The Collection of Uranium from Sea Water with Hydrous Metal Oxide. II. The Mechanism of Uranium Adsorption on Hydrous Titanium(IV) Oxide

Hisao YAMASHITA,* Yoshihiro OZAWA,** Fumito NAKAJIMA, and Toshifumi MURATA**

Hitachi Research Laboratory, Hitachi Ltd., Kujimachi, Hitachi 319-12

***Energy Research Laboratory, Hitachi Ltd., Moriyama-cho, Hitachi 316*

(Received January 6, 1979)

The mechanism of uranium adsorption from sea water by hydrous titanium(IV) oxide was investigated. The uranium adsorption experiments were conducted using a solution containing NaCl, $NaHCO_3$, and uranium. Thermochemical calculation showed that the tris(carbonato)dioxouranate(VI) ion $[UO_2(CO_3)_3]^{4-}$ found in sea water existed in the solution at pH 8 and 25 °C. The uranium uptake varied with the pH of the solution, exhibiting a minimum value at pH 8. The enthalpy change, ΔH, and the activation energy, E, of the uranium adsorption were found to be 23.6 kJ mol^{-1} and 52.7 kJ mol^{-1} respectively. The analysis of carbonate in the adsorbent showed that the carbonate ion in $[UO_2(CO_3)_3]^{4-}$ was released into the solution during the uranium adsorption. On the basis of the present experimental results, the mechanism of uranium adsorption was discussed.

Many studies have been made on extracting uranium from sea water by adsorption on hydrous titanium(IV) oxide.[1-3] Previous investigations of the uranium adsorption have, however, dealt almost exclusively with the adsorption capacity. Only a few investigations have been carried out on the mechanism of uranium adsorption. Keen[4] reported that uranium was adsorbed by hydrous titanium(IV) oxide as the UO_2^{2+} cation. Ogata *et al.*[5] proposed that the uranium was adsorbed by a coordinate bond on hydrous titanium(IV) oxide.

In the present work, the enthalpy change, rate constant, and activation energy of the uranium adsorption by hydrous titanium(IV) oxide were determined, and the adsorption mechanism was discussed.

Experimental

Preparation of Hydrous Titanium(IV) Oxide. The hydrous titanium(IV) oxide was prepared in the following manner. Into 200 ml of a 0.6 mol dm^{-3} $TiCl_4$ solution under stirring and heating at 90 °C, a 7% NH_3 solution was added at a rate of 3.5 ml/min until the pH of the solution reached 5. After it had then aged for 1 h, the precipitate was filtered, washed several times with water, and dried for about a week at room temperature. The dried samples were crushed and sieved, a portion of 400—600 mesh being used in following experiments. The water content of the dried sample was determined by measuring the ignition loss at 800 °C and found to be 18%, which corresponds to that of $TiO(OH)_2$.

Adsorption Experiment. In the uranium adsorption experiments, 0.04 g of hydrous titanium(IV) oxide was introduced into 1000 ml of a solution containing 0.72 mol dm^{-3} NaCl, 0—5×10^{-3} mol dm^{-3} $NaHCO_3$, and 10—500 ppb of uranium. The concentration of NaCl was taken to be 0.72 mol dm^{-3} in order for it to have the same ionic strength as that of sea water. The concentration of $NaHCO_3$ was nearly equal to that of sea water. The solution was stirred vigorously by means of a vertical stirrer. After adsorption equilibrium has been attained, the solution was filtered and the uranium concentration was measured. The uranium uptake by the adsorbent was determined from the change in the uranium concentration in the solution. The pH of the solution was changed from 4 to 12 with an HCl or NaOH solution. The determination of carbonate uptake was carried out by the following procedure. One fifth of a gram of hydrous titanium(IV) oxide was equilibrated with 5000 ml of a 0.72 mol dm^{-3} NaCl+5×10^{-3} mol dm^{-3} $NaHCO_3$ solution containing 40—500 ppb of uranium at pH 8 and 25 °C. After 5 h adsorption, the hydrous titanium(IV) oxide was separated from the solution, and the carbonate adsorbed in the adsorbent was determined.

Analytical Method. The uranium in the sloution was determined spectrophotometrically with Arsenazo III as the indicator.[6] The determination of carbonate in the adsorbent was carried out by the following procedure. The carbonate was decomposed with an HCl solution, and the carbon dioxide thus produced was measured by coulomatic titration with a Kokusai Denki VK-l-type "Coulomatic C."

Results and Discussion

Adsorption Equilibrium. The uranium uptake as a function of the adsorption time with hydrous titanium(IV) oxide of different particle sizes is shown in Fig. 1. The smaller granules showed a faster rate of the uranium uptake than the larger granules. It was found that an adsorption equilibrium was attained within 3 h using the adsorbent smaller than 300 mesh. A portion of 400—600 mesh adsorbent was used, and the adsorption time of 5 h was chosen for the following

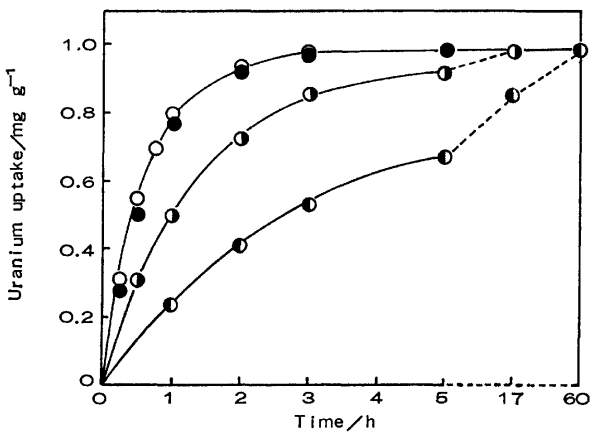

Fig. 1. Uranium uptake as a function of adsorption time.
Adsorption temperature: 25 °C, pH of the solution: 8.0, NaCl: 0.72 mol dm^{-3}, $NaHCO_3$: 2.3×10^{-3} mol dm^{-3}, uranium: 60 ppb. Mesh size of adsorbent, ○: 400—600 ●: 300—400 ◑: 100—200 ◐: 50—100.

TABLE 1. STABILITY CONSTANTS (K) OF URANYL(VI) COMPLEXES[5]

Reaction	log K	Reaction	log K
$UO_2^{2+}+H_2O=[UO_2OH]^+ + H^+$	−5.0	$2UO_2^{2+}+H_2O=[(UO_2)_2(OH)]^{3+}+H^+$	−4.2
$UO_2^{2+}+2H_2O=UO_2(OH)_2+2H^+$	−11.2	$4UO_2^{2+}+7H_2O=[(UO_2)_4(OH)_7]^+ +7H^+$	−24.9
$UO_2^{2+}+3H_2O=[UO_2(OH)_3]^- +3H^+$	−17.1	$UO_2^{2+}+Cl^-=[UO_2Cl]^+$	−0.1
$2UO_2^{2+}+2H_2O=[(UO_2)_2(OH)_2]^{2+}+2H^+$	−5.96	$UO_2^{2+}+2Cl^-=UO_2Cl_2$	−0.91
$3UO_2^{2+}+4H_2O=[(UO_2)_3(OH)_4]^{2+}+4H^+$	−12.8	$UO_2^{2+}+3Cl^-=[UO_2Cl_3]^-$	−2.6
$4UO_2^{2+}+2H_2O=[(UO_2)_4(OH)_2]^{6+}+2H^+$	−1.26	$UO_2^{2+}+CO_3^{2-}=UO_2CO_3$	9.11
$4UO_2^{2+}+6H_2O=[(UO_2)_4(OH)_6]^{2+}+6H^+$	−20.0	$UO_2^{2+}+2CO_3^{2-}=[UO_2(CO_3)_2]^{2-}$	15.57
$3UO_2^{2+}+5H_2O=[(UO_2)_3(OH)_5]^+ +5H^+$	−16.21	$UO_2^{2+}+3CO_3^{2-}=[UO_2(CO_3)_3]^{4-}$	22.8
$5UO_2^{2+}+8H_2O=[(UO_2)_5(OH)_8]^{2+}+8H^+$	−32.14		

experiments.

Effect of pH. The effect of the pH on the uranium uptake by the hydrous titanium(IV) oxide is shown in Fig. 2. The uranium uptake is significantly influenced by the pH of the solution, showing a minimum at pH 8. The same adsorption curve as that in Fig. 2 was obtained in the adsorption experiment with sea water in the present work.

The variation in the uranium uptake with the pH is supposed to result from the fact that the species of uranyl(VI) ions changes with the pH. Under the present experimental conditions, the uranyl(VI) ion may exist in the form of *hydroxo-*, *chloro-*, and *carbonato-*complexes, the stability constants (K) of which are summarized in Table 1.[5] The distributions of the uranyl(VI) species in the NaCl–$NaHCO_3$ solution at various pH values, as calculated from the stability constants, are shown in Table 2. Tris(carbonato)-dioxouranate(VI) ion which is present in sea water is a predominant species at pH 8—10, while the uranyl and chloro complex ion in an acidic solution and the hydroxo complex ion in an alkaline solution are stable. The uranium uptake reaches its minimum at pH 8, where predominant uranyl(VI) species in the solution is $[UO_2(CO_3)_3]^{4-}$.

Effect of Carbonate Ions. In order to investigate the effect of carbonate ions in the solution, the uranium uptake was measured with a solution containing 0.72 mol dm^{-3} NaCl, 60 ppb uranium, and 0—5×10^{-3} mol dm^{-3} $NaHCO_3$ at pH 8. The results are shown in Fig. 3. The distribution of uranyl(VI) species in the NaCl–$NaHCO_3$ solution used in the experiments is summarized in Table 3. It may be found from Fig. 3 and Table 3 that the uranium uptake decreases with an increase in $[UO_2(CO_3)_3]^{4-}$. That is, the uranium uptake is larger from the tris(hydroxo)dioxouranate(VI) $[UO_2(OH)_3]^-$ solution than from the $[UO_2(CO_3)_3]^{4-}$ solution. It is considered that the

TABLE 2. DISTRIBUTION OF URANYL(VI) COMPLEXES WITH VARIOUS pH VALUES

(%)

Species	pH				
	4	6	8	10	12
UO_2^{2+}	57.6	3.9	0	0	0
$[UO_2(OH)]^+$	5.8	38.6	0	0	0
$UO_2(OH)_2$	0	24.3	0.1	0	0
$[UO_2(OH)_3]^-$	0	30.7	14.1	39.8	100
$[UO_2Cl]^+$	32.9	2.2	0	0	0
UO_2Cl_2	3.6	0.3	0	0	0
$[UO_2Cl_3]^-$	0.1	0	0	0	0
UO_2CO_3	0	0	0	0	0
$[UO_2(CO_3)_2]^{2-}$	0	0	0.9	0	0
$[UO_2(CO_3)_3]^{4-}$	0	0	84.9	60.2	0

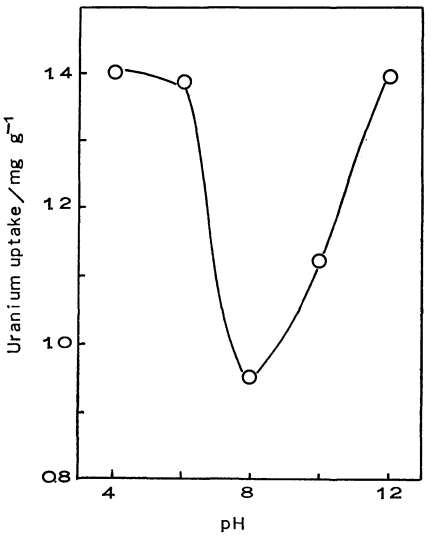

Fig. 2. Effect of pH on uranium uptake.
Adsorption temperature: 25 °C, NaCl: 0.72 mol dm^{-3}, $NaHCO_3$: 2.3×10^{-3} mol dm^{-3}, uranium: 60 ppb.

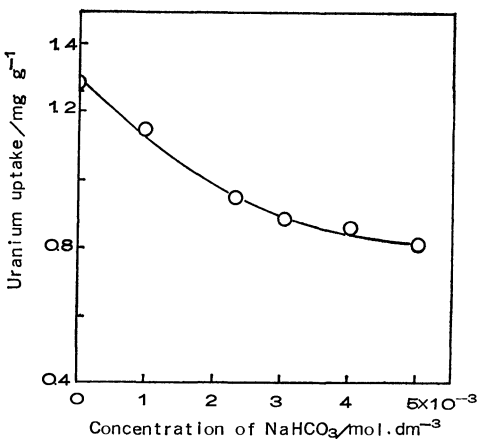

Fig. 3. Effect of carbonate ions on uranium uptake.
Adsorption temperature: 25 °C, pH of the solution: 8.0, NaCl: 0.72 mol dm^{-3}, uranium: 60 ppb.

Table 3. Distribution of uranyl(VI) complexes with various concentrations of $NaHCO_3$ (%)

Species	$[NaHCO_3]$/mol dm^{-3}			
	0	10^{-3}	2.3×10^{-3}	5×10^{-3}
$[UO_2(OH)_3]^-$	100	66.7	14.1	0
$[UO_2(CO_3)_3]^{4-}$	0	31	84.9	98.5

uranium uptake is reduced by the presence of $NaHCO_3$ because carbonate ions behave as a masking agent to uranium adsorption. The uranium uptake from a 5×10^{-3} mol dm^{-3} $NaHCO_3$ solution in which uranyl(VI) species is present in the form of $[UO_2(CO_3)_3]^{4-}$ (98.5%) is found to be 0.82 mg g^{-1} as is shown in Fig. 3. The results indicate that uranium adsorption takes place from the $[UO_2(CO_3)_3]^{4-}$ solution by means of hydrous titanium(IV) oxide.

Effect of Temperature. The effect of the temperature on the uranium uptake of hydrous titanium(IV) oxide is shown in Fig. 4. It is shown that the uranium uptake increases with the adsorption temperature. In order to obtain the enthalpy change of the adsorption, ΔH, the distribution coefficient, K_d, was calculated from the data. The distribution coefficient is defined as C_s/C_l, where C_s is the uranium adsorbed in the adsorbent per gram, and C_l the uranium in the solution per ml at equilibrium. The enthalpy change of the adsorption can be expressed as follows:[7]

$$\frac{d\ln K_d}{dT}=\frac{\Delta H}{RT^2}. \quad (1)$$

By integrating Eq. 1, we obtain

$$\log K_d = -\frac{\Delta H}{2.3R}\cdot\frac{1}{T}+\text{const}, \quad (2)$$

where T is the adsorption temperature, and R, the gas constant. As is shown in Fig. 4, the distribution coefficient increases markedly with the adsorption temperature. A plot of log K_d *versus* $1/T$ is shown in Fig.

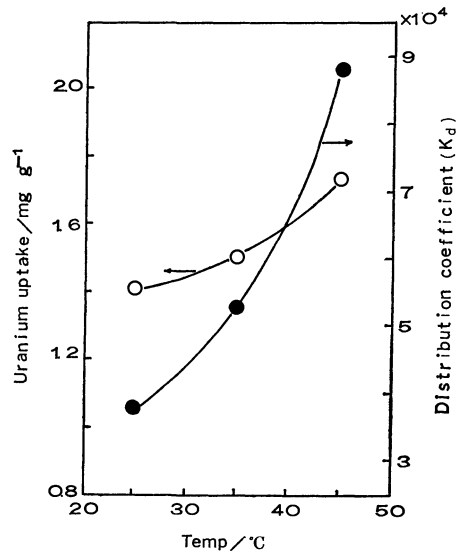

Fig. 4. Effect of temperature on uranium uptake.
pH of the solution: 8.0, NaCl: 0.72 mol dm^{-3}, $NaHCO_3$: 2.3×10^{-3} mol dm^{-3}, uranium: 90 ppb.

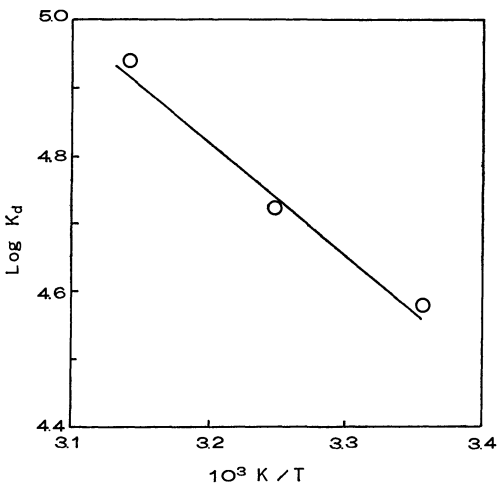

Fig. 5. Plot of log K_d *vs.* $1/T$.

5. The enthalpy change in the adsorption, ΔH, was found to be 23.6 kJ mol^{-1}. This value suggests that the uranium adsorption is neither physical adsorption nor an ion-exchange reaction. The physical adsorption is ordinarily exothermic, and the enthalpy change of the ion-exchange reaction is said to be -8.4—-12.6 kJ mol^{-1}.[7]

It may, therefore, be considered that the uranium adsorption proceeds *via* a certain complex chemical reaction.

Kinetics of Adsorption. The rate constant, k, and the activation energy, E, of the uranium adsorption were also determined. The variation in the uranium uptake with time is shown in Fig. 6. The rate of the uranium adsorption is larger at higher temperatures. The following equation is assumed:

$$\frac{dv}{dt}=k(v_e-v), \quad (3)$$

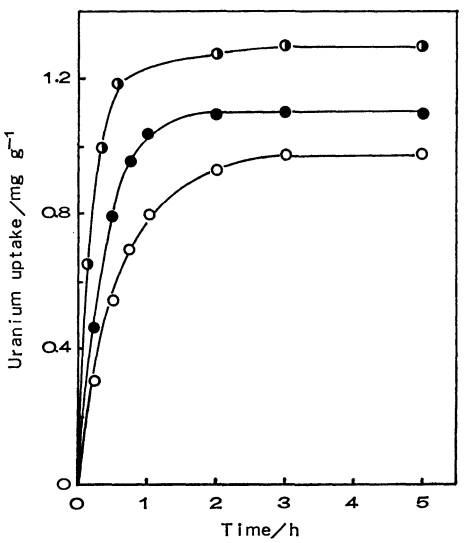

Fig. 6. Variation of uranium uptake with adsorption time.
pH of the solution: 8.0, NaCl: 0.72 mol dm^{-3}, $NaHCO_3$: 2.3×10^{-3} mol dm^{-3}, uranium: 60 ppb. Adsorption temperature, ○: 25 °C ●: 35 °C ◑: 45 °C.

where v_e is the adsorption capacity at equilibrium, and v, the adsorption capacity at time t. By integrating Eq. 3, Eq. 4 is obtained:

$$\ln\frac{1}{1-\theta} = kt, \quad (4)$$

where θ is the extent of adsorption (v/v_e). A plot of $\log 1/(1-\theta)$ *versus* t will give a straight line if the adsorption rate is represented by Eq. 3. As is shown in Fig. 7, the relation between $\log 1/(1-\theta)$ and t is nearly linear. The rate constants calculated from the slope were 0.0113 min^{-1} at 25 °C, 0.0217 min^{-1} at 35 °C, and 0.038 min^{-1} at 45 °C.

The activation energy, E, was determined by using the Arrhenius equation. A plot of $\log k$ *versus* $1/T$ is shown in Fig. 8, which gives an activation energy of 52.7 kJ mol^{-1}.

Mechanism of Adsorption. The adsorption mechanism of $[UO_2(CO_3)_3]^{4-}$ found in sea water will now

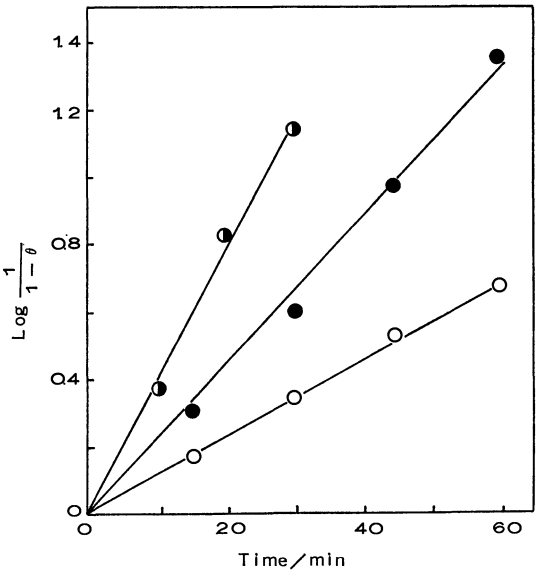

Fig. 7. Plot of $\log 1/(1-\theta)$ *vs.* t.
Adsorption temperature, ○: 25 °C, ●: 35 °C, ◑: 45 °C.

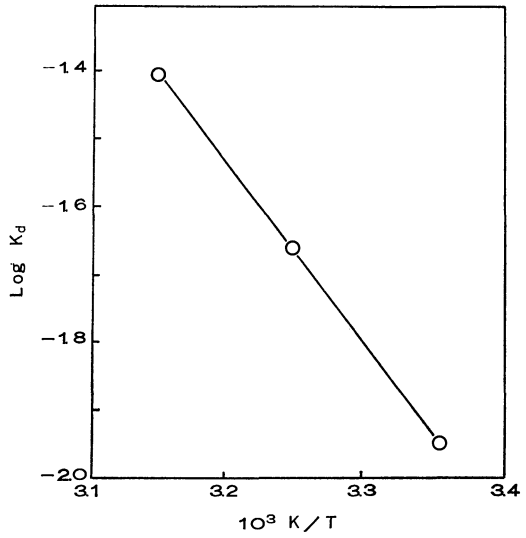

Fig. 8. Plot of $\log k$ *vs.* $1/T$.

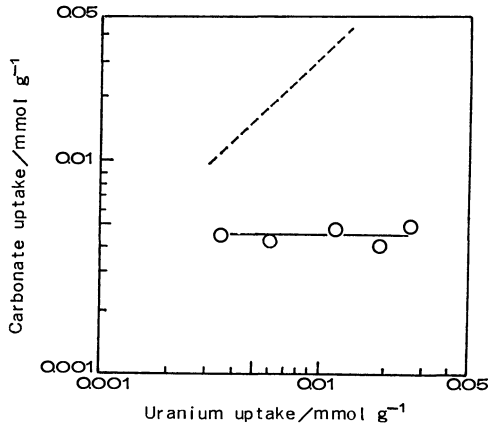

Fig. 9. Relation between uranium and carbonate uptake.
Adsorption temperature: 25 °C, pH of the solution: 8.0, NaCl: 0.72 mol dm^{-3}, $NaHCO_3$: 5×10^{-3} mol dm^{-3}.
Solid line: Experimental value.
Broken line: Calculated value of carbonate adsorbed as $[UO_2(CO_3)_3]^{4-}$.

be discussed. Uranium adsorption takes place from the solution containing 0.72 mol dm^{-3} NaCl and 5×10^{-3} mol dm^{-3} $NaHCO_3$ by means of the hydrous titanium(IV) oxide mentioned before. In order to investigate the form of uranium adsorbed from the $[UO_2(CO_3)_3]^{4-}$ solution on the adsorbent, the uranium and carbonate uptake from the solution containing 0.72 mol dm^{-3} NaCl, 5×10^{-3} mol dm^{-3} $NaHCO_3$, and 40—500 ppb uranium are measured. The results are shown in Fig. 9. If the uranium form adsorbed on the adsorbent is $[UO_2(CO_3)_3]^{4-}$, the carbonate uptake should increase with the uranium uptake, as is shown by the broken line in Fig. 9. However, the carbonate uptake remains constant regardless of the uranium uptake. It is considered from the results that carbonate in $[UO_2(CO_3)_3]^{4-}$ is released into the solution, so that carbonate is not taken up by the adsorbent when uranium adsorption takes place from the tris(carbonato)dioxouranate(VI) solution.

In an alkaline solution, the surface hydroxo group [–Ti–OH] of hydrous titanium(IV) oxide dissociates into –Ti–O^-, which tends to undergo a cation exchange.[8] The amount of –Ti–OH in hydrous titanium(IV) oxide, as determined by the adsorption of fluoride ions, and that of –Ti–O^-, as determined by the ion-exchange reaction of potassium ions at pH 8, were found to be 1.7 mmol g^{-1} and 0.4 mmol g^{-1} respectively.[9] Although –Ti–OH and –Ti–O^- are present in the NaCl–$NaHCO_3$ solution at pH 8, it is unlikely that $[UO_2(CO_3)_3]^{4-}$ reacts with –Ti–O^- because they have the same electric charge. Therefore, the adsorption site of hydrous titanium(IV) oxide for the uranium is supposed to be –Ti–OH. Based on the present experimental results, the adsorption mechanism of $[UO_2(CO_3)_3]^{4-}$ is represented by

$$TiO(OH)_2 + [UO_2(CO_3)_3]^{4-} = TiO_3\cdot UO_2 + 2HCO_3^- + CO_3^{2-}. \quad (5)$$

The decrease in the concentration of $NaHCO_3$ in

the solution raises the uranium uptake, as is shown in Fig. 3. This may be attributable to the increase in $[UO_2(OH)_3]^-$, which shows a higher adsorbability than $[UO_2(CO_3)_3]^{4-}$. The adsorption mechanism of $[UO_2(OH)_3]^-$ is deduced to be as follows:

$$TiO(OH)_2 + [UO_2(OH)_3]^- = TiO_3 \cdot UO_2 + 2H_2O + OH^- . \quad (6)$$

It is considered that the competitive adsorption presented by the reaction of (5) and (6) takes place when $[UO_2(CO_3)_3]^{4-}$ and $[UO_2(OH)_3]^-$ coexist in the solution. However, with respect to the adsorption mechanism of $[UO_2(OH)_3]^-$, hydrolysis adsorption has been suggested by Katoh *et al.*[10] Therefore, further experiments will be made in the future with regard to the adsorption of $[UO_2(OH)_3]^-$.

In the present work, the mechanism of uranium adsorption from sea water, *i.e.*, a $[UO_2(CO_3)_3]^{4-}$ solution, was investigated. It is important to determine the adsorption mechanisms of all the uranyl(VI) species. However, the data for verifying the assumption of the adsorption mechanism cannot be obtained because various uranyl(VI) species coexist in the solutions of pH 4—8 under the present experimental conditions. Further study is required on this point.

The authors wish to thank Professor Shosuke Imoto of Osaka University for his many helpful discussions and suggestions.

References

1) R. V. Davies, J. Kennedy, R. W. McIlroy, R. Spence, and K. M. Hill, *Nature*, **203**, 1110 (1964).
2) N. Ogata and H. Kakihana, *J. At. Energy Soc. Jpn.*, **11**, 82 (1969).
3) M. Kanno, Y. Ozawa, and T. Mukaibo, *J. At. Energy Soc. Jpn.*, **12**, 708 (1970).
4) N. J. Keen, *J. Brit. Nucl. Energy Soc.*, **7**, 178 (1968).
5) N. Ogata, N. Inoue, and H. Kakihana, *J. At. Energy Soc. Jpn.*, **13**, 560 (1971).
6) Y. Miyake, Y. Sugimura, and T. Uchida, *Recod. Oceanog. Works. Jpn.*, **11**, 53 (1972).
7) F. Helfferich, "Ion Exchange," McGraw-Hill (1962), p. 166.
8) D. Britz and G. H. Nancollas, *J. Inorg. Nucl. Chem.*, **31**, 3861 (1961).
9) H. Yamashita, Y. Ozawa, F. Nakajima, and T. Murata, *Nippon Kagaku Kaishi*, **1978**, 1057.
10) S. Katoh, K. Sugasaka, A. Fujii, N. Takagi, and Y. Miyai, *Nippon Kaisui Gakkai Shi.*, **30**, 118 (1976).

Catalytic Property of Calcined Iron Sulfate Treated with Hydrogen Chloride in Alkylation of Toluene and Benzene with Alkyl Chlorides[1)]

Kazushi ARATA,* Makoto HINO,† and Katsumasa YABE††
Hokkaido University of Education, Hachiman-cho, Hakodate 040
† *Hakodate Technical College, Tokura-cho, Hakodate 042*
†† *Government Industrial Development Laboratory, Hokkaido, Sapporo 061-01*
(Received January 6, 1979)

Alkylation was carried out at room temperature over catalysts prepared by calcination of $FeSO_4$, Fe_2O_3, and $Fe(OH)_3$ in the air at various temperatures and subsequent exposure to HCl at room temperature for 20 min. The $FeSO_4$–HCl catalysts heat-treated at 700 and 750 °C showed very high activity and selectivity, the other catalysts except for the sulfate treated at 800 °C being almost inactive. The $FeSO_4$(700 °C)–HCl catalyst was found to consist of $FeCl_3$ and α-Fe_2O_3 by means of Mössbauer effect, the absorption peak areas being 14 and 86% for portions of iron based on the chloride and oxide, respectively. The results of DTA and TGA experiments suggest that the coordinate bond of water molecule on $FeCl_3$ of the $FeSO_4$(700 °C)–HCl catalyst is stronger than that on $FeCl_3$ of the $FeSO_4$ (600, 800, and 900 °C)–HCl and commercial $FeCl_3$. The $FeSO_4$(700 °C)–HCl catalyst showed a much higher activity than pure $FeCl_3$. The iron(III) chloride formed by reaction of HCl and α-Fe_2O_3 obtained by thermal decomposition of the sulfate at 700 or 750 °C was found to be a very strong Lewis acid catalyst.

t-Butylation and isopropylation of toluene and benzene with *t*-butyl and isopropyl chlorides are generally catalyzed by Lewis acids such as anhydrous aluminum chloride[2)] and boron trifluoride.[3)] This type of catalyst has been mostly used for the Friedel-Crafts reaction.[4)]

No data are available on the alkylation catalyzed by solid acids such as SiO_2–Al_2O_3 and metal sulfates at room temperature. We examined the reactions over heat-treated $FeSO_4$, which showed high catalytic activity and selectivity for benzylation and benzoylation of toluene with the corresponding chlorides in comparison with those of other solid acid catalysts, $NiSO_4$, SiO_2–Al_2O_3, *etc.*,[5)] although the catalyst was inactive for alkylation at room temperature. However, treatment with HCl remarkably promoted catalytic activity. The $FeSO_4$ catalyst prepared by calcination in the air at a certain temperature followed by treatment with HCl was found to show exceedingly high activity, its activity being higher than that of anhydrous $FeCl_3$.

Experimental

Materials and Catalysts. Toluene and benzene (guaranteed reagents) were purified by distillation over sodium metal. *t*-Butyl and isopropyl chlorides (guaranteed reagents, Tokyo Kasei Kogyo Co.) were used without further purification. Catalysts were prepared as follows: $FeSO_4 \cdot 7H_2O$ (guaranteed reagent, Kanto Chemicals Co.), Fe_2O_3 (Wako Pure Chemical Co.) and $Fe(OH)_3$ (Kokusan Chemical Works, Ltd.) were heated at 150 °C in the air for 1 h, and powdered below 100 mesh size. They were then calcined in Pyrex or quartz glass tubing at various temperatures in the air for 3 h and kept in sealed glass tubings. Catalysts thus prepared were exposed to a stream of mixed gas of N_2 (20 ml/min) and HCl (26 ml/min) for 20 min and finally to N_2 gas for 30 min. Hydrogen chloride gas was obtained by dropping concd hydrochloric acid into concd sulfuric acid, followed by passing the gas through concd sulfuric acid twice and cooling to −72 °C three times for drying. The catalyst thus prepared was sealed in an ampoule.

Procedure for Reaction. The reaction was carried out by stirring a mixture of weighed catalyst and 50 ml of 0.5 M toluene solution of *t*-butyl or isopropyl chlorides at room temperature. At appropriate time intervals, a small amount of the sample was taken out with a 1 ml syringe, separated from the catalyst, and analyzed by gas-liquid chromatography with a TCD detector using a 5 m column of tricresyl phosphate on Celite 545 (110 °C; He, 3.0 kg/cm^2). The yields of products were estimated on the basis of unreacted chloride and calculated by measurement of GLC peak areas (corrected). The competitive *t*-butylation of benzene and toluene was carried out with 0.5 M *t*-butyl chloride in equimolar amounts of benzene and toluene.

Physical Measurements. Differential thermal analysis (DTA) and thermal gravimetrical analysis (TGA) diagram were recorded at a heating rate of 10 °C/min from room temperature to 720 °C with a Rigaku CN8002. Infrared spectra were obtained with a Hitachi EPI-G2 spectrophotometer using Nujol and KBr tablets. Mössbauer spectra were recorded on an Elron Mössbauer effect radiation analyzer, using a ^{57}Co–Cu source at room temperature. The spectrum of the 90% ^{57}Fe-enriched iron foil was used for calibration of velocity scale.

Results and Discussion

No report seems to be available concerning the Friedel-Crafts *t*-butylation and isopropylation of aromatics with *t*-butyl and isopropyl halides as the alkylation reagents catalyzed by solid acids such as Al_2O_3 and SiO_2–Al_2O_3. No alkylation of toluene with *t*-butyl and isopropyl chlorides took place at room temperature over calcined $FeSO_4$, a solid acid. However, remarkable increase in the catalytic activity of $FeSO_4$ was caused by treatment with HCl, in which $FeSO_4$ was exposed to HCl gas at room temperature for 20 min after calcination. The catalytic activity and product distribution for the reactions at room temperature over catalysts prepared by calcination of $FeSO_4$ in the air at various temperatures, followed by treatment with HCl are given in Tables 1 and 2. The catalytic activity changed markedly with the calcination temperature of $FeSO_4$. The sulfates heat-treated at 700 and 750 °C showed strikingly high activity, $FeSO_4$ (800 °C)–HCl** being also highly active for *t*-butyla-

** This indicates a HCl-treated catalyst of $FeSO_4$ calcined at the temperature in parentheses.

Table 1. *t*-Butylation of toluene over iron salts treated with hydrogen chloride at room temperature (catalyst : 0.1 g)

Catalyst	Temp of calcn./°C	Reaction time/h	Conversion/%	Yield of *t*-butyltoluene/%		
				ortho-	*meta-*	*para-*
$FeSO_4$–HCl	500	3	7.0			
	600	3	8.5			
	650	3	14.6			
	700	3 min	29.7			
	700	10 min	86.2	—	5.2	94.8
	750	3 min	38.5			
	750	10 min	100.0	—	5.8	94.1
	800	20 min	14.6	—	4.1	95.9
	900	3	5.2			
$FeSO_4$[a)]	700	24	0			
Fe_2O_3–HCl	500	3	0.5			
	700	3	9.4			
	900	3	0.5			
$Fe(OH)_3$–HCl	700	3	5.3			

a) No treatment with HCl.

Table 2. Isopropylation of toluene over iron salts treated with hydrogen chloride at room temperature (catalyst : 0.5 g)

Catalyst	Temp of calcn./°C	Reaction time/h	Conversion/%	Yield of *i*-propyltoluene/%		
				ortho-	*meta-*	*para-*
$FeSO_4$–HCl	500	3	trace			
	700	10 min	6.3			
	700	30 min	73.1	45.7	21.7	32.6
	750	10 min	8.0			
	750	30 min	98.6	43.5	22.7	33.8
	800	3	1.7			
$FeSO_4$[a)]	700	24	0			
Fe_2O_3–HCl	500	3	trace			
	700	3	trace			
	900	3	trace			

a) No treatment with HCl.

tion. Figure 1 shows the time course of both reactions over these catalysts. In the case of *t*-butylation over $FeSO_4$ (700 °C and 750 °C)–HCl, the progress of reaction was linear with time up to over 50% completion,

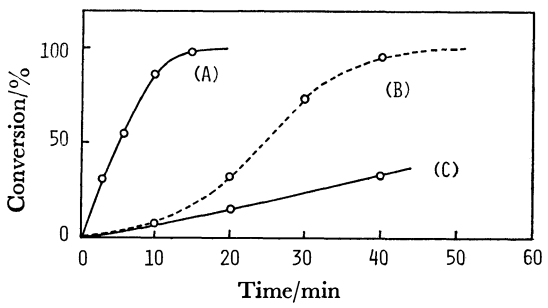

Fig. 1. *t*-Butylation and isopropylation of toluene over $FeSO_4$ treated with HCl at room temperature. *t*-Butylation (——), isopropylation (---). Heat-treatment of $FeSO_4$: 700 °C for (A) and (B); 800 °C for (C). Catalyst amount: 0.1 g for (A) and (C); 0.5 g for (B).

the reaction afterwards following first-order kinetics with respect to the *t*-butyl chloride concentration. Some of the reactions showed S-shaped curves, probably owing to the promotion effect of HCl formed by the reaction.

The reaction mixture after the 100% completion of the reaction was quite clear, no products other than listed in the Tables being detected. The isomer distributions of *t*-butyltoluenes and isopropyltoluenes did not change at 0 °C reaction temperature and were also the same as those observed for the general Friedel-Crafts Lewis catalysts such as $AlCl_3$[2)] and BF_3.[3)]

The activity of $FeSO_4$–HCl is low at 650 °C calcination as compared with the remarkable activity at 700 °C treatment. $FeSO_4$ decomposes completely to form α-Fe_2O_3 at temperatures in the range 675—700 °C, crystallization proceeding rapidly afterwards.[6)] Commercially available Fe_2O_3 and $Fe(OH)_3$ were calcined around 700 °C and treated with HCl, but the catalysts were almost inactive for both reactions (Tables 1 and 2).

The present catalysts were examined in the *t*-butyla-

tion and isopropylation of benzene with *t*-butyl and isopropyl chlorides at room temperature under the same reaction conditions, the following results being obtained: $FeSO_4$ (700 °C)–HCl and $FeSO_4$(800 °C)–HCl gave 94.3% *t*-butylbenzene in 10 min and 84.6% in 30 min, respectively, 85.5% isopropylbenzene being produced by $FeSO_4$(700 °C)–HCl in 5 min.[7] The sulfates–HCl heat-treated at 500, 600, and 900 °C showed conversion below 4% for *t*-butylation and isopropylation.

When a large amount of $FeSO_4$(700 °C)–HCl was used for *t*-butylation of toluene, isomerization of *t*-butyltoluene took place; *i.e.* isomerization from the *para*- to the *meta*-position up to the equilibrium composition of 64% *m*- and 36% *p*-*t*-butyltoluene.[2] The reaction with 1.0 g catalyst at room temperature gave 23.9% *m*- and 76.1% *p*-isomer at 5 min, 40.4 and 59.6 at 15 min, and 61.5 and 38.5 at 60 min, respectively. No isomerization was observed even over a period of 3 h when the catalyst amount was 0.1 g.

The competitive *t*-butylation of benzene and toluene at room temperature was carried out with 0.5 g of the above catalyst in equimolar amount. The secondary reactions such as transalkylation between *t*-butyltoluene and benzene and the isomerization of *t*-butyltoluene took place. The apparent k_T/k_B value (the relative rate of toluene to benzene, estimated from yields of *t*-butyltoluene and *t*-butylbenzene) decreased with time as was observed by Shimada.[8] The k_T/k_B value obtained was 14.7 at 1 min, 8.7 at 3 min, 4.8 at 10 min, and 1.5 at 60 min. The isomer distribution of *t*-butyltoluene was 6.6% *m*- and 93.4% *p*-form at 1 min and 52.7% *m*- and 47.3% *p*-form at 60 min.

On exposure to HCl at room temperature, the sulfates calcined at 700 and 750 °C evolved heat violently in 10 min, but $FeSO_4$ treated at 800 °C only slightly. The heat evolution seems to be related with the catalytic activity, since other materials except for the sulfates treated at 700, 750, and 800 °C evolved no heat. Even the $FeSO_4$(700 °C)–HCl was inactive when HCl treatment was stopped before heat generation. Figure 2 shows the catalytic activity of $FeSO_4$ (700 °C) with various periods of the HCl treatment for the isopropylation of benzene. The activity increases with duration of the treatment after the beginning of heat generation. The catalyst before the generation of heat was extremely low in activity even for the *t*-butylation of toluene, an easier reaction than isopropylation, though its activity was still high in comparison with that without any HCl treatment (Tables 1 and 2).

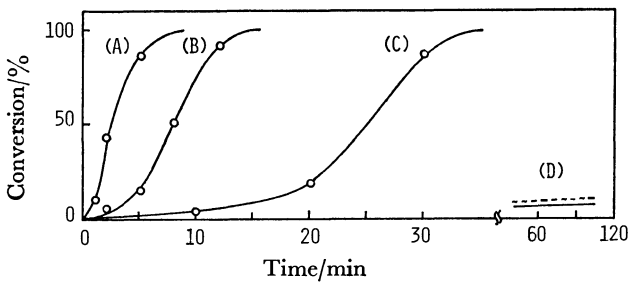

Fig. 2. Catalytic activity of $FeSO_4$ (700 °C) with different periods of the HCl treatment for the isopropylation of benzene at room temperature (catalyst: 1.1 g). The HCl treatment was ceased 10 min (A), 1 min (B), at once (C) after beginning of the heat generation and before (D) the generation. (---): *t*-butylation of toluene (catalyst: 0.1 g).

Heat generation by HCl treatment is considered to be due to the formation of $FeCl_3$ on the surface. In order to confirm the existence of $FeCl_3$, Mössbauer experiment on $FeSO_4$(700 °C)–HCl was carried out. The spectrum obtained is shown in Fig. 3. The spectrum consists of a single peak around zero velocity and other six peaks showing magnetic hyperfine splitting. The single peak is attributed to $FeCl_3$, the isomer shift 0.45±0.05 mm/s being close to 0.37 mm/s for commercial $FeCl_3$ and 0.36 mm/s for the value obtained by DeBenedetti *et al.*[9] The other six lines are attributed to α-Fe_2O_3,[5] indicating that $FeSO_4$ is decomposed to form Fe_2O_3 at 700 °C calcination. From absorption peak areas, the portions of iron based on $FeCl_3$ and α-Fe_2O_3 were found to be 14 and 86%, respectively.

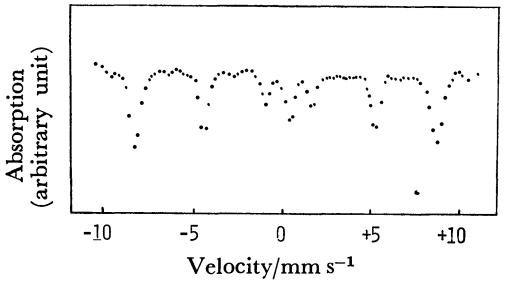

Fig. 3. Mössbauer spectrum of $FeSO_4$ (700 °C)–HCl. Isomer shift referred to metallic iron.

IR spectrum of $FeSO_4$(700 °C)–HCl showed an absorption band at 1600 cm^{-1}, which is assigned to a water molecule coordinated to $FeCl_3$.[10] The intensity of the band decreased when the substance was dried in the air at 150 °C for 2 h. The catalytic activity of the dried catalyst was higher than that of $FeSO_4$ (700 °C)–HCl, not subjected to drying, *viz.*, conversion for *t*-butylation of toluene at room temperature was 34.2% at 3 min, and 100% at 10 min (*cf.* Table 1).[11]

DTA and TGA of the catalysts were measured as shown in Fig. 4. The endothermic peaks appearing at 130—160 °C in all the samples are ascribed to the desorption of water molecule bonded coordinately to $FeCl_3$ formed by HCl treatment. A similar peak was observed around 140 °C in the case of pure anhydrous $FeCl_3$, a corresponding sharp decrease in weight being observed. Endothermic desorption of the water molecules is observed at much higher temperature, 160 °C for $FeSO_4$(700 °C)–HCl, and at a slightly higher one, 144 °C, for $FeSO_4$(800 °C)–HCl than that for other materials treated at 600 and 900 °C. The difference in temperature is connected with their catalytic activities (Table 1). The activity of the $FeSO_4$(700 °C)–HCl catalyst was much higher than that of anhydrous $FeCl_3$ (guaranteed reagent, Wako Pure Chemical Co.) for isopropylation, the activity

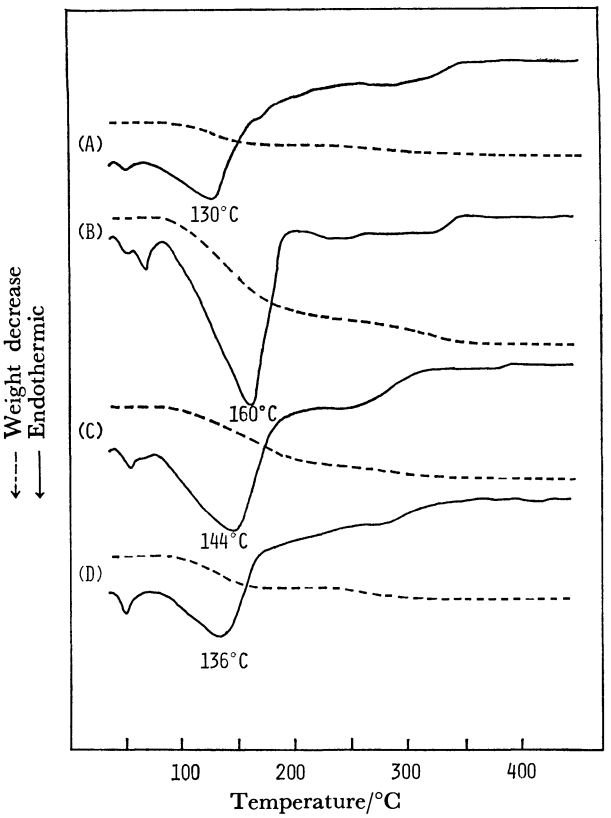

Fig. 4. DTA (——) and TGA (---) curves of $FeSO_4$ heat-treated at various temperatures, followed by treating with HCl. (A): 600 °C (21.7 mg), (B): 700 °C (25.3 mg), (C): 800 °C (30.0 mg), (D): 900 °C (30.0 mg).

ratio being greater than 10. The former also showed marked activity for the reaction of toluene with methanesulfonyl chloride at 100 °C, but not $FeCl_3$. It seems that the high temperature of desorption of water is based on the strong coordinate bond between water and the surface $FeCl_3$. Thus, the iron(III) chloride formed by reaction of HCl and α-Fe_2O_3, prepared by the thermal decomposition of the sulfate at 700 or 750 °C, could be a quite strong Lewis acid catalyst.

Gradual decrease in weight was observed in the temperature range 200—350 °C. This seems to be due to the sublimation of $FeCl_3$. The weight decrease was estimated as 1.6, 7.8, 3.5, and 2.0% for the 600, 700, 800, and 900 °C catalysts, respectively (adsorbed water observed up to 200 °C in TGA was not included in calculation).

References

1) For a preliminary communication see M. Hino and K. Arata, *Chem. Lett.*, **1977**, 277.
2) G. A. Olah, S. H. Flood, and M. E. Moffatt, *J. Am. Chem. Soc.*, **86**, 1060 (1964).
3) R. Nakane, O. Kurihara, and A. Takematsu, *J. Org. Chem.*, **36**, 2753 (1971).
4) G. A. Olah, "Friedel-Crafts and Related Reactions," Wiley-Interscience, New York and London (1963, 1964), Vols. I—IV.
5) K. Arata, K. Yabe, and I. Toyoshima, *J. Catal.*, **44**, 385 (1976).
6) K. Yabe, K. Arata, and I. Toyoshima, *J. Catal.*, **57**, 231 (1979).
7) Catalyst amount used was 0.20 g for *t*-butylation and 1.1 g for isopropylation.
8) K. Shimada, *Bull. Chem. Soc. Jpn.*, **49**, 1375 (1976).
9) S. DeBenedetti, G. Lang, and R. Ingalls, *Phys. Rev. Lett.*, **6**, 60 (1961).
10) F. A. Miller and C. H. Wilkins, *Anal. Chem.*, **24**, 1253 (1952).
11) The catalysts dried at 250 and 350 °C gave 21.7% conversion at 2.5 h and 17.2% at 3 h, respectively. The cause of low activities might be due to the sublimation of $FeCl_3$ on the surface, since some black-colored substance, seemingly $FeCl_3$, was observed on the upper wall of a test tube used for drying.

The Crystal Structure of (Acetylacetonato)bis(diethylamine)palladium(II) Acetylacetonate at −170 °C

Shoji Kotake, Tsuyoshi Sei, Kunio Miki, Yasushi Kai, Noritake Yasuoka, and Nobutami Kasai*

Department of Applied Chemistry, Faculty of Engineering, Osaka University, Yamadakami, Suita, Osaka 565

(Received February 22, 1979)

The crystal structure of $[\{Pd(acac)(NHEt_2)_2\}^+(acac)^-]$ at −170 °C was determined by means of X-ray diffraction. The crystal belongs to monoclinic system: $a=13.905(3)$, $b=12.901(4)$, $c=12.205(3)$ Å, $\beta=96.28(2)°$, space group I2/c with $Z=4$. The structure was established by the heavy atom method and refined anisotropically by the least-squares procedure; $R=0.044$ for 1558 non-zero reflections. Both the $\{Pd(acac)(NHEt_2)_2\}^+$ cation and $(acac)^-$ anion lie on the crystallographic two-fold axis. The cation and anion lying on the same two-fold axis are bound together by two hydrogen bonds [N–H···O(2)=N′–H′···O(2′)=2.871(4) Å] to form an ion-pair. Two ion-pairs mutually related by the crystallographic center of symmetry make a packing unit of the crystal.

Okeya *et al.*[1] obtained (acetylacetonato)bis(diethylamine)palladium(II) acetylacetonate (**2**) by the reaction between (acetylacetonatoacetylacetonyl)(diethylamine)palladium(II) (**1**) and diethylamine. They observed that ligand exchange and Pd–C bond formation take place when the complex is dissolved in dichloromethane.

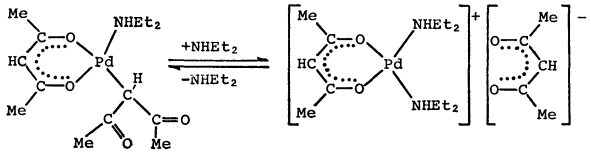

1 **2**

Crystals of **2** are unstable at room temperature, and by liberating a diethylamine molecule, Pd–C bond formation takes place in the solid state. Since the spatial disposition of anions and cations in the crystal seemed to be of interest in relation to ligand exchange and Pd–C bond formation reactions, the crystal structure analysis of the present complex was undertaken.

Experimental

The crystals are unstable at room temperature and easily decompose in a few days. A crystal, *ca.* 0.25×0.23×0.25 mm, was mounted on a Rigaku automated, four-circle single crystal diffractometer. The unit-cell parameters were determined at 20 and −170 °C, respectively. Crystal data are given in Table 1.

Intensity data were collected at −170 °C on the Rigaku diffractometer. Low temperature was attained by the gas flow method using liquid N_2. Graphite-monochromatized Mo $K\alpha$ radiation was used, the θ-2θ scan technique, with scan rate 4° min^{-1} and asymmetric scan width $\Delta(2\theta)=(2.0+0.7\tan\theta_c)°$, where θ_c is the calculated value of the Bragg angle using λ(Mo $K\alpha_1$)(=0.70926 Å), being employed. Background count was obtained by averaging the values measured for 7.5 s at both ends of a scan. For weak reflections with $|F|<3\sigma(F)$ the peak scan was repeated up to four times depending on their intensities. Four standard reflections (404, 640, 314, and 080) were measured after every 60 reflections, no intensity decrease being observed during the course of experiment. Numbers of reflections scanned ($2\theta\leqq48°$), observed, and unobserved were 1804, 1558, and 246, respectively. Correction for the usual Lp effect was made, the absorption correction being ignored (μ(Mo $K\alpha$)=8.61 cm^{-1}).

Table 1. Crystal data of $[\{Pd(acac)(NHEt_2)_2\}^+(acac)^-]$ ($C_{18}H_{36}N_2O_4Pd$, *F.W.* 450.9)

	−170 °C	20 °C
Crystal system	Monoclinic	Monoclinic
Space group	I2/c	I2/c
a/Å	13.905 (3)	14.455 (3)
b/Å	12.901 (4)	12.863 (3)
c/Å	12.205 (3)	12.210 (2)
β/°	96.28 (2)	95.56 (2)
V/Å^3	2176.2 (8)	2259.3 (7)
Z	4	4
D_c/g cm^{-3}	1.376	1.325
μ(Mo $K\alpha$)/cm^{-1}	8.61	8.30

Structure Determination and Refinement

The structure was solved by the heavy atom method. Since the space group is I2/c (No. 15) and the number of formula units per unit-cell is four, both the $\{Pd(acac)(NHEt_2)_2\}^+$ and $(acac)^-$ ions should lie on a two-fold axis. The coordinates of the Pd atom were determined from a three-dimensional Patterson function. Locations of all the remaining non-hydrogen atoms were determined by the Fourier synthesis. All the H atoms were located from the subsequent difference Fourier map.

The structure was refined by the block-diagonal least-squares procedure (*HBLS* V)[2] minimizing $\Sigma w\cdot(\Delta F)^2$. Anisotropic thermal parameters were considered for Pd, C, O, and N and isotropic ones for H. The final R value is 0.044 for 1558 observed (0.057 for all) reflections. The weighting scheme used was $w=(\sigma_{cs}+a|F_o|+b|F_o|^2)^{-1}$ for $|F_o|>0$ and $w=c$ for $|F_o|=0$, where σ_{cs} is the standard deviation obtained from the counting statistics, the values of a, b, and c used in the final refinement being −0.0162, 0.0037, and 2.7537, respectively. All the atomic scattering factors used were taken from International Tables for X-Ray Crystallography, Vol. IV.[3] The final atomic parameters are given in Table 2.†

TABLE 2. FINAL ATOMIC PARAMETERS (e.s.d.'s in parentheses)
Positional parameters in fraction of cell edges and anisotropic and isotropic thermal parameters in the form of $\exp\{-(\beta_{11}h^2+\beta_{22}k^2+\beta_{33}l^2+\beta_{12}hk+\beta_{13}hl+\beta_{23}kl)\}$ and $\exp\{-B(\sin\theta/\lambda)^2\}$, respectively.

Atom	x	y	z	β_{11} or B	β_{22}	β_{33}	β_{12}	β_{13}	β_{23}
Pd	0.0	0.00329(3)	0.25	0.00249(2)	0.00128(2)	0.00351(3)	0.0	0.00078(4)	0.0
O(1)	0.0876(2)	−0.1024(2)	0.1935(2)	0.0031(1)	0.0025(2)	0.0049(2)	0.0008(3)	−0.0000(3)	−0.0023(3)
O(2)	0.0744(2)	0.2889(2)	0.3461(2)	0.0034(2)	0.0017(2)	0.0039(2)	0.0004(2)	−0.0005(3)	−0.0005(3)
N	0.0905(2)	0.1153(2)	0.2020(2)	0.0022(2)	0.0019(2)	0.0027(2)	0.0003(3)	0.0007(3)	−0.0001(3)
C(1)	0.0732(3)	−0.1999(3)	0.1992(3)	0.0051(3)	0.0024(2)	0.0038(3)	0.0029(4)	−0.0027(5)	−0.0002(4)
C(2)	0.0	−0.2467(4)	0.25	0.0081(5)	0.0008(3)	0.0042(4)	0.0	−0.0045(7)	0.0
C(3)	0.1412(4)	−0.2641(3)	0.1404(4)	0.0081(4)	0.0030(3)	0.0054(4)	0.0058(5)	−0.0023(6)	−0.0021(5)
C(4)	0.0600(3)	0.3839(3)	0.3353(3)	0.0019(2)	0.0025(2)	0.0037(3)	−0.0002(3)	0.0012(4)	−0.0012(4)
C(5)	0.0	0.4321(4)	0.25	0.0030(3)	0.0009(3)	0.0048(4)	0.0	−0.0002(6)	0.0
C(6)	0.1117(3)	0.4545(3)	0.4235(3)	0.0035(2)	0.0020(2)	0.0042(3)	−0.0006(4)	−0.0001(4)	−0.0004(4)
C(7)	0.1935(2)	0.0927(3)	0.2438(3)	0.0017(2)	0.0027(2)	0.0054(2)	0.0005(3)	0.0007(3)	0.0006(4)
C(8)	0.0765(3)	0.1283(3)	0.0796(3)	0.0028(2)	0.0035(2)	0.0026(3)	0.0003(4)	0.0008(4)	0.0012(4)
C(9)	0.2060(3)	0.0698(3)	0.3656(4)	0.0024(2)	0.0035(3)	0.0054(3)	−0.0001(4)	−0.0016(4)	0.0020(5)
C(10)	0.1296(3)	0.2203(3)	0.0397(4)	0.0033(2)	0.0056(2)	0.0050(3)	−0.0006(3)	0.0014(5)	0.0040(5)
H(2)	0.0	−0.314(5)	0.25	5.8(17)					
H(3A)	0.141(3)	−0.322(4)	0.158(3)	3.6(10)					
H(3B)	0.128(3)	−0.267(3)	0.066(4)	3.4(9)					
H(3C)	0.204(3)	−0.234(4)	0.153(4)	5.3(11)					
H(5)	0.0	0.505(3)	0.25	1.2(10)					
H(6A)	0.180(3)	0.427(3)	0.454(3)	2.8(9)					
H(6B)	0.074(3)	0.459(3)	0.488(3)	2.7(8)					
H(6C)	0.117(3)	0.505(2)	0.406(3)	1.4(8)					
H(7A)	0.216(3)	0.037(3)	0.203(3)	0.9(7)					
H(7B)	0.224(2)	0.146(2)	0.223(3)	0.8(7)					
H(8A)	0.098(2)	0.057(3)	0.054(3)	2.1(8)					
H(8B)	0.006(3)	0.140(3)	0.055(3)	2.2(8)					
H(9A)	0.176(2)	0.003(2)	0.368(3)	1.3(8)					
H(9B)	0.265(3)	0.066(4)	0.389(3)	4.2(11)					
H(9C)	0.180(2)	0.127(3)	0.404(3)	2.3(9)					
H(10A)	0.199(2)	0.206(3)	0.052(3)	2.3(8)					
H(10B)	0.110(3)	0.279(4)	0.069(4)	4.9(12)					
H(10C)	0.117(3)	0.218(3)	−0.046(3)	2.8(9)					
H(N1)	0.075(2)	0.168(3)	0.231(3)	1.7(8)					

Results and Discussions

An *ORTEP*[4] drawing of an ion-pair of the present complex and the numbering scheme of the atoms are shown in Fig. 1. The bond lengths and bond angles are given in Table 3. Some least-squares planes, deviations of atoms from the plane, and dihedral angles are given in Table 4. The most remarkable feature of the structure is that both the $\{Pd(NHEt_2)_2(acac)\}^+$ cation and $(acac)^-$ anion lie on the crystallographic two-fold axis.

In the cation the geometry around the Pd atom is square-planar. The Pd, N, O(1), N′, and O(1′) atoms lie on nearly the same plane, the maximum deviation being 0.054 Å. The Pd–O(1) distance [2.000(3) Å] is almost equal to that in $Pd(acac)_2$ at −170 °C [1.991(3) and 1.988(3) Å].[7] However, it is shorter than in mono-β-diketonate complexes.[5,6] The

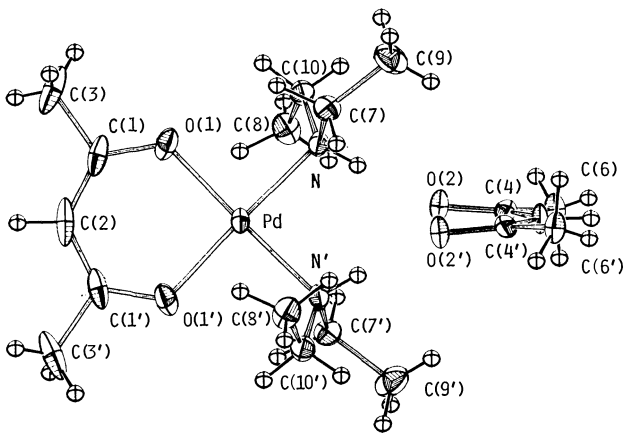

Fig. 1. An *ORTEP* drawing of the $\{Pd(acac)(NHEt_2)_2\}^+(acac)^-$ ion-pair with the numbering scheme of non-hydrogen atoms.
Non-hydrogen atoms are drawn as thermal ellipsoids with 50% probability level, and hydrogen atoms are drawn as spheres with 0.1 Å radius.

† The Tables of structure factors are kept in the Chemical Society of Japan as Document No. 8014.

TABLE 3. BOND LENGTHS, BOND ANGLES, AND HYDROGEN BONDS IN $[\{Pd(NHEt_2)_2(acac)\}^+(acac)^-]$ (e.s.d.'s in parentheses)

Bond length [l/Å]					
$\{Pd(NHEt_2)_2(acac)\}^+$					
Pd	-O(1)	2.000(3)	Pd	-N	2.044(3)
C(1)	-O(1)	1.277(5)	C(1)	-C(2)	1.386(7)
C(1)	-C(3)	1.498(7)	N	-C(7)	1.497(5)
N	-C(8)	1.494(5)	C(7)	-C(9)	1.506(6)
C(8)	-C(10)	1.507(6)			
C(2)	-H(2)	0.86(7)	C(3)	-H(3A)	0.78(5)
C(3)	-H(3B)	0.91(4)	C(3)	-H(3C)	0.95(5)
C(7)	-H(7A)	0.95(4)	C(7)	-H(7B)	0.86(3)
C(8)	-H(8A)	1.03(4)	C(8)	-H(8B)	1.01(4)
C(9)	-H(9A)	0.97(4)	C(9)	-H(9B)	0.85(5)
C(9)	-H(9C)	0.98(4)	C(10)	-H(10A)	0.97(4)
C(10)	-H(10B)	0.89(5)	C(10)	-H(10C)	1.04(4)
N	-H(N)	0.81(4)			
$(acac)^-$					
C(4)	-C(5)	1.406(6)	C(4)	-C(6)	1.528(6)
O(2)	-C(4)	1.246(5)			
C(5)	-H(5)	0.95(4)	C(6)	-H(6A)	1.04(4)
C(6)	-H(6B)	1.00(4)	C(6)	-H(6C)	0.69(4)
Bond angle [ϕ/°]					
$\{Pd(NHEt_2)_2(acac)\}^+$					
O(1)	-Pd -N	88.1(2)	N	-Pd -N'	90.0(2)
O(1)	-Pd -O(1')	94.0(2)	Pd	-O(1) -C(1)	123.2(3)
Pd	-N -C(7)	111.1(2)	Pd	-N -C(8)	110.4(2)
O(1)	-C(1) -C(2)	125.4(5)	O(1)	-C(1) -C(3)	114.1(4)
C(1)	-C(2) -C(1')	128.4(5)	C(2)	-C(1) -C(3)	120.5(4)
N	-C(7) -C(9)	112.2(3)	N	-C(8) -C(10)	113.4(3)
C(7)	-N -C(8)	112.2(3)			
C(1)	-C(2) -H(2)	116(5)	C(1)	-C(3) -H(3A)	112(3)
C(1)	-C(3) -H(3B)	116(3)	C(1)	-C(3) -H(3C)	108(3)
H(3A)	-C(3) -H(3B)	103(4)	H(3A)	-C(3) -H(3C)	112(5)
H(3B)	-C(3) -H(3C)	105(4)			
Pd	-N -H(N)	106(3)	N	-C(7) -H(7A)	109(2)
N	-C(7) -H(7B)	103(2)	N	-C(8) -H(8A)	101(2)
N	-C(8) -H(8B)	109(2)	C(7)	-C(9) -H(9A)	101(2)
C(7)	-C(9) -H(9B)	111(3)	C(7)	-C(9) -H(9C)	109(2)
C(8)	-C(10) -H(10A)	108(2)	C(8)	-C(10) -H(10B)	111(3)
C(8)	-C(10) -H(10C)	105(2)	C(7)	-N -H(N)	108(3)
C(8)	-N -H(N)	109(3)	C(9)	-C(7) -H(7A)	112(2)
C(9)	-C(7) -H(7B)	116(2)	C(10)	-C(8) -H(8A)	116(2)
C(10)	-C(8) -H(8B)	106(2)			
H(7A)	-C(7) -H(7B)	104(3)	H(8A)	-C(8) -H(8B)	111(3)
H(9A)	-C(9) -H(9B)	110(4)	H(9A)	-C(9) -H(9C)	118(3)
H(9B)	-C(9) -H(9C)	107(4)	H(10A)	-C(10) -H(10B)	116(4)
H(10A)	-C(10) -H(10C)	102(3)	H(10B)	-C(10) -H(10C)	114(4)
$(acac)^-$					
O(2)	-C(4) -C(6)	117.0(3)	C(5)	-C(4) -C(6)	116.9(4)
O(2)	-C(4) -C(5)	126.1(4)	C(4)	-C(5) -C(4')	127.5(4)
C(4)	-C(5) -H(5)	116(2)	C(4)	-C(6) -H(6A)	113(2)
C(4)	-C(6) -H(6B)	110(2)	C(4)	-C(6) -H(6C)	114(4)
H(6A)	-C(6) -H(6B)	106(3)	H(6A)	-C(6) -H(6C)	107(4)
H(6B)	-C(6) -H(6C)	106(4)			
Hydrogen bonding [l/Å and ϕ/°]					
H(N)····O(2)		2.10(4)			
N····O(2)		2.871(4)			
N-H(N)···O(2)		160(4)			

TABLE 4. LEAST-SQUARES PLANES AND DIHEDRAL ANGLES

Equation of the plane is of the form $AX+BY+CZ+D=0$,
where X, Y, Z, and D are measured in Å units; $X=ax+cz\cos\beta$, $Y=by$ and $Z=cz\sin\beta$.

(1) Coordination plane (Pd, O(1), O(1′), N(1), N(1′))
$-0.4360X-0.9000Z+2.5848=0$

	Pd	O(1)	O(1′)	N(1)	N(1′)
Δ[a]	0.001	0.054	−0.054	−0.051	0.053

(2) (acac) ligand (C(1), C(2), C(3), C(1′), C(3′), O(1), O(1′))
$-0.5127X+0.0038Y-0.8586Z+2.4434=0$

	C(1)	C(2)	C(3)	C(1′)	C(3′)	O(1)	O(1′)
Δ[a]	−0.026	−0.001	0.057	0.028	−0.062	−0.069	0.080

(3) $(acac)^-$ ion (C(4), C(5), C(6), C(4′), C(6′), O(2), O(2′))
$0.8187X+0.0155Y-0.5740Z+1.9572=0$

	C(4)	C(5)	C(6)	C(4′)	C(5′)	O(2)	O(2′)
Δ[a]	0.016	0.030	−0.092	0.024	0.030	0.074	−0.072

Dihedral angles [ϕ/°]

between planes		
(1) & (2)	5.0
(1) & (3)	80.8
(2) & (3)	85.8

a) Δ: Deviations of atoms [l/Å] from the plane.

O(1)–Pd–O(1′) angle [94.0(2)°] is slightly smaller than that in $Pd(acac)_2$ [95.04(10)°]. The Pd–N bond length is 2.044(3) Å. The N–Pd–N′ and O(1)–Pd–N angles are 90.0(2)° and 88.2(2)°, respectively. All the bond lengths and bond angles for the acac ligand in the cation are equal within the limits of errors to the corresponding values in $Pd(acac)_2$ (Fig. 2).

Two diethylamines *cis*-coordinated to the Pd atom are mutually related by the two-fold axis. The N–C bond lengths are equal [1.497(5) and 1.498(7) Å], comparable with those in $RhCl(CO)(C_2H_4)(NHEt_2)$[8] [1.507 and 1.508 Å]. One of the methyl groups in a diethylamine group takes the most stable *trans* conformation, the other being in a *gauche* conformation. This seems to be caused by the steric hindrance between the $C(9)H_3$ and $C(8')H_3$ or the $C(8)H_3$ and $C(9')H_3$ methyl groups.

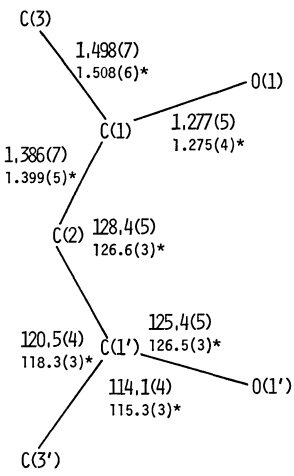

Fig. 2. Structure of the (acac) moiety *O,O′*-chelated to the Pd atom (−170 °C).
Average values the corresponding bond lengths and bond angles in $Pd(acac)_2$[7] are also given with asterisks.

In the $(acac)^-$ anion the O(2)–C(4) bond length of 1.246(5) Å is *ca.* 0.03 Å shorter than the corresponding length [1.277(5) Å] for the (acac)-*O,O′*-chelate. On the other hand, the C(4)–C(5) and C(4)–C(6) bond lengths [1.406(6) and 1.528(6) Å] are respectively equal to the corresponding lengths in the *O,O′*-chelate.

The cation and the anion lying on the same two-fold axis are bound together by hydrogen bonds, N–H···O(2) and N′–H′···O(2′) [both 2.871(4) Å], to form a ion-pair. The other two N–H···O(2′) and N′–H′···O(2) distances [both 3.213(4) Å] are rather short, and comparable with the largest value of the N–H···O hydrogen bond distances determined by means of neutron diffraction.[9]

An *ORTEP* drawing of the crystal structure is given in Fig. 3. Two ion-pairs mutually related by the crystallographic center of symmetry make a packing

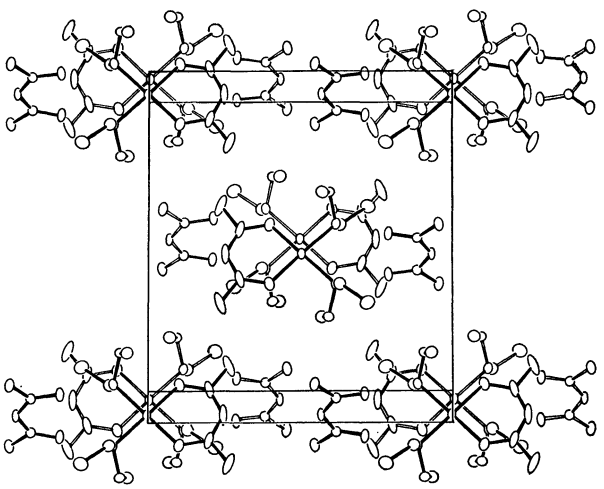

Fig. 3. Crystal structure of $[\{Pd(acac)(NHEt_2)_2\}^+(acac)^-]$ projected onto the ab plane.

unit of the crystal. No close atomic contact was found between these ion-pairs. No anion is located above or below the Pd atom of the cation. No explanation can be obtained for the ligand exchange reaction from **2** to **1**.

The authors wish to express their thanks to Prof. Shinichi Kawaguchi, Osaka City University, and Prof. Seichi Okeya, Wakayama University, for their valuable discussions and the supply of crystals. Computations were carried out on an ACOS Series 77 NEAC System 800 computer at Osaka University.

References

1) S. Okeya, H. Sazaki, Y. Nakamura, and S. Kawaguchi, 36th National Meeting of the Chemical Society of Japan, Osaka, April 1977, Abstr. 3E05.

2) T. Ashida, *The Universal Crystallographic Computing System-Osaka*, The Computation Center, Osaka University (1973), p. 55.

3) "International Tables for X-Ray Crystallography," The Kynoch Press, Birmingham (1974), Vol. IV, p. 71.

4) C. K. Johnson, "*ORTEP* II, Report ORNL-5138," Oak Ridge National Laboratory, Tennessee (1976).

5) M. Horike, Y. Kai, N. Yasuoka, and N. Kasai, *J. Organomet. Chem.*, **72**, 441 (1974).

6) Y. Zenitani, K. Inoue, Y. Kai, N. Yasuoka, and N. Kasai, *Bull. Chem. Soc. Jpn.*, **49**, 1531 (1976).

7) M. Sato, K. Miki, Y. Kai, N. Tanaka, N. Yasuoka, and N. Kasai, unpublished data.

8) J.-J. Bonnet, Y. Jeannin, A. Maisonnat, P. Kalck, and R. Poilblanc, *C. R. Acad. Sci., Ser. C.*, **281**, 15 (1975).

9) E. O. Schlemper and W. C. Hamilton, *J. Chem. Phys.*, **44**, 4498 (1966).

The Dissociation Rate of S_2 Produced from COS Pyrolysis

Tetsuo HIGASHIHARA, Ko SAITO,* and Ichiro MURAKAMI
Department of Chemistry, Faculty of Science, Hiroshima University, Higashisenda-machi, Hiroshima 730

(Received February 23, 1979)

The disappearance rate of S_2, which was produced from the pyrolysis of COS, was measured behind incident shock waves by monitoring the UV emission in the temperature range of 4500—6000 K and in the pressure range of 0.32—0.5 atm. It was found that two processes could possibly account for the disappearance of S_2:

$$S_2 + Ar \longrightarrow 2S + Ar \quad (3)$$

and

$$\begin{cases} S_2 + Ar \longrightarrow S_2^* + Ar & (4) \\ S_2^* + Ar \longrightarrow 2S + Ar & (5) \end{cases}$$

and the following rate equation was obtained:

$$-d[S_2]/dt = k_{II}[S_2][Ar] \text{ mol cm}^{-3} \text{ s}^{-1}$$

where

$$k_{II} = 10^{13.68} \exp(-77 \text{ kcal}/RT) \text{ cm}^3 \text{ mol}^{-1} \text{ s}^{-1}.$$

The recombination of S atoms and the dissociation of the S_2 molecule play important roles in the combustion system of sulfur-containing compounds. Despite the importance of these reactions, there are no data for the rate of S_2 dissociation. At room temperature, some authors[1-3] have determined the rate constant for the recombination of S atoms, but the values determined were very different from one another. Fair and Thrush[1] generated ground-state sulfur atoms in a discharge-flow system by means of a rapid reaction between H and H_2S in order to observe the emission from the radiative recombination of S atoms; they determined the rate constant of S atom recombination from the emission intensity and the Franck-Condon factor as:

$$k_{-5} = 1 \times 10^{15} \text{ cm}^6 \text{ mol}^{-2} \text{ s}^{-1}.$$

This may be the most reliable data, since the rate constant of atom recombination is generally of the order of 10^{15} cm^6 mol^{-2} s^{-1} at room temperature.

The thermal decomposition of carbonyl sulfide was studied by Hay and Belford[4] and by Schecker and Wagner[5] in the temperature range of 1550—3200 K. The results of these studies showed that S_2 was mainly produced by these reactions:

$$COS + Ar \longrightarrow CO + S + Ar \quad (1)$$

$$COS + S \longrightarrow CO + S_2, \quad (2)$$

and that the rate constants for Reaction 1 determined by these two groups agreed with each other. Thus, the mechanism of COS pyrolysis is rather simple compared with those of the other sulfur-containing compounds and the concentration of S_2 formed during the reaction can be easily calculated under the conditions presently studied.

The purpose of this study is to investigate the behavior of the S_2 molecule at higher temperatures (above 4500 K). There are two spectrophotometric methods for monitoring the concentration change of S_2. The absorption method is preferable for the measurement of the ground-state sulfur molecules. However, this method was not successful because of the very strong interference of S_2 emission at temperatures above 4500 K. Therefore, in this study the concentration change of S_2 in the $B^3\Sigma_u^-$ state (S_2^*) was followed by monitoring the UV emission at 392.5 nm.

Experimental

The shock tube was 3.8 cm in internal diameter, with a 2.5-m test section and a 1.5-m driver section. The system was pumped off by means of an oil-diffusion pump to less than 1×10^{-4} Torr before each run. All experiments were performed behind incident shock waves which were generated by high-pressure hydrogen. The UV emission at 392.5 nm, selected by means of a grating monochromator, was detected by means of a photomultiplier through a quartz window which was placed at a position 2.1 m downstream from the diaphragm. Only the S_2 molecule has an emission band around this wavelength corresponding to the $B^3\Sigma_u^- \rightarrow X^3\Sigma_g^-$ transition.

Carbonyl sulfide obtained from a commercial cylinder was degassed at the temperature of liquid N_2–ethanol slash and purified by fractional distillations between this temperature and −197 °C. The gas mixtures studied were 0.5 and 1% COS in Ar. The post shock pressure and temperature were in the 0.32—0.5 atm and 4500—5800 K ranges, respectively. The temperature drop due to the pyrolysis of COS was estimated to be about 100 K for 1% COS and about 50 K for 0.5% COS in Ar mixture. The boundary-layer effects on the particle time, temperature, and density were estimated by the method of Mirels.[6] It was found that at $t_1 = 30$ μs (at the end of the observation time) the maximum time correction was 20%, the maximum temperature shift was 6.2%, and the maximum density increase was 9.4%.

Results and Discussion

At temperatures above 4500 K, the emission intensity reached a maximum value within 5 μs of laboratory time and then decreased exponentially to a steady value. A typical oscillogram is shown in Fig. 1 (a).

If S_2^* (the $B^3\Sigma_u^-$ state of S_2) was mainly produced by the recombination of S atoms, the emission intensity should maintain the equilibrium value observed by Bott and Jacobs[7] at relatively lower temperatures (2300—4800 K) and high pressures (10—20 atm), since the S atom concentration did not overshoot

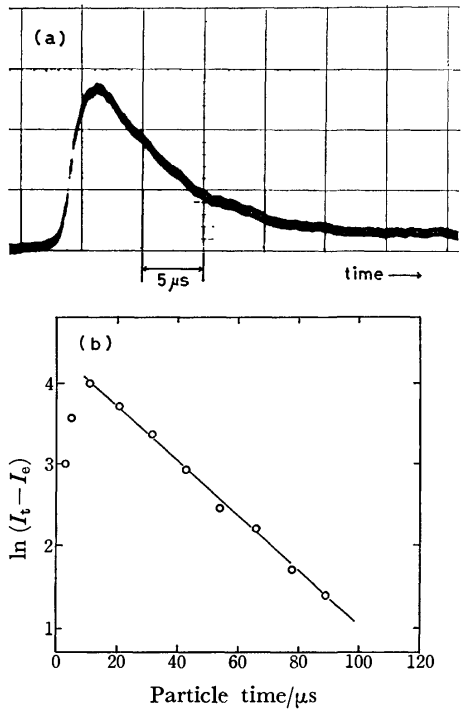

Fig. 1. (a): Typical oscilloscopic trace of S_2 emission at 392.5 nm, 0.5% COS in Ar mixture; post shock temperature=5507 K. (b): Plot of ln ($I_t - I_e$) *vs.* particle time.

behind the shock front, as is shown in Fig. 6. Therefore, the phenomenon shown in Fig. 1 (a) should be due to the thermal excitation from the ground electronic state of S_2. If so, the temperature dependence of the peak intensity per unit of S_2 concentration should give the energy difference between the ground and excited electronic states (90.6 kcal/mol). Figure 2 shows the Arrhenius plot of the peak intensity per unit of the initial concentration of COS. The apparent activation energy of this plot is 72.6 kcal/mol, smaller by about 20 kcal/mol than the energy difference of the two electronic states. This can reasonably be explained by considering that the yield of S_2 at the peak is temperature-dependent. If we plot the peak intensity per unit of S_2 concentration against $1/T$ (broken line of Fig. 2), where the S_2 concentration was calculated by using Reactions 1 and 2, the apparent activation energy becomes 114 kcal/mol, greater by about 20 kcal/mol than the energy difference of the two electronic states of S_2. However, if we use a value of $k_2=10^{13.92}$ exp (-27.2 kcal/RT) cm^3 mol^{-1} s^{-1} for the rate constant of Reaction 2, which was estimated by Kondratiev,[10] the apparent activation energy of the peak intensity becomes about 90 kcal/mol. Thus, the yield of S_2 (and the resulting apparent activation energy) is strongly influenced by the rate constants of Reactions 1 and 2. Unfortunately, since we have no reliable rate constants for these reactions at higher temperatures, we could not decide whether or not, at the peak, the thermal equilibrium between the $^3\Sigma_u^-$ and $^3\Sigma_g^-$ states of S_2 was maintained, but it may be reasonable to assume that the equilibrium was maintained. If such is the case, the

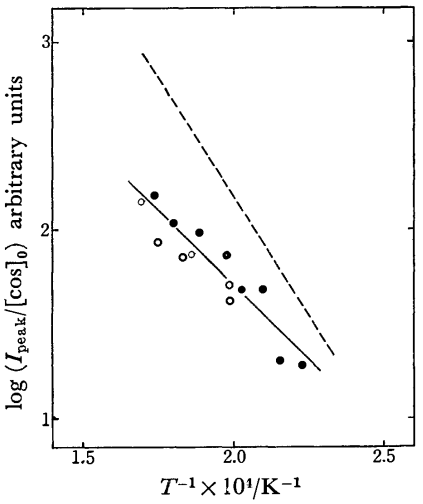

Fig. 2. ○ and ●: Arrhenius plot of peak intensity per unit initial concentration of COS, ○: 1% COS in Ar mixture; ●: 0.5% COS in Ar mixture. ----: Arrhenius plot of peak intensity per unit S_2 concentration.

decrease in the emission intensity after the peak corresponds to the dissociation rate of the S_2 molecule. Similar phenomena were observed for the emission of C_2 during the pyrolysis of CH_4, CCl_4, CF_4, and C_2H_2 by Fairbarn[8] and of C_2H_2 by Beck and Mackie.[9] In those studies, it was found that the thermal equilibrium between the electronically ground and excited states of C_2 was maintained.

The emission intensity is proportional to the concentration of S_2*. As is shown in Fig. 1 (b), since a semilogarismic plot of ($I_t - I_e$) *vs.* the time gives a straight line after the maximum, the variation in the S_2* concentration with the time is expressed by the following relation:

$$\ln (I_t - I_e) \propto \ln ([S_2^*]_t - [S_2^*]_e) = k_I t,$$

where the subscripts t and e denote the time t and the time needed to reach an equilibrium respectively. Although the emission intensity profile as experimentally recorded reflects the time variations in the gas temperature and density, in this study these corrections were not carried out and the mean temperature and density were used for the date reduction, since the observation time was very limited (from about 5 μs to about 20 μs laboratory time). Since COS decomposes almost completely at the time when the emission intensity reaches a peak (see Fig. 6), there is no need to consider the effect of S_2 formation on the rate of S_2 disappearance. Thus, the value of k_I gives a quasi-first-order rate constant of S_2 disappearance. Furthermore, taking into consideration the fact that S_2 disappears mainly as a result of the collision with Ar, the second-order rate constant of S_2 disappearance (k_{II}) is obtained from the $k_{II}=k_I/$[Ar] equation. The Arrhenius plot of k_{II} thus obtained is shown in Fig. 3 for 0.5 and 1% COS in Ar mixtures. The best-fitting line gives:

$$k_{II} = 10^{13.68} \exp (-77 \text{ kcal}/RT) \text{ cm}^3 \text{ mol}^{-1} \text{ s}^{-1}.$$

The formation and disappearance of S_2 were considered to be governed by the reactions listed in Table

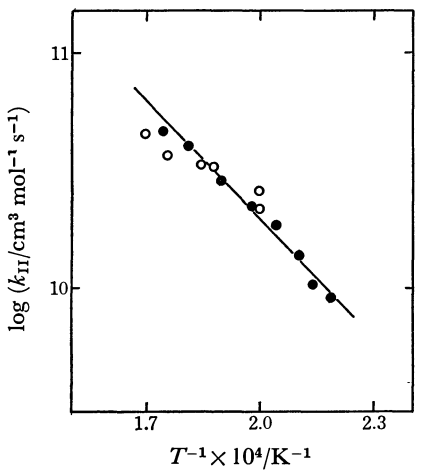

Fig. 3. Arrhenius plot of k_{II}, ○: 1% COS in Ar mixture; ●: 0.5% COS in Ar mixture.

1. In order to check the reliability of the assumption of the equilibrium between S_2 and S_2* and the resultant rate constant, k_{II}, for the S_2 disappearance, the concentration change of S_2* with the time was calculated at the temperatures of 5025 and 5753 K by using a reaction mechanism including the 11 elementary reactions listed in Table 1, and was compared with that obtained experimentally. The values of k_1,[4,5] k_2,[10] k_{-4}[1] at 298 K, k_{-5}[1] at 298 K, k_6[1] have been determined by other investigators, but there are no rate data for the rest. Therefore, the rate constants of these reactions were estimated in the following way. The rate constants of Reaction 4 were calculated from the simple collision theory, by assuming that the molecular diameters of S_2, S_2*, and Ar were 3.88, 4.47, and 3.42 Å respectively, as

$$k_4 = \lambda_4 \times 8.46 \times 10^{12}\, T^{1/2} \exp(-90.6\,\text{kcal}/RT)\ \text{cm}^3\,\text{mol}^{-1}\,\text{s}^{-1}$$

$$k_{-4} = \lambda_{-4} \times 9.89 \times 10^{12}\, T^{1/2}\ \text{cm}^3\,\text{mol}^{-1}\,\text{s}^{-1}.$$

The equilibrium constant for these reactions was expressed as

$$K_4 = k_4/k_{-4} = (Q_{S_2}*/Q_{S_2}) \exp(-90.6\,\text{kcal}/RT),$$

where Q_{S_2}* and Q_{S_2} are the partition functions of the electronically excited and ground states of S_2. The ratio of $Q_{S_2}*/Q_{S_2}$ can be calculated from the molecular constants; it is given as 2.15 at 5000 K. From this value, the λ_4/λ_{-4}=2.5 ratio was obtained. In general, the efficiency of electronic excitation is large; therefore, in this study λ_4=1 was assumed, and λ_{-4}=0.4 was thus obtained. Fair and Thrush[1] determined the value of k_{-4} at 298 K as

$$k_{-4} = 1.5\times10^{14}\ \text{cm}^3\,\text{mol}^{-1}\,\text{s}^{-1}.$$

The collision efficiency, λ_{-4}, was calculated from this value as λ_{-4}=0.88 at 298 K, in good agreement with that value obtained by assuming λ_4=1. Fair and Thrush also obtained values of k_{-5} at 298 K and k_6 as

$$k_{-5} = 10^{15}\ \text{cm}^6\,\text{mol}^{-2}\,\text{s}^{-1}$$

$$k_6 = 10^{7.48}\ \text{s}^{-1}.$$

Assuming that the rate constant of recombination reaction was inversely proportional to the temperature, k_{-5} was expressed as

$$k_{-5} = 10^{17.47}/T\ \text{cm}^6\,\text{mol}^{-2}\,\text{s}^{-1}.$$

The value of k_5 was obtained from k_{-5} by combining it with the equilibrium constant as

$$k_5 = 10^{13.95} \exp(-6\,\text{kcal}/RT)\ \text{cm}^3\,\text{mol}^{-1}\,\text{s}^{-1}.$$

The value of k_3 was assumed to be the same as that of k_{II}, and from the value of k_3 and the equilibrium constant, the value of k_{-3} was calculated. Now, we have all the rate constants needed to calculate the concentration changes in COS, CO, S, S_2, and S_2* with the time. Figures 4 and 5 present comparisons of the experimental (circle) and calculated histories of S_2* by using different sets of rate constants. As is shown in these figures, if a value of k_3 is set as equal to that of k_{II}(Case a), the calculated rate of S_2* disappearance becomes larger than that observed. This means that Reaction 4, followed by Reaction 5, contributes to the consumption of S_2. Therefore, the value of k_3 was changed to one-half the value of k_{II} and the concentration change of S_2* was recalculated (Case b). Although the agreement with the experiment seems to be improved, there remains some difference with regard to the equilibrium concentration of S_2*. Therefore, in order to check the influence of the values of k_4, k_{-4}, k_5, and k_{-5} on the

Table 1. Reaction mechanism

	Reaction	Rate expression[a]	Ref.
1)	$COS + Ar \underset{k_{-1}}{\overset{k_1}{\rightleftharpoons}} CO + S + Ar$	$k_1 = 10^{14.2} \exp(-61\,\text{kcal}/RT)$	5
2)	$COS + S \underset{k_{-2}}{\overset{k_2}{\rightleftharpoons}} CO + S_2$	$k_2 = 10^{12.23} \exp(-4.0\,\text{kcal}/RT)$	10
3)	$S_2 + Ar \underset{k_{-3}}{\overset{k_3}{\rightleftharpoons}} 2S + Ar$	See text	
4)	$S_2 + Ar \underset{k_{-4}}{\overset{k_4}{\rightleftharpoons}} S_2* + Ar$	See text	
5)	$S_2* + Ar \underset{k_{-5}}{\overset{k_5}{\rightleftharpoons}} 2S + Ar$	See text	
6)	$S_2* \xrightarrow{k_6} S_2 + h\nu$	$k_6 = 10^{7.48}$	1

a) Units: mol/cm^3 for concentration, s for time.

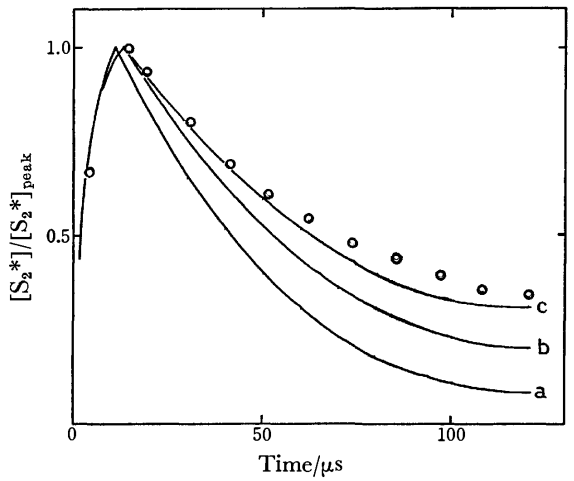

Fig. 4. Comparison of S_2* profils between the experiment (O) and the calculations (—), 1% COS in Ar mixture; post shock temperature=4851 K; mean temperature between 5 and 20 μs laboratory time=5025 K.

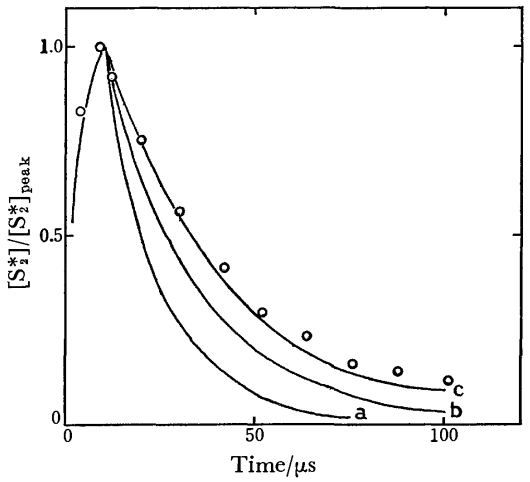

Fig. 5. Comparison of S_2* profiles between the experiment (O) and the calculations (—), 0.5% COS in Ar mixture; post shock temperature=5507 K; mean temperature between 5 and 20 μs laboratory time=5753 K.

equilibrium concentration of S_2*, the values of k_4 and k_{-4} were divided by 10, while those of k_5 and k_{-5} were multiplied by 10, leaving $k_3=1/2\ k_{II}$, and then the concentration change of S_2* was recalculated (Case c). The results of the calculations are shown in Figs. 4 and 5; the agreement is very satisfactory. Thus, if a set of proper rate constants was selected for Reactions 3, 4, and 5, the concentration change in S_2* could be reasonably reproduced, but the rate constant for Reaction 3 could not be determined precisely, since the exact values of k_4 and k_5 are not yet available. Therefore, we have the limiting relation, $k_{II}=k_3$, when the rates of Reactions 4 and 5 are negligibly small; we may conclude that the value of k_{II} is the upper limit of k_3.

Figure 6 shows the concentration profiles of COS, S, S_2, and S_2* with the time; these profiles were calculated by using the rate constants of Case c. As is

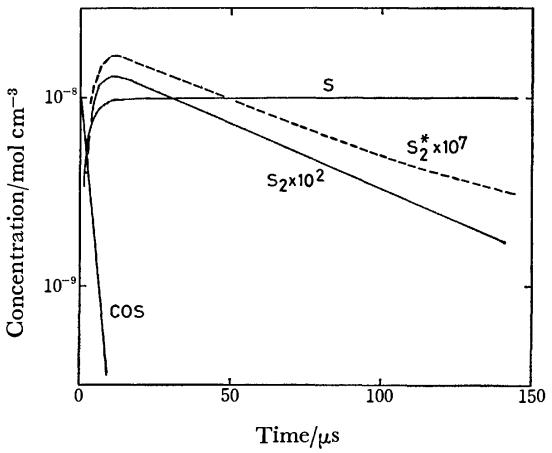

Fig. 6. Time dependent concentration changes of COS, S, S_2, and S_2*. Experimental conditions are the same as those of Fig. 4.

shown in this figure, although the equilibrium between the concentrations of S_2 and S_2* was not maintained precisely, it was found that the assumption of the equilibrium did not introduce many errors in estimating the disappearance rate of S_2 from the change in the emission intensity with the time.

The following three reactions are also possible in the decomposition of COS:

$$COS + S \longrightarrow CS + SO \quad (7)$$

$$COS + SO \longrightarrow CO_2 + S_2 \quad (8)$$

$$CS + SO \longrightarrow CO + S_2. \quad (9)$$

The influence of these reactions on k_{II} were examined. Since there are no rate data for Reaction 7, a value of 10^{12} cm^3 mol^{-1} s^{-1} was assumed for k_7. Using values of 10^{11} and 10^9 cm^3 mol^{-1} s^{-1} for k_8[10] and k_9[10] respectively, the history of S_2* was calculated. It was found from this calculation that the concentration of S_2* was slightly influenced by these reactions, but that the value of k_{II} so determined was not influenced.

References

1) R. W. Fair and B. A. Thrush, *Trans. Faraday Soc.*, **65**, 1208 (1969).
2) N. Basco and A. E. Pearson, *Trans. Faraday Soc.*, **63**, 2684 (1967).
3) P. Fowles, M. de Sorgo, A. J. Yarwood, O. P. Strausz, and H. E. Gunnig, *J. Am. Chem. Soc.*, **89**, 1352 (1967).
4) A. J. Hay and R. L. Belford, *J. Chem. Phys.*, **47**, 1352 (1967).
5) H. G. Schecker and H. Gg. Wagner, *Int. J. Chem. Kinet.*, **1**, 541 (1969).
6) H. Mirels, Proc. 8th Int. Shock Tube Symp., Chapman and Hall, London (1971), Paper 6.
7) J. F. Bott and T. A. Jacobs, *J. Chem. Phys.*, **52**, 3545 (1970).
8) A. R. Fairbarn, *Proc. R. Soc. London, Ser. A*, **312**, 229 (1969).
9) W. H. Beck and J. C. Mackie, *J. Chem. Soc., Faraday Trans. 1*, **71**, 1363 (1975).
10) D. L. Baulch, D. D. Drysdale, J. Duxbury, and S. J. Grant, "Evaluated Kinetic Data for High Temperature Reactions," Butterworths (1976), Vol. 3.

Diffusion Coefficients of Bolaform Electrolytes. Part II.† Diffusion Coefficients of Magnesium 1,2-Ethanedisulfonate and Magnesium 1,4-Butanedisulfonate in Aqueous Solution

Hisashi UEDAIRA* and Hatsuho UEDAIRA

Research Institute for Polymers and Textiles, 1-1-4 Yatabe-Higashi, Tsukuba, Ibaraki 305

(Received May 11, 1979)

The diffusion coefficients of magnesium 1,2-ethanedisulfonate and magnesium 1,4-butanedisulfonate in aqueous solutions have been measured at 25 °C. The concentration dependence of the diffusion coefficients of these salts was larger than those of the corresponding sodium salts. It has been shown that the 2:2 bolaform electrolyte behaves approximately like an ordinary 2:2 electrolyte. From these and previous results, it has been concluded that the diffusion behavior of bolaform electrolytes distinctively depend on the valency of the counterion.

In a previous report,[1] it was reported that diffusion of the 2:1 bolaform electrolyte, *i. e.*, the salt composed of a bolion[2] and two monovalent counterions, showed a peculiar behavior: the diffusion coefficients were significantly larger than that calculated according to the theory of diffusion of ordinary 2:1 electrolytes. The results were interpreted by assuming that the bolaform electrolyte behaves like an ordinary 1:1 electrolyte in the concentration range where the ionic atmosphere around each charged group is independent.

The spin-lattice relaxation time of ^{23}Na in aqueous solutions of sodium sulfonates has been reported.[3] The relaxation rate of ^{23}Na in ethanedisulfonate solution was reported to be smaller than that in butandisulfonate solution. If the both terminal sulfonic groups contribute to the relaxation rate of the Na^+ ion, the ^{23}Na relaxation rate in ethanedisulfonate solution should be larger. This result indicates that the Na^+ ions crowd separately around each sulfonic group and the electrostatic interaction between each crowd and the sulfonic group at one end is independent from the other terminal group.

In the case of the 2:2 bolaform electrolyte, the situation appears to be different. It is expected that the concentration dependence of the diffusion coefficients of 2:2 salts are larger than that of 2:1 salts. The diffusion coefficients of magnesium 1,2-ethanedisulfonate (MgEDS) and magnesium 1,4-butanedisulfonate (MgBuDS) in aqueous solution at 25 °C are presented and the effect of the valency of the counterion is discussed.

Experimental

MgEDS and MgBuDS (G. R., Tokyo Kasei Co.,) were recrystallized from water four times.

The diffusion experiments were performed at 25±0.01 °C using a Spinco Model H diffusion apparatus as Rayleigh interferometer. Details of the measurements are described elesewhere.[4]

Water, which was distilled after deionization, was used as the solvent. All the solutions were prepared by weight with the appropriate vacuum correction. The molar concentrations of the solutions were calculated from the densities, which were measured with a densimeter DMA O2C (Anton Paar Co.,) at 25±0.001 °C.

† For Part I in this series see Ref. 1.

Results and Discussion

The mean concentration in each diffusion experiment and the corresponding value of the diffusion coefficient are given in Table 1. The diffusion coefficient of each salt at infinite dilution was calculated from the

TABLE 1. DIFFUSION COEFFICIENTS OF BOLAFORM ELECTROLYTES IN WATER AT 25 °C

Electrolytes	$c\times10^2$ / mol l^{-1}	$D\times10^5$ / $cm^2\ s^{-1}$
1,2-MgEDS	0	0.7713
	0.4658	0.6695
	2.2667	0.6368
	3.0158	0.6338
	8.7935	0.6205
	12.4196	0.6211
	16.4742	0.6218
1,4-MgBuDS	0	0.7058
	0.7526	0.6314
	2.2524	0.6088
	4.0967	0.5985
	6.3088	0.5960
	8.9845	0.5921
	15.8497	0.5872

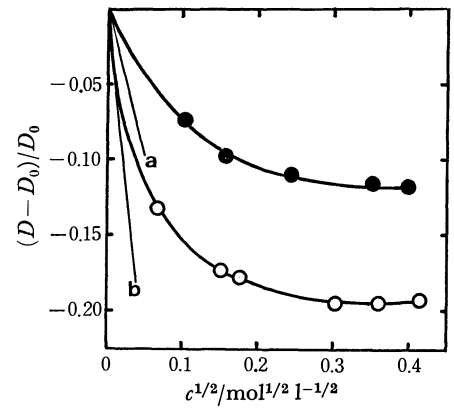

Fig. 1. Relative diffusion coefficients of MgEDS and Na_2EDS in aqueous solutions.
—●— Na_2EDS, —○— MgEDS.
a; The limiting slope for Na_2EDS, b; the limiting slope for MgEDS.

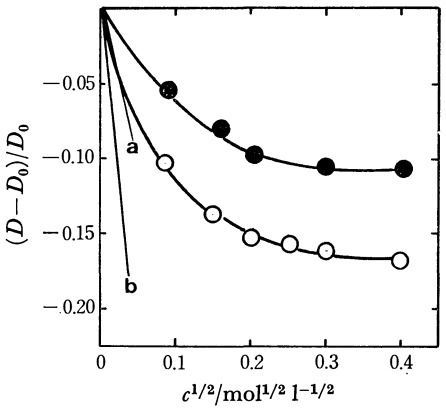

Fig. 2. Relative diffusion coefficients of MgBuDS and Na_2BuDS in aqueous solutions.
—●— Na_2BuDS, —○— MgBuDS.
a; The limiting slope for Na_2BuDS, b; the limiting slope for MgBuDS.

limiting mobilities of the relevant ions by the Nernst equation. The limiting mobilities of EDS^{2-}, $BuDS^{2-}$, and Mg^{2+} ions are 63.9[1] 63.1,[1] and 50.03[5] $cm^2\ \Omega^{-1}$ $equiv^{-1}$, respectively.

Figures 1 and 2 show plot of $(D-D_0)/D_0$ against $c^{1/2}$ for ethanedisulfonates and butanedisulfonates, respectively. The concentration dependence of the diffusion coefficients of the magnesium salts is larger than that of the sodium salts as expected. For the magnesium salts as well as the sodium salts, the dependence is smaller for butanedisulfonate than for ethanedisulfonate.

The diffusion coefficient of an electrolyte in aqueous solution may be given by

$$D = (D_0+\Delta_1)\left(1+c\frac{\mathrm{d}\ln y}{\mathrm{d}c}\right) \quad (1)$$

where D_0 is the Nernst limiting value of the diffusion coefficient, c the molarity and y the activity coefficient in molarity scale. Δ_1 is the first-order electrophoretic term.

The limiting equation for the diffusion coefficient may be obtained from the limiting mobilities of the cation and bolaform anion;[6]

$$D = D_0 - 3.63 \times 10^{-5}\sqrt{c} \quad (2)$$

for MgEDS, and

$$D = D_0 - 3.32 \times 10^{-5}\sqrt{c} \quad (3)$$

for MgBuDS.

In Figs. 1 and 2, the limiting slopes for 2:1 and 2:2 bolaform electrolyte are shown. The curves drawn through the experimental values approach asymptotically to the limiting slope only for the 2:2 bolaform electrolyte.

For 2:2 electrolytes, Δ_1 and the rational activity coefficient $f_\pm$ at 25 °C may be expressed by following relations, respectively.[5]

$$\Delta_1 = -8.07 \times 10^{-6}\frac{(\lambda_0^+-\lambda_0^-)^2}{\lambda_0^2}\cdot\frac{\sqrt{c}}{1+\kappa a} \quad (4)$$

$$\ln f_\pm = -\frac{9.42\sqrt{c}}{1+0.658a\sqrt{c}} + bc \quad (5)$$

where λ_0^+ and λ_0^- are the limiting mobilities of the cation and bolion, respectively. $\lambda_0=\lambda_0^++\lambda_0^-$. a and b are the constants adjustable to fit the experimental curve of the activity coefficient. κ has the usual meaning. The experimental data for the activity coefficients for MgEDS and MgBuDS are, however, not available at present. Consequently the values of a and b in Eq. 5 were estimated as follows.

In a previous report,[1] a was reported as 0.396 nm for Na_2EDS. Since a is related to the closest distance between the cation and the charged group of bolion, a is given as 0.553 nm for MgEDS by employing the Stokes radius for the cations.[5] The empirical relation given by Davis[5] $b=0.1\ |z_+z_-|$, was then employed, where z_+ and z_- are the valencies of the cation and anion, respectively.

The calculated diffusion coefficient for MgEDS is compared with the experimental value in Fig. 3. The decrease of the diffusion coefficient comes from that of the activity coefficient, since the Δ_1 value is of the order 10^{-8}—10^{-9} $cm^2\ s^{-1}$ and negligible compared with D_0. Similarly, the second-order electrophoretic term Δ_2 is of the order 10^{-9} $cm^2\ s^{-1}$ and of negligible contribution.

The density term of the activity coefficient $\ln y$ is small and contributes *ca.* 2% to the diffusion coefficient at 0.16 mol l^{-1}, becoming negligible below 0.07 mol l^{-1}.

The experimental and calculated values show greater agreement for MgEDS than for Na_2EDS, *i. e.*, at c=0.16 mol l^{-1}, the ratio of these values is 1.5 for Na_2EDS, but only 1.04 for MgEDS. The experimental determination of the activity coefficient of MgEDS will bring the calculated coefficient closer to the experimental one, since the correct value of b for MgEDS is probably larger than 0.4 as judged from 0.335 for Na_2EDS.[1]

A 2:1 bolaform electrolyte behaves approximately as a 1:1 electrolyte,[1] when the ionic atmosphere around each charged group is independent under the condition $\kappa R>1$, where R is the charge distance of the bolion. That is to say, a bolion behaves like two monovalent ions

If the 2:2 boalform electrolyte behaved like the 2:1 bolaform electrolyte under the conditions $\kappa R>1$, it would behave like an ordinary 1:2 electrolyte.

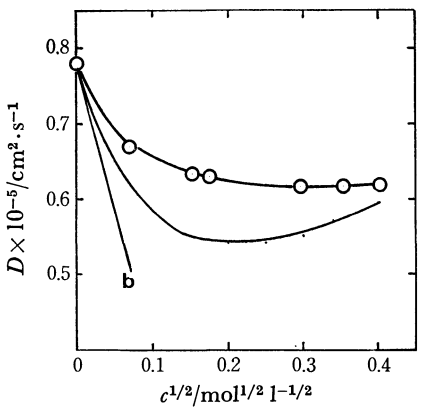

Fig. 3. Diffusion coefficients of MgEDS in aqueous solution.
—○— Experimental values, ——— calculated values, b; limiting slope.

From Figs. 1, 2, and 3, it is evident that the behavior of 2:2 bolaform electrolytes are quite different from that of the ordinary 1:2 electrolytes but resemble the ordinary 2:2 electrolytes. This is reasonable since the divalent counterion must contribute to the formation of the ionic atmospheres around the two charged groups of a bolion or bolions.

The motion of a charged group in a bolion is restricted by the other one connected to the skelton. In the diffusion process, the cation and anion move with the same velocity; hence a divalent counterion and two charged groups of two bolions or a counterion and a bolion move with the same velocity, *i.e.*, a counterion and a bolion move with the same velocty. That is, the 2:2 bolaform electrolyte behaves approximately like an ordinary 2:2 electrolyte.

There is a difference between the concentration dependence of the diffusion coefficient of the 2:2 bolaform electrolyte and that of the ordinary 2:2 electrolyte. The diffusion coefficient of the latter shows a minimum but that of the former shows a monotonical tendency to approach a constant value. Rice[7] pointed out that the assymmetry of the ion atmosphere leads to an additional retarding effect which will compensate for the increase in the diffusion coefficient by the thermodynamic term.

The concentration dependence of the diffusion coefficients of magnesium salts is larger than that of sodium salts. The explanation for this is that the concentration dependence of the activity coefficient of magnesium salts is larger than that of the sodium salts (compare Eq. 5 with Eq. 5 Ref. 1). And this is due to the ionic distribution which depends strongly on the valency of the counterion.

In the case of 2:1 bolaform electrolytes, Thomson *et al.*[8] found that the diffusion coefficients of potassium *p*-benzenedisulfonate and potassium 4,4'-biphenyldisulfonate in aqueous solution show no concentration dependence. The authors have shown that the sodium salts of several alkyl and aromatic disulfonic acids behave like 1:1 electrolytes rather than 2:1 electrolytes. The origin of this difference in diffusion has not yet been clarified. Such peculiar diffusion behavior probably only occurs in the case of 2:1 bolaform electrolytes with monoatomic counterions.

The authors would like to thank Dr. J. Komiyama (Tokyo Institute of Technology) for his interesting and helpful discussions.

References

1) H. Uedaira, *Bull. Chem. Soc. Jpn.*, **46**, 401 (1973).
2) R. M. Fuoss, *J. Am. Chem. Soc.*, **77**, 198 (1955).
3) H. Uedaira and H. Uedaira, 38th National Meeting of the Chemical Society of Japan, Nagoya, October 1978, Abstr. No. 2T11.
4) H. Uedaira and H. Uedaira, *Bull. Chem. Soc. Jpn.*, **42**, 2140 (1969).
5) R. A. Robinson and R. H. Stokes, "Electrolyte Solutions," 2nd ed Butterworths, London (1959).
6) H. S. Harned and B. B. Owen, "The Physical Chemistry of Electrolyte Solutions," 3rd ed Reinhold, New York (1958).
7) S. A. Rice, *J. Am. Chem. Soc.*, **80**, 3207 (1958).
8) G. Thomson, S. A. Rice, and M. Nagasawa, *J. Am. Chem. Soc.*, **85**, 2537 (1963).

The Crystal and Molecular Structure of γ-Metasantonin

Hideo UEDA,** Chuji KATAYAMA, and Jiro TANAKA*

Department of Chemistry, Faculty of Science, Nagoya University, Chikusa, Nagoya 464

(Received April 4, 1979)

The crystal and molecular structure of γ-metasantonin has been determined by the X-ray method. The crystal is orthorhombic, $P2_12_12_1$, with lattice parameters $a=10.371(1)$, $b=7.904(1)$, $c=15.975(1)$ Å. The molecule has two independent α,β-unsaturated ketone chromophores which take a chiral configuration. The chromophores show good planarity. A/B ring fusion is *cis*.

Many investigations concerning the stereochemistry of santonin(I) and its related compounds have been made by the chemical methods,[1,2] NMR,[3,4] CD,[5,6] and X-ray analysis.[7-9] γ-Metasantonin, 6β-hydroxy-3-oxo-5β-eudesma-1,7(11)-dien-12-oic acid γ-lactone, is obtained by the reaction of concentrated sulfuric acid on santonic acid or metasantonic acid. Woodward and Yates[1] assigned the gross structure (II) to γ-metasantonin.

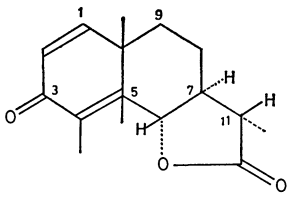

I

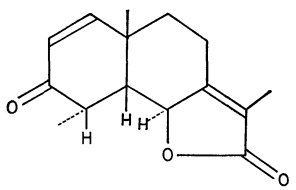

II

Hortman, Daniel, and Schaefer[3] and McMurry and Rane[4] confirmed the structure (II) by NMR. The conformation of this molecule, containing two separated α,β-unsaturated ketones, is interesting from the viewpoint of CD analysis. We determined the structure by X-ray analysis.

Experimental

The crystals are of transparent prismatic forms. The space group was determined as $P2_12_12_1$ from the oscillation and Weissenberg photographs. The density was measured by the flotation method with aqueous KI solution. The unit-cell parameters were determined by the least-squares methods, using twelve reflections measured on a Hilger & Watts four circle diffractometer with Zr-filtered Mo $K\alpha$ radiation ($\lambda=0.71069$ Å). The intensity data were collected on the diffractometer with the 2θ-ω scanning mode ($2\theta \leqq 54°$). The size of the crystal used was $0.2\times0.3\times0.1$ mm. The crystal used for X-ray measurement was mounted in a glass capillary. The intensities of three standard reflections were monitored after every 50 reflections. They were stable to 1% from their mean values. Neither absorption nor extinction correction was made. The crystal data are given in Table 1.

TABLE 1. CRYSTAL DATA

$C_{15}H_{18}O_3$
M.W.: 246.31
Space group: $P2_12_12_1$; $Z=4$
$a=10.371(1)$, $b=7.904(1)$, $c=15.975(1)$ Å
$D_m=1.244$, $D_c=1.249$ g cm^{-3}
$\mu=0.92$ cm^{-1} (for Mo $K\alpha$ radiation)

Determination and Refinement of the Structure

The structure was determined by the direct method with the program MULTAN[10] using 201 reflections

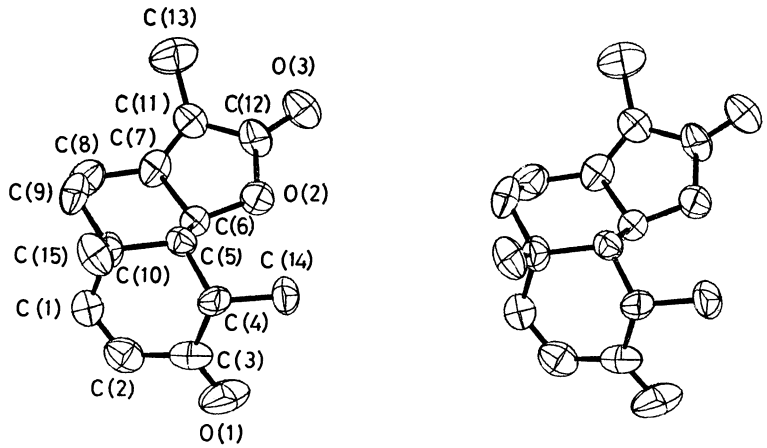

Fig. 1. The atomic labelings and a stereoscopic view of γ-metasantonin. Carbon and oxygen atoms are represented as thermal ellipsoids of a size such that the vibrating atoms have a 50% probability of being found within them. The absolute configuration of the molecule was drawn to be in conformity with the established configuration by a chemical correlation method.

** Present address: Central Research Laboratory, Ube Industries Ltd., Nishihon-machi, Ube, Yamaguchi 755.

with $|E| \geqq 1.30$. An E map computed from the phase set with the highest figure of merit ($FOM = 1.12$) revealed a partial structure containing a lactone ring. Other atoms were found by the succesive Fourier synthesis. Refinement of the structure was performed by the block-diagonal least-squares method with 752 independent reflections of $|F_o| \geqq 3\sigma$. R-index converged to 0.065 with an equal weight for each reflection. The atomic scattering factors were taken from "International Tables for X-Ray Crystallography."[11] The program HBLS-IV coded by Ashida in UNICS was utilized for the refinement. The program ORTEP[12] was used for drawing Figs. 1 and 2. A part of computation was performed at the Nagoya University Computation Center. The observed and calculated structure factors are given in Table 2.[13]

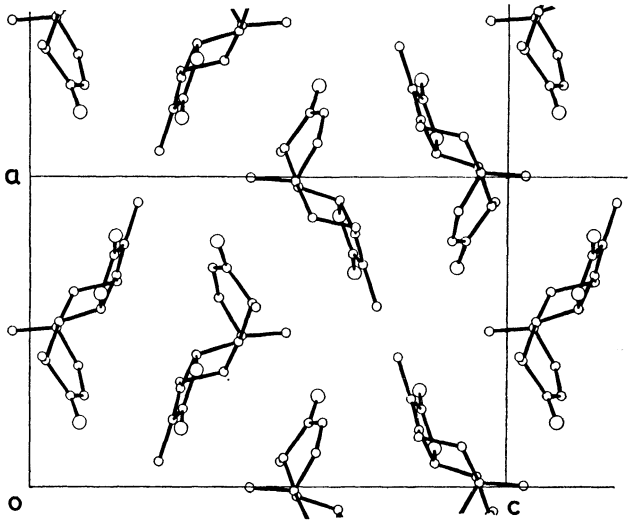

Fig. 2. The projection of the crystal structure along the b-axis. Carbon atoms are depicted as small circles and oxygen atoms as large circles. The configuration is the same as in Fig. 1.

Results and Discussion

The molecular structure, atomic labelings, and thermal ellipsoids are shown in Fig. 1. The positional and thermal parameters of non-hydrogen atoms with their standard deviations are given in Tables 3 and 4, respectively. The coordinates and isotropic thermal parameters of hydrogen atoms are given in Table 5.

Molecular Structure. The bond lengths and angles

Table 3. Atomic coordinates and their standard deviations[a]

	x	y	z
O(1)	0.2078 (6)	0.2162 (11)	0.1052 (5)
O(2)	0.6235 (6)	0.3066 (7)	0.1489 (4)
O(3)	0.8099 (6)	0.4320 (8)	0.1809 (4)
C(1)	0.3909 (9)	−0.1630 (11)	0.1018 (6)
C(2)	0.2935 (9)	−0.0586 (12)	0.1150 (6)
C(3)	0.2937 (8)	0.1204 (12)	0.0860 (5)
C(4)	0.4074 (8)	0.1723 (11)	0.0330 (5)
C(5)	0.5319 (8)	0.0844 (11)	0.0616 (5)
C(6)	0.7544 (8)	0.1362 (10)	0.1488 (5)
C(7)	0.6825 (8)	0.0318 (10)	0.1820 (4)
C(8)	0.6612 (9)	−0.1557 (13)	0.1830 (6)
C(9)	0.6294 (10)	−0.2056 (11)	0.0920 (6)
C(10)	0.5131 (9)	−0.1129 (10)	0.0557 (5)
C(11)	0.7831 (8)	0.1310 (11)	0.1990 (5)
C(12)	0.7483 (8)	0.3051 (11)	0.1775 (5)
C(13)	0.9181 (10)	0.0868 (16)	0.2276 (7)
C(14)	0.4196 (10)	0.3659 (11)	0.0260 (7)
C(15)	0.5029 (10)	−0.1681 (12)	−0.0369 (5)

a) The estimated standard deviations are given in parentheses and refer to the last decimal position of respective values.

Table 4. Anisotropic thermal factors[a] ($\times 10^4$) and their standard deviations of heavy-atoms

	B_{11}	B_{22}	B_{33}	B_{12}	B_{23}	B_{31}
O(1)	105 (8)	405 (21)	85 (4)	136 (25)	13 (19)	55 (11)
O(2)	101 (7)	171 (11)	53 (3)	−1 (17)	−27 (11)	−46 (8)
O(3)	132 (8)	221 (13)	58 (3)	−114 (21)	−33 (13)	−29 (9)
C(1)	111 (11)	156 (18)	61 (5)	−14 (25)	1 (17)	0 (13)
C(2)	114 (11)	254 (22)	45 (4)	−59 (30)	10 (19)	−24 (12)
C(3)	70 (9)	290 (24)	41 (4)	−4 (28)	−47 (18)	2 (11)
C(4)	78 (9)	172 (18)	45 (4)	32 (24)	3 (15)	−50 (10)
C(5)	75 (8)	143 (16)	35 (3)	−23 (21)	−11 (13)	−6 (10)
C(6)	80 (9)	138 (15)	41 (4)	5 (22)	−6 (14)	3 (10)
C(7)	119 (10)	168 (16)	19 (3)	45 (24)	47 (13)	−7 (10)
C(8)	114 (12)	231 (22)	74 (6)	76 (30)	53 (21)	−15 (15)
C(9)	155 (13)	131 (16)	56 (5)	82 (29)	−21 (16)	14 (14)
C(10)	113 (11)	118 (15)	48 (4)	−14 (23)	17 (14)	16 (12)
C(11)	108 (10)	182 (17)	35 (4)	−41 (25)	6 (15)	3 (11)
C(12)	131 (11)	166 (17)	34 (4)	−78 (26)	−41 (16)	−40 (11)
C(13)	118 (13)	361 (30)	69 (6)	70 (36)	24 (25)	−39 (15)
C(14)	129 (13)	122 (16)	88 (7)	−37 (27)	61 (18)	−55 (15)
C(15)	169 (14)	197 (21)	36 (4)	−119 (32)	−66 (15)	2 (13)

a) The anisotropic thermal factors are of the form $\exp\{-(h^2B_{11}+k^2B_{22}+l^2B_{33}+hkB_{12}+hlB_{31}+klB_{23})\}$.

are given in Tables 6 and 7, respectively. The various types of bond have lengths in good agreement with those reported for santonins.[7-9] The bond angles are all normal. The torsion angle O(1)–C(3)–C(2)–C(1) is −174°, and the maximum deviation from the least-squares plane containing these atoms is 0.031 Å at O(1), showing the good planarity of the α,β-unsaturated ketone group in the six-membered ring. The cyclohexenone ring A is puckered, C(5) being displaced by *ca.* 0.7 Å from the plane. The methyl group attached to C(4) is equatorial.

The molecule has a *cis* A/B ring fusion, and the ring B has a chair conformation. The mean endocyclic torsion angle for B is 54°, which is between santonins and *epi*-santonins,[9] and the value is similar to those for steroids.[14,18] The torsion angle C(6)–C(5)–C(10)–C(9) is −49° and the rotation around the bond C(5)–C(10) is in the opposite direction compared with the *epi*-santonins, the mean value being 47°.

Table 5. Hydrogen atoms and their standard deviations

	x	*y*	*z*	*B*/Å²
H(C1)	0.379(8)	−0.290(11)	0.116(5)	4.2(2.4)
H(C2)	0.206(9)	−0.119(11)	0.158(5)	4.6(2.4)
H(C4)	0.387(7)	0.117(9)	−0.028(4)	1.4(1.8)
H(C5)	0.601(7)	0.106(9)	0.022(4)	1.9(1.9)
H(C6)	0.496(6)	0.119(9)	0.192(4)	0.7(1.6)
H(C8a)	0.731(7)	−0.201(11)	0.196(4)	2.7(2.0)
H(C8b)	0.583(7)	−0.183(10)	0.232(4)	2.3(2.0)
H(C9a)	0.710(9)	−0.194(12)	0.047(5)	4.7(2.5)
H(C9b)	0.627(8)	−0.328(10)	0.093(4)	2.6(2.0)
H(C13a)	0.924(8)	−0.037(12)	0.246(6)	5.3(2.6)
H(C13b)	0.969(9)	0.079(12)	0.190(5)	6.2(2.7)
H(C13c)	0.936(8)	0.144(12)	0.282(5)	4.7(2.5)
H(C14a)	0.490(8)	0.403(11)	0.001(5)	3.6(2.2)
H(C14b)	0.341(8)	0.422(10)	−0.011(5)	3.6(2.3)
H(C14c)	0.443(9)	0.417(12)	0.077(5)	4.9(2.6)
H(C15a)	0.477(2)	−0.283(10)	−0.051(4)	3.0(2.1)
H(C15b)	0.598(7)	−0.163(10)	−0.071(4)	2.2(1.9)
H(C15c)	0.423(10)	−0.096(13)	−0.072(6)	6.7(2.9)

Table 6. Bond lengths and their standard deviations

O(1)–C(3)	1.210(14) Å	O(2)–C(6)	1.439(10) Å
O(2)–C(12)	1.373(11)	O(3)–C(12)	1.190(11)
C(1)–C(2)	1.322(14)	C(1)–C(10)	1.519(13)
C(2)–C(3)	1.488(15)	C(3)–C(4)	1.508(13)
C(4)–C(5)	1.537(12)	C(4)–C(14)	1.539(14)
C(5)–C(6)	1.516(12)	C(5)–C(10)	1.575(13)
C(6)–C(7)	1.489(12)	C(7)–C(8)	1.498(13)
C(7)–C(11)	1.333(13)	C(8)–C(9)	1.539(14)
C(9)–C(10)	1.523(14)	C(10)–C(15)	1.545(14)
C(11)–C(12)	1.463(13)	C(11)–C(13)	1.514(16)
C(*i*)–H(*i*)			
average	1.02(9)		
range	0.83—1.24		

The α,β-unsaturated lactone of γ-metasantonin is perfectly planar. The torsion angle O(3)–C(12)–C(11)–C(7) is −178°, the largest endocyclic torsion angle being 1.4°, and the maximum deviation from a least-squares plane of the conjugated double bond is 0.034 Å at O(2).

Some empirical rules[15,16] related to the sign of Cotton effect and the chirality of α,β-unsaturated lactones were reported. McMurry and his coworkers[17] investigated that the sign of $n\rightarrow\pi^*$ transition of the photolysis products of 4-hydroxysantonene, which had the same conformation as the lactone ring of γ-metasantonin, agreed with the rules. The CD spectrum of this molecule shows no peak due to $n\rightarrow\pi^*$ transition, presumably because of the planarity of the unsaturated ketone chromophore.[4] The CD spectrum shows a negative band around 230 nm and a positive one at 205 nm due to the coupled $\pi\rightarrow\pi^*$ transition.[19] Two independent chromophores, of which dihedral angle is 48°, take a chiral configuration, and the CD bands might appear owing to this configuration

Crystal Structure. Figure 2 shows the arran-

Table 7. Bond angles and their standard deviations

C(6)–O(2)–C(12)	109.1(6)°	C(2)–C(1)–C(10)	123.5(9)°
C(1)–C(2)–C(3)	122.9(10)	C(2)–C(3)–C(4)	115.8(9)
O(1)–C(3)–C(2)	121.0(10)	O(1)–C(3)–C(4)	123.3(9)
C(3)–C(4)–C(5)	111.5(7)	C(3)–C(4)–C(14)	112.1(8)
C(5)–C(4)–C(14)	113.7(7)	C(4)–C(5)–C(6)	113.3(7)
C(4)–C(5)–C(10)	109.0(7)	C(6)–C(5)–C(10)	111.1(7)
C(5)–C(6)–C(7)	113.3(7)	O(2)–C(6)–C(5)	110.9(7)
O(2)–C(6)–C(7)	104.4(7)	C(6)–C(7)–C(11)	109.6(8)
C(6)–C(7)–C(8)	116.2(8)	C(8)–C(7)–C(11)	134.0(9)
C(7)–C(8)–C(9)	105.7(8)	C(8)–C(9)–C(10)	114.2(8)
C(1)–C(10)–C(5)	109.4(7)	C(1)–C(10)–C(9)	110.6(8)
C(1)–C(10)–C(15)	109.5(8)	C(5)–C(10)–C(9)	110.5(8)
C(5)–C(10)–C(15)	110.2(8)	C(9)–C(10)–C(15)	106.6(8)
C(7)–C(11)–C(12)	108.2(8)	C(7)–C(11)–C(13)	130.5(9)
C(12)–C(11)–C(13)	121.0(9)	O(2)–C(12)–O(3)	120.9(8)
O(2)–C(12)–C(11)	108.5(7)	O(3)–C(12)–C(11)	130.5(9)

Table 8. Short van der Waals contacts

The Roman numerals represent the symmetry operators relevant to the atoms listed second.

C(10)-O(3)^{i}	3.605(12) Å	O(3)-C(14)^{ii}	3.575(13) Å
C(11)-O(3)^{ii}	3.594(11)	O(3)-C(2)^{iii}	3.454(13)
C(9)-C(2)^{iii}	3.513(14)	O(3)-C(15)^{iv}	3.404(14)

Symmetry code

Superscript	Symmetry operator		
i)	x	$-1+y$	z
ii)	$1/2+x$	$1/2-y$	$-z$
iii)	$1-x$	$1/2+y$	$1/2-z$
iv)	$2-x$	$1/2+y$	$1/2-z$

gement of molecules in the crystal, viewed along the b-axis. The intermolecular contacts shown in Table 8 are all greater than 3.4 Å and correspond to normal van der Waals interactions; the shortest separations involve the oxygen atom O(3).

References

1) R. B. Woodward and P. Yates, *J. Am. Chem. Soc.*, **85**, 551 (1963).
2) T. B. H. McMurry and R. R. Talekar, *J. Chem. Soc., Perkin Trans. 1*, **1976**, 442.
3) A. G. Hortmann and D. S. Daniel, *J. Org. Chem.*, **33**, 3988 (1968).
4) D. S. R. East, T. B. H. McMurry, and R. C. Mollan, *J. Chem. Soc., C*, **1970**, 2012.
5) C. Djerassi, R. Riniker, and B. Riniker, *J. Am. Chem. Soc.*, **78**, 6362 (1956).
6) L. Bartlett, P. M. Scopes, T. B. H. McMurry, and R. C. Mollan, *J. Chem. Soc., C*, **1969**, 1088.
7) J. D. M. Asher and G. A. Sim, *J. Chem. Soc.*, **1965**, 6041.
8) P. Coggon and G. A. Sim, *J. Chem. Soc., B*, **1969**, 237.
9) D. N. J. White and G. A. Sim, *J. Chem. Soc., Perkin Trans. 2*, **1975**, 1826.
10) G. Germain, P. Main, and M. M. Woolfson, *Acta Crystallogr., Sect. A*, **27**, 368 (1971).
11) "International Tables for X-Ray Crystallography," Birmingham, Kynoch Press (1974), Vol. IV, pp. 72—98.
12) C. K. Johnson, "ORTEP, Report ORNL-3794," Oak Ridge National Laboratory, Tennessee, 1965.
13) Table 2 is kept at the Office of the Chemical Society of Japan (Document No. 8001).
14) G. Ferguson, R. J. Restivo, G. A. Lane, J. M. Midgley, and W. B. Whalley, *J. Chem. Soc., Perkin Trans. 2*, **1978**, 1038.
15) A. F. Beecham, *Tetrahedron*, **28**, 5542 (1972).
16) I. Uchida and K. Kuriyama, *Tetrahedron Lett.*, **43**, 3761 (1974).
17) D. S. R. East, T. B. H. McMurry, and R. R. Taleker, *J. Chem. Soc., Perkin Trans. 1*, **1976**, 433.
18) D. C. Rohrer, P. D. Strong, W. L. Daux, and A. Segaloff, *Acta Crystallogr., Sect. B*, **34**, 2913 (1978).
19) J. Tanaka, unpublished work.

Spherical Particles and Their Surface Properties. I. Interaction of Water with the Surface of Spherical Silica

Tetsuo MORIMOTO, Toshie KADOTA, Hiroshi YANAZAWA,* and Shigeharu KITTAKA**

Department of Chemistry, Faculty of Science, Okayama University, Tsushima, Okayama 700

**Central Research Laboratory, Hitachi Ltd., Kokubunji, Tokyo 185*

***Department of Chemistry, Faculty of Science, Okayama College of Science, 1-1 Ridaicho, Okayama 700*

(Received May 21, 1979)

Spherical particles of silica were prepared by passing fine silica material through the O_2–H_2 flame. Spherical particles obtained were amorphous, creviceless, and very large in size compared to those of the starting material which indicates that spheres are made by complete comelting of a large number of fine particles. Water adsorption measurements showed that the rate of rehydration of the dehydroxylated silica surface is very slow, especially at low water pressures, and that the spherical silica has a heterogeneous surface, this heterogeneity being enhanced when the sample is heated at elevated temperatures. The ratio of the number of water molecules adsorbed in the first physisorption layer to that of the underlying surface hydroxyls was found to be 1:1.

Particles of most powders employed in industry and surface chemical researches have irregular shapes and inhomogeneous surfaces. Since an ideally spherical particle of any solid substance, if available, will have a physically and chemically homogeneous surface, the usage of such a particle should simplify the surface phenomena and therefore permit exact theoretical treatment. Thus, spherical particles will represent the reference sample for the surface chemistry of powders.

The preparation of spherical particles can be carried out by two methods. The first is the reaction in the liquid phase, that is, the precipitaion of sparingly soluble salts,[1,2] hydrous metal oxides,[3–5] and polystyrene lattices.[6] The particles formed by this method usually contain reagents and by-products as impurities. The second method consists of melting of powders at elevated temperature and solidification on cooling at a lower temperature.[7,8] This procedure should give particles whose purity depends on the purity of the raw materials.

Silica is used in a variety of industrial fields as mixed catalysts, carriers of catalyst, fillers and drying materials, and has been extensively studied from the surface-chemical stand point. Generally, surface hydroxyls are present on metal oxides as the result of chemisorption of water in the atmosphere,[9–11] and it has been found that surface hydroxyls on silica show characteristic behavior[11] which differs from that of most oxides[10,11] in the following points: a small rate of hydroxylation, a small surface density of the hydroxyls, and the 1:1 ratio between the amounts of physisorbed water and the underlying hydroxyls. In the present work we have undertaken the preparation of spherical silica particles by passing fine silica powders through the O_2–H_2 flame in order to investigate the interaction of the surface with water.

Experimental

Preparation of Spherical Particles of Silica. The apparatus for preparing spherical particles is illustrated schematically in Fig. 1. Raw material of silica was melted by the O_2–H_2 flame in a cylindrical furnace tube made of high alumina, 30 mm in diameter and 250 mm in length, where O_2 and H_2 were introduced at the rate of 14 and 10 l min^{-1}, respectively. A sample bucket was vibrated electrically to permit the sample to fall through the 150 mesh sieve placed at the bottom of the bucket, and the sample was passed into the furnace by the O_2 stream. H_2 was emitted into the furnace at the entrance. After passing through the furnace, the sample was pumped out; the major part of spherical particles formed sedimented on the bottom of the ducts D_1, D_2, and D_3, of 1000 mm each in length, and a minor part was collected on the 100 mesh stainless steel net N and cotton gauze G.

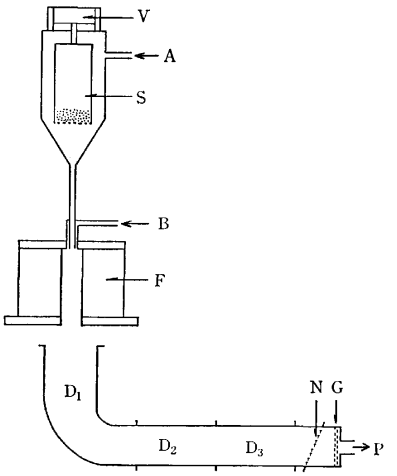

Fig. 1. Diagram of the apparatus for preparing spherical particles by fusion in the O_2–H_2 flame. A, O_2 inlet tube; B, H_2 inlet tube; V, vibrator; S, sample bucket (with 150 mesh net); F, furnace; D_1, D_2, D_3, ducts; N, stainless steel net (100 mesh); G, cotton gauze; P, pump.

Materials. The raw material of silica used in this study was Aerosil 200 made by Japan Aerosil Co., having a specific surface area of about 200 m^2 g^{-1}. Since the sample was too light to pass through the sieving mesh, it was sintered by heating it at 1220 °C for 3 h in an electric furnace; the particles formed had a specific surface area of about 31 m^2 g^{-1}, and could pass easily through the mesh.

Measurement of the Water Adsorption Isotherm and Surface Water Content. The adsorption isotherm of water on spherical silica was measured volumetrically by using a conventional adsorption apparatus equipped with an oil manometer. Prior to the adsorption measurement, the spherical sample was treated at 25, 300, 500, 900, and 1200 °C,

respectively for 4 h each in a vacuum of 10^{-6} Torr.† After the measurement of the water adsorption isotherm at 25 °C, the sample was exposed to the saturated water vapor for 12 h at room temperature in order to ensure the complete hydroxylation of the surface, followed by the evacuation at 40 °C to leave chemisorbed water on the surface. The second adsorption isotherm was then measured on the fully hydroxylated surface of silica. In order to obtain the isosteric heat of physisorption of water, the second adsorption isotherm was measured over a range of temperatures 10, 15, 20, and 25 °C. The time required of reaching the adsorption equilibrium was about 2 h and 30 min for the first and second adsorption, respectively.

The surface water content was measured by means of the successive-ignition-loss method,[12] and the N_2-BET method was used for the determination of surface area. Electron microscopes were Hitachi HU-11E and JEOL JSM-35.

Results and Discussion

Formation of Spherical Silica. Electron micrographs of sintered silica used as starting material and of spherical silica particles obtained are shown in Fig. 2. It is clear from Fig. 2 that the spherical particles obtained have smooth surfaces. Furthermore, observation of fracture of crushed particles of spherical silica under the field of a scanning electron microscope showed the inner part of the particle to have no crevices, in contrast to TiO_2.[13] X-Ray analysis proved the spherical particles of silica to be amorphous. The mean surface area of the particles obtained was 0.315 $m^2 g^{-1}$ as shown in Table 1, indicating that the size of the spherical particles is very much larger than that of the sintered sample. This fact manifests that a large number of sintered particles form a drop of melted silica in the flame, and the state of agglomeration of silica at the time when it enters the furnace determines the size of the silica sphere formed.

Adsorption Isotherm of Water and Isosteric Heat of Adsorption. The adsorption isotherm of water on spherical silica is given in Fig. 3. It can be seen from Fig. 3 that the isotherms belong to type II according to Brunauer's classification,[14] and that the second adsorption isotherms on the same sample almost coincide with each other when they are plotted against the relative pressure of water. Furthermore, Fig. 3 shows that the first adsorption isotherm lies above the second one except for the sample treated at 25.0 °C. In addition, the first and second adsorption isotherms measured at the same temperature do not go parallel, but deviate from each other with increasing relative pressure.

This can be explained by the idea that the rate of rehydration of the siloxane surface formed by dehydration of silanols is very slow at lower pressure and gradually increases with increasing relative humidity. This is in contrast to the behavior of most metal oxides where the two isotherms go parallel because of fast rehydration of the dehydrated surface

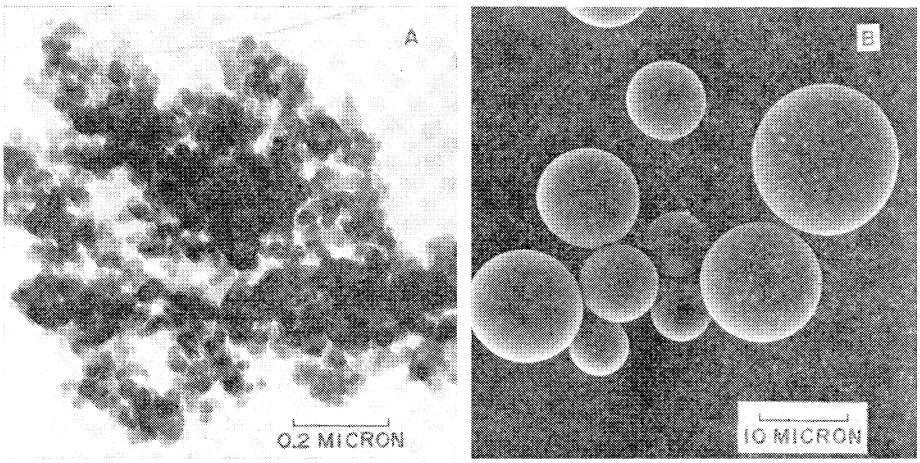

Fig. 2. Electron micrograph of starting material of SiO_2(A) and scanning electron micrograph of spherical SiO_2(B).

Table 1. Relation between the amounts of physisorbed and chemisorbed water on spherical SiO_2

Treatment temperature °C	Specific surface area $m^2 g^{-1}$	V_m $ml(STP)m^{-2}$	V_p $H_2Os \cdot nm^{-2}$	V_c	V_h	V_c+V_h $OHs \cdot nm^{-2}$	$\frac{V_p}{V_c+V_h}$ $(H_2O)\cdot(OH)^{-1}$
25	0.315	0.0948	2.55	0	2.63	2.63	0.970
300	0.315	0.1391	2.56	2.36	0.35	2.71	0.945
500	0.300	0.1439	2.59	2.56	0	2.56	1.012
900	0.279	0.1500	2.60	2.91	0	2.91	0.893
1200	0.231	0.1349	2.36	2.52	0	2.52	0.937
500[a]	31.1	0.0868	2.34	0	—	—	—

a) Starting material of SiO_2 (sintered).

† 1 Torr=133.322 Pa.

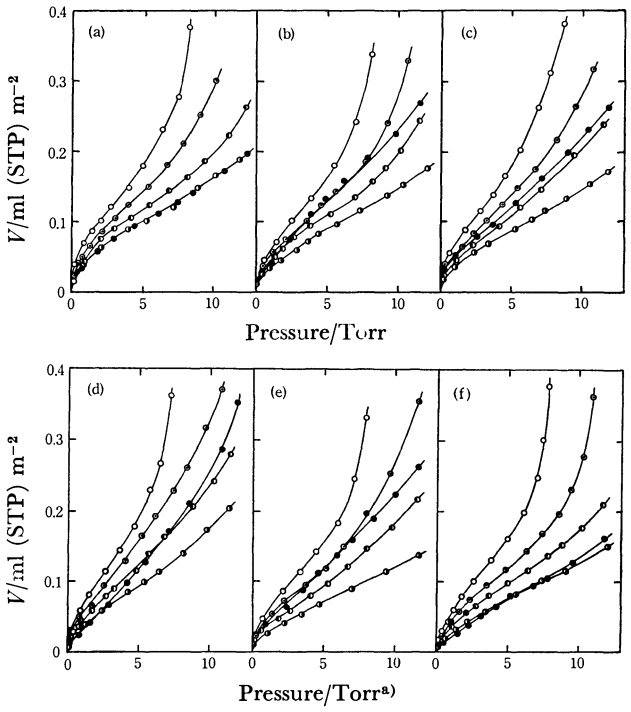

Fig. 3. Adsorption isotherms of water on spherical SiO_2 pretreated at (a) 25, (b) 300, (c) 500, (d) 900, (e) 1200 °C, and (f) starting material of SiO_2 treated at 500 °C. First adsorption ● at 25 °C; second adsorption ○ at 10 °C, ⊙ at 15 °C, ◐ at 20 °C, and ◑ at 25 °C. a) 1 Torr=133.322 Pa.

even at the initial pressure of water.[10]

For comparison, the water adsorption isotherms measured on the sintered silica are illustrated in Fig. 3. The results show that the adsorbed amounts for the second isotherm are almost equal to those in the case of spherical silica, but the first adsorption isotherm lies below that of the spherical silica. In other words, the extent of rehydroxylation differs from sample to sample, and the rehydroxylation rate is faster for the spherical sample than for the sintered one. This better hydrophilicity of spherical silica may be due to the history of the sample, *i.e.* the steam treatment by the O_2–H_2 flame at a very high temperature during the preparation.

As stated above, the first adsorption isotherm obtained includes physisorption and chemisorption of water, the latter of which is irreversible and increases in quantity with increasing pressure of water. This leads to a conclusion that the measurement of isosteric heat of adsorption q_{st} from the first adsorption isotherms by applying the Clausius-Clapeyron equation is unexpectable. On the other hand, the second adsorption isotherm measured on the fully hydroxylated surface of metal oxide has been found to be reversible and reproducible. Thus, we usually measure q_{st} values of water on the fully hydroxylated surface of metal oxide, though the surface heterogeneity discussed by the q_{st} values might be a little of quite different from that on the bare surface.

By applying the Clausius-Clapeyron equation to the second adsorption isotherm in Fig. 3, we can obtain the isosteric heat of adsorption q_{st} as given in

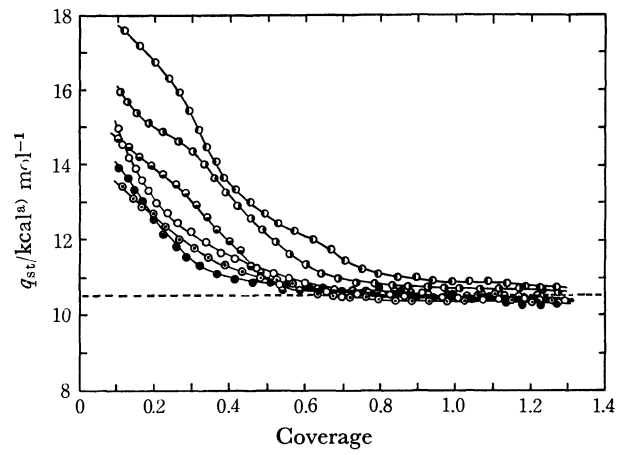

Fig. 4. Isosteric heat of adsorption of water on spherical SiO_2 pretreated at ○ 25 °C, ● 300 °C, ⊙ 500 °C, ◑ 900 °C, ◐ 1200 °C, and ◒ starting material of SiO_2 treated at 500 °C. Broken line represents the heat of liquefaction of water 25 °C. a) 1 cal (thermochemical)=4.184 J.

Fig. 4. The results reveal that the adsorption energy of water onto the hydroxylated surface of the original spherical silica decreases with the coverage of water indicating some heterogeneity of the surface, and that the extent of heterogeneity depends on the pretreatment temperature of the sample. The q_{st} curves change little until the pretreatment temperature of 500 °C is reached, but further increase in temperature raises the q_{st} values. Additional data of the q_{st} value of the sintered silica give an intermediate curve as shown in Fig. 4, which indicates that the surface heterogeneity of silica was clearly decreased by the formation of spheres. Thus, it is found that the surface activity and surface heterogeneity of fully hydroxylated surface of spherical silica for water adsorption were less than that of the raw material, though they were not so low as those expected. This can be elucidated as follows. When liquid spherical particles of silica melted in the O_2–H_2 flame are quenched, the solid particles formed will have surface state close to that of the liquid, including a small amount of water from the environment. Also on the fully hydroxylated surface of the spherical silica, there will exist the network of SiO_2 including Si atoms of the coordination number 4, which have at least one or two hydroxyls per Si atom. The variety of the direction and surface density of these hydroxyls can be considered to bring about the heterogeneity of hydroxylated spherical silica surface for water adsorption.

It is interesting to note that the surface becomes more active when spherical silica is treated at higher temperature *in vacuo*. The heat treatment at higher temperature naturally causes the migration of atoms in solid toward the direction of more stable state of the solid, *i.e.* toward crystallization, though it be very slow, accompanied by the evolution of bonded water molecules. This may produce more active sites such as corners and edges on the surface.

Surface Water Content on Spherical Silica. Figure 5 gives the surface water content on the spherical silica

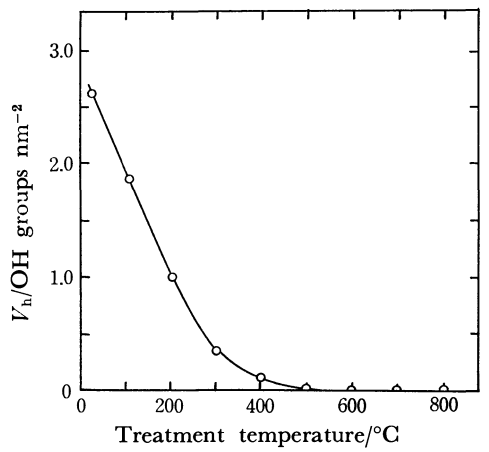

Fig. 5. Surface water content of spherical SiO_2.

which was obtained by the successive-ignition-loss method. The data obtained show that the surface water content at room temperature is almost the same as that reported on various other silica samples,[11] and very much smaller than that on most metal oxides.[10,11] The value 2.55 is almost one half of the calculated theoretical value.

Relation between the Amounts of Physisorbed Water and the Underlying Hydroxyls. The data obtained by the analysis of water adsorption isotherms of spherical silica are listed in Table 1. V_m and V_p are the monolayer capacities obtained by applying the BET method to the first and second isotherms, respectively. V_p contains only the physisorbed amount, but V_m both physisorbed and chemisorbed ones, and the difference between V_p and V_m therefore represents the amount of chemisorption V_c. We have another component of chemisorbed water, that is, the surface water content V_h which exists on the surface before the measurement of the first adsorption isotherm.

The sum V_c+V_h, therefore, represents the total amount of chemisorbed water. In the last column in Table 1, we can see the ratio of H_2O:OH to be 1:1, which shows a good agreement with the value obtained on fine silica particles.[11] In other words, a water molecule is physisorbed on a surface silanol group by hydrogen bonding on any kind of silica, contrary to the case of metal oxides, where a water molecule is adsorbed by two surface hydroxyls forming a tetrahedral coordination of the oxygen atom in an adsorbed water molecule. This interesting phenomenon of the silica surface may be attributed to a dilute population of surface silanols on the surface as was stated above, so that the neighboring two hydroxyls on silica are located too far apart for the bridging of a water molecule by two hydroxyls.

The present work was partially supported by a Grant-in-Aid for Development Research from the Ministry of Education.

References

1) M. Miura, Y. Tsuchiya, and Y. Murakami, *J. Sci. Hiroshima Univ., Ser. A-II*, **26**, 151 (1963).
2) Y. Nakahara and K. Miyata, *Nippon Kagaku Zasshi*, **1979**, 727.
3) W. Stöber and A. Fink, *J. Colloid Interface Sci.*, **26**, 62 (1968).
4) A. Bell and E. Matijević, *J. Phys. Chem.*, **78**, 2621 (1974).
5) E. Matijević, M. Budnik, and L. Meites, *J. Colloid Interface Sci.*, **61**, 302 (1977).
6) K. Furusawa, W. Norde, and J. Lyklema, *Kolloid-Z. Z. Polymere*, **250**, 908 (1972).
7) N. J. Themelis and W. H. Gauvin, *AIChE J.*, **8**, 437 (1962).
8) L. S. Nelson, S. R. Skaggs, and N. L. Richardson, *Laser J.*, March/April (1971), p. 12.
9) H. P. Boehm, *Angew. Chem.*, **78**, 617 (1966).
10) T. Morimoto, M. Nagao, and F. Tokuda, *J. Phys. Chem.*, **73**, 243 (1969).
11) T. Morimoto, M. Nagao, and J. Imai, *Bull. Chem. Soc. Jpn.*, **44**, 1282 (1971).
12) T. Morimoto and H. Naono, *Bull. Chem. Soc. Jpn.*, **46**, 2000 (1973).
13) To be published.
14) S. Brunauer, L. E. Copeland, and D. L. Kantro, in "The Solid-Gas Interface," ed by E. A. Flood, Marcel Dekker, Inc., New York (1966), Vol. 1, p. 86.

Structure of α Form of L-Glutamic Acid. α-β Transition

Noriaki HIRAYAMA,* Kunikatsu SHIRAHATA, Yuji OHASHI,† and Yoshio SASADA†

Tokyo Research Laboratory, Kyowa Hakko Kogyo Co., Ltd., 3-6-6, Asahimachi, Machida, Tokyo 194

†*Laboratory of Chemistry for Natural Products, Tokyo Institute of Technology, Nagatsuta, Midori-ku, Yokohama 227*

(Received May 22, 1979)

An X-ray analysis of the α form of L-glutamic acid, $C_5H_9NO_4$, has been carried out. The space group is $P2_12_12_1$ with $a=7.068(1)$, $b=10.277(1)$, $c=8.755(1)$ Å and $Z=4$. The structure was solved by the direct method, and least-squares refinement using 855 reflexions led to the final R value of 0.034. The molecule is in a zwitter ion form, and there is a strong OH···O intermolecular hydrogen bond with the O···O distance of 2.578(2) Å. The conformation of L-glutamic acid in the α form is quite different from that in the β form. The occurence frequency in various crystal structures containing glutamic acid residues shows that the conformation in the β crystal is more stable and favourable than that in the α crystal. The transition of the α form to the β form of L-glutamic acid in the mother liquor and the conditions for obtaining the α crystals are discussed based on the crystal and molecular structures of the two polymorphs.

L-Glutamic acid crystallizes in two polymorphic forms; they are designated α and β forms by Hirokawa.[1] In industrial processes, the α form is more advantageous to handle. The α crystal, however, is converted to the β when the α crystal is placed in solution for a long time. The β crystal is also obtained when it is grown slowly. Consequently, various kinds of investigations have been undertaken to find the conditions for crystallization of L-glutamic acid in the α form and to elucidate the mechanism of the α-β transition.[2-5] It was found empirically that addition of trace amount of some amino acids or other special compounds causes formation of the α form.[2,4,5] To clarify these problems, however, it is inevitable to know the difference in the crystal and molecular structure between the two polymorphs. While the refined crystal structure of the β form was obtained from neutron diffraction,[6] only crystal data for the α form has been reported by Bernal.[7] We have, therefore, undertaken an X-ray analysis of the α form of L-glutamic acid.

Experimental and Structure Determination

Prismatic crystals were obtained from an aqueous solution. A crystal, 0.5×0.4×0.3 mm in size, was used for data collection on a Rigaku four-circle automated diffractometer with graphite monochromated Mo $K\alpha$ radiation ($\lambda=0.71069$ Å). Preliminary unit cell dimensions and space group were obtained from photographs. The space group was determined from the systematic absences ($h00$, $2n+1$; $0k0$, $2n+1$; 001, $2n+1$). Accurate cell dimensions were determined by the least-squares method using the 2θ values of 15 high angle reflexions, measured on the diffractometer. Crystal data are summarized in Table 1. All reflexions within the range of $2\theta \leqq 55°$ were collected by the use of the ω-2θ scan mode with a scanning rate of $4°(2\theta)$ min^{-1}. Stationary background counts were accumulated for 10 s before and after each scan. A total of 874 independent reflexions were obtained, of which 17 ($|F_o|<3.0\sigma(|F_o|)$) were considered as unobserved. A Lorentz-polarization correction was made as usual but absorption effect was neglected.

Table 1. Crystal data

$C_5H_9NO_4$	$V=637.5$ Å^3
$M.W.=147.13$	$D_x=1.533$ g·cm^{-3}
Orthorhombic	$Z=4$
$P2_12_12_1$	μ(Mo $K\alpha$) $=3.426$ cm^{-1}
$a=7.068(1)$ Å	
$b=10.277(1)$	
$c=8.775(1)$	

The phases for 191 reflexions with $|E_o|\geqq 1.2$ were assigned with MULTAN.[8] An E map computed with the phase set of the lowest R_k revealed the positions of 10 non-hydrogen atoms.** All hydrogen atoms were located from the difference synthesis. The structural parameters were refined by the block-diagonal least-squares method. The function minimized was $\sum w(|F_o|-|F_c|)^2$ with unit weight.

Table 2a. Final positional parameters multiplied by 10^4 for non-hydrogen atoms and by 10^3 for hydrogen atoms

Estimated standard deviations are given in parentheses.

Atom	x	y	z
O(1)	4566(3)	2360(2)	5129(2)
O(2)	4232(3)	3718(1)	3154(2)
C(1)	4180(3)	3438(2)	4568(2)
C(2)	3607(3)	4528(2)	5657(2)
N	2088(3)	4018(2)	6681(2)
C(3)	5261(3)	4991(2)	6650(3)
C(4)	6956(3)	5509(2)	5742(3)
C(5)	6509(3)	6768(2)	4957(2)
O(3)	6244(3)	6651(2)	3467(2)
O(4)	6368(3)	7805(2)	5610(2)
HC(2)	306(4)	528(3)	502(3)
HN1	112(3)	357(2)	610(2)
HN2	253(4)	349(2)	720(3)
HN3	165(4)	465(3)	736(3)
H1C(3)	565(4)	420(2)	730(3)
H2C(3)	478(4)	572(2)	743(3)
H1C(4)	740(5)	481(3)	492(3)
H2C(4)	807(4)	583(3)	647(3)
HO(3)	582(5)	751(3)	292(4)

** It was informed that Matsuzaki reported in his Ms thesis[9] the structure analysis of the α form as one example of successful applications of the symbolic addition method.

Table 2b. Final thermal parameters multiplied by 10^4 for non-hydrogen atoms and by 10^3 for hydrogen atoms

Estimated standard deviations are given in parentheses.

Atom	U_{11} or U	U_{22}	U_{33}	U_{12}	U_{13}	U_{23}
O(1)	417(9)	191(7)	234(8)	98(8)	47(8)	34(6)
O(2)	394(9)	211(7)	152(7)	9(7)	19(8)	−1(6)
C(1)	183(9)	189(9)	184(9)	−9(8)	10(8)	−23(8)
C(2)	208(9)	159(8)	158(8)	9(8)	15(9)	4(8)
N	239(8)	179(8)	175(8)	−12(8)	31(8)	−4(7)
C(3)	285(11)	240(10)	178(9)	−58(9)	−31(9)	18(9)
C(4)	225(10)	252(10)	282(11)	−31(9)	−34(9)	39(10)
C(5)	221(10)	224(10)	212(9)	−64(9)	11(9)	0(9)
O(3)	446(10)	228(7)	201(7)	−12(8)	−53(8)	−6(6)
O(4)	618(12)	237(7)	247(8)	−51(9)	−18(10)	−35(7)
HC(2)	38(8)					
HN1	18(6)					
HN2	29(7)					
HN3	58(10)					
H1C(3)	38(8)					
H2C(3)	27(7)					
H1C(4)	48(9)					
H2C(4)	47(9)					
HO(3)	67(10)					

Two strong reflexions, (2 1 0) and (1 2 1) were excluded because they seemed to suffer from secondary extinction. The final R value was 0.034 for 855 reflexions. Atomic scattering factors were taken from "International Tables for X-Ray Crystallography."[10] The final positional and thermal parameters are given in Table 2.***

Description of the Structure

Hydrogen Bond. The crystal structure viewed along the a axis is drawn in Fig. 1, where the numbering of the atoms are shown. Here O(1) of α-carboxylate group is denoted to the oxygen atom whose torsional angle of O(1)–C(1)–C(2)–C(3) is negative. All of the hydrogen donors, OH and NH_3, participate in hydrogen bonds. The distances and angles of the hydrogen bonds are given in Table 3. A strong OH···O bond between the α- and γ-carboxyl groups links the molecules to form a chain along the b axis. The chains are interlinked by the three NH··· O hydrogen bonds to make a three-dimensional network. This scheme is similar, in general, to that of the β crystal. The difference is that in α O(2) accepts the hydrogen bonds from the γ-carboxyl and the NH_3^+ group and O(1) links to another NH_3^+ group while in β O(2) is the hydrogen bond acceptor from two NH_3^+'s and O(1) links to OH. The OH··· O distance in α is 0.06 Å longer than that in β, whereas the average of three NH···O distance in the former are 0.06 Å shorter than those of the latter.

Conformation. Figure 2 shows a stereoscopic drawing of the present molecule. The torsional angles are listed in Table 4. The conformations around the C(2)–C(3) and C(3)–C(4) bonds in the α form are both *gauche*, whereas those in the β form are *trans-gauche*. Such folded conformation of the molecule has

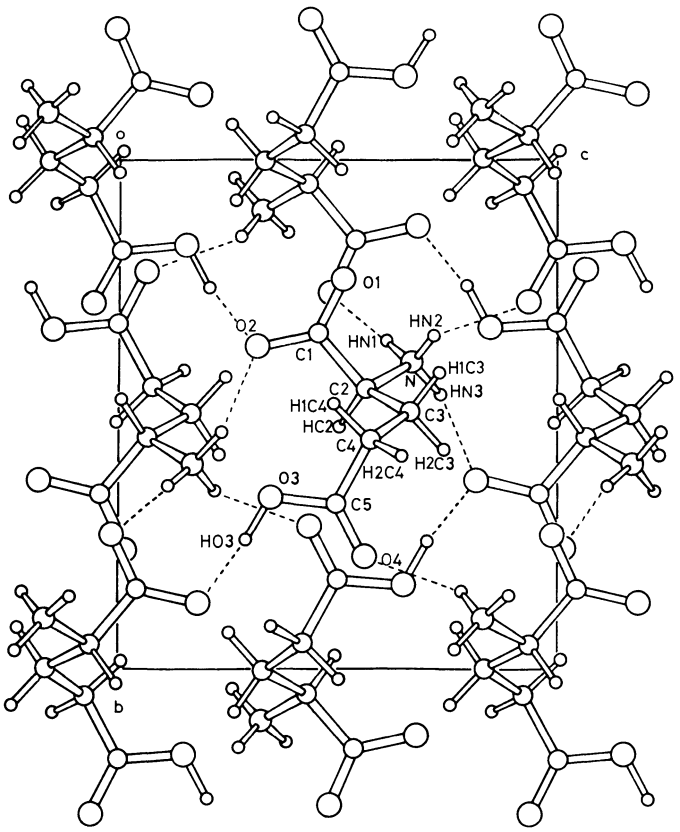

Fig. 1. A crystal structure viewed along the a axis with the numbering system of L-glutamic acid molecule.

***Lists of the observed and calculated structure factors are kept as Document No. 8002 at the Chemical Society of Japan.

not been observed in the crystal structures of the related compounds so far determined. Some torsional angles are compared with those of the related compounds in Table 5, in which the torsional angle nomenclature of IUPAC-IUB commission[11] are also given.

The conformation around the C(1)–C(2) bond in the α form is similar to that of the β form; the O(1)–C(1)–C(2)–N torsional angles for α and β are −50.3 and −42.3°, respectively. Similar negative values are usually observed in L-amino acids.[21] This would be brought about by the fact that both oxygen atoms of the α-carboxylate group should avoid C(3) and N which are bulky substituents. The torsional angles, χ^{31} and χ^{32}, in α are different from those in β, although the values in β are similar to those of the other compounds.

Table 3. INTERMOLECULAR HYDROGEN BOND LENGTHS (l/Å) AND ANGLES (ϕ/°)

A-H···B	H···B	A···B	∠A-H···B
O(3)-HO(3)···O(2)^{I}	1.56(3)	2.578(2)	163(3)
N-HN3···O(2)^{II}	1.93(3)	2.820(2)	161(3)
N-HN2···O(4)^{III}	2.19(3)	2.898(3)	152(3)
N-HN3···O(1)^{IV}	1.82(2)	2.776(3)	172(2)
I. $(1.0-x$	$0.5+y$	$0.5-z)$	
II. $(0.5-x$	$1.0-y$	$0.5+z)$	
III. $(1.0-x$	$-0.5+y$	$1.5-z)$	
IV. $(-0.5+x$	$0.5-y$	$1.0-z)$	

Bond Lengths and Angles. Bond lengths and angles are listed in Table 6, in which the corresponding values of the related compounds are also shown. As found in the β form, L-glutamic acid in the α form exists as a zwitter ion; a proton transfers from the α-carboxyl group to the amino group. The C(1)–O(1) and C(1)–O(2) distances of 1.242(3) and 1.275(3) Å, respectively, are the values of the ionized carboxyl group. The discrepancy of 0.03 Å between them can be attributed to differences of their intermolecular hydrogen bonds. As mentioned above, O(2) makes a very short hydrogen bond with the OH group and a NH···O hydrogen bond with the NH_3^+ group, while O(1) makes one NH···O bond with NH_3^+.

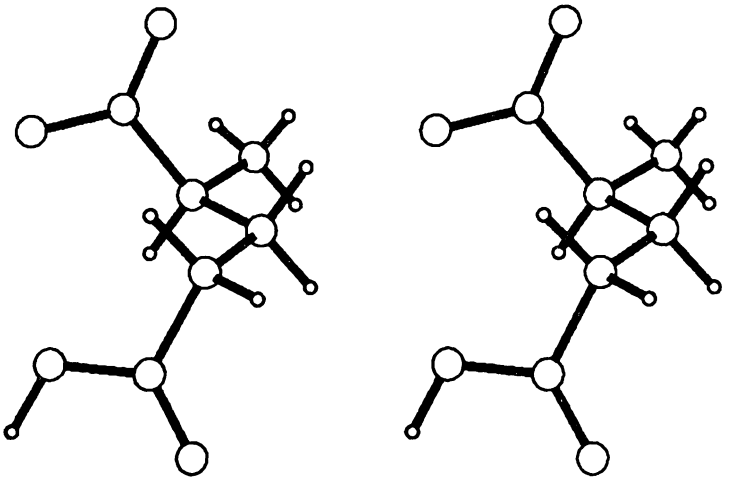

Fig. 2. A stereoscopic drawing of L-glutamic acid in the α form.

Table 4. TORSIONAL ANGLES (ϕ/°)

O(1)-C(1)-C(2)-C(3)	69.0	HC(2)-C(2)-C(3)-H1C(3)	175.8
O(2)-C(1)-C(2)-C(3)	−110.6	HC(2)-C(2)-C(3)-H2C(3)	61.5
O(1)-C(1)-C(2)-N	−50.3	N-C(2)-C(3)-H1C(3)	56.4
O(2)-C(1)-C(2)-N	130.0	N-C(2)-C(3)-H2C(3)	−57.9
O(1)-C(1)-C(2)-HC(2)	−167.9	C(2)-C(3)-C(4)-C(5)	68.8
O(2)-C(1)-C(2)-HC(2)	12.4	H1C(3)-C(3)-C(4)-H1C(4)	66.2
C(1)-C(2)-N-HN1	−47.4	H1C(3)-C(3)-C(4)-H2C(4)	−61.2
C(1)-C(2)-N-HN2	67.2	H2C(3)-C(3)-C(4)-H1C(4)	−176.7
C(1)-C(2)-N-HN3	178.6	H2C(3)-C(3)-C(4)-H2C(4)	55.9
HC(2)-C(2)-N-HN1	69.8	C(3)-C(4)-C(5)-O(4)	−105.0
HC(2)-C(2)-N-HN2	−175.6	C(3)-C(4)-C(5)-O(3)	73.9
HC(2)-C(2)-N-HN3	−61.4	H1C(4)-C(4)-C(5)-O(3)	17.6
C(3)-C(2)-N-HN1	−170.3	H1C(4)-C(4)-C(5)-O(4)	−163.5
C(3)-C(2)-N-HN2	−54.7	H2C(4)-C(4)-C(5)-O(3)	136.9
C(3)-C(2)-N-HN3	59.5	H2C(4)-C(4)-C(5)-O(4)	−44.2
C(1)-C(2)-C(3)-C(4)	59.1	O(4)-C(5)-O(3)-HO(3)	−3.7
N-C(2)-C(3)-C(4)	178.4	C(4)-C(5)-O(3)-HO(3)	175.2
HC(2)-C(2)-C(3)-C(4)	−62.2		

Table 5. Selected torsional anagles (ϕ/°) in the α form L-glutamic acid and other related crystal structures

IUPAC-IUB nomenclature	N-C2-C3-C4 χ^1	C2-C3-C4-C5 χ^2	C3-C4-C5-O3 χ^{32}	C3-C4-C5-O4 χ^{31}	Ref. 11
L-Glutamic acid α form	178.4	68.8	−105.0	73.9	present work
L-Glutamic acid β form	−51.8	−73.1	−160.7	18.8	6
L-Glutamic acid·HCl	−68.9	−173.1	−167.0	15.0	12
L-Arginine L-glutamate	−57	−172	180	−3	13
1:1 Mixed crystal of L-glutamic acid and L-pyroglutamic acid	−55.9	−65.2	−173.3	3.8	14
N-Tosyl-L-glutamic acid					15
A molecule	−51.9	−164.1	176.2	−3.2	
B molecule	−55.6	174.0	−174.2	7.5	
Phthaloyl-DL-glutamic acid					16
A molecule	−144.8	69.0	−162.4	16.9	
B molecule	−61.3	−65.5	154.3	−25.4	
Cu L-Glutamate·H_2O	67.8	−177.1	−171.2	6.7	17
Zn L-Glutamate·H_2O	67.0	−176.6	−170.1	7.8	18
Ca L-Glutamate·$3H_2O$	179.4	174.6	−169.1	12.3	19
L-glutamatobis(ethylenediamine) cobalt(III) perchlorate	70.6	−92.3	−122.7	54.8	20

Table 6. Bond lengths (l/Å) and angles (ϕ/°)
Estimated standard deviations are given in parentheses.

	α form	β form[10]	HCl salt[11]		α form	β form[10]	HCl salt[11]
C(1)-O(1)	1.242(3)	1.263(2)	1.221(9)	C(3)-C(4)-C(5)	111.9(2)	116.1(1)	112.0(4)
C(1)-O(2)	1.275(3)	1.243(2)	1.296(8)	C(4)-C(5)-O(3)	113.9(2)	112.2(1)	114.9(5)
C(1)-C(2)	1.527(3)	1.533(2)	1.535(7)	C(4)-C(5)-O(4)	123.9(2)	124.1(1)	122.7(5)
C(2)-N	1.495(3)	1.490(2)	1.482(6)	O(3)-C(5)-O(4)	122.3(2)	123.7(2)	122.4(5)
C(2)-C(3)	1.534(3)	1.530(2)	1.537(6)	C(5)-O(3)-HO(3)	115(2)	115.1(2)	114.7(9)
C(3)-C(4)	1.534(3)	1.523(2)	1.526(7)	C(2)-N-HN1	111(1)	110.8(2)	109.8(7)
C(4)-C(5)	1.500(3)	1.501(2)	1.476(7)	C(2)-N-HN2	108(2)	110.1(2)	110.0(8)
C(5)-O(4)	1.214(3)	1.219(2)	1.225(9)	C(2)-N-HN3	112(2)	112.3(2)	108.9(6)
C(5)-O(3)	1.327(3)	1.312(2)	1.315(8)	HN1-N-HN2	105(2)	108.6(3)	109.5(10)
N-HN1	0.97(2)	1.038(3)	1.04(1)	HN2-N-HN3	116(2)	107.1(2)	107.2(9)
N-HN2	0.77(3)	1.038(4)	1.06(1)	HN2-N-HN3	104(3)	107.8(3)	110.4(9)
N-HN3	0.93(3)	1.027(3)	1.08(1)	HC(2)-C(2)-N	109(1)	107.5(2)	108.2(7)
C(2)-HC(2)	1.03(3)	1.091(3)	1.085(10)	HC(2)-C(2)-C(1)	108(1)	110.5(2)	108.4(7)
C(3)-H1C(3)	1.03(3)	1.102(4)	1.08(1)	HC(2)-C(2)-C(3)	111(1)	110.9(2)	110.9(7)
C(3)-H2C(3)	1.07(3)	1.079(4)	1.07(1)	H1C(3)-C(3)-C(2)	106(1)	107.9(2)	108.4(8)
C(4)-H1C(4)	1.07(3)	1.080(4)	1.10(1)	H1C(3)-C(3)-C(4)	111(1)	107.0(2)	109.1(8)
C(4)-H2C(4)	1.06(3)	1.086(4)	1.11(1)	H2C(3)-C(3)-C(2)	110(1)	107.1(3)	108.0(7)
O(3)-HO(3)	1.04(3)	1.050(2)	0.98(1)	H2C(3)-C(3)-C(4)	110(1)	109.9(2)	108.4(8)
O(1)-C(1)-O(2)	125.5(2)	126.0(2)	125.4(6)	H1C(3)-C(3)-H2C(3)	106(2)	106.5(3)	106.7(12)
O(1)-C(1)-C(2)	117.7(2)	115.6(1)	122.0(5)	H1C(4)-C(4)-C(3)	110(2)	108.0(2)	112.7(8)
O(2)-C(1)-C(2)	116.8(2)	118.3(1)	112.6(5)	H1C(4)-C(4)-C(5)	109(2)	106.6(2)	109.0(7)
C(1)-C(2)-N	108.1(2)	109.3(1)	108.8(4)	H2C(4)-C(4)-C(3)	112(1)	112.8(2)	108.5(7)
C(1)-C(2)-C(3)	112.4(2)	107.3(1)	107.7(4)	H2C(4)-C(4)-C(5)	96(1)	106.8(2)	109.2(8)
N-C(2)-C(3)	108.3(2)	111.5(1)	112.6(3)	H1C(4)-C(4)-H2C(4)	114(2)	105.9(4)	105.2(13)
C(2)-C(3)-C(4)	114.1(2)	117.8(1)	115.8(4)				

Such a discrepancy is also found in the β form. The O(1) atom forms one OH···O hydrogen bond, whereas O(2) participates in two NH···O hydrogen bonds. The C(1)–O(1) bond is 0.02 Å longer than C(1)–O(2). This seems to indicate that the OH···O hydrogen bond is predominant in the L-glutamic acid crystals.

In the γ-carboxyl group, the lengths of C(5)–O(4) and C(5)–O(3), 1.214(3) and 1.327(3) Å, respectively, indicate that it is unionized. Other bond lengths and angles are normal.

The bond angles around C(2), C(3), and C(4) in the α form are significantly different from the corresponding ones in the β form. Such discrepancies may be resulted from the steric repulsions which are due to the conformational difference.

Discussion

In glutamic acid, χ^1 and χ^2 represent rotation about C(sp^3)–C(sp^3) bonds. Each of them is likely to have values in the neighbourhood of 60, 180, and $-60°$ which are designated by g, t, and $\bar{g}$, respectively. According to the conformational energy calculation,[22] favourable combinations χ^1 and χ^2 should be ($\bar{g}$, $\bar{g}$), (g, t), ($\bar{g}$, t), (t, t), and (t, g). The corresponding minimum conformational energies are 0.00, 0.21, 0.23, 0.40, and 0.43 kcal/mol. Judging from these values, glutamic acid in the β form is of the ($\bar{g}$, $\bar{g}$) conformer with the lowest energy, whereas that of the α form is of the (t, g) conformer with the highest energy. From the NMR study, Ham suggested that six conformers of L-glutamic acid can exist in solution.[23,24] Their populations are 0.27, 0.27, 0.18, 0.18, 0.06, and 0.04 for ($\bar{g}$, t), (g, t), ($\bar{g}$, g), (g, g), (t, t), and (t, g), respectively.

Six distinct conformations have been observed in the crystal structures so far reported as seen from Table 5. There are four, three, two, two, one, and one crystal structures containing conformers of ($\bar{g}$, t), ($\bar{g}$, $\bar{g}$), (g, t), (t, g), (g, $\bar{g}$), and (t, t), respectively. The occurence frequency in the crystal structures is in qualitative correspondence to the minimum conformational energy and the population in solution. This coincidence seems to indicate that the occurence frequency of each conformer is not biased to much extent by different crystalline fields or different substituents. Therefore, the occurence frequency may reflect the inherent relative stability of the conformations, and be used as a measure of the stability of the conformers if the considerable number of the related crystal structures can be obtained. These three measures suggest that the conformation in the β crystal is more stable and favourable than in the α crystal. The difference in conformational energy should be responsible for the transition from the α to β form.

Two types of chains or molecular arrangements, which are observed in the α and β crystals, are shown in Fig. 3, a and b, respectively. As mentioned above,

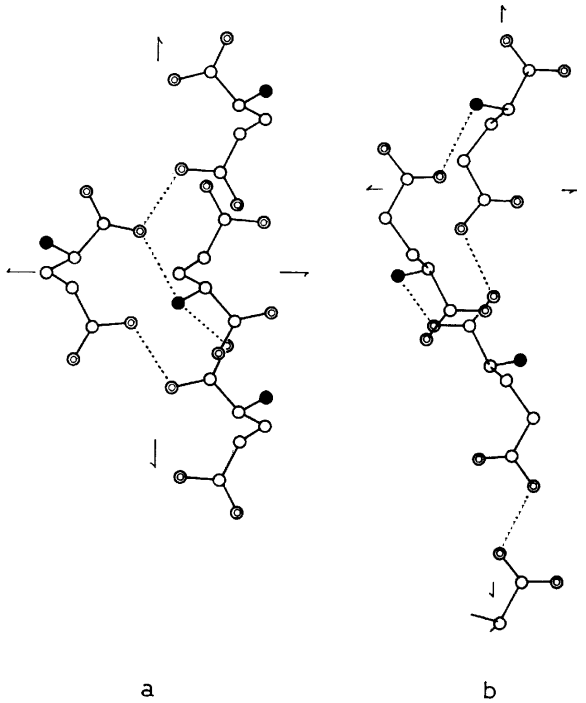

Fig. 3. A comparison of the hydrogen bond systems and the molecular arrangements in the α form (a) and the β form (b) crystals.

the OH···O bond seems to be most predominant among the four hydrogen bonds. Therefore, it is reasonable to assume that the considerable amounts of molecules are connected by the OH···O hydrogen bond to form chains in solution. The neighbouring chains can be connected by the NH···O hydrogen bonds and the conformation and the arrangement of the molecules are stabilized by these hydrogen bonds.

The α to β transition can be explained as shown in Fig. 4, in which the OH···O hydrogen bond is conserved. Here a and e correspond, respectively, to the initial α and the final β conformation. The b, c, and d conformers are hypothetical intermediates rotated stepwisely around the C–C single bonds. The

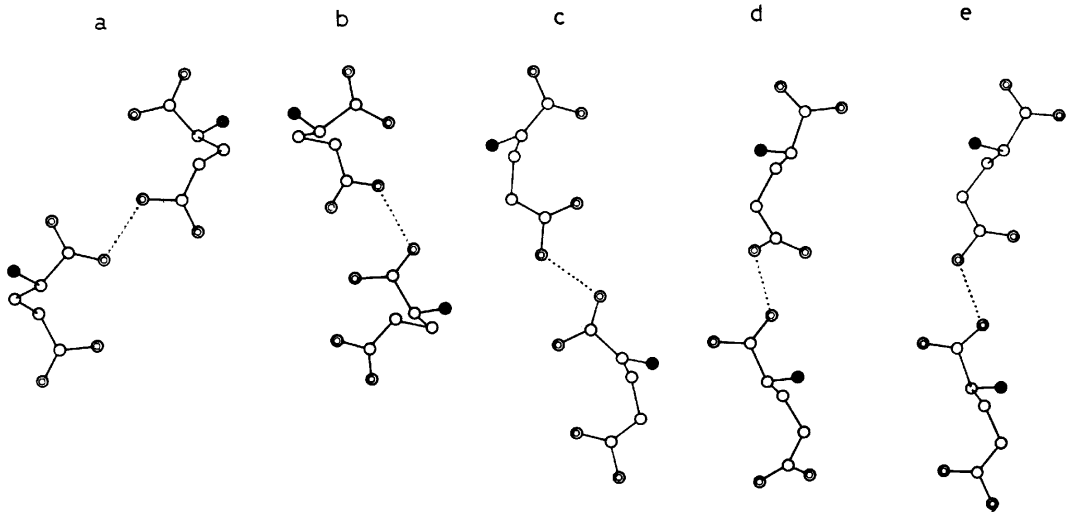

Fig. 4. A schematic drawing of the α to β transition.

actual conformational change might occur cooperatively. The α conformation would change to the β conformation, from a to e spontaneously rearranging the NH···O hydrogen bonds in solution.

Figure 4 also gives us an idea how the trace amount of the specific amino acids facilitates the crystallization of L-glutamic acid in the α form. Conformation of such amino acids would be suitable to make the NH···O hydrogen bonds with OH···O hydrogen bonded L-glutamic acid chains in the state a, and the nuclei generated in this way may trigger the initial stage of the crystallization to grow the α crystal.

References

1) S. Hirokawa, *Acta Crystallogr.*, **8**, 637 (1955).
2) M. Hasegawa, N. Fukuda, H. Higuchi, and I. Matsubara, *Agric. Biol. Chem.*, **41**, 49 (1977).
3) Y. Sakata, *Agric. Biol. Chem.*, **25**, 829 (1961).
4) S. Hiramatsu, *Nippon Nogei Kagaku Kaishi*, **51**, 27 (1977).
5) S. Hiramatsu, *Nippon Nogei Kagaku Kaishi*, **51**, 39 (1977).
6) M. S. Lehman, T. F. Koetzle, and W. C. Hamilton, *J. Cryst. Mol. Struct.*, **2**, 225 (1972).
7) J. D. Bernal, *Z. Kristallogr.*, **78**, 363 (1931).
8) G. Germain, P. Main, and M. M. Woolfson, *Acta Crystallogr., Sect. A*, **27**, 368 (1971).
9) T. Matsuzaki, Ms thesis (University of Tokyo, 1970).
10) "International Tables for X-Ray Crystallography," Kynoch Press, Birmingham (1974), Vol. IV, pp. 72—102.
11) IUPAC-IUB Commission on Biochemical Nomenclature Tentative Rules (1969), *J. Mol. Biol.*, **52**, 1 (1970).
12) A. Sequeira, H. Rajagopal, and R. Chidambaram, *Acta Crystallogr., Sect. B*, **28**, 2514 (1972).
13) T. N. Bhat and M. Vijayan, *Acta Crystallogr., Sect. B*, **33**, 1754 (1977).
14) Z. Taira and W. H. Watson, *Acta Crystallogr., Sect. B*, **33**, 3823 (1977).
15) M. Ohki, A. Takenaka, H. Shimanouchi, and Y. Sasada, *Bull. Chem. Soc. Jpn.*, **49**, 3493 (1976).
16) M. Ohki, A. Takenaka, H. Shimanouchi, and Y. Sasada, *Bull. Chem. Soc. Jpn.*, **50**, 90 (1977).
17) C. M. Gramaccioli and R. E. Marsh, *Acta Crystallogr.*, **21**, 594 (1966).
18) C. M. Gramaccioli and R. E. Marsh, *Acta Crystallogr.*, **21**, 600 (1966).
19) H. Einspahr and E. B. Charles, *Acta Crystallogr., Sect. B*, **30**, 1037 (1974).
20) R. D. Gillard, N. C. Payne, and G. B. Robertson, *J. Chem. Soc., A*, 2579 (1970).
21) A. V. Lakshminarayanan, V. Sasisekharan and G. N. Ramachandran, "Conformation of Biopolymers," Academic Press, New York (1967), Vol. 1, p. 61.
22) P. K. Ponnuswamy and V. Sasisekharan, *Int. J. Protein Res.*, **3**, 9 (1971).
23) N. S. Ham, "Molecular and Quantum Pharmacology," D. Reidel Publishing Co., Dordrecht (1974), pp. 261—268.
24) It seems that Ham assumed the conformers with $\chi^2=-60°$ are identical to those with $\chi^2=60°$. Therefore, the ($\bar{g}$, g) conformer is essentially equal to the ($\bar{g}$, $\bar{g}$) conformer in this discussion.

Resonance Raman Spectra of Tetracyanoethylene Anion Dimers

Kenji YOKOYAMA, Shiro MAEDA,* Chisumi ETOH,† Susumu MATSUZAKI,† and Koichi TOYODA†

Research Laboratory of Resources Utilization, Tokyo Institute of Technology, Midori-ku, Yokohama 227

†*Department of Chemistry, Faculty of Science, Kumamoto University, Kumamoto 860*

(Received May 22, 1979)

The resonance Raman spectra of $TCNE^-M^+$ (M=Na, K, Rb, Cs) in MTHF solutions have been measured at 100 K by exciting radiations within the long wavelength absorption band characteristic of the dimer $(TCNE^-)_2$. Two remarkably resonant lines have been observed at about 180 cm^{-1} and 150 cm^{-1}, showing an obvious change of the relative intensity depending on the counter cation species. The resonance behavior definitely indicates that the stretching vibration of interradical bond is responsible for these lines. Formation of two different types of dimer salts has been proposed as the most probable interpretation of the observed spectral behaviors.

A number of aromatic radical ions have been known to form the dimers under appropriate conditions of temperature and concentration. The formation of dimers is manifested by the temperature dependence of ESR and electronic spectra, which have been quantitatively investigated in several systems to discuss the monomer-dimer equilibrium.[1-4] Recently we studied the vibrational spectra of the dimers of some Würster's cations[5] and of *p*-benzosemiquinone anion,[6] by taking advantage of the resonance Raman effect. The spectra were obtained by exciting radiations close to the new long wave absorption bands characteristic of the dimer formation. In each case, a new resonant Raman line was observed at a low frequency and was assigned to the stretching vibration of interradical bond of the dimer, because of its remarkable and exclusive resonance enhancement by the dimer's characteristic absorption.

Tetracyanoethylene radical anion($TCNE^-$) has been shown to form the dimer at low temperatures.[7] Itoh[4] carried out quantitative investigations of the ESR and electronic spectra, from which he obtained the heat of dimer formation for several counter alkali metal ions and for varied solvent compositions. He also measured the electronic spectra of solid salts, noticing the spectral similarity between the room temperature solids and low temperature solutions. Hinkel *et al.*[8] measured the resonance Raman spectra of $TCNE^-Na^+$ and $TCNE^-K^+$ solid films by exciting radiations within the broad low frequency absorption band. They observed a very broad and intense Raman band at about 170 cm^{-1} with the features sensitive to the condition of sample deposition. Making reference to the behavior of overtone progression, they assigned the band to several librational lattice modes, by assuming mixed formation of different crystal structures with changeable composition.

In this paper, we present the resonance Raman spectra of $TCNE^-$ dimers observed in the low temperature solutions, and discuss the results in connection with the existing experimental data mentioned above.

Experimental

$TCNE^-M^+$ (M=Na, K, Rb, Cs) was prepared by contacting 2-methyltetrahydrofuran(MTHF) solution of TCNE with an alkali metal film in an evacuated manifold. The Raman spectra were recorded for the solution at 100±2 K, where the sample was still kept fluid, by cooling with a regulated flow of cold nitrogen gas in a vacuum cell. The condition of spectroscopic measurement was almost equal to the previous studies.[5,6]

Results and Discussion

The Raman spectra of about 3×10^{-3} mol dm^{-3} $TCNE^-Rb^+$ solution in MTHF at 100 K are shown in Fig. 1 for some Ar^+ laser exciting radiations. These laser lines are located on the higher frequency side within the long wave absorption band characteristic of the dimer, as shown in Fig. 2. As the laser wavelength approaches the absorption maximum at about 540 nm, new Raman lines emerge at 180 cm^{-1} and 150 cm^{-1} with remarkable resonance enhancement, both showing the depolarization ratio of about 0.35. No monomer lines have appreciable intensity in the same conditions.

The aspect of things is essentially similar to the previous observations on Würster's cations[5] and *p*-

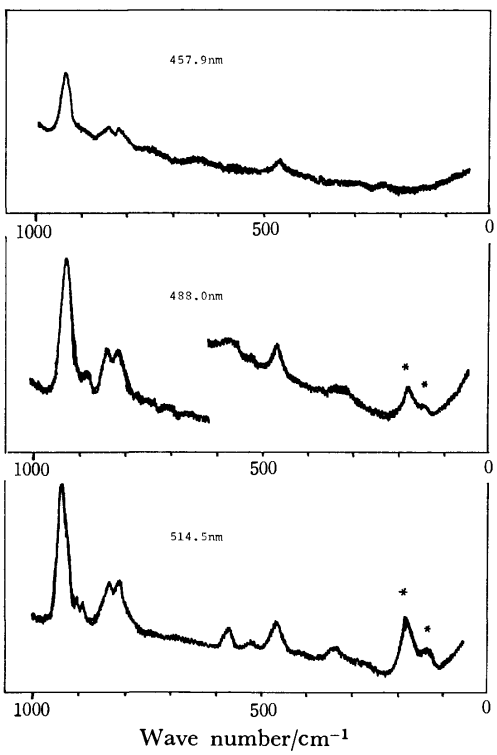

Fig. 1. Raman spectra of $TCNE^-Rb^+$ in MTHF solutions at 100±2 K. *Lines of the dimer.

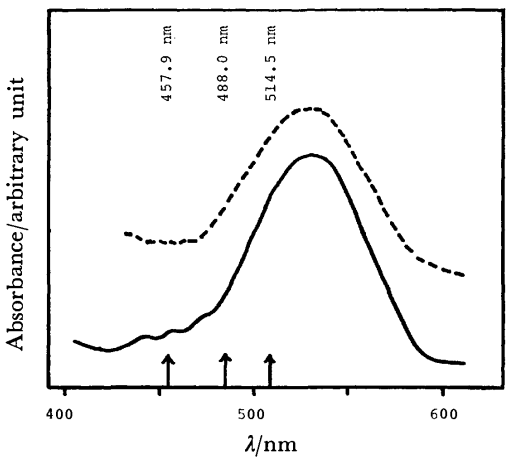

Fig. 2. Visible absorption spectra of $TCNE^-Na^+$ (solid line) and $TCNE^-Cs^+$ (broken line) in MTHF solutions at 100±2 K.

benzosemiquinone anion,[6] except that two well resolved new lines, instead of one, have been observed in the present spectra. Namely, it is little questionable that the 540 nm absorption band is attributed to the charge transfer type transition between $TCNE^-$ moieties of the dimer. The resonance Raman effect associated with this transition is most reasonably considered to originate in the Franck-Condon type term of the scattering tensor,[9] which is raised by the shift in the minimum position of interradical potential curves between the ground and excited states. Then, the strongly resonant low frequency lines obtained above are most likely associated with the stretching vibration of interradical bond. Here, we have tacitly assumed a parallel D_{2h} configuration of the dimer, by reason of the maximum overlap between the π-orbitals of both moieties. It may be noticed, however, that the electrostatic repulsion between the charge distributions on monomer ions is certainly against the D_{2h} structure, and the effect of attached counter cations brings further complexity.

Now, the appearance of two low frequency lines may possibly be due to the coupling of a low frequency dimer mode, composed of monomers' internal motion, with the strongly resonant interradical stretching mode. Such a coupling may be most probable for the symmetric combination of infrared active out-of-plane vibrations of monomers, and the Raman intensity of coupled modes is brought from the incorporated interradical motion. However, by measuring the spectra of other alkali metal salts under the same conditions, it has been found out that the intensity ratio of those two Raman lines changes remarkably depending on the counter cation species, as shown in Fig. 3. If we assume the coupled mode scheme as above, the observed intensity behavior signifies that the mixing ratio of internal and interradical mode amplitudes changes considerably by cation species, necessarily being attended by the corresponding frequency changes.

In the observed spectra, the higher frequency line is almost unchanged in the maximum position for different counter cation species, while a slight shift can be noticed for the lower frequency one, as shown

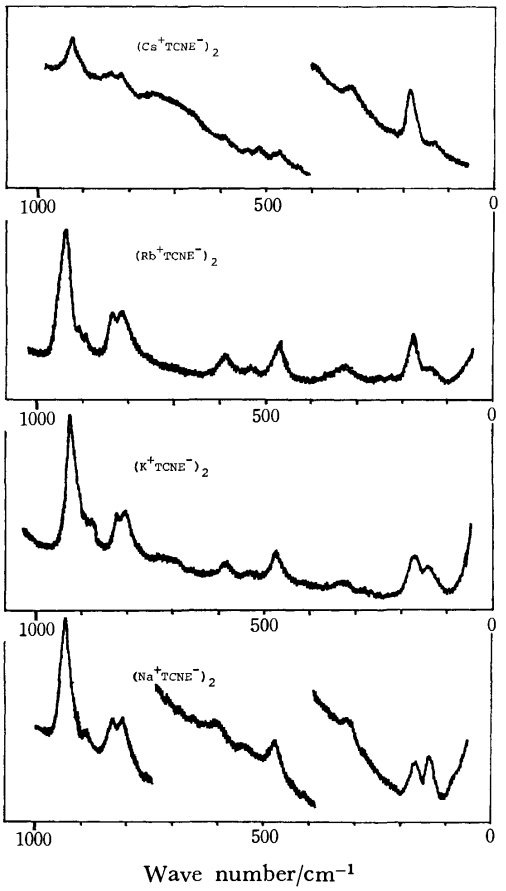

Fig. 3. Raman spectra of $TCNE^-M^+$ (M=Na, K, Rb, Cs) in MTHF solutions at 100±2 K with a 514.5 nm exciting radiation. The concentration is about 3×10^{-3} mol dm^{-3} for Na, K, and Rb salt and about 6×10^{-3} mol dm^{-3} for Cs salt.

in Fig. 4. A simple mechanical consideration shows that such a frequency behavior is rather unlikely in the above coupling scheme, and, even if admitted, cannot possibly be consistent with the observed intensity trend.

There may arise another argument that the two Raman lines are assigned to separate interradical modes with different origins of electronic resonance, so that the relative intensity changes due to the gradual shift of resonance origins from Na to Cs salts. However, this does not seem probable either, because the resonant 540 nm absorption band is essentially unchanged for different counter cations as observed in Fig. 2, and also because the relative intensity of two Raman lines hardly changes by altering the exciting radiation from 514.5 nm to 488.0 nm. The scarce sensitivity of the dimer's characteristic absorption to the counter cation species may be realized by the fact that the associated transition, illustrated in Fig. 5, gives rise to no substantial change in charge distribution, unlike the other transitions between different monomer orbitals.

Thus, we are led to conclude that the dimer molecules are distributed in two different forms, so that the observed intensity change may be interpreted as due to the population change in those forms effected by replacing the counter cation. In view of the ordinary and unchangeable features of 540 nm absorp-

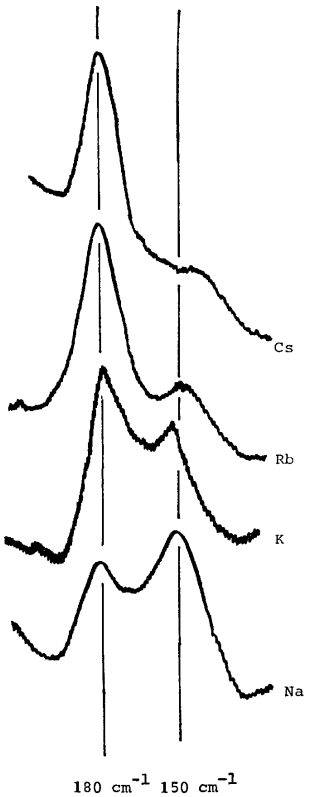

Fig. 4. Change of low frequency Raman features by counter cations in the spectra by 514.5 nm excitation.

tion band, the distinction between the two dimer forms may not consist in any notable difference in the interradical binding nature, but may be due to chemically less significant factors.

By investigating the temperature dependence of ESR and electronic absorption intensities, Itoh[4] showed that the heat of dimer formation($-\Delta H$) in MTHF solutions is appreciably dependent on counter cation species in the order $Na^+ > K^+ > Rb^+ > Cs^+$. He also showed that the $-\Delta H$ tends to be smaller for increasing solvation effect, from the same investigation by using THF/MTHF mixed solvents. The latter observation may be incorporated with the normally expected order of solvation strength, $Na^+ > K^+ > Rb^+ > Cs^+$, to suggest that the principal factor to give the above order of counter cation effect on $-\Delta H$ is not the solvation but more probably be ionic interactions. This is favorable for the supposition that two different modes of interaction between $(TCNE^-)_2$ and counter cations are responsible for the observed two Raman lines.

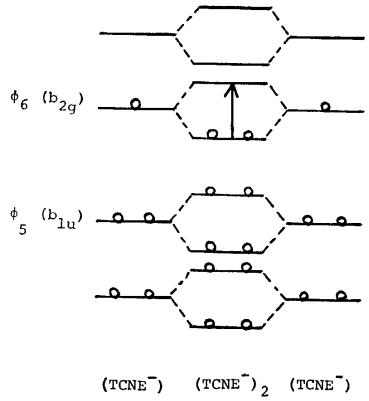

Fig. 5. MO scheme of $(TCNE^-)_2$ dimer formation. The arrow indicates the transition of 540 nm absorption.

Conceivable schemes may be the pair of $M^+(TCNE^-)_2$-M^+ and $M^+(TCNE^-)_2//M^+$, where // represents intervening solvent molecules, or two different geometrical arrangements in $M^+(TCNE^-)_2M^+$, *etc.*, but further investigations are required for discussing those schemes significantly.

On the other hand, it may be noticed that the observed low frequency Raman lines are in good correspondence to those of solid salts[8] in the frequencies and resonant behavior. Accordingly, it seems fairly probable that the solid lines have essentially the same origin as the present solution lines rather than the librational modes in the previous assignment[8]. This observation gives support to the formerly given suggestion that the structure unit of the crystal is the dimer[4].

References

1) S. Nakagawa and K. Suzuki, *Bull. Chem. Soc. Jpn.*, **46**, 3694 (1973).
2) K. Kimura, T. Yamazaki, and S. Katsumata, *J. Phys. Chem.*, **75**, 1768 (1971).
3) R. H. Boyd and W. D. Phyllips, *J. Chem. Phys.*, **43**, 2927 (1965).
4) M. Itoh, *Bull. Chem. Soc. Jpn.*, **45**, 1947 (1972).
5) K. Yokoyama and S. Maeda, *Chem. Phys. Lett.*, **48**, 59 (1977).
6) S. Yamaguchi, K. Yokoyama and S. Maeda, *Bull. Chem. Soc. Jpn.*, **51**, 3193 (1978).
7) R. Chang, *J. Phys. Chem.*, **74**, 2029 (1970).
8) J. J. Hinkel and J. P. Devlin, *J. Chem. Phys.*, **58**, 4750 (1973).
9) A. C. Albrecht, *J. Chem. Phys.*, **34**, 1476 (1961).

Classification of the External Magnetic Field Effects on the Photodecomposition Reaction of Dibenzoyl Peroxide

Yoshio SAKAGUCHI, Hisaharu HAYASHI,† and Saburo NAGAKURA*

The Institute for Solid State Physics, The University of Tokyo, Roppongi, Minato, Tokyo 106

† *The Institute of Physical and Chemical Research, Wako, Saitama 351*

(Received May 28, 1979)

The external magnetic field effects upon product yields in the singlet sensitized photolysis of dibenzoyl peroxide in toluene were studied. The observed field dependencies were classified into four types, and were interpreted in terms of the electronic Zeeman and hyperfine interactions in the intermediate radical pair. Especially large magnetic field effects were observed for the yields of dimethylbiphenyls, new products in this reaction.

Studies of external magnetic field effects upon intramolecular and intermolecular dynamical processes, have recently made much progress. New phenomena have been observed concerning intramolecular and intermolecular energy transfer[1] and also concerning chemical reactions[2-9] and their mechanisms have been clarified for some cases. Many problems, however, are still left unsolved in this field. The external magnetic field effect upon chemical reactions may be expected to be fruitful research field to be developed in future.

In a previous paper,[6] we first observed an external magnetic field effect upon the product yield of a photochemical reaction in solution, taking as an example the singlet sensitized photodecomposition reaction of dibenzoyl peroxide in the presence of magnetic field range, 1.0—4.3 T. We found the effect upon the yield of phenyl benzoate and interpreted the result in terms of the electronic Zeeman interaction in an intermediate radical pair. On the other hand, product yields and reaction intermediates for some other reactions through radical pairs have been found to be influenced by hyperfine interactions in low magnetic fields below 0.1 T.[7,8] Recently, we have published the theoretical study of external magnetic field effects on chemical reaction in solutions which occurs through radical pair formation,[10] and have classified them into three types.

In the present study, we have studied the photodecomposition reaction of dibenzoyl peroxide in the presence not only of high fields (4.3 and 6 T) but also of low fields below 78 mT. In the course of this study, we have found some new products and have succeeded in observing several different types of magnetic field effects on the product yields.[11]

Experimental

Toluene solutions (0.5 ml) of dibenzoyl peroxide (0.04 M) containing chrysene (0.002 M) as a singlet sensitizer[12] in Pyrex glass cells were degassed with the freeze-thaw technique, and were sealed under a nitrogen atmosphere. In the low magnetic field experiment below 78 mT the cells were placed in a hand-made coil which was cooled in a water bath, the temperature being kept 16.5±0.3 °C. The solution was irradiated with a 1 kW high pressure mercury lamp through a water filter and Pyrex glass. The decrease of dibenzoyl peroxide was monitored by iodometric titration of an aliquot and the half life under our experimental conditions was determined to be 11 min. Therefore the irradiation time was set to be 80 min in such a way that the dibenzoyl peroxide decomposed almost completely. In the high magnetic-field experiment, ternary solutions containing dibenzoyl peroxide and chrysene in toluene were irradiated in the presence of a magnetic field of 4.3 or 6 T induced by a superconducting magnet, and the details of the experiment were the same as described before.[6] The products were identified by GC-MS and VPC by comparing their retention times with those of the corresponding authentic samples. The yield, $P(H)$, of each product in the presence of an external magnetic field, H, was determined by VPC using 1,4-dicyanobenzene as an internal standard.

The viscosity dependence of the magnetic field effect upon the yield of phenyl benzoate was examined by changing the solvent viscosity. The viscosity was increased by the addition of polystyrene to the solvent. Polystyrene (Wako Pure Chemical Industries Ltd. polymerization degree 1600—1800) was purified by repeating twice precipitation from its toluene solution by methanol. The viscosity was measured by Ostwald's viscometer.

Results and Discussion

The singlet sensitized photolysis of dibenzoyl peroxide proceeds as follows:

$$\begin{aligned} &PhCO_2OCOPh^* \longrightarrow \\ &\quad \overline{PhCO_2\cdot + Ph\cdot} + CO_2 \longrightarrow \\ &\qquad \downarrow \qquad PhCO_2Ph \text{ (cage product)} + CO_2 \\ &PhCO_2\cdot + Ph\cdot \text{(escaping radicals)} + CO_2 \qquad (1) \\ &\qquad\qquad \downarrow \\ &\qquad\qquad \text{escape products} \end{aligned}$$

For this reaction in toluene, we identified 14 products the molecular weights of which are less than 212.[13] They are listed in Table 1 together with their yields. Among them *m,n'*-dimethylbiphenyls (**6**'s) were found in this study for the first time, although the others had already been detected.[14]

Phenyl benzoate (**2**) and biphenyl (**1**) are cage products[15] and the others in Table 1 are considered to be escape ones. From Table 1 we can see the following characteristic features of the yields of dimethylbiphenyls (**6**). Firstly, the dimethylbiphenyls with a methyl group on the 4-position are not observed. Secondly, the yield is larger for 3,3'-**6** than for 2,2'-**6** and 2,3'-**6**.

The simplest possible mechanism for the formation of dimethylbiphenyls in the present system is the tolylation of toluene which proceeds as follows;

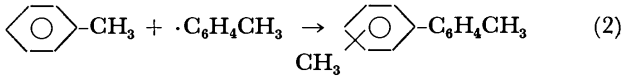

(2)

Table 1. Identified products and their yields in the presence of 0.3 mT

	Products	Yield[a)]
Cage products	biphenyl (**1**)	0.9
	phenyl benzoate (**2**)	11.6
Escape products	benzoic acid (**3**)	---[b)]
	o-methylbiphenyl (*o*-**4**)	6.4
	m-methylbiphenyl (*m*-**4**) *p*-methylbiphenyl (*p*-**4**) 1,2-diphenylethane (1,2-**5**)	18.9[c)]
	2,2′-dimethylbiphenyl (2,2′-**6**)	0.1
	2,3′-dimethylbiphenyl (2,3′-**6**)	0.8
	3,3′-dimethylbiphenyl (3,3′-**6**)	1.4
	o-tolyl benzoate (*o*-**7**)	2.6
	m-tolyl benzoate (*m*-**7**)	---[b)]
	p-tolyl benzoate (*p*-**7**)	---[b)]
	benzyl benzoate (**8**)	---[b)]

a) In mol% of dibenzoyl peroxide. b) --- indicates that their yields were not measured because of the incomplete separation between these compounds under our VPC conditions. c) Only the sum of the yields of these compounds was measured because they were not resolved from one another under our VPC conditions.

However, the partial rate factors (F_i) for this reaction determined by Ito *et al.*[16] ($F_o:F_m:F_p=3.3:1.0:1.3$) are completely different from the present results in Table 1. Thus the tolylation mechanism is disregarded.

Another possible mechanism for the formation of **6**'s is an assisted reaction[17] by $PhCO_2\cdot$ radicals. For example, 3,3′-**6** can be formed through (*o*-benzoyloxy)-methylcyclohexadienyl radical (*o*-**9**):

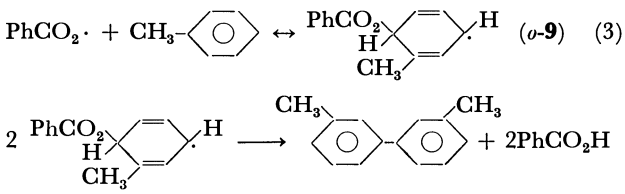

(*o*-**9**) (3)

The benzoyloxylation of toluene may preferably occur on the *o*-position through the hyperconjugation of the methyl group. The steric hindrance of the benzoyloxyl group is considered to disturb formation of the dimethylbiphenyls with a methyl group on the 4-position (2,4′-, 3,4′-, and 4,4′-dimethylbiphenyls). Thus, the assisted reaction scheme explains the observed yields of the dimethylbiphenyls. According to this mechanism, dimethylbiphenyls are escape products. This conclusion is also supported by the changes of the yields of dimethylbiphenyls due to dissolved oxygen and due to the excitation light intensity.[18]

From the magnetic field dependence of the measured $P(H)$ values listed in Table 1, the products can be classified into four groups.

[1] phenyl benzoate (**2**)

[2] 1,2-diphenylethane (1,2-**5**), *o*-, *m*-, and *p*-methylbiphenyls (*o*-, *m*-, and *p*-**4**'s) and biphenyl (**1**)

[3a] 2,2′-, 2,3′-, and 3,3′-dimethylbiphenyls (**6**'s)

[3b] *o*-tolyl benzoate (*o*-**7**)[19]

The observed relative change, $R(H)$, of the yield of the typical product in each group is plotted against log H in Fig. 1. Here $R(H)$ is defined

$$R(H) = [P(H)-P(0)]/P(0)$$

Here, $P(0)$ is the yield without an external magnetic field (in actuality, under the residual field (0.3 mT) of the magnets).

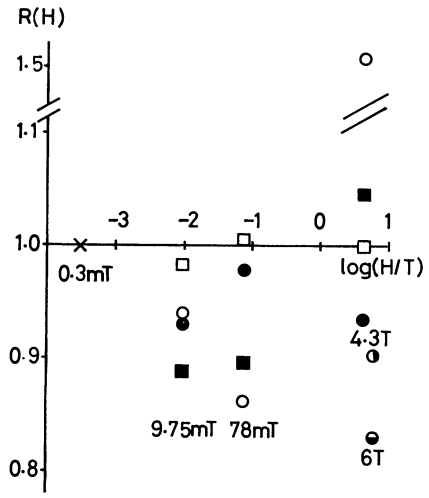

Fig. 1. $R(H)$-H plots in toluene and the viscosity dependence of R_2 (6 T): ● $R(H)$ for **2** (type 1); □ $R(H)$ for mixture of 1,2-**5**, *m*-**4**, and *p*-**4** (type 2); ○ $R(H)$ for 3,3′-**6** (type 3a); ■ $R(H)$ for *o*-**7** (type 3b); ◑ R_2 (6 T) for $\eta_r=3.6$; ◒ R_2 (6 T) for $\eta_r=8.8$. Here, $\eta_r=\eta_{solvent}/\eta_{toluene}$.

According to the theory of the external magnetic field effect on chemical reactions through a radical pair,[10] the field dependence of $P(H)$ for cage or escape products from Γ-precursors (Γ is singlet, triplet, or free radical) can be represented qualitatively as shown in Fig. 2.[20]

Case (a) in Fig. 2. can be applied to reactions in which the energy separation, $|2J|$, between the singlet, S, and triplet, T_m ($m=0, \pm1$), states of the intermediate radical pair is smaller than or comparable to the largest

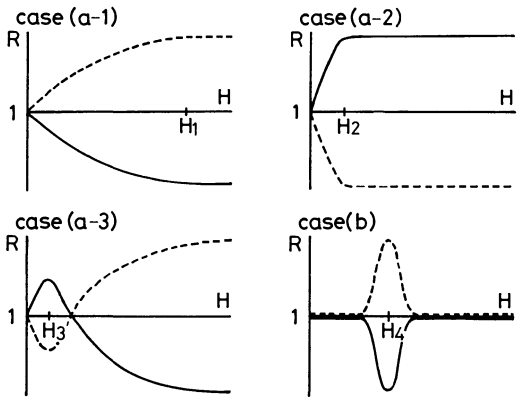

Fig. 2. Theoretical classifications of the magnetic field dependences on the product yields. The full curves indicate the magnetic field dependence of the cage (escape) product from a singlet (triplet or free radical) precursor; the broken curves indicate the magnetic field dependence of the escape (cage) product from a singlet (triplet or free radical) precursor. See text for H_1, H_2, H_3, and H_4.

off-diagonal matrix element between S and T_m. Case (a) is further divided into three sub-groups according to the effective off-diagonal matrix elements: (a-1) electronic Zeeman interaction between S and T_0 (the first term in Eq. 2 of the previous paper[10]) is effective; (a-2) hyperfine interactions between S and T_m (the second and third terms in Eq. 2 and Eqs. 3 and 4 of the previous paper[10]) are effective; (a-3) both interactions are effective. Here we added a new situation (case (b)) which is applicable to reactions where $|2J|$ is larger than the largest off-diagonal matrix element.

Let us summarise the field dependence of $P(H)$ for the cage (escape) product from a singlet (triplet or free radical) precursor (full curves in Fig. 2). In case (a-1), $P(H)$ decreases with increasing magnetic field by the S-T_0 conversion through the electronic Zeeman term[10] and converges into a constant at a high magnetic field H_1. In case (a-2), $P(H)$ increases suddenly at a low field, H_2, and remains almost constant above H_2. In case (a-3), $P(H)$ first increases with the increasing magnetic field but begins to decrease from a fairly low magnetic field, H_3. In case (b), $P(H)$ suddenly decreases at a level-crossing field, $H_4=|2J|/(g\beta)$, through a sudden increase of the S-T_m ($m=1$ or -1) conversion in the radical pair.[2] Here g is the mean value of the isotropic g-factors of the component radicals. $P(H)$ for the cage (escape) product from a triplet or free radical (singlet) precursor can be represented as shown by the broken curves in Fig. 2.

Let us consider the $R(H)$ values observed in this study (Fig. 1) on the basis of the above-mentioned theoretical classification. We can see from Fig. 1 that $R(H)$ of **2** (group [1]) decreases with increasing magnetic field, and those of the products in group [2] are nearly constant independent of the applied field within the limits of experimental error. **2** is a cage product from the singlet radical pair containing Ph· and $PhCO_2$·, and the products in group [2] except for **1** are the escape products from the radical pairs shown in Eq. 1. The $R(H)$ values of **2**, *o*-**4**, *p*-**4**, and 1,2-**5** at the high field region, 1—4.3 T, were measured and analysed theoretically in the previous paper,[6] being classified to case (a-1). According to the present results at the low field region below 78 mT, no appreciable hyperfine effect (case (a-2)) could be detected for the products in groups [1] and [2]. Thus $R(H)$'s of **2** in the whole magnetic field region under the measurements are well explained in terms of the electronic Zeeman effect and **2** is regarded as one of the typical examples belonging to case (a-1).

1 is a cage product as **2**, but its $R(H)$ is independent of the applied field within the limits of experimental error. Thus **1** belongs to group [2]. The electronic Zeeman effect may be disregarded for this case because Δg is equal to zero for the radical pair containing the two phenyl radicals.

The $R(H)$ values of the products in groups [3a] and [3b] are smaller than 1.0 in the low field region and larger than 1.0 at the field of 4.3 T (Fig. 1). Actually $R_{3,3'\text{-}6}$ (78 mT) was determined to be as small as 0.86 and $R_{3,3'\text{-}6}$ (4.3 T) as large as 1.51. The latter is one of the largest external magnetic field effects upon the reaction yields observed so far. The above-mentioned field dependence of the $R(H)$ for the products of groups [3a] and [3b] clearly corresponds to the broken curve of case (a-3) in Fig. 2. Therefore they are regarded as escape products, since the present photodecomposition reaction occurs from the singlet precursor. This conclusion is supported by the following facts: (1) **6**'s are considered to be produced through dimerization of the **9** radical as is shown in Eq. 3. (2) According to Nakata *et al.*,[14] **7**'s are formed by the reaction between the **9** radical and the escaping (R·) radical. For example, *o*-**7** can be formed through the following reaction.

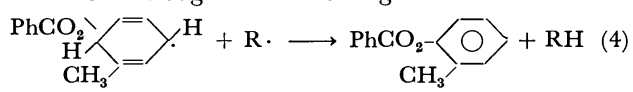

(4)

(3) The **9** radical is formed from the escaping benzoyloxyl radical as is shown in Eq. 3.

Thus, the magnetic field dependence of $R(H)$ for the products of groups [3a] and [3b] is explained in terms of the mixed effects of the electronic Zeeman and hyperfine interaction. Precisely speaking, the $R(H)$ value at 4.3 T is much smaller for *o*-**7** than for **6**'s, while in the low field region the values are similar to each other for *o*-**7** and **6**'s (see Fig. 1). This might be due to the fact that the yields of each **7** is proportional to the concentration of the corresponding(benzoyloxy)-methylcyclohexadienyl radical but that of *m*,*n*'-**6** is proportional to the product of the concentrations of *m*''- and *n*''-**9**.

We measured the viscosity dependence of $R(H)$ for **2**. The viscosity was increased by addition of polystyrene to the solvent (toluene). We can see from Fig. 1 that $R(6\text{ T})$ for **2** at $\eta_r=8.8$ was determined to be as small as 0.83, and the decrease in the yield of the cage product due to a magnetic field was proved to be enhanced by solvent viscosity.

The authors wish to express their sincere thanks to Prof. K. Tokumaru and Dr. H. Sakuragi, The University of Tsukuba and Prof. M. Yoshida, The University of Tokyo for helpful discussions and for supplying some of the authentic samples.

References

1) for example, P. W. Atkins and T. P. Lambert, *Ann. Rep. Prog. Chem. A*, **72**, 67 (1975); A. Matsuzaki and S. Nagakura, *Helv. Chim. Acta*, **61**, 675 (1978).
2) N. Hata, *Chem. Lett.*, **1976**, 547.
3) R. Z. Sagdeev, Yu. N. Molin, K. K. Salikhov, T. V. Leshina, M. A. Kamha, and S. M. Shein, *Org. Magn. Reson.*, **5**, 603 (1973).
4) A. V. Podoplelov, R. Z. Sagdeev. T. V. Leshina, Yu. A. Grishin, and Yu. N. Molin, *Dokl. Akad. Nauk. SSSR*, **225**, 866 (1975).
5) H. Sakuragi, M. Sakuragi, T. Mishima, S. Watanabe, M. Hasegawa, and K. Tokumaru, *Chem. Lett.*, **1975**, 231.
6) Y. Tanimoto, H. Hayashi, S. Nagakura, H. Sakuragi, and K. Tokumaru, *Chem. Phys. Lett.*, **41**, 267 (1976).
7) H. J. Werner, H. Staerk, and A. Weller, *J. Chem. Phys.*, **68**, 2419 (1978).

8) M. E. Michel-Beyerle, R. Haberkorn, W. Bube, E. Bube, E. Steffens, H. Schroder, H. J. Neusser, and E. W. Schlang, *Chem. Phys.*, **17**, 139 (1976).
9) N. J. Turro and B. Kraeutler, *J. Am. Chem. Soc.*, **100**, 7432 (1978).
10) H. Hayashi and S. Nagakura, *Bull. Chem. Soc. Jpn.*, **51**, 2862 (1978).
11) Preliminary result, Y. Sakaguchi, H. Hayashi, and S. Nagakura, Proc. VII IUPAC Symposium on Photochemistry, Heverlee (Belgium), July 1978, p. 291.
12) T. Nakata and K. Tokumaru, *Bull. Chem. Soc. Jpn.*, **43**, 3315 (1970).
13) According to analysis of the irradiated solution by the GC-MS, the products with the molecular weights larger than 212 were also found, although their yields were not measured.
14) T. Nakata, K. Tokumaru, and O. Simamura, *Tetrahedron Lett.*, **1967**, 3303.
15) E. M. Schulman, R. D. Bertrand, D. M. Grant, A. R. Lepley, and C. Walling, *J. Am. Chem. Soc.*, **94**, 5972 (1972).
16) R. Ito, T. Migita, N. Morikawa, and O. Simamura, *Tetrahedron*, **21**, 955 (1965).
17) T. Suehiro, S. Igeta, O. Kuwabara, and M. Hirai, *Tetrahedron*, **26**, 963 (1970).
18) Y. Sakaguchi, H. Hayashi, and S. Nagakura, Abstract of Papers, Symposium on Photochemistry: Kyoto, Nov. 1978, p. 26.
19) *m*-and *p*-**7**'s may belong to this group. Since these compounds were not resolved from **8** under our VPC conditions, their $P(H)$ could not be measured.
20) In Fig. 2, we show the yields of the products which are given only from singlet states. Those of other reactions can similarly be analysed.

 © 1980 The Chemical Society of Japan Bull. Chem. Soc. Jpn., 53, 43—47 (1980)

Picosecond Spectroscopy Studies of the Intersystem Crossing of Aromatic Carbonyl and Nitro Compounds in Solution

Hiroyuki OHTANI, Takayoshi KOBAYASHI,† Kaoru SUZUKI, and Saburo NAGAKURA*

Institute for Solid State Physics, The University of Tokyo, Roppongi, Minato, Tokyo, 106

†*The Institute of Physical and Chemical Research, Wako, Saitama 351*

(Received July 16, 1979)

The build-up time constants of $T_n \leftarrow T_1$ transition bands were measured with 4-hydroxybenzophenone, Michler's ketone, 2-nitrofluorene, 1-nitropyrene, and 9-nitroanthracene in solution with the aid of picosecond spectroscopy. All the compounds exhibit fast build-up of the $T_n \leftarrow T_1$ absorption with the time constants smaller than 100 ps. The picosecond kinetics of these nonfluorescent compounds are interpreted in terms of the electronic structures of initial and final states relevant to radiationless transitions.

Aromatic carbonyl and nitro compounds are well known to be nonfluorescent.[1-3] Benzophenone exhibits strong phosphorescence, the quantum yield of the triplet formation being unity.[3] Therefore, the nonfluorescent property of benzophenone is caused by the fast S-T intersystem crossing. The quantum yields of the triplet formation are 0.63 and 0.83[4] for 1- and 2-nitronaphthalenes which are nonfluorescent and show weak phosphorescence, respectively.[2] Since the yield of fluorescence, $\Phi_F (=k_f/(k_f+k_{nr})$, $k_f=10^6$—$10^7\ s^{-1})$ is smaller than 10^{-4} for these molecules, the nonradiative rate constant, k_{nr}, is larger than $10^{10}\ s^{-1}$ and the nonradiative relaxation process occurs in the time scale of subnanosecond.

Nonradiative decay time constants of aromatic carbonyl compounds,[5-9] nitronaphthalene,[6] acridine,[10,11] and phenazine[10] have been measured so far by monitoring $T_n \leftarrow T_1$ absorption with picosecond time-resolved spectroscopy.

In a previous paper[7] we reported the intersystem crossing rate of anthrone and fluorenone. In anthrone the break-down of the El-Sayed rule was explained by the second order perturbation theory considering the vibronic interactions between appropriate states. In the present paper the nonradiative decay processes of excited singlet states have been studied for 4-hydroxybenzophenone, Michler's ketone (4,4'-bis(dimethylamino)benzophenone), 2-nitrofluorene, 1-nitropyrene, and 9-nitroanthracene.

Experimental

Picosecond Experiments. Figure 1 shows a picosecond time-resolved spectroscopy apparatus which is similar to the one described in the previous paper.[7] We used one OMA instead of two. The double-beam method[7,12] is effective for reducing deviations caused by the shot by shot change in spatial intensity distribution of the picosecond pulse. The frequency of a single pulse (694.3 nm, 30±3 ps pulse width, several giga watts) selected from a pulse train from a mode-locked ruby laser was doubled with a phase-matched ADP crystal. The frequency-doubled pulse (347.2 nm) was used for the excitation of samples through a pinhole (0.9 mm in diameter) of a sample cell holder. By passing the fundamental pulse through a phosphoric acid cell (20 mm in diameter, 100 mm in light path) a picosecond pulse of continuum light was generated. The pulse was divided into 14 pulses by an echelon with the time interval of 19.0 ps between the neighbouring pulses. These pulses were divided into two sets by a beam splitter.

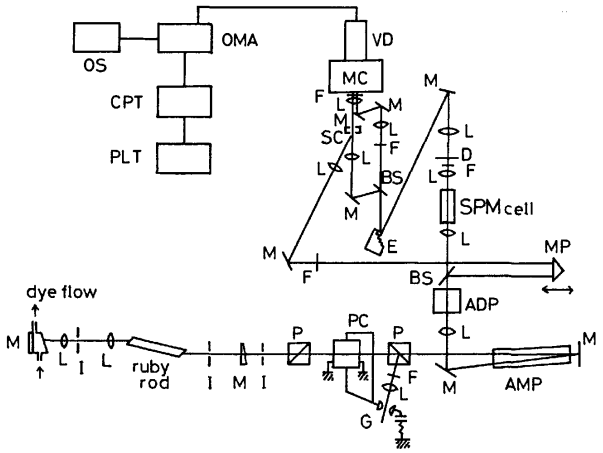

Fig. 1. The block diagram of the picosecond spectroscopy apparatus.
M: Mirror, L: lens, I: iris, P: polarizer, PC: Pockels cell, G: spark gap, BS: beam splitter, MP: movable prism, F: filter, SPM cell: self-phase modulation cell, D: diffuser, E: echelon, SC: sample cell, MC: monochromator, VD: vidicon, OMA: optical multichannel analyzer, OS: oscilloscope, CPT: computer, PLT: plotter.

One set passed through the Pyrex sample cell (light path 2.0 mm) and another set was used as reference. The observation wavelength was selected by a Shimadzu grating polychromator. Light intensities were detected by a vidicon head (PAR 1205 I) of an OMA (PAR 1205), digitized, and memorized in an OMA console (PAR 1205 A). The data were recorded in the digital cassette tapes and analyzed with a YHP 9825A desk-top computer. The results were printed out with the internal thermal printer of the computer or plotted with a YHP 9862A X-Y plotter.

Materials. 4-Hydroxybenzophenone (Tokyo Kasei), Michler's ketone (4,4'-bis(dimethylamino)benzophenone) (Tokyo Kasei), 2-nitrofluorene and 9-nitroanthracene (Aldrich) were purified by repeated recrystallizations and/or column chromatography. 1-Nitropyrene kindly supplied by Prof. T. Yamaoka, Chiba University was purified by repeated recrystallizations from ethanol. Ethanol (Wako, spectrograde) and benzene (Tokyo Kasei, UVIR grade) were used without further purification. Concentrations of samples were set in such ways that the absorbances at 337.1 nm were 1.0 in a 1 mm cell for nanosecond time-resolved spectroscopy experiments and those at 347.2 nm were at least 1.5 in a 1 mm cell for picosecond time-resolved spectroscopy experiments.

Results

Nanosecond Time-resolved Spectroscopy Experiments. Since the $T_n \leftarrow T_1$ spectra of 2-nitrofluorene, 9-nitroanthracene and Michler's ketone in benzene have never been reported, we measured their spectra with the nanosecond apparatus.[7] The strong absorption of Michler's ketone was observed between 420 nm and 600 nm in benzene solution. 2-Nitrofluorene exhibits strong absorption between 400 nm and 650 nm with a peak at 510—550 nm. The $T_n \leftarrow T_1$ absorption spectrum of 9-nitroanthracene resembles that of anthracene. All these transient absorption are assigned to $T_n \leftarrow T_1$ transitions, since the transient species are quenched by oxygen.

Picosecond Time-resolved Spectroscopy Experiments. Figures 2—6 show the time dependence of the $T_n \leftarrow T_1$ absorption intensity. Data of 7—14 shots are averaged for each point. Error bars in these figures represent standard deviations. The time constants were determined by the computer simulation on the assumptions described below. Before the measurement of the build-up of the $T_n \leftarrow T_1$ absorption of each sample we observed the build-up of the $S_n \leftarrow S_1$ absorption of coronene to determine the time resolution of the apparatus under the same monitoring wavelength and optical allignment. With the aid of formulas (1) and (2) we made computer simulation to determine the pulse width of the light source and the arrival time difference between the excitation pulse and the monitoring pulse train:

$$A(t) = -\log\left[\int_{-\infty}^{\infty} I(t-t')10^{-S(t')}\mathrm{d}t' \Big/ \int_{-\infty}^{\infty} I(t-t')\mathrm{d}t'\right] \quad (1)$$

$$S(t') = \Delta S \int_{-\infty}^{t'} I_{ex}(t''-t_0)\mathrm{d}t''$$

$$= \Delta S \int_{-\infty}^{t'} \frac{1}{\sqrt{\pi}G} e^{-(t''-t_0)^2/G^2}\mathrm{d}t'' \quad (2)$$

Here $A(t)$ is the absorbance for the $S_n \leftarrow S_1$ transition of coronene at time t, $I(t-t')$ is the monitoring pulse intensity at time t' which has the maximum at time t, ΔS is an experimentally determined parameter corresponding to the absorbance for the $S_n \leftarrow S_1$ transition of coronene at $t=\infty$, and $I_{ex}(t''-t_0)$ is the excitation pulse intensity at time t'' which has the maximum at time t_0. We assumed that excitation and monitoring pulses are gaussian and have the same pulse width (fwhm is $2 \ln G$). The time constant of the build-up of the $T_n \leftarrow T_1$ absorption (τ) and the contribution of $S_n \leftarrow S_1$ absorption (W) were obtained by the simulation of $A(t)$ to the observed curve by formulas (3) and (4),

$$A(t) = -\log\left[\int_{-\infty}^{\infty} I(t'-t)10^{-T(t')}\mathrm{d}t' \Big/ \int_{-\infty}^{\infty} I(t'-t)\mathrm{d}t'\right] \quad (3)$$

$$T(t') = \Delta A \int_{-\infty}^{t'} I_{ex}(t''-t_0)[W+(1-W)(1-e^{-(t-t'')/\tau})]\mathrm{d}t'' \quad (4)$$

where $T(t')$ is the transient absorption at time t' and consists of the $S_n \leftarrow S_1$ absorption and $T_n \leftarrow T_1$ absorption at the monitoring wavelength and ΔA is an experimentally determined parameter corresponding to the absorption for the transient absorption at $t=\infty$. The best-fit curve for each sample is shown in Figs. 2—6. The $T_n \leftarrow T_1$ build-up time constants thus determined are tabulated in Table 1. Error limits of

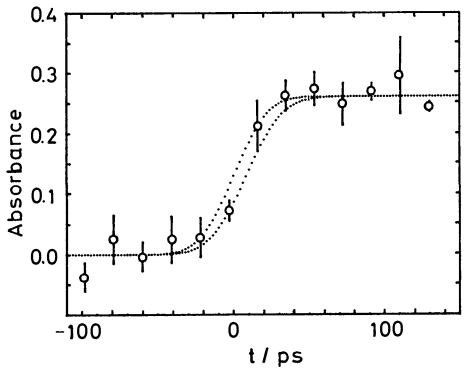

Fig. 2. Kinetics of $T_n \leftarrow T_1$ absorption at 550 nm for 4-hydroxybenzophenone in benzene. The time constants are 0 ps for •••• (upper) and 8 ps for •••• (lower).
The fraction of $S_n \leftarrow S_1$ absorption (W) is 0.0.

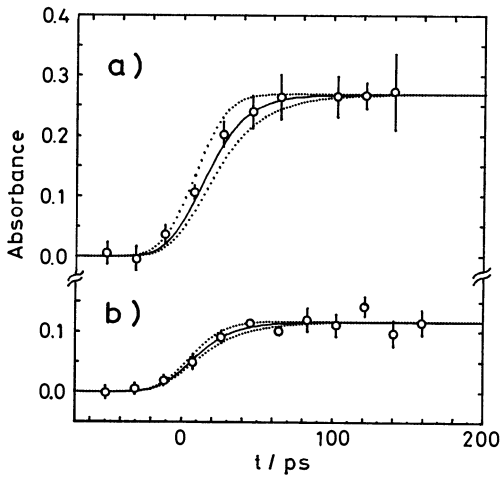

Fig. 3. Kinetics of $T_n \leftarrow T_1$ absorption at 550 nm for Michler's ketone: a) in benzene; b) in ethanol.
The time constants are 10 ps •••• (upper), 18 ps for —, and 26 ps for •••• (lower) in both a) and b).
The contribution of $S_n \leftarrow S_1$ absorption, is 0.0 for a) and 0.3 for b).

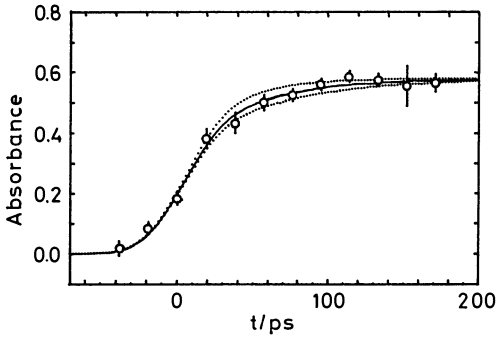

Fig. 4. Kinetics of $T_n \leftarrow T_1$ absorption at 520 nm for 2-nitrofluorene in benzene.
The time constants are 30 ps for •••• (upper), 45 ps for —, and 60 ps for •••• (lower), W being 0.6.

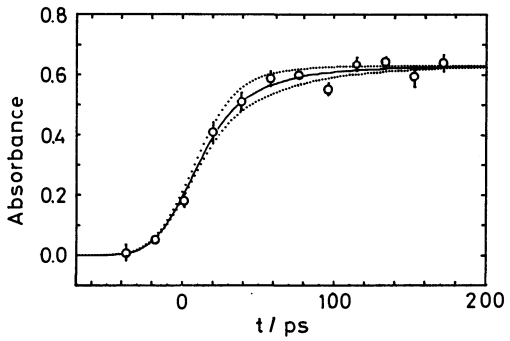

Fig. 5. Kinetics of $T_n \leftarrow T_1$ absorption at 520 nm for 1-nitropyrene in benzene.
The time constants are 20 ps for •••• (upper), 33 ps for —, and 46 ps for •••• (lower), W being 0.5.

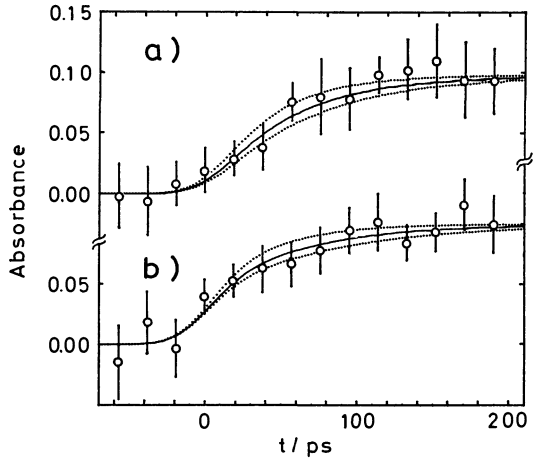

Fig. 6. Kinetics of $T_n \leftarrow T_1$ absorption for 9-nitroanthracene in benzene: a) observed at 450 nm where the $T_n \leftarrow T_1$ absorption is strong but the probing light intensity is reduced by the $S_1 \leftarrow S_0$ absorption tail: b) observed at 490 nm where the $T_n \leftarrow T_1$ absorption is weak the $S_1 \leftarrow S_0$ absorption intensity is negligibly small.
The time constants are 37 ps for •••• (upper), 50 ps for —, and 63 ps for •••• (lower) in a); 38 ps for •••• (upper), 58 ps for —, and 78 ps for •••• (lower) in b). The W value is 0.4 for both a) and b).

the time constants were determined in the following way. Simulation curves for the total absorbance of $T_n \leftarrow T_1$ and $S_n \leftarrow S_1$ absorptions were obtained with various build-up time constants of the triplet formation. The determined $\Delta\tau$ is the maximum of $\delta\tau$ which satisfies the following conditions; at least one of the two simulated curves with the time constants of $\tau+\delta\tau$ and $\tau-\delta\tau$ crosses all the error bars of absorbances at the respective steps of the echelon in the build-up part of the observed rising curves.

Discussion

The rate of the intersystem crossing depends on the matrix elements of the spin-orbit interaction between initial and final states. The selection rules for the radiationless transitions between electronic states with different spin-multiplicities were derived by El-Sayed.[13] The El-Sayed rule is applicable to the intersystem crossing process of many organic compounds. The break-down of this rule, however, has been observed for some cases: for example, benzophenone[14] and 9,10-diazaphenanthrene.[15] In the following we discuss the observed intersystem crossing rates in terms of the electronic structures of initial and final states relevant to the intersystem crossing.

Table 1. $T_n \leftarrow T_1$ build-up time constants at 347.2 nm excitation (room temperature)

Molecule	Solvent	λ_{obsd} / nm	τ [a] / ps	
			This work	Other authors
4-Hydroxy-benzophenone	Benzene	550	<8	
Michler's ketone	Benzene	550	18±8	
	Ethanol	550	18±8	
1-Nitronaphthalene	Benzene	533	—	12±5[b]
2-Nitronaphthalene	Benzene	533	—	10±2[b]
2-Nitrofluorene	Benzene	520	45±15	
1-Nitropyrene	Benzene	520	33±13	
9-Nitroanthracene	Benzene	450	50±13	
	Benzene	490	58±20	

a) τ is the $T_n \leftarrow T_1$ build-up time constant. b) λ_{ex} = 355 nm, λ_{obsd} = 533 nm.[6]

Aromatic Carbonyl Compounds. The intersystem crossing is a dominant deactivation process for benzophenone and 4-hydroxybenzophenone because its quantum yield, Φ_{ISC}, is unity and 0.9 for the former and the latter, respectively.[16] As for Michler's ketone, Φ_{ISC} is large in benzene (1.0) but small in ethanol (0.08).[17]

The $T_n \leftarrow T_1$ build-up time constant of benzophenone has been observed by several authors.[5,6,9] Recently, Hochstrasser and collaborators determined the value to be 12±2 ps in the benzene solution.[18] In the present study the $T_n \leftarrow T_1$ build-up time constant of 4-hydroxybenzophenone was found to be smaller than that of benzophenone, although the value was smaller than the time resolution of our apparatus. The energy level diagram of 4-hydroxybenzophenone is similar to that of benzophenone[19–23] and the lowest excited singlet state and the lowest triplet state have the n-π^* characters for both compounds. Therefore, 4-hydroxybenzophenone is another example deviating from the El-Sayed rule for the intersystem crossing rate. Its fast intersystem crossing may be explained, as in the cases of benzophenone and anthrone,[7] by the second order perturbation theory which considers vibronic couplings between the S_1 and S_2 states and also between the T_1 and T_2 states.[24,25]

The energy level diagram of Michler's ketone[26] in ethanol and in benzene are shown in Fig. 7; the diagram for the benzene solution is assumed to be the same as in hexane.[26] Since the yield of triplet formation is unity for Michler's ketone in benzene,[17] the observed time constant (18 ps) corresponds to the intersystem crossing rate constant. From the El-Sayed rule, we can expect the large spin-orbit coupling and the fast intersystem crossing for Michler's ketone in benzene,

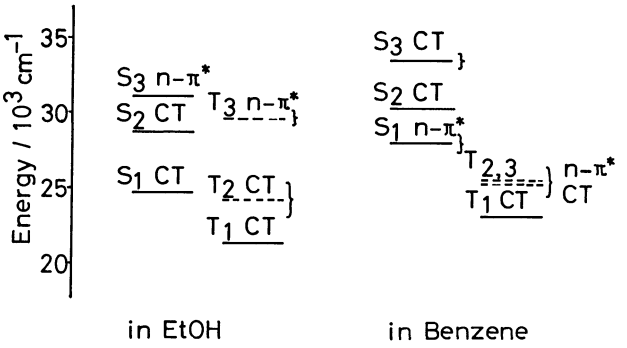

Fig. 7. Energy level diagrams of Michler's ketone in benzene and in ethanol.

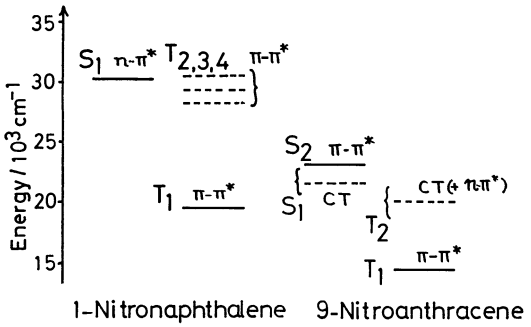

Fig. 8. Energy level diagrams of 1-nitronaphthalene and 9-nitroanthracene.
a) 1-Nitronaphthalene: S_1, determined from the absorption spectrum,[31] the triplet (π-π^*) states near S_1, estimated by the CNDO-CI calculation;[31] T_1 determined from the phosphorescence spectrum.[1,2]
b) 9-Nitroanthracene: S_1 and S_2, determined from the absorption spectrum.[32] The triplet state, determined from the $T \leftarrow S_0$ absorption spectrum.[33]
——: Experimentally determined level, ----: calculated level.

since the initial state is S_1(n-π^*) the final state is T_2 (CT).

Concerning Michler's ketone in ethanol the yield of triplet formation is 0.08[17] and the quantum yield of the photochemical reaction is below 10^{-4}.[17] This means that for this case the internal conversion to the ground state (S_0) is a main decay process of the lowest excited singlet state (S_1). The time constant of the intersystem crossing (k_{ISC}^{-1}) and that of the internal conversion (k_{IC}^{-1}) were determined to be 225 ps and 19 ps, respectively, by the use of the observed rate constant, $\tau^{-1}(=k_{IC}+k_{ISC})$ and the yield of triplet formation, $\Phi_T(=0.08)$.[17] The time constant of the intersystem crossing in ethanol (225 ps) is greater than that for benzene solution (18 ps). This fact is understandable, since the initial and final states are both of CT character in the ethanol solution (Fig. 7).

The rapid $S_1 \rightarrow S_0$ internal conversion (19 ps) of Michler's ketone in ethanol may be interpreted in terms of the proton transfer; the hydrogen bond is formed between Michler's ketone and ethanol in the ground state and the equilibrium position of hydrogen is changed in the excited state. Recently the proton-induced enhancement of the intersystem crossing[27] and the fluorescence quenching by proton transfer have been reported.[28,29]

Aromatic Nitro Compounds. The quantum yields of triplet formation are high for aromatic nitro compounds: 0.63 for 1-nitronaphthalene,[4] 0.83 for 2-nitronaphthalene,[4] and 0.6 for 1-nitropyrene.[30] These compounds exhibit strong $T_n \leftarrow T_1$ absorption. Therefore, the intersystem crossing is the important decay process of their singlet states. In aromatic nitro compounds the position of the CT state among other electronic states determines the rate of the intersystem crossing. Figure 8 shows the energy level diagrams of 1-nitronaphthalene[1,2,31] and 9-nitroanthracene.[1,2,32,33] Anderson *et al.*[6] reported the $T_n \leftarrow T_1$ build-up time constants of 1- and 2-nitronaphthalenes. Time constants of 1-nitronaphthalene in benzene and in ethanol are 10 ps and 12 ps, respectively. Using the quantum yields of triplet formation the time constants of the intersystem crossing for 1- and 2-nitronaphthalenes were determined to be 15.9 ps and 14.5 ps, respectively. Mikula *et al.*[31] calculated transition energies of 1-nitronaphthalene and reported that two π-π^* states and an n-π^* state are located 26300—37700 cm^{-1} corresponding to absorption band. The initial state of the intersystem crossing is the ^{1}n-π^*[2] state and the final state is the $^3\pi$-π^* states nearby.[31] The effective intersystem crossing causes the rapid build-up of the $T_n \leftarrow T_1$ absorption.

The ionization potential of naphthalene is 8.15 eV[34] and the CT state of 1-nitronaphthalene lies in the higher energy region. The CT state of 9-nitroanthracene lies under the ^{1}n-π^* states because the ionization potential of anthracene (7.47 eV)[35] is smaller than that of naphthalene. Thus the initial state of the intersystem crossing of 9-nitroanthracene is S_1(CT) and its final state is ^{3}CT or $^3\pi$-π^*. Since the yield of triplet formation may be less than unity for 9-nitroanthracene, the time constant of the intersystem crossing, k_{ISC}^{-1} is larger than the $T_n \leftarrow T_1$ build-up time constant, 50 ps. This time constant is larger than that of 1-nitronaphthalene and is reasonable for the intersystem crossing from ^{1}CT to $^3\pi$-π^* or ^{3}CT.

2-Nitrofluorene and 1-nitropyrene may be assumed to be intermediate cases between 1-nitronaphthalene and 9-nitroanthracene, since the ionization potentials of fluorene and pyrene (7.93 eV[36] and 7.53 eV,[37] respectively) lie between those of naphthalene and anthracene. The observed $T_n \leftarrow T_1$ build-up time constants of 2-nitrofluorene and 1-nitropyrene fall in between those of 1-nitronaphthalene and 9-nitroanthracene.

The authors wish to thank Professor Tsuguo Yamaoka, Chiba University for his kind gift of 1-nitropyrene.

References

1) C. J. Seliskar, O. S. Khalil, and S. P. McGlynn, "Excited States," ed by E. C. Lim, Academic Press, New York (1974), p. 231.
2) O. S. Khalil, H. G. Bach, and S. P. McGlynn, *J. Mol. Spectrosc.*, **35**, 455 (1970).
3) A. A. Lamola and G. S. Hammond, *J. Chem. Phys.*,

43, 2129 (1965).
4) R. Hurley and A. C. Testa, *J. Am. Chem. Soc.*, **90**, 1949 (1968); R. Rusakowicz and A. C. Testa, *Spectrochim. Acta, Part A*, **27**, 787 (1971).
5) P. M. Rentzepis and C. J. Mitschele, *Anal. Chem.*, **42**, 20 (1970).
6) R. W. Anderson, Jr., R. M. Hochstrasser, H. Lutz, and G. W. Scott, *Chem. Phys. Lett.*, **28**, 153 (1974).
7) T. Kobayashi and S. Nagakura, *Chem. Phys. Lett.*, **43**, 429 (1976).
8) S. Hirayama and T. Kobayashi, *Chem. Phys. Lett.*, **52**, 55 (1977).
9) D. E. Damschen, C. D. Merritt, D. L. Perry, G. W. Scott, and L. D. Talley, *J. Phys. Chem.*, **82**, 2268 (1978).
10) Y. Hirata and I. Tanaka, *Chem. Phys.*, **25**, 381 (1977).
11) V. Sundstrom, P. M. Rentzepis, and E. C. Lim, *J. Chem. Phys.*, **66**, 4287 (1977); L. J. Noe, E. O. Degenkolb, and P. M. Rentzepis, *J. Chem. Phys.*, **68**, 4435 (1978).
12) T. L. Netzel and P. M. Rentzepis, *Chem. Phys. Lett.*, **29**, 337 (1974).
13) M. A. El-Sayed, *J. Chem. Phys.*, **38**, 2834 (1963); S. K. Lower and M. A. El-Sayed, *Chem. Rev.*, **66**, 199 (1966).
14) S. Dym and R. M. Hochstrasser, *J. Chem. Phys.*, **51**, 2458 (1969).
15) C. T. Lin and J. A. Stikeleather, *Chem. Phys. Lett.*, **38**, 561 (1976).
16) A. A. Lamola and L. J. Sharp, *J. Phys. Chem.*, **70**, 2634 (1966).
17) D. I. Schuster, M. D. Goldstein, and P. Bane, *J. Am. Chem. Soc.*, **99**, 187 (1977).
18) G. W. Scott, R. W. Anderson, Jr., R. M. Hochstrasser, and H. Lutz, *Bull. Am. Phys. Soc.*, **20**, 46 (1975).
19) R. M. Hochstrasser and J. E. Wessel, *Chem. Phys. Lett.*, **19**, 156 (1973).
20) W. L. Dilling, *J. Org. Chem.*, **31**, 1045 (1966).
21) P. J. Wagner, M. J. May, A. Haug, and D. R. Graber, *J. Am. Chem. Soc.*, **92**, 5269 (1970).
22) G. Porter and P. Suppan, *Trans. Faraday Soc.*, **61**, 1664 (1965).
23) D. R. Kearns and W. A. Case, *J. Am. Chem. Soc.*, **88**, 5087 (1966).
24) N. Kanamaru, *Sci. Papers I.P.C.R.*, **71**, 85 (1977).
25) N. Shimakura, Y. Fujimura, and T. Nakajima, *Chem. Phys.*, **19**, 155 (1977).
26) E. J. J. Groenen and W. N. Koelman, *J. Chem. Soc., Faraday Trans. 2*, **74**, 58 (1978); *ibid.*, **74**, 69 (1978).
27) H. Shizuka, Y. Ishii, and T. Morita, *Chem. Phys. Lett.*, **51**, 40 (1977).
28) K. Tsutsumi and H. Shizuka, *Chem. Phys. Lett.*, **52**, 485 (1977).
29) M. A. El-Bayoumi, P. Avouris, and W. R. Ware, *J. Chem. Phys.*, **62**, 2499 (1975).
30) R. Scheerer and A. Henglein, *Ber. Bunsenges. Phys. Chem.*, **81**, 1234 (1977).
31) J. J. Mikula, R. W. Anderson, L. E. Harris, and E. W. Stuebing, *J. Mol. Spectrosc.*, **42**, 350 (1972).
32) L. Skulski and J. M. Kanabus, *Bull. Acad. Pol. Sci. Ser. Sci. Chim.*, **17**, 311 (1969).
33) J. B. Birks, "Photophysics of Aromatic Molecules," Willey-Interscience, New York (1970), p. 268.
34) F. Brogli, E. Heilbronner, and T. Kobayashi, *Helv. Chim. Acta*, **55**, 274 (1972).
35) R. Boschi, J. N. Murrell, and W. Schmidt, *Discuss. Faraday Soc.*, **54**, 116 (1972).
36) J. P. Maier and D. W. Turner, *Discuss. Faraday Soc.*, **54**, 149 (1972).
37) E. S. Pysh and N. C. Yang, *J. Am. Chem. Soc.*, **85**, 2124 (1963).

Ab Initio Calculation of Force Constants of Hydroxylamine

Yoshiaki HAMADA, Masamichi TSUBOI,* and Hideaki UMEYAMA**

Faculty of Pharmaceutical Sciences, The University of Tokyo, 7-3-1, Hongo, Bunkyo-ku, Tokyo 113

***School of Pharmaceutical Sciences, Kitasato University, 5-9-1, Shirokane, Minato-ku, Tokyo 108*

(Received June 7, 1979)

Ab initio molecular orbital calculation has been applied to hydroxylamine molecule to reach a reliable set of force constants by the use of the 4-31G basis set. This approach was found to be an enlightening way to solve a problem of the so far undeterminable amino twisting frequency. For this, the value of 1250 ± 100 cm^{-1} was estimated. A few comments are also given on the theoretical and experimental values of force constants.

The amino group $-NH_2$ has three bending vibrational modes. They are scissoring, wagging, and twisting modes. The vibrational frequecies of the scissoring and wagging modes have been conclusively fixed in most of the primary amines. Figure 1 shows the established bending frequencies and approximate vibrational modes for three representative molecules. These are ammonia derivatives in each of which one of the hydrogen atoms is replaced by methyl, amino, or hydroxyl group. As are indicated in the figure, the twisting frequencies of methylamine and hydroxylamine have not been determined. In the twisting vibration, two XNH angles open and close alternately. Therefore, as long as the two NH bonds are equivalent to each other this vibration causes almost no change in the dipole moment, and only very weak absorption in the infrared spectrum. The twisiting modes of hydrazine give exceptionally strong absorptions, probably because the two NH bonds are not equivalent in this molecule.[1]

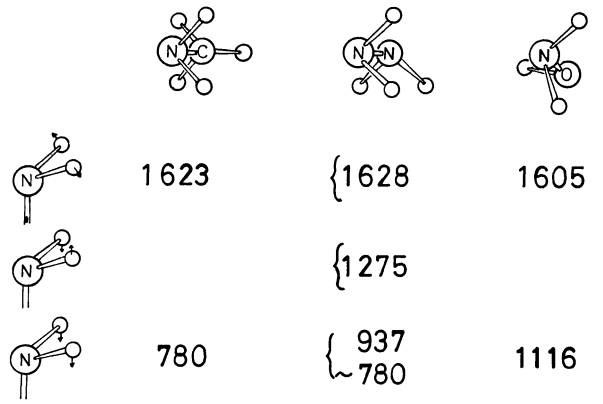

Fig. 1. Amino-scissoring, twisting, and wagging frequencies in cm^{-1}. Small circles indicate hydrogen atoms.

The weakness of the twisting bands of methylamine and hydroxylamine is one of the causes of a long-term debate[2–5] on the twisting frequency, whether it is in the vicinity of 1300 cm^{-1} or below 1000 cm^{-1}. Although there have been many normal coordinate treatments on the variety of assumptions, the results were not yet satisfactory. The off-diagonal elements of the potential energy matrix **F** for the XNH bending coordinates have never been determined on the basis of the experimental data. The infrared spectrum of hydroxylamine in gas phase was first observed by Giguere and Liu in 1952.[6] They assigned the perpendicular type band at 750 cm^{-1} to the amino twisting mode. However this band was shown later to be the first overtone of torsional vibration at 390 cm^{-1}.[7] Thus, the amino twisting frequency is now yet to be established.

The purpose of the present work is to fix the amino twisting frequency of hydroxylamine on the basis of *ab initio* molecular orbital calculation by the use of the 4-31 G basis set.[8]

Much effort has been made to obtain the meaningful set of force constants through various applications of molecular orbital theory. Unfortunately the semiempirical method such as the CNDO/2 method[9] has given the values two to three times as great as the experimental ones, and was scarcely fit for practical purpose, except for a work of estimating an order of magnitude of a vibrational frequency.[10] *Ab initio* molecular orbital calculations, on the other hand, have recently proved to be more reliable in estimating force constants of some small molecules. Particularly the "force method" developed by Pulay[11] seems to be the most useful in terms of both precision and computing time. The examples of its application are nicely reviewed by Duncan.[12]

Calculations of force constants using the 4-31 G basis set have been done by Bernhard-Schlegel *et al.*[13] The estimated error of the diagonal elements of stretching force constants is about 6%, and that of bending force constants is about 15% when the bonds involve hydrogen and second- or third-row elements. This means that the errors in frequencies are 3 and 8% for stretching and bending modes, respectively. In general, an advantage of application of *ab initio* calculation to a force field problem is that we can estimate the off-diagonal elements with the same precision as that for the diagonal elements. By experimental ways, off-diagonal elements of **F** matrix are often hard to evaluate even for small molecules.

Calculation

In this study, we used the 4-31 G split valence shell basis set in the Gaussian 70 program system.[14] The calculations were performed with a HITAC 8700/8800 in the computer center, University of Tokyo.

The internal coordinates are defined as shown in Fig. 2. There are six A′ modes and three A″ modes.

Starting from the experimental values determined by microwave spectroscopy,[15] one of the six internal coordinates belonging to the A′ symmetry species was changed, and we find the optimized point to

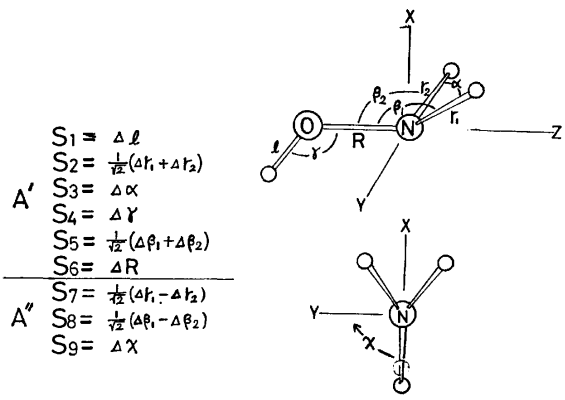

Fig. 2. Denotations of the bond lengths, bond angles, and internal rotation angle (χ); and definitions of symmetry coordinates **S** for the hydroxylamine molecule.

minimize the total energy. This procedure was repeated stepwise for other five coordinates to reach a calculated equilibrium structure (Process I).

From the process of geometry optimization we can estimate approximate values of diagonal force constants. To obtain off-diagonal force constants (or coupling constants), we need to calculate total energies at various combinations of six internal coordinates in question. A special attention was paid to have important coupling constants determined effectively (Process II).

Totally 77 sets of coordinates were chosen. Among them, the maximum deviations were ±0.04 Å in the bond lengths, and ±5° in the bond angles from the calculated equilibrium geometry. The 77 values of the total energy were used to obtain, by the least squares fit, the elements F_{ij} of the potential energy matrix in the expression,

$$V = V_0 + \sum_{i,j} \frac{1}{2} F_{ij}(R_i - R_i^0)(R_j - R_j^0), \qquad (1)$$

where R are internal coordinates (for which the total energy was calculated) and R^0 are those for the equilibrium geometry. By this procedure, we can obtain the minimum total energy (V_0), 6 parameters (R_j^0) of the "final" equilibrium geometry, and 21 force constants (F_{ij}) belonging to the A′ symmetry species.

A few comments will now be given below on the results of the calculations, so far described.

1) The total energy −130.791865(9) Hartrees at the equilibrium geometry is less than −130.78729 Hartrees obtained by Radom *et al.*[16] using the same computing program. This means that our optimization is better than theirs. (The figure given in the parenthesis gives the standard deviation in the unit corresponding to the last significant figures).

2) As shown in Table 1, the equilibrium geometry calculated by Process I is significantly different from that calculated by Process II. In the Process I, only one coordinate is changed with others fixed in finding the coordinate value that gives energy minimum. In the Process II, on the other hand, several coordinates are changed simultaneously with a proper assumption

Table 1. Equilibrium geometry of the NH_2OH molecule

	Calculated		Observed(r_0)
	Process I	Process II	
NO	1.4636(Å)	1.4432(4)[a]	1.453(2)[a]
OH	0.9528	0.9519(3)	0.962(5)
∠HON	104.98(deg)	106.00(6)	101.37(50)
∠HNH	110.86	111.28(7)	107.1(5)
NH	0.9987	0.9992(1)	1.016(8)
∠ONH	105.2	105.84(2)	103.25(50)

a) The figure in the parenthesis gives 1σ (standard deviation) in the unit corresponding to the last significant figure.

on the coupling among the coordinates. Probably, the most reliable geometry is reached by repeating the Process I in a systematic manner, but this will take a great amount of computer time.

3) The optimized structural parameters (Table 1) are found to be within the stated precision.[17,18] It should be realized that the calculated geometry is that for equilibrium or the geometry in which the total energy is minimized, while the experimental set of values determined by microwave spectroscopy, for example, are often that for vibrational ground state and for $J=K=0$ level. The former corresponds to the so-called r_e-structure, while the latter r_0-structure. Table 2 gives some examples, showing the differences of r_e- and r_0-structures. Taking probale differences between the r_e and r_0 structures of NH_2OH into account, it may be concluded that our *ab initio* calculations could reproduce the bond lengths quite satisfactorily, but the calculated bond angles are all larger than the experimental angles by about 5°.

Next, the internal symmetry coordinates belonging to the A″ symmetry species were subjected to our examination. After the equilibrium coordinates were determined, the three A″ internal coordinates were changed within the range of distortion where anharmonicities do not become influential. Six force constants were obtained from 15 data sets in a similar way to those of the A′ symmetry species.

Table 2. A few examples of the r_e- and r_0-structures actually found in some small molecules

Molecule	Bond or bond angle	r_e-Structure	r_0-Structure
HF[a]	HF	0.9170(Å)	0.9257
OH[a]	OH	0.9707	0.9800
$^{12}C^{16}O$[a]	CO	1.1282	1.1309
NH_3[a]	NH	1.0124	1.0136
	∠HNH	106.68 (deg.)	107.05
HNO($\tilde{A}$)[b]	HN	1.020	1.036
	NO	1.239	1.241
	∠HNO	114.42	116.25

a) W. Gordy and R. Cook, "Microwave Molecular Spectra," Wiley (1970). b) Landolt-Börnstein, New Series Vol. 7, Springer-Verlag (1976).

TABLE 3. CALCULATED FORCE CONSTANT MATRIX ELEMENTS[a]

	S_1(OH)	S_2(NH)	$S_3(\alpha)$	$S_4(\gamma)$	$S_5(\beta)$	S_6(NO)	S_7(NH)	$S_8(\beta)$	$S_9(\chi)$
S_1	8.042(226)[b]	0.002(108)	−0.048(53)	−0.011(64)	0.100(50)	−0.224(134)			
S_2		8.077(86)	0.302(34)	0.039(49)	0.195(19)	0.062(69)			
S_3			0.743(8)	−0.018(10)	−0.027(6)	−0.049(27)			
S_4				1.000(6)	0.181(12)	0.754(53)			
S_5					1.054(7)	0.837(25)			
S_6						5.427(106)			
S_7							7.894(37)	0.021(7)	0.042(8)
S_8								1.027(10)	0.061(4)
S_9									0.072(5)

a) Units are as follows. str.-str.: 10^5 (dyn/cm), str.-bend.: 10^{-3} (dyn), bend.-bend.: 10^{-11} (dyn cm). b) The figure in the parenthesis gives 1σ (standard deviation) in the unit corresponding to the last significant figure.

Force Constants and Normal Frequencies

Table 3 shows the force constants obtained for the two symmetry species. Some off-diagonal elements are not found to be determinable from our 77 sets. All of these, however, are taken to be actually very small judged from their physical meanings. The coupling constant between S_3 and S_5 has been found to be as small as -0.03×10^{-11} dyne cm. The corresponding off-diagonal element of methylamine was once estimated to be as big as 0.123×10^{-11} dyne cm[2] (see Table 4). This should now be revised; an *ab initio* study on methylamine by Pulay and Török[19] also gave a very small value to this off-diagonal element.

In the process of experimental force-constant determination, the definitions of non-totally symmetrical coordinates are sometimes ambiguous. Particularly the physical meanings of off-diagonal elements and their signs are not usually the subject of investigation. On the other hand, in the case of calculation using molecular orbital theory as in this study, the definitions of coordinates and related force constants with their signs are determined unambiguously in principle. This is another merit of such a theoretical study.

The calculated normal frequencies, ω, are shown in Table 5, where experimental geometry was used to calculate **G**-matrix (inverse kinetic energy matrix). We have no data of experimental normal frequencies to compare, except for torsional oscillation. Here a rather nice agreement has been obtained, *i.e.* $\omega_{obsd}=407$ cm^{-1} [7] while $\omega_{calcd}=457$ cm^{-1}.

In comparing the observed and calculated frequencies, the frequency difference between the normal and fundamental frequencies, which is caused by anharmonicity, should be taken into account. For a correction, Pulay & Török[19] reduced 10% of diagonal stretching force constants and 20% of diagonal bending force constants, with off-diagonal force constants fixed. With this correction to include the anharmonicity effectively, they reproduced the observed frequencies within the deviation of 40 cm^{-1} for the fundamental frequencies below 2000 cm^{-1}. We adopted the same empirical way in changing the calculated normal frequencies into "calculated fundamental frequencies." The results are given in Table 5 (see also Table 4).

NH_2 stretching and wagging have deviations as much as 100—200 cm^{-1}. The anharmonicity for the former might be underestimated, and that for the latter overestimated. These discrepancies may be removed by including polarization functions and or by configura-

TABLE 4. SOME OF THE AMINO-DEFORMATION FORCE CONSTANTS

CH_3NH_2[a]	S_2(NH_2 str.)	S_3(NH_2 sci.)	S_5(NH_2 wag.)
$S_2(\nu_2=3360$ cm$^{-1})$	6.444	0.305	0.034
$S_3(\nu_3=1623$ cm$^{-1})$		0.453	0.123
$S_5(\nu_5=780$ cm$^{-1})$			0.774
NH_2OH[b]	S_2	S_3	S_5
$S_2(\nu_2=3297$ cm$^{-1})$	7.269	0.302	0.195
$S_3(\nu_3=1605$ cm$^{-1})$		0.594	−0.027
$S_5(\nu_5=1115$ cm$^{-1})$			0.843

a) Determined by Hirakawa *et al.*[2] b) Calculated in the present work, and corrected on the basis of the Pulay & Török's proposal.[19]

TABLE 5. OBSERVED AND CALCULATED FUNDAMENTAL FREQUENCIES (ν_i) AND CALCULATED NORMAL FREQUENCIES (ω_i) OF HYDROXYLAMINE
(The potential energy distribution calculated on the force constant values obtained in the present work are also shown.)

A′	ν_i(obsd)	3656	3297	1605	1357	1115	895
	ν_i(calcd)	3602	3578	1569	1341	1021	888
	ω_i(calcd)	3797	3764	1836	1483	1125	981
S_1	OH-str.	99.6	0.2	0.1	0.2	0.0	0.5
S_2	NH-str.	0.2	99.9	0.5	0.6	1.2	0.4
S_3	HNH-bend.	0.0	0.0	61.4	24.2	15.6	1.4
S_4	NOH-bend.	0.0	0.0	3.3	55.8	42.2	16.5
S_5	ONH-bend.	0.0	0.0	28.8	3.0	64.7	26.1
S_6	NO-str.	0.0	0.0	0.0	3.0	1.3	131.2

A″	ν_i(obsd)	3350	—	386
	ν_i(calcd)	3618	1233	391
	ω_i(calcd)	3823	1409	457
S_7	NH-str.	99.9	0.0	0.5
S_8	NH_2 twist	0.1	97.6	10.8
S_9	Torsion	0.0	0.2	108.8

tion interaction calculation.

Now we can predict the twisting frequency in question. Estimating the maximum error, we predict that the frequency should be 1250±100 cm^{-1}. Giguére and Liu[6] observed, in their IR spectrum, a weak absorption at 1297 cm^{-1} on the shoulder of the OH bending band centered at 1350 cm^{-1}. They assigned this to $\nu_6+\nu_9$ combination band. In a solid state spectrum, a very weak absorption at 1287 cm^{-1} was assigned to $\nu_8+\nu_9$. It is possible, however, to assign these to the twisting mode. An *ab initio* MO study on methylamine by Pulay and Török[19] shows that NH_2 twisting mode and CH_3 rocking mode are so severely coupled to give positive combination of the two modes at 1335 cm^{-1}, and negative combination somewhere in the 880—1000 cm^{-1} region, with uncoupled original position around 1170 cm^{-1}. Therefore it is now certain that NH_2 twisting mode contributes to a band in the region of 1300 cm^{-1}.

The first order centrifugal distortion constants directly reflect the harmonic force field, and these were also calculated in our present study. The results are shown in Table 6. The most of the calculated values are in agreement with the experimental values at least in the order of magnitude.

Table 6. Centrifugal distortion constants (MHz)

	Obsd[15]	Calcd[a]
τ' aaaa	−17.306	−10.14
τ' bbbb	−0.3257	−0.263
τ' cccc	−0.2895	−0.251
T_1	−3.3744	−1.14
T_2	−0.31212	−1.78

a) Procedure II.

Dipole Moment Derivatives

The intensity of infrared fundamental band is represented by the formula,

$$A_i = \frac{N\pi g_i}{3c^2}\left|\frac{\partial^2 P}{\partial Q_i^2}\right|^2 \qquad (2)$$

where N is Avogadro's number, g_i the degeneracy of the i-th normal vibration, c the light velocity, P the dipole moment, and Q_i the normal coordinate of the i-th normal vibration. Therefore, $(\partial^2 P/\partial Q_i^2)^2$ is the experimentally determinable value. To investigate the physical meaning of the intensity we need to know $\partial P/\partial R_i$ which is related to $\partial P/\partial Q_i$ by the following formula,

$$\frac{\partial P}{\partial R_j} = \sum_i \left(\frac{\partial P}{\partial Q_i}\right) L_{ij}^{-1}, \qquad (3)$$

where $\boldsymbol{L}$ is the transformation matrix between internal (symmetry) coordinate R and normal coordinate Q, and can be obtained accurately when the vibrational analysis is completed.

Since it is difficult to determine the sign of $\partial P/\partial Q_i$ experimentally, and there is in general some ambiguity in the values of the off-diagonal elements $\boldsymbol{L}_{ij}$, the determination of the size of dipole moment derivative $\partial P/\partial R_j$ and its sign by *ab initio* calculations would have some significance. For example, near-Hartree-Fock calculation on NH_3[20] and CH_4[21] by Meyer and Pulay gave satisfactory results determining a set of signs of dipole moment derivatives. They stated that the dipole moment derivatives by *ab initio* calculations for bending coordinates are fairly stable for the choise of basis set, and estimated error is 20—30%.

Table 7. Dipole moment and its derivatives at equilibrium geometry

	μ_{total}	μ_x	μ_z
Expl.	0.592	0.060	0.582
ab initio	0.9181(5)	−0.0048(5)	0.9185(3)
A′-symmetry			
$\mu'_i=\frac{\partial\mu}{\partial S_i}$	μ'_{total}	μ'_x	μ'_z
1(OH str.)	−0.616(33)	−0.727(37)	−0.544(22)
2(NH_2 str.)	0.050(18)	0.245(21)	0.088(12)
3(NH_2 sci.)	0.588(12)	−1.267(13)	0.578(8)
4(OH bend.)	−1.290(11)	0.173(12)	−1.287(7)
5(NH_2 wag.)	1.443(6)	−1.189(7)	1.409(4)
6(NO str.)	1.515(21)	0.364(23)	1.457(13)
A″-symmetry			
$\mu'_i=\frac{\partial\mu}{\partial S_i}$	μ_{total}	μ'_x	μ'_y	μ'_z
7(NH_2 str.)	0.012(12)	−0.005(6)	0.268(5)	0.006(7)
8(NH_2 twist.)	0.017(6)	−0.005(3)	0.088(3)	0.012(4)
9(torsion)	0.011(8)	−0.015(4)	−1.195(4)	−0.004(5)

We present our results on NH_2OH in Tables 7 and 8. The dipole moment μ at various sets of coordinates were calculated, and by the use of an equation,

$$\mu = \mu_0 + \sum_i \left(\frac{\partial\mu}{\partial S_i}\right)\Delta S_i + \frac{1}{2}\sum_{i,j}\left(\frac{\partial^2\mu}{\partial S_i \partial S_j}\right)\Delta S_i \Delta S_j, \qquad (4)$$

the values of μ_0, $\partial\mu/\partial S_i$, and $\partial^2\mu/\partial S_i\partial S_j$ were determined by a least squares fit. The third term, with the second derivatives, was included (see Table 8) because some of them were determinable from our data set. The x, y, z axes were defined as in Fig. 2.

Strong intensities of OH bending and NH_2 wagging bands are obvious, and almost no intensity for NH_2 twisting is just as expected. It would be worthwhile to give the following two comments here:

1) The derivatives of the dipole components $\partial\mu_x/\partial S_i$, $\partial\mu_y/\partial S_i$,····· can be used to determine the band type —parallel or perpendicular—of each fundamental band, or, if it is a hybrid band, to determine the amount of contribution from each type.

2) When the amplitude of a stretching mode is set greater than 10^{-2} Å, the contribution from the second derivative is found to be appreciable. This can be accurate up to a few percent. This would allow us to estimate an intensity of some overtone and combination bands. To an intensity factor of overtone or combination transitions, the electrical anharmonicity (second derivative of dipole moment) and mechanical anharmonicity (anharmonicity of potential surface) are possible to contribute. So far,

TABLE 8. EXAMPLES OF SECOND DERIVATIVES OF DIPOLE MOMENT

$\frac{1}{2}\partial^2\mu_x/\partial S_i\partial S_j$					
OH str.	NH_2 str.	NH_2 sci.	OH bend.	NH_2 wag.	NO str.
−0.47(158)	−0.81(151)	−0.02(74)	3.06(90)	−2.01(35)	−0.16(187)
	−2.00(60)	0.44(48)	1.47(68)	−0.10(27)	0.20(96)
		−0.78(6)	0.13(14)	−1.90(8)	−0.02(38)
			0.68(4)	−0.17(16)	−1.91(74)
				−1.82(5)	1.49(35)
					1.45(75)

however, no systematic investigation has been done on them. We hope that *ab initio* calculation is valuable also in this field of research.

References

1) See, for example, a recent electron diffraction study made by K. Kohata, Doctor Thesis, the University of Tokyo, 1979.
2) A. Y. Hirakawa, M. Tsuboi, and T. Shimanouchi, *J. Chem. Phys.*, **57**, 1236 (1972).
3) H. Wolff and H. Ludwig, *J. Chem. Phys.*, **56**, 5278 (1972).
4) A. P. Gray and R. C. Lord, *J. Chem. Phys.*, **26**, 690 (1957).
5) C. J. Purnell, A. J. Barnes, S. Suzuki, D. F. Ball, and W. J. Orville-Thomas, *Chem. Phys.*, **12**, 77 (1976).
6) R. A. Giguere and I. D. Liu, *Can. J. Chem.*, **30**, 948 (1952).
7) K. Tamagake, Y. Hamada, J. Yamaguchi, A. Y. Hirakawa, and M. Tsuboi, *J. Mol. Spectrosc.*, **49**, 232 (1974).
8) R. Ditchfield, W. J. Hehre, and J. A. Pople, *J. Chem. Phys.*, **51**, 2657 (1969).
9) J. A. Pople, D. P. Santry, and G. A. Segal, *J. Chem. Phys.*, **43**, 5129 (1965).
10) J. A. Pople and D. L. Beveridge, "Approximate Molecular Orbital Theory," McGraw-Hill Book Co. (1970), p. 89.
11) P. Pulay, *Mol. Phys.*, **17**, 197 (1969).
12) J. L. Duncan, "Specialist Periodical Reports, Molecular Spectroscopy Vol. 3," The Chemical Society (London) (1975).
13) H. Bernhard-Schlegel, S. Wolfe, and F. Bernardi, *J. Chem. Phys.*, **67**, 4181 (1977).
14) W. J. Hehre, W. A. Lathan, R. Ditchfield, M. D. Newton, and J. A. Pople, Gaussian 70, Quantum Chemistry Program Exchange, Indiana University (1974).
15) S. Tsunekawa, *J. Phys. Soc. Jpn.*, **33**, 167 (1972).
16) L. Radom, W. J. Hehre, and J. A. Pople, *J. Am. Chem. Soc.*, **94**, 2371 (1972).
17) J. A. Pople, "Computational Methods for Large Molecules and Localized States in Solid," Plenum Press., (1973).
18) S. Huzinaga, "Precise and Accurate Measurements in Chemistry (in Japanese), Kagaku Sosetsu No. 10," The Chemical Society of Japan (1976), pp. 264—272.
19) P. Pulay and F. Török, *J. Mol. Structure*, **29**, 239 (1975).
20) P. Pulay and W. Meyer, *J. Chem. Phys.*, **57**, 3337 (1972).
21) W. Meyer and P. Pulay, *J. Chem. Phys.*, **56**, 2109 (1972).

Light Scattering Study of Local Structure in Solutions. Importance of Temperature Dependency Measurements

Tadashi KATO, Katsuaki YANO, and Tsunetake FUJIYAMA*

Department of Chemistry, Faculty of Science, Tokyo Metropolitan University, Fukasawa, Setagaya-ku, Tokyo 158

(Received June 26, 1979)

Light scattering spectra have been observed for binary solutions of acetic acid and carbon tetrachloride at several concentrations and temperatures. The Rayleigh intensities were reduced to concentration fluctuations. The observed concentration and temperature dependencies of concentration fluctuation were interpreted by assuming association equilibria involving both cyclic dimers and linear polymers. The simultaneous measurement of concentration and temperature dependencies of concentration fluctuation are necessary to determine local structures in solutions where different types of local structure coexist.

The local fluctuation of concentration can aid understanding the mixing of liquids from the molecular viewpoint. Based on this, studies on the temperature and concentration dependencies of concentration fluctuation through observations of light scattering spectra have been initiated.[1]

The relationship between concentration fluctuation and Rayleigh intensities have been theoretically established[2] and a method proposed for determining the local structures[3] existing in associated solutions from observed concentration fluctuation.[4,5] The validity of the method has been checked for the diethyl ether–chloroform system in which local structures of the (A-B)type (A and B represent diethyl ether and chloroform molecules, respectively) are expected. The method has been extended to the systems in which several types of local structures are formed. The use of infrared and light scattering spectra is complementary and useful to determine local structures for the system in which local structures of the A_l and A_lB types are expected (A_l represents an aggregate which is made up of l molecules of A, and A_lB represents an aggregate which is made up of l molecules of A and one molecule of B). The simultaneous use of microscopic and macroscopic information is necessary to understand the state of mixing in solutions. In certain cases, however, microscopic information such as infrared spectra cannot be obtained for solutions, particularly at high concentration.

In the present report, it will be shown that the simultaneous measurement of concentration and temperature dependnecies of concentration fluctuation can determine local structures in solutions where different types of local structures coexist. The acetic acid–carbon tetrachloride system was chosen because acetic acid molecules have been known to form both cyclic dimers and linear polymers in nonpolar solvents.[7]

Experimental

Light scattering spectra were observed at 22.5, 37, and 51 °C using a spectrometer designed and constructed in this laboratory.[1] The spectrometer is composed of a He–Ne gas laser source (NEC, GLG 108) and a pressure scanning Fabry-Perot interferometer. The temperature of the samples was controlled by a high temperature cell developed in this laboratory. A temperature constancy of ±0.1 °C was obtained with the apparatus. The refractive indicies of the samples were measured by an Abbe refractometer (Atago).

The samples used in the present study were commercial products and used without further purification. The binary solution of acetic acid and carbon tetrachloride was made dust-free by the use of a milipore filter FG of 0.2 μm pore size.

Results and Discussion

Light Scattering Spectra and Concentration Fluctuation. Figure 1 illustrates the observed light scattering spectra for the acetic acid–carbon tetrachloride system at 22.5 °C. After separating the Rayleigh part from the observed spectra, the Rayleigh intensity was expressed relative to the Rayleigh intensity of pure carbon tetrachloride. The concentration fluctuation, $N\langle(\Delta X_A)^2\rangle$, was calculated from the relation,[2]

$$N\langle(\Delta X_A)^2\rangle = \frac{N_A\rho}{M}\left(\frac{\lambda^4}{\pi^2}\right)\frac{1}{4n^2\left(\frac{\partial n}{\partial X_A}\right)^2}\{(R_{90})_R-(R_{90})_S\},$$

where N is the total number of molecules included in the field within which the concentration fluctuation is considered, N_A the Avogadro number, M the mean molecular weight, n the refractive index, ρ the density, λ the wavelength of the incident light, X_A the mole fraction of acetic acid, and $(R_{90})_R$ the Rayleigh ratio for a Rayleigh line. $(R_{90})_S$ is the Rayleigh ratio for entropy fluctuation and is expressed by the relationship:

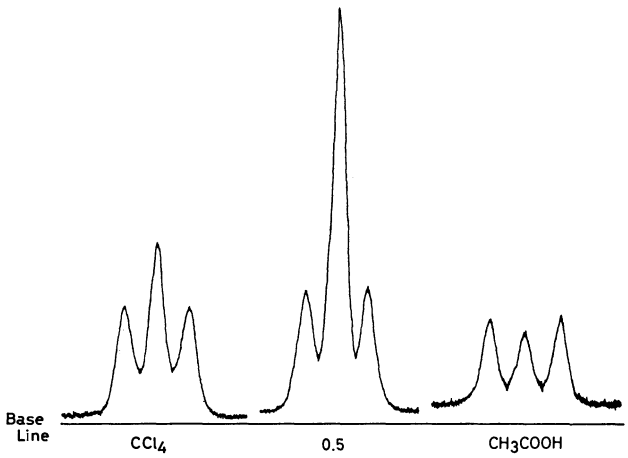

Fig. 1. Observed light scattering spectra for acetic acid-carbon tetrachloride system at 22.5 °C. Concentration is expressed in terms of mole fraction of acetic acid.

$$(R_{90})_S = \frac{\pi^2}{\lambda^4}\frac{4kn^2T^2}{C_{p_g}}\left(\frac{\partial n}{\partial T}\right)^2,$$

where k is the Boltzmann's constant, T the absolute temperature and C_{p_g} the isobaric heat capacity per gram. The values of $(R_{90})_S$ at each mole fraction were calculated from the physical quantities observed or obtained from the literature.[8]

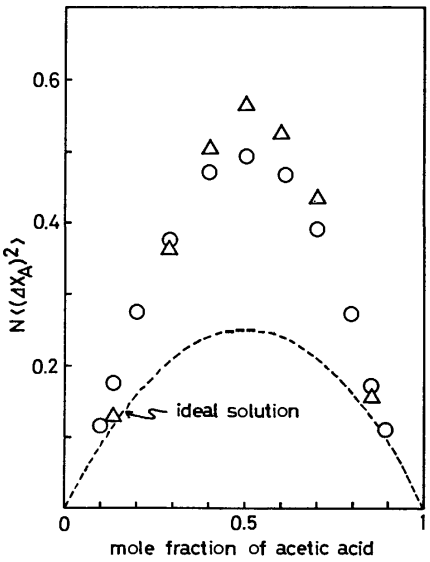

Fig. 2. Observed concentration fluctuation for acetic acid–carbon tetrachloride system at different temperatures: (○) 22.5 °C, (△) 51 °C.

In Fig. 2, the concentration fluctuations thus obtained are plotted against the mole fraction of acetic acid for different temperatures. The dashed line in Fig. 2 corresponds to the concentration fluctuation expected for an ideal solution. It is seen from the figure that the observed concentration fluctuation is larger than that of an ideal solution at all concentrations and the magnitude of concentration fluctuation increases with increasing temperature.

Analysis of Concentration Fluctuation. The method for determining local structures from the observed concentration fluctuation has been reported elsewhere.[4-6] In this method, an ideal associated complex model[9] was employed. This model assumes that the local structure can be treated as an associated complex and the solution regarded as an ideal solution whose components are free molecules and associated complex molecules.

As acetic acid molecules are associated with each other through hydrogen bonding, it may be assumed that associated molecules of the A_l type exist in the solution where A represents the acetic acid molecule and l is an association number. In this case, the concentration fluctuation is expressed by[6]

$$N\langle(\Delta X_A)^2\rangle = X_A(1-X_A)\{(1-X_A)\langle l\rangle + X_A\},$$
$$\langle l\rangle \equiv \frac{\sum_l l^2 n_{A_l}}{\sum_l l n_{A_l}}, \quad (1)$$

where n_{A_l} is the number of A_l molecules and $\langle l\rangle$ is the mean association number. Equation 1 qualitatively explains the present results in the sense that the concentration fluctuation is always larger than that of an ideal solution, $X_A(1-X_A)$. Therefore, the concentration and temperature dependencies of $\langle l\rangle$ may be determined by choosing an appropriate association equilibria model.

Acetic acid molecules are known to form both cyclic dimers and linear polymers. Therefore, $N\langle(\Delta X_A)^2\rangle$ will be calculated for the following types of model systems;

(a) cyclic dimer model,
(b) linear polymer model, and
(c) cyclic dimer-linear polymer model,

and calculated results will be compared with the observed values.

(a) Cyclic Dimer Model: It is assumed that the following species coexist in solutions;

$$A_1,\ A_2^c,\ B, \quad (2)$$

where A_1 and A_2^c represent a monomer and a cyclic dimer of acetic acid, respectively, and B represents a carbon tetrachloride molecule. In this model, the mean association number $\langle l\rangle$ is defined as

$$\langle l\rangle \equiv \frac{n_1+4n_2^c}{n_1+2n_2^c}, \quad (3)$$

where n_1 and n_2^c are the number of species A_1 and A_2^c, respectively. The mean concentrations of these species are related to each other by the equilibrium constant, K^c,

$$\frac{x_2^c}{x_1^2} = \frac{q_2^c}{q_1^2} \equiv K^c, \quad (4)$$

where q_i is a partition function of an i-th species,[6] which depends on temperature and not on concentration. x_i is the mole fraction of the i-th species, namely,

$$x_i = \frac{n_i}{n_1+n_2^c+n_B}, \quad (5)$$

where n_i is the number of carbon tetrachloride molecules. In the special case where $K^c=0$ and $K^c=\infty$, the mean association number may be written as

$$\langle l\rangle = 1 \quad \text{for } K^c = 0,$$
$$\langle l\rangle = 2 \quad \text{for } K^c = \infty. \quad (6)$$

In Fig. 3, the $N\langle(\Delta X_A)^2\rangle$ values calculated for $K^c=0$ and $K^c=\infty$ are compared with the observed values. In the case where $0<K^c<\infty$, the concentration fluctuation takes the values between the values calculated for $K^c=0$ and $K^c=\infty$. It is seen from the figure that the observed values are generally larger than the calculated values for $K^c=\infty$ except for in the low concentration range indicating the existence of a polymer whose association number is larger than two.

(b) Linear Polymer Model: The coexistence of the following species is assumed:

$$A_1,\ A_2,\ A_3,\ \ldots,\ A_l,\ldots$$
$$B \quad (7)$$

In this model, $\langle l\rangle$ is expressed as

$$\langle l\rangle = \frac{\sum_l l^2 n_l}{\sum_l l n_l} \quad (8)$$

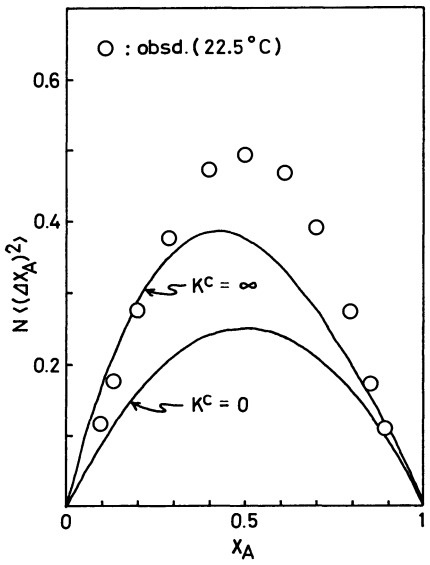

Fig. 3. Theoretical values of concentration fluctuation calculated from Eqs. 1, 3, and 4 for $K^c=0$ and $K^c=\infty$.

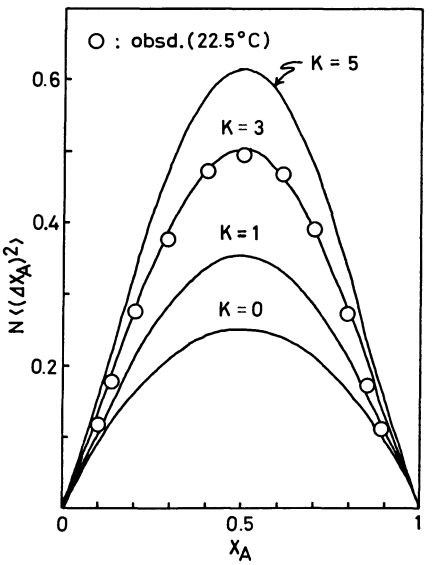

Fig. 4. Theoretical values of concentration fluctuation calculated from Eqs. 1 and 8—10 for $K=0$, 1, 3, and 5.

where n_l is the number of species A_l. The following equilibrium constants are thus defined;

$$\frac{x_3}{x_1^2}=\frac{q_2}{q_1^2}\equiv K_1,$$

$$\frac{x_3}{x_2x_1}=\frac{q_3}{q_2q_1}\equiv K_2,$$

$$\vdots \qquad \vdots \qquad \vdots$$

$$\frac{x_{l+1}}{x_lx_1}=\frac{q_{l+1}}{q_lq_1}\equiv K_l, \tag{9}$$

and it is assumed that

$$K_1=K_2=\ldots=K_l\equiv K. \tag{10}$$

In Fig. 4, the $N\langle(\Delta X_A)^2\rangle$ values calculated for different K values are compared with the observed values. From the figure it is apparent that the concentration fluctuation takes larger values for larger K. Therefore, the equilibrium constant, K, should increase with increasing temperature, since the observed concentration fluctuation increases as the temperature increases. This is inconsistent since the formation enthalpy of hydrogen bonding is negative. Therefore, this model cannot be applied to the present system, although the calculated values for $K=3$ agree well with the observed values at 22.5 °C.

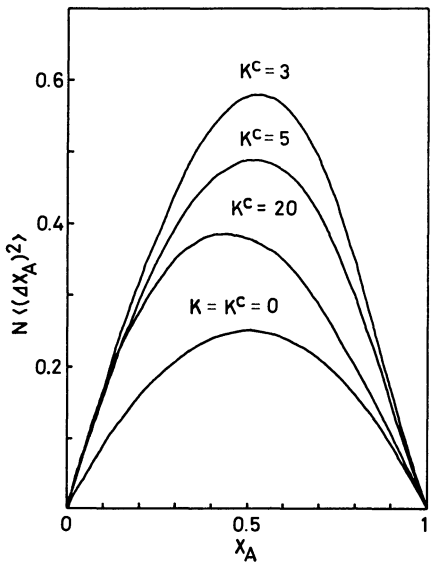

Fig. 5. Theoretical values of concentration fluctuation calculated from Eqs. 1, 12, and 13 for $K=10$ and various K^c values.

(c) Cyclic Dimer-Linear Polymer Model: It is assumed that cyclic dimers and linear polymers coexist in solution, that is, the following species:

$$\begin{matrix} A_2^c \\ A_1,\ A_2,\ A_3,\ \ldots,\ A_l,\ \ldots. \\ B \end{matrix} \tag{11}$$

The mean association number and equilibrium constants are

$$\langle l\rangle=\frac{4n_2^c+\sum_l l^2n_l}{2n_2^c+\sum ln_l}, \tag{12}$$

$$\frac{x_2^c}{x_1^2}=K^c,$$

$$\frac{x_2}{x_1^2}=\frac{x_3}{x_2x_1}=\ldots=\frac{X_{l+1}}{x_lx_1}=\ldots=K. \tag{13}$$

Figure 5 demonstrates the concentration dependencies of the concentration fluctuation calculated for $K=10$ and several K^c values. It is seen from the figure that the concentration fluctuation increases in magnitude with decrease in K^c. This suggests that the observed temperature dependence of concentration fluctuation arises from a difference in temperature dependencies of K and K^c. The best fit between the calculated and observed concentration fluctuation was obtained by setting $K=13$ and $K^c=90$ for 22.5 °C and $K=8$ and $K^c=20$ for 51 °C. The final results for the theoretical calculation are shown in Figs. 6 and 7.

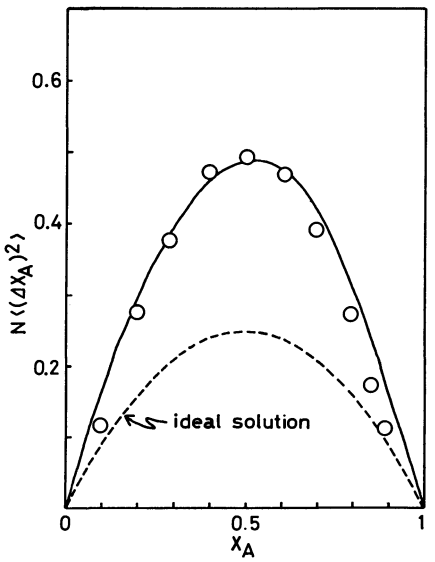

Fig. 6. Final results for theoretical calculations corresponding to experimental values at 22.5 °C.

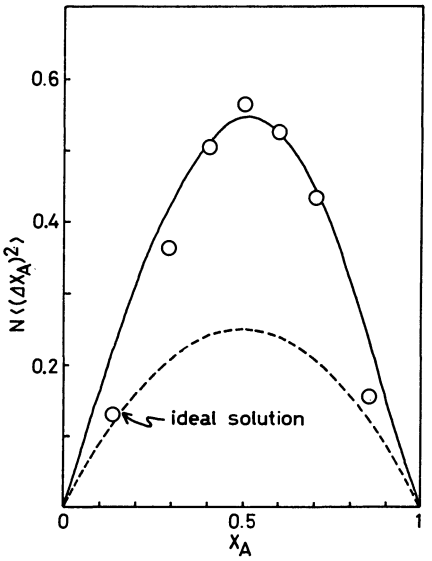

Fig. 7. Final results for theoretical calculations corresponding to experimental values at 51 °C.

The formation enthalpy of an associated complex may be calculated from the relationships;

$$\Delta H^{c} = RT^{2}\frac{\partial \ln K^{c}}{\partial T}, \qquad \Delta H = RT^{2}\frac{\partial \ln K}{\partial T}, \tag{14}$$

where ΔH^{c} and ΔH are the enthalpy change for the reaction, $A_1+A_1 \rightleftarrows A_2^c$ and $A_l+A_1 \rightleftarrows A_{l+1}$, respectively. The obtained values of ΔH^{c} and ΔH and the related entropy change, ΔS^{c} and ΔS, are given in Table 1.

The number ratio of the molecules forming an associated complex to the total acetic acid molecules,

$$\Phi_2^c = \frac{2n_2^c}{2n_2^c+\sum_l ln_l} \quad \text{(cyclic dimers)}$$

or (15)

$$\Phi_l = \frac{ln_l}{2n_2^c+\sum_l ln_l} \quad \text{(linear polymers)}$$

may be calculated from Eq. 13. Figure 8 illustrates the temperature and concentration dependencies of Φ_2^c and Φ_l. It is seen from the figure that almost all the acetic acid molecules form cyclic dimers at low concentrations. At higher concentrations, however, the number of molecules forming linear polymers ($l>2$) is larger than the number of molecules forming cyclic dimers. As the temperature increases, the number of molecules forming cyclic dimers decreases and the molecules forming linear polymers increase. The number of monomers increases with the increase of temperature.

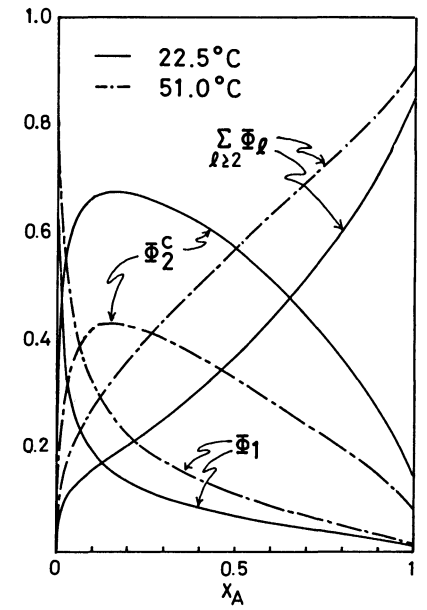

Fig. 8. Concentration and temperature dependencies of Φ^{c} and Φ_l calculated from Eq. 15.

TABLE 1. THE ENTHALPY AND ENTROPY CHANGES CALCULATED FROM EQ. 14

The equilibrium constants at the temperatures of 22.5, 37, and 51 °C have been used in the calculation.

Enthalpy/kcal mol^{-1}		Entropy/cal deg^{-1} mol^{-1}	
ΔH^{c}	10.1	ΔS^{c}	25.1
ΔH	3.2	ΔS	5.9

Goldman and Emerson[10] have quantitatively analyzed the NMR chemical shift of the acid proton of acetic acid in carbon tetrachloride solution at several concentrations and temperatures. The present results are consistent with their results qualitatively, although they used three equilibrium constants.

Conclusions. In the preceding paragraphs, the observed concentration fluctuation has been analyzed using three different models of association equilibria. Model(a) is excluded because it could not explain the observed concentration dependence of concentration fluctuation whereas Model (b) and (c) could explain the observed concentration dependence of concentration fluctuation. The observed temperature dependence of concentration fluctuation could not how-

ever be explained by model (b). Only model (c) explained the observed concentration and temperature dependencies of concentration fluctuation, simultaneously. It must be emphasized that the mean association number itself can be determined directly from Eq. 1. The introduction of the concept of association equilibria will furnish additional information about the concentration and temperature dependencies of the concentration fluctuation. In determining local structures in solutions where various types of local structures are expected, however, an appropriate model of association equilibria has to be selected from the various plausible models which give the same mean association number. The present results indicate the possibility of determining local structures uniquely by observing both concentration and temperature dependencies for concentration fluctuation.

The authors wish to express their sincere thanks to miss Masako Yudasaka for her helpful advice on the light scattering measurements.

References

1) K. Iwasaki, M. Tanaka, and T. Fujiyama, *Bunko Kenkyu*, **25**, 1346 (1976).
2) K. Iwasaki, M. Tanaka, and T. Fujiyama, *Bull. Chem. Soc. Jpn.*, **49**, 2719 (1976).
3) "Local structure" is defined here as a group of molecules which form a specific local configuration with finite life-time by strong intermolecular interactions such as hydrogen bonding.
4) K. Iwasaki, Y. Katayanagi, and T. Fujiyama, *Bull. Chem. Soc. Jpn.*, **49**, 2988 (1976).
5) T. Kato and T. Fujiyama, *J. Phys. Chem.*, **80**, 2771 (1976).
6) T. Kato, S. Hyodo, and T. Fujiyama, *J. Phys. Chem.*, **82**, 1010 (1978).
7) See for example, M. D. Joesten and L. J. Schaad, "Hydrogen Bonding," Marcel Dekker, Inc., New York (1974), p. 287.
8) J. Timmermans, "The Physico-chemical Constants of Binary Systems," Intersciene, New York (1959).
9) I. Prigogine and R. Defay, "Chemical Thermodynamics," Longmans Green and Co., London (1954), Chap. 26.
10) M. A. Goldman and M. T. Emerson, *J. Phys. Chem.*, **77**, 2295 (1973).

TABLE 2. ION-EXCHANGE CAPACITY OF SOLUBLE PRUSSIAN BLUE CAGED IN THE GEL FOR METAL IONS (BATCH OPERATION)
(unit: 10^{-4} g-ion dm^{-3})

Metal ions[a]			Fe^{3+}	Cr^{3+}	Co^{2+}	Ni^{2+}	Ca^{2+}	Sr^{2+}	Ba^{2+}	Mn^{2+}	Cu^{2+}	Zn^{2+}	Cd^{2+}	Pb^{2+}
Original concentration of metal ions			2.0 (3.2)	2.0 (3.8)	3.0 (5.3)	3.0 (5.9)	3.0 (6.0)	3.0 (5.6)	3.0 (5.8)	3.0 (6.0)	3.0 (5.1)	3.0 (5.6)	3.0 (5.6)	3.0 (4.9)
Equilibrium concentration of metal ions in the presence of the gels examined	Sephadex G-75 gel	Gel only	1.0 (5.2)	1.6 (5.4)	2.1 (6.7)	2.8 (6.6)	2.4 (7.7)	2.7 (7.8)	1.8 (6.7)	2.6 (7.7)	2.4 (6.1)	2.2 (6.5)	2.4 (6.7)	2.1 (6.1)
		Gel containing P.b.	0.3 (3.3)	0.2 (3.4)	0.3 (3.5)	0.1 (3.4)	0.6 (4.2)	0.9 (4.2)	0.7 (4.2)	0.5 (3.8)	0.1 (3.3)	0.1 (3.4)	0.1 (3.5)	0.4 (4.0)
	Agar gel	Gel only	1.8 (5.5)	0.5 (6.2)	0.8 (6.8)	0.9 (6.9)	2.4 (7.4)	0.3 (7.3)	0.7 (7.0)	0.8 (7.1)	0.4 (6.1)	0.5 (6.8)	0.3 (6.7)	0.1 (5.8)
		Gel containing P.b.	1.8[b] (3.3)	0.0 (3.4)	0.0 (3.6)	0.0 (3.6)	0.3 (3.7)	0.0 (3.6)	0.0 (3.7)	0.0 (3.6)	0.0 (3.4)	0.0 (3.5)	0.0 (3.6)	0.0 (3.6)

a) Test solutions of the individual metal ions were prepared from their nitrate salts and were used in the test without the addition of any buffer agent. The figures in the parentheses beneath the analytical results indicate the pH values of the intact sample solution and the equilibrium solutions in each case. b) In this case, the Fe^{3+} ion in the red-colored sample solution was considered to have been partially hydrolysed and to exist as the colloidal state iron(III) nitrate hydroxide, it might be unable to diffuse into gel particles.

was no longer blue. The resulting blue particles of gel were preserved in water or dried.

The analytical results on the soluble Prussian blue in the system prepared are shown in Table 1. The high level of potassium content is considered to be proof of the fact that the majority of the blue is soluble Prussian blue. Under the conditions used in this work to prepare the system, among a variety of Sephadex gels (G-10, 15, 25, 50, 75, and 150) G-75 gel was the most suitable as a material for the preparation.

A microscopic photograph of the frozen slice of the Sephadex G-75 gel containing the soluble Prussian blue is shown in Fig. 1, from which it can be found that Prussian blue is well prepared in the network structure of gel. From the electron-microscopic photograph shown in Fig. 2, it is found that the Prussian blue is preserved as particles of 5 to 50 nm in size in the gel particle. In view of the fact that soluble Prussian blue is non-adsorptive to Sephadex gel,[4] these two photographs demonstrate that the soluble Prussian blue is caged in the gel particle.

When the system was swollen in water, a batch of it vividly captured various heavy metal ions. Tests of the ability of this system to capture the heavy metal ions in an aqueous solution in the batch procedure were carried out by using 0.1 g of each dry gel and 5 cm^3 of a solution containing the metal ions in the concentrations shown in Table 2. After having been allowed to stand overnight, the supernatants were taken for chemical analyses. The analytical results revealed a strong activity of the system in capturing heavy metal ions (Table 2).

Fig. 1. Microscopic photograph of the frozen slice of the Sephadex G-75 gel particles in which the soluble Prussian blue is caged.

Discussion

Our original expectation that a very soluble reagent of a large molecular size could be caged in the network structure of gel, and that it could be confined in the gel particle, was successfully realized in the preparation of this system.

On such a novel system in which intact soluble Prussian blue is caged, it had been further expected that the system would be an excellent capturer of heavy metal ions in an aqueous solution, since soluble Prussian blue reacts with ions of various heavy metals to form precipitates. The heavy metal ion in the solution would be able to diffuse into the gel particle through the network structure in the gel particle, and would then collide with the molecule of soluble Prussian blue residing there and react with the blue to be trapped. Thus, the heavy metal ion would not be able to return to the outside solution. This expectation as to the system was materialized, also, by the observation of its ability as a heavy-metal-ion capturer.

Recently, a way of combining two polymers to form such systems called "interpenetrating polymer network systems", has come to attract chemists' interest as a third possible way of combining two different types of polymers for the purpose of modifying the properties of individual polymers,[5] coming to supplement the conventional mechanical blending and copolymerization. This third way has, however, been used mostly to combine the elastomer-type polymer and the glassy-type polymer.

In the present work we accomplished the preparation of a new art of macromolecular system, in which the water soluble macromolecular electrolyte of an inorganic metal complex was confined within the swollen gel. The intriguing features of the structure and

10 μm

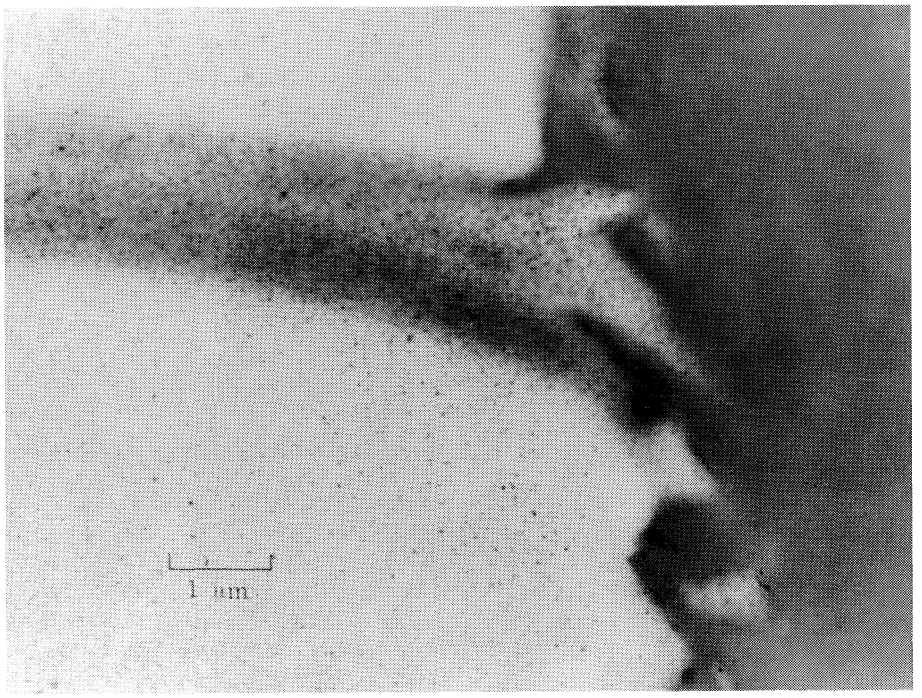

Fig. 2. Electron-microscopic photograph of soluble Prussian blue caged in the Sephadex G-75 gel. The sample system was embedded in Epon 812 after dehydrated with Durcupan.

nature, as well as the practical utility of the system, were also experimentally ascertained in this work.

The authors are very grateful for the aid of Dr. Ichiro Yamamoto, Professor of Pathology in Kitasato University, and Dr. Shinkichi Akao, Faculty of Medicine, Keio University, in preparing the electron-microscopic photographs of the gels.

References

1) Partly presented orally at the 17th International Conference on Coordination Chemistry held in Hamburg, Sept. 8th, 1976.
2) Y. Matsumoto, M. Shirai, and H. Saito, *Bull. Chem. Soc. Jpn.*, **41**, 2542 (1968).
3) T. G. Spiro, *J. Am. Chem. Soc.*, **88**, 2721 (1966).
4) H. Saito and Y. Matsumoto, *J. Chromatogr.*, **168**, 227 (1979).
5) D. Klempner, *Angew. Chem. Int. Ed. Engl.*, **17**, 97 (1978).

Ab Initio Studies of the Hydrogen Atom Addition to Ethylene

Okio NOMURA,* and Suehiro IWATA

Institute of Physical and Chemical Research, Hirosawa 2-1, Wakoh, Saitama 351

(Received June 6, 1979)

The ethyl radical formation from hydrogen and ethylene was studied with *ab initio* open shell SCF and CI methods. At first, the minimal basis set (STO-6G) was used to determine a minimal energy path. The calculated exothermicity and the height of the barrier were 72.3 kcal/mol† and 16.9 kcal/mol, respectively. After the full geometry optimization with the double zeta basis set the calculated exothermicity became 38.3 kcal/mol, which is in agreement with the experimental value (40.1 kcal/mol), but the barrier height (16.5 kcal/mol) was no better than that obtained by the minimal basis set. After the extensive CI calculations along Sloane and Hase's path with the minimal basis set, the calculated height of the barrier became only 5.1 kcal/mol. The small but finite barrier height is important in this reaction. The successive hydrogenation to form ethane was also studied and no barrier was found in the reaction.

The addition of hydrogen to ethylene (1),

$$H\cdot + C_2H_4 \rightleftharpoons C_2H_5\cdot{}^* \longrightarrow C_2H_5\cdot \qquad (1)$$

has long been a concern to chemists as a fundamental model of addition reaction of alkyl to olefins. In recent years several powerful experimental techniques have been developed for studying free radical formation. The analysis of kinetic data clarifies the reaction mechanism and has made activation energy reliable in some important radical reactions within the error of a few kilocalories.[1-4] The experimental activation energy falls between 0.5 and 7 kcal/mol.[1,†] Sato and his collaborators[5] observed the isotopic effect and they suggested that there is a barrier, however small it might be. The exothermicity of the reaction is obtained experimentally as 40.1 kcal/mol,[6] which is equal to the theoretical value obtained by Lathan *et al.*[7] This agreement may be fortuitous, though the heat of formation is not difficult to estimate in the SCF (self-consistent field) calculation as demonstrated by Pople.[8] It is, however, difficult to evaluate the barrier height of radical reactions in which a bonded pair and an unshared electron are exchanged between reactants and products,[9] such as

$$A\text{-}B + C\cdot \longrightarrow A\cdot + B\text{-}C. \qquad (2)$$

The hydrogen exchange reaction H_2+H[10] and the reactions of hydrogen and fluorine, such as $H+F_2$, $H+HF$, and $F+H_2$[11] are among examples for which the barrier height is successfully evaluated by very extensive *ab initio* CI calculations. Another reaction studied theoretically is $H+N_2$,[12] in which three atoms are found not to lie on a line. In this case change of hybridization in the course of reaction plays a significant role.

A more complicated reaction may be an addition of hydrogen (H*) to ethylene. This can be regarded as a model of radical reaction of conjugated hydrocarbons. The reaction has characteristics in change of geometry as well as of hybridization along the reaction path. Bending the CH_2 moiety off the molecular plane is expected to be one of the most important changes in geometry to form a methyl moiety. The transfer of an unpaired electron occurs from the attacking hydrogen to the other side of carbon to which the hydrogen is not attached. Shih *et al.*[13] studied the reaction of $NH_2+C_2H_4$ from a similar point of view. The UHF method might be a convenient tool in discussing the reaction mechanism because it, in many cases, predicts proper dissociation products of a ground state in a single determinant approach at the cost of vitiating the spin symmetry. Sloane and Hase[14a] calculated the potential surfaces of the Reaction 1 using the UHF method with STO-3G and 4-31G. Though geometry optimization was made at each point, they could not find a barrier. Since experimentally the barrier is known to exist in the reaction, in the recent paper,[14b] they had to use the "experimental barrier height" (3.5 kcal/mol at r_{CH^*}= 2.0 Å) to derive the analytic potential energy surface. On the other hand, Nagase and Kern,[15a] and Kato and Morokuma[15b] found a very small barrier after careful geometry optimization with the 4-31 G UHF calculations. In the present paper the restricted open shell SCF and CI methods are used for the study of the Reaction 1. At first, several model reaction paths are examined to clarify the change of the electronic structure along the path, and then geometrical parameters are optimized. Finally careful CI calculations along the reaction path determined by Sloane and Hase are performed to compare with the UHF results. The barrier is found both in the restricted SCF and in the CI calculations.

Methods

Restricted SCF Method (RHF): The restricted SCF method for open shell (hereafter it is called RHF as traditionally is) used is essentially equivalent to the two-Hamiltonian method by Davidson.[16] The program written by one of the present authors (S. I.) was linked with GAUSSIAN 70 at the University of Rochester. Since it is also capable of solving the three-Hamiltonian method, the program can be applied to an excited singlet state belonging to an irreducible representation different from that of the closed shell ground state configuration. The closed shell SCF of a cation ($[C_2H_4]H^+$) is first solved to obtain an initial set of orbitals for determining the RHF MO of the radical ($[C_2H_4]H\cdot$). The set of doubly occupied orbitals (ϕ_i, $i=1,\cdots,7$) are first determined and then an electron is added to the vacant orbitals (ϕ_8 or ϕ_9) depending on the state of the radical. The matrix equations to be solved at the $(\nu+1)$th

† 1cal=4.184 J.

cycle are

$$G_C^{\nu} b_C^{\nu+1} \equiv \{F_C^{\nu} - (n_O/n_C)(P_O^{\nu} F_O^{\nu} + F_O^{\nu} P_O^{\nu})\} b_C^{\nu+1} = \varepsilon b_C^{\nu+1}, \quad (3)$$

$$(1-P_C^{\nu+1}) F_O^{\nu} (1-P_C^{\nu+1}) b_O^{\nu+1} = \varepsilon b_O^{\nu+1}, \quad (4)$$

where the occupation numbers, n_C and n_O, in this case, are equal to 2 and 1, respectively. Fock matrices F_C^{ν} of a closed shell and F_O^{ν} of an open shell are defined in terms of the ν-th cycle MO's $\{\phi_k^{\nu}\}$ as

$$(F_C^{\nu})_{jk} = \langle \phi_j^{\nu} | h + 2J_C - K_C + 2J_O - K_O | \phi_k^{\nu} \rangle, \quad (5)$$

$$(F_O^{\nu})_{jk} = \langle \phi_j^{\nu} | h + 2J_C - K_C | \phi_k^{\nu} \rangle, \quad (6)$$

respectively, where J_C and K_C, and J_O and K_O are the coulomb and exchange operators of the closed shell and of the open shell orbitals, respectively. The projection operators P_O^{ν} and $P_C^{\nu+1}$ are defined in the present case as

$$P_O^{\nu} = |\phi_s^{\nu}\rangle\langle\phi_s^{\nu}|, \quad P_C^{\nu+1} = \sum_{k=1}^{7} |\phi_k^{\nu+1}\rangle\langle\phi_k^{\nu+1}|. \quad (7)$$

The transformation of the operator F_O in Eq. 4 by the projection operator $(1-P_C)$ implies that the open shell orbital and the virtual orbitals are determined outside the space spanned by the closed shell orbitals. The orbital energies of both the closed shell and the open shell orbitals satisfy Koopmans' theorem. Generally speaking, convergence is slower than in the closed shell SCF procedure. The orbital set after about fifteen cycles is used as a basis for the MRBW and CI calculations; the energy convergence is about 10^{-4} hartree.

MRBW Method: Even for a system which can be satisfactorily described by a single Slater determinant around its stable geometry, several electronic configurations are required for correct description when the geometry changes to a transition state in a reaction path. The CI calculation may be the best way but it is time-consuming. To estimate the characteristics of the potential energy surface, the second order Brillouin-Wigner perturbation with several reference states is used. The essential idea has been proposed by Löwdin[17] by partitioning a full Hamiltonian matrix into reference (R) and its quotient (Q).

$$H_{\mathrm{eff}}(E) = H_{RR} + H_{RQ}(E - H_{QQ})^{-1} H_{QR} \quad (8)$$

A careful choice of a reference space, R, allows us to regard Eq. 8 as the effective Hamiltonian projected onto the space R. By neglecting the off-diagonal elements of H_{QQ}, the effective Hamiltonian reduces to a simple form,

$$H_{\mathrm{eff}}^{\mathrm{MRBW}}(E) = H_{RR} + H_{RQ}(E - E_Q^{\mathrm{diag}})^{-1} H_{QR}, \quad (9)$$

where H_{RR} and H_{RQ} are the Hamiltonian matrix among reference states and between the reference and the quotient states, respectively. E_Q^{diag} is the diagonal element of H_{QQ}. This perturbation expansion may be called the multi-reference Brillouin-Wigner (MRBW), which is equivalent to the B_k method of Gershgorn and Shavitt[18] and to the method proposed by Segal *et al.*[19] Obviously, in MRBW, the choice of the reference CSF's (configuration state function) is important to obtain the approximate results to the large CI calculation.

CI (Configuration Interaction): A CI program named EFCI[20] consists of six modules as follows.

Link 1. Reading a symmetry table of MO and transforming integrals from AO to MO basis.

Link 2. Generation of electronic configurations. A set of MO's are partitioned into four groups:

i) the fixed core orbitals (which are always doubly occupied),

ii) the core orbitals (hereafter abbreviated as $\{c\}$)

iii) the valence orbitals $\{v\}$, and

iv) the excited orbitals $\{e\}$.

The electronic configurations generated are grouped into nine types. (1) The "valence" CSF: First, all of $\{c\}$ are doubly occupied, and then, the rest of electrons are filled in $\{v\}$. All the possible CSF's are generated without filling electrons in $\{e\}$. The "valence" CSF's are usually the reference states for MRBW and for the configuration selection procedure. The dominant CSF's in the states which are being studied should be included in this type. The other eight types of CSF's are single and double excitations from the "valence" CSF's. (2) $v^2 \rightarrow e^2$ (3) $v \rightarrow e$ (4) $cv \rightarrow e^2$ (5) $c \rightarrow e$ (6) $c^2 \rightarrow e^2$ (7) $c \rightarrow v$ (8) $c^2 \rightarrow ve$ (9) $c^2 \rightarrow v^2$.

Link 3. Evaluation of matrix elements in H_{RR}, H_{RQ} and the diagonal of H_{QQ}, and selection of CSF's in Q using the second-order multi-reference Rayleigh-Schrödinger perturbation expansion (A_k method).[18]

Link 4. Performing MRBW and analysis of the result.

Link 5. Evaluation of off-diagonal matrix elements in H_{QQ}.

Link 6. Solving the eigenvalue problem and analysis of the electron correlation.[21] Davidson's method modified by S. I. is used.[22]

In some cases the type of excitations $c^2 \rightarrow e^2$, though inclusion of this type lowers the total energy considerably, can be neglected because this type of excitations contributes only to the pair correlation energy of the core electrons by shifting all the "valence" states almost uniformly.[21] Care should be taken of the choice of valence orbitals and the threshold value of configuration selection. On a similar account the size of CI is also paid attention to. Hereafter the size of CI calculation is denoted as $[M_{\mathrm{root}}/N_R, N_{\mathrm{Qsel}}/N_{\mathrm{Qgen}}]$, where N_R stands for the number of reference CSF's (which consist, in most cases, of the "valence" states) and M_{root} denotes the number of the eigenstates of H_{RR}, which are used for the CSF selection procedure. N_{Qgen} and N_{Qsel} are the numbers of CSF's generated for the Q space and of selected CSF's for the CI calculation, respectively. If the CSF selection procedure is not applied, the CI size is given by $[N_R, N_{\mathrm{Qsel}}]$.

A deliberate choice of valence orbitals is necessary to take into account a well-balanced correlation along the reaction path. Those orbitals (frontier orbitals) which play an important role in a bond formation or bond exchange should be taken into account in the valence orbitals $\{v\}$. It is necessary to include the antibonding orbitals which suffer considerable changes in the new bond formation, even if they lie much higher than the lowest vacant orbitals.

Results and Discussion

First the SCF calculations are performed along several model paths with a planar ethylene of fixed geometry as shown in Fig. 1. A hydrogen atom attacks an

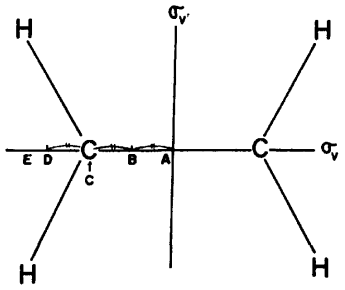

Fig. 1. Attacking points of a hydrogen on the planar ethylene (D_{2h} symmetry) in model calculations. (Only the attack on A has C_{2v} symmetry. Others have C_s symmetry.)

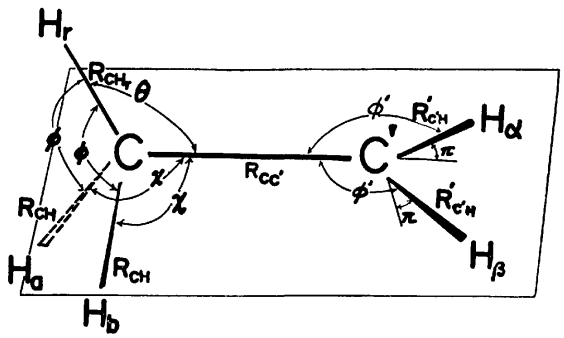

Fig. 2. Parameters of the ethyl for geometry optimization. (C_s symmetry is kept.)

ethylene vertically in the model paths. The vertical approach to the middle point of the C–C bond (path A in Fig. 1) has C_{2v} symmetry. In the paths, B to E, the hydrogen approaches the planar ethylene above the positions shown in Fig. 1. The partial geometry optimization is also performed for these models. These paths are useful for elucidating the origin of the barrier and change of the electron distribution in the course of reaction. Subsequently to the model calculations, the geometrical parameters which are critical to the reaction are optimized. In methyl formation, optimization of the angles ϕ and χ as well as θ defined in Fig. 2 is found to be important. This accounts for the change of hybridization of the carbon atom from sp^2 to sp^3. Sloane and Hase's path[14] is also examined to compare our RHF and CI results with their UHF's. In addition, careful optimization of geometries is made using the RHF method with the double zeta basis set for several important HC_1 distance.

Model A: The potential energy curves for Model A are shown in Fig. 3. In this model the repulsive $^2A_1$ state is dissociated to the ground state ethylene ($^1A_{1g}$) and hydrogen atom (^2S). The other state $^2B_2$ is correlated with the ionic products, $C_2H_4^+(^2B_{1u})+H^-$ in the RHF picture. If the UHF methode is used to describe the dissociation process, this state should be correlated with $C_2H_4(^3B_{2u})+H$. If the C–C bond length, R_{CC} is optimized along with the distance R_{HP} between H and the ethylene plane, the energy is lowered by 18.7 kcal/mol at $R_{HP}=1.1$ Å (see the curve b in Fig. 3). Even after the optimization of R_{CC} the energy minimum of the potential energy curve of $^2B_2$ in model A is found to be higher than the dissociation limit

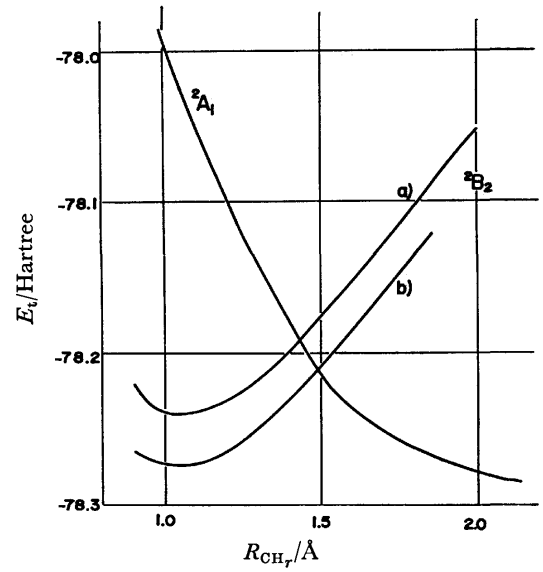

Fig. 3. Potential energy curves of the planar ethyl formation (model A).
a) In $^2B_2$, R_{CC} is fixed at 1.34 Å.
b) In $^2B_2$, R_{CC} is optimized with respect to R_{CH}.

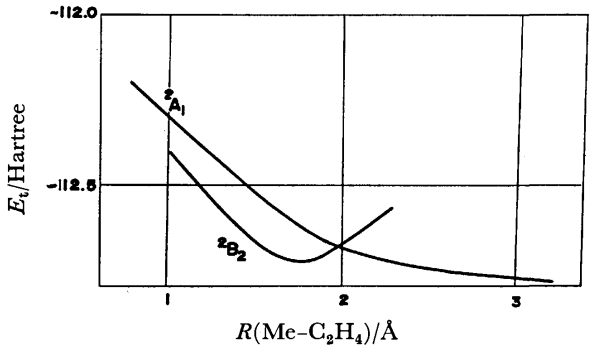

Fig. 4. Potential energy curves of $CH_3+C_2H_4\rightarrow C_3H_7$. Methyl radical approaches the planar ethylene perpendicularly to the middle of the C–C bond. $^2A'$ and $^2A''$ corresponds to the $^2A_1$ and $^2B_2$ in the C_{2v} $H+C_2H_4$ model system.

of C_2H_4+H. The optimization of the out-of-plane angles of CH_2 moieties does not change this conclusion. Although an experimental analysis suggests that CF_3 and CH_3 radicals might give rise to bridged adducts with substituted ethylenes,[23] no stable structures are found in bridged form (model A path) in our SCF calculation for $C_2H_4+CH_3$, as is shown in Fig. 4. This type of symmetric insertion is orbital-symmetry forbidden.[24–26]

Model B—E: In these models, because of the lower symmetry, the states $^2A_1$ and $^2B_2$ in model A can interact with each other. Consequently, at longer R_{HP}, the $^2A_1$ character is dominant in the lowest state while the bonding $^2B_2$ becomes a main component at shorter R_{HP}. At an intermediate R_{HP} the character of the lowest state suddenly changes. Around that distance a hump is expected to be found. The calculated potential energy curves are shown in Fig. 5. In models C, D, and E, C_2H_5 is more stable than the dissociation limit, C_2H_4+H. Among them, the most plausible path of the hydrogen to the planar ethylene is the

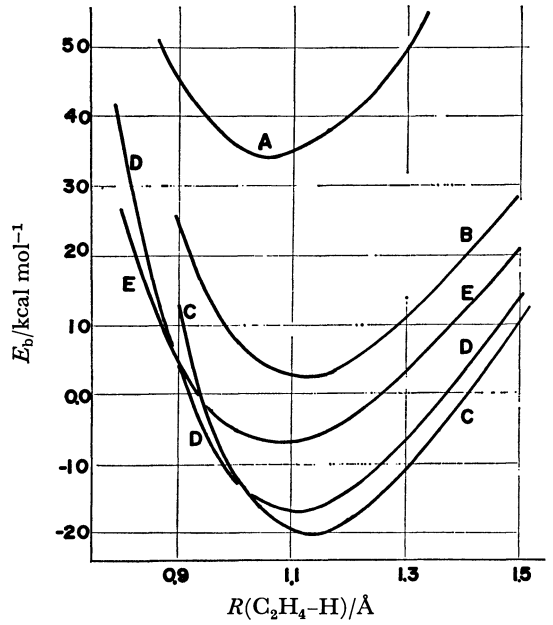

Fig. 5. Potential energy curves of $H+C_2H_4 \rightarrow C_2H_5$ model system (*cf.* Fig. 1). The energy is relative to the dissociation limit.

attack from above a carbon atom (path C). When a hydrogen atom attacks one of the carbon atom C_1, while a new H–C bond is formed, the C–C π bond breaks and an unpaired electron is localized at the other side of carbon C_2. The most stable R_{HC_1} is 1.15 Å; it is a little longer than a usual C–H bond length. As is expected, the hump is found at $R_{HC_1} \approx 1.8$ Å and its height is 20 kcal/mol, which is about several times larger than the experimentally estimated activation energy (see below).

Geometry Optimization: First, three geometry parameters (R_{CC}, θ, and χ) are optimized for each R_{HC_1} along the path C, using STO-6G and open shell RHF; the results are given in Table 1. It is notable that the C–C double bond is suddenly lengthened to become a single bond at the vicinity of the hump of the potential curve. As is mentioned above, at these R_{HC_1}, the main character of the ground state has changed. A similar feature is reported for R_{CN} in the reaction $C_2H_4+NH_2$.[13] Full geometry optimization is carried out using the double zeta basis set and the open shell RHF method at the bottom ($R_{HC_1}=1.1$ Å) and the hump (1.8 Å) determined above by the minimum basis set RHF calculations. The results are given in

Table 1. Optimized geometries
$C_2H_4 + H \rightarrow C_2H_5$ Case C

R/Å	R(C–C)/Å	θ/°	χ/°	E_T/a.u.
0.8	1.512	108.5	110.5	−78.29816
1.0	1.516	109.5	109.3	−78.40805
1.1	1.515	108.8	110.2	−78.41495
1.3	1.505	108.2	110.6	−78.38732
1.5	1.495	105.2	108.8	−78.33173
1.65	1.487	106.0	111.8	−78.29389
1.8	1.365	93.1	118.4	−78.27281
3.0	1.308	89.5	120.2	−78.29760

Table 2. Geometry of the ethyl radical

Parameter[a]	Ours	NK[b]	PD[c]	LHP[d]
R_{HC_1}/Å	1.1	1.089	1.090	1.09
$R_{C_1C_2}$/Å	1.511	1.496	1.498	1.516
$R_{C_1H_\beta}$/Å	1.094	1.084	1.086	1.087
$R_{C_2H_\alpha}$/Å	1.085	1.073	1.076	1.083
θ/°	111.0	111.7	112.01	111.2
χ/°	110.5	111.4	111.42	110.4
π/°	4.8	8.4	6.19	22.9
ϕ/°	108.0	107.1	—	107.8
ϕ'/°	121.1	120.7	120.6	118.9

a) See Fig. 2 as to the parameter. b) Ref. 29. c) Ref. 27. d) Ref. 7.

Table 3. Geometry of the ethyl at transition state

Parameter[a]	Ours	NK[b]
R_{CH}/Å	1.80	2.015
R_{CC}/Å	1.480	1.357
$R_{C_1H_\beta}$/Å	1.109	1.072
$R_{C_2H_\alpha}$/Å	1.088	1.072
θ/°	111.2	106.2
ϕ/°	104.8	93.0
χ/°	108.6	121.4
ϕ'/°	120.0	121.6
π/°	10.8	1.9

a) See Fig. 2 as to the parameter. b) Ref. 29.

Tables 2 and 3, and are compared with parameters determined by other workers. The angle π in Fig. 2 is the bending angle of nonreacting CH_2 moiety off the ethylene plane. The geometry of free ethylene with the same basis set is determined as $R_{CC}=1.342$ Å, $R_{CH}=1.084$ Å and $\angle CCH=121.7°$. Previously, Pacansky and Dupuis (PD),[27] Lathan *et al.* (LHP),[7] and Nagase and Kern (NK)[15a] optimized the structure parameters of the ethyl radical C_2H_5. PD used the triple zeta basis set for the RHF calculation and a larger set with polarization functions for the UHF calculation. They found no appreciable difference in the RHF and UHF structures. NK and LHP employed the 4-31G and STO-3G set, respectively and both used UHF method. Agreement between our parameter set and theirs is rather good except for the out-of-plane angle, π, for the $C_2H_\alpha H_\beta$, which is much smaller (4.8°) in ours, then increases in PD's and NK's, and is the largest in LHP's (22.9 °).

The exothermicity calculated by RHF with STO-6G is 72.3 kcal/mol; too large in comparison with the experimental value, 40±1 kcal/mol. The UHF method also overestimates the exothermicity (59.1 kcal/mol by Lathan *et al.*[7] and 76.1 kcal/mol by Sloane and Hase,[14a] if the minimal basis set is used. The use of the double zeta basis set improves this value substantially, which is 38.3 kcal/mol in our calculation and 40.1 kcal/mol in 4-31G UHF calculation by LHP and NK.

The calculated hump height is 12.76 kcal/mol at $R_{CH_1}=1.8$ Å for the STO-6G set and 16.5 kcal/mol at

the same bond length for the double zeta basis set, when the RHF method is applied. On the other hand, Sloane and Hase reported that they found no hump in their UHF potential energy curve.[14a] Very recently Kato and Morokuma,[15b] also using the UHF method and the 4-31G set, optimized the structure of C_2H_5 along the reaction path and found the hump with 2 kcal/mol at $R_{HC_1}=2.1$ Å, while NK obtained the same barrier at 2.015 Å.[15a] Experimentally, it has been known that the barrier exists in the reaction. Although the experimental activation energies reviewed by Teng *et al.*[1] are scattered from 7.2 to 0.5 kcal/mol, the most probable value may be *ca.* 3 kcal/mol. Our calculated heights are considerably higher than the experimental activation energy. Difficulty in calculating the hump height by RHF is not surprising, because the single electron configuration description such as RHF should fail at the hump region as model calculations (A—E) indicate. To obtain more reliable calculated hump height, the CI calculation is required.

CI Calculations: To compare Sloan and Hase (SH)'s UHF results, the CI calculations are performed along the reaction path determined by SH. The various schemes of the generation of the CSF list are examined. In this series of CI calculations, the STO-6G set is used. The molecular orbitals used are the open shell RHF MO's for the lowest state of ethyl radical. To test the MO set dependence, the closed shell SCF MO's for $C_2H_5^+$ are also used. The convergence is faster in the open shell MO-CI than in the closed shell MO-CI. Below, only the former results are discussed.

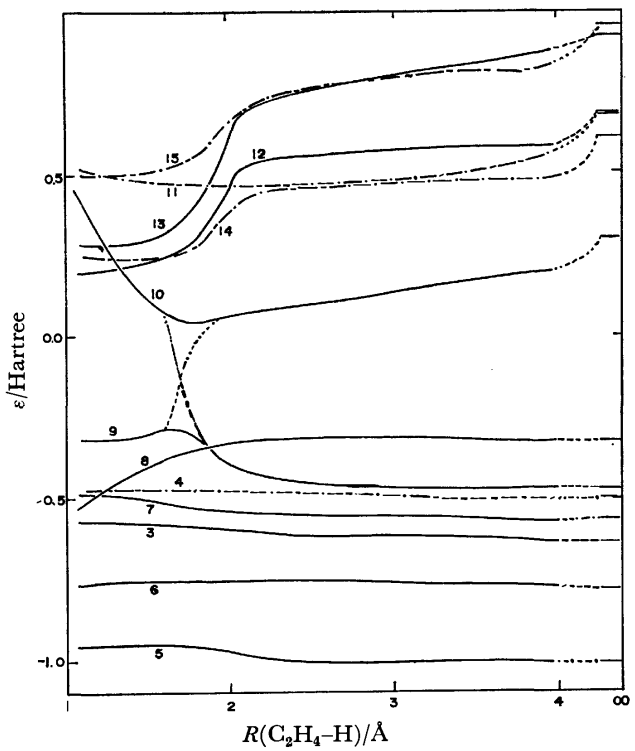

Fig. 6. Orbital correlation diagram for $H+C_2H_4\rightarrow C_2H_5$ (STO-6G RHF ground state), along the Sloane and Hase's path. Broken lines are for a″ and solid lines for a′.

To obtain even qualitatively correct potential energy surfaces in the CI calculations, it is very important how to generate the SCF list. In our terminology defined in the previous section, the CI results are dependent on the division of the set of MO's into $\{c\}$, $\{v\}$, and $\{e\}$. In Fig. 6 the change of the orbital energies is shown along the path. Note that the number given to each orbital is not the order of the orbital energy. For $R>1.9$ Å, the half filled orbital is the orbital 8, while at $R<1.9$ Å it switches to the orbital 9. Furthermore the character of the orbital 9 changes around the hump; at the shorter distance, the half filled orbital 9 becomes a localized π orbital on C_2. It is worth emphasizing the necessity of drawing the orbital correlation diagram before CI calculations for the potential energy surface. The MO coefficients in Table 4 show change of charracter of the frontier orbitals (ϕ_8, ϕ_9, and ϕ_{10}) as the hydrogen approaches. At $R_{HC_1}=4.079$ Å, the orbitals ϕ_8 and ϕ_{10} are the bonding and antibonding π of C_2H_4, and ϕ_9 is hydrogen ls. Just after the hump ($R_{HC_1}=1.7$ Å), where the bond formation between the hydrogen and the C_1 is almost completed, the half filled orbital ϕ_9 becomes localized on the $2p\pi$ lobe of the carbon C_2. The bonding π character of ϕ_8 disappears and the orbital becomes the $H-C_1$ bonding character. This is also reflected in the $H-C_1$ antibonding character in ϕ_{10}.

In PCI-1, ECI, and LCI shown in Table 5, the orbitals, 8, 9, and 10 are chosen as the "valence" orbitals, $\{v\}$, and the other occupied and vacant

Table 4. Frontier Orbitals of ethyl radical (Open shell SCF STO-6G)

$R(H-C_1)$		1.079 Å		
MO		7	9(half)	10
C_1	$2p\pi$	0.5709	−0.0520	1.1178
	$2p\sigma$	0.0121	0.0001	0.0247
C_2	$2p\pi$	0.0723	0.9987	−0.1704
	$2p\sigma$	−0.0112	−0.0004	−0.0288
H*		−0.4845	0.1703	1.0118
$H(C_1)$		0.2390	−0.0847	−0.4821
$R(H-C_1)$		1.700 Å		
MO		8	9(half)	10
C_1	$2p\pi$	0.5739	0.0293	0.8244
	$2p\sigma$	0.1041	−0.0034	0.1327
C_2	$2p\pi$	0.1936	−0.9439	−0.3281
	$2p\sigma$	−0.0775	−0.0118	−0.3429
H*		−0.6004	−0.3815	0.7754
$H(C_1)$		0.0954	0.0793	−0.0040
$R(H-C_1)$		4.079 Å		
MO		8	9(half)	10
C_1	$2p\pi$	0.6314	−0.0043	0.8179
	$2p\sigma$	−0.0000	−0.0006	−0.0036
C_2	$2p\pi$	0.6324	−0.0052	−0.8171
	$2p\sigma$	0.0000	0.0000	−0.0052
H*		−0.0042	−1.0000	0.0015
$H(C_1)$		0.0000	0.0006	0.0115

TABLE 5. THE POTENTIAL ENERGIES OF $H+C_2H_4 \rightarrow C_2H_5$ ALONG THE SLOANE AND HASE'S PATH

	RHF	UHF[a)]	PCI-0	[8, 0] PCI-1	[1/8, 1225/4077] ECI	[8, 4077] LCI	[490, 0] PCI-2	[8, 4099] MRBW
1.079	−73.97	−76.1	−74.08	−51.22	−52.6	−52.14	−40.27	−51.28
1.400	−41.58	−45.0	−41.76	−17.89	−38.13	−28.28	−7.22	−36.14
1.700	12.76	−10.5	1.24	1.36	0.84	2.66	23.21	0.71
2.079	8.19	−2.1	6.16	6.08	4.48	5.15	20.20	3.22
4.079	−1.22	0.0	−1.21	1.04	1.45	1.84	24.98	−0.20
$E(\infty)$	−78.2979	−77.54	−78.2979	−78.3431	−78.3778	−78.4562	−78.3778	−78.3772

a) see Ref. 16.

orbitals in the RHF electron configuration are the "core" $\{c\}$ and "excited" $\{e\}$ orbitals along the reaction path. Eight CSF's are constructed by filling three electrons in three "valence states". In LCI, all possible single and double electron excitations ($N_{Qgen}=4077$) from the "valence states" are taken into account. In ECI the CSF selection procedure are performed with a threshold value (10^{-4} h). These three CI potential curves agree qualitatively with each other as shown in Table 2, although the total electron energies in three calculations differ substantially. The MRBW calculations reproduce the ECI results except at $R_{HC_1}=4.079$ Å. There are several differences in the CI and RHF curves. The exothermicity and hump height are improved, and in addition, the hump position moves to a longer R_{HC_1}. Since our basis set used in CI is minimal, the calculated exothermicity (52 kcal/mol) and hump height (5 kcal/mol) may be satisfactorily in good agreement with the experiments. Surprisingly, the very small CI (PCI-1) among 8 CSF's can produce the qualitatively correct potential curve. This is because our choice of the "valence orbitals" are suitable for the potential curve calculations; in this sense, the orbitals, 8, 9, and 10, given in Table 2 can be called the "reaction orbitals".[25]

Our CI potential curves are differnt even qualitatively from the UHF curve obtained by Sloan and Hase, even though the reaction path is the same. As Yamaguchi[25] pointed out, the UHF (different orbitals for different spins, DODS) wavefunction for three electron-three orbital model, $|\psi_{1\alpha}\ \psi_{2\alpha}\ \overline{\psi}_{1\beta}|$ can be expanded in terms of four electron configurations, $|\chi_a\overline{\chi}_a\psi_{2\alpha}|$, $|\chi_b\overline{\chi}_b\psi_{2\alpha}|$, $|\chi_a\overline{\chi}_b\psi_{2\alpha}|$, and $|\chi_b\overline{\chi}_a\psi_{2\alpha}|$, where χ_a and χ_b are linear combinations of $\psi_{1\alpha}$ and $\psi_{1\beta}$, but the coefficients of these four Slater determinants are severely restricted in the UHF wavefunction. To compare the UHF results, the 3×3 CI calculations among $|\psi_8\overline{\psi}_8\psi_9|$, $|\psi_{10}\overline{\psi}_{10}\psi_9|$ and $1/\sqrt{2}[|\psi_8\overline{\psi}_{10}\psi_9|+|\psi_{10}\overline{\psi}_8\psi_9|]$ are carried out and the energies are shown as PCI-0 in Table 5. Again, the potential curve behaves correctly. These results clearly show that the CI or MCSCF calculations combined with an appropriate choice of the "reaction orbitals" are suitable for the study of the reaction potential curves. As another example of the importance of a careful selection of the "reaction orbitals", is given the PCI-2 calculations in Table 5, where 490 CSF's are created by filling nine electrons in seven orbitals (3a'—9a'). The potential curve thus obtained is absurd.

Ethane Formation: Addition of hydrogen to ethyl radical is studied to see the feature of the successive hydrogenation of ethylene,

$$C_2H_5 + H \longrightarrow C_2H_6^* \longrightarrow C_2H_6. \qquad (9)$$

Two curves are obtained in the SCF calculations. One (b in Fig. 7) is the result by the closed shell RHF which is correlated with the ethane formation. The other (a) is the curve obtained by the open shell RHF which leads to the dissociation product. The latter curve is already flat at the intersection of two curves. This implies that the dissociation is an almost complete at the bond length as short as 2 Å (Fig. 7) and that there may be no activation barrier in the ethane formation. In fact, the potential energy curve (c) obtained by CI shows no barrier. It is in conformity with the experimental facts that the rate of the ethane formation is hundred times as fast as that of the ethyl radical formation and that the abstraction of hydrogen by the ethyl easily occurs.

The MO basis set for CI at shorter C–H distance was obtained by the closed shell SCF. The ground electron configuration is $(1a')^2\cdots(5a')^2(1a'')^2(6a')^2(7a')^2(2a'')^2$. The next important configurations are a pair excitation to an antibonding orbital 8a' from the 7a' orbital with mixed character of C–H and C–C bonding, and the double excitation from 1a''

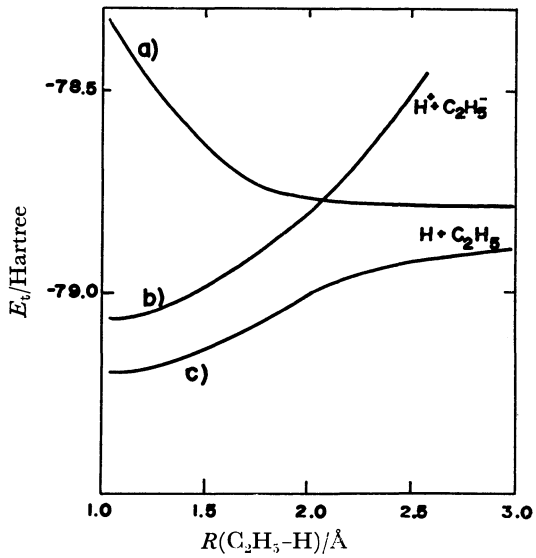

Fig. 7. Potential energy curves of ethane formation. a) Open shell SCF, b) closed shell SCF, c) CI.

and 2a'' to 3a'' and 4a''.These configurations are used as the reference states in the large CI calculation. At R_{HC_1}=2 Å the open shell SCF energy is slightly lower than that of the closed shell SCF. The highest occupied MO 7a' and the lowest vacant MO 8a' in the closed SCF MO are of the character of C–H bonding and C–H antibonding, respectively. Because of restriction of the double occupancy, the wavefuction is of too strong an ionic character. The open shell SCF makes it possible to localize electronic charge on each atom by a linear transformation of the orbitals. The frontier orbitals obtained by the open shell SCF take the form of hydrogen 1s orbital and unpaired pπ orbital on the carbon. The small energy difference between the two configurations suggests considerable configuration mixing. The CI based on the open shell SCF MO shows that the open shell electronic structure (i) $\Lambda_2(5a')^2(6a')^2(2a'')^2(7a')^1(8a')^1$ is dominant. The complementary ones are composed of closed shell structures (ii) $\Lambda_2(5a')^2(6a')^2(2a'')^2(7a')^2$ and (iii) $\Lambda_2(5a')^2(6a')^2(2a'')^2(8a')^2$, where $\Lambda_2=(1a')^2(2a')^2(3a')^2(4a')^2(1a'')^2$. The wavefunction can be approximated as: Ψ=0.90 (i) −0.29 (ii) −0.24 (iii). A linear transformation of the relevant orbitals among the major three configurations reduces to a single configuration wavefunction $\Psi=^1(\phi,\phi)$, with orbitals ϕ=0.97(pπ)−0.07 h and ϕ=1.02 h−0.05(pπ), where h and pπ denote the hydrogen ls orbital and the unpaired pπ on a carbon, respectively. On the other hand, the half filled orbitals determined by the open shell SCF are of the pure pπ and h character. Further decrease of the interaction between the hydrogen and the carbon changes the orbital character. At R_{HC_1}=3 Å the molecule can be regarded as a mixed system composed of a hydrogen atom and an ethyl radical, since 7a' and 8a' have characters of pure hydrogen ls orbital and of an unpaired pπ orbital, respectively. The orbital energy of the 7a' differs no more than 2 kcal/mol from the free hydrogen atom. The predominant configuration is $\Lambda_2(5a')^2(6a')^2(2a'')^2(7a')^1(8a')^1$. The complementary configurations are used to improve the other methyl moiety by promoting one or two electrons in the 6a' orbital (σ C–H) to the 11a' (σ^* C–C).

We wish to express our thanks to generous hospitality and suggestions given by Professor Keiji Morokuma and the members in his laboratory at the Institite of Molecular Science in Okazaki. Computation is performed with FACOM 230-75 (Fujitsu Co., Ltd.) in our Institute. Part of the work was supported by the Scientific Grant from Ministry of Education (No. 154144 and 254148).

References

1) W. E. Jones, S. D. Macknight, and L. Teng, *Chem. Rev.*, **73**, 407 (1973).
2) V. V. Voevodskii and V. N. Kondrat'ev, *Progr. React. Kinet.*, **1**, 41 (1961).
3) K. Yang, *J. Am. Chem. Soc.*, **84**, 719 (1962).
4) V. V. Azatyan, A. B. Nalbandyan, and M. Y. Ts'ui, *Dokl. Akad. Nauk SSSR*, **149**, 1095 (1963).
5) Y. Ishikawa, M. Yamabe, A. Noda, and S. Sato, *Bull. Chem. Soc. Jpn.*, **51**, 2488 (1978).
6) J. L. Franklin, J. G. Dillard, H. M. Rosenstock, J. T. Herron, and K. Draxel, NSRDS-NBS-26, National Bureau of Standards (Estimation of the heat of formation is based on the data).
7) W. A. Lathan, W. J. Hehre, and J. A. Pople, *J. Am. Chem. Soc.*, **93**, 808 (1971).
8) "MTP International Review of Scienec," ed by W. B. Brown, Butterworth & Co. London (1972), Vol. 1.
9) "Theoretical Chemistry," ed by R. N. Dixon and C. Thomson, Chem. Soc., London (1975), Vol. 2.
10) B. Liu, *J. Chem. Phys.*, **58**, 1925 (1973).
11) a) C. F. Bender, P. K. Pearson, S. V. O'Neil, and H. F. Schaefer III, *J. Chem. Phys.*, **56**, 4626 (1972); *Science*, **176**, 1412 (1972); b) S. V. O'Neil, P. K. Pearson, H. F. Schaefer III, and C. F. Bender, *J. Chem. Phys.*, **58**, 1126 (1973).
12) K. Vasudevan, S. D. Peyerimhoff, and R. J. Buenker, *J. Mol. Struct.*, **29**, 285 (1975).
13) S. Shih, R. J. Buenker, S. D. Peyerimhoff, and C. J. Michejda, *J. Am. Chem. Soc.*, **94**, 7620 (1972).
14) a) C. C. Sloane and W. L. Hase, *Discuss. Faraday Soc.*, **62**, 210 (1977). In fact, even in their calculation, a very low hump is found, if the energy at the dissociation limit (C_2H_4+H) is correctly evaluated. They took R_{HC_1}= 4.079 Å as the dissociation limit; b) W. L. Hase, G. Mrowka, R. J. Brudzynski, and C. S. Sloane, *J. Chem. Phys.*, **69**, 3548 (1978).
15) a) S. Nagase and C. W. Kern, *J. Am. Chem. Soc.*, to be appeared. b) S. Kato and K. Morokuma, *J. Chem. Phys.*, in press.
16) E. R. Davidson, *Chem. Phys. Lett.*, **21**, 565 (1973).
17) P.-O. Löwdin, *J. Mol. Spectrosc.*, **10**, 12 (1963); **13**, 326 (1964).
18) Z. Gershgorn and I. Shavitt, *Int. J. Quantum Chem.*, **2**, 751 (1968).
19) G. A. Segal, R. W. Wetmore, and K. Wolf, *Chem. Phys.*, **30**, 269 (1978).
20) Coding of EFCI started when S. I. stayed at University of Chicago. He is grateful to Prof. K. Freed for his support and suggestion.
21) N. Kosugi, H. Kuroda, and S. Iwata, *Chem. Phys.*, **39**, 337 (1979).
22) E. R. Davidson, *J. Comp. Phys.*, **17**, 87 (1975).
23) A. P. Stefani, L-Y. Y. Chuang, and H. E. Todd, *J. Am. Chem. Soc.*, **92**, 4168 (1970).
24) K. Yamaguchi, *Chem. Phys. Lett.*, **28**, 93 (1974).
25) K. Yamaguchi, *Chem. Phys.*, **25**, 215 (1977).
26) V. Bonacic-Koutecky, J. Koutecky, and L. Salem, *J. Am. Chem. Soc.*, **99**, 842 (1977).
27) J. Pacansky and M. Dupuis, *J. Chem. Phys.*, **68**, 4276 (1978).

 © 1980 The Chemical Society of Japan Bull. Chem. Soc. Jpn., 53, 68—71 (1980) [Vol. 53, No. 1

Effect of Pressure on Proton Jumps in Methanol at 25 °C

Masaru NAKAHARA,* Yoshio KUMO-OKA,** and Jiro OSUGI

Department of Chemistry, Faculty of Science, Kyoto University, Oiwake-cho, Kitashirakawa, Sakyo-ku, Kyoto 606

(Received July 19, 1979)

Conductivities of HCl and KCl in methanol containing traces (0.12 to 0.40 mol%) of water have been measured in the concentration range of ≈0.4 to ≈5 mmol dm^{-3} at 25 °C up to 2000 kg cm^{-2}. The limiting equivalent conductance ($\Lambda°$) for HCl and KCl decreased with increasing pressure. The excess proton conductance due to the proton-jump mechanism has been measured by $\Lambda°$(HCl)—$\Lambda°$(KCl) and found to increase with increasing pressure in nearly and absolutely pure methanol. The acceleration of proton jumps by pressure indicates that the rotation of methanol molecules about the longer molecular axis becomes faster at higher pressure. This anomaly is attributed to distortion with pressure of hydrogen bonds in methanol and to an increase in the repulsive field exerted by the proton on the molecule to rotate.

It is one of the most interesting ionic transport phenomena that protons in hydrogen-bonded solvents have the anomalous (excess) conductance due to proton jumps in addition to the normal hydrodynamic one. Since the rotation of solvent molecules is regarded as the rate-determining step in the proton-jump mechanism,[1,2] the excess proton conductance can be used as a probe for a dynamic study of liquid structure of hydrogen-bonded solvents. Following this line, the effect of pressure on the reorientation of water molecules was investigated at various temperatures in our previous papers;[2,3] the water reorientation was promoted by pressure, and the larger the pressure effect, the lower the temperature. When a hydrogen atom in H_2O is replaced by a methyl group CH_3, the way of hydrogen bonding is simplified; methanol in the solid state contains linear chains of O–H···O hydrogen bonds,[4] while the various types of ice have three-dimensional networks of hydrogen bonds.[5] The present authors attempt here to elucidate the influence of pressure upon proton jumps in methanol hydrogen-bonded in a way simpler than water. Since proton jumps in methanol are markedly influenced by water contained in the solvent, it is to be clarified how the effect of pressure on proton jumps is varied with the content of water. After making it clear whether proton jumps in methanol are accelerated by pressure or not, the effect of pressure on the rotation of methanol molecules is discussed in view of hydrogen bonds in methanol.

Experimental

Methanol of guaranteed reagent grade (Nakarai Chemicals Co., Ltd.) was refluxed over sodium methoxide and silver nitrate and fractionally distilled. The central fraction collected was dried with aluminum amalgam and distilled again. By drying further with molecular sieves (3A, Nakarai) and distilling, methanol for conductivity measurements was prepared. Methanol just after the purification showed a water content of 0.02 mol % in the Karl Fischer test, but easily absorbed moisture from air without special care. The conductivity of methanol was less than 3×10^{-7} Ω^{-1} cm^{-1} in any case. Potassium chloride salt of high purity was obtained from Merck and dried above 150 °C. Methanol solutions of this salt were prepared by use of calibrated pipets and measuring flasks. The stock solution of HCl was obtained by allowing purified methanol absorb dry HCl gas; the HCl gas was generated by the addition of a concentrated aqueous HCl solution to a concentrated H_2SO_4, condensed at −90 °C to remove water, and then slowly evaporated. The concentration was determined by careful titration with carbonate-free NaOH solution standardized against potassium hydrogen phthalate (ultra-pure, Merck) solution.

The density (ρ)[6] and viscosity (η)[7] data of Bridgman for methanol at elevated pressures at various temperatures were interpolated to the required temperature and pressure. The dielectric constant (ε) was cited from Ref. 8. The properties of methanol at high pressure at 25 °C are listed in Table 1.

The high-pressure system for conductivity measurement is illustrated in Fig. 1. Pressure generated by the hand pump (1) was measured to ±1 kg cm^{-2} (1 kg cm^{-2}=0.9807 $\times10^5$ Pa) by a Heise Bourdon gage (3). The temperature of the oil bath (3) was kept constant at 25±0.03 °C. The conductivity cell (8) was put in the vessel (4) and resistances of methanol and solutions in the cell were measured by a commercially available instrument (Yanagimoto MY 7). The cell constant of the conductivity cell was determined at

Table 1. Properties of methanol at 25 °C

P/kg cm^{-2}	ρ/g cm^{-3}	$\eta/10^{-3}$ Pa s	ε
1	0.7870	0.5445	32.65
500	0.8216	0.6838	34.29
1000	0.8470	0.8134	35.55
1500	0.8702	0.9416	36.58
2000	0.8888	1.072	37.48

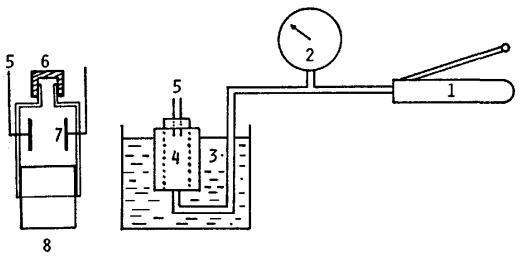

Fig. 1. High-pressure system for conductivity measurement.
1, Hand pump; 2, Heise Bourdon gage; 3, oil bath; 4, high-pressure vessel; 5, leading wire; 6, Teflon cap; 7, platinum electrode; 8, conductivity cell of a syringe type.

** Present address: Explosion Section, National Research Institute of Police Science, 6 Sanban-cho, Chiyoda-ku, Tokyo 102.

Table 2. The values of $\Lambda/\Omega^{-1}\,cm^2\,equiv^{-1}$ and $K_A/mol^{-1}\,dm^3$ for KCl

$10^4\,C$[a] / mol dm^{-3}	P/kg cm^{-2} 1	500	1000	1500	2000
0	104.4 (±0.1)	90.6 (±0.1)	81.5 (±0.1)	74.0 (±0.1)	68.0 (±0.1)
4.994	98.7	86.3	77.4	70.8	65.3
9.961	96.8	84.6	76.4	69.6	64.1
14.99	95.1	83.5	75.3	68.6	63.4
19.99	93.5	82.2	74.3	67.8	62.4
24.99	92.3	80.9	73.4	67.0	61.9
29.99	91.4	80.4	72.8	66.7	61.6
40.03	89.3	78.8	71.5	65.4	60.5
50.04	87.8	77.8	70.5	64.5	59.7
K_A	6.2 (±0.3)	3.4 (±0.6)	2.8 (±0.1)	1.9 (±0.3)	1.5 (±0.4)

a) Concentrations at 1 kg cm^{-2}.

atmospheric pressure from the conductivity of 0.01 mol dm^{-3} KCl solution,[9] and assumed invariant with pressure.

Results

The equivalent conductances Λ of KCl and HCl in Tables 2 and 3 were obtained by subtracting the solvenct conductivity and assuming that densities of dilute KCl and HCl solutions were equal to the methanol density at each pressure. The Shedlovsky equation,[10]

$$1/\Lambda S(z) = 1/\Lambda^\circ + K_A C\Lambda S(z) f^2/\Lambda^{\circ 2},$$

where

$$S(z) = \{z/2+\sqrt{1+(z/2)^2}\}^2, \quad (2)$$

$$Z = 8.204\times10^5\,\Lambda^\circ/(\varepsilon T)^{3/2} + 82.50/\eta(\varepsilon T)^{1/2}\}\sqrt{C\Lambda/\Lambda^{\circ 3}}, \quad (3)$$

and

$$-\ln f^2 = 3.649\times10^6(\varepsilon T)^{3/2}\sqrt{C\Lambda S(z)/\Lambda^\circ}, \quad (4)$$

has been employed to obtain the limiting equivalent conductance Λ° from Λ; here, K_A, C, f^2, η, ε, and T are the association constant, concentration, Debye-Hückel limiting activity coefficient of the solute, the viscosity and dielectric constant of the solvent, and temperature, respectively. The present value of Λ° (KCl)/Ω^{-1} cm^2 equiv^{-1}, 104.4 at atmospheric pressure is comparable with the more accurate ones, 104.78[4] and 104.93[11] in literature.

As known well,[1,12,13] Λ(HCl) in methanol drops very sharply with the increase of the amount of water contained in contrast to Λ(KCl) insensitive to the impurity water, because protons bound to H_2O molecules (H_3O^+) will not tend to jump to neighboring CH_3OH molecules of lower dipole moment and the fraction of protons bound to CH_3OH molecules (CH_3OH^+) decreases on the addition of water to methanol. Hence, three sets of HCl solutions, which are different in the amount of water absorbed, were investigated. The mole fraction x[14] of water contained in methanol has been estimated at atmospheric pressure by means of Strehlow's equation,[13]

Table 3. The values of $\Lambda/\Omega^{-1}\,cm^2\,equiv^{-1}$ and $K_A/mol^{-1}\,dm^3$ for HCl

$10^4\,C$[a] / mol dm^{-3}	P/kg cm^{-2} 1	500	1000	1500	2000
	x=0.12 mol %				
0	180.0 (±0.3)	169.2 (±0.2)	161.0 (±0.3)	154.2 (±0.3)	148.6 (±0.2)
3.958	173.5	163.7	156.3	150.0	144.7
7.923	171.5	162.0	154.6	148.8	143.6
11.88	168.9	159.4	152.4	146.5	141.9
15.85	166.3	157.8	151.4	145.8	140.8
19.80	165.6	157.2	151.3	145.4	140.5
23.17	163.6	155.3	149.7	144.1	139.5
27.73	162.8	154.9	149.1	143.8	139.2
31.70	161.6	153.2	147.4	142.3	137.9
39.62	159.1	151.5	146.1	141.1	136.7
K_A	7.4 (±0.7)	6.1 (±0.6)	3.2 (±0.8)	2.3 (±0.7)	1.7 (±0.5)
	x=0.31 mol %				
0	168.0 (±0.2)	157.9 (±0.2)	150.8 (±0.2)	144.5 (±0.2)	139.3 (±0.3)
3.555	161.9	152.8	146.4	140.5	135.6
7.117	159.5	150.5	144.3	138.8	134.1
14.23	155.2	147.4	141.7	136.3	131.8
21.35	152.1	145.2	139.8	134.8	130.7
28.47	149.5	142.6	137.6	133.0	128.8
35.59	147.6	140.7	135.8	131.1	127.0
K_A	11.8 (±0.5)	8.7 (±0.5)	7.0 (±0.5)	5.5 (±0.5)	4.9 (±0.8)
	x=0.40 mol %				
0	162.6 (±0.2)	152.3 (±0.3)	145.2 (±0.3)	139.0 (±0.3)	134.0 (±0.2)
8.142	153.9	145.6	139.4	133.8	129.1
12.21	151.9	143.6	137.4	131.9	127.6
16.28	150.3	142.0	136.2	131.0	126.8
20.36	148.4	140.6	135.1	130.1	125.8
24.43	147.5	139.7	133.6	128.8	124.8
28.50	146.1	139.2	133.9	129.1	124.9
32.57	145.2	138.3	132.8	127.8	123.8
36.64	143.8	137.2	132.0	127.1	123.1
K_A	6.9 (±0.6)	3.8 (±0.8)	3.3 (±1.0)	2.7 (±0.9)	2.4 (±0.7)

a) Concentrations at 1 kg cm^{-2}.

$$\Lambda_x^\circ(\mathrm{HCl}) = \lambda^\circ(CH_3OH_2^+) + \lambda^\circ(Cl^-) - \{\lambda^\circ(CH_3OH_2^+) - \lambda^\circ(H_3O^+)\}Kx/\{1+(K-1)x\}, \quad (5)$$

where

$$K = x_1(1-x)/(1-x_1)x, \quad (6)$$

for the equilibrium,

$$CH_3OH_2^+ + H_2O \rightleftharpoons H_3O^+ + CH_3OH,$$

($1-x_1$, x, x_1, $1-x$)

and

$$\Lambda_x^\circ(\mathrm{HCl}) = x_1\lambda^\circ(H_3O^+) + (1-x)\lambda^\circ(CH_3OH_2^+) + \lambda^\circ(Cl^-). \quad (8)$$

Here, $\lambda^\circ(H_3O^+)$, $\lambda^\circ(CH_3OH^+)$, and $\lambda^\circ(Cl^-)$ are, respectively, the limiting equivalent conductances of H^+ bound to H_2O with the mole fraction x_1, H^+

TABLE 4. THE VALUES OF $t°(K^+)$, $\lambda°/\Omega^{-1}\,cm^2\,equiv^{-1}$, AND $\lambda°\eta/\Omega^{-1}\,cm^2\,equiv^{-1}\,mPa\,s$

	P/kg cm^{-2}				
	1	500	1000	1500	2000
$t°(K^+)$	0.500	0.493	0.487	0.481	0.475
$\lambda°(H^+)$[a]	127.8	123.3	119.2	115.8	112.9
$\lambda°(K^+)$	52.2	44.7	39.7	35.6	32.3
$\lambda°(Cl^-)$	52.2	45.9	41.8	38.4	35.7
$\lambda°(H^+)^{a)}\eta$	69.6	84.3	97.0	109.0	121.0
$\lambda°(K^+)\eta$	28.4	30.6	32.3	33.5	34.6
$\lambda°(Cl^-)\eta$	28.4	31.4	34.0	36.2	38.3

a) In methanol containing 0.12 mol % water.

bound to CH_3OH, and Cl^- in nearly pure methanol. The parameters in Eq. 5 are determined at atmospheric pressure at 25 °C as

$$\Lambda_x°(HCl) = 198.5 - 1.39\times10^4 x/(1+138x). \quad (9)$$

The limiting equivalent conductances of KCl and HCl were divided into their ionic components as in Table 4, using the limiting transference numbers $t°(K^+)$ in KCl solution at atmospheric pressure[15] and those at high pressure which were obtained from Fig. 13 in Ref. 16. The ions decrease their mobilities with the rise in pressure as the methanol viscosity increases with increasing pressure, but initially increase in water qualitatively in parallel with the pressure dependence of the water viscosity.[2] In a quantitative sense, however, the pressure dependence of $\lambda°$ is not exactly parallel with that of the solvent fluidity η^{-1} because the Walden products of the ions $\lambda°\eta$ are not constant at high pressures as seen in Table 4. The effect of pressure on the Walden products of the ions is in the sequence,

$$H^+ > Cl^- > K^+.$$

Any of these ions has a much larger positive pressure coefficient of the Walden product in methanol than in water.[2,17]

The proton conductance in hydrogen-bonded solvents is due to the parallel series of the proton-jump and hydrodynamic processes.[1,18] However, no exact way to measure exclusively the anomalous conductance due to the proton-jump has been invented, and an empirical method is often used. The quantity,

$$\lambda_x°^{E} = \Lambda_x°(HCl) - \Lambda°(KCl), \quad (10)$$

is taken here as a measure of the anomalous conductance. Altough Li^+ and Na^+ are chosen elsewhere[1,19] instead of K^+ as a measure of the hydrodynamic conductance of the protonated species, H_3O^+ and CH_3OH^+, K^+ would be more appropriate because its ionic size is closer to H_3O^+ and CH_3OH^+ than the smaller ions.[20] The values of $\lambda_x°^{E}$ are plotted against pressure in Fig. 2. It is to be noted that $\lambda_x°^{E}$ increases with increasing pressure in methanol as $\lambda°^{E}$ in water.[2] The tendency is observed not only at infinite dilution but also at finite concentrations covered by the present work, while a decrease with pressure in the excess conductance measured at 2.5 mmol kg^{-1} by Λ(HBr)—Λ(NaBr) was reported[19] and later, an increase at infinite dilution was suggested.[21] The reason for the

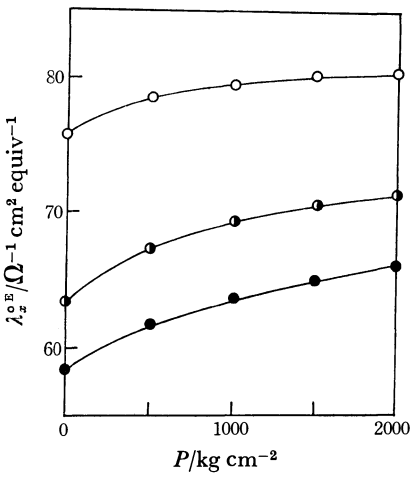

Fig. 2. Pressure dependence of excess proton conductances.
○, x=0.12 mol %; ◑, x=0.31 mol %; ●, x=0.40 mol %.

pressure-induced acceleration of proton jumps will be considered in the following section. On the other hand, the overall proton conductance decreases in methanol but increases in water.[2] The difference is explained in view of the facts that the contribution of the anomalous conductance to the overall proton conductance is much larger in the three-dimensionally hydrogen-bonded solvent (water) than in the one-dimensionally hydrogen-bonded solvent (methanol) and that the anomalous proton conductance is increased by pressure in both solvents but the hydrodynamic conductance is not initially promoted by pressure in methanol.

Discussion

It is important, first of all, to prove that the increase with pressure in the excess proton conductance at infinite dilution occurs in absolutely pure methanol as well as in methanol containing water. Using Eqs. 5 and 10 and assuming $\lambda°(H_3O^+)=\lambda°(K^+)$, We can derive the equation,

$$\lambda_x°^{E} = \lambda°^{E}(1-x)/\{1+(K-1)x\} \approx \lambda°^{E}/\{1+(K-1)x\}, \quad (11)$$

where the limiting excess proton conductance in pure methanol, $\lambda°^{E}$ is expressed as

$$\lambda°^{E} = \lambda°(CH_3OH_2^+) - \lambda°(K^+). \quad (12)$$

The differentiation of Eq. 11 with respect to pressure leads to the equation,

$$\partial\lambda°^{E}/\partial P = \{1+(K-1)x\}\partial\lambda_x°^{E}/\partial P + \lambda°^{E}\{1+(K-1)x\}^{-1}x\partial K/\partial P. \quad (13)$$

Since $\partial\lambda_x°^{E}/\partial P$ around 1 kg cm^{-2} is positive as seen in Fig. 2 and K at 1 kg cm^{-2} 139,[13] the first term in the right-hand side of Eq. 13 is positive. The second term is positive more or less because the equilibrium (7) is supposed to be shifted by pressure in some degree toward the right-hand side where the proton is bound to the stronger dipole and would have a smaller volume. Althogh the present data

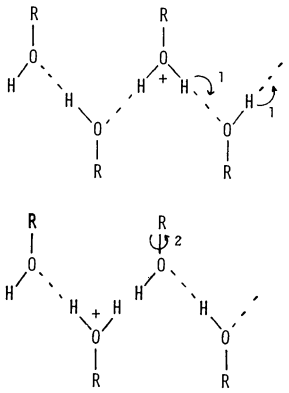

Fig. 3. Model for proton jump in methanol.
1, Proton transfer; 2, molecular rotation; R, methyl group.

are not enough to obtain quantitative information on $\partial\lambda^{\circ E}/\partial P$, they clearly exhibit through Eq. 13 that proton jumps in pure methanol are promoted by pressure to a larger extent than in methanol containing water.

The mechanism of proton jumps in alcohols has been proposed by Conway *et al.*[1] on the basis of the comparison between the excess proton conductance and the dielectric relaxation time in water and a few alcohols; there are two elementary processes, the proton transfer and the rotation of solvent molecules, the latter being the rate-determining step as in water. The same mechanism is assumed here and the molecular model is illustrated in Fig. 3. According to this mechanism, the increase with pressure in the excess proton conductance in methanol indicates that the rotation of methanol molecules about the longer molecular axis is promoted by pressure in spite of the increase in the density and the number of the hydrogen bonds.[22] When methanol is subjected to high pressure, the system is compressed to a denser state, irrespective of gain or loss in energy. For compression of the chain shown in the second row of Fig. 3, the following two factors are to be considered: (1) pushing the molecules above and below the plane of the chain so that the methyl groups may get closer, pressure distorts or bends the hydrogen bonds and weakens the strength; (2) keeping the molecules in the chain on the same plane, pressure decreases the intermolecular distance between the molecule to rotate and the hydrogen-bonded molecule (on the right side) and that between the molecule to rotate and the protonated molecule (on the left side). In the latter case, pressure gives more repulsive field to the molecule to rotate in favor of the rotation and at the same time, the strengthened hydrogen bond increases in some degree the potential barrier to the rotation. Although any conclusion on the relative importance of these factors must meet more straightforward studies, such as dielectric relaxation, NMR relaxation, and spectroscopic measurements at high pressure, at least, the factor (1) could not be neglected. As a matter of fact, the static dielectric constant of methanol increases and the Kirkwood correlation factor g decreases as methanol is compressed.[8] The increase in the dielectric constant is dominated by the density increase due to compression, but the decrease in the correlation factor suggests that such kind of distortion of the hydrogen bonds occurs that reduces the sum[23] of the average cosines of the angles between the dipoles of the correlated molecules in the hydrogen-bond chain.

References

1) B. E. Conway, J. O'M. Bockris, and H. Linton, *J. Chem. Phys.*, **24**, 834 (1956).
2) M. Nakahara and J. Osugi, *Rev. Phys. Chem. Jpn.*, **47**, 1 (1977).
3) M. Ueno, M. Nakahara, and J. Osugi, *J. Solution Chem.*, **8**, 881 (1979).
4) K. J. Tauer and W. N. Lipscomb, *Acta Crystallogr.*, **5**, 606 (1952).
5) D. Eisenberg and W. Kauzmann, "The Structure and Properties of Water," Oxford Universirty Press, London (1969).
6) P. W. Bridgman, *Proc. Am. Acad. Arts Sci.*, **49**, 3 (1913).
7) P. W. Bridgman, *Proc. Am. Acad. Arts Sci.*, **77**, 117 (1949).
8) K. R. Srinivasan and R. L. Kay, *J. Solution Chem.*, **4**, 299 (1975).
9) J. P. Butler, H. I. Schiff, and A. R. Gordon, *J. Chem. Phys.*, **19**, 752 (1951).
10) T. Shedlovsky, *J. Franklin Inst.*, **225**, 739 (1938); R. M. Fuoss and T. Shedlovsky, *J. Am. Chem. Soc.*, **71**, 1496 (1949).
11) E. C. Evers and A. G. Knox, *J. Am. Chem. Soc.*, **73**, 1739 (1951).
12) T. Shedlovsky and R. L. Kay, *J. Phys. Chem.*, **60**, 151 (1956).
13) H. Strehlow, *Z. Phys. Chem., N. F.*, **24**, 240 (1960).
14) Water in HCl solution exists in the forms H_2O and H_3O^+, as expressed in Fig. 7. However, the contribution of the latter form to the total concentration is negligible at infinite dilution where proton conductances are considered.
15) J. A. Davies, R. L. Kay, and A. R. Gordon, *J. Chem. Phys.*, **19**, 749 (1951).
16) B. Watson and R. L. Kay, cited by Kay in "Water," ed by F. Franks, Plenum, New York (1973), Vol. 3, Chap. 4.
17) M. Nakahara, K. Shimizu, and J. Osugi, *Rev. Phys. Chem. Jpn.*, **42**, 12 (1972).
18) T. Erdey-Grúz and S. Lengyel, "Modern Aspects of Electrochemistry," ed by J. O'M. Bockris and B. E. Conway Plenum, New York (1977), Chap. 1.
19) W. Strauss, *Aust. J. Chem.*, **10**, 277 (1957).
20) According to Ref. 16, the smaller ions Li^+ and Na^+ and the larger ion Me_4N^+ decrease their mobilities to a larger extent than K^+ as pressure increases. Therefore, to replace K^+ in Eq. 10 by Li^+, Na^+, or Me_4N^+ makes more positive the pressure coefficient of $\lambda_x^{\circ E}$.
21) J. F. Cukurins and W. Strauss, *Aust. J. Chem.*, **29**, 249 (1976).
22) E. Fishman and H. G. Drickamer, *J. Chem. Phys.*, **24**, 548 (1956); S. D. Hamann, "High Pressure Physics and Chemistry," ed by R. S. Bradley, Academic press, London (1963), Vol. 2, P. 144.
23) G. Oster and J. G. Kirkwood, *J. Chem. Phys.*, **11**, 175 (1943).

A Conductance Study of Alkali Metal Ion–15-Crown-5, 18-Crown-6, and Dibenzo-24-crown-8 Complexes in Propylene Carbonate

Yasuyuki TAKEDA,* Hisao YANO, Masayuki ISHIBASHI, and Hiroshi ISOZUMI

Department of Chemistry, Faculty of Science, Chiba University, Yayoi-chō, Chiba 260

(Received July 23, 1979)

The formation constants, K_{ML^+}, for 1:1 complexes of 15-crown-5 (15C5), 18-crown-6 (18C6), and dibenzo-24-crown-8 (DB24C8) with alkali metal ions and the limiting ionic molar conductivities, $\lambda°$, of the complexed cations in propylene carbonate have been determined at 25 °C conductometrically. The K_{ML^+} value series about the same alkali metal ion among the crown ethers are given in the order 18C6 $\gg$ DB24C8 > 15C5. The K_{ML^+} sequences of the alkali metal ions with 15C5, 18C6, and DB24C8 are $Li^+ > Na^+ > K^+ > Rb^+ > Cs^+$, $K^+ > Na^+ > Rb^+ \gg Cs^+$, and $Na^+ > K^+ > Rb^+ \geq Cs^+$, respectively. The indication is that the ability of the alkali metal ions to form complexes with the three crown ethers is not always affected primarily by the relative sizes of the alkali metal ions and the crown ether cavity. In each case of 18C6 and DB24C8 the $\lambda°$ values of the alkali metal ions are nearly equal, while in the case of 15C5 there are considerably differences, suggesting that in the former case the charge of the alkali metal ion trapped in the crown ether cavity is effectively shielded. This is not true in the latter case.

It is known that crown ethers interact with certain cations, especially with alkali and alkaline earth metal ions, to form stable stoichiometric complexes. The stability of the complexes is governed by the solvent medium, the relative sizes of the cation and the crown ether cavity, the number of binding sites in the crown ether ring, and the flexibility of the crown ether.[1] The crown ether complexes in the crystalline state have been investigated by X-ray crystallography[2] and those in solution by spectroscopy[3] and conductimetry.[1h,4] The studies show that in many cases the cation is held in the crown ether cavity and surrounded by the oxygen atoms of the crown ether ring. The structure of the complex in solution is not always however the same as in the crystalline state.

The crown ethers used in this work are 15-crown-5 (15C5), 18-crown-6 (18C6), and dibenzo-24-crown-8 (DB24C8). The sizes, the cavity sizes, and the number of donor oxygen atoms of these three compounds are different from one another. Moreover, 15C5 and 18C6, whose oxygen atoms are coplanar and symmetrically distributed in the crown ether ring, are rigid crown ethers, while DB24C8, whose configuration is termed cylindrically symmetrical, is a flexible crown ether.[1a] In this paper, the formation constants for 1:1 complexes of 15C5, 18C6, and DB24C8 with alkali metal ions and the limiting ionic molar conductivities of the complexed cations in propylene carbonate (PC) have been determined conductometrically in order to study the factors influencing complex formation between crown ethers and alkali metal ions and the behavior of the complexed cations in PC, respectively. PC has a high dielectric constant (ε_r = 64 at 25 °C[5]) and moderate Lewis base and weak Lewis acid properties.[6] PC was used as the solvent since almost all univalent metal perchlorates are nearly completely dissociated in PC solution.[5,6b]

Experimental

Materials. 15C5, 18C6, and DB24C8 were obtained from Nisso Co., Ltd. 15C5 was purified by distillation under vacuum (bp 115—129 °C, 1.5 mmHg). 18C6 was recrystallized from acetonitrile and, prior to use, dried at 70 °C in a vacuum oven. The method of purification of DB24C8 was previously described.[7] Rubidium and caesium perchlorates were prepared by adding an equimolar perchloric acid solution to an aqueous solution of rubidium bromide and caesium hydroxide respectively. Lithium, sodium, and potassium perchlorates were purchased commercially. All perchlorates were recrystallized from water five times and, prior to use, dried at 150 °C in a vacuum oven. PC was distilled twice under nitrogen at approx. 12 mmHg. The middle 70% of the distillate was used. The water content of the finally purified PC determined by Karl Fischer titration was less than 0.01%. The conductivity of the final product was less than $5 \times 10^{-8}\ \Omega^{-1}\ cm^{-1}$.

Apparatus and Procedure. The conductance measurements were conducted on a Yanagimoto conductivity apparatus, model MY-7, in a water bath thermostated at 25.00±0.01 °C. Two cells were used with cell constants of 0.09317_1 and $0.2046_7\ cm^{-1}$.

The experimental procedure to obtain formation constants of crown ether complexes with alkali metal ions is as follows; a PC solution of the alkali metal perchlorate (4×10^{-4}—5×10^{-4} M, 200 cm^3) was placed in the cell (volume 300 cm^3) and the resistance of the solution measured. A step-by-step increase in the crown ether concentration was effected by a rapid transfer from the PC solution of the crown ether (5×10^{-3}—2×10^{-2} M) to the cell using a pipet, until the total concentration of the crown ether was approx. five times as large as that of the alkali metal perchlorate. The resistance of the solution in the cell was remeasured after each transfer.

The experimental procedure to obtain limiting ionic molar conductivities of the alkali metal ion–crown ether complexes was as follows; a PC solution of the crown ether (2×10^{-3} M, 200 cm^3) was placed in the cell and the resistance of the solution measured. Then a step-by-step increase in the alkali metal perchlorate concentration was effected by a rapid transfer from the PC solution of the alkali metal perchlorate (2×10^{-2} M) to the cell with a pipet, until the total concentration of the alkali metal perchlorate was approx. twice as large as that of the crown ether. The resistance of the solution in the cell was remeasured after each transfer.

Results

The molar conductivity, Λ, *vs.* $[L]_t/[M]_t$ plots in PC at 25 °C are given in Figs. 1—3, where $[L]_t$ and $[M]_t$ are the total concentrations of the crown ether

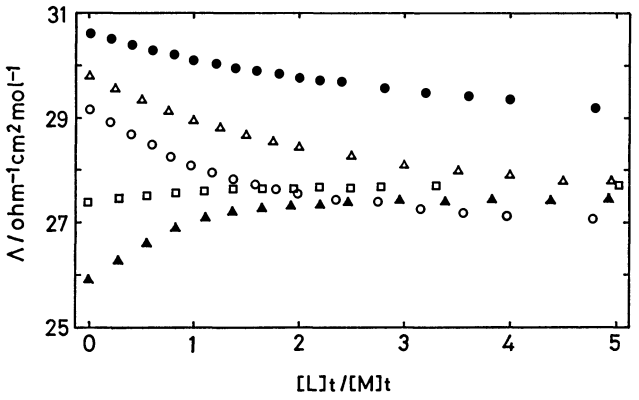

Fig. 1. Λ *vs.* $[L]_t/[M]_t$ curves for 15C5-alkali metal perchlorate systems in PC at 25 °C.
▲: Li^+, □: Na^+, ○: K^+, △: Rb^+, ●: Cs^+, $[M]_t = 5\times10^{-4}$ M.

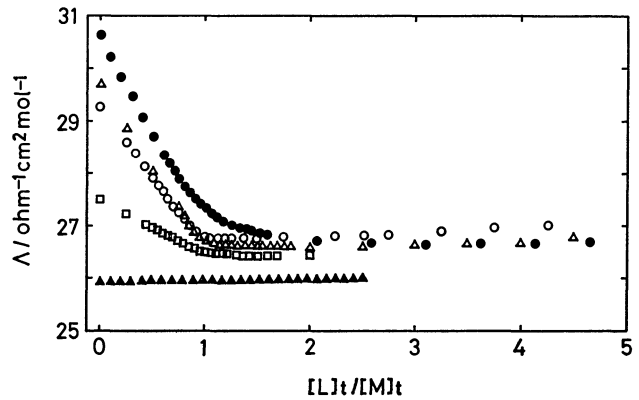

Fig. 2. Λ *vs.* $[L]_t/[M]_t$ curves for 18C6-alkali metal perchlorate systems in PC at 25 °C.
▲: Li^+, □: Na^+, ○: K^+, △: Rb^+, ●: Cs^+, $[M]_t = 5\times10^{-4}$ M.

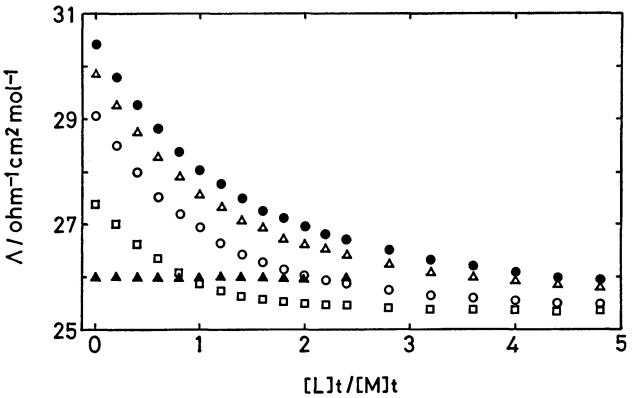

Fig. 3. Λ *vs.* $[L]_t/[M]_t$ curves for DB24C8-alkali metal perchlorate systems in PC at 25 °C.
▲: Li^+, □: Na^+, ○: K^+, △: Rb^+, ●: Cs^+, $[M]_t = 4\times10^{-4}$ M.

and the alkali metal ion respectively. Figures 1, 2, and 3 correspond to the cases of 15C5, 18C6, and DB24C8 respectively. The Λ *vs.* $[L]_t/[M]_t$ plots in Figs. 1—3 show a decrease of Λ with an increase in the crown ether concentration except for the 15C5-Li^+ and Na^+ and the Li^+–18C6 and DB24C8 systems. Those for the 15C5–Li^+ and Na^+ systems show an increase of Λ as the 15C5 concentration increases. In the Li^+–18C6 and DB24C8 systems, there is a negligible change in Λ in spite of an increase in the crown ether concentration, consequently the conductometric determination of the complex formation constant was impossible. The association between a cation, *i.e.*, an alkali metal ion and a tetraalkylammonium ion, and a perchlorate ion in PC is negligible,[5,6b] and therefore it is assumed on this basis that the association between the alkali metal ion–crown ether complex and the perchlorate ion in PC is also negligible under the highly dilute experimental conditions mentioned above. From Figs. 1—3, in the cases of the 15C5–Li^+ and Na^+, the 18C6–Na^+, K^+, Rb^+, and Cs^+, and the DB24C8–Na^+ systems, the slope of each curve changes sharply at the point when $[L]_t/[M]_t=1$, indicating that the crown ether forms a 1:1 complex with the alkali metal ion in PC under these experimental conditions.[8] For the 15C5 and DB24C8–K^+, Rb^+, and Cs^+ systems, no such clear breaking point was observed. From the literature[1b,1c,1f,1g] however, it is assumed that 15C5 and DB24C8 form 1:1 complexes with K^+, Rb^+, and Cs^+ in PC under these experimental conditions.

The equilibrium equation is given by

$$\begin{array}{ccccc} M^+ & + & L & \rightleftharpoons & ML^+ \\ \alpha[M]_t & & [L]_t-(1-\alpha)[M]_t & & (1-\alpha)[M]_t, \end{array} \quad (1)$$

where M^+, L, and α are the alkali metal ion, the crown ether, and the fraction of free alkali metal ions respectively. Accordingly, the complex formation constant, K_{ML^+}, is defined by

$$K_{ML^+} = \frac{[ML^+]}{[M^+][L]} = \frac{1-\alpha}{\alpha[L]}. \quad (2)$$

The observed conductivity, κ, is written as

$$\kappa = \kappa_{MClO_4} + \kappa_{MLClO_4}, \quad (3)$$

where κ_{MClO_4} and κ_{MLClO_4} are the conductivities of the alkali metal perchlorate and alkali metal crown ether perchlorate respectively. The molar conductivities are given by

$$\Lambda_{MClO_4} = \frac{\kappa_{MClO_4}}{[M^+]} = \frac{\kappa_{MClO_4}}{\alpha[M]_t}, \quad (4)$$

$$\Lambda_{MLClO_4} = \frac{\kappa_{MLClO_4}}{[ML^+]} = \frac{\kappa_{MLClO_4}}{(1-\alpha)[M]_t}, \quad (5)$$

where Λ_{MClO_4} and Λ_{MLClO_4} are the molar conductivities of the alkali metal perchlorate and alkali metal crown ether perchlorate respectively. Equation 3 may be transformed *via* Eqs. 4 and 5 to give

$$\Lambda = \frac{\kappa}{[M]_t} = \alpha\Lambda_{MClO_4} + (1-\alpha)\Lambda_{MLClO_4}. \quad (6)$$

Since the crown ether concentration was kept low ($<2.5\times10^{-3}$ M), corrections for viscosity changes were neglected. Substituting from Eq. 6 into Eq. 2 gives

$$K_{ML^+} = \frac{\Lambda_{MClO_4}-\Lambda}{(\Lambda-\Lambda_{MLClO_4})[L]}, \quad (7)$$

where

$$[L] = [L]_t - \frac{[M]_t(\Lambda_{MClO_4}-\Lambda)}{\Lambda_{MClO_4}-\Lambda_{MLClO_4}}.$$

Table 1. $\log (K_{ML^+}/mol^{-1}\,dm^3)$ values at 25 °C

	15C5		18C6		DB24C8	
	PC	H_2O[1b]	PC	H_2O[1b]	PC	70 wt% CH_3OH in H_2O[1c]
Li^+	4.2_6	—	—	—	—	—
Na^+	3.7	0.70	5.6_8	0.80	4.1_6	1.54
K^+	3.4_1	0.74	6.2_4	2.03	3.7_3	2.42
Rb^+	3.0_4	0.62	5.3_2	1.56	3.5_5	2.55
Cs^+	2.6_9	0.8	4.4_8	0.99	3.4_6	2.48

The procedure for obtaining the K_{ML^+} value is as follows. The Λ_{MLClO_4} value is estimated from the Λ values at the points of large $[L]_t$ to $[M]_t$ ratios. Using this Λ_{MLClO_4} value, the K_{ML^+} values in Eq. 7 is calculated. The actual K_{ML^+} and Λ_{MLClO_4} values are calculated by a nonlinear least-squares analysis.[1h] The log K_{ML^+} values are listed in Table 1.

The procedure for obtaining the limiting ionic molar conductivity, λ°, of the alkali metal ion–crown ether complex is as follows. The mass balances are

$$[M]_t = [M^+] + [ML^+], \quad (8)$$

$$[L]_t = [L] + [ML^+]. \quad (9)$$

From Eqs. 2, 8, and 9, the following quadratic equation follows;

$$K_{ML^+}[ML^+]^2 - \{1 + K_{ML^+}([M]_t + [L]_t)\}[ML^+] + K_{ML^+}[M]_t[L]_t = 0. \quad (10)$$

The $[M^+]$ value is obtained from Eq. 8 using the $[ML^+]$ value calculated from Eq. 10. The κ_{MClO_4} value in Eq. 3 at this $[M^+]$ point can be obtained from the previous $\Lambda_{MClO_4}-[MClO_4]^{1/2}$ plots in PC at 25 °C.[1i] Then, the Λ_{MLClO_4} value at this $[ML^+]$ point can be calculated from Eqs. 3 and 5 using this κ_{MClO_4} value. The limiting molar conductivity, Λ°, of the alkali metal crown ether perchlorate is determined by extrapolation of the calculated Λ_{MLClO_4} values from $\Lambda_{MLClO_4}-[MLClO_4]^{1/2}$ plots for ten-odd concentration points. From this Λ° value, the λ° value of the alkali metal ion–crown ether complex in PC at 25 °C is computed, using the λ° value of the perchlorate ion, $\lambda^\circ = 18.2_8\ \Omega^{-1}\,cm^2\,mol^{-1}$.[5] The λ° values of the alkali metal ion–crown ether complexes are given in Table 2, together with the λ° values of the alkali metal ions in PC at 25 °C.

Discussion

The log K_{ML^+} value series about the same alkali metal ion among the crown ethers in PC are from Table 1 in the order 18C6≫DB24C8>15C5. A complex is more stable the greater the number of oxygen atoms, provided the oxygens are coplanar and symmetrically distributed in the crown ether ring.[1a] 15C5 and 18C6 structurally obey these criteria and the log K_{ML^+} values of 15C5 and 18C6 in both PC and aqueous solutions (Table 1) show the same tendency as stated above. The log K_{ML^+} values of DB24C8 in PC (Table 1) are smaller than expected based on the greater number of donor oxygen atoms (eight) compared to those of 15C5 and 18C6 (five and six respectively), as found in the calorimetric titration study of the DB24C8 complexes with cations.[1c] This may be largely attributed to the entropy contribution due to the ring flexibility[1a] of DB24C8.

The log K_{ML^+} values of 15C5, 18C6, and DB24C8 for the alkali metal ions have been plotted as a function of the crystal ionic radius in Fig. 4. Figure 4 shows that the log K_{ML^+} values of these crown ethers for the same alkali metal ion are much larger for PC than for aqueous and 70 wt% CH_3OH solutions. This indicates that the alkali metal ions are more strongly solvated by water and methanol than PC. The data in Fig. 4 together with the fact that the dielectric constant, ε_r, value sequences of the three solvents are H_2O (ε_r=78 at 25 °C[1c])>PC (ε_r=64 at 25 °C[5c])> 70 wt% CH_3OH (ε_r=47 at 25 °C[1c]) indicates that the dielectric constant of the solvent is not always a

Table 2. $(\lambda^\circ/\Omega^{-1}\,cm^2\,mol^{-1})$ values of alkali metal ion–crown ether complexes and alkali metal ions in PC at 25 °C

		15C5	18C6	DB24C8
Li^+	8.5_5	9.2_7	—	—
Na^+	9.7_6	$10._1$	8.5_1	7.5_4
K^+	11.9_8	8.6_6	8.9_1	7.4_2
Rb^+	12.4_9	8.3_7	8.8_6	7.3
Cs^+	13.2_9	9.4_3	8.7_8	7.3

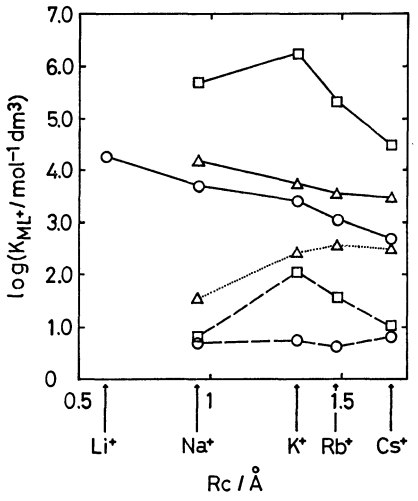

Fig. 4. Plots of log K_{ML^+} at 25 °C *vs.* crystal ionic radius, $R_c(M^+)$, of alkali metal.
○: 15C5, □: 18C6, △: DB24C8.
——: PC, present work, — —: H_2O, Ref. 1b,
----: 70 wt% CH_3OH in H_2O, Ref. 1c.

Table 3. Crystal ionic radii of alkali metals and cavity radii of crown ethers (Å)

Cation	Crystal ionic radius[9]	Crown ether	Cavity radius[10]
Li^+	0.60	15C5	0.85—1.1
Na^+	0.95	18C6	1.3—1.6
K^+	1.33	DB24C8	2.25—2.5
Rb^+	1.48		
Cs^+	1.69		

dominant factor in the alkali metal ion–crown ether complexing. The $\log K_{ML^+}$ series of 15C5 for the alkali metal ions in PC are in the order $Li^+ > Na^+ > K^+ > Rb^+ > Cs^+$ (Table 1), showing that the ability of the alkali metal ions to form complexes with 15C5 in PC is sensitive to the ratio of the ionic size to the cavity size except in the case of Li^+ (Table 3), while that in the aqueous solution is not (Fig. 4 and Table 3). The differences in the $\log K_{ML^+}$ values of 15C5 for the neighboring alkali metal ions increase from water to PC (Table 1). It is interesting that Li^+ forms a more stable complex with 15C5 than Na^+ in PC, although Li^+ is more strongly solvated by PC than Na^+[6a] and Na^+ fits more closely into the 15C5 cavity than Li^+ (Tables 1 and 3). From Table 1, the $\log K_{ML^+}$ sequences of the alkali metal ions with 18C6 in PC and aqueous solutions are $K^+ > Na^+ > Rb^+ \gg Cs^+$ and $K^+ > Rb^+ > Cs^+ > Na^+$ respectively, indicating that the selectivity of 18C6 for the alkali metal ions in PC and aqueous solutions primarily depends on the ratio of the ionic size to the cavity size of 18C6 (Table 3) and that the $\log K_{ML^+}$ sequences of the complex in PC differ from those in the aqueous solution. The $\log K_{ML^+}$ series of DB24C8 for the alkali metal ions in PC are given in the order $Na^+ > K^+ > Rb^+ \geq Cs^+$, although the more the size of the alkali metal ion decreases, the more strongly it is solvated by PC[6a] and as the size of the alkali metal ion increases, the crystal radius approaches the cavity radius of DB24C8 (Tables 1 and 3). The $\log K_{ML^+}$ sequences of the complex with DB24C8 in PC entirely differ from those in the 70 wt% CH_3OH solvent. It may be seen from Table 1 that in the case of each crown ether system an increase in $\log K_{ML^+}$ in moving from aqueous and 70 wt% CH_3OH solutions to PC increases with a decrease in the size of the alkali metal ion. Based on the above observations, both the stabilities and selectivities on complexation appear to reflect the competition between ligand coordination and solvation.

As can be seen from Table 2, the λ° value of the alkali metal ion is much larger than that of the corresponding alkali metal ion–crown ether complex except for the cases of 15C5-Li^+ and Na^+ systems, indicating that the size of the moving entity in PC is much larger for the alkali metal ion–crown ether complex than for the corresponding alkali metal ion. On the contrary the Li^+ and Na^+ ions are bulkier than the complexes of 15C5 with these ions in PC respectively. The λ° values of the alkali metal ion–crown ether complexes are larger for 18C6 than for DB24C8 and the size of DB24C8 is larger than that of 18C6. It thus appears that the relative sizes of the two crown ethers are the main factor influencing the mobilities. The λ° values of the complexes of 15C5 with Na^+ and Cs^+ are larger than those of 18C6 with Na^+ and Cs^+ respectively, which is the same tendency as that found in the 18C6 and DB24C8 systems. Those of 15C5 with K^+ and Rb^+ are smaller than those of 18C6 with K^+ and Rb^+ respectively, although the size of 15C5 is smaller than that of 18C6.

In each case of 18C6 and DB24C8 the λ° values of the alkali metal ions are nearly equal (Table 2), suggesting that the charge of the alkali metal ion trapped in the crown ether cavity is effectively shielded by the crown ether and that in each case of 18C6 and DB24C8 the complexes with the alkali metal ions are approximately equal to each other in size. That the λ° values of 15C5 for the alkali metal ions are considerably different from each other is in remarkable contrast to the cases of the 18C6 and DB24C8 systems (Table 2). A possible explanation for this is that it may be impossible for 15C5 to effectively screen the surface charge of the alkali metal ion held in its cavity because of its smaller size compared to 18C6 and DB24C8 (Table 3). Thus the 15C5 complexes with the alkali metal ions would more strongly undergo specific solvation by PC molecules than would 18C6 and DB24C8. It is of interest to note that in the cases of the 15C5 and 18C6 systems the Na^+ and K^+ complexes, where Na^+ and K^+ most closely fit into the cavities of 15C5 and 18C6 respectively (Table 3), have the largest mobilities of all the alkali metal ion complexes respectively (Table 2).

According to Lehn[11] and Boileau *et al.*,[4] the crystal ionic radii, $R_c(ML^+)$, of the alkali metal ion–15C5 and 18C6 complexes have been approximately evaluated from the crystal ionic radii $R_c(M^+)$, of the cations located within the central molecular cavity and from the ligand volume V_L:

$$R_c(ML^+) = \{R_c(M^+)^3 + 3V_L/4\pi\}^{1/3}$$

V_L may be approximated by summing the van der Waals volumes of the atoms or groups forming the ligand. Values of $R_c(ML^+)$ are given in Table 4 together with the calculated Stokes' radii, $R_s(ML^+)$, of the alkali metal ion-15C5 and 18C6 complexes from the equation $R_s(ML^+) = 0.819/\eta_0\lambda^\circ$, where η_0 is the viscosity of the pure solvent. Table 4 shows that the $R_s(ML^+)$ value about the same alkali metal ion in PC is much smaller than the $R_c(ML^+)$ one for 15C5 and 18C6, which is the same and opposite trends

Table 4. Stokes' radii, R_s, and crystal ionic radii, R_c, of alkali metal ion–crown ether complexes (Å)

Cation	15C5		18C6	
	R_s	R_c	R_s	R_c
Li^+	3.4_9	4.5	—	—
Na^+	3.2_1	4.6	3.8_0	4.8
K^+	3.7_4	4.6	3.6_3	4.9
Rb^+	3.8_7	4.6	3.6_5	4.9
Cs^+	3.4_3	4.6	3.6_9	4.9

for tetraalkylammonium ($R_s \ll R_c$) and alkali metal ions ($R_s \gg R_c$) in PC respectively.[5] The crystal ionic radii of the alkali metal ion–15C5 and 18C6 complexes are nearly identical with those of tetrapropylammonium (4.52 Å[12]) and tetrabutylammonium ions (4.94 Å[12]) respectively (Table 4). The λ° values of the alkali metal ion–15C5 and 18C6 complexes are however smaller than those of tetrapropylammonium (11.0_0[5]) and tetrabutylammonium ions (9.32_5[5]) respectively (Table 2).

References

1) (a) C. J. Pedersen, *J. Am. Chem. Soc.*, **89**, 7017 (1967); (b) R. M. Izatt, R. E. Terry, B. L. Haymore, L. D. Hansen, N. K. Dalley, A. G. Avondet, and J. J. Christensen, *J. Am. Chem. Soc.*, **98**, 7620 (1976); (c) R. M. Izatt, R. E. Terry, D. P. Nelson, Y. Chan, D. J. Eatough, J. S. Bradshaw, L. D. Hansen, and J. J. Christensen, *J. Am. Chem. Soc.*, **98**, 7626 (1976); (d) H. K. Frensdorff, *J. Am. Chem. Soc.*, **93**, 600 (1971); (e) C. J. Pedersen, *Fed. Proc., Fed. Am. Soc. Exp. Biol.*, **27**, 1305 (1968); (f) Y. Takeda and H. Gotō, *Bull. Chem. Soc. Jpn.*, **52**, 1920 (1979); (g) Y. Takeda, *Bull. Chem. Soc. Jpn.*, **52**, 2501 (1979); (h) D. F. Evans, S. L. Wellington, J. A. Nadis, and E. L. Cussler, *J. Solution Chem.*, **1**, 499 (1972); (i) N. Matsuura, K. Umemoto, Y. Takeda, and A. Sasaki, *Bull. Chem. Soc. Jpn.*, **49**, 1246 (1976).

2) M. R. Truter and C. J. Pedersen, *Endeavour*, **30**, 142 (1971).

3) D. Live and S. I. Chan, *J. Am. Chem. Soc.*, **98**, 3769 (1976).

4) S. Boileau, P. Hemery, and J. C. Justice, *J. Solution Chem.*, **4**, 873 (1975).

5) N. Matsuura, K. Umemoto, and Y. Takeda, *Bull. Chem. Soc. Jpn.*, **48**, 2253 (1975).

6) (a) N. Matsuura, K. Umemoto, M. Waki, Z. Takeuchi, and M. Omoto, *Bull. Chem. Soc. Jpn.*, **47**, 806 (1974); (b) M. L. Jansen and H. L. Yeager, *J. Phys. Chem.*, **77**, 3089 (1973).

7) Y. Takeda, K. Oshio, and Y. Segawa, *Chem. Lett.*, **1979**, 601.

8) H. K. Frensdorff, *J. Am. Chem. Soc.*, **93**, 4684 (1971).

9) L. Pauling, "The Nature of the Chemical Bond," 3rd ed, Cornell Univ. Press (1960).

10) C. J. Pedersen, *J. Am. Chem. Soc.*, **92**, 386 (1970).

11) J. M. Lehn, *Struct. Bonding*, **16**, 1 (1973).

12) D. E. Arrington and E. Griswold, *J. Phys. Chem.*, **74**, 123 (1970).

Preparation and Stereochemistry of Cobalt(III) Complexes with Tetramines Derived from 1-(2-Pyridyl)ethylamine

Toshishige M. Suzuki,* Tetsuo Kimura, and Junnosuke Fujita†

Government Industrial Research Institute, Tohoku, Nigatake, Haranomachi, Sendai 983

†*Department of Chemistry, Faculty of Science, Nagoya University, Chikusa, Nagoya 464*

(Received May 14, 1979)

The optically active ligands, (2*S*,7*S*)-2,7-di(2-pyridyl)-3,6-diazaoctane (*S*,*S*-peaen) and (2*R*,8*R*)-2,8-di(2-pyridyl)-3,7-diazanonane (*R*,*R*-peatn) have been prepared. The dichlorocobalt(III) complexes of these ligands have been prepared and several isomers isolated. The ligand, *S*,*S*-peaen yielded one *cis*-α and two types of *cis*-β isomers, while the *R*,*R*-peatn gave only one *cis*-β isomer. Oxalato and dinitro derivatives of the *R*,*R*-peatn complexes have been isolated and characterized and the stereochemistry of the isolated complexes discussed.

Extensive investigations have been conducted on the stereochemistry of cobalt (III) complexes containing trien (triethylenetetramine) or its methyl substituted derivatives.[1] Tetramines derived from heteroaromatic ligands are quite limited however.[2–5] The quadridentate ligand, 1,6-di(2-pyridyl)-2,5-diazahexane (bispicen) is one of the representative tetramine ligands having pyridyl groups on the terminal arms. There are three topological ways for coordination of the tetramine type ligands to a cobalt(III) ion, *i.e.* *cis*-α, *cis*-β, and *trans*. Gibson and McKenzie isolated and characterized the *cis*-α and *cis*-β isomers of the dichlorocobalt(III) complex of bispicen for the first time.[2] Very recently Utsuno *et al.*, isolated the *cis*-α and two types of *cis*-β isomers of the cobalt(III) complex containing bispicen and ethylenedianime.[5]

Optically active centers may be introduced into the tetramine chain by methyl substitution on the skeletal carbons. The optically active derivatives of bispicen, $(+)_D$-1,6-di(2-pyridyl)-3-methyl-2,5-diazahexane (picpn)[3] and $(+)_D$-1,6-di(2-pyridyl)-3,4-dimethyl-2,5-diazahexane (bnpic)[4] are examples of such ligands having substituent(s) in the central bridge. Stereospecific coordination to a cobalt(III) ion giving a Δ-*cis*-β configuration has been found for these ligands.[3,4] The stereospecificity has been explained in relation to the restricted conformation of the central diamine chelate of picpn and bnpic.

The ligands prepared in the present study, (2*S*,7*S*)-2,7-di(2-pyridyl)-3,6-diazaoctane (*S*,*S*-peaen) and (2*R*,8*R*)-2,8-di(2-pyridyl)-3,7-diazanonane (*R*,*R*-peatn) derived from 1-(2-pyridyl)ethylamine (pea) have two methyl groups in the terminal arms as illustrated in Fig. 1. The terminal pea moiety has a structure intermediate between 1,2-propanediamine and 2,2′-bipyridine. It has been demonstrated that the *S*-pea chelate tends to assume a δ-conformation on complexation with the methyl group occupying an equatorial position.[6,7] Therefore on coordination both of the terminal chelate rings of *S*,*S*-peaen and *R*,*R*-peatn may be fixed giving a sterically prefered configuration about the metal ion.

The preparation and isolation of the isomers of cobalt(III) complexes containing *S*,*S*-peaen and *R*,*R*-peatn are given in this paper and the stereochemistry of the complexes discussed.

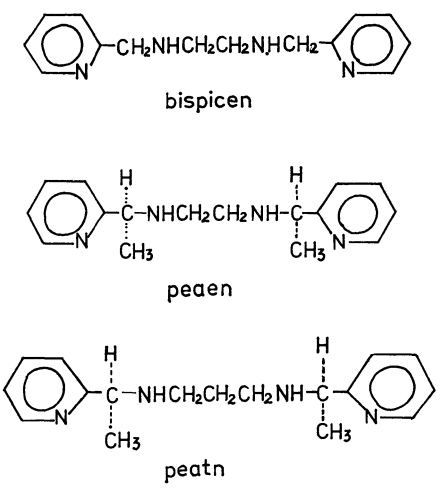

Fig. 1. Abbreviation and structure of ligands.

Experimental

Preparation of Ligands. Optically active 1-(2-pyridyl)-ethylamine (pea) used as the starting materials in the preparation of the tetramines were synthesized according to a method similar to that given by Michelsen.[8] The $(+)_D$-isomer of pea is known to have an *R* configuration.[9]

(2S,7S)-2,7-Di(2-pyridyl)-3,6-diazaoctane (S,S-peaen). To a vigorously stirred solution of *S*-pea (30.54 g, 0.25 mol) in ethanol (300 cm³) was added dropwise 1,2-dibromoethane (9.40 g, 0.05 mol) over a period of 2 h under nitrogen atmosphere at 50 °C. The mixture was heated to reflux with vigorous stirring under nitrogen for 18 h. The end point of the condensation was correlated with the disappearance of the 1,2-dibromoethane peak found from gas chromatography. The reaction mixture was subsequently cooled to room temperature. To the stirred solution was added granulated metallic sodium (2.3 g) in small portions. The mixture was stirred at 50 °C for a further 2 h and cooled to room temperature. After filtration, the ethanol and excess *S*-pea was removed by distillation under reduced pressure. The residue was purified by alumina column chromatography using hexane as an eluent. After removal of the solvent, a brown syrup (6.8 g) was obtained. Yield 50.3%. The tetramine was isolated as its hydrochloride by the addition of concd HCl (10 cm³) and ethanol (100 cm³). Yield 7.85 g.

Found: C, 46.33; H, 6.31; N, 13.56%. Calcd for $C_{16}H_{22}N_4 \cdot 4HCl$: C, 46.15; H, 6.25; N, 13.46%.

(2R,8R)-2,8-Di(2-pyridyl)-3,7-diazanonane (R,R-peatn). This ligand was prepared according to a method similar to that for *S*,*S*-peaen using *R*-pea and 1,3-dibromopropane and isolated as the hydrochloride. Yield 48.6%.

Found: C, 47.33; H, 6.82; N, 12.97%. Calcd for $C_{17}H_{24}N_4 \cdot 4HCl$: C, 47.45; H, 6.56; N, 13.02%.

cis-*β-I*-[*CoCl*$_2$(S,S-*peaen*)]*ClO*$_4 \cdot H_2O$. A stream of air was bubbled through a solution of the *S,S*-peaen·4HCl (2.08 g), $LiOH \cdot H_2O$ (0.65 g) and $CoCl_2 \cdot 6H_2O$ (1.2 g) in water (50 cm^3) for 3 h. To the solution was added concd HCl (8 cm^3) and 70% $HClO_4$ (2 cm^3). The resulting red solution was evaporated to 30 cm^3 on a water bath (60 °C) and stored in a refrigerator overnight. The violet crystals deposited were filtered, washed with water, ethanol and ether. Yield: 350 mg. The second crop of crystals which were identical with those of the first crop were obtained by evaporating the filtrate to 20 cm^3. Yield: 240 mg.

Found: C, 36.91; H, 4.86; N, 10.69%. Calcd for $C_{16}H_{24}N_4O_5Cl_3Co$: C, 37.17; H, 4.64; N, 10.82%.

cis-*β-II*-[*CoCl*$_2$(S,S-*peaen*)]*ClO*$_4 \cdot 1/2H_2O$. The filtrate from the separation of *cis-β*-I was stored in a refrigerator for 3 h. The reddish-purple crystals deposited were filtered, washed with a water–ethanol mixture (1:1), ethanol and ether, and air dried. Yield: 200 mg.

Found: C, 37.89; H, 4.60; N, 10.87%. Calcd for $C_{16}H_{22}N_4O_4Cl_3Co \cdot 1/2H_2O$: C, 37.73; H, 4.52; N, 11.01%.

cis-α-[*CoCl*$_2$(S,S-*peaen*)]*ClO*$_4 \cdot 3/2H_2O$. $CoCl_2 \cdot 6H_2O$ (1.2 g) in water (10 cm^3) and 30% H_2O_2 (1 cm^3) were mixed in an ice bath and added dropwise to a solution of $NaHCO_3$ (2.8 g in 50 cm^3 of water) at 0 °C for 30 min.[10] To the solution was added a mixture of *S,S*-peaen·4HCl (2.08 g) and $LiOH \cdot H_2O$ (0.63 g) in water (10 cm^3). The resulting red solution, concd HCl (10 cm^3) and 70% $HClO_4$ (1 cm^3) were added and heated at 80 °C for 20 min, and allowed to stand at room temperature overnight. The violet crystals deposited were filtered, washed with water, ethanol and finally ether. Yield: 300 mg. The crystals were identical with *cis-β*-I obtained by the air oxidation method. The filtrate from the separation of *cis-β*-I was poured onto a column of cation exchanger Dowex 50W-X8 (H^+ form) (ϕ 3.0× 20 cm). The column was washed with water, and the adsorbed product was eluted with 5 M HCl. The reddish-purple eluate was evaporated to dryness. The purple residue was dissolved in 5 M HCl (15 cm^3) and the solution filtered. After the addition of 70% $HClO_4$ (1 cm^3), the solution was stored in a refrigerator for three days. The purple crystals deposited were filtered, washed with a water–ethanol mixture (1:1), ethanol and finally ether. Yield: 240 mg.

Found: C, 36.63; H, 4.56; N, 10.64%. Calcd for $C_{16}H_{22}N_4O_4Co \cdot 3/2H_2O$: C, 36.49; H, 4.75; N, 10.63%.

cis-α-[*Co(ox)*(S,S-*peaen*)]*ClO*$_4 \cdot H_2O$. A mixture of *cis*-α-[$CoCl_2$(*S,S*-peaen)]$ClO_4 \cdot 3/2H_2O$ (0.5 g) and sodium oxalate (0.2 g) in water (30 cm^3) was heated at 80 °C for 30 min. The orange solution was evaporated to 10 cm^3 and stored at room temperature. The orange crystals deposited were collected and recrystallized from hot water.

Found: C, 40.58; H, 4.96; N, 10.39%. Calcd for $C_{18}H_{22}N_4O_8ClCo \cdot H_2O$: C, 40.43; H, 4.48; N, 10.48%.

cis-*β*-[*CoCl*$_2$(R,R-*peatn*)]*ClO*$_4 \cdot H_2O$. The procedure used here was analogous to the preparation of [$CoCl_2$(*S,S*-peaen)]$ClO_4 \cdot H_2O$. A stream of air was bubbled through a solution of *R,R*-peatn·4HCl (2.15 g), $LiOH \cdot H_2O$ (0.65 g) and $CoCl_2 \cdot 6H_2O$ (1.2 g) in water (50 cm^3) for 4 h. To the dark brown solution was added concd HCl (8 cm^3) and 70% $HClO_4$ (2 cm^3). The resulting solution was evaporated to 20 cm^3 on a water bath. On standing at room temperature for 1 h deep violet crystals deposited. The crystals were collected, washed with a small amount of water, acetone and air dried. Yield 1.64 g. The filtrate was poured onto a column of SP-Sephadex (ϕ 3.0×42 cm). The adsorbed band was eluted with 2 M HCl. The eluatant of the purple band was fractionated and the CD spectra recorded. All the fractions gave an identical CD spectra with that of the isolated complex. No indication of the presence of the other isomer was found. The so-called tricarbonato method[10] was also employed in the preparation of dichloro(*R,R*-peatn) complexes. The obtained complex was identical with that prepared by the air oxidation method.

Found: C, 38.28; H, 5.21; N, 10.37%. Calcd for $C_{17}H_{24}N_4Cl_3Co \cdot H_2O$: C, 38.40; H, 4.94; N, 10.53%.

cis-*β*-[*Co*(NO_2)$_2$(R,R-*peatn*)]*ClO*$_4$. Sodium nitrate (0.2 g) was added to a hot solution of *cis-β*-[$CoCl_2$(*R,R*-peatn)]ClO_4 (0.4 g) in water (10 cm^3). The solution was heated at 70 °C for 30 min. On cooling to room temperature for 1 h, the orange-yellow crystals were filtered and washed with water, ethanol and finally ether. Yield: 310 mg.

Found: C, 38.15; H, 4.54; N, 15.84%. Calcd for $C_{17}H_{24}N_6O_8ClCo$: C, 38.18; H, 4.52; N, 15.71%.

cis-*β*-[*Co(ox)*(R,R-*peatn*)]*ClO*$_4 \cdot 1/2H_2O$. A solution of *cis-β*-[$CoCl_2$(*R,R*-peatn)]ClO_4 (0.52 g) and sodium oxalate (0.2 g) in water (10 cm^3) was heated at 50 °C for 2 h. The cherry-red crystals deposited were collected and recrystallized from hot water. Yield: 220 mg.

Found: C, 42.06; H, 4.61; N, 10.38%. Calcd for $C_{19}H_{24}N_4O_8ClCo \cdot 1/2H_2O$: C, 42.27; H, 4.67; N, 10.38%.

Measurements. The visible and ultraviolet absorption were recorded with a Shimadzu Double 40-R spectrophotometer. The CD spectra were recorded on a JASCO J-20 spectropolarimeter. The spectra of the dichloro complexes were recorded in concd HCl, while those of the other complexes were recorded in water. The PMR spectra in DMSO-d_6 were obtained with a JNM-PMX60 spectrometer using tetramethylsilane (TMS) as an internal standard. All the measurements were conducted at room temperature.

Results and Discussion

Ligands. The quadridentate ligands, *S,S*-peaen and *R,R*-peatn were prepared from optically active 1-(2-pyridyl)ethylamine (pea) with 1,2-dibromoethane and 1,3-dibromopropane, respectively. The absolute configuration of the tetramine ligands is expected to be the same as that of the mother pea whose absolute configuration has been determined.[9]

S,S-*Peaen Complexes.* Dichlorocobalt(III) complexes of *S,S*-peaen were prepared according to the reaction scheme:

1) $Na_3[Co(CO_3)_3]$ + *S,S*-peaen

$$\xrightarrow[HClO_4]{HCl} \begin{cases} \textit{cis-α}\text{-}[CoCl_2(S,S\text{-peaen})]^+ \\ \quad \text{(purple)} \\ \textit{cis-β}\text{-I-}[CoCl_2(S,S\text{-peaen})]^+ \\ \quad \text{(violet)} \end{cases}$$

2) $Co(II)Cl_2 \cdot 6H_2O$ + *S,S*-peaen

$$\xrightarrow[HCl,\ HClO_4]{O_2} \begin{cases} \textit{cis-β}\text{-I-}[CoCl_2(S,S\text{-peaen})]^+ \\ \quad \text{(violet)} \\ \textit{cis-β}\text{-II-}[CoCl_2(S,S\text{-peaen})]^+ \\ \quad \text{(reddish-purple)} \end{cases}$$

Two types of stereoisomers were isolated by fractional crystallization from both reactions. The violet isomer (*cis-β*-I) was a major product in both reactions. Elemental analyses of the isomers are in good accord with the formulation and the geometrical configura-

tions were confirmed by visible absorption and PMR spectral data. No *trans*(Cl–Cl) isomer was obtained. The trans geometry of the peaen complex would be unstable presumably due to steric hindrance between the hydrogen atoms of the two terminal pyridine residues. The PMR spectra of the isolated isomers measured in deuterated DMSO are given in Fig. 2. The purple isomer which was obtained *via* tricarbonatocobaltate(III) showed a single methyl doublet at approximately 1.9 ppm, indicating that the two methyl groups of peaen are equivalent; the geometrical configuration is therefore *cis*-α. The violet (*cis*-β-I) and reddish-purple (*cis*-β-II) complexes gave signals for the two types of methyl groups. Thus, the geometries may be assigned as *cis*-β. For the *cis*-α isomer of the cobalt(III) complex of the trien type ligand, only one enantiomer is possible,

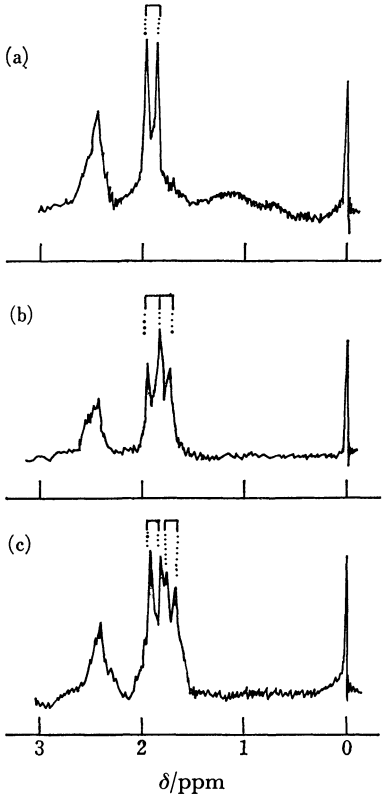

Fig. 2. PMR spectra of (a) *cis*-α-$[CoCl_2(S,S\text{-peaen})]^+$, (b) *cis*-β-I-$[CoCl_2(S,S\text{-peaen})]^+$ and (c) *cis*-β-II-$[CoCl_2(S,S\text{-peaen})]^+$ in DMSO(d_6).

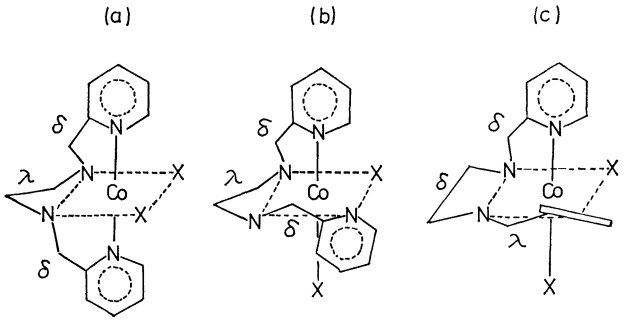

Fig. 3. Three diastereomers of *cis*-$[CoX_2(\text{bispicen})]^+$. (a) *Λ-cis*-α-($R_N$,$R_N$), (b) *Δ-cis*-β-($R_N$,$S_N$), (c) *Δ-cis*-β-($R_N$,$R_N$).

whereas two types of diastereomers are expected for the *cis*-β geometry. The two *cis*-β geometries arise from a combination of the configuration of the coordinated secondary nitrogen atoms.[11] Similar isomers are expected for the complexes of bispicen type ligands as shown in Fig. 3.[12]

According to a recent X-ray analysis of *Λ-fac*-$[Co(S\text{-pea})_3](ClO_4)_3\cdot H_2O$, the *S*-pea chelate has been shown to take a puckered δ-conformation with the C-methyl group occupying an equatorial position.[6] The terminal chelate rings of *S,S*-peaen in the present complex would also favour the δ-conformation in a similar manner to the chelate ring of the mother *S*-pea. A molecular model predicts that whenever the terminal chelates of *S,S*-peaen are fixed in a δ-conformation, the *cis*-α and *cis*-β geometries uniquely yield *Λ-cis*-α-(R_N,R_N) and *Δ-cis*-β-(R_N,S_N) configuration, respectively. Thus the present *cis*-α and one of the *cis*-β isomers are most likely to have the above configurations, respectively. Since two types of *cis*-β isomers were obtained in the present study, one must be either the *Δ-cis*-β-(R_N,R_N) or the *Λ-cis*-β-(S_N,S_N) (see Fig. 3-c). In these enantiomeric configurations, the two outer chelate rings should have opposed conformations, *i.e.*, one of the terminal chelate rings should take a λ-conformation in which the methyl group takes an axial position.

The electronic absorption and CD spectra of the *Λ-cis*-α dichloro(*S,S*-peaen) complex and its oxalato derivative are shown in Fig. 4. The *Λ-cis*-α dichloro-(*S,S*-peaen) complex shows a well defined shoulder at the longer wavelength side of the first absorption band. A similar feature in the first absorption band has been observed for the *cis*-α dichloro complex of trien[13] and methyl substituted trien.[14] The CD spectrum in the first absorption band region gives positive and negative components with nearly equal

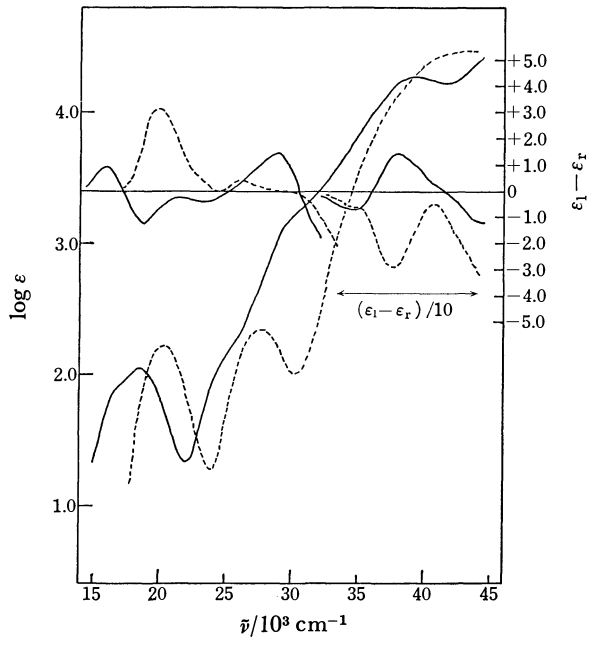

Fig. 4. Absorption and CD spectra of *cis*-α-$[CoCl_2(S,S\text{-peaen})]^+$ (——) in concd hydrochloric acid and *cis*-α-$[Co(ox)(S,S\text{-peaen})]^+$ (----) in water.

intensity from the longer to shorter wavelength. This CD pattern is vertually enantiomeric with that of *Λ-cis-α*-[$CoCl_2$(trien)]$^+$,[13] and *Λ-cis-α*-[$CoCl_2$(3*S*,8*S*-dimetrien)]$^+$ (3*S*,8*S*-dimetrien=(2*S*,7*S*)-2,7-dimethyl-3,6-diazaoctane-1,8-diamine).[14] The *cis-α* oxalato (*S*,*S*-peaen) complex which was obtained from the dichloro complex by a treatment with sodium oxalate in aqueous solution gave CD spectrum very similar to that of *Λ-cis-α*-[Co(ox)(trien)]$^+$.[15] The PMR spectrun of the oxalato complex showed a singel methyl doublet, indicating that the *cis-α* configuration is maintained in the course of reaction.

The absorption and CD spectra of the two types of *cis-β* isomers are shown in Fig. 5. Obviously these *cis-β* isomers give different absorption and CD spectra in the first absorption band region. The absorption maximum of *cis-β*-I appears at a longer wavelength than that of *cis-β*-II and the band has a well defined shoulder on the longer wavelength side. The CD associated with the first absorption band of *cis-β*-I gives two components, positive and negative Cotton effects from longer to shorter wavelength, while that of *cis-β*-II gives only one negative CD component. In contrast to the *S*,*S*-peaen complex only one *cis-β* isomer of structure *Λ-cis-β*-(R_N,S_N) has been obtained for the dichlorocobalt(III) complexes of 3*S*,8*S*-dimetrien and 2*S*,9*S*-dimetrien (2*S*,9*S*-dimetrien=(1*S*,8*S*)-1,8-dimethyl-3,6-diazaoctane-1,8-diamine).[14] The absorption and CD spectra in the first absorption band region for these *cis-β* complexes resembles those of the *cis-β*-II isomer rather than the *cis-β*-I isomer in the following points: (1) no shoulder of the first absorption band was detected; (2) only one negative CD peak was observed in the first absorption band region. Thus, the present *cis-β*-II isomer is most likely to have a *Λ-cis-β*-(R_N,S_N) configuration in which both of the two outer chelates have a *δ*-conformation.

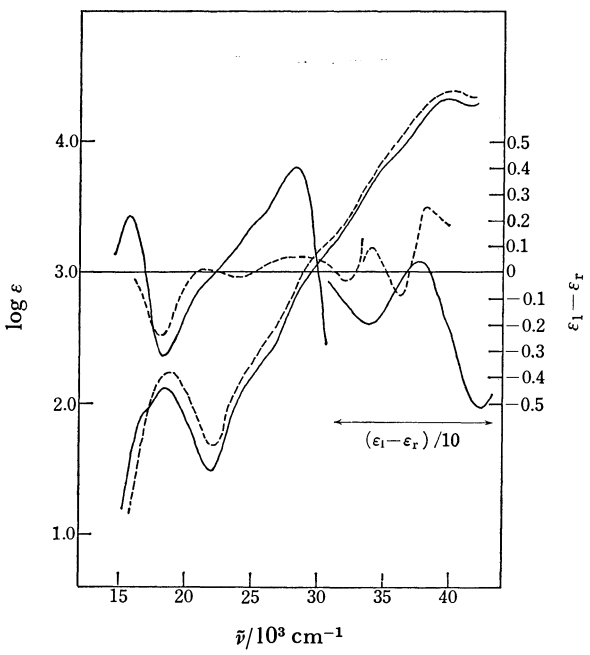

Fig. 5. Absorption and CD spectra of *cis-β*-I-[$CoCl_2$-(*S*,*S*-peaen)]$^+$ (——) and *cis-β*-II-[$CoCl_2$(*S*,*S*-peaen)]$^+$ (----) in concd hydrochloric acid.

The absorption spectra and CD pattern of the *cis-β*-I isomer resemble the *cis-α* more than the *cis-β* II, although the CD magnitude of the *cis-β*-I is smaller than that of *cis-α*. At present it is impossible to be unambiguous about the absolute configuration of the *cis-β*-I based on the CD pattern. Saburi *et al.*, have isolated a novel *cis-β* isomer of dinitro and carbonato (3*S*,8*S*-dimetrien)cobalt(III) complexes whose absolute configuration has been deduced to be *Λ-cis-β*-(S_N,S_N) on the basis of the PMR and CD spectra.[16] The molecular structure of *Λ-cis-β*-[Co(CO_3)(3*S*,8*S*-dimetrien)]-ClO_4 has been determined by the X-ray diffraction method[17] where it has been shown that the methyl group on the apically ligated chelate ring has an axial orientation. It is said that the apically ligated chelate ring inthe *cis-β*-(trien) complexes is less restricted than the side chelate ring coplanar with the central chelate.[1] Thus the structure of the present *cis-β*-I would also be in a *Λ-cis-β*-(S_N,S_N) configuration.

R,R-*peatn Complexes.* Dichlorocobalt(III) complexes with *R*,*R*-peatn were prepared according to the same method as those of the peaen complexes. In both methods, only one purple isomer was stereospecifically obtained. The PMR spectra of the dichloro complex shown in Fig. 6 gives two types of methyl doublets due to the terminal pea in the 1.8—2.0 ppm region, indicating that the complex has *cis-β* geometry.

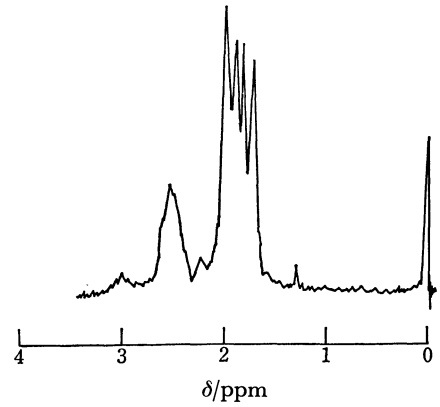

Fig. 6. PMR spectra of *cis-β*-[$CoCl_2$(*R*,*R*-peatn)]$^+$ in DMSO(d_6).

The central diamine moiety of *R*,*R*-peatn forms a six-membered chelate ring on complex formation. The conformational behavior of the six-membered chelate ring parallels that of cyclohexane. Among the three possible conformers of the six-membered chelate, *i.e.*, chair, skew and boat, the chair conformation is known to be most stable.[18–20] For the *cis-β* configuration of *R*,*R*-peatn complex, the following isomers are possible, *Λ-cis-β*-(S_N,S_N), *Λ-cis-β*-(R_N,R_N), *Λ-cis-β*-(R_N,S_N) and *Λ-cis-β*-(S_N,R_N). An examination of the molecular models indicates that for the *Λ-cis-β*-(S_N,S_N) configuration, the central six-membered ring can assume the chair conformation and at the same time both *R*-pea chelates take an *λ*-conformation with the methyl groups occupying equatorial positions. Accordingly, the most probable configuration of the *cis-β*-(*R*,*R*-peatn) complex is *Λ-cis-β*-(S_N,S_N).

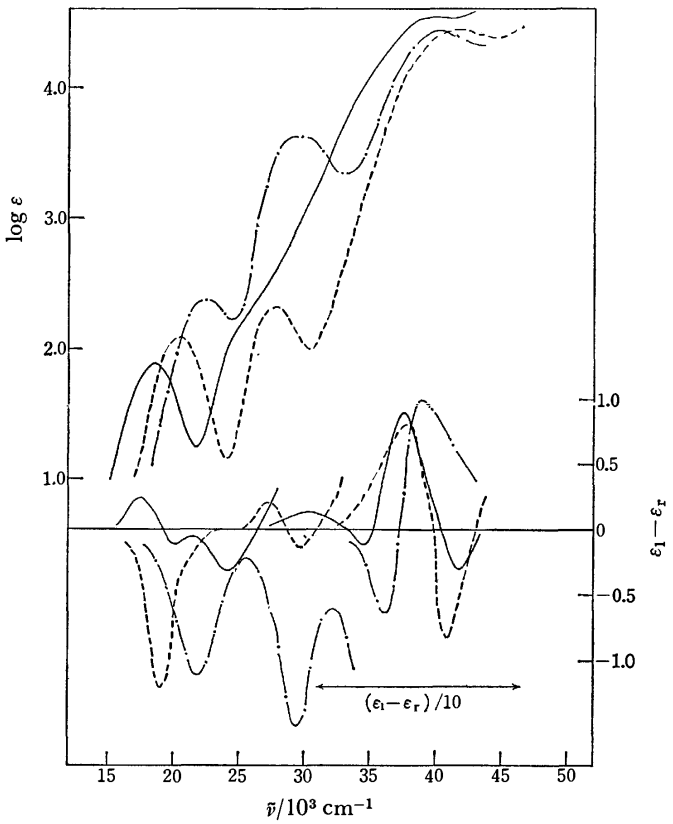

Fig. 7. Absorption and CD spectra of *cis*-β-[$CoCl_2$(*R*,*R*-peatn)]$^+$ (——) in concd hydrochloric acid, *cis*-β-[Co(ox)(*R*,*R*-peatn)]$^+$ (----) and *cis*-β-[$Co(NO_2)_2$-(*R*,*R*-peatn)]$^+$ (—·—·) in water.

The cis dinitro and oxalato complexes of *R*,*R*-peatn were prepared from *cis*-β-[$CoCl_2$(*R*,*R*-peatn)]ClO_4 by heating an aqueous solution of the complex with sodium nitrate or sodium oxalate, respectively. In all cases, absorption and CD spectra of the reacted solution were identical with those obtained for the isolated complexes and no other isomers were formed. Thus, it appears that the relative configurations of the dinitro and oxalato complexes are the same as that of the dichloro species.

The absorption and CD curves of dichloro, dinitro and oxalato complexes are shown in Fig. 7. The CD corresponding to the first absorption band of the dichloro complex gives two components, positive and negative signs from longer to shorter wavelengths. In contrast, the dinitro and oxalato complexes of *R*,*R*-peatn give one negative component in the first absorption band region. The Δ-configuration can be assigned for these complexes on the basis of the signs of the dominants CD peaks in the first absorption band region.[21] This assignment is in accord with that based on the stereomodels.

It has been revealed that the stereochemical behavior of the peaen and peatn complexes is very similar to the corresponding complexes of methyl substituted trien[14,16,22] and 2′,3,2′-tet ligands.[23] This indicates that the conformational effects of the terminal pea chelate moieties of peaen and peatn complexes are essentially the same as those of the chiral diamine chelates.

References

1) M. Saburi and S. Yoshikawa, "Chemistry of Octahedral Complexes (in Japanese); Kagaku Sosetsu, No. 13," ed by the Chemical Society of Japan (1976), p. 109.
2) J. G. Gibson and E. D. McKenzie, *J. Chem. Soc., A*, **1971**, 1666.
3) J. Cragel Jr., and G. R. Brubaker, *Inorg. Chem.*, **11**, 303 (1972).
4) B. Bosnich and W. R. Kneen, *Inorg. Chem.*, **9**, 2191 (1970).
5) S. Utsuno, A. Hayashi, S. Kondo, and M. Utsumi, *Chem. Lett.*, **1979**, 351.
6) E. Bang, *Acta Chim. Scand., A*, **31**, 495 (1977).
7) K. Michelsen and E. Pedersen, *Acta Chim. Scand., A*, **32**, 847 (1978).
8) K. Michelsen, *Acta Chim. Scand., A*, **28**, 428 (1974).
9) H. E. Smith, L. J. Schaad, R. B. Banks, C. J. Wiant, and C. F. Jordan, *J. Am. Chem. Soc.*, **95**, 811 (1973).
10) M. Shibata, *Nippon Kagaku Zasshi*, **87**, 771 (1966).
11) D. A. Buckingham, P. A. Marzilli, and A. M. Sargeson, *Inorg. Chem.*, **6**, 1032 (1967).
12) In this paper, the absolute configuration of the coordinated secondary nitrogen is represented by R_N and S_N, neglecting the substituted methyl groups in order to avoid complications.
13) A. M. Sargeson and G. H. Searle, *Inorg. Chem.*, **4**, 45 (1965).
14) M. Saburi and S. Yoshikawa, *Bull. Chem. Soc. Jpn.*, **45**, 806, (1972).
15) G. R. Brubaker and D. P. Schaefer, *Inorg. Chem.*, **10**, 968, (1971).
16) M. Saburi, T. Sato, and S. Yoshikawa, *Bull. Chem. Soc. Jpn.*, **49**, 2100 (1976).
17) K. Toriumi and Y. Saito, *Acta Crystallogr., Sect. B*, **31**, 1247 (1975).
18) J. R. Gollogly and C. J. Hawkins, *Inorg. Chem.*, **11**, 156 (1972).
19) Y. Saito, T. Nomura, and F. Marumo, *Bull. Chem. Soc. Jpn.*, **41**, 530 (1968).
20) R. J. Geue and M. R. Snow, *J. Chem. Soc., A*, **1971**, 2981.
21) A. J. MacCaffery, S. F. Mason, and B. J. Norman, *J. Chem. Soc.*, **1965**, 5094.
22) M. Saburi, T. Sawai, and S. Yoshikawa, *Bull. Chem. Soc. Jpn.*, **45**, 1086 (1972).
23) P. C. Harrington, S. Linke, and M. D. Alexander, *Inorg. Chem.*, **12**, 168 (1973).

Kinetics and Mechanisms of Ligand Exchange Reactions of Tris(acetylacetonato)-chromium(III), -cobalt(III), -ruthenium(III), and -rhodium(III) in Acetylacetone

Hiroaki KIDO

Chemistry Department, Faculty of Science, Tohoku University, Aramaki, Aoba, Sendai 980

(Received May 15, 1979)

Tris(acetylacetonato[2-^{14}C])-cobalt(III), -chromium(III), -ruthenium(III), and -rhodium(III) undergo ligand exchange in acetylacetone(Hacac) at 85—190 °C without decomposition of the complexes. The exchange rate is proportional to the complex concentration, and the first-order rate constant k_0 decreases in the sequence Co(III) > Cr(III) > Ru(III) > Rh(III), $k_0/10^{-5}$ s^{-1} being 2.4 (93 °C), 5.6 (117 °C), 9.5 (158 °C), and 2.4 (185 °C), respectively. The activation enthalpies and entropies and deuterium isotope effect on k_0 are significantly different between the Co(III) and the Cr(III), Ru(III) and Rh(III) complexes. An intermediate involving an one-ended acetylacetonate and a solvent molecule(Hacac) is concluded to be formed in the rate-determining step. The S_N1 and the S_N2 mechanism are assigned to the exchange reactions of the Co(III) complex and the others, respectively, for the rate-determining steps.

The exchange reaction of solvo ligands with solvent molecules has been scarecely studied with bidentate ligands, although the reaction is profitable for the assignment of the substitution mechanisms. Pearson and Lanier[1] observed, as a unique example, the rate and the rate limits for the exchange of ethylene glycol coordinated to bivalent transition metal ions in ethylene glycol. In this work, the ligand exchange reactions of tris(acetylacetonato) complexes of tervalent transition metal ions(M(acac)$_3$; M(III)=Cr(III), Co(III), Ru(III), and Rh(III)) have been investigated in a reaction system consisting of only two components, the labelled complex as solute and acetylacetone (Hacac) as solvent.

In the previous papers, we have proposed the mechanisms of the ligand exchange reactions of Cr(acac)$_3$ and Co(acac)$_3$ in acetonitrile.[2,3] However, there remains an ambiguity in the mechanisms concerning participation of solvent molecule. In the present work, we have simplified the reaction system, confirmed the mechanisms of the reactions and suggested relative rates of individual steps in the substitution processes of the bidentate.

The ligand substitution kinetics of Co(III), Ru(III), and Rh(III) complexes containing O_6 core have been hardly studied,[3-5] although those of the N_5O type complexes represented by $[M^{III}(NH_3)_5H_2O]^{3+}$ containing the present metal ions have been systematically studied.[6,7] Therefore, we have also a unique opportunity of comparing the substitution mechanisms of the present exchange of the O_6 type complexes with those of the water exchange of the N_5O type complexes.[8-11]

Experimental

Materials. The labelled species, Hacac[2-^{14}C],[12] Hacac[*methylene*-$^2H_2$],[2] Co(acac[2-^{14}C])$_3$[3] and Cr(acac[2-^{14}C])$_3$[2] have been prepared and purified by the reported methods. The labelled complex, Ru(acac[2-^{14}C])$_3$, was prepared from ruthenium(III) chloride and Hacac[2-^{14}C] by the method of Wilkinson[13] and sublimed *in vacuo* (140 °C, 1 mmHg; 1 mmHg≒133 Pa). Both radioactive and non-active Rh(acac)$_3$ were prepared as follows; Hacac[2-^{14}C] or the ordinary Hacac (3 ml), and a few drops of water added to a mixture of rhodium(III) chloride trihydrate (0.5 g) and potassium hydroxide (0.3 g), and refluxed for 10 h at 110 °C and then for 2 h at 120 °C, with stirring. The Hacac and water were evaporated off from the resulting mixture, under a reduced pressure at room temperature. Light yellow crystals (0.3 g) were sublimed from the residue at 170 °C under 1 mmHg. Anal. (for the non-active Rh(acac)$_3$) Found; C, 44.71; H, 5.38%. Calcd for $RhC_{15}H_{21}O_6$; C, 45.01; H, 5.29%. Mp 262 °C for both the complexes (lit[14] 260 °C).

The deuterium content of Hacac[*methylene*-$^2H_2$] in the methylene moiety was determined to be 80% by PMR spectroscopy. Specific activities of Hacac[2-^{14}C] and the labelled complexes were *ca.* 10^4 and 10^3 dpm mg^{-1}, respectively. The solvent Hacac was dried over anhydrous sodium sulfate and distilled.

Kinetic Procedure. Aliquots of the solution of the labelled complex (0.003—0.009 M; 1 M=1 mol dm^{-3}) in Hacac or Hacac[*methylene*-$^2H_2$] containing 0.01—0.1 M water were sealed in 5 to 10 Pyrex glass tubes (10 mm in diameter, 50 mm in length) after degassing, and heated in a thermostated oil bath at 85—190 °C. The tubes were withdrawn one by one at appropriate time intervals and put into a cold water bath. From a given amount of the solution in each tube, the solvent was evaporated *in vacuo* at room temperature to recover the complex quantitatively in the original tube. The total amount of the recovered complex was dissolved in a given volume of acetonitrile and a given part of the solution was dissolved in toluene containing 0.1% *p*-terphenyl and 0.04% *p*-bis(5-phenyl-2-oxazolyl)benzene (POPOP) for scintillation pulse counting with a Nuclear Chicago Unilux IIA Liquid Scintillation Counter. The water content was determined for each portion of the solution by Karl Fischer titration.

Calculation of the Exchange Rate. The rates were calculated by the McKay equation

$$\text{Rate} = \frac{3[M][Hacac]}{3[M]+[Hacac]} \frac{\ln[(x_0-x_\infty)/(x_t-x_\infty)]}{t} \fallingdotseq 3[M]\ln(x_0/x_t)/t \quad ([Hacac] \gg [M],\ x_\infty \fallingdotseq 0) \qquad (1)$$

where [M] and [Hacac] stand for the concentration of the complex and acetylacetone, respectively. The x's are the specific counting rates of the complex for the time indicated by the subscripts.

Hacac is in tautomeric equilibrium between enol and keto forms, but the interconversion rate in neat Hacac is significantly greater[15] than the present exchange rates in the given temperature ranges; the tautomers are not kinetically distinguishable. Therefore, the overall concentration of

Hacac was used in the kinetic treatment.

Results

Verification of the Exchange Reactions. In the case of the Cr(III) and Co(III) complexes, the McKay plots gave straight lines up to at least 50—60% of the completion of exchange (Fig. 1) and the visible absorption spectra and the water content of the reaction mixture did not vary throughout the reaction. Hence, no other reaction than the exchange takes place.

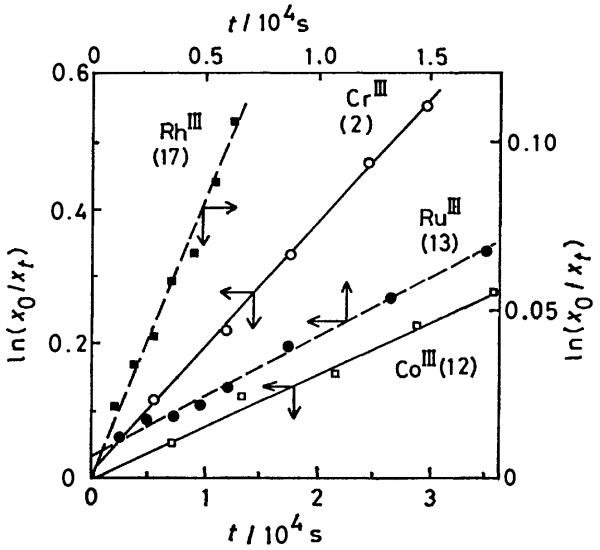

Fig. 1. Typical McKay plots for the ligand exchange of $M^{III}(acac)_3$ in acetylacetone. Numbers in parentheses stand for the experimental numbers in Table 1.

When the reaction mixture of the Ru(III) complex was heated at the given temperature, yellow substances were formed in the solution and water content increased gradually with time (Table 1). However, the visible absorption spectra of the solution did not change throughout the reaction. The linear McKay plots were obtained up to at least 50% of the completion of exchange. When the solvent was evaporated from 1 ml of the solution which had been heated for 3×10^4 s, a small amount of yellow oil (*ca.* a few mg at most) and the complex were left in the original tube. The oil was separated from the complex by vacuum distillation at 100 °C. The counting rate (^{14}C) of the oil was nearly zero. These facts show that the yellow substances should be formed not from the complex but from the solvent (probably, condensation polymerization of acetylacetone to give water as a by-product).

In the case of the Rh(III) complex, the similar changes in the color (the formation of the oil) and in the water content of the reaction mixture were observed as in the case of the Ru(III) complex. The counting rate of the oil recovered from the solution (heated for 10^4 s) was also nearly zero. The fact shows that the complex did not decompose. The McKay plots gave straight lines up to 10% of the completion of exchange and then the slopes of the plots increased steeply. The exchange rates were determined from the plots at the initial stage.

These facts show that the decrease of the specific counting rate of the complexes shown in Fig. 1 corresponds to the exchange of acetylacetonate between the complex and the solvent,

$$M^{III}(\overset{*}{acac})_3 + Hacac \rightleftharpoons M^{III}(acac)_3 + H\overset{*}{acac} \quad (2)$$

where asterisks denote ^{14}C labelling.

Kinetic Data. The exchange rate was proportional to the concentration of the complex, [M], (Table 1) and expressed by

$$\text{Rate} = k_o[M] \quad (3)$$

where k_o is the observed first-order rate constant.[16] The k_o values were independent of $[H_2O]$ for the Cr(III) and Co(III) systems (Table 1). For the Ru(III) and Rh(III) systems, the McKay plots gave straight lines, regardless of the increase in water concentration with the progress of the exchange (Fig. 1 and Table 1). Hence, the k_o values can be reckoned to be independent of $[H_2O]$.

When Hacac[*methylene-*$^2H_2$] was used as the solvent in place of the ordinary Hacac, the k_o values for the Cr(III) and Rh(III) systems decreased but those for the Co(III) system did not (Table 1). Ratio of the rate constants $k_o(H)/k_o(D)$ are calculated and given in Table 2, together with the activation parameters.

Discussion

Reaction Route of the Exchange. Since k_o was independent of $[H_2O]$, the chemical species participating in the rate-determining step should be only M(acac)$_3$ and Hacac. Consequently probable reaction routes are very much restricted. Equation 4 can be assumed almost exclusively as a common route for these exchange reactions,

$$\underset{I^*}{M(O,\overset{*}{O})} + Hacac \underset{k_{-1}}{\overset{k_1}{\rightleftharpoons}} \underset{II^*}{M(acacH,O\text{–}\overset{*}{O})} \xrightarrow{k_2} \underset{II}{M(O\text{–}O,\overset{*}{acacH})} \xrightarrow{k_{-1}} \underset{I}{M(O,O)} + \overset{*}{Hacac} \quad (4)$$

where O–O and I* denote $acac^-$ and $M(\overset{*}{acac})_3$, respectively. (Two $acac^-$ chelates are omitted in these species.) The original complex I* and a solvent molecule(Hacac) produce an intermediate II*, which is converted into II through the proton transfer, and then II changes into I and $H\overset{*}{acac}$. The intermediate II* involves an one-ended bidentate and a solvent molecule as unidentates. Such a type of the intermediate is generally accepted as an intermediate for dissociation and formation reactions of chelates in octahedral complexes in coordinating solvents.[17–19] Acetylacetone, with a donor number *ca.* 17,[20] can be regarded as coordinating solvent. Therefore, the formation of II* is considered to be reasonable.

The k_1 step in Eq. 4 should be the rate-determining step. If k_2 were smaller than k_1, the proton transfer process would be the rate-determining step. However, such a mechanism does not interpret the different

TABLE 1. RATES AND FIRST-ORDER OBSERVED RATE CONSTANTS FOR THE LIGAND EXCHANGE OF $M^{III}(acac)_3$ IN Hacac

Exp. No.	M(III)	T / °C	[M] / 10^{-3} M	[H_2O] / M	Rate / 10^{-7} M s^{-1}	k_o / 10^{-5} s^{-1}
1	Cr(III)	108.9	3.04	0.035		2.4 ±0.3
2		117.1	2.98	0.025	1.6	5.4 ±0.3
3			5.67	0.025	3.4	6.0 ±0.3
4			3.00	0.086		5.6 ±0.5
5			2.95	0.013		4.0 ±0.4[b]
6		124.9	2.87	0.043		11.2 ±0.3
7	Co(III)	85.0	4.28	0.048		0.73±0.08
8		93.0	4.32	0.048	1.0	2.4 ±0.3
9			8.01	0.030	2.4	2.3 ±0.3
10			4.33	0.077		2.3 ±0.2
11			4.40	0.028		2.3 ±0.1[b]
12		101.1	4.28	0.048		6.8 ±0.6
13	Ru(III)	150.0	3.11	0.01—0.03[a]		5.2 ±0.2
14		157.5	3.11	*ca.* 0.03		9.5 ±0.3
15		165.1	3.11	*ca.* 0.04		16.3 ±0.5
16	Rh(III)	179.7	4.35	0.04—0.07[a]		1.60±0.09
17		185.2	4.35	0.02—0.07[a]	1.0	2.37±0.17
18			8.55	*ca.* 0.05		2.39±0.12
19			4.33	*ca.* 0.05		2.23±0.13[c]
20			4.27	*ca.* 0.03		1.85±0.13[b]
21		190.2	4.35	0.03—0.05[a]		3.33±0.30

a) Increased with time. b) In Hacac[*methylene*-$^2H_2$] (deuterium content: 80%). c) In Hacac[*methylene*-$^2H_2$] (deuterium content: 37%).

TABLE 2. ACTIVATION PARAMETERS AND DEUTERIUM ISOTOPE EFFECT ON RATE FOR THE LIGAND EXCHANGE OF $M^{III}(acac)_3$ IN Hacac

M(III)	ΔH^* / kcal mol^{-1}	ΔS^* / cal K^{-1} mol^{-1}	k_o(H)[a] / k_o(D)
Cr(III)	28.8±0.7	−5.0±2.2	1.5
Co(III)	36.4±2.2	+19.2±6.1	1.0
Ru(III)	27.4±1.8	−14.6±4.5	—
Rh(III)	28.3±0.5	−19.0±1.4	1.4

a) The ratio of the rate constants of the exchange in normal and deuterated acetylacetone(Hacac[*methylene*-$^2H_2$]).

values of the kinetic parameters shown in Tables 1 and 2 among the complexes(*vide infra*).

Besides the k_2 process, an alternative route (Eqs. 5—7) containing the complete dissociation of the coordinated $\overset{*}{a}cac^-$ might be considered between II* and II in Eq. 4. (Notations are identical with those for Eq. 4.)

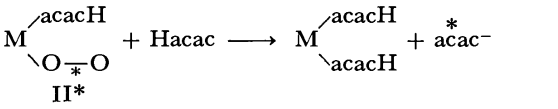

(5)

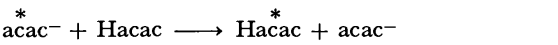

(6)

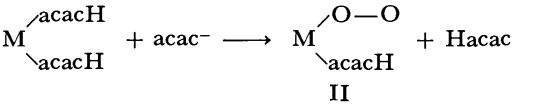

(7)

However, the route is not consistent with the observed k_o(H)/k_o(D) values for the Cr(III) and Rh(III) systems (Table 2), since it is unlikely that the k_o values are governed by the proton transfer process (Eq. 6) which is considered to be much faster than the dissociation process (Eq. 5). For the Co(III) complex, the complete dissociation of $acac^-$ (Eq. 5) has been suggested to be much slower than the exchange in acetonitrile.[3] Therefore, the k_2 process in Eq. 4 must be indispensable for the exchange to take place.

So far as k_1 is very small as compared with k_{-1} and k_2 and the stationary-state condition is assumed for II* in Eq. 4, k_o is expressed by Eq. 8,

$$k_o = k_1 \frac{k_2}{k_{-1}+k_2} \tag{8}$$

where k_1 is taken to be first-order ([M]≪[Hacac]). The k_1 process represents the rate-determining step, and the term $k_2/(k_{-1}+k_2)$ indicates a branching ratio for the accomplishment of the exchange from II*.

Substitution Mechanisms of the Rate-determining Step. Table 2 shows that the Co(III) complex gives different activation parameters and k_o(H)/k_o(D) values from those of the other complexes. The ΔH^* value for the Co(III) complex is distinctly higher than those for the others. The ΔH^* values for substitution processes of complexes containing the present tervalent metal ions are reported to be in similar ranges to one another.[6] The Co(III) complex has positive ΔS^*, whereas others have negative values. The difference reaches 24—38 cal K^{-1} mol^{-1}. These facts suggest the different mechanisms between the Co(III) and the other com-

plexes. Since the rate-determining step is reckoned to be the k_1 process, the acitivation parameters should reflect mostly those for this step. It is most likely that the intermediate II* in Eq. 4 is formed by the S_N1 and the S_N2 mechanism for the Co(III) and the other complexes, respectively.[21]

The difference in $k_o(H)/k_o(D)$ values in Table 2 is also interpreted on the basis of the same assignment of the mechanism. The Co(III) complex gives no isotope effect, whereas the Cr(III) and Rh(III) complexes have the ratio more than unity. If $k_{-1} \ll k_2$ in Eq. 8,

$$k_o = k_1 \quad (9)$$

If $k_{-1} \gg k_2$

$$k_o = k_1 k_2 / k_{-1} \quad (10)$$

Since the deuterium isotope effect on k_o must be attributable to that on k_2, Eqs. 9 and 10 should be applicable to the Co(III) and the other complexes with their inequalities, respectively. The rate constant k_{-1} can be assumed to be much more susceptible to the nature of M^{III} than k_2 is, since the k_{-1} process contains the dissociation and formation processes of M^{III}–O bonds, whereas the k_2 process does not. So far as k_2 for these metal complexes remains without big difference, the rate constant for the ring closure, k_{-1}, should be responsible for the difference in the inequalities [k_{-1}(for Co(III)) $\ll k_2 \ll k_{-1}$(for Cr(III) and Rh(III))]. The relatively high k_{-1} values assumed for the Cr(III) and Rh(III) complexes might be related to the labilization of cis position by the S_N2 action of unbound atom of a ligand (cis anchimeric effect).[22] Some fast substitution of Cr(III) complexes was interpreted by this effect. Therefore, an intermediate of S_N2 type (IV in Fig. 2) with a structure similar to that proposed for the effect[23] is suggested to be formed on going from I* to II*. On the contrary, such an effect is not expected for the S_N1 substitution. The relatively small k_{-1} assumed for the Co(III) complex is thus accounted for. An intermediate such as III in Fig. 2 may be present in the Co(III) system.

On the other hand, on the assumption that the proton transfer (k_2) in Eq. 4 is the rate-determining step, the following kinetic results are not interpreted; i) the different values of the activation parameters and $k_o(H)/k_o(D)$ for the Co(III) complex with those for the others and ii) a common sequence of the M(acac)$_3$ for the rates of the present exchange and the racemization in chlorobenzene (*vide infra*, the racemization cannot contain such a proton transfer process.)

The two unidentates in II* and II should be cis to each other, at least when the proton is transferred. The presence of trans isomer cannot be excluded, but it does not seem to play important role in the exchange reactions. It may be a dead end species, even if it is formed.

Therefore, the mechanisms illustrated in Fig. 2 can be proposed. The relatively slow and fast ring-closure processes (the k_{-1} step) compared with the proton transfer process (the k_2 step) are suggested for the Co(III) and the other complexes, respectively.

Comparison of Rates with Racemization. The Arrhenius plots for the exchange (k_o) and the racemization(k_{rac}, in chlorobenzene)[24] of the complexes are given in Fig. 3. The rates of both the reactions decrease in the sequence under the given conditions.

$$Co(III) > Cr(III) > Ru(III) > Rh(III)$$

The common sequence suggests that each M(acac)$_3$ has similar reactivities for both the inter- and intramolecular processes.

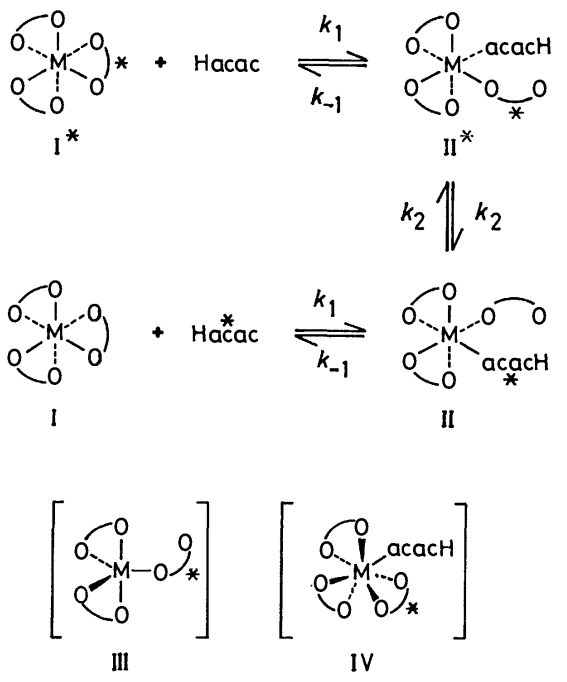

Fig. 2. Mechanisms of the ligand exchange of M^{III}(acac)$_3$ (I) in acetylacetone. The routes I*→III→II* (S_N1) and I*→IV→II*(S_N2) are proposed for the Co(III) and the Cr(III), Ru(III), and Rh(III) complexes, respectively. (The structures of III and IV are only provisional.)

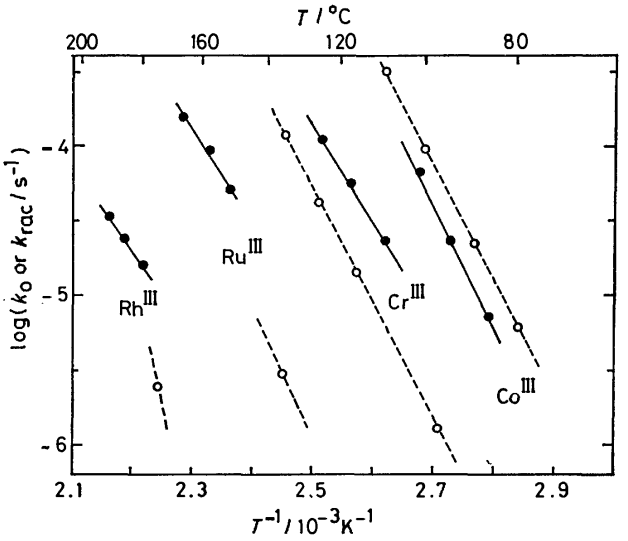

Fig. 3. Arrhenius plots for the reactions of $M^{III}(acac)_3$. Full circles with a solid line: the ligand exchange in acetylacetone (k_o). Open circles with a broken line: the racemization in chlorobenzene(k_{rac}, appoximate values for Ru(III) and Rh(III)[24]).

However, the correlation of the Arrhenius plots of both the reactions for the Co(III) complex is different from that for the other complexes; $k_o > k_{rac}$ and the less steep slopes for k_o in the Cr(III), Ru(III), and Rh(III) complexes, whereas $k_o \fallingdotseq k_{rac}$ (k_{rac} is rather slightly bigger than k_o) and similar gradient of the slopes for the Co(III) complex. A common S_N1 mechanism for both the exchange in acetonitrile and the racemization in chlorobenzene has been concluded for the Co(III) complex, despite of the difference of the solvent.[3] These facts and the conclusion support the difference in the proposed mechanisms for the exchange reactions, so far as the one-ended bond-rupture mechanism(S_N1)[25] opperates commonly in the racemization of these complexes.

Comparisons of the Mechanisms with Related Reactions. The substitution mechanisms for the present exchange reactions can be compared with those of the substitution reactions of unidentates in the tervalent metal complexes, since the rate-determining step of the former reactions is concluded to be the replacement of one of coordinated oxygen atoms in a chelate ring by an Hacac molecule and is comparably simple with that of the latter ones.

Comparison of Mechanisms with Those for Complexes Containing N_5O Core: The water exchange and the anation of various ligands to pentaammineaqua complexes of Co(III),[7,9] Cr(III),[7,10,26-28] Ru(III)[29,30] and Rh(III)[31-36] have been systematically studied in aqueous solutions. The S_N1 and the S_N2 mechanisms were predominantly assigned to the reactions of the Co(III) and the other complexes, respectively. Especially, the mechanisms assigned to the water exchange on the basis of ΔV^* values are generally accepted to be most convincing.[8-11] The Co(III) complexes have a rather exceptional mechanism[37] commonly in both the present and the reported exchange systems, despite of the difference in the charge of the complexes, the assortment of the coordinating atoms, the dentate number of the leaving and entering ligands and the property of the solvents. The ionic radius of M^{III} [11,38] (Co^{III}:52.5, Cr^{III}:61.5, Ru^{III}:68, Rh^{III}:66.5 pm)[41] seems to be commonly an important factor in determining the mechanisms of the exchange reactions of these complexes containing O_6 and N_5O cores.

Comparison of Mechanism among Complexes Containing O_6 Core: The S_N2 mechanism for the present exchange of $Cr(acac)_3$ is consistent with that for the solvent exchange of $Cr(H_2O)_6^{3+}$ [37], $Cr(dmf)_6^{3+}$ [38] and $Cr(dmso)_6^{3+}$ [39] (dmf=*N*,*N*-dimethyformamide, dmso=dimethyl sulfoxide) and for the anation of various ligands to hexaaqua complex ion.[40] The S_N2 mechanism is considered to commonly operate in these reactions of the $Cr^{III}O_6$ complex.

Little information is available concerning the substitution mechanism of the $M^{III}O_6$ type complexes of Co(III), Ru(III), and Rh(III). An S_N2 mechanism is concluded in the exchange of $Rh(acac)_3$, but an S_N1 mechanism was proposed for the water exchange and the bromide anation of $Rh(H_2O)_6^{3+}$.[4,5] The proposed mechanisms for the present Co(III) and Ru(III) complexes may be the first examples for O_6 type complexes of Co(III) and Ru(III), and should be compared with other examples in future.

The author wishes to thank Professor Kazuo Saito for helpful discussions. This work was supported by the Grant-in-Aid from the Ministry of Education.

References

1) R. G. Pearson and R. D. Lanier, *J. Am. Chem. Soc.*, **86**, 765 (1964).
2) H. Kido and K. Saito, *Inorg. Chem.*, **16**, 397 (1977).
3) H. Kido and K. Saito, *Bull. Chem. Soc. Jpn.*, **52**, 3544 (1979).
4) W. Plumb and G. M. Harris, *Inorg. Chem.*, **3**, 542 (1964).
5) R. J. Buchacek and G. M. Harris, *Inorg. Chem.*, **15**, 926 (1976).
6) J. O. Edwards, F. Monacelli and G. Ortaggi, *Inorg. Chim. Acta*, **11**, 47 (1974).
7) T. W. Swaddle, *Coord. Chem. Rev.*, **14**, 217 (1974).
8) F. Monacelli and E. Veil, *Inorg. Chim. Acta*, **1**, 467 (1967).
9) H. R. Hunt and H. Taube, *J. Am. Chem. Soc.*, **80**, 2642 (1958).
10) T. W. Swaddle and D. R. Stranks, *J. Am. Chem. Soc.*, **94**, 8357 (1972).
11) S. B. Tong and T. W. Swaddle, *Inorg. Chem.*, **13**, 1538 (1974).
12) K. Saito and K. Masuda, *Bull. Chem. Soc. Jpn.*, **41**, 384 (1968).
13) G. Wilkinson, *J. Am. Chem. Soc.*, **74**, 6146 (1952).
14) F. P. Dwyer and A. M. Sargeson, *J. Am. Chem. Soc.*, **75**, 984 (1953).
15) M. Kato, private communication.
16) The equation is estimated for the Ru(III) complex.
17) F. Basolo and R. G. Pearson, "Mechanisms of Inorganic Reactions," 2nd ed, J. Wiley and Sons Inc., New York (1967), p. 223.
18) R. G. Wilkins, *Acc. Chem. Res.*, **3**, 408 (1970).
19) U. Nickel, H. Hoffmann and W. Jaenicke, *Ber. Bunsenges. Phys. Chem.*, **72**, 526 (1968).
20) M. Nishizawa, private communication.
21) For the S_N2 exchange reactions, the equation $k_o = k_o'$[Hacac] ([Hacac]=9.7 M) is suggested. The ΔS^* values calculated for k_o' are −7.3, −17.4 and −23.8 cal K^{-1} mol^{-1} for the Cr(III), Ru(III), and Rh(III) complexes, respectively, being slightly more negative than those for k_o.
22) H. Ogino, T. Watanabe and N. Tanaka, *Inorg. Chem.*, **14**, 2093 (1975) and references cited therein.
23) S. N. Choi and D. W. Carlyle, *Inorg. Chem.*, **13**, 1818 (1974).
24) R. C. Fay, A. Y. Girgis and U. Klabunde, *J. Am. Chem. Soc.*, **92**, 7056 (1970).
25) A. Y. Girgis and R. C. Fay, *J. Am. Chem. Soc.*, **92**, 7061 (1970).
26) G. Guastalla and T. W. Swaddle, *Can. J. Chem.*, **51**, 821 (1973).
27) T. Ramasami and A. G. Sykes, *Inorg. Chem.*, **15**, 2885 (1976) and references cited therein.
28) L. Mønsted, *Acta Chem. Scand.*, **A**, **32**, 377 (1978).
29) J. A. Broomhead, L. Kane-Maguire and D. Wilson, *Inorg. Chem.*, **14**, 2575 (1975) and references cited therein.
30) H. Sakamoto, K. Yoshikuni, S. Ohno, K. Ohkubo, and A. Ohyoshi, *Chem. Lett.*, **1974**, 1309 and references cited therein.
31) F. Monacelli, *Inorg. Chim. Acta*, **2**, 263 (1968).
32) H. L. Bott, A. J. Poë and K. Shaw, *J. Chem. Soc.*,

Sect. A, **1970**, 1745.
33) C. Chatterjee and P. Chaudhuri, *Indian J. Chem.*, **11**, 777 (1973).
34) E. Borghi and F. Monacelli, *Inorg. Chim. Acta*, **23**, 53 (1977).
35) S. C. Chan, *Aust. J. Chem.*, **20**, 61 (1967).
36) R. van Eldik, *Z. Anorg. Allg. Chem.*, **416**, 88 (1975).
37) D. R. Stranks and T. W. Swaddle, *J. Am. Chem. Soc.*, **93**, 2783 (1971).
38) S. T. D. Lo and T. W. Swaddle, *Inorg. Chem.*, **14**, 1878 (1975).
39) D. L. Carle and T. W. Swaddle, *Can. J. Chem.*, **51**, 3795 (1973).
40) D. Thusius, *Inorg. Chem.*, **10**, 1106 (1971) and references cited therein.
41) R. D. Shannon and C. T. Prewitt, *Acta Crystallogr., Sect. B*, **25**, 925 (1969), **26**, 1046 (1970).

A Nephelometric Analysis of Mercury(II) with Potassium Salt of α,α′-Bis(dithiocarboxyoxy)-*p*-xylene

Daijiro YAMAMOTO, Masamichi TSUKADA,* Yasuaki HIROTA,† and Haruo MIZUNO††

Department of Agricultural Chemistry, Faculty of Agriculture, Meiji University, 5158, Ikuta, Tama-ku, Kawasaki, Kanagawa 214

††*Department of Food Science and Technology, Tokyo University of Fisheries, 4, Konan, Minato-ku, Tokyo 108*

(Received May 15, 1979)

Potassium salt of α,α′-bis(dithiocarboxyoxy)-*p*-xylene (abbreviated as K_2-XDX) was synthesized as a chelating agent with *p*-xylene-α,α′-diol, carbon disulfide, and potassium hydroxide. Since a mercury(II)–XDX chelate complex suspension scattered pearl-blue light strongly because of the formation of a colloidal solution, the nephelometric analysis of small amounts of mercury(II) was undertaken. The calibration curve was found to be linear in the two ranges of 0.03—1.00 and 0.50—25.00 μg cm^{-3} of the mercury(II) ion respectively, but no suitable masking agents for interfering metal ions were found. The mole ratio of mercury(II) to XDX in the complex was found to be 1 to 1. These data for the complex suggested that XDX and mercury(II) combined alternately to form the $(-Hg-XDX-)_n$ complex. The molecular weight of this complex could be calculated as about 2×10^7 from the Zimm plot on the basis of the light-scattering method.

The formation of chelate complexes between a number of metals and dithiocarbonic acid derivatives is well known. Since the derivatives with a dithiocarboxyoxy group as a functional group can readily be prepared, and since they have a good reactivity with many metal ions, they have been used for other analytical studies as well as for absorptiometric analysis.[1–7] If the two hydrogen atoms of dihydroxy-compounds can be replaced by some functional groups, we can assume that the dithiocarbonic acid derivatives react with each of the different kinds of metal ions to form polynuclear metal complex salts in which a successive and alternate arrangement of metal and ligand is found. Provided that these chelate complexes become large and colloidal in form, those solutions may be used in the nephelometric determination of trace amounts of the metal ions.

According to the above-mentioned idea, potassium salt of α,α′-bis(dithiocarboxyoxy)-*p*-xylene, (K_2-XDX), was prepared from *p*-xylene-α,α′-diol. This derivative reacted with many ions and produced light-scattering colloidal solutions. Among these, the mercury(II)–XDX solution scattered very remarkable pearl-blue light. This colloidal solution was very stable for a long time. The substance could be extracted into 1-octanol and 3-heptanone, which were good solvents for some organic polymers. The solution was colloidal and scattered light as well as in the case of an aqueous solution. This colloidal solution was also very stable for a long time.

This solution could be used in the determination of mercury(II) by the nephelometric method, and the amount of the mercury(II) ion (from 0.03—25.00 μg cm^{-3}) was detectable. The molecular weight of the mercury(II)–XDX chelate was measured by the light-scattering method and found to be about 2×10^7. Therefore, a polynuclear chelate compound might be produced.

Although there have been reported several nephelometric methods for the determination of such metals as Ag, Ba, and Zn, nephelometry with a colloidal solution of polymeric polynuclear chelate has not yet been reported.[8] It should be emphasized that this analytical method may be a new tool for trace analysis.

Experimental

Reagents. Dust-free water was obtained by distilling deionized water with an all-quartz distillation apparatus and by then filtering it through a G-5 glass filter, it has been used throughout all the processes. Mercury(II) chloride was purified by sublimation. All the other reagents were of a chemically pure grade and were used without further purification. Each of the reagents was dissolved with the dust-free water until it became the desired concentration and then filtered through the G-5 glass filter.

Buffer Solution. Among many kinds of buffer solutions, the most rapid clearance of the reaction mixture was observed in the case of Walpole's buffer solution. At pH values of 3.8 or below, XDX^{2-} was decomposed rapidly, while above this pH, even in an alkaline solution, it was stable. This buffer solution was prepared by mixing hydrochloric acid and a sodium acetate solution. The maximum intensity of the scattering light from the chelate complex suspension was obtained at about pH 4.0.

Synthesis of K_2-XDX. This was synthesized according to the method given by Price.[9] The procedure was as follows: one gram of *p*-xylene-α,α′-diol (α,α′-dihydroxy-*p*-xylene) was dissolved in 6 cm^3 of a 15% potassium hydroxide solution, and then the mixture was added to 5 cm^3 of carbon disulfide. The mixture was stirred for 16 h, with the temperature kept at 5 °C. After the surplus carbon disulfide had been removed by filtration, ethanol was added to the solution until a slightly yellow crystalline was produced. The precipitate was filtered out, washed by ethanol, and recrystallized by dissolving them in a minimum amount of water and adding ethanol. The resulting product was filtered, washed with ethanol, and dried at room temperature under reduced pressure.

Properties of K_2-XDX. The K_2-XDX synthesized was not changed when kept for at least 50 days in a brown desiccator at reduced pressure. It is very soluble in water and acetone, and insoluble in carbon tetrachloride, ethanol, and benzene.

Some of its physicochemical properties were as follows.

† Present address: AMCO Co., Ltd., Iidabashi, Chiyoda-ku, Tokyo 102.

The ultraviolet spectrum of an aqueous solution of this compound in a neutral medium showed an absorption maximum at 303 nm. This is due to the replacement of a hydrogen atom by a carbodithioic group.[10]

The infrared spectra of the compound was measured in a KBr disc, and the bands were assigned (cm^{-1}) to the stretching vibrations of C=S (1150), and C–S (915, 870, and 650).[11,12] The ^1H NMR spectrum of a deuterium oxide solution of *p*-xylene-α,α'-diol (the starting material) showed a peak at 4.55 ppm by the existence of two protons of $-R-CH_2-O-$. In the case of this derivative, however, the identical peak was shifted to 5.48 ppm by substitution with the dithiocarboxyoxy group.

According to the data presented above, the structural formula was determined to be as follows:

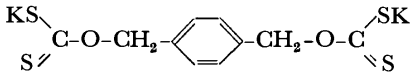

The purity of this compound was determined to be over 99.7% by the method of JIS-K8269.

Stability of the Reagent Solution. The absorbance of the aqueous solution adjusted at pH 6.8 was measured at the wavelength of 303 nm. It showed little change for at least 120 min. After 24 h, however, it decreased 30%. On the basis of the results, all the measurements were designed to be completed within 30 min.

Apparatus. For the measurement of the intensity of the scattering light, a Hitachi EPS-3T recording spectrophotometer with an L-3 model fluorometer was used. As a light source, an ultra-high pressure lamp was used. Two monochromatic rays of 365 nm, through a ultraviolet filter, and 546 nm, through a green interference filter, were used in order to excite the sample. The intensity of the scattering light from the sample was measured perpendicular to the incident light. A greater intensity was always obtained in the case of 365 nm than in that of 546 nm.

For the estimation of the molecular weight, a Fica 4200 model light-scattering spectrophotometer was used.

Procedure for the Determination of Mercury(II). All the measurements were carried out at room temperature. The general procedure for the determination of mercury was as follows: 10-cm^3 portions of the sample solutions containing 0.06—50.00 μg cm^{-3} of the mercury(II) ion, which had been prepared from 100 μg cm^{-3} of the mercury(II) ion stock solution, were placed in a 30 cm^3-test tube fitted with a ground-glass stopper. 5 cm^3 of an acetate buffer solution (pH 4.0) and 5 cm^3 of an XDX^{2-} solution (150 mg dm^{-3} of K_2-XDX) were added. The XDX^{2-} solution was prepared afresh each time. The test tube was vigorously shaken and then allowed to stand for 10 min. The intensities of the scattering light were measured at 365 nm. The constant regulation of the slit width and the photomultiplier sensitivity was necessary in order to choose the best conditions between the concentration range of the mercury(II) ion and the intensity of the scattering light.

Results and Discussion

Reactions of XDX^{2-}. As is shown in Table 1, in the reactions between XDX^{2-} and various kinds of metal ions, the coloration was often similar to those which were observed in a reaction with the ethylxanthate ion. In an aqueous solution, however, XDX^{2-} differed from the ethylxanthate ion, in which turbidity or a precipitate more often appears when a kind of metal ion is mixed with it. The apparent values of the molar absorption coefficients, (ε), shown in the table might be slightly higher because of the influence of light scattering. They are, however, lower than those obtained by the use of ethylxanthate.[13] From the graph of the calibration curve prepared for each metal ion except Mo^{5+}, we obtained a straight line passing a point near to zero.

Calibration Curve. The two linear calibration curves were obtained for the concentration ranges of 0.03—1.00 μg cm^{-3} and of 0.50—25.00 μg cm^{-3}.

Solvent Extraction. Twenty-one kinds of generally available polar and nonpolar organic extractants were examined for the selective extraction of the mercury(II)–XDX chelate polymer. The polymer could be extracted into only 1-octanol and 3-heptanone, as is shown in Table 1. The light scattering was observed by this extracted sample, and the intensity of the scattered light was the same as in the aqueous solution. Other kinds of metal chelates, such as Co(II)–, Ni(II)–, Cu(II)–, and Cd(II)–XDX, were also extracted into both solvents.

Effect of Diverse Ions. For the study of the tolerance limits for diverse ions, 1 cm^3 of a 5.00 μg cm^{-3} mercury(II) ion solution was mixed with 1 cm^3

Table 1. Reactions of metal ions with XDX^{2-}

Ion	Color	λ_{max} / nm	ε / $dm^{-3}\,mol^{-1}\,cm^{-1}$	Extractant[a]
Fe^{2+}	Brown (unstable)	—	—	None
Co^{2+}	Pale-blue	360	1.5×10^4	3-Hept., 1-Oct.
Ni^{2+}	Brown-yellow	430	2.6×10^3	3-Hept., 1-Oct.
Cu^{2+}	Yellow	408[b]	3.5×10^3	3-Hept., 1-Oct.
As^{3+}	Colorless (precipitate)	—	—	None
Bi^{2+}	Yellow (precipitate)	—	—	None
Cd^{2+}	Pearl-blue	305	2.8×10^3	3-Hept., 1-Oct.
Hg^{2+}	Pearl-blue	295	2.8×10^3	3-Hept., 1-Oct.
Mo^{5+} [c]	Reddish-orange	521	5.8×10^3	None
V^{5+}	Yellow (precipitate)	—	—	None
UO_2^{2+}	Reddish-orange (precipitate)	—	—	None

a) 3-Hept. is 3-heptanone. 1-Oct. is 1-octanol. b) In the case of Cu^{2+}, undistinct peak of absorption was found.
c) Reduced MoO_4^{2-} with hydrazine sulfate.

of another ion solution in different concentrations. To each of these solutions 3 cm^3 of the buffer solution (pH 4.0), 2 cm^3 of the EDTA solution (3.7% of Na_2 edta) as a masking agent, and 3 cm^3 of the XDX^{2-} solution (150 mg dm^{-3} of K_2–XDX) were added. Then, in order to extract the mercury(II)–XDX chelate polymer, these were vigorously shaken with 10 cm^3 of 1-octanol.

According to the result, a large excess (300 $\mu g\ cm^{-3}$ each) of the following ions—Ag^+, Al^{3+}, Ba^{2+}, Be^{2+}, Ca^{2+}, Cr^{3+}, Mg^{2+}, Mn^{2+}, MoO_4^{2-}, and Sr^{2+}—had no effect on the intensity of the scattering light. Co^{2+}, Fe^{2+}, Fe^{3+}, Mo^{5+}, UO_2^{2+}, and Zn^{2+} did not interfere in concentrations 30 times or less that of the Hg^{2+}. Even if, in the same concentration as that of the Hg^{2+}, Cd^{2+} caused a positive interference, As^{3+}, Bi^{2+}, $Cr_2O_7^{2-}$, Cu^{2+}, Pb^{2+}, and V^{5+} showed a negative interference. The reason for the negative interference is probably that, in the case of Cu^{2+}, the solution formed with XDX^{2-} has a broad absorption band in the near-ultraviolet region, and the exciting and scattering lights are absorbed by the solution. In the cases of As^{3+}, Bi^{2+}, $Cr_2O_7^{2-}$, Pb^{2+}, and V^{5+}, they co-precipitate the Hg–XDX polymer. The addition of Na_2edta as a masking agent for these ions was not effective.

Composition of the Chelate. A continuous-variation method by means of nephelometry was carried out. Both mercury(II) and XDX ion solutions were adjusted to 5×10^{-3} mol dm^{-3} in concentration, (Hg:10 $\mu g\ cm^{-3}$), they were mixed in proper proportions, and a 4-cm^3 portion of a buffer solution (pH 4.0) was added. The total volume of this solution was finally made up to 14 cm^3, and then we measured the intensity of the scattering light. The results are shown in Fig. 1.

Since the maximum intensity was obtained with a concentration ratio of 0.5, the ratio of mercury(II) to XDX in this polymer was confirmed to be 1 to 1.

Estimation of the Molecular Weight of the Polymer. The molecular weight of the colloidal polymer can be determined by light-scattering spectrophotometry at the wavelength of 546 nm. The variation in the refractive index at various concentrations, (dn/dc), was

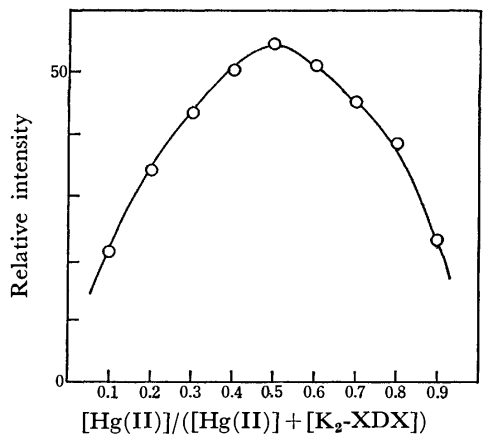

Fig. 1. Continuous variation method for Hg–XDX complex. This was obtained by means of nephelometry using the excitation at 365 nm. [Hg(II)]+[K_2-XDX]: 3.6×10^{-5} mol dm^{-3}.

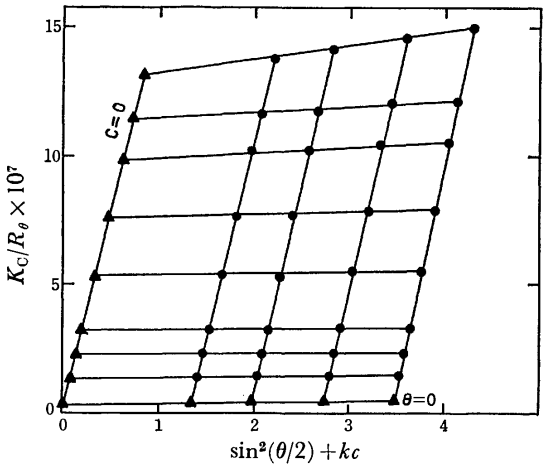

Fig. 2. Zimm plot for 1-octanol suspension of Hg–XDX complex.

obtained by using a differential refractometer (Narumi Co., Ltd.). To obtain a dust-free sample, pretreatment by centrifuging (10000 rpm) was necessary. Because the aqueous solution, however, had too low a viscosity to maintain the suspension, the sample extracted by high viscous 1-octanol was used.

From the measurements carried out on solutions ranging in concentration from 1.3×10^{-2} to 6.6×10^{-2} mg cm^{-3}, the dn/dc was calculated to be 1.65 $cm^3\ g^{-1}$. As is shown in Fig. 2, the molecular weight estimated by extrapolating into the Zimm plot was about 2×10^7. It is thus proved that the intense light scattering is due to the formation of a large molecule which can be considered to be a kind of colloid.

The authors wish to express their deep thanks to Assistant Professor Naomichi Iso of the Tokyo University of Fisheries for his many helpful discussions.

References

1) M. Aihara and M. Kiboku, *Bunseki Kagaku*, **26**, 559 (1977).
2) Y. Tanaka and S. Yoshiki, *Bunseki Kagaku*, **23**, 1190 (1978).
3) Y. Sasaki, *Bunseki Kagaku*, **27**, 237 (1978).
4) K. Hayashi, Y. Sasaki, S. Tagashira, and E. Yamate, *Bunseki Kagaku*, **27**, 712 (1978).
5) E. M. Donaldson, *Talanta*, **23**, 411 (1976).
6) E. M. Donaldson, *Talanta*, **24**, 441 (1977).
7) Y. Yamamoto, H. Murata, and S. Ueda, *Talanta*, **25**, 696 (1978).
8) H. J. G. Challis, "Handbook of Analytical Chemistry," 1st ed, ed by Louis Meites, McGraw-Hill, New York (1963), pp. 6—174.
9) C. C. Price and G. W. Stancy, *Org. Synth.*, **28**, 82 (1948).
10) I. Iwasaki and S. R. B. Cooke, *J. Am. Chem. Soc.*, **80**, 285 (1958).
11) L. J. Bellamy, "Advances in Infrared Group Frequencies," (translated into Japanese), Methuen & Co., England (1968).
12) M. L. Shankaranarayana and C. C. Patel, *Can. J. Chem.*, **39**, 1633 (1961).
13) K. Hayashi, Y. Sasaki, and E. Nagano, *Bunseki Kagaku*, **20**, 727 (1971).

 © 1980 The Chemical Society of Japan Bull. Chem. Soc. Jpn., 53, 91—95 (1980)

Formation and Spectral Properties of Some Bis(β-diketonato)-copper(II)–Diazole Complexes

Tamizo KOGANE* and Reiko HIROTA**

Industrial Research Institute of Kanagawa Prefecture, Showa-machi, Kanazawa-ku, Yokohama 236

***Faculty of Science, Rikkyo University, Nishi-ikebukuro, Toshima-ku, Tokyo 171*

(Received May 19, 1979)

The reactions of bis(β-diketonato)copper(II) with pyrazole and imidazole gave the diazole adducts Cu(β-dik)$_2$(Hdzl) (β-dik=β-diketonate anion; Hdzl=diazole) and/or the μ-diazolato complexes [Cu(β-dik)(dzl)]$_n$ (n=2,4,....). The complexation reactions are very sensitive to the nature of the diazole and to the reaction conditions, sometimes giving different products depending upon the solvent used. In chloroform, Cu(β-dik)$_2$–pyrazole and Cu(β-dik)$_2$–imidazole complexes exhibited characteristic absorption maxima at approximately 570 and 555 nm, respectively, which are much shorter than the λ_{max} values of the starting Cu(β-dik)$_2$ chelates.

Nitrogen heterocycles react with bis(β-diketonato)-copper(II) complexes in different solvents forming 1:1 or 1:2 adducts.[1] There have been several reports concerning the reactions of bis(β-diketonato)copper(II) with bidentate ligands containing similar nitrogen atoms. For example, the ethylenediamine complex with bis(2,4-pentanedionato)copper(II),[2] as well as the 2,2′-bipyridine,[3] pyrazine,[4] 1,5-naphthyridine,[5] and 1,10-phenanthroline[6] complexes with bis(1,1,1,5,5,5-hexafluoro-2,4-pentanedionato)copper(II), has been isolated and identified. Few papers have been published, however, on the reactions of bis(β-diketonato)copper(II) with heterocyclic bidentate ligands containing dissimilar nitrogen atoms.[7,8]

Pyrazole (Hpz) and imidazole (Him) are known to be versatile ligands which produce complexes with many metal ions or Lewis acids. These diazoles behave differently from pyridine and other six-membered nitrogen heterocycles in complex formation, since the NH protons are acidic and easily dissociate to give the corresponding anions.[9,10]

Diazole adducts of the bis(β-diketonato)copper(II) complexes, such as imidazole adducts of bis(fluorinated β-diketonato)copper(II)[7,8] and Cu$_2$(acac)$_2$(pz)$_2$ and Cu$_2$(acac)$_2$(OH)(pz) have been reported.[11] The reactions of diazoles with bis(β-diketonato)copper(II) in general, however, have not been studied systematically. The results of such studies and the behavior of the mixed complexes obtained, will be reported here.

Experimental

Materials. The β-diketonato chelates of copper(II) employed were Cu(dpm)$_2$, Cu(dibm)$_2$, Cu(dnbm)$_2$, Cu(dprm)$_2$, Cu(acac)$_2$, Cu(bzac)$_2$, Cu(tac)$_2$, Cu(fac)$_2$, and Cu(tfac)$_2$, where dpm, dibm, dnbm, dprm, acac, bazc, tac, fac, and tfac designate the anions of 2,2,6,6-tetramethyl-3,5-heptanedione, 2,6-dimethyl-3,5-heptanedione, 4,6-nonanedione, 3,5-heptanedione, 2,4-pentanedione, 1-phenyl-1,3-butanedione, 1-(2-thienyl)-1,3-butanedione, 1-(2-furyl)-1,3-butanedione, and 1,1,1-trifluoro-2,4-pentanedione, respectively. The chelates were prepared by mixing copper(II) acetate (1 mol) in aqueous solution with β-diketone (2 mol) in ethanol under stirring. The precipitate formed was filtered, dried, and recrystallized from chloroform or from a chloroform–ethanol mixture. Other materials and solvents were purified by standard procedures.

Syntheses of Pyrazolato and Imidazolato Mixed Complexes (Substitution Complexes). Cu$_2$(acac)$_2$(pz)$_2$, Cu$_2$(dprm)$_2$(pz)$_2$, and Cu$_2$(dnbm)$_2$(pz)$_2$ were obtained by reacting the β-diketonato complex with equimolar pyrazole in suitable solvents such as chloroform, acetone and ethanol. Cu(β-dik)(im) was obtained as a precipitate by the reaction of Cu(β-dik)$_2$ with an excess of imidazole in ethanol. The results of elemental analyses are given in Tables 1 and 3.

Synthesis of Pyrazole Adduct. Cu(bzac)$_2$(Hpz) and Cu(tfac)$_2$(Hpz): Cu(bzac)$_2$ or Cu(tfac)$_2$ was allowed to react with an equimolar quantity of pyrazole in cyclohexane under reflux for 5 min. After cooling, a light green or green precipitate was separated by filtration and dried *in vacuo*. Found: C, 60.88; H, 4.75; N, 5.95%. Calcd for $CuC_{23}H_{22}N_2O_4$: C, 60.85; H, 4.88; N, 6.17%. Found: C, 35.77; H, 2.62; N, 6.23%. Calcd for $CuC_{13}F_6H_{12}N_2O_4$: C, 35.67; H, 2.76; N, 6.40%.

Cu(tac)$_2$(Hpz) and Cu(fac)$_2$(Hpz): An equimolar mixture of pyrazole and Cu(tac)$_2$ or Cu(fac)$_2$ was dissolved in dichloromethane. The solvent was allowed to evaporate *in vacuo* and a green or light green solid was obtained as a residue. Found: C, 49.25; H, 4.04; N, 5.96%. Calcd for $CuC_{19}H_{18}N_2O_4S_2$: C, 48.97; H, 3.89; N, 6.01%. Found: C, 52.01; H, 4.09; N, 6.28%. Calcd for $CuC_{19}H_{18}N_2O_6$: C, 52.59; H, 4.18; N, 6.46%.

Spectra Measurement. The electronic absorption and diffuse reflectance spectra were recorded on a Hitachi Model 356 spectrophotometer and IR on a Hitachi Model 225 grating infrared spectrophotometer. ^{1}H-NMR spectra were obtained on a JEOL JNM C-60H spectrometer. Mass spectra were measured on a Hitachi RMU-6L mass spectrometer by introducing the sample through a direct inlet system.

Results and Discussion

The bis(β-diketonato)copper(II) complexes were treated with diazoles in solutions, and one or both of the reactions (a), (b) shown in Scheme 1 took place. Reaction (a) forms five or six coordinated bis(β-diketonato)copper(II) adducts, Cu(β-dik)$_2$(Hdzl) or Cu(β-dik)$_2$(Hdzl)$_2$, while (b) is a substitution reaction forming mononuclear Cu(β-dik)(Hdzl)(dzl) or polynuclear [Cu(β-dik)(dzl)]$_n$.[12]

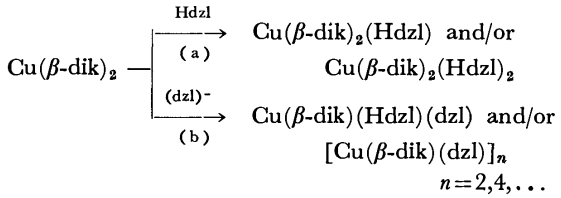

Scheme 1. Reaction paths of bis(β-diketonato)copper(II) with diazoles.

The complexation reactions are very sensitive to the nature of the solvent and to the reaction conditions, giving different products depending upon the solvent used. Hereafter, reactions (a) and (b) are referred to as addition and substitution reactions, respectively. The former proceeds *via* coordination of the neutral diazole molecules to the apical positions of the chelate, while the latter proceeds apparently by replacement of a β-diketonate anion of the chelate with one or two molecules of the diazolate anion.

The Pyrazole Complexes. Equimolar amounts of pyrazole and $Cu(acac)_2$ were mixed in chloroform, which gave $Cu_2(acac)_2(pz)_2$ (**1**) which was isolated as a light blue precipitate. The precipitate was identified by elemental analysis and spectroscopy, the results of which are in accordance with those previously reported by Barraclough *et al.*[11] who showed that it is a binuclear complex. The reaction of pyrazole with $Cu(dprm)_2$ and $Cu(dnbm)_2$ also gave the pyrazolato complexes **2** and **3**, respectively (Table 1).

TABLE 1. THE DIFFUSE REFLECTANCE SPECTRA AND CHEMICAL ANALYSES OF THE PYRAZOLATO COMPLEXES

Complex	λ_{max}/nm	Found (Calcd) (%)		
		C	H	N
$Cu_2(acac)_2(pz)_2$	630	41.72 (41.83)	4.37 (4.39)	12.37 (12.19)
$Cu_2(dprm)_2(pz)_2$	618	46.54 (46.59)	5.60 (5.47)	10.65 (10.87)
$Cu_2(dnbm)_2(pz)_2$	635	50.19 (50.43)	6.13 (6.35)	9.97 (9.80)

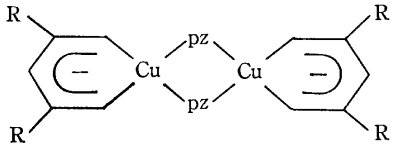

1 R=CH_3
2 R=C_2H_5
3 R=n-C_3H_7

The other bis(β-diketonato)copper(II) complexes examined gave no pyrazolato complexes of this type. Bis(β-diketonato)copper(II) complexes with bulky substituents such as isopropyl and *t*-butyl resist the formation of pyrazolato complexes, probably because of steric hindrance.

In order to investigate the substitution reactions further, the NMR spectra of ternary $Cu(\beta\text{-dik})_2$–diazole–chloroform-*d* system were measured. The signals of the OH and CH protons (*ca.* 16.0 ppm and 5.7 ppm, respectively) characteristic of the intramolecularly hydrogen-bonded enolic form of β-diketone are observed when diazole is added to $Cu(\beta\text{-dik})_2$ in chloroform. The signals are attributed to the β-diketone liberated during the reaction of $Cu(\beta\text{-dik})_2$ with diazole. The enolic CH and OH signals are also observed in cases when the substituents are bulky and the solid substitution products are not isolated. For example, the system $Cu(dpm)_2$–Hpz shows the following signals: ($CDCl_3$) δ=1.2 (s, *t*-butyl), 4.3 (br, ring), 5.73 (s, CH), and 16 (br, OH), suggesting that pyrazole, in solution, is coordinated in the anionic form even to the $Cu(\beta\text{-dik})_2$ chelates with bulky alkyl group, liberating the β-diketone.

The reaction of $Cu(bzac)_2$ with equimolar pyrazole in cyclohexane gave a light green precipitate, which was shown to be a 1:1 addition complex, $Cu(bzac)_2$-(Hpz).[13] The product undergoes extremely slow breakdown on standing for several months to give measurable amounts of $Cu(bzac)_2$ and pyrazole. $Cu(bzac)_2$(Hpz) exhibits a rather broad band at 3310 cm^{-1} which has been assigned to ν(N–H), showing that pyrazole is present as the neutral ligand in this complex. An analogous addition complex is also obtained by reacting pyrazole with $Cu(tfac)_2$ in cyclohexane. The diffuse reflectance spectra of the pyrazole complexes are shown Fig. 1. $Cu(bzac)_2$(Hpz) has a broad maximum at 675 nm, while that of $Cu(tfac)_2$-(Hpz) is broader and somewhat split, with the maximum at >700 nm. In general, the addition of a nitrogen base to bis(β-diketonato)copper(II) causes a shift in the visible absorption maximum of the original copper chelate to a longer wavelength, when the base is coordinated at an apical position.[14,15]

The electronic absorption spectrum of the ternary system, $Cu(tfac)_2$–pyrazole–chloroform, showed two isosbestic points at 597 and 483 nm, when the amount of pyrazole was altered. $Cu(tfac)_2$(Hpz) was also obtained from this ternary system. This addition complex has an absorption maximum at 700 nm in chloroform. The addition complex $Cu(bzac)_2$(Hzp), however, behaves differently from $Cu(tfac)_2$(Hzp) in the same solvent, having an absorption maximum at 568 nm (Fig. 2). In this case, no isosbestic point was

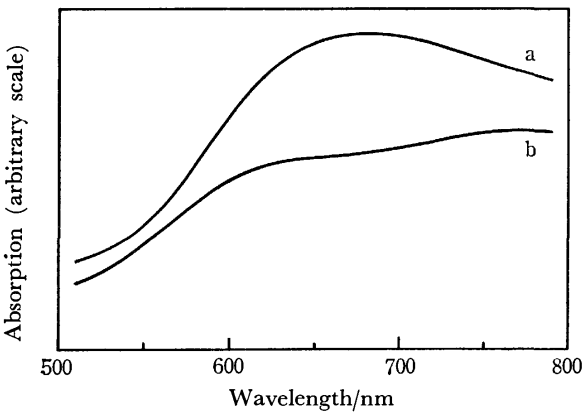

Fig. 1. The diffuse reflectance spectra of $Cu(bzac)_2$-(Hpz) (a) and $Cu(tfac)_2$(Hpz) (b).

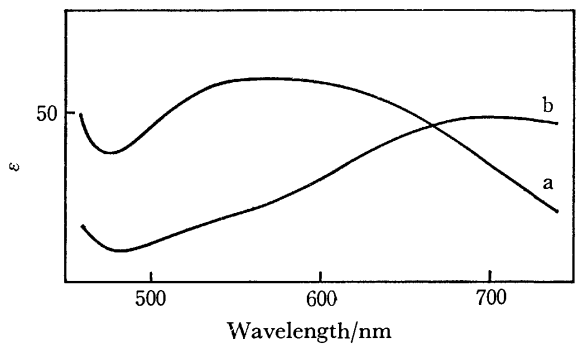

Fig. 2. The electronic spectra of $Cu(bzac)_2$(Hpz) (a) and $Cu(tfac)_2$(Hpz) (b) in chlorofrom.

observed with successive additions of pyrazole to a solution of $Cu(bzac)_2$. The spectral behavior suggests some structural change in the adduct, *e.g.* isomerization or partial dissociation, probably accompanied by apical-equatorial transfer of Hpz. Evaporation of chloroform, however, left a residue composed mainly of normal $Cu(bzac)_2(Hpz)$ and therefore the structural change in solution is apparently reversible.

As mentioned above, the adduct is obtained when the β-diketonato ligand is Hbzac and not when the ligands are aliphatic β-diketone. This suggests that the adduct $Cu(bzac)_2(Hpz)$ is more stable than the pyrazole adducts of bis(1,5-dialkyl-2,4-pentanedionato)-copper(II) chelates. This is in agreement with conclusions from the stability constants[15] of the $Cu(\beta\text{-dik})_2$(pyridine) and probably due to the contribution of phenyl group to the resonance stabilization of the adduct.[16]

Similarly, $Cu(tac)_2$ and $Cu(fac)_2$ formed stable 1:1 adducts with pyrazole. Equimolar quantities of pyrazole and either $Cu(tac)_2$ or $Cu(fac)_2$ were dissolved in dichloromethane. Evaporation of the solvent *in vacuo* left a green or light green residue, which was a 1:1 adduct of $Cu(tac)_2(Hpz)$ or $Cu(fac)_2(Hpz)$. The adducts lost pyrazole on standing for a long period in the atmosphere. The spectral data of the addition complexes are shown in Table 2, where it may be seen that the spectra are similar to that of $Cu(bzac)_2(Hpz)$, showing again characteristic absorption maxima at *ca.* 570 nm in solution.

The Imidazole Complexes. Using imidazole, 1:1 and 1:2 adducts of bis(fluorinated β-diketonato)copper-(II) have been isolated.[7] Those without fluorine substituents have, however, not been isolated because of their instability. An equimolar mixture of imidazole and $Cu(acac)_2$ in chloroform, when refluxed for 1 h, gave crystals which were isolated and shown to have a composition corresponding to Cu(acac)(im) by elemental analysis, IR and mass spectra. By the successive addition of imidazole to a solution of $Cu(acac)_2$ in chloroform, further displacement occurs. The product has not been identified, however. The displacement reaction in ethanol, however, gave Cu(acac)(im) exclusively. Consequently, $Cu(\beta\text{-dik})$(im) was prepared by the reaction of the bis(β-diketonato)copper-(II) complex with an excess of imidazole in ethanol. Characteristic data on the substitution complexes are given in Table 3.

Table 2. The electronic and IR spectra of the pyrazole adducts

Adduct	Electronic: Reflectance λ_{max}/nm	Electronic: In chloroform λ_{max}/nm	Electronic: In chloroform ε_a[a]	IR ν^{KBr}_{N-H}/cm^{-1}
$Cu(bzac)_2(Hpz)$	675	568	60	3310
$Cu(tac)_2(Hpz)$	673	567	56	3310
$Cu(fac)_2(Hpz)$	685	569	51	3300
$Cu(tfac)_2(Hpz)$	—	700	48[b]	3310

a) Apparent molar absorptivity. b) This value appears to correspond to the true molar absorptivity, since the addition complex is, probably, the only chemical species present in solution under the experimental conditions.

Cu(acac)(im) exhibits no N–H absorption band in the infrared spectra, and imidazole is shown to be present as the imidazolate anion. This complex has a magnetic moment of 1.59 BM which is less than the spin-only value of 1.73 BM for bivalent copper. The value of the magnetic moment is similar to that of a blue (1.57 BM) or a green (1.62 BM) modification of bis(imidazolato)copper(II).[17] The subnormal magnetic moment suggests the exsistence of spin interaction between the copper atoms through imidazole rings in the complex. The imidazolate anion thus acts as a bridging bidentate ligand linking two copper ions. Cu(acac)(im) was insoluble in ordinary solvents and is thus suspected to be polymeric, or tetranuclear as reported on a similar complex,[18] in structure rather than binuclear as in **1**.

The diffuse reflectance spectra of Cu(acac)(im) and **1** are shown in Fig. 3. The former complex has a maximum at 540 nm, while the latter has at 630 nm (Table 1). The binuclear complex $Cu_2(acac)_2(pz)_2$

Table 3. Characteristic data on the imidazolato complexes

Complex	Color	Found (Calcd) (%) C	H	N	Diffuse reflectance spectra λ_{max}/nm
Cu(acac)(im)	violet	41.74 (41.83)	4.41 (4.39)	12.28 (12.19)	540
Cu(dprm)(im)	purple	46.37 (46.59)	5.49 (5.47)	10.88 (10.87)	542
Cu(dnbm)(im)	black	50.36 (50.43)	6.22 (6.35)	9.65 (9.80)	563
Cu(dibm)(im)	dark blue	50.53 (50.43)	6.56 (6.35)	9.68 (9.80)	580
Cu(dpm)(im)	dark blue	53.38 (53.57)	7.07 (7.06)	8.91 (8.92)	554
Cu(bzac)(im)	dark green	53.50 (53.51)	4.12 (4.15)	9.52 (9.60)	572
Cu(tac)(im)	dark green	44.27 (44.36)	3.26 (3.38)	9.10 (9.41)	574
Cu(fac)(im)	gray	47.22 (46.89)	3.67 (3.58)	9.83 (9.94)	559

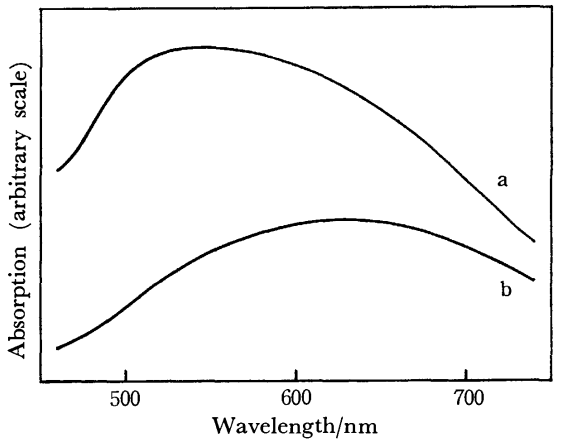

Fig. 3. The diffuse reflectance spectra of Cu(acac)(im) (a) and $Cu_2(acac)_2(pz)_2$ (b).

was assumed to take a square-planar configuration.[11] The electronic spectra in Fig. 3 show that the coordination around the copper atom of the imidazolato complex is clearly different from that of the pyrazolato complex. Square-planar coordination around each copper atom with a coplanar arrangement of the two imidazole rings and one 2,4-pentanedionato ligand appears sterically difficult, and the coordination around the copper atom may be considerably distorted from square-planar towards a tetrahedral. The similarity of the spectra in the series of Cu(β-dik)(im) suggests similar structures. The spectra in chloroform solutions[19] (Fig. 4) are also similar to the corresponding solid spectra, so the arrangement of the ligands around the copper(II) ions in such solutions is assumed to be analogous to that in the solid complexes.

The reaction of $Cu(tfac)_2$ with diazoles gave the diazole adducts, and did not yield the μ-diazolato complexes under the experimental conditions described above. The introduction of a CF_3 group into β-diketone greatly increases the stability of Lewis base adducts of the chelates,[16,20] making it difficult to transform to the μ-diazolato complexes. 2-Methylimidazole and 3-methylpyrazole exclusively form addition

TABLE 4. PRODUCTS OF THE REACTION OF $Cu(RCOCHCOR')_2$ WITH NITROGEN BASES

Substituent		Base			
		Pyrazole		Imidazole	
R	R′	Path	Product	Path	Product
CH_3	CH_3	(b)	binuclear	(b)	polynuclear
C_2H_5	C_2H_5	(b)	binuclear	(b)	polynuclear
n-C_3H_7	n-C_3H_7	(b)	binuclear	(b)	polynuclear
i-C_3H_7	i-C_3H_7	(b)	(substitution)[a]	(b)	polynuclear
t-C_4H_9	t-C_4H_9	(b)	(substitution)[a]	(b)	polynuclear
C_6H_5	CH_3	(a)	1:1 adduct	(b)	polynuclear
C_4H_3S	CH_3	(a)	1:1 adduct	(b)	polynuclear
C_4H_3O	CH_3	(a)	1:1 adduct	(b)	polynuclear
CF_3	CH_3	(a)	1:1 adduct	(a)	1:1 and 1:2 adducts[b]

a) Reaction was found to proceed in solution. No solid product was isolated, however. b) Ref. 7.

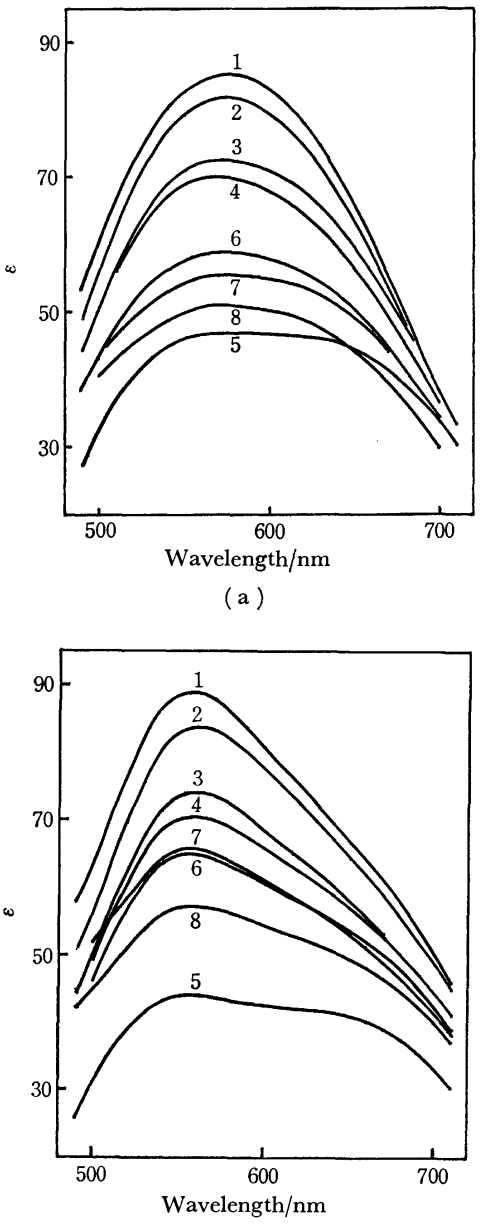

Fig. 4. The electronic spectra of $Cu(\beta\text{-dik})_2$–pyrazole (4a) and $Cu(\beta\text{-dik})_2$–imidazole (4b) complexes in chloroform: $Cu(\beta\text{-dik})_2$ chelates are (1), $Cu(dpm)_2$; (2), $Cu(dibm)_2$; (3), $Cu(dnbm)_2$; (4), $Cu(dprm)_2$; (5), $Cu(acac)_2$; (6), $Cu(bzac)_2$; (7), $Cu(tac)_2$; (8), $Cu(fac)_2$.

complexes when reacted with $Cu(bzac)_2$. In these cases, the isomerization and the formation of substitution complex are prevented probably by steric hindrance.

In conclusion, the reactions of $Cu(\beta\text{-dik})_2$ with diazoles proceed differently depending upon the nature of the substitutions on the β-diketonato ligands and also on the nature of nitrogen bases. The investigated nitrogen bases (pyrazole and imidazole) have both pyridine-like and imino nitrogen atoms in the same molecule, which enable them to react through two alternate paths here referred to as the addition and substitution reactions (Scheme 1). In the case of a

fluorinated β-diketonato ligand, the addition complex is favored irrespective to the nature of the nitrogen base. The substitution complex is always produced, on the contrary, when the β-diketone is aliphatic. The structures of the complexes appear to be different, however, depending on the nature of the bases in cases when aroyl- or hetaroylacetonato chelates are allowed to react. Addition complexes are obtained from pyrazole and substitution complexes from imidazole (Table 4). The greater ease of formation of the addition complexes in the former cases may be due to the π-donating power of the neighboring imino group in pyrazole.[16)]

The authors are grateful to Mr. Katsuo Hara of Yokohama National University for the measurement of ^{1}H-NMR spectra.

References

1) D. P. Graddon, *Coord. Chem. Rev.*, **4**, 1 (1969).
2) T. Kurauchi, M. Matsui, Y. Nakamura, S. Ooi, S. Kawaguchi, and H. Kuroya, *Bull. Chem. Soc. Jpn.*, **47**, 3049 (1974).
3) M. V. Veidis, G. H. Schreiber, T. E. Gough, and G. J. Palenik, *J. Am. Chem. Soc.*, **91**, 1859 (1969).
4) R. C. E. Belford, D. E. Fenton, and M. R. Truter, *J. Chem. Soc., Dalton Trans.*, **1974**, 17.
5) H. W. Richardson, J. R. Wasson, and W. E. Hatfield, *Inorg. Chem.*, **16**, 484 (1977).
6) D. E. Fenton, R. S. Nyholm, and M. R. Truter, *J. Chem. Soc., A*, **1971**, 1577.
7) J. T. Chen and S. M. Wang, *J. Chin. Chem. Soc.*, **18**, 213 (1971).
8) S. M. Wang and J. T. Chen, *J. Chin. Chem. Soc.*, **22**, 179 (1975).
9) S. Trofimenko, *Chem. Rev.*, **72**, 497 (1972).
10) R. J. Sundberg and R. B. Martin, *Chem. Rev.*, **74**, 471 (1974).
11) C. G. Barraclough, R. W. Brookes, and R. L. Martin, *Aust. J. Chem.*, **27**, 1843 (1974).
12) Hereafter diazole and β-diketone are abbreviated as Hdzl and Hβ-dik, respectively. Hβ-dik is used to designate non-fluorinated β-diketones in this report.
13) When the same reaction was conducted in chloroform, the reaction proceeds only partly and a mixture of the addition product and the starting materials was obtained.
14) R. L. Belford, M. Calvin, and G. Belford, *J. Chem. Phys.*, **26**, 1165 (1957).
15) D. P. Graddon and E. C. Watton, *J. Inorg. Nucl. Chem.*, **21**, 49 (1961).
16) K. Ueda, *Bull. Chem. Soc. Jpn.*, **51**, 805 (1978).
17) M. Inoue, M. Kishita, and M. Kubo, *Bull. Chem. Soc. Jpn.*, **39**, 1352 (1966).
18) G. Kolks, C. R. Frihart, H. N. Rabinowitz, and S. J. Lippard, *J. Am. Chem. Soc.*, **98**, 5720 (1976).
19) Since the polymeric solid of Cu(β-dik)(im) is sparingly soluble in chloroform, the spectra were obtained with 1:1 mixtures of $Cu(\beta\text{-dik})_2$ and imidazole. The spectra did not change in the course of polymerization and final deposition of the solid. The differences in the solubilities of these complexes may thus be ascribed to the differences in the degree of polymerization in the solids.
20) D. P. Graddon and W. K. Ong, *Aust. J. Chem.*, **27**, 741 (1974).

Syntheses and Magnetic Properties of Three Modifications of Dichloro[2-(hydroxymethyl)pyridine *N*-oxide]copper(II)

Yoneichiro Muto,* Tadashi Tokii, Michio Nakashima,
Michinobu Kato,† and Hans B. Jonassen††

Department of Chemistry, Faculty of Science and Engineering, Saga University, Saga 840
†*Aichi Prefectural University, Mizuho-ku, Nagoya 467*
††*Department of Chemistry, Tulane University, New Orleans, Louisiana, U. S. A.*

(Received June 4, 1979)

Three modifications of dichloro[2-(hydroxymethyl)pyridine *N*-oxide]copper(II), $CuCl_2(2\text{-}CH_2OH\cdot pyo)$, were prepared and characterized by the temperature dependences of their magnetic susceptibilities and their IR spectra. The greenish-yellow modification shows ferromagnetic behavior (θ/K = +20), whereas both the yellow and deep-green modifications exhibit a dimer type of antiferromagnetism ($J/cm^{-1} = -585$ and -565). The hemi adducts with the empirical formula of $CuCl_2(2\text{-}CH_2OH\cdot pyo)\cdot 1/2L$, where $L = C_2H_5OH$ and H_2O, were also isolated. The structural assignments for the three modifications and the two adducts were made on the basis of the similarity of their magnetic and spectral properties to those of dimeric copper(II) pyridine *N*-oxide complexes, and the whole preparative scheme of these complexes was interpreted in terms of their structural features.

In a previous study of copper(II) halide complexes with substituted pyridine *N*-oxides,[1] we found that dichloro[2-(hydroxymethyl)pyridine *N*-oxide]copper-(II), $CuCl_2(2\text{-}CH_2OH\cdot pyo)$,[2] formed two magnetically different modifications: a greenish-yellow modification with a normal magnetic moment at room temperature and a yellow one with a subnormal moment. The normal moment is unusual, since many 1:1 complexes of copper(II) chloride with substituted pyridine *N*-oxides, including 3-and 4-(hydroxymethyl)pyridine *N*-oxides, exhibit antiferromagnetic interaction between the copper ions.[1]

This study was initiated in order to investigate the factors which cause such a difference in the magnetic properties. We have now prepared another modification and its hemi adducts with ethanol or water. A complex with the empirical formula of $Cu(2\text{-}CH_2OH\cdot pyo)_2(ClO_4)_2$ has also been prepared to help the investigation of the structural differences among the three modifications. We wish to report here the results of our preparative, IR spectral, and cryomagnetic studies of these complexes.

Results and Discussion

Preparation Scheme. The preparation scheme of the complexes studied in this work is shown diagrammatically in Fig. 1, together with the colors and the room-temperature magnetic moments. Compound **1** was easily converted into **2** either by keeping it over calcium chloride in a vacuum desiccator at room temperature for about one month[1] or by recrystallizing it from 1-butanol. On the other hand, attempts to convert **2** into **1** were unsuccessful. Compound **5** was readily converted into the hydrated form, **4**, on standing in the air at room temperature, whereas **1** and

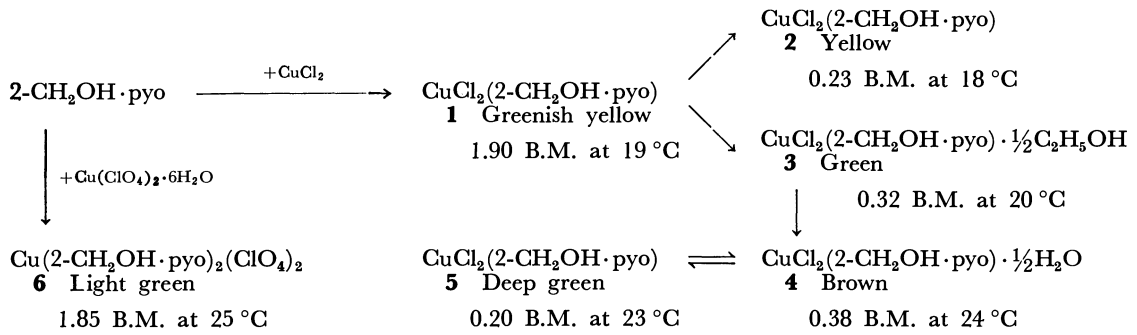

Fig. 1. Preparation scheme of complexes.

Table 1. Analytical data

	Complex	Found (%)				Calcd (%)			
		C	H	N	Cu	C	H	N	Cu
1	$CuCl_2(2\text{-}CH_2OH\cdot pyo)$	27.73	2.81	5.42	24.54	27.76	2.72	5.40	24.48
2	$CuCl_2(2\text{-}CH_2OH\cdot pyo)$	27.66	2.72	5.30	24.48	27.76	2.72	5.40	24.48
3	$CuCl_2(2\text{-}CH_2OH\cdot pyo)\cdot \frac{1}{2}C_2H_5OH$	27.72	2.66	5.45	22.46	29.75	3.57	4.96	22.48
4	$CuCl_2(2\text{-}CH_2OH\cdot pyo)\cdot \frac{1}{2}H_2O$	26.84	2.96	5.15	23.65	26.83	3.00	5.22	23.66
5	$CuCl_2(2\text{-}CH_2OH\cdot pyo)$	27.58	2.66	5.33	24.64	27.76	2.72	5.40	24.48
6	$Cu(2\text{-}CH_2OH\cdot pyo)_2(ClO_4)_2$	27.83	2.69	5.29	12.46	28.11	2.75	5.46	12.39

2 do not form such a hydrate under the same conditions.

In contrast with 2-(hydroxymethyl)pyridine *N*-oxide, 3- and 4-(hydroxymethyl)pyridine *N*-oxides form only one kind of 1:1 complex with copper(II) chloride; these complexes show subnormal magnetic moments.[1] This difference in the formation of 1:1 complexes may be due to the different ligand natures of the oxides: 2-(hydroxymethyl)pyridine *N*-oxide may coordinate to a metal ion by both the *N*-oxide and alcohol oxygens to form a six-membered chelate ring, whereas 3- and 4-(hydroxymethyl)pyridine *N*-oxides are not able to form such a chelate. This was confirmed by the observation that 2-(hydroxymethyl)pyridine *N*-oxide forms a 2:1 complex with copper(II) perchlorate (Compound **6**), unlike other aromatic amine *N*-oxides, which generally form 4:1 or 6:1 complexes with copper(II) perchlorate.[1,3-5]

The ethanol adduct, **3**, readily loses its ethanol and absorbs water in the air to give Compound **4**. As a consequence, the analytical data of carbon, nitrogen, and hydrogen for this compound were unsatisfactory. However, the copper analysis carried out immediately after the preparation indicated the formulation of **3**; the weight loss after the sample had stood in the air for 24 h at room temperature also agreed with that calculated on the basis of the structural change from **3** to **4** (*cf.* Table 1).

IR Spectra. The IR spectra of Compounds **1**, **2**, **4**, **5**, and **6** were measured in order to obtain information about the coordination mode of $2\text{-}CH_2OH\cdot pyo$ in these complexes. The IR frequencies pertaining to the alcohol- and *N*-oxide-oxygen atoms may be correlated with the geometric structures of the complexes and with the strength in the oxygen–metal coordination bond. The results for the O–H stretching vibration (νO–H), the N–O stretching vibration (νN–O), and the N–O bending vibration (δN–O) are shown in Fig. 2. For comparison, Fig. 2 also includes the IR spectrum of the copper(II) chloride complex with 2-ethylpyridine *N*-oxide, $CuCl_2(2\text{-}C_2H_5\cdot pyo)$, to which an oxygen-bridged binuclear structure has been assigned.[1]

These complexes can be classified into two groups based on the observed IR spectra and their magnetic moments: A) Compounds **2**, **4**, and **5**, which show subnormal magnetic moments, and B) Compounds **1** and **6**, which exhibit normal moments.

νO–H: In each of the complexes the strong band observed in the 3100—3500 cm^{-1} region may be assigned to the O–H stretching vibration of the CH_2OH group.[6,7] In support of this assignment, no band is observed in this region for the $CuCl_2(2\text{-}C_2H_5\cdot pyo)$ complex(*cf.* Fig. 2). There is a significant difference in the band position between the A and B groups; *i.e.*, the B compounds show the band at a frequency of less than 3300 cm^{-1}, whereas the A compounds exhibit it at *ca.* 3400 cm^{-1}(*cf.* Fig. 2). This fact suggests that the coordination mode of the OH group in the Group A complexes differs from that in the Group B complexes. The other band, at 3500 cm^{-1} in Compound **4**, may be due to the O–H stretching vibration of the water in this compound, because this band is absent in the spectrum of the anhydrous compound, **5**.

νN–O and δN–O: In the spectra of dimeric copper-

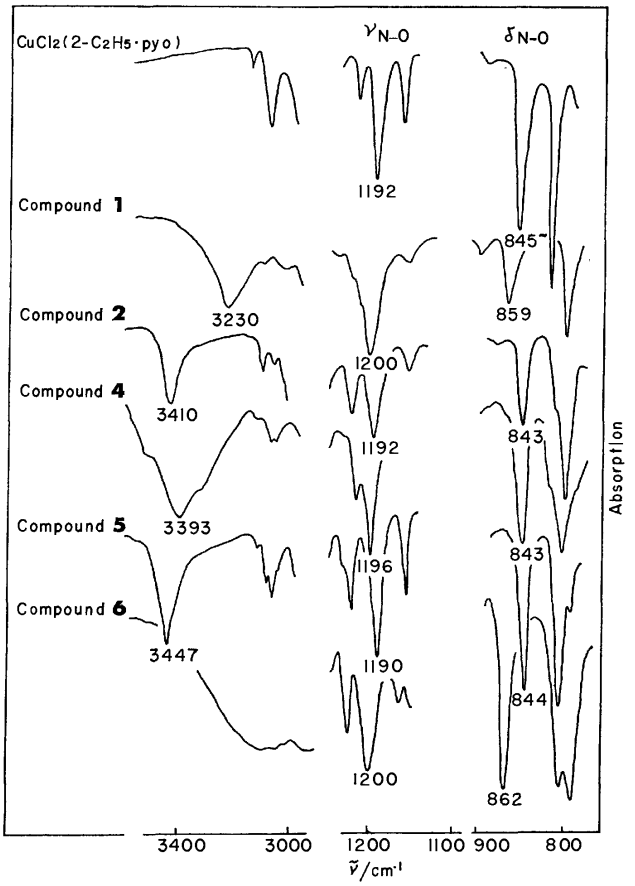

Fig. 2. IR spectra of complexes.

(II) halide complexes with aromatic amine *N*-oxides, a strong and sharp band at *ca.* 1200 cm^{-1} was assigned to the stretching vibration of the N–O group bridging two copper ions by the oxygen atom.[8,9] The present complexes exhibit the N–O band at 1190—1200 cm^{-1}. Figure 2 shows that the band frequencies in the Group A compounds (1190—1196 cm^{-1}) are lower than those in the Group B componds (1200 cm^{-1}). The lowering of νN–O is possibly due to a decrease in the N–O double-bond character,[9,10] resulting from stronger Cu–O–Cu bridging bonds formation for the A complexes than for the B complexes. The same trend was observed in the frequencies of the δN–O band of these complexes in the region of 840—860 cm^{-1}(*cf.* Fig. 2):[8] the band appeared at *ca.* 843 cm^{-1} for the A complexes and at *ca.* 860 cm^{-1} for the B complexes.

The IR spectrum of Compound **6** shows a broad and strong band around 1100 cm^{-1}, indicating the presence of an uncoordinated perchlorate ion.

For Compound **3**, accurate IR measurements could not be carried out because of its instability in the air.

Magnetic Susceptibility. The magnetic susceptibilities of Compounds **1**—**6** were measured in the temperature range of 80—300 K; the results are shown in Figs. 3 and 4. Their room-temperature magnetic moments, given in Fig. 1, were calculated from this expression:

$$\mu_{eff} = 2.83\sqrt{(\chi_A - N\alpha)\cdot T} \qquad (1)$$

where χ_A is the molar magnetic susceptibility corrected

for the diamagnetism of the constituted atoms using Pascal's constants (2-CH_2OH·pyo, −70; C_2H_5OH, −34; H_2O, −13; Cu^{2+}, −11; Cl^-, −26; ClO^-_4, −34 in 10^{-6} cgs emu mol^{-1})[11] and, where $N\alpha$ is the temperature-independent paramagnetism per gram-ion of copper(II).** The $N\alpha$ values for Compounds **2**, **3**, **4**, and **5** were obtained from the analyses of their χ_A *vs.* T data (see below). For the other compounds, $N\alpha$ was assumed to be 60×10^{-6} cgs emu.[12]

The susceptibility data of Compound **1** follow the Curie-Weiss law in the temperature range studied(*cf.* Fig. 3). The positive Weiss constant, $\theta/K=+20$, estimated from the slope of the $(\chi_A-N\alpha)^{-1}$ *vs.* T plots, indicates the existence of a ferromagnetic interaction between the copper ions in this complex.

The susceptibilities of Compounds **2**—**5** over the temperature range are very low(*cf.* Fig. 4), indicating the existence of a very strong antiferromagnetic interaction in these complexes. Their cryomagnetic data are represented by the Bleaney-Bowers equation 2[13] for isotropic exchange in a copper(II) dimer (*cf.* Fig. 4):

$$\chi_A=\frac{N\beta^2g^2}{3kT}\left[1+\frac{1}{3}\exp\frac{-2J}{kT}\right]^{-1}(1-P)+\frac{N\beta^2g_1^2}{4kT}\cdot P+N\alpha \qquad (2)$$

where N is Avogadro's number, g is the average g factor of the binuclear complex, β is the Bohr magneton, k is the Boltzmann constant, J is the exchange integral, P is the mole fraction of the noncoupled Cu(II) impurity, and g_1 is the average g factor for the impurity. The second term in Eq. 2 was added to account for the presence of the small amount of a paramagnetic impurity, which was assumed to obey the Curie law.

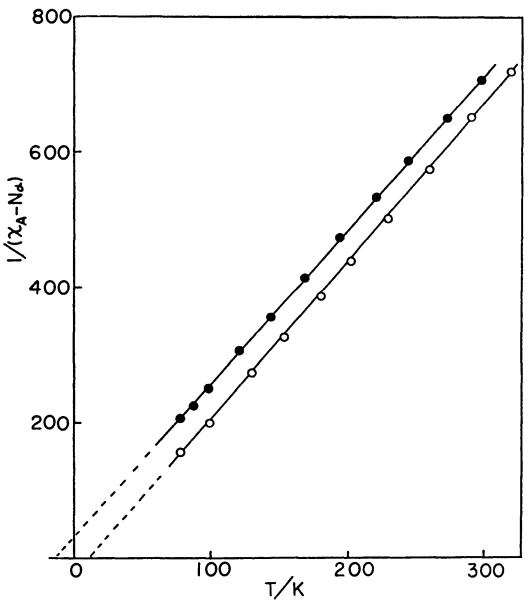

Fig. 3. Variation of reciprocal magnetic susceptibilities with temperature. ○=Compound **1**, ●=Compound **6**.

** The value of the molar magnetic susceptibility in m^3 mol^{-1} (SI) can be obtained by multiplying the value in cm^3 mol^{-1} (cgs) by $4\pi\times10^{-6}$.

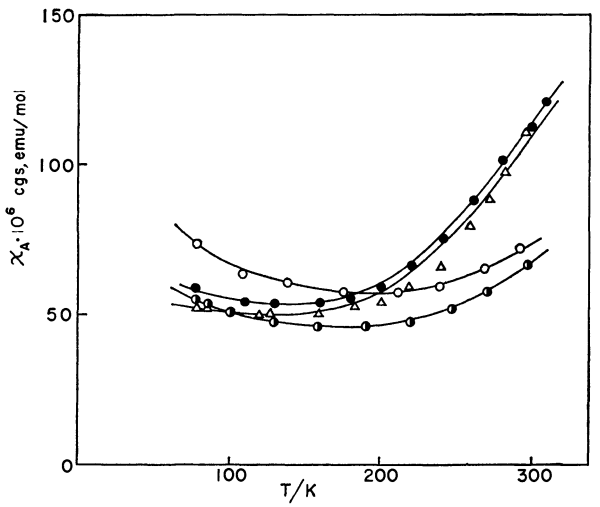

Fig. 4. Temperature dependence of magnetic susceptibilities of (○) Compound **2**, (●) Compound **3**, (△) Compound **4**, and (◑) Compound **5**.
The solid curves were calculated from Eq. 2 using the parameters listed in Table 2.

The J, $N\alpha$, and P values listed in Table 2 were estimated from the best fit of their cryomagnetic data to Eq. 2, assuming $g=g_1=2.20$. It is noteworthy that the values of $N\alpha(37\times10^{-6}$—46×10^{-6} cgs emu) are much smaller than that generally accepted in published works (60×10^{-6} cgs emu). However, it should also be pointed out that the magnitude of $N\alpha$ is dependent on the ligand-field strength, the stereochemistry around the metal ion, and the covalency of the bond between the metal ion and the ligand. The similarity of the magnetic properties of these complexes to those of a number of 1:1 aromatic amine *N*-oxide copper(II) halide complexes indicates that they are composed of binuclear structural units in crystals similar to that of dichloro(pyridine *N*-oxide)copper(II), $CuCl_2$(pyo).[14,15]

The χ_A *vs.* T data of Compound **6** follow the Curie-Weiss law with a small value of the Weiss constant, $\theta/K=-5$(*cf.* Fig. 3), indicating the absence of any appreciable antiferromagnetic interaction in this compound. It is thus probable that Compound **6** is composed of the monomeric structural units shown in (6). The IR spectral data are also consistent with this assignment.

Structure and Magnetism. On the basis of the experimental results and discussions described in the preceding sections, structural assignments for the three modifications(Compounds **1**, **2**, and **5**) may be made as follows. The most probable structure for Compound **1** is either (1) in which the monomeric $CuCl_2$(2-CH_2-OH·pyo) units are bridged by the Cu–O out-of-plane bonds or (2) in which the copper ions are bridged with chloride ions from the adjacent monomer moieties. The possible structures for both Compounds **2** and **5** are either (3) in which the pyridine rings are nearly perpendicular to the plane, in a manner similar to that in the $CuCl_2$(pyo) complex[14,15] or (4) in which the rings are parallel to the coordination

Table 2. Magnetic parameters

		J/cm^{-1}	$N\alpha$/cgs emu	P/mol
2	$CuCl_2(2\text{-}CH_2OH\cdot pyo)$	−585	44×10^{-6}	5×10^{-3}
3	$CuCl_2(2\text{-}CH_2OH\cdot pyo)\cdot\frac{1}{2}C_2H_5OH$	−470	46×10^{-6}	2×10^{-3}
4	$CuCl_2(2\text{-}CH_2OH\cdot pyo)\cdot\frac{1}{2}H_2O$	−475	46×10^{-6}	1×10^{-3}
5	$CuCl_2(2\text{-}CH_2OH\cdot pyo)$	−565	37×10^{-6}	3×10^{-3}

plane. However, a binuclear structure bridging copper ions with chloride ions is very unlikely for both Compounds **2** and **5**, since dimeric or polymeric copper(II) complexes containing a chloride bridge do not show any strong antiferromagnetism.[16,17] For Compound **1**, consequently, Structure (1) is considered to be more probable than (2), based on the ready conversion of **1** into **2**: the structural change from (1) to (3) or (4) is accompanied by no breaking of chemical bonds, while the change from (2) to (3) or (4) require a breaking and recombination of the coordinate bonds; thus, the former process may take place more easily than the latter. The ferromagnetism observed in Compound **1** may, therefore, be explained, as in the case

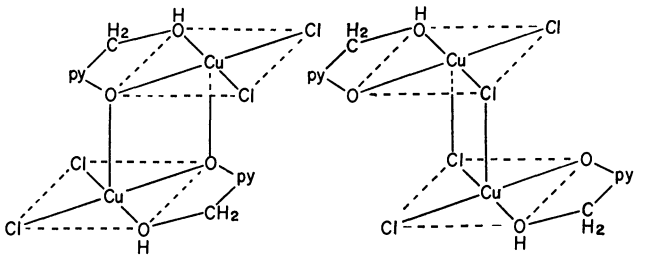

(1) (2)

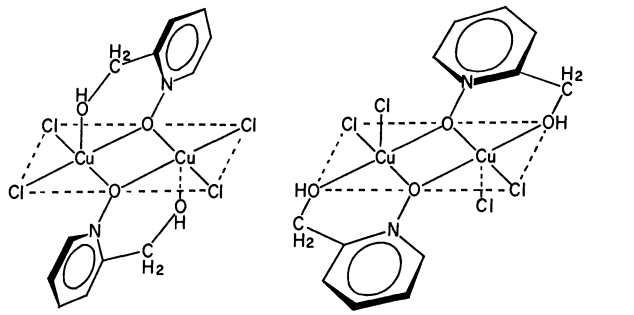

(3) (4)

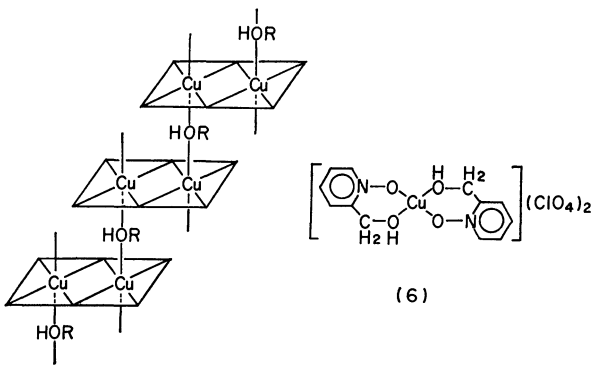

R=H or C_2H_5

(5)

(6)

of $[Cu(NO_3)_2(pyo)_2]_2$,[18] in terms of the 90° cation-anion-cation type of superexchange interaction discussed by Goodenough[19] and Kanamori.[20] The pathway is given by Ginsbergs' notation[21] as follows:

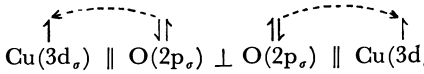

$Cu(3d_\sigma) \parallel O(2p_\sigma) \perp O(2p_\sigma) \parallel Cu(3d_\sigma)$

where $\parallel$ and $\perp$ indicate spin parallel and antiparallel interactions through orbitals in non-orthogonality and orthogonality respectively and, where the dashed arrows indicate partial electron transfer through the overlapping orbitals. The scheme represents the simultaneous partial electron transfer from a bridging oxygen atom to the pair of copper ions and the successive intra-atomic spin coupling on the oxygen atom. On the other hand, unambiguous structural assignments for Compounds **2** and **5** to either (3) or (4) are not possible on the basis of the present IR and magnetic data. However, the strong antiferromagnetism observed in these complexes may be interpreted on the basis of structure (3) or (4) in essentially the same manner as in the case of $CuCl_2(pyo)$, where we have previously emphasized the σ-type exchange pathway of $Cu(3d_\sigma)$-$O(2p_\sigma)$-$Cu(3d_\sigma)$.[1]

The bridging structure of the adducts, **3** and **4**, is considered to be essentially the same as that of the non-adducts with low magnetic moments, judging from their very similar magnetic behavior and the easy interconversion between Compounds **4** and **5**(*cf.* Fig. 1). The easy conversion of the ethanol adduct to the water adduct in the air suggests that the frameworks of the structures of the two compounds are the same; the adding molecules occupy the same position in each structure. The polymeric structure of type (5) can explain all these facts consistently since (a) this structure requires the one-adding-molecule—one-dimer relation, *i.e.*, the formation of hemi adducts, and (b) a water molecule of a higher coordinating ability replaces an ethanol molecule of a lower coordinating ability at the same coordination site of a dimer without destroying the framework of the whole polymeric structure. The **3** and **4** adducts exhibit a definitely weaker antiferromagnetic interaction than the two non-adducts, **2** and **5**, perhaps because the formation of an additional coordinate bond by a ligand at the fifth or sixth coordination site of Cu(II) weakens the in-plane coordinate bonds through which the spin coupling takes place, leading to a weaker antiferromagnetic interaction.

Experimental

Syntheses. *Compound 1*: A solution of $CuCl_2$ (1.57 g, 11 mmol) in ethanol (50 ml) was added to a solution of 2-

CH_2OH·pyo (1.25 g, 10 mmol) in ethanol (50 ml). The mixed solution was stirred at *ca.* 70 °C for 1/2 h. The greenish-yellow microcrystals thus produced were filtered off, washed with ethanol, and dried at 70—80 °C.

Compound **2**: This was obtained by recrystallizing compound **1** from 1-butanol.

Compound **3**: A solution of Compound **1** (1 g) in ethanol (500 ml) was allowed to stand for several days at *ca.* 5 °C in a freezer. After this period, green crystals were produced. The crystals separated were washed with ethanol and dried in a vacuum desiccator over calcium chloride at room temperature.

Compound **4**: This was obtained when Compound **3** was allowed to stand overnight in the air.

Compound **5**: This was obtained when the hydrate complex **4** was dehydrated in a vacuum desiccator at 70 °C over phosphorus pentaoxide.

Compound **6**: A solution of $Cu(ClO_4)_2 \cdot 6H_2O$ (1.08 g, 3 mmol) in ethanol (30 ml) was added to a solution of 2-CH_2OH·pyo (0.75 g, 6 mmol) in ethanol (30 ml). After the mixed solution has been concentrated to a third of its volume, it was allowed to stand for few days at *ca.* 5 °C in a freezer. The green crystals thus precipitated were collected, washed twice with a small quantity of ethanol and once with ether, and dried at *ca.* 70 °C.

The results of the elemental analyses are given in Table 1.

Physical Measurements. The IR spectral measurements were made with a Hitachi EPI-G2 spectrophotometer in 400—4000 cm^{-1} region on Nujol mulls. The magnetic susceptibilities in the temperature range of 80—300 K were determined by the Gouy method for Compounds **1**, **2**, **4**, **5**, and **6** and by the Faraday method for Compound **3**.

References

1) Y. Muto, M. Kato, H. B. Jonassen, and L. C. Cusachs, *Bull. Chem. Soc. Jpn.*, **42**, 417 (1969).

2) ·pyo is used as abbreviation for the C_5H_4NO group, and pyo, for unsubstituted pyridine *N*-oxide.

3) R. L. Carlin, *J. Am. Chem. Soc.*, **83**, 3773 (1967).

4) R. Whyman, W. E. Hatfield, and J. S. Paschal, *Inorg. Chim. Acta*, **1**, 113 (1967).

5) Recently, Okawa *et al.* reported the preparation of $Cu(2\text{-}CH_2OH\text{·pyo})_n(ClO_4)_2$ (n=2 and 4): H. Okawa, H. Matsubara, T. Higuchi, and S. Kida, *Memoirs of the Faculty of Science, Kyushu University, Series C, Chemistry*, **9**, 223 (1975).

6) D. Knetsch and W. L. Croeneveld, *Inorg. Chim. Acta*, **7**, 81 (1973).

7) J. O. Miners and E. Sinn, *Bull. Chem. Soc. Jpn.*, **46**, 1457 (1973).

8) S. Kida, J. V. Quagliano, J. A. Walmsley, and S. Y. Tyree, *Spectrochim. Acta*, **19**, 189 (1963).

9) Y. Muto and H. B. Jonassen, *Bull. Chem. Soc. Jpn.*, **39**, 58 (1966).

10) W. E. Hatfield, Y. Muto, H. B. Jonassen, and J. S. Paschal, *Inorg. Chem.*, **4**, 97 (1965).

11) P. W. Selwood, "Magnetochemistry," Interscience Publishers, New York (1956), pp. 78, 91.

12) B. N. Figgis and R. L. Martin, *J. Chem. Soc.*, **1959**, 1359.

13) B. Bleaney and K. D. Bowers, *Proc. R. Soc. London, Ser. A*, **214**, 451 (1952).

14) H. L. Schafer, J. C. Morrow, and H. M. Smith, *J. Chem. Phys.*, **42**, 504 (1965).

15) R. S. Sager, R. J. Williams, and W. H. Watson, *Inorg. Chem.*, **6**, 951 (1967).

16) R. D. Willet, C. Dwiggins, Jr., R. F. Kruh, and R. E. Rundle, *J. Chem. Phys.*, **38**, 2429 (1963).

17) M. Kato, H. B. Jonassen, and J. C. Fanning, *Chem. Rev.*, **64**, 99 (1964).

18) W. E. Hatfield, J. A. Barnes, D. Y. Jeter, R. Whyman, and E. R. Jones, Jr., *J. Am. Chem. Soc.*, **92**, 4982 (1970).

19) J. B. Goodenough, "Magnetism and the Chemical Bond," Interscience Publishers, New York (1963), p. 180.

20) J. Kanamori, *J. Phys. Chem. Solids*, **10**, 87 (1959).

21) A. P. Ginsberg, *Inorg. Chem. Acta Rev.*, **5**, 45 (1971).

The Proton-transfer Reactions of the Univalent Anions of *ortho*-Hydroxy Azo Compounds in Dioxane–Water Media†

Noboru YOSHIDA and Masatoshi FUJIMOTO*

Department of Chemistry, Faculty of Science, Hokkaido University, Sapporo 060

(Received June 13, 1979)

The proton-transfer reactions of the univalent anions of 4-(2-pyridylazo)resorcinol (PAR) and 4-(2-hydroxy-5-ethylphenylazo)benzenesulfonic acid (HEB) with hydroxide ion in dioxane–water media, $HA^- + OH^- \underset{k_r}{\overset{k_f}{\rightleftharpoons}} A^{2-} + H_2O$, were studied by means of temperature-jump method. The dependencies of the rate constants, k_f and k_r, on the solvent compositions were interpreted by a mechanism involving the breaking of an intramolecular hydrogen-bond.

In the previous papers we reported the proton-transfer reactions in mixed solvents of some anionic ortho-hydroxy azo compounds having a strong intramolecular hydrogen-bond.[1,2] These studies have brought us some important informations for the elucidation of mechanisms of proton-transfer reactions of these compounds in aqueous and/or in non-aqueous systems.

Recently Jost *et al.*[3] extensively studied the pressure effects on the proton-transfer reaction of 4-(*p*-nitrophenylazo)resorcinol (MAG) in aqueous solution; they gave the values of activation volumes, $\Delta\vec{V}^* = -(3.9 \pm 0.5)$ cm^3 mol^{-1} and $\Delta\overleftarrow{V}^* = -(3.1 \pm 1)$ cm^3 mol^{-1} for the forward and the backward reaction, respectively, and supported a mechanism involving the breaking of the intramolecular hydrogen-bond which will be discussed here.

In the present paper we studied the proton-transfer reactions between OH^- ion and the uninegative Brønsted acids, a slightly water-soluble acid PAR and a water-soluble acid HEB, in dioxane–water media by a temperature-jump method in order to clarify the difference of the behavior observed for PAR and HEB of the same charge-type. For kinetics of the proton-transfer reactions in dioxane–water media, the definite difference depending on the water-solubility of the reactant was observed. Although PAR and HEB behave as univalent anions, the dependence of the forward rate constant of PAR on the dielectric constant is considerably different from that of HEB.

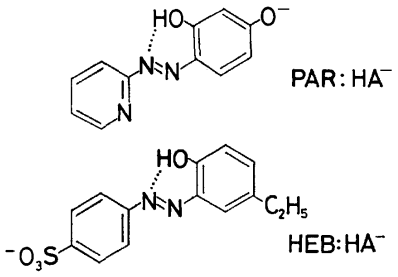

Experimental

Measurements. Kinetic measurements were carried out at 25 °C and $I = 0.1$ mol dm^{-3} (KNO_3) with a Union Giken co-axial-cable temperature-jump apparatus Model RA-105 equipped with a pressurizing apparatus. The relaxation signal was recorded using a Tektronix oscilloscope Type 545B. The absorption spectra were measured with a Hitachi recording spectrophotometer Model EPS-3T. The pH-measurements in dioxane-water media were reported in a previous paper.[1]

Materials. Water was deionized and distilled. Dioxane was distilled and used without further purification. PAR was synthesized according to the literature[4] and recrystallized from hot ethanol–water. The purity was confirmed by elemental analysis. HEB was synthesized by the azo-coupling of *p*-ethylphenol and sulfanilic acid, and recrystallized from hot ethanol-water. Found: C, 49.31; H, 4.15; N, 8.18; S, 9.74; Na, 6.03%. Calcd for $C_{14}H_{13}N_2O_4SNa \cdot 0.5H_2O$: C, 49.85; H, 4.18; N, 8.30; S, 9.50; Na, 6.82%. Stock solutions of the dyes were prepared by dissolving a desired amount in water.

Results and Discussion

The overall equilibrium for the acid dissociation of the univalent anions of HEB and PAR, HA^-, is represented as follows:

$$HA^- \overset{K_a^c(s)}{\rightleftharpoons} A^{2-} + H^+. \quad (1)$$

The acid-dissociation constant, $K_a^c(s)$, is determined from the pH-dependence of the absorbance of HEB and PAR in solutions.[1] The values of $K_a^c(s)$ for HEB and PAR in various dioxane-contents are summarized in Table 1. The changes in the values of $pK_a^c(s)$ for

Table 1. Acid-dissociation constants for the reaction of PAR and HEB, $HA^- \rightleftharpoons A^{2-} + H^+$ in dioxane-water media at 25 °C and $I = 0.1$ mol dm^{-3} (KNO_3)

x_{dlox}	$pK_a^c(s) = -\log(K_a^c(s)/\text{mol dm}^{-3})$	
	HEB	PAR
0.000	9.04	12.11 (12.66)[a]
0.023	9.25	12.47 (12.22)
0.050	9.69	12.76 (12.78)
0.083	10.11	13.15 (13.18)
0.123	10.49	13.54 (13.66)
0.174	10.81	13.94 (13.91)

a) The value of pK_a^c in parentheses obtained from the relationship, $pK_a^c = pC_H + \log\{(D_B - D)/(D - D_A)\}$, where D is the absorbance, and A and B is the subscript for the acid and the base form of PAR and HEB, respectively.

† Presented in part at the 1977 Winter Meeting in Hokkaido of the Chemical Society of Japan and the Japan Society for Analytical Chemistry, Sapporo, February 2, 1977, Abstract, p. 6.

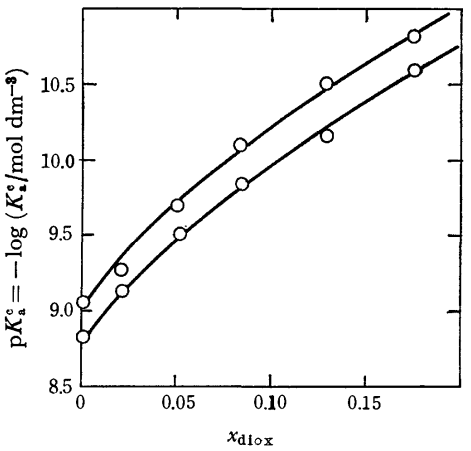

Fig. 1. Dependence of the acid-dissociation comstants, K_a^c, of HEB on the mole fractions of dioxane, x_{dlox}. At 25 °C and $I = 0.1$ mol dm^{-3} (KNO_3). (a) The plot of pK_a^c(s) *vs.* x_{dlox}. (b) The plot of pK_a^c(k) *vs.* x_{dlox}.

the change in mole fractions of dioxane, x_{dlox}, from 0 to 0.174 are evaluated to be +1.77 and +1.83 for HEB and PAR, respectively. The corresponding values for the bivalent anions of *o*-hydroxy azo compounds, 7-hydroxy-8-phenylazo-1,3-naphthalenedisulfonic acid and 4-(2,4-dihydroxyphenylazo)benzenesulfonic acid, were reported to be +2.31 and +2.27, respectively.[2] In Fig. 1, the negative logarithms of the acid-dissociation constants of HEB ($pK_a^c(s) = -\log(K_a^c(s)/\text{mol dm}^{-3})$) are plotted as a function of x_{dlox}. Increasing dioxane content in the medium leads to a decrease in K_a^c(s) of HEB as expected. Similar tendency is observed in the pK_a^c(s) of PAR.

For the proton-transfer reactions between univalent anions of Brønsted acids and OH^- ion in dioxane–water media,

$$HA^- + OH^- \underset{k_r}{\overset{k_f}{\rightleftharpoons}} A^{2-} + H_2O, \qquad (2)$$

with the equilibrium constant $K_b^c = k_f/k_r' = \bar{C}_A/\bar{C}_{HA}\bar{C}_{OH}$, the relaxation time, τ, is expressed by

$$\tau^{-1} = k_f(\bar{C}_{OH} + \bar{C}_{HA}) + k_r', \qquad (3)$$

where k_r' equals $k_r[H_2O]$ and the bar over the concentration symbols denotes equilibrium concentrations. Table 2 shows the dependence of the reciprocal relaxation time on the analytical concentrations of HEB and pH*. Figure 2 shows the plots of τ^{-1} *vs.* $\bar{C}_{OH}$, giving k_f and k_r of PAR from the slope and the intercept, respectively. The values of k_f, k_r', pK_a^c(k), and K_b^c are summarized in Tables 3 (HEB) and 4 (PAR). In Fig. 1, pK_a^c(k)'s of HEB evaluated as $K_a^c(k) = K_b^c K_w^c$ from the kinetic data are plotted against x_{dlox}, where K_w^c denotes the apparent ionic product

Table 2. The reciprocal relaxation time of the proton-transfer reaction of HEB in aqueous solution at 25 °C and I=0.1 mol dm^{-3} (KNO_3)

$C^\circ/10^{-5}$ mol dm^{-3} a)	pH* b)	$\tau^{-1}/10^4$ s^{-1}
1.81	8.99	6.1
3.62	8.77	8.3
3.76	8.77	9.5
5.77	8.56	12.6
2.68	9.23	9.3

a) C° is the total concentration of HEB. b) pH* denotes the pH-meter readings.

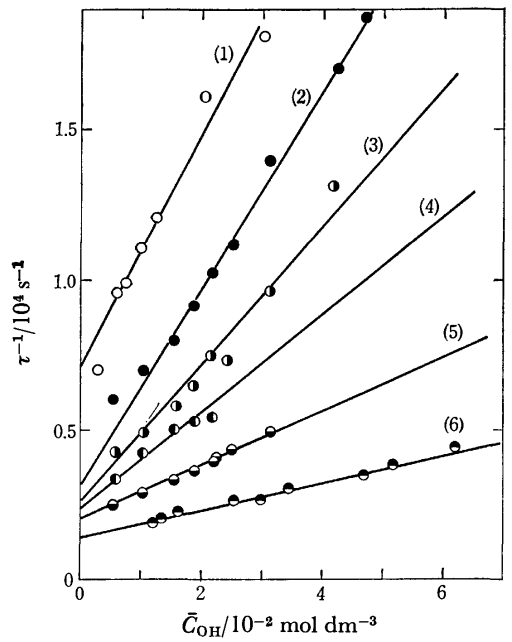

Fig. 2. Plots of reciprocal relaxation time, τ^{-1}, *vs.* $\bar{C}_{OH}$ in dioxane–water media. The mole fraction of dioxane: (1) 0.000, (2) 0.023, (3) 0.050, (4) 0.083, (5) 0.123, and (6) 0.174. At 25 °C and $I = 0.1$ mol dm^{-3} (KNO_3).

Table 3. Rate and equilibrium constants for the proton-transfer reaction of HEB, $HA^- + OH^- \underset{k_r}{\overset{k_f}{\rightleftharpoons}} A^{2-} + H_2O$, in dioxane–water media at 25 °C and I=0.1 mol dm^{-3} (KNO_3)

x_{dlox}	k_f/mol^{-1} dm^3 s^{-1}	k_r'/s^{-1}	K_b^c/mol^{-1} dm^3	pK_a^c(k)
0.000	1.8×10^9	2.0×10^4	9.0×10^4	8.8
0.023	1.6×10^9	2.0×10^4	8.0×10^4	9.1
0.050	1.4×10^9	2.3×10^4	6.1×10^4	9.5
0.083	9.6×10^8	1.7×10^4	5.6×10^4	9.8
0.123	6.9×10^8	1.1×10^4	6.3×10^4	10.2
0.174	6.0×10^8	1.1×10^4	5.5×10^4	10.6

Table 4. Rate and equilibrium constants for the proton-transfer reaction of PAR, $HA^- + OH^- \underset{k_r}{\overset{k_f}{\rightleftharpoons}} A^{2-} + H_2O$, in dioxane–water media at 25 °C and I=0.1 mol dm^{-3} (KNO_3)

x_{dlox}	k_f/mol^{-1} dm^3 s^{-1}	k_r'/s^{-1}	K_b^c/mol^{-1} dm^3	pK_a^c(k)
0.000	3.8×10^5	7.1×10^3	54	11.99
0.023	3.4×10^5	3.2×10^3	106	12.02
0.050	2.3×10^5	2.7×10^3	85	12.34
0.083	1.6×10^5	2.3×10^3	70	12.69
0.123	8.8×10^4	2.0×10^3	44	13.33
0.174	4.4×10^4	1.4×10^3	31	13.82

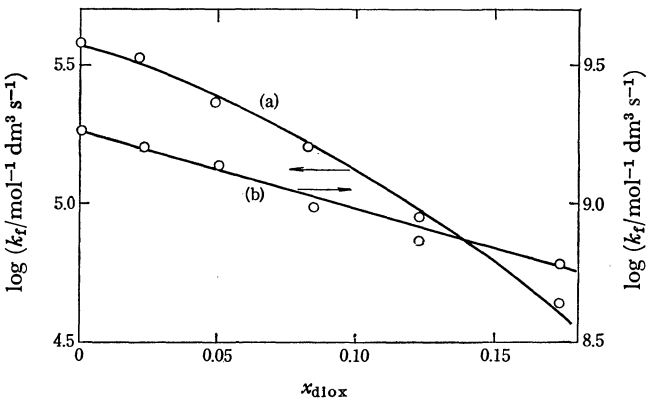

Fig. 3. Dependence of the recombination rate constants k_f on the x_{dlox} at 25 °C and $I = 0.1$ mol dm^{-3} (KNO_3) for PAR (a) and HEB (b).

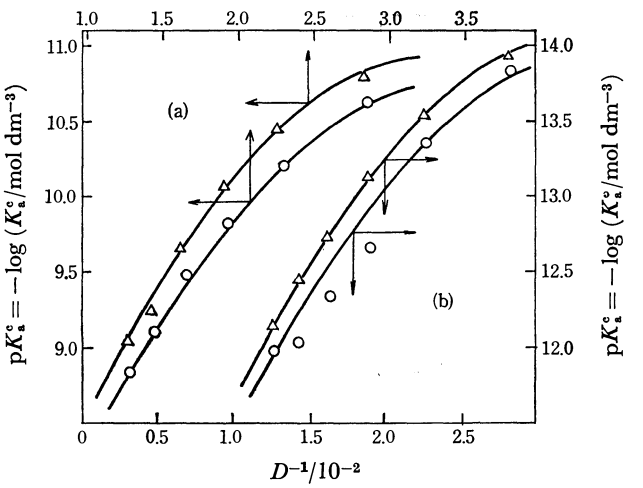

Fig. 4. Dependence of the acid-dissociation constants, K_a^c, of HEB (a) and PAR (b) on the dielectric constant of the medium at 25 °C and $I = 0.1$ mol dm^{-3} (KNO_3). ○: The plot of pK_a^c(k) *vs.* D^{-1}. △: The plot of pK_a^c(s) *vs.* D^{-1}.

of water. The differences in values between pK_a^c(k) and pK_a^c(s) of HEB and PAR are found to be small as compared with those of the bivalent anions of azo compounds. Figure 3 shows a dependence of log k_f on x_{dlox}. The recombination rate constants of HEB and PAR with OH^- ion decrease with increasing x_{dlox} (Fig. 3).

In Fig. 4 the values of pK_a^c(k) and pK_a^c(s) are plotted against the inverse macroscopic dielectric constant of medium, D^{-1}; the dependence is not linear. The simple electrostatic effect of the Born type is not observed.

The value of pK_a^c of HEB having no para O^--substituent with respect to the azo group is smaller by three orders of magnitude than that of PAR having a para O^--substituent. This is due to the difference in the stabilities of the acid form, HA^-, of HEB and PAR.

The recombination of OH^- ion and a univalent anion of HEB was found to proceed with the rate constants in the order of magnitude 10^9 mol^{-1} dm^3 s^{-1} (Table 3). However, the reaction of PAR proceeds considerably slowly, the rate constant k_f being in the order of magnitude 10^5 mol^{-1} dm^3 s^{-1}. These facts would be interpreted by the thermodynamic stability of the intramolecular hydrogen-bond and the increased double-bond character of a C–N bond between an azo nitrogen and the benzene ring owing to the resonance contribution from the para O^--substituent.[1]

A reaction mechanism

$$HA^- \underset{k_{21}}{\overset{k_{12}}{\rightleftharpoons}} HA^{*-} \tag{4}$$

$$HA^{*-} + OH^- \underset{k_{32}}{\overset{k_{23}}{\rightleftharpoons}} HA^{*-}\cdots(H_2O)_n\cdots OH^- \tag{5}$$

$$HA^{*-}\cdots(H_2O)_n\cdots OH^- \underset{k_{43}}{\overset{k_{34}}{\rightleftharpoons}} A^{2-} + H_2O \tag{6}$$

postulated previously[1] for the proton-transfer reactions in dioxane–water media is applicable also to that of HEB and PAR. Equation 4 suggests the equilibrium between two isomeric species of the acid form of *o*-hydroxy azo compounds, *viz.*, an HA^- species having an intramolecular hydrogen-bond and an intermediate species HA^{*-} having no intramolecular hydrogen-bond. The intermediate species can interact with the surrounding water molecules as the normal Brønsted acids do.

The relaxation time for the above reaction, τ, is given[1] by

$$\tau^{-1} = K_{12}k_{23}(\bar{C}_{OH} + \bar{C}_{HA}) + k_{32}/K_{34}. \tag{7}$$

The overall rate constants, k_f and k'_r, are shown by Eqs. 8 and 9.

$$k_f = K_{12}k_{23} = (k_{12}/k_{21})k_{23} \tag{8}$$

and

$$k'_r = k_{32}/K_{34} = k_{32}/(k_{34}/k_{43}) \tag{9}$$

Although no data on the equilibrium constant, $K_{12} = [HA^{*-}]/[HA^-]$, have been reported so far, the values of K_{12} can be estimated to be 10^{-5}—10^{-6} for PAR and 10^{-1}—10^{-2} for HEB provided that the rate constant k_{23} is in the order of magnitude 10^{10} mol^{-1} dm^3 s^{-1} (diffusion-controlled). Since the K_{12} is the equilibrium constant involving the step where HA^- interacts with the surrounding water molecules in the vicinity of reaction site, the larger value of K_{12} in the case of HEB indicates that the HA^- species of HEB can more easily interact with the surrounding water molecules than that of PAR.[5]

By neglecting the ionic-atmosphere term in Christiansen-Scatchard equation[7,8] we obtain

$$\ln (k_f/k_f^\circ) = -z_i z_j e^2/kTr^*D, \tag{10}$$

where z_i and z_j represent the charge of the reactants, D is the macroscopic dielectric constant of the medium, k the Boltzmann's constant, T the absolute temperature, r^* the reaction distance, e the elementary charge, and k_f° the rate constant at infinite dielectric constant. As shown in Fig. 5, the plot of log k_f *vs.* D^{-1} is linear. The forward rate constant k_f for the proton-transfer reaction is equal to $K_{12}k_{23}$ (see Eq. 8). Since, in the case of a sparingly water-soluble Brønsted acid, PAR, the value of K_{12} decreases with the decrease of the dielectric constant as observed in the case of 4-(*p*-

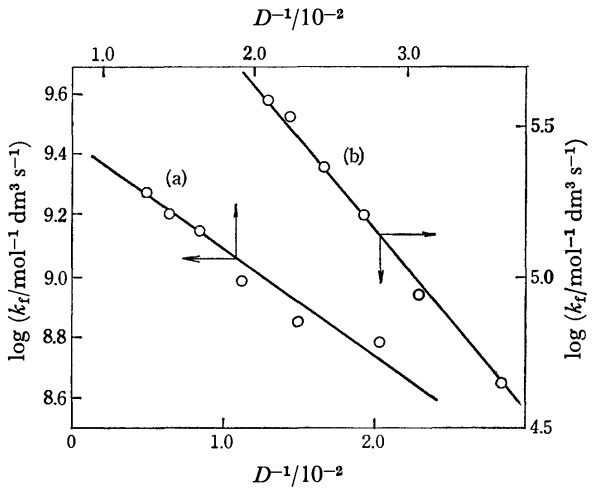

Fig. 5. Dependence of the log k_f of HEB (a) and PAR (b) on the dielectric constant, D, of the medium at 25 °C and $I = 0.1$ mol dm^{-3} (KNO_3).

nitrophenylazo)resorcinol,[1] we obtain an expectedly small value for r^* to be 3.8 Å (Fig. 5). Since in the case of a water-soluble Brønsted acid, HEB, the term K_{12} is assumed to be nearly constant, the slope in Fig. 5 is reduced to Eq. 11.

$$\begin{aligned} &\mathrm{d}\log(k_f/\mathrm{mol^{-1}\,dm^3\,s^{-1}})/\mathrm{d}\,D^{-1} \\ &= \mathrm{d}\log(k_{23}/\mathrm{mol^{-1}\,dm^3\,s^{-1}})/\mathrm{d}\,D^{-1} \\ &= -(z_i z_j e^2)/(kTr^*). \end{aligned} \tag{11}$$

From the slope for HEB in Fig. 5, we obtain the value of r^* to be 7.2 Å. The value of r^* was reported to be 8 Å for the neutralization reaction between hydrated proton $H_9O_4^+$ and hydrated hydroxide ion $H_7O_4^-$ in aqueous solution.[9,10] From the data mentioned above the intervening water molecules would be involved in the encounter complex, $HA^{*-}\cdots(H_2O)_n\cdots OH^-$.

Figure 6 leads to the linear relationships between log k_f and pK_a^c for HEB:

$$\log k_f = -0.27\mathrm{p}K_a^c(\mathrm{k}) + 11.65, \tag{12}$$

and

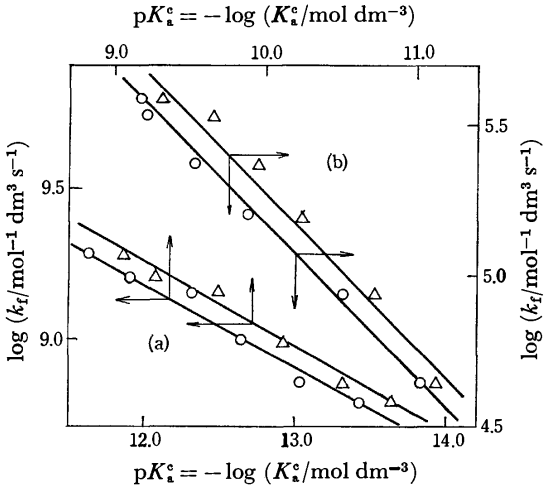

Fig. 6. Dependence of the log k_f on the pK_a^c of HEB (a) and PAR (b) in dioxane-water media at 25 °C and $I = 0.1$ mol dm^{-3} (KNO_3). ○: The plot of log k_f *vs.* pK_a^c(k). △: The plot of log k_f *vs.* pK_a^c(s).

$$\log k_f = -0.28\mathrm{p}K_a^c(\mathrm{s}) + 11.81, \tag{13}$$

and for PAR;

$$\log k_f = -0.51\mathrm{p}K_a^c(\mathrm{k}) + 11.70, \tag{14}$$

and

$$\log k_f = -0.51\mathrm{p}K_a^c(\mathrm{s}) + 11.80. \tag{15}$$

From the empirical equations 12, 13, 14, and 15, the following Brønsted type relation is found to hold between k_f and K_a^c upon changing the solvent composition:

$$k_f = G(K_a^c)^\alpha \tag{16}$$

and

$$0<\alpha<1. \tag{17}$$

Equations 16 and 17 indicates a correlation between the reactivity of HA^- with OH^- ion and the proton-donor strength of HA^- upon changing the solvent composition.

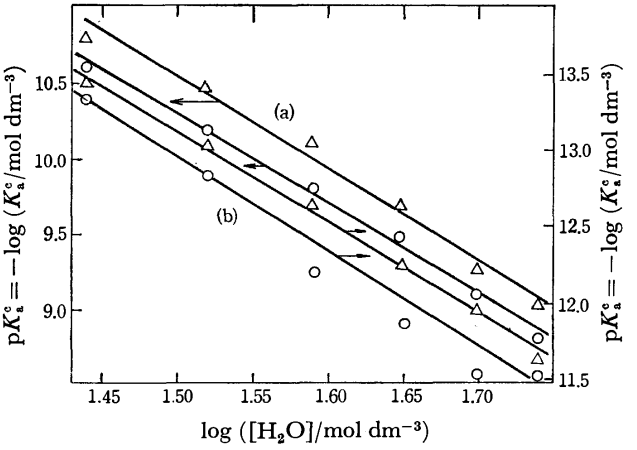

Fig. 7. Dependence of pK_a^c of HEB (a) and PAR (b) on the log [H_2O] in dioxane-water media at 25 °C and $I = 0.1$ mol dm^{-3} (KNO_3). △: The plot of pK_a^c(s) *vs.* log [H_2O]. ○: The plot of pK_a^c(k) *vs.* log [H_2O].

Figure 7 shows the linear relationship between pK_a^c and the logarithms of the concentrations of water, log[H_2O], for HEB:

$$\mathrm{p}K_a^c(\mathrm{k}) = -5.87\log[H_2O] + 19.08, \tag{18}$$

and

$$\mathrm{p}K_a^c(\mathrm{s}) = -6.13\log[H_2O] + 19.74, \tag{19}$$

and for PAR:

$$\mathrm{p}K_a^c(\mathrm{k}) = -6.27\log[H_2O] + 22.87, \tag{20}$$

and

$$\mathrm{p}K_a^c(\mathrm{s}) = -6.00\log[H_2O] + 22.74. \tag{21}$$

If the following simple acid dissociation of HA^- is postulated,

$$HA^- + n\ H_2O \overset{K}{\rightleftharpoons} H(H_2O)_x^+ + A(H_2O)_y^{2-} \tag{22}$$

with the equilibrium constant $K=[H^+_{aq}][A^{2-}_{aq}]/\{[HA^-]\cdot[H_2O]^n\}$, the acid-dissociation constant of HA^-, K_a^c, is defined as

$$K_a^c = [H^+_{aq}][A^{2-}_{aq}]/[HA^-] = K[H_2O]^n. \tag{23}$$

Therefore the following relationship could be expected:

$$\mathrm{p}K_a^c = -n\log[H_2O] + \mathrm{p}K. \tag{24}$$

From the empirical equations 18, 19, 20, and 21, the value of n is estimated to be 6 for the acid dissociation of the univalent anions, HA^-, of HEB and PAR.[11]

References

1) N. Yoshida and M. Fujimoto, *Bull. Chem. Soc. Jpn.*, **50**, 1328 (1977).
2) N. Yoshida and M. Fujimoto, *Bull. Chem. Soc. Jpn.*, **52**, 2527 (1979).
3) K. G. Liphard and A. Jost, *Ber. Bunsenges. Phys. Chem.*, **82**, 707 (1978).
4) F. H. Pollard, P. Hansen, and W. J. Geary, *Anal. Chim. Acta*, **20**, 26 (1959).
5) ^1H NMR data show the presence of the intramolecular hydrogen-bond in HA^- of HEB. As for the intramolecular hydrogen-bond in HA^- of PAR, see Ref. 6.
6) K. Mochizuki, T. Ito, and M. Fujimoto, *Bull. Chem. Soc. Jpn.*, **52**, 441 (1979).
7) J. A. Christiansen, *Z. Phys. Chem.*, **113**, 35 (1924).
8) G. Scatchard, *Chem. Rev.*, **10**, 229 (1932).
9) M. Eigen and L. De Maeyer, "The Structure of Electrolytic Solutions," ed by W. J. Hamer, Wiley, New York, N. Y. (1959), Chap. 5, p. 70.
10) M. Eigen and L. De Maeyer, *Proc. R. Soc. London, Ser. A*, **247**, 505 (1958).
11) Since Bell suggested that H_3O^+ is probably further hydrated with 3 molecules of solvent,[12] the values of x and y was estimated to be 4 and 2, respectively. Glover reported the value of n as 6 for benzoic acid.[13]
12) R. P. Bell, "The Proton in Chemistry," Cornell University Press, Ithaca, N. Y. (1959), p. 83.
13) D. J. Glover, *J. Am. Chem. Soc.*, **67**, 5275 (1965).

Solution Equilibria of Histidine-containing Ternary Amino Acid–Copper(II) Complexes in 20 v/v% Dioxane–Water

Osamu YAMAUCHI,* Toshikazu TAKABA, and Takeshi SAKURAI†

Faculty of Pharmaceutical Sciences, Osaka University, Yamadakami, Suita, Osaka 565

†*Institute of Chemistry, College of General Education, Osaka University, Toyonaka, Osaka 560*

(Received June 13, 1979)

Equilibria of histidine-containing ternary amino acid–copper(II) systems have been investigated by potentiometric titration in acid—neutral solution in 20 v/v% dioxane–water containing 0.1 M KNO_3 (1 M=1 mol dm^{-3}) at 25 °C. The stability constants of the binary complexes of histidine (his) and other amino acids (A) with a polar or a nonpolar side chain (A: serine, threonine, homoserine, asparagine, glutamine, citrulline, glycine, alanine, or valine) and the ternary complexes Cu(his)(A) have been calculated by the method of nonlinear least-squares. The overall stability constants for CuA, CuA_2, and Cu(his)(A) are higher than the values reported for the corresponding complexes in water, those for Cu(his) and $Cu(his)_2$ remaining unaffected. The stability constants (log β_{1110}) for Cu(his)(A) are in the range 17.4—18.0, no difference in stability being observed between the diastereomers Cu(L-his)(L-A) and Cu(D-his)(L-A). Species distribution as a function of pH reveals that Cu(his)(A) predominates in the neutral region. The stability constants have been compared with various theoretical values and found to be higher than the statistically estimated ones.

Copper(II) in human blood serum has been reported to form histidine-containing ternary complexes preferentially with threonine (thr), asparagine (asn), and glutamine (gln).[1] In fact a ternary complex, L-histidinato-L-threoninatocopper(II), has been detected by thin-layer chromatography using ^{64}Cu and ^{14}C as tracers.[2] Such low-molecular-weight copper(II) complexes are involved in the copper(II) transport in biological systems.[3,4] Computer simulation of the multimetal-multiligand equilibria in blood plasma indicates that copper(II) exists predominantly as binary and ternary complexes containing histidine (his),[5] supporting the reported involvement of histidine in copper(II) complex formation.

X-Ray crystal structure analysis of [Cu(L-his)(L-thr)(H_2O)]·H_2O shows that histidine coordinates to copper(II) through its amine and imidazole nitrogens with the carboxylate oxygen in the apical position and that threonine occupies the rest of the coordination plane with a glycine-like chelation in a *cis*-configuration with respect to the amino groups.[6]

On the basis of the molecular structure disclosed, the results of synthesis of ternary copper(II) complexes containing histidine and an amino acid with a polar side chain, such as asparagine and serine, and optical resolution of racemic histidine through ternary complex formation, we inferred that such a combination of ligands around copper(II) facilitates the crystallization of the ternary complexes probably owing to ligand-ligand interactions between the carboxylate oxygen of histidine and the polar side group of the other amino acid.[7,8] Very recently the structures of two modifications of L-asparaginato-L-histidinatocopper(II), isolated from water and from aqueous ethanol, have been revealed by X-ray analysis to have different side chain conformations of L-asparagine,[9] showing that the conformation is flexible and affected by the crystalline environment. Since the polar side groups of histidine and asparagine can have access to each other to within a hydrogen bond distance by the conformational change, the structures suggest that ligand-ligand interactions may take place under favorable conditions.

In order to obtain information on the ternary complex formation and ligand-ligand interactions in a medium with low polarity, we have investigated by potentiometric titration in 20 v/v% dioxane–water the equilibria of copper(II) complexes containing histidine and/or other amino acids (A) with a polar or a nonpolar side chain and compared the results with those reported for the systems in water. Comparison was also made between the stability constants for the diastereomers Cu(L-his)(L-A) and Cu(D-his)(L-A) and between the experimental and theoretical values for Cu(L-his)(L-A).

Experimental

Materials. L-Homoserine (L-hmser), L-glutamine, L-citrulline (L-cit), glycine (gly), L-alanine (L-ala), and L-valine (L-val) were obtained from Nakarai Chemicals, Ltd., and L- and D-histidine hydrochloride monohydrate, L-threonine, and L-serine (L-ser) from Ajinomoto Chemical Co. Dioxane (Nakarai Chemicals, Ltd.) was purified by distillation after refluxing for two hours over calcium hydride. All the materials were of analytical reagent grade or of highest grade available. Water was distilled and deionized.

Potentiometric Titrations. *Reagents*: Carbonate-free potassium hydroxide (0.1 M (M=mol dm^{-3})) was prepared by the method of Armstrong[10] and standardized against potassium hydrogen phthalate. Copper (II) nitrate (0.01 M) was standardized by chelatometric titration using EDTA with 1-(2-pyridylazo)-2-naphthol (PAN) as an indicator. Zinc (JIS primary standard) was used for standardization of 0.01 M EDTA.

Apparatus: Measurement of pH was made with an Orion Research 801A digital pH meter equipped with a 90-01-00 glass electrode and a 91-02-00 double junction reference electrode. The meter was standardized with Horiba standard buffer solutions (4.01, 6.86, and 9.18 at 25 °C).

Correction of pH *Meter Reading*: The pH meter readings in 20 v/v% dioxane–water were corrected according to Van Uitert and Haas[11] by titrating HNO_3 in 0.1 M KNO_3 (ionic strength (I)=0.1 M) with 0.1 M KOH. The correction factor C was calculated by means of the relation

$$-\log [H^+] = pH_M + C,$$

where $[H^+]$ and pH_M denote the analytical hydrogen ion concentration and the pH meter reading in 20 v/v% dioxane–

water, respectively. Thus, the hydrogen ion concentration was given by $10^{-pH_M}/0.66$. The ion product of water (pK_w') in this medium (I=0.1 M (KNO_3)) was determined to be 14.61 by varying the hydroxide ion concentration with 0.1 M KOH.

Determination of Equilibrium Constants: For determination of the acid dissociation constant (pK_a), a 4×10^{-3}M solution of an amino acid containing an excessive amount of nitric acid was titrated with 0.1 M KOH at 25±0.05 °C under a nitrogen atmosphere. The data for determination of the stability constants of the binary and ternary complexes were obtained by titrating 1:2 Cu(II)–amino acid systems and 1:1:1 Cu(II)–his–A systems, respectively, under the same conditions, the initial total concentration of copper(II) being 2×10^{-3} M. Dioxane was added at each addition of 0.1 M KOH to maintain the solvent composition. The pH value was measured after each addition of 0.1 M KOH and dioxane. Reproducibility of the titration was checked by multiplicate runs.

Calculations. The equilibria of the present systems in general are expressed by Eq. 1 and the equilibrium constant β_{pqrs} (Eq. 2):

$$pCu + q\text{his} + rA + sH \overset{\beta_{pqrs}}{\rightleftharpoons} Cu_p(\text{his})_q(A)_r(H)_s, \quad (1)$$

$$\beta_{pqrs} = \frac{[Cu_p(\text{his})_q(A)_r(H)_s]}{[Cu]^p[\text{his}]^q[A]^r[H]^s}, \quad (2)$$

where p, q, r, and s refer to the numbers of Cu(II), his, A, and H contained in the complex, respectively, and the charges are omitted. The β_{pqrs} values were calculated by the method of nonlinear least-squares by using the computer program SCOGS.[12] The acid dissociation constants were calculated by the usual method and refined by least-squares treatment when necessary.

Results

Acid Dissociation Constants. Typical titration curves for ligands alone are illustrated in Fig. 1, and the acid dissociation constants calculated from the data are summarized in Table 1, where pK_{COOH}, pK_{Im}, and pK_{NH_2}, referring to the pK_a's of the carboxyl, the imidazole, and the amino group, respectively, are compared with the corresponding values determined in water.[13] The pK_{COOH} values are less reliable owing to the low concentrations of the solutions, the standard deviations being *ca.* ±0.05 log unit. Whereas the constants for the amino groups, pK_{NH_2}, in aqueous dioxane are higher than those in water by 0.1—0.2 log unit,[13] the imidazole group exhibits a slightly lower pK_a value.

Stability Constants. Binary and ternary copper(II)–amino acid systems give the titration curves shown in Fig. 2, which reveals that coordination of the amino acids are nearly complete at neutral pH. The calculated stability constants ($\log\beta_{pqrs}$) for the binary and the ternary complexes are listed in Tables 2 and 3, respectively. In the computation we took into account the complex species, CuA, CuA_2, Cu(his), $Cu(his)_2$, Cu(his)(H), $Cu(his)_2(H)$, $Cu(his)_2(H)_2$, and Cu(his)(A). The stability constants thus determined reproduce the experimental curves satisfactorily (Fig. 3), with the standard deviations expressed in titer in the binary and ternary systems usually less than 0.5 and 1% of the total volume of 0.1 M KOH used,

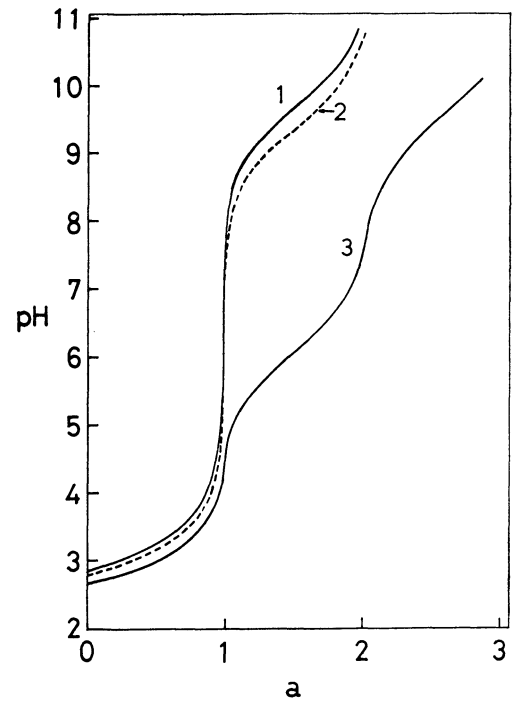

Fig. 1. Typical titration curves for ligands (25 °C; I=0.1M (KNO_3)). Curve 1, L-cit; curve 2, L-ser; curve 3, L-his. Initial total concentration: 0.004000 M. a: Moles of KOH added per mole of amino acid.

Table 1. Acid dissociation constants of amino acids in 20 v/v% dioxane-water (25 °C; I=0.1 M (KNO_3))[a]

Amino acid	Acid dissociation constant[b]		
	pK_{COOH}	pK_{Im}	pK_{NH_2}
gly	2.6_7 (2.36)		9.74 (9.57)
L-ala	2.6_4 (2.30)		9.82 (9.69)
L-val	2.6_2 (2.26)		9.68 (9.49)
L-asn	2.4_6 (2.14)		8.89 (8.72)
L-gln	2.4_5 (2.17)		9.14 (9.01)
L-cit	2.5_8 (2.43)		9.49 (9.41)
L-ser	2.4_4 (2.13)		9.16 (9.06)
L-thr	2.5_0 (2.21)		9.07 (8.97)
L-hmser	2.4_6 (2.27)		9.44 (9.28)
L-his	1.8 (1.70)	5.93 (6.02)[c]	9.23 (9.08)[c]

a) Standard deviations are <0.05 for pK_{COOH} and <0.01 for pK_{Im} and pK_{NH_2}. b) Corresponding values in water taken from Ref. 13 are shown in parentheses. c) We obtained the following values in water: pK_{Im}=6.03; pK_{NH_2}=9.11 (25 °C; I=0.1M (KNO_3)).

respectively. We see from Table 2 that the binary complexes, CuA and CuA_2, and the protonated complexes of histidine exhibit higher stability constants in aqueous dioxane than in water,[13,14] while Cu(his) and $Cu(his)_2$ remain equally stable in both media. The ternary complexes Cu(his)(A) have the $\log\beta_{1110}$ values of 17.4—18.0 (Table 3), which are also higher than the corresponding values in water.[8,14] The diastereomers Cu(L-his)(L-A) and Cu(D-his)(L-A) have $\log\beta_{1110}$ values which agree with each other to within experimental errors, apparently showing no stereo-

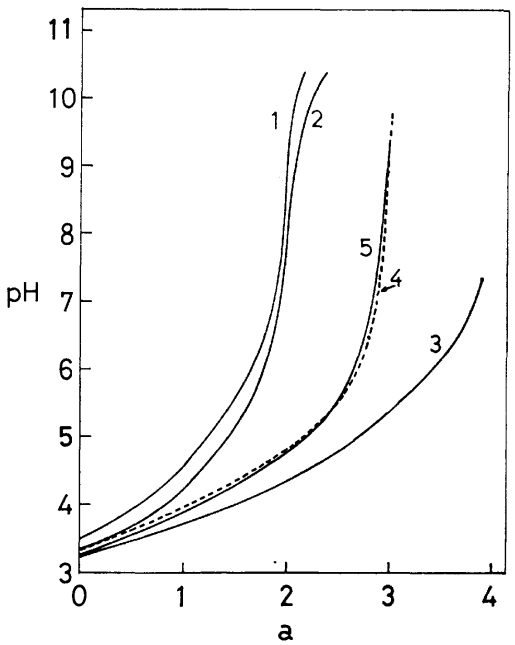

Fig. 2. Typical titration curves for binary and ternary copper(II)-amino acid systems (25°C; I=0.1 M (KNO_3)). Curves 1—5 correspond to the following systems: 1, 1:2 Cu(II)-L-hmser; 2, 1:2 Cu(II)-L-asn; 3, 1:2 Cu(II)-L-his; 4, 1:1:1 Cu(II)-L-his-L-hmser; 5, 1:1:1 Cu(II)-L-his-L-asn.
Initial total concentrations are as follows:
(i) Binary systems Cu(II)=0.002016 M; his or A=0.004000 M.
(ii) Ternary systems Cu(II)=0.002016 M; his=0.002000 M; A=0.002000 M.
a: Moles of KOH added per mole of Cu(II).

TABLE 2. STABILITY CONSTANTS OF BINARY COPPER(II) COMPLEXES IN 20 v/v% DIOXANE-WATER (25°C; I=0.1 M(KNO_3))[a]

Amino acid	Stability constant[b]	
	$\log \beta_{1010}$	$\log \beta_{1020}$
gly	8.55(8.15)	15.64(15.03)
L-ala	8.40(8.13)	15.45(14.92)
L-val	8.39(8.11)	15.52(14.90)
L-asn	8.20(7.86)	14.95(14.42)
L-gln	8.02(7.75)	14.80(14.23)
L-cit	8.29(7.92)	15.19(14.39)
L-ser	8.14(7.89)	14.98(14.48)
L-thr	8.28(8.01)	15.21(14.73)
L-hmser	8.32(7.97)	15.24(14.69)
L-his[c]	10.13(10.10)	18.13(18.10)

a) Standard deviations are <0.01 for CuA and CuA_2 and 0.02—0.04 for the histidine complexes. b) Corresponding values in water taken from Ref. 13 are shown in parentheses. The values for the histidine complexes were taken from Ref. 14. c) $\log \beta_{1100}$ and $\log \beta_{1200}$ values. The stability constants for the protonated complexes are as follows: $\log \beta_{1101}$=14.31 (14.00); $\log \beta_{1201}$=24.07 (23.88); $\log \beta_{1202}$=27.83 (27.56).

selectivity in complex formation. In this connection, Freeman and Martin[15] and Brookes and Pettit[14] also reported that no stereoselectivity is observed between the diastereomers of Cu(his)(thr) in water, but the latter observed a small stability difference (0.06 log unit) between Cu(L-his)(L-val) and Cu(D-his)(L-val).

TABLE 3. STABILITY CONSTANTS OF TERNARY COMPLEXES $Cu_p(his)_q(A)_r(H)_s$ IN 20 v/v% DIOXANE-WATER (25 °C; I=0.1 M (KNO_3))[a]

Amino acid	Stability constant ($\log \beta_{1110}$)	
	Cu(L-his)(A)	Cu(D-his)(A)
gly	17.78(0.01)	
L-ala	17.83(0.01)	17.80(0.01)
L-val	18.01(0.01)	18.04(0.02)
L-asn	17.53(0.03)	17.54(0.03)
L-gln	17.42(0.01)	17.45(0.01)
L-cit	17.67(0.02)	17.64(0.02)
L-ser	17.51(0.02)	17.54(0.02)
L-thr	17.57(0.02)	17.59(0.02)
L-hmser	17.64(0.01)	17.68(0.01)

a) Standard deviations are shown in parentheses.

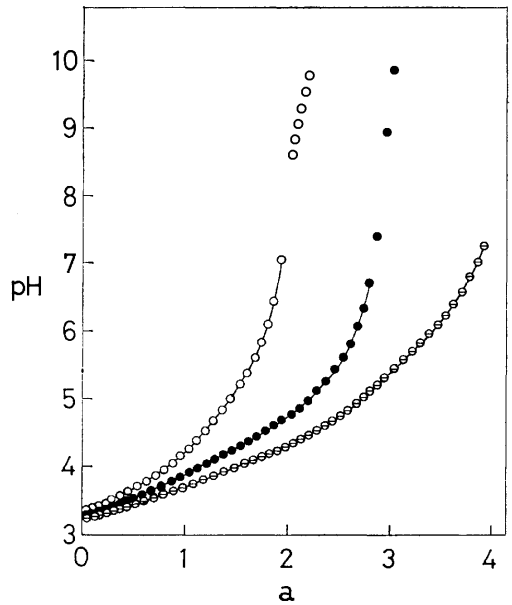

Fig. 3. Fit of the theoretical titration curves to the experimental.
Experimental: ○ 1:2 Cu(II)-L-asn, ⊖ 1:2 Cu(II)-L-his, ● 1:1:1 Cu(II)-L-his-L-asn.
Theoretical ——.

Discussion

Equilibrium Constants in 20 v/v% Dioxane-Water. *Binary Systems*: Depending on the structure of molecules involved, the polarity of the medium affects their behavior in different ways. The use of aqueous dioxane in place of water could approximate biological fluids, where the polarity may be lower because of proteins and other dissolved molecules and the difference in the stability of complexes could be more pronounced. The slightly lower pK_a value of the imidazole group of histidine as compared with the value in water may be explained by the result of a recent NMR study of histidine in aqueous solution,[16] which indicates that neutral histidine favors the struc-

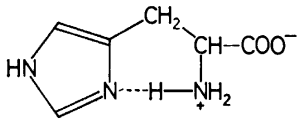

1

ture with an intramolecular hydrogen bonding (**1**). Deprotonation from the imidazolium group of monoprotonated histidine is probably more favorable in aqueous dioxane and in hydrophobic regions in biological systems where the hydrogen bonding in **1** is more stabilized than in water. Analogously the higher log β_{1010} and log β_{1020} values of the complexes CuA and CuA_2 are interpreted as due to stabilization of the glycine-like mode of coordination involving a metal-carboxylate bonding with ionic character.

On the other hand, the copper(II)–histidine complexes behave differently; Cu(his) and $Cu(his)_2$ have approximately the same stability constants as those in water. This is what we expect for the two nitrogen–copper(II) bonds with covalent character through the amino group and the imidazole moiety. Formation of Cu(his)(H) and $Cu(his)_2(H)$ from Cu(his) and $Cu(his)_2$, respectively, is accompanied by stability enhancement (*ca.* 0.3 log unit) due to the solvent effect. This suggests that the carboxylate oxygen of histidine is involved in the coordination plane of copper(II).[17–20]

Ternary Systems: For the ternary complexes to have an intramolecular ligand-ligand interaction, the active complex Cu(L-his)(L-A) should assume a *cis*-configuration and the *meso* complex Cu(D-his)(L-A) a *trans*-configuration with respect to the amino groups, because of the steric requirement for the interaction. Lack of stereoselectivity may implicate either that the intramolecular interaction is too weak to affect the stability and/or *cis-trans* isomerism to an appreciable extent under the present conditions or that the proposed *cis*- and *trans*-isomers have the same stability. For the ternary systems with an acidic amino acid (Ac) and a basic amino acid (B) such as Cu(lys)(glu)(H), where lys and glu refer to lysine and glutamic acid, respectively, the difference log β_{1111} − log β_{1110} is larger than that for the system involving alanine instead of Ac.[21] This has been interpreted as due to the intramolecular electrostatic interaction between the oppositely charged groups of the side chains of Ac and B, because it makes the deprotonation from the ω-ammonium group of B more unfavorable than when Ac is replaced with alanine. However, no stereoselectivity has been detected between the diastereomers of Cu(Ac)(B)(H). Considering that the intramolecular hydrogen bonding proposed for Cu(his)(A) is weaker than the electrostatic interactions in Cu(Ac)(B)(H), it may not affect the stability constants appreciably even in 20 v/v% dioxane-water.

Information is lacking about the structures in solution of the ternary complexes, especially the *meso* complexes; they might exist as mixtures of geometric isomers. As regards the active complexes, however, the X-ray crystal structure analyses,[6,9] which have disclosed that all the three histidine-containing ternary copper(II) complexes have a *cis*-arrangement of the amino groups, may indicate their plausible structures in solution.[8]

Preferential Formation of Ternary Complexes. The species distributions as a function of pH, illustrated for Cu(L-his)(L-ala), Cu(L-his)(L-hmser), and Cu(L-his)(L-cit) in Fig. 4, show that the ternary complex Cu(his)(A) predominates in the neutral region.

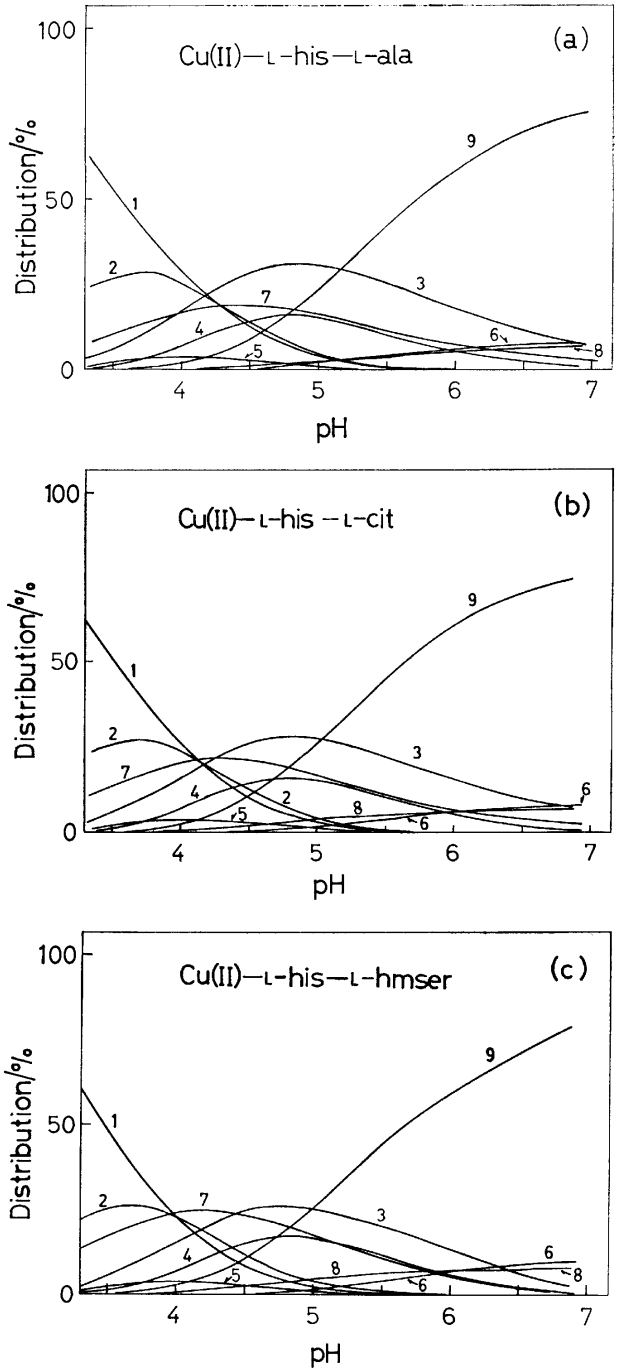

Fig. 4. Species distributions in the ternary systems as a function of pH(25 °C; I=0.1 M (KNO_3)).
(a) 1:1:1 Cu(II)–L-his–L-ala; (b) 1:1:1 Cu(II)–L-his–L-cit; (c) 1:1:1 Cu(II)–L-his–L-hmser.
Curves 1—9 correspond to the following species:1, Cu(II); 2, Cu(L-his)(H); 3, Cu(L-his); 4, $Cu(L\text{-his})_2(H)$; 5, $Cu(L\text{-his})_2(H)_2$; 6, $Cu(L\text{-his})_2$; 7, Cu(L-A); 8, $Cu(L\text{-A})_2$; 9, Cu(L-his)-(L-A).
Initial total concentrations: Cu(II)=0.002016 M; L-his=0.002000 M; L-A=0.002000 M.

Whether the formation of a ternary complex is favored or not as compared with that of binary complexes can be estimated in various ways. We use here log X and log β_{stat} defined by Eqs. 4 and 5, respectively:

$$Cu(his)_2 + CuA_2 \overset{X}{\rightleftharpoons} 2Cu(his)(A), \quad (3)$$

$$\log X = 2\log\beta_{1110} - (\log\beta_{1200} + \log\beta_{1020}), \quad (4)$$

$$\log\beta_{stat} = 1/2(\log\beta_{1200} + \log\beta_{1020}) + \log 2, \quad (5)$$

$$\Delta\log\beta = \log\beta_{1110} - \log\beta_{stat}. \quad (6)$$

We prefer the use of log X to $\Delta\log K$ ($=\log\beta_{1110} - (\log\beta_{1100} + \log\beta_{1010})$), because electrostatic factors cancel in the log X formulation for the present amino acid–copper(II) complexes where the charges of the two ligands are equal to each other.[22] The situation is regarded as the same in the log β_{stat} formulation. The observed values of log X and log β_{1110} can be compared with the statistical values of 0.6[23,24] and log β_{stat},[25] respectively. For all the systems investigated the values are larger than the statistical values (log $X>0.6$ and $\Delta\log\beta>0$) (Table 4). Thus, the formation of the ternary complexes with histidine is favored irrespective of the group contained in the side chain of A. This is partly ascribable to the favorable combination of the π-system of imidazole with a ligand with an oxygen donor.[26]

An interesting approach to the estimation of stability constants has been made by Tanaka,[27,28] who evaluated them on the basis of mechanistic considerations and by introduction of several parameters describing possible ligand-ligand interactions through the central metal ion. For copper(II) complexes with at least one neutral amine nitrogen as a ligand, the following relationship is derived:[28]

$$Cu(his) + A \overset{K}{\rightleftharpoons} Cu(his)(A), \quad (7)$$

$$\log K_{calcd} = \log\beta_{1010} + \sum^{I}\sum^{J}\delta_{ij}X_i(his)Y_j(A), \quad (8)$$

where δ_{ij} is the ligand interaction term allowing for the effect of the donor atom X_i of his on the donor atom Y_j of A, and X_i(his) and Y_j(A) are the numbers of donor atoms X_i and Y_j, respectively. Since log $K=\log\beta_{1110}-\log\beta_{1100}$, we have from Eq. 8

$$\log\beta_{1110\,calcd} = \log\beta_{1100} + \log\beta_{1010} + \sum^{I}\sum^{J}\delta_{ij}X_i(his)Y_j(A). \quad (9)$$

The δ_{ij} values have been determined by a detailed survey of reported stability constants.[28] For Cu(his)(A) with an aromatic nitrogen (N_{Im}) and an aliphatic nitrogen (N_{Am}) of histidine and an oxygen and an aliphatic nitrogen of A in the coordination plane, the expected values $\log\beta_{1110\,calcd}$ can be calculated by using $\delta_{N_{Im}N_{Am}}=-0.25$, $\delta_{N_{Im}N_{Im}}=-0.39$, $\delta_{N_{Im}O}=0.09$, $\delta_{N_{Am}N_{Am}}=-0.35$, and $\delta_{N_{Am}O}=-0.26$. Although these δ_{ij} values refer to the systems in water, we have calculated the $\log\beta_{1110\,calcd}$ values according to Eq. 9 by assuming that the δ_{ij} values are the same in 20 v/v% dioxane–water as in water because they are essentially the differences between the calculated and experimental stability constants. We see from Table 4 that the estimated values for Cu(his)(A) are in excellent agreement with the experimental ones, indicating that the δ_{ij} values hold in 20 v/v% dioxane–water and that the stability of these complexes could be affected by the electronic ligand-ligand interactions mediated by copper(II).

For the binary complexes, CuA_2, the values calculated by Eq. 10[28] are also close to those determined experimentally:

$$\log\beta_{1020\,calcd} = 2\log\beta_{1010} + \sum^{I}\sum^{J}\delta_{ij}X_i(A)Y_j(A) - \log 2. \quad (10)$$

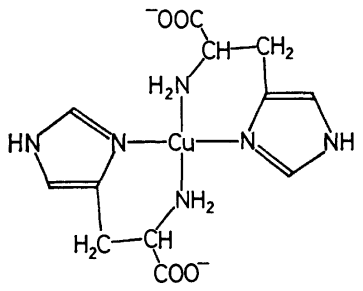

2

Table 4. Comparison of stability constants with theoretical values

Amino acid	Cu(L-his)(L-A)					Cu(L-amino acid)$_2$	
	$\log\beta_{1110}$	$\log\beta_{1110\,calcd}$[a]	$\log\beta_{stat}$[b]	$\Delta\log\beta$[c]	$\log X$[d]	$\log\beta_{1020}$	$\log\beta_{1020\,calcd}$
gly	17.78	17.91	17.18	0.60	1.79	15.64	15.64
ala	17.83	17.76	17.09	0.74	2.08	15.45	15.34
val	18.01	17.75	17.13	0.88	2.37	15.52	15.32
asn	17.53	17.56	16.84	0.69	1.98	14.95	14.94
gln	17.42	17.38	16.77	0.65	1.91	14.80	14.58
cit	17.67	17.65	16.96	0.71	2.02	15.19	15.12
ser	17.51	17.50	16.86	0.65	1.91	14.98	14.82
thr	17.57	17.64	16.97	0.60	1.80	15.21	15.10
hmser	17.64	17.68	16.99	0.65	1.91	15.24	15.18
his[f]						18.13	18.72[g]
							19.19[h]

a) Calculated according to Eq. 9. b) Calculated according to Eq. 5. c) Calculated according to Eq. 6. d) Calculated according to Eq. 4. e) Calculated according to Eq. 10. f) $\log\beta_{1200}$ and $\log\beta_{1200\,calcd}$ values. g) Two (N_{Im})(N_{Am}) coordinations assumed. h) One (N_{Im})(N_{Am}) and one (N_{Am})(O) coordination assumed.

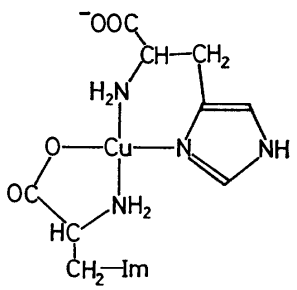

3

Interestingly $Cu(his)_2$ has a $\log \beta_{1200}$ value much smaller than the values estimated from $\log \beta_{1100}$ by Eq. 10 for two sets of donor atoms in the coordination plane, *i.e.*, two $(N_{Im})(N_{Am})$ coordinations (**2**) and one $(N_{Im})(N_{Am})$ and one $(N_{Am})(O)$ coordination (**3**). This suggests that the sterically and/or electronically unfavorable combination of donor groups in $Cu(his)_2$ contributes to the formation of ternary complexes.

We gratefully acknowledge the valuable suggestion and discussion by Prof. Motoharu Tanaka, Nagoya University. We wish to thank Profs. Akitsugu Nakahara and Yoshio Sasaki, Osaka University, for their helpful discussions, and the members of the Osaka University Computer Center for computation of the stability constants. This work was supported in part by a Grant-in-Aid from the Ministry of Education.

References

1) P. Z. Neumann and A. Sass-Kortsak, *J. Clin. Invest.*, **46**, 646 (1967).
2) B. Sarkar and T. P. A. Kruck, "The Biochemistry of Copper," ed by J. Peisach, P. Aisen, and W. E. Blumberg, Academic Press, New York and London (1966), p. 183.
3) B. Sarkar and Y. Wigfield, *Can. J. Biochem.*, **46**, 601 (1968).
4) S.-J. Lau and B. Sarkar, *J. Biol. Chem.*, **246**, 5938 (1971).
5) P. M. May, P. W. Linder, and D. R. Williams, *J. Chem. Soc., Dalton Trans.*, **1977**, 588; G. Berthon, P. M. May, and D. R. Williams, *ibid.*, **1978**, 1433.
6) H. C. Freeman, J. M. Guss, M. J. Healy, R.-P. Martin, C. E. Nockolds, and B. Sarkar, *Chem. Commun.*, **1969**, 225.
7) T. Sakurai, O. Yamauchi, and A. Nakahara, *J. Chem. Soc., Chem. Commun.*, **1977**, 718
8) O. Yamauchi, T. Sakurai, and A. Nakahara, *J. Am. Chem. Soc.*, **101**, 4164 (1979).
9) T. Ono, H. Shimanouchi, Y. Sasada, T. Sakurai, O. Yamauchi, and A. Nakahara, *Bull. Chem. Soc. Jpn.*, **52**, 2229 (1979).
10) D. M. G. Armstrong, *Chem. Ind. (London)*, **1955**, 1405.
11) L. G. Van Uitert and C. G. Haas, *J. Am. Chem. Soc.*, **75**, 451 (1953).
12) I. G. Sayce, *Talanta*, **15**, 1397 (1968).
13) A. E. Martell and R. M. Smith, "Critical Stability Constants," Plenum Press, New York (1974), Vol. 1.
14) G. Brookes and L. D. Pettit, *J. Chem. Soc., Dalton Trans.*, **1977**, 1918.
15) H. C. Freeman and R.-P. Martin, *J. Biol. Chem.*, **244**, 4823 (1969).
16) F. Blomberg, W. Maurer, and H. Rüterjans, *J. Am. Chem. Soc.*, **99**, 8149 (1977).
17) E. W. Wilson, Jr., M. H. Kasperian, and R. B. Martin, *J. Am. Chem. Soc.*, **92**, 5365 (1970).
18) R. J. Sundberg and R. B. Martin, *Chem. Rev.*, **74**, 471 (1974).
19) D. R. Williams, *J. Chem. Soc., Dalton Trans.*, **1972**, 790.
20) T. P. A. Kruck and B. Sarkar, *Can. J. Chem.*, **51**, 3563 (1973).
21) T. Sakurai, O. Yamauchi, and A. Nakahara, *Bull. Chem. Soc. Jpn.*, **51**, 3203 (1978).
22) R. B. Martin and R. Prados, *J. Inorg. Nucl. Chem.*, **36**, 1665 (1974).
23) R. DeWitt and J. I. Watters, *J. Am. Chem. Soc.*, **76**, 3810 (1954).
24) S. Kida, *Bull. Chem. Soc. Jpn.*, **29**, 805 (1956).
25) V. S. Sharma and J. Schubert, *J. Chem. Educ.*, **46**, 506 (1969).
26) H. Sigel, *Angew. Chem. Int. Ed. Engl.*, **14**, 394 (1975).
27) M. Tanaka, *J. Inorg. Nucl. Chem.*, **35**, 965 (1973).
28) M. Tanaka, *J. Inorg. Nucl. Chem.*, **36**, 151 (1974).

Polarographic Catalytic Currents Produced by Cytochromes c in Ammoniacal Buffers Containing Cobalt Ions. I. Significance of Heme Group

Tokuji IKEDA, Hideaki KINOSHITA,** Yoshiyuki YAMANE, and Mitsugi SENDA*

Department of Agricultural Chemistry, Kyoto University, Sakyo-ku, Kyoto 606

***Department of Chemistry, Kwassui Women's College, Higashi-yamate, Nagasaki 850*

(Received June 29, 1979)

Polarographic behavior of the Brdička current (catalytic current produced by proteins in ammoniacal buffers containing cobalt ions) of cytochromes c from five sources (horse, chicken, and tuna hearts, *C. krusei* and *S. cerevisiae*) and of modified horse cytochromes (metal-substituted, metal-free, and heme-free cytochrome, and carboxymethylated cytochrome at methionyl residues) was investigated at dme and hmde. The results indicate that the heme group and its sixth ligand are important in determining the Brdička current-activity of cytochromes c. Replacement of the sixth heme ligand from Met to Lys reduced the Brdička current-activity by about one-half. Brdička current of *D. vulgaris* cytochrome c_3 was interpreted as due to four Lys-liganded heme groups.

Polarographic catalytic currents produced by cytochrome c in ammoniacal buffers containing cobalt ions have been studied by Carruthers[1] and Carruthers and Suntzeff[2] with a dropping mercury electrode (dme) and by Kuznetsov[3] with a hanging mercury drop electrode (hmde). They attributed the catalytic activity of cytochrome c to the cysteine residues in its molecule, as usually recognized with SS- and/or SH-containing proteins. In cytochrome c, however, the two residues of cysteine are linked to the heme group to form heme c and are not present as SS- or SH-groups. We have investigated the polarographic and voltammetric behavior of the catalytic currents, *i.e.* the Brdička currents, of cytochromes c from five sources (horse, chicken, and tuna hearts, *Candida krusei*, and *Saccharomyces cerevisiae*) and of modified horse heart cytochromes (metal-substituted, metal-free, and heme-free cytochrome, and carboxymethylated cytochrome at methionyl residues) and found that the heme group and its sixth ligand are important in the Brdička current-activity of cytochrome c. Brdička current-activity of *Desulfovibrio vulgaris* cytochrome c_3 was interpreted as due to four Lys-liganded heme groups.

Experimental

Materials. Horse heart cytochrome c (horse cyt-c), chicken heart cytochrome c (chicken cyt-c), tuna heart cytochrome c (tuna cyt-c), *Candida krusei* yeast cytochrome c (*C. krusei* cyt-c), and *Saccharomyces cerevisiae* yeast cytochrome c (*S. cerevisiae* cyt-c) were products of Sigma Chemicals Co. The purity of these cytochromes c was checked by means of cellulose acetate membrane electrophoresis. Stock solutions, usually 0.5% in cytochrome c were stored at 5 °C. The concentrations were checked spectrophotometrically.[4] Carboxymethylated cytochrome c (CM-cyt-c) was prepared by carboxymethylation of methionyl residues of horse cyt-c by the method of Babul and Stellwagen, identified by absorption spectroscopy, and its concentration determined spectrophotometrically with an absorbance coefficient 127 $mM^{-1}\,cm^{-1}$ at 406 nm.[5] Porphyrin cytochrome c (porphyrin cyt-c) was prepared by the method of Robinson and Kamen.[6] The product was further purified by the gel filtration method according to Dickerson and Chien.[7] The purified porphyrin cyt-c was identified by absorption spectroscopy, and its concentration determined spectrophotometrically with an absorbance coefficient 81 $mM^{-1}\,cm^{-1}$ at 404 nm.[8] Since porphyrin cyt-c is unstable,[7] freshly prepared porphyrin cyt-c was used for electrochemical measurements within the day. Cobalt cytochrome c (Co-cyt-c) was prepared by the method of Dickerson and Chien, identified by absorption spectroscopy, and its concentration determined spectrophotometrically with an absorbance coefficient 106 $mM^{-1}\,cm^{-1}$ at 426 nm.[7] Apocytochrome c (apo-cyt-c) was prepared by the method of Stellwagen and Rysavy.[9] The apoprotein exhibited no absorption in the visible region, indicating the absence of heme moiety. The concentration of apo-cyt-c was determined spectrophotometrically with an absorbance 0.92 ml $mg^{-1}\,cm^{-1}$ at 277 nm.[9] The purity of all these modified cytochromes was further checked by means of SDS-disk electrophoresis. *Desulfovibrio vulgaris* Miyasaki cytochrome c_3 (*D. vulgaris* cyt-c_3) supplied by T. Yagi was used. All other chemicals used were of reagent grade.

Instruments. Voltage sweep voltammograms and cyclic voltammograms at hmde were recorded on a Yanagimoto P8-MS6C polarograph and a Riken Denshi F42C X-Y recorder or a Yanagimoto PE21-TB2S potentiostat with a built-in sweep voltage generator and a Yokogawa 3077 X-Y recorder. A Metrohm E410 mercury drop electrode was used, its surface area being $0.0187\pm0.0003\ cm^2$. D.c. polarograms were recorded on a Yanagimoto P8 polarograph. In most cases a dme having the characteristics $m=1.43$ mg/s and $\tau=4.6$ s at open circuit in ammoniacal buffer at 74 cm height of mercury reservoir (h) was used. In some cases a dme having the characteristics $m=1.60$ mg/s and $\tau=6.3$ s at $h=70$ cm was used.

Electrochemical Measurements. All measurements were made in an H-type cell. All potentials were measured against a saturated calomel electrode (SCE). A buffer solution containing 0.1 M NH_3, 0.1 M NH_4Cl, and 0.1 M KCl (pH 9.4, ionic strength 0.2 mol/dm^3) was used as the base solution. 10 ml of the base solution was transferred to the cell and deaerated by passing nitrogen gas through the solution, which had been previously passed through a solution of the same composition as the base solution. An aliquot of each of the stock solutions of 0.05 M $Co(NH_3)_6Cl_3$ and 0.5% cytochromes c was then introduced into the base solution with a microsyringe under nitrogen atmosphere. In the measurements with hmde a mercury drop freshly formed at the tip of hmde was exposed to the test solution for a given period of time, referred to as exposure time (t_{exp}), during which the electrode potential was kept controlled at the initial voltage (E_i), voltammo-

grams being then run from $E_i = -0.1$ V with a sweep rate, $v = -0.2$ V/s. In determining the current intensities of the catalytic currents an extrapolated theoretical trace of degradating curve of the cobalt peak was subtracted from the current measured at the proper potential. In the measurements with dme, current intensities at the maximum growth of each mercury drop were taken and the catalytic currents measured from the cobalt limiting current. The measurements were carried out at 25 °C unless otherwise stated.

Results

Brdička Current of Horse Cyt-c. Horse cyt-c gave characteristic catalytic current, *viz.*, Brdička current in ammoniacal buffers containing hexaamminecobalt-(III) ion, Co(III), at both dme and hmde. Figure 1 shows d.c. polarograms of (a) 2×10^{-4} M Co(III) in the base solution (0.1 M NH_3, 0.1 M NH_4Cl, and 0.1 M KCl, pH 9.4) and (b—e) horse cyt-c at four different concentrations in (a) at the dme. Figure 2 shows cyclic voltammograms of (a) 2×10^{-4} M Co-(III) in the base solution and (b and c) 10^{-6} M horse cyt-c in (a) at two exposure times at the hmde. Detailed analysis of the polarographic and voltammetric

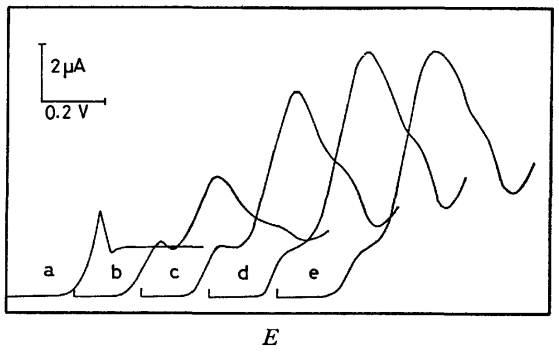

Fig. 1. D.c. polarograms of (a) 2.0×10^{-4} M Co(III) in the base solution and of horse cyt-c at (b) 4.0×10^{-7}, (c) 2.0×10^{-6}, (d) 4.0×10^{-6}, and (e) 5.7×10^{-6} M in (a). Polarograms are recorded from −0.9 V.

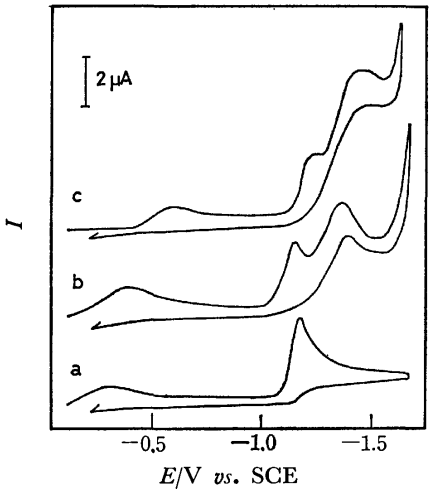

Fig. 2. Cyclic voltammograms of (a) 2.0×10^{-4} M Co(III) in the base solution and of (b and c) 1.0×10^{-6} M horse cyt-c in (a) exposuretim e: 4 s and 64 s, respectively, at the hmde.

behavior of the Brdička current produced by horse cyt-c at the dme and hmde has shown[10] that the dependence of the Brdička current-intensity at a given potential on various factors such as concentrations of the protein and Co(III), exposure time at hmde and drop time at dme is the same as that of the Brdička current produced by SS- and/or SH-containing proteins;[10,11] also that the Brdička current, i_B, at lower concentrations of Co(III), lower than 2×10^{-4} M in this case, can be expressed by

$$i_B = AFk_B\Gamma f_{Co} \quad (1)$$

where A is the electrode surface area, F Faraday constant, k_B a constant representing the Brdička current-activity of the protein studied, Γ the surface concentration of the protein adsorbed on the electrode surface, and f_{Co} the flux of cobalt ion at the electrode surface. It has also been shown[10,11] that the adsorption of protein on the mercury electrode surface at −1.4 V is controlled by diffusion and that Γ can be estimated by Koryta's equation.[12] The cobalt ion flux at the dme is given by Ilkovič theory. Thus the k_B value of horse cyt-c was determined by applying Eq. 1 to the Brdička current produced by horse cyt-c at −1.4 V, the diffusion coefficients of horse cyt-c and Co(III) being taken as 1.3×10^{-6} cm^2/s[13] and 7.5×10^{-6} cm^2/s,[11] respectively. The result is given in Table 1.

Figure 3 shows the temperature dependence of the polarograms of Brdička current produced by horse cyt-c from 10 °C to 25 °C. The current intensity at its maximum height (at −1.35 to −1.4 V) increased with rise in temperature. In contrast, it decreased at its shoulder at −1.5 V. The behavior is similar to that of SS- and/or SH-containing proteins.[10,14]

Brdička Current of Horse Cyt-c in the Presence of Other Metal Ions. In the presence of Co(II), cobaltous chloride, in place of Co(III), horse cyt-c gave a characteristic catalytic current practically the same in shape but slightly smaller in height than the catalytic current produced by horse cyt-c in the presence of Co(III). In the presence of Ni(II), nickel chloride,

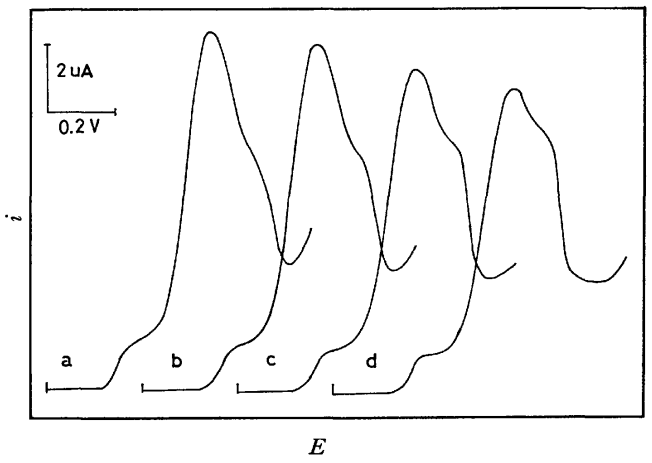

Fig. 3. Temperature dependence of d.c. polarograms of Brdička current of 4.0×10^{-6} M horse cyt-c in the base solution containing 2.0×10^{-4} M Co(III); temperature: (a) 25, (b) 20, (c) 15, and (d) 10 °C. Polarogramsa re recorded from −0.9 V.

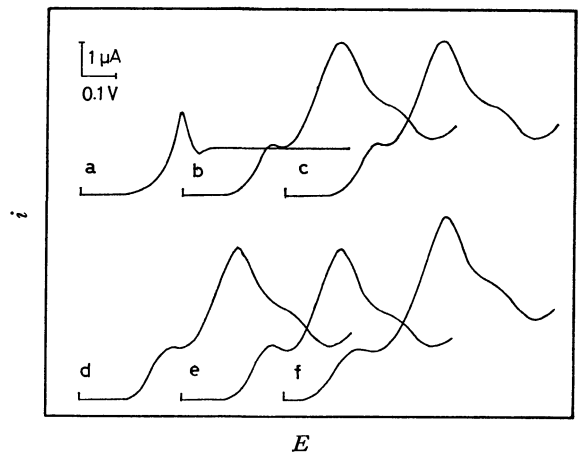

Fig. 4. D.c. polarograms of (a) 2.0×10^{-4} M Co(III) in the base solution and of 4.0×10^{-7} M cyt-c from (b) horse, (c) chicken, (d) tuna, (e) *C. krusei*, and (f) *S. cerevisiae* in (a). Polarograms are recorded from -0.9 V.

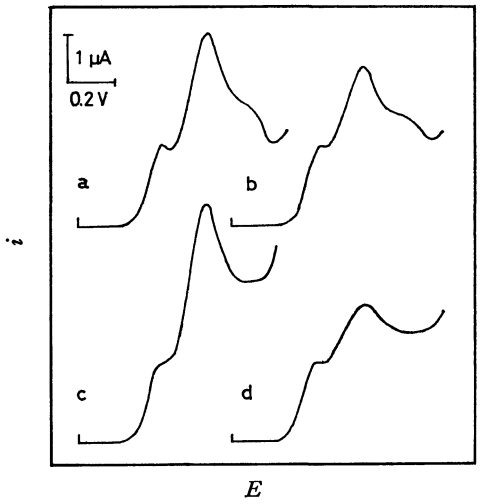

Fig. 5. D.c. polarograms of (a) native horse cyt-c, (b) CM-Cyt-c, (c) Co-cyt-c, and (d) porphyrin cyt-c each at 4.0×10^{-7} M in the base solution containing 2.0×10^{-4} M Co(III). Polarograms are recorded from -0.8 V.

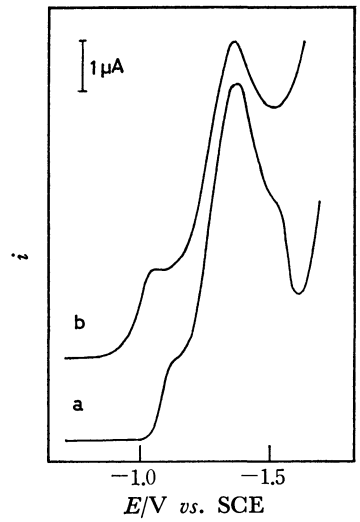

Fig. 6. D.c. polarograms of (a) 4.0×10^{-6} M native horse cyt-c and (b) 4.0×10^{-6} M apo-cyt-c in the base solution containing 2.0×10^{-4} M Co(III).

also catalytic current, though rather small, was produced. No catalytic current was observed when Co(III) was replaced by Cu(II), cupric nitrate, Zn(II), zinc chloride, and Mn(II), manganese chloride, each of 2×10^{-4} M.

Brdička Current of Cytochromes c from Other Sources. Figure 4 shows d.c. polarograms of cyt-c from five different sources at 4×10^{-7} M in a base soution containing 2×10^{-4} M Co(III). Chicken cyt-c and tuna cyt-c (Fig. 4, c and d) gave polarograms practically the same in both shape and height as horse cyt-c (Fig. 4b). *C. krusei* cyt-c also gave polarograms practically the same as horse cyt-c (Fig. 4e). At higher concentrations ($>2\times10^{-6}$ M), however, polarograms of *C. krusei* cyt-c were appreciably smaller in height as compared with those of horse cyt-c. *S. cerevisiae* cyt-c (Fig. 4f) gave polarograms which were different in shape and height from the four cytochromes mentioned above. The difference should be attributed to the existence of a free thiol group due to another cysteine residue.[15] k_B-values of these proteins determined by applying Eq. 1 to their Brdička currents at -1.4 V are given in Table 1.

Brdička Current of Modified Horse Heart Cytochromes. Figure 5 shows d.c. polarograms produced by (a) native horse cyt-c, (b) CM-cyt-c, (c) Co-cyt-c, and (d) porphyrin cyt-c each of 4×10^{-7} M in a base solution containing 2×10^{-4} M Co(III). The Brdička current of CM-cyt-c was very similar in shape to but smaller in height than that of native horse cyt-c. The Brdička currents of Co-cyt-c and porphyrin cyt-c differed more or less in shape and height from that of native horse cyt-c. Brdička currents of these modified proteins also have been found to follow Eq. 1. Their k_B values at -1.4 V are summarized in Table 1.

Apo-cyt-c gave Brdička current characteristic of denatured SS- and/or SH-containing proteins[10] (Fig. 6).

Brdička Current of D. vulgalis Cyt-c_3. Figure 7 and 8 show d.c. polarograms of *D. vulgaris* cyt-c_3 at four different concentrations in a base soution containing 2×10^{-4} M Co(III) at the dme and voltammograms of 4×10^{-7} M *D. vulgaris* cyt-c_3 at two exposure times at the hmde, respectively. Voltammograms of native cyt-c are also shown in Fig. 8. At lower surface concentration of adsorbed protein, *i.e.* at low bulk concentration with the dme or at smaller exposure time with the hmde, the polarograms (Fig. 7) and voltammograms (Fig. 8) of *D. vulgaris* cyt-c_3 were very similar in shape to but about double in height as compared with those of horse cyt-c. k_B-value of *D. vulgaris* cyt-c_3 determined at low protein concentrations at -1.4 V is given in Table 1. At high surface concentration of adsorbed protein, however, appreciable difference was observed especially at negative potential region (Figs. 1, 7, and 8).

Discussion

The polarograms of the Brdička current produced by Brdička current-active proteins are characteristic

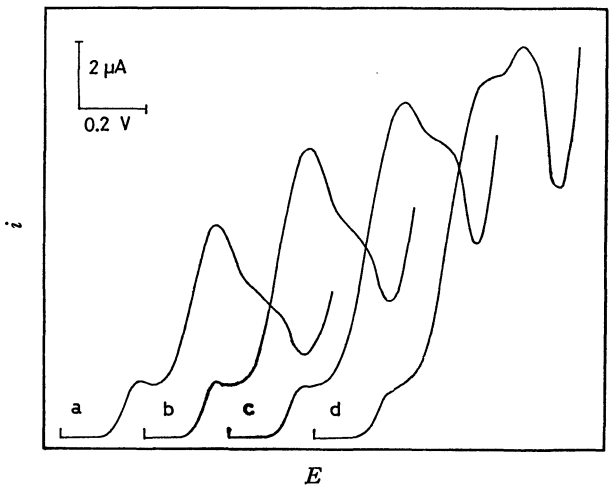

Fig. 7. D.c. polarograms of Brdička current of *D. vulgaris* cyt-c_3 at (a) 5.7×10^{-7}, (b) 1.7×10^{-6}, (c) 3.6×10^{-6}, and (d) 6.4×10^{-6} M in the base solution containing 2.0×10^{-4} M Co(III). Polarograms are recorded from −0.9 V.

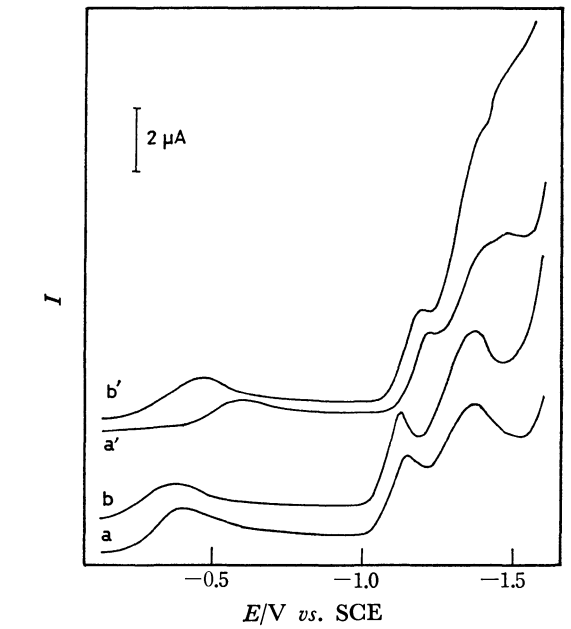

Fig. 8. Voltage-sweep voltammograms of (a and a') 4.0×10^{-7} M horse cyt-c at exposure time: 30 and 60 s, respectively and of (b and b') 4.0×10^{-7} M *D. vulgaris* cyt-c_3 at exposure time: 30 and 60s, respectively in the base solution containing 2.0×10^{-4} M Co(III) at the hmde.

of the proteins examined under specified conditions. Equation 1 predicts that the Brdička current is controlled by two factors, k_B and Γ. At and near −1.4 V the proteins we studied are very strongly adsorbed on the mercury electrode surface. At low bulk concentrations of the proteins, Γ at the dme surface can be evaluated by Koryta's equation, $\Gamma=(6/7)(D_p t_d/(3\pi/7))^{1/2}c_p$ *i.e.* as a function of the bulk concentration, c_p, and the diffusion constant, D_p, of the protein and the age of a mercury drop, t_d, at the dme. With increasing negative potential, however, the proteins become less strongly adsorbed on mercury electrode surface and Γ can no longer be evaluated by Koryta's equation. Evaluation of Γ, which is now a function also of the electrode potential, becomes very difficult.[10] In the following, quantitative analysis of the Brdička current-activities of the proteins is limited to k_B-values at −1.4 V, where Koryta's equation is valid to evaluate Γ. It is noted, however, the potential dependence of Γ and that of k_B are responsible for determining the polarographic wave-form of Brdička current characteristic of the proteins examined, especially at negative potential region.

Table 1. Polarographic catalytic activities at −1.4 V of cytochromes c at pH 9.4

Protein	n_H	n_S	k_B / 10^{12} cm^2 mol^{-1}	6th ligand
Cytochrome c				
horse	1	0	4.2	Met[15]
chicken	1	0	4.2	Met
tuna	1	0	4.2	Met
C. krusei	1	0	4.2	Met
S. cerevisiae	1	1	5.8	Met
Modified cytochrome (horse)				
CM-cyt-c	1	0	2.3	Lys[19]
Co-cyt-c	1	0	4.7	Met[21]
porphyrin cyt-c	1	0	1.4	—
apo-cyt-c	0	2	2.2	—
Cytochrome c_3				
D. vurgaris	4	0	8.8	Lys[22] or His[23]

k_B(−1.4 V)-values of various proteins are given in Table 1, in which n_H and n_S are the numbers of heme groups and SH (plus 2×SS) groups, respectively, in one protein molecule. D.c. polarograms (Fig. 4) and k_B(−1.4 V)-values of horse, chicken, and tuna cyt-c indicate that the Brdička current-activities of these mitochondrial cytochromes are the same in spite of a difference in amino acid composition among these proteins. This indicates that the Brdička current-activity with these cytochromes is primarilly due to the heme group in their molecules.

C. krusei cyt-c also has the same activity as that of mitochondrial cytochromes at lower surface concentration of the adsorbed proteins (Fig. 4 and Table 1). At high surface concentration, however, a difference in Brdička current-activity was observed between *C. krusei* cyt-c and the mitochondrial cytochromes. This might be due to the fact[15] that the amino acid composition of *C. krusei* cyt-c differs from that of mitochondrial cytochromes and is characterized by a high content of proline. When proteins are adsorbed on mercury electrode surface, their conformational states change more or less.[16,17] The conformational state of protein adsorbed on water-air interface is highly dependent on the concentration of protein in the bulk of solution, from which the adsorption of proteins takes place.[18]

The difference in amino acid composition between *C. krusei* cyt-c and mitochondrial cytochromes c may cause a difference in the conformation of the proteins adsorbed on mercury electrode surface. The Brdička current can be interpreted to be due to the catalytic action of Co(0)-protein complex formed on electrode surface. The k_B-value depends on the intrinsic catalytic activity and stability of the Co(0)-protein complex, which are determined by the conformational state of protein adsorbed on the electrode surface.

The Brdička current-activity of *S. cerevisiae* cyt-c should be interpreted as the sum of the activity of a heme group and that of an SH group. The average $k_B(-1.4\ V)/n_S$ value of five SS- and/or SH-containing proteins (bovine serum albumin, lysozyme, ribonuclease, trypsin, and pepsin) was determined to be $1.4\pm0.2\times10^{12}$ cm^2/mol.[10] Thus $k_B(-1.4\ V)=5.8\times10^{12}$ cm^2/mol of *S. cerevisiae* cyt-c can be interpreted as the sum of $k_B(-1.4\ V)=4.2\times10^{12}$ cm^2/mol of the heme group and $k_B(-1.4\ V)=1.6\times10^{12}$ cm^2/mol of the SH group.

In the presence of adsorbed SS- and/or SH-containing protein on the electrode surface the reduction step Co(II) to Co(0) shifts positively by 0.2 V.[11,14] An interesting feature of d.c. polarograms and voltammograms of the Brdička current of horse cyt-c is that the reduction potential of Co(II) to Co(0) is not or only slightly (less than ±30 mV) affected by the presence of the adsorbed protein on electrode surface. When SS and/or SH groups coexist, as in the case of *S. cerevisiae* cyt-c (Fig. 4), the reduction step Co(II) to Co(0) shifts a great deal to positive potential (Fig. 6). The results indicate that the Brdička current produced by the cytochromes is due to the heme group in them.

When the heme group of horse cyt-c was modified, the Brdička current-activities of the proteins were drastically changed as expected from the above conclusion. The removal of the central metal atom from the heme reduced the activity to about one-third and also changed the shape of the Brdička current. Replacement of the sixth ligand of the heme iron from Met to Lys[19] also reduced the activity to almost one-half of the original value. At the potential where Brdička current is produced ferricytochrome c is reduced to ferrocytochrome c on electrode surface. This was confirmed by potential-controlled electrolysis of horse ferricytochrome c at -1.4 V on mercury pool electrode, the electrolyzed solution showing an absorption spectrum characteristic of ferrocytochrome c.[4]

The sixth heme ligand of ferricytochrome c can change from Met to Lys, depending on the proton dissociation of ε-amino group of lysine with $pK=9.3$.[15] Upon reducing ferricytochrome c with dithionite or hydrated electron[15,20] in a basic solution (pH 11) a ferro-form having lysine as the sixth ligand is produced transiently, with a subsequent relaxation step to Met-liganded ferrocytochrome c within several hundred milliseconds. We may thus conclude that the Met-liganded ferrocytochrome c plays a dominant role in producing the Brdička current of native cytochromes in ammoniacal buffer of pH 9.4. Replacement of the central metal atom from iron to cobalt resulted in a slight increase in the Brdička current-activity of cytochrome. The sixth ligand is methionine for both cobalti- and cobalto-forms of Co-cyt-c.[21]

The fact that $k_B(-1.4\ V)$-value of CM-cyt-c is about one-half of $k_B(-1.4\ V)$-value of native cytochromes is of interest in view of the result that the $k_B(-1.4\ V)$-value of *D. vulgaris* cyt-c_3, 8.8×10^{12} cm^2/mol, is approximately equal to $4\times k_B(-1.4\ V)$-value of CM-cyt-c, $4\times2.3\times10^{12}$ cm^2/mol, indicating that the sixth ligands of four hemes of *D. vulgaris* cyt-c_3 are lysine. This is in line with the proposed sixth ligands of the four hemes on the basis of laser raman spectroscopy,[22] though a proposed His-liganded cytochrome c_3[23] is not excluded since the polarographic effect of replacement of the sixth ligand from Met to His is not clear at present. The observed difference between polarograms and voltammograms of cyt-c_3 and cyt-c at higher concentrations should be interpreted in a similar way to that discussed above on Brdička current of *C. krusei* cyt-c.

We are grateful to Prof. Seiyo Sano for his help in preparing porphyrin cyt-c, and to Prof. Tatsuhiko Yagi, Shizuoka University, for the supply of *D. vulgaris* cyt-c_3. This work was supported by a Grant-in-Aid from the Ministry of Education.

References

1) C. Carruthers, *J. Biol. Chem.*, **171**, 641 (1947).
2) C. Carruthers and V. Suntzeff, *Anal. Biochem.*, **17**, 261 (1948).
3) B. A. Kuznetsov, *Experientia Suppl.*, **18**, 381 (1971).
4) W. D. Butt and D. Keillin, F. R. S., *Proc. R. Soc. London, Ser. B*, **156**, 429 (1962).
5) J. Babul and E. Stellwagen, *Biochemistry*, **11**, 1195 (1972).
6) A. B. Robinson and M. D. Kamen, "Structure and Function of Cytochromes," ed by K. Okunuki, M. D. Kamen, and I. Sekuzu, University of Tokyo Press, Tokyo (1968), p. 383.
7) L. C. Dickerson and J. C. W. Chien, *Biochemistry*, **14**, 3526 (1975).
8) J. M. Vanderkool, F. Adar, and M. Erecinska, *Eur. J. Biochem.*, **64**, 381 (1976).
9) E. Stellwagen and R. Rysavy, *J. Biol. Chem.*, **247**, 8074 (1972).
10) H. Kinoshita, Ph. D. Thesis, University of Kyoto, Kyoto, 1979.
11) M. Senda, T. Ikeda, and H. Kinoshita, *Bioelectrochem. Bioenerg.*, **3**, 257 (1976).
12) J. Koryta, *Collect. Czech. Chem. Commun.*, **18**, 206 (1953).
13) "CRC Handbook of Biochemistry," The Chem. Rubber Co., Cleaveland, Ohio, 1968.
14) B. Alexander, M. Brezina, and V. Kalous, *Collect. Czech. Chem. Commun.*, **28**, 210 (1963).
15) R. E. Dickerson and R. Timkovich, "The Enzymes XI," ed by P. Boyer, Academic Press, New York (1975), p. 397.
16) F. Sheller, M. Jänchen, and H-Jörg Prümke, *Biopolymers*, **14**, 1533 (1975).
17) T. Ikeda, K. Toriyama, and M. Senda, *Bull. Chem. Soc. Jpn.*, **52**, 1937 (1979).
18) a) H. B. Bull, *Adv. Protein. Chem.*, **3**, 95 (1947); b) L. K. James and L. G. Augenstein, *Adv. Enzym.*, **28**, 1 (1966).

19) a) M. Brunori, M. T. Wilson, and E. Antonini, *J. Biol. Chem.*, **247**, 6076 (1972); b) R. T. Eakin, L. O. Morgan, and N. A. Metmiyoff, *Biochemistry*, **14**, 4538 (1975).
20) I. Pecht and M. Faraggi, *Proc. Natl. Acad. Sci. U.S.A.*, **69**, 902 (1972).
21) L. C. Dickerson and J. C. W. Chien, *Biochemistry*, **14**, 3534 (1975).
22) T. Kitagawa, Y. Ozaki, J. Teraoka, Y. Kyogoku, and T. Yamanaka, *Biochim. Biophys. Acta*, **494**, 100 (1977).
23) a) C. M. Dobson, N. J. Hoyle, C. F. Geraldes, M. Bruschi, J. LeGall, P. E. Wright, and R. J. P. Williams, *Nature*, **249**, 425 (1974); b) C. C. McDonald, W. D. Phillips, and J. LeGall, *Biochemistry*, **13**, 1952 (1974).

Halogenotriphenyltin(IV) Adducts of Tetrakis(*t*-butyl isocyanide)-rhodium(I) Perchlorate. Preparation and Kinetics

Ryosho KUWAE and Toshio TANAKA*

Department of Applied Chemistry, Faculty of Engineering, Osaka University, Suita, Osaka 565

(Received July 3, 1979)

$[Rh(t\text{-BuNC})_4]ClO_4$ undergoes oxidative addition reactions with Ph_3SnX (X=Cl, Br) to give *cis*-$[Rh(Ph_3Sn)X(t\text{-BuNC})_4]ClO_4$. The adducts partly dissociate in solution to exist as an equilibrium mixture with the Rh(I) substrate and the addendum. Kinetics of the equilibrium reactions in three different organic solvents were studied spectrophotometrically under pseudo-first-order conditions with excess Ph_3SnX. Rate constants for the forward reaction (k_f) are strongly dependent on the solvent polarity; k_f increases in the order of 1,2-dichloroethane<acetone<acetonitrile, whereas those for the backward reaction are little dependent on the solvents. Activation parameters also were obtained for the X=Cl system in acetonitrile; ΔS^* for the forward reaction is $-99.2\ J\ mol^{-1}\ K^{-1}$, while that for the backward reaction is $+24.9\ J\ mol^{-1}\ K^{-1}$. These results indicate that the addition reactions proceed *via* a three-center transition state formed by the nucleophilic attack of the Rh(I) ion to the tin atom.

Low-valent square planar rhodium(I) and iridium(I) complexes are known to undergo oxidative addition reactions with alkyl, aryl, and metal halides to afford octahedral rhodium(III) and iridium(III) complexes.[1-4] Some of these reactions have been studied kinetically.[5-11] As the results, the oxidative addition reactions may be classified mechanistically into the following three types; (i) a mechanism similar to the Menschutkin type reaction,[5-7] (ii) radical mechanisms,[8,9] and (iii) the mechanism involving a three-center transition state.[10] These reactions kinetically studied so far, however, were all irreversible. The present work was undertaken to study some reversible oxidative addition reactions, which will give more clear insight into transition states of the reactions.

This paper reports the preparation and configuration of chloro- and bromotriphenyltin(IV) adducts with tetrakis(*t*-butyl isocyanide)rhodium(I) perchlorate, and the kinetic study on the adduct formation

Experimental

Materials. $[Rh(t\text{-BuNC})_4]ClO_4$ was prepared as described elsewhere.[12] Chloro- and bromotriphenyltin(IV) were prepared and purified according to the literature methods, mp 105—106 °C (lit,[13] 104—106 °C) and 122—123 °C (lit,[14] 120—121 °C), respectively. Acetonitrile and acetone used as the solvents for kinetic measurements were dried over P_2O_5 and $CaSO_4$, respectively, followed by distillation. 1,2-Dichloroethane used for the same purpose was purified by the usual method.[15]

Isolation of $[Rh(Ph_3Sn)X(t\text{-BuNC})_4]ClO_4$ *(X=Cl, Br).* An acetone (7 cm^3) solution containing $[Rh(t\text{-BuNC})_4]ClO_4$ (0.75 mmol) and Ph_3SnCl (2.3 mmol) was stirred for 4 h at room temperature, followed by the addition of ligroin (*ca.* 15 cm^3). The solution was allowed to stand for 2 d in a refrigerator to afford white plates of $[Rh(Ph_3Sn)Cl(t\text{-BuNC})_4]ClO_4$, which were collected by filtration and dried *in vacuo*. From the filtrate, the adduct was further obtained by the addition of ligroin (*ca.* 15 cm^3), followed by the same procedure, 60% yield as a whole. ν(Rh–Cl), 301 cm^{-1}. Found: C, 49.47; H, 5.60; N, 6.08%. Calcd for $C_{38}H_{51}Cl_2N_4O_4RhSn$: C, 49.59; H, 5.59; N, 6.09%. The Ph_3SnBr adduct, $[Rh(Ph_3Sn)Br(t\text{-BuNC})_4]ClO_4$, was similarly obtained as white needles in a 65% yield by the reaction of $[Rh(t\text{-BuNC})_4]ClO_4$ with Ph_3SnBr at the mole ratio of 1:3. Found: C, 47.13; H, 5.36; N, 5.82%. Calcd for $C_{38}H_{51}BrClN_4O_4RhSn$: C, 47.31; H, 5.33; N, 5.81%.

Kinetic and Other Measurements. Kinetic measurements were performed using a Union Giken SM-401 spectrophotometer and a 10 mm quartz cell equipped with a Union Giken MX-7 mixing apparatus thermostated to ±0.2 °C. Two reactant solutions were rapidly introduced into the cell by the mixing apparatus. The initial concentration of the Rh(I) substrate was 8.0×10^{-5} mol dm^{-3}. All the reactions were carried out under pseudo-first-order conditions, using at least twenty-fold excess of Ph_3SnX. The rate of reaction was determined by following the decay of absorbances at 381 nm (absorption maximum of the Rh(I) substrate in acetonitrile) or at 383 nm (absorption maxima in acetone and in 1,2-dichloroethane) with time.

Infrared and ^1H NMR spectra were recorded as described elsewhere.[12]

Results and Discussion

Configuration of the Adducts. The infrared spectrum of $[Rh(Ph_3Sn)Cl(t\text{-BuNC})_4]ClO_4$ in acetone (2.0×10^{-2} mol dm^{-3}) showed three ν(N≡C) bands at 2156, 2202, and 2230 cm^{-1}. The same spectrum was observed in an equimolar mixture (2.0×10^{-2} mol dm^{-3}) of $[Rh(t\text{-BuNC})_4]ClO_4$ with Ph_3SnCl in acetone. The 2156 cm^{-1} band was assigned to the Rh(I) substrate with a square planar configuration, on the basis of its coincidence with the ν(N≡C) frequency observed in an acetone solution containing $[Rh(t\text{-BuNC})_4]ClO_4$ alone. On the other hand, the 2202 and 2230 cm^{-1} bands are due to the adduct, because of their proximity in positions to the ν(N≡C) bands exhibited by the adduct in Nujol mulls(2205 and 2238 cm^{-1}). When one more equivalent Ph_3SnCl was added to the equimolar solution, the two high frequency bands were intensified at the expense of the low frequency one. It is therefore suggested that the adduct partly dissociates in acetone to exist as an equilibrium mixture with the Rh(I) substrate and the addendum. The appearance of the two ν(N≡C) bands assignable to the adduct indicates its *cis* configuration in an octahedral geometry around the rhodium ion, as shown in **1**. This configuration was confirmed also by ^1H NMR spectra. A chloroform-d_1 solution of $[Rh(t\text{-BuNC})_4]ClO_4$ (5.0×10^{-2} mol dm^{-3}) exhibited a triplet signal due to the *t*-BuNC protons at δ 1.58 ($J(H-^{14}N)=2$ Hz). Upon addition of excess Ph_3SnCl (5.0×10^{-1}

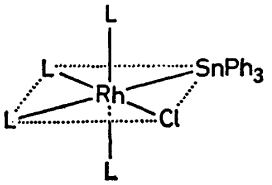

1: L=*t*-BuNC

mol dm^{-3}) to the solution, the triplet signal disappeared, instead three singlets[16] occurred at δ 1.27, 1.55, and 1.67 with the relative intensities of 2:1:1, which is compatible with the *cis* configuration of the adduct involving four *t*-BuNC placed in three magnetically different environments from one another. The same configuration is suggested also for the Ph_3SnBr adduct from its infrared and ^1H NMR spectra in acetone. Thus, the stoichiometry of the adduct formation is expressed as follow,

$$[Rh(t\text{-BuNC})_4]^+ + Ph_3SnX \rightleftharpoons [Rh(Ph_3Sn)X(t\text{-BuNC})_4]^+. \quad (1)$$

Kinetics and Mechanism. Figure 1 depicts the decay of the 381 nm band after mixing the Rh(I) substrate with Ph_3SnCl in acetonitrile. Plots of $\ln(A_t - A_\infty)$ *vs.* time, where A_t and A_∞ are absorbances at a time t and at the end of reaction respectively, showed a good linearity. Pseudo-first-order rate constants, k_{obsd}, were calculated by the least squares

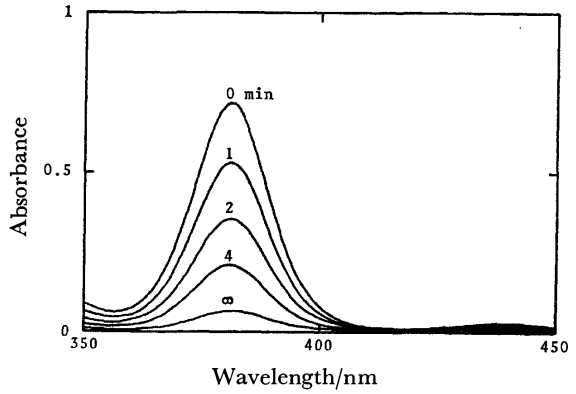

Fig. 1. Decay of the absorbance with time after mixing $[Rh(t\text{-BuNC})_4]ClO_4$ (8.0×10^{-5} mol dm^{-3}) with Ph_3SnCl (4.8×10^{-3} mol dm^{-3}) in acetonitrile at 25 °C, cell length = 10 mm.

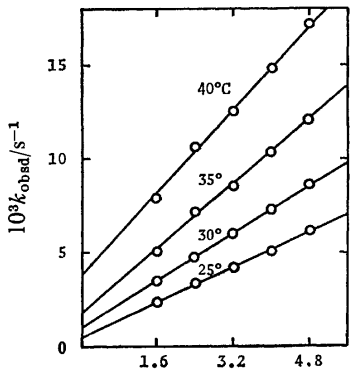

Fig. 2. Plots of k_{obsd} *vs.* $[Ph_3SnCl]$ for the reactions of $[Rh(t\text{-BuNC})_4]ClO_4$ (8.0×10^{-5} mol dm^{-3}) with Ph_3SnCl in acetonitrile at various temperatures.

method. As shown in Fig. 2, plots of k_{obsd} *vs.* the concentration of Ph_3SnCl at each temperature give a straight line with non-zero intercept which is characteristic of reversible reactions. In the presence of excess Ph_3SnCl, k_{obsd} is expressed as,[17]

$$k_{obsd} = k_f[Ph_3SnCl] + k_b \quad (2)$$

where k_f and k_b stand for the rate constants of forward and backward reactions of Eq. 1, respectively. The k_f and k_b values were obtained from the slope and intercept of the straight lines, respectively (Fig. 2). The rate constants for the $[Ph(t\text{-BuNC})_4]ClO_4$–$Ph_3SnCl$ system in acetone and 1,2-dichloroethane and for the $[Ph(t\text{-BuNC})_4]ClO_4$–$Ph_3SnBr$ system in three different solvents were similarly obtained. The results are listed in Table 1, which contains also equilibrium constants $K(=k_f/k_b)$. The ClO_4^- anion may not participate in the reactions, because the rate of reactions was little influenced by the presence of excess ClO_4^-. The reaction rate was hardly altered also by changing the slit width of the spectrophotometer. Thus, the light intensity has no appreciable effect upon the reaction rate, confirming that radical mechanisms may be ruled out for the present reactions.

The rate constant of forward reactions is strongly dependent on the solvent; k_f increases in the order 1,2-dichloroethane<acetone<acetonitrile in the two reaction systems. On the contrary, the rate constant of backward reactions is little dependent on solvent

Table 1. Rate and equilibrium constants for the reactions of $[Rh(t\text{-BuNC})_4]ClO_4$ with Ph_3SnX

X	Solvent	Temp °C	k_f[a] dm^3 mol^{-1} s^{-1}	10^3k_b[a] s^{-1}	K dm^3 mol^{-1}
Cl	Acetonitrile	25	1.18 ±0.01	0.502±0.014	2350± 70
		30	1.57 ±0.01	1.02 ±0.01	1540± 10
		35	2.16 ±0.04	1.78 ±0.14	1220±100
		40	2.80 ±0.06	3.68 ±0.19	762± 43
	Acetone	35	0.416±0.012	1.70 ±0.04	245± 9
	1,2-Dichloroethane	35	0.275±0.004	1.39 ±0.01	198± 3
Br	Acetonitrile	35	1.39 ±0.02	1.03 ±0.06	1340± 80
	Acetone	35	0.297±0.006	0.855±0.018	348± 10
	1,2-Dichloroethane	35	0.134±0.003	0.724±0.009	185± 5

a) k_f and k_b stand for rate constants of the forward and backward reactions, respectively.

TABLE 2. ACTIVATION AND THERMODYNAMIC PARAMETERS FOR THE REACTION OF $[Rh(t\text{-BuNC})_4]ClO_4$ WITH Ph_3SnCl IN ACETONITRILE AT 25 °C

Reaction	E_a / kJ mol^{-1}	ΔH^* or ΔH° / kJ mol^{-1}	ΔS^* or ΔS° / J mol^{-1} K^{-1}	ΔG^* or ΔG° / kJ mol^{-1}
Forward	45.8±0.8	43.3±0.8	−99.2± 2.6	72.9± 2.3
Backward	102 ±3	99.5±2.5	24.9± 8.1	92.1±30.0
Equilibrium	—	−56.2±3.7	−124 ±12	−19.2± 2.2

polarity (Table 1). Accordingly, the equilibrium constant, K, undergoes the solvent effect to the same extent as k_f. This result suggests that an activated complex in the transition state has virtually the same polarity as the final product.

Table 2 lists activation and thermodynamic parameters for the $[Rh(t\text{-BuNC})_4]ClO_4$–$Ph_3SnCl$ system in acetonitrile at 25 °C. The entropy of activation, ΔS^*, for the forward reaction is large negative value, which implies that the activated complex is subjected to stereochemical restriction in the transition state. On the other hand, the ΔS^* value for the backward reaction is small, suggesting the activated complex may assume a structure which resembles that of the adduct. It is well known that low-valent transition metal complexes function as nucleophiles.[2] In the present reaction the Rh(I) ion of $[Rh(t\text{-BuNC})_4]ClO_4$ may initially attack the tin atom which is an electron deficient part of the addendum. In the Menschutkin-type oxidative addition reactions which have been suggested to proceed *via* a linear transition state $M^{\delta+}\cdots R\cdots X^{\delta-}$ (M=metal complex, RX=alkyl halide), the rate constant of the reaction for X=Br has been reported to be several hundred times larger than that for X=Cl.[6] In contrast to this, the k_f value in the present reactions is larger in Ph_3SnCl than in Ph_3SnBr in any solvents (Table 1), suggesting that the transition state may be different from that of the Menschutkin-type reactions. Thus, the oxidative addition of Ph_3SnX toward $[Rh(t\text{-BuNC})_4]ClO_4$ may proceed *via* a three-center (asymmetric) transition state which may involve deformation of the $[Rh(t\text{-BuNC})_4]^+$ moiety from a square planar configuration to some extent as follow.

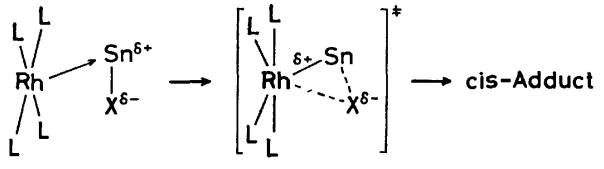

L=*t*-BuNC

Similar transition states have been proposed for the reactions of $IrCl(CO)(PR_3)_2$ (R=alkyl, aryl) with MeI and $PhCH_2X$ (X=Cl, Br).[10]

The authors are grateful to the Ministry of Education for support of this work through Grant-in-Aid for Scientific Research, No. 147074.

References

1) J. P. Collman and W. R. Roper, *Adv. Organomet. Chem.*, **7**, 53 (1968).
2) D. F. Shriver, *Acc. Chem. Res.*, **3**, 231 (1970).
3) J. Halpern, *Acc. Chem. Res.*, **3**, 386 (1970).
4) J. W. Dart, M. K. Lloyd, R. Mason, and J. A. McCleverty, *J. Chem. Soc., Dalton Trans.*, **1973**, 2046.
5) P. B. Chock and J. Halpern, *J. Am. Chem. Soc.*, **88**, 3511 (1966).
6) A. J. Hart-Davis and W. A. G. Graham, *Inorg. Chem.*, **10**, 1653 (1971).
7) M. Kubota, G. W. Kiefer, R. M. Ishikawa, and K. E. Bencala, *Inorg. Chim. Acta*, **7**, 195 (1973).
8) J. S. Bradley, D. E. Connor, D. Dolphin, J. A. Labinger, and J. A. Osborn, *J. Am. Chem. Soc.*, **94**, 4043 (1972).
9) S. Otsuka and K. Ataka, *Bull. Chem. Soc. Jpn.*, **50**, 1118 (1977).
10) R. Ugo, A. Pasini, A. Fusi, and S. Cenini, *J. Am. Chem. Soc.*, **94**, 7364 (1972).
11) W. H. Thompson and C. T. Sears, Jr., *Inorg. Chem.*, **16**, 769 (1977).
12) R. Kuwae and T. Tanaka, *Bull. Chem. Soc. Jpn.*, **52**, 1067 (1979).
13) H. Gilman and S. D. Rosenberg, *J. Am. Chem. Soc.*, **74**, 5580 (1952).
14) J. B. Pedley and H. A. Skinner, *Trans. Faraday Soc.*, **55**, 544 (1959).
15) J. A. Riddick and E. E. Toops, Jr., "Technique of Organic Chemistry," Interscience, New York (1955), Vol. 7, p. 415.
16) Spin-spin couplings of the isocyanide-protons with the ^{14}N nucleus in some isocyanide metal complexes are often not observed; T. Sawai and R. J. Angelici, *J. Organomet. Chem.*, **80**, 91 (1974).
17) A. A. Frost and R. G. Pearson, "Kinetics and Mechanism," 2nd ed, Wiley, New York (1961), p. 186.

Synthetic Inorganic Ion-exchange Materials. XXVI. Ion-exchange Properties of Crystalline Antimonic(V) Acid towards Noble Metals in Nitric Acid Media

Mitsuo ABE* and Mitsuo AKIMOTO**

Department of Chemistry, Faculty of Science, Tokyo Institute of Technology, Ookayama, Meguro-ku, Tokyo 152

(Received July 7, 1979)

A study of the distribution coefficients on crystalline antimonic(V) acid (C-SbA) shows an unusual affinity series {Pt(IV) < Au(III) < Pd(II) ≪ Hg(I), Hg(II), Ag(I)} for microamounts of noble metal ions in nitric acid solution, as compared with ion-exchange resins in strong acid type. Extremely high adsorptive properties are found on the exchange system of Hg(II) and Ag(I), even in relatively high concentrations of nitric acid solution. The ion-exchange studies for macroamounts indicate that a solid solution forms for the system of the Ag(I) ions and hydrogen ions in C-SbA, while two solid phases are presented for the system of Hg(II) ions and hydrogen ions.

There has been a large amount of research on synthetic inorganic ion-exchange materials because of their thermal stability and resistance to radiation, and high selectivities for certain elements.[1-6]

Among these inorganic ion-exchangers, crystalline antimonic(V) acid (C-SbA) has been of interest in the last decade due to its high cation-exchange capacity and high selectivities for certain elements.[7-10] The increasing order of selectivities for microquantities show; $Li^+ < K^+ < Cs^+ < Rb^+ < Na^+$ for alkali metals,[8,10] $Mg^{2+} < Ba^{2+} < Ca^{2+} < Sr^{2+}$ for alkaline earth metals,[11] and $Ni^{2+} < Mn^{2+} < Zn^{2+} < Co^{2+} < Cu^{2+} < Cd^{2+}$ for transition metals[12] in nitric acid media. Extremely high absorptive ability was found for Na^+, Ca^{2+}, Sr^{2+}, and Cd^{2+} on C-SbA. The large differences in the distribution coefficients have been observed for several pairs of the elements. Some mutual separations can be achieved effectively for alkali metals,[8,10,13] Mg^{2+}–Ba^{2+}, Ba^{2+}–Sr^{2+}, Cs^+–Sr^{2+},[11] Ni^{2+}–Zn^{2+}, and Zn^{2+}–Cd^{2+} pairs[12] by using a relatively small C-SbA column.

Similar compounds to C-SbA have been reported, *e.g.* polyantimonic acid (PAA) by Lefebrve *et. al.*[14,15] and Baetsle and Huys,[16] and hydrated antimony pentoxide (HAP) by Girardi *et al.*[17]

This paper describes the ion-exchange properties of C-SbA for noble metal ions.

Experimental

Reagents. The antimony pentachloride (Yotsuhata Chemical Co., Ltd.) was used without further purification. The other reagents used were all analytical grade.

A solution of Ag(I), Hg(I), and Pd(II) was prepared by dissolving the corresponding nitrate salts with water and a solution of Hg(II) was prepared by dissolving the nitrate salt in 0.1 M (1 M = 1 mol dm^{-3}) nitric acid solution in order to prevent hydrolysis of Hg^{2+}. Tetrachloroauric(III) acid and hexachloroplatinic(IV) acid were used for preparing the solutions of Au(III) and Pt(IV).

Preparation of C-SbA as an Ion-exchange Material. C-SbA was prepared as described previously:[10,11] the precipitate obtained by the hydrolysis of antimony pentachloride was kept in the mother solution at 40 °C for more than 20 d. The precipitate was washed with cold demineralized water in a centrifuge (10000 rpm) until free from chloride ions, dried and the product ground and sieved (100—200 mesh size). The collected sample was rewashed with demineralized water in order to obtain a clear supernatant solution following batch equilibrium experiments and to improve the elution-flow rate.

Distribution Coefficients (K_d). The values for K_d for the noble metal ions were determined by batch operation as follows. C-SbA (0.250 g) was immersed in nitric acid solution (25.0 cm^3) containing 1×10^{-4} M of the metal ions at 30±0.1 °C with occasional shaking. The amount of metal ions adsorbed was determined from the changes in the concentration of the metal ions relative to the initial concentrations of the solution after equilibration. The concentrations of the metal ions were determined spectrometrically with *p*-diethylaminobenzalrhodanine for Ag(I), Hg(I), Hg(II), and Au(III), with tin(II) chloride for Pt(IV) and with sodium iodide and sodium sulfite for Pd(II).[18,19] The emf titration method was employed for determining the hydrogen ion concentration by means of a standardized sodium hydroxide solution.

Preparation of the Ion-exchanged C-SbA. The C-SbA ion-exchanged with Ag(I) in different degree was prepared by immersing C-SbA in 0.1 M $AgNO_3$ solution of which the volume contained amounts corresponding to 25, 50, or 80% of its theoretical capacity. The theoretical capacity (5.06 meq/g) may be estimated from the empirical formula $Sb_2O_5 \cdot 4H_2O$ assuming that one antimony atom gives one hydrogen ion available for ion-exchange.[20] In the case of C-SbA ion-exchanged with Hg(II), a solution containing 0.05 M $Hg(NO_3)_2$ in 0.1 M nitric acid solution was used. The fully ion-exchanged C-SbA with Ag(I) and Hg(II) was prepared by a breakthrough experiment as follows; a 0.1 M $AgNO_3$ was passed continuously through the C-SbA column of 0.5 g with a flow rate of 0.3 cm^3/min, and a 0.05 M $Hg(NO_3)_2$ solution containing 0.1 M HNO_3 was used for the fully ion-exchanged C-SbA. Injection was continued until the change in the concentration of metal ions between influent and effluent was negligible within the experimental error.

X-Ray Diffraction Analysis. The X-ray diffractions for the ion-exchanged C-SbA were determined using a JEOL X-ray Diffractometer Model, JDX-7E, with Ni-filtered Cu$K\alpha$ radiation.

Results and Discussion

The results of the TGA, DTA, and X-ray studies on C-SbA in the hydrogen ion form showed good

**Present address: Kugoh Middle School, 5-81, Kugoh-chō, Yokosuka-shi, Kanagawa 238.

agreement with earlier data.[10,20]

Adsorption of Noble Metal Ions. The time dependence on the adsorption of different metals was measured qualitatively in order to determine the equilibrium distribution coefficients (Fig. 1). Equilibrium was attained within 3, 4, and 7 d for Pd(II), Au(III), and Pt(IV) respectively. Complete adsorption (99—100%) was achieved for Ag(I), Hg(I), and Hg(II) within 24 h.

Distribution Coefficients. The equilibrium distribution coefficients of noble metal ions on C-SbA are shown in Fig. 2 as log-log plots of K_d *vs.* [HNO_3]. The slope, d log K_d/d log [HNO_3], for the Pd(II)–H^+ system is approximately 2 in the concentration range 0.5—2 M HNO_3 and approximately 1 in the range 0.05—0.5 M. Similar behavior has been found on Dowex 50W-X8, indicating the "ideal 2:1 ion-exchange reaction" of Pd^{2+}/H^+ at relatively high concentration of nitric acid solution. The reduction in slope may be explained in terms of the ion-exchange reaction of the $Pd(OH)^+$–H^+, since the $Pd(OH)^+$ species increases with decreasing concentration of hydrogen ions below 0.5 M HNO_3 from studies of the stability constant of the Pd(II)–OH^- system.[21] The slope was approximately 2 for the Pt(IV)–H^+ system, while the K_d value for Au(III) was independent of the concentration of nitric acid. It is known that in perchloric acid solution, the Pt(IV) ion is unaffected by cation-exchange resins such as Dowex 50, while in chloride solution the Pt(IV) ion gives stable chloride

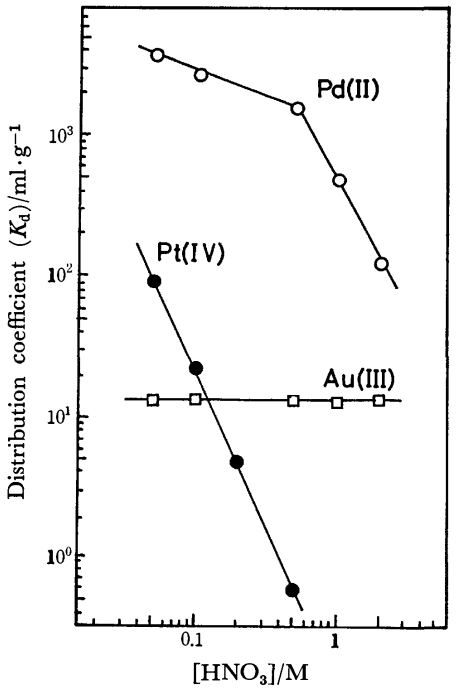

Fig. 2. Distribution coefficients of noble metals on C-SbA at different concentration of nitric acid solution. Initial concentration of the metals, $1.\times10^{-4}$ M. C-SbA, 0.250 g. Total volmue, 25.0 cm^3. Temperature, 30±0.1 °C.

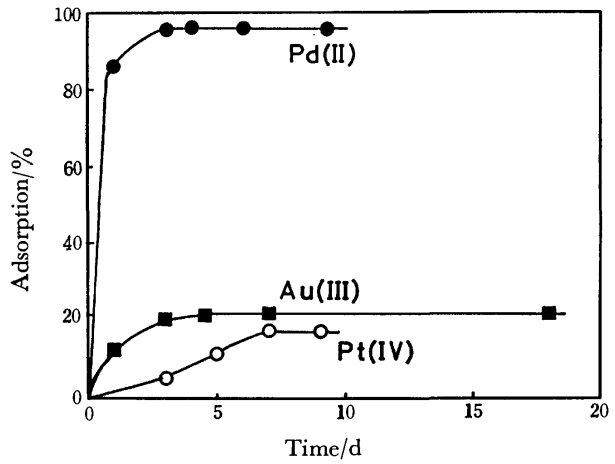

Fig. 1. Time dependence of the adsorption of noble metals on C-SbA in 0.2 M nitric acid solution. Initial concentration of metal ions, 1×10^{-4} M, C-SbA, 0.250 g. Total volume, 25.0 cm^3. Temperature, 30±0.1 °C.

complexes which can be retained quantitatively by anion-exchange resins.[22] On the ion-exchange system in aqueous solution, cationic species of Pt(IV) can not be found in the literature known so far. It has been reported that chloride and nitrate ions are unaffected by antimonic(V) acid in most media, but that phosphate ions can be adsorbed in phosphoric acid solutions.[23] The adsorptive behavior of Pt(IV) and Au(III) may be due to a difference in mechanism in the cation-exchange reaction.

The K_d values obtained are summarized in Table 1, the values on cation-exchange resin being included for comparison. The results obtained on Dowex 50W-X8 are in fairly good agreement with the results reported by Strelow *et al.*[24] Extremely high values of $K_d(>10^4)$ were observed for Ag(I), Hg(I), and Hg(II) on C-SbA in the concentration range 0.05—2 M HNO_3, compared with the ion-exchange resins. The following affinity series was found for C-SbA: Pt(IV)<Au(III)<Pd(II)≪Hg(I), Hg(II), Ag(I) in 0.5 M HNO_3 solution.

TABLE 1. DISTRIBUTION COEFFICIENTS FOR NOBLE METALS ON C-SbA IN 0.5 M HNO_3

Ion-exchanger	Pt(IV)	Au(III)	Pd(II)	Hg(I)	Hg(II)	Ag(I)
C-SbA	0.56	32	1.5×10^3	$>10^4$	$>10^4$	$>10^5$
	Pt(IV)	Ag(I)	Au(III)	Hg(II)	Hg(I)	Pd(II)
Dowex 50W-X8	—	35	2.1×10^2	3.2×10^2	7.2×10^2	1.4×10^3
BIO-RAD AG50W-X8[a]	—	36.0	—	1.21×10^2	6.4×10^2	23.5

a) Data from Ref. 24.

Preparation of the Ion-exchanged C-SbA with Ag(I) and Hg(II). A solution containing Ag(I) or Hg(II) of macroamounts, corresponding to 25, 50, or 80% of the theoretical capacity when added to C-SbA, the liberated hydrogen ions were found to be equivalent to the metal ions added. This indicates that complete adsorption was achieved in both systems in the determination of metals and hydrogen ions within experimental error. In the batch system of Hg(II)–H^+, especially a very small quantity ($\simeq 10^{-6}$ M) of Hg(II) was observed in the supernatant solution equilibrated with C-SbA.

The breakthrough curves show that hydrogen ions are liberated quantitatively for an equivalent uptake of Hg(II) and Ag(I) ions (Fig. 3). The curves obtained are steep, indicating a reasonable rate of ion-exchange for the metal ions. The breakthrough capacities were found to be 4.95 meq/g for Ag(I) and 5.06 meq/g for Hg(II), which are in good agreement with the theoretical capacity for C-SbA. A similar result for Ag(I) has been reported; 5.0 meq/g by Lefebrve and Gaymard[15] and 5.1±0.5 meq/g by Baetsle and Huys.[16] The color of the C-SbA in the H^+ form changed from which to yellow on complete exchange of Ag(I) or Hg(II).

The addition of a 5 M nitric acid solution to the fully exchanged C-SbA with Hg(II) produced very small quantities ($\simeq 10^{-5}$ M) of Hg(II) which were found in the supernatant solution (50 cm^3).

X-Ray Analysis. The X-ray diffraction patterns of the C-SbA ion-exchanged with Hg(II) revealed two solid phases present on the C-SbA exchanged

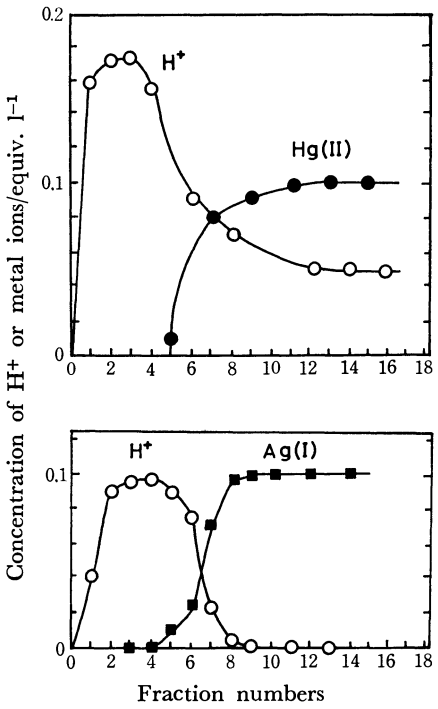

Fig. 3. Breakthrough curves for Hg(II) and Ag(I) on C-SbA. C-SbA column, 0.5 g. Flow rate, 0.3 cm^3/min.
Influent: Hg(II), 0.05 M $Hg(NO_3)_2$ in 0.1 M HNO_3, Ag(I); 0.1 M $AgNO_3$. -○-: H^+, -●-: Hg(II), -■-: Ag(I).

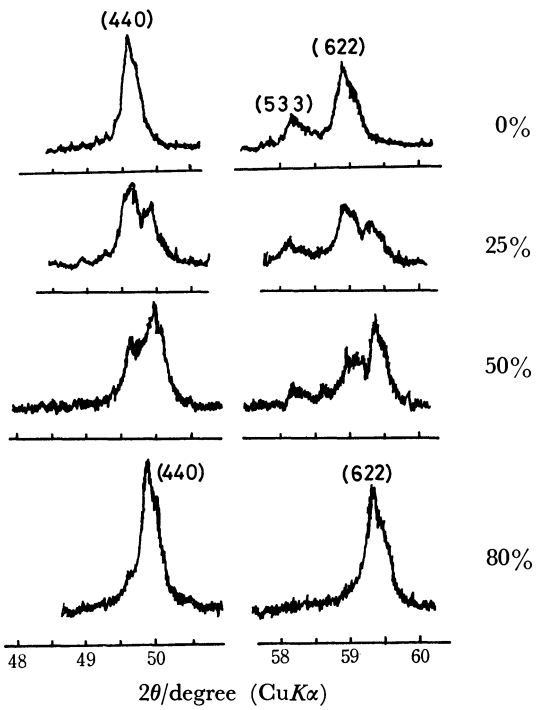

Fig. 4. Schmatic diagrams of X-ray diffraction patterns for (444), (533), and (622) planes of the C-SbA ion-exchanged with Hg(II) at different loading.

by approximately 10—80%. Typical patterns *viz.* (440), (533), and (622) are illustrated in Fig. 4. Both phases belong to the crystal system of Fd3m with a lattice constant of 10.37_5 and 10.31_4 Å. The former phase may be identified as the unexchanged C-SbA in the H^+ form. The diffraction intensities of the latter phase increase with increasing degree of ion-exchanging Hg(II) ions while those of the former decrease simultaneously. A single phase was observed for the C-SbA ion-exchanged by several metal ions, such as the alkali metals,[25] the alkaline earth metals,[26] and transition metals.[27] It has been established that the presence of two phases during ion-exchange is often observed in the system of ion-exchange on crystalline zirconium- or titanium-phosphate exchangers.[28–30] The presence of two solid phases is however the first case in the ion-exchange systems of C-SbA.

The calculated lattice constants for the C-SbA ion-exchanged with Hg(II) and Ag(I) are plotted against the loading of the ion-exchanging metal ions in Fig. 5. The lattice constants of the C-SbA ion-exchanged with Ag(I) decreased continuously with the degree of exchanging Ag(I) ions indicating that a solid solution forms for the ion-exchange system of the Ag^+ and hydrogen ions in the C-SbA. The X-ray diffraction data for the fully ion-exchanged C-SbA with Ag(I) and Hg(II) ions are summarized in Table 2. A remarkable decrease on the diffraction intensities of the (111) and (311) planes was observed for both ion-exchanged C-SbA, while the (222) plane increased simultaneously. Similar behavior was observed on the C-SbA ion-exchanged with relatively heavy metal ions sucn as Ag^+, Rb^+, Cs^+, Sr^{2+}, and Ba^{2+}.[25,26,31] Further ion-exchange studies Hg(II) with

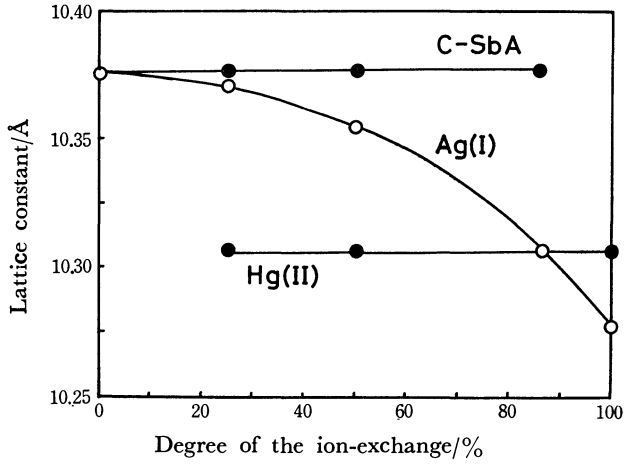

Fig. 5. Lattice constants as a function of the loading of the C-SbA ion-exchanged with Hg(II) or Ag(I). -○-: Ion-exchanged with Ag(I), -●-: ion-exchanged with Hg(II).

TABLE 2. X-RAY DIFFRACTION DATA OF THE C-SbA EXCHANGED WITH Ag(I) AND Hg(II)

Exchanged	H^+		Ag(I)		Hg(II)	
hkl	*d*/Å	I/I_0	*d*/Å	I/I_0	*d*/Å	I/I_0
111	5.970	100	5.953	2		
311	3.127	54	3.098	2		
222	2.995	62	2.964	100	2.977_5	100
400	2.594	13	2.567_9	40	2.579_0	34
331	2.377_9	11				
422	2.118_0	2				
333	1.995_6	16				
440	1.833_0	29	1.818_3	43	1.823_4	48
531	1.753_0	21	1.737_1	43		
533	1.582_4	9				
622	1.563_5	23	1.549_5	33	1.555_0	62
444	1.497_5	5	1.483_2	9	1.489_7	8
711	1.452_6	13	1.439_7	1		
713	1.350_6	10				
ā[a]	10.37_5		10.28_0		10.31_4	

a) ā: Mean lattice constant.

regard to irreversibility will be published at a later date.[32]

References

1) V. Veselý and V. Pekárek, *Talanta*, **19**, 219 (1972).
2) V. Pekárek and Veselý, *Talanta*, **19**, 1245 (1972).
3) M. Abe, *Bunseki Kagaku*, **23**, 1254 (1974).
4) M. Abe, *Bunseki Kagaku*, **23**, 1561 (1974).
5) M. Qureshi, S. Z. Qureshi, J. P. Gupta, and H. S. Rathore, *Sep. Sci.*, **7**, 615 (1972).
6) A. K. De and A. K. Sen, *Sep. Sci. Technol.*, **13**, 519 (1978).
7) M. Abe and T. Ito, *Nippon Kagaku Zasshi*, **86**, 1259 (1965).
8) M. Abe and T. Ito, *Nippon Kagaku Zasshi*, **87**, 1174 (1966).
9) M. Abe and T. Ito, *Bull. Chem. Soc. Jpn.*, **40**, 1013 (1967).
10) M. Abe and T. Ito, *Bull. Chem. Soc. Jpn.*, **41**, 333 (1968).
11) M. Abe and K. Uno, *Sep. Sci. Technol.*, **14**, 355 (1979).
12) M. Abe and K. Kasai, *Sep. Sci. Technol.*, **14**, 895 (1979).
13) M. Abe, *Sep. Sci. Technol.*, **13**, 347 (1978).
14) J. Lefbrve, *C. R. Hebd. Seances Acad. Sci.*, **260**, 5575 (1965).
15) J. Lefbrve and F. Gaymard, *C. R. Hebd. Seances Acad. Sci.*, **260**, 6911 (1965).
16) L. H. Baetsle and D. Huys, *J. Inorg. Nucl. Chem.*, 30, **639** (1968).
17) F. Girardi, R. Pietra, and E. Sabbioni, *J. Radioanal. Chem.*, **5**, 141 (1970).
18) E. B. Sandell, "Colorimetric Determination of Trace Metals," 3rd ed, Interscience, New York (1959), p. 726.
19) N. Strafford and P. F. Wyatt, *Analyst*, **61**, 528 (1936).
20) M. Abe and T. Ito, *Bull. Chem. Soc. Jpn.*, **41**, 2366 (1968).
21) E. Martell and L. G. Sillén, "Stability Constants of Metal-ion Complexes," Special Publication No. 25, The Chem. Soc. Burlington House, London (1971), p. 25.
22) P. C. Stevenson, A. A. Franke, R. Borg, and W. Nervik, *J. Am. Chem. Soc.*, **75**, 4876 (1953).
23) M. Abe and T. Ito, *Denki Kagaku*, **33**, 175 (1965).
24) F. W. E. Strelow, R. Rethemeyer, and C. J. C. Bothma, *Anal. Chem.*, **37**, 106 (1965).
25) M. Abe, *J. Inorg. Nucl. Chem.*, **41**, 85 (1979).
26) M. Abe, *Bull. Chem. Soc. Jpn.*, **52**, 1386 (1979).
27) M. Abe and K. Sudoh, *J. Inorg. Nucl. Chem.*, in press.
28) A. Clearfild, W. L. Daux, A. S. Media, G. D. Smith, and J. R. Thomas, *J. Phys. Chem.*, **73**, 3424 (1969).
29) G. Alberti, P. Cardini-Galli, U. Costantino, and E. Torracca, *J. Inorg. Nucl. Chem.*, **29**, 571 (1969).
30) K. Takaguchi and I. Tomita, *J. Chromatogr.*, **118**, 263 (1976).
31) B. G. Novikov, F. A. Belinskaya, and E. A. Materova, *Vestn. Liningrad Univ. Fiz. Khim.*, **1971**, No. 4, 29.
32) M. Abe and M. Tsuji, 37th National Meeting of the Chemical Society of Japan, Yokohama, April 1978, Abstr. p. 60.

Structural Study of Optical Resolution. VII. The Crystal Structure of $(-)_{589}$-Oxalatobis(ethylenediamine)cobalt(III) Hydrogen-*d*-tartrate Dihydrate and Comparison between the Crystal Structures of the More- and Less-soluble Diastereoisomers

Masahiro KURAMOTO, Yoshihiko KUSHI, and Hayami YONEDA*

Department of Chemistry, Faculty of Science, Hiroshima University, Higashi-senda-machi, Hiroshima 730

(Received August 14, 1978)

The single crystals of the more-soluble diastereoisomeric salt including the hydrogen-*d*-tartrate anion as a resolving agent, $(-)_{589}$-[Co(ox)en_2]H-*d*-tart·$2H_2O$, have been newly obtained, and the crystal structure has been determined by three-dimensional X-ray analysis. The crystals are orthorhombic, space group $P2_12_12$, $Z=4$, $a=16.583(5)$, $b=14.186(5)$, and $c=7.403(2)$ Å. The structure was solved by the heavy-atom method and refined by the block-diagonal least-squares method to a conventional *R*-value of 0.044 for the 1907 independent reflections. One of the two ethylenediamine rings is of the *ob* form. The other ring has a conformational disorder, the proportion of the *ob* to the *lel* form being 50:50. The absolute configuration of the complex cation is denoted as $\Delta[(50\%\text{-}\delta, 50\%\text{-}\lambda)\delta]$. The framework of the crystal structure is built up of a stack of complex cations and H-*d*-tart anions along the c-axis in a "head-to-tail" arrangement. The shortest interatomic distance between the H-*d*-tart anions is 2.473 Å(O–H···O), while that between the complex cations is 2.995 Å (N–H···O). A comparison of the crystal structure of the more-soluble diastereoisomer with that of the less-soluble one revealed that the $\{\text{H-}d\text{-tart}\}_\infty$ chain is structurally different from that in the latter; the chain is spiral in the latter, but not in the former. The structural feature in the $\{\text{H-}d\text{-tart}\}_\infty$ chain is considered to play an important role in the discrimination of the chirality of the $[Co(ox)en_2]^+$ cation. The conformational disorder is discussed in connection with the dehydration of crystals.

Recently, we reported the crystal structure of the less-soluble diastereoisomeric salt, $(+)_{589}$-[Co(ox)en_2] H-*d*-tart·H_2O,[1] which is obtained as an intermediate in the course of the optical resolution of the $[Co(ox)en_2]^+$ cation using the hydrogen-*d*-tartrate anion (d-$C_4H_5O_6^-$, abbr. H-*d*-tart) as a resolving agent.[2] The optically active complex cation, Λ-$\delta\lambda$-$(+)_{589}$-$[Co(ox)en_2]^+$, was found to be locked in the right-handed spiral chains of $\{\text{H-}d\text{-tart}\}_\infty$.[1]

It has been thought that the comparison of a pair of crystal structures of less- and more-soluble diastereoisomeric salts would give valuable information on the mechanism of optical resolution. Therefore, we have attempted to determine the crystal structure of the more-soluble diastereoisomer, $(-)_{589}$-[Co(ox)en_2] H-*d*-tart·$2H_2O$, and to compare it with the structure of the less-soluble diastereoisomer, $(+)_{589}$-[Co(ox)en_2] H-*d*-tart·H_2O.

Experimental

The preparation of the more-soluble diastereoisomer, $(-)_{589}$-[Co(ox)en_2]H-*d*-tart·$2H_2O$, was reported in our earlier paper.[1] A red crystal with dimensions of $0.15\times0.15\times0.30$ mm³ was used for the X-ray analysis. The unit-cell dimensions were determined by the least-squares refinement of the angular settings of 25 reflections measured on a diffractometer. The crystal data are as follows: $C_{10}H_{25}O_{12}N_4Co$, orthorhombic, $P2_12_12$, $a=16.583(5)$, $b=14.186(5)$, $c=7.403(2)$ Å, $D_m=1.72$(by flotation in $CHCl_3$–$CHBr_3$), and $D_x=1.73(1)$ g cm^{-3} for $Z=4(\mu(\text{Mo }K\alpha)=11.0$ cm^{-1}).

The intensity data were measured on an automatic Rigaku AFC-5 four-circle diffractometer, equipped with a rotating anode(50 kV, 170 mA), using graphite-monochromated Mo-$K\alpha$ radiation ($\lambda=0.71069$ Å) and a monitor-counting technique. The ω-2θ scan mode with a scan rate of 16° min^{-1} employed. The θ scan range was $(1.0+0.45\tan\theta)°$. The intensity data of 2034 independent reflections were collected with $(\sin\theta)/\lambda\leq0.65$ Å^{-1}; of these, 1907 were measured with $|F_o|\geq3\sigma|F_o|$ and used in the present X-ray analysis. No absorption correction was applied.

Determination and Refinement of Crystal Structure

The position of the Co atom was determined from the Patterson map. Successive Fourier refinements with phases based initially on the Co atom revealed the locations of the remaining 27 nonhydrogen atoms. Block-diagonal least-squares refinement with anisotropic thermal parameters for these atoms converged to $R=0.101$ ($R=\Sigma||F_o|-|F_c||/\Sigma|F_o|$). The different synthesis showed the "50%-*ob*, 50%-*lel*" type conformational disorder in one of the etylenediamine chelate rings.[3] The subsequent refinement for all the nonhydrogen atoms gave $R=0.063$. All the hydrogen-atom coordinates were found from the difference map; these 35 hydrogen atoms with fixed positional and isotropic thermal ($B=3.5$ Å^2) parameters were included in the final refinement. The convergence was attained at $R=0.044$. The final difference map showed no peaks higehr than 0.4 electron/Å^3. The quantity minimized was $\Sigma w(|F_o|-k|F_c|)^2$, where $w=1/(a+|F_o|+b|F_o|^2)$ with $a=16.0$ and $b=0.012$.[4] The atomic scattering factors from the International Tables for X-Ray Crystallography[5] were used. The effect of the anomalous dispersion of the Co atom was included in the calculation.[6] All the computations were carried out by a HITAC-8700 computer at the Hiroshima University Computer Center. The computer programs used were FOUR-MMM (Fourier synthesis)[7] and HBLS-IV (Least-square calculation), with a slight modification.[8] The final atomic parameters, the temperature factors (with their estimated standard deviations), and the occupation numbers are listed in Tables 1a, 1b, and 2 respectively. Complete lists of the $10|F_o|$ and $10|F_c|$ values have been

TABLE 1a. OCCUPATION NUMBERS(o), FINAL ATOMIC PARAMETERS, AND TEMPERATURE FACTORS (WITH THEIR e.s.d.'s)

Atom	o	x	y	z	B/Å^2
Co	1.0	0.25184(5)	0.55094(4)	0.91996(10)	a)
O(X1)	1.0	0.2749(4)	0.8093(3)	0.7571(9)	a)
O(X2)	1.0	0.2602(3)	0.6875(3)	0.4656(6)	a)
O(X3)	1.0	0.2596(3)	0.6851(3)	0.9386(6)	a)
O(X4)	1.0	0.2538(3)	0.5706(3)	0.6639(5)	a)
O(T1)	1.0	0.4269(3)	0.8715(3)	0.0416(6)	a)
O(T2)	1.0	0.4722(3)	0.7250(3)	0.0118(6)	a)
O(T3)	1.0	0.3823(3)	0.8389(3)	0.3872(6)	a)
O(T4)	1.0	0.5585(3)	0.8078(3)	0.3735(6)	a)
O(T5)	1.0	0.5163(3)	0.7588(4)	0.6993(6)	a)
O(T6)	1.0	0.4369(3)	0.6411(3)	0.6113(6)	a)
N(1)	1.0	0.3695(3)	0.5406(4)	0.9255(8)	a)
N(2)	1.0	0.1343(3)	0.5588(3)	0.9205(7)	a)
N(3)	1.0	0.2434(3)	0.5384(4)	1.1817(7)	a)
N(4)	1.0	0.2520(4)	0.4153(3)	0.8829(8)	a)
C(E1A)(*ob*)	0.5	0.3949(7)	0.4467(8)	0.8684(16)	2.1(2)
C(E1B)(*lel*)	0.5	0.3928(10)	0.4399(11)	0.9167(23)	4.1(3)
C(E2)	1.0	0.1084(3)	0.5822(4)	1.1080(9)	a)
C(E3)	1.0	0.1584(4)	0.5233(5)	1.2355(9)	a)
C(E4A)(*ob*)	0.5	0.3367(9)	0.3788(11)	0.9383(22)	3.7(3)
C(E4B)(*lel*)	0.5	0.3280(10)	0.3874(12)	0.7948(24)	4.1(3)
C(X1)	1.0	0.2652(4)	0.7247(4)	0.7835(9)	a)
C(X2)	1.0	0.2591(4)	0.6570(4)	0.6193(8)	a)
C(T1)	1.0	0.4401(3)	0.7936(4)	0.1016(7)	a)
C(T2)	1.0	0.4210(3)	0.7645(4)	0.2929(8)	a)
C(T3)	1.0	0.5003(4)	0.7344(4)	0.3840(7)	a)
C(T4)	1.0	0.4832(3)	0.7094(4)	0.5839(7)	a)
O(W1)	0.5	0.0000(0)	0.5000(0)	0.5276(21)	a)
O(W2)	1.0	0.4138(3)	0.5130(4)	0.3322(8)	a)
O(W3)	0.5	0.3302(9)	0.3692(10)	0.5055(20)	5.7(3)

a) See Table 2.

TABLE 1b. OCCUPATION NUMBERS(o) AND POSITIONAL PARAMETERS OF HYDROGEN ATOMS

Atom	o	x	y	z	Atom	o	x	y	z
H(OT2)	1.0	0.483	0.740	−0.125	H(N41)[a]	0.5	0.240	0.399	0.752
H(OT3)	1.0	0.343	0.800	0.450	H(N42)[a]	0.5	0.210	0.383	0.959
H(OT4)	1.0	0.612	0.784	0.435	H(N43)[b]	0.5	0.204	0.396	0.808
H(W11)	0.5	0.037	0.540	0.545	H(N44)[b]	0.5	0.249	0.381	1.000
H(W12)	0.5	0.028	0.450	0.515	H(C11)[a]	0.5	0.453	0.431	0.906
H(W21)	1.0	0.462	0.512	0.325	H(C12)[a]	0.5	0.393	0.445	0.720
H(W22)	1.0	0.407	0.532	0.430	H(C13)[b]	0.5	0.391	0.408	1.051
H(W31)	0.5	0.305	0.432	0.460	H(C14)[b]	0.5	0.453	0.429	0.871
H(W32)	0.5	0.340	0.338	0.615	H(C21)	1.0	0.047	0.568	1.125
H(N11)[a]	0.5	0.391	0.551	1.052	H(C22)	1.0	0.119	0.654	1.136
H(N12)[a]	0.5	0.395	0.591	0.846	H(C31)	1.0	0.146	0.544	1.369
H(N13)[b]	0.5	0.392	0.572	1.039	H(C32)	1.0	0.141	0.452	1.220
H(N14)[b]	0.5	0.394	0.575	0.820	H(C41)[a]	0.5	0.349	0.313	0.879
H(N21)	1.0	0.110	0.498	0.881	H(C42)[a]	0.5	0.344	0.376	1.075
H(N22)	1.0	0.115	0.610	0.836	H(C43)[b]	0.5	0.329	0.417	0.654
H(N31)	1.0	0.265	0.598	1.241	H(C44)[b]	0.5	0.335	0.315	0.776
H(N32)	1.0	0.278	0.485	1.225	H(CT2)	1.0	0.382	0.708	0.280
					H(CT3)	1.0	0.524	0.675	0.312

a) These hydrogens belong to the *ob* ring. b) These hydrogens belong to the *lel* ring.

TABLE 2. ANISOTROPIC TEMPERATURE FACTORS ($\times 10^3$ Å^2) EXPRESSED IN THE FORM $\exp[-2\pi^2(U_{11}h^2a^{*2}+U_{22}k^2b^{*2}+U_{33}l^2c^{*2}+2U_{12}hka^*b^*+2U_{13}hla^*c^*+2U_{23}klb^*c^*)]$

Atom	U_{11}	U_{22}	U_{33}	U_{12}	U_{13}	U_{23}
Co	23.2(2)	18.5(3)	28.1(3)	1.1(3)	2.7(4)	−1.2(3)
O(X1)	104(5)	21(2)	72(4)	−15(3)	−27(4)	8(2)
O(X2)	45(3)	51(3)	34(2)	−4(2)	0(3)	11(2)
O(X3)	39(2)	23(2)	39(2)	−2(2)	−9(2)	−4(2)
O(X4)	41(2)	26(2)	29(2)	−4(2)	4(2)	−6(1)
O(T1)	46(2)	38(2)	34(2)	17(2)	13(2)	13(2)
O(T2)	63(3)	31(2)	19(2)	7(2)	8(2)	1(2)
O(T3)	39(2)	36(2)	36(2)	10(2)	13(2)	0(2)
O(T4)	34(2)	50(3)	28(2)	−18(2)	−3(2)	11(2)
O(T5)	60(3)	53(3)	21(2)	−15(3)	−1(2)	−9(2)
O(T6)	51(3)	33(2)	27(2)	−12(2)	5(2)	6(2)
N(1)	26(2)	32(2)	48(3)	−2(2)	−3(2)	13(3)
N(2)	24(2)	29(2)	33(2)	0(2)	−8(2)	−2(2)
N(3)	27(2)	43(3)	33(2)	10(2)	−6(2)	6(2)
N(4)	40(3)	19(2)	64(4)	−4(2)	26(4)	2(2)
C(E2)	26(3)	33(3)	36(3)	4(2)	3(3)	−6(3)
C(E3)	32(3)	39(3)	31(3)	3(2)	3(3)	−7(3)
C(X1)	37(4)	21(2)	42(2)	−6(2)	−17(3)	1(2)
C(X2)	34(3)	32(3)	30(3)	−2(3)	−2(3)	1(2)
C(T1)	22(2)	25(2)	23(3)	−5(2)	−4(2)	4(2)
C(T2)	28(3)	23(3)	24(2)	−3(2)	3(2)	1(2)
C(T3)	32(3)	32(3)	20(2)	−1(2)	1(2)	1(2)
C(T4)	28(3)	32(3)	18(2)	4(2)	1(2)	10(2)
O(W1)	120(10)	91(8)	127(11)	22(7)	0(0)	0(0)
O(W2)	45(3)	62(3)	55(3)	12(3)	−11(3)	−15(3)

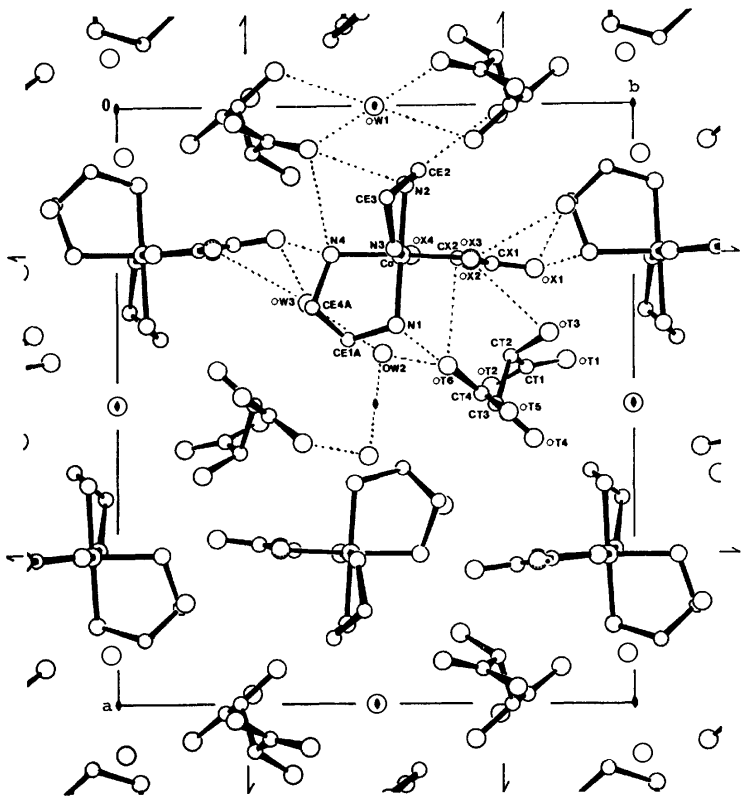

Fig. 1. A perspective drawing of the contents of the unit cell viewed down the c-axis. Possible hydrogen bonds and short contacts are indicated by broken lines. The carbon atoms of the *lel* ring, C(E1B)-C(E4B), are omitted for clarity.

preserved by the Chemical Society of Japan (Document No. 8004).

Results and Discussion

Figures 1 and 2 show the projections of the crystal structure along the c- and b- axes respectively. The structure consists of discrete $(-)_{589}$-$[Co(ox)en_2]^+$ cations, H-*d*-tart anions, and water molecules. The bond distances and angles in the complex cation and the H-*d*-tart anion are listed in Table 3.

Cation and Anion Geometries. The absolute configuration of the $(-)_{589}$-$[Co(ox)en_2]^+$ cation is identified as Δ based on that of the H-*d*-tart anion.[9] This is in accordance with the absolute configuration of $(-)_{589}$-$[Co(ox)en_2]^+$ reported by Aoki *et al.*[10] and Toriumi *et al.*[11] However, in the present complex cation, one ethylenediamine ring is in the "50%-*ob*(N(1)–C(E1A)–C(E4A)–N(4)), 50%-*lel*(N(1)–C(E-1B)–C(E4B)–N(4))" form, as was described in the last section. The other ethylenediamine ring(N(2)–C(E2)–C(E3)–N(3)) is in the *ob* form. Thus, the absolute configuration should be denoted as $\Delta[50\%\text{-}\delta,50\%\text{-}\lambda)\delta]$. The structure is illustrated in Fig. 3.

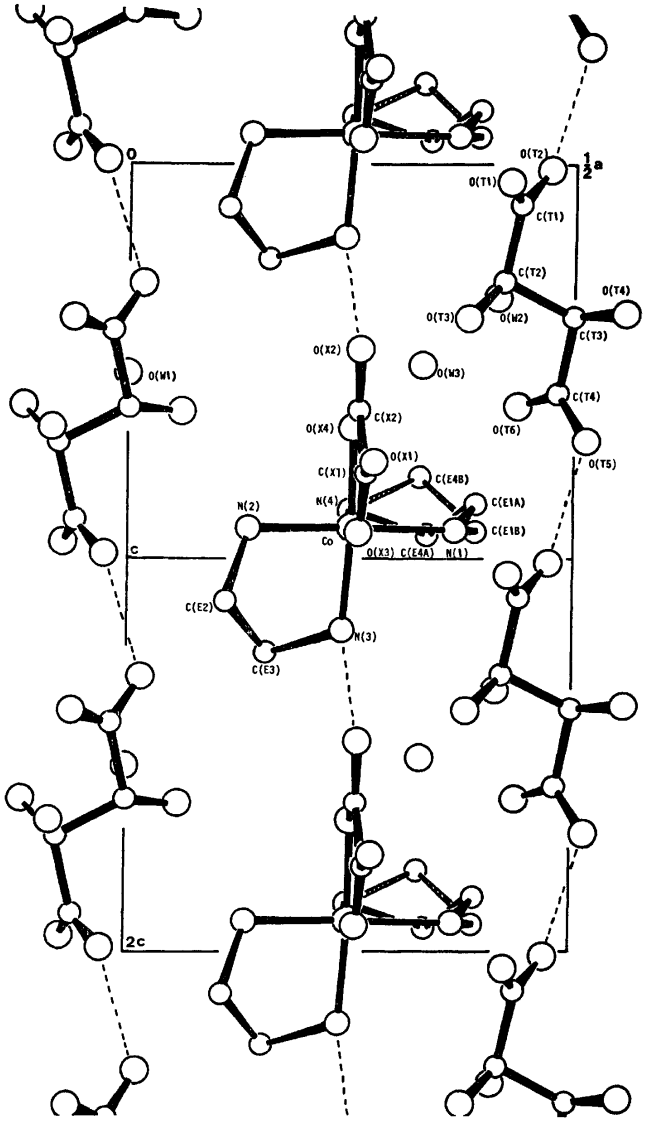

Fig. 2. A boundary projection of the crystal structure viewed along the b-axis.

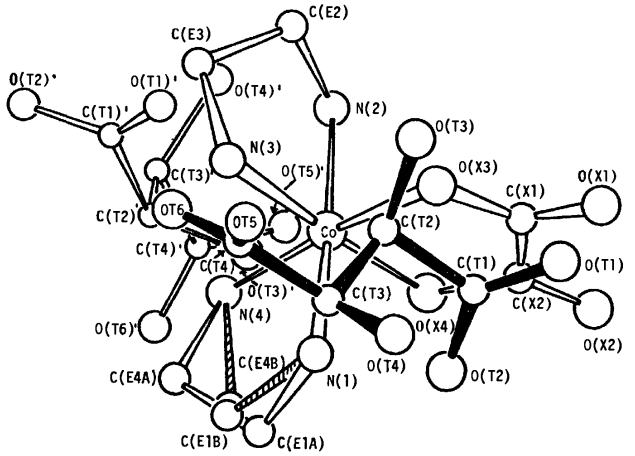

Fig. 3. The arrangement of the complex cation and H-*d*-tart anions projected down the quasi-threefold axis of the complex cation.

Crystal Packing. The intermolecular bond distances and angles are summarized in Table 4. The H-*d*-tart anions are arranged to make a "head-to-tail" chain structure in which two adjacent anions related by the translation along the c-axis (Fig. 2). The hydrogen-bond distance of $O(T2)^{II}\cdots O(T5)$ is 2.473 Å. This value is close to the corresponding one in $(+)_{589}$-$[Co(ox)en_2]$H-*d*-tart·H_2O(2.44 Å).[1] Along the c-axis, there is also a chain of complex cations which are joined by the $N(3)\cdots O(X2)^{II}$ hydrogen bond (2.995 Å). The chain of H-*d*-tart anions and that of the complex cations have the following short contacts: $N(1)\cdots O(T6)$, $N(2)\cdots O(T1)^{I}$, $N(4)\cdots O(T1)^{I}$, $O(X2)\cdots O(T3)$, $C(X2)\cdots O(T6)$, and $C(E2)\cdots O(T5)^{IV}$. Moreover, adjacent H-*d*-tart anions are connected through water molecules(O(W1) and O(W2)): $O(T3)^{V}\cdots O(W1)$, $O(T4)^{V}\cdots O(W1)$, and $O(T6)\cdots O(W2)$. There is no short contact between the complex cation and the water molecule lying on the twofold axis(O(W1)).

Figure 3 shows the relative arrangement of the $(-)_{589}$-$[Co(ox)en_2]^+$ cation and the H-*d*-tart anions projected down the quasi-threefold axis of the complex cation. The close contacts are: $N(1)\cdots O(T2)^{II}$, $N(4)\cdots O(T1)^{I}$, $N(4)\cdots O(T3)^{I}$, and $N(2)\cdots O(T1)^{I}$. In this case, the "face-to-face"-type close contact found in the $[CoXY(en)_2]^{n+}\cdots$*d*-bcs^{-}[15,16] and $[M(en)_3]^{3+}\cdots$*d*-$tart^{2-}$ systems[17–19] does not exist between any triangular face of the octahedral complex cation and the H-*d*-tart anion. This lack of any "face-to-face"-type close contact seems to be true of all salts containing the H-*d*-tart anion. In fact, the "face-to-face"-type close contact was not found in the structures of $(+)_{589}$-

TABLE 3. BOND DISTANCES AND ANGLES (e.s.d.'s IN PARENTHESES)

(a) Bond distances/Å

Co-N(1)	1.957(6)	N(4)-C(E4A)	1.552(18)	O(T1)-C(T1)	1.211(7)
Co-N(2)	1.952(5)	N(4)-C(E4B)	1.474(19)	O(T2)-C(T1)	1.294(8)
Co-N(3)	1.951(5)	O(X1)-C(X1)	1.226(10)	O(T3)-C(T2)	1.419(7)
Co-N(4)	1.944(6)	O(X2)-C(X2)	1.217(8)	O(T4)-C(T3)	1.422(8)
Co-O(X3)	1.913(4)	O(X3)-C(X1)	1.281(8)	O(T5)-C(T4)	1.234(8)
Co-O(X4)	1.917(5)	O(X4)-C(X2)	1.274(8)	O(T6)-C(T4)	1.253(7)
N(1)-C(E1A)	1.458(13)	C(E1A)-C(E4A)	1.459(20)	C(T1)-C(T2)	1.509(8)
N(1)-C(E1B)	1.481(18)	C(E1B)-C(E4B)	1.588(25)	C(T2)-C(T3)	1.537(8)
N(2)-C(E2)	1.490(8)	C(E2)-C(E3)	1.508(9)	C(T3)-C(T4)	1.548(8)
N(3)-C(E3)	1.481(8)	C(X1)-C(X2)	1.552(9)		

(b) Bond angles/°

N(1)-Co-N(4)	85.9(3)	N(1)-C(E1A)-C(E4A)	108.0(10)
N(2)-Co-N(3)	86.1(2)	N(1)-C(E1B)-C(E4B)	107.5(13)
O(X3)-Co-O(X4)	85.7(2)	N(2)-C(E2)-C(E3)	107.5(5)
Co-N(1)-C(E1A)	110.5(6)	N(3)-C(E3)-C(E2)	105.9(5)
Co-N(1)-C(E1B)	109.4(8)	N(4)-C(E4A)-C(E1A)	106.5(11)
Co-N(2)-C(E2)	107.6(4)	N(4)-C(E4B)-C(E1B)	101.6(13)
Co-N(3)-C(E3)	110.4(4)	O(X1)-C(X1)-C(X2)	119.2(6)
Co-N(4)-C(E4A)	107.1(7)	O(X2)-C(X2)-C(X1)	120.8(6)
Co-N(4)-C(E4B)	109.2(8)	O(X3)-C(X1)-C(X2)	115.2(6)
Co-O(X3)-C(X1)	112.1(4)	O(X4)-C(X2)-C(X1)	113.4(5)
Co-O(X4)-C(X2)	113.4(4)	O(X1)-C(X1)-O(X3)	125.5(7)
		O(X2)-C(X2)-O(X4)	125.8(6)
O(T1)-C(T1)-O(T2)	124.9(6)	O(T5)-C(T4)-O(T6)	126.8(6)
O(T1)-C(T1)-C(T2)	123.8(5)	O(T2)-C(T1)-C(T2)	111.3(5)
O(T3)-C(T2)-C(T1)	110.7(5)	O(T3)-C(T2)-C(T3)	112.1(5)
O(T4)-C(T3)-C(T2)	110.7(5)	O(T4)-C(T3)-C(T4)	110.1(5)
O(T5)-C(T4)-C(T3)	116.8(5)	O(T6)-C(T4)-C(T3)	116.4(5)
C(T1)-C(T2)-C(T3)	108.0(5)	C(T2)-C(T3)-C(T4)	109.1(5)

[Co(ox)en$_2$]H-*d*-tart·H$_2$O[1] and the less- and more-soluble *trans*(*O*)-[Co(gly)$_2$en]H-*d*-tart·*n*H$_2$O.[20] In the case of the H-*d*-tart anion, the chiral discrimination is effected in a different way from the "face-to-face"-type compact fit.[1]

*Comparison between the Crystal Structures of the More-soluble Salt, $(-)_{589}$-[Co(ox)en$_2$]H-*d*-tart·2H$_2$O, and the Less-soluble Salt, $(+)_{589}$-[Co(ox)en$_2$]H-*d*-tart·H$_2$O.*[1] The crystal structures of more- and less-soluble diastereoisomers are shown schematically in Figs. 4 and 5, where the ions are represented simply by cylinders. It is noticeable that, in a broad sense, there are some resemblances in the packing features of the two structures in Fig. 4: (1) The H-*d*-tart anions in both crystals are stacked along the axis of the cylinder and make the {H-*d*-tart}$_\infty$ chain of the "head-to-tail" type.[1,12] (2) The complex cations are also stacked along the cylinder axis and form a chain parallel to the chain of the H-*d*-tart anion. (3) The effective lengths of the unit cylinders of the H-*d*-tart anion are quite similar: 7.403 Å for the more-soluble salt and 7.294 Å for the less-soluble salt. There are, however, some different features between the crystal structures: (1) The H-*d*-tart chain denoted as A is formed by the stacking of H-*d*-tart anions related by the translation along the c-axis, but the A′ chain is formed by the stacking of H-*d*-tart anions related by the twofold screw axis. (2) The chain of the *Δ*-$(-)_{589}$-complex cation in Fig. 4(a) is formed by the repetition of translations of the complex cation, but that of the *Δ*-$(+)_{589}$-complex cation in Fig. 4(b) is formed by the linkages of the complex cation along the twofold screw axis.

The projected views along the c-axis of the $(-)_{589}$-salt and along the b-axis of the $(+)_{589}$-salt are illustrated in Fig. 5. The column of complex cations in each structure is surrounded by four columns of H-*d*-tart anions. The parallelogramic frames shown by the broken and solid lines are depicted by connecting the four H-*d*-tart chains. The size of the parallelogram of the $(-)_{589}$-salt ($8.292\times7.196\times\sin(100.6°)$) is similar to that of the $(+)_{589}$-salt ($8.256\times7.009\times\sin(104.7°)$),[21] though the space groups are different. The water molecules in the more-soluble $(-)_{589}$-salt serve to connect the B and C chains or the A and D chains, but not the A and B chains or the C and D chains. This situation is quite similar to that with the less-soluble $(+)_{589}$-salt, though the number of water molecules different from that in the more-soluble salt.

The close contacts between the ions in both salts are summarized in Table 5. The $(+)_{589}$-salt has more short contacts than the $(-)_{589}$-salt. This suggests that the complex cation in the more-soluble $(-)_{589}$-salt is more loosely packed than that in the less-soluble $(+)_{589}$-salt. This situation is reflected in the difference between their densities (1.73(1) g cm^{-3} in the $(-)_{589}$-salt *vs.* 1.77(1) g cm^{-3} in the $(+)_{589}$-salt). The tight

TABLE 4. INTERMOLECULAR DISTANCES AND ANGLES

X–H···Y or X···Y	X···Y Å	H···Y Å	X–H···Y °	X–H···Y or X···Y	X···Y Å	H···Y Å	X–H···Y °
N(1)–H(N12)···O(T2)^{II}	3.187(8)	2.60	117	C(E1B)–H(C13)···O(W2)^{II}	3.264(18)	2.58	120
N(1)–H(N13)···O(T2)^{II}	3.187(8)	2.56	119	N(3)–H(N31)···O(X2)^{II}	2.995(7) a)	2.09	146
N(1)–H(N12)···O(T6)	2.948(8) a)	2.00	153	N(4)–H(N42)···O(X1)^{III}	3.092(9) a)	2.36	129
N(1)–H(N14)···O(T6)	2.948(8) a)	1.94	177	N(4)–H(N44)···O(X1)^{III}	3.092(9) a)	2.10	172
N(2)–H(N21)···O(T1)^{I}	2.858(7) a)	1.98	145	C(E4A)–H(C42)···O(X1)^{III}	3.079(18)	2.51	115
N(2)–H(N22)···O(T4)^{V}	3.147(7) a)	2.16	166	C(E3)–H(C32)···O(X1)^{III}	3.233(10)	2.46	128
N(4)–H(N42)···O(T1)^{I}	3.082(8) a)	2.28	136	C(E1A)–H(C12)···O(W3)	3.095(19)	2.18	139
N(4)–H(N43)···O(T1)^{I}	3.082(8)	2.46	119	C(E4A)–(C44)···O(W3)	3.209(22)	2.15	122
N(4)–H(N41)···O(T3)^{I}	3.183(8) a)	2.43	130	C(E2)···O(T1)^{I}	3.241(8)	—	—
N(4)–H(N43)···O(NT3)^{I}	3.183(8) a)	2.18	168	C(E2)–H(C22)···O(T5)^{IV}	3.075(9)	2.43	119
O(T3)–H(OT3)···O(X1)	3.294(8)	2.54	134	C(X2)···O(T6)	2.957(8)	—	—
O(T3)–H(OT3)···O(X2)	3.009(7) a)	2.11	153	O(T3)^{V}···O(W1)	3.070(16)	—	—
O(X2)···O(T6)	3.191(7)	—	—	O(W1)–H(W11)···O(T4)^{V}	2.985(17) a)	2.27	142
O(X4)···O(T6)	3.220(7)	—	—	O(T4)–H(OT4)···O(W3)^{VII}	3.266(16)	2.43	135
C(T2)–H(CT2)···O(X2)	3.153(8)	2.46	124	O(W2)–H(W22)···O(T6)	2.778(8) a)	2.11	144
N(1)–H(N11)···O(W2)^{II}	3.124(9) a)	2.18	155	O(T2)^{II}–H(OT2)···O(T5)	2.473(8) a)	1.44	166
N(1)–H(N13)···O(W2)^{II}	3.124(9) a)	2.35	132	O(T6)···O(T2)^{II}	3.248(7)	—	—
N(3)–H(N32)···O(W2)^{II}	3.059(8)	2.41	121	O(T5)···C(T1)^{II}	3.272(8)	—	—
N(4)–H(N41)···O(W3)	3.150(16) a)	2.40	130	O(T2)···C(T4)^{VI}	3.181(8)	—	—
O(X1)···O(W3)^{VIII}	2.746(17)	—	—	O(W2)^{VII}–H(W21)···O(W2)	2.883(12) a)	2.09	170
O(X2)···O(W3)^{VIII}	2.989(16)	—	—	O(W3)–H(W31)···O(W2)	2.780(16)	2.34	104

Roman numerals as superscripts refer to the following equivalent positions relative to the reference molecule at x, y, z:

I $(1/2-x, -1/2+y, 1-z)$, II $(x, y, 1-z)$
III $(1/2-x, -1/2+y, 2-z)$, IV $(-1/2+x, 3/2-y, 2-z)$
V $(-1/2+x, 3/2-y, 1-z)$, VI $(x, y, -1+z)$
VII $(1-x, 1-y, z)$, VIII $(1/2-x, 1/2+y, 1-z)$

a) Possible hydrogen bonds.

TABLE 5. SHORT CONTACTS BETWEEN COMPLEX CATION AND H-*d*-TART ANION FOR $(-)_{589}$-[Co(ox)en$_2$]H-*d*-tart·2H$_2$O (The corresponding distances for $(+)_{589}$-[Co(ox)en$_2$]H-*d*-tart·H$_2$O[1] are shown in square brackets.)

Complex	H-*d*-tartrate					
	O(T1)	O(T2)	O(T3)	O(T4)	O(T5)	O(T6)
N(1)	— [2.91]	3.187 (Å) [3.12]				2.948 [—]
N(2)	2.858 [—]			3.147 [2.97]		— [2.89]
N(4)	3.082 [—]		3.183 [3.24]			— [3.00]
O(X1)			3.294 [3.01]			
O(X2)	— [3.10]		3.009 [2.90]			3.191 [—]
O(X4)						3.220 [—]
C(E2)	3.241 [—]				3.075 [—]	
C(X1)				— [3.02]		
C(X2)	— [2.94]			— [3.06]		2.957 [—]

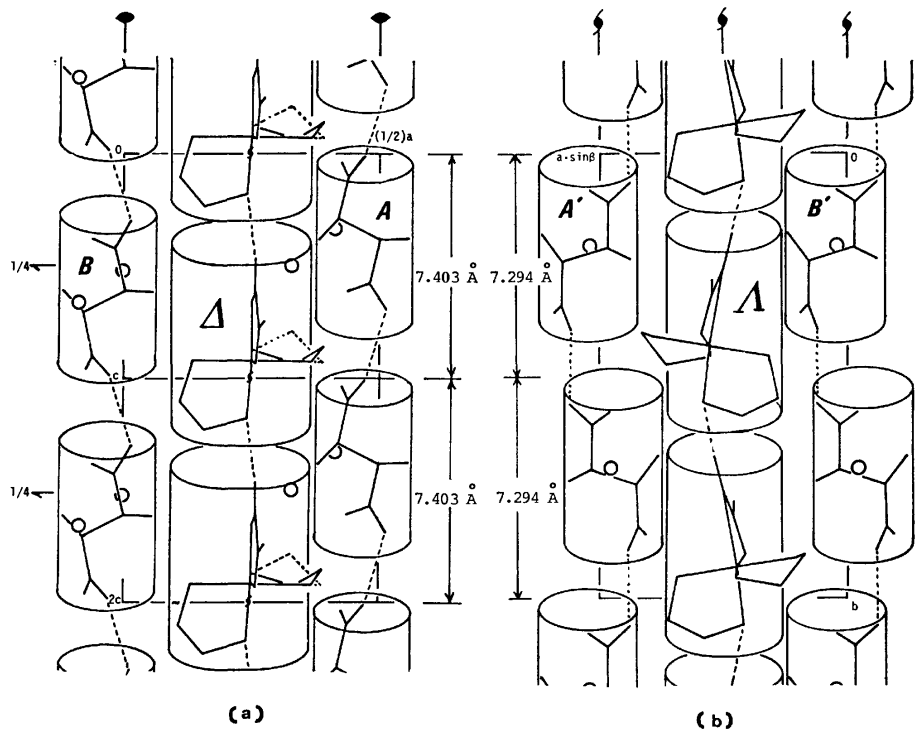

Fig. 4. A schematic drawing of the crystal structures of the more- and the less-soluble diastereoisomeric salts. Broken lines denote hydrogen bonds and disorder of the ethylenediamine ring. Circles indicate water molecules:
(a) $(-)_{589}$-[Co(ox)en_2]H-*d*-tart·$2H_2O$, (b) $(+)_{589}$-[Co(ox)en_2]H-*d*-tart·H_2O(all the *y* parameters in the less-soluble salt are shifted 3.10 Å along the b-axis from the reported values[1] for the purpose of the comparison).

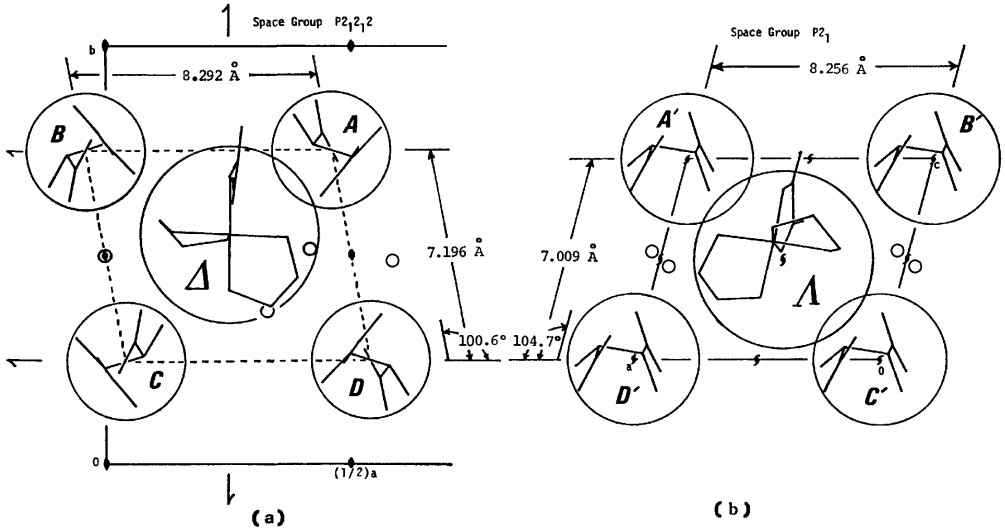

Fig. 5. A comparison of the arrangements of the H-*d*-tart anions and the complex cations.
(a) $(-)_{589}$-[Co(ox)en_2]H-*d*-tart·$2H_2O$, (b) $(+)_{589}$-[Co(ox)en_2]H-*d*-tart·H_2O.

packing in the less-soluble salt is thought to be caused by the twofold spiral chain of {H-*d*-tart}∞. Indeed, the spiral chains of {H-*d*-tart}∞ were always found in several less-soluble diastereoisomeric salt, $(+)_{589}$-*trans*(*O*)-[Co(gly)$_2$en]H-*d*-tart·$3H_2O$,[20] (−)-adrenalinium H-*d*-tart,[12] (+)-[(−)-1-methy-3-benzoylpiperidinium H-*d*-tart]H_2O,[13] and (−)-[(−)-1-methyl-3-ethyl-3-benzoylpiperidinium H-*d*-tart].[14] Although the present more-soluble salt also has a {H-*d*-tart}∞ chain, the chain is in a non-spiral form. The discrimination of the optically active $[Co(ox)en_2]^+$ cation by the H-*d*-tart anion is attributable to such a structural difference in the {H-*d*-tart}∞ columns.

Dehydration of the Water of Crystallization and Conformational Disorder. The water molecule O(W3) with a one-half weight is located at an unusually short distance (2.16 Å) from the C(E4B) (*lel* form) in the disordered ethylenediamine ring. On the other

hand, the distance from O(W3) to C(E4A) (*ob* form) is normal (3.12 Å). If this water molecule exists with weight one (this imaginary compound corresponds to 2.5 hydrate), the conformation of the ethylenediamine ring (N(1)–C(E1)–C(E4)–N(4)) is thought to be restricted to the *ob* form in order to avoid such an abnormal short contact between the O(W3) and C(E4B) atoms. In other words, the change in conformation from *ob* to *lel* seems to be related to the partial loss of this water(O(W3)) of crystallization. Shimura and Tsutsui[22] reported that the more-soluble $(-)_{589}$-salt contains 2.5 mol of the water of crystallization. If the crystal of $(-)_{589}$-salt·$2.5H_2O$ is isomorphous to the $(-)_{589}$-salt·$2H_2O$, the complex cation in the former crystal is confirmed to have the *ob-ob* form exclusively.

Recntly, Brouty *et al.* reported the crystal structures of (±)-$[Cr(en)_3](SCN)_3 \cdot 0.75H_2O$[23,24] and [(+)-Co(en)$_3$(−)-Cr(en)$_3$](SCN)$_3 \cdot nH_2O$[25] at 293 K and 133 K respectively. They found that, in both cases, one ethylenediamine ring in the $[Cr(en)_3]^{3+}$ cation is in conformational disorder at 293 K. They mentioned that the partial loss of the water of crystallization plays some role in causing the change in conformation from *lel* to *ob*. However, in $(-)_{589}$-$[Co(ox)en_2]$-H-*d*-tart·$2H_2O$, such a loss causes the confromational change from *ob* to *lel*. The reason for such a difference still remains unsolved.

We wish to thank the Hiroshima University Computer Center for its generous allocation of computer time and acknowledge a Grant-in-Aid for Scientific Research from the Ministry of Education.

References

1) M. Kuramoto, Y. Kushi, and H. Yoneda, *Bull. Chem. Soc. Jpn.*, **51**, 3251 (1978).
2) W. T. Jordan, B. J. Brennan, L. R. Froebe, and B. E. Douglas, *Inorg. Chem.*, **12**, 1827 (1973).
3) C. J. Hawkins, "Absolute Configuration of Metal Complexes," Wiley-Interscience, New York (1971), p. 129. The "*lel*, *ob*" notation was introduced by E. J. Corey and J. C. Bailar, Jr.(E. J. Corey and J. C. Bailar, Jr., *J. Am. Chem. Soc.*, **81**, 2620 (1959)).
4) D. W. J. Cruickshank, "Computing Methods and the Phase Problem in X-Ray Crystal Analysis," ed by R. Pepinsky, J. M. Robertson, and J. C. Speakman, Pergamon Press, Oxford (1961), p. 45.
5) "International Tables for X-Ray Crystallography," Kynoch Press, Birmingham (1968), Vol. III, pp. 201—206.
6) "International Tables for X-Ray Crystallography," Kynoch Press, Birmingham (1974), Vol. IV, p. 148.
7) Y. Kushi, unpublished work.
8) T. Ashida, "The Universal Crystallographic Computation Program System." ed by T. Sakurai, The Crystallographic Society of Janan (1967).
9) A. J. van Bommel and J. M. Bijvoet, *Acta Crystallogr.*, **11**, 61 (1958).
10) T. Aoki, K. Matsumoto, S. Ooi, and H. Kuroya, *Bull. Chem. Soc. Jpn.*, **46**, 159 (1973).
11) K. Toriumi, S. Sato, and Y. Saito, *Acta Crystallogr., Sect. B*, **33**, 1378 (1977).
12) D. Carlstrøm, *Acta Crystallogr,. Sect. B*, **29**, 161 (1973).
13) G. Hite and J. R. Soares, *Acta Crystallogr., Sect. B*, **29**, 2935 (1973).
14) J. R. Ruble, G. Hite, and J. R. Soares, *Acta Crystallogr., Sect. B*, **32**, 136 (1976).
15) Y. Kushi, M. Kuramoto, and H. Yoneda, *Chem. Lett.*, **1976**, 663.
16) M. Kuramoto, Y. Kushi, and H. Yoneda, *Bull. Chem. Soc. Jpn.*, **51**, 3196 (1978).
17) Y. Kushi, M. Kuramoto, and H. Yoneda, *Chem. Lett.*, **1976**, 135.
18) Y. Kushi, M. Kuramoto, and H. Yoneda, *Chem. Lett.*, **1976**, 339.
19) T. Tada, Y. Kushi, and H. Yoneda, *Chem. Lett.*, **1977**, 379.
20) M. Kuramoto, *Bull. Chem. Soc. Jpn.*, in press.
21) The crystal data of $(+)_{589}$-$[Co(ox)en_2]H$-*d*-tart·H_2O were remeasured on a Syntex R3 computer-controlled four-circle diffractometer; $a=8.256(3)$, $b=14.588(4)$, $c=7.009(1)$ Å, $\beta=104.73(2)°$, $P2_1$, and $Z=2$.
22) Y. Shimura and K. Tsutsui, *Bull. Chem. Soc. Jpn.*, **50**, 145 (1977).
23) C. Brouty, P. Spinat, A. Whuler, and P. Herpin, *Acta Crystallogr., Sect. B*, **33**, 1913 (1977).
24) C. Brouty, P. Spinat, A. Whuler, and P. Herpin, *Acta Crystallogr., Sect. B*, **33**, 1920 (1977).
25) C. Brouty, A. Whuler, P. Spinat, and P. Herpin, *Acta Crystallogr., Sect. B*, **33**, 2563 (1977).

 © 1980 The Chemical Society of Japan Bull. Chem. Soc. Jpn., 53, 133—138 (1980)

Partition of Tris(acetylacetonato)chromium(III) and Its Temperature Dependence in the Systems of Dodecane/(Water–Organic Solvent Mixture)

Hiroshi Awano,** Hitoshi Watarai, and Nobuo Suzuki*

Department of Chemistry, Faculty of Science, Tohoku University, Sendai 980

(Received July 31, 1979)

The partition constants $K_t^{\ominus}$ of tris(acetylacetonato)chromium(III) between dodecane and water–organic solvent mixtures have been measured. The organic solvents used as co-solvents were acetonitrile, *N,N*-dimethylformamide, methanol, ethylene glycol, and dimethyl sulfoxide which are all miscible with water but not with dodecane. From the temperature dependence of $K_t^{\ominus}$ the thermodynamic parameters for the transfer of the complex from dodecane to the mixed solvents have been determined. The dependences of the partition constants on solvent composition of the aqueous phase have been interpreted in terms of changes in the internal pressure and the volume upon mixing of water with the organic co-solvents. The standard transfer enthalpies have been correlated with the excess enthalpies of the mixed solvents.

The solvent extraction of metal chelates is one of the most useful methods for the separation or enrichment of metal ions. The effects of organic phases on the partition behavior of chelating reagents and their metal chelates have been interpreted in terms of the regular solution theory.[1] Quantitative interpretation of the effects of the aqueous phase on the partition behavior is however difficult. This is largely due to strong interactions such as hydrogen bonding or dipole-dipole interactions between solute and solvent molecules in the aqueous phase of the partition system. In spite of the important role of the aqueous phase in solvent extraction, few studies have been made on this subject. Yoshimura and Suzuki[2] examined the effects of some electrolytes on the standard chemical potential of benzoylacetone and benzoyltrifluoroacetone in aqueous solutions, and discussed the changes in the cohesive forces of water and the structure of water.

The present authors reported the partition equilibrium of acetylacetone complexes of chromium(III), cobalt(III), and rhodium(III)[3] in the heptane/(water–dimethyl sulfoxide (DMSO)) system. The dependence of the partition constants on the composition of the mixtures was discussed in terms of the extended McDevit-Long theory.[4] It was found that the partition constant variation with solvent composition was governed by the strong interactions between water and DMSO.

In this study, the partition constants of $[Cr(acac)_3]$ have been measured in the partition systems consisting of water–organic solvent mixtures and dodecane, which is less soluble in the polar solvents than heptane. Acetonitrile (AN), *N,N*-dimethylformamide (DMF), DMSO, methanol (MeOH), and ethylene glycol (EG) have been used as co-solvents in the aqueous mixtures. The temperature dependence of the partition constants have been examined, and the thermodynamic parameters for the transfer from dodecane to the solvent mixtures estimated. The partition constants and the standard transfer enthalpies are discussed in terms of the solvent-solvent interactions.

Experimental

Reagents. Tris(acetylacetonato)chromium(III) ($[Cr(acac)_3]$) was prepared by the method reported by Fernelius and Blanch.[5] Recrystallization from benzene and petroleum ether was repeated twice and the products sublimed under reduced pressure (*ca.* 10^{-3} mmHg, 100—150 °C). Mp, 214.0—215 °C; lit, 216 °C.[5] Found: C, 51,68; H, 6.02%. Calcd for $C_{15}H_{21}O_6Cr$: C, 51.81; H, 6.06%.

Dodecane (Tokyo Kasei, GR) was washed with a mixture of concd sulfuric acid and fuming sulfuric acid, an aqueous solution of sodium hydroxide, and water. After drying with calcium hydride, the dodecane was distilled under reduced pressure (less than 20 mmHg, 105 °C). Waste dodecane was recovered and purified by the same treatment. Acetonitrile (Wako, GR) was stirred with calcium hydride for 24 h and distilled in the presence of phosphorus pentaoxide under ambient pressure (61 °C). *N,N*-Dimethylformamide (Kanto, GR) was dried by stirring with molecular sieve 4A for 24 h, and distilled under reduced pressure under an atmosphere of N_2 (less than 20 mmHg, 62.5 °C). Dimethyl sulfoxide (Wako, GR) was stirred with calcium hydride overnight to dryness and distilled under reduced pressure (17 mmHg, 74 °C). Methanol (Kanto, GR) was distilled under ambient pressure. Ethylene glycol (Kanto, GR) was dried with molecular sieve 4A and distilled under reduced pressure (less than 20 mmHg, 106 °C). These very hygroscopic solvents were preserved in a desiccator over silica gel. Doubly distilled water was used throughout.

The water-organic solvent mixtures were prepared by weight.

Partition Measurements. A specified volume of a dodecane solution of $[Cr(acac)_3]$ ($1—4\times10^{-4}$ mol dm^{-3}) and a specified volume of mixed solvent were stirred for 30 min in a partition vessel which was equipped with a water jacket and thermostated at the desired temperature within $\pm$0.02 K. The partition constants in the system of dodecane/(water–acetonitrile), dodecane/(water-DMF), dodecane/(water-MeOH), and dodecane/(water-ethylene glycol) were measured at 278.15 K, 288.15 K, and 298.15 K, and those in dodecane/(water-DMSO system) were measured at 288.15 K, 293.15 K, and 298.15 K. The equilibrated dodecane phase was isolated, and the concentration at (298.15$\pm$0.2)K determined spectrophotometrically from the absorbance at 336 nm ($\varepsilon=1.715\times10^4$ dm^3 mol^{-1} cm^{-1}). The absorbance was measured by a Hitachi 356 or JASCO Uvidec 2 spectrophotometer. In this study, a partition constant is defined as an equilibrium

** Present address: The Chemical Research Institute of Non-aqueous Solutions, Tohoku University, Sendai 980.

constant for the transfer process from the nonpolar phase to the polar phase. The partition constant was determined from the following relationship:

$$K_t\ominus = \frac{x_s^p}{x_s^n} = \frac{C_{s,\mathrm{init}}^n - C_s^n}{C_s^n}\frac{V^n}{V^p}\frac{v_p}{v_n}, \quad (1)$$

where x_s^n and x_s^p are the mole fractions of the solute in the nonpolar (dodecane) and polar (mixed solvent) phase, $C_{s,\mathrm{init}}^n$ and C_s^n are the initial and equilibrium concentrations in the dodecane phase, V^n and V^p are the volumes of the nonpolar and polar phases, and v_n and v_p are the molar volumes of the nonpolar and polar phases, respectively. Literature values[6] for v_n and v_p were used for the calculation $K_t\ominus$. More than five minutes' stirring made the ratio, $(C_{s,\mathrm{init}}^n - C_s^n)/C_s^n$, independent of the stirring time. The reversed partition experiment (a transfer of the solute from the mixed solvent phase to the dodecane phase) gave an equal value for $K_t\ominus$ with the normal partition experiment. Stirring for 24 h caused no change in spectra of both phases, and so it has been assumed that the decomposition

TABLE 1. PARTITION CONSTANTS OF TRIS(ACETYLACETONATO)CHROMIUM(III) BETWEEN DODECANE AND WATER–DIMETHYL SULFOXIDE

	$K_t\ominus$					$K_t\ominus$			
	278.15K	288.15K	293.15K	298.15K		278.15K	288.15K	293.15K	298.15K
x_{AN}					x_{MeOH}				
0.000	2.22	0.937		0.427	0.000	2.22	0.937		0.427
0.025	1.50	0.739		0.392	0.025	2.07	0.913		0.476
0.050	1.27	0.694		0.407	0.050	1.81	0.894		0.509
0.100	1.73	1.08		0.684	0.100	1.54	0.924		0.595
0.200	5.49	3.42		2.18	0.150	1.62	1.06		0.744
0.300	14.6	9.00		5.88	0.200	1.84	1.36		0.966
0.400	27.4	17.0		11.1	0.250	2.46	1.83		1.36
0.500	41.8	25.8		18.0	0.300	3.36	2.52		1.87
0.600	58.7	37.3		25.1	0.400	5.95	4.43		3.33
0.700	78.1	50.0		33.8	0.500	9.67	7.17	5.98	4.89[a]
0.800	95.8	61.6		41.7	0.600	13.1	9.90	8.12	6.41[a]
0.900	110	67.7		45.9	0.700	16.4	12.1	10.1	8.22[a]
0.950	112	68.0		43.6	0.800	16.9	12.6	9.94	7.39[a]
1.000	105	67.0		40.6	0.900	15.2	12.3	9.28	6.23[a]
					1.000	12.2	9.70	7.77	5.82[a]
x_{DMF}									
0.000	2.22	0.937		0.427	x_{EG}				
0.025	2.15	1.06		0.587	0.000	2.22	0.937		0.427
0.050	2.15	1.18		0.723	0.050	1.23	0.636		0.354
0.100	2.19	1.46		1.03	0.100	0.836	0.505		0.316
0.200	3.02	2.32		1.86	0.150	0.685	0.461		0.317
0.300	5.48	4.29		3.47	0.200	0.635	0.441		0.333
0.400	11.0	8.37		6.59	0.300	0.699	0.517		0.413
0.600	39.9	27.9		19.7	0.400	0.856	0.651		0.527
0.800	95.2	64.6	52.6	43.2[a]	0.600	1.31	0.984		0.824
1.000	167	103	80.0	62.8[a]	0.800	1.82	1.38		1.16
					0.900	2.05	1.61		1.32
					1.000	2.31	1.79		1.52
x_{DMSO}									
0.000		0.937	0.638	0.427					
0.025		0.840	0.593	0.445					
0.050		0.723	0.510	0.424					
0.100		0.570	0.442	0.388					
0.150		0.489	0.409	0.385					
0.200		0.514	0.447	0.435					
0.300		0.940	0.812	0.810					
0.400		2.38	2.03	1.95					
0.600		12.8	10.8	9.94					
0.800		41.1	34.1	30.8					
0.900		64.5	54.0	44.5					
1.000		102[a]	78.3	61.0					

a) $K_t\ominus = x_s^p/x_s^n$. b) Estimated value (see text).

of $[Cr(acac)_3]$ is negligible. Thirty minutes' stirring was taken as sufficient to place the system into partition equilibrium. For each system at least three runs were conducted.

Results

Partition Constants. Table 1 illustrates the partition constants $K_t^{\ominus}$ of $[Cr(acac)_3]$ in dodecane/(water–organic solvent mixture) systems observed at several temperatures. All the values have a relative standard deviation within ±5%. Partition constants in the systems of $x_{DMF} \geq 0.8$ and $x_{MeOH} \geq 0.5$ at 298.15 K are the estimated values based on the quadratic regression for the experimental values at the lower temperatures given in the table, because of unsatisfactory phase separation at 298.15 K. For the system of $x_{DMSO}=1.0$ at 288.15 K, this is below the freezing point of DMSO 18.54 °C,[7] and so a hypothetical value was estimated by applying a linear regression for the observed values at 298.15 K and 293.15 K given in the table.

In Figs. 1(a) to 1(e), $-\log K_t^{\ominus}$ is shown as a function of the mole fraction of the organic co-solvent in the solvent mixture, x_2, in which the subscript 2 denotes the co-solvent. All the curves indicate that the partition constant decreases with increase in temperature and that the partition constant increases with an increase in x_2. In most systems, the curves have maxima in the water-rich regions.

The Thermodynamic Parameters. From the partition constants, the standard transfer chemical potential $\Delta_t\mu^{\ominus}$ of $[Cr(acac)_3]$ from dodecane to the water–organic solvent mixtures at different temperatures were calculated based on the following equation:

$$\Delta_t\mu^{\ominus} = -RT \ln K_t^{\ominus}. \quad (2)$$

From the expression for the temperature dependence of $\Delta_t\mu^{\ominus}$ as a quadratic function of temperature, the standard transfer enthalpy $\Delta_t h^{\ominus}$ and the standard transfer entropy $\Delta_t s^{\ominus}$ from dodecane to the solvent mixtures were calculated as follows:

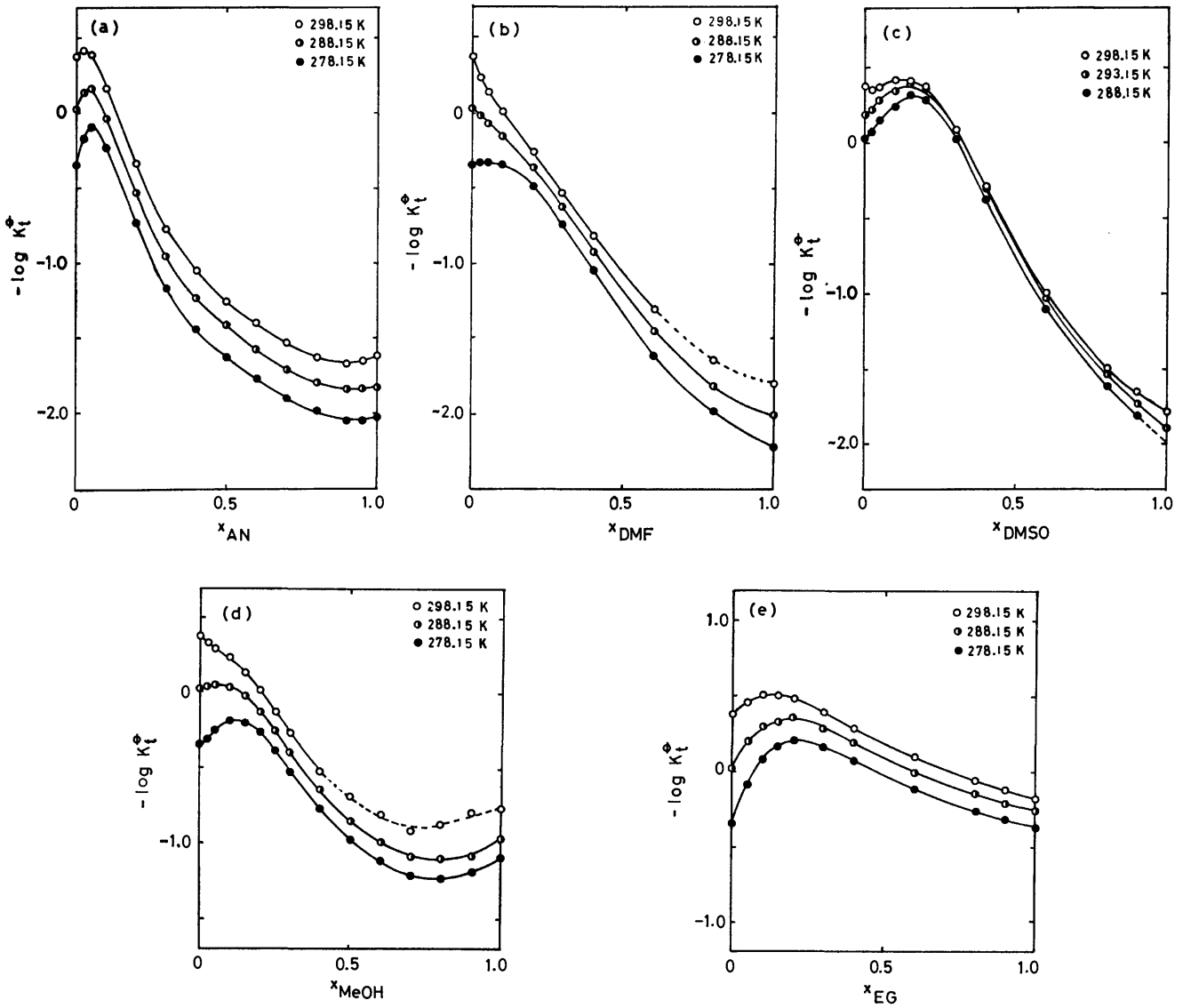

Fig. 1. Variation of the partition constants of $[Cr(acac)_3]$ in dodecane/(water–organic solvent mixtures) with mole fraction of the co-solvent; (a) acetonitrile, (b) dimethylformamide, (c) dimethyl sulfoxide, (d) methanol, (e) ethylene glycol.

$$\Delta_t h^{\ominus} = -T^2\left[\frac{\partial(\Delta_t\mu^{\ominus}/T)}{\partial T}\right]_p, \quad (3)$$

$$\Delta_t s^{\ominus} = -\left(\frac{\partial\Delta_t\mu^{\ominus}}{\partial T}\right)_p. \quad (4)$$

The calculated $\Delta_t h^{\ominus}$ and $\Delta_t s^{\ominus}$ at 298.15 K are shown in Figs. 2(a) to 2(e) as function of the mole fraction of the organic co-solvent. The standard transfer entropies are given in the term, $-T\Delta_t s^{\ominus}$.

The figures show that the transfer of $[Cr(acac)_3]$ from dodecane to water is accompanied by a very large decrease in the standard enthalpy (−55.0 kJ mol^{-1}), and that, in most systems variation in the thermodynamic values is remarkable in the water-rich regions. Cancellation of the large negative $\Delta_t h^{\ominus}$ with the large negative $T\Delta_t s^{\ominus}$ causes the small $\Delta_t\mu^{\ominus}$ values.

Discussion

Partition Constants in the Systems of Dodecane/Pure Solvent. The partition constant $K_t^{\ominus}$ in various systems of dodecane/pure solvent increases in the order: water<ethylene glycol<methanol<acetonitrile<DMSO≃DMF. Less work is needed for solute transfer into solvents with strong solute-solvent interactions and more work is required for solute transfer into solvents with strong solvent-solvent interactions. The dipole moment of solvent molecules is a measure of the electrostatic and polarization interaction between solute and solvent

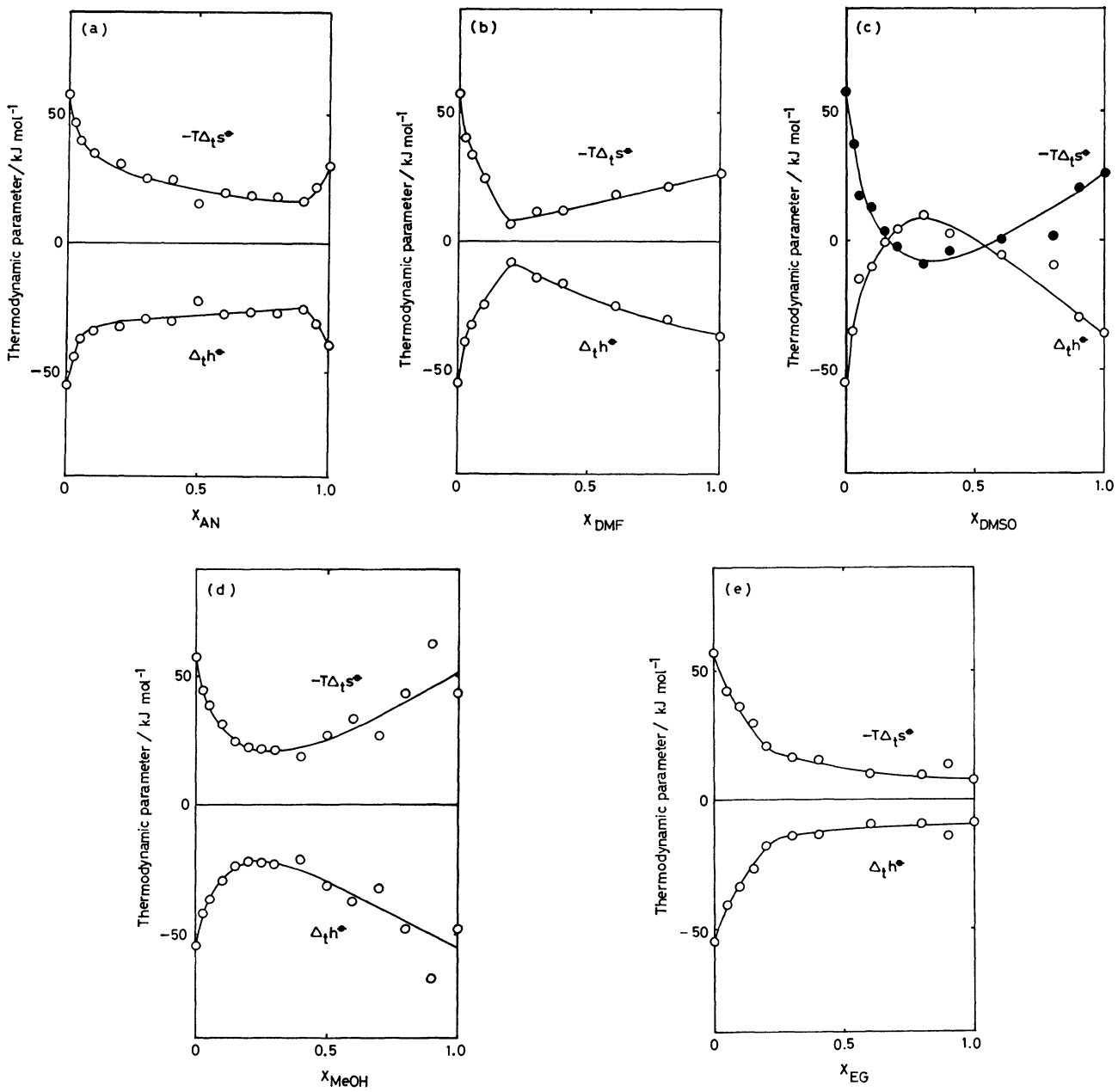

Fig. 2. Thermodynamic parameters for transfer of $[Cr(acac)_3]$ from dodecane to water-organic solvent mixtures at 298.15 K. Co-solvents are (a) acetonitrile, (b) dimethylformamide, (c) dimethyl sulfoxide, (d) methanol and (e) ethylene glycol.

Table 2. Dipole moment and cohesive energy density of the polar solvents studied[a)]

Solvent	Dipole moment D[b)]	Cohesive energy density MPa
Water	1.94	2302
Ethylene glycol	2.28	892
Methanol	2.87	874
Acetonitrile	3.44	582
DMSO	3.9	705
DMF	3.86	582

a) J. A. Riddick and W. B. Bunger, "Organic Solvents," 3rd ed, Wiley, New York (1970). b) $1D = 3.333 \times 10^{-30}$ C m.

and cohesive energy density is a measure of the solvent-solvent interaction. It has been found that the increase in value of $K_t^{\ominus}$ or the decrease in value of $\Delta_t\mu^{\ominus}$ corresponds approximately to the increase in dipole moment of the solvent molecules and to the decrease in cohesive energy density of the solvent (see Table 2).

Dependence of the Partition Constant on the Composition of the Solvent Mixture. The pressure-volume approach has been previously proposed in order to interpret the solvent effect of water–organic mixture on the partition constants of acetone, acetylacetone,[4)] and several metal(III) acetylacetonates[3)] in heptane/(water–DMSO) systems. This approach is essentially an extension of the McDevit-Long theory,[7)] introduced to predict the activity coefficients of nonelectrolytes in water–organic solvent mixtures. The pressure-volume approach assumes that the non-ideal change in internal pressure and volume upon mixing two solvents causes a change in chemical potential or activity coefficient of the solute. According to this approach, the following relationship holds for a nonelectrolyte solute in a solvent mixture.[4)]

$$\ln f_s = -k\frac{P_i}{\alpha T}\frac{v^E}{v}, \qquad (5)$$

where f_s is the activity coefficient of the solute on the basis of the ideal mixing of the solvent mixture, and α, P_i, v, and v^E are the isobaric thermal expansivity, the internal pressure, the molar volume, and the excess molar volume of the solvent mixture, respectively. k is a proportional constant. In the partition systems studied here, it is acceptable to define the activity coefficient of the solute as

$$\ln f_s = -\ln K_t^{\ominus} + \phi_1 \ln K_{t,1}^{\ominus} + \phi_2 \ln K_{t,2}^{\ominus}, \qquad (6)$$

where $K_t^{\ominus}$, $K_{t,1}^{\ominus}$, and $K_{t,2}^{\ominus}$ are the partition constants in dodecane/mixed solvent, dodecane/solvent 1, and dodecane/solvent 2, respectively, and ϕ_1 and ϕ_2 are the volume fractions of the components 1 and 2. In this study, solvent 1 and solvent 2 refer to water and the organic co-solvent, respectively.

In dodecane/(water–DMSO) system, a plot of log f_s against the pressure factor $-(P_i/\alpha T)(v^E/v)$ gives reasonably good linearity as shown in Fig. 3. The observed partition behavior of [Cr(acac)$_3$], which is characterized by the minima of the partition constant (Fig. 1), is interpreted from the change in the internal

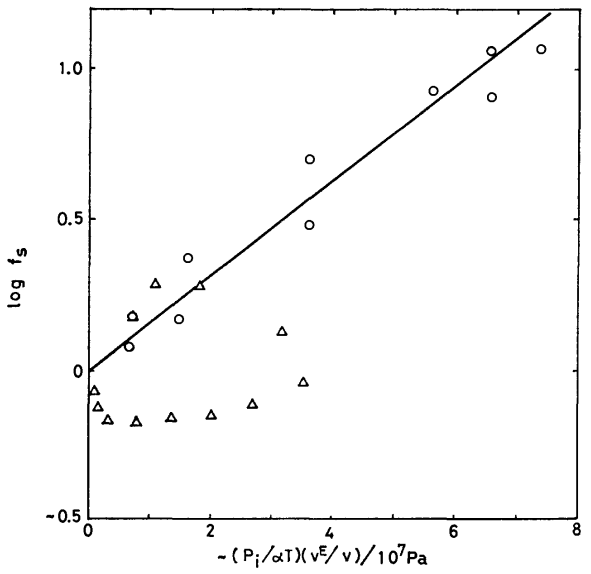

Fig. 3 Plot of logarithms of the activity coefficients of [Cr(acac)$_3$] against the pressure factors of the mixed solvent phase; ○, water–DMSO and △, water-AN.

pressure and the volume upon mixing which are caused by a strong interaction between water and DMSO, since the pressure-volume approach takes account of a solvent-solvent interaction as the only factor in the solvent effect.

In dodecane/(water–acetonitrile) system, a plot of log f_s against the pressure factor calculated from the internal pressure and density data reported by Grant-Taylor and Macdonald[8)] does not give a linear plot. In the region of $x_{AN} \leq 0.1$, however the slope of the best line is close to that for the water–DMSO system. A quite large scattering observed in the region $x_{AN} > 0.1$ may be due to the addition of acetonitrile to water causing not only an increase in the internal pressure but also destruction of the solvent structure. The destruction of the solvent structure causes an increase in the activity coefficient of water and acetonitrile. The abrupt increase in $K_t^{\ominus}$ in the region from $x_{AN} = 0.05$ to 0.4 or more corresponds to the abrupt structure-breaking of the polar phase upon mixing water and acetonitrile (h^E is positive in this region[9)]). The partition constant has a minimum in the region of $x_{AN} \leq 0.05$, which may be attributed to structure-making of the solvent upon mixing water and acetonitrile (h^E is negative in this region[9)]).

As shown in Fig. 1, a maximum in the $-\log K_t^{\ominus}$ *vs.* x_2 curve becomes remarkable as the temperature is lowered. As the temperature is lowered the interaction between water and the co-solvent becomes stronger, so that transfer of the solute from dodecane to the water-rich mixture becomes more unfavorable. It is expected that the interaction between water and the co-solvent affects the partition behavior of [Cr(acac)$_3$] in a similar fashion in every system except dodecane/(water–acetonitrile), because the h^E's of the mixed solvent have negative values in order of H_2O–EG> H_2O–MeOH> H_2O–DMF> H_2O–DMSO except for the water–acetonitrile system. The lack of data of

internal pressure and/or isobaric thermal expansivity, prohibits application of the pressure-volume approach to the other systems.

Dependence of the Standard Transfer Enthalpy of the Composition of the Solvent Mixture. It has been noted that a mixed solvent with a large negative value of h^E shows a large value of $\Delta_t h^\ominus$. A semi-quantitative formulation to represent this observation is developed by assuming that if 1 mol of the solute molecule is transferred from dodecane to the water–organic solvent mixture, then the interactions among the mixed solvent molecules included in volume V_s would be broken. The "excess" transfer enthalpy $\Delta_t h^{\ominus E}$ which is defined as

$$\Delta_t h^{\ominus E} = \Delta_t h^\ominus - x_1 \Delta_t h^\ominus(1) - x_2 \Delta_t h^\ominus(2), \quad (7)$$

where $\Delta_t h^\ominus(1)$ and $\Delta_t h^\ominus(2)$ are the standard transfer enthalpies from dodecane to solvent 1 and solvent 2, respectively will be proportional to the excess cohesive energy density, $-h^E/v$, *i.e.*,

$$\Delta_t h^{\ominus E} = V_s\left(-\frac{h^E}{v}\right), \quad (8)$$

where v refers to the mean molar volume of the solvent mixture. A plot of the calculated $\Delta_t h^{\ominus E}$ values against $(-h^E/v)$ gives a linear correlation, as shown in Fig. 4. From the slope the parameter V_s has been estimated as 616 $cm^3\ mol^{-1}$. This value is about 2.2 times larger than the molar volume of $[Cr(acac)_3]$ in the crystalline state, 275.3 $cm^3\ mol^{-1}$.[10] This observation may reflect the distance of closest approach of the solvent molecule to the complex molecule is larger than the radius of the complex molecule.

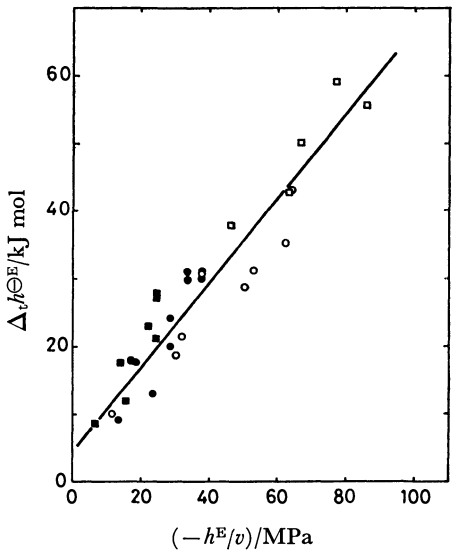

Fig. 4 Plot of the "excess" transfer enthalpy of $[Cr(acac)_3]$ against the excess cohesive energy density of water-organic solvent mixture; ○, water-DMF,[11] □, water-DMSO,[6,d] ●, water-methanol,[12] ■, water-ethylene glycol.[13]

Conclusion

In this study, it has been found that the activity coefficient derived from the partition coefficient may be correlated linearly with the pressure factor of the solvent mixture in Eq. 5 in the water–DMSO system, but not in the water–AN. This apparent discrepancy may be result from differences in the types of interactions, that is, the aqueous mixture is structure-making ($h^E<0$) or structure-breaking ($h^E>0$). It has been found that, in dodecane/aqueous mixtures with DMF, DMSO, MeOH, and EG, which are structure-making, the "excess" transfer enthalpy defined in Eq. 7 can be correlated linearly with the excess cohesive energy density. These findings show the importance of the solvophobic interaction between $[Cr(acac)_3]$ and polar solvent molecules in the aqueous mixed solvent phase.

References

1) T. Wakahayashi, S. Oki, T. Omori, and N. Suzuki, *J. Inorg. Nucl. Chem.*, **26**, 2255 (1964) and literature cited in H. M. N. H. Irving, "Ion Exchange and Solvent Extraction," ed by J. A. Marinsky and Y. Marcus, Mercel Dekker, New York (1974), Vol. 6, p. 139.

2) Y. Yoshimura and N. Suzuki, *Bull. Chem. Soc. Jpn.*, **51**, 2002 (1978).

3) H. Awano, H. Watarai, and N. Suzuki, *J. Inorg. Nucl. Chem.*, **41**, 124 (1979).

4) H. Watarai and N. Suzuki, *Chem. Lett.*, **1977**, 321.

5) W. C. Fernelius and J. E. Blanch, *Inorg. Synth.*, **5**, 130 (1957).

6) a) For dodecane, J. A. Riddick and W. B. Bunger, "Organic Solvents," 3rd ed, Wiley-Interscience, New York (1970); b) For water-acetonitrile, D. F. Grant-Taylor and D. D. Macdonald, *Can. J. Chem.*, **54**, 2813 (1976): c) For water-DMF, S. Saphon and H. -J. Bittrich, *Z. Phys. Chem., (Leipzig)*, **252**, 113 (1973); d) For water-DMSO, J. M. G. Cowie and P. M. Toporowski, *Can. J. Chem.*, **39**, 2240 (1961); e) For water-methanol, V. S. Griffiths, *J. Chem. Soc.*, **1954**, 860; f) For water-ethylene glycol, M. F. Schwers, *Rev. Trav. Chim.*, **28**, 42 (1909).

7) W. F. McDevit and F. A. Long, *J. Am. Chem. Soc.*, **74**, 1773 (1952).

8) D. F. Grant-Taylor and D. D. Macdonald, *Can. J. Chem.*, **54**, 2813 (1976).

9) K. M. Morcom and R. W. Smith, *J. Chem. Thermodynamics*, **1**, 503 (1969).

10) M. M. Jones, A. T. Davila, J. E. Hix, Jr., and R. V. Dilts, *J. Inorg. Nucl. Chem.*, **25**, 369 (1963).

11) H. Peters and E. Tappe, *Monatsber. Deut. Akad. Wiss. Berlin*, **9**, 692 (1967).

12) L. Benjamin and G. C. Benson, *J. Phys. Chem.*, **67**, 858 (1963).

13) H. -G. Konnecka, H. Steinert, and E. Leibnitz, *Z. Phys. Chem. (Leipzig)*, **208**, 147 (1957).

Organonickel(II) Complexes Containing Carbon-bonded Heterocycles as a Ligand

Kiyoshi Isobe, Yukio Nakamura, and Shinichi Kawaguchi*

Department of Chemistry, Faculty of Science, Osaka City University, Sumiyoshi-ku, Osaka 558

(Received August 14, 1979)

Oxidative addition reactions of 2- and 3-chloropyridines and of 2-chloropyrazine to tetrakis(triphenylphosphine)nickel(0) occurred in toluene at ambient temperature to afford dinuclear nickel(II) complexes containing carbon-bonded heterocycles as a ligand. They are quite stable and the bridging chloride was readily substituted by other halides and pseudohalides preserving the dinuclear structure. 8-Chloroquinoline yielded a mononuclear complex as an exception. These novel organonickel(II) complexes were characterized by analytical and molecular weight data together with IR, ^{1}H NMR, and ^{13}C NMR spectra. Di-μ-chloro-bis(2-pyridyl)bis(triphenylphosphine)dinickel(II) was found to be an excellent catalyst for selective cross coupling of 2-chloropyridine with methylmagnesium bromide.

Organonickel complexes have attracted interest of many investigators in coordination chemistry, synthetic chemistry, and other related fields.[1] The transition metal–carbon bond is not so unstable as was formerly considered. Thus the *trans*-NiX(aryl)$(PR_3)_2$ complexes, which are prepared conveniently by the oxidative addition reactions of aryl halides with tetrakis(tertiary phosphine)nickel(0),[2] are stable especially when the aryl ligand bears an *ortho*-substituent.[3] Benzyl,[4] vinyl, and acyl[5] halides also react with the nickel(0) complexes to afford similar square-planar organonickel(II) complexes which are isolable though they are less stable than the aryl complexes.

Cross coupling of alkyl, aryl, and alkenyl Grignard reagents with aryl and alkenyl halides was found by Kumada and his coworkers to be catalyzed by the dichlorodiphosphinenickel(II) complexes and the diorganonickel(II) complexes were presumed to be important intermediates.[6] The efficient method of carbon–carbon bond formation was successfully applied to halogenopyridines.[7] The σ-pyridyl nickel(II) complexes must be included in the catalytic turn-over in these reactions, although they have not yet been isolated.

Only a few examples of the carbon-bonded pyridyl complexes with transition metals have been reported. Stable (2-pyridyl)pentacyanocobaltate(III) was obtained by the reaction between 2-iodopyridine with pentacyanocobaltate(II).[8] Reactions of perfluoropyridine with several metal carbonyl compounds afforded the perfluoro-4-pyridyl complexes.[9] 2-Pyridylgold(I) was obtained by the reaction of chloro(triphenylarsine)gold(I) with 2-pyridyllithium and assumed to be a cyclic trimer.[10] 2-Methyl-, 2-phenyl-, and 2-vinylpyridines reacted with bis(η-cyclopentadienyl)methyltitanium(III) to give a 6-pyridyl complex, in which the nitrogen atom also interacts with the metal atom to form a three-membered titanocycle.[11] This paper reports very stable nickel(II) complexes containing carbon-bonded pyridines and two other nitrogen heterocycles as a ligand.

Experimental

Unless otherwise stated, air-sensitive materials were handled under a nitrogen atmosphere. Solvents were distilled under nitrogen and other reagents purged with nitrogen before use. Tetrakis(triphenylphosphine)nickel(0) and tetrakis(triphenyl phosphite)nickel(0) were prepared by the methods of Schunn,[12] and McLaughlin.[13] 2-Pyridyllithium was prepared according to Gilman and Spatz,[14] and sodium acetylacetonate by the reaction of acetylacetone with metallic sodium in methanol. Halopyridines, tertiary phosphines, and Grignard reagents were purchased and used without further purification.

*Preparation of Di-μ-halogeno-bis(2-pyridyl)bis(triphenylphosphine)dinickel(II) Complexes, $[NiX(C_5H_4N\text{-}C^2)(PPh_3)]_2$, where X=Cl (**1a**), Br(**1b**), and I(**1c**).* To a solution of tetrakis(triphenylphosphine)nickel(0) (2.5 g, 2.3 mmol) in toluene (100 ml) was added dropwise 2-chloropyridine (0.46 g, 4.0 mmol) or 2-bromopyridine (0.58 g, 3.7 mmol). The reaction proceeded quickly at ambient temperature to deposit an orange-red precipitate. After stirring for 3 h, the product was filtered, washed with methanol, and dried *in vacuo*. The yields were 60% for **1a** and 55% for **1b**. The crude product (*ca.* 0.4 g) of **1a** or **1b** was dissolved in dichloromethane (10 ml). After filtration, methanol (*ca.* 40 ml) was added slowly to the filtrate to precipitate glittery brownish yellow crystals, which were filtered, washed with diethyl ether, and dried *in vacuo*.

Compound **1c** was prepared by metathesis of **1a**. Compound **1a** (0.5 g, 0.6 mmol) was dissolved in dichloromethane (30 ml), and methanol (15 ml) was added slowly to the solution. A methanol solution (15 ml) of an excess amount (1.8 g, 12 mmol) of sodium iodide was then added slowly and the mixture was stirred for 2 h at room temperature. After evaporation of the solvent under reduced pressure, the concentrate (*ca.* 20 ml) was left standing for 2 h. An orange-red precipitate of **1c** was filtered and washed with methanol several times and with diethyl ether. The yield was 80%. Complex **1b** was also derived from **1a** by the same method in a 90% yield.

*Preparation of Di-μ-chloro-bis(6-chloro-2-pyridyl)- and Di-μ-chloro-bis(5-chloro-3-pyridyl)-bis(triphenylphosphine)dinickel(II) Complexes, $[NiCl(R)(PPh_3)]_2$, where $R=C_5H_3(6\text{-}Cl)N\text{-}C^2$ (**2a**) and $C_5H_3(5\text{-}Cl)N\text{-}C^3$ (**2b**).* The reaction of tetrakis(triphenylphosphine)nickel(0) (2.5 g, 2.3 mmol) with 2,6- or 3,5-dichloropyridine (1.5 g, 10 mmol) was carried out in toluene (140 ml) at ambient temperature in a similar manner as above. After stirring for 5 h, compound **2a** was obtained as an orange-red precipitate in a 90% yield. The reaction for **2b** was remarkably slow and allowed to proceed for 3 d to deposit a brown precipitate in a 70% yield.

*Preparation of Di-μ-chloro-bis(3-pyridyl)-, Di-μ-chloro-bis(2-pyrazinyl)-, and Di-μ-chloro-bis(6-methoxy-2-pyridyl)-bis(triphenylphosphine)nickel(II) Complexes, $[NiCl(C_5H_4N\text{-}C^3)(PPh_3)]_2$ (**3**), $[NiCl(C_4H_3N_2\text{-}C^2)(PPh_3)]_2$ (**4**), and $[NiCl(C_5H_3\text{-}(6\text{-}CH_3O)\text{-}N\text{-}C^2)(PPh_3)]_2$ (**5**).* Compounds **3**, **4**, and **5** were prepared by the method analogous to that for **1a**. The

reaction finished within 1 h in the case of **4** and **5**, but it took about 24 h for **3**. Yields of crude products were 40, 90, and 80% for **3**, **4**, and **5**, respectively. On recrystallization from dichloromethane–methanol **3** and **5** were obtained as orange-yellow crystals and **4** was orange-red. Compound **3** is less stable in air and prompt handling is necessary.

Preparation of Chloro(8-quinolyl)bis(triphenylphosphine)nickel(II), [NiCl(C_9H_6N-C^8)(PPh_3)$_2$]. A toluene solution (40 ml) of 8-chloroquinoline (1.6 g, 10 mmol) was added drop by drop to a solution of tetrakis(triphenylphosphine)nickel(0) (2.5 g, 2.3 mmol) in toluene (100 ml). After stirring for 3 h, a yellow precipitate was filtered, washed with diethyl ether, and dried *in vacuo*. The yield was 90%.

*Preparation of Di-μ-pseudohalogeno-bis(6-substituted 2-pyridyl)-bis(triphenylphosphine)dinickel(II) Complexes, [NiX(R)(PPh_3)]$_2$, where R=C_5H_3(6-CH_3O)N-C^2, X=N_3 (**7a**), OCN (**7b**), SCN (**7c**), and SeCN (**7d**); R=C_5H_3(6-Cl)N-C^2, X=N_3 (**7a'**), OCN (**7b'**), and SCN (**7c'**).* Complex **5** or **2a** (0.4 g, 0.4 mmol) was dissolved in dichloromethane (40 ml) and methanol (15 ml) was added slowly to the solution. A methanol solution (15 ml) of sodium azide (0.3 g, 4 mmol), sodium cyanate (0.3 g, 4 mmol), sodium thiocyanate (0.3 g, 4 mmol), or potassium selenocyanate (0.6 g, 4 mmol) was added drop by drop to the complex solution. (Sodium cyanate was dissolved in 5 ml of water and then methanol was added to make up a 15 ml solution.) After stirring for 2 h, the reaction mixture was concentrated to about 20 ml by evaporation under reduced pressure to deposit an orange-yellow or orange-red precipitate in 65 (**7a**), 75 (**7b**), 90 (**7c**), 47 (**7d**), 70 (**7a'**), 75 (**7b'**), and 92% (**7c'**) yields, respectively. Glittery crystals of each complex were obtained by recrystallization from dichloromethane–methanol.

*Preparation of Bis(acetylacetonato)bis(6-chloro-2-pyridyl)dinickel(II), [Ni(C_5H_3(6-Cl)N-C^2)(acac)]$_2$ (**8**).* Complex **2a** (0.5 g, 0.5 mmol) was dissolved in dichloromethane (30 ml) and methanol (10 ml) was added slowly to it. A methanol solution (15 ml) of sodium acetylacetonate was added dropwise to the complex solution. After stirring for 7 h, the reaction mixture was concentrated to 20 ml by evaporation at ambient temperature under reduced pressure, and left standing for 30 min. A precipitate was separated by filtration and dissolved in dichloromethane (10 ml) and a blue insoluble residue was filtered off. Methanol (30 ml) was added to the filtrate and the solution was again evaporated to 20 ml to deposit yellow-orange crystals in a 60% yield. The blue residue was identified as sodium tris(acetylacetonato)-nickelate(II) (yield, 7%) on the basis of elemental analysis and IR spectrum.

*Reaction of Compound **8** with Triphenyl Phosphite.* Triphenyl phosphite (1.0 g, 3 mmol) was added to a suspension of compound **8** (0.3 g, 0.6 mmol) in methanol (40 ml) and the mixture was heated under reflux for 3 h. A precipitate was filtered off during hot and the filtrate was concentrated to 20 ml under reduced pressure and allowed to stand for 2 d to deposit a white precipitate of 6,6'-dichloro-2,2'-bipyridine. The product was dissolved in dichloromethane (5 ml) and methanol (20 ml) was added to the solution to separate out a less soluble contaminant. This procedure of purification was repeated several times to remove a small amount of tetrakis(triphenyl phosphite)nickel(0) (Found: C, 66.04; H, 4.81%. Calcd for $C_{72}H_{60}P_4O_{12}Ni$: C, 66.53; H, 4.65%). The yield of the coupling product was 60%. Found: C, 53.03; H, 2.66; N, 12.33%; parent mass peak (*m/e*), 223.90. Calcd for $C_{10}H_6N_2Cl_2$: C, 53.36; H, 2.69; N, 12.45%; *m/e*, 223.90.

*Cross Coupling of Methylmagnesium Bromide to 2-Chloropyridine Catalyzed by Compound **1a**.* Compound **1a** (0.7 g, 0.9 mmol) was added to a tetrahydrofuran (THF) solution (100 ml) of 2-chloropyridine (5.4 g, 48 mmol). To this solution was added dropwise a THF solution (60 ml) of methylmagnesium bromide (6.6 g, 60 mmol). The reaction proceeded quickly at ambient temperature, producing a precipitate of magnesium bromide chloride and color of the solution changing from yellowish brown to deep green. 2-Methylpyridine was yielded quantitatively and absence of unreacted 2-chloropyridine and other coupling products was confirmed by the gas-liquid chromatography.

Measurements. IR spectra were recorded in Nujol on JASCO IR-E (4000—650 cm^{-1}), Hitachi EPI-L (700—200 cm^{-1}) and FIS-3 (400—30 cm^{-1}) spectrophotometers. JEOL JNM C60-HL and PS-100 spectrometers were used to obtain ^1H NMR spectra at 60 and 100 MHz, respectively, in CD_2Cl_2 with tetramethylsilane as external reference. ^{13}C NMR spectra were taken in CD_2Cl_2 with a JEOL JNM-FX60 spectrometer at 15.0 MHz. Tetramethylsilane was used again as external reference. The molecular weight was determined by vapor pressure osmometry in dichloromethane at 25 °C with an instrument manufactured by Knauer in Berlin, Germany. Mass spectra were measured with a Hitachi GC-mass-spectrometer M-52 and gas chromatography was performed on a Varian Aerograph Model 920 through a column of Silicon OV 17 with helium as a carrier gas. The injection temperature was 100 °C.

Results and Discussion

Tetrakis(triphenylphosphine)nickel(0) has frequently been used as a starting material for preparation of the aryl and other organonickel compounds, and proved now to react readily with halogenated nitrogen heterocycles such as 2- and 3-halogenopyridines, 2,6- and 3,5-dichloropyridines, 2-chloro-6-methoxypyridine, 2-chloropyrazine, and 8-chloroquinoline. In each case the reaction occurred at room temperature and the time necessary for completion of reaction increased in the sequence of 2-bromopyridine<2-chloropyrazine ≈ 2-chloropyridine < 2-chloro-6-methoxypyridine ≈ 2,6-dichloropyridine < 3-chloropyridine < 3,5-dichloropyridine, indicating that the reactivity of pyridine at the C^2 position with nickel(0) is appreciably higher than at the C^3 position. 2-Chlorothiophene did not react with $Ni(PPh_3)_4$. 2-Chlorobenzothiazole did react, but gave no organonickel compound, producing dichlorobis(triphenylphosphine)nickel(II). The reaction of tetrakis(triphenyl phosphite)nickel(0) with 2-chloropyridine was examined, but refluxing in toluene for 10 h showed no sign of reaction.

Characterization of the Di-μ-halogeno-bis(σ-pyridyl)bis(triphenylphosphine)dinickel(II) Complexes. The analytical and molecular weight data of these complexes are collected in Table 1. The 3-pyridyl complex (**3**) is less stable than the 2-pyridyl complexes and decomposes gradually on exposure to air, thus giving unsatisfactory analysis. The complexes in Table 1 are all diamagnetic and have the square-planar structure, indicating the effect of π-bonding between the carbon-bonded pyridine ring and the nickel(II) ion, since dichlorobis(triphenylphosphine)nickel(II) has a tetrahedral structure.[15]

The molecular weight data indicate that all complexes except **6** are dinuclear. Characteristic IR data for these complexes are summarized in Tables 2 and

Table 1. Analytical data for the σ-pyridyl nickel(II) complexes

Complex		Found (Calcd)			
		C(%)	H(%)	N(%)	mol wt[a]
$[NiCl(C_5H_4N\text{-}C^2)(PPh_3)]_2$	**1a**	62.67 (63.57)	4.57 (4.40)	3.31 (3.23)	829 (869)
$[NiBr(C_5H_4N\text{-}C^2)(PPh_3)]_2$	**1b**	58.04 (57.67)	4.10 (4.00)	2.99 (2.93)	790 (958)
$[NiI(C_5H_4N\text{-}C^2)(PPh_3)]_2$	**1c**	51.68 (52.52)	3.65 (3.64)	2.63 (2.66)	840 (1052)
$[NiCl(C_5H_3(6\text{-}Cl)N\text{-}C^2)(PPh_3)]_2$	**2a**	58.41 (58.90)	3.84 (3.87)	3.11 (2.99)	947 (940)
$[NiCl(C_5H_3(5\text{-}Cl)N\text{-}C^3)(PPh_3)]_2$	**2b**	59.55 (58.90)	4.10 (3.87)	3.20 (2.99)	890 (940)
$[NiCl(C_5H_4N\text{-}C^3)(PPh_3)]_2$	**3**	61.54 (63.57)	4.35 (4.40)	3.12 (3.23)	
$[NiCl(C_4H_3N_2\text{-}C^2)(PPh_3)]_2$	**4**	59.78 (60.67)	4.06 (4.16)	6.24 (6.43)	857 (871)
$[NiCl(C_5H_3(6\text{-}CH_3O)N\text{-}C^2)(PPh_3)]_2$	**5**	62.04 (62.05)	4.48 (4.56)	3.00 (3.01)	881 (927)
$[NiCl(C_9H_6N\text{-}C^8)(PPh_3)_2]$	**6**	72.11 (72.36)	4·80 (4.86)	1.77 (1.88)	710 (747)
$[NiN_3(C_5H_3(6\text{-}CH_3O)N\text{-}C^2)(PPh_3)]_2$	**7a**	60.73 (61.12)	4.47 (4.59)	11.75 (11.88)	910 (943)
$[NiNCO(C_5H_3(6\text{-}CH_3O)N\text{-}C^2)(PPh_3)]_2$	**7b**	62.46 (63.67)	4.43 (4.59)	5.89 (5.94)	940 (943)
$[NiNCS(C_5H_3(6\text{-}CH_3O)N\text{-}C^2)(PPh_3)]_2$	**7c**	61.44 (61.57)	4.32 (4.44)	5.80 (5.74)	970 (975)
$[NiNCSe(C_5H_3(6\text{-}CH_3O)N\text{-}C^2)(PPh_3)]_2$	**7d**	55.11 (56.17)	3.90 (4.05)	5.19 (5.24)	990 (1069)
$[NiN_3(C_5H_3(6\text{-}Cl)N\text{-}C^2)(PPh_3)]_2$	**7a′**	56.57 (56.52)	3.78 (3.96)	12.55 (11·46)	923 (951)
$[NiNCO(C_5H_3(6\text{-}Cl)N\text{-}C^2)(PPh_3)]_2$	**7b′**	60.68 (60.62)	3.88 (3.82)	6.04 (5.89)	924 (951)
$[NiNCS(C_5H_3(6\text{-}Cl)N\text{-}C^2)(PPh_3)]_2$	**7c′**	58.44 (58.64)	3.68 (3.69)	5.74 (5.70)	956 (983)
$[Ni(acac)(C_5H_3(6\text{-}Cl)N\text{-}C^2)]_2$	**8**	44.19 (44.43)	4.10 (3.72)	4.82 (5.18)	528 (541)

a) In dichloromethane at 25 °C.

3. As is seen in Table 2, two distinct ν(Ni–X) bands are observed for each complex and the frequencies are reasonable for the bridging halides.[16,17] The IR spectra in the lower frequency region also exhibit one band each at about 340 cm^{-1} which is assigned unambiguously to the ν(Ni–P) vibration. These IR-spectral patterns strongly support the following C_{2h} *trans* structure for the dinuclear complexes.[18]

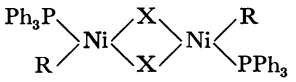

Since the alkyl and aryl ligands are usually considered to exert a stronger *trans* influence than the tertiary phosphines,[19] the higher frequency one of the two ν(Ni–X) bands may be assigned to the vibration of the Ni–X bond *trans* to triphenylphosphine. The ν(Ni–Cl) frequencies (289 and 248 cm^{-1}) for **1a** are similar to but appreciably lower than those (302 and 280 cm^{-1}) for $[NiCl(CH_3)(PMe_3)]_2$,[17] probably indicating a stronger *trans* influence of the 2-pyridyl ligand than that of the methyl group. The ν(Ni–Cl):ν(Ni–Br):ν(Ni–I) ratio (1:0.67:0.53) for **1a**, **1b**, and **1c** is appreciably different from the values found for other halogenonickel(II) complexes, *e.g.* 1:0.83:0.70 for NiX_2(1,2-bis(diphenylphosphino)ethane).[20] The reason is not certain why the halogen-discriminating ability of nickel(II) is enhanced in the present complexes. As is expected from the order of *trans* influence of halide ions, the ν(Ni–P) frequencies slightly decrease in the sequence of **1a**>**1b**>**1c**.

Table 2. Decomposition temperatures and some FIR data

Complex	Dec. temp °C	ν(Ni–X) cm^{-1}		ν(Ni–P) cm^{-1}
1a	187	289 s	248 s	338 s
1b	170	191 s	170 m	337 s
1c	160	152 m	134 m	329 s
2a	194	305 m	250 m	355 m
2b	140	283 s	246 s	337 w
3	124	310 w	245 w	360 s
4	193	290 s	245 m	335 m
5	187	290 s	250 s	340 w
6	170	352 s		290 m

When 2,6- or 3,5-dichloropyridine is used as a reactant, it may be expected to react with two molecules of tetrakis(triphenylphosphine)nickel(0) to afford a dinuclear complex in which the pyridine links to nickel atoms *via* two ring carbons. In reality compounds **2a** and **2b** were obtained, which showed no sign of reaction with another nickel(0) compound. On coordination to a metal atom, electron density of the pyridine ring may be increased by the π-bonding so as to prevent the oxidative addition to another nickel(0).

All complexes listed in Table 2 except compounds **2b** and **3** are stable on long-time exposure to air and their decomposition temperatures are higher than that of *trans*-chloro(phenyl)bis(triphenylphosphine)nickel(II) (122—3 °C).[2b] The thermal stability diminishes in the sequence of Cl>Br>I and 6-chloro-2-pyridyl≈2-pyrazinyl>2-pyridyl≈6-methoxy-2-pyridyl>5-chloro-3-pyridyl>3-pyridyl. The former sequence suggests the operation of antisymbiotic effect,[21] increasing softness of the halide ions weakening the *trans* Ni–C bond. Similarly, the lowest π* level becomes higher[22] and the M→L π-bonding ability decreases in the sequence of pyrazinyl>pyridyl>phenyl. Instability of the 3-pyridyl complexes relative to the 2-pyridyl complexes may be caused by the larger electron density at the 3-position of pyridine than at the 2-position[23] which lowers the acceptor ability.

Data of ^1H NMR spectra for the chloro complexes are included in Table 4. In each case the ring protons

Table 3. Characteristic IR data for the μ-pseudohalogeno complexes[a)]

Complex	ν(CN) or ν_a(NNN)	ν(CY) or ν_s(NNN)	δ(NCY) or δ(NNN)	ν(Ni-N)	ν(Ni-Y)	ν(Ni-P)
7a	2060 s	1340 w	590 w	410 m	398 m	343 w
7b	2226 s	1332 m	598 m	398 m	373 m	333 w
7c	2100 vs	b)	b)	400 m	347 w	337 w
7d	2110 vs	620 w, 590 w	b)	367 m	b)	320 m
7a′	2080 vs	1347 m	585 w	413 m	413 m	323 m
7b′	2245 vs	1345 m	602 m	415 m	375 m	329 m
7c′	2100 vs	b)	b)	395 m	350 m	323 m

a) Y=O, S, or Se. b) Indiscernible.

Table 4. Proton chemical shifts from external TMS in dichloromethane

	Hetero-ring proton at the position				Phenyl ring proton at the position		Methyl proton
	3	4	5	6	*meta* and *para*	*ortho*	
1a	6.33 m	6.79 m	6.27 m	8.57 m	7.30 m	7.90 m	
2a	6.45 d	6.21 t	6.65 d		7.31 m	8.03 m	
4	8.52 m		a)	a)	7.34 m	7.88 m	
5		(6.16 m, 5.76 m)[b)]			7.35 m	8.16 m	4.00 s
6[c)]	a)	a)			(7.50 m)[b)]		
7a	6.27 m	5.83 m	6.27 m		7.35 m	7.95 m	4.05 s
7b	6.29 m	5.82 m	6.29 m		7.40 m	8.04 m	4.02 s
7c	6.35 s	5.84 m	6.35 s		7.47 m	8.00 m	4.04 s
7d	6.33 s	5.86 m	6.33 s		7.46 m	7.96 m	4.06 s
7c′	6.72 d	6.34 t	6.54 d		7.50 m	7.90 m	
8	7.30 d	6.70 t	7.00 d				1.90 s, 2.00 s

s=singlet, d=doublet, t=triplet, m=multiplet
a) Masked by the signals of phenyl protons. b) Unassignable. c) H^2 and H^6 resonate at 8.82(m) and 6.75(m) ppm, respectively.

of triphenylphosphine resonate as two multiplets with the area ratio of 3:2 in the 7.30—7.50 and 7.88—8.16 ppm regions, respectively. The higher-field signal is assigned to the *meta* and *para* protons and the lower-field one to the *ortho* protons.[24)] The pyridine-ring protons of **1a** exhibit an ABCX-type signals at 6.27, 6.33, 6.79, and 8.57 ppm, showing large up-field shifts as compared with those at 7.18 (H^3), 7.55 (H^4), and 8.69(H^2) ppm for uncoordinated pyridine. The M→L π-bonding in the present complexes may be much more extensive than in *trans*-$NiBr(C_6H_5)(PEt_3)_2$, since the chemical shifts of the phenyl protons (6.90 and 7.40 ppm) in this complex are not so different from that of benzene (7.15 ppm).[25)]

When H^2 of pyridine is substituted by an electron-releasing group, similar up-field shifts of the ring proton signals are observed. Thus ring protons of 2-methylpyridine resonate at 6.92 (H^5), 7.00 (H^3), 7.43 (H^4), and 8.51 (H^6) ppm and those of 2-aminopyridine at 6.60 (H^5), 6.70 (H^3), 7.44 (H^4), and 8.11 (H^6) ppm.[26)] By reference to these data the pyridyl proton signals were assigned as shown in Table 4. A similar trend was also observed for $[Co(CN)_5(2\text{-pyridyl})]^{3-}$ but the up-field shifts are not so large as for the present complexes.[9)]

As is seen in Fig. 1, the pyridine-ring protons of **2a** show a triplet at 6.21 ppm and two doublets at 6.45 and 6.65 ppm. They are tentatively assigned to H^4, H^3, and H^5, respectively, on the assumption of

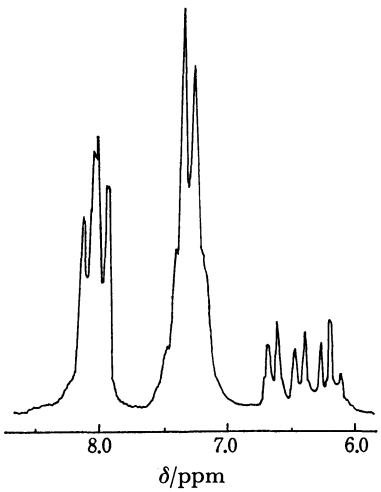

Fig. 1. The ^1H NMR spectrum of $[NiCl(C_5H_3(6\text{-Cl})\text{-}N\text{-}C^2)(PPh_3)]_2$ (**2a**) in CD_2Cl_2 with external TMS.

the first-order ABC spin system.[27)] In the case of uncoordinated 2-chloropyridine, signals for the corresponding protons are observed at 7.83, 7.39, and 7.49 ppm, respectively.[26)] A great deal of the up-field shifts of the ring-proton signals on coordination are again noted, the shift at H^4 (*meta* position from the metal) being the largest. Table 5 collects the ^{13}C NMR data for complex **2a** together with those for triphenylphosphine[28)] and 2-chloropyridine[29)] for

TABLE 5. ^{13}C NMR DATA

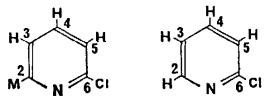

Compound	Chemical shift (δ/ppm)					Coupling constant/Hz
$P(C_6H_5)_3$	C^1 138.3	C^2 134.4	C^3 129.2	C^4 129.3		$J(P-C^1)=21$, $J(P-C^2)=20$ $J(P-C^3)=7$, $J(P-C^4)<1$
2-Cl-C_5H_4N[a]	C^2 151.1	C^3 123.9	C^4 138.5	C^5 122.4	C^6 149.7	
2a Phenyl carbon	C^1 134.2	C^2 135.7	C^3 128.5	C^4 130.5		$J(P-C^1)\simeq 20$, $J(P-C^2)=12$ $J(P-C^3)=10$, $J(P-C^4)=0$
2a Pyridyl carbon	C^2 131.8	C^3 118.8	C^4 128.7	C^5 128.1	C^6 130.5	

a) Ring carbons are numbered by reference to the complex as above.

comparison. Tentative assignments are given on the basis of the relative intensity and the J(P-C) value of each carbon and also by reference to the above literature data. In a similar manner as the proton resonances, the pyridine-ring carbons exhibit remarkable up-field shifts on coordination.

The pyridine-ring protons of compound **5** show two broad signals at 5.76 and 6.16 ppm, the methoxy protons resonating at 4.00 ppm. The corresponding proton signals for uncoordinated 2-methoxypyridine are observed at 6.62 (H^3), 7.40 (H^4), 6.70 (H^5), and 3.84 (CH_3) ppm. It is noteworthy that the methoxy protons show a down-field shift, while the pyridine-ring protons up-field shifts on coordination.

Properties of Chloro(8-quinolyl)bis(triphenylphosphine)-nickel(II) (6). As stated already only 8-chloroquinoline gave the mononuclear complex **6** on reaction with $Ni(PPh_3)_4$. Complex **6** exhibits a single ν(Ni–Cl) band at 350 cm^{-1} and a ν(Ni–P) band at about 290 cm^{-1}. The ν(Ni–Cl) frequency is quite similar to those observed for the *trans*-$NiCl(aryl)(PR_3)_2$ complexes,[2b,5] and the ν(Ni–P) frequency is a little higher than that observed for *trans*-$NiCl_2(PEt_3)_2$ (273.4 cm^{-1})[30] probably due to the weaker *trans* influence of PPh_3 as compared to PEt_3.[19] Thus complex **6** is considered to have the *trans* structure. It is stable in the air and the decomposition temperature (170 °C) is much higher than that of *trans*-$NiCl(C_6H_5)(PPh_3)_2$ (122—123 °C).[2b] The remarkable stability of **6** may be caused partly by the "*ortho* effect" [3] exerted by the fused pyridine ring in the 8-quinolyl ligand.

Proton NMR data for **6** are included in Table 4. In contrast with other dinuclear complexes, **6** exhibits a broad signal at about 7.50 ppm due to the phenyl protons. Of the quinoline-ring protons H^2 and H^6 resonate at 8.82 and 6.75 ppm, respectively, other proton signals being masked by those of the phenyl protons. Compared with the chemical shifts of H^2 (8.81 ppm) and H^6 (7.44 ppm) of uncoordinated quinoline,[26] the signal of H^6 which is in the *meta* position from the metal shows a remarkable up-field shift on ligation.

Characterization of the Di-μ-pseudohalogeno-bis(σ-pyridyl)-bis(triphenylphosphine)dinickel(II) Complexes. The bridging chloride ions in complexes **2a** and **5** were readily replaced by the azide, cyanate, thiocyanate, and selenocyanate ions to afford two series of compounds **7** in a mixture of dichloromethane and methanol at room temperature, the yields decreasing in the sequence of $SCN^- > OCN^- > N_3^-$ for both series. The analytical and molecular weight data listed in Table 1 together with the diamagnetic behavior indicate that the dinuclear square-planar structure is preserved in these complexes. Many dinuclear transition metal complexes containing pseudohalides as the bridging ligands have been prepared so far,[31–33] but no example of the square-planar nickel(II) complexes of this kind has been reported to our knowledge.

Of various bridging modes of the pseudohalide anions, the "one-end" bridge (A) and the "end-to-end" bridge (B) are most widely recognized. In the case

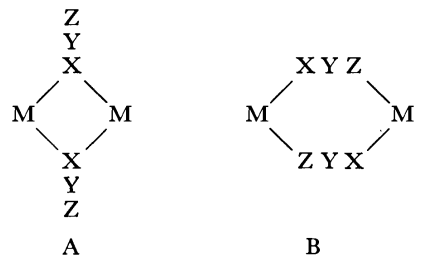

of the di-μ-azido complexes, X-ray analysis revealed that some complexes such as $[AsPh_4]_2[Pd_2(N_3)_6]$[34] and $NEt_4[Mn_2(N_3)_3(CO)_6]$[35] have the type A structure and the azide ion in $[Rh_2N_3(\eta^5\text{-}C_5Me_5)\text{-}(N_3C_4F_6)_3]$ is also one-end bridging,[36] while $[Cu(N_3)\text{-}(PPh_3)_2]_2$[37] and $[Cu_2(N_3)_2(Me_5dien)_2](BPh_4)_2$[38] have the type B structure. However both of the di-μ-azido structures have the local D_{2h} symmetry and it is impossible to distinguish between them only from the IR-spectral information. The cyanate ion usually coordinates to transition metals through the nitrogen atom,[31,33] and only one pair of linkage isomers has been reported in the solid state.[39] When the cyanate ion is involved in a dinuclear complex, one-end bridging at the nitrogen atom (type A) is common and the type B bridging has been found only in $[Ni_2(NCO)_2(tren)_2](BPh_4)_2$,[40] where tren is $N(CH_2\text{-}CH_2NH_2)_3$, and $(C_6H_5)_3TeNCO\cdot 0.5CHCl_3$.[41] In the case of thiocyanate and selenocyanate ions, however, the bridging mode of type B is usually preferred to type A,[31,33] although the one-end bridging both at

nitrogen[42] and sulfur[43] atoms has been exemplified.

Each of compounds **7a**—**7d** containing the 6-methoxy-2-pyridyl ligand exhibits a single sharp signal assignable to the methyl protons, indicating that neither geometrical nor linkage isomers are involved in each case. As is seen in Table 4 the pattern of ^{1}H NMR spectra for **7a**—**7d** and the chemical shifts of phenyl and pyridyl ring protons in these complexes show a striking resemblance to each other irrespective of the nature of the pseudohalide anions, suggesting the existence of a common bridging mode. We would like to tentatively assume the end-to-end bridging with the *trans* configuration (C). The IR spectral data in

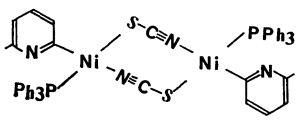

C

Table 3 are not diagnostic but conform to the presumed structure.

Characterization of Compound **8**. The analytical and molecular weight data in Table 1 indicate that compound **8** is dinuclear. The ν(C=O) and ν(C=C=C) bands are observed at 1565 and 1514 cm^{-1}, respectively, resembling those of $Ni_3(acac)_6$ at 1598 and 1520 cm^{-1}. Figure 2 shows the ^{1}H NMR spectrum of **8** in CD_2Cl_2. Two kinds of methyl signals are observed at 1.90 and 2.00 ppm. The pyridyl protons resonate at 6.70, 7.00, and 7.30 ppm. The coupling constants to each other are equal to those for **2a**, but the down-field shifts of these signals are remarkable as compared with those of **2a** although they still exist in higher field than proton signals of uncoordinated 2-chloropyridine. All pieces of the spectral information well conform to the proposed structure. To our knowledge this is the first example of the square-planar NiO_3C-type complexes, although the NiO_2CP-type complexes such as $NiC_2H_5(acac)$-PPh_3[44] have been reported. Again the strong effect of

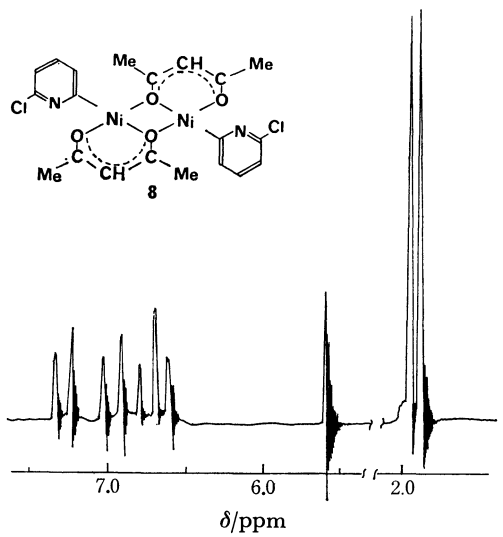

Fig. 2. The ^{1}H NMR spectrum of [Ni(acac)(C_5H_3-(6-Cl)N-C^2)]$_2$ (**8**) in CD_2Cl_2 with external TMS.

π-bonding between the pyridyl ligand and the nickel ion upon stabilizing the σ-carbon-bonded complex is noted.

Reactions of the σ*-Pyridyl Complexes.* Reactions of **1** with excess triphenylphosphine, thiourea, and pyridine were tried in vain at room temperature, ending in recovery of **1**. Refluxing of a solution of **1a** in neat pyridine for 2 h gave dichlorobis(pyridine)-nickel(II) in a 40% yield. Complex **6** reacted with acetylacetone to produce $Ni(acac)_2(C_9H_7N)_2$ in a 55% yield. Found: C, 64.78; H, 5.46; N, 5.19%. Calcd for $C_{28}H_{28}N_2O_4Ni$: C, 65.27; H, 5.48; N,5.44%. Presumably acetylacetone acted as an acid to split the nickel–quinolyl bond, the conjugate base (acac anion) replacing the chloride ion. It is noteworthy that bis(acetylacetonato)nickel(II) preferred quinoline to triphenylphosphine as a base in the adduct formation.

The reactions of bases such as pyridine and triphenylphosphine with **8** to break the dinuclear structure were unsuccessful at ambient temperature, but refluxing in a mixture of dichloromethane and methanol effected decomposition of **8** to yield unidentified products. When triphenyl phosphite was employed as a base, refluxing in methanol gave rise to 6,6′-dichloro-2,2′-bipyridine and tetrakis(triphenyl phosphite)nickel(0). Reductive elimination has occurred to yield a homocoupled product and the nickel(0) complex. The other product containing the acetylacetonate moiety has not been identified.

When Grignard reagents RMgBr (R=CH_3 or C_6H_5) and 2-pyridyllithium were reacted with **1a**, the diorganonickel complexes were not obtained, but instead 2-methylpyridine was yielded in the case of methylmagnesium bromide. On the contrary to the extraordinary stability of the σ-pyridyl nickel(II) complexes, the diorganonickel complex must be unstable, immediately undergoing a coupling reaction. As was described in the Experimental section, complex **1a** was found to be an excellent catalyst for the cross coupling of 2-chloropyridine with methylmagnesium bromide in THF at ambient temperature to produce 2-methylpyridine quantitatively. The pathway of the catalytic turn-over may be visualized by the proposed Scheme. The intermediates in brackets have not

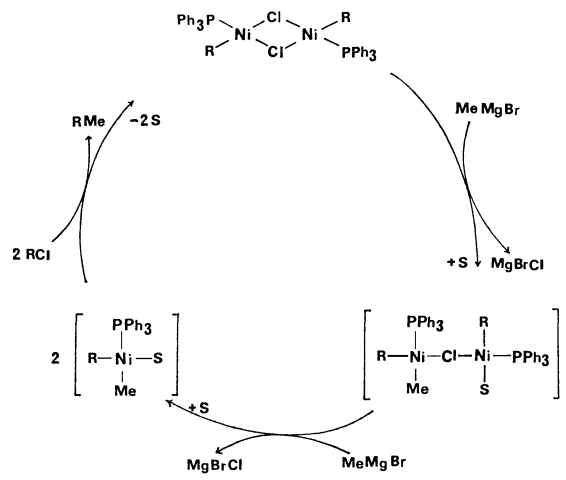

Scheme.

been isolated but just presumed. A molecule S is used for bookkeeping of the coordination number and may be either the solvent or *N*-bonded 2-chloropyridine.

Morrell and Kochi[25] prepared *trans*-methylphenyl(and *o*-tolyl)bis(triethylphosphine)nickel(II) and determined the rates of reductive elimination to yield toluene and *o*-xylene, respectively. These rates were found to be too slow to allow for a catalytic process probably because of the *trans* structure. Oxidative addition of aryl halides to nickel(0) species usually affords trans products, showing no sign of isomerization to either a *cis* isomer or a tetrahedral species.[25] These results offer a trouble to understanding of the cross coupling mechanism. In the present case, on the other hand, the dinuclear structure of **1a** is quite favorable for the catalytic steps, allowing the *cis* arrangement of the two organic ligands as depicted in Scheme.

The authors wish to thank Mr. Junichi Gohda for the elemental analysis, and Drs. Kyo Abe and Takamasa Kinoshita for NMR measurements. They are also grateful to the Ministry of Education for the Grant-in-Aid for Special Project Research (No. 311706).

References

1) P. W. Jolly and G. Wilke, "The Organic Chemistry of Nickel," Academic Press, Vol. I (1974), Vol. II (1975).
2) (a) D. R. Fahey, *J. Am. Chem. Soc.*, **90**, 402 (1970); (b) M. Hidai, T. Kashiwagi, T. Ikeuchi, and Y. Uchida, *J. Organomet. Chem.*, **30**, 279 (1971).
3) J. Chatt and B. L. Shaw, *J. Chem. Soc.*, **1960**, 1718.
4) J. K. Stille and A. B. Cowell, *J. Organomet. Chem.*, **124**, 253 (1977).
5) D. R. Fahey and J. E. Mahan, *J. Am. Chem. Soc.*, **99**, 2501 (1977).
6) K. Tamao, K. Sumitani, and M. Kumada, *J. Am. Chem. Soc.*, **94**, 4374 (1972); K. Tamao, K. Sumitani, Y. Kiso, M. Zembayashi, A. Fujioka, S. Kodama, I. Nakajima, A. Minato, and M. Kumada, *Bull. Chem. Soc. Jpn.*, **49**, 1958 (1976).
7) (a) K. Tamao, S. Kodama, T. Nakatsuka, Y. Kiso, and M. Kumada, *J. Am. Chem. Soc.*, **97**, 4405 (1975); (b) L. N. Pridgen, *J. Heterocyclic Chem.*, **12**, 443 (1975).
8) J. Halpern and J. P. Maher, *J. Am. Chem. Soc.*, **87**, 5361 (1965).
9) J. Cook, M. Green, and F. G. A. Stone, *J. Chem. Soc., A*, **1968**, 173.
10) L. G. Vaughan, *J. Am. Chem. Soc.*, **92**, 730 (1970).
11) B. Klei and J. H. Teuben, *J. Chem. Soc., Chem. Commun.*, **1978**, 659.
12) R. A. Schunn, *Inorg. Synth.*, **13**, 124 (1972).
13) J. R. McLaughlin, *Inorg. Nucl. Chem. Lett.*, **9**, 565 (1973).
14) H. Gilman and S. M. Spatz, *J. Org. Chem.*, **16**, 1485 (1951).
15) G. Garton, D. E. Henn, H. M. Powell, and L. M. Venanzi, *J. Chem. Soc.*, **1963**, 3625.
16) K. Nakamoto, "Infrared and Raman Spectra of Inorganic and Coordination Compounds," 3rd ed, Wiley-Interscience (1978), p. 322.
17) H. F. Klein and H. H. Karsch, *Chem. Ber.*, **106**, 1433 (1973).
18) R. J. Goodfellow, P. L. Goggin, and L. M. Venanzi, *J. Chem. Soc., A*, **1967**, 1897; R. J. Goodfellow, J. G. Evans, P. L. Goggin, and D. A. Duddell, *ibid.*, **1968**, 1604.
19) F. H. Allen and S. N. Sze, *J. Chem. Soc., A*, **1971**, 2054.
20) C. Udovich, J. Takemoto, and K. Nakamoto, *J. Coord. Chem.*, **1**, 89 (1971).
21) R. G. Pearson, *Inorg. Chem.*, **12**, 712 (1973).
22) W. L. Jorgensen and L. Salem, "The Organic Chemist's Book of Orbitals," Academic Press (London), 1973.
23) E. Clementi, *J. Chem. Phys.*, **46**, 4731 (1967).
24) R. Keat, *Chem. Ind. (London)*, **1968**, 1362.
25) D. G. Morrell and J. K. Kochi, *J. Am. Chem. Soc.*, **97**, 7262 (1975).
26) T. J. Batterham, "NMR Spectra of Simple Heterocycles," Wiley, New York (1973), p. 31.
27) W. Brügel, *Z. Elektrochem., Ber. Bunsenges. Phys. Chem.*, **66**, 159 (1962).
28) O. A. Gansow and B. Y. Kimura, *Chem. Commun.*, **1970**, 1621.
29) H. L. Retcofsky and R. A. Friedel, *J. Phys. Chem.*, **72**, 2619 (1968).
30) K. Shobatake and K. Nakamoto, *J. Am. Chem. Soc.*, **92**, 3332 (1970).
31) R. A. Bailey, S. L. Kozak, T. W. Michelsen, and W. N. Mills, *Coord. Chem. Rev.*, **6**, 407 (1971).
32) U. Müller, *Struct. Bonding*, **14**, 141 (1973).
33) A. H. Norbury, *Adv. Inorg. Chem. Radiochem.*, **17**, 231 (1975).
34) W. P. Fehlhammer and L. F. Dahl, *J. Am. Chem. Soc.*, **94**, 3377 (1972).
35) R. Mason, G. A. Rusholme, W. Beck, H. Englemann, K. Joos, B. Lindenberg, and H. S. Smedal, *Chem. Commun.*, **1971**, 496.
36) W. Rigby, P. M. Bailey, J. A. McCleverty, and P. M. Maitlis, *J. Chem. Soc., Dalton Trans.*, **1979**, 371.
37) R. F. Ziolo, A. P. Gaughan, Z. Dori, C. G. Pierpont, and R. Eisenberg, *Inorg. Chem.*, **10**, 1289 (1971).
38) T. R. Felthouse, E. J. Laskowski, D. S. Bieksza, and D. N. Hendrickson, *J. Chem. Soc., Chem. Commun.*, **1976**, 777.
39) S. J. Anderson, A. H. Norburg, and J. Sonstad, *J. Chem. Soc., Chem. Commun.*, **1974**, 37.
40) D. M. Duggan and D. N. Hendrickson, *Inorg. Chem.*, **13**, 2056, 2929 (1974).
41) D. D. Titus, J.-S. Lee, and R. F. Ziolo, *J. Organomet. Chem.*, **120**, 381 (1976).
42) G. D. Andreetti, L. Coghi, M. Nardelli, and P. Sgarabotto, *J. Cryst. Mol. Struct.*, **1**, 147 (1971); M. Cannas, G. Carta, and G. Marongiu, *J. Chem. Soc., Dalton Trans.*, **1973**, 251.
43) A. Mawby and G. E. Pringle, *Chem. Commun.*, **1970**, 385.
44) F. A. Cotton, B. A. Frenz, and D. L. Huater, *J. Am. Chem. Soc.*, **96**, 4820 (1974); A. Yamamoto, T. Yamamoto, T. Saruyama, and Y. Nakamura, *ibid.*, **95** 4073 (1973).

The Chemistry of 1,3-Glycol Derivatives. III. The Preparation of 1,1-Bis(1-hydroxyalkyl)cyclopropanes and Their Halogenation

Osamu Itoh,* Yoshiro Kohmura, Yasunori Ichikawa, Makoto Umezu, Tsutomu Okita, and Katsuhiko Ichikawa

Department of Hydrocarbon Chemistry, Faculty of Engineering, Kyoto University, Yoshida, Kyoto 606

(Received December 27, 1978)

By the reduction of 1,1-diacylcyclopropanes and their related compounds, several kinds of 1,1-bis(1-hydroxyalkyl)cyclopropanes have been prepared. Some of the stereoisomers were separated, and their configurations were determined by the NMR study of the 1,3-dioxanes prepared by the acetallization of the diols. The diols were subjected to halogenation. Although the reactions of *meso*- and *dl*-bis(1-hydroxyethyl)cyclopropanes with thionyl chloride and phosphorus pentachloride gave normal dichlorides, accompanied by slight skeletal rearrangements, the stereospecificities were rather low. With $ZnCl_2$–HCl, the specificities were lost completely and large amounts of the homoallyl derivative were formed. The reaction mechanism is discussed.

Stereoisomers of several kinds of aliphatic 1,3-glycol and their derivatives, including cyclic orthoacetates, were prepared and their reactions reported previously.[1] In this paper, an extension of the study to 1,3-glycols, whose C-2 carbons are cyclopropane-ring carbons, will be reported, since the preparation of this type of compound has not yet been reported except for one case of 1,1-bis(hydroxymethyl)cyclopropane.[2]

The glycols have been prepared by the reduction of 1,1-diacylcyclopropanes. Some of the stereoisomers have been separated and their conformations have been determined by the ^1H and ^{13}C NMR study of the glycols and their corresponding acetals. The diols were subjected to halogenation under various conditions to examine the stereospecificities and the skeletal rearrangements.

The starting materials and the glycols obtained (including several kinds of related compounds) are listed in Table 1.

According to conventional methods, the reductions were carried out with lithium aluminium hydride in tetrahydrofuran at 0 °C, with sodium borohydride in methanol at room temperature, and with aluminium isopropoxide in 2-propanol under reflux. Normal results were obtained, and no unusual phenomena such as those observed in the case of spiro-diketone[3] were encountered.

By reducing the reagent/substrate ratio, mono alcohols could be obtained. In the Meerwein-Pondorf-Verly reduction of the reference compound **6**, only glycol was obtained; no mono-alcohol could be isolated, not even with a smaller ratio of reagent/substrate (2/3) and with a shorter reaction time (0.5 h). No detectable amount of any by-product was obtained except 2-methyl-2,4-pentanediol, which was the aldol condensation product of acetone from the reducing reagent.[4] The results of the reduction are summarized in Table 2.

Since glycol **10** contains two asymmetric carbons, there should be *meso*- and *dl*-isomers. These were separated successfully by the following procedure. When a carbon tetrachloride solution of **10** was kept in a refrigerator at about −16 °C overnight, crystals (found to be *meso*-**10**, as will be described later) were formed. After filtration and evaporating the solvent, the liquid part of **10** (*dl*-**10**) was obtained. However, NMR analysis showed that the purity of the liquid part was as low as 70%. Since the solubility of *meso*-**10** was found to be slightly greater than that of the *dl*-form in water, the liquid portion was shaken with an ether–water mixture to remove the *meso*. After repeating the procedure, a *dl*-form with a purity of more than 80% was obtained.

Glycol **12** also has two asymmetric carbons and has *erythro*- and *threo*-forms. From crude **12**, crystals were formed after it had stood at room temperature for three months. Using the crystals as the seeds, a crystalline isomer of **12** (found to be *erythro*-**12**, as will be described later) were obtained from the ethereal solution of crude **12** at −30 °C. The residual part was *threo*-**12**, containing about 25% *erythro*-form.

Glycol **13** has *cis*- and *trans*-isomers in addition to *meso*- and *dl*-isomers, and all attempts at separation were unsuccessful. The isomer separation of *meso*- and *dl*-**15** was unsuccessful too, although the NMR assignments could be made in this case.

The structural assignments of the isomers of **10** and **12** were carried out by NMR analyses of the corresponding acetals obtained by the reactions with acetaldehyde and benzaldehyde (in the presence of calcium chloride and catalytic amounts of *p*-toluenesulfonic acid[5] in the same way as was reported previously.[1]

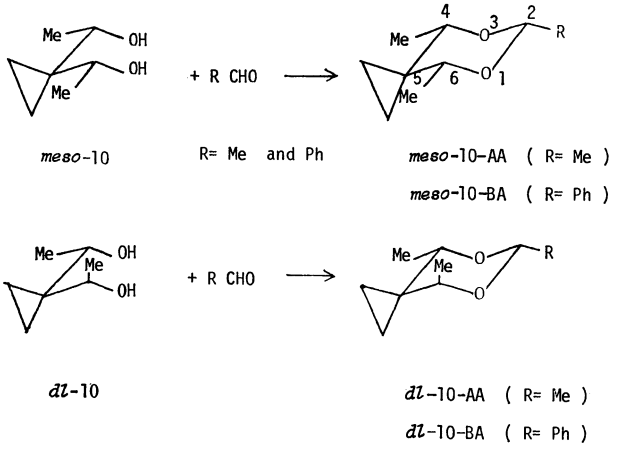

The physical properties of the acetals obtained are listed in Table 3.

The discussion of the NMR data of 1,3-dioxanes

Table 1. Physical properties of the diols obtained

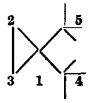

Starting material	Diol	Bp °C/mmHg (Mp/°C)	NMR data of diol in $CDCl_3$, δ/ppm						
			Ring CH_2	H on C^4	H on C^5	CH_3 on C^4	CH_3 on C^5	OH	Others
1	**7**	111—115/6	0.5, s, 4H	3.59, s, 4H				3.84, s, 2H	
2	**8**	91—92/4.7	0.32, m, 4H	3.45, q, 1H J=6.3	3.19, d, 1H J=11.3 4.02, d, 1H J=11.3	1.26, d, 3H J=6.3		3.28, s, 2H	
2	**9**	89—91/11.3	0.84—1.27 m, 4H	3.72, q, 1H J=7.0		1.26, d, 3H J=7.0		3.40, s, 2H	3.66, s, 3H (CH_3O)
3	*meso*-**10**	118—121/11 (62.8—63.0)	0.5, s, 4H	3.91, q, 2H J=6.8		1.15, d, 6H J=6.8		2.56, s, 2H	
3	*dl*-**10**	118—121/11	0.48, m, 4H	3.85, q, 2H J=6.8		1.13, d, 6H J=6.8		3.03, s, 2H	
3	**11**	110/15	0.86—1.29 m, 4H	3.90, q, 1H J=7.2		1.38, d, 3H J=7.2	1.91, s, 3H	3.60, 1H	
4	*erythro*-**12**	146—156/6 (84.5—85.1)	0.09—0.63 m, 4H	3.79, q, 1H J=6.0	4.84, s, 1H	0.95, d, 3H J=6.0	Ph, 7.20 s, 5H	3.14, 2H	
4	*threo*-**12**		0.09—0.63 m, 4H	1,00, d, 1H J=6.0	4.74, s, 1H	3.61, q, 1H J=6.0	Ph, 7.25 s, 5H	3.61, 2H	
5	**13**	164—170/11.5							
5	**14**	167/14	1.20—1.40 m, 2H PhCH 1.89, d of d, J=14, 7 2.71, d of d, J=17, 14	3.43, q J=6 4.23, q J=6 } 1H 1H		1.24, d J=6 1.31, d J=6 } 3H	1.53, s 1.54, s } 3H	2.95, 1H	7.17, m, 5H Ph

1: 1,1-Bis(ethoxycarbonyl)cyclopropane,**2** : 1-acetyl-1-(methoxycarbonyl)cyclopropane, **3**: 1,1-diacetylcyclopropane, **4**: 1-acetyl-1-benzoylcyclopropane, **5**: 1,1-diacetyl-2-phenylcyclopropane, **6**: 1,1-diacetyl-2-phenylethylene, **7**: 1,1-bis(hydroxymethyl)cyclopropane, **8**: 1-(1-hydroxyethyl)-1-(hydroxymethyl)cyclopropane, **9**: 1-(1-hydroxyethyl)-1-(methoxycarbonyl)cyclopropane, **10**: 1,1-bis(1-hydroxyethyl)cyclopropane, **11**: 1-(1-hydroxyethyl)-1-(acetyl)cyclopropane, **12**: 1-(1-hydroxyethyl)-1-(1-hydroxybenzyl)cyclopropane, **13**: 1,1-bis(1-hydroxyethyl)-2-phenylcyclopropane, **14**: 1-acetyl-1-(1-hydroxyethyl)-2-phenylcyclopropane, **15**: 1,1-bis(1-hydroxyethyl)-2-phenylethylene

which were obtained by the reactions of aliphatic 1,3-glycols with orthoacetate[1] can be applied to the present case without any change except that the cyclopropane ring anisotropy shifts the signals of equatorial hydrogens and methyl hydrogens at C^4 and C^6 to higher magnetic fields. The data in Table 3 can be explained reasonably in terms of the configurations described in the table. In the case of **8**, the NMR data showed that the acetallization gave a mixture of isomers due to axial and equatorial methyl derivatives in a ratio of 12:88.

Table 2. The results of the reduction

Substrate	Reducing reagent and Substrate/reagent mol ratio in mmol	Product (yield)
1	$LiAlH_4$ in THF 63/63	**7** (88%)
2	$LiAlH_4$ in THF 21/56	**8** (84%)
2	$NaBH_4$ in MeOH 70/53	**9** (70%)
3	$LiAlH_4$ in THF 380/330	**10** (77%) (*meso*:*dl*=63:37)
3	$LiAlH_4$ in THF 80/50	**3**+**10**+**11** (8:74:18)
3	$Al(i\text{-}PrO)_3$ in *i*-PrOH 25/82	**10** (88%) (*meso*:*dl*=79:21)
3	$Al(i\text{-}PrO)_3$ in *i*-PrOH 25/17	**11** (30%)
4	$LiAlH_4$ in THF 145/87	**12** (93%) (*threo*:*erythro*=1:1)
5	$Al(i\text{-}PrO)_3$ in *i*-PrOH 25/82	**13** (65%) mixture of 4 isomers
5	$Al(i\text{-}PrO)_3$ in *i*-PrOH 25/17	**14** (20%)
6	$Al(i\text{-}PrO)_3$ in *i*-PrOH 25/82	**15** (31%)

The following characteristic features of the NMR signals of benzaldehyde acetals can be pointed out. 1. Acetal-ring methylene protons give signals at about δ=4.21—4.31 for axial ones, and at δ=3.21—3.39 for equatorial ones. 2. Methine protons at C^4 and C^6 give signals at δ=4.16—4.54 for axial ones, and at δ=3.21—3.68 for equatorial ones. 3. Methyl protons at C^4 and C^6 give signals at δ=1.32—1.61 for axial ones, and at δ=0.90—1.05 for equatorial ones. These facts can be explained by the anisotropic effects of cyclopropane and phenyl rings.

The structures of *meso*- and *dl*-**10** were confirmed further by ^{13}C NMR. The *meso*-form gave signals at δ=4.4 and 9.0 (ring CH_2), 20.0 (CH_3), 29.5 (ring head C), and 71.2 (CHOH). The *dl*-form gave signals at δ=7.7 (ring CH_2), 18.9 (CH_3), 28.6 (ring head C), and 71.2 (CHOH) ppm downfield from the internal TMS. The major differences between the spectra of the two isomers are those due to the ring methylene carbons. The fact that the ring methylene carbons of *meso*-**10** gave two signals, while those of *dl*-**10** gave only one signal, shows that the former carbons are not equivalent, while the latter is equivalent, and that all can be well understood in terms of their structures.[6]

Among the physical properties of **10**, it should be

Table 3. Physical properties of the acetals obtained by the reactions

Acetal	Bp °C/mmHg (Mp/°C)	e-H on C^4	a-H on C^4	e-H on C^6
7-AA	60/25	3.21, d, 1H J=11.6	4.21, d, 1H J=11.6	3.21, d, 1H J=11.6
7-BA	150/25	3.39, d, 1H J=11.8	4.31, d, 1H J=11.8	3.39, d, 1H J=11.8
8-BA-a			4.41, q, 1H J=7.0	3.34, d, 1H J=12.0
8-BA-b		3.68, q, 1H J=7.0		3.29, d, 1H J=12.0
meso-**10-AA**	80/23		4.16, q, 1H J=6.0	
dl-**10-AA**	68/22		4.37, q, 1H J=6.0	3.37, q, 1H J=6.0
meso-**10-BA**	98—104/4		4.30, q, 1H J=6.0	
dl-**10-BA**	100—104/4		4.50, q, 1H J=6.0	3.48, q, 1H J=6.0
erythro-**12-AA**	(88.5—89.0)		5.04, s, 1H	
threo-**12-AA**			5.15, s, 1H	3.44, q, 1H J=6.5
erythro-**12-BA**	180/5		5.24, s, 1H	
threo-**12-BA**	162/3		5.34, s, 1H	3.59, q, 1H J=7.0

noted that the *meso*-form is crystalline and that the *dl*-form is liquid, while Pritchard reported that the crystalline form (mp 48—49 °C) was *dl* and the liquid one was *meso* in the case of 2,4-pentanediol.[7]

It is well known that the halogenation of cyclopropylalkanols is accompanied by skeletal rearrangements. For example, the reaction of cyclopropylmethanol with thionyl chloride gave cyclopropylmethyl chloride, cyclobutyl chloride, and homoallyl chloride.[8] We examined whether or not the behavior of bis(1-hydroxyalkyl)cyclopropanes is the same as that of mono-(1-hydroxyalkyl)cyclopropanes.

Thionyl chloride is the most frequently used reagent in the chlorination of a cyclopropylalkanol system. Therefore, the reaction with this reagent has been examined first.

Cyclic Sulfite Formation. Pritchard and his coworkers demonstrated that the reaction of 2,4-pentanediol with thionyl chloride gave a cyclic sulfite.[7] Similarly, **10** gave cyclic sulfites. In pyridine at 0 °C, *meso*-**10** formed two kinds of sulfite, crystalline and liquid (7:3).

Six-membered cyclic sulfites have stereoconformers, as in the case of cyclohexane derivatives. Since the C–O bonds of the glycol are not broken in the sulfite formation, the configurations of the carbons of C–O in the sulfites should be the same as those in the starting glycol. The two methyl groups at C-4 and C-6 of the cyclic sulfites from *meso*-**10** should both be equatorial or both axial. Apparently, the diaxial conformer should be much more unstable, and the product should have a di-equatorial conformation. The fact that the two kinds of product were obtained appears to have resulted from the axial and equatorial forms of S=O bond. Since the S=O bond shows an anisotropic effect,[9] NMR data can be used to clarify the structures. The axial S=O should shift the signals of the axial protons at C-4 and C-6 to lower fields, but not the equatorial S=O. All NMR data can be explained reasonably in terms of the structures depicted; they exclude the possibility of the twisted boat form.

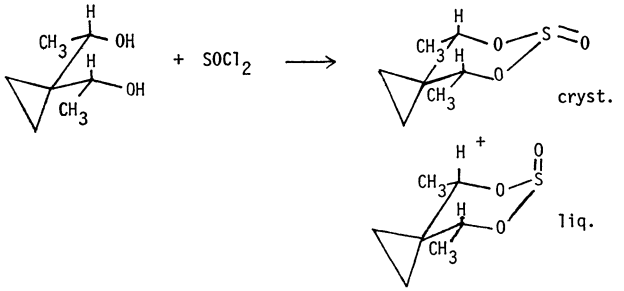

There are two conflicting reports on the IR spectra of S=O. Pritchard and his coworkers assigned the absorptions of cyclic sulfite of 2,4-pentanediol at 1240 and 1188 cm^{-1} to axial and equatorial S=O respectively,[7] while Hellier and his coworkers assigned the absorptions of the same compound at 1230 and 1190 cm^{-1} to equatorial and axial respectively.[9,10] Our conclusion agreed with the latter assignment. *dl*-**10** gave only one cyclic sulfite, and the S=O bond was found to be axial from the NMR and IR data.

The cyclic sulfites obtained are listed in Table 4.

WITH ACETALDEHYDE (AA) AND BENZALDEHYDE (BA)

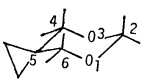

NMR data in $CDCl_3$, δ/ppm

a-H on C⁶	e-CH_3 on C⁴	a-CH_3 on C⁴	e-CH_3 on C⁶	a-CH_3 on C⁶
4.21, d, 1H J=11.6				
4.31, d, 1H J=11.8				
4.33, d, 1H J=12.0			0.95, d, 3H J=7.0	
4.32, d, 1H J=12.0		1.43, d, 3H J=7.0		
4.16, q, 1H J=6.0	0.91, d, 3H J=6.0		0.91, d, 3H J=6.0	
	0.90, d, 3H J=6.0			1.40, d, 3H J=6.0
4.30, q, 1H J=6.0	0.93, d, 3H J=6.0		0.93, d, 3H J=6.0	
	0.95, d, 3H J=6.0			1.44, d, 3H J=6.0
4.30, q, 1H J=6.0	C_6H_5-, 7.20		0.98, d, 3H J=6.0	
	C_6H_5-, 7.18			1.50, d, 3H J=6.5
4.54, q, 1H J=7.0	C_6H_5-, 6.82 —7.45, m		1.05, d, 3H J=7.0	
	C_6H_5-, 7.14 —7.32, m			1.61, d, 3H J=7.0

Table 4. Physical properties of the

Sulfite	Bp °C/mmHg (Mp/°C)	e-H on C^4	a-H on C^4	e-H on C^6
7-S	78—82/13 (72.4—73.4)	3.04, d, 1H J=12.0	5.24, d, 1H J=12.0	3.04, d, 1H J=12.0
	IR of S=O, 1178 cm^{-1}, axial			
8-S-a	65/24	4.22, q, 1H J=6.5		3.72, d, 1H J=12.0
	IR of S=O, 1230 cm^{-1}, equatorial			
8-S-b			5.61, q, 1H J=7.5	3.00, d, 1H J=12.0
	IR of S=O, 1180 cm^{-1}, axial			
meso-**10-S**-e	(80.8—81.2)		5.01, q, 1H J=6.0	
	IR of S=O, 1230 cm^{-1}, equatorial			
meso-**10-S**-a			5.63, q, 1H J=6.0	
	IR of S=O, 1190 cm^{-1}, axial			
dl-**10-S**	112—120/22	3.89, q, 1H J=7.5		
	IR of S=O, 1180 cm^{-1}, axial			

Diol **8** gave the sulfite containing two conformers.

Reaction of Cyclic Sulfite with Thionyl Chloride. The reaction of alkyl sulfite with thionyl chloride is believed to proceed according to the following equation.[11]

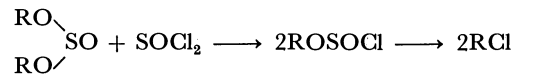

In the present case, the equation is as follows:

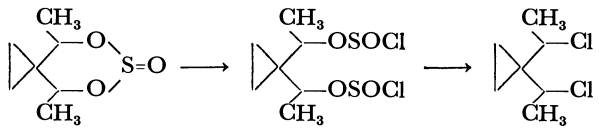

The configuration of the chloride is determined in the second step of the above equation, since the first step does not involve the breaking of the C–O bond.

The results of the reaction of sulfites with thionyl chloride are listed in Table 5.

The sulfite of *meso*-**10** (*meso*-**10-S**) reacted much slower than that of *dl*-**10**. Since the rates of the second step should be the same in both the stereoisomers, the difference must have resulted from the first step. The results can reasonably be explained by considering that the backsides of both O–SO bonds are blocked by two methyl groups to S_N2 attack on O in the case of the *meso*-isomer, while one of the backsides is open in the case of the *dl*-isomer.

The final dichloride (**10-Cl**) has stereoisomers of *meso* and *dl*, whose structural assignments will be described later. In a chloroform solution, *meso*-**10-S** gave *meso*-**10-Cl** and *dl*-**10-S** gave *dl*-**10-Cl** predominantly, but the stereospecificities were about 70%. If the reactions of the two C–O–SO groups are of the S_Ni type (which is believed to be the case in the absence of a base), the specificities should be 100%. The addition of pyridine changes the reaction to S_N2, but the results should be the same by double inversion. The formation of 5-chloro-3-(1-chloroethyl)-2-pentene (homoallyl-**Cl**), although the yields were very low, appears to show that the cyclopropylmethyl cation intervenes in the reaction, as in the chlorination of the usual cyclopropylmethanol. The addition of pyridine to the reaction system resulted in the further loss of the specificity and in the larger yield of homoallyl-**Cl**. These results will be discussed in the following section.

Halogenation of meso- *and* dl-***10*** *under Various Conditions.* The results of the halogenation of *meso*- and *dl*-**10** are listed in Table 6.

It is difficult to reach a clean-cut conclusion as to the steric course of the reactions with thionyl chloride and phosphorus pentachloride except that slight retentions of configuration were observed. It has been pointed out that the stereospecificity of the chlorination of alcohol with thionyl chloride depends on the experimental technique.[12] Therefore, we reexamined the reaction of *meso*-2,4-pentanediol reported by Pritchard[7] and confirmed that the reaction gave a product with a stereospecificity of more 98%, showing that the above results had not resulted from our experimental technique.

The formation of a homoallyl derivative, which indicates the intervention of the cyclopropylmethyl cation, was observed in all cases. Its yields were higher in a chloroform solution than in donor solvents such as benzene, dioxane, ether, carbon disulfide, and acetonitrile, but not pyridine. These results may be explained on the assumptions that the cyclopropylmethyl cation is stabilized by solvation with the basic solvent and that the rearrangement to the homoallyl derivative is suppressed. In the presence of pyridine, the hydrogen chloride formed reacts to form ionic pyridine hydrochloride, which may favor the formation of the cation and the rearrangement to the homoallyl

CYCLIC SULFITE OF THE DIOLS 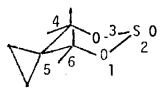

NMR data in $CDCl_3$, δ/ppm				
a-H on C^6	e-CH_3 on C^4	a-CH_3 on C^4	e-CH_3 on C^6	Propane ring
5.24, d, 1H J=12.0				0.43—0.87, m
4.64, d, 1H J=12.0		1.51, d, 3H J=6.5		0.25—0.75, m
5.30, d, 1H J=12.0	0.98, d, 3H J=7.5			0.25—0.75, m
5.01, q, 1H J=6.0	1.12, d, 3H J=6.0		1.12, d, 3H J=6.0	0.20—1.10, m
5.63, q, 1H J=6.0	1.00, d, 3H J=6.0		1.00, d, 3H J=6.0	0.15—1.10, m
5.49, q, 1H J=6.0		1.59, d, 3H J=7.5	1.11, d, 3H J=6.0	0.23—0.96, m

TABLE 5. REACTIONS OF *meso*- AND *dl*-**10** SULFITES WITH THIONYL CHLORIDE IN CHLOROFORM

Sulfite	Temp °C	Time h	Isomer distribution		
			meso-**10-Cl**	*dl*-**10-Cl**	homoallyl-**Cl**
meso-**10-S** crystal	60	8	71	29	trace
meso-**10-S** liquid	25	90	70	30	trace
dl-**10-S**	25	1	27	73	trace
dl-**10-S**[a)]	25	1	46	50	4

a) Pyridine was added to the chloroform.

derivative. The loss of the stereospecificity in the normal dichloride formation appears also to have resulted from the formation of the cation. Another possible reason for the loss of specificity might be that one of the two chlorine atoms is introduced by S_N2, and the other by S_N1. This possibility, however, appears to be excluded by the fact that the changes in the medium did not change the results appreciably.

In the case of the $ZnCl_2$–HCl system, the stereospecificity was lost almost completely and a large amount of the homoallyl product was formed, showing the formation of the cyclopropylmethyl cation.

The bromination of the same substrates resulted in further losses of specificity than in the case of chlorination and in larger yields of the homoallyl product.

Structural Assignments of meso- *and* dl-***10-X*** *and Homoallyl Chloride.* Attempts at the structural assignments of *meso*- and *dl*-**10** by PMR and IR were unsuccessful. However, ^{13}C NMR could clearly discriminate the two isomers by analogy with the case of diols mentioned in the early part of this paper. The cyclopropane-ring methylene carbons of the *dl*-isomer were equivalent (δ:11.3), but not those of the *meso*-isomer (δ:12.4 and 15.5).

The NMR data of homoallyl-**10-Cl** show that the structure should be the one depicted in Table 4. [δ: 1.60 (d, J=7.0, 3H, C^7H_3), 1.69 (d, J=7.0, 3H, C^1H_3), 2.66 (t, J=8.0, 2H, C^5H_2), 3.58 (m, 2H, C^4H_2), 4.59 (q, J=7.0, 1H, C^6H), and 5.73 (q, J=7.0, 1H, C^2H)]. Whether this compound has the structure of E or that of Z could not be determined, however.

Experimental

Materials. According to the method reported by Dox and Yoder,[13] **1** was prepared by the reaction of diethyl malonate with 1,2-dibromoethane in the presence of sodium ethoxide. The use of 2 M NaOH instead of the previously reported *n*-$BuNH_2$ to remove the unreacted diethyl molonate from the reaction product gave better results. Compounds **2**—**5** were prepared by the reaction of oxymercuration products of olefins with β-diketo compounds followed by demercuration, as had been reported previously.[14] Compound **6** was prepared from benzaldehyde and acetylacetone in the presence of picoline.[15]

Reduction. The reductions were carried out by the conventional methods;[3] no special technique was used except in the product isolations of **7**, **11**, and **14**. The reported poor yields of **7**[2] was greatly improved by the following procedure. After the hydrolysis of the reduction mixture, the aluminium hydroxide was filtered and washed

Table 6. Halogenation of *meso*- and *dl*-**10**[a]

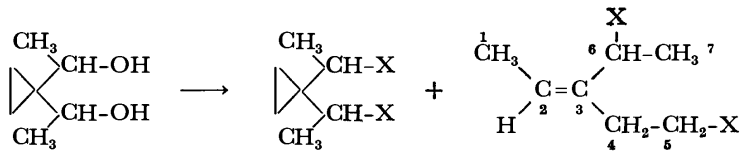

meso- and *dl*-**10** → *meso*- and *dl*-**10-X** (X=Cl or Br) + homoallyl-**X**

Diol-**10**	Reagent	Solvent	Temp °C	Time h	Isomer distribution of the product *meso*-**10-X**	*dl*-**10-X**	homoallyl-**X**
meso	$SOCl_2$	$CHCl_3$	0	1	50	45	5
dl	$SOCl_2$		0	1	44	52	4
meso	$SOCl_2$	$CHCl_3$+Py[b]	0	1	50	34	16
dl	$SOCl_2$	$CHCl_3$+Py[b]	0	1	42	49	9
meso	$SOCl_2$	$CHCl_3$	−70	1	63	25	12
meso	$SOCl_2$	C_6H_6	0	1	60	40	trace
dl	$SOCl_2$	C_6H_6	0	1	50	50	trace
meso	$SOCl_2$	dioxane	60	20	68	32	trace
dl	$SOCl_2$	dioxane	60	20	41	59	trace
meso	$SOCl_2$	CH_3CN	25	1	62	38	trace
meso	$SOCl_2$	Et_2O	25	1	65	35	trace
meso	$SOCl_2$	CS_2	25	1	57	43	trace
meso	$SOCl_2$	CCl_4	25	1	51	49	trace
meso	PCl_5	C_6H_6	0	2	73	22	5
dl	PCl_5	C_6H_6	0	2	36	60	4
meso	$ZnCl_2$–HCl	concd HCl	0	1	37	33	30
dl	$ZnCl_2$–HCl	concd HCl	0	1	27	26	47
meso	$SOBr_2$	$CHCl_3$	0	2	40	35	25
dl	$SOBr_2$	$CHCl_3$	0	2	45	45	10
meso	PBr_3	$CHCl_3$	25	1	57	39	4
dl	PBr_3	$CHCl_3$	25	1	42	48	10

a) The *dl*-**10** substrate contained 20% *meso*. The combined yields of the halides were about 80—90%. b) The ratio of $CHCl_3$:pyridine:$SOCl_2$=6.7:0.38:0.42 (mol).

Table 7. Analytical data

Compound	Calcd for	C, %	H, %	Cl, Br, or S, %	Found C, %	H, %	Cl, Br, or S, %
8	$C_6H_{12}O_2$	62.04	10.41		61.87	10.66	
9[a]	$C_7H_{12}O_3$	58.31	8.39		57.81	8.35	
meso-**10**	$C_7H_{14}O_2$	64.58	10.84		64.62	11.11	
dl-**10**	$C_7H_{14}O_2$	64.58	10.84		64.40	11.11	
11	$C_7H_{12}O_2$	65.59	9.44		63.86	9.69	
erythro-**12**[a]	$C_{12}H_{16}O_2$	74.97	8.37		74.29	8.38	
threo-**12**	$C_{12}H_{16}O_2$	74.97	8.37		75.30	8.66	
13	$C_{13}H_{18}O_2$	75.69	8.80		75.50	8.86	
14	$C_{13}H_{16}O_2$	76.44	7.90		76.29	8.18	
15	$C_{12}H_{16}O_2$	74.97	8.39		75.10	8.11	
meso-**10-BA**	$C_{14}H_{18}O_2$	77.03	8.11		77.00	8.14	
dl-**10-BA**	$C_{14}H_{18}O_2$	77.03	8.11		77.02	8.24	
erythro-**12-AA**	$C_{14}H_{18}O_2$	77.03	8.11		77.07	8.29	
threo-**12-BA**	$C_{19}H_{20}O_2$	81.39	7.19		81.25	7·30	
7-S[b]	$C_5H_8O_3S$	40.52	5.44	21.63	39.90	4.96	
8-S-(a+b)[b]	$C_6H_{10}O_3S$	44.44	6.22	19.74	44.77	6.35	19.12
meso-**10-S**-a	$C_7H_{12}O_3S$	47.72	6.87	18.17	47.19	6.88	17.54
dl-**10-S**	$C_7H_{12}O_3S$	47.72	6.87	18.17	47.88	7.00	17.91
meso-**10-Cl**	$C_7H_{12}Cl_2$	50.32	7.24	42.44	50.04	7.19	41.91
meso-**10-Br**	$C_7H_{12}Br_2$	33.84	4.73	62.43	33.12	4.69	62.14

a) Very hygroscopic. b) Unstable to atmospheric moisture and light.

with water. When the water was removed from the filtrate by the use of rotatory evaporator, aluminium hydroxide precipitated again. After filtering again, the filtrate was distilled under reduced pressure. It appears that the second removal of aluminium hydroxide improved the isolation yield.

In order to isolate **11** (IR, $\nu_{C=O}$ at 1670 cm^{-1}), the distillate which had been obtained by the usual work-up was subjected to column chromatography (Wakogel C-200 $2\phi \times 20$ cm; 1. hexane–ethyl acetate (95 : 5), 2. hexane–ethyl ether (70 : 30), 3. ethyl ether). Similarly, **14** (IR, $\nu_{C=O}$ at 1680 cm^{-1}) was isolated by column chromatography (Silicic acid, Mallinckrodt, $2\phi \times 15$ cm; 1. hexane–ethyl ether (95 : 5), 2. hexane–ethyl ether (70 : 30), 3. ethyl ether).

Acetallization. The acetaldehyde acetal and benzaldehyde acetals were prepared by the method by Eliel and his coworkers.[16]

Cyclic Sulfite. The following example shows a typical experimental procedure. Into a pyridine (20 ml) solution of diol **10** (2.6 g, 20 mmol), we stirred thionyl chloride (4.76 g, 40 mmol), drop by drop in an ice bath. After 1 h, the crystalline pyridine hydrochloride formed was removed by filtration, and then pyridine was removed by distillation under reduced pressure. Ether was added to the residue, which was then washed with 6 M HCl, a saturated $NaHCO_3$ solution, and then with water, and dried over Na_2SO_4. After the ether had been removed, the residue (2.5 g, 71% yield) was recrystallized from CCl_4 to give crystalline *meso*-**10-S** (mp 80.8—81.2 °C). The liquid part was purified by column chromatography with Wakogel C-200, using $CHCl_3$ as the solvent (bp 112—120 °C). The ratio of the crystalline to the liquid part was 7 : 3. The same procedure gave the cyclic sulfite of **8** (bp 65 °C/24 mmHg).

Formation of Dihalides. The experimental procedure is shown by the following example. Into a chloroform (800 g) solution of diol **10** (29.6 g, 0.374 mol) we stirred a pyridine (29.6 g, 0.374 mol) solution of thionyl chloride (50.0 g, 0.42 mol) in an ice bath. After 10 h, the reaction mixture was washed with 2 M HCl, saturated $NaHCO_3$ and then water, and dried over Na_2SO_4. After the chloroform had then been removed, the residue was distilled under reduced pressure to give a mixture of *dl*- and *meso*-dichloride and homoallyl chloride (bp 84—86 °C/20 mmHg; yield, 90%), which was analyzed by GLC. Upon cooling in a dry ice–acetone bath, the mixture gave crystalline *meso*-**10-Cl**. The liquid part was *dl*-**10-Cl**, containing a small amount of homoallyl-**Cl**.

*Reaction of Diol-**10** with $ZnCl_2$–HCl.* Into concd hydrochloric acid (1 ml) containing $ZnCl_2$ (0.22 g) we stirred **10** (0.3 g) at 0. °C. After 5 h, the product was extracted with benzene, washed with saturated $NaHCO_3$ and water, dried over Na_2SO_4, and analyzed by GLC.

The analytical data are shown in Table 7.

The IR spectra were recorded on a HITACHI EPI-G2 apparatus. The NMR spectra (in deuteriochloroform, with TMS as the internal standard) were recorded on a Varian Associates HR-220 apparatus at 220 MHz at room temperature. The ^{13}C NMR spectra (in deuteriochloroform, with TMS as the internal standard) were obtained by the use of a JNM FX-100 spectrometer.

This work was partially supported by a Grant-in-Aid from the Ministry of Education, Japan (S-52-243019).

References

1) O. Itoh, Y. Ichikawa, H. Katano, and K. Ichikawa, *Bull. Chem. Soc. Jpn.*, **49**, 1353 (1976).
2) P. von Schleyer, *J. Am. Chem. Soc.*, **83**, 1368 (1961).
3) O. Itoh, T. Okita, M. Umezu, M. Inoue, and K. Ichikawa, *Bull. Chem. Soc. Jpn.*, **50**, 1549 (1977).
4) C. H. Snyder, *J. Org. Chem.*, **32**, 2904 (1967).
5) Private communication from Dr. M. Inoue.
6) C. J. Carman, A. R. Tarpley, Jr., and J. H. Goldstein, *J. Am. Chem. Soc.*, **93**, 2864 (1971).
7) J. G. Pritchard and R. L. Vollmer, *J. Org. Chem.*, **28**, 1545 (1963).
8) J. D. Roberts and R. H. Mazur, *J. Am. Chem. Soc.*, **73**, 2509 (1951); M. C. Caserio, W H. Graham, and J. D. Roberts, *Tetrahedron*, **11**, 171 (1960).
9) C. H. Green and D. G. Hellier, *J. Chem. Soc., Perkin Trans. 2*, **1972**, 458.
10) B. A. Arbuzov and Yu. Yu. Samitov, *Tetrahedron Lett.*, **1963**, 473.
11) M. J. Frazer, W. Gerrard, G. Machell, and B. D. Shephered, *Chem. Ind. (London)*, **1954**, 931.
12) See, for example, "Reagents for Organic Synthesis," ed by L. F. Fieser and M. Fieser, Wiley (1967), Vol. 1, p. 1158.
13) A. W. Dox and L. Yoder, *J. Am. Chem. Soc.*, **43**, 2097 (1921).
14) K. Ichikawa, O. Itoh, T. Kawamura, M. Fujiwara, and T. Ueno, *J. Org. Chem.*, **31**, 447 (1966); O. Itoh, N. Yamamoto, K. Nakano, T. Sugita, and K. Ichikawa, *Bull. Chem. Soc. Jpn.*, **48**, 3968 (1975).
15) B. D. Wilson, *J. Org. Chem.*, **28**, 314 (1963).
16) E. L. Eliel and M. C. Knoeber, *J. Am. Chem. Soc.*, **90**, 3444 (1968).

Solvent Effects on the Photoamination of 1-Amino-2,4-dibromoanthraquinone. II. Dual Mode of the Photoamination in Ethanol *via* the $S_1(^1CT)$ and $T_1(^3CT)$ States

Haruo INOUE,* Tsutomu SHINODA,† and Mitsuhiko HIDA

Department of Industrial Chemistry, Faculty of Technology, Tokyo Metropolitan University, Fukazawa, Setagaya-ku, Tokyo 158

† *Organic Division, The Tokyo Metropolitan Industrial Technic Institute, 3-13-10, Nishigaoka, Kita-ku, Tokyo 115*

(Received February 17, 1979)

The photoamination of 1-amino-2,4-dibromoanthraquinone (**1**) by butylamine in ethanol was investigated. The reaction was accelerated under an air atmosphere ($\Phi_{air}=1.7\times10^{-3}$, $\Phi_{N_2}=2.3\times10^{-4}$, where [butylamine]$=5.00\times10^{-2}$ mol/dm^3). A detailed kinetic study indicated that, under nitrogen, the photoamination proceeded *via* the $T_1(^3CT)$ state populated by the intersystem crossing from the $S_1(^1CT)$ state, while under air it proceeded *via* both the $T_1(^3CT)$ and the $S_1(^1CT)$ states. The latter pathway under air included an interaction between the $S_1(^1CT)$ state and oxygen to form an exciplex or a collisional complex such as $[AQ^{\delta+}\cdots O_2^{\delta-}]$. The deactivation constant from the $T_1(^3CT)$ of **1** in ethanol was revealed to be one order of magnitude smaller than that in benzene and one order magnitude larger than that of 1-aminoanthraquinone in benzene. These results were discuessd in relation to the energy diagram in the excited state and the intramolecular heavy-atom effect of bromine in **1**.

It has long been emphasized that the excited triplet $n\pi^*$ state is reactive in almost all the photochemical reactions of anthraquinone derivatives, while the intramolecular CT state has little reactivity.[1] It has also been proved that the excited triplet $n\pi^*$ state is reactive even in the photoreduction of 2-piperidinoanthraquinone by an electron transfer from the hydroxide ion in aqueous 2-propanol,[2] which had been postulated to proceed *via* the intramolecular CT level.[3] However, we recently reported an interesting new photosubstitution reaction of aminoanthraquinones as the first example of a reaction actually demonstrated to proceed *via* the CT level.[4]

In the preceding paper we reported the striking solvent effects on the photoamination of 1-amino-2,4-dibromoanthraquinone (**1**) by butylamine.[5] In ethanol, 1) the dissolved oxygen promoted the photoamination of **1** and 2) the yield (%) of the aminated product (**2**) was not equivalent to the conversion (%) of **1** and the ratio (0.79) between them was unchanged during the photoreaction. The last result suggests that the photodecomposition of **1** and its photoamination took place simultaneously, as was previously observed in the photoamination of sodium 1-amino-4-bromoanthraquinone-2-sulfonate (**3**) in aqueous 2-propanol.[4] In benzene, 1) oxygen acted as a strong quencher to the reaction and 2) the yield of **2** was equal to the conversion of **1**, suggesting that the photoamination of **1** proceeded quantitatively.[5] On the basis of the postulated energy diagram of the excited **1** shown in Fig. 1, it was suggested that, in benzene, the photoamination proceeded through the $T_1(^3CT)$ level without the aid of oxygen because of a dominant population on the T_1 level by means of a close contiguity or an inversion in the disposition of $S_1(^1CT)$ and $T_2(^3n\pi^*)$ levels. In this paper we will report on our detailed kinetic analysis of the photoamination of **1** in ethanol and will propose a reaction mechanism with a dual mode from the $S_1(^1CT)$ and the $T_1(^3CT)$ levels of **1** in contrast with the single mode in benzene.

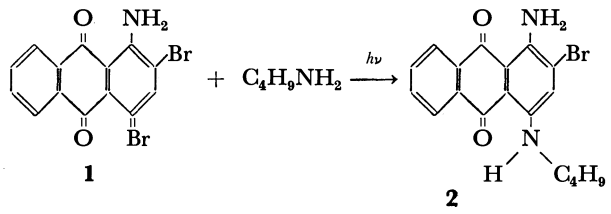

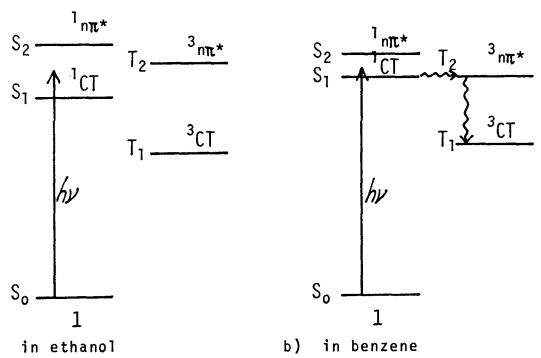

Fig. 1. Energy diagram of the excited state of **1**.

Experimental

The 1-amino-2,4-dibromoanthraquinone (**1**) was prepared and purified as reported in the preceding paper.[5] A Shimadzu UV-200 spectrophotometer and a Hitachi MPF-4 spectrofluorometer were used for the measurement of the UV and visible absorption spectra and the fluorescence emission spectra respectively. Irradiation was carried out by the use of a 500-W xenon lamp (USHIO UXL 500 DKO) through the following filter system: a soda glass for the irradiation of $\lambda>300$ nm, a Toshiba interference filter KL-40 for the monochromatic irradiation of $\lambda=400$ nm, a Toshida glass filter VY-42 for $\lambda>420$ nm, and VY-45 and KL-47 filters for the light of $\lambda=470$ nm. The amount of the aminated product (**2**) generated in the irradiated reaction mixture was determined by colorimetric analysis of the first absorption band of **2** ($\lambda_{max}=625$ nm, $\varepsilon=1.40\times10^5$ dm^2/mol). The number of photons absorbed by the reaction mixture was determined by the use of the chemical actinometer of potas-

sium tris(oxalato)ferrate(III). The amount of hydrogen peroxide in the irradiated reaction mixture was determined by colorimetric analysis of the absorption intensity at 357 nm, which is characteristic of the I_3^- generated by the addition of an aqueous solution of potassium iodide to an acidified reaction mixture.

Results and Discussion

The Photoamination of ***1*** *in Ethanol under a Nitrogen Atmosphere.* The photoamination of **3** in a 2-propanol–water (4 : 1 v/v) mixture proceeded through an exciplex formation between the excited **3** in its ^{1}CT state and the ground state oxygen; the reaction was hardly observed at all under a nitrogen atmosphere.[4] On the other hand, the photoamination of **1** in ethanol does proceed even under nitrogen, though the reactivity is about one-seventh of that under air ($\Phi_{air}=1.7\times10^{-3}$, $\Phi_{N_2}=2.3\times10^{-4}$, where [butylamine]$=5.00\times10^{-2}$ mol/dm^3). The previous study of the photoamination of **1** in benzene revealed that the ^{3}CT level of **1** is also responsible for the photoamination. Hence, the photoamination of **1** in ethanol under nitrogen may be explained by either of the following suggestions: 1) a direct photoamination proceeds *via* the ^{1}CT level of **1** without the aid of oxygen, or 2) the ^{3}CT level of **1** is responsible for the reaction.

In Table 1 the 0-0 level of the $S_1(^1CT)$ state and the relative fluorescence intensity of **1** in ethanol are compared with those of other aminoanthraquinones. Since the $S_1(^1CT)$ states of aminoanthraquinones (**3**—**5**) have much the same energy as that of **1**, and since the $n\pi^*$ levels of anthraquinones have been thought to be hardly affected by the introduction of substituents,[1] it may be accepted that the excited states of **3**—**5** have energy diagrams similar to that of **1**. On the other hand, the relative intensity of the fluorescence decreased with the increase in $\sum\zeta^2$, the sum of the squares of the spin-orbit coupling factors over all the atoms in the corresponding molecule. These results suggest that the intersystem crossing between the $S_1(^1CT)$ and the $T_1(^3CT)$ levels in **1** might be enhanced by the spin-orbit interaction promoted by the heavy-atom effect of the two bromine atoms as compared with those of other aminoanthraquinones. In order to make clear the multiplicity of the reactive excited state of **1** in the photoamination in ethanol under a nitrogen atmosphere, the effect of a triplet quencher, cyclooctatetraene (COT)($E_T=163$ kJ/mol), was investigated. As is shown in Fig. 2, a good linear Stern-Volmer plot was obtained with a slope of 54.0 dm^3/mol. This clearly indicated that the photoamination of **1** under nitrogen proceeded *via* only one pathway. Since COT was confirmed to act as a triplet quencher by the fact that the fluorescence intensity of **1** in ethanol was hardly affected at all by the presence of COT (5.0×10^{-2} mol/dm^3), it seems that the photoamination proceeded through the triplet ^{3}CT level of **1**.

A plot of the reciprocal of the quantum yield of the photoamination of **1** versus the reciprocal of the concentration of butylamine gave a fairly straight line (Fig. 3), indicating the presence of a collisional process between the excited **1** and butylamine in the photoamination in ethanol under a nitrogen atmosphere. The ratio of the slope to the intercept in Fig. 3 was 3.7×10^{-3} mol/dm^3. When the photoamination reac-

Table 1. 0-0 levels of the 1st absorption bands[a] and relative fluorescence intensities of aminoanthraquinones in ethanol

Aminoanthraquinones		0-0 level kJ/mol	Relative fluorescence intensity	$\sum\zeta^2$ cm^{-1}
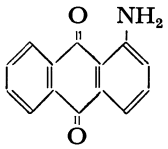	(**4**)	218	100	6.21×10^3
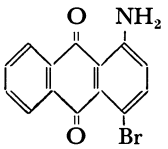	(**5**)	216	49	6.11×10^6
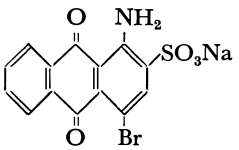	(**3**)	216	36	6.33×10^6
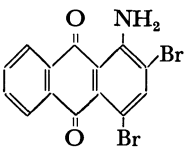	(**1**)	218	18	1.22×10^7

a) The 0-0 levels of aminoanthraquinones were estimated from the intersections of the corresponding absorption and fluorescence spectra in a mirror image.

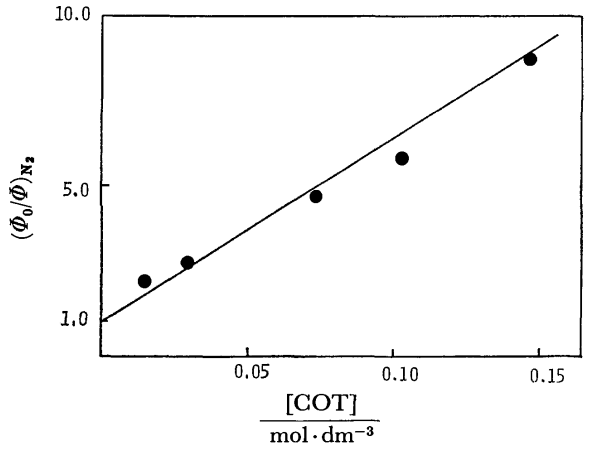

Fig. 2. Stern-Volmer plot for the quenching effect of cyclooctatetraene on the photoamination of **1** (1.00×10^{-4} mol/dm³) by butylamine (5.00×10^{-2} mol/dm³) in ethanol under nitrogen atmosphere by the irradiation of the light of $\lambda=470$ nm.

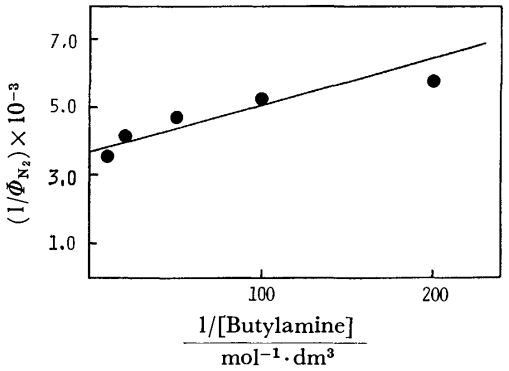

Fig. 3. Effect of the concentration of butylamine on the photoamination of **1** (1.00×10^{-4} mol/dm³) in ethanol under nitrogen atmosphere by the irradiation of the light of $\lambda=470$ nm.

tion of **1** (1.00×10^{-4} mol/dm³) was carried out in the presence of fluorenone ($E_T=226$ kJ/mol) (1×10^{-2} mol/dm³) as a triplet sensitizer under the irradiation of a light of $\lambda>300$ nm,[6] a good linear relationship was also found between the reciprocals of the quantum yield and the concentration of butylamine, with the value of the ratio of the slope to the intercept being 4.3×10^{-3} mol/dm³. The good agreement between these values obtained from the direct-irradiation experiment and the triplet-sensitizing experiment also strongly suggested that the photoamination proceeded through the $T_1(^3CT)$ level of **1** under a nitrogen atmosphere. When the fluorenone-sensitizing photoamination was carried out under air-saturated conditions, the reciprocals of the quantum yield and the concentration of amine also gave a good linear relationship. However, the ratio of the slope to the intercept, determined to be 39.1×10^{-3} mol/dm³, was much larger than that determined under a nitrogen atmosphere. Since the ratio of the slope to the intercept of the plot corresponds to the ratio of the rate constant of the deactivation to the reaction of the excited **1**, which is reactive to amine, the larger value of the ratio in

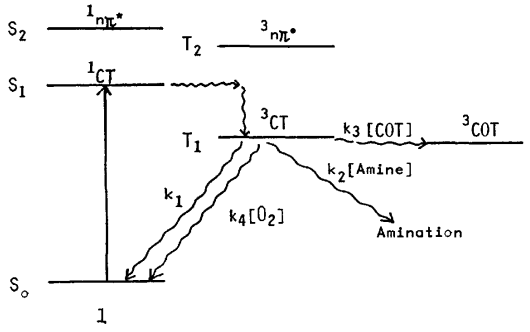

Fig. 4. Reaction scheme of the photoamination of **1** by butylamine under nitrogen atmosphere in ethanol.

the plot implies a larger deactivation from the excited **1** (^3CT) under air. This is in accord with the fact that the $T_1(^3CT)$ level of **1** was efficently quenched by the dissolved oxygen in benzene.[5]

The Reaction Mechanism of the Photoamination of ***1*** *in Ethanol under a Nitrogen Atmosphere.* On the basis of the above experimental results, the reaction scheme of the photoamination of **1** in ethanol under a nitrogen atmosphere may be depicted as in Fig. 4. The excited **1** in its $T_1(^3CT)$ state, populated by the intersystem crossing from the $S_1(^1CT)$ state, interacts directly with the amine to produce the aminated product, **2** (k_2). The $T_1(^3CT)$ state decays with the rate constant of k_1 and is quenched by COT (k_3). The reciprocal of the quantum yield of the photoamination under nitrogen *via* the $T_1(^3CT)$ level of **1**, $\Phi_{N_2}(^3CT)$, can be written as

$$1/\Phi_{N_2}(^3CT) = \frac{1}{\Phi_{isc}}\cdot\left(1+\frac{k_1}{k_2[A]}\right)\cdot\frac{1}{\alpha}, \quad (1)$$

where Φ_{isc}=the efficiency of the intersystem crossing of $S_1(^1CT)\rightarrow T_1(^3CT)$, α=the yield of the aminated product, **2**, for every collision between the amine and **1** in its $T_1(^3CT)$ level.

The Stern-Volmer plot with COT present under a nitrogen atmosphere is expressed by

$$(\Phi_0/\Phi)_{N_2} = 1 + \frac{k_3[COT]}{k_1+k_2[A]}. \quad (2)$$

Moreover, the reciprocal of the quantum yield, $\Phi^s_{N_2}(^3CT)$, of the photoamination in the fluorenone-sensitizing experiment under a nitrogen atmosphere can be written as

$$1/\Phi^s_{N_2}(^3CT) = \frac{1}{\Phi_{ET}}\cdot\left(1+\frac{k_1}{k_2[A]}\right)\cdot\frac{1}{\alpha}, \quad (3)$$

where Φ_{ET}=the triplet yield of **1** in the fluorenone-sensitizing experiment under a nitrogen atmosphere and under these conditions.

When the fluorenone-sensitizing experiment is carried out under air-saturated conditions, Eq. 3 is modified to Eq. 4 because of the quenching effect of oxygen on the $T_1(^3CT)$ level of **1**:

$$1/\Phi^s_{air}(^3CT) = \frac{1}{\Phi'_{ET}}\cdot\left(1+\frac{k_1+k_4[O_2]}{k_2[A]}\right)\cdot\frac{1}{\alpha}, \quad (4)$$

where Φ'_{ET}=the triplet yield of **1** in the fluorenone-sensitizing experiment under air-saturated conditions.

The value of the ratio of the slope to the intercept in Fig. 3 and Eq. 1, and the slope in Fig. 2 and Eq. 2 indicate the following relations:

$$k_1/k_2 = 3.7 \times 10^{-3}\ \text{mol/dm}^3,$$

$$k_3/(k_1+k_2[\text{A}]) = 54.0\ \text{dm}^3/\text{mol}.$$

The results of the fluorenone-sensitizing experiment under air-saturated conditions and Eq. 4 may also indicate that:

$$(k_1+k_4[\text{O}_2]_{\text{air}})/k_2 = 39.1 \times 10^{-3}\ \text{mol/dm}^3.$$

The concentration of the dissolved oxygen in air-saturated ethanol, $[\text{O}_2]_{\text{air}}$, was taken to be 2.07×10^{-3} mol/dm^3,[7] and $[\text{A}]=5.0\times 10^{-2}$ mol/dm^3. If the quenching rate constant of the $T_1(^3\text{CT})$ state by the dissolved oxygen is assumed to be $k_4=9.2\times 10^9$ dm^3 mol^{-1} s^{-1} (a diffusion-controlled one), the rate constants may be calculated as $k_1=2.0\times 10^6$ s^{-1}, $k_2=5.4\times 10^8$ dm^3 mol^{-1} s^{-1}, and $k_3=1.6\times 10^9$ dm^3 mol^{-1} s^{-1}. The value of the quenching rate constant (k_3) of the $T_1(^3\text{CT})$ state by COT coincides well with that obtained in a benzene solution (1.6×10^9 dm^3 mol^{-1} s^{-1}).[5]

The Photoamination of **1** *under an Air Atmosphere.* As has been stated before, the photoamination reaction in ethanol was remarkably accelerated under an air atmosphere. By comparison with the photoamination of **3** in a 2-propanol–water (4 : 1 v/v) mixture,[4] it might be immediately concluded that the reaction in ethanol proceeded through the interaction between **1** in its ^{1}CT state and the ground-state oxygen. However, our observation of the photoamination under a nitrogen atmosphere implies that the photoamination of **1** under air has a dual reaction mode: the reaction without the aid of oxygen through the $T_1(^3\text{CT})$ level of **1**, and the reaction *via* its $S_1(^1\text{CT})$ level with the aid of oxygen. Hence, the following kinetic treatment of the photoamination *via* the $S_1(^1\text{CT})$ level of **1** under an air atmosphere was developed for the quantum yield, $\Phi_{\text{air}}(^1\text{CT})$, calculated by Eq. 5:

$$\Phi_{\text{air}}(^1\text{CT}) = \Phi_{\text{air}} - \Phi_{\text{air}}(^3\text{CT}), \tag{5}$$

where Φ_{air} denotes the observed quantum yield of the photoamination under air, and $\Phi_{\text{air}}(^3\text{CT})$, the quantum yield of the reaction *via* the $T_1(^3\text{CT})$ level of **1** under air, which can be calculated by means of Eq. 6:[8]

$$\Phi_{\text{air}}(^3\text{CT}) = \Phi_{\text{isc}}\left(\frac{k_2[\text{A}]}{k_1+k_4[\text{O}_2]+k_2[\text{A}]}\right)\alpha. \tag{6}$$

As is shown in Fig. 5, a plot of the reciprocal of the quantum yield $\Phi_{\text{air}}(^1\text{CT})$ versus the reciprocal of the concentration of the dissolved oxygen gave a good straight line. This clearly indicated the presence of a collisional process between the excited **1** and the dissolved oxygen, leading to the aminated product, **2**. This is contrary to the case of the reaction *via* the $T_1(^3\text{CT})$ level of **1**, in which the dissolved oxygen acts as a strong quencher to the reaction. With respect to the fate of the oxygen, it was revealed that hydrogen peroxide was produced during the photoamination.[9] These results strongly suggested that the photoamination under air *via* the $S_1(^1\text{CT})$ proceeded through an exciplex or a collisional complex formation between the excited **1** in its ^{1}CT state and the ground-state

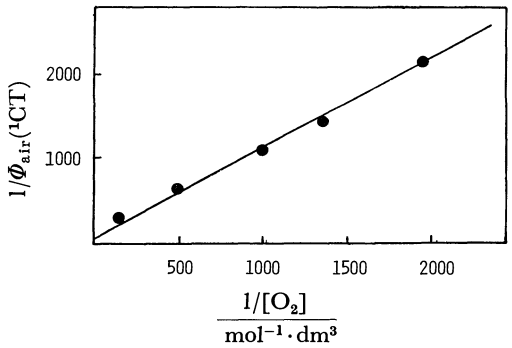

Fig. 5. Effect of the concentration of oxygen on the quantum yield $\Phi_{\text{air}}(^1\text{CT})$ calculated by Eq. 5; [1]: 1.00×10^{-4} mol/dm^3, [butylamine]: 5.00×10^{-2} mol/dm^3 in ethanol; irradiation light: $\lambda=470$ nm.

oxygen, designated $[\text{AQ}^{\delta+}\cdots\text{O}_2{}^{\delta-}]$. However, the intercept in Fig. 5 has a very small value, suggesting that the low quantum yield of the photoamination (in the order of 10^{-3}) is mainly due to the low efficiency of the reaction process between the excited **1** in its ^{1}CT state and oxygen. This is in accord with the fact that the fluorescence of **1** is not affected by the dissolved oxygen.

A double reciprocal plot between the quantum yield of the photoamination, $\Phi_{\text{air}}(^1\text{CT})$, and the concentration of butylamine also gave a good straight line, with the ratio of the slope to the intercept of 2.5×10^{-2} mol/dm^3 (Fig. 6), suggesting that, on the reaction pathway, butylamine collided with an intermediate which could be treated with the steady-state approximation. When COT was added to the reaction system, the photoamination was retarded and the Stern-Volmer plot gave a good straight line with a slope of 41 dm^3/mol (Fig. 7), indicating that COT also acted as a quencher molecule to the photoamination *via* the $S_1(^1\text{CT})$ level of **1** under air. Moreover, 1,3-cyclohexadiene (CHD), which has a higher triplet level ($E_T=226$ kJ/mol) than the $T_1(^3\text{CT})$ level of **1** ($E_T=163$—176 kJ/mol in benzene), also quenched the photoamination of **1** under air. Since COT and CHD hardly quenched the fluorescence of **1** at all, it appears that such olefins as COT and CHD did not interact with the excited **1** in its $S_1(^1\text{CT})$ state, but interacted

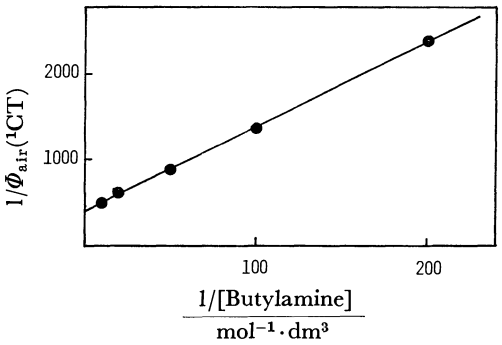

Fig. 6. Effect of the concentration of butylamine on the quantum yield $\Phi_{\text{air}}(^1\text{CT})$ calculated by Eq. 5; [1]: 1.00×10^{-4} mol/dm^3 in air-saturated ethanol; irradiation light: $\lambda=470$ nm.

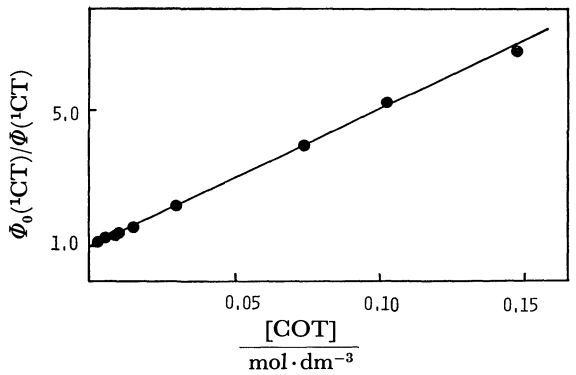

Fig. 7. Stern-Volmer plot for the quenching effect of cyclooctatetraene on the quantum yield of the photoamination under air; $\Phi_{air}(^1CT)$ was calculated by

$$\Phi_{air}(^1CT) = \Phi_{air} - \Phi_{isc}\cdot\left(\frac{k_2[A]}{k_1+k_3[COT]+k_4[O_2]+k_2[A]}\right)\cdot\alpha$$

[**1**]: 1.00×10^{-4} mol/dm^3, [butylamine]: 5.00×10^{-2} mol/dm^3 in air-saturated ethanol; irradiation light λ=470 nm.

with another intermediate on the reaction pathway of the photoamination *via* the $S_1(^1CT)$ level of **1** under air. Recently it has been reported that some exciplexes happen to be quenched by a third molecule (exciplex quenching).[10] The quenching effects of COT and CHD on the photoamination under air might be reasonably explained by assuming that these olefins interacted with the exciplex $[AQ^{\delta+}\cdots O_2^{\delta-}]$ to result in the quenching of the photoamination of **1** under air.

The Reaction Mechanism of the Photoamination of ***1*** *in Ethanol under Air.* The reaction scheme of the photoamination of **1** in ethanol under air may be depicted as in Fig. 8. The photoamination of **1** in ethanol has two possible reaction pathways. One is *via* the $S_1(^1CT)$ level of **1**. After being excited by the irradiation to the 1st absorption band of **1** (λ_{max}= 473 nm), **1** in its $S_1(^1CT)$ state interacts with the ground-state oxygen (k_5) to form an exciplex or a collisional complex, $[AQ^{\delta+}\cdots O_2^{\delta-}]$. The exciplex decays with the rate constant k_6 and is attacked by butylamine to produce the aminated product, **2** (k_7). The exciplex also interacts with such olefins as COT or CHD to be quenched (k_8; exciplex quenching). The quantum yield of the photoamination *via* the $S_1(^1CT)$, $\Phi_{air}(^1CT)$, can be written as Eq. 7:

$$\Phi_{air}(^1CT) = \left(\frac{k_5[O_2]}{1/\tau_s+k_5[O_2]}\right)\left(\frac{k_7[A]}{k_6+k_7[A]}\right)\beta, \quad (7)$$

where A=butylamine, τ_s=the lifetime of the $S_1(^1CT)$ state, and β=the yield of the aminated product, **2**, for every collision between the exciplex and the amine. The reciprocal of the quantum yield is thus expressed by

$$1/\Phi_{air}(^1CT) = \left(1+\frac{1}{\tau_s\cdot k_5[O_2]}\right)\left(1+\frac{k_6}{k_7[A]}\right)\frac{1}{\beta}. \quad (8)$$

When COT is present, the Stern-Volmer equation may be expressed by

$$\Phi_0(^1CT)/\Phi(^1CT) = 1 + \frac{k_8[COT]}{k_6+k_7[A]}. \quad (9)$$

Hence, the following values are estimated from the ratio of the slope to the intercept in the linear plot of Fig. 6 and Eq. 8, and from the slope in the Stern-Volmer plot of Fig. 7 and Eq. 9:

$k_6/k_7 = 2.5\times10^{-2}$ mol/dm^3, $k_8/(k_6+k_7[A]) = 41$ dm^3/mol,

where $A=5.0\times10^{-2}$ mol/dm^3.

Assuming the exciplex quenching rate constant, k_8, to be diffusion-controlled (9.2×10^9 dm^3 mol^{-1} s^{-1}), k_6 and k_7 may be calculated to be 7.5×10^7 s^{-1} and 3.0×10^9 dm^3 mol^{-1} s^{-1} respectively. Thus, the lifetime of the exciplex $[AQ^{\delta+}\cdots O_2^{\delta-}]$ was estimated to be about 13 ns. It may be significant that the lifetime of an exciplex such as $[AQ^{\delta+}\cdots O_2^{\delta-}]$ could be successfully estimated by means of this kinetic treatment, though in most cases the exsistence of a 'non-emmisive exciplex' on the reaction pathway is difficult to verify and its lifetime can hardly be estimated at all. The other reaction pathway is the photoamination *via* the $T_1(^3CT)$ level of **1**.[12] The quantum yield can be expressed by Eq. 6.

In Table 2 the rate constants obtained in this study are compared with those obtained in benzene, together with the rate constants in the case of 1-amino-4-bromo-

Table 2. Rate constants in the photoamination of **1** and **5** by butylamine

Anthraquinones		k_1 / s^{-1}	k_2 / dm^3/mol s	k_6 / s^{-1}	k_7 / dm^3/mol s
1	in ethanol	2.0×10^5	5.4×10^8	7.5×10^7	3.0×10^9
	in benzene	2.8×10^7	5.7×10^7	——	——
5	in ethanol	——	——	1.8×10^8	9.0×10^9
	in benzene	2.1×10^7	2.1×10^8	——	——

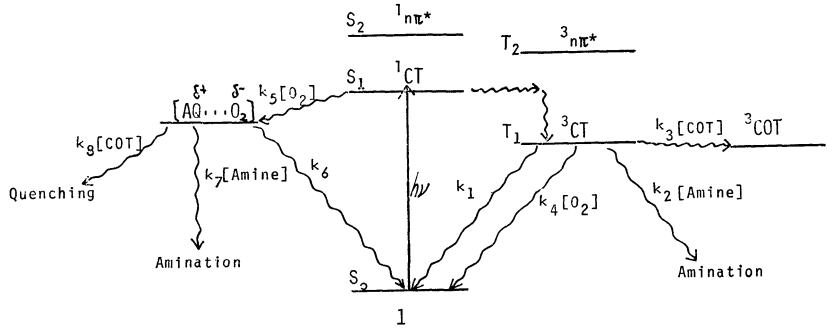

Fig. 8. Reaction scheme of the photoamiantion of **1** by butylamine under air atmosphere in ethanol.

anthraquinone (**5**) estimated by a similar kinetic treatment.

Contrary to the usual solvent effect, the deactivation constant, k_1, from the $T_1(^3CT)$ level is revealed to be one order of magnitude smaller in ethanol than that in benzene. This may be well correlated with the energy diagram of the excited state of **1** in ethanol and benzene shown in Fig. 1. In benzene, the $S_1(^1CT)$ state is supposed to interact more strongly with the $T_2(^3n\pi^*)$ state than in ethanol because of a close contiguity or a reversal of the disposition of $S_1(^1CT)$ and $T_2(^3n\pi^*)$, as is depicted in Fig. 1b). Hence, the $S_1(^1CT)$ state may interact more strongly with the $T_1(^3CT)$ state in benzene than in ethanol through the interaction among $S_1(^1CT)$, $T_2(^3n\pi^*)$, and $T_1(^3CT)$ states. The deactivation process (k_1) from the $T_1(^3CT)$ to the ground state, S_0, may borrow a part of the transition moment between the S_0 and the $S_1(^1CT)$ as a result of the mixing of the $S_1(^1CT)$ and $T_1(^3CT)$ states. Therefore, a larger deactivation from the $T_1(^3CT)$ may occur in benzene than in ethanol. It may also be noted that the deactivation constants, k_1, from the $T_1(^3CT)$ state of **1** and **5** in both ethanol and benzene are one or two orders of magnitude larger than that of 1-aminoanthraquinone (**4**) ($k_1=2\times10^5\ s^{-1}$),[11] which has no bromine atom in the molecule. These results clearly support the postulate that the heavy-atom effect on the spin-orbit interaction may be enhanced in **1**, which bears two bromine atoms. As has been reported in an earlier paper, the fluorescence intensity of **1** in benzene decreased by a factor of one-tenth as compared with that in ethanol.[6] This could also be successfully explained by the difference in the energy diagram with the alteration in the nature of the solvent (Fig. 1). On the other hand, the fluorescence intensity of **4** in benzene increased by a factor of 1.5 as compared with that in ethanol, in accordance with the usual solvent effect. Since **4** is supposed to have much the same energy diagram as that of **1** as has been stated before, this contradicting solvent effect on the fluorescence intensity may indicate that the close contiguity of the disposition of $S_1(^1CT)$ and $T_2(^3n\pi^*)$ and the spin-orbit interaction promoted by the intramolecular heavy-atom effect both play significant roles in the enhanced intersystem crossing between the $S_1(^1CT)$ and the $T_2(^3n\pi^*)$ of **1** in benzene.

References

1) J. M. Bruce, *Quart. Rev.*, **21** 405 (1967); D. Schulte-Frohlinde and C. V. Sonntag, *Zh. Phys. Chem.*, **44**, 314 (1965); H. Inoue and M. Hida, *Yuki Gosei Kagaku Kyokai Shi*, **32**, 348 (1974).

2) H. Inoue, K. Kawabe, N. Kitamura, and M. Hida, *Chem. Lett.*, **1977**, 987.

3) G. O. Phillips, A. K. Davies, and J. F. McKellar, *Chem. Commun.*, **1970**, 519; A. K. Davies, J. F. McKellar, and G. O. Phillips, *Proc. R. Soc. London. Ser. A*, **323**, 69 (1971); A. K. Davies, G. A. Gee, J. F. McKellar, and G. O. Phillips, *J. Chem. Soc., Perkin Trans. 2*, **1972**, 923.

4) H. Inoue, T. D. Tuong, M. Hida, and T. Murata, *J. Chem. Soc., Chem. Commun.*, **1971**, 1347; H. Inoue, T. D. Tuong, M. Hida, and T. Murata, *Bull. Chem. Soc. Jpn.*, **46**, 1759 (1973); H. Inoue, K. Nakamura, S. Kato, and M. Hida, *Bull. Chem. Soc. Jpn.*, **48**, 2872 (1975); H. Inoue and M. Hida, *Chem. Lett.*, **1974**, 255.

5) H. Inoue and M. Hida, *Bull. Chem. Soc. Jpn.*, **51**, 1793 (1978).

6) Under these conditions, fluorenone molecules absorb the incident light exclusively.

7) S. L. Murov, "Handbook of Photochemistry," Marcel Dekker (1973), p. 89.

8) Since the fluorescence of **1** was not affected by the dissolved oxygen, Φ_{isc} was supposed to have the same value under both nitrogen and air atmospheres, and $\Phi_{isc}\cdot\alpha$ was estimated to be 2.7×10^{-4} (the reciprocal of the intercept (3.7×10^3) in Fig. 3).

9) When **1** (1.00×10^{-4} mol/dm^3) and butylamine (5.00×10^{-2} mol/dm^3) in aerated ethanol were irradiated by light of $\lambda=470$ nm for 13 minutes, hydrogen peroxide was produced in an amount (0.6×10^{-4} mol/dm^3) equimolar with that of the aminated product, **2** (0.5×10^{-4} mol/dm^3).

10) R. A. Caldwell and L. Smith, *J. Am. Chem. Soc.*, **96**, 2994 (1974); D. Creed and R. A. Caldwell, *J. Am. Chem. Soc.*, **96**, 7369 (1974); R. A. Caldwell, D. Creed, and H. Ohta, *J. Am. Chem. Soc.*, **97**, 3246 (1975); H. Ohta, D. Creed, P. H. Wine, R. A. Caldwell, and L. A. Melton, *J. Am. Chem. Soc.*, **98**, 2002 (1976); D. Creed, R. A. Caldwell, H. Ohta, and D. C. DeMareo, *J. Am. Chem. Soc.*, **99**, 277 (1977); R. A. Caldwell, N. I. Ghali, C. K. Chien, D. DeMareo, and L. Smith, *J. Am. Chem. Soc.*, **100**, 2857 (1978); T. Majima, C. Pac, and H. Sakurai, *Bull. Chem. Soc. Jpn.*, **51**, 1811 (1978).

11) B. E. Hulme, E. J. Land, and G. O. Phillips, *J. Chem. Soc., Faraday Trans. 1*, **68**, 2003 (1972).

12) It was revealed that $\Phi_{air}(^1CT):\Phi_{air}(^3CT)=11:1$ in the photoamination of **1** in ethanol under air-saturated conditions where $[A]=5.00\times10^{-2}$ mol/dm^3.

Synthesis of (±)-Dihydrofomannosin Acetate[1)]

Hiroshi Kosugi* and Hisashi Uda

Chemical Research Institute of Non-aqueous Solutions, Tohoku University, Katahira-2, Sendai 980

(Received April 19, 1979)

The synthesis of (±)-dihydrofomannosin acetate [5-acetoxymethyl-1-(4,4-dimethyl-2-oxocyclopentyl)-3-oxabicyclo[4.2.0]oct-5-en-4-one] is described. Photocycloaddition of 4-(2-acetoxy-4,4-dimethylcyclopentyl)-2(5*H*)-furanone to ethylene gave 5-(2-acetoxy-4,4-dimethylcyclopentyl)-3-oxabicyclo[3.2.0]heptan-2-one, which was converted into ethyl [2-acetoxymethyl-2-(2-acetoxy-4,4-dimethylcyclopentyl)cyclobutyl]glyoxylate by the reaction with 2-methylthio-1,3-dithiane, followed by acetylation and ethanolysis. Introduction of an additional one carbon unit to the glyoxylate was accomplished by the Wittig reaction, and the subsequent hydrolysis and lactonization afforded 1-(2-hydroxy-4,4-dimethylcyclopentyl)-5-methylene-3-oxabicyclo[4.2.0]octan-4-one, which was transformed into 5-acetoxymethyl-5-hydroxy-1-[4,4-dimethyl-2-(tetrahydropyranyloxy)cyclopentyl]-3-oxabicyclo[4.2.0]-octan-4-one. Mesylation followed by elimination and oxidation led to (±)-dihydrofomannosin acetate.

Fomannosin (**1**) is a biologically active sesquiterpene first isolated from the still culture of the wood-rotting fungus Basidiomycete *Fomes annosus* (Fr.) Karst[2)] and subsequently from *Fomitopsis insularis*,[3)] and has been found toxic toward *Pinus tadea* seedlings, *Chlorella pyrenoidosa*, and some bacteria.[4)] The unusual B-*seco*-protoilludane structure of fomannosin was determined by an X-ray study of the *p*-bromobenzoylurethane derivative of dihydrofomannosin (**2**).[2)] Recently, X-ray crystallography of the (−)-camphenate of **2** led to the establishment of its absolute configuration.[5)] The synthesis of fomannosin and its derivative seems to be of interest from structural and biological points of view. However, fomannosin is very unstable,[2)] and our initial efforts in synthetic studies have been directed towards the synthesis of dihydrofomannosin (**2**) or its acetate **3**. In view of the recent work on

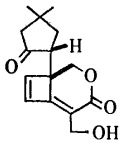

1

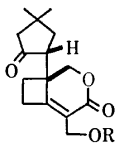

2 : R=H
3 : R=Ac

the photocycloaddition reaction of $\Delta^{\alpha,\beta}$-butenolides [2(5*H*)-furanones] with ethylene,[6)] we adopted Scheme 1 involving the photo-process on a suitably substituted butenolide **4** and the ring enlargement of a γ-lactonic photo-adduct to a δ-lactone system for construction of the fomannosin skeleton.[7)]

Our first step was to prepare the β-substituted $\Delta^{\alpha,\beta}$-butenolide **13** as a key intermediate. Three routes (Schemes 2—4) were examined for this purpose. Firstly, the intramolecular Reformatsky reaction of (bromoacetoxy)methyl ketones,[8)] a method for the synthesis of β-substituted butenolides, was applied. 2-Ethoxycarbonyl-4,4-dimethylcyclopentanone (**5**) was converted into the acetoxy carboxylic acid **8** by the usual procedure. The carboxyl group of **8** could be then transformed into the (bromoacetoxy)methyl ketone function through the standard steps[8)] to give the desired ketone **11** (Scheme 2). The Reformatsky reaction of **11** in the presence of ethyl bromoacetate[8)] followed by dehydration of the resulting hydroxy lactone **12** with alumina afforded the key butenolide **13** in 60% yield. In practice, however, this route appeared to be disadvantageous because of the low yield (<9.6% overall from **5**), requiring multistage operations and separation.

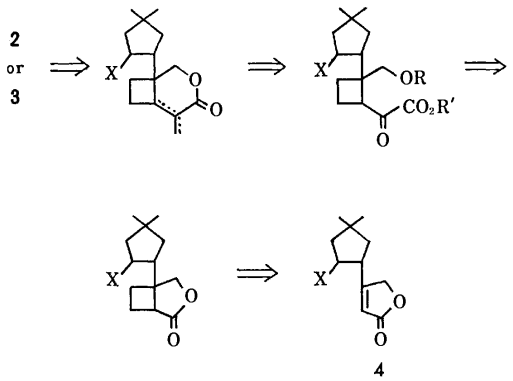

Scheme 1.

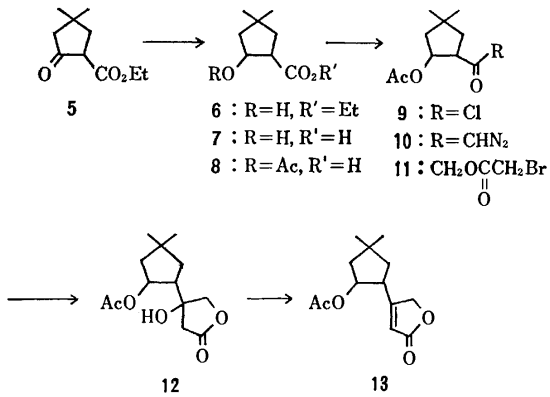

Scheme 2.

We adopted, as the second Scheme, introduction of the double bond at the α,β-position of a suitable γ-butyrolactone derivative such as **18** or **19**. The Michael reaction of **5** with γ-crotonolactone (**14**) afforded the adduct **15** in 66% yield, use of excess **14** being essential for a good yield of **15**. The adduct **15** was decarboxylated to give the keto lactone **16** in 74% yield, which was reduced to the hydroxy lactone **17**. Attempt to introduce unsaturation to the lactone moiety of the acetate **18** by the usual bromination-dehydrobromination was unsuccessful; bromination gave an intractable mixture. We examined the sulfenylation-dehydrosulfenylation procedure recently developed by Trost *et al.*[9)] Reaction of the enolate of the tetrahydropyranyl ether derivative **19** with

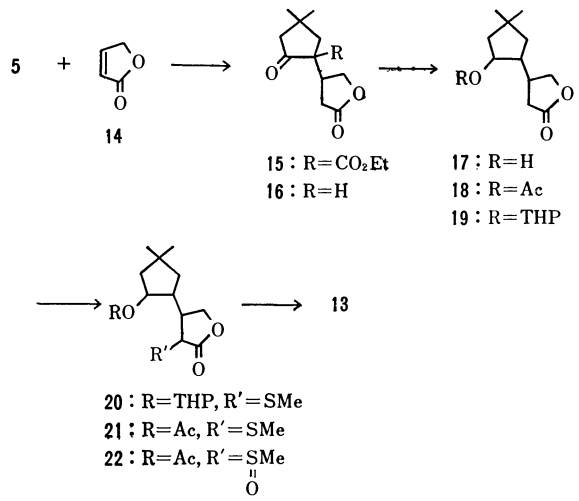

Scheme 3.

dimethyl disulfide afforded the α-methylthio lactone **20** in 60% yield. From the fact that a tetrahydropyranyloxy group is somewhat sensitive to UV irradiation (partial decomposition) at this stage, the protecting group was exchanged by an acetyl group. Oxidation of the acetoxy derivative **21** and subsequent pyrolysis of the resulting sulfoxide **22** gave **13** in 60% yield from **20** (Scheme 3). Thus, the desired compound **13** was available in moderate yield. However, the route also seems to be practically inconvenient for the preparation of **13** on a larger scale.

During the course of this study, it was found that α-phenylthio- (**23**) or α-phenylsulfinyl-$\Delta^{\alpha,\beta}$-butenolide (**24**) is an efficient carbanion acceptor in the Michael reactions and the use of **23** or **24** provides a high-yield and convenient method for the synthesis of butenolides having various substituents at the β-position.[10] The method should be applicable to the present case. Reaction of the enolate of **5** with either of **23** or **24** resulted in the formation of only self-polymerization product of **23** or **24**, indicating that the enolate of **5** acts as a base rather than the Michael addend.[10] This suggests that a much stronger nucleophilic enolate should be employed as an addend to achieve the Michael reaction. 3,3-Dimethylcyclopentanone (**25**) was chosen for this purpose. The Michael reaction of **24** with the lithium enolate of **25** proceeded smoothly at −68 °C, as expected, to produce the adduct **26** and **27**, which was dehydrosulfenylated, without separation, in refluxing toluene giving two separable keto butenolides **28** and **29** in 54 and 18% yields, respectively (Scheme 4). In the NMR spectra, the methine proton α to the keto group was observed as a broad triplet (J=10.5 Hz) at δ 3.45 in the major product **28**, but as a broad singlet at δ 3.40 in the minor one **29**, indicating that **28** is the desired compound and **29** the regioisomer. On the other hand, the reaction of the α-phenylthio lactone **23** with **25** gave a singel adduct (38% yield), which was confirmed to be the phenylthio analogue of **26** by transformation into **13** *via* **28**. The precursor **27** of the minor isomer **29** should be sterically less favorable than the major precursor **26**. The actual formation of **27** can be attributed to the formation of

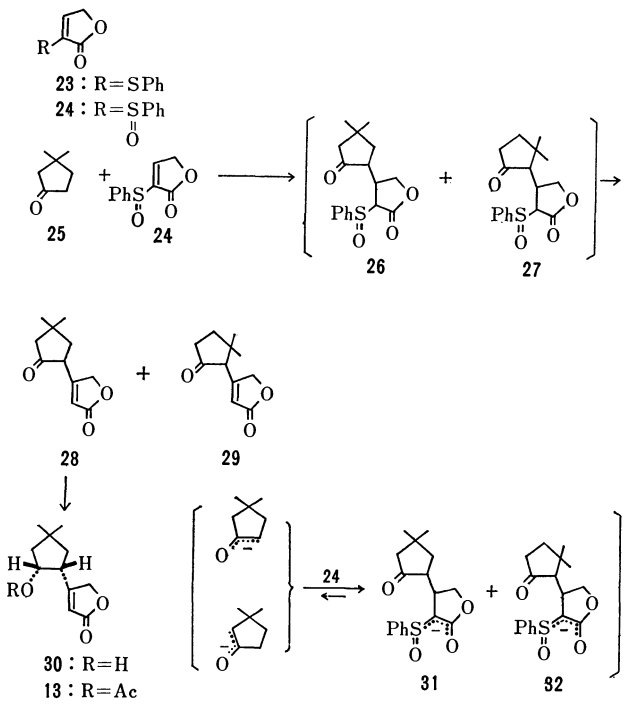

Scheme 4.

the relatively tight bonding between lithium cation and the effectively stabilized carbanion intermediate **32** together with **31**[10] from the equilibrated enolate of **25**. Such a tight bonding would prevent the reversible process (**32**→**24**+**25**) under the conditions employed, resulting in slight loss of the regioselectivity in the reaction. Reduction of **28** with sodium borohydride afforded the single crystalline hydroxy butenolide **30**, mp 36—37 °C, which was acetylated to give **13** in 74% yield. The spectral properties were compatible with the assigned structure **13**. Assignment of the *cis* configuration of two vicinal substituents on the cyclopentane ring of **13** follows from the steric course of the reaction and the NMR coupling pattern of the proton at the carbon atom bearing the acetoxyl group: doublet (J=6.0 Hz, *trans* coupling) of triplet (J=7.5 Hz, *cis* coupling) at δ 5.12.

According to the procedure of Kosugi *et al.*,[6] a solution of **13** in acetone with moderately rapid introduction of ethylene was irradiated at −50— −60 °C with a 500 W high-pressure mercury lamp without filter giving an 85% yield of the 1:1 photoadduct **33** (Scheme 5). From the NMR spectrum, the photoadduct was found to be a mixture of stereoisomers **33a** and **33b**. The ratio of **33a** and **33b** could not be determined at this stage, since the product was homogeneous on thin layer chromatography, and the NMR spectrum revealed no distinctly separated signals. Actual separation of the stereoisomers was carried out at a later stage.

The next step to elaborate the fomannosin skeleton was one carbon elongation of the lactone-carbonyl position. Among a number of agents, 2-methylthio-1,3-dithiane[11] was chosen as a carboxyl equivalent. The photoadduct **33** was treated with lithiated 2-methylthio-1,3-dithiane, followed by acetylation giving the ring-opened product **34** in 74% yield. Mercury(II) ion-

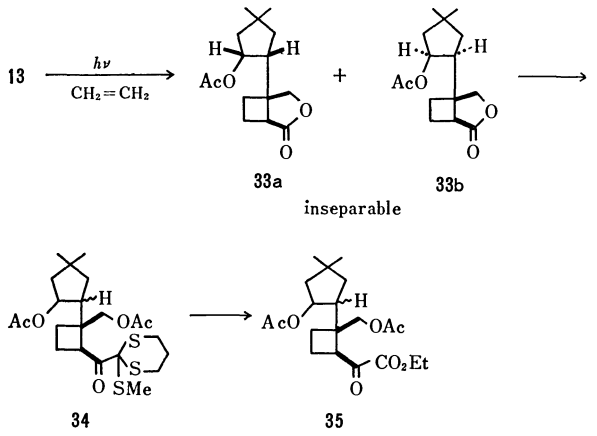

Scheme 5.

catalyzed ethanolysis of **34** gave the glyoxylate **35** in high yield, which apparently consists of about equal amounts of two stereoisomers as detected by the NMR spectrum. The prominent peaks were observed as the pairs with about equal intensities. Although an α-methylene-δ-lactone structural unit has been found to a lesser extent than an α-methylene-γ-lactone unit in naturally occurring compounds, it is of growing importance from the viewpoint of its biological activities, *e.g.*, vernolepin. The glyoxylate **35** can be easily converted into an α-methylene-δ-lactone derivative **37**. The sequential reactions developed in the present study [(i) nucleophilic attack of the anion of 2-methylthio-1,3-dithiane, (ii) acetylation and ethanolysis, (iii) a Wittig reaction, and (iv) hydrolysis and lactonization] would provide a convenient method for the synthesis of α-methylene-δ-lactones from readily available γ-lactones.[12]

The next step was to extend the keto group of **35** by an additional one-carbon unit. A methylene function would be most suitable for leading to the final functionality, an allylic hydroxy- or acetoxymethyl grouping, of the synthetic targets, and would be introduced easily by the Wittig reaction.[13] However, it was found that the reaction of **35** with methylenetriphenylphosphorane in the standard way (generated by dimsylsodium in dimethyl sulfoxide or butyllithium in ether) is unsatisfactory because of very low yields of the product. Observation of the rapid consumption of the starting material **35** and of the low recovery after work-up in the above experiments suggests that the use of polar media probably caused further undesirable side reactions. A less polar medium, benzene, was employed as a co-solvent for the reaction. Inverse slow addition of a reagent solution in dimethyl sulfoxide to a solution of **35** in benzene afforded a high yield of the product **36**. At this stage, the stereoisomers could be separated by preparative thin layer chromatography to give the α-methylene esters **36a** and **36b** in 33 and 32% yields, respectively. Each isomer **36a** or **36b** was hydrolyzed with potassium hydroxide, and the resulting dihydroxy carboxylic acid was treated with *p*-toluenesulfonic acid in refluxing benzene giving, without double bond isomerization, the α-methylene-δ-lactone **37a** or **37b** in a high yield. The observed significant differences in the physical properties of

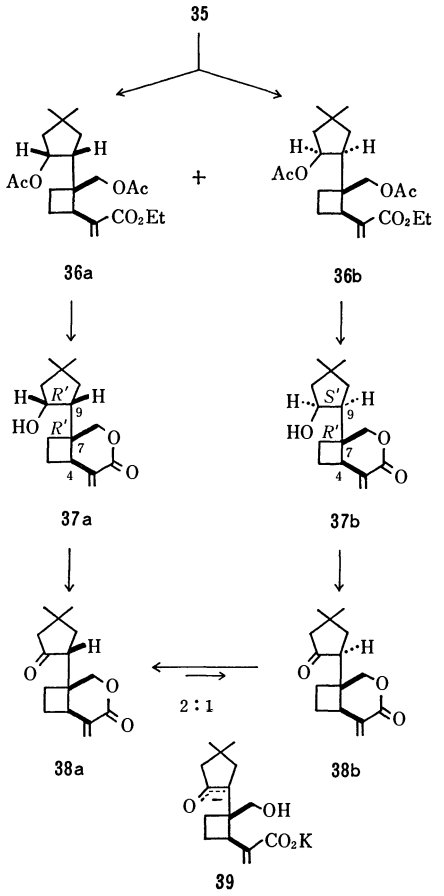

Scheme 6.

these isomers were the NMR coupling patterns of the lactonic methylene protons (–CH_2–O–CO–): an AB type quartet (J=12 Hz) at δ 4.20 in **37a** and a singlet at δ 4.07 in **37b**, and the chemical shift values of the allylic methine protons: δ 3.14 (dd) in **37a** and 3.43 (dd) in **37b**. Such characteristics were also observed in the corresponding keto lactones **38**: the lactonic methylene protons appeared as an AB type quartet (J=11 Hz) at δ 4.16 in **38a**, while a singlet at δ *ca.* 3.90 in **38b**, and the allylic methine protons appeared at δ 3.10 (br s) in **38a** and at δ *ca.* 3.80 (br s) in **38b**, respectively.

We now considered the stereochemical features of these isomeric lactone derivatives with Dreiding models, in order to establish whether the a-series or b-series lactone would possess the same stereochemistry as that of fomannosin. As shown in Scheme 6, one series has the same (7*R*′,9*R*′)[14] configuration as that of fomannosin,[16] the other having the (7*R*′,9*S*′) configuration. In both series, the conformations, in which the cyclopentane ring (especially the part of

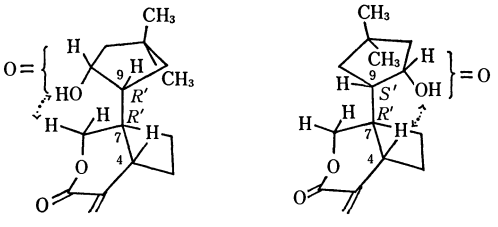

37a, 38a **37b, 38b**

the dimethyl groups) is so oriented as to be far from the bicyclic lactone ring system, the lactone ring being bisected by the methine hydrogen on the cyclopentane ring, could be postulated to be the sterically favorable conformations as shown by the stereoformulae. If so, in the (7*R*′,9*R*′)-series compounds the hydroxyl or carbonyl group on the cyclopentane ring is located close to the lactonic methylene group and apart from the allylic methine hydrogen at C-4, and therefore, the anisotropic effect of the oxygen-functions may cause a somewhat large difference in the chemical shifts of two methylene protons, resulting in the appearance as an AB type quartet. Almost no shift would be expected in the signal of the allylic methine proton upon conversion of the hydroxyl into the keto group. Contrary to the (7*R*′,9*R*′)-series, in the case of the (7*R*′,9*S*′)-series compounds the hydroxyl or carbonyl group on the cyclopentane ring should be far from the lactonic methylene group, approaching to the allylic methine hydrogen. Thus, lactonic methylene protons would appear as a singlet (alomost same chemical shifts), and the allylic proton signal at a lower field than that of the corresponding (7*R*′,9*R*′)-isomer, shifting markedly upon conversion of the hydroxyl into the keto group. The compounds (a-series) exhibiting an AB type quartet methylene signal should be the desired (7*R*′,9*R*′)-stereoisomers **37a** and **38a**. The assignment was confirmed by completion of the synthesis of dihydrofomannosin acetate from **37a**.[17] The spectral properties of the b-series compounds **37b** and **38b** were also in good agreement with expectation for the (7*R*′,9*S*′)-configuration.

At this point a remark regarding the relative stabilities between the stereoisomers is appropriate. After treatment of pure **38b** with excess potassium hydroxide in aqueous dioxane–methanol at room temperature overnight, the keto lactone **38** was recovered through acidification and lactonization. The recovered material was found to be a *ca.* 2:1 mixture of **38a** and **38b** as determined by a comparison of the NMR peak areas of the respective lactonic methylene protons. Thus, in the ring-opened state **39** the (7*R*′,9*R*′)-stereoisomer leading to **38a** was slightly more stable than the (7*R*′,9*S*′)-one.

Of the compounds **37a** and **38a**, both having the proper stereochemistry and functionalities for the synthesis, **37a** appeared to be the better precursor, since the use of **38a** would cause some complexity (epimerization *etc.*) upon subsequent operations. For the remaining functional group manipulation, 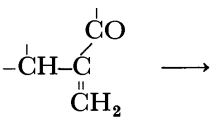 ⟶ 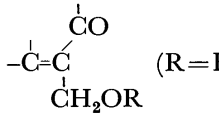 (R=H or Ac), allylic oxidation-rearrangement with singlet oxygen[18] or selenium dioxide[19] would be the most promising procedure. However, all attempts to achieve the allylic oxidation-rearrangement of **37a** or the acetate with singlet oxygen or selenium dioxide under various conditions were unsuccessful. Thus, a stepwise scheme (Scheme 7) was adopted.

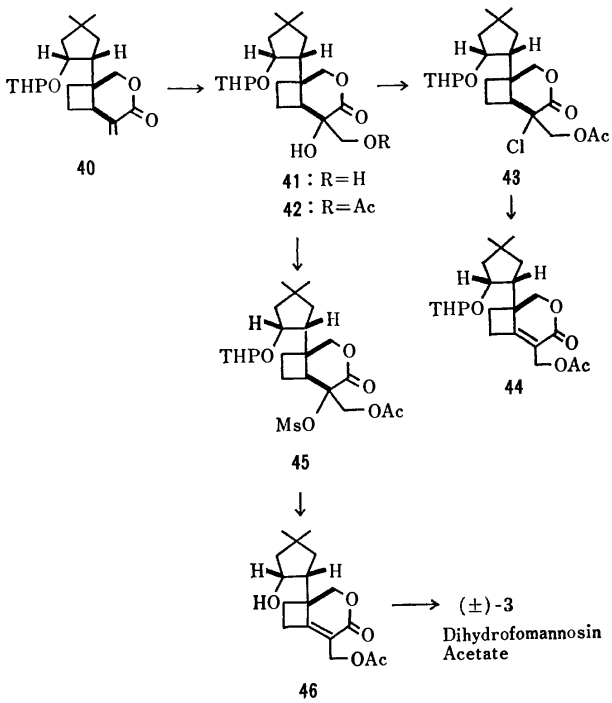

Scheme 7.

The tetrahydropyranyl ether **40**, derived from **37a**, was hydroxylated with osmium tetraoxide-pyridine in ether, and the resulting dihydroxy lactone **41** was acetylated to the monoacetate **42** in 69% yield. Dehydration of **42** with the common agents (thionyl chloride or phosphoryl chloride in pyridine) was found to be quite troublesome. The reactions were extremely slow and the chloride **43** initially formed resisted subsequent dehydrochlorination enormously giving only a trace of the unsaturated lactone **44**. Compound **42** was then treated with methanesulfonyl chloride in the presence of triethylamine to give quantitatively the unstable mesylate **45**. Demesylation of crude **45** was accomplished by heating with lithium chloride-lithium carbonate in *N*,*N*-dimethylformamide, providing directly the unsaturated hydroxy lactone **46** along with several by-products. The Jones oxidation of **46**, without isolation, gave after chromatographic separation, (±)-dihydrofomannosin acetate (**3**), mp 102—103 °C, in 20% yield from **45**. The spectral [IR, NMR (60 and 100 MHz), and mass] and chromatographic behaviors were identical with those of the authentic sample prepared from dihydrofomannosin derived from natural fomannosin. Furthermore, we examined the preparation of (±)-dihydrofomannosin (**2**) itself. It was found that **3** and **2** seem to be base-sensitive; saponification of **3** resulted in the formation of a complex mixture.

An attempt to synthesize (±)-deoxydihydrofomannosin (**50a**) should be mentioned (Scheme 8). Treatment of the glyoxylate **35** with methyllithium gave the hydroxy ester **47**, which was converted into the dihydroxy lactone **48** through hydrolysis and lactonization in the same manner; there was no indication of cyclization to a tetrahydrofuran derivative. The Jones oxidation of **48** afforded the hydroxy keto lactone **49**. In the case of **49**, dehydration with thionyl chlo-

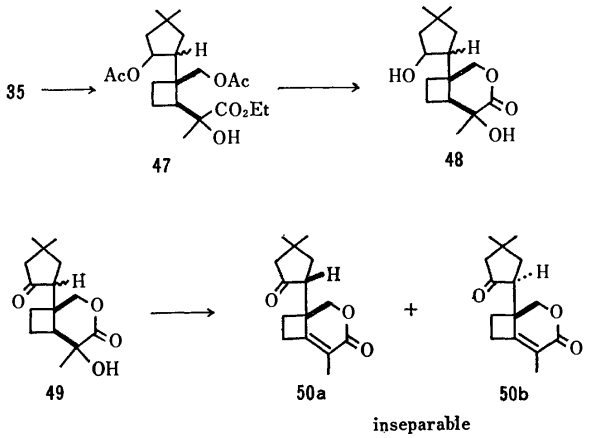

Scheme 8.

ride–pyridine proceeded well to give selectively the *endo*-unsaturated lactone. The product was apparently a *ca.* 1:1 mixture of the stereoisomers **50a** and **50b**, which were inseparable. In the NMR spectrum, the signals due to the lactonic methylene protons were observed as a set of an AB type quartet and a singlet. The isomer revealing an AB type quartet should be (±)-deoxydihydrofomannosin (**50a**).

Experimental

All melting points were taken on a Yamato melting point apparatus and are uncorrected. Small amounts of liquid products were purified by evaporative short-path distillation; oil-bath temperatures are recorded. IR spectra were obtained with a Hitachi EPI-S2 or G2 spectrophotometer, NMR spectra with a JEOL PMX-60 (60 MHz), C-60HL (60 MHz), or PS-100 (100 MHz) instrument with TMS as an internal standard, coupling constants being given in Hz, and mass spectra with a Shimadzu LKB-9000 spectrometer at 70 eV. Silica gel (Merck GF-254) was used for preparative and analytical thin-layer chromatography (TLC); solvent systems are indicated in parentheses. Microanalyses were carried out at this Institute.

*4-(2-Acetoxy-4,4-dimethylcyclopentyl)-2(5H)-furanone (**13**).* *Route a*: 2-Acetoxy-4,4-dimethylcyclopentyl (bromoacetoxy)-methyl ketone (**11**) was prepared from 2-ethoxycarbonyl-4,4-dimethylcyclopentanone (**5**)[20] in 16% overall yield through six steps by a procedure similar to that reported.[8] Activated zinc powder (1.56 g, 3 equiv) was added portionwise under stirring and gentle refluxing to a solution of **11** (2.65 g, 8 mmol), ethyl bromoacetate (1.0 g, 0.6 mmol), and iodine (a catalytic amount) in anhydrous benzene (40 ml). After vigorous reaction ceased, refluxing and stirring were continued for 2 h. Acetic acid (2 ml) and methanol (1 ml) were added in succession to the cooled reaction mixture, and the resulting mixture was diluted with water. The water layer was extracted with ether. The combined organic layers were washed with an aqueous solution of sodium hydrogencarbonate, water, and saturated brine, and dried over anhydrous sodium sulfate. After removal of the solvent, the oily residue (1.6 g) was dissolved in acetic anhydride (20 ml) and heated under reflux for 24 h. Concentration of the solution under reduced pressure and chromatography of the concentrate on silica gel (50 g) using $CHCl_3$ as an eluant gave **13** (437 mg, 48%).

Route b: To a slurry of potassium *t*-butoxide (4.93 g, 44 mmol) in anhydrous benzene (25 ml) was added dropwise a solution of **5** (7.4 g, 40 mmol) in anhydrous benzene (35 ml) at room temperature under nitrogen. After stirring at room temperature for 2 h, the solution was concentrated under reduced pressure, and the concentrated enolate was dissolved in DMSO (25 ml). To this solution was added dropwise a solution of γ-crotonolactone (**14**) (8.2 g, 0.1 mol, 2.5 equiv) in DMSO (25 ml) with ice-water cooling under nitrogen. After being stirred at room temperature for 12 h, the reaction mixture was poured into ice-water, neutralized with 10% sulfuric acid, and extracted with ether. The combined extracts were washed with water and brine, and dried. Evaporation of the solvent gave a stereoisomeric mixture of 4-(1-ethoxycarbonyl-4,4-dimethyl-2-oxocyclopentyl)tetrahydro-2-furanone (**15**) (6.06 g, 66%): bp 160—165 °C/1.5 Torr; IR ($CHCl_3$) 1780, 1750, 1720, 1180, and 1020 cm^{-1}; NMR ($CDCl_3$) δ 1.16 (6H, s) 1.28 (3H, t, J=7.0), 1.70—3.40 (7H, m), 4.20—4.75 (2H, m), and 4.25 (2H, q, J=7.0). Found: *m/e* 268 (M^+). Calcd for $C_{14}H_{20}O_5$: M 268.

A mixture of **15** (3.82 g) and an aqueous 20% perchloric acid solution was heated at 80—90 °C with vigorous stirring for 12 h and then at the refluxing temperature for 1 h. After cooling, the product was extracted with ether. The combined extracts were washed with water and brine, and freed from the solvent. Distillation of the oil remaining afforded 4-(4,4-dimethyl-2-oxocyclopentyl)tetrahydro-2-furanone (**16**): bp 135—145 °C/1.5 Torr; IR (CCl_4) 1780, 1740, 1170, and 1030 cm^{-1}; NMR ($CDCl_3$) δ 1.07 (3H, s), 1.20 (3H, s), and 3.90—4.90 (2H, m). Found: C, 67.21; H, 7.90%. Calcd for $C_{11}H_{16}O_3$: C, 67.32; H, 8.22%.

To a solution of **16** (2.0 g, 10 mmol) in methanol (80 ml) was added portionwise sodium borohydride (550 mg, 15 mmol) under cooling in an ice–water bath, and the reaction mixture was stirred at 0 °C for 1.5 h and at room temperature for 1 h. After the reaction was quenched by the addition of dilute hydrochloric acid (2 M), the solution was concentrated under reduced pressure. The residual semi-solid was dissolved in $CHCl_3$, the resulting solution being washed with brine. Evaporation of the solvent and distillation of the residue gave 4-(2-hydroxy-4,4-dimethylcyclopentyl)tetrahydro-2-furanone (**17**) (1.52 g, 77%): bp 145—155 °C/1.5 Torr; IR ($CHCl_3$) 3450 and 1760 cm^{-1}; NMR ($CDCl_3$) δ 1.02 (3H, s), 1.10 (3H, s), 2.40 (1H, s, OH), and 3.70—4.70 (3H, m). Found: C, 66.75; H, 8.95%. Calcd for $C_{11}H_{18}O_3$: C, 66.64; H, 9.15%.

A solution of tetrahydropyranyl ether **19** (2.83 g, 10 mmol), prepared from **17** by the standard method, in THF (6 ml) was added dropwise at −60 °C over a period of 10 min under nitrogen to a solution of lithium diisopropylamide (20 mmol) in anhydrous ether (14 ml) and THF (5 ml). After stirring at −60 °C to −40 °C for 1 h, the reaction mixture was added dropwise to a solution of dimethyl disulfide (2 ml, 20 mmol) in THF (6 ml) at −35 °C, and the resulting mixture was allowed to warm slowly to room temperature over a period of 2 h with stirring. A saturated aqueous solution of ammonium chloride was added, the water layer being separated and extracted with ether. The combined organic layers were washed with water and brine, dried, and freed from ether. Chromatography of the residue (3.26 g) on silica gel (75 g) using petroleum ether–ether (the amount of ether was gradually increased, the final ratio being 2:1.) as an eluant gave 4-[4,4-dimethyl-2-(tetrahydropyranyloxy)cyclopentyl]-3-(methylthio)tetrahydro-2-furanone (**20**) (1.88 g, 60%): IR ($CHCl_3$) 1760, 1025, and 1015 cm^{-1}; NMR (CCl_4) δ 1.04 and 1.10 (total 6H, each s), 2.15 and 2.25 (total 3H), and 3.00—4.80 (7H, m). Found: C, 62.44; H, 8.92%. Calcd for $C_{17}H_{28}O_4S$: C, 62.17; H, 8.59%.

A solution of **20** (3.1 g) and hydrochloric acid (1 M, 4 ml)

in methanol (50 ml) was allowed to stand at room temperature for 4 h. The reaction mixture subjected to the usual work-up (dilution with water and extraction with ether) gave 4-(2-hydroxy-4,4-dimethylcyclopentyl)-3-(methylthio)tetrahydro-2-furanone (1.95 g, 84%): bp 120 °C/0.5 Torr; IR ($CHCl_3$) 3400, 1760, 1160, and 1015 cm^{-1}; NMR ($CDCl_3$) δ 1.00 (3H, s), 1.07 (3H, s), 2.25 and 2.27 (total 3H, each s), and 3.80—4.70 (3H, m). Found: C, 59.02; H, 8.55%. Calcd for $C_{12}H_{20}O_3S$: C, 59.00; H, 8.25%.

The above hydroxy lactone was acetylated in the usual way with acetic anhydride and pyridine to afford 4-(2-acetoxy-4,4-dimethylcyclopentyl)-3-(methylthio)tetrahydro-2-furanone (**21**): IR ($CHCl_3$) 1770, 1725, and 1020 cm^{-1}; NMR (CCl_4) δ 1.07 (6H, s), 1.98 (3H, s), 2.22 (3H, s), 3.20 (1H, m), 3.90—4.70 (2H, m), and 5.00 (1H, m).

A solution of sodium periodate (1.7 g, 8 mmol) in water (15 ml) was added dropwise at 0 °C to a solution of **21** (1.94 g, 6.8 mmol) in methanol (15 ml), and the reaction mixture was stirred at room temperature overnight. After removal of inorganic material by filtration, the filtrate was extracted with $CHCl_3$ three times. The combined extracts were washed with water and brine, dried, and evaporated. The residual oil was dissolved in pyridine (20 ml), and the resulting solution was heated under reflux for 3 h and evaporated under reduced pressure. The residue was dissolved in ether, the ethereal solution being washed with dilute hydrochloric acid, water, and brine, and evaporated. The residue was passed through a short column of silica gel with the aid of 1:1 petroleum ether–ether and distilled to give **13** (1.23 g, 76% from **21**): bp 140 °C/1 Torr.

Route c: To a solution of lithium diisopropylamide (0.03 mol) in anhydrous THF (20 ml) and hexane (20 ml) was added dropwise a solution of 3,3-dimethylcyclopentanone (**25**)[21] (3.36 g, 0.03 mol) in anhydrous THF (10 ml) at −60 °C under nitrogen, and the reaction mixture was stirred at −60 °C for 1 h. A solution of 3-phenylsulfinyl-2(5*H*)-furanone (**24**)[10] (6.9 g, 0.03 mol) in anhydrous THF (35 ml) was added to the above solution at −78 °C with stirring. After stirring at this temperature for 2 h, a saturated aqueous solution of ammonium chloride was added. The resulting solution was then neutralized with dilute sulfuric acid and extracted with ether three times. The combined extracts were washed with water and brine, dried, and evaporated. The residue was dissolved in toluene (150 ml), and the solution was heated under reflux for 30 min. Evaporation of the solvent under reduced pressure and chromatography on silica gel (150 g) using 4:6 petroleum ether–ether as an eluant gave 4-(4,4-dimethyl-2-oxocyclopentyl)-2(5*H*)-furanone (**28**) (3.17 g, 54%, faster eluted fraction): IR ($CHCl_3$) 1790, 1758, 1750, and 1638 cm^{-1}; NMR ($CDCl_3$) δ 1.15 (3H, s), 1.26 (3H, s), 2.24 (2H, s), 1.80—2.50 (2H, m), 3.45 (1H, br t, J=10.5), 4.80 (1H, a part of AB type q, finely split, J=18.0), 5.12 (1H, a part of AB type q, finely split, J=18.0), and 5.88 (1H, q, J=2.2), and 4-(2,2-dimethyl-5-oxocyclopentyl)-2(5*H*)-furanone (**29**): IR ($CHCl_3$) 1785, 1765, 1745, and 1630 cm^{-1}; NMR ($CDCl_3$) δ 0.93 (3H, s), 1.30 (3H, s), 1.70—2.70 (4H, m), 3.40 (1H, br s), 4.76 (1H, a part of AB type q, finely split, J=18.0), 5.00 (1H, a part of AB type q, finely split, J=18.0), and 5.96 (1H, q, J=2.2). Both **28** and **29** were fairly unstable, decomposing on storage, giving no satisfactory analytical data.

To a solution of **28** (2.31 g, 12 mmol) in anhydrous methanol (60 ml) was added portionwise sodium borohydride (464 mg, 12 mmol) at −15 °C over a period of 30 min, and the reaction mixture was stirred at −15 °C for 30 min. A few drops of glacial acetic acid was added, and the resulting solution was concentrated under reduced pressure. The residue was dissolved in $CHCl_3$, and the solution successively washed with dilute sulfuric acid, water, and brine. Evaporation of the solvent left the single crystalline product, 4-(2-hydroxy-4,4-dimethylcyclopentyl)-2(5*H*)-furanone (**30**) (2.01 g, 89%). An analytical sample was purified by preparative TLC (1:1 $CHCl_3$–ether) and then by recrystallization from 4:1:1 CCl_4–ether–petroleum ether: mp 36—38 °C; IR ($CHCl_3$) 3450, 1780, 1745, 1630, and 1030 cm^{-1}; NMR ($CDCl_3$) δ 1.12 (3H, s), 1.19 (3H, s), 1.30—2.20 (4H, m), 2.97 (1H, m), 3.55 (1H, OH), 4.13 (1H, q, J=9.5), 4.92 (2H, t, J=2.5), and 5.85 (1H, q, J=2.5). Found: C, 66.90; H, 8.39%. Calcd for $C_{11}H_{16}O_3$: C, 67.32; H, 8.22%.

Compound **30** (1.79 g) was treated with pyridine (20 ml) and acetic anhydride (20 ml), and the reaction mixture was allowed to stand at 0 °C overnight. The usual work-up and purification by chromatography on silica gel (50 g) using 1:1 petroleum ether–ether as an eluant gave **13** (1.78 g, 82%): bp 120—130 °C/1 Torr; IR (CCl_4) 1785, 1745, and 1640 cm^{-1}; NMR (CCl_4) δ 1.12 (3H, s), 1.15 (3H, s), 2.00 (3H, s), 3.16 (1H, dt, J=10.5 and 7.5), 4.77 (2H, d, J=2.2), 5.12 (1H, td, J=7.5 and 6.0), and 5.83 (1H, td, J=2.2 and 1.2). Found: C, 65.45; H, 7.64%. Calcd for $C_{13}H_{18}O_4$: C, 65.53; H, 7.61%.

*5-(2-Acetoxy-4,4-dimethylcyclopentyl)-3-oxabicyclo[3.2.0]heptan-2-one (**33**).* A solution of **13** (1.9 g) in freshly distilled acetone (600 ml) was irradiated with a 500 W high-pressure mercury lamp (immersed, no filter) at −50—−60 °C with continuous introduction of finely dispersed ethylene. On this scale, the reaction was essentially completed within 3—5 h. Evaporation of the solvent left the product (2.4 g) which was chromatographed on silica gel (70 g) using petroleum ether–ether (the amount of ether was gradually increased, the final ratio being 6:4.) as an eluant to give an inseparable stereoisomeric mixture of **33** (1.80 g, 85%): bp 110—120 °C/1 Torr; IR (CCl_4) 1775, 1732, 1233, and 1020 cm^{-1}; NMR (CCl_4) δ 1.08 and 1.12 (total 6H, each s), 2.00 (total 3H, two singlets), 4.10 (2H, m), and 5.00 (1H, m). Found: C, 68.03; H, 8.10%. Calcd for $C_{15}H_{22}O_4$: C, 67.64; H, 8.33%.

*Ethyl [2-Acetoxymethyl-2-(2-acetoxy-4,4-dimethylcyclopentyl)cyclobutyl]glyoxylate (**35**).* 2-Methylthio-1,3-dithiane was prepared according to the procedure given by Ellison *et al.*:[11] bp 130—150 °C/4—5 Torr; NMR (CCl_4) δ 2.10 (3H, s) and 4.75 (1H, s). To a solution of 2-methylthio-1,3-dithiane (1.80 g, 11 mmol) in anhydrous THF (10 ml) was added dropwise a solution of butyllithium in hexane (5.7 ml of 1.9 M solution, 11 mmol) at −60 °C under nitrogen, and the mixture was stirred at −60 °C for 0.5 h. A solution of **33** (850 mg, 3.2 mmol) in anhydrous THF (8 ml) was added dropwise to the above solution at −60 °C, and the reaction mixture was allowed to warm to 0 °C over a period of several hours with stirring. A saturated aqueous solution of ammonium chloride was added, and the product was extracted with ether. The combined extracts were washed with water and brine, and dried. Evaporation of the solvent left an oily material which was treated with a mixture of acetic anhydride (18 ml) and pyridine (18 ml) at room temperature overnight. The mixture was evaporated to dryness under reduced pressure. Chromatography of the oil remaining on silica gel (50 g) using 2:1 petroleum ether–ether as an eluant gave the ring-opened product **34** (1.08 g, 71%): IR ($CHCl_3$) 1725 cm^{-1}; NMR (CCl_4) δ 1.10 (6H), 1.87 (3H), 2.04 (3H), 4.05 (2H), and 4.30—5.50 (1H). Found: *m/e* 474 (M^+). Calcd for $C_{22}H_{34}O_5S_3$: M 474.

To a slurry of mercury(II) chloride (3.31 g, 12.2 mmol) and mercury(II) oxide (1.35 g, 6.2 mmol) in 95% ethanol

(50 ml)[11] was added a solution of **34** (1.43 g, 3.0 mmol) in 95% ethanol (20 ml), and the reaction mixture was vigorously stirred at 80—90 °C for 2 h. After cooling to room temperature, inorganic material was removed by filtration and the filtrate concentrated under reduced pressure. The residue was dissolved in ether, the ethereal solution being washed with water and brine. Evaporation of the ether gave colorless oily **35** (990 mg, 85%), which was sufficiently pure to be used for subsequent treatment. An analytical sample was purified by preparative TLC (6:4 petroleum ether–ether) and then distilled: bp 120—130 °C/0.5 Torr; IR ($CHCl_3$) 1730 (sh) and 1720 cm^{-1}; NMR ($CDCl_3$) δ 1.07, 1.13, and 1.18 (total 6H, each s), 1.38 and 1.41 (total 3H, each t, J=7.0), 1.95 and 2.12 (total 6H, each s), 3.60—4.20 (3H, m), 4.35 (2H, q, J=7.0), and 4.77 and 5.33 (total 1H, each m). Found: C, 62.76; H, 8.02%. Calcd for $C_{20}H_{30}O_7$: C, 62.81; H, 7.90%.

*Ethyl 2-[2-Acetoxymethyl-2-(2-acetoxy-4,4-dimethylcyclopentyl)-cyclobutyl]propenoate (**36**).* A solution of methylenetriphenylphosphorane in DMSO (2.8 ml of 0.5 M solution, 1.4 mmol), prepared according to the procedure given by Greenwald *et al.*,[22] was added to a solution of **35** (420 mg, 1.1 mmol) in anhydrous benzene (10 ml) at 0 °C under nitrogen. After stirring at room temperature for 1—2 h, the reaction mixture was poured into ice–water containing a few drops of 2 M sulfuric acid, and the product was extracted with ether. The combined extracts were washed with water and brine, dried and freed from ether. Preparative TLC (6:4 petroleum ether–ether) of the residue (710 mg) gave **36a** (R_f 0.58, 137 mg, 33%) and **36b** (R_f 0.67, 124 mg, 32%). The analytical samples were purified by distillation, bp 110—120 °C/0.5 Torr. Isomer **36a** had IR ($CHCl_3$) 1720, 1624, and 1035 cm^{-1}; NMR (CCl_4) δ 1.10 (3H, s), 1.13 (3H, s), 1.32 (3H, t, J=7.5), 1.85 (6H, s), 2.70 (1H, m), 3.30 (1H, br t, J=*ca.* 8.0), 3.84 (2H, s), 4.17 (2H, q, J=7.5), 4.63 (1H, m), 5.40 (1H, m), and 6.13 (1H, m). Found: C, 66.04; H, 8.73%. Calcd for $C_{21}H_{32}O_6$: C, 66.30; H, 8.48%. Isomer **36b** had mp 51—53 °C (crystallized sample); IR ($CHCl_3$) 1718, 1625, and 1030 cm^{-1}; NMR ($CDCl_3$) δ 1.05 (3H, s), 1.13 (3H, s), 1.33 (3H, t, J=7.0), 1.90 (3H, s), 1.97 (3H, s), 3.47 (1H, br t, J=7.5), 3.70 and 4.00 (1H each, AB type q, J=7.0), 4.22 (2H, q, J=7.0), 5.47 (2H, br s), and 6.13 (1H, br s). Found: C, 66.55; H, 8.44%.

*1-(2-Hydroxy-4,4-dimethylcyclopentyl)-5-methylene-3-oxabicyclo-[4.2.0]octan-4-one (**37**).* A solution of **36a** (221 mg) in a mixture of dioxane (4 ml), an aqueous solution of potassium hydroxide (200 mg in 4 ml of water), and methanol (1 ml) was allowed to stand at room temperature overnight. After acidification with dilute sulfuric acid, the product was thoroughly extracted with $CHCl_3$. The combined extracts were washed with brine, and evaporated. The residue was dissolved in benzene (5 ml) containing a catalytic amount of fused *p*-toluenesulfonic acid, and the resulting solution was heated under reflux for 1 h. The reaction mixture was diluted with ether and washed successively with an aqueous solution of sodium hydrogencarbonate, water, and brine, and dried. Evaporation of the solvent under reduced pressure gave **37a** (146 mg, quantitative). A pure sample was obtained by preparative TLC (1:4 petroleum ether–ether), but further purification by distillation caused decomposition. Compound **37a** had IR ($CHCl_3$) 3400, 1720, 1628, 1030, and 940 cm^{-1}; NMR ($CDCl_3$) δ 1.04 (3H, s), 1.18 (3H, s), 2.50 (1H, OH), 3.14 (1H, dd, J=9.0 and 6.0), 4.10 (1H, m), 4.02 and 4.38 (1H each, AB type q, J=10.0), 5.36 (1H, br s), and 5.95 (1H, br s). Found: *m/e* 250 (M^+). Calcd for $C_{15}H_{22}O_3$: M 250.

In the same manner, isomeric **37b** was obtained from **36b** and had IR ($CHCl_3$) 3400, 1720, 1625, 1030, and 940 cm^{-1}; NMR ($CDCl_3$) δ 1.05 (3H, s), 1.15 (3H, s), 2.42 (1H, OH), 3.43 (1H, dd, J=9.9 and 6.0), 4.07 (2H, s), 4.20 (1H, m), 5.43 (1H, br s), and 5.96 (1H, br s). Found: *m/e* 250 (M^+).

*1-(4,4-Dimethyl-2-oxocyclopentyl)-5-methylene-3-oxabicyclo-[4.2.0]octan-4-one (**38**).* The hydroxy lactone **37a** (90 mg) was oxidized with Jones reagent[23] in the standard way to afford **38a** (81 mg, 91%). Similarly, isomeric **38b** (74 mg, 90%) was obtained from **37b** (81 mg). The analytical samples were purified by preparative TLC (1:1 petroleum ether–ether) and by distillation, bp 130—140 °C/0.1 Torr. Isomer **38a** had IR ($CHCl_3$) 1730, 1725, 1640, 1625, 1140, 1040, and 950 cm^{-1}; NMR (CCl_4) δ 1.06 (3H, s), 1.23 (3H, s), 3.10 (1H, br s), 3.94 and 4.38 (1H each, AB type q, J=11.0), 5.26 (1H, br s), and 5.83 (1H, br s). Found: C, 72.77; H, 7.99%. Calcd for $C_{15}H_{20}O_3$: C, 72.55; H, 8.12%. Isomer **38b** had IR ($CHCl_3$) 1740, 1730, 1640, 1625, 1140, 1042, and 950 cm^{-1}; NMR (CCl_4) δ 1.03 (3H, s), 1.10 (3H, s), *ca.* 3.90 [total 3H, br, two singlets of 2H and 1H (centered at *ca.* 3.80) were overlapped], 5.30 (1H, br s), and 5.90 (1H, br s). Found: C, 72.47; H, 7.77%.

A solution of **38b** (50 mg, 0.2 mmol) in a mixture of dioxane (1 ml), methanol (2 ml), and water (2 ml) containing potassium hydroxide (56 mg, 1 mmol, 5 equiv) was left at room temperature overnight. Work-up and the subsequent lactonization of the acidic product (52 mg) in the same way as described in the preceding experiment gave a *ca.* 2:1 mixture of **38a** and **38b** [total product (50 mg) isolated by passing through a short column of silica gel with the aid of ether] as determined by the NMR spectrum.

*1-[4,4-Dimethyl-2-(tetrahydropyranyloxy)cyclopentyl]-5-methylene-3-oxabicyclo[4.2.0]octan-4-one (**40**).* A solution of **37a** (59 mg, 0.23 mmol), dihydropyrane (21 mg, 0.28 mmol), fused *p*-toluenesulfonic acid (a catalytic amount) in CH_2Cl_2 (2 ml) was stirred at 0 °C for 1 h. After addition of a few drops of pyridine, the usual work-up and purification by chromatography on silica gel with ether gave **40** (70 mg, 92%): IR ($CHCl_3$) 1720, 1630, 1150, 1130, and 1028 cm^{-1}; NMR (CCl_4) δ 1.07 and 1.12 (total 6H, each s), 4.47 (1H), 5.27 (1H, br s), and 5.83 (1H, br s). Found: *m/e* 334 (M^+). Calcd for $C_{20}H_{30}O_4$: M 334.

*(±)-Dihydrofomannosin Acetate (**3**).* To a solution of **40** (180 mg, 0.53 mmol) and pyridine (536 mg, 6.5 mmol) in ether (3 ml) was added dropwise a solution of osmium tetraoxide (165 mg, 0.65 mmol) in ether (1.5 ml) at 0 °C under nitrogen,[24] and the reaction mixture was stirred at room temperature overnight. Pyridine (2.5 ml) and then an aqueous solution of sodium hydrogensulfite (270 mg in 3.5 ml) were added to the stirred mixture at 0 °C, and the stirring was continued at room temperature for 1 h. Water was added, and the product was thoroughly extracted with a 1:2:1 mixture of $CHCl_3$–ether–ethyl acetate. The combined extracts were successively washed with dilute sulfuric acid, water, and brine, and dried. The solvent was evaporated to leave the diol **41** (225 mg): IR ($CHCl_3$) 3500—3200 and 1720 cm^{-1}; NMR ($CDCl_3$) δ 1.03 and 1.11 (total 6H, each s).

This crude diol **41**, without further purification, was dissolved in a mixture of acetic anhydride (0.6 ml) and pyridine (1 ml) at 0 °C, and the mixture was allowed to stand at the same temperature for 1 h. The usual work-up and purification by preparative TLC (2:3 petroleum ether–ether) gave 5-acetoxymethyl-5-hydroxy-1-[4,4-dimethyl-2-(tetrahydropyranyloxy)cyclopentyl]-3-oxabicyclo[4.2.0]octan-4-one (**42**) (148 mg, 68%) as a mixture of stereoisomers:

IR ($CHCl_3$) 3300 and 1735 cm^{-1}; NMR ($CDCl_3$) δ 1.03 and 1.12 (total 6H, each s), 2.10 (3H, s), and 3.20—5.50 (9H). Found: *m/e* 410 (M^+). Calcd for $C_{22}H_{34}O_7$: M 410.

To a solution of **42** (144 mg, 0.35 mmol) and triethylamine (54 mg, 0.53 mmol) in CH_2Cl_2 (2 ml) was added dropwise a solution of methanesulfonyl chloride (48 mg, 0.42 mmol) in CH_2Cl_2 (1 ml) at 0 °C, and the reaction mixture was stirred at 0 °C for 45 min. The mixture was poured into ice–water, and the water layer was extracted with a 2:1:1 mixture of ether–CH_2Cl_2–ethyl acetate. The combined organic layers were washed with water and brine, and dried. Removal of the solvent gave the unstable mesylate **45** (180 mg, quantitative): IR ($CHCl_3$) 1740 cm^{-1}; NMR ($CDCl_3$) δ 1.10 and 1.17 (total 6H), 2.13 (3H, s), and 3.17 (3H, s).

A mixture of **45** (187 mg, 0.38 mmol), lithium chloride (160 mg), and lithium carbonate (112 mg) in DMF (3.5 ml)[25] was heated with stirring at 110 °C for 1 h and then at 160 °C for 2 h. After cooling, the reaction mixture was poured into ice–water and acidified with dilute sulfuric acid, and the product was extracted with a 1:1 mixture of ether–ethyl acetate. The extracts were washed with water and brine, and dried. Removal of the solvent left an oily **46** (128 mg), which was immediately dissolved in acetone and treated with Jones reagene at 0 °C by the standard procedure. The reaction mixture was diluted with water and extracted with a 1:1 mixture of ether–ethyl acetate. The combined extracts were washed with water and brine, dried, and evaporated to dryness. Preparative TLC (4:6 petroleum ether–ether) of the residue gave (±)-**3** (23 mg, 20%): mp 102—103 °C. The IR, NMR, and mass spectra and chromatographic behavior were identical with those of the authentic sample, which was prepared by acetylation of dihydrofomannosin (2 mg), derived from natural fomannosin, with acetic anhydride (0.1 ml) and pyridine (0.1 ml) at room temperature for 4 h.

*Deoxydihydrofomannosin (**50a**) and the Stereoisomer (**50b**).* To a solution of **35** (413 mg, 1.04 mmol) in anhydrous ether (10 ml) was added dropwise a solution of methyllithium in ether (1.5 ml of 1.0 M solution, 1.5 mmol) at −60 °C under nitrogen. The reaction mixture was stirred at −60 °C for 1 h and the reaction was quenched by the addition of a saturated aqueous solution of ammonium chloride. After the usual work-up, the crude product **47** (400 mg) was dissolved in dilute methanol (75%, 4 ml) containing potassium hydroxide (290 mg), and the resulting solution was heated at 68—70 °C for 2 h. Acidification with 4 M sulfuric acid to pH 1—2 and the usual work-up gave an acidic product (280 mg). A solution of this product in benzene (10 ml) containing a catalytic amount of fused *p*-toluenesulfonic acid was heated under reflux for 2 h. The solution was diluted with ether and washed with an aqueous solution of sodium hydrogencarbonate, water, and brine. Evaporation of the solvent left the dihydroxy lactone **48** (243 mg): IR ($CHCl_3$) 3580, 3500, 1730, and 1160 cm^{-1}.

The total crude **48** was oxidized with Jones reagent by the standard procedure gave the hydroxy keto lactone **49** (240 mg). An analytical sample was purified by preparative TLC (1:3 petroleum ether–ether) and then by distillation: bp 160—170 °C/0.05 Torr; IR ($CHCl_3$) 3520, 1735, 1160, 1140, and 1035 cm^{-1}; NMR ($CDCl_3$) δ 1.03 and 1.10 (total 3H), 1.25 and 1.27 (total 3H), 1.42 and 1.46 (total 3H), 3.65 (1H, OH), and 4.00 (d, J=12.0), 4.25 (d, J=12.0), 4.57 (d, J=12.0), and 4.68 (d, J=12.0) [total 2H, two pairs of AB type q]. Found: C, 67.44; H, 8.45%; *m/e* 266 (M^+). Calcd for $C_{15}H_{22}O_4$: C, 67.64; H, 8.86%, M 266.

Thionyl chloride (0.2 ml) was added to a solution of **49** (227 mg) in pyridine (2 ml) and the reaction mixture was heated at 60 °C for 1 h. The usual work-up gave an inseparable stereoisomeric mixture (*ca.* 1:1) of **50** (171 mg, 81%). An analytical sample was purified by preparative TLC (1:2 petroleum ether–ether) and then by distillation: bp 130—140 °C/0.05 Torr; IR ($CHCl_3$) 1730 and 1030 cm^{-1}; NMR (CCl_4) δ 1.10 and 1.12 (total 3H, each s), 1.25 (3H, s), 1.72 (3H, br. s), and 4.10 and 4.72 (a pair of AB type q, J=10.5, isomer **50a**) and 4.10 (s, isomer **50b**) [total 2H]. Found: C, 72.35; H, 8.05%. Calcd for $C_{15}H_{20}O_3$: C, 72.55; H, 8.12%.

We are grateful to Dr. J. K. Kepler, Research Triangle Institute, for the supply of dihydrofomannosin derived from natural fomannosin. This work was supported by a Grant-in-Aid for Encouragement of Young Scientist No. 974158 (for HK) and a Grant-in-Aid for Scientific Research No. 147028 (for HU) from the Ministry of Education.

References

1) Preliminary report, H. Kosugi and H. Uda, *Chem. Lett.*, **1977**, 1491.

2) J. A. Kepler, M. E. Wall, J. E. Mason, C. Basset, A. T. McPhail, and G. A. Sim, *J. Am. Chem. Soc.*, **89**, 1260 (1967); A. T. McPhail and G. A. Sim, *J. Chem. Soc., B*, **1968**, 1104.

3) S. Nozoe, H. Matsumoto, and S. Urano, *Tetrahedron Lett.*, **1971**, 3125.

4) C. Basset, R. T. Sherwood, J. A. Kepler, and P. B. Hamilton, *Phytopathology*, **57**, 1046 (1967).

5) D. E. Cane, R. B. Nachbar, J. Clardy, and J. Finer, *Tetrahedron Lett.*, **1977**, 4277.

6) H. Kosugi, S. Sekiguchi, R. Sekita, and H. Uda, *Bull. Chem. Soc. Jpn.*, **49**, 520 (1976).

7) For the first synthesis of the fomannosin skeleton, see K. Miyano, Y. Ohfune, S. Azuma, and T. Matsumoto, *Tetrahedron Lett.*, **1974**, 1545.

8) P. A. Plattner and H. Heusser, *Helv. Chim. Acta*, **28**, 1044 (1945); F. Weygand and H. J. Bestmann, "Newer Methods of Preparative Organic Chemistry," ed by W. Foerst, Academic Press, New York and London (1964), Vol. III, p. 499.

9) B. M. Trost and T. N. Salzmann, *J. Am. Chem. Soc.*, **95**, 6840 (1973); B. M. Trost, T. N. Salzmann, and K. Hiroi, *ibid.*, **98**, 4887 (1976).

10) a) K. Iwai, H. Kosugi, and H. Uda, *Chem. Lett.*, **1975**, 981; K. Iwai, H. Kosugi, H. Uda, and M. Kawai, *Bull. Chem. Soc. Jpn.*, **50**, 242 (1977); b) M. Watanabe, K. Shirai, and T. Kumamoto, *Chem. Lett.*, **1975**, 855.

11) R. A. Ellison, W. D. Woessner, and C. C. Williams, *J. Org. Chem.*, **37**, 2757 (1972); **39**, 1430 (1974); W. D. Woessner, *Chem. Lett.*, **1976**, 43.

12) For an alternative route for the synthesis of an α-methylene-δ-lactone unit from a γ-lactone using aldehyde equivalent agents ($CH_3SOCH_2^-$ or $PhS\overline{C}HOCH_3$), *cf.* B. M. Trost and C. H. Miller, *J. Am. Chem. Soc.*, **97**, 7182, (1975).

13) For the Wittig reaction of glyoxylates, see R. Raap, C. G. Chin, and R. G. Micetich, *Can. J. Chem.*, **49**, 2143 (1971).

14) For the sake of convenience, the numbering in references 5 and 15 was employed.

15) D. E. Cane and R. B. Nachbar, *J. Am. Chem. Soc.*, **100**, 3208 (1978).

16) The absolute configuration of both fomannosin and dihydrofomannosin was established as 7*S*,9*R*. The opposite designation at C-7 is due to the unsaturation at C-4.
17) The AB type quartet pattern of the lactonic methylene protons was also observed in natural fomannosin and dihydrofomannosin.[2)]
18) A. Schönberg, "Preparative Organic Photochemistry," Springer-Verlag, Berlin (1968), p. 373.
19) C. S. F. Tang, C. J. Morrow, and H. Rapoport, *J. Am. Chem. Soc.*, **97**, 159 (1975).
20) R. N. Chakravarti, *J. Chem. Soc.*, **1947**, 1028.
21) G. A. Hiegel and P. Burk, *J. Org. Chem.*, **38**, 3637 (1973). Methyllithium was employed instead of methylmagnesium iodide.
22) R. Greenwald, M. Chaykovsky, and E. J. Corey, *J. Org. Chem.*, **28**, 1128 (1963).
23) K. Bowden, I. M. Heilbron, E. R. H. Jones, and B. C. L. Weedon, *J. Chem. Soc.*, **1946**, 39; A. Bowers, T. G. Halsall, E. R. H. Jones, and A. J. Lemin, *ibid.*, **1953**, 2548.
24) E. J. Corey, M. Ohno, R. B. Mitra, and P. A. Vatakencherry, *J. Am. Chem. Soc.*, **86**, 478 (1964).
25) L. F. Fieser and M. Fieser, "Reagents for Organic Synthesis," John Wiley and Sons, Inc., New York, N. Y. (1967), p. 606.

Abnormal Nazarov Reaction. A New Synthetic Approach to 2,3-Disubstituted 2-Cyclopentenones

Shigeo HIRANO, Seiji TAKAGI, Tamejiro HIYAMA,* and Hitosi NOZAKI
Department of Industrial Chemistry, Kyoto University, Yoshida, Kyoto 606
(Received July 3, 1979)

Acid-catalyzed reaction of β,β′-disubstituted cross conjugated dienones or the corresponding ethylene acetals gives mainly 2,3-disubstituted 2-cyclopentenones in stead of the simple Nazarov cyclization products, 3,4-disubstituted 2-cyclopentenones. This transformation is explained in terms of electrocyclic ring-closure, addition of hydroxylic solvent(s), tautomerization of the resulting 2-hydroxycyclopentanone intermediates, followed by solvolysis and isomerization. Based on this working hypothesis a new route to jasmonoids is disclosed which involves acid-treatment of the acyloin disilyl ethers derived from substituted glutarates.

Conjugated cyclopentenones[1] are the key compounds for the synthesis of natural products such as jasmonoids,[2] prostanoids,[3] and muscone[4] as well as of [*n*]-metacyclophanes.[5] Among various kinds of approach[1] to 2-cyclopentenones the Nazarov reaction[6] seemed attractive with respect to its simple operation, ready availability of the starting material and also to the mechanistic view point. We have studied the acid-catalyzed cyclization of β,β′-disubstituted cross-conjugated dienones or their ethylene acetals and observed the cyclization accompanied by transposition of the carbonyl group.[7] This unusual Nazarov reaction led us to explore an additional route to 2,3-disubstituted 2-cyclopentenones from 2-hydroxycyclopentanones or their enol disilyl ethers.

Acid-catalyzed Cyclization of Cross-conjugated Dienones ***1*** *or Their Ethylene Acetals* ***2*** *to 2-Cyclopentenones* ***3***. The starting dienones **1a**, **1b**, **1d** were prepared by usual hydrolysis of the corresponding ethylene acetals **2**[8] obtained by dibromination[9] and duplicated dehydrobromination of the saturated ketone acetals. Upon exposure to acidic conditions either **1** or **2**[10] afforded 2,3-dialkyl-2-cyclopentenones **3** in good yield (Scheme 1). Two acid systems, namely (A) phosphoric acid–formic acid (1:1) and (B) hydrobromic acid–acetic acid (1:3), were studied and the results are summarized in Table 1. Depending on the conditions and the substrates the Nazarov products, 3,4-dialkyl-2-cyclopentenones **4**, were produced to some extent, whose formation is understood by deprotonation of the oxyallyl cation **6** (Scheme 2) which is derived from the oxypentadienyl cation **5**[11] by electrocyclic conrotatory ring closure. The formal "shift" of the carbonyl group in the production of **3** is rationalized by assuming the attack of the hydroxylic solvents, such as water or carboxylic acids, onto **6** to yield **7**, which is subsequently converted to acyloin (and/or equivalents) **8** by tautomerization. Elimination of hydroxyl group

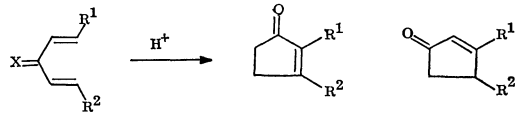

1, X=O
2, X=OCH_2CH_2O

3 **4**

a, $R^1=R^2=Et$
b, $R^1=R^2=-(CH_2)_7-$
c, $R^1=R^2=-(CH_2)_5-$
d, $R^1=n\text{-}C_5H_{11}$, $R^2=H$

Scheme 1.

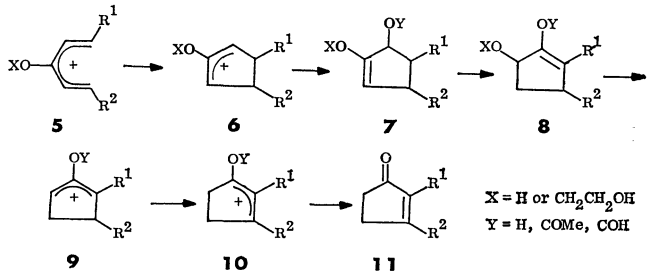

5 **6** **7** **8**

9 **10** **11**

X = H or CH_2CH_2OH
Y = H, COMe, COH

Scheme 2.

Table 1. 2-Cyclopentenones *via* acid-catalyzed cyclization of cross-conjugated dienones and the corresponding ethylene acetals

Starting material	Procedure[a]	Product (yield/%)[b]	
		3a	**4a**
1a (X = O)	A	77	-
	B	55 (41)[c]	15 (11)[c]
2a (X = OCH_2CH_2O)	A	67	-
	B	43	9
		3b	**4b**
1b (X = O)	B	41[c]	5[c]
2b (X = OCH_2CH_2O)	A	67 (63)[c]	-
	B	55	6
		3c	**4c**
2c (X = OCH_2CH_2O)	A	58	6
	B	47	37
		3d	**4d**
1d (X = O)	A[d]	18	2
2d (X = OCH_2CH_2O)	A	14	1

a) Details are in the experimental part. b) Estimated by GLC unless otherwise stated. c) Isolation yield. d) Treatment of **1d** with phosphoric acid gave **3d** (22%) and **4d** (13%).

and isomerization of the resulting oxyallyl cation **9** afford the most stable one **10**, deprotonation of which should give **3**. The driving force of this cyclopentenone formation is ascribed to the thermal cyclization of pentadienyl cation **5** to cyclopentenyl cation **6** and the subsequent isomerization to the most stable allylic cation **10**. Notably, when the reaction was carried out in less nucleophilic solvent or procedure B, the yield of the by-product **4** increased considerably. Hereby deprotonation of **6** is probably competing with the solvent attack. Previous study on the Nazarov reaction[6] has dealt only with α,β-disubstituted cross-conjugated dienone system wherein the cyclized form **6** is easily deprotonated to give a thermodynamically most favorable dienone of type **4**. The β,β'-disubstituted dienones studied here appear to have never been subjected to the acidic conditions before.[12] The proposed mechanism has been confirmed by the regioselective dehydration of alternatively synthesized **8** affording **3** as described below.

Regioselective Synthesis of 2-Cyclopentenones **3** via *Acid-catalyzed Dehydration of 2-Hydroxycyclopentanones.* In general, acyloins are hardly dehydrated to the corresponding α,β-enones. However, the proposed mechanism shown in Scheme 2 involves dehydration of the acyloin (and/or equivalents) **8**. In order to verify this 2,3-dialkylglutarates **11** were transformed to enediol disilyl ethers **12**, which were exposed to phosphoric acid. Both hydrolysis and dehydration[14] took place in one pot to give 2,3-dialkyl-2-cyclopentenones **3**. The results are summarized in Table 2. Disilyl ethers **12d** and **12e** were preferentially transformed to **3d** and **3e** respectively and their regioisomers **4d**, **4e**, were not isolated (entry 1, 2). This process gives dihydrojasmone (**3f**) in good yields. The substrates having olefinic appendage turned out rather unstable under these conditions and gave allethrone (**3g**) and *cis*-jasmone (**3h**) in somewhat lower yields.[15]

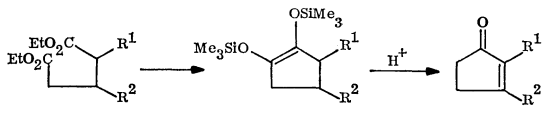

11 **12** **3**

d: $R^1=n$-C_5H_{11}, $R^2=H$
e: $R^1=Me$, $R^2=H$
f: $R^1=n$-C_5H_{11}, $R^2=Me$
g: $R^1=CH_2=CHCH_2$, $R^2=Me$
h: $R^1=cis$-2-pentenyl, $R^2=Me$

Scheme 3.

Experimental

All the temperatures are uncorrected. PMR spectra were taken on a JEOL JNM-PMX 60 or Varian EM 390 spectrometer and chemical shifts are recorded in ppm unit. IR spectra were recorded on a Shimadzu IR-27G spectrometer, and MS on a Hitachi RMU-6L spectrometer with 70 eV.

Dibromination of Ketone Ethylene Acetals. A General Procedure. Bromine (100 mmol) was added dropwise to a solution of the saturated ketone acetal (50 mmol) in dry ether (100 ml) under cooling with water bath. The mixture was neutralized with monosodium ethylene glycolate (prepared from sodium (2.5 g) and ethylene glycol (100 ml)) and worked up as usual. The yield and physical properties of α,α'-dibromo ketone ethylene acetals are given in the following order: R^1, R^2 of $R^1CHBrC(O_2C_2H_2)CHBrCH_2R^2$, yield(%), bp or mp, IR, PMR, elemental analysis. $R^1=R^2=Et$ (see Ref. 9). R^1, $R^2=-(CH_2)_7-$, 99%, mp 133—134 °C (ethyl acetate), IR (Nujol): 1185, 1047, 957 cm^{-1}, PMR ($CDCl_3$): δ 1.1—2.2 (m, 18H), 4.35 (s, 4H), 4.48 (t, 2H), (Found: C, 43.8; H, 6.4%. Calcd for $C_{14}H_{24}Br_2O_2$: C, 43.8; H, 6.3%). R^1, $R^2=-(CH_2)_5-$, 100%, mp 76—77.5 °C (ethyl acetate), IR (Nujol): 1045, 949 cm^{-1}, PMR ($CDCl_3$): 1.3—1.9 (m, 10H), 2.0—2.5 (m, 4H), 4.4 (s, 4H), 4.70 (t, $J=6$ Hz, 2H), (Found: C, 40.3; H, 5.7%. Calcd for $C_{12}H_{20}Br_2O_2$: C; 40.5; H, 5.7%). $R^1=n$-C_5H_{11}, $R^2=H$, *ca.* 96%, bp 135 °C/0.08 Torr, IR (neat): 1198, 1076, 954 cm^{-1}, PMR (CCl_4): 0.7—1.1 (m, 3H), 1.70 (d, $J=6.5$ Hz, 3H), 1.1—2.0 (m, 10H), 4.25 (s, 4H), 4.0—4.7 (m, 2H), (Found: C, 40.0; H, 6.5%. Calcd for $C_{12}H_{22}Br_2O_2$: C, 40.3; H, 6.2%).

Cross-conjugated Dienone Ethylene Acetals **2**. A solution of α,α'-dibromo acetal (30 mmol) dissolved in dry DMSO (120 ml) was admixed with finely powdered potassium *t*-butoxide (100 mmol) and the mixture stirred for 3 h at room temperature for acyclic bromides or at 50 °C for cyclic ones. The resulting dark-brown mixture was treated with water (200 ml) and the product extracted with benzene. Product, yield (%) were as follows: **2a**, 88; **2b**, 97; **2c**, 91; **2d**, 85 (based on the acetal). Physical properties of these are listed in Table 3.

Cross-conjugated Dienones **1**. Dienone acetal **2** (5 mmol) dissolved in THF (30 ml) was vigorously shaken with 10% sulfuric acid at room temperature for 2 h. The resulting mixture was saturated with sodium chloride and the product was extracted with ether. Product, yield (%): **1a**, 97; **1b**, 96; **1d**, 62. Physical properties are summarized in Table 3.

Acid-catalyzed Cyclization of Cross-conjugated Dienones **1** *or Their Ethylene Acetals* **2** *into 2-Cyclopentenones* **3**. *Procedure A*: A mixture of dienone **1** or its ethylene acetal **2** (1.0 mmol), 85% phosphoric acid (2.5 ml), and 90% formic acid (2.5 ml) was stirred at 90 °C for 2—3 h under a nitrogen atmosphere. The resulting brown solution was quenched with water (15 ml) and stirred for additional 0.5 h. After extraction with benzene the extract was washed with water, aq sodium hydrogencarbonate solution and brine, then dried over sodium sulfate. Preparative TLC on silica gel or GLC (SE 30 or Dowfax 9N9 on Chromosorb) gave pure **3** and **4** (Table 1). The structural assignment is based upon either comparison with the respective authentic samples or spectrometric analysis (see Table 4).

TABLE 2. 2-CYCLOPENTENONES *via* DEHYDRATION OF 2-HYDROXYCYCLOPENTANONE DERIVATIVES

Entry	Glutarate	2-Hydroxycyclopentanone enol disilyl ether Yield/%[a]	2-Cyclopentenone Yield/%[a]
1	**11d**	**12d**, 80	**3d**, 64
2	**11e**	**12e**, 87	**3e**, 73[b]
3	**11f**	**12f**, 85	**3f**, 74
4	**11g**	**12g**, 81	**3g**, 46
5	**11h**	**12h**, 81	**3h**, 39[c]

a) Isolation yield. b) The dehydration was carried out by simple distillation. c) This was prepared by the acid hydrolysis and the subsequent treatment of the resulting acyloin with *p*-toluenesulfonic acid in *N,N*-dimethylformamide at 60 °C for 20 h.

Table 3. Physical properties of dienones **1** and their ethylene acetals **2**

Compound	Bp (°C/Torr)	IR (cm^{-1})[a]	PMR (δ)[b]
1a[c]	100/14	1669, 1640, 1617 1199, 980	1.12 (t, J=7 Hz, 6H), 2.27 (td, J=7, 1 Hz, 4H), 6.22 (dt, J=15, 1 Hz, 2H), 6.88 (dt, J=15, 6 Hz, 2H)
1b[d]	110/0.4	1657, 1224, 992 744	0.9—1.9 (m, 10H), 1.9—2.7 (m, 4H), 5.45—6.37 (m, 2H), 6.13 (dd, J=16, *ca.* 1 Hz, 1H), 6.89 (dt, J=16, 6.5 Hz, 2H)
1d[e]	80/3.5	1668, 1635, 1614 1216, 986	0.7—1.1 (m, 3H), 1.1—1.7 (m, 6H), 2.2—2.5 (m, 2H), 5.6—7.1 (m, 5H)
2a[f]	95/13	1671, 1037, 968	1.0 (t, J=6.5 Hz, 6H), 1.6—2.35 (m, 4H), 3.65 (s, 4H), 4.8—5.7 (m, 4H)
2b[g]	125/5	3024, 1036, 978	1.0—1.8 (m, 10H), 1.8—2.7 (m, 4H) 3.84 (m, 4H), 5.2—6.2 (m, 4H)
2c[h]	150/5	1177, 1043, 979, 729	0.9—2.8 (m, 10H), 3.90 (s, 4H), 5.1—6.1 (m, 4H)
2d[i]	90/5	1672, 1057, 939	0.7—1.1 (m, 3H), 1.0—1.6 (m, 6H), 1.8—2.3 (m, 2H), 3.80 (s, 4H), 5.0—6.0 (m, 5H)

a) Neat liquid film. b) Recorded in CCl_4 solution. c) MS *m/e* (rel intensity): 139 (M^+, 9), 83 (100). Found: C, 78.3; H, 10.0%. Calcd for $C_9H_{14}O$: C, 78.2; H, 10.2%. d) MS *m/e* (rel intensity): 178 (M^+, 12), 107 (100), 81 (98). Found: C, 80.9; H, 9.9%. Calcd for $C_{12}H_{18}O$: C, 80.9; H, 10.2%. e) MS *m/e* (rel intensity): 152 (M^+, 1), 55 (100). Found: C, 78.7; H, 10.4%. Calcd for $C_{10}H_{16}O$: C, 78.9; H, 10.6%. f) MS *m/e* (rel intensity): 182 (M^+, 1), 127 (100), 83 (53). Found: C, 72.4; H, 9.8%. Calcd for $C_{11}H_{18}O_2$: C, 72.5; H, 10.0%. g) MS *m/e* (rel intensity): 222 (M^+, 23), 125 (100), 91 (68). Found: C, 75.8; H, 9.8%. Calcd for $C_{14}H_{22}O_2$: C, 75.6; H, 10.0%. h) MS *m/e* (rel intensity): 194 (M^+, 25), 125 (81), 112 (100). Found: C, 74.1; H, 9.4%. Calcd for $C_{12}H_{18}O_2$: C, 74.2; H, 9.3%. i) MS *m/e* (rel intensity): 196 (M^+, 1), 169 (36), 139 (72), 99 (100). Found: C, 73.6; H, 10.5%. Calcd for $C_{12}H_{20}O_2$: C, 73.4; H, 10.3%.

Table 4. Physical properties of cyclopentenones **3** and **4**

Compound	IR (cm^{-1})[a]	PMR (δ)[b]
3a[c]	1698, 1644, 1175, 936	0.97 (t, J=7.5 Hz, 3H), 1.15 (t, J=7.5 Hz, 3H), 1.9—2.7 (m, 8H)
3b[d]	1696, 1646, 1298, 1155 1070	1.2—2.0 (m, 10H), 2.0—2.7 (m, 8H)
3c[e]	1695, 1646, 1286, 1064 990, 816	1.3—2.1 (m, 6H), 2.1—2.7 (m, 8H)
3d[f]	1705, 1633, 1000, 788	0.7—1.1 (t, 3H), 1.0—1.8 (m, 6H), 1.8—2.7 (m, 6H), 7.15 (br s, 1H)
3e[g]	1702, 1640, 1067, 791	1.74 (m, 3H), 2.1—2.7 (m, 4H), 7.3 (m, 1H)
3f[h]	1701, 1640, 1178, 1075	0.90 (t, 3H), 1.0—1.8 (m, 6H), 1.9—2.6 (m+s (δ 2.03), 9H)
3g[i]	1695, 1640	2.00 (s, 3H), 2.1—2.6 (m, 4H), 2.90 (d, J=6.5 Hz, 2H), 4.7—5.1 (m, 2H), 5.3—6.0 (m, 1H)
3h[j]	1700, 1647, 1177, 1070	0.98 (t, J=7.0 Hz, 3H), 2.03 (s, 3H), 1.9—2.65 (m, 6H), 2.85 (d, 2H), 4.9—5.55 (m, 2H)
4a[k]	1685, 1613, 858[l]	0.7—1.4 (m, 6H), 1.5—2.9 (m, 7H), 5.9 (m, 1H)
4b[m]	1682, 1610, 854[l]	1.1—2.0 (m, 12H), 2.0—3.1 (m, 5H), 5.95 (br s, 1H)
4c[n]	1680, 1603, 910,[l] 853	1.1—2.3 (m, 18H), 2.3—3.1 (m, 5H), 5.80 (br s, 1H)
4d[o]	1707, 1677, 1616, 1181 864, 840	0.7—1.1 (m, 3H, 3H), 1.1—1.7 (m, 6H), 2.1—2.7 (m, 6H), 5.8 (m, 1H)

a) Neat liquid film unless otherwise stated. b) Recorded in CCl_4 solution. c) MS *m/e* (rel intensity): 138 (M^+, 100), 123 (69), 109 (74), 95 (38), 81 (72). Found: C, 77.9; H, 10.0%. Calcd for $C_9H_{14}O$: C, 78.2; H, 10.2%. d) Bp 95 °C/2 Torr, MS *m/e* (rel intensity): 178 (M^+, 51), 149 (33), 135 (100); see Ref. 5. e) Bp 104 °C/4 Torr; MS *m/e* (rel intensity): 150 (M^+, 73), 122 (100), 79 (52). Found: C, 79.8; H, 9.3%. Calcd for $C_{10}H_{14}O$; C, 80.0; H, 9.4%. f) Bp 115 °C/3.5 Torr; MS *m/e* (rel intensity): 152 (M^+, 65), 123 (88), 97 (100), see Ref. 2d. g) Bp 135 °C/95 Torr; MS *m/e* (rel intensity): 96 (M^+, 96), 67 (100), see Ref. 11d. h) MS *m/e* (rel intensity): 166 (M^+, 16), 151 (57), 110 (100), see Ref. 2. i) MS *m/e* (rel intensity): 136 (M^+, 100), 121 (88), see Ref. 2d. j) MS *m/e* (rel intensity): 164 (M^+, 67), 149 (52), 110 (59), 79 (73), 55 (100), see Refs. 2a—d. k) MS *m/e* (rel intensity): 138 (M^+, 35), 110 (100), 95 (53). Found: C, 78.3; H, 10.0%. Calcd for $C_9H_{14}O$: C, 78.2; H, 10.2%. l) Determined in $CHCl_3$. m) Bp 150 °C/5 Torr; MS *m/e* (rel intensity): 178 (M^+, 72), 135 (84), 79 (100). Found: C, 80.7; H, 10.0%. Calcd for $C_{12}H_{18}O$: C, 80.9; H, 10.2%. n) MS *m/e* (rel intensity): 150 (M^+, 100), 107 (94). Found: C, 79.7; H, 9.2%. Calcd for $C_{10}H_{14}O$: C, 80.0; H, 9.4%. o) MS *m/e* (rel intensity): 152 (M^+, 24), 96 (100), see P. M. McCurry, Jr., and R. K. Singh, *J. Org. Chem.*, **39**, 2317 (1974).

TABLE 5. PHYSYCAL PROPERTIES OF GLUTARATES **11** AND 1,2-BIS(TRIMETHYLSILYLOXY)CYCLOPENTENES **12**

Compound	Bp (°C/Torr)	IR (cm^{-1})[a]	PMR (δ)[b]
11c	78—80/0.009	1732	0.85 (t, 3H), 0.92 (t, J=6.5 Hz, 6H), 1.0—2.4 (m, 13H), 4.00 (q, J=6.5 Hz, 4H)
11f[d]	140—145/0.2	1736, 1177, 1030	1.27 (t, J=7 Hz, 6H), 0.7—2.5 (m, 18H), 4.08 (q, J=7 Hz, 4H)
11g[e]	145/20	1735, 1643	0.95 (m, 3H), 1.25 (t, J=7 Hz, 6H), 1.8—2.6 (m, 6H), 4.10 (q, J=7 Hz, 4H), 4.8—5.3 (m, 2H), 5.3—6.1 (m, 1H)
11h[f]	115—120/0.07	1737, 1176, 1095 1030	0.9—1.1 (m+t (δ 0.96, J=7.5 Hz), 6H), 1.25 (t, J=7 Hz, 6H), 1.3—2.7 (m, 8H), 4.10 (q, J=7 Hz, 4H), 4.8—5.6 (m, 2H)
12d[g]	95—120/0.15	1702, 1250, 840	0.10 (s, 18H), 0.90 (t, 3H), 1.1—1.9 (m, 10H), 2.0—2.5 (m, 3H)
12e[h]	108/25	1700, 1249, 840	0.15 (s, 18H), 0.95 (d, J=6 Hz, 3H), 1.0—1.4 (m, 1H), 1.8—2.5 (m, 4H)
12f[i]	120/0.2	1704, 1252, 914 843, 754	0.15 (s, 18H), 0.7—2.7 (m, 18H, main peaks at δ 2.2, 1.8, 1.3, 1.1, 0.97, 0.90)
12g[j]	75/4	1697, 1635	0.15 (s, 18H), 1.0 (m, 3H), 1.4—2.8 (m, 6H), 4.8—5.3 m, 2H), 5.3—6.1 (m, 1H)
12h[k]	115—120/0.07	3007, 1703, 1251 841, 753	0.15 (s, 18H), 0.7—2.9 (m, 14H), 5.2—5.7 (m, 2H)

a) Neat liquid film. b) Recorded in carbon tetrachloride solution. c) MS *m/e* 213 (M^+—OEt). Found: C, 64.9; H, 10.2%. Calcd for $C_{14}H_{26}O_4$: C, 65.1; H, 10.1%. d) MS *m/e* (rel intensity): 227 (M^+—OEt, 35), 69 (100). Found: C, 66.0; H, 10.4%. Calcd for $C_{15}H_{28}O_4$: C, 66.1; H, 10.4%. e) MS *m/e* 197 (M^+—OEt). Found: C, 64.2; H, 9.1%. Calcd for $C_{13}H_{22}O_4$: C, 64.4; H, 9.2%. f) MS *m/e* (rel intensity): 225 (M^+—OEt, 46), 196 (80), 109 (100). Found: C, 66.5; H, 9.9%. Calcd for $C_{15}H_{26}O_4$: C, 66.6; H, 9.7%. g) MS *m/e* (rel intensity): 314 (M^+, 13), 293 (55), 91 (100). h) MS *m/e* 258 (M^+). i) MS *m/e* (rel intensity): 328 (M^+, 18), 257 (100). j) MS *m/e* (rel intensity): 298 (M^+, 6), 256 (79), 73 (100). k) MS *m/e* (rel intensity): 326 (M^+, 11), 257 (100).

Procedure B: Dienone **1** or its ethylene acetal **2** (1.0 mmol) was cyclized by treatment with a mixture of 47% hydrobromic acid (2 ml) and acetic acid (6 ml) at 80—90 °C for 2 to 3 h. Work-up and product analysis were carried out as described above.

*2-Cyclopentenone **3** from 2-Hydroxycyclopentanone Enol Disilyl Ether **12**.* A mixture of acyloin disilyl ether **12** (1.0 mmol) and 57% phosphoric acid (4.5 ml) was stirred at 50—60 °C for 1.5—3 h under a nitrogen atmosphere. Work-up followed by preparative TLC on silica gel gave analytically pure **3** (Tables 2 and 4).

Diethyl 2-Alkyl-2-ethoxycarbonyl-3-methylglutarate. Introduction of Allylic Group: Into a suspension of sodium hydride (22 mmol) in dry 1,2-dimethoxyethane (20 ml) diethyl 2-ethoxycarbonyl-3-methylglutarate[16] (5.48 g, 20 mmol) dissolved in the same solvent (10 ml) was added over a period of 10 min under cooling with a water bath. After 1 h allyl bromide or *cis*-2-pentenyl bromide (22 mmol) was added and the mixture was stirred overnight. Work-up gave the desired products: diethyl 2-allyl-2-ethoxycarbonyl-3-methylglutarate, 79% yield, bp 135 °C/5 Torr; IR (neat): 1739, 1635 cm^{-1}; MS *m/e* 269 (M^+—OEt); (Found: C, 61.1; H, 8.5%. Calcd for $C_{16}H_{26}O_6$: C, 61.1; H, 8.3%); diethyl 2-ethoxycarbonyl-3-methyl-2-(*cis*-2-pentenyl)glutarate, 86% yield, bp 130—135 °C/0.07 Torr, IR (neat): 1739, 1728, 1187, 860 cm^{-1}, MS *m/e* 297 (M^+—OEt). (Found: C, 63.2; H, 9.0%. Calcd for $C_{18}H_{30}O_6$: C, 63.1; H, 8.8%).

Reaction with 1-Iodopentane: The anion of the triester was prepared as above and to the anion solution hexamethylphosphoric triamide (30 ml) and successively 1-iodopentane (22 mmol) were added. Work-up gave diethyl 2-pentyl-2-ethoxycarbonyl-3-methylglutarate in 82% yield. Bp 150—160 °C/0.17 Torr; IR (neat): 1735, 1240, 1218, 1189, 1033 cm^{-1}; MS *m/e* 299 (M^+—OEt). Found: C, 62.6; H, 9.4%. Calcd for $C_{18}H_{32}O_6$: C, 62.8; H, 9.4%.

*Diethyl 2-Alkyl-3-methylglutarate (**11**).* A mixture of the above triester (10 mmol) and aqueous sodium hydroxide (50 mmol in 30 ml of water) was vigorously stirred at 100 °C for 10 h, the resulting clear solution being acidified (pH *ca.* 5) with 4 mol dm^{-3} hydrochloric acid and then subjected to thermal decarboxylation at bath temperature as high as 150—160 °C for 3—4 h under a nitrogen atmosphere. The reaction mixture was treated with 6 mol dm^{-3} hydrochloric acid and the separated free dicarboxylic acid was extracted with ether. The crude acid was esterified by treating with refluxing ethanol (50 ml) and benzene (60 ml) in the presence of a catalytic amount of *p*-toluenesulfonic acid under continuous removal of water with molecular sieves (3A). Product, % yield were as follows: **11f**, 84; **11g**, 85; **11h**, 81%. Physical properties of these are listed in Table 5.

*Diethyl 2-Pentylglutarate (**11d**).* Diethyl pentylmalonate[17] (400 mg, 2.0 mmol) was added to sodium hydride (3 mmol) suspended in dimethoxyethane (4 ml) and the resulting mixture was stirred for 30 min. Ethyl acrylate (300 mg, 3 mmol) dissolved in dimethoxyethane (2 ml) was added and the mixture stirred for an additional 30 min. Work-up followed by distillation afforded the recovered malonate (20 mg) and diethyl 2-pentyl-2-ethoxycarbonylglutarate (501 mg, 76% yield based on the consumed starting malonate), bp 120—122 °C/0.01 Torr, IR (neat): 1712 cm^{-1}. Found: C, 61.8; H, 9.3%. Calcd for $C_{17}H_{30}O_6$: C, 61.8; H, 9.2%. Decarboxylation of the triester to **11d** was performed as described above in 67% yield (see Table 5).

*3,4-Dialkyl-1,2-bis(trimethylsilyloxy)cyclopentene (**12**).* To sodium dispersion (276 mg, 12 mmol) stirred vigorously in dry toluene (25 ml) a mixture of glutarate **11** (2.0 mmol), chlorotrimethylsilane (1.30 g, 12 mmol) and toluene (10 ml) was added dropwise over a period of 20 min at 110 °C under an argon atmosphere. After 30 min the insoluble material was filtered off and solvent was evaporated *in vacuo*. Distillation gave the product listed in Table 5.

References

1) R. A. Ellison, *Synthesis*, **1973**, 397.

2) T. L. Ho, *Synth. Commun.*, **4**, 265 (1974).

3) a) A. Mitra, "The Synthesis of Prostaglandins," John Wiley and Sons, New York (1977); b) W. Bartmann, *Angew. Chem.*, **87**, 14 3(1975); c) P. Crabbé, *Chem. Brit.*, **11**, 132 (1975).

4) a) D. Felix, J. Schreiber, G. Ohloff, and A. Eschenmoser, *Helv. Chim. Acta*, **54**, 2896 (1971); b) R. W. Gray and A. S. Dreiding, *ibid.*, **60**, 1969 (1977).

5) S. Hirano, H. Hara, T. Hiyama, S. Fujita, and H. Nozaki, *Tetrahedron*, **31**, 2219 (1975).

6) a) I. N. Nazarov, I. I. Zaretskaya, and T. I. Sorkina, *Zh. Obshch. Khim.*, **30**, 746 (1960); *Chem. Abstr.*, **55**, 524h (1961); b) E. A. Braude and J. A. Coles, *J. Chem. Soc.*, **1952**, 1430; c) J. -M. Conia and M. L. Leriverend, *Bull. Soc. Chim. Fr.*, **1970**, 2918.

7) For the preliminary report, see S. Hirano, T. Hiyama, and H. Nozaki, *Tetrahedron Lett.*, **1974**, 1429.

8) E. W. Garbisch, Jr., *J. Org. Chem.*, **30**, 2109 (1965).

9) G. Giusti and C. Morales, *Bull. Chem. Soc. Fr.*, **1973**, 382.

10) Acetal **2** rather than dienone **1** is readily available and preferable. Ten-membered cyclic dienone could not be obtained by usual acid hydrolysis of **2c**.

11) a) R. B. Woodward and R. Hoffmann, "The Conservation of Orbital Symmetry," Academic Press, New York, N. Y. (1970), p. 58; b) C. W. Shoppee and B. J. A. Cooke, *J. Chem. Soc. Perkin Trans. 1*, **1972**, 2271. For the cyclization reaction of pentadienyl cations, see c) P. H. Campbell, N. W. K. Deugau, I. J. Miller, and T. S. Sorensen, *J. Am. Chem. Soc.*, **91**, 6404 (1969); d) T. Hiyama, M. Tsukanaka, and H. Nozaki, *ibid.*, **96**, 3713 (1974); e) T. Hiyama, M. Shinoda, and H. Nozaki, *Tetrahedron Lett.*, **1978**, 771; *J. Am. Chem. Soc.*, **101**, 1599 (1979); f) R. M. Jacobson and G. P. Lahm, *J. Org. Chem.*, **44**, 462 (1979). For the photo-induced cyclization reaction of hydroxypentadienyl cations, see R. Noyori, Y. Ohnishi, and M. Kato, *J. Am. Chem. Soc.*, **97**, 928 (1975).

12) Thus we can predict that the acid-catalyzed cyclization of 2,5-heptadien-4-one should afford 2,3-dimethyl-2-cyclopentenone instead of the recorded isomer, 3,4-dimethyl-2-cyclopentenone, see N. Jones and H. T. Taylor, *J. Chem. Soc.*, **1961**, 1345. Actually, a question on the previously assigned structure has been raised, see Ref. 6c.

13) K. Rühlmann, *Synthesis*, **1971**, 236.

14) a) G. P. Pollini, G. de Giuli, G. Traverso, and A. Barco, *Chim. Ind. (Milan)*, **52**, 1205 (1970); b) T. Mukaiyama, S. Kobayashi, K. Kamio, and H. Takei, *Chem. Lett.*, **1972**, 237; c) A. J. Bellamy, *J. Chem. Soc., B*, **1969**, 449; d) T. Wakamatsu, K. Hashimoto, M. Ogura, and Y. Ban, *Synth. Commun.*, **8**, 319 (1978).

15) The relatively low yield of **3g** and **3h** was ascribed to the transient formation of "unstable" exocylic dienone derivatives, which were major products in the reaction of the corresponding acyloins with polyphosphate ester (PPE) (*cf.* L. F. Fieser and M. Fieser, "Reagents for Organic Synthesis," John Wiley and Sons, Inc., New York (1967), p. 892). Allylic olefin isomerization of the resulting conjugated dienones afforded **3g** and **3h** under the acidic conditions, respectively, although considerable resinification had occurred.

16) J. Cason, *Org. Synth.*, Coll. Vol. 4, 630 (1967).

17) R. Adams and R. M. Kamm, *Org. Synth.*, Coll. Vol. 1, 250 (1967).

Regio- and Stereoselective Cross-aldol Reactions *via* Dialkylboryl Triflates

Tan INOUE and Teruaki MUKAIYAMA*

Department of Chemistry, Faculty of Science, The University of Tokyo, Hongo, Bunkyo-ku, Tokyo 113

(Recieved April 25, 1979)

New borylating reagents, (Bu_2BOTf and 9-BBNOTf), were prepared in high yields. The triflates reacted with enolizable ketones in the presence of tertiary amines to generate selectively one of the regioisomers of vinyloxyboranes by the choice of the reagents (the dialkylboryl triflates and tertiary amines) under mild reaction conditions. Vinyloxyboranes thus generated showed remarkable reactivity toward aldehydes to give only one regioisomer of the corresponding cross-aldols in good yields. High stereoselectivity was also observed in these reactions.

Recently, attention is focussed on the cross-aldol reaction, a most useful means of organic synthesis, and various efficient intermediates such as enolates and their equivalents have been worked out.[1] Nevertheless, the methods so far reported are not generally feasible because of difficulties in regio- and stereoselective generation of the enolates from one of carbonyl compounds.

Vinyloxyboranes react easily with various carbonyl compounds to give corresponding β-hydroxy ketones and β-hydroxy esters under mild conditions.[2] Despite the synthetic use of vinyloxyboranes, no general and convenient methods for the direct formation of these key intermediates from ketones was reported until 1976.[3]

We prepared dialkylboryl triflates, a new class of borylation reagents, from borane derivatives and trifluoromethanesulfonic acid. The triflates (trifluoromethanesulfonates) react smoothly with various ketones in the presence of tertiary amines, giving the corresponding vinyloxyboranes. The reactions using these enolates represent new regioselective cross-aldol reactions under mild conditions.[3] In this paper, we wish to report on the extension of our works.

Results and Discussion

Design and Synthesis of Dialkylboryl Triflates. We prepared a new borylation reagent which has potential utility for the formation of vinyloxyboranes with enolizable ketones under mild conditions. Dialkylboryl carboxylates, derivatives of dialkylboric acids, were reported to be easily formed by the reaction of trialkylboranes with carboxylic acids.[4] This promoted us to prepare dialkylboryl triflate which has a better leaving group than dialkylboryl carboxylate by the reaction of equimolar amount of borane derivatives and trifluoromethanesulfonic acid.

$Bu_3B + TfOH \longrightarrow Bu_2BOTf$ 84%

9-BBN + TfOH ⟶ 9-BBNOTf 85%

(9-Borabicyclo[3,3,1]nonane)

Scheme 1.

The reactions proceeded quite smoothly at room temperature, the corresponding dialkylboryl triflates being isolated in high yields by distillation.[5] We attempted to prepare anologous compounds by the combined use of borane derivatives or trialkylaluminum and various sulfonic acids (*e.g.* Bu_3B–$MeSO_3H$, Bu_3B–TsOH, Bu_3B–FSO_3H, Et_3B–TfOH, catecholborane–TfOH, 2,3-dimethylboracyclopentane–TfOH, Et_3Al–TfOH, *i*-Bu_3Al–TfOH). However, the desired boron and aluminum compounds were too unstable to be isolated in pure form for the generation of enolates.

Formation of Vinyloxyboranes from Ketones. 1-Pheny-1-butanone was treated with dibutylboryl triflate in the presence of 2,6-lutidine at room temperature. The NMR spectrum of the reaction mixture showed a signal at δ 5.4 assigned to a vinyl proton of dibutyl (1-phenyl-1-butenyloxy)borane, indicating that tertiary amine promotes the condensation reaction between ketones and dibutylboryl triflate and acts as the proton accepter (Scheme 2).

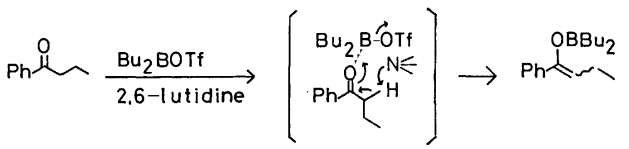

Scheme 2.

This is the first example for the formation of enolate from ketone by the combined use of Lewis acid and Lewis base.

The vinyloxyborane thus generated in situ was allowed to react with 3-phenylpropanal at room temperature for the formation of the cross-aldol (**1**) (Table 1).

Table 1. Effects of amines and solvents on the yield of 1,5-diphenyl-2-ethyl-3-hydroxy-1-pentanone[a]

Amine	Solvent	Yield of **1**/%
2,6-Lutidine	Hexane	83
	Diethyl ether	77
	Tetrachloromethane	70
N,*N*-Diisopropylethylamine	Hexane	74
Tributylamine	Hexane	65
Protonsponge	Hexane	38

a) The reactions were carried out at room temperature overnight.

The combined use of 2,6-lutidine and hexane afforded the corresponding aldol in the highest yield. The reaction conditions were applied to the reactions of cyclic ketones such as cyclopentanone or cyclohexanone with 3-phenylpropanal. However, no corresponding cross-aldols could be obtained in satisfactory yield, presumably because of the self-aldol type reactions of starting ketones. In order to avoid such undesirable side reactions, preparation of the vinyloxyboranes and

Table 2. Synthesis of aldols using dibutylboryl triflate from ketones and aldehydes

	Ketone	Aldehyde	Product (Yield/%)	
4	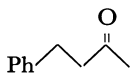	PhCHO	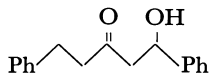 (84)	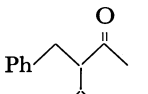 (≈0)
5	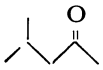	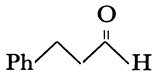	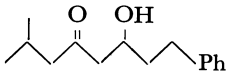 (82)	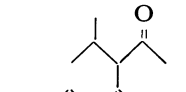 (≈0)
6	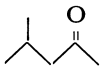	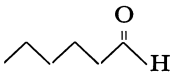	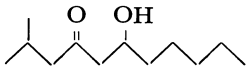 (70)	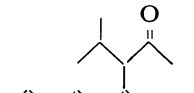 (≈0)
7	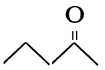	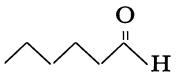	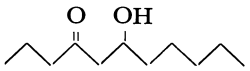 (65)	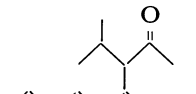 (≈0)

the subsequent reaction with aldehydes were carried out at lower temperature (−78 °C).

This gave better results in the formation of the cross-aldols (Scheme 3).

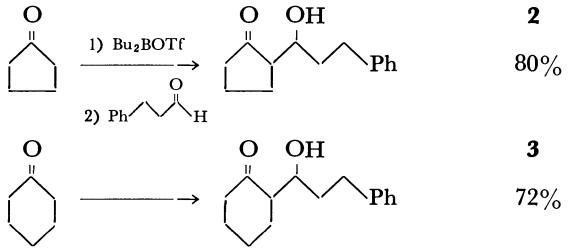

Scheme 3.

Regioselectivity. In order to examine the regioselection of the new method, methyl ketones were allowed to react with aldehydes using dibutylboryl triflate under similar conditions. The results are given in Table 2.

Only one of the regioisomers of cross-aldols was product without being accompanied by detectable amount of the other regioisomers. The results are interpreted by considering vinyloxyboranes to be generated through kinetically controlled steps.

The regioselectivity was examined by changing the combination of the triflates and amines in the reaction of 4-phenyl-2-butanone with benzaldehyde in ether at −78 °C (Table 3).

The results show that the ratio (**A**/**B**) of regioisomers great depends on the properties of the triflates and amines employed. The use of 9-BBNOTf and 2,6-lutidine afforded a remarkably high ratio (**A**/**B**=12/88) in contrast with the ratio of Bu_2BOTf and *N*,*N*-diisopropylethylamine (**A**/**B**=100/0).

Tertiary amines employed in the borylation also affected the yield and selectivity of the produced aldol greatly (Table 4).

Table 3. Ratios of regioisomers of the cross-aldol (**8**) by the combination of triflates and amines[a)]

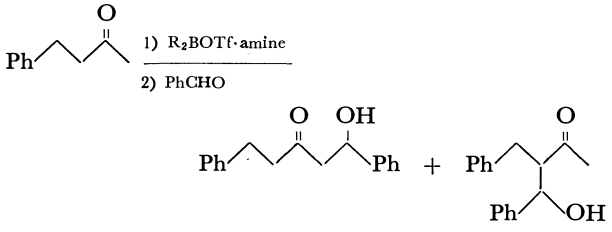

Triflate	Amine	Ratio(**8A**:**8B**)
Bu_2BOTf	*N*,*N*-Diisopropylethylamine	100: 0
	2,6-Lutidine	69:31
9-BBNOTf	*N*,*N*-Diisopropylethylamine	38:62
	2,6-Lutidine	12:88

a) The reaction time for the generation of vinyloxyborane was 15 min and for the subsequent reaction with benzaldehyde 3 h at −78 °C.

Table 4. Ratio of regioisomers by the combination of 9-BBNOTf and amine[a)]

Amine	Temp/°C	Yield/%	Ratio(**8A**:**8B**)
2,6-Lutidine	−78	70	12:88
	−50	44	18:82
Tributylamine	−78	72	19:81
N,*N*-Diisopropylethylamine	−78	73	38:62
2,5-Lutidine	−78	34	56:44
Pyridine	−78	30	36:64

a) Reaction conditions the same as those in Table 3.

It was confirmed that the use of 2,6-lutidine at −78 °C gives a satisfactory yield and the highest ratio. For the formation of vinyloxyborane, the ef-

Table 5. The effect of time on the ratios of the regioisomers by the use of 9-BBNOTf at −78 °C[a)]

Time/h	Yield/%	Ratio(**8A**:**8B**)
0.25	70	12:88
2	80	6:94
3	90	2:98
4	92	1:99
16	96	0:100

a) Reaction conditions the same as those in Table 3.

fect of reaction time was studied in the same reaction (Table 5).

The synthetic yield and selectivity increased with increase in reaction time, complete reverse of selectivity being achieved in a different way from the case in which dibutylboryl triflate was used under kinetic controlled conditions. This revealed the fact that the vinyloxyborane kinetically formed isomerizes easily to the other more stable isomer. No such complete isomerization has been reported, though kinetically controlled enolates or enol ethers isomerize to thermodynamically stable ones in the presence of proton donor till two isomers equilibrate.[6)]

The method using 9-BBNOTf with 2,6-lutidine was applied to the reactions of other methyl ketones with various carbonyl compounds (Table 6).

The procedure provides an efficient method for the preparation of one regioisomer of cross-aldols from thermodynamically stable enolates of methyl ketones.

Stereoselectivity. The aldol reaction was subjected to kinetic stereoselection, with (*Z*)-enolate giving predominantly the erythro aldol, and (*E*)-enolate leading preferentially to threo isomer.[7)] This suggests that high stereoselection takes place in the present aldol reaction, since the key intermediate, vinyloxyborane, might be generated stereoselectively under suitable conditions. Thus, the reaction of 3-pentanone with benzaldehyde was taken as a model for examining selectivity. The results obtained under various conditions are summarized in Table 7.

It is apparent that reaction temperature is the most important factor to affect the selectivity. The reaction at lower temperature (−78 °C) gave rise to a remarkably high stereoselection (erythro/threo=96:4), and a fairly good selection at room temperature. The high selectivity of the reaction is explained by assuming that the initial generation of vinyloxyborane and subsequent reaction with benzaldehyde proceed in stereoselective manner at low temperature (Scheme 4).

Attempted Reactions of Vinyloxyboranes to Some Electrophiles.

The reactivity of vinyloxyboranes generated from

Table 6. Synthesis of aldols by the use of 9-BBNOTf from ketones and carbonyl compounds

	Ketone	Carbonyl compounds	Product (Yield/%)	
9	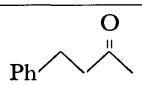		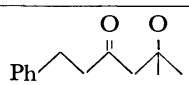 (≈0)	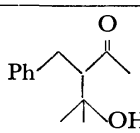 (63)
10	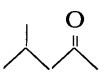	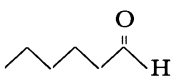	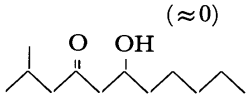 (≈0)	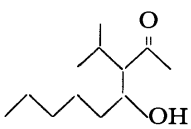 (67)
11	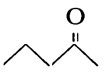	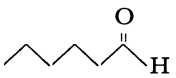	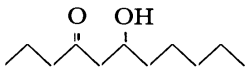 (≈0)	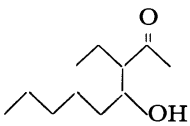 (78)

Table 7. Effect of the triflates and amines on the ratios of the stereoisomers

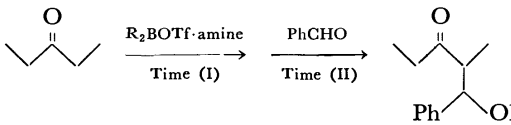

(**12**)

R_2BOTf	Amine	Solvent	Temp	Time (I)	Time (II)	Yield/%	e : t [a)]
Bu_2BOTf		Hexane	r.t.	1 min	overnight	60	70:30
9-BBNOTf	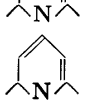	Hexane	r.t.	1 min	overnight	49	75:25
Bu_2BOTf	Et_3N	Ether	−78 °C	15 min	3 min	92	96: 4
9-BBNOTf		Ether	−78 °C	16 h	3 min	79	96: 4

a) The ratios (erythro:threo) were determined on the basis of their NMR spectra.

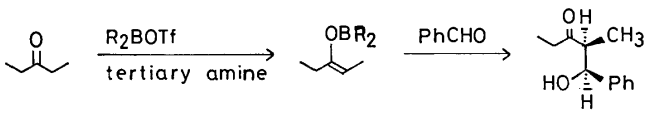

Scheme 4.

3-pentanone was examined for various electrophiles such as ethyl acetate, acetic anhydride, acetal, 1-phenyl-1-propanone and benzyl bromide. The electrophiles were recovered nearly quantitatively when the reactions were carried out by the two methods (Tables 2 and 6). The utility of the present procedure in the preparation of vinyloxyboranes is shown clearly in the difference of reactivity toward aldehydes and other electrophiles.

The reaction with γ-cyclocitral was achieved in 71% yield without any isomerization of the vinyl group (Scheme 5).[8]

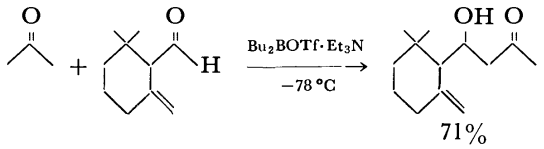

Scheme 5.

In this case, use of alkali metal enolates or titanium tetrachloride with silyl enol ether of acetone on an acid or base sensitive double bond of γ-cyclocitral was unsatisfactory, the desired product not being obtained in satisfactory yield. The present methods might provide the mildest conditions among the procedures so far employed.

Summary. Various directed cross-aldols with high regio- and stereoselectivities were prepared in good yields starting from ketones with aldehydes by using dialkylboryl triflates and tertiary amines.

Experimental

Materials. Tributylborane was prepared from boron trifluoride etherate and butylmagnesium bromide in dry ether under argon. 9-BBN was prepared from borane–THF complex and 1,5-cyclooctadiene in dry THF under argon. Commercially available trifluoromethanesulfonic acid was distilled under argon before use.

Dibutylboryl Triflate.[5] Trifluoromethanesulfonic acid (12.51 g, 83.3 mmol) was added to tributylborane (15.16 g, 83.3 mmol) at room temperature under argon. After being stirred for 3 h, the reaction mixture was distilled *in vacuo* under argon. Bp 37 °C/0.12 mmHg, 19.15 g (84%). IR (CCl_4): 1405, 1380, 1320, 1200, 1150 cm^{-1}.

9-BBN Triflate. Trifluoromethanesulfonic acid (18.75 g, 125 mmol) was added to 9-BBN (15.33 g, 127 mmol) in hexane (100 ml) under argon. After being stirred overnight, the reaction mixture was concentrated and distilled *in vacuo* under argon. Bp 38 °C/0.03 mmHg, 28.84 g (85%). IR (CCl_4): 1400, 1240, 1080 cm^{-1}.

Reaction of 1-Phenyl-1-butanone with 3-Phenylpropanal Using Dibutylboryl Triflate (1). To a hexane solution (2 ml) of dibutylboryl triflate (0.253 g, 0.92 mmol) and 2,6-lutidine (0.099 g, 0.92 mmol) was added a hexane solution (1 ml) of 1-phenyl-1-butanone (0.137 g, 0.92 mmol) under argon at room temperature. After stirring for 10 min, a hexane solution (1 ml) of 3-phenylpropanal (0.124 g, 0.92 mmol) was added at room temperature and the reaction mixture was allowed to stand overnight. The mixture was added to phosphate buffer (pH 7.0) and extracted with ether. After removal of ether, the mixture was treated with 30% H_2O_2 (1 ml) in MeOH (3 ml) for 2 h and water was added. The mixture was concentrated *in vacuo* in order to remove most of the methanol and extracted with ether. The ethereal layer was washed with a 5% solution of $NaHCO_3$ and a saturated solution of NaCl, and dried over Na_2SO_4, the solvent being removed. The crude oil was purified by preparative TLC to give 1,5-diphenyl-2-ethyl-3-hydroxy-1-pentanone (0.233 g, 83%).

IR (neat); 1670 cm^{-1}: NMR (CCl_4) δ 7.20—8.10 (broad, 5H), 7.10 (s, 5H), 3.91 (m, 1H), 3.50 (m, 2H), 2.40—3.10 (broad, 2H), 1.40—2.10 (broad, 4H), 0.81 (t, 3H, J=6 Hz). The other reactions given in Table 1 were carried out according to the same procedure.

Reaction of 2-Methyl-4-pentanone with 3-Phenylpropanal Using Dibutylboryl Triflate (5). To an ether solution (1.5 ml) of dibutylboryl triflate (0.301 g, 1.1 mmol) and *N,N*-diisopropylethylamine (0.142 g, 1.1 mmol) was added dropwise an ether solution (1.5 ml) of 2-methyl-4-pentanone (0.100 g, 1.0 mmol) at −78 °C under argon. After being stirred for 30 min, an ether solution (1.5 ml) of 3-phenylpropanal (0.134 g, 1.0 mmol) was added at that temperature. The reaction mixture was allowed to stand for 1 h, then added to phosphate buffer (pH 7.0) at room temperature and extracted with ether. After removal of ether, the crude oil was treated as described above and purified by TLC to give 6-hydroxy-2-methyl-8-phenyl-4-octanone (0.192 g, 82%). IR (neat); 1695 cm^{-1}: NMR (CCl_4); δ 7.11 (s, 5H), 4.00 (m, 1H), 3.05 (broad, s, 1H), 2.06—2.92 (m, 6H), 1.70—2.00 (m, 3H), 0.86 (d, 6H), J=7 Hz.

The other reactions **2**, **3**, **4**, **6**, and **7** (Scheme 2 and Table 2), were carried out according to the same procedure (triethylamine was used as proton accepter in Reactions **4**, **6**, and **7** instead of *N,N*-diisopropylethylamine.), the physical and analytical data being given in Table 8. Absence of the regioisomers was determined by NMR or GLC (10% QF_1 at 130 °C).

Examination of Regioselectivity. Reaction of 4-Phenyl-2-butanone with Benzaldehyde (8). All the reactions (Tables, 3, 4, and 5) were carried out as follows: To a mixture of dialkylboryl triflate (2.00 mmol) and tertiary amine (2.00 mmol) in a solvent (3 ml) was added a solution (1.5 ml) of 4-phenyl-2-butanone (2.00 mmol) under argon. A solution (2 ml) of benzaldehyde (2.00 mmol) was added to the above mixture and allowed to stand for 3 h. The reaction mixture was added into phosphate buffer of pH 7.0 (5.0 ml), methanol (10 ml) and 30% H_2O_2 (5 ml) at 0 °C. After 15 min, the mixture was concentrated *in vacuo* in order to remove most of the methanol, extracted with dichloromethane and dried over $MgSO_4$, the solvent being then removed. The crude oil was purified by TLC, the regioisomers ((**8A**) and (**8B**)) being separated.

Reaction of 4-Phenyl-2-butanone with Benzaldehyde Using 9-BBN Triflate (8). To a solution of 9-BBN triflate (0.551 g, 2.04 mmol) and 2,6-lutidine (0.218 g, 2.04 mmol) in ether (6 ml) was added a solution of 4-phenyl-2-butanone (0.302 g, 2.04 mmol) in ether (3 ml) at −78 °C under argon. After the mixture had been stirred for 4 h, benzaldehyde (0.216 g, 2.04 mmol) in ether (3 ml) was added at the same temperature. The reaction mixture was left to stand for 3 h and worked up as described above. The resulting crude oil was purified by TLC to give 1-hydroxy-1,5-diphenyl-3-pentanone (**8A**) (0.006 g, 1%) and 3-benzyl-4-hydroxy 4-phenyl-2-butanone (**8B**) (0.476 g, 92%. (**8A**): IR (neat);

Table 8. Physical and analytical data for the products

Product	IR(C=O) ν/cm^{-1}	NMR (CCl_4), δ	Found(Calcd), % C	H
2	1725	7.12(s, 5H), 3.38—4.12(m, 1H), 3.60—4.12 (broad, 1H), 1.20—2.87 (broad, 11H)	76.67 (77.03)	8.46 (8.31)
3	1700	7.00(s, 5H), 3.95—4.20(broad, 1H), 3.20—3.72(m, 1H), 1.20—3.20 (broad, 13H)	77.42 (77.55)	8.79 (8.68)
4	1700	7.17(s, 5H), 7.08(s, 5H), 4.98(t, 1H), J=7.5 Hz, 3.24—3.64(broad s, 1H), 2.25—3.12(m, 6H)	80.12 (80.28)	7.54 (7.13)
6	1700	3.50—4.06(m, 1H), 3.00—3.50(broad, 1H), 2.38(t, 2H), J=7 Hz, 2.43(d, 2H), J=6 Hz	71.84 (71.94)	12.23 (12.09)
7	1700	3.61—4.21(m, 1H), 3.03—3.35(broad, 1H), 2.42(d, 2H), J=6 Hz, 2.30(t, 2H), J=6 Hz, 0.63—1.78(broad, 16H)	70.81 (70.92)	12.04 (11.90)
9	1700	7.14(s, 5H), 2.60—3.11(broad, 4H), 1.24(s, 6H)		
10	1700	3.53—4.07(broad, 1H), 3.00—3.53(broad, 1H), 2.31—2.90(m, 1H), 2.13(s, 3H), 0.60—1.73(m, 18H)	71.79 (71.94)	12.40 (12.09)
11	1700	3.40—4.30(m, 1H), 3.09—3.52(broad, 1H), 2.23—2.77 (m, 1H), 2.10(s, 3H), 0.60—1.97(m, 16H)	71.16 (70.92)	12.08 (11.90)

1700 cm^{-1}: NMR; 7.17 (s, 5H), 7.08 (s, 5H), 4.98 (t, 1H), J=7.5 Hz, 3.24—3.64 (broad s, 1H), 2.25—3.12 (m, 6H). Found; C, 80.12; H, 7.54%. Calcd for $C_{17}H_{18}O_2$; C, 80.28; H 7.13%. (**8B**): IR (neat); 1700 cm^{-1}: NMR (CCl_4); 7.22 (s, 5H), 7.05 (s, 5H), 4.63 (d, 0.96 H, J=5 Hz), 4.53 (d, 0.04 H, J=8 Hz), 3.70—4.20 (broad, 1H), 2.60—3.42 (broad, 3H), 1.73 (s, 0.12 H), 1.34 (s, 2.88 H). Found: C 80.12; H 7.50%. Calcd for $C_{17}H_{18}O_2$; C 80.28; H 7.13%. Reactions **9**, **10**, and **11**, listed (Table 6) were carried out according to the same procedure. Physical and analytical data are given in Table 8. Absence of the regioisomers was determined by GLC (QF$_1$, 130 °C).

*Examination of Stereoselectivity. Reaction of 3-Pentanone with Benzaldehyde (**12**).* The reactions were carried out by the same procedure as described in 2 mmol scale. IR (neat); 1695 cm^{-1}: NMR (CCl_4); 7.13 (s, 5H), 4.81 (d, 0.70—0.96 H), J=6 Hz, 4.55 (d, 0.04—0.30 H), J=9 Hz, 3.50—3.85 (broad, 1H), 1.78—2.95 (m, 3H), 0.60—1.10 (m, 6H). Found; C, 74.50; H 8.88%. Calcd for $C_{12}H_{16}O_2$; C 74.97; H 8.39%.

References

1) Reviews: a) A. T. Nielsen and W. H. Houlihan, *Org. React.*, **16**, 1 (1968); b) H. O. House, "Modern Synthetic Reactions," 2nd ed, W. A. Benjamin, Menlo Park, Calif., 1972, pp. 629—682; c) M. E. Jung, *Tetrahedron*, **32**, 3 (1976); d) J. d'Angelo, *ibid.*, **32**, 2979 (1976); e) T. Mukaiyama, *Angew. Chem., Int. Ed. Engl.*, **16**, 817 (1977). Recent papers: H. O. House, D. S. Crumrine, A. Y. Teranishi, and H. D. Olmstead, *J. Am. Chem. Soc.*, **95**, 3310 (1973); T. Mukaiyama, T. Sato, S. Suzuki, T. Inoue, and H. Nakamura, *Chem. Lett.*, **1976**, 95; I. Kuwajima, T. Sato, M. Arai, and N. Minami, *Tetrahedron Lett.*, **1976**, 1817; R. Noyori, K. Yokoyama, J. Sakata, I. Kuwajima, E. Nakamura, and M. Shimizu, *J. Am. Chem. Soc.*, **99**, 1265 (1977); K. Maruoka, S. Hashimoto, Y. Kitagawa, H. H. Yamamoto, and H. Nozaki, *ibid.*, **99**, 7705 (1977); I. Kuwajima, T. Inoue, and T. Sato, *Tetrahedron Lett.*, **1978**, 4887; and references cited there in.

2) T. Mukaiyama, K. Inomata, and M. Muraki, *Bull. Chem. Soc. Jpn.*, **46**, 1807 (1973).

3) T. Mukaiyama and T. Inoue, *Chem. Lett.*, **1976**, 559; T. Inoue, T. Uchimaru and T. Mukaiyama, *ibid.*, **1977**, 153.

4) E. Negishi, *J. Chem. Ed.*, **52**, 159 (1975).

5) The reactions may proceed through a radical chain path, since they do not ccur in the absence of oxygen and can be initiated by the injection of air.

6) Ref. 1 b), pp. 546—570; H. O. House, L. J. Czuba, M. Gall, and H. D. Olmstead, *J. Org. Chem.*, **34**, 2324 (1969).

7) J.-E. Dubois and M. Dubois, *Tetrahedron Lett.*, **1967**, 4215; J.-E. Dubois and P. Fellmann, *C. R. Acad. Sci.*, **274**, 1307 (1972); *Tetrahedron Lett.*, **1975**, 1225; W. Fenzl and R. Köster, *Liebigs Ann. Chem.*, **1975**, 1322.

8) T. Mukaiyama, K. Saigo and O. Takazawa, *Chem. Lett.*, **1976**, 1033.

The Oxidation of (*E*)-α-Phenylcinnamic Acids with Manganese(III) Acetate

Kazuki Oishi and Kazu Kurosawa*

Department of Chemistry, Faculty of Science, Kumamoto University, Kurokami 2-39-1, Kumamoto 860

(Received April 27, 1979)

The oxidation of eight (*E*)-α-phenylcinnamic acids with manganese(III) acetate in boiling acetic acid containing acetic anhydride gave 3-phenylcoumarins, 3-phenyl-1-oxaspiro[4.5]deca-3,7,9-triene-2,6-diones, 2-phenylbenzofurans, 3-(acetoxymethyl)-2-phenylbenzofurans, 3-formyl-2-phenylbenzofuran, 2-acetoxy-2-phenyl-3(2*H*)-benzofuranones, (*Z*)-α-acetoxystilbenes, 2-acetoxy-1,2-diphenylethanones, 5-acetoxy-4,5-diphenyl-2(5*H*)-furanones, and diphenylacetylene. The reaction pathways are discussed.

In the reaction of lead(IV) acetate and manganese(III) acetate with phenolic compounds in which a hydroxyl group and a double bond are located in spatially suitable positions, an oxidative cyclization has often been observed.[1-7] Davies *et al.* have reported that 2′-substituted biphenyl-2-carboxylic acid was oxidized with lead(IV) acetate to give 3,4-benzocoumarin as a cyclized product.[8] This result prompted us to examine the oxidation of α-phenylcinnamic acids with manganese(III) acetate, in the hope to obtain 3-phenylcoumarins.

(*E*)-α-Phenylcinnamic acids (**1a**—**h**) were prepared from the corresponding phenylacetic acid and benzaldehyde by the Perkin condensation; the (*Z*)-acid (**2f**) was also obtained in the reaction as a minor product. The structures of the new α-phenylcinnamic acids were confirmed by examining their NMR[9] and IR spectra, and by elemental analyses. The (*E*)-α-phenylcinnamic acids which were examined were (*E*)-2-methoxy-α-phenylcinnamic acid (**1a**), (*E*)-2,4-dimethoxy-α-phenylcinnamic acid (**1b**), (*E*)-2,3,4-trimethoxy-α-phenylcinnamic acid (**1c**), (*E*)-2-methoxy-α-(2-methoxyphenyl)-cinnamic acid (**1d**), (*E*)-2,4-dimethoxy-α-(2-methoxyphenyl)cinnamic acid (**1e**), (*E*)-2-methoxy-α-(4-methoxyphenyl)cinnamic acid (**1f**), (*E*)-2,4-dimethoxy-α-(4-methoxyphenyl)cinnamic acid (**1g**), and (*E*)-3,4-dimethoxy-α-(4-methoxyphenyl)cinnamic acid (**1h**). When the (*E*)-α-phenylcinnamic acids (**1a**—**h**) were oxidized with manganese(III) acetate, several products (**3**—**12**) were isolated. The structures of the products were determined again by examining their NMR, IR, and mass spectra, by elemental analyses, and by unambiguous syntheses.

The reactions of **1a**—**h** were carried out using two, four, and five equivalents of manganese(III) acetate in acetic acid containing acetic anhydride at the reflux temperature until the color of manganese(III) acetate disappeared (Fig. 1 and Table 1).

*3-Phenylcoumarins (**3**) and Spiro Lactones (**4**).* The manganese(III) acetate oxidation of methoxy-substituted (*E*)-α-phenylcinnamic acids (**1**), in which α- and β-phenyl groups are *cis*, afforded 3-phenylcoumarins (**3**) and spiro lactones (**4**), both with a *trans* double bond as to two phenyl groups in **3** and the six-menbered ring and a phenyl group in **4**. This indicates that the isomerization of **1** to **2** is involved and that then **2** is oxidized with manganese(III) acetate to give a carbonyloxy radical (I). Subsequently, the (I) radical cyclizes either at the 2-position with the elimination of a methoxyl radical, or at the 6-position with the elimination of hydrogen, while the attack at the 1-position yields **4** with the elimination of the methyl radical (Scheme 1). The pathway would be similar to that of the oxidation of 2′-substituted biphenyl-2-carboxylic acid with lead(IV) acetate.[8] It seems that the cyclization can occur when **1** possesses more than two methoxyl groups in the β-phenyl moiety (**1b**, **1c**, **1e**, and **1h**). An exception is **1g**.

*2-Phenylbenzofurans (**5**), 3-(Acetoxymethyl)-2-phenylbenzofurans (**6**), 3-Formyl-2-phenylbenzofuran (**7**), and 2-Acetoxy-2-phenyl-3(2H)-benzofuranone (**8**).* These compounds were obtained in the reaction of **1** substances which have a methoxyl group at the 2-position in the β-phenyl ring (**1a**, **1b**, **1d**, **1e**, **1f**, and **1g**). An exception is **1c**. Thus, the reaction may proceed through the pathway shown in Scheme 2. The vinylic radical (II), which is formed on the oxidative decarboxylation of the parent acid (**1**), is further oxidized to give a vinylic cation (III). The 2-methoxyl group in **1** attacks the cationic center of III intramolecularly, and then **5** is formed by the removal of the methyl cation. A similar reaction has been known to occur in the solvolysis of 1-aryl-2,2-bis(2-methoxyphenyl)vinyl halides.[10] In the oxidation of **1f**, the yield of **5f** decreased from 34 to 15%, and that of **6f** increased from 2 to 14%, where the amount of manganese(III) acetate was increased, and **7** and **8f** were isolated in the reaction in a molar ratio of 1:5 (Table 1, entries 8 and 9). This suggests that **6f**, **7**, and **8f** can be formed *via* the oxidation of **5f**. In fact, when 2-phenylbenzofuran (**5a**) was oxidized with manganese(III) acetate, 3-(acetoxymethyl)-2-phenylbenzofuran (**6a**, 30%) and 2-acetoxy-2-phenyl-3(2*H*)-benzofuranone (**8a**, 25%) were obtained. Therefore, the reaction may proceed as shown in Scheme 2. **7** can be formed by the further oxidation of **6**, followed by hydrolysis during the work-up. Acetoxymethylation has been reported to occur in the reaction of aromatic compounds with manganese(III) acetate.[11-15]

*(Z)-α-Acetoxystilbenes (**9**), 2-Acetoxy-1,2-diphenylethanones (**10**), and 5-Acetoxy-4,5-diphenyl-2(5H)-furanone (**11**).* The structures of **9** were elucidated by a comparison of their UV spectra with those of (*E*)- and (*Z*)-α-acetoxystilbenes.[16] (*Z*)-α-Acetoxy-3′,4,4′-trimethoxystilbene (**9h**) was synthesized from the corresponding benzyl aryl ketone and was found to be identical. The reaction which gave **9** may proceed through one of the following pathways: a) an acetoxyl radical attacks the vinylic radical (II) to form **9**, or b) the vinylic cation (III) reacts with acetic acid to yield **9**, with the elimination of a proton. The absence of dimeric compounds and stilbenes, which could be

formed from II, in the products suggests that the b pathway is preferable to the a pathway. As to the formation of **10**, again two pathways can be considered: c) the oxidation of **9** gives **10**, or d) the oxidation of benzyl aryl ketone, which might be formed *via* the solvolysis of **9**, gives **10**. In order to distinguish the c and d pathways, **9h** was oxidized with two equivalents of manganese(III) acetate. 2-Acetoxy-1-(4-methoxyphenyl)-2-(3,4-dimethoxyphenyl)ethanone (**10h**) was obtained in a good yield (67%), together with unchanged **9h** (22%) (Table 2, entry 1). However, when **9h** was heated without the oxidant, **9h** was recovered quantitatively. The fact that 3,4-dimethoxybenzyl 4-methoxyphenyl ketone, which might be formed by the solvolysis of **9h**, was not found in the products of these reactions, even though a substantial amount of **9h** was recovered, leads to the conclusion that the 2-acetoxy-1,2-diphenylethanones (**10**) were formed through the c pathway. It is worth noting that the acetoxyl group in 2-acetoxy-1,2-diphenylethanone (**10**) obtained in the reaction of (*E*)-α-phenylcinnamic acid was located at the α-position in the parent acids and that the yield of **10i** was much improved in the reaction of **9i** in acetic acid (Table 2, entry 4). This suggests that the manganese(III) acetate oxidation of **1** can be utilized as a regiospecific synthesis of 2-acetoxy-1,2-diphenylethanones which have different aryl groups from (*E*)-α-phenylcinnamic acids (**1**), although the formation of α-acetoxy ketones from enol acetates by lead(IV) acetate[17] and by anodic oxidation[18] have been reported.

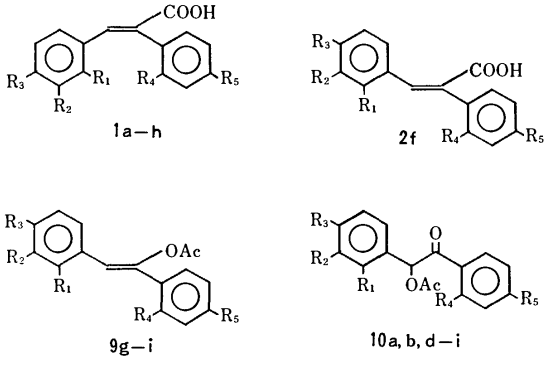

a: $R_1=OCH_3$, $R_2=R_3=R_4=R_5=H$
b: $R_1=R_3=OCH_3$, $R_2=R_4=R_5=H$
c: $R_1=R_2=R_3=OCH_3$, $R_4=R_5=H$
d: $R_1=R_4=OCH_3$, $R_2=R_3=R_5=H$
e: $R_1=R_3=R_4=OCH_3$, $R_2=R_5=H$
f: $R_1=R_5=OCH_3$, $R_2=R_3=R_4=H$
g: $R_1=R_3=R_5=OCH_3$, $R_2=R_4=H$
h: $R_2=R_3=R_5=OCH_3$, $R_1=R_4=H$
i: $R_1=R_2=R_3=R_4=R_5=H$

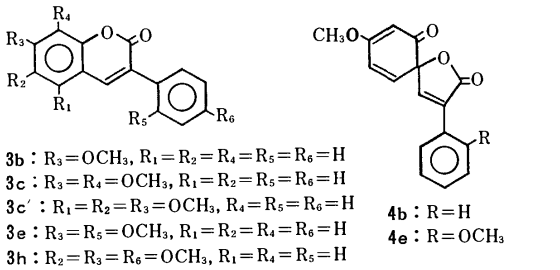

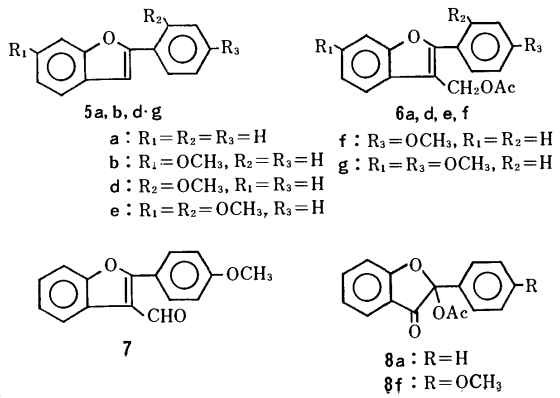

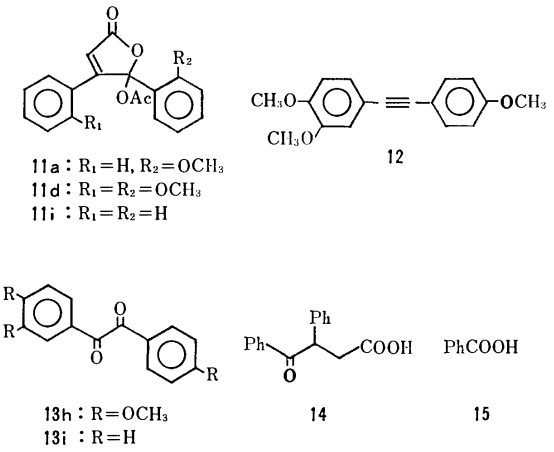

Fig. 1.

When **9h** was oxidized with five equivalents of manganese(III) acetate, 3,4,4′-trimethoxybenzil (**13h**) was obtained, together with **10h** (Table 2, entry 2). Two reaction pathways (e and f) which could give **13h** may be envisaged: e) the oxidation of **9h** gives **13h**, or f) the oxidation of 2-acetoxy-1-(4-methoxy-

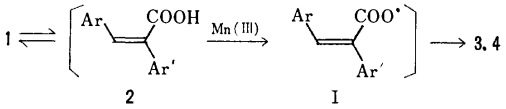

Scheme 1.

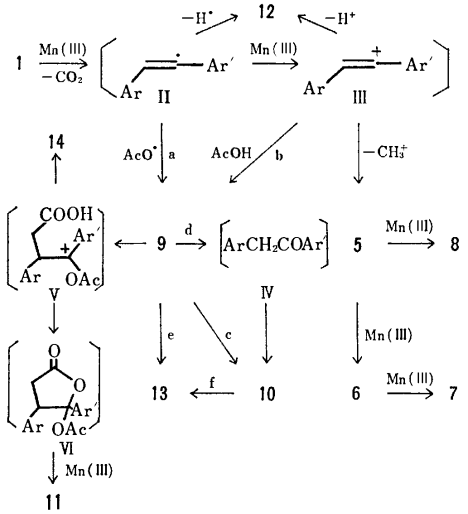

Scheme 2.

[17] J. Kurosawa and K. Kurosawa, *Bull. Chem. Soc. Jpn.*, **52**, 1967 (1979).
[18] K. Kurosawa, *Bull. Chem. Soc. Jpn.*, **53**, 1 (1980).

Table 1. Oxidation of α-phenylcinnamic acids with manganese(III) acetate in boiling acetic acid containing acetic anhydride

Entry	Substrate	Reaction conditions: Molar ratio	Reaction conditions: Time/min	Products (yield/%)[a]	Recovered substrate
1	**1a**[20]	1 : 5	18	**5a** (5) **6a** (10) **10a** (7) **11a**(12)	**1a** (43)
2	**1b**[21]	1 : 2	13	**3b** (17) **4b** (14) **5b** (2) **10b** (19)	**1b** (20)
3	**1c**[22]	1 : 2	16	**3c** (10) **3c′** (8)	**1c** (30)
4	**1c**	1 : 4	25	**3c** (4) **3c′** (17)	**1c** (16)
5	**1c**	1 : 5	40	**3c** (3) **3c′** (15)	**1c** (12)
6	**1d**[23]	1 : 5	11	**5d** (5) **6d** (20) **10d** (9) **11d**(12)	**1d** (34)
7	**1e**	1 : 5	12	**3e** (6) **4e** (15) **5e** (2) **6e** (7) **10e** (25)	**1e** (18)
8	**1f**[24]	1 : 2	10	**5f** (34) **6f** (2) **10f** (16)	**1f** (16)
9	**1f**	1 : 5	30	**5f** (15) **6f** (14) **7** (5) **8f** (6) **10f** (32)	**1f** (2)
10	**1g**	1 : 2	6	**5g** (9) **9g** (20) **10g** (21)	**1g** (31)
11	**1h**[25]	1 : 2	3	**3h** (3) **9h** (3) **10h** (25) **12** (9)	**1h** (48)
12	**1h**	1 : 5	8	**3h** (10) **10h** (64) **12** (12)	**1h** (3)

a) The yield is based on the amount of substrate used.

Table 2. Oxidation of (*Z*)-α-acetoxystilbenes (**9**) with manganese(III) acetate

Entry	Substrate	Reaction conditions[a]: Molar ratio of **9** : oxidant	Reaction conditions[a]: Solvent	Reaction conditions[a]: Time/min	Product (yield/%)[b]	Recovered substrate
1	**9h**	1 : 2	AcOH, Ac_2O	2	**10h** (67)	**9h** (22)
2	**9h**	1 : 5	AcOH, Ac_2O	30	**10h** (70) **13h** (6)	
3	**9i**	1 : 3	AcOH, Ac_2O	12	**10i** (13) **11i** (12) **14** (26)	**9i** (34)
4	**9i**	1 : 3	AcOH	95	**10i** (43) **11i** (2) **15** (7)	

a) The reactions were carried out at reflux temperature. b) The yield is based on the amount of the substrate used.

phenyl)-2-(3,4-dimethoxyphenyl)ethanone (**10h**) gives **13h**. In order to establish the true pathway, 2-acetoxy-1,2-diphenylethanone (**10i**) was oxidized with manganese(III) acetate to give **13i** in a 15% yield. The result showed that 3,4,4′-trimethoxybenzil (**13h**) was formed through the f pathway.

The formation of 5-acetoxy-4,5-diphenyl-2(5*H*)-furanones (**11**) from **1** is very interesting, as it may be formed by another reaction of (*Z*)-α-acetoxystilbene (**9**) with manganese(III) acetate. The reaction of (*Z*)-α-acetoxystilbene (**9i**) with manganese(III) acetate did give 5-acetoxy-4,5-diphenyl-2(5*H*)-furanone (**11i**), along with 3,4-diphenyl-4-oxobutanoic acid (**14**) (Table 2, entry 3). The reaction pathway could be explained as follows. The reaction of **9** with the carboxymethyl radical would give a radical. This radical is oxidized to a cation, V, which gives a γ-lactone (VI). The VI would then be oxidized to give **11** via acetoxylation at the 4-position of VI, followed by the elimination of acetic acid. The V cation also reacts with acetic acid and then eliminates acetic anhydride, giving **14** (Scheme 2). It has been mentioned earlier that the yield of **10i** was increased when **9i** was oxidized in acetic acid, but that of **11i** decreased (Table 2, entry 4). This may suggest that diacetoxylation took place[2b] under the present reaction conditions and that the carboxymethyl radicals were produced in smaller amounts. It has previously been reported that the reaction of olefins with manganese(III) acetate under anhydrous conditions gave γ-lactones.[19]

*1-(3,4-Dimethoxyphenyl)-2-(4-methoxyphenyl)acetylene (**12**).* This compound may be formed either from the vinylic radical (II) with a loss of hydrogen or from the vinylic cation (III) with the removal of the proton (Scheme 2).

In conclusion, it was shown that the reactions of (*E*)-α-phenylcinnamic acid (**1**) with manganese (III) acetate could be explained by assuming two radicals, I and II, two cations, III and V, and the lactone VI as the reaction intermediates.

Experimental

All the ^1H NMR spectra were recorded with a Hitachi Perkin-Elmer R-24 spectrometer, with tetramethylsilane as the internal reference. The IR spectra were taken on a JASCO IRA-1 grating spectrometer, while the UV spectra were recorded for the methanol solution with a Hitachi EPS-3T spectrophotometer. The mass spectra were recorded with JMS-01 SG-2 and Hitachi RMU-7M 002CPU mass spectrometers. The melting points were determined with a Yanagimoto micro-melting point apparatus and were not corrected.

*Preparation of α-Phenylcinnamic Acids (**1a—h**).* The general procedure for the preparation of α-phenylcinnamic acids was as follows. A mixture of a benzaldehyde (45 mmol), a phenylacetic acid (36 mmol), triethylamine (30

ml), and acetic anhydride (60 ml) was heated under reflux for 4 h. The reaction mixture was acidified with concd hydrochloric acid (40 ml) and extracted with benzene. This solution was washed with water and then extracted several times with 2 M aqueous sodium hydroxide. The combined extract was then acidified to a pH of 5.9 (the pH adjustment was checked with a Hitachi-Horiba F-5 pH meter) with concd hydrochloric acid. The precipitate was collected by filtration. The crude acid was purified by recrystallization to give (*E*)-α-phenylcinnamic acid. The (*Z*)-isomer was precipitated by the further addition of concd hydrochloric acid to the filtrate. The crude (*Z*)-acid was collected by filtration and recrystallized.

*(E)-2,4-Dimethoxy-α-(2-methoxyphenyl)cinnamic Acid (**1e**)*: Mp 177.5—179 °C (benzene); 20% yield; IR (KBr) 2950 and 1697 cm^{-1} (COOH); UV λ_{max} (log ε) 239^{sh} (4.09), 294 (4.08), and 331 nm (4.23); NMR ($CDCl_3$) δ=3.71 (3H, s, OCH_3), 3.75 (3H, s, OCH_3), 3.81 (3H, s, OCH_3), 6.11 (1H, dd, J=9 and 2.5 Hz, $H_{(5)}$), 6.37 (1H, d, J=2.5 Hz, $H_{(3)}$), 6.74 (1H, d, J=9 Hz, $H_{(6)}$), 6.7—7.5 (4H, m, $H_{(3'-6')}$), 8.24 (1H, s, =CH), and 9.9—11 (1H, br, COOH). Found; C, 68.60; H, 5.82%. Calcd for $C_{18}H_{18}O_5$; C, 68.78; H, 5.77%.

*(Z)-2-Methoxy-α-(4-methoxyphenyl)cinnamic Acid (**2f**)*: Mp 129.5—131 °C (benzene–light petroleum); 0.3% yield; IR (KBr) 2960 and 1705 cm^{-1} (COOH); UV λ_{max} (log ε) 236^{sh} (4.12), 290^{sh} (4.22), and 321 nm (4.25); NMR ($CDCl_3$) δ=3.82 (6H, s, 2×OCH_3), 6.89 (2H, m, $H_{(3')}$ and $H_{(5')}$), 7.46 (2H, m, $H_{(2')}$ and $H_{(6')}$), 6.7—7.6 (4H, m, $H_{(3-6)}$), 7.19 (1H, s, =CH), and 10.57 (1H, br s, COOH). (Found; C, 71.67; H, 5.73%. Calcd for $C_{17}H_{16}O_4$; C, 71.82; H, 5.67%.

*(E)-2,4-Dimethoxy-α-(4-methoxyphenyl)cinnamic Acid (**1g**)*: Mp 217.5—220.5 °C (EtOH); 27% yield; IR (KBr) 2940 and 1680 cm^{-1} (COOH); UV λ_{max} (log ε) 240 (4.17), 295 (4.07), and 336 nm (4.23); NMR (DMSO-d_6) δ=3.72 (3H, s, OCH_3), 3.76 (3H, s, OCH_3), 3.86 (3H, s, OCH_3), 6.20 (1H, dd, J=9 and 2.5 Hz, $H_{(5)}$), 6.54 (1H, d, J=2.5 Hz, $H_{(3)}$), 6.59 (1H, d, J=9 Hz, $H_{(6)}$), 6.90 (2H, m, $H_{(3')}$ and $H_{(5')}$), 7.07 (2H, m, $H_{(2')}$ and $H_{(6')}$), 7.93 (1H, s, =CH), and 11.5 (1H, br, COOH). Found; C, 68.62; H, 5.81%. Calcd for $C_{18}H_{18}O_5$; C, 68.78; H, 5.77%.

*Oxidation of (E)-α-Phenylcinnamic Acids (**1a—h**) with Manganese(III) Acetate.* The general procedure for the oxidation of (*E*)-α-phenylcinnamic acids was as follows. To a hot solution of an (*E*)-α-phenylcinnamic acid (2 mmol) in acetic acid (35 ml) containing acetic anhydride (5 ml), we added manganese(III) acetate dihydrate.[26] The solution was then heated under reflux until the dark color of the Mn(III) ions disappeared. After the removal of the solvent *in vacuo*, the resulting mixture was triturated with water and extracted with chloroform. The chloroform solution was washed with aqueous sodium carbonate, dried over sodium sulfate, and evaporated under reduced pressure. The products were chromatogrammed on TLC (Wakogel B-10) with chloroform and then ether as developing solvents, and recrystallized. The yields are summarized in Table 1. The aqueous sodium carbonate solution was acidified with concd hydrochloric acid and extracted with ethyl acetate. The ethyl acetate solution was dried and evaporated. The IR spectrum of the resulting substance was superimposible on that of the (*E*)-α-phenylcinnamic acid. The acid was also recovered on TLC. The recovery of the (*E*)-α-phenylcinnamic acid in Table 1 was the sum of them.

*Oxidation Products of **1a**. 2-Phenylbenzofuran (**5a**)*: Mp 120—121 °C (EtOH) (lit,[27] mp 120 °C).

*3-(Acetoxymethyl)-2-phenylbenzofuran (**6a**)*: Liquid; IR ($CHCl_3$) 1750 cm^{-1} (OAc); NMR (CCl_4) δ=2.03 (3H, s, OAc), 5.32 (2H, s, $-CH_2-$), and 6.9—8.0 (9H, m, aromatic). Found; *m/e* 266.0921. Calcd for $C_{17}H_{14}O_3$; M, 266.0943.

*2-Acetoxy-1-phenyl-2-(2-methoxyphenyl)ethanone (**10a**)*: Liquid; IR ($CHCl_3$) 1752 (OAc) and 1715 cm^{-1} (C=O); NMR (CCl_4) δ=2.08 (3H, s, OAc), 3.84 (3H, s, OCH_3), 6.6—7.5 (8H, m, >CH– and aromatic), and 7.7—8.0 (2H, m, $H_{(2)}$ and $H_{(6)}$). Found; *m/e* 284.1041. Calcd for $C_{17}H_{16}O_4$; M, 284.1049.

*5-Acetoxy-4-(2-methoxyphenyl)-5-phenyl-2(5H)-furanone (**11a**)*: Mp 150—152 °C (aq MeOH); IR ($CHCl_3$) 1770 cm^{-1} (α,β-unsaturated γ-lactone[28]); UV λ_{max} (log ε) 236^{sh} (4.03), 283 (4.19), and 334 nm (3.89); NMR ($CDCl_3$) δ=2.12 (3H, s, OAc), 3.89 (3H, s, OCH_3), 6.5—7.9 (9H, m, aromatic), and 7.13 (1H, s, $H_{(3)}$); MS *m/e* 324 (M^+), 282, 265, 254, 237, 177, 132, 105, and 77. Found; C, 70.20; H, 4.96%. Calcd for $C_{19}H_{16}O_5$; C, 70.36; H, 4.98%.

*Oxidation Products of **1b**. 7-Methoxy-3-phenylcoumarin (**3b**)*: Mp 122—123 °C (EtOH) (lit,[29] mp 124 °C).

*8-Methoxy-3-phenyl-1-oxaspiro[4.5]deca-3,7,9-triene-2,6-dione (**4b**)*: Mp 135—137.5 °C (benzene–light petroleum); IR (KBr) 1770 (γ-lactone) and 1675 cm^{-1} (C=O); UV λ_{max} (log ε) 225 (4.38) and 276 nm (4.26); NMR ($CDCl_3$) δ=3.75 (3H, s, OCH_3), 5.73 (1H, s, $H_{(7)}$), 6.38 (2H, s, $H_{(9)}$ and $H_{(10)}$), 7.25 (1H, s, $H_{(4)}$), 7.3—7.6 (3H, m, $H_{(3'-5')}$), and 7.7—8.1 (2H, m, $H_{(2')}$ and $H_{(6')}$); MS *m/e* 268 (M^+). Found; C, 71.51; H, 4.50%. Calcd for $C_{16}H_{12}O_4$; C, 71.63; H, 4.51%.

*6-Methoxy-2-phenylbenzofuran (**5b**)*: IR and NMR spectra of **5b** separated on TLC were identical with those of an authentic sample.[4]

*2-Acetoxy-1-phenyl-2-(2,4-dimethoxyphenyl)ethanone (**10b**)*: Mp 112—113 °C (benzene–light petroleum); IR (KBr) 1753 (OAc) and 1715 cm^{-1} (C=O); UV λ_{max} (log ε) 239 (4.23), 283 (3.75) and 289^{sh} nm (3.71); NMR ($CDCl_3$) δ=2.18 (3H, s, OAc), 3.77 (3H, s, OCH_3), 3.89 (3H, s, OCH_3), 6.3—6.6 (2H, m, $H_{(3')}$ and $H_{(5')}$), 7.1—7.6 (5H, m, >CH– and aromatic), and 7.8—8.1 (2H, m, $H_{(2)}$ and $H_{(6)}$). Found; C, 68.83; H, 5.86%. Calcd for $C_{18}H_{18}O_5$; C, 68.78; H, 5.77%.

*Oxidation Products of **1c**. 7,8-Dimethoxy-3-phenylcoumarin (**3c**)*: Mp 135.5—136 °C (EtOH) (lit,[30] mp 142—144 °C).

*5,6,7-Trimethoxy-3-phenylcoumarin (**3c'**)*: Mp 143—143.5 °C (MeOH); IR ($CHCl_3$) 1730 cm^{-1} (C=O); UV λ_{max} (log ε) 232^{sh} (4.32), 251^{sh} (4.04), and 351 nm (4.33); NMR ($CDCl_3$) δ=3.85 (3H, s, OCH_3), 3.91 (3H, s, OCH_3), 4.04 (3H, s, OCH_3), 6.64 (1H, s, $H_{(8)}$), 7.2—7.8 (5H, m, Ph), and 8.01 (1H, s, $H_{(4)}$). Found: C, 69.02; H, 5.15%. Calcd for $C_{18}H_{16}O_5$; C, 69.22; H, 5.16%.

*Oxidation Products of **1d**. 2-(2-Methoxyphenyl)benzofuran (**5d**)*: Mp 78.5—80 °C (EtOH) (lit,[31] mp 82—83 °C).

*3-(Acetoxymethyl)-2-(2-methoxyphenyl)benzofuran (**6d**)*: Liquid; IR ($CHCl_3$) 1748 cm^{-1} (OAc); NMR (CCl_4) δ=1.93 (3H, s, OAc), 3.69 (3H, s, OCH_3), 5.12 (2H, s, $-CH_2-$), and 6.7—7.7 (8H, m, aromatic). Found; *m/e* 296.1059. Calcd for $C_{18}H_{16}O_4$; M, 296.1049.

*2-Acetoxy-1,2-bis(2-methoxyphenyl)ethanone (**10d**)*: Mp 101—102 °C (cyclohexane) (lit,[32] mp 102 °C).

*5-Acetoxy-4,5-bis(2-methoxyphenyl)-2(5H)-furanone (**11d**)*: Mp 143.5—146 °C (MeOH); IR ($CHCl_3$) 1770 cm^{-1} (α,β-unsaturated γ-lactone[28]); UV λ_{max} (log ε) 281 (4.21) and 330 nm (3.89); NMR ($CDCl_3$) δ=2.11 (3H, s, OAc), 3.61 (3H, s, OCH_3), 3.85 (3H, s, OCH_3), 7.06 (1H, s, $H_{(3)}$), 6.6—7.6 (7H, m, aromatic), and 7.79 (1H, dd, J=7.5 and 2 Hz, $H_{(6')}$); MS *m/e* 354 (M^+), 312, 295, 253, 177, 135, 132, 92, 89, and 77. Found; C, 67.81; H, 5.12%. Calcd for $C_{20}H_{18}O_6$; C, 67.79; H, 5.12%.

Oxidation Products of ***1e****.* *7-Methoxy-3-(2-methoxyphenyl)-coumarin (**3e**)*: Mp 134—135 °C (benzene–light petroleum) (lit,[33] mp 136 °C).

*8-Methoxy-3-(2-methoxyphenyl)-1-oxaspiro[4.5]deca-3,7,9-triene-2,6-dione (**4e**)*: Mp 171—172 °C (CCl_4); IR ($CHCl_3$) 1775 (γ-lactone) and 1680 cm^{-1} (C=O); UV λ_{max} (log ε) 224 (4.40), 240^{sh} (4.30), 277 (4.19), and 311^{sh} nm (3.88); NMR ($CDCl_3$) δ=3.72 (3H, s, OCH_3), 3.89 (3H, s, OCH_3), 5.68 (1H, s, $H_{(7)}$), 6.38 (2H, s, $H_{(9)}$ and $H_{(10)}$), 6.8—7.5 (3H, m, $H_{(3'-5')}$), 7.59 (1H, s, $H_{(4)}$), and 8.40 (1H, dd, J=8 and 2 Hz, $H_{(6')}$); MS *m/e* 298 (M^+). Found; C, 68.25; H, 4.70%. Calcd for $C_{17}H_{14}O_5$; C, 68.45; H, 4.73%.

*6-Methoxy-2-(2-methoxyphenyl)benzofuran (**5e**)*: Mp 87—88 °C (aq EtOH); IR (KBr) 1555, 947, and 910 cm^{-1} (C=C); NMR (CCl_4) δ=3.79 (3H, s, OCH_3), 3.90 (3H, s, OCH_3), 6.5—7.5 (6H, m, aromatic), 7.13 (1H, s, $H_{(3)}$), and 7.96 (1H, dd, J=7.5 and 2.5 Hz, $H_{(6')}$). Found; C, 75.42; H, 5.58%. Calcd for $C_{16}H_{14}O_3$; C, 75.57; H, 5.55%.

*3-(Acetoxymethyl)-6-methoxy-2-(2-methoxyphenyl)benzofuran (**6e**)*: Liquid; IR ($CHCl_3$) 1745 cm^{-1} (OAc); NMR (CCl_4) δ=1.97 (3H, s, OAc), 3.79 (6H, s, 2×OCH_3), 5.10 (2H, s, $-CH_2-$), and 6.6—7.7 (7H, m, aromatic). Found; *m/e* 326.1166. Calcd for $C_{19}H_{18}O_5$; M, 326.1154.

*2-Acetoxy-1-(2-methoxyphenyl)-2-(2,4-dimethoxyphenyl)ethanone (**10e**)*: Mp 111.5—112 °C (ether); IR ($CHCl_3$) 1745 (OAc) and 1698 cm^{-1} (C=O); UV λ_{max} (log ε) 236^{sh} (4.05), 253 (3.94), 288 (3.65), and 313 nm (3.58); NMR ($CDCl_3$) δ= 2.14 (3H, s, OAc), 3.67 (3H, s, OCH_3), 3.71 (6H, s, 2× OCH_3), 6.2—6.5 (2H, m, $H_{(3')}$ and $H_{(5')}$), 6.6—7.5 (4H, m, aromatic), 7.14 (1H, s, >CH–), and 7.69 (1H, dd, J= 8.5 and 2 Hz, $H_{(6)}$). Found; C, 66.34; H, 5.58%. Calcd for $C_{19}H_{20}O_6$; C, 66.27; H, 5.85%.

Oxidation Products of ***1f****.* *2-(4-Methoxyphenyl)benzofuran (**5f**)*: Mp 146—147 °C (EtOH) (lit,[4] mp 146 °C).

*3-(Acetoxymethyl)-2-(4-methoxyphenyl)benzofuran (**6f**)*: Mp 72—73 °C (light petroleum); IR ($CHCl_3$) 1740 cm^{-1} (OAc); UV λ_{max} (log ε) 305 nm (4.47); NMR ($CDCl_3$) δ=2.09 (3H, s, OAc), 3.84 (3H, s, OCH_3), 5.38 (2H, s, $-CH_2-$), 6.98 (2H, m, $H_{(3')}$ and $H_{(5')}$), 7.74 (2H, m, $H_{(2')}$ and $H_{(6')}$), and 7.0—7.8 (4H, m, $H_{(4-7)}$). Found: C, 72.85; H, 5.45%. Calcd for $C_{18}H_{16}O_4$; C, 72.96; H, 5.44%.

*3-Formyl-2-(4-methoxyphenyl)benzofuran (**7**)*: Mp 114.5—115.5 °C (cyclohexane); IR ($CHCl_3$) 1678 cm^{-1} (CHO); UV λ_{max} (log ε) 251 (4.28) and 331 nm (4.26); NMR ($CDCl_3$) δ=3.88 (3H, s, OCH_3), 7.08 (2H, m, $H_{(3')}$ and $H_{(5')}$), 7.2—7.7 (3H, m, $H_{(5-7)}$), 7.83 (2H, m, $H_{(2')}$ and $H_{(6')}$), 8.2—8.5 (1H, m, $H_{(4)}$), and 10.25 (1H, s, CHO); MS *m/e* 252 (M^+). Found; C, 76.19; H, 4.84%. Calcd for $C_{16}H_{12}O_3$; C, 76.18; H, 4.80%.

*2-Acetoxy-2-(4-methoxyphenyl)-3(2H)-benzofuranone (**8f**)*: Mp 112.5—113.5 °C (benzene–light petroleum); IR ($CHCl_3$) 1770^{sh} (C=O) and 1747 cm^{-1} (OAc); UV λ_{max} (log ε) 225^{sh} (4.32), 259 (4.11), 283^{sh} (3.58), and 330 nm (3.69); NMR ($CDCl_3$) δ=2.15 (3H, s, OAc), 3.74 (3H, s, OCH_3), 6.83 (2H, m, $H_{(3')}$ and $H_{(5')}$), 7.10 (2H, m, aromatic), 7.48 (2H, m, $H_{(2')}$ and $H_{(6')}$), and 7.3—7.8 (2H, m, aromatic); MS *m/e* 298 (M^+). Found; C, 68.49; H, 4.74%. Calcd for $C_{17}H_{14}O_5$; C, 68.45; H, 4.73%.

*2-Acetoxy-1-(4-methoxyphenyl)-2-(2-methoxyphenyl)ethanone (**10f**)*: Mp 81.5—83.5 °C (hexane); IR ($CHCl_3$) 1745 (OAc) and 1705 cm^{-1} (C=O); UV λ_{max} (log ε) 222 (4.25) and 286 nm (4.27); NMR ($CDCl_3$) δ=2.17 (3H, s, OAc), 3.80 (3H, s, OCH_3), 3.91 (3H, s, OCH_3), 6.83 (2H, m, $H_{(3)}$ and $H_{(5)}$), 6.7—7.5 (4H, m, aromatic), 7.36 (1H, s, >CH–), and 7.97 (2H, m, $H_{(2)}$ and $H_{(6)}$). Found; C, 68.89; H, 5.87%. Calcd for $C_{18}H_{18}O_5$; C, 68.78; H, 5.77%.

Oxidation Products of ***1g****.* *6-Methoxy-2-(4-methoxyphenyl)-benzofuran (**5g**)*: Mp 156.5—158 °C (EtOH) (lit,[4] mp 159 °C).

*(Z)-α-Acetoxy-2',4,4'-trimethoxystilbene (**9g**)*: Mp 105.5—108.5 °C (benzene–light petroleum); IR ($CHCl_3$) 1762 cm^{-1} (OAc); UV λ_{max} (log ε) 237^{sh} (4.05), 300^{sh} (4.33), and 325 nm (4.41); NMR ($CDCl_3$) δ=2.24 (3H, s, OAc), 3.80 (9H, s, 3×OCH_3), 6.4—6.7 (2H, m, $H_{(3')}$ and $H_{(5')}$), 6.87 (1H, s, =CH), 6.92 (2H, m, $H_{(3)}$ and $H_{(5)}$), 7.48 (2H, m, $H_{(2)}$ and $H_{(6)}$), and 7.56 (1H, m, $H_{(6')}$). Found; C, 69.58; H, 6.27%. Calcd for $C_{19}H_{20}O_5$; C, 69.50; H, 6.14%.

*2-Acetoxy-1-(4-methoxyphenyl)-2-(2,4-dimethoxyphenyl)ethanone (**10g**)*: Liquid; IR ($CHCl_3$) 1750 (OAc) and 1705 cm^{-1} (C=O); NMR ($CDCl_3$) δ=2.16 (3H, s, OAc), 3.74 (3H, s, OCH_3), 3.77 (3H, s, OCH_3), 3.88 (3H, s, OCH_3), 6.2—6.6 (2H, m, $H_{(3')}$ and $H_{(5')}$), 6.81 (2H, m, $H_{(3)}$ and $H_{(5)}$), 7.21 (1H, m, $H_{(6')}$), 7.23 (1H, s, >CH–), and 7.89 (2H, m, $H_{(2)}$ and $H_{(6)}$). Found; *m/e* 344.1235. Calcd for $C_{19}H_{20}O_6$; M, 344.1260.

Oxidation Products of ***1h****.* *6,7-Dimethoxy-3-(4-methoxyphenyl)coumarin (**3h**)*: Mp 172—173 °C (EtOH); IR ($CHCl_3$) 1730 cm^{-1} (C=O); UV λ_{max} (log ε) 230 (4.42), 249^{sh} (4.15), and 370 nm (4.36); NMR ($CDCl_3$) δ=3.84 (3H, s, OCH_3), 3.92 (3H, s, OCH_3), 3.94 (3H, s, OCH_3), 6.7—7.1 (4H, m, aromatic), 7.67 (2H, m, $H_{(2')}$ and $H_{(6')}$), and 7.68 (1H, s, $H_{(4)}$). Found; C, 69.10; H, 5.26%. Calcd for $C_{18}H_{16}O_5$; C, 69.22; H, 5.16%.

*(Z)-α-Acetoxy-3',4,4'-trimethoxystilbene (**9h**)*: Mp 108.5—109 °C (benzene–light petroleum); IR ($CHCl_3$) 1760 cm^{-1} (OAc); UV λ_{max} (log ε) 320 nm (4.48); NMR ($CDCl_3$) δ=2.28 (3H, s, OAc), 3.82 (3H, s, OCH_3), 3.89 (6H, s, 2×OCH_3), 6.52 (1H, s, =CH–), 6.88 (2H, m, $H_{(3)}$ and $H_{(5)}$), 6.7—7.2 (3H, m, $H_{(2')}$, $H_{(5')}$, and $H_{(6')}$), and 7.46 (2H, m, $H_{(2)}$ and $H_{(6)}$). Found; C, 69.21; H, 6.20%. Calcd for $C_{19}H_{20}O_5$; C, 69.50; H, 6.14%.

*2-Acetoxy-1-(4-methoxyphenyl)-2-(3,4-dimethoxyphenyl)ethanone (**10h**)*: Liquid; IR ($CHCl_3$) 1750 (OAc) and 1705 cm^{-1} (C=O); NMR (CCl_4) δ=2.07 (3H, s, OAc), 3.66 (6H, s, 2×OCH_3), 3.69 (3H, s, OCH_3), 6.68 (2H, m, $H_{(3)}$ and $H_{(5)}$), 6.5—7.0 (4H, m, >CH– and aromatic), and 7.77 (2H, m, $H_{(2)}$ and $H_{(6)}$). Found; *m/e* 344.1238. Calcd for $C_{19}H_{20}O_6$; M, 344.1260.

*1-(3,4-Dimethoxyphenyl)-2-(4-methoxyphenyl)acetylene (**12**)*: Mp 107—107.5 °C (EtOH); IR ($CHCl_3$) 2840 cm^{-1} (OCH_3); UV λ_{max} (log ε) 247^{sh} (4.04), 298 (4.49), 310 (4.46), and 319 nm (4.46); NMR ($CDCl_3$) δ=3.78 (3H, s, OCH_3), 3.86 (6H, s, 2×OCH_3), 6.83 (2H, m, $H_{(3')}$ and $H_{(5')}$), 6.7—7.3 (3H, m, $H_{(2)}$, $H_{(5)}$, and $H_{(6)}$), and 7.41 (2H, m, $H_{(2')}$ and $H_{(6')}$); MS *m/e* 268 (M^+). Found; C, 75.90; H, 6.12%. Calcd for $C_{17}H_{16}O_3$; C, 76.10; H, 6.01%.

*Oxidation of 2-Phenylbenzofuran (**5a**).* A mixture of 2-phenylbenzofuran (**5a**)[27] (194 mg), manganese(III) acetate dihydrate (2.68 g), acetic acid (30 ml), and acetic anhydride (2 ml) was heated under reflux for 2.5 h. After the removal of the acetic acid *in vacuo*, the resulting mixture was triturated with chloroform and filtered. The filtrate was concentrated and separated on TLC, giving **5a** (25 mg), 3-(acetoxymethyl)-2-phenylbenzofuran (**6a**) (86.7 mg, 30%), and 2-acetoxy-2-phenyl-3(2*H*)-furanone (**8a**) (67.7 mg, 25%); mp 128—129 °C (light petroleum); IR ($CHCl_3$) 1770 (C=O) and 1748 cm^{-1} (OAc); UV λ_{max} (log ε) 257 (4.11) and 329 nm (3.55); NMR ($CDCl_3$) δ=2.14 (3H, s, OAc) and 6.9—7.8 (9H, m, aromatic) (Found: C, 71.80; H, 4.41%. Calcd for $C_{16}H_{12}O_4$; C, 71.63; H, 4.51%).

*Preparation of (Z)-α-Acetoxy-3',4,4'-trimethoxystilibene (**9h**).* A mixture of 3,4-dimethoxybenzyl 4-methoxyphenyl ketone[34] (1.8 g), freshly fused potassium acetate (3.6 g), and acetic anhydride (60 ml) was heated under reflux for 5 h. After

the removal of the acetic anhydride *in vacuo*, the residue was extracted with chloroform. The chloroform solution was washed with aqueous sodium hydrogencarbonate, dried, and evaporated. The crude product was purified on TLC, using chloroform as the developing solvent, and by recrystallization, giving colorless needles (900 mg, 44%), mp 108.5—109 °C (MeOH).

Oxidation of (Z)-α-Acetoxystilbene (9). The general procedure for the oxidation of (*Z*)-α-acetoxystilbene (**9**) was as follows. A mixture of **9** (1 mmol), manganese(III) acetate dihydrate (2—5 mmol), and a solvent (20 ml) was heated under reflux for the time shown in Table 2. After being worked-up in a manner similar to that used in the oxidation of (*E*)-α-phenylcinnamic acids (**1**), the following products were obtained (the yields are summarized in Table 2): (*Z*)-α-Acetoxy-3′,4,4′-trimethoxystilbene (**9h**) gave **10h** and 3,4,4′-trimethoxybenzil (**13h**); mp 123—124 °C (EtOH); IR ($CHCl_3$) 1670 cm^{-1} (C=O); UV λ_{max} (log ε) 228 (4.29), 295 (4.36), and 322^{sh} nm (4.23); NMR ($CDCl_3$) δ=3.87 (3H, s, OCH_3), 3.93 (6H, s, 2×OCH_3), 6.89 (1H, d, J=7.5 Hz, $H_{(5)}$), 6.95 (2H, m, $H_{(3')}$ and $H_{(5')}$), 7.3—7.6 (2H, m, $H_{(2)}$ and $H_{(6)}$), and 7.92 (2H, m, $H_{(2')}$ and $H_{(6')}$) (Found; C, 68.05; H, 5.48%. Calcd for $C_{17}H_{16}O_5$; C, 67.99; H, 5.37%). (*Z*)-α-Acetoxystilbene (**9i**)[35] yielded 2-acetoxy-1,2-diphenylethanone (**10i**); mp 81.5—82.5 °C (benzene–hexane) (lit,[36] mp 83 °C); 5-acetoxy-4,5-diphenyl-2(5*H*)-furanone (**11i**); liquid; IR ($CHCl_3$) 1770 cm^{-1}; NMR ($CDCl_3$) δ=2.16 (3H, s, OAc), 6.61 (1H, s, $H_{(3)}$), and 7.2—7.7 (10H, m, 2×Ph); MS *m/e* 294 (M^+), 252, 235, 147, 105, 102, and 77, and 3,4-diphenyl-4-oxobutanoic acid (**14**); mp 148—149 °C (benzene–light petroleum) (lit,[37] mp 161 °C); IR ($CHCl_3$) 1705 (C=O), 1735 (COOH), and 2400—3600 cm^{-1} (COOH); NMR ($CDCl_3$) δ=2.72 (1H, dd, J=18 and 6 Hz, -CH-), 3.41 (1H, dd, J=18 and 9 Hz, -CH-), 5.05 (1H, dd, J=9 and 6 Hz, >CH-), 7.0—7.6 (8H, m, aromatic), 7.90 (2H, m, aromatic), and 9.95 (1H, br, s, COOH), and benzoic acid (**15**).

Oxidation of 2-Acetoxy-1,2-diphenylethanone (10h). A mixture of **10h** (254 mg), manganese(III) acetate dihydrate (536 mg), acetic acid (20 ml), and acetic anhydride (0.4 ml) was heated under reflux for 3 h. After the removal of the solvent, the resulting mixture was extracted with chloroform. The chloroform solution was concentrated and the resulting substance was chromatogrammed on TLC by developing with chloroform, giving **13i** (31 mg, 15%) and unchanged **10i** (173 mg, 68%).

The authors wish to thank Mr. Shuichi Ueda at the Taiho Pharmaceutical Co., Ltd., Tokushima, and Dr. Shinzaburo Hishida at Hitachi, Ltd., Katsuda, for their measurements of the mass spectra.

References

1) F. F. Stephens and J. D. Bower, *J. Chem. Soc.*, **1949**, 2971.
2) a) K. Kurosawa, *Bull. Chem. Soc. Jpn.*, **42**, 1456 (1969); b) K. Kurosawa and J. Higuchi, *ibid.*, **45**, 1132 (1972).
3) K. Kurosawa, Y. Sasaki, and M. Ikeda, *Bull. Chem. Soc. Jpn.*, **46**, 1498 (1973); S. Ueda and K. Kurosawa, *ibid.*, **50**, 193 (1977).
4) K. Nogami and K. Kurosawa, *Bull. Chem. Soc. Jpn.*, **47**, 505 (1974).
5) K. Kurosawa and K. Nogami, *Bull. Chem. Soc. Jpn.*, **49**, 1955 (1976).
6) K. Kurosawa and F. Araki, *Bull. Chem. Soc. Jpn.*, **52**, 529 (1979).
7) R. N. Butler, "Synthetic Reagents," ed by J. S. Pizey, Ellis Horwood, Ltd., England (1977), Vol. 3, p. 277.
8) D. I. Davies and C. Waring, *Chem. Commun.*, **1965**, 263; D. I. Davies and C. Waring, *J. Chem. Soc., C*, **1967**, 1639; W. R. Moove and H. Arzoumanian, *J. Org. Chem.*, **27**, 4667 (1962).
9) Z. Buczkowski and S. Maciaszek, *Bull. Acad. Pol. Sci., Ser. Sci. Chim.*, **1970**, 577; *Chem. Abstr.*, **74**, 111159f (1971).
10) T. Sonoda, S. Kobayashi, and H. Taniguchi, *Bull. Chem. Soc. Jpn.*, **49**, 2560 (1976).
11) T. Aratani and M. J. S. Dewar, *J. Am. Chem. Soc.*, **88**, 5479 (1966).
12) E. I. Heiba, R. M. Dessau, and W. J. Koehl, Jr., *J. Am. Chem. Soc.*, **91**, 138 (1969).
13) E. I. Heiba, R. M. Dessau, and W. J. Koehl, Jr., *J. Am. Chem. Soc.*, **91**, 6830 (1969).
14) A. Kasahara, T. Izumi, A. Suzuki, and T. Takeda, *Bull. Chem. Soc. Jpn.*, **49**, 3711 (1976).
15) K. Kurosawa and H. Harada, *Bull. Chem. Soc. Jpn.*, **52**, 2386 (1979).
16) D. S. Noyce and A. M. Myers, *J. Org. Chem.*, **35**, 2460 (1970).
17) S. Moon and H. Bohm, *J. Org. Chem.*, **37**, 4338 (1972).
18) T. Shono, Y. Matsumura, and Y. Nakagawa, *J. Am. Chem. Soc.*, **96**, 3532 (1974); T. Shono, M. Okawa, and I. Nishiguchi, *J. Am. Chem. Soc.*, **97**, 6144 (1975).
19) J. B. Bush, Jr., and H. Finkbeiner, *J. Am. Chem. Soc.*, **90**, 5903 (1968); E. I. Heiba, R. M. Dessau, and W. J. Koehl, Jr., *J. Am. Chem. Soc.*, **90**, 5905 (1968); E. I. Heiba, R. M. Dessau, and P. G. Rodewald, *J. Am. Chem. Soc.*, **96**, 7977 (1974); M. Okano, *Bull. Chem. Soc. Jpn.*, **49**, 1041 (1976).
20) C. Funk and St. v. Kostanecki, *Ber.*, **38**, 939 (1905).
21) H. Kauffmann, *Ber.*, **52**, 1432 (1919).
22) N. R. Krishnasway, T. R. Seshadri, and B. R. Sharma, *Indian J. Chem.*, **2**, 182 (1964).
23) C. Weygand and T. Siebenmark, *Ber.*, **73B**, 765 (1940).
24) H. C. Caldwell, J. A. Finkelstein, P. P. Goldman, A. J. Sivak, J. Schlosser, C. Pelikan, and W. G. Groves, *J. Med. Chem.*, **13**, 1076 (1970).
25) D. Papa, E. Klingsberg, and E. Schwenk, U. S. Patent 2606922 (1952); *Chem. Abstr.*, **47**, 6442h (1953).
26) P. J. Andrulis, Jr., M. J. S. Dewar, R. Dietz, and R. L. Hunt, *J. Am. Chem. Soc.*, **88**, 5473 (1966).
27) S. Kawai, T. Nakamura, and N. Sugiyama, *Pro. Imp. Akad. (Tokyo)*, **15**, 45 (1939); S. Kawai, T. Nakamura, and N. Sugiyama, *Nippon Kagaku Zasshi*, **60**, 513 (1939).
28) K. Nakanishi, "Sekigaisen Kyushu Supekutoru, Teisei-hen," Nankodo, Tokyo (1960), p. 50.
29) W. Baker, *J. Chem. Soc.*, **1927**, 2898.
30) G. Bargellini, *Gazz. Chim. Ital.*, **57**, 457 (1927).
31) J. N. Chatterjea, K. Achari, and N. C. Jain, *J. Indian Chem. Soc.*, **47**, 590 (1970).
32) R. P. Barnes and W. M. Lucas, *J. Am. Chem. Soc.*, **64**, 2258 (1942).
33) C. A. Anirudhan, W. B. Whalley, and M. M. E. Bardan, *J. Chem. Soc., C*, **1966**, 629.
34) J. C. Cain, J. L. Simonsen, and C. Smith, *J. Chem. Soc.*, **103**, 1035 (1913).
35) R. P. Barnes, S. R. Cooper, V. J. Tulane, and H. Delaney, *J. Org. Chem.*, **8**, 153 (1943).
36) B. B. Corson and N. A. Saliani, *Org. Synth.*, Coll. Vol. 2, 69 (1948).
37) E. R. Japp and A. C. Michie, *J. Chem. Soc.*, **1903**, 291.

 © 1980 The Chemical Society of Japan Bull. Chem. Soc. Jpn., 53, 185—188 (1980)

Molecular Dynamical Studies on Nitrobenzene in Solutions of Tetraethyl and Tetrabutylammonium Bromides

Hiroyasu NOMURA,* Yoshiaki TSUKAMOTO, and Yutaka MIYAHARA

Department of Chemical Engineering, Faculty of Engineering, Nagoya University, Chikusa-ku, Nagoya 464

(Received May 15, 1979)

The concentration and temperature dependences of the reorientational correlation times of nitrobenzene in solutions of tetraethyl(TEABr) and tetrabutylammonium bromides(TBuABr) have been determined by Raman line shape analysis. Pure liquid nitrobenzene was evaluated for comparison. The reorientational correlation times of nitrobenzene in solutions decreased with increasing concentration of the salts and the apparent activation enthalpy of τ_{or} of nitrobenzene in solutions was larger than in that pure nitrobenzene. From the experimental results, the solution structure of TEABr and TBuABr in nitrobenzene are discussed.

It the studies of ionic association in nonaqueous solvents, nitrobenzene has an important role, because of its high viscosity and high dielectric constant. In these studies, the ionic association constant and the kinetic parameters have been determined by means of various techniques, such as electrical conductance[1-3] and ultrasonic absorption measurements.[4] It has been shown that the association of ions in nitrobenzene type was of the solvent-separated type.

Hyne proposed a model for the specific solvation of the n-$Bu_4N^+Br^-$ ion pair in nitrobenzene.[5] Considering the relative dimensions and the charge distributions of the n-$Bu_4N^+Br^-$ ion-pair and nitrobenzene molecule, it was concluded that it was not improbable that the nitrobenzene acts as a "template for the absorption" of n-$Bu_4N^+Br^-$ ion-pairs and this was comfirmed by NMR studies.

Recently, several molecular dynamical studies of liquid nitrobenzene have been reported using nuclear magnetic resonance[6,7] and depolarized Rayleigh scattering.[7,8] In these studies, the reorientational correlation times of nitrobenzene have been determined and the liquid structure of nitrobenzene discussed.

One of the most powerful tools in determining the reorientational correlation times is Raman spectroscopy. It is expected that the reorientational correlation times of the nitrobenzene molecule is a sensitive measure of the solute-solvent interaction, especially the local structure, in solutions.

In this paper, the temperature dependence of the reorientational correlation time of nitrobenzene and the concentration dependence in tetraethyl and tetrabutylammonium bromides–nitrobenzene solutions will be reported. In addition, in order to discuss the effects of viscosity and molecular volume on reorientational motion, the viscosity and partial molar volumes of tetraethyl and tetrabutylammonium bromides in nitrobenzene have been evaluated.

Experimental and Data Analysis

Sample. Nitrobenzene was a commercial product (extra-pure-grade reagent) and was distilled under reduced pressure, after drying by molecular sieves. Tetraethylammonium bromide and tetrabutylammonium bromide, hereafter abbreviated TEABr and TBuABr, respectively, were of extra-pure-grade.

Viscosity and Density Measurements. The density and viscosity were measured, respectively, with an Ostwald type pycnometer and viscometer at 30 °C.

Raman Spectroscopy. The apparatus used consisted of an argon ion laser (800 mW 488 nm) produced by the Coherent Radiation Co., Ltd., and a Laser Raman Spectrometer of JRS-Ul type, JEOL Ltd., Japan.

In order to obtain the reorientational correlation times, the Raman line shape of the ν_{12} (a_1) fundamental mode of ring-stretching,[9] 1004 cm^{-1}, was analyzed. The Raman spectrum was observed at 90° scattering with respect to the linearly polarized incident light. The intensities $I_{isot}(\omega)$ and $I_{anis}(\omega)$ may be determined from the spectra obtained by polarizing the scattered beam parallely, $I_{\parallel}(\omega)$ and perpendicularly, $I_{\perp}(\omega)$ to the electric field vector E of incident light:

$$I_{isot}(\omega) = I_{\parallel}(\omega) - 4/3 I_{\perp}(\omega) \quad (1)$$

$$I_{anis}(\omega) = I_{\perp}(\omega) \quad (2)$$

$I_{isot}(\omega)$ represents the intrinsic vibrational line shape and $I_{anis}(\omega)$ is a convolution of the vibrational line shape and the reorientational spectrum.

The Raman bands measured are broadened by the instrumental slit width and the spectrum obtained is a convolution of the true Lorentzian spectrum and the slit function, $S(\omega)$. The spectral slit function is well approximated by a Gaussian function,[10] and thus:

$$I'(\omega) = N\int_{-\infty}^{\infty} \frac{1}{\beta_L{}^2 + (\omega-\omega')^2} \exp\left\{-\left(\frac{\omega'}{\beta_G}\right)^2\right\} d\omega', \quad (3)$$

where β_L is the true half-width and $\beta_G = S/2\sqrt{\ln 2}$, where, S is the spectral slit width.

An approximate analytical expression for $I'(\omega)$ in Eq. 3, has been proposed by Kielkopf.[12] It is preferable to estimate the apparent spectral line-width as a function of mechanical slit width by means of the direct calculation of Eq. 3 for each β_L value.

For example, the Raman line shape of the $\nu_{12}(a_1)$ band of nitrobenzene is shown in Fig. 1. The spectral half-width of the Raman line of the $\nu_{12}(a_1)$ band of nitrobenzene was measured as a function of the mechanical slit width S. Figure 2 shows a plot of the apparent spectral line width obatined *vs.* the mechanical slit width of the spectrometer used. In Fig. 2, the solid line shows the relation between the apparent spectral line width calculated by Eq. 3 and the mechanical slit width, $\beta_G = S/2\sqrt{\ln 2}$, assuming the true half-width, β_L, of Lorentzian spectrum. As seen in Fig. 2, the agreement between the values observed and those calculated is extremely good. This indicates that the isotropic and anisotropic line shapes of Raman scattering of the $\nu_{12}(a_1)$ fundamental mode of nitrobenzene is adequately described by the Lorentzian function and the slit function, $S(\omega)$, of the spectrometer used may be well approximated by the Gaussian function. The true half-width, β_L, by fitting the observed spectrum with one calculated from Eq. 3 using the

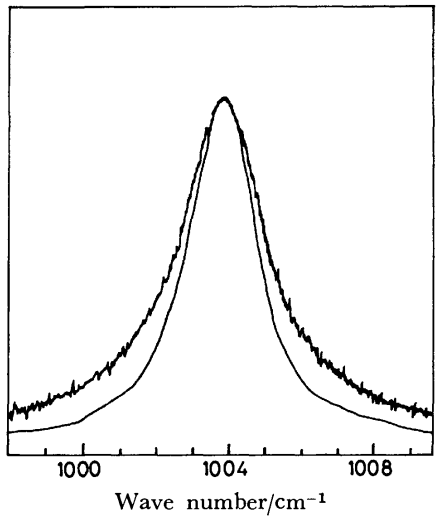

Fig. 1. Raman line shape of isotropic (∥) and anisotropic (⊥) parts of $\nu_{12}(a_1)$ mode (1004 cm^{-1}) of nitrobenzene in tne solution of TBuABr, 0.025 mol/l. (the intensities were normalized each other.)

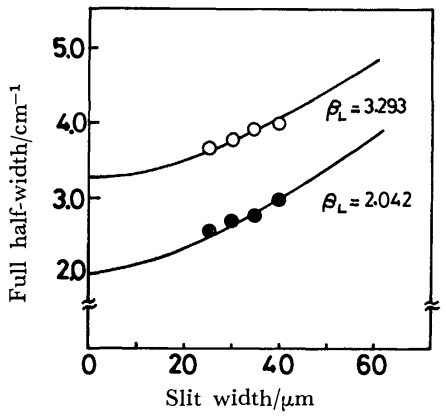

Fig. 2. Plots of apparent spectral slit-width *vs.* mechanical slit-width of the spectrometer used. Solid lines show the calculated ones from Eq. 4. (0.05 mol/l; TBuABr-nitrobenzene solution).
○; Anisotropic, ●; isotropic.

spectral slit width, β_G, under the conditions of measurement. Hereafter, instead of β_L, $\omega_{isot}(1/2)$ and $\omega_{anis}(1/2)$ refer to the true half-width of isotropic and anisotropic Raman line shape.

Thus, the vibrational and reorientational correlation times may be estimated from the half-width of anisotropic and isotropic Raman line shape as follows;

$$\tau_v = (\pi c \omega_{isot}(1/2))^{-1}, \quad (4)$$

$$\tau_{or} = (\pi c \omega_{or}(1/2))^{-1}, \quad (5)$$

where, $\omega_{or}(1/2) = \omega_{anis}(1/2) - \omega_{isot}(1/2)$.

Results

The polts of $\omega_{isot}(1/2)$ and $\omega_{anis}(1/2)$ against the concentration of TEABr and TBuABr are shown in Fig. 3. The differences in these values of TEABr and TBuABr can not be observed. The values of $\omega_{anis}(1/2)$ increase with increasing concentration, but at higher concentration, the increment increase of $\omega_{anis}(1/2)$ with concentration becomes small. The

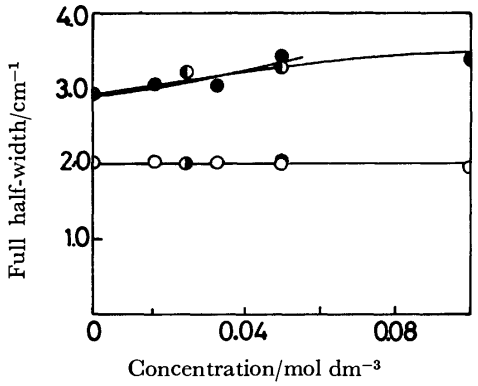

Fig. 3. Concentration dependences of the full half-width of isotropic, $\omega_{isot}(1/2)$, and anisotropic. $\omega_{anis}(1/2)$, parts.
○; $\omega_{isot}(1/2)$, ●: $\omega_{anis}(1/2)$, TEABr-nitrobenzene.
◑; $\omega_{isot}(1/2)$, ◐; $\omega_{anis}(1/2)$, TBuABr-nitrobenzene.

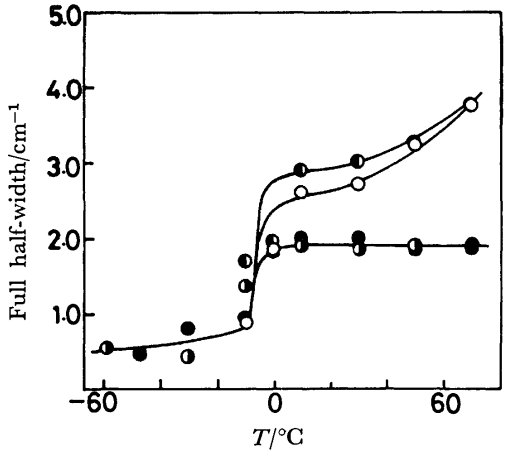

Fig. 4. Temperature dependences of the full half-width.
●; $\omega_{isot}(1/2)$, ○; $\omega_{anis}(1/2)$, neat nitrobenzene,
◑; $\omega_{isot}(1/2)$, ◐; $\omega_{anis}(1/2)$, 0.0333 mol/l, TEABr-nitrobenzene solution.

values of $\omega_{isot}(1/2)$ are however independent of concentration, indicating that the solute molecules, TEABr and TBuABr, do not contribute to the vibrational correlation times of the $\nu_{12}(a_1)$ mode of nitrobenzene in the solutions.

The temperature dependence of $\omega_{anis}(1/2)$ and $\omega_{isot}(1/2)$ of nitrobenzene and nitrobenzene in solutions of TEABr are shown in Fig. 4. As seen, the differences in value of $\omega_{isot}(1/2)$ in pure nitrobenzene and in the solutions could not be observed in the temperature ranges, but at the transition point from solid to liquid phases, the values of $\omega_{isot}(1/2)$ change drastically. This line broadening is thought due to a molecular dephasing process accompanied by molecular collisions in the liquid and/or solution. This mechanism is independent of the solute ions in solutions. The values of $\omega_{anis}(1/2)$ in the liquid phase increase with increasing temperature.

In Table 1, the partial molar volumes and the viscosity *B* coefficients of TEABr and TBuABr in nitrobenzene, obtained from density and viscosity measurements, are summarized together with those in aqueous solutions.

Table 1. Partial molar volumes and B coefficient of TEABr and TBuABr in nitrobenzene

	ϕ_v°/l mol^{-1}		B/l mol^{-1}		$B-2.5\,\phi_v^\circ$/l mol^{-1}	
	Nitrobenzene	Water	Nitrobenzene	Water	Nitrobenzene	Water
TEABr	0.1660	0.1738[a)]	0.88_8	0.338[a)]	0.473	−0.097
TBuABr	0.3012	0.3004[a)]	1.07_7	1.238[a)]	0.324	0.487

a) "Water and Aqueous Solutions: Structure, Thermodynamics, and Transport Processes," ed by R. A. Horne, Wiley-Interscience, New York (1971).

Discussion

The molecular symmetry of nitrobenzene belongs to the class C_{2v}. In the present work, the $\nu_{12}(a_1)$ mode of nitrobenzene, the ring stretching mode, was used to determine the reorientational correlation time of nitrobenzene by line shape analysis. As clearly indicated by Nafie and Peticolas,[13] the normalized correlation function obtained from the Raman line shape analysis of this mode may be expressed as follows;

$$C(t) = (a^2+b^2+c^2-ac-ab-bc)^{-1} \times \{(b-a)^2\boldsymbol{P}_2[\boldsymbol{u}^y(0)\boldsymbol{u}^y(t)] + (c-a)^2\boldsymbol{P}_2[\boldsymbol{u}^z(0)\boldsymbol{u}^z(t)] + (b-a)(c-a)\boldsymbol{P}_2[\boldsymbol{u}^z(0)\boldsymbol{u}^y(t)] + \boldsymbol{P}_2[\boldsymbol{u}^y(0)\boldsymbol{u}^z(t)]\}, \quad (6)$$

where $\boldsymbol{u}^z(0)$ is unit vector indicating the direction of the molecular z axis at time $t=0$, $\boldsymbol{u}^z(t)$ indicates the direction of the same axis at time t and a, b, and c refer to the Raman tensors of α_{xx}, α_{yy}, and α_{zz}, respectively. Therefore, at this stage, the reorientational correlation time, τ_{or}, obtained from the Raman line shape analysis of the ν_{12} mode of nitrobenzene can not explicitly assigned to a rotational diffusion tensor. Bauer *et al.* concluded by comparison with NMR measurements that the reorientation about the z axis is at least twice as fast as reorientation about the other axis.[7,8] The reorientational motion of nitrobenzene is mainly concerned with motion about the z axis and the τ_{or} obtained, here, is a measure of the local motion of nitrobenznene in the liquid and solutions.

Influence of TEABr and TBuABr on the Molecular Motion of Nitrobenzene. As seen in Fig. 3, the values of $\omega_{isot}(1/2)$, which are related to the vibrational correlation times of nitrobenzene, are independent of the concentration of tetraalkylammonium bromide and its chain length. This indicates that the solute molecules do not affect the molecular vibrational correlation times of nitrobenzene as a solvent.

The plots of reorientational correlation time against the concentration of TEABr and TBuABr are shown in Fig. 5. The reorientational correlation time of nitrobenzene, τ_{or}, as a solvent decreases with increasing concentration of solute, indicating that the interaction between nitrobenzenes is stronger than that between nitrobenzene and TEABr and/or TBuABr. As seen in Table 1, the partial molar volumes of TEABr and TBuABr in nitrobenzene do not greatly differ from in aqueous solutions. This indicates that the molecular diameter and volumes of the tetraalkylammonium ion in nitrobenzene are comparable to those in aqueous solutions. The viscosity B coefficients of both solutions

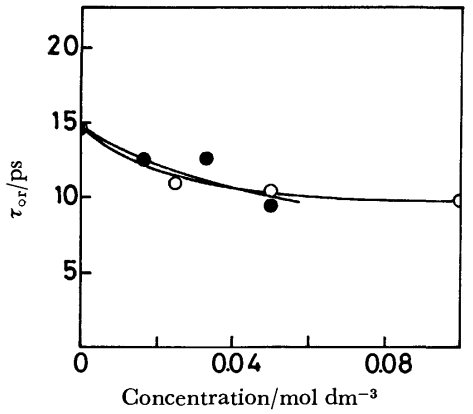

Fig. 5. Plots of τ_{or} *vs.* concentration of salts in solutions.
●; τ_{or} of nitrobenzene in TEABr,
○; τ_{or} of nitrobenzene in TBuABr.

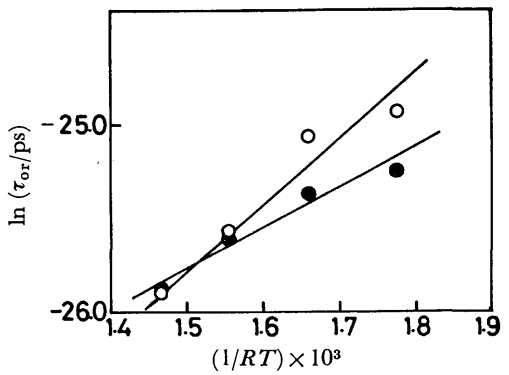

Fig. 6. Plots of $\ln\tau_{or}$ *vs.* $1/RT$.
○; τ_{or} of nitrobenzene in 0.0333 mol/l TEABr solution.
●; τ_{or} of neat nitrobezene.

are positive.

The values of $(B-\phi_{ion}^\circ)$ which are a measure of the ion-solvent interactions do not differ indicating that the ion-solvent interactions remain in TEABr and TBuABr–nitrobenzene solutions. The results mentioned above do not agree with the model proposed by Hyne for specific solvation of n-$Bu_4N^+Br^-$ ion-pairs and nitrobenzene.

Temperature Dependence of Reorientational Correlation Times of Nitrobenzene in the Pure and Solution States. The relationships between the reorientational correlation times of nitrobenzene in the pure and solution states, τ_{or}, and $1/RT$ are shown in Fig. 6. As seen in Fig. 6, τ_{or} can be expressed by the equation

$$\tau_{or} = \tau_{or}^\circ \exp(U/RT), \quad (7)$$

TABLE 2. REORIENTATIONAL RELAXATION TIMES DETERMINED BY VARIOUS TECHNIQUES

T/°C	τ_{or}(Raman)	τ_{1s}	$\tau_{NMR,p}(C^{13})$	$\tau_{NMR,o,m}(C^{13})$	$\tau_{NMR}(N^{14})$
10	14.8[a]				
20	17.6[e]	40.83[e]			
24		36.0[b]	12.5[b]	8.1[b]	
30	13.1[a]				3.45 (25 °C)[d]
38			9.6[c]	6.6[c]	
50	8.0[a]				
70	5.7[a]				

a) This work. b) Ref. 7. c) G. C. Levy, J. D. Cargioli, and F. A. L. Anet, *J. Am. Chem. Soc.*, **95**, 1527 (1973). d) Ref. 6. e) A. M. Amorim, D. Costa, M. A. Norman, and J. H. Rclarke, *Mol. Phys.*, **29**, 191 (1975).

where U refers to the apparent activation energy. The apparent activation energies, U, estimated from the plots of τ_{or} *vs.* $1/RT$ are 3.5 kcal/mol and 2.2 kcal/mol in the pure and solution states, respectively. The value of U, 3.5 kcal/mol, for pure liquid nitrobenzene is in good agreement with those obtained from the temperature dependence of "quadrupolar" correlation times for the molecular reorientation of liquid nitrobenzene by means of nuclear relaxation experiment of N^{14} [6] and are also comparable to those obtained from the temperature dependence of viscosity of nitrobenzene.

The reorientational correlation times of nitrobenzene in the solution of TEABr (0.0333 mol/l) are shorter than that in the pure liquid state in the temperature ranges and the apparent activation energy of τ_{or} in the solution state is smaller than that in pure liquid state. This indicates that the molecular motion of nitrobenzene is easier in solution than in the pure liquid state.

Bauer *et al.*[8] considered that nitrobenzene forms a "weak" dimer which hinders rotation. The addition of TEABr and/or TBuABr in nitrobenzene breaks the "weak" dimer and consequently nitrobenzene molecule can rotate more freely.

Comparison with Other Relaxation Times. The reorientational relaxation time obtained from the depolarized light scattering spectrum, τ_{LS}, relates to the single particle reorientational relaxation time, τ_s, which can be determined directly by means of Raman line shape analysis:[8]

$$\tau_{LS} = \left(\frac{1+fN}{1+gN}\right)\tau_s, \qquad (8)$$

where the parameter, fN and gN, refer to the static and dynamic orientational pair correlation terms, respectively.

The relaxation times determined by several techniques are summarized in Table 2. Alms *et al.*[8] estimated the values of fN and gN as 1.30 ± 0.05 and 0.1 ± 0.0 for neat nitrobenzene. Using the value of τ_{LS}, 36.0 ps, and these values of fN and gN, the single particle relaxation time, τ_s, has been estimated to be 15.8 ± 0.5 ps. This value is in good agreement with those of τ_{or} obtained from the Raman line shape analysis.

References

1) H. Sadek and R. M. Fuoss, *J. Chem. Phys.*, **72**, 301 (1950).
2) R. M. Fuoss and F. Accascina, "Electrolyte Conductance," International Publishers Inc. New York. N. Y. (1959).
3) R. M. Fuoss and H. Sadek, *J. Am. Chem. Soc.*, **81**, 4507 (1959).
4) S. Petrucci and M. Battistini, *J. Chem. Phys.*, **71**, 1181 (1967).
5) J. B. Hyne, *J. Am. Chem. Soc.*, **85**, 304 (1963).
6) W. B. Moniz and H. S. Gutowsky, *J. Chem. Phys.*, **38**, 1155 (1963).
7) G. R. Alms, D. R. Bauer, J. I. Brauman, and R. Pecora., *J. Chem. Phys.*, **59**, 5310 (1973).
8) D. R. Bauer, G. R. Alms, J. I. Brauman, and R. Pecora, *J. Chem. Phys.*, **61**, 2255 (1974).
9) J. H. Green, W. Kynaston, and A. S. Lindsey., *Spectrochim. Acta*, **17**, 486 (1961).
10) R. E. Meredith, *J. Quant. Spectrosc. Radiat. Transfer.*, **12**, 455 (1972).
11) J. S. Seshadri and R. Norman Jones, *Spectrochim. Acta*, **19**, 1013 (1963).
12) J. F. Kielkopf, *J. Opt. Soc. Am.*, **63**, 987 (1973).
13) L. A. Nafie and W. L. Peticolas. *J. Chem. Phys.*, **57**, 3145 (1972).
14) H. C. Lucas, D. A. Jackson, J. G. Powles, and B. Simic-Glavaski, *Mol. Phys.*, **18**, 505 (1970).

Branched-chain Sugars. XIX. On the Application of ^{13}C NMR Spectroscopy to the Configurational Assignment of 3-*C*-Substituents of Aldohexopyranose Derivatives[1)]

Ken-ichi SATO, Masafumi MATSUZAWA, Katsumi AJISAKA,† and Juji YOSHIMURA*

Laboratory of Chemistry for Natural Products, Faculty of Science, Tokyo Institute of Technology, Nagatsuta, Midori-ku, Yokohama 227

(Received May 18, 1979)

It was found that ^{13}C NMR spectroscopy is applicable to the unequivocal configurational assignment at the quarternary carbon in seven pairs of 3-*C*-substituted-hexopyranose derivatives. The configuration of methyl 4,6-*O*-benzylidene-3-*C*-nitromethyl-2-*O*-*p*-tolylsulfonyl-α-D-glucopyranoside reported by Jordaan *et al.* is revised to D-*allo* by a chemical method.

Determination of the configuration of a branching carbon atom in branched-chain sugars having no hydrogen atom at the branching point is difficult, no simple and reliable method being available. In our work on the subject, chemical derivations, cuprammonium complex formation,[1)] and the chemical shift of tertiary acetoxyl protons[3)] have been used. However, some exceptions in ^1H NMR method have been found in the case of branched-chain sugars.[4-6)]

Recently, lanthanoid-induced changes in the chemical shifts of ^1H NMR[7)] and the ^{13}C chemical shift differences between axial and equatorial carbons[8)] have been used to elucidate the configuration of tertiary alcoholic centers of several branched-chain sugars.

In the lanthanoid method, the magnitude of the shift gradient (proportional shift of the concentration to shift reagent) for each identifiable proton resonance of a tertiary alcoholic derivative is compared with that of the corresponding secondary alcohol of known stereochemistry. The uniform correspondence of the entire set of shift gradients is taken as evidence of their same relative configuration.[7)] However, during the course of examination of the method for branched-chain sugars synthesized in our laboratory, we found that it is ambiguous in a few instances; the configuration of methyl 4,6-*O*-benzenzylidene-3-*C*-nitromethyl-2-*O*-*p*-tolylsulfonyl-α-D-glucopyranoside (**1**)[9)] assigned by this method[6)] has been revised to D-*allo* (**2**).

More data seemed necessary to establish the ^{13}C NMR method. In this paper, the above structure revision and consistent results in the examination of the ^{13}C NMR method for seven pairs of 3-*C*-substituted hexopyranose derivatives having various functional groups at the branching point are described.

Results and Discussion

Methyl 4,6-*O*-benzylidene-3-*C*-(benzoylaminomethyl)-α-D-allopyranoside (**3**) was obtained by the reaction of methyl 4,6-*O*-benzylidene-2-*O*-benzoyl-α-D-*ribo*-hexopyranosid-3-ulose with nitromethane, followed by hydrogenation which was accompanied by O→N benzoyl migration.[10)] The configuration of **3** was confirmed by comparison of the rotational change in cuprammonium solution with that of its 3-epimer synthesized from the same 3-ulose by the successive reactions; spiro-epoxidation with diazomethane, epoxy-ring opening with ammonia, and then *N*-benzoylation. From the results, the assignment of D-*gluco* configuration to a 3-*C*-nitromethyl derivative from nitromethane and 2-*O*-*p*-tolylsulfonyl analogue of the above 3-ulose was highly doubtful. From the reaction conditions the 3-*C*-nitromethyl derivatives were considered to be thermodynamically stable products. Consequently, **1** preparaed according to the method of Jordaan *et al.*[9)] was hydrogenated in the presence of well-washed Raney nickel and then subjected to *N*-benzoylation with benzoic anhydride to give the corresponding 3-*C*-(benzoylaminomethyl) derivative (**4**). Treatment of **3** in pyridine with equimolar *p*-toluenesulfonyl chloride also gave **4**. Thus, the D-*gluco* configuration of **1** assigned by shift reagent method was revised to D-*allo* (**2**) by the chemical method.

The fact that equatorially oriented branching carbons are deshielded with respect to axially oriented carbons in ^{13}C NMR for the configurational assignment of branched-chain pyranoses has been shown by examination of three epimeric pairs of 4-*C*-methyl,[11)] two pairs of 3-*C*-hydroxymethyl,[8)] one pair of 3-*C*-methyl derivatives[8)] possessing an hydroxyl group at the quarternary carbon, and one pair of 2-deoxy-2-*C*-methyl derivatives.[11)] We have examined seven epimeric pairs of 3-*C*-substituted derivatives: methyl 2-*O*-acetyl-4,6-*O*-benzylidene-3-*C*-methyl-α-D-allo- (**5**) and -glucopyranoside (**6**),[10)] their 3-*O*-acetyl derivatives (**7** and **8**),[10)] methyl 4,6-*O*-benzylidene-3-*C*-methyl-2-*O*-methyl-α-D-allo- (**9**) and glucopyranoside (**10**),[4a)] methyl 4,6-*O*-benzylidene-3-*C*-methyl-2-*O*-methyl-α-D-altro- (**11**) and -mannopyranoside (**12**),[4a)] methyl 2-*O*-acetyl-3-*C*-(benzoylaminomethyl)-4,6-*O*-benzylidene-α-D-allo- (**13**)[10)] and -glucopyranoside (**14**), methyl 3-acetylamino-2,3,6-trideoxy-3-*C*-methyl-4-*O*-methyl-α-L-*ribo*- (**15**) and -*arabino*-hexopyranoside (**16**),[1)] 2,3,6-trideoxy-3-*C*-methyl-4-*O*-methyl-3-nitro-L-*ribo*- (**17**) and -*arabino*-hexose (**18**),[1)] and one pair of 2-*C*-methyl derivatives; methyl 4,6-*O*-benzylidene-2-*C*-methyl-3-*O*-methyl-α-D-altro- (**19**) and -allopyranoside (**20**).[4b)] Among these compounds, only **14** was newly synthesized by acetylation of the 3-epimer of **3**[10)] in pyridine with acetic anhydride.

Chemical shifts of the chain carbons and 3-*C*-branching carbon of hexopyranoses and shift differences between axially and equatorially oriented carbons at C_3 in **5**—**18** and at C_2 in **19** and **20** are summarized in Table 1. The carbon shifts were distinguished

† Present address: Ajinomoto Co., Inc., Central Research Laboratories, 1-1 Suzuki-cho, Kawasaki-ku, Kawasaki 210.

from other carbon shifts in phenyl, methine, methoxyl, and acetyl groups on the basis of their position, multiplicity and consistency.[7,8,11-13] The methyl signals of the same chemical shift in a pair of 3-epimers were assigned to confusing methyl carbons in acetyl groups.

Of the carbon shifts given, C_1, C_6, quarternary carbon atoms and branching carbon atoms were identified

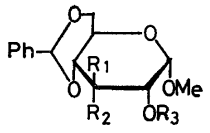

	R_1	R_2	R_3
1	OH	CH_2NO_2	Ts
2	CH_2NO_2	OH	Ts
3	CH_2NHBz	OH	H
4	CH_2NHBz	OH	Ts
5	Me	OH	Ac
6	OH	Me	Ac
7	Me	OAc	Ac
8	OAc	Me	Ac
9	Me	OH	Me
10	OH	Me	Me
13	CH_2NHBz	OH	Ac
14	OH	CH_2NHBz	Ac

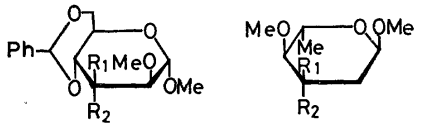

	R_1	R_2		R_1	R_2
11	Me	OH	**15**	NHAc	Me
12	OH	Me	**16**	Me	NHAc

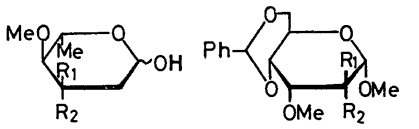

	R_1	R_2		R_1	R_2
17	NO_2	Me	**19**	OH	Me
18	Me	NO_2	**20**	Me	OH

from their chemical shifts and single frequency off-resonance decoupled spectra, the other carbons being assigned from their chemical shifts. The effect of acetylation of the tertiary hydroxyl group[14] was observed on the chemical shifts of C_3 and branching carbons in **7** and **8**, as compared with those in **5** and **6**. The deshielding effect[12] by *O*-methylation is also prominent in the chemical shifts of C_2 in **9**—**12**, C_4 in **15** and **17**, and C_3 in **19** and **20**, but very small in the cases of **16** and **18**. The lower field shifts from the usual position of branching carbons in **13** and **14**, and of C_3 in **15**—**18** are attributed to the deshielding effects of the groups attached to them; the chemical shifts of C_2 and C_5 in **15**—**18** are reasonable for the deoxy carbon atoms of 2,6-dideoxy-4-*O*-methylhexoses.[13] Data of **17** and **18** support the ^1H NMR spectra which show that **17** exists almost completely in the β-form, whereas **18** exists in an α,β-mixture of nearly equal amounts.

The resonance due to the equatorial carbon atoms of 3-*C*-branching chains is always at a field lower than that of the axial carbons for the seven pairs of 3-*C*-substituted sugars examined (Table 1). Consistent results were also obtained for the sugars containing a benzoylaminomethyl group or a nitro group at quar-

TABLE 1. ^{13}C CHEMICAL SHIFTS OF CHAIN CARBON ATOMS AND BRANCHING CARBON ATOMS OF BRANCHED-CHAIN SUGARS AND THE CHEMICAL SHIFT DIFFERENCES BETWEEN AXIALLY AND EQUATORIALLY ORIENTED CARBON ATOMS (ppm from Me_4Si in $CDCl_3$)

Hexoses (configuration)	C_1	C_2	C_3	C_4	C_5	C_6	C_3-CH_3 (C_3-CH_2NHBz)	$\Delta(e-a)$
5 (D-*allo*)	98.1	72.3	71.6	81.8	59.2	68.9	20.7	3.7
6 (D-*gluco*)	97.7	74.8	72.5	83.5	61.3	69.0	17.0	
7 (D-*allo*)	97.9	72.9	79.9	82.7	58.9	69.1	19.3	3.2
8 (D-*gluco*)	98.4	70.2	83.3	78.1	61.4	69.1	16.1	
9 (D-*allo*)	97.8	80.3[a]	72.1	81.8[a]	58.9	68.8	20.6	3.9
10 (D-*gluco*)	97.9	83.0[a]	73.8	83.3[a]	61.0	69.0	16.7	
11 (D-*altro*)	99.0	79.6	71.1	82.8	59.7	68.9	21.0	2.5
12 (D-*manno*)	98.9	82.0	70.7	84.9	62.4	69.0	18.5	
13 (D-*allo*)	98.2	70.0	72.6	80.0	59.0	68.9	(43.1)	1.9
14 (D-*gluco*)	97.7	73.0	75.1	84.5	61.5	69.0	(41.2)	
15 (L-*ribo*)	99.7	38.5	56.7	87.9	69.7	18.4	24.7	4.6
16 (L-*arabino*)	99.7	40.5	56.4	82.9	70.3	19.0	20.1	
17 (L-*ribo*)	91.8	42.7	89.3	85.8	70.1	18.7	25.4	8.8
18 (L-*arabino*)	92.4 90.5	44.2 40.9	90.3 89.8	84.4 84.7	71.2 66.1	18.4[a]	16.6 18.6[a]	6.8
19 (D-*altro*)	104.8	73.4	77.9	82.2	58.1	69.2	22.5	−1.5
20 (D-*allo*)	104.7	69.0	78.7	83.7	58.1	69.4	24.0	

a) Assignments may be reversed although those given here are preferred.

ternary carbon. It was established for seven pairs of 3-*C*-substituted sugars that the $\Delta(e-a)$ values in the ^{13}C NMR spectra permit the configurational assignment at the 3-*C* position. Inconsistent results for the 2-*C*-methyl derivatives **19** and **20** seem to be related to their conformations. At present only a somewhat flattened configuration can be deduced from the $J_{3,4}=2.0$ Hz value for **20**, more data being needed for 2-*C*-branching sugars.

Experimental

^{13}C NMR spectra of branched-chain sugars, **5**, **6**, **9**—**12**, **19**, and **20** were obtained at 30 °C on a JEOL JNM FX-100 spectrometer in pulse Fourier transform/proton noise decoupled mode at 25.15 MHz in deuteriochloroform. The corresponding spectra of **7**, **8**, and **13**—**18** were similarly recorded 32 °C on a Varian XL-100-15-FT spectrometer. Each spectrum was obtained after 1000 transients with a spectral width of 5000 Hz, a computer data memory size for the free induction decay of 8 K, an acquisition time of 0.8 s, a pulse delay of 0.8 s, and pulse angle of 45°. ^1H NMR spectra were measured on a JEOL PS-100 spectrometer with a CW mode. All measurments were carried out in a $CDCl_3$ solution containing a drop of TMS as an internal standard. Optical rotations were measured in 0.2-dm tubes in a Carl Zeiss LEP-A1 polarimeter. IR spectra were recorded with a Hitachi Model EPI-G2 spectrometer.

Chemical shifts and coupling constants in ^1H NMR were recorded in δ(ppm) and Hz, respectively, and IR frequencies in cm^{-1}.

Methyl 3-C-(benzoylaminomethyl)-4,6-O-benzylidene-2-O-p-tolylsulfonyl-α-D-allopyranoside (4). *a)*: Methyl 4,6-*O*-benzylidene-3-*C*-nitromethyl-2-*O*-*p*-tolylsulfonyl-α-D-allopyranoside [300 mg, mp 143—145 °C, $[\alpha]_D$ +39.5° (*c* 1.01, $CHCl_3$)] prepared by the method of Jordaan *et al.* [lit,[9] mp 143—144 °C, $[\alpha]_D^{24}$ +41.6° (*c* 1, $CHCl_3$)] was hydrogenated in ethanol in the presence of well-washed Raney nickel at room temperature, and then filtered. The filtrate was evaporated under reduced pressure. The residue was *N*-benzoylated with benzoic anhydride (150 mg) in ethanol to give **4** (121 mg) in 35% yields. Mp 184—185 °C (from ethanol), $[\alpha]_D^{22}$ +13.3° (*c* 1.8, $CHCl_3$), IR: 3450 (NH), 3340 (OH), 1636 (NHBz), NMR: 8.00—7.24 (Ph:m), 7.10 (NH), 5.57 (PhCH), 4.74 (H_1: d, $J_{1,2}=4.0$), 4.61 (H_2: d), 4.36 (H_6: q, $J_{5,6}=4.0$), 4.28—3.95 (CH_2: m), 3.95 ($H_{6'}$: t, $J_{5,6'}=J_{6,6'}=9.0$), 3.38 (H_5: m), 3.35 (OMe), 2.43 ($PhCH_3$).

Found: C, 61.01; H, 5.35; N, 2.41; S, 5.58%. Calcd for $C_{29}H_{31}NO_9S$: C, 61.15; H, 5.49; N, 2.46; S, 5.63%.

b): Tosylation of methyl 3-*C*-(benzoylaminomethyl)-4,6-*O*-benzylidene-α-D-allopyranoside[10] in pyridine with 1.2 equimolar *p*-toluenesulfonyl chloride gave **4** in 82% yield.

Methyl 2-O-Acetyl-3-C-(benzoylaminomethyl)-4,6-O-benzylidene-α-D-glucopyranoside (14). Acetylation of methyl 3-*C*-(benzoylaminomethyl)-4,6-*O*-benzylidene-α-D-glucopyranoside[10] in pyridine with acetic anhydride in the usual manner gave the corresponding 2-acetate as a sirup in 93% yield; it was purified by silica-gel column chromatography. $[\alpha]_D^{22}$ +15.8° (*c* 1.2, $CHCl_3$), NMR: 7.00—7.60 (Ph: m), 5.53 (PhCH), 4.98 (H_1:d, $J_{1,2}=3.5$ Hz), 4.90 (H_2:d), 4.70—3.60 (H_4, H_5, H_6, $H_{6'}$, CH_2:m), 3.40 (OMe), 2.20 (Ac).

Found: C, 63.23; H, 5.25; N, 3.06%. Calcd for $C_{24}H_{23}NO_8$: C, 63.57; H, 5.11; N, 3.09%.

The work was carried out with a Grant-in-Aid (No. 347023, 474244) from the Ministry of Education. The authors with to thank Mr. Y. Nakamura for the measurements of a part of the ^{13}C NMR spectra.

References

1) Part XVIII. J. Yoshimura, M. Matsuzawa, K. Sato, and Y. Nagasawa, *Carbohydr. Res.*, **76**, 67 (1979).
2) R. E. Reeves, *Adv. Carbohydr. Chem.*, **6**, 131 (1951).
3) F. W. Lichtenthaler, *Fortschr. Chem. Forsch.*, **14**, 556 (1970); F. W. Lichtenthaler and P. Emig, *Tetrahedron Lett.*, **1967**, 577.
4) a) K. Sato and J. Yoshimura, *Bull. Chem. Soc. Jpn.*, **51**, 2116 (1978); b) K. Sato and J. Yoshimura, *Carbohydr. Res.*, **73**, 75 (1979).
5) G. B. Howarth, W. A. Szarek, and J. K. N. Jones, *Can. J. Chem.*, **46**, 3376 (1968).
6) J. J. Nieuwenhuis and J. H. Jordaan, *Carbohydr. Res.*, **51**, 207 (1976).
7) S. D. Gero, D. Horton, A.-M. Sepulchre, and J. D. Wander, *J. Org. Chem.*, **40**, 1061 (1975) and previous papers cited therein.
8) P. M. Collins and V. R. N. Munasinghe, *Carbohydr. Res.*, **62**, 19 (1978) and references cited therein.
9) J. H. Jordaan, J. J. Nieuwenhuis, and G. J. Lourences, *Carbohydr. Res.*, **51**, 195 (1976).
10) J. Yoshimura, K. Sato, K. Kobayashi, and C. Shin, *Bull. Chem. Soc. Jpn.*, **46**, 1516 (1973).
11) M. Miljkovic, M. Gligorijevic, T. Satoh, D. Glisin, and R. D. Pitcher, *J. Org. Chem.*, **39**, 3847 (1974).
12) D. E. Dorman and J. D. Roberts, *J. Am. Chem. Soc.*, **92**, 1355 (1970).
13) S. Omura, A. Nakagawa, A. Neszmelyi, S. D. Gero, A.-M. Sepulchre, F. Piriou, and G. Lukacs, *J. Am. Chem. Soc.*, **97**, 4001 (1975).
14) A.-M. Sepulchre, B. Septe, G. Lukacs, and S. D. Gero, *Tetrahedron*, **30**, 905 (1974).

Synthesis of a Partial Sequence of Proinsulin Using the A-Chain of Natural Insulin. II.[1] Synthesis of a Peptide Corresponding to Positions 53—81 of Bovine Proinsulin

Hiroko AIBA and Yasutsugu SHIMONISHI*

Institute for Protein Research, Osaka University, Yamada-kami, Suita, Osaka 565

(Received May 23, 1979)

For the synthesis of bovine proinsulin, the *S*-sulfonate of the A-chain of bovine insulin was elongated by two single-step reactions using Boc-Arg(Tos)-ONSu and Boc-Leu-Glu(OBu^t)-Gly-Pro-Pro-Gln-Lys[Z(2-Cl)]-N_3. The *S*-sulfonate of the Leu-Glu-Gly-Pro-Pro-Gln-Lys[Z(2-Cl)]-Arg-A-chain, corresponding to positions 53—81 of bovine proinsulin, was obtained after removal of the protecting groups. The *S*-sulfonates of the elongated derivatives of the A-chain were shown to be very soluble not only in water, but also in organic solvents such as DMF and DMSO in the presence of water. Therefore, these *S*-sulfonates could react with protected peptides in homogeneous solution. Furthermore, the *S*-sulfonates could easily be purified by ion-exchange chromatography. The *S*-sulfonates of the A-chain and its elongated derivatives are thus useful intermediates for the synthesis of proinsulin.

Weinert *et al.*[2] proposed that the *S*-sulfonate of the des-Gly^1-A-chain, prepared by the Edman degradation of the A-chain of natural insulin, can be used as starting material for the synthesis of proinsulin. The procedure has the advantage that the des-Gly^1-A-chain can be coupled by various methods with protected peptides which have a glycine residue at the carboxyl end. However, the procedure is complicated, since the des-Gly^1-A-chain must be prepared from the A-chain by a laborious degradation process. One of the authors (Y.S.)[1] reported the synthesis of a partial sequence of proinsulin using the *S*-sulfonate of the A-chain[3,4] prepared by sulfitolysis of natural insulin. The procedure merits special attention as a method for direct elongation of the A-chain.

We are working on further elongation of the peptide chain of the A-chain of bovine insulin using our procedure for the synthesis of proinsulin. This paper describes the synthesis of a partial sequence corresponding to positions 53—81 of bovine proinsulin[5] (Fig. 1). First, Boc-Leu-Glu(OBu^t)-Gly-Pro-Pro-Gln-Lys-[Z(2-Cl)]-N_2H_3[6] (X) was synthesized (Fig. 2), two fragments, Boc-Leu-Glu(OBu^t)-Gly-OH (IV) and Boc-Pro-Pro-Gln-Lys[Z(2-Cl)]-OMe (VIII), being synthesized separately and coupled together to give the heptapeptide methyl ester (IX), which was then converted to the corresponding hydrazide (X). The tripeptide (IV) was synthesized by two routes. (a) Z-Glu(OBu^t)-ONSu[7] was coupled with H-Gly-OEt to give Z-Glu(OBu^t)-Gly-OEt (I). The dipeptide ethyl ester (I) was then catalytically hydrogenated. The resulting dipeptide ester was not isolated, but coupled directly with Boc-Leu-ONSu[8] to give Boc-Leu-Glu(OBu^t)-Gly-OEt (II). The resulting tripeptide ester was converted to the corresponding acid (IV) by saponification. (b) Z-Glu(OBu^t)-ONSu[7] was condensed with H-Gly-OBzl to give Z-Glu(OBu^t)-Gly-OBzl (III). The dipeptide benzyl ester (III) was catalytically hydrogenated and the resulting dipeptide was condensed with Boc-Leu-ONSu[8] to give IV.

The synthesis of the tetrapeptide, Boc-Pro-Pro-Gln-Lys[Z(2-Cl)]-OMe (VIII), was started by condensing Boc-Gln-ONp[9] with H-Lys[Z(2-Cl)]-OMe (V) to give Boc-Gln-Lys[Z(2-Cl)]-OMe (VI). VI was then treated with TFA and the resulting dipeptide ester was coupled with Boc-Pro-Pro-ONSu (VII) prepared by condensing Boc-Pro-Pro-OH[10] with HONSu using DCC, to give Boc-Pro-Pro-Gln-Lys[Z(2-Cl)]-OMe (VIII). The tetrapeptide (VIII) thus synthesized was treated with TFA and the resulting tetrapeptide ester was condensed with the tripeptide (IV) using DCC in the presence of HOBt.[11] The isolated Boc-Leu-Glu(OBu^t)-Gly-Pro-Pro-Gln-Lys[Z(2-Cl)]-OMe (IX) was converted to the corresponding hydrazide (X) by the usual method of hydrazinolysis.

The *S*-sulfonate of the Arg-A-chain[2] was synthesized by coupling the *S*-sulfonate of the A-chain with Boc-Arg(Tos)-ONSu and removing the protecting group of the arginine residue of the *S*-sulfonate of the Boc-Arg(Tos)-A-chain with anhydrous liquid hydrogen fluoride.[12] In the preceding work,[1] the *S*-sulfonate of the protected Arg-A-chain, Boc-Arg(NO_2)-A-chain, was used directly without removal of the guanidino protecting group of the arginine residue. However, when Boc-Arg(Tos)-ONSu was used for acylation of the *S*-sulfonate of the A-chain, no quantitative coupling of the A-chain could be attained. Thus, in this work the protecting group of the arginine residue was removed from the *S*-sulfonate of the crude Boc-Arg(Tos)-A-chain, the *S*-sulfonate of Arg-A-chain[2] being purified by chromatography on DEAE-Sephadex A-25[13] (Fig. 3).

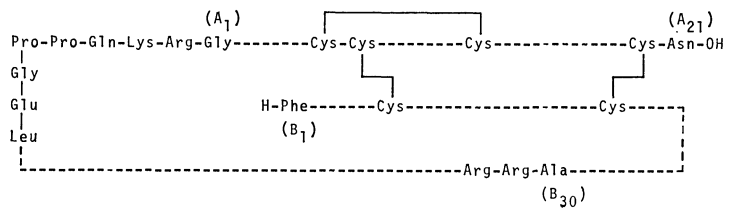

Fig. 1. Structural model of bovine proinsulin.[5]

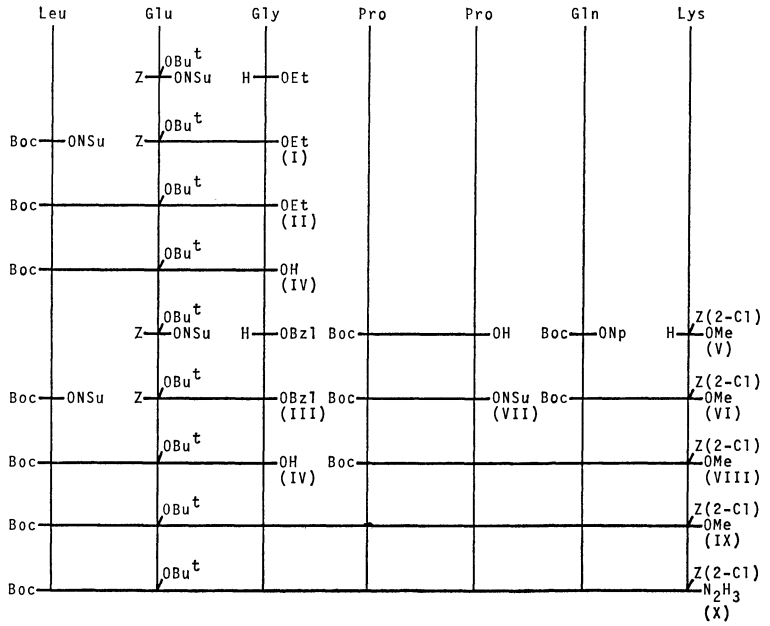

Fig. 2. Scheme for synthesis of protected heptapeptide (sequence corresponding to positions C_{21} to CA_1 in bovine proinsulin).

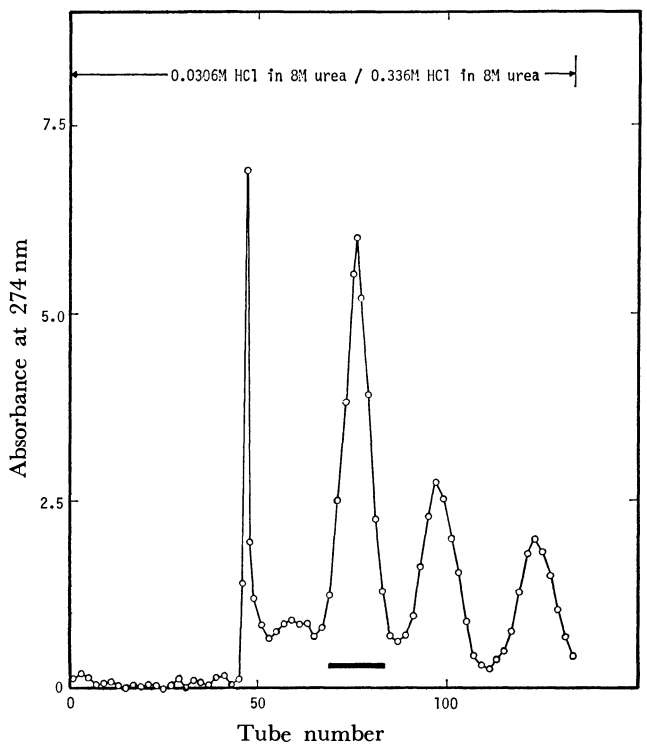

Fig. 3. Chromatogram of the *S*-sulfonate of Arg-A-chain on DEAE-Sephadex A-25 under the conditions described in the text.

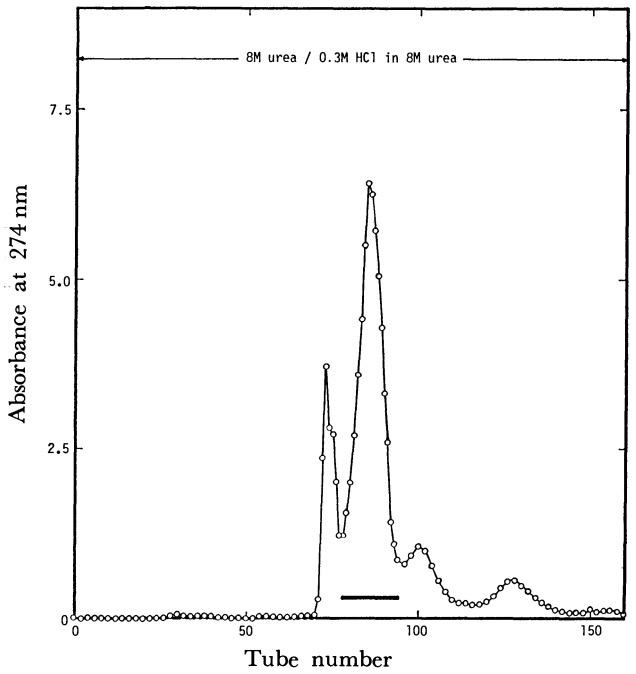

Fig. 4. Chromatogram of the *S*-sulfonate of Leu-Glu-Gly-Pro-Pro-Gln-Lys[Z(2-Cl)]-Arg-A-chain on DEAE-Sephadex A-25 under the conditions described in the text.

The *S*-sulfonate of Arg-A-chain was acylated by protected peptide azides with the sequence, Leu-Glu-Gly-Pro-Pro-Gln-Lys. The *S*-sulfonate of the Arg-A-chain was coupled with Boc-Leu-Glu(OBu^t)-Gly-Pro-Pro-Gln-Lys(Z)-N_3, prepared from the corresponding hydrazide. Considerable cleavage of the N$^\varepsilon$-Z group from the lysine residue occurred when the isolated *S*-sulfonate of the Boc-Leu-Glu(OBu^t)-Gly-Pro-Pro-Gln-Lys(Z)-Arg-A-chain was treated with TFA to remove the Boc group at the amino terminus. The *S*-sulfonate of the Arg-A-chain was then condensed with Boc-Leu-Glu(OBu^t)-Gly-Pro-Pro-Gln-Lys-[Z(2-Cl)]-N_3 protected at the lysine residue with the Z(2-Cl) group,[14] which is more stable than the Z group. The condensation reaction was examined using ratios of 5, 7.5 and 10 equivalents of the protected peptide azide to the *S*-sulfonate of the Arg-A-chain under the conditions described below. The resulting

TABLE 1. AMINO ACID CONTENTS OF DERIVATIVES OF THE A-CHAIN[a]

Amino acid	I[b]	II[b]	III[b]
Lys			1.00 (1)
Arg		1.01 (1)	1.00 (1)
Asp	1.99 (2)	1.96 (2)	1.94 (2)
Ser	1.82 (2)	1.58 (2)	1.79 (2)
Glu	4.35 (4)	4.23 (4)	6.73 (6)
Pro			2.09 (2)
Gly	1.02 (1)	0.99 (1)	1.95 (2)
Ala	1.00 (1)	1.00 (1)	1.00 (1)
Cys	nd[c]	nd[c]	nd[c]
Val	1.59 (2)	1.80 (2)	1.59 (2)
Ile	0.60 (1)	0.84 (1)	0.63 (1)
Leu	2.03 (2)	2.00 (2)	2.96 (3)
Tyr	2.12 (2)	1.94 (2)	1.94 (2)

a) Molar ratios of individual amino acid are shown relative to that of alanine. Numbers in parentheses are theoretical values. b) Compounds I, II, and III are the *S*-sulfonates of the A-chain, Arg-A-chain and Leu-Glu-Gly-Pro-Pro-Gln-Lys[Z(2-Cl)]-Arg-A-chain, respectively. c) Cystine was not determined.

S-sulfonate of Boc-Leu-Glu(OBu^t)-Gly-Pro-Pro-Gln-Lys[Z(2-Cl)]-Arg-A-chain was treated with TFA and the *S*-sulfonate obtained was subjected to chromatography on DEAE-Sephadex A-25[13] (Fig. 4). The best result was obtained with use of 7.5 equivalents of the protected peptide azide.

The N-terminal amino acid residues of the purified *S*-sulfonates of the Arg- and Leu-Glu-Gly-Pro-Pro-Gln-Lys[Z(2-Cl)]-Arg-A-chains were detected as arginine and leucine, respectively, by dinitrophenylation.[15] Amino acid analyses of acid hydrolysates of the purified *S*-sulfonates gave satisfactory results (Table 1).

Thus, the *S*-sulfonate of the A-chain of bovine insulin was elongated by reactions with acylamino acid active ester and acylpeptide azides. During the procedure it became clear that the *S*-sulfonates of the elongated derivatives of the A-chain thus synthesized are very soluble in buffers and organic solvents such as DMF and DMSO containing water, and can react with acylpeptide in homogeneous solution and be purified by chromatography on ion-exchange resin. These *S*-sulfonates seem to be useful intermediates for synthesis of proinsulin. Results on the further elongation of the derivatives obtained will be described in subsequent papers.[16,17]

Experimental

Crystalline bovine insulin was obtained from the Chemical Research Laboratories, Takeda Chemical Industries, Ltd. (Osaka), by courtesy of Dr. M. Fujino. Sephadex was purchased from Pharmacia Co. (Uppsala). All chemicals were of reagent grade and used without further purification. Thin layer chromatography was performed on silica gel G (Merck) using the following solvent systems (volume ratios); $CHCl_3$: MeOH : AcOH (95 : 5 : 3), *n*-BuOH : AcOH : H_2O (4 : 1 : 1), $CHCl_3$: MeOH : AcOH : H_2O (10 : 10 : 1 : 10, lower phase). Peptide samples were hydrolyzed in 6 M HCl in sealed tubes at 105 °C for 48 h, amino acids in the hydrolysates being analyzed in a Hitachi KLA-5 analyzer by the method of Moore *et al.*[18] Optical rotations were determined with a Perkin-Elmer Model 241 polarimeter. Melting points were measured by the capillary method and are given as uncorrected values. 1 M = 1 mol dm^{-3}.

Z-Glu(OBu^t)-Gly-OEt (I). H-Gly-OEt·HCl (7.50 g, 53.6 mmol) and TEA (7.6 ml) were dissolved in a mixture of DMF (100 ml) and $CHCl_3$ (100 ml), and then Z-Glu (OBu^t)-ONSu[7] (19.5 g, 44.9 mmol) was added to the solution. The solution was stirred at room temperature for a day and then concentrated to a syrup *in vacuo*. The syrup was dissolved in AcOEt, and the solution was washed successively with 0.1 M HCl and 5% aqueous $NaHCO_3$ and then dried over Na_2SO_4. The dried solution was concentrated to a syrup *in vacuo*; crystals formed on storage in a refrigerator. The crude crystals were collected by filtration with hexane; wt 18.2 g (95.8%). The crude material was recrystallized from AcOEt and hexane; wt 15.6 g (82.1%), mp 76.5—78 °C, $[\alpha]_D^{20}$ −7.3° (*c* 2.0, DMF).

Found: C, 59.63; H, 7.15; N, 6.78%. Calcd for $C_{21}H_{30}O_7N_2$: C, 59.70; H, 7.16; N, 6.63%.

Boc-Leu-Glu(OBu^t)-Gly-OEt (II). Compound I (8.45 g, 20.0 mmol) was dissolved in EtOH (100 ml) and hydrogenated over 5% palladium-charcoal catalyst under atmospheric pressure for 2.5 h. The catalyst was filtered off and washed with EtOH. The filtrate and washings were combined and concentrated to a solid under reduced pressure. The solid was dissolved with Boc-Leu-ONSu[8] (7.20 g, 22.0 mmol) in a mixture of DMF (50 ml) and CH_2Cl_2 (50 ml). The solution was stirred at room temperature for 1 h and then concentrated to a semi-solid residue. The residue was dissolved in $CHCl_3$ and the solution was washed successively with 0.1 M HCl, 5% aqueous $NaHCO_3$ and water. The washed solution was dried and then concentrated to a solid. The solid was collected by filtration with hexane; wt 9.00 g. The crude material was recrystallized from AcOEt and hexane; wt 6.70 g (67.0%), mp 128—130 °C, $[\alpha]_D^{20}$ −22.6° (*c* 1.0, DMF).

Found: C, 57.37; H, 8.94; N, 8.33%. Calcd for $C_{24}H_{43}O_8N_3$: C, 57.46; H, 8.64; N, 8.38%.

Z-Glu(OBu^t)-Gly-OBzl (III). H-Gly-OBzl·TosOH (12.1 g, 35.9 mmol) was suspended in THF (200 ml) and mixed with TEA (5.0 ml). The clear solution thus obtained was mixed with Z-Glu(OBu^t)-ONSu[7] (13.0 g, 30.0 mmol). The mixture was stirred at room temperature for 4 d and then concentrated to a syrupy residue, and the residue was dissolved in AcOEt. The solution was washed successively with 0.1 M HCl, 5% aqueous $NaHCO_3$ and water. The washed solution was dried and then concentrated to an oil. The oil was triturated in AcOEt and hexane; wt 13.5 g. The crude product was recrystallized from AcOEt and hexane; wt 12.0 g (82.2%), mp 59.5—61.5 °C, $[\alpha]_D^{19}$ −6.0° (*c* 2.0, DMF). (lit,[19] mp 45—47 °C, $[\alpha]_D^{25}$ −15.9° (*c* 1.01, MeOH)).

Found: C, 64.46; H, 6.65; N, 5.82%. Calcd for $C_{26}H_{32}O_7N_2$: C, 64.45; H, 6.66; N, 5.78%.

Boc-Leu-Glu(OBu^t)-Gly-OH·DCHA (IV). a) Compound II (6.52 g, 13.0 mmol) was dissolved in dioxane (100 ml). To the solution was added 1 M NaOH (15.6 ml) dropwise under cooling with ice-water. The solution was stirred at room temperature for 2 h and then neutralized with 1 M HCl and the dioxane was evaporated off. The residue was mixed with 5% aqueous $NaHCO_3$ and AcOEt. The aqueous layer was separated from the organic layer and acidified with 1 M HCl. The product was extracted several times with AcOEt. The extracts were combined,

dried and concentrated to a syrup; wt *ca.* 5.5 g.

b) Compound III (12.1 g, 24.9 mmol) was dissolved in MeOH (300 ml) and hydrogenated over 5% palladium–charcoal catalyst at 35 °C for 2.5 h. The catalyst was filtered off and the filtrate was concentrated to a solid. The solid was mixed with Boc–Leu–ONSu[8] (9.00 g, 27.4 mmol) and TEA (3.5 ml) in $CHCl_3$ (200 ml), and then stirred at room temperature for 3 d. The reaction mixture was concentrated to a residue, which was dissolved in AcOEt. The solution was washed with 0.1 M HCl and water, dried and concentrated to a syrupy residue. The residue was dissolved with DCHA (5.0 g) in AcOEt. Hexane was added to the soultion and the precipitate formed was collected by filtration; wt 16.0 g. The crude product was crystallized from AcOEt and hexane; wt 13.5 g (82.8%), mp 137—140 °C, $[\alpha]_D^{15.5}$ −13.5° (*c* 1.0, DMF).

Found: C, 62.04; H, 9.78; N, 8.42%. Calcd for $C_{34}H_{62}O_8N_4$: C, 62.35; H, 9.54; N, 8.56%.

H–Lys[Z(2-Cl)]–OMe·HCl (V). Thionyl chloride (8.7 g) was added dropwise in MeOH below −10 °C. To the solution was added H–Lys[Z(2-Cl)]–OH[14] (22.0 g, 69.8 mmol). The mixture was stirred at room temperature for 3 d and concentrated to a syrup, which was crystallized from MeOH and ether; wt 22.5 g. The crude material was recrystallized from MeOH and ether; wt 18.0 g (70.6%), mp 119—121 °C, $[\alpha]_D^{19}$ +12.0° (*c* 2.0, DMF).

Found: C, 49.19; H, 6.04; N, 7.90; Cl, 19.64%. Calcd for $C_{15}H_{22}O_4N_2Cl_2$: C, 49.32; H, 6.07; N, 7.67; Cl, 19.41%.

Boc–Gln–Lys[Z(2-Cl)]–OMe (VI). Compound V (1.80 g, 4.93 mmol) was dissolved in DMF (30 ml) and mixed with TEA (0.7 ml). The mixture was stirred with Boc–Gln–ONp[9] (2.00 g, 5.45 mmol) at room temperature for 1 d and then concentrated to dryness. The residue was dissolved in AcOEt and washed successively with 0.1 M HCl, 1 M Na_2CO_3 and water. The washed solution was dried and then concentrated to a syrup, which was crystallized from AcOEt and hexane; wt 2.33 g. The crude material was recrystallized from AcOEt and hexane; wt 2.30 g (83.6%), mp 95.5—97.5 °C, $[\alpha]_D^{19}$ −7.6° (*c* 2.0, DMF).

Found: C, 53.91; H, 6.93; N, 9.87; Cl, 6.40%. Calcd for $C_{25}H_{37}O_8N_4Cl$: C, 53.90; H, 6.70; N, 10.06; Cl, 6.37%.

Boc–Pro–Pro–ONSu (VII). A solution of Boc–Pro–Pro–OH[10] (25.0 g, 80.1 mmol) and HONSu (10.0 g, 87.0 mmol) in THF (400 ml) was cooled to −10—−20 °C, DCC (16.5 g, 80.1 mmol) then being added. The solution was stirred at the same temperature for 1 h and at room temperature overnight and the resulting precipitate was filtered off. The filtrate was concentrated to a syrup, which was dissolved in AcOEt. The solution was washed with 5% aqueous $NaHCO_3$ and water saturated with NaCl, dried, and concentrated to a syrup, which was crystallized from AcOEt and hexane; wt 24.6 g. The crude material was recrystallized from 2-propanol; wt 23.5 g (71.6%), mp 147.5—149.5 °C, $[\alpha]_D^{19}$ −90.0° (*c* 2.0, DMF).

Found: C, 55.72; H, 6.63; N, 10.33%. Calcd for $C_{19}H_{27}O_7N_3$: C, 55.73; H, 6.65; N, 10.26%.

Boc–Pro–Pro–Gln–Lys[Z(2-Cl)]–OMe (VIII). Compound VI (11.1 g, 19.9 mmol) was dissolved in TFA (30 ml). The solution was stirred at room temperature for 40 min and concentrated to a syrup, which was washed with ether and dried over NaOH. The dried material was dissolved in THF (100 ml), mixed successively with TEA (3.4 ml) and compound VII (9.0 g, 22.0 mmol), and stirred at room temperature for 1 d. The mixture was stirred with TEA (1.2 ml) and compound VII (4.0 g, 9.8 mmol) at room temperature for 2 d and then concentrated to an oil. The oil was dissolved in AcOEt and washed successively with 0.1 M HCl, 5% aqueous $NaHCO_3$ and water. The washed solution was dried and concentrated to a syrup, The syrup was solidified in a mixture of AcOEt and hexane, and reprecipitated from AcOEt and hexane; wt 12.5 g (83.9%), mp 70.5—72.5 °C, $[\alpha]_D^{16.5}$ −55.2° (*c* 1.0, DMF).

Found: C, 55,65; H, 6.96; N, 10.88; Cl, 4.63%. Calcd for $C_{35}H_{51}O_{10}N_6Cl$: C, 55.95; H, 6.84; N, 11.19; Cl, 4.72%.

Boc–Leu–Glu(OBu^t)–Gly–Pro–Pro–Gln–Lys[Z(2-Cl)]–OMe (IX). Compound VIII (2.25 g, 3.00 mmol) was dissolved in TFA (7 ml). The solution was stirred at room temperature for 60 min and then concentrated to a syrup. The syrup was solidified in ether and dried over NaOH. The dried solid was dissolved in THF (80 ml) with Boc–Leu–Glu(OBu^t)–Gly–OH, which was prepared from compound IV (2.00 g, 3.05 mmol). The solution was mixed with *N*-methylmorpholine (0.64 ml) and cooled to 0 °C. To the solution were added HOBt (0.60 g, 4.44 mmol) and DCC (0.68 g, 3.30 mmol). The mixture was stirred at 0 °C for 1 h and at room temperature for 1 d and then HOBt (0.2 g) and DCC (0.3 g) were added. The precipitate formed was filtered off after 3 d, and the filtrate was concentrated to dryness. The residue was dissolved in AcOEt, washed successively with 0.1 M HCl, 5% aqueous $NaHCO_3$ and water, and concentrated to a residue, which was crystallized from AcOEt and hexane; wt 2.81 g. The crude product was recrystallized from AcOEt and hexane; wt 2.57 g (77.4%), mp 96—98 °C, $[\alpha]_D^{16.5}$ −53.6° (*c* 1.0, DMF). Amino acid ratio in the acid hydrolysate: Glu, 2.22 (2); Gly, 1.00 (1); Pro, 2.21 (2); Leu, 0.99 (1); Lys, 1.10 (1).

Found: C, 56.21; H, 7.49; N, 11.19; Cl, 3.23%. Calcd for $C_{52}H_{80}O_{15}N_9Cl$: C, 56.43; H, 7.29; N, 11.39; Cl, 3.20%.

Boc–Leu–Glu(OBu^t)–Gly–Pro–Pro–Gln–Lys[Z(2-Cl)]–N_2H_3 (X). Compound IX (5.53 g, 5.00 mmol) was dissolved in MeOH (50 ml) and mixed with $NH_2NH_2 \cdot H_2O$ (2.5 g). The solution was stirred at room temperature for 3 d and concentrated to a residue, which was collected with ether; wt 5.76 g. The crude material was reprecipitated from $CHCl_3$ and ether; wt 3.82 g (67.0%), mp 114.5—117.5 °C.

Found: C, 53.83; H, 7.36; N, 13.61; Cl, 3.66%. Calcd for $C_{51}H_{80}O_{14}N_{11}Cl \cdot 2H_2O$: C, 53.79; H, 7.44; N, 13.18; Cl, 3.11%.

S-Sulfonate of the A-Chain. The *S*-sulfonate of the A-chain was prepared by the method of Zahn and Drechsel[4] with some modifications. Bovine insulin (1.0 g) was suspended in a solution of 0.05 M NaOAc (36 ml) and dioxane (26 ml). To the suspension was added EDTA·2Na (0.08 g) to give a clear solution, which was adjusted to pH 7.6 with NaOH. Then a solution (10.4 ml) containing Na_2SO_3 (2.3 g) at pH 7.6 and a solution (10.4 ml) containing $Na_2S_4O_6$ (5 g) at pH 7.6 were added at 37—38 °C alternately over a period of 30 min. The *S*-sulfonate of the A-chain was separated from the *S*-sulfonate of the B-chain as follows: The solution was stirred at 37—38 °C for 2 h and at room temperature for 1 d. The resulting precipitate, mainly consisting of the *S*-sulfonate of the B-chain, was removed by centrifugation, and the upper phase, mainly containing the *S*-sulfonate of the A-chain, was desalted on a column of Sephadex G-25 using 0.1 M NH_4HCO_3. The eluate with absorption at 274 nm was lyophilized; wt 493 mg. The lyophilized powder was charged on a column of Dowex 50×2 (1.7×11 cm) equilibrated with 10% HCOOH and 10% AcOH in 8 M urea, and the *S*-sulfonate of the A-chain was eluted with the same buffer. The eluate with absorption at 274 nm was desalted on a column of Sephadex G-25 and lyophilized; wt 361.1 mg. The *S*-sulfonate of the A-chain was also recovered from the precipitate consisting mainly of the *S*-sulfonate of the B-chain during purification of the

latter on a column of carboxymethylcellulose;[20] wt 88.1 mg. For amino acid ratio in the acid hydrolystae, see Table 1.

S-Sulfonate of Arg-A-Chain. *a) Boc-Arg(Tos)-ONSu.* Boc-Arg(Tos)-OH[21] (8.75 g, 20.4 mmol) was dissolved with HONSu (2.80 g, 24.3 mmol) and DCC (4.10 g, 19.9 mmol) in THF (350 ml) below 0 °C. The solution was stirred at the same temperature for 1 h and at room temperature for 3.5 h. The precipitate formed was filtered off and the filtrate was concentrated to a syrup, which was crystallized from AcOEt; wt 6.70 g (62.6%). Although the product contained some impurities, it was used without further purification.

b) S-*Sulfonate of Arg-A-Chain.* The *S*-sulfonate of the A-chain (546 mg) was dissolved in a mixture of DMF (3 ml) and DMSO (3 ml). The solution was mixed with TEA (0.14 ml) and then with a solution of Boc-Arg(Tos)-ONSu (1.10 g) in DMF (4 ml) and DMSO (1 ml). The mixture was stirred at room temperature for 1 d and then mixed with TEA (0.1 ml) and a solution of Boc-Arg(Tos)-ONSu (0.50 g) in DMSO (2 ml). The mixture was stirred at room temperature for 3 d and then mixed with 0.1 M NH_4HCO_3. The precipitate formed was removed by centrifugation and the upper phase was charged on a column of Sephadex G-25 equilibrated with 0.1 M NH_4HCO_3. The column was eluted with 0.1 M NH_4HCO_3 and the eluate with absorption at 274 nm was collected and lyophilized; wt 517.1 mg. Amino acid ratio in the acid hydrolysate: Asp, 1.97 (2); Ser, 1.75 (2); Glu, 4.29 (4); Gly, 1.01 (1); Ala, 1.00 (1); Val, 1.64 (2); Ile, 0.62 (1); Leu, 2.01 (2); Tyr, 2.30 (2); Arg, 0.83 (1). The lyophilized powder and anisole (0.64 ml) were put into the Daiflon-cylinder of an HF-reaction apparatus.[12] Anhydrous hydrogen fluoride (15 ml) was distilled into the cylinder cooled to −78 °C. The mixture was stirred at 0 °C for 90 min and then hydrogen fluoride was evaporated off. The residue was dissolved in 8 M urea (40 ml) with Na_2SO_3 (1.6 g), $Na_2S_4O_6$ (1.6 g) and EDTA·2Na (24 mg) and the solution was adjusted to pH 8 and stirred at room temperature for 3 d. It was then charged on a column (3×77 cm) of Sephadex G-25 equilibrated with 0.1 M NH_4HCO_3, and the column was eluted with 0.1 M NH_4HCO_3. The eluate with absorption at 274 nm was collected and lyophilized; wt 455.1 mg. The lyophilized powder (449.4 mg) was charged on a column (1.6×21 cm) of DEAE-Sephadex A-25 (acetate cycle) previously equilibrated with 8 M urea, and fractionated with a liner gradient of 0.0306 M HCl in 8 M urea (250 ml) to 0.336 M HCl in 8 M urea (250 ml) (Fig. 3). The fraction with absorption at 274 nm (shown by a bar) was collected, desalted on a column (3×57 cm) of Sephadex G-25, and lyophilized; wt 252.7 mg. For amino acid ratio in the acid hydrolysate, see Table 1.

S-Sulfonate of Leu-Glu-Gly-Pro-Pro-Gln-Lys[Z(2-Cl)]-Arg-A-Chain. Compound X (2.01 g, 1.76 mmol) was dissolved in DMF (7.5 ml) and cooled to below −40 °C. The cooled solution was mixed with 4.0 M HCl in dioxane (2.25 ml) and isopentyl nitrite (0.25 g, 2.11 mmol), and then stirred at the same temperature for 75 min. To the mixture were added *N*-methylmorpholine (1.10 ml) and a solution of the *S*-sulfonate of Arg-A-chain (0.68 g) in a mixture of DMSO (10 ml) and water (3.3 ml). The mixture was stirred at 2—3 °C in a refrigerator for 5 d and then 0.1 M NH_4HCO_3 was added. The resulting syrupy material was centrifuged and the supernatant was charged on a column of Sephadex G-25 equilibrated with 0.1 M NH_4HCO_3. The eluate with absorption at 274 nm was lyophilized; wt 848 mg. Amino acid ratio in the acid hydrolysate: Asp, 1.96 (2); Ser, 1.81 (2); Glu, 6.64 (6); Pro, 1.94 (2); Gly, 1.94 (2); Ala, 1.00 (1); Val, 1.63 (2); Ile, 0.62 (1); Leu, 2.89 (3); Tyr, 1.94 (2); Lys, 0.96 (1); Arg, 0.97 (1). The lyophilized powder was dissolved in TFA (20 ml) under cooling in an ice-water bath. The solution was stirred at room temperature for 60 min and then concentrated to a syrup. The syrup was dissolved in 0.1 M ammonium water at pH 8.0, and the solution was lyophilized. The resulting powder was dissolved in 8 M urea (50 ml) with Na_2SO_3 (2.0 g), $Na_2S_4O_6$ (2.0 g) and EDTA·2Na (0.04 g). The solution was stirred at room temperature for 2 d and then desalted using a column of Sephadex G-25 in 0.1 M NH_4HCO_3. The eluate with absorption at 274 nm was lyophilized; wt 770 mg. The lyophilized powder (329 mg) was charged on a column (1.6×15 cm) of DEAE-Sephadex A-25 (acetate cycle) equilibrated with 8 M urea, and the column was eluted with a linear gradient of 8 M urea (250 ml) to 0.3 M HCl in 8 M urea (250 ml) (Fig. 4). The fraction shown by a bar was collected, desalted and lyophilized; wt 213 mg. For amino acid ratio in the acid hydrolysate, see Table 1.

References

1) Y. Shimonishi, *Bull. Chem. Soc. Jpn.*, **43**, 3251 (1970).
2) M. Weinert, D. Brandenburg, and H. Zahn, *Hoppe-Seyler's Z. Physiol. Chem.*, **350**, 1566 (1969).
3) J. L. Bailey and R. D. Cole, *J. Biol. Chem.*, **234**, 1733 (1959).
4) H. Zahn and E. Drechsel, *Hoppe-Seyler's Z. Physiol. Chem.*, **349**, 359 (1969).
5) D. F. Steiner, S. Cho, P. E. Oyer, S. Terris, J. D. Peterson, and A. H. Rubenstein, *J. Biol. Chem.*, **246**, 1365 (1971).
6) The abbreviations used are those recommended by the IUPAC-IUB: *J. Biol. Chem.*, **247**, 977 (1972). Additional abbreviations: TFA, trifluoroacetic acid; DCC, dicyclohexylcarbodiimide; HOBt, 1-hydroxybenzotriazole; TEA, triethylamine; DMF, *N,N*-dimethylformamide; THF, tetrahydrofuran, DCHA, dicyclohexylamine; DMSO, dimethyl sulfoxide.
7) J. Beacham, G. Cupuis, F. M. Finn, H. T. Storey, C, Yanaihara, N, Yanaihara, and K. Hofmann, *J. Am. Chem. Soc.*, **93**, 5526 (1971).
8) G. W. Anderson, J. E. Zimmerman, and F. M. Callahan, *J. Am. Chem. Soc.*, **86**, 1839 (1964).
9) H. C. Beyerman, C. A. M. Boers-Boonekamp, and H. Maassen van den Brink-Zimmermannova, *Rec. Trav. Chim. Pays-Bas*, **87**, 257 (1968).
10) G. R. Pettit and S. K. Das Gupta, *Can. J. Chem.*, **45**, 1600 (1967).
11) W. König and R. Geiger, *Chem. Ber.*, **103**, 788 (1970).
12) S. Sakakibara, Y. Shimonishi, Y. Kishida, M. Okada, and H. Sugihara, *Bull. Chem. Soc. Jpn.*, **40**, 2164 (1967).
13) Y. Shimonishi and H. Zahn, *Biochim. Biophys. Acta*, **154**, 598 (1968).
14) B. W. Erickson and R. B. Merrifield, *J. Am. Chem. Soc.*, **95**, 3757 (1973).
15) K. Narita, H. Matsuo, and T. Nakajima, "Protein Sequence Determination, "ed by S. B. Needleman, Springer-Verlag, Berlin (1975), p. 39.
16) H. Aiba and Y. Shimonishi, *Bull. Chem. Soc. Jpn.*, **53**, 197 (1980).
17) H. Aiba and Y. Shimonishi, *Bull. Chem. Soc. Jpn.*, **53**, 201 (1980).
18) S. Moore, D. H. Spackman, and W. Stein, *Anal. Chem.*, **30**, 1185 (1958).
19) V. K. Naithani, *Hoppe-Seyler's Z. Physiol. Chem.*, **354**, 67 (1973).
20) P. G. Katsoyannis, A. Tometsko, C. Zalut, S. Johnson, and A. C. Trakatellis, *Biochemistry*, **6**, 2635 (1967).
21) J. Ramachandran and C. H. Li, *J. Org. Chem.*, **27**, 4006 (1962).

Synthesis of a Partial Sequence of Proinsulin Using the A-Chain of Natural Insulin. III.[1] Synthesis of a Peptide Corresponding to Positions 41—81 of Bovine Proinsulin

Hiroko AIBA and Yasutsugu SHIMONISHI*

Institute for Protein Research, Osaka University, Yamada-kami, Suita, Osaka 565

(Received May 23, 1979)

For the synthesis of bovine proinsulin, the *S*-sulfonate of the Leu-Glu-Gly-Pro-Pro-Gln-Lys[Z(2-Cl)]-Arg-A-chain, which was synthesized using the *S*-sulfonate of the A-chain of natural bovine insulin and which corresponds to positions 53—81 of bovine proinsulin, was coupled with Boc-Ala-Leu-Glu(OBu^t)-Leu-Ala-Gly-Gly-Pro-Gly-Ala-Gly-Gly-N_3. After removal of the protecting groups from the resulting material the *S*-sulfonate of the Ala-Leu-Glu-Leu-Ala-Gly-Gly-Pro-Gly-Ala-Gly-Gly-Leu-Glu-Gly-Pro-Pro-Gln-Lys[Z(2-Cl)]-Arg-A-chain, corresponding to positions 41—81 of bovine proinsulin, was purified by chromatography on QAE-Sephadex A-25.

In the preceding paper[1] we reported the synthesis of a peptide corresponding to positions 53—81 of bovine proinsulin,[2] the *S*-sulfonate of the Leu-Glu-Gly-Pro-Pro-Gln-Lys[Z(2-Cl)]-Arg-A-chain,[3] using the *S*-sulfonate of the A-chain of natural bovine insulin. The synthesis has the merit that the *S*-sulfonates not only of the A-chain but also of its elongated derivatives can react with acylpeptides in homogeneous solution, since they are very soluble in organic solvents such as DMF and DMSO in the presence of water. The solubility of the reaction products makes it easy to purify them, and pure products can be obtained free from starting materials and side-reaction products by chromatography. The present paper reports the synthesis of a 41-amino acid sequence corresponding to positions 41—81 of bovine proinsulin by this procedure, as a step in the synthesis of the prohormone.

In the synthesis of this partial sequence of the prohormone, shown in Fig. 1, the *S*-sulfonate of the Leu-Glu-Gly-Pro-Pro-Gln-Lys[Z(2-Cl)]-Arg-A-chain[1] was allowed to react with a protected peptide azide with the sequence, Ala-Leu-Glu-Leu-Ala-Gly-Gly-Pro-Gly-Ala-Gly-Gly. Boc-Ala-Leu-Glu(OBu^t)-Leu-Ala-Gly-Gly-Pro-Gly-Ala-Gly-Gly-OBzl (X) was synthesized, according to the scheme shown in Fig. 2. Before synthesis of this protected dodecapeptide, its two building fragments, Boc-Ala-Leu-Glu(OBu^t)-Leu-Ala-Gly-OH (V) and Boc-Gly-Pro-Gly-Ala-Gly-Gly-OBzl (IX) were synthesized separately. The synthesis of the former hexapeptide (V) was started by coupling Boc-Ala-OH[4] with H-Gly-OBzl by DCC to give Boc-Ala-Gly-OBzl (I). The protecting group on the amino terminus was removed by TFA and the peptide chain was elongated further by two single-reactions using Boc-Leu-ONSu[5] and Z-Glu(OBu^t)-ONSu[6] for acylation. The tetrapeptide, Z-Glu(OBu^t)-Leu-Ala-Gly-OBzl (III), thus synthesized was catalytically hydrogenated and the resulting free tetrapeptide was condensed *in situ* with Z-Leu-ONSu[5] to give Z-Leu-Glu(OBu^t)-Leu-Ala-Gly-OH (IV). The protected pentapeptide (IV) was once again catalytically hydrogenated and the resulting peptide was allowed to react with Boc-Ala-ONSu[5] to give the hexapeptide (V), Boc-Ala-Leu-Glu(OBu^t)-Leu-Ala-Gly-OH.

The hexapeptide (IX), Boc-Gly-Pro-Gly-Ala-Gly-Gly-OBzl, was synthesized by the condensation of Boc-Gly-Pro-OH[7] with the tetrapeptide benzyl ester, which was prepared by treatment of Boc-Gly-Ala-Gly-Gly-OBzl (VIII) with TFA, by DCC. The tetrapeptide (VIII) was synthesized from Boc-Gly-Gly-OBzl (VI), which was prepared by coupling Boc-Gly-OH[4] with H-Gly-OBzl by DCC, by a stepwise elongation procedure using Boc-amino acid *N*-hydroxysuccinimide ester. The hexapeptide (IX) thus synthesized was treated with TFA. The resulting peptide was not isolated, but coupled directly with the hexapeptide (V) by DCC in the presence of HOBt.[8] The crude material was purified on a column of LH-20 to give pure Boc-Ala-Leu-Glu(OBu^t)-Leu-Ala-Gly-Gly-Pro-Gly-Ala-Gly-Gly-OBzl (X).

The *S*-sulfonate of Leu-Glu-Gly-Pro-Pro-Gln-Lys-[Z(2-Cl)]-Arg-A-chain[1] was coupled with a protected peptide with the sequence Ala-Leu-Glu-Leu-Ala-Gly-Gly-Pro-Gly-Ala-Gly-Gly. The dodecapeptide benzyl ester (X) was converted to the corresponding acid (XI) by catalytic hydrogenation. Attempts were made to couple the dodecapeptide acid (XI) thus obtained with HONSu in the presence of DCC in order to obtain the corresponding active ester. However, pure active ester could not be obtained. The dodecapeptide ester (X) was converted to its corresponding

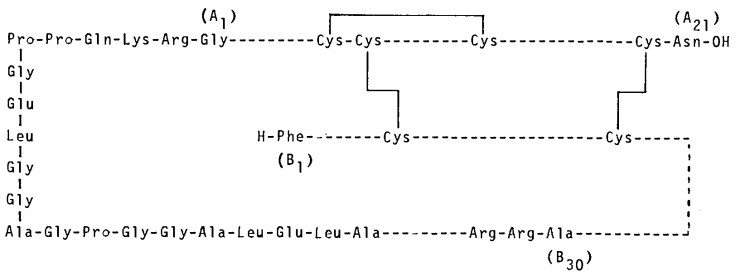

Fig. 1. Strutural model of bovine proinsulin.[2]

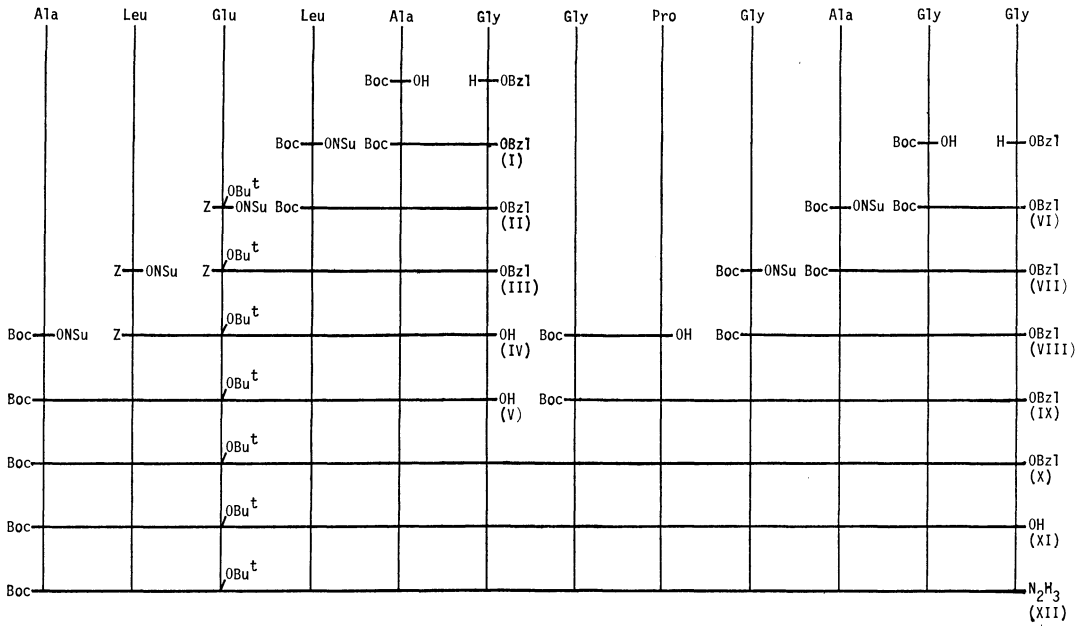

Fig. 2. Scheme for synthesis of protected dodecapeptide (sequence corresponding to positions C_9 to C_{20} in bovine proinsulin).

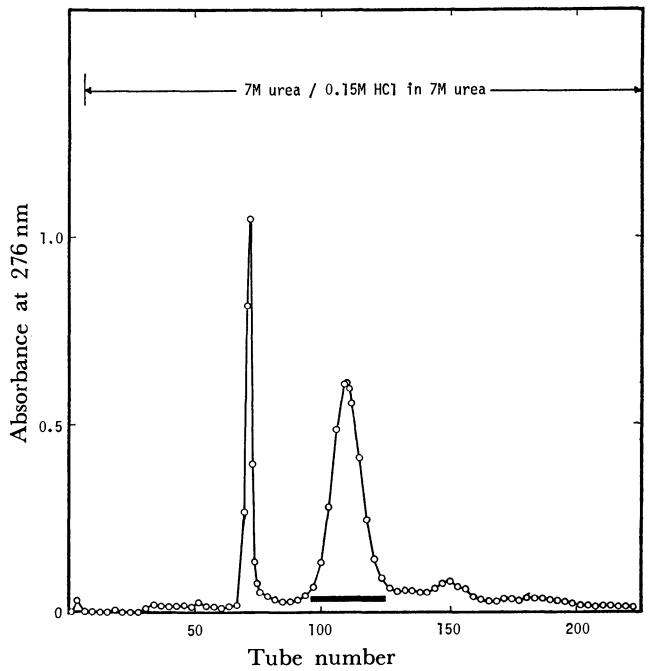

Fig. 3. Chromatogram of the *S*-sulfonate of the Ala–Leu–Glu–Leu–Ala–Gly–Gly–Pro–Gly–Ala–Gly–Gly–Leu–Glu–Gly–Pro–Pro–Gln–Lys[Z(2-Cl)]–Arg–A-chain on QAE-Sephadex A-25 obtained under the conditions described in the text.

hydrazide (XII) by the usual method of hydrazinolysis, and the hydrazide (XII) was converted to the corresponding azide by Rudinger's method[9]. The peptide azide was allowed to react *in situ* with the *S*-sulfonate of the Leu–Glu–Gly–Pro–Pro–Gln–Lys[Z(2-Cl)]–Arg–A-chain. The resulting *S*-sulfonate of the Boc–Ala–Leu–Glu(OBu^t)–Leu–Ala–Gly–Gly–Pro–Gly–Ala–Gly–Gly–Leu–Glu–Gly–Pro–Pro–Gln–Lys[Z-(2-Cl)]–Arg–A-chain was treated with TFA and then

TABLE 1. AMINO ACID RATIO OF PEPTIDES SYNTHESIZED[a]

Amino acid	Protected [41—53]	*S*-Sulfonate of [53—81][b]	*S*-Sulfonate of [41—81]
Lys		1.00 (1)	1.00 (1)
Arg		1.00 (1)	1.00 (1)
Asp		1.94 (2)	2.09 (2)
Ser		1.79 (2)	1.98 (2)
Glu	1.03 (1)	6.73 (6)	8.39 (7)
Pro	1.06 (1)	2.09 (2)	3.04 (3)
Gly	4.85 (5)	1.95 (2)	7.40 (7)
Ala	3.00 (3)	1.00 (1)	4.00 (4)
Cys		nd[c]	nd[c]
Val		1.59 (2)	1.60 (2)
Ile		0.63 (1)	0.55 (1)
Leu	1.92 (2)	2.96 (3)	5.09 (5)
Tyr		1.94 (2)	1.86 (2)

a) Molar ratios of individual amino acids are shown relative to that of alanine. Numbers in parentheses are theoretical values. b) Values are cited from Ref. 1. c) Cystine was not determined.

subjected to chromatography on QAE-Sephadex A-25 (Fig. 3). The amino acid ratio of the acid hydrolysate of the *S*-sulfonate synthesized is given in Table 1. The N-terminal amino acid residue of the purified *S*-sulfonate was identified as alanine by dinitrophenylation.[10]

Thus, the *S*-sulfonate of a peptide corresponding to positions 41—81 of bovine proinsulin was synthesized and purified. Studies on the further elongation of this peptide will be described in the subsequent paper.[11]

Experimental

The general experimental and analytical methods used were described in the preceding paper.[1]

Boc–Ala–Gly–OBzl (I). H–Gly–OBzl·TosOH (40.4 g,

120 mmol) and TEA (16.8 ml) were dissolved in a mixture of DMF (100 ml) and THF (200 ml). The solution was mixed with Boc-Ala-OH[4] (18.9 g, 100 mmol) and cooled to −5 °C—−10 °C. DCC (20.6 g, 100 mmol) was added to the cooled mixture. The mixture was stirred at the same temperature for 1 h and at room temperature for 1 d. The precipitate formed was filtered off and the filtrate was concentrated to a syrup under reduced pressure. The syrup was dissolved in AcOEt and washed successively with 0.1 M HCl, 5% aqueous $NaHCO_3$ and water. The washed solution was dried over Na_2SO_4 and concentrated to a syrup *in vacuo*. The syrup was crystallized from AcOEt and hexane; wt 26.0 g (77.4%). The crude material was recrystallized from AcOEt and hexane; wt 21.5 g (64.0%), mp 86—88 °C, $[\alpha]_D^{18}$ −11.7° (*c* 2.2, DMF).

Found: C, 60.75; H, 7.34; N, 8.65%. Calcd for $C_{17}H_{24}O_5N_2$: C, 60.70; H, 7.19; N, 8.33%.

Boc-Leu-Ala-Gly-OBzl (II). Compound I (20.2 g, 60.1 mmol) was dissolved in TFA (40 ml). The solution was stirred at room temperature for 90 min and then concentrated to a syrup. The syrup was washed with ether and redissolved with TEA (8.4 ml) and Boc-Leu-ONSu[5] (21.0 g, 64.0 mmol) in THF (200 ml). The solution was stirred for 2 d and then concentrated to a syrup. The syrup was dissolved in AcOEt and washed successively with 0.1 M HCl, 5% aqueous $NaHCO_3$ and water. The washed solution was dried and concentrated to an oily residue, which was crystallized from a mixture of AcOEt, ether and hexane; wt 26.5 g. The crude material was recrystallized from ether; wt 20.5 g (75.9%), mp 83—86 °C, $[\alpha]_D^{18}$ −19.2° (*c* 2.0, DMF).

Found: C, 61.24; H, 7.88; N, 9.52%. Calcd for $C_{23}H_{35}O_6N_3$: C, 61.45; H, 7.85; N, 9.35%.

Z-Glu(OBu^t)-Leu-Ala-Gly-OBzl (III). Compound II (18.0 g, 40.0 mmol) was dissolved in TFA (50 ml), stirred at room temperature for 90 min and then concentrated to a syrup. The syrup was solidified in ether, dissolved with TEA (5.6 ml) and Z-Glu(OBu^t)-ONSu[6] (18.4 g, 42.4 mmol) in $CHCl_3$ (300 ml), and stirred at room temperature for 2 d. The solution was diluted with $CHCl_3$, washed successively with 0.1 M HCl, 5% aqueous $NaHCO_3$ and water, dried, and then concentrated to a solid. The solid was crystallized from AcOEt and hexane; wt 23.5 g. Recrystallization of the crude product from AcOEt and hexane gave 23.0 g of material (85.8% yield), mp 162—164 °C, $[\alpha]_D^{18}$ −17.5° (*c* 2.0, DMF).

Found: C, 62.68; H, 7.25; N, 8.52%. Calcd for $C_{35}H_{48}O_9N_4$: C, 62.85; H, 7.24; N, 8.38%.

Z-Leu-Glu(OBu^t)-Leu-Ala-Gly-OH (IV). Compound III (6.70 g, 10.0 mmol) was dissolved in hot MeOH (150 ml), cooled to room temperature and mixed with AcOH (50 ml). Catalytic hydrogenation was carried out over 5% palladium-charcoal catalyst at atmospheric pressure. The catalyst was filtered off and the filtrate was concentrated to a solid. The solid was suspended with TEA (2 ml) and Z-Leu-ONSu[5] (4.32 g, 11.9 mmol) in a mixture of DMF (100 ml) and THF (50 ml), and dissolved gradually during the course of stirring. The solution was stirred overnight at room temperature and concentrated to a solid, which was suspended in AcOEt and washed with 0.1 M HCl and water. The organic layer was concentrated to a solid, which was crystallized from EtOH; wt 5.10 g. The crude material was recrystallized from EtOH; wt 4.58 g (66.2%), mp 226—228 °C (dec), $[\alpha]_D^{20}$ −26.0° (*c* 2.0, DMF).

Found: C, 58.90; H, 7.84; N, 10.18%. Calcd for $C_{34}H_{53}O_{10}N_5$: C, 59.03; H, 7.72; N, 10.12%.

Boc-Ala-Leu-Glu(OBu^t)-Leu-Ala-Gly-OH (V). Compound IV (4.15 g, 6.00 mmol) was dissolved in hot MeOH (150 ml), cooled to room temperature, and hydrogenated in the presence of AcOH (50 ml) and 5% palladium-charcoal catalyst. AcOH (100 ml) was added to dissolve the solid formed during the course of hydrogenation. The catalyst was filtered off and the filtrate was concentrated to a solid. The solid was suspended with Boc-Ala-ONSu[5] (2.00 g, 6.99 mmol) in DMF (300 ml) and stirred at room temperature for 3 d. The solution thus obtained was concentrated to a gelatinous solid, which was collected by filtration with $CHCl_3$. The crude material was recrystallized from MeOH; wt 3.52 g (79.5%), mp 230 °C (dec), $[\alpha]_D^{20}$ −34.2° (*c* 2.0, DMF). Amino acid ratio in the acid hydrolysate: Glu, 1.10 (1); Gly, 1.00 (1); Ala, 2.00 (2); Leu, 2.00 (2).

Found: C, 55.07; H, 8.25; N, 11.38%. Calcd for $C_{34}H_{60}O_{11}N_6 \cdot 1/2H_2O$: C, 55.34; H, 8.33; N, 11.39%.

Boc-Gly-Gly-OBzl (VI). H-Gly-OBzl·TosOH (24.3 g, 72.1 mmol) was dissolved with TEA (10.1 ml) and Boc-Gly-OH[4] (10.5 g, 60.0 mmol) in THF (300 ml). The solution was cooled to 0 °C, mixed with a solution of DCC (12.4 g, 60.2 mmol) in THF (50 ml), and stirred overnight at room temperature. The precipitate formed was filtered off and the filtrate was concentrated to an oily residue. The residue was dissolved in AcOEt, washed successively with 0.1 M HCl, 5% aqueous $NaHCO_3$ and water, dried, and concentrated to a syrup. The syrup was crystallized from a mixture of AcOEt and hexane; wt 16.5 g. The crude material was recrystallized from AcOEt and hexane; wt 16.0 g (82.9%), mp 83—84.5 °C.

Found: C, 59.78; H, 7.02; N, 8.84%. Calcd for $C_{16}H_{22}O_5N_2$: C, 59.61; H, 6.88; N, 8.69%.

Boc-Ala-Gly-Gly-OBzl (VII). Compound VI (13.0 g, 40.4 mmol) was dissolved in 3.55 M HCl in dioxane (113 ml) and stirred at room temperature for 1 h. The crystalline material formed was collected by filtration with ether and dissolved with TEA (5.4 ml) and Boc-Ala-ONSu[5] (13.7 g, 47.9 mmol) in a mixture of $CHCl_3$ (200 ml) and DMF (100 ml). The solution was stirred at room temperature for 1 d and then concentrated to a syrup. The syrup was dissolved in AcOEt and washed successively with 0.1 M HCl, 5% aqueous $NaHCO_3$ and water, dried and then concentrated to an oil. The oil was triturated in a mixture of AcOEt and hexane; wt 14.0 g. The crude material was recrystallized from AcOEt and hexane; wt 13.9 g (87.4%), mp 108.5—110.5 °C, $[\alpha]_D^{17}$ +0.2° (*c* 2.0, DMF).

Found: C, 58.21; H, 6.70; N, 10.69%. Calcd for $C_{19}H_{27}O_6N_3$: C, 58.00; H, 6.92; N, 10.68%.

Boc-Gly-Ala-Gly-Gly-OBzl (VIII). Compound VII (9.80 g, 24.9 mmol) was dissolved in 3.90 M HCl in dioxane (47.5 ml), stirred at room temperature for 60 min and concentrated to an oily residue. The oil was triturated in ether and dissolved with TEA (3.5 ml) and Boc-Gly-ONSu[5] (8.20 g, 30.1 mmol) in a mixture of DMF (100 ml) and $CHCl_3$ (100 ml). The solution was stirred overnight at room temperature and concentrated to a syrup. The syrup was dissolved in AcOEt, washed successively with 0.1 M HCl, 5% aqueous $NaHCO_3$ and water, dried, and concentrated to a crystalline solid. The solid was collected by filtration with a mixture of AcOEt and hexane; wt 9.00 g. The crude material was recrystallized from AcOEt and hexane; wt 8.54 g (76.3%), mp 126—128 °C, $[\alpha]_D^{17}$ −1.0° (*c* 2.0, DMF).

Found: C, 55.74; H, 6.84; N, 11.96%. Calcd for $C_{21}H_{30}O_7N_4$: C, 55.99; H, 6.71; N, 12.44%.

Boc-Gly-Pro-Gly-Ala-Gly-Gly-OBzl (IX). Compound VIII (4.05 g, 9.00 mmol) was dissolved in 4.0 M HCl in dioxane (25 ml), stirred at room temperature for

60 min and then concentrated to a crystalline residue. The residue was collected by filtration with ether and dried over NaOH. The crystalline material was dissolved with *N*-methylmorpholine (1.0 ml), Boc-Gly-Pro-OH[7] (2.45 g, 9.01 mmol) and HOBt (2.02 g, 15.0 mmol) in DMF (40 ml). The mixture was cooled to 0 °C, mixed with DCC (2.30 g, 11.2 mmol), and then stirred at the same temperature for 1 h and at room temperature overnight. The precipitate formed was filtered off and the filtrate was concentrated to dryness. The residue was dissolved in $CHCl_3$, washed successively with 0.1 M HCl, 5% aqueous $NaHCO_3$ and water, dried, and concentrated to a syrup. The syrup was crystallized from AcOEt, EtOH, and hexane; wt 5.17 g. The crude product was recrystallized from AcOEt, EtOH, and hexane; wt 4.73 g (86.8%), mp 164 °C, $[\alpha]_D^{18}$ −21.0° (*c* 2.0, DMF). Amino acid ratio in the acid hydrolysate: Gly, 3.84 (4); Ala, 1.00 (1); Pro, 1.02 (1).

Found: C, 55.67; H, 6.78; N, 13.83%. Calcd for $C_{28}H_{40}O_9N_6$: C, 55.62; H, 6.67; N, 13.90%.

Boc-Ala-Leu-Glu(OBu^t)-Leu-Ala-Gly-Gly-Pro-Gly-Ala-Gly-Gly-OBzl (X). Compound IX (3.00 g, 4.96 mmol) was dissolved in TFA (10 ml), stirred at room temperature for 30 min and concentrated to a syrup, which was triturated with ether. The solid was dissolved with *N*-methylmorpholine (0.85 ml), compound V (3.70 g, 5.01 mmol) and HOBt (1.00 g, 7.41 mmol) in DMF (300 ml) and cooled below 0 °C. The solution was stirred with DCC (1.00 g, 4.85 mmol) at the same temperature for 1 h and at room temperature for 1 d. The solution was stirred with HOBt (0.30 g, 2.2 mmol) and DCC (0.5 g, 2.4 mmol) at room temperature for 3 d. The precipitate formed was filtered off and the filtrate was concentrated to dryness. The residue was taken up in DMF and water and purified on a column (3×50 cm) of LH-20 using DMF as a solvent. The fractions containing the product were collected and concentrated to a solid, which was filtered with hot AcOEt; wt 4.09 g (67.4%), mp 210 °C (sintered) and 227 °C (dec), $[\alpha]_D^{20}$ −31.0° (*c* 2.0, DMF). Amino acid ratio in the acid hydrolysate: Glu, 1.03 (1); Pro, 1.06 (1); Gly, 4.85 (5); Ala, 3.00 (3); Leu, 1.92 (2).

Found: C, 55.86; H, 7.64; N, 13.68%. Calcd for $C_{57}H_{90}O_{17}N_{12}\cdot 1/2H_2O$: C, 55.91; H, 7.49; N, 13.73%.

Boc-Ala-Leu-Glu(OBu^t)-Leu-Ala-Gly-Gly-Pro-Gly-Ala-Gly-Gly-OH (XI). Compound X (1.22 g, 1.00 mmol) was dissolved in DMF (100 ml) by gentle heating and hydrogenated over 5% palladium-charcoal catalyst in a water bath at 35 °C. The catalyst was filtered off and the filtrate was concentrated to a solid, which was collected with AcOEt by filtration; wt 1.14 g. The crude product was reprecipitated from DMF and AcOEt; wt 1.12 g (97.4%), mp 217 °C (dec), $[\alpha]_D^{16.5}$ −25.9° (*c* 1.0, DMF).

Found: C, 52.16; H, 7.43; N, 14.51%. Calcd for $C_{50}H_{84}O_{17}N_{12}\cdot 3/2H_2O$: C, 52.11; H, 7.61; N, 14.59%.

Boc-Ala-Leu-Glu(OBu^t)-Leu-Ala-Gly-Gly-Pro-Gly-Ala-Gly-Gly-N_2H_3 (XII). Compound X (2.79 g, 2.28 mmol) was dissolved in *N*-methylpyrrolidone (20 ml) by gentle heating. The solution was cooled to room temperature, mixed with hydrazine hydrate (1.2 ml) and stirred at room temperature overnight. The precipitate formed was filtered and dried; wt 2.26 g (81.0%), mp 222—224 °C (dec).

Found: C, 51.89; H, 7.62; N, 16.79%. Calcd for $C_{50}H_{86}O_{16}N_{14}\cdot H_2O$: C, 51.89; H, 7.66; N, 16.95%.

S-Sulfonate of the Ala-Leu-Glu-Leu-Ala-Gly-Gly-Pro-Gly-Ala-Gly-Gly-Leu-Glu-Gly-Pro-Pro-Gln-Lys[Z(2-Cl)]-Arg-A-Chain. Compound XII (1.68 g, 1.38 mmol) was suspended in *N*-methylpyrrolidone (20 ml), cooled to −20 °C—−30 °C and mixed with 3.0 M HCl in dioxane (2.3 ml). The solution thus obtained was mixed with isopentyl nitrite (0.19 g, 1.66 mmol) and stirred at −15 °C—−20 °C for 60 min. The *S*-sulfonate of the Leu-Glu-Gly-Pro-Pro-Gln-Lys[Z(2-Cl)]-Arg-A-chain (510 mg) in water (2 ml) was added and its solution was stirred at 2 °C—3 °C in a refrigerator for 5 d and then poured into 0.1 M NH_4HCO_3 (100 ml). The precipitate formed was centrifuged, dissolved in DMSO, mixed with 0.1 M NH_4HCO_3 and filtered through a column of Sephadex G-25 (3×60 cm). The supernatant was also filtered through a similar Sephadex G-25 column. The eluates with absorption at 280 nm were pooled and lyophilized; wt 639 mg. Amino acid ratio in the acid hydrolysate: Lys, 1.00 (1); Arg, 1.00 (1); Asp, 2.09 (2); Ser, 1.98 (2); Glu, 8.39 (7); Pro, 3.04 (3); Gly, 7.40 (7); Ala, 4.00 (4); Cys, not determined; Val, 1.60 (2); Ile, 0.55 (1); Leu, 5.09 (5); Tyr, 1.86 (2). The powder (325 mg) was dissolved in TFA (10 ml) in an ice-water bath, stirred at room temperature for 60 min and concentrated to a syrup. The syrup was dissolved in 0.1 M NH_4HCO_3 (pH *ca.* 8.0) and lyophilized. The powder was dissolved with Na_2SO_3 (0.5 g), $Na_2S_4O_6$ (0.5 g) and EDTA·2Na (0.01 g) in 8 M urea (12.5 ml). The solution was adjusted to pH 8.0 and stirred at room temperature for 2 d. Then it was charged on Sephadex G-25 (3×60 cm) and the material was eluted with 0.1 M NH_4HCO_3. Fractions with absorption at 280 nm were collected and lyophilized; wt 287 mg. The lyophilized powder (49.1 mg) was charged on a column (0.9×8 cm) of QAE-Sephadex A-25 (acetate cycle) equilibrated with 7 M urea, and the material was eluted with a linear gradient of 7 M urea (250 ml) to 0.15 M HCl in 7 M urea (250 ml), as shown in Fig. 3. The fraction with an absorption at 276 nm, shown by a bar in Fig. 3, was collected and desalted on a column (3×60 cm) of Sephadex G-25 using 0.1 M NH_4HCO_3 and lyophilized; wt 38.3 mg.

References

1) Part II: H. Aiba and Y. Shimonishi, *Bull. Chem. Soc. Jpn.*, **53**, 192 (1980).
2) D. F. Steiner, S. Cho, P. E. Oyer, S. Terris, J. D. Peterson, and A. H. Rubenstein, *J. Biol. Chem.*, **246**, 1365 (1971).
3) The abbreviations used are those recommended by the IUPAC-IUB: *J. Biol. Chem.*, **247**, 977 (1972). Additional abbreviations: DCC, dicyclohexylcarbodiimide; TFA, trifluoroacetic acid; HOBt, 1-hydroxybenzotriazole; TEA, triethylamine; DMF, *N,N*-dimethylformamide; THF, tetrahydrofuran.
4) G. W. Anderson and A. C. McGregor, *J. Am. Chem. Soc.*, **79**, 6180 (1957).
5) G. W. Anderson, J. E. Zimmerman, and F. M. Callahan, *J. Am. Chem. Soc.*, **86**, 1839 (1964).
6) J. Beacham, G. Cupuis, F. M. Finn, H. T. Storey, C. Yanaihara, N. Yanaihara, and K. Hofmann, *J. Am. Chem. Soc.*, **93**, 5526 (1971).
7) J. C. Anderson, M. A. Barton, P. M. Hardy, G. W. Kenner, J. Preston, and R. C. Sheppard, *J. Chem. Soc.*, **1967**, 108.
8) W. König and R. Geiger, *Chem. Ber.*, **103**, 788 (1970).
9) J. Honzl and J. Rudinger, *Collect. Czech. Chem. Commun.*, **26**, 2333 (1961).
10) K. Narita, H. Matsuo, and T. Nakajima, "Protein Sequence Determination," ed by S. B. Needleman, Springer-Verlag, Berlin (1975), p. 39.
11) H. Aiba and Y. Shimonishi, *Bull. Chem. Soc. Jpn.*, **53**, 201 (1980).

 © 1980 The Chemical Society of Japan Bull. Chem. Soc. Jpn., 53, 201—204 (1980)

Synthesis of a Partial Sequence of Proinsulin Using the A-Chain of Natural Insulin. IV.[1] Synthesis of a Peptide Corresponding to Positions 31—81 of Bovine Proinsulin

Hiroko AIBA and Yasutsugu SHIMONISHI*

Institute for Protein Research, Osaka University, Yamada-kami, Suita, Osaka 565

(Received May 23, 1979)

For the synthesis of bovine proinsulin, the *S*-sulfonate of the Ala–Leu–Glu–Leu–Ala–Gly–Gly–Pro–Gly–Ala–Gly–Gly–Leu–Glu–Gly–Pro–Pro–Gln–Lys[Z(2-Cl)]–Arg–A-chain, which corresponds to positions 41—81 of bovine proinsulin, was coupled with Boc–Arg(Tos)–Arg(Tos)–Glu(OBu^t)–Val–Glu(OBu^t)–Gly–Pro–Gln–Val–Gly–N_3. The *S*-sulfonate of the Arg(Tos)–Arg(Tos)–Glu–Val–Glu–Gly–Pro–Gln–Val–Gly–Ala–Leu–Glu–Leu–Ala–Gly–Gly–Pro–Gly–Ala–Gly–Gly–Leu–Glu–Gly–Pro–Pro–Gln–Lys[Z(2-Cl)]–Arg–A-chain, correspoding to positions 31—81 of bovine proinsulin, was obtained in a pure form by removal of the protecting groups from the coupled product and chromatography on QAE-Sephadex A-25.

In preceding papers[1-3] we reported the synthesis of the *S*-sulfonates of the Arg–A-chain,[2] Leu–Glu–Gly–Pro–Pro–Gln–Lys[Z(2-Cl)]–Arg–A-chain[3] and Ala–Leu–Glu–Leu–Ala–Gly–Gly–Pro–Gly–Ala–Gly–Gly–Leu–Glu–Gly–Pro–Pro–Gln–Lys[Z(2-Cl)]–Arg–A-chain,[1] which correspond to positions 60—81, 53—81, and 41—81 respectively, of bovine proinsulin,[4] using the *S*-sulfonate of the A-chain of natural bovine insulin as a starting material. In the conventional procedure, the low solubility of larger polypeptides protected with hydrophobic groups causes serious problems not only in their reactivity in solution but also in purification. Attempts have been made to find protecting groups that increase the solubility of larger protected polypeptides. The Bunte-salt[2,5] was found to be suitable as both a protecting group for cysteine residues in the A-chain of insulin, as well as for increasing the solubility of the A-chain and its elongated derivatives in buffers and organic solvents such as DMF and DMSO[6] in the presence of water. It was found feasible to carry out the elongation reaction of the A-chain in homogeneous solution and purification of the product by ion-exchange chromatography. In the present work, the procedure was applied to the synthesis of the *S*-sulfonate of the sequence corresponding to positions 31—81 of bovine proinsulin (Fig. 1). The synthesis was carried out as a step in the synthesis of the prohormone.

The synthesis was performed by the reaction of the *S*-sulfonate of sequence 41—81 of bovine proinsulin[1] with a protected peptide azide with the sequence, Arg–Arg–Glu–Val–Glu–Gly–Pro–Gln–Val–Gly, which corresponds to positions 31—40 of the prohormone. Boc–Arg(Tos)–Arg(Tos)–Glu(OBu^t)–Val–Glu(OBu^t)–Gly–Pro–Gln–Val–Gly–OBzl[6] (IX) was synthesized (Fig. 2), the protected decapeptide being constructed from two appropriately protected smaller fragments (V) and (VIII). The synthesis of (V), Boc–Arg(Tos)–Arg(Tos)–Glu(OBu^t)–Val–Glu(OBu^t)–Gly–OH, was started by condensing Z–Val–ONSu[7] with H–Glu(OBu^t)–Gly–OH, obtained by catalytic hydrogenation of its corresponding Z derivative[3] and used directly without isolation. The tripeptide (I) Z–Val–Glu(OBu^t)–Gly–OEt, thus synthesized, was catalytically hydrogenated. The resulting tripeptide ester was not isolated, but coupled directly with Z–Glu(OBu^t)–ONp[8] to give Z–Glu(OBu^t)–Val–Glu(OBu^t)–Gly–OEt (II). The Z group of the protected tetrapeptide (II) was then removed by catalytic hydrogenation, and the resulting tetrapeptide ester was acylated with Z–Arg(Tos)–OH[9] by means of DCC to give Z–Arg(Tos)–Glu(OBu^t)–Val–Glu(OBu^t)–Gly–OEt (III). The protected pentapeptide (III) was once again catalytically hydrogenated and allowed to react with Boc–Arg(Tos)–ONSu[3] to give the protected hexapeptide (IV), Boc–Arg(Tos)–Arg(Tos)–Glu(OBu^t)–Val–Glu(OBu^t)–Gly–OEt. IV was saponified under the usual conditions to give the corresponding acid (V). Synthesis of the latter fragment (VIII), Boc–Pro–Gln–Val–Gly–OBzl, was started by coupling Boc–Val–OH[10] with H–Gly–OBzl by DCC. The dipeptide derivative (VI) thus synthesized was treated with TFA. The resulting dipeptide ester was not isolated, but directly elongated by two further single-reactions using Boc–Gln–ONp[11] and Boc–Pro–ONSu[7] for acylation. The protected tetrapeptide (VIII), Boc–Pro–Gln–Val–Gly–OBzl, thus obtained was treated with TFA. The resulting peptide ester was not isolated, but directly coupled with the

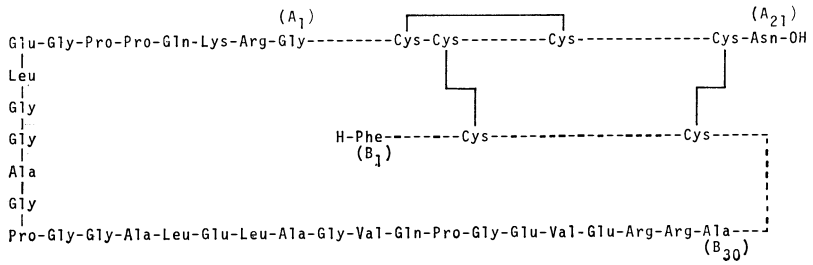

Fig. 1. Structural model of bovine proinsulin.

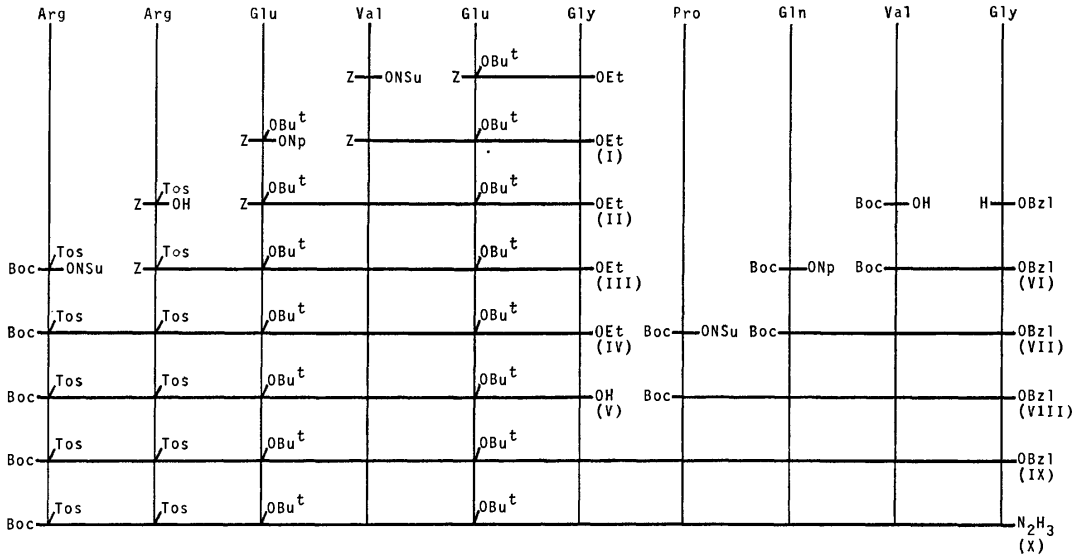

Fig. 2. Scheme for synthesis of protected decapeptide (sequence corresponding to positions BC_1 to C_8 in bovine proinsulin).

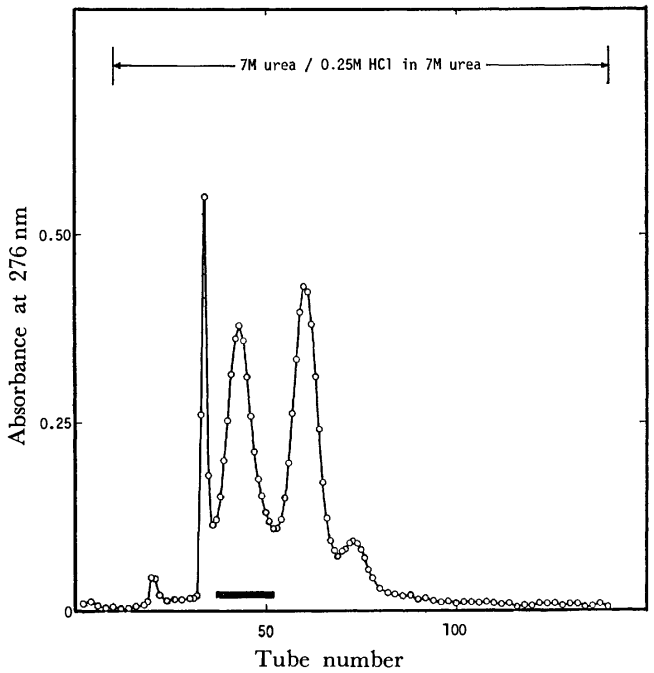

Fig. 3. Chromatography of the *S*-sulfonate of the Arg(Tos)-Arg(Tos)-Glu-Val-Glu-Gly-Pro-Gln-Val-Gly-Ala-Leu-Glu-Leu-Ala-Gly-Gly-Pro-Gly-Ala-Gly-Gly-Leu-Glu-Gly-Pro-Pro-Gln-Lys[Z(2-Cl)]-Arg-A-chain on QAE-Sephadex A-25 under the conditions described in the text.

hexapeptide acid V by DCC in the presence of HOBt[12] to give the protected decapeptide ester (IX), Boc-Arg(Tos)-Arg(Tos)-Glu(OBu^t)-Val-Glu(OBu^t)-Gly-Pro-Gln-Val-Gly-OBzl, which was then converted to its corresponding hydrazide (X) by the usual method.

Boc-Arg(Tos)-Arg(Tos)-Glu(OBu^t)-Val-Glu(OBu^t)-Gly-Pro-Gln-Val-Gly-N_3, prepared from its corresponding hydrazide (X) by Rudinger's method[13] without being isolated, was coupled with the *S*-sulfonate of the Ala-Leu-Glu-Leu-Ala-Gly-Gly-Pro-Gly-Ala-Gly-Gly-Leu-Glu-Gly-Pro-Pro-Gln-Lys[Z(2-Cl)]-Arg-A-cahin.[1] Azide couplings in the synthesis of peptides corresponding to positions 53—81[3] and 41—81[1] of bovine proinsulin mainly gave the target material, leaving only a little unchanged starting material. On the other hand, on azide coupling starting material remained considerably unreacted, even though the coupling reaction was performed under similar conditions to those described in the preceding papers.[1,3] However, the target product ,the *S*-sulfonate of a peptide corresponding to positions 31—81 of bovine proinsulin, Arg(Tos)-Arg(Tos)-Glu-Val-Glu-Gly-Pro-Gln-Val-Gly-Ala-Leu-Glu-Leu-Ala-Gly-Gly-Pro-Gly-Ala-Gly-Gly-Leu-Glu-Gly-Pro-Pro-Gln-Lys[Z(2-Cl)]-Arg-A-chain, could be easily separated from the starting material and the side-reaction product by ion-exchange chromatography on QAE-Sephadex A-25 after treatment of the reaction product with TFA (Fig. 3). The amino acid ratio of the acid

Table 1. Amino acid ratios of peptides synthesized[a]

Amino acid	Protected [31—40]	*S*-Sulfonate of [41—81][b]	*S*-Sulfonate of [31—81]
Lys		0.92(1)	1.00(1)
Arg	1.87(2)	1.00(1)	2.76(3)
Asp		1.96(2)	2.04(2)
Ser		1.94(2)	1.99(2)
Glu	3.14(3)	7.62(7)	11.27(10)
Pro	1.02(1)	2.88(3)	4.40(4)
Gly	2.00(2)	7.10(7)	9.15(9)
Ala		4.00(4)	4.00(4)
Cys		nd[c]	1.39(2)
Val	2.09(2)	1.67(2)	3.52(4)
Ile		0.55(1)	0.60(1)
Leu		5.00(5)	5.23(5)
Tyr		1.72(2)	1.98(2)

a) Molar ratios of individual amino acids are shown relative to that of glycine or alanine. Numbers in parentheses are theoretical values. b) Cited from Ref. 1. c) Cystine was not determined.

hydrolysate of the purified *S*-sulfonate is given in Table 1. Edman-degradation[14] of the purified material released the phenylthiohydantoin derivative of ω-tosylarginine as the N-terminal amino acid residue, which was identified on polyamide thin-layer by comparison with an authentic sample.

Thus a peptide with 51 amino acid residues, which shares a little over 62% of the 81 amino acid residues of bovine proinsulin, could be prepared in a homogeneous reaction system and purified easily by chromatography on an ion-exchanger.

Experimental

The general experimental and analytical methods are the same as reported.[3] UV-Absorption spectra were recorded on a Hitachi-spectrophotometer, type-124 and ^{1}H-NMR spectra on a JEOL PFT-100 pulse Fourier transform NMR spectrometer locked in deuterium and equipped with an FT-1a pulse control system. Chemical shifts were measured with TMS as an internal reference.

5-[3-[3-(p-Tolylsulfonyl)guanidino]propyl]-3-phenyl-2-thiohydantoin Hydrochloride (PTH-derivative of H-Arg(Tos)-OH). The title compound was prepared from H-Arg(Tos)-OH,[9] as reported[14]; mp 139—141 °C; $[\alpha]_D^{20}$ −9.7° (*c* 0.6, EtOH); UV (EtOH): λ_{max} 269.5 nm ($\varepsilon=15.1\times10^3$), λ_{min} 252 (8.6×10^3); ^{1}H-NMR (D_2O in DMSO-d_6): CH_2-CH_2(1, 2) δ 1.47—1.75 (4H, m), CH_3(aromatic) 2.32 (3H, s), CH_2(3) 3.11 (2H, t), CH(ring) 4.41 (1H, t), H(aromatic) 7.23—7.68 (9H, m); (DMSO-d_6): NH(ring) 10.57 (1H, s) ppm. Found: C, 49.47; H, 4.80; N, 14.50; S, 13.57; Cl, 7.05%. Calcd for $C_{20}H_{23}O_3N_5S_2\cdot HCl$: C, 49.83; H, 5.02; N, 14.53; S, 13.30; Cl, 7.36%.

Z-Val-Glu(OBu^t)-Gly-OEt (I). Z-Glu(OBu^t)-Gly-OEt[3] (16.5 g, 39.1 mmol) was dissolved in EtOH (250 ml) and hydrogenated over 5% palladium-charcoal catalyst. The catalyst was filtered off and the filtrate was concentrated to an oil under reduced pressure. The oil was dissolved with Z-Val-ONSu[7] (13.0 g, 37.4 mmol) in $CHCl_3$ (150 ml), stirred at room temperature for 2 d and then concentrated to a syrup. The syrup was dissolved in AcOEt and washed successively with 0.1 M HCl, 5% aqueous $NaHCO_3$ and water, dried and then concentrated to a crystalline solid, which was collected with AcOEt and hexane; wt 17.5 g. The crude material was recrystallized from EtOH; wt 16.2 g (83.1%), mp 141—143 °C, $[\alpha]_D^{27}$ −31.6° (*c* 2.2, EtOH).

Found: C, 59.89; H, 7.75; N, 8.09%. Calcd for $C_{26}H_{39}O_8N_3$: C, 59.87; H, 7.54; N, 8.06%.

Z-Glu(OBu^t)-Val-Glu(OBu^t)-Gly-OEt (II). Compound I (13.0 g, 24.9 mmol) was suspended in EtOH (250 ml), and hydrogenated over 5% palladium-charcoal at 40 °C. The catalyst was filtered off and the filtrate was concentrated to an oil. The oil was dissolved with Z-Glu(OBu^t)-ONp[8] (12.0 g, 26.2 mmol) in $CHCl_3$ (150 ml) and stirred at room temperature for a day, The solution was washed successively with 0.1M HCl, 5% aqueous $NaHCO_3$ and water, dried and then concentrated to a syrup. The syrup was triturated with hexane; wt 14.3 g. The crude material was recrystallized from AcOEt and hexane; wt 14.1 g (80.1%), mp 149—150 °C, $[\alpha]_D^{27}$ −8.8° (*c* 2.0, DMF).

Found: C, 59.33; H, 7.95; N, 7.83%. Calcd for $C_{35}H_{54}O_{11}N_4$: C, 59.47; H, 7.70; N, 7.93%.

Z-Arg(Tos)-Glu(OBu^t)-Val-Glu(OBu^t)-Gly-OEt (III). Compound II (2.80 g, 3.96 mmol) was dissolved in hot MeOH (150 ml), and hydrogenated over 5% palladium-charcoal catalyst at room temperature. The catalyst was filtered off and the filtrate was concentrated to a solid. The solid was dissolved in THF (100 ml) with Z-Arg(Tos)-OH, which was prepared from its cyclohexylammonium salt[9] (2.50 g, 4.45 mmol), cooled to −5 °C— −10 °C and mixed with HOBt (0.8 g, 5.93 mmol) and DCC (0.9 g, 4.37 mmol). The mixture was stirred at the same temperature for 1 h and at room temperature for 1 d. The precipitate formed was filtered off and the filtrate was concentrated to a syrup. The syrup was dissolved in AcOEt, washed successively with 0.1M HCl, 5% aqueous $NaHCO_3$ and water, dried and concentrated to a crystalline residue; wt 3.60 g. The crude product was recrystallized from EtOH and hexane; wt 3.48 g (86.4%), mp 179.5—181.5 °C, $[\alpha]_D^{21}$ −7.5° (*c* 2.0, DMF).

Found: C, 56.51; H, 7.13; N, 10.95; S, 3.44%. Calcd for $C_{48}H_{72}O_{14}N_8S$: C, 56.67; H, 7.14; N, 11.02; S, 3.15%.

Boc-Arg(Tos)-Arg(Tos)-Glu(OBu^t)-Val-Glu(OBu^t)-Gly-OEt (IV). Compound III (5.10 g, 5.01 mmol) was dissolved in hot MeOH (200 ml) and hydrogenated over 5% palladium-charcoal catalsyt at 35 °C. The catalyst was filtered off and the filtrate was concentrated to a solid. The solid was dissolved with Boc-Arg(Tos)-ONSu[3] (3.90 g, 7.41 mmol) in DMF (50 ml), stirred at room temperature for 1 d and then concentrated to a residue. The residue was dissolved in $CHCl_3$ and washed successively with 0.1M HCl, 5% aqueous $NaHCO_3$ and water, dried, and concentrated to a residue. The residue was collected from $CHCl_3$ and ether; wt 6.06 g. The crude product was reprecipitated from $CHCl_3$ and ether; wt 4.69 g (70.4%), mp 141—142 °C, $[\alpha]_D^{21}$ −8.1° (*c* 2.0, DMF). Amino acid ratio in the acid hydrolysate: Glu, 2.13 (2); Gly, 1.00 (1); Val, 1.04 (1); Arg, 1.95 (2).

Found: C, 52.30; H, 7.15; N, 12.80; S, 4.91%. Calcd for $C_{58}H_{92}O_{17}N_{12}S_2\cdot 2H_2O$: C, 52.39; H, 7.28; N, 12.64; S, 4.82%.

Boc-Arg(Tos)-Arg(Tos)-Glu(OBu^t)-Val-Glu(OBu^t)-Gly-OH (V). Compound IV (1.30 g, 0.977 mmol) was dissolved in MeOH (30 ml) and 1 M NaOH (3 ml) was added to the solution. The solution was stirred at room temperature for 2 h and then neutralized with 1 M HCl. MeOH was evaporated from the solution and the residue was mixed with 0.1 M HCl. The precipitate formed was filtered and reprecipitated from MeOH and ether; wt 1.20 g (94.5%), mp 136—139 °C, $[\alpha]_D^{21}$ −7.5° (*c* 2.0, DMF).

Found: C, 51.46; H, 6.81; N, 12.86; S, 5.04%. Calcd for $C_{56}H_{88}O_{17}N_{12}S_2\cdot 2H_2O$: C, 51.67; H, 7.12; N, 12.92; S, 4.93%.

Boc-Val-Gly-OBzl (IV). Boc-Val-OH prepared from its dicyclohexylammonium salt[10] (20.0 g, 50.1 mmol) was added to a solution of H-Gly-OBzl·TosOH (20.2 g, 59.9 mmol) and TEA (8.4 ml) in THF (200 ml). The solution was cooled below 0 °C, mixed with a solution of DCC (11.3 g, 54.9 mmol) in THF (50 ml) and stirred at the same temperature for 1 h and at room temperature for 1 d. It was then concentrated to a syrupy residue, dissolved in AcOEt and washed successively with 0.1 M HCl, 5% aqueous $NaHCO_3$ and water. The washed solution was dried and then concentrated to a syrup, which was crystallized from hexane; wt 16.0 g. The crude material was recrystallized from EtOH and hexane; wt 10.5 g (57.7%), mp 74.5—76.5 °C, $[\alpha]_D^{20}$ −8.3° (*c* 2.0, DMF).

Found: C, 62.78; H, 7.97; N, 7.75%. Calcd for $C_{19}H_{28}O_5N_2$: C, 62.62; H, 7.74; N, 7.69%.

Boc-Gln-Val-Gly-OBzl (VII). Compound VI (8.40 g, 23.1 mmol) was dissolved in 3.65 M HCl in dioxane (63 ml) and stirred at room temperature. After 1 h the solution was mixed with 3.65 M HCl in dioxane (10 ml) and stirred at room temperature for 30 min. The solution then was

concentrated to a syrup, which was solidified in ether. The solid was dissolved with TEA (3.2 ml) and Boc-Gln-ONp[11] (8.40 g, 22.9 mmol) in DMF (200 ml), stirred at room temperature for 2 d and then concentrated to dryness. The residue was suspended in $CHCl_3$, washed successively with 0.1 M HCl, 5% aqueous $NaHCO_3$ and water, filtered, and then dried; wt 10.0 g. The crude material was crystallized from a mixture of EtOH and MeOH; wt 9.50 g (84.1%), mp 203.5—204.5 °C, $[\alpha]_D^{20}$ −17.3° (*c* 2.0 DMF).

Found: C, 58.68; H, 7.35; N, 11.48%. Calcd for $C_{24}H_{36}O_7N_4$: C, 58.52; H, 7.37; N, 11.38%.

Boc-Pro-Gln-Val-Gly-OBzl (VIII). Compound VII (9.40 g, 19.1 mmol) was dissolved in 3.65 M HCl in dioxane (52 ml), stirred at room temperature for 60 min and then concentrated to a syrup. The syrup was triturated in ether, dissolved with TEA (2.7 ml) and Boc-Pro-ONSu[7] (7.10 g, 22.8 mmol) in DMF (150 ml), stirred at room temperature for 2 d and then concentrated to a solid. The solid was suspended in $CHCl_3$, washed successively with 0.1 M HCl, 5% aqueous $NaHCO_3$ and water, filtered, and dried over P_2O_5; wt 9.71 g. The crude material was reprecipitated from DMF, EtOH, and water; wt 8.66 g (76.7%), mp 210 °C (sintered) and 216—217 °C (decomp), $[\alpha]_D^{20}$ −38.2° (*c* 2.0, DMF). Amino acid ratio in the acid hydrolysate: Glu, 1.12 (1); Pro, 0.99 (1); Gly, 1.00 (1); Val, 1.04 (1).

Found: C, 59.02; H, 7.33; N, 11.89%. Calcd for $C_{29}H_{43}O_8N_5$; C, 59.07; H, 7.35; N, 11.88%.

Boc-Arg(Tos)-Arg(Tos)-Glu(OBu^t)-Val-Glu(OBu^t)-Gly-Pro-Gln-Val-Gly-OBzl (IX). Compound VIII (1.95 g, 3.31 mmol) was stirred in TFA (7 ml) at room temperature for 60 min. The solution was concentrated to a syrupy residue, which was triturated in ether. The material was dissolved wtih compound V (3.88 g, 2.98 mmol), *N*-methylmorpholine (0.43 ml) and HOBt (0.6 g) in DMF (50 ml). The solution was cooled below 0 °C, mixed with a solution of DCC (0.68 g, 3.30 mmol) in DMF (20 ml) and stirred at the same temperature for 1 h and at room temperature for 1 d. The mixture was stirred with HOBt (0.2 g), *N*-methylmorpholine (0.25 ml) and DCC (0.3 g) at room temperature for 2 d. The precipitate formed was filtered off and the filtrate was concentrated to dryness. The residue was collected with DMF and water and reprecipitated from MeOH and AcOEt; wt 4.54 g (86.0%), mp 201.5—203.5 °C (melt and dec), $[\alpha]_D^{20}$ −30.8° (*c* 1.0, DMF).

Found: C, 54.31; H, 7.02; N, 13.07; S, 3.74%. Calcd for $C_{80}H_{121}O_{22}N_{17}S_2 \cdot 2H_2O$: C, 54.19; H, 7.10; N, 13.43; S, 3.62%.

Boc-Arg(Tos)-Arg(Tos)-Glu(OBu^t)-Val-Glu(OBu^t)-Gly-Pro-Gln-Val-Gly-N_2H_3 (X). Compound IX (1.42 g, 0.802 mmol) was dissolved in DMF (10 ml) and mixed with 100% hydrazine hydrate (0.5 g). The solution was stirred at room temperature for 4 h and concentrated to a syrup, which was triturated in ether; wt 1.35 g (100%), mp 207.5—209.5 °C (dec).

Found: C, 52.07; H, 7.34; N, 16.07; S, 4.01%. Calcd for $C_{73}H_{117}O_{21}N_{19}S_2 \cdot H_2O$: C, 52.22; H, 7.14; N, 15.85; S, 3.82%.

S-Sulfonate of the Arg(Tos)-Arg(Tos)-Glu-Val-Glu-Gly-Pro-Gln-Val-Gly-Ala-Leu-Glu-Leu-Ala-Gly-Gly-Pro-Gly-Ala-Gly-Gly-Leu-Glu-Gly-Pro-Pro-Gln-Lys[Z(2-Cl)]-Arg-A-Chain. Compound X (0.83 g, 0.5 mmol) was dissolved in *N*-methylpyrrolidone (8 ml) and mixed with 3.0 M HCl in dioxane (1 ml) and then isopentyl nitrite (70 mg) in *N*-methylpyrrolidone (1 ml) at −20 °C. The solution was stirred at −20 °C——25 °C for 75 min, mixed with *N*-methylmorpholine (0.4 ml) and the *S*-sulfonate of the Ala-Leu-Glu-Leu-Ala-Gly-Gly-Pro-Gly-Ala-Gly-Gly-Leu-Glu-Gly-Pro-Pro-Gln-Lys[Z(2-Cl)]-Arg-A-chain[1] (236 mg, *ca.* 50 μmol), and stirred at 2—3 °C for a week in a refrigerator.

The solution then was mixed with 0.1M NH_4HCO_3 (20 ml) and subjected to gel-filtration on Sephadex G-25 (3×60 cm) in 0.1M NH_4HCO_3. The eluate with absorption at 280 nm was collected and lyophilized. The lyophilized material was dissolved in TFA (10 ml) in an ice-water bath, stirred at room temperature for an hour and concentrated to a syrup. The syrupy material was dissolved in 0.1 M NH_4HCO_3 (50 ml) with a small amount of ammonia water, lyophilized and redissolved with Na_2SO_3 (0.4 g), $Na_2S_4O_6$ (0.4 g) and EDTA·2Na (0.01 g) in 8 M urea (10 ml) at pH 8.0. The solution was stirred at room temperature for 2 d and then charged on a column (3×60 cm) of Sephadex G-25 in 0.1 M NH_4HCO_3. The eluate with absorption at 280 nm was collected and lyophilized. The lyophilized material was charged on a column (9×140 mm) of QAE-Sephadex A-25 (acetate cycle), equilibrated with 7 M urea, and material was eluted with a linear gradient of 7 M urea (250 ml) to 0.25 M HCl in 7 M urea (250 ml) (Fig. 3). The fraction (shown by a bar), with an absorption at 276 nm, was desalted on a column (3×60 cm) of Sephadex G-25 using 0.1 M NH_4HCO_3 and lyophilized; 87.6 mg.

References

1) Part III: H. Aiba and Y. Shimonishi, *Bull. Chem. Soc. Jpn.*, **53**, 197 (1980).
2) Y. Shimonishi, *Bull. Chem. Soc. Jpn.*, **43**, 3251 (1970).
3) H. Aiba and Y. Shimonishi, *Bull. Chem. Soc. Jpn.*, **53**, 192 (1980).
4) D. F. Steiner, S. Cho, P. E. Oyer, S. Terris, J. D. Peterson, and A. H. Rubenstein, *J. Biol. Chem.*, **246**, 1365 (1971).
5) M. Weinert, D. Brandenburg, and H. Zahn, *Hoppe-Seyler's Z. Physiol. Chem.*, **350**, 1566 (1969).
6) The abbreviations used are as follows: DMF, *N,N*-dimtheylformamide: DMSO, dimethyl sulfoxide; DCC, dicyclohexylcarbodiimide; HOBt, 1-hydroxybenzotriazole; TFA, trifluoroacetic acid; THF, tetrahydrofuran; TEA, triethylamine; Other abbreviations used are those recommended by the IUPAC-IUB: *J. Biol. Chem.*, **247**, 977 (1972).
7) G. W. Anderson, J. E. Zimmerman, and F. M. Callahan, *J. Am. Chem. Soc.*, **86**, 1839 (1964).
8) E. Scoffone, R, Rocchi, G. Vidali, A. Scatturin, and F. Marchiori, *Gazz. Chim. Ital.*, **94**, 743 (1964).
9) J. Ramachandran and C. H. Li, *J. Org. Chem.*, **27**, 4006 (1962).
10) G. W. Anderson and A. McGregor, *J. Am. Chem. Soc.*, **79**, 6180 (1957).
11) H. C. Beyerman, C. A. M. Boers-Boonekamp, and H. Maassen van den Brink-Zimmermannova, *Recl. Trav. Chim. Pays-Bas*, **87**, 257 (1968).
12) W. König and R. Geiger, *Chem. Ber.*, **103**, 788 (1970).
13) J. Honzl and J. Rudinger, *Collect. Czech. Chem. Commun.*, **26**, 2333 (1961).
14) P. Edman and K. Lauber, *Acta Chem. Scand.*, **10**, 466 (1956).

Chemistry of *N*-Thiosulfinylanilines. V.[1] Reactions of *N*-Thiosulfinylanilines with Nucleophilic Reagents

Yoshio Inagaki, Takeo Hosogai, Renji Okazaki, and Naoki Inamoto*

Department of Chemistry, Faculty of Science, The University of Tokyo, Hongo, Bunkyo-ku, Tokyo 113

(Received May 24, 1979)

2,4-Di-*t*-butyl-6-methyl-*N*-(thiosulfinyl)aniline (**1**) gave 2,4-di-*t*-butyl-6-methylaniline in the reactions with such reagents as alkylamines, thiourea, butyllithium, alkylmagnesium halides, 1-(1-pyrrolidinyl)cyclopentene, and hydrogen sulfide. Triphenylphosphine reacted with **1** to give (2,4-di-*t*-butyl-6-methylphenylimino)triphenylphosphorane and bis(2,4-di-*t*-butyl-6-methylphenyl)sulfur diimide. Reaction of triphenylphosphine with 2,4,6-tri-*t*-butyl-7,8-dithia-9-azabicyclo[4.3.0]nona-2,4,9-triene afforded 2,4,6-tri-*t*-butylaniline, bis(2,4,6-tri-*t*-butylphenyl)-sulfur diimide, and 2,4,6-tri-*t*-butyl-*N*-sulfinylaniline (**7**). The sulfur diimide was considered to be formed *via* intermediary 2,4,6-tri-*t*-butylthionitrosobenzene, which was trapped by oxygen to give the *N*-sulfinyl derivative **7**.

It is an interesting subject which atom of a thiocumulene of the type X=S=Y is attacked by a nucleophile. Some thiocumulenes are attacked on the central sulfur atom (*e.g.* sulfur dioxide,[2] sulfinylamines,[3] sulfur diimides,[4] and sulfines[5]), while some others are attacked on the terminal atom, X or Y (*e.g.* thiocarbonyl imines[6] and sulfines[7]). The latter type of reaction is known to occur when the difference in electronegativity between the two ligand atoms, X and Y, is small.[8] We became interested in the attacking point of a nucleophile in the case of an *N*-thiosulfinyl group. There seem three conceivable modes as depicted in Scheme 1, and the formation of Nu=S and Nu=S=S is of interest from the standpoint of utilization of thiosulfinylamino compounds as thiotransfer reagents.

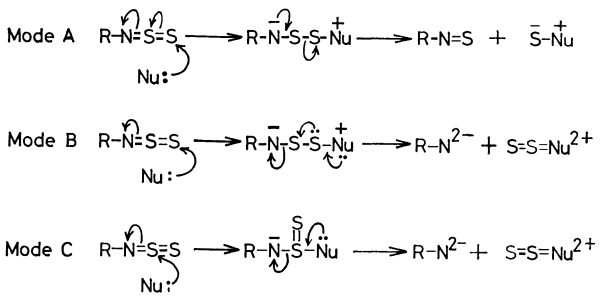

Scheme 1.

This paper describes the reactions of *N*-thiosulfinylanilines with various nucleophilic reagents in relation to these problems.

Results and Discussion

Reactions with Triphenylphosphine. We described previously[9] that one of the possible decomposition pathways of a thiosulfinylamino compounds was extrusion of one sulfur atom leading to sulfur diimide *via* thionitroso intermediate and that this explained the instability of the thiosulfinylamino group.

$$\mathrm{Ar{-}N{=}S{=}S} \xrightarrow{-S} \mathrm{Ar{-}N{=}S} \xrightarrow{-S} 1/2\,\mathrm{Ar{-}N{=}S{=}N{-}Ar}$$

It is conceivable, therefore, that elimination of one sulfur atom from thiosulfinylamino group by phosphines would also afford sulfur diimide. In order to examine such a possibility, desulfurization of *N*-thiosulfinylanilines with triphenylphosphine was investigated.

Reactions of 2,4-di-*t*-butyl-6-methyl-*N*-thiosulfinylaniline (**1**) or 2,4,6-tri-*t*-butyl-7,8-dithia-9-azabicyclo-[4.3.0]nona-2,4,9-triene (**4**) with an equimolar amount of triphenylphosphine proceeded even at −78 °C to give products shown in Scheme 2. Since about 50% of **1** or **4** was recovered in these reactions, the yields of the products were calculated based on the consumed **1** or **4**.

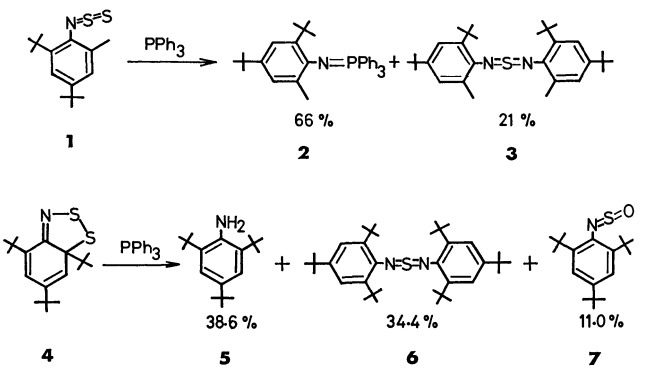

Scheme 2.

Reaction of **4** with trimethyl phosphite proceeded very slowly even at room temperature; reaction with 3.9 molar excess of trimethyl phosphite at room temperature for 3 days afforded the phosphoramidate (**8**) in 56% yield.

$$\mathbf{4} \xrightarrow{\mathrm{P(OMe)_3}} \mathrm{Ar^1NHP(O)(OMe)_2} \quad \mathbf{8}$$

$\mathrm{Ar^1 = 2,4,6\text{-}(t\text{-}Bu)_3C_6H_2}$

The reactivity of the *N*-thiosulfinylanilines is in striking contrast to that of *N*-sulfinylanilines, which do not react with trivalent phosphorus compounds; for example, 2,4,6-tri-*t*-butyl-*N*-sulfinylaniline (**7**) reacted with neither triphenylphosphine nor trimethyl phosphite.

When the reaction of **4** with triphenylphosphine was carried out under a stream of oxygen, the sulfur diimide (**6**) was not produced, but the yield of the *N*-sulfinylaniline (**7**) increased up to 38.6% instead. Since **4** did not react with oxygen under the reaction conditions, this result suggests

$$\mathbf{4} \xrightarrow[-78\,^\circ\mathrm{C}]{\mathrm{Ph_3P,\ O_2}} \mathrm{Ar^1{-}NH_2} + \mathrm{Ar^1{-}N{=}S{=}O}$$

5, 35.4% **7**, 38.6%

that the sulfur diimide (**6**) and the *N*-sulfinylaniline

(**7**) were produced *via* a common intermediate, thionitrosobenzene (**9**) (Ar^1–N=S), which could be trapped by oxygen.

Reactions of sterically hindered nitrosobenzenes (**10** and **13**) with trialkylphosphines afford products which are considered to be formed *via* nitrene[10,11] (Scheme 3).

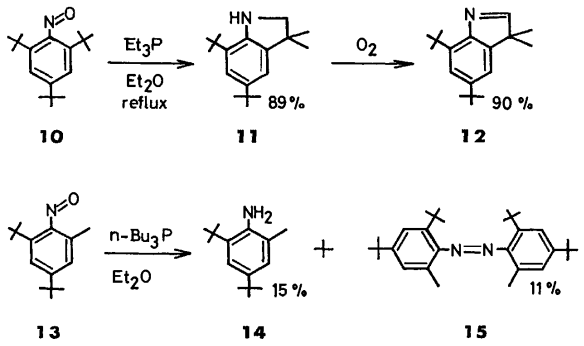

Scheme 3.

Absence of **11** or **15** in the prodcuts obtained by the reaction of **1** or **4** with triphenylphosphine excludes the nitrene formation. Therefore, the probable reaction mechanism can be depicted as in Scheme 4. Nucleophilic attack of triphenylphosphine on **1** or **4** affords zwitterion **16**, which gives the iminophosphorane **17** when R is methyl. When R is more bulky *t*-butyl, elimination of triphenylphosphine sulfide from **16** to give the thionitrosobenzene (**18**) is a predominant pathway. The thionitroso derivative gives **22** *via* cyclization into **20** or **21** followed by extrusion of sulfur. Formation mechanism of 2,4,6-tri-*t*-butylaniline (**5**) is not clear but one possible route is hydrolysis of the zwitterion **16**.

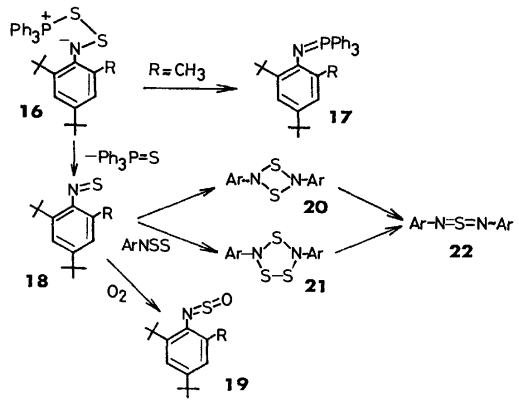

Scheme 4.

Reactions with Amines. A sulfinyl group of a sulfinylamine has been reported to be transferred to a primary amine.[12]

$$R\text{-}N{=}S{=}O + R'\text{-}NH_2 \longrightarrow R\text{-}NH_2 + R'\text{-}N{=}S{=}O$$

In the hope that a similar transfer might occur in the case of thiosulfinylamino compounds, the reactions of the *N*-thiosulfinylaniline (**1**) with amines were attempted. Reactions of **1** with alkylamines afforded 2,4-di-*t*-butyl-6-methylaniline (**14**) together with other products which could not be identified because of difficulty in purification. The results are summarized in Table (see also Experimental).

Table 1. Yields of **14**

R-NH_2	Reaction time	Solvent	Molar ratio R-NH_2/**1**	Yield of **14** %
n-$BuNH_2$	88 h	EtOH	1.08	41.1
t-$BuNH_2$	22 h	Et_2O	1.39	30.6
1-$AdNH_2$[a]	11 days	CH_2Cl_2	1.01	81.1
$PhNH_2$	1 week	Et_2O	0.94	no reaction
Pyrr.[b]	2.5 h	CH_2Cl_2	2.23	63.7

a) 1-Ad denotes 1-adamantyl. b) Pyrr. stands for pyrrolidine.

Similar reduction of **1** also took place with thiourea in ethanol for a day at room temperature in 87.7% yield.

Reactions with Organometallic Compounds. Reaction of **1** with an equimolar amount of methylmagnesium iodide afforded the aniline (**14**) (65.2%) and the sulfur diimide (**3**) (8.5%). In the reaction with an equimolar amount of butyllithium the products were also **14** (54.1%) and **3** (23.6%). Reaction of **1** with excess isopropylmagnesium bromide gave **14** in 59.6% yield. These reactions proceeded smoothly and **1** was almost completely consumed. In contrast to

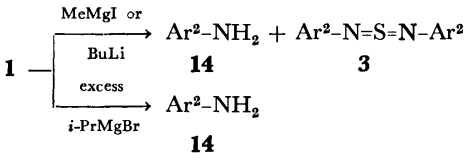

Ar^2 = 2,4-(*t*-Bu)$_2$-6-MeC_6H_2

these reactions, reactions of 2,4,6-tri-*t*-butyl-*N*-sulfinylaniline (**7**) with isopropylmagnesium bromide afforded 63.0% of *N*-(2,4,6-tri-*t*-butylphenyl)-1-methylethanesulfinamide (**23**),

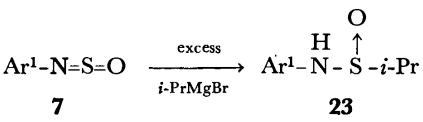

the structure of which was established by hydrolysis giving the aniline (**5**) as well as its spectral and analytical data.

Reaction with an Enamine. Reaction of **1** with 1-(1-pyrrolidinyl)cyclopentene was carried out in the hope of obtaining 1 : 1 cycloadduct. Although the reaction proceeded immediately even at −78 °C to give the aniline (**14**) (57.7%), the reaction mechanism is not clear at present. Absence of the cycloadduct may be attributable to steric hindrance around the nitrogen atom of **1** and to lability of the N–S bond against nucleophilic attack.[13]

Reaction with Hydrogen Sulfide. Reaction of **1** with hydrogen sulfide in benzene followed by chromatographic treatment on silica gel afforded 50.8% of the aniline (**14**) and another compound which was unstable to decompose into **14** on further chromatographic treatment on alumina.

Conclusion. In all these reactions described above, 1:1 adducts appeared too unstable to be isolated. Since any product containing sulfur atom(s) could

not be isolated except for the case of triphenylphosphine, the detailed reaction mechanism remains to be determined. However, it is clear that the thiosulfinylamino group has thiotransfer ability judging from the formation of the corresponding reduced compounds.

Experimental

All melting points were uncorrected. The IR and UV spectra were recorded with Hitachi EPI-G2 and EPS-3 spectrophotometers, respectively. The NMR spectra were measured with a Hitachi R-20B (60 MHz) spectrometer using tetramethylsilane as an internal standard. The mass spectra were recorded with a Hitachi RMU-6L mass spectrometer (70 eV). Chromatographic treatment was carried out using dry column chromatography (Woelm silica gel for dry column chromatography) unless otherwise stated.

*Reaction of 2,4-Di-t-butyl-6-methyl-*N*-(thiosufinyl)aniline (**1**) with Triphenylphosphine.* To an ethereal solution (25 ml) of **1** (634 mg, 1.90 mmol)[14] was added an ethereal solution (15 ml) of triphenylphosphine (498 mg, 1.90 mmol) at −78 °C under nitrogen. After the mixture was stirred for 4 h at −78 °C, the temperature was raised gradually up to −5 °C over a 13.5 h period. Removal of the solvent followed by treatment with hexane gave white precipitates. They were recrystallized once from ethanol to give triphenylphosphine sulfide (mp 166.5—167.0 °C), which was identified by means of IR. Hexane-soluble part was subjected to dry column chromatography (DCC) (silica gel, hexane) to give three fractions. From the first fraction was recovered 287 mg (53.7%) of **1**. The second fraction gave 51 mg of orange tar, which was purified by DCC to give 43 mg (21.0% based on consumed **1**) of bis(2,4-di-*t*-butyl-6-methylphenyl)sulfur diimide (**3**) (NMR and IR).[9] The third fraction afforded 278 mg (66.0% based on consumed **1**) of (2,4-di-*t*-butyl-6-methylphenylimino)triphenylphosphorane (**2**) as pale yellow crystals, which were recrystallized five times from hexane to give colorless crystals, mp 171—172.5 °C; IR (KBr): 1110 (P–Ph) cm^{-1}; NMR (CCl_4): δ 1.24 (s, 9H), 1.31 (s, 9H), 1.61 (s, 3H), 6.6 (broad, 1H), 7.01 (broad, 1H), and 7.13—7.93 (m, 15H); MS: *m/e* 479 (M^+, 31.5%), 464 (43.5), 262 ($Ph_3P^{+\cdot}$, 50.0), 252 (45.4), and 185 (Ph_2P^+, 100). Found: C, 82.42; H, 8.14; N, 2.84%. Calcd for $C_{33}H_{38}NP$: C, 82.64; H, 7.99; N, 2.92%.

*Reaction of 2,4,6-Tri-t-butyl-7,8-dithia-9-azabicyclo[4.3.0]nona-2,4,9-triene (**4**) with Triphenylphosphine.* To an ethereal solution (20 ml) of **4** (426 mg, 1.32 mmol)[14] was added an ethereal solution (12 ml) of triphenylphosphine (351 mg, 1.34 mmol) at −78 °C under nitrogen. The mixture was stirred for 1.5 h at −78 °C, for 2 h at 0 °C, and 3 h at room temperature. Removal of the solvent followed by treatment with hexane afforded triphenylphosphine sulfide (mp 161—163 °C), which was identifical by means of IR. The hexane-soluble part was chromatographed (silica gel, hexane) to give four fractions. The first fraction afforded recovered **4** (225 mg, 52.8%). The second fraction was rechromatographed (silica gel, CCl_4) to give 59 mg (34.4% based on consumed **4**) of bis(2,4,6-tri-*t*-butylphenyl)sulfur diimide (**6**) and 21 mg (11.0% based on consumed **4**) of *N*-sulfinyl-2,4,6-tri-*t*-butylaniline (**7**). These products were identified by comparing the IR and NMR spectra with those of authentic samples.[9] The third fraction gave 63 mg (38.6% based on consumed **4**) of 2,4,6-tri-*t*-butylaniline (**5**) which was identified by IR and NMR. The fourth fraction gave 21 mg of pale yellow tarry material, which could not be purified.

*Reaction of **4** with Triphenylphosphine under a Stream of Oxygen.* After oxygen was bubbled into 40 ml of ether at −78 °C for 30 min, 804 mg (2.49 mmol) of **4** was dissolved. To this solution was added an ethereal solution (39 ml) of triphenylphosphine (652 mg, 2.49 mmol). The reaction mixture was stirred under an oxygen stream for 5 h at −78 °C, for 2 h at 0 °C, and similar work-up to the preceding experiment gave **4** (409 mg, 50.9% recovery), **7** (145 mg, 38.6% based on consumed **4**) and **5** (113 mg, 35.4% based on consumed **4**).

*Reaction of **4** with Trimethyl Phosphite.* A solution of **4** (560 mg, 1.73 mmol) and trimethyl phosphite (332 mg, 8.04 mmol) in ether (45 ml) was stirred for 3 days at room temperature. After ether and excess trimethyl phosphite were removed under reduced pressure, the resulting residue was treated with hexane to give 357 mg (56%) of *O,O*-dimethyl *N*-(2,4,6-tri-*t*-butylphenyl)phosphoramidate (**8**) as colorless needles, which were recrystallized six times from hexane and once from methanol, mp 182 °C; IR (KBr): 3170 (broad, NH), 1140 (PO), and 825 cm^{-1} ($POCH_3$); NMR (CCl_4): δ 1.31 (s, 9H), 1.52 (s, 18H), 3.56 (d, J= 11 Hz, 6H), 4.35 (broad, 1H), and 7.33 (s, 2H); MS: *m/e* 369 (M^+, 20.6%), 298 (41.3), 242 (40.0), 57 (100), and 41 (87.0). Found: C, 64.74; H, 10.03; N, 3.73%. Calcd for $C_{20}H_{36}NO_3P$: C, 65.02; H, 9.82; N, 3.79%.

*Reaction of 2,4,6-Tri-t-butylnitrosobenzene (**10**) with Triethylphosphine.* To an ethereal solution (50 ml) of **10**[15] (8.43 g, 27 mmol), was added triethylphosphine (6.4 g, 54 mmol) dissolved in 50 ml of ether under nitrogen. The solution was then refluxed for 18 h. The solvent and the remaining triethylphosphine were removed under reduced pressure. Crude 3,3-dimethyl-5,7-di-*t*-butylindoline (**11**) was obtained by DCC on silica gel. The yield was 6.2 g (89%). The crude material dissolved in petroleum ether was shaken with aq hydrochloric acid. The precipitated hydrochloride salt was washed with petroleum ether. The free indoline (**11**) was obtained by treatment of the salt with aq sodium carbonate. The above purification was repeated four times to yield pure **11** (2.6 g, 34%), mp 100—102 °C; NMR (CCl_4): δ 1.25 and 1.31 (24H), 3.20 (2s, H), 3.69 (br, 1H), 6.77 (d, J=4 Hz, 1H), and 6.92 (d, J=4 Hz, 1H); IR (KBr): 3300 cm^{-1} (NH). Found: C, 83.10; H, 11.43; N, 5.50%. Calcd for $C_{18}H_{29}N$: C, 83.33; H, 11.27; N, 5.40%. This compound was also purified by recrystallization from ethanol. The dihydroindole (**11**) (0.41 g, 1.6 mmol) dissolved in 25 ml of 90% ethanol was heated at reflux for 11 h in the presence of active charcoal (1 g) under a stream of oxygen. The active charcoal was filtered off from the warm solution and then the crude 3*H*-indole (**12**) (0.36 g, 90%) was obtained by removal of the solvent. The pure material was obtained by repeated recrystallization from 80% ethanol. The yield was 0.2 g (50%), mp 128—129 °C; NMR (CCl_4): δ 1.29 and 1.35 (s, 15H), 1.50 (s, 9H), 7.04 (d, J=4 Hz, 1H), 7.17 (d, J=4 Hz, 1H), and 7.77 (s, 1H); IR (KBr): 1590 cm^{-1} (C=N); UV_{max} (C_2H_5OH): 224 (log ε 4.2), 231 (4.1), and 266 nm (3.9). Found: C, 83.86; H, 10.51; N, 5.28%. M^+ 257. Calcd for $C_{18}H_{27}N$: C, 83.99; H, 10.57; N, 5.44%. M^+ 257.

*Reaction of 2,4-Di-t-butyl-6-methylnitrosobenzene (**13**) with Tributylphosphine.* To an ethereal solution (20 ml) of tributylphosphine (2 g, 9.9 mmol) was added an ethereal solution (15 ml) of **13** (0.996 g, 4.27 mmol).[15] The mixture was stirred for 70 min at room temperature, and then stirred with sulfur (170 mg) for 40 min. After removal of the solvent, the residue was chromatographed on silica gel. Elution with benzene afforded a red fraction (Fraction A) and a yellow one (Fraction B). Fraction A was chromatographed

on silica gel with CCl_4 as eluent to afford 97.5 mg (0.224 mmol, 10.5%) of 2,2′,4,4′-tetra-*t*-butyl-6,6′-dimethylazobenzene (**15**), which was recrystallized from aq methanol; mp 156—158 °C. NMR (CCl_4): δ 1.37 (s, 36H), 2.24 (s, 6H), 7.04 (d, J=2 Hz, 2H), and 7.32 (d, J=2 Hz, 2H); UV_{max} (hexane): 238 (ε 9040), 247 (sh) (8570), 312 (15650), and 486 nm (1750); MS: *m/e* 434 (M^+, 5.4%), 217 (35), and 57 (100).

Fraction B was chromatographed on alumina with hexane as eluent to give 140 mg (0.638 mmol, 15.0%) of 2,4-di-*t*-butyl-6-methylaniline (**14**).

Reactions of **1** *with Amines.* Reactions were carried out under nitrogen or argon.

Reaction with Butylamine: A mixture of **1** (400 mg, 1.42 mmol) and butylamine (112 mg, 1.53 mmol) in 10 ml of ethanol was stirred for 88 h at room temperature. The reaction mixture was filtered to give 62 mg of colorless crystals, which melted at 107.5—108.5 °C after twice recrystallization from ethanol; IR (KBr): 3420, 870, 725, 605, and 590 cm^{-1}; NMR (CCl_4): δ 1.27 (s, 9H), 1.48 (s, 9H), 2.42 (s, 3H), and 7.05 (ABq, J=2 Hz, $\Delta\delta$=0.09, 2H); MS: *m/e* 267 (3.6%), 233 (3.6), 225 (17.2), 220 (17.5), and 205 (100). Found: C, 59.90; H, 8.44; N, 4.54; S, 26.58%, which requires $C_{15.4}H_{25.8}NS_{2.6}$, but the structure was not determined.

The filtrate was treated with DCC (silica gel, CCl_4). A reddish fraction gave 116 mg of tarry mixture, which could not be purified and identified; IR (neat): 3430 and 3340 cm^{-1} (broad); NMR (CCl_4): δ 1.26 (s, *ca.* 18H), 1.44 (s, 18H), 2.35 (s, *ca.* 3H), 2.41 (broad s, *ca.* 3H), 5.24 (broad, 1H), 5.37 (broad, 1H), 6.92 (m, 2H), and 7.07 (m, 2H). A colorless fraction gave 128 mg (41.1%) of **14**.

Reaction with t-*Butylamine*: A mixture of **1** (399 mg, 1.42 mmol) and *t*-butylamine (145 mg, 1.98 mmol) in 5 ml of ether was stirred for 22 h at room temperature. Removal of the solvent followed by treatment with hexane afforded 62 mg of colorless precipitates; IR (KBr): 2600—2500 (broad band), 1200, 1110, and 640 cm^{-1}; NMR ($CDCl_3$): δ 1.31 (s, 9H), 1.47 (s, 18H), 2.50 (s, 3H), 5.62 (broad s, 1H), 6.05 (broad s, 4H), 7.15 (m, 1H), and 7.33 (m, 1H). The hexane-soluble part was treated with DCC (silica gel, hexane) to give 117 mg (29.3%) of **1**, 116 mg of tarry mixture, which could not be purified, and 95 mg (30.6%) of **14**.

Reaction with 1-Adamantylamine: A solution of **1** (565 mg, 2.01 mmol), 380 mg (2.03 mmol) of 1-adamantylammonium chloride, and triethylamine (255 mg, 2.52 mmol) in dichloromethane (15 ml) was stirred for 11 days at room temperature. The reaction mixture was washed with water and dried over $MgSO_4$. Removal of the solvent followed by treatment with pentane afforded 110 mg of sparingly soluble colorless powder, which sublimed at 315—350 °C; IR (KBr): 3345 (NH), 3250—2500 (broad band), 1210, 1190, 1025, and 640 cm^{-1}; NMR (acetone-d_6): δ 1.55—1.92 (m) and 2.00—2.25 (m), the intensity ratio was 12:3; MS: *m/e* 264 (2.6%), 330 (1.1), 307 (1.1), 297 (0.9), 284 (0.9), 213 (2.2), 204 (4.8), 197 (3.0), 151 (1-$AdNH_2^{+\cdot}$, 100), 135 (Ad^+, 62), and 108 (32).

Found (recrystallized once from acetone): C, 52.00; H, 7.15; N, 5.82; S, 22.31%, which requires $C_{10.4}H_{17.0}N_{1.0}O_{1.9}S_{1.7}$, but the structure could not be identified.

The pentane-soluble part was treated with DCC (silica gel, hexane) to give 72 mg (12.7%) of **1** in a purple fraction, and 357 mg (81.1%) of **14**. The other products could not be isolated, but a tarry mixture (104 mg) obtained from a fraction next to an orange-yellow fraction exhibited following spectral data; IR (neat): 3410 (sharp), 3475, and 3300 cm^{-1} (broad); NMR (CCl_4): δ 1.18 (s, 9H), 1.38 (s, 9H), 1.46—1.88 (m, 11—12H), 1.82—2.20 (m, 3H), 2.36 (s, 3H), 3.46 (broad, 1H), 5.40 (broad, 1H), 6.39 (d, J=2 Hz, 1H), and 7.15 (d, J=2 Hz, 1H); MS: *m/e* 380 (trace), 352 (trace), 330 (trace), 262 (trace), 247 (6.6%), 232 (23.8), 219 (18.9), 204 (100), 151 (13.9), 148 (7.8), 94 (86.9), and 64 (75.4).

Reaction with Pyrrolidine: A solution of **1** (302 mg, 1.07 mmol) and pyrrolidine (170 mg, 2.39 mmol) in dichloromethane (5 ml) was stirred for 2.5 h at room temperature to give a yellowish orange solution, which was washed with water and dried over $MgSO_4$. Removal of the solvent followed by DCC (silica gel, hexane) gave 150 mg (63.7%) of **14**. The other products could not be isolated.

Reaction of **1** *with Thiourea.* Ethanol solution (10 ml) of 404 mg (1.44 mmol) of **1** and 109 mg (1.44 mmol) of thiourea was stirred for 24 h at room temperature. The reaction mixture was filtered to give 83 mg (2.58 mg-atom) of sulfur and reddish brown solution. After removal of the solvent, the residue was treated with hexane to give colorless crystals which seemed to be a mixture containing thiourea mainly on the basis of the IR spectrum, but could not be purified. The hexane-soluble part was subjected to DCC (silica gel, hexane) to give 276 mg (87.7%) of **14**.

Reaction of **1** *with Organometallic Compounds.* Reactions were carried out under nitrogen. Concentration of organometallic reagents were determined by titration with 2-butanol in xylene using 1,10-phenanthroline as an indicator.[16]

Reaction of **1** *with Methylmagnesium Iodide.* To an ethereal solution (10 ml) of **1** (440 mg, 1.56 mmol) cooled to *ca.* 0 °C was added an ethereal solution (1.63 ml) of CH_3MgI (0.98 M). After being stirred for 30 min at 0 °C, the reaction mixture was treated with aq NH_4Cl (5 ml) to give orange solution, which was washed with water and dried over $MgSO_4$. Removal of the solvent followed by DCC (silica gel, hexane) afforded 23 mg (5.3% recovery) of **1** in a purple fraction. The subsequent fraction gave 25 mg of slightly colored tarry material, which partly decomposed into purple substance (probably **1**) on treatment with TLC (silica gel). This tarry material afforded following spectral data; IR (neat): 3420 cm^{-1}; NMR (CCl_4): δ 1.28 (s, 9H), 1.49 (s, 9H), 1.94 (s, 3H), 5.46 (broad s, 1H), 7.00 (d, J=2 Hz, 1H), and 7.15 (d, J=2 Hz, 1H); MS: *m/e* 247 (3%), 232 (13), 219 (19), and 204 (100).

The orange fraction gave 118 mg of orange crystalline material, which was recrystallized once from acetone to give 31 mg (8.5%) of the sulfur diimide **3**.

The most polar fraction gave 224 mg (65.2%) of **14**.

Reaction of **1** *with Isopropylmagnesium Bromide.* To an ethereal solution of the Grignard reagent prepared from 871 mg (7.08 mmol) of isopropyl bromide and cooled with an ice bath, 160 mg (6.59 mmol) of magnesium, and 11 ml of ether, was added an ethereal solution (11 ml) of **1** (198 mg, 0.703 mmol) dropwise over a period of 10 min. After being stirred for 1 h at 0 °C, the reaction mixture was hydrolyzed by aq NH_4Cl. After the usual work up, the residue was treated with DCC (silica gel, hexane) to give 32 mg of orange tar, which gave 15 mg of **14** on purification by TLC (silica gel, CCl_4–hexane; 4:1), and 112 mg of pale yellow tar, which was treated with DCC (silica gel, CCl_4). From a colorless fraction, 77 mg of **14** was obtained. Thus the yield of **14** was 92 mg (59.6%).

Reaction of **1** *with Butyllithium.* To a pentane solution (5 ml) of **1** (501 mg, 1.78 mmol) was added 1.15 ml of hexane solution of butyllithium (1.55 M) at 0 °C over a 5 min period. After being stirred for 1 h at 0 °C, the reaction mixture was hydrolyzed by 5 ml of aq NH_4Cl, washed with water, dried over $MgSO_4$. After the solvent was removed, the residual orange tar was washed with 3 ml of methanol to give 98 mg (23.6%) of **3** as orange crystals. The methanol-soluble part

was treated with DCC (silica gel, hexane) to give 211 mg (54.1%) of **14**.

Reaction of 2,4,6-Tri-t-butyl-N-sulfinylaniline (7) with Isopropylmagnesium Bromide. To the Grignard reagent prepared from 391 mg (16.1 mmol) of magnesium, 2.00 g (16.3 mmol) of isopropyl bromide, and 25 ml of ether and cooled with an ice bath, was added an ethereal solution (10 ml) of **7** (501 mg, 1.63 mmol) dropwise with stirring. After additional stirring for 40 min, the reaction mixture was hydrolyzed by aq NH_4Cl, washed with water, and dried over $MgSO_4$. Removal of the solvent gave 569 mg of colorless crystals, which were recrystallized once from aq methanol to give 261 mg (63.0%) of the sulfinamide **23** (mp 100.5—101 °C (dec)), which was recrystallized three times from hexane to give colorless needles, mp 101 °C (dec); IR (KBr): 3290 (broad, νNH) and 1075 cm^{-1} (νSO); NMR ($CDCl_3$): δ 1.33 (s, 9H), 1.45 (d, J=7 Hz, 6H), 1.50 (s, 18H), 3.21 (sep, J=7 Hz, 1H), 6.12 (broad s, 1H), and 7.39 (s, 2H); MS: *m/e* 261 ($M^+ - (CH_3)_2C{=}S{=}O$, 16.3%) and 246 (100). Found: C, 71.87; H, 10.84; N, 3.92; S, 8.94%. Calcd for $C_{21}H_{37}NOS$: C, 71.74; H, 10.61; N, 3.98; S, 9.12%.

A solution of **23** (42 mg, 0.12 mmol) in 10 ml of methanol containing 1 drop of trifluoroacetic acid was allowed to stand for 3 days at room temperature. Removal of the solvent followed by preparative TLC purification (silica gel, CCl_4) gave 17 mg (54%) of **14**.

Reaction of 1 with 1-(1-Pyrrolidinyl)cyclopentene. To a CH_2Cl_2 solution (15 ml) of **1** (880 mg, 3.13 mmol) was added a solution of the enamine[12] (4.38 mg, 3.19 mmol) in 10 ml of CH_2Cl_2 at −78 °C. The color of **1** (red-purple) disappeared immediately. After removal of the solvent, the residue was chromatographed on silica gel. Elution with benzene afforded 396 mg (57.7%) of **14**.

Reaction of 1 with Hydrogen Sulfide. Hydrogen sulfide was bubbled into a benzene solution (15 ml) of **1** (306 mg, 1.09 mmol) at *ca.* 10 °C for 3.5 h. Removal of the solvent followed by preparative TLC (silica gel, CCl_4) gave two fractions. The first fraction was rechromatographed (TLC, silica gel, hexane) to give 131 mg of brown tar, which gave **14** (57 mg) on treatment with TLC (alumina, hexane). The second fraction gave 121 mg (50.8%) of **14** (mp 33.5—35.5 °C).

References

1) For Part IV, see Y. Inagaki, R. Okazaki, and N. Inamoto, *Bull. Chem. Soc. Jpn.*, **52**, 3615 (1979).

2) H. G. Houlton and H. V. Tartar, *J. Am. Chem. Soc.*, **60**, 544 (1938); C. S. Marvel and R. S. Johnson, *J. Org. Chem.*, **13**, 822 (1948); P. Allen, Jr., *ibid.*, **7**, 23 (1942).

3) H. Gilman and H. H. Morris, *J. Am. Chem. Soc.*, **48**, 2399 (1926); A. Son and E. Achmidt, *Ber.*, **57**, 1355 (1924); D. Klamann, C. Sass, and M. Zelenka, *ibid.*, **92**, 1910 (1959); W. T. Smith, Jr., P. A. Thiu, and M. Grasley, *J. Org. Chem.*, **27**, 629 (1962).

4) J. Kuyper and K. Vrieze, *J. Chem. Soc., Chem. Commun.*, **1976**, 64; G. Kresze and N. Schönberger, *Justus Liebigs Ann. Chem.*, **1974**, 847.

5) G. Schulz and R. H. Schlessinger, *J. Chem., Soc., Chem. Commun.*, **1970**, 747.

6) S. Holm, J. A. Boerma, N. H. Nilson, and A. Sennig, *Chem. Ber.*, **109**, 1069 (1976).

7) J. Strating, L. Thijs, and B. Zwanenburg, *Recl. Trav. Chim. Pays-Bas*, **86**, 641 (1967); G. E. Veenstra and B. Zwanenburg, *ibid.*, **95**, 28 and 195 (1976).

8) Y. Inagaki and R. Okazaki, *Yuki Gosei Kagaku Kyokai Shi*, **36**, 1 (1978).

9) Y. Inagaki, R. Okazaki, and N. Inamoto, *Bull. Chem. Soc. Jpn.*, **52**, 2002 (1979).

10) Under similar conditions, such reagents as triethyl phosphite, triphenylphosphine, and phosphorus trichloride did not react with **10**. When **10** and an excess amount of triethylphosphine were mixed in ether under nitrogen at 0 °C, the solution gradually turned red with concomitant appearance of a set of persistent ESR signals (g=2.004, a_N=9.7 G, $a_H(2)$=2.2 G; a triplet of triplet). When the solution was shaken under air, the red color as well as the ESR signals disappeared with concurrent recovery of the green color due to **10**. The same phenomena were observed when tributylphosphine was used in place of triethylphosphine. When the nitrosobenzene **13** was allowed to react with tributylphosphine, strong ESR signals were also observed, albeit they were less stable than that observed for **10**, bearing much complex features presumably due to the presence of some species.

11) Reaction of **10** with triethyl phosphite under more forcing conditions has recently been reported. L. R. C. Barcley, P. G. Khazanie, K. A. H. Adams, and E. Reid, *Can. J. Chem.*, **55**, 3273 (1977).

12) G. Kresze, A. Maschke, R. Albrecht, K. Bederke, P. Patzschke, H. Smalla, and A. Trede, *Angew. Chem.*, **74**, 135 (1962).

13) An S–N bond is cleaved even by thiols; F. A. Davis, *Int. J. Sulfur Chem.*, **8**, 71 (1973).

14) Y. Inagaki, R. Okazaki, and N. Inamoto, *Bull. Chem. Soc. Jpn.*, **52**, 1998 (1979).

15) R. Okazaki, T. Hosogai, E. Iwadare, M. Hashimoto, and N. Inamoto, *Bull. Chem. Soc. Jpn.*, **42**, 3611 (1969).

16) R. A. Ellison, R. Griffin, and F. N. Kotsonis, *J. Organomet. Chem.*, **36**, 209 (1972).

The Transformation of Jervine into 18-Functional *C*-Nor-*D*-homosteroids[1)]

Hiroshi SUGINOME,* Norihisa YONEKURA, and Tadashi MASAMUNE*
Department of Chemistry, Faculty of Science, Hokkaido University, Sapporo 060
(Received June 2, 1979)

N,O-Diacetyldeoxojervine, obtained by the Wolff-Kishner reduction of jervine followed by acetylation, has been catalytically hydrogenated to (22*S*,25*S*)-*N*,3-*O*-diacetyl-5α-veratranine-3β,23β-diol. Irradiation in benzene containing mercury(II) oxide and iodine afforded 20-formyl-17β-ethyl-12α-etiojervan-3β-ol 3-acetate which was converted into 17β-ethyl-3β-hydroxy-12α-etiojervan-20-one 3-acetate by dye-sensitized photo-oxygenation of the corresponding morpholine enamine. Reduction to 17β-ethyl-12α-etiojervane-3β,20β-diol 3-acetate with sodium borohydride followed by irradiation in benzene in the presence of mercury(II) oxide and iodine afforded an 18-functional *C*-nor-*D*-homosteroid, (20*R*)-18,20-epoxy-17β-ethyl-12α-etiojervane-3β,20β-diol. The configuration of the methyl group on the tetrahydrofuran ring has been shown to be α on the basis of the NMR spectrum, confirming a previous assignment.

In a previous paper, the transformation of deoxojervine, a jerveratrum alkaloid, into an 18-functional *C*-nor-*D*-homosteroid was reported.[2)] The transformation involved the catalytic hydrogenolysis of deoxojervine[3)] to a veratranin-23β-ol (**5**), removal of the piperidine ring by a procedure devised by Franck and Johnson to afford 17β-ethyl-3β-hydroxy-12α-etiojervan-20-one, reduction to 17β-ethyl-12α-etiojervane-3β,20β-diol 3-acetate (**10**) with sodium borohydride, and a functionalization of the inactive 13β-methyl group by an intramolecular radical process.

In this paper, an alternative method for the transformation of deoxojervine derived from jervine into the 18-functional *C*-nor-*D*-homosteroid (**11**) is described which utilizes photo-induced reactions as the key steps.

Results

Jervine (**1**), an abundantly available jerveratrum alkaloid, was used as the starting material. The previous severe conditions for the removal of the hindered 11-oxo group[3)] was found to be unnecessary and the 11-oxo group was smoothly removed either by the Huang-Minlon or by the Nagata-Itasaki[4)] modification of the Wolff-Kishner reduction to yield deoxojervine (approximate yield 50%).

In previous experiments, the transformation of deoxojervine into (22*S*,25*S*)-5α-veratranine was achieved in a rather poor yield by catalytic hydrogenation of deoxojervine itself.[2)] This has now been significantly improved by the use of the *N,O*-diacetyl derivative (**2**). Thus, catalytic hydrogenation of the diacetate **2**[3)] in glacial acetic acid in the presence of Adams platinum oxide (25% weight of the substrate) afforded an amorphous product which showed a single spot on TLC and which was identified as (22*S*,25*S*)-*N*,3-*O*-diacetyl-5α-veratr-13(17)-enine-3β,23β-diol (**3**) by NMR analysis (see Experimental). Hydrogenation conducted with less catalyst (10% weight of the substrate) gave (22*S*,25*S*)-*N*-3-*O*-diacetylveratr-5,13(17)-dienine-3β,23β-diol (**4**) as the major product; the product was identified by NMR analysis.

The hindered tetrasubstituted double bond of the 23β-ols **3** or **4** was hydrogenated catalytically using a rhodium–platinum catalyst as reported in a previous paper[2)] to yield an amorphous perhydro derivative (**6**) as the exclusive product. The stereochemistries at the C-13 and the C-17 were identified by its transformation into 17β-ethyl-3β-hydroxy-12α-etiojervan-20-one 3-acetate obtained in previous experiments.[2,5)]

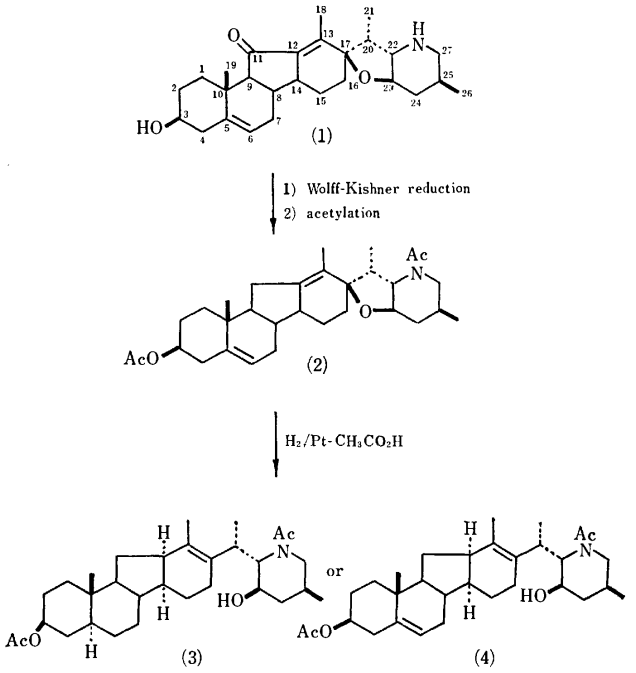

Scheme 1.

The removal of a heterocyclic ring of veratranine **6** was executed by a method involving a radical fragmentation developed by the authors.[6)] Thus, (22*S*,25*S*)-*N*,3-*O*-diacetyl-5α-veratranine-3β,23β-diol (**6**) in benzene containing mercury(II) oxide and iodine was irradiated for 13 h with a high pressure Hg arc. The product was passed through a column of silica gel and the most mobile fraction collected to afford crystalline 20-formyl-17β-ethyl-3β-hydroxy-12α-etiojervan-20-one 3-acetate **7** in 35% yield. As noted previously, this fragmentation reaction is considered to be a radical counterpart of an ionic fragmentation[7)] and is useful in removing the piperidine ring from *N*-acetylveratranine at room temperature under neutral conditions.

The transformation of the aldehyde into 17β-ethyl-3β-hydroxy-12α-etiojervan-20-one 3-acetate (**9**) was conducted by a photochemical method. The aldehyde **7**, obtained as above, was converted into a morpholine enamine (**8**) which was immediately subjected to dye-sensitized photo-oxygenation as reported by Huber[8)]

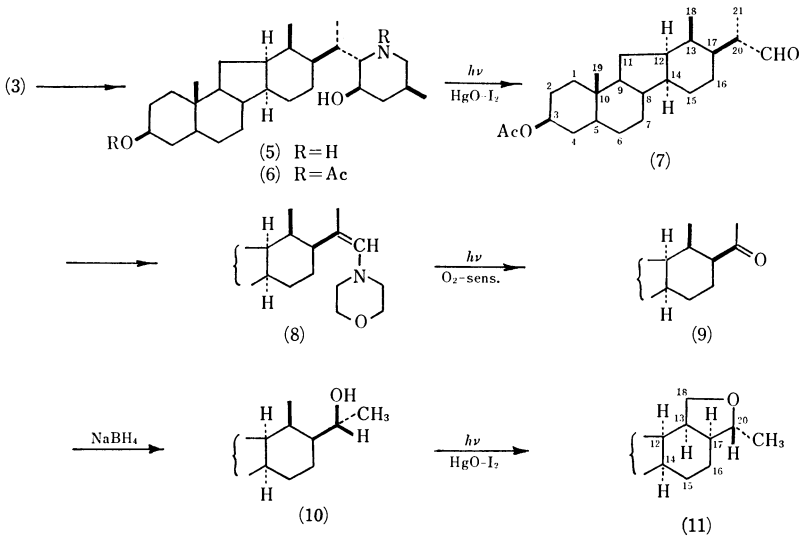

Scheme 2.

and Foote.[9] Irradiation of a benzene solution of the enamine **8** containing Rose Bengal with a 100-W high pressure Hg arc for 10 h with oxygen bubbling slowly through afforded 17β-ethyl-3β-hydroxy-12α-etiojervan-20-one 3-acetate (**9**), identical with a specimen obtained by a nonphotochemical procedure[2] as a single product in 83% yield. As previously reported,[2] reduction of the methyl ketone **9** with sodium borohydride afforded nearly a single alcohol (**10**). The configuration of the 20-hydroxyl group of this compound was assumed to be β on the basis of the consideration of the steric course of the reduction with complex metal hydrides.[2]

Irradiation of 20β-ol **10** in benzene containing mercury(II) oxide and iodine[10] gave an amorphous 18-functional *C*-nor-*D*-homosteroid **11** in 47% yield after purification by column chromatography. The yield was much greater than that in the previous experiments in which lead tetraacetate was used instead of mercury-(II) oxide.

An analysis of the NMR spectrum of the cyclic ether **11** with the aid of spin-decoupling confirmed the structure to be (20*R*)-18,20-epoxy-17β-ethyl-12α-etiojervane-3β,20β-diol acetate **11**, confirming the β-configuration of the C-20 hydroxyl of the starting C-20-ol **10**. Thus, the epoxide **11** showed a 3H singlet at τ 9.27 (19-H), a 3H doublet centered at τ 8.79 (J=6.0 Hz, C-20-methyl), a 3H singlet at τ 8.01 and a broad signal centered at τ 5.34 due to 3α-H. Besides these signals, the spectrum exhibited signals attributable to a methine and methylene protons adjacent to the oxygen of a tetrahydrofuran ring. The methine proton appeared as a 1H broad octet centered at τ 6.39 and the methylene proton as two triplets at τ 6.06 (J= 8 Hz) and 6.58 (J=8 Hz). Irradiation at the center of the doublet at τ 8.79 due to C-20 methyl caused a collapse of the broad octet to a doublet (J=6.5 Hz). Inspection of the Dreiding molecular model indicated that the dihedral angle between the 17α-H and the 20β-H is approximately 130° in epoxide (**11**) having 20 (*R*) configuration. The observed coupling constant is in agreement with this configuration.

Irradiation at τ 7.42 corresponding to a signal due to 13α-H caused a collapse of two triplets into two doublets with J=8 Hz. This decoupling defines the couplings between 13α-H and 18β-H as well as 13α-H and 18α-H to be approximately the same and 8 Hz. These results are summarized in a formula (**12**).

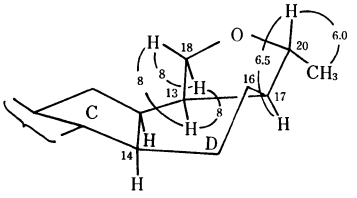

(**12**)

Experimental

All melting points were determined with a hot-plate apparatus (Yanagimoto micro melting point apparatus) and are uncorrected. Unless stated otherwise, IR spectra were determined in Nujol with a JASCO model IR-E spectrophotometer. NMR spectra were determined with a JEOL PS-100 high-resolution spectrometer (solvent $CDCl_3$; Me_4Si as internal reference). TLC was conducted on Wakogel B-5. Mass spectra and elemental analyses were taken by the staff of the Faculty of Pharmaceutical Sciences of this University, the MS with a Hitachi RMU-6E spectrometer.

Reduction of Jervine **1** *to Deoxojervine. i) By Nagata-Itazaki Procedure*:[4] Jervine (30 g) in triethylene glycol (900 ml) containing hydrazine hydrochloride (54 g) and 80% hydrazine hydrate (216 ml) was refluxed for 3 h and the solution cooled to room temperature. To this solution, potassium hydroxide (81 g) was added and the solution concentrated and refluxed for a further 3 h (bath temp 240—260 °C) and poured into water. The crystals, collected by filtration, were dissolved in chloroform and the chloroform solution washed with water and dried (Na_2SO_4). The residue was recrystallized from methanol to yield deoxojervine (14.4 g, 49%) in three crops.

ii) By Huang-Minlon Procedure: Jervine **1** (2 g) in triethylene glycol (60 ml) containing hydrazine hydrate (12 ml) and potassium hydroxide (5.4 g) was refluxed for 1 h (bath temp

120 °C). To the solution, triethylene glycol (100 ml) was added and the solution refluxed for 1 h. The solution was concentrated at bath temperature 200 °C and refluxed for 3 h. The solution was poured into water and extracted with chloroform and the chloroform solution worked up in the usual way. The residue was recrystallized from methanol to yield deoxojervine (0.98 g, 51%) in three crops.

Catalytic Hydrogenation of N,O-*Diacetyldeoxojervine* **2** *in the Presence of Adams Platinum Oxide.* i) *N*,3-*O*-Diacetyl-11-deoxojervine (1 g) in acetic acid (10 ml) containing platinum oxide (250 mg) was hydrogenated under atmospheric pressure until absorption of hydrogen gas ceased. After removal of the catalyst and the solvent, the residue was neutralized with aq sodium hydrogencarbonate and extracted with chloroform. The chloroform solution was washed with water and dried (Na_2SO_4). The residue (1.01 g) showed a single spot on TLC. Crystallization could not be induced and the solution was immediately used for the next step. IR 3387 (OH), 1740 (OAc), 1620 (NAc), 1239, 1027, and 762 cm^{-1}; NMR 9.29 (1H, s, 19-H), 8.94 (3H, d, J=6.8, 26-H), 8.79 (3H, d, J=6.8, 21-H), 8.34 (3H, s, 18-H), 7.98 and 7.93 (each 3H, s, NAc and OAc), 7.03 (1H, m, 2-H), 6.74 (2H, br. s, 27-H), 5.92 (1H, br. s, $W_{1/2}$=8.4, 23β-H), 5.33 (1H, d, J=10.5, 22β-H) and 5.33 (1H, br. overlapped with 22α-H).

ii) *N*,3-*O*-Diacetyl-11-deoxojervine **2** (1 g) in acetic acid (10 ml) containing platinum oxide (100 mg) was hydrogenated as described above until absorption of hydrogen gas ceased. Work-up of the solution afforded (22*S*,25*S*)-*N*,3-*O*-diacetylveratr-5,13(17)-dienine-3β,23β-diol **4**. Crystallization of the diol was not possible. IR 3394 (OH), 1743 (OAc), 1618 (NAc), 1239, and 1029 cm^{-1}. NMR τ 9.08 (3H, s, 19-H), 8.95 (3H, d, J=7.5, 26-H), 8.65 (3H, d, J=7.5, 21-H), 8.32 (3H, s, 18-H), 7.98 (6H, s, NAc, and OAc), 6.74 (2H, s, br. s, 27-H), 5.93 (1H, br. s, $W_{1/2}$= 9.0, 23β-H), 5.34 (1H, d, J=11.9, 22β-H), and 4.64 (1H, br. s, 6-H).

This diacetate was immediately used for the next step.

*Catalytic Hydrogenation of (22S,25S)-*N-*3-*O-*Diacetylveratr-13-(17)-enine-3β,23β-diol* (**3**) *in the Presence of Rhodium–Platinum Catalyst.* The rhodium–platinum catalyst (800 mg) in glacial acetic acid (10 ml) was hydrogenated until approximately 200 ml of hydrogen gas were absorbed. To this solution, 400 mg of (22*S*,25*S*)-*N*,3-*O*-diacetylveratr-13(17)-enine-3β,23β-diol (**3**) was added and the solution hydrogenated for 91 h under atmospheric pressure. The usual work-up of the solution afforded an amorphous (22*S*,25*S*)-*N*,3-*O*-diacetyl-5α-veratranine-3β,23β-diol (**6**) (410 mg). IR 3367 (OH), 1739 (OAc), 1617 (NAc), 1238, 1025, and 775 cm^{-1}; NMR 9.26 (3H, s, 19-H), 9.26 (3H, d, J=6.9), 9.10 (3H, d, J=6.0), and 8.92 (3H, d, J=6.9) (three secondary methyl groups at C-13, C-20, and C-25), 8.03 (3H, s, NAc), 7.91 (3H, s, OAc), 6.80 (1H, d, 22β-H), 6.00 (1H, br. s, 23α-H), and 5.47 (1H, br. 3α-H).

Preparation of 20-Formyl-17β-ethyl-12α-etiojervan-3β-ol Acetate by Irradiation of 23β-ol **6** *in Benzene in the Presence of Mercury(II) Oxide and Iodine.* (22*S*,25*S*)-*N*,3-*O*-Diacetyl-5α-veratranine-3β,23β-diol (**6**) (1 g) in dry benzene (50 ml) containing mercury(II) oxide (1.3 g) and iodine (2.4 g) was placed in a Pyrex vessel and the solution irradiated with a 100-W high pressure Hg arc under an atmosphere of argon for 13 h. After removal of the inorganic materials by filtration, the solvent was evaporated and the residue subjected to column chromatography (Wakogel C-200). Elution with benzene afforded a residue which was dissolved in dichloromethane. The solution was washed with aq sodium thiosulfate and water successively and dried (Na_2SO_4). Evaporation of the solvent left the crystalline aldehyde **7** (259 mg). NMR 9.19 (3H, s, 19-H), 9.21 (3H, d, J=6.9, 18-H), 8.98 (3H, d, J=7.2, 21-H), 7.99 (3H, s, OAc), 5.34 (1H, broad signal, 3α-H), and 0.49 (1H, d, J=4.1, CHO). In this reaction, a tarry polymerized material accompanied the aldehyde.

Morpholine Enamine **8** *of Aldehyde* **7**. The aldehyde **7** as obtained above (210 mg) together with morpholine (0.5 ml) and *p*-toluenesulfonic acid (10 mg) in benzene (40 ml) were refluxed for 3 h in a vessel equipped with a Dean-Stark apparatus. The solvent was removed by a rotary evaporator and the residue dissolved in dichloromethane. The solution was washed with 5% aq sodium hydrogencarbonate solution and water successively and dried (Na_2SO_4). Evaporation of the solvent by a rotatory evaporator left an amorphous enamine **8** (250 mg) which was immediately used for the next step. NMR 9.38 (3H, d, J=7.5, 18-H), 9.26 (3H, s, 19-H), 8.41 (3H, s, CH_3–C=C–N), 8.07 (3H, s, OAc), 7.35 (4H, m, $-CH_2-O-CH_2-$), 6.36 (4H, m, $-CH_2-N-CH_2-$), 5.38 (1H, broad signal, 3α-H), and 5.79 (1H, d, J=2.7, C=CH–N–).

Preparation of 17β-Ethyl-3β-hydroxy-12α-etiojervan-20-one Acetate from Enamine **8** *by Dye-sensitized Oxygenation.* Morpholine enamine **8** (250 mg) in dry benzene (35 ml) containing Rose Bengal (6 mg) in a Pyrex vessel was irradiated with a 100-W high pressure Hg arc through a Pyrex filter for 10 h while oxygen was bubbled slowly though. After removal of the solvent, the residue was dissolved in dichloromethane and the solution worked up in the usual way. The residue was subjected to column chromatography (alumina) to remove the Rose Bengal. Elutions with a 6:1 mixture of benzene and diethyl ether afforded a crude 17β-ethyl-3β-hydroxy-12α-etiojervan-20-one acetate (**9**) which was recrystallized from methanol to afford the pure acetate (171 mg). This was identical with the specimen obtained by a non-photochemical procedure.

Reduction of 17β-Ethyl-3β-hydroxy-12α-etiojervan-20-one Acetate (**9**) *with Sodium Borohydride.* 17β-Ethyl-3β-hydroxy-12α-etiojervan-20-one acetate **9** (1.56 g) and sodium borohydride (640 mg) in ethanol containing ethyl acetate (6 ml) were stirred for 4 h at room temperature. After the addition of acetic acid, the solvent was evaporated and the residue extracted with dichloromethane. The solution was washed with water and dried to afford an amorphous alcohol (1.44 g) which was virtually a single compound. This was recrystallized from a hexane–diethyl ether mixture.

The Hypoiodite Reaction of 17β-Ethyl-12α-etiojervane-3β,20β-diol 3-Acetate (**10**) *with Mercury(II) Oxide and Iodine.* Etiojervan-20β-ol **10** (550 mg) in dry benzene (100 ml) containing mercury(II) oxide (825 mg) and iodine (1.1 g) was irradiated with a high pressure mercury arc generated by Rayonet RPR-208 preparative photochemical reactor through Pyrex for 3 h under an argon atmosphere with stirring. The solution was filtered and a further amount of benzene added. The solution was washed with 5% sodium thiosulfate and water successively and dried. The amorphous residue (575 mg) was subjected to column chromatography (silica gel). Elution with a 20:1 mixture of benzene and diethyl ether afforded an amorphous 18,20-epoxide **11** (260 mg) identical with a specimen obtained previously.[2] It had mp 80.5—81.5 °C after recrystallization from methanol. For NMR spectrum see text.

The authors would like to thank Mrs. Tomoko Okayama of this laboratory for the NMR measurements and spin-decoupling.

References

1) Photoinduced Transformations. Part 45. Part 44, H. Suginome and T. Uchida, *J. Chem. Soc., Perkin Trans. 1*, in press.

2) H. Suginome, N. Sato, and T. Masamune, *Tetrahedron Lett.*, **1969**, 2671; *Bull. Chem. Soc. Jpn.*, **52**, 3043 (1979).

3) T. Masamune, Y. Mori, M. Takasugi, A. Murai, S. Ohuchi, N. Sato, and N. Katsui, *Bull. Chem. Soc. Jpn.*, **38**, 1374 (1965).

4) W. Nagata and H. Itazaki, *Chem. Ind.*, **1964**, 1194.

5) For nomenclature of *C*-nor-*D*-homosteroids see S. M. Kupchan and M. J. Abu El-Haj, *J. Org. Chem.*, **33**, 647 (1968); F. C. Chang and R. C. Ebersole, *Tetrahedron Lett.*, **1968**, 3521.

6) H. Suginome, H. Umeda, S. Sugiura, and T. Masamune, *J. Chem. Res.* (*S*), 380, (*M*), 4520 (1978).

7) R. W. Franck and W. S. Johnson, *Tetrahedron Lett.*, **1963**, 545; R. W. Franck, G. P. Rizzi, and W. S. Johnson, *Steroids*, **1964**, 463.

8) J. E. Huber, *Tetrahedron Lett.*, **1968**, 3271.

9) C. S. Foote and J. W. P. Lin, *Tetrahedron Lett.*, **1968**, 3267.

10) For review of the hypoiodite reaction see J. Kalvoda and K. Heusler, *Synthesis*, **1971**, 501; For mercury(II) oxide–iodine reagent see M. Akhtar and D. H. R. Barton, *J. Am. Chem. Soc.*, **86**, 1528 (1964).

Homogeneous Hydroformylation of Methyl Acrylate Catalyzed by $Co_2(CO)_8$–Di(tertiary phosphine) Complexes

Kazuhisa MURATA* and Akio MATSUDA

National Chemical Laboratory for Industry, 1-1, Higashi, Yatabe-Machi, Tsukuba-Gun, Ibaraki, Japan

(Recieved June 7, 1979)

Some complexes prepared *in situ* from $Co_2(CO)_8$ and various di(tertiary phosphine)s as ligands have been found to be more active than $Co_2(CO)_8$ for the hydroformylation of methyl acrylate. The activity decreased in the order; $Ph_2P(CH_2)_2PPh_2 > Ph_2PC{\equiv}CPPh_2 >$ *cis*-$Ph_2PCH{=}CHPPh_2 > Ph_2P(CH_2)_3PPh_2 >$ none $> Ph_2PCH_2PPh_2 > Ph_2P(CH_2)_4PPh$. The most active catalyst (I) was obtained when a molar ratio of $Ph_2P(CH_2)_2PPh_2$ to $Co_2(CO)_8$ was *ca.* 0.5. The catalyst (I) is also active even at low pressure, where the decomposition of $Co_2(CO)_8$ occurs.

Many efforts have been made to enhance the catalytic activity in the hydroformylation of olefin using $Co_2(CO)_8$ catalyst.[1] It is well known that the presence of small amounts of organic amines such as pyridine increases the rate of cobalt-catalyzed hydroformylation.

From the reaction of cyclohexene in methylcyclohexane as solvent, for example, Wender *et al.* found a small rate increase for pyridine/$Co_2(CO)_8$ ratios between 0.15 and 1.2, the maximum being around 0.15.[2] For the hydroformylation of methyl acrylate in benzene, Iwanaga reported that the relative rate increased up to 3.14 times at 100 °C using pyridine/Co ratios of 10.[3]

On the other hand, recently, it has been reported by Sanger that the rate of hydroformylation of 1-hexene with $RhH(CO)(PPh_3)_3$ was enhanced by the addition of a small amount of a di- or tri(tertiary phosphine) to this system.[4] In the case of cobalt catalyst, however, the presence of phosphines such as PPh_3, PBu_3, $Ph_2P(CH_2)_nPPh_2$ (n=2,4,5) drastically decreased the rate, although a slight increase in product linearity was observed.[5]

We have found for the first time that complexes prepared *in situ* from $Co_2(CO)_8$ and some di(tertiary phosphine)s are more active catalysts for the homogeneous hydroformylation of methyl acrylate than $Co_2(CO)_8$. Now we would like to report on some of the interesting findings that have been obtained.

Experimental

Materials. Methyl acrylate, phosphines and toluene were obtained commercially and used with no further purifications. Cobalt carbonyl cluster ($CH_3CCo_3(CO)_9$) was prepared from $Co_2(CO)_8$, according to a procedure based on that given by Pályi.[6]

Reaction Procedure. The hydroformylation reactions were carried out in the 100 ml stainless-steel autoclave, in which methyl acrylate, $Co_2(CO)_8$, toluene, and phosphine were placed. After the vessel was sealed, a mixture of hydrogen and carbon monoxide (*ca.* 1/1 ratio) was introduced. The system was then brought to the desired reaction temperature and pressure by the additional charging of the same gas under heating. Stirring was begun and the reaction took place. The total pressure was kept constant during the reaction by supplying the gas from a 100 ml pressure storage vessel through a pressure regulator, and the reaction temperature was controlled within a range of ±1 °C. The amount of syn-gas supplied at constant pressure during the reaction was calculated from pressure drop in the storage.

Analysis of the Products. Liquid products were analyzed by gas chromatography. A gas chromatograph, equipped with a 6 m column of squalane was used at 100 °C. The IR spectra of catalyst solutions were recorded on a Hitachi-215 type spectrometer.

Determination of Molar Ratios of CO to Co, CO/Co, in Complexes Formed in the Catalytic System. Aliquat samples of catalyst solutions were withdrawn at definite times through a stainless-steel tube into a glass reciever in ice. After nitrogen of a high purity had been bubbled through these samples to purge the dissolved CO, the sample was heated with 3.6 M-H_2SO_4. The gas thus liberated was measured in volume and analyzed for CO by gas chromatography, while the resulting cobalt ions was determined by an EDTA-titration method.

Results

Effect of Some Diphosphorus Ligands. A hydroformylation catalyst was prepared *in situ* from $Co_2(CO)_8$ and a complementary diphosphine. As shown in Table 1, where the initial rate of gas consumption was taken, remarkable ligand effects on the activity were observed; 1,2-bis(diphenylphosphino)ethane (hereafter, abbreviated as diphos) was found to be the most effective ligand, and in this case the activity was *ca.* 3 times that in $Co_2(CO)_8$ (Run 1, 3).

For comparison, the use of bis(2-diphenylphosphinoethyl) phenylphosphine results in the slight increase in the activity (Run 9), but triphenylphosphine is an unfavorable ligand (Run 10). A cobaltcarbonyl cluster ($CH_3CCo_3(CO)_9$) instead of $Co_2(CO)_8$ appears to be undesirable as a catalyst precursor (Run 4).

The results of analysis of the products are also listed in Table 1. The competitive hydrogenation to give methyl propionate occurred very little (Run 3), and little difference between Run 1 ($Co_2(CO)_8$) and Run 3 ($Co_2(CO)_8$–diphos) was observed in the α/β ratio.

Effect of Diphos to $Co_2(CO)_8$ Ratio on the Activity. The results tested under standard conditions are illustrated in Fig. 1, where the amount of $Co_2(CO)_8$ was kept constant at 0.25 mmol. The maximum activity was achieved when the molar ratio was *ca.* 0.5 and subsequent addition of diphos drastically decreased the activity. (Thereafter, the complex showing the maximum activity will be called 'cobalt–diphos catalyst'.)

Another feature of the cobalt–diphos catalyst is that it is active even under lower pressure than $Co_2(CO)_8$; as shown in Table 2, for instance, at 110 °C under 30 kg/cm² of total pressure (CO/H_2=1) aldehyde($\alpha+\beta$) is produced in *ca.* 77% yield after 107 min-reaction

Table 1. Hydroformylation of methyl acrylate catalyzed by $Co_2(CO)_8$ with some diphosphines
$Co_2(CO)_8$ 0.25 mmol, phosphine 0.125 mmol, toluene (solvent) 50 ml
methyl acrylate 50 mmol, $H_2/CO=1$, 50 kg/cm² (const.), temp 120 °C.

Run No.	Added phosphine	Initial rate of gas consumption / mmol min⁻¹	Time / min	β+α[a] yield/%[b]	Methyl Propionate yield/%	β/α[c]
1	None	1.3	132	77.0	0.6	19.4
2	$Ph_2PCH_2PPh_2$	1.2	—	—	—	—
3	$Ph_2P(CH_2)_2PPh_2$	3.8	35	84.1	1.4	18.3
4	$Ph_2P(CH_2)_2PPh_2$[d),e)]	1.5	—	—	—	—
5	$Ph_2P(CH_2)_3PPh_2$	1.8	—	—	—	—
6	$Ph_2P(CH_2)_4PPh_2$	0.4	—	—	—	—
7	*cis*-$Ph_2PCH{=}CHPPh_2$	2.7	—	—	—	—
8	$Ph_2PC{\equiv}CPPh_2$	2.8	—	—	—	—
9	$PhP(CH_2CH_2PPh_2)_2$	1.8	—	—	—	—
10	PPh_3	0.6	252	85.0	0.5	17.9

a) α, β denote methyl α-formylpropionate and methyl β-formylpropionate, respectively. b) Aldehydes produced/methyl acrylate initially added (50 mmol). c) The molar ratio of β-isomer to α. d) Cobalt carbonyl cluster ($CH_3CCo_3(CO)_9$, 0.25 mmol) in place of $Co_2(CO)_8$ was used as catalyst precursor. e) The value of this rate was 0.6 (mmol/min) when diphos was absent.

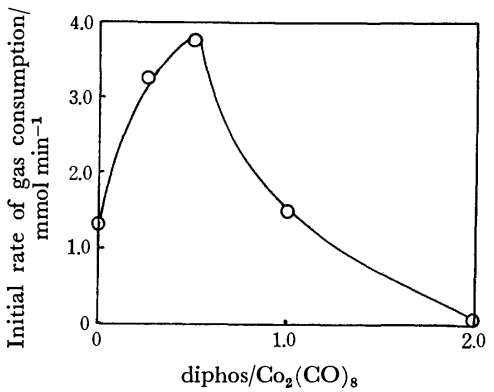

Fig. 1. Effect of diphos/$Co_2(CO)_8$ ratio on the activity.
$Co_2(CO)_8$ 0.25 mmol, methyl acrylate 50 mmol, toluene 50 ml, $CO/H_2=1$, 50 kg/cm²(const), 120 °C.

Table 2. Comparison of cobalt-diphos catalyst with $Co_2(CO)_8$ with some pressures
$Co_2(CO)_8$ 0.25 mmol, diphos 0.125 mmol (Run 1, 2), toluene 50 ml, methyl acrylate 50 mmol, temp 110 °C.

Run No.	Pressure kg/cm² CO	Pressure kg/cm² H_2	Time / min	α+β[b] yield/%	Methyl propionate yield/%
1	25	10	168	86	0.6
2	15	15	107	77	0.2
3[a)]	25	10	553	45	—
4[a)]	15	15	372	34	—

a) Without diphos. b) See footnotes in Table 1.

with the resulting catalyst solution remaining homogeneous (Run 2), whereas confined yield in aldehyde is significantly low in $Co_2(CO)_8$ under the same conditions, because the catalyst decomposition occurs completely during the course of the reaction (Run 4).

Effect of Reaction Parameters. Using both cobalt-diphos and $Co_2(CO)_8$ catalysts kinetic properties were examined, the purpose of which is to shed light on the reasons for the promoting effect of diphos in this cobalt-catalyzed hydroformylation.

For the calculation of the reaction rate, the correlation between the amount of reacted methyl acrylate (MA) and that of the gas ($CO/H_2=1$), which was supplied during the reaction, must be known. In order to obtain information on change in the amount of aldehyde formation with time, the reactions at 100—110 °C under 50 kg/cm² (const., $CO/H_2=1$) were carried out and aliquot samples were withdrawn from autoclave at several reaction times and analyzed.

As can be seen from a comparison of Fig. 2A(○) with Fig. 2B(○), the amount of total aldehydes ([TA]) was approximately equal to one-half that of the corresponding gas uptake ([C]), indicating that the hydroformylation (but not hydrogenation) principally occurs under these conditions. Also, [TA] increases with time with a first order behavior with respect to the concentration of (MA), similar to [C], according to Eq. 1,

$$r = -\mathrm{d}[\mathrm{MA}]_t/\mathrm{d}t = k[\mathrm{MA}]_t, \quad (1)$$

where r, k, and [MA] stand for the overall rate, apparent rate constant and the concentration of (MA) at time 't', respectively. These observations on cobalt-diphos catalyst allow us to assume that [TA]=[C]/2. Thus $[\mathrm{MA}]_t$ in Eq. 1 can be expressed as follows;

$$[\mathrm{MA}]_{\mathrm{initial}} = 50(\mathrm{mmol}) = [\mathrm{MA}]_t + [\mathrm{C}]/2. \quad (2)$$

Good linear plots of $\ln(50/[\mathrm{MA}]_t)$ *vs.* time are provided in Fig. 2B(●, ▲), apparent rate constant, k, being calculated from the slope.[7]

In case of $Co_2(CO)_8$, on the other hand, Figs. 2A(△), C(○, △) show rather zero order behavior with respect to the concentration of (MA), though the hydroformylation predominantly occurs. Thus, apparent rate constant, k', was calculated from the slope, according to Eq. 3;

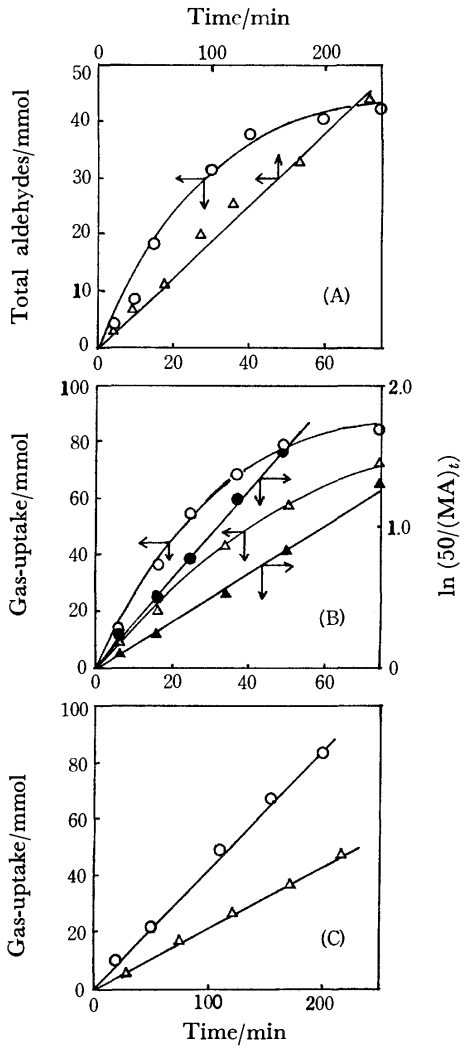

Fig. 2. Results plotted against time.
$Co_2(CO)_8$ 0.25 mmol, diphos 0.125 mmol (A,B), toluene 50 ml, $CO/H_2=1$, 50 kg/cm^2(const.), methyl acrylate 50 mmol.
(A) Total aldehydes (mmol), temp 110 °C.
—○—: Cobalt-diphos, —△—: $Co_2(CO)_8$.
(B) Cobalt-diphos
—○—, —●—: 110 °C; —△—, —▲—: 100 °C.
(C) $Co_2(CO)_8$
—○—: 110 °C, —△—: 100 °C.

$$k't = ([MA]_{initial} - [MA]_t) = [C]/2. \quad (3)$$

Good Arrhenius plots of the rate constants, k or k', provide the apparent activation energies, respectively; the values obtained when the reactions were carried out in the temperature range from 90 to 120 °C were 23.0 kcal/mol with respect to k, 26.7 kcal/mol to k'.

Effects of catalyst concentrations on k or k' were examined under total pressure of 50 kg/cm^2 ($CO/H_2=1$) with the diphos/$Co_2(CO)_8$ molar ratio kept constant at 0.5 in the case of cobalt-diphos catalyst. Figure 3 reveals first order dependence of k as well as k' on the catalyst concentration over this range.

Effects of partial pressure of hydrogen (carbon monoxide) on k or k' were examined, where carbon monoxide (hydrogen) partial pressure in each run was adjusted to 25±2 kg/cm^2 and syn-gas ($CO/H_2=1$) was supplied during the reaction. The rate constants, k or k', were calculated from the slopes as mentioned above. As shown in Fig. 4, these constants increase with the increase in hydrogen pressure. Also, Figure 5 shows that k value tends to decrease more greatly with the increased CO pressure than does k', in the range from 25 to 77 kg/cm^2.

Change in the CO/Co Molar Ratio with Time. The CO/Co molar ratio, which was determined by withdrawing samples from the vessel at definite time, may give some hints to discuss the promoting effect of diphos on the reaction. Interestingly, the ratio for the cobalt-diphos catalyst slightly increases from a value of *ca.* 1.5 to 2, as the reaction proceeds, and it is apparently lower than that for $Co_2(CO)_8$ (from 3 to 4).

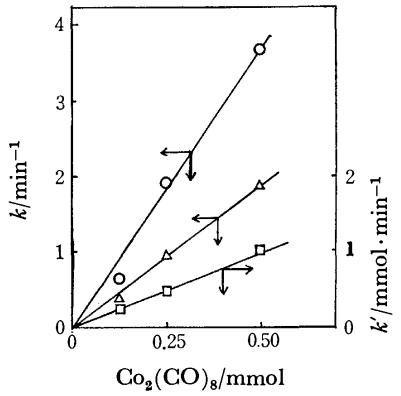

Fig. 3. Effect of catalyst concentration.
Methyl acrylate 50 mmol, toluene 50 ml, $CO/H_2=1$, 50 kg/cm^2(const.), —○—: 110 °C, cobalt-diphos (diphos/$Co_2(CO)_8=0.5$ (const.)). —△—: 100 °C, cobalt-diphos(diphos/$Co_2(CO)_8=0.5$(const.)). —□—: 110 °C, $Co_2(CO)_8$.

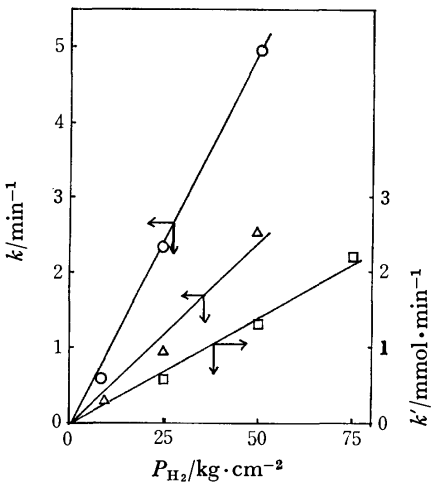

Fig. 4. Effect of partial pressure of hydrogen.
$Co_2(CO)_8$ 0.25 mmol, toluene 50 ml, P_{CO} 25 kg/cm^2 (const.), cobalt-diphos (diphos 0.125 mmol). (const.), —○—: 110 °C, cobalt-diphos (diphos 0.125 mmol). —△—: 100 °C, cobalt-diphos (diphos 0.125 mmol). —□—: 110 °C, $Co_2(CO)_8$.

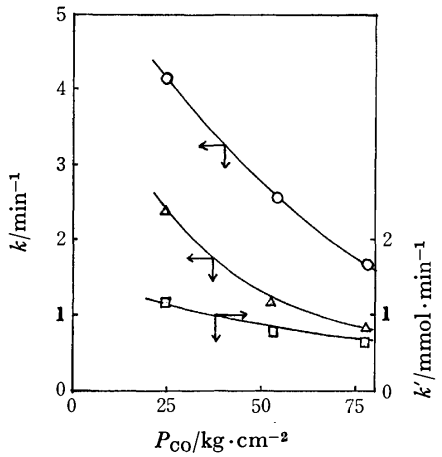

Fig. 5. Effect of partial pressure of CO.
$Co_2(CO)_8$ 0.25 mmol, toluene 50 ml, P_{H_2} 25 kg/cm² (const.), —○—: 120 °C, cobalt-diphos (diphos 0.25 mmol). —△—: 110 °C, cobalt-diphos (diphos 0.25 mmol). —□—: 120 °C, $Co_2(CO)_8$.

Discussion

By numerous workers effects of different phosphines on the rate of $Co_2(CO)_8$-catalyzed hydroformylation have been already investigated, and the general conclusion obtained was that the addition of phosphorus ligands always decreases the rate, though certain ligands such as PBu_3 are favorable for high product linearity.[1,5] Of all these reports, that published by Slaugh and Mullineaux is interesting to us, since $Co_2(CO)_8$ complex with diphos ligand has been used as a catalyst for the hydroformylation of 1-pentene.[5a] The catalytic features of both our system(A) and Slaugh(B) may be summarized as in Table 3.

Our catalyst system (cobalt–diphos) is relatively favorable for the measurement of the hydroformylation rate, because little hydrogenation of methyl acrylate occurs under the conditions employed. As shown in Figs. 2—5, cobalt–diphos catalyst gave similar kinetic behavior to $Co_2(CO)_8$, except for first order with respect to the concentration of (MA).

However, these do not always appear to mean the participation of active species such as $HCo(CO)_x$ (x= 3 or 4),[8] since the CO/Co molar ratio obtained for this catalyst is apparently lower than that for $Co_2(CO)_8$, and since different IR spectral patterns during the reaction were observed for these catalyst solutions.[9] This view may be also supported by the finding that cobalt-diphos catalyst is active even under lower pressure than $Co_2(CO)_8$. (Table 2).

Thus, $HCo(CO)_2$(P–P), (**A**), which is responsible for the increase in the activity, may be postulated as one of principal active catalysts. Though attempts to isolate the species **A** and to identify it were not successful, following two facts would prompt us greatly;

1) The treatment of $Co_2(CO)_8$ with trialkylphosphine(PR_3) under the hydroformylation reaction conditions leads to the formation of $HCo(CO)_3(PR_3)$, which is an active catalyst for the reaction.[5b,c,10]

2) Apparently, diphos acts as a bidentate ligand.[11,12] In fact, Ikariya and Yamamoto have reported the preparation and properties of **A**, $HCo(CO)_2$(P–P), which has been characterized by elemental analysis and IR spectrum.[13]

A speculative reaction scheme and rate equation containing the species **A** is given in *Appendix*, where a rate law of the form in Eq. 7 is derived. According to Eq. 7, r is first order in [MA] and decreases as the CO pressure is increased (Fig. 5). Also, according to Eq. 7, the overall rate, r, is closely related to the concentration of both $HCo(CO)_2$(P–P) and $HCo(CO)$-(P–P). Namely, the mean ratio of CO coordinated to cobalt atom, (CO/Co), should be of the value between 1 and 2 so long as a steady state is reached, and should approach to 2 at the end of the reaction, since steps [1], [7] are still present.; these are in accordance with the foregoing results.

Equation 7, however, does not necessarily justify the first order behavior in catalyst concentration (Fig. 3) and in hydrogen pressure (Fig. 4). Therefore, these facts reveal that cobalt–diphos system is very complex, and that more than one active species or other reaction schemes are probably involved.

The reason for the drastic decrease in the activity, which is shown in Fig. 1, cannot be explained by paths [1]—[7]. Therefore, another paths leading to, probably, the formation of inactive catalyst species consisting of $Co_2(CO)_8$ and diphos, would be also present.[11,14]

Appendix

Overall possible reaction scheme may be postulated as follows;

$$Co_2(CO)_8 + H_2 + 2P\text{-}P \longrightarrow \underset{\mathbf{A}}{2HCo(CO)_2(P\text{-}P)} + 4CO \qquad [1]$$

Table 3. Comparison of our catalyst system(A) with Slaugh(B)

		(A)	(B)
1)	Olefin	Methyl acrylate	1-Pentene
2)	Diphos/$Co_2(CO)_8$ ratio	0—1.0 (0.5 for the most active catalyst, Fig. 1)	4.0
3)	Temperature	90—120 °C	150—200 °C
4)	Catalytic activity in comparison with $Co_2(CO)_8$	*ca.* 3 times active (Table 1, Fig. 1)	Less active by a factor of, at least, 100
5)	Main products	Aldehydes (Table 1, 2)	Alcohols
6)	Thermal stability	Active at 110 °C under 30 kg/cm² (CO/H_2=1) (Table 2)	Active at 150—200 °C under 7—20 kg/cm²

$$HCo(CO)_2(P\text{-}P) + H_2C{=}CH\text{-}COOMe \underset{k_{-2}}{\overset{k_2}{\rightleftharpoons}} HCo(CO)(P\text{-}P) + CO \quad [2]$$

$$H_2C{=}CH\text{-}COOMe$$

1

$$\mathbf{1} \underset{k_{-3}}{\overset{k_3}{\rightleftharpoons}} MeOOC\text{-}CH_2\text{-}CH_2\text{-}Co(CO)(P\text{-}P) \quad [3]$$

2

$$\mathbf{2} + CO \underset{k_{-4}}{\overset{k_4}{\rightleftharpoons}} MeOOC\text{-}CH_2\text{-}CH_2\text{-}\overset{O}{\overset{\|}{C}}\text{-}Co(CO)(P\text{-}P) \quad [4]$$

3

$$\mathbf{3} + H_2 \xrightarrow{k_5} MeOOC\text{-}CH_2\text{-}CH_2\text{-}CHO + HCo(CO)(P\text{-}P) \quad [5]$$

$$HCo(CO)(P\text{-}P) + H_2C{=}CH\text{-}COOMe \underset{k_{-6}}{\overset{k_6}{\rightleftharpoons}} \mathbf{1} \quad [6]$$

$$HCo(CO)(P\text{-}P) + CO \xrightarrow{k_7} HCo(CO)_2(P\text{-}P), \quad [7]$$

where P-P stands for diphos.

An active species **A** is formed by step [1], and the step is not probably rate determining, because no induction period was observed at the beginning of the reaction (Fig. 2A) and rate constant, k, is first order in [MA] (Fig. 2B).

Subsequent steps [2]—[7] are similar to that presented previously by Heck.[8] That the reversal of step [5] is negligible under the conditions employed has been already confirmed by an additional experiment.[9] Also, if the reversal of step [7] is present, the CO/Co molar ratio would be still of the value between 1 and 2 at the end of the reaction; our result is not consistent with this. Thus, steps [5], [7] are proposed as irreversible steps.

The overall rate, r, is expressed as in Eq. 4;

$$r = k_5[\mathbf{3}]P_{H_2}, \quad (4)$$

where [**3**] stands for the concentration of an intermediate ***3***. A rate law of the form in Eq. 5 would be obtained, provided that steady state concentrations for intermediates ***1***, ***2***, ***3*** are assumed, respectively;

$$r = \frac{k_3k_4P_{CO}(k_2[HCo(CO)_2(P\text{-}P)] + k_6[HCo(CO)(P\text{-}P)]) \cdot [MA] \cdot k_5P_{H_2}}{(k_{-2}k_{-3}k_{-4}P_{CO} + k_{-3}k_{-4}k_{-6}) + k_5P_{H_2}[k_{-3}k_{-6} + (k_{-2}k_{-3} + k_3k_4 + k_4k_{-6} + k_{-2}k_4P_{CO})P_{CO}} \quad (5)$$

where $[HCo(CO)_2(P\text{-}P)]$, $[HCo(CO)(P\text{-}P)]$ stand for the concentrations of species $HCo(CO)_2(P\text{-}P)$, $HCo(CO)(P\text{-}P)$, respectively. Here, if the second term in the denominator is assumed to be much larger than the first one, Eq. 6 is obtained;

$$r = \frac{k_3k_4P_{CO}(k_2[HCo(CO)_2(P\text{-}P)] + k_6[HCo(CO)(P\text{-}P)]) \cdot [MA]}{k_{-3}k_{-6} + (k_{-2}k_{-3} + k_3k_4 + k_4k_{-6} + k_{-2}k_4P_{CO})P_{CO}}. \quad (6)$$

Furthermore, if $k_{-3}k_{-6} \ll (k_{-2}k_{-3} + k_3k_4 + k_4k_{-6} + k_{-2}k_4P_{CO})P_{CO}$, the overall rate, r, is expressed as Eq. 7;

$$r = \frac{k_3k_4[MA](k_2[HCo(CO)_2(P\text{-}P)] + k_6[HCo(CO)(P\text{-}P)])}{(k_{-2}k_{-3} + k_3k_4 + k_{4-6}) + k_{-2}k_4P_{CO}}. \quad (7)$$

References

1) I. Wender and P. Pino, "Organic Synthesis *via* Metal Carbonyls," Wiley, New York (1977), Vol. 2.

2) I. Wender, H. W. Sternberg and M. Orchin, "Catalysis Vol. V," Reinhold, New York (1957).

3) R. Iwanaga, *Bull. Chem. Soc. Jpn.*, **35**, 865 (1962).

4) A. R. Sanger, *J. Mol. Catal.*, **3**, 221 (1977/78).

5) a) L. H. Slaugh and R. D. Mullineaux, *J. Organomet. Chem.*, **13**, 469 (1968), b) E. R. Tucci, *Ind. Eng. Chem. Prod. Res. Dev.*, **9**, 4 (1970), c) E. R. Tucci, *ibid.*, **7**, 1 (1968).

6) G. Pályi, F. Piacenti and L. Markó, *Inorg. Chim. Acta Rev.*, **1970**, 109.

7) The value of k obtained when 30 mmol of (MA) was initially introduced, was in good accordance with that of k in Fig. 2B(●).

8) R. F. Heck, *Adv. Organomet. Chem.*, **4**, 243 (1966).

9) K. Murata, A. Matsuda and Y. Sugi, Inorg. Chem. No. 271 ACS/CSJ Chemical Congress, Hawaii, April 1979.

10) G. F. Pregaglia, A. Andreetta, G. Gregorio, G. F. Ferrari, G. Montrasi and R. Ugo, *Chim. Ind.*, **55**, 2, 203 (1973).

11) D. J. Thornhill and A. R. Manning, *J. Chem. Soc., Dalton*, **1973**, 2086.

12) a) A. R. Sanger, *J. Chem. Soc., Dalton*, **1977**, 1971 b) A. R. Sanger, *J. Chem. Soc., Chem. Commun.*, **1975**, 893.

13) T. Ikariya and A. Yamamoto, *J. Organomet. Chem.*, **116**, 231 (1976).

14) We also have failed in explaining the reason why a maximum activity was achieved when a ratio diphos/$Co_2(CO)_8$ was 0.5.

 © 1980 The Chemical Society of Japan Bull. Chem. Soc. Jpn., 53, 219—221 (1980)

Photo-induced Alkoxybromination of Olefins by *N,N'*-Dibromo-2,5-piperazinedione

Akira Sera,* Hiroshi Yamada, and Kuniaki Itoh

Department of Chemistry, Faculty of Science, Kobe University, Kobe 657

(Received June 28, 1979)

Irradiation of *N,N'*-dibromo-2,5-piperazinedione in dichloromethane in the presence of an alcohol induced alkoxybromination of cyclohexene to give *trans*-1-bromo-2-alkoxycyclohexane in a good yield. The reaction was thought to proceed through an ionic mechanism.

N-Bromosuccinimide(NBS) and related active *N*-halogeno compounds have been prepared and their reactivity has been thoroughly examined.[1] They have been employed as the versatile allylic brominating and oxidizing reagents in many organic syntheses. Although reactions of NBS with simple olefins in water or in acetic acid gave corresponding bromohydrins or bromoacetoxylated compounds, photoreactions of NBS with olefins in aprotic solvents gave exclusively allylic brominated products, 1,2-addition products, and in some instances rearranged products, which were all produced through the well established free radical reaction mechanism. Related reactions of *N*-halogenated amines or imides,[1] sulfoximides,[2,3] have been examined, however, nothing has been investigated on the reaction of *N*-halogeno derivatives of 2,5-piperazinedione, a cyclic anhydride of glycine. This paper concerns with some particular reactions of *N,N'*-dibromo-2,5-piperazinedione (NBP, **1**).

Results and Discussion

Bromination of 2,5-piperazinedione gave NBP in a good yield. NBP showed free radical reactivities similar to those of NBS. For example, a benzoyl peroxide induced reaction of NBP with cyclohexene in boiling carbon tetrachloride gave 3-bromocyclohexene (70—75%) and a small amount of 1,2-dibromocyclohexane. No *N*-(2-bromocyclohexyl)-2,5-piperazinedione was obtained in this case, while quite recently Skell[4] reported the formation of the corresponding free radical adducts,[5] *N*-(2-halocyclohexyl)succinimide, in a similar reaction of *N*-halosuccinimide with cyclohexene.

Irradiation of NBP with cyclohexene in dichloromethane[6] gave neither photo-decomposition product nor substitution product in an appreciable amount. In the presence of added ethanol (5 mol equivalent to NBP), however, the reaction gave 3-bromocyclohexene (12%) and *trans*-1-bromo-2-ethoxycyclohexane (37%, **2**). No *cis* isomer was detected (NMR). The stereochemistry of **2** was determined by comparison of its spectral characteristics with those of authentic specimen.[7] An increased yield of **2** was achieved by adding a small amount of a free radical inhibitor, 2,6-di-*t*-butyl-*p*-cresol (BHT, 0.1 mol equivalent to NBP). The free radical inhibitor depressed the formation of 3-bromocyclohexene which was thought to be produced by the free radical mechanism as was observed for the allylic bromination by NBS. Instead, 1,2-dibromocyclohexane was obtained in a considerable yield. This dibromide could be resulted from an addition of bromine which was produced from NBP through an ionic process.[8]

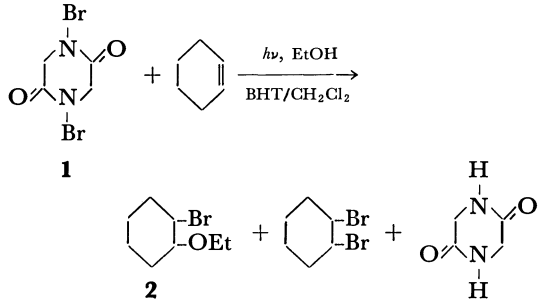

The reaction was examined using variable sets of alcohol–olefin or –vinyl ether pair. The reactivity of the photoalkoxybromination decreased in the order of primary, secondary, and tertiary alcohols (see Table 1). With an increased amount of added ethanol (or by the use of an ethanol as the solvent), **2** was obtained in a nearly quantitative yield. Although the alkoxybromination of olefins was observed in dark conditions,[9] the reaction was actually accelerated by a UV irradiation. A representative case was the bromo-*t*-butoxylation of cyclohexene by NBP–*t*-butyl alcohol, where the irradiation gave a nearly 20-fold yield of 1-bromo-2-*t*-butoxycyclohexane in comparison with that in the dark reaction.

In the cases of less reactive alcohols, isopropyl and *t*-butyl alcohols, small amounts of *N,N'*-bis(2-bromocyclohexyl)-2,5-piperadinedione (**3**) and 2,6-di-*t*-butyl-4-formylphenol (**4**) were isolated in addition to alkoxybromides. The former is one of the free radical reaction products,[10] while the latter is considered to be produced by the oxidation of the free radical inhibitor, BHT.

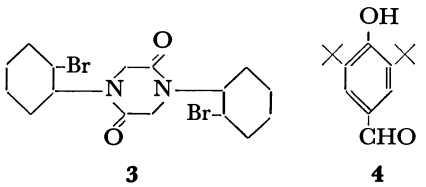

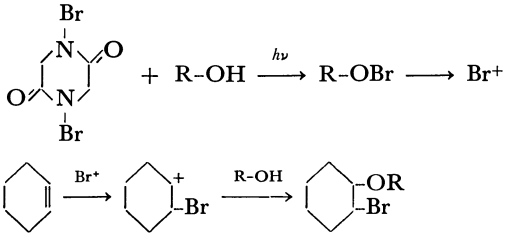

1-Hexene and 3,4-dihydro-2*H*-pyran were also ethoxy-

TABLE 1. ALKOXYBROMINATION OF OLEFINS BY NBP[a]

Olefins (2 mmol)	ROH, added mmol		Product yields/% Br OR -C-C-	Br Br -C-C-	Others
Cyclohexene		—	0	0	3-bromocyclohexene (trace)
Cyclohexene	EtOH	10[b]	37	trace	3-bromocyclohexene (12%)
Cyclohexene	MeOH	10	73	12	
Cyclohexene	MeOH	10	43	4	(dark reaction)
Cyclohexene	EtOH	10	73	13	
Cyclohexene	EtOH	10	20	0	(dark reaction)
Cyclohexene	EtOH	30	95	5	
Cyclohexene	*n*-BuOH	10	73	17	
Cyclohexene	*i*-PrOH	10	44	32	small amounts of **3** and **4**
Cyclohexene	*t*-BuOH	10	11	11	small amounts of **3** and **4**
Cyclohexene	*t*-BuOH	10	0.6	0	(dark reaction)
1-Hexene	EtOH	10	62[c]	29	
Dihydropyran	EtOH	10	100[d]	0	
t-Bu-CH=CH_2	EtOH	10	11[e]	20	
C_4H_9-O-CH=CH_2	EtOH	10	18[f]	5	small amounts of **3** and **4**

a) Irradiation with 1 mmol of NBP in 5 ml of dichloromethane containing 0.1 mmol of 2,6-di-*t*-butyl-*p*-cresol for 30 min. b) Without 2,6-di-*t*-butyl-*p*-cresol. c) 1-Bromo-2-ethoxyhexane. d) *trans*-3-Bromo-2-ethoxytetrahydropyran. e) 2-Bromo-1-ethoxy-3,3-dimethylbutane. f) 2-Bromo-1-ethoxy-1-butoxyethane.

brominated in the same conditions to give 1-bromo-2-ethoxyhexane and 3-bromo-2-ethoxytetrahydropyran, respectively. These two products were undoubtedly the Markovnikov addition products, and hence the formation of these two products indicated that the reaction should proceed through an ionic mechanism.[11] Accordingly one can assume that the photoreaction of NBP with an alcohol gives an alkyl hypobromite intermediate[12] which in turn decomposes to give bromine cation. An addition of bromine cation to cyclohexene yields a new carbon centered cation. Following reaction of the cation with alcohol finally produces the alkoxybrominated product. Intervention of the alkyl hypobromite or bromine cation in the reaction can rationalize the formation of **4** as a by-product, because Cohen[13] reported that **4** was obtained from 2,6-di-*t*-butyl-*p*-cresol by treatment with bromine in *t*-butyl alcohol or acetic acid. The photoethoxybromination of *t*-butylethylene gave 2-bromo-1-ethoxy-3,3-dimethylbutane which was seemingly an *anti*-Markovnikov adduct. However, this observation implied the intervention of an intermediate bridged bromonium cation[14] on which a nucleophilic attack of ethanol occurred from less hindered site.[15] Photoreactions with electron poor olefins (methyl acrylate, stilbene *etc.*) gave little or no alkoxybromides, but yielded dibromides exclusively. In the photo-induced ionic addition of alcohols, Marshall[16] reported that cyclohexenes and cycloheptenes showed marked reactivities to give Markovnikov addition products. As seen in the Table, cycloolefins (cyclohexene and 3,4-dihydro-2*H*-pyran) gave alkoxybromides in higher yield than corresponding acyclic olefins (1-hexene and vinyl ether) did. All of these results agree the proposed ionic addition mechanism where the electrophilic attack of bromine cation plays a key role in determining regioselectivity of the reaction.

Experimental

The olefins used were dried over Molecular Sieves 4A and distilled over copper chloride(I) prior to use. Alcohols were dried over Molecular Sieves 4A and distilled. Dichloromethane was washed successively with sulfuric acid, sodium hydroxide solution and water, dried over calcium chloride and distilled. IR and NMR spectra were measured on a JASCO IRA-1 and a JEOL JNN-PMX 60 spectrometers, respectively. GLC analysis was carried out by a Hitachi Model 063; column (1 m×3 mm); A, 10% Carbowax 20 M on 60—80 mesh Shimalite W; B, 15% Diethylene Glycol Succinate Polyester on 60—80 mesh Chromosorb W. All irradiations were conducted through a Pyrex filter using an Ushio Model UI-501e high-pressure mercury lamp (500 W).

Preparation of NBP:[17] To a solution of 3.5 g of sodium carbonate in 100 ml of water was added 3.3 g of 2,5-piperazinedione. The mixture was stirred as bromine was added dropwise. After the reaction mixture had been stirred for 2 h, the pale yellow solid was collected by filtration, washed with water, and dried under vacuum. Yield, 5.7 g, white powder, recrystallizable from hot pyridine; insoluble in carbon tetrachloride, dichloromethane, acetone, benzene; slightly soluble in ethanol, acetonitrile, DMF and DMSO.

NBP–Cyclohexene–Ethanol Reaction. The typical experimental procedure employed in all the reactions is described. Irradiation of a mixture[6] containing 272 mg (1 mmol) of NBP, 164 mg (2 mmol) of cyclohexene, 461 mg (10 mmol) of ethanol, 22 mg (0.1 mmol) of BHT in 5 ml of dichloromethane was carried out under stirring at ambient temperature for 30 min. The products were determined by GLC using methyl benzoate as the internal standard. The reaction mixtures (3—4 runs) were combined, and after removal of solvent, the products were separated on a silica-gel column (benzene→benzene:ethyl acetate/4 : 1). 1,2-Dibromocyclohexane: liquid; NMR (CCl_4) δ=4.40 (2H, s), 1.0—2.8 ppm (8H, m); IR, ν_{C-Br} 680 cm^{-1}. *trans*-1-Bromo-2-ethoxycyclohexane: MS, *m/e*, 208 and 206 (M^+), 127, 81 57; NMR (CCl_4) δ=1.14 (3H, t), 3.48 (2H, q),

3.1—3.5 (1H, m), 3.6—4.1 (1H, m), 1.0—2.5 ppm (8H, m): IR, ν_{C-O} 1110, ν_{C-Br} 690 cm^{-1}. The stereochemistry of the products was determined to be *trans* judging from comparison with the authentic specimen.

NBP–Cyclohexene–t-BuOH Reaction. Irradiation of a mixture[6] containing 272 mg (1 mmol) of NBP, 164 mg (2 mmol) of cyclohexene, 741 mg (10 mmol) of *t*-butyl alcohol, 22 mg (0.1 mmol) of BHT in 5 ml of dichloromethane was carried out as above. The products: 1-Bromo-2-*t*-butoxycyclohexane: NMR (CCl_4) δ=1.20 (9H, s), 3.1—3.5 (1H, m), 3.7—4.0 (1H, m), 1.0—2.5 ppm (8H, m); IR, ν_{C-O} 1100, ν_{C-Br} 690 cm^{-1}. *N,N'*-Bis(2-bromocyclohexyl)-2,5-piperadinedione: mp 211.2—211.5 °C; NMR ($CDCl_3$) δ= 1.1—2.6 (16H, m), 3.90 (4H, s), 3.9—4.5 (4H, m); IR, $\nu_{C=O}$ 1680, ν_{C-N} 1080, ν_{C-Br} 680 cm^{-1}. 2,6-Di-*t*-butyl-4-formylphenol: mp 191.5—192.5 °C (Ref.[18] mp 189—190 °C); NMR (CCl_4) δ=1.50 (18H, s), 5.72 (1H, s), 7.60 (2H, s), 9.71 (1H, s); IR, ν_{O-H} 3440, ν_{C-H} 2810 and 2730, $\nu_{C=O}$ 1665, ν_{C-O} 1100 cm^{-1}.

Products from Other Reactions: *trans*-1-Bromo-2-methoxycyclohexane: NMR (CCl_4) δ=3.35 (1H, s), 3.1—3.5 (1H, m), 3.7—4.1 (1H, m), 1.0—2.5 ppm (8H, m); IR, ν_{C-O} 1110, ν_{C-Br} 690 cm^{-1}.

trans-1-Bromo-2-isopropoxylcycloxane: NMR(CCl_4) δ= 1.12 (6H, dd), 3.67 (1H, m), 3.1—3.5 (1H, m), 3.7—4.0 (1H, m), 1.0—2.5 ppm (8H, m); IR, ν_{C-O} 1110, ν_{C-Br} 680 cm^{-1}.

trans-1-Bromo-2-butoxycyclohexane: NMR (CCl_4) δ=0.95 (3H, t), 1.0—2.5 (4H, m), 3.44 (3H, t), 3.1—3.5 (1H, m), 3.7—4.1 (1H, m), 1.0—2.5 ppm (8H, m); IR, ν_{C-O} 1110, ν_{C-Br} 690 cm^{-1}.

1-Bromo-2-ethoxyhexane: NMR (CCl_4) δ=1.13 (3H, t), 3.45 (2H, q), 3.2—3.4 (2H, m), 3.5—4.0 (1H, m), 1.03 (3H, t), 0.6—2.1 ppm (6H, m); IR, ν_{C-O} 1100, ν_{C-Br} 670 cm^{-1}.

trans-3-Bromo-2-ethoxytetrahydropyan: NMR (CCl_4) δ= 1.18 (3H, t), 3.63 (2H, q), 3.7—4.1 (1H, m), 4.50 (1H, d), 3.2—4.1 (2H, m), 1.2—2.7 ppm (4H, m); IR, ν_{C-O} 1100, ν_{C-Br} 670 cm^{-1}.

2-Bromo-1-ethoxy-3,3-dimethylbutane: NMR (CCl_4) δ= 1.17 (3H, t), 3.42 (2H, q), 3.62 (2H, dd), 3.82 (1H, t), 1.07 ppm (9H, s); IR, ν_{C-O} 1110, ν_{C-Br} 660 cm^{-1}.

(2-Bromo-1-ethoxyethyl)benzene: NMR (CCl_4) δ=1.16 (3H, t), 3.30 (2H, q), 3.28 (2H, d), 4.30 (1H, t), 7.08 ppm (5H, s); IR, ν_{C-O} 1120, ν_{C-Br} 690 cm^{-1}.

2-Bromo-1-ethoxy-1-butoxyethane: NMR (CCl_4) δ=1.16 (3H, t), 3.48 (2H, q), 3.22 (2H, d), 4.53 (1H, t), 1.06 (3H, t), 0.7—2.1 ppm (6H, m); IR, ν_{C-O} 1120, ν_{C-Br} 680 cm^{-1}.

The present work has been supported in part by a Grant-in-Aid for Scientific Research (No. 247021, 1977) from the Ministry of Education.

References

1) J. S. Pizey, "Synthetic Reagents," Ellis Horwood Ltd., Chichester (1974), Vol. 2, p. 1.
2) H. Morita, H. Itoh, N. Furukawa, and S. Oae, *Chem. Lett.*, **1978**, 817.
3) T. Akasaka, N. Furukawa, and S. Oae, *Chem. Lett.*, **1979**, 529.
4) J. C. Day, M. G. Katsaros, W. D. Kocher, A. E. Scott, and P. S. Skell, *J. Am. Chem. Soc.*, **100**, 1950 (1978).
5) A similar 1,2-adduct was reported in the reaction of diphenyl *N*-bromosulfoximide with cyclohexene.[3]
6) Non-homogeneous mixture, most of NBP being undissolved.
7) W. H. Puterbaugh and M. S. Newman, *J. Am. Chem. Soc.*, **79**, 3469 (1957).
8) L. Horner and E. H. Winkelmann, "Newer Methods of Preparative Organic Chemistry," (1964), Vol. 3, p. 151.
9) Similar reactions of NBS in alcohols were reported: A. Jovtscheff, H. Reinheckel, K. Haage, and R. Pomakotsh, *Monatsh. Chem.*, **97**, 1620 (1966).
10) Details of the photo-induced free radical reactions of NBP with olefins will be reported elsewhere.
11) While the free radical addition of methyl hypobromite to 1-hexene gave 2-bromo-1-methoxyhexane as the main adduct (85%), the reaction under ionic condition gave 1-bromo-2-methoxyhexane in 71% yield; V. L. Heasley, C. L. Frye, G. E. Heasley, K. A. Martin, D. A. Redfield, and P. S. Wilday, *Tetrahedron Lett.*, **1970**, 1573.
12) Irradiation accelerated the formation of alkyl hypobromites, while the reactions of alkyl hypobromites with 1-hexene could proceed in the dark conditions.[11]
13) L. A. Cohen, *J. Org. Chem.*, **22**, 1333 (1957).
14) V. L. Heaslay and R. A. Skidgel, *J. Org. Chem.*, **26**, 3953 (1974).
15) The addition reaction of bromine to *t*-butylethylene in methanol also gave 2-bromo-1-methoxy-3,3-dimethylbutane (44%) besides 1,2-dibromo-3,3-dimethylbutane (45%).[7]
16) J. A. Marshall, *Acc. Chem. Res.*, **2**, 33 (1969).
17) M. T. Tetembaum and E. R. Dessinger, U. S. Patent 3692908, Sep. 19, 1972.
18) G. M. Coppinger and T. W. Campbell, *J. Am. Chem. Soc.*, **75**, 734 (1953).

The Use of Grignard Reagents in the Synthesis of Carbohydrates. I.[1] The Synthesis of Deoxy and Branched-chain Deoxy Sugars

Masajiro KAWANA* and Sakae EMOTO

The Institute of Physical and Chemical Research, Wako-shi, Saitama 351

(Received July 2, 1979)

Two branched-chain deoxy sugars, methyl 5,6-*O*-cyclohexylidene-3-deoxy-2-*C*-methyl-β-D-*arabino*-hexofuranoside and its α-D-*ribo* isomer, were easily prepared by the one-step reaction of methyl 5,6-*O*-cyclohexylidene-3-*O*-mesyl-β-D-allofuranoside (**3a**) with methylmagnesium iodide. Similarly, the corresponding α-mesylate (**4a**) gave methyl 5,6-*O*-cyclohexylidene-3-deoxy-2-*C*-methyl-α-D-*ribo*-hexofuranoside. It was demonstrated that these reactions involved 1,2-hydride shifts. The reaction of **3a** and **4a** with *t*-butylmagnesium bromide yielded two deoxy sugars, methyl 5,6-*O*-cyclohexylidene-3-deoxy-β-D-*arabino*-hexofuranoside and the corresponding α-D-*ribo* isomer, respectively. Under certain reaction conditions with the Grignard reagents, the sulfonate (**3a**) afforded dimeric compounds, in which two furanose rings were directly bound with a carbon–carbon bond. A convenient method for the preparation of the sulfonates (**3a** and **4a**) is also reported.

The synthesis of deoxy and branched-chain sugars has recently received increased attention because these sugars are found in nature as glycoside-components of an important class of antibiotics.[2] We would like to describe here the details of a new method previously reported in only preliminary form[3] for the one-step synthesis of deoxy and branched-chain deoxy sugars starting from sugar sulfonates with Grignard reagents; we will also report some observations made during this work.

The starting point for the present work was our finding of a convenient method for the preparation of the starting sulfonates, methyl 5,6-*O*-cyclohexylidene-3-*O*-mesyl-β-D-allofuranoside (**3a**) and the corresponding α-anomer (**4a**), in good yields. Thus, a methanolic solution of a 3-*O*-mesyl derivative (**2** in Fig. 1) prepared from 1,2:5,6-di-*O*-cyclohexylidene-α-D-allofuranose[4a] (**1**) was refluxed in the presence of an acid, after which the mixture was diluted with benzene. In order to complete this reaction, a large amount of the methanol was evaporated to give a mixture (92%) of **3a** and **4a** in a ratio of 2:1; those anomers were easily separated by fractional crystallization.

The structures of both mesylates were established by means of their elemental analyses and spectrocsopic data (see Experimental). Their mass spectra showed strong peaks at *m/e* 141 characteristic of the dioxolane ring at C-4, thus indicating the furanose structures of these mesylates.[5]

The branched-chain deoxy sugars were obtained very easily when these mesylates were treated with an excess of methylmagnesium iodide (MeMgI). Thus **3a** was added to an ethereal solution of a 3-molar excess of MeMgI to give, in one step, methyl 5,6-*O*-cyclohexylidene-3-deoxy-2-*C*-methyl-β-D-*arabino*-hexofuranoside (**6a**) and the corresponding *ribo* isomer

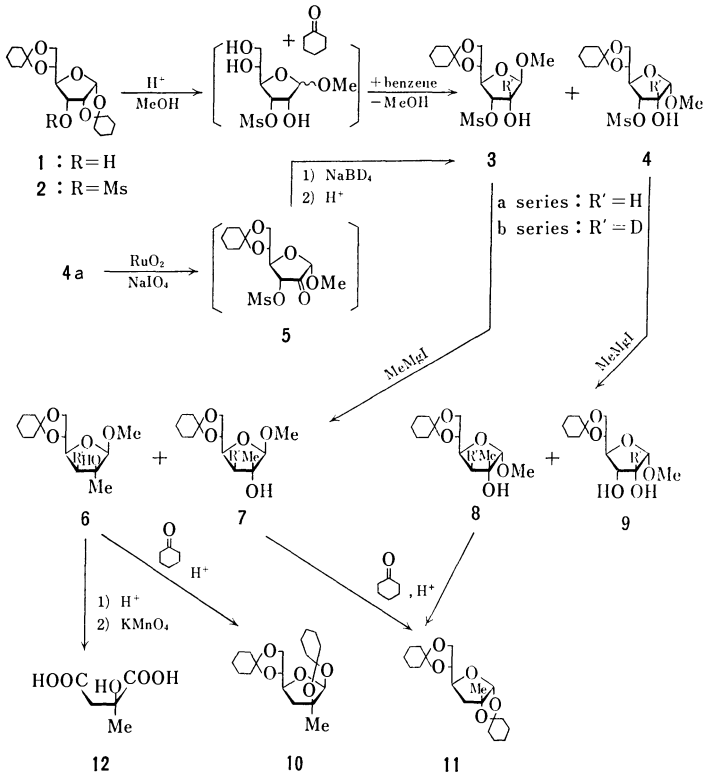

Fig. 1.

(**7a**) in 86 and 4% yields respectively. When **4a** was treated with MeMgI, methyl 5,6-*O*-cyclohexylidene-3-deoxy-2-*C*-methyl-α-D-*ribo*-hexofuranoside (**8a**) was obtained in a 29% yield, besides methyl 5,6-*O*-cyclohexylidene-α-D-allofuranoside (**9a**) in a 37% yield, the cleavage of the mesyl group in **4a** being predominant in this case.

The structures of the newly synthesized branched-chain deoxy sugars were established on the basis of their analytical and spectroscopic data and the chemical conversion. The ^{1}H NMR spectrum of each sugar derivative (**6a**—**8a**) showed a singlet due to the anomeric proton and a pair of quartets characteristic of the AB parts of an ABX system; these phenomena were assignable to H_{3a} (A), H_{3b} (B), and H_4 (X).[6] The relatively large values (8.6—6.4 Hz) of the coupling constants for H_{3a}–H_4 and H_{3b}–H_4 in **6a**—**8a** suggested that these sugars most probably existed in C_3-*endo* conformations.[7] For example, the C_3-*endo* conformation of **6a** can be depicted as in Fig. 2, in which H_{3a} and the methyl group at C-2 as well as H_{3a} and H_4 consititute an axial-quasi axial pair. Spin-spin decoupling experiments demonstrated that the methyl protons in the former pair were coupled to H_{3a} (J=0.8 Hz) because of their W-shaped arrangement.

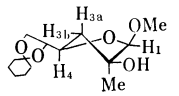

Fig. 2. C_3-*endo* conformation of **6a**.

The ^{13}C NMR spectra of **6a**—**8a** were also taken (Table 1). The signal due to the methyl carbon at C-2 of **7a** appeared at fields higher by 2.7 and 4.6 ppm than those for **6a** and **8a** respectively. This indicated that the methyl group at C-2 in **7a** was located vicinal to the methoxyl group at C-1 in a *cis* manner.[8] These ^{1}H and ^{13}C NMR spectral data are consistent with the proposed structures for **6a**, **7a**, and **8a**.

Both compounds, **7a** and **8a**, gave 1,2:5,6-di-*O*-cyclohexylidene-3-deoxy-2-*C*-methyl-α-D-*ribo*-hexofuranose (**11**) when they were treated with cyclohexanone in the presence of an acid. Similarly, the corresponding β-D-*arabino* isomer (**10**) could be obtained from **6a**. The mass spectra of **10** and **11** showed strong peaks at *m/e* 141 attributable to the dioxolane ring at C-4, thus indicating the furanose structures of these compounds.[5] Their anomeric configurations were also assigned on the basis of the sign of the optical rotation; **10** had a negative sign, whereas **11** had a positive one.[9] From these results, it was concluded that **7a** and **8a** were a pair of anomers, and that the configurations at C-2 for these anomers were different from that for **6a**.

Furthermore, the absolute configuration of the branching point at the C-2 position of **6a** was determined by chemical degradation. Thus, **6a** was treated with an acid to hydrolyze the acetal protecting group and the glycoside, after which the resulting free sugar was oxidized with potassium permanganate to yield the known 2-methylmalic acid (**12**), which had the *S* configuration at its asymmetric center.[10a]

Salaün and Conia[11] have reported that when 2-tosyloxycyclobutanone was treated with MeMgI, the resulting Grignard adduct, 1-methyl-2-*O*-tosyl-1,2-cyclobutanediol, underwent a skeletal rearrengement of the cyclobutane ring to give cyclopropyl methyl ketone. Sasaki *et al.*[12] have obtained 3-deoxy-2-keto sugar-nucleosides by the reaction of 3′-*O*-sulfonates of nucleosides with sodium benzoate in *N*,*N*-dimethylformamide; they assumed that these reactions proceeded *via* the 1,2-elimination of the sulfonyloxyl group at C-3′ and of the proton at C-2′. In the present reactions, it was considered that the 3-deoxy-2-keto sugars (**B** in Fig. 3) were formed as intermediates from **3a** and **4a** by the elimination of the mesyloxyl groups at C-3 concomitant with the 1,2-hydride shifts from C-2 to C-3.

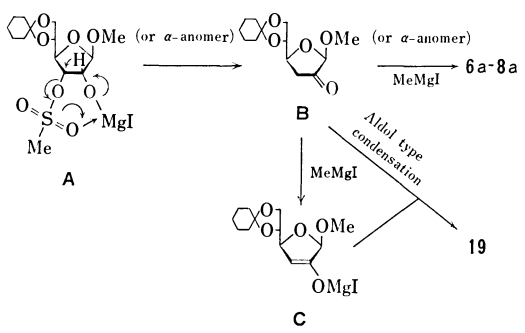

Fig. 3.

In order to demonstrate the hydride shifts in our case, the C-2 deuterated analogs of **3a** and **4a** were prepared. The oxidation of **4a** with ruthenium dioxide-sodium metaperiodate gave an ulose (**5**), which, without purification, was then reduced with sodium borodeuteride to give the C-2 deuterated analog (**4b**). The corresponding β-anomer (**3b**) was obtained by the anomerization of **4b** with an acid.

The deuterated analogs (**3b** and **4b**) thus obtained were subjected to the same Grignard reactions to give the corresponding deuterated products (**6b**—**8b**). The mass spectra of these products showed that the deuterium contents of the starting materials were almost entirely retained in the products. Their ^{1}H NMR spectra indicated that the deuteriums at C-2 in the starting materials had been transferred to the C-3 position of the products. As the ^{1}H NMR analysis distinguished between H_{3a} and H_{3b} in **6a**, the *S* configuration could be assigned to the C-3 position of **6b**. Therefore, the 1,2-deuteride shift in **3b** occurred stereoselectively by way of the intramolecular S_N2 displacement of the mesyloxyl group at C-3.

On the basis of these observations it can be assumed that the present Grignard reactions proceed through a postulated intermediate (**A** in Fig. 3) in which the oxygen atom of the sulfone moiety is coordinated to the magnesium atom to form a cyclic seven-membered ring. The formation of the keto group, the 1,2-hydride shift, and the elimination of the mesyloxyl group then occurs in a concerted manner to give the 3-deoxy-2-keto sugar (**B**), which, in turn, reacts with another MeMgI, mainly from the opposite side of the methoxyl group at C-1, to yield the branched-chain deoxy sugars.

TABLE 1. THE ^{13}C NMR CHEMICAL SHIFTS OF DEOXY AND BRANCHED-CHAIN DEOXY SUGARS[a]

Product	Carbon positions[b]											
	C_1	C_2	C_3	C_4	C_5	C_6	C-Me	O-Me	$C_{1'}$	$C_{2',6'}$	$C_{3',4',6'}$	
6a	106.56	77.60	41.18	78.66[c]	78.78[c]	66.72	23.80	54.90	109.88	34.84 36.51	23.80 24.00	25.14
7a	109.81	80.51	41.39	79.87	79.05	67.20	21.10	54.54	109.81	34.98 36.52	23.86 24.02	25.16
8a	107.38	77.51	40.66	78.00	76.94	66.72	25.73	55.43	110.06	34.74 36.20	23.78 23.94	25.16
13a	101.82	72.33	35.02	78.08[c]	78.59[c]	66.65	—	54.86	109.67	34.78 36.42	23.77 23.97	25.09
14a	102.56	71.69	33.60	77.03[c]	77.69[c]	66.43	—	55.24	110.13	34.62 36.17	23.74 23.98	25.14

a) The spectra were run in $CDCl_3$ and were completely decoupled. The shifts are given in parts per million relative to the internal tetramethylsilane. b) C_1-C_6 refer to the carbon atoms of the sugars, while $C_{1'}$-$C_{6'}$ refer to the cyclohexylidene carbon atoms. c) The assignment of the signals to C_4 and C_5 may be reversed.

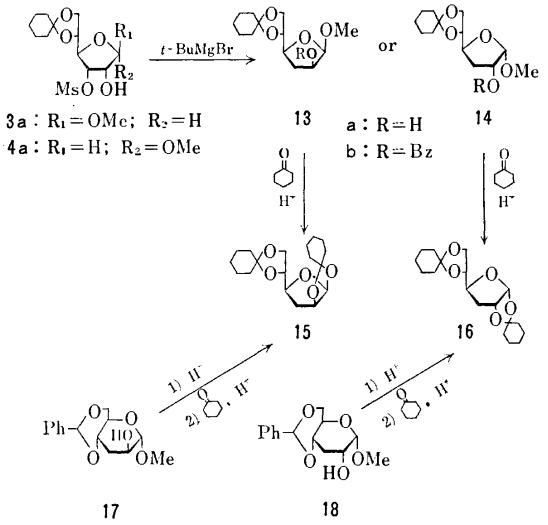

Fig. 4.

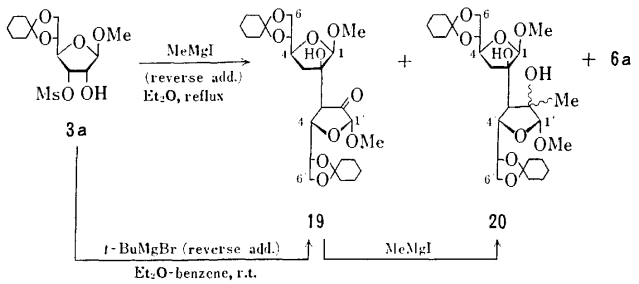

Fig. 5.

With the hope of obtaining exclusively the 3-deoxy-2-keto sugars in the present reactions, we attempted to use sterically bulky *t*-butylmagnesium bromide (*t*-BuMgBr) instead of MeMgI. However, the reaction of **3a** or **4a** with *t*-BuMgBr did not stop at the stage of the formation of the desired sugar derivative, but proceeded further to afford methyl 5,6-*O*-cyclohexylidene-3-deoxy-β-D-*arabino*-hexofuranoside (**13a**) or the corresponding α-D-*ribo* isomer (**14a**) in an 87 or 75% yield respectively after column chromatography (Fig. 4). The Grignard reduction by *t*-BuMgBr was effective in this case. An attempt to reduce 1,2:5,6-di-*O*-cyclohexylidene-α-D-*ribo*-hexofuranos-3-ulose[4b] with *t*-BuMgBr under similar conditions gave a mixture (91:9) of the corresponding *allo*- and *gluco*-furanose in a 78% yield.

The structures of **13a** and **14a** as well as their monobenzoates (**13b** and **14b**) were characterized by their elemental analyses and spectroscopic data, including the ^{13}C NMR spectra (Table 1). Furthermore, the treatment of **13a** and **14a** with cyclohexanone in the presence of an acid gave 1,2:5,6-di-*O*-cyclohexylidene-3-deoxy-β-D-*arabino*-hexofuranose (**15**) and the corresponding α-D-*ribo* isomer (**16**) respectively, their furanose structures being tentatively assigned. However, the physical properties of **15** and **16** were identical with those of the specimens prepared from known compounds, methyl 4,6-*O*-benzylidene-3-deoxy-α-D-*arabino*-hexopyoranoside[13] (**17**) and the corresponding α-D-*ribo* isomer[14] (**18**) respectively.

When an ethereal solution of MeMgI was very gradually added to a refluxing solution of **3a** in ether, it gave two dimeric compounds, **19** and **20**, in 3 and 44% yields respectively, besides **6a** (29%)(Fig. 5). Using *t*-BuMgBr, we obtained **19** in a moderate yield, upon subsequent treatment with MeMgI, this gave **20**.

The structures and the stereochemistry of the binding sites of the two furanose rings for **19** and **20** were deduced to be as is shown in the scheme on the basis of their spectral data as well as an inspection of the CPK molecular model, but the configuration of the methyl and hydroxyl groups in **20** is not clear at this time. These reactions are considered to be Aldol-type condensations of the ketone (**B**, β-anomer) and its enolate (**C**) (Fig. 3); the slow addition of MeMgI to a solution of **3a** would result in the survival of a relatively large amount of unreacted ketone (**B**), some of which would be isomerized with MeMgI to **C**. Similar reactions have been reported by Horton and Just[15a] and others.[15b,c]

Experimental

The boiling and melting points are uncorrected. The optical rotations were measured with a Perkin-Elmer Model 141 polarimeter. The IR spectra were recorded on a Shimadzu IR-27 instrument. The mass spectra were obtained

with a Japan Optics Lab. Model JMS-01SG instrument. The ^{1}H NMR spectra were recorded on a Varian HA-100D apparatus, with tetramethylsilane as the internal standard. The proton noise-decoupling ^{13}C NMR spectra were obtained on a JEOL FX-60 FT.

Merck silica gel 60 (0.063—0.20 mm) was used for the column chromatography, and silica gel GF_{254} was used for the analytical TLC; visualization was effected by the use of a methanol–sulfuric acid–*p*-methoxybenzaldehyde (85:10:5, v/v) spray, followed by heating. The elemental analyses were performed by this Institute. The sodium borodeuteride (98% min deuterium content) was purchased from Merck.

1,2:5,6-Di-O-Cyclohexylidene-3-O-mesyl-α-D-allofuranose (2). Mesyl chloride (5.5 ml) was added to a stirred solution of I[4a] (17 g, 0.05 mol) in a mixture of dry pyridine (30 ml) and benzene (30 ml) at 0—5 °C (bath temperature). The mixture was then stirred at room temperature overnight. After cooling, iced water was added and the mixture was extracted with chloroform. The extract was washed with water, dried ($MgSO_4$), and concentrated. The pyridine was removed by co-evaporation with xylene. The residue was diluted with methanol to give **2** (88%) as crystals. An analytically pure sample was obtained by recrystallization from methanol: mp 119.5—121.5 °C; $[\alpha]_D^{23}$ +82.2° (*c* 1.3, $CHCl_3$). IR (KBr): 1358 (S=O), 1179 (S=O) cm^{-1}. ^{1}H NMR ($CDCl_3$): δ 1.0—2.0 (20H, m, CH_2 of the cyclohexylidene groups), 3.8—4.4 (4H, m), 4.7—4.9 (2H, m), 5.82 (1H, dd, J=3.8 Hz, J=0.8 Hz, H-3).

Found: C, 54.68; H, 6.98; S, 7.67%. Calcd for $C_{19}H_{30}O_8S$: C, 54.53; H, 7.23; S, 7.66%.

Methyl 5,6-O-Cyclohexylidene-3-O-mesyl-β-D-allofuranoside (3a) and Its α-Anomer (4a). A mixture of **2** (16.8 g, 0.04 mol) and concd sulfuric acid (0.2 ml) in dry methanol (120 ml) was stirred at 75—80 °C (bath temperature) for 3 h. The methanol was then removed below 35 °C *in vacuo* until crystals appeared. Dry benzene (60 ml) was added, and the mixture was concentrated to *ca.* 30 ml. This procedure (the addition of benzene and the concentration of the mixture) was repeated once again. Calcium hydroxide (4 g) was then added, and the mixture was diluted with chloroform. After the crystalline materials had been removed by filtration, the chloroform solution was washed successively with aqueous sodium hydrogencarbonate and water, and dried ($MgSO_4$). The removal of the solvent gave crude products, the ^{1}H NMR spectrum of which showed that the ratio of **3a** and **4a** was approximately 2:1. The products were triturated with hot hexane (80 ml). After the mixture had been cooled, the crystalline compounds were collected and washed with hexane. Recrystallization from benzene–diisopropyl ether gave **3a** (8.1 g, 57%). The mother liquor was concentrated, and the residue was submitted to fractional crystallization from diisopropyl ether, giving **4a** (3.95 g, 28%) and another crop of **3a** (0.98 g, 7%).

The recrystallization of the crude **3a** from methanol gave an analytically pure sample as needles: mp 138—140 °C; $[\alpha]_D^{24}$ −44.6° (*c* 1, $CHCl_3$). IR (KBr): 3470 (OH), 1353 (S=O), 1173 (S=O) cm^{-1}. MS: *m/e* 352 (M^+), 141 (the dioxolane ring at C-4). ^{1}H NMR ($CDCl_3$): δ 1.2—1.8 (10H, m, CH_2 of the cyclohexylidene groups), 2.50 (1H, br s, OH), 3.16 (3H, s, SCH_3), 3.35 (3H, s, OCH_3), 3.9—4.2 (4H, m), 4.31 (1H, dd, $J_{1,2}$=1.4 Hz, $J_{2,3}$=4.6 Hz, H-2), 4.87 (1H, d, $J_{1,2}$=1.4 Hz, H-1), 5.10 (1H, m, H-3).

Found: C, 47.73; H, 6.84; S, 9.00%. Calcd for $C_{14}H_{24}O_8S$: C, 47.72; H, 6.78; S, 9.10%.

The recrystallization of the crude **4a** from benzene–diisopropyl ether gave an analytically pure sample as prisms: mp 118—119 °C; $[\alpha]_D^{22}$ +97.7° (*c* 1, $CHCl_3$). IR (KBr): 3500 (OH), 1353 (S=O), 1172 (S=O) cm^{-1}. MS: *m/e* 352 (M^+), 141 (the dioxolane ring at C-4). ^{1}H NMR ($CDCl_3$): δ 1.2—2.0 (10H, m, CH_2 of the cyclohexylidene groups), 3.12 (3H, s, SCH_3), 3.47 (3H, s, OCH_3), 3.7—4.4 (5H, m) 4.93 (1H, d, $J_{1,2}$=4.8 Hz, H-1), 5.0 (1H, m, H-3).

Found: C, 47.53; H, 6.83; S, 9.13%. Calcd for $C_{14}H_{24}O_8S$: C, 47.72; H, 6.87; S, 9.10%.

Methyl 5,6-O-Cyclohexylidene-3-O-mesyl-β-D-allofuranoside-2-d (3b) and Its α-Anomer (4b). A mixture of **4a** (2.27 g, 6.45 mmol), sodium metaperiodate (6.8 g), ruthenium dioxide (400 mg), and potassium carbonate (720 mg) in alcohol-free chloroform (80 ml) and water (80 ml) was vigorously stirred at room temperature for 8 h.[16] After the excess of ruthenium tetraoxide had then been decomposed with 2-propanol, the undissolved materials were filtered through a Celite pad and washed with chloroform. The filtrate was dried ($MgSO_4$) and concentrated to give a syrupy ketone (**5**, 1.85 g) which was almost pure, judging from its TLC analysis, and IR and ^{1}H NMR spectral data; this product was found to be converted to almost pure **4a** by reduction with sodium borohydride under conditions similar to those described below.

Sodium borodeuteride (200 mg) was added to a stirred solution of this crude **5** (1.75 g) in methanol (15 ml) at 0—5 °C (bath temperature) over a period of 5 min. After 1 h, the mixture was diluted with ether, and the solution was washed with water and dried ($MgSO_4$). The evaporation of the solvent gave a crystalline product, which was triturated with hot diisopropyl ether to give **4b** (1.48 g, 69% from **4a**); the deuterium content was found to be 91% on the basis of the mass spectrometric analysis. MS: *m/e* 353 (M^+). ^{1}H NMR ($CDCl_3$): δ 1.1—1.8 (10H, m, CH_2 of the cyclohexylidene group), 3.11 (3H, s, SCH_3), 3.46 (3H, s, OCH_3), 3.9—4.3 (4, 1H, m), 4.92 (1H, s, H-1), 4.97 (1H, m, H-3).

A stirred mixture of **4b** (1.3 g) and concd sulfuric acid (0.03 ml) was refluxed at 80—85 °C (bath temperature) for 3 h. The solution was treated in a manner to that described for the synthesis of **3a** to give a mixture (1.2 g) of **3b** and **4b** in a ratio of 2:1, from which **3b** (500 mg, 38%) was isolated. Recrystallization from benzene–diisopropyl ether gave **3b**; the deuterium content was found to be 87% on the basis of the mass spectrometric analysis. MS: *m/e* 353 (M^+). ^{1}H NMR ($CDCl_3$): δ 1.1—1.9 (10H, m, CH_2 of the cyclohexylidene group), 3.16 (3H, s, SCH_3), 3.36 (3H, s, OCH_3), 3.8—4.2 (4H, m), 4.3 (0.1H, m, H-2), 4.87 (1H, s, H-1), 5.1 (1H, m, H-3).

Methyl 5,6-O-Cyclohexylidene-3-deoxy-2-C-methyl-β-D-arabino-hexofuranoside (6a) and Methyl 5,6-O-Cyclohexylidene-3-deoxy-2-C-methyl-β-D-ribo-hexofuranoside (7a). To a stirred solution of MeMgI (6 mmol) in ether (20 ml) we added **3a** (705 mg, 2 mmol) at 0—5 °C (bath temperature) under a dry nitrogen atmosphere over a period of 5 min, after which the mixture was stirred at room temperature for 2 h. After the mixture had been cooled, aqueous ammonium chloride was added. The mixture was then extracted with ether. The extract was washed with water, dried ($MgSO_4$), and concentrated to give crystalline products, which were recrystallized from water–ethanol on seeding to afford **6a** (262 mg, 48%): mp 69—70 °C; $[\alpha]_D^{25}$ −69.4° (*c* 1, $CHCl_3$). IR (KBr): 3500 (OH) cm^{-1}. MS: *m/e* 272 (M^+). ^{1}H NMR[6] ($CDCl_3$): δ 1.2—1.7 (10H, m, CH_2 of the cyclohexylidene group), 1.32 (3H, d, $J_{3a,Me}$=0.8 Hz, C-CH_3), 1.88 (1H, q, $J_{3a,3b}$=11.5 Hz, $J_{3a,4}$=8.0 Hz, H-3a), 2.09 (1H, q, $J_{3a,3b}$=11.5 Hz, $J_{3b,4}$=6.5 Hz, H-3b), 2.72 (1H, br s, OH), 3.40 (3H, s, OCH_3), 3.7—4.2 (4H, m), 4.35 (1H, s, H-1).

Found: C, 62.00; H, 8.70%. Calcd for $C_{14}H_{24}O_5$: C,

61.74; H, 8.88%.

The mother liquor was concentrated, and the residue was chromatographed on a silica-gel column with hexane–ether (2:1) to give a ketonic compound (11 mg) which was not characterized, another crop of **6a** (209 mg, 38%), and the C-2 epimer (**7a**, 22 mg, 4%) as crystals: mp 90—92 °C; $[\alpha]_D^{20}$ −80.2° (*c* 0.3, $CHCl_3$). IR (KBr): 3280 (OH) cm^{-1}. MS: *m/e* 272 (M^+). ^1H NMR[6] ($CDCl_3$): δ 1.1—1.7 (10H, m, CH_2 of the cyclohexylidene group), 1.36 (3H, s, C-CH_3), 1.91 (1H, q, $J_{3a,3b}=13.1$ Hz, $J_{3a,4}=8.6$ Hz, H-3a), 2.09 (1H, q, $J_{3a,3b}=13.1$ Hz, $J_{3b,4}=6.6$ Hz, H-3b), 2.23 (1H, br s, OH), 3.32 (3H, s, OCH_3), 3.8—4.4 (4H, m), 4.51 (1H, s, H-1).

Found: C, 61.96; H, 8.97%. Calcd for $C_{14}H_{24}O_5$: C, 61.74; H, 8.88%.

*Methyl 5,6-*O*-Cyclohexylidene-3-deoxy-2-*C*-methyl-α-*D*-ribo-hexofuranoside (**8a**) and Methyl 5,6-*O*-Cyclohexylidene-α-*D*-allofuranoside (**9a**).* A solution of MeMgI (18 mmol) in ether (15 ml) was gradually added to a stirred suspension of powdered **4a** (1.06 g, 3 mmol) in ether (20 ml) at −3—0 °C (bath temperature) under a dry nitrogen atmosphere over a period of 30 min; when powdered **4a** was added to the solution of MeMgI under conditions similar to those described for the synthesis of **6a**, gummy materials were formed to decrease the yield of **8a**. After the mixture had then been stirred at room temperature for 7 h, it was poured into a cold solution of ammonium chloride (1 g) in water (30 ml) and extracted with ether (250 ml). The extract was washed with water (40 ml×8), dried ($MgSO_4$), and concentrated. The residue was chromatographed on a silica-gel column with hexane–ether to give **8a** (240 mg, 29%) as a syrup. An analytically pure sample was obtained by distillation: bp 128—130 °C (bath temperature)/2 mmHg; $[\alpha]_D^{21}$ +75.2° (*c* 1, $CHCl_3$). IR (neat): 3530 (OH) cm^{-1}. MS: *m/e* 272 (M^+). ^1H NMR[6] ($CDCl_3$): δ 1.2—1.7 (10H, m, CH_2 of the cyclohexylidene group), 1.37 (3H, s, C-CH_3), 1.93 (1H, q, $J_{3a,3b}=12.4$ Hz, $J_{3a,4}=6.4$ Hz, H-3a), 2.11 (1H, q, $J_{3a,3b}=12.4$ Hz, $J_{3b,4}=7.0$ Hz, H-3b), 2.74 (1H, br s, OH), 3.47 (3H, s, OCH_3), 3.8 (1H, m), 3.9—4.3 (3H, m), 4.53 (1H, s, H-1).

Found: C, 61.86; 8.89%. Calcd for $C_{14}H_{24}O_5$: C, 61.74; H, 8.88%.

The aqueous ammonium chloride and washings were combined and concentrated. The residue was triturated with chloroform, and the undissolved materials were removed by filtration. The chloroform was evaporated to give a syrup, which was then chromatographed on a silica-gel column with chloroform–methanol (98:2) to afford **9a** (304 mg, 37%) as a syrup: $[\alpha]_D^{21}$ +100° (*c* 1, $CHCl_3$). IR (neat): 3450 (OH) cm^{-1}. MS: *m/e* 274 (M^+). ^1H NMR ($CDCl_3$): δ 1.1—2.0 (10H, m, CH_2 of the cyclohexylidene group), 2.85 (2H, s, two hydroxyl protons), 3.48 (3H, s, OCH_3), 3.7—4.3 (6H, m), 4.9 (1H, m, H-1); (benzene-d_6) δ 3.11 (3H, s, OCH_3), 4.60 (1H, d, $J_{1,2}=4.2$ Hz, H-1).

Found: C, 56.90; H, 7.95%. Calcd for $C_{13}H_{22}O_6$: C, 56.92; H, 8.08%.

*Methyl 5,6-*O*-Cyclohexylidene-3-deoxy-2-*C*-methyl-β-*D*-arabino-hexofuranoside-3-*d* (**6b**) and Its C-2 Epimer (**7b**).* The deuterated analog (**3b**, 300 mg, 0.85 mmol) was treated with MeMgI (5.1 mmol) in a manner similar to that described for the synthesis of **6a** to give, after chromatography, **6b** (192 mg, 83%) and **7b** (5 mg, 2.2%). The mass spectra of these products indicated that their deuterium contents were 87%.

6b. MS: *m/e* 273 (M^+). ^1H NMR[6] ($CDCl_3$): δ 1.34 (3H, s, C-CH_3), 1.2—1.8 (10H, m, CH_2 of the cyclohexylidene group), 1.9 (0.15H, m, H-3a), 2.1 (1H, m, H-3b), 2.79 (1H, s, OH), 3.42 (3H, s, OCH_3), 3.8—4.2 (4H, m), 4.36 (1H, s, H-1).

7b. MS: *m/e* 273 (M^+). ^1H NMR[6] ($CDCl_3$): δ 1.1—1.8 (10H, m, CH_2 of the cyclohexylidene group), 1.34 (3H, s, C-CH_3), 1.9 (0.15H, m, H-3a), 2.1 (1H, m, H-3b), 3.30 (3H, s, OCH_3), 3.8—4.3 (4H, m), 4.50 (1H, s, H-1).

*Methyl 5,6-*O*-Cyclohexylidene-3-deoxy-2-*C*-methyl-α-*D*-ribo-hexofuranoside-3-*d* (**8b**) and Methyl 5,6-*O*-Cyclohexylidene-α-*D*-allofuranoside-2-*d* (**9b**).* The deuterated analog (**4b**, 282 mg, 0.8 mmol) was treated with MeMgI (4.8 mmol) in a manner similar to that described for the synthesis of **8a**. After the reaction had been completed, a small amount of cold aqueous ammonium chloride was added to the cooled reaction mixture and the products were extracted with ether and dried ($MgSO_4$). The residue was chromatographed on a silica-gel column with hexane–ether (1:1) to give **8b** (63 mg, 29%) and **9b** (59 mg, 27%). The mass spectra of **8b** and **9b** indicated that their deuterium contents were 86 and 90% respectively.

8b. MS: *m/e* 273 (M^+). ^1H NMR[6] ($CDCl_3$): δ 1.2—1.8 (10H, m, CH_2 of the cyclohexylidene group), 1.36 (3H, s, C-CH_3), 1.9 (0.15H, m, H-3a), 2.1 (1H, m, H-3b), 2.94 (1H, s, OH), 3.46 (3H, s, OCH_3), 3.7—3.9 (1H, m), 4.0—4.2 (3H, m), 4.52 (1H, s, H-1).

9b. MS: *m/e* 257 (M^+). ^1H NMR ($CDCl_3$): δ 1.1—1.8 (10H, m, CH_2 of the cyclohexylidene group), 2.79 (1H, br d, $J=7.4$ Hz, OH at C-3), 3.01 (1H, br s, OH at C-2), 3.47 (3H, s, OCH_3), 3.7—4.3 (5.1H, m), 4.91 (1H, s, H-1).

*1,2:5,6-Di-*O*-cyclohexylidene-3-deoxy-2-*C*-methyl-β-*D*-arabino-hexofuranose (**10**).* A mixture of **6a**, cyclohexanone (0.4 ml), and concd sulfuric acid (*ca.* 40 mg) in dry benzene (2 ml) was vigorously stirred at room temperature for 30 h. During this reaction time, the following procedure was repeated several times: the mixture was concentrated below 30 °C *in vacuo*, followed by the addition of dry benzene in order to remove the methanol and water produced. The mixture was then diluted with dry benzene and neutralized with calcium hydroxide. The undissolved material was filtered and washed with chloroform. The chloroform solution was washed successively with aqueous sodium hydrogencarbonate and water, and then dried ($MgSO_4$). The subsequent evaporation of the solvent gave a syrup, which was chromatographed on a silica-gel column with hexane–ether (8:2) to give **10** (180 mg, 58%). An analytically pure sample was obtained by distillation: bp 167—170 °C (bath temperature)/1 mmHg; $[\alpha]_D^{23}$ −21.0° (*c* 1, $CHCl_3$). IR (neat): no OH absorption. MS: *m/e* 338 (M^+), 141 (the dioxolane ring at C-4). ^1H NMR[6] ($CDCl_3$): δ 1.1—1.9 (10H, m, CH_2 of the cyclohexylidene group), 1.48 (3H, s, C-CH_3), 2.09 (1H, q, $J_{3a,3b}=13.8$ Hz, $J_{3a,4}=7.8$ Hz, H-3a), 2.34 (1H, q, $J_{3a,3b}=13.8$ Hz, $J_{3b,4}=6.8$ Hz, H-3b), 3.6—4.4 (4H, m), 5.35 (1H, s, H-1).

Found: C, 67.59; H, 8.70%. Calcd for $C_{19}H_{30}O_5$: C, 67.43; H, 8.94%.

*1,2:5,6-Di-*O*-cyclohexylidene-3-deoxy-2-*C*-methyl-α-*D*-ribo-hexofuranose (**11**).* *From **8a***: A mixture of **8a** (130 mg, 0.48 mmol), cyclohexanone (0.4 ml), and concd sulfuric acid (*ca.* 40 mg) in dry benzene (2 ml) was vigorously stirred at room temperature for 2.5 h; the benzene was then removed below 30 °C *in vacuo*. The residue was treated in a manner similar to that described for the synthesis of **10** to afford, after column chromatography, **11** (140 mg, 86%). An analytically pure sample was obtained by distillation: bp 173—175 °C (bath temperature)/1.5 mmHg; $[\alpha]_D^{22}$ +10.3° (*c* 1, $CHCl_3$). IR (neat): no OH absorption. MS: *m/e* 338 (M^+), 141 (the dioxolane ring at C-4). ^1H NMR ($CDCl_3$): δ 1.1—1.9 (10H, m, CH_2 of the cyclohexylidene group),

1.50 (3H, s, C-CH_3), 2.1—2.5 (2H, m, H-3a and H-3b), 3.7—4.3 (4H, m), 5.48 (1H, s, H-1).

Found: C, 67.63; H, 8.75%. Calcd for $C_{19}H_{30}O_5$: C, 67.43; H, 8.94%.

From **7a**. The compound (**7a**, 5 mg, 0.018 mmol) was treated with cyclohexanone in a manner similar to that described for the synthesis of **11** from **8a**, giving a syrupy **11** (5 mg, 82%). The physical properties (IR, ^1H NMR, and the specific rotation) of this material were identical with those of the specimen prepared from **8a**.

(S)-(+)-2-Methylmalic Acid (12). Dowex 50W-X8 (H^+ form, 6 ml) was added to a solution of **6a** (1.32 g, 4.85 mmol) in a mixture of dioxane (10 ml) and water (16 ml), after which was stirred at 90 °C (bath temperature) for 1 h. The resin was removed by filtration and washed with water. The combined filtrate and washings were concentrated. The residue was chromatographed on a silica-gel column with chloroform–methanol (8:2) to give a syrupy product (740 mg). To a solution of this syrup (350 mg) and potassium hydroxide (200 mg) in water (50 ml), there was added powdered potassium permanganate (1.3 g) at 4—5 °C over a period of 1 h. After the mixture had been stirred at this temperature for another 1 h, 15% hydrogen peroxide (*ca.* 5 ml) was added to decompose the excess potassium permanganate. The mixture was then diluted with water and treated with charcoal. The undissolved materials were removed by filtration through a Celite pad and washed with water. The combined filtrate and washings were acidified with Dowex 50W-X8 (H^+ form). After the removal of the resin, the solution was concentrated. The residue was chromatographed on a column of Dowex-X8 (H^+ form, 100—200 mesh, 300 ml, 2.8×66 cm) with water; a 6-ml fraction was thus collected. Fractions No. 31—38 were combined and concentrated to give a syrup, which was taken up in ethyl acetate. A small amount of the undissolved material was filtered, and the filtrate was concentrated. The water which remained in the residue was removed by repeated co-evaporation with ethyl acetate–benzene to give, after drying (P_2O_5) at 57 °C *in vacuo* for 4 h, **12** as a syrup (190 mg, 56% from **6a**): $[\alpha]_D^{27}$ +21.2° (*c* 1.2, H_2O) [lit,[10b] $[\alpha]_D^{22}$ +23° (*c* 6.316, H_2O)]; $[\alpha]_D^{27}$ +1300° [*c* 0.1, in a mixture of H_2O (2.5 ml), 0.25 M sodium citrate (2.5 ml), 29% ammonium molybdate (4.5 ml), and acetic acid (0.5 ml)] [lit,[10c] $[\alpha]_D^{18}$ −1335°: This optical rotation was measured in a mixture of 0.01 M (−)-2-methylmalic acid (2.5 ml), 0.25 M sodium citrate (2.5 ml), 29% ammonium molybdate (4.5 ml), and acetic acid (0.5 ml)]. The ^1H NMR spectrum of **12** was completely identical with that of an authentic sample of racemic **12**.

A solution of the syrupy **12** (47 mg) and brucine (136 mg) in water (0.3 ml) was allowed to stand at 3 °C overnight to give an analytically pure brucine salt of **12** as crystals (67 mg, 41%): mp 216—217 °C (dec under rapid heating) [lit,[10b] 222 °C (dec)]; $[\alpha]_D^{26}$ −7.3° (*c* 0.44, 50% MeOH). The IR spectrum of this salt was completely identical with that of an authentic sample.

*Methyl 5,6-O-Cyclohexylidene-3-deoxy-β-*D-arabino-*hexofuranoside (13a)*. Into a solution of *t*-BuMgBr (24 mmol) in a mixuter of ether (20 ml) and benzene (10 ml) we stirred **3a** (704 mg, 2 mmol) at room temperature under a dry nitrogen atmosphere over a period of 30 min. The mixture was stirred for another 30 min and then cooled to 5 °C. Cold aqueous ammonium chloride was added, and the mixture was extracted with ether. The extract was washed with water, dried ($MgSO_4$), and then concentrated. The residue was chromatographed on a silica-gel column with benzene–ethyl acetate (9:1) to give **13a** (447 mg, 87%) as a syrup: $[\alpha]_D^{25}$ −86.0° (*c* 0.8, $CHCl_3$). IR (neat): 3480 (OH) cm^{-1}. MS: *m/e* 258 (M^+). ^1H NMR ($CDCl_3$): δ 1.2—1.9 (10H, m, CH_2 of the cyclohexylidene group), 2.2—2.6 (2H, m, H-3a and H-3b), 3.39 (3H, s, OCH_3), 3.8—4.4 (5H, m), 4.71 (1H, d, $J_{1,2}$=4.3 Hz, H-1).

Found: C, 60.27; H, 8.55%. Calcd for $C_{13}H_{22}O_5$: C, 60.44; H, 8.59%.

*Methyl 5,6-O-Cyclohexylidene-3-deoxy-α-*D-ribo-*hexofuranoside (14a)*. To a stirred solution of *t*-BuMgBr (24 mmol) in a mixture of ether (20 ml) and benzene (10 ml) we added **4a** (704 mg, 2 mmol) at 60—65 °C (bath temperature) under a dry nitrogen atmosphere over a period of 15 min. The stirring was continued at this temperature for another 25 min. The usual work-up gave a syrupy product, which was chromatographed on a silica-gel column with hexane–ether (6:4) to give **14a** (387 mg, 75%) as a syrup: $[\alpha]_D^{25}$ +93.6° (*c* 1, $CHCl_3$). IR (neat): 3500 (OH) cm^{-1}. MS: *m/e* 258 (M^+). ^1H NMR ($CDCl_3$): δ 1.1—1.9 (10H, m, CH_2 of the cyclohexylidene group), 1.7—2.4 (2H m, H-3a and H-3b), 2.46 (1H, d, J=8.6 Hz, OH), 3.43 (3H, s, OCH_3), 3.72 (1H, m), 3.9—4.5 (4H, m), 4.83 (1H, d, $J_{1,2}$=4.5 Hz, H-1).

Found: C, 60.48; H, 8.55%. Calcd for $C_{13}H_{22}O_5$: C, 60.44; H, 8.59%.

*Methyl 2-O-Benzoyl-5,6-O-cyclohexylidene-3-deoxy-β-*D-arabino-*hexofuranoside (13b)*. Benzoyl chloride (0.3 ml) was stirred into a cold (0—5 °C) solution of **13a** (147 mg, 0.57 mmol) in dry pyridine (1.5 ml). The mixture was stirred at room temperature for 10 min and then cooled. Iced water was added, and the mixture was extracted with ether. The extract was washed with water, dried ($MgSO_4$), and then concentrated to give a syrup, which was chromatographed on a silica-gel column with benzene–ethyl acetate (9:1) to give **13b** as crystals in a quantitative yield: mp 86.0—86.5 °C; $[\alpha]_D^{25}$ −88.4° (*c* 1.2, $CHCl_3$). IR (KBr): 1724 (C=O) cm^{-1}. MS: *m/e* 362 (M^+). ^1H NMR ($CDCl_3$): δ 1.1—1.9 (10H, m, CH_2 of the cyclohexylidene group), 2.0—2.8 (2H, m, H-3a and H-3b), 3.32 (3H, s, OCH_3), 3.8—4.3 (4H, m), 5.0—5.3 (2H, m, H-1 and H-2), 7.2—7.7 (3H, m, the phenyl protons), 7.9—8.2 (2H, m, the phenyl protons).

Found: C, 66.38; H, 7.17%. Calcd for $C_{20}H_{26}O_6$: C, 66.28; H, 7.23%.

*Methyl 2-O-Benzoyl-5,6-O-cyclohexylidene-3-deoxy-α-*D-ribo-*hexofuranoside (14b)*. Benzoyl chloride (0.3 ml) was stirred into a cold (0—5 °C) solution of **14a** (160 mg, 0.62 mmol) in dry pyridine (1.5 ml). The mixture was then stirred at room temperature for 10 min. The usual work-up gave a syrup, which was subsequently chromatographed on a silica-gel column with hexane–ether (8:2) to afford **14b** (185 mg, 83%) as a syrup: $[\alpha]_D^{25}$ +96.0° (*c* 1, $CHCl_3$). IR (neat): 1721 (C=O) cm^{-1}. ^1H NMR ($CDCl_3$): δ 1.2—1.8 (10H, m, CH_2 of the cyclohexylidene group), 2.2—2.5 (2H, m, H-3a and H-3b), 3.36 (3H, s, OCH_3), 3.78 (1H, m), 4.0—4.3 (3H, m), 5.1—5.3 (2H, m, H-1 and H-2), 7.2—7.7 (3H, m, the phenyl protons), 7.9—8.2 (2H, m, the phenyl protons).

Found: C, 66.30; H, 7.27%. Calcd for $C_{20}H_{26}O_6$: C, 66.28; H, 7.23%.

*The Reaction of 1,2:5,6-Di-O-cyclohexylidene-α-*D-ribo-*hexofuranos-3-ulose with* t-*BuMgBr*. To a stirred solution of *t*-BuMgBr (6 mmol) in ether (8 ml) and benzene (4 ml), there was added a solution of the title compound[4b] (172 mg, 0.51 mmol) at room temperature under a dry nitrogen atmosphere over a period of 5 min. The mixture was then stirred for 15 min. The usual work-up gave crystalline products, which were recrystallized from ligroin to give a mixture (154 mg, 89%) of 1,2:5,6-di-*O*-cyclohexylidene-α-D-allofuranose and the corresponding gluco isomer in a ratio of approximately 91:9, judging from the ^1H NMR

spectroscopy.

*1,2:5,6-Di-O-cyclohexylidene-3-deoxy-β-D-arabino-hexofuranose (**15**).* *From **13a***: A mixutre of **13a** (100 mg, 0.39 mmol), cyclohexanone (0.3 ml), and concd sulfuric acid (*ca.* 40 mg) in dry benzene (1.5 ml) was stirred at room temperature for 4 h. Calcium hydroxide was then added, and the undissolved material was filtered off and washed with methanol. The combined filtrate and washings were treated with sodium borohydride at 0—5 °C (bath temperature) to reduce the excess cyclohexanone. The mixture was then extracted with ether. The extract was washed with water, dried ($MgSO_4$), and concentrated to give a syrup, which was subsequently chromatographed on a silica-gel column with hexane–ether (9:1) to afford **15** (80 mg, 63%) as a syrup: $[\alpha]_D^{24}$ +6.1° (*c* 1.4, $CHCl_3$). IR (neat): no OH absorption. MS: *m/e* 324 (M^+). ^1H NMR ($CDCl_3$): δ 1.2—1.9 (20H, m, CH_2 of the cyclohexylidene groups), 2.0—2.5 (2H, m, H-3a and H-3b), 3.7—4.5 (4H, m), 4.72 (1H, m), 5.75 (1H, d, $J_{1,2}$=4.0 Hz, H-1).

Found: C, 66.58; H, 8.59%. Calcd for $C_{18}H_{28}O_5$: C, 66.64; H, 8.70%.

*From **17***: A mixture of **17**[13] (500 mg, 1.9 mmol) and Dowex 50W-X8 (H^+ form, 4 ml) in dioxane (10 ml) and water (4 ml) was stirred at room temperature for 23 h. The resin was removed by filtration through a Celite pad, and washed successively with dioxane and water. The combined filtrate and washings were concentrated. The residue was chromatographed on a silica-gel column with chloroform–methanol (9:2) to give a syrupy product (350 mg). A stirred mixture of this product (100 mg), cyclohexanone (0.35 ml), and concd sulfuric acid (*ca.* 80 mg) was heated at 65—70 °C (bath temperature) for 30 min. After cooling, calcium hydroxide was added, and the undissolved material was removed by filtration and washed with methanol (6 ml). The combined filtrate and washings were cooled (0—5 °C) and treated with sodium borohydride (230 mg) for 5 min to reduce the excess of cyclohexanone. The mixture was then diluted with ether. The solution was washed with water, dried ($MgSO_4$), and concentrated to give syrup, which was subsequently chromatographed on a silica-gel column with hexane–ether (9:1), thus affording **15** (74 mg, 41% from **17**). An analytically pure sample was obtained by distillation: bp 172—175 °C (bath temperature)/1 mmHg. This product was identical in all respects (IR, ^1H NMR, and the specific rotation) with a specimen prepared from **13a**.

*1,2:5,6-Di-O-cyclohexylidene-3-deoxy-α-D-ribo-hexofuranose (**16**).* *From **14a***: A mixture of **14a** (63 mg, 0.24 mmol), cyclohexanone (0.3 ml), and concd sulfuric acid (*ca.* 40 mg) in dry benzene (1.5 ml) was stirred at room temperature for 1.5 h and then treated in a manner similar to that described for the synthesis of **15** from **13a**, thus giving **16** (75 mg, 95%) as a syrup: $[\alpha]_D^{26}$ +1.4° (*c* 1.2, $CHCl_3$). IR (neat): no OH absorption. MS: *m/e* 324 (M^+). ^1H NMR ($CDCl_3$): δ 1.1—2.0 (20H, m, CH_2 of the cyclohexylidene groups), 2.0—2.4 (2H, m, H-3a and H-3b), 3.6—4.3 (4H, m), 4.72 (1H, m) 5.80 (1H, d, $J_{1,2}$=3.7 Hz, H-1).

Found: C, 66.64; H, 8.67%. Calcd for $C_{18}H_{28}O_5$: C, 66.64; H, 8.70%.

*From **18a***: The sugar derivative (**18**,[14] 500 mg, 2 mmol) was treated with Dowex 50W-X8 (H^+ form, 4 ml) at room temperature for 20 h in a manner similar to that described for the synthesis of **15** from **17** to yield a syrupy product (300 mg) after chromatography. This product (100 mg) was treated with cyclohexanone (0.35 ml) in dry benzene (1.5 ml) in the persence of concd sulfuric acid at 70 °C (bath temperature) for 5 min. Subsequent reduction with sodium borohydride, followed by column chromatography, gave analyticaly pure **16** (104 mg, 49% from **18**). The physical properties (IR, ^1H NMR, and the specific rotation) of this product were identical with those of a specimen prepared from **14a**.

*The Dimer (**19**).* To a stirred solution of **3a** (352 mg, 1 mmol) in a mixture of ether (10 ml) and benzene (10 ml) we added, drop by drop, a solution of *t*-BuMgBr (6 mmol) in a mixture of ether (10 ml) and benzene (5 ml) at room temperature under a dry nitrogen atmosphere over a period of 1 h; the mixture was then stirred for another 1 h. After cooling, cold aqueous ammonium chloride was added and the mixture was extracted with ether. The extract was washed with water, dried ($MgSO_4$), and concentrated. The residue was chromatographed on a silica-gel column with hexane–ether (6:4) to give **19** (143 mg, 56%) as crystals. An analytically pure sample was obtained by recrystallization from hexane–benzene: mp 151—153 °C; $[\alpha]_D^{20}$ −49.6° (*c* 0.8, $CHCl_3$). IR (KBr): 3480 (OH), 1773 (C=O) cm^{-1}. MS: *m/e* 512 (M^+). ^1H NMR ($CDCl_3$): δ 1.1—1.9 (20H, m, CH_2 of the cyclohexylidene groups), 1.90 (1H, m, H-3a), 2.53 (1H, m, H-3b), 2.65 (1H, d, $J_{3',4'}$=3.0 Hz, H-3′), 2.83 (1H, br s, OH), 3.41 and 3.43 (each 3H, s, OCH_3), 3.6—4.3 (7H, m), 4.3—4.6 (1H, m, H-4′), 4.68 and 5.31 (each 1H, s, H-1 and H-1′).

Found: C, 61.08; H, 7.71%. Calcd for $C_{26}H_{40}O_5$: C, 60.92; H, 7.87%.

*The Dimer (**20**).* *From **3a***: To a refluxing suspension of **3a** (1.06 mg, 3 mmol) in ether (25 ml) we added, drop by drop, a solution of MeMgI (12 mmol) in ether (20 ml) under a dry nitrogen atmosphere over a period of 1 h. The mixture was further refluxed for another 10 min and then treated with aqueous ammonium chloride and extracted with chloroform. The extract was washed with water, dried ($MgSO_4$), and concentrated. The resulting crystalline products were triturated with a small amount of hexane. The undissolved crystals were collected by filtration, washed with cold hexane, and dried.

The hexane-insoluble crystals were recrystallized from benzene to give **20** (350 mg. 44%) as crystals. An analytically pure sample was obtained by silica-gel column chromatography with chloroform–ether (9:1): mp 155—156 °C; $[\alpha]_D^{25}$ −83.2° (*c* 1, $CHCl_3$). IR (KBr): 3460 (OH) cm^{-1}. MS: *m/e* 528 (M^+). ^1H NMR ($CDCl_3$): δ 1.2—1.9 (20H, m, CH_2 of the cyclohexylidene groups), 1.36 (3H, s, C-CH_3), 1.76 (1H, q, $J_{3a,3b}$=12.0 Hz, $J_{3a,4}$=7.8 Hz, H-3a), 2.22 (1H, d, $J_{3a',4'}$=4.0 Hz, H-3a′), 2.92 (1H, q, $J_{3a,3b}$=12 Hz, $J_{3b,4}$=6.4 Hz, H-3b), 3.30 and 3.44 (each 3H, s, OCH_3), 3.8—4.5 (8H, m), 4.58 and 5.10 (each 1H, s, H-1 and H-1′).

Found: C, 61.53; H, 8.19%. Calcd for $C_{27}H_{44}O_{10}$: C, 61.34; H, 8.39%.

The mother liquor, from which **20** had been isolated, was concentrated, and the residue was chromatographed on a silica-gel column with chloroform–ether (9:1), thus giving **19** (26 mg, 3%).

The hexane-soluble material was chromatographed on a silica-gel column with hexane–ether (4:6) to afford **6a** (240 mg, 29%).

*From **19***. The dimer (**19**, 50 mg, 0.098 mmol) was added to a stirred solution of MeMgI (1 mmol) in ether (4 ml) at room temperature under a dry nitrogen atmosphere, after which the mixture was stirred for 30 min. After cooling, cold aqueous ammonium chloride was added, and the mixture was extracted with chloroform. The extract was washed with water, dried ($MgSO_4$), and concentrated. The residue was chromatographed on a silica-gel column with chloroform–methanol (99.5:0.5) to give **20** (45 mg, 87%). The

IR spectrum of this material was completely identical with that of a sample prepared from **3a**.

We wish to thank Dr. Haruo Homma and his staff for the elemental analyses, Dr. Jun Uzawa and Mrs. Tamiko Chijimatsu for measuring the NMR spectra, and Mr. Yasuaki Ezumi and Miss Kyoko Sugita for their measurment of the mass spectra. We are also grateful to Drs. Hiroyoshi Kuzuhara and Hiroshi Ohrui for their valuable discussions.

References

1) Portions of this work have been reported at (a) the 32nd National Meeting of the Chemical Society of Japan, Tokyo, April 1975, Abstr. III., p. 1724, and (b) the 9th International Symposium of Carbohydrate Chemistry, London, April 1978, Abstr. p. 111.

2) F. Shafizadeh, "Advances in Carbohydrate Chemistry," ed by M. L. Wolfrom and R. S. Tipson, Academic Press, New York (1956), Vol. 11, p. 263; S. Hanessian, *ibid.*, (1966), Vol. 21, p. 143; J. S. Brimacombe, *Angew. Chem.*, **81**, 415 (1969).

3) M. Kawana and S. Emoto, *Tetrahedron Lett.*, **1975**, 3395; M. Kawana and S. Emoto, *Chem. Lett.*, **1977**, 597.

4) (a) M. Kawana, H. Ohrui, and S. Emoto, *Bull. Chem. Soc. Jpn.*, **41**, 2199 (1968); (b) K. James, A. R. Tatchell, and P. K. Ray, *J. Chem. Soc., C*, **1967**, 2681.

5) A. N. de Belder, "Advances in Carbohydrate Chemistry and Biochemistry," ed by R. S. Tipson and D. Horton, Academic Press, New York (1977), Vol 34, p. 179.

6) The configurational relations among H_{3a}, H_{3b}, and H_4 in the sugars obtained are the same as those among the corresponding protons in Fig. 2.

7) C. D. Jardetzky, *J. Am. Chem. Soc.*, **84**, 62 (1962).

8) M. Christle, H. J. Reich, and J. D. Roberts, *J. Am. Chem. Soc.*, **93**, 3463 (1971); H. Ohrui, G. H. Jones, J. G. Moffatt, M. L. Maddox, A. T. Christensen, and S. K. Byram, *ibid.*, **97**, 4602 (1975), and the references cited therein,

9) C. S. Hudson, *J. Am. Chem. Soc.*, **31**, 66 (1909); E.L. Eliel, "Stereochemistry of Carbon Compounds," McGraw-Hill Book Co., New York (1962), p. 110.

10) (a) P. A. Stadler, A. J. Frey, and A. Hofmann, *Helv. Chim. Acta*, **46**, 2300 (1963); they quote the results of G. Settimy, H. Weber, and D. Arigoni; (b) E. B. Abbot, E.A. Kidney, and A. McKenzie, *Chem. Ber.*, **71**, 1210 (1938); (c) H. A. Krebs and L. V. Eggleston, *Biochem. J.*, **37**, 334 (1943).

11) J. Salaün and J. M. Conia, *Chem. Commun.*, **1970**, 1358.

12) T. Sasaki, K Minamoto, and K. Hattori, *Tetrahedron*, **30**, 2689 (1974), and the references cited therein; Y. Mizuno, Y. Watanabe, K. Ikeda, and J. A. McCloskey, *Chem. Pharm. Bull.*, **23**, 1411 (1975).

13) D. A. Prins, *J. Am. Chem. Soc.*, **70**, 3955 (1948).

14) E. Vis and P. Karrer, *Helv. Chim. Acta*, **37**, 378 (1954).

15) (a) D. Horton and E. K. Just, *Carbohydr. Res.*, **9**, 129 (1969); (b) J. M. J. Tronchet and M. J. Tronchet, *Helv. Chim. Acta*, **53**, 1174 (1970); (c) P. M. Collins and R. Iyer, *Carbohydr. Res.*, **46**, 277 (1976).

16) D. C. Baker, D. Horton, and C. G. Tindall, Jr., *Carbohydr. Res.*, **24**, 192 (1972).

The Use of Grignard Reagents in the Synthesis of Carbohydrates. II.[1] The Cleavage of Acetal Protecting Groups in Sugar Derivatives

Masajiro KAWANA* and Sakae EMOTO

The Institute of Physical and Chemical Research, Wako-shi, Saitama 351

(Received July 2, 1979)

The selective reaction of acetal protecting groups in sugars with Grignard reagents is described. The treatment of 1,2:5,6-di-*O*-cyclohexylidene-α-D-glucofuranose (**1**) with methylmagnesium iodide in benzene–ether at about 85 °C gave 1,2-*O*-cyclohexylidene-6-*O*-(1-methylcyclohexyl)-α-D-glucofuranose. When isopropylmagnesium iodide or *t*-butylmagnesium bromide was used instead of methylmagnesium iodide, **1** gave 1,2-*O*-cyclohexylidene-6-*O*-(cyclohex-1-enyl)-α-D-glucofuranose and the corresponding 6-*O*-cyclohexyl derivative. The selective cleavage of the acetal protecting groups in some other sugars with the Grignard reagents is also described.

It is considered that acetals are generally stable under Grignard reaction conditions. However, when benzene was used as a solvent, the Grignard reagent formed a complex with the acetal, resulting in the cleavage of the acetal carbon–oxygen bond.[2] For example, the treatment of 1,4-dioxaspiro[4.5]decane (cyclohexanone ethylene acetal) with methylmagnesium iodide (MeMgI) in a benzene solution at 75 °C gave 2-(1-methylcyclohexyloxy)ethanol in a 91% yield.[2a] In the course of our work on the synthesis of sugar derivatives with Grignard reagents, we found that the acetal protecting groups in the sugar derivatives were also cleaved by these reagents to be transformed into *O*-alkyl or -alkenyl protecting groups. Independently, Fischer and Horton[3] have found a similar phenomenon in the carbohydrate field. They treated 1,2:5,6-di-*O*-isopropylidene-α-D-*ribo*-hexofuranos-3-ulose with phenylmagnesium bromide under usual Grignard reaction conditions to obtain two normal Grignard adducts, along with a small amout of the 5,6-*O*-isopropylidene ring-opening product. In this paper we wish to describe our results concerning the cleavage of cyclohexylidene and isopropylidene groups in the sugars with several kinds of Grignard reagents.

When a mixture of 1,2:5,6-di-*O*-cyclohexylidene-α-D-glucofuranose[4] (**1**) and 4 molar equivalent of MeMgI in benzene–ether was heated under reflux at about 85 °C (Method A, Table 1) for 20 h, the 5,6-*O*-cyclohexylidene group of **1** was selectively cleaved and the methyl group of the Grignard reagent was introduced into the cyclohexyl moiety to form 1,2-*O*-cyclohexylidene-6-*O*-(1-methylcyclohexyl)-α-D-glucofuranose (**3**) in a 58% yield (Fig. 1); under these reaction conditions, the ether had very gradually been evaporated through a refluxing condenser. Its reaction time was shortened to about 1 h when the reaction mixture in a flask without a refluxing condenser was heated at the same temperature and the ether was allowed to evaporate (Method B).

The structural assignment of **3** was done on the basis of its elemental analysis and spectral properties (Tables 2 and 3). The ^{1}H NMR spectrum of **3** in dimethyl-d_6 sulfoxide showed a singlet at δ 1.04 due to the methyl protons and two doublets at δ 4.50 and 5.07 due to two secondary hydroxyl protons. The signals due to the methylene protons at C-6 for **3** shifted by *ca.* 0.3 ppm to a higher field than those for **1**. This shift was diagnostic for the *O*-alkylation at C-6 of the aldohexofuranoses prepared in the present work. On the other hand, the chemical shifts and coupling constants of the anomeric and C-2 protons of **3** were

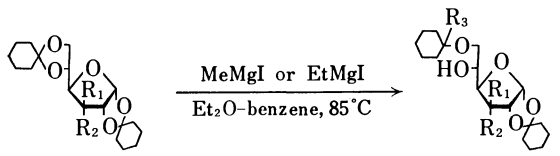

1 : R_1=OH; R_2=H
2 : R_1=H; R_2=OH
3 : R_1=OH; R_2=H; R_3=Me
4 : R_1=OH; R_2=H; R_3=Et
5 : R_1=H; R_2=OH; R_3=Me

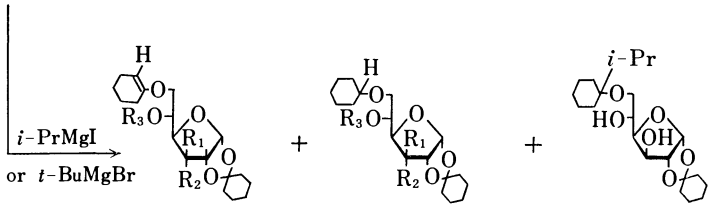

6 : R_1=OH; R_2, R_3=H
7 : R_1=OAc; R_2=H; R_3=Ac
8 : R_1=H; R_2=OH; R_3=H
9 : R_1=OH; R_2, R_3=H
10 : R_1=OAc; R_2=H; R_3=Ac
11 : R_1=H; R_2=OH; R_3=H
12

Fig. 1.

Table 1. The reactions of the sugar derivatives with the Grignard reagents

Starting material (mmol)	Reagent (mmol)	Solvent[a] benzene–ether (ml)	Method[b]	Reaction time h	Product	Yield %	Chromatography[c] benzene–AcOEt (v/v)
1 (2)	MeMgI (8)	10—10	A	20	**3**	58	($CHCl_3$)
1 (1)	MeMgI (4)	15—5	B	1.25	**3**	67	($CHCl_3$)
1 (1)	EtMgI (4)	15—5	B	1.4	**4**	67	8 : 2
1 (2)	*i*-PrMgI (8)	30—10	B	1.3	**6** / **9** / **12**	60 / 11 / 8	7 : 3
1 (1)	*t*-BuMgBr (8)	15—10	B	0.6	**6**[d]	(87)	—
2 (2)	MeMgI (8)	10—10	A	6.8	**5**	75	($CHCl_3$)
2 (1)	MeMgI (4)	15—5	B	0.5	**5**	84	85 : 15
2 (1)	*i*-PrMgI (4)	15—5	B	0.7	**8** / **11**	53 / 14	8 : 2
2 (1)	*t*-BuMgBr (16)	30—20	B	0.3	**11**	92	7 : 3
13 (3)	MeMgI (12)	10—10	A	6	**15**	79	8 : 2
13 (1)	MeMgI (4)	15—5	B	1.2	**15**	54	7 : 3
14 (3)	MeMgI (12)	10—10	A	3.8	**16**	54	1 : 1
14 (1)	MeMgI (4)	15—5	B	0.2	**16**	56	1 : 1
17 (1)	MeMgI (4)	5—5	A	3	**19**	73	8 : 2
18 (0.19)	MeMgI (1.6)	5—5	A	4	**20**	64	9 : 1
21 (3)	MeMgI (12)	10—10	A	20	**22**	58	9 : 1
21 (2)	*i*-PrMgI (8)	10—20	B	1.75	**23a** / **24a**	52 / 22	8 : 2
21 (1)	*t*-BuMgBr (8)	20—10	B	2	**23a** / **24a**	21 / 71	8 : 2

a) Anhydrous solvents were used. b) A: A reaction mixture in a flask equipped with a condenser was refluxed at 80—85 °C for the given reaction time. B: A reaction mixture was heated at the same temperature without a refluxing condenser to remove the ether by distillation. c) Crude products were purified by chromatography on a silica-gel column with the given solvent system. d) This product was not isolated, acetylated to **7** (see Experimental).

almost the same as those for **1**, thus indicating that the 1,2-*O*-cyclohexylidene moiety of **1** was unchanged in this product. These observations were consistent with the proposed structure for **3**.

The reaction of **1** with ethylmagnesium iodide similarly gave a 1-ethylcyclohexyl derivative (**4**). Using isopropylmagnesium iodide (*i*-PrMgI), however, we obtained 6-*O*-cyclohexenyl and -cyclohexyl[5] derivatives (**6** and **9**) in 60 and 11% yields respectively, along with a small amount of a 6-*O*-(1-isopropylcyclohexyl) derivative (**12**).

The compound (**6**), with the enol group, could not be purified because of its instability at room temperature. When *t*-butylmagnesium bromide (*t*-BuMgBr) was used in this reaction, **6** was also produced; it was later acetylated to give the corresponding diacetyl derivative (**7**) in an 87% overall yield. The ^1H NMR spectrum of **7** showed a multiplet at δ 4.60 due to a vinyl proton at C-2′. On catalytic hydrogenation, **7** was converted into 3,5-di-*O*-acetyl-6-*O*-cyclohexyl-1,2-*O*-cyclohexylidene-α-D-glucofuranose (**10**), which was identical with the specimen prepared from **9** by acetylation.

Similarly, 1,2:5,6-di-*O*-cyclohexylidene-α-D-allofuranose[6] (**2**) reacted with MeMgI to yield a 6-*O*-(1-methylcyclohexyl) derivative (**5**). When **2** was treated with *i*-PrMgI, a 6-*O*-cyclohexenyl derivative (**8**) was obtained in a good yield as crystals, which could be purified by recrystallization.

The formation of 6-*O*-alkyl and -alkenyl derivatives can be explained by means of a postulated intermediacy (**A**), which involves a cyclohexyl cation[2b] formed

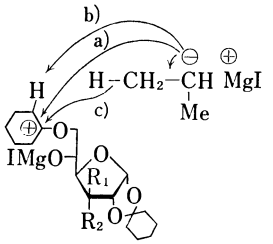

A

by the ring-opening of the 5,6-*O*-cyclohexylidene group. The attack of the alkyl anion of the Grignard reagent on the center of this cation (Path a) gave the 1-alkylcyclohexyl derivatives (**3**—**5** and **12**). When a sterically bulky reagent, such as *i*-PrMgI or *t*-BuMgBr, was used in this reaction, the direct attack of the bulky alkyl group of this reagent on the center of the cyclohexyl cation was largely prevented, so that the abstraction of a proton α to the cation (Path b) and the reduction of this cation (Path c) by the reagent preferably occurred to afford the cyclohexenyl compounds (**6** and **8**) and the cyclohexyl compounds (**9** and **11**) respectively.

The isopropylidene groups also reacted with the Grignard reagents. Thus, the treatment of 1,2:5,6-

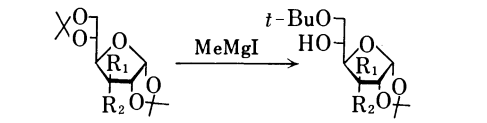

13 : R_1=OH; R_2=H 15 : R_1=OH; R_2=H
14 : R_1=H; R_2=OH 16 : R_1=H; R_2=OH

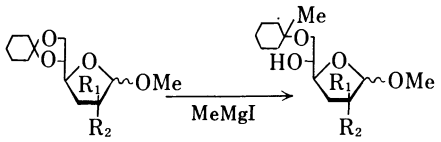

17 : R_1=OH; R_2=Me; (β) 19 : R_1=OH; R_2=Me; (β)
18 : R_1=Me; R_2=OH; (α) 20 : R_1=Me; R_2=OH; (α)

Fig. 2.

di-*O*-isopropylidene-α-D-gluco-[7] and -allofuranose[8] (**13** and **14**) with MeMgI gave the corresponding 6-*O*-*t*-butyl derivatives (**15** and **16** respectively) (Fig. 2). Here again, the 1,2-*O*-isopropylidene group remained intact, but the one at the 5,6-position was selectively cleaved, while the secondary hydroxyl group at C-5 was freed. This selectivity was the same as that observed by Fischer and Horton.[3]

Branched-chain deoxy sugars, [1a,9] methyl 5,6-*O*-cyclohexylidene-3-deoxy-2-*C*-methyl-β-D-*arabino*-hexofuranoside (**17**), and the corresponding α-D-*ribo* isomer (**18**) yielded, upon treatment with MeMgI, the corresponding 6-*O*-(1-methylcyclohexyl) derivatives, **19** and **20** respectively.

The same reaction was applied to an acetal protecting aldopentose; 1,2:3,5-di-*O*-cyclohexylidene-α-D-xylofuranose[10] (**21**) reacted with MeMgI to give 1,2-*O*-cyclohexylidene-3-*O*-(1-methylcyclohexyl)-α-D-xylofuranose (**22**) in a 58% yield (Fig. 3). The cleavage of the carbon–oxygen bond between O-5 and the cyclohexyl carbon in **21** was confirmed by means of ^{1}H NMR spectroscopy. On the treatment of **21** with *i*-PrMgI, 3-*O*-(cyclohex-1-enyl)-1,2-*O*-cyclohexylidene-α-D-xylofuranose (**23a**) was obtained as the main product (52%), but with *t*-BuMgBr the corresponding 3-*O*-cyclohexyl derivative (**24a**) was the major one (71%). The former product was characterized as its acetate (**23b**); thus, it was hydrogenated to give 5-*O*-acetyl-3-*O*-cyclohexyl-1,2-*O*-cyclohexylidene-α-D-xylofuranose (**24b**), which was identical with the sample prepared by the acetylation of **24a**.

In all cases of the aldohexofuranoses tested in the present experiments, their 5,6-*O*-acetal protecting groups were selectively cleaved and the secondary hydroxyl groups at C-5 were selectively freed. The latter selectivity is, however, different from that observed for the previously reported experiments with a steroidal derivative (**25**), in which the acetal ring was opened to form the primary hydroxyl group.[2b] It has been assumed that, in this case, the Grignard reagent would predominantly attack the sterically less hindered primary hydroxyl oxygen of the acetal ring. This is the case for the reaction of the pentofuranose (**21**). One possible explanation for the observed selectivity in the hexofuranose is as follows.

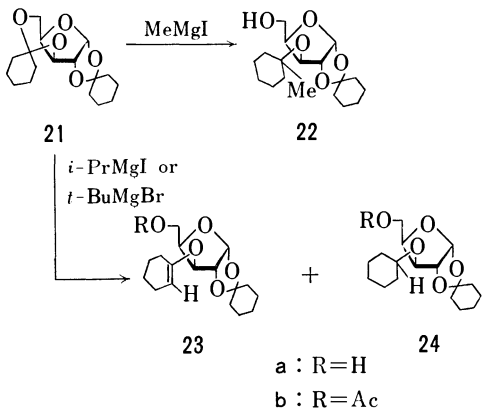

Fig. 3.

The magnesium atom of the Grignard reagent would be coordinated with both oxygen atoms of C-5 and the furanose ring (see **26**);[11] these oxygens were, therefore, activated to cleave the bond between O-5 and the cyclohexyl carbon in this case.[12] The same chelation as in **26** would also be possible for **21** to explain the observed selectivity.

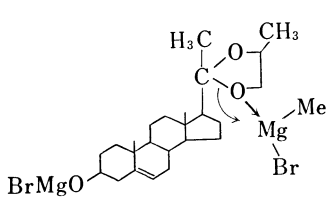

25

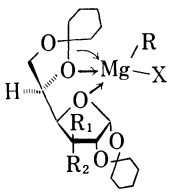

26

Experimental

The melting points are uncorrected. The optical rotations were determined with a Perkin-Elmer 241 MC polarimeter. The IR spectra were recorded on a Shimadzu IR-27 instrument. The mass spectra were obtained with a Japan Optics Lab. Model JMS-OlSG instrument. The ^{1}H NMR spectra were recorded on a Varian HA-100D apparatus, with tetramethylsilane as the internal standerd. Merck silica gel GF_{254} was used for the TLC, and the compounds were detected by heating after spraying them with a methanol–sulfuric acid–*p*-methoxylbenzaldehyde (85:10:5, v/v) mixture. Merck silica gel 60 (0.063—0.29 mm) was used for column chromatography. The elemental analyses were performed by this Institute.

The results of the elemental analysis and the physical properties of the compounds obtained are summarized in Tables 2 and 3.

General Method for the Reaction of the Acetal Protecting Sugars with the Grignard Reagents. Some of the reaction conditions are described in Table 1. A crystalline sugar derivative or a solution of a syrupy sugar derivative in a small amount of dry benzene was added to a solution of the Grignard reagent in dry benzene–ether in a flask equipped with a condenser (Method A) or without a condenser (Method B) at room temperature under a dry nitrogen atmosphere. The mixture was then heated at 80—85 °C (bath temperature) for a given period; in the case of Method B, the ether was distilled out. After cooling, aqueous ammonium chloride was added, and the mixture was extracted with ether. The extract was washed with water, dried ($MgSO_4$), and con-

Table 2. The spectral data (MS, IR, and ^{1}H NMR) of the products

Product	MS, *m/e* (M^+)	IR(neat) (cm^{-1})	^{1}H NMR (δ)
3	356	—	DMSO-d_6: 1.04(3H, s, CH_3), 1.0—1.9(20H, m, cyclohexane ring protons), 3.1—3.5(2H, m, H-6), 4.36(1H, d, J=3.8 Hz, H-2), 4.50(1H, d, J=6.4 Hz, OH), 5.07(1H, d, J=4.4 Hz, OH), 5.79(1H, d, J=3.8 Hz, H-1)
4	370	—	$CDCl_3$: 0.82(3H, t, J=7.2 Hz, CH_3), 1.0—1.2(22H, m, cyclohexane ring protons and $CH_3C\underline{H}_2$), 3.3—3.7 (2H, m, H-6), 4.53(1H, d, J=4.0 Hz, H-2), 5.97 (1H, d, J=4.0 Hz, H-1)
5	356	—	DMSO-d_6: 1.04(3H, s, CH_3), 1.1—1.2(20H, m, cyclohexane ring protons), 3.1—3.5(2H, m, H-6), 4.44(1H, t, J=4.0 Hz, H-2), 4.64(1H, d, J=5.0 Hz, OH), 4.69(1H, d, J=6.4 Hz, OH), 5.65(1H, d, J=4.0 Hz, H-1)
6	—	1672 (C=C)	$CDCl_3$: 1.2—2.2(18H, m, CH_2 of cyclohexane and cyclohexene rings), 3.16(1H, br d, J=3.6 Hz, OH), 3.54 (1H, br s, OH), 4.52(1H, d, J=3.7 Hz, H-2), 4.68 (1H, m, vinyl proton), 5.96(1H, d, J=3.7 Hz, H-1)
7	427	1755 (C=O) 1672 (C=C)	$CDCl_3$: 1.2—2.2(18H, m, CH_2 of cyclohexane and cyclohexene rings), 2.00 and 2.04(3H, each s, CH_3), 3.82 and 3.95(1H, each q, H-6), 4.48(1H, d, J=4.0 Hz, H-2), 4.60(2H, m, H-4 and vinyl proton), 5.22(1H, m, H-5), 5.38(1H, d, J=2.6 Hz, H-3), 5.92(1H, d, J=4.0 Hz, H-1)
8	340	1668[b] (C=C)	$CDCl_3$: 1.2—2.3(18H, m, CH_2 of cyclohexane and cyclohexene rings), 2.54(1H, d, J=3.3 Hz, OH), 2.76 (1H, d, J=8.6 Hz, OH), 4.5—4.8(2H, m, H-2 and vinyl proton), 5.81 (1H, d, J=4.0 Hz, H-1)
9	342	—	DMSO-d_6: 1.0—1.2(20H, m, CH_2 of cyclohexane ring), 3.1—3.7(3H, m, H-6 and CH of cyclohexane ring), 4.36 (1H, d, J=3.6 Hz, H-2), 4.62(1H, d, J=5.6 Hz, OH), 5.07(1H, d, J=4.8 Hz, OH), 5.79(1H, d, J= 3.6 Hz, H-1)
10	426	1743[b] (C=O)	$CDCl_3$: 1.0—2.0(20H, m, CH_2 of cyclohexane ring), 2.00 and 2.02(3H, each s, CH_3), 3.3(1H, m, CH of cyclohexane ring), 3.62 and 3.79(1H, each q, H-6), 4.46(1H, d, J=3.7 Hz, H-2), 5.1(1H, m, H-5), 4.37 (1H, d, J=2.6 Hz, H-3), 5.92(1H, d, J=3.7 Hz, H-1)
11	342	—	$CDCl_3$: 1.0—2.1(20H, m, CH_2 of cyclohexane rings), 1.69 (1H, d, J=3.8 Hz, OH), 3.34(1H, m, CH of cyclohexane ring), 3.44(1H, d, J=6.2 Hz, OH), 3.64(2H, m, H-6), 4.62(1H, t, J=4.0 Hz, H-2), 5.78(1H, d, J=4.0 Hz, H-1)
12	342	—	$CDCl_3$: 0.86(6H, d, J=6.6 Hz, $CH_3\times2$), 1.0—1.1(21H, m, CH_2 of cyclohexane rings and CH of isopropyl group), 3.23(1H, br d, J=3 Hz, OH), 3.3—3.36(2H, m, H-6), 3.78(1H, br d, J=3 Hz, OH), 4.52(1H, d, J=3.7 Hz, H-2), 5.96(1H, d, J=3.7 Hz, H-1)
15	261[a]	—	DMSO-d_6: 1.11(9H, s, *t*-butyl protons), 1.22 and 1.36(3H, each s, isopropylidene protons), 3.1—3.6(2H, m, H-6), 4.36(1H, d, J=4.0 Hz, H-2), 4.52(1H, d, J=5.5 Hz, OH), 5.06(1H, d, J=4.8 Hz, OH), 5.78(1H, d, J=4.0 Hz, H-1)

TABLE 2. Continued

Product	MS, *m/e* (M^+)	IR(neat) (cm^{-1})	^1H NMR (δ)
16	261[a]	—	DMSO-d_6: 1.11(9H, s, *t*-butyl protons), 1.26 and 1.44(3H, each s, isopropylidene protons), 3.14—3.54(2H, m, H-6), 4.45(1H, t, J=4.0 Hz, H-2), 4.65(1H, d, J=4.8 Hz, OH), 4.74(1H, d, J=7.2 Hz, OH), 5.64(1H, d, J=4.0 Hz, H-1)
19	288	—	DMSO-d_6: 1.05 and 1.16(3H, each s, CH_3), 1.1—2.1(12H, m, H-3 and CH_2 of cyclohexane ring), 2.0—3.6(3H, m, H-6 and H-5), 3.27(3H, s, CH_3), 3.85(1H, br q, H-4), 4.23(1H, s, H-1), 4.41(1H, d, J=5 Hz, OH at C-5), 4.43(1H, s, OH at C-2)
20	288	—	$CDCl_3$: 1.09(3H, s, CH_3 at C-1'), 1.34(3H, s, CH_3 at C-2), 2.0(2H, m, H-3), 2.54(1H, d, J=4.0 Hz, OH at C-5), 2.94(1H, s, OH at C-2), 3.2—3.4(2H, m, H-6), 3.44(3H, s, OCH_3), 3.72(1H, m, H-5), 4.2 (1H, m, H-4), 4.50(1H, s, H-1)
22	326	—	DMSO-d_6: 1.0—1.9(20H, m, CH_2 of cyclohexane rings), 1.13 (3H, s, CH_3), 4.41(1H, d, J=4.0 Hz, H-2), 4.51 (1H, t, J=5.6 Hz, OH), 5.79(1H, d, J=4.0 Hz, H-1)
23a	—	1673 (C=C)	DMSO-d_6: 1.0—2.2(18H, m, CH_2 of cyclohexane and cyclohexene rings), 3.58(2H, m, H-5), 4.47(1H, d, J= 4.0 Hz, H-2), 4.65(1H, t, J=5.6 Hz, OH), 4.75(1H, m, vinyl proton), 5.82(1H, d, J=4.0 Hz, H-1)
23b	352	1745 (C=O) 1670 (C=C)	$CDCl_3$: 1.1—2.2(18H, m, CH_2 of cyclohexane and cyclohexene rings), 2.08(3H, s, CH_3), 4.55(1H, d, J= 4.0 Hz, H-2), 4.78(1H, br t, vinyl proton), 5.95(1H, d, J=4.0 Hz, H-1)
24a	312	—	DMSO-d_6: 1.0—1.9(20H, m, CH_2 of cyclohexane rings), 3.37 (1H, m, CH of cyclohexane ring), 4.44(1H, d, J= 4.0 Hz, H-2), 4.56(1H, t, J=5.6 Hz, OH), 5.80(1H, d, J=4.0 Hz, H-1)
24b	354	1744 (C=O)	$CDCl_3$: 1.2—2.0(20H, m, CH_2 of cyclohexane rings), 2.08 (3H, s, CH_3), 3.34(1H, br s, CH of cyclohexane ring), 3.98(1H, d, J=2.8 Hz, H-3), 4.45(1H, d, J= 3.8 Hz, H-2), 5.93(1H, d, J=3.8 Hz, H-1)

a) M^+-CH_3. b) KBr.

centrated. The crude product was purified by silica-gel column chromatography using a given solvent system.

3,5-Di-O-acetyl-6-O-(cyclohex-1-enyl)-1,2-O-cyclohexylidene-α-D-glucofuranose (7). A powdered sugar derivative (**1**,[4] 340 mg, 1 mmol) was stirred into a solution of MeMgI (8 mmol) in benzene (15 ml)–ether (10 ml) under a dry nitrogen atmosphere, after which the mixture was heated at 80—85 °C (bath temperature) for 35 min to remove the ether. After the mixture had been cooled, dry pyridine (0.2 ml) was added, followed by the addition of aqueous ammonium chloride. The mixture was then extracted with ether. The extract was washed with water, dried ($MgSO_4$), and concentrated below 35 °C *in vacuo*. The water was removed by co-evaporation with benzene below 35 °C *in vacuo*. The residue was then taken up in dry pyridine (5 ml) and cooled to about 5 °C. To this cold solution, we added acetic anhydride (1.5 ml), after which the mixture was stirred at room temperature for 6 h. After the usual work-up, the mixture was extracted with ether. The extract was washed with water, dried ($MgSO_4$), and concentrated. The pyridine was removed by co-evaporation with xylene. The residue was chromatographed on a silica-gel column with benzene–ethyl acetate (9:1) to give **7** (370 mg, 87%).

3,5-Di-O-acetyl-6-O-cyclohexyl-1,2-O-cyclohexylidene-α-D-glucofuranose (10). *From* ***9***: Acetic anhydride (0.3 ml) was added to a cold (0—5 °C) solution of **9** (95 mg, 0.28 mmol) in dry pyridine (1 ml), and the mixture was stirred at room temperature overnight. The usual work-up gave a crude product, which was chromatographed on a silica-gel column with benzene–ethyl acetate (9:1) to give **10** (112 mg, 95%) as crystals.

From ***7***: The sugar derivative (**7**, 130 mg, 0.3 mmol) was hydrogenated in methanol (20 ml) in the presence of 10% Pd on charcoal (80 mg) with a Parr apparatus at 2.8 kg/cm^2 at room temperature for 7 h. The catalyst was removed by filtration through a Celite pad and washed with methanol. The combined filtrate and washings were concentrated below 35 °C. The residue was chromatographed on a silica-gel column with benzene–ethyl acetate (95:5) to give **10** (80 mg, 61%) as crystals. The physical properties (mp, IR, MS,

Table 3. The physical properties and elemental analyses of the products

Compound	Mp °C	$[\alpha]_D$ (c, $CHCl_3$)	Temp/°C	Formula	Found (%) C	Found (%) H	Calcd (%) C	Calcd (%) H
3	92—93[a]	+1.1° (1.0)	22	$C_{19}H_{32}O_6$	63.90	8.92	64.02	9.05
4	syrup	−1.4° (1.0)	21	$C_{20}H_{34}O_6$	64.92	9.31	64.84	9.25
5	78—80[b]	+33.2° (1.0)	22	$C_{19}H_{32}O_6$	64.06	8.97	64.02	9.05
7	syrup	+0.5° (2.2)	24	$C_{22}H_{32}O_8$	62.31	7.61	62.25	7.60
8	122—124[c]	+41.8° (1.1)	24	$C_{18}H_{28}O_6$	63.57	8.18	63.51	8.29
9	syrup	−5.1° (0.95)[e]	21	$C_{18}H_{30}O_6$	63.14	8.83	63.13	8.83
10	79—81	+6.6° (1.2)	25	$C_{22}H_{34}O_8$	61.93	8.01	61.95	8.04
11	93.0—94.5[d]	+37.3° (0.8)	24	$C_{18}H_{30}O_6$	63.18	8.85	63.13	8.83
12	syrup	−2.2° (0.9)	21	$C_{21}H_{36}O_6$	65.70	9.43	65.59	9.44
15	79—80[b]	−6.4° (1.0)	22	$C_{13}H_{24}O_6$	56.40	8.50	56.50	8.76
16	80.5—81.5[a]	+30.7° (1.0)	22	$C_{13}H_{24}O_6$	56.51	8.66	56.50	8.76
19	syrup	−66.5° (1.1)	23	$C_{15}H_{28}O_5$	62.51	9.61	62.47	9.79
20	syrup	+67.3° (1.2)	18	$C_{15}H_{28}O_5$	62.50	9.76	62.47	9.79
22	syrup	−10.5° (0.3)	20	$C_{18}H_{30}O_5$	66.25	9.20	66.23	9.26
23b	syrup	−12.3° (0.95)	23	$C_{19}H_{28}O_6$	64.63	7.85	64.75	8.01
24a	syrup	−31.7° (1.2)	25	$C_{17}H_{28}O_5$	65.35	9.18	65.36	9.03
24b	syrup	−17.6° (1.0)	23	$C_{19}H_{30}O_6$	64.60	8.52	64.38	8.53

a) Recrystallization from hexane. b) Diisopropyl ether. c) Benzene. d) Benzene–hexane. e) The solvent was ethanol: lit, Ref. 5, $[\alpha]_D^{25}$ −3.7° (c 0.5, EtOH).

and ^1H NMR) of this product were identical with those of the sample prepared from **9**.

*5-O-Acetyl-3-O-(cyclohex-1-enyl)-1,2-O-cyclohexylidene-α-D-xylofuranose (**23b**).* Acetic anhydride (0.3 ml) was added to a cold (0—5 °C) solution of **23a** (140 mg, 0.45 mmol) in dry pyridine (2 ml), and the mixture was stirred at room temperature for 4 h. The usual work-up gave a syrup, which was subsequently chromatographed on a silica-gel column with benzene–ethyl acetate (95:5) to give **23b** (147 mg, 93%) as a syrup.

*5-O-Acetyl-3-O-cyclohexyl-1,2-O-cyclohexylidene-α-D-xylofuranose (**24b**).* *From **24a***: Acetic anhydride (0.3 ml) was added to a cold (0—5 °C) solution of **24a** (220 mg, 0.71 mmol) in dry pyridine (2 ml), after which the mixture was allowed to stand at room temperature overnight. The usual work-up gave a syrup, which was subsequently chromatographed on a silica-gel column with benzene–ethyl acetate (95:5) to give **24b** (245 mg, 95%) as a syrup.

*From **23b***: The sugar derivative (**23b**, 50 mg, 0.14 mmol) was hydrogenated with a Parr apparatus at 3 kg/cm² in methanol (15 ml) in the presence of 10% Pd on charcoal (95 mg) at room temperature for 7 h. The catalyst was removed by filtration through a Celite pad, and washed with methanol. The combined filtrate and washing were concentrated below 35 °C *in vacuo*, and the residue was chromatographed on a silica-gel column with benzene–ethyl acetate (98:2) to afford **24b** (36 mg, 72%) as a syrup. The physical properties (IR and ^1H NMR) of this product was identical with those of the sample prepared from **24a**.

We are indebted to Dr. Haruo Homma and his staff for the elemental analyses, to Dr. Jun Uzawa and Mrs. Tamiko Chijimatsu for measuring the NMR spectra, and to Mr. Yasuaki Ezumi and Miss Kyoko Sugita for their measurement of the mass spectra. Grateful acknowledgment is also made to Drs. Hiroyoshi Kuzuhara and Hiroshi Ohrui for their helpful discussions.

References

1) a) Part 1: M. Kawana and S. Emoto, *Bull. Chem. Soc. Jpn.*, **53**, 222 (1980); b) Portions of this work have been reported at the 36th National Meeting of the Chemical Society of Japan, Osaka, April 1977, Abstr. II, p. 1176, and the 9th International Symposium of Carbohydrate Chemistry, London, April 1978, Abstr. p. 111.

2) a) R. A. Mallory, S. Rovisnki, and I. Scheer, *Proc. Chem. Soc.*, **1964**, 416; b) R. A. Mallory, S. Rovinski, F. Kohen, and I, Scheer, *J. Org. Chem.*, **32**, 1417 (1976), and the references cited therein.

3) J.-C. Fischer and D. Horton, *Carbohydr. Res.*, **59**, 477 (1977).

4) R. C. Hockett, R. E. Miller, and A. Scattergood, *J. Am. Chem. Soc.*, **71**, 3072 (1949).

5) S. S. Bhattacharjee and P. A. J. Gorin, *Can. J. Chem.*, **47**, 1195 (1969).

6) K. James, A. R. Tatchell, and P. K. Ray, *J. Chem. Soc., C*, **1967**, 2681; M. Kawana, H. Ohrui, and S. Emoto, *Bull. Chem. Soc. Jpn.*, **41**, 2199 (1968).

7) W. L. Glen, G. S. Myers, and G. A. Grant, *J. Chem. Soc.*, **1951**, 2568.

8) D. C. Baker, D. Horton, and C. G. Tindall, Jr., *Carbohydr. Res.*, **24**, 192 (1972).

9) M. Kawana and S. Emoto, *Tetrahedron Lett.*, **1975**, 3395.

10) K. Heyns and J. Lenz, *Chem. Ber.*, **94**, 348 (1961).

11) M. L. Wolfrom and S. Hanessian, *J. Org. Chem.*, **27**, 1800 (1962).

12) Recently, we have found an example of the cleavage of the furanose ring with Grignard reagents; M. Kawana and S. Emoto, *Tetrahedron Lett.*, **1978**, 1561.

The Sensitized Photooxidation of Methoxycycloheptatrienes. The Synthesis of α-, β-, and γ-Tropolones[1]

Morio YAGIHARA,[2] (the late) Yoshio KITAHARA, and Toyonobu ASAO*,†

Department of Chemistry, Faculty of Science, Tohoku University, Aramaki Aoba, Sendai 980

† *Department of Chemistry, College of General Education, Tohoku University, Kawauchi, Sendai 980*

(Received July 2, 1979)

The sensitized photooxidation of 7-methoxycycloheptatriene (7-methoxytropilidene) afforded [4+2] cycloadduct (**2**), tropone, benzaldehyde and their 2-methoxy derivatives. Thermal isomerization of **2** followed by the treatment with alumina yielded 4-methoxytropone. The photooxidation of 1-methoxytropilidene gave 4-hydroxytropone and *o*-methoxybenzaldehyde, and the photooxidation of 3-methoxytropilidene followed by the treatment with triethylamine afforded 3-methoxytropone, tropone, and *o*-methoxybenzaldehyde. Characterization of the products and the mechanisms of the reactions are discussed.

Recently, we have reported that the oxidation of cycloheptatriene (tropilidene) by photochemically generated singlet oxygen afforded [4+2] cycloadduct, and other products derived from [6+2] cycloadduct, and that tropone can be efficiently obtained *via* the photooxidation of tropilidene.[3]

Mori and Takeshita have also reported on the photooxidation of tropilidene, methoxytropilidene, and bitropyl sensitized by α-dicarbonyl compounds to isolate [4+2] and [6+2] cycloadducts.[4]

More recently, Adam and Balci have isolated [6+2] cycloadduct and two kinds of [4+2] cycloadducts derived from norcaradiene and cycloheptatirene by the separation of photooxidation product of tropilidene at low temperature.[5]

We have studied the photooxidation of three kinds of methoxytropilidenes to isolate and characterize the oxidation products and to derive to hydroxytropones, especially to 3- and 4-hydroxytropones (β- and γ-tropolones, respectively) which have been prepared with some difficulty. The results are reported in this paper.

Results and Discussion

Photooxidation of 7-Methoxytropilidene. The photooxidation of 7-methoxytropilidene (**1**) was performed in acetone with visible light (60 W×3) at room temperature in the presence of hematoporphyrin as sensitizer, and the products were separated by silica gel chromatography to afford five products; [4+2] cycloadduct (**2**, 40—50%), benzaldehyde (**3**, 10%), *o*-methoxybenzaldehyde (**4**, 5%), tropone (**5**, trace), and 2-methoxytropone (**6**, trace). The compounds (**3**—**6**)

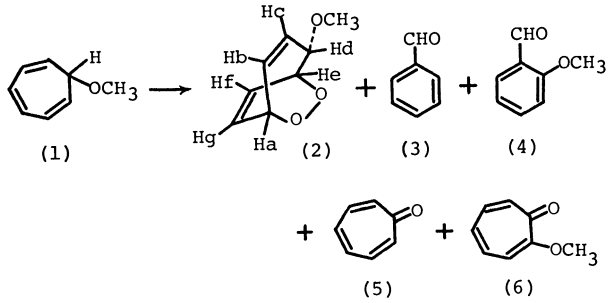

were characterized by direct comparison of their spectroscopic data with those of the authentic samples. The compound (**2**) was obtained as colorless oil, shows a parent ion peak at 154 in the mass spectrum, and strong IR absorption bands (neat) at 1085, 970, and 750 cm^{-1}. ^{1}H-NMR spectrum of **2** in $CDCl_3$ is shown in Fig. 1 and the each signal and coupling constant can be assigned with the help of double resonance

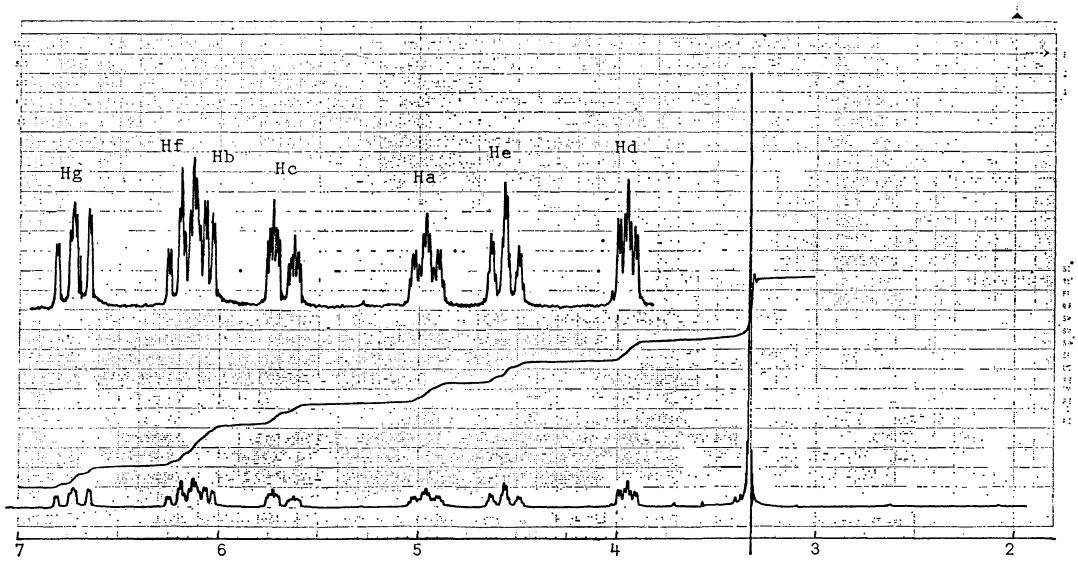

Fig. 1. ^{1}H-NMR spectrum of 2 in $CDCl_3$ (100 MHz).

experiments, and the parameters are shown in Table 1. From these data the structure of the compound (**2**) was determined as [4+2] cycloadduct, 4-methoxy-6,7-dioxabicyclo[3.2.2]nona-2,8-diene, shown in scheme including a stereochemistry of methoxyl group.

We tentatively proposed the mechanisms, involving peroxides and [6+2] cycloadduct as intermediates, of the formation of the products (**3**—**6**) as follows.

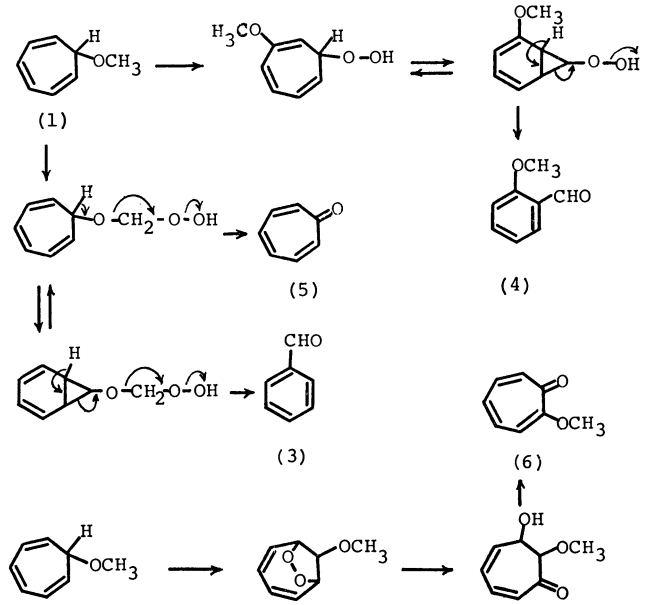

The adduct (**2**) was thermally isomerized in xylene to give 4-hydroxy-5-methoxy-2,6-cycloheptadien-1-one (**7**) in 60% yield, whose structure including a stereochemistry was determined by ^{1}H-NMR spectrum data shown in Table 1. The compound (**7**) is considered to be formed *via* diepoxide (**8**) which could not be isolated in this case.[6] The treatment of **7** with alumina afforded 4-methoxytropone (**9**)[7,8] in 58% yield. Furthermore, the treatment of **2** with triethylamine afforded **7** (34%) and 2-methoxytropone (**6**) (34%).

From these results, it was found that 4-methoxytropone (**9**) can be effectively synthesized in moderate yield starting from 7-methoxytropilidene *via* photooxidation.

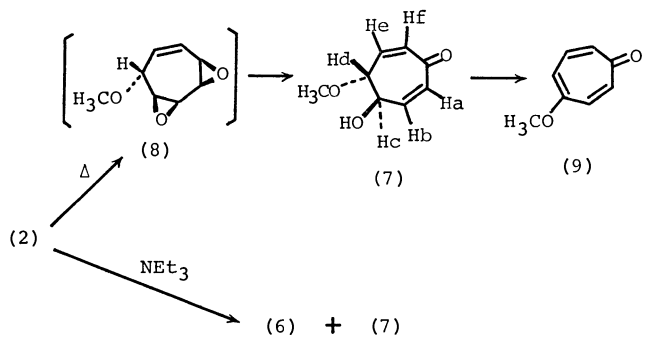

Photooxidation of 1-Methoxytropilidene. The photooxidation of 1-methoxytropilidene (**10**)[9] was performed in a similar manner to 7-methoxytropilidene in acetone in the presence of hematoporphyrin. The removal of the solvent just after the oxidation was completed caused explosion, and no clear product was obtained. However, working up after the solution of the oxidation was allowed to stand at room temperature for a week, gave two products; 4-hydroxytropone (γ-tropolone) (**11**)[7,8] and *o*-methoxybenzaldehyde (**4**) in 34% and 12% yields, respectively by chromatographic separation, and any *endo*-peroxides could not be isolated. The mechanisms of the formation of these compounds were tentatively proposed as follows.

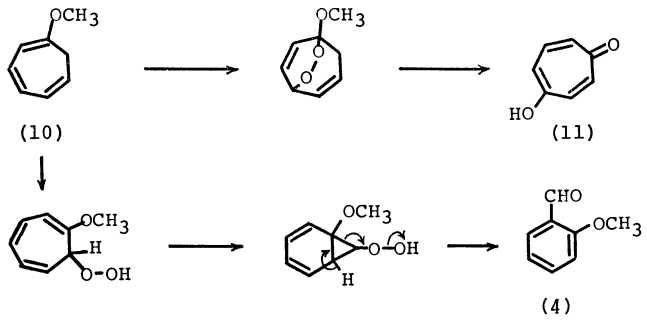

Photooxidation of 3-Methoxytropilidene. The photooxidation of 3-methoxytropilidene[9] in methanol in the presence of Methylene Blue afforded only *o*-methoxybenzaldehyde after the direct separation using silica gel chromatography. However, the treatment of the crude photooxidation products with triethylamine afforded 3-methoxytropone (**13**),[8,10] tropone (**5**), and *o*-methoxybenzaldehyde in 16%, 24%, and 5% yield, respectively. 3-Methoxytropone (**13**) can be easily hydrolyzed by acids to give 3-hydroxytropone (β-tropolone) (**14**).[10a] The mechanism of the formation of the tropones was tentatively considered as follows which involves the formation of [4+2] or [6+2] cycloadduct and peroxide at methoxyl carbon as intermediates.

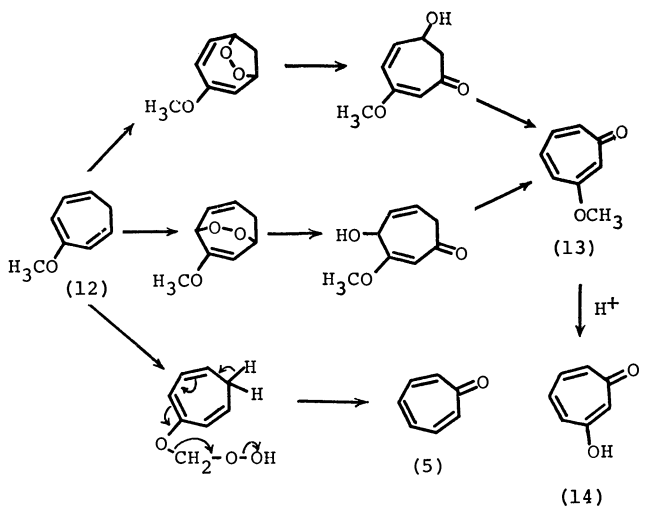

Experimental

The mp values are uncorrected. The IR spectra were recorded with Hitachi EPI 510 and Hitachi 215 grating spectrophotometer. The mass spectra were obtained with Hitachi RMU 60 mass spectrometer. The NMR spectra were recorded on Varian HA-100, A-60, and Hitachi R-20 spectrometers.

TABLE 1. ^{1}H-NMR PARAMETERS OF **2** AND **7**

Compound	^{1}H-NMR parameters (δ values, J in Hz)[a]
2[b]	3.34 (OCH_3), 3.93 (H_d), 4.55 (H_c), 4.96 (H_a), 5.68 (H_e), 6.07 (H_f), 6.18 (H_b), 6.78 (H_g) $J_{ab}=7.0$, $J_{ac}=1.3$, $J_{af}=1.2$, $J_{ag}=7.0$, $J_{bc}=10.5$, $J_{bd}=1.8$, $J_{bg}=0.5$, $J_{cd}=3.5$, $J_{ce}=1.5$, $J_{de}=6.5$, $J_{df}=0.5$, $J_{ef}=7.0$, $J_{eg}=1.1$, $J_{fg}=9.0$
7[c]	2.9 (OH), 3.51 (OCH_3), 3.48, 3.65 (H_c, H_d), 5.92, 5.97 (H_a, H_f), 6.47, 6.50 (H_b, H_e) $J_{ab}=13.0$, $J_{ac}=2.0$, $J_{af}=2.0$, $J_{bc}=2.0$, $J_{cd}=10.5$, $J_{de}=2.0$, $J_{df}=2.0$, $J_{ef}=13.0$

a) Refer the scheme for proton numberings. b) In $CDCl_3$. c) In CCl_4.

Sensitized Photooxidation of 7-Methoxytropilidene. A solution of 7-methoxytropilidene (10.0 g, 0.082 mol) and hematoporphyrin (132 mg) in acetone (400 ml) was irradiated by visible light (60 W×3) for 6 days at below 30 °C by cooling with water while oxygen was slowly passed through the solution. The solvent was removed under reduced pressure, the residue was submitted to column chromatography on silica gel and eluted with chloroform. From the effluents, benzaldehyde (869 mg, 8.2 mmol, 10%), *o*-methoxybenzaldehyde (558 mg, 4.1 mmol, 5%), an adduct (**2**, 5.44 g, 34.3 mmol, 43.5%), tropone (trace), and 2-methoxytropone (trace) were obtained by the order of the effluents. **2**; Colorless oil, IR (neat) 1085, 970, 750 cm^{-1}; MS *m/e* 154 (M^+, 18), 122 (57), 94 (100), 84 (71), 81 (52), 68 (73), 66 (73); Found: C, 62.42; H, 6.46%. Calcd for $C_8H_{10}O_3$: C, 62.32; H, 6.54%.

Thermal Reaction of 2. A solution of **2** (600 mg, 3.9 mmol) in anhydrous xylene (30 ml) was refluxed under nitrogen atmosphere for 15 h. The solvent was removed under reduced pressure, the residue was submitted to column chromatography on silica gel and eluted with chloroform, and keto alcohol (**7**, 360 mg, 2.34 mmol, 60%) was obtained. **7**; Colorless oil, IR (neat) 3450, 1660, 1618 cm^{-1}; MS *m/e* 154 (M^+, 2.9), 122 (47.1), 109 (35.3), 95 (35.3), 94 (100). 2,4-Dinitrophenylhydrazone; reddish crystals, mp 156—157 °C, Found: C, 50.17; H, 4.14; N, 16.71%. Calcd for $C_{14}H_{14}O_6N_4$: C, 50.30; H, 4.22; N, 16.76%.

Treatment of 7 with Alumina. A solution of **7** (200 mg, 1.3 mmol) in chloroform was adsorbed on alumina column (10 g). After 2 h, the column was eluted with ethyl acetate to give 4-methoxytropone (102 mg, 0.75 mmol, 58%), colorless crystals, mp 28—29 °C, which was identified by direct comparison of spectroscopic data with those of the authentic sample.

Reaction of 2 with Triethylamine. A solution of **2** (429 mg, 3.2 mmol) in dichloromethane (30 ml) was refluxed for 25 h in the presence of triethylamine (5 drops). The solvent was removed under reduced pressure, a solution of the residue in chloroform was submitted to chromatography on silica gel and eluted with chloroform–methanol (2%). From the effluents, keto alcohol (**7**, 158 mg, 1.1 mmol, 34.4%) and 2-methoxytropone (138 mg, 1.1 mmol, 34.4%) were obtained.

Sensitized Photooxidation of 1-Methoxytropilidene. A solution of 1-methoxytropilidene (1.0 g, 8.2 mmol) and hematoporphyrin (30 mg) in acetone (100 ml) was photochemically oxidized for 2 days in a similar manner to 7-methoxytropilidene. After the oxidation, the solution was allowed to stand at room temperature for a week. The solvent was removed under reduced pressure and 4-hydroxytropone (**11**, 382 mg, 34.1%), mp 211 °C (dec) was obtained as crystalline substance. The residue was separated by chromatography on silica gel and *o*-methoxybenzaldehyde (137.5 mg, 12.3%) was obtained. 4-Hydroxytropone (**11**) was identified by direct comparison of the physical data with those of the authentic sample.

Photooxidation of 3-Methoxytropilidene. A solution of 3-methoxytropilidene (**12**, 1.0 g, 8.2 mmol) and Methylene Blue (50 mg) in methanol (100 ml) was photochemically oxidized for 2 days in a similar manner to 7-methoxytropilidene. The solvent was removed under reduced pressure. A solution of the residue in methanol (70 ml) was added triethylamine (1.5 ml) and allowed to stand at room temperature for 10 h. The solvent was removed under reduced pressure, the residue was submitted to chromatography on alumina and eluted with chloroform. From the effluents, *o*-methoxybenzaldehyde (55.8 mg, 5%), tropone (213 mg, 24%), and 3-methoxytropone (**13**, 210.5 mg, 16%), colorless oil, were obtained. 3-Methoxytropone (**13**) was identified by the comparison of the spectroscopic data with those of the authentic sample.

References

1) This paper was presented at the National Meeting of Chemical Society of Japan, Tokyo, April, 1975.

2) Present Address; Fuji Photofilm Co., Minami-ashigara, Kanagawa.

3) T. Asao, M. Yagihara, and Y. Kitahara, *Bull. Chem. Soc. Jpn.*, **51**, 2131 (1978).

4) A. Mori and H. Takeshita, *Chem. Lett.*, **1978**, 395.

5) W. Adam and M. Balci, *Angew. Chem., Int. Ed., Engl.*, **17**, 954 (1978).

6) In the similar thermal isomerization of [4+2] cycloadduct of tropilidene and oxygen, diepoxide corresponding to **8** which is assumed to be a primaly product could be isolated as well as keto alcohol corresponding to **7**; Ref. 3.

7) T. Nozoe, T. Mukai, Y. Ikegami, and T. Toda, *Chem. Ind. (London)*, **1955**, 66; O. L. Chapman and P. Fitton, *J. Am. Chem. Soc.*, **85**, 41 (1963); J. Font, F. Serratosa, and J. Valls, *Chem. Commun.*, **1970**, 721.

8) Y. Kitahara, T. Asao, and M. Oda, in "Chemistry of Novel Aromatic Compounds," Kagaku-sosetsu, No. 15, ed by S. Ito, (Chemical Society of Japan), Tokyo University Press, Tokyo (1977) p. 101.

9) T. Nozoe and K. Takahashi, *Bull. Chem. Soc. Jpn.*, **38**, 665 (1965).

10) a) R. B. Johns, A. W. Johnson, and M. Tisler, *J. Chem. Soc.*, **1954**, 4605. b) W. G. Dauben, K. Koch, S. L. Smith, and O. L. Chapman, *J. Am. Chem. Soc.*, **85**, 2615 (1963); A. J. Birch and R. Keeton, *Aust. J. Chem.*, **24**, 331 (1971).

The Temperature Dependence of Carbon-13 Chemical Shifts of Retinal Isomers and Their Related Compounds

Yoshito HANAFUSA, Masakazu TODA, Yoshio INOUE, and Riichiro CHÛJÔ*

Department of Polymer Chemistry, Tokyo Institute of Technology, O-okayama, Meguro-ku, Tokyo 152

(Received April 25, 1979)

The temperature dependence of carbon-13 chemical shifts has been studied for retinal isomers, *N-all-trans*-retinylidenebutylamine(*all-trans*-NRB) and *N-all-trans*-retinylidenebutylammonium chloride(*all-trans*-NRB·HCl). The change in the chemical shift was discussed in terms of the temperature dependences of the polarizability and conformation of the polyene-chain. In 11-*cis*-retinal, the coplanarity between the two parts of polyene-chain separated by the cis bond increases with a lowering of the temperature. The equilibrium between 12-*s*-*cis* and 12-*s*-*trans* conformers in 11-*cis*-retinal was studied and it was shown the latter conformer is preferable at low temperatures. In *all-trans*-NRB and *all-trans*-NRB·HCl, the temperature dependences of the chemical shifts are similar to those in *all-trans*-retinal. The extents of the chemical shift changes are in the following order: NRB·HCl<NRB <retinal. This trend can be correlated with the order of the red shifts of the absorption spectra.

The carotenoid compound, 11-*cis*-retinal, acts as a photoreceptor in a visual system. The primary event in the visual process in vertebrate retinas is the photochemical isomerization of the bound 11-*cis*-retinal to the *all-trans* form (Fig. 1). Other succeeding transformations in the retina are known to occur in the dark.[1,2]

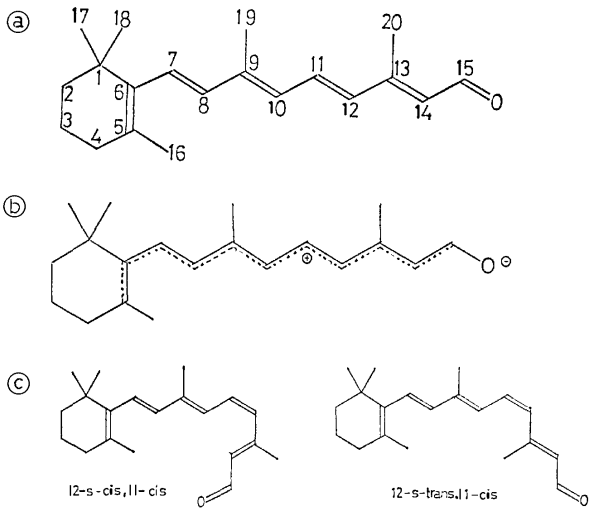

Fig. 1. a) Structural formula of *all-trans*-retinal.
b) Resonance structure of *all-trans*-retinal.
c) Structural formulas of 12-*s*-*cis* and 12-*s*-*trans* conformers in 11-*cis*-retinal.

The conformations of retinal isomers and related compounds have been studied by means of the UV spectra at lower temperatures because of the instability of the transient intermediates in the visual process at ambient temperatures. The absorption maxima of the retinal isomers and their Schiff bases reveal a red (bathochromic) shift upon the lowering of the temperature.[2-4]

The conjugated polyene-chain of 11-*cis*-retinal twists around the C12–C13 single bond as a result of the severe steric hindrance, while that of *all-trans*-retinal is planar. The 11-*cis*-retinal may exist as an equilibrium mixture of distorted 12-*s*-*cis* and 12-*s*-*trans* conformers as is shown in Fig. 1c; this indicates much larger absorption and intensity changes in the UV spectra than in the cases of the other retinal isomers for the same range of temperatures and solvent polarity.[3] Such a conformational equilibrium is a possible key to interpreting the temperature dependence of the spectroscopic parameter in the molecular level. We will study the temperature dependence of the carbon-13 NMR spectra of retinal and its related compounds. Both proton and carbon-13 NMR spectra of these compounds have been widely studied by many including the present authors.[5-10] Rowan *et al.*[7] have investigated the temperature dependence of the proton NMR spectrum of 11-*cis*-retinal; they concluded the 12-*s*-*trans* to be the preferred conformer in the 11-*cis* isomer in acetone at lower temperatures. Since the carbon-13 chemical shift is related to the electron density of the corresponding carbon atom, it makes possible a study of the charge delocalization in conjugated polyene carbons of the retinal Schiff base.[8,10]

In this investigation, the carbon-13 chemical shifts of retinal isomers and their Schiff bases were observed in the temperature range from −50 °C to +30 °C. The temperature dependences of the chemical shifts will be discussed in terms of the changes in the electronic structure. The degree of the delocalization of the positive charge (Fig. 1b) will be related with the conformational changes in the conjugated polyene-chain of 11-*cis*-retinal at lower temperatures. This relation will be used to explain the degree of the red shift of the absorption maximum in the absorption spectra of corresponding compounds at lower temperatures. It has been widely accepted that, in the rhodopsin, a protonated Schiff-base linkage exists between the retinal chromophore and the protein opsin *via* an ε-amino group of the lysin residue.[11] Therefore, the protonated Schiff base with *n*-butylamine was chosen as a pertinent model for the rhodopsin.

Experimental

All of the retinal compounds used were prepared by a procedure described elsewhere.[9]

The UV spectra were observed in methanol with a Beckman-25 spectrometer. The carbon-13 NMR spectra were measured in the dark, using a JNM JEOL PS-100 spectrometer equipped with a PFT-100 Fourier transform system at 25.15 MHz and in the temperature range of −50 °C—+30 °C. The 90°-pulse recycle times were chosen to be at least five times the longest spin-lattice relaxation time of the carbon atoms. The number of accumulations were chosen to be 128—1024. The concentrations of the retinal

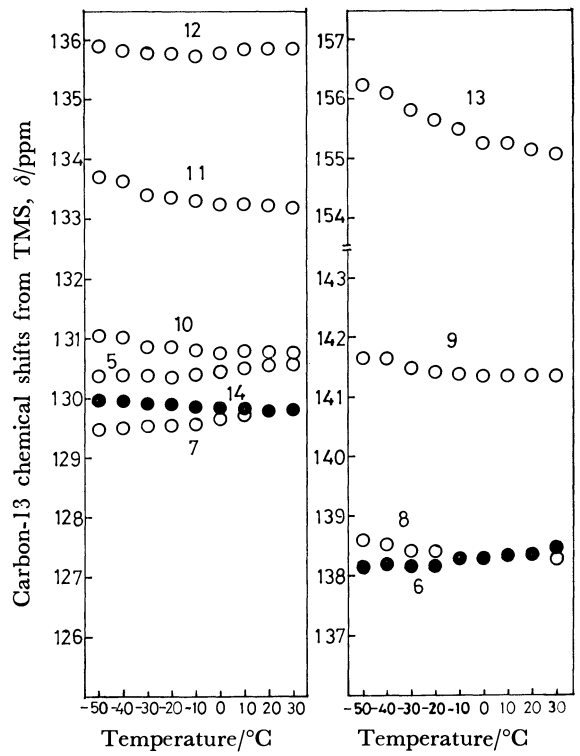

Fig. 2. Temperature dependence of chemical shifts for each of conjugated polyene-chain carbons of *all-trans*-retinal in acetone.

compounds were 0.3—0.5 mol dm^{-3} in a solution of acetone-d_6 and chloroform-*d*. The chemical shifts were expressed in ppm as downfield shifts from internal tetramethylsilane (TMS). The maximum experimental error of the chemical shift was within ±0.06 ppm.

Results

The carbon-13 NMR spectra have been assigned by the use of various techniques shown in previous papers.[6,9,10] Figure 2 shows the temperature dependence of the chemical shift for each of the conjugated polyene-chain carbons in *all-trans*-retinal in an acetone solution. Similar temperature dependences were also obtained for the same isomer in a chloroform solution and for the 11-*cis* isomer in acetone and chloroform solutions. The carbon atoms are numbered as is shown in Fig. 1a; the numbers indicated in Fig. 2 correspond to this numbering.

Tables 1 and 2 are tabulated the chemical shifts at room and lower temperatures and the differences, $\Delta\delta$, between the chemical shifts at these two temperatures for identical carbons. The plus and minus signs in $\Delta\delta$ indicate the downfield and upfield shifts respectively upon a lowering of the temperature. According to the UV analysis[3,4] and solvent theory,[12] the conformational change of the retinal isomer increases with an increase the polarity of the solvent. Therefore, acetone and chloroform were used in this work as representative polar and non polar solvents respectively.

From these two tables, a general trend was observed for downfield shifts to be observed with a lowering of the temperature for the conjugated polyene-chain carbons of both *all-trans*- and 11-*cis*-retinal. This trend

Table 1. The chemical shifts of *all-trans*-retinal and 11-*cis*-retinal temperatures in acetone

Carbon number	*all-trans*-Retinal			11-*cis*-Retinal		
	29 °C	−50 °C	$\Delta\delta$[a]	28 °C	−50 °C	$\Delta\delta$[a]
1	34.82	34.70	−0.12	34.82	34.64	−0.18
2	40.28	39.55	−0.73	40.22	39.61	−0.61
3	19.83	19.65	−0.18	19.83	19.59	−0.24
4	33.61	33.36	−0.25	33.55	33.30	−0.25
5	130.56	130.38	−0.18	130.62	130.32	−0.30
6	138.45	138.14	−0.31	138.26	138.20	−0.06
7	129.77	129.47	−0.30	129.77	129.59	−0.18
8	138.26	138.57	+0.31	138.51	138.81	+0.30
9	141.36	141.66	+0.30	141.66	142.33	+0.67
10	130.74	131.04	+0.30	126.92	127.28	+0.36
11	133.17	133.71	+0.54	131.59	132.44	+0.85
12	135.84	135.90	+0.06	131.59	131.53	−0.06
13	155.07	156.22	+1.15	155.93	156.89	+0.96
14	129.77	129.95	+0.18	130.62	131.04	+0.42
15	191.11	192.20	+1.09	191.17	192.02	+0.85
16	21.96	22.38	+0.42	21.90	22.26	+0.36
17, 18	—	—	—	—	—	—
19	12.98	12.98	±0	12.25	12.31	+0.06
20	12.98	12.98	±0	17.95	17.77	−0.18

a) The change in the chemical shift in going from room temperatures to −50 °C.

Table 2. The $\Delta\delta$ of polyene-chain carbons of retinal isomers in $CHCl_3$

Carbon number	*all-trans*-Retinal	*all-trans*-NRB	*all-trans*-NRB·HCl
	$\Delta\delta$[a]	$\Delta\delta$[a]	$\Delta\delta$[b]
1	−0.30	−0.24	−0.18
2	−0.79	−0.79	−0.48
3	−0.43	−0.37	−0.25
4	−0.24	−0.24	−0.06
5	+0.18	+0.18	±0
6	−0.49	−0.43	−0.19
7	−0.30	−0.31	−0.12
8	+0.06	−0.19	+0.12
9	+0.36	+0.24	±0
10	±0	−0.18	−0.06
11	+0.30	+0.06	+0.12
12	−0.30	−0.18	−0.12
13	+1.21	+0.60	+0.06
14	−0.12	−0.49	−0.25
15	+0.91	+0.48	±0

a) The chemical-shift changes between room temperature and −40 °C. b) The chemical-shift changes between room temperature and −20 °C.

is clear in acetone, though it is rather ambiguous in chloroform. The β-ionone-ring carbons indicate a upfield shift with a lowering of the temperature in both solvents. The relatively large upfield shift of C2 is remarkable. Among conjugated polyene-chain carbons, the downfield shifts are remarkable for the odd-numbered carbons, while they are not so clear for the even-numbered carbons. The same experimen-

tal result, that the chemical-shift changes of polyene-chain carbons can be classified into two types according to whether the numbering on the carbon is even or odd, is also found in the chemical-shift changes on going from retinal isomers to their Schiff bases and from Schiff bases to protonated Schiff bases.[9,10]

Table 2 also shows the chemical-shift changes, $\Delta\delta$, of the conjugated polyene-chain carbons of *all-trans*-NRB and *all-trans*-NRB·HCl in chloroform. The chemical shift changes in the carbons of *all-trans*-NRB are generally smaller than those in the carbons of *all-trans*-retinal, while those of *all-trans*-NRB·HCl are smaller than those of *all-trans*-NRB.

Discussion

Origin of the Temperature Dependence of Chemical Shifts. Several contributions can be pointed out as the causes of the temperature dependences of chemical shifts. Firstly, the effect of the temperature-dependent polarizability of the solvent must be examined, since the changes in the carbon-13 chemical shifts of polyene carbons of retinal are connected with the changes in electron density.[8-10] Wyman[13] has reported that the dielectric constant and the polarizability of the solvent increase with a lowering of the temperature. An increase in the polarizability of the solvent induces an increase in that of the retinal carbonyl group.[14] As has been shown in previous papers,[9,10] the positive charge at the polyene-chain-end atom tends to be distributed onto the polyene-chain carbons(Fig. 1b); this delocalization of the positive charge results in the downfield shifts for these carbons. Thus, the downfield shifts(Table 1) of the odd-numbered polyene carbons in *all-trans*- and 11-*cis*-retinal with a lowering of the temperature may be attributed to the delocalization of the positive charge at the polyene-chain end resulting from an increase in the polarizability of the retinal carbonyl group. Such downfield shifts are especially clear in the C13 and C15. The large $\Delta\delta$'s of the C9 and C11 in 11-*cis*-retinal imply a larger delocalization of the positive charge compared with that of the same carbons in *all-trans*-retinal.

The overall decrease in the electron density of the polyene-chain can be explained in terms of the intramolecular polarizability, which produces an increase in the electron density in the β-ionone-ring carbons. These carbons show upfield shifts. Thus, at least a part of the origin of the chemical-shift changes, $\Delta\delta$'s, can be explained by the changes in polarizability. However we have to consider other factors besides polarizability, since the polyene carbons of 11-*cis*-retinal show very different $\Delta\delta$'s from those of *all-trans*-retinal, as is indicated in Fig. 3. The peculiarity of $\Delta\delta$ of 11-*cis*-retinal can be explained by the conformational changes of its conjugated polyene-chain.

The following two conformational changes can be induced by lowering the temperature. One is due to a decrease in the skewness in the conjugated polyene-chain, while the other is due to the rotation around the C12–C13 single bond.

In 11-*cis*-retinal, the steric hidrance between the C10-hydrogen and C20-methyl group is relieved by a skew geometry around the C12–C13 single bond at

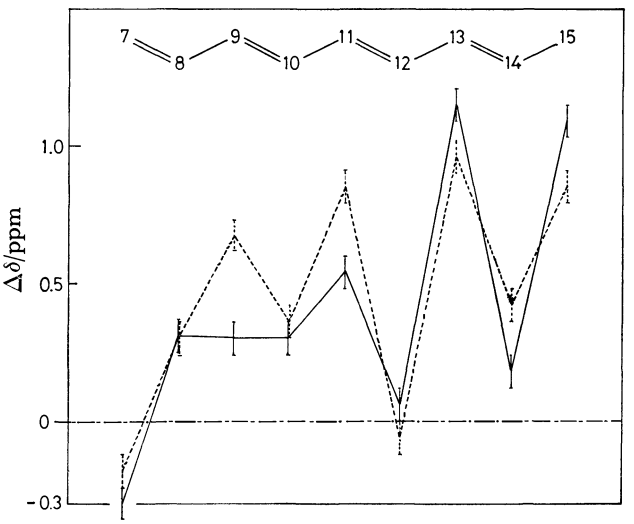

Fig. 3. The plot of the chemical-shift differences $\Delta\delta$ *vs.* carbon number of *all-trans*-retinal (—) and 11-*cis*-retinal (---) in acetone.

room temperature.[5,7] Patel[5] suggested that it is more difficult to distribute the positive charge in 11-*cis*-retinal than in *all-trans*-retinal, judging from the proton chemical-shift differences in the two retinal isomers at room temperature. In Table 1, the $\Delta\delta$'s in acetone of the C9 and C11 in 11-*cis*-retinal are +0.67 and +0.85 ppm respectively, while those in *all-trans*-retinal are +0.30 and +0.54 ppm. The $\Delta\delta$'s of the C15 and C13 in *all-trans*-retinal are about 1.1 ppm, while those in 11-*cis*-retinal are about 0.9 ppm. These trends indicate an increase in the degree of the delocalization of the positive charge on C15 upon a lowering of the temperature. The decrease in the skewness produces an increase in planarity(an increase in the resonance structure) of the 11-*cis* polyene-chain and results in an increase in the delocalization of the positive charge. Therefore, the larger downfield shitfs of C9 and C11 of 11-*cis*-retinal as compared with those of *all-trans*-retinal may be due to a decrease in the skewness of the conjugated polyene-chain upon a lowering of the temperature. This explanation is consistent with that of UV analysis at lower temperatures.[3,15]

The other origin of chemical-shift change is the change in equilibrium between the 12-*s-cis* and 12-*s-trans* conformers of 11-*cis*-retinal. It has been reported that the relative stabilities of the two conformers in 11-*cis*-retinal change with temperature[7] and the kind of solvent.[12] The chemical shifts of sterically perturbed carbon atoms are generally found at higher magnetic fields than those of similar carbons which are not spatially crowded. This steric perturbation of the carbon-13 chemical shifts is known as the γ-effect.[16] The chemical shifts of C10, and C20 may be affected by the γ-effect resulting from the steric hindrance between the C10-hydrogen and C20-methyl or C14-hydrogen, depending on the equilibrium between the two conformers. As is shown in Table 1, the $\Delta\delta$ of C10 in 11-*cis*-retinal in acetone is nearly equal to that of *all-trans*-retinal. The 14 and 20 carbons of 11-*cis*-retinal show a downfield shift of 0.42 ppm and an upfield shift of 0.18 ppm respectively, while those of

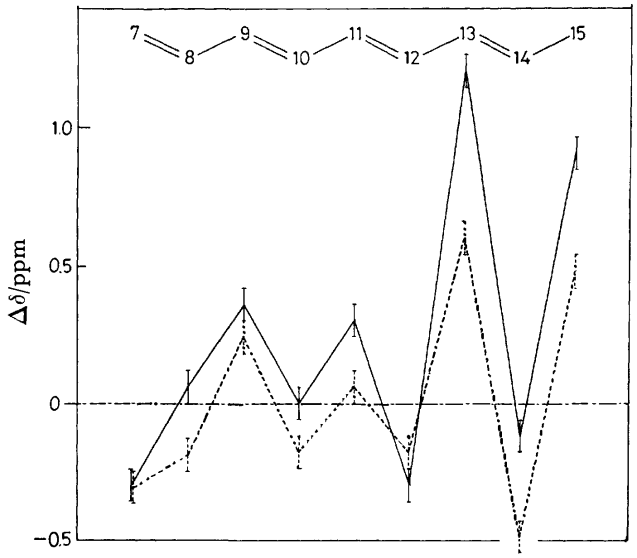

Fig. 4. The plot of the chemical shift differences $\Delta\delta$ *vs.* carbon number of *all-trans*-retinal(—) and *all-trans*-NRB(---) in chloroform.

all-trans-retinal remain in nearly the same positions. These results reveal that, in 11-*cis*-retinal, the 12-*s-trans* conformer is preferred over the 12-*s-cis* one in acetone at low temperatures. These results are consistent with the proton-NMR analysis,[7] which indicates a higher population of the 12-*s-trans* conformer in acetone at −52 °C. At present, however, we can not evaluate the population of each conformer.

In *all-trans*-NRB, the smaller downfield shifts for C13 and C15 as compared with those of *all-trans*-retinal might be due to a decrease in the delocalization of the positive-charge density induced by a decrease in the electronegativity of the terminal group,[9] because $\Delta\delta$'s of the β-ionone ring carbons are approximately equal to those of *all-trans*-retinal(Table 2 and Fig. 4).

Correlation between the UV Red Shift and the Carbon-13 Chemical Shift. It has previously been reported that the blue shift with a magnitude of about 20 nm on going from *all-trans*-retinal to *all-trans*-NRB is due mainly to the delocalization of the π-electron density,[9] and that the large red shift (about 80 nm) by the N-protonation on NRB is due mainly to the collapse of the bond alternation[9] and the delocalization of the positive charge.[9,17,18] Schaffer *et al.*[4] have indicated that 11-*cis*-retinal shows a larger red shift than other retinal isomers and that the magnitudes of the red shifts of retinal isomers are somewhat larger than those of the corresponding Schiff bases on going from room to lower temperatures. These phenomena are explained by the carbon-13 NMR analysis as follows.

The red shifts in retinal compounds at lower temperatures may be due to an increase in the degree of delocalization of the positive charge as a result of an increase in the degree of polarizability. The difference in the magnitude of the red shift in *all-trans*-retinal and 11-*cis*-retinal can be related to the magnitude of the chemical-shift changes of C9 and C11 resulting from the delocalization of the positive charge induced by an increase in planarity in the conjugated polyene-chain of 11-*cis*-retinal upon a lowering of the temperature.

The small chemical-shift changes of *all-trans*-NRB as compared with those of *all-trans*-retinal explain why *all-trans*-retinal shows a larger red shift than does *all-trans*-NRB on going from room to lower temperatures. For *all-trans*-NRB·HCl, the smaller red shift[4] corresponds to the smaller chemical-shift changes. Thus, the chemical-shift changes are correlated with the UV red shift.

From the present work, it is clear that the temperature dependences of the carbon-13 chemical shifts of the retinal isomers and related compounds are explainable in terms of the changes in the polarizability and conformation of the polyene chain, although this explanation is more or less qualitative. To give a quantitative explanation of the experimental results, a theoretical investigation by means of CNDO calculation is now in progress and will be reported elsewhere.

The present work was partially supported by a Grant-in-Aid for Scientific Research from the Ministry of Education(No. 311809).

References

1) R. Hubbard and A. Kropf, *Proc. Natl. Acad. Sci. U. S.*, **44**, 130 (1958).
2) G. Wald, *Science*, **162**, 230 (1968).
3) W. Speerling and C. N. Rafferty, *Nature (London)*, **224**, 591 (1969).
4) A. M. Schaffer, W. H. Waddell, and R. S. Becker, *J. Am. Chem. Soc.*, **96**, 2063 (1974); **99**, 8456 (1977).
5) D. J. Patel, *Nature (London)*, **221**, 825 (1969).
6) R. Rowan and B. D. Sykes, *J. Am. Chem. Soc.*, **96**, 7000 (1974); Y. Tokito, Y. Inoue, R. Chûjô, and Y. Miyoshi, *Org. Magn. Reson.*, **7**, 485 (1975).
7) R. Rowan, A. Warshel, B. D. Sykes, and M. Karplus, *Biochemistry*, **13**, 970 (1974).
8) J. Shriver, E. W. Abrahamson, and G. D. Matteescu, *J. Am. Chem. Soc.*, **98**, 2407 (1976).
9) Y. Inoue, Y. Tokito, R. Chûjô, and Y. Miyoshi, *J. Am. Chem. Soc.*, **99**, 5592 (1977).
10) Y. Inoue, Y. Tokito, S. Tomonoh, and R. Chûjô, *Bull. Chem. Soc. Jpn.*, **52**, 265 (1979).
11) D. Bownds, *Nature (London)*, **216**, 1178 (1967); M. Akhtar, P. T. Blosse, and P. B. Dewhurst, *Chem. Commun.*, **1967**, 631; M. O. Hall and A. D. E. Bacharach, *Nature (London)*, **225**, 637 (1970); W. J. DeGrip, S. L. Bonting, and F. J. M. Daemen, *Biochim. Biophys. Acta*, **303**, 189 (1973).
12) R. R. Birge, M. J. Sulliran, and B. E. Kohler, *J. Am. Chem. Soc.*, **98**, 358 (1976).
13) J. Wyman, *J. Am. Chem. Soc.*, **58**, 1482 (1936).
14) T. Suzuki and Y. Kito, *Photochem. Photobiol.*, **15**, 275 (1972).
15) R. S. Becker, K. Inuzuka, and D. E. Balke, *J. Am. Chem. Soc.*, **93**, 38 (1971).
16) D. M. Grant and E. G. Paul, *J. Am. Chem. Soc.*, **86**, 2984 (1964); W. R. Woolfendon and D. M. Grant, *J. Am. Chem. Soc.*, **88**, 1496 (1966); D. M. Grant and B. V. Cheney, *J. Am. Chem. Soc.*, **89**, 5315 and 5319 (1967).
17) B. Honig, A. D. Greenberg, U. Dinur, and T. G. Ebrey, *Biochemistry*, **15**, 4593 (1976).
18) D. S. Kliger, S. J. Milder, and E. A. Dratz, *Photochem. Photobiol.*, **25**, 277 (1977).

12,13-Epoxy-*C*-nor-*D*-homosteroids. VI.[1] Reaction of 17-Oxygenated 12,13-Epoxyetiojervanes with Boron Trifluoride Etherate[2]

Akio MURAI, Noriaki IWASA, Masami TAKEDA, and Tadashi MASAMUNE*

Department of Chemistry, Faculty of Science, Hokkaido University, Sapporo 060

(Received July 11, 1979)

17-Oxygenated 12,13-epoxyetiojerv-5-en-3-one 3,3-ethylene acetals (**1A—10A**) were treated with boron trifluoride etherate in benzene at room temperature. The epoxy ring cleavage reactions proceeded slowly with increase of electronegativity of the 17-substituents without and/or with deacetalization to give a variety of compounds including rearranged products (**23A** and **23B**). The results summarized in Table 1 indicated that the reactions produced compounds formed by initial cleavage at less electronegative C-12 rather than at C-13 except several compounds (**11A**, **20A**, **20B**, and **34A**). Formation of the latter compounds was attributed by hydride shift or neighboring participation of the 17-acetoxyl groups.

In a previous paper[3] we reported the synthesis and stereochemistry of 17-oxygenated 12,13-epoxyetiojervanes. As a continuing study on the reactions of 12,13-epoxy-*C*-nor-*D*-homosteroids, involving formation of novel rearranged products,[4] we have examined reactions of 17-oxygenated 12α,13α- and 12β,13β-epoxyetiojervanes with boron trifluoride etherate, keeping in mind that the epoxy ring cleavage of the 11-oxygenated 12,13-epoxides varied, depending on electronegativity of the 11-substituents rather than conformation of the epoxy groups.[4] In this paper we describe the results, including interesting participation of neighboring groups.

The reactions of 17α-hydroxy-[3] (**1A**), 17α-acetoxy-[3] (**2A**), 17β-hydroxy-[3] (**3A**), 17β-acetoxy-[3] (**4A**), and 17-oxo derivatives of 12α,13α-epoxyetiojerv-5-en-3-one 3,3-ethylene acetals[3] (**5A**), and the corresponding 12β, 13β-epoxides[3] (**6A—10A**) with boron trifluoride etherate were carried out in benzene at room temperature, and the results are summarized in Table 1. The structure of each product was assigned on the basis of the chemical and spectral evidence. The functional groups in the A and B rings, Δ^5-3,3-ethylenedioxy ($S=S_A$) and Δ^4-3-oxo groups ($S=S_B$), the latter being formed by deacetalization of the former under the acidic conditions, were defined clearly on the spectral grounds: (i) S_A, δ ≈3.94 (4H, s, $OC\underline{H}_2C\underline{H}_2O$) and ≈5.40 (1H, br, W_H=8 Hz, 6-H): S_B, λ_{max} 235 nm (ε ≈10000); ν_{max} ≈1660 and ≈1615 cm^{-1}; δ ≈5.78 (1H, s, 4-H), and (ii) difference in chemical shift of 19-methyl protons of several pairs of compounds differing only in these functional groups, $\Delta\delta_{obsd}$ 0.14—0.18; $\Delta\delta_{calcd}$ 0.16.[5]

Table 1. Reaction results of 17-oxygenated 12α,13α-epoxy- (**1A—5A**) and 12β,13β-epoxy-13-epietiojerv-5-en-3-one 3,3-ethylene acetals (**6A—10A**) with boron trifluoride etherate[a]

Epoxide	Reaction time	Products (yield/%)[b]
1A	30 s	**11A** (30), **12A** (10), **17A** (5)
2A	30 s	**17A** (16), **17B** (19), **18A** (6)
3A	30 s	**19A** (60), **19B** (22)
4A	20 min	**20A** (34), **20B** (40)
5A	1 h	**5B** (25), **23A** (5), **23B** (25), **24B** (15)
6A	30 s	**25A** (45), **25B** (25), **30A** (15), **30B** (4)
7A	30 s	**26A** (51), **26B** (20)
8A	30 s	**31A** (33), **31B** (28), **32A** (20)
9A	1 min	**34A** (16), **35A** (25)
10A	20 min	**28B** (80)

a) Carried out in benzene at room temperature. b) Isolated yields.

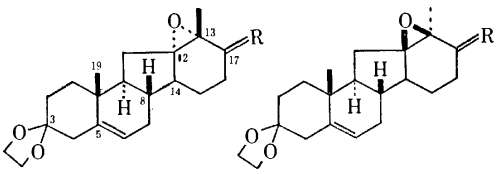

1A R=···OH, −H
2A R=···OAc, −H
3A R=−OH, ···H
4A R=−OAc, ···H
5A R=O

6A R=−OH, ···H
7A R=−OAc, ···H
8A R=···OH, −H
9A R=···OAc, −H
10A R=O

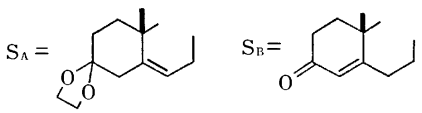

Compound **11A**, mp 132—134 °C, a major product of **1A**, had a molecular formula $C_{21}H_{28}O_3$ corresponding to a dehydration product of **1A**. The IR (ν_{max} 1720 cm^{-1}) and NMR spectra [δ 1.21 (3H, d, J=7 Hz, 18-H)] suggested the presence of a $\Delta^{12(14)}$-17-carbonyl moiety on the six-membered *D* ring. Indeed, compound **11A**, when treated with base (KOH in aq CH_3OH, room temp, 1 h), was converted quantitatively into a known compound, etiojerva-5,12-diene-3,17-dione ethylene acetal[3] (**12A**). The configuration of the 13-methyl group was deduced from the negative Cotton effect (a=+15°) as illustrated in Fig. 1. All these facts establishes that the compound is represented by formula **11A**. The deshielding effect ($\Delta\delta$ 0.12) of a double bond at C-12–C-14 to the chemical shift of the 19-methyl protons [δ_{obsd} 1.10 for **11A**; δ_{calcd} 0.98 and 1.03 for 12β- and 12α-etiojerv-4-en-3-one ethylene acetals[5] (**13A** and **14A**)] was in good accord with the corresponding difference (0.11) between 12β,13α-dihydroacetyljervine[6] (**15**) (δ 1.02) and "diacetyl-Δ^{13}-jervine"[6,7] (**16**) (δ 1.13).

The structure of compound **17A** ($C_{21}H_{26}O_2$), mp 116—118 °C, was based on the spectral data, which gave indications of an aromatic *D* ring: λ_{max} 273 nm

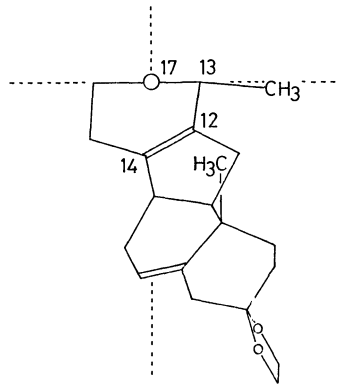

Fig. 1

(ε 300) and 264 (300); δ 2.26 (3H, s, 18-H) and 6.96 (3H, m, W_H=5 Hz, 15-, 16-, and 17-H). The compound (**17A**), on treatment with acid (p-TsOH in a 3:1 mixture of acetone and water, reflux, 4 h) afforded its deacetalization product, Δ^4-3-ketone (**17B**), mp 129—130 °C, in good yield. Naturally, the chemical shifts (δ 1.16 and 1.30) of 19-methyl protons of **17A** and **17B** coincided with those (δ 1.17 and 1.31) of the related veratramine derivatives,[5,8] indicating the deshielding effect of an aromatic D ring to be $\Delta\delta$ 0.17 [1.16 (δ_{obsd} of **17A**)—0.98 (δ_{calcd} of **13A**) or 1.30 (δ_{obsd} of **17B**)—1.14 (δ_{calcd} of **13B**)].

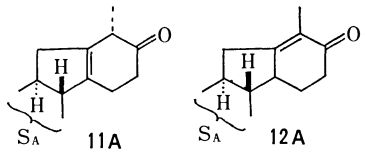

11A

12A

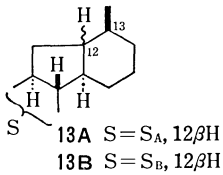

13A S=SA, 12βH
13B S=SB, 12βH
14A S=SA, 12αH

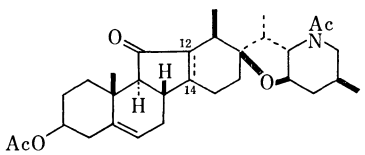

15 12βH, 14αH
16 $\Delta^{12(14)}$

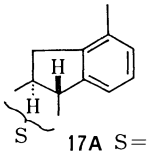

17A S=SA
17B S=SB

The reaction of 17α-acetoxy-12α,13α-epoxide (**2A**) afforded fluorohydrin (**18A**), mp 186—189 °C, as a minor product besides the two aromatic compounds (**17A** and **17B**). The molecular formula $C_{23}H_{33}O_5F$ suggested that **18A** would be a compound formed by simple cleavage of the epoxy ring by a fluoride anion.[9] A 12β-fluoro-13α-hydroxyetiojervane formula (**18A**) was assigned to the compound by analogy of the NMR spectra of the related compounds: 13β-fluoro-12α-hydroxyetiojervanes[10] and the corresponding *C*-nor-*D*-homospirostanes[10,11] exhibited three-proton singlets due to the 18-methyl protons at δ 1.47—1.58, while 12β-fluoro-13α-hydroxyetiojervane,[12] the corresponding spirostan,[11,12] and the relevant compound (**18A**) displayed the singlets at higher fields, δ 1.27, 1.29, and 1.25, respectively.

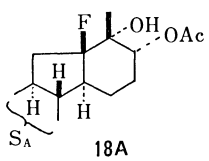

18A

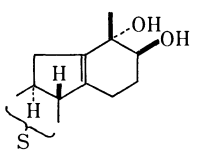

19A S=SA
19B S=SB

Compound **19A**, mp 201—203 °C, obtained as a major reaction product of 17β-hydroxy-12α,13α-epoxide (**3A**), had the same molecular formula $C_{21}H_{30}O_4$ as **3A**. The NMR spectrum revealed a broad singlet (1H, W_H=7 Hz) due to a proton on the carbon (probably C-17) bearing an axial secondary hydroxyl group at δ 3.93 and two singlets (each 3H) due to the 19- and 18-methyl protons at δ 1.08 and 1.35, respectively. In view of the absence of evidence supporting any skeletal rearrangement (no absorption maxima in the carbonyl region), the appearance of the 19- and 18-methyl protons at such low fields indicated the presence of the afore-mentioned double bond at C-12–C-14 (δ_{calcd} 1.10[5] for 19-H). Hence the remaining oxygen atom would have to constitute a tertiary hydroxyl group most probably at C-13. Since the compound did not form the acetonide under the conditions described later, it was formulated as structure **19A**. On the other hand, a minor product, mp 174—177 °C, was readily assigned the corresponding Δ^4-3-ketone formula (**19B**) from the spectral data (Experimental).

The acid treatment of 17β-acetoxy-12α,13α-epoxide (**4A**) gave two compounds (**20A** and **20B**) as major products. The former (**20A**), mp 204—206 °C, had a molecular formula $C_{23}H_{34}O_6$ corresponding to a hydration product of **4A**, suggesting formation of two new hydroxyl groups. Compound **20A**, formulated as monoacetate [δ 2.06 (3H, s, OCOCH$_3$) and 5.00 (1H, br, W_H=9 Hz, 17-H)], resisted mild acetylation and oxidation with periodic acid. Hydrolysis of **20A** with base (K_2CO_3 in aq CH_3OH, room temp, 3 h) gave triol (**21A**), mp 197—199 °C [δ 3.82 (1H, br, W_H=10 Hz, 17-H)], in 80% yield, which on treatment with acetone and acid ($HClO_4$, room temp, 4 h) underwent acetonide formation with concomitant deacetalization, giving Δ^4-3-oxo triol 13β,17β-acetonide (**22B**), amorphous, in 70% yield [δ 1.44 (9H, s, 18-H and acetonide CH$_3$) and 4.19 (1H, m, W_H=12 Hz,

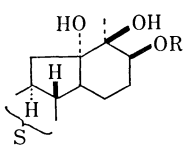

20A S=SA, R=Ac
20B S=SB, R=Ac
21A S=SA, R=H
21B S=SB, R=H

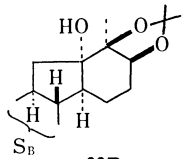

22B

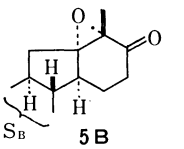

5B

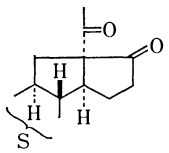

23A S=SA
23B S=SB

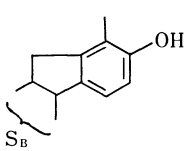

24B

17-H)]. All these facts indicate that the compound is represented favorably by formula **20A**. The latter compound (**20B**), mp 182—184 °C, was also formulated as monoacetate [δ 2.07 (3H, s, $OCOCH_3$) and 5.01 (1H, br, W_H=9 Hz, 17-H)] and was converted under the afore-mentioned basic conditions into triol (**21B**), mp 217—218 °C, in 90% yield, which formed the corresponding acetonide by the same treatment as **21A** in 80% yield. This acetonide was identical with that (**22B**) derived from **20B**, and hence formula **20B** was assigned to the compound. The β-configurational assignment to the 13-hydroxyl group in **20A** and **20B** was understood reasonably by neighboring participation[13] of the *trans*-17β-acetoxyl group adjacent to the relevant α-epoxy group, as discussed later.

Prolonged treatment of 17-oxo-12α,13α-epoxide (**5A**) with the acid produced four compounds. The first compound (**5B**), mp 185—187 °C, was identified easily as a deacetalization product of **5A** by comparison of the spectral data. The second (**23A**), mp 124—125 °C, had the same molecular formula $C_{21}H_{28}O_4$ as **5A**. The spectra revealed that acetyl [ν_{max} 1715 cm^{-1}; δ 2.20 (3H, s)] and five-membered ring carbonyl groups (ν_{max} 1734 cm^{-1}) were newly formed, suggesting cleavage of the C-12–O bond and contraction of the D ring. These data, combined with analogous examples,[4,11] led to assignment of formula **23A** to the compound. The configuration of the acetyl group was deduced from recently reported mechanism on rearrangement of epoxy ketones,[14] as discussed later. The third compound (**23B**), mp 112—113 °C, was identified as a deacetalization product of **23A** on the spectral ground. The fourth compound, mp 289—291 °C, was assigned formula **24B** on the basis of the spectral data indicating the presence of a phenol ring: λ_{max} 285 nm (sh) (ε 900) and 279 (1100); δ 2.15 (3H, s, 18-H), and 6.58 and 6.79 (each 1H, ABq, J=8 Hz, 16- and 15-H).

One (**25A**), mp 102—104 °C, of two major products in the reaction of 17β-hydroxy-12β,13β-epoxide (**6A**) had the same molecular formula as **6A** and gave its monoacetate (**26A**), mp 232—234 °C. The IR and NMR spectra of **25A** and **26A** revealed the presence of secondary (equatorial) and tertiary hydroxyl groups at C-17 and C-13, respectively: **25A**, δ 1.23 (3H, s, 18-H) and 3.41 (1H, br m, W_H=25 Hz, 17-H): **26A**, ν_{max} 3507, 1719, and 1260 cm^{-1}; δ 1.13 (3H, s, 18-H) and 4.77 (1H, do d, J=10 and 5 Hz, 17-H). Compound **25A**, when treated with acid (*p*-TsOH in aq acetone, reflux, 2 h), underwent deacetalization to give another major product (**25B**), mp 185—187 °C, in 80% yield, which also formed its monoacetate (**26B**), mp 123—124 °C. Further treatment of **25B** with acetone and acid ($HClO_4$, room temp, 0.5 h) afforded the corresponding 13β,17β-acetonide (**27B**), oily, though in low yield: δ 1.33 and 1.40 (each 3H, s, acetonide CH_3), and 4.14 (1H, br m, 17-H). Mild oxidation of **25B** with chromium(VI) oxide in pyridine afforded the corresponding 17-ketone (**28B**), mp 178—180 °C, in low yield together with a major product, amorphous, assigned tentatively formula **29B** on the spectral ground (Experimental): **28B**, ν_{max} 3370 and 1717 cm^{-1}. All these facts indicated the presence of 13β- and 17β-hydroxylgroups in **25A** and **25B**. Contrary to the expectation that the remaining double bond would be located at C-12–C-14 as in the case of **19A**, the 19-methyl protons of **25A** and **26A** appeared at abnormally high fields, δ 0.91 and 0.92, compared with those of other usual etiojervanes: δ_{obsd} 1.04, 1.10, 1.08, and 1.02 for **6A**, **11A**, **19A**, and **18A**; δ_{calcd} 0.98 and 1.03 for **13A** and **14A**. The chemical shifts in question were consistent with disposition of a double bond at C-8–C-14, since the shielding effect ($\Delta\delta$ −0.12= 0.91–1.03) of a $\Delta^{8(14)}$-system to the relevant chemical shift has been demonstrated for normal[15] ($\Delta\delta$ 0.117) and *C*-nor-*D*-homosteroids.[11] It is also emphasized that the absorption maximum due to the double bond in question was observed at 208 nm (ε 10000).[16] Hence the compound is represented reasonably by formula **25A**, in which the configuration at C-12 was assigned from the mechanistic ground (hydride shift from C-14 as well as by analogy of the related reactions,[11] as discussed later).

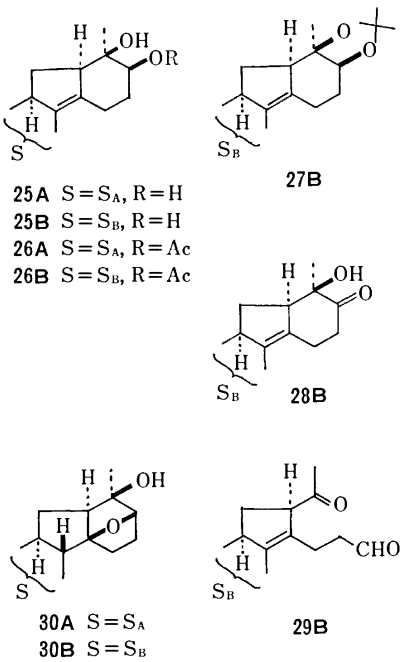

Two minor products, **30A**, mp 207—208 °C, and its deacetalization product (**30B**), mp 136—138 °C, were assigned hydroxy oxolane structures. The former (**30A**), with the same molecular formula $C_{21}H_{30}O_4$ as **6A**, resisted acetylation and oxidation with periodic acid under the usual conditions. While the spectra revealed the presence of a $-CH_3(C)(OH)-$ moiety, in which (C) denotes a quaternary carbon [*m/e* 346 (M^+), 331, and 328; ν_{max} 3580 cm^{-1}; δ 1.30 (3H, s, 18-H)], a one-proton doublet (J=5 Hz) was observed at a relatively low field, δ 4.06. This signal could be ascribed to a proton on the carbon (probably C-17) bearing an ether oxygen atom because of the absence of absorption maxima at 205—210 nm and also at the carbonyl region in the UV and IR spectra. In view of the splitting pattern of the 17-proton (*cf.*, W_H=25 Hz for 17-H of **25A**), the *D*-ring would be deformed considerably and the 17-oxygen atom would constitute an ether bond between C-17 and either one of C-12, C-14, and C-8. The formation of an

oxetane or an oxane ring (C-12 or C-8) would be eliminated by examination of the Dreiding model and also by inertness to hydride reduction of **30A** ($LiAlH_4$ in THF–dioxane, reflux, 4 h).[17] The compound is therefore be represented favorably by formula **30A**. In view of the fact that interconversion between **25A** and **30A** did not take place under the acidic conditions, compound **30A** would presumably be formed by cleavage of the C-12–O bond, hydride shift of the 14α-hydrogen to C-12, and subsequent intramolecular attack of the 17β-hydroxyl group to the relevant 14-carbenium ion.

Two reaction products of 17β-acetoxy-12β,13β-epoxide (**7A**) were identified as the above-described $\Delta^{8(14)}$-13β,17β-diol 17-acetate (**26A**) and its deacetalization compound (**26B**), respectively, by direct comparison. Naturally, compounds corresponding to **30A** and **30B** could not be detected.

Two major products, **31A**, mp 174—175 °C, and its deacetalization product (**31B**), amorphous, in the reaction of 17α-hydroxy-12β,13β-epoxide (**8A**) were assigned $\Delta^{8(14)}$-13β,17α-diol formulas as follows. The former (**31A**), with the same molecular formula $C_{21}H_{30}O_4$ as **8A**, displayed essentially the same mass and UV spectra as **25A** with the $\Delta^{8(14)}$-13β,17β-dihydroxy moiety: λ_{max} 207 nm (ε 9000). The NMR spectrum also resembled that of **25A**, except a signal due to the 17-proton [δ 3.70 (1H, br, W_H=8 Hz)], indicating that **31A** differed from **25A** only in configuration of the 17-hydroxyl group. The same situation held for the relation between **31B** and **25B**. Indeed, compound **31B**, when oxidized with chromium(VI) oxide in pyridine (room temp, 0.6 h) afforded the afore-mentioned hydroxy ketone (**28B**), mp 178—180 °C, confirming the assigned structures to compounds **31A** and **31B**. A minor product (**32A**), mp 169—171 °C, with the same molecular formula as **8A**, gave its monoacetate (**33A**), mp 119—121 °C, which still showed an absorption maximum at 3440 cm^{-1} due to a hydroxyl group. These facts, coupled with the mass spectrum [**32A**, *m/e* 346 (M^+), 331, 328, 302 (M^+—$CH(OH)CH_2$), and 234], suggested that **32A** would probably possess a partial formula of –(CH_3)(C)(OH)CH(OH)CH_2– on the D ring. However, the UV (no absorption maximum above 205 nm) and NMR spectra [δ 1.12 and 1.29 (each 3H, s, 19- and 18-H)] differed clearly from those of **31A** [δ 0.90 and 1.20 (each 3H, s, 19- and 18-H)]. These spectra were consistent with disposition of a double bond at C-12–C-14: δ_{calcd} 1.10 and 0.91 for 19-H of **32A** and **31A**. Hence the $\Delta^{12(14)}$-13β,17α-diol structure (**32A**) was assigned to the minor compound.

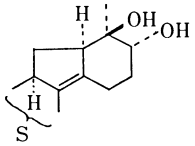

31A S=S_A
31B S=S_B

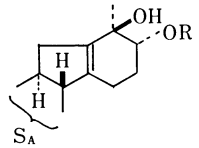

32A R=H
33A R=Ac

The reaction of 17α-acetoxy-12β,13β-epoxide (**9A**) with the acid gave rise to a complex mixture, from which two compounds (**34A** and **35A**) were isolated with a mixture of the respective deacetalization products. The former (**34A**), mp 217—219 °C, had a molecular formula $C_{23}H_{34}O_6$ corresponding to that of a hydration product of **9A**. The NMR spectrum exhibited a three-proton singlet due to 18-methyl protons at δ 1.22 and a broad multiplet (1H, W_H= 17 Hz) due to a proton on the 17-carbon bearing an equatorial acetoxyl group at δ 5.14. Compound **34A**, when hydrolyzed with base (KOH in CH_3OH, room temp, 5 h), yielded triol (**36A**), mp 207.5—208.5 °C, showing no carbonyl band in the IR spectrum. This triol (**36A**), on treatment with acetone and acid under the same conditions as described above, gave Δ^4-3-oxo triol 13α,17α-acetonide (**37B**), amorphous, whose spectra (Experimental) were in good accord with the assigned structure. All these facts, combined with the formation of **20A** from **4A**, led to assignment of formula **34A** to the compound. On the other hand, compound **35A**, amorphous, had the same molecular formula as **34A** and displayed three three-proton singlets at δ 1.02, 1.18, and 2.08 and a broad multiplet (1H, W_H=22 Hz) at δ 3.72, which were attributed to 19-, 18-, acetoxyl methyl protons and a proton at C-17, respectively. The compound (**35A**) was hydrolyzed by base treatment to give triol (**38A**), mp 199.5—201.5 °C [δ 2.60, 2.66, and 2.71 (each 1H, s, 3OH) and 3.68 (1H, br, W_H=14 Hz, and 6 Hz on addition of D_2O, 17-H), which on treatment with acid (*p*-TsOH in aq acetone, reflux, 2 h) gave the corresponding Δ^4-3-ketone (**38B**), mp 197—198 °C. Oxidation of **38B** with chromium(VI) oxide in pyridine afforded 17-ketone (**39B**), mp 171.5—173 °C: ν_{max} 3605, 3510, and 1715 cm^{-1}; δ 1.58 and 3.66 (each 1H, s, 2OH). The same 17-ketone was also obtained by oxidation of **21B** (12α,13β,17β-triol) under the same conditions as that of **38B**, establishing the presence of a 12α,13β,17α-trihydroxy moiety in compound **38B**. These facts, coupled with neighboring participation of the 17α-acetoxyl group, indicated that the compound is represented favorably by formula **35A**.

The epoxy cleavage reaction of 17-oxo-12β,13β-epoxide (**10A**) with the acid proceeded rather slowly with concomitant deacetalization to give ketone, mp 178—180 °C, in 80% yield as a sole product, which

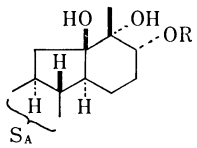

34A R=Ac
36A R=H

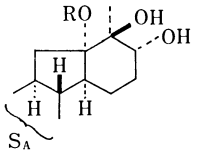

35A S=S_A, R=Ac
38A S=S_A, R=H
38B S=S_B, R=H

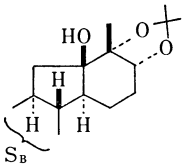

37B

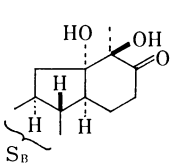

39B

was identified as the afore-mentioned $\Delta^{8(14)}$-13β-hydroxy-17-ketone (**28B**).

The results in Table 1 are summarized as follows. The reactions gave rise to products resulting from the epoxy ring cleavage at C-12 rather than C-13 for all the starting epoxides (**1A**—**10A**) except those **11A**, **20A**, **20B**, and **34A**. The preferential C-12–O bond cleavage, combined with the previously reported analogous results on acid treatment of 11-oxygenated 17α-aceytl-12,13-epoxides,[4] is understood well by the difference in stability of incipient carbenium ions at C-12 and C-13 formed by the epoxide opening. The fact that the reactions proceeded slowly with increase of electronegativity of the 17-substituents is also in good accord with the preferential cleavage of the C-12–O bond. These results are discussed in more details in the following.

(i) The formation of aromatic compounds (**17A**, **17B**, and **24B**) is rationalized well by assuming the initial cleavage of the C-12–O bond (Scheme 1). The route a (initial cleavage of the C-12–O bond) would give a 12-carbenium ion (I) (step a-1), which would be transformed smoothly *via* diene alcohol (IIa) or its acetate (IIb) into the aromatic compounds (step a-2). The reaction of 17α-acetate (**2A**) leading to the predominant formation of **17A** and **17B**, compared with the formation of **17A** from 17α-alcohol (**1A**) as a minor product, is ascribed to facile removal of the acetoxyl function as a leaving group (step a-2). On the other hand, the route b (initial cleavage of the C-13-O bond) must involve relatively unstable 13-carbenium ions (III) or (IV) (step b-1). Moreover, conversion of dienol (Va) or dienol acetate (Vb), formed from III, into IIa or IIb (step b-2) would not easily proceed under the acidic conditions.

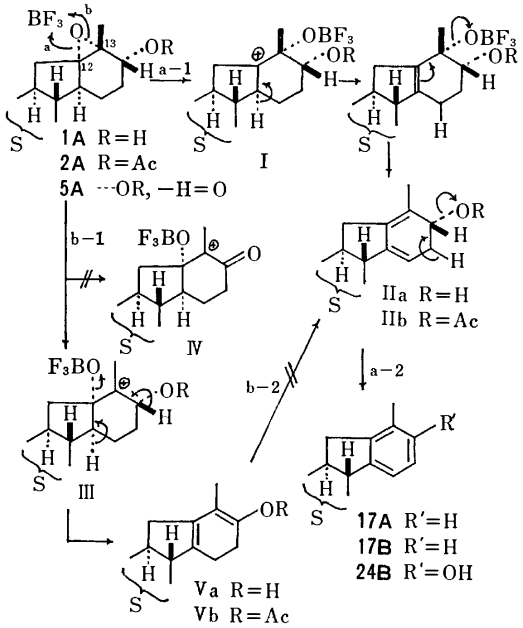

Scheme 1. Pathway for formation of **17A**, **17B**, and **24B**.

(ii) The reaction results of **4A** and **9A**, in which the 17-acetoxyl groups are oriented *trans* to the 12,13-epoxy groups, are explained reasonably on the basis of participation of the acetoxyl groups to epoxy bond cleavage leading to formation of acetoxonium ion intermediates (VI—VIII) (Scheme 2). While we have a few of analogous precedents[13] regarding the relevant participation controlling epoxy ring opening, the formation of **35A** from **9A** is very noteworthy in the sense that a 1,3-diaxial acetoxonium ion (VIII) is required as an intermediate, resulting from attack of the 17β-acetoxy function to an alternate, not adjacent, epoxy carbon atom (C-12). Moreover, the difference in reactivity between **4A** and **9A** would be attributed to that between conformations of the respective 17-acetoxyl groups, as suggested by the Dreiding model and demonstrated by the NMR spectra (17-H, W_H=6 Hz for **4A** and 14 Hz for **9A**).

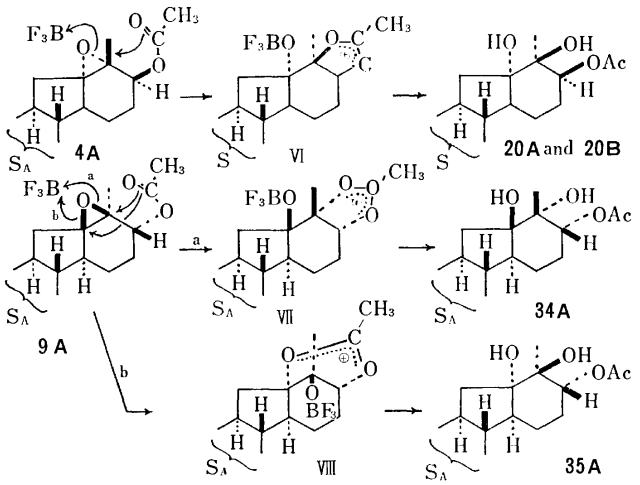

Scheme 2. Pathways for formation of **20A**, **34A**, and **35A**.

(iii) The reaction of 17α-hydroxy-12α,13α-epoxide (**1A**). especially the formation of β,γ-unsaturated ketone (**11A**), was examined in more detail. Reduction of 12α,13α-epoxy-17-ketone (**5A**) with sodium borodeuteride (>98%) afforded alcohol-17-*d* (**40A**), mp 169—171 °C, and its 17-epimer (**41A**), mp 154.5—157 °C, in 79 and 20% yields, respectively. These alcohols showed almost the same parent peaks at *m/e* 347 (0.59 and 0.66%) in the mass spectra and the same R_f values on TLC as **1A** and **3A**, respectively. Naturally, these alcohols (**40A** and **41A**) were reconverted by oxidation with chromium(VI) oxide in pyridine into the original ketone (**5A**). Reaction of **40A**, a 17-*d* derivative of **1A**, under the same acidic conditions as that of **1A** resulted in isolation of two deuterated compounds (**42A** and **43A**), mp 133—135 °C and 116—118.5 °C, which were corresponding to **11A** and **17A**, respectively. In accordance with the assigned structures, the former (**42A**) (isotope content, >75% by MS and NMR) exhibited a parent peak at *m/e* 329 (1.73%) and a singlet due to the 18-methyl protons at δ 1.21 in the mass and NMR spectra, while the latter (**43A**) (>98%) displayed a parent peak at *m/e* 311 (2.48%) and an AB type quartet (J=8 Hz) due to the 15- and 16-protons at δ 6.97 and 7.06. Furthermore, compound **42A**, when treated with base under the afore-mentioned conditions, was transformed into the undeuterated α,β-unsaturated ketone (**12A**).

These results established that (i) formation of **11A** resulted from cleavage of the epoxy ring at more electronegative C-13 and hydride shift of the 17β-hydrogen to C-13 in a concerted manner,[18] and (ii) reaction of **1A** to the aromatic compound (**17A**) proceeded *via* route a but not route b (Scheme 1).

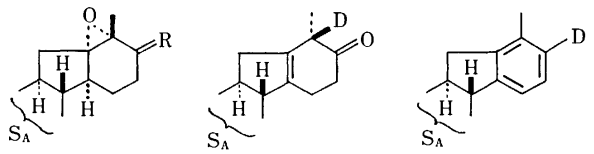

40A R=···OH, −D
41A R=−OH, ···D

42A

43A

(iv) The reaction of 17-oxo-12α,13α-epoxide (**5A**) gave rise to rearranged products (**23A** and **23B**), which evidently resulted from migration of the C-17–C-13 bond (acyl) to C-12 *via* an intermediate (IX) formed by cleavage of the C-12–O bond (Scheme 3). It has been reported that the acyl migration[19] is preferred over a hydrogen or a primary alkyl shift[19b] and occurs in aprotic solvents in a concerted manner with inversion of the configuration at the migration terminus.[14] The configuration of **23A** and **23B** was deduced from these mechanistic grounds. The fact that no rearranged product was obtained in the reaction of 17-oxo-12β,13β-epoxide (**10A**) would probably be ascribed to difficult formation of *trans*-fusion of two five-membered (*C*/*D*) rings.

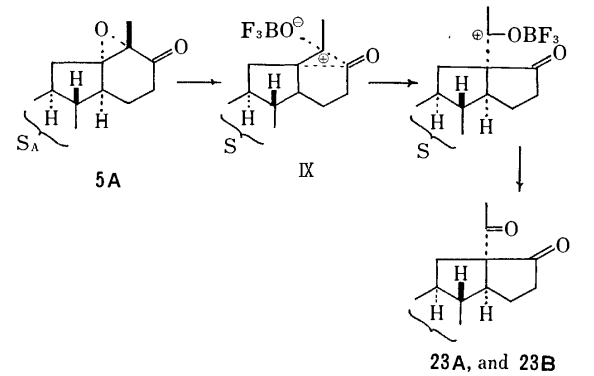

5A IX **23A**, and **23B**

Scheme 3.

In summary we again emphasize that all the reactions, except those involving the hydride shift and neighboring participation of the acetoxyl groups, were initiated by the epoxy ring cleavage at the less electronegative C-12. It is also noteworthy that the products with a double bond at C-12–C-14 were isolated only from the 12β,13β-epoxides.

Experimental

All the melting points were uncorrected. The homogeneity of each compound was always checked by TLC on silica gel (Wakogel B-5) with various solvent systems, and the spots were developed with cerium(IV) in dil sulfuric acid and/or iodine. Column chromatography was carried out over silica gel (Merck, Kieselgel 60, 70—230 mesh) or over alumina (Merck, Aluminiumoxid G. Type E), and preparative TLC over silica gel (Wakogel B-5F, 20×20 cm^2), unless otherwise stated. The optical rotations, UV, and IR spectra were measured in chloroform, ethanol, and Nujol, respectively, unless otherwise stated. The NMR spectra were obtained in chloroform-*d* at 100 MHz, TMS being used as an internal reference. The abbreviations, "s, d, q, m, br, do, and sh," in the NMR and IR spectra denote "singlet, doublet, quartet, multiplet, broad, double, and shoulder," respectively.

Reaction of 12α,13α-Epoxy-17α-hydroxyetiojerv-5-en-3-one 3,3-Ethylene Acetal (1A) with Boron Trifluoride Etherate (BF_3). To a benzene solution (100 ml) of **1A** (450 mg) was added rapidly BF_3 (0.2 ml) in benzene (3 ml) under stirring, and the resulting dark-blue solution was stirred at room temperature for 30 s. The reaction was ceased by rapid addition of ether (70 ml) and 5% aq sodium hydrogencarbonate ($NaHCO_3$, 70 ml), when the mixture became yellow. The benzene-ether solution was washed with 5% aq $NaHCO_3$ (3×80 ml) and water (3×100 ml), dried over anhydrous sodium sulfate and evaporated to dryness to leave resinous substance (430 mg), which was separated by chromatography over silica gel (25 g), benzene-ether mixtures being used as solvents. Fractions eluted with benzene–ether (10:1) gave etiojerva-5,12,14,16-tetraen-3-one 3,3-ethylene acetal (**17A**, 25 mg), mp 116—118 °C (from ether) and $[\alpha]_D$ −84.7°; MS, *m/e* 310 (M^+); UV, λ_{max} 273 nm (ε 300), 264 (300), 220 (sh) (5000), 215 (sh) (6300), and 205 (9000); IR, ν_{max} 1108 and 1095 cm^{-1}; NMR, δ 1.16 and 2.26 (each 3H, s, 19- and 18-H), 3.94 (4H, s, OC_2H_4O), 5.47 (1H, br, W_H=10 Hz, 6-H), and 6.96 (3H, m, W_H=5 Hz, 15-, 16-. and 17-H). Found: C, 80.81; H, 8.57%. Calcd for $C_{21}H_{26}O_2$: C, 81.25; H, 8.44. Fractions eluted with benzene–ether (10:2) gave 13-epietiojerva-5,12(14)-diene-3,17-dione 3,3-ethylene acetal (**11A**, 118 mg), mp 132—134 °C (from ether) and $[\alpha]_D$ −55.6°; ORD (dioxane), $[\phi]_{322}^{trough}$ −1540°, $[\phi]_{293}^{peak}$ 0°, and a=+15°, MS, *m/e* 328 (M^+), 313, 300, and 286; IR, ν_{max} 1720, 1113, and 1101 cm^{-1}; NMR, δ 1.10 (3H, s, 19-H), 1.21 (3H, d, J=7 Hz, 18-H), 3.97 (4H, s, OC_2H_4O), and 5.41 (1H, br, W_H=10 Hz, 6-H). Found: C, 76.49; H, 8.80%. Calcd for $C_{21}H_{28}O_3$: C, 76.79; H, 8.59%. Fractions eluted with benzene-ether (2:1) afforded α,β-unsaturated ketone (22 mg), mp 162—164 °C, which was identical with an authentic sample of etiojerva-5,12-diene-3,17-dione 3,3-ethylene acetal[3] (**12A**) (UV, IR, NMR, and TLC).

Compound **11A** (25 mg) was treated with 5% potassium hydroxide (KOH) in methanol (1 ml) at room temperature for 1 h. After removal of the solvent, the residue was mixed with water and 2M hydrochloric acid (pH≈6) and extracted with chloroform (4×10 ml). The chloroform solution was washed with 5% aq $NaHCO_3$ (2×20 ml) and water (2×20 ml), dried and evaporated to leave amorphous substance (23 mg), showing a single spot, which was purified by preparative TLC (1 plate) over silica gel with benzene-ether (3:1) to yield **12A** (14 mg), which had mp 164—165 °C on trituration with isopropyl ether.

Reaction of 12α,13α-Epoxy-17α-hydroxyetiojerv-5-en-3-one 17-Acetate 3,3-Ethylene Acetal (2A) with BF_3. A solution of **2A** (250 mg) in benzene (25 ml) was stirred with BF_3 (0.25 ml) at room temperature for 30 s. After addition of ether (50 ml) and 5% aq $NaHCO_3$ (50 ml), the benzene-ether solution was worked up as mentioned above to leave resinous substance, showing several spots on TLC, which was separated into three fractions by chromatography over silica gel (15 g) as usual. Most mobile fractions gave **17A** (32 mg), mp 114—116 °C (from ether). Middle fractions afforded etiojerva-4,12,14,16-tetraen-3-one (**17B**, 27 mg), mp 129—130 °C (from ether) and $[\alpha]_D$ +75.6°; MS, *m/e* 266 (M^+);

UV, λ_{max} 272 nm (ε 300), 237 (8400), and 219 (7600); IR, ν_{max} 1665 and 1613 cm^{-1}; NMR, δ 1.30 and 2.26 (each 3H, s, 19- and 18-H), 5.79 (1H, s, 4-H), and 6.97 (3H, s, W_H= 5 Hz, 15-, 16-, and 17-H). Found: C, 85.79; H, 8.19%. Calcd for $C_{19}H_{22}O$: C, 85.67; H, 8.33%. Least mobile fractions gave 12β-fluoro-13α,17α-dihydroxyetiojerv-5-en-3-one 17-acetate 3,3-ethylene acetal (**18A**, 15 mg), mp 186—189 °C (from ether) and $[\alpha]_D$ −53.0°; MS, *m/e* 408 (M^+), 388 (M^+−HF), and 364; IR, ν_{max} 3500, 1718, 1260, and 1110 cm^{-1}; NMR, δ 1.02, 1.25, and 2.10 (each 3H, s, 19- and 18-H, and OCOCH_3), 3.94 (4H, s, OC_2H_4O), 4.94 (1H, br, W_H=20 Hz, 17-H), and 5.36 (1H, br, W_H=10 Hz, 6-H). Found: C, 67.89; H, 8.16%. Calcd for $C_{23}H_{33}O_5F$: C, 67.62; H, 8.08%.

*Reaction of 12α,13α-Epoxy-17β-hydroxyetiojerv-5-ene-3,17-dione 3,3-Ethylene Acetal (**3A**) with BF_3.* Compound **3A** (110 mg) was treated with BF_3 (0.04 ml) in benzene (27 ml) at room temperature for 30 s under stirring. The reaction mixture was worked up as mentioned above to leave amorphous substance (130 mg), showing two main spots on TLC, which was separated by preparative TLC (6 plates) over silica gel with benzene–ether (1:3). A fraction with higher R_f value gave 13α,17β-dihydroxyetiojerva-5,12(14)-dien-3-one 3,3-ethylene acetal (**19A**, 60 mg), mp 201—203 °C and $[\alpha]_D$ −50.8°; MS, *m/e* 346 (M^+) and 303; IR, ν_{max} 3535, 3380, and 1095 cm^{-1}; NMR, δ 1.08 and 1.35 (each 3H, s, 19- and 18-H); 3.93 (5H, br s, W_H=7 Hz, 17-H and OC_2H_4O), and 5.36 (1H, br, W_H=10 Hz, 6-H). Found: C, 72.95; H, 8.85%. Calcd for $C_{21}H_{30}O_4$: C, 72.80; H, 8.73%. A fraction with lower R_f value afforded 13α,17β-dihydroxyetiojerva-4,12(14)-dien-3-one (**19B**, 23 mg), mp 174—177 °C (from ether) and $[\alpha]_D$ +57.2°; MS, *m/e* 302 (M^+) and 259; UV, λ_{max} 237 nm (ε 9600); IR, ν_{max} ($CHCl_3$) 3640, 3460, 1662, 1613, 1110, 1010, and 960 cm^{-1}; NMR, δ 1.24 and 1.36 (each 3H, s, 19- and 18-H), 3.96 (1H, br, W_H=7 Hz, 17-H), and 5.75 (1H, s, 4-H). Found: C, 75.38; H, 8.77%. Calcd for $C_{19}H_{26}O_3$: C, 75.46; H, 8.67%.

*Reaction of 12α,13α-Epoxy-17β-hydroxyetiojerv-5-en-3-one 17-Acetate 3,3-Ethylene Acetal (**4A**) with BF_3.* To a benzene solution (80 ml) of **4A** (320 mg) was added BF_3 (0.2 ml) in benzene (2 ml) under stirring. The resulting dark-green mixture was stirred at room temperature for 20 min. The reaction was ceased by addition of 5% aq $NaHCO_3$ (80 ml), when the mixture became yellow. The benzene solution was worked up as usual to leave resinous substance (320 mg), which was separated into three fractions by chromatography over silica gel (90 g) with benzene–ether mixtures. Initial fractions eluted with benzene–ether (1:1) gave the unreacted epoxide (**4A**, 43 mg). Early fractions eluted with benzene–ether (1:1) afforded 12α,13β,17β-trihydroxy-13-epietiojerv-5-en-3-one 17-acetate 3,3-ethylene acetal (**20A**, 115 mg), mp 204—206 °C (from ether–acetone) and $[\alpha]_D$ −25.4°; MS, *m/e* 406 (M^+), 388, 370, and 346; IR, ν_{max} 3530, 3460, 3350, 1730, 1267, 1105, 1090, and 1020 cm^{-1}; NMR, δ 1.02, 1.20, and 2.06 (each 3H, s, 19- and 18-H, and OCOCH_3), 3.93 (4H, s, OC_2H_4O), 5.00 (1H, br, W_H=9 Hz, 17-H), and 5.34 (1H, br, W_H=10 Hz, 6-H). Found: C, 67.59; H, 8.68%. Calcd for $C_{23}H_{34}O_6$: C, 67.95; H, 8.43%. Later fractions eluted with benzene–ether (1:1) gave 12α,13β,17β-trihydroxy-13-epietiojerv-4-en-3-one 17-acetate (**20B**, 140 mg), mp 182—184 °C (from ether–acetone) and $[\alpha]_D$ +124°; MS, *m/e* 362 (M^+), 344, 302, 284, and 266; UV, λ_{max} 239 nm (ε 9700); IR, ν_{max} 3490, 3400, 1712, 1668, 1610, 1263, and 1024 cm^{-1}; NMR, δ 1.17, 1.20, and 2.07 (each 3H, s, 19- and 18-H, and OCOCH_3), 5.01 (1H, br, W_H=9 Hz, 17-H), and 5.74 (1H, s, 4-H). Found: C, 69.83; H, 8.35%. Calcd for $C_{21}H_{30}O_5$; C, 69.58; H, 8.34%.

Compound **20A** (20 mg) was treated with potassium carbonate (K_2CO_3, 8 mg) in water (2 ml) at room temperature for 3 h under stirring. The reaction mixture was mixed with saturated brine (40 ml) and extracted with chloroform (3×10 ml). The chloroform solution was washed with water (3×20 ml), dried and evaporated to leave amorphous residue, showing a single spot on TLC, which was purified by preparative TLC (1 plate) over silica gel with ether, giving 12α,13β,17β-trihydroxy-13-epietiojerv-5-en-3-one 3,3-ethylene acetal (**21A**, 14 mg), mp 197—199 °C (from acetone) and $[\alpha]_D$ −33.2°; MS, *m/e* 364 (M^+), 346, and 328; IR, ν_{max} 3460, 3360, 1117, 1100, 1023, and 990 cm^{-1}; NMR, δ 1.05 and 1.29 (each 3H, 19- and 18-H), 3.82 (1H, br, W_H=10 Hz, 17-H), 3.94 (3H, s, OC_2H_4O), and 5.37 (1H, br, W_H=10 Hz, 6-H). Found: C, 69.23; H, 8.84%. Calcd for $C_{21}H_{32}O_5$: C, 69.20; H, 8.85%.

Compound **20B** (20 mg) in methanol (8 ml) was treated with K_2CO_3 (8 mg) in water (2 ml) in the same manner as **20A**. The reaction mixture was worked up as described above to yield 12α,13β,17β-trihydroxy-13-epietiojerv-4-en-3-one (**21B**, 13 mg), mp 217—218 °C (from acetone) and $[\alpha]_D$ +79.4°; MS, *m/e* 320 (M^+), 302, 284, and 266; UV, λ_{max} 239 nm (11000); IR, ν_{max} 3470, 1638, and 990 cm^{-1}; NMR, δ 1.20 and 1.30 (each 3H, s, 19- and 18-H), 3.82 (1H, br, W_H =11 Hz, 17-H), and 5.76 (1H, s, 4-H). Found: C, 70.87; H, 8.88%. Calcd for $C_{19}H_{28}O_4$: C, 71.22; H, 8.81%.

A solution of **21A** (37 mg) in acetone (8 ml) was stirred with 60% aq perchloric acid ($HClO_4$, 0.5 ml) at room temperature for 4 h. The solution was mixed with 5% aq $NaHCO_3$ (2 ml) and saturated brine (2 ml), and extracted with chloroform (4×10 ml). The chloroform extracts were washed with water (3×10 ml), dried and evaporated to yield amorphous residue, which was purified by preparative TLC (2 plates) over silica gel with ether–ethyl acetate (5:1) to give 12α,13β,17β-trihydroxy-13-epietiojerv-4-en-3-one 13β,17β-acetonide (**22B**, 25 mg), showing a single spot, amorphous and $[\alpha]_D$ +88.0 °; MS, *m/e* 360 (M^+), 345, 327, 302 (M^+−C_3H_6O), 284, and 267; UV, λ_{max} 239 nm (ε 12000); IR, ν_{max} ($CHCl_3$) 3580, 3440, 1660, 1615, 1380, 1376, and 1071 cm^{-1}; NMR, δ 1.17 (3H, s, 19-H) and 1.44 (9H, s, 18-H and acetonide CH_3), 4.19 (1H, br, W_H=12 Hz, 17-H), and 5.76 (1H, s, 4-H). Found: C, 72.99; H, 9.39%. Calcd for $C_{22}H_{32}O_4$: C, 73.30; H, 8.95%.

Compound **21B** (8 mg) in acetone (2 ml) was stirred with 60% aq $HClO_4$ (0.1 ml) in the same manner as **21A**. The reaction mixture was worked up as usual to give the amorphous acetonide (7 mg) identical with **22B** (UV, IR, NMR, and TLC).

*Reaction of 12α,13α-Epoxyetiojerv-5-ene-3,17-dione 3,3-Ethylene Acetal (**5A**) with BF_3.* Compound **5A** (400 mg) in benzene (100 ml) was treated with BF_3 (0.36 ml) in benzene (3 ml) at room temperature for 1 h under stirring, when a small spot of **5A** was still detected on TLC. After addition of ether (50 ml) and 5% aq $NaHCO_3$, the mixture was separated into the benzene–ether and aqueous solutions. The former was worked up as usual to a resinous mixture, which was separated and purified by chromatography over silica gel (25 g) with benzene–ether mixtures. Initial two fractions eluted with benzene–ether (6:1) afforded the unchanged epoxide (**5A**, 24 mg) and 13α-acethyl-18,*C*-dinorcholest-5-ene-3,17-dione 3,3-ethylene acetal (**23A**, 20 mg), mp 124—125 °C (from ether) and $[\alpha]_D$ −72.1°; MS, *m/e* 344 (M^+) and 301; IR, ν_{max} 1734, 1715, 1361, and 1105 cm^{-1}; NMR, δ 0.96 and 2.20 (each 3H, s, 19-H and $COCH_3$), 3.94 (4H, s, OC_2H_4O), and 5.38 (1H, br, W_H=11 Hz, 6-H). Found: C, 73.08; H, 8.31%. Calcd for $C_{21}H_{28}O_4$: C, 73.22; H, 8.19%. Next two fractions eluted with benzene–ether (6:

1) gave 17-hydroxyetiojerva-4,12,14,16-tetraen-3-one (**24B**, 60 mg), mp 289—291 °C (from $CHCl_3$) and $[\alpha]_D$ +48.4°, and 12α,13α-epoxyetiojerv-4-ene-3,17-dione (**5B**, 90 mg), mp 185—187 °C and $[\alpha]_D$ +82.9°. **24B**, MS, *m/e* 282 (M^+) and 160; UV, λ_{max} 285 nm (sh) (ε 900), 279 (1100), and 234 (9000); IR ν_{max} 3280, 1648, 1600, and 830 cm^{-1}; NMR, δ 1.28 and 2.15 (each 3H, 19- and 18-H), 5.78 (1H, s, 4-H), 6.58 and 6.79 (each 1H, ABq, J=8 Hz, 16- and 15-H). Found: C, 80.60; H, 7.72%. Calcd for $C_{19}H_{22}O_3$: C, 80.81; H, 7.85%. **5B**, MS, *m/e* 300 (M^+), 285, 257, and 214; UV, λ_{max} 237 nm (ε 9500); IR ν_{max} 1716, 1673, and 1613 cm^{-1}; NMR, δ 1.20 and 1.36 (each 3H, s, 19- and 18-H), and 5.80 (1H, s, 4-H). Found: C, 75.68; H, 8.16%. Calcd for $C_{19}H_{24}O_3$: C, 75.94; H, 8.05%. Fractions eluted with benzene-ether (4:1) afforded 13α-acetyl-*C*,18-dinorcholest-4-ene-3,17-dione (**23B**, 90 mg), mp 112—113 °C (from ether) and $[\alpha]_D$ +74.0°; MS, *m/e* 300 (M^+), 285 and 257, UV, λ_{max} 237 nm (ε 10000), IR, ν_{max} 1733, 1700, 1679, 1615, and 1365 cm^{-1}; NMR, δ 1.14 and 2.20 (each 3H, s, 19-H and $COCH_3$), and 5.73 (1H, s, 4-H). Found: C, 75.82; H, 8.06%. Calcd for $C_{19}H_{24}O_3$: C, 75.97; H, 8.05%.

*Reaction of 12α,13β-Epoxy-17β-hydroxy-13-epietiojerv-5-en-3-one 3,3-Ethylene Acetal (**6A**) with BF_3.* To a benzene solution (50 ml) of **6A** (200 mg) was added rapidly BF_3 (0.06 ml) in benzene (2 ml) under stirring, and the dark-blue solution was stirred at room temperature for 30 s, when the solution became brown. The reaction was ceased by addition of ether (50 ml) and 5% aq $NaHCO_3$ (50 ml). The benzene-ether solution was worked up as mentioned above to leave amorphous substance, which was separated roughly by chromatography over silica gel (8 g) with a 2:1 mixture of benzene and ether. Early eluates contained two compounds, which were separated by preparative TLC (6 plates) over silica gel with ether to give 14β,17β-epoxy-13β-hydroxy-12α,13-epietiojerv-5-en-3-one 3,3-ethylene acetal (**30A**, 29 mg), mp 207—208 °C and $[\alpha]_D$ −45.2°, and 13β,17β-dihydroxy-12α,13-epietiojerva-5,8(14)-dien-3-one 3,3-ethylene acetal (**25A**, 90 mg), mp 102—104 °C (from ether-hexane) and $[\alpha]_D$ −37.2°. **30A**, MS, *m/e* 346 (M^+), 331, 328, and 303; IR, ν_{max} 3580, 1200, 1140, 1130, 1100, 1080, 1060, 1040, 970, and 940 cm^{-1}; NMR, δ 1.08 and 1.30 (each 3H, s, 19- and 18-H), 3.95 (4H, s, OC_2H_4O), 4.06 (1H, d, J=5 Hz, 17-H), and 5.38 (1H, br, W_H=10 Hz, 6-H). Found: C, 72.84; H, 8.71%. Calcd for $C_{21}H_{30}O_4$: C, 72.80; H, 8.73%. **25A**, MS, *m/e* 346 (M^+), 331, 328, and 313; UV, λ_{max} 208 nm (ε 10000); IR, ν_{max} 3420, 1095, and 1018 cm^{-1}; NMR, δ 0.91 and 1.23 (each 3H, s, 19- and 18-H), 3.41 (1H, br, W_H= 25 Hz, 17-H), 3.94 (4H, s, OC_2H_4O), and 5.34 (1H, br, W_H=8 Hz, 6-H). Found: C, 73.15; H, 8.32%. Calcd for $C_{21}H_{30}O_4$: C, 72.80; H, 8.73%. Later eluates also consisted of at least two compounds, from which the following were isolated by preparative TLC (3 plates over silica gel with ether. 13β,17β-Dihydroxy-12α,13-epietiojerva-4,8(14)-dien-3-one (**25B**, 49 mg), mp 185—187 °C and $[\alpha]_D$ +83.3°; MS, *m/e* 302 (M^+) and 284; UV, λ_{max} 234 nm (ε 12000) and 208 (10000); IR, ν_{max} 3530, 3380, 1650, 1618, 1120, 1060, and 1002 cm^{-1}; NMR, δ 1.07 and 1.24 (each 3H, s, 19- and 18-H), 3.45 (1H, br, W_H=22 Hz, 17-H), and 5.82 (1H, s, 4-H). Found: C, 74.99; H, 8.57%. Calcd for $C_{19}H_{26}O_3$: C, 75.46; H, 8.67%. 14β,17β-Epoxy-13β-hydroxy-12α,13-epietiojerv-5-en-3-one (**30B**, 13 mg), mp 136—138 °C (from ether-hexane) and $[\alpha]_D$ +60.2°; MS, *m/e* 302(M^+), 287, 284, and 259; UV, λ_{max} 237 nm (ε 11000); IR, ν_{max} 3460, 1660, 1610, 1010, 990, 952, and 912 cm^{-1}; NMR, δ 1.23 and 1.31 (each 3H, s, 19- and 18-H), 4.07 (1H, d, J=5 Hz, 17-H), and 5.75 (1H, s, 4-H). Found: C, 75.81; H, 8.60%. Calcd for $C_{19}H_{26}O_3$: C, 75.46; H, 8.67%.

Compounds **25A** (12 mg) and **25B** (12 mg) were treated with acetic anhydride (0.6 ml) and pyridine (0.12 ml) at room temperature for 20 h under stirring. The respective reaction mixtures were mixed with cold water (5 ml) and extracted with chloroform (3×10 ml). The extracts were washed with 5% aq $NaHCO_3$ to give the corresponding monoacetates (**26A**, 9 mg, and **26B**, 10 mg), which were identical with the reaction products of **7A** described later.

Compound **25A** (42 mg) was refluxed with *p*-toluenesulfonic acid (*p*-TsOH, 22 mg) in acetone (13 ml) and water (2 ml) for 2 h under stirring. The mixture was evaporated to leave amorphous residue, which was treated with 5% aq $NaHCO_3$ and chloroform. The chloroform extracts were worked up as usual to leave crystalline residue (41 mg), which was purified by preparative TLC (1 plate) over silica gel with ether–benzene (1:1) to yield a crystalline substance (32.5 mg), which was identical with an authentic sample of **25B** in all respects.

Compound **25B** (32 mg) was treated with acetone (5 ml) and 60% aq $HClO_4$ (0.05 ml) at room temperature for 30 min under stirring. The mixture was evaporated below 30 °C, made alkaline with 6 M aq ammonia, and extracted with dichloromethane (4×10 ml). The extracts were worked up as usual to leave oily residue (22 mg), containing **25B** regenerated during work-up, which was submitted to chromatography over alumina (3 g). Less polar fractions eluted with benzene gave an oily material (2.3 mg), showing a single spot on TLC, which was identified as the corresponding acetonide (**27B**), oily; MS, *m/e* 342 (M^+), 327, 284, and 269; IR, ν_{max} ($CHCl_3$) 1665 and 1618 cm^{-1}; NMR, δ 1.07 and 1.26 (each 3H, s, 19- and 18-H), 1.33 and 1.40 (each 3H, s, acetonide CH_3), 4.14 (1H, br, W_H=14 Hz, 17-H), and 5.81 (1H, s, 4-H). Eluates with chloroform afforded the unchanged glycol (**25B**, 17 mg).

To a suspended mixture of chromium(VI) oxide (CrO_3, 27 mg) in dichloromethane (0.3 ml) and pyridine (2 drops) was added **25B** (6.3 mg) in dichloromethane (0.3 ml). The mixture was stirred at room temperature for 30 min and then diluted with ether (10 ml). The ether-dichloromethane solution was washed 5% aq sodium hydroxide, 2M hydrochloric acid (HCl), 5% aq $NaHCO_3$, and saturated brine, dried and evaporated to leave oily residue (6.7 mg), showing 3 spots on TLC. The mixture was separated by preparative TLC (10×20 cm^2, 1 plate) with benzene–ether (1:1). A less polar fraction gave a crystalline substanec (0.4 mg), which was identical with the reaction product (**28B**) of **10A** described later. A more polar fraction yielded formyl ketone (**29B**, 2.0 mg), oily, showing a single spot on TLC, which exhibited the following spectra; MS, *m/e* 300 (M^+), 257, 256, and 213; IR, ν_{max} ($CHCl_3$) 2700, 1723, 1710, 1668, and 1620 cm^{-1}; NMR, δ 1.02 and 2.20 (each 3H, s, 19-H and CH_3CO), 3.65 (1H, br, W_H=12 Hz, 12-H), 5.85 (1H, s, 4-H), and 9.74 (1H, d, J=5 Hz, CHO). A most polar fraction gave the starting glycol (**25B**, 1.3 mg).

*Reaction of 12β,13β-Epoxy-17β-hydroxy-13-epietiojerv-5-en-3-one 17-Acetate 3,3-Ethylene Acetal (**7A**) with BF_3.* Compound **7A** (100 mg) was treated with BF_3 (0.03 ml) in benzene (40 ml) at room temperature for 30 s under stirring, when the spot of **7A** had disappeared on TLC. The reaction mixture was worked up as described above to leave amorphous residue, which was separated roughly into two fractions by chromatography over silica gel (5 g) with benzene–ether mixtures. Fractions eluted with benzene–ether (3:1) were further purified by preparative TLC (3 plates) over silica gel with benzene–ether (2:1) to give 17-acetate (**26A**, 51 mg) of **25A**,

mp 232—234 °C (from ether) and $[\alpha]_D$ +19.2°; MS, 388 (M^+), 373, 370, 355, 328, and 313; UV, λ_{max} 205 nm (ε 6000); IR, ν_{max} 3507, 1719, 1260, 1105, 1088, 1028, and 1019 cm^{-1}; NMR, δ 0.92, 1.13, and 2.09 (each, 3H, s, 19- and 18-H, and OCOCH$_3$), 3.94 (4H, s, OC$_2$H$_4$O), 4.77 (1H, do d, J=10 and 5 Hz, 17-H), and 5.30 (1H, br, W_H=8 Hz, 6-H). Found: C, 70.82; H, 8.21%. Calcd for $C_{23}H_{32}O_5$: C, 71.10; H, 8.30%. Fractions eluted with benzene–ether (2:1 and 1:1) were purified in the same manner as mentioned above to give 17-acetate (**26B**, 20 mg) of **25B**, mp 123—124 °C (from ether) and $[\alpha]_D$ +88.0°; MS, *m/e* 344 (M^+), 326, 284, and 266; UV, λ_{max} 232 nm (ε 12000) and 210 (12000); IR, ν_{max} 3400, 1748, 1673, 1250, 1050, and 1040 cm^{-1}; NMR, δ 1.09, 1.15, and 2.08 (each 3H, s, 19- and 18-H, and OCOCH$_3$), 4.78 (1H, do d, J=10 and 5 Hz, 17-H), and 5.77 (1H, s, 4-H). Found: C, 72.89; H, 8.12%. Calcd for $C_{21}H_{28}O_4$: C, 73.22; H, 8.19%.

Reaction of 12β,13β-Epoxy-17α-hydroxy-13-epietiojerv-5-en-3-one 3,3-Ethylene Acetal (8A) with BF_3. To a benzene solution (50 ml) of **8A** (150 mg) was added BF_3 (0.05 ml) in benzene (2 ml) under stirring. The solution was stirred at room temperature for 30 s, when the starting alcohol (**8A**) had disappeared on TLC. After addition of ether (25 ml) and 5% aq $NaHCO_3$ (25 ml), the benzene–ether mixture was worked up as usual to leave resinous material, which was submitted to chromatography over silica gel (8 g) with benzene–ether mixtures. Early fractions eluted with benzene–ether (2:1) gave 13β,17α-dihydroxy-12α,13-epietiojerva-5,8(14)-dien-3-one 3,3-ethylene acetal (**31A**, 50 mg), mp 174—175 °C (from ether) and $[\alpha]_D$ −45.8°; MS, *m/e* 346 (M^+), 331, 328, 313, and 284; UV, λ_{max} 207 nm (ε 9000); IR, ν_{max} 3550, 3480, 1100, 1075, 1032, and 1022 cm^{-1}; NMR, δ 0.90 and 1.20 (each 3H, s, 19- and 18-H), 3.70 (1H, br, W_H=8 Hz, 17-H), 3.94 (4H, s, OC$_2$H$_4$O), and 5.34 (1H, br, W_H=8 Hz, 6-H). Found: C, 72.83; H, 8.97%. Calcd for $C_{21}H_{30}O_4$: C, 72.80; H, 8.73%. Later fractions eluted with benzene–ether (2:1) afforded 13β,17α-dihydroxy-13-epietiojerva-5,12(14)-dien-3-one 3,3-ethylene acetal (**32A**, 30 mg), mp 169—171 °C (from acetone–ether) and $[\alpha]_D$ −3.7°; MS, *m/e* 346 (M^+), 331, 328, 313, 302, and 234; IR, ν_{max} 3400, 1095, and 1058 cm^{-1}; NMR, δ 1.12 and 1.29 (each 3H, s, 19- and 18-H), 3.58 (1H, br, W_H=5 Hz, 17-H), 3.95 (4H, s, OC$_2$H$_4$O), and 5.44 (1H, br, W_H=7 Hz, 6-H). Found: C, 72.68; H, 8.90%. Calcd for $C_{21}H_{30}O_4$: C, 72.80; H, 8.73%. Fractions eluted with benzene–ether (1:1) gave 13β,17α-dihydroxy-12α,13-epietiojerva-4,8(14)-dien-3-one (**31B**, 42 mg), showing a single spot on TLC, amorphous and $[\alpha]_D$ +59.7°; MS, *m/e* 302 (M^+), 284, and 266; UV, λ_{max} 234 nm (ε 11000) and 208 (9000); IR, ν_{max} 3400, 1650, 1070, and 1018 cm^{-1}; NMR, δ 1.08 and 1.25 (each 3H, s, 19- and 18-H), 3.76 (1H, br, W_H=7 Hz, 17-H), and 5.84 (1H, s, 4-H). Found: C, 75.89; H, 8.34%. Calcd for $C_{19}H_{26}O_3$: C, 75.46; H, 8.67%.

Compound **31A** (6 mg) was treated with *p*-TsOH (2 mg) in acetone (2 ml) and water (0.5 ml) under reflux for 2 h. The mixture was worked up as usual to give an amorphous substance, showing a single spot on TLC, which was identical with a sample of **31B** (MS, IR, NMR, and TLC).

Compound **32A** (8 mg) was treated with acetic anhydride (0.05 ml) and pyridine (0.1 ml) at room temperature for 24 h under stirring. The mixture was worked up as usual to give 17-acetate (**33A**, 6 mg), mp 119—121 °C (ether) and $[\alpha]_D$ −15.2°; MS, *m/e* 388 (M^+), 373, and 310; IR, ν_{max} 3440, 1735, 1248, and 1100 cm^{-1}; NMR, δ 1.13, 1.20, and 2.05 (each 3H, s, 19- and 18-H, and OCOCH$_3$), 3.96 (4H, s, OC$_2$H$_4$O), 4.77 and 5.44 (each 1H, br, W_H=7 Hz, 17- and 7-H).

To a suspended mixture of CrO_3 (20 mg) in dichloromethane (0.3 ml) and pyridine (2 drops) was added **31B** (6 mg) in dichloromethane (0.4 ml) under stirring. The mixture was stirred vigorously at room temperature for 40 min and diluted with ether. The whole mixture was worked up as described before to leave crystalline residue (5.4 mg), which was purified by preparative TLC (10× 20 cm^2, 1 plate) over silica gel with benzene–ether (1:1). A major fraction gave hydroxy ketone (2.3 mg), mp 176—179 °C, which was identical with a sample of **28B** described before in all respects.

Reaction of 12β,13β-Epoxy-17α-hydroxy-13-epietiojerv-5-en-3-one 17-Acetate 3,3-Ethylene Acetal (9A) with BF_3. Compound **9A** (140 mg) was treated with BF_3 (0.04 ml) in benzene (50 ml) at room temperature for 1 min under stirring, when the solution became violet. After addition of ether (25 ml) and 5% aq $NaHCO_3$ (25 ml), the mixture was separated into the benzene–ether and aqueous solutions. The former was washed with 5% aq $NaHCO_3$ (50 ml) and water (3× 50 ml), dried and evaporated to leave a complex mixture, which was separated roughly into two fractions by chromatography over silica gel (5 g) with a 1:1 benzene–ether mixture. Early and later eluates (33 and 65 mg) were further purified by preparative TLC (2 and 4 plates) over silica gel, respectively, giving 12α,13β,17α-trihydroxy-13-epietiojerv-5-en-3-one 12-acetate 3,3-ethylene acetal (**35A**, 33 mg) and 12β,13α,17α-trihydroxyetiojerv-5-en-3-one 17-acetate 3,3-ethylene acetal (**34A**, 24 mg). **35A**, amorphous and $[\alpha]_D$ −14.6°; MS, 406 (M^+), 388, 346, and 328; IR, ν_{max} ($CHCl_3$) 3640, 3510, 1708, 1280, 1100, 1010, and 980 cm^{-1}; NMR, δ 1.02, 1.18, and 2.08 (each 3H, s, 19- and 18-H, and OCOCH$_3$), 3.72 (1H, br, W_H=22 Hz, 17-H), 3.95 (4H, s, OC$_2$H$_4$O), and 5.38 (1H, br, W_H=8 Hz, 6-H). Found: C, 67.40; H, 8.77%. Calcd for $C_{23}H_{34}O_6$: C, 67.95; H, 8.43%. **34A**, mp 217—219 °C (from ether) and $[\alpha]_D$ −22.5°; MS, *m/e* 406 (M^+), 388, 346, and 328; IR, ν_{max} 3608, 3550, 1728, 1260, 1110, 1023, and 990 cm^{-1}; NMR, δ 1.03, 1.22, and 2.09 (each 3H, s, 19- and 18-H, and OCOCH$_3$), 3.95 (4H, s, OC$_2$H$_4$O), 5.14 (1H, br, W_H=17 Hz, 17-H), and 5.41 (1H, br, W_H=8 Hz, 6-H). Found: C, 67.92; H, 8.55%. Calcd for $C_{23}H_{34}O_6$: C, 67.95; H, 8.43%.

Compound **34A** (6 mg) was treated with 5% KOH in methanol (1 ml) at room temperature for 5 h under stirring. The reaction mixture was worked up as usual to leave crystalline residue (4.8 mg), which was recrystallized from ether to give the corresponding triol (**36A**), mp 207.5—208.5 °C; MS, *m/e* 364 (M^+), 346, 328, and 99; IR, ν_{max} ($CHCl_3$) 3605, 3470, 1101, 1017, and 987 cm^{-1}; NMR, δ 1.02 and 1.32 (each 3H, s, 19- and 18-H), 3.87 (1H, br m, W_H= 24 Hz, 17-H), 3.94 (4H, s, OC$_2$H$_4$O), and 5.39 (1H, br, W_H=8 Hz, 6-H). The triol (**36A**, 4.8 mg) was then treated with acetone (2 ml) and 60% aq $HClO_4$ (2 drops, 0.035 ml) at room temperature for 20 h under stirring. The reaction mixture was worked up as usual to give the corresponding 13α,17α-acetonide (**37B**, 4.6 mg), amorphous; MS, *m/e* 360 (M^+), 320, 302, 284; IR, ν_{max} ($CHCl_3$) 3690, 3480, 1661, and 1614 cm^{-1}; NMR, δ 1.14 (3H, s, 19-H), 1.24 and 1.29 (6H, and 3H, each s, 18-H and acetonide CH$_3$), 4.22 (1H, br, W_H=20 Hz, 17-H), and 5.77 (1H, s, 4-H).

Compound **35A** (36 mg) was hydrolyzed with 5% KOH in methanol (2 ml) at room temperature for 20.5 h to give the corresponding triol (**38A**, 26 mg), mp 199.5—201.5 °C (from benzene) and $[\alpha]_D$ −51.7°; MS, *m/e* 364 (M^+), 346, 328, and 99; IR, ν_{max} 3460, 3425 (sh), 1084, 1013, and 985 cm^{-1}; ν_{max} ($CHCl_3$) 3615, 3490, 1105, 1088, 1059, 1019, and 997 cm^{-1}; NMR, δ 1.04 and 1.36 (each 3H, s, 19- and 18-H), 2.60, 2.66, and 2.71 (each 1H, s, 3OH), 3.68 (1H,

br, W_H=14 Hz, and 6 Hz on addition of D_2O, 17-H), 3.94 (4H, s, $OC_2\underline{H}_4O$), and 5.36 (1H, br, W_H=9 Hz, 6-H). The triol (**38A**, 13 mg) was also treated with *p*-TsOH (3 mg) in acetone (2 ml) and water (0.5 ml) under reflux for 2 h. The mixture was worked up as described already to leave crystalline residue (12 mg), which on recrystallization from benzene-diisopropyl ether gave 12α,13β,17α-trihydroxy-13-epietiojerv-4-en-3-one (**38B**, 5.0 mg), mp 197—198 °C and $[\alpha]_D$ +76.6°; MS, *m/e* 320 (M^+), 302, 284, 266, and 84; IR, ν_{max} ($CHCl_3$) 3645, 3455, 1667, 1617, 1060, 1016, and 937 cm^{-1}; NMR, δ 1.14 and 1.37 (each 3H, s, 19- and 18-H), 3.03 (1H, br s, OH), 3.68 (1H, br, W_H=21 Hz, and 9 Hz on addition of D_2O, 17-H), and 5.73 (1H, s, 4-H).

To a suspended mixture of CrO_3 (30 mg) in dichloromethane (0.3 ml) and pyridine (3 drops) was added **38B** (10 mg) in pyridine (0.5 ml). The mixture was stirred at room temperature for 40 min. After addition of ether (50 ml) the reaction mixture was worked up as described before to leave oily residue (6 mg), which was submitted to prepararive TLC (20×10 cm^2, 1 plate) over silica gel to give the starting alcohol (**38B**, 1.3 mg) and 12α,13β-dihydroxy-13-epietiojerv-4-ene-3,17-dione (**39B**, 1.7 mg), mp 171.5—173 °C (from benzene-diisopropyl ether); MS, *m/e* 318 (M^+) and 300; IR, ν_{max} ($CHCl_3$) 3605, 3510, 1715, 1669, and 1619 cm^{-1}; NMR, δ 1.08 and 1.47 (each 3H, s, 19- and 18-H), 1.58 and 3.66 (each 1H, s, 2OH), and 5.79 (1H, s, 4-H). Compound **21B** (9.2 mg) was likewise oxidized with CrO_3 (25 mg) in dichloromethane (0.6 ml) and pyridine (0.2 ml) at room temperature for 45 min under stirring. The reaction mixture was worked up as usual and purified by preparative TLC (1 plate) over silica gel with ether to give the starting alcohol (**21B**, 0.5 mg) and hydroxy ketone, mp 168.5—170 °C, which was identical with a sample of **39B** (MS, IR, NMR, and TLC).

*Reaction of 12β,13β-Epoxy-13-epietiojerv-5-ene-3,17-dione 3,3-Ethylene Acetal (**10A**) with BF_3.* Compound **10A** (50 mg) was treated with BF_3 (0.02 ml) in benzene (20 ml) at room temperature for 20 min under stirring, when the spot of **10A** had disappeared on TLC. The reaction was ceased by addition of ether (10 ml) and 5% aq $NaHCO_3$ (10 ml), and the mixture was worked up as mentioned above to leave amorphous residue, showing essentially a single spot on TLC, which was purified by preparative TLC (3 plates) over silica gel with a 6:4:1 mixture of benzene, ether, and chloroform to give 13β-hydroxy-12α,13-epietiojerva-4,8(14)-diene-3,17-dione (**28B**, 35 mg), mp 178—180 °C and $[\alpha]_D$ +178.2°; MS, *m/e* 300 (M^+), 282 and 214; UV, λ_{max} 232 nm (ε 10000) and 206 (8000); IR, ν_{max} 3370, 1717, 1650, 1610, 1112, and 1083 cm^{-1}; NMR, δ 1.14 and 1.27 (each 3H, s, 19- and 18-H), and 5.83 (1H, s, 4-H). Found: C, 75.69; H, 7.85%. Calcd for $C_{19}H_{24}O_3$: C, 75.97; H, 8.05%. The compound (**28B**) was identified as the aforementioned oxidation product of **25B** by direct comparison of both the samples.

*Reduction of **5A** with Sodium Borodeuteride ($NaBD_4$).* Compound **5A** (1.12 g) was treated with $NaBD_4$ (Merck, D-content 98%, 160 mg) in methanol (100 ml) at room temperature for 30 min under stirring. After addition of acetic acid to decompose excess of the $NaBD_4$, the mixture was made alkaline with 6 M aq ammonia, evaporated below 30 °C, mixed with water and extracted with chloroform. The chloroform extracts were worked up as usual to leave foamy residue (1.27 g), showing two spots on TLC, which was submitted to chromatography over silica gel (80 g) with benzene-ether mixtures. Less polar fractions (220 mg) eluted with benzene-ether (2:1) afforded 12α,13α-epoxy-17β-hydroxyetiojerv-5-en-3-one-17-*d* 3,3-ethylene acetal (**41A**, 161 mg), mp 154.5—157 °C (from benzene-diisopropyl ether) and $[\alpha]_D$ −75.2°; MS, *m/e* 348 (0.25%), 347 (M^+, 0.66%), 329 (0.27%), and 99 (base); IR, ν_{max} 3470, 1115, 1100, 1028, 997, and 963 cm^{-1}; NMR, δ 1.00 and 1.37 (each 3H, s, 19- and 18-H), 1.60 (1H, s, OH), 3.95 (4H, s, $OC_2\underline{H}_4O$), and 5.38 (1H, br, W_H=11 Hz, 6-H). More polar fractions eluted with benzene-ether (2:1 and 1:1) gave a 17β-epimer (α-OH) (**40A**, 890 mg), mp 169—171 °C (from benzene-diisopropyl ether) and $[\alpha]_D$ −57.8°; MS, *m/e* 348 (0.24%), 347 (M^+, 0.59%), 329 (0.33%), and 99 (base); IR, ν_{max} 3480, 1136, 1090, 1070, 1047, 961, and 946 cm^{-1}; NMR, δ 1.00 and 1.39 (each 3H, s, 19- and 18-H), 1.68 (1H, s, OH), 3.95 (4H, s, $OC_2\underline{H}_4O$), and 5.38 (1H, br, W_H=10 Hz, 6-H). The R_f values of **40A** and **41A** on TLC were identical with those of **1A** and **3A**, respectively.

Compound **40A** (20 mg) was oxidized with CrO_3 (242 mg) in pyridine (5.1 ml) at room temperature for 17 h under stirring. The reaction mixture was worked up as mentioned above to leave oily residue (21 mg), showing two spots on TLC, which was separated by chromatography over silica gel (1.5 g) with benzene–ether (2:1). Less polar fractions gave a crystalline substance (6.7 mg) on trituration with diisopropyl ether, which had mp 143.5—144 °C and was identified as **5A** by direct comparison of both the samples. More polar fractions afforded the unchanged alcohol (**40A**, 12.3 mg). Compound **41A** (15 mg) was likewise oxidized with CrO_3 (173 mg) in pyridine (4.5 ml) at room temperature for 17 h to give **5A** (8.2 mg), mp 143.5—144 °C, and the unchanged alcohol (**41A**, 6 mg).

*Reaction of **40A** with BF_3.* To a benzene solution (100 ml) of **40A** (452 mg) cooled with ice-water was added rapidly BF_3 (0.2 ml), freshly distilled over calcium hydride, in benzene (3 ml) under stirring. The mixture was stirred at room temperature for 30 s. The reaction was ceased by addition of 5% aq $NaHCO_3$ (50 ml). The whole mixture was separated into the benzene and aqueous layers, and the latter was shaken with ether (2×50 ml). The benzene and ether solutions were combined, washed with 5% aq $NaHCO_3$ (3×30 ml) and saturated brine (3×30 ml), dried and evaporated below 30 °C to leave foamy residue (437 mg), showing two major spots on TLC, which was separated by chromatography over silica gel (30 g) with benzene–ether (19:1). Less polar fractions afforded a crystalline substance (51 mg) on trituration with diisopropyl ether–hexane, which on recrystallization from ether gave a 17-*d* derivative (**43A**, 13 mg) of **17A**, mp 116—118.5 °C and $[\alpha]_D$ −81.0°; MS, *m/e* 312 (0.87%), 311 (M^+, 2.48%), 310 (0.20%), and 99 (base); IR, ν_{max} ($CHCl_3$) 1104 and 1094 cm^{-1}; NMR, δ 1.16 and 2.27 (each 3H, s, 19- and 18-H), 3.95 (4H, s, $OC_2\underline{H}_4O$), 5.49 (1H, br, W_H=10 Hz, 6-H), 6.97 and 7.06 (each 1H, ABq, J=8 Hz, 15- and 16-H). More polar fractions afforded a crystalline substance (79 mg) on trituration with diisopropyl ether, which was recrystallized from ether to give a 13-*d* derivative (**42A**, 24 mg) of **11A**, mp 133—135 °C and $[\alpha]_D$ −63.2°; MS, *m/e* 330 (0.67%), 329 (M^+, 1.73%), 328 (0.50%), and 99 (base); IR, ν_{max} 1722, 1109, and 1096 cm^{-1}; NMR, δ 1.09 and 1.21 (each 3H, s, 19- and 18-H), 3.96 (4H, s, $OC_2\underline{H}_4O$), and 5.43 (1H, br, W_H=10 Hz, 6-H).

Compound **42A** (25 mg) was treated with 5% KOH in methanol (1 ml) at room temperature for 1 h. The reaction mixture was evaporated, diluted with water, acidified to pH 6 with 2 M aq HCl, and extracted with chloroform (4×10 ml). The chloroform extracts were worked up as usual to leave amorphous residue (23 mg), which was purified by preparative TLC over silica gel (1 plate) with benzene-ether (3:1). Major fractions gave a crystalline substance

(13 mg) on trituration with diisopropyl ether, which had mp 164.5—166 °C and was identical with a sample of **12A** (MS, IR, NMR, and TLC).

References

1) Part V, A. Murai, N. Iwasa, and T. Masamune, *Chem. Lett.*, **1978**, 235.

2) Part XXXIII of "*C*-Nor-*D*-homosteroids and Related Alkaloids;" Part XXXII, A. Murai, H. Sasamori, and T. Masamune, *Bull. Chem. Soc. Jpn.*, **51**, 243 (1978).

3) A. Murai, N. Iwasa, M. Takeda, H. Sasamori, and T. Masamune, *Bull. Chem. Soc. Jpn.*, **50**, 429 (1977).

4) A. Murai, H. Sasamori, and T. Masamune, *Bull. Chem. Soc. Jpn.*, **50**, 437 (1977).

5) T. Masamune, A. Murai, K. Nishizakura, T. Orito, S. Numata, and H. Sasamori, *Bull. Chem. Soc. Jpn.*, **49**, 1622 (1976).

6) T. Masamune, N. Sato, K. Kobayashi, I. Yamazaki, and Y. Mori, *Tetrahedron*, **23**, 1591 (1967).

7) B. M. Iselin and O. Wintersteiner, *J. Am. Chem. Soc.*, **77**, 5318 (1955).

8) T. Masamune, I. Yamazaki, K. Orito, and M. Takasugi, *Tetrahedron*, **27**, 3387 (1971).

9) D. N. Kirk and M. P. Hartshorn, "Steroid Reaction Mechanisms," Elsevier Publ. Co., London (1968), p. 353.

10) Compounds **2**, **2a**, **6**, and **18** in Ref. 4.

11) J. M. Coxon, M. P. Hartshorn, and D. N. Kirk, *Tetrahedron*, **21**, 2489 (1965).

12) Compounds **17** and **19** in Ref. 4.

13) T. H. Campion, G. A. Morrison, and J. B. Wilkinson, *J. Chem. Soc., Perkin Trans. 1*, **1976**, 2508, and references cited therein; E. Glotler, P. Krinsky, M. Rejto, and M. Weissenberg, *ibid.*, **1976**, 1442.

14) J. M. Domagala and R. D. Bach, *J. Am. Chem. Soc.*, **100**, 1605 (1978), and references cited therein; J. M. Domagala, R. D. Bach, and J. Wemple, *ibid.*, **98**, 1975 (1976).

15) N. S. Bhacca and D. H. Williams, "Application of NMR Spectroscopy in Organic Chemistry," Holden-Day Inc., San Francisco, California (1964), p. 20.

16) *Cf.*, D. W. Turner, *J. Chem. Soc.*, **1959**, 30; P. S. Ellington and G. D. Meakins, *ibid.*, **1960**, 697 and references cited therein.

17) A. Murai, M. Ono, and T. Masamune, *Bull. Chem. Soc. Jpn.*, **50**, 1226 (1977), and related refs cited therein.

18) a) Ref. 9, p. 355; b) C. D. Nenitzescu, "Carbonium Ions," ed by G. A. Olah and P. von R. Schleyer, Wiley-Interscience, New York (1970), Vol. II, p. 463; G. J. Karabatos and J. L. Fry, *ibid.*, p. 521; c) B. N. Blackett, J. M. Coxon, M. P. Hartshorn, and K. E. Richards, *Tetrahedron Lett.*, **1969**, 1737; J. M. Coxon, M. P. Hartshorn, C. N. Muir, and K. E. Richards, *ibid.*, **1967**, 3725; d) E. J. Parish, M. E. Newcomer, G. L. Gilliland, F. A. Quischo, and G. J. Schroepfer, Jr., *Tetrahedron Lett.*, **1976**, 4401.

19) a) S. P. Singh and J. Kagan, *J. Am. Chem. Soc.*, **91**, 6198 (1969); b) H. O. House and D. J. Reif, *J. Am. Chem. Soc.*, **79**, 6451 (1957); *ibid.*, **77**, 6525 (1955); H. O. House, *ibid.*, **76**, 1235 (1954); c) A. M. Maione, I. Torrini, and A. Romeo, *J. Chem. Soc., Perkin Trans. 1*, **1976**, 2363; d) M. Niwa, M. Iguchi, and S. Yamamura, *Tetrahedron Lett.*, **1975**, 3661.

12,13-Epoxy-*C*-nor-*D*-homosteroids. VII.[1] Reaction of 11-Oxygenated 17α-Acetyl-12β,13β-epoxy-13-epietiojervanes with Boron Trifluoride Etherate and Potassium Hydroxide[2]

Akio MURAI, Hiroshi SASAMORI, and Tadashi MASAMUNE*

Department of Chemistry, Faculty of Science, Hokkaido University, Sapporo 060

(Received July 11, 1979)

The title compounds were treated with boron trifluoride etherate in benzene at room temperature. 11β-Hydroxy- and 11-oxo-12β,13β-epoxides (**1** and **14**) underwent cleavage of the epoxy group at C-13 by the acid treatment to give the corresponding fluorohydrins (**2** and **5**) as the respective major products, while the former (**1**) also afforded a 13β-pregnane derivative (**3**) with a normal steroid skeleton. On the other hand, several 11-oxygenated 12α,13α- and 12β,13β-epoxides (**17**, **17a**, **19**, **21**, **1**, and **23**) were treated with potassium hydroxide in aqueous methanol at room temperature. All epoxides gave the corresponding $\Delta^{13(17)}$-20-ketones, and only 11-hydroxy- and 11-acetoxy-12α,13α-epoxides (**17**, **19**, and **17a**) were further transformed into a 13α-pregnane derivative (**12**).

In a previous paper[3] we reported the synthesis and stereochemistry of 17α-acetyl-12,13-epoxyetiojervanes. As a continuing study aimed at the preparation of normal steroids from jervine, we have examined reactions of 11-oxygenated 17α-acetyl-12β,13β-epoxy-13-epietiojervanes[3] with boron trifluoride etherate and potassium hydroxide, considering the reaction of the corresponding 12α,13α-epoxyetiojervanes.[4] In the present paper we describe the result, which involves transformation into a compound with a pregnane skeleton.

Acid Treatment. Treatment of 17α-acetyl-12β,13β-epoxy-11β-hydroxy-13-etiojerv-4-en-3-one[3] (**1**) with boron trifluoride etherate (BF_3) in benzene at room temperature for 30 s produced a mixture, from which three compounds (**2**—**4**) were isolated after careful chromatography in 38, 16 and 10% yields, respectively. The major product (**2**), mp 228—230 °C, was assigned on the basis of the following evidence. The mass [*m/e* 364 (M^+), 344 (M^+-HF), and 301 (344—$COCH_3$)] and NMR spectra [δ 2.22 (3H, s, 21-H), 3.29 (1H, d, J=6 Hz, 11-OH), 3.72 (1H, s, OH)] revealed the presence of one fluorine atom, one acetyl (at C-17) and two hydroxyl groups. These spectra, coupled with the UV [λ_{max} 239 nm (ε 11000)] and IR spectra (ν_{max} 1702 cm^{-1}), indicated that the A ring and 17-side chain remained unchanged. The NMR spectrum also exhibited two three-proton singlets at δ 1.40 and 1.42 (19- and 18-H or *vice versa*) and one-proton doublet (J=8 Hz) due to a proton on the carbon atom (at C-11) bearing the hydroxyl group at δ 4.57. Compound **2**, when oxidized with the Jones reagent, was converted into hydroxy ketone (**5**), mp 198—200 °C, in 75% yield, which showed a strong absorption maximum at 1748 cm^{-1} in the IR spectrum, indicating the secondary hydroxyl group is located on a five-membered (C) ring. Compound **2** also formed the acetonide (**6**), oil, by prolonged treatment (42 h) with acetone and acid ($HClO_4$) in 47% yield, with the recovered fluorohydrin (**2**, 50%), indicative of the presence of a *cis*-glycol moiety. Moreover, the fluorohydrin (**2**) underwent dehydrofluorination by treatment with base (KOH in aq CH_3OH, room temp, 3.5 h) to give $\Delta^{13(17)}$-20-ketone (**7**), mp 154—156 °C, showing an absorption maximum at 245 nm (ε 17000) and two three-proton singlets at δ 1.39 and 1.86 (19- and 18-H) in the UV and NMR spectra. This compound (**7**), when treated with BF_3 at room temperature for 30 s, was transformed into a known Δ^{12}-11,17-dione[3] (**8**) in 40% yield. All these facts indicate that the major compound should be assigned formula **2**, excluding an alternate structure (**2'**). The configuration of the fluorine atom at C-13 was assigned by analogy of *trans*-fluorohydrin formation[4] resulting from the epoxide cleavage by the S_N2 type of nucleophilic attack of a fluoride anion.[5]

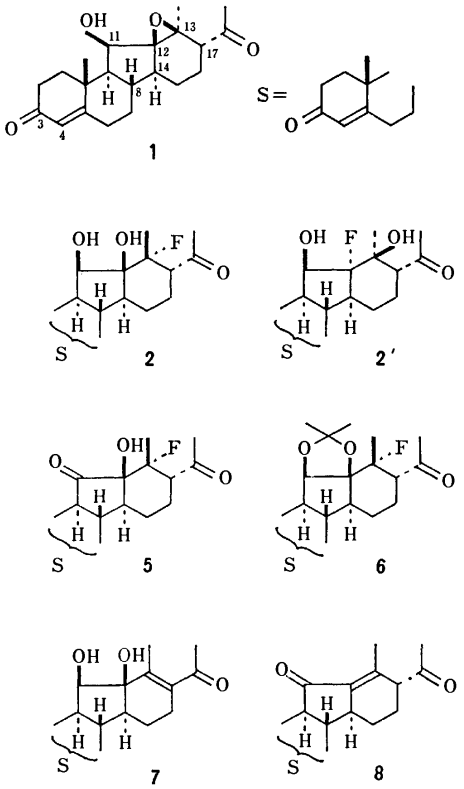

The second product (**3**), oil, had the same molecular formula $C_{21}H_{28}O_4$ as the starting epoxide (**1**), and its spectra revealed the presence of hydroxyl, acetyl, and Δ^4-3-carbonyl groups: OH, *m/e* 344 (M^+) and 326 (M^+-H_2O); ν_{max} 3483 cm^{-1}; δ 3.80 (1H, d, J=4 Hz, OH): CH_3C=O, ν_{max} 1713 cm^{-1}; δ 2.18 (3H, s, 21-H): Δ^4-3-C=O, λ_{max} 239 nm (ε 13000); ν_{max} 1664

and 1616 cm^{-1}; δ 5.72 (1H, s, 4-H). Hence the remaining oxygen atom would consititute a carbonyl group on a six-membered ring, whose absorption maximum might overlap with that of the acetyl carbonyl group (1713 cm^{-1}),[6] or an ether oxygen function. The possibility of the latter was excluded by the following facts. Compound **3**, when oxidized with the Jones reagent, was converted into diosphenol (**9**), mp 142—144 °C, in 75% yield. The diosphenol structure was characterized by the spectra of **9** and its acetate (**9a**): **9**, λ_{max} 284 nm (ε 7000);[7] ν_{max} 3400, 1664, and 1620 cm^{-1}; δ 6.91 (1H, s, OH) and no signal due to a proton at C-11: **9a**, λ_{max} 243 nm (ε 20000) ($\Delta^{9(11)}$-12-C=O and Δ^{4}-3-C=O); ν_{max} 1766, 1621, and 1225 cm^{-1}; δ 2.28 (3H, s, $OCOCH_3$), 1.12 and 1.53 (each 3H, s, 18- and 19-H), and 3.55 (1H, do d, J=12.5 and 6 Hz, 17-H). The formation of diosphenol **9** suggested strongly that an α-ketol group is located in a six-membered ring in **3** and hence the compound (**3**) must possess a normal steroid skeleton. In order to confirm the structure, compound **3** was treated with base (KOH in aq CH_3OH, room temp, 16 h) with expectation that **3** would be transformed into a known steroidal compound[8] (**10**). However, the treatment led to formation of hemiacetal (**11**). oil, in 40% yield, whose structure was deduced from the spectral data; ν_{max} 3600, 3430, 1718, 1667, and 1614 cm^{-1}; δ 1.13, 1.32 and 1.41 (each 3H, s, 18-, 19- and 21-H, or *vice versa*), 4.22 and 5.72 (each 1H, s, 12- and 4-H). The spectra were similar to but not identical with those of the corresponding 13α-pregnane[4] (**12**). The compound (**3**) is therefore represented by the 13β-pregnane formula (**3**) most favorably. The formation of hemiacetal **11** rather than **10** would probably result from facile epimerization of the α-ketol system under the basic conditions, compared with that of the 17-acetyl group.

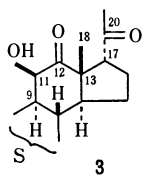

3

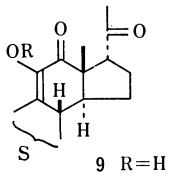

9 R=H
9a R=Ac

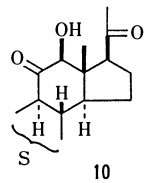

10

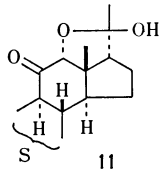

11

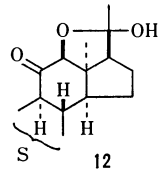

12

The third product (**4**), mp 188—190 °C, was tentatively assigned formula **4**. The molecular formula $C_{21}H_{30}O_5$ [(**1**) $C_{21}H_{28}O_3+H_2O$], coupled with the spectral data, suggested that the compound would be formed by hydrolysis of the epoxy group and formulated by **4** or **4'**: OH, *m/e* 362 (M^+), 344 (M^+-H_2O) and 326 (M^+-2H_2O); ν_{max} 3360 cm^{-1}; δ 4.46 (1H, d, J=6 Hz, 11-H) and 1.34 (3H, s, 18-H): 17-$COCH_3$, ν_{max} 1693 cm^{-1}; δ 3.15 (1H, br, W_H=18 Hz, 17-H) and 2.26 (3H, s, 21-H): Δ^{4}-3-C=O, λ_{max} 239 nm (ε 13000); ν_{max} 1661 and 1613 cm^{-1}; δ 1.38 (3H, s, 19-H) and 5.70 (1H, s, 4-H). Oxidation of **4** with chromium(VI) oxide gave a five-membered hydroxy ketone (**13**), mp 198—200 °C, showing an absorption maximum at 1747 cm^{-1} in the IR spectrum. The compoumd (**4**) was then treated with periodic acid (aq dioxane, room temp, 18 h), when none of the acid had been consumed. Moreover, it did not give the acetonide under the same conditions as **2**. These results are in good accord with formula **4** with two *trans*-glycol systems for the third compound. The formation of **4** would probably take place in acidic media during the work-up.

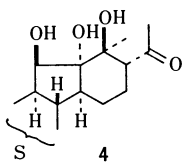

4

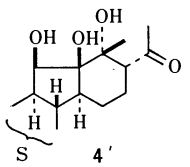

4'

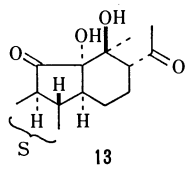

13

Similar and slightly prolonged (10 min) treatment of 17α-acetyl-12β,13β-epoxy-13-epietiojerv-4-ene-3,11-dione[3] (**14**) with BF_3 producted two compounds in 63 and 18% yields. The major product, mp 198—200 °C, was identified as fluorohydrin **5** described already. The minor product (**15**), mp 221—223 °C, had a molecular formula $C_{21}H_{38}O_4$ [(**14**) $C_{21}H_{26}O_3+H_2O$] and displayed the mass, UV, and IR spectra (except the finger print region) similar closely to those of compound **13**. However, the NMR spectrum revealed the presence of two hydroxyl groups at δ 4.20 and 7.24 (each 1H, s) and differed clearly from that of **13**. These data led to tentative assignment of formula **15** to the compound. It is beyond our comprehension that 12β,13β-epoxyetiojervanes (**1** and **14**) gave compounds formulated by simple hydrolysis products (**13** and **15**) though in low yield, while such compounds were not isolated from 12α,13α-epoxyetiojervanes.[4] In summary, the reactions of 12β,13β-epoxyetiojervanes with the acid resembled those of the corresponding 12α,13α-epimers as far as the predominant formation of fluoro-

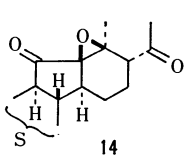

14

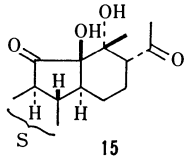

15

hydrins concerns, but differed definitely in the one-step transformation into the 13β-pregnane derivative (**3**).

Base Treatment. We previously reported that base treatment of 17α-acetyl-13β-fluoro-11α,12α-dihydroxy-13-epietiojerv-4-en-3-one (**16**), a major product obtained by the BF_3 treatment of the corresponding 12α,13α-epoxide (**17**), gave rise to a 13α-pregnane derivative (**12**) *via* 11α,12α-dihydroxy-$\Delta^{13(17)}$-20-ketone (**18**).[4] In connection with the interesting rearrangement, we examined reactions of several 11-oxygenated 17α-acetyl-12,13-epoxyetiojervanes with base. The results (Table 1) are summarized as follows.

Table 1. The reaction of 11-oxygenated 17α-acetyl-12,13-epoxyetiojervanes with base[a]

Starting 12,13-epoxide	Reaction time/h	Products (isolated yield/%) $\Delta^{13(17)}$-20-ketone		13-pregnane	
11α-OH, α-epoxide (**17**)	2.5	(**18**)	15	(**12**)	65
	19	(**18**)	0	(**12**)	75
11α-OAc, α-epoxide (**17a**)	1.6	(**18**)	56	(**12**)	40
	19	(**18**)	10	(**12**)	67
11β-OH, α-epoxide (**19**)	1.6	(**20**)	70	(**12**)	20
	2.5	(**20**)	55	(**12**)	25
	19	(**20**)	0	(**12**)	75
11-deoxo, α-epoxide (**21**)	1.6	(**22**)	100		0
	19	(**22**)	70		0
11β-OH, β-epoxide (**1**)	1.6	(**7**)	90		0
	19	(**7**)	75		0
11α-OAc, β-epoxide (**23**)	19	(**24**)	70		0

a) KOH in aq CH_3OH, room temp.

(i) The base treatment of 11α-hydroxy-12α,13α-epoxide[3] (**17**) and its 11-acetate[3] (**17a**) afforded **18** and **12**. Likewise, 11β-hydroxy-12α,13α-epoxide[3] (**19**) was converted into the corresponding 11β,12α-dihydroxy-$\Delta^{13(17)}$-20-ketone (**20**) and **12**. However, (ii) the reaction of 11-unsubstituted 12α,13α-epoxide[3] (**21**) resulted in formation of only the corresponding $\Delta^{13(17)}$-20-ketone (**22**). Moreover, 11β-hydroxy-12β,13β-epoxide (**1**) and its 11α-acetoxy isomer[3] (**23**) produced only 11β,12β- and 11α,12β-dihydroxy-$\Delta^{13(17)}$-20-ketones (**7** and **24**) under almost the same conditions, no 13β-pregnane derivatives (**3** and **11**) being isolated. The structure of these new compounds (**20**, **22**, and **24**) were deduced from their spectral data. Compounds **20**, mp 221—223 °C, **22**, mp 169.5—171.5 °C, and **24**, mp 212—214 °C, exhibited the same absorption maximum at 245 nm (ε 17000) as the known $\Delta^{13(17)}$-20-ketones (**7** and **18**) and also three three-proton singlets at δ 1.36, 1.91, and 2.29 (19-, 18- and 21-H), δ 1.07, 1.90, and 2.25, and δ 1.21, 1.97, and 2.25, respectively. The configuration of 11-hydroxyl groups in **20** and **24** were drawn from the chemical shifts of the respective 19-methyl protons (δ_{calcd} 1.36 for **20** and 1.17 for **24**), the contribution of 12-hydroxyl groups being neglected.[9]

Detailed examination of Table 1 reveals the following points. (i) All the epoxides (**17**, **17a**, **19**, **21**, **1**, and **23**) readily gave the respective $\Delta^{13(17)}$-20-ketones (**18**, **18**, **20**, **22**, **7**, and **24**) by base treatment, and the former

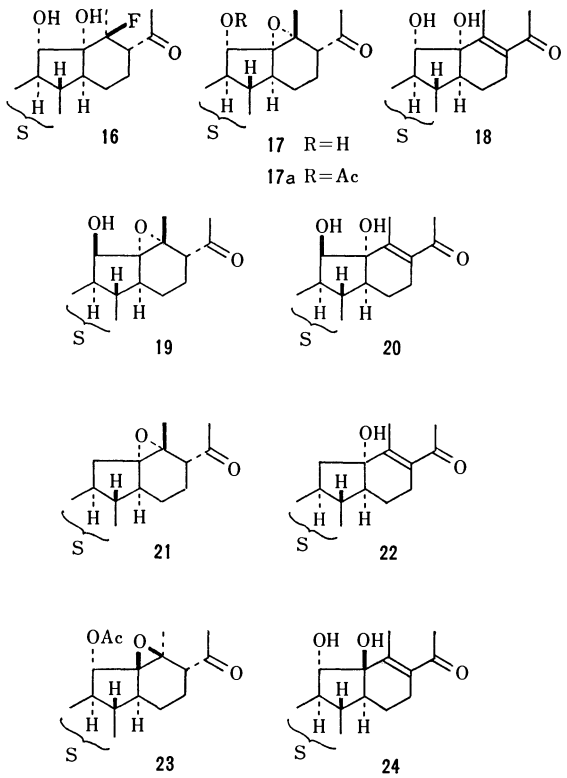

two (**18** and **20**) were intermediates for the formation of the 13α-pregnane (**12**). (ii) The reaction of 11α-acetoxy-12α,13α-epoxide (**17a**) proceeded slowly than that of 11α-hydroxy-12α,13α-epoxide (**17**), because the former involved hydrolysis of the 11α-hydroxyl group as the first step. (iii) It should be noted that (a) the formation of 13α-pregnane **12** required the presence of not only a 12α-hydroxyl group but also a hydroxyl group at C-11, whatever the configuration was, and (b) the rearrangement of *cis* (11α,12α)-glycol (**18**) took place more rapidly than *trans* (11β,12α)-glycol (**20**), indicative of serious participation of the 11-hydroxyl group in the rearrangement. The fact that only the compounds possessing 11- and 12α-hydroxyl groups were transformed into the rearranged product (**12**) would be interpreted by assuming that the cleavage of the C-12–C-14 bond and formation of the C-13–C-14 bond would occur from the β-side of the molecule in a concerted manner. We again emphasize that the 13β-pregnane (**3**) was produced from the 11β-hydroxy-12β,13β-epoxide (**1**) only by acid treatment but not by base treatment, while the 13α-pregnane (**12**) from the 11-hydroxy-12α,13α-epoxides (**17** and **19**) only by base treatment.

Experimental

All the melting points were uncorrected. The homogeneity of each compound was always checked by TLC on silica gel (Wakogel B-5) with various solvent systems, and the spots were developed with cerium(IV) sulfate in dil sulfuric acid and/or iodine. The optical rotations, UV, and IR spectra were measured in chloroform, ethanol, and chloroform, respectively, unless otherwise stated. The NMR spectra were obtained in chloroform-*d* at 100 MHz, and the chemical shifts were given in δ-values, TMS being used as an internal reference. The abbreviations "s, d, t, br, and

do" in the NMR and IR spectra denote "singlet, doublet, broad, and double," respectively.

Treatment of 17α-Acetyl-12β,13β-epoxy-11β-hydroxy-13-epietiojerv-4-en-3-one (1) with Boron Trifluoride Etherate (BF_3). A solution of **1** (90 mg) in anhydrous benzene (9 ml) was stirred with BF_3 (0.18 ml), freshly distilled over calcium hydride, at room temperature for 30 s. The solution was mixed with ether (5 ml), washed with 5% aq sodium hydrogencarbonate and water, dried over anhydrous sodium sulfate, and evaporated to leave amorphous residue (100 mg), which was separated into three fractions by preparative TLC over silica gel (Wakogel B-5F, 10 plates) with ether. A most mobile fraction gave a crystalline substance, which was recrystallized from ether to yield 17α-acetyl-13α-fluoro-11β,12β-dihydroxyetiojerv-4-en-3-one (**2**, 35 mg), mp 228—230 °C and $[\alpha]_D$ +156°; MS, UV, IR, and NMR, in the text. Found: C, 69.35; H, 8.20%. Calcd for $C_{21}H_{29}O_4F$: C, 69.20; H, 8.02%. A middle fraction afforded 11β-hydroxy-17-epipregn-4-ene-3,12,20-trione (**3**, 14 mg), oil, $[\alpha]_D$ +45°; MS, UV, IR, and NMR, in the text; NMR, δ 1.51 and 1.21 (each 3H, s, 19- and 18-H), 3.80 and 4.08 (each 1H, d, J= 4 Hz, OH and 11-H). Found: C, 73.03; H, 8.40%. Calcd for $C_{21}H_{28}O_4$: C, 73.22; H, 8.19%. A least mobile fraction gave 17α-acetyl-11β,12α,13β-trihydroxy-13-epietiojerv-4-en-3-one (**4**, 10 mg), mp 188—190 °C (from diisopropyl ether–acetone) and $[\alpha]_D$ +129°; MS, UV, IR, and NMR, in the text.

17α-Acetyl-13α-fluoro-12β-hydroxy-etiojerv-4-ene-3,11-dione (5). A solution of **2** (20 mg) in dry acetone (4 ml) was stirred with the Jones reagent (0.24 ml) for 1 h under cooling with ice. After addition of ethanol, the solution was evaporated and shaken with water and chloroform. The chloroform solution was worked up as usual to leave a crystalline substance, showing a single spot, which was recrystallized from acetone-hexane to give **5** (15 mg), mp 198—200 °C and $[\alpha]_D$ −5.5°; ORD, $[\phi]_{344}^{trough}$ −3900°, $[\phi]_{300}^{peak}$ +4250°, a= −82°; MS, *m/e* 362 (M^+), 344 (M^+-H_2O), 342 (M^+−HF), and 299 (342−$COCH_3$); UV, λ_{max} 235 nm (ε 10000); IR, ν_{max} 3400, 1748, 1707, 1664, and 1614 cm^{-1}; NMR, δ 1.21, 1.50 and 2.20 (each 3H, s, 19-, 18- and 21-H), and 5.80 (1H, s, 4-H).

11,12-Acetonide (6) of 2. A solution of **2** (40 mg) in acetone (8 ml) was stirred with 60% aq perchloric acid (0.4 ml) for 42 h. The solution was made alkaline with 5% aq sodium hydrogencarbonate, evaporated and extracted with chloroform. The chloroform solution, after being worked up as usual, left an oily residue (50 mg), showing two spots, which was separated into two fractions by preparative TLC over silica gel (Wakogel B-5F, 2 plates) with ether. A less polar fraction gave **6** (20 mg), oil; IR, ν_{max} 1705, 1664, 1615, 1384, and 1373 cm^{-1}; NMR, δ 1.39 and 2.17 (6H and 3H, each s, 19-, 18- and 21-H), 1.47 and 1.55 (each 3H, s, acetonide 2CH_3), 3.00 (1H, br, W_H=20 Hz, 17-H), 4.74 (1H, d, J=4 Hz, 11-H), and 5.71 (1H, s, 4-H). Found: C, 71.33; H, 8.07%. Calcd for $C_{24}H_{33}O_4F$: C, 71.26; H, 8.22%. A more polar fraction (20 mg) was identified as the starting fluorohydrin (**2**).

17-Acetyl-11β,12β-dihydroxyetiojerva-4,13(17)-dien-3-one (7). a) A solution of **2** (10 mg) in methanol (2.5 ml) containing 5% potassium hydroxide was stirred at room temperature for 3.5 h. The solution was made neutral with 10% aq acetic acid, evaporated below 40 °C, and shaken with water and chloroform. The chloroform solution gave a crystalline substance, showing a single spot, which was recrystallized from diisopropyl ether–acetone to yield **7**, (8 mg), mp 154—156 °C; MS, *m/e* 344 (M^+), 326, and 311; UV, λ_{max} 245 nm (ε 17000); IR, ν_{max} 3624, 3450, 1680 (br), 1658, and 1612 cm^{-1}; NMR, δ 1.39, 1.86, and 2.25 (each 3H, s, 19-, 18-, and 21-H), 3.36 (1H, d, J=9 Hz, OH), 4.33 (1H, t, J= 9 Hz, 11-H), and 5.67 (1H, s, 4-H).

b) A solution of **7** (20 mg) in anhydrous benzene (2 ml) was stirred with freshly distilled BF_3 (0.04 ml) at room temperature for 30 s. The solution was worked up as usual to leave an oily residue (19 mg), which was separated by preparative TLC over silica gel (Wakogel B-5F, one plate) with ether. A major fraction was crystallized on trituration with diisopropyl ether–acetone and recrystallized from the same solvent mixture to give Δ^{12}-11,20-dione (**8**, 7 mg), which was identified as the known compound.[3]

11-Hydroxy-17-epipregna-3,11-diene-3,12,20-trione (9) and Its 11-Acetate (9a). a) A solution of **3** (8 mg) in dry acetone (1.5 ml) was stirred with the Jones reagent (0.05 ml) for 1 h under cooling with ice. The reaction mixture was worked up as described before to leave an oily substance, which was purified by preparative TLC to yield diosphenol (**9**, 6 mg), mp 142—144 °C; UV, λ_{max} 237 nm (ε 12000) and 284 (7000); IR, ν_{max}3400, 1712, 1664, 1620, and 1613 cm^{-1}; NMR, δ 1.11, 1.53, and 2.14 (each 3H, s, 18-, 19-, and 21-H), 5.77 (1H, s, 4-H), and 6.91 (1H, s, OH). Found: C, 73.41; H, 7.86%. Calcd for $C_{21}H_{26}O_4$: C, 73.66; H, 7.66%.

b) Compound **9** (6 mg) was stirred with acetic anhydride (0.2 ml) and pyridine (0.4 ml) at room temperature for 12 h. The reaction mixture was worked up as usual to give enol acetate (**9a**, 6.4 mg), oil; UV, IR, and NMR, in the text.

12α-Hydroxy-17-epipregn-4-ene-3,11,20-trione 12,20-Hemiacetal (11). A solution of **3** (10 mg) in methanol (2.5 ml) containing 5% potassium hydroxide was stirred at room temperature for 16 h. The reaction mixture was made neutral, evaporated, and shaken with water and chloroform. The chloroform solution was worked up as usual to leave an oily substance, which was purified by preparative TLC to give hemiacetal (**11**, 4 mg), oil and $[\alpha]_D$ +96°; MS, *m/e* 344 (M^+), 326, 311, 301, 284, 283, and 256; UV, λ_{max} 237 nm (ε 10000); IR and NMR, in the text.

17α-Acetyl-12α,13β-dihydroxy-13-epietiojerv-4-ene-3,11-dione (13). To a stirred suspension of chromium(VI) oxide (15 mg) in dry dichloromethane (0.4 ml) and pyridine (0.025 ml) was added a solution of **4** (8 mg) in dichloromethane (0.1 ml). The mixture was stirred at room temperature for 15 min and filtered, then precipitates were washed with ether. The filtrate and ether washings were combined, washed with 5% aq sodium hydroxide and saturated aq sodium chloride, dried and evaporated to leave a crystalline substance (7 mg), which was recrystallized from ether to yield **13** (4 mg), mp 198—200 °C; MS, *m/e* 360 (M^+), 342, 318, 300, and 285; UV, λ_{max} 238 nm (ε 12000); IR, ν_{max} 3440, 1747, 1710, 1665, and 1612 cm^{-1}; NMR, δ 1.23, 1.46, and 2.20 (each 3H, s, 19-, 18- and 21-H), 4.20 (1H, s, OH), 5.76 (1H, s, 4-H), and 7.24 (1H, s, OH).

Treatment of 17α-Acetyl-12β,13β-epoxy-13-epietiojerv-4-ene-3,11-dione (14) with BF_3. Compound **4** (30 mg) in benzene (3 ml) was treated with BF_3 (0.07 ml) at room temperature for 10 min. The reaction mixture was worked up as described before to give oily residue (34 mg), which was separated into two fractions by preparative TLC over silica gel (Wakogel B-5F, 2 plates) with ether. A less polar fraction gave 11-oxo fluorohydrin (20 mg), mp 198—200 °C (from acetone–hexane), which was identified as **5**. A more polar fraction afforded 17α-acetyl-12β,13α-dihydroxyetiojerv-4-ene-3,11-dione (**15**, 6 mg), mp 221—223 °C and $[\alpha]_D$ −2.2°; MS, *m/e* 360 (M^+), 342, 318, 300, and 285; UV, λ_{max} 238 nm (ε 12000); IR, ν_{max} 3443, 1743, 1713, 1664, and 1614 cm^{-1};

NMR, δ 1.18, 1.46, and 2.20 (each 3H, s, 19-, 18- and 21-H), 4.20 (1H, s, OH), 5.76 (1H, s, 4-H), and 7.24 (1H, s, OH).

*Base Treatment of 11-Oxygenated 17α-Acetyl-12,13-epoxyetiojervanes (**17**, **17a**, **19**, **21**, **1**, and **23**).* The results are summarized in Table 1, and a few representative examples are described below. a) A solution of 11α-hydroxy-12α,13α-epoxide[3] (**17**, 20 mg) in methanol (5 ml) containing 5% potassium hydroxide was stirred at room temperature for 2.5 h. The reaction mixture was made neutral with 10% aq acetic acid under cooling, evaporated below 40 °C, and shaken with water and chloroform. The chloroform solution was worked up as usual to leave oily residue, showing two spots on TLC, which was separated into two fractions by preparative TLC over silica gel (Wakogel B-5F, one plate). A less polar fraction (13 mg) was identified as a known 13α-pregnane derivative[4] (**12**) by direct comparison with the sample (MS, NMR, IR, and TLC). A more polar fraction (3 mg) was also identified as 11α,12α-dihydroxy-$\Delta^{13(17)}$-20-ketone[4] (**18**).

b) Treatment of 11β-hydroxy-12α,13α-epoxide[3] (**19**, 20 mg) with potassium hydroxide under the same conditions (2.5 h) as mentioned above afforded **12** (5 mg) and 11β,12α-dihydroxy-$\Delta^{13(17)}$-20-ketone (**20**, 11 mg) after preparative TLC, mp 221—223 °C; MS, *m/e* 344 (M^+); UV, λ_{max} 245 nm (ε 16000); IR, ν_{max} 3540, 3380, 1690 (br), 1655, and 1608 cm^{-1}; NMR, δ 1.36, 1.91, and 2.29 (each 3H, s, 19-, 18-, and 21-H), 4.10 (1H, d, J=4 Hz, 11-H), and 5.71 (1H, s, 4-H).

c) Treatment of 11-unsubstituted 12α,13α-epoxide[3] (**21**, 20 mg) and 11α-acetoxy-12β,13β-epoxide[3] (**23**, 20 mg) were treated with potassium hydroxide under the same conditions (19 h) as described above. The respective reaction mixture was worked up as usual to give 12α-hydroxy- (**22**, 13 mg) and 11α,12β-dihydroxy-$\Delta^{13(17)}$-20-ketones (**24**, 13 mg), 13α- and 13β-pregnane derivatives being not detected on TLC: **22**, mp 169.5—171.5 °C; MS, *m/e* 328 (M^+); UV, λ_{max} 245 nm (ε 17000); IR, ν_{max} 3610, 3444, 1680 (br), 1660, and 1614 cm^{-1}; NMR, δ 1.07, 1.90, and 2.25 (each 3H, s, 19-, 18-, and 21-H), and 5.73 (1H, s, 4-H): **24**, mp 212—214 °C; MS, *m/e* 344 (M^+), 326, 311, and 301; UV, λ_{max} 245 nm (ε 17000); IR, ν_{max} 3624, 3444, 1680 (br), 1660, and 1610 cm^{-1}; NMR, δ 1.21, 1.97, and 2.25 (each 3H, s, 19-, 18-, and 21-H), 3.97 (1H, br, W_H=10 Hz, 11-H), and 5.75 (1H, s, 4-H).

References

1) Part VI, A. Murai, N. Iwasa, M. Takeda, and T. Masamune, *Bull. Chem. Soc. Jpn.*, **53**, 243 (1980).
2) Part XXXIV of "*C*-Nor-*D*-homosteroids and Related Alkaloids," Part XXXIII, Ref. 1.
3) A. Murai, H. Sasamori, and T. Masamune, *Bull. Chem. Soc. Jpn*, **51**, 234 (1978).
4) A. Murai, H. Sasamori, and T. Masamune, *Bull. Chem. Soc. Jpn.*, **50**, 437 (1977).
5) D. N. Kirk and M. P. Hartshorn, "Steroid Reaction Mechanisms," Elsevier Publ. Co., London, (1968), p. 353.
6) A. I. Cohen, B. T. Keeler, E. J. Becker, and P. A. Diassi, *J. Org. Chem.*, **30**, 2175 (1965).
7) L. Dorfman, *Chem. Rev.*, **53**, 47 (1953).
8) E. J. Becker, R. M. Palmere, A. I. Cohen, and P. A. Diassi, *J. Org. Chem.*, **30**, 2169 (1965).
9) T. Masamune, A. Murai, K. Nishizakura, T. Orito, S. Numata, and H. Sasamori, *Bull. Chem. Soc. Jpn.*, **49**, 1622 (1976).

12,13-Epoxy-*C*-nor-*D*-homosteroids. VIII.[1] Transformation of 12α,13α-Epoxyetiojerv-5-ene-3,17-dione 3,3-Ethylene Acetal into Testosterone[2]

Akio Murai, Noriaki Iwasa, and Tadashi Masamune*

Department of Chemistry, Faculty of Science, Hokkaido University, Sapporo 060

(Received July 11, 1979)

Transformation of the title epoxy ketone (**2**) into testosterone (**1**), which implies synthesis of the hormone **1** from jervine, is described. Irradiation of **2** by a low-pressure lamp in dioxane afforded an androstane-12,17-dione derivative, which was reduced regioselectively with lithium tri-*t*-butoxyaluminium hydride to give 12β-hydroxy ketone (**5**). The compound **5** was transformed *via* a four-step process into androstan-4-ene-3,17-dione, which was converted into **1** by a known procedure. The overall yield amounted to 1.8% from jervine.

In a recent preliminary communication[3] we reported the synthesis of testosterone (**1**) from jervine *via* the title epoxy ketone (**2**) as a result of continuing studies on the preparation of biologically active steroid hormones from jervine, one of the most readily available veratrum alkaloids. In the present paper we describe the details of the transformation from **2** into **1**, since the preparation of **2** had already been reported.

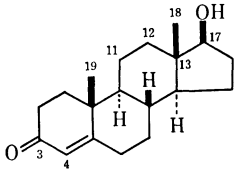

1

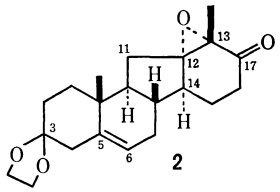

2

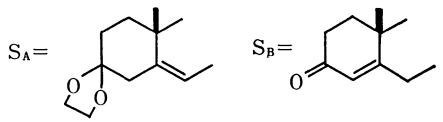

Photo-transformation of α,β-epoxy ketones has been investigated extensively and demonstrated to give a variety of products including rearranged 1,3-diketones.[5] With the expectation that the title 12α,13α-epoxy 17-ketone (**2**) would be transformed into an androstane-12,17-dione derivative, we examined the photolysis of **2** under various conditions (Experimental, Table 1). It was found that irradiation of **2** by a low pressure lamp in dioxane produced two isomeric 1,3-diketones (**3**), mp 253—254 °C, and (**4**), mp 181—183 °C, in 14 and 10% yields, respectively, a considerable amount (67%) of the starting material (**2**) being recovered unchanged. In accordance with the assigned structures, the respective compounds (**3** and **4**) had the same molecular formula $C_{21}H_{28}O_4$ as **2** and exhibited two absorption maxima at the carbonyl region and two three-proton singlets at high field in the IR and NMR spectra: **3**, ν_{max} 1756 and 1707 cm^{-1}; δ 1.13 and 1.23 (19- and 18-H): **4**, ν_{max} 1745 and 1708 cm^{-1}; δ 0.97 and 1.23. The calculated δ-values (1.167 and 1.293) for 19- and 18-methyl protons[6] and mechanistic considerations[5] indicated that a normal steroid skeleton could be assigned to the former (**3**), while a bicyclo-[3.3.1]nonane-2,9-dione partial structure to the latter (**4**). The former was then obtained in 40% yield by the repeated photo-transformations.

Table 1. Photolysis of **2**[a]

Solvent	Time	Products (yield/%)						
		2	**3**	**4**	**15**	**17**	**18**	**19**
Dioxane	1 d	67	14	10	—	—	—	—
Ether	1 d	76	5	5	—	—	—	—
DME[b]	1 d	67	10	6	—	—	—	—
Cyclohexane	1 d	75	4	3	—	—	—	—
THF	1 d	70	7	4	—	—	—	—
CH_3CN	10 h	35	6	5	18[d]	—	—	—
CCl_4[c]	3.5 h	84	—	—	4[d]	—	—	—
CCl_4+O_2[e]	20 h	27	—	—	38	—	—	—
Benzene[d]	10 h	24	—	—	—	19	8	22

a) Carried out by a 15-W low pressure mercury lamp at room temperature. b) DME, 1,2-dimethoxyethane. c) By a 100-W high pressure lamp. d) Formation of **15** would be attributed to the presence of oxygen gas contaminated in the solvents. e) Carried out in stream of oxygen.

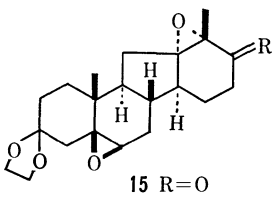

15 R=O
16 R=⋯OH, —H

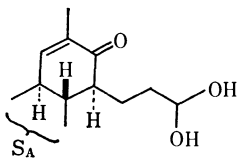

17

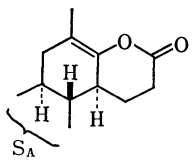

18

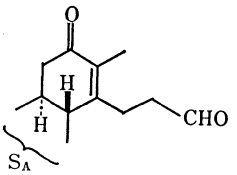

19

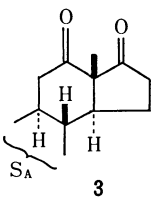

3

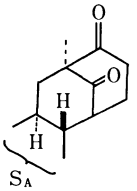

4

Transformation of the 12,17-diketone (**3**) into **1** was carried out by two usual routes. Reduction of **3** with lithium tri-*t*-butoxyaluminium hydride in tetrahydrofuran (THF) proceeded regioselectively to give 12β-hydroxy 17-ketone (**5**), mp 195—197 °C [ν_{max} 1736 cm^{-1}; δ 3.81 (1H, do d, J=10 and 5 Hz, 12-H)], in 96% yield, which was converted readily into the corresponding 12β-mesylate (**6**), mp 156—158 °C. Attempted reductive elimination of the mesyl group by treatment with lithium aluminium hydride resulted in the S–O bond cleavage of the group to give only 12β,17β-diol (**7**), mp 186—188 °C [δ 3.52 (1H, do d, J=10 and 5 Hz, 12-H) and 3.88 (1H, t, J=8 Hz, 17-H)]. The diol (**7**) was also obtained by direct reduction of **3** with the hydride reagent in 94% yield.[7] Partial acetylation of **7**, however, led to formation of a 3:2 mixture of the 17β- and 12β-monoacetates (**8a** and **8b**), which without further purification was oxidized with chromium(VI) oxide (CrO_3) in pyridine to yield a 1:1 mixture of the corresponding 17-oxo 12-acetate (**9a**) and 12-oxo 17-acetate (**9b**). The mixture was then submitted to the Wolff-Kishner reduction followed by purification by preparative TLC to give 17β-hydroxyandrost-5-en-3-one 3,3-ethylene acetal[8] (**10**) in low (12%) yield from **3**. This compound (**10**) underwent deacetalization by a known procedure[8] to yield testosterone (**1**).

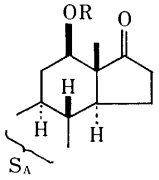

5 R=H
6 R=CH_3SO_2
9a R=Ac
10 RO=H

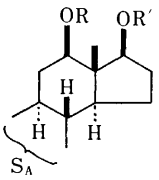

7 R=R'=H
8a R=H, R'=Ac
8b R=Ac, R'=H

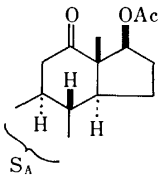

9b

An alternate and improved transformation of **3** into **1** was commenced by acetalization of 12β-hydroxy 17-ketone (**5**) with ethylene glycol and acid (p-TsOH). The resulting acetal (**11**), mp 219—220 °C, was oxidized by the usual procedure (CrO_3 in Py) to 12,17-diketone 17-acetal (**12**), mp 215—216 °C, in 66% yield from **5**. The Wolff-Kishner reduction of **12** produced 3,17-diacetal (**13**), mp 175—176 °C, which on deacetalization with the acid in aqueous acetone gave androst-4-ene-3,17-dione[8] (**14**), mp 175—176 °C, in 85% yield from **12**. This diketone (**14**) was transformed by a known procedure[8] into testosterone (**1**). The overall yield amounted to 35% from the photolysis product (**3**) and 1.8% from jervine.

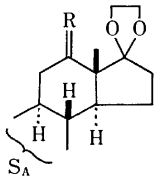

11 R=—OH, ···H
12 R=O
13 R=H_2

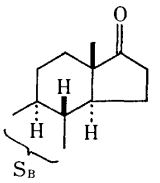

14

Experimental

All the melting points were uncorrected. The homogeneity of each compound was always checked by TLC on silica gel (Wakogel B-5) with various solvent systems, and the spots were developed with cerium(IV) in dil sulfuric acid and/or iodine. Column chromatography was carried out over silica gel (Merck, Kieselgel 60, 70—230 mesh) and preparative TLC over silica gel (Wakogel B-5F, 20×20 cm^2). The optical rotations, UV, IR, and NMR (100 MHz) spectra were measured in chloroform, ethanol, Nujol, and chloroform-*d*, respectively, unless otherwise stated. The abbreviations "s, d, t, m, br, and do" in the NMR spectra denote "singlet, doublet, triplet, multiplet, broad, and double," respectively.

Photolysis of 12α,13α-Epoxyetiojerv-5-ene-3,17-dione 3,3-Ethylene Acetal (2). The photolysis was examined under various conditions and the results were summarized in Table 1. A few representative examples were described below. i) Compound **2** (1.12 g) in dioxane (200 ml) was irradiated by a 15-W low-pressure mercury lamp at room temperature for 2 d under nitrogen. The reaction mixture was evaporated to leave resinous material (1.10 g), which was separated by chromatography over silica gel (35 g) with benzene-ether mixtures. Elution with benzene-ether (5:1) led to recovery of **2** (750 mg). Early fractions eluted with benzene-ether (2:1) afforded semi-crystalline substance, which was purified by preparative TLC (6 plates) over silica gel with benzene–ether (3:2) to give a bicyclo [3.3.1]nonane-2,9-dione derivative (**4**, 120 mg), mp 181—183 °C (from ether) and $[\alpha]_D$ −24.2°; MS, *m/e* 344 (M^+); IR, ν_{max} 1745, 1708, 1275, and 1095 cm^{-1}; NMR, δ 0.97 and 1.23 (19- and angular CH$_3$), 3.94 (4H, s, OC_2H_4O), and 5.42 (1H, br, W_H=10 Hz, 6-H). Found: C, 73.19; H, 7.98%. Calcd for $C_{21}H_{28}O_4$: C, 73.22; H, 8.19%. Later fractions eluted with benzene–ether (1:1) gave a crystalline substance, which was also purified by preparative TLC (8 plates) under the same conditions as mentioned above to give androst-5-ene-3,12,17-trione 3,3-ethylene acetal (**3**, 157 mg), mp 242—243 °C and 253—254 °C (from acetone) and $[\alpha]_D$ +68.4°; MS, *m/e* 344 (M^+) and 149; IR, ν_{max} 1756, 1707, 1291, and 1095 cm^{-1}; NMR, δ 1.13 and 1.23 (each 3H, s, 19- and 18-H), 3.94 (4H, s, OC_2H_4O), and 5.41 (1H, br, W_H=10 Hz, 6-H). Found: C, 73.00; H, 8.38%. Calcd for $C_{21}H_{28}O_4$: C, 73.22; H, 8.19%.

ii) An acetonitrile solution (20 ml) of **2** (200 mg) was irradiated for 10 h under the same conditions. The mixture

was worked up as usual to leave amorphous residue (190 mg), which was submitted to chromatography over silica gel (15 g) to give **2** (70 mg), **4** (10 mg), a new compound (**15**, 35 mg), and **3** (12 mg) as benzene–ether eluates (5:1, 10:3, 10:4, and 1:1), respectively. The new compound (**15**), 5β,6β:12α,13α-diepoxyetiojervane-3,17-dione 3,3-ethylene acetal, mp 129—130 °C (from diisopropyl ether) and $[\alpha]_D$ −37°; MS, *m/e* 360 (M^+); IR, ν_{max} 1720, 1125, 1104, 1075, and 1015 cm^{-1}; NMR, δ 0.98 and 1.30 (each 3H, s, 19- and 18-H), 3.14 (1H, d, J=2 Hz, 6-H), and 3.92 (4H, s, OC_2H_4O). This diepoxide was obtained by oxidation of a known compound, 5β,6β:12α,13α-diepoxy-17α-hydroxyetiojervan-3-one 3,3-ethylene acetal[4] (**16**) as follows. To a suspended mixture of CrO_3 (1.0 g) in pyridine (10 ml) was added **16** (100 mg) in pyridine (1 ml) under stirring. The mixture was stirred at room temperature for 4 h. After addition of ether (20 ml), the mixture was worked up as usual to leave amorphous residue, which was purified by passing through a silica gel column (6 g) to give **15** (70 mg), mp 129—130 °C. This was identical with one of the photolysis products in acetonitrile (MS, IR, NMR, and TLC).

iii) Compound **2** (170 mg) was irradiated in benzene (thiophene-free, 30 ml) under the afore-mentioned conditions for 10 h. The mixture, after being worked up as usual, left a complex mixture (205 mg), which was separated by chromatography over silica gel (7.0 g) with benzene–ether mixtures. While eluates with benzene–ether (20:1) gave **2** (40 mg), those with benzene–ether (10:1, 5:1, and 5:2) were further purified by preparative TLC (each 2, plates) over silica gel with a 3:2 mixture of benzene–ether, respectively, to yield three new compounds (**17**, 34 mg), (**18**, 16 mg), and (**19**, 37 mg), respectively. These compounds were tentatively assigned the respective formulas on the basis of the following spectral data: **17**, amorphous; MS, *m/e* 344 (M^+−18), 316, 301, 288, and 256; UV, λ_{max} 237 nm (ε 6500); IR, ν_{max} (neat) 3440, 1673, 1115, 1095, and 1020 cm^{-1}; NMR, δ 1.06 and 1.76 (19-H and CH_3), 3.92 (4H, s, OC_2H_4O), 5.36 (1H, br, W_H=9 Hz, 6-H), and 6.43 (1H, br, W_H=10 Hz, $CH(OH)_2$]; **18**, amorphous, MS, *m/e* 344 (M^+); IR, ν_{max} ($CHCl_3$) 1749, 1714, 1265, 1162, and 1110 cm^{-1}; NMR, δ 1.00 and 1.70 (each 3H, s, 19-H and CH_3), 3.95 (4H, s, OC_2H_4O), and 5.34 (1H, br, W_H=10 Hz, 6-H): **19**, amorphous, MS, *m/e* 344 (M^+), 316, 300, and 272; UV, λ_{max} 244 nm (ε 10000); IR, ν_{max} ($CHCl_3$), 2725, 1731, 1663, 1615, and 1097 cm^{-1}; NMR, δ 1.07 and 1.84 (each 3H, s, 19-H and CH_3), 3.97 (4H, s, OC_2H_4O), 5.46 (1H, br, W_H=10 Hz, 6-H), and 9.78 (1H, s, CHO).

12β-Hydroxyandrost-5-ene-3,17-dione 3,3-Ethylene Acetal (5). A THF solution (12 ml) of **3** (100 mg) was stirred with lithium tri-*t*-butoxyaluminium hydride (160 mg) at room temperature for 8 h. The reaction was ceased by addition of aq ammonium sulfate, and the mixture was filtered. The filtrate was concentrated, mixed with water, and extracted with chloroform (3×30 ml). The chloroform solution was washed with water, dried over anhydrous sodium sulfate and evaporated to leave a crystalline substance, which was recrystallized from acetone to yield **5** (97 mg), mp 195—197 °C and $[\alpha]_D$ +2.8°; MS, *m/e* 346 (M^+), IR, ν_{max} 3500, 1736, 1133, 1119, and 1100 cm^{-1}; NMR, δ 0.98 and 1.07 (each 3H, s, 18- and 19-H), 3.81 (1H, do d, J=10 and 5 Hz, 12-H), 3.95 (4H, s, OC_2H_4O), and 5.37 (1H, br, W_H=10 Hz, 6-H). Found: C, 72.61; H, 8.77%. Calcd for $C_{21}H_{30}O_4$: C, 72.80; H, 8.73%.

12β,17β-Dihydroxyandrost-5-en-3-one 3,3-Ethylene Acetal (7). i) To a dichloromethane solution (4 ml) of **5** (60 mg) cooled at −8 °C (ice-water-NaCl) was added dropwise triethylamine (0.07 ml) and then methanesulfonyl chloride (0.02 ml) under stirring. The mixture was stirred at the temperature for 2 h and then diluted with dichloromethane (20 ml). The solution was washed with water (20 ml), 2 M hydrochloric acid (HCl, 20 ml), 5% aq sodium hydrogencarbonate ($NaHCO_3$, 2×20 ml), and water (3×20 ml), dried and evaporated to leave a crystalline substance (50 mg), which was purified by passing through a silica gel column (3 g) to give the 12β-mesylate (**6**, 32 mg) of **5**, mp 156—158 °C (from ether): NMR, δ 1.04 and 1.07 (each 3H, s, 18- and 19-H), 3.22 (3H, s, CH_3SO_2), 3.95 (4H, s, OC_2H_4O), 4.40 (1H, do d, J=10 and 5 Hz, 12-H), and 5.38 (1H, br, W_H=10 Hz, 6-H).

To a suspended mixture of lithium aluminium hydride (LAH, 26 mg) in THF (10 ml) cooled with ice-water was added **6** (30 mg) in THF (10 ml) under stirring, and the mixture was refluxed for 3 h under nitrogen and then cooled. After dropwise addition of water (4 ml) and 4 M aq sodium hydroxide (1 ml) under cooling with ice-water, the mixture was filtered. The filtrate was concentrated, mixed with water and extracted with chloroform (4×50 ml). The extracts were worked up as usual to leave a crystalline substance, which was purified by passing through a silica gel column (2.0 g) to yield **7** (23 mg), mp 186—188 °C (from diisopropyl ether) and $[\alpha]_D$ −31.9°; MS, *m/e* 348 (M^+); IR, ν_{max} 3400, 1140, 1102, 1062, and 1025 cm^{-1}; NMR, δ 0.82 and 1.06 (each 3H, s, 18- and 19-H), 3.52 (1H, do d, J=10 and 5 Hz, 12-H), 3.88 (1H, t, J=8 Hz, 17-H), 3.95 (4H, s, OC_2H_4O), and 5.32 (1H, br, W_H=10 Hz, 6-H). Found: C, 70.33; H, 9.11%. Calcd for $C_{21}H_{32}O_4 \cdot 1/2H_2O$: C, 70.55, H, 9.31%.

ii) To a mixture of LAH (40 mg) in THF (8 ml) cooled with ice-water was added **3** (50 mg) in THF (30 ml) under stirring, and the whole mixture was refluxed for 3 h. The reaction mixture was worked up and purified as described above to give **7** (45 mg), mp 186—188 °C, which was identical with a sample of the afore-mentioned diol (**7**) (IR, NMR, and TLC).

17β-Hydroxyandrost-5-en-3-one 3,3-Ethylene Acetal (10). A benzene solution (3 ml) of **7** (55 mg) was treated with acetic anhydride (0.1 ml) and pyridine (0.1 ml) at room temperature for 31 h. The solution was diluted with ether (100 ml) and worked up as usual to give a mixture of the 12β- and 17β-monoacetates (**8a** and **8b**, total 34 mg) of **7**; amorphous; NMR, δ 0.80 and 0.86 (total 3H, 3:2, each s, 18-H), 1.06 (3H, s, 19-H), 2.09 and 2.07 (total 3H, 3:2, each s, $OCOCH_3$), 3.58 (2/3H, do d, J=10 and 5 Hz, 12-H), 3.96 (≈4H, s, OC_2H_4O and 17-H), 4.75 (1H, br m, W_H=24 Hz, 12- and 17-H), and 5.36 (1H, br, W_H=10 Hz, 6-H).

The mixture (**8a** and **8b**, 34 mg) in pyridine (2 ml) was treated with CrO_3 (340 mg) in pyridine (3.4 ml) at room temperature for 1.5 h under stirring. The reaction mixture was worked up as usual to give a 1:1 mixture of 17- and 12-ketones (**9a** and **9b**), amorphous: **9a**, 0.97 and 1.06 (each 1.5H, s, 18- and 19-H), 2.09 (1.5H, $OCOCH_3$), and 4.96 (0.5H, br, W_H=16 Hz, 12-H); **9b**, 1.14 and 1.19 (each 1.5H, s, 19- and 18-H), 2.04 (1.5H, s, $OCOCH_3$), and 5.06 (0.5H, br, W_H=20 Hz, 17-H); **9a** and **9b**, 3.94 (3H, s, OC_2H_4O) and 5.37 (1H, br, W_H=10 Hz, 6-H).

To a solution of the mixture (**9a** and **9b**, 24 mg) in ethylene glycol (6 ml) was added 85% aq hydrazine hydrate (0.18 ml) and powdered potassium hydroxide (KOH, 0.32 g). The solution was heated at 100—110 °C for 1.5 h and then refluxed at 180—190 °C for 18.5 h. The reaction mixture was cooled, poured into ice-water, and extracted with chloroform (3×40 ml). The chloroform solution was washed with 2 M HCl (2×50 ml) and water (4×80 ml), dried and evaporated

under reduced pressure to leave amorphous residue (23 mg), which was separated by preparative TLC (2 plates) over silica gel with benzene–ether (2:1). A fraction with the highest R_f value gave a crystalline substance, which was recrystallized from acetone to yield **10** (7.1 mg), mp 188—189 °C and $[\alpha]_D$ −45.6°; MS, *m/e* 332 (M^+); IR, ν_{max} 3260, 1136, 1097, 1055, and 1025 cm^{-1}; NMR, δ 0.76 and 1.05 (each 3H, s, 18- and 19-H), 3.65 (1H, t, J=8 Hz, 17-H), 3.96 (4H, s, OC_2H_4O), and 5.34 (1H, br, W_H=10 Hz, 6-H). This sample was identical with an authentic specimen[8] obtained by acetalization of **1**.

*12β-Hydroxyandrost-5-ene-3,17-dione 3,3-Ethylene Acetal (**11**).* Compound **5** (42 mg) was dissolved in benzene (20 ml) and ethylene glycol (2 ml) containing *p*-toluenesulfonic acid (*p*-TsOH, 3 mg), and the solution was refluxed (oil-bath temperature, 100±5 °C) for 16 h under stirring, water being removed under a Dean-Stark apparatus. The mixture was washed with 5% aq $NaHCO_3$ (3×50 ml) and water (3×40 ml), dried and evaporated to leave a crystalline substance, which was purified by passing through a silica gel column (1.8 g) to give **11** (31 mg), mp 219—220 °C (from ether) and $[\alpha]_D$ −70.8°; MS, *m/e* 390 (M^+) and 372; IR, ν_{max} 3540, 1105, 1028, 995, and 945 cm^{-1}; NMR, δ 0.93 and 1.05 (each 3H, s, 18- and 19-H), 3.96 (8H, br, s, $2OC_2H_4O$), and 5.35 (1H, br, W_H=10 Hz, 6-H). Found: C, 70.56; H, 8.75%. Calcd for $C_{23}H_{34}O_5$: C, 70.74; H, 8.78%.

*Androst-5-ene-3,12,17-trione 3,3:17,17-Bis(ethylene acetal) (**12**).* To a suspended mixture of CrO_3 (300 mg) in pyridine (3 ml) was added **11** (30 mg) in pyridine (2 ml) under stirring. The mixture was stirred at room temperature for 1.5 h, cooled and then filtered. The filtrate and precipitates were washed with ethyl acetate (4×50 ml and 50 ml), respectively. All the ethyl acetate solutions were worked up as described above to leave a crystalline substance, which was purified by passing through a silica gel column (1.5 g) to give **12** (21 mg), mp 215—216 °C (from ether) and $[\alpha]_D$ +10.5°; MS, *m/e* 388 (M^+); IR, ν_{max} 1715, 1100, 1025, and 990 cm^{-1}; NMR, δ 1.08 and 1.11 (each 3H, s, 18- and 19-H), 3.94 (4H, s, 3-OC_2H_4O), 4.02 (4H, m, 17-OC_2H_4O), and 5.39 (1H, br, W_H=10 Hz, 6-H). Found: C, 71.06; H, 8.32%. Calcd for $C_{23}H_{32}O_5$: C, 71.10; H, 8.30%.

*Androst-5-ene-3,17-dione 3,3:17,17-Bis(ethylene acetal) (**13**) and Androst-5-ene-3,17-dione 3,3-Ethylene Acetal (**14**).* i) An ethylene glycol solution (3 ml) of **12** (9 mg) was heated with 85% aq hydrazine hydrate (0.08 ml) and KOH (0.08 g) at 100—110 °C (bath temp) for 1 h and then refluxed (bath temp, 180—200 °C) for 20 h. After being cooled, the mixture was poured into ice–water (20 ml) and then extracted with chloroform (4×40 ml). The chloroform extracts were worked up as mentioned above to yield amorphous residue (9 mg), which was purified by passing through a silica gel column (0.5 g) and crystallized on trituration with ether. Recrystallization from ethanol–ether afforded **13** (7.4 mg), mp 174—176 °C and $[\alpha]_D$ −64.0°; MS, *m/e* 374 (M^+); IR, ν_{max} 1100, 1037, 1025, and 990 cm^{-1}; NMR, δ 0.86 and 1.04 (each 3H, s, 18- and 19-H), 3.89 and 3.94 (each 4H, s, 17- and 3-OC_2H_4O). Found: C, 73.62; H, 9.17%. Calcd for $C_{23}H_{34}O_4$: C, 73.76; H, 9.15%.

Compound **13** (45 mg) was heated with *p*-TsOH (15 mg) in acetone (15 ml) and water (3 ml) under reflux for 17 h. After being cooled, the mixture was evaporated, mixed with water and then extracted with chloroform (4×20 ml). The chloroform extracts were worked up as mentioned above to leave amorphous residue (59 mg), which was purified by passing through a silica gel column (3 g) and crystallized on trituration with ether. This was recrystallized from ether to give **14** (29 mg), mp 175—176 °C and $[\alpha]_D$ +198.8°; MS, *m/e* 286 (M^+) and 244; UV, λ_{max} 239 nm (ε 12000); IR, ν_{max} 1740, 1662, and 1613 cm^{-1}; NMR δ 0.93 and 1.23 (each 3H, s, 18- and 19-H), and 5.74 (1H, s, 4-H). Found: C, 79.49; H, 9.28%. Calcd for $C_{19}H_{26}O_2$: C, 79.68; H, 9.15%. This compound (**14**) was identical with an authentic sample obtained by oxidation of **1** (MS, UV, IR, NMR, TLC, and mixed mp), and was converted into **1** by a known procedure.[8]

References

1) Part VII, A. Murai, H. Sasamori, and T. Masamune, *Bull. Chem. Soc. Jpn.*, **53**, 254 (1980).

2) Part XXXV of "*C*-Nor-*D*-homosteroids and Related Alkaloids;" Part XXXIV, Ref. 1.

3) A. Murai, N. Iwasa, and T. Masamune, *Chem. Lett.*, **1977**, 235.

4) A. Murai, N. Iwasa, M. Takeda, H. Sasamori, and T. Masamune, *Bull. Chem. Soc. Jpn.*, **50**, 429 (1977).

5) a) A. Padwa, "Organic Photochemistry," ed by O. L. Chapman, Marcel Dekker, Inc., New York, N. Y. (1967), Vol. 1, p. 91; b) M. Debono, R. M. Molloy, D. Bauer, T. Iizuka, K. Schaffner, and O. Jeger, *J. Am. Chem. Soc.*, **92**, 420 (1970); H. Wehrli, C. Lehmann, T. Iizuka, K. Schaffner, and O. Jeger, *Helv. Chim. Acta*, **50**, 2403 (1967); H. Wehrli, C. Lehmann, P. Keller, J. J. Bonet, K. Schaffner, and O. Jeger, *ibid.*, **49**, 2218 (1966); H. Wehrli, C. Lehmann, K. Schaffner, and O. Jeger, *ibid.*, **47**, 1336 (1964); c) H. Hart, Cheng-tai Peng, and Eng-mu Shih, *Tetrahedron Lett.*, **1977**, 1641; H. Hart, Cheng-tai Peng, and Eng-mu Shih, *J. Org. Chem.*, **42**, 3635 (1977); J. Muzart and J. P. Pete, *Tetrahedron Lett.*, **1977**, 303, 307; D. J. Dewar and R. G. Sutherland, *J. Chem. Soc., Perkin Trans. 2*, **1977**, 1522; *cf.*, R. K. Murray, Jr., T. K. Morgan, Jr., J. A. S. Polley, C. A. Andruskiewicz, Jr., and D. L. Goff, *J. Am. Chem. Soc.*, **97**, 940 (1975).

6) N. S. Bhacca and D. H. Williams, "Application of NMR Spectroscopy in Organic Chemistry," Holden-Day, Inc., San Francisco, California (1964), p. 19.

7) *Cf.*, J. K. Norymberski and G. F. Woods, *J. Chem. Soc.*, **1955**, 3426.

8) H. L. Herzog, M. A. Jevnik, M. E. Tully, and E. B. Hershberg, *J. Am. Chem. Soc.*, **75**, 4425 (1953); H. J. Dauben, Jr., B. Löken, and H. J. Ringold, *ibid.*, **76**, 1359 (1954); W. S. Johnson, B. Bannister, R. Pappo, and J. E. Pike, *ibid.*, **78**, 6354 (1956).

© The Chemical Society of Japan

NOTES

Bull. Chem. Soc. Jpn., 53, 263—264 (1980)

The Catalytic Reactions on Hafnium Dioxide

Yoshito Onishi,* Yasuo Iizuka, and Takuya Hamamura
Department of Chemistry, Faculty of Industrial Arts, Kyoto Technical University, Matsugasaki, Sakyo-ku, Kyoto 606

(Received May 18, 1979)

Synopsis. The mechanisms of the catalytic oxidations of carbon monoxide and hydrogen on hafnium dioxide are similar to those on titanium dioxide (anatase and rutile) and zirconium dioxide, and the activation energies of these reactions have been correlated with the oxygen bond energies of these four oxides.

In previous papers, the catalytic reactions on zirconium dioxide were reported in comparison with those on titanium dioxide. There exist however little data on the catalytic reactions on hafnium dioxide.[1,2] This paper will report the catalytic reactions on hafnium dioxide in connection with those on titanium dioxide and zirconium dioxide.

Experimental

The procedure and apparatus employed were almost the same as those used previously.[3] Hafnium dioxide obtained from Ventron Alfa Products Corporation was employed as the catalyst. The sample was of spectroscopic grade and free from zirconia. From X-ray powder analysis, the specimen was shown to exist in the monoclinic form. The BET surface area was 0.66 m^2/g (N_2 at −196 °C). Hafnium dioxide (9.5 g) was used as the catalyst.

Prior to measurement, the sample in the reaction tube was evacuated to 10^{-6} mmHg** and subsequently heated at 870 °C in oxygen (75 mmHg) for 3 h to clean the surface. A mixture of carbon monoxide and oxygen or a mixture of hydrogen and oxygen when introduced to the heated hafnium dioxide produced cataytic oxidation giving carbon dioxide or water, which then condensed into the liquid nitrogen cooled traps. The reaction rate was determined by measuring the decrease in the total pressure.

Results and Discussion

Kinetic studies of the carbon monoxide oxidation on hafnium dioxide were conducted using a mixed gas of carbon monoxide and oxygen in the temperature range 400—550 °C and in the pressure range 10^{-3}—100 mmHg. The oxidation rate was proportional to the carbon monoxide pressure and independent of the oxygen pressure. Therefore, the reaction rate may be expressed by the following equation:

$$d(CO_2)/dt = k_{CO_2} \cdot P_{CO}, \quad (1)$$

where k_{CO_2} is the oxidation rate constant of carbon monoxide on hafnium dioxide.

The oxidation rate of hydrogen on hafnium dioxide was measured using a mixed gas of hydrogen and oxygen in the temperature range 450—600 °C and in the pressure range 10^{-3}—10^{-1} mmHg. The reaction rate may be expressed as follows:

$$d(H_2O)/dt = k_{H_2O} \cdot P_{H_2}, \quad (2)$$

where k_{H_2O} is the oxidation rate constant of hydrogen on hafnium dioxide.

The catalyst pretreated in oxygen (75 mmHg) at 870 °C for 3 h was cooled to the reaction temperature and evacuated. Carbon monoxide or hydrogen, at a pressure of approximately 10^{-2} mmHg, was introduced into the reaction system, whereby it reacted with the active oxygen of the catalyst and the formed carbon dioxide or water was caught in the traps. The rate of the formation of carbon dioxide and water was found to be proportional to P_{CO} or P_{H_2}, respectively:

$$d(CO_2)/dt = k_{CO} \cdot P_{CO}, \quad (3)$$

$$d(H_2O)/dt = k_{H_2} \cdot P_{H_2}, \quad (4)$$

where k_{CO} and k_{H_2} are the rate constants of the reductions of hafnium dioxide by carbon monoxide and hydrogen, respectively. The Arrhenius plots of k_{CO} and k_{H_2} are shown in Fig. 1 together with those of the oxidation rate constants k_{CO_2} and k_{H_2O}. It may be seen that k_{CO} reasonably agrees with k_{CO_2}, and k_{H_2} with k_{H_2O} at each corresponding temperature.

The catalyst was reduced by carbon monoxide at approximately 40 mmHg for 1 h. Oxygen at approximately 10^{-2} mmHg was then introduced to measure the oxidation rate of the reduced hafnium dioxide by oxygen. The oxidation rates were 1100—5300 times as large as the reduction rates of hafnium dioxide by carbon monoxide and hydrogen in the temperature range 450—600 °C.

Thus the mechanism of the oxidation of carbon monoxide on hafnium dioxide may be expressed by the following equations:

$$CO(g) + O(s) \xrightarrow{h\nu} CO_2(g) + (s), \quad (5)$$

$$(s) + 1/2\,O_2(g) \longrightarrow O(s), \quad (6)$$

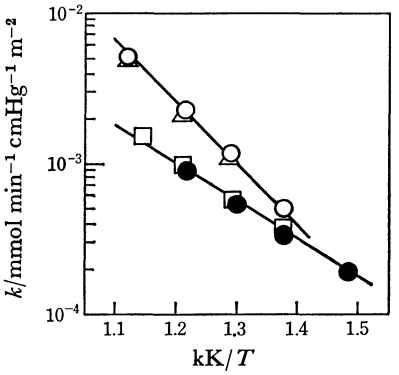

Fig. 1. Effect of temperature on the rate constant. ●: k_{CO_2}, ○: k_{H_2O}, □: k_{CO}, △: k_{H_2}.

**1 mmHg=133.322 Pa.

where O(s) refers to the active oxygen of the catalyst and (s) the oxygen defect on the surface. Step (6) is much faster than step (5), so that step (5) becomes the rate-determining step of the overall reaction. This mechanism is closely analogous to those for titanium dioxide[3] and zirconium dioxide.[4]

The oxidation of hydrogen on hafnium dioxide may be expressed as follows:

$$H_2(g) + O(s) \xrightarrow{\text{slow}} H_2O(g) + (s), \quad (7)$$

$$(s) + 1/2\,O_2(g) \longrightarrow O(s), \quad (8)$$

and similar mechanisms have been published on titanium dioxide[5] and zirconium dioxide.[6]

The thermodesorption rate of oxygen from hafnium dioxide was measured by a procedure described in previous papers.[3,4]

The activation energies of the two oxidation reactions and that of the thermodesorption of oxygen from hafnium dioxide are summarized in Table 1 together with those on anatase, rutile, and zirconium dioxide. It may be seen from Table 1 that hafnium dioxide agrees well with zirconium dioxide in the activation energies not only on the oxidations of carbon monoxide and hydrogen but also on the thermodesorption of oxygen. This is possibly a direct result of the remarkable resemblances between hafnium dioxide and zirconium dioxide in crystal structures.[7]

There have been several studies to elucidate the correlations between the strength of the metal oxygen bond of the oxidation catalysts and their activities in the several types of oxidation reaction. According to Seiyama,[8] the reactivity of oxygen on the metal oxide catalyst may be estimated by determining the equilibrium oxygen pressures of the oxide at several temperatures. Sachtler *et al.*[9,10] studied the catalytic oxidation reactions on several metal oxides, and concluded that the activity of the oxide is related to its ability to release oxygen. Boreskov *et al.*[11–15] investigated the catalytic properties of Period IV transition metal oxides, and stated that the rates of the catalytic oxidations of carbon monoxide depend upon the surface oxygen bond energies of these oxides estimated by the thermodesorption method and that a linear correlation is established between the oxygen bond energies and the activation energies of the catalytic oxidations of hydrogen and methane.

Table 1. Activation energies (E/kcal$_{th}$ mol^{-1})[a] for the oxidations of CO and H_2 and those for the thermodesorption of oxygen

Catalyst	Oxidation of CO	Oxidation of H_2	Thermodesorption of oxygen
Hafnia	11.7	19.8	42.8
Zirconia	12.5	22.6	44.0
Anatase	16.0	29.2	57.8
Rutile	6.7	17.8	38.4

a) 1 cal$_{th}$=4.184 J.

From Table 1, it may be seen that the four oxides can be arranged in the same order anatase zirconia hafnia rutile with respect to their activation energies in the catalytic oxidations of carbon monoxide and hydrogen and the thermodesorption rate of oxygen. Consequently, the activation energies of the oxidations of carbon monoxide and hydrogen on anatase, rutile, zirconium dioxide, and hafnium dioxide may be correlated with the oxygen bond energies of these four oxides.

References

1) E. R. S. Winter, *J. Catal.*, **19**, 32 (1970).
2) I. I. Ioffe, V. S. Fedorov, B. Yu. Gurevich, M. A. Ustraikh, I. S. Fuks, and K. K. Mukhenberg, *Proc. Int. Congr. Catal. 4th*, **2**, 216 (1968).
3) Y. Onishi and T, Hamamura, *Bull. Chem. Soc. Jpn.*, **43**, 996 (1970).
4) T. Hamamura, Y. Onishi, and Y. Iizuka, *Bull. Chem. Soc. Jpn.*, **45**, 1288 (1972).
5) Y. Onishi, *Bull. Chem. Soc. Jpn.*, **44**, 912 (1971).
6) T. Hamamura, Y. Onishi, and Y. Iizuka, *Bull. Chem. Soc. Jpn.*, **46**, 2592 (1973).
7) C. E. Curtis, L. M. Doney, and J. R. Johnson, *J. Am. Ceram. Soc.*, **37**, 458 (1954).
8) T. Seiyama, "Kinzoku Sankabutsu To Sono Shokubai Sayoo," Koodansha, Japan (1978), p. 20.
9) W. M. H. Sachtler, G. J. H. Dorgelo, J. Fahrenfort, and R. J. H. Voorhoeve, *Proc. Int. Congr. Catal. 4th*, **1**, 454 (1968).
10) W. M. H. Sachtler, G. J. H. Dorgelo, J. Fahrenfort, and R. J. H. Voorhoeve, *Recl. Trav. Chim. Pays-Bas*, **89**, 460 (1970); *Chem. Abstr.*, **73**, 24693 m (1970).
11) G. K. Boreskov, *Discuss. Faraday Soc.*, **41**, 263 (1966).
12) G. K. Boreskov, V. A. Sazonov, and V. V. Popovskii, *Dokl. Akad. Nauk. SSSR*, **176**, 1331 (1967).
13) G. K. Boreskov, *Kinet. Katal.*, **8**, 1020 (1967).
14) B. A. Sazonov, V. V. Popovskii, and G. K. Boreskov, *Kinet. Katal.*, **9**, 312 (1968).
15) V. I. Marshneva and G. K. Boreskov, *Reac. Kinet. Catal. Lett.*, **1**, 15 (1974).

Liquid Crystalline Properties of *N*-(4-Alkoxybenzylidene)-4-halogenoanilines

Sakumitsu SAKAGAMI* and Minoru NAKAMIZO
National Industrial Research Institute of Kyushu, Tosu, Saga 841

(Received July 3, 1979)

Synopsis. *N*-(4-Alkoxybenzylidene)-4-halogenoanilines have been synthesized, and the phase transitions determined using a differential scanning calorimeter and a polarizing microscope. Smectic and nematic phases have been observed for fluoro and chloro derivatives whereas bromo and iodo derivatives exhibit only a smectic phase.

A number of investigations have been conducted on the relationship between molecular structure and liquid crystallinity.[1-4] The vast majority of compounds exhibiting a liquid crystalline phase may be regarded as consisting of a rigid central group and a flexible end group.[4] In order to understand the relationship between liquid crystallinity and terminal substituents, the homologous series of *N*-(4-alkoxybenzylidene)-4-halogenoanilines has been synthesized. The members of this homologous series having the generallized structural formula have been given the

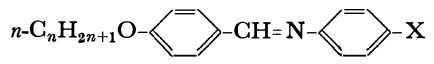

abbreviation *n*-O-X, in which the value of *n* ranges from 1 to 8 and X denotes a halogen atom.

Experimental

Materials. The *N*-(4-alkoxybenzylidene)-4-halogenoanilines were prepared by condensing 4-halogenoaniline with an equimolar amount of 4-alkoxybenzaldehyde in absolute ethanol. The reaction mixture was refluxed for one hour after which the product was collected as a solid crystalline precipitate. The product was recrystallized two or three times from ethanol and benzene.

Measurements. The liquid crystalline texture and the transition temperatures were determined by a Nikon polarizing microscope equipped with a Mettler FP 52 microfurnace and control unit. Checks on the transition temperatures and the measurement of enthalpies of transitions were made using a Rigaku differential scanning calorimeter.

Results and Discussion

The transition temperatures and the heats of transition in the case of the homologous series *n*-O-F are given in Table 1. In this series the only methoxy member shows no mesomorphic property, all the other higher members exhibiting a smectic II phase. The pentyloxy and hexyloxy members of this series show an enantiotropic smectic II phase although the smectic II phases of the other members occur monotropically. With increasing alkoxyl chain another feature is found on the appearance of the smectic phase, *i.e.*, a smectic I phase is enantiotropically observed for the hexyloxy to octyloxy members. On cooling the nematic state of the hexyloxy member, focal conic or fan texture may be observed for the smectic I phase. In addition, the focal conic or fan textures are easily changed to a pseudo-isotropic texture (homeotropic alignment) by cover slip displacement. The characteristic behavior of the textures indicates that the smectic I phase can be identified as smectic A.[5] In the phase transition from smectic I to smectic II transition bars are temporarily formed. On further cooling the transition bars disappear, and mosaic or fan-shaped textures similar to those observed for the smectic I phase are found. It should be emphasized that on cooling the smectic I phase with homeotropic alignment, the homeotropic alignment is also maintained in the smectic II phase. From these characteristic changes in microscopic textures, it follows that the smectic II phase can be classified as smectic B.[5] Smectic polymorphism is not unusual, and has been frequently observed as the alkoxyl chain length increases in other homologous series of liquid crystalline materials.[4]

Table 1. Thermodynamic data for the homologous series, *n*-O-F

n	Smectic B(II)	Smectic A(I)	Nematic	Isotropic
1				63.0 4800
2	(56.0) (1800)		(62.5) (140)	72.2 4900
3	(55.0) (1800)			62.1 5400
4	(58.0) (1700)		(59.6) (130)	64.5 6300
5	51.5 3800			57.4 1900
6	52.3 5200	55.0 640	59.3 770	61.1 150
7	(56.4) (640)	57.0 7200		61.6 1100
8	(54.3) (590)	60.0 7700		63.6 1000

The upper value indicates the transition temperature (°C) and the lower value the heat of transition (cal/mol). 1 cal=4.184 J. The parentheses show the monotropic transition.

Furthermore, it should be noted that a nematic phase occurs only for ethoxy, butoxy, and hexyloxy members. That the nematic phase can only be observed for homologues with even numbers of carbon atoms in alkoxyl chain is not surprising, and can be explained by considering the chain-order parameter of the end alkoxyl group with respect to the molecular axis.[6]

The phase transition temperatures of the homologous series *n*-O-Cl are given in Table 2. In this series the appearance of liquid crystalline phases is similar to that observed for *n*-O-F as stated above. As the length of the alkoxyl chain is increased, two smectic phases, *i.e.*, smectic A and B phases are found. It should be emphasized however that the nematic phase is monotropically observed for only ethoxy member. This indicates that increasing the ionic radius of the terminal substituent tends to destroy the parallel orientation of the molecules. This observation is more

Table 2. Thermodynamic data for the homologous series, *n*-O-Cl

n	Smectic B	Smectic A	Nematic	Isotropic
1				90.2 8300
2			(85.0) (151)	94.0 6500
3	(81.5) (1900)			82.0[a]
4	83.5 5000	88.6 900		89.4 1200
5	58.5 4400	90.7 840		92.8 1300
6	56.5 5200	88.7 750		96.3 1300
7	59.4 6500	89.4 770		97.5 1300
8	61.0 6100	87.7 740		98.5 1300

a) The heat of transition could not be determined due to complex crystal-to-crystal transitions.

Table 3. Thermodynamic data for the homologous series, *n*-O-Br

n	Smectic B	Smectic A	Isotropic
1			115.0 5000
2			103.1 4100
3	(92.2) (2200)		94.1 4500
4	78.5 4500		99.1 2300
5	71.9 5100	100.5 850	103.2 1500
6	72.1 5100	100.4 830	103.3 1400
7	64.5 6600	100.7 870	103.8 1600
8	65.4 6100	100.1 860	104.9 1600

readily demonstrated in Tables 3 and 4 which show the phase transition temperatures for *n*-O-Br and *n*-O-I, respectively. In both homologous series the nematic phase is no longer found. In the homologous series, *n*-O-I, the smectic B phase alone is observed

Table 4. Thermodynamic data for the homologous series, *n*-O-I

n	Smectic B	Isotropic
1		149.5 6800
2		132.8 5100
3		117.0 4300
4	78.0 3000	111.4 2600
5	72.7 4300	108.5 2500
6	85.7 5400	110.3 2600
7	80.1 6300	110.7 2600
8	79.0 6500	110.8 2700

while in the series *n*-O-Br both the smectic A and B phases are exhibited depending on the length of the alkoxyl chain.[7]

References

1) G. W. Gray, "Molecular Structure and Properties of Liquid Crystals," Academic Press, New York (1962).
2) G. H. Brown, J. W. Doane, and V. D. Neff, "A Review of the Structure and Physical Properties of Liquid Crystals," Chemical Rubber Co., Cleveland (1971).
3) G. W. Gray, "Liquid Crystals and Plastic Crystals," ed by G. W. Gray and P. A. Winsor, Ellis Horwood, Chichester (1974), Vol. 1, p. 103.
4) D. Demus, H. Demus, and H. Zaschke, "Fluessige Kristalle in Tabellen," Verlag, Leipzig (1974).
5) D. Demus and L. Richter, "Textures of Liquid Crystals," Verlag, Leipzig (1978).
6) D. P. Pink, *J. Chem. Phys.*, **63**, 2533 (1975).
7) Vora has recently studied the phase transitions of the series *n*-O-Br. There is an essential discrepancy between his and the present data besides the slight difference in transition temperatures. According to Vora the smectic B phase may be observed only for the hexyloxy member which is in contrast with the results reported here. This discrepancy could be ascribed to the fact that the authors determined the phase transitions from both the DSC measurements and microscopic observations while Vora employed only an optical microscope to identify the smectic phases. R. A. Vora, *Mol. Cryst. Liq. Cryst.*, **44**, 83 (1978).

On the Nature of the 5,10-Dimethyl-5,10-dihydrophenazine–Tetracyanoquinodimethane

Isao FUJITA and Yoshio MATSUNAGA*

Department of Chemistry, Faculty of Science, Hokkaido University, Sapporo 060

(Received July 18, 1979)

Synopsis. The 5,10-dimethyl-5,10-dihydrophenazine–tetracyanoquinodimethane appears to be largely ionic at room temperature. The results of various physical measurements of this compound can be explained without the reversible nonionic-to-ionic transition proposed by Soos *et al.*

The 1:1 compound between 5,10-dimethyl-5,10-dihydrophenazine (DMPH) and tetracyanoquinodimethane (TCNQ) has been prepared by Melby by the treatment of $DMPH^+I^-$ in hot absolute ethanol with a boiling solution of Li^+TCNQ^- dissolved in the same solvent.[1] He has suggested that the solid compound is represented as a pi-complex rather than as an ion-radical salt. The structure and the packing arrangement of this compound have been studied by Goldberg and Shmueli.[2] The structure consists of stacks in which the DMPH and TCNQ molecules alternate along the c axis. On the basis of the intrastack contacts and the molecular geometry of TCNQ, these authors have postulated the presence of rather strong charge transfer interactions.

Recently, Soos *et al.* have reported measurements of the ESR spectrum.[3] At room temperature, DMPH–TCNQ powder exhibits a very weak ESR signal at $g=2.0026$. An additional exchange-narrowed signal at $g=2.0035$ appears on heating. The intensity of the latter increases rapidly with a rise in the temperature. They have considered the compound to be largely neutral and diamagnetic at 300 K and to undergo an unusual reversible transition to a paramagnetic state at 390 K. The same group has reported an increase in the activation energy for semiconduction around 360 K.[4] Earlier, one of the present authors isolated two differently-colored forms of 7-methylbenzo[*a*]phenazinium–TCNQ.[5] The violet form is largely ionic, while the green form is not. Although the transformation of the green form to the violet one was observed in the presence of a solvent, the crystals were found to be stable once they were isolated. As it seemed unlikely to us that the nonionic-to-ionic transition proposed by Soos *et al.* occurs without hysteresis, a further study of this compound was undertaken.

5,10-Dimethyl-5,10-dihydrophenazine was prepared by means of the method described by Gilman and Dietrich[6] and was subsequently purified by sublimation in a vacuum. By the treatment of the phenazine with one equivalent of TCNQ separately dissolved in hot acetonitrile, dark violet DMPH–TCNQ crystals were precipitated. Found: C, 75.54; H, 4.37; N, 20.07%. Calcd for $C_{14}H_{14}N_2$–$C_{12}H_4N_4$: C, 75.28; H, 4.38; N, 20.28%.

The temperature dependence of the ESR signals examined at the X band exactly reproduced the observation described by Soos *et al.* Furthermore, three pairs of resonance lines characteristic of triplet-spin excitons could be recorded with the polycrystalline sample. The zero-field splitting parameters, $|D/g\beta|$ and $|E/g\beta|$, are 149 and 21 G (1 G=10^{-4}T) at 327 K. As the temperature is increased, the lines are broadened and the splittings become less, the values at 380 K being 135 and 18 G. Our observation reasonably agrees with the results reported by Nöthe *et al.*, namely, 144 and 20 G at 339 K[4]. The room temperature resistivity of polycrystalline compactions measured by a four-probe method is in accord with the value of 6×10^6 ohm cm reported by Melby. The activation energy for semiconduction is 0.51 eV below 350 K and 0.65 eV in the higher-temperature region. The former value is in good agreement with the value of 0.50 eV obtained by two-probe single crystal measurements.[4] Consequently, we suppose that our DMPH–TCNQ sample is identical with that prepared by Soos *et al.*

The vibrational spectrum of TCNQ is known to be considerably modified by the addition of an extra electron;[7] therefore, it is not difficult to distinguish between the nonionic and ionic complexes by examining the spectrum. In Fig. 1, the spectrum of DMPH–TCNQ is compared with those of TCNQ and K^+-$TCNQ^-$, all examined as Nujol mineral oil mulls at room temperature. As the bands appearing at 1580, 1520, 1320, 1167, 844, and 710 cm^{-1} approximately constitute the pattern of the $TCNQ^-$ ion, the compound appears to be largely ionic under the conditions ex-

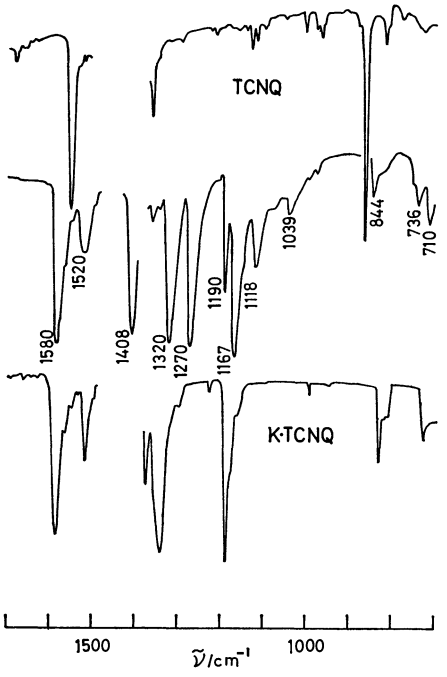

Fig. 1. Vibrational spectrum of the 5,10-dimethyl-5,10-dihydrophenazine–tetracyanoquinodimethane compared with those of TCNQ and K^+TCNQ^-.

amined. The measurements were performed at several temperatures up to 410 K; however, no change could be observed except for slight shifts to the lower-energy side.

As a distinct difference in the electronic spectrum has been seen between the nonionic and ionic forms of 7-methylbenzo[*a*]phenazinium–TCNQ, some changes may be expected in the specrtum of DMPH–TCNQ if the proposed transition takes place upon an increase in the temperature. The spectrum recorded as Nujol mineral oil mulls at room temperature shows absorption maxima at 6.8×10^3, about 16×10^3, and 27.5×10^3 cm^{-1}, with a shoulder around 23×10^3 cm^{-1}. These spectral features could be reproduced by diffuse-reflectance measurements of a sample diluted with sodium chloride. The maxima are located at 6.8×10^3, 17.2×10^3, and 27.5×10^3 cm^{-1}, with a shoulder around 24×10^{-3} cm^{-1}. By means of the latter technique, we examined the spectrum at several temperatures up to 473 K; nonetheless, no change could be detected in the spectral pattern.

The Seebeck coefficient, as measured with a polycrystalline compaction, is negative throughout the range from room temperature to 385 K, as is shown in Fig. 2. The open and shaded circles indicate points taken in the processes of increasing and decreasing the temperature respectively. A broad minimum of about -100 μV K^{-1} is located near 350 K. Such a change in the slope is commonly found when the contribution of impurities or imperfections cannot be ignored in the lower-temperature region.[8] If this interpretation is correct, the change in the activation energy of semiconduction may be attributed to the extrinsic conduction dominant below 350 K rather than to the nonionic-to-ionic transition around that temperature.

Differential scanning calorimetric measurements carried out up to 420 K showed that no enthalpy change takes place, at least not in a relatively narrow temperature range. Moreover, the X-ray diffraction pattern of the polycrystalline sample recorded at about 390 K was found to be the same as that recorded at room temperature.

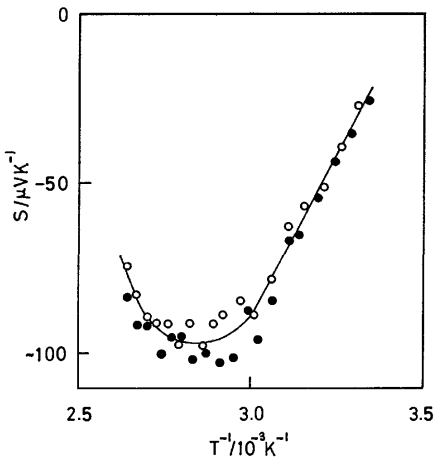

Fig. 2. Seebeck coefficient of the 5,10-dimethyl-5,10-dihydrophenazine-tetracyanoquinodimethane.

The newly obtained results lead to the conclusions that, basically, the DMPH–TCNQ is ionic at room temperature and that the nonionic-to-ionic transition does not occur in this solid complex. The former conclusion seems, though, to be inconsistent with the number of electrons per TCNQ molecule (0.30) estimated by Flandrois and Chasseau based on the bond lengths in the TCNQ molecule determined by Goldberg and Shmueli.[9] The ground state of the DMPH–TCNQ is supposed to be singlet because of an antiferromagnetic exchange interaction, as has been found for a number of ionic charge-transfer complexes. A change in the weak ESR signals appearing near $g=2.00$ with the temperature is not unknown for such complexes. Faucher and Robert have examined the ESR spectrum of powder and single crystals of the *p*-phenylenediamine–*p*-chloranil and have found two magnetic species in it.[10] One of them has an isotropic *g*-factor of 2.0035, and its intensity varies following the classic Curie law. The other species exhibits temperature-dependent *g*-factor splittings, and the spin density shows an exponential dependence with an activation energy of 0.22 eV. Because of this complication, the powder spectrum is markedly dependent on the temperature.

The observations described above were supplemented with some measurements of a related compound; that is, the 5,10-diethyl-5,10-dihydrophenazine–TCNQ is largely ionic, judging from the vibrational spectrum. Triplet-spin excitons can also be found in this compound. The zero-field splitting parameters are 147 and 19 G at 310 K and 141 and 18 G at 380 K. In this case, too, a weak signal in the $g=2.00$ region at room temperature is reversibly replaced by a rapidly growing signal with a little larger *g*-value when the temperature is increased. The zero-field splitting parameters obtained here compare well with those observed for the ionic form of 7-methylbenzo[*a*]-phenazinium–TCNQ and also with those reported for a number of simple TCNQ salts.

This work was supported by a Grant-in-Aid for Scientific Research from the Ministry of Education, Science, and Culture (No. 234028).

References

1) L. R. Melby, *Can. J. Chem.*, **43**, 1448 (1965).
2) I. Goldberg and U. Shmueli, *Acta Crystallogr., Sect. B*, **29**, 421 (1973).
3) Z. G. Soos, H. J. Keller, W. Moroni, and D. Nöthe, *J. Am. Chem. Soc.*, **99**, 5040 (1977).
4) D. Nöthe, W. Moroni, H. J. Keller, Z. G. Soos, and S. Mazumdar, *Solid State Commun.*, **26**, 713 (1978).
5) Y. Matsunaga, *Bull. Chem. Soc. Jpn.*, **51**, 3071 (1978).
6) H. Gilman and J. J. Dietrich, *J. Am. Chem. Soc.*, **79**, 6178 (1957).
7) M. Kinoshita and H. Akamatu, *Nature*, **207**, 291 (1965).
8) G. Busch and U. Winkler, *Ergeb. Exakt. Naturw.*, **29**, 145 (1956).
9) S. Flandrois and D. Chasseau, *Acta Crystallogr., Sect. B*, **33**, 2744 (1977).
10) J. P. Faucher and H. Robert, *C. R. Acad. Sci., Ser. B*, **267**, 522 (1968).

Reaction between Aluminium Trichloride and Oxygen in the Vapor Phase and Properties of the Aluminium Oxide Formed

Yuichi SHOJI, Kimikazu TATSUMI, Ryoko MATSUZAKI, and Yuzo SAEKI*

Research Laboratory of Resources Utilization, Tokyo Institute of Technology, 4259, Nagatsuta-cho, Midori-ku, Yokohama 227

(Received April 23, 1979)

Synopsis. The reaction between gaseous $AlCl_3$ and oxygen occurs at above *ca.* 400 °C and proceeds appreciably above *ca.* 800 °C to form Al_2O_3 and chlorine. The Al_2O_3 formed is amorphous Al_2O_3 at 800 °C, γ-Al_2O_3 containing amorphous Al_2O_3 at 900 and 950 °C, and γ-Al_2O_3 at 1000 °C. The phase transition of the Al_2O_3 formed is discussed.

There is limited data on the reaction between gaseous aluminium trichloride($AlCl_3$) and oxygen. Kato *et al.*[1] have studied the modification and the particle size distribution of the aluminium oxide(Al_2O_3) prepared by the reaction between gaseous $AlCl_3$ and oxygen mainly at 1100 °C and the thermal transition of δ-Al_2O_3 formed. In this paper, the reaction between gaseous $AlCl_3$ and oxygen at temperatures below 1000 °C, and the products formed have been examined by X-ray analysis, thermogravimetry(TG), differential thermal analysis(DTA), and electron microscopy.

Experimental

The $AlCl_3$ used was prepared by the reaction between pure aluminium (Al: 99.99%) and chlorine at 400 °C, and confirmed as $AlCl_3$ by X-ray analysis.[2] Found: Al, 20.2; Cl, 79.8%. Calcd for $AlCl_3$: Al, 20.24; Cl, 79.76%.

A transparent quartz reaction tube (1000 mm length) with an inner concentric tube was used. Gaseous $AlCl_3$ was formed by heating $AlCl_3$ placed in the inner tube at 150 °C, and was carried by a stream of argon (40 cm^3/min) to the reaction zone (27 mm i.d. and 250 mm length) held at a specified temperature. In the meantime, pre-dried oxygen was introduced through a separate tube into the reaction zone at a flow-rate of 100 cm^3/min. The mean flow-rate of the $AlCl_3$ was approximately 3.8 cm^3 Al_2Cl_6(g)/min. The reaction was allowed to proceed for 2 h.

The amount of chlorine formed during the reaction was determined by iodometry after being absorbed in potassium iodide solution.

The unreacted $AlCl_3$ which was deposited together with the Al_2O_3 formed was separated by heating the mixture in an argon stream at 250 °C, a temperature higher than the sublimation point of $AlCl_3$ (180 °C).[3] Removal of the $AlCl_3$ adsorbed on Al_2O_3, which could not be removed by the above heating procedure, was conducted as follows: The Al_2O_3 (0.5—1.0 g) was washed with ethanol (100 cm^3) in an Erlenmeyer flask with a reflux condenser at boiling point for 2 h with stirring. The Al_2O_3 was separated from the ethanol phase by a centrifuge. The washing was repeated until no chlorine could be detected in the ethanol phase. The aluminium content in the ethanol phase was determined by chelatometric titration,[4] and the chlorine content by a Corning-ELL Chloride Meter Model 921.

Throughout this work, $AlCl_3$ was handled in an argon atmosphere to prevent any contamination with moisture in the air.

X-Ray analysis of the solid product was performed with an X-ray powder diffractometer, equipped with a proportional counter, using Ni filtered Cu radiation. TG and DTA were performed in an argon stream and a heating rate of 5 °C/min was employed. The sensitivity of the quartz helix used for TG was approximately 71 mm/g. α-Al_2O_3 was used as a reference for DTA.

The percentage of the reacted $AlCl_3$ was calculated from the amount of chlorine formed, the value also being evaluated from the amount of Al_2O_3 formed. Both values showed good agreement with each other.

Results and Discussion

The formation of chlorine by the reaction between gaseous $AlCl_3$ and oxygen was observed above 400 °C. The percentages of the reacted $AlCl_3$ at various temperatures are shown in Fig. 1. The percentage of reacted $AlCl_3$ was very low below 700 °C (less than 2.5%), and the reaction between gaseous $AlCl_3$ and oxygen proceeded appreciably above 800 °C.

The products formed above 800 °C were examined by X-ray analysis and TG after removal of the unreacted $AlCl_3$.

The products formed at 800 and 900 °C could not be identified by X-ray analysis, because the former gave no diffraction line and the latter gave a faint and diffuse diffraction line (2θ=67°) alone. The products obtained at 950 and 1000 °C gave diffraction lines corresponding to γ-Al_2O_3.[5,6]

The products formed at 800, 900, and 950 °C gradually lost weight in the temperature range 350—900 °C, and the final weight losses were 18, 10, and 5%, respectively. It was observed that a white powder was deposited on a cooler part during the weight loss. The product formed at 1000 °C showed no weight change. The white powder mentioned above was identified as $AlCl_3$ by chemical analysis in a sub-

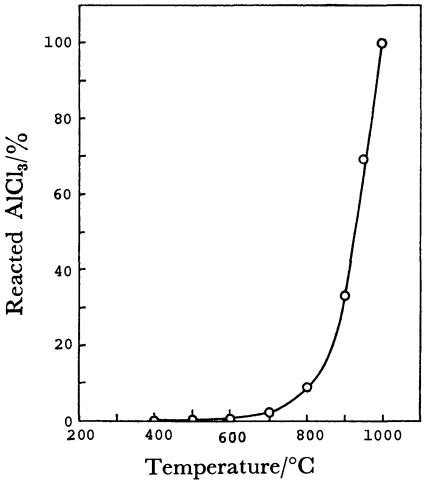

Fig. 1. Reaction rates of $AlCl_3$ with oxygen at various temperatures.

sequent experiment. From the results, it may be assumed that the $AlCl_3$ adsorbed on the fine powders of Al_2O_3 formed by the reaction between gaseous $AlCl_3$ and oxygen vaporized when the Al_2O_3 was heated above approximately 350 °C.

The removal of the $AlCl_3$ adsorbed on the products formed at 800—950 °C was conducted by washing the products with ethanol, in order to prepare the sample for examination. From the chemical analysis of the Al and Cl contents in the ethanol phase, it was confirmed that $AlCl_3$ was dissolved in the ethanol phase. The X-ray diffraction patterns of the products after the washing showed no change in comparison with those of the products before the washing. The products freed from $AlCl_3$ were examined by TG. All prodcuts showed no weight change.

The Al_2O_3 formed by the reaction between gaseous $AlCl_3$ and oxygen at various temperatures were examined by electron microscopy. The Al_2O_3 formed was found to be an ultrafine powder with diameters of the order of 1/100 μm. Electron micrographs of the Al_2O_3 formed at 900 and 1000 °C are shown in Fig. 2.

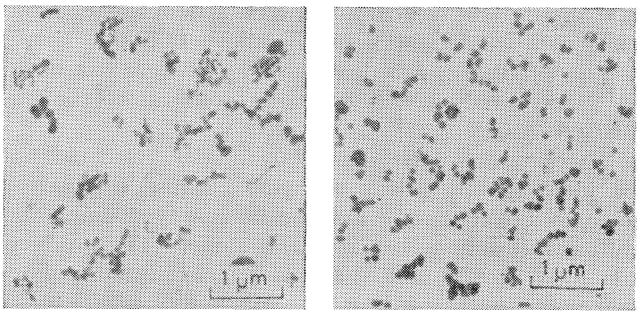

(a) (b)

Fig. 2. Electron micrographs of the Al_2O_3 formed. (a): 900 °C, (b): 1000 °C.

The Al_2O_3 formed at various temperatures were examined by DTA. The DTA curves of the Al_2O_3 formed at 800, 900, and 950 °C showed a weak exothermic effect in the vicinity of 820 °C. The sample after heating the Al_2O_3 formed at 800 °C up to 900 °C was found by X-ray analysis to be χ-Al_2O_3.[5,7] The samples after heating the Al_2O_3 formed at 900 and 950 °C were found to be a mixture of χ-Al_2O_3 and γ-Al_2O_3. The Al_2O_3 formed at 1000 °C showed no thermal effect in the DTA cuvre, and gave no change in X-ray diffraction pattern (γ-Al_2O_3) on heating.

The Al_2O_3 obtained by heating the Al_2O_3 formed at 800—1000 °C at a specified temperature for 2 h was examined by X-ray analysis. The results are summarized in Table 1.

From the experimental results above, the Al_2O_3 formed by the reaction between gaseous $AlCl_3$ and oxygen at 800 °C is amorphous Al_2O_3. On heating the amorphous Al_2O_3, the amorphous→χ→κ→α transition occurs. The Al_2O_3 formed by the reaction at 1000 °C is γ-Al_2O_3. On heating the γ-Al_2O_3, the γ→δ→θ→α transition occurs.

Table 1. Thermal transitions of Al_2O_3 formed at various temperatures

Heating temp/°C	Formation temperature of Al_2O_3			
	800 °C	900 °C	950 °C	1000 °C
Room temp	Amorphous	γ	γ	γ
600	Amorphous	γ	γ	—
700	χ	χ, γ	$\gamma>\chi$	—
800	$\chi>\kappa$	$\chi>\gamma>\kappa$	$\gamma>\chi\gg\kappa$	—
900	χ, κ	$\chi>\gamma$, κ	$\gamma>\chi$, κ	γ
1000	$\kappa>\alpha$	κ, $\delta>\alpha$	$\delta>\alpha$, κ	γ, δ
1100	$\alpha>\kappa$	α, $\theta>\delta$	δ, θ, α	δ, $\theta\gg\alpha$
1200	α	$\alpha>\theta$	α, θ	$\theta>\alpha$
1300		$\alpha>\theta$	$\alpha>\theta$	α, θ

Amorphous=amorphous Al_2O_3, γ=γ-Al_2O_3, χ=χ-Al_2O_3, κ=κ-Al_2O_3,[5,8] α=α-Al_2O_3,[9] δ=δ-Al_2O_3,[5,10] θ=θ-Al_2O_3.[11]

As mentioned before, the Al_2O_3 formed at 900 °C gave a faint and diffuse diffraction line (2θ=67°; corresponding to the strongest line of γ-Al_2O_3) alone. The Al_2O_3 formed at 950 °C showed diffraction lines corresponding to γ-Al_2O_3. The DTA curves of both the Al_2O_3 formed at 900 and 950 °C showed a weak exothermic effect due to the crystallization of amorphous Al_2O_3 to χ-Al_2O_3. As shown in Table 1, on heating the Al_2O_3 formed at 900 and 950 °C, the both amorphous→χ→κ→α and γ→δ→θ→α transitions occurred. Thus the Al_2O_3 formed by the reaction between gaseous $AlCl_3$ and oxygen at 900 °C comprises amorphous Al_2O_3 and γ-Al_2O_3 and the Al_2O_3 formed by the reaction at 950 °C is γ-Al_2O_3 containing amorphous Al_2O_3.

The thermal transition of amorphous Al_2O_3 formed by the reaction between gaseous $AlCl_3$ and oxygen differs from the thermal transition of amorphous Al_2O_3 prepared by the thermal decomposition of $Al(NO_3)_3\cdot 9H_2O$, $AlCl_3\cdot 6H_2O$, and $Al(CH_3COO)_3$ in which the transition has been reported to be the amorphous→γ→δ→θ→α.[12]

References

1) A. Kato, S. Kawazoe, and I. Mochida, *Zairyo*, **21**, 540 (1972).
2) JCPDS, Powder Diffraction File, 22-10.
3) O. Kubaschewski, E. LL. Evans, and C. B. Alcock, "Metallurgical Thermochemistry," 4 th ed, Pergamon Press (1967).
4) H. Flaschka and H. Abdine, *Z. Anal. Chem.*, **152**, 77 (1956).
5) K. Funaki and Y. Shimizu, *Denki Kagaku*, **35**, 8 (1960).
6) ASTM, Powder Diffraction File, 10-425.
7) JCPDS, Powder Diffraction File, 13-373.
8) ASTM, X-Ray Powder Data File, 4-878.
9) ASTM, Powder Diffraction File, 10-173.
10) JCPDS, Powder Diffraction File, 16-394.
11) JCPDS, Powder Diffraction File, 11-517.
12) K. Funaki and Y. Shimizu, *Kogyo Kagaku Zasshi*, **62**, 788 (1959).

Electron Spin Resonance Spectra of Square Planar Cobalt(II) Complexes with Various N_4-Macrocyclic Ligands

Yuzo NISHIDA,* Kazuki HAYASHIDA, Akira SUMITA, and Sigeo KIDA
Department of Chemistry, Faculty of Science, Kyushu University 33, Fukuoka 812
(Received May 18, 1979)

Synopsis. ESR spectra of square planar cobalt(II) complexes with various N_4-macrocyclic ligands were measured, the results being discussed in relation to the π-basicity and π-conjugation of the macrocyclic ligands.

Square planar low-spin cobalt(II) complexes can be classified into complexes of the $(d_{xy})^2(d_{z^2})^1$ ground state(Type I) and those of the $(d_{xy})^2(d_{yz})^1$ ground state(Type II).[1-5] The diagnosis of the compounds can be carried out by means of ESR spectra; $|A_3|$ (g_3 is the ESR peak observed at the highest field) is always larger than 100×10^{-4} cm^{-1} in Type I complexes but much smaller than this in Type II compounds. A number of compounds were subjected to analysis on this basis. From the results, it was found that complexes with electrically neutral ligands, phthalocyanine and porphyrins belong to Type I, and those with dinegatively charged ligands to Type II. This is interpreted as Type I complexes being formed with π-neutral or very weak π-basic ligands, and Type II complexes with fairly strong π-bases.[6]

In this study, we have measured the ESR spectra of square planar cobalt(II) complexes with tetraaza-macrocyclic ligands (Fig. 1 (e)—(j)) in order to confirm this view.

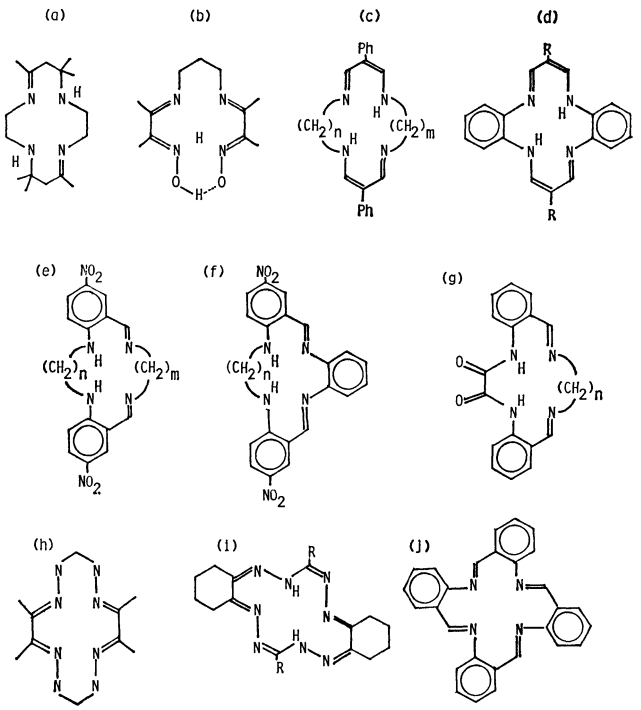

Fig. 1. N_4-Macrocyclic ligands cited in this paper. Abbreviations are: (a); (a-14), (b); H(b-14), (c); H_2(c-14), $n=m=2$, H_2(c-15), $n=2$, $m=3$, (d); H_2(d-14), R=phenyl, H_2(d-14′), R=*p*-tolyl, (e); H_2(e-14), $n=m=2$, H_2(e-15), $n=2$, $m=3$, H_2(e-15′), $n=3$, $m=2$, (f); H_2(f-14), $n=2$, H_2(f-15), $n=3$ (g); H_2(g-14), $n=2$, H_2(g-15), $n=3$, (h); (h-14), (i); H_2(i-14), R=CH_3, H_2(i-14′), R=C_2H_5, (j); (j-16).

Experimental

Preparation. The ligands and their metal complexes were prepared according to the methods reported. ((e),[7] (f),[7] (g),[8] (h),[9] (i),[10] and (j)[11]). New compounds were prepared as follows.

[Co(i-14)]: To a methanol solution (20 ml) of cobalt(II) acetate (0.001 mol) was added a benzene solution (10 ml) of the ligand, H_2 (i-14) (*cf.* Fig. 1, R=CH_3) (0.001 mol) under an atmosphere of nitrogen, and the resulting solution was warmed at 60 °C for 1 h. After the solution had been cooled, violet crystals deposited.

H_2 (f-14) and H_2 (f-15): A DMF solution (100 ml) of $[Mn(py)_4(NCS)_2]$[12] (0.001 mol), *N,N′*-bis(2-formayl-4-nitrophenyl)ethylenediamine[7] (0.001 mol) (or its 1,3-propanediamine derivative) and *o*-phenylenediamine (0.002 mol) was refluxed for several hours. After the solution had beed cooled, yellow crystals deposited. Analytical data of the compounds are given in Table 1.

Table 1. Analytical data of the new compounds

Compound	Found (Calcd) (%)		
	C	H	N
H_2(f-14)	61.19(61.39)	4.18(4.22)	19.47(19.52)
H_2(f-15)	61.89(62.16)	4.50(4.54)	18.90(18.90)
[Co(f-14)][a]	53.76(53.79)	3.32(3.35)	17.32(17.11)
[Co(f-15)][a]	55.02(54.58)	3.62(3.59)	16.79(16.63)
[Co(i-14)]	50.10(49.87)	5.92(5.75)	29.53(29.08)
[Co(i-14′)]	52.81(52.30)	6.43(6.34)	27.44(27.11)

a) Obtained by the use of free ligands obtained in this study, and not a new complex.

Measurements. ESR spectra were obtained with a JEOL ESR apparatus model MEX-3X at liquid nitrogen temperature. For ESR measurements, all the cobalt(II) complexes were diluted in the corresponding nickel(II) complexes. The diluted samples were obtained by the use of template reactions except for [Co(f-14)] and [Co(f-15)]. For the latter complexes, the free ligands we prepared were used for obtaining diluted samples.

Results and Discussion

The ESR parameters are summarized in Table 2 together with some related data.[2-4] It is seen that the complexes are satisfactorily classified into Types I and II by their $|A_3|$ values. The results are completely in line with our view that all the complexes with dinegatively charged ligands belong to Type II.

In some Type II pairs of compounds, [Co(c-14)] and [Co(d-14)], [Co(e-14)], and [Co(f-14)], and [Co(e-15)] and [Co(f-15)], π-conjugation is assumed to be

Table 2. ESR parameters of cobalt(II) complexes

Type	Complex	g_1	g_2	g_3	$\|A_1\|$	$\|A_2\|$	$\|A_3\|$	Ref.
					10^{-4} cm^{-1}			
I	$[Co(a\text{-}14)]^{2+}$	2.57	2.37	2.02	102	83	138	3
	$[Co(b\text{-}14)]^{+}$	2.88	2.28	2.04	199	97	173	4
	$[Co(h\text{-}14)](ClO_4)_2$	2.47	2.33	1.93	82	60	120	a)
	$[Co(j\text{-}16)](ClO_4)_2$	2.62	b)	2.02	106	b)	130	a)
II	[Co(c-14)]	2.676	b)	1.97	0	b)	32	4
	[Co(d-14)]	4.256	1.71	1.53	397	30	55	2
	[Co(d-14′)]	4.057	1.70	1.55	352	b)	b)	2
	[Co(e-14)]	3.07	b)	b)	122	b)	b)	a)
	[Co(f-14)]	3.45	1.84	1.84	206	30	30	a)
	[Co(g-14)]	3.862	b)	b)	330	b)	b)	a)
	[Co(i-14)]	3.91	1.67	1.56	341	28	55	a)
	[Co(i-14′)]	3.30	1.91	1.90	165	b)	28	a)
	[Co(c-15)]	2.874	2.04	1.94	47	b)	35	4
	[Co(e-15)]	2.98	2.02	1.99	92	41	22	a)
	[Co(e-15′)]	3.19	1.99	1.90	139	29	24	a)
	[Co(f-15)]	4.00	b)	b)	365	b)	b)	a)
	[Co(g-15)]	3.25	2.16	1.97	190	55	54	a)

a) This work. b) Accurate values not obtained.

more developed in the latter than in the former, because ethylenediamine-ring is substituted for *o*-phenylenediamine-ring in the latter complexes. g_1 and $|A_1|$ (the ESR peak observed at the lowest field) of the latter complexes are larger than those of former complexes. This can be explained by the theoretical interpretation of g and $|A|$ values for square planar cobalt(II) complexes.[3] We showed that g_1 (and also $|A_1|$) corresponds to g_x ($|A_x|$) in Type II complexes, increasing considerably with decrease in Δ_{z^2}, which denotes the energy difference between $(d_{xy})^2(d_{z^2})^1$ and $(d_{xy})^2(d_{yz})^1$ states (*cf.* Fig. 2 in Ref. 3). From the results of X-ray crystal structure determination on analogous complexes,[13] it can be expected that all the 14-membered macrocyclic metal complexes such as [Co(c-14)], [Co(d-14)], [Co(f-14)], and [Co(i-14)], have essentially a planar structure. Thus, the present ESR results suggest that the increase of π-conjugation brings about the decrease of the energy difference between $(d_{xy})^2(d_{z^2})^1$ and $(d_{xy})^2(d_{yz})^1$, *i.e.*, the ground state of Type II compound approaches the cross-over region between Type I and Type II, when π-conjugation of the ligand increases.

References

1) Y. Nishida, A. Sumita, and S. Kida, *Bull. Chem. Soc. Jpn.*, **50**, 759 (1977).
2) Y. Nishida, A. Sumita, and S. Kida, *Bull. Chem. Soc. Jpn.*, **50**, 2485 (1977).
3) Y. Nishida and S. Kida, *Bull. Chem. Soc. Jpn.*, **51**, 143 (1978).
4) Y. Nishida, K. Hayashida, A. Sumita, and S. Kida, *Inorg. Chim. Acta*, **31**, 19 (1978).
5) Y. Nishida and S. Kida, *J. Inorg. Nucl. Chem.*, **40**, 1331 (1978).
6) Y. Nishida and S. Kida, *Coord. Chem. Rev.*, **27**, 275 (1979).
7) D. St. Black and M. J. Lane, *Aust. J. Chem.*, **23**, 2039 (1970).
8) D. St. Black, C. H. Bos Vanderzalm, and A. J. Hartshown, *Inorg. Nucl. Chem. Lett.*, **12**, 657 (1976).
9) S-M. Peng, G. C. Gordon, and V. L. Goedken, *Inorg. Chem.*, **17**, 119 (1978).
10) N. Neunhoeffer and L. Motitschke, *Tetrahedron Lett.*, **1970**, 655.
11) G. A. Melson and D. H. Busch, *J. Am. Chem. Soc.*, **86**, 4830 (1964).
12) G. B. Kaufman, A. A. Albers, and F. L. Harlan, *Inorg. Synth.*, **12**, 251 (1970).
13) For example, *cf.* M. C. Weiss, G. Gordon, and V. L. Goedken, *Inorg. Chem.*, **16**, 305 (1977); R. G. Little, J. A. Ibers, and J. E. Baldwin, *J. Am. Chem. Soc.*, **97**, 7049 (1975); S-M. Peng, J. A. Ibers, M. Millar, and R. H. Holm, *ibid.*, **98**, 8037 (1976).

Induced Circular Dichroism Spectra of Some Racemic *cis*-Bis(ethylenediamine)cobalt(III) Complexes in Aqueous (*R,R*)-Tartrate and (*R,R*)-Tartratoantimonate(III) Solutions and Their Optical Resolution by Ion-exchange Chromatography

Hiroshi NAKAZAWA, Chang Eon OH, Katsuhiko MIYOSHI, and Hayami YONEDA*

Department of Chemistry, Faculty of Science, Hiroshima University, Hiroshima 730

(Received June 25, 1979)

Synopsis. Induced circular dichroism (induced CD) was measured for some racemic cobalt(III) complexes in aqueous (*R,R*)-tartrate and (*R,R*)-tartratoantimonate(III) solutions, and correlation was examined between the sign of their induced CD spectra and their elution order in ion-exchange chromatography.

In a previous paper,[1] it was demonstrated that relatively weak circular dichroism (CD) induced in the first d-d transition region for a series of racemic tervalent cobalt(III) complexes of the type *cis*-[Co(RNH$_2$)$_2$(en)$_2$]$^{3+}$ in aqueous (*R,R*)-tartrate (*d*-tart^{2-}) and (*R,R*)-tartratoantimonate(III) (Sb$_2$*d*-tart$_2^{2-}$) solutions owes its origin to the differential CD change between the two enantiomers of each complex upon the addition of these chiral anions. It was proposed that the induced CD spectrum serves as a measure of chiral discrimination effected by *d*-tart^{2-} or Sb$_2$*d*-tart$_2^{2-}$. An attempt was made to correlate the sign of the induced CD spectrum of a racemic complex with the elution order in its chromatographic resolution on an ion-exchange column with *d*-tart^{2-} or Sb$_2$*d*-tart$_2^{2-}$ as an eluent. In the present study, a similar attempt was made for some bi- and univalent bis(ethylenediamine)cobalt(III) complexes whose absolute configurations were established by X-ray diffraction and/or assigned on the basis of their CD spectra.

Experimental

Metal Complexes. Metal complexes [Co(tn)$_3$]$^{3+}$,[2] [Co(gly)(en)$_2$]$^{2+}$,[3] [Co(β-ala)(en)$_2$]$^{2+}$,[3] [Co(acac)(en)$_2$]$^{2+}$,[4] [Co(ox)(en)$_2$]$^{+}$,[5] [Co(mal)(en)$_2$]$^{+}$,[5] *cis*-[Co(CN)$_2$(en)$_2$]$^{+}$,[6] *cis*-[Co(NO$_2$)$_2$(en)$_2$]$^{+}$,[6,7] *cis*-[Co(NCS)$_2$(en)$_2$]$^{+}$,[7] and *cis*-[Co(N$_3$)$_2$(en)$_2$]$^{+}$,[6,7] were prepared as appropriate salts and, when necessary resolved by pertinent methods. They were found to be chromatographically pure and were identified by their absorption and/or CD spectra.

Chromatographic Resolution and Measurements. Chromatographic resolution was carried out in the same way as reported,[1,3] and found incomplete for most of the complexes. Since partial resolution is often attained on an SP-Sephadex column even with achiral eluents owing to the chirality of the resin,[8] Dowex 50W-X2 resin was used to confirm that the resulting elution order was not determined by the chirality of SP-Sephadex resin. Induced CD spectra were recorded for racemic complexes (0.01 mol dm^{-3}) in aqueous solutions containing sodium (*R,R*)-tartrate (0.1 mol dm^{-3}) or sodium (*R,R*)-tartratoantimonate(III) (0.1 mol dm^{-3}) at ambient temperature.

Results and Discussion

Figure 1 shows the induced CD spectra in the first d-d transition region obtained for all the racemic complexes in aqueous *d*-tart^{2-} and Sb$_2$*d*-tart$_2^{2-}$ solutions. Only one CD component is induced for all of the tris-chelate complexes. Their Λ-enantiomers except for [Co(tn)$_3$]$^{3+}$ have in common a positive main CD component[3-6] in the first d-d transition region, its magnitude being diminished upon the addition of *d*-tart^{2-} or Sb$_2$*d*-tart$_2^{2-}$. Thus negative and positive induced CD obtained for these complexes indicates that the Λ- and Δ-enantiomers, respectively, are subjected to a greater CD change upon addition of *d*-tart^{2-} or Sb$_2$*d*-tart$_2^{2-}$.[1] The enantiomer for which the eluent has a stronger affinity should be eluted faster in ion-exchange chromatography. It is thus possible to predict the elution order from the sign of the induced CD if stronger interaction of these chiral anions with the complex leads to a greater change in its natural CD spectrum.

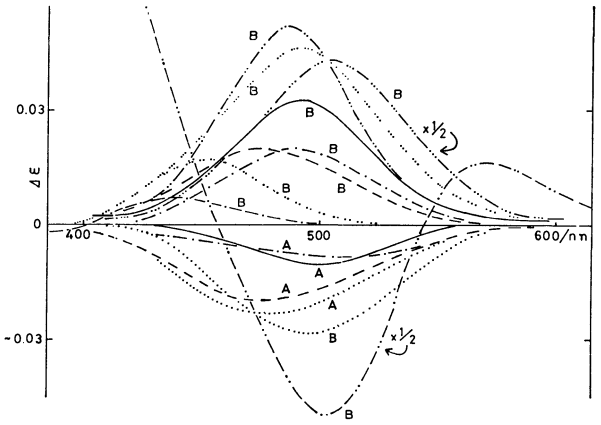

Fig. 1. Induced CD spectra in the first d-d transition region for racemic complexes in aqueous *d*-tart^{2-} (A) and Sb$_2$*d*-tart$_2^{2-}$ (B) solutions; [Co(tn)$_3$]$^{3+}$(———), [Co(gly)(en)$_2$]$^{2+}$ (·····), [Co(β-ala)(en)$_2$]$^{2+}$ (— — —), [Co(acac)(en)$_2$]$^{2+}$ (—·—·), [Co(ox)(en)$_2$]$^{+}$ (—···—···), [Co(mal)(en)$_2$]$^{+}$ (—··—··), *cis*-[Co(CN)$_2$(en)$_2$]$^{+}$ (— —·— —), *cis*-[Co(NO$_2$)$_2$(en)$_2$]$^{+}$ (·· ·· ·· ··), *cis*-[Co(NCS)$_2$(en)$_2$]$^{+}$ (··· ··· ··· ···), and *cis*-[Co(N$_3$)$_2$(en)$_2$]$^{+}$ (— —·· — —).

In Table 1 are summarized the sign of the induced CD spectra and the absolute configurations of the enantiomers for which *d*-tart^{2-} or Sb$_2$*d*-tart$_2^{2-}$ is expected to have a greater affinity as judged from the signs of the corresponding induced CD spectra for tris-chelate complexes. Also given in Table 1 are the absolute configurations of the enantiomers eluted faster in ion-exchange chromatography with *d*-tart^{2-} or Sb$_2$*d*-tart$_2^{2-}$ as an eluent. It is confirmed that, when *d*-tart^{2-} is used, the elution order[3] is in complete agreement with the prediction from the sign of the induced CD spectrum for all the tris-chelate complexes. On the other hand, when Sb$_2$*d*-tart$_2^{2-}$ is used, the induced

Table 1. Elution order and sign of induced CD spectra

		Chromatography[a]	Induced CD	(Affinity)[d]
Na_2*d*-tart	$[Co(tn)_3]^{3+}$	$(-)_D$-*Λ*	negative	(*Λ*)
	$[Co(gly)(en)_2]^{2+}$	$(+)_D$-*Λ*	negative	(*Λ*)
	$[Co(\beta\text{-ala})(en)_2]^{2+}$	$(+)_D$-*Λ*	negative	(*Λ*)
	$[Co(acac)(en)_2]^{2+}$	$(+)_D$-*Λ*	negative	(*Λ*)
	$[Co(ox)(en)_2]^{+}$	$(+)_D$-*Λ*	negative[e]	(*Λ*)
	$[Co(mal)(en)_2]^{+}$	$(+)_D$-*Λ*	negative[e]	(*Λ*)
	cis-$[Co(CN)_2(en)_2]^{+}$	$(+)_D$-*Λ*	negative[e]	
	cis-$[Co(NO_2)_2(en)_2]^{+}$	$(+)_D$-*Λ*	—[f]	
	cis-$[Co(NCS)_2(en)_2]^{+}$	—[b]	negative[e]	
	cis-$[Co(N_3)_2(en)_2]^{+}$	$(+)_D$-*Λ*[c]	negative[e]	
Na_2Sb_2*d*-$tart_2$	$[Co(tn)_3]^{3+}$	$(+)_D$-*Λ*	positive	(*Δ*)
	$[Co(gly)(en)_2]^{2+}$	$(+)_D$-*Λ*	negative	(Λ)
	$[Co(\beta\text{-ala})(en)_2]^{2+}$	$(+)_D$-*Λ*	positive	(*Δ*)
	$[Co(acac)(en)_2]^{2+}$	$(+)_D$-*Λ*	positive	(*Δ*)
	$[Co(ox)(en)_2]^{+}$	$(-)_D$-*Δ*	positive	(*Δ*)
	$[Co(mal)(en)_2]^{+}$	$(-)_D$-*Δ*	positive	(*Δ*)
	cis-$[Co(CN)_2(en)_2]^{+}$	$(-)_D$-*Δ*	g)	
	cis-$[Co(NO_2)_2(en)_2]^{+}$	$(-)_D$-*Δ*	positive	
	cis-$[Co(NCS)_2(en)_2]^{+}$	$(+)_D$-*Δ*	positive	
	cis-$[Co(N_3)_2(en)_2]^{+}$	$(+)_D$-*Λ*[c]	g)	

a) Absolute configuration of the enantiomer eluted faster. b) No resolution. c) Absolute configuration assigned not by its CD spectrum. See Ref. 8. d) Absolute configuration of the enantiomer expected to have a greater affinity for the eluent. e) Very weak. f) No induced CD detected. g) See Fig. 1.

CD exceptionally fails to predict a correct elution order for $[Co(\beta\text{-ala})(en)_2]^{2+}$ and $[Co(acac)(en)_2]^{2+}$ only. A similar apparent discrepancy was observed for *cis*-$[Co(NH_3)_2(en)_2]^{3+}$ with Sb_2*d*-$tart_2^{2-}$ as an eluent.[1] It seems that Sb_2*d*-$tart_2^{2-}$ associates more easily with the *Λ*-enantiomers of the two complexes, their CD spectra not being so affected in comparison with those of the *Δ*-enantiomers, *i.e.*, the stronger interaction with Sb_2*d*-$tart_2^{2-}$ does not lead to a greater CD change for the two complexes.[1] This suggests that the discriminating interaction with these cobalt(III) complexes essentially differs for *d*-$tart^{2-}$ and Sb_2*d*-$tart_2^{2-}$.[9,10]

In the case of $[Co(tn)_3]^{3+}$ (Table 1) its *Λ*-enantiomer has a *negative* main CD component in the first d-d transition region unlike other tris-chelate complexes. However, its magnitude is enhanced upon addition of *d*-$tart^{2-}$ or Sb_2*d*-$tart_2^{2-}$, so that negative and positive induced CD suggest stronger interaction of *d*-$tart^{2-}$ or Sb_2*d*-$tart_2^{2-}$ with the *Λ*- and *Δ*-enantiomers, respectively. Thus the induced CD also correctly predicts the elution order[11] for $[Co(tn)_3]^{3+}$.

The induced CD spectra of bis-chelate complexes of the type *cis*-$[Co(X)_2(en)_2]^{+}$ are complicated (Fig. 1 and Table 1). Their natural CD spectra are enhanced in magnitude for some complexes and are diminished for others upon the addition of *d*-$tart^{2-}$, Sb_2*d*-$tart_2^{2-}$, or oxoanions.[6,12] It is impossible to predict the elution order from the induced CD spectra for *cis*-$[Co(X)_2(en)_2]^{+}$ complexes.

On the other hand, there seems to be a general trend in the elution order (Table 1) in the present chromatographic resolution. When *d*-$tart^{2-}$ is used, the *Λ*-enantiomers are eluted faster for all the bis(ethylenediamine) complexes including the tervalent complexes[1] and $[Co(tn)_3]^{3+}$. When Sb_2*d*-$tart_2^{2-}$ is used, the *Λ*- and *Δ*-enantiomers are eluted faster for the bivalent and univalent bis(ethylenediamine) complexes, respectively, except for the diazido complex. The exceptional chromatographic behavior of the diazido complex has been discussed separately.[8] However, it is not possible at present to interpret the elution order obtained for *cis*-$[Co(X)_2(en)_2]^{+}$ complexes.

References

1) K. Miyoshi, C. E. Oh, H. Nakazawa, and H. Yoneda, *Bull. Chem. Soc. Jpn.*, **51**, 2946 (1978).
2) J. C. Bailar, Jr., and J. B. Work, *J. Am. Chem. Soc.*, **68**, 232 (1946).
3) M. Kojima, H. Takayanagi, and J. Fujita, *Bull. Chem. Soc. Jpn.*, **50**, 1891 (1977), and references cited therein.
4) L. J. Boucher, *Inorg. Chim. Acta*, **6**, 29 (1972).
5) W. T. Jordan, B. J. Brennan, L. R. Froebe, and B. E. Douglas, *Inorg. Chem.*, **12**, 1827 (1973), and references cited therein.
6) A. J. McCaffery, S. F. Mason, and B. J. Norman, *J. Chem. Soc.*, **1965**, 5094, and references cited therein.
7) K. Yamasaki, J. Hidaka, and Y. Shimura, *Bull. Chem. Soc. Jpn.*, **49**, 3060 (1976), and references cited therein.
8) S. Yamazaki and H. Yoneda, *J. Chromatogr.*, **177**, 227 (1979).
9) H. Nakazawa and H. Yoneda, *J. Chromatogr.*, **160**, 89 (1978).
10) H. Yoneda, *J. Liquid Chromatogr.*, **2**, 1157 (1979).
11) M. Kojima, H. Yamada, H. Ogino, and J. Fujita, *Bull. Chem. Soc. Jpn.*, **50**, 2325 (1977).
12) H. L. Smith and B. E. Douglas, *Inorg. Chem.*, **5**, 784 (1966).

Formation of Sr_2SiO_4 and $SrSiO_3$ from Strontium Silicate Hydrate Prepared by the Alkoxy Method

Osamu YAMAGUCHI,* Yoshifumi ITO, and Kiyoshi SHIMIZU*

Department of Applied Chemistry, Faculty of Engineering, Doshisha University, Karasuma Imadegawa, Kamigyo-ku, Kyoto 602

(Received August 1, 1979)

Synopsis. Sr_2SiO_4 and metastable $SrSiO_3$ were formed directly at low temperatures from $3SrO \cdot 2SiO_2 \cdot 3H_2O$ prepared by the alkoxy method. The transformation of metastable into stable $SrSiO_3$ was observed at 900—980 °C. A kinetic study was made on the formation of Sr_2SiO_4.

Strontium silicon oxide exists in three forms, $SrSiO_3$ (monoclinic), Sr_2SiO_4(monoclinic), and Sr_3SiO_5(tetragonal). Though $SrSiO_3$ has been known only in the pseudo-wollastonite modification,[1] Takamori and Roy[2] obtained a compound of new modification by heating $SrSiO_3$ glass. Yamaguchi *et al.*[3] found that the metastable compound is formed from an amorphous substance prepared by the alkoxy method, and carried out kinetic studies on the formation of metastable $SrSiO_3$ and the transformation of metastable into stable $SrSiO_3$. Their studies on the solid state reaction of an equimolar mixture between strontium carbonate and amorphous silica showed that stable $SrSiO_3$ is formed *via* two processes: (a) transformation of metastable into stable $SrSiO_3$; (b) solid state reaction between Sr_2SiO_4 and SiO_2.[4] This study was undertaken to elucidate the reaction mechanism in the heating process of the alkoxy-derived $3SrO \cdot 2SiO_2 \cdot 3H_2O$ and the kinetics of formation of Sr_2SiO_4.

Experimental

Silicon ethoxide of guaranteed purity was used. Strontium methoxide was synthesized by heating strontium metal, purity 99.9%, in an excessive amount of dehydrated methanol at 65 °C for 5 h. A mixture of these alkoxides with mole ratio $Sr^{2+}/Si^{4+}=3:2$ was prepared, and then poured into aqueous ammonia solution at 30 °C. The temperature was slowly raised up to 85 °C with stirring. The resulting mixed powder was washed repeatedly with hot water and dried at 65 °C under reduced pressure. The product was identified as $3SrO \cdot 2SiO_2 \cdot 3H_2O$[1] by X-ray diffraction analysis using nickel filtered copper $K\alpha$.

Results and Discussion

DTA was carried out at a heating rate of 10 °C/min. A large endothermic peak corresponding to dehydration was observed at 270—410 °C. The specimen turned amorphous after the completion of dehydration. Three exothermic reactions were observed at 700—815 °C, 815—860 °C, and 900—980 °C. X-Ray diffraction analysis confirmed that the first exothermic peak (700—815 °C) is due to the formation of Sr_2SiO_4, the second (815—860 °C) to that of metastable $SrSiO_3$, and the third (900—980 °C) to the transformation of metastable into stable $SrSiO_3$. The result is in line with that reported, *viz.*, Sr_2SiO_4 is always the first product obtained in solid state reaction,[4-7] regardless of the Sr/Si ratio.

Figure 1 shows the results of X-ray diffraction analysis of the specimens heated at 870 °C with various reaction times. The specimen was pre-heated at 450 °C for 30 min. The fractions of Sr_2SiO_4, metastable $SrSiO_3$, and stable $SrSiO_3$ were determined from heights d=2.80 Å, d=2.68 Å, and d=3.57 Å, respectively, in comparison with those of the well-formed products obtained by heating the specimens at 900 °C 1 h for Sr_2SiO_4, 860 °C 30 min for metastable $SrSiO_3$, and 1000 °C 1 h for stable $SrSiO_3$. The fractions of Sr_2SiO_4 and metastable $SrSiO_3$ attained a constant value in a short time. This suggests that both products are formed directly from the starting substance. No change was observed in the fraction of Sr_2SiO_4. On the other hand, the transformation of metastable into stable $SrSiO_3$ was observed with lapse of time. From the results as well as DTA data, the reaction mechanism can be postulated as shown in Fig. 2. More than one compound were observed during the course of solid state reaction in silicate systems; the final product can be predicted from the initial composition by referring to the equilibrium phase diagram. Results of the solid state reaction between strontium carbonate

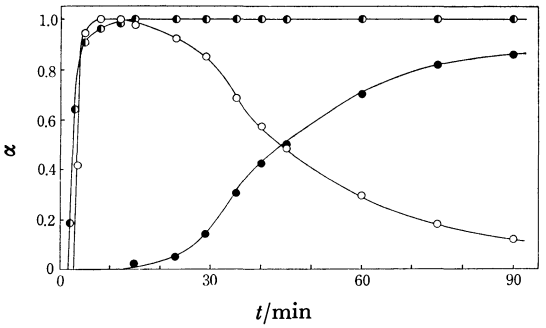

Fig. 1. Results of X-ray diffraction analysis during the reaction at 870 °C.
○: Metastable $SrSiO_3$, ●: stable $SrSiO_3$, ◐: Sr_2SiO_4.

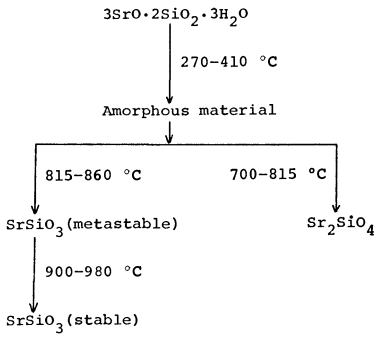

Fig. 2. Reaction scheme to the formation of $SrSiO_3$ and Sr_2SiO_4 from $3SrO \cdot 2SiO_2 \cdot 3H_2O$ as a raw material.

and amorphous silica (Sr/Si=3:2), mixed by ball-milling for 20 h, showed that metastable and stable $SrSiO_3$, Sr_2SiO_4, Sr_3SiO_5, and free SrO are formed during the course of heating. The discrepancy in the two results should be attributed to the difference in the contact between reactant between particles.

The fraction of Sr_2SiO_4 formation was determined by the lapse of time, since it is a function of time at different temperatures. The starting powder was pre-heated under the same conditions as mentioned above. The fraction of formation of each specimen was determined from the height d=2.80 Å (2θ=31.9°), the strongest line of the Sr_2SiO_4 spectrum as observed by X-ray diffraction. Alpha-crystobalite was used as an internal standard. Short induction periods were observed, attempts being made to fit the results to kinetic laws by considering the induction periods. As shown in Fig. 3, formation isotherms are best described by the first-order equation $-\ln(1-\alpha)=k(t-t_0)$, where α is the fraction of formation, t time and t_0 induction period. The rate constants were determined from the slopes of the straight lines. Activation energies calculated from the Arrhenius plot were 142 kJ/mol and 113 kJ/mol for initial and final stages, respectively. They might represent activation energies employed for establishing a nucleation process and a propagation process, respectively.[8]

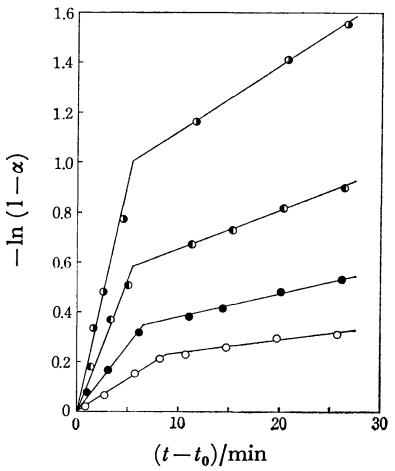

Fig. 3. Plots of $-\ln(1-\alpha)$ *vs.* time $t-t_0$.
○: 680 °C, ●: 720 °C, ◐: 760 °C, ◑: 800 °C.

References

1) E. T. Carson and L. S. Wells, *J. Res. Nat. Bur. Stand.*, **51**, 73 (1953).
2) T. Takamori and R. Roy, *J. Am. Ceram. Soc.*, **58**, 348 (1975).
3) O. Yamaguchi, K. Matumoto, and K. Shimizu, *Bull. Chem. Soc. Jpn.*, **52**, 237 (1979).
4) O. Yamaguchi, K. Yabuno, K. Takeoka, and K. Shimizu, *Chem. Lett.*, **1979**, 401.
5) W. Jander and J. Wuhrer, *Z. Anorg. Allg. Chem.*, **226**, 225 (1936).
6) V. B. Glushkova, *Zh. Neorg. Khim.*, **2**, 2438 (1957).
7) V. B. Glushkova and E. K. Keler, *Zh. Prikl. Khim.*, **30**, 517 (1957).
8) *E.g. cf.* Y. Kotera and M. Yonemura, *Trans. Faraday Soc.*, **59**, 147 (1963).

N-Alkylation of Cytosine and Its Nucleosides with Trialkyl Phosphates

Masahiro HAYASHI,* Kiyoshi YAMAUCHI, and Masayoshi KINOSHITA
Department of Applied Chemistry, Osaka City University, Sumiyoshi-ku, Osaka 558
(Received March 22, 1979)

Synopsis. Cytosine has been readily alkylated with trialkyl phosphates to give the corresponding *N*-alkyl derivatives, trimethyl phosphate being especially useful for the *N*-methylation of the base moiety of cytosine nucleosides.

The alkylation of nucleic acid components has been the subject of deep interest in organic and biological fields because of the induced physiological effects of alkylated products. The conventional alkylating agents used have been diazomethane,[1] dimethyl sulfate,[2] and alkyl halides.[3]

The alkylation of purines, pyrimidines, imidazole analogs, and pyridones with the alkyl esters of oxoacids of phosphorus,[4] have been reported where it was found that these agents were useful for the alkylation of nitrogen-containing heterocyclic compounds. This paper deals with an application of the method to the alkylation of cytosine and its nucleosides using trialkyl phosphates.

Results and Discussion

The reaction conditions and results are shown in Table 1. Upon heating cytosine (I) with trimethyl phosphate(TMP), I went gradually into solution to give three products, 1-methylcytosine (IIa), 3-methylcytosine (IIIa), and 1,3-dimethylcytosine (IVa, main). Triethyl and triallyl phosphate also converted I into a mixture of the corresponding 1-alkyl-, 3-alkyl-, and 1,3-dialkylcytosines. In general, the reactivity of trialkyl phosphates as alkylating agents appeared in the following order; methyl>allyl>ethyl.

In methylations using *N*,*N*-dimethylformamide (DMF) as the solvent in the presence of triethylamine, the reaction time was considerably reduced and the yield of IIa increased. The employment of protic solvents such as ethanol resulted in decreasing yields of alkylated products, in spite of the addition of triethylamine.

The methylation of I with dimethyl sulfate has been reported to produce only IIIa (25%) and IVa (5%);[2a] the authors have found however this reaction afforded IIa (9%) in addition to IIIa (42%) and IVa (15%) under the same conditions described in the literature[2a] (100 °C, 1 h, sulfate/I=2). The product distribution observed is somewhat different from that in the reaction with TMP (see Table), suggesting that TMP more readily methylates *N*-1 of I than dimethyl sulfate does.

Table 1. Alkylation of cytosine (I) with trialkyl phosphates[a]

R in $(RO)_3PO$	Time h	Temp °C	Solvent	Products yield/% II	III	IV	V
Me	27	100	—	6	10	74	0
	31	80	EtOH	4	20	11	10
	12	90	DMF	18	8	22	0
	12	88	DMF Et_3N	36	4	38	0
	34	100	DMF[b]	16	10	53	0
Et	37	130	—	13	3	71	0
Allyl	56	100	—	16	11	44	0
	17	110	DMF	21	8	36	0

a) Phosphate/I=4, b) Phosphate/I=8.

In the formation of IVa, two pathways (I→IIIa→IVa and I→IIa→IVa) are possible and this was examined briefly. The time-course of the reaction of I with TMP in DMF is depicted in Fig. 1. Figure 2 shows the reactions of IIa or IIIa with TMP under conditions similar to that used for reactions described in Fig. 1, indicating that IIIa is converted to IVa faster than IIa. Since IIa and IIIa are produced in similar yields in the reaction mixture of I and TMP (see Fig. 1), IVa should be produced largely *via* IIIa rather than IIa.

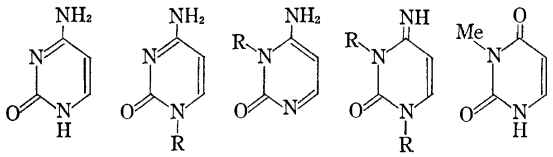

I IIa—c IIIa—c IVa—c V
a: R=Me, b: R=Et, c: R=allyl.

The *N*-1 of IIIa, which exists in the form of a 4-amino-2-oxo structure, is known to be more basic and less sterically hindered than the *N*-3 of IIa,[5] suggesting the former site is more reactive than the latter. The faster rate of formation of IVa from IIIa than from IIa (Fig. 2) may be attributable to these factors.

The methylation of cytidine (VIa) and 2'-deoxycytidine (VIb) was examined using TMP, which appeared to be the most reactive alkylating agent of the trialkyl phosphates studied.

Under neutral conditions in water or anhydrous solvent, alkylating agents such as diazomethane, benzyl

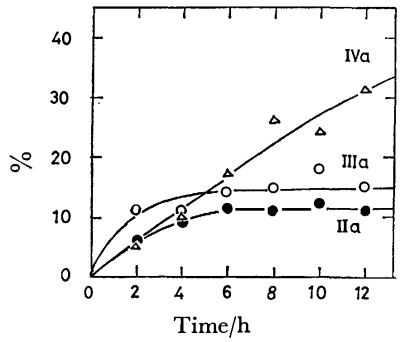

Fig. 1. The reaction of cytosine (I) with trimethyl phosphate (TMP) in DMF at 100 °C. TMP/I=8.

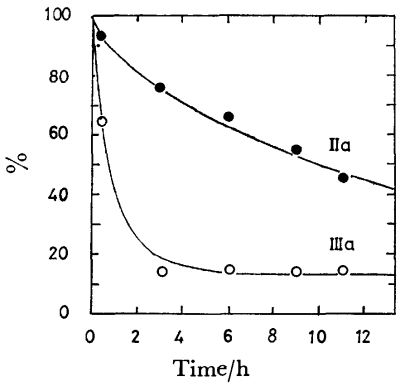

Fig. 2. The reaction of 1-methylcytosine (IIa) and 3-methylcytosine (IIIa) with trimethyl phosphate (TMP) in DMF at 100 °C. TMP:IIa:IIIa=8:1:1.

iodide, dimethyl sulfate, and nitrogen mustard have been shown to give the *N*-3-alkylated derivatives.[1,2a,3a,3b,6] Under alkaline conditions these alkylating agents predominantly alkylate the carbohydrate hydroxyls.[2b,7]

In the reaction with TMP (10 mol-equiv.) in DMF (70 °C; 32 h), compound VIa was smoothly methylated only at the *N*-3 position to give 3-methylcytidine (VIIa) in 81% yield. Under similar conditions, VIb was converted to 3-methyl-2′-deoxycytidine (VIIb; 52 %), but unlike the 4-amino group of VIa, VIb was also methylated to generate N^4-methyl-2′-deoxycytidine (VIII; 11%) as a by-product.[8] Under the present conditions, TLC analysis of the reaction mixture did not show any products which were methylated at the carbohydrate hydroxyls of VIa and VIb.

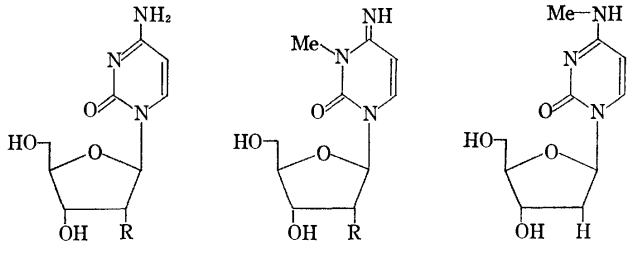

VIa,b VIIa,b VIII

a: R=OH, b: R=H.

The methylation of VIa with dimethyl sulfate gave VIIa in a yield comparable with that of TMP. Methylations with diazomethane and methyl iodide have been known to be less efficient than dimethyl sulfate or TMP. Thus, the present method would be useful particularly for the *N*-methylation of cytosine and its nucleosides.

Experimental

Commercial reagents were used without further purification. Triallyl phosphate was prepared by the procedure of Toy *et al.*[9] The reaction procedures and product isolations were in a manner similar to that of previous work.[4c] The yields of the reaction products were obtained spectroscopically similarly to that used in the former study.[4d] Results and reaction conditions are given in Table 1.

The majority of the products isolated agreed with the literature values (mp, UV, and NMR).[2a,3b,10,12,13,14]

Physical Constants. IVb; mp 262—264 °C (HCl salt), 237—239 °C (methanol–ether), NMR (D_2O) δ 1.32 (t, J=8 Hz, 3H, CH_3), 1.34 (t, J=8 Hz, 3H, CH_3), 3.96 (q, J=8 Hz, 2H, $-CH_2-$), 4.12 (q, J=8 Hz, 2H, $-CH_2-$), 6.22 (d, J=8 Hz, 1H, C-5), and 7.87 ppm (d, J=8 Hz, 1H, C-6), UV, λ_{max} 277, λ_{min} 242 mμ (pH 7), MS, *m/e* 167 (M^+ for $C_8H_{13}N_3O$): IIc; mp 242—245 °C (ethanol), NMR (D_2O) δ 4.46 (m, 2H, $-CH_2-$), 5.36 (m, 2H, $=CH_2$), 6.10 (d, J=7.5 Hz, 1H, C-5), 6.13 (m, 1H, $-CH=$), and 7.64 ppm (d, J=7.5 Hz, 1-H, C-6), UV, λ_{max} 274, λ_{min} 252 mμ (pH 7), MS, *m/e* 151 (M^+ for $C_7H_9N_3O$): IIIc; UV, λ_{max} 296, λ_{min} 255 mμ (pH 7): IVc; mp 242—244 °C (HCl salt), NMR (D_2O) δ 4.55 (m, 4H, $-CH_2-$), 5.27 (m, 4H, $=CH_2$), 5.95 (m, 2H, $-CH=$), 6.30 (d, J=8 Hz, 1H, C-5), and 7.88 ppm (d, J=8 Hz, 1H, C-6), UV, λ_{max} 277, λ_{min} 243 mμ (pH 7), MS, *m/e* 191 (M^+ for $C_{10}H_{13}N_3O$): VIIb; mp 174—176 °C ($CHCl_3$), NMR (D_2O) δ 2.50 (m, 2H, 2′-H), 3.57 (s, 3H, CH_3), 3.83 (d, J=2 Hz, 1H, 5′-H), 3.93 (s, 1H, 5′-H), 4.18 (m, 1H, 4′-H), 4.53 (m, 1H, 3′H), 6.30 (t, J=7 Hz, 1H, 1′-H), 6.38 (d, J=8 Hz, 1H, C-5), and 8.17 ppm (d, J=8 Hz, 1H, C-6), UV, λ_{max}, λ_{min} mμ (pH), 279, 245 (1), 279, 245 (7), 267, 246 (13), MS, *m/e* 241 (M^+ for $C_{10}H_{15}N_3O_4$).

References

1) J. A. Haines, C. B. Reese, and L. Todd, *J. Chem. Soc.*, **1964**, 1406.

2) a) P. Brookes and P. D. Lawley, *J. Chem. Soc.*, **1962**, 1348; b) J. T. Kuśmierek, J. Giziewcz, and D. Shugar, *Biochemistry*, **12**, 194 (1973).

3) a) P. Brookes, A. Dipple, and P. D. Lawley, *J. Chem. Soc., C*, **1968**, 2026; b) L. Sun and B. Singer, *Biochemistry*, **13**, 1905 (1974); c) G. E. Hilbert, *J. Am. Chem. Soc.*, **56**, 190 (1934); d) G. W. Kenner, C. B. Reese, and A. R. Todd, *J. Chem. Soc.*, **1955**, 855.

4) a) K. Yamauchi and M. Kinoshita, *J. Chem. Soc., Perkin Trans. 1*, **1973**, 391, 2506; b) K. Yamauchi, M. Hayashi, and M. Kinoshita, *J. Org. Chem.*, **40**, 385 (1975); c) M. Hayashi, K. Yamauchi, and M. Kinoshita, *Bull. Chem. Soc. Jpn.*, **49**, 283 (1976) and **50**, 1510 (1977); d) K. Yamauchi, T. Tanabe, and M. Kinoshita, *J. Org. Chem.*, **41**, 369 (1976); e) T. Tanabe, K. Yamauchi, and M. Kinoshita, *Bull. Chem. Soc. Jpn.*, **49**, 3224 (1976) and **50**, 3021 (1977).

5) T. Ueda and J. J. Fox, *J. Am. Chem. Soc.*, **85**, 4024 (1963).

6) C. C. Price, G. M. Gaucher, P. Koneru, R. Shibakawa, J. R. Sowa, and M. Yamaguchi, *Biochim. Biophys. Acta*, **166**, 327 (1968).

7) D. M. G. Martin, C. B. Reese, and G. F. Stephenson, *Biochemistry*, **7**, 1406 (1968).

8) The reaction of 2′-deoxycytidine hydrochloride with TMP resulted in decreasing the yield of products (VIIb; 38% and VIII; 6%).

9) A. D. F. Toy and J. R. Costello, U. S. Patent 2 754 315 (1950).

10) A. R. Katritzky and A. J. Waring, *J. Chem. Soc.*, **1963**, 3046.

11) J. J. Fox and D. Shugar, *Biochim. Biophys. Acta*, **9**, 369 (1952).

12) K. Senga, F. Yoneda, and S. Nishigaki, *J. Org. Chem.*, **36**, 1829 (1971).

13) L. Doub and U. Krolls, *J. Heterocyclic Chem.*, **7**, 527 (1970).

14) J. J. Fox, *J. Am. Chem. Soc.*, **83**, 4755 (1961).

Effect of Polyether Linkages on the Carboxylation of Sodium Phenoxide

Tsutomu SAKAKIBARA* and Kazuyo HARAGUCHI
Institute of Chemistry, College of Liberal Arts, Kagoshima University, Korimoto, Kagoshima 890

(Received April 23, 1979)

Synopsis. In the carboxylation of sodium phenoxide under mild conditions, the crown compound or polyethers with three to five ether linkages caused carboxylation to give *o*- and *p*-hydroxybenzoic acids, but not ethers with one or two linkages. The chelation of sodium phenoxide with polyethers changed the formation ratio of isomers.

It is well known that various polyethers have properties in which a neutral molecule encircles metal ions or related cation, and changes the chemical or physical charactor of metal ion or the paired anion, such as reactivity, solubility, or catalytic activity.[1] With potassium phenoxides, chelation with crown ethers achieves conversion of phenols into their chalcones,[2] the chelation increasing the reactivity of potassium phenoxide.

In the Kolbe-Schmitt reactions, sodium phenoxide exclusively gives *o*-hydroxybenzoic acid (salicylic acid).[3] Preferential formation of *o*-isomer is explained in terms of intramolecular chelation in the intermediate (**1**) (Eq. 1).

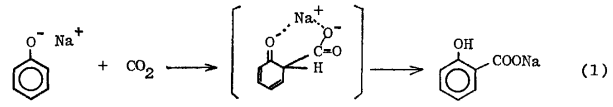

(1)

1

So far, only a few reports have appeared on the effect of polyethers on the carboxylation of sodium phenoxide. In this report, we will show how the chelation with polyethers influences the reaction of sodium phenoxide with carbon dioxide under mild conditions.

In a typical experiment, 0.03 mol of sodium phenoxide in dry diglyme (1.0 mol) was stirred under carbon dioxide atmosphere at 80 °C for 10 h. After work-up of the reaction mixture, pure *o*-hydroxybenzoic acid was isolated in 5% yield as the sole product. Similar reactions were carried out in some polyether solvents. The results are summarized in Table 1.

The conversion of the reactant was low due to the mild reaction conditions. However, the results indicate that the number of ether linkages in solvent molecule influences the carboxylation of sodium phenoxide. A solvent with three to five ether linkages in a molecule gave rise to carboxylation of aromatic ring, but not a solvent with one or two. Use of tetraglyme in the reaction resulted in the formation of *p*-hydroxybenzoic acid, in spite of the preferential formation of *o*-isomer under the usual Kolbe-Schmitt conditions, *i.e.*, under high temperature and high pressure of carbon dioxide.[3]

Sodium phenoxide in monoglyme solvent gives no aromatic acids (Table 1). However, in the presence of a small amount of dibenzo-18-crown-6, carboxylation

TABLE 1. EFFECT OF POLYETHERS ON THE CARBOXYLATION OF SODIUM PHENOXIDE

Polyethers	Yield/%		
	Yield of hydroxybenzoic acid[a]	Composition	
		o-isomer,	*p*-isomer
Tetrahydrofuran	0	0	0
2,2′-Bi(tetrahydrofuranyl)	0	0	0
$H_3CO(CH_2CH_2O)_nCH_3$			
$n=1$	0	0	0
2	5	100	0
2	7	97	3
3	5	80	20
4	4	20	80
4	3	25	75

a) Based on the amount of sodium phenoxide.

slowly proceeds in monoglyme to give a mixture of *o*-hydroxybenzoic acid and the *p*-isomer. Thus, a mixture of sodium phenoxide (0.03 mol) and dibenzo-18-crown-6 (0.005 mol) was stirred in monoglyme (1.0 mol) at 80 °C for 10 h under carbon dioxide atmosphere. After neutralization of the reaction products, a mixture of aromatic acids was isolated in a 3.5% yield, which contained *o*- (56%) and *p*-acid (44%). The 1:1 formation of *o*- and *p*-isomers is in line with the expected reactivity at *o*- and *p*-positions of free phenoxide ion.[4] This shows that the carboxylation may proceed *via* a phenoxide ion separated from the paired sodium ion by chelation with crown ether (Eq. 2).

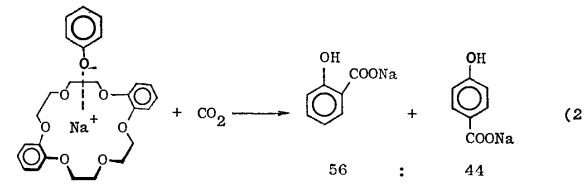

(2)

2

The results of reactions in noncyclic polyethers are also explained in terms of the chelation of sodium phenoxide with polyethers. Diglyme and triglyme may activate sodium phenoxide to react with carbon dioxide, but cannot form free phenoxide ion because of their weak chelation ability. The formation of probable intermediate (**3**) may lead to *o*-isomer. On the other hand, tetraglyme completely binds sodium ion to form an analogous intermediate (**4**) to **2**. The complex (**4**) might have a less coplanar chelating ring as compared with that in **2** due to the terminal methyl groups. The preferential formation of *p*-isomer might show the steric effect at *o*-position by methyl groups.

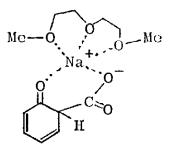

3

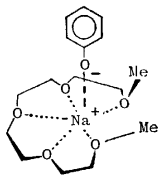

4

Experimental

Materials. Sodium phenoxide and dibenzo-18-crown-6 were prepared according to the methods described by Mori *et al.*,[5] and Pedersen,[6] respectively. 2,2'-Bi(tetrahydrofuranyl) was prepared in a 24% yield by the photoreduction of acetone in tetrahydrofuran (molar ratio of acetone/THF; 1/10): n_D^{23} 1.4572 (lit,[7] n_D^{20} 1.4512), Mass (*m/e*); 142 (M^+), 71 ($M^+/2$). The IR and NMR were identical with those of authentic material. Commercially available monoglyme, diglyme, triglyme, and tetraglyme were distilled on sodium under reduced pressure before use.

Carboxylation of Sodium Phenoxide in Diglyme. A mixture of 3.48 g of sodium phenoxide (0.03 mol) and 134 g of diglyme (1.0 mol) was stirred at 80 °C for 10 h bubbling with dried carbon dioxide in a dried four necked flask, equipped with a stirrer sealed by liquid paraffin, a Dimroht condenser with calcium chloride tube, a thermometer, and an introducing tube of carbon dioxide. After the reaction, 40 ml of 15% aqueous sodium hydroxide was added to the reaction mixture and the organic solvent was separated in a separating funnel. The aqueous layer was washed with a small amount of diethyl ether and afterwards was acidified with concd HCl, followed by extraction with diethyl ether. After the ether solution had been dried on anhydrous sodium sulfate, evaporation of ether gave 207 mg of pure salicylic acid, which was identified with the authentic material by mp measurement, IR, and NMR.

Similar reactions using tri- or tetraglyme, or dibenzo-18-crown-6 gave a mixutre of organic acids, in which the formation ratio of *o*- and *p*-isomers was determined by GLC using OV-101 column (182 °C, carrier gas; H_2).

The authors wish to express their thanks to Prof. T. Hase, Kagoshima University, for his valuable aid.

References

1) C. J. Pedersen and H. F. Frensdorff, *Angew. Chem. Int. Ed. Engl.*, **11**, 16 (1972).

2) G. J. H. Rall, M. E. Oberholzer, D. Ferreira, and D. G. Roux, *Tetrahedron Lett.*, **1976**, 1033.

3) A. S. Linsey and H. Jeskey, *Chem. Rev.*, **57**, 583 (1957).

4) When benzyl anion is considered as a model of phenoxide ion, the total π-electron density at *p*-position is somewhat larger than that at *o*-position (*o*/*p*=1.142/1.144), the Frontier electron densities being almost equal at both positions. Thus, the reaction of phenoxide ion with carbon dioxide, known as a hard acid, should give a considerable large *o*/2*p* ratio when the steric effect is neglected. In the present reaction. the *o*/2*p* ratio was 0.63; see I. Fleming, "Frontier Orbitals and Organic Chemical Reactions," Japanese Edition (translated by K. Fukui *et al.*), Kodansha Co., Ltd., (1978), pp. 40—77.

5) H. Mori, H. Yamamoto, and T. Kwan, *Chem. Pharm. Bull.*, **20**, 2440 (1972).

6) C. J. Pedersen, *J. Am. Chem. Soc.*, **89**, 7017 (1967).

7) T. Sakakibara and Y. Odaira, *J. Org. Chem.*, **36**, 3664 (1971).

Preparation of Methoxy-substituted Diaryl Ketone Anils *via* Phenyliminodimagnesium Intermediate

Masao Ōkubo* and Sonoko Ueda

Department of Chemistry, Faculty of Science and Engineering, Saga University, Honjō-machi, Saga 840

(Received May 18, 1979)

Synopsis. Phenyliminodimagnesium reagent ($PhN(MgBr)_2$) and its *o*- and *p*-methoxy derivatives, prepared in THF by treatment of anilines with EtMgBr, were found to be effective for condensation with benzophenones and fluorenone. The corresponding anils (*N*-(diarylmethylene)-anilines) were prepared in good yields.

In the course of studies on the Grignard reaction with a carbon-nitrogen double bond, it was found necessary to prepare the unknown *o*-methoxybenzophenone anil (*N*-(phenyl-2-methoxyphenylmethylene)-aniline) as a model compound for examining the S_{RN}-type reaction of the methoxyl group with phenylmagnesium bromide.[1] While benzaldehydes can be condensed with anilines without any catalyst,[2] the condensation of ketones with amines requires a catalyst such as $ZnCl_2$,[3,4] HBr,[5] $POCl_3$,[6] BF_3,[7] $TiCl_4$,[8] or molecular sieves.[9] The first four catalysts have been used for the condensation of diaryl ketones with anilines, but they can cause side reactions such as cleavage of ether linkage, making their applicability to the desired condensation of *o*-methoxybenzophenone with aniline impracticable.

The three catalytic methods gave anils in poor yields (Table 1). The very high yield of anil **4** obtained by the condensation of fluorenone with *p*-methoxyaniline(c-4)[7] might show the effectiveness of BF_3, which, however, gave no satisfactory results in other cases. None or only trace amounts of the expected anils were detected by TLC in experiments b-2, c-2, c-6, and c-7. From the results and from successful BF_3-catalysis reported on the condensation of nitro-substituted fluorenones with anilines,[7] it is apparent that the strongly electron-donating methoxyl group especially at *ortho*-position of both benzophenones and anilines is unfavorable for catalytic condensation. Since benzaldehyde and *o*-methoxybenzaldehyde can be condensed respectively with *o*-methoxyaniline and aniline,[10] the bulkiness of the carbonyl component is another obstructive factor.

In our search for some other method involving a procedure to activate the NH-bond of aniline molecule, the anilinomagnesium (PhNHMgBr) and phenyliminodimagnesium($PhN(MgBr)_2$) reagents supplied us with a clue. The former reagent and its *N*-methyl derivative have been used as catalysts for aldol condensation;[11] the latter has been used as the intermediate for preparing trimethylsilylated amino compounds[12] and for converting carboxylic esters into amides.[13] The dimagnesium intermediate seems effective for achieving dehydrative condensation. The expected reaction is shown in Scheme 1.

Phenyliminodimagnesium reagent(**A**) and its *o*- and *p*-methoxy derivatives were prepared according to step i) and subsequently condensed with benzophenones and fluorenone (Table 1, d-1 to d-7). The yields

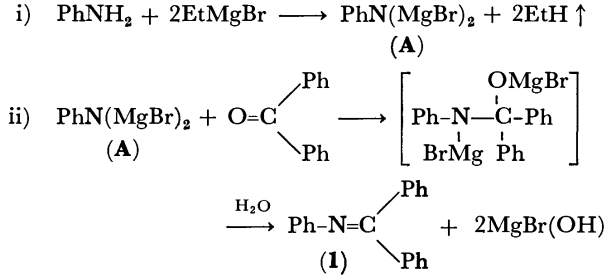

Scheme 1.

of anils **1**[3] and **2**[5] were markedly improved though the reaction conditions were not optimized. However, the desired preparation of *o*-methoxybenzophenone anil was not successful even by this method(d-6), since the methoxyl group was replaced by the PhN(MgBr)-group leading to the formation of **6**. This is apparently due to a S_{RN}-type reaction similar to that proposed for the Grignard reaction of hindered benzophenone derivatives.[1] The low yield of **6** is due to the consumption of two molar equivalents of **A**. The successful preparation of **7** by the condensation of 4,4'-bis(dimethylamino)benzophenone with *p*-methoxyaniline(d-7), both of which have strongly electron-donating substituents, shows the usefulness of the method. The *ortho*-effect of the methoxyl group on the aniline component was substantially overcome as indicated by the fair yields of **3** and **5**. The anils **3**, **5**, **6**, and **7** are new compounds.

The reaction conditions of the method are much milder compared to those of the previous ones requiring higher temperature for the fusion of the reaction mixtures or for the removal of the formed water. The THF solution of **A** is extremely air-sensitive, the solution turning reddish purple rapidly by only a slight intrusion of air. The mechanism of step ii) remains equivocal, since there is another possibility that the $O(MgBr)_2$ species leaves directly from the addition complex prior to treatment with water. Since it is not applicable to nitro-substituted diaryl ketones and aniline, this method and BF_3-catalysis[7] are complementary to each other.

Experimental

Procedures. The phenyliminodimagnesium reagent (**A**, 0.03 mol) in THF (35 ml) was prepared under nitrogen by the addition of aniline to a solution of ethylmagnesium bromide (0.06 mol) at room temperature. The mixture was stirred at 50—55 °C for 30 min to complete the evolution of the latter half equivalent of ethane. Slight heat evolution took place with the subsequent addition of equimolar benzophenone (0.03 mol in 10 ml THF). The reaction mixture turned yellow and then reddish brown. The colored mixture was stirred at 50—55 °C for 30 min and at room temperature overnight, and then treated with saturated aqueous NH_4Cl.

Table 1. Yields of methoxy-substituted ketone anils

Anils No.	Structure	Ketones	Anilines	Yields of anils (a) $ZnCl_2$	(b) $POCl_3$	(c) BF_3	(d) $ArN(MgBr)_2$
1	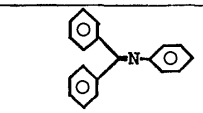	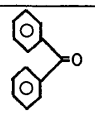		28	27	—	68
2	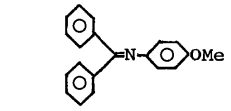	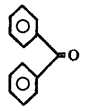	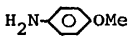	10.1 1.3 7.5	not isolated	not isolated	72
3	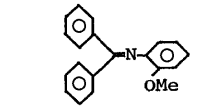	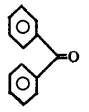		—	3.6	—	36
4	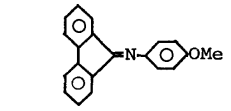	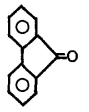	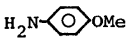	—	—	81	82
5	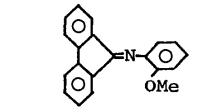	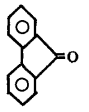		—	—	10.2	54
6	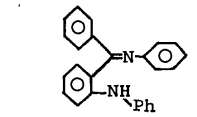	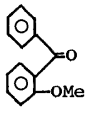	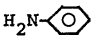	—	—	not isolated	39
7	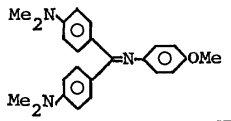	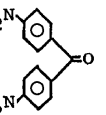	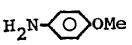	—	—	not isolated	59

Extraction of the resulting mixture with diethyl ether or benzene, drying of the combined extracts with $MgSO_4$, and evaporation of the solvent under reduced pressure afforded a dark yellow crystalline mass. Recrystallization from methyl alcohol afforded 5.0 g (68%) of **1** in a pure form.

The other anils were prepared similarly. Anils **3** and **6** were isolated from the respective product mixture by column chromatography on silica gel (Wakogel C-200, petroleum ether:diethyl ether:benzene=10:1:1).

Melting points (uncorrected), NMR data for methyl and NH protons, and results of the elemental analysis (for only new anils) are given below. All the aromatic protons in NMR appear in the range 6.40—7.95 ppm.

Anil **1**. Mp 116 °C (lit,[3] 116 °C), —.

Anil **2**. Mp 70—72 °C (lit,[4] 70 °C), δ=3.62(s).

Anil **3**. Mp 61—62 °C, δ=3.52(s). Found: C, 83.81; H, 5.85; N, 4.67%. Calcd for $C_{20}H_{17}NO$: C, 83.60; H, 5.96; N, 4.87%.

Anil **4**. Mp 135—138 °C (lit,[4,7] 135—136 °C), δ=3.80(s).

Anil **5**. Mp 141—142 °C, δ=3.70(s). Found: C, 83.97; H, 5.28; N, 4.81%. Calcd for $C_{20}H_{15}NO$: C, 84.19; H, 5.30; N, 4.91%.

Anil **6**. Oil, δ=10.02(s, NH). Found: C, 86.23; H, 5.76; N, 8.07%. Calcd for $C_{22}H_{20}N_2$: C, 86.18; H, 5.79; N, 8.04%.

Anil **7**. Mp 174—175 °C, δ=3.64 (3H, s) and 3.90 (12H, d). Found: C, 77.15; H, 7.31; N, 11.22%. Calcd for $C_{24}H_{27}N_3O$: C, 77.18; H, 7.29; N, 11.26%.

From the control experiments for measuring the volume of evolved ethane, the yield of intermediate **A** was estimated to be 85—92%.

References

1) M. Ōkubo, *Bull. Chem. Soc. Jpn.*, **50**, 2379 (1977).

2) L. A. Bigelow and H. Eatough, *Org. Synth.*, Coll. Vol. I, 80 (1956).

3) G. Reddelien, *Chem. Ber.*, **42**, 4759 (1909).

4) J. H. Billman and K. M. Tai, *J. Org. Chem.*, **23**, 535 (1958).

5) G. Reddelien, *Chem. Ber.*, **47**, 1355 (1914); Ref. 4.

6) A. W. Weston and R. J. Michaels, Jr., *J. Am. Chem. Soc.*, **73**, 1381 (1951).

7) M. Taylor and T. L. Fletcher, *J. Org. Chem.*, **26**, 940 (1961).

8) H. Weingarten, J. P. Chupp, and W. A. White, *J. Org. Chem.*, **32**, 3246 (1967); I. Moretti and G. Torre, *Synthesis*, **1970**, 141.

9) K. Taguchi and F. H. Westheimer, *J. Org. Chem.*, **36**, 1570 (1971).

10) M. Ōkubo and S. Ueda, *Bull. Chem. Soc. Jpn.*, **52**, 3346 (1979).

11) A. T. Nielsen, C. Gibbons, and C. A. Zimmerman, *J. Am. Chem. Soc.*, **73**, 4696 (1951); W. D. Garden and F. D. Gunstone, *J. Chem. Soc.*, **1952**, 2650; and references cited therein.

12) E. W. Abel and G. R. Wiley, *J. Chem. Soc.*, **1964**, 1528; D. R. M. Walton, *ibid., C*, **1966**, 1706.

13) P. A. Petyunin and V. V. Boltov, *Zh. Org. Khim.*, **9**, 836 (1973); *Chem. Abstr.*, **79**, 53130 (1973): D. I. Uvarov and M. E. Konshin, *Khim. Geterotsikl. Soedin*, **1973**, 1084; *Chem. Abstr.*, **79**, 126282 (1973).

Studies on 2-Aziridinecarboxylic Acid. III. Reaction of 1-Acyl-2-aziridinecarboxylic Acid Peptide with Amines

Kiichiro NAKAJIMA, Takumi TANAKA, Kaoru MORITA, and Kenji OKAWA*

Department of Chemistry, Faculty of Science, Kwansei Gakuin University, Nishinomiya 662

(Received June 6, 1979)

Synopsis. The reaction of Z-Gly-Azy-Gly-OBzl with amines was studied. With primary amines, the 1-acyl group (Z-Gly) of the aziridine peptide mainly migrated to the reactant amine with cleaving of the amide bond between glycine and aziridine, whereas aniline and diethylamine gave diaminopropionic acid derivatives *via* the ring opening reaction.

The present study is a part of an investigation of the reactivity of 1-acylaziridine peptides. It was shown that 1-acylaziridine peptides afford the *O*-esters as a result of the ring opening reaction with carboxylic acids.[1]

In this communication, we wish to give the results of a study of the reactivity of Z-Gly-Azy-Gly-OBzl(**1**)[2] with amines. Ammonia, benzylamine, ethylenediamine, amino acid esters, aniline, and diethylamine were used as the amines.

1-Acylaziridine derivatives generally undergo the ring opening reaction with primary or secondary amine, giving the following ethylenediamine derivatives.[3]

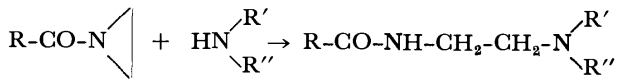

All amines examined, however, caused migration of the 1-acyl group (Z-Gly) from **1** to the reactant amines except aniline and diethylamine. Consequently, the fragment peptides (Z-Gly-NH-R(**2**) and Azy-Gly-OBzl(**3**)) were obtained in quantitative yields (Scheme 1 and Table 1). The results indicate that the reactivity of 1-acylaziridine peptide is independent of both the amount of amine and the reaction temperature. Evidently, the carbonyl carbon of the acyl group on 1-acylaziridine peptide is more positive than that of ordinary amides. The aziridine ring has an electron withdrawing or quasi-aromatic character.[4] A similar property is recognized in a nitrogen-containing heterocyclic ring system as amide component, such as pyrazolides, imidazolides and triazolides. The competitive reaction between migration and the ring opening reaction occurred to give the fragment peptides (**2**, **3**) and diaminopropionic acid derivative (A_2pr; **4**) in aniline. In contrast, only diaminopropionic acid derivative (**5**) was obtained *via* the ring opening reaction in the case of diethylamine. It seems that the reaction is specific for secondary amine.

TABLE 1. REACTION OF **1** WITH AMINES

Exp. No.	Reactant amines	Eq. amt. of amines	Temp °C	Time h	Yield/% 2	3	4 or 5
a	NH_3	excess	−5	1	94.5	92.8	0
b	NH_3	excess	r.t.	1	95.1	92.2	0
c	$PhCH_2NH_2$	20	r.t.	24	77.7	99.5[a]	0
d	$PhCH_2NH_2$	5	r.t.	24	90.4	79.0[a]	0
e	$PhCH_2NH_2$	5	45	24	99.4	41.6[a]	0
f	$(H_2N\text{-}CH_2)_2$	0.5	r.t.	24	77.7	64.6	0
g	$CH_2(NH_2)CO_2Bu^t$	8	r.t.	24	84.8	100	0
h	D-$PhCH(NH_2)CO_2Bu^t$	1.4	r.t.	72	100	100	0
i	$PhNH_2$	20	r.t.	24	14.1	15.0	27.8
j	$PhNH_2$	5	r.t.	72	36.2	28.0	43.7
k	$PhNH_2$	5	45	24	11.5	19.0	51.9
l	$HN(C_2H_5)_2$	20	r.t.	72	0	0	88.5

a) Total yield of both products Azy-Gly-OBzl and Ary-Gly-$NHCH_2Ph$.

Experimental

All melting points are uncorrected. NMR spectra were compatible for all products isolated. The purity of products was confirmed by thin layer chromatography on silica gel G.

Z-Gly-Azy-Gly-OBzl (1). Compound **1** prepared from serine derivative[5] was crystallized from THF–ether; mp 118—119 °C, $[\alpha]_D^{23}$ −52.2° (*c* 1.0, MeOH). NMR (acetone-d_6): δ 2.38 (1H q, J=1.5, 2.9 Hz, aziridine β-proton), 2.52 (1H, q, J=1.5, 5.9 Hz, aziridine β-proton), 3.29 (1H, q, J=2.9, 5.9 Hz, aziridine α-proton), 4.01 (2H t, J=5.0, -NH-CH_2-CO-). Found: C, 61.92; H, 5.57; N, 10.07%. Calcd for $C_{22}H_{23}O_6N_3$: C, 62.16; H, 5.45; N, 9.88%.

Reaction of 1 with Amines. *By Ammonia (a)*: Dry ammonia gas was bubbled into a solution of **1** (106 mg, 0.25 mmol) in CH_2Cl_2 (3 ml) at −5 °C until saturation. After being kept at the same temperature for 1 h, the solvent was removed. Dry ether was added to the residual product.

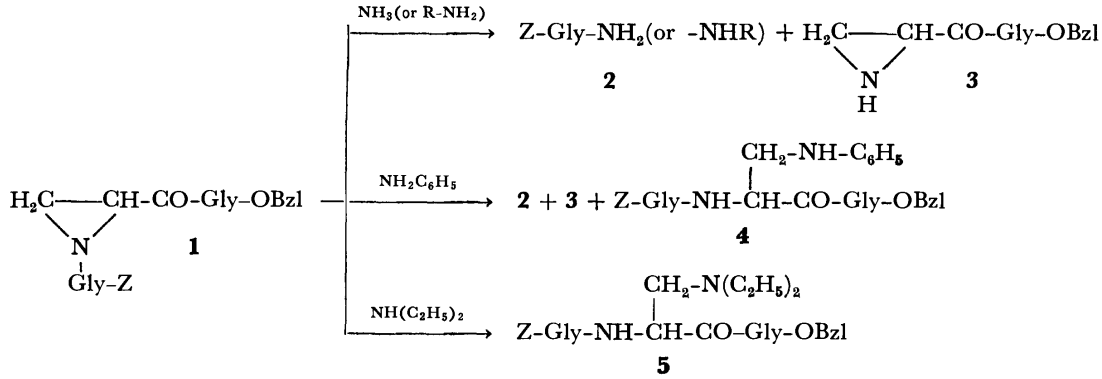

Scheme 1.

Crystals which appeared were collected by filtration, and identified as Z-Gly-NH_2; 52 mg (94.5%), mp 135—136 °C (lit,[6] mp 138—139 °C). From the filtrate, Azy-Gly-OBzl was isolated as crystals from $CHCl_3$-ether-hexane; 54.3 mg (92.8%), mp 118—119 °C, $[\alpha]_D^{23}$ −21.0° (*c* 1.0, $CHCl_3$). Found: C, 61.48; H, 5.97; N, 11.83%. Calcd for $C_{12}H_{14}O_3N_2$: C, 61.52; H, 6.02; N, 11.96%.

By Ammonia (b): Dry ammonia gas was bubbled into a solution of **1** (100 mg, 0.23 mmol) in CH_2Cl_2 (3 ml) at room temperature. After 1 h, the products were isolated as described for (a). Z-Gly-NH_2; 54.3 mg (95.1%). Azy-Gly-OBzl; 56 mg (92.2%).

By Benzylamine (c): Benzylamine (0.56 ml, 5.2 mmol) was added with stirring to a solution of **1** (110 mg, 0.26 mmol) in CH_2Cl_2 (3 ml) at room temperature. After 24 h, ether was added to the reaction mixture. Crystals which appeared were collected by filtration, and identified as Z-Gly-NH-CH_2-C_6H_5; 58 mg (77.7%), mp 118—119 °C (lit,[7] mp 119—120 °C). The filtrate was concentrated *in vacuo*, the residual product being crystallized from MeOH-ether-hexane. The first crop of crystals was Azy-Gly-NH-CH_2-C_6H_5; 53.6 mg (91.6%), mp 140—141 °C, $[\alpha]_D^{23}$ −22.0° (*c* 1.0, MeOH). Found: C, 61.98; H, 6.48; N, 17.87%. Calcd for $C_{12}H_{15}O_2N_3$: C, 61.78; H, 6.48; N, 18.02%. The second crop was Azy-Gly-OBzl; 4.4 mg (7.9%).

By Benzylamine (d): Compound **1** (106 mg, 0.25 mmol) and benzylamine (0.14 ml, 1.25 mmol) were reacted in CH_2Cl_2 (3 ml) at room temperature for 24 h. The products were isolated as described for (c). Z-Gly-NH-CH_2-C_6H_5; 67 mg (90.4%), Azy-Gly-NH-CH_2-C_6H_5 and Azy-Gly-OBzl; 57 mg (79.0%).

By Benzylamine (e): Compound **1** (212 mg, 0.5 mmol) and benzylamine (0.27 ml, 2.5 mmol) were reacted in CH_2Cl_2 (3 ml) at 45 °C for 24 h. The products were isolated as described for (c). Z-Gly-NH-CH_2-C_6H_5; 148.2 mg (99.4 %), Azy-Gly-NH-CH_2-C_6H_5 and Azy-Gly-OBzl; 61 mg (41.6%).

By Ethylenediamine (f): Ethylenediamine (12.4 mg, 0.21 mmol) was added with stirring to a solution of **1** (176 mg, 0.4 mmol) in CH_2Cl_2 (3 ml) at room temperature. After 24 h, crystals which appeared were collected by filtration, and identified as (Z-Gly-NH-CH_2-)$_2$; 71.1 mg (77.7%), mp 206 °C (dec). Found: C, 59.65; H, 5.88; N, 12.47%. Calcd for $C_{22}H_{26}O_6N_4$: C, 59.72; H, 5.92; N, 12.66%. From the filtrate, Azy-Gly-OBzl was obtained; 65.8 mg (64.6%).

By Gly-OBu^t (g): Gly-OBu^t (525 mg, 4 mmol) was added to a solution of **1** (212 mg, 0.5 mmol) in CH_2Cl_2 (3 ml) at room temperature. After 24 h, the solvent was removed *in vacuo*. The residual oily product was subjected to silica gel column chromatography with ethyl acetate-$CHCl_3$ (1:1 v/v). Z-Gly-Gly-OBu^t; 135 mg (84.8%), oil. Found: C, 59.48; H, 6.98; N, 8.72%. Calcd for $C_{16}H_{22}O_5N_2$: C, 59.61; H, 6.88; N, 8.69%. Azy-Gly-OBzl; 125 mg (100%).

By D-Gly(ph)-OBu^t (h): D-Gly(ph)-OBu^t (72 mg, 0.35 mmol) was added to a solution of **1** (106 mg, 0.25 mmol) in CH_2Cl_2 (3 ml) at room temperature. After 72 h, the products were isolated as described for (g). Z-Gly-D-Gly-(ph)-OBu^t; 99.6 mg (100%), oil, $[\alpha]_D^{23}$ −88.8° (*c* 1.0, $CHCl_3$). Found: C, 66.09; H, 6.96; N, 7.40%. Calcd for $C_{22}H_{26}O_5N_2$: C, 66.39; H, 7.09; N, 7.04%. Azy-Gly-OBzl; 62.5 mg (100%).

By Aniline (i): Aniline (0.88 ml, 10 mmol) was added to a solution of **1** (212 mg, 0.5 mmol) in CH_2Cl_2 (3 ml) at room temperature. After 24 h, the solvent was removed *in vacuo*. Ether was added to the residue, and crystals which appeared were collected by filtration. The crystals were identified as Z-Gly-NH-C_6H_5; 40.5 mg (14.1%), mp 144.5—146.5 °C (lit,[8] mp 145—146 °C). The filtrate was subjected to silica gel column chromatography with ethyl acetate-$CHCl_3$ (1:1 v/v). Azy-Gly-OBzl; 38.7 mg (15.0%). Z-Gly-A_2pr(NHph)-Gly-OBzl; 71.5 mg (27.8%), mp 80—81.5 °C, $[\alpha]_D^{23}$ +6.5° (*c* 0.25, MeOH). Found: C, 64.75; H, 5.84; N, 10.51%. Calcd for $C_{28}H_{30}O_6N_4$: C, 64.85; H, 5.84; N, 10.80%.

By Aniline (j): Compound **1** (212 mg, 0.5 mmol) and aniline (0.22 ml, 2.5 mmol) were reacted in CH_2Cl_2 (3 ml) at room temperature for 72 h. The products were isolated as described for (i). Z-Gly-NH-C_6H_5; 104 mg (36.2%), Azy-Gly-OBzl; 72.2 mg (28.0%), and Z-Gly-A_2pr(NHph)-Gly-OBzl; 112 mg (43.7%).

By Aniline (k): Compound **1** (212 mg, 0.5 mmol) and aniline (0.22 ml, 2.5 mmol) were reacted in CH_2Cl_2 (3 ml) at 45 °C for 24 h. The products were isolated as described for (i). Z-Gly-NH-C_6H_5; 33 mg (11.5%), Azy-Gly-OBzl; 49 mg (19.0%), and Z-Gly-A_2pr(NHph)-Gly-OBzl; 134 mg (51.9%).

By Diethylamine (l): Diethylamine (1.02 ml, 10 mmol) was added to a solution of **1** (212 mg, 0.5 mmol) in CH_2Cl_2 (3 ml) at room temperature. After 72 h, the solvent was removed *in vacuo*. The residual oily product was subjected to silica gel column chromatography with MeOH-$CHCl_3$ (1:20 v/v). Z-Gly-A_2pr(NEt_2)-Gly-OBzl was obtained as oil; 221 mg (88.5%), $[\alpha]_D^{23}$ −5.1° (*c* 0.4, MeOH). Found: C, 61.67; H, 6.76; N, 10.14%. Calcd for $C_{26}H_{34}O_6N_4 \cdot 1/2H_2O$: C, 61.52; H, 6.95; N, 10.15%.

References

1) Part II; T. Tanaka, K. Nakajima, T. Maeda, A. Nakamura, N. Hayashi, and K. Okawa, *Bull. Chem. Soc. Jpn.*, **52**, 3579 (1979).

2) Abbreviations according to IUPAC-IUB commission, *J. Biol. Chem.*, **247**, 977 (1972), are used. Z: benzyloxycarbonyl, Bzl: benzyl ester, OBu^t: *t*-butoxy, Gly(ph): α-phenylglycine, A_2pr: 2,3-diaminopropionic acid. "Azyline" is used as the name of an 2-aziridinecarboxylic acid, "Azy" being its abbreviation.

3) O. C. Dermer and G. E. Ham, "Ethyleneimine and other Aziridines," Academic Press, New York and London (1969), p. 262.

4) S. Searles, M. Tamres, F. Block, and L. A. Quarterman, *J. Am. Chem. Soc.*, **78**, 4917 (1956).

5) K. Okawa, K. Nakajima, T. Tanaka, and Y. Kawana, *Chem. Lett.*, **1975**, 591.

6) R. Camble, R. Garner, and G. T. Young, *J. Chem. Soc.*, **1969**, 1911.

7) D. J. Woodman, L. C. Butler, and J. Stewart, *Tetrahedron Lett.*, **1973**, 1557.

8) A. Cosmatos, I. Photaki, and L. Zervas, *Chem. Ber.*, **94**, 2644 (1961).

Kinetics of the Tungstate-catalyzed H_2O_2 Oxidation of Amines in Aqueous Methanol. Acidity Effect[1)]

Yoshiro OGATA,* Kohtaro TOMIZAWA, and Hirokazu MAEDA

Department of Applied Chemistry, Faculty of Engineering, Nagoya University, Chikusa-ku, Nagoya 464

(Received June 13, 1979)

Synopsis. Oxidation of *N,N*-dimethylaniline and benzylamine with H_2O_2 catalyzed by Na_2WO_4 has been kinetically studied in buffered 50% aqueous methanol at 25 °C. The rates with a catalytic amount of Na_2WO_4 fit Eq.: $v=k[\text{amine}]_t[Na_2WO_4]_t[H_2O_2]^0$ and the pH profile of rate constant shows no dissociation of peroxotungstate at pH 5—10. *N,N*-Dimethylaniline gives *N*-oxide (73%) and benzylamine gives benzaldehyde oxime (65%) under the present kinetic conditions.

The oxidation reactions with hydrogen peroxide catalyzed by metallic salts (*e.g.*, molybdate, tungstate and vanadate) have been reported with epoxidation of fumaric[2)] and maleic[3)] acids and allyl alcohol[4)] and also oxidation of amines.[5,6)] The tungstate-catalyzed oxidation of primary and secondary amines gives the corresponding oximes, hydroxylamines and hydroxamic acids, while the same oxidation of tertiary amines gives the corresponding *N*-oxides. Russian workers reported that the rate expression was shown as: $k_{obsd}=k[\text{amine}]^1[WO_4^{2-}]^1[H_2O_2]^0$, which was discussed mainly as to the steric effect of amines.[5,6)] The present paper summarizes our kinetic data and probable mechanisms based on the acidity effect on the oxidation of *N,N*-dimethylaniline forming *N*-oxide and that of benzylamine forming benzaldehyde oxime in aqueous methanol.

Results and Discussion

The Na_2WO_4-catalyzed H_2O_2 oxidation of *N,N*-dimethylaniline gave *N*-oxide in a yield of 73%. The same reaction of benzylamine gave benzaldehyde oxime in a yield of 65%. These reactions do not occur without the catalyst, hence the active oxidant, peroxotungstate, may be formed by the reaction of Na_2WO_4 and H_2O_2.

The rates were measured with various initial concentrations of amines and H_2O_2 (*i.e.*, $[PhMe_2N]_0=3.95-7.89\times10^{-3}$ M, $[H_2O_2]_0=9.21-18.6\times10^{-3}$ M, $[Na_2WO_4]_0=1.00\times10^{-3}$ M at pH 5.80 and $[PhCH_2NH_2]_0=4.53-18.3\times10^{-3}$ M, $[H_2O_2]_0=9.10-17.8\times10^{-3}$ M, $[Na_2WO]_0=1.00\times10^{-3}$ M at pH 9.40; all data for difinite molar ratio of reactants fit the rate equation (1) previously reported,[5)] where $[\ ]_t$ means the stoichiometric concentration.

$$v=k_{obsd}[\text{amine}]_t[Na_2WO_4]_t \quad (1)$$

The values of k_{obsd} were $1.20\pm0.1\times10^{-2}$ M^{-1} s^{-1} for $PhMe_2N$ and $5.90\pm0.2\times10^{-2}$ M^{-1} s^{-1} for $PhCH_2NH_2$ in 50% aq MeOH at 25 °C.

The rates were measured at various initial concentrations of Na_2WO_4 and H_2O_2 for the oxidation of *N,N*-dimethylaniline and thus the rate is practically independent of the concentration ($4.60-27.6\times10^{-3}$ M) of H_2O_2 in this range of $0.20-3.20\times10^{-3}$ M Na_2WO_4; *i.e.*, at initial molar ratio $[Na_2WO_4]_0/[H_2O_2]_0$ below 1/9; but as the ratio approaches to unity, the rate deviates from the first-order dependence on $[Na_2WO_4]_0$. The similar result was obtained for the oxidation of benzylamine. This deviation may be attributed to the decrease of rate of reproducing peroxotungstate with decreasing concentration of H_2O_2.

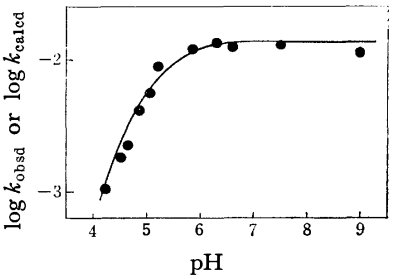

Fig. 1. pH profile for the Na_2WO_4-catalyzed H_2O_2 oxidation of *N,N*-dimethylaniline in 50% aq MeOH at 25 °C. $[PhMe_2N]=7.00\times10^{-3}$ M, $[H_2O_2]=18.1\times10^{-3}$ M, $[Na_2WO_4]=1.00\times10^{-3}$ M.
● $\log k_{obsd}$, $-\log k_{calcd}$.

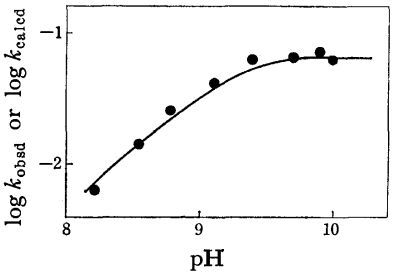

Fig. 2. pH profile for the Na_2WO_4-catalyzed H_2O_2 oxidation of benzylamine in 50% aq MeOH at 25 °C. $[PhCH_2NH_2]=9.61\times10^{-3}$ M, $[H_2O_2]=13.5\times10^{-3}$ M, $[Na_2WO_4]=1.00\times10^{-3}$ M.
● $\log k_{obsd}$, $-\log k_{calcd}$.

The effects of acidity of solution on the second-order rate constant k_{obsd} are shown in Figs. 1 and 2. As apparent from the figures, the rate constants decrease with increasing acidity at pH below 5 for *N,N*-dimethylaniline and at pH below 9 for benzylamine. Since the basicity constants, $K_H=[BH^+]/([B][H^+])$, are 1.15×10^5 for *N,N*-dimethylaniline[7)] and 2.19×10^9 for benzylamine,[7)] the decrease of k_{obsd} is ascribed to the deactivation of amines by protonation of amino nitrogen.

These results suggest a mechanism for *N,N*-dimethylaniline oxidation, where T means WO_3^-, WO_4^-, or WO_6^-. ($m=1$, 2, 4, $n=0$, 1, 3)[8)]

$$Na_2WO_4 \underset{\text{fast}}{\rightleftharpoons} 2Na^+ + WO_4^{2-} \quad (2)$$

$$WO_4^{2-} + mH_2O_2 \underset{\text{fast}}{\rightleftharpoons} T\text{-}OOH + OH^- + nH_2O \quad (3)$$

$$PhMe_2N + H^+ \underset{\text{fast}}{\overset{K_H}{\rightleftharpoons}} PhMe_2\overset{+}{N}H \quad (4)$$

$$PhMe_2N + T\text{-}OOH \xrightarrow[\text{slow}]{k_1} PhMe_2\overset{+}{N}OH + T\text{-}O^- \quad (5)$$

$$PhMe_2\overset{+}{N}OH \underset{\text{fast}}{\rightleftharpoons} PhMe_2N{\rightarrow}O + H^+ \quad (6)$$

Since the rate is determined by step 5 as in the case of analogous oxidation of amines, the rate is expressed as

$$v = k_1[PhMe_2N][T\text{-}OOH]. \quad (7)$$

Here,

$$[PhMe_2N] = [PhMe_2N]_t/(1+K_H[H^+]). \quad (8)$$

$[PhMe_2N]_t$ means stoichiometric or total concentration, *i.e.*, $[PhMe_2N]_t=[PhMe_2N]+[PhMe_2\overset{+}{N}H]$. Sodium tungstate reacts rapidly with excess H_2O_2 giving quantitatively peroxotungstate, T–OOH, whose structure is still ambiguous, *i.e.*, T–OOH may be HWO_5^-, HWO_6^-, HWO_8^-, *etc.*[8] Hence, Eq. 7 can be transformed into

$$v = \frac{k_1}{1+K_H[H^+]}[PhMe_2N]_t[Na_2WO_4]_t. \quad (9)$$

Introduction of the value of $K_H=1.15\times10^5\ M^{-1}$ and an average observed value of $k_1=1.25\times10^{-2}\ M^{-1}\ s^{-1}$ at pH independent region ($6\leq pH\leq8$) gave the value of $k_1/(1+K_H[H^+])$ or k_{calcd}. A plot of log k_{calcd} *vs.* pH is shown as a solid line in Fig. 1, on which lies the values of log k_{obsd} and this supports the mechanism.

Analogously, a mechanism for benzylamine is proposed as follows:

$$PhCH_2NH_2 + T\text{-}OOH \xrightarrow[\text{slow}]{k_2} PhCH_2\overset{+}{N}H_2OH + T\text{-}O^- \quad (10)$$

$$PhCH_2\overset{+}{N}H_2OH \underset{\text{fast}}{\rightleftharpoons} PhCH_2NHOH + H^+ \quad (11)$$

$$PhCH_2NHOH + H_2O_2 \xrightarrow[\text{fast}]{} PhCH{=}NOH + 2H_2O \quad (12)$$

Although benzylhydroxylamine cannot be isolated in the oxidation of benzylamine, the rapid uncatalyzed oxidation of prepared benzylhydroxylamine to benzaldehyde oxime with rate constant $k_{obsd}\approx10^{-2}\ s^{-1}$ at 25 °C was confirmed. Therefore, the rate for the rate-determining step is expressed as

$$v = \frac{k_2}{1+K_H[H^+]}[PhCH_2NH_2]_t[Na_2WO_4]_t. \quad (13)$$

Here, K_H is $1.2\times10^9\ M^{-1}$ and an average k_2 value was calculated to be $7.24\times10^{-2}\ M^{-1}\ s^{-1}$, which is comparable to that in water ($8.4\times10^{-2}\ M^{-1}\ s^{-1}$).[5] By the similar treatments as above, it was found that the observed values of k_{obsd} lie on the calculated solid line in Fig. 2, hence the above mechanism is supported.

In conclusion, the present reaction involves a rate-determining electrophilic attack of HO– (or $\begin{matrix}O\\|\\O\end{matrix}$) from peroxotungstate on neutral amino nitrogen of amine. The rate for *N,N*-dimethylaniline (log $k_{obsd}=-1.9$) is smaller than the rate with H_2SO_5 oxidation (log $k_{obsd}=1.5$)[9] and the rate with H_3PO_5 (log $k_{obsd}=-0.7$).[10] *N,N*-Dimethylaniline is less reactive than benzylamine, which is expected from the lower basicity of *N,N*-dimethylaniline ($K_H=1.15\times10^5\ M^{-1}$) compared with that of benzylamine ($K_H=2.19\times10^9\ M^{-1}$).

Experimental

Materials. *N,N*-Dimethylaniline, bp 192—194 °C, and benzylamine, bp 185 °C, used were of guaranteed grade. Sodium tungstate was also of guaranteed grade. Benzylhydroxylamine was prepared by the reaction of benzyl chloride with hydroxylamine hydrochloride in alkaline aqueous ethanol, mp 54—56 °C (lit,[11] 57 °C).

Aqueous hydrogen peroxide for kinetic experiments was prepared by dilution of guaranteed 90% H_2O_2 purchased from Mitsubishi Gas Chem. Co.

Products. *N,N*-Dimethylaniline was oxidized with 3 equivalents of 90% H_2O_2 in the presence of catalytic amount of Na_2WO_4 in 50% aqueous MeOH to yield *N,N*-dimethylaniline *N*-oxide, λ_{max}^{MeOH} 254 nm (log ε 2.40), mp 150—152 °C (lit,[12] mp 151—152 °C). Benzylamine, λ_{max}^{MeOH} 253 nm (log ε 2.38) was oxidized with 3 equivalents of 90% H_2O_2 in the presence of Na_2WO_4 at below 20 °C, yielding benzaldehyde oxime, bp 78—79 °C/1 mmHg (lit,[5] 104 °C/5 mmHg). Benzylhydroxylamine was oxidized analogously to give quantitative yield of benzaldehyde oxime, bp 78—79 °C/1 mmHg. These products were identified by comparison of NMR peaks with those of authentic specimen.

Kinetics. The kinetic experiments were conducted in buffered 50% aqueous MeOH at 25 °C. The reaction was started by the addition of aqueous methanol solution of H_2O_2 (5 ml) to thermostated aqueous methanol Na_2WO_4 solution (45 ml). The rate was followed by iodometric titration of H_2O_2 and also by UV spectrophotometry of the pipetted out aliquots. The rates observed by both methods agreed satisfactorily. In the UV spectrophotometry, the decrease of absorption of *N,N*-dimethylaniline at λ_{max}^{MeOH} 251 nm (log ε 4.10) and the increase of absorption of benzaldehyde oxime at λ_{max}^{MeOH} 250 nm (log ε 4.14) were measured. The buffer solutions were made of AcONa–HCl, AcONa–AcOH, or KH_2PO_4–Na_2HPO_4.

References

1) Contribution No. 264.
2) M. A. Beg and I. Ahmad, *J. Catal.*, **39**, 260 (1975).
3) G. G. Allan and A. N. Neogi, *J. Catal.*, **16**, 197 (1970).
4) Z. Raciszewski, *J. Am. Chem. Soc.*, **82**, 1267 (1960).
5) K. Kahr and C. Berther, *Chem. Ber.*, **93**, 132 (1960).
6) O. L. Lebedev and S. N. Kazarnoski, *Zh. Obshch. Khim.*, **30**, 1631, 3105 (1960).
7) N. F. Hall and M. R. Sprinkle, *J. Am. Chem. Soc.*, **54**, 1928 (1932).
8) K. F. Jahr and E. Lother, *Ber.*, **71**, 894, 903, 1127 (1938).
9) Y. Ogata and I. Tabushi, *Bull. Chem. Soc. Jpn.*, **31**, 969 (1958).
10) Y. Ogata, K. Tomizawa, and T. Morikawa, *J. Org. Chem.*, **44**, 352 (1979).
11) L. W. Jones and M. C. Sneed, *J. Am. Chem. Soc.*, **39**, 674 (1917).
12) A. C. Cope and P. H. Towle, *J. Am. Chem. Soc.*, **71**, 3423 (1949).

Reaction of Bis(dimethylglyoximato)(pyridine)styrylcobalt(III) Derivatives with Arenesulfenyl Chloride

Masaru TADA,* Hiraku SHINOZAKI, and Kyo MIURA
Department of Chemistry, School of Science and Engineering, Waseda University, Shinjuku, Tokyo 160

(Received June 25, 1979)

Synopsis. *cis*-Styryl and *trans*-styryl-type cobaloximes, having a *para*-substituent on the styrene moiety, give the corresponding *cis*- and *trans*-(styrylthio)benzene derivatives in excellent yields by the reaction with 2,4-dinitrobenzenesulfenyl chloride. The substitution proceeds stereospecifically with retention of configuration except for the case of *cis*-(*p*-cyanostyryl)cobaloxime.

Bis(dimethylglyoximato)(pyridine)cobalt(III) derivatives (the conventional name styryl-type cobaloxime is used hereafter) are converted to styryl-type halides and mercurials by reaction with bromine and mercury(II) acetate, respectively. The substitution proceeds stereospecifically with retention of configuration.[1,2] In this report the substitution of styryl-type cobaloximes with 2,4-dinitrobenzenesulfenyl chloride will be discussed. The reaction gives styryl-type sulfides, which may be utilized as a synthetic intermediate.[3] This reaction is an addition to the new synthetic routes for sulfides,[4-8] and the preparation of styryl-type cobaloxime is relatively simple.

cis- and *trans*-Styryl-type cobaloximes (**1**, **2**, and **3**) were synthesized from the corresponding styryl-type halides and the cobaloxime anion prepared *in situ* from dimethylglyoxime, pyridine, cobalt(II) chloride, and sodium borohydride.[1] Treatment of one of the *cis*-(**1c**, **2c**, and **3c**) or *trans*-styryl-cobaloximes (**1t**, **2t**, and **3t**) with 2,4-dinitrobenzenesulfenyl chloride in dichloromethane gave *cis*- (**4c**, **5c**, and **6c**) and *trans*-2,4-dinitro-1-(styrylthio)benzene (**4t**, **5t**, and **6t**), respectively, in excellent yields (see Table 1). The structures of the products were detected by elemental analyses and spectroscopy. The stereochemistry of the products was readily assigned by the coupling constants of vinyl hydrogens in the NMR spectra (J=11 Hz for *cis*-isomers and J=16 Hz for *trans*-isomers). The displacement of the cobaloxime moiety with 2,4-dinitrobenzenesulfenyl group proceeds with retention except in the reaction of *cis*-(*p*-cyanostyryl)cobaloxime (**1c**), in which a mixtures of *cis*- and *trans*-2,4-dinitro-1-(*p*-cyanostyrylthio)benzene (**4c** and **4t**) was obtained. As reported in an earlier paper,[1] the reaction of *cis*-(*p*-cyanostyryl)cobaloxime (**1c**) with bromine gave *cis*- and *trans*-styryl bromides. The formation of *trans*-styryl bromide was shown to be due to the isomerization of the *cis*-*p*-cyanostyryl bromide formed initially. The non-stereospecificity of the reaction of **1c** in the present study, therefore, is thought due to the isomerization of *cis*-2,4-dinitro-1-(*p*-cyanostyrylthio)benzene (**4c**) to the *trans*-isomer (**4t**) under the reaction conditions.

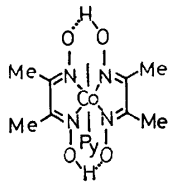

(**Co**)

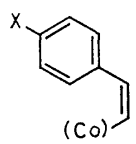

1c, **2c**, **3c**

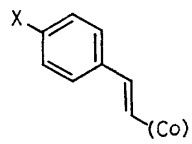

1t, **2t**, **3t**

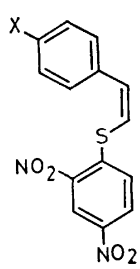

4c, **5c**, **6c**

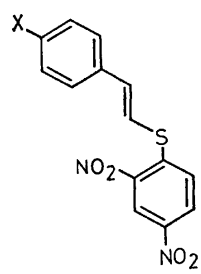

4t, **5t**, **6t**

(**1c**, **1t**, **4c**, **4t**): X=CN (**2c**, **2t**, **5c**, **5t**): X=H
(**3c**, **3t**, **6c**, **6t**): X=OCH_3

Table 1. Products and yields of the sulfenylation of styryl-type cobaloxime

Starting material	Product	Yield %	Starting material	Product	Yield %
1c	**4c**, **4t** (44 : 56)	98	**1t**	**4t**	95
2c	**5c**	*ca.* 100	**2t**	**5t**	*ca.* 100
3c	**6c**	*ca.* 100	**3t**	**6t**	*ca.* 100

The basic nature of the present reaction is thought to be the same as that of bromination. The steric consequence of bromination has been discussed in some detail[1] in which the interaction between the benzylic cation and cobalt(III) by p_π-d_π[9] or σ-π conjugation[10] was important. Bond rotation is hindered in the intermediates **5** and **6** in the reaction scheme due to this type of interaction. The mechanistic feature of the present sulfenylation, therefore, can be shown correctly by the scheme shown here. The reaction of **1**, **2**, and **3** with benzenesulfenyl chloride gave (styrylthio)benzenes in the same manner but with less stereospecificity.

In the experiments it was found that styryl-type

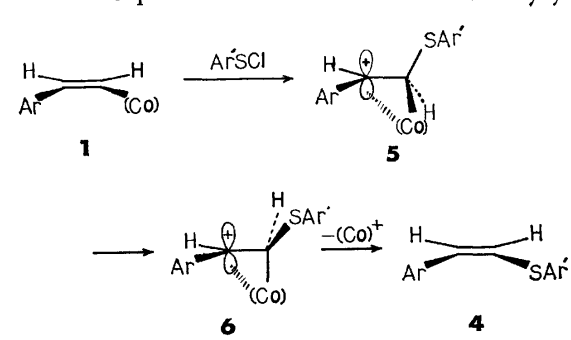

Scheme 1.

cobaloximes do not react with hard electrophiles[11] such as isoamyl nitrite and ethyl chloroformate. Soft but weak electrophiles, such as diphenyl disulfide and *N*-(phenylthio)succinimide, again do not react with styryl-type cobaloximes. This property of styryl-type cobaloximes can be attributed to the soft nature and p_π-d_π interaction of cobalt(III). The olefinic carbon of styryl-type cobaloxime, therefore, must acquire a more soft and less nucleophilic property, a property stemming from p_π*-d_π back-donation from cobalt(III) which diminishes the reactivity of the olefinic carbon towards electrophiles.

In conclusion, soft and strong electrophiles, such as bromine, mercury(II) acetate, and arenesulfenyl chloride, smoothly substitute the cobaloxime group of styryl-type cobaloximes *via* an addition-elimination mechanism as shown in the scheme.

Experimental

Styryl-type cobaloximes (**1**, **2**, and **3**) were prepared by the methods reported[1] and 2,4-dinitrobenzenesulfenyl chloride was prepared by the method of Kharasch and Langford[12] from 2,4-dinitrochlorobenzene. Melting points are not corrected and IR spectra were measured using KBr disks. The NMR spectra were measured in DMSO-d_6 and chemical shifts have been expressed by δ values using sodium 3-(trimethylsilyl)propanoate-d_4 as an internal standard.

Reaction of Cobaloximes with 2,4-Dinitrobenzenesulfenyl Chloride. To a solution of one of the styryl-type cobaloximes (0.25×10^{-3} mol) in dichloromethane (10 ml) was added dropwise 2,4-dinitrobenzenesulfenyl chloride (0.28×10^{-3} mol) dissolved in dichloromethane (2 ml) with magnetic stirring. The reaction mixture was stirred for 1 h after addition of the reagent under nitrogen at ambient temperature (*ca.* 27 °C). The reaction mixture was passed through an alumina column (Merck act. II—III) and the column further eluted by chloroform. Condensation of the combined eluates gave 2,4-dinitro-1-(styrylthio)benzenes (Table 1). Recrystallization of the products from DMF–ethanol gave the pure sulfides. In the case of **1c** the product was a mixture of isomers, which was separated into **4c** and **4t** by chromatography on silica gel eluted by chloroform and recrystallization from DMF–ethanol. **4c**: Mp 149—151 °C. High resolution mass, Found: *m/e* 327.0300. Calcd for $C_{15}H_9N_3O_4S$: *m/e* 327.0313. IR, 2230, 1600, 1340, 920, 900, 850, 830, 745, and 730 cm^{-1}. NMR, 7.18, 7.46 (2H, AB-type, J= 11 Hz), 7.96 (4H, s), and 8.0—9.1 (3H, dinitrobenzene moiety). **4t**: Mp 219—219.5 °C. Found: C, 55.28; H, 2.72; N, 13.02%. Calcd for $C_{15}H_9N_3O_4S$: C, 55.05; H, 2.77; N, 12.84%. IR, 2225, 1595, 1340, 960, 950, 800, 745, and 730 cm^{-1}. NMR, 7.44, 7.72 ((2H, AB-type, J= 16 Hz), 7.96 (4H, s), and 8.0—9.1 (3H, dinitrobenzene moiety). **5c**: Mp 104—105 °C. High resolution mass, Found: *m/e* 302.0381. Calcd for $C_{14}H_{10}N_2O_4S$: *m/e* 302.0361. IR, 1595, 1340, 837, 793, 730, and 695 cm^{-1}. NMR, 6.86, 7.36 (2H, AB-type, J=11.0 Hz), 7.44—7.88 (5H, m), and 8.0—9.2 (3H, dinitrobenzene moiety). **5t**: Mp 166.5—168 °C. High resolution mass, Found: *m/e* 302.0381. Calcd for $C_{14}H_{10}N_2O_4S$: *m/e* 302.0361. IR, 1590, 1335, 825, 750, 733, and 695 cm^{-1}. NMR, 7.48 (2H, t, J=16 Hz), 7.60—7.90 (5H, m), and 8.0—9.1 (3H, dinitrobenzene moiety). **6c**: Mp 160—161 °C. Found: C, 54.85; H, 3.31; N, 8.51%. Calcd for $C_{15}H_{12}N_2O_5S$: C, 54.22; H, 3.64; N, 8.43%. IR, 1594, 1334, 1310, 1260, 830, 770, 745, and 735 cm^{-1}. NMR, 3.82 (3H, s), 6.62, 7.23 (2H, AB-type, J=11 Hz), 7.03, 7.62 (4H, AA'BB'-type, J=9 Hz), and 7.9—9.0 (3H, dinitrobenzene moiety). **6t**: Mp 203—204 °C. Found: C, 54.33; H, 3.54; N, 8.48%. Calcd for $C_{15}H_{12}N_2O_5S$: C, 54.22; H, 3.64; N, 8.43%. IR, 1598, 1340, 1315, 1255, 830, 800, 750, and 735 cm^{-1}. NMR, 3.87 (3H, s), 7.04, 7.68 (4H, AA'BB'-type, J=9.5 Hz), 7.10, 7.30 (2H, AB-type, J=16 Hz), and 7.8—9.2 (3H, dinitrobenzene moiety).

References

1) H. Shinozaki, M. Kubota, O. Yagi, and M. Tada, *Bull. Chem. Soc. Jpn.*, **49**, 2280 (1976).
2) D. Dodd, M. D. Johnson, B. S. Meeks, D. M. Tichmarsh, K. N. V. Duong, and A. Gaudemer, *J. Chem. Soc., Perkin Trans. 2*, **1976**, 1262.
3) K. Oshima, K. Shimoji, H. Takahashi, H. Yamamoto, and H. Nozaki, *J. Am. Chem. Soc.*, **95**, 2694 (1973).
4) N. Furukawa, S. Oae, and T. Masuda, *Chem. Ind. (London)*, **1975**, 396.
5) M. Mikolajaczyk, S. Grezeiszczak, and A. Zatorski, *J. Org. Chem.*, **40**, 1979 (1975).
6) P. Vermeer, J. Meijer, C. Eylander, and L. Brandsma, *Recl. Trav. Chim. Pays-Bas*, **95**, 25 (1976).
7) T. Mukaiyama and M. Inomata, *Chem. Lett.*, **1978**, 413.
8) M. Hojo, R. Masuda, and S. Takagi, *Synthesis*, **1978**, 254.
9) G. E. Coats, M. L. H. Green, and K. Wade, "Organometallic Compounds," Methuen, London (1968), Vol. 2, p. 215.
10) T. G. Traylor, W. Hanstein, H. J. Berwin, N. A. Clinton, and R. S. Brown, *J. Am. Chem. Soc.*, **93**, 5715 (1971).
11) T-L. Ho, "Hard and Soft Acids and Bases Principle in Organic Chemistry," Academic Press, New York (1977).
12) N. Kharasch and R. S. Langford, *Org. Synth.*, **44**, 47 (1964).

Synthesis of 3-(*p*-Hydroxycinnamoyl)-5-methylfilicinic Acid and Dehydro-3,3′-diacetyl-5,5′-methylenedifilicinic Acid[1)]

Heitaro Obara,* Jun-ichi Onodera, Satoshi Abe, and Takashi Saito
Department of Applied Chemistry, Faculty of Engineering, Yamagata University, Yonezawa 992
(Received June 28, 1979)

Synopsis. In connection with studies on the structure of carthamin (**1**), two analogous compounds of **1**, 3-(*p*-hydroxycinnamoyl)-5-methylfilicinic acid and dehydro-3,3′-diacetyl-5,5′-methylenedifilicinic acid have been synthesized.

The structure for carthamin **1**, the red coloring matter of the flowers of Safflower (*Carthamus tinctorius* L.) has recently been proposed on the basis of spectroscopic evidence and hydrolytic behavior.[1)] In this paper, the synthesis of two compounds, 3-(*p*-hydroxycinnamoyl)-5-methylfilicinic acid (**3**) and dehydro-3,3′-diacetyl-5,5′-methylenedifilicinic acid (**6**), will be reported. These compounds have been offered as the analogs of **1** in a previous communication.[1)]

3-(*p*-Hydroxycinnamoyl)-5-methylfilicinic acid (**3**) was synthesized by the condensation of 3-acetyl-5-methylfilicinic acid (**2**),[2)] obtained by the methylation of phloroacetophenone, with *p*-hydroxybenzaldehyde in the presence of piperidine[3)] by reference to the synthesis of ceroptene. Dehydro-3,3′-diacetyl-5,5′-methylenedifilicinic acid (**6**) was prepared by the condensation of 3-acetyl-5-formylfilicinic acid (**4**), obtained by the methylation of formylphloroacetophenone,[4)] with acetylfilicinic acid (**5**)[2)] and 1% aqueous potassium hydroxide solution at −10— −15 °C. The structures of **3** and **6** were confirmed by IR, PMR, and mass spectra, and elemental analysis.

Compounds **3** and **6** both showed a characteristic enol proton signal at very low field (19.30 and 18.38 ppm) in the PMR spectra, which have been observed in other enolized 1,3,5-triketone structure.[5)] Hydrogenation of **6** gave 3,3′-diacetyl-5,5′-methylenedifilicinic acid (**7**), which was identical to the specimen obtained by the condensation of **5** with formaldehyde.

Compound **6**, light yellow crystals, exhibited an absorption maximum at 350 nm in chloroform solution, but shifted to the long-wavelength region, 490 nm, in ethanol solution. The unusual red shift has been ascribed to the formation of the stable enol anion of **6** in ethanol.

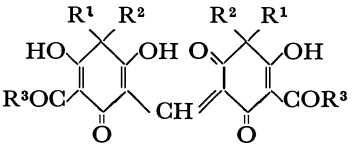

1 R^1=Gl, R^2=OH, R^3=-CH=CH-⟨○⟩-OH

6 R^1=R^2=R^3=Me

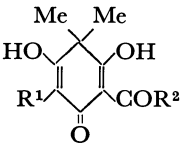

2 R^1=R^2=Me

3 R^1=Me, R^2=-CH=CH-⟨○⟩-OH

4 R^1=CHO, R^2=Me

5 R^1=H, R^2=Me

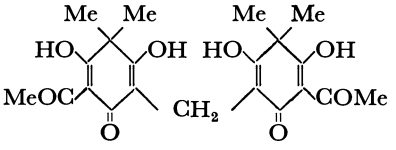

7

Experimental

All melting points are uncorrected. The UV and IR spectra were recorded on a Hitachi 135 and a Hitachi EPI-S2 spectrophotometer, respectively. The PMR spectra were measured with a Hitachi R-22 spectrometer (90 MHz), using tetramethylsilane as an internal standard. The mass spectra were obtained on a Hitachi RMU-6M mass spectrometer.

3-(p-Hydroxycinnamoyl)-5-methylfilicinic Acid (3). A mixture of 3-acetyl-5-methylfilicinic acid (**2**) (2.0 g), *p*-hydroxybenzaldehyde (6.0 g), and piperidine (2 ml) was heated on a water bath for 1 h. The reaction mixture was poured into dilute hydrochloric acid and extracted with ethyl acetate. The ethyl acetate solution was washed with water, dried over anhydrous Na_2SO_4, and evaporated *in vacuo*. The residue was chromatographed on a silica-gel column with benzene–ethyl acetate (4:1) to give crude crystals, which were further chromatographed with a benzene–ethyl acetate–acetic acid mixture (80:20:1). Recrystallization from methanol gave **3** (380 mg, 13%) as yellow needles, mp 215—216 °C. UV_{max} (EtOH) 350 and 415 nm; IR (KBr) 1600, 1624, and 1663 cm^{-1}; PMR (acetone-d_6) δ 1.39 (6H, s, $C_{3'}$-Me×2), 1.87 (3H, s, $C_{5'}$-Me), 6.90 (2H, d, J=8.5 Hz, $C_{3,5}$-H), 7.58 (2H, d, J=8.5 Hz, $C_{2,6}$-H), 7.80 (1H, d, J=16 Hz, C_α-H), 8.22 (1H, d, J=16 Hz, C_β-H), 19.30 (s, OH). Found: C, 68.55; H, 5.80%; M^+, 314. Calcd for $C_{18}H_{18}O_5$: C, 68.78; H, 5.77%; M, 314.

Diacetate, mp 152—153 °C; IR (KBr) 1673, 1662, 1650, and 1600 cm^{-1}. Found: C, 66.32; H, 5.63%; M^+, 398. Calcd for $C_{22}H_{22}O_7$: C, 66.32; H, 5.57%; M, 398.

3-Acetyl-5-formylfilicinic Acid (4). To a solution of formylphloroacetophenone (4.9 g)[4)] in dried methanol (25 ml) was added a sodium methylate solution, which was prepared from sodium (1.8 g), methanol (40 ml), and methyl iodide (21 g). The reaction mixture was allowed to stand for 3 days in the dark at room temperature. Removal of the solvent *in vacuo* gave a residue. The residue, after the addition of 1 M hydrochloric acid, was extracted with ethyl acetate. The ethyl acetate solution was washed with water, dried over anhydrous Na_2SO_4 and evaporated *in vacuo* to yield a viscous oil, which on crystallization from ligroin, gave compound **4** (1.85 g, 33%), mp 56—58 °C; IR (KBr) 1675 and 1625 cm^{-1}. Found: C, 58.94; H, 5.45%; M^+, 224. Calcd for $C_{11}H_{12}O_5$: C, 58.92; H, 5.40%; M, 224.

Dehydro-3,3′-diacetyl-5,5′-methylenedifilicinic Acid (6). A

mixed solution of 3-acetylfilicinic acid (**5**)[2] (600 mg) and **4** (860 mg) in 1% aqueous potassium hydroxide solution (17 ml) was allowed to stand for 12 h at −10—−15 °C. The reaction mixture was acidified with 2 M hydrochloric acid and extracted with ether. Removal of the solvent from the ether solution gave a residue, which was extracted with ethyl acetate. The ethyl acetate, on removal of the solvent *in vacuo*, gave a residue. The residue gave **6** (550 mg, 44%) as yellow needles, which on recrystallization from benzene showed a mp 173—174.5 °C. UV_{max} ($CHCl_3$) 350 nm (log ε=4.33), UV_{max} (EtOH) 300 and 490 nm (log ε= 4.17 and 4.85); IR (KBr) 1670, 1648, and 1628 cm^{-1}; PMR (DMSO-d_6) δ 1.28 (12H, s, $-CH_3\times4$), 2.57 (6H, s, $-COCH_3\times2$), 7.95 (1H, s, -CH=), 18.38 (2H, br s, $-OH\times2$). Found: C, 62.73; H, 5.59%; M^+, 402. Calcd for $C_{21}H_{22}O_8$: C, 62.68; H, 5.51%; M, 402.

*3,3'-Diacetyl-5,5'-methylenedifilicinic Acid (**7**).* To a solution of 3-acetylfilicinic acid[2] (100 mg) in 1% aqueous potassium hydroxide solution (0.4 ml) was added paraformaldehyde (25 mg) under cooling with ice–water and the mixture allowed to stand for 30 min. The reaction mixture was acidified with 2 M hydrochloric acid and extracted with ether. The ether solution was evaporated and the residue was recrystallized from methanol to give **7** (40 mg, 19%), mp 170—172 °C. IR (KBr) 1640 cm^{-1} (C=O); PMR (pyridine-d_5) δ 1.53 (12H, s, $-CH_3\times4$), 2.72 (6H, s, $-COCH_3\times2$), 3.96 (2H, s, $-CH_2-$), 18.47 (2H, s, $-OH\times2$). Found: C, 62.16; H, 6.13%; M^+, 404. Calcd for $C_{21}H_{24}O_8$: C, 62.37; H, 5.98%; M, 404.

*Reduction of **6**.* Compound **6** (80 mg) was hydrogenated in methanol (8 ml) with 4% aqueous palladium chloride solution (1.5 ml) for 5 h. The reaction mixture was filtered and the filtrate cooled to give a small amount of colorless prisms, mp 170—172 °C. The IR spectrum of this reduction product was identical with that of a synthetic sample of **7**.

The present work was partly supported by a Grant-in-Aid for Scientific Research from the Ministry of Education, Science and Culture.

References

1) Preliminary communication; H. Obara and J. Onodera, *Chem. Lett.*, **1979**, 201.

2) W. Riedl, J. Nickl, K. H. Risse, and R. Mitteldorf, *Chem. Ber.*, **89**, 1849 (1956); W. Riedl and K. H. Risse, *Ann.*, **585**, 209 (1954).

3) M. Nilsson, *Acta Chem. Scand.*, **13**, 750 (1959).

4) H. A. Shah and R. C. Shah, *J. Chem. Soc.*, **1939**, 949.

5) S. Forsén and M. Nilsson, *Acta Chem. Scand.*, **13**, 1383 (1959); S. Forsén, M. Nilsson, and C. A. Wachtmeister, *ibid.*, **16**, 583 (1962); D. De. Keukeleile and M. Verzele, *Tetrahedron*, **26**, 385 (1970).

Synthesis, Absolute Configuration, and Chiroptical Property of (+)-*cis*-4b,5,9b,10-Tetrahydroindeno[2,1-*a*]indene-5,10-dione

Fumio OGURA,*,** Akio NAKAO, and Masazumi NAKAGAWA
Department of Chemistry, Faculty of Science, Osaka University, Toyonaka, Osaka 560
(Received June 30, 1979)

Synopsis. The title compound having the (4b*S*,9b*S*) configuration was prepared from (2*S*,3*S*)-(+)-2,3-diphenylsuccinic acid, and the circular dichroic property was discussed.

The title compound (I) has a fairly rigid *cis*-bicyclo-[3.3.0]octane skeleton and holds two 1-indanone chromophores in a twisted spacial position. This paper deals with the synthesis, determination of the absolute configuration, and the chiroptical property of (+)-I.

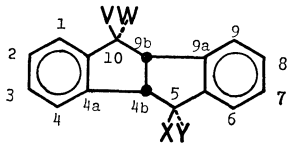

I, V+W = X+Y = O
II, V = W = H, X+Y = O
III, V = W = X = Y = H

The route of synthesis was outlined in Scheme 1. (2*S*,3*S*)-(+)-2,3-Diphenylsuccinic acid (IV)[1,2] was converted to the dichloride, which was subjected to the Friedel-Crafts reaction to yield (+)-I. Thus, the absolute configuration of (+)-I was determined to be (4b*S*,9b*S*). As a by-product of the cylization, (−)-keto acid (V) was obtained. The keto acid was subjected again to the same cyclization reaction, but virtually recovered unchanged. Under the more drastic condition using hot polyphosphoric acid, (−)-V afforded (+)-I having somewhat low optical purity. The only product isolated from the same Friedel-Crafts reaction of *meso*-IV was *rac*-V. On the basis of these facts, (−)-V was tentatively assigned to be (1*S*,2*S*)-(−)-3-oxo-2-phenyl-1-indancarboxylic acid, in which the configuration between the phenyl and carboxyl groups would be trans, being unable to proceed to further cyclization. The trans isomer seemed to be thermodynamically more stable than the cis one and to be produced from (+)-IV during the course of transformation (not before but after the half cyclization) by epimerization at the C-2 chiral center α to both phenyl and carbonyl groups. The Clemmensen reduction of (+)-I gave monoketone (II) and hydrocarbon (III), both of which had (4b*S*,9b*S*) configuration.

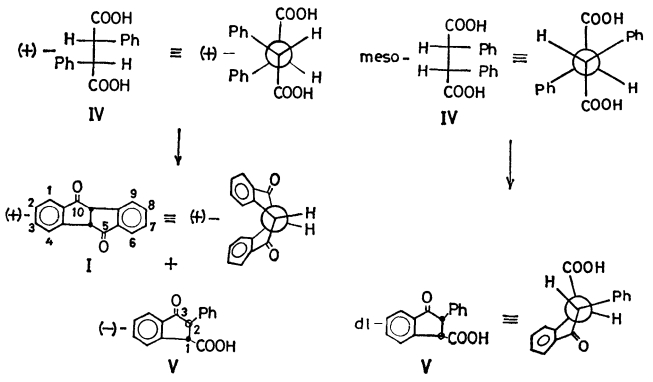

Scheme 1.

The UV and CD spectra of (+)-I are shown in Fig. 1. A negative CD band with fine structure and a positive one were observed in the n-π* and $^1B_{2u}$ regions, respectively. A typical negative couplet centered at near 40000 cm^{-1} was attributed to an exciton couplet due to the interaction of so-called intramolecular CT band of two benzoyl chromophores. From a consideration using the Dreiding molecular model with the (4b*S*,9b*S*)-configuration, the negative and positive peaks could be assigned to the transitions from the ground to the excited states with A and B symmetry, respectively. The transition moment of the monomeric indanone chromophores was assumed to lie in the center of the benzene ring and to be directed to the oxygen atom. This interpretation was supported by UV intensity distribution *versus* wavelength in the band, and with the lack of a CD couplet in the same absorption region of monoketone II.[3]

Thus, the absolute configuration deduced from the CD analysis was in accord with the chemically established (4b*S*,9b*S*) configuration.

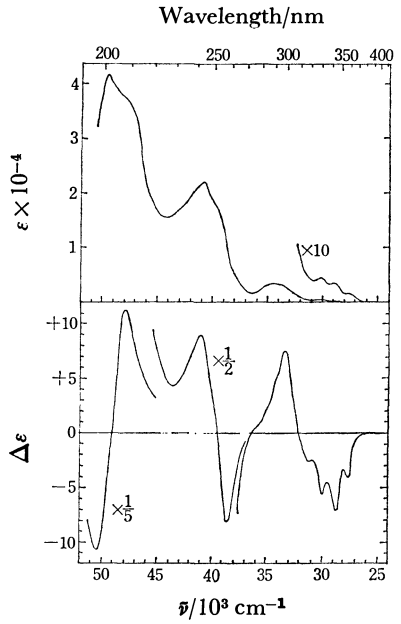

Fig. 1. UV (top) and CD (bottom) spectra of (4b*S*,9b*S*)-(+)-*cis*-4b,5,9b,10-tetrahydroindeno[2,1-*a*]-indene-5,10-dione (I) in 99% EtOH.

** Present address: Department of Applied Chemistry, Faculty of Engineering, Hiroshima University, Hiroshima 730.

Experimental

Melting points were measured on a Mettler FP2 apparatus and were uncorrected. IR spectra (Nujol mull) were obtained on a Hitachi EPI-2, EPI-G_3, or a JASCO DS-301 spectrometer, and UV spectra on a Hitachi EPS-3T spectrometer. ^{1}H-NMR spectra of $CDCl_3$ solutions were obtained on a Varian XL-100 or A-60D spectrometer, and chemical shifts from internal TMS are given in δ-unit. Optical rotations were measured on a Union Giken Polarimeter PM-71 at 20 °C, and CD spectra on a JASCO J-20 spectrometer. Shoulders and inflections are denoted by an asterisk.

2,3-Diphenylsuccinic Acid (IV): *dl*-Form,[1] recrystallized from water, melted once at 184—185 °C, immediately resolidified and melted again at 233—236 °C, and had IR: 1700 ($\nu_{c=o}$)cm^{-1}, ^{1}H-NMR: 4.38 (s, 2H, methine), 7.27 (s, 10H, aromatic), 7.40 (s, 2H, COOH). *meso*-Form,[1] recrystallized from 99% EtOH, melted at 248—252 °C, and had IR: 1690 ($\nu_{c=o}$)cm^{-1}, ^{1}H-NMR (DMSO-d_6): 4.26 (s, 2H, methine), 7.20—7.54 (m, 10H, aromatic), 12.22 (br s, 2H, COOH).

The racemate was resolved *via* bis-brucine salt.[1] An optically pure salt melted at 154.5—155.5 °C. Found: C, 64.59; H, 6.92; N, 4.69%. Calcd for $C_{62}H_{66}N_4O_{12}\cdot 5H_2O$: C, 64.79; H, 6.67; N, 4.87%. (*S*)-(+)-Form,[1,2] recrystallized from water, melted once at 170—180 °C, resolidified immediately and melted again at 210—220 °C. The hygroscopic acid was analysed immediately after drying at 100 °C for 17 h *in vacuo*, and had $[\alpha]_D$ +361.0° (*c* 1.457, 99% EtOH). Found: C, 70.82; H, 5.29%. Calcd for $C_{16}H_{14}O_4$: C, 71.10; H, 5.22%.

*(4bS,9bS)-(+)-*cis*-4b,5,9b,10-Tetrahydroindeno[2,1-*a*]indene-5,10-dione (I) and (−)-3-Oxo-2-phenyl-1-indancarboxylic Acid (V)*: A mixture of (*S*)-(+)-IV (0.655 g, 2.34 mmol) and PCl_5 (1.2 g, 5.8 mmol) was warmed on a boiling water bath for 30 min. After removal of $POCl_3$ *in vacuo*, the residue was dissolved in CS_2 (65 ml) and cooled in an ice bath. Freshly powdered $AlCl_3$ (1 g) was added at once, and the mixture was heated under reflux for 30 min with stirring. The reaction was quenched carefully by addition of ice water and 3M-HCl, and the product was extracted with ether. The combined organic layers were washed three times with aq 5% $NaHCO_3$ and dried over Na_2SO_4. The solvents were removed under reduced pressure to afford crude crystals (0.277 g) of (+)-I, which were recrystallized from EtOH. (*S*)-(+)-Diketone (I) sublimed at *ca.* 240 °C, melted at 253.5—254.5 °C, and had $[\alpha]_D$ +51.1°, $[\alpha]_{405}$ −600° (*c* 0.0572, 99% EtOH); IR: 1710 ($\nu_{c=o}$) cm^{-1}; UV: $\lambda_{max}^{99\%\ EtOH}$ (ε) 364 (164), 346 (346), 332.5 (392), 297* (3220), 291 (3310), 253* (17000), 245.5 (21300), 237* (23500), 210* (36800), 202 (42500) nm; CD: $\lambda_{max}^{99\%\ EtOH}$ ($\Delta\varepsilon$) 362 (−4.00), 348 (−7.12), 333 (−5.42), 320 (−2.60), 299 (+7.29), 258.5 (−16.8), 243.5 (+18.9), 209 (+56.8), 198 (−54.8) nm. Found: C, 81.96; H, 4.27%. Calcd for $C_{16}H_{10}O_2$: C, 82.04; H, 4.30%. The combined $NaHCO_3$ washings were acidified with concd HCl, and light yellow solid (0.273 g) thus obtained was recrystallized from CCl_4 to yield (−)-V; mp 138—139 °C; $[\alpha]_D$ −150.3°; $[\alpha]_{405}$ −496.9° (*c* 0.192, 99% EtOH); IR: 1725 ($\nu_{c=o}$, ketone), 1690 ($\nu_{c=o}$) cm^{-1}; ^{1}H-NMR (DMSO-d_6): 4.26 (d, J=4.5 Hz, 1H, methine), 4.42 (d, J=4.5 Hz, 1H, methine), 7.10—7.94 (m, 9H, aromatic); UV: $\lambda_{max}^{99\%\ EtOH}$ (ε) 335* (110), 293 (1820), 287* (1800), 244 (9500), 208 (24200) nm; CD: $\lambda_{max}^{99\%\ EtOH}$ ($\Delta\varepsilon$) 345* (−0.76), 331 (−1.06), 318 (−0.96), 292.5 (−0.86), 285 (−0.78), 269 (−0.35), 244 (−6.12), 220 (+7.58), 210 (+6.66) nm. Found: C, 76.07; H, 4.76%. Calcd for $C_{16}H_{12}O_3$: C, 76.18; H, 4.80%.

(−)-Keto acid (V, 110 mg) was converted to the acid chloride with $SOCl_2$ in benzene and subjected again to the same cyclization. Only a minor amount (11 mg) of (+)-I was isolated, and almost all of (−)-V was recovered.

Polyphosphoric acid (5 g) was mixed with (−)-V (50.3 mg) and heated on a boiling water bath for 15 h. After ordinary work up, (+)-I (40.3 mg, optical purity *ca.* 40%) was obtained as a neutral product.

rac-*3-Oxo-2-phenyl-1-indancarboxylic Acid (V)*: By the essentially same cyclization reaction of *meso*-IV as in the case of (*S*)-(+)-IV, *dl*-V was obtained, mp 124—126 °C. Neither *dl*-I nor its *trans*-isomer was isolated.

*(4bS,9bS)-*cis*-4b,5,9b,10-Tetrahydroindeno[2,1-*a*]indene (III) and -5-one (II)*: (*S*)-(+)-Diketone (I, 200 mg) was dissolved in benzene (5 ml) and added to a mixture of water (1 ml), concd HCl (1 ml), and amalgamated Zn, which was prepared by the standard procedure from granules of Zn (1 g). The reaction mixture was refluxed for 6 h with stirring, and the product was extracted with CH_2Cl_2 after dilution with water. After usual work up, the solvent was removed *in vacuo*, and the residue was chromatographed on a column of silica gel (20 g) using benzene as an eluant. Hydrocarbon III (30 mg), monoketone II (55 mg), and recovered I (90 mg) were eluted successively. Both of II and III were purified by vacuum sublimation and then recrystallization from EtOH. Hydrocarbon III showed mp 140 °C; ^{1}H-NMR: 2.9—4.2 (m, 6H, aliphatic), 7.0—7.7 (m, 8H, aromatic); UV: $\lambda_{max}^{99\%\ EtOH}$ (ε) 273.5 (3880), 267 (2970), 261 (1780), 254 (890), 217.5 (17200), 212.5 (18900), 209 (20200), 196 (64800) nm; CD: $\lambda_{max}^{99\%\ EtOH}$ ($\Delta\varepsilon$) 272.5 (−1.7), 265 (−1.4), 260 (−1.0), 220.5 (+12), 197 (+67.4) nm. Found: C, 93.24; H, 6.81%. Calcd for $C_{16}H_{14}$: C, 93.16; H, 6.84%.

Monoketone II melted at 120 °C, and had ^{1}H-NMR: 3.0—4.1 (m, 4H, methylene and methine), 7.0—7.4 (m, 8H, aromatic); UV: $\lambda_{max}^{99\%\ EtOH}$ (ε) 332 (295), 294 (2200), 286 (2160), 276 (3100), 269 (2630), 247 (12400), 208.5 (29500) nm; CD: $\lambda_{max}^{99\%\ EtOH}$ ($\Delta\varepsilon$) 362 (+0.15), 346 (+0.39), 331 (+0.50), 316 (+0.46), 305 (+0.37), 291 (+1.2), 285* (+0.98), 275 (−3.4), 268 (−3.9), 251 (−7.2), 230* (+1.4), 206 (+38.1) nm.

References

1) H. Wren and C. J. Still, *J. Chem. Soc.*, **107**, 444 (1915).

2) R. Buchan and M. B. Watson, *J. Chem. Soc., C*, **1968**, 2465; N. D. Berova and B. J. Kurtev, *Tetrahedron*, **25**, 2301 (1969).

3) A positive couplet was anticipated for an exciton interaction of the short axis polarized transition of two 1-indanones. The strongest positive couplet observed at near 49000 cm^{-1} and the positive peak in $^1B_{2u}$ band might be attributed to the coupling of this nature. However, further interpretation of CD is reserved until the exact molecular structural parameters and nature of the electronic transition are clarified.

Synthetic Studies *via* Arene-Metal Compounds. An Application to the Regioselective Synthesis of a Natural Phthalide

Motokazu UEMURA,* Naomi NISHIKAWA, Satoru TOKUYAMA, and Yuji HAYASHI

Department of Chemistry, Faculty of Science, Osaka City University, Sugimoto-cho, Sumiyoshi-ku, Osaka 558

(Received July 3, 1979)

Synopsis. A naturally occuring methoxyphthalide derivative, a constituent of *Othonna Cylindrica Dc*, was synthesized by employing stereoselective carbonyl reduction of (η-arene)tricarbonylchromium complex and regioselective lithiation of 7-methoxy-2-(1-hydroxyethyl)-1-tetralol.

The 3-methoxybenzyl alcohol derivatives and related compounds were lithiated mostly at 2-position of the aromatic ring on the basis of coordination between the lithium cation and the two proximal oxygen atoms.[1] In case of such a molecule that the benzylic hydroxyl group is fixed by a rigid conformation as in 7-methoxy-1-tetralol, this selective metallation is more facilitated by further stabilization of the cyclic lithio compound. This paper reports an application of this reaction to the synthesis to (**1**),[2] a constituent of *Othonna Cylindrica Dc*, combined with the stereoselective carbonyl reduction of tricarbonyl (2-substituted 7-methoxy-1-tetralol) chromium complex.

Refluxing of 7-methoxy-1-tetralone with hexacarbonylchromium in heptane and dibutyl ether gave a red colored (η-arene) tricarbonylchromium complex (**2**) in a 65% yield. The reaction of the complex **2** with *N*-trimethylsilyldiethylamine in the presence of *p*-toluenesulfonic acid,[3] followed by cross-aldol condensation[4] with paraldehyde and titanium tetrachloride, afforded a mixture of diastereomeric keto alcohols (**3**).[5] The compound **3** was reduced with diisobutylaluminum hydride (Dibal) to give the chromium complex (**4**) of *trans* substituted diol. No trace of the corresponding *cis* isomer was detected. In this reaction, the hydroxyethyl and hydride addition selectively took place from the other side of the tricarbonylchromium group.[6] Decomplexation of the chromium metal (by exposure to sunlight) gave the *trans* diol (**5**), which was chracterized as a diacetyl compound (**6-A**).

When the carbonyl reduction of the trimethylsilyl ether of the keto alcohol (**7**), prepared from 7-methoxy-1-tetralone by an analogous procedure, was performed without complexation by $Cr(CO)_3$ group, the product (80% yield) was a mixture of *trans* and *cis* alcohols in an approximate ratio of 12:88. The stereochemistry (C-1 and C-2) of both compounds was elucidated by the comparison of the ^{1}H-NMR spectra of the corresponding diacetates, **6-A** and **6-B**, derived by deprotection of trimethylsilyl group and acetylation. In this reduction, the *cis* isomer was formed predominantly, in contrast to the reduction of the (η-arene) tricarbonylchromium complex.

Treatment of the *trans* compound **5**[5] with butyl lithium and tetramethylethylenediamine (TMEDA) in hexane, followed by carboxylation with solid carbon dioxide, gave a hydroxy γ-lactone, which, without purification, was oxidized with Collins reagent to a

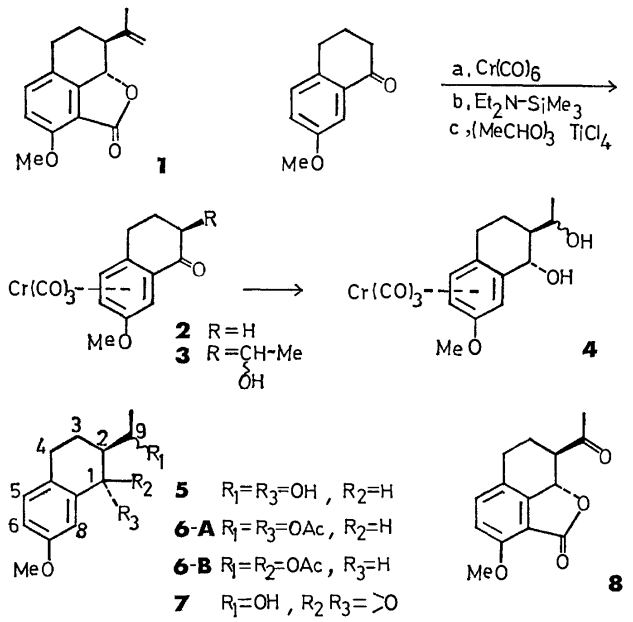

trans keto lactone (**8**)[7] as a sole isolable product in a 20% overall yield, unaccompanied with any other carboxylated products. Reaction of the *trans* keto lactone (**8**) with methylenetriphenylphosphorane gave **1**, which exhibited the same spectral data as those of the reported natural product.[2]

Experimental

Tricarbonyl(η-7-methoxy-1-tetralone)chromium Complex (2). A mixture of 7-methoxy-1-tetralone (1 g, 3.67 mmol), $Cr(CO)_6$ (2 g, 5.87 mmol), α-picoline (0.54 g, 5.87 mmol), heptane (20 ml) and dibutyl ether (100 ml) was refluxed under nitrogen for 24 h in a Strohmeier type apparatus. After filtration and evaporation *in vacuo*, a crude product was chromatographed on silica gel. Elution with ether–petroleum ether (1 : 4) gave a 1.15 g (65%) of **2**. IR ($CHCl_3$): 1975, 1920—1880, 1683 cm^{-1}. NMR ($CDCl_3$)δ: 3.66 (s, 3H, OMe), 5.36(d, J=6 Hz, 1H), 5.49 (dd, J=2, 6 Hz, 1H), 5.66 (d, J=2 Hz, 1H).

Tricarbonyl[η-7-methoxy-2-(1-hydroxyethyl)-1-tetralone]chromium Complex (3). A mixture of **2** (997 mg, 3.2 mmol), *N*-trimethylsilyldiethylamine (1.856 g, 12.8 mmol) and catalytic amount of *p*-TsOH was stirred at 35 °C in dry dichloromethane (15 ml) for 24 h. After evaporation at a reduced pressure, a residue was triturated with dry pentane. Evaporation of the pentane solution gave an oily enolsilyl ether (811 mg, 66%), which was used for next step without further purification. IR(neat): 1955, 1885—1855, 1640, 1605 cm^{-1}. NMR($CDCl_3$)δ: 0.19(s, 9H, $SiMe_3$), 3.68(s, 3H, OMe), 4.96—5.44(m, 4H). A solution of the crude enolsilyl ether (811 mg) in dry dichloromethane (10 ml) was added dropwise into a mixture of paraldehyde (169 mg, 0.84 mmol) and titanium tetrachloride (480 mg, 2.52 mmol) in dry dichlo-

romethane (10 ml) under argon atmosphere at −78 °C, and the reaction mixture was stirred for 7 h at the same temperature. After hydrolysis with water, the reaction mixture was extracted with dichloromethane. The extract was washed with brine and dried over Na_2SO_4. The solvent was evaporated under reduced pressure, and the residue was purified by silica gel chromatography. Elution with ether–petroleum ether (1 : 3) afforded a diastereomeric mixture of **3** (428 mg, 57% yield). IR ($CHCl_3$): 3440, 1970, 1910, 1890, 1660 cm^{-1}. NMR ($CDCl_3$)δ: 1.23 (d, J=7 Hz) and 1.26 (d, J=7 Hz) (2 : 3 ratio, 3H, CHMe), 3.66 (s, 3H, OMe), 5.39 (d, J=6 Hz, 1H), 5.55 (dd, J=2, 6 Hz, 1H), 5.72 (d, J=2 Hz).

trans-*7-Methoxy-2-(1-hydroxyethyl)-1-tetralol (**5**).* Diisobutylaluminum hydride in toluene (0.186 M solution, 3.0 ml, 5.28 mmol) was added to a solution of **3** (510 mg, 1.43 mmol) in dry THF (10 ml) under argon atmosphere at −78 °C. After stirring for 3 h, acetone (1 ml) and then, water (10 ml) were added, After filtration and evaporation of the organic solvents under reduced pressure, the reaction mixture was extracted with ether. The extract was worked up as usual to leave *trans* compound **4** as a yellow oil which was used for next step without further purification. A solution of the *trans* compound **4** in ether (10 ml) was exposed to sunlight for 2 h. The precipitate was filtered and washed with ether. The ether solution was concentrated *in vacuo*, leaving a crude product which was purified by silica-gel chromatography (elution with ether–petroleum ether; 1:3) to give **5** as a colorless oil (250 mg, 79% from **3**). IR(CCl_4): 3210, 1610, 1580, 1505 cm^{-1}. NMR(CCl_4)δ: 1.18(d, J=7 Hz) and 1.21(d, J=7 Hz) (2 : 3 ratio, 3H, CHMe), 3.77(s, 3H, OMe), 6.76(dd, J=3, 7 Hz, 1H,) 7.03(d, J=7 Hz, 1H), 7.16(d, J=3 Hz, 1H).

trans *Keto Lactone (**8**).* A solution of the *trans* diol **5** (730 mg, 3.29 mmol) in dry ether (3 ml) was added into a mixture of butyllithium (1.3 M in hexane solution, 8.0 ml, 10.4 mmol), TMEDA (1.206 g, 10.4 mmol) in dry hexane (10 ml) under nitrogen, and the reaction mixture was heated at 60 °C for 5 h. The resulting dark red reaction mixture, after cooling to −78 °C, was treated with large excess of Dry Ice (in small pieces). After standing overnight, the reaction mixture was acidified with 2 M-HCl, heated at 50 °C for 30 min, and extracted with ethyl acetate. The extract was washed with brine, and dried over Na_2SO_4. Evaporation of the solvent gave an oily product, which was used for next oxidation step without purification. A solution of the product in dry dichloromethane (2 ml) was added to stirred Collins reagent (prepared from 1.2 g of chromium trioxide, and 1.9 g of pyridine in 25 ml of dry dichloromethane) at 0 °C. After stirring at that temperature for 3 h, ether (10 ml) was added. The solution was filtrated from the residue, which was washed with ether. The combined organic solution was washed with 2M-HCl, saturated aq $NaHCO_3$, and brine and then, dried over Na_2SO_4. Evaporation of the solvent at reduced pressure afforded 290 mg of an oily product, which was purified over silica gel column chromatography to give a crystalline compound **8** (159 mg, 20% from **5**). Recrystallization from ether–petroleum ether gave colorless needles; mp 148—149 °C. IR($CHCl_3$): 1750, 1710, 1640, 1605, 1510 cm^{-1}. NMR($CDCl_3$)δ: 2.32(s, 3H, COMe), 3.92(s, 3H, OMe), 5.22(d, J=10 Hz, CHOC=O), 6.82(d, J=8 Hz, 1H), 7.31(d, J=8 Hz, 1H). Found: C, 68.23; H, 5.76%. Calcd for $C_{14}H_{14}O_4$: C, 68.28; H, 5.73%.

*Wittig Reaction of **8**.* Butyllithium (1.3 M in hexane solution, 0.29 ml, 0.382 mmol) was added to a mixture of methyltriphenylphosphonium bromide (151 mg, 0.42 mmol) in dry THF (2 ml) at 0 °C under nitrogen atmosphere. After stirring for 1 h, a solution of **8** (77 mg, 0.313 mmol) in dry THF (5 ml) was added to the above Wittig reagent, and the reaction mixture was stirred for 3 h at 0 °C. After addition of 2M-HCl, the product was extrated with ether as usual. The crude product was purified by silica gel column chromatography to give crystalline compound **1** (25 mg). MS *m/e*: 244, 176. IR($CHCl_3$): 2940, 1750, 1660, 1605, 1510 cm^{-1}. NMR($CDCl_3$)δ: 1.86(s, 3H, MeC=), 3.97(s, 3H, OMe), 4.94(broad s, 2H, H_2C=C), 5.12(d, J=10 Hz, 1H, O=COCH–), 6.85(d, J=8 Hz, 1H), 7.32(d, J=8 Hz, 1H). UV(EtOH) max: 215, 241, 305 nm. These data were well consistent to the spectral data reported for the natural product.[2]

trans-*Diacetate (**6-A**).* This acetate was prepared with acetic anhydride and pyridine by usual method. IR (CCl_4): 1740, 1615, 1505, 1245 cm^{-1}. NMR(CCl_4)δ: 1.25(d, J=7 Hz) and 1.29(d, J=7 Hz) (3:2 ratio, 3H, CHMeOAc), 1.97(s) and 2.01(s) (2:3 ratio, 3H, OAc), 2.13(s, 3H, OAc), 4.80—5.10(m, 1H, MeCHOAc), 5.95(d, J=8 Hz, 1H, CHOAc), 6.63(d, J=3 Hz, 1H), 6.77(dd, J=3, 8 Hz, 1H), 7.01(d, J=8 Hz, 1H).

cis-*Diacetate (**6-B**).* A mixture of **7** (110 mg, 0.5 mmol) and hexamethyldisilazane (242 mg, 1.5 mmol) was heated at 50 °C for 24 h. Evaporation at reduced pressure gave an oily silylated product in a quantitative yield. IR(neat): 1680, 1610, 1500 cm^{-1}. NMR($CDCl_3$)δ: 0.21(s) and 0.18(s) (2:3 ratio, 9H, $OSiMe_3$), 1.18(d, J=7 Hz) and 1.32(d, J=7 Hz) (3:2 ratio, 3H, CHMe), 3.88(s, 3H, OMe), 4.70(m, 1H, MeCHO–), 7.08(dd, J=2, 7 Hz, 1H), 7.20(d, J=7 Hz, 1H), 7.54(d, J=2 Hz, 1H). The keto silylated product was reduced with Dibal (THF, −78 °C), to giva a hydroxy silylated compound, which was converted to a diacetylated product by deprotection of silyl group (aq AcOH, THF, rt) and then acetylation (acetic anhydride, pyridine, rt) in a 80% yield. Pure *cis* isomer was obtained by preparative TLC. IR(CCl_4): 1740, 1615, 1505, 1245 cm^{-1}. NMR (CCl_4)δ: 1.26(d, J=7 Hz, 3H, CHMeOAc), 1.91(s) and 1.98(s) (3:2 ratio, 3H, OAc), 1.95(s) and 2.00(s) (3:2 ratio, 3H, OAc), 3.74(s, 3H, OMe), 4.80—5.05(m, 1H, MeCHOAc), 6.05(d, J=7 Hz, 1H, CHOAc), 6.70—6.82(m, 2H), 6.97 (broad d, J=8 Hz, 1H).

References

1) M. Uemura, S. Tokuyama, and T. Sakan, *Chem. Lett.*, **1975**, 1195.

2) F. Bohlmann and M. Grenz, *Tetrahedron Lett.*, **1974**, 1681.

3) L. H. Hellberg and A. Juarez, *Tetrahedron Lett.*, **1974**, 3553.

4) T. Mukaiyama, K. Banno, and K. Narasaka, *J. Am. Chem. Soc.*, **96**, 7503 (1974).

5) An epimeric mixture at C-9. Since the epimeric center will be removed by oxidation to a C-9 keto compound at the later step, this diastereomeric mixture was used for a series of reaction without separation.

6) G. Jaouen and A. Meyer, *J. Am. Chem. Soc.*, **97**, 4667 (1975); B. Caro and G. Jaouen, *Tetrahedron Lett.*, **1974**, 1229.

7) Similarly, an isomeric *cis* keto lactone was obtained from a corresponding *cis* alcohol by lithiation, carboxylation, and then Collins oxidation. Mp 126 °C. IR($CHCl_3$): 1760, 1710, 1640, 1510 cm^{-1}. NMR($CDCl_3$)δ: 2.08(s, 3H, COMe), 3.95(s, 3H, OMe), 5.40(d, J=7 Hz, 1H, CHOC=O), 6.84(d, J=8 Hz, 1H), 7.32(d, J=8 Hz, 1H).

A Novel Synthesis of 2-(1-Imidazolyl)benzophenones

Yasutaka KAYAMA, Takeshi HARA,* and Tamiko SUNAMI
Teijin Institute for Bio-medical Research, Asahigaoka, Hino, Tokyo 191

(Received July 5, 1979)

Synopsis. 2-(1-Imidazolyl)benzophenones were prepared from 3-(2,2-dialkoxyethyl)-3,4-dihydro-4-hydroxy-4-phenylquinazolines and a corresponding 4-alkoxy derivative by heating in formic acid or in sulfuric acid–ethanol.

2-(1-Imidazolyl)benzophenones with appropriate substituents are themselves pharmacologically active compounds[1,2] or important intermediates for the synthesis of 6-phenyl-4*H*-imidazo[1,2-*a*][1,4]benzodiazepines[3] or 6-phenyl-4*H*-imidazo[1,5-*a*][1,4]benzodiazepines.[4] This type of compounds have so far been prepared by nucleophilic reaction of imidazolide anions with 2-halobenzophenones,[2] oxidation of 1-(2-benzylphenyl)-1*H*-imidazoles[5] or seven-membered ring cleavage of 6-phenyl-4*H*-imidazo[1,2-*a*][1,4]benzodiazepines.[1,4,6] We now wish to report a novel synthesis of 2-(1-imidazolyl)benzophenones.

When 3-(2,2-dialkoxyethyl)-3,4-dihydro-4-hydroxy-4-phenylquinazolines **3a**, **c** prepared by the reaction[7] of aminoacetaldehyde dialkyl acetals (**2**) with 2-(1-alkoxyethylideneamino)benzophenones (**1**) were heated with formic acid, ring opening and recyclization occured to afford the 2-(1-imidazolyl)benzophenones **5a**, **b** in good yields (Table 1).

The conversion of **3c** to **5b** could also be carried out with sulfuric acid, but in a decreased yield. As we previously reported,[7] the 4-hydroxydihydroquinazolines **3** formed by refluxing an ethanolic solution of **1** and **2** are converted to the corresponding 4-ethoxy derivatives **4** under the reaction conditions, and the latters can be isolated as such avoiding acidic treatment such as silica gel chromatography; the chromatography converted **4** to **3**. So, next we examined the conversion of **4** to **5**. Treatment of **4b** with formic acid also afforded **5b** in 81% yield. The 2-(1-imidazolyl)benzophenones **5a**, **b** thus obtained gave satisfactory elemental analysis and IR and NMR spectral properties. Ring opening and recyclization of dihydroquinazolines to yield 2-(4*H*-1,2,4-triazol-4-yl)benzophenones, a reaction similar to the one reported herein, was previously reported.[8]

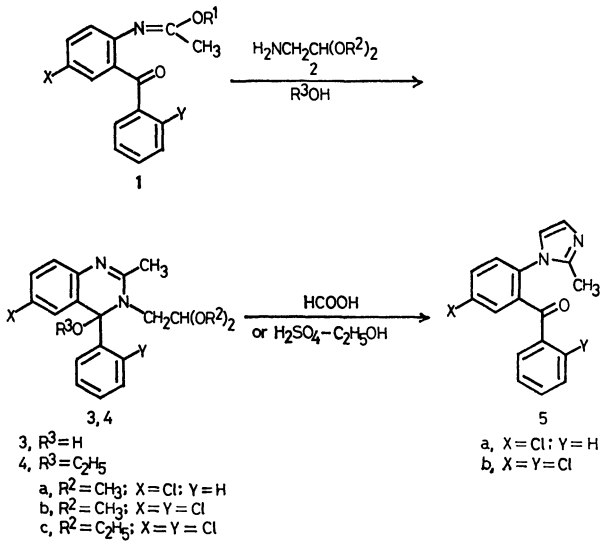

TABLE 1. CONVERSION OF QUINAZOLINES (**3**, **4**) TO IMIDAZOLYLBENZOPHENONES (**5**)

Run	Starting material	Catalyst-solvent	Refluxing period/h	Product	Yield/%
1	**3a**	80% HCO_2H[a]	3	**5a**	83
2	**3c**	99% HCO_2H[a]	1	**5b**	85
3	**3c**	H_2SO_4–C_2H_5OH	3	**5b**	55
4	**4b**	85% HCO_2H[a]	3	**5b**	81

a) Formic acid was employed as solvent as well as catalyst.

Experimental

Melting points were taken with a Yanagimoto hot-stage apparatus and are uncorrected. Combustion analyses were carried out by the Analytical Chemistry Laboratory of Central Research Institute, Teijin Limited. IR spectra were measured on a Hitachi EPI-S2 spectrophotometer. NMR spectra were obtained on a JEOL JNM-MH-100 spectrometer, and chemical shifts are expressed in parts per million (δ) relative to TMS as an internal standard.

*5-Chloro-2-(2-methyl-1-imidazolyl)benzophenone (**5a**).*

A solution of 6-chloro-4-hydroxy-3-(2,2-dimethoxyethyl)-2-methyl-4-phenyl-3,4-dihydroquinazoline (**3a**) (2.03 g, 5.62 mmol) in 80% formic acid (10 ml) was refluxed for 3 h. The formic acid was evaporated. Ice–water (10 g) was added to the residue, and the mixture was made alkaline with 4 M (1M=1 mol dm^{-3}) NaOH and extracted with dichloromethane (40 ml). The extract was washed with brine, dried (Na_2SO_4), and evaporated. The residue was crystallized with ether and triturated after addition of a small amount of hexane. The crystals were collected on a filter, washed with ether–hexane, and dried to give 1.40 g (83%) of **5a** as colorless crystals. Recrystallization from ether–hexane gave colorless plates: mp 115.5—117.0 °C; IR (KBr) 1656, 1596, 1485, 1414, 1303, 1284, 1242, 827, 737, 711; NMR ($CDCl_3$) δ 2.18 (s, 3H), 6.73 (s, 2H), 7.24—7.67 (m, 8H).

Found: C, 68.51; H, 4.24; N, 9.60%. Calcd for $C_{17}H_{13}N_2OCl$: C, 68.80, H, 4.42; N, 9.44%.

*2',5-Dichloro-2-(2-methyl-1-imidazolyl)benzophenone (**5b**).*

a) Compound **5b** isolated by silica gel column chromatography [eluent; dichloromethane–ethyl acetate (2:1)] of the product mixture in Run 2 of Table 1 was recrystallized from dichloromethane–hexane to give colorless prisms: mp 112—113.5 °C; IR (KBr) 1665, 1591, 1482, 1415, 1298, 1258, 1238, 837, 747; NMR ($CDCl_3$) δ 2.12 (s, 3H), 6.69 (m, 2H), 7.20—7.34 (m, 5H), 7.61 (dd, J=8.0 and 2.5 Hz, 1H), 7.71 (d, J=2.5 Hz, 1H).

Found: C, 61.65; H, 3.48; N, 8.43%. Calcd for $C_{17}H_{12}N_2OCl_2$: C, 61.65; H, 3.65; N, 8.46%.

b) A mixture of 6-chloro-4-(2-chlorophenyl)-3-(2,2-diethoxyethyl)-3,4-dihydro-4-hydroxy-3-methylquinazoline (**4b**) (1.00 g, 2.36 mmol), ethanol (5 ml), and 9 M H_2SO_4 (5 ml) was refluxed for 3 h. To the reaction mixture, after evapora-

tion of ethanol, was added ice–water (10 g) and dichloromethane (30 ml), and the resulting mixture was made alkaline with 4 M NaOH. The layers were separated, and the organic layer was washed with brine, dried (Na_2SO_4), and evaporated. The residue was chromatographed on silica gel with benzene–ethyl acetate (2:1 to 0:1) as eluent to give 0.427 g (55%) of **5b** as yellowish crystals. Recrystallization from dichloromethane–hexane gave colorless prisms of mp 112.5—113 °C, showing identical IR and NMR spectra with those of **5b** prepared in Run 2 of Table 1.

The authors wish to thank Miss A. Mineo for NMR spectral measurement. Particular appreciation is expressed to Dr. T. Noguchi for his encouragement during the course of this work.

References

1) M. Gall, J. B. Nester, Jr., A. D. Rudzik, and R. A Lahti, *J. Med. Chem.*, **19**, 1057 (1976).

2) a) M. Nakanishi, T. Yokobe, T. Arai, and M. Abe (to Yoshitomi Pharm. Ind. Ltd.), Japanese Patent Kokai 74-117 466 (1974); *Chem. Abstr.*, **84**, 44045g (1976); b) M. Nakanishi, T. Yokobe, T. Arai, and M. Abe, Japanese Patent Kokai 75-41 860 (1975); *Chem. Abstr.*, **83**, 193312y (1975).

3) M. Gall (to Upjohn Co.), U.S. Patent 3 941 803 (1976); *Chem. Abstr.*, **85**, 21368w (1976).

4) M. Gall (to Upjohn Co.), U. S. Patent 4 005 099 (1977); *Chem. Abstr.*, **86**, 190029n (1977).

5) a) T. Yokobe, T. Arai, and M. Abe (to Yoshitomi Pharm. Ind. Ltd.), Japanese Patent Kokai 75-95 264 (1975); *Chem. Abstr.*, **84**, 105590e (1976); b) M. Gall (to Upjohn Co.), U. S. Patent 3 941 802 (1976); *Chem. Abstr.*, **85**, 63067c (1976).

6) J. P. Maffrand, G. Ferrand, and F. Eloy, *Tetrahedron Lett.*, **1973**, 3449.

7) T. Hara, Y. Kayama, and T. Sunami, *J. Org. Chem.*, **43**, 4865 (1978).

8) a) M. E. Derieg, R. Ian Fryer, and S. S. Hillery, *J. Heterocycl. Chem.*, **8**, 181 (1971); b) Y. Kuwada, K. Meguro, and H. Tawada (to Takeda Chem. Ind. Ltd.), Japanese Patent Kokai 73-5 796 (1973); *Chem. Abstr.*, **78**, 97730j (1973).

New Routes to the Pyrrolo[2,1-*a*]isoquinoline System

Masatomo Iwao* and Tsukasa Kuraishi

Department of Chemistry, Faculty of Liberal Arts, Nagasaki University, 1-14 Bunkyo-machi, Nagasaki 852

(Received July 12, 1979)

Synopsis. Some derivatives of the title ring system were prepared from methyl α-(1-isoquinolyl)-β-aminocrotonate and ethyl α-(1-isoquinolyl)-β-amino-β-ethoxyacrylate in moderate to good yields *via* their quaternary salts.

Although several methods for the preparation of pyrrolo[2,1-*a*]isoquinoline system have been reported, the yields of the products are usually poor.[1)]

In the course of our recent study of the convenient synthesis of heteroarylacetic esters, methyl α-(1-isoquinolyl)-β-aminocrotonate (**1**) was prepared in a moderate yield (58%) as an intermediate compound for methyl 1-isoquinolylacetate, from isoquinoline 2-oxide and methyl β-aminocrotonate in the presence of benzoyl chloride.[2)] The ready availability of **1** and its unique

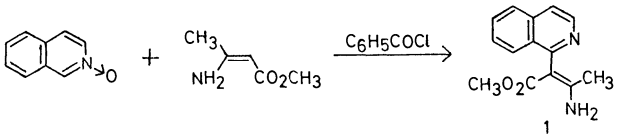

structure, possessing a reactive enaminic substituent at the 1-position of the isoquinoline ring, prompted us to determine the utility of this compound for the synthesis of fused isoquinoline systems. In this paper, we wish to describe the efficient synthesis of pyrrolo-[2,1-*a*]isoquinoline system from **1**. In addition, a related synthesis of the same system from ethyl α-(1-isoquinolyl)-β-amino-β-ethoxyacrylate(**7**) will also be described.

Compound **1** was allowed to react with phenacyl bormide or bromoacetone in chloroform under reflux for 1 h to give quaternary salts **2a**, **b** in about 90% yields. When these salts were treated with excess triethylamine in methanol in order to generate the ylides, **3**, a successive cyclization occurred and two pyrrolo[2,1-*a*]isoquinoline derivatives, **4a** and **4b**, were obtained in 93% and 77% yields respectively. This cyclization can be well explained in terms of the intramolecular nucleophilic attack of the ylidic carbanion on a β-carbon atom in the crotonate moiety, followed by the elimination of ammonia. The intermediacy of the ylides was shown by the development of a deep-red color at the initial stage of the reactions. Although the yield was not satisfactory (23%), Compound **4c** was obtained in a similar manner from **1** and *p*-nitrobenzyl bromide without isolating the intermediate quaternary salt, **2c**.

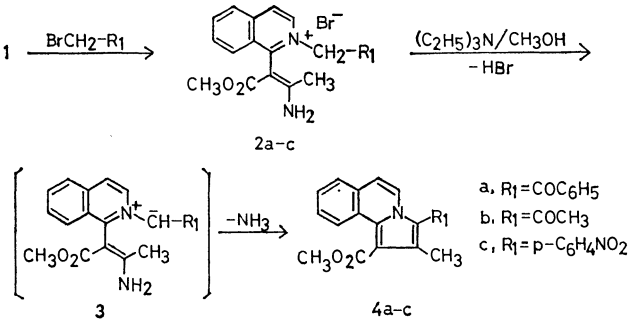

On the other hand, when quaternary salts **2a** and **2b** were heated in methanol under the reflux temperature for an appropriate time, pyrrolo[2,1-*a*]isoquinoline derivatives of another type, **6a** and **6b**, were obtained in 85% and 92% yields respectively. The structures of these unexpected compounds were fully supported by the results of microanalyses and the spectral data. In addition, the Compound **6b** thus obtained was completely identical with an authentic sample prepared from methyl 1-isoquinolylacetate and bromoacetone using Bragg's method.[3)] Although we have not conducted experiments to establish the reaction mechanism, it is reasonable to assume that the reaction is initiated by the nucleophilic attack of methanol on a β-carbon of **2**, which causes the elimination of methyl acetimidate. The intermediate enamine, **5**, thus formed gives **6** by spontaneous dehydrative cyclization.

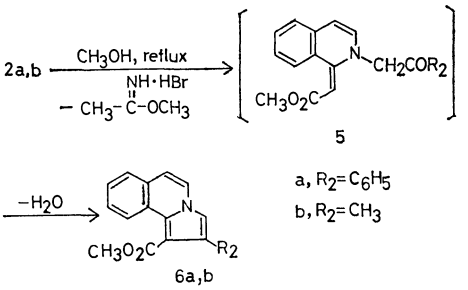

Recently, Yamanaka *et al.* reported the synthesis of ethyl α-(1-isoquinolyl)-β-amino-β-ethoxyacrylate(**7**).[4)] The structural resemblance of **7** to **1** suggested that the above cyclization methods are also applicable to this compound. In fact, the quaternization of **7** with phenacyl bromide and subsequent treatment with triethylamine afforded 2-aminopyrrolo[2,1-*a*]isoquinoline derivative **8** in a 66% yield. In this case, the elimination of ethanol occurred in preference to that of ammonia.

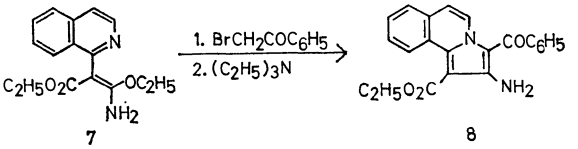

Experimental

All the melting points are uncorrected. The NMR spectra were recorded on a Hitachi R-20B spectrometer for a solution in deuteriochloroform, using TMS as the internal standard. The IR spectra were obtained in Nujol mulls with a Hitachi EPI-2 spectrometer. The UV spectra were determined for solutions in 95% ethanol with a Hitachi 323 spectrometer.

*Preparation of Quaternary Salts (**2a, b**). General Procedure*: A solution of 2.51 g (10 mmol) of hemihydrate of **1** and the appropriate α-bromoketone (10 mmol) in 25 ml of chloroform was refluxed for 1 h. The precipitated yellow solid of **2** was collected by filtration, washed with ether, and then recrystallized from methanol–ether. If the quaternary salt was not precipitates from the reaction mixture, the chloroform was removed by evaporation and the residual oil was crystallized by trituration with ether. The quaternary salt **2a** was thus obtained in a 92% yield; mp 190.5 °C (dec). IR: 3330, 3230, and 3160 cm^{-1} (NH_2), 1692 and 1672 cm^{-1} (C=O). The quaternary salt **2b** was obtained in a 90% yield; mp 148—149 °C (dec). IR: 3350, 3240, and 3160 cm^{-1} (NH_2), 1723 and 1672 cm^{-1} (C=O).

*Methyl 3-Benzoyl-2-methylpyrrolo[2,1-a]isoquinoline-1-carboxylate (**4a**).* Triethylamine (2 ml) was added to a solution of 1.00 g of **2a** in 20 ml of chloroform. The solution turned a deep red and was gradually decolorized. After several minutes, a crystalline compound began to precipitate. After having been allowed to stand overnight, the precipitates were collected by filtration, giving 0.72 g (94%) of **4a** as pale yellow needles. An analytical sample was purified by recrystallization from ethanol; mp 151.5—152.5 °C. IR: 1695 and 1612 cm^{-1} (C=O). UV max: 216^{sh} (log ε 4.40), 273 (4.60), 320 (4.13), 368^{sh} (4.12), and 382 nm (4.18). NMR; δ 2.07 (s, 3H, CH_3), 3.95 (s, 3H, $COOCH_3$), 7.01 (d, 1H, H-6, J=7.5 Hz), 7.3—7.9 (m, 5H arom, 3H, H-7, H-8, H-9), 8.6—8.9 (m, 1H, H-10), and 8.94 ppm (d, 1H, H-5, J=7.5 Hz). Found; C, 77.02; H, 4.92; N, 4.11%. Calcd for $C_{22}H_{17}NO_3$: C, 76.95; H, 4.99; N, 4.08%.

*Methyl 3-Acetyl-2-methylpyrrolo[2,1-a]isoquinoline-1-carboxylate (**4b**).* This compound was prepared from **2b** in a 77% yield in a manner similar to that described above; colorless prisms; mp 124.5—125.5 °C. IR: 1702 and 1623 cm^{-1} (C=O). UV max: 224^{sh} (log ε 4.19), 249 (4.30), 274 (4.57), 284 (4.48), 323 (4.11), 340 (3.91), 357 (4.15), and 375 nm (4.12). NMR: δ 2.51 (s, 3H, CH_3 or $COCH_3$), 2.53 (s, 3H, $COCH_3$ or CH_3), 3.96 (s, 3H, $COOCH_3$), 6.94 (d, 1H, H-6, J=7.5 Hz), 7.35—7.6 (m, 3H, H-7, H-8, H-9), 8.2—8.5 (m, 1H, H-10), and 9.52 ppm (d, 1H, H-5, J=7.5 Hz). Found: C, 72.43; H, 5.32; N, 5.07%. Calcd for $C_{17}H_{15}NO_3$: C, 72.58; H, 5.37; N, 4.98%.

*Methyl 2-Methyl-3-(p-nitrobenzyl)pyrrolo[2,1-a]isoquinoline-1-carboxylate (**4c**).* A mixture of 2.51 g (10 mmol) of hemihydrate of **1**, 2.16 g (10 mmol) of *p*-nitrobenzyl bromide, and 25 ml of chloroform was refluxed for 3 h. The chloroform was then removed by evaporation, and the residual oil was dissolved in 20 ml of methanol. Triethylamine (4 ml) was added to the solution, and the reaction mixture was allowed to stand at room temperature for 2d. The precipitated orange prisms were collected by filtration to give 0.72 g of **4c**; mp 192.5—193.5 °C. The filtrate was evaporated, and the residue was passed through a colum of silica gel, using chloroform as the eluent. From the first orange band, an additional 0.09 g of **4c** was obtained; mp 189—192.5 °C. The total yield was 0.81 g (23%). An analytical sample was purified by recrystallization from ethanol; mp 192.5—193.5 °C. IR: 1682 cm^{-1} (C=O), 1510 and 1346 cm^{-1} (NO_2). UV max: 253^{sh} (log ε 4.42), 269^{sh} (4.55), 277 (4.65), 332 (4.11), and 388 nm (4.00). NMR: δ 2.30 (s, 3H, CH_3), 3.96 (s, 3H, $COOCH_3$), 6.80 (d, 1H, H-6. J=7.5 Hz), 7.3—7.7 (m, 2H arom, 4H, H-5, H-7, H-8, H-9). 8.31 (near d, 2H arom) and 8.9—9.1 ppm (m, 1H, H-10). Found: C, 70.15; H, 4.50; N, 7.77%. Calcd for $C_{21}H_{16}N_2O_4$: C, 69.99; H, 4.48; N, 7.77%.

*Methyl 2-Phenylpyrrolo[2,1-a]isoquinoline-1-carboxylate (**6a**).* A solution of 0.5 g of **2a** in 20 ml of methanol was refluxed for 2 d. The solution was then evaporated, and the residue was extracted with chloroform. The extract was washed with water, dried over sodium sulfate, and evaporated. The residue was recystallized from methanol to give 0.29 g (85%) of **6b** as colorless plates; mp 91.5—92.5 °C. IR: 1690 cm^{-1} (C=O). UV max: 253^{sh} (log ε 4.42), 274^{sh} (4.62), 281 (4.68), and 329 nm (4.08). NMR: δ 3.65 (s, 3H, $COOCH_3$), 6.62 (d, 1H, H-6, J=7.5 Hz), 7.03 (s, 1H, H-3), 7.1—7.7 (m, 5H arom, 4H, H-5, H-7, H-8, H-9), and 8.7—8.95 ppm (m, 1H, H-10). Found: C, 79.62; H, 4.90; N, 4.69%. Calcd for $C_{20}H_{15}NO_2$: C, 79.71; H, 5.02; N, 4.65%.

*Methyl 2-Methylpyrrolo[2,1-a]isoquinoline-1-carboxylate (**6b**).* A solution of 0.5 g of **2b** in 20 ml of methanol was refluxed for 17 h and then worked up in a manner similar to that described for **6a**. Recrystallization from methanol afforded 0.29 g (92%) of **6b** as colorless needles; mp 139—140 °C. IR: 1675 cm^{-1} (C=O). UV max; 223 (log ε 4.44), 243 (4.15), 272^{sh} (4.45), 281 (4.62), and 331 nm (4.06). NMR: δ 2.30 (s, 3H, CH_3), 3.88 (s, 3H, $COOCH_3$), 6.64 (d, 1H, H-6, J=7.5 Hz), 6.80 (s, 1H, H-3), 7.3—7.6 (m, 4H, H-5, H-7, H-8, H-9), and 9.15—9.4 ppm (m, 1H, H-10). Found: C, 75.56; H, 5.50; N, 5.93%. Calcd for $C_{15}H_{13}NO_2$: C, 75.30; H, 5.48; N, 5.85%.

Unequivocal Synthesis of Methyl 2-Methylpyrrolo[2,1-a]isoquinoline-1-carboxylate. A solution of 2.24 g (11 mmol) of methyl 1-isoquinolylacetate and 0.77 g (5.5 mmol) of bromoaceone in 10 ml of acetone was refluxed for 17 h. The solution was then evaporated, and the residue was extracted with chloroform. The extract was washed with water, dried over sodium sulfate, and evaporated. The residue was subsequently recrystallized from methanol, giving 0.67 g (50%) of methyl 2-methylpyrrolo[2,1-*a*]isoquinoline-1-carboxylate; mp 138—140 °C. This compound was shown to be identical with Compound **6b** by a comparison of the IR spectra and by a mixed-melting-point determination.

*Ethyl 2-Amino-3-benzoylpyrrolo[2,1-a]isoquinoline-1-carboxylate (**8**).* A solution of 2.86 g (10 mmol) of **7** and 1.99 g (10 mmol) of phenacyl bromide in 25 ml of chloroform was refluxed for 1 h. The solution was then evaporated, and the residual oil was dissolved in 20 ml of methanol. After triethylamine (4 ml) has been added to this solution, the reaction mixture was allowed to stand overnight at room temperature. The yellow needles thus precipitated were collected by filtration to give 2.38 g (66%) of **8**; mp 155—156 °C. An analytical sample was purified by recrystallization from ethanol; mp 155—156 °C. IR: 3450 and 3300 cm^{-1} (NH_2), 1683 cm^{-1} (C=O). UV max: 214^{sh} (log ε 4.46), 228^{sh} (4.40), 287 (4.62), and 362 nm (4.30). NMR: δ 1.39 (t, 3H, $COOCH_2C\underline{H}_3$, J=7 Hz), 4.38 (q, 2H $COOC\underline{H}_2CH_3$, J=7 Hz), 5.97 (broad s, 2H, NH_2), 6.80 (d, 1H, H-6, J=7.5 Hz), 7.3—7.7 (m, 5H arom, 3H, H-7, H-8, H-9), 8.56 (d, 1H, H-5, J=7.5 Hz) and 9.0—9.25 ppm (m, 1H, H-10). Found: C, 73.93; H, 5.06; N, 7.90%. Calcd for $C_{22}H_{18}N_2O_3$: C, 73.73; H, 5.06; N, 7.82%.

References

1) For a review, see: T. Uchida and K. Matsumōto, *Synthesis*, **1976**, 209.

2) M. Iwao and T. Kuraishi, *J. Heterocycl. Chem.*, **15**, 1425 (1978).

3) D. R. Bragg and D. G. Wibberley, *J. Chem. Soc.*, **1962**, 2627.

4) H. Yamanaka, M. Komatsu, S. Ogawa, and S. Konno, *Chem. Pharm. Bull.*, **27**, 806 (1979).

Isomerization of Cyclohexene Oxide over Solid Acids and Bases[1)]

Kazushi ARATA and Kozo TANABE*,**

Hokkaido University of Education, Hachiman-cho, Hakodate 040

***Department of Chemistry, Faculty of Science, Hokkaido University, Sapporo 060*

(Received December 19, 1978)

The reaction of cyclohexene oxide over solid acids and bases at 108 °C gave five main products, 1,3-cyclohexadiene (**1**), cyclohexanone (**2**), cyclohexanol (**3**), 2-cyclohexen-1-one (**4**), and 2-cyclohexen-1-ol (**5**). SiO_2–TiO_2 and SiO_2–TiO_2–MgO were highly active for the isomerization, giving a large amount of **1**. TiO_2–ZrO_2 mainly showed selectivity for the formation of **5**, and other catalysts formed both **2** and **5**. Of the alumina prepared in four different ways, two were highly active, giving **5** predominantly. The results were discussed in comparison with those for an oxide containing a methyl group on the oxide ring, 1-methylcyclohexene oxide. By the experiment using the deuterated epoxide, 1,2-epoxycyclohexane-3,3,6,6-d_4, isotope effects for the formation of **2**, **3**, **4**, and **5** over Al_2O_3's, SiO_2–TiO_2 and solid H_3PO_4 were observed. It has been concluded that the epoxide is adsorbed on both acidic and basic sites, and that allyl alcohol is formed when both the opening of the epoxide ring and the hydrogen abstraction take place simultaneously, while ketone is formed when the former precedes the latter.

Studies on the rearrangement of cyclohexene oxide have been made. Nagvi and his coworkers reported for the first time that the oxide undergoes rearrangement in the presence of magnesium bromide etherate to *trans*-2-bromocyclohexanol and cyclopentanecarbaldehyde, a ring-contracted aldehyde.[2)] The aldehyde formation from the oxide has been demonstrated using molten salts, low-melting binary or ternary eutectic salts as catalysts, *i.e.*, in the presence of lithium bromide or perchlorate with tributylphosphine oxide or hexamethylphosphoric triamide as reported by Rickborn and Gerkin,[3)] or over lithium bromide–rubidium bromide eutectic supported on firebrick similar to the gas chromatography column reported by Kennedy and Buse.[4)]

The isomerization of cyclohexene oxide to the uncontracted products has also been reported. Cyclohexanone was readily formed in alcoholic solutions of octacarbonyldicobalt(0),[5)] 2-cyclohexenol being predominantly given by various lithium monoalkylamides and dialkylamides as strong bases.[6,7)] The oxide was also converted into both cyclohexanone and 2-cyclohexenol by thermal gas-phase isomerization over the temperature range 407—464 °C under pressures 1.6—6 Torr (1 Torr=133.322 Pa).[8)]

In contrast to the above observations on the homogeneous system, Al_2O_3 was used as a catalyst in the heterogeneous system.[9)] However, diols or hydrated dimers were obtained instead of the isomerized products, probably owing to the incomplete dehydration of Al_2O_3 or adsorption of moisture caused by careless treatment.[10)] Use of solid catalysts under heterogeneous conditions has the advantage of allowing easy separation of products from catalyst.

We have recently studied the isomerization of 1-methylcyclohexene oxide and *d*-limonene oxide catalyzed by solid acids and bases in a heterogeneous solid–liquid system, and observed the markedly different selectivities which depend on the type of catalyst.[11)] Since only alumina has been investigated for the isomerization of cyclohexene oxide, the epoxide has now been isomerized over several solid acids and bases in order to see how the activity and selectivity differ according to the type of catalyst.

Experimental

Cyclohexene oxide (Tokyo Kasei Kogyo Co.) was more than 98% pure and toluene (guaranteed reagent) used as solvent was purified by distillation over sodium metal. 1,2-Epoxycyclohexane-3,3,6,6-d_4 (supplied by Dr. M. C. Flowers) was used. Purity of the epoxide was 99.5%, and isotopic purity was about 90% $C_6H_6D_4O$.

Standard Procedure for Reaction. The reaction was carried out at 108 °C in the presence of toluene as a solvent. A mixture of 0.5 ml of the epoxide, 2.5 ml of toluene, and about 0.3 g of catalyst, ground to below 100 mesh, was stirred in a reaction vessel with a magnetic stirrer. At appropriate time intervals, a small amount of the sample was taken out with a 1 ml syringe, separated from the catalyst by means of centrifuge, and analyzed by gas-liquid chromatography with a TCD detector using a 3-m column of 20% polyethylene glycol 20 M on Celite 545 SK (180 °C, He 1.0 kg/cm²). The yields of products were based on the epoxide and calculated by measurement of GLC areas (uncorrected). The competitive isomerization of the deuterated and undeuterated cyclohexene oxide was carried out with a mixture of 0.1 ml of both oxides in equivalent amount, 0.5 ml of toluene and 60 mg of catalyst. The products were analyzed by combined gas chromatography-mass spectrometry (Hitachi RM50GC) with a 2-m column of PEG 20M.

Catalysts. SiO_2–Al_2O_3 [N361(L)(Al_2O_3; 15 wt %) of Nikki Chemical Co.] was calcined at 500 °C. SiO_2–TiO_2 (molar ratio=1:1) was prepared by coprecipitation of a mixed solution of ethyl orthosilicate and titanium tetrachloride with aqueous ammonia. The precipitate was aged over a water bath for 1 h, washed with distilled water until no chloride ion was detected, dried at 100 °C for 20 h and calcined at 500 °C. SiO_2–TiO_2–MgO (molar ratio=1:1:1) was prepared by kneading SiO_2–TiO_2 (1:1) and magnesium hydroxide together with an appropriate amount of water for 2 h, followed by drying at 120 °C for 1 d and calcining at 500 °C. Magnesium hydroxide was prepared by hydrolysis of magnesium chloride with aqueous ammonia, followed by washing and drying as above. $LiClO_4 \cdot 3H_2O$ (guaranteed reagent, Nakarai Chemical Co.) was dried at 120 °C for 3 d. H_2SO_4/SiO_2 was prepared as follows: 10 g of granular silica gel was immersed in 12 ml of 0.5 M H_2SO_4, evaporated, dried and then calcined at 150 °C. $FeSO_4$ and $NiSO_4$ were prepared by calcining their heptahydrates (guaranteed) at 500 and 350 °C, respectively. Solid phosphoric acid (N501, Nikki Chemical Co.) was calcined at 300 °C. TiO_2–ZrO_2

(molar ratio= 1 : 1) was prepared by thermal decomposition, at 500 °C, of H_4TiO_4–$Zr(OH)_4$, which was precipitated by heating a mixed aqueous solution of titanium tetrachloride, zirconium dichloride oxide, and an excess amount of urea on a boiling water bath, followed by washing thoroughly with distilled water until no chloride ions were detected in the filtrate and drying in the air at 110 °C. Al_2O_3 A (KAT 6, Nishio Chemical Co.) was heat-treated at 500 °C. Al_2O_3 B, C, and D, Albes FF, Albes FE and Albes C, respectively, (Showa Tansan Kaisha, Ltd.) were calcined at 500 °C. All the catalysts were heat-treated in air for 3 h and stored in sealed ampoules.

Identification of Products. Reaction products were identified by the observed gas-chromatographic retention time and their mass spectra, obtained by combined gas chromatography-mass spectrometry, by comparison with authentic samples. A mixture of cyclohexene oxide (0.1 ml) and toluene (0.4 ml) was reacted over 60 mg of Al_2O_3 A at 110 °C for 2 h. The products were 5% of **1**, 2% of **2**, 6% of **3**, 30% of **5**, and 8% of **4** as the order of elution on a GLC PEG 20 M column at 180 °C. Their mass spectra at 70 eV of ionization voltage are as follows: important ions at *m/e* of **1**: 80 (M^+), 79 (100 %), 40 (78%), 80 (61%), 77 (36%), 78 (14%); **2**: 98 (M^+), 41 (100%), 55 (98%), 69 (82%), 42 (76%), 70 (35%); **3**: 100 (M^+), 57 (100%), 40 (51%), 82 (49%), 44 (38%), 67 (23%); **4**: 96 (M^+), 68 (100%), 40 (46%), 96 (42%), 39 (19%), 42 (10%); **5**: 98 (M^+), 70 (100%), 98 (50%), 97 (34%), 83 (30%), 39, (23%), 41 (22%).

Results and Discussion

The reaction of cyclohexene oxide catalyzed by solid acids and bases gave 1,3-cyclohexadiene (**1**), cyclohexanone (**2**), cyclohexanol (**3**), 2-cyclohexen-1-one (**4**) 2-cyclohexen-1-ol (**5**), and other compounds.

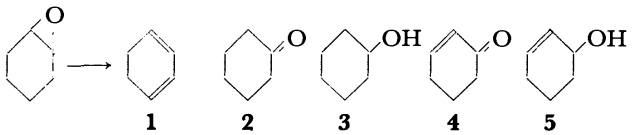

1 **2** **3** **4** **5**

The products are substances expected from studies on the rearrangement of 1-methylcyclohexene oxide (A).[11a] Cyclopentanecarbaldehyde, a ring-contacted aldehyde, which was formed as the main product over molten salts or binary eutectic salts,[3,4] could not be detected, though the corresponding aldehydes were observed on the rearrangements of *d*-limonene (B) and carvomenthene oxides (C) over some of the present catalysts under the same reaction conditions.[11c,g]

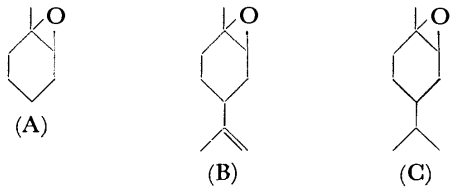

(A) (B) (C)

The catalytic activity and selectivity of several solid acids and bases at 108 °C are given in Table 1. The catalysts were chosen on the basis of activity and selectivity for isomerization of 1-methylcyclohexene[11a,b] and carvomenthene oxides.[11g] The isomerization of 1-methylcyclohexene oxide was suggested to proceed *via* a carbonium ion intermediate.[2] Thus, cyclohexene oxide is considered to require a longer reaction time for the formation of secondary carbonium ions by cleavage of carbon–oxygen bond than 1-methylcyclohexene oxide which forms tertiary carbonium ions on carbon atoms bearing methyl groups. The results meet this expectation.

The time of reaction was so selected that appropriate conversion levels could be achieved. An example of

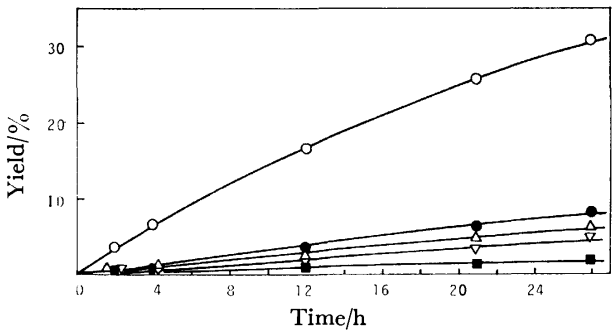

Fig. 1. Isomerization of cyclohexene oxide over TiO_2–ZrO_2 at 108 °C.
1 (△), **2** (■), **3** (▽), **4** (●), **5** (○).

TABLE 1. ISOMERIZATION OF CYCLOHEXENE OXIDE OVER VARIOUS SOLID ACID AND BASE CATALYSTS AT 108 °C

Catalyst	Catalyst amount	Reaction time	Total conversion	Product yields/%					
	g	h	%	**1**	**2**	**3**	**4**	**5**	others
SiO_2–Al_2O_3	0.36	12	29	2	7	1	2	6	12
H_2SO_4/SiO_2	0.26	24	6				1	0.5	5
$FeSO_4$	0.30	34	23	1	6		5	10	1
Solid H_3PO_4	0.41	21	28		7		4	15	1
$LiClO_4$	0.32	3	18	3	10				3
SiO_2–TiO_2	0.24	4	90	40	13	1	4	26	6
SiO_2–TiO_2–MgO	0.28	2	95	48	14	2	5	19	6
$NiSO_4$	0.42	48	11	1	5		1	4	
TiO_2–ZrO_2	0.32	27	51	6	2	5	7	31	
Al_2O_3 A	0.30	1	28	1	1	3	4	19	
Al_2O_3 B	0.18	2	30	1	3	3	6	16	1
Al_2O_3 C	0.39	12	29	2	8	1	10	7	1
Al_2O_3 D	0.20	4	39	3	10	1	8	16	1

time-variation of the products is shown in Fig. 1, where the catalyst is TiO_2–ZrO_2. The yields of all products increased almost parallel to each other during the course of reaction. A similar time-variation was observed for the other catalysts.

Cyclohexanol (**3**) was presumably formed by a hydrogen transfer from **4**, since the corresponding alcohol and α,β-unsaturated ketone were observed with approximately the same yield in the case of 1-methylcyclohexene oxide.[11b] **3** was formed with less yield in comparison with **4** in every case and at any time of reaction. **3** was probably converted into cyclohexene by its readsorption and dehydration on the catalyst surface during reaction periods. However, trace amount of cyclohexene was detected on GLC analysis. The olefin having a lower boiling point (82 °C) as compared with reaction temperature might have evaporated out of the reaction vessel.

In the case of 1-methylcyclohexene oxide, ketone was predominantly formed over SiO_2–Al_2O_3, H_2SO_4/SiO_2, $FeSO_4$, solid H_3PO_4, $LiClO_4$, SiO_2–TiO_2, and SiO_2–TiO_2–MgO, and allyl alcohol over TiO_2–ZrO_2 and Al_2O_3 A, the selectivities being more than 80% in both groups.[11a,b,f] $NiSO_4$ gave both products in the same amount. In the present work, the former catalysts produced unexpectedly large amounts of allyl alcohol, while the three latter catalysts, TiO_2–ZrO_2, Al_2O_3 A, and $NiSO_4$, showed catalytic actions analogous to the case of 1-methylcyclohexene oxide. Allyl alcohol formation is explained by an acid-base bifunctional mechanism.[11b] Strong acid sites are active for the selective formation of ketone,[11a] SiO_2–Al_2O_3,[12] SiO_2–TiO_2,[13] and SiO_2–TiO_2–MgO[11f] being known to have acid sites stronger than $pK_a = -8.2$ on their surfaces. In the present reaction, basic sites on these catalysts seem to play an important role. The slow reaction rate of the epoxide is due to the greater difficulty in formation of secondary carbonium ion intermediates on acid sites than that of the tertiary one for the case of 1-methylcyclohexene oxide. It is likely that the basic sites cause hydrogen abstraction during the course of cleavage of a carbon–oxygen bond by acid sites, even though the basic sites are weak.

In the case of *d*-limonene oxide,[11e] of the fibrillar aluminas Al_2O_3 B, C, and D, Al_2O_3 B predominantly formed allyl alcohols and Al_2O_3 D carbonyl compounds (ring-contracted aldehyde and ketone), both selectivities exceeding 75%, while Al_2O_3 C formed both products in the same amount. In the present case, however, Al_2O_3 D produced a considerable amount of allyl alcohol which can be understood by the above mechanism explaining the formation of allyl alcohol. The selectivities of Al_2O_3 B and C are comparatively close to those expected from the results on *d*-limonene oxide. Al_2O_3 A and B were extremely active for the present isomerization.

A large amount of diene **1** was formed over SiO_2–TiO_2 and SiO_2–TiO_2–MgO, and also in the isomerization of cyclohexene oxide catalyzed by solid acids and bases in gas phase, the diene formation being interpreted by the dehydration of 2-cyclohexen-1-ol.[11d] The results on cyclohexene oxide differ from those on 1-methylcyclohexene oxide. The difference might be caused by the easier readsorption of the present allyl alcohol on the catalyst surface to form the diene as compared with the case of the allyl alcohols formed from 1-methylcyclohexene oxide, because of the steric hindrance of the methyl group for readsorption of the hydroxyl group of the allyl alcohol. The interpretation leads to the observation of a smaller yield of **3** than that of **4**, *viz.*, easy dehydration of **3** on the catalyst surface. The reaction of cyclohexene oxide seems to occur in the following series of parallel and consecutive steps,

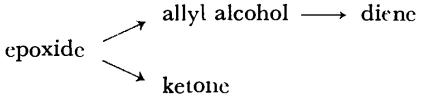

In order to obtain further information on the reaction mechanism, the isomerization of cyclohexene oxide deuterated at the 3 and 6 positions, 1,2-epoxycyclohexane-3,3,6,6-d_4, was performed over Al_2O_3 A and the products were analyzed by combined gas chromatography-mass spectrometry. The product distribution and parent mass number of products are given in Table 2, the reaction scheme being as follows.

Table 2. Isomerization of 1,2-epoxycyclohexane-3,3,6,6-d_4 over Al_2O_3 A[a] and mass number of parent peak of products

Product	**2′**	**3′**	**4′**	**5′**
Yield/%	2	7	10	22
Mass number of parent peak	102	104	99	101

a) The reaction was carried out with 0.1 ml of the epoxide in toluene (0.4 ml) over the catalyst (60 mg) at 108 °C for 2 h. b) 2% of 1,3-cyclohexadiene was observed.

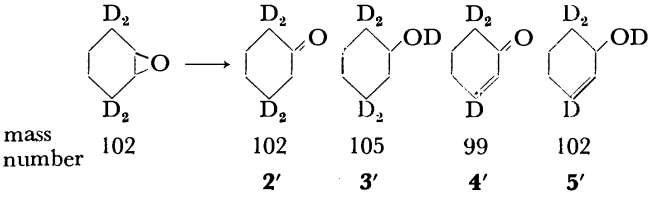

The mass numbers 104 and 101 shown for **3′** and **5′**, respectively, seem to be due to the alcoholic proton D^+ of **3′** and **5′** being exchanged with outer proton H^+ during the course of reaction and analysis. Al_2O_3 A consists of Lewis acid sites.[14] Thus, the exchange of proton between the epoxide and the catalyst surface could be excluded. **3′** and **4′** are considered to be formed by hydrogen (HD) transfers between two molecules of the oxide. Therefore, the above reaction scheme seems to be reasonable.

In order to obtain isotope effects for isomerization over catalysts, the competitive isomerization of deuterated and undeuterated cyclohexene oxide in equiamount was carried out over several catalysts, the products being analyzed by GLC-MS (Table 3). The d_0/d value was taken as the isotope effect for the isomerization of cyclohexene oxide. The primary isotope effect

TABLE 3. COMPETITIVE ISOMERIZATION OF 1,2-EPOXYCYCLOHEXANE AND 1,2-EPOXYCYCLOHEXANE-3,3,6,6-d_4 OVER SEVERAL SOLID ACID AND BASE CATALYSTS AT 108 °C FOR 1 h

Catalyst		Product 2	3	4	5
Al_2O_3 A	Yield/%	3	4	5	18
	d_0/d[a]	4.7	1.2	4.1	2.1
Al_2O_3 D[b]	Yield/%	3		1	2
	d_0/d	3.1		4.6	2.9
SiO_2–TiO_2	Yield/%	12			12
	d_0/d	2.8			3.1
Solid H_3PO_4[c]	Yield/%	16			2
	d_0/d	1.7			

a) Relative intensity of parent peak between undeuterated and deuterated products. b) For 2 h. c) Heat-treated at 200 °C.

of the 3 or 6 position of cyclohexane ring can be seen for the formation of **2**, **4**, and **5**.

The allyl alcohol formation was interpreted in terms of the correlation between activity and acid-base property of catalyst by an acid-base bifunctional mechanism, where an oxygen of epoxide is adsorbed on an acidic site and a hydrogen atom of the methylene group on a basic site.[11] The present isotope effect for **5** supports the reaction mechanism. The isotope effect for dehydration of isobutyl alcohol over Al_2O_3 by acid-base bifunctional mechanism determined to be 2.55 at 170 °C[15] is close to our value.

Ketone formation, however, showed an unexpected primary isotope effect, indicating interaction between a hydrogen at the 3 or 6 position and a basic site on the catalyst surface. The formation of ketone is explained by the isomerization on strong acid sites in consideration of correlation between acid and base properties of catalyst and its selectivity.[11] The cleavage of the oxygen bond takes place by adsorption of oxygen on a strong acid site with a subsequent shift of a hydrogen attached to a carbon atom bearing another oxygen bond. However, the isotope effect decreases in the order Al_2O_3 A, Al_2O_3 D, SiO_2–TiO_2, and solid H_3PO_4 with increase in the selectivity for ketone (Table 3). It can be concluded that ketone is formed selectively when acid sites play a more important role as compared with basic sites. In other words, a molecule of epoxide adsorbs on both an acid and a basic site, the extent of both adsorptions determining the selectivity. When both modes of adsorption are such that both the opening of the epoxide ring and the hydrogen abstraction take place simultaneously, allyl alcohol would be formed, while the cleavage of oxygen bond prior to the hydrogen abstraction would occur to form ketone if the acid is too strong.

Values of the isotope effect for **2** over Al_2O_3 A and D are comparatively large. These catalysts, especially Al_2O_3 A, probably affect the strong interaction between a hydrogen at the 3 or 6 position and a relatively strong basic site on the surface, together with the weak one between an oxygen and a weak acid site. Consequently, the anion formed on carbon would facilitate cleavage of the oxygen bond. However, this case seems to be limited, judging from the low yield of **2** on both aluminas. Since MgO and CaO catalysts, which have a stronger basic character than alumina, were inactive for the isomerization of 1-methylcyclohexene and *d*-limonene oxides,[11] it seems that the oxide ring can not be opened by a basic site only without the effect of an acid site.

The reaction mechanism for the isomerization of cyclohexene oxide over solid acid and base catalysts is shown in the following.

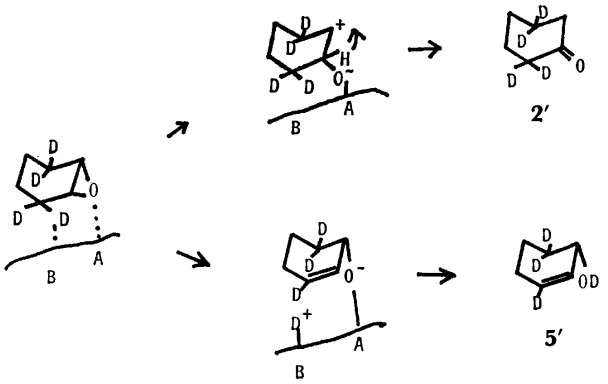

The fact that the isotope effect for **4** is large but that for **3** is small seems to be reasonable in view of the deuterium distributions of products **3'** and **4'** which indicate the HD migration from a molecule of the oxide to another. The products of **3** and **4** were observed over the catalysts giving preferential formation of allyl alcohol. Thus, the intermediate species is considered to be related with the formation of both products.

The authors are indebted to Dr. M. C. Flowers, The University of Southampton, England, for the supply of the sample of 1,2-epoxycyclohexane-3,3,6,6-d_4.

References

1) Epoxide Rearrangement XII. Part XI, see K. Arata J. O. Bledsoe, Jr., and K. Tanabe, *J. Org. Chem.*, **43**, 1660 (1978).

2) S. M. Nagvi, J. P. Horwitz, and R. Filler, *J. Am. Chem. Soc.*, **79**, 6283 (1957).

3) B. Rickborn and R. M. Gerkin, *J. Am. Chem. Soc.*, **90**, 4193 (1968); b) B. Rickborn and R. M. Gerkin, *ibid.*, **93**, 1693 (1971).

4) J. H. Kennedy and C. Buse, *J. Org. Chem.*, **36**, 3135 (1971).

5) J. L. Eisenmann, *J. Org. Chem.*, **27**, 2706 (1962).

6) J. K. Crandall and L. H. Chang, *J. Org. Chem.*, **32**, 435 (1967).

7) C. L. Kissel and B. Rickborn, *J. Org. Chem.*, **37**, 2061 (1972).

8) M. C. Flowers, D. E. Penny, and J. C. Pommelet, *Int. J. Chem. Kinet.*, **5**, 353 (1973).

9) V. S. Joshi, N. P. Damodaran, and S. Dev, *Tetrahedron*, **27**, 459 (1971).

10) K. Tanabe, "Solid Acids and Bases," Academic Press, New York/London (1970).

11) (a) K. Arata, S. Akutagawa, and K. Tanabe, *Bull. Chem. Soc. Jpn.*, **48**, 1097 (1975); (b) K. Arata, S. Akutagawa, and K. Tanabe, *ibid.*, **49**, 390 (1976); (c) K. Arata, S. Akutagawa and K. Tanabe *J. Catal.*, **41**, 173 (1976); (d) K. Arata, K. Kato, and K. Tanabe, *Bull. Chem. Soc. Jpn.*, **49**, 563 (1976); (e) K. Arata and K. Tanabe, *Chem. Lett.*, **1976**, 321; (f) T. Yamada, K. Arata, M. Itoh, H. Hattori, and K. Tanabe, *Bull. Chem. Soc. Jpn.*, **49**, 2946 (1976); (g) K. Arata, S. Akutagawa, and K. Tanabe, *ibid.*, **51**, 2289 (1978).

12) H. A. Benesi, *J. Phys. Chem.*, **61**, 970 (1957).

13) M. Itoh, H. Hattori, and K. Tanabe, *J. Catal.*, **35**, 225 (1974).

14) Ref. 10, p. 48.

15) H. Knözinger and A. Scheglila, *J. Catal.*, **17**, 252 (1970).

Isomeric Transition-activated ^{80}Br and ^{82}Br Reactions in the Gaseous CH_3Br–HBr System

Kenjiro KONDO** and Masuo YAGI*

Laboratory of Nuclear Science, Faculty of Science, Tohoku University, Mikamine 1, Sendai 982

(Received February 9, 1979)

The isomeric transition(IT)-activated ^{80}Br and ^{82}Br reactions in the gaseous $H^{80m}Br$–CH_3Br and $H^{82m}Br$–CH_3Br systems have been compared and the roles of the charge and kinetic energy imparted to ^{80}Br and ^{82}Br in recombina tion reactions studied using a Kr moderator. The products CH_3Br, CH_2Br_2, $CHBr_3$, and CH_3CH_2Br in both reactions are only formed *via* thermal ionic processes. This differs from the $^{82m}BrBr$–CH_3Br system, in which the reaction products are only formed through excess kinetic energy processes. The difference between the two reactions has been explained on the basis of the cross sections for charge neutralization and ion molecule reactions of Br^+ ions as a function of the kinetic energy initially imparted to the ^{80}Br or ^{82}Br atoms. An isotope effect has been observed between the IT-activated ^{80}Br and ^{82}Br reactions with CH_3Br, and attributed to the difference in the decay modes of ^{80m}Br and ^{82m}Br. Furthermore, the analysis of product yields due to the successive internal conversion process in ^{80m}Br suggested that the second Auger process from the excited ^{80}Br occurs in a liquid-like condition such as ion-clusters.

Generally, the radioactive bromine atoms produced by a variety of nuclear transformations have an appreciable recoil kinetic energy and charges. Many investigations have been made in order to evaluate and interpret the kinetic energy and charges in the recombination reactions of radioactive bromine atoms in the gas phase.[1-11] It has been demonstrated that the formation of the C–*Br bond by the reactions of (n,γ)[11-13] and/or fission[14] activated energetic bromine with CH_4 proceeds principally through kinetic energy processes, and that not only kinetic energy but also the charges of IT-activated ^{80}Br and ^{82}Br in the $^{80m}Br_2$ and/or $^{82m}Br_2$–CH_4 system play important roles in determining the chemical reactions of these atoms.[5-9] Furthermore the authors have recently reported that IT-activated ^{80}Br and ^{82}Br in the $H^{80m}Br$–CH_4 and $H^{82m}Br$–CH_4 systems undergo only thermal ionic reactions (kinetic energy independent).[1-4] Since the kinetic energy imparted to the ^{80}Br and ^{82}Br by molecular explosion processes following the internal conversion in HBr molecule is 0.75 eV on average,[15] being very small compared with that (40.3 eV)[16] for the IT in $^{80m}Br_2$ and/or $^{82m}Br_2$, this indicates that the organic yields by thermal ionic processes are largely dependent on the kinetic energy of the positively charged $*Br^+$ ion.

This paper will report the contribution of the charge and kinetic energy of IT-activated ^{80}Br and ^{82}Br to the organic product yields in the $H^{80m}Br$–CH_3Br and $H^{82m}Br$–CH_3Br systems, by comparing the results previously reported for the reactions of CH_3Br with *Br activated by (n,γ)[11] and IT[11,17,18] in Br_2. An isotope effect between thermal ionic ^{80}Br and ^{82}Br reactions has been found in the $H^{80m}Br$–CH_4 and $H^{82m}Br$–CH_4 systems,[1] and a similar isotope effect between the IT-activated ^{80}Br and ^{82}Br reactions with CH_3Br using HBr as a source molecule will be reported.

Experimental

Materials. The listed purities of gaseous reagents, supplied by Takachiho Chemical Co., were 99.95% for Kr and 99.5% for CH_3Br. Krypton gas was used without further purification and CH_3Br was purified by a vacuum distillation technique so that the impurity was reduced below less than 0.1% for gas chromatographic analysis. The ^{80m}Br and ^{82m}Br labeled HBr were prepared by procedures described previously.[1,2,4]

Sample Preparation. The gaseous samples were prepared in the same manner as reported elsewhere.[1,2,4] The reaction mixtures were sealed in cylindrical Pyrex glass ampoules or breakable glass tubes using a vaccum line. The ratio of HBr to CH_3Br and the total pressure were maintained constant at 0.1 ± 0.01 and 660 ± 30 mmHg,† respectively, throughout the series of gas phase experiments. In the solid phase experiments, the reaction gases of HBr (^{80m}Br-labeled) (200 mmHg) and CH_3Br (700 mmHg) were mixed thoroughly by the freeze-thaw method and solidified at liquid nitrogen temperature.

Product Analysis and Yield Determination. The details concerning product analysis and yield determination have been reported elsewhere.[1,2,4]

The experimental errors due to the standard deviation for counting statistics and chemical procedures were estimated as 5—9% for the organic yields in the ^{80m}Br-experiments and less than 10% for those in the ^{82m}Br-experiments.

Results and Discussion

Role of Charge and Kinetic Energy of IT-Activated ^{80}Br and ^{82}Br in Product Formation. The conventional method for discriminating between the charge contribution and the kinetic energy of bromine in the reactions of product formation is the addition of an inert gas to the system. The yield of products formed through kinetic energy processes is expected to decrease by the addition of an inert gas due to the removal of Br kinetic energy by the moderation effect. Hence, a yield which is insensitive to the addition of an inert gas is considered to be due to thermal ionic processes.

Krypton was used as the moderator which has an ionization potential of 13.99 eV, (Br (11.84 eV)), and a mass almost equal to that of Br. Kr therefore appears to be the most effective moderator for energetic Br atoms and appropriate for distinguishing between the yields

** Present address: National Laboratory for High Energy Physics, Oho-machi, Tsukuba-gun, Ibaraki 300-12.

† 1 mmHg≈133.3 Pa.

from kinetic processes and thermal ionic processes.

The effect of Kr as an additive on the product yield distributions in the $H^{80m}Br$–CH_3Br and $H^{82m}Br$–CH_3Br systems is summarized in Tables 1 and 2, and also illustrated in Figs. 1 and 2. The ^{80}Br and ^{82}Br labeled CH_3Br, CH_2Br_2, C_2H_5Br, and $CHBr_3$ were identified as the reaction products in both systems. The products

Table 1. Percentage of ^{80}Br stabilized in organic combinations in a gaseous mixture of HBr, CH_3Br, and Kr[a]

X_{Kr}[b]	Product yield %			Org. yield %
	CH_3Br	CH_2Br_2	Other	
0	2.6±0.2	1.3±0.1	0.8±0.1	4.8±0.2
0	2.4±0.1	1.5±0.1	0.6±0.1	4.5±0.2
0	—	—	—	4.5±0.2
0	2.5±0.1	1.3±0.1	0.5±0.1	4.3±0.4
0.1	2.1±0.2	1.4±0.1	0.6±0.1	4.1±0.2
0.1	2.4±0.2	1.4±0.1	0.8±0.1	4.6±0.2
0.1	2.4±0.2	1.3±0.1	0.7±0.1	4.4±0.3
0.2	2.3±0.1	1.3±0.1	0.8±0.1	4.4±0.4
0.3	2.5±0.2	1.3±0.1	0.5±0.1	4.2±0.4
0.3	—	—	—	4.1±0.4
0.4	2.4±0.2	1.3±0.1	0.8±0.1	4.5±0.3
0.5	2.5±0.2	1.5±0.1	0.6±0.1	4.6±0.3
0.5	—	—	—	4.4±0.3
0.6	2.2±0.1	1.7±0.1	0.4±0.1	4.3±0.2
0.7	1.7±0.1	2.1±0.2	0.3±0.1	4.2±0.3
0.7	—	—	—	4.3±0.3
0.8	1.9±0.1	2.2±0.2	0.5±0.1	4.6±0.3

a) $H^{80m}Br/CH_3Br=0.1\pm0.01$. b) Mole fraction of krypton.

Table 2. Percentage of ^{82}Br stabilized in organic combinations in a gaseous mixture of HBr, CH_3Br, and Kr[a]

X_{Kr}[b]	Product yield %			Org. yield %
	CH_3Br	CH_2Br_2	Other	
0	3.9±0.2	1.1±0.1	0.3±0.1	5.3±0.2
0	3.9±0.3	1.3±0.1	0.2±0.1	5.4±0.2
0	—	—	—	5.4±0.3
0	3.5±0.2	1.4±0.1	0.1±0.1	4.9±0.2
0.1	3.8±0.2	1.1±0.1	0.2±0.1	5.1±0.2
0.2	—	—	—	5.0±0.4
0.2	3.4±0.3	1.4±0.1	0.2±0.1	5.1±0.3
0.3	3.8±0.3	1.4±0.1	0.2±0.1	5.4±0.3
0.3	3.6±0.3	1.3±0.1	0.4±0.1	5.3±0.2
0.3	—	—	—	5.5±0.5
0.4	3.7±0.2	1.2±0.1	0.3±0.1	5.2±0.2
0.5	3.8±0.3	0.9±0.1	0.1±0.1	4.8±0.2
0.5	3.5±0.3	1.5±0.1	0.3±0.1	5.3±0.2
0.6	—	—	—	5.0±0.4
0.6	3.7±0.3	1.2±0.1	0.2±0.1	5.1±0.3
0.7	—	—	—	5.4±0.5
0.7	3.4±0.3	1.3±0.1	0.3±0.1	5.0±0.2

a) $H^{82m}Br/CH_3Br=0.1\pm0.01$. b) Mole fraction of krypton.

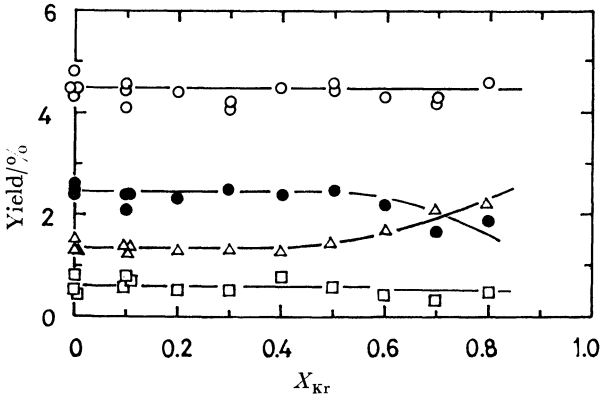

Fig. 1. Effect of Kr additive on the yield distribution in the $H^{80m}Br$–CH_3Br system.
$HBr/CH_3Br=0.1\pm0.01$, ○: organic yield, ●: $CH_3{}^{80}Br$, △: $CH_2{}^{80}BrBr$, □: other.

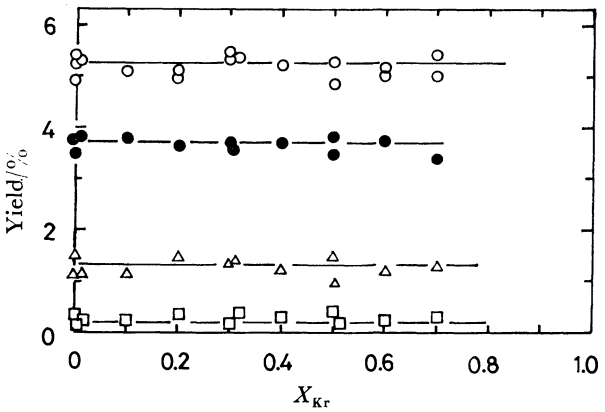

Fig. 2. Effect of Kr additive on the yield distributions in the $H^{82m}Br$–CH_3Br system.
$HBr/CH_3Br=0.1\pm0.01$, ○: organic yield, ●: $CH_3{}^{82}Br$, △: $CH_2{}^{82}BrBr$, □: other.

were similar to those found previously for (n,γ)-[11] and IT-[17,18] activated ^{80}Br and ^{82}Br reactions in the Br_2–CH_3Br system. The C_2H_5Br and $CHBr_3$ yields are listed as the other product yield (the 4th column) in the Tables. The $C_2H_5{}^{82}Br$ yields were less than 0.1% in most cases, while the $CHBr_2{}^{80}Br$ yields were approximately 60 to 80% of the other yield. As is shown in Figs. 1 and 2, the product yield distributions was not altered by the addition of Kr in the range 0—0.5 mole fraction indicating that the reaction products in both systems are formed only through thermal ionic processes, similar to the results observed in the $H^{80m}Br$–CH_4[1] and $H^{82m}Br$–CH_4[2] systems. The thermal ionic yields of CH_3Br and CH_2Br_2 at 0 mole fraction of Kr were 3.8% and 1.3% for the ^{82m}Br system, and 2.4% and 1.5% for the ^{80m}Br system, respectively.

Oate *et al.*,[17] and Okamoto and Tachikawa[18] have reported that the IT-activated ^{82}Br in the $^{82m}BrBr$–CH_3Br system undergoes only kinetic energy dependent reactions. Similarly, Spicer and Gordus[11] have pointed out that the (n,γ)-activated ^{80}Br in the same system reacts to give the products through kinetic energy processes. The present results are however largely different from the above earlier findings. The present

Table 3. Percentage yields of organic products due to kinetic and thermal ionic processes in the IT and (n,γ) experiments[a]

		$H^{82m}Br$–CH_3Br[b]	$H^{80m}Br$–CH_3Br	$^{82m}BrBr$–CH_3Br		(n,γ)-Activated[e] ^{80}Br–CH_3Br
E_{max}/eV		1.3	1.3	158		417
Org. yield/%		5.3	4.5	2.3[c]	5.9[d]	4.0
Kinetic process	CH_3Br/%	0	0	1.5[c]	4.6[d]	3.0
	CH_2Br_2/%	0	0	0.8[c]	1.3[d]	1.0
Thermal ionic process	CH_3Br/%	3.8	2.4	0	0	0
	CH_2Br_2/%	1.3	1.4	0	0	0

a) HBr or $Br_2/CH_3Br=0.1\pm0.01$. b) Present work. c) Ref. 17. d) Ref. 18. e) Ref. 11, $Br_2=0.0254$ mole fraction.

authors have pointed out that the product yields due to both kinetic and thermal ionic processes largely depend on the Br kinetic energy acquired initially as results of a nuclear event.[1,2] The maximum kinetic energies (E_{max})[15] of Br for (n,γ) and IT in HBr and Br_2 are shown in Table 3. In contrast to the present results, there is no contribution of thermal ionic reaction to the product formation in both (n,γ)[11] and IT[17,18] in Br_2 because of the large values of E_{max}. This difference suggests that there is a close relationship between the kinetic energy of Br and the yields due to both thermal ionic and kinetic energy processes. The yields due to thermal ionic reactions are largely dependent on the number of Br^+ ions reaching the thermal energy region by escaping from the charge neutralization.[1-4] Therefore it is of paramount importance to estimate the cross sections for charge neutralization and ion-molecule (capture collision) reactions as a function of the kinetic energy of Br^+ in the present systems. These relationships are shown in Fig. 3. The cross sections (σ) for capture collision between Br^+ and CH_3Br were calculated from the following equation,[20] which is applicable for ions with a kinetic energy <1 eV.

$$\sigma = (2\pi e/v)(\alpha/\beta) + (2\pi e/v^2)(\mu/m)$$

where v is the relative velocity of Br^+, e the charge on the ion, α the polarizability of CH_3Br (2.8×10^{-24} cm^3/mol),[21] m the mass of Br^+, β the reduced mass of collision pair, and μ the dipole moment of CH_3Br (1.45×10^{-18} esu. cm).[22] The cross sections for resonant charge transfer reaction between Br^+ and Br, which are the highest of several types of charge neutralization concerning Br^+, were obtained by interpolating the resonant charge transfer cross sections at intermediate impact velocity (10^5—10^8 cm/s) as calculated by Rapp and Francis using the semi-classical impact-parameter method.[23] Furthermore, V_{max}, giving the maximum cross sections for asymmetric charge transfer reactions of ground state Br^+ with CH_3Br, Kr, and HBr, were calculated from the "adiabatic rule."[24] V_{max} for CH_3Br is 2.2×10^7 cm/s, 3.5×10^6 for HBr, and 3.6×10^7 for Kr. The threshold velocity (V_{th})[25] of Br^+ for endo-energetic charge transfer reaction with Kr was obtained as 2.3×10^5 cm/s. The dotted line in Fig. 3, showing the velocity dependence of cross sections for the charge transfer reactions of Br^+ with Kr, is drawn on the basis of values of V_{max} and V_{th}, assuming that the asymmetric charge transfer cross section is close to that for the resonance charge transfer at velocities above V_{max}.[23] The charge transfer reactions of the ground state Br^+ with HBr and CH_3Br are exothermic, 0.2 and 1.3 eV respectively. In consideration of the vibrationally excited states of those molecules, it is expected that the charge neutralization of Br^+ takes place effectively, and its cross section is close to that of the resonant charge transfer between Br^+ and Br. The thus formed neutral Br cannot however enter into chemical combination *via* kinetic energy processes because the kinetic energy is not sufficient to substitute for H and/or Br in the CH_3Br molecule. The values of E_{max} for (n,γ) and IT in HBr and Br_2 are shown by arrows in the upper abscissa of the Fig. 3.

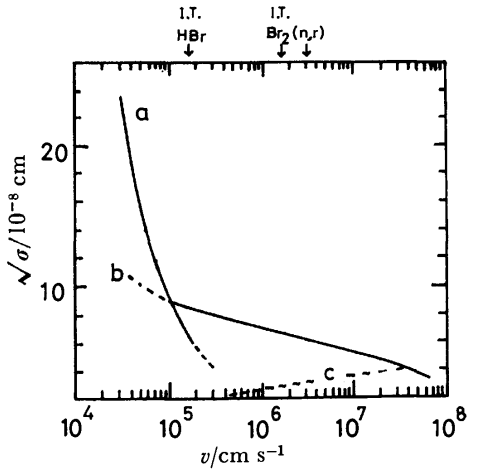

Fig. 3. Relationship between the velocity of $*Br^+$ and cross sections for capture collision and charge neutralization.
a: Capture collision; $*Br^+ + CH_3Br \rightarrow CH_3Br*Br^+$, b: resonant charge transfer; $*Br^+ + Br \rightarrow *Br + Br^+$, c: $Br^+(^3P_2) + Kr \rightarrow Br + Kr^+$.

Figure 3 indicates that the charge transfer reactions occur predominantly in the energy range >1 eV, while the formation of the capture collision complex is favoured at energies <1 eV. It is readily seen therefore that the Br atoms produced by (n,γ) and IT in Br_2 undergo charge neutralization before reaching the reaction range because of the large values of E_{max}. The average kinetic energy of Br in the case of IT in HBr is only 0.75 eV,[15] which is very small compared with that for (n,γ) and IT in Br_2. It is presumed therefore that the formation of the capture collision complex competes with the charge neutralization under the present experimental

systems using HBr as a source molecule, and a part of $*Br^+$ which escapes charge neutralization reacts with CH_3Br to form the capture collision complex, CH_3Br*Br^+. This complex ion is thought to be a precursor for product formation *via* a thermal ionic process as will be described in the following section.

Isotope Effect in the Reactions of IT-Activated ^{80}Br and ^{82}Br with CH_3Br. As Figs. 1 and 2 illustrate, the organic yields were a little larger in the $H^{82m}Br$–CH_3Br system than in the $H^{80m}Br$–CH_3Br system. An outstanding difference between the results in both systems was found in the yield distribution of individual products. The yield ratios of CH_3Br to CH_2Br_2 were 3.0±0.5 for ^{82m}Br and 1.8±0.2 for ^{80m}Br at 0 mole fraction of Kr. Evidently there is an isotope effect between the thermal ionic reactions of IT-activated ^{80}Br and ^{82}Br in the gaseous HBr–CH_3Br system. The mass difference between ^{80}Br and ^{82}Br cannot be considered to be responsible for the above isotope effect and therefore the isotope effect may be attributed to the differences in the decay modes of ^{80m}Br and ^{82m}Br.[19]

The de-excitation of ^{82m}Br to the ground state occurs in a single step and is fully converted. The ^{80m}Br however is de-excited in two successive steps through an intermediate state with a half-life of 7.4 ns; the first step is fully converted and the second, partially converted (61%). Since the first de-excitation step of ^{80m}Br is essentially the same as that of ^{82m}Br, the charge and kinetic energy distribution on the excited ^{80}Br should be identical with those on the ^{82}Br. Furthermore, the excited ^{80}Br undergoes successive de-excitation to the ground state; 61% of the excited ^{80}Br is de-excited through the second internal conversion process, while the remaining 39% is directly de-excited to the ground state by means of a 37 keV gamma-ray emission. The chemical effect due to this gamma-emission is however considered to be negligible since the kinetic energy achieved on the ^{80}Br is of the order of 10^{-2} eV. On the basis of the foregoing the reaction processes of IT-activated ^{80}Br may be classified into two types:[1,3]

Process (A); 39%, internal conversion (IC)
+ 37 keV gamma-ray emmission

Process (B); 61%, IC + IC

The chemical effects due to process (A) are essentially identical with those of the ^{82m}Br, and therefore the yields due to process (A) are equal to 39% of those obtained in the ^{82m}Br. Hence the normalized yields due to process (B) may be calculated by the following equation.

Yield/% due to process (B) = 100/61(^{80m}Br-yield − 39% of ^{82m}Br-yield)

and are depicted in Fig. 4. The isotope effect in both systems may be elucidated by comparing the yields due to process (B) with those due to the ^{82m}Br.

As Fig. 4 shows, the $CH_3{}^{80}Br$ and $CH_2{}^{80}BrBr$ yields were constant in the range 0—0.6 mole fraction of Kr, indicating that the products due to process (B) are also formed through kinetic energy independent processes. The yield ratio of CH_3Br to CH_2Br_2 was between 0.9

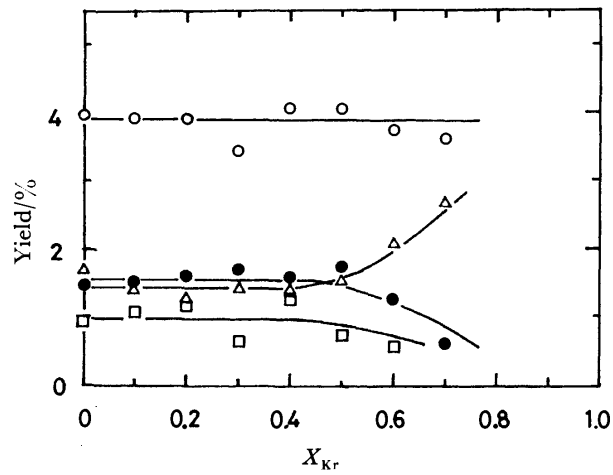

Fig. 4. Effect of Kr additive on the product yield distributions due to process (B).
○: Organic yield, ●: $CH_3{}^{80}Br$, △: $CH_2{}^{80}BrBr$, □: other.

and 1.3 for 0.6 mole fraction of Kr, being largely different from that due to the ^{82m}Br (3.0). The other product yields due to process (B) were much higher compared to those due to the ^{82m}Br.

Assuming the excited ^{80}Br does not react within its life time (1.1×10^{-8} s), and/or assuming that the excited ^{80}Br forms chemical combinations, such as $H*Br$, H_2*Br, $H*Br^+$, *etc.*, the chemical effect due to the successive IC (process B) should also be identical to that due to the ^{82m}Br because the following IC leads to an additional build-up of the charge on the free atom, and/or the kinetic energy of ^{80}Br resulting from the molecular explosion in such a species is very small. In this case, an isotope effect will be absent.

Assuming the excited ^{80}Br reacts with the surroundings to form a C–*Br and/or Br–*Br combination prior to the second IC, the resulting ^{80}Br by successive IC acquires an appreciable kinetic energy and undergoes kinetic energy dependent reactions. As Fig. 4 illustrates, the experimental results show that there is no contribution to the yield by excess kinetic energy processes, *i.e.*, these chemical species will not be present in process (B). The existence of an isotope effect suggests that the life-time of the excited $^{80}Br^+$ (1.1×10^{-8} s) is sufficiently long to form some chemical species containing the excited $^{80}Br^+$. The environment surrounding the excited ^{80}Br is thought to be different from those for the ions present as single species. Accordingly, it has been concluded that the $^{82}Br^+$ and excited $^{80}Br^+$ undergo capture collision complex formation (Reactions 1a and 2). Typically this type of ion-molecule reaction does not require any activation energies.[1,2]

$$*Br^+ + CH_3Br \longrightarrow CH_3Br*Br^+ \quad (1a)$$

$$*Br^+ + HBr \longrightarrow HBr*Br^+ \quad (2)$$

Furthermore, the thermal complex ions have an ample opportunity to interact with the surroundings within the life-time of the excited ^{80}Br[26] since the life-time is relatively long compared to the collision time under the present experimental conditions.[27]

It is generally known that at high pressure thermal ions preferentially form ion-clusters by electro-static forces.[28-30] The authors have demonstrated that the isotope effect observed in the $H^{80m}Br$–CH_4 and $H^{82m}Br$–CH_4 systems may be explained by introducing the above cluster model.[1,3] The complex ions formed by the above reactions undergo successive attachment reactions with surrounding molecules to form ion-clusters, and the second IT in process (B) proceeds in a liquid-like condition such as ion-clusters. Thus the chemical effect due to process (B) is expected to be very similar to that in the condensed phase. Table 4 shows the results obtained in the solidified $H^{80m}Br$–CH_3Br system. The yield ratio of CH_3Br to CH_2Br_2 was 0.8, which compare favourably with the values of 0.9–1.3 for process (B). This indicates that the chemical effect due to process (B) is very similar to that in the solid phase, which qualitatively supports the above cluster model. The large amount of energy evolved from the second molecular explosion in process (B) is dissipated to the rigid sphere of the cluster and used in the formation of ions, radicals and excited species, which contribute directly or indirectly to individual product formation.

TABLE 4. THE YIELD RATIO OF INDIVIDUAL PRODUCTS RELATIVE TO CH_3Br IN THE SOLIDIFIED $H^{80m}Br$–CH_3Br SYSTEM

Product	CH_3Br	C_2H_5Br	CH_2Br_2	$C_2H_4Br_2$	$CHBr_3$
Relative yield ratio	1	<0.1	1.3	0.2	0.4

There is little precise information on the ion-molecule reactions leading to the $CH_3{}^*Br$ and $CH_2Br{}^*Br$ in process (A) because of a lack of knowledge concerning the chemical behaviour of the complex ion ($CH_3Br{}^*Br^+$) under high pressure. The following reactions are considered to be possible reaction routes for the formation of the above products from thermodynamics.

$$CH_3Br{}^*Br^+ \longrightarrow CH_3{}^*Br^+ + Br \qquad (1b)$$

$$CH_3Br{}^*Br^+ + HBr \longrightarrow CH_2Br{}^*Br + H_2Br^+ \qquad (3)$$

$$CH_3Br{}^*Br^+ + CH_3Br \longrightarrow CH_2Br{}^*Br + CH_4Br^+ \qquad (4)$$

The heat of reaction for the above reactions has been calculated approximately as 29, 65, and 87 $kcal_{th}$††/mol (exothermic) for Reactions 1a, 1b, 3, and 4, respectively.[32]

The second IC in process (B) proceeds *via* an ion-cluster, so that the molecular explosion following the second IC is responsible for the chemical effect due to process (B). Although no information on the IT-activated ^{80}Br reactions under such specific conditions is available, both ion-molecule reactions and the reactions concerning radicals and excited species produced in the clusters appear to be responsible for product formation in analogy with the results previously obtained in the $H^{80m}Br$–CH_4 system.[1,3] The details of such reactions must however await further analysis.

The authors would like to thank the staff of the Hot Laboratory, Research Reactor Institute, Kyoto University, who assisted in the neutron irradiations and provided the research facilities.

†† 1 cal_{th} = 4.184 J.

References

1) K. Kondo and M. Yagi, *Bull. Chem. Soc. Jpn.*, **51**, 1284 (1978).
2) K. Kondo and M. Yagi, *Bull. Chem. Soc. Jpn.*, **51**, 372 (1978).
3) K. Kondo and M. Yagi, *Bull. Chem. Soc. Jpn.*, **52**, 225 (1979).
4) M. Yagi and K. Kondo, *Radiochem. Radioanal. Lett.*, **14**, 123 (1973).
5) M. Yagi, K. Kondo, and T. Kobayashi, *Bull. Chem. Soc. Jpn.*, **44**, 580 (1971).
6) J. B. Nicholas and E. P. Rack, *J. Chem. Phys.*, **48**, 4085 (1968).
7) E. Tachikawa and T. Kahara, *Bull. Chem. Soc. Jpn.*, **43**, 1293 (1970).
8) E. Tachikawa, *Bull. Chem. Soc. Jpn.*, **42**, 2304 (1970).
9) E. Tachikawa and J. Okamoto, *Radiochim. Acta*, **13**, 159 (1970).
10) E. Tachikawa, *Bull. Chem. Soc. Jpn.*, **43**, 63 (1970).
11) L. D. Spicer and A. A. Gordus, "Symposium on Chemical Effects Associated with Nuclear Reactions and Radioactive Transformations," IAEA, Vienna (1965), Vol. 1, p. 185.
12) E. P. Rack and A. A. Gordus, *J. Phys. Chem.*, **65**, 944 (1961).
13) M. Saeki, K. Numakura, and E. Tachikawa, *Bull. Chem. Soc. Jpn.*, **45**, 1715 (1962).
14) H. D. Sirblet and R. H. Tomlinson, *Radiochim. Acta*, **5**, 217 (1966).
15) M. E. Berg, W. H. Grauer, R. W. Helton, and E. P. Rack, *J. Phys. Chem.*, **79**, 1327 (1975).
16) A. R. Kazanjian and W. F. Libby, *J. Chem. Phys.*, **42**, 277 (1965).
17) D. W. Oates, R. L. Ayers, R. W. Helton, K. S. Schwarts, and E. P. Rack, *Radiochem. Radioanal. Lett.*, **4**, 123 (1970).
18) J. Okamoto and E. Tachikawa, *Bull. Chem. Soc. Jpn.*, **42**, 1504 (1969).
19) C. M. Leaderer, J. M. Hollander and I. Perlman, "Table of Isotopes," John Wiley and Sons, New York (1968), pp. 215, 217.
20) J. V. Dugan, Jr., and J. L. Magee, *J. Chem. Phys.*, **47**, 3103 (1967).
21) The value (σ) was calculated using the Clausius-Mossotti equation; dielectric const ε for CH_3Br = 1.00095.
22) W. J. Moor, "Physical Chemistry," (Japanese Translation), Tokyo Kagakudojin (1961), p. 337.
23) D. Rapp and W. E. Francis, *J. Chem. Phys.*, **37**, 2631 (1962).
24) D. Seewald and R. Wolfgang, *J. Chem. Phys.*, **47**, 143 (1967).
25) C. F. Giese and W. B. Maier, *J. Chem. Phys.*, **39**, 197 (1963).
26) "Mass Spectrometry of Organic Ions," ed by F. Mclafferty, Academic Press, New York (1963), p. 65.
27) M. Burton and J. L. Magee, *J. Phys. Chem.*, **56**, 842 (1952).
28) S. C. Lind, "The Chemical Effects of Alpha Particles

and Electrons," Chemical Catalog Co., New York (1928), p. 663.
29) "Ion Molecule Reactions," ed by J. L. Franklin, Plenum Press, New York (1972), Vol. 1, p. 315.
30) J. L. Magee and L. Funabashi, *Radiat. Res.*, **10**, 633 (1959).
31) S. Bloom and H. Margenau, *Phys. Rev.*, **85**, 670 (1952).
32) The thermodynamic values used for the calculation were taken from the following references: a) J. L. Beauchamp, *Ann. Rev. Phys. Chem.*, **22**, 527 (1971); b) V. I. Vedoneyev, L. V. Guvvich, V. N. Kondratyev, V. A. Medvedev, and Ye. L. Frankevich, "Bond Energies, Ionization-Potentials and Electron Affinities," (English Translation), Edward Arnold Ltd., London (1966); c) F. W. Lampe, J. L. Franklin, and F. H. Field, "Progress in Reaction Kinetics," ed by G. Porter, Pergamon Press, New York (1961), Vol. 1, p. 67.

The Isomerization of *cis*-2-Butene over SO_2-adsorbing $Mg(OH)_2$ and MgO

Kiyoshi Otsuka,* Kimiaki Tanaka, and Akira Morikawa

Department of Chemical Engineering, Tokyo Institute of Technology, Ookayama, Meguro-ku, Tokyo 152

(Received April 18, 1979)

The reaction of butenes caused by the surface compounds formed from SO_2 on $Mg(OH)_2$ or MgO has been studied. It has been shown that the cis-trans isomerization of 2-butene is selectively induced by the sulfur compounds. This specific isomerization has been explained by the previously proposed mechanism that the reaction is accompanied by the copolymerization of 2-butene and SO_2. The infrared spectroscopic study on the sulfur compounds formed on $Mg(OH)_2$ or on MgO has demonstrated the presence of SO_3^{2-}, SO_4^{2-}, or sulfinato complexes. The formation of these surface species may cause a strong electrostatic field on the surface, resulting in the polarization of reactant molecules, which is necessary for the initiation of the copolymerization or of the cis-trans isomerization. It has been shown, however, that the presence of weakly adsorbed SO_2 is essential for determining the catalytic activities of the solids in the SO_2-induced isomerization.

The need to understand gas-aerosol reactions in the atmosphere stems from the potential impact of such reactions on atmospheric chemistry, as well as their contribution to atmospheric haze formation and health effects attributable to aerosols in the respirable size range. Heterogeneous reactions of SO_2 and the contribution of the reactions to atmospheric sulfate aerosol are considered to be important to the over all pollution problem.[1-4] There are many reports which relate to the reactions between SO_2 and various solid particulates likely to be found in the polluted atmosphere.[5-12] However, very little is known about the possible, thermal reactions of SO_2 with hydrocarbons over solid particulates.

Preliminary experiments showed that the addition of SO_2 onto such solids as SiO_2, Al_2O_3, Fe_2O_3, CaO, $Ca(OH)_2$, MgO, or $Mg(OH)_2$, all of which are likely to be found in urban aerosols, causes the isomerization of butene. The most active solids to the reaction were MgO and $Mg(OH)_2$. Hence, we intend to report here the reaction over $Mg(OH)_2$ and MgO in the presence of the sulfur compounds on their surfaces formed from SO_2, which were confirmed by infrared spectroscopic measurement. The reaction mechanism and the nature of the active sites will also be discussed.

Experimental

Materials. The $Mg(OH)_2$ used in these experiments was reagent-grade powder from the Kanto Chemical Co., Inc. The reagent SO_2 gas, of anhydrous grade and supplied by the Matheson Chemical Co., and *cis*-2-butene gas, a high-purity product of the Phillips Petroleum Co., were purified by the freeze-pump technique.

Procedure. In the infrared spectroscopic experiments, a self-supporting $Mg(OH)_2$ wafer was made by pressing powder (about 15 mg) in 2-cm-diameter stainless steel discs at 2.7 t/cm^2. The wafer was then placed into the IR-cell for pretreatment and spectroscopic measurements. The sample wafer was degassed in a vacuum with increasing temperature to a required value between 100 and 600 °C. The rate of heating was 10 °C/min. Evacuation was further kept at the fixed temperature for 2 h. After the base-line spectrum of the wafer had been recorded at 20 °C, a known amount of SO_2 was adsorbed onto the wafer at the same temperature. Then the wafer was degassed in a vacuum for 3 min through a cold trap immersed in liquid nitrogen. After these procedures, the spectra of the sulfur compounds on the wafer were recorded. The amount of SO_2 remaining on the solid was calculated by the mass valance of the amount of SO_2 introduced and the amount of collected in a liquid nitrogen trap. A Shimadzu IR-430 grating spectrometer was used for all the infrared measurements.

The relative absorbance of the sulfur compounds, OD_s, on an unit surface area of the wafer was calculated by assuming the following, modified Lambert-Beer law equation,

$$OD_s = \left(\log \frac{I_0}{I}\right) \Big/ A = \varepsilon CW/A \qquad (1)$$

where I_0 represents the light intensity transmitted through the wafer of W in weight with a surface area of A (cm^2/g) in the absence of SO_2, I is the intensity of light transmitted through the wafer which contains the sulfur compounds of the concentration C (mol/g), and ε is the molar extinction coefficient.

The adsorption experiments were carried out volumetrically using a conventional closed system 119 cm^3 in volume. The BET surface area of the $Mg(OH)_2$ pretreated at different temperatures were determined by means of the nitrogen adsorption. The molecular cross sections of N_2 and SO_2 were taken as 16.2 and 19.2 Å^2 respectively.[13]

The isomerization of *cis*-2-butene in the presence or absence of SO_2 was carried out in a gas-circulation system with a volume of 210 cm^3. After the pretreatment of $Mg(OH)_2$ ($\approx$0.20 g), the reaction was started at 20 °C by feeding and circulating *cis*-2-butene gas at the pressure of 85 Torr, through the catalyst bed. A small amount of the reactant gas was periodically sampled and analyzed by gas chromatography. The initial rates of the isomerization were calculated from the concentration of the butene isomers formed in the initial 3 min. In the case of the SO_2-induced isomerization, a required amount of SO_2 was preadsorbed on the solid at 20 °C after the pretreatment of $Mg(OH)_2$. The solid was then evacuated slightly for 3 min before the addition of the reactant gas.

Results and Discussion

The State of the Catalyst after the Pretreatment. The state of the $Mg(OH)_2$ after evacuation pretreatment for 3 h at different temperatures has been examined by X-ray analysis. The results are summarized in Table 1, together with the surface areas of the samples. The

Table 1. The form of the solid and the BET surface area after the pretreatment

Pretreatment temperature/°C	Surface area $m^2\ g^{-1}$	The form of solid from X-ray analysis
100	21.4	$Mg(OH)_2$
200	27.4	$Mg(OH)_2$
300	295.0	MgO
400	282.0	MgO
500	251.0	MgO
600	221.0	MgO

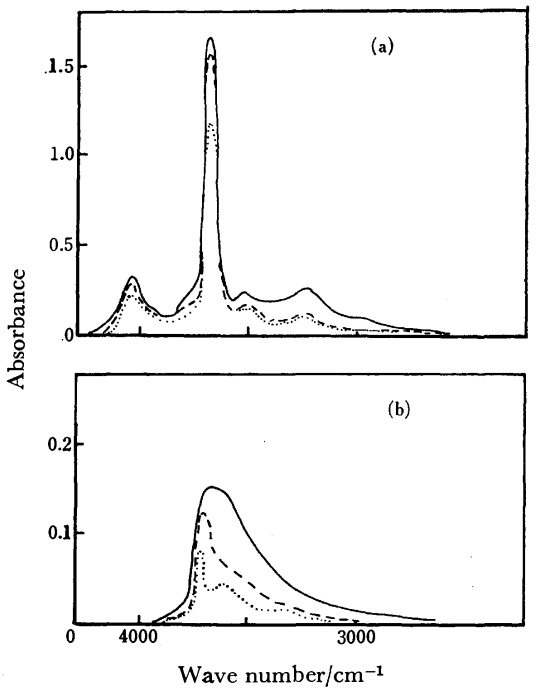

Fig. 1. Infrared spectra of hydroxyl groups for the samples pretreated at different temperatures.
The pretreatment temperatures: (a) —100 °C, ---200 °C, ···300 °C, (b) —400 °C, ---500 °C, ···600 °C.

X-ray data have shown that the $Mg(OH)_2$ dehydrated at the temperatures higher than 300 °C were converted into MgO face-centered cubic crystals. The surface areas were also drastically changed above 300 °C. Figure 1 shows the infrared spectra for the sample wafers in the wave number range of the stretching bands of hydroxyl groups. Only a slight decrease in the intensities of the hydroxyl bands was observed when the pretreatment temperature was increased from 200 to 300 °C, as is indicated in Fig. 1-a. These facts from the X-ray and infrared data imply that, under the dehydration conditions at 300 °C, only a part of the individual $Mg(OH)_2$ grains has been converted to MgO, while the $Mg(OH)_2$ grains are covered by MgO layers at the surface. The information from the X-ray analysis is limited to these surface MgO layers. A decrease in the intensity of hydroxyl groups is obvious at temperatures higher than 400 °C, suggesting that a further dehydration progresses into bulk $Mg(OH)_2$.

The SO_2-induced Cis-Trans Isomerization of cis*-2-Butene.* The catalytic activity of $Mg(OH)_2$ at 20 °C for the isomerization of *cis*-2-butene emerged when the sample was pretreated at temperatures above ≈400 °C. The steep increase in the catalytic activity as raising the activation temperatures above ≈400 °C is a general observation for the isomerization of olefin catalyzed by MgO[14–16] or CaO.[15,16] The catalytically active centers for the reaction, presumably the strongly basic O^{2-} ions, are considered to be created as a result of the removal of H_2O and/or CO_2 as raising the pretreatment temperatures for the catalysts.[14–16]

For the $Mg(OH)_2$ pretreated at the temperatures lower than 400 °C, the addition of SO_2 onto the surface induced the cis-trans isomerization of *cis*-2-butene without causing any double-bond migration to 1-butene. The absence of the double-bond migration has been confirmed using 1-butene as the starting olefin. The addition of SO_2 to the MgO prepared from $Mg(OH)_2$ by dehydration at 500 and 600 °C rather retarded the two isomerizations which proceeded with an appreciable rate in the absence of SO_2. The addition of SO_2 (5.4×10^{-10} mol/cm^2) to a sample pretreated at 600 °C stopped the progress of both the isomerizations. Further addition of SO_2, however, enhanced the rate of cis-trans isomerization selectively.

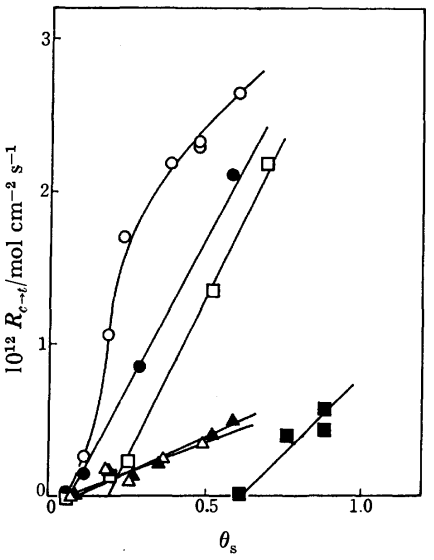

Fig. 2. The rate of SO_2-induced isomerization as a function of θ_s. The samples were pretreated at the following temperatures; (▲) 100 °C, (△) 200 °C, (●) 300 °C, (○) 400 °C, (□) 500 °C, (■) 600 °C.

The rates of SO_2-induced cis-trans isomerization on the catalysts pretreated at 100—600 °C have been plotted in Fig. 2 as a function of the apparent surface coverage of SO_2, θ_s.[17] The specific isomerization did not proceed until a critical amount of SO_2 had been preadsorbed. These values in θ_s are ≈0.1, ≈0.2, and ≈0.6 for the samples pretreated at 100—400 °C, at 500 °C, and at 600 °C, respectively. Beyond the critical θ_s, the rates of the reaction increased sharply.

The temperature effects on the rates of the SO_2-induced isomerization for the samples activated at 100 and 400 °C have been examined under the initial pressures of 85 and 49 Torr for *cis*-2-butene and SO_2 respectively. For both samples, the rates increased as

the reaction temperatures were raised until 25 °C, but decreased above this temperature. The addition of a small amount of NO (less than 10% of the amount of SO_2) strongly inhibited the cis-trans conversion. These results suggest that the reaction proceeds by means of the polysulfone-accompanying mechanism proposed previously:[18-20]

cis- or *trans*-2-butene + $\cdot SO_2[CH(CH_3)CH(CH_3)SO_2]_n$
$\rightleftarrows \cdot CH(CH_3)CH(CH_3)\text{-}SO_2[CH(CH_3)CH(CH_3)SO_2]_n$ (2)

The specific cis-trans isomerization proceeds *via* the addition and elimination of 2-butene molecules at the terminal of the polymer formed in the adsorption layer. The attempt to confirm the polysulfone production at 20 °C by infrared spectroscopic measurement was unsuccessful because the ceiling temperature for the copolymerization lies at about 25 °C.[19] The formation has, however, been confirmed using MgO in the reaction at −10 °C under 280 Torr of the *cis*-2-butene and SO_2 (1: 1) gas mixture. The infrared spectra of the water of this sample have exhibited the two characteristic absorption bands ascribed to the polysulfone from *cis*-2-butene, one at 1300 cm^{-1} and the other at 1105—1140 cm^{-1}, attributable to the symmetrical and asymmetrical stretching vibrations of the sulfone groups respectively.[21]

Surface Sulfur Compounds from SO_2. Figure 3 shows the infrared spectra of the sulfur compounds on the samples pretreated at 100—600 °C, where OD_s was calculated by means of Eq. 1. At least eleven bands are apparent in the (b)-spectrum of Fig. 3. As the pretreatment temperature is raised from 300 to 600 °C, these resolved bands are diminished, but at least three broad bands, at 1030, 950, and 800 cm^{-1} are observed.

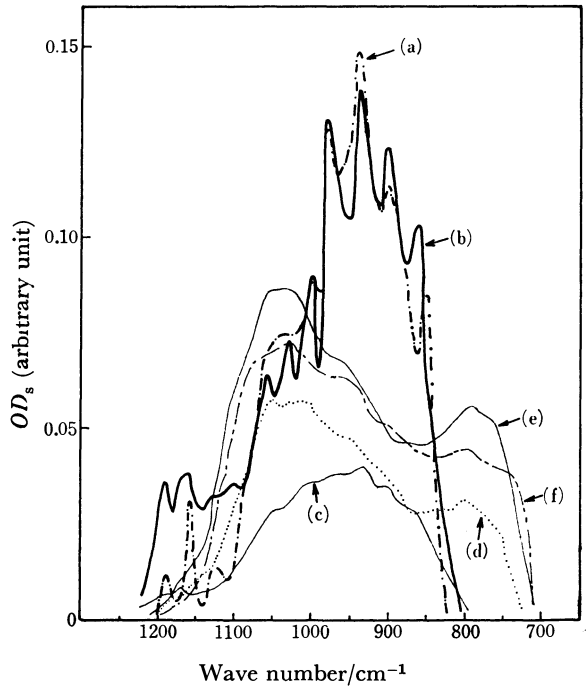

Fig. 3. The infrared spectra of the surface sulfur compounds on the samples pretreated at 100—600 °C. (a) Pretreatment temperature (T_p) 100 °C, θ_s=0.26, (b) T_p 200 °C, θ_s=0.26, (c) T_p 300 °C, θ_s=0.23, (d) T_p 400 °C, θ_s=0.17, (e) T_p 500 °C, θ_s=0.17, (f) T_p 600 °C, θ_s=0.19. SO_2-preadsorption at 20 °C.

Some bands from $Mg(OH)_2$ can be identified with reference to the work on MgO.[6,8] Schoonheydt and Lunsford have observed two different SO_3^{2-} species on MgO pretreated at 500 °C, one is an unidentate sulfito complex coordinated through an oxygen atom and the other a bidentate sulfito complex coordinated through its sulfur and oxygen atoms.[8] The former has absorption bands at 895, 925, and 975 cm^{-1}, and the latter, at 975, 1040, and 1070 cm^{-1}. The frequencies of the pair bands at 900, 940, and 980 cm^{-1} and those at 980, 1030, and 1060 cm^{-1} for the (a)- and (b)-spectra agree reasonably well with those of the pair bands observed by Schoonheydt and Lunsford. Thus, the bands between 900—1100 cm^{-1} in the (a)- and (b)-spectra can be assigned to the SO_3^{2-} species.

SO_3 species, including the sulfito complex, free SO_3^{2-} ions and free SO_3, do not exhibit absorption bands in 1100—1200 cm^{-1} region. The bands observed at this region and at 850—860 and 1000 cm^{-1} for Spectrum(a) or (b) may be ascribed to the formation of various SO_4^{2-} species which have been proposed by Goodsel *et al.*[6] and by Schoonheydt and Lunsford,[8] on MgO. Although the exact assignment of these surface sulfato complexes on $Mg(OH)_2$ cannot be verified from our experiments, the production of the SO_4^{2-} species at room temperature is a surprising observation, since the higher temperatures than 500 °C are usually needed for the formation of SO_4^{2-} species on alkaline earth metal oxides.[5,6,8]

In the case of the samples evacuated at high temperatures (>400 °C) (MgO), the broad bands between 700—1200 cm^{-1} do not allow the identification of the possible sulfur compounds. Schoonheydts and Lunsford speculated that SO_2 is present in the form of a sulfinato complexes on MgO at room temperature.[8] Goodsel and coworkers suggested the formation of unidentate- and bidentate-like sulfito complexes on the surface.[6] The broad bands in the (c)—(f) spectra may be attributed to these surface complexes.

Drastic changes in the spectra such as was shown in Fig. 3 when the pretreatment temperature was increased from 200 to 300 °C imply that the surface reactive species responsible for the SO_2—surface reactions may change in their nature between $Mg(OH)_2$ and MgO. Electron-donor centers associated with OH^- groups for $Mg(OH)_2$ or strongly basic O^{2-} ions for MgO may be necessary for the generation of the surface sulfur complexes described above.[14,22] The poisoning effect of SO_2 at low θ_s on the butene isomerizations observed on the samples activated at 500 and 600 °C can be ascribed to the consumption of the active centers, *i.e.*, the basic O^{2-} ions, by SO_2, producing sulfinato or SO_3^{2-} species.

Contribution of the Weakly Adsorbed SO_2 to the Isomerization of cis*-2-Butene.* It has been suggested that the polysulfone-accompanying cis-trans isomerization of 2-butenes (Eq. 2) is initiated through the strong polarization of the butene–SO_2 charge-transfer complexes

under the influence of the electrostatic field on the catalyst surface.[19,20] The charge-transfer complex necessary for the reaction is formed from the butene and SO_2 molecules physisorbed. Therefore, knowledge about the sulfur compound remaining on the surface in the form of SO_2 is required to explain the peculiar feature of the reaction rates as a function of θ_s as is indicated in Fig. 2.

Goodsel *et al.* have observed the bands due to chemisorbed SO_2 on MgO at 1140 (ν_1) and 1322 cm^{-1} (ν_2), and those of the physisorbed SO_2 at 1149 and 1336 cm^{-1}.[6] In the present work the bands at 1140 and 1330 cm^{-1} becomes observable when θ_s increases beyond 0.50 in the case of the samples pretreated at 500 and 600 °C. For the samples pretreated at the temperature below 400 °C, the bands due to adsorbed SO_2, however, were not detected, probably because the weak band around 1140 cm^{-1} was hidden in the bands of SO_4^{2-} species and the band around 1330 cm^{-1} was obscured by the broad, strong band at 1290—1340 cm^{-1} attributable to carbonated species contained in $Mg(OH)_2$ as an unavoidable impurity.

Since the information about the sulfur compound in the form of SO_2 derived from infrared spectroscopic experiments was scarce, a volumetric study has been carried out. The amount of SO_2 desorbed at 50 °C in 30 min from a surface with a fixed value of θ_s was measured by collecting the desorbed SO_2 by cold trap at 77 K. The amount of the weakly adsorbed SO_2 thus measured, $[SO_2]_a$, has been plotted as a function of θ_s in Figs. 4 and 5 for the samples activated at 100 and 400 °C respectively. The rates of the SO_2-induced isomerization of *cis*-2-butene are also shown by dotted curves in the figures. It is noticeable that the reaction rate and the amount of the weakly adsorbed SO_2 depend on θ_s in very similar ways. The correlation between the rate of the SO_2-induced isomerization and the amount of weakly adsorbed SO_2 has been examined

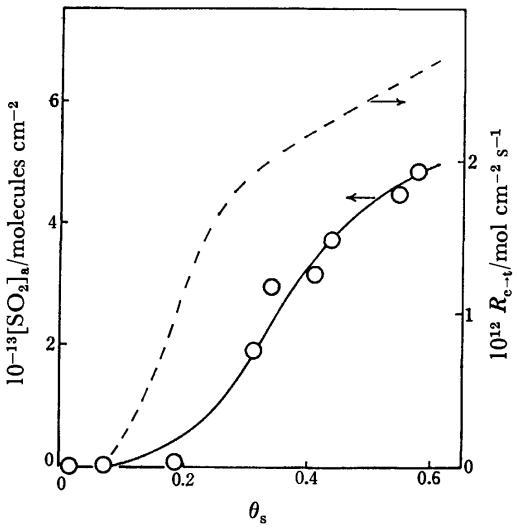

Fig. 5. The amount of weakly adsorbed SO_2 and the rate of isomerization of *cis*-2-butene over MgO as a function of θ_s: The sample was activated at 400 °C. —; The amount of weakly adsorbed SO_2, ---; the rate of cis-trans isomerization.

at the fixed θ_s of 0.57. The results are shown in Figs. 6 and 7 for $Mg(OH)_2$ and MgO respectively. Here also a good correlation between the rate and the amount of weakly adsorbed SO_2 has been demonstrated.

The ratios of the amount of weakly adsorbed SO_2 to that of the total sulfur compounds at θ_s of 0.57, on the basis of the sulfur atoms, are 0.25 and 0.015 for the samples pretreated at 100 and 600 °C respectively. Most of the sulfur compounds remaining on the surface after desorption treatment must be in the form of the SO_3^{2-}, SO_4^{2-}, or sulfinato complexes described previously. At a low θ_s the added SO_2 must have been converted to these sulfur compounds as a result of the reaction with the solid, leaving no physisorbed SO_2 necessary for the specific isomerization. The absence

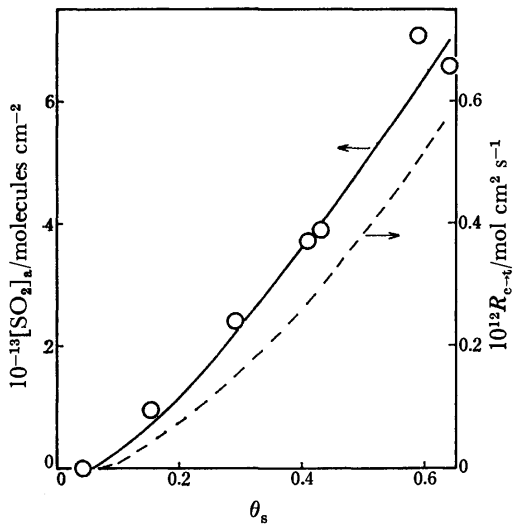

Fig. 4. The amount of weakly adsorbed SO_2 and the rate of cis-trans isomerization of *cis*-2-butene on $Mg(OH)_2$, as a function of θ_s: The sample was activated at 100 °C. —; The amount of weakly adsorbed SO_2, ---; the rate of cis-trans isomerization.

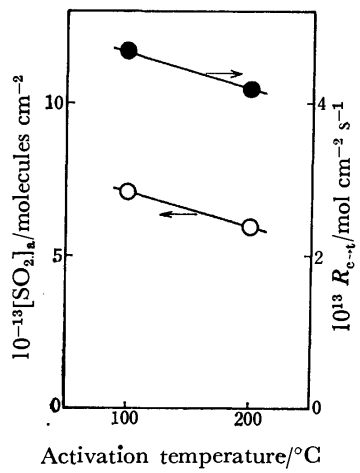

Fig. 6. The amount of weakly adsorbed SO_2 and the rate of isomerization of *cis*-2-butene on $Mg(OH)_2$ as a function of pretreatment temperatures: (●); the rate of cis-trans isomerization, (○); the amount of weakly adsorbed SO_2. θ_s=0.57.

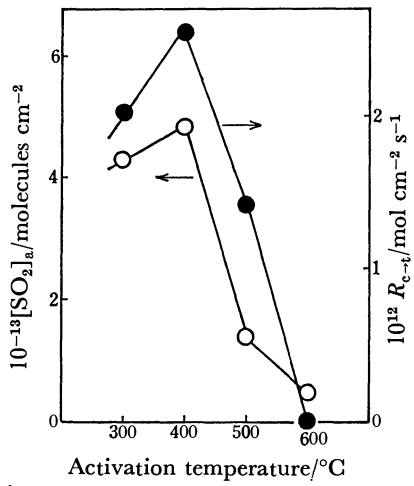

Fig. 7. The amount of weakly adsorbed SO_2 and the rate of isomerization of *cis*-2-butene on MgO as a function of pretreatment temperatures: (●); The rate of cis-trans isomerization, (○); the amount of weakly adsorbed SO_2. θ_s=0.57.

of the reaction at the θ_s less than the critical values shown in Fig. 2 can be ascribed to the absence of the weakly adsorbed SO_2, as has been described above.

The amount of *cis*-2-butene adsorbed per unit of the surface area did not change with the θ_s for the samples activated at 100—600 °C; for example, it was $20.0\pm 1.2\times10^{13}$ molecules/cm^2 for the samples activated at 300—600 °C over the range of θ_s of 0.05—0.60. Therefore, the change in the rate of the cis-trans isomerization shown in Figs. 2, 6, and 7 cannot be ascribed to that in the amount of the adsorbed *cis*-2-butene. A good correlation between the isomerization rate and the amount of weakly adsorbed SO_2 (Figs. 4—7) indicates that the activities of the solids for the polysulfone-accompanying isomerization are determined by the concentration of the weakly adsorbed SO_2 remaining on the surface.

The picture of the initiation step of the copolymerization, and accordingly of the cis-trans isomerization, that we have in mind is the polarization of the SO_2–butene charge-transfer complex under the influence of electrostatic field due to exposed surface ions.[20] As a consequence of the formation of the SO_3^{2-}, SO_4^{2-} species or sulfinato complexes, the surface magnesium will be positively charged due to electron transfer from the surface to these ionic species, and a strong electrostatic field would be formed. The concerted action of the negatively charged sulfur complexes—magnesium cation pairs may promote the strong polarization of the charge-transfer complex, causing the initiation of the copolymerization.

References

1) H. S. Judeikis and S. Siegel, *Atmos. Environ.*, **7**, 619 (1973).
2) Environmental Protection Agency, "Position paper on regulation of atmospheric sulfates," U. S. Department of Commerce, National Technical Information Service, PB-245760, September, 1975.
3) A. Liberti, D. Brocco, and M. Possanzini, *Atmos. Environ.*, **12**, 255 (1978).
4) H. S. Judeikis, T. B. Stewart, and A. G. Wren, *Atmos. Environ.*, **12**, 1633 (1978).
5) M. J. D. Low, A. J. Goodsel, and N. Takezawa, *Environ. Sci. Technol.*, **5**, 1191 (1971).
6) A. J. Goodsel, M. J. D. Low, and N. Takezawa, *Environ. Sci. Technol.*, **6**, 268 (1972).
7) R. A. Schoonheydt and J. H. Lunsford, *J. Phys. Chem.*, **76**, 323 (1972).
8) R. A. Schoonheydt and J. H. Lunsford, *J. Catal.*, **26**, 261 (1972).
9) M. J. Lin and J. H. Lunsford, *J. Phys. Chem.*, **79**, 892 (1975).
10) T. Novakov, S. G. Chang, and A. B. Harker, *Science*, **186**, 259 (1974).
11) B. Barbaray, J. P. Contour, and G. Mouvier, *Atmos. Environ.*, **11**, 351 (1977).
12) K. Otsuka, K. Tanaka, and A. Morikawa, *Bull. Chem. Soc. Jpn.*, **52**, 2069 (1979).
13) D. M. Young and A. D. Crowell, "Physical Adsorption of Gases," Butterworths, London, England (1962), p. 226.
14) M. J. Baird and J. H. Lunsford, *J. Catal.*, **26**, 440 (1972).
15) H. Hattori, N. Yoshii, and K. Tanabe, *Proc. Inter. Congr. Catal., 5th*, 10-233 (1973).
16) K. Shimazu, H. Hattori, and K. Tanabe, *J. Catal.*, **48**, 302 (1977).
17) The molecular cross section of SO_2 (19.2 Å^2) was tentatively adopted in the calculation of θ_s. The θ_s indicates the apparent coverage, since most of the SO_2 added reacts with the surface, forming various surface complexes, as will be described later.
18) K. Otsuka and A. Morikawa, *J. Catal.*, **46**, 71 (1977).
19) K. Otsuka, T. Tanabe, and A. Morikawa, *J. Catal.*, **48**, 333 (1977).
20) K. Otsuka and A. Morikawa, *J. Catal.*, **56**, 88 (1979).
21) R. E. Cook, F. S. Dainton, and K. J. Ivin, *J. Polym. Sci.*, **26**, 351 (1957).
22) M. Che, C. Naccache, and B. Imelik, *J. Catal.*, **24**, 328 (1972).

On the Excimer Formation of Pyrene in Electrochemiluminescenece

Takeshi SUMINAGA and Sohachiro HAYAKAWA*

Department of Applied Physics, Tokyo Institute of Technology, Ookayama, Meguro-ku, Tokyo 152

(Received April 20, 1979)

Temperature effect in electrochemiluminescenece (ECL) of pyrene was investigated in order to clarify the formation of excimers. The ratio of intensity of excimer to monomer emission was measured on solutions of pyrene in *N,N*-dimethylformamide (DMF) at various temperatures from the decay curves of excimer emission due to pulse excitation with a nitrogen laser. The temperature change of concentration dependence of the ratio was derived from the rate equations for the respective direct and indirect formation of excimers. The mechanism of direct excimer formation was confirmed in ECL of pyrene more clearly by analysis of the temperature effect than by that of the concentration effect at a certain temperature.

Electrochemiluminescence (ECL) from pyrene has been studied by several workers since Hercules[1] first recognized the blue emission in *N,N*-dimethylformamide (DMF). Fleet *et al.*[2] reported on ECL spectra containing an excimer emission. Kihara *et al.*[3] proposed the formation of the excited state of pyrene *via* anion-cation annihilation in acetonitrile, but carried out measurements only at room temperature. Very few measurements have been made on the temperature effect on ECL. Recently, we reported on the temperature dependence of the red emission in ECL of pyrene.[4] The temperature effect in ECL of pyrene from monomer and excimers does not seem to have been measured.

This paper deals with the excimer formation process by the temperature effect in emission intensity and relevant rate constants. The rate constants can be analyzed from the decay curves of the excited state of pyrene in DMF under pulse excitation with a nitrogen laser.

Experimental

Pyrene was recrystallized carefully from benzen solution. Tetrabutylammonium bromide (TBAB) used as a supporting electrolyte was recrystallized from ethyl acetate solution. The ECL was observed in a pyrex glass cell equipped with two Pt wire electrodes. The cell was cooled by cold N_2 gas through a copper tube around the cell. ECL spectrum was measured with a fluorescence spectrophotometer (Hitachi MPF-2A) at room temperature and a Hamamatsu T.V. R375 photomultiplier and a photon counting system through interference filter (center wavelength: 386 nm, half width: 13 nm) at low temperatures. The decay curve of excimer emission by nitrogen laser excitation was measured with an oscilloscope, the result being analyzed following the method of Birks.[5] The measurement was performed under the same conditions as those for ECL measurements, a solution degassed by N_2 gas and containing 1×10^{-2} mol dm^{-3} supporting electrolyte being used. Transmittance of the interference filter was compensated by the spectrum measured with MPF-2A at room temperature.

Results and Discussion

The relationship between ECL emission and the formation of anion-cation was investigated by means of a double potential step and/or triangular potential sweep. Emission with steady intensity was obtained with applied voltage DC 4 V, the solution being stirred.

Figure 1 shows the ECL spectrum and the fluorescence spectra. The concentration dependence of the emission

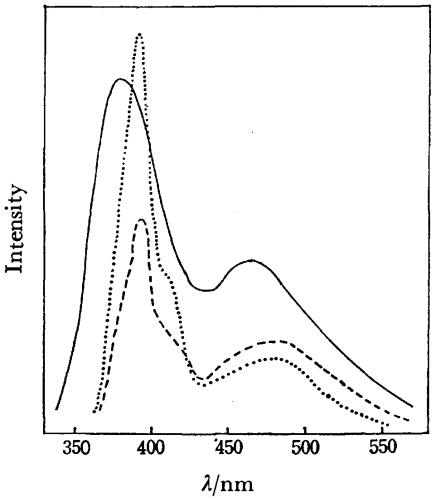

Fig. 1. Emission spectra of pyrene.
——: ECL spectrum at room temperature, pyrene 0.8×10^{-3} mol dm^{-3}, ——: fluorescence spectrum at room temperature, pyrene 6×10^{-3} mol dm^{-3}, ……: fluorescence spectrum at −38 °C, pyrene 6×10^{-3} mol dm^{-3}.

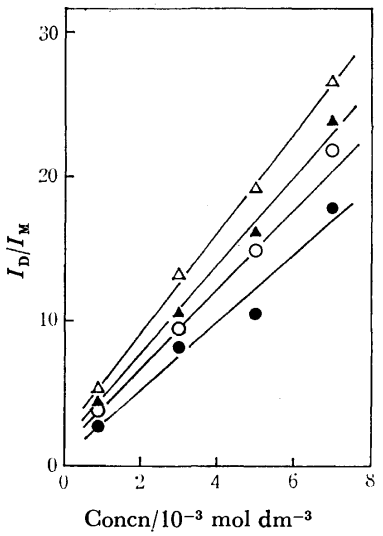

Fig. 2. Concentration dependence of the ratio excimer to monomer emission in ECL at various temperatures.
●: 20 °C, ○: 0 °C, ▲: −10 °C, △: −30 °C.

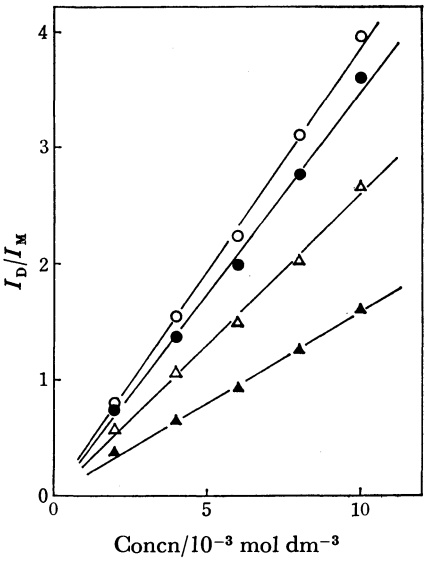

Fig. 3. Concentration dependence of the ratio of excimer to monomer emission in case of photoexcitation at various temperatures.
○: 20 °C, ●: 0 °C, △: −20 °C, ▲: −40 °C.

intensity ratio of excimer to monomer (I_D/I_M) on temperature is shown for ECL and emission by photoexcitation in Figs. 2 and 3, respectively. The results show linearity as regards concentration. The results were analyzed assuming the following reaction scheme:[3]

$$M^+ + M^- \xrightarrow{k_A} M^* + M, \quad (1)$$

$$M^+ + M^- \xrightarrow{k_B} D^*, \quad (2)$$

$$M^* \xrightarrow{k_{FM}} M + h\nu \qquad M^* \xrightarrow{k_{GM}} M, \quad (3)$$

$$D^* \xrightarrow{k_{FD}} 2M + h\nu' \qquad D^* \xrightarrow{k_{GD}} 2M, \quad (4)$$

$$M^* + M \underset{k_{MD}}{\overset{k_{DM}}{\rightleftharpoons}} D^*, \quad (5)$$

where M, M^+, M^-, and D^+ denote the pyrene molecule, its cation, anion, and excimer, respectively, and k denotes the rate constants of each reaction.

In the steady state we have

$$\frac{d[M^*]}{dt} = 0, \qquad \frac{d[D^*]}{dt} = 0. \quad (6)$$

Thus

$$\frac{I_D}{I_M} = \frac{k_{FD}}{k_{FM}} \frac{ak_M + (1+a)k_{DM}[M]}{k_D + (1+a)k_{MD}} \equiv K + K'[M], \quad (7)$$

where

$$\frac{I_D}{I_M} = \frac{k_{FD}[D^*]}{k_{FM}[M^*]},$$

and

$$k_M = k_{FM} + k_{GM},\ k_D = k_{FD} + k_{GD},\ k_B/k_A = a. \quad (8)$$

On the other hand, k_B is zero in the case of photoexcitation, since excited states are given by the following process instead of processes (1) and (2):

$$M + h\nu \longrightarrow M^*.$$

Thus

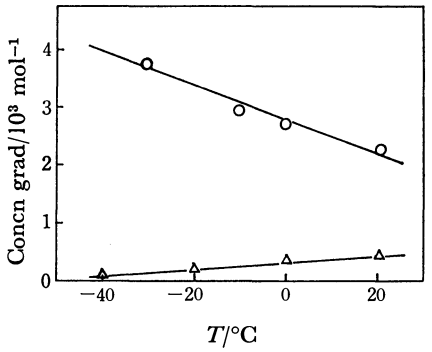

Fig. 4. Temperature dependence of concentration gradient obtained from Figs. 2 and 3.
○: ECL, △: photoexcitation.

$$\frac{I_D}{I_M} = \frac{k_{FD}}{k_{FM}} \frac{k_{DM}[M]}{k_D + k_{MD}} \equiv K''[M]. \quad (9)$$

From Eqs. 7 and 9 and experimental results (Figs. 2 and 3), the formation of the excited state *via* anion-cation annihilation is suggested. Plots of the gradient of I_D/I_M *vs.* temperature from data in Figs. 2 and 3 are shown in Fig. 4. The gradient increases in the case of ECL with fall in temperature but decreases in the case of photoexcitation.

From Eqs. 7 and 9, Kihara *et al.*[3] put

$$K'/K = (1+a^{-1})k_{DM}k_M, \quad (10)$$

$$K'/K'' = 1 + 1/[a^{-1} + (1+a^{-1})k_{MD}k_D], \quad (11)$$

and evaluated a from the data of k_M, k_D, k_{DM}, k_{MD} of pyrene in cyclohexane or 95% ethanol in substitution for them in acetonitrile. The value of K was estimated by extrapolation. The estimation seems erroneous for the following reasons: estimation of k values from the solutions different from the actual ones of ECL, and the erroneous extrapolation from the relationships I_D/I_M *vs.* concentration.

We postulate the following process for excimer formation in order to analyze the temperature effect on the concentration dependence of I_D/I_M.

From Eqs. 3, 4, 5, and 8, we have

$$\frac{d[M^*]}{dt} = k_{MD}[D^*] - (k_M + k_{DM}[M^*])[M^*]$$

$$\frac{d[D^*]}{dt} = k_{DM}[M][M^*] - (k_D + k_{MD})[D^*].$$

Let us consider the case in which the initial state is a monomer-state. Putting $[M^*]=[M^*]_0$, $[D^*]=0$ at $t=0$, we get

$$[M^*] = \frac{[M^*]_0}{\lambda_2 - \lambda_1}(c_1 e^{-\lambda_1 t} + c_2 e^{-\lambda_2 t}),$$

$$[D^*] = \frac{k_{DM}[M][M^*]_0}{\lambda_2 - \lambda_1}(e^{-\lambda_1 t} - e^{-\lambda_2 t}),$$

where

$$\lambda_1 = \frac{1}{2}\{k_M + k_{DM}[M] + k_D + k_{DM} - \sqrt{s}\},$$

$$\lambda_2 = \frac{1}{2}\{k_M + k_{DM}[M] + k_D + k_{MD} + \sqrt{s}\},$$

$$s = (k_D + k_{MD} - k_M - k_{DM}[M])^2 - 4k_{MD}k_{DM}[M],$$

$$c_1 = \lambda_2 - k_M - k_{DM}[M],$$
$$c_2 = k_M + k_{DM}[M] - \lambda_1.$$

Substituting them into the equation

$$\frac{I_D}{I_M} = \frac{k_D \int [D^*]dt}{k_M \int [M^*]dt},$$

we get

$$\frac{I_D}{I_M} = \frac{k_D k_{DM}[M]}{k_M(k_D + k_{MD})}. \quad (12)$$

Putting $[M^*]=0$, $[D^*]=[D^*]_0$ at $t=0$, we get

$$[M^*] = \frac{[D^*]_0(\lambda_2 - y)(y - \lambda_1)}{k_{DM}[M](\lambda_2 - \lambda_1)}(e^{-\lambda_1 t} - e^{-\lambda_2 t}),$$

$$[D^*] = \frac{[D^*]_0}{\lambda_2 - \lambda_1}[(\lambda_2 - y)e^{-\lambda_1 t} + (y - \lambda_1)e^{-\lambda_2 t}],$$

and

$$\frac{I_D}{I_M} = \frac{k_D(k_M + k_{DM}[M])}{k_M k_{MD}}, \quad (13)$$

where

$$y = k_D + k_{MD}.$$

The decay parameters λ_1 and λ_2, obtained experimentally are given Figs. 5 and 6. The values of the rate constants k_M, k_D, k_{DM}, and k_{MD} can be obtained by use of the parameters. The constants in DMF at 20 °C, 0 °C, −20 °C, and −40 °C are given in Table 1. The temperature dependence of $k_D k_{DM}/k_M(k_D + k_{MD})$ and

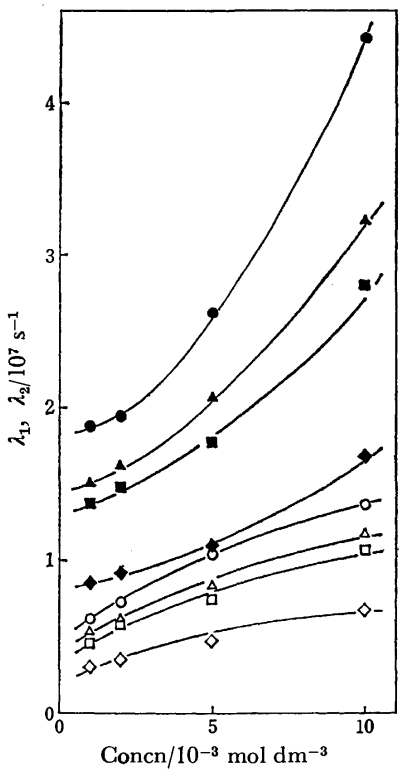

Fig. 5. Plots of decay parameters λ_1 and λ_2 against molar concentration, obtained by pulse excitation on the DMF solution of pyrene at various temperatures.
λ_1: ○ 20 °C, △ 0 °C, □ −20 °C, ◇ −40 °C.
λ_2: ● 20 °C, ▲ 0 °C, ■ −20 °C, ◆ −40 °C.

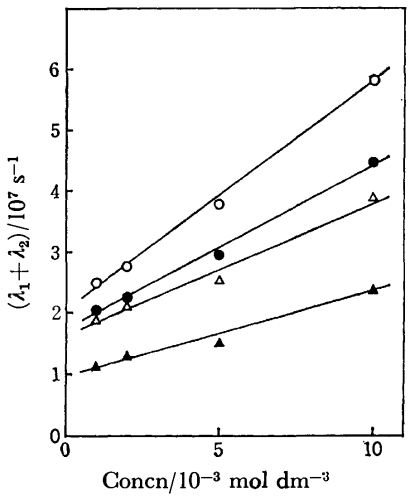

Fig. 6. Dependence of $\lambda_1+\lambda_2$ against molar concentration at various temperatures.
○: 20 °C, ●: 0 °C, △: −20 °C, ▲: −40 °C.

Table 1. Rate constants obtained by pulse excitation of the DMF solution of pyrene at various temperatures

Temp/°C	k_M / 10^{-7} s^{-1}	k_D / 10^{-7} s^{-1}	k_{DM} / 10^{-9} M^{-1} s^{-1}	k_{MD} / 10^{-7} s^{-1}
20	0.5	1.4	3.8	0.4
0	0.4	1.2	2.6	0.4
−20	0.35	1.1	2.1	0.2
−40	0.25	0.7	1.4	0.1

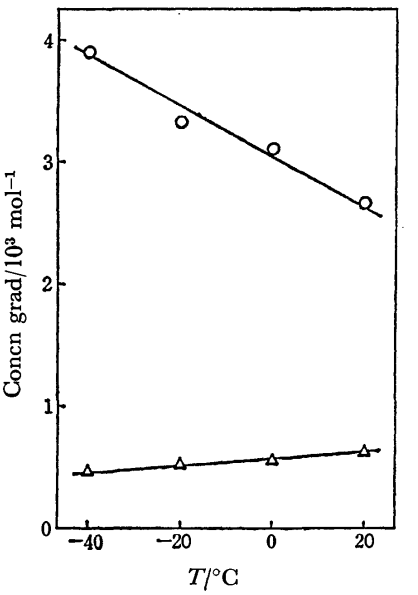

Fig. 7. Temperature dependence of concentration gradient calculated from Eqs. 12, 13, and Table 1.
○: Initial conditions $[M^*]=0$, △: initial conditions $[D^*]=0$.

$k_D k_{DM}/k_M k_{MD}$ is calculated by means of Eqs. 12 or 13 and the values given in Table 1. The results are shown in Fig. 7. By comparison of the curves in Figs. 4 and 7,

we see that the curves for photoexcitation and for ECL (Fig. 4) correspond respectively to the curves for Eqs. 12 and 13. $[D^*]=0$ at $t=0$ in case of photoexcitation, and $[M^*]=0$ at $t=0$ (excimers are directly generated from anion-cation annihilation) in case of ECL. Mechanism of direct excimer formation is confirmed in ECL of pyrene through analysis of temperature and concentration dependence of I_D/I_M. The present approach is more advantageous than the conventional one, utilizing the value K of I_D/I_M at $[M]=0$, which is often erroneous.

The authors wish to express their sincere thanks to Mr. Tadamasa Akutagawa and Mr. Katsuhiko Abe for their valuable advice and help in the course of the study.

References

1) D. M. Hercules, *Science*, **145**, 808 (1964).
2) B. Fleet, G. F. Kirkbright, and C. J. Pickford, *J. Electroanal. Chem.*, **30**, 115 (1971).
3) T. Kihara, M. Sukigara, and K. Honda, *J. Electroanal. Chem.*, **47**, 161 (1973).
4) T. Suminaga and S. Hayakawa, *J. Electrochem. Soc.*, **124**, 1075 (1977).
5) J. B. Birks, "Photophysics of Aromatic Molecules," Wiley-Interscience, London (1970), Chap. 7.

The Crystal and Molecular Structure of Palythine Trihydrate

Akio FURUSAKI,* Takeshi MATSUMOTO, Isami TSUJINO,† and Isao SEKIKAWA††

Department of Chemistry, Faculty of Science, Hokkaido University, Sapporo 060

†*Department of Chemistry, Faculty of Fisheries, Hokkaido University, Hakodate 041*

††*Institute of Immunological Science, Hokkaido University, Sapporo 060*

(Received May 1, 1979)

The molecular structure of palythine, $C_{10}H_{16}N_2O_5$, has been confirmed by means of an X-ray crystal analysis of its trihydrate. The crystals are monoclinic, with two formula units in a unit cell with dimensions of $a=10.499$, $b=12.812$, $c=5.322$ Å, and $\beta=98.53°$; the space group is $P2_1$. 1377 unique intensity data were collected on a four-circle diffractometer with LiF-monochromated Cu $K\alpha$ radiation. The structure was solved by the Monte Carlo direct method, using the 20 strongest reflections as a starting set, and was refined by the block-diagonal least-squares method. The final R value was 3.1%. The molecular structure thus obtained corresponds to that proposed by Tsujino *et al.* and Takano *et al.* on the basis of the chemical evidence. Palythine exists as a zwitter ion in the crystal. The palythine and water molecules are connected by twelve types of hydrogen bonds, forming a three-dimensional hydrogen-bonded structure.

Palythine is a new amino acid isolated from the red alga *Chondrus yendoi* and the zoanthid *Palythoa tuberculosa*.[1,2] On the basis of the chemical evidence, the **1** structure has been proposed for this compound. However, because of the remarkable lability of palythine, there was some doubt about the proposed structure. Therefore, in order to confirm **1**, we have now undertaken an X-ray crystallographic study of palythine trihydrate.

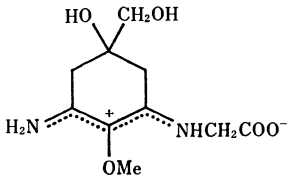

1

Experimental

Colorless, single crystals of palythine trihydrate were obtained from an aqueous solution. A crystal with dimensions of about $0.1\times0.3\times0.4$ mm³ was used for the X-ray measurement. The crystal data are summarized in Table 1. The cell dimensions and diffraction intensities were measured on an automatic, four-circle diffractometer using Cu $K\alpha$ radiation ($\lambda=1.5418$ Å) monochromatized with an LiF crystal. The intensity measurement was made by using an ω-2θ continuous scan at a rate of about 1°(ω)/min; the background was measured for 20—30 s at each end of the scan range. The intensities thus obtained were corrected for the Lorentz and polarization factors, but not for the absorption or the extinction effect. In the range of 2θ values up to 140°, 1377 unique structure factor magnitudes above $2\sigma(F)$ were selected for the structure determination.

Table 1. The crystal data

Formula	$C_{10}H_{16}N_2O_5\cdot3H_2O$
Formula weight	298.29
Crystal system	Monoclinic
Space group	$P2_1$
Cell dimensions	$a=10.499(5)$ Å
	$b=12.812(6)$
	$c=5.322(3)$
	$\beta=98.53(5)°$
	$V=708.0$ Å³
Z	2
D_x	1.399 g cm⁻³

Structure Determination

At the early stage of the structure determination, attempts were made to solve the structure by the symbolic-addition method.[3] Although a phase set which showed a low R_K value of 32.8% ($R_K=\Sigma||E_o|-k|E_c||/\Sigma|E_o|$) gave an E-map which contained a six-membered ring, it did not lead to the elucidation of the whole structure. It was found afterwards that the six-membered ring in the E-map deviated from its correct position, nearly perpendicular to the ($\bar{2}$ 0 1) plane by

Table 2. The 54th random phase set and correct phases (in $10^{-3}\pi$)

	h	k	l	$\|E\|$	No. 54	Correct	ϕ[a]
1	$\bar{1}0$	0	2	3.79	1000	0	0
2	$\bar{3}$	8	2	2.93	1000	1012	1021
3	3	0	5	2.79	0	0	1000
4	$\bar{2}$	4	3	2.73	0	4	10
5	7	8	0	2.52	750	953	1021
6	4	0	2	2.46	0	0	0
7	$\bar{3}$	4	1	2.46	750	587	1009
8	4	2	5	2.46	1250	1002	1006
9	$\bar{5}$	10	1	2.39	0	261	25
10	$\bar{2}$	3	2	2.38	1000	1288	1506
11	6	6	2	2.35	1000	949	1015
12	$\bar{1}\bar{1}$	6	1	2.27	1250	912	1016
13	1	12	1	2.27	1750	1286	1032
14	$\bar{1}\bar{1}$	6	2	2.27	250	489	1013
15	$\bar{4}$	1	5	2.25	1250	1388	1502
16	$\bar{6}$	0	3	2.24	0	0	0
17	8	3	0	2.24	1250	1461	1507
18	$\bar{1}0$	1	2	2.21	500	880	1501
19	$\bar{5}$	4	5	2.16	1750	995	1010
20	$\bar{5}$	1	4	2.16	1250	650	502

a) Phase values obtained from the starting phase set, different from the 54th set only in the phase of $\bar{1}0$ 0 2.

about 1.1 Å. The structure was finally elucidated by the Monte Carlo direct method.[4] The 20 strongest reflections given in Table 2 were chosen as members of a starting set. The tentative phase values for the starting reflections were derived from successively-generated random numbers. In order to extend this tentative phase set, 10 cycles of the tangent procedure were performed using 331 $|E|$ values above 1.20; during the first 5 cycles, the phases of the starting reflections were kept constant. Since the 54th phase set showed a low R_K value of 28.2%,** 6 additional cycles of the tangent procedure were carried out. Consequently, the R_K value was reduced to 18.8%. An E-map based on 329 phases clearly revealed the locations of all 20 non-hydrogen atoms.

The 54th random phase set and the correct phases calculated with the final atomic parameters are given in Table 2. The two corresponding phase values are in substantial agreement with each other except for the $\bar{1}0\ 0\ 2$, $\bar{5}\ 4\ 5$, and $\bar{5}\ 1\ 4$ reflections. However, it should be noted that the phase value assigned to the strongest $\bar{1}0\ 0\ 2$ reflection is different from the correct phase by π. It was ascertained that, when this phase value was replaced by the correct one in the initial stage of the tangent procedure, the 54th random phase set no longer led to the correct solution. Of the phase values calculated in such a way, those for the starting reflections are given in the last column of Table 2. Especially great deviations from the correct phases can be seen for the $3\ 0\ 5$, $\bar{3}\ 4\ 1$, $\bar{1}\bar{1}\ 6\ 2$, and $\bar{1}0\ 1\ 2$ reflections, those derivations being π, $0.422\,\pi$, $0.524\,\pi$, and $0.621\,\pi$ respectively. Since none of the 24 most probable phase relationships ($\kappa=2\sigma_3\sigma_2^{-3/2}|E_hE_kE_{h-k}>3.5$) associated with the $\bar{1}0\ 0\ 2$ reflection contain errors greater than

Table 3. The final atomic parameters and estimated standard deviations

(1) The non-hydrogen atoms

The positional and thermal parameters are multiplied by 10^4 and 10^5 respectively. The latter ones are defined as $\exp[-(\beta_{11}h^2+\beta_{22}k^2+\beta_{33}l^2+\beta_{12}hk+\beta_{13}hl+\beta_{23}kl)]$.

Atom	x	y	z	β_{11}	β_{22}	β_{33}	β_{12}	β_{13}	β_{23}
C(1)	−1030(2)	1458(1)	938(3)	50(1)	31(1)	185(5)	−1(2)	26(4)	19(4)
C(2)	−663(2)	2325(1)	2450(3)	50(1)	29(1)	219(6)	8(2)	45(5)	4(4)
C(3)	617(2)	2498(1)	3506(3)	53(1)	25(1)	194(5)	−6(2)	39(4)	11(4)
C(4)	1664(2)	1792(1)	2860(4)	47(1)	30(1)	250(6)	−6(2)	38(5)	−12(4)
C(5)	1186(2)	700(1)	2062(3)	46(1)	28(1)	202(5)	2(2)	39(4)	2(4)
C(6)	−34(2)	752(2)	114(4)	49(1)	36(1)	205(5)	4(2)	26(4)	−27(4)
C(7)	2232(2)	75(2)	1008(4)	56(2)	33(1)	214(6)	10(2)	38(5)	−4(4)
C(8)	−2183(2)	2716(2)	5141(5)	71(2)	50(1)	335(8)	−17(3)	125(6)	−53(5)
C(9)	2174(2)	3583(2)	6346(4)	60(2)	33(1)	210(6)	−23(2)	23(5)	−16(4)
C(10)	2954(2)	4225(2)	4682(4)	64(2)	34(1)	301(7)	−3(2)	78(5)	23(4)
N(1)	−2248(2)	1247(1)	116(3)	49(1)	37(1)	258(6)	3(2)	14(4)	−31(4)
N(2)	898(2)	3294(1)	5087(3)	53(1)	32(1)	280(6)	−7(2)	54(4)	−22(4)
O(1)	−1603(1)	3011(1)	2972(3)	55(1)	32(1)	271(5)	15(1)	59(4)	9(3)
O(2)	841(1)	131(1)	4182(3)	62(1)	37(1)	207(4)	−8(2)	49(3)	16(3)
O(3)	2549(1)	551(1)	−1239(3)	54(1)	53(1)	248(4)	12(2)	79(3)	16(4)
O(4)	2552(2)	4317(2)	2406(3)	109(2)	54(1)	289(5)	−8(2)	90(5)	64(4)
O(5)	3990(2)	4595(2)	5790(5)	88(2)	92(2)	500(9)	−97(3)	8(6)	88(6)
O(W1)	4754(2)	1462(2)	5129(4)	93(2)	62(1)	472(8)	36(3)	4(6)	20(5)
O(W2)	4873(2)	−533(2)	−684(4)	76(1)	64(1)	417(7)	25(2)	153(5)	26(5)
O(W3)	4702(2)	−2731(2)	−323(4)	96(2)	51(1)	477(8)	−22(2)	101(6)	21(5)

(2) The hydrogen atoms

The positional and thermal parameters are multiplied by 10^3 and 10 respectively.

Atom	x	y	z	B(Å^2)	Atom	x	y	z	B(Å^2)
H(4a)	231(3)	173(2)	432(5)	27(5)	H(N1a)	−242(3)	71(2)	−82(5)	27(5)
H(4b)	201(3)	211(2)	143(5)	24(4)	H(N1b)	−283(3)	166(3)	52(6)	33(6)
H(6a)	−36(3)	2(3)	−19(6)	35(6)	H(N2)	29(3)	371(3)	534(6)	31(5)
H(6b)	19(3)	106(3)	−135(6)	37(6)	H(O2)	140(3)	24(2)	552(5)	26(5)
H(7a)	189(3)	−59(2)	57(5)	23(4)	H(O3)	320(4)	28(3)	−156(7)	42(7)
H(7b)	295(2)	5(2)	228(5)	20(4)	H(W1a)	517(5)	101(4)	509(9)	53(8)
H(8a)	−290(4)	323(3)	523(7)	47(7)	H(W1b)	490(5)	172(4)	665(9)	59(10)
H(8b)	−153(3)	282(3)	667(6)	38(6)	H(W2a)	539(4)	−52(4)	−167(8)	51(8)
H(8c)	−249(4)	198(3)	496(7)	43(7)	H(W2b)	529(4)	−49(4)	83(8)	53(8)
H(9a)	211(3)	397(2)	786(6)	29(5)	H(W3a)	506(5)	−294(4)	−150(9)	57(9)
H(9b)	265(3)	299(3)	685(7)	40(6)	H(W3b)	476(5)	−214(5)	−40(10)	65(11)

** The second lowest of the R_K values for the 54 sets was 30.7%.

$\pi/3$, such serious deviations may be due to the accidental accumulation of rather large errors produced by these phase relationships.

The structure thus obtained was refined by the block-diagonal-matrix least-squares method, first with isotropic and then with anisotropic temperature factors. After all the 22 hydrogen atoms had been located in a difference Fourier map, further least-squares refinement including these hydrogen atoms with isotropic temperature factors was carried out. For this refinement, the following weighting scheme was used:

$$W = 1/\{\sigma(F)^2 \exp(AX^2+BY^2+CXY+DX+EY)\}$$

where $X=|F_o|$ and $Y=\sin\theta/\lambda$. The A, B, C, D, and E coefficients are constants which were determined from the $(\Delta F)^2$ values in each cycle of the refinement. In this manner, the R value reached 3.1%. The atomic parameters thus obtained are listed in Table 3. The tables of the observed and calculated structure factors are kept at the Chemical Society of Japan (Document No. 8003).

All the calculations were performed on a FACOM 230-75 computer at the Hokkaido University Computing Center, using our own programs. Random numbers were generated by calling a function RANDOM which existed in a program library of the Computing Center. The atomic scattering factors were taken from the International Tables.[5]

Results and Discussion

Molecular Structure. The molecular structure of palythine is illustrated in Fig. 1, where each atom is represented as a thermal ellipsoid enclosing a 50% probability. As can be seen in Fig. 1, the molecular framework obtained corresponds to the structure **1**. Since the proton of the carboxyl group is transferred to the nitrogen atom, in the crystalline state palythine exists as a zwitter ion which is stabilized by resonance between the two nearly-equivalent structures, **2a** and **2b**. The bond distances and angles and the dihedral angles are listed in Tables 4 and 5 respectively. If the H(N1a) atom and the CH_2COO^- group are excluded,

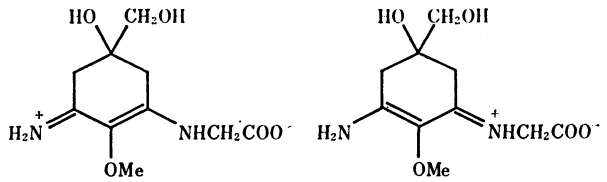

2a **2b**

TABLE 4. THE BOND DISTANCES (l/Å) AND ANGLES (ϕ/°), WITH THEIR STANDARD DEVIATIONS
The standard deviations given in parentheses refer to the last decimal position.

C(1)–C(2)	1.392(2)	O(W1)–H(W1a)	0.73(5)	C(5)–C(7)–O(3)	110.7(2)
C(1)–C(6)	1.496(3)	O(W1)–H(W1b)	0.87(5)	C(5)–C(7)–H(7a)	107(2)
C(1)–N(1)	1.317(2)	O(W2)–H(W2a)	0.81(5)	C(5)–C(7)–H(7b)	107(2)
C(2)–C(3)	1.394(2)	O(W2)–H(W2b)	0.86(4)	O(3)–C(7)–H(7a)	108(2)
C(2)–O(1)	1.381(2)	O(W3)–H(W3a)	0.82(5)	O(3)–C(7)–H(7b)	111(2)
C(3)–C(4)	1.503(3)	O(W3)–H(W3b)	0.76(6)	H(7a)–C(7)–H(7b)	113(2)
C(3)–N(2)	1.327(2)	C(2)–C(1)–C(6)	120.4(2)	O(1)–C(8)–H(8a)	106(2)
C(4)–C(5)	1.525(3)	C(2)–C(1)–N(1)	121.9(2)	O(1)–C(8)–H(8b)	107(2)
C(4)–H(4a)	0.96(3)	C(6)–C(1)–N(1)	117.7(2)	O(1)–C(8)–H(8c)	110(2)
C(4)–H(4b)	0.98(3)	C(1)–C(2)–C(3)	121.8(2)	H(8a)–C(8)–H(8b)	108(3)
C(5)–C(6)	1.525(2)	C(1)–C(2)–O(1)	118.6(2)	H(8a)–C(8)–H(8c)	113(3)
C(5)–C(7)	1.531(3)	C(3)–C(2)–O(1)	119.5(2)	H(8b)–C(8)–H(8c)	113(3)
C(5)–O(2)	1.434(2)	C(2)–C(3)–C(4)	120.4(2)	C(10)–C(9)–N(2)	113.9(2)
C(6)–H(6a)	1.01(4)	C(2)–C(3)–N(2)	119.2(2)	C(10)–C(9)–H(9a)	108(2)
C(6)–H(6b)	0.93(4)	C(4)–C(3)–N(2)	120.4(2)	C(10)–C(9)–H(9b)	107(2)
C(7)–O(3)	1.425(2)	C(3)–C(4)–C(5)	113.2(2)	N(2)–C(9)–H(9a)	110(2)
C(7)–H(7a)	0.94(3)	C(3)–C(4)–H(4a)	109(2)	N(2)–C(9)–H(9b)	110(2)
C(7)–H(7b)	0.93(2)	C(3)–C(4)–H(4b)	107(2)	H(9a)–C(9)–H(9b)	107(3)
C(8)–O(1)	1.433(3)	C(5)–C(4)–H(4a)	108(2)	C(9)–C(10)–O(4)	119.1(2)
C(8)–H(8a)	1.01(4)	C(5)–C(4)–H(4b)	108(2)	C(9)–C(10)–O(5)	115.6(2)
C(8)–H(8b)	0.99(3)	H(4a)–C(4)–H(4b)	112(2)	O(4)–C(10)–O(5)	125.2(2)
C(8)–H(8c)	1.00(4)	C(4)–C(5)–C(6)	111.0(1)	C(1)–N(1)–H(N1a)	118(2)
C(9)–C(10)	1.531(3)	C(4)–C(5)–C(7)	110.9(2)	C(1)–N(1)–H(N1b)	119(2)
C(9)–N(2)	1.455(2)	C(4)–C(5)–O(2)	111.0(1)	H(N1a)–N(1)–H(N1b)	123(3)
C(9)–H(9a)	0.96(3)	C(6)–C(5)–C(7)	110.5(1)	C(3)–N(2)–C(9)	126.2(2)
C(9)–H(9b)	0.93(4)	C(6)–C(5)–O(2)	105.8(1)	C(3)–N(2)–H(N2)	119(2)
C(10)–O(4)	1.228(3)	C(7)–C(5)–O(2)	107.5(1)	C(9)–N(2)–H(N2)	115(2)
C(10)–O(5)	1.251(3)	C(1)–C(6)–C(5)	112.3(2)	C(2)–O(1)–C(8)	113.3(2)
N(1)–H(N1a)	0.86(3)	C(1)–C(6)–H(6a)	112(2)	C(5)–O(2)–H(O2)	110(2)
N(1)–H(N1b)	0.86(3)	C(1)–C(6)–H(6b)	105(2)	C(7)–O(3)–H(O3)	108(3)
N(2)–H(N2)	0.86(3)	C(5)–C(6)–H(6a)	108(2)	H(W1a)–O(W1)–H(W1b)	108(5)
O(2)–H(O2)	0.86(3)	C(5)–C(6)–H(6b)	107(2)	H(W2a)–O(W2)–H(W2b)	108(4)
O(3)–H(O3)	0.80(4)	H(6a)–C(6)–H(6b)	113(3)	H(W3a)–O(W3)–H(W3b)	103(6)

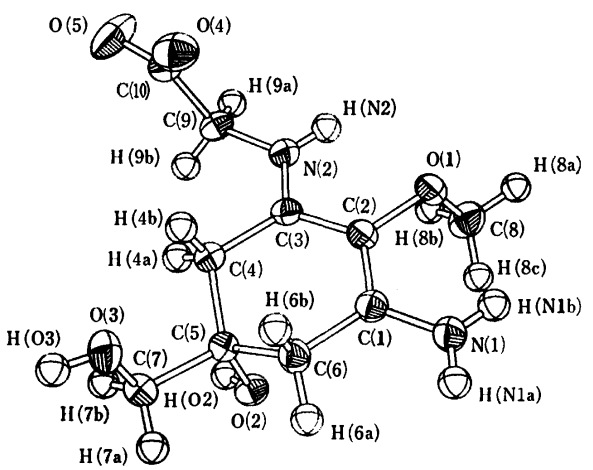

Fig. 1. A perspective view of the palythine molecule. For hydrogen atoms, a B value of 2 Å^2 was used.

the zwitter ion is almost symmetrical with respect to the plane determined by the C(2), C(5), and O(2) atoms.

The six-membered ring takes an envelope-like form in which the C(5) atom is 0.579 Å apart from the least-squares plane for the other five atoms. The deviations of the other atoms from this plane are as follows: C(1), 0.039 Å; C(2), −0.031 Å; C(3), 0.006 Å; C(4), 0.009 Å; C(6), −0.023 Å; N(1), 0.117 Å; N(2), 0.038 Å; O(1), −0.097 Å. All the bond distances in the ring are normal. The average of the C(1)-N(1) and C(3)-N(2) bond distances is 1.322 Å, which is somewhat small compared with the C–N distances (1.334 Å) in pyrazine[6] and 1,2,4,5-tetrazine,[7] and almost equal to the lengths of amide linkages, CO–NH.[8] This bond shortening may be related to the cationic nature of the conjugated system, since the C–NH part in amides also carries a considerable positive charge.

In a crystalline state, a carbon atom of a methoxyl group attached to an aromatic ring usually lies nearly on the ring plane. However, since the present molecule has amino or imino groups at both of the two positions *ortho* to the methoxyl group, the C(8) atom deviates remarkably from the C(1)-C(2)-C(3) plane in the same direction as the O(2) atom. The H(N1b) and H(N2) atoms are situated at distances of 2.42 and 2.37 Å from the O(1) atom respectively. An NMR study of 2-substituted 1,3-phenylenediamines and their *N,N'*-diacyl derivatives has revealed that, for the 2-methoxy compound in a deuterochloroform solution, a weak, but still effective, dual intramolecular hydrogen bonding is formed.[9] Accordingly, the N(1)···O(1) and N(2)···O(1) contacts in the palythine molecule can be taken as intramolecular hydrogen bonds.

Of the two groups bonded to the C(5) atom, the larger, CH_2OH group occupies the equatorial position, and the smaller, OH group, the axial. Although, from the standpoint of steric repulsion, a structure in which the O(3)H group takes a *trans* conformation with one of the two bulky methylene groups around the C(5)-C(7) bond can be expected to be the most stable, in fact,

Table 5. The dihedral angles (ϕ/°)
The A–B–C–D angle is positive if, when looking along B to C, A has to be rotated clockwise to eclipse D.

C(6)-C(1)-C(2)-C(3)	−8.0	C(4)-C(5)-C(6)-C(1)	−49.9
C(6)-C(1)-C(2)-O(1)	174.0	C(4)-C(5)-C(6)-H(6a)	−173
N(1)-C(1)-C(2)-C(3)	174.2	C(4)-C(5)-C(6)-H(6b)	65
C(2)-C(1)-C(6)-C(5)	31.1	C(7)-C(5)-C(6)-C(1)	−173.3
C(2)-C(1)-C(6)-H(6a)	152	O(2)-C(5)-C(6)-C(1)	70.6
C(2)-C(1)-C(6)-H(6b)	−85	C(4)-C(5)-O(2)-H(O2)	−42
N(1)-C(1)-C(6)-C(5)	−151.1	C(6)-C(5)-O(2)-H(O2)	−162
C(2)-C(1)-N(1)-H(N1a)	179	C(7)-C(5)-O(2)-H(O2)	80
C(2)-C(1)-N(1)-H(N1b)	0	C(4)-C(5)-C(7)-O(3)	−63.3
C(6)-C(1)-N(1)-H(N1a)	2	C(4)-C(5)-C(7)-H(7a)	179
C(1)-C(2)-C(3)-C(4)	5.1	C(4)-C(5)-C(7)-H(7b)	58
C(1)-C(2)-C(3)-N(2)	−174.9	C(6)-C(5)-C(7)-O(3)	60.2
O(1)-C(2)-C(3)-C(4)	−177.0	O(2)-C(5)-C(7)-O(3)	175.2
C(1)-C(2)-O(1)-C(8)	86.5	C(2)-O(1)-C(8)-H(8a)	−175
C(3)-C(2)-O(1)-C(8)	−91.5	C(2)-O(1)-C(8)-H(8b)	70
C(2)-C(3)-C(4)-C(5)	−25.6	C(2)-O(1)-C(8)-H(8c)	−53
C(2)-C(3)-C(4)-H(4a)	−146	C(3)-N(2)-C(9)-C(10)	81.7
C(2)-C(3)-C(4)-H(4b)	93	C(3)-N(2)-C(9)-H(9a)	−156
N(2)-C(3)-C(4)-C(5)	154.4	C(3)-N(2)-C(9)-H(9b)	−39
C(2)-C(3)-N(2)-C(9)	180.0	H(N2)-N(2)-C(9)-C(10)	−94
C(2)-C(3)-N(2)-H(N2)	−5	N(2)-C(9)-C(10)-O(4)	−10.2
C(4)-C(3)-N(2)-C(9)	0.1	N(2)-C(9)-C(10)-O(5)	171.7
C(3)-C(4)-C(5)-C(6)	47.4	H(9a)-C(9)-C(10)-O(4)	−133
C(3)-C(4)-C(5)-C(7)	170.6	H(9b)-C(9)-C(10)-O(4)	112
C(3)-C(4)-C(5)-O(2)	−70.0	C(5)-C(7)-O(3)-H(O3)	168
H(4a)-C(4)-C(5)-C(6)	168	H(7a)-C(7)-O(3)-H(O3)	−75
H(4b)-C(4)-C(5)-C(6)	−71	H(7b)-C(7)-O(3)-H(O3)	49

the O(3)H group has *gauche* relations with both of the methylene groups. The preference of the present conformation may be due not only to the electrostatic repulsion between the negatively-charged atoms, O(2) and O(3), but also to the hydrogen-bond formation of the O(3)H group with adjacent molecules.

The carboxylate ion group is placed on the opposite side of the mean plane for the N(1)–C(1)–C(2)–C(3)–N(2) conjugated system to the $C(8)H_3$ group. The carboxylate plane is approximately perpendicular to the C(3)–N(2)–C(9) plane, and the O(4) atom nearly eclipses the N(2) atom around the C(9)–C(10) bond. As a result, the H(4a) and H(9b) atoms are very close to each other, the distance between them being only 2.10 Å.

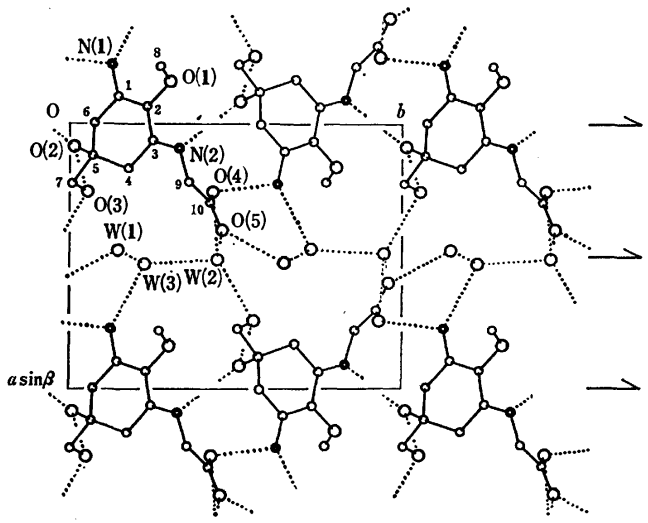

Fig. 2. The crystal structure viewed along the c axis.

TABLE 6. THE HYDROGEN BONDS, X–H···Y

X	Y	X···Y (*l*/Å)	H···Y (*l*/Å)	X–H···Y (*φ*/°)
(1) intramolecular				
N(1)	O(1)	2.751(2)	2.42(3)	104(2)
N(2)	O(1)	2.723(2)	2.37(3)	105(2)
(2) intermolecular				
N(1)	O(4)[b]	2.809(3)	1.97(3)	167(3)
N(1)	O(W3)[c]	2.906(3)	2.11(3)	156(3)
N(2)	O(2)[d]	3.039(2)	2.20(3)	163(3)
O(2)	O(3)[e]	2.855(2)	1.99(3)	174(3)
O(3)	O(W2)[a]	2.785(2)	2.04(4)	154(4)
O(W1)	O(5)[f]	2.810(3)	2.10(5)	166(5)
O(W1)	O(W3)[g]	2.927(3)	2.06(5)	177(5)
O(W2)	O(4)[h]	2.987(3)	2.26(4)	149(4)
O(W2)	O(5)[h]	3.130(3)	2.38(4)	154(4)
O(W2)	O(5)[f]	2.704(3)	1.85(4)	174(5)
O(W3)	O(W1)[h]	2.893(3)	2.12(5)	159(4)
O(W3)	O(W2)[a]	2.831(3)	2.07(6)	178(5)

The symmetry codes are: a) x, y, z (given in Table 3); b) $-x, -1/2+y, -z$; c) $-x, 1/2+y, -z$; d) $-x, 1/2+y, 1-z$; e) $x, y, 1+z$; f) $1-x, -1/2+y, 1-z$; g) $1-x, 1/2+y, 1-z$; h) $1-x, -1/2+y, -z$.

Crystal Structure. The projection of the crystal structure viewed along the c axis is shown in Fig. 2, while the details of the hydrogen bonds are given in Table 6. The palythine and water molecules are joined together into a three-dimensional hydrogen-bonded structure by twelve types of hydrogen bonds. Three groups, N(1)–H(N1b), N(2)–H(N2), and O(W2)–H(W2a), take part in bifurcated hydrogen bonds.[10] The first two make intermolecular hydrogen bonds with the O(W3)[c] and O(2)[d] atoms respectively, besides intramolecular ones with the O(1) atom. The last group donates its proton, H(W2a), to both of the two oxygen atoms in the same carboxylate group, O(4)[h] and O(5)[h]. Although the O(W2)···O(4)[h] and O(W2)···O(5)[h] distances are somewhat different, the O(W2)–H(W2a)···O(4)[h] and O(W2)–H(W2a)···O(5)[h] angles are nearly equal to each other, 149 and 154° respectively.

References

1) I. Tsujino, K. Yabe, I. Sekikawa, and N. Hamanaka, *Tetrahedron Lett.*, **1978**, 1401.
2) S. Takano, D. Uemura, and Y. Hirata, *Tetrahedron Lett.*, **1978**, 2299.
3) J. Karle and I. L. Karle, *Acta Crystallogr.*, **21**, 849 (1966).
4) A. Furusaki, *Acta Crystallogr., Sect. A*, **35**, 220 (1979).
5) "International Tables for X-Ray Crystallography," The Kynoch Press, Birmingham (1974), Vol. IV.
6) P. J. Wheatley, *Acta Crystallogr.*, **10**, 182 (1957).
7) F. Bertinotti, G. Giacomello, and A. M. Liquori, *Acta Crystallogr.*, **9**, 510 (1956).
8) "Molecular Structures and Dimensions," ed by O. Kennard, D. G. Watson, F. H. Allen, N. W. Isaacs, W. D. S. Motherwell, R. C. Pettersen, and W. G. Town, The International Union of Crystallography and The Crystallographic Data Center, Cambridge, England (1972), Vol. A1.
9) B. D. Andrews and I. D. Rae, *Aust. J. Chem.*, **24**, 413 (1971).
10) G. A. Albrecht and R. B. Corey, *J. Am. Chem. Soc.*, **61**, 1087 (1939).

Catalytic Properties of Iron Oxides. II.[1] Isotopic Exchange of Oxygen, Oxidation of Carbon Monoxide, and Reduction-Oxidation Mechanism

Kanji SAKATA, Fumio UEDA, Makoto MISONO,* and Yukio YONEDA

Department of Synthetic Chemistry, Faculty of Engineering, The University of Tokyo, Hongo, Bunkyo-ku, Tokyo 113

(Received May 4, 1979)

The reactivity and mobility of the lattice oxygen of iron oxide, in particular γ-Fe_2O_3, has been investigated by ^{18}O-exchange with CO_2 and CO oxidation by $^{18}O_2$. The low mobility of the lattice oxygen is in agreement with the reduction-oxidation mechanism of γ-Fe_2O_3 bulk, which proceeds by Fe ion migration without diffusion of the lattice oxygen. The rapid diffusion of the Fe ion makes the redox cycles of γ-Fe_2O_3 easy and explains, together with the cation deficient structure, the high reactivity and selectivity of lattice oxygen. Thus, γ-Fe_2O_3 may be regarded as a new prototype of selective catalyst for allylic oxidation.

Iron oxide catalyst is widely used either as a single metal oxide or as a mixed oxide in industrial processes such as dehydrogenation (*e.g.* ethylbenzene to styrene and methanol to formaldehyde), the water gas shift reaction, and the reduction of nitrogen monoxide.[2] Among the oxides of the first transition metals, iron oxide exhibits intermediate activity in the complete oxidation of methane, carbon monoxide, and isotopic equilibration of oxygen,[3] but is not a good catalyst in the partial oxidation of hydrocarbons.[4,5]

It has been demonstrated that iron oxide becomes very active and selective in the oxidative dehydrogenation of butenes, when the structure of iron oxide is transformed from the α-form (hematite; a corundum structure) to the γ-form (maghemite; an inverse spinel).[6] This high activity and selectivity of γ-Fe_2O_3 was confirmed in catalytic reactions in both pulse and flow reactors at 250—300 °C.[6c] This temperature range is considerably lower than that employed for Bi_2O_3–MoO_3 catalysts.[7]

The importance of structural factors and the oxidation state of iron oxide catalysts may be inferred from the following. In the dehydrogenation of ethylbenzene, the addition of alkali metal to or the pre-reduction of iron oxide increases the selectivity significantly. It has been suggested that this effect is not only electronic but also structural.[8] In this reaction, the oxidation state of iron oxide has been reported to be important.[9] Changes in structure under the reaction conditions of oxidative dehydrogenation of butenes was observed by Sazonova *et al.*,[10] who attributed this change to the reduction of α-Fe_2O_3 to Fe_3O_4. This change is probably however a transformation to γ-Fe_2O_3 based on our results. In ferrite catalysts, distribution of metal ions into tetrahedral (Td) sites and octahedral (Oh) sites appears to be connected to the catalytic activity for the dehydrogenation of butenes.[11]

In a previous report the catalytic activity of iron oxide in the oxidation of butene was investigated as a function of the structure and oxidation state, the results of which are summarized as follows:

(i) The activity for butadiene formation varies markedly with the bulk structure and the oxidation state, *i.e.* γ-$Fe_2O_3 > \alpha$-$Fe_2O_3 \gg Fe_3O_4$.[6]

(ii) Lattice oxygen is the reactive oxygen species and the redox mechanism which comprises reduction-oxidation cycles of iron oxide is operative.[6]

(iii) The allylic species is probably the reaction intermediate in view of the substituent effect of the reactant.[6b]

The last two facts apparently coincide with those reported for Bi_2O_3–MoO_3.** In Bi_2O_3–MoO_3, oxygen tracer studies coupled with kinetic studies have revealed that oxidation proceeds by redox cycles of catalyst and the lattice oxygen is directly involved in the reaction.[7,12] The importance of the high mobility of oxygen in the bulk oxide has been pointed out in this oxide and also for other related mixed oxides.[13] These mixed oxides form one group of oxidation catalysts, in which Bi_2O_3–MoO_3 may be considered a prototype.

The aim of the present study has been to investigate the reactivity and mobility of the lattice oxygen of iron oxide, particularly in γ-Fe_2O_3, and to elucidate the redox process which is pertinent to the catalytic oxidation. Stress has been placed on the similarity and contrasts of iron oxide to Bi_2O_3–MoO_3, to provide a new prototype of oxidation catalyst, comprising a single metal oxide.

Experimental

Apparatus. A conventional pulse reactor and a closed circulation reactor were used for the reactions. The pulse technique used was the same as described elsewhere.[6] Oxygen impurities in the He carrier gas were removed by a molecular-sieve trap kept at the temperature of liquid-nitrogen. The closed circulation system, equipped with a mercury manometer, a magnetic circulation pump, and a gas-sampling valve for the measurement of mass spectra, had a volume of *ca.* 200 cm^3 and was readily evacuated to 10^{-3} Pa by a rotary pump and an oil diffusion pump.

Catalysts and Reagents. α-Fe_2O_3 (BET surface area: 10 $m^2\,g^{-1}$) was prepared from $Fe(NO_3)_3$ (Kishida Chemical Co.) as described previously.[6] γ-Fe_2O_3 was prepared from α-Fe_2O_3 by two methods. In the pulse reactor, α-Fe_2O_3 was reduced

** Both iron oxide and Bi_2O_3–MoO_3 are selective catalysts for butene oxidation, but the former is not a selective catalyst for the oxidation of propene to acrolein. This difference may be attributed to the low activity of iron oxide in the reaction step of oxygen addition to the allylic intermediate. Both oxides are however very similar for the allyl formation (abstraction of an allyl hydrogen by oxygen on metal oxides). This step is often considered the key reaction of allylic oxidation.

by CO pulses to Fe_3O_4 and then re-oxidized by O_2 or N_2O pulses to γ-Fe_2O_3 at 200—300 °C. The structures of α- and γ-Fe_2O_3 prepared by this procedure were confirmed by X-ray powder diffraction patterns and Mössbauer spectra. γ-Fe_2O_3 was also prepared in the closed circulation system by reducing α-Fe_2O_3 to Fe_3O_4 with pure CO or mixtures of CO and CO_2, followed by re-oxidation with O_2. As described in the following section the reduction of iron oxide by CO in a closed system appeared to partially form Fe metal and Fe carbide.

O_2 enriched in ^{18}O(^{18}O: 20 or 70 atom %) was purchased from Japan Radioisotope Association. $C^{18}O_2$(^{18}O: 10 or 35 atom %) was prepared by oxidizing CO with ^{18}O-enriched O_2 over iron oxide at 300 °C and used without further treatment.

Procedures. Both ^{18}O-exchange between CO_2(or O_2) and iron oxide and CO oxidation over iron oxide using $^{18}O_2$ were conducted in the closed circulation reactor. Prior to reaction, the iron oxide samples (300 or 600 mg) were evacuated in the closed system for 1 h at 300 °C, treated with pure O_2 (13 kPa) at 300 °C (with circulation and a liquid nitrogen trap), and finally evacuated for 1 h at the reaction temperature. ^{18}O distributions in CO, O_2, and CO_2 in the gas phase was analyzed by a mass spectrometer (Hitachi Co, Ltd.) after intermittent sampling. After the run, the catalyst was subjected to X-ray powder diffraction analysis by a Geigerflex ECP-TG (Rigaku Denki Co.) with Cu $K\alpha$ irradiation. Analysis showed that the structure of the catalyst did not change before and after the run.

Results

Oxygen-18 Exchange between CO_2 or O_2 and Iron Oxide. The reactivity of the lattice oxygen of the iron oxide was investigated by ^{18}O-exchange between ^{18}O-labeled CO_2 (10 Torr) and iron oxide (600 mg). Figure 1 illustrates the changes of ^{18}O content (atomic fraction) in CO_2 with reaction time, where the ^{18}O contents relative to the initial ^{18}O content are given. The reaction temperature was raised in steps from 150 °C to 300 °C as indicated in the figure. The times required to raise the temperature from 150 to 220 °C and from 220 to 300 °C were 10—15 min each.

From Fig. 1 it may be seen that the ^{18}O content became constant within 5 min after the introduction of CO_2 over both α- and γ-Fe_2O_3 at 150 °C. In all runs, the ^{18}O distributions in CO_2 in the gas phase were always in equilibrium, *i.e.* $[C^{16}O^{18}O]^2/\{[C^{18}O_2]\times[C^{16}O_2]\}=4$. In the case of α-Fe_2O_3, a small decrease of the ^{18}O content in CO_2 with reaction time was observed at 220 and 300 °C (Fig. 1), but this decrease was very small and negligible compared with the total change of the ^{18}O content in CO_2.

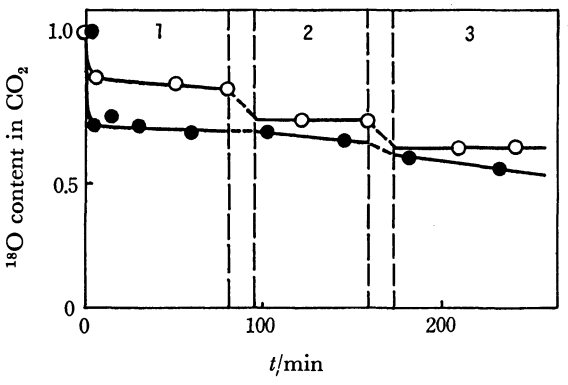

Fig. 1. Isotopic exchange of oxygen between $C^{18}O_2$ and Fe_2O_3.
React. temp (°C), 1: 150, 2: 220, 3: 300.
○: γ-Fe_2O_3, ●: α-Fe_2O_3, Fe_2O_3: 0.6 g, P_{CO_2}: 1 cmHg. ^{18}O content is relative to the initial content.

The indication is that oxygens of the iron oxides exchange rapidly with CO_2, but the degree of exchange is very small: 1.4 cm^3 NTP g^{-1} (0.5) for α-Fe_2O_3 and 0.9 cm^3 NTP g^{-1} (0.3) for γ-Fe_2O_3 at 150 °C. At 300 °C, the values are 3.5 (1.3) and 2.7 cm^3 NTP g^{-1} (1.0) for α- and γ-Fe_2O_3, respectively. The numbers in parentheses are the amounts of exchangeable oxygen in terms of surface layers, calculated by assuming the number of oxygen in one layer to be 1.5×10^{19} atom m^{-2} (see Discussion). Consequently, the amounts of exchangeable oxygen are comparable to or smaller than one surface layer.

Oxygen exchange between $^{18}O_2$ and iron oxide was very slow, *e.g.* 0.6 cm^3 NTP g^{-1} (0.2 surface layer) exchanged after 4 h at 300 °C and the isotope distributions in O_2 remained far from equilibrium, indicating that isotopic equilibration of O_2 was also very slow. Therefore, the activation of molecular oxygen on iron oxides in the fully oxidized state is a slow process.

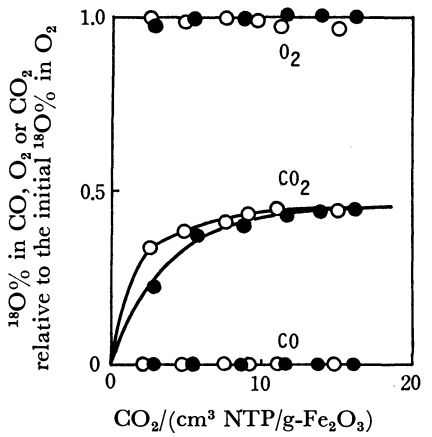

Fig. 2. ^{18}O contents in CO, O_2 and CO_2 during CO oxidation by $^{18}O_2$ over α- and γ-Fe_2O_3 at 150 °C.
○: γ-Fe_2O_3, ●: α-Fe_2O_3.

CO Oxidation by $^{18}O_2$. CO oxidation by $^{18}O_2$ was conducted at 150 °C, to determine the amount of oxygen atoms in iron oxide participating in catalytic oxidation. The ^{18}O contents in CO, O_2, and CO_2 are plotted in Fig. 2 as a function of the amount of CO_2 produced, where the ^{18}O contents are all normalized to the initial ^{18}O content in O_2. Over both α- and γ-Fe_2O_3, the ^{18}O content in CO_2 produced at the initial stage was low and then gradually increased with reaction time as shown in Fig. 2. The ^{18}O distributions in CO_2 were always in equilibrium during the reaction. In contrast to CO_2, ^{18}O-exchange between CO or O_2 and iron oxide did not occur at all, as seen from the constant ^{18}O contents in O_2 and CO during the reaction. Isotopic equilibration in O_2 was also absent.

From these data, it is possible to calculate the amount

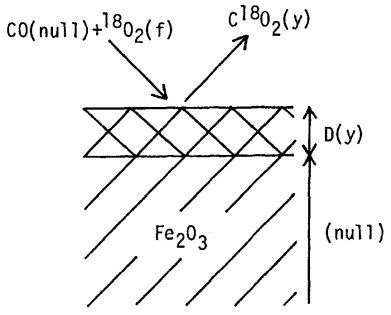

Fig. 3. Model for calculation of the amount of lattice oxygen participating in CO oxidation by $^{18}O_2$.
( ): ^{18}O content (%)
D: the amount of lattice oxygen participating in CO oxidation (see text).
f and y are ^{18}O% in O_2 and CO_2, respectively.

of oxygen atoms in iron oxide, which participate in the CO oxidation. Since the ^{18}O-exchange between CO_2 and iron oxide was very rapid as shown in Fig. 1, the amount of oxygen atoms calculated here includes those which participated only in the ^{18}O-exchange between CO_2 and iron oxide, in addition to the lattice (or surface) oxygen atoms which were incorporated into CO_2 directly by the oxidation reaction. In other words, only the upper limit of the lattice (or surface) oxygen atoms which have participated directly in CO oxidation can be determined. The calculation was conducted in the following manner. Since the oxygen exchange between the surface and CO_2 is rapid, it is reasonable to place the ^{18}O content in the catalyst surface equal to the ^{18}O content in CO_2 at each reaction time. The model for CO oxidation by $^{18}O_2$ over iron oxide is shown in Fig. 3. It was assumed that the surface layer of the catalyst which participates equally in the reaction has a uniform ^{18}O concentration to a depth of D (expressed in $cm^3\,NTP\,g^{-1}$) and that the lattice oxygen in the bulk deeper than this layer (depth$>D$) does not participate in the reaction (^{18}O: 0%). The method reported by Miura *et al.*[14] was subsequently applied for the calculation, where the contribution from ^{18}O-exchange between CO_2 and catalyst surface was additionally taken into account. In Fig. 3, p, y, and f represent the amount ($cm^3\,NTP\,g^{-1}$) of CO_2 produced, the ^{18}O content (%) in CO_2 at reaction time t (min), and the ^{18}O content (%) in O_2, respectively. The mass balance of the ^{18}O in the catalyst surface layer D at reaction time t is represented by Eq. 1.

$$D\mathrm{d}y = f\mathrm{d}p - 2\mathrm{d}(py) \quad (1)$$

$$p = D\cdot y/(f-2y) \quad (2)$$

Integration of Eq. 1 at the initial conditions of $p=0$ and $y=0$ gives Eq. 2. Equation 2 shows that a plot of p against $y/(f-2y)$ gives a slope ($=D$) which represents the amount of oxygen in the catalyst participating in CO oxidation (oxygen atom, $cm^3\,NTP\,g^{-1}$). The results in Fig. 2 are plotted in Fig. 4, according to Eq. 2. From the slopes of the linear plots in this figure, the amounts of oxygen at 150 °C have been calculated as 3.3 (1.2) and 2.0 $cm^3\,NTP\,g^{-1}$ (0.7 surface layers) for α- and γ-Fe_2O_3, respectively (numbers in parentheses are in terms of surface layers). These values are comparable with the amount of exchangeable oxygen with

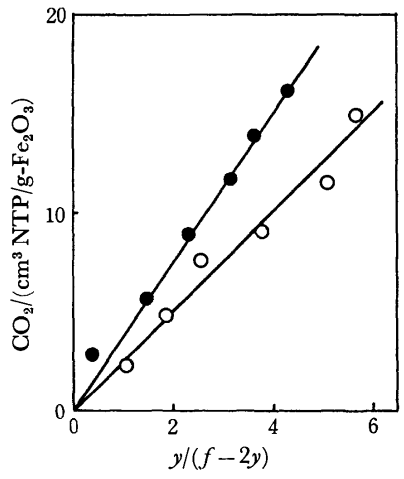

Fig. 4. Plots of CO_2 produced *vs.* $y/(f-2y)$ (Eq. 2) for the calculation of the amount (D) of lattice oxygen participating in CO oxidation by $^{18}O_2$.
○: γ-Fe_2O_3, ●: α-Fe_2O_3
Slope of linear plot gives D.
f and y are the same as in Fig. 3.

CO_2 and demonstrate that the amount of oxygen participating directly in the reaction is at most one or two surface layers even during the CO oxidation.

Reduction-Oxidation (Redox) Mechanism of γ-Fe_2O_3. The reduction and re-oxidation of the bulk of iron oxide was very rapid, and this rapid redox process appeared connected with the high activity and selectivity observed for oxidative dehydrogenation.[6] The results indicate however that the lattice oxygen has low mobility in the bulk. Therefore, an attempt was made to determine which ion (O^{2-} or Fe^{3+}) diffused during the redox process. The method is schematically drawn in Scheme 1. γ-$Fe_2{}^{18}O_3$ prepared by the re-oxidation of Fe_3O_4 by

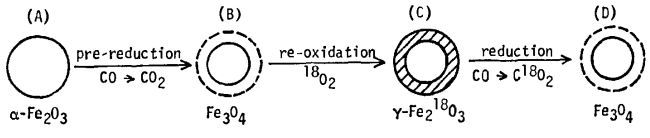

Scheme 1. Changes of one sample particle are schematically drawn. Shaded area is the layer formed by re-oxidation, which is eliminated by subsequent reduction.

$^{18}O_2$ (Scheme 1, A→B→C) was gradually reduced by CO (Scheme 1, C→D), in which the ^{18}O contents of CO_2 produced were measured as a function of the degree of reduction, x in γ-Fe_2O_{3-x}. The degree of reduction, x, has been evaluated from the amount of CO_2 produced (x of Fe_3O_4=0.33). The ^{18}O recovery is defined as

$$^{18}O\text{ recovery} = 2\times[^{18}O\%\text{ in }CO_2\text{ produced during the reduction by CO}]/[^{18}O\%\text{ in }O_2\text{ used for the re-oxidation}] \quad (3)$$

The ^{18}O recovery is expected to be as follows, depending on the rate of oxygen diffusion. (1) If lattice oxygen does not migrate during the $^{18}O_2$ re-oxidation and the subsequent CO reduction, ^{18}O should be uniformly contained only in the surface layer formed by the re-oxidation, the ^{18}O content in this layer being identical

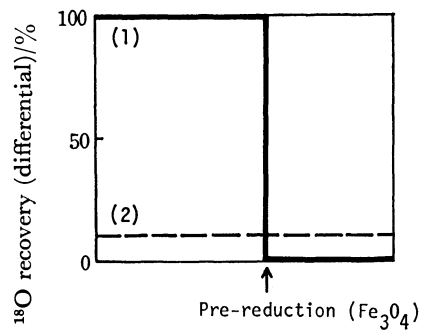

Fig. 5. ^{18}O recovery (differential) expected for the process C→D in Scheme 1 for two extreme cases.
(1) No oxygen diffusion,
(2) rapid oxygen diffusion.

to that in $^{18}O_2$ used for the re-oxidation. Therefore, the differential ^{18}O recovery, which is defined as the ^{18}O recovery for a small increment of CO_2 formation, should be 100% until the γ-$Fe_2{}^{18}O_3$ is reduced to the state of the pre-reduction (Scheme 1, B), and nil (zero) on further reduction (Fig. 5, full line). (2) If lattice oxygen diffuses very rapidly (complete mixing of lattice oxygens), the differential ^{18}O recovery is constant and equal to the amount determined by the reaction stoichiometry: 11% for γ-Fe_2O_3 in the present experiment (Fig. 5, broken line). Thus the ^{18}O recovery reflects the change in the ^{18}O concentration from the surface to the center and, therefore, the rate of diffusion of the oxide ion (Fig. 6).

In Exp. 1, both the CO reduction and $^{18}O_2$ re-oxidation were performed in a closed circulation system at 250 °C. The ^{18}O recovery was 66% after corrections for the ^{18}O-exchange between iron oxide and CO_2. The migration of lattice oxygen was slow but not negligible. This rather low recovery of ^{18}O may be attributed to a diffusion of lattice oxygen accelerated by the increase of temperature caused by the exothermic re-oxidation step. Therefore, the reaction temperature of the re-oxidation step was lowered from 250 °C to 150 °C in Exp. 2, but there was only a small increase in ^{18}O recovery (65—71%). Another possible explanation for the low ^{18}O recovery is the formation of iron metal or iron carbide in the reduction step ($CO+Fe_2O_3 \rightarrow CO_2+Fe$, FeC_n). In Exp. 3, reduction was carried out with a mixture of CO and CO_2. The ^{18}O recovery increased slightly (72—73%) but the formation of iron metal and iron carbide was still indicated since the reduction-oxidation was not completely stoichiometric and a small amount of CO_2 was formed on re-oxidation. Finally, CO reduction (both pre-reduction and final reduction) was performed with the pulse method and re-oxidation by $^{18}O_2$ with the closed circulation system (Exp. 4), by transferring the sample between the two systems without exposing it to air. In this method, the reduction and subsequent re-oxidation of α-$Fe_2O_3 \rightarrow Fe_3O_4 \rightarrow \gamma$-$Fe_2O_3$ was confirmed at each step stoichiometrically and by X-ray diffraction analysis and Mössbauer spectroscopy. Further, there was no change in surface area.

As shown in Fig. 6, by using γ-$Fe_2{}^{18}O_3$ thus prepared the ^{18}O recovery increased to 91% at the reduction stage of $x=0.25$ and was 83% at $x=0.33$ (reduction to Fe_3O_4). Therefore, it may be assumed that little diffusion of lattice oxygen took place during the redox cycle.

Exp.	Redox conditions: Re-oxid.	Red.	Total recovery of ^{18}O (%)
	$^{18}O_2$	CO	
1	250°C	250°C	62 - 66
	C	C	
	$^{18}O_2$	CO	
2	150°C	230°C	65 - 71
	C	C	
	$^{18}O_2$/He	CO+CO_2	
3	200°C	270°C	72 - 73
	C	C	
	$^{18}O_2$	CO/He	
4	200°C	300°C	82 - 83
	C	P	

C: circulation system
P: pulse reactor

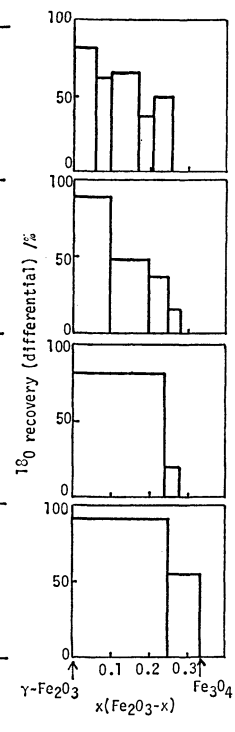

Fig. 6. ^{18}O recovery into CO_2 for the process, γ-$Fe_2{}^{18}O_2 + CO \rightarrow Fe_3O_4 + C^{18}O_2$.

Discussion

Mobility of Lattice Oxygen in Iron Oxide. As shown by the isotopic exchange of oxygen with CO_2 (Fig. 1) and the CO oxidation by $^{18}O_2$ (Figs. 2—4), the amount of lattice (surface) oxygen of iron oxide, which participates in these reactions was 0.9—3.5 cm^3 NTP/g-Fe_2O_3. This amount is equivalent to 0.4—1.4% of the total lattice oxygen and is very small compared with Bi_2O_3–MoO_3, for which the amount of oxygen participating in CO oxidation was about 20% of total lattice oxygen.[14] A remarkable contrast exists, therefore, between iron oxide and Bi_2O_3–MoO_3, although both catalysts are very similar.

Although iron oxide is not very active for the activation of the O_2 molecule below 300 °C, as seen from the very small rate observed in the ^{18}O-exchange with O_2, the ^{18}O-exchange between surface oxygen and CO_2 was rapid and equilibrium was reached almost instantaneously. The agreement of the amounts of exchangeable oxygen calculated for CO_2 exchange (Fig. 1) and CO oxidation (Fig. 4) may be due to the fact that both were determined by the same reaction, that is, the ^{18}O-exchange between CO_2 and iron oxide surface. This reaction is generally considered to proceed *via* a surface carbonate complex.[15] Over iron oxide the formation of surface carbonate from CO_2 has actually been detected

by infrared spectrometry.[16]

The amount of exchangeable oxygen of iron oxide calculated from the ^{18}O concentration of CO_2 after a long period of the reaction was 3.5 and 2.7 cm^3 NTP/g-Fe_2O_3 at 300 °C for α- and γ-Fe_2O_3, respectively. These values may be represented in terms of the number of surface layers and compared with those reported in the literature. Assuming the surface of iron oxide is composed of the maximum packing of oxide ion, the surface density is thus 1.5×10^{19} atom m^{-2} for the (111) surface (radius of O^{2-}; 1.40 Å). The actual surface density of oxide ion may be lower than this value, since the metal oxide surface is not fully covered with oxide ion. In general, the surface atom density is given as $1—2\times10^{19}$ atom m^{-2}.[17] Assuming the value of 1.5×10^{19} atom m^{-2}, the exchangeable oxygen at 300 °C obtained in the present work corresponds to 1.3 and 1.0 surface layers for α- and γ-Fe_2O_3, respectively. Based on the work of Nováková using Winter's data,[18] the amount of oxygen exchangeable with O_2 is 1.5—4 layers for α-Fe_2O_3 at 260—400 °C, the surface oxide density being assumed 0.6×10^{19} atom m^{-2}.[15] Boreskov *et al.* reported that 1.8 surface layers were exchangeable with O_2 at 350 °C (surface oxide density; 1.28×10^{19} atom m^{-2}).[19] The present results are in reasonable agreement with those reported values and demonstrate that the diffusion of the lattice oxygen of iron oxide between the surface layer (1—2 layers) and inner bulk is a very slow process during both CO_2-oxygen isotopic exchange and CO oxidation. It is thus concluded that the mobility of the lattice oxygen is small in the bulk of iron oxide under the conditions of catalytic oxidation.

Mechanism of CO Oxidation over Iron Oxide. The oxidation state of the iron oxide catalyst may be regarded as in the fully oxidized state (Fe_2O_3) when CO oxidation is taking place, on the basis of the following. The re-oxidation process of partially reduced iron oxide by O_2 was much faster than the reduction of iron oxide by CO when measured in the circulation system. Furthermore, the rate of CO oxidation was of zero order with respect to O_2 pressure. The iron oxide catalyst under the working conditions was also found to be Fe_2O_3 (α- or γ-) in the case of the oxidative dehydrogenation of butenes in the flow reactor and the reaction was of zero order in O_2 pressure.[6c]

The reactive oxygen species on the surface of iron oxide does not desorb into the gas phase unless reaction occurs with CO to form CO_2, *i.e.* the adsorption of oxygen is irreversible and probably dissociative. In Fig. 2 neither ^{18}O-exchange between O_2, CO, and the catalyst nor the equilibration of the oxygen isotope in gaseous O_2 was observed during the CO oxidation by $^{18}O_2$. Reversible and molecularly adsorbed oxygen that might explain the facts in Fig. 2 does not seem sufficiently reactive to participate directly in the CO oxidation, even if it exists. The irreversible adsorption process of oxygen can be the oxidation of the bulk to form lattice oxygen as discussed below.

From the agreement of the reactions of butene pulses with and without O_2 it was concurred that the lattice oxygen of iron oxide is the oxygen species responsible for oxidative dehydrogenation of butenes below 300 °C.[6a] The lattice oxygen is also probably the main oxygen species involved directly in the CO oxidation. The reactivity of γ-Fe_2O_3 with CO (non-catalytic) was examined and found independent of the oxidation state from γ-Fe_2O_3 to $Fe_2O_{2.8}$. This relationship between the reactivity and the extent of reduction was very similar to that observed for the oxidative dehydrogenation of butenes. Over γ-Fe_2O_3 however the rate of oxidation of CO pulsed together with O_2 was 1.6 times greater than that without O_2, indicating that the contribution of adsorbed oxygen to the activity can not be neglected. Therefore, both the lattice oxygen and adsorbed oxygen, although these are sometimes difficult to distinguish, must be considered in the mechanism of CO oxidation. The amount of adsorbed oxygen on α-Fe_2O_3 measured by thermal desorption was approx. 2.0% of one surface layer.[20]

The CO oxidation necessitates the transfer of two electrons. In the case that lattice oxygen is the active species, a two-centered mechanism which involves two Fe^{3+} ions operates. This is a typical redox mechanism of catalytic oxidation:

$$CO + 2Fe^{3+} + O^{2-}(\text{lattice}) \longrightarrow CO_2 + 2Fe^{2+}, \quad (4)$$

$$1/2O_2 + 2Fe^{2+} \longrightarrow 2Fe^{3+} + O^{2-}(\text{lattice}). \quad (5)$$

A one-centered mechanism is for an adsorbed O^- and a Fe^{3+} ion, *i.e.* the mechanism proposed for butene dehydrogenation over ferrite catalysts:[23]

$$CO + Fe^{3+} + O^- \longrightarrow CO_2 + Fe^{2+}, \quad (6)$$

$$1/2O_2 + Fe^{2+} \longrightarrow Fe^{3+} + O^-. \quad (7)$$

In both mechanisms, CO_2 is formed by the reaction of CO and the surface oxygen species to form vacant sites which are reoccupied by the oxygen from the gas phase. The second step, (5) or (7), is always instantaneous and irreversible. The two-centered mechanism, which is probably responsible for the major part of the reaction, occurs readily, since the electron exchange in iron oxide must be very easy owing to its high electric conductivity. The ease of the electron transfer or exchange must be an important factor in some catalytic oxidations.

Reduction-Oxidation Mechanism of Bulk Iron Oxide and Catalytic Activity. In this section, the catalytic activity and the reduction-oxidation (redox) mechanism of γ-Fe_2O_3 is discussed in terms of structural characteristics, particularly the similarity of its crystal structure to Fe_3O_4. While α-Fe_2O_3 has a corundum-type structure (oxide ions form a hexagonal close-packed array with Fe^{3+} ions occupying octahedral (Oh) interstices), both γ-Fe_2O_3 and Fe_3O_4 have an inverse-spinel structure (cubic close-packed array (ccp) of oxide ion).[24] For Fe_3O_4, two-thirds of the iron cations are Fe^{3+} ions which are distributed at Td sites and Oh sites. For γ-Fe_2O_3, one-ninth of the total cation sites are vacant, probably in Oh sites.[25] The dimension of the unit cell of γ-Fe_2O_3 is 8.350 Å, which is slightly smaller than that of Fe_3O_4 (8.390 Å).

The structural characteristics suggest the following redox process between γ-Fe_2O_3 and Fe_3O_4, in which the packing structure of oxide ion remains unchanged.

The oxidation of Fe_3O_4 to γ-Fe_2O_3 proceeds by the addition of oxygen atoms on the surface to form new oxide layers which have the same packing structure as in Fe_3O_4 (ccp). This process is accompanied by the migration of iron cations from the bulk into the newly formed oxide layer to compensate for the charge, forming cation vacancies. The reduction of γ-Fe_2O_3 to Fe_3O_4 may be exactly the reverse process: removal of the oxide layer and migration of iron cations inward to fill the vacancies in the bulk. Thus, in the case of γ-Fe_2O_3, only iron cation diffuses during the reduction-oxidation of the bulk.

Experimentally this was confirmed by Exp. 4 shown in Fig. 6. The redox model of γ-Fe_2O_3, discussed above, is shown schematically in Fig. 7. The redox mechanism of γ-Fe_2O_3 bulk without the diffusion of lattice oxygen is in agreement with the results shown in Figs. 1—4, which demonstrate the very slow diffusion of lattice oxygen. Therefore, the ready interconversion between Fe^{2+} and Fe^{3+}, and the comparatively rapid diffusion of iron cations between bulk and surface layer perhaps make the redox cycles of γ-Fe_2O_3 easy. In addition to the easy redox cycles, the high energetic lattice oxygen induced by cation vacancy (low coordination number of iron)[21] may also be responsible for the high reactivity of lattice oxygen in γ-Fe_2O_3.

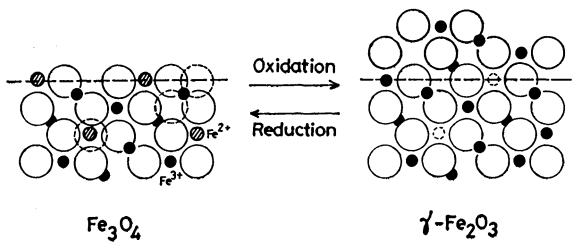

Fig. 7. Redox model of iron oxide for selective oxidation.

As discussed above, the oxidative dehydrogenation of butenes over γ-Fe_2O_3 resembles that over Bi_2O_3–MoO_3. The rapid diffusion of lattice oxygen in Bi_2O_3–MoO_3 originating from its layered structure[22] was however not observed for γ-Fe_2O_3. In the case of γ-Fe_2O_3 rapid diffusion of iron cations makes the redox cycles easy. Although the high reactivity and selectivity of both γ-Fe_2O_3 and Bi_2O_3–MoO_3 is attributed to the easy redox cycles of bulk and the high reactivity of lattice oxygen for allyl-type oxidation, their origin is quite different. Thus, γ-Fe_2O_3 may be regarded as another catalysts prototype for selective allylic oxidation.

References

1) Part I: M. Misono, Y. Nozawa, and Y. Yoneda, *Proc. 6th Int. Congr. Catal., London, 1976*, The Chemical Society (1977), p. 386.

2) M. Misono, "Kinzoku-sankabutsu To Fukugo-sankabutsu," ed by K. Tanabe, T. Seiyama, and K. Fueki, Kodansha, Tokyo (1978), p. 242.

3) G. K. Boreskov, V. V. Povovskii, and V. A. Sazonov, *Proc. 4th Int. Congr. Catal., Moskow, 1968*, Akademiai Kaido, Budapest (1971), p. 439; G. K. Boreskov, *Adv. Catal.*, **15**, 285 (1964).

4) T. Seiyama, N. Yamazoe, and M. Egashira, *Proc. 5th Int. Congr. Catal., Florida, 1972*, North-Holland Publishing Co. (1973), p. 997.

5) V. Fattore, Z. A. Fuhrman, G. Manara, and B. Notari, *J. Catal.*, **37**, 215 (1975).

6) a) M. Misono, Y. Nozawa, and Y. Yoneda, *Proc. 6th Int. Congr. Catal., London, 1976*, The Chemical Society (1977), p. 386; b) M. Misono, Y. Nozawa, and Y. Yoneda, *Shokubai*, **18**, 30 (1976); c) M. Misono, F. Ueda, K. Sakata, and Y. Yoneda, Ann. Symp. Catal. Soc. Japan, Toyama, 1977, C-17.

7) D. J. Hucknall, "Selective Oxidation of Hydrocarbons," Academic Press, London (1974).

8) E. H. Lee, *Catal. Rev.*, **8**, 285 (1974).

9) T. Hattori, Y. Murakami, M. Ii, and H. Uchida, *Kogyo Kagaku Zasshi*, **72**, 2188 (1969).

10) N. N. Sazonova, S. A. Venyaminov, and G. K. Boreskov, *Kinet. Katal.*, **14**, 1169 (1972).

11) R. J. Rennard and W. Kehl, *J. Catal.*, **21**, 282 (1971); U. S. Patent 3450787 (1969).

12) P. A. Batist, H. J. Prette, and G. C. A. Schuit, *J. Catal.*, **15**, 267 (1969); M. Egashira, H. Sumie, T. Sakamoto, and T. Seiyama, *Kogyo Kagaku Zasshi*, **73**, 860 (1970).

13) P. Pendleton and D. Taylor, *J. Chem. Soc., Faraday Trans. 1*, **72**, 1114 (1976).

14) H. Miura, Y. Morikawa, and T. Shirasaki, *Nippon Kagaku Kaishi*, **1975**, 1985.

15) J. Nováková, *Catal. Rev.*, **4**, 77 (1970).

16) V. G. Amerikov and L. A. Kasatkina, *Kinet. Katal.*, **12**, 165 (1969).

17) J. R. Anderson, "Structure of Metallic Catalysts," Academic Press Inc., London (1975), p. 296.

18) E. R. S. Winter, *J. Chem. Soc.*, **1968**, 2889.

19) G. K. Boreskov, L. A. Kasatkina, and V. G. Amerikov, *Kinet. Katal.*, **10**, 102 (1968).

20) a) T. Seiyama, "Kinzoku-sankabutsu To Sono Shokubai-sayo," Kodansha, Tokyo (1978), p. 169; b) M. Iwamoto, Y. Yoda, N. Yamazoe, and T. Seiyama, *Bull. Chem. Soc. Jpn.*, **51**, 2765 (1978).

21) Ref. 20 a), p. 41.

22) Ref. 20 a), p. 48.

23) F. E. Massoth and D. A. Scarpiello, *J. Catal.*, **21**, 294 (1971).

24) A. F. Wells, "Structural Inorganic Chemistry," 3rd ed, Clarendon Press (1967).

25) R. J. Armstrong, A. H. Morrish, and D. A. Savatzky, *Phys. Lett.*, **23**, 414 (1966). It is not confirmed which cation vacancies are distributed at Td or Oh sites. *Cf.* M. Nakahira, "Kessho Kagaku-Muki Zaishitsu Kenkyu No Shuppatsu Ten," Kodansha, Tokyo (1973), p. 185.

A Kinetic Study of the Reaction of 1-Propyl-1,4-dihydronicotinamide with Hexacyanoferrate(III)

Tadashi Okamoto,* Atsuyoshi Ohno, and Shinzaburo Oka
Institute for Chemical Research, Kyoto University, Gokasho, Uji 611
(Received May 15, 1979)

The reaction of 1-propyl-1,4-dihydronicotinamide with hexacyanoferrate(III) in 20% aqueous methanol follows a second-order rate law with first order with respect to each reactant concentration. Kinetic parameters are $\Delta H^{\neq}$: $(8.8\pm0.4)\times10^3$ J mol^{-1} and $\Delta S^{\neq}$: -1.8×10^2 J mol^{-1} K^{-1}, the observed kinetic isotope effect, k_H/k_D, being 1.51. The mechanism of the reaction is discussed.

The reaction of unsaturated organic compounds by *N*-substituted dihydronicotinamide has been extensively investigated as a model of reduction by coenzymes NADH and NADPH.[1] The formation of an intermediate complex(es) during the course of the reaction has been reported for various systems.[2] The facility of electron-transfer mechanism for such a net hydride-transfer reaction in biological systems was suggested.[3]

However, the mechanism of this apparent hydride-transfer reaction has not yet been clarified: an initial electron-transfer followed by a hydrogen (as a hydrogen atom, or a proton and an electron) on one hand and a hydride-transfer on the other.[1a] Argument was given as to the single- or multi-step character of the reduction.[4]

In the present paper, we would like to report the details of a kinetic study of the electron-transfer reaction of 1-propyl-1,4-dihydronicotinamide (PNAH) with hexacyanoferrate(III),[5] showing the mechanism of a simplified reduction by PNAH together with some parameters of the reaction.

Experimental

Materials. PNAH-4,4-d_2 was prepared by the repeated reduction of 1-propyl-3-carbamoylpyridinium salt with alkaline dithionite in D_2O and re-oxidation of the resulting dihydronicotinamide with ethyl benzoylformate three times. The deuterium content was estimated by the integral ratios of NMR signals (deuterium purity; 94±5%). Solvents for spectroscopic measurement were Dotait spectro-grade reagents and used after distillation under nitrogen. Inorganic reagents (analytically pure reagents, Nakarai Chem. Co.) were used.

Kinetic Measurement. The solution for kinetic measurement was prepared by injecting 10 μl of a 1.00×10^{-2} M-methanol solution of PNAH into a 4.0 ml portion of 20% aqueous methanol containing $2.00—8.00\times10^{-4}$ M of $K_3Fe(CN)_6$ and $0.75—1.00\times10^{-2}$ M of K_2CO_3 in a serum-capped optical cuvett under nitrogen. Solutions of Li_2CO_3 and KCN, or solid $K_4Fe(CN)_6$ were added when necessary. Reaction rates were measured by the spectroscopic method monitoring the absorbance change at 356 nm on a thermostatted Union Giken SM 401 spectrophotometer. The concentration of potassium ion was adjusted by using potassium chloride.

Results

Stoichiometry. The stoichiometry of the reaction was determined by titration of a 4.0 ml portion of the solution of $K_3Fe(CN)_6$ (2.00×10^{-3} M) and K_2CO_3 (1.00×10^{-2} M) with 1.25×10^{-4} M equivalents of PNAH in 20% aqueous methanol (Fig. 1). Two moles

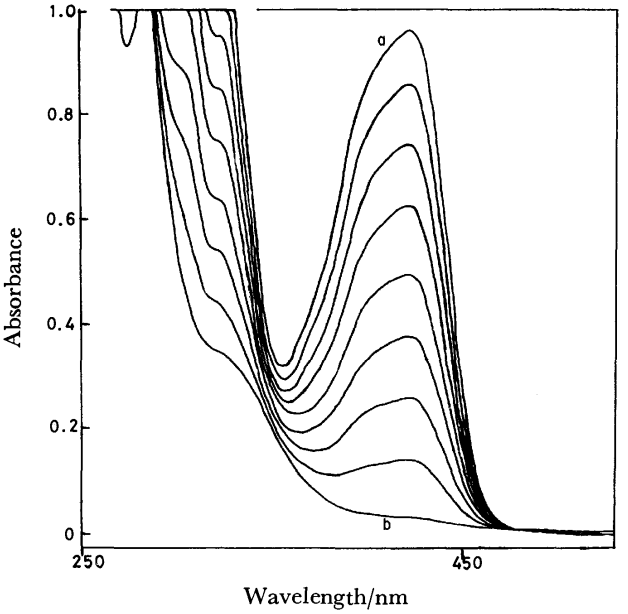

Fig. 1. Spectra of titration.
$[Fe(CN)_6^{3-}]$, 2.00×10^{-3} M; [PNAH], 1.25×10^{-4} M equivalent each at 298 K in 20% aqueous methanol. a, Initial spectrum; b, end spectrum.

of hexacyanoferrate(III) were consumed by 1 mol of PNAH giving rise to the product solution, the spectrum of which was identical with that of the authentic sample of 1-propyl-3-carbamoylpyridinium salt (PNA^+) and hexacyanoferrate(II).

$$PNAH + 2Fe(CN)_6^{3-} \longrightarrow PNA^+ + 2Fe(CN)_6^{4-} + H^+ \quad (1)$$

Kinetic Study. A good pseudo-first-order kinetics (correlation coefficient: $\gamma>0.999$) was observed throughout the experiments for over 90% of the reaction with an excess of hexacyanoferrate(III). However, the reproducibility of the rates of different batches was not very good, suggesting the presence of some impurity which affects the reaction rate. The results are given in Table 1. The apparent rate constants thus obtained are linearly correlated with the concentration of hexacyanoferrate(III) by a straight line that passes through the origin ($\gamma=0.9994$) indicating the second-order rate law with the rate constant (k) of $(6.68\pm0.08)\times10$ M^{-1} s^{-1} ($[K^+]$ of 1.80×10^{-2} M, $[CO_3^{2-}]$ of 0.750×10^{-2} M, and pH of 10.92). The change of basicity of the solution, and the addition of hexa-

TABLE 1. RATE CONSTANTS OF THE REACTION OF PNAH WITH $K_3Fe(CN)_6$[a)]

$[Fe(CN)_6^{3-}]$ / 10^{-3} M	[PNAH] / 10^{-5} M	$[K^+]$ / 10^{-2} M	$[CO_3^{2-}]$ / 10^{-2} M	k_{obsd} / 10^{-2} s^{-1}	k / 10 M^{-1} s^{-1}	Remarks
0.500	2.50	0.650	0.250	1.50	3.01	
0.500	2.50	0.650	0.250	1.02	2.03	PNAH-d_2
0.800	2.50	1.80	0.750	5.24	6.55	
0.700	2.50	1.80	0.750	4.70	6.71	
0.600	2.50	1.80	0.750	4.04	6.73	
0.500	2.50	1.80	0.750	3.26	6.52	
0.400	2.50	1.80	0.750	2.66	6.65	
0.300	2.50	1.80	0.750	2.01	6.70	
0.200	2.50	1.80	0.750	1.32	6.60	
0.500	2.50	1.80	0.750	2.86	5.72	[KCN], 1.50×10^{-3} M
2.00	5.00	2.60	1.00	3.71	1.85	
2.00	5.00	2.60	1.00	3.65	1.82	[PNA$^+$Br$^-$], 4.60×10^{-3} M
0.500	2.50	2.15	1.00	3.25	6.51	298 K
0.500	2.50	2.15	1.00	3.47	6.93	303 K
0.500	2.50	2.15	1.00	3.72	7.43	308 K
0.500	2.50	2.15	1.00	4.07	8.15	313 K
0.500	2.50	2.15	1.00	4.32	8.65	318 K

a) Reaction rate was measured at 298 K under nitrogen in 20% aqueous methanol unless otherwise stated.

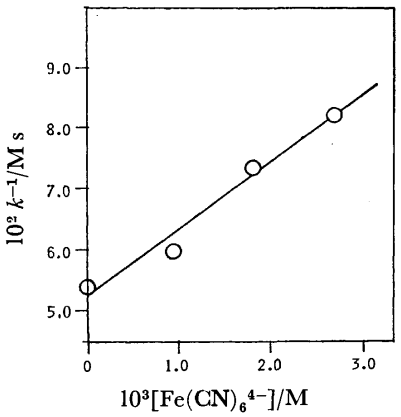

Fig. 2. Dependence of the rate on $Fe(CN)_6^{4-}$ concentrations.
[PNAH], 5.00×10^{-5} M; $[K_2CO_3]$, 1.00×10^{-2} M (pH = 10.97), $[Fe(CN)_6^{3-}]$, 2.00×10^{-3} M at 298 K in 20% aqueous methanol under nitrogen.

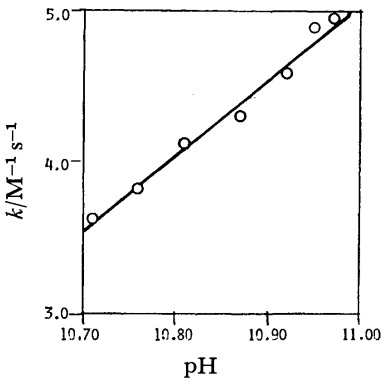

Fig. 3. Effect of the basicity.
$[K_3Fe(CN)_6]$, 5.00×10^{-4} M; [PNAH], 2.50×10^{-5} M; $[K_2CO_3]$, 2.50×10^{-3} M; $[Li_2CO_3]$, 0.00—0.75×10^{-2} M at 298 K in 20% aqueous methanol under nitrogen.

$$-\frac{d[PNAH]}{dt} = k_{obsd}[PNAH] = k[Fe(CN)_6^{3-}][PNAH] \quad (2)$$

cyanoferrate(II) or some alkali-metal ions[6)] affected the reaction rate. Slight retardation took place by addition of cyanide ion, but not by that of other anions such as chloride and perchlorate. Ionic strength had almost no effect either.[6,7)] Linear relationship holds between the reciprocal of the rate constant and the concentration of hexacyanoferrate(II) (Fig. 2). The dependence of rate on basicity was measured with the use of lithium carbonate, since lithium ion does not affect the reaction rate, in contrast to other alkali-metal ions.[6)] The rate was accelerated by increasing basicity (Fig. 3).

Kinetic Parameters. Kinetic parameters measured in the temperature range 298 K—318 K were ΔH^*: $(8.8\pm0.4)\times10^3$ J mol^{-1} and ΔS^*: -1.8×10^2 J mol^{-1} K^{-1} (γ=0.997) at pH of 10.97 and potassium ion concentration of 2.15×10^{-2} M.

The kinetic deuterium isotope effect observed by using PNAH-4,4-d_2 at 298 K was 1.51 ± 0.03.[8)]

Discussion

Only a hydride ion, a hydrogen atom, and an electron give rise to the reducing equivalent of the reduction by PNAH. However, the mechanism is complicated. The hydride-transfer mechanism is simple; the reduction itself should be a single-step reaction no matter whether there is a step for the complex-formation preceding the reduction. A single-step transfer of hydrogen and a reducing equivalent, however, does not necessarily indicate the hydride-transfer mechanism (*vide infra*). The electron-transfer mechanism, in contrast, has many possibilities. The reducing equivalent could be transferred to a substrate at the initial step or after a certain modification of the reductant in a slow step

or in an equilibrium preceding the slow step. Even when an electron is transferred at the initial slow step, the hydrogen at the C_4-position of PNAH could be transferred as a hydrogen atom or a proton in the succeeding step. These elementary steps might occur simultaneously at different reaction sites.

Since hexacyanoferrate(III) is inert for substitution reaction in the ordinary time scale,[9] the possibility of direct hydride-transfer yielding an iron hydride is eliminated. A certain retarding effect by cyanide ion is observed but it is too small for a mass law effect on a reactive intermediate existing in very low concentration. A mechanism with the initial fast equilibrium generating a hydride ion, which reduces hexacyanoferrate(III) in a slow step, is unlikely in the light of hydride chemistry. Since the rate increases with the basicity of solution, one might expect a process of deprotonation of PNAH preceding the net reduction. This mechanism is discarded by the absence of deuterium exchange between PNAH and D_2O under basic conditions and also by the small deuterium isotope effect. The difficulty of deprotonation from such an electron-rich compound would be easily expected.

The above discussion leads to the initial electron-transfer mechanism as the only reasonable possibility for the present reaction shown in the following.

$$\mathrm{PNAH} + \mathrm{Fe(CN)_6^{3-}} \xrightarrow[\text{slow}]{k} \mathrm{PNAH^{\cdot+}} + \mathrm{Fe(CN)_6^{4-}} \quad (3)$$

$$\mathrm{PNAH^{\cdot+}} \longrightarrow \mathrm{PNA^{\cdot}} + \mathrm{H^+} \quad (4)$$

$$\mathrm{PNA^{\cdot}} + \mathrm{Fe(CN)_6^{3-}} \xrightarrow[\text{fast}]{} \mathrm{PNA^+} + \mathrm{Fe(CN)_6^{4-}} \quad (5)$$

The linear dependence of the reciprocal of the rate constant on the concentration of hexacyanoferrate(II) suggests that Eq. 3 is reversible at high concentrations of hexacyanoferrate(II). However, under the usual reaction conditions with no extra hexacyanoferrate(II), the ratio of the rate of the back reaction of Eq. 3 to that of Eq. 4, calculated from the slope of Fig. 2, is 2×10^{-2} even at the end of the reaction. So the net reaction under the usual reaction conditions proceeds according to the reaction sequences presented above. The good correlation coefficient for the pseudo-first order kinetics observed throughout the experiments supports the conclusion.

The values of $\Delta H^{\ddagger}$ and $\Delta S^{\ddagger}$ lie within the region of outer-sphere electron-transfer reaction,[10] which could be taken as evidence of the mechanism presented. The reaction of radical species with hexacyanoferrate(III), corresponding to Eq. 5, is fast.[11]

The acceleration of the reaction by increasing basicity suggests that the deprotonation step also participates in the rate-determining step. In this context, the work of electrochemical oxidation of dihydronicotinamide presents an important evidence.[12] The oxidation potential of dihydronicotinamide is slightly lowered in the presence of a base, indicating the assistance of a base for the initial electron-transfer step. A possible picture of the transition state of the electron-transfer reaction is shown in Fig. 4. Expectation of the base working

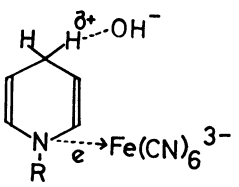

Fig. 4. A possible sketch of the transition state.

only in the step of Eq. 4 which competes with the back reaction of Eq. 3 is not in line with our result quantitatively.

The observed value of the kinetic deuterium isotope effect is too large to be accounted for by the normal secondary isotope effect, and too small to be the rate-determining deprotonation. However, it should be noted that a similar value (1.4) of deuterium isotope effect was reported for the oxidation of tetracyanodiamineferrate(III) into diimine complex,[13] which proceeds through the rate-determining electron-transfer reaction followed by the loss of hydrogen.

The present study has revealed that the reduction by PNAH under weakly basic conditions proceeds through a mechanism with an electron-transfer followed by a proton-transfer and that the transfer of a proton participates in the initial rate-determining electron-transfer step, though slightly. The transfer of the second electron is fast.

This work was supported by a Scientific Research Grant from the Ministry of Education.

References

1) (a) R. H. Ables, R. F. Hutton, and F. H. Westheimer, *J. Am. Chem. Soc.*, **79**, 712 (1957); (b) D. C. Dittmer, A. Lombardo, F. H. Botzold, and C. S. Greene, *J. Org. Chem.*, **41**, 2976 (1976), and references cited therein; (c) D. J. Creighton, J. Hajdu, and D. S. Sigman, *J. Am. Chem. Soc.*, **98**, 4619 (1976) and references cited therein; (d) Y. Onishi, M. Kagami, and A. Ohno, *J. Am. Chem. Soc.*, **97**, 4766 (1975); (e) J. J. Steffens and D. M. Chipman, *J. Am. Chem. Soc.*, **93**, 6694 (1971); (f) R. A. Gase, G. Boxhoorn, and U. K. Pandit, *Tetrahedron Lett.*, **1976**, 2889, and so on.

2) T. Kimura, A. Ohno, Y. Yamamoto, and S. Oka, ACS/CSJ Chemical Congress, ORG 369, Honolulu, Hawaii, April, 1979.

3) E. Zeffren and P. L. Hall, "The Study of Enzyme Mechanism," John Wiley and Sons, Inc., New York (1973), Chap. 10.

4) S. Shinkai, T. Ide, H. Hamada, O. Manabe, and T. Kunitake, *J. Chem. Soc., Chem. Commun.*, **1977**, 848.

5) A part of the results is communicated already; T. Okamoto, A. Ohno, and S. Oka, *J. Chem. Soc., Chem. Commun.*, **1977**, 181.

6) T. Okamoto, A. Ohno, and S. Oka, *J. Chem. Soc., Chem. Commun.*, **1977**, 784.

7) A similar observation was reported for the electron-transfer reaction of thallium(III) with hydrazine; *cf.* B. M. Thakuria and Y. K. Gupta, *J. Chem. Soc., Dalton Trans.*, **1975**, 2541.

8) The figure given in the preliminary communication was erroneous.

9) H. Taube, *Inorg. Radiochem.*, **1**, 1 (1959).

10) See F. Basolo and R. G. Pearson, "Mechanisms of Inorganic Reactions," 2nd ed, John Wiley and Sons, Inc., New York (1967), p. 454.
11) S. Matsuda, A. Yamagishi, and M. Fujimoto, Abstract of the 26th Symposium of Coordination Chemistry of Japan, Sapporo, 1976, p. 254.
12) W. J. Blaedel and R. G. Haas, *Anal. Chem.*, **42**, 918 (1970).
13) M. Goto, M. Takeshita, and T. Sakai, ACS/CSJ Chemical Congress, Honolulu, Hawaii, INOR 366, April 1979.

An Investigation of the Power Characteristics in Heterogeneous Electrochemical Photovoltaic Cells for Solar-energy Utilization

Tooru INOUE,* Claude WEBER, Akira FUJISHIMA, and Kenichi HONDA

Department of Synthetic Chemistry, Faculty of Engineering, The University of Tokyo, 7-3-1 Hongo, Bunkyo-ku, Tokyo 113

(Received May 23, 1979)

A heterogeneous electrochemical photovoltaic cell was constructed using the system of cadmium sulfide(CdS)/sulfides reducing agents//oxidizing agents/platinum. The output power characteristics were investigated focusing upon the redox potentials of the oxidizing agents in the cathodic half-cell and then discussed from the point of view of the solution-electrode junction. Though this type of cell intrinsically has a negative free energy for redox reactions of redox agents in an anodic and a cathodic compartment, it has a characteristic point that a larger open-circuit output than the intrinsical electromotive force determined by a redox couple was obtainable in operation under illumination. For example, in the CdS/S^{2-}/S//$Fe^{2+/3+}$/Pt system we found the open-circuit photovoltage of *ca.* 2.0 V, which is *ca.* 83% of a band gap (2.4 eV) of CdS. These measurements showed that a larger open-circuit photovoltage was obtained, though, of course, it was smaller than the band-gap energy of CdS, when the oxidizing agent of the more positive redox potential was dissolved in the cathodic compartment.

The conception of solar-energy conversion to chemical energy and/or electrical energy has been actualized by the use of such electrochemical photocells as photoelectrolytic cells[1-8] and regenerative photovoltaic cells.[9-11] As these photocells have a Schottky-type junction of a semiconductor/solution interface, photoinduced electron-hole pairs are separated by the electric field in the space-charge layer and react with redox agents in an electrolyte solution. For the efficient conversion of solar energy, much information has been presented on the reactions at semiconductor electrodes under illumination.[12] The stabilization of a photoelectrode with a small bandgap is a key problem and is attained by the competitive reaction of redox agents in an electrolyte solution.[12-16] For a regenerative photovoltaic cell after it has been stabilized by a strong reducing agent, its output photovoltage was small with respect to the bandgap value of the semiconductor employed. In order to obtain good output-power characteristics in a regenerative photovoltaic cell, a variety of combinations of semiconductors and solution species have been employed and then discussed, focusing upon the solar-conversion efficiency.[17-19]

Cadmium sulfide (CdS) is a promising material because its bandgap (2.4 eV) is suitable for the conversion of solar light and because its flatband potential (E_{fb}) is sufficiently negative, in particular in a sulfide solution.[14,20-22] However, the output voltage of the regenerative photovoltaic cell constituted by the single compartment of the CdS/redox species/Pt system is limitted to about 600 mV,[18] as determined by the potential difference between the flatband potential of CdS and the reduction potential of the oxidized species. When the low value of the photovoltage is compared with the CdS bandgap of 2.4 eV, one can understand that it limits the electric-output power efficiency.

In order to increase the electric-output power, it may be advantageous to employ a photovoltaic cell constructed by two separated half cells: CdS/sulfide solution//oxidizing solution/Pt. In this case, such a cell can be expected to overcome the photovoltage limitation (*ca.* 600 mV) by means of the positive reduction potentials of the oxidizing agent dissolved in the cathodic compartment, while stabilizing the CdS photoanode by means of the sulfide solution. The evaluation of the power characteristics of such systems is the subject of the present study.

Experimental

The cadmium sulfide electrode was an n-type single crystal (Teikoku Tsushin Kogyo Co., Ltd.) with a resistivity of 0.26 Ω·cm and a carrier density of 8×10^{16} cm^{-3} (as determined by the company). The irradiated face (001) had an area of 0.85 cm^2. This face was polished by alumina powder and etched in concentrated HCl for 10 s. Ohmic contact for a copper wire was made by means of indium and silver paste, and the electrode was isolated on a glass rod by means of epoxy resin. As a cathode, platinum foil (1.7 cm^2) was used. Before the experiment, the platinum electrode was treated with concentrated HNO_3. The solution for stabilizing CdS was 0.5 M Na_2S+0.1 M NaOH (M=mol/cm^3). The aqueous solutions in the cathode compartment were as follows: (1) 0.1 M NaOH+0.5 M Na_2S+0.01 M S; (2) 0.2 M Na_2SO_4; (3) 0.5 M $K_3Fe(CN)_6$; (4) 0.5 M $Fe(NO_3)_3$; (5) 0.5 M KI +0.1 M I_2+0.2 M Na_2SO_4. All the chemicals used were reagent-grade. The light source was a 500-W Xe lamp (Ushio Electric UXL Type). The incident light was filtered by means of a UV-D2 (Toshiba Kasei) glass filter, which lets the wavelengths of 300—400 nm pass through and which has a peak transmittance of 80% for the wavelength of 360—370 nm. The power output characteristics were measured by using a compensated electrometer (Kowa Electronics VM-208) and an ammeter (Nikko Keisoku NZ-1). The anode and cathode compartments were separated with an agar-agar salt bridge containing saturated KCl.

Results and Discussion

Figure 1 shows the current-potential curves at the illuminated CdS electrode and at the platinum electrode obtained under potentiostatic conditions. The anodic photocurrent (Curve 1) appears at a potential more positive than −1.13 V *vs.* NHE at the CdS photoelectrode in the electrolyte solution containing sulfide ions. When the platinum counter electrode is set in an electrolyte solution containing oxidizing agents ($K_3Fe(CN)_6$), the cathodic current appears at the

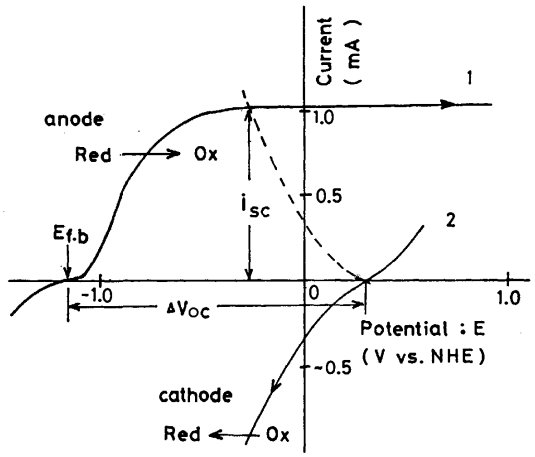

Fig. 1. Current-potential curves at a CdS photoanode and a platinum cathode.
Solid line 1: at CdS in 0.5 M Na_2S+0.1 M NaOH+0.01 M S aqueous solution, solid line 2: at Pt in 0.5 M $K_3Fe(CN)_6$+0.2 M Na_2SO_4 aqueous solution, dashed line: rewriting of a negative part of a solid line 2 with absolute values

potential of *ca.* 0.37 V *vs.* NHE. This cathodic onset potential is more positive than the onset potential of the cathodic current which appears at the Pt electrode in the solution containing sulfides. Considering the limitation of the open-circuit photovoltage determined by the potential difference between anodic and cathodic onset potentials, one can see that the larger electric-output power will be obtained when the cathode is set in the solution with the stronger oxidizing agent.

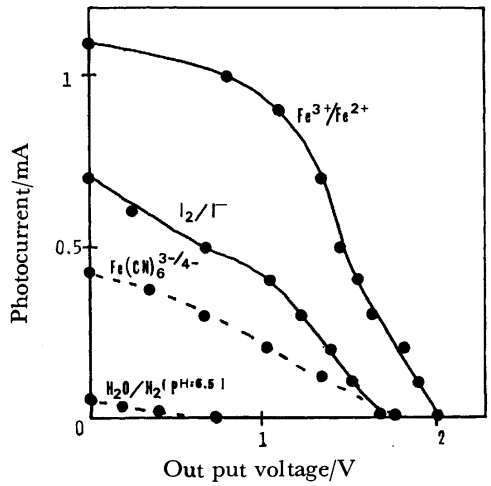

Fig 2. Output power characteristics (current-voltage curves) in heterogeneous photovoltaic cells of CdS/0.5 M+0.1 M NaOH/0.5 M oxidizing agent/Pt systems. Oxidizing agents: 1, H_2O (pH=6.5); 2, $K_3Fe(CN)_6$; 3, I_3^-; 4, $Fe_2(SO_4)_3$.

In Fig. 2 we present some output power characteristics for [a CdS/0.5 M Na_2S+0.01 M S+0.1 M NaOH aqueous solution//solution containing oxidizing agents/Pt] photovoltaic cell. The actual output power was in the order of $Fe^{3+}>I_2(I_3^-)>Fe(CN)_6^{3-}>H_2O$, so the maximum of the open-circuit photovoltage was about 2.0 V, which was *ca.* 83% of the bandgap (2.4 eV) of CdS. This suggests that the output power increases with the more positive shift of the redox potential of an oxidizing agent.

We examined the open-circuit output voltages in the dark and under illumination when various oxidizing agents were introduced in the solution. The results are shown as functions of their redox potentials in Fig. 3.

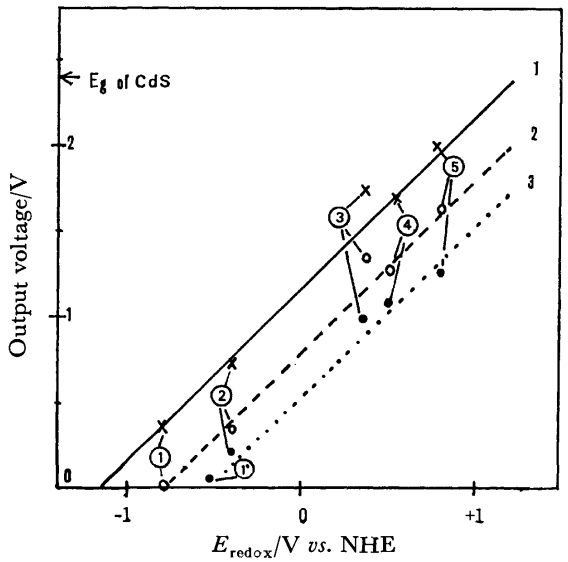

Fig. 3. Open-circuit voltage in heterogeneous photovoltaic cells as a function of the redox potentials of oxidizing agents in cathodic compartments.[25]
1: H_2O/H_2 (pH=13.5), 1′: S^{2-}/S_2^{2-}, 2: H_2O/H_2 (pH=6.5), 3: $Fe(CN)_6^{3-/4-}$, 4: I_2/I^-, 5: $Fe^{3+/2+}$.
×, Solid line 1; output photovoltage between CdS and Pt, ○, dashed line 2; output voltage (dark) between CdS and Pt ●, dotted line 3; output voltage between Pt and Pt.

The dashed line 2 represents the output voltages in dark conditions, its slope is *ca.* 1.0. The intersection of this line with the abscissa is at the potential of −0.8 V *vs.* NHE, which is close to the water reduction potential (hydrogen evolution) at this pH value (13.5). The solid line 1 represents the output voltages obtained under irradiation. The value of its slope is also 1.0, and the intersection of the line with the abscissa is at the potential of −1.16 V *vs.* NHE, corresponding to the flatband potential of the CdS electrode under these conditions. As for the flatband potential (E_{fb}), Minoura *et al.*[20] have reported $E_{fb}\fallingdotseq-1.13$ V *vs.* NHE for a 0.1 M Na_2S+1 M Na_2SO_4 solution, Ginley and Butler[21] have reported $E_{fb}\fallingdotseq-1.05$ V *vs.* NHE for a 0.9 M Na_2S+0.05 M KOH solution, while we ourselves[22] have presented $E_{fb}\fallingdotseq-1.09$ V *vs.* NHE for a 0.1 M Na_2S+0.2 M Na_2SO_4 solution. The dotted line 3 in Fig. 3 represents the relation between the open-circuit output voltage and the redox potentials of the oxidizing agents when we employed the Pt electrode instead of the CdS electrode in the anodic compartment (pH=13.5). The intersection of this line with the abscissa is at the potential ($E_{redox,1}=-0.52$ V *vs.*

NHE) of a S^{2-}/S system.

The open-circuit output voltage (ΔV_{oc}) of the electrochemical photovoltaic cell arises from the difference between the flatband potential of the semiconductor photoanode and the redox potential ($E_{redox,2}$) of an oxidizing agent (O_x) at a cathode:

$$\Delta V_{oc} = |E_{fb} - E_{redox,2}| \quad (1)$$

$$2S^{2-} \longrightarrow S_2^{2-} + 2e^- \text{ (at an anode)} \quad (2)$$

$$O_x + ne^- \longrightarrow \text{Red (at a cathode)} \quad (3)$$

Some investigations have also reported as the output characteristics in the electrochemical photovoltaic cell determined using a CdS electrode, as are shown in Table 1. The upper four electrochemical photovoltaic cells are composed of a single compartment with a redox couple, so they are regenerative. The last two electrochemical photovoltaic cells are similar to ours and are not regenerative. From the data in Fig. 3 and Table 1, we can conclude that the relation (Eq. 1) is applicable to the output voltage in the electrochemical photovoltaic cell.

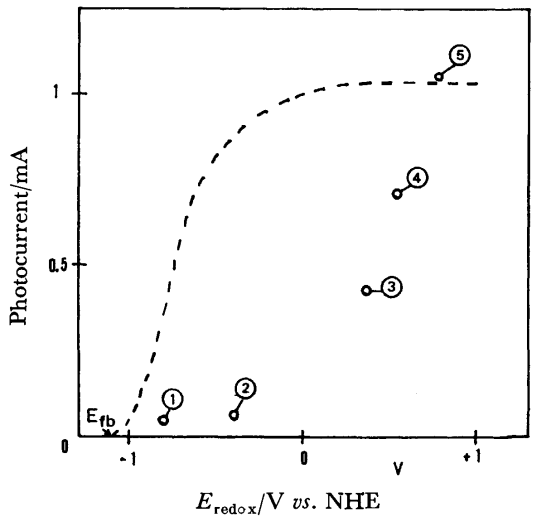

Fig. 4. Short-circuit currents in heterogeneous photovoltaic cells as a function of the redox potentials of oxidizing agents in cathodic compartments.[25] A dashed line shows a current-potential curve of a CdS photoanode. All numbers are the same as those in Fig. 3.

Figure 4 shows the short-circuit output currents as functions of the redox potentials of oxidizing agents dissolved in the cathodic compartment. The dashed curve represented the anodic photocurrent at a CdS electrode obtained under potentiostatic conditions. The currents actually obtained are smaller than the CdS anodic photocurrent observed under the potentiostatic conditions. The difference in photocurrents between the value from this dashed curve and that from the experimental results may come from polarization losses in an operation. Therefore, if the redox couples in the cathodic half-cell are infinitely reversible, and also if all losses in the semiconductor bulk and surface can be neglected, these plots will lie on the ideal dashed curve. The fact that the losses diminish with an increase in the redox potential can be explained the fact that the increase in the cell electromotive force advantageously affects the polarization characteristics of both electrode reactions. It can be assumed that the limited photocurrent determined by the light absorption of CdS can be obtained in this cell when an oxidizing agent with a redox potential more positive than a $Fe^{2+/3+}$ couple is dissolved in the cathodic compartment.

Figure 5 shows the output power in the electrochemical photovoltaic cells as functions of the redox potentials of the oxidizing agents. The dashed line represents the maximum output power (P_{max}) obtainable for a particular redox system, it is calculated by the following procedure:

$$P_{max} = i[E_F](E_{redox} - E_F) \quad (4)$$

where E_F denotes the semiconductor Fermi level, *i.e.*, the electrode potential in an operation; E_{redox}, the redox potential of an oxidizing agent in a cathodic compartment; and $i[E_F]$, the output current determined from the photocurrent at the potential of E_F. Figure 6 explains the calculation procedure of P_{max} schematically, where the magnitude of the current is determined by means of the polarization of CdS. The output power observed is plotted in Fig. 5 and is reflected in the

TABLE 1. VARIOUS ELECTROCHEMICAL PHOTOVOLTAIC CELLS USING CdS

Workers	No.		ΔVexp	$U_{fb} - E_{redox}$[a]	Ref.
Gerischer and Gobrecht	1	$CdS/Fe(CN)_6^{3-/4-}/Pt$	0.97	0.99	6
	2	$CdS / \begin{matrix} S_2O_3^{2-} \\ S_4O_6^{2-} \end{matrix} / Pt$	0.82	0.85	6
Heller, Chang, and Miller	3	$CdS / \begin{matrix} Na_2S \\ NaOH \end{matrix} / C$	0.60	0.59	10
Minoura, Tsuiki, and Oki	4	$CdS / \begin{matrix} Na_2S \\ Na_2SO_3 \end{matrix} / Pt$	0.38	0.38	16
	5	$CdS / \begin{matrix} Na_2S \\ Na_2SO_3 \end{matrix} / \begin{matrix} Na_2SO_4 \\ pH=7 \end{matrix} / Pt$	0.78	0.74	16
	6	$CdS / \begin{matrix} Na_2S \\ Na_2SO_3 \end{matrix} / \begin{matrix} Na_2SO_4 \\ pH=1 \end{matrix} / Pt$	1.15	1.10	16

a) The potentials (E_{redox}) of various oxidizing agents were calculated by consulting Ref. 23.

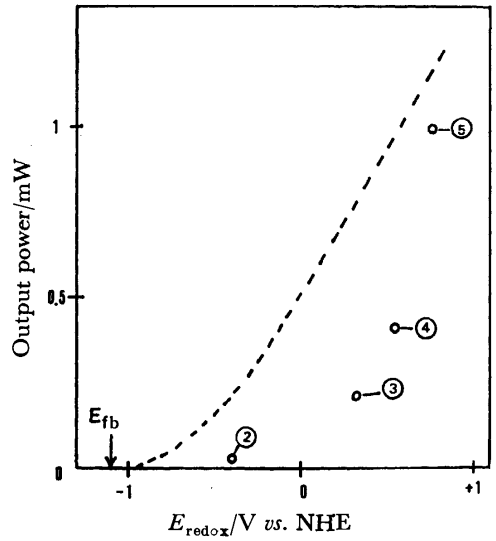

Fig. 5. Maximum electric output power in heterogeneous photovoltaic cells as a function of the redox potential of oxidizing agents in cathodic compartments.[25] Dashed line was calculated by Eq. 4. All numbers are same in Fig. 3.

characteristics shown in Fig. 4. The calculated power, P_{max}, increases with the variation in the redox potential and will be saturated at the potentials near the valence-band potential (*ca.* 1.4 V *vs.* NHE) of CdS.

In conclusion, we have shown the power characteristics in the heterogeneous electrochemical photovoltaic cell. This type of photovoltaic cell has two kinds of redox systems. Sulfides as a reducing agent shift the flatband potential of CdS and are oxidized at the CdS photoanode. Oxidizing agents are reduced at the Pt electrode. The characteristic point is that a large open-circuit voltage is obtainable with respect to the bandgap (2.4 V) of CdS. For the elucidation of the

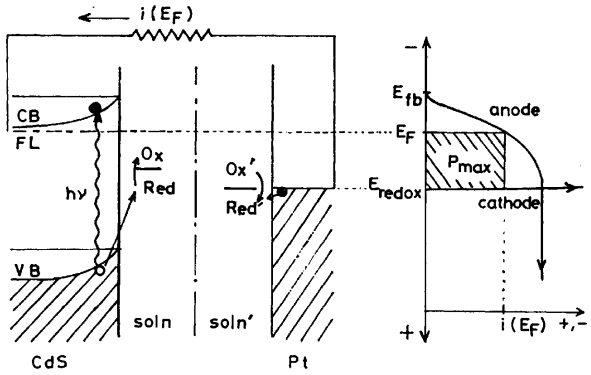

Fig. 6. Schematic explanation for calculation of P_{max} according to Eq. 4.

heterogeneous photovoltaic cell, we show in Fig. 7 a schematic illustration of the potential variations in the solution-electrode junctions in comparison with other types of electrochemical photocells. We can classify the electrochemical photocells into three types from the point of view of the difference (ΔE) in redox potentials at an anode and a cathode:

$$\Delta E = E_{redox,1} - E_{redox,2} \quad (5)$$

First, when the value of ΔE is positive, the electrochemical photocell works as a photoelectrolytic cell which can convert the light energy to chemical and/or electrical energy and also store the chemical energy. Second, when the value of ΔE is zero, it works as a regenerative photovoltaic cell which can convert the light energy only to electrical energy. Third, when the value of ΔE is negative, it works as a heterogeneous photovoltaic cell which can convert both the light and the chemical energy to electrical energy and which can generally give the largest output photovoltage of these three electrochemical photocells.

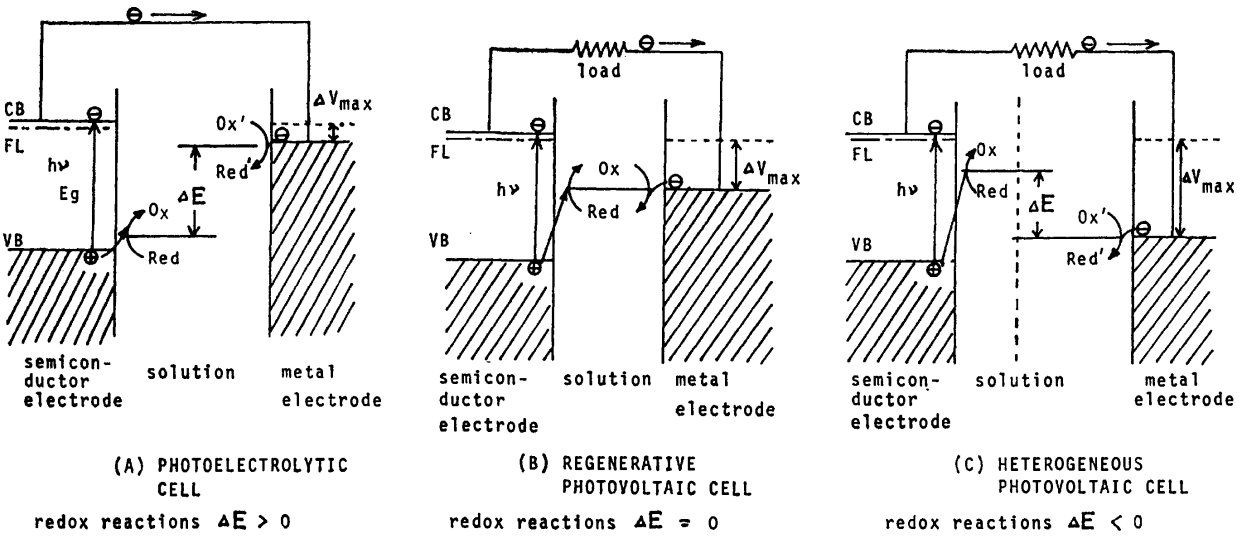

Fig. 7. Schematic illustrations of the semiconductor electrode-solution junctions for three typesof electrochemical photocells.
(A) Photoelectrolytic cell (Refs. 4, 6, 7, 8), free energy of a redox reaction is positive.
(B) Regenerative photovoltaic cell (Refs. 7—11), free energy of a redox reaction is zero.
(C) Heterogeneous photovoltaic cell (this study), free energy of a redox reaction is negative.

References

1) A. Fujishima, K. Kohayakawa, and K. Honda, *Bull. Chem. Soc. Jpn.*, **48**, 1041 (1975).
2) M. Yoneyama, S. Mayumi, and H. Tamura, *J. Electrochem. Soc.*, **125**, 68 (1978).
3) T. Ohnishi, Y. Nakato, and H. Tsubomura, *Ber. Bunsenges. Phys. Chem.*, **79**, 523 (1975).
4) M. S. Wrighton, A. B. Ellis, P. T. Wolczanski, D. L. Morse, H. B. Abrahamson, and D. S. Ginley, *J. Am. Chem. Soc.*, **98**, 2774 (1976).
5) S. N. Frank and A. J. Bard, *J. Am. Chem. Soc.*, **99**, 4667 (1977).
6) T. Watanabe, A. Fujishima, and K. Honda, *Bull. Chem. Soc. Jpn.*, **49**, 355 (1976).
7) A. Fujishima, T. Inoue, and K. Honda, *J. Am. Chem. Soc.*, **101**, 5582 (1979).
8) T. Inoue, A. Fujishima, and K. Honda, "Proceedings of a Conference on Energy Conversion," ed by The Institute of Electrical Engineers of Japan, EDD-79-31, CH-79-17 (1979), p. 63.
9) H. Gerischer and J. Gobrecht, *Ber. Bunsenges. Phys. Chem.*, **80**, 377 (1976).
10) H. Tributch, *J. Electrochem. Soc.*, **125**, 1086 (1978).
11) A. B. Ellis, J. M. Bolts, S. W. Kaiser, and M. S. Wrighton, *J. Am. Chem. Soc.*, **99**, 2848 (1977).
12) "Semiconductor-Liquid Junction Solar Cells: Proceedings of a Conference on the Electrochemistry and Physics of Semiconductor-Liquid Interfaces under Illumination," 77-3, ed by A. Heller, Electrochem. Soc., Princeton (1977).
13) T. Inoue, T. Watanabe, A. Fujishima, K. Honda, and K. Kohayakawa, *J. Electrochem. Soc.*, **124**, 719 (1977).
14) T. Inoue, T. Watanabe, A. Fujishima, and K. Honda, *Bull. Chem. Soc. Jpn.*, **52**, 1243 (1979).
15) A. Fujishima, T. Inoue, T. Watanabe, and K. Honda, *Chem. Lett.*, **1978**, 357.
16) H. Minoura, M. Tsuiki, and T. Oki, *Ber. Bunsenges. Phys. Chem.*, **81**, 588 (1977).
17) A. Heller, G. P. Shwartz, R. G. Vadimsky, S. Menezes, and B. Miller, *J. Electrochem. Soc.*, **125**, 1156 (1978).
18) J. R. Owen, *Nature*, **267**, 504 (1977).
19) K. Rajeshwar, P. Singh, and J. DuBow, *Electrochim. Acta*, **23**, 1117 (1978).
20) H. Minoura, T. Watanabe, T. Oki, and M. Tsuiki, *Jpn. J. Appl. Phys.*, **16**, 865 (1977).
21) D. S. Ginley and M. A. Butler, *J. Electrochem. Soc.*, **125**, 1968 (1978).
22) T. Inoue, T. Watanabe, A. Fujishima, and K. Honda, in Ref. 12, p. 210.
23) M. Pourbaix, "Atlas d'equilibres electrochimiques," Gauthier-Villars, Paris (1973).
24) A. J. Bard, *J. Photochem.*, **10**, 59 (1979).
25) The redox potentials of the oxidizing agents are represented by their standard redox potentials.

Formation of Chiral Aggregates of Acylamino Acids in Solutions

Kazutami SAKAMOTO* and Masahiro HATANO**

Central Research Laboratories, Ajinomoto Co., Inc., Suzuki-cho, Kawasaki-ku, Kawasaki, Kanagawa 210

***The Chemical Research Institute of Non-aqueous Solutions, Tohoku University, Katahira 2-2-1, Sendai, Miyagi 980*

(Received May 29, 1979)

An alcoholic solution of optically active acylamino acid (AAA) was found to show a circular dichroism (CD) band at 212 nm. The CD band should be inherent to the solution system, since AAA and alcohol *per se* have no absorption band at this wavelength. The CD band intensity decreased on addition of urea and rise in temperature. This is attributed to the formation of chiral aggregate through hydrogen bonds among AAA molecules. Hydrophobic interaction seems to be of minor importance for the formation of the chiral aggregate in alcoholic solution, since the variation of the chain length in the acyl group or addition of myristic acid did not affect the magnitude of profile of the CD band. In aqueous solutions, salts of optically active AAA formed micelles with hydrophobic interactions among the molecules, and only in the case of optically active monosodium salt of *N*-acylglutamic acid (AGS) showed a CD band at 220 nm resulting from the formation of chiral hydrogen bonds at concentrations above the critical micelle concentration (CMC). This type of chiral aggregation may be caused by the existence of free carboxyl group in the optically active AGS molecule.

New lyotropic cholesteric liquid crystals consisting of *N*-acyl-L-glutamic acid (L-AGA) and aromatic solvents were found recently,[1] and a discussion was given on the origin of the circular dichroism (CD) and the iridescent color observed in these liquid crystals.[2] It was deduced that optically active acylamino acids (AAA's) can form lyotropic cholesteric liquid crystals when they are suspended in the solvents in which the acids do not dissolve but undergo swelling. During the course of swelling in some solvents, the optically active AAA molecules are oriented to form a helix.

On the other hand, when L-AGA was completely dissolved in methanol, no iridescent color or CD band around 300—400 nm was observed. However, a new CD band around 200—250 nm was observed for the isotropic solution. Since L-LGA and methanol *per se* have no absorption in this wavelength region, the new CD band should be inherent to the solution systems. The CD band indicates the formation of a chiral aggregate of L-AGA molecules in alcoholic solution, which might result from the asymmetrical interaction between molecules and have a correlation with the formation of cholesteric liquid crystals of L-AGA.

AGA is somewhat similar to protein, having an acyl group neighboring an asymmetric carbon of amino acid and being sufficiently amphiphilic to interact with both hydrophobic and hydrophilic surroundings. Thus an investigation of the chiral aggregate of AGA would be of interest as regards the structure and function of protein.

The function of protein depends on its stereochemical structure, the local structure of proteins, such as α-helix or β-sheet, being determined essentially by their sensitivity toward molecular environments. Some local structures exhibit optical activity similar to that of AAA aggregates by the formation of chiral hydrogen bonding between amino acid residues.

Tachibana and Oda showed that the chirality of the amino acid residue in the polyglutamate determines the asymmetric structure of higher ordered aggregates such as fibrous aggregates[3] and cholesteric films.[4] Saeva and Olin reported that the helical sense of the cholesteric liquid crystals consisting of polyglutamate also depends on the chirality of glutamic acid residue.[5] The higher ordered structures of polyglutamate also result from the hydrogen bond formation among chiral amino acid residues. AGA forms higher ordered chiral structures such as cholesteric liquid crystals[1,2] and chiral aggregates, similar to polyglutamates. They might result from the hydrogen bond formation among molecules since AGA has the same glutamic acid residue which can form hydrogen bond as in polyglutamates. Parthasarthy *et al.* reported the formation of a hydrogen bond among AAA molecules in crystals by means of X-ray diffraction but gave no discussion in view of chirality.[6–8]

We have analysed the CD spectrum of the aggregates of optically active acylamino acids (AAA's) and their salts in isotropic reaction in terms of chiral hydrogen bonding. The results are given in this paper.

Experimental

The AAA's we used are the same as those reported by Takehara *et al.*[9] Their sodium salts can be prepared through neutralization of the corresponding AAA's by the addition of an equivalent quantity of sodium hydroxide.[10] The CD spectra of samples were recorded on a JASCO J-20A spectropolarimeter. Spectral measurements were carried out at constant temperature, the temperature being adjusted by circulation of thermostated water. Solvents used were of spectral grade and used without further purification.

Results and Discussion

Formation of Chiral Aggregate in Alcoholic Solutions. Optically active *N*-lauroylglutamic acid (L- or D-LGA) dissolved in methanol shows a CD band at 212 nm (Fig. 1). The CD band should be inherent to the mixture, since LGA and methanol have no absorption at around 212 nm. L-Enantiomer (L-LGA) and D-enantiomer (D-LGA) have opposite signs and their CD bands should thus be due to the different chiral configuration of LGA. CD bands were also obtained for L-LGA in other solvents such as 1-propanol or 1-octanol, in which L-LGA was apparently completely dissolved (Table 1). Similar CD bands around 212 nm were

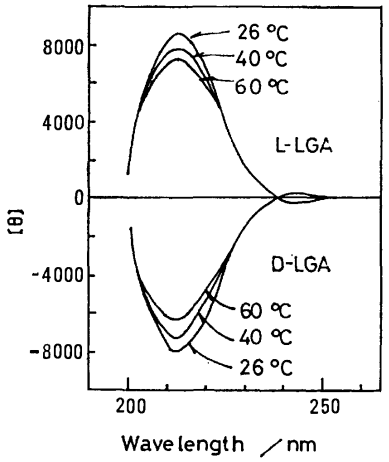

Fig. 1. The CD spectra of optically active *N*-lauroyl-glutamic acid (LGA) in methanol; concentration is 1.0×10^{-2} M.

TABLE 1. EFFECT OF SOLVENTS OR ADDITIVES ON $[\theta]_{212}$ OF L-LGA, 6.1×10^{-3} M, AT 26° C

Solvent	Additive		$[\theta]_{212}$
Methanol	—		8.9×103
	Urea	6.0×10^{-1} M	6.9
	Myristic acid	8.8×10^{-3} M	9.2
1-Propanol	—		9.3
1-Octanol	—		8.8

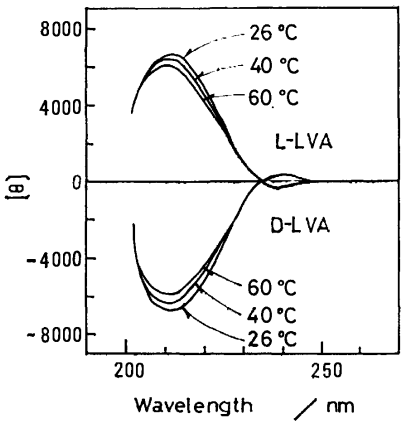

Fig. 2. The CD spectra of optically active *N*-lauroyl-valine (LVA) in methanol; concentration is 1.0×10^{-2} M.

observed in the alcoholic solutions of optically active *N*-lauroylvaline (L- or D-LVA) (Fig. 2). They differ entirely from those of the lyotropic cholesteric liquid crystals consisting of optically active AAA's and solvents,[2] since the wavelengths of the CD band maxima and the spectral profiles differ a great deal in the two cases.[11] The alcoholic solutions showed no birefringence toward the polarized light. The CD bands at 212 nm disappeared at a concentration below 1×10^{-4}, indicating a chiral structure through aggregation. We therefore examined in detail the concentration effect on the CD bands of LGA in alcohols.

Effect of Concentration. The magnitude of the CD band at 212 nm was found to be independent of the concentration of L-LGA or L-LVA in methanol at concentrations higher than 1×10^{-4} M (Fig. 3). This indicates that the number of molecules per aggregate is independent of the concentration of AAA. A concentrated solution of L-LGA (>*ca.* 1×10^{-1} M) in methanol showed birefringence together with a CD band at 212 nm due to the formation of liquid crystaline phase.[12]

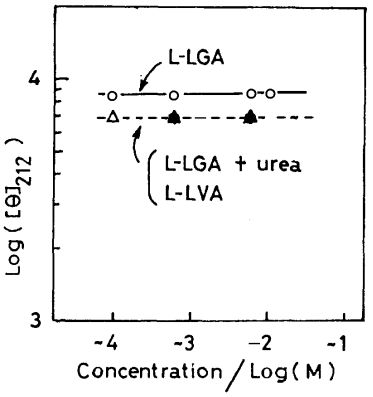

Fig. 3. Relation between concentration of *N*-acyl-L-amino acid and the magnitude of CD in methanol solution at 26 °C.
○: L-LGA, ●: L-LGA+0.6 M urea, △: L-LVA.

Since alcohols have higher affinity to both hydrophobic and hydrophilic parts in the solute molecule, most amphiphilic substances can not form any micelle in alcohols. AAA's have amphiphilic structure in themselves, and the aggregates of AAA's in alcohols do not seem to be micelle.

TABLE 2. $[\theta]_{212}$ IN METHANOL SOLUTION OF *N*-ACYL-L-AMINO ACIDS (L-AAA), 1×10^{-2} M, AT 26 °C

L-AAA	Amino acid residue	Carbon number in the acyl group	$[\theta]_{212}$
L-LGA	Glutamic acid	12	8.5×10^{3}
L-MGA		14	8.5
L-PGA		16	8.0
L-P_3VA	Valine	3	6.7
L-LVA		12	6.7
L-MVA		14	7.9
L-PVA		16	5.9

Hydrophobic Interactions among the Acyl Long Chains. Since AAA has amphiphilic structure, we examined the effect of hydrophobic counterpart in an AAA molecule on the CD spectral profile. In both cases of L-AGA and *N*-acyl-L-valine (L-AVA) the magnitude of CD band at 212 nm ($[\theta]_{212}$) was almost independent of the chain length of acyl groups in each series (Table 2). In the case of L-AVA, chiral aggregation occurred even for *N*-propionyl-L-valine which seems to have a too short acyl chain to form micelle by the hydrophobic interaction between its acyl side chains. Addition of myristic acid to the methanol solution of L-LGA, by which

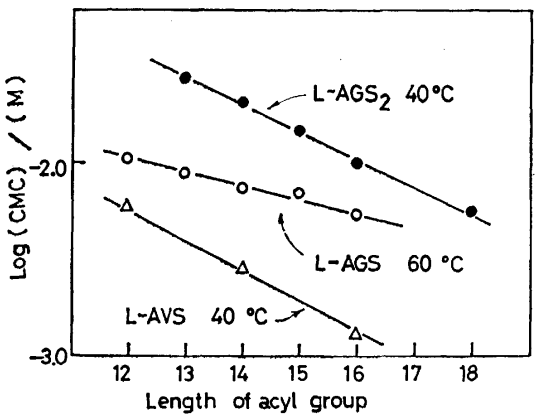

Fig. 4. Relation between log CMC and number of carbon atoms in acyl-group.
○: Monosodium *N*-acyl-L-glutamate (L-AGS),
●: disodium *N*-acyl-L-glutamate (L-AGS$_2$),
△: sodium *N*-acyl-L-valinate (L-AVS).
The CMC data were observed by conductivity method at 60 °C for L-AGS and at 40 °C for L-AGS$_2$ and L-AGS.

perturbation of the hydrophobic interaction between the acyl groups was expected to take place, showed no effect on the value of $[\theta]_{212}$ (Table 1).

The results suggest that hydrophobic interaction is less important for the formation of chiral aggregates. On the other hand, values of critical micelle concentration (CMC) in aqueous solutions of AAA were dependent on the lengths of acyl groups (Fig. 4)[10,13] and hydrophobic interaction was essential for the micelle formation. The structure of the chiral aggregates in alcoholic solutions should be quite different from the micelle structure in aqueous solutions.

Aggregation by Hydrogen Bonding. On addition of urea, which tends to break hydrogen bonds in the proteins,[14] the values of $[\theta]_{212}$ for the alcoholic solutions of AAA decreased (Table 1 and Fig. 3). L-LGA and L-LVA showed no CD band at 212 nm in trifluoroacetic acid, a hydrogen bond breaker stronger than urea. The formation of chiral aggregates of optically active AAA in alcohols may be caused by the hydrogen bond formation between AAA molecules themselves. The decrease in the value of $[\theta]_{212}$ at higher temperatures may be caused by hydrogen bonds rupture in the aggregates (Figs. 1 and 2).

Proteins form second order structure with the hydrogen bond between NH-group and CO-group in the molecule[15] and its helical sense is partially determined by the asymmetric carbon in the amino acid residue. The α-helical conformation, including the hydrogen bonds, results in the appearance of CD bands at 191, 209, and 222 nm.[16] From these properties of proteins, it was assumed that the CD band at 212 nm in alcoholic solutions of optically active AAA indicates the formation of the intermolecular chiral hydrogen bond.

Two possible hydrogen donors in AAA, NH in amide group and OH in carboxyl group, can be considered. The latter may have no contribution to the hydrogen bond formation, since a similar CD band at 212 nm was observed in the methanol solution of

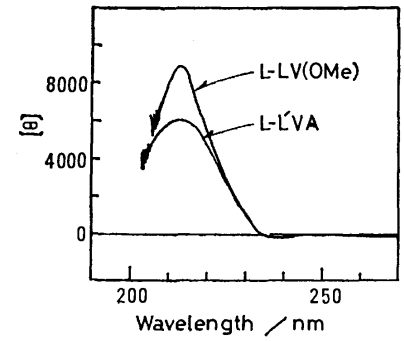

Fig. 5. CD spectra of *N*-lauryl-L-valine (L-L'VA) and methyl ester of *N*-lauroyl-L-valine(L-LV(OMe)) in methanol; at 40 °C and 1.0×10^{-2} M.

methyl ester of L-LVA (Fig. 5). We can also expect two types of hydrogen acceptor in AAA, amide carbonyl and carbonyl of carboxylic group. CO in the amide group may have no participation for the hydrogen bond formation, since the CD band at 212 nm could not be detected for the methanol solution of *N*-lauryl-L-valine(L-L'VA), an *N*-alkylated amino acid without amide group (Fig. 5). An intermolecular chiral hydrogen bond may occur between NH in amide group and CO in carboxyl group of AAA. Mutual orientation between the NH and CO groups is determined by the configuration of the asymmetric carbon being adjacent to both. In the case of racemic mixture of AAA in methanol, no CD band could be detected. Thus, the aggregation of optically active AAA in alcoholic solution occurrs through the chiral hydrogen bonds among AAA molecules.

Table 3. Critical micelle concentration (CMC) of monosodium *N*-acyl-L-glutamate (L-AGS) and disodium *N*-acyl-L-glutamate (L-AGS$_2$)

	Carbon number in the acyl group	CMC/mM	
		By conductivity method[10]	By CD method
L-AGS	12	10.6[a]	9[a]
	14	7.2[b]	8[b]
	16	5—6[b]	5[b]
L-AGS$_2$	14	21[a]	—
	16	9.8[a]	—

a) At 40 °C. b) At 60 °C.

CD of Optically Active AAA in Aqueous Solution. The sodium salts of optically active AAA's form micelles in aqueous solutions at concentrations above their CMC (Table 3).[10] If the chiral aggregation occurrs together with micelle formation, the existence of a CD band and its concentration dependence are expected for the aqueous solutions of the sodium salts of optically active AAA's. Only monosodium salt of *N*-acylglutamic acid (L- or D-AGA) shows a CD band at 220 nm (Fig. 6). The concentration dependency of this CD magnitude was found to be correlated with its CMC (Fig. 7 and Table 3). For example, the magnitude of CD band at 220 nm, $[\theta]_{220}$, observed for the aqueous solution of monosodium salt of *N*-lauroyl-L-glutamic acid (L-LGS)

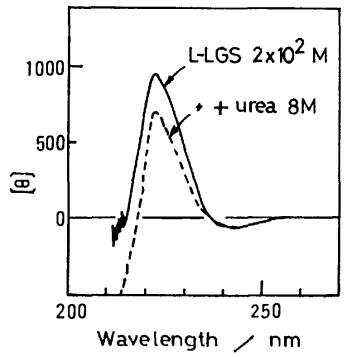

Fig. 6. The CD spectra of monosodium *N*-lauroyl-L-glutamate (L-LGS) in water at 40 °C.
Solid line: L-LGS, 2×10^{-2} M.
Broken line: L-LGS, 2×10^{-2} M and urea, 8 M.

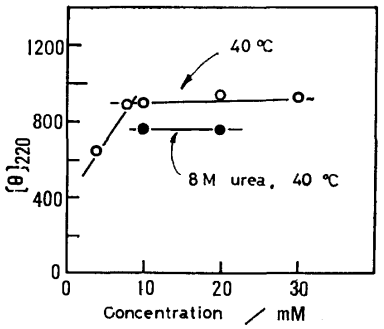

Fig. 7. Relation between $[\theta]_{220}$ and concentration of monosodium *N*-lauroyl-L-glutamate(L-LGS) in water, at 40 °C.

increased with increase in the concentration of L-LGS upto about 1×10^{-2} M which corresponds to its CMC. At concentrations above 1×10^{-2} M, $[\theta]_{220}$ was approximately constant (Fig. 7). Addition of urea to the aqueous solution of L-LGS decreased the CD magnitude in a similar way to that in the case of alcoholic solution (Figs. 4, 6, and 7). Thus, the CD band at 220 nm observed for optically active AGS in aqueous solutions suggests the occurrence of micelle formation together with the formation of chiral hydrogen bond.

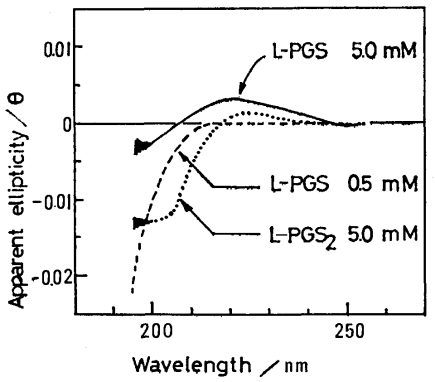

Fig. 8. The CD spectra of sodium and disodium *N*-palmitoyl-L-glutamate (L-PGS and L-PGS_2).
Solid line: L-PGS, 5.0 mM (above CMC), at 60 °C.
Broken line: L-PGS, 0.5 mM (below CMC), at 60 °C.
Dotted line: L-PGS_2, 5.0 mM (below CMC), at 40 °C.

At concentrations lower than CMC, L-AGS shows another CD band at *ca.* 200 nm with the opposite sign to that of the CD band at *ca.* 220 nm (Fig. 8). On the other hand, the aqueous solutions of optically active disodium *N*-acylglutamates (L- or D-AGS_2) and optically active sodium *N*-acylvalinates (L- or D-AVS) show a CD band only at *ca.* 200 nm irrespective of their concentration. From the results, the CD band at 200 nm is attributable to the asymmetric structure of the optically active AGS, AGS_2, and AVS themselves. Since CMC's of these surfactants are dependent on the length of acyl groups (Fig. 4 and Table 3), the micelle formation might be caused by the hydrophobic interaction among acyl chains. On the surface of micelles, amino acid residues of these surfactants can not be brought close enough to form hydrogen bonds because of the repulsive interaction among the carboxylate anions. In the case of L-AGS the decrease in CMC with increase of the acyl chain length is a little smaller than in the case of L-AGS_2 and L-AVS (Fig. 4). This suggests that the hydrophobic interaction is less in L-AGS than in L-AGS_2 and L-AVS. The mutual repulsion between amino acid residues on the surface of L-AGS micelles might be relaxed by the existence of a free carboxyl group. The free carboxyl group in L-AGS is assumed to form chiral hydrogen bond, which may be correlated to the CD band at 220 nm.

The structure of the aggregates of optically active AAA's or their salts are determined by solvent. In alcoholic solutions, AAA's form a different aggregate from micelle through the chiral hydrogen bonding among AAA molecules. However, in aqueous solutions, salts of optically active AAA's form micelles by the hydrophobic interaction among their side chains; the hydrophobic interaction induces hydrogen bond formation in the parts of the hydrophilic moiety of L-AGS.

Conclusion

A CD band at 212 nm was found in alcoholic solutions of optically active AAA's. Hydrophobic interaction among the long chains of acyl groups of AAA molecules is of minor importance to the formation of their aggregates, since the spectral profile and magnitude of the CD bands are independent of the lengths of the acyl groups in the AAA molecules and of their concentrations. Hydrogen bonds might break under certain conditions. The addition of urea and rise in temperature decrease the magnitude of the CD bands, and thus the aggregate may result from the chiral hydrogen bond formation among AAA molecules.

On the other hand, in aqueous solutions, salts of optically active AAA's form micelles with hydrophobic interaction among the molecuels, and show a CD band at 220 nm at concentrations above its CMC only in the case of optically active AGS. The CD band at 220 nm corresponds to the formation of chiral hydrogen bond caused by the existence of a free carboxyl group.

AAA's have a certain similarity to proteins, having acyl group juxtaposition to the asymmetric carbon and becoming amphiphilic to interact both with hydrophobic and hydrophilic surroundings. Proteins em-

bedded in biological membranes reveal two different features. Inside membranes where hydrophobic environment is predominant, the embedded proteins behave like a polar solute in lipid, being forced to form intramolecular hydrogen bonding inside the proteins. In contrast, at the surface of membranes where hydrophilic environment is predominant, the buried proteins are hydrated and seem to be suppressed to form a chiral hydrogen bond. The chiral aggregation or micelle formation of AAA's, which reflects the interaction of AAA's with environmental solvents, may help us to understand the behavior of proteins embedded in membranes.

References

1) K. Sakamoto, R. Yoshida, and M. Hatano, *Chem. Lett.*, **1976**, 1401.
2) K. Sakamoto, R. Yoshida, M. Hatano, and T. Tachibana, *J. Am. Chem. Soc.*, **100**, 6898 (1978).
3) T. Tachibana and H. Kambara, *Kolloid Z. Z. Polym.*, **219**, 40 (1967).
4) T. Tachibana and E. Oda, *Bull. Chem. Soc.. Jpn.*, **46**, 2583 (1973).
5) F. D. Saeva and G. R. Olin, *J. Am. Chem. Soc.*, **95**, 7882 (1973).
6) R. Parthasarathy, B. Paul, and W. Korythnk, *J. Am. Chem. Soc.*, **98**, 6634 (1976).
7) C. S. Chen and R. Parthasarathy, *Acta Crystallogr., Sect. B*, **33**, 3332 (1977).
8) C. S. Chen and R. Parthasarathy, *Int. J. Peptide Protein Res.*, **11**, 9 (1978).
9) M. Takehara, I. Yoshimura, K. Takizawa, and R. Yoshida, *J. Am. Oil Chem. Soc.*, **49**, 157 (1972).
10) M. Takehara, K. Sakamoto, and R. Yoshida, *Yukagaku*, **24**, 538 (1975).
11) The maximum wavelength of CD band attributable to the cholesteric helical structure for the L-LGA–benzene system appears at *ca.* 300—400 nm, its spectral profile being more broad than that of the CD band at 212 nm for the L-LGA–methanol solution.
12) The liquid crystal showed no CD band corresponding to the cholesteric structure, and was assumed to be another type of lyotropic liquid crystal differing from the L-LGA–benzene system.
13) M. Takehara, K. Sakamoto, and R. Yoshida, *Yukagaku*, **25**, 789 (1976).
14) "Poly-α-amino Acids," ed by G. D. Fasman, Marcel Dekker, Inc., New York (1967), p. 704.
15) L. Pauling, R. Corey, and H. Branson, *Proc. Natl. Acad. Sci. U. S. A.*, **37**, 205 (1951).
16) G. Holzwarth and P. Doty, *J. Am. Chem. Soc.*, **87**, 218 (1965).

Adsorption of Alkaline Earth Cations on Mercury as Studied with the Perbromate Kinetic Probe

Tetsuya OSAKA*,** and Robert DE LEVIE
Department of Chemistry, Georgetown University, Washington, D. C., 20057, U. S. A.
(Received June 8, 1979)

Reduction of perbromate was used as a kinetic probe of double layer parameters for weak specific adsorption of double layer parameters for weak specific adsorption of alkaline earth cations at the mercury/electrolyte solutions interface. The results are interpreted as evidence for weak specific adsorption of Sr^{2+} and particularly Ba^{2+} in 10 mM solutions at negative electrode charge densities. The limitation of the use of an anionic probe for the quantitation of cation specific adsorption is discussed.

The weak specific adsorption of alkali metal cations at the interface between mercury and aqueous electrolyte solutions has given rise to controversy because of the seemingly conflicting results obtained from various experimental methods.[1-10] Damaskin[11] showed that such results are, in fact, quite to be expected for subequivalent specific adsorption of ions, for which the usual thermodynamic method is not sufficiently sensitive. A similar situation applies to alkaline earth cations, for which Frumkin and Nikolaeva-Fedorovich[12] reported a slight increase in the rate of peroxydisulfate reduction in going from Ca^{2+} to Ba^{2+}, whereas Parsons *et al.*[13,14] observed approximate agreement between experimental data and double layer calculations assuming the absence of specific adsorption for both Mg^{2+} and Ba^{2+}. In the present communication, we report results similar to those of Frumkin and Nikolaeva-Fedorovich, using perbromate as a kinetic double layer probe.

Experimental

The dc, ac, and pulse polarograms were obtained on an instrument described earlier[15-17] which features phase-resolved ac polarograms, IR compensation and a simple integral pulse circuit based on the 60 Hz line frequency. Chemicals of reagent grade were used without further purification. The rate constants $k_c^\ominus$'s were calculated from dc polarograms using the Koutecký formalism[18-21] and from integral pulse polarograms using an equivalent method based on the relations of Brinkman and Los.[22] Polarographic maxima of the first kind in the dc polarograms were avoided by using low perbromate concentrations ($\leqslant$0.1 mM), and maxima of the second kind by using low mercury flow rates ($\approx$0.15 mg s^{-1}); maxima on the integral pulse polarograms such as reported by Fonds *et al.*[23] were initially observed, but were eliminated by proper IR compensation. Charge densities were obtained by integration of capacitance data from IR-compensated quadrature ac polarograms at 159 Hz ($\omega = 10^3$ rad s^{-1}). The potentials of zero charge required as integration constants were taken at the diffuse layer minima in the capacitance curves. Comparison with electrocapillary measurements in 10 mM LiCl and 10 mM $MgSO_4$ showed agreement within 1 and 2 μC cm^{-2}, respectively. All potentials are referred to a saturated calomel electrode (SCE), measurements being made at 25.0 °C.

Results and Discussion

The dc polarograms of perbromate in 10 mM alkali halide solutions exhibit pronounced minima, but the corresponding minima in 10 mM solutions of alkaline earth halides or sulfates are too shallow to allow accurate numerical evaluation. Thus, integral pulse polarograms were used instead to provide sufficiently accurate rate parameters. Figure 1 shows the dependence of the ratio i/i_l on the reaction rate constant $k_c^\ominus$ for the dc and integral pulse polarograms. Heterogeneous rate constants up to *ca.* 0.05 cm s^{-1} could be obtained with reasonable accuracy from pulse-polarographic i/i_l ratios. Where the pulse-polarographic limiting current was not directly observable, and its value was calculated from the dc limiting current and the known ratio of dc and pulse-polarographic limiting currents in our instrument as determined with Cd^{2+} and Zn^{2+} ions. The results for 10 mM alkaline earth chlorides and for 10 mM $MgSO_4$ are shown in Fig. 2, and compared with rate constants calculated for a 2,2-electrolyte such as $MgSO_4$ on the basis of measured rate constants for 10 mM LiCl assuming the absence of specific adsorption

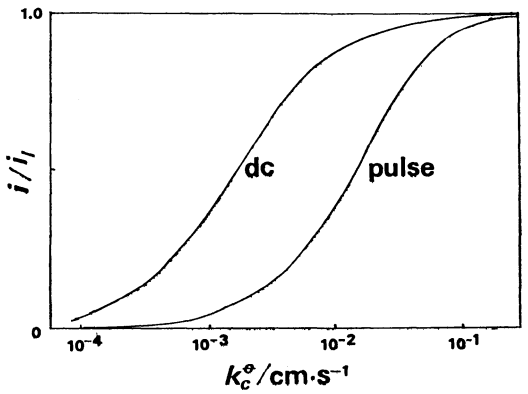

Fig. 1. The ratio of current i to limiting current i_l as a function of rate constant $k_c^\ominus$ for an irreversible reduction or oxidation in dc and integral pulse polarography respectively. The curves were calculated with the following specific parameter: $D = 2.5 \times 10^{-5}$ cm^2 s^{-1}, sampling time (for dc and pulse) 4.2 s after drop birth, sampling interval from 16.7 to 33.3 ms after application of the pulse.

** Present address: Department of Applied Chemistry, Waseda University, Shinjuku-ku, Tokyo 160.

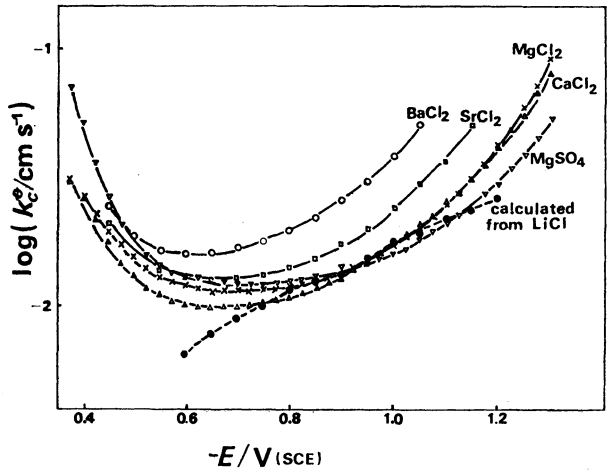

Fig. 2. Rate constants calculated from the integral pulse polarograms of 0.06 mM $KBrO_4$ in 10 mM aqueous alkaline earth electrolytes.

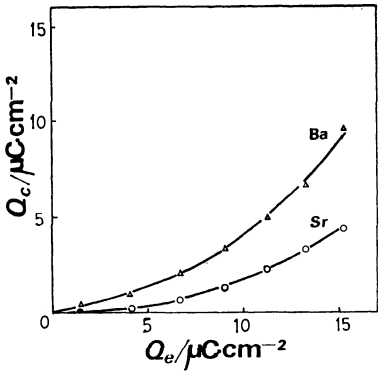

Fig. 3. Specifically adsorbed charge density Q_c as a function of electronic charge density Q_e, calculated from the data of Fig. 2 for 10 mM $SrCl_2$ and $BaCl_2$ on the assumptions that the Gouy-Chapman-Stern theory and simple Frumkin correction apply and that Mg^{2+} is not at all specifically adsorbed from 10 mM aqueous $MgCl_2$.

of both Li^+ and Mg^{2+}.† At potentials more negative than −0.8 V *vs.* SCE, the data for $MgSO_4$ coincide with those calculated from LiCl within experimental error. Comparison of the results for $MgSO_4$ and $MgCl_2$ indicates that the nature of the anion is not very important at sufficiently negative potentials, where the double layer predominantly contains cations. Coincidence of the curves for $MgCl_2$ and $CaCl_2$ suggests that Ca^{2+} is not specifically adsorbed to any appreciable extent from 10 mM aqueous halide solutions either. However, Sr^{2+} and particularly Ba^{2+} appear to be specifically adsorbed. Estimation of such specific adsorption can be made on the assumption that $MgCl_2$ is not specifically adsorbed at all. The results are shown in Fig. 3. Calculation of the specifically adsorbed charge densities Q_c of Sr^{2+} and Ba^{2+} from the difference of their measured rate constants was made by assuming complete absence of specific adsorption of Mg^{2+} as follows.

$$\Delta\phi_0 = \frac{RT}{(1+2\alpha)F} \ln \Delta k_c^\circ \quad (1)$$

$$Q_d = \left\{A\sum_i c_i \left\{\exp\left(-\frac{Z_i F}{RT}\phi_0\right) - 1\right\}\right\}^{1/2} \quad (2)$$

$$Q_c = -(Q_d + Q_e) \quad (3)$$

where Q_d and Q_e are the diffusion double layer and electronic charge densities, respectively. Since the charge transfer coefficient α is potential-dependent, each value was determined graphically with the use of k_{corr} *vs.* $(E-\phi_0)$ curve of perbromate reduction.†† In both cases of Sr^{2+} and Ba^{2+}, the estimates indicate weak specific adsorption, considerably less than in amount equivalent to the electronic charge density Q_e.

In an earlier work with perbromate,[9] quite good agreement with data reported was obtained for specifically adsorbed anions. However, the estimates for alkali ion adsorption were a factor of two higher than those obtained with the mixed-electrolyte approach.[6-8] Damaskin[11,24] reported a similar discrepancy with MnO_4^-, $S_4O_6^{2-}$, $S_2O_8^{2-}$, PtF_6^{2-}, and $Fe(CN)_6^{3-}$ in studying alkali ion adsorption, but good agreement when H^+ was used. It appears that the probe ion is attracted electostatically by the specifically adsorbed ion, and preferentially reduced close to the latter if the two have charge of opposite sign. The probe ion would undergo stronger specific adsorption than accounted for by the Frumkin correction. Because of this dynamic discreteness-of-charge effect, the data in the present communication should be qualitative.

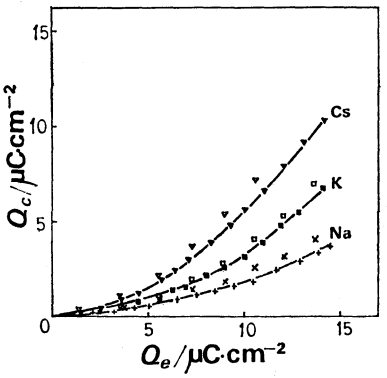

Fig. 4. Specifically adsorbed charge density Q_c as a function of electronic charge density Q_e, calculated from dc and integral pulse polarograms in 10 mM and 0.1 M aqueous alkali halide solutions respectively, based on Gouy-Chapman-Stern theory, Frumkin correction and the absence of specific adsorption of Li^+. Symbols used: +, ■ and ▼: 10 mM NaF, KCl, and CsCl respectively; ×, □ and ▽: 0.1 M NaCl, KCl, and CsCl respectively.

† The rate constants calculated for a 2,2-electrolyte such as $MgSO_4$ were derived from the rate constant with the Frumkin correction $k_{corr}(\log k_{calcd} = \log k_{corr} + (F/2.3RT)\phi_0$, *cf.* Ref. 9) in 10 mM LiCl, and the double layer potential ϕ_0 (mean potential of OHP) was calculated by means of Gouy-Chapman-Stern theory using the electronic charge density in 10 mM LiF and 10 mM $MgSO_4$ obtained by integrating capacitance.

†† A more detailed discussion is given in Ref. 9. The value of α is sufficiently small to justify this procedure.

The same applies to the slight extension of the work of de Levie and Nemes on alkali cations (Fig. 4), where the earlier dc-polarographic results for 10 mM solutions are combined with new pulse-polarographic data for 0.1 M. The amount of specific adsorption is approximately independent of the ten-fold increase in concentration, in agreement with the observations of Damaskin and Ivanova[8] and with the buffering effect of the double layer on weak specific adsorption of cations.[11,25] The results appear to be qualitatively correct, although the specific values obtained are likely to be too high in view of the dynamic discreteness-of-charge effect. Other possible sources of systematic error, of cource, result from all other assumptions in the Gouy-Chapman-Stern theory and the Frumkin correction, specifically the assumption that the average potential at the reaction plane coincides with that of the outer Helmholtz plane.

The authors thank Mr. James F. Garvey for construction of the pulse-polarographic attachment, Drs. Srinivasan Sarangapani and Paul F. Seelig for their help in the calculations, and Dr. E. H. Appelman, Argonne National Laboratories, for the supply of $KBrO_4$. The work was carried out with Grants 76-3027 and GM 2296-03 from AFOSR and NIH, respectively.

References

1) D. C. Grahame, A. E. Higginbotham, and F. R. M. Deane, Trans. Symp. on Electrode Processes, Philadelphia (1959), p. 197.
2) A. N. Frumkin, O. A. Petry, and N. V. Nikolaeva-Fedorovich, *Electrochim. Acta*, **8**, 177 (1963).
3) H. Wroblova, Z. Kovač, and J. O'M. Bockris, *Trans. Faraday Soc.*, **61**, 1523 (1965).
4) L. Gierst, E. Nicholas, and L. Tytgat-Vandenberghen, *Croat. Chim. Acta*, **42**, 117 (1970).
5) R. V. Ivanova, B. B. Damaskin, and S. Mazurek, *Elektrokhim.*, **6**, 1041 (1970).
6) R. Parsons and A. Stockton, *J. Electroanal. Chem.*, **25**, A10 (1970).
7) R. V. Ivanova, *Elektrokhim.*, **9**, 1565 (1973).
8) B. B. Damaskin and R. V. Ivanova, *Elektrokhim.*, **9**, 1569 (1973).
9) R. de Levie and M. Nemes, *J. Electroanal. Chem.*, **58**, 123 (1975).
10) A. N. Frumkin, N. V. Nikolaeva-Fedorovich, N. P. Berezina, and Kh. E. Keis, *J. Electroanal. Chem.*, **58**, 189 (1975).
11) B. B. Damaskin, *J. Electroanal. Chem.*, **65**, 799 (1975).
12) A. N. Frumkin and N. V. Nikolaeva-Fedorovich, "Progress in Polarography" Interscience Publisher, New York, London (1962), Vol. 1, p. 229.
13) K. M. Joshi and R. Parsons, *Electrochim. Acta*, **4**, 129 (1961).
14) R. Parsons and S. Trasatti, *Trans. Faraday Soc.*, **65**, 3314 (1969).
15) R. de Levie and A. A. Husovsky, *J. Electroanal. Chem.*, **20**, 181 (1969).
16) T. Ohsaka and R. de Levie, *J. Electroanal. Chem.*, **99**, 255 (1979).
17) R. de Levie and T. Ohsaka, Trans. 3rd Symp. on Electrode Processes, Boston (1979), in press.
18) N. Meiman, *Zh. Fiz. Khim.*, **22**, 1415 (1948).
19) J. Koutecký, *Collect. Czech. Chem. Commun.*, **18**, 597 (1953).
20) H. Matsuda and Y. Ayabe, *Bull. Chem. Soc. Jpn.*, **28**, 422 (1955).
21) D. E. Smith, T. G. McCord, and H. L. Hung, *Anal. Chem.*, **39**, 144 (1967).
22) A. A. A. M. Brinkman and J. M. Los, *J. Electroanal. Chem.*, **14**, 269 (1967).
23) A. W. Fonds, A. A. A. M. Brinkman, and J. M. Los, *J. Electroanal. Chem.*, **14**, 43 (1967).
24) B. B. Damaskin and N. V. Fedorovich, *Electrokhim.*, **11**, 999 (1975).
25) R. de Levie, *J. Electrochem. Soc.*, **118**, 185C (1971).

The Micelle-promoted Selective Hydrolysis of Anionic and Nonionic Ester Substrates by Hydroxamic Acids and Histidine Derivatives

Ryuichi UEOKA,* Hidehiko MATSUURA, Syuji NAKAHATA, and Katsutoshi OHKUBO**

Department of Industrial Chemistry, Kumamoto Institute of Technology, Kumamoto 860
***Department of Synthetic Chemistry, Faculty of Engineering, Kumamoto University, Kumamoto 860*

(Received June 11, 1979)

The hydrolyses of anionic 3-nitro-4-acyloxybenzoic acid (S_2^-–S_{16}^-) and nonionic *p*-nitrophenyl carboxylate (S_2—S_{16}) substrates catalyzed by hydroxamic acids (C_6—C_{12}) and histidine derivatives (AcetHis and LauHis) were performed with and without alkyltrimethylammonium (DTAC, CTAB, and OTAC) surfactants at pH 7.45. The present reaction was characterized by the selectively efficient hydrolysis of the same substrate of S_6^- or S_{10} by the comicellar C_m (m=8, 10, or 12)–CTAB (or OTAC) or LauHis–CTAB (or OTAC) catalysts. Relevant factors to such a selective hydrolysis of a specific substrate by the comicellar catalysts were discussed by taking notice of the electrostatic-charge-attraction force, steric hindrance, and hydrophobic interaction. The investigation of the binding constants in the present micellar reaction system demonstrated the importance of an appropriate hydrophobic interaction between a substrate and micelles for the selective rate enhacement of ester-hydrolysis.

The contribution of hydrophobic (apolar) forces and micellar effects to the rate enhancement of enzyme-model reactions has recently received considerable attention, especially in connection with the hydrolysis of ester substrates by synthetic catalysts involving the hydroxamate group (a model of the Ser-195 part in chymotrypsin),[1–11] imidazolyl group (a model of the His-57 part in chymotrypsin),[12–24] both of them (bifunctional catalysts),[6,25–27] or with *N*-alkylamines,[28–30] amino acids,[31] polyelectrolytes,[32] surfactants,[33–38] and surfactants having imidazole derivatives.[39–43] The magnitude of the hydrophobic interaction between a substrate and a catalyst is well kown to be directly dependent on their apolar alkyl-chain lengths and on the micellar effects of the species participating in the reaction. In this regard, the micellar effects of catalysts, surfactants, and/or substrates on the rate enhancement of ester-hydrolyses have no yet been treated systematically by changing the hydrophobic alkyl-chain length in the above species, even though the micellar effects on the ester-hydrolyses have been discussed in many of the ealier investigations.[44]

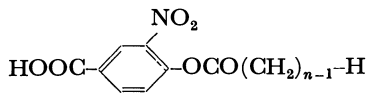

S_n^- (n=2, 4, 6, 10, 12, and 16)

S_n (n=2, 4, 6, 10, 12, and 16)

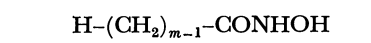

C_m (m=6, 8, 10, and 12)

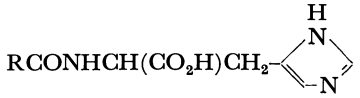

AcetHis (R=CH_3) and LauHis (R=$C_{11}H_{23}$)

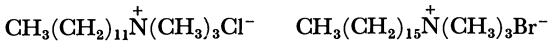

DTAC CTAB

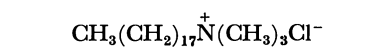

OTAC

The present work has been undertaken in an attempt to investigate how the systematic change in hydrophobic chain lengths in substrates, catalysts, and surfactants influences the hydrolyses of anionic 3-nitro-4-acyloxybenzoic acids (S_n^-) and nonionic *p*-nitrophenyl carboxylates (S_n) by hydroxamic acids (C_m) or L-histidine derivatives (AcetHis and LauHis) with and without cationic-surfactant (DTAC, CTAB, or OTAC) micelles.

Experimental

Material. 3-Nitro-4-acyloxybenzoic acids (S_2^-—S_{16}^-) were prepared in accordance with the method of Overberger *et al.*[18] Satisfactory elementary analyses were obtained for S_n^- (n=2—16), and those for new compounds are shown below: S_4^-: mp 113—114 °C. Found: C, 52.47; H, 4.25; N, 5.64%. Calcd: C, 52.17; H, 4.35; N, 5.53%. S_6^-: mp 75.0—76.0 °C. Found: C, 54.86; H, 5.29; N, 4.94%. Calcd: C, 55.51; H, 5.38; N, 4.98%. S_{10}^-: mp 70.1—72.0 °C. Found: C, 60.29; H, 6.79; N, 4.10%. Calcd: C, 60.52; H, 6.87; N, 4.15%. S_{16}^-: mp 87.1—89.0 °C. Found: C, 65.24; H, 8.21; N, 3.66%. Calcd: C, 65.53; H, 8.37; N, 3.32%.

p-Nitrophenyl acetate (S_2) was prepared by the acylation of *p*-nitrophenol with acetic anhydride, while the other *p*-nitrophenyl carboxylates (S_2—S_{12}) were obtained by the condensation of the corresponding acid chloride with *p*-nitrophenol. *p*-Nitrophenyl hexadecanoate (S_{16}) was commercially available and was used without further purification, because the elementary analysis of S_{16} gave satisfactory results. The results of the elementary analyses of synthetic S_n (n=2—12) were as follows: S_2: Found: C, 52.85; H, 3.66; N, 7.65%. Calcd: C, 53.00; H, 3.86; N,7.74%. S_4: Found: C, 57.74; H, 5.32; N, 6.90%. Calcd: C, 57.50; H, 5.32; N, 6.72%. S_6: Found: C, 60.75; H, 6.37; N, 5.90%. Calcd: C, 60.90; H, 6.32; N, 5.93%. S_{10}: Found: C, 65.65; H, 7.77; N, 4.68%. Calcd: C, 65.50; H, 7.85; N, 4.78%. S_{12}: Found: C, 67.71; H, 8.69; N, 4.41%. Calcd: C, 67.26; H, 8.47; N, 4.36%.

N^{α}-Lauroyl-L-histidine (LauHis) was obtained by the reaction of L-histidine and lauroyl chloride:[14] mp 162 °C (lit,[31] mp 160—161 °C). Found: C, 64.03; H, 9.27; N, 12.11%. Calcd: C, 64.06; H, 9.26; N, 12.45%. The N^{α}-acetyl-L-histidine (AcetHis) used in the present work was supplied by the Sigma Chemical Company.

The hydroxamic acids (C_6—C_{12}) were prepared from H–$(CH_2)_{m-1}$–$CO_2C_2H_5$ (m=6—12) and hydroxylamine, and

satisfactory elementary analyses were obtained: C_6: mp 45—47 °C. Found: C, 55.53; H, 9.78; N, 10.40%. Calcd: C, 54.94; H, 9.99; N, 10.68%. C_8: mp 75.6—77.2 °C. Found: C, 60.55; H, 10.52; N, 8.58%. Calcd: C, 60.34; H, 10.76; N, 8.80%. C_{10}: mp 85.9—86.7 °C. Found: C, 64.96; H, 11.10; N, 7.41%. Calcd C, 64.13; H, 11.30; N, 7.48%. C_{12}: mp 96—97 °C. Found: C, 67.13; H, 11.53; N, 6.26%. Calcd for: C, 66.98; H, 11.63; N, 6.51%.

Commercially available dodecyltrimethylammonium chloride (DTAC), hexadecyltrimethylammonium bromide (CTAB), and octadecyltrimethylammonium chloride (OTAC) were recrystallized from an anhydrous ethanol–ether mixture.

Hydrolysis. The hydrolyses of anionic S_n^- and nonionic S_n substrates ($(2—5)\times10^{-5}$ M; 1 M=1 mol dm^{-3}) by the C_m and LauHis (and/or AcetHis) catalysts ($(1—5)\times10^{-4}$ M) with or without a surfactant of DTAC (3.3×10^{-2} M), CTAB (5×10^{-3} M), or OTAC (5×10^{-3} M) were carried out at 31.0 °C, pH 7.45, in a 0.083 M tris(hydroxymethyl)aminomethane buffer (Tris) involving 0.083 M KCl (μ=0.083) in 10%(v/v) CH_3CN–H_2O; the reactions were followed spectrophotometrically by means of the phenolate-anion formation at 410 nm (for S_n^-) and 400 nm (for S_n). In the above procedure, the concentrations of the surfactants are higher than their critical micelle concentrations (CMC).

Determination of Critical Micelle Concentration (CMC). The CMC values for the substrates (S_n^-), the catalysts (C_m or LauHis), or the surfactants were measured by means of the usual conductivity method; a remarkable change in the conductivities of the above species upon an increase in their concentrations was found in the cases of S_n^- (n=12 and 16), C_m (m=8, 10, and 12), and all of the surfactants (DTAC, CTAB, and OTAC) employed for the present work. The CMC values obtained under the present reaction conditions are summarized below: $S_{12}^-=(1—3)\times10^{-4}$ M, $S_{16}^-=2\times10^{-5}$ M, $C_8=1\times10^{-4}$ M, $C_{10}=(1.3—2.0)\times10^{-5}$ M, $C_{12}=1\times10^{-5}$ M, LauHis=5×10^{-5} M, DTAC=1.5×10^{-2} M, CTAB=1×10^{-3} M, and OTAC=1.3×10^{-4} M at 31 °C, pH 7.45, in a 0.083 M Tris–KCl buffer in 10%(v/v) CH_3CN–H_2O.

Results and Discussion

Pseudo-first-order Hydrolysis. The hydrolysis of the S_n^- or S_n (n=2—16) substrates by the C_m (m=6—12) or LauHis (and/or AcetHis) catalysts, with and without the surfactants, obeys the usual pseudo-first-order rate law, which is substantiated by the linear relationship between log $(A_\infty-A_t)$ and the reaction time (t), where A_∞ and A_t denote the absorbances of the phenolate anion formed at an infinite time and at t respectively. The second-order rate constant (k_{cat}) for the deacylation of the ester substrates was evaluated as an average value obtained from the reactions repeated three times under identical conditions:

$$k_{cat} = (k_{total}-k_{spont})/[Cat]_0,$$

where k_{total} and k_{spont} (less than 5% of the k_{total}[45]) indicate, respectively, the first-order rate constant for the S_n^- (or S_n) hydrolysis with or without the catalyst, and where $[Cat]_0$ indicates the initial catalyst concentration. The catalytic efficiency of mixed catalysts was, then, compared on the basis of the k_{cat} values obtained at a fixed surfactant concentration (DTAC=3.3×10^{-2} M, CTAB=5×10^{-3} M, and OTAC=5×10^{-3} M).

Hydrolysis of Anionic S_n^- by C_m. The effects of the hydrophobic acyl- or alkyl-chain lengths of substrates, catalysts, or surfactants on the ester-hydrolysis reaction will first be discussed by comparing the rate constants obtained in the S_n^- (n=2—16) hydrolysis by C_m (m=6—12) with or without the surfactant (DTAC, CTAB, or OTAC); since the pK_a values of the hydroxamic acids (C_m) tested are around 9.5,[46] the hydrolyzing activity of the C_m catalyst is weaker in a neutral region (pH≈7) than in a basic solution.

In the absence of the surfactant micelles, an increase in the alkyl-chain length in the C_m catalyst from m=6 to m=10 results in a monotonous rate-enhancement for the S_n^- (n=2—16) hydrolysis because of the increase in the hydrophobic interaction between S_n^- and C_m; such a rate enhancement came to be especially great when the catalyst was changed from C_{10} to C_{12}.

On the other hand, the change in the acyl-chain length of the substrates also influenced the rate of S_n^- (n=2—16) hydrolysis by C_m (m=6—12). The increase in the acyl-chain length in S_n^- (n=2—16) for the S_n^- hydrolysis by C_6, which has no CMC, retarded the hydrolysis rate monotonously, probably because of the steric hindrance of the long acyl chain (in S_n^-);[18,19] this trend was also observed in the cases of the S_n^- (n=2—6) hydrolysis by the C_m (m=8—12) catalysts. However, in the hydrolysis of S_n^- (n=10—16), which possesses a relatively long acyl-chain length, by the C_{10} and C_{12} (especially by C_{12}), the contribution of the hydrophobic forces to the hydrolysis acceleration can be recognized (Table 1).

Table 1. k_{cat}(M^{-1} s^{-1}) values for the hydrolyses of S_n^- by C_m at pH 7.45

Catalyst	S_2^-	S_4^-	S_6^-	S_{10}^-	S_{12}^-	S_{16}^-
C_6	0.88	0.27	0.27	0.26	0.21	0.0
C_6+DTAC	1.83	0.46	0.44	0.39	0.37	0.34
C_6+CTAB	2.30	0.82	0.80	0.70	0.67	0.54
C_6+OTAC	2.15	0.67	0.93	0.66	0.70	0.52
C_8	0.99	0.29	0.30	0.41	0.32	0.00$_3$
C_8+DTAC	4.30	1.45	1.32	1.07	1.01	1.00
C_8+CTAB	13.6	5.59	5.91	4.76	4.03	3.28
C_8+OTAC	13.7	6.13	6.28	4.96	4.30	3.85
C_{10}	0.94	0.37	0.39	0.47	0.42	0.56
C_{10}+DTAC	6.22	2.57	2.53	2.44	2.54	2.21
C_{10}+CTAB	41.5	21.4	31.4	20.6	14.5	17.6
C_{10}+OTAC	11.7	6.80	8.77	5.91	6.94	4.48
C_{12}	4.91	1.98	0.82	2.27	4.15	7.73
C_{12}+DTAC	5.82	2.37	2.56	1.77	1.77	2.26
C_{12}+CTAB	33.6	19.3	20.0	16.8	13.8	5.10
C_{12}+OTAC	52.3	21.9	26.5	23.8	21.3	15.8

In the presence of the surfactant micelles, the comicellar catalysis was recognized in the S_n^- (n=2—16) hydrolysis, which was fairly much accelerated by condensing the anionic S_n^- substrates on the cationic micelles through electrostatic and hydrophobic forces. In this respect, the extent of the rate acceleration by the surfactant micelles, which was the most remarkable in the S_n^- (n=2—16) hydrolysis by the mixed micelles of the C_m (m=10 or 12)–CTAB (or OTAC) system,

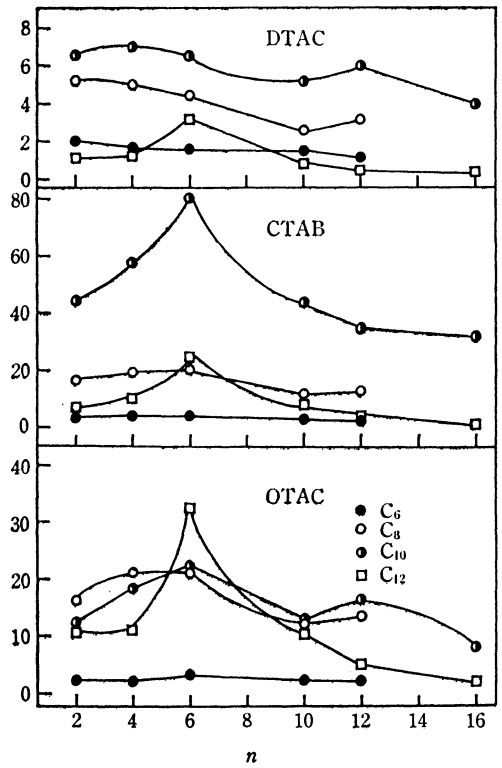

Fig. 1. Dependence of r value on the acyl chain length (n) in S_n^-.

was not monotonously increased by lengthening the hydrophobic acyl or alkyl chain in the catalyst, substrate, or surfactant (Table 1). Here, we can notice the magnitude of the micellar influence of the surfactant on the hydrolysis acceleration, which can be measured by the ratio (r) of the k_{cat} value in the presence of the surfactant to that in its absence, and the dependence of the r value on the acyl-chain length in S_n^- is shown in Fig. 1. As Fig. 1 indicates, a remarkable enhancement of the hydrolysis rate by the comicellar catalyst was realized in the S_6^- hydrolysis by C_{10}–CTAB or C_{12}–OTAC; that is, the hydrolyzing activities of C_{10} and C_{12} in the S_6^- hydrolysis are elevated by the respective surfactants (CTAB and OTAC) to *ca.* 80 and 32 times as great as those of C_{10} and C_{12} themselves. Such a selective enhancement of S_6^- hydrolysis by the above comicellar catalysts has also been observed in the S_n^- hydrolysis at pH 9.06.[10] The efficient activities of the mixed micelles of C_m (m=8, 10, and 12) –CTAB (or OTAC) for the selective enhancement in the hydrolysis of the same specific substrate (S_6^-) might result from the cooperative forces appearing in the following factors, in view of the fact that the alkyl-chain lengths in CTAB and OTAC are not so very different: (a) a favorable arrangement of the active nucleophilic group in C_m on the micellar surface for selectively accelerating the hydrolysis of a substrate possessing an appropriate acyl chain length and/or (b) a balance between the steric hindrance and the hydrophobic forces of the acyl-chain length (in S_n^-) in the condensation of S_n^- by the comicellar catalysts. Since the C_{10}–CTAB (or C_{12}–OTAC) catalyst showed great activity for the rate

Table 2. k_{cat}(M^{-1} s^{-1}) values for the hydrolyses of S_n^-(or S_n) by AcetHis and LauHis

Catalyst	S_2^-	S_4^-	S_6^-	S_{10}^-	S_{12}^-	S_{16}^-
AcetHis	0.45 (0.12)	0.41 (0.20)	0.34 (0.23)	0.23 (0.17)	0.35 (0.17)	0.06 (0.02)
AcetHis+ DTAC	0.18	0.05	0.03	0.03	0.02	0.07
AcetHis+ CTAB	0.27 (0.11)	0.05 (0.08)	0.03 (0.04)	0.01 (0.01)	0.02 (0.01)	0.07 (0.01)
AcetHis+ OTAC	0.24	0.06	0.01	0.01	0.02	0.06
LauHis	0.73 (0.58)	0.47 (1.02)	0.59 (0.91)	1.49 (1.64)	1.99 (2.36)	3.47 (10.3)
LauHis+ DTAC	3.31 (2.10)	2.37 (2.20)	2.52 (2.03)	2.27 (2.42)	2.48 (2.57)	2.62 (2.92)
LauHis+ CTAB	6.40 (3.65)	6.00 (4.99)	7.14 (6.08)	6.00 (9.76)	5.59 (9.54)	5.45 (6.64)
LauHis+ OTAC	5.20 (3.27)	4.83 (5.19)	5.07 (8.03)	4.49 (9.51)	3.98 (9.31)	3.73 (9.20)

The values in parentheses are those for the S_n hydrolyses.

enhancement in all the hydrolyses of S_n^-, the latter factor (b) seems to play a predominant role in such a selective enhancement of S_6^- hydrolysis.

Hydrolysis of S_n^- and S_n by AcetHis and LauHis. In order to investigate the effects of different substrates and catalysts on the above-mentioned selective hydrolysis acceleration, the hydrolyses of the anionic S_n^- and nonionic S_n (n=2—16) substrates by an AcetHis (with no CMC) or micellar LauHis catalyst were performed with or without surfactants.

Although the relatively small activity of AcetHis, as compared with that of LauHis, was considerably diminished by the addition of the surfactant (DTAC, CTAB, or OTAC), the micellar or comicellar catalysis for the hydrolysis acceleration was also recognized in the S_n^- (or S_n) hydrolysis by a LauHis or LauHis-surfactant system (Table 2). The LauHis catalyst hydrolyzed both kinds of substrates (S_n^- and S_n) more easily, as the hydrophobic acyl-chain length in the substrates varied from n=4 in S_n^- (or n=6 in S_n) to n=16 through the hydrophobic forces. The extent of the change in the hydrolysis rates by lengthening the acyl chain in S_n (or S_n^-) is different between LauHis–DTAC and LauHis–CTAB (or OTAC); that is, the former comicellar catalyst increases the rate of S_n or S_n^- (n=10—16) hydrolyses monotonously, in parallel with the increase in the acyl-chain length (n), but the latter one results in a rate decrease in the S_n (n=10—16) or S_n^- (n=6—16) hydrolyses. Such a difference in catalysis between LauHis–DTAC and LauHis–CTAB (or OTAC) is also reflected in the following observations: the latter catalyst brought about a rate enhancement for the hydrolysis of anionic S_6^- and nonionic S_{10} selectively (this is probably due to the force expressed by the (b) factor mentioned before, even though such a selective rate enhancement was not realized by the former one. At any rate, it is worthy of notice that the same selective rate enhancement of S_n^- (especially S_6^-) hydrolysis by LauHis–CTAB and C_{10}–CTAB catalysts was observed in spite of the different functional groups between LauHis and C_{10}.

Binding Constants for the Selective Hydrolysis of S_n.

The present selective hydrolysis of a substrate possessing an appropriate acyl-chain length by the comicellar catalysts will be briefly discussed by taking notice of the binding constants obtained for the present hydrolyses of S_n (n=2, 6, 10, and 16) by the LauHis–OTAC comicelles at pH 7.45. The present micellar reactions can be given the following steps:

$$S_n + M \overset{K_b}{\rightleftharpoons} MS_n \overset{k}{\longrightarrow} P$$

(on the miceller surface)

$$S_n \overset{k_{spont}}{\longrightarrow} P$$

(in the bulk solution)

where M=comicelles of LauHis–OTAC; MS_n=micelle-substrate complex; P=*p*-nitrophenol; K_b=binding constant.

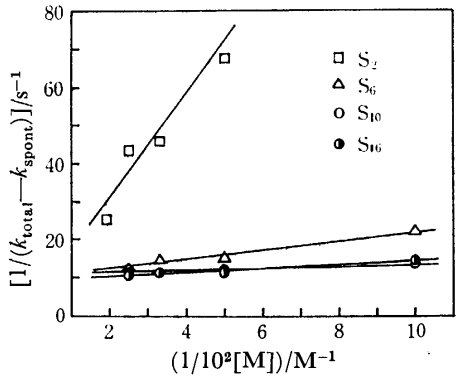

Fig. 2. Linear relationships between the reciprocal values of (k_{total}—k_{spont}) and [M] in the hydrolyses of S_n by LauHis in the presence of OTAC.

In the present study, the experiments were carried out under the following conditions: [OTAC]≫CMC, and [OTAC]>[LauHis]>[S_n], at 31 °C, pH 7.45, in a 0.083 M Tris-KCl buffer in 10%(v/v) CH_3CN–H_2O. The linear relationships between the reciprocal value of ($k_{total}-k_{spont}$) and [M] ([M]=[OTAC]+[LauHis]−[OTAC]$_{CMC}$; [OTAC]$_{CMC}$ is 1.3×10^{-4} M) were obtained as is indicated in Fig. 2. The K_b/N and k values were, then, evaluated from the following equation according to the previous techniques:[31,34]

$$1/(k_{total}-k_{spont}) = N/K_b(k-k_{spont})[M] + 1/(k-k_{spont})$$

where N=aggregation number.

In estimating the K_b/N and k values listed in Table 3, the monotonous increase in the former value with an increase in the acyl-chain length in S_n from n=2 to n=16 suggests that the formation of MS_n by the condensation of S_n by the comicelles is favored in the hydrolysis of S_n with a longer hydrophobic acyl-chain length. However, no appreciable change in the k value with an increase in the acyl-chain length in S_n was observed.

It may be deduced, therefore, that the selective S_{10} hydrolysis by the LauHis+OTAC comicelles cannot be explained well by only the binding constant, and the present selective hydrolysis of a specific substrate with an appropriate acyl chain can be understood as a result of the approximation effect which makes the nucleophile and the substrate come close to each other.

Table 3. Estimated constants for the binding system in the hydrolysis of S_n by a comicellar catalyst (LauHis+OTAC)

	S_2	S_6	S_{10}	S_{16}
$(K_b/N)M^{-1}$	52.8	811	1829	2772
k/min^{-1}	0.149	0.100	0.106	0.099

References

1) W. B. Gruhn and M. L. Bender, *J. Am. Chem. Soc.*, **91**, 5883 (1969).
2) R. Hershfield and M. L. Bender, *J. Am. Chem. Soc.*, **94**, 1376 (1972).
3) I. Tabushi, Y. Kuroda, and S. Kita, *Tetrahedron Lett.*, **1974**, 643.
4) I. Tabushi and Y. Kuroda, *Tetrahedron Lett.*, **1974**, 3613.
5) T. Kunitake, Y. Okahata, and R. Ando, *Bull. Chem. Soc. Jpn.*, **47**, 1509 (1974).
6) T. Kunitake, Y. Okahata, and T. Sakamoto, *J. Am. Chem. Soc.*, **98**, 7799 (1976).
7) T. Kunitake, S. Shinkai, and Y. Okahata, *Bull. Chem. Soc. Jpn.*, **49**, 540 (1976).
8) R. Ueoka, M. Kato, and K. Ohkubo, *Tetrahedron Lett.*, **1977**, 2163.
9) R. Ueoka, K. Shimamoto, Y. Maezato, and K. Ohkubo, *J. Org. Chem.*, **43**, 1815 (1978).
10) R. Ueoka and K. Ohkubo, *Tetrahedron Lett.*, **1978**, 4131.
11) R. Ueoka, H. Mori, K. Yonezawa, M. Kato, H. Ohtsuka, and K. Yamada, *Nippon Kagaku Kaishi*, **1979**, 522.
12) C. G. Overberger, T. P. Pierre, C. Yaroslavsky, and S. Yaroslavsky, *J. Am. Chem. Soc.*, **88**, 1184 (1966).
13) A. Ochoa-Solano, R. Romero, and C. Gitler, *Science*, **156**, 1243 (1967).
14) C. Gitler and A. Ochoa-Solano, *J. Am. Chem. Soc.*, **90**, 5004 (1968).
15) J. R. Knowles and C. A. Parsons, *Nature*, **221**, 53 (1969).
16) T. Kunitake and S. Shinkai, *J. Am. Chem. Soc.*, **93**, 4256 (1971).
17) C. A. Blyth and J. R. Knowles, *J. Am. Chem. Soc.*, **93**, 3021 (1971).
18) C. G. Overberger, R. C. Glowaky, and P.-H. Vandewyer, *J. Am. Chem. Soc.*, **95**, 6008 (1973).
19) C. G. Overberger and R. C. Glowaky, *J. Am. Chem. Soc.*, **95**, 6014 (1973).
20) D. G. Oakenfull and D. E. Fenwick, *J. Phys. Chem.* **78**, 1759 (1974).
21) K. Martineck, A. T. Ositov, A. K. Yatsimirski, and I. V. Berezin, *Tetrahedron*, **31**, 709 (1975).
22) W. Tagaki, S. Kobayashi, and D. Fukushima, *Chem. Commun.*, **1977**, 29.
23) C. G. Overberger and T. W. Smith, *Macromolecules*, **8**, 416 (1975).
24) U. Tonellato, *J. Chem. Soc., Perkin Trans. 2*, **1976**, 771.
25) T. Kunitake, Y. Okahata, and T. Sakamoto, *Chem. Lett.*, **1975**, 459.
26) T. Kunitake and S. Horie, *Bull. Chem. Soc. Jpn.*, **48**, 1304 (1975).
27) T. Kunitake and Y. Okahata, *J. Am. Chem. Soc.*, **98**, 7793 (1976).

28) D. G. Oakenfull, *Chem. Commun.*, **1970**, 1655; *J. Chem. Soc., Perkin Trans. 2*, **1973**, 1006.
29) C. G. Blyth and J. R. Knowles, *J. Am. Chem. Soc.*, **93**, 3017 (1971).
30) C. A. Bunton, S. Diaz, J. M. Hellyer, Y. Ihara, and L. G. Inonscu, *J. Org. Chem.*, **38**, 3120 (1973).
31) T. Inoue, K. Nomura, and H. Kimizuka, *Bull. Chem. Soc. Jpn.*, **49**, 719 (1976).
32) T. Okubo and N. Ise, *J. Am. Chem. Soc.*, **95**, 2293 (1973).
33) M. T. A. Behme and E. H. Cordes, *J. Am. Chem. Soc.*, **87**, 260 (1965).
34) F. M. Menger and C. E. Portnoy, *J. Am. Chem. Soc.*, **89**, 4698 (1967).
35) R. B. Dunlap and E. H. Cordes, *J. Am. Chem. Soc.*, **90**, 4395 (1968).
36) L. R. Romsted and E. H. Cordes, *J. Am. Chem. Soc.*, **90**, 4404 (1968).
37) T. C. Bruice, J. Katzhendler, and L. R. Fedor, *J. Phys. Chem.*, **71**, 1961 (1967); *J. Am. Chem. Soc.*, **90**, 1097, 1333 (1968).
38) C. A. Bunton, L. Robinson, J. Schaak, and M. F. Stam, *J. Org. Chem.*, **36**, 2346 (1971).
39) R. G. Shorenstein, C. S. Pratt, Chen-Jung Hsu, and T. E. Wagner, *J. Am. Chem. Soc.*, **90**, 6199 (1968).
40) W. Tagaki, M. Chigira, T. Amada, and Y. Yano, *Chem. Commun.*, **1972**, 219.
41) J. M. Brown and C. A. Bunton, *J. Chem. Soc., Chem. Commun.*, **1974**, 969.
42) J. M. Brown, C. A. Bunton, and S. Diaz, *J. Chem. Soc., Chem. Commun.*, **1974**, 971.
43) R. A. Moss, R. C. Nahas, and S. Ramaswami, *J. Am. Chem. Soc.*, **99**, 627 (1977).
44) With regard to the micellar effects on the ester hydrolyses, the following articles are also important: H. Nogami, S. Awazu, and N. Nakajima, *Chem. Pharm. Bull.*, **10**, 503 (1962); P. Heitman, *Eur. J. Biochem.*, **5**, 305 (1968); E. J. Menger and M. J. McGreery, *J. Am. Chem. Soc.*, **96**, 121 (1974); C. A. Bunton, A. A. Kamego, M. J. Minch, and J. L. Wright, *J. Org. Chem.*, **40**, 1321 (1975).
45) In the case of the S_n^- (or S_n) hydrolysis by AcetHis with or without the surfactant, the k_{spont} value comes to be about 20% of the k_{total} value because of the low activity of AcetHis.
46) See Refs. 3 and 7. In our experiments, the pH dependence of the k_{cat} value in the C_m (m=6—12)-CTAB (or OTAC) system indicated a pK_a value of *ca.* 9 for the C_m catalysts.

A Development in Polarization Experiments; Emission Spectra of Anthracene, Dibenzothiophene, and Xanthone in Stretched Polyethylene Films[1)]

Tomoyuki TERADA, Motohiko KOYANAGI,* and Yoshiya KANDA
Department of Chemistry, Faculty of Science, Kyushu University, Hakozaki, Higashi-ku, Fukuoka 812
(Received June 15, 1979)

The polarized emission spectra of anthracene, dibenzothiophene, and xanthone have been studied in stretched polyethylene films at 77 and 4.2 K. Applicability and advantage of this method are examined by virtue of conventional polarization technique and modulation technique. The latter leads us to finding of an important role of a nontotally symmetric vibration, the b_{3g} ring vibration at 1655 cm^{-1}, in the fluorescence spectrum of anthracene. An assignment for several prominent vibrational bands in the phosphorescence spectrum of dibenzothiophene is proposed from detailed analysis of the modulation polarization spectrum at 77 K. The phosphorescence properties of xanthone are also investigated.

A number of polarization measurements of electronic transitions of molecules have been carried out mainly in crystal systems[2–5)] and in glasses[6–10)] using the single crystal technique and the photoselection technique, respectively. During the present decade another polarization technique has been developed through the measurements of the absorption[11–15)] and emission[16,17)] spectra of oblate or prolate organic molecules oriented in stretched polymer films.

Main advantages of the emission polarization measurements in the stretched polyethylene film over conventional photoselection and mixed-crystal methods are in wider range of the degree of polarization and less ambiguous environmental effects. In the present work a modulation polarization technique is applied to these film systems and its applicability and advantage are shown in several examples of emission spectra. An application of the similar techniques to the single crystal systems has been reported elsewhere.[18,19)]

Experimental

Materials. Commercial extra-pure-grade heptane and zone refined anthracene, both obtained from Tokyo Kasei Co. Ltd., were used without further purification. Dibenzothiophene and xanthone, products of the same company, were purified by zone-refining after several vacuum sublimations. Commercial polyethylene films of 0.15 mm in thickness were swollen in heptane for a few days before measurements. The films treated in this way showed no background emission at 77 K.

Apparatus. The optical arrangement employed in this work is schematically shown in Fig. 1. Light from a 500 W xenon arc lamp (**1**) passed through a condensing lens (**2**) and a combination filter system (**3**), *i.e.*, a Corning glass of type 7—54 of 3 mm in thickness and a 30% $NiSO_4$ aqueous solution of 30 mm in pathlength. The sample film (**4**) was set in a Dewar (**5**) with an aluminum cell holder. The direction of the stretching axis of the film was then inclined by 45° from the vertical axis of the Dewar for possible diminution of the systematic error of polarization coming from the curvature of the Dewar wall. The emission from the sample film passed through a lens (**6**), a standing polarizer (**7**) (and, if necessary, a rotating polarizer system (**8**) according to two different methods of polarization measurements as mentioned below), and a slit of a 3/4 m Czerny-Turner Nalumi grating spectrometer (**9**) in order. The polarization emission spectra were

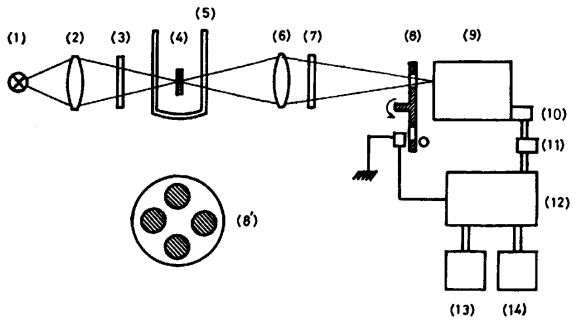

Fig. 1. Optical arrangement. For the notations (**1**)—(**10**) see descriptions in the Experimental section of this paper. Other notations are: (**11**), preamplifier; (**12**), lock-in-amplifier; (**13**), Iwatsu Dual beam oscilloscope type DS-5016; and (**14**), Hitachi recorder type 056. The drawing (**8'**) shows the front view of (**8**).

recorded on the spectrometer in the first order with an HTV R-375 photomultiplier tube (**10**). An HN 22 polaroid sheet employed in the polarizer systems (**7** and **8**) showed transmittance of about 8% at 375 nm and 28% at 500 nm.

Measurements. Two kinds of techniques were employed for polarization measurements. One is the same as given by Dekkers *et al.*:[16)] Two intensities $I_{//}$ and $I_{\perp}$ are measured independently and compared each other against wavelength. Here $I_{//}$ and $I_{\perp}$, respectively, refer to the intensity of an emission with the electric vector parallel to the direction of the stretching axis of the sample film and that perpendicular to it. We shall call this type of experiment *the DP method* and the spectrum *the DP spectrum* hereafter. The other method is an application of the modulation technique to the polarization experiments. The rotating-polarizer system (**8**) consists of a 120 mmϕ aluminum chopper with four holes (20 mmϕ) to which one each HN 22 polarizer sheet was fixed in such a way that the axis of the analyzing polarizer appears alternatively either parallel to or perpendicular to the stretching axis of the film. The emission signals were thus modulated at 100 Hz and fed to a lock-in-amplifier type NF model-LI-572B. If an appropriate phase relation is selected between the sample and reference signals, the output voltage of the lock-in-amplifier will be proportional to the difference between two intensities of interest, *i.e.*, $I_{//}-I_{\perp}$. This method will be called *the MP method* after its modulation polarization technique. The spectrum obtained by this method will also be *the MP spectrum.*

There is a problem in the case of analysis of the MP spectrum. The extremum of the MP spectrum does not always signify the existence of a band ! An apparent maximum is

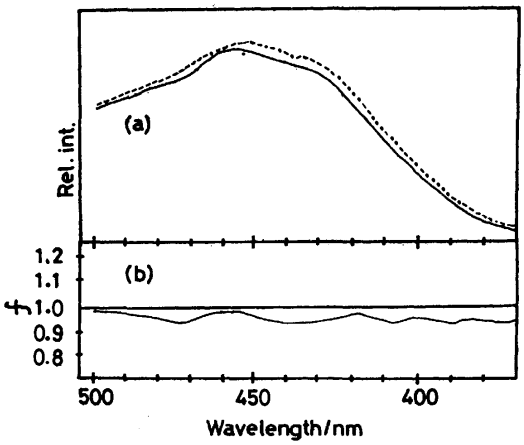

Fig. 2. (a) The self-polarization of the optical system employed. The solid curve denotes the polarization parallel to the stretching direction of polyethylene films and the dotted one that perpendicular to the film direction. (b) The dispersion curve of the correction factor f $(=I_{//}/I_{\perp})_{\text{system}}$ against wavelength.

formed among overlapping bands on rare occasions. A maximum appears sometimes near a minimum position between two emission bands, while another occurs in a region where the $I_{//}-I_{\perp}$ signal of a certain band competes with those of neighboring bands. Therefore, it is very meaningful to compare the MP spectrum with a well-resolved spectrum such as that in a Shpolskii matrix.[20]

Correction. In polarization experiments we sometimes encounter a problem of instrumental self-polarizations; in this work these come largely from a Dewar, lenses, and a spectrometer. The correction for the self-polarizations was carried out according to a conventional method.[21] As shown in Fig. 2, the correction factor in our system was found to vary little over a wide range of wavelength and to be nearly equal to 0.95 on an average. The correction factor of 0.95 was thus adopted for the DP experiments.

In principle, of course, the MP spectrum should also be corrected through 5% attenuation of $I_{\perp}$-component intensity. However, the actual correction of the MP spectrum leads to only a little increase in intensity toward the (+) parity direction and, accordingly, a little change in the band feature. Consequently, no correction was applied for the MP spectra in this work.

Sample Preparation. Swollen in heptane for a few days, a polyethylene film of 3×6 cm^2 was immersed in a solution of sample of 10^{-3} M in heptane. After natural evaporation of the solvent in the atmosphere, it was fixed on a stretching machine and extended by 500% in length at room temperature. Then the stretched sample film was set on an aluminum cell-holder.

Results and Discussion

Anthracene. The fluorescence and its polarization spectra of anthracene in polyethylene film systems are shown in Fig. 3, together with the fluorescence spectrum in heptane matrix. The spectroscopic data are also given in Table 1. The DP spectra shown in Fig. 3a are in good agreement with those reported by Dekkers *et al.*[16] It should be noted that the minima of bands shown in Fig. 3c just correspond to the band locations of the short-molecular-axis polarized spectrum (see also the dotted curve in Fig. 3a); and that the MP spectral line crosses the base line at the same wavelength position as the $I_{//}$ curve does the $I_{\perp}$ one in the DP spectra. This means that there is a one-to-one correspondence between the DP and MP spectra. The MP spectrum shows several extrema at 386.4 (α in Fig. 3c), 406.4 (γ),

Table 1. Vibrational analysis of the fluorescence spectrum of anthracene at 77 K

Stretched polyethylene[a]			Heptane		Assignment[c]	
ν/cm^{-1}	$\Delta\nu$/cm^{-1}	Sign[b]	ν/cm^{-1}	$\Delta\nu$/cm^{-1}		
26265	0	− (*o*)	26212	0	0−0 of $^1B_{1u}$-^1A_g	
25870	395	− (α)	25819	393	0−393	a_g
25505	765	−	25458	754	0−754	a_g
			25425	787	0−2×393(−1)	A_g
			25201	1011	0−1011	
			25056	1156	0−1156	
			24956	1256	0−1256	
24855	1410	− (β)	24807	1405	0−1405	a_g
			24648	1564	0−1564	a_g?
24610	1655	+ (γ)	24575	1637	0−1637	b_{3g}
24445	1820	− (δ)	24413	1799	0−1405−393(−1)	A_g
			24253	1959	0−1564−393(−2)	A_g?
24220	2045	+ (ε)	24183	2029	0−1637−393(+1)	B_{3g}
24020	2245	−	24020	2192	0−1405−787(0)	A_g
			23792	2420	0−1405−1011(−4)	
			23643	2569	0−1405−1156(−8)	
			23545	2667	0−1405−1256(−6)	
23470	2795	− (θ)	23402	2810	0−2×1405(0)	A_g
			23244	2968	0−1405−1564(+1)	
23180	3085	+ (η)	23171	3041	0−1637−1405(+1)	B_{3g}

a) Results obtained with the MP method. b) The sign "+" means a maximum peak of $I_{//}-I_{\perp}$ signal in the MP spectrum and the "−" a minimum one. Band designations to the figures are given in parenthesis by greek letters. c) Deviation in cm^{-1} units from the first fundamental combinations is given in parenthesis.

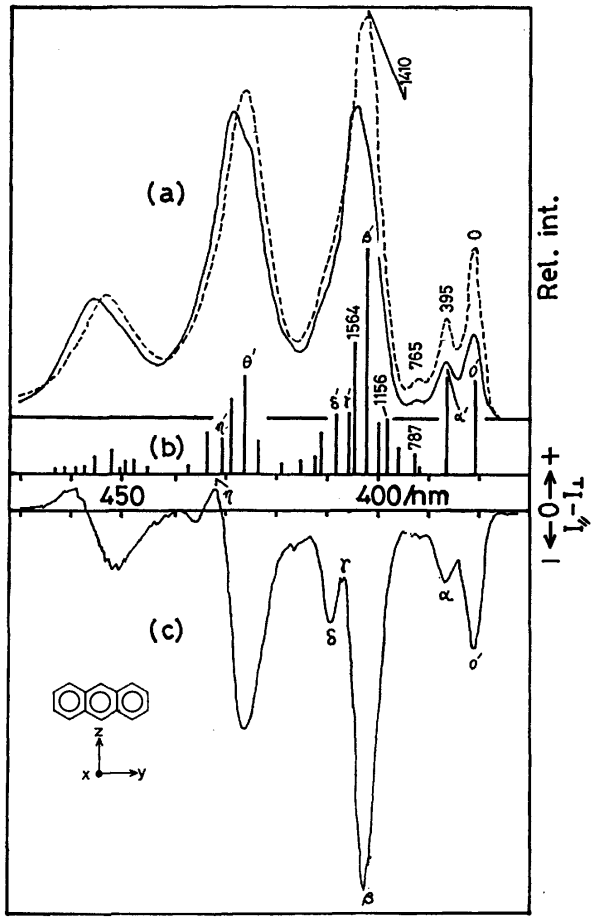

Fig. 3. The fluorescence and its polarization spectra of anthracene at 77 K. (a) The DP spectra in stretched polyethylene film systems; the solid curve denotes the polarization parallel to the stretching direction of polyethylene films and the dotted one that perpendicular to the film direction. (b) The fluorescence spectrum in heptane matrix (schematic). (c) The MP spectrum. Band notations are defined in Table 1.

and 409.0 nm (δ). These extrema are difficult to be identified in the DP spectra because of the band broadness. Among them the first two extrema in the MP spectrum are attributed to several vibrational bands in comparison with the spectrum in a Shpolskii solvent, heptane (see Fig. 3b). In view of concentrations employed a considerable weakness of the origin band in intensity is ascribed to the reabsorption effect of the 0—0 band.[22,23]

The DP and MP spectra show that the origin band of the fluorescence spectrum of anthracene is polarized along the short axis of the molecule under an assumption of *nice* molecular orientations in stretched polymer systems. This result is in good agreement with those from other experimental[24-26] and theoretical[27-29] works.

The band at 386.4 nm in the DP spectra, *i.e.*, the 0—395 cm^{-1} ($\pm$15 cm^{-1}) band in Table 1 and Fig. 3a, is assigned to be of an a_g-vibration, based on the band behavior in the MP spectrum. Dekkers *et al.* reported $P=-0.39$ for the 0—0 band and $P=-0.30$ for the 0—395 cm^{-1} band from their DP spectra and inferred that the latter came from accidental overlapping of a totally symmetric a_g-mode and a nontotally symmetric b_{3g}-mode. The MP spectrum also supports such an assignment from the intensity consideration.

The weak band at 392.0 nm, *i.e.*, the 0—765 cm^{-1} band in Fig. 3a, is ascribed to an a_g-fundamental vibration or an overtone of the a_g-vibration at 394 cm^{-1}.[25] Although the corresponding band also appears in the MP spectrum, it is too weak to discriminate between these assignments.

The strong band at 402.2 nm in the DP spectrum, *i.e.*, the 0—1410 cm^{-1} band, consists of several overlapping bands as can be seen from the broad band feature. Therefore, detailed discussion for the "band" is not possible with the DP spectra. However, it is an experimental fact that $I_{//}$ (max) appears at a longer wavelength than $I_{\perp}$ (max) does. Through the vibrational analysis of the fluorescence spectrum in heptane matrix (see Table 1), $I_{\perp}$ (max) is attributed mainly due to the band of 0—1405 cm^{-1} ($\pm$5 cm^{-1}) and $I_{//}$ (max) due to those of 0—1564 cm^{-1} ($\pm$5 cm^{-1}), 0—1637 cm^{-1} ($\pm$5 cm^{-1}), and 0—1799 cm^{-1} ($\pm$5 cm^{-1}) as Dekkers *et al.* suggested.[16]

On the other hand, the MP spectrum clearly discriminates among three bands of 0—1410 cm^{-1} ($\pm$15 cm^{-1}), 0—1655 cm^{-1} ($\pm$15 cm^{-1}), and 0—1820 cm^{-1} ($\pm$15 cm^{-1}) which are designated as β, γ, and δ in Fig. 3c and correspond to those of 0—1405 cm^{-1}, 0—1637 cm^{-1}, and 0—1799 cm^{-1} in the fluorescence spectrum in heptane matrix, respectively. From their polarization behaviors we attribute these bands to a_g, b_{3g}, and a_g fundamentals, respectively, in good correspondence with suggestions inferred from the experiments in the crystal systems.[30] The band of 0—1564 cm^{-1} in heptane matrix does not correspond to any maximum or minimum position in the MP spectrum. However, it is suggested that this band would be based on an a_g fundamental mode from viewpoints of the band shape of the MP spectrum.

Although the fluorescence polarization spectrum of anthracene has been studied in naphthalene crystals at 4.2 K, no positive evidence has been found for the existence of long-molecular-axis polarized bands, possibly due to strong crystal effects.[24] We also confirmed this in our mixed crystal systems at 4.2 K. Only one report has been given for observation of the long-molecular-axis polarized fluorescence spectrum of anthracene in fluorene at 20 K.[25] However, the band system is complicated reflecting site emissions and no precise data concerning polarization intensities is available. Thus it should be noted that the present work gives a clear-cut evidence for a participation of the b_{3g} vibration in the $S_1 \rightarrow S_0$ fluorescence process. This observation is in good agreement with finding of the band intensification observed in the pre-resonance Raman effect of anthracene by Ohta and Ito.[31]

Dibenzothiophene. The phosphorescence spectrum of dibenzothiophene (DBTH in abbreviated form) in heptane at 77 K is shown in Fig. 4, together with the DP spectra in stretched polyethylene film systems. A considerable polarization of the origin band observed in the DP spectra establishes that DBTH molecules are sufficiently oriented in the systems in such a way that

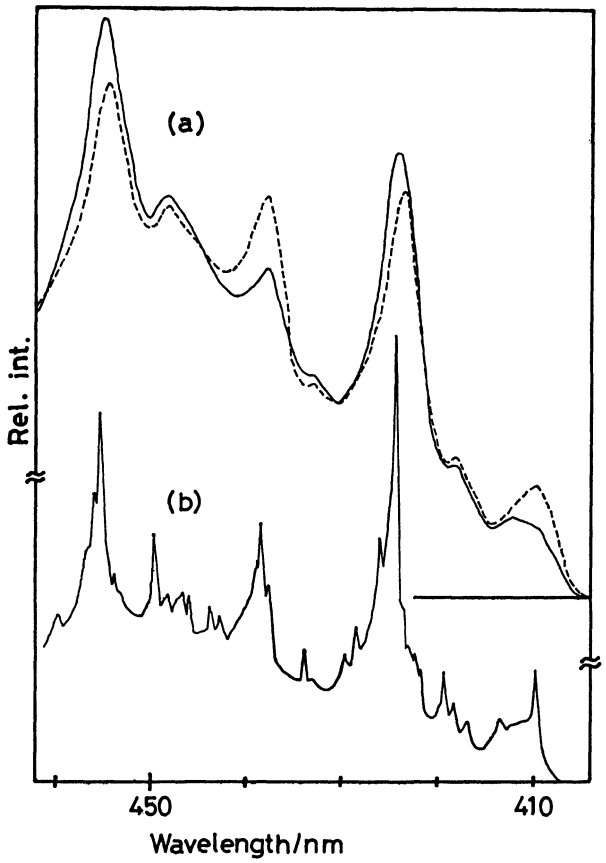

Fig. 4. (a) The phosphorescence polarization spectrum of DBTH in stretched polyethylene film systems at 77 K with the DP method; the solid curve represents the spectrum polarized parallel to the stretching direction of the films and the dotted one that perpendicular to the film direction. (b) The phosphorescence spectrum of DBTH in heptane at 77 K.

the long-molecular-axis is parallel to the stretching axis of the film.

The MP spectrum is compared with the phosphorescence spectrum in heptane matrix in Fig. 5, where the

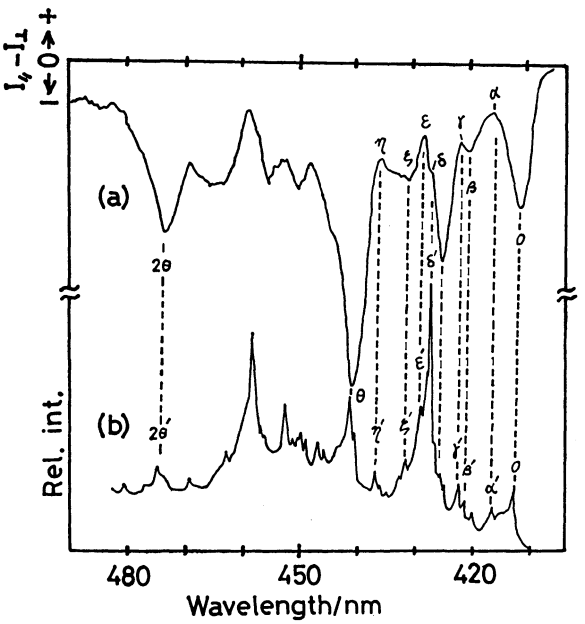

Fig. 5. (a) The MP phosphorescence spectrum of DBTH in polyethylene film systems at 77 K and (b) the phosphorescence spectrum of DBTH in heptane at 77 K. Band notations are given in Table 2.

positions of the origin bands are adjusted to be identical. A tentative vibrational assignment for the first main bands is also given in Table 2. As shown in Fig. 5a, the origin band (designated as *o* in the figure) is polarized normal to the long axis of the molecule, *i.e.*, along the x- or z-axis in the molecular coordinates shown in Fig. 6. Since the emission is certainly ascribed to be of $\pi\pi^*$ in the nature from the long lifetime of 0.5 s, the origin band is assumed to be polarized along the out-of-plane axis of the molecule, *i.e.*, the x-axis, on the basis of the predominant first-order spin-orbit coupling mechanism illustrated schematically in Fig. 6a.

As shown in Fig. 5a, the 0—240 cm^{-1} (± 15 cm^{-1}) band (α) in the MP spectrum is polarized along the

Table 2. Vibrational analysis of the phosphorescence spectrum of DBTH at 77 K[a)]

Streched polyethylene[b)]			Heptane		Assignment		
ν/cm^{-1}	$\Delta\nu$/cm^{-1}	Sign[c)]	ν/cm^{-1}	$\Delta\nu$/cm^{-1}	Present work		Bree and Zwarich[d)]
24260	0	— (o)	24413	0	0—0 of $^3A_1$-$^1A_1$		0—0 of $^3A_1$-$^1A_1$
24020	240	+ (α)	24184	229	0—229	b_1	a_1(0—210/221)
			23991	422	0—422	?	b_1
23760	500	— (β)	23911	502	0—502	a_1	a_1
23690	570	+ (γ)	23848	565	0—565	a_2	b_2
			23701	712	0—712	a_1?	a_1
			23668	745	0—745	?	b_1
23490	770	—	23640	773	0—773	a_1	a_1
23410	850	+ (δ)	23562	851	0—851	b_1	b_2
23325	935	+ (ε)	23479	934	0—934	b_1	b_1
23185	1075	— (ζ)	23347	1066	0—1066	a_1	a_1
23120	1140	—	23282	1131	0—1131	a_1	a_1
22910	1350	+ (η)	23062	1351	0—851—502(+2)	B_1	B_2
22655	1605	— (θ)	22806	1607	0—1607	a_1	a_1

a) For brevity we list only the assignment of bands sufficient enough to show the vibronic pattern. b) See Table 1, footnote a. c) See Table 1, footnote b. d) Data taken from Ref. 32.

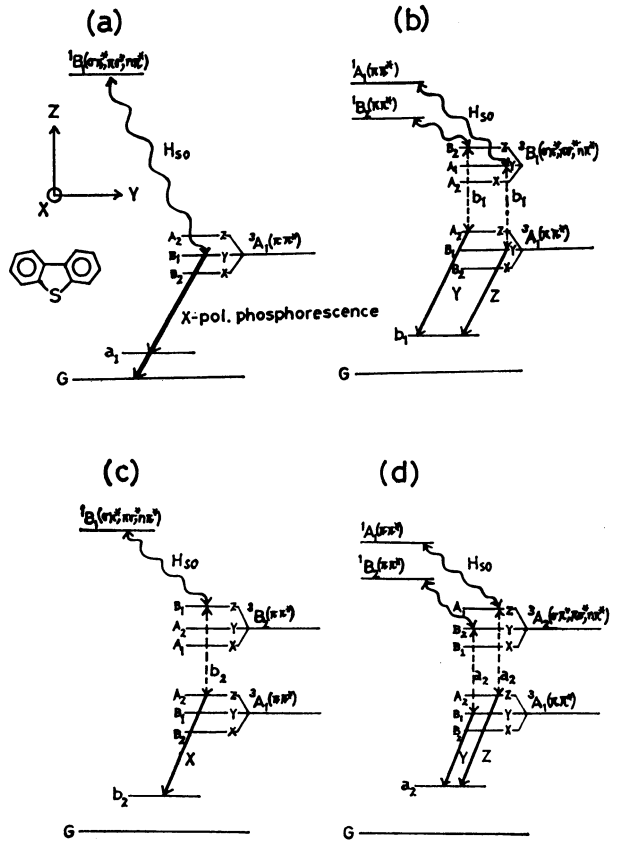

Fig. 6. Main coupling mechanisms in the phosphorescence process of DBTH. (a): 1st-order spin-orbit coupling. (b), (c), and (d): 2nd-order spin-orbit-vibronic couplings due to b_1, b_2, and a_2 vibrations, respectively. Here are described only vibronic couplings between triplet manifold for the saving of the space. Similar schemes, of course, hold for singlet manifold.

y-axis. It is evident from the coupling schemes given for triplet manifold (see Figs. 6b and 6d) and from the similar ones for singlet manifold that the y-axis polarized transition is caused by nontotally symmetric b_1 and/or a_2 vibrations through the second-order spin-orbit-vibronic coupling mechanisms under the assumption that the first-order spin-orbit-vibronic couplings are negligibly small.[32] The spacing of 0—240 cm^{-1} observed in the MP spectrum is found to correspond to a b_1-fundamental vibration of 226 cm^{-1} assigned from the observed IR and Raman spectra.[33]

The 0—500 cm^{-1} (± 15 cm^{-1}) band (β) in the MP spectrum is polarized perpendicular to the long axis of the molecule. This band is close in wavenumber to the 0—502 cm^{-1} (± 5 cm^{-1}) band in the phosphorescence in heptane matrix (see also Table 2). Several coupling schemes are possible for such transitions that are polarized perpendicular to the long axis, as shown in Fig. 6. According to the vibrational analysis, a band at 498 cm^{-1} in the IR spectrum of crystalline DBTH has been assigned as an a_1 fundamental.[33] If this vibration is employed, the 0—500 cm^{-1} band in the MP spectrum is to be polarized along the x-axis. Similarly, many other bands are assigned on the basis of the IR and Raman data.

The vibrational assignment for most of the bands are in accord with that given by Bree and Zwarich (hereafter referred to BZ).[32] However, several prominent bands are assigned here in a different way: They are the bands of 0—229 cm^{-1} (α' in Fig. 5b), 0—565 cm^{-1} (γ'), 0—851 cm^{-1} (δ'), and 0—1351 cm^{-1} (η') in the phosphorescence spectrum in heptane matrix at 77 K, as designated by greek symbols in Fig. 5b. In an energy region of 200—300 cm^{-1} from the origin band of the phosphorescence of DBTH in heptane at 15 K, BZ observed two main bands at 210 cm^{-1} and 221 cm^{-1} and assigned as (a_1) and (a_1+phonon) modes, respectively, in comparison with the assignment to the X-trap emission of DBTH in the crystal at the same temperature. We also studied the phosphorescence spectrum in heptane at 4.2 K and obtained a similar band pattern to that reported by BZ. We find that the band system contains several site emissions and that the 0—210 cm^{-1} band reported by BZ is ascribed to an emission from a different site. On the other hand, the phosphorescence of DBTH in heptane at 77 K is found to be mainly due to one site as shown in Fig. 5b, although it is not clear at present what is the origin of those sites in heptane matrix at low temperatures. The 0—229 cm^{-1} band (α') in heptane matrix at 77 K, *i.e.*, the main band between 200 and 300 cm^{-1} from the origin band (o') should thus correspond to a maximum position in the MP spectrum (α in Fig. 5a) which is here ascribed to a b_1 fundamental vibration as mentioned above.

The 0—565 cm^{-1} band (γ') in heptane matrix was attributed to a b_2 symmetry mode by BZ. However, the corresponding MP band is found at 570 cm^{-1} from the origin peak (o) and has a nature of the (+) parity polarization. This property is in contrast with the predicted (—) polarization if the BZ's b_2-assignment would be accepted for the band (*e.g.*, see Fig. 6c). The coupling schemes (**b**) and/or (**d**), however, suggest such (+) polarization behaviors. Thus we assign this band as due to an a_2 mode which is only out-of-plane fundamental vibration predicted in a wavelength region of 500—650 cm^{-1}.[33]

The 0—851 cm^{-1} band (δ') is the strongest one in the phosphorescence system of DBTH. Observing an IR active b_2 vibrational band at 868 cm^{-1}, BZ attributed this phosphorescence band to the b_2 mode. However, the result of the MP spectrum indicates that the band should be out-of-plane vibration from the same reason as mentioned in the case of the 0—565 cm^{-1} band. In a wavenumber region of 800—900 cm^{-1} only one out-of-plane vibration was observed at 859 cm^{-1} (b_1) by BZ! The b_1 assignment is thus preferable. This revised assignment leads us to another prediction that the 0—1351 cm^{-1} band (η'), which can be assigned here as a combination band of 851+502 cm^{-1} ($b_1 \times a_1 = B_1$) in accord with the assignment by BZ, might manifest a similar polarization behavior to that of the 0—851 cm^{-1} band. The MP spectrum shown in Fig. 5a endorses this prediction.

Xanthone. The phosphorescence spectrum of xanthone (hereafter XTH) in 3-methylpentane and EPA has been reported to be very sensitive to temperature.[34,35] This is also confirmed to be the case

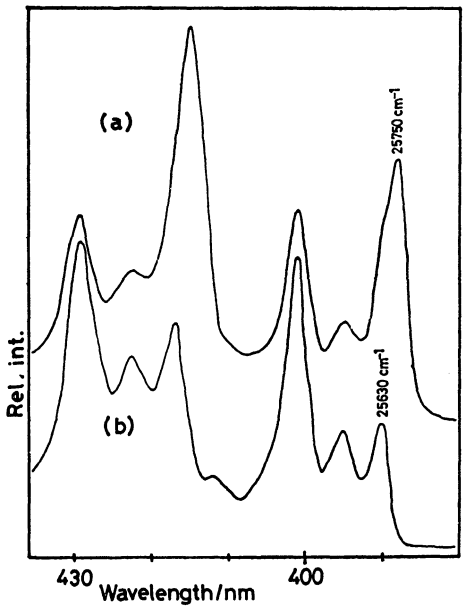

Fig. 7. The phosphorescence spectrum of XTH in polyethylene polymer systems (a) at 77 K and (b) at 4.2 K.

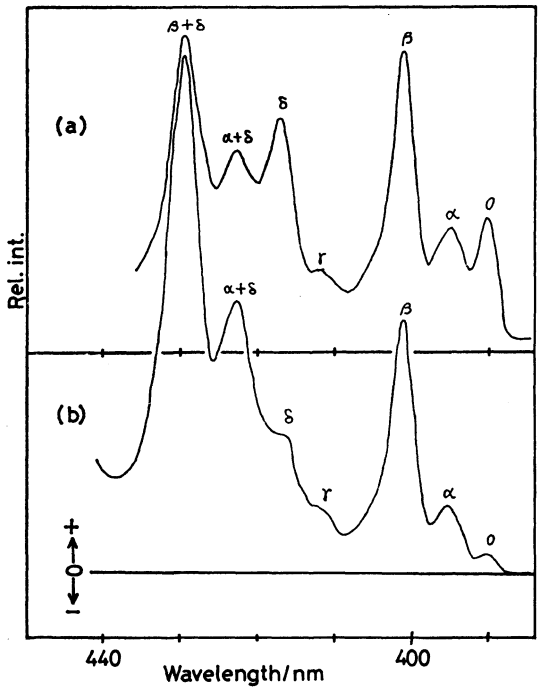

Fig. 8. (a) The phosphorescence spectrum of XTH in polyethylene polymer systems at 4.2 K. (b) The phosphorescence polarization spectrum of XTH with the MP method at 4.2 K. Band notations are given in the Text.

in polyethylene matrix; *e.g.*, the spectra at 4.2 and 77 K as illustrated in Fig. 7. On account of a small energy separation between $^3\pi\pi^*$ and $^3n\pi^*$ levels and a general existence of molecules at different sites the phosphorescence spectrum of XTH in aliphatic hydrocarbons has generally been found to manifest complicated band-patterns.[34-36] Especially, a statistical distribution of emission sites in polyethylene film systems seems to increase the complication of the spectrum, as can be seen in too much deviation from an exponential decay relationship of the phosphorescence lifetime at 77 K.

On the other hand, the phosphorescence at 4.2 K is observed to decay nearly exponentially and to show little change in intensity with a decrease in temperature to 1.5 K. The strong activeness of several out-of-plane vibronic bands and the rather long lifetime of the order of $\approx 10^{-1}$ s are manifestations that the lowest excited triplet state of almost all the emission sites in polyethylene matrix is of $\pi\pi^*$ type. These features resemble those reported in the spectra of XTH in the crystal and in diphenylmethane matrix at 1.5 K by Chakrabarti and Hirota,[37] although there is a big difference in the T_1-T_2 energy separation between their systems and ours, possibly based on environmental difference (*e.g.*, $\Delta E(T_2\text{-}T_1) \approx 1680\ cm^{-1}$ in their diphenylmethane matrix and $\Delta E(T_2\text{-}T_1) \approx 140\ cm^{-1}$ in the present work). Thus, we confine ourselves to the spectrum at 4.2 K in this paper. The phosphorescence spectrum of XTH in polyethylene film systems and its MP spectrum are shown in Fig. 8. Except for some combination bands, the band system consists mainly of the origin band (band notation *o* in Fig. 8) and several fundamental bands such as $0-320\ cm^{-1}$ ($\pm 20\ cm^{-1}$) (α), $0-700\ cm^{-1}$ ($\pm 20\ cm^{-1}$) (β), $0-1320\ cm^{-1}$ ($\pm 20\ cm^{-1}$) (γ), and $0-1670\ cm^{-1}$ ($\pm 20\ cm^{-1}$) (δ). It is found that the bands α, β, γ, $\alpha+\delta$, and $\beta+\delta$ are strongly polarized along the long axis of the molecule (P: 0.40—0.50). The origin band itself and the $0-\nu(C{=}O)$ band (δ) are also polarized along the long-molecular-axis, but their degrees of polarization are considerably small (P=0.10). The great degrees of polarization along the long-molecular-axis observed in the bands α, β, γ, $\alpha+\delta$, and $\beta+\delta$ support a large contribution to the overall phosphorescence system through the second-order spin-orbit-vibronic mixings *via* the magnetic z-sublevel.[37] However, it is difficult to mention from only the present work which coupling scheme plays a predominant role in the phosphorescence process for such a close-energy-system *via* singlet manifold or *via* triplet manifold. As has been suggested in the case of the phosphorescence spectrum of *p*-methoxybenzaldehyde in *p*-dimethoxybenzene,[19] remarkable degrees of the depolarization of the bands *o* and δ may be attributed to the existence of the competitive processes of the environmental direct coupling between $^3\pi\pi^*$ and $^3n\pi^*$ and the first-order spin-orbit coupling between $^3\pi\pi^*$ and $^1\sigma\pi^*$.

Concluding Remarks

The DP method in stretched polymer film systems has extensively been employed for absorption and emission polarization measurements. The method is attractive certainly in simplicity of the experiment, but it is unfortunately subject to a limitation in its applicability. In general the wide band-width originating from a statistical distribution of emission sites in those polymer film systems prevents us from finding out a weak band near a strong band and from discriminating a band from the overlapping bands. Despite the

unavoidable problem of the band broadness in stretched polyethylene film systems, the MP method is found to improve the band resolution remarkably. The high S/N ratio in the MP method promises a future development in the application to other molecules.

The authors acknowledge helpful discussions with Prof. R. J. Zwarich. This work has been supported by the Kurata Foundation Fund awarded to one of the authors (M. K.) and by a Grant-in-Aid for Scientific Research from the Ministry of Education, Science and Culture.

References

1) A preliminary report of this work was presented at the 26th IUPAC congress, Tokyo, 1977.
2) D. S. McClure, *Solid State Phys.*, **8**, 1 (1959); *ibid.*, **9**, 399 (1959).
3) H. C. Wolf, *Solid State Phys.*, **9**, 1 (1959).
4) D. P. Craig and S. H. Walmsley, "Excitons in Molecular Crystals," Benjamin Inc., New York (1968).
5) R. M. Hochstrasser, *Rev. Mod. Phys.*, **34**, 531 (1962).
6) A. C. Albrecht, *J. Mol. Spectrosc.*, **6**, 84 (1961).
7) A. H. Kalantar and A. C. Albrecht, *Ber. Bunsenges. Phys. Chem.*, **68**, 361 (1964).
8) R. Shimada and L. Goodman, *J. Chem. Phys.*, **43**, 2027 (1965).
9) E. C. Lim and J. M. H. Yu, *J. Chem. Phys.*, **49**, 3878 (1968).
10) F. Dörr, *Angew. Chem.*, **78**, 457 (1966).
11) P. M. Johnson and A. C. Albrecht, *J. Chem. Phys.*, **48**, 851 (1968).
12) Y. Tanizaki, H. Inoue, and N. Ando, *J. Mol. Spectrosc.*, **17**, 156 (1965); H. Hiratsuka, Y. Tanizaki, and T. Hoshi, *Spectrochim. Acta, Part A*, **28**, 2375 (1972).
13) E. W. Thulstrup and J. H. Eggers, *Chem. Phys. Lett.*, **1**, 690 (1968); E. W. Thulstrup, J. Michl, and J. H. Eggers, *J. Phys. Chem.*, **74**, 3868 (1970).
14) Å. Davidsson and B. Nordén, *Chem. Phys. Lett.*, **28**, 221 (1974).
15) Y. Tanizaki and H. Hiratsuka, *J. Spectrosc. Soc. Jpn.*, **25**, 205 (1976) and references cited therein.
16) J. J. Dekkers, G. Ph. Hoornweg, C. MacLean, and N. H. Velthorst, *Chem. Phys.*, **5**, 393 (1974); *Chem. Phys. Lett.*, **19**, 517 (1973).
17) J. J. Dekkers, G. Ph. Hoornweg, K. J. Terpstra, C. MacLean, and N. H. Velthorst, *Chem. Phys.*, **34**, 253 (1978).
18) K. Ohno and H. Inokuchi, *Chem. Phys.*, **33**, 585 (1975).
19) M. Koyanagi, K. Higashi, and Y. Kanda, *Chem. Phys. Lett.*, **52**, 184 (1977).
20) E. V. Shpolskii, *Usp. Fiz. Nauk.*, **80**, 255 (1963) [*Sov. Phys. Usp.*, **6**, 411 (1963)].
21) T. Azumi and S. P. McGlynn, *J. Chem. Phys.*, **37**, 2413 (1962).
22) W. H. Wright, *Chem. Rev.*, **67**, 581 (1967).
23) M. Nakamizo and Y. Kanda, *Spectrochim. Acta*, **19**, 1235 (1963).
24) J. W. Sidman, *J. Chem. Phys.*, **25**, 115 (1956).
25) A. V. Bree and S. Katagiri, *J. Mol. Spectrosc.*, **17**, 24 (1965).
26) C. D. Akon and D. P. Craig, *Trans. Faraday Soc.*, **62**, 1673 (1966).
27) J. R. Platt, *J. Chem. Phys.*, **17**, 484 (1949).
28) R. Pariser, *J. Chem. Phys.*, **24**, 250 (1956).
29) J. A. Pople, *Proc. Phys. Soc. (London), Ser. A*, **68**, 81 (1955).
30) R. M. Macnab and K. Sauer, *J. Chem. Phys.*, **53**, 2805 (1970).
31) N. Ohta and M. Ito, *Chem. Phys.*, **20**, 71 (1977).
32) A. V. Bree and R. J. Zwarich, *Spectrochim. Acta, Part A*, **27**, 621 (1971).
33) A. V. Bree and R. J. Zwarich, *Spectrochim. Acta, Part A*, **27**, 599 (1971).
34) H. J. Pownall, R. E. Connors, and J. R. Huber, *Chem. Phys. Lett.*, **22**, 403 (1973).
35) H. J. Pownall and W. W. Mantulin, *Mol. Phys.*, **31**, 1393 (1976).
36) H. J. Pownall and J. R. Huber, *J. Am. Chem. Soc.*, **93**, 6429 (1971).
37) A. Chakrabarti and N. Hirota, *J. Phys. Chem.*, **80**, 2966 (1976).

 © 1980 The Chemical Society of Japan Bull. Chem. Soc. Jpn., 53, 359—361 (1980)

The Molecular Structure of 1-Phenoxy-1,2,2a,8b-tetrahydrocyclobuta[*a*]naphthalene-8b-carbonitrile

Hideaki MATSUURA,† Yasushi KAI, Noritake YASUOKA,†† and Nobutami KASAI*

Department of Applied Chemistry, Faculty of Engineering, Osaka University, Yamadakami, Suita, Osaka 565

(Received June 16, 1979)

The molecular structure of the sole photocycloaddition product of α-naphthonitrile with phenyl vinyl ether, $C_{18}H_{15}ON$ was determined by means of X-ray diffraction. The crystals are monoclinic, space group $P2_1/c$, unit-cell dimensions are $a=11.563(2)$, $b=9.826(1)$, $c=14.324(2)$ Å, $\beta=113.46(1)°$, $Z=4$. The structure was solved by the direct method, the final R value being 0.042 for 2022 non-zero reflections. The molecule has an *endo*-configuration, and the cyclobutane ring is puckered.

Recently, Pac and co-workers found that the photoreaction of α-naphthonitrile with alkyl vinyl ethers (CH_2=CHOR, R: Me or Et) affords both the *endo*- and *exo*-cycloadducts,[1] whereas the (4+4) photocycloaddition of furan to α-naphthonitrile is highly stereoselective and remarkably dependent on solvent used.[2] These facts suggested the enhanced stereoselectivity on the photocycloaddition of α-naphthonitrile with phenyl vinyl ether.

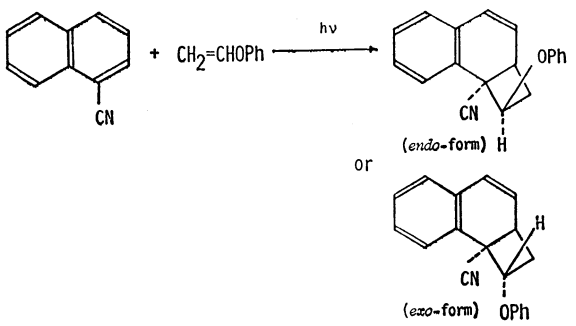

A sole cycloadduct has been obtained by the phtoreaction in question.[3] However, spectroscopic studies failed to characterize the cycloadduct to have *endo*- or *exo*-form (Scheme), and X-ray crystal structure analysis of the cycloadduct has been carried out in order to determine the exact configuration.

Experimental

Crystal Data. $C_{19}H_{15}ON$, mp 115.5—116.5 °C, *F.W.* 273.3, $F(000)=576$, monoclinic, space group $P2_1/c$, $a=11.563(2)$, $b=9.826(1)$, $c=14.324(2)$ Å, $\beta=113.46(1)°$, $V=1493.1(3)$ Å^3, $D_m=1.22$ g cm^{-3} (25 °C, aqueous solution of potassium tartarate), $Z=4$, $D_c=1.22$ g cm^{-3}.

Unit-cell dimensions and reflection intensities were measured on a Rigaku automated, four-circle diffractometer using graphite monochromatized Cu $K\alpha$ radiation. A parallelepiped, transparent crystal with dimensions of *ca.* $0.2\times0.3\times0.1$ mm^3 was used.

The θ-2θ scan technique was employed for the intensity data collection at a 2θ rate of 2° min^{-1}. Backgrounds were measured for 7.5 s before and after the scan of each peak. In total 2209 independent reflections were collected up to $2\theta\leqq120°$, of which 184 were considered unobserved. Intensity data were corrected for Lp effect but not for absorption [μ(Cu)=6.08 cm^{-1}].

Solution and Refinement of the Structure

The structure was solved by the direct method. From the Wilson plot average temperature factor and scale factor were obtained. A set of 284 $|E|$'s($|E|\geqq1.5$) were used with the *MULTAN* program[4] to establish the phase relationship. From the E map (ABSFOM 1.2422) all the non-hydrogen atoms could be located. The positional and isotropic thermal parameters of these atoms were refined by the block-diagonal least-squares procedure (*HBLS* V[5]). After eight cycles of refinement ($R=0.158$), anisotropic thermal parameters were introduced; five cycles of refinement reduced the R to 0.094. All the H atoms were located on a difference Fourier map. The refinement was continued including these H atoms with isotropic thermal parameters. The function minimized was $(\sum w|F_o|-k|F_c|)^2$, where k is a single scale factor and $w=\{\sigma_{cs}(F_o)+a|F_o|+b|F_o|^2\}^{-1}$ (σ_{cs}: standard deviation determined from the counting statistics). The R value converged to 0.053. However, in the range $7.0\leqq|F_o|\leqq20.0$ the quantity minimized showed an anomaly. The $30\bar{2}$, 111, and 402 reflections which have extraordinarily large $|F|$'s were then excluded, and the weights of Hughes,[6] $w=(F_{max}/|F_o|)^{-2}$ for $|F_o|>F_{max}$ and $w=1$ for $|F_o|\leqq F_{max}$ ($F_{max}=15.0$ in the present study), were introduced in the next stage. The refinement converged normally to $R=0.042$ ($R_w=0.052$). Atomic scattering factors for C, N, and O were taken from those of Hanson and coworkers,[7] and that of H from Stewart and coworkers.[8] The final atomic parameters are given in Table 1.†††

Results and Discussion

Figure 1 shows an *ORTEP* plot[9] of the molecule. Bond lengths and bond angles are given in Fig. 2.

The remarkable feature of the structure is that the photocycloadduct of α-naphthonitrile with phenyl vinyl ether has the *endo*-configuration (Scheme). This result suggests an existence of the exciplex of the phenyl vinyl ether as a photoreaction intermediate.[3]

† Present address: Ehime Works, Sumitomo Chemical Co., Ltd., Niihama, Ehime 795.

†† Present address: Institute for Protein Research, Osaka University, Yamadakami, Suita, Osaka 565.

††† The Table of observed and calculated structure factors are kept as Document No. 8007 at the Chemical Society of Japan.

TABLE 1. FRACTIONAL ATOMIC COORDINATES ($\times 10^4$ for C, N, and O atoms and $\times 10^3$ for H atoms) AND THERMAL PARAMETERS WITH e.s.d.'s IN PARENTHESES

Anisotropic thermal parameters ($\times 10^4$) expressed in the form:
$\exp\{-(\beta_{11}h^2+\beta_{22}k^2+\beta_{33}l^2+\beta_{12}hk+\beta_{13}hl+\beta_{23}kl)\}$.

	x	y	z	β_{11}	β_{22}	β_{33}	β_{12}	β_{13}	β_{23}
O	2868(1)	1495(1)	4099(1)	74(1)	94(1)	55(1)	−11(2)	19(1)	2(2)
N	3786(2)	5716(2)	5313(1)	110(2)	141(2)	111(1)	−73(3)	100(3)	−82(3)
C(1)	2446(1)	4069(2)	3855(1)	74(1)	88(2)	57(1)	−9(3)	51(2)	3(2)
C(2)	1157(1)	3853(2)	3883(1)	70(1)	92(2)	57(1)	−5(3)	43(2)	−22(2)
C(3)	75(2)	4354(2)	3084(1)	77(2)	103(2)	80(1)	25(3)	37(2)	−21(3)
C(4)	173(2)	5058(2)	2212(2)	131(2)	142(3)	79(1)	92(4)	31(3)	59(3)
C(5)	1223(2)	5117(2)	2070(2)	159(3)	147(3)	84(2)	74(4)	90(3)	93(3)
C(6)	2379(2)	4435(2)	2771(1)	115(2)	124(2)	71(1)	6(3)	88(3)	42(3)
C(7)	2551(2)	2909(2)	2604(1)	118(2)	145(2)	56(1)	37(4)	80(3)	9(3)
C(8)	3145(1)	2737(2)	3751(1)	69(1)	102(2)	55(1)	−1(3)	46(2)	4(2)
C(9)	3190(2)	4998(2)	4674(1)	76(2)	103(2)	80(1)	−22(3)	74(2)	−19(3)
C(10)	1058(2)	3231(2)	4708(1)	84(1)	125(2)	63(1)	−26(3)	64(2)	−31(3)
C(11)	−113(2)	3081(2)	4755(2)	123(2)	155(3)	88(2)	−76(4)	130(3)	−71(3)
C(12)	−1179(2)	3572(2)	3963(2)	76(2)	165(3)	129(2)	−45(4)	102(3)	−122(4)
C(13)	−1077(2)	4196(2)	3148(2)	77(2)	154(3)	108(2)	19(4)	53(3)	−52(4)
C(14)	3624(1)	1052(2)	5066(1)	69(1)	95(2)	54(1)	25(3)	47(2)	−3(2)
C(15)	4527(2)	1840(2)	5790(1)	88(2)	111(2)	63(1)	24(3)	27(2)	−18(3)
C(16)	5238(2)	1264(2)	6734(1)	110(2)	174(3)	59(1)	82(4)	22(3)	−39(3)
C(17)	5051(2)	−51(2)	6953(2)	157(3)	178(3)	60(1)	151(5)	80(3)	41(3)
C(18)	4148(2)	−821(2)	6223(2)	162(3)	134(3)	82(1)	73(4)	122(3)	58(3)
C(19)	3433(2)	−275(2)	5283(1)	114(2)	107(2)	72(1)	7(3)	81(3)	10(3)
H(4)	−61(2)	550(3)	172(2)	8.2(6)					
H(5)	125(2)	556(3)	144(2)	7.6(6)					
H(6)	318(2)	496(2)	287(2)	5.8(5)					
H(7A)	304(2)	270(2)	221(2)	5.6(5)					
H(7B)	169(2)	242(2)	232(2)	5.0(5)					
H(8)	408(2)	293(2)	403(2)	3.5(4)					
H(10)	183(2)	289(2)	526(2)	3.9(5)					
H(11)	−14(2)	265(2)	535(2)	5.4(5)					
H(12)	−199(2)	349(3)	403(2)	7.0(5)					
H(13)	−187(2)	454(2)	257(2)	6.3(4)					
H(15)	466(2)	277(2)	565(2)	4.6(4)					
H(16)	586(2)	186(3)	724(2)	7.0(6)					
H(17)	551(2)	−44(3)	763(2)	7.7(6)					
H(18)	402(2)	−178(3)	635(2)	7.8(6)					
H(19)	279(2)	−82(2)	476(2)	5.7(5)					

Fig. 1. A stereoscopic drawing of the molecule.
Non-hydrogen atoms are drawn as thermal ellipsoids with 30% probability and H atoms are circles with $B=1.2$ Å^2

The cyclobutane ring C is puckered, dihedral angle between the plane defined by C(6), C(1), and C(8) and the plane of C(6), C(7), and C(8) being 31.3°. A significant lengthening of C(1)–C(6) [1.565(3) Å] and C(1)–C(8) bonds [1.577(2) Å] is clearly observed. On the other hand C(7)–C(8) bond shows a shortening [1.516(3) Å]. As a result of the cyclobutane ring formation, ring B of the naphthonitrile moiety is no more planar, the C(1) and C(6) atoms are deviated by 0.10 and −0.14 Å out of the mean plane, respectively. Both rings A and D are planar within 0.002 Å and have normal structures. Concerning the ether

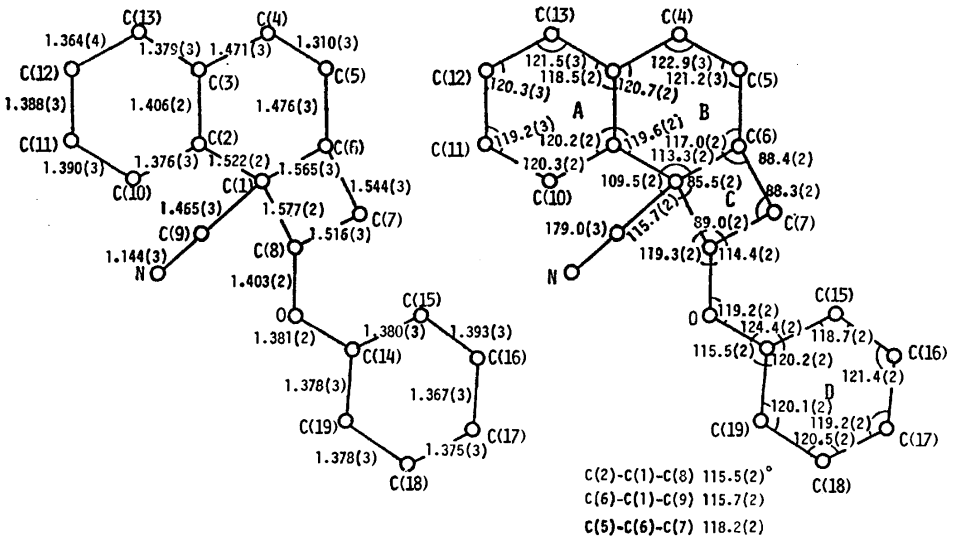

Fig. 2. Bond lengths and bond angles with e.s.d's in parentheses.

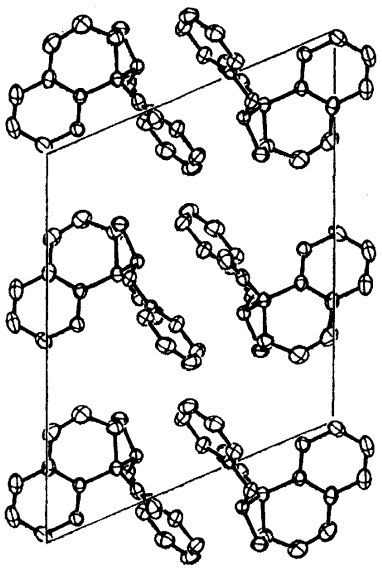

Fig. 3. Crystal structure projected along the b axis.

bond, the C(8)–O bond length [1.403(2) Å] is longer than the C(14)–O [1.381 (2) Å]. The torsion angle C(8)–O–C(14)–C(15) is −10.9°. This is considered as due to the steric interaction between H(8) and H(15) [H(8)···H(15)=2.13(3) Å].

Figure 3 shows the crystal structure projected along the b axis. No close intermolecular contact less than usual van der Waals distance is observed.

The authors wish to express their deep thanks to Professor Hiroshi Sakurai and Dr. C.-J. Pac of the Institute of Scientific and Industrial Research, Osaka University for crystals. Thanks are also due to Mr. Kunio Miki for his helpful discussions. All the numerical computations were done on a NEAC 2200-700 computer at the Osaka University.

References

1) C.-J. Pac, T. Sugioka, K. Mizuno, and H. Sakurai, *Bull. Chem. Soc. Jpn.*, **46**, 238 (1973).
2) C.-J. Pac, T. Sugioka, and H. Sakurai, *Chem. Lett.*, **1972**, 39.
3) C.-J. Pac, K. Mizuno, T. Sugioka, and H. Sakurai, *Chem. Lett.*, **1972**, 187.
4) G. Germain, P. Main, and M. M. Woolfson, *Acta Crystallogr., Sect. A*, **27**, 368 (1971).
5) T. Ashida, The Universal Crystallographic Computing System-Osaka, The Computation Center, Osaka Univ. (1973) p. 55.
6) E. W. Hughes, *J. Am. Chem. Soc.*, **63**, 1737 (1941).
7) H. P. Hanson, F. Herman, J. D. Lea, and S. Skillman, *Acta Crystallogr., Sect. B*, **32**, 625 (1976).
8) R. F. Stewart, E. R. Davidson, and W. T. Simpson, *J. Chem. Phys.*, **42**, 3175 (1965).
9) C. K. Johnson, *ORTEP* II, Report ORNL-5138. Oak Ridge National Laboratory, Tennessee (1976).

Direct Measurement of the Interaction Energy between Solids and Gases. V. Change of the Differential Heats of Adsorption of Ammonia with Specific Poisoning on Silica-Alumina

Hitofumi TANIGUCHI,* Tatsuo MASUDA, Kazuo TSUTSUMI, and Hiroshi TAKAHASHI
Institute of Industrial Science, The University of Tokyo, Roppongi, Minato-ku, Tokyo 106
(Received June 18, 1979)

Heats of adsorption of ammonia on specifically poisoned silica–alumina were measured by use of a twin-conduction-type calorimeter in order to elucidate the adsorption energy and acid strength distributions for both Brönsted (hereafter referred to as B) and Lewis (L) acid sites. Infrared spectra of adsorbed pyridine and cumene cracking activity for the poisoned sample were also examined. Sodium alcoholate–alcohol solution was used as the reagent poisoning only B sites. The use of sodium 2-propanolate–2-propanole dilute solution of which sodium contents was approximately equal to the expected amount of proton on silica–alumina surface caused a large portion of B sites to be poisoned without the decrease in the number of L sites. The following conclusions could be drawn from the experimental results that i) above 115 kJ/mol of the differential heat of adsorption of ammonia no B acid sites were present but only L acid sites, and ii) B acid sites existed chiefly in the vicinity of the adsorption energy distribution of 110 kJ/mol.

The acid strength distribution of dehydrated silica–alumina was determined by amine titration using Hammett indicators[1] or by gas adsorption calorimetric titration[2] and the relation between these two methods was clarified.[3] However, bases such as butylamine and ammonia are adsorbed on both L and B acid sites so that the acid strength distribution of one kind of acid sites has been still uncertain.

On the basis of the inference that B acid sites are generated by the addition of water to L acid sites,[4,5] heats of adsorption of ammonia on the latter may be higher than that on the former. However, a number of other models of acid sites of silica–alumina have been proposed[4–7] and the real silica–alumina surface seems to be more complex.

In this study, heats of adsorption of ammonia on specifically poisoned sample were calorimetrically determined in order to evaluate the acid strength distribution of only L acid sites or B sites. An ion exchange method has been mainly adopted so as to poison B acid sites. Since the exchange technique using aqueous solution such as aq sodium acetate is unsuitable for the specific poisoning of B sites because of the new generation of B sites accompanied by the addition of water molecules to L sites, sodium alcoholate–alcohol solution was used as exchange reagent of proton. Sodium alcoholate reacts easily with the hydroxyl group and has been known as the reagent for the determination of active hydrogen content on the surface. Triphenylchloromethane–hexane solution was used as the reagent poisoning L acid sites.[8,9]

Experimental

Materials. Commercial FCC silica–alumina (Catalysts & Chemicals Ind. Co., Ltd.: alumina 13 wt%) was used as a starting material. Sodium exchanged silica–aluminas (NaSA series) were obtained by impregnation of a starting material into sodium alcoholate–alcohol solutions after pretreatment at 400 °C under 10^{-3} Pa for 5 h. Silica–alumina of which L acid sites were poisoned (TSA) was prepared by impregnation of pretreated original silica–alumina into triphenylchloromethane–hexane solution. The poisoned samples were washed with corresponding alcohol or hexane and subsequently freed from the solvent by the evacuation at 400 °C.

Apparatus and Procedure. Heats of adsorption were determined by a twin-conduction-type microcalorimeter (Tokyo Riko Co., Ltd.) with a conventional vacuum system.[10] In order to measure the differential heat of adsorption, about 0.5 g of the sample was weighed into the sample cell which was evacuated at 400 °C under 10^{-3} Pa for 5 h and placed in the calorimeter. The heat of adsorption of ammonia was measured at 25 °C.

Cumene cracking activity tests were performed by use of a micro pulsereactor connected to a conventional gas chromatography assembly. One hundred and fifty milligrams of the sample was packed in a stainless steel tube and pretreated at 400 °C for 3 h in a stream of helium gas as a carrier. The helium flow rate was 30 cm^3/min. Catalytic activity was given in terms of the conversion ratio of cumene to propylene and benzene during the first pulse reaction.

Infrared spectra of the adsorbed pyridine were measured in an *in situ* quartz cell connected to a vacuum system. Twenty milligrams of sample was pressed to a thin wafer and set in the cell. After evacuation at 400 °C under 10^{-3} Pa for 3 h, pyridine was adsorbed with an equilibrium pressure of 1.3 kPa at room temperature. Then the sample was evacuated at 150 °C for 1 h in order to remove physisorbed pyridine. The spectral measurement was carried out at room temperature.

Specific surface area was determined by the BET nitrogen adsorption method.

Results and Discussion

Silica–alumina was treated with sodium methanolate, sodium 2-propanolate and sodium 2-methyl-2-propanolate in order to clarify the effect of the chain length and the steric conformation of the alkyl group on the amount of sodium exchange. The properties of NaSA series samples were shown in Table 1. NaSA(I), (III), and (IV) were obtained by the impregnation of pretreated silica–alumina into the concentrated sodium alcoholate–alcohol solutions in which sodium contents were in large excess in relation to the expected proton contents of silica–alumina surfaces. On the other hand, NaSA(II) was obtained by treatment with sodium 2-propanolate–2-propanole dilute solution in which

Table 1. Samples

Sample	Specific surface area, $S/m^2\ g^{-1}$	Na content / mmol g^{-1}	Treatment[b]
SA-13[a]	410	0	none
NaSA(I)	374	0.25	$(CH_3)_3CONa$–$(CH_3)_3COH$, concn
NaSA(II)	404	0.52	$(CH_3)_2CHONa$–$(CH_3)_2CHOH$, dilute
NaSA(III)	361	0.97	$(CH_3)_2CHONa$–$(CH_3)_2CHOH$, concn
NaSA(IV)	390	1.64	CH_3ONa–CH_3OH, concn

a) Commercial FCC silica-alumina. b) Each poisoned sample was obtained by impregnation with sodium alcoholate–alcohol solution at room temperature.

sodium content was nearly equal to the expected proton content. The amount of sodium exchange was maximum in case of NaSA(IV) which was treated with sodium methanolate and decrease with an increase in the steric hindrance of the alkyl group. Since no remarkable reduction of specific surface area with the treatment of sodium alcoholate was observed for each sample, the surface structure of the original silica–alumina remained unchanged after the treatment.

Figure 2 shows the differential heats of adsorption of ammonia on sodium exchanged samples. With an increase in sodium content, the heat of adsorption of ammonia decreased. The initial heats of adsorption of ammonia on NaSA(I) and (II) were approximately equal to that on original silica-alumina, however, those on NaSA(III) and (IV) were remarkably reduced. Ammonia gas adsorption energy distributions are shown in Fig. 3. In cases of NaSA(I) and (II), the distribution around 110 kJ/mol of the heat of adsorption became markedly lower with an increase in sodium content, while that above 115 kJ/mol remained unchanged compared with original silica-alumina. In cases of NaSA(III) and (IV), however, the adsorption sites distribution became lower in a whole range above 80 kJ/mol. It is noteworthy that this range for original silica-alumina was also influenced by the heat treatment as shown in Fig. 1. The effect of the treatment with sodium 2-methyl-2-propanolate–2-methyl-2-propanol solution or sodium 2-propanolate–2-propanol dilute solution differed from that with sodium methanolate–methanol solution or sodium 2-propanolate–2-propanol concentrated solution.

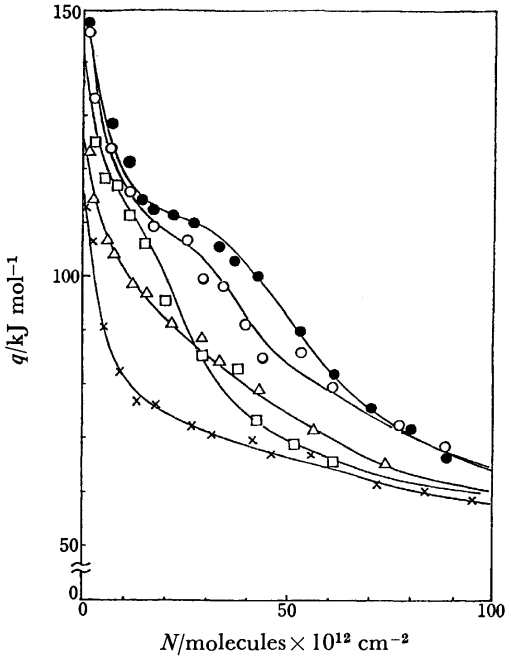

Fig. 2. Differential heat of adsorption of ammonia on silica-alumina poisoned with sodium alcoholate.
● SA-13, ○ NaSA(I), □ NaSA(II), △ NaSA(III), × NaSA(IV).

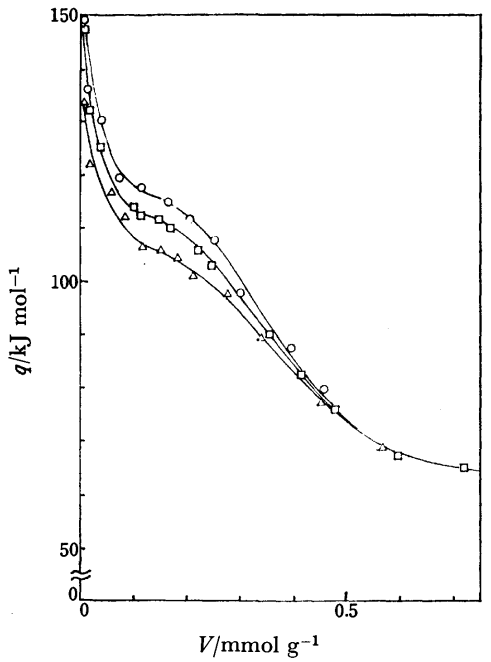

Fig. 1. Effect of pretreatment temperature on differential heat of adsorption of ammonia on silica-alumina.
○ 600, □ 400, △ 150 C.

Infrared spectra of pyridine adsorbed on sodium exchanged samples were shown in Fig. 4. Both absorption peaks for B acid sites (1540 cm^{-1}) and for L acid sites (1450 cm^{-1}) were observed on original silica-alumina. However, the former was remarkably reduced for NaSA(I) and disappeared for other exchanged samples, which suggests that B acid sites almost or completely disappeared by the treatment with sodium alcoholate. On the other hand, the reduction of the latter peak occurred particularly for NaSA(IV). This fact suggests that sodium methanolate reacted not only with surface active proton but was coordinated with L acid sites. The formation of the coordinative bond must require the small steric hindrance and the strong basicity of the coordinated species. Therefore it is

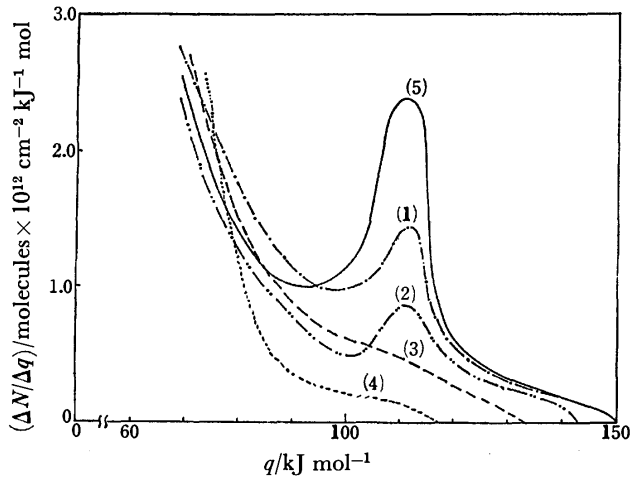

Fig. 3. Adsorption energy distribution on silica-alumina poisoned with sodium alcoholate.
(1) NaSA(I), (2) NaSA(II), (3) NaSA(III), (4) NaSA(IV), (5) SA-13.

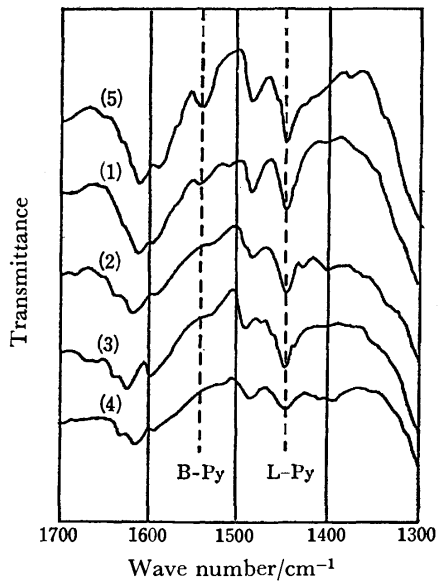

Fig. 4. Infrared spectra of adsorbed pyridine.
(1) NaSA(I), (2) NaSA(II), (3) NaSA(III), (4) NaSA(IV), (5) SA-13.

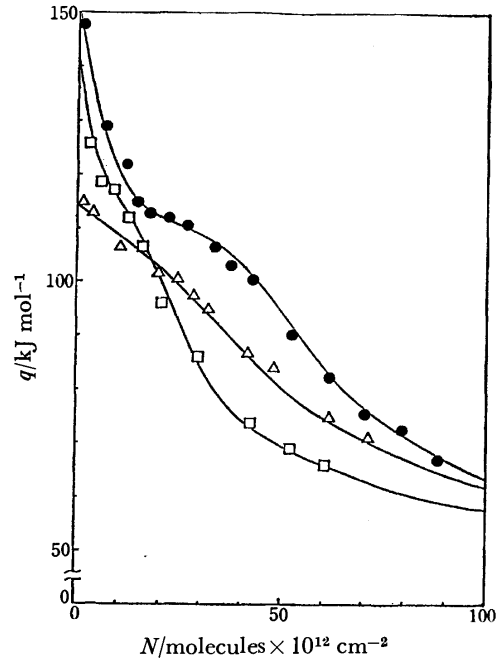

Fig. 5. Comparison of differential heat of adsorption on NaSA(II), (□), with TSA, (△), (poisoned with triphenylchloromethane). SA-13 (●).

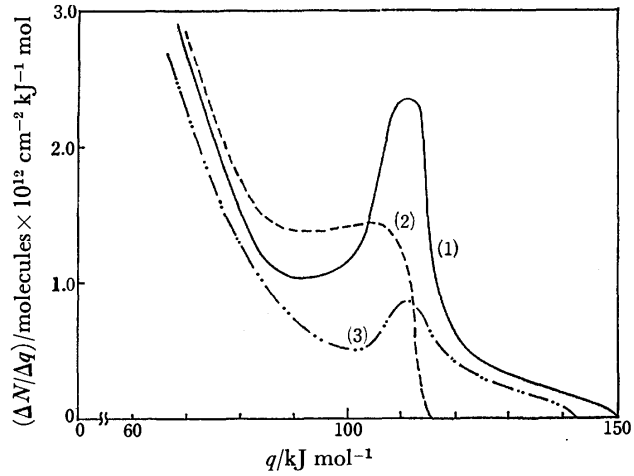

Fig. 6. Adsorption energy distributions on NaSA(II), (3), TSA, (2), and SA-13, (1).

reasonable that the larger the alkyl group of sodium alcoholate is, the more difficult the formation of the coordinative bond with L acid site becomes. On the sample treated with sodium 2-methyl-2-propanolate, even a part of B sites still remained besides L sites.

The adsorbed amount of ammonia having the heat of adsorption below 115 kJ/mol, chiefly in the vicinity of 110 kJ/mol, decreased by sodium exchange. When the coordination of sodium alcoholate with L acid sites occurred besides sodium exchange, even the adsorbed amount of ammonia above 115 kJ/mol decreased together with the reduction of initial heat of adsorption. Hence, B acid sites seem to distribute mainly in the adsorption energy region below 115 kJ/mol.

In Fig. 5 the differential heat of adsorption of ammonia on silica-alumina poisoned with triphenylchloromethane (TSA) is shown together with those on SA-13 and on NaSA(II). The initial heat of adsorption of ammonia on TSA, 115 kJ/mol, was much lower than that on original silica-alumina, while that on NaSA(II) was approximately equal to that on original sample. Furthermore, as shown in Fig. 6, ammonia adsorption sites on TSA existed below 115 kJ/mol of the differential heat of adsorption, which was markedly different from the case of NaSA(II). This supports the above-mentioned suggestion that only L acid sites exist above 115 kJ/mol of the differential heat of adsorption. The number of ammonia adsorption sites above 115 kJ/mol for NaSA(III) or (IV) was smaller than that for NaSA-(II) or original silica-alumina, as a result of a decrease in the number of L acid sites.

It is possible to consider that L acid sites are stronger

than B sites in silica–alumina from the finding[11] that pyridine adsorbed on B sites was completely removed by evaculation at 300 °C while pyridine on L sites remained after evacuation even at 400 °C. As shown in Fig. 1, the adsorbed amount of ammonia above 115 kJ/mol on silica–alumina pretreated at 600 °C was about twice as much as that on the sample pretreated at 400 °C, which can therefore be ascribed to the increase in the number of L acid sites. The results are similar to those found in Y type zeolites.[12]

Table 2. Relations among cumene conversion ratio, sodium content and calorimetrically determined *acidity*

Sample	*Acidity* mmol g^{-1}	Na content mmol g^{-1}	Cumene conversion ratio/%
SA-13	0.35	0	87
NaSA(I)	0.31	0.25	78
NaSA(II)	0.22	0.52	31
NaSA(III)	0.21	0.97	23
NaSA(IV)	0.08	1.64	0

Cumene cracking activity of the catalyst has been known to arise from B acidity and its dependence on the calorimetrically determined surface acidity was reported previously in detail.[13] We now define the adsorbed amount of ammonia between 80 and 115 kJ/mol as *acidity* which seems to be the difference between total acidity and a large portion of L acidity. In Table 2 the relations among *acidity*, sodium content and cumene cracking activity are shown. With an increase in sodium content, both *acidity* and activity decreased. This fact suggests that the treatment with sodium alcoholate reduced B acidity.

The conclusions based on the above experiments are that B acid sites of silica–alumina studied here are distributed below 115 kJ/mol of the differential heat of adsorption of ammonia, mainly in the vicinity of 110 kJ/mol, and above 115 kJ/mol only L acid sites exist. A part of L acid sites may be present below 115 kJ/mol.

Considering a poisoning technique, it was shown that ion exchange in aq solution was unsuitable for the purpose of poisoning only B acid sites. Because the shape of q-N curve and the adsorption energy distribution curve of silica–alumina treated with aq sodium acetate solution were close to those of NaSA(IV); the amount of L sites of the latter decreased to about one-third of that of original silica–alumina.

This work was partly supported by a Grant-in-Aid for Science Research from the Ministry of Education.

References

1) H. A. Benesi, *J. Am. Chem. Soc.*, **78**, 5490 (1956).
2) T. Masuda, H. Taniguchi, K. Tsutsumi, and H. Takahashi, *Bull. Chem. Soc. Jpn.*, **51**, 1965 (1978).
3) H. Taniguchi, T. Masuda, K. Tsutsumi, and H. Takahashi, *Bull. Chem. Soc. Jpn.*, **51**, 1970 (1978).
4) M. W. Tamele, *Discuss. Faraday Soc.*, **8**, 270 (1950).
5) M. R. Basila, T. R. Kantner, and K. H. Rhee, *J. Phys. Chem.*, **68**, 3197 (1964).
6) J. D. Danforth, *J. Phys. Chem.*, **59**, 564 (1955).
7) P. Cloos, A. J. Leonard, J. P. Moreau, A. Herbillon, and J. J. Fripiat, *Clays and Clay Minerals*, **17**, 279 (1969).
8) H. P. Leftin and W. K. Hall, *Actes Congr. Intern. Catalyse, 2e, Paris*, II, No. 65 (1960).
9) H. Taniguchi, T. Masuda, K. Tsutsumi, and H. Takahashi, *Bull. Chem. Soc. Jpn.*, **52**, 2195 (1979).
10) T. Masuda, H. Taniguchi, K. Tsutsumi, and H. Takahashi, *Bull. Chem. Soc. Jpn.*, **51**, 633 (1978).
11) J. Take, T. Ueda, and Y. Yoneda, 28 th National Meeting of Chem. Soc. Jpn., Tokyo, April 1973, Abstr. No. 2C 38.
12) J. W. Ward, *J. Catal.*, **9**, 225 (1967).
13) T. Masuda, H. Taniguchi, K. Tsutsumi, and H. Takahashi, *J. Jpn. Petro. Inst.*, **22**, 67 (1979).

High Temperature Hard Anodizing with Tartaric Acid-Oxalic Acid-Triethanolamine Bath

Yoshio FUKUDA* and Toshiro FUKUSHIMA

Corrosion Division, National Research Institute for Metals, 2-3-12, Nakameguro, Meguro-ku, Tokyo 153

(Received July 9, 1979)

Tartaric acid does not produce uniform films on A6063 alloy (Al–Mg–Si). Uniform films are formed when oxalic acid is added to the tartaric acid bath, but hardness above Hv 400 cannot be obtained at a voltage below 100 V. When 1 mol dm^{-3} tartaric acid–0.4—0.6 mol dm^{-3} oxalic acid baths were adjusted with triethanolamine (0.26—0.54 mol dm^{-3}) to pH 1.00 and 1.25, crack-free films with hardness above Hv 430 were formed at 40 °C in the range 65—85 V. The hardness of the film is independent of the anion content of the film, increasing with increase in the thickness of cell wall and lowering in porosity.

In general, hard anodizing of aluminum has been carried out in sulfuric acid at low temperatures below 10 °C.[1] It is considered that compact films can be obtained at low temperatures because of high formation voltages and that thick films can be obtained because of the low rate of dissolution of porous layers during the course of anodization. However, this process requires special facilities for refrigeration, and the films are cracked. A process operating at moderate temperatures is desirable.

For this purpose, (a) dilute sulfuric acid or (b) organic acid whose solvent action on the oxide film is weak above ordinary temperatures, are suitable as electrolyte, because hard films which possess large cells and a small number of pores can be formed on account of high voltage. (a) is liable to produce pitting,[2] and (b) to produce uniform films.[3,4] However, study on hard anodizing above ordinary temperatures has seldom been reported. Although malonic acid yields hard films at temperatures 40—60 °C,[5] it is liable to decompose into CH_3COOH and CO_2 at high temperatures.[6]

Recently, it was found[7,8] that crack-free films with hardness above Hv 500 are formed in tartaric or malic acid baths at temperatures above 60 °C. However, the acids have the disadvantages that the bath voltage is too high (above 150 V for high purity aluminum) and uniform films cannot be formed on alloys such as A6063 (Al–Mg–Si). Additives for overcoming the difficulty were investigated.[9] By addition of 0.2 mol dm^{-3} oxalic acid to 1 mol dm^{-3} tartaric or malic acid, films with hardness Hv 300—420 were obtained on A6063 alloy at 40—50 °C.[10] However, the bath voltage was still high (105—140 V at 5.65 A dm^{-2}).

The bath voltage can be lowered by further addition of oxalic acid, but the dissolution of the cell wall during anodization is accelerated, leading to a decrease in the hardness of the film. Simultaneous attainment of the increase in hardness and decrease in bath voltage is impossible.

With the aim of producing film with hardness above Hv 400 at voltages below 100 V, tartaric–oxalic acid electrolyte was improved. The dependence of the hardness on the anion content and porous structure of the film was also investigated.

Effect of pH and Oxalic Acid Concentration

The rise in the pH of electrolyte is necessary to reduce the rate of chemical dissolution of the porous layer during the course of anodization above room temperature. However, the rise in bath voltage, which follows the rise in pH and induces burning, should be suppressed as much as possible. There are two means for raising the pH, dilution of acid and addition of a base without dilution. In a dilute oxalic acid bath of high pH, the bath voltage is so high that burning is liable to occur, whereas in a bath with high oxalic acid concentration, adjusted to the same pH, the voltage is lower than in the dilute acid bath.[11,12] The lower the pH and the higher the oxalic acid concentration, the more the oxalate is involved in the film. The chemical dissolution rate of the film is independent of the oxalate concentration of the bath, and the film becomes soluble when the oxalate content of the film is higher and the pH of the bath lower. It seems that the barrier layer formed in a bath with concentrated oxalic acid, adjusted to a high pH, contains more oxalate than that formed in a dilute acid bath of the same pH so that the electrochemical dissolution of the layer is accelerated, lowering the bath voltage at a constant current density. This might occur also in the case of oxalic acid mixed with tartaric or malic acid. In a tartaric or malic acid bath with high oxalic acid concentration, adjusted to a high pH, the bath voltage would be lower than that in a bath with low oxalic acid concentration. Even if the bath voltage is decreased, the rate of dissolution of the cell wall is relatively low because of a high pH so that the hardness of the film would not decrease remarkably.

Experimental

Plates of extruded aluminium alloy A6063-T5,[13] 3 mm thick and 40 mm wide, were cut into 100 mm lengths (surface area $=88.4$ cm^2). Each of them was racked to a holder made of pre-anodized tantalum wire, 1 mm diam., and treated with an aqueous solution of 1.25 mol dm^{-3} NaOH at 80 °C for 30 s. They were then successively rinsed, neutralized with 15% HNO_3, rinsed and anodized. A 5 dm^3 beaker was used as an electrolytic cell, cathodes being made of two plates of carbon ($250\times 50\times 10$ mm).

Tartaric acid which can produce film at lower voltage than malic acid was used as the primary ingredient of the electrolyte

Table 1. Composition and pH of electrolytes

Tartaric acid / mol dm^{-3}	Oxalic acid / mol dm^{-3}	Triethanolamine / mol dm^{-3}	pH (at 25 °C)
1	0.2	0	0.80
1	0.2	0.13	1.00
1	0.2	0.22	1.25
1	0.4	0	0.67
1	0.4	0.26	1.00
1	0.4	0.34	1.25
1	0.6	0	0.60
1	0.6	0.43	1.00
1	0.6	0.54	1.25
1	0	0	1.28

and was mixed with oxalic acid or oxalic acid and triethanolamine[14] (Table 1). The bath temperature was kept at 30, 40, and 50±1 °C. While the solution was stirred with a propeller at about 330 min^{-1}, galvanostatic anodization using a three-phase full-wave rectifier was carried out at 2.26 A dm^{-2} for 50 min and at 5.65 A dm^{-2} for 20 min. Current was controlled to a specified value within 15 s after switching on.

The hardness was measured on the surfaces of two anodized specimens at three points each, using a micro Vickers hardness tester with a load of 100 g. The average of six readings was taken. The microstructure of the anodized surface was observed with an electron microscope using a one-step carbon replica at an accelerated voltage of 50 kV. The carbon content of the film was determined by analysis of CO_2 gas produced by combustion (1300 °C, carrier gas O_2) of the film.[12] The film was isolated by the cathodic reduction method.

Results

States of the Anodized Surface. When anodizing was carried out in a bath with 0.2 mol dm^{-3} oxalic acid, adjusted to pH 1.00 and 1.25, at 5.65 A dm^{-2}, burning occurred. Under all other conditions uniform films were formed. The thickness of each film was about 35 μm. Films were colored, no cracks being observed. The color of the films formed at 2.26 A dm^{-2} was grayish yellow and that of the films formed at 5.65 A dm^{-2} reddish dark yellow. The lightness of the color increased with increase in oxalic acid concentration and rise in temperature.

Bath Voltage. The time dependence of the bath voltage is shown in Fig. 1. The voltage dropped after

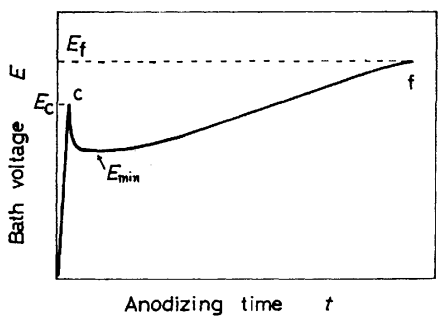

Fig. 1. Time dependence of bath voltage under galvanostatic anodizing.

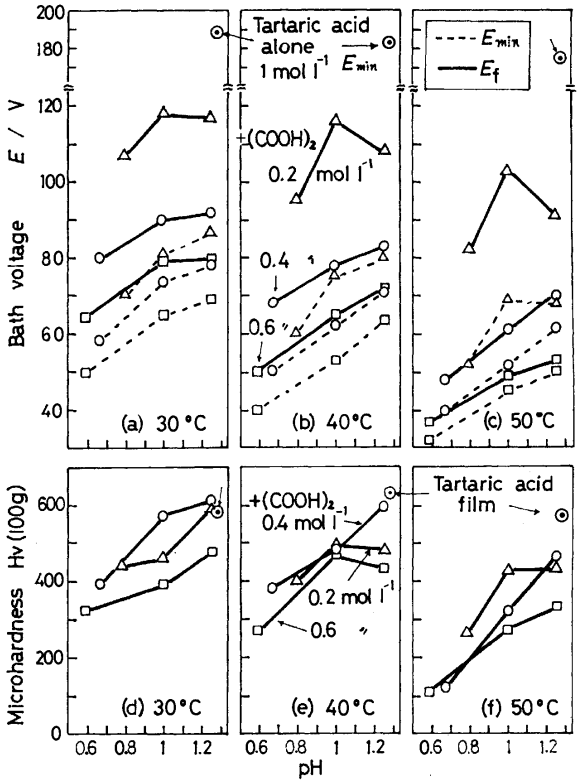

Fig. 2. Dependence of bath voltage and hardness of films on pH of electrolytes at various temperatures and oxalic acid concentrations(2.26 A dm^{-2}, 50 min, A6063 alloy).

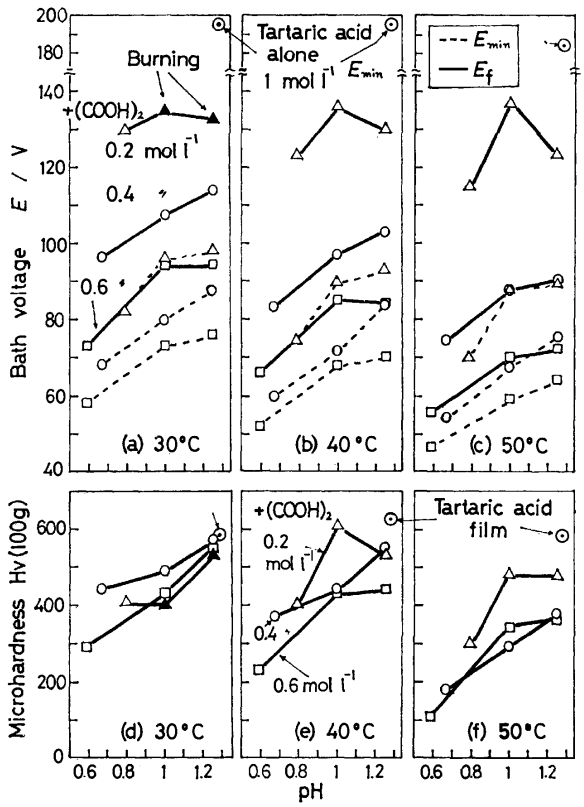

Fig. 3. Dependence of bath voltage and hardness of films on pH of electrolytes at various temperatures and oxalic acid concentrations(5.65 A dm^{-2}, 20 min, A6063 alloy).

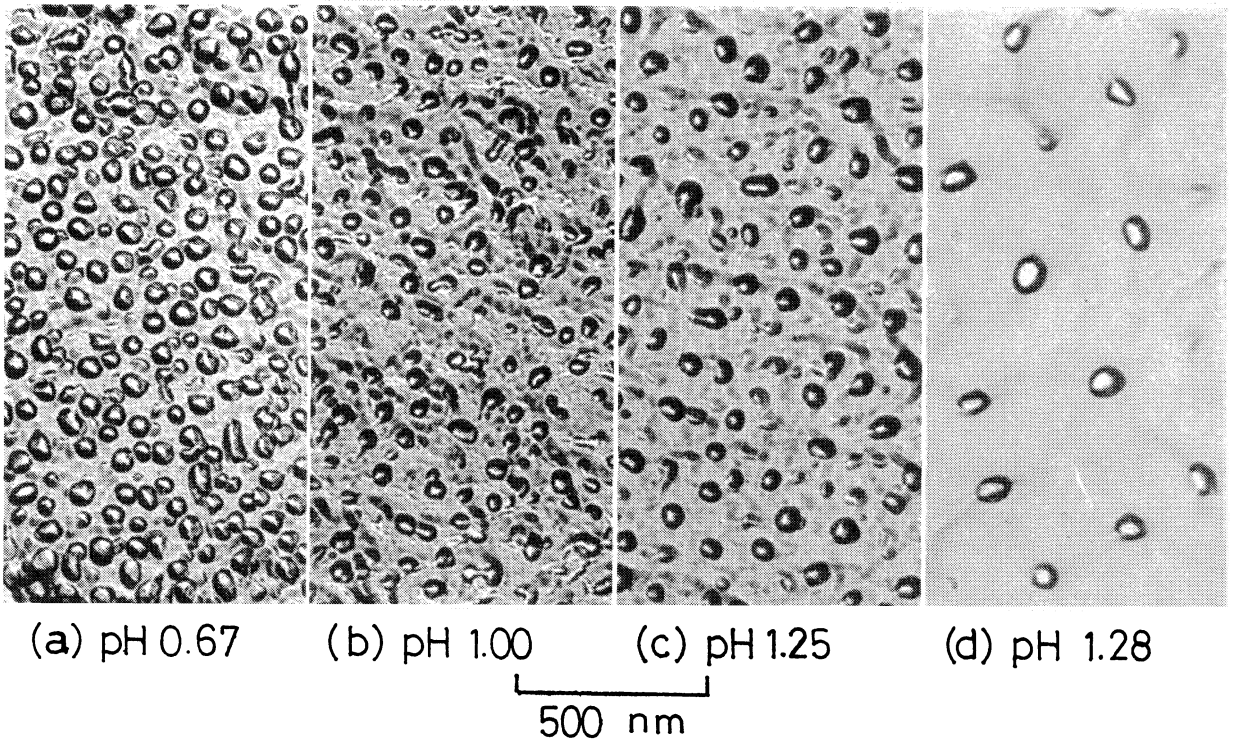

Fig. 4. Replica electron micrographs of film formed in (a) 1 mol dm^{-3} tartaric acid -0.4 mol dm^{-3} oxalic acid, (b) (a) $+0.26$ mol dm^{-3} triethanolamine, (c) (a) $+0.34$ mol dm^{-3} triethanolamine and (d) 1 mol dm^{-3} tartaric acid at 40 °C and 2.26 A dm^{-2} for 50 min.

the critical point "c" and then rose gradually. The slope of the voltage-time curve after point "c" decreased with increase in oxalic acid concentration, rise in temperature and lowering in current density.

The minimum bath voltage immediately after the critical point (E_{min}) increased with increase in pH and decreased with increase in oxalic acid concentration (broken line, Figs. 2a—c and 3a—c). The tendency was recognized also in the case of the final voltage (E_f, solid line). However, when oxalic acid concentration was 0.2 mol dm^{-3}, the E_f at pH 1.25 was lower than that at pH 1.00. The bath voltage decreased with rise in temperature and increased with increase in current density.

Hardness of the Film. As shown in Figs. 2d—f and 3d—f, the hardness increased with increase in pH and decreased with rise in temperature. At constant pH and temperature, the hardness decreased with

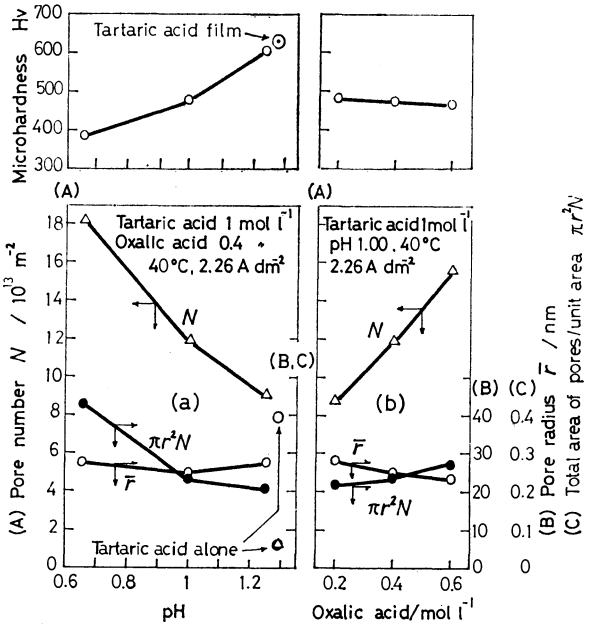

Fig. 5. Dependence of number, radius and total area of pores on pH and oxalic acid concentration of electrolytes.

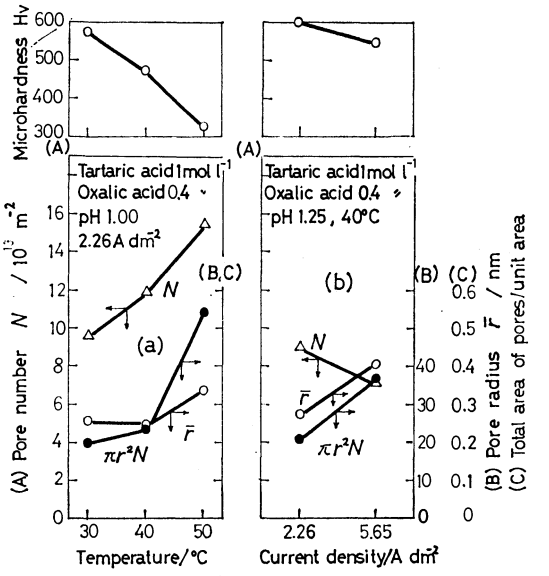

Fig. 6. Dependence of number, radius and total area of pores on temperature and current density.

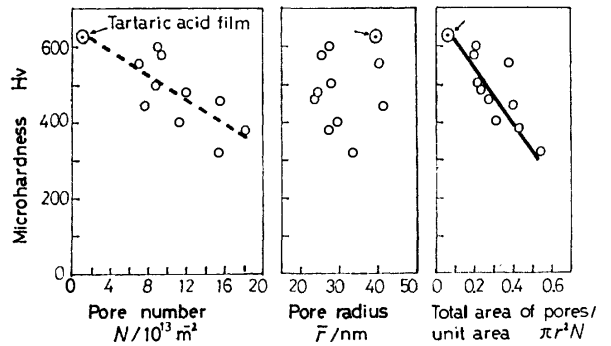

Fig. 7. Dependence of hardness of films on number, radius and total area of pores.

oxalic acid concentration. There was little change in the hardness with current density. By comparing the hardness with bath voltage, it was found that films with hardness above Hv 430 are formed in 1 mol dm^{-3} tartaric acid–0.4—0.6 mol dm^{-3} oxalic acid baths of pH 1.00 and 1.25 with voltage 65—85 V at 40 °C.

Carbon Content and Hardness of the Film. The carbon content of the film was determined in order to examine the effect of electrolyte anions on the hardness of the film. The hardness was independent of the carbon content of the film.

Microstructure and Hardness of the Film. Replica images of the film surface are given in Fig. 4. The number of pores in the films formed with mixed baths (a—c) is larger than that of pores in the film formed with tartaric acid alone (d). There is a difference in the number and radius of pores among the films shown in Figs. 4a—c. The number (surface density, m^{-2}) and radius (nm) of pores were measured on the photographs and the total area of pores was calculated. The parameters are plotted against the anodizing variables (Figs. 5 and 6) and the hardness of the film (Fig. 7). The hardness increased with decrease in the number and area of pores, but was not correlated with the radius of pores.

Discussion

When the pH of tartaric–oxalic acid electrolyte is raised by addition of triethanolamine, the electrochemical dissolution of the barrier layer is so suppressed that the bath voltage generally increases to maintain the current flow constant. The role of triethanolamine in this case is considered to be only the suppression of dissolution of the film by reducing the acidity of the tartaric–oxalic acid electrolyte as in the oxalic acid–triethanolamine bath.[12]

Porous layer contains a considerable amount of electrolyte anions,[15] the anion content of the phosphoric,[16] oxalic,[11] or sulfuric[17] acid film becoming maximum at a point between the wall/solution interface and the cell boundary. Electrolyte anions are considered to migrate through the barrier layer. Assuming that electrolyte anions are immobile, the porous layer arising from the barrier layer formed only by anion (O^{2-} and OH^-) migration[18] would contain no electrolyte anions.

The radius of oxalate ions seems to be smaller than that of tartrate ions. Thus oxalate ions are more mobile in the barrier layer than tartrate ions. The solvent action of oxalic acid on the oxide film is stronger than that of tartaric acid. The bath voltage rises gradually with anodizing time (Fig. 1). As the porous layer grows, the supply of oxalic acid by diffusion from the bulk of the solution to the surface of the barrier layer is retarded[19] and the dissolution of the barrier layer is suppressed and the layer becomes thick gradually, leading to gradual rise in bath voltage. In baths with 0.2 mol dm^{-3} oxalic acid, the E_f at pH 1.25 is lower than that at pH 1.00. At pH 1.25, a local rise in temperature of the anode might occur[20] owing to uneven current distribution. However, apparently uniform films were formed.

According to the theory of ionic equilibria,[21] in the pH range 0—1.25, little tartaric acid dissociates, while 5—48% of the oxalic acid dissociates to $HC_2O_4^-$ ions. For instance, at pH 1.00, 99% of the tartaric acid remains undissociated, while 65% of the oxalic acid remains undissociated and 35% of the oxalic acid is present as $HC_2O_4^-$ ions. Even if this mixed acid has the same pH value, undissociated oxalic acid concentration increases with the addition of oxalic acid, causing the decrease in bath voltage.

No cracks were observed in the films obtained by high temperature process. From the fact[22] that cracks increase as the anode warms up to room temperature after withdrawal, the film formed by the low temperature process may easily be cracked under the influence of tensile stress caused by expansion of the anode. On the other hand, in the case of the high temperature process, when the anode is cooled to room temperature after withdrawal, the film undergoes compressive stress by contraction of the anode but it can withstand the stress.

The hardness of the film is controlled by the geometrical structure of the film, but not the carbon or anion content of the film. The hardness of the film is closely related to its porosity,[23] but the porosity varies with the number and radius of pores. Hardness seems to be related to the wall thickness. The relation between these parameters and the hardness was examined in detail.

Higher pH gave a harder film with a smaller number of pores and smaller area of pores, or lower porosity (Fig. 5a). The distance between the pores, or wall thickness, increases with increase in pH (Fig. 4). Lower oxalic acid concentration gave a harder film with a smaller number of pores and lower porosity (Fig. 5b), the cell wall becoming thick. Lower temperature also gave a harder film with a smaller number of pores and lower porosity (Fig. 6a). The cell wall became thick with fall in temperature, the parameters changing with current density (Fig. 6b). When the current density was high, the number of pores was small but the porosity was high and the hardness value small. In this case, the relation between the number of pores and the hardness was opposite to that obtained in the other cases. The bath voltage at 5.65 A dm^{-2} was higher than at 2.26 A dm^{-2} so that the cell wall near the pore base should be thicker. However, the thicknesses of the walls near

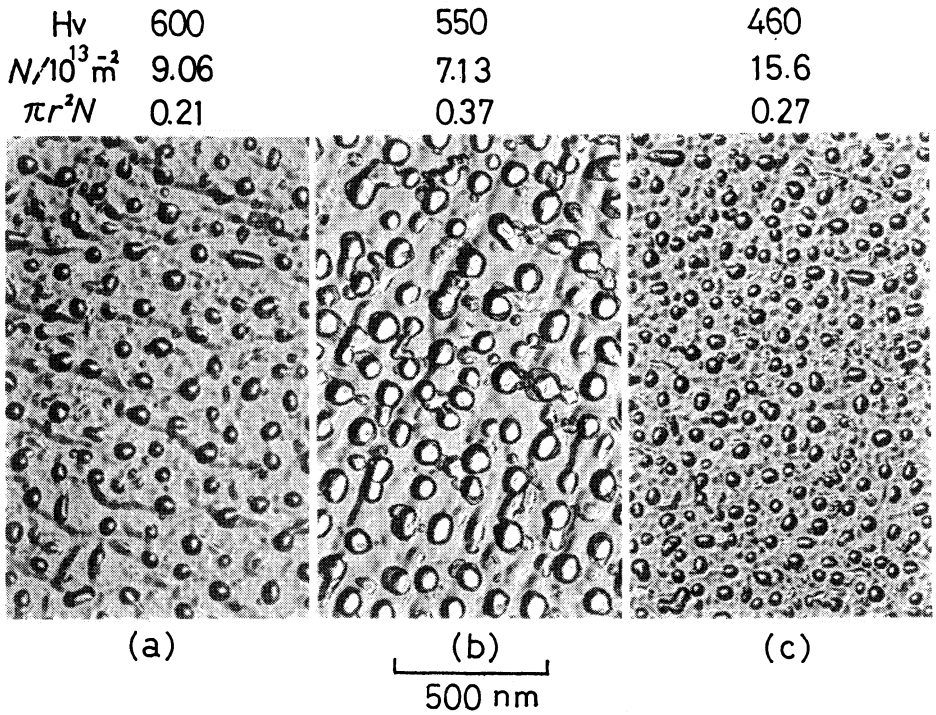

Fig. 8. Porous structure (replica image) and hardness of film.
(a) 1 mol dm^{-3} tartaric acid —0.4 mol dm^{-3} oxalic acid —0.34 mol dm^{-3} triethanolamine, pH 1.25, 40 °C, 2.26 A dm^{-2}, 50 min.
(b) The same bath as (a), 5.65 A dm^{-2}, 20 min.
(c) 1 mol dm^{-3} tartaric acid—0.6 mol dm^{-3} oxalic acid—0.43 mol dm^{-3} triethanolamine, pH 1.00, 40 °C, 2.26 A dm^{-2}, 50 min.

the surface were nearly the same as those of the walls of the film formed at 2.26 A dm^{-2} (Fig. 8b). When the current density is high, considerable heat is generated from the anode, making heat transmission insufficient and causing easy dissolution of the film. No definite relation exists between hardness and the radius of pores (Fig. 7).

When the bath voltage was raised, the cell wall as well as the barrier layer became thick and the number of pores decreased (Fig. 9), leading to a decrease in porosity and increase in hardness. Thus, in many cases, hardness was related to pore number, wall thickness and porosity. However, the number of pores is not closely related to hardness (Fig. 7). As shown in Fig. 8, film (a) is harder than film (b), while (a) has a larger number of pores than (b). This is due to the lower porosity of (a). Film (b) is harder than film (c), while (b) has a higher porosity than (c). This is due to the thicker wall of (b).

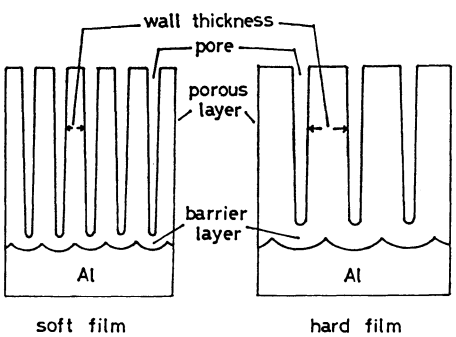

Fig. 9. Porous structure (cross section) and hardness of film.

The hardness of the film is controlled by wall thickness and porosity of the film, but not the anion content of the film; the thicker the wall and the lower the porosity, the harder the film.

Conclusions

High temperature hard anodizing of A6063 alloy was tested in 1 mol dm^{-3} tartaric acid–0.2—0.6 mol dm^{-3} oxalic acid–0—0.54 mol dm^{-3} triethanolamine baths at temperatures 30—50 °C and current densities 2.26 and 5.65 A dm^{-2}. The results are as follows:

1) In tartaric–oxalic acid baths, the films formed by addition of 0.2 mol dm^{-3} oxalic acid gave hardness above Hv 400, but the bath voltage was too high (above 100 V). When oxalic acid concentration was increased to 0.4—0.6 mol dm^{-3}, the hardness of film as well as the bath voltage decreased.

2) When 1 mol dm^{-3} tartaric acid–0.4—0.6 mol dm^{-3} oxalic acid baths were adjusted with triethanolamine (0.26—0.54 mol dm^{-3}) to pH 1.00 and 1.25, crack-free films with hardness above Hv 430 were formed at 40 °C with voltage 65—85 V.

3) The hardness of the film is independent of the anion content of the film, increasing with increase in the thickness of cell wall and decrease in porosity.

References

1) S. Wernick and R. Pinner, "The Surface Treatment and Finishing of Aluminium and Its Alloys," 4th ed, Robert Draper Ltd., Teddington (1972), Vol. 2, p. 566.
2) P. Csokán and M. Holló, *Werkst. Korros.*, **12**, 288 (1961).
3) S. Tajima, S. Itoh, and T. Fukushima, *Denki Kagaku*, **23**, 342, 395 (1955).
4) T. L. Sharma and Y. N. Trehan, *NML Technical Journal (India)*, **18**, 54 (1976).
5) J. M. Kape, *Metallurgia (Brit.)*, **60**, 181 (1959).
6) J. M. Kape, Brit. Patent 1173597 (1965).
7) T. Fukushima and Y. Fukuda, Japan, Patent 705694 (1973).
8) Y. Fukuda, *J. Metal Fin. Soc. Jpn.*, **27**, 398 (1976).
9) Y. Fukuda, *J. Metal Fin. Soc. Jpn.*, **27**, 681 (1976).
10) Y. Fukuda, *J. Metal Fin. Soc. Jpn.*, **29**, 33 (1978).
11) Y. Fukuda, *Nippon Kagaku Kaishi*, **1974**, 1868; *Trans. Nat. Res. Inst. Metals*, **17**, 239 (1975).
12) Y. Fukuda, *Nippon Kagaku Kaishi*, **1975**, 1299; *Trans. Nat. Res. Inst. Metals*, **18**, 197 (1976).
13) JIS-H4100, alloy composition; Mg, 0.57; Fe, 0.19; Si, 0.23; Mn, 0.03; Cu, 0.008%. T 5; quenched from high temperature during extrusion and followed by tempering (*ca.* 205 °C, 1 h).
14) When NaOH was added to solutions containing 0.2 mol dm^{-3} or more oxalic acid, precipitate was observed.
15) S. Tajima, "Advance in Corrosion Science and Technology," ed by M. G. Fontana and R. W. Staehle, Plenum Press, New York (1971), Vol. 1, p. 281.
16) H. Takahashi and M. Nagayama, *Nippon Kagaku Kaishi*, **1974**, 453.
17) Y. Fukuda and T. Fukushima, Preprint for 52th Lecture Meeting of Metal Fin. Soc. Jpn., p. 80 (1975).
18) J. Siejka and C. Ortega, *J. Electrochem. Soc.*, **124**, 883 (1977).
19) S. Hoshino, T. Imamura, S. Matsumoto, and K. Kojima, *J. Metal Fin. Soc. Jpn.*, **28**, 167 (1977).
20) I. Mizuki, N. Baba, and S. Tajima, *J. Metal Fin. Soc. Jpn.*, **28**, 30 (1977).
21) H. Freiser and Q. Fernando, "Ionic Equilibria in Analytical Chemistry," translated into Japanese by T. Fujinaga and E. Sekido, Kagaku Dojin, Kyoto (1972), p. 65.
22) Ref. 1, p. 592.
23) F. Keller, M. S. Hunter, and D. L. Robinson, *J. Electrochem. Soc.*, **100**, 411 (1953).

Studies of Spin Labeled Sodium Dodecyl Sulfate. I. Synthesis and Properties

Takeo YAMAGUCHI,* Akira YAMAUCHI,† Eiji KIMOTO, and Hideo KIMIZUKA†

Department of Chemistry, Faculty of Science, Fukuoka University, Nanakuma, Fukuoka 814

†*Department of Chemistry, Faculty of Science, Kyushu University 33, Hakozaki, Fukuoka 812*

(Received July 20, 1979)

Nitroxide spin labeled surfactant, sodium salt of 2-ethyl-2-[9-(hydroxysulfonyloxy)nonyl]-4,4-dimethyloxazolidin-3-yloxyl, was synthesized and some properties of the compound were studied by means of ESR and conductivity measurements. From conductivity measurements it was found that the critical micelle concentration of the compound was 21.6 mmol kg^{-1} at 25.0±0.1 °C and the micelle consisted of a small number of labeled surfactant ions. The ESR spectra of the labeled surfactant were measured as a function of concentration and temperature. These spectra showed a typical pattern interpreted in terms of spin exchange. Regarding spin exchange as chemical reaction, second order rate constant was determined from the analysis of line width and compared with the values obtained by diffusion controlled model.

Spin label method[1] developed by Ohnishi and McConnell[2] has become more important because the ESR spectrum reflects sensitively the rotational motion in the wide range, *i.e.*, 10^{-11}—10^{-3} s,[3] the local environment, and the orientation of labeled compound. In particular, the application to biological system has offered many valuable information concerning the dynamic properties.[4]

In general, it is well known that surfactant molecules form the ordered aggregates known as micelles. Since a dynamic study of micellar solution by means of ESR was first attempted by Waggoner *et al.*,[5] many studies of micellar solution have been examined.[6-8] However, most of the studies have been performed by spin probe method. In order to obtain more detailed information on micelle, it is desirable to use the sample of micellar solution which consists of the spin labeled surfactant molecules only. So, a nitroxide spin label compound,[9] sodium salt of 2-ethyl-2-[9-(hydroxysulfonyloxy)nonyl]-4,4-dimethyloxazolidin-3-yloxyl (SL-SDS)

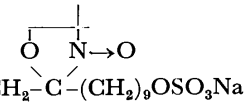

$CH_3CH_2-C-(CH_2)_9OSO_3Na$ (SL-SDS)

was synthesized and examined whether this compound is able to form micelle, characteristic of surface active molecule, or not.

In this paper, the results of a study of SL-SDS solution by means of ESR and conductivity measurements will be presented.

Experimental

Materials. Preparation of SL-SDS.[9] Dimethyl decanedioate was prepared by refluxing a mixture of 202 g (1 mol) of decanedioic acid, 800 ml of methanol, and 80 ml of concentrated sulfuric acid for 3 h. The reaction mixture was diluted with water of 3 times volume and the diester was extracted with 2000 ml benzene. After the removal of benzene under reduced pressure, the residue was transferred to a flask containing 85.6 g (0.5 mol) of anhydrous barium hydroxide in 1000 ml methanol. The flask was quickly closed with a soda-lime tube and the mixture was allowed to stand for 24 h with stirring at room temperature. The white barium salt collected by filtration was washed with two 200 ml portions of methanol and was shaken with a mixture of 1000 ml of 4 M HCl and 1000 ml of ether in a separatory funnel. The ether extract was washed with three 1000 ml portions of water. The ether was removed by evaporation and the residue was distilled under reduced pressure. The yield of methyl hydrogen decanedioate was 130 g (60%).

In a flask were placed 130 g (0.6 mol) of methyl hydrogen decanedioate and 143 g (1.2 mol) of thionyl chloride. The solution was gently warmed at 30—40 °C for 3 h and allowed to stand for 12 h at room temperature. The excess thionyl chloride was removed under reduced pressure and the residue was distilled, yielding 127 g (70%) of 9-(methoxycarbonyl)-nonanoyl chloride.

A solution of ethyl bromide 30.2 g (0.2 mol) in 100 ml of anhydrous ether was added to the 100 ml ether solution containing a 0.2 g atom of magnesium turnings and the mixture was refluxed for 30 min longer. To the mixture was portion-wise added 18.3 g (0.1 mol) of anhydrous cadmium chloride at 0 °C. The mixture was refluxed until a Gilman test[10] for the Grignard reagent was negative. The ether was completely removed and 200 ml of anhydrous benzene was added. The mixture in benzene was refluxed for 1 h. A solution of acid chloride, 9-(methoxycarbonyl)nonanoyl chloride 47 g (0.2 mol), dissolved in 50 ml anhydrous benzene was slowly added to the solution of the organo-cadmium compound and refluxed with stirring for an additional hour. The reaction product was cooled in an ice bath and decomposed by dropping of 50 ml of ice water, followed by an addition of 20% sulfuric acid sufficient to produce two transparent layers. The benzene solution was washed successively with 100 ml of water, 100 ml of 5% sodium hydrogencarbonate, 100 ml of water, and 50 ml of saturated sodium chloride. Then, the benzene solution was dried on anhydrous sodium sulfate. After removal of benzene, the reaction product was distilled (bp 115—117 °C/399 Pa), yielding 32 g (70%) of methyl 10-oxododecanoate; IR 1710 (C=O) and 1735 cm^{-1} (ester C=O); NMR (CCl_4) δ=0.99 (3H, t, J=7.6 Hz, CH_3).

To 500 ml of toluene were dissolved 22.8 g (0.1 mol) of the methyl 10-oxododecanoate, 89 g (1.0 mol) of 2-amino-2-methyl-1-propanol, and 100 mg (0.5 mmol) of *p*-toluenesulfonic acid monohydrate. The mixture was refluxed for 3 days using a Dean-Stark trap for continuous water removal. The toluene solution was washed 6 times with 200 ml portions of saturated sodium hydrogencarbonate solution and 4 times with 200 ml portions of water and dried through a column of anhydrous sodium sulfate. The toluene was then removed with a rotary evaporator. The residue containing the oxazolidine derivative was directly used to the following reaction for oxidation. Identification of oxazolidine was as

follows: NMR (CCl_4) δ=3.43 (2H, s, CH_2O); IR 1080—1190 cm^{-1} (triplet bands).[11]

A 15 g of the mixture containing the oxazolidine was dissolved in 300 ml of anhydrous ether and cooled at 0 °C in an ice bath. A cold solution of 100 ml ether containing 9 g (0.05 mol) of *m*-chloroperbenzoic acid was added drop-wise to the oxazolidine solution over a period of 2 h. The mixture was allowed to stand for 48 h with stirring at room temperature. The ether solution was then washed 4 times with 200 ml portions of saturated sodium hydrogencarbonate solution and water successively, and dried on anhydrous sodium sulfate. After removing ether under reduced pressure, a yellow oil was eluted with hexane–ether (7: 3) through a column of activated alumina. The yield of 2-ethyl-2-[8-(methoxycarbonyl)octyl]-4,4-dimethyloxazolidin-3-yloxyl based on methyl 10-oxododecanoate was 40%.

10 ml anhydrous ether solution containing 17.5 mg (0.46 mmol) of $LiAlH_4$ was cautiously added to 20 ml anhydrous ether solution of 144 mg (0.46 mmol) of 2-ethyl-2-[8-(methoxycarbonyl)octyl]-4,4-dimethyloxazolidin-3-yloxyl at −15——20 °C and the mixed solution was allowed to stand for 30 min at 0 °C. Then, to the solution were carefully added 5 ml of cold water and 10 ml of 5% sulfuric acid at −15——5 °C. After separation of the ether layer, the aqueous layer was extracted with two 30 ml portions of ether. The ether solutions were dried over anhydrous sodium sulfate. After removing the ether, a yellow oil was eluted with hexane–ether (1: 1) through a column of activated alumina. The nitroxide alcohol, 2-ethyl-2-(9-hydroxynonyl)-4,4-dimethyloxazolidin-3-yloxyl, was obtained in 70% yield after eluting the nitroxide ester. Found: C, 66.90; H, 11.30; N, 4.70%. Calcd for $C_{16}H_{32}O_3N$: C, 67.09; H, 11.26; N, 4.88%; mol wt 286.4.

In a 10 ml flask equipped with a magnetic stirrer were placed 100 mg (0.35 mmol) of nitroxide alcohol, 1 ml of anhydrous dioxane and 0.02 ml of anhydrous pyridine. The solution was stirred and sulfur trioxide-pyridine,[12] 55.5 mg (0.35 mmol), was portion-wise added over a period of 5—10 min at 20—25 °C. Thereafter, the mixture was allowed to stand for 24 h with stirring at 30—40 °C, then cooled, neutralized with 10% sodium hydroxide and poured into 10 ml of cold methanol. After filtration, solvents were evaporated under reduced pressure. A paste-like residue was washed many times with 2 ml portions of ether, dissolved in the ethanol of 10 ml, and filtered. Removing the ethanol, SL-SDS was obtained as the yellow solid in 25% yield. Found: C, 48.88; H, 8.07; N, 3.50%. Calcd for $C_{16}H_{31}O_6NSNa$:C, 49.46; H, 8.04; N, 3.60%; mol wt 388.4.

Sodium dodecyl sulfate (SDS), sodium decyl sulfate (SDeS), and Würster's blue perchlorate were prepared by conventional methods.

3-Carbamoyl-2,2,5,5-tetramethyl-3-pyrrolin-1-yloxy (CTMPY) was purchased from Aldrich Chemical Co.

Measurement of ESR and Conductivity. The samples for ESR measurement were carefully deoxygenated by the repetitive freeze-thaw technique and then substituted by dry nitrogen gas. ESR spectra were recorded on JEOLCO model PE-1X spectrometer equipped with a variable temperature accessory. The temperature control was checked with a copper-constantan thermocouple and found to be stable within ±0.5 °C. The magnetic field sweep was calibrated by a Würster's blue perchlorate sample.[13] The measurements of electrolytic conductivity were carried out by means of Yokogawa-Hewlett-Packard (YHP) model 4255A conductivity outfit connecting 4440B decade capacitor (YHP) at 25.0±0.1 °C.

Results and Discussion

The relations of conductivity against concentration for SL-SDS and SDS are shown in Fig. 1. The kink point in the conductivity curve indicated that the critical micelle concentration (CMC) of SL-SDS was 21.6 mmol kg^{-1} at 25.0±0.1 °C. The CMC of SL-SDS lies between those of SDS (8.3 mmol kg^{-1}) and SDeS (33.2 mmol kg^{-1}). It is found at first sight that the slope of a straight line below the CMC of SL-SDS is almost the same as that of SDS, but above CMC the slope of the line for SL-SDS is greater than that for SDS. The difference in the slope of conductivity *vs.* concentration for these surfactants above CMC may be largely dependent on the strength of hydrophobic interaction among the surfactant ions. That is, the smaller slope for SDS will be attributed to the strong hydrophobic interaction which gives rise to the rigid micelle with larger aggregation number, while the greater slope for SL-SDS will represent the weak hydrophobic interaction which produces the soft micelle with smaller aggregation number. The weak hydrophobic interaction of SL-SDS may be ascribed to hydrophilic oxazolidine ring introduced into the hydrocarbon chain.

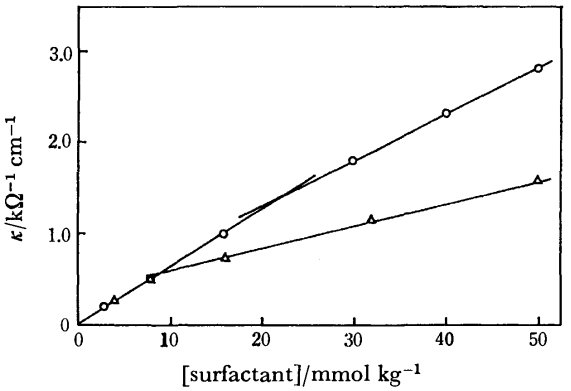

Fig. 1. Relation of specific conductivity *vs.* concentration for SL-SDS(○) and SDS(△) at 25.0±0.1 °C.

Kimizuka and Satake[14] presented the equation for estimating aggregation number from conductivity data as follows:

$$\left(\frac{\Lambda_0-\Lambda}{\Lambda_0-\Lambda_m}\right)^2 = \left\{(z_d-z_c)+(z_d+z_c)\frac{m}{m_m}\right\}\Big/(z_g+z_d), \quad (1)$$

where Λ_0 and Λ_m are the equivalent conductivities at infinite dilution and CMC, respectively. Further, z_g and z_d denote the charges of gegen and detergent ions, respectively, m, the concentration in the gram formula weight per kilogram, m_m, critical micelle concentration, and z_c, the aggregation number of micelle. For SL-SDS, Λ_0=69.4, Λ_m=63.6, $|z_g|=|z_d|=1$ and m_m=21.6 mmol kg^{-1} were obtained respectively. The aggregation number of SL-SDS micelle, $z_c\simeq 6$, was evaluated by inserting these values in Eq. 1. This value is very small as compared with the aggregation number ($z_c\simeq 60$) of SDS. The increase in CMC and the decrease in micellar aggregation number of SL-SDS compared with SDS indicate that the micelles are formed under the influence

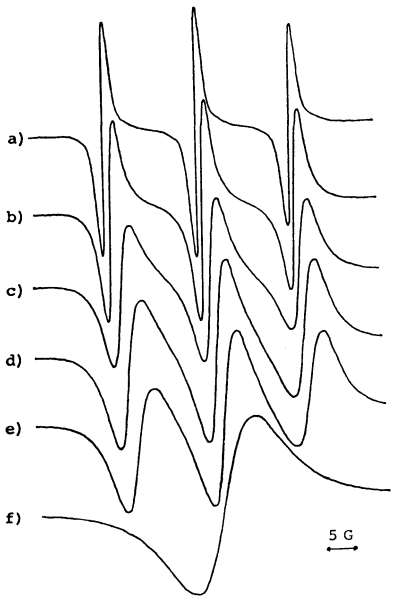

Fig. 2. ESR spectra of SL-SDS in a) 8, b) 16, c) 30, d) 40, e) 50, and f) 250 mmol kg^{-1}, respectively, at 25 °C.

of the weak hydrophobic interaction as well as the steric hindrance due to oxazolidine ring.

Figure 2 represents the ESR spectra of SL-SDS as a function of concentration at 25 °C. As the concentration of SL-SDS increases, each line width of nitroxide radical becomes broader and two side bands ($M=\pm 1$ lines, where M is the nuclear spin quantum number) shift gradually to the center of the spectrum so that the individual lines coalesce into one broad line at about 250 mmol kg^{-1}. These phenomena can be well interpreted in terms of spin exchange which results from the collision among the radical molecules.[15]

Above CMC, the ESR spectrum of micellar solution with both large aggregation number and low CMC may indicate the superposition of the three sharp lines and single broad line caused by singly dispersed and micellar surfactants, respectively.[16] However, in the case of SL-SDS the superposed monomer-micelle signal was not observed. On the other hand, the ESR spectrum of SL-SDS solution containing 1 mol kg^{-1} NaCl gave rise

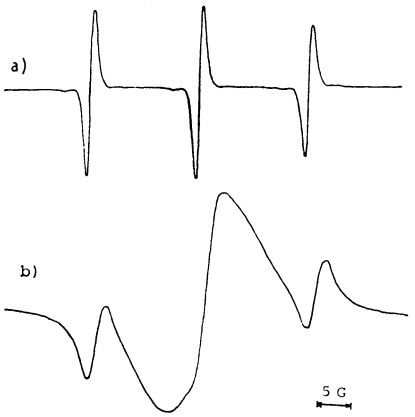

Fig. 3. ESR spectra of SL-SDS solution containing 1 mol kg^{-1} NaCl in a) 8 and b) 100 mmol kg^{-1} at 25 °C.

to the superposed signal as shown in Fig. 3. This implies that the aggregation number of the micelle increases by the added salt. Therefore, the fact that the superposed signal is not observed in SL-SDS solution may be ascribed to a small aggregation number of SL-SDS micelle in agreement with the result of the conductivity measurement. Taking account of the results mentioned above, the observed spectra in (c)—(f) of Fig. 2 are explained as the effect of spin exchange caused by the interaction between the singly dispersed surfactant ions and the surfactant ions of a soft micelle with a small aggregation number.

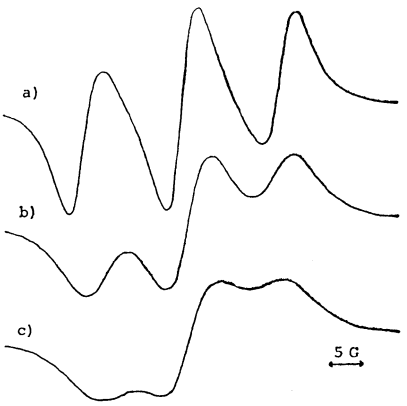

Fig. 4. ESR spectra of 50 mmol kg^{-1} SL-SDS solution at a) 25 °C, b) 55 °C, and c) 70 °C.

The ESR spectra recorded at various temperature are shown in Fig. 4. The broadening of the line width and the shift reflect mainly the effect of spin exchange due to the rise in temperature.

Generally, the analysis of line width offers the important information on the dynamic state of the molecule. In SL-SDS solution, the variation of line width as a function of temperature and concentration may be mainly dependent on spin rotation,[17] dipolar interaction, spin exchange, and monomer-micelle exchange effect.

Foremost spin rotational relaxation is caused by the interaction between the rotational magnetic moment of a paramagnetic molecule and its spin magnetic moment. In order to examine the contribution to the line width of spin rotational relaxation, the line width was plotted against a function T/η, where η is the viscosity of the medium and T is the absolute temperature. For this system, the solution of 5×10^{-5} mol kg^{-1} was used so that the other relaxation effects except spin rotation could be ignored. As shown in Fig. 5, the relation between line width ($M=+1$ line) and T/η exhibits a small contribution to line width of spin rotational relaxation. In Fig. 5, in order to inquire the effect of small spherical molecule, the line width of CTMPY is also plotted against T/η. Clearly, the relaxation due to spin rotation of the latter was more dominant as compared with the former. However, it can be said that the effect of spin rotation of SL-SDS, is slightly dependent upon radical concentration.

Secondly, when radical concentration increases, it

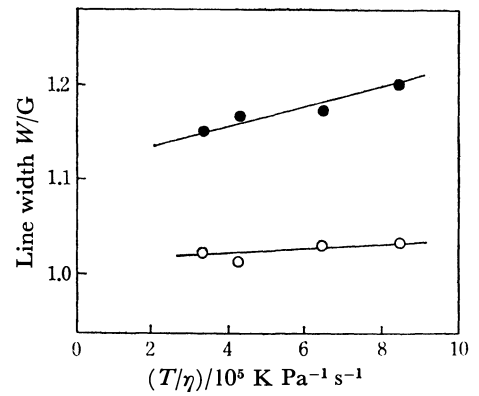

Fig. 5. Width of the $M=+1$ line *vs.* T/η for SL-SDS(○) and CTMPY(●) at each 5×10^{-5} mol kg^{-1} solution.

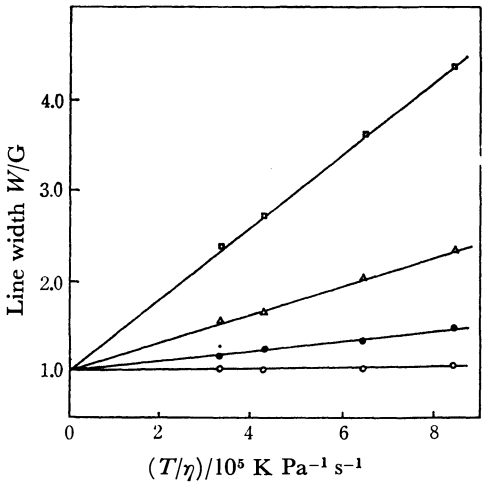

Fig. 6. Width of the $M=+1$ line *vs.* T/η for SL-SDS in 0.05 (○), 4 (●), 8 (△), and 18 mmol kg^{-1} (□), respectively.

will be necessary to consider the contribution to the line width by electron spin dipolar interaction and spin exchange.[18,19] Electron-electron intermolecular dipolar interaction should be proportional to η/T, while spin exchange interaction should be proportional to T/η. The observed line width in the concentration range from 0.05 to 20 mmol kg^{-1} showed the dependence on T/η and the intercept in each concentration coincides with each another, as shown in Fig. 6. This indicates that the relaxation by spin exchange is predominant in this concentration range. As a result, it may be concluded that the dipolar interaction would not exist in the above concentration range. Furthermore, the fourth effect, *i.e.*, monomer-micelle exchange is taken into consideration for the analysis of line width indicated below.

In Fig. 7, widths of $M=+1$ line *vs.* concentration of SL-SDS for each temperature are given, in which the line width is given by subtracting the line width ($W(0)$) due to spin rotation at 5×10^{-5} mol kg^{-1} SL-SDS from the observed line width (W). The line width ($W-W(0)$) remains almost constant below about 2 mmol kg^{-1} but increases linearly with concentration in the range of 2—20 mmol kg^{-1} due to spin exchange effect. Spin exchange effect is also dependent on temperature and the width increases with the rise in temperature. Above

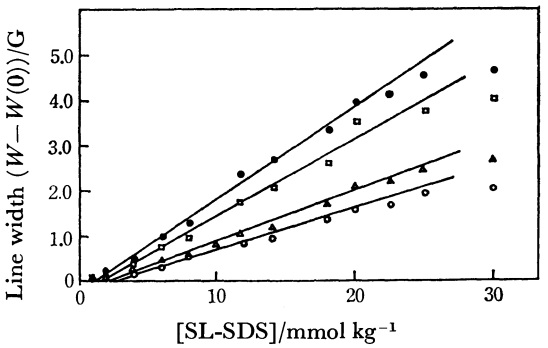

Fig. 7. Width of the $M=+1$ line *vs.* concentration of SL-SDS at 25 °C (○), 35 °C (△), 55 °C (□), and 70 °C (●).

about 20 mmol kg^{-1}, which corresponds to CMC of SL-SDS obtained from the conductivity measurement, the plot of line width *vs.* concentration deviates from a straight line. The effect of monomer-micelle exchange on the line width is not clear because of the signal distortion above 20 mmol kg^{-1} and the small aggregation number of the micelle.

In order to understand the behavior of the surfactant ions at molecular level, it is desirable and valuable to know the rate constant of spin exchange. Here, provided that spin exchange is regarded as a second order chemical reaction, a second order rate constant can be obtained from the line width.[19] Therefore, according to the method of Eastman *et al.*,[19] the rate constant was estimated and was compared with that obtained from the treatment of the diffusion controlled model.[20]

According to their theory, the second order rate constant k_2 is given as follows:

$$k_2 = \frac{3\sqrt{3}}{4}|\gamma_e|h, \qquad (2)$$

where γ_e is a magnetogyric ratio of a free electron, and h is the slope of a linear plot of the line width *vs.* concentration at a constant temperature in Fig. 7. The values of k_2 at various temperatures were obtained from Eq. 2 and are given in Table 1.

Table 1. Values of second order rate constant for spin exchange

T / K	$k_2\times10^{-9}$ / kg mol^{-1} s^{-1}	$k_2'\times10^{-9}$ / kg mol^{-1} s^{-1}
289	2.2	3.6
308	2.7	4.7
328	4.0	7.1
343	5.0	9.3

On the other hand, when the probability of spin exchange between two spins during an encounter is close to unity, the reaction limited by the rate of encounters is described as diffusion controlled.[20] Under these conditions, the second order rate constant k_2' is determined by the collision frequency among the radicals. On using the Stokes-Einstein relation for the Brownian diffusion of SL-SDS molecules in the solution, the following equation for collision frequency ν can be

obtained,

$$\nu = \frac{4kT}{3\eta} n^2, \quad (3)$$

where n is equal to the radical concentration, η, solvent viscosity, and k, Boltzmann constant. In this case the second order rate constant k_2' is given by

$$k_2' = \frac{N_A}{1000\rho} \frac{4kT}{3\eta}, \quad (4)$$

where N_A is the Avogadro number and ρ, density of the solution. The calculated values using Eq. 4 are also represented in Table 1.

In Table 1, the values of k_2 and k_2' at various temperatures are summarized. The dependence of these values on temperature is accounted as the increase of collision between spin molecules. These orders of k_2 and k_2', 10^9 kg mol^{-1} s^{-1}, are well consistent with the spin exchange rates for several free radicals in solution.[19,21] This consistency indicates that spin exchange between SL-SDS molecules in this study also can be regarded as diffusion controlled process. However, though k_2 and k_2' are of the same order, the values of the latter are approximately twice as large as those of the former. The fact that k_2 is not exactly in accord with k_2' may be ascribed to the approximation in which SL-SDS molecule is assumed as small spherical one. In the case of long chain molecule such as SL-SDS, it is a problem whether Stokes-Einstein relation can be simply applied to the system or not. It is probable that diffusion constant of SL-SDS is slightly smaller than that of the simple spherical molecule. On the other hand, regarding SL-SDS molecule as a spherical one in using Stokes-Einstein relation, diffusion constant of SL-SDS becomes more or less larger than true diffusion constant. Therefore, the difference of k_2 and k_2' may be ascribed to the incorrect estimation of diffusion constant. Considering the crudeness of the relation described above, the agreement would be satisfactorily good. In the end, it is concluded that the spin exchange for SL-SDS molecules is the same bimolecular reaction as that for small organic free radicals interpreted by diffusion controlled model.[21]

The authors wish to thank Dr. Junji Inanaga of Kyushu University for his helpful suggestions for SL-SDS preparation. We are also grateful to Dr. Sunao Tokii of Saga University for permitting us to use an ESR apparatus.

References

1) "Spin Labeling: Theory and Applications," ed by L. J. Berliner, Academic press, New York and London (1975).
2) S. Ohnishi and H. M. McConnell, *J. Am. Chem. Soc.*, **87**, 2293 (1965).
3) L. R. Dalton, P. Coffey, L. A. Dalton, B. H. Robinson, and A. D. Keith, *Phys. Rev. A*, **11**, 488 (1975).
4) D. D. Thomas, J. C. Seidel, J. S. Hyde, and J. Gergely, *Proc. Nat. Acad. Sci. U.S.A.*, **72**, 1729 (1975).
5) A. S. Waggoner, O. H. Griffith, and C. R. Christensen, *Proc. Nat. Acad. Sci. U.S.A.*, **57**, 1198 (1967).
6) S. Ohnishi, T. J. R. Cyr, and H. Fukushima, *Bull. Chem. Soc. Jpn.*, **43**, 673 (1970).
7) T. Nakagawa and H. Jizomoto, *Kolloid Z. Z. Polym.*, **250**, 594 (1972).
8) N. M. Atherton and S. J. Strach, *J. Chem. Soc., Faraday Trans. 2*, **68**, 374 (1972).
9) T. Yamaguchi, A. Yamauchi, and H. Kimizuka, *Chem. Lett.*, **1978**, 941.
10) H. Gilman and F. Schulze, *J. Am. Chem. Soc.*, **47**, 2002 (1925).
11) E. D. Bergmann, D. Lavie, and S. Pinchas, *J. Am. Chem. Soc.*, **73**, 5662 (1951).
12) H. H. Sisler and L. F. Audrieth, *Inorg. Synth.*, Vol. II, 173 (1946).
13) W. R. Knolle, Ph. D. thesis, University of Minnesota, 1970.
14) H. Kimizuka and I. Satake, *Bull. Chem. Soc. Jpn.*, **35**, 251 (1962).
15) A. Carrington and A. D. McLachlan, "Introduction to Magnetic Resonance," Harper and Row (1967), Chap. 11.
16) K. K. Fox, *Trans. Faraday Soc.*, **67**, 2802 (1971).
17) P. W. Atkins and D. Kivelson, *J. Chem. Phys.*, **44**, 169 (1966).
18) M. Aizawa, T. Komatsu, and T. Nakagawa, *Bull. Chem. Soc. Jpn.*, **52**, 980 (1979).
19) M. P. Eastman, R. G. Kooser, M. R. Das, and J. H. Freed, *J. Chem. Phys.*, **51**, 2690 (1969).
20) E. A. Moelwyn-Hughes, "The Chemical Statics and Kinetics of Solutions," Academic Press, New York and London (1971) Chap. 5.
21) T. A. Miller and R. N. Adams, *J. Am. Chem. Soc.*, **88**, 5713 (1966).

Infrared and ESR Spectra of Reaction Intermediates Formed from 1,1-Diphenylethylene Adsorbed on Oxides

Noriko TANI, Asako KAWAMORI, and Haruka YAMADA*

Faculty of Science, Kwansei Gakuin University, Nishinomiya, Hyogo 662

(Received July 26, 1979)

When 1,1-diphenylethylene (DPE) was adsorbed on porous Vycor glass (PVG) or silica–alumina, some unstable reaction intermediates, blue, green, and yellow species, were formed. The blue species produced on the silica–alumina showed a characteristic band at 1525 cm^{-1}, assigned to the shifted C=C stretching band, which disappeared in the green and yellow samples; it also showed an ESR signal. This indicates that the unstable blue species is probably a cation radical $\left[\begin{matrix}\Phi\\ \Phi\end{matrix}\!\!>\!C\!-\!CH_2\right]^+$. The infrared spectra of the green and yellow species on the silica–alumina showed new bands, ascribed to the $-CH_3$ and $-CH_2-$ vibrations, which were in good agreement with the resonance Raman bands of the carbonium ions formed on the PVG. The green and yellow intermediates, therefore, should be two kinds of carbonium ions. The structures, formation mechanisms, and surface coverages of these intermediates are discussed.

We first applied the resonance Raman technique to the study of a small amount of surface species; the resonance Raman spectra could be successfully obtained for halogens adsorbed on silicas,[1] reaction intermediates on porous Vycor glass,[2] dye adsorbed on a working ZnO electrode[3] and pyridines adsorbed on various oxides.[4]

When 1,1-diphenylethylene (DPE) was adsorbed on porous Vycor glass (PVG) treated at 500 °C, two carbonium ions, reaction intermediates, were detected by means of the resonance Raman spectra.[2] In the present work, the infrared and ESR spectra of the reaction intermediates formed from DPE adsorbed on oxides have been studied in order to obtain more precise information about the vibrational spectra of the reaction intermediates and also about the adsorption mechanism. As adsorbents PVG treated at a higher temperature (800 °C) and silica–alumina were used in this study; they had more Lewis or Brönsted acid sites than the PVG treated at 500 °C.

On the other hand, reaction intermediates produced by the adsorption of DPE on silica–alumina were studied by measuring the ESR and electronic spectra.[5–10] The structures of the intermediates, however, are still in question. Some radical species were really found on silica–alumina by observing the ESR signal. However, it is uncertain whether the radical is produced directly from the DPE adsorbed or whether it is concerned with any impurity involved.

Experimental

The porous Vycor glass used was obtained from Corning Glass Works, No. 7930; 1 mm thick transparent sheet, containing 96.3% SiO_2 and 2.9% B_2O_3. It was cut into 20×10 mm sections. Then it was pretreated in the same way as that for the resonance Raman measurements;[2] it was heated at 500 °C in 500 Torr** oxygen for 4 h and then degassed at 800 °C for 10 h. The surface area was 130 m^2/g,[11] compared with 170 m^2/g[1] for the PVG treated at 500 °C.

The silica–alumina was obtained from the Catalysts and Chemicals Ind. Co.; it was 13.8% Al_2O_3 and 85.9% SiO_2 and consisted of particles 60 μm in diameter. It was pressed into disks (10 or 20 mm in diameter) whose optical thickness was about 10 mg/cm^2. This was heated at 500 °C in 500 Torr** oxygen and then degassed at 400 °C (or 500 °C) for 3 h.

The 1,1-diphenylethylene used was obtained from Nakarai Chemicals (99.8%) and also from Wako Chemicals and Tokyo Chemicals (99%). This DPE was used after having been degassed by alternate freezing and thawing. The infrared spectra of these three DPE's did not show any difference from one another, and the 99% DPE did not show any appreciable OH stretching band.

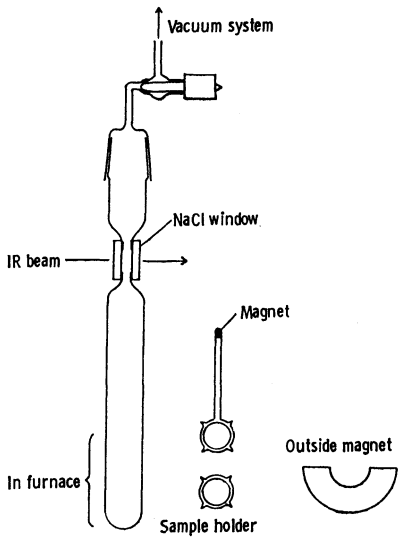

Fig. 1. Infrared absorption cell made of quartz. Sample was fixed in the holder with platinum wire and placed into the cell tube.

An infrared cell made of quartz was specially designed, as is shown in Fig. 1; it consisted of a tube and a sample holder. There were NaCl windows where infrared light passed through. The distance between these two plates was only 5 mm, so that atmospheric vapors could hardly interfere at all with the spectra obtained. A small magnet was enclosed in the tip of the holder, so a sample fixed in the holder could be moved up to the window for the infrared measurement. Greaseless stopcocks and a connector were used.

The infrared spectra were measured with a JASCO DS-402

** 1 Torr ≃ 133.3 Pa.

G infrared spectrophotometer and a modified JASCO DS-3 0 1 infrared spectrophotometer especially designed for the use with small samples.[12] The ESR measurements were carried out with a JEOL-JES 3B-type X-band spectrometer using 100 kHz modulation.

Results and Discussion

PVG. When the vapor of DPE was adsorbed onto PVG, some unstable intermediates were produced. First, a blue species was found, and then it gradually changed to a green species and then to a yellow species. Finally, the sample became reddish brown. The blue, green, and yellow species, therefore, might be reaction intermediates. The color development observed was the same for both DPE's; 99.8% and 99%. Since the PVG (1 mm) absorbed infrared light strongly in the region below 2000 cm^{-1}, only the >2000 cm^{-1} region could be used for the measurements of the reaction intermediates. When a disk (*ca.* 0.1 mm thick) made of PVG powder was used instead of 1 mm PVG, it was fairly transparent in the <2000 cm^{-1} region. However, no band assigned to the unstable species adsorbed on that disk could be detected, so the number of surface species adsorbed on it must be quite small.

The infrared spectra for the blue, green, and yellow samples are shown in Fig. 2. (a) shows the spectrum of PVG pretreated at 800 °C as a background. The two bands at 3747 and 3703 cm^{-1} are assigned to the free surface OH groups.[13] The spectra for the colored samples are shown in (b), (c), and (d). For comparison, the liquid spectrum of DPE is also given in Fig. 2.

A new OH band at 3610 cm^{-1} appeared in these (b), (c), and (d) spectra. This is a shifted OH band due to the interaction of surface OH groups with the π-electrons of DPE. Further, these spectra showed new bands at 2966 and 2926 cm^{-1}; these bands increased in intensity in the order of (b), (c), and (d). An additional band at 2865 cm^{-1} appeared in the (c) and (d) spectra. These three new bands can be assigned to the CH stretching vibrations of $-CH_3$ and $-CH_2-$ groups. On the other hand, the olefinic band at 3083 cm^{-1} decreased. That is to say, the bond order of the olefinic C=C decreased upon adsorption, while new surface species with aliphatic $-CH_3$ and $-CH_2-$ groups were formed on the PVG. In Table 1 the absorption peak frequencies observed for the DPE adsorbed on PVG

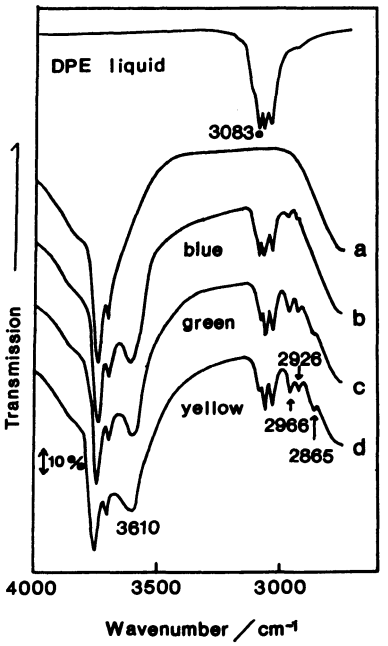

Fig. 2. Infrared spectra of DPE adsorbed on PVG pretreated at 800 °C for 10 h; (a) background, (b) blue, (c) green, and (d) yellow samples.

are listed, with the relative intensities in parentheses. The amounts of the intermediates produced on the PVG are rather small, so only the bands in the 3 μm region can be detected by using the 1 mm thick PVG. The blue species is probably a kind of radical, because the ESR signal was observed for the blue sample.[2]

Silica–Alumina. When the 99.8% DPE was adsorbed on the silica–alumina pretreated at 400 °C for 3 h, the sample appeared blue or blue-green immediately and then changed to a deeper color as the amount of adsorbed species increased. After the sample had been kept at 80 °C for 20 h, it turned green and then to yellow (after several days), and finally it became brown. Much more reaction intermediates were produced on the silica–alumina than on the PVG. When the 99.8% DPE was adsorbed on the silica–alumina pretreated at 500 °C for 3 h, the sample showed a rather green color at first, while when the 99% DPE was used instead of the 99.8% DPE on the silica–alumina pretreated at 500 °C, the sample appeared rather blue at first. All the blue samples gradually changed in

Table 1. Peak frequencies of absorption bands of DPE adsorbed on PVG (cm^{-1})

Sample adsorbed			Liquid	Assignment
Blue	Green	Yellow		
≈3610	≈3610	≈3610		OH···π
			3100 sh	
3083 (78)	3083 (53)	3086 (48)	3083 (101)	$=CH_2$ ν_{CH}
3062 (100)	3063 (100)	3064 (100)	3061 (100)	Φ ν_{CH}
3028 (82)	3029 (82)	3028 (77)	3029 (90)	Φ ν_{CH}
2967[i] (13)	2965[i] (63)	2966[i] (86)	2932 (4)	$-CH_3$ ν_{CH}
2927[i] (6)	2927[i] (15)	2926[i] (26)		$-CH_2-$ ν_{CH}
	2862[i] (26)	2865[i] (33)		$-CH_3$, $-CH_2-$ ν_{CH}

i) Band ascribed to an intermediate or a product.

color in the order of green, yellow, and brown when they were kept at room or a higher temperature. Thus, the blue, green, and yellow species formed on the silica-alumina must be reaction intermediates, though there was a little difference in the color development of the samples. Dollish and Hall[10] reported that lemon yellow appeared on the silica-alumina pretreated at 540 °C for 24 h; they pretreated the silica-alumina at a higher

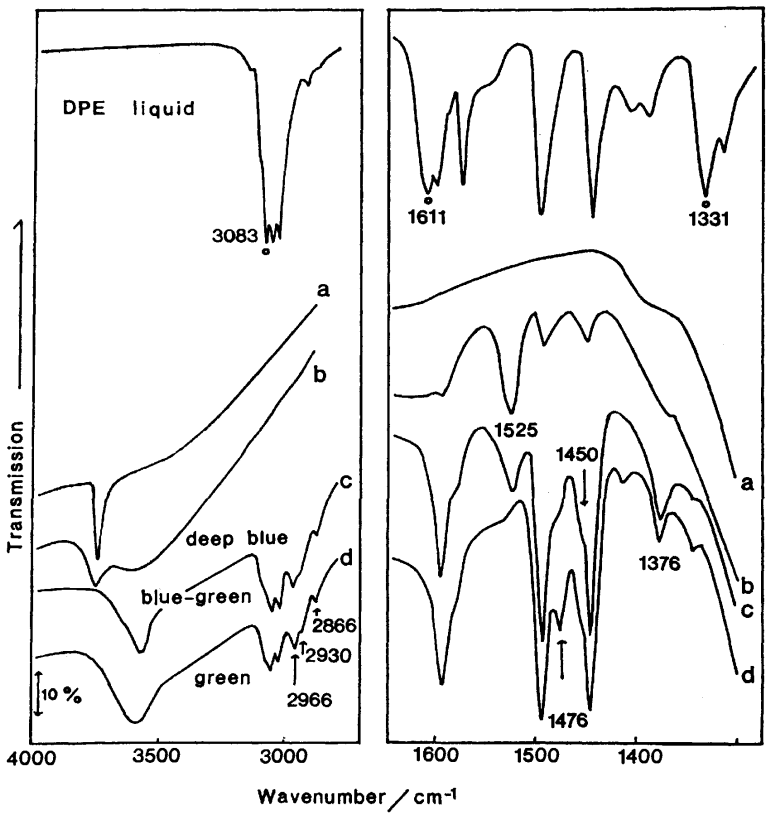

Fig. 3. Infrared spectra of DPE adsorbed on silica-alumina pretreated at 500 °C for 3 h; (a) background, (b) deep blue, (c) blue-green, and (d) green samples.

Table 2. Peak frequencies of absorption bands of DPE adsorbed on silica-alumina (cm^{-1})

Sample adsorbed				Liquid	Assignment
Deep blue	Blue-green	Green	Yellow		
	≈3570	≈3580			OH···π
			3000—3600		
				3100 sh	
	3082 (82)	3080 sh		3083 (101)	$=CH_2$ ν_{CH}
≈3058	3060 (100)	3058 (100)		3061 (100)	Φ ν_{CH}
≈3035	3025 (100)	3026 (98)		3029 (90)	Φ ν_{CH}
≈2983[i]	2963[i] (83)	2966[i] (88)	2963[i]	2932 (4)	$-CH_3$ ν_{CH}
	2930[i] sh	2930[i] sh	2933[i]		$-CH_2-$ ν_{CH}
	2873[i] (27)	2866[i] (38)	2870[i]		$-CH_3$, $-CH_2-$ ν_{CH}
				1611 (47)	$C=CH_2$ ν_{CC}
1595	1594 (54)	1596 (56)	1596 (30)	1602 (38)	Φ
	1577 sh	1580 sh	1580 sh	1575 (34)	Φ
1525[i] (100)	1525[i] (23)	1540[i] sh			radical ν_{CC}
1492 (32)	1492 (116)	1494 (117)	1494 (117)	1494 (110)	Φ
1476[i] sh	1480[i] sh	1476[i] (14)	1476[i] (17)		$-CH_2-$ δ_{CH}
1450[i] (32)	1450[i] sh	1450[i] sh	1450[i] sh		$-CH_3$ δ_{CH}
	1444 (100)	1446 (100)	1445 (100)	1445 (100)	Φ
		1414[i] (3)			
1366[i] (8)	1376[i] (26)	1376[i] (14)	1374[i] (13)		$-CH_3$ δ_{CH}
	1343[i] (4)	1344[i] (7)			
				1331 (49)	$=CH_2$ δ_{CH}

i) Band ascribed to an intermediate or a product.

temperature and for a longer period than in the present work.

Figure 3 shows the observed spectra for the colored samples on the silica–alumina pretreated at 500 °C. The spectrum of the yellow sample was similar to (d). The spectra observed for the adsorbed species differed from that of liquid DPE as follows: Three new bands appeared at 2966, 2930, and 2866 cm^{-1}; they were assigned to the aliphatic CH stretching bands. On the other hand, the olefinic CH band of DPE at 3083 cm^{-1} decreased in intensity in the 3 μm region. In the region below 1700 cm^{-1} the blue sample showed a characteristic new band at 1525 cm^{-1} (b). This band was also found for the blue-green sample (c), but it disappeared for the green sample (d). The (c) and (d) spectra showed distinct bands at 1476 and 1376 cm^{-1} which could be assigned to the aliphatic CH bending vibrations. On the other hand, the 1611 and 1331 cm^{-1} bands of DPE almost disappeared for the adsorbed species. The 1611 and 1331 cm^{-1} bands can be assigned to the olefinic C=C stretching and CH deformation vibrations respectively. Since these bands disappear in (b), (c), and (d), it follows that the double bond might vanish for the adsorbed species. In Table 2 the absorption peak frequencies observed for the DPE adsorbed on the silica–alumina are listed, with the relative intensities in parentheses.

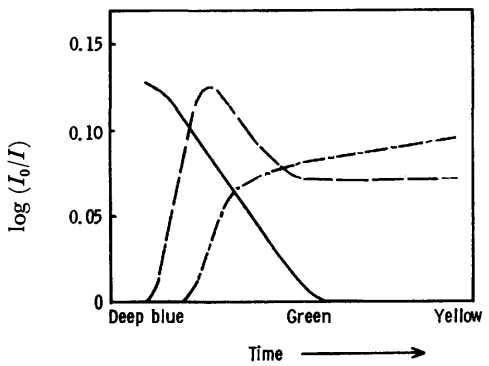

Fig. 4. Intensity changes accompanied with color development; (——) 1525 cm^{-1} band ascribed to radical species, (-•••-) 1476 cm^{-1} band assigned to $-CH_2-$ bending vibration and (----) 1376 cm^{-1} band assigned to $-CH_3$ bending vibration.

The relationship between the color development of the sample and the infrared band intensities can be seen in Fig. 4. The abscissa shows the color change with the time after the DPE has been adsorbed, while the ordinate shows the relative peak height of each band. As the blue species decreased, the 1525 cm^{-1} band rapidly dropped, while the 1476 cm^{-1} band increased in intensity. The 1476 cm^{-1} band could be assigned to the $-CH_2-$ deformation, and the 1376 cm^{-1} band, to the $-CH_3$ deformation. These two bands (1476 and 1376 cm^{-1}) must be ascribed to the unstable reaction intermediates. The present infrared spectra observed for the blue-green, green, and yellow samples are in good harmony with the results of the resonance Raman spectra for DPE adsorbed on the PVG. The reaction intermediates, therefore, must be the carbonium ions;[2]

where A represents the adsorbent.

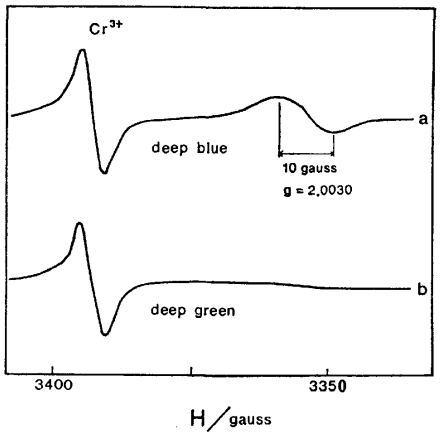

Fig. 5. ESR spectra of DPE adsorbed on silica–alumina pretreated at 500 °C for 3 h (9 GHz); (a) deep blue and (b) deep green samples.

In order to ascertain whether the reaction intermediates were paramagnetic or not, we measured the ESR spectra for these samples. Figure 5 shows the ESR spectra obtained for the blue and green samples with the signal belonging to the Cr^{3+} ion (g=1.9800) doped in MgO added as a standard material. The blue sample had a broad signal centered at g=2.0030, whose half-width was about 10 G,*** while the green sample did not show any ESR signal. Consequently, it is found that the blue sample certainly included some radical. The ESR signal observed for the blue sample was also observed for the deep blue or blue-green samples, but not for the green sample. This ESR signal coincides well with that observed by Leftin *et al.* for the blue sample on silica–alumina.[7]

Since the infrared 1525 cm^{-1} band characteristic of the blue species was observed, the 1525 cm^{-1} band must be ascribed to a radical which showed the ESR signal. For this radical the following structure must be considered;

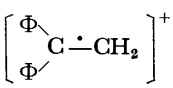

which is consistent with the results of the observed infrared and ESR spectra. When the DPE changes to this radical, the C=C band has to shift to the lower-frequency side. The band observed at 1525 cm^{-1} is lower than the 1611 cm^{-1} band by 90 cm^{-1}; this shift corresponds well to this change:

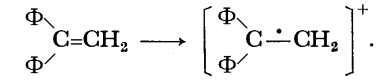

It is the first time that the vibrational spectrum of this unstable radical has been detected.

Now we have actually found these three reaction intermediates formed on the silica–alumina, a cation

*** 1 G = 10^{-4} T.

radical, and two carbonium ions. We shall now proceed to consider the formation mechanism of these reaction intermediates. When DPE was adsorbed on the Lewis acid site, the cation radical could be formed. If the proton was accepted by the DPE on the Brönsted acid site, the carbonium ion, $\Phi\diagdown\atop\Phi\diagup$C$^+$–CH$_3$, could be formed. The cation radical combined with the Lewis acid site changes to the carbonium ion, $\Phi\diagdown\atop\Phi\diagup$C$^+$–CH$_2$–A. More

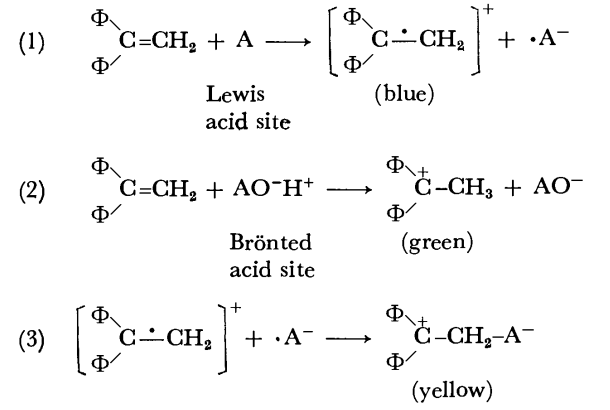

blue species were formed when the silica-alumina was pretreated at a lower temperature or for a shorter period. Therefore, it seems likely that the surface OH groups play an important role in the formation of the blue species. However, it is not clear whether or not this role of the OH groups is catalytic. For the cation radical, a modified C=C stretching vibration was observed, while for the carbonium ions, $-CH_3$ and $-CH_2-$ stretching and deformation vibrations were observed. The CH stretching bands for the carbonium ions are in good agreement with those of the resonance Raman spectra of the carbonium ions formed on the PVG.

Now we would like to consider the coverage of the intermediates. When DPE was adsorbed on PVG or silica-alumina, the reaction intermediates with physically adsorbed DPE were formed. The CH stretching vibration of the phenyl group at 3061 cm^{-1} is supposed to be hardly changed when the DPE is changed to the three intermediates described above or a physically adsorbed species. Therefore, if the absorption intensities of the 3061 cm^{-1} bands for all the adsorbed species are the same as that of the liquid DPE, the total amount of the adsorbed species can be estimated from the observed intensities; 0.05 molecule/nm^2 for the PVG treated at 800 °C and $\approx$1.4 molecule/nm^2 for the silica-alumina treated at 500 °C. The intensity decrease of the olefinic band at 3083 cm^{-1} may be proportional to the amount of the intermediates. For the DPE on the PVG, this decrease was $\approx$10% for the blue sample, $\approx$20% for the blue-green sample, and 30—40% for the green or yellow sample. The intensity of the 3061 cm^{-1} band was almost constant during this color changing of the sample. For the DPE on the silica-alumina, the intensity decrease of the 3083 cm^{-1} band was found to be $\approx$70% for all the samples (blue to yellow). Therefore, the coverage of the intermediates and products should be 0.005—0.02 molecule/nm^2 on the PVG and $\approx$1 molecule/nm^2 on the silica-alumina in Table 3, judging from the surface areas of 130 m^2/g on the PVG and $\approx$500 m^2/g on the silica-alumina.[14]

Table 3. Coverage of surface intermediates formed from DPE

(molecules/nm^2)

Adsorbent	θ (total)	θ (intermediates and products)
PVG(800 °C)	0.05	0.005—0.02
Silica-alumina (500 °C)	$\approx$1.4	$\approx$1

Table 4. Numbers of Lewis and Brönsted acid sites obtained from the adsorbed pyridine

(molecules/nm^2)

Adsorbent	Lewis acid site	Brönsted acid site
PVG (800 °C)	0.05	Not observed
Silica-alumina (500 °C)	0.2	0.04

Let us now compare these coverages with the numbers of Lewis and Brönsted acid sites[15] which could be found from the experiments on adsorbed pyridines (Table 4). The numbers of Lewis acid sites were estimated by comparing the intensities of the 1629 cm^{-1} (on the PVG) and 1452 cm^{-1} (on the silica-alumina) bands with those of the 1610 cm^{-1} (ν_{8a}) and 1450 cm^{-1} (ν_{19a}) bands[16] of pyridine respectively in the (pyridine)$_2$–$ZnCl_2$ complex. Also, the number of Brönsted acid sites on the silica-alumina was obtained by comparing the intensity of the 1545 cm^{-1} band of adsorbed pyridine with that of the 1528 cm^{-1} (ν_{19b}) band[16] of pyridine in the pyridine-HCl complex. The coverage of the intermediates on the PVG is comparable to the number of Lewis acid sites, while the coverage on the silica-alumina seems much more than that of the Lewis or Brönsted acid sites.

References

1) T. Nagasao and H. Yamada, *J. Raman Spectrosc.*, **3**, 153 (1975).
2) Y. Yamamoto and H. Yamada, *J. Chem. Soc., Faraday Trans. 1*, **74**, 1562 (1978).
3) H. Yamada, T. Amamiya, and H. Tsubomura, *Chem. Phys. Lett.*, **56**, 591 (1978).
4) H. Yamada and Y. Yamamoto, *J. Chem. Soc., Faraday Trans. 1*, **75**, 1215 (1979).
5) H. P. Leftin and W. K. Hall, *J. Phys. Chem.*, **64**, 382 (1960).
6) H. P. Leftin, *J. Phys. Chem.*, **64**, 1714 (1960).
7) H. P. Leftin, M. C. Hobson, and J. S. Leigh, *J. Phys. Chem.*, **66**, 1214 (1962).
8) J. J. Rooney and R. C. Pink, *Trans. Faraday Soc.*, **58**, 1632 (1962).
9) J. J. Rooney and B. J. Hathaway, *J. Catal.*, **3**, 447 (1964).
10) F. R. Dollish and W. K. Hall, *J. Phys. Chem.*, **69**, 4402 (1965).
11) M. J. D. Low and N. Ramasubramanian, *J. Phys. Chem.*, **71**, 730 (1967).

12) H. Yamada and M. Kawamori, *Spectrochim. Acta, Part A*, **27**, 2425 (1971).
13) M. J. D. Low and N. Ramasubramanian, *J. Phys. Chem.*, **70**, 2740 (1966).
14) Technical Data, Catalysts and Chemicals Ind. Co., Ltd., 1978.
15) N. Tani, Master Thesis, Kwansei Gakuin University, Nishinomiya, 1979; N. Tani, Y. Yamamoto, and H. Yamada, The ACS/CSJ Chemical Congress, Hawaii, April 1979, Colloid and Surface Chemistry, Abstr. No. 182.
16) N. S. Gill, R. H. Nuttall, D. E. Scaife, and D. W. A. Sharp, *J. Inorg. Nucl. Chem.*, **18**, 79 (1961); E. P. Parry, *J. Catal.*, **2**, 371 (1963); M. R. Basila, T. R. Kantner, and K. H. Rhee, *J. Phys. Chem.*, **68**, 3197 (1964).

Structures and Properties of 5-Substituted Cytosines. II.** The Crystal Structure of 5-Methylcytosine Hemihydrate

Akio TAKENAKA,* Masuhiro KATO, and Yoshio SASADA*

Laboratory of Chemistry for Natural Products, Tokyo Institute of Technology, Nagatsuta, Midori-ku, Yokohama 227

(Received July 30, 1979)

The crystal structure of 5-methylcytosine hemihydrate has been determined by an X-ray analysis to investigate the substitution effect on the cytosine moiety. The space group is C2/c, with unit-cell dimensions $a=17.832(4)$, $b=8.261(2)$, $c=10.641(3)$ Å, $\beta=125.12(1)°$, and $Z=8$. The hydrogen bonding scheme is quite different from that of cytosine, its monohydrate, 5-bromocytosine, and its dioxane hemi-solvate. This is ascribed to the packing effect of the methyl group. A comparison with the cytosine structure indicates some deviations in bond lengths and angles, which are due to the steric and electronic effects caused by methylation. The similar values of the C(2)–N(3)–C(4) angle in cytosine and 5-methylcytosine can be related to a resemblance of their pK_a values.

In the course of the studies on the protein: nucleic acid interaction, we have found two different interaction modes of acidic amino acids with cytosine and 5-bromocytosine.[1-4] To interpret this in terms of the molecular structure of the component, crystal structures of 5-substituted cytosines have been determined by X-ray analyses.

Previously it was revealed that the geometrical change of cytosine upon bromination at C(5) is related to its physico-chemical property in solution.[5] The present paper deals with the crystal structure of 5-methylcytosine. Since its substituent has almost the same van der Waals radius[6] as bromine but electronically opposite effect, the comparison of their structures will give some additional supports to the view mentioned in the previous paper.[5]

Experimental and Structure Determination

5-Methylcytosine was purchased from Aldrich Chemical Co. Crystals were obtained from an aqueous solution. Density was measured by flotation in a mixture of cyclohexane and carbon tetrachloride. Weissenberg photographs showed the systematic absences, hkl for $h+k=2n+1$ and $h0l$ for $l=2n+1$, indicating the space group to be C2/c or Cc. A crystal $0.3\times0.3\times0.4$ mm was used for data collection on a Rigaku four-circle diffractometer with graphite-monochromated Mo $K\alpha$ radiation ($\lambda=0.71069$ Å). The unit-cell dimensions were determined with 24 high angle reflexions. Intensities were measured in the ω-2θ scan mode with a scan width of 1.25° (in ω) plus α_1-α_2 divergence and a scan speed of 4° (in 2θ) min^{-1}. Four reference reflexions showed no significant intensity deterioration throughout the data collection. The intensities were corrected for Lorentz and polarization factors but not for absorption effects. Of 850 independent reflexions in the range $2<2\theta<55°$, 93 reflexions with F_o less than $3\sigma_P(F_o)$ were considered zero reflexions, where $\sigma_P(F_o)$ is evaluated by counting statistics; the observational threshold value, F_{llm}, was 3.70. The standard deviations were estimated by the equation of $\sigma^2(F_o)=\sigma_P^2(F_o)+qF_o^2$, where q, 3×10^{-5}, was derived from the variations of the monitored reflexions.[7] Crystal data are summarized in Table 1.

Normalized structure factor statistics strongly indicated the space group to be centrosymmetric, C2/c. The structure was solved by the direct method and its parameters were refined by the full-matrix least-squares method. All the hydrogen atoms, found on a difference map, were included. The quantity minimized was $\sum w(|F_o|-|F_c|)^2$, with $w=1/\sigma^2(F_o)$. The zero reflexions were included in least-squares calculation by assuming $F_o=F_{llm}$ and $w=w(F_{llm})$; those for which $|F_c|<F_{llm}$ were omitted. The final R was 0.066 ($R=0.056$ for $F_o>3\sigma(F_o)$); the maximum shift of parameters in the last cycle was 0.02σ for C, N, and O, and 0.18σ for H atoms. Atomic scattering factors used were taken from International Tables for X-ray Crystallography.[8] Atomic parameters are listed in Table 2, and observed and calculated structure factors in Table 3.[9]

Table 1. Crystal data

5-Methylcytosine hemihydrate	
$C_5H_7N_3O\cdot1/2H_2O$	
Space group: C2/c	
$a=17.832(4)$ Å	$Z=8$
$b=8.261(2)$	$D_x=1.39$ g cm^{-3}
$c=10.641(3)$	$D_m=1.39$
$\beta=125.12(1)°$	
$U=1282.1(6)$ Å^3	

Results and Discussion

Crystal Structure. Figure 1 shows the crystal structure. Hydrogen bond distances and angles are given in Table 4 (as for atomic numbering, see Fig. 2). Two N(4)–H(4A)···N(3) hydrogen bonds between molecules related by the inversion at (1/4, 1/4, 1/2) constitute a cytosine dimer. This pattern is similar to the dimer component of the cytosine ribbon found in 5-bromocytosine: *N*-tosyl-L-glutamic acid and 5-bromocytosine: *N*-phthaloyl-DL-glutamic acid complexes.[1,2] The carbonyl oxygen, O(2), is an acceptor of hydrogen bond from the remaining N(4)–H(4B) group of the adjacent molecule to form a layer of the dimers. The water molecule, the oxygen, O(W), of which is located on the two-fold axis, links the cytosine layers with two O(W)–H(W)···O(2) and two O(W)···H(1)–N(1) hydrogen bonds in tetrahedral disposition.

The hydrogen bonding scheme found in the present crystal is quite different from that of cytosine,[10] its monohydrate,[11] 5-bromocytosine,[5] and its hemi-dioxane solvate,[12] in which cytosines form a ribbon by the two hydrogen bonds, N(4)–H···O(2) and N(3)···H–N(1), along the 2_1 axis. This difference is ascribed to the

** Part I of this series is Ref. 5.

TABLE 2. FINAL POSITIONAL AND THERMAL PARAMETERS

Standard deviations are given in parentheses. The anisotropic thermal factor has the form $\exp[-(\beta_{11}h^2+\beta_{22}k^2+\beta_{33}l^2+\beta_{12}hk+\beta_{13}hl+\beta_{23}kl)]$.

Atom	x*	y*	z*	β_{11}**	β_{22}**	β_{33}**	β_{12}**	β_{13}**	β_{23}**
N(1)	35236(17)	12576(35)	44937(25)	295(11)	1668(44)	580(26)	186(34)	263(28)	335(52)
C(2)	36833(18)	16817(36)	34169(29)	259(11)	1358(41)	647(29)	82(34)	320(30)	−92(54)
N(3)	29618(16)	19130(33)	19417(25)	278(10)	1583(40)	683(27)	56(31)	439(29)	222(50)
C(4)	21085(17)	17728(32)	15676(29)	267(11)	1029(34)	706(29)	49(30)	401(30)	−63(49)
C(5)	19115(18)	13174(36)	26539(30)	304(11)	1279(39)	715(29)	22(35)	517(32)	85(55)
C(6)	26538(20)	10495(37)	40990(30)	361(13)	1373(42)	710(30)	165(36)	618(34)	306(56)
O(2)	44933(14)	18279(34)	38273(26)	259(9)	2121(44)	978(27)	−60(31)	−77(26)	−264(55)
N(4)	14207(17)	20461(38)	1015(28)	265(11)	2032(52)	688(28)	134(37)	376(30)	495(59)
C(7)	9478(22)	10805(51)	22025(41)	342(14)	1941(61)	1234(43)	81(47)	787(42)	461(87)
O(W)	50000	2345(44)	75000	315(13)	1575(52)	864(37)	0	442(38)	0

Atom	x**	y**	z**	B(/Å^2)
H(1)	4033(36)	1019(61)	5485(60)	2.93(0.93)
H(4A)	1567(27)	2308(48)	−459(48)	1.30(0.67)
H(4B)	855(33)	2149(51)	−204(52)	1.99(0.76)
H(6)	2613(30)	669(51)	4925(51)	1.79(0.74)
H(7A)	947(33)	780(58)	3117(56)	2.72(0.90)
H(7B)	582(41)	2088(72)	1688(68)	4.02(1.18)
H(7C)	669(39)	226(68)	1493(66)	3.35(1.03)
H(W)	5204(37)	−323(62)	7163(62)	3.09(1.04)

*$\times 10^5$, **$\times 10^4$.

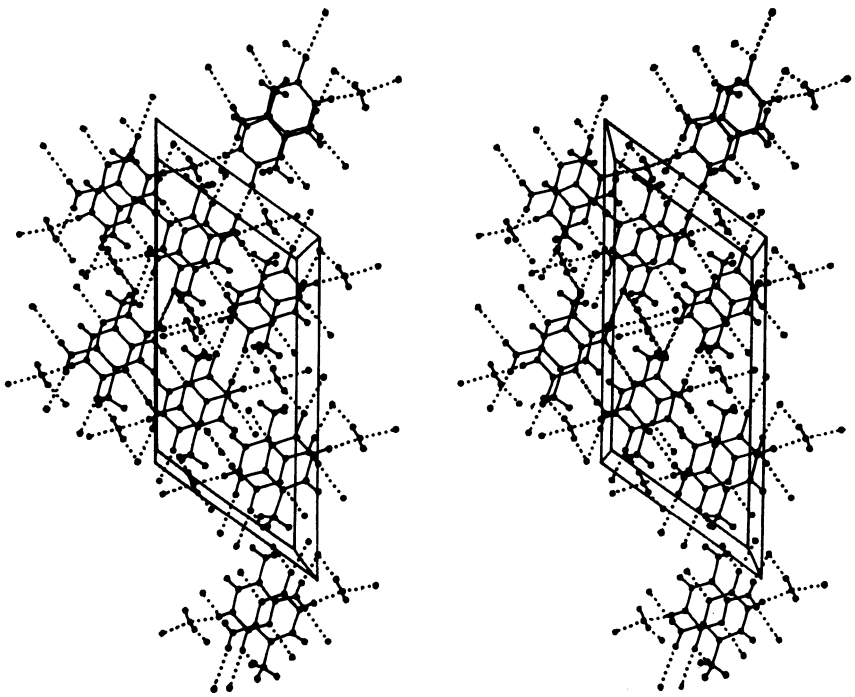

Fig. 1. Stereoscopic diagram showing the molecular packing and the hydrogen-bond network. The origin is at the upper right rear corner, *b* points to the viewer, *a* downward, and *c* leftward.

steric effect of methyl group at C(5) atom. A hypothetical model of 5-methylcytosine crystal was constructed using the parameters of 5-bromocytosine crystal by an interactive computer graphics,[13] and intermolecular atomic distances were calculated by rotating the methyl group around the C(5)–C(7) bond. Such an examination showed that the hydrogen atoms of the methyl group could be put considerably far from the surrounding atoms by an appropriate rotation, owing to the shorter C–CH_3 bond distance than C–Br bond, though van der Waals radii of bromine and methyl group are nearly the same.[6] In this crystal, therefore,

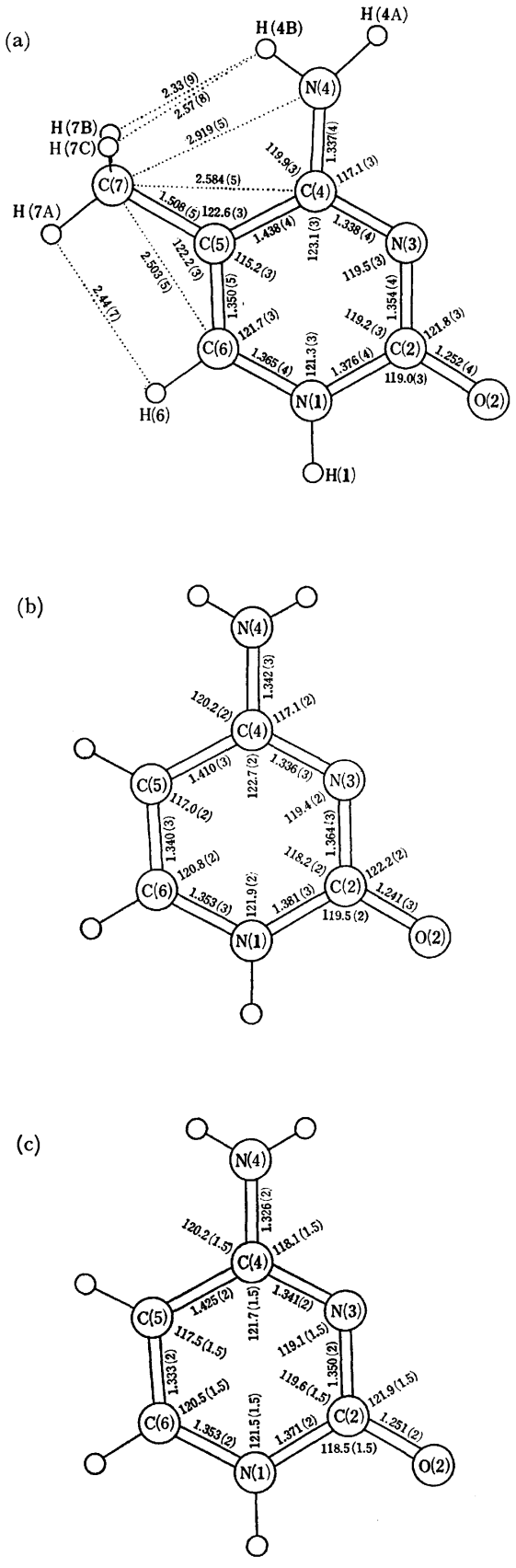

Fig. 2. Bond lengths (l/Å) and angles (ϕ/°), and their standard deviations in parentheses. (a) The present work, 5-methylcytosine. Some non-bonded distances (l/Å) from the methyl group are also shown. (b) Cytosine. (c) Cytosine monohydrate.

TABLE 4. HYDROGEN BOND DISTANCES AND ANGLES
Standard deviations are given in parentheses.

Distances (l/Å)	
N(4)···N(3)[a]	3.072(4)
H(4A)···N(3)[a]	2.27(4)
N(1)···O(W)	2.861(3)
H(1)···O(W)	1.93(5)
N(4)···O(2)[b]	3.026(4)
H(4B)···O(2)[b]	2.19(4)
O(2)···O(W)[c]	2.680(3)
O(2)···H(W)[c]	1.90(5)

Angles (ϕ/°)	
N(4)–H(4A)···N(3)[a]	177(4)
N(4)–H(4B)···O(2)[b]	161(5)
C(4)–N(4)···N(3)[a]	114.3(2)
C(4)–N(4)···O(2)[b]	128.2(2)
N(3)[a]···N(4)···O(2)[b]	112.0(1)
C(2)–N(3)···N(4)[a]	111.8(2)
C(2)–N(3)···H(4A)[a]	111(1)
C(4)–N(3)···N(4)[a]	128.6(2)
C(4)–N(3)···H(4A)[a]	129(1)
C(2)–O(2)···N(4)[d]	166.3(2)
C(2)–O(2)···H(4B)[d]	161(1)
C(2)–O(2)···O(W)[c]	115.2(2)
C(2)–O(2)···H(W)[c]	113(2)
N(4)[d]···O(2)···O(W)[c]	77.9(1)
H(4B)[d]···O(2)···H(W)[c]	85(2)
N(1)–H(1)···O(W)	172(5)
C(2)–N(1)···O(W)	120.5(2)
C(6)–N(1)···O(W)	117.3(2)
O(W)–H(W)···O(2)[c]	171(6)
N(1)···O(W)···N(1)[e]	145.6(1)
N(1)···O(W)···O(2)[c]	88.3(1)
N(1)···O(W)···O(2)[f]	113.9(1)
O(2)[c]···O(W)···O(2)[f]	101.1(1)
H(1)···O(W)–H(W)	92(5)
H(1)···O(W)–H(W)[e]	111(4)
H(1)···O(W)···H(1)[e]	141(2)

Symmetry codes
(a) $1/2-x, 1/2-y, -z$
(b) $-1/2+x, 1/2-y, -1/2+z$
(c) $1-x, -y, 1-z$
(d) $1/2+x, 1/2-y, 1/2+z$
(e) $1-x, y, 3/2-z$
(f) $x, -y, 1/2+z$

the packing of 5-methylcytosine molecules is thought to be looser than that of 5-bromocytosine.† Such a hypothetical loose packing of 5-methylcytosine is actual-

† Crystal structure of 5-bromocytosine closely resembles that of cytosine. In both crystals, the molecules form ribbons with hydrogen bonds along the two-fold screw axis. The only difference is the lacking of inter-ribbon hydrogen bonds in the former due to bromine substituents.[5] It is argued, therefore, that the former crystal is less stable than the latter one. This is supported by the fact that recrystallization of 5-bromocytosine from a water–dioxane mixture gives a complex with dioxane, in which the dioxane molecule links the 5-bromocytosine ribbons.[12] The screwed ribbon structure is thought to be barely allowed to be taken in the 5-bromocytosine crystal which was the basis of the present simulation.

TABLE 5. BOND LENGTHS AND ANGLES INVOLVING HYDROGEN ATOMS
Standard deviations are given in parentheses.

Distance (l/Å)		Angle(ϕ/°)	
N(1)–H(1)	0.94(6)	C(2)–N(1)–H(1)	117(4)
N(4)–H(4A)	0.81(5)	C(6)–N(1)–H(1)	121(4)
N(4)–H(4B)	0.87(5)	C(4)–N(4)–H(4A)	116(3)
C(6)–H(6)	0.97(5)	C(4)–N(4)–H(4B)	123(4)
C(7)–H(7A)	1.01(6)	H(4A)–N(4)–H(4B)	120(5)
C(7)–H(7B)	1.00(7)	C(5)–C(6)–H(6)	123(3)
C(7)–H(7C)	0.94(7)	N(1)–C(6)–H(6)	115(3)
O(W)–H(W)	0.79(6)	C(5)–C(7)–H(7A)	111(3)
		C(5)–C(7)–H(7B)	109(4)
Symmetry code		C(5)–C(7)–H(7C)	109(4)
(e) $1-x, y, 3/2-z$		H(7A)–C(7)–H(7B)	112(5)
		H(7A)–C(7)–H(7C)	107(5)
		H(7B)–C(7)–H(7C)	108(6)
		H(W)–O(W)–H(W)[e]	109(5)

ly forbidden and replaced by a different hydrogen-bond network involving the water in order that the molecules pack more effectively.

Molecular Structure. Bond lengths and angles are shown in Fig. 2 together with those of cytosine[14] and its monohydrate[14] for comparison. The bond lengths and angles involving the hydrogen atoms are given in Table 5. The deviations from the cytosine values may be attributed to the steric and electronic effects caused by methylation. After an interpretation of benzene ring deformation on the basis of the valence-shell electron-pair repulsion theory,[15] the electron-releasing group attached to C(5) atom makes the C(4)–C(5)–C(6) angle smaller. In addition, the lengthening of C(5)–C(4) and C(5)–C(6) bonds, which are due to repulsions between C(7) and C(4) or C(6) atoms, may allow to narrow the C(4)–C(5)–C(6) angle accompanied by the slight expansions of C(5)–C(4)–N(3) and C(5)–C(6)–N(1) angles. Although the distance between the C(7) and N(4) atoms looks rather short, there are no abnormal contacts between their hydrogen atoms. Steric hindrance between the methyl and amino groups is relieved by an appropriate rotation of the former around the C(5)–C(7) bond, so that the deviation of C(5)–C(4)–N(4) angle becomes small. The steric effect of the methyl group thus is buffered and does not extend to N(3), while that of bromine in 5-bromocytosine makes the C(2)–N(3)–C(4) angle slightly expand. The C(2)–N(3)–C(4) angle, which is varied little by the methyl substitution, suggests no significant change of the effective charge of lone-pair lobe at N(3), and this seems to be related to similar pK_a values of cytosine and 5-methylcytosine [4.58 and 4.6, respectively].[16] Table 6 shows the atomic net charges calculated by CNDO approximation[17] for cytosine and its 5-methyl derivative. Invariant charge at N(3) upon methylation supports the above interpretation.

As compared with cytosine structure, the shortening of the C(2)–N(3) and C(4)–N(4) bonds, and the lengthening of the C(2)–O(2) bond accompanied by the increase of N(1)–C(2)–N(3) angle are observed. These changes, though small, suggests the increase of the contribution from the canonical formula in which the amino nitrogen and the carbonyl oxygen carry positive and negative charges, respectively. Such an increase may be induced by the strong hydrogen bond from water molecule to the carbonyl oxygen. Similar trend is also observed in cytosine monohydrate, in which the water molecule participates in the same way.[11,14]

TABLE 6. NET CHARGE DISTRIBUTION

Cytosine		5-Methylcytosine	
N(1)	−0.182	N(1)	−0.183
C(2)	0.417	C(2)	0.415
O(2)	−0.425	O(2)	−0.426
N(3)	−0.337	N(3)	−0.334
C(4)	0.322	C(4)	0.308
N(4)	−0.259	N(4)	−0.259
C(5)	−0.172	C(5)	−0.111
C(6)	0.187	C(6)	0.160
H(5)	0.135	C(7)	−0.024
H(1)	0.031	H(1)	0.134
H(4A)	0.135	H(4A)	0.147
H(4B)	0.136	H(4B)	0.135
H(6)	0.001	H(6)	0.002
		H(7A)	0.009
		H(7B)	0.013
		H(7C)	0.014

TABLE 7. LEAST-SQUARES PLANE FOR PYRIMIDINE RING
X, Y, and Z are in Å along a^*, b, and c, respectively. Asterisks denote atoms defining the plane. Standard deviations are given in parentheses.

Equation

$$-0.0110(13)X+0.96519(33)Y+0.2613(12)Z-1.2394(54)=0$$

Deviations (l/Å) of atoms from the plane			
N(1)*	0.012	C(7)	−0.035
C(2)*	0.005	H(1)	−0.05
N(3)*	−0.016	H(6)	−0.08
C(4)*	0.011	H(4A)	0.03
C(5)*	0.006	H(4B)	0.17
C(6)*	−0.017	H(7A)	−0.02
O(2)	0.005	H(7B)	0.73
N(4)	0.016	H(7C)	−0.83

The least-squares plane of 5-methylcytosine together with the deviations of atoms from the plane is listed in Table 7. Although the pyrimidine ring with amino nitrogen N(4) and carbonyl oxygen O(2) is planar within 0.017 Å, the small deviations of atoms show the slight bending of the ring around the N(3)–C(6) axis. The methyl C(7) atom deviates on the opposite side of the plane to the amino group. This deviation is rather small as compared with that of bromine in 5-bromocytosine because of the relief of short contacts by an appropriate rotation of the methyl group mentioned above.

Figure 1 was drawn by TSD: XTAL, which is a computer-graphics interactive modelling programme for the NOVA 3 computer.[13]

The present work was partially supported by a Grant-in-Aid for Scientific Research from the Ministry of Education and by the Kawakami Foundation, to which the authors' thanks are due.

References

1) M. Ohki, A. Takenaka, H. Shimanouchi, and Y. Sasada, *Bull. Chem. Soc. Jpn.*, **49**, 3493 (1976).
2) M. Ohki, A. Takenaka, H. Shimanouchi, and Y. Sasada, *Bull. Chem. Soc. Jpn.*, **50**, 90 (1977).
3) A. Takenaka, M. Ohki, and Y. Sasada, 36th National Meeting of the Chemical Society of Japan, Osaka, April 1977, Abstr. I, 4M10.
4) T. Hata, M. Yoshikawa, S. Sato, and C. Tamura, *Acta Crystallogr., Sect. B*, **31**, 312 (1975).
5) M. Kato, A. Takenaka, and Y. Sasada, *Bull. Chem. Soc. Jpn.*, **52**, 49 (1979).
6) L. Pauling, "The Nature of Chemical Bond," 3rd ed, Cornel Univ. Press, New York (1960), p. 260.
7) L. E. McCandlish and G. H. Staut, *Acta Crystallogr., Sect. A*, **31**, 245 (1975).
8) "International Tables for X-Ray Crystallography," Kynoch Press, Birmingham (1974), Vol. IV, p. 71.
9) Table 3 has been deposited as Document No. 8008, at the Office of the Bulletin of the Chemical Society of Japan.
10) D. L. Barker and R. E. Marsh, *Acta Crystallogr.*, **17**, 1581 (1964).
11) G. A. Jefferey and Y. Kinoshita, *Acta Crystallogr.*, **16**, 20 (1963).
12) M. Kato, A. Takenaka, and Y. Sasada, unpublished.
13) A. Takenaka and Y. Sasada, Annual Meeting of the Crystallographic Society of Japan, Hiroshima, November 1978, Abstr. p. 32.
14) R. J. McClure and B. M. Craven, *Acta Crystallogr., Sect. B*, **29**, 1234 (1973).
15) A. Domenicano, A. Vaciago, and C. A. Coulson, *Acta Crystallogr., Sect. B*, **31**, 1630 (1975).
16) A. Albert, "Synthetic Procedures in Nucleic Acid Chemistry," ed by W. W. Zorbach and R. S. Tipson, John Wiley and Sons, Inc., New York (1973), p. 1.
17) J. A. Pople and D. L. Beveridge, "Approximate Molecular Orbital Theory," McGraw-Hill Book Company, New York (1970).

Effect of Ultraviolet Ray on Graphite Fluoride in Organic Solvents

Nobuatsu WATANABE* and Kazuo UENO

Department of Industrial Chemistry, Faculty of Engineering, Kyoto University, Yoshida, Sakyo-ku, Kyoto 606

(Received March 16, 1979)

Graphite fluoride, $(CF)_n$, was photolyzed in alcohols and hydrocarbons. Hydrogen fluoride was formed in each case. Alcohols were partially converted into the corresponding carbonyl compounds by the reaction $2(C\text{–}F)+RR'CHOH \xrightarrow{h\nu} 2(C)+2HF+RR'C{=}O$. ESCA measurement revealed that the fluorine at the surface decreases more rapidly than that of the inner region of $(CF)_n$ particle, the inner region being also photolyzed. Results of DTA measurement indicate that the irradiation reduces the thermostability of $(CF)_n$.

Graphite fluoride, $(CF)_n$, is prepared by the reaction of fluorine gas with various carbon materials at high temperature. The crystalline structure consists of condensed cyclohexane-like carbon rings with fluorine atoms occupying the fourth coordination site of the sp^3-hybridized carbon atom.[1–3] Recently, the compound has been used as a superior lubricant[4–6] under extreme conditions of high temperature and high vacuum. It has also been found to be a cathodic depolarizer in high energy density batteries.[7–9] However, little is known about its chemical reactivity towards organic compounds. This paper deals with the effect of ultraviolet irradiation on graphite fluoride in various hydrocarbons and alcohols.

Experimental

Graphite fluoride with a F/C molar ratio of 1.16 was prepared by the direct fluorination of petroleum coke,[10] fine white powder with particle size greater than 400 mesh being obtained. All organic solvents were of reagent grade and used without further purification. Graphite fluoride dispersed in the solvent was irradiated at room temperature in a 500 ml photochemical reactor (Ushio Denki Co.) with a high pressure mercury lamp of 100 W (UM-102) put into a water cooling jacket made of Pyrex glass. The lamp emits ultraviolet rays (the output is indicated in parentheses) 3132 Å (2.10 W), 3650—3663 Å (3.08 W), 4047—4078 Å (1.26 W), and other rays with smaller power. The suspension was stirred with a magnetic stirrer during the course of irradiation. The oxygen dissolved in the solvent was removed by bubbling nitogen for half an hour before irradiation. After the irradiation, $(CF)_n$ was separated from the solvent by centrifugation, and then dried in a vauum. The sample was analyzed by means of X-ray photoelectron spectroscopy (ESCA), X-ray diffraction, and differential thermal analysis (DTA). The content of carbon, hydrogen and fluorine was determined by the usual method.[11]

Results and Discussion

Photochemical Decomposition of $(CF)_n$. The F/C molar ratio of $(CF)_n$, which was allowed to stand in MeOH without irradiation for more than six months remained almost unchanged. On the other hand, by ultraviolet irradiation for several hours, the color of $(CF)_n$ in organic solvent turned black or brown from white, the F/C ratio decreasing with increasing irradiation time. Thus, the decomposition of $(CF)_n$ by ultraviolet irradiation would proceed only in a solvent, considering the fact that $(CF)_n$ is photochemically stable in the air.

Since the F/C ratio decreased by irradiation, the photolysis of $(CF)_n$ may lead to the cleavage of a C–F bond rather than a C–C bond. In thermal decomposition of $(CF)_n$ in a vacuum or in inert gas, the initial step of the reaction may be the rupture of C–C bonds rather than C–F bonds.[12]

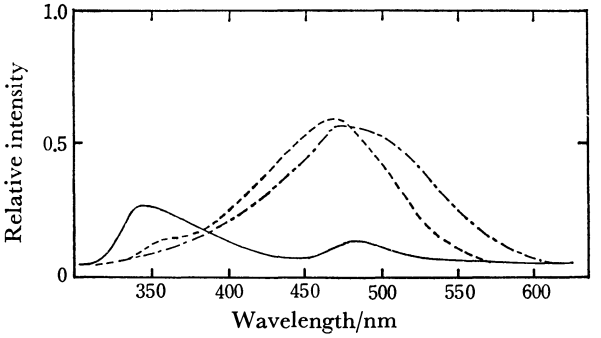

Fig. 1. Emission spectra of $(CF)_n$. Exciting wavelength is 290 nm. ——: in air, ——: in paraffin, –·–: in MeOH.

Figure 1 shows the emission spectra of $(CF)_n$ in the air, MeOH, and in liquid paraffin. The peak areas of the spectra both in MeOH and in paraffin were 3 times greater than those in the air. The coloration of $(CF)_n$ turns slightly dark when it is put into MeOH and paraffin, *viz.* solvatochromism takes place. The absorption spectrum of a solution changes with solvent without chemical reaction between solute and solvent. In the case of $(CF)_n$, the main peak in its emission spectra shifted to lower wavelength with increasing solvent polarity. Compounds which show such bathochromic effect are, in general, more polar in excited state than in the ground state.

Parry[13] calculated the band structure of $(CF)_n$ on the basis of the self-consistent semi-empirical LCMO method, and found that the direct band gap at the center of the Brillouin zone for a layer of $(CF)_n$ is 8.4 eV, *viz.*, 147.6 nm. The emission spectra were not in line with his results. This may be attributed to the $(CF)_n$ we prepared which has mechanical distortions and crystal defects such as exfoliation and crack, being far from Parry's ideal crystal.

The F/C ratio and decomposition ratio (α) of $(CF)_n$ after photolysis in various alcohols and hydrocarbons for 24 h are given in Table 1. The decomposition ratio,

Table 1. F/C ratio and decomposition ratio of graphite fluoride photolyzed for 24 h in various alcohols and hydrocarbons

Solvent	F/C[a)]	Decomposition ratio/%	Dielectric constant
MeOH	0.94	7.3	32.6
n-PrOH	0.97	6.3	20.1
i-PrOH	0.99	5.5	18.3
n-BuOH	1.01	4.9	17.8
t-BuOH	1.08	2.5	10.9
Hexane[b)]	1.09	2.3	1.9
Cyclohexane[b)]	1.07	2.8	2.0

a) Value of original $(CF)_n$ 1.16. b) Irradiation time 20 h.

α, is defined by

$$\alpha = \frac{F_0 - F}{F_0} \times 100,$$

where F_0 and F are the fluorine content of original sample and that of the sample photolyzed, respectively. Graphite fluoride was decomposed to a greater extent in alcohols than in hydrocarbons. α is proportional to the dielectric constant of the solvent. Thus, $(CF)_n$ seems to be polar at the transition state of the reaction. This is supported by the solvent effect of the emission spectra, if the excited state is the transition state of the reaction.

Photochemical Reaction in Alcohols. When photolysis was carried out for a longer time, the reaction mixture became acidic by the formation of hydrogen fluoride. When it was neutralized with aqueous sodium hydroxide, precipitation of sodium fluoride took place. This was confirmed by means of X-ray diffraction. The amount of hydrogen fluoride coincided with the net decrease of fluorine in $(CF)_n$.

The solvent was subjected to gas chromatography with Porapak R (Water Associates Inc.) as a separating packing. In *i*-PrOH and *n*-BuOH, the corresponding carbonyl compounds, acetone and butyraldehyde, respectively, were detected. From the results, photochemical decomposition of $(CF)_n$ in alcohols can be presented by

$$2(C\text{–}F) + RR'CHOH \xrightarrow{h\nu} 2(C) + 2HF + RR'C{=}O,$$

where R and R′ are either hydrogen or alkyl group.

ESCA Measurement. ESCA measurement was made on $(CF)_n$ photolyzed in MeOH for 27, 72, and 96 h (Fig. 2). The spectra show, in addition to the main peak at 290 eV (A_1), a broad shoulder at 292.4 eV (A_2) and a low intensity tail at *ca.* 294.4 eV (A_3), which are assigned to the carbon having $>CF$, $>CF_2$, and $-CF_3$ bonds, respectively.[14,15] After photolysis, the peaks became smaller, while a new peak appeared at *ca.* 286 eV (A_4), which may be the carbons having no C–F bond.[16] The peak at 285 eV is due to hydrocarbon contamination, and regarded to have approximately the same intensity in each run.

The relative peak area of these peaks, the F/C ratio calculated from above relative peak area, and that determined by elemental analysis are given in Table 2.

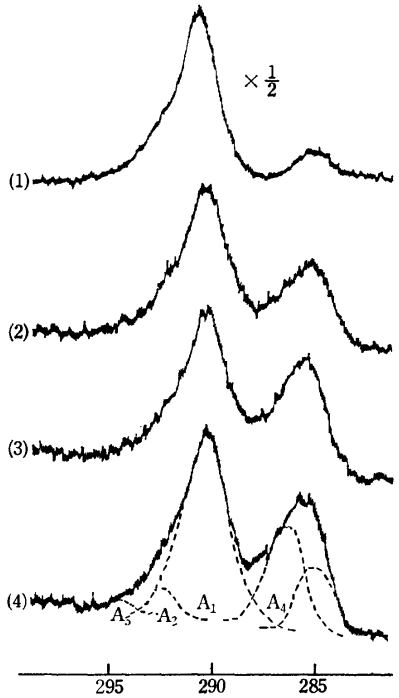

Fig. 2. The change in ESCA spectra of C_{1s} photoelectron of $(CF)_n$ photolyzed for various times in MeOH. (1) Original sample, (2) 27 h, (3) 72 h, (4) 96 h.

Table 2. Influence of time on the relative peak area of C_{1s} and F/C ratio of $(CF)_n$ photolyzed in methanol

Irradiation time h	C_{1s} peak/%				F/C ratio	
	A_1	A_2	A_3	A_4	(a)	(b)
0	79.4	16.0	4.6	0	1.33	1.16
27	67.3	5.0	4.6	23.1	0.91	0.93
72	59.5	4.4	3.8	32.3	0.80	0.86
96	60.9	3.6	2.7	32.8	0.76	0.84

a) Determined by means of ESCA spectrum. b) Determined by chemical analysis.

In the original $(CF)_n$, the F/C ratio calculated from the ESCA spectrum is higher than that from elemental analysis. This indicates that there are many $>CF_2$ and $-CF_3$ groups at the surface of the $(CF)_n$ particle. Since the electron escape depth for C_{1s} photoelectron is *ca.* 10 Å,[17] and the $(CF)_n$ particle has a diameter of several micrometers, only the surface region of solid can be examined by ESCA. By photolysis, the amount of fluorine at the surface decreased more rapidly than that of the inner region of the particle (Table 2). However, after photolysis for even 96 h, many fluorine atoms remained undecomposed at the surface as shown in Fig. 2, the F/C ratio at the surface no differing from that of the total particle. The reaction may proceed not only at the surface but also in the inner region of the solid, especially at cracks and mechanically distorted parts where the solvent can permeate.

Effects on the Structure of $(CF)_n$. No remarkable changes of the structure of $(CF)_n$ due to photolysis

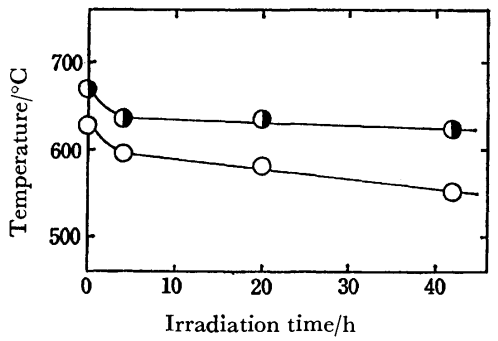

Fig. 3. The variation of the starting temperature, T_s, and of the peak maximum temperature, T_m, with the irradiation time.
○: T_s, ◑: T_m.

were observed by means of X-ray diffraction. A DTA curve of $(CF)_n$ prepared from flaky natural graphite showed an exothermic peak at *ca.* 670 °C. Figure 3 shows variation of the peak starting temperature, T_s, and of the peak maximum temperature, T_m, with irradiation time. Photolysis was carried out in MeOH, the DTA being measured in a vacuum. Both T_s and T_m decreased linearly, the peak being broadened with increasing irradiation time. The irradiated sample undergoes thermal decomposition at lower temperature as compared with the original one. The thermostability of $(CF)_n$ is reduced by irradiation.

References

1) V. K. Mahajan, R. B. Badachhape, and J. L. Margrave, *Inorg. Nucl. Chem. Lett.*, **10**, 1103 (1974).
2) L. B. Ebert, J. I. Brauman, and R. A. Huggins, *J. Am. Chem. Soc.*, **96**, 7841 (1974).
3) M. Takashima and N. Watanabe, *Nippon Kagaku Kaishi*, **1975**, 432.
4) R. L. Fusaro and H. E. Sliney, *A. S. L. E. Trans.*, **13**, 56 (1970).
5) H. Gisser, M. Petronio, and A. Shapiro, *Lubric. Eng.*, **28**, 161 (1972).
6) Ch. Martin, J. Sullean, and M. Roussel, *Wear*, **34**, 215 (1973).
7) W. Tiedemann, *J. Electrochem. Soc.*, **121**, 1308 (1974).
8) M. S. Whittingham, *J. Electrochem. Soc.*, **122**, 526 (1975).
9) H. F. Hunger and J. E. Ellison, *J. Electrochem. Soc.*, **122**, 1288 (1975).
10) Petroleum coke was fluorinated at *ca.* 400 °C for several hours.
11) K. Hozumi and N. Akimoto, *Jpn. Analyst*, **20**, 467 (1971).
12) P. Kamarchik, Jr., and J. L. Margrave, *J. Therm. Anal.*, **11**, 259 (1977).
13) D. E. Parry, *J. Chem. Soc., Faraday Trans., 2*, **73**, 774 (1977).
14) P. Cadman, J. D. Scott, and J. M. Thomas, *J. Chem. Soc., Chem. Commun.*, **1975**, 654.
15) P. Cadman, J. D. Scott, and J. M. Thomas, *Carbon*, **15**, 75 (1977).
16) D. T. Clark and J. Peeling, *J. Polym. Sci., Polym. Chem. Ed.*, **14**, 2941 (1976).
17) D. T. Clark, W. J. Feast, W. K. R. Musgrave, and I. Ritchie, *J. Polym. Sci., Polym. Chem. Ed.*, **13**, 857 (1975).

Photoacoustic Spectrometry of Solid Samples. III. Microdetermination of Mercury as Hg Diphenylcarbazone Complex

Seiji KAWAMOTO, Yu YOKOYAMA,* and Shigero IKEDA
Department of Chemistry, Faculty of Science, Osaka University, Toyonaka, Osaka 560
(Received April 12, 1979)

Photoacoustic spectrometry was applied to the determination of michroamount of Hg diphenylcarbazone complex. The photoacoustic spectrum and diffuse reflectance spectrum almost agree with each other, showing an absorption maximum at 560 nm, as in the absorption spectrum of the complex in benzene solution. Determination of Hg was performed by measuring the intensity of photoacoustic signal at 560 nm. The normalized signal intensity increased linearly with the amount of mercury ion up to 100 ng, deviating from linear relationship downwards above 100 ng. The photoacoustic signal saturation caused by strong absorption of radiation was investigated.

Photoacoustic spectrometry of solid substances was applied to the determination of Ni, Cu, and Al as Ni dimethylglyoxime complex, Cu thiooxine complex, and Al quinalizarin lake, respectively.[1,2] The complex or lake was formed on filter paper according to the procedure of spot test and the signal intensity by the photoacoustic effect of colored substances was measured. As the amount of the colored substance increased beyond a certain limit, the relation between the amount of substance and normalized signal intensity was no longer linear and the intensity deviated from linear relationship downwards.

Mercury ion forms a strongly colored insoluble complex with diphenylcarbazone. The complex shows violet to blue color and is contrasted with reagent blank in acidic medium. It has been used as a color reagent of mercury in both extraction spectrophotometric determination and spot test. Dithizone is also a very sensitive color reagent, but the reagent itself is intensely colored. The present work was undertaken for a study on the determination of microamount of mercury with diphenylcarbazone and the photoacoustic signal saturation.

Experimental

Apparatus. The photoacoustic spectrometer assembly for this work was the same as previously reported.[1,2] Absorption spectra and diffuse reflectance spectra were measured with a Hitachi 124 type spectrophotometer and a Hitachi 323 type recording spectrophotometer with integrating sphere, respectively.

Reagent. The stock solution of mercury was prepared by dissolving distilled mercury metal in concentrated nitric acid and by diluting the solution with deionized water. The concentration of mercury and nitric acid were adjusted to 1150 ppm and 0.1 mol dm^{-3}, respectively. Standard solutions were prepared by diluting the stock solution and by adjusting the concentration of nitric acid to 0.02 mol dm^{-3}.

Diphenylcarbazone solution was prepared by dissolving 100 mg of diphenylcarbazone in 10 cm^3 ethanol immediately before use.

Other reagents were of reagent grade and were used without further purification. Water was deionized through ion exchange resin after distillation. Carbon black paper was prepared by smoking benzene soot on filter paper.

Procedure. Diphenylcarbazone test paper was prepared by impregnating filter paper with alcoholic solution of diphenylcarbazone. Hg diphenylcarbazone complex was formed by dropping 5 mm^3 of mercury standard solution on a diphenylcarbazone test paper of 10 mm in diameter. The test paper was immediately mounted on the sample holder by use of transparent double-sided adhensive tape and then photoacoustic signal intensity was measured.

Acidity. The sensitivity of mercury determination with diphenylcarbazone depends on the acidity of solution, decreasing with increasing acidity. However, in neutral or weakly acidic solution, other heavy metals also give colored compounds with diphenylcarbazone. With increasing acidity, interference of other ions decreases, and in 0.2 mol dm^{-3} nitric acid solution the diphenylcarbazone reaction is almost specific for mercury.[3] The acidity of solution should be chosen according to the circumstances, especialy in consideration of foreign ions. In the case of high acidity, Hg diphenylcarbazone complex formed on filter paper gradually decomposed to decolorize because of concentration of acid due to evaporation of water. In addition nitric acid vapor attacks the diaphragm of the microphone. Therefore in the present study, the concentration of nitric acid in mercury solution was adjusted to 0.02 mol dm^{-3} and the signal intensity was measured immediately after complex formation.

When sulfuric acid was used, the photoacoustic signal intensity of blank was higher and Hg diphenylcarbazone complex was less stable than in nitric acid medium.

Results and Discussion

Photoacoustic Spectrum of Hg Diphenylcarbazone Complex. The photoacoustic spectrum was obtained by calculating the normalized intensity (I_n) at each wavelength and by plotting the value against wavelength.[1,2] The photoacoustic spectrum of Hg diphenylcarbazone complex thus obtained is shown in Fig. 1. The absorption maximum appears at *ca.* 560 nm and the photoacoustic spectrum of benzene solution of the complex except for broadening of the absorption band. It also agrees with

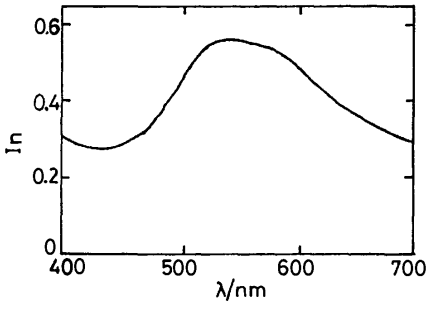

Fig. 1. Photoacoustic spectrum of Hg diphenylcarbazone complex.

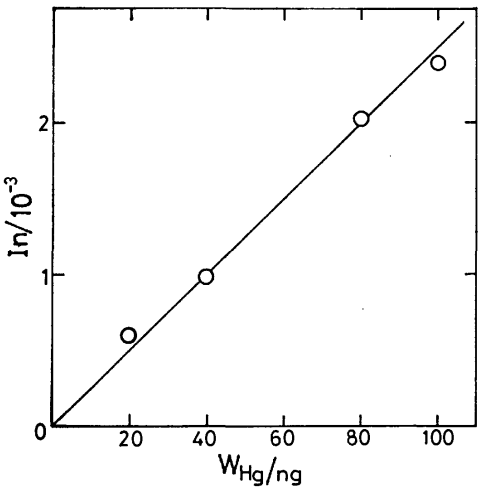

Fig. 2. Calibration curve for mercury. Wavelength: 560 nm.

the diffuse reflectance spectrum.

Determination of Microamounts of Mercury by Photoacoustic Spectrometry. Hg diphenylcarbazone complex was formed by the analytical procedure on diphenylcarbazone test paper. A blank diphenylcarbazone test paper was prepared by dropping 5 mm^3 of 0.02 mol dm^{-3} nitric acid. The photoacoustic signal intensity of sample, blank and carbon black were measured at 560 nm, and the normalized signal intensity was calculated. The calibration curve obtained by plotting the normalized signal intensity against mercury amount was linear from 20 to 100 ng as shown in Fig. 2. The detection limit for mercury (20 ng) was lower than for diffuse reflectance spectrometry of the complex (40 ng),[4] and that for extraction photometry of the complex in benzene (5 μg).[5]

TABLE 1. DETERMINATION OF Hg

Taken W_{Hg} / ng	Found W_{Hg} / ng		
20	26	22	26
40	38	37	42
80	84	84	76
100	100	92	92

By use of the calibration curve, determination of Hg was carried out. The results are summarized in Table 1. Samples containing 20 ng of Hg showed comparatively higher results. The error was within ±8% for samples containing Hg from 40 to 100 ng.

Saturation of Photoacoustic Signal. The photoacoustic effect of solid sample was analyzed theoretically by Rosencwaig and Gersho.[6] The expression giving the amplitude of pressure fluctuation by photoacoustic effect in a cell is simplified, when the thermal diffusion length of the sample (μ_s) and the optical absorption length ($\mu_\beta = 1/\beta$) are appreciably larger than the sample thickness (l). Thus the amplitude of pressure fluctuation in the cell is given by

$$Q = A[1-\exp(-\beta l)], \quad (1)$$

where A is a constant which depends on thermal property of the sample cell and of the filler gas, geometrical structure of the cell, intensity of the incident monochromatic light and the ambient pressure and volume, and β denotes the optical absorption coefficient of the solid sample (in cm^{-1}) for the wavelength λ, and is $2.3\times\varepsilon C$ where ε is the molar extinction coefficient of the sample and C is the sample concentration. Since the exponential term of Eq. 1 is approximated by $1-\beta l$ for a very small value of βl, Eq. 1 becomes

$$Q \cong A\beta l = 2.3A\varepsilon Cl. \quad (2)$$

It is obvious from Eq. 2 that the calibration curve obtained by plotting the signal intensity against sample amount is linear for a small amount of sample. For a higher value of βl, however, the higher order terms of expantion terms of $\exp(-\beta l)$ can be ignored. When $\exp(-\beta l)$ is developed up to the second order term, Eq. 1 becomes

$$Q = A\beta l\left(1-\frac{\beta l}{4}\right). \quad (3)$$

When βl increases infinitely and the sample absorbs most part of the incident light, $\exp(-\beta l)$ nearly equals zero and therefore Eq. 1 becomes

$$Q = A. \quad (4)$$

It is obvious from Eqs. 3 and 4 that, as the absorption coefficient increases or sample thickness becomes larger, saturation of the signal intensity occures. As a result, the signal intensity approaches gradually to a constant value independent of the absorption coefficient and the sample thickness.

Since carbon black might be assumed to be an approximately black body absorbing visible light perfectly, the normalized signal intensity (I_n) obtained by taking the ratio of the signal intensity of the sample to that of carbon black is given as follows by means of Eqs. 1 and 4.

$$I_n = \frac{S_s}{S_b}[1-\exp(-\beta l)], \quad (5)$$

where the coefficient S_s/S_b is a correction term introduced by considering that the photoacoustic signal intensity is proportional to surface area of the substance, and S_s and S_b are surface areas of samples and carbon black, respectively.

Since Eq. 5 was derived on the assumption that $\mu_s > l$, it is necessary to examine the validity of assumption. Experiments were carried out with Hg diphenylcarbazone complex formed on filter paper. Rosencwaig and Gersho[6] showed that in the case of $\mu_s > l$ and $\mu_\beta > l$, the photoacoustic signal intensity (I) is proportional to the reciprocal of chopping frequency of the incident light (ω^{-1}), but the signal intensity is proportional to $\omega^{-3/2}$ in the case of $\mu_s < l$ and $\mu_\beta > l$. Thus the dependence of the photoacoustic signal intensity of Hg diphenylcarbazone complex on the chopping frequency was investigated. The relation between photoacoustic signal intensity (in μV) and ω^{-1} is shown for the range of the chopping frequency from 17—125 Hz in Fig. 3. In this chopping frequency range the signal intensity is proportional to ω^{-1}. It is concluded that Hg diphenylcarbazone complex prepared in this way satisfies $\mu_s > l$.

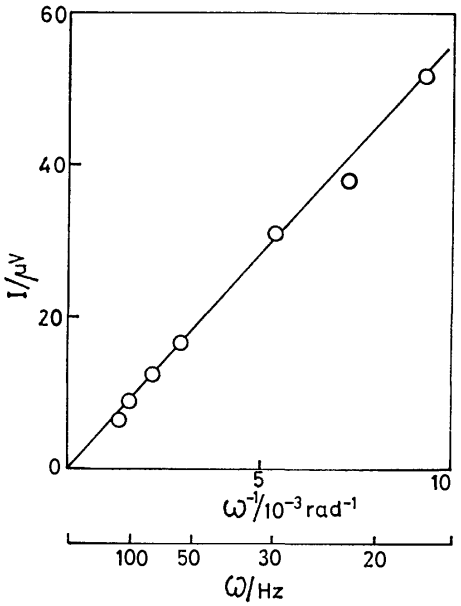

Fig. 3. Photoacoustic signal intensity of Hg diphenylcarbazone complex *versus* reciprocal of the chopping frequency.

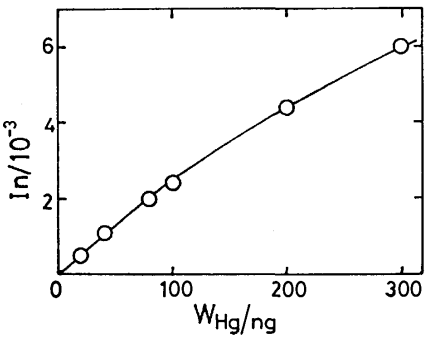

Fig. 4. Observed normalized signal intensity of Hg diphenylcarbazone complex *versus* weight of Hg in complex.

The relation between the photoacoustic signal intensity and mercury amount dropped onto filter paper was linear for 20—100 ng of Hg, as shown in Fig. 2. In order to examine the relation above 100 ng of Hg, measurements were extended up to 300 ng of Hg. The results are shown in Fig. 4. The normarized signal intensity of sample containing Hg above 100 ng deviates from linear relationship downwards. The normalized signal intensity was calculated from Eq. 5 by substituting the following values; the molar extinction coefficient ($\varepsilon=4.5\times10^4$), which was determined on benzene extract of the Hg complex, S_s which was measured on the spot of complex, $S_b=0.785$ cm^2, the concentration of complex in filter paper (C), which was calculated from mercury amount dropped onto test paper and the volume of spot [$S_s\times$thickness of filter paper (l)]. The normalized signal intensity calculated by use of these parameters is plotted against the mercury amount in Fig. 5. Figures 4 and 5 almost agree with each other except for the scale of the ordinate. And it is understood that the saturation of normalized signal

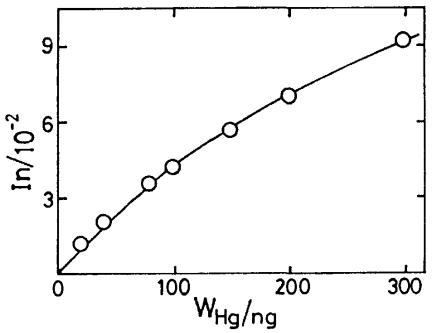

Fig. 5. Calculated normalized signal intensity of Hg diphenylcarbazone complex *versus* weight of Hg

intensity is mainly due to the terms of higher order of $[1-\exp(-\beta l)]$ in Eq. 5.

Disagreement between the calculated and the observed intensities might be explained by some of the following factors: 1) Validity of the assumption that carbon black paper used is a black body, 2) estimation of the term βl, and 3) estimation of the effective particle size of solid samples.

When the black standard is not a perfectly black body, it is expected that the observed value is larger than the calculated value. Since this is not the case, the experimental results can not be explained by this factor. A light absorber having a microscopically heterogeneous distribution in a dispersed system should show apparently a smaller absorption coefficient than that shown in a homogeneous system. The value of ε measured in homogeneous solution would be too high to used in Eq. 5, giving a higher calculated photoacoustic intensity. In fact the calculated intensity is one order higher than the observed one. On the other hand, since the incident beam reflects repeatedly within texture of filter paper before passing through it, the effective optical path length would be greater than the sample thickness (l). Therefore lowering of I_n caused by decrease in apparent absorption coefficient would be cancelled partially by increase in effective optical path length.

Absorption by particles is largely affected by particle size, the smaller the particle size, the higher the photoacoustic intensity. Usually the particle size of soot produsd by burning is approximately 50—500 nm. Crystals (approximately 1—30 μm) of Hg diphenylcarbazone complex formed in filter paper can be observed by microscopy. Effective surface area of benzene soot seems to be at least one order larger than that of the complex. This might be the principal cause for the difference between the observed and the calculated intensities.

Saturation of the photoacoustic signal should influence the shape of photoacoustic spectrum as well as calibration curve. As is obvious from Eq. 2, the photoacoustic spectrum can reflect wavelength dependency of β for a small value of βl. However, when the photoacoustic intensity is beyond the range of proportionality around the absorption maximum, the center of the absorption band should be flattened for saturation of absorption. Therefore in measurement of the photoacoustic spec-

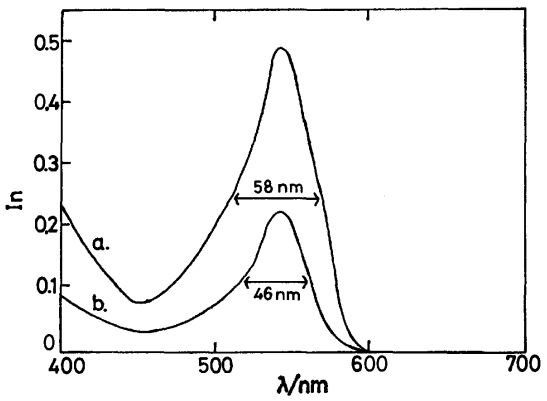

Fig. 6. Photoacoustic spectra of Ni dimethylglyoxime complex.
(a) $W_{Ni}=3$ μg, (b) $W_{Ni}=0.7$ μg.

trum, it is desirable to restrict the value of βl within the proportionality range by reducing the concentration of absorber and/or the thickness of samples. The phenomenon of saturation could easily be demonstrated by photoacoustic spectra of Ni dimethylglyoxime complex. Figure 6 show the spectra of samples containing 0.7 and 3 μg of Ni. The former belongs to the linear part of calibration curve for nickel and the latter to the saturation part. The half maximum width of the absorption band at 545 nm was 46 and 58 nm for the former and the latter samples, respectively. The absorption band is broadened due to saturation of photoacoustic signal.

References

1) Y. Yokoyama and N. Nakamura, *Bunseki Kagaku*, **28**, 97 (1979).
2) S. Kawamoto, Y. Yokoyama, and S. Ikeda, *Bunseki Kagaku*, **28**, 142 (1979).
3) F. Feigl, "Spot Test. I. Inorganic Application," Elsevier, New York (1954), p. 61.
4) R. Reisfeld, E. Greenberg, and W. J. Leven, *Anal. Chim. Acta*, **74**, 253 (1975).
5) H. Seno and Y. Kakida, *Nippon Kagaku Zasshi*, **82**, 452 (1961).
6) A. Rosencwaig and A. Gersho, *J. Appl. Phys.*, **47**, 64 (1976).

 © 1980 The Chemical Society of Japan Bull. Chem. Soc. Jpn., 53, 395—401 (1980)

Metal Complexes Coordinating Pyridine Derivatives. I. Preparation and Circular Dichroism Spectra of *cis*-α Isomers of [(*S*)-*N*,*N*′-Bis(2-pyridylmethyl)propylenediamine]dihalogenochromium(III) and -cobalt(III) Complexes

Yukihiro YAMAMOTO* and Yoichi SHIMURA

Department of Chemistry, Faculty of Science, Osaka University, Toyonaka, Osaka 560

(Received April 23, 1979)

Several chromium(III) and cobalt(III) complexes with (*S*)-*N*,*N*′-bis(2-pyridylmethyl)propylenediamine (*S*-picpn) were prepared and their structures assigned. The $[CoCl_2(S\text{-picpn})]^+$ complex was reassigned to have *cis*-α configuration. The *Δ* and *Λ* diastereomers of $[CrX_2(S\text{-picpn})]^+$ of *cis*-α configuration were obtained (X=Cl^- and Br^-) and their absorption and circular dichroism spectra were discussed.

The structural assignment of $[CoX_2(S\text{-picpn})]^+$ complexes, where *S*-picpn is the abbreviation for (*S*)-*N*,*N*′-bis(2-pyridylmethyl)propylenediamine and X^- stands for an aniono ligand such as Cl^- or Br^- has been the subject of controversy. In 1967 Bosnich prepared several complexes and discussed their circular dichroism (CD) spectra in terms of *cis*-α configuration (Fig. 1).[1] Cragel and Brubaker[2] studied the stereospecific formation of such complexes from racemic or resolved picpn ligand, and concluded that in contrast most of the cobalt(III) complexes have *cis*-β configuration. Studies on strain energy minimization and conformational analysis[3] of six possible isomers of $[Co(ox)(S\text{-picpn})]^+$ have shown that the strain energy of a *cis*-α isomer is the lowest of the six isomers, although the strain energy of some *cis*-β isomers differs from that of the lowest α-isomer by only a few percent.

The corresponding ethylenediamine analogue ligand, *N*,*N*′-bis(2-pyridylmethyl)ethylenediamine (abbrev. picen), also forms several cobalt(III) complexes.[4] The structures of two isomers of dichloro complex $[CoCl_2(picen)]^+$, a purple and a cherry-red one, were definitely assigned by Gibson and McKenzie to *cis*-α and *cis*-β configurations, respectively, from their PMR spectra.[4a] Michelsen[5] prepared the *cis*-α and *cis*-β isomers of dichloro chromium(III) complexes, and also studied chromium(III) complexes of some analogous bidentate ligands, *i.e.*, 2-pyridylmethylamine[6] and 1-(2-pyridyl)ethylamine.[7]

The present paper deals with the preparation of several dianiono *S*-picpn chromium(III) and cobalt(III) complexes, their structures being discussed along with the absorption and CD spectra.

Experimental

Ligands. The ligands *S*-picpn and picen were prepared from (*S*)-propylenediamine or ethylenediamine and 2-pyridinecarbaldehyde by the method of Goodwin and Lions.[8]

Cobalt(III) Complexes. $(+)^{CD}_{600}$-$[CoCl_2(S\text{-picpn})]Cl\cdot H_2O$: A portion of $Na_3[Co(NO_2)_6]$ was dissolved in water, and an equimolar amount of *S*-picpn was added with stirring. A yellowish orange precipitate was formed. This is supposed to be $[Co(NO_2)_2(S\text{-picpn})]NO_2$. After cooling in an ice bath, the product was collected and washed with ether; this was suspended in a small amount of concd hydrochloric acid and evaporated to dryness on a steam bath. The violet residue was dissolved in warm dilute hydrochloric acid (*ca.* 6 M (1 M= 1 mol dm^{-3})) and cooled in an ice bath. Violet crystals were obtained; $\Delta\varepsilon_{600}=+1.67$. Found: C, 41.29; H, 4.84; N, 12.85%. Calcd for $CoC_{15}H_{20}N_4Cl_3\cdot H_2O$: C, 40.98; H, 5.04; N, 12.74%. The CD spectrum in the region of 15000—50000 cm^{-1} was the same as that of a $[CoCl_2(S\text{-picpn})]^+$ complex which was erroneously assigned to *cis*-β configuration by Cragel and Brubaker.[2]

$(+)^{CD}_{600}$-$[CoCl_2(S\text{-picpn})]ClO_4$: The violet residue mentioned above was dissolved in water to which was added sodium perchlorate. After the solution had been left to stand overnight in a refrigerator, violet crystals were obtained. Recrystallization was performed from a small amount of warm dilute hydrochloric acid; $\Delta\varepsilon_{600}=+1.67$. Found: C, 36.89; H, 4.20; N, 11.55%. Calcd for $CoC_{15}H_{20}N_4O_4Cl_3$: C, 37.10; H, 4.15; N, 11.54%.

cis-α-$[CoCl_2(picen)]Cl$: The complex, prepared by the method of Michelsen[5] and for which the *cis*-α configuration has been confirmed,[4a] was partially resolved on an SP-Sephadex C-25 column when eluted with a 0.25 M sodium antimony(III) $(+)_{589}$-tartrate aqueous solution. The CD spectrum of the former fractions of the eluted band is opposite in the sign to that of $(+)^{CD}_{600}$-$[CoCl_2(S\text{-picpn})]Cl$, showing a negative band at 16670, positive ones at 19230 and 23810, and a negative one at 30300 cm^{-1} (Fig. 3). The latter fractions exhibited the same CD pattern of opposite sign.

Chromium(III) Complexes. $(-)^{CD}_{600}$-$[CrF_2(S\text{-picpn})]Br\cdot LiBr\cdot 3H_2O$: *S*-picpn (2.5 g, 9.9 mmol) was dissolved in a solution of *trans*-$[CrF_2(py)_4]Br\cdot 2H_2O$[9] (5.17 g, 9.9 mmol) and 20 cm^3 of 2-methoxyethanol. The solution was heated on a water bath with occasional stirring until it became sticky. To the resulting solution were added a small amount of water, an ethanol solution (20 cm^3) of 10 g LiBr, and then 50 cm^3 of an ethanol–ether mixture (1:1). After standing the solution overnight in a refrigerator, a violet precipitate was filtered, the precipitate mainly consisting of the starting complex, *trans*-$[CrF_2(py)_4]Br$. To the filtrate were added 20 cm^3 of methanol and 400 cm^3 of acetone, and an oily material obtained by decantation was dissolved in 10 cm^3 of water; then an ethanol solution (20 cm^3) of 10 g LiBr and 150 cm^3 of acetone were added. By scratching with a glass rod and cooling, the desired violet crystals were precipitated, the precipitate showing a CD spectrum. The violet crystals were washed with acetone and dried in the air. The substance was adsorbed on an SP-Sephadex C-25 column ($\phi 10\times 200$ mm) and eluted with a 0.1 M sodium chloride aqueous solution in order to confirm the purity of the complex; all fractions showed the same CD spectra: $\Delta\varepsilon_{600}=-1.61$. Found: C, 31.78; H, 4.71; N, 9.84%. Calcd for $CrC_{15}H_{20}N_4F_2Br\cdot LiBr\cdot 3H_2O$: C, 31.77; H, 4.62; N, 9.88%.

$(-)^{CD}_{600}$-$[CrCl_2(S\text{-picpn})]Cl\cdot 0.5NaCl$: In dimethyl sulfoxide

(10 cm³) was suspended anhydrous chromium(III) chloride (3.2 g, 20 mmol), and *S*-picpn (5.07 g, 20 mmol) was added to it with stirring at room temperature. After 1 h, the unreacted chromium(III) chloride was filtered off and washed with a small amount of water. The filtrate and washings were adsorbed on an SP-Sephadex C-25 column (ϕ45×600 mm) and eluted with a 0.1 M sodium chloride aqueous solution acidified with hydrochloric acid (0.12 M). Four colored bands, (i) violet, (ii) red-violet, (iii) blue-violet, and (iv) dirty violet, were eluted in this order. A dark green band appearing between bands (i) and (ii) turned red after being eluted from the column. Eluate (i) was condensed to a small volume with a vacuum rotary evaporator below 40 °C, red-violet crystals being separated. They were filtered and washed with cold water and ether: $\Delta\varepsilon_{600}=-1.26$. Found: C, 40.13; H, 4.54; N, 12.54%. Calcd for $CrC_{15}H_{20}N_4Cl_3\cdot 0.5NaCl$: C, 40.58; H, 4.54; N, 12.62%. The CD spectrum of the latter half of eluate (i) showed the opposite sign to that of the former half, indicating that the band contains two diastereomers. However, the crystals obtained above showed the same CD spectrum as that of the former half of eluate (i). Eluate (ii) was condensed to a small volume. The crystals obtained were collected but no pure crystals obtained in spite of repeated recrystallization. Their absorption spectrum indicates that band (ii) contains $[Cr(OH)(H_2O)(S\text{-picpn})]^{2+}$ ions. Eluate (iii) and (iv) were adsorbed so tightly to the Sephadex column that they could not be eluted with a 0.1 M sodium chloride aqueous solution. They were eluted with a 0.25 M sodium chloride aqueous solution, but broadened through the column. They may be some polynuclear complexes.

(−)$^{CD}_{600}$-[CrCl$_2$(S-picpn)]ClO$_4$: (−)$^{CD}_{600}$-[$CrCl_2$(*S*-picpn)]Cl·0.5NaCl was dissolved in water, and sodium perchlorate was added to the solution. A dark violet precipitate was soon formed. After filtering and washing with ethanol and ether, the product was air-dried: $\Delta\varepsilon_{600}=-1.26$. Found: C, 37.44; H, 4.21; N, 11.61%. Calcd for $CrC_{15}H_{20}N_4O_4Cl_3$: C, 37.64; H, 4.21; N, 11.70%.

(−)$^{CD}_{600}$-[CrCl$_2$(S-picpn)]I: (−)$^{CD}_{600}$-[CrF_2(*S*-picpn)]Br·LiBr·3H$_2$O was dissolved in a small volume of concd hydrochloric acid in a flask (50 cm³). The mixture was saturated with gaseous hydrogen chloride below −13 °C, and the flask was stoppered tightly and left to stand at room temperature for 3 d. After cooling, the flask was opened. Sodium iodide was added to the red-violet solution with stirring, the violet precipitate being filtered promptly and washed with acetone. Recrystallization was carried out by dissolving it in hot water (70 °C): $\Delta\varepsilon_{600}=-1.26$. Found: C, 35.31; H, 3.94; N, 11.08%. Calcd for $CrC_{15}H_{20}N_4Cl_2I$: C, 35.59; H, 3.98; N, 11.07%.

(+)$^{CD}_{600}$-[CrCl$_2$(S-picpn)]I·0.5H$_2$O: One gram of chromium shot (19.2 mmol) was dissolved in a 50 cm³ flask containing 15 cm³ of concd hydrochloric acid under a current of nitrogen. The resulting solution was evaporated and heated to dryness in a vacuum rotary evaporator to obtain chronium(II) chloride. To the flask was added *S*-picpn (4.9 g, 19.4 mmol, in 20 cm³ pyridine) and the mixture was heated, a solution of iodine (2.4 g, 9.5 mmol, in 8 cm³ pyridine) being added. The reaction was carried out by refluxing for 20 min. After cooling, the violet precipitate was filtered and washed with ethanol. The crude product (0.78 g) was suspended in 10 cm³ of water, and 0.2 g of freshly prepared silver chloride was added with stirring. The silver salt precipitated was filtered off. The filtrate was adsorbed on an SP-Sephadex C-25 column (ϕ20×300 mm) and eluted with a 0.1 M sodium chloride aqueous solution acidified with hydrochloric acid (0.1 M), only one band being eluted. The band was collected in 15 fractions, all fractions except for the last two showing the same CD pattern. The first 13 fractions were combined and condensed with a rotary evaporator below 40 °C. To the concentrated solution was added sodium iodide. On cooling, violet crystals were obtained. They were recrystallized from water: $\Delta\varepsilon_{600}=+0.89$. Found: C, 33.87; H, 3.94; N, 10.55%. Calcd for $CrC_{15}H_{20}N_4Cl_2I\cdot 0.5H_2O$: C, 34.97; H, 4.11; N, 10.88%.

(+)$^{CD}_{600}$-[CrCl$_2$(S-picpn)]Cl·0.5H$_2$O: The dichloro iodide, (+)$^{CD}_{600}$-[$CrCl_2$(*S*-picpn)]I, was suspended in water and silver chloride was added to it. The silver salt was filtered. Concd hydrochloric acid was added to the filtrate and the solution was cooled in an ice bath. Violet crystals were obtained. $\Delta\varepsilon_{600}=+0.89$. Found: C, 42.61; H, 4.87; N, 13.12%. Calcd for $CrC_{15}H_{20}N_4Cl_3\cdot 0.5H_2O$: C, 42.52; H, 5.00; N, 13.22%.

(−)$^{CD}_{600}$-[CrBr$_2$(S-picpn)]Br·0.5LiBr·0.5H$_2$O: The difluoro bromide, (−)$^{CD}_{600}$-[CrF_2(*S*-picpn)]Br·LiBr·3H$_2$O (1.15 g), was suspended in a small amount of 47% hydrobromic acid in a flask. Gaseous hydrogen bromide was bubbled into the mixture below −13 °C for 5 min, and the flask was stoppered tightly and left to stand at room temperature for 3 d. After cooling, the violet precipitate was filtered and washed with ethanol and ether. By adding a mixture of ethanol–ether (1:1) to the filtrate, more crystals were obtained. Recrystallization was carried out by dissolving the combined precipitate in hot water (70 °C) acidified with 47% hydrobromic acid (1 M). The bromide salt was sparingly soluble in water: $\Delta\varepsilon_{600}=-1.10$. Found: C, 29.94; H, 3.48; N, 9.22%. Calcd for $CrC_{15}H_{20}N_4Br_3\cdot 0.5\ LiBr\cdot 0.5H_2O$: C, 30.00; H, 3.52; N, 9.33%.

(+)$^{CD}_{600}$-[CrBr$_2$(S-picpn)]I·0.25H$_2$O: One gram (19.2 mmol) of chromium shot was dissolved in a 50 cm³ flask containing a mixture of 47% hydrobromic acid (3 cm³) and water (2 cm³) under a current of nitrogen. The resulting solution was evaporated in a vacuum rotary evaporator to give chromium(II) bromide which was heated to dryness. To the flask was added *S*-picpn (4.8 g, 19.2 mmol, in 30 cm³ pyridine) and the mixture was heated and then a solution of iodine (2.4 g, 9.5 mmol, in 8 cm³ pyridine) was added. The reaction was carried out by refluxing for 20 min. After cooling, the red violet precipitate was filtered. This was mainly "diol complex," $[\{Cr(OH)(S\text{-picpn})\}_2]I_4$, which was characterized by elemental analysis, absorption, and CD spectrum.[5] Found: C, 29.21; H, 3.84; N, 9.10%. Calcd for $Cr_2C_{30}H_{42}N_8O_2I_4\cdot 2.5H_2O$: C, 29.94; H, 3.94; N, 9.31%.

To the filtrate was added *ca.* 30 cm³ of ethanol, a small amount of violet precipitate being obtained. This was (−)$^{CD}_{600}$-[$CrBr_2$(*S*-picpn)]I. More ethanol was added and the precipitate obtained was filtered. After standing the filtrate for a month, violet powder less soluble in water than the (−)$^{CD}_{600}$-[$CrBr_2$(*S*-picpn)]I complex was precipitated. The crude product was washed on a glass filter with a small amount of water (70 °C), the residue being extracted with a large amount of hot water (70 °C). To the extracted solution was added sodium iodide and the resulting solution was cooled in an ice bath. The violet crystals obtained were washed with ethanol–ether (1:1) and then air-dried: $\Delta\varepsilon_{600}=+0.78$. Found: C, 29.48; H, 3.35; N, 9.19%. Calcd for $CrC_{15}H_{20}N_4Br_2I\cdot 0.25H_2O$: C, 30.05; H, 3.45; N, 9.35%.

(−)$^{CD}_{600}$-[Cr(NCS)$_2$(S-picpn)]SCN: The dichloro chloride, (−)$^{CD}_{600}$-[$CrCl_2$(*S*-picpn)]Cl (0.5 g), and an excess potassium thiocyanate were dissolved in water, and the solution was heated to boiling. The original violet solution turned red. After cooling, the precipitate was filtered and recristallized twice from water; $\Delta\varepsilon_{600}=-0.08$. Found: C, 44.97; H, 4.20; N, 20.48%. Calcd for $CrC_{18}H_{20}N_7S_3$: C, 44.80; H, 4.18; N, 20.32%.

cis-α-[*CrCl*$_2$*(picen)*]*Cl*: The complex prepared by the method of Michelsen[5] was partially resolved by the same method as for *cis*-α-[CoCl$_2$(picen)]Cl. The CD spectrum of the former part of the eluted band showed a negative value at 17150, a positive one at 19420, a negative one at 36360, and a negative one at 37310 cm^{-1} (Fig. 4); this is similar to the spectra of $(-)_{589}$-[CrCl$_2$(picen)]ClO$_4$[7] and $(-)^{CD}_{600}$-[CrCl$_2$(*S*-picpn)]Cl.

cis-α-[*CrCl*$_2$*(trien)*]*Cl*: The complex[10] was partially resolved by the same method as for *cis*-α-[CoCl$_2$(picen)]Cl. The complex was adsorbed on an SP-Sephadex C-25 column (ϕ15×300 mm) and eluted with a 0.25 M sodium antimony(III) $(+)_{589}$-tartrate aqueous solution. The CD spectrum of the former fractions was opposite in sign to that of the latter fractions (Fig. 4).

Measurements. The visible and ultraviolet absorption spectra were obtained with a Shimadzu UV-200 spectrophotometer and the CD spectra with a JASCO MOE-1 spectropolarimeter. The absorption and CD spectra were measured in 0.1 M hydrochloric acid for the dichloro and dibromo complexes, and in water for the other complexes. The X-ray powder patterns were measured with Cu *K*α radiation for the chromium(III) complexes and with Co *K*α radiation for the cobalt(III) complexes. The IR spectra were run as nujol mulls on a JASCO DS-402G spectrophotometer.

Results and Discussion

Structural Assignments. $(+)^{CD}_{600}$-[*CoCl*$_2$*(S-picpn)*]$^+$: Three geometrical configurations, *cis*-α, *cis*-β, and *trans* (Fig. 1)[11] are possible in general for an octahedral

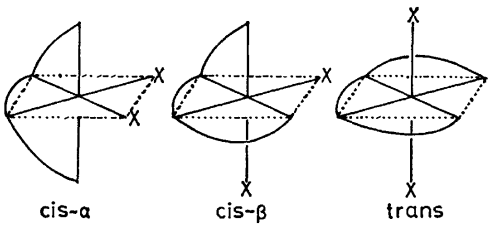

Fig. 1. Three geometrical isomers of [MX$_2$(linear tetradentate)]$^+$.

complex coordinating a linear tetradentate ligand. Both *cis*-α and *cis*-β configurations have several optically active isomers and their classifications is made in two steps. (1) In a [MX$_2$(picen)]$^+$ complex, *Δ* and *Λ* configurations exist for each of the *cis*-α and *cis*-β isomers. (2) Chirality of the coordinated secondary amine nitrogens should be considered for each configuration, *viz.*, only one (*R*,*R*) pair of asymmetric nitrogen is possible for the *Δ*-*cis*-α configuration and only one (*S*,*S*) for the *Λ*-*cis*-α. In the *cis*-β configuration, the two nitrogen atoms differ from each other and are distinguished by numbering N$_1$ and N$_2$ for those located at the center of N–N–N moieties coordinated facially and meridionally, respectively. Thus (R^1,R^2) and (R^1,S^2) isomers exist for the *Λ*-*cis*-β configuration, and (S^1,S^2) and (S^1,R^2) for the *Δ*-*cis*-β. For the case of [CoCl$_2$(*S*-picpn)]$^+$, the number of possible isomers of the *cis*-β configuration doubles the above number because of non-symmetrical disposition of the methyl substituent. Thus two structures are possible for the *cis*-α configuration and eight for *cis*-β. It is well established that the

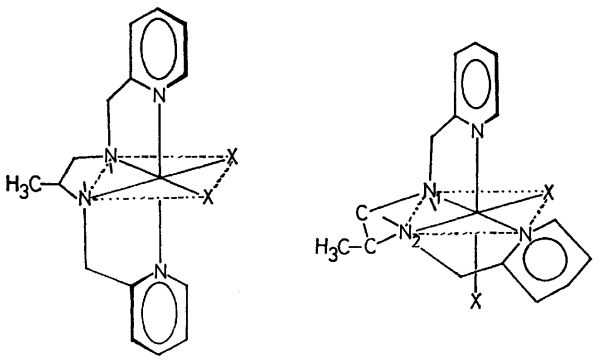

Fig. 2. Two configurations of [MX$_2$(*S*-picpn)]$^+$ (a) *Λ*-*cis*-α-(*SR*): this corresponds to the (*S*,*S*) isomer of picen complex. (b) *Δ*-*cis*-β-(S^1,R^2): this corresponds to the (S^1,S^2) isomer of picen complex.

methyl substituent of propylenediamine type moiety prefers the equatorial orientation in octahedral complexes.[12] Two of the ten possible isomers are shown in Fig. 2.

The CD spectrum of $(+)^{CD}_{600}$-[CoCl$_2$(*S*-picpn)]Cl prepared in the present study (Fig. 3) is in good agreement with the data of Cragel and Brubaker on their "*cis*-β" form.[2] On the other hand, the *cis*-α-[CoCl$_2$(picen)]$^+$ complex, assigned to this configuration,[4a] was resolved by SP-Sephadex column chromatography, and the CD spectrum (dotted line) is very similar in pattern to that of the $(+)^{CD}_{600}$-[CoCl$_2$(*S*-picpn)]Cl complex. Thus, the $(+)^{CD}_{600}$-[CoCl$_2$(*S*-picpn)]Cl complex is considered to take the *cis*-α configuration. The "*cis*-β" assignment by Cragel and Brubaker for this complex seems to be incorrect.

The CD spectrum of $(+)^{CD}_{600}$-[CoCl$_2$(*S*-picpn)]Cl shows a positive (longer wavelength) and a negative (shorter wavelength) extremum in the first absorption band region. In order to assign the absolute configuration

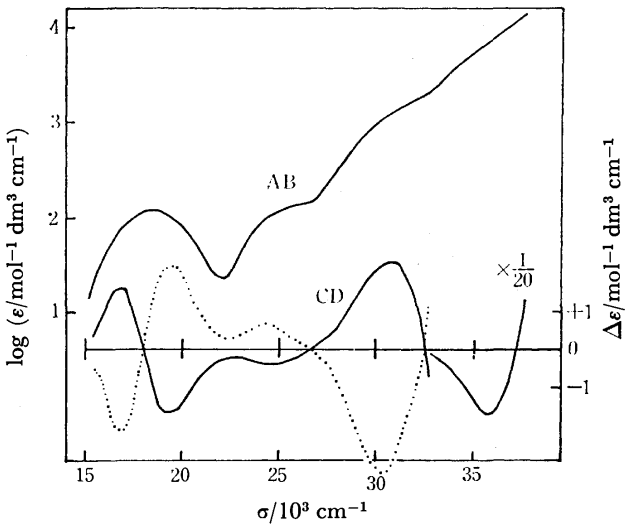

Fig. 3. The absorption (AB) and CD spectra of $(+)^{CD}_{600}$-[CoCl$_2$(*S*-picpn)]Cl (——), and the qualitative CD spectrum of former fraction of [CoCl$_2$(picen)]$^+$ eluted with sodium antimony(III) $(+)_{589}$-tartrate (···).

TABLE 1. ABSORPTION AND CD DATA OF *cis*-α- AND *cis*-β-[$CoCl_2$(tetradentate)]$^+$ COMPLEXES[a)]

Ligand	Configuration	Absorption		CD		Ref.
		σ_{max}/cm^{-1}	logε[d)]	σ_{ext}/cm^{-1}	$\Delta\varepsilon$[d)]	
(*S*)-picpn	*Δ*-*cis*-α	18520	2.10	16670	+1.67	b)
				19230	−1.65	
		26040 sh	2.13	24510	−0.41	
				30490	+2.34	
(3*S*,8*S*)-dimetrien	*Λ*-*cis*-α	18450	2.09	16340	−1.49	13)
				18940	+2.78	
		26040	2.02	24270	+0.59	
				27100	−0.57	
(2*S*,9*S*)-dimetrien	*Λ*-*cis*-α	18350	2.09	16290	−1.71	13)
				18690	+2.19	
		25970	2.04	24100	+0.35	
				26810	−0.89	
(3*S*,8*S*)-dimetrien	*Δ*-*cis*-β	18420	2.11	18690	−1.18	13)
		25190	2.10	24330	−0.60	
(2*S*,9*S*)-dimetrien	*Δ*-*cis*-β	18800	2.21	19050	−1.55	13)
		25320	2.18	24630	−0.40	
bnpic	*Δ*-*cis*-β	19000		17000	−0.31	15)[c)]
				20000	−0.80	

a) Abbreviations of ligands: (3*S*,8*S*)-dimetrien= (2*S*,7*S*)-2,7-dimethyl-3,6-diazaoctane-1,8-diamine; (2*S*,9*S*)-dimetrien= (1*S*,8*S*)-1,8-dimethyl-3,6-diazaoctane-1,8-diamine; bnpic= (2*S*,3*S*)-*N*,*N*′-bis(2-pyridylmethyl)-2,3-butanebiamine. b) This work; sh=shoulder. c) Values taken from the figure in the paper. d) Given in mol^{-1} dm^3 cm^{-1} unit.

of this complex, the CD spectrum was compared with those of the *cis*-α-[$CoCl_2$(dimetrien)]$^+$ (dimetrien= dimethyl derivative of triethylenetetramine) complexes (Table 1). The *Λ*-*cis*-α-[$CoCl_2$(dimetrien)]$^+$ complexes show a negative and then a positive CD extremum from the lower energy side in the first absorption band region, while the corresponding *cis*-β complex show no such dispersion type pattern.[13,14] Thus, it is confirmed that the $(+)^{CD}_{600}$-[$CoCl_2$(*S*-picpn)]$^+$ complex has *Λ*-*cis*-α configuration. Bosnich and Kneen prepared the *Λ*-*cis*-β-[$CoCl_2$(bnpic)]Cl complex,[15] which shows no dispersion type CD pattern (bnpic=(2*S*,3*S*)-*N*,*N*′-bis(2-pyridylmethyl)-2,3-butanediamine). Gibson and McKenzie,[4a] and Michelsen[5] prepared the *cis*-β dichloro complex with the picen ligand, but the *cis*-β complex of the *S*-picpn ligand was not formed by our methods. The reason why the *cis*-β complex could not be prepared for this ligand is unknown.

$(+)^{CD}_{600}$- and $(-)^{CD}_{600}$-[$CrCl_2$(S-picpn)]Cl: The CD spectrum of $(+)^{CD}_{600}$-[$CrCl_2$(*S*-picpn)]Cl shown in Fig. 4 (broken line) is quite enantiomeric to the qualitative CD spectrum (dotted line) of *cis*-α-[$CrCl_2$(picen)],[5]

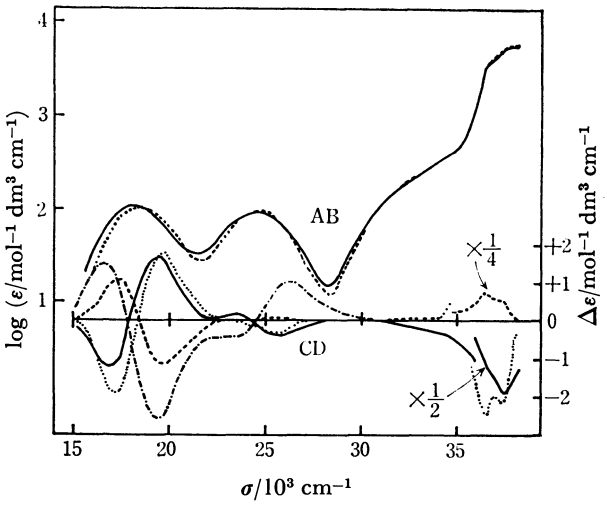

Fig. 4. The absorption (AB) and CD spectra of $(+)^{CD}_{600}$-[$CrCl_2$(*S*-picpn)]Cl (----), and $(-)^{CD}_{600}$-[$CrCl_2$(*S*-picpn)]Cl (——); and the qualitative CD spectra of *cis*-α-[$CrCl_2$(picen)]$^+$ (····) and *cis*-α-[$CrCl_2$(trien)]$^+$ (latter fraction) (-·-·-).

TABLE 2. INFRARED ABSORPTION OF [MCl_2(*S*-picpn)] Cl COMPLEXES (M=Co and Cr)

	$(+)^{CD}_{600}$-Co	$(+)^{CD}_{600}$-Cr	$(-)^{CD}_{600}$-Cr
CH_2-rocking	868	868	885
(860—940 cm^{-1})	932	932	901
CH_2-twisting	1005	1008	
(980—1100 cm^{-1})	1035	1033	1028
	1060	1057	1040
	1072	1070	1057
	1098	1095	

which was resolved by a chromatographic method. Thus, the $(+)^{CD}_{600}$-[$CrCl_2$(*S*-picpn)]Cl complex is assigned to the *cis*-α configuration. The IR spectra of the two complexes, $(+)^{CD}_{600}$-[$CoCl_2$(*S*-picpn)]Cl and $(+)^{CD}_{600}$-[$CrCl_2$(*S*-picpn)]Cl, were measured, and the wave numbers of the absorption bands corresponding to the CH_2-rocking and -twisting are given in Table 2. The peak positions of the two complexes almost agree. The IR data of another complex, $(-)^{CD}_{600}$-[$CrCl_2$(*S*-picpn)]Cl, also given in Table 2, differ from those of the former two

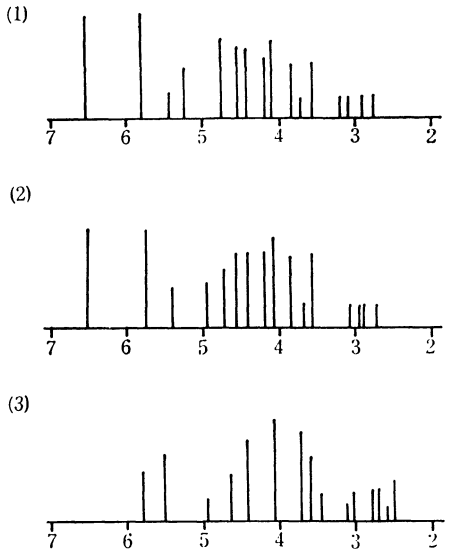

Fig. 5. The X-ray powder patterns: The *d*-spacings (in Å) of the complexes, $(+)^{CD}_{600}$-$[CoCl_2(S\text{-picpn})]ClO_4$ (1), $(+)^{CD}_{600}$-$[CrCl_2(S\text{-picpn})]ClO_4$ (2), and $(-)^{CD}_{600}$-$[CrCl_2(S\text{-picpn})]ClO_4$ (3).

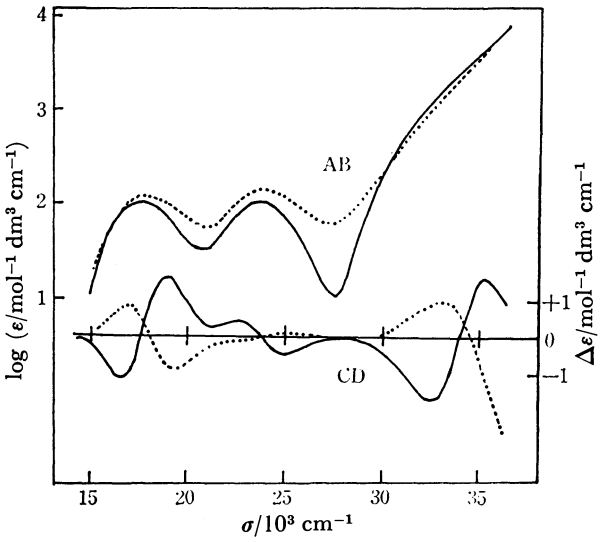

Fig. 6. The absorption (AB) and CD spectra of $(+)^{CD}_{600}$-$[CrBr_2(S\text{-picpn})]I$ (——) and $(-)^{CD}_{600}$-$[CrBr_2(S\text{-picpn})]Br$ (——).

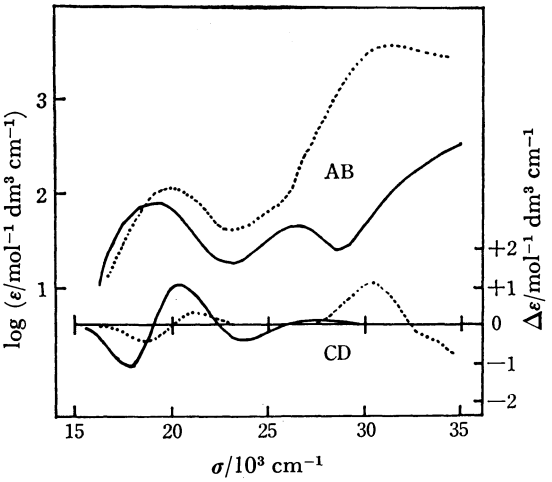

Fig. 7. The absorption (AB) and CD spectra of $(-)^{CD}_{600}$-$[CrF_2(S\text{-picpn})]Br$ (——) and $(-)^{CD}_{600}$-$[Cr(NCS)_2(S\text{-picpn})]SCN$ (——).

$(+)^{CD}_{600}$ complexes. Results of measurement of X-ray powder patterns of the three complexes (perchlorate salts) are shown in Fig. 5. The patterns of the cobalt(III) and the $(+)^{CD}_{600}$ chromium(III) complexes are very similar but that of the $(-)^{CD}_{600}$ chromium(III) complex is different. The CD spectra of the *Δ-cis-α*-$(+)^{CD}_{600}$-$[CoCl_2(S\text{-picpn})]Cl$, $(+)^{CD}_{600}$-$[CrCl_2(S\text{-picpn})]Cl$, and *cis-α*-$[CrCl_2(trien)]^+$ (latter fractions) complexes show a similar pattern (a positive and then a negative sign from the lower energy side) in the first absorption band region but that of the $(-)^{CD}_{600}$-$[CrCl_2(S\text{-picpn})]Cl$ complex shows the opposite dispersion type pattern (Fig. 4). It can be concluded that the former three complexes have the same *Δ-cis-α* configuration and the latter one *Λ-cis-α*. The latter *Λ-cis-α* configuration has been expected to be more unstable than the *Δ-cis-α* configuration from a strain energy minimization calculation.[3] This trend is reflected on the observed positions of the first absorption bands, *viz.*, the first absorption band (18180 cm^{-1}) of the *Λ* complex is in the slightly lower energy side than that (18520 cm^{-1}) of the *Δ* complex.

The Other Complexes: Absorption and CD spectra are shown on Figs. 6 and 7; the data are given in Table 3. Since the fluoro, chloro, bromo, and isothiocyanato ligands lie in the same (weaker) side on the spectrochemical series as compared with organic amine ligands,[16] the CD patterns of the fluoro, bromo, and isothiocyanato complexes are expected to resemble those of the corresponding chloro complexes in the first absorption band region, as seen in Table 3. All the complexes are assigned to the *cis-α* configuration, and the complexes which show a positive and then a negative CD extremum from the lower energy side in the first absorption band region to the *Δ-cis-α* configuration. The complexes with the inverse sign can be assigned to the *Λ-cis-α* configuration.

Spectral Properties: The wave number of the first absorption band maximum of the *Λ-cis-α*-$[CrBr_2(S\text{-picpn})]^+$ complex is slightly smaller than that of the *Δ-cis-α*-$[CrBr_2(S\text{-picpn})]^+$ complex (Table 3). The same trend was observed between the corresponding dichloro complexes, suggesting that the *S*-picpn ligand is strained to a greater extent in the *Λ-cis-α* configuration than in the *Δ-cis-α* one. The CD strength in the first absorption band region increases in the order NCS< F<Br<Cl.

The complexes $[CrCl_2(S\text{-picpn})]^+$ and $[CrF_2(S\text{-picpn})]^+$ show a broad absorption band of low intensity (log ε=1.2—2.6) in the region 30000—35000 cm^{-1}, where weak CD bands are observed. The low intensity absorption band might correspond to the third d-d band due to two electron excitation. An alternative explanation is to assign it to a d→π^* transition.[17] A similar band was observed in the $[Ni(phen)_3]^{2+}$ and $[Ni(bpy)_3]^{2+}$ complexes[18] in the region 22200—28600 cm^{-1} (phen=1,10-phenanthroline and bpy=2,2′-bi-

TABLE 3. ABSORPTION AND CD DATA OF CHROMIUM(III) COMPLEXES OF *cis*-α CONFIGURATION

Complex	Absorption		CD	
	σ_{max}/cm^{-1}	log ε[a)]	σ_{ext}/cm^{-1}	$\Delta\varepsilon$[a)]
Λ-[$CrCl_2$(*S*-picpn)]Cl	18520	2.01	17240	+1.13
			19610	−1.21
	24630	2.01	25250	+0.08
			36230	+3.13
			37040	+2.44
Λ-[$CrBr_2$(*S*-picpn)]I	17910	2.07	16950	+0.82
			19270	−0.87
	23920	2.16	25060	+0.08
			33000	+0.95
Λ-[$CrCl_2$(picen)]ClO_4	18350	2.02	17240	+1.15
			19610	−1.16
	24510	2.01	25510	+0.12
			36320	+2.79
			36900	+2.28
			37230	+2.57
Λ-[CrF_2(*S*-picpn)]Br	19120	1.91	17450	−1.13
			22620	+1.08
	26460	1.69	23580	−0.43
			27550	+0.08
Λ-[$CrCl_2$(*S*-picpn)]Cl	18180	2.00	16890	−1.29
			19230	+1.70
	24510	1.97	23420	+0.19
			25450	−0.42
			37310	−7.96
Λ-[$CrBr_2$(*S*-picpn)]Br	17700	2.02	16530	−1.12
			18870	+1.60
	23810	2.03	22680	+0.43
			24840	−0.50
Λ-[$Cr(NCS)_2$(*S*-picpn)]-SCN	19960	2.07	18690	−0.42
			21190	+0.34
			30300	+1.11
	31350	3.59		

a) Given in mol^{-1} dm^3 cm^{-1} unit.

pyridine). The bands in the present chromium(III) complexes seem to correspond to the "Ir(III)–pyridine band."[17] No such band is observed in the [$CrBr_2$(*S*-picpn)]$^+$ and [$CoCl_2$(*S*-picpn)]$^+$ complexes, in which the band is covered by charge transfer bands due to the bromo or chloro ligands.[19]

In the [CrX_2(*S*-picpn)]$^+$ complex, three kinds of chiralities should be considered: configurational (*Δ* and *Λ*), asymmetric carbon atoms (*S*), and conformational of the central chelate ring (*δ* and *λ*). Since the chiralities of the secondary amine nitrogen atoms in the *cis*-α complex depend on configurational chirality, the contributions of these two chiral nitrogen atoms are combined with that of the chirality *Δ* or *Λ*.

By applying the additivity rule,[20] CD contributions for the three complexes, *Λ*-*cis*-α-[$CrCl_2$(*S*-picpn)]$^+$ (1), *Λ*-*cis*-α-[$CrCl_2$(*S*-picpn)]$^+$ (2), and *Λ*-*cis*-α-[$CrCl_2$-(picen)]$^+$ (3), are written as follows.

$$\Delta\varepsilon(1) = \Lambda + \delta + S \quad \text{(i)}$$

$$\Delta\varepsilon(2) = \Lambda + \delta + S \quad \text{(ii)}$$

$$\Delta\varepsilon(3) = \Lambda + \lambda \quad \text{(iii)}$$

The vicinal contribution ($\delta+S$) of the ligand *S*-picpn is calculated by 1/2{(1)+(2)}:

$$\frac{1}{2}\{\Delta\varepsilon(1)+\Delta\varepsilon(2)\} = \delta + S$$

The configurational contribution (*Λ*) is calculated by 1/2{(1)−(2)}:

$$\frac{1}{2}\{\Delta\varepsilon(1)-\Delta\varepsilon(2)\} = \Lambda \quad \text{(iv)}$$

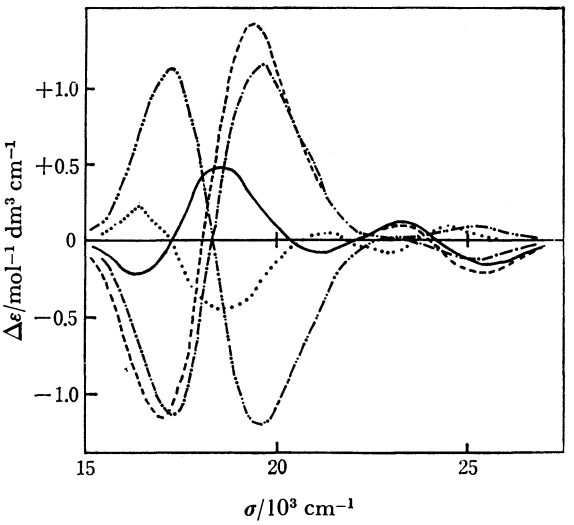

Fig. 8. Configurational and vicinal CD curves: configurational *Λ* (——), vicinal $\delta+S$ (——), and conformational *λ* (····). The observed CD curves of *Λ*-*cis*-α-[$CrCl_2$(*S*-picpn)]$^+$ (-·-·-·-) and *Λ*-*cis*-α-[$CrCl_2$(picen)]$^+$ (-····-) are also shown for comparison.

The calculated curves are shown in Fig. 8. We then obtain from (iii) and (iv) the conformational contribution (*λ*) (dotted line) of the central chelate ring,

$$\Delta\varepsilon(3) - \frac{1}{2}\{\Delta\varepsilon(1)-\Delta\varepsilon(2)\} = \lambda$$

This is nearly enantiomeric to the $\delta+S$ vicinal curve, indicating that the contribution of asymmetric atoms (*S*) is negligibly small. This is also substantiated by the fact that the observed CD curve of the *Λ*-*cis*-α-[$CrCl_2$(*S*-picpn)]$^+$ is almost identical to that of the *Λ*-*cis*-α-[$CrCl_2$-(picen)]$^+$ (Table 3). Similar CD curves for the vicinal and the configurational contributions can be calculated for the dibromo complexes.

We are grateful to Dr. Shinichi Kikkawa and Mr. Hideo Kusuyama for measuring the X-ray powder patterns.

References

1) B. Bosnich, *Proc. R. Soc. London, Ser. A*, **297**, 88 (1967).
2) J. Cragel, Jr., and G. R. Brubaker, *Inorg. Chem.*, **11**, 303 (1972).
3) G. R. Brubaker and R. A. Euler, *Inorg. Chem.*, **11**, 2357 (1972).
4) a) J. G. Gibson and E. D. McKenzie, *J. Chem. Soc., A*, **1971**, 1666; b) S. Utsuno, A. Hayashi, S. Kondo, and M. Utsumi, *Chem. Lett.*, **1979**, 351.

5) K. Michelsen, *Acta Chem. Scand.*, *A*, **31**, 429 (1977).
6) K. Michelsen, *Acta Chem. Scand.*, *A*, **30**, 521 (1976).
7) K. Michelsen, *Acta Chem. Scand.*, *A*, **32**, 847 (1978).
8) H. A. Goodwin and F. Lions, *J. Am. Chem. Soc.*, **82**, 5021 (1960).
9) J. Glerup, J. Josephsen, K. Michelsen, E. Pedersen, and C. E. Schäffer, *Acta Chem. Scand.*, **24**, 247 (1970).
10) D. A. House and C. S. Garner, *J. Am. Chem. Soc.*, **88**, 2156 (1966).
11) F. Basolo, *J. Am. Chem. Soc.*, **70**, 2634 (1948).
12) D. A. Buckingham and D. Jones, *Inorg. Chem.*, **4**, 1387 (1965). A. M. Sargeson, *Transition Metal Chem.*, **3**, 303 (1966).
13) M. Saburi and S. Yoshikawa, *Bull. Chem. Soc. Jpn.*, **45**, 806 (1972).
14) M. Goto, H. Matsushita, M. Saburi, and S. Yoshikawa, *Inorg. Chem.*, **12**, 1498 (1973).
15) B. Bosnich and W. R. Kneen, *Inorg. Chem.*, **9**, 2191 (1970).
16) R. Tsuchida, *Bull. Chem. Soc. Jpn.*, **13**, 388 (1938); Y. Shimura and R. Tsuchida, *ibid.*, **29**, 311 (1956).
17) C. K. Jørgensen, *Acta Chem. Scand.*, **11**, 151, 166 (1957); "Absorption Spectra and Chemical Bonding in Complexes," Pergamon Press (1962), p. 191.
18) J. Hidaka and B. E. Douglas, *Inorg. Chem.*, **3**, 1180 (1964).
19) H. Yamatera, *J. Inorg. Nucl. Chem.*, **15**, 50 (1960); V. M. Miskowski and H. B. Gray, *Inorg. Chem.*, **14**, 401 (1975).
20) C. T. Liu and B. E. Douglas, *Inorg. Chem.*, **3**, 1356 (1964); N. Matsuoka, J. Hidaka, and Y. Shimura, *ibid.*, **9**, 719 (1970); K. Okamoto, J. Hidaka, and Y. Shimura, *Bull. Chem. Soc. Jpn.*, **46**, 3134 (1973).

Adsorption of Orthophosphate on a Synthetic Silica-Alumina

Shuzo TOKUNAGA* and Jiro SHIOKAWA**

National Chemical Laboratory for Industry, Yatabe, Ibaraki 305

***Department of Applied Chemistry, Faculty of Engineering, Osaka University, Yamada-kami, Suita, Osaka 565*

(Received April 25, 1979)

The characteristics and mechanism of the adsorption of orthophosphate on a commercial synthetic silica–alumina, Neobead D, were studied. The adsorption rate increased with decrease in pH and increase in the dose of silica–alumina below the concentration of 4 g dm^{-3}. The adsorption almost terminated in 24 h, but a very slow reaction was observed even after 3 d. The adsorption isotherm follows the Freundlich equation, the inflection in the log-log plot indicating difference in the adsorption mechanism between low and high phosphate concentrations. The adsorption capacity increased with decrease in pH, being the highest at an initial pH of 3.0. The silica–alumina exhibited buffer action, phosphate-free solutions of pH 4—10 showing pH of *ca.* 6 after 24 h. In coincidence with and in proportion to the adsorption, release of hydroxide, sulfate and silicate ions occurred in the reaction of initial pH of 4.7. The sum of the equivalents of the three anions released could well account for the moles of phosphate adsorbed. The adsorption thus proceeds mainly through the ion-exchange process between phosphate in solution and the anions on the solid, univalent phosphate ions taking part in the reaction.

Recently eutrophication of enclosed water areas has caused problems in fishery, agriculture and other industries, and development of effective methods for removal of nutrients has become necessary.

In order to remove phosphate from water, coagulation, chemical and biological methods have been utilized conventionally. Ion-exchange is also effective for removal of phosphate, but does not seem advantageous since ordinary organic anion-exchange resins remove not only phosphate ions but also other anions. Yee[1] proposed a selective ion-exchange process using a packed bed of acid-treated alumina, with which orthophosphate, pyrophosphate, triphosphate, and hexametaphosphate can be removed efficiently. Regeneration of the alumina consumed was conducted with small amounts of sodium hydroxide and nitric acid. Columnar studies[2-4] made on the activated alumina process have shown that it has advantages such as high selectivity for phosphate, simplicity in operation, easy regeneration and production of small amounts of solid waste.

The phosphate adsorption capacity of alumina is increased by addition of silica, which suppresses crystallization of alumina and increases its surface area, mechanical strength and heat resistance. Takimoto *et al.*[5] showed that silica–alumina containing 10% silica by weight exhibits the highest phosphate adsorption capacity.

In order to study the removal of phosphate from aqueous solution, we used a commercial synthetic silica–alumina. Useful information was obtained about the characteristics and mechanism of adsorption of phosphate.

Experimental

Synthetic Silica–Alumina. Neobead D (Mizusawa Industrial Chemicals Ltd.) was pulverized to 105—250 μm in diameter. This is an X-ray amorphous hydrogel having the composition 79.4% Al_2O_3, 11.5% SiO_2, 1.1% SO_4, and 8.0% ignition loss, and a specific surface area of *ca.* 330 $m^2\ g^{-1}$.

Phosphate Solution. Potassium dihydrogenphosphate, KH_2PO_4 (reagent grade) was dissolved in water, the pH being adjusted with hydrochloric acid or sodium hydroxide.

Orthophosphate was chosen as a model phosphate, since other forms of phosphates proved to be also adsorbed on alumina,[1] and readily converted into orthophosphate in natural water through chemical and biological reactions.

Analysis. JIS K 0102† was applied to the determination of phosphate, sulfate (the barium–chromate colorimetric method) and aluminum ions, and JIS K 0101†† to that of silicate (the molybdenum blue method). Sulfate and silicate were determined after removing phosphate as calcium phosphate in order to avoid its interference which became appreciable from a phosphate concentration of *ca.* 0.03 mmol dm^{-3} in the sulfate determination and *ca.* 2 mmol dm^{-3} in the silicate determination.

Adsorption Rate. 3—12 g of the silica–alumina was added to 3 dm^3 of 1.05-mmol dm^{-3} phosphate solution, and stirred at 25 °C. An aliquot was taken at intervals and centrifuged, phosphate, sulfate, silicate, aluminum, and pH being determined for the supernatant.

Adsorption Equilibrium. Eighty cm^3 of 0—8.42-mmol dm^{-3} phosphate solution was placed in a 100-cm^3 glass-stoppered Erlenmeyer flask, to which 0.2 g of the silica–alumina was added. This was shaken in a 25 °C water bath for 24 h and centrifuged, and then phosphate, sulfate, silicate, aluminum, and pH were determined for the supernatant.

Results and Discussion

Adsorption Rate. Since adsorption of phosphate on silica–alumina is a solid-liquid reaction, the adsorption rate is strongly dependent on the total surface area of the solid, or solid concentration. Figure 1 shows decrease of phosphate concentration in solution at an initial pH of 5.0 with addition of 1.0—4.0 g dm^{-3} of the silica–alumina. The adsorption rate was extremely great immediately after the addition of the silica–alumina. The reaction seemed to almost terminate in 24 h, but the phosphate concentration decreased very slowly even after 3 d. Such a slow reaction was observed in the reaction between phosphate ions and alumina or kaolinite by Chen *et al.*[6] who postulated that it follows the first-order reaction rate law and

† Japanese Industrial Standard, "Testing Methods for Industrial Waste Water."

†† Japanese Industrial Standard, "Testing Method for Industrial Water."

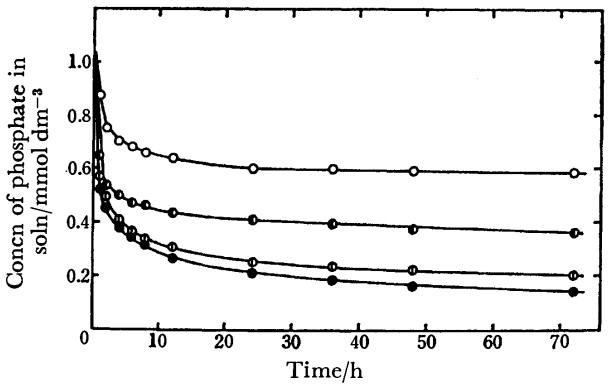

Fig. 1. Relation between adsorption rate and concentration of the silica–alumina.
Initial phosphate concentration: 1.05 mmol dm^{-3}, initial pH: 5.0, temperature: 25 °C, concentration of the silica–alumina (g dm^{-3}); ○: 1.0, ◐: 2.0, ⓘ: 3.0, ●: 4.0.

continues as long as for 60 d. The initial adsorption rate increased with increase in solid concentration, but this tendency became unappreciable with addition of a large amount of solid, indicating that diffusional effects become significant.

Effects of initial pH on the adsorption rate are shown in Figs. 2 and 3. The adsorption rate decreased considerably with increase in the initial pH value from 5.0 to 8.5. The pH variation and release of sulfate, silicate and aluminum ions were determined with the progress of phosphate adsorption. The release of sulfate rapidly reached a plateau possibly due to depletion of sulfate group on the solid. The release of the other ions was almost in line with the adsorption of phosphate. The pH variation in the alkaline solution seems independent of phosphate adsorption.

Adsorption Isotherm. Though phosphate concentration decreased very slowly even after 3 d, the adsorption rate was much higher at the initial stage, the greater part of the reaction having proceeded in several hours.

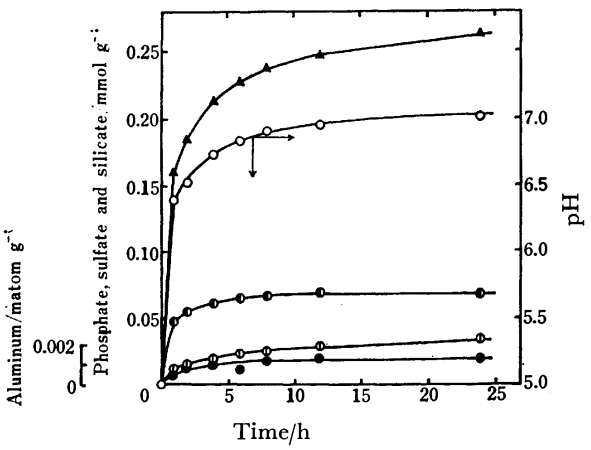

Fig. 2. Release of sulfate, silicate, and aluminum ions and pH variation concomitant with the adsorption of phosphate at an initial pH of 5.0.
▲: Amount of phosphate adsorbed (mmol g^{-1}), ◐: amount of sulfate released (mmol g^{-1}), ⓘ: amount of silicate released (mmol g^{-1}), ●: amount of aluminum released (matom g^{-1}, on the enlarged scale on the left), ○: pH (on the right scale).

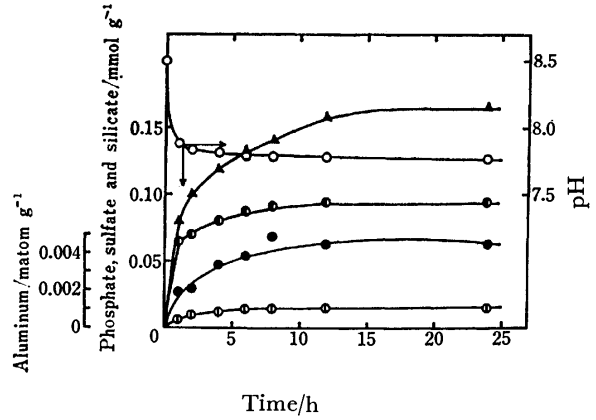

Fig. 3. Release of sulfate, silicate, and aluminum ions and pH variation concomitant with the adsorption of phosphate at an initial pH of 8.5.
▲: Amount of phosphate adsorbed (mmol g^{-1}), ◐: amount of sulfate released (mmol g^{-1}), ⓘ: amount of silicate released (mmol g^{-1}), ●: amount of aluminum released (matom g^{-1}, on the enlarged scale on the left), ○: pH (on the right scale).

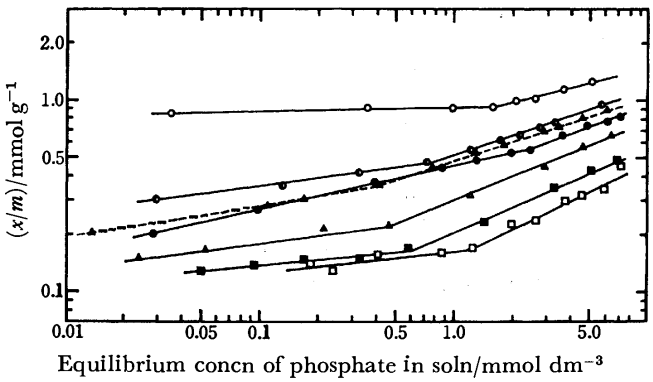

Fig. 4. log-log plots of adsorption isotherm data at 25 °C.
Initial pH; ●: 2.0, ○: 3.0, ◐: 4.0, ▲: 4.7, △: 7.2, ■: 8.5, □: 10.0.

Adsorption isotherms at 25 °C at initial pH 2.0—10.0 are shown in Fig. 4. The amount of phosphate adsorbed is plotted against the equilibrium concentration of phosphate in solution in logarithmic scale. A linear relationship was obtained. There is an inflection at a phosphate concentration of 0.38—2.58 mmol dm^{-3}. The linear relationship indicates that the adsorption reaction is of Freundlich type:

$$\log x/m = 1/n \log c + k,$$

where

x/m = quantity of phosphate adsorbed per unit mass of silica–alumina, mmol g^{-1},
c = equilibrium concentration of phosphate in solution, mmol g^{-1}, and
k and $1/n$ = constants.

The inflection in the isotherms indicates the difference in the adsorption mechanism between low and high

Table 1. Isotherms of phosphate adsorption on silica–alumina

Initial pH	Inflection point (mmol dm^{-3})	Low concn		High concn	
		$1/n$	$-k$	$1/n$	$-k$
2.0	2.58	0.217	0.350	0.387	0.420
3.0	1.75	0.050	0.033	0.264	0.085
4.0	0.70	0.152	0.310	0.307	0.286
4.7	0.38	0.154	0.400	0.349	0.318
7.2	0.50	0.102	0.620	0.417	0.525
8.5	0.59	0.092	0.776	0.417	0.701
10.0	1.31	0.130	0.783	0.509	0.828

Freundlich's adsorption equation: $\log x/m = 1/n \log c + k$.

phosphate concentrations. The values of the slope ($1/n$), intercept (k) and inflection of each isotherm are given in Table 1. The higher values of $1/n$ at higher phosphate concentrations indicate greater increase in phosphate adsorption value with increase in phosphate concentration. On the other hand, the lower values of $1/n$ and the higher values of intercepts at lower concentrations indicate that relatively high phosphate adsorption still takes place at lower concentrations of phosphate.

The quantity of phosphate adsorbed per unit mass of the silica–alumina was very small in alkaline solutions. It increased with decrease in pH value, becoming the greatest (>1 mmol g^{-1}) at an initial pH of 3.0. However, it was very low at an initial pH of 2.0.

The effects of pH in this system seem to change with the species of phosphate in solution and the adsorption reaction. The pH of the solutions varied during the course of reaction, the initial pH values 3.0, 4.0, and 4.7, at which high adsorption values were attained, finally increasing up to 4.2—5.5, 6.3—7.0, and 6.3—7.0, respectively, depending on adsorption values. The dissociation constants of orthophosphoric acid††† indicate that the univalent phosphate species, $H_2PO_4^-$, predominates in this range of pH. It can thus be said that univalent phosphate ion is most easily adsorbed, while molecular phosphoric acid and ionic species of higher valence are adsorbed with difficulty or not at all. Acidic condition seems to favor the adsorption of phosphate, since the highest adsorption values were obtained at an initial pH of 3.0.

Release of Hydroxide, Sulfate, Silicate, and Aluminum Ions. Increase in pH and release of sulfate, silicate, and aluminum ions were observed coincidently with the adsorption of phosphate. This is discussed for the case of initial pH of 4.7, where $H_2PO_4^-$ is the predominant form of phosphate and high adsorption values were obtained, and for that of initial pH 8.5 for comparison.

At zero phosphate-adsorption where the silica–alumina was added to phosphate-free water, the initial pH values 4.0, 4.7, 7.2, 8.5, and 10.0 turned to 5.7, 5.8, 6.0, 6.2, and 6.2, respectively ater 24 h. Sacconi[7] reported such surface buffer action for pure activated alumina in acid or salt solution and explained that it is due to displacement of Al^{3+} ions with H^+ ions in the solution. However, we found no such evidence in our silica–alumina study. The phenomenon can be explained in terms of adsorption and desorption of hydroxide ions on and from the silica–alumina, *i.e.*, desorption of hydroxide ions in acidic solution causes increase in pH, adsorption in alkaline solution a decrease.

††† $pk_1=2.2$, $pk_2=7.2$, and $pk_3=12.3$.

Table 2. Approximate value of hydroxide-ion release

Phosphate concn μmol dm^{-3}			pH		Δeq/mol[a] ratio	ΔOH[b]
Init. (*A*)	Fin. (*B*)	(*A*+*B*)/2	Init.	Fin.	(*C*)	μeq g^{-1}
0	0	0	4.73	5.80	—	0
526	14	270	4.72	6.70	0.41	44
790	113	452	4.79	6.94	0.54	98
948	170	559	4.76	7.00	0.58	130
1316	418	867	4.73	7.04	0.60	208
1974	776	1375	4.77	6.92	0.52	286
2632	1323	1979	4.79	6.83	0.46	364
3291	1812	2552	4.70	6.71	0.40	408
4607	2854	3731	4.73	6.54	0.30	448
5265	3412	4339	4.68	6.49	0.29	503
6581	4615	5598	4.78	6.41	0.23	515
8424	6143	7284	4.76	6.32	0.20	583

a) Increment of (OH equivalent: PO_4 mole) ratio corresponding to difference in pH, obtained on the titration curve. b) Equals $\frac{(A+B)}{2} \times C \times 0.08 \div 0.2$ (volume of sample solution=0.08 dm^3, and amount of the silica–alumina added=0.2 g).

In the phosphate solutions, the final pH increased with the adsorption of phosphate, indicating that hydroxide ions were released. Due to the buffer action

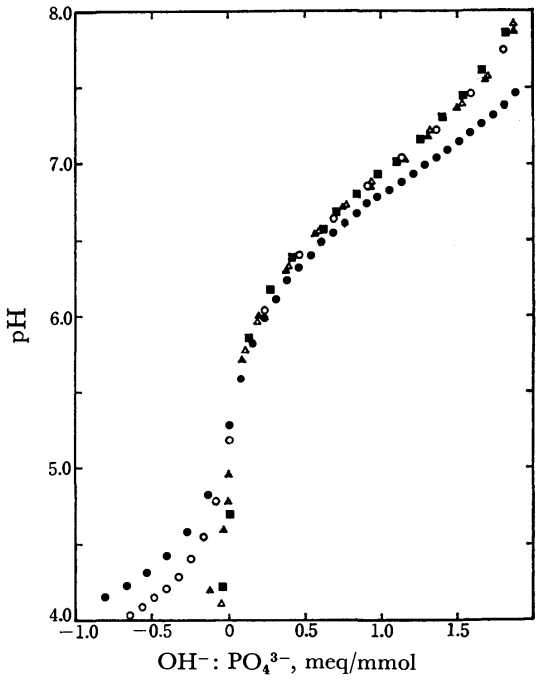

Fig. 5. Titration curves of dihydrogenphosphate solutions. (The positive and negative abscissae correspond to the titration with NaOH and HCl, respectively.) Phosphate concentration (mmol dm^{-3}); ●: 0.15, ○: 0.25, ▲: 1.00, △: 4.00, ■: 8.00.

of phosphate solution and decrease in phosphate concentration during the course of reaction, the amount of hydroxide ions released can not be calculated only from the initial and final pH values. If phosphate concentration remains constant during the course of reaction and pH increases, the amount of hydroxide ions released can be calculated using a titration curve of phosphate solution. The actual amount of hydroxide ions released should be between the value calculated from the initial phosphate concentration and that from the final concentration. We have calculated the approximate values of the hydroxide-ion release as follows (Table 2). The arithmetical mean value of the initial and final phosphate concentrations $((A+B)/2)$ was chosen to represent phosphate concentrations during the course of adsorption. This was multiplied by the increment of the ratio of hydroxide-ion equivalent and phosphate-ion mole $((C))$ corresponding to the difference between the initial and final pH values on the titration curves (Fig. 5). The curve was prepared by means of titration, adding sodium hydroxide or hydrochloric acid stepwisely to dihydrogenphosphate solutions of various concentrations. The shapes of the curves are almost the same in the pH range 5—8 and phosphate concentrations 0.25—8.0 mmol dm^{-3}.

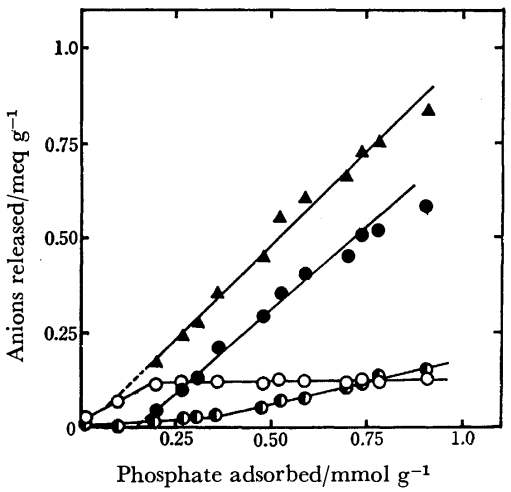

Fig. 6. Relation between adsorption of phosphate and release of hydroxide, sulfate and silicate ions at an initial pH of 4.7.
Amount of anions released (meq g^{-1}); ●: hydroxide ion (approximate value), ○: sulfate ion, ◐: silicate ion, ▲: sum of the equivalents of the three anions.

The calculated values together with the amounts of sulfate and silicate released* are plotted in Fig. 6 against the amounts of phosphate adsorbed. From an adsorption value of *ca.* 0.2 mmol g^{-1}, the release of hydroxide ions is in a linear relation with the adsorption of phosphate, indicating that phosphate ions in solution were exchanged with hydroxide group on the solid. However, at high adsorption values, it deviated downward from the linear relation, suggesting the existence of weakly and strongly bonded hydroxide groups on the silica–alumina, as reported by Takimoto *et al.*[5]

The silica–alumina originally contains *ca.* 0.2 meq g^{-1} of sulfate derived from aluminum sulfate. When it was brought into contact with neutral phosphate-free solution, *ca.* 0.06 meq g^{-1} of sulfate ions was released. In alkaline solution, sulfate release increased up to 0.2 meq g^{-1}, the total amount of sulfate contained in the silica–alumina. In acidic phosphate solutions, sulfate ions are released in proportion to the adsorption of phosphate, the release becoming constant as the sulfate on the solid is depleted. Thus the exchange process with sulfate ions is significant only at low phosphate adsorption values less than *ca.* 0.2 mmol g^{-1}. In alkaline phosphate solutions, on the other hand, a constant amount of sulfate ions, *ca.* 0.2 meq g^{-1}, was brought into solution irrespective of the phosphate adsorption, the sulfate ions undergoing exchange only with hydroxide ions.

The release of silicate ions was insignificant in alkaline phosphate solutions. In acidic phosphate solutions, it was very small in quantity at low adsorption values, but increased in proportion to the adsorption of phosphate above an adsorption value of *ca.* 0.2 mmol g^{-1}. In general, silicate tends to polymerize in aqueous solution, making determination by the molybdenum blue procedure impossible.[8] However, silicate determination before and after the sodium-carbonate fusion on the same sample gave almost the same results, indicating that the silicate exists in the monomeric state. Silicate groups at the terminal of the structure of the silica–alumina seem to be easily exchangeable with phosphate ions in solution, and consequently released as univalent anions such as $H_3SiO_4^-$.

From the coincidence of the release of the three anions with the adsorption of phosphate and the proportionality between the amounts of phosphate adsorbed and the three anions released, it is certain that the adsorption reaction involves an ion-exchange process between phosphate ions in solution and the three anions on the solid.

In consideration of the contribution of the three anions to the adsorption reaction, we see that the sulfate group plays the greatest role in the ion-exchange reaction for adsorption values less than *ca.* 0.2 mmol g^{-1}, while the contribution of sulfate rapidly decreases with increase in adsorption value due to depletion of the effective sulfate group on the solid. The contribution of hydroxide and silicate ions to the exchange reaction increases at higher adsorption values.

For a better understanding of the process of phosphate adsorption on silica–alumina, we should consider the species of phosphate adsorbed on the solid. By X-ray study Cole and Jackson[9] found that crystalline aluminum dihydroxide dihydrogenphosphate, $Al(OH)_2H_2PO_4$, is obtained by the reaction between aluminum oxide and potassium dihydrogenphosphate in acidic solution. It was suggested that phosphatized silica–alumina contains the H_2PO_4 group. However, we found no decisive evidence for the formation of crystalline material by means of X-ray diffraction.

We made stoichiometrical discussion on the basis of the release of the anions. The sums of the equivalents

* Blank values for phosphate-free solution were subtracted from individual measured values for phosphate solutions.

of the three anions released are plotted against moles of phosphate adsorbed (Fig. 6). These plots give a straight line with a 1.0 slope almost passing through the origin, indicating that the sum values can account for the moles of phosphate adsorbed. It can be concluded that the adsorption of phosphate on the silica–alumina proceeds mainly through the ion-exchange reaction between phosphate ions in solution and hydroxide, sulfate and silicate ions on the solid, and that the phosphate ions adsorbed should be univalent, the latter conclusion being supported by the results obtained from a similar study with an ion-exchange resin, Amberlite IRA-410 in the Cl^--form, in pH 4.0 solutions. The exchange ratio of phosphate and chloride ions was 1 : 1, indicating that phosphate ions taking part in the exchange reaction are univalent.

The amount of the release of aluminum ions was small, *ca.* 1/5—1/10 that of silicate ions. Aluminum ions were determined also by the atomic absorption method, which gave almost identical results with those obtained by the colorimetric method, indicating that the values obtained represent the total amount of aluminum ions which may be present in solution in various species. It tended to increase with the adsorption of phosphate and was greater in alkaline solutions, but was at most less than 0.08% of the total aluminum of the silica–alumina. It seems that the solubility of alumina hydrogel increases with increase in the concentration of phosphate.

References

1) W. C. Yee, *J. Am. Water Works Assoc.*, **58**, 239 (1966).
2) R. D. Neufeld and G. Thodos, *Environ. Sci. Technol.*, **3**, 661 (1969).
3) L. L. Ames and R. B. Dean, *J. Water Poll. Control Fed.*, **42**, R 161 (1970).
4) B. F. Winkler and G. Thodos, *J. Water Pollut. Control. Fed.*, **43**, 474 (1971).
5) K. Takimoto, A. Fujita, and S. Tsuda, *Bull. Chem. Soc. Jpn.*, **50**, 2479 (1977).
6) Y. S. R. Chen, J. N. Butler, and W. Stumm, *Environ. Sci. Technol.*, **7**, 327 (1973).
7) L. Sacconi, *Discuss. Faraday Soc.*, **1949**, 173.
8) M. Koyama and T. Hori, *Kagaku*, **29**, 59 (1974).
9) C. V. Cole and M. L. Jackson, *J. Phys. Colloid Chem.*, **54**, 128 (1950).

Lifetimes of *ortho*-Positronium in Benzene Solutions of β-Diketonates of Iron(III) and Cobalt(III)

Kazutoyo ENDO,* Michiaki FURUKAWA,† Hideo YAMATERA,† and Hirotoshi SANO

Department of Chemistry, Faculty of Science, Tokyo Metropolitan University, Fukazawa, Setagaya, Tokyo 158

†*Department of Chemistry, Faculty of Science, Nagoya University, Chikusa, Nagoya 464*

(Received May 21, 1979)

The lifetimes of *ortho*-positronium (*o*-Ps) have been measured in benzene solutions of β-diketonates of iron(III) and cobalt(III). A trend in substituent effect on the acceleration of *o*-Ps decay has been found. A substituent such as trifluoromethyl, that tends to withdraw electrons from the chelate ring, greatly accelerated *o*-Ps decay; the greatest rate constant observed was 33.8×10^9 M^{-1} s^{-1} for tris(hexafluoroacetylacetonato)iron(III). An electron-releasing substituent such as *t*-butyl accelerated *o*-Ps decay to a lesser extent, *e.g.* 10.5×10^9 M^{-1} s^{-1} for tris(dipivaloylmethanato)iron(III). The extent to which a complex accelerated *o*-Ps decay was largely related to the redox potential, which was observed by cyclic voltammetry. Complexes with phenyl substituents in the ligand showed slightly smaller effects than that suggested by their redox potentials.

Chemical reactions of *ortho*-positronium (*o*-Ps) in aqueous solutions have been investigated by many workers,[1–9] who have shown that the reactions of *o*-Ps with solute species can be characterized essentially as one or the other type: oxidation of *o*-Ps, and spin-conversion of *o*-Ps to *para*-positronium (*p*-Ps) and *vice versa*. Highly oxidizing ions such as MnO_4^- and CrO_4^{2-} oxidized *o*-Ps, resulting in a decrease in the lifetime and intensity of *o*-Ps.[2,3] Bartal and Ache[7] reported that the reactions of *o*-Ps show some similarities to those of the hydrogen atom in aqueous solutions of Werner-type cobalt(III) complexes. In nonaqueous systems, however, the interaction of *o*-Ps has not been systematically investigated. In nonaqueous solvents such as benzene, positrons and positronium as well as solute species are solvated to a lesser extent than in aqueous solutions. There is no evidence to prove whether positrons and positronium in benzene are solvated or not, but molecular orbital calculations have shown that the positron is barely bound to benzene.[10,11] Thus *o*-Ps will react with solute species in a way more characteristic of dissolved species. In a previous paper,[12] it was shown that *o*-Ps is oxidized by acetylacetonates and dipivaloylmethanates of iron(III) and manganese(III), and that the decay rate constant strongly depends on the redox potential of the solute. The reaction of *o*-Ps with solutes may however be influenced by the outer constituent of the solute molecule and the reaction mechanism may not be so simple. Thus, it is of interest to study the reaction of *o*-Ps with a series of complexes which are identical in the first coordination sphere but differ in the periphery.

A series of β-diketones form chelates of similar structure with a variety of metal ions. Among them, iron(III) forms tris chelates of high-spin ($S=5/2$) type, while cobalt(III) forms chelates of low-spin ($S=0$) type. In the present study, the lifetimes of positrons and positronium decaying in benzene solutions of β-diketonates of iron(III) and cobalt(III) have been measured. These complexes have different electronic densities at the metal center with different substituents in the ligands, thus showing different redox potentials. Another type of acceleration of *o*-Ps decay, due to spin-conversion mechanism, may occur in the presence of unpaired electrons. A comparison of the reaction rates for diamagnetic cobalt(III) and paramagnetic iron(III) complexes will enable the mechanism of *o*-Ps decay to be elucidated.

Experimental

Preparation of β-Diketonates. The following chemicals of reagent grade were used for the preparation of iron and cobalt complexes without further purification: acetylacetone (Hacac), dipivaloylmethane (Hdpm), trifluoroacetylacetone (Htfa), hexafluoroacetylacetone (Hhfa), 2-thenoyltrifluoroacetone (Htta), benzoyltrifluoroacetone (Hbta), dibenzoylmethane (Hdbm), benzoylacetone (Hbza), and 3-phenylacetylacetone (Hpaa).

Tris(β-diketonato)iron(III) complexes were prepared by the reaction of iron(III) sulfate or nitrate with the corresponding β-diketones.[13,14] $Fe(hfa)_3$, $Fe(tfa)_3$, $Fe(acac)_3$, and $Fe(dpm)_3$ were purified by repeated vacuum sublimations. $Fe(tta)_3$, $Fe(dbm)_3$, $Fe(bta)_3$, $Fe(bza)_3$, and $Fe(paa)_3$ were recrystallized from a benzene–hexane mixture. The preparation of aluminium complexes was essentially the same as that for the corresponding iron compounds. $Co(acac)_3$ was synthesized by the method of Moeller,[13] and $Fe(dpm)_3$ by Hammond *et al.*[14] $Co(tfa)_3$ and $Co(bza)_3$ were prepared from $Na_3[Co(CO_3)_3]3H_2O$, and purified on an alumina column.[15]

Lifetime Measurements. A specified amount of each complex was dissolved in benzene, and the solution was kept in a Pyrex-glass tube which contained a positron source of nearly 6 μCi of ^{22}Na(NaCl) of high specific activity. The ^{22}Na(NaCl) was sealed with aluminium foil, such that annihilation of positrons in the foil was negligibly small. The sample solution was degassed by repeated vacuum freeze-thaw treatments. The lifetime of positrons and positronium was measured with a fast-slow coincidence system constructed by the authors, the details of which were reported elsewhere.[16] The time resolution of the system was determined to be 750 ps (full width at half maximum) with prompt γ-rays of ^{60}Co under the same condition as that for positron measurements. The lifetime of *o*-Ps was obtained from the slope in the lifetime spectrum.

Cyclic Voltammetry. Cyclic-voltammetric measurements were made on β-diketonates of iron(III) and cobalt(III) in *N,N*-dimethylformamide (DMF), using 0.1 M tetrabutylammonium perchlorate (TBAP) as the supporting electrolyte. The measurement was conducted in a three-necked cell at room temperature. A platinum inlay electrode (Beckman 32273) was used as the working electrode; the counter electrode was a piece of platinum wire. A saturated Ag/AgCl

electrode as reference was connected to the cell by the two salt bridges: saturated KCl in water, and 0.1 M TBAP in DMF. A Hokuto Denko Model HA-101 potentiostat and a Hokuto Denko Model HB-107 function generator were used. Voltammograms were recorded on a Rikadenki X-Y recorder Model BW-133.

Results and Discussion

Benzene–Acetylacetone System. The lifetime spectra of positrons and positronium were measured in mixture of benzene and acetylacetone (Hacac). The lifetime (τ_2) of *o*-Ps in the mixture was essentially the same irrespective of the molar fraction of acetylacetone, whereas the *o*-Ps intensity (I_2) decreased with increasing molar fraction of Hacac (from 34.4% for pure benzene to 10.4% for pure acetylacetone), as shown in Fig. 1. The ionization and UV spectroscopy data suggest that no remarkable difference in the Oré gap model exists between benzene and acetylacetone, and thus the observed trend in I_2 values is not explainable by a simple Oré model.

Assuming the compounds of the mixture behave additively in the formation of *o*-Ps, the I_2 value for a mixture containing acetylacetone at a molar fraction of x may be expressed by

$$I_2 = \frac{\lambda_{pb}(1-x)+\lambda_{pa}x}{(\lambda_{pb}+\lambda_{qb})(1-x)+(\lambda_{pa}+\lambda_{qa})x}, \quad (1)$$

where λ_{pb} and λ_{qb} are respectively the average rate of *o*-Ps formation and that of annihilation without forming *o*-Ps in pure benzene, and λ_{pa} and λ_{qa} are those in pure acetylacetone. The curve in Fig. 1 shows the I_2 values calculated from Eq. 1, assuming $\lambda_{qb}/\lambda_{pb}=2$, $\lambda_{pa}/\lambda_{pb}=4$, and $\lambda_{qa}/\lambda_{pb}=34$. Within the experimental error, the curve fits the results except for one data point. This indicates that acetylacetone is ten times more reactive against positrons compared with benzene. The probability of *o*-Ps formation is however lower in the former case.

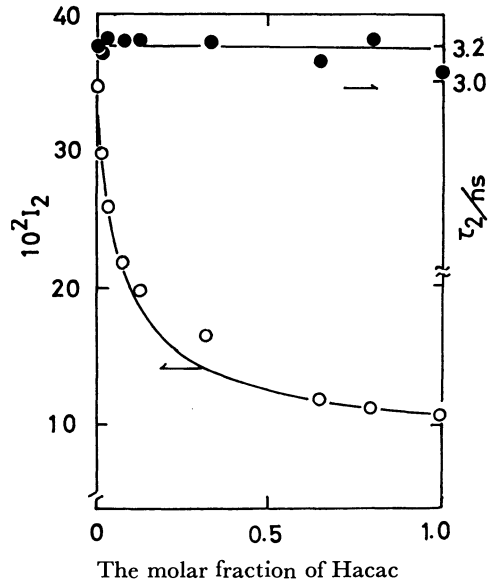

Fig. 1. Dependence of the lifetime(τ_2) and intensity(I_2) of *o*-Ps on the molar fraction of acetylacetone in acetylacetone–benzene mixture.

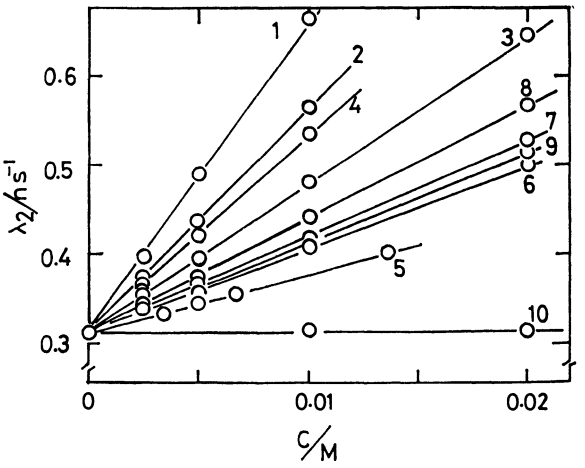

Fig. 2. Decay constant, $\lambda_2(\tau_2^{-1})$ of *o*-Ps in benzene solutions of β-diketonates of iron(III) as a function of the chelate concentration: (1) $Fe(hfa)_3$, (2) $Fe(tta)_3$, (3) $Fe(bta)_3$, (4) $Fe(tfa)_3$, (5) $Fe(dbm)_3$, (6) $Fe(bza)_3$, (7) $Fe(paa)_3$, (8) $Fe(acac)_3$, (9) $Fe(dpm)_3$, (10) $Al(bta)_3$ (as reference).

Effects of Ligating β-Diketonate Anion on the Lifetime of o-Ps. As reported in a previous paper,[12] $Al(dpm)_3$ and $Al(acac)_3$ do not affect the lifetime of *o*-Ps. Neither phenyl nor trifluoromethyl substituents changed the lifetime of *o*-Ps at 0.06 M, which was proved by the use of $Al(bza)_3$ and $Al(tfa)_3$. Therefore, the change in the lifetime of *o*-Ps in solutions of their complexes may be attributed to the effect of the central metal ions.

Lifetimes in Benzene Solutions of β-Diketonates of Iron(III) and Cobalt(III). The lifetime spectra of positrons and positronium were measured in benzene solutions of β-diketonato complexes at several concentrations. Figure 2 shows the plot of the observed decay constant, $\lambda_2(=\tau_2^{-1})$ against the solute concentration. For each compound, the following linear relationship was observed

$$\lambda_2 = 0.313 + k[C],$$

where 0.313 is the pick-off rate constant of *o*-Ps in pure benzene, [C] the molar concentration of the complex, and k the rate constant for *o*-Ps decay induced by the solute. The observed rate constants are given in Table 1. Apparently, the acceleration of *o*-Ps decay is greatest for compounds which have the trifluoromethyl group in the ligands. The trend is clearly shown in Fig. 3, where the rate constants of β-diketonates with different substituents are compared. For a series of β-diketonates with one common substituent, the acceleration of *o*-Ps decay increased in the same sequence of the other substituents. The sequence is closely related to the electron attracting or releasing properties of the substituents. For a more quantitative estimation of the latter property, the cyclic voltammograms were measured in DMF. Typical voltammograms are shown in Fig. 4. The voltammogram of $Fe(dbm)_3$ showed an almost reversible wave, whereas those of the other iron(III) compounds were found to be irreversible; the

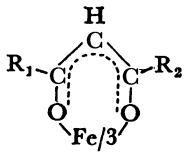

Common substituent	The sequence of the other substituent with regard to the acceleration of the *o*-Ps decay
CF_3	CF_3>thenoyl>CH_3>phenyl
phenyl	CF_3>CH_3>phenyl
CH_3	CF_3>CH_3>phenyl

Fig. 3. Schematic drawing of the molecular structure of tris(β-diketonato)M(III) (M=Co, Fe) and the sequence of the substituents with respect to the effects on the *o*-Ps decay.

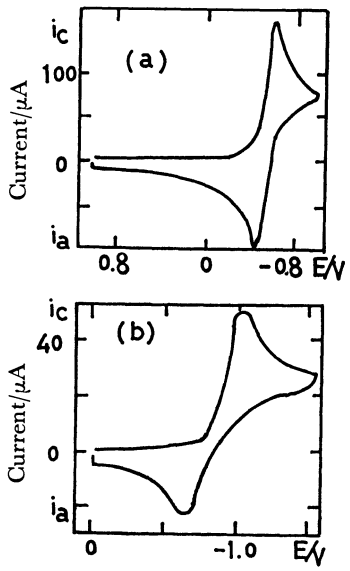

Fig. 4. Cyclic voltammograms for 5 mM β-diketonates of Fe(III) in *N*,*N*-dimethylformamide with 0.1 M tetrabutylammonium perchlorate: (a) $Fe(bza)_3$, (b) $Fe(dpm)_3$. Scan rate was 100 mV/s and the potential was measured against a saturated Ag/AgCl electrode.

irreversibility was highest for the wave of $Fe(dpm)_3$ among the iron(III) compounds studied, the results of which are summarized in Table 1. Figure 5 gives a plot of log *k* against *E*, the redox potential (the average of the peak potentials of the reduction and oxidation waves) of the complex. As expected, a greater acceleration of *o*-Ps decay was in general observed for a complex of less negative redox potential. The trifluoromethyl group tends to withdraw σ-electrons from the chelate ring, and therefore makes the reduction of the complex easier, both at the electrode and by *o*-Ps. Dipivaloylmethane has electron-releasing methyl substituents, and thus the increased electron density at the iron(III) atom of the dipivaloylmethanate makes the addition of an electron less easy. As seen in Fig. 5, exceptions were found for those compounds with phenyl substituents. In spite of the more positive or less negative redox potentials, the values of the rate constants were lower for $Fe(bta)_3$ and $Co(bta)_3$ than for $Fe(tfa)_3$ and $Co(tfa)_3$, respectively. The compounds, $Fe(dbm)_3$, $Fe(bza)_3$,

Table 1. Rate constants of *o*-Ps reaction and the cathodic and anodic potentials of cyclic voltammograms for β-diketonates of iron(III) and cobalt(III)

	$10^{-9}\,k/M^{-1}\,s^{-1}$	E_{pc}/V[a]	E_{pa}/V[a]
$Fe(hfa)_3$	33.8±0.8	0.50	0.72
$Fe(tta)_3$	24.6±0.5	0.06	0.19
$Fe(bta)_3$	19.6±0.5	0.07	0.21
$Fe(tfa)_3$	22.1±0.7	0.00	0.19
$Fe(dbm)_3$	7.1±0.4	−0.55*	−0.49*
$Fe(bza)_3$	9.6±0.3	−0.61	−0.47
$Fe(paa)_3$	10.1±0.4	−0.69	−0.55
$Fe(acac)_3$	15.6±0.6	−0.68	−0.55
$Fe(dpm)_3$	10.5±0.4	−1.16	−0.66
$Co(bta)_3$	16.6±0.7	−0.07	1.12
$Co(tfa)_3$	17.0±0.6	−0.05	1.10
$Co(bza)_3$	0.5±0.1	−0.93	0.53
$Co(acac)_3$	1.1±0.2	−1.04	0.47
$Co(dpm)_3$	0.0±0.1	—[b]	—[b]

a) The scan rate was 100 mV/s except for the data with an asterisk for which the scan rate was 500 mV/s, and the reproducibility of the potential was within±0.04 V on each sample. b) No reliable data were obtained because of the limited solubility of $Co(dpm)_3$.

$Fe(paa)_3$, and $Co(bza)_3$ also contain phenyl groups and showed lower *k* values than expected from the reduction potentials.

The *o*-Ps decay was also accelerated by most cobalt(III) complexes, but to a lesser extent than by the iron(III) analogues. This can primarily be attributed to the more negative reduction potentials of the cobalt(III) complexes. The reduction potential however cannot fully explain the very slow rate of reaction between *o*-Ps and the complex, and the electronic structure of the cobalt(III) complex may be partly responsible for the slow rates. Unlike the iron(III) β-diketonate of the high-spin type ($S=5/2$), all the cobalt(III) complexes investigated are of low-spin type ($S=0$). In the reduced state, however, the high-spin configuration should be preferred by the cobalt complexes ($S=3/2$) as well as the iron complexes ($S=2$). Thus, an extra activation energy will be required in the reduction of the cobalt complexes. Activation energy is essential in a kinetic process such as the reaction of *o*-Ps, but rarely important in the equilibrium. Voltammetry measures an equilibrium property rather than a kinetic one, although the latter is to some extent involved when irreversible waves occur. Thus the extra activation energy required in the reduction of cobalt(III) complexes will make the rate of the reaction with *o*-Ps considerably lower than expected from the redox potential.

An approximately linear relationship was observed between log *k* and *E* (Fig. 5); however, the slope or the value of $\Delta\log k/\Delta E$ was unusally small. A linear free energy relationship is often observed between logarithms of the rate and equilibrium constants of interrelated reactions, with a coefficient of $\Delta\log k_A/\Delta\log K_{A'}$, usually ranging from 0.3 to 0.9.[17] The $\Delta\log k/\Delta E$ value of 0.33

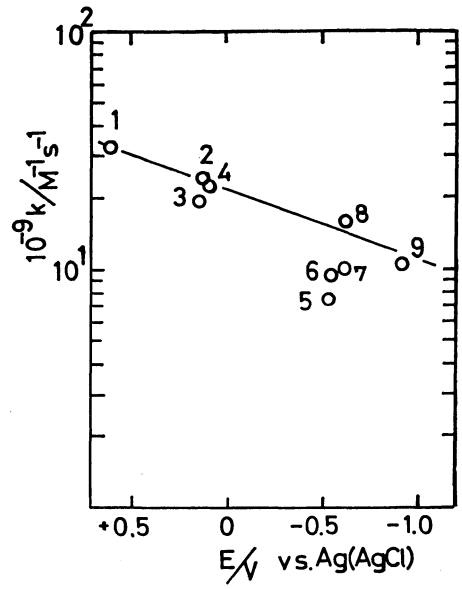

Fig. 5. Rate constants for the reactions of *o*-Ps with *β*-diketonates of iron(III) *vs.* the half-wave potentials measured with cyclic voltammetry in *N,N*-dimethylformamide with 0.1 M tetrabutylammonium perchlorate: (1) $Fe(hfa)_3$, (2) $Fe(tta)_3$, (3) $Fe(bta)_3$, (4) $Fe(tfa)_3$, (5) $Fe(dbm)_3$, (6) $Fe(bza)_3$, (7) $Fe(paa)_3$, (8) $Fe(acac)_3$, (9) $Fe(dpm)_3$.

observed here corresponds to a $\Delta\log k/\Delta\log K$ value of approx. 0.02.

No definite explanation can be made at present for this unusually small value. A possible explanation is that the rate constants were observed in a region where the rate is close to diffusion controlled. Assuming this to be the case, the $\Delta\log k/\Delta E$ value can be unusually small, but cannot be constant over such a wide range as covered in Fig. 5. Another possibility is that the difference between activation energies for the reactions of *o*-Ps and the iron(III) complexes is much less than that between the free energy changes for the electrode reactions of the complexes. This may occur if the structure of the complex undergoes only slight changes during the process of the reaction with the *o*-Ps atom, a very soft atom, from the initial to the transition state. A third possibility cannot be excluded, *i.e.* that the observed linear relationship is incidental and results from a mixing of the various effects including the steric effect of the substituent groups.

The acceleration of *o*-Ps decay can also occur through the spin-conversion mechanism in the presence of unpaired electrons. In the present case, this mechanism may not be important, since it has been previously shown that *o*-Ps decay by way of spin-conversion process makes only a minor contribution when both spin-conversion and oxidation processes are possible.[18]

The authors wish to thank Prof. I. Motoyama for his valuable advice on cyclic voltammetry.

References

1) For positronium chemistry, the following review papers and monographs are important: (a) J. Green and J. Lee, "Positronium Chemistry," Academic Press, New York, N. Y. (1964); (b) J. D. McGervey "Positron Annihilation," ed by A. T. Stewart and L. O. Roellig, Academic Press, New York, N. Y. (1967); (c) S. J. Tao and J. H. Green, *J. Chem. Soc., A*, **1968**, 408; (d) H. J. Ache, *Angew. Chem., Int. Ed. Engl.*, **11**, 179 (1972); (e) J. A. Merrigan, J. H. Green, and S. J. Tao, "Physical Methods of Chemistry," ed by A. Weissberger and B. W. Rossiter, Wiley, New York, N. Y. (1972), Vol. 1, Part III D; (f) S. H. Massey, *Phys. Today*, **42**, March (1976).

2) J. E. Jackson and J. D. McGervey, *J. Chem. Phys.*, **38**, 300 (1963).

3) V. I. Goldanskii and V. P. Shantarovich, *Appl. Phys.*, **3**, 335 (1974).

4) V. I. Goldanskii, T. A. Solonenko, and V. P. Shantarovich, *Dokl, Akad, Nauk SSSR*, **151**, 608 (1963).

5) J. B. Nicholas, R. E. Wild, L. J. Bartal, and H. J. Ache, *J. Phys. Chem.*, **77**, 178 (1973).

6) L. J. Bartal, J. B. Nicholas, and H. J. Ache, *J. Phys. Chem.*, **76**, 1124 (1972).

7) L. J. Bartal and H. J. Ache, *J. Inorg. Nucl. Chem.*, **36**, 267 (1974).

8) A. L. Nichols, R. E. Wild, L. J. Bartal, and H. J. Ache, *Appl. Phys.*, **4**, 37 (1974).

9) R. E. Wild and H. J. Ache, *J. Chem. Phys.*, **65**, 247 (1976).

10) W. J. Madia, J. C. Schug, A. L. Nichols, and H. J. Ache, *J. Phys. Chem.*, **78**, 2682 (1974).

11) D. M. Schrader and C. M. Wang, *J. Phys. Chem.*, **80**, 2507 (1976).

12) K. Endo, M. Furukawa, and H. Yamatera, *J. Phys. Chem.*, **80**, 1540 (1976).

13) For acac complexes, see for example, W. C. Fernelius and J. E. Blanch, *Inorg. Synth.*, **5**, 130 (1957); R. C. Young, *ibid.*, **2**, 25 (1946).

14) G. S. Hammond, D. C. Nonhebel, and Chin-Hua. S. Wu, *Inorg. Chem.*, **2**, 73 (1963).

15) R. C. Fay and T. S. Piper, *J. Am. Chem. Soc.*, **85**, 500 (1963).

16) K. Endo, K. Sasaki, M. Furukawa, and H. Yamatera, *Nucl. Instr. Meth.*, **141**, 273 (1977).

17) See for example, A. A. Frost and R. G. Peason, "Kinetics and Mechanism," 2nd ed, John Wiley and Sons, Inc., New York and London (1961) p. 223.

18) K. Endo, M. Furukawa, H. Yamatera, and H. Sano, *Bull. Chem. Soc. Jpn.*, **51**, 2566 (1978).

 © 1980 The Chemical Society of Japan Bull. Chem. Soc. Jpn., 53, 411—415 (1980)

The Precipitation of Traces of Copper, Cadmium, and Lead with 6-Anilino-1,3,5-triazine-2,4-dithiol and Its Application to X-Ray Fluorescence Spectrometry

Hiroto WATANABE* and Takashi UEDA

Department of Applied Chemistry, Muroran Institute of Technology, Mizumoto-cho, Muroran 050

(Received June 15, 1979)

A selective enrichment procedure for copper, cadmium, and lead is described. This method is based on precipitating the three elements with 6-anilino-1,3,5-triazine-2,4-dithiol (ATD) or with a combination of ATD and benzyldimethyltetradecylammonium chloride (BMTAC), filtering the precipitates to form a suitable X-ray sample, and then analyzing the sample by means of X-ray fluorescence. Microgram amounts of the three elements were precipitated quantitatively with ATD from 50 cm^3 or less of aqueous solutions of pH 7. Several to several tens mg amounts of such other elements as aluminium, iron(III), vanadium(V), zinc, arsenic(III, V), nickel, cobalt, and manganese(II) do not form any precipitates in the presence of citrate. Quantitative recoveries of the three elements from aqueous solutions ranging from 200 to 500 cm^3 were also possible when BMTAC was present as a coagulant aid. ATD was used for the determination of the three elements in reference materials (Orchard Leaves and Pepperbush Leaves). The results agreed with the certified values and with those obtained by isotope-dilution mass-spectrometry, and the precisions were satisfactory. The three elements in hot-spring water at levels from several to several tens ppb were determined by using a combination of ATD and BMTAC.

Various 6-substituted 1,3,5-triazine-2,4-dithiols react with relatively limited numbers of metal ions to give precipitates which are sparingly soluble in water.[1] One of the most remarkable properties of the dithiols is their extraordinary stability. They are not readily oxidized on exposure to air and are stable in either an alkaline or an acid solution.[1] This is quite different from the properties of other sulfur-containing ligands, such as dithiocarbamates, which react rather nonspecifically with a wide variety of metal ions. The dithiols have proved to be very effective in precipitating copper(II), cadmium(II), lead(II), and mercury(II) in industrial waste waters.[2]

Precipitation has long been used for the concentration and separation of trace elements in aqueous samples. Recently emphasis has been placed on the use of polymeric precipitating reagents. Muzzarelli[3] used a naturally occurring chelating polymer, chitosan, and Buono *et al.*[4] employed poly(5-vinyl-8-hydroxyquinoline). However, there has been little mention of utilizing organic ligands which give rise to polynuclear complexes. It is well known that dithiooxamide (DTO) reacts with copper to form a bridged polymer consisting of a series of five-membered rings.[5] Unfortunately, DTO is unstable and readily undergoes hydrolysis to hydrogen sulfide, so that metal ions, such as zinc, cadmium, lead, and mercury, are precipitated as their sulfides.[6] In this respect, the dithiols seem to be potential precipitants. As has been reported by Chudy and Dalziel[7] and by Mori *et al.*,[8] the dithiols are also capable of forming polymeric complexes with metal ions.

Of the commercially available dithiols, 6-anilino-1,3,5-triazine-2,4-dithiol (ATD) was chosen in this study because it gave the most insoluble precipitates. This report will deal with the application of ATD as a precipitant for the determination of copper, cadmium, and lead in conjunction with X-ray fluorescence (XRF) spectrometry.

Experimental

Materials. A 1.0% (w/w) ATD solution was prepared by dissolving 1.0 g of the compound (sodium hydrogen 6-anilino-1,3,5-triazine-2,4-dithiolate tetrahydrate; Sankyo Kasei Co., Ltd., Osaka) in 50 cm^3 of 2 mol dm^{-3} aqueous sodium hydroxide and by then diluting the mixture to 100 g with water.

A 0.001 mol dm^{-3} aqueous solution of benzyldimethyltetradecylammonium chloride (BMTAC) was prepared by using a commercial material (Dojindo Co., Ltd., Kumamoto).

Standard solutions containing 1 g dm^{-3} portions of a number of elements were prepared by dissolving weighed quantities of the high-purity metal, oxide or salt in a minimum amount of acid and then diluting the mixtures to known volumes. Working solutions containing the cations at concentrations of from 1 to 100 $\mu g\ cm^{-3}$ were prepared by dilution.

A buffer solution of pH 7.0 was made by mixing 0.5 mol dm^{-3} of sodium dihydrogenphosphate and 0.5 mol dm^{-3} of disodium hydrogenphosphate.

A 0.5 mol dm^{-3} portion of sodium citrate was prepared by dissolving the compound in water.

The citrate and the buffer solutions were cleansed of metal contaminants by precipitation with ATD, as in Method A described below.

The other reagents, such as nitric, hydrochloric, hydrofluoric, and perchloric acids, were purified by sub-boiling distillation.[9]

Apparatus. A Rigaku model SX X-ray fluorescence spectrometer with a tungsten target tube, a LiF(200) crystal, and a NaI(Tl) scintillation counter was used. However, in the determination of cadmium, it was necessary to use a chromium target tube, an EDDT crystal, and a flow proportional counter. The X-ray tubes were operated at 40 kV and 35 mA. Both sample and spectrometer chambers were evacuated to a pressure of less than 13.3 Pa.

Procedure. Precipitation of Copper, Cadmium, and Lead with ATD (Method A): To a test solution (usually 25 cm^3) containing 10 μg or less of the respective element, 1 cm^3 of a 1.0% ATD solution and 1 cm^3 of 0.5 mol dm^{-3} sodium citrate were added. Then the pH was adjusted to 7.0 with 2 cm^3 of the phosphate buffer and, if necessary, with an appropriate amount of ammonium hydroxide or hydrochloric

acid. The resulting mixture was allowed to stand for 20 min at room temperature and then filtered under suction through a Millipore filter disk (25 mm diameter, 0.45 μm pore size). The precipitate on the filter disk was washed with a small amount of water and subsequently allowed to dry at 60 °C for 10 min. The XRF specimens thus prepared were placed between 6 μm Mylar films in an XRF sample holder. A titanium disk was inserted into the holder to keep the filter flat. The XRF intensities were then measured at the *Kα* line of copper (45.02°) and the *Lα* lines of cadmium (53.38°) and lead (33.92°). The counting times were 40 s except in the case of cadmium, for which the counting time was 100 s. The background counts were measured at the following 2θ values: copper (44.52°, 45.52°), cadmium (52.38°, 54.38°), lead (33.72°, 34.12°).

Precipitation of the Three Elements with a Combination of ATD and BMTAC (Method B): To a test solution (usually 200 cm^3) containing 10 μg or less of the respective element, 1 cm^3 of a 1.0% ATD solution, 1 cm^3 of 0.5 mol dm^{-3} sodium citrate, 1 cm^3 of 0.001 mol dm^{-3} BMTAC, and 2 cm^3 of the phosphate buffer were added successively. Precipitation and XRF sample preparation were then performed as in Method A, but the time of precipitation was extended to 25 min. These methods were selected in view of the results of the optimization study to be described in the next section.

Throughout the present study, the recovery yields of the three elements (5.0 μg each) were expressed as ratios of the net counts of samples prepared under various conditions to that of a reference sample. The reference sample was prepared by applying Method A to a 25 cm^3 aqueous solution containing 5.0 μg of the respective element. For the reference sample, the recoveries of the three elements were confirmed to be quantitative by determining the three elements remaining in the filtrates. Atomic absorption spectrometry was used for this purpose.

Results and Discussion

Effect of the pH *on the Precipitation of Various Elements.* The recovery yields of various elements from 25 cm^3 of aqueous solutions were examined as a function of the pH in the absence of BMTAC. This procedure was practically the same as Method A except that no buffer was used and filtration was done 60 min after precipitation. Copper was precipitated over the pH range of 4—9, while the range for cadmium and lead was 6 to 9, as is shown in Fig. 1. Thus, a pH value of 7 was chosen in Method A. The precipitates thus formed were easily filtered and did not adhere to glass.

Ten micrograms of other elements, such as cobalt, nickel, arsenic(III, V), manganese(II), vanadium(V), zinc, aluminium, iron(II, III), bismuth, calcium, and magnesium, gave no precipitates over the entire pH range studied. In the absence of citrate aluminium, iron(III) and bismuth were precipitated, but their precipitates seemed to be hydroxides because the precipitation of these elements was also observed for solutions from which ATD was omitted. When the pH was adjusted to 7 by using the phosphate buffer in the presence of citrate, the other elements did not form any precipitates.

Although it has been pointed out that mercury(II) forms a highly insoluble precipitate with ATD,[1,2] the sensitivity of XRF for mercury is low, thus precluding its determination in the present study. ATD itself

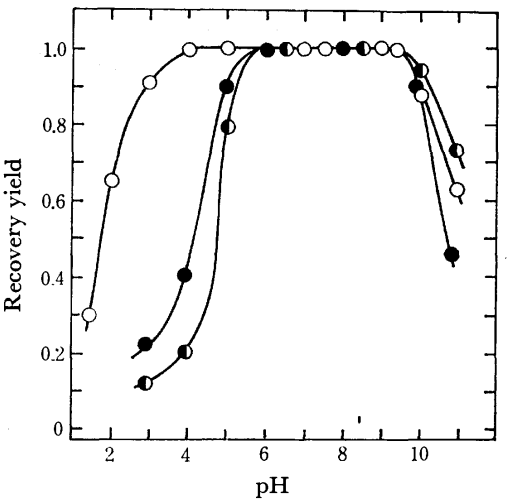

Fig. 1. Effect of pH on the precipitation of copper(II), cadmium(II), and lead(II) with ATD.
○: Cu, ●: Cd, ◐: Pb.
Counting time: 10 s. Total volume of aqueous solutions: 25 cm^3. Amount of each of the three elements: 5.0 μg.

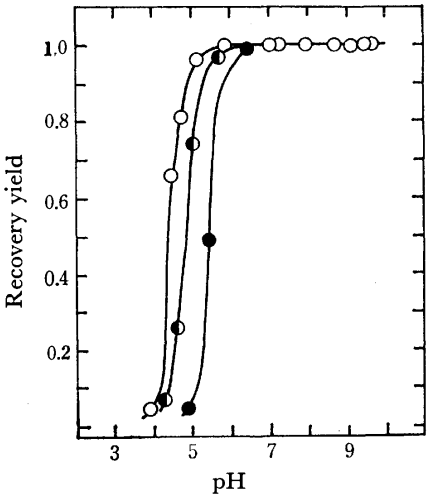

Fig. 2. Effect of pH on the precipitation of copper(II), cadmium(II), and lead(II) with the ATD–BMTAC combination.
○: Cu, ●: Cd, ◐: Pb.
Counting time: 40 s for Cu and Pb, 100 s for Cd. Total volume of aqueous solutions: 200 cm^3. Amount of each of the three elements: 5.0 μg.

did not precipitate at pH 7, but it was precipitated below pH 4. This is due to the insolubility of the protonated form of ATD.

Figure 2 shows the effect of the pH on the collection of the three elements from 200 cm^3 portions of aqueous solutions containing BMTAC. For this purpose, Method B, from which the phosphate buffer had been omitted, was used. The recoveries of the three elements were quantitative over the pH range of 6—9. Working at pH values greater than 9 appeared to be time-consuming for filtration (>30 min): thus, no further studies were carried out. For the filtration of 200 cm^3 portions of the

aqueous solutions prepared over the pH range of 6—9, a period of 5 min was required. For experimental convenience, a pH value of 7 was also chosen in Method B.

ATD itself did not form any precipitates with BMTAC. This was verified by the fact that no intensities due to sulfur $K\alpha$ line were observed for samples from which the three elements had been omitted.

Effect of ATD. Ten-μg amounts of the three elements were precipitated from 25 cm³ (Method A) or 200 cm³ (Method B) of test solutions containing various amounts of ATD. The recoveries were independent of the amounts of the ATD solution in the range >0.8 cm³. Thus, 1 cm³ of the ATD solution was used for both methods.

Effect of Time. The minimum time required to obtain quantitative precipitation was determined by varying the time of precipitation. Method A was used for several 25 cm³ solutions, filtration being done for a specified period of time ranging from 5 min to 24 h. It was found that filtration should be performed after 20 min in Method A.

Method B was applied to several 200 cm³ portions of test solutions. After the addition of the ATD solution and the phosphate buffer to the test solutions, the mixtures were allowed to stand for from 5 to 60 min. Twenty-five min was found to be adequate for the completion of the precipitation of the three elements.

Table 1. Effect of sample volume on the recovery yields of the three elements[a] at pH 7

Method A				Method B			
Volume cm³	Recovery yield Cu	Pb	Cd	Volume cm³	Recovery yield Cu	Pb	Cd
10	1.00	1.00	1.00	200	1.00	1.00	1.00
25	1.00	1.00	1.00	300	0.99	0.98	0.99
50	1.00	1.00	1.00	400	1.01	0.99	1.00
100	1.00	0.98	0.81	500	1.00	1.00	0.99
150	0.74	0.66	0.51				

a) A 5-μg portion of the respective element was used.

Effect of Sample Volume. Method A was applied to various volumes (10—150 cm³) of test solutions. The results, shown in Table 1, indicate that the influence of the sample volume is significant. It is thus recommended that the sample volume should be made up to 50 cm³ or less for the simultaneous determination of the three elements.

On the other hand, when BMTAC was present, the recovery yields were essentially independent of the sample volume, as is shown in Table 1. A 5 μg portion of the respective element was precipitated quantitatively even from 500 cm³ of aqueous solutions. This fact makes it possible to determine the three elements present in water at levels of from several to several tens ppb. This marked effect of BMTAC is probably due to the formation of a large anionic polynuclear complex of ATD. This interpretation seems to be consistent with the failure of a usual organic solvent such as *N,N*-dimethylformamide to dissolve the precipitates prepared by Method A. Working with sample volumes larger than 500 cm³ was not done, but it appeared to be too time-consuming to be practical.

Effect of BMTAC. The three elements were collected from 200 cm³ portions of aqueous solutions containing various amounts of BMTAC. When the amount of the BMTAC solution added was 1 cm³ or larger, the recoveries were quantitative. However, a longer period (>30 min) was required for filtration because of the dispersing action when 3 cm³ or more of the BMTAC solution was added. When 1 cm³ of the BMTAC solution was added to test solutions ranging from 200 to 500 cm³, a period of 5 to 10 min was required for filtering off the precipitates. Thus, in Method B a 1 cm³ portion of the solution was employed.

Table 2. Effect of foreign ions on the determination of the three elements[a]

Foreign ion	Added mg	Method A Cu	Pb	Cd	Method B Cu	Pb	Cd
Fe(III)	1.0				0.97	0.98	0.96
	10	1.01	1.03	0.97			
Mn(II)	2.0				1.01	1.00	1.00
	40	1.00	1.01	0.99			
Zn(II)	2.0				1.00	1.01	1.01
	10	1.00	0.98	1.02			
Co(II)	2.0				0.99	0.99	0.98
	10	0.98	0.97	0.96			
Ni(II)	2.0				1.01	1.02	1.00
	10	1.00	0.99	0.98			
V(V)	5	0.98	0.97	0.96			
Bi(III)	0.3	1.03	1.02	1.01			
Al(III)	1.0				0.96	0.97	0.98
	20	0.99	0.98	0.99			
Ca(II)	20				1.00	1.01	1.00
	30	0.97	0.97	0.98			
Mg(II)	20				1.00	1.00	1.01
	50	0.97	0.98	0.98			

a) A 5-μg portion of the respective element was used.

Effect of Foreign Ions. Test solutions containing 5.0 μg of the respective element and various amounts of a foreign ion were analysed. The results are summarized in Table 2. Lower results were obtained when foreign ions other than calcium, magnesium, and arsenic(III, V) were present in amounts higher than those indicated in Table 2. In Method A, several to several tens mg of foreign ions do not interfere with the determination of the three elements. It is well known that arsenic interferes seriously with the determination of lead because of mutual line interference. However, ATD does not react with arsenic(III, V), so the interference for lead is thus eliminated. At least 1 mg of arsenic was tolerable for the determination of 5 μg of lead.

In Method B the tolerance limits of foreign ions are lower than those in Method A. This is due to the precipitation of foreign ions to such an extent that the

XRF intensities of the three elements are lowered significantly. For example, when 1 mg of iron(III) was added about 10 μg portions of iron were found on the filter disk by measuring the XRF intensity of the iron $K\alpha$ line. The precipitation of iron(III) becomes more significant as the quantities of iron(III) exceed 1 mg. This precipitation of iron(III) may be caused by the reaction between a citrate complex of iron(III) and BMTAC, for a similar tendency was observed on samples prepared by Method B from which the ATD solution and the buffer had been omitted. The precipitate of iron(III) has a very small grain size; hence, filtration is made more time-consuming (>30 min). Though it was not shown in Table 2, the recoveries of the three elements were quantitative from test solutions (200—500 cm^3) of any salinity up to that of seawater.

Mutual interferences among the three elements must also be taken into account. When one of the three elements was present in an amount higher than 100 μg, the XRF intensities for the other two elements were reduced. The total amounts of the three elements in an aliquot should be below 100 μg for both methods.

TABLE 3. SENSITIVITY AND PRECISION

	Cu	Pb	Cd
Sensitivity (counts/s)/μg	253	42.1	38.7
Background counts/s	1100	1113	19.9
95% confidence limit[a] μg	5.05±0.10[b]	5.05±0.11[b]	5.02±0.05[b]
	5.03±0.20[c]	5.02±0.24[c]	5.03±0.13[c]
Limit of detection μg	0.04	0.24	0.03

a) Confidence limit (95%) for the median of the eleven samples used for the preparation of the calibration curves. The median sample contains 5.00 μg of the respective element. b) Method A. c) Method B.

Calibration Curve. Linear calibration functions were obtained for the three elements in the concentration range of up to 10 μg. Table 3 lists the sensitivity of the XRF measurements; the background counts; the confidence limits (95%), C, for the median of the eleven samples used for the preparation of the calibration curves, and the limit of detection, D. The limit of detection at the 95% confidence level was calculated from the $D=3C\sqrt{B}M^{-1}$ relationship, where M is the slope of the calibration curves, and B, the background counts, based on a 40 s counting period for copper and lead or a 100 s counting period for cadmium. From this table it may be seen that the precision of the two methods is satisfactory.

Application of the Present Methods. Method A was applied to the determination of the three elements in NBS Orchard Leaves (National Bureau of Standards, U.S.A., Standard No. 1571). A weighed sample (3.0896 g) was placed in a Teflon beaker, together with 30 cm^3 of 14 mol dm^{-3} nitric acid, 5 cm^3 of 26 mol dm^{-3} hydrofluoric acid, and 4 cm^3 of 8 mol dm^{-3} perchloric acid. This mixture was warmed until a clear solution was obtained. The solution was then gently evaporated to dryness. The residue was dissolved in 5 cm^3 of 1 mol dm^{-3} hydrochloric acid and finally diluted to 100 cm^3 with water. A 15 cm^3 aliquot of this solution was used for the determination of the three elements. The confidence limits (95%) for the average of five determinations are shown in Table 4. In the table the present results are also compared with the values obtained by Murozumi[10] by isotope-dilution mass-spectrometry and those given by the NBS.[11] The data indicate a very satisfactory agreement between the present results and the others.

Method A was also used for the determination of the three elements in a reference sample, NIES Pepperbush Leaves (*Clethra barbinervis Sieb. et Zucc.*), distributed by the National Institute for Environmental Study, Japan. The sample (0.9788 g) was decomposed in the same manner as the Orchard Leaves. The results are presented in Table 4, in which the values given by Murozumi[10] are also included. They are in acceptable agreement.

The three elements in a sample of hot-spring water were also determined by Method B. Two 150 g aliquots of the sample, both alone and with 2.0 μg of the respec-

TABLE 5. ANALYSIS OF HOT-SPRING WATER

Sample taken g	Element	Added μg	Element found: Total μg	Element found: In water μg/kg[a]	C.V.[b] %
150	Cu	—	3.00	20.0	4.6
	Cd	—	0.94	6.3	4.0
	Pb	—	5.80	38.6	4.6
150	Cu	2.00	5.13	20.8	2.7
	Cd	2.00	2.95	6.3	5.6
	Pb	2.00	7.92	39.8	2.9

a) Average of five determinations. b) Coefficient of variation.

TABLE 4. ANALYSIS OF ENVIRONMENTAL SAMPLES[a]

	NBS orchard leaves μg/g			NIES pepperbush leaves μg/g		
	Cu	Cd	Pb	Cu	Cd	Pb
Present method (Method A)	12.2±0.1	0.12±0.01[b]	46.3±1.2	11.6±0.2	6.89±0.11	5.4±0.3
Isotope-dilution mass-spectrometry[10]	12.7±0.2	0.122±0.003	47.4±1.1	11.4±0.2	6.66±0.03	5.35±0.04
NBS[11]	11±1	0.11±0.01	45±3			

a) The samples were dried at 120 °C for 24 h before the determinations. b) Counting time: 400 s.

tive element added, were analysed. The samples were placed in a polyethylene bottle (1 dm^3) containing 1 g of 6 mol dm^{-3} hydrochloric acid, and the mixture was allowed to stand overnight prior to the determination. It is apparent from Table 5 that from several to several tens ppb level of the three elements in water can be determined with fairly satisfactory precision.

Conclusion

Sodium diethyldithiocarbamate,[12,13] ammonium 1-pyrrolidinecarbodithioate,[14,15] 1-(2-pyridylazo)-2-naphthol,[13,16,17] and sodium dibenzyldithiocarbamate[18] are currently used in the preparation of suitable XRF samples. These organic reagents ordinarily react with a wide range of metal ions. Therefore, as has been reported by Hellman,[19] it is necessary to select certain masking conditions if a limited number of elements are to be precipitated by means of a nonspecific reagent. In this respect, the specificity of ATD toward copper, cadmium, and lead can be useful for separating μg amounts of the three elements from large amounts of other elements. Especially, there are few simple and selective methods for the separation of cadmium and lead, so ATD will be one of the most suitable reagents for their enrichment from multicomponent solutions.

Takemoto *et al.*[20] were the first to introduce a coagulant aid for the precipitation of heavy metal ions as dithiocarbamates. Microgram amounts of heavy metal ions were rapidly and quantitatively precipitated in the presence of dibenzylidene-D-sorbitol. Recently Panayappan *et al.*[21] have reported that a combination of poly(*N*-vinylpyrrolidone) and *N*-(2-naphthyl)mercaptoacetamide was excellent in precipitating heavy metal ions rapidly and forming insoluble compounds. These methods are convenient for the simultaneous precipitation of a variety of metal ions. The combination of ATD and BMTAC proposed in this study is particularly suited for the selective enrichment of the three elements from large volumes of aqueous samples containing considerable amounts of other elements. A number of coagulant aids currently used for water and waste-water purification, in combination with ATD, were tested, but they did not show any promise of being as effective as the ATD-BMTAC combination.

The authors wish to thank Professor Masayo Murozumi of this laboratory for his offer of reference materials (Orchard Leaves and Pepperbush Leaves) and for his kindness in letting us use a part of his analytical results obtained on the samples by means of isotope-dilution mass spectrometry. The XRF measurements were made on the spectrometer in the laboratory of Mr. Katsumasa Yabe, the Goverment Industrial Development Laboratory, Hokkaido, to whom the authors wish to express their gratitude. We also would like to thank Mr. Akira Umehara, Sankyo Kasei Co., Ltd., for kindly supplying a sample of ATD.

References

1) K. Mori and Y. Nakamura, *Kagaku Kojo*, **19**, 81 (1975).
2) T. Kono, T. Sugisawa, Y. Nakamura, and K. Mori, *Kogai*, **7**, 257 (1972).
3) R. A. A. Muzzarelli, *Anal. Chim. Acta*, **54**, 133 (1971).
4) J. A. Buono, J. C. Buono, and J. L. Fasching, *Anal. Chem.*, **47**, 1926 (1975).
5) S. Kanda and S. Kawaguchi, *J. Chem. Phys.*, **34**, 1070 (1961).
6) D. D. Perrin, "Organic Complexing Reagents: Structures, Behavior, and Application to Inorganic Analysis," in "Chemical Analysis: A Series of Monographs on Analytical Chemistry and Its Applications," ed by P. J. Elving and I. M. Kolthoff, Interscience Publishers, New York (1966), Vol. XVIII, p. 174.
7) J. C. Chudy and J. A. W. Dalziel, *J. Inorg. Nucl. Chem.*, **37**, 2459 (1975).
8) K. Mori, Y. Nakamura, M. Okumura, and M. Miyazaki, *Nippon Kagaku Kaishi*, **1977**, 786.
9) M. Murozumi, S. Nakamura, and M. Yuasa, *Bunseki Kagaku*, **26**, 626 (1977).
10) In Table 4, the values obtained by means of isotope-dilution mass spectrometry (surface ionization) are those reported by M. Murozumi of this laboratory (private communication, 1979).
11) Catalog of Standard Reference Materials, NBS Special Publication, 260, July (1970).
12) C. W. Luke, *Anal. Chim. Acta*, **41**, 237 (1968).
13) H. Watanabe, S. Berman, and D. S. Russell, *Talanta*, **19**, 1363 (1972).
14) J. F. Elder, S. K. Perry, and F.P. Brady, *Environ. Sci. Technol.*, **9**, 1039 (1975).
15) Y. Yamamoto, H. Yamagishi, and S. Ueda, *Nippon Kagaku Kaishi*, **1975**, 78.
16) R. Püschel, *Talanta*, **16**, 351 (1969).
17) M. G. Vanderstappen and R. E. Van Grieken, *Talanta*, **25**, 653 (1978).
18) H. R. Linder, H. D. Seltner, and B. Schreiber, *Anal. Chem.*, **50**, 896 (1978).
19) H. Hellmann, *Fresenius' Z. Anal. Chem.*, **289**, 24 (1978).
20) S. Takemoto, H. Kitamura, Y. Kuge, S. Nakagawa, M. Murata, and S. Ikeda, *Bunseki Kagaku*, **25**, 40 (1976).
21) R. Panayappan, D. L. Venezky, J. V. Gilfrich, and L. S. Birks, *Anal. Chem.*, **50**, 1125 (1978).

Polarographic Trace Analysis of Cadmium(II) after Solvent Extraction Using the Salting-out Method

Taitiro FUJINAGA and Yukio NAGAOSA*

Faculty of Science, Kyoto University, Kitashirakawa, Sakyo-ku, Kyoto 606
**Faculty of Engineering, Fukui University, 3-chome, Bunkyo, Fukui 910*

(Received June 16, 1979)

A selective and sensitive method is presented for the determination of cadmium(II), based on polarography after salting-out extraction into acetonitrile. The effect of nonaqueous solvents, salting-out agents, and the concentration of reagents has been studied. Under the conditions established, the cadmium(II) iodide complex extracted into the solvent gives a well-defined d.c. wave and a sharp a.c. peak, with $E_{1/2}$ and $E_p = -0.72$ V *vs.* SCE respectively. Down to 0.50 ppm of cadmium(II) in the original aqueous solution can be determined by the proposed method. Lead(II) and In(III) do not interfere up to a 1000-fold amount relative to Cd(II). Interference from Fe(III) and Tl(III) can be eliminated by the addition of ascorbic acid.

The polarographic behavior of metal complexes in nonaqueous solvents has been reported in various papers.[1,2] As for analytical applications, the polarographic analysis of methods after extraction have been studied using chloroform,[3] 4-methyl-2-pentanone (MIBK),[4] and benzyl alcohol,[5] in which cases the extract has been diluted with other polar solvents, such as water, methyl cellosolve, or methanol, to obtain a higher conductivity of the medium. Recently, Kitagawa and Ichimura[6] have reported the d.c. polarographic determination of metals in the MIBK extract. These methods, however, still seem insufficient with respect to the sensitivity and selectivity of the determination.

The salting-out effect is useful for analytical purposes in order to increase the extractability of species and to facilitate phase separation in the liquid-liquid extraction. Matkovich and Christian[7] have used the salting-out phenomenon in the separation of acetone from an aqueous solution and have determined the cobalt(II) in the extract by means of atomic-absorption spectrophotometry. Kawamoto and Akaiwa[8] have also studied a spectrophotometric determination of iron(III) after extraction into 2-propanol by the salting-out method.

In a previous paper,[9] an attempt has been made to utilize the salting-out technique for the extraction-polarographic method of analysis, in which both extraction and polarography have been carried out with acetonitrile. In the present paper, the phase separation of various organic solvents from an aqueous solution has been investigated and has been used for the polarographic determination of cadmium(II) after the salting-out extraction of the iodide complex. Acetonitrile as the solvent has a relatively low viscosity (0.345 cP) and a high dielectric constant (37.5), and it dissolves many ion-pair compounds, particularly tetraalkylammonium salts as supporting electrolytes; the resulting solution has a high conductivity. Further, the solvent is easily salted-out from an aqueous solution with various inorganic compounds. With ammonium sulfate as the salting-out, cadmium(II) in an aqueous solution can be extracted quantitatively into the acetonitrile phase as the ion-pair of tetrabutylammonium tetraiodocadmate, $NR_4[CdI_4]$; tetrabutylammonium iodide (TBAI) has been added not only as the reagent to form the tetraiodocadmate(II) complex, but also as the supporting electrolyte for the polarographic measurements. The present method constitutes a useful means of solving some problems in polarographic analysis.

Experimental

Reagents. Standard cadmium(II) solution (100 ppm): 0.247 g of cadmium(II) nitrate was dissolved in 20 cm^3 of 0.1 mol dm^{-3} nitric acid, after which the solution was diluted to 1 dm^3 with water. The acetonitrile was purified by distillation once from phosphorus pentaoxide. The ammonium sulfate (Wako Junyaku Co., Ltd.) for atomic-absorption spectrometry, the TBAI (Tokyo Kasei Co., Ltd.), and the Karl Fisher reagent (Mitsubishi Kasei Co., Ltd.) were used without further purification. The other chemicals were of guaranteed grade. Redistilled water was used throughout this study.

Apparatus. Two Yanagimoto polarographs, Model P8-D with a three-electrode system and PA-102, were used for the d.c. and a.c. polarographic measurements. In the a.c. polarographic measurements, a capacitor of 100 μF was inserted between the platinum wire counter electrode and the aqueous saturated calomel reference electrode. The DME had the following characteristics at a mercury head of 60 cm: $m = 0.783$ mg s^{-1}, $t = 3.98$ s in acetonitrile with an open circuit. A Toa Denpa pH meter, Model HM-5A, was used for the pH measurements.

Salting-out Experiment. Aliquots of water and an organic solvent were placed in a 50.0-cm^3 stoppered volumetric cylinder which had been calibrated before use. After a salting-out agent had been added to the mixture, the volume of the two phases was measured and the amount of the water present in the organic phase was determined by the Karl Fisher titration method.

Procedure. An aliquot of the standard cadmium(II) solution was placed in a 50.0-cm^3 stoppered centrifuge tube, and the volume was adjusted to 20.0 cm^3 with water. After 10.0 cm^3 of a 0.1 mol dm^{-3} TBAI solution in acetonitrile had then been added to it, the mixture was shaken with 10.0 g of ammonium sulfate for 1 min and then allowed to stand for 1 min. A portion of the extract was placed in a polarographic cell and deaerated for 3 min. The d.c. and a.c. polarograms were recorded against SCE at (25±0.1) °C.

Results and Discussion

Solvent for Polarographic Use. The phase separation of various organic solvents suitable for the polarography after salting-out extraction was investigated with ammonium sulfate. Table 1 summarizes the salting-out

Table 1. Salting-out data with ammonium sulfate for water-miscible solvents

Solvent	Organic phase-volume recovered/cm³	Water content of organic phase/(v/v %)	Dielectric constant	Viscosity/cP
Acetonitrile	10.2	9.8	37.5	0.325
Acetone	12.2	29.1	20.7	0.304
Dioxane	10.0	35.6	2.2	1.087
Tetrahydrofuran	10.0	6.2	7.5	0.460
Ethanol	14.5	50.6	24.6	1.078
1-Propanol	12.5	19.5	20.3	2.004
1-Butanol	10.3	7.7	17.5	2.271
2-Methoxyethanol	15.5	44.3	29.6	1.85
2-Buthoxyethanol	10.4	10.6	9.3	3.12
1,2-Dimethoxyethane	13.7	43.4	7.2	0.455
Propylene carbonate	9.9	4.7	64.4	2.53

The initial volumes of the water and the non-aqueous solvent were 10.0 cm³ each. The phase separations were carried out from a saturated ammonium sulfate solution.

data: the volume and the water content of the organic phase after phase separation, together with the dielectric constant and the viscosity of the pure solvents. In the polarography after extraction, it is considered preferable for the solvent to have such properties as a low mutual solubility with water, a high dissociation constant of extracted species, and a high conductivity. Acetonitrile was found to be the most useful among the solvents examined. Propylene carbonate and 1-butanol seem fairly useful, provided a suitable salting-out agent is present. Methanol, *N,N*-dimethylformamide, dimethyl sulfoxide, and pyridine did not cause any phase separation.

Salting-out Agent. Various inorganic salts were investigated as possible salting-out agents for the phase separation of acetonitrile from aqueous solution. Table 2 summarizes the minimum salt quantities required to cause phase separation, and also the volume and the water content of the acetonitrile phase after saturation with the salt. It may be concluded from Table 2 that the phase separation takes place more easily with the salt of multivalent ions than with that of univalent ions. The water content of the acetonitrile phase decreased in this order: alkali ion>alkaline earth ion> aluminum ion, with respect to their chloride salts. Among the inorganic salts tested, all the sodium and ammonium salts showed a water content of about 10%, except for sodium acetate. Ammonium sulfate as a salting-out agent is useful for the polarographic determination of cadmium(II) because of the high extractability of the complex.

Volume Ratio after Phase Separation. The initial volume of water was varied from 10.0 to 50 cm³ against 10.0 cm³ of acetonitrile. The aqueous and acetonitrile phase-volumes were measured after the mixture was saturated with ammonium sulfate. The results are shown in Table 3, from which it may be found that the acetonitrile phase-volume recovered decreased with an increase in the volume of the aqueous solution and that the water content remained almost constant under the conditions studied; this can be presumed from the fact that the amount of acetonitrile dissolved in the aqueous phase increases with the volume of the aqueous solution taken initially. The addition of TBAI to this system

Table 2. Salting-out data for inorganic compounds causing phase separation in the acetonitrile–water system

Compound	Minimum quantity causing phase separation/mmol	Acetonitrile phase-volume recovered from sat. salt solution/cm³	Water content of acetonitrile phase/(v/v %)
$AlCl_3$	2.48	7.52	0.81
$SrCl_2$	3.23	7.70	1.37
$BaCl_2$	3.36	6.69	1.32
$MgCl_2$	3.93	6.75	1.36
$CaCl_2$	4.08	6.85	1.30
NaCl	6.86	8.30	14.2
KCl	8.05	7.43	11.4
NH_4Cl	11.2	7.05	10.4
LiCl	11.8	5.95	6.70
Na_2SO_4	2.81	10.5	11.2
$Na_2S_2O_3$	2.82	9.26	—
Na_2CO_3	2.83	10.3	18.3
CH_3COONa	6.80	8.17	4.30
NaBr	14.5	5.62	14.7
$NaNO_3$	23.5	6.51	12.1
$(NH_4)_2SO_4$	3.03	10.2	9.87

The initial volumes of the water and the acetonitrile were 10.0 cm³ each.

Table 3. Effect of initial volume ratio on phase separation

Initial volume ratio (V_w/V_o)	Acetonitrile phase-volume recovered/cm³	Aqueous phase-volume recovered/cm³	Water content of acetonitrile phase/(v/v %)
1	10.2	13.0	9.87
2	9.7	27.2	9.32
3	9.2	40.5	10.0
4	8.5	54.3	10.0
5	7.7	68.3	9.32

The initial volume of the acetonitrile was 10.0 cm³. The phase separations were carried out from a saturated ammonium sulfate solution.

Table 4. Effect of amount of ammonium sulfate on phase separation

$(NH_4)_2SO_4$/g	Acetonitrile phase-volume recovered/cm³	Water content of acetonitrile phase/(v/v %)
1.5	9.9	24.2
2.0	10.1	20.5
2.5	10.2	18.0
3.0	10.2	16.6
3.5	10.3	15.0
4.0	10.1	14.6
4.5	10.2	13.8
5.0	10.3	11.5
5.5	10.1	10.6
6.6	10.2	9.8

The initial volumes of the water and the acetonitrile were 10.0 cm³ each.

caused a slight increase in the final acetonitrile phase-volume because of a salting-in effect.

Varying amounts of ammonium sulfate (1.5—6.0 g) were added to a mixture of acetonitrile (10.0 cm³) and water (10.0 cm³), and the phase-volumes were measured after the phase separation. According to the results shown in Table 4, the phase separation was initiated by the addition of 1.2 g of the ammonium salt, while the final acetonitrile phase-volume became almost constant (10.2 cm³) with a salt amount of more than 1.5 g. The content of water present in the acetonitrile phase decreased with an increase in the salt amount added. In this extraction system, the addition of a large amount of a salting-out agent is desirable to accelerate the phase separation and to increase the extractability of the species, provided no significant contamination with the coexisting impurities results. The volumes of the two phases were measured under varying experimental conditions. On the basis of the results, a ternary-phase diagram composed of acetonitrile, water, and ammonium sulfate was obtained, as is shown in Fig. 1. The solid lines of 1—4 in Fig. 1 represent the volume ratio of the two phases recovered

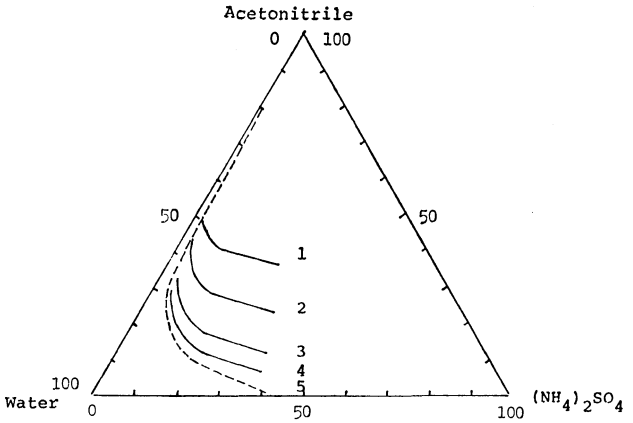

Fig. 1. Phase diagram of acetonitrile/water/ammonium sulfate 1, $V_w/V_o=1$; 2, $V_w/V_o=2$; 3, $V_w/V_o=5$; 4, $V_w/V_o=10$; 5 represents a line producing a homogeneous solution.

after the separation. A homogeneous solution is produced on the left side of the dotted line.

Polarography of the Cadmium(II) Iodide Extracted into Organic Solvents. The polarographic constants were determined for the cadmium(II) complex extracted into the four solvents with ammonium sulfate as the salting-out agent. As the results in Table 5 show, the largest

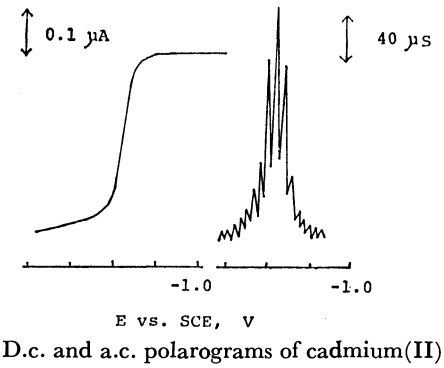

Fig. 2. D.c. and a.c. polarograms of cadmium(II) iodide extracted into acetonitrile. Cd(II) taken: 100 μg.

Table 5. Polarographic data with various solvents
Cd(II): 100 μg

Solvent	D.c. wave height μA	A.c. peak height μS	$E_{1/2}$/V *vs.* SCE	Volume of extract cm³
Acetonitrile	0.495	239	−0.82	10.0
Acetone	0.214	143	−0.77	12.5
Ethanol	0.108	156	−0.73	13.0
Propylene carbonate	0.145	48	−0.80	10.0

Table 6. Effect of TBAI concentration
Cd(II): 100 μg

Concn of TBAI / mol dm^{-3}	D.c. wave height / μA	A.c. peak height / μS	$E_{1/2}$/V *vs.* SCE	Volume of extract / cm^3
0.030	0.302	157	−0.77	9.5
0.040	0.395	220	−0.78	9.8
0.050	0.507	247	−0.79	9.9
0.075	0.498	246	−0.81	10.0
0.100	0.495	239	−0.82	10.0
0.125	0.495	226	−0.83	10.0
0.150	0.493	215	−0.85	10.1
0.200	0.463	180	−0.86	10.2

d.c. wave and a.c. peak heights were obtained in the case of the acetonitrile extraction; this suggests that acetonitrile is the best solvent to obtain a good sensitivity. Under the conditions established, the cadmium(II) complex gave a well-defined d.c. wave and a sharp a.c. peak usable for the polarographic determination, as can be seen in Fig. 2. The available potential range was from −0.53 to −1.47 V *vs.* SCE, between which potentials no metal except for cadmium(II) gave polarographic waves. The half-wave potential of the cadmium(II) complex varied with the solvent; this is presumably a result of the difference in the liquid junction potential between SCE and the organic solvent, or to that in the electrode reaction.

Effect of pH. Extractions were carried out at varying pH values, while the other experimental conditions were kept constant. It was found that the d.c. wave and the a.c. peak heights were approximately constant at pH values between 1.7 and 6.8, in which range there was no shift of the half-wave potential. Beyond this pH range, the final acetonitrile phase-volume was decreased somewhat by salting-out with added hydrochloric acid or sodium hydroxide.

Effect of TBAI Concentration. Hitherto, TBAI has often been used as a complexing agent[10] for the formation of metal iodides in acetonitrile, a supporting electrolyte[11] for the polarographic measurement in the solvent, and an extraction reagent[5] after ion-pairing with anions. In the present study, it was examined whether or not TBAI simultaneously played the three roles over the concentration range from 0.03 to 2.00 mol dm^{-3}. The results in Table 6 show that a well-defined d.c. polarogram and a sharp a.c. polarogram of cadmium(II) were observed at all the TBAI concentrations studied. The d.c. wave and the a.c. peak heights decreased gradually with an increase in the TBAI concentration above 0.05 mol dm^{-3}, probably because of the increase in the final volume and in the viscosity of the acetonitrile phase. As the TBAI concentration was increased, the half-wave potential shifted toward negative values and the content of water in the acetonitrile phase increased. The negative shift may be interpreted as resulting from the increase in the concentrations of the complexing agent and the supporting electrolyte. The extractability of TBAI into acetonitrile in the absence of cadmium(II) was determined by the titration method[12] to be 98.9%. The electrolytic conductivity and the viscosity of the acetonitrile extract obtained under the conditions of the procedure were 1.07×10^{-2} S cm^{-1} and 0.439 cP respectively. A 0.1

Table 7. Effect of amount of ammonium sulfate
Cd(II): 100 μg

$(NH_4)_2SO_4$ / g	D.c. wave height / μA	A.c. peak height / μS	$E_{1/2}$/V *vs.* SCE	Volume of extract / cm^3
2.0	0.654	291	−0.76	6.3
3.0	0.586	270	−0.75	7.5
4.0	0.540	264	−0.78	8.7
6.0	0.525	253	−0.80	9.3
8.0	0.503	244	−0.81	9.8
10.0	0.495	239	−0.82	10.0
12.0	0.492	236	−0.82	10.1

Table 8. Effect of volume of aqueous solution taken initially
Cd(II): 100 μg

Volume of aqueous solution / cm^3	D.c. wave height / μA	A.c. peak height / μS	$E_{1/2}$/V *vs.* SCE	Volume of extract / cm^3
10	0.479	220	−0.83	10.6
15	0.486	223	−0.83	10.4
20	0.495	239	−0.82	10.0
25	0.541	251	−0.82	9.6
30	0.623	277	−0.81	8.4

mol dm^{-3} TBAI solution in acetonitrile was used in the present investigation.

Effect of Amount of Ammonium Sulfate. Preliminary experiments indicated that ammonium sulfate was effective in obtaining a high extractability of the cadmium(II) complex, in addition to being a good salting-out agent for the phase separation. Table 7 shows the polarographic data obtained with varying amounts of ammonium sulfate. The d.c. wave and the a.c. peak heights decreased linearly with an increase in the salt concentration. This is mainly caused by the increase in the final volume of the extract. The half-wave potential shifted toward more negative values with an increase in the salt concentration. The amount of the ammonium sulfate involved in the acetonitrile extract was determined to be below 0.1 mg cm^{-3} after evaporating under reduced pressure and drying at 110 °C. Approximately constant heights of the d.c. wave and the a.c. peak were obtained when ammonium sulfate was added in the range between 8.0 and 12.0 g; 10.0 g of the salt was chosen for the determination of cadmium(II).

Effect of Volume of Aqueous Solution. The initial volume of the aqueous solution was varied from 10.0 to 30.0 cm^3 against 10.0 cm^3 of acetonitrile, while the other conditions were kept constant. As can be seen from Table 8, the d.c. wave and the a.c. peak heights of the cadmium(II) complex increased as the initial volume of the aqueous solution was increased; in the volume range, the degree of extraction is quantitative. The extracted cadmium(II) complex is enriched at a higher concentration as the acetonitrile phase-volume recovered is decreased. A slight shift of the half-wave potential was observed. The initial volume of the aqueous solution was adjusted to a constant volume of 20.0 cm^3.

Calibration Curves. Under the established procedure, the d.c. wave and the a.c. peak heights were determined at varying amounts of cadmium(II). The calibration curves constructed were linear over the concentration range from 0.05 to 10.0 ppm cadmium(II) in the original aqueous solution. The sensitivity of the proposed method was about twice as much as that obtained in a 1.0 mol dm^{-3} KI solution.[13] The relative standard deviation for 100 μg of cadmium(II) were 1.8% and 1.5% in the d.c. and a.c. methods respectively. The extractability of cadmium(II) was >99% over the working range. The polarographic parameters were determined to be 30 mV for the slope of the plot of $\log [i/(i_d-i)]$ *vs.* E and 5.20 $\mu A \cdot dm^3 \cdot mmol^{-1} \cdot mg^{-2/3} \cdot s^{1/2}$ for the diffusion-current constant; this indicates that the cadmium(II) complex extracted into acetonitrile is reduced by two-electron transfer.

Effect of Diverse Ions. The interference from coexisting ions was studied for the a.c. polarographic determination of 100 μg of cadmium(II). The results are summarized in Table 9. Each ten-fold amount of Bi(III), Hg(II), Fe(II), Cu(II), and Tl(III) did not interfere; Fe(III) and Tl(III) were tolerable up to 100 mg in the presence of 1 g of ascorbic acid. Indium(III) and Pb(II), both non-extractable into acetonitrile, had no effect up to 100 mg, but interfered on the addition of 0.5 g of KI. None of the metals such as Mn(II), Co(II), Ni(II), and Zn(II) interfered. Of the anions examined, MoO_4^{2-}, $S_2O_4^{2-}$, and EDTA showed a serious interference, even with the same amount of cadmium(II).

Table 9. Effect of diverse ions on the determination of Cd(II)

Element added	Amount of ion added mg	Cd(II) found μg	Error %
Bi(III)*	1.0	103.0	+3.4
Hg(II)*	1.0	97.7	−2.3
Tl(III)	1.0	96.0	−4.0
Tl(III)+1 g ascorbic acid	100.0	100.5	+0.5
Fe(III)*	1.0	100.2	+0.2
Fe(III)+1 g ascorbic acid	100.0	102.8	+2.8
Cu(II)*	1.0	96.7	−3.3
In(III)	100.0	101.8	+1.8
Pb(II)	100.0	98.4	−1.6
Cr(III)	15.0	100.9	+0.9
Sn(IV)	2.0	101.0	+1.1
Zn(II)	10.0	97.2	−2.8
Ni(II)	10.0	101.2	+1.2
Co(II)	10.0	99.5	−0.5
Mn(II)	10.0	100.7	+0.7
Cl^-	100.0	96.9	−3.1
Br^-	100.0	96.3	−3.7
I^-	100.0	100.6	+0.6
PO_4^{3-}	10.0	98.6	−1.4
F^-	10.0	102.8	+2.8
SCN^-	11.4	102.0	+2.0
ClO_4^-	13.0	96.9	−3.1
WO_4^{2-}	10.0	98.7	−1.3
VO_4^-	10.0	103.4	+3.4
Na·Citrate	20.0	99.5	−0.5
Na·Tartrate	20.0	101.1	+1.1

Cd(II) taken: 100 μg;* denotes the maximum amount tolerable, within an error of ±4%.

References

1) I. M. Kolthoff, *J. Polarogr. Soc.*, **10**, 22 (1964).
2) T. Fujinaga, K. Izutsu, K. Umemoto, T. Arai, and K. Takaoka, *Nippon Kagaku Zasshi*, **89**, 105 (1968).
3) T. Fujinaga, K. Izutsu, T. Nomura, and S. Komatsu, *Nippon Kagaku Zasshi*, **90**, 1143 (1969).
4) R. M. Dagnall and S. K. Hasanuddin, *Talanta*, **15**, 1025 (1968).
5) K. Hasebe, T. Ohtsuki, and T. Kambara, *Bull. Chem, Soc. Jpn.*, **48**, 1786 (1975).
6) T. Kitagawa and A. Ichimura, *Bunseki Kagaku*, **24**. 41 (1975).
7) C. E. Matkovich and G. D. Christian, *Anal. Chem.*, **46**, 102 (1974).
8) H. Kawamoto and H. Akaiwa, *Chem. Lett.*, **1973**, 259.
9) T. Fujinaga and Y. Nagaosa, *Chem. Lett.*, **1978**, 587.
10) M. Aihara and S. Misumi, *Bull. Chem. Soc. Jpn.*, **46**, 1964 (1973).
11) I. M. Kolthoff and J. F. Coetzee, *J. Am. Chem. Soc.*, **79**, 870 (1957).
12) H. Boden, *Chemist-Analyst*, **52**, 112 (1963).
13) I. A. Korshunov, N. I. Malyugia, and O. M. Balabanova, *J. Gen. Chem. (U.S.S.R.)*, **21**, 685 (1951).

Benzo-15-crown-5-Aluminium Chloride Complexes of Unusual Stability

Fumio WADA* and Tsutomu MATSUDA

Department of Organic Synthesis, Faculty of Engineering, Kyushu University, Hakozaki, Higashi-ku, Fukuoka 812

(Received June 25, 1979)

Among twelve crown ethers of 12, 15, 18, and 21 rings only benzo-15-crown-5 and those with an electron-releasing substituent formed the complexes with aluminium chloride which were stable in methanol.

The halides of group III elements, such as boron trifluoride and aluminium chloride, are typical Lewis acids and known to form stable adducts with ether and tertiary amine in nonpolar solvents. The common feature of the ether adducts so far known is easy exchange of the donated ether molecule(s) with other donative molecule (Eq. 1) or substitution of the halide ion by protic molecule such as methanol (Eq. 2).[1] Though the extent of the processes depends on the nature of

$$R_2O{\rightarrow}AlX_3 + R_2'O \longrightarrow R_2'O{\rightarrow}AlX_3 + R_2O \quad (1)$$

$$R_2O{\rightarrow}AlX_3 + R'OH \longrightarrow R'OAlX_2 + HX + R_2O \quad (2)$$

the halide and the donating molecule, there is no ether–aluminium halide adduct (or complex) which is stable in protic solvent as far as we know.

In the course of our study to introduce various substituents into the benzene ring of benzocrown ethers, attempted Friedel-Crafts acylation catalyzed by aluminium chloride was proved to be unpractical. The failure of the reaction can be reasonably explained in terms of the formation of a stable crown ether adduct with the aluminium chloride, and resulting deactivation of the catalyst.[2] However, this study led us to a novel finding that a complex containing aluminium chloride was obtained even after usual hydrolysis of the reaction mixture and successive recrystallization from methanol. The unusual feature of the complex has prompted us to study behavior of typical Lewis acids to various crown ethers (**1** to **8**). It should be noted that despite of a large number of studies on the chemistry of the crown ether complexes with group I and II element cations as well as ammonium-type ions there have been few papers concerned with those of group III element halides.[3]

This paper described a specific feature of benzo-15-crown-5 and some of its derivatives with an electron-releasing group, those ethers which afford stable 1 : 1 complexes with aluminium chloride in methanol. Though elucidation of the relationship between their structures and the unusual stability has to await X-ray crystallography, the present observations would shed light to the study for the crown ether complexes with neutral Lewis acids.

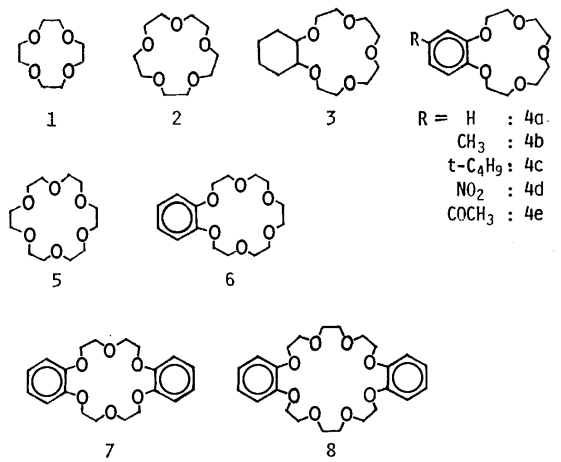

Results and Discussion

Slow addition of benzo-15-crown-5 (**4a**) (3 mmol) in benzene into an ethereal aluminium chloride (6 mmol) produced white precipitates (**9**) in a quantitative yield (>95%), which proved to be an 1 : 2 adduct of the crown ether and aluminium chloride (Eq. 3). The same adduct was obtained even when the ratio of the starting materials was changed to 1 : 1. The reaction in more donative solvent, THF or nitromethane, afforded viscous oil, which offered difficulty for further treatment. The adduct **9** was sparingly soluble in methanol, and attempted recrystallization from the solvent gave a complex (**10**), white powders, mp 147—148 °C, in 77% yield (Eq. 4). Longer heating of **9** in methanol brought about slow decomposition to liberate the crown ether. The interaction between

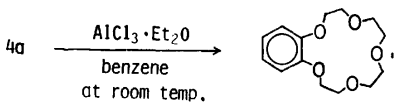

(3)

9

EA: calcd for $C_{14}H_{20}O_5Al_2Cl_6$:

	C%	H%
Found	31.02	3.90
Calcd	31.42	3.74

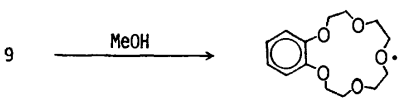

(4)

10

EA: calcd for $C_{14}H_{20}O_5AlCl_3$:

	C%	H%
Found	41.74	5.06
Calcd	41.86	5.02

the ether oxygens and aluminium in both **9** and **10** was shown by bathochromic shift in the IR absorptions of ether linkages (Fig. 1). The adduct **9** was also proved to be transformed easily into **10** on dissolution in methanol, and thus **9** and **10** gave the same NMR spectrum in methanol-d_4 (Fig. 2). The larger down-field shift in methylene signals ($\Delta\delta$ 0.4—0.6 ppm) than those of aromatic protons ($\Delta\delta$ *ca.* 0.32 ppm)

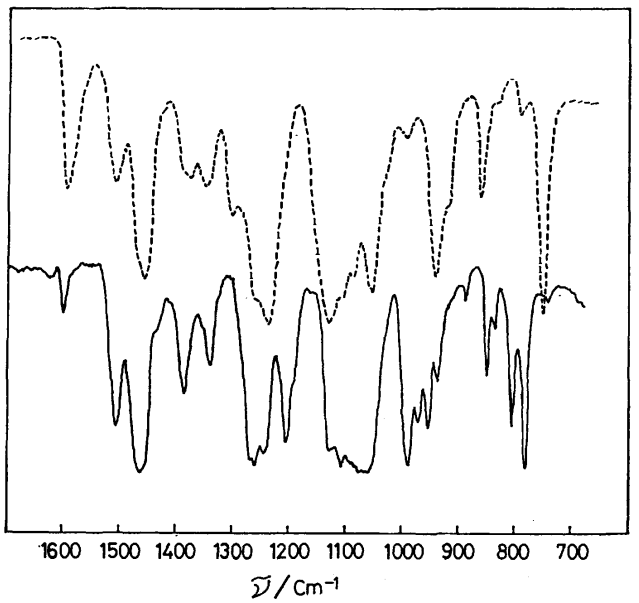

Fig. 1. Infrared spectra of benzo-15-crown-5 and complex **10**. ——: Benzo-15-crown-5, ——: complex **10**.

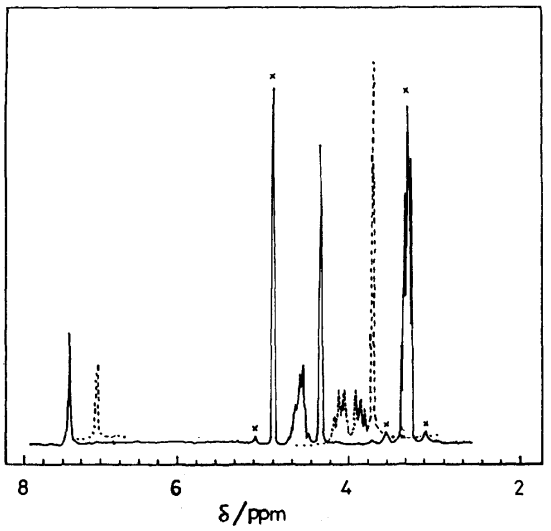

Fig. 2. ^{1}H NMR (90 MHz) spectra of benzo-15-crown-5 and complex **10** in methanol-d_4.
——: Benzo-15-crown-5, ——: complex **10**, ×: impurities in methanol-d_4.

is indicative of the preferential coordination of aluminium with the ether oxygens. The fact that the similar treatment of **9** with ethanol gave **10** (NMR and EA; Found: C, 41.55; H, 5.00%) reasonably ruled out the possibility that **10** was one of the products derived by substitution of the chloride ion(s) by the alcohols. The complex **10** is insoluble in most solvents but shows a small solubility in methanol (*ca.* 6×10^{-3} mol/l). Molecular weight determination by means of vapor pressure depression technique gave an average value of 403 ± 10 (calcd for $C_{14}H_{20}O_5AlCl_3$: 401.3), indicating that **10** was monomeric in methanol. None of useful information was obtained in MS analysis. The reactions of **4a** with boron trifluoride etherate, aluminium bromide and indium chloride under the similar conditions gave white precipitates, but on dissolution in methanol they liberated the crown ether. Thus, the following experiments were conducted with use of aluminium chloride. Aluminium chloride adducts of **1**, **5**, **6**, and **8** were again proved to decompose in methanol and **7** did not afford any solid adduct. Although **2** and **3** seem to be favorable ligands than **4a** in terms of their increased basicity of the ether oxygens, the methanol-d_4 solutions of their 1:2 adducts showed the NMR spectra coincided with those of the free crown ethers.

Since these experiments led us to the presumption that the ability of forming stable complex with aluminium chloride was limited to benzo-15-crown-5 structure, we proceeded to examine whether the feature was common among substituted benzo-15-crown-5 ethers. The adducts obtained from **4d** and **4e** bearing an electron-withdrawing group were found to liberate the corresponding crown ether in methanol-d_4, even when the amount of aluminium chloride was increased to 10 molar excess taking account of possible donation of the substituent to the halide. **4b** and **4c** with an electron-releasing group gave semi-solid and viscous oil, respectively, in the reaction with 2 equivalents of aluminium chloride. White powders were obtained by evaporation of the solvent, and their NMR spectra in methanol-d_4 demonstrated the formation of the complexes which showed the similar signals to that of **10**. However, attempts to isolate them as crystals failed. The down-field deviation of ^{1}H signals in the three complexes in the solvent at room temperature are summarized in Table 1. From these data it could be

Table 1. The down-field shifts of ^{1}H signals of benzo-15-crown-5–aluminium chloride in methanol-d_4

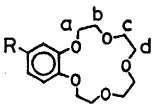

R	$\Delta(\delta_{complex}-\delta_{free})$/ppm[a)]				
	Aromatic proton	Methylene proton			
		a	b	c	d
H	0.32	0.42	0.62	0.59	0.59
CH_3	0.33	0.43	0.63	0.60	0.60
t-C_4H	0.29 0.31	0.44	0.62	0.59	0.59

a) δ_{free} and $\delta_{complex}$ stand for chemical shifts of free crown ethers and their aluminium chloride complexes, respectively.

deduced that the aluminium atom in the complexes does not equally interact with the five ether oxygens, but preferentially does with the three located remote from the benzene ring. The deduction is also in line with the less basicity of the phenol ether oxygens than other aliphatic ones.

It is noteworthy that the formation of the crown ether–aluminium chloride complexes which are stable in methanol is limited only to benzo-15-crown-5 and

those with an electron-releasing group. Moreover, there is no precedent of such peculiar properties among known ether–aluminium chloride adducts (or complexes). The stability of various crown ether complexes with cation is known to be determined principally by the basicity of crown ethers and matching of their cavities with the size of a guest cation. The present results, however, seem to indicate that the similar generalization does not necessarily hold for the aluminium chloride complex, a complex with neutral species, in view of the behaviors that the adducts of **2** and **3** are more susceptible to the decomposition. The presence of the benzo moiety might be one of the reasons for the increased stability of **10** and the complexes of **4b** and **4c**, leading to increased conformational rigidity of the crown ether ring and the resulting steric hindrance toward the attack by methanol.

Experimental

Materials. 12-Crown-4, 15-crown-5, and 18-crown-6 were of commercial origin (Bokusuy Brown Co.). 4′-Acetobenzo-15-crown-5 (mp 94.2—95.4 °C) was obtained by acetylation of **4a** with acetic anhydride in polyphosphoric acid–acetic acid mixture. Other crown ethers were prepared according to the published procedures[4] (lit, 5 for **4d**). Indium chloride (extra pure) was used as received, and other Lewis acids used were purified by the known procedure: sublimation for aluminium chloride and distillation for aluminium bromide and boron trifluoride etherate. Solvents were dehydrated over sodium–potassium alloy and distilled under nitrogen.

General Procedure. The preparations of the adducts and the complex (**10**) were carried out in a closed system and under nitrogen. ^{1}H NMR spectra in methanol-d_4 were recorded using Brucker WH 90 FT spectrometer (90 MHz) at room temperature. The following procedure for the preparation of **9** and **10** was also used in the other combinations of the Lewis acid and the crown ether. To a solution of **4a** (3 mmol) in benzene (6 ml) aluminium chloride (6 mmol) in ether (3 ml) was slowly added. The adduct (**9**) precipitated was collected and thoroughly washed with ether, and dried under vacuum. The treatment of **9** with methanol (or ethanol) gave **10**.

References

1) S. Patai, "The Chemistry of the Ether Linkage," John Wiley and Sons, New York (1967), p. 243.

2) W. W. Parish, P. E. Stott, and C. W. Mclausland, *J. Org. Chem.*, **43**, 4577 (1978).

3) A study for complex formation of iodine with several crown ethers showed that the equilibrium constants were only 2 or 3 times larger than those for mono- and di-ethers. H. P. Hopkins, Jr., D. V. Jahagirdar, and F. J. Windler, III, *J. Phys. Chem.*, **82**, 1254 (1978).

4) C. J. Pedersen, *J. Am. Chem. Soc.*, **89**, 2495 (1967).

5) R. Ungaro, B. El Haj, and J. Smid., *J. Am. Chem. Soc.*, **98**, 5198 (1976).

Kinetics and Mechanism of Ligand Exchange of Tris(acetylacetonato)-iron(III) in Acetylacetone

Hiroaki KIDO* and Kazuo SAITO*

Chemistry Department, Faculty of Science, Tohoku University, Aramaki, Aoba, Sendai 980

(Received August 9, 1979)

Tris(acetylacetonato[2-^{14}C])iron(III) undergoes ligand exchange in acetylacetone at 4—16 °C without side reactions. The exchange rate is expressed by Rate$=(k_a+k_b[H_2O])$[complex]([complex]$\approx$0.01 M, [H_2O]$\approx$0.05 M), and the rate constant (10.2 °C) and activation parameters are $k_a=(8.9\pm1.2)\times10^{-4}$ s^{-1}, $\Delta H^{\ddagger}=14.4\pm0.9$ kcal mol^{-1}, $\Delta S^{\ddagger}=-22\pm3$ cal K^{-1} mol^{-1} and $k_b=(2.22\pm0.20)\times10^{-2}$ M^{-1} s^{-1}, $\Delta H^{\ddagger}=16.9\pm0.4$ kcal mol^{-1}, $\Delta S^{\ddagger}=-6.1\pm1.3$ cal K^{-1} mol^{-1} (1 cal$=$4.18 J, 1 M$=$1 mol dm^{-3}). No deuterium isotope effect on the rate. The rate-determining steps seem to correspond to the formation of intermediates containing a one-ended acac$^-$ and an Hacac molecule (the k_a path), and the anion and a water molecule (the k_b path), by the S_N2 mechanism.

Although numerous studies of ligand substitution reactions of Fe^{III} complexes have been reported,[1] almost all the studies are concerned with $[Fe(H_2O)_6]^{3+}$ and $[Fe(dmso)_6]^{3+}$ (dmso=dimethyl sulfoxide). These complexes undergo labile solvent exchange and anation reactions with various ligands, and both the S_N1 and the S_N2 mechanism have been proposed to these substitution processes. However, little information is available concerning the kinetics of Fe^{III} complexes containing bidentate ligands. Recently, the rate of the ligand substitution of tris(acetylacetonato)iron(III) with 2-thenoyltrifluoroacetone has been reported in organic solvents such as carbon tetrachloride and benzene, but the mechanism was not definitely proposed.[2]

The reaction systems consisting of two components, tris(acetylacetonato)complexes of Cr^{III}, Co^{III}, Ru^{III}, or Rh^{III} as solute and acetylacetone (Hacac) as solvent, are suitable for understanding the mechanism of the ligand exchange between the two species.[3] On extending of the kinetic studies of these systems, we have found a slow exchange of $Fe(acac)_3$ in Hacac at 10 °C. This paper deals with the kinetics and the mechanism of this exchange reaction examined by the isotopic labelling method.

Experimental

Materials. The labelled acetylacetone, Hacac[2-^{14}C][4] and Hacac[*methylene*-$^2H_2$] (the deuterium content in the methylene moiety: 80%)[5] were prepared and purified by the reported methods. Tris(acetylacetonato)iron(III), $Fe(acac)_3$, was prepared from ammonium iron(III) sulfate dodecahydrate (1.9 g), acetylacetone (1.5 ml) and sodium hydrogencarbonate (1.3 g) in water (40 ml) at room temperature. The labelled complex, $Fe(acac[2\text{-}^{14}C])_3$, was prepared from Hacac[2-^{14}C] and $Fe(acac)_3$ by the ligand exchange method. The solution of $Fe(acac)_3$ (300 mg) in a mixed solvent of Hacac[2-^{14}C] (1 ml) and acetonitrile (0.5 ml) was heated at 80 °C for 1 h and evaporated to dryness under reduced pressure at room temperature to give orange crystals (*ca.* 300 mg of $Fe(acac[2\text{-}^{14}C])_3$), which were recrystalized from benzene–petroleum ether. Its UV and visible absorption spectra in acetonitrile coincided with the reported data.[6] The specific activity of the complex was 0.005 μCi/mg.

The solvents, Hacac and acetonitrile, were purified by the reported method.[5] Guaranteed grade of hexane was used without purification.

Kinetic Procedure. The free Hacac was separated from the complex in the reaction mixtures by the solvent extraction with hexane. The labelled complex (*ca.* 12 mg) and the solvent (6 ml of Hacac, Hacac[*methylene*-$^2H_2$] or Hacac diluted with acetonitrile) were placed separately in the two sections of a glass-stoppered flask with a branched bottom. The flask was kept in a thermostat (4.4±0.1, 10.2±0.1, or 16.2±0.1 °C) for *ca.* 30 min and rotated to unite the contents of the two sections. The complex dissolved within 10 s. Portions (0.5 ml) of the solution were taken out at appropriate time intervals and swiftly (<10 s) poured into a chilled (−30 °C) hexane layer (10 ml), which floated on a pure acetonitrile layer (1 ml) in a glass-stoppered thin test tube. The tube was shaken vigourously for 10 s and allowed to stand for *ca.* 1 min at −30 °C. A 1 ml portion of the acetonitrile layer was taken out and washed twice with hexane (10 ml) at −30 °C in a similar manner to be made free from Hacac. The complex is insoluble in hexane and present only in the acetonitrile layer. This acetonitrile solution contained sufficient amount of $Fe(acac)_3$ for kinetic analysis (*ca.* 70% of that in the original Hacac solution) and a negligible amount of Hacac. Spectrophotometry at 434 nm and the liquid scintillation counting of this acetonitrile solution gave the specific counting rate of the recovered complex. The exchange rate R was calculated by the McKay equation

$$R=\frac{3[Fe][Hacac]}{3[Fe]+[Hacac]}\frac{\ln[(x_0-x_\infty)/(x_t-x_\infty)]}{t}$$
$$\approx 3[Fe]\ln(x_0/x_t)/t \quad ([Hacac]\gg[Fe],\ x_\infty\approx0) \qquad (1)$$

where [Fe] and [Hacac] stand for the concentration of the complex and acetylacetone, respectively. The x's are the specific counting rates of the recovered complex at the times indicated by the subscripts.

The water contents (0.2—0.8 M; 1 M$=$1 mol dm^{-3}) of the reaction mixture were determined by the Karl Fischer titration.

Results

The visible absorption spectra of the reaction mixture containing the given amount of H_2O remained unchanged throughout the reaction, and were identical with those of the complex in anhydrous Hacac and in anhydrous acetonitrile ([H_2O]<0.01 M) within experimental errors at room temperature ($\lambda_{max}=434\pm0.5$ nm, log $\varepsilon=3.55\pm0.02$). The water content also remained unchanged. The McKay plots gave straight lines up to at least 50% completion of the exchange (Fig. 1). No significant zero-time exchange was observed. Therefore, the decrease of the specific counting rate of

the recovered complex corresponds exclusively to the exchange reaction (2).

$$Fe(\overset{*}{acac})_3 + Hacac \rightleftharpoons Fe(acac)_3 + H\overset{*}{acac} \quad (2)$$

The R in neat acetylacetone was proportional to the concentration of the complex (Table 1) and is given by

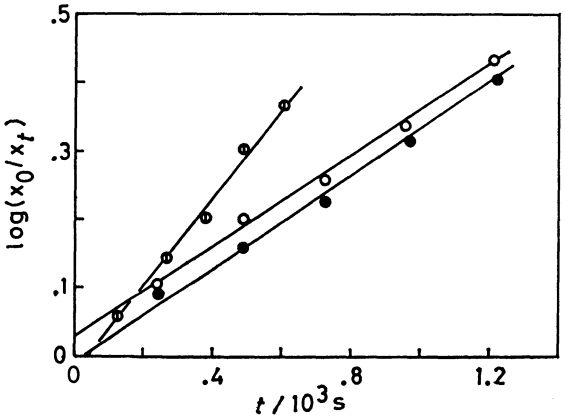

Fig. 1. Typical McKay plots for the ligand exchange of $Fe(acac)_3$ in acetylacetone (○, ⓘ) and in acetylacetone[*methylene*-$^2H_2$](●) at 10.2(ⓘ) and 16.2(○,●) °C ([Fe]≈0.006 M).

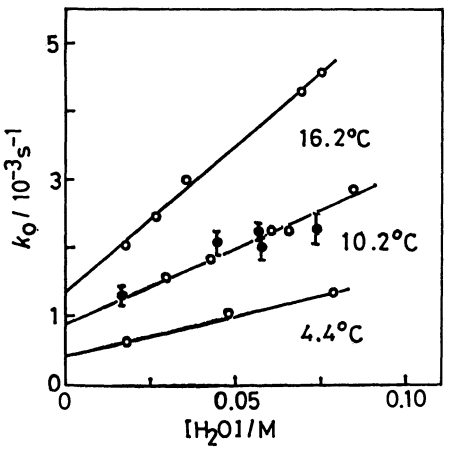

Fig. 2. Influence of the water concentration and the deuterium isotope effect on the exchange rate constant (k_o) of $Fe(acac)_3$ in acetylacetone(○) and in acetylacetone[*methylene*-$^2H_2$](●)([Fe]≃0.006 M).

Table 1. Ligand exchange rate of Fe(acac-[2-$^{14}C_3$])$_3$ in acetylacetone at 4.4 °C

[Fe] / 10^{-3} M	[H_2O] / M	R / 10^{-6} M s^{-1}	k_o / 10^{-4} s^{-1}
5.78	0.018	3.7±0.1	6.4±0.2
9.75	0.021	6.5±0.2	6.7±0.2

$$R = k_o[Fe] \quad (3)$$

where k_o is the observed first-order rate constant. The k_o value was dependent on [H_2O] (Fig. 2), and expressed by Eq. 4 in the given concentration range,

$$k_o = k_a + k_b[H_2O]. \quad (4)$$

The k_a and k_b values were obtained from the intercepts and the slopes of the lines in Fig. 2, respectively, and are shown in Table 2, together with the activation parameters.

When Hacac[*methylene*-$^2H_2$] was used as the solvent at 10.2 °C in place of the ordinary Hacac, the k_o values coincided with those in Hacac within the experimental errors (Fig. 2).

The k_o value increased linearly with the increase in concentration of Hacac in the mixed solvent with acetonitrile up to 9.7 M (in neat acetylacetone) under a given concentration of the complex and water (Fig. 3). The k_o *vs.* [Hacac] plot has a very small intercept.

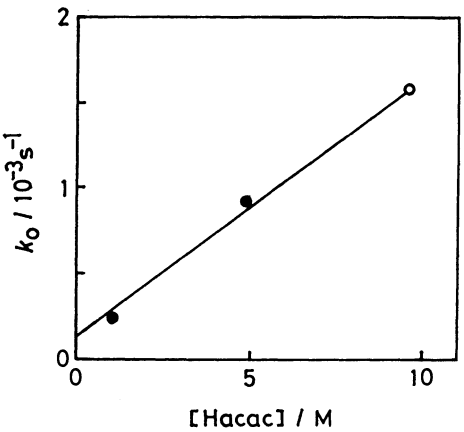

Fig. 3. Influence of the free ligand concentration on the exchange rate constant (k_o) of $Fe(acac)_3$ in acetylacetone(○) and in acetonitrile(●)([Fe]≃0.006 M, [H_2O]=0.03 M, 10.2 °C).

Discussion

Equation 4 indicates that the exchange in Hacac (Eq. 2) proceeds by two paths (the k_a and k_b path) in the presence of water. The linear plot of k_o *vs.* [Hacac] (Fig. 3) suggests that the exchange reactions in Hacac and in the mixed solvent are essentially the same and expressed by Eq. 5 in the concentration region from 1 to 9.7 M of Hacac,

$$k_o = k_o'[Hacac]. \quad (5)$$

If either k_a or k_b in Eq. 4 were independent of [Hacac], the k_o *vs.* [Hacac] plot would not have such a small intercept shown in Fig. 3, because the k_a and k_b terms give comparable contributions to k_o under the given

Table 2. Kinetic data for the ligand exchange of Fe(acac[2-^{14}C])$_3$ in acetylacetone

Parameters	Rate constants 4.4 °C	10.2 °C	16.2 °C	$\Delta H^{\ddagger}$ / kcal mol^{-1}	$\Delta S^{\ddagger}$ / cal K^{-1} mol^{-1}
k_a/10^{-3} s^{-1}	0.44±0.04	0.89±0.12	1.35±0.10	14.4±0.9	−22±3
k_b/10^{-2} M^{-1} s^{-1}	1.16±0.08	2.22±0.20	4.24±0.19	16.9±0.4	−6.1±1.3

conditions (*cf.* Fig. 2, $[H_2O] \simeq 0.03$ M). Hence Eq. 6 holds at least in the vicinity of [Hacac]=9.7 M (in Hacac),

$$k_o \approx (k_a' + k_b'[H_2O])[\text{Hacac}]. \quad (6)$$

Equations 3 and 6 suggest that one $Fe(acac)_3$ and one Hacac molecule participate in the k_a and k_b paths and one H_2O molecule also does in the k_b path.

Possible Reaction Routes of the k_a and k_b Paths. Varieties of probable reaction routes for the k_a path are very much limited, since the reaction system is very simple and the chemical species participating in the rate-determining step should be only $Fe(acac)_3$ and Hacac. Scheme 1 can be assumed almost exclusively as possible routes for the k_a path,[3]

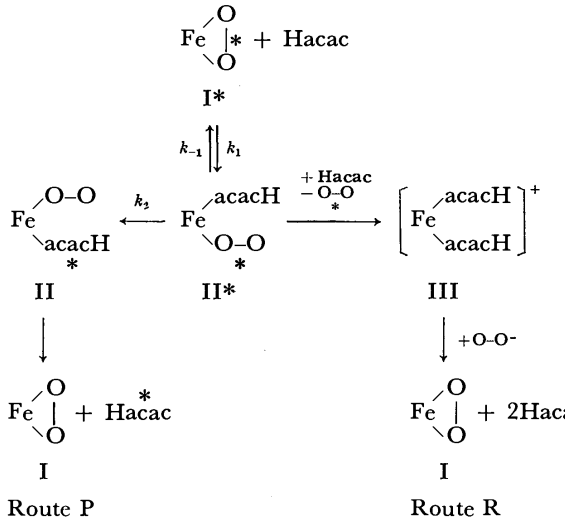

Scheme 1.

where O–O and I* denote $acac^-$ and $Fe(acac)_3$, respectively, and two $acac^-$ chelates are omitted from each species. The intermediate II* is formed from I* and Hacac. (II* corresponds to an intermediate containing a one-ended bidentate and a solvent molecule; such a type of intermediate is generally accepted in substitution processes of bidentates.[3]) In the Route P, II* is converted into II through the proton transfer between the unidentate ligands, $O^*\text{–}O^-$ and Hacac, and II turns to I and Hacac*. In the Route R, II* changes into another cationic intermediate III by the replacement of unidentate $O^*\text{–}O^-$ by free Hacac (III corresponds to a bis-chelate-type intermediate containing two solvent molecules, $[Fe(acac)_2(solvent)_2]^+$), and III produces I by the ligation of $O^*\text{–}O^-$ which is formed by the proton exchange between $O^*\text{–}O^-$ and Hacac in the bulk or in the second coordination sphere of the complex.

Similar routes are possible for the k_b path shown in Scheme 2. I* and a water molecule produce an intermediate IV*. When H_2O or the unidentate $O^*\text{–}O$ in IV* is replaced by the free Hacac, II*′ or III′ is formed, respectively. The intermediates II*′ and III′ undergo similar changes as in the P and R Routes in Scheme 1, to turn to I through the P′ and R′ Routes, respectively.

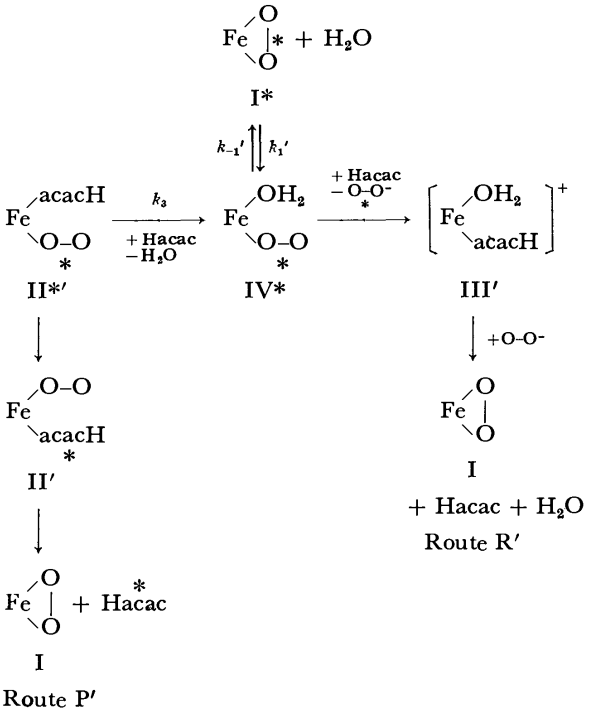

Scheme 2.

Reaction Mechanism. The activation enthalpies and entropies for k_a and k_b can be reckoned to have similar tendency to each other (Table 2). Hence both the paths are suggested to have similar reaction routes and rate-determining steps to each other. If the similar routes are P and P′ and the k_1 and the k_1' step are the slowest in each path, stationary-state conditions to II* and IV*, can be reasonably assumed to give Eqs. 7 and 8,

$$k_a = k_1[\text{Hacac}]\frac{k_2}{k_{-1}+k_2} \quad (7)$$

$$k_b[H_2O] = k_1'[H_2O]\frac{k_3[\text{Hacac}]}{k_3[\text{Hacac}]+k_{-1}'} \quad (8)$$

Concentrations of the intermediates should be negligible as compared with those of I* and I, since the visible absorption spectra of the complex in the reaction mixture, in Hacac and in acetonitrile are almost identical to one another (*vide supra*). On the assumptions, $k_{-1} \ll k_2$ and $k_{-1}' \gg k_3[\text{Hacac}]$, Eqs. 7 and 8 are further converted into Eqs. 9 and 10, respectively.

$$k_a = k_1[\text{Hacac}] \simeq k_a'[\text{Hacac}] \quad (9)$$

$$k_b[H_2O] = k_1'[H_2O]\frac{k_3[\text{Hacac}]}{k_{-1}'} \simeq k_b'[H_2O][\text{Hacac}] \quad (10)$$

These assumptions are not unreasonable. The proton transfer process(k_2) can be much faster than the ring-closure process(k_{-1}). On the contrary, if k_2 were much smaller than k_{-1}, k_a should be affected by k_2 (*cf.* Eq. 7) and deuterium isotope effect on the exchange rate should be observed as in the exchange of $Cr(acac)_3$ in Hacac.[5] Moreover, replacement of H_2O in IV* by the free end of one-ended acetylacetonate ligand (k_{-1}', intramolecular) can be much faster than that by the free Hacac (k_3[Hacac], intermolecular).

Equations 9 and 10 are consistent with Eq. 6. The k_1 and k_1' steps correspond to the rate-determining steps and the term $k_3[Hacac]/k_{-1}'$ represents a branching ratio for the accomplishment of the exchange from IV*.

On the contrary, the combination of the R and R' Routes does not seem adequate. When the first steps, I*→II* and I*→IV*, are considered to be the rate-determining steps, the first-order dependency of [Hacac] in the k_b term in Eq. 6 cannot be interpreted. On the other hand, when the second steps (II*→III, IV*→III', *i.e.*, replacement of acetylacetonate unidentate by Hacac or H_2O) are assumed to be rate-determining or to be concerned in determining the rate as in the P' Route mentioned above, the k_a term must have the second-order dependency with respect to [Hacac], which conflicts with the observation (Eq. 6). Such a type of one-ended acetylacetonate in II* and IV* has been claimed to be stablized towards replacement by free ligands such as Hacac, H_2O and acetonitrile in the exchange of $Co(acac)_3$ in acetonitrile. The stability has been attributed to the conjugated structure of the ligand, *i.e.*, concentration of negative charge on the coordinated oxygen (Co–O–C(CH_3)=CH–C(CH_3)=O).[7]

Alternative Routes. Besides the combination of the routes mentioned above, other sets of routes for the k_a and k_b paths can satisfy Eq. 6; a) the P Route for the k_a path and a water-assisted route, in which a water molecule assists the proton transfer in the P Route (II*→II in Scheme 1), for the k_b path, and b) catalytic action of Hacac or H_2O as a proton donor to the original complex or to some of the intermediates, *e.g.*, the formation of II* in the P Route without and with the aid of a proton of H_2O for the k_a and k_b paths, respectively. However, if these routes operated in the exchange, the deuterium isotope effect on k_a and k_b might be observed. In the exchange of $Cr(acac)_3$[5] and $Co(acac)_3$[7] in acetonitrile, the effect was significant in a water-assisted ($k_H/k_D=1.5$) and an acid-catalyzed ($k_H/k_D=0.4$) processes, respectively. Hence the routes shown in a) and b) are considered to be unlikely on the basis of the absence of the isotope effect in both k_a and k_b.

Therefore, the P and P' Routes are concluded to be the most plausible mechanisms and illustrated again in Fig. 4.

Substitution Mechanism in the Rate-determining Steps. An S_N2 mechanism can be assigned to the rate-determining k_1 step on the basis of the negative value of $\Delta S^{\ddagger}$ (Table 2) and the first-order dependency of k_a on [Hacac] (Fig. 3). In the exchange of $Co(acac)_3$ in acetonitrile[7] and in Hacac,[3] $\Delta S^{\ddagger}$ has large positive values and the rate is independent of [Hacac]. An S_N1 mechanism has been clearly assigned to the exchange of the Co^{III} complex on the basis of these features and the almost identical rate of the exchange with that of the racemization.[8]

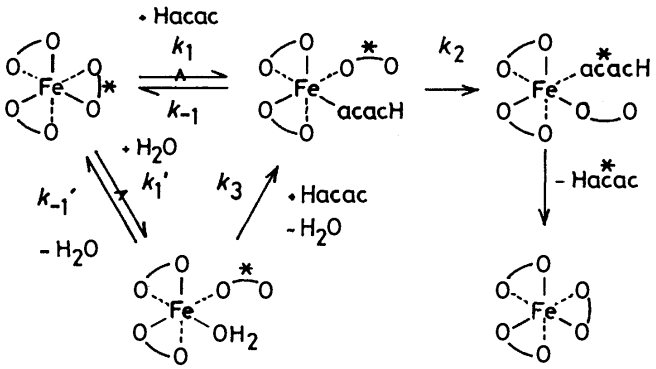

Fig. 4. Plausible mechanism of the ligand exchange of $Fe(acac)_3$ in acetylacetone.

The negative value of $\Delta S^{\ddagger}$ for k_b also suggests an S_N2 attack of H_2O in the k_1' step.

The $\Delta S^{\ddagger}$ value for k_b is less negative than that for k_a by *ca.* 16 cal K^{-1} mol^{-1}, while the $\Delta H^{\ddagger}$ value for k_b is slightly larger than that for k_b. On the other hand, the contributions of the k_a and the k_b term for the rate are comparable, while the concentration of H_2O (0.02—0.1 M) is much less than that of Hacac (9.7 M). The result suggests the prevailing nucleophilicity of H_2O over that of Hacac. Such a difference may be attributable to the steric factor of the nucleophiles.

Comparison with Related Reactions. Kinetic parameters of the present exchange and the solvent exchange reactions of $Fe^{III}O_6$ type complexes are collected in Table 3. The present k_o is different from that of the other reactions involving unidentate ligands, the ratio amounting to 10^4. Such a marked inertness in substitution of bidentate ligands in iron(III) complexes has been also found in the aquation of $[Fe(C_2O_4)(H_2O)_4]^+$ ($k=3\times10^{-3}$ s^{-1} at 25 °C)[1d] and in the replacement of $acac^-$ in $Fe(acac)_3$ by 2-thenoyltrifluoroacetonate in CCl_4 ($k=6\times10^{-3}$ s^{-1} at 25 °C).[2]

On the other hand, the reactions in Table 3 exhibit a common tendency in the values of the activation parameters. There seems to be a common trend that these exchange reactions proceed *via* an S_N2 mechanism, regardless of the dentate number of the ligands. The assignment is consistent with the recent assignment

Table 3. First-order rate constants and activation parameters of the ligand exchange reactions of iron(III) complexes at 25 °C

Complex	Solvent	k_1/s^{-1}	$\Delta H^{\ddagger}$/kcal mol^{-1}	$\Delta S^{\ddagger}$/cal K^{-1} mol^{-1}	Reference
$Fe(acac)_3$	Hacac	0.0033(k_a)	14.4±0.9	−22±3	This work
$[Fe(H_2O)_6]^{3+}$	H_2O	150	—	—	a)
$[Fe(dmf)_6]^{3+}$	DMF	33	12.5±1.5	−10±5	b)
		61	10.1±1	−16.5±3.0	c)
$[Fe(dmso)_6]^{3+}$	DMSO	50	10±2	−11±4	d)

DMF=*N*,*N*-Dimethylformamide, DMSO=Dimethyl sulfoxide. a) Ref. 1e(*cf.* Ref. 1g). b) Ref. 1g. c) Ref. 1i. d) Ref. 1f.

of an S_N2 mechanism to the anation of NCS^- and Cl^- upon $[Fe(H_2O)_6]^{3+}$ on the basis of the values of the activation volume.[1p,q]

The authors wish to thank the Ministry of Education for the Grant-in-Aid.

References

1) a) J. F. Below, Jr., R. E. Connick, and C. P. Coppel, *J. Am. Chem. Soc.*, **80**, 2961 (1958). b) D. Seawald and N. Sutin, *Inorg. Chem.*, **2**, 643 (1963). c) R. E. Bauer and W. MacF. Smith, *Can. J. Chem.*, **43**, 2763 (1965). d) E. G. Moorhead and N. Sutin, *Inorg. Chem.*, **5**, 1866 (1966). e) M. R. Judkins, Ph. D. Thesis, Univ. of Calf., May, 1967. f) C. H. Langford and F. M. Chung, *J. Am. Chem. Soc.*, **90**, 4485 (1968). g) F. W. Brivogel, Jr., *J. Phys. Chem.*, **73**, 4203 (1969). h) F. P. Cavasino and E. Di Dio, *J. Chem. Soc., Sect. A*, **1971**, 3176. i) J. Hodgkinson and R. B. Jordan, *J. Am. Chem. Soc.*, **95**, 763 (1973). j) E. Mentasti and Pelizzetti, *J. Chem. Soc., Dalton Trans.*, **1973**, 2605. k) D. H. Devia and D. W. Watts, *Inorg. Chim. Acta*, **7**, 691 (1973). l) K. Nakamura, T. Tsuchida, A. Yamagishi, and M. Fujimoto, *Bull. Chem. Soc. Jpn.*, **46**, 456 (1973). m) S. Funahashi, S. Adachi, and M. Tanaka, *Bull. Chem. Soc. Jpn.*, **46**, 479 (1973). n) G. Wada and Y. Kobayashi, *Bull. Chem. Soc. Jpn.*, **48**, 2451 (1975). o) S. Gouger and J. Stuehr, *Inorg. Chem.*, **13**, 379 (1974). p) A. Jost, *Ber. Bunsenges. Phys. Chem.*, **80**, 316 (1976). q) B. B. Hasinoff, *Can. J. Chem.*, **54**, 1820 (1976).

2) T. Sekine, H. Honda, M. Kokiso, and T. Tosaka, *Bull. Chem. Soc. Jpn.*, **52**, 1046 (1979).

3) H. Kido, *Bull. Chem. Soc. Jpn.*, **53**, 82 (1980).

4) K. Saito and K. Masuda, *Bull. Chem. Soc. Jpn.*, **41** 384 (1968).

5) H. Kido and K. Saito, Inorg. *Chem.*, **16**, 397 (1977).

6) D. W. Barnum, *J. Inorg. Nucl. Chem.*, **21**, 221 (1961).

7) H. Kido and K. Saito, *Bull. Chem. Soc. Jpn.*, **52**, 3545 (1979).

8) R. C. Fay, A. Y. Girgis, and U. Klabunde, *J. Am. Chem. Soc.*, **92**, 7056 (1970).

Intramolecular Cycloaddition Reactions of *N*-Sulfonyl Nitrile Imides Bearing Alkenyl Groups

Tomio SHIMIZU,* Yoshiyuki HAYASHI, Yoshio NAGANO, and Kazuhiro TERAMURA

Department of Dyeing, Faculty of Industrial Arts, Kyoto Technical University, Matsugasaki, Sakyo-ku, Kyoto 606

(Received February 15, 1979)

The reaction of the *p*-tolyl(or phenyl)sulfonylhydrazones of some 2-(alkenyloxy)benzaldehydes with lead tetraacetate leads, *via* the nitrile imide intermediates, Ar–C(+)=N–N(−)–SO_2–C_6H_4–X-*p*, to intramolecular 1,3-dipolar cycloadducts and 1-acetyl-2-aroyl-1-[*p*-tolyl(or phenyl)sulfonyl]hydrazines in 20—65% and 7—70% yields respectively, while the intermolecular reactions of the benzaldehyde *p*-tolylsulfonylhydrazone with a dipolarophile such as acrylonitrile or styrene in the presence of lead tetraacetate gives only 1-acetyl-2-benzoyl-1-(*p*-tolylsulfonyl)-hydrazine. The treatment of the *N*-(*p*-tolylsulfonyl)-*o*-(allyloxy)benzohydrazonoyl chloride (**10**) with triethylamine or by refluxing a benzene solution of **10** also gives an intramolecular 1,3-dipolar cycloadduct in a good yield.

1,3-Dipolar cycloaddition reactions are one of the most useful methods for the preparation of five-membered heterocyclic rings.[1] These reactions are usually regarded as concerted reactions,[2] but sometimes a diradical intermediate has been postulated.[3] The stereochemistry of the dipolarophiles is usually maintained, and the orientation phenomena can be ascribed to frontier orbital interactions.[4]

In this decade, many studies of intramolecular 1,3-dipolar cycloaddition reactions have been reported.[5-10] The most interesting aspects of these reactions are as follows: first, the reaction products are complex polycyclic, annelated, and fused ring molecules which are difficult to prepare by any other methods. Second, a comparison of the results of an intermolecular reaction with that of an intramolecular reaction suggests several things. For example, much information has been obtained from the various intramolecular cycloadditions of nitrile oxides,[5] nitrile imines,[6] nitrones,[7] nitrile ylides,[8] azides,[9] diazoalkanes,[10] and azomethine imines[6b,7b] as dipoles.

Except for a few instances, most dipoles are prepared by multistep reactions and, consequently, in low yields. For example, nitrile imines are generally generated (i) from hydrazonyl halides by treatment with a base[11] or (ii) from the thermal decomposition of 2,5-disubstituted tetrazoles.[12] These methods, while moderately satisfactory, are rather combersome. However, a new method (iii) reported by Gladstone[13] has been shown to be a simpler preparative method for nitrile imines.

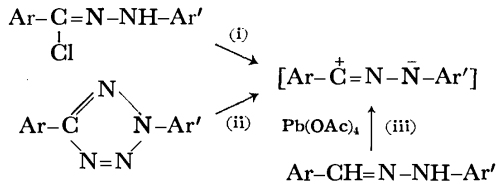

Several attempts to prepare the *N*-sulfonyl nitrile imide (**4**) have been made.[14,15] It has been reported that the reaction of *N*-sulfonyl hydrazonoyl chloride (**1**) with triethylamine gave only a dimer (**3**) *via* the intermediate (**2**).[14] On the other hand, when a toluene solution of **1** and a dipolarophile was refluxed, the 1,3-dipolar cycloadduct (**5**) was obtained.[15] We found

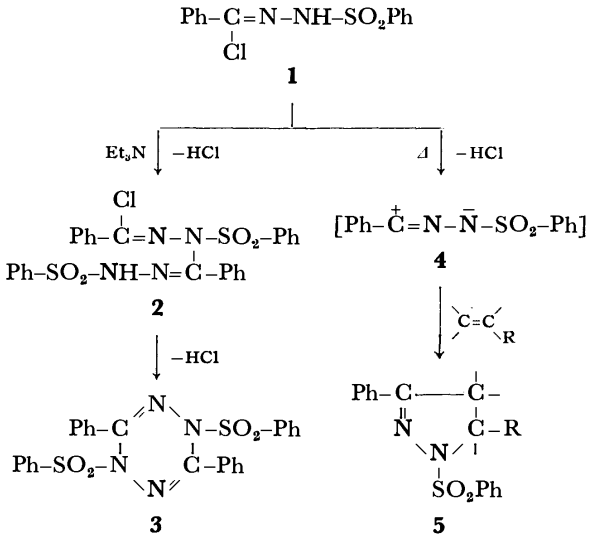

that the new method reported by Gladstone was equally useful for the preparation of *N*-sulfonyl nitrile imide from *p*-tolylsulfonylhydrazone of aromatic aldehyde.

$$\text{Ar–CH=N–NH–SO}_2\text{–Tol-}p \xrightarrow{\text{Pb(OAc)}_4} \mathbf{4'}$$

This paper will describe some smooth intramolecular cycloaddition reactions using these sulfonylhydrazones.

Results and Discussion

An expected intramolecular cycloadduct, 2,3,3a,4-tetrahydro-2-*p*-tolylsulfonyl[1]benzopyrano[4,3-*c*]-pyrazole (**7a**), and the unexpected 1-acetyl-2-(*o*-allyloxy)benzoyl-1-*p*-tolylsulfonylhydrazine (**8a**) were isolated from a reaction mixture of *p*-tolylsulfonylhydrazone of 2-(*o*-allyloxy)benzaldehyde (**6a**) and lead tetraacetate by fractional recrystallization and/or column chromatography. Some of the hydrazones (**6**), shown in Table 1, also gave the intramolecular cycloadducts (**7**) and *N*-acetylated hydrazines (**8**). These results are shown in Tables 2 and 3 respectively.

The structure of **7a** was established on the basis of elemental analysis and the spectral data, IR (cm^{-1}): 1180 (N–SO_2); NMR ($CDCl_3$) δ: 2.40 (3H, s, CH_3), 2.60—4.70 (4H, m), 6.7—7.5 (5H, m), and 7.7—7.95 (3H, m). The assignment of the structure **7a** was further

TABLE 1. YIELDS AND MELTING POINTS OF THE HYDRAZONES (**6**)[a]

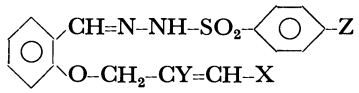

6	X	Y	Z	Mp/°C	Yield/%
a	H	H	CH_3	116—117[b]	quanti.
b	H	H	H	141—142	95
c	Ph	H	CH_3	128—130	quanti.
d	Ph	H	H	113—114	83
e	H	Br	CH_3	114—115	52
f	H	Br	H	144—145	50
g	CN	H	CH_3	144—146	quanti.
h	CN	H	H	165—167	81
i	CH_3	H	CH_3	127—128	66
j	CH_3	H	H	136—137	88

a) Satisfactory analytical data were obtained for new compounds. b) Lit,[10c] mp 119 °C.

TABLE 2. YIELDS, MELTING POINTS, AND ANALYTICAL DATA OF THE PYRAZOLINES (**7**)

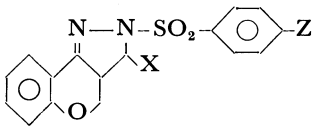

7	X	Z	Mp/°C	Yield/%	Found (%) (Calcd (%)) H	C	N
a	H	CH_3	205—207	40	4.93 (4.91	62.56 62.19	8.35 8.53)
b	H	H	252—254	30	4.42 (4.49	61.17 61.14	8.83 8.91)
c	Ph	CH_3	243—246	20	5.00 (4.99	67.45 68.30	6.68 6.93)
d	Ph	H	206—210	65	4.60 (4.65	67.23 67.67	7.02 7.17)
g	CN	CH_3	204—206	20	4.17 (4.28	61.20 61.18	11.67 11.89)
h	CN	H	212—215	25	3.68 (3.83	60.32 60.17	12.46 12.38)
i	CH_3	CH_3	183—188	24	5.16 (5.30	62.87 63.14	8.10 8.18)
j	CH_3	H	191—194	20	4.94 (4.91	62.53 62.18	8.44 8.53)

supported by the following experiment: the hydrolysis and then the dehydrogenation of **7a** by treatment with potassium hydroxide gave 2,4-dihydro[1]benzopyrano-[4,3-*c*]pyrazole (**9a**), IR (cm^{-1}): 3210 (NH); NMR ($CDCl_3$) δ: 5.24 (2H, s), 6.7—7.35 (4H, m), and 7.5—7.7 (1H, m) (see Table 4). The NMR spectra of pyrazolines (**7**) and pyrazoles (**9**) are consistent with those of analogous polycyclic pyrazolines and pyrazoles reported in the literature.[6b-d] These results show that the new method is satisfactory for the preparation of benzopyranopyrazoles (**7** and **9**).

Although no appreciable difference in reactivity was observed when the substituent of X and Z on **6** was varied, the introduction of bromine at the Y position

TABLE 3. YIELD AND MELTING POINTS OF THE *N*-ACETYLATED COMPOUNDS (**8**)[a]

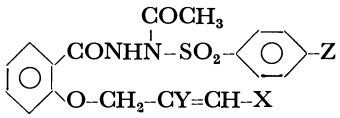

8	X	Y	Z	Mp/°C	Yield/%
a	H	H	CH_3	—	—
b	H	H	H	108—109	7
c	Ph	H	CH_3	—	—
d	Ph	H	H	≃100	trace
e	H	Br	CH_3	136—138	17
f	H	Br	H	139—141	70
g	CN	H	CH_3	180—181	27
h	CN	H	H	145—148	37
i	CH_3	H	CH_3	110—111	21
j	CH_3	H	H	126—128	20

a) Satisfactory analytical data were obtained for these compounds.

TABLE 4. MELTING POINTS AND ANALYTICAL DATA OF THE PYRAZOLES (**9**)

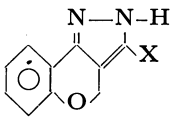

9	X	Mp/°C	Found (%) (Calcd (%)) H	C	N
a,b	H	171—173	4.69 (4.68	71.23 69.75	16.11 16.27)
c,d	Ph	230—233	5.00 (4.87	76.10 77.40	10.99 11.28)
g,h	$CONH_2$	≃305	4.17 (4.22	58.69 61.39	18.07 19.53)
i,j	CH_3	197—202	5.30 (5.41	71.24 70.95	14.31 15.04)

gave only *N*-acetylated compounds (**8e** and **8f**); no 1,3-dipolar cycloadducts could be detected. Our method described above gave **7a** in 40% total yield *via* only two reaction steps from salicylaldehyde. Though Compound **7a** was also prepared in a 26% overall yield *via* hydrazonoyl chloride (**10**) from methyl salicylate (see Scheme 1), this method is rather combersome because it involves six reaction steps. It is interesting that *N*-sulfonyl hydrazonoyl chloride (**10**), another precursor of the nitrile imide for the cycloadduct, also gave the cycloadduct (**7a**) when treated with triethylamine. Even in the absence of triethylamine, the precursor (**10**) yielded **7a** with liberating hydrogen chloride when subjected to reflux in a benzene solution. In these reactions, no dimer like **3** was detected; this indicates a favorable intramolecular cycloaddition reaction.

The structure of the *N*-acetylated compound (**8a**) was assigned on the basis of a comparison of the spectra with those of analogous compounds reported by Scott *et al.*[16] The following results also support the structure

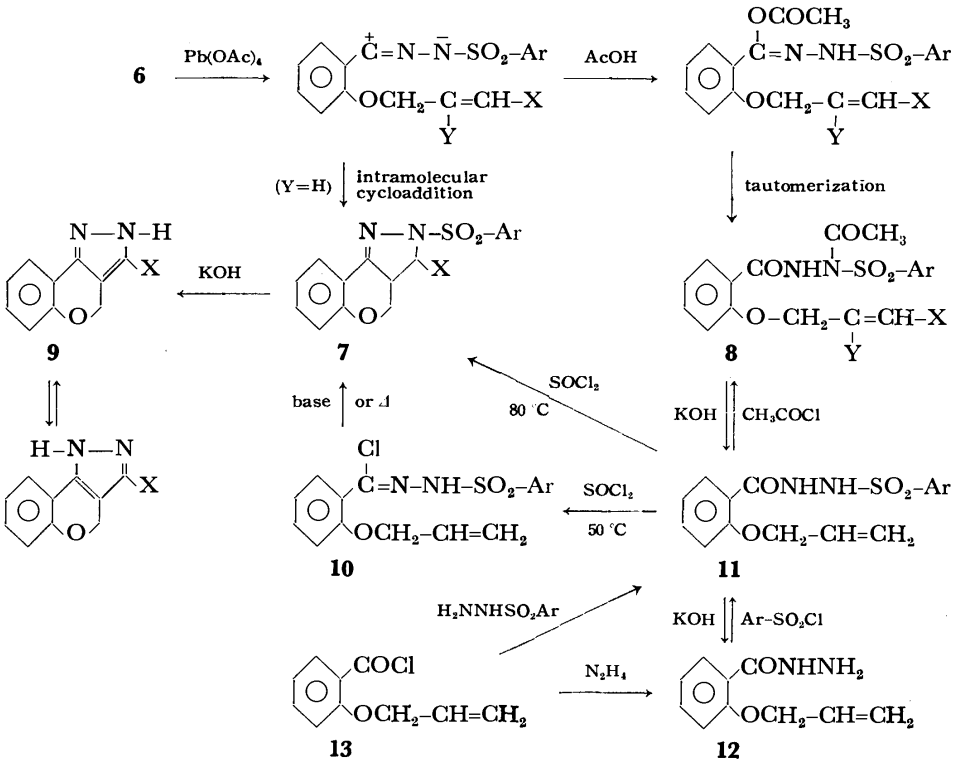

Scheme 1.

(**8a**): the deacetylation of **8a** with aqueous potassium hydroxide under mild conditions gave 2-[*o*-(allyloxy)-benzoyl]-1-(*p*-tolylsulfonyl)hydrazine (**11a**), which was then further hydrolyzed to [*o*-(allyloxy)benzoyl]-hydrazine (**12a**) under more severe conditions. These compounds, **11a** and **12a**, have properties identical with those of authentic specimens prepared by the reaction of *o*-(allyloxy)benzoyl chloride (**13**) with *p*-tolylsulfonylhydrazine or hydrazine hydrate respectively. **8a** can be prepared by the reaction of **11a** with acetyl chloride.

Since the intramolecular 1,3-dipolar cycloadducts (**7**) were obtained from the reaction of sulfonylhydrazones (**6**) with lead tetraacetate, the possibility of the intermolecular cycloaddition reactions was examined under the same conditions. When benzaldehyde *p*-tolylsulfonylhydrazone (**14**) was treated with lead tetraacetate in a dipolarophile such as styrene, acrylonitrile, diethyl maleate, diethyl fumarate or allyl phenyl ether, no cycloadducts were obtained; the only isolated compound was the *N*-acetylated compound (**15**) in any case. These results suggest that *N*-sulfonyl nitrile

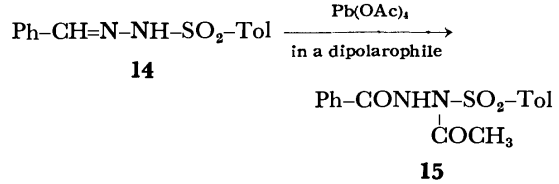

imide is less reactive for 1,3-dipolar cycloaddition reactions and, consequently, undergoes an entropically favored reaction as intramolecular cycloaddition[7b] or the reaction with the acetic acid which exists near the nitrile imide when it is generated. A similar reaction was carried out using the compound bearing a cinnamoyl (**16**) or propargyl group (**17**), which groups are usually more reactive dipolarophiles toward nitrile imine, but *N*-acetylated compounds (**18** and **19**) were the only products isolated from the reaction mixture in each case. There may be many explanations for this result, but

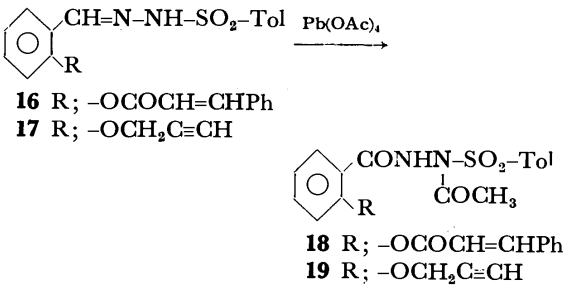

we have no definitive information in this connection. While the carbonyl absorption of phenyl cinnamate appears at 1730 cm^{-1}, that of **16** does so at 1695 cm^{-1}. The broad NH absorption of the hydrazone (**16**) at 3130 cm^{-1} is in sharp contrast with that of the compounds (**6**) which show a sharp absorption at 3200 cm^{-1}. This is presumably a result of an intramolecular hydrogen bonding such as **16'**, in which case the double bond of **16** is relatively remote from the hydrazone group.

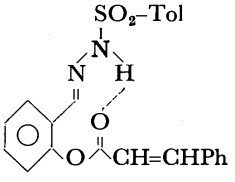

It is thought that compound (**17**) can not attain the optimum overlap needed for cycloaddition reaction because the propargyl group has a linear configuration. While the diaryl nitrile imine, which has a propargyl group, really gave the intramolecular cycloadduct,[6c] no cycloadducts were isolated from the reaction of *N*-sulfonyl hydrazonoyl chloride (**1**) with phenylacetylene or ethyl propiolate.[15]

These results may be explained on the basis of the strong electron-withdrawing property of the sulfonyl group. Thus, the *N*-sulfonyl nitrile imide should function as an electron-accepting one and should react with electron-rich olefins in the dipole-LUMO controlled manner,[20] not with an electron-poor one such as cinnamate.

Though the successful intramolecular cycloadditions may be interpreted in terms of a dipole-LUMO controlled 1,3-dipolar cycloaddition reaction with an allyloxy group which is moderately electron-rich, a step-by-step mechanism can also be considered. An interesting reaction of **1** with enamines (**20**) has been reported.[14] Though the cycloadducts **21** are obtained from the reaction mixture in good yields, this pyrazole

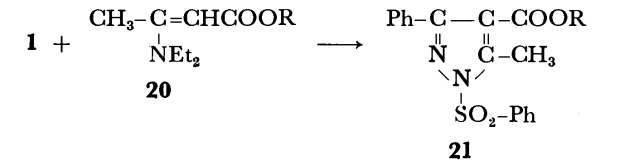

20 **21**

formation is interpreted in terms of a step-by-step process involving the nucleophilic attack of the enamines on the hydrazonoyl chloride.

Finally, we may resonably suppose that the intermediate in the reaction of **6** to **7** and **8** is the 1,3-dipole shown in Scheme 1 and that the *N*-sulfonyl nitrile imides which are prepared by the reaction of **6** with lead tetraacetate usually do not undergo 1,3-dipolar cycloadditions except for the case of an intramolecular reaction which is entropically favored.

Experimental

All the melting and boiling points are uncorrected. The IR spectra were determined on a Hitachi 215 Infrared Spectrophotometer. The PMR spectra were measured on a Varian T-60A instrument with TMS as an internal standard.

Materials. The lead tetraacetate (90.6%) was commercially obtained (Nakarai Chem. Co.) and was used without further purification. The (*o*-alkenyloxy)benzaldehydes were prepared from salicylaldehyde and 1-substituted 3-bromopropenes according to the method in the literature.[5,18] The *N*-(phenylsulfonyl)benzohydrazonoyl chloride (**1**) was prepared by the method of Ito *et al.*[14]

Preparation of the Sulfonylhydrazone. The sulfonylhydrazones (**6**) were prepared by the method of Kirmse *et al.*[10c] The structure of **8b—j** was confirmed on the basis of IR and NMR; IR (Nujol): 3175—3200 (NH), 1160—1172 ($N-SO_2$) and 2240 cm^{-1} (CN); NMR ($CDCl_3$) δ: 8.2—8.3 (s, NH), 4.4—4.8 ($O-CH_2-$), 2.3—2.4 [s, $-CH_3(Z)$] and 1.70 [d, J=4 Hz, $-CH_3(X)$].

*Reaction of Sulfonylhydrazones (**6**) with Lead Tetraacetate. General Procedure*: To a stirred solution of lead tetraacetate (15 mmol) in chloroform (300 ml), we added, drop by drop, a solution of sulfonylhydrazone (**6**) (10 mmol) in chloroform (100 ml) at 0 °C over a period of 30 min. The mixture was stirred at the same temperature for 1 h and then at room temperature overnight. The insoluble material thus precipitated was filtered off using a Celite bed. The filtrate was washed with water (500 ml), and the mixture was filtered using the Celite bed. The organic layer was washed with additional water several times and dried over magnesium sulfate. The subsequent evaporation of the organic layer yielded a viscous oil which solidified upon scraching with a glass rod. Recrystallization from ethanol gave colorless needles of the cycloadduct (**7**) and then an *N*-acetylated compound (**8**). The residue of the concentration of the filtrate from the recrystallization was chromatographed (silica gel) with chloroform to give additional needles, **7** and **8**. For **7a**, the spectral data are shown in the text; the other compounds (**7b—j**) show similar spectral data with an absence of NH absorption in the IR spectrum and an absence of olefinic protons in the NMR spectrum. The spectral data for **8** were as follows: IR (Nujol): 3350—3395 (NH), 1720—1725 (-CONH-), 1675—1690 (CON), 1165—1170 ($N-SO_2$) and 2240 cm^{-1} (CN), and NMR (DMSO-d_6) δ: 10.2 (s, NH), 2.10 (s, $-COCH_3$), 2.40 [s, $-CH_3(Z)$] and 1.80 [d, J=4 Hz, $-CH_3(X)$].

*Reaction of **16** with Lead Tetraacetate.* The reaction was carried out by the General Procedure. 4.4 g (10 mmol) of **16** were treated with lead tetraacetate (10 g, 20 mmol) to give white crystals (**18**) in a 62% yield; mp 185 °C (from ethanol). IR (Nujol): 3375 (NH), 1730 and 1685 (three carbonyl groups), and 1160 cm^{-1} ($N-SO_2$); NMR ($CDCl_3$) δ: 2.10 (s, 3H, $-COCH_3$), 2.37 (s, 3H, $-CH_3$), 6.68 (d, 1H, J=16 Hz, =CH-Ph), 7.1—8.1 (m, 14H, aromatic protons and -CO-CH=) and 9.06 (s, 1H, NH). Found: C, 63.24; H, 4.75; N, 5.78%. Calcd for $C_{25}H_{22}O_6N_2S$; C, 62.75; H, 4.63; N, 5.85%.

*Reaction of **17** with Lead Tetraacetate.* The reaction was carried out by the General Procedure. 3.3 g (10 mmol) of **17** were treated with lead tetraacetate (9 g, 18 mmol) to give white crystals (**19**) in a 30% yield; mp 166—168 °C (from ethanol). IR (Nujol): 3400 (NH), 3300 (≡CH), 2130 (C≡C), 1730 and 1690(two carbonyl groups) and 1170 cm^{-1}($N-SO_2$); NMR ($CDCl_3$) δ: 2.13 (s, 3H, $-COCH_3$), 2.43 (s, 3H, CH_3), 2.63 (t, J=2.6 Hz, 1H, ≡CH), 4.93 (d, J=2.6 Hz, 2H, $-CH_2-$), 7.0—7.73 (m, 5H, aromatic protons), 7.90—8.27 (m, 3H, aromatic protons) and 9.97 (s, 1H, NH). Found: C, 59.61; H, 4.92%. Calcd for $C_{19}H_{18}O_5N_2S$; C, 59.06; H, 4.70%.

*Treatment of **14** with Lead Tetraacetate in Dipolarophiles.* To a stirred solution of lead tetraacetate in 100 ml of dipolarophile and benzene (1: 1) we added, drop by drop, a solution of hydrazone (**14**) (10 mmol) in benzene (50 ml) at room temperature. The mixture was then stirred at room temperature overnight. After the usual work-up, shown in the General Procedure, a 70% yield of 1-acetyl-2-benzoyl-1-(*p*-tolylsulfonyl)hydrazine (**15**) was obtained; mp 204—205 °C (from ethanol) [lit,[16] mp 197—198 °C]; IR (Nujol): 3310 (NH), 1723 and 1675 (two carbonyl groups) and 1160 cm^{-1} ($N-SO_2$); NMR (DMSO-d_6) δ: 2.10 (s, 3H, $-COCH_3$), 2.40 (s, 3H, $-CH_3$), 7.26—8.21 (m, 9H, aromatic protons) and 11.6 (s, 1H, NH).

*Hydrolysis of the Cycloadducts (**7**) with Potassium Hydroxide.* To a solution of potassium hydroxide (2 g, 36 mmol) in 95% aqueous ethanol (60 ml) we added 300 mg of **7**, after which the mixture was stirred for 1 h under refluxing. After the evaporation of the solvent of the reaction mixture, the residue was treated with water (60 ml) and extracted with benzene (50 ml). The organic layer was dried over anhydrous sodium sulfate. The subsequent evaporation of the solvent yielded the pyrazoles (**9**) in 90—95% yields; they were recrystallized from ethanol to give colorless substances. The spectral data for these pyrazoles were as follows: IR (Nujol): 3100—3120

(NH), 3230 [NH_2(**9g, h**)] and 1705 cm^{-1} [CON(**9g, h**)], and NMR ($CDCl_3$) δ: 5.24—5.5 (s, 2H, $-CH_2O-$) and 9.33—11.4 (br NH).

Hydrolysis of the N-*Acetylated Compound (8a) with Potassium Hydroxide.* To a solution of potassium hydroxide (600 mg, 11 mmol) in 95% aqueous ethanol (50 ml) we added **8a** (300 mg, 0.77 mmol), after which the mixture was stirred for 1 h under refluxing. After the subsequent removal of the solvent from the reaction mixture, the residue was treated with water (50 ml) and extracted with ether (50 ml). The ethereal layer was then dried over anhydrous sodium sulfate. The evaporation of the solvent yielded 150 mg (56%) of **11a**; mp 127—128 °C (from ethanol). IR (Nujol): 3370, 3140 (NH) and 1160 cm^{-1} ($N-SO_2$); NMR ($CDCl_3$) δ: 2.34 (s, 3H, $-CH_3$), 4.72 (d, J=6 Hz, $-OCH_2-$), 5.13—5.66 (m, 2H, $=CH_2$), 5.8—6.5 (m, 1H, $-CH=$), 5.8—6.5 (m, 1H, $-CH=$), 6.80—8.00 (m, 9H, aromatic protons and NH) and 9.66 (d, J=6 Hz, NH).

Hydrolysis of 11a with Potassium Hydroxide. To a solution of potassium hydroxide (2 g, 36 mmol) in 95% aqueous ethanol (50 ml) we added **11a** (150 mg, 0.43 mmol), after which the mixture was refluxed for 1 h with stirring. After the subsequent removal of the solvent from the mixture, the residue was treated with water (50 ml) and extracted with ether (50 ml). The evaporation of the solvent yielded 50 mg (60%) of **12a**; mp 51—54 °C. IR (Nujol): 3250 (NH) and 1615 cm^{-1} (C=O); NMR ($CDCl_3$) δ: 4.17 (s, 2H, NH_2), 4.57 (d, J=5 Hz, 2H, $-CH_2-$), 5.07—5.55 (m, 2H, $=CH_2$), 5.67—6.33 (m, 1H, $-CH=$), 6.67—7.50 (m, 3H, aromatic protons), 7.90—8.23 (m, 1H, aromatic proton) and 8.87 (s, 1H, NH).

Methyl o-*(Allyloxy)benzoate.* To a mixture of methyl salicylate (76 g, 0.5 mol), allyl bromide (70 g, 0.58 mol) and acetone (250 ml) we added potassium carbonate (100 g, 0.72 mol), after which the mixture was refluxed overnight with stirring. After the filtration of the inorganic salts and the evaporation of the acetone, the residue was distilled *in vacuo* to give the ester; bp 147—151 °C/19 mmHg; 96 g (quantitative).

o-*(Allyloxy)benzoic Acid.* To a solution of sodium hydroxide (50 g, 1.25 mol) in 90% aqueous ethanol (300 ml) we added methyl *o*-(allyloxy)benzoate (80 g, 0.42 mol), after which the mixture was refluxed overnight with stirring. The reaction mixture was acidified with hydrochloric acid and extracted with benzene (200 ml). The subsequent evaporation of the solvent yielded 69 g (95%) of *o*-(allyloxy)benzoic acid; mp 85 °C (lit,[8a] 64—65 °C). The NMR spectra of this compound agreed with the previously reported one.[8a]

o-*(Allyloxy)benzoyl Chloride (13).* This compound was prepared by the reaction of the corresponding carboxylic acid and thionyl chloride by the method of Padwa *et al.*[8a]

Reaction of 13 with p-*Tolylsulfonylhydrazine.* To a mixture of *p*-tolylsulfonylhydrazine (19 g, 0.1 mol) and triethylamine (20 g, 0.2 mol) in benzene (150 ml) we added, drop by drop, a solution of **13** (15 g, 76 mmol) in benzene over a period of 30 min at room temperature. The mixture was then refluxed for 3 h with stirring. After the filtration of the triethylamine hydrochloride, the filtrate was washed with water and dried over anhydrous sodium sulfate. The subsequent evaporation of the solvent gave **11a** in a 57% (15 g) yield; it was recrystallized from ethanol to give a colorless substance; mp 127—128 °C. IR (Nujol): 3380, 3150 (NH), 1650 (C=O) and 1163 cm^{-1} ($N-SO_2$); NMR ($CDCl_3$) δ: 2.34 (s, 3H, $-CH_3$), 4.72 (d, J=6 Hz, 2H, $-CH_2-$), 5.23—5.66 (m, 2H, $=CH_2$), 5.83—6.53 (m, 1H, $-CH=$), 6.83—7.63 (m, 5H, aromatic protons), 7.63—8.00 (m, 4H, aromatic protons and NH) and 9.71 (d, J=6 Hz, 1H, NH).

Reaction of 11a with Acetyl Chloride. A solution of **11a** (2 g, 5.78 mmol) in acetic acid–acetyl chloride (1: 1) (100 ml) was refluxed for 1 h. The reaction mixture was poured into the water (200 ml) and extracted with ether (150 ml). The ethereal layer was dried over anhydrous sodium sulfate and evaporated to give **8a** in a 54% (1.2 g) yield; mp 122—123 °C (from ethanol).

Reaction of 11a with Thionyl Chloride. (A) A mixture of **11a** (3 g, 8.67 mmol) and thionyl chloride (5 g, 42 mmol) was refluxed for 4 h. After cooling, ethanol (20 ml) and then water (100 ml) were added to the reaction mixture, and it was extracted with ether (70 ml). The subsequent evaporation of the solvent gave **7a** in a 21% (0.7 g) yield; mp 199—200 °C (from ethanol). (B) A mixture of **11a** (2.3 g, 6.65 mmol) and thionyl chloride (5 g, 42 mmol) was stirred at 50—60 °C for 3 h. After cooling, the reaction mixture was added, drop by drop, to ice water and then extracted with chloroform (50 ml). The subsequent evaporation of the solvent gave **10** in a 78% (1.9 g) yield; mp 199—201 °C.

Reaction of Methyl o-*(Allyloxy)benzoate with Hydrazine Hydrate.* A mixture of methyl *o*-(allyloxy)benzoate (15.2 g, 0.1 mol), hydrazine hydrate (50 g, 1 mol), and methanol (50 ml) was refluxed for 6 h. After the distillation of the methanol and the hydrazine hydrate, the residue was solidified to give [*o*-(allyloxy)benzoyl]hydrazine (**12**) in a 75% (11.4 g) yield.

References

1) R. Huisgen, *Angew. Chem. Int. Ed. Engl.*, **2**, 565, 633 (1963).

2) R. Huisgen, *J. Org. Chem.*, **33**, 2291 (1968); **41**, 403 (1976).

3) R. A. Firestone, *J. Org. Chem.*, **33**, 2285 (1968); **37**, 2181 (1972); *J. Chem. Soc., A*, **1970**, 1570; *Tetrahedron*, **33**, 3009 (1977).

4) K. Fukui, "Theory of Orientation and Stereoselection," Springer-Verlag, Berlin (1975); K. N. Houk, *Acc. Chem. Res.*, **8**, 361 (1975).

5) R. Fusco, L. Garanti, and G. Zecchi, *Chim. Ind. (Milan)*, **57**, 16 (1975); L. Garanti, A. Sala, and G. Zecchi, *J. Org. Chem.*, **40**, 2403 (1975).

6) (a) L. Garanti, A. Scandroglio, and G. Zecchi, *J. Heterocycl. Chem.*, **13**, 1339 (1976); L. Garanti and G. Zecchi, *Tetrahedron Lett.*, **1976**, 1339; *Synthsis*, **1974**, 814; *J. Org. Chem.*, **43**, 2077 (1978), and the references cited therein; (b) H. Meier, H. Heimgartner, and H. Schmidt, *Helv. Chim. Acta*, **60**, 1087 (1977); H. Meier and H. Heimgartner, *ibid.*, **60**, 3035 (1977); (c) G. Schmidt and B. Laude, *Tetrahedron Lett*, **1978**, 3727; (d) A. Padwa, S. Nahm, and E. Sato, *J. Org. Chem.*, **43**, 1664 (1978); (e) C. Wentrup, A. Damarius, and W. Reichen, *ibid.*, **43**, 2037 (1978).

7) (a) W. Oppolzer and K. Keller, *Tetrahedron Lett.*, **1970**, 1117, 4313; W. Oppolzer and H. P. Weber, *ibid.*, **1970**, 1121; (b) W. Oppolzer, *Angew. Chem. Int. Ed. Engl.*, **16**, 10 (1977); (c) W. C. Lumma Jr., *J. Am. Chem. Soc.*, **91**, 2820 (1969); (d) N. A. LeBel and E. G. Banucci, *J. Org. Chem.*, **36**,2440 (1971); N. A. LeBel, N. D. Ojha, J. R. Menke, and R. J. Newland, *ibid.*, **37**, 2896 (1972); (e) A. Padwa, H. Ku, and A. Mazzu, *ibid.*, **43**, 381 (1978).

8) (a) A. Padwa, P. H. J. Calsen, and A. Ku, *J. Am. Chem. Soc.*, **99**, 2798 (1977); **100**, 3494 (1978); (b) L. Garanti, G. Padova, and G. Zecchi, *J. Heterocycl. Chem.*, **14**, 947 (1977).

9) (a) R. Fusco, L. Garanti, and G. Zecchi, *J. Org. Chem.*, **40**, 1906 (1975); O. Tsuge, K. Ueno, and A. Inaba, *Heterocycles*, **4**, 1 (1976); (b) A. Padwa, A. Ku, H. Ku, and A. Mazzu, *J. Org. Chem.*, **43**, 66 (1978); *Tetrahedron Lett.*, **1977**, 551; (c) M. Bartrand, J. P. Dulcere, and M. Santelli, *ibid.*, **1977**, 1783; (d) A. L. Logothetis, *J. Am. Chem. Soc.*, **87**, 749 (1965).

10) (a) J. L. Brewbaker and H. Hart, *J. Am. Chem. Soc.*, **91**, 711 (1969); (b) A. Ledwith and D. Parry, *J. Chem. Soc., B*, **1967**, 41; (c) W. Kirmse and H. Dietrich, *Chem. Ber.*, **100**, 2710 (1967).

11) R. Huisgen, M. Siedel, G. Wallbillich, and H. Knupfer, *Tetrahedron*, **17**, 3 (1962)

12) R. Huisgen, M. Siedel, J. Sauer, J. W. McFarland, and G. Wallbillich, *J. Org. Chem.*, **24**, 892 (1959); R. Huisgen, J. Sauer, and M. Siedel, *Chem. Ber.*, **94**, 2503 (1961); R. Huisgen, R. Grashey, E. Aufder haar, and R. Kunz, *ibid.*, **98**, 642 (1965); J. S. Clovis, A. Eckell, R. Huisgen, and R. Sustmann, *ibid.*, **100**, 60 (1967); A. Eckell, R. Huisgen, R. Sustmann, G. Wallbillich, D. Grashey, and E. Spindler, *ibid.*, **100**, 2192 (1967).

13) W. A. F. Gladstone, *J. Chem. Soc., Chem. Commum.*, **1969**, 179; W. A. F. Gladstone, J. B. Aylward, and R. O. C. Norman, *J. Chem. Soc., C*, **1969**, 2587.

14) S. Wawzonek and J. N. Kellen, *J. Org. Chem.*, **38**, 3627 (1973); S. Ito, T. Tanaka, A. Kakehi, and H. Miyazawa, *Bull. Chem. Soc. Jpn.*, **50**, 2969 (1977); S. Ito, T. Tanaka, A. Kakehi, and T. Matsumoto, *ibid.*, **51**, 327 (1978).

15) Y. Tanaka, S. Eguchi, and T. Sasaki, 38th National Meeting of the Chemical Society of Japan, Nagoya, October 1978, Abstr. Vol. II, 348.

16) F. L. Scott and R. N. Butler, *J. Chem. Soc., C*, **1966**, 1202; A. Bhati, *J. Chem. Soc.*, **1965**, 1020.

17) C. Grundmann and P. Grünanger, "The Nitrile Oxides," Springer-Verlag, Berlin (1971), p. 92.

18) J. Ide and I. Iwai, *Chem. Pharm. Bull.*, **11**, 1042 (1963).

19) F. M. Dean and S. Marray, *J. Chem. Soc., Parkin Trans., 1*, **1975**, 1706.

20) I. Fleming, "Frontier Orbitals and Organic Chemical Reactions," John Wiley and Sons, New York (1476), p. 150.

 © 1980 The Chemical Society of Japan Bull. Chem. Soc. Jpn., 53, 435—437 (1980)

Syntheses and Reactions of Optically Active Alkoxyaminosulfonium Salts

Kentaro Okuma, the late Hiroshi Minato, and Michio Kobayashi*

Department of Chemistry, Tokyo Metropolitan University, Fukazawa, Setagaya, Tokyo 158

(Received March 28, 1979)

The optically active methoxymorpholino-*p*-tolylsulfonium salt has been synthesized by the reaction of optically active *N*-*p*-toluenesulfinylmorpholine with methyl trifluoromethanesulfonate. The sulfonium ion methylated benzylethylphenylamine and benzyl ethyl sulfide with asymmetric induction to give the optically active benzylethylmethylphenylammonium ion and benzylethylmethylsulfonium ion respectively. The optically active methoxymorpholino-*p*-tolylsulfonium salt and diaminosulfonium salts have been prepared in a one pot reaction between *N*-*p*-toluenesulfenylmorpholine and 1-chlorobenzotriazole with methanol in the presence of 1-menthol at −80 °C.

Stereochemically, the sulfonium ions are of great interest. The absolute configuration of the ethylmethylphenylsulfonium ion has been reported,[1] and the syntheses and absolute configuration of the oxosulfonium ions have been reported.[2-4] Johnson and Schroeck have studied the syntheses of optically active sulfoximines and the reactions of aminooxosulfonium methylide with carbonyl compounds.[5]

Several kinds of alkoxyaminosulfonium salts have been reported and it has been found that the sulfonium ions alkylate amines and sulfides to give the corresponding ammonium and sulfonium salts in high yields.[6] It is expected that the optically active alkoxyaminosulfonium ions alkylate amines and sulfides with asymmetric induction. In this paper, the syntheses of optically active alkoxyamino- and diaminosulfonium salts and their optical resolution will be described.

Results and Discussion

(−)-(*S*)-Menthyl *p*-toluenesulfinate ($[\alpha]_D^{20}$ −198°)(**1**) was treated with morpholinomagnesium bromide according to the literature[7] to give the optically active *N*-*p*-toluenesulfinylmorpholine (**2**); $[\alpha]_D^{23}$ +115°. In the handling of **2**, it was necessary to work below room temperature in the absence of light and oxygen in order to prevent optical deterioration. The treatment of **2** with phenyllithium gave phenyl *p*-tolyl sulfoxide in good yields; $[\alpha]_D^{23}$ −16.2°. Mislow prepared phenyl *p*-tolyl sulfoxide ($[\alpha]_D$ +21.1°) by the reaction of **1** with phenyllithium, and determined its absolute configuration to be (+)-(*R*).[8] Therefore, the absolute configuration of phenyl *p*-tolyl sulfoxide ($[\alpha]_D^{23}$ −16.2°) obtained in this reaction should be (−)-(*S*), and the optical purity was calculated as 76%. The reaction of sulfinamide with organolithium compounds is known to proceed with 100% inversion of configuration around the sulfur atom,[9] and consequently the absolute configuration of **2** obtained in the reaction of **1** with morpholinomagnesium bromide should be (+)-(*S*), with an assumed optical purity of 76%. The configurational relationships between the sulfinic ester, the sulfinamide and the sulfoxide are illustrated in the following scheme.

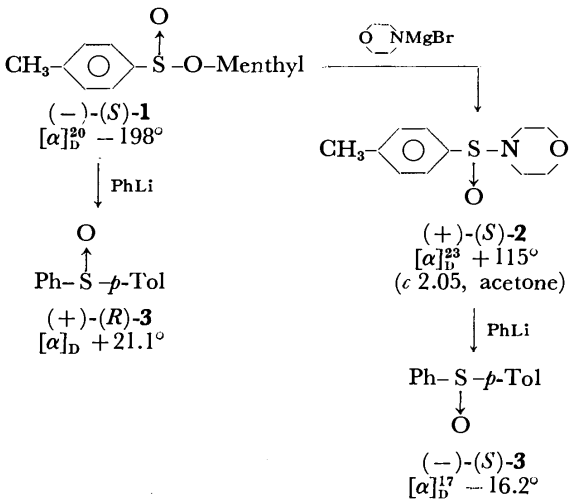

It has been reported that alkoxyaminosulfonium ions alkylate amines and sulfides quantitatively.[6] With optically active sulfonium ions, asymmetric induction is to be expected and this has been investigated by the reactions of optically active methoxymorpholino-*p*-tolylsulfonium tetraphenylborate (**4**) with benzylethylphenylamine and benzyl ethyl sulfide.

Optically active **4** ($[\alpha]_D^{24}$ +17°) was prepared by the methylation of optically active (+)-(*S*)-**2** with methyl trifluoromethanesulfonate in nitromethane at 0 °C for 5 h followed by the anion exchange reaction with sodium tetraphenylborate. Assuming the optical purity of the sample is the same as the starting sulfinamide, the optical activity of pure (+)-(*S*)-**4** is estimated to be $[\alpha]_D^{24}$ +22.2°.

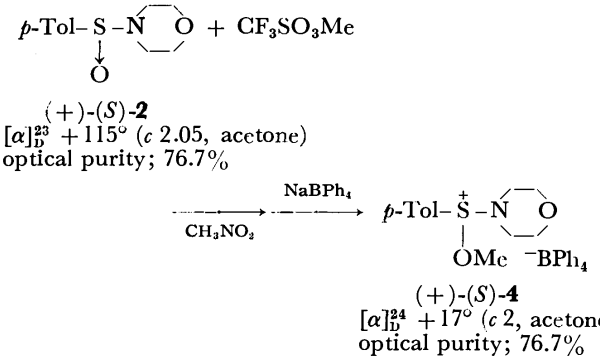

Optically active **4** ($[\alpha]_D^{24}$ +17°) was treated with benzylethylphenylamine in nitromethane at room temperature for 7 d and a salt-like product was obtained. This was shown to be benzylethylmethylphenylammonium tetraphenylborate (**5**), the optical activity of which was found to be $[\alpha]_D^{23}$ −4.0°. Optically pure (+)-**5** was prepared separately by the anion exchange

reaction of optically pure benzylethylmethylphenylammonium *d*-camphorsulfonate with sodium tetraphenylborate,[9] $[\alpha]_D^{20}$ +6.5°. Assuming $[\alpha]_D^{20}$ −6.5° for the optically pure (−)-**5**, the optical purity of the methylated amine by the reaction of **4** with benzylethylphenylamine was estimated as 62%.

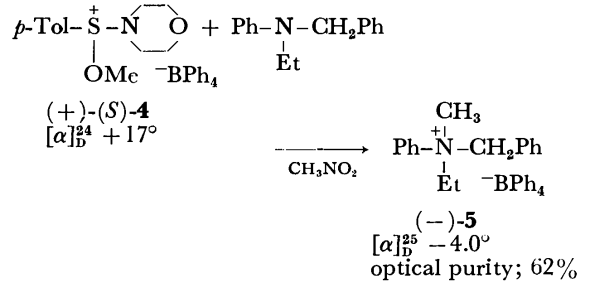

Opically active **4** ($[\alpha]_D^{24}$ +17°) was allowed to react with benzyl ethyl sulfide in nitromethane at room temperature for 5 h and asymmetric benzylethylsulfonium tetraphenylborate (**6**) was formed. The optical activity of the salt (**6**) was determined; $[\alpha]_D^{23}$ −4°.

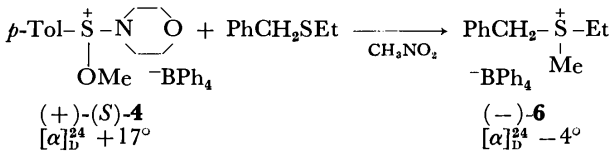

Oae and coworkers reported the syntheses of optically active diarylsulfilimines by the reaction of diarylsulfides and *t*-butyl hypochlorite in the presence of l-menthol, followed by treatment with sodium *N*-tosylamide.[10] The asymmetric syntheses of **4** were investigated by applying the method of Oae. *N-p*-toluenesulfenylmorpholine was treated with 1-chlorobenzotriazole in dichloromethane at −80 °C for 10 min and l-menthol was added to this solution. The subsequent addition of methanol and sodium tetraphenylborate gave **4**, exhibited optical activity; $[\alpha]_D^{25}$ +5° (*c* 2, acetone).

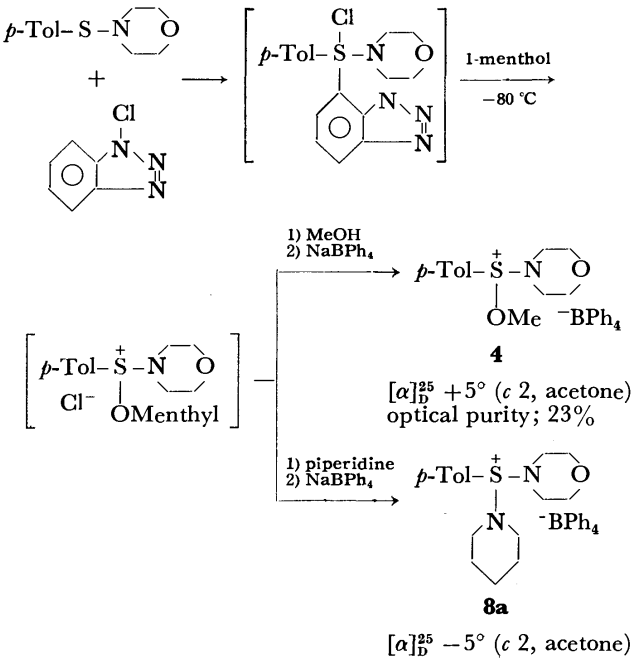

The optical purity of **4** thus obtained was only 23%. This synthetic method for optically active sulfonium salts has an advantage however in that the reaction can be conducted in one pot. **8a** was prepared in a similar method by the addition of piperidine replacing methanol; $[\alpha]_D^{25}$ −5° (*c* 2, acetone). This is the first example of the optically active diaminosulfonium ion (**8**).

On the basis of these findings, the optically active alkoxyaminosulfonium ion appears to be more useful for asymmetric inducing alkylation for amines and sulfides than the optically active alkoxysulfonium ion.[11]

Experimental

General. Optical rotation was measured on a Applied Electric Lab. MP-1T polarimeter using a 0.5-dm cell. Infrared spectra were obtained on a Hitachi EPI-G_2 spectrometer. NMR spectra were recorded on a Hitachi R-20B spectrometer. Melting points are uncorrected.

Materials. (−)-(*S*)-Menthyl *p*-toluenesulfinate was prepared according to the usual manner; $[\alpha]_D^{20}$ −198° (*c* 2, acetone); lit,[8] $[\alpha]_D^{25}$ −202° (*c* 2, acetone). 1-Chlorobenzotriazole was prepared from benzotriazole and 10% aq NaOCl solution according to the method in the literature.[12] *N-p*-toluenesulfenylmorpholine was prepared by the method reported previously; bp 80 °C/4.5 mmHg, mp 39—42 °C.[13]

Preparation of Optically Active N-p-*Toluenesulfinylmorpholine* (*2*). An anhydrous THF solution (30 ml) of morpholinomagnesium bromide (20 mmol), which was prepared by the reaction of phenylmagnesium bromide (3.73 g; 20 mmol) with morpholine (1.74 g; 20 mmol) was added dropwise to a stirred ether solution (80 ml) of **1** (5.88 g; 20 mmol) for 1 h at 0 °C. The reaction mixture was stirred at 0 °C for an additional 3 h. A saturated ammonium chloride solution (100 ml) was added to the above solution and the ether–THF layer separated. The aqueous layer was extracted three times, with dichloromethane (20 ml), and the combined extracts were concentrated under reduced pressure below 30 °C to give a pale yellow oil. The residue subjected to elution chromatography on silica gel (hexane–ether eluent) afforded 1.24 g of (+)-**2** (5.54 mmol; 28%); $[\alpha]_D^{23}$ +115° (*c* 2.05, acetone).

To ascertain the optical purity, the reaction of **2** with phenyllithium was conducted. An anhydrous ether solution (30 ml) of phenyllithium (10 mmol) was added dropwise to a stirred ether solution (20 ml) of **2** (500 mg; 2.4 mmol) for 30 min at 0 °C. The mixture was stirred at 0 °C for an additional 1 h. A saturated sodium chloride solution (40 ml) was added to the reaction mixture, and the ether layer separated. The aqueous layer was extracted three times with ether. The combined extracts were dried over anhydrous magnesium sulfate, and the solvent evaporated to give oil. The residual oil was separated by column chromatography on silica gel (hexane–ether eluent) to afford (−)-(*S*)-**3**; 150 mg (29%), $[\alpha]_D^{17}$ +21.1° (*c* 1.64, acetone).[8] These rsults indicate that (−)-**2**, which was obtained by the reaction of (−)-(*S*)-**1** with morpholinomagnesium bromide, has 76% optical purity.

*Preparation of Optically Active Methoxymorpholino-*p-*tolylsulfonium Tetraphenylborate (4).* A nitromethane solution (10 ml) of (+)-(*S*)-**2** (620 mg; 2.76 mmol) and methyl trifluoromethanesulfonate was stirred for 5 h at 0 °C. To this orange solution a nitromethane solution (10 ml) of sodium tetraphenylborate (950 mg; 2.8 mmol) was added. The addition of ether (30 ml) to the reaction mixture formed a precipiatate of sodium trifluoromethanesulfonate, which was removed by

filtration. The further addition of ether (60 ml) to the filtrate resulted in the precipitation of **4**; 650 mg, 1.16 mmol (42%). Found: C, 77.37; H, 7.06; N, 2.74%. Calcd for $C_{36}H_{38}NO_2SB$: C, 77.27; H, 6.84; N, 2.56%. $[\alpha]_D^{24}$ +17° (*c* 2, acetone).

Preparation of Optically Active 4. A dichloromethane solution (10 ml) of *N-p*-toluenesulfenylmorpholine (3 mmol) and a dichloromethane solution (10 ml) of 1-chlorobenzotriazole (3 mmol) were mixed at −80 °C to give yellow solution. A dichloromethane solution (10 ml) of l-menthol (3 mmol) and methanol (10 ml) was added to this solution at −80 °C. A cooled acetonitrile solution (10 ml) of sodium tetraphenylborate (3 mmol) was added to this solution at −80 °C, and the addition of ether caused the precipitation of a mixture of **4** and sodium chloride which was removed by filtration. Ether was added to the acetone solution to give **4** as colorless needles; 1.05 mmol, yield, 35%, $[\alpha]_D^{25}$ −5° (*c* 2, acetone), mp 149—150 °C.

Preparation of Optically Active 8. A dichloromethane solution (10 ml) of *N-p*-toluenesulfenylmorpholine (3 mmol) and a dichloromethane solution (10 ml) of 1-chlorobenzotriazole (3 mmol) were mixed at −80 °C. The addition of a dichloromethane solution (5 ml) of l-menthol (3 mmol) to this yellow solution at −80 °C caused the solution to lose color. A dichloromethane solution (10 ml) of piperidine (3 mmol) was added immediately to this solution, and the solution warmed to room temperature. A nitromethane solution (15 ml) of sodium tetraphenylborate (3 mmol) was added to this pale yellow solution. After 3 h, the addition of ether precipitated a mixture of sodium chloride and morpholino-piperidino-*p*-tolylsulfonium tetraphenylborate (**8a**), which dissolved in acetone–ether to give colorless crystals of **8a**; 200 mg (0.32 mmol; 11.1%), mp 220.5—222 °C, $[\alpha]_D^{25}$ −5° (*c* 2, acetone). Found: C, 78.88; H, 7.04; N, 4.07%. Calcd for $C_{40}H_{45}N_2OSB$: C, 78.41; H, 7.40: N, 4.57%. Optically active *N*-methylphenylaminomorpholino-*p*-tolylsulfonium tetraphenylborate (**8b**), (0.79 mmol, 26%) was prepared in a similar manner from *N-p*-toluenesulfenylmorpholine (3 mmol) and *N*-methylaniline (3 mmol), mp 155—156 °C, $[\alpha]_D^{25}$ −4.8° (*c* 2.4, acetone). Found: C, 79.26; H, 6.70, N, 4.41%. Calcd for $C_{42}H_{43}N_2OSB$: C, 79.48; H, 6.83; N, 4.42%.

References

1) K. K. Andersen, R. L. Caret, and D. L. Ladd, *J. Org. Chem.*, **41**, 3096 (1976).

2) M. Kobayashi, K. Kamiyama, H. Minato, Y. Oishi, and Y. Hattori, *Chem. Commun.*, **1971**, 1577.

3) M. Kobayashi, K. Kamiyama, H. Minato, Y. Oishi, Y. Takada, and Y. Hattori, *Bull. Chem. Soc. Jpn.*, **45**, 3703 (1972).

4) K. Kamiyama, H. Minato, and M. Kobayashi, *Bull. Chem. Soc. Jpn.*, **46**, 3895 (1973).

5) C. R. Johnson and C. W. Schroeck, *J. Am. Chem. Soc.*, **93**, 5303 (1971).

6) H. Minato, K. Yamaguchi, K. Okuma, and M. Kobayashi, *Bull. Chem. Soc. Jpn.*, **49**, 2590 (1976).

7) A. Nudelman and D. J. Cram, *J. Am. Chem. Soc.*, **90**, 3869 (1968).

8) K. Mislow, M. M. Green, P. Laur, J. T. Mellilo, T. Simmons, and A. L. Ternay, Jr., *J. Am. Chem. Soc.*, **87**, 1958 (1965).

9) S. Colonna, R. Giovini, and F. Montanari, *Chem. Commun.*, **1968**, 865.

10) M. Moriyama, T. Yoshimura, N. Furukawa, T. Numata, and S. Oae, *Tetrahedron*, **32**, 3003 (1976).

11) K. Tsumori, H. Minato, and M. Kobayashi, *Bull. Chem. Soc. Jpn.*, **46**, 3158 (1973).

12) C. R. Johnson, C. C. Bacon, and W. D. Kingsbury, *Tetrahedron Lett.*, **1972**, 501.

13) N. Kharasch, S. J. Potempa, and H. L. Wehrmeister, *Chem. Rev.*, **39**, 269 (1946).

14) H. O. Jones, *J. Chem. Soc.*, **85**, 227 (1904).

Mechanisms of Stannyl-Carbon Bond Cleavages by Reactions with Benzoyl Peroxide

Seizi KOZUKA,* Ikuya NARIBAYASHI, Jun-ichi NAKAGAMI, and Kenji OGINO

Department of Applied Chemistry, Faculty of Engineering, Osaka City University, Sugimotocho, Sumiyoshi, Osaka 558

(Received April 23, 1979)

The mechanism for the process giving trimethyl(benzoyloxy)stannane by the reaction of benzoyl peroxide with trimethylphenylstannane or tetramethylstannane has been investigated. The kinetic results exclude the possibility that the decomposition of the peroxide is induced by the stannanes. The addition of dicyclohexylcarbodiimide as a trapping agent for benzoic acid markedly depressed the yield of the benzoyloxystannane by the reaction of trimethylphenylstannane, suggesting that the benzoyloxystannane is mainly or exclusively produced by the protodestannylation reaction of trimethylphenylstannane with benzoic acid. In the reaction of tetramethylstannane with benzoyl peroxide, trimethyl(benzoyloxy)stannane was formed only when a large excess of the stannane was used, and dicyclohexylcarbodiimide showed no significant effect upon the formation of the benzoyloxystannane. A homolytic process has been suggested for the reaction giving the benzoyloxystannane from tetramethylstannane.

There are many reactions which have been established to involve homolytic cleavages of the stannyl–carbon bond caused by free-radical attack.[1] An example is the reaction of diacyl peroxide with tetraalkylstannane or trialkylarylstannane.[2] The thermal decomposition of benzoyl peroxide in trimethylphenylstannane was examined by Razuvaev *et al.*; they found carbon dioxide, benzene, biphenyl, and trimethyl(benzoyloxy)stannane as the products. Since the formation of carbon dioxide and the hydrocarbons was thought to strongly suggest the generation of the benzoyloxyl radical through the thermolysis of the benzoyl peroxide, the formation of trimethyl(benzoyloxy)stannane was explained in terms of the attack of the benzoyloxyl radical on the stannane.[2a,b] However, there was no definite evidence

$$(PhC(=O)-O-)_2 \longrightarrow PhC(=O)-O\cdot \xrightarrow{Me_3SnPh} PhC(=O)-O-SnMe_3 + Ph\cdot$$

in support of their mechanism for the process giving trimethyl(benzoyloxy)stannane from trimethylphenylstannane. Some other mechanisms are possible; for example, the reaction of diacyl peroxide with the stannane by way of the coordination of the tin atom to the carbonyl oxygen of the peroxide, analogous to the Lewis acid-catalyzed decomposition,[3] may produce the benzoyloxystannane. A somewhat modified cyclic coordination process has been suggested for the reaction of allyltrimethylstannane with benzoyl peroxide giving allyl benzoate and trimethyl(benzoyloxy)stannane; this suggestion was based on the observations that the rate of the decomposition was apparently dependent on the concentration of the stannane, a large negative entropy value, and that only 1-methylallyl benzoate was formed from 2-butenyltrimethylstannane.[4]

Secondly, since carboxylic acid has been known to be formed by the thermolysis of diacyl peroxide in a hydrocarbon solvent,[5] protodestannylation of organostannane with the carboxylic acid is also a possible route to give acyloxystannane,[6] as has been suggested preliminarily.[7]

Such a tetraalkylstannane as tetraethylstannane has also been known to give trialkyl(benzoyloxy)stannane by means of a reaction with benzoyl peroxide.[2a] A stannane not bearing a phenyl group would resist the protodestannylation process,[8] though; hence a different mechanism would be expected for the process giving triethyl(benzoyloxy)stannane in the reaction of tetraethylstannane with benzoyl peroxide. In this paper we wish to discuss the mechanisms of the processes giving trialkyl(benzoyloxy)stannane from trialkylphenyl- and tetraalkylstannanes by means of reactions with benzoyl peroxide.

Results and Discussion

Trialkyl(benzoyloxy)stannane from Trialkylphenylstannane.[9] In order to elucidate the mechanism for the process giving trimethyl(benzoyloxy)stannane, the thermal decompositions of benzoyl peroxide were carried out under several different conditions. Reactions were carried out in evacuated sealed tubes except for that analyzing the amount of carbon dioxide formed by the thermolysis of benzoyl peroxide. Although the formations of other products such as benzene, benzoic acid, and biphenyl were observed, only the yields of carbon dioxide and trimethyl(benzoyloxy)stannane will be noted in the present study since a detailed product analysis of the reaction had been reported by Razuvaev *et al.*[2]

The rate of the thermal decomposition of benzoyl peroxide was measured in the presence and in the absence of trimethylphenylstannane. Although cyclohexane has often been used as the solvent for the thermolysis,[5] a cyclohexane–chloroform mixed solvent was used for the present kinetic study because of the poor solubility of the other additives in the hydrocarbon solvent. The rate of the decomposition was substantially depressed in the presence of styrene, while the presence of the stannane was found neither to depress nor enhance the rate of the decomposition of benzoyl peroxide. The results, given in Table 1, suggest that trimethylphenylstannane does not take a part in the decomposition of benzoyl peroxide. The possibility of the reaction giving the benzoyloxy stannane directly from trimethylphenylstannane and benzoyl peroxide can thus be ruled out.

Table 1. Rate constants for the decomposition of benzoyl peroxide (0.01 mol/dm³) in chloroform–cyclohexane (1 : 1 v/v) at 80 °C with or without an additive

Additive	Mole ratio Add./BPO	Rate constant $k_1 \times 10^5/s^{-1}$
None		4.91±0.15
$PhCH{=}CH_2$	10	3.05±0.10
Me_3SnPh	10	4.34±0.29
Me_4Sn	10	4.69±0.18
DCC[a]	2[b]	5.92±0.28
PhCOOCOPh	10	4.92±0.30
DCU[c]	2[b]	3.43±0.33

a) Dicyclohexylcarbodiimide. b) Experiments with higher concentrations could not be performed because of the limited solubility of the additive. c) *N,N'*-Dicyclohexylurea.

Dicyclohexylcarbodiimide (DCC) was added to the reaction system in order to trap the benzoic acid formed by the thermolysis of benzoyl peroxide in the hydrocarbon solvent. *N,N'*-dicyclohexylurea (DCU) was isolated by the TLC separation of the reaction mixture. The yield of trimethyl(benzoyloxy)stannane was depressed by the addition of DCC in a cyclohexane–chloroform solution. The themolysis of benzoyl peroxide in a cyclohexane–tetrahydrofuran solution in the presence of DCC gave no detectable amount of trimethyl(benzoyloxy)stannane. The amount of carbon dioxide formed by the thermolysis, however, was not affected by the addition of DCC, suggesting that DCC does not intercept the benzoyloxyl radicals during the thermolysis, although a carbodiimide has been known to intercept radicals.[10] The results shown in Table 2 indicate that the decomposition of benzoyl peroxide was not affected by the addition of DCC, they also suggest that benzoic acid might be an intermediate to give trimethyl(benzoyloxy)stannane.

In a control experiment, benzoic acid was heated with trimethylphenylstannane at 85—90 °C for 16 h.

Table 2. Reaction of benzoyl peroxide (BPO) with trimethylphenylstannane (TPSn) at 85—90 °C for 16 h

Initial concentration mol/dm³			Solvent[a]	Product yield/%[b]	
BPO	TPSn	DCC		CO_2	$Me_3SnOCOPh$
0.03	0	0	C_6H_{12}–$CHCl_3$	58	—
0.03	0	0.03	C_6H_{12}–$CHCl_3$	55	—
0.03	0.06	0	C_6H_{12}–$CHCl_3$	55	34
0.03	0.06	0.03	C_6H_{12}–$CHCl_3$	54	20
0.03	0	0	C_6H_{12}–THF	27	—
0.03	0	0.03	C_6H_{12}–THF	27	—
0.03	0.06	0	C_6H_{12}–THF	26	15
0.03	0.06	0.03	C_6H_{12}–THF	27	0
0.21	4.2	0	$CHCl_3$	—[c]	103
0.21	4.2	0.21	$CHCl_3$	—[c]	30

a) 1 : 1 v/v mixture, C_6H_{12}=cyclohexane, THF=tetrahydrofuran. b) Based on mole of BPO. c) Not analyzed.

Table 3. Reaction of benzoic acid (BA) with trimethylphenylstannane (TPSn) or tetramethylstannane (TMSn) at 85—90 °C for 16 h

Initial concentration/(mol/dm³)				Solvent[b]	Yield/%[a]
BA	TPSn	TMSn	DCC		$Me_3SnOCOPh$
0.03	0.06	0	0	C_6H_{12}–$CHCl_3$	26
0.03	0.06	0	0.03	C_6H_{12}–$CHCl_3$	0
0.03	0.06	0	0	C_6H_{12}–THF	11
0.03	0.06	0	0.03	C_6H_{12}–THF	trace
0.3[c]	0	6.0[c]	0	none	0

a) Based on mole of BA. b) 1 : 1 v/v mixture, C_6H_{12}=cyclohexane, THF=tetrahydrofuran. c) Millimoles used for neat reaction.

Trimethyl(benzoyloxy)stannane was formed in yields comparable with those obtained by the reactions with benzoyl peroxide in both the solvents examined. Here again, the presence of DCC completely depressed the formation of trimethyl(benzoyloxy)stannane. These results are shown in Table 3. No serious effect of these additives, *i.e.*, DCC, DCU, and benzoic anhydride, on the rate of the decomposition of benzoyl peroxide was observed, although a slight acceleration and a little depression of the rate of the decompositions were observed in the presence of DCC and DCU respectively. The kinetic results are summarized in Table 1. These results also reveal that the thermolysis of benzoyl peroxide was not seriously affected in the presence of DCC.

On the basis of these observations, the mechanism for the process giving trimethyl(benzoyloxy)stannane may be concluded to involve the protodestannylation reaction of trimethylphenylstannane with benzoic acid, at least partially in a cyclohexane–chloroform solution or a high-concentration reaction in chloroform, and exclusively in a cyclohexane–tetrahydrofuran solution. In the reactions carried out in chloroform-containing solutions, it is not clear whether another competing process (for example, the radical process suggested by Razuvaev *et al.*[2]) was also operative concurrently or whether DCC could not effectively trap all the benzoic acid.

The mechanism for the formation of trimethyl(benzoyloxy)stannane by means of the reaction of benzoyl peroxide with trimethylphenylstannane in a cyclohexane–tetrahydrofuran solution (and the main process in the other solvent) is shown below. The observation that only the aryl–Sn bond is cleaved by

$$(PhCOO)_2 \longrightarrow 2PhCOO\cdot$$

$$PhCOO\cdot + R\text{–}H \longrightarrow PhCOOH + Ph\text{–}H,\ CO_2,\ Ph\text{–}Ph\ etc.$$

$$PhCOOH + Me_3SnPh \xrightarrow{\text{Protodestannylation}} Me_3SnOCOPh + Ph\text{–}H$$

the reaction of trimethylphenylstannane with benzoyl peroxide, giving trimethyl(benzoyloxy)stannane as the sole benzoyloxystannane, is also in accordance with the proposed mechanism.[8]

Trialkyl(acyloxy)stannane from Tetraalkylstannane. Tetraethylstannane has been known to give triethyl(benzoyloxy)stannane by the reaction with benzoyl peroxide, along with such other products as carbon dioxide, ethane, ethene, butane, and benzoic acid.[2b,d] In our present study, tetramethylstannane instead of tetraethylstannane was chosen as the tetraalkylstannane for two reasons: 1) the recovered tetramethylstannane can easily be removed from the reaction mixture by evaporation, and 2) both the starting stannane and the product, trimethyl(benzoyloxy)stannane, exhibit sharp singlet methyl signals in the NMR spectra and so can conveniently be detected.

Table 4. Reaction of benzoyl peroxide (BPO) with tetramethyl stannane (TMSn) at 85—90 °C for 16 h

Initial concentration mol/dm³			Solvent[a]	Yield/%[b] $Me_3SnOCOPh$
BPO	TMSn	DCC		
0.03	0.06	0	C_6H_{12}–$CHCl_3$	0
0.03	0.06	0	C_6H_{12}–THF	0
0.03	0.24	0	C_6H_{12}–$CHCl_3$	0
0.21	4.2	0	$CHCl_3$	20
0.21	4.2	0.21	$CHCl_3$	18
0.3[c]	6.0[c]	0	none	24
0.3[c]	6.0[c]	0.3[c]	none	23

a) C_6H_{12} = cyclohexane, THF = tetrahydrofuran. Mixed solvents are 1:1 v/v mixtures. b) Based on mol of BPO. c) Millimoles used for neat reactions.

The rate of the thermal decomposition of benzoyl peroxide was measured in both the presence and absence of tetramethylstannane. The results are summarized in Table 1. Neither the acceleration nor the retardation of the rate in the presence of tetramethylstannane was observed. The results suggest that the stannane does not take part in the decomposition of benzoyl peroxide. On the other hand, no detectable amount of trimethyl(benzoyloxy)stannane was formed by the thermolysis of the peroxide in the presence of tetramethylstannane under the same reaction conditions as those used for the thermolysis of benzoyl peroxide in the presence of trimethylphenylstannane. The benzoyloxystannane was formed in a moderate yield only when a large excess and a high concentration of tetramethylstannane were used. The reaction of benzoyl peroxide with tetramethylstannane without the use of the solvent gave trimethyl(benzoyloxy)stannane in a similar yield.[11] Under these conditions, DCC showed no significant effect upon the formation of trimethyl(benzoyloxy)stannane. These results are given in Table 4. Furthermore, the heating of benzoic acid with tetramethylstannane gave no detectable amount of trimethyl(benzoyloxy)stannane under any reaction conditions used for the thermal decomposition of benzoyl peroxide in the presence of the stannane. This result, together with the lack of any effect of DCC on the formation of trimethyl(benzoyloxy)stannane and the lack of any effect of tetramethylstannane on the rate of the decomposition of benzoyl peroxide, rules out the possibility that the benzoyloxystannane was formed by the decomposition of the peroxide by way of the coordination mechanism. The same results would also rule out the possibility of the benzoyloxystannane being given by the protodestannylation reaction of tetramethylstannane with benzoic acid under the reaction conditions examined. A possible mechanism for the formation of the benzoyloxystannane is a radical attack, as has been suggested by Razuvaev *et al.*[2] The formation of butane by the reaction of benzoyl peroxide with tetraethylstannane[2b,d] is clear evidence in support of the generation of the ethyl radical through the radical attack on the stannane.

$$PhCOO\cdot + Me_4Sn \longrightarrow Me_3SnOCOPh + Me\cdot$$

$$2Me\cdot \longrightarrow C_2H_6 \text{ or } \xrightarrow{R\text{-}H} CH_4 + R\cdot$$

The reactions of benzoyl peroxide with trialkylphenylstannane and with tetraalkylstannane, both giving trialkyl(benzoyloxy)stannane, have thus been found to be quite different in their mechanisms. The formation of trialkyl(benzoyloxy)stannane from trialkylphenylstannane is a more facile reaction than that from tetraalkylstannane. The reaction of tetraalkylstannane with benzoyl peroxide gives trialkyl(benzoyloxy)stannane in a moderate yield only when a high concentration of the stannane is used. The difference is undoubtedly due to the different reactivities of tetraalkyl- and trialkylphenylstannanes to a protodestannylation reaction. The phenyl–Sn bond is reactive enough to be cleaved by the reaction with benzoic acid under the conditions used for the thermolysis of benzoyl peroxide. The alkyl–Sn bond, on the other hand, is stable enough in the reaction with benzoic acid under the same conditions and is cleaved by radical attack only when a high concentration of the stannane is used.

The reaction of benzoyl peroxide with allyltrimethylstannane[4] seems to be an exception, since the stannane has two coordination centers, *i.e.*, the tin atom and the double bond, and can form a cyclic complex with the peroxide. Although trimethylphenylstannane also bears an unsaturated moiety, the interaction of the phenyl group with the electrophile might be weaker than that of the allyl group, and the formation of a cyclic complex of trimethylphenylstannane with the peroxide would not be conformationally favored. Thus, trimethylphenylstannane does not promote the decomposition of benzoyl peroxide.

Experimental

Materials. The tetramethylstannane and trimethylphenylstannane were prepared in according to the literature.[12] Commercial benzoyl peroxide was recrystallized from chloroform–ethanol before use. The solvents were purified by usual procedures

Kinetics. Six evaporated sealed tubes, each containing 2 ml of the peroxide solution (0.01 mol/dm³), were prepared for each run. The tubes were dipped in a constant-temperature bath (80 °C) and then taken up at intervals. The rate of the decomposition was calculated by measuring the remaining amount of the peroxide, which was obtained by iodometry. Experiments in the presence of additives were carried out similarly. The results are given in Table 1.

Reaction of Benzoyl Peroxide with Trimethylphenylstannane or Tetramethylstannane. Benzoyl peroxide (72.7 mg, 0.3 mmol) and trimethylphenylstannane (145 mg, 0.6 mmol) were dissolved in a chloroform–cyclohexane mixed solvent (1 : 1 v/v mixture; total, 10 ml) and sealed in an evacuated tube with or without addition of DCC.

The tube was then heated for 16 h at 85—90 °C. After heating, the solvent and volatile products were evaporated. The residue was weighed and dissolved in chloroform-*d*. A known amount of dichloromethane was added to the solution, and the whole solution was submitted to NMR analysis. The amount of trimethyl(benzoyloxy)stannane was determined by the integration of the trimethyl signal (δ 0.62 ppm) relative to that of dichloromethane (δ 5.21 ppm). A substantial amount of trimethyl(benzoyloxy)stannane (34, 15, and 103% yields in C_6H_{12}–$CHCl_3$, C_6H_{12}–THF, and $CHCl_3$ respectively) was detected by the reaction with trimethylphenylstannane, though the yield was markedly affected by the addition of DCC. The formation of trimethyl(benzoyloxy)stannane was not observed at all in the reaction with tetramethylstannane under the same conditions as that of trimethylphenylstannane. Trimethyl(benzoyloxy)stannane was formed from tetramethylstannane in a 20% yield when an excess of the stannane (1 g, 4.2 mmol) in a high concentration was allowed to react with benzoyl peroxide (51 mg, 0.21 mmol) in chloroform (10 ml); it was also formed in an 18% yield in the presence of DCC (39 mg, 0.21 mmol). The neat reaction of benzoyl peroxide (73 mg, 0.3 mmol) with tetramethylstannane (1.45 g, 6.0 mmol) gave trimethyl(benzoyloxy)stannane in a 24% yield; the yield was not affected by the addition of DCC (55 mg, 0.3 mmol). The NMR signal of trimethyl(benzoyloxy)stannane was confirmed by examining the spectrum of the authentic sample prepared from bromotrimethylstannane and silver benzoate.[13] The amount of carbon dioxide formed during thermolysis (reflux, 16 h) was measured by bubbling a nitrogen stream into the reaction solution, which was then introduced into aqueous barium hydroxide (0.1 mol/dm^3, 10 ml). After the decomposition of the peroxide, the aqueous solution was titrated by dil HCl (0.1 mol/dm^3), and the amount of carbon dioxide was obtained from the comsumption of barium hydroxide. The results are shown in Tables 2 and 4.

Reaction of Benzoic Acid with Trimethylphenylstannane or Tetramethylstannane. The acid (37 mg, 0.3 mmol) and trimethylphenylstannane (145 mg, 0.6 mmol) were dissolved in chloroform–cyclohexane (1 : 1 v/v, total, 10 ml), and then the solution was allowed to react at 85—90 °C for 16 h. The amount of trimethyl(benzoyloxy)stannane was determined by the method as described above. Trimethyl(benzoyloxy)stannane was obtained by the reaction with trimethylphenylstannane in a 26% yield, with a 74% recovery of the starting stannane. No reaction of tetramethylstannane with benzoic acid was observed, even without the use of the solvent. For example, both the starting materials were recovered nearly quantitatively after the heating of benzoic acid (37 mg, 0.3 mmol) with tetramethylstannane (1.45 g, 6.0 mmol) for 16 h at 85—90 °C. The results are given in Table 3.

References

1) See, for general reference: W. P. Newman, "The Organic Chemistry of Tin," John Wiley and Sons, New York (1967), p. 38.

2) a) G. A. Razuvaev, O. S. D'yachkovskaya, N. S. Vyazankin, and O. A. Shchepetkova, *Dokl. Akad. Nauk SSSR*, **137**, 618 (1961); b) G. A. Razuvaev, N. S. Vyazankin, and O. S. D'yachkovskaya, *Zh. Obshch. Khim.*, **32**, 2161 (1962); c) G. A. Razuvaev, N. S. Vyazankin, and O. A. Shchepetokova, *Tetrahedron*, **18**, 667 (1962); d) G. A. Razuvaev and N. S. Vyazankin, *Khim. Perekisnkh Soedin, Akad. Nauk. SSSR, Inst. Obshch. i Neorgan. Khim.*, **1963**, 289.

3) T. Kashiwagi and S. Oae, *Tetrahedron*, **26**, 3631 (1970).

4) M. Kosugi, P. Q. Hanh, M. Nakayama, and T. Migita, *Chem. Lett.*, **1978**, 927.

5) C. G. Swain, L. J. Schaad, and A. J. Kresge, *J. Am. Chem. Soc.*, **80**, 5313 (1958).

6) J. Nasielsky, O. Buchman, M. Grosjean, and M. Jaquet, *J. Organomet. Chem.*, **19**, 353 (1969), and the references cited therein. The mechanism of Sn–C bond fission by electrophilic attack has been widely investigated, see M. A. Cook, C Eaborn, and D. R. M. Walton, *J. Organomet. Chem.*, **23**, 85 (1970); C. Eaborn, A. R. Thompson, and D. R. M. Walton, *J. Organomet. Chem.*, **29**, 257 (1971); M. H. Abraham, D. F. Dadjour, and C. J. Holloway, *J. Organomet. Chem.*, **52**, C27 (1973).

7) S. Kozuka and J. Nakagami, *J. Organomet. Chem.*, **135**, C1 (1977).

8) The reaction of Me_3SnPh with AcOH giving Me_3SnOAc has been known to proceed at room temperature, $k_{(s^{-1})} = 4.26 \times 10^{-5}$ at 25 °C,[5] while alkyl–Sn bond cleavage by carboxylic acid proceeds much slower; *e.g.*, Et_4Sn (bp 181 °C) + PhCOOH reflux for 3 h gave $Et_3SnOCOPh$ in only 18% yield. See R. Sasin and G. S. Sasin, *J. Org. Chem.*, **20**, 770 (1955), and the rate of the reaction: $Me_3SnOCOCH_3$ + $HCOOH \rightarrow Me_2Sn(OCHO)_2$, $k_{(s^{-1})} = 2.63 \times 10^{-5}$ at 99.5 °C. See S. Kozuka, N. Kobayashi, and K. Ogino, *Memoirs of the Faculty of Engin., Osaka City Univ.*, **18**, 89 (1977).

9) Preliminary results were reported in Ref. 7.

10) G. Brunton, J. F. Taylor, and K. U. Ingold, *J. Am. Chem. Soc.*, **98**, 4879 (1976).

11) This is pretty close to the reaction conditions of Razuvaev *et al.*[2]

12) a) C. E. Waring and W. S. Horton, *J. Am. Chem. Soc.*, **67**, 540 (1945); b) R. H. Bullard and W. B. Robinson, *J. Am. Chem. Soc.*, **49**, 1368 (1927).

13) H. H. Anderson, *Inorg. Chem.*, **3**, 912 (1964).

Reactions of α-Aminoacetonitriles with Isothiocyanates. Synthesis of 1,3-Disubstituted 5-Imino-2-thiohydantoins

Takeshi KINOSHITA,* Hiroko WATANABE, Sadao SATO, and Chihiro TAMURA

Central Research Laboratories, Sankyo Co., Ltd., Hiromachi, Shinagawa-ku, Tokyo 140

(Received April 24, 1979)

The reactions of α-aminoacetonitriles with isothiocyanates gave 1-cyanomethyl-1,3-disubstituted thioureas or 1,3-disubstituted 4-amino-4-imidazoline-2-thiones depending upon the reaction conditions. In the presence of polar organic solvents such as methanol the former products were easily cyclized to the latter. 1,3-Disubstituted 4-amino-4-imidazoline-2-thiones were autoxidized in methanol affording 1,3-disubstituted 5-imino-2-thiohydantoins.

A number of reports have been published concerning the synthesis of 1,3-disubstituted 5-iminohydantoins.[1-3] However, no synthetic study on 1,3-disubstituted 5-imino-2-thiohydantoins seems to have been reported except for the work of Kinoshita *et al.*[4] In a previous paper,[5] a report was given on the crystal structure of 1,3-dimethyl-5-imino-2-thiohydantoin prepared by the reaction of methylaminoacetonitrile with methyl isothiocyanate in the presence of atmospheric oxygen. This paper deals with the synthesis of 1,3-disubstituted 5-imino-2-thiohydantoins and the mechanism of the reaction of isothiocyanates with α-aminoacetonitriles.

Results and Discussion

Various types of isothiocyanates were allowed to react with α-aminoacetonitriles. The most basic compounds for this reaction are methyl isothiocyanate and equimolar quantities of methylaminoacetonitrile, which gave compound **1a** in methanol solution (85% yield). The structure of **1a** was confirmed to be 1,3-dimethyl-5-imino-2-thiohydantoin by the spectra data.

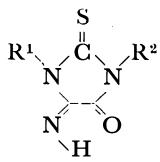

1, a: $R^1=R^2=CH_3$

The structure of the ring system has been established by X-ray analysis of **1a**.[5] However, the above reaction was carried out using benzene as a solvent to give compound **2a** (77% yield). The structure of **2a** was determined to be 1-cyanomethyl-1,3-dimethylthiourea by the spectral data.

When the reaction was undertaken using toluene as a solvent, compound **3a** was quantitatively precipitated (91% yield). However, when phenyl isothiocyanate

TABLE 1. YIELDS AND ANALYTICAL DATA OF 1,3-DISUBSTITUTED 5-IMINO-2-THIOHIDANTOINS (**1**)

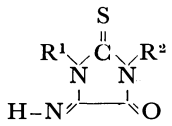

Compd	R^1	R^2	Yield[a] %	Mp °C	Molecular[b] formula	Found (Calcd) C%	H%	N%	S%
1a	CH_3	CH_3	85	112	$C_5H_7N_3OS$	38.21 (38.21	4.52 4.49	26.62 26.73	20.52 20.40)
1b	C_6H_5	CH_3	75	170	$C_{10}H_9N_3OS$	54.85 (54.78	4.19 4.14	19.08 19.16	14.76 14.62)
1c	$C_6H_5CH_2$	CH_3	88	113	$C_{11}H_{11}N_3OS$	56.59 (56.63	4.71 4.75	18.13 18.01	13.62 13.74)
1d	$CH_3(CH_2)_3$	CH_3CH_2	40	78	$C_9H_{15}N_3OS$	50.46 (50.68	6.93 7.09	19.55 19.70	15.12 15.03)
1e	$C_6H_5CH_2$	CH_3CH_2	58	115	$C_{12}H_{13}N_3OS$	58.53 (58.28	5.16 5.30	16.88 16.77	13.24 13.28)
1f	$C_6H_5CH_2$	$CH_3CH_2CH_2$	42	67	$C_{13}H_{15}N_3OS$	59.49 (59.75	5.59 5.79	16.12 16.08	12.42 12.27)
1g	$C_6H_5CH_2$	$CH_3(CH_2)_3$	35	75	$C_{14}H_{17}N_3OS$	60.95 (61.06	6.03 6.22	15.29 15.26	11.72 11.64)
1h	$C_6H_5CH_2$	C_6H_5	14	196	$C_{16}H_{13}N_3OS$	64.94 (65.07	4.36 4.44	14.32 14.23	11.00 10.85)
1i	CH_3	$C_6H_5CH_2$	34	103	$C_{11}H_{11}N_3OS$	56.45 (56.63	4.61 4.75	18.04 18.01	13.83 13.74)
1j	$CH_3(CH_2)_3$	$C_6H_5CH_2$	70	73	$C_{14}H_{17}N_3OS$	61.07 (61.06	6.25 6.22	15.22 15.26	11.41 11.64)

a) Isolated yields. b) Determined by high resolution mass spectrometry.

Table 2. Physical properties of 1,3-disubstituted 5-imino-2-thiohydantoins (**1**)

Compd	IR[a] ν/cm^{-1} C=N	C=O	N-H	UV[b] $\lambda_{max}(\varepsilon)$/nm	^{1}H NMR[c] of N-H, N-CH_2, and N-CH_3 (δ/ppm)
1a	1680	1755	3250	309 (11400)	3.23 (s, 3H, CH_3), 3.37 (s, 3H, CH_3), 10.10 (s, 1H, NH)
1b	1680	1745	3260	300 (14600)	3.30 (s, 3H, CH_3), 10.01 (s, 1H, NH)
1c	1680	1745 1754*	3260	308.5 (15600)	3.30 (s, 3H, CH_3), 5.19 (s, 2H, CH_2), 9.09 (s, 1H, NH)
1d	1678	1748	3260	312 (16000)	3.95 (q, J=7 Hz, 2H, CH_2), 4.03 (t, J=7 Hz, 2H, CH_2) 8.93 (s, 1H, NH)
1e	1680	1745	3250	309 (15700)	3.95 (q, J=7 Hz, 2H, CH_2), 5.19 (s, 2H, CH_2), 9.03 (s, 1H, NH)
1f	1680	1745	3250	309.5 (15800)	3.82 (t, J=7 Hz, 2H, CH_2), 5.16 (s, 2H, CH_2), 9.04 (s, 1H, NH)
1g	1680	1750	3250	310 (15200)	3.85 (t, J=7 Hz, 2H, CH_2), 5.16 (s, 2H, CH_2), 9.04 (s, 1H, NH)
1h	1678	1753	3260	310 (15800)	5.30 (s, 2H, CH_2), 9.17 (s, 1H, NH)
1i	1678	1750	3260	310 (15900)	3.43 (s, 3H, CH_3), 5.00 (s, 2H, CH_2), 8.99 (s, 1H, NH)
1j	1678	1745	3270	314 (14900)	4.01 (t, J=7 Hz, 2H, CH_2), 4.98 (s, 2H, CH_2), 8.97 (s, 1H, NH)

a) Measured in Nujol mulls (* shoulder). b) Observed in EtOH. c) Observed in DMSO-d_6 (**1** and **1b**), and CCl_4 (**1c**—**j**).

was used instead of methyl isothiocyanate, **2b** was not isolated even in a nonpolar solvent (benzene), **3b** being obtained in 88% yield. Whether the reaction gives **2** or **3** seems to depend upon the subtle difference in the overall polarity of the reaction system. Actually **2** was easily cyclized to **3** in a polar solvent. The structure of **3** was deduced to be 1,3-disubstituted 4-amino-4-imidazoline-2-thione by the spectral data.

In 1948, Cook *et al.*[6] examined the reaction of aminoacetonitrile with methyl isothiocyanate to give 5-amino-2-(methylamino)thiazole (**4**). It appears that the isomer **5** is also possible as the structure of **3**.

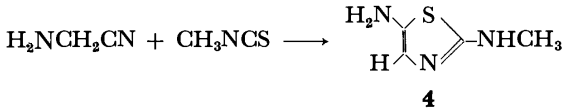

4

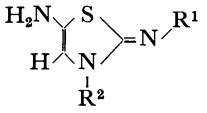

5, **a**: $R^1=R^2=CH_3$
b: $R^1=C_6H_5$, $R^2=CH_3$

However, convincing proof for the structure of **3** could be given by the pyrolysis of **6** prepared by the reduction of **1b** with $LiAlH_4$. The main products derived from the pyrolysis of **6** at the injection port of a gas chromatograph were determined to be a dehydration compound, 1-methyl-3-phenyl-4-amino-4-imidazoline-2-thione and a deamination compound, 1-phenyl-3-methyl-2-thiohydantoin by gas chromatography mass spectrometry (Fig. 1).

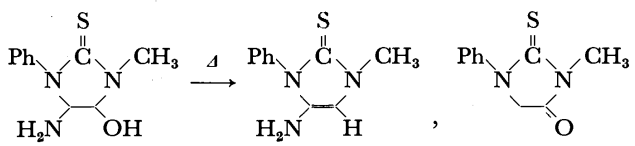

6 (*cis*/*trans*)

The retention time and the mass spectrum of the dehydration peak 2 in Fig. 1 were identical with those of **3b** (Fig. 2). Compound **3b** underwent no ring-isomerization,[7] the starting material being recovered after heating at 230 °C. The structure of **3** should be similar to that of the dehydration compound of **6**, but not that of **5**. However, we have found no definite evidence for

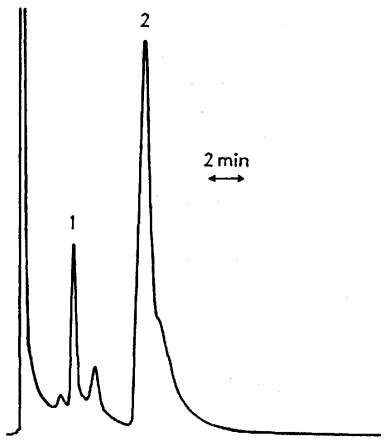

Fig. 1. Gas chromatogram of the products derived from the pyrolysis of *cis*-**6** taken by total ion current of GC-MS. Column of 2% Silicone OV-17 on Gas Chrom Q, 1 m×2 mm i.d. glass column, col. temp: 200 °C, inj. temp: 230 °C, flow rate: 23 ml/min He.

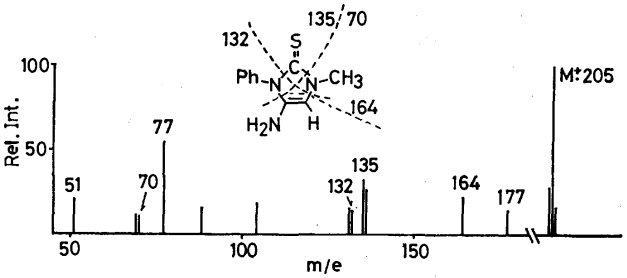

Fig. 2. Mass spectrum of peak 2 in Fig. 1.

the isomerization of **5** to **3** not occurring in the reaction process.

Even the solid of **3** is labile and turns dark-red on exposure to air producing a dimeric compound (**7**) which is insoluble in benzene, toluene, or cold methanol. Compound **7** is slightly soluble in hot methanol and is autoxidized to give **1**. Figure 3 shows the gas chromatogram derived from the autoxidation of **3a** in methanol solution. From the mass spectrum of GLC peak 2

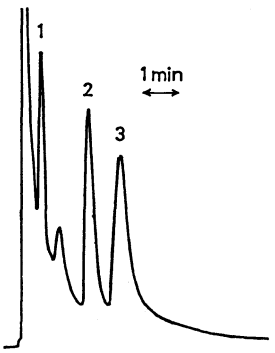

Fig. 3. Gas chromatogram of the products derived from the methanol solution of **3a** (after stirring 35 min at room temperature). Column of 2% Silicone OV-17 on Gas Chrom Q, 1 m×2 mm i.d. glass column, col. temp: 170 °C, inj. temp: 230 °C, flow rate: 32 ml/min He.

shown in Fig. 3, it was found that the peak is due to a new intermediate compound (**8a**). Attempts to isolate **8a** were unsuccessful. However, the intermediate **8b** could be isolated from the methanol solution of **3b**. In the presence of atmospheric oxygen **8b** was converted into **1b** quantitatively in a methanol solution at room temperature. The structure of **8b** was determined to be 5-amino-3-methyl-1-phenyl-2-thiohydantoin.

A plausible mechanism of the reaction of α-amino-acetonitriles with isothiocyanates in methanol is given in Scheme 1. 5-Imino-2-thiohydantoins (**1**) can be prepared from the autoxidation of two intermediate compounds (**7** and **8**) derived from the autoxidation of **3**.

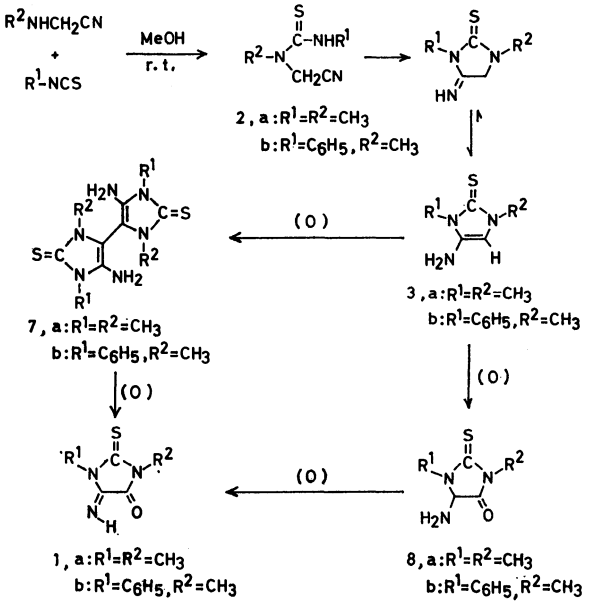

Scheme 1.

The above reaction is applicable to the synthesis of 5-iminohydantoin derivatives such as 1,3-dimethyl-5-iminohydantoin (**9**) obtained by the reaction of methyl-aminoacetonitrile with methyl isocyanate. However, the reaction was extremely slow under conditions similar to those for the reaction in the preparation of **1**.

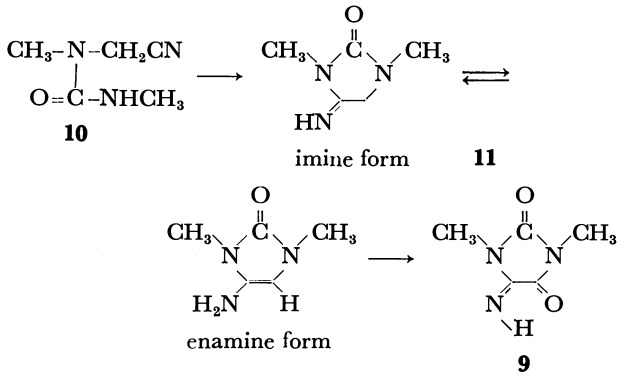

It was found that the cyclization reaction of **10** to **11** requires some kind of catalytic base such as pyridine or triethylamine, and the autoxidation of **11** to **9** requires a long period of time (*ca.* two weeks). The low reactivity of **11** toward atmospheric oxygen can be attributed to the fact that the equilibrium of **11** lies toward the imine form, whereas that of **3** lies toward the enamine form. Information on these tautomers was obtained from NMR spectra.

Experimental

All melting points are uncorrected. IR spectra were obtained on a JASCO IRA-2 spectrometer, UV spectra on a Cary 14 spectrometer, NMR spectra on a Varian A-60D spectrometer using tetramethylsilane as an internal standard, and high resolution mass spectra on a JEOL JMS-01SG mass spectrometer using a direct insertion probe and an ionization energy of 75 eV. GLC analyses were carried out on a JEOL JGC-20KFP gas chromatograph and GC-MS analyses on a JEOL JMS D-100 gas chromatograph mass spectrometer.

Materials. Commercial methyl, ethyl, butyl, phenyl, benzyl isothiocyanates, methyl isocyanate, methylaminoacetonitrile, and amines of reagent grade were used. α-Aminoacetonitriles were prepared according to the reported method.[8]

*Preparation of 1-Cyanomethyl-1,3-dimethylthiourea (**2a**).* A solution of methyl isothiocyanate (1.46 g, 20 mmol) in benzene (30 ml) was added dropwise to a solution of methylaminoacetonitrile (1.4 g, 20 mmol) in benzene (30 ml) at 5—10 °C, and the reaction mixture was stirred at 5—10 °C for 15 min and then filtered to give a colorless crystalline product (**2a**) (2.2 g, 77%); mp 75°C; MS, M. W. obsd=143.051, M. W. calcd=143.052 for $C_5H_9N_3S$; IR (Nujol), 3400 (N–H), 2270 (C≡N), 1542 (–NHCSN<) cm^{-1}; NMR (δ, ppm, DMSO-d_6), 7.91 (broad, 1H), 4.95 (s, 2H), 3.13 (s, 3H), 2.95 (d, J=4.5 Hz, 3H). Found: C, 42.09; H, 6.35; N, 29.31; S, 22.17%. Calcd for $C_5H_9N_3S$: C, 41.94; H, 6.33; N, 29.34; S, 22.39%.

*Preparation of 1,3-Dimethyl-4-amino-4-imidazoline-2-thione (**3a**).* A solution of methyl isothiocyanate (1.46 g, 20 mmol) in toluene (30 ml) was added dropwise to a solution of methyl-aminoacetonitrile (1.4 g, 20 mmol) in toluene (30 ml) at room temperature, and the reaction mixture was stirred at room temperature for 30 min and then filtered to give colorless needles (**3a**) (2.6 g, 91%); mp 96 °C; MS, M. W. obsd=143.050, M. W. calcd=143.052 for $C_5H_9N_3S$; IR (Nujol), 3320, 1645 cm^{-1}; UV (EtOH), λ_{max} 266.5 nm; NMR (δ, ppm, DMSO-d_6), 6.16 (s, 1H), 4.73 (broad, 2H), 3.38 (s, 3H), 3.33 (s, 3H); Found: C, 41.89; H, 6.47; N, 29.23; S, 22.28%. Calcd for $C_5H_9N_3S$: C, 41.94; H, 6.33; N, 29.34

S, 22.39%. In another experiment run exactly as above, except that benzene–triethylamine (27: 3) was used in place of toluene, the yield of **3a** was 2.5 g (88%).

Preparation of 1-Methyl-3-phenyl-4-amino-4-imidazoline-2-thione (3b). A solution of phenyl isothiocyanate (2.7 g, 20 mmol) in benzene (30 ml) was added dropwise to a solution of methylaminoacetonitrile (1.4 g, 20 mmol) in benzene (30 ml) at room temperature, and the reaction mixture was stirred at room temperature for 30 min and then filtered to give a pale yellow product (**3b**) (3.6 g, 88%); mp 113 °C; MS, M. W. obsd=205.067, M. W. calcd=205.068 for $C_{10}H_{11}N_3S$; IR (Nujol), 3350, 3260, 1645 cm^{-1}: NMR (δ, ppm, DMSO-d_6), 7.43 (5H, C_6H_5), 6.31 (1H, =CH–), 4.40 (2H, NH_2), 3.43 (3H, CH_3); Found: C, 58.73; H, 5.40; N, 20.23; S, 15.42%. Calcd for $C_{10}H_{11}N_3S$: C, 58.51; H, 5.40; N, 20.47; S, 15.62%.

Preparation of 1,3-Disubstituted 5-Imino-2-thiohydantoins (1). The following procedure illustrates the general method. A solution of methyl isothiocyanate (1.46 g, 20 mmol) in MeOH (30 ml) was added dropwise to a solution of methylaminoacetonitrile (1.82 g, 26 mmol) in MeOH (30 ml) at room temperature, and the reaction mixture was stirred at room temperature for 48 h in the presence of atmospheric oxygen. The solvent was evaporated *in vacuo*, and the residue was dissolved in hot ethanol, and filtered to remove the insoluble dimer (**7a**). The filtrate was then cooled to *ca.* 10 °C and filtered to give **1a** (2.67 g). An analytical sample was recrystallized from ethanol. Analytical data and physical properties of **1a** are summarized in Tables 1 and 2, respectively, along with the other derivatives (**1b**—**j**).

Isolation of the Intermediary Compound 7a. A solution of **3a** (1.5 g) in MeOH (40 ml) was stirred at room temperature for 4 h, and the solution was filtered to give a grayish product (**7a**) (230 mg, 15%); mp 246—248 °C (dec); MS, M. W. obsd=284.086, M. W. calcd=284.088 for $C_{10}H_{16}N_6S_2$; IR (Nujol), 3300, 3170, 1680, 1640 cm^{-1}; UV (EtOH), 288 nm; NMR (δ, ppm, DMSO-d_6), 5.05 (s, 4H), 3.42 (s, 6H), 3.20 (s, 6H); Found: C, 42.14; H, 5.75; N, 29.51; S, 22.47%. Calcd for $C_{10}H_{16}N_6S_2$: C, 42.23; H, 5.67; N, 29.55; S, 22.55%.

Isolation of the Intermediary Compound 8b. A solution of **3b** (0.5 g) in MeOH (20 ml) was stirred at room temperature for 4 h, and the solvent was evaporated *in vacuo*. The residue was subjected to preparative TLC on silica gel eluting with petroleum ether–benzene–ethanol (12: 4: 3) to give 5-amino-3-methyl-1-phenyl-2-thiohydantoin (**8b**) (60 mg, 11%); colorless plastic solid; MS, M. W. obsd=221.063, M. W. calcd=221.062 for $C_{10}H_{11}N_3OS$; IR (Nujol), 3390, 3310, 1747 cm^{-1}; NMR (δ, ppm, CCl_4), 7.24 (s, 5H), 4.82 (s, 1H), 3.18 (s, 3H), 1.76 (broad, 2H), Found: C, 54.08; H, 5.10; N, 18.87; S, 14.41%. Calcd for $C_{10}H_{11}N_3OS$: C, 54.28; H, 5.01; N, 18.99; S, 14.49%.

Reduction of 1b. A solution of **1b** (1.31 g, 6 mmol) in dry THF (40 ml) was added dropwise to a suspension of lithium aluminum hydride (0.5 g, 13 mmol) in dry THF (40 ml) at a rate such as to produce gentle reflux. After completing the addition, sufficient water was added dropwise with ice–water cooling to decompose the excess hydride. The reaction mixture was filtered and extracted with CH_2Cl_2, and the solution was dried over sodium sulfate and concentrated under reduced pressure. The residue was chromatographed on silica gel ($CHCl_3$–EtOH, 40: 1) to give 240 mg of *cis*-4-amino-5-hydroxy-1-methyl-3-phenylimidazolidine-2-thione(*cis*-**6**) and 20 mg of *trans*-**6**.

cis-**6**: Mp 102—103.5 °C; MS, M. W. obsd=223.079, M. W. calcd=223.078 for $C_{10}H_{13}N_3OS$; IR ($CHCl_3$), 3400, 3340 cm^{-1}; NMR (δ, ppm, DMSO-d_6), 7.35 (5H, C_6H_5), 5.12 (d, J=6 Hz, 1H, CH), 5.05 (d, J=6 Hz, 1H, CH), 3.5—3.0 (broad, 3H), 3.11 (s, 3H, CH_3). Found: C, 53.81; H, 5.66; N, 18.77; S, 14.30%. Calcd for $C_{10}H_{13}N_3OS$: C, 53.79; H, 5.87; N, 18.82; S, 14.36%.

trans-**6**: Mp 145.5—146.5 °C; MS, M^+ 223; IR ($CHCl_3$), 3380, 3330 cm^{-1}; NMR (δ, ppm, DMSO-d_6), 7.40 (5H, C_6H_5), 4.85 (d, J=3 Hz, 1H, CH), 4.63 (d, J=3 Hz, 1H, CH), 3.4—3.0 (broad, 3H), 3.08 (s, 3H, CH_3). Found: C, 53.62; H, 5.94; N, 18.71; S, 14.27%. Calcd for $C_{10}H_{13}N_3OS$: C, 53.79; H, 5.87; N, 18.82; S, 14.36%.

The assignments of *cis*/*trans*-**6** were carried out according to the reported method.[9]

Reaction of Methylaminoacetonitrile with Methyl Isocyanate. A solution of methyl isocyanate (1.6 g, 28 mmol) in benzene (30 ml) was added dropwise to a solution of methylaminoacetonitrile (2 g, 28.6 mmol) at 5—10 °C, and the reaction mixture was stirred at 5—10 °C for 10 min and then filtered to give 1-cyanomethyl-1,3-dimethylurea (**10**) (2.8 g, 78%); mp 83—83.5 °C; MS, M^+ 127; IR (Nujol), 3370 (N–H), 2250 (C≡N), 1640, 1550 cm^{-1}; NMR (δ, ppm, DMSO-d_6) 6.58 (broad, 1H, NH), 4.28 (s, 2H, CH_2), 2.84 (s, 3H, CH_3), 2.61 (d, J=4.5 Hz, 3H, CH_3). Found: C, 47.30; H, 7.09; N, 33.01%. Calcd for $C_5H_9N_3O$: C, 47.23; H, 7.13; N, 33.05%. A solution of **10** (2.54 g, 20 mmol) in methanol–triethylamine (50 ml: 5 ml) was stirred at room temperature for 24 h, and the solvent was evaporated *in vacuo* to give 1,3-dimethyl-4-iminoimidazolidine-2-one (**11**) (2.3 g, 91%); mp 35—37 °C; MS, M^+ 127; IR (Nujol), 3290 (N–H), 1740, 1716, 1668 cm^{-1}; NMR (δ, ppm, DMSO-d_6), 4.26 (s, 1H, NH), 3.92 (s, 2H, CH_2), 2.84 (s, 3H, CH_3), 2.79 (s, 3H, CH_3). Found: C, 47.18; H, 7.25; N, 33.00%. Calcd for $C_5H_9N_3O$: C, 47.23; H, 7.13; N, 33.05%. A solution of **11** (0.5 g, 4 mmol) in pyridine (20 ml) was stirred at room temperature for two weeks and separated by column chromatography (silica gel) to give 1,3-dimethyl-5-iminohydantoin (**9**) (110 mg, 20%); mp 117—118 °C (lit,[1] 119—120 °C); IR (Nujol), 3255 (N–H), 1735 (C=O), 1730 (C=O), 1665 (C=N) cm^{-1}; NMR (δ, ppm, $CDCl_3$), 8.85 (s, 1H, NH), 3.22 (s, 3H, CH_3), 3.12 (s, 3H, CH_3). Found: C, 42.49; H, 5.05; N, 29.86%. Calcd for $C_5H_7N_3O_2$: C, 42.55; H, 5.00; N, 29.77%.

References

1) T. L. Patton, *J. Org. Chem.*, **32**, 383 (1967).
2) I. Ojima, S. Inaba, and Y. Nagai, *J. Chem. Soc., Chem. Commun.*, **1974**, 826.
3) Y. Nagai, A. Maki, K. Natsuka, and S. Umemoto, *Chem. Pharm. Bull. Jpn.*, **24**, 1179 (1976).
4) T. Kinoshita, S. Sato, and C. Tamura, *Tetrahedron Lett.*, **1971**, 3695.
5) S. Sato, T. Kinoshita, T. Hata, and C. Tamura, *Acta Crystallogr., Sect. B*, **32**, 918 (1976).
6) A. H. Cook, J. D. Downer, and Sir Ian Heilbron, *J. Chem. Soc.*, **1948**, 2028.
7) Y. Ueno, T. Nakai, and M. Okawara, *Bull. Chem. Soc. Jpn.*, **43**, 162 (1970).
8) K. Pfister III, S. Plains, and J. Weijlard, United States Patent 2650221, Aug. 25, 1953.
9) K. Tori, Y. Hamashima, and A. Takamizawa, *Chem. Pharm. Bull. Jpn.*, **12**, 924 (1964).

The Acetylation of Toluene and Benzene with Acetyl Chloride and Bromide and Acetic Anhydride Catalyzed by Calcined Iron Sulfate Activated by Exposure to a Mixture of Benzyl Chloride and the Aromatics[1)]

Kazushi ARATA* and Makoto HINO†
Hokkaido University of Education, Hachiman-cho, Hakodate 040
†*Hakodate Technical College, Tokura-cho, Hakodate 042*

(Received May 4, 1979)

The acetylations of toluene and benzene with acetyl halides and acetic anhydride were studied over catalysts prepared by heat-treating $FeSO_4$ in air, followed by activation on exposure to benzyl chloride in toluene or benzene at 40—80 °C for 1 h, together with $FeCl_3$ and $AlCl_3$. The sulfates treated at 700 and 800 °C showed high activity. The former, activated at 60 °C, gave 68% methylacetophenones, and the latter, more than 90%, with an isomer distribution of 2% *ortho*-, 1% *meta*-, and 97% *para*-form in the reaction of toluene with acetyl halides at room temperature, while the maximum yield was 24% with $FeCl_3$ and 29% with $AlCl_3$. A high yield of acetophenone, 77%, was obtained over the $FeSO_4$ (700 °C) catalyst in the reaction of benzene with acetyl bromide at 60 °C for 1 h. The present catalysts were also highly active for the acetylation of toluene with acetic anhydride; *e.g.*, 55% methylacetophenones were obtained over the $FeSO_4$ (800 °C) catalyst at 100 °C for 5 h. $FeCl_3$ and $AlCl_3$ gave quite low yield compared with the present catalysts.

The Friedel-Crafts acylation of aromatics with acid anhydrides and acyl halides in the presence of acidic halide catalysts has been the subject of a great many investigations during the hundred years since the discovery of the reaction. Extensive reviews have discussed the reaction mechanism.[2-5)] Alkylation with alkyl halides requires only catalytic amounts of catalysts, whereas acylation affords ketones in yields which are proportional to the amount of catalysts. The reaction is complete when little more than a molecular proportion of catalyst is used. On the other hand, more than two moles of the Lewis catalyst are consumed in the case of acid anhydride as an acylating agent.

The acetylation of toluene and benzene with acetyl halides or acetic anhydride has also been performed with, at least, an equimolar amount of a catalyst for an acetylating agent by using such Lewis catalysts as anhydrous aluminum chloride, boron trifluoride, and iron(III) chloride.[6-11)] We have found that the acetylation of toluene and benzene with acetyl halides or acetic anhydride with a new catalyst at room temperature under the heterogeneous system gave methylacetophenones and acetophenone in good yields.

Experimental

The toluene and benzene, guaranteed reagents, were purified by distillation over sodium metal. The acetyl chloride, acetyl bromide, and acetic anhydride, all guaranteed reagents of the Wako Pure Chemical Co., were used without further purification. The acetyl chloride and bromide were stored in sealed ampoules until use in order to prevent hydrolysis. The catalysts were prepared as follows: $FeSO_4 \cdot 7H_2O$ (guaranteed grade of the Kanto Chemical Co.) was heated at 150 °C for 1 h, powdered below 100 mesh, and then calcined in a Pyrex or quartz glass tube at various temperatures in air for 3 h. The prepared catalyst was sealed in an ampoule until use. The activation of the catalyst was performed by heating a mixture of 50 ml of toluene or benzene, 1 g of the catalyst, and 1 ml of benzyl chloride at 60—100 °C. After the mixture has been cooled, an acetylating reagent (0.025 mol) was added, and the whole mixture was stirred at room temperature for 15—360 min. The catalyst was then removed by filtration, and the filtrate was washed with water several times and dried over anhydrous calcium chloride. The products were identified by means of a gas-chromatographic comparison with commercially available authentic samples and analyzed, using benzene (for the acetylation of toluene) or toluene (for the reaction of benzene) as the internal standard (a 1-m column of tritolyl phosphate on Celite 545, 110 °C, He: 1.0 kg/cm²).

Results and Discussion

It was previously reported[12,13)] that the benzylation of toluene with benzyl chloride was markedly catalyzed by iron sulfates, which belong to the solid-acid type of catalysts, such as SiO–Al_2O_3 and $NiSO_4$. The iron sulfates also catalyzed the benzoylation of toluene with benzoyl chloride.[14)] The catalysts heat-treated at 700 °C showed the maximum activity in both reactions. The reaction rate in the benzoylation was, however, quite low. It took more than 50 min to complete the 30% conversion at 110 °C over the most active catalyst. Thus, the reaction rate of the acetylation of toluene with acetyl halides can be expected to be quite low because of the weak electrophilicity of the acetyl cation, CH_3CO^+. In fact, no product was detected in the gas-chromatographic analysis in the reaction of toluene with acetyl chloride at the reaction temperature of 50 °C, close to the boiling point of the chloride, over $FeSO_4$ heat-treated at 700 °C. However, the catalyst was found to be highly activated by exposure to benzyl chloride in toluene, and the acetylation proceeded at room temperature.

An example of the reaction by the activated catalyst is as follows. A mixture of toluene (50 ml), benzyl chloride (0.5 ml), and 1 g of $FeSO_4$ calcined at 700 °C was heated at 60 °C for 1 h; after cooling, acetyl chloride (0.025 mol) was added to the mixture, after which the whole mixture was stirred at room temperature. Thus, the aromatic compound for the acetylation is the toluene used in the activation of the catalyst. A

TABLE 1. YIELD(%) FOR ACETYLATION OF TOLUENE WITH ACETYL CHLORIDE AND BROMIDE AT ROOM TEMPERATURE[a)]

Catalyst	Temp of calcn./°C	Acetylating reagent	Yield/%							Isomer distribution/%		
			15 min	30 min	60 min	90 min	120 min	150 min	180 min	*o*-,	*m*-,	*p*-
$FeSO_4$	500	CH_3COCl	12	13								
	600	CH_3COCl	17		16							
	700	CH_3COCl	52		68		68			2	1	97
	700	CH_3COBr	61	65	67					2	1	97
	700[b)]	CH_3COBr							0			
	700[c)]	CH_3COBr		70	78							
	750	CH_3COCl		53	77		82					
	800	CH_3COCl			31	54	88	90	90	2	1	97
	800	CH_3COBr	13	34	87		92			2	1	97
	900	CH_3COCl			1		8					
$FeCl_3$		CH_3COCl	23	22	22					3	1	96
$FeCl_3$		CH_3COBr	24									
$AlCl_3$		CH_3COCl	26		29					2	2	96
$AlCl_3$		CH_3COBr	22									

a) Activated at 60 °C by the addition of 1 ml of benzyl chloride; catalyst amount: 1 g. b) Without treatment with benzyl chloride, 0% for 300 min. c) Reacted at 60 °C.

mixture of *o*-, *m*-, and *p*-methylacetophenone was obtained in a 21% yield after 60 min. The longer the period of reaction the more products were given: 31% for 120 min and 34% for 180 min. The reaction with acetyl bromide under the same conditions gave a 40% yield in 30 min and a 42% yield in 60 min.

The catalytic activity was dependent on the temperature of activation; *i.e.*, mixtures of methylacetophenones were obtained in 11, 21, 29, and 30% yields for 3 h when activated at 40, 50, 70, and 80 °C respectively, 60 °C thus being the most activating temperature (34% for 3 h). The acetylation with the chloride was performed over $AlCl_3$ and $FeCl_3$, but the product amount was only 9% for 3 h with both catalysts and 11% for even a period of 11 h with $FeCl_3$ under the same reaction conditions.

Table 1 shows the yields of the products for the acetylation of toluene with acetyl chloride and bromide at room temperature catalyzed by iron sulfates calcined at various temperatures, followed by activation with benzyl chloride at 60 °C; the yields obtained with $FeCl_3$ and $AlCl_3$ are also shown for comparison. As has already been mentioned, iron sulfate calcined at any temperature was completely inactive for the acetylation at room temperature unless otherwise activated. The catalytic activity of activated $FeSO_4$ changed remarkably with the calcination temperature. The sulfates calcined at 500, 600, and 900 °C showed low activity. However, a considerable amount, 68%, of methylacetophenones was obtained over the catalyst prepared by calcining at 700 °C with both acetyl chloride and bromide, and the sulfate calcined at 800 °C gave methylacetophenones in more than a 90% yield, though its reaction rate was slower than that when using the catalyst calcined at 700 °C. $FeSO_4$(750 °C)** falls into the intermediate range between the above two catalysts. The catalysts treated at 500 and 600 °C were found to be dissolved in the reaction mixture, and $FeSO_4$(700 °C) was slightly dissolved, while the materials calcined at 800 °C and 900 °C were insoluble.

When $FeCl_3$ and $AlCl_3$ were used instead of the present catalysts under similar conditions, the maximum yields were 24% and 29% respectively, quite close to the expected maximum yields estimated from the molar amounts of these catalysts and the acetylating reagent.

The acetylations was carried out with acetic anhydride as the acetylating agent over the sulfates treated at 700 °C and 800 °C, as is shown in Table 2. The reaction was performed over 60 °C because of the slow rate of the reaction. Whereas $FeCl_3$ and $AlCl_3$ produced less than 15% of methylacetophenones in 3 h at 80 °C, $FeSO_4$(700 °C) gave a 38% yield under the same conditions and even 44% in 5 h. It should be noted that 55% methylacetophenones were obtained over $FeSO_4$(800 °C) at 100 °C in 5 h. The selectivity was lower than that in the case of acetyl halides, whose isomer distribution was 2% *ortho*-, 1% *meta*-, and 97% *para*-methylacetophenone (Table 1).

The acetylation of benzene was performed with highly active catalysts, $FeSO_4$(700 °C) and $FeSO_4$(800 °C). The results are shown in Table 3. Since the reaction rate was quite low, the reaction temperature taken was 50 °C and 60 °C in the cases of the chloride and bromide respectively, both temperatures close to their boiling points. The catalysts were almost inactive for this reaction with acetic anhydride at 80 °C. The activity of $FeSO_3$(700 °C) was higher than that of $FeSO_4$(800 °C) in contrast with the observations of the reaction of toluene. Although the reaction with acetyl chloride showed a slower rate than that with the bromide, as was seen also in the case of toluene, the $FeSO_4$(700 °C) catalyst gave a 49% conversion to acetophenone in 6 h. A high yield, 77%, was obtained over this catalyst with acetyl bromide over a period of 1 h. $FeCl_3$ and $AlCl_3$ afforded 20% and 16% yield respectively when reacted with the bromide for 1 h.

On the exposure of the catalysts to a mixture of

** Numbers in parentheses here and elsewhere indicate the calcination temperatures.

TABLE 2. YIELD (%) FOR ACETYLATION OF TOLUENE WITH ACETIC ANHYDRIDE[a)]

Catalyst	Temp of calcn./°C	Reaction temp/°C	Yield/% 1.0 h	3.0 h	5.0 h	Isomer distribution/% o-,	m-,	p-
$FeSO_4$	700	room temp[b)]			4			
	700[c)]	60		17				
	700	80	15	38	44			
	700	100		39		15	3	82
	800	80			33			
	800	100		48	55	14	2	84
$FeCl_3$		80		15		8	2	90
$AlCl_3$		80		11		4	6	90

a) Activated at the reaction temperature by the addition of 1 ml of benzyl chloride; catalyst amount: 1 g.
b) Activated at 60 °C. c) 22% for 22 h.

TABLE 3. YIELD (%) OF ACETOPHENONE FOR ACETYLATION OF BENZENE WITH ACETYL CHLORIDE, ACETYL BROMIDE, AND ACETIC ANHYDRIDE[a)]

Catalyst	Temp of calcn./°C	Acetylating reagent	Reaction temp/°C	Yield/% 1.0 h	1.5 h	2.0 h	6.0 h
$FeSO_4$	700	CH_3COCl	50			27	49
	700	CH_3COBr	room temp		21		
	700	CH_3COBr	60	77			
	700[b)]	$(CH_3CO)_2O$	80				0.3
	800	CH_3COCl	50			13	26
	800	CH_3COBr	60	45			

a) Activated at 60 °C by the addition of 1 ml of benzyl chloride; catalyst amount: 1 g. b) Activated at 80 °C.

benzyl chloride and toluene or benzene, it appears likely that iron chloride was newly formed on the catalyst surface because of the HCl evolved by the benzylation of toluene or benzene with benzyl chloride, the iron chloride thus acting as a catalyst. After the activation of the catalysts, gas-chromatographic (GC) analysis showed the benzylation of toluene and benzene to be 100% complete. The $FeSO_4$(700 °C) catalyst was separated from the mixture of benzyl chloride and toluene after the activation, washed with toluene, and dried, and finally its IR spectrum was taken, together with that of commercial $FeCl_3$ for reference.*** The spectra showed an absorption band at 1600 cm^{-1} which is assigned to water molecule coordinated to $FeCl_3$. However, this separated catalyst produced only 10% of methylacetophenones in a reaction of 2 h with acetyl chloride. The differently prepared HCl-treated catalyst, which had been prepared by exposing $FeSO_4$(700 °C) to a stream of the mixed gas of N_2 (20 ml/min) and HCl (26 ml/min) for 20 min and then to N_2 gas for 30 min,[15] gave a 28% conversion at the highest in the acetylation of toluene with acetyl chloride. It may, therefore, be considered that the catalyst surface was activated by complicated interactions with benzyl chloride and HCl evolved by the benzylation. As for alkyl halides other than benzyl chloride, *t*-butyl and isopropyl chlorides were examined, but these halides did not activate the catalysts. GC analysis revealed that the catalysts are not active at all for the *t*-butylation and isopropylation of toluene or benzene.

The Friedel-Crafts acylation of aromatic hydrocarbons such as toluene and benzene is characterized by a generally high selectivity of the reactions reflected in high substrate-rate ratios (usually $k_{toluene}/k_{benzene} > 100$) and related predominant *para*-substitution. The competitive acetylation of toluene and benzene was studied over the present catalysts. The obtained values of k_T/k_B, the relative rate between toluene and benzene, were 99.2 with $FeSO_4$(700 °C) and CH_3COCl, 98.6 with $FeSO_4$(800 °C) and CH_3COCl, 33.6 with $FeSO_4$(800 °C) and CH_3COBr, and 65.2 with $FeSO_4$-(800 °C) and $(CH_3CO)_2O$.[16] Several workers have determined the k_T/k_B value to be 121—141 over Lewis catalysts with a high para positional selectivity (95.5—98.3% *para* isomer).[6,17,18] These high values reflect the week electrophilic nature of the acetyl cation. The present values are relatively small in comparison with those literature values, especially that in the $FeSO_4$-(800 °C) and the CH_3COBr system, in spite of the high para selectivity. This suggests that the present acetylation was not just catalyzed by iron chlorides on the catalyst surface.

*** The infrared spectra were obtained using Nujol and KBr tablets.

References

1) For preliminary communication, see M. Hino and K. Arata, *Chem. Lett.*, **1978**, 325.
2) G. A. Olah, "Friedel-Crafts and Related Reactions," Vols. I—IV, Wiley-Interscience, New York and London

(1963—1964).
3) G. A. Olah, "Friedel-Crafts Chemistry," Wiley-Interscience, New York and London (1973).
4) K. Tanabe and T. Takeshita, "Acid-Base Catalysis," Sangyo Tosho, Tokyo (1966), pp. 357—367.
5) M. Tashiro, *Yuki Gosei Kagaku Kyokai Shi*, **36**, 426 (1978); K. Nakane, *ibid.*, **36**, 440 (1978); K. Muneyuke and H. Tanida, *ibid.*, **36**, 454 (1978).
6) G. A. Olah, M. E. Moffatt, S. J. Kuhn, and B. A. Hardie, *J. Am. Chem. Soc.*, **86**, 2198 (1964).
7) E. H. Man and C. R. Hauser, *J. Org. Chem.*, **17**, 397 (1952).
8) G. A. Olah and S. Kobayashi, *J. Am. Chem. Soc.*, **93**, 6964 (1971).
9) E. J. Salmi and E. Väihkönen, *Suom. Kemistil. B*, **19**, 132 (1946); *Chem. Abstr.*, 5481c (1947).
10) E. Koike and K. Ohkawa, *Nippon Kagaku Zasshi*, **75**, 83 (1954).
11) Y. Takegami, K. Azuma, and H. Niimiya, *Kogyo Kagaku Zasshi*, **55**, 630 (1952).
12) K. Arata and I. Toyoshima, *Chem. Lett.*, **1974**, 929.
13) K. Arata, K. Sato, and I. Toyoshima, *J. Catal.*, **42**, 221 (1976).
14) K. Arata, K. Yabe, and I. Toyoshima, *J. Catal.*, **44**, 385 (1976).
15) M. Hino and K. Arata, *Chem. Lett.*, **1977**, 277.
16) The reaction was carried out with a 0.5 M acetylating reagent in an equimolar amount of benzene and toluene at room temperature for acetyl chloride and bromide and at 80 °C for acetic anhydride. The products were analyzed after reaction of 30 min.
17) G. A. Olah, S. J. Kuhn, S. H. Flood, and B. A. Hardie, *J. Am. Chem. Soc.*, **86**, 2203 (1964).
18) H. C. Brown and G. Marino, *J. Am. Chem. Soc.*, **81**, 5611 (1959).

A ^{13}C NMR and CNDO/2 Calculation Study of the Transannular Interaction in [2.2]Cyclophanes[1)]

Kazushi TOKITA, Tetsuo TAKEMURA, Shoichi KONDO, and Nobuo MORI*

Department of Chemistry, Science University of Tokyo, Shinjuku-ku, Tokyo 162

(Received May 14, 1979)

The relationships between the aryl carbon chemical shifts and the CNDO/2 electron densities for several [2.2]cyclophanes are reported. Plots of the chemical shifts against the excess total electron densities indicate additional downfield shifts of 6—9 ppm on the average for those aryl carbons that are in close proximity to other aryl carbons. A plot of the ^{13}C shielding constant, calculated using the Karplus-Pople theory, against the chemical shift shows a downfield shift of a similar magnitude for the proximate carbons relative to the others. It is found that this difference can be essentially eliminated simply by adjusting the ΔE parameter in the Karplus-Pople equation from 10.0 eV to 9.7 eV for the proximate carbon atoms.

Although the transannular interactions in [2.2]-cyclophanes of electronically excited states have been thoroughly investigated, the interactions in the ground electronic states are still not well understood. In their photoelectron spectral study of the [2.2]para- and [2.2]-metacyclophanes, **7** and **10**, Boschi and Schmidt[2)] suggested that the interaction in **7** takes place between all the facing aryl carbons, whereas in **10** it is confined to C(8) and C(16), which are in the closest proximity to each other. In the ground state, however, no such interaction could be detected by means of ^{13}C NMR spectroscopy.[3)] Recent ^{13}C NMR results for **7** and **10**[4)] have indicated that the interacting carbons, especially C(8) and C(16) in **10**, are noticeably deshielded compared with open-chain models. Similar deshieldings were observed for other facing unsaturated carbons whose p-orbital axes were nearly colinear.[4-6)]

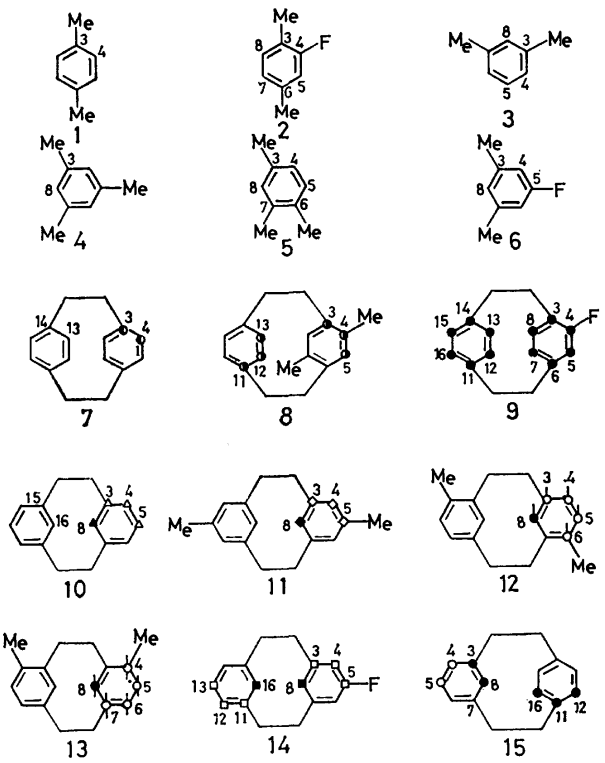

Fig. 1. The reference and [2.2]cyclophane compounds examined. The positions in **1**—**6** are numbered so as to correspond to those in **7**—**15**.

In an attempt to explain these observations we have first investigated the relationships between the aryl carbon chemical shifts and the CNDO/2 electron densities in the nine [2.2]cyclophanes, **7**—**15**, shown in Fig. 1, and in six monocyclic reference compounds, **1**—**6**. Then we have compared the observed chemical shifts with the shielding constants calculated using the Karplus-Pople theory.[7)]

Calculation

The theoretical ^{13}C shielding for an atom, σ, was calculated in terms of the Karplus-Pople theory[7)] using:

$$\sigma = \sigma_d + \sigma_p, \quad (1)$$

but the local diamagnetic term, σ_d, was estimated using:[8)]

$$\sigma_d = 4.45Zq^t, \quad (2)$$

where Z is the effective nuclear charge estimated according to Slater's rules and q^t is the total electron density on the atom. The electron densities and bond orders used in these calculations were those estimated by the CNDO/2-Molecular Orbital method.[9)] In the MO calculations for all the cyclophanes, the geometry parameters of the parent unsubstituted compounds[10)] were used in defining the input geometries, but the standard geometry parameters[11)] were used for the methyl and fluorine substituents in the methyl- and fluorocyclophanes, **8**, **9**, and **11**—**14**, and for all the monocyclic compounds.

All the computations were performed on a HITAC-8800/8700 computer at the Computer Centre of the University of Tokyo.

Results and Discussion

Table 1 gives the excess π- and total electron densities, Δq^π and Δq^t, as calculated by the CNDO/2 approximation,[9)] together with the observed and calculated aryl carbon chemical shifts, δ and σ from Eq. 1 using 10.0 eV[12)] as ΔE for all compounds.

In Models **1**—**6**, the δ value was found to bear a better linear relationship with the Δq^t than with the Δq^π value. The least-squares graph of the correlation ($r^{**}=0.972$) is drawn in Figs. 2—4, together with similar plots for the cyclophanes. The line ($s^{**}=153$) is very

** r: correlation coefficient; s: slope of the line.

Table 1. ^{13}C Chemical shifts and excess total electron densities

Compd	Carbon[h]	$\delta(^{13}C)$[a] ppm	$\Delta q^{\pi}\times 10^3$	$\Delta q^{t}\times 10^3$	$-\sigma_p$ ppm	$-\sigma$ ppm
1[b]	(3)	134.5	12	38	273.4	215.9
	(4)	129.1	−11	6	260.0	202.2
2[c]	(3)	121.5	−27	−11	—	—
	(4)	161.0	16	225	—	—
	(5)	115.7	−44	−51	—	—
	(6)	137.5	31	58	—	—
	(7)	124.6	−34	−13	—	—
	(8)	131.2	7	24	—	—
3[b]	(3)	137.5	34	50	275.1	217.7
	(4)	126.4	−34	−7	258.3	200.4
	(5)	128.3	19	24	258.4	200.5
	(8)	130.1	−42	−13	261.6	204.0
4[b]	(3)	137.6	42	52	275.6	218.2
	(8)	127.4	−55	−22	257.3	199.3
5[b]	(3)	135.2	14	42	274.2	216.0
	(4)	126.7	−21	−3	258.9	201.0
	(5)	129.8	−10	9	260.6	202.8
	(6)	133.4	6	24	272.3	214.7
	(7)	136.3	7	36	276.8	219.3
	(8)	130.5	−30	−9	258.9	201.0
6[c]	(3)	140.2	54	70	—	—
	(4)	113.0	−79	−65	—	—
	(5)	163.2	47	245	—	—
	(8)	125.7	−67	−33	—	—
7[d]	(3)	139.4	31	29	274.9	217.3
	(4)	132.8	−22	−10	259.7	201.8
8[e]	(3)	137.7	21	26	—	—
	(4)	134.5	−7	24	—	—
	(5)	131.2	−36	−18	—	—
	(11)	139.2	31	26	—	—
	(12)	128.4	−22	−8	—	—
	(13)	132.4	−22	−7	—	—
9[f]	(3)	125.8	−12	−23	—	—
	(4)	161.1	12	218	—	—
	(5)	122.2	−70	−68	—	—
	(6)	142.8	49	51	—	—
	(7)	128.0	−46	−29	—	—
	(8)	135.4	0	10	—	—
	(11)	138.8	26	27	—	—
	(12)	132.9	−21	−11	—	—
	(13)	129.2	−22	−11	—	—
	(14)	139.7	29	29	—	—
	(15)	132.5	−20	−12	—	—
	(16)	133.5	−20	−11	—	—
10[d]	(3)	138.6	42	39	281.8	224.3
	(4)	125.1	−47	−30	259.6	201.5
	(5)	128.6	9	2	264.0	206.0
	(8)	136.3	−33	−22	258.1	200.1
11[d]	(3)	138.7	53	46	—	—
	(4)	125.7	−72	−48	—	—
	(5)	137.8	39	45	—	—
	(8)	133.9	−48	−32	—	—
12[d]	(3)	136.2	29	31	—	—
	(4)	125.3	−36	−25	—	—
	(5)	130.0	−16	−16	—	—
	(6)	132.3	−17	13	—	—
	(8)	136.6	−2	−16	—	—
13[d]	(4)	132.5	−17	13	—	—
	(5)	130.0	−15	−15	—	—
	(6)	125.1	−36	−25	—	—
	(7)	136.4	30	32	—	—
	(8)	136.6	−22	−16	—	—
14[c]	(3)	141.0	65	63	—	—
	(4)	112.0	−100	−89	—	—
	(5)	163.0	43	232	—	—
	(8)	132.6	−61	−44	—	—
	(11)	138.6	41	40	—	—
	(12)	125.5	−46	−30	—	—
	(13)	128.6	9	1	—	—
	(16)	136.2	−46	−22	—	—
15[g]	(3)	140.6	53	48	278.4	220.9
	(4)	124.7	−48	−32	259.1	201.0
	(5)	126.8	21	11	264.1	206.3
	(8)	133.0	−56	−38	258.6	200.4
	(11)	138.5	31	16	272.6	214.9
	(12)	129.7	−26	−38	255.5	197.3
	(16)	128.2	−22	−35	254.0	195.9

a) Downfield from internal TMS (all data in $CDCl_3$). b) δ taken from J. B. Stothers, "Carbon-13 NMR Spectroscopy," Academic Press, New York (1972), p. 95. c) Obtained in this work (Ref. 15). d) Taken from Ref. 4. e) Taken from H. Horita, H. Takemitsu, T. Otsubo, Y. Sakata, S. Misumi, M. Mishima, and Y. Tsuno, Abstract presented at the 32 nd Annual Meeting of the Chemical Society of Japan, Tokyo, April, 1975. f) δ taken from T. Takemura and N. Mori, *Chem. Lett.*, **1978**, 857. g) Taken from Ref. 1. h) Numbering as in Fig. 1.

close to that ($s=160$) shown by Bloor and Breen[12] for monosubstituted benzenes. Also, the correlation graph obtained between the σ and δ values of **1**, **3**, **4**, and **5** is shown in Fig. 5.

Figures 2—4 show plots of the δ against the Δq^{t} values for the **7**—**9**, **10**—**14**, and **15** cyclophanes respectively. It should be noticed in any of the figures that the aryl carbons proximate to each other show a linear relationship different from that for the remote or non-interacting carbons, as will be discussed further below (see Table 2).

In Fig. 2, the plots for all the facing carbons of the paracyclophanes lie roughly on the same correlation line,

Table 2. The least-squares linear relationships between δ and Δq^{t} for Compounds **1**—**15**

$\delta = a\Delta q^{t} + b$

Compd	a[a]	b[a]	r[b]
1—**6**	153	128.0	0.972
7—**9**	(138)	(133.4)	(0.951)
10—**14**	153 (153)	130.4 (139.4)	0.980 (0.980)
15	(113)	(135.9)	(0.953)

a) The values in parentheses are those for the proximate carbons. b) Correlation coefficient.

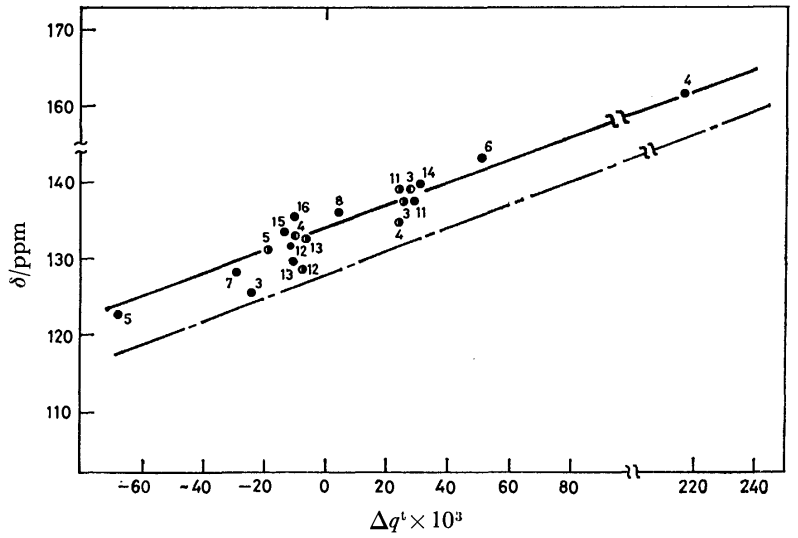

Fig. 2. Plots of δ *vs.* Δq^t for [2.2]paracyclophanes **7**—**9**. Numbering and designations as in Fig. 1. Reference line for **1**—**6**: — — —.

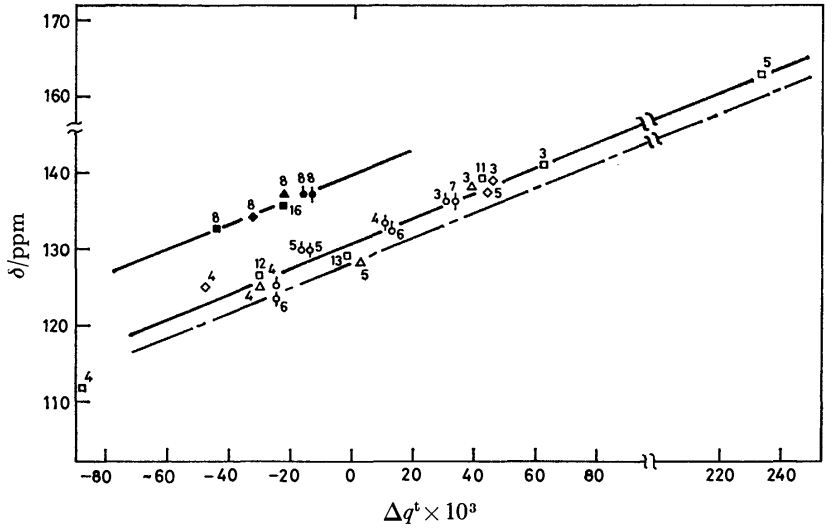

Fig. 3. Plots of δ *vs.* Δq^t for metacyclophanes **10**—**14**. Numbering and designations as in Fig. 1. Reference line for **1**—**6**: — — —.

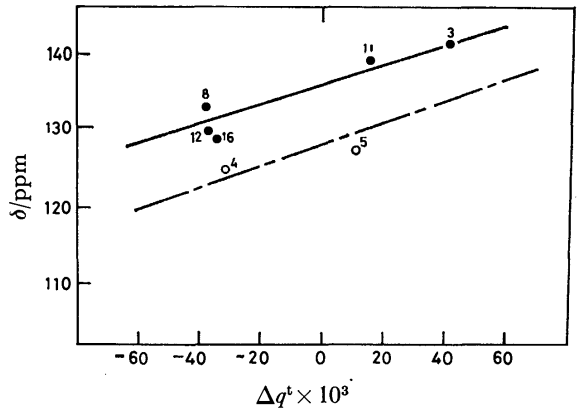

Fig. 4. Plots of δ *vs.* Δq^t for metaparacyclophane **15**. Numbering and designations as in Fig. 1. Reference line for **1**—**6**: — — —.

which is *ca.* 6 ppm upward (or downfield) from the line for the reference monocycles. Figure 3 indicates that the inner, C(8) and C(16), and the outer carbons, C(3)—C(5), of the metacyclophanes are distinguished by two separate linear relationships. The least-squares lines are parallel and are 9.0 ppm apart. The lower line for the outer carbons is only 2 ppm away from the reference line. This slight discrepancy between the latter two is unimportant, if one considers the approximate nature of the theory used to calculate the electron densities and the fact that the observed data are uncorrected for the ring current and other anisotropic shielding effects. Figure 4 shows that, in metaparacyclophane **15**, the plots for the outer carbons, C(4) and C(5), of the meta ring fall on the reference line, whereas those for the rest of the aryl carbons are on a separate line which is *ca.* 8 ppm away from the reference. From these results it may be concluded that the proximate carbons

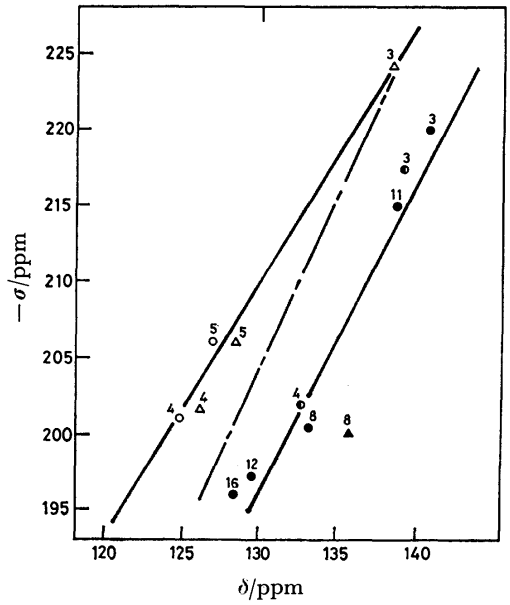

Fig. 5. Plots of σ *vs.* δ for [2.2]cyclophanes **7**, **10**, and **15**, using 10.0 eV as ΔE for all carbons. Numbering and designations as in Fig. 1. Reference line for **1**, **3**, **4**, and **5**: — - —

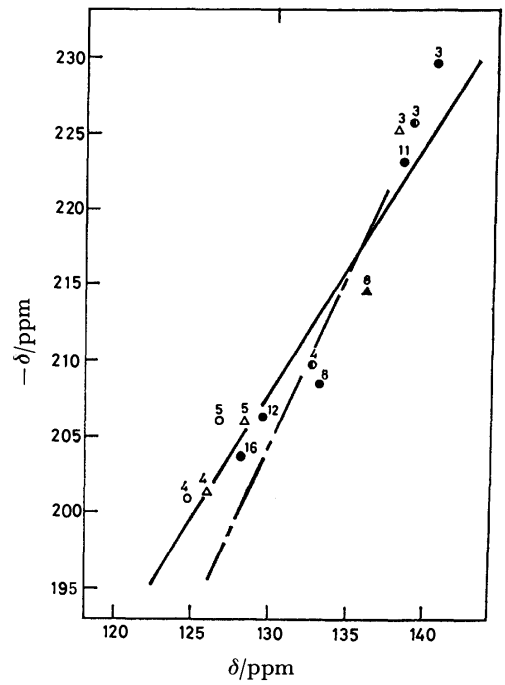

Fig. 6. The effect of using decreased ΔE for the proximate carbons, 9.5 eV for C(8) of **10** and 9.7 eV for all the others.

are shifted downfield compared with the remote carbons with the same total electron densities. The magnitude of the downfield shifts varies with the type of the cyclophane series within the range of *ca.* 6—9 ppm. This is probably attributable to decreases in the excitation energy term, ΔE, of the paramagnetic shielding expression, σ_p, as will be interpreted below.

Figure 5 shows plots of the σ values predicted from Eq. 1, using 10.0 eV as ΔE, against the δ values for the **7**, **10**, and **15** cyclophanes. Apparently, there are two different linear relationships, which are characteristic of the proximate and the remote carbons. The least-squares lines are nearly parallel, with a space of *ca.* 10 ppm between; both are in poor agreement with the reference line. Exactly, the use of the ΔE value of 10.0 eV leads to an estimation of the chemical shifts for the proximate carbons 8—12 ppm smaller than those for the remote carbons, except for the inner C(8) of **10** and **15**, which are underestimated by 20 and 14 ppm respectively (similar results were obtained by using 8.0 eV as the ΔE). The magnitude of the underestimation is seemingly correlated with the interatomic distance between the interacting carbons and the relative orientation of the p-orbitals concerned, as Table 3 shows. A possible explanation for the underestimation can be obtained by assuming decreases in ΔE caused by a transannular interaction.[13] Such decreases in the meta- and metaparacyclophanes must be highly local (Karplus and Pople[7b] suggest the possibility of localized excitations). For example, a decrease in the ΔE from 10.0 to 9.7 eV changes the σ value for C(3) of **7** from −217.3 to −225.8 ppm. The graph of Fig. 6 shows the effect of using the ΔE of 9.7 eV for all the proximate carbons except for C(8) of **10**, for which 9.5 eV is used. All the points now lie roughly on the same line, which is closer to the reference than in Fig. 5. The assumption of the local decreases in ΔE can also explain the downfield-shift trend of the proximate carbon resonances shown in Figs. 2—4, because a decrease in ΔE should cause a downfield shift. Recent studies of smaller molecules[14] indicate that the correlation between theory and experiment for ^{13}C chemical shifts is improved by using different excitation energies for individual carbons in calculating their chemical shifts.

TABLE 3. UNDERESTIMATED CHEMICAL SHIFTS, $\Delta\sigma$ AND INTERATOMIC DISTANCES, l, FOR THE PROXIMATE CARBONS

Compd	Centers	l/Å	$\Delta\sigma$/ppm[a]
7	C(3)-C(14)	2.77[10c]	8
	C(4)-C(13)	3.09	12
10	C(8)-C(16)	2.69[10a]	20
	C(3)-C(15)	3.02	0
15	C(8)-C(12)	3.1[10b]	14 for C(8)
	C(8)-C(11)	3.0	12 for C(12)
	C(7)-C(11)	2.7	10 for C(11)
			9 for C(7)

a) Predicted chemical shift difference of the proximate from the remote carbon.

The authors wish to thank Professor Masatami Takeda of Science University of Tokyo for his advice.

References

1) For a preliminary report of this work, see T. Takemura, K. Tokita, S. Kondo, and N. Mori, *Chem. Lett.*, **1977**, 865.
2) R. Boschi and W. Schmidt, *Angew. Chem., Int. Ed., Engl.*, **12**, 402 (1973).
3) T. Takemura, K. Tokita, S. Kondo, and N. Mori, *J. Chem. Res. (S)*, **1978**, 452.

4) T. Sato, T. Takemura, and M. Kainosho, *J. Chem. Soc., Chem. Commun.*, **1974**, 97; T. Takemura and T. Sato, *Can. J. Chem.*, **54**, 3412 (1976).

5) T. Sato, H. Matsui, and R. Komaki, *J. Chem. Soc., Perkin Trans.* **1**, **1976**, 2053.

6) E. Kloster-Jensen and J. Wirz, *Angew. Chem.*, Int. Ed., Engl., **12**, 671 (1973).

7) (a) J. A. Pople, *J. Chem. Phys.*, **37**, 53 (1962); (b) M. Karplus and J. A. Pople, *ibid.*, **38**, 2803 (1963).

8) T. Yonezawa, I. Morishima, and H. Kato, *Bull. Chem. Soc. Jpn.*, **39**, 1398 (1965).

9) J. A. Pople and D. L. Beveridge, "Approximate Molecular Orbital Theory," McGraw-Hill, New York (1970).

10) (a) C. J. Brown, *J. Chem. Soc.*, **1953**, 3278; (b) D. T. Hefelfinger and D. J. Cram, *J. Am. Chem. Soc.*, **93**, 4754 (1971); (c) H. Hope, J. Berstein, and K. N. Trueblood, *Acta Crystallogr., Sect. B*, **28**, 1933 (1972).

11) J. A. Pople and M. Gordon, *J. Am. Chem. Soc.*, **89**, 4253 (1967).

12) J. E. Bloor and D. L. Breen, *J. Phys. Chem.*, **72**, 716 (1968).

13) L. L. Ingraham, *J. Chem. Phys.*, **18**, 988 (1950) and **27**, 1228 (1957); N. L. Allinger, M. A. Da Rooge and R. B. Hermann, *J. Am. Chem. Soc.*, **83**, 1974 (1961).

14) K. Takahashi, I. Ando, M. Kondo, R. Chujo, and A. Nishioka, *Bull. Chem. Soc. Jpn.*, **47**, 1559 (1974); N. C. Baird and K. C. Teo, *J. Magn. Reson.*, **24**, 87 (1976).

15) The ^{13}C and ^{1}H FT NMR spectra of Compounds **2**, **6**, and **14** were measured in 0.2—0.3 mol dm^{-1} solutions in $CDCl_3$, using a JEOL-PFT-100/JNM-PS-100 spectrometer operating at 25 and 100 MHz respectively, in the Fourier transform mode, as has previously been described.[3] The ^{13}C chemical shifts were assigned by means of selective decouplings using the ^{1}H data and by taking account of the J_{C-F} coupling pattern.[16]

16) W. Adcock, B. D. Gupta, and T. C. Khor, *J. Org. Chem.*, **41**, 751 (1976).

 © 1980 The Chemical Society of Japan Bull. Chem. Soc. Jpn., 53, 455—457 (1980)

Pseudo-sugars. 5. Synthesis of DL-Validatol and DL-Deoxyvalidatol, and Their Epimers[1,2]

Seiichiro OGAWA,* Tatsushi TOYOKUNI, Masaji OMATA,
Noritaka CHIDA, and Tetsuo SUAMI
Department of Applied Chemistry, Faculty of Engineering, Keio University, Hiyoshi, Yokohama 223
(Received May 21, 1979)

New cyclitols, validatol and deoxyvalidatol, derived by hydrogenolysis of antibiotic validamycin A, were synthesized as the racemates from readily available tri-*O*-acetyl-(1,3/2,4,6)-4-bromo-6-bromomethyl-1,2,3-cyclohexanetriol.

In connection with a previous work,[3] we wish to report the first synthesis of racemic validatol and deoxyvalidatol, the degradation products of validamycin A,[4] from readily available tri-*O*-acetyl-(1,3/2,4,6)-4-bromo-6-bromomethyl-1,2,3-cyclohexanetriol (**1**).[2]

Treatment of **1** with 1.2 molar equivalent of silver fluoride in dry pyridine at ambient temperature overnight gave exclusively tri-*O*-acetyl-(1,3/2,4)-4-bromo-6-methylene-1,2,3-cyclohexanetriol (**2**) in 60% yield. The ^{1}H NMR spectrum showed the signals of C-5 methylene protons as a one-proton broad triplet (J=12 and 14 Hz) at δ 2.61 and a one-proton doublet of doublets (J=5 and 14 Hz) at δ 3.01, confirming the assigned structure. Debromination of **2** with tributyltin(IV) hydride in toluene in the presence of α,α'-azobisisobutyronitrile gave tri-*O*-acetyl-(1,3/2)-4-methylene-1,2,3-cyclohexanetriol (**3**) in 60% yield. On the other hand, exhaustive dehydrobromination of **1** was effected by treatment with 1,5-diazabicyclo[5.4.0]undec-5-ene (DBU) in toluene to give an exocyclic diolefin, tri-*O*-acetyl-(1,3/2)-4-methylene-5-cyclohexene-1,2,3-triol (**4**)[5] in 45% yield, which was identical with the compound obtained from **2** in a similar way in 51% yield. Its structure was determined by the ^{1}H NMR spectrum, which revealed the signals of the exocyclic methylene protons as two broad singlets at δ 5.08 and 5.21. Compounds **2**, **3**, and **4** thus obtained might be useful intermediates for the preparation of unsaturated branched cyclitols.

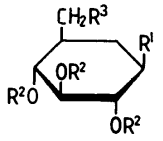

	R^1	R^2	R^3
1	Br	Ac	Br
7	H	Ac	H
8	H	H	H
9	Br	Ac	OAc
10	H	Ac	OAc
11	H	H	OH

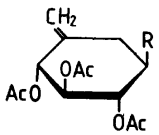

2 R=Br
3 R=H

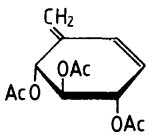

4

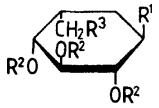

	R^1	R^2	R^3
5	H	Ac	H
6	H	H	H
12	Br	Ac	OAc
13	H	Ac	OAc
14	H	H	OH

Catalytic reduction of **3** or **4** in ethyl acetate with platinum oxide gave preferentially tri-*O*-acetyl-(1,3,4/2)-4-methyl-1,2,3-cyclohexanetriol (**5**) in a high yield, the ^{1}H NMR spectral data of which were identical with those of an optically active sample reported by Horii and Kameda.[6] A 4-epimer (**7**) of **5** was also prepared by hydrogenolysis of **1** with Raney nickel T-4[7] in ethyl acetate in the presence of Amberlite IR-45 (OH^-) in 92% yield. *O*-Deacetylation of **5** and **7** with methanolic sodium methoxide gave crystalline triol **6** (deoxyvalidatol) and **8**, respectively.

(1,3,4/2)-4-Hydroxymethyl-1,2,3-cyclohexanetriol (validatol) (**14**) was synthesized from **2** or **3** by hydroboration followed by the usual sequence of reactions. First, (1,3/2,4)-4-hydroxymethyl-1,2,3-cyclohexanetriol (**11**) was prepared from **1** as a reference compound. Tetra-*O*-acetyl-(1,3/2,4,6)-4-bromo-6-hydroxymethyl-1,2,3-cyclohexanetriol (**9**)[2] derived by treatment of **1** with sodium acetate in aqueous 2-methoxyethanol was hydrogenolyzed with Raney nickel in the usual way to give a crystalline tetraacetate (**10**) of **11** in 96% yield. *O*-Deacetylation gave a crystalline **11** in 97% yield.

Hydroboration of **2** with sodium borohydride and boron trifluoride in tetrahydrofuran (THF) followed by treatment with hydrogen peroxide[8] and successive acetylation gave, after purification on a silica-gel column, a homogeneous syrupy product in 30% yield. Comparison of the ^{1}H NMR spectrum with that of **9** showed that the product consists of **9** and tetra-*O*-acetyl-(1,3,6/2,4)-4-bromo-6-hydroxymethyl-1,2,3-cyclohexanetriol (**12**) in a 1:2 ratio. Without separation, the mixture was hydrogenolyzed in the usual way to give a syrup, which was found by ^{1}H NMR spectroscopy to consist of **10** and validatol tetraacetate (**13**) in a 1:2 ratio. Compound **3** was also subjected to hydroboration similarly followed by acetylation to give a 1:2.5 mixture of **10** and **13** in 29% yield. Since both compounds showed a similar mobility on TLC in various solvent systems, separation was carried out by converting them into tetrols **11** and **14**. *O*-Deacetylated mixture was successfully fractionated by chromatography on silica gel to give **11** as crystals and **14** as a homogeneous syrup. Acetylation of **14** gave a syrupy **13** whose

^{1}H NMR spectrum was superimposable on that of an authentic optically active sample reported.[4b]

Experimental

Melting points were determined in a capillary in a silicone bath and are uncorrected. Solutions were evaporated under reduced pressure at 40—50 °C. Unless otherwise stated, the ^{1}H NMR spectra were taken on a Varian EM 360A (60 MHz) or HA 100D (100 MHz) in deuteriochloroform ($CDCl_3$) with reference to tetramethylsilane as an internal standard, the peak positions being given in terms of δ-values. Values given for coupling constants are of first-order. TLC was performed on pre-coated silica gel 60 F-254 plaques (Merck, Darmstadt; 0.25 mm thickness). Silica gel (Wakogel C-300, Wako Pure Chemical Industries, Ltd.) was used for column chromatography.

Tri-O-acetyl-(1,3/2,4)-4-bromo-6-methylene-1,2,3-cyclohexanetriol (2). A mixture of tri-*O*-acetyl-(1,3/2,4,6)-4-bromo-6-bromomethyl-1,2,3-cyclohexanetriol (**1**)[2] (1 g) and silver fluoride (0.36 g, 1.2 molar equiv.) in dry pyridine (20 ml) was stirred at ambient temperature for 20 h. The brown reaction mixture was diluted with ether (100 ml) and the precipitates were removed by filtration. The filtrate was evaporated and the product purified by passage through a short column of alumina with chloroform. The eluate was evaporated and the residue was crystallized from ethanol to give **2** (0.49 g, 60%) as needles: mp 124—125 °C: ^{1}H NMR (60 MHz) δ 2.00 (3H, s), 2.05 (3H, s), and 2.10 (3H, s) (OAc), 2.61 (1H, broad t, $J_{4,5ax}=12$ Hz, $J_{5gem}=14$ Hz, H-5ax), 3.01 (1H, dd, $J_{4,5eq}=5$ Hz, H-5eq), 3.80 (1H, ddd, $J_{3,4}=9.5$ Hz, H-4), 4.7—5.5 (5H, m, H-1, H-2, H-3, and exocyclic methylene).

Found: C, 44.43; H, 4.87; Br, 23.12%. Calcd for $C_{13}H_{17}O_6Br$: C, 44.71; H, 4.91; Br, 22.88%.

Tri-O-acetyl-(1,3/2)-4-methylene-1,2,3-cyclohexanetriol (3). A solution of **2** (1.65 g) in dry toluene (50 ml) was treated with tributyltin(IV) hydride (1.6 ml) in the presence of a trace of α,α'-azobisisobutyronitrile at 80 °C for 30 min under a nitrogen stream. The reaction mixture was then evaporated and the residue was crystallized from ligroin to give **3** (0.76 g, 60%) as prisms: mp 69—71 °C; ^{1}H NMR (60 MHz) δ 1.15 (4H, m, ring methylene), 2.00 (3H, s), 2.01 (3H, s), and 2.10 (3H, s) (OAc), 4.7—5.5 (5H, m, H-1, H-2, H-3, and exocyclic methylene).

Found: C, 57.56; H, 6.71%. Calcd for $C_{13}H_{18}O_6$: C, 57.77; H, 6.71%.

Tri-O-acetyl-(1,3/2)-4-methylene-5-cyclohexene-1,2,3-triol (4). a) A solution of **1** (1 g) and DBU (1.8 ml, 5 molar equiv.) in toluene (10 ml) was refluxed for 30 min. After cooling, the precipitates were removed by decantation. The solution was evaporated and the residue dissolved in ethyl acetate (50 ml). The solution was washed with 0.2 M hydrochloric acid, aqueous saturated sodium hydrogencarbonate, and water, successively, dried over anhydrous sodium sulfate, and filtered through a short column of alumina. The filtrate was evaporated and the residue was crystallized from ethanol to give **4** (0.28 g, 45%) as needles: mp 67—68 °C; ^{1}H NMR (100 MHz) δ 2.06 (3H, s), 2.08 (3H, s), and 2.15 (3H, s) (OAc), 5.08 (1H, broad s) and 5.21 (1H, broad s) (exocyclic methylene), 5.28 (1H, dd, $J=7.5$ Hz, $J=10.5$ Hz, H-2), 5.6 —5.8 (3H, m, H-1, H-3, and H-5), 6.31 (1H, m, H-6).

Found: C, 57.97; H, 5.96%. Calcd for $C_{13}H_{16}O_6$: C, 58.26; H, 6.01%.

b) A solution of **2** (1 g) and DBU (0.52 ml, 1.2 molar equiv.) in toluene (20 ml) was refluxed for 6 h. After cooling, the precipitates were removed by filtration and the filtrate was treated as described above. Crystallization of the crude product from ethanol gave **4** (0.4 g, 51%): mp 66—67.5 °C, identical with the compound obtained above.

Tri-O-acetyl-(1,3,4/2)-4-methyl-1,2,3-cyclohexanetriol (Deoxyvalidatol) (5). a) A solution of **3** (0.1 g) in ethyl acetate (10 ml) was hydrogenated in a Parr shaker apparatus in the presence of platinum oxide (10 mg) under an initial hydrogen pressure of 3 kg cm^{-2} at ambient temperature overnight. The catalyst was removed by filtration and the filtrate was evaporated to give **5** (77 mg, 76%) as a chromatographically homogeneous syrup: ^{1}H NMR (100 MHz) δ 1.05 (3H, d, $J=7$ Hz, methyl), 1.1—1.9 (4H, m, two ring methylene), 2.01 (6H, s) and 2.05 (3H, s) (OAc), 2.21 (1H, m, H-4), 4.83 (1H, dd, $J_{2,3}=9$ Hz, $J_{3,4}=5$ Hz, H-3), 5.23 (1H, t, $J_{1,2}=9$ Hz, H-2). The ^{1}H NMR spectral data were almost identical with those of an optically active sample reported,[6] showing that **5** contains a trace of its 4-epimer (**7**). (Found: C, 56.75; H, 7.31%).

b) Compound **4** (65 mg) was hydrogenated in ethyl acetate (5 ml) in a similar way to that described above to give a syrupy mixture (56 mg, 85%) of **5** and **7** in the ratio of 3: 1.

(1,3,4/2)-4-Methyl-1,2,3-cyclohexanetriol (Deoxyvalidatol) (6). A solution of crude **5** (0.1 g) in methanol (10 ml) was treated with 1 M methanolic sodium methoxide (0.2 ml) and allowed to stand at ambient temperature overnight. The mixture was then treated with Amberlite IR-120 (H^+) and concentrated to give a crystalline residue. Recrystallization from ethanol–ether gave **6** (46 mg, 86%) as colorless crystals: mp 109.5 °C (after melting partly at 93 °C). ^{1}H NMR (60 MHz in D_2O with sodium 4,4-dimethyl-4-silapentane-1-sulfonate as an internal standard) δ 0.92 (3H, d, $J=7$ Hz, methyl), 1.12—2.27 (5H, m, two ring methylene and H-4), 3.06—3.76 (3H, m, H-1, H-2, and H-3).

Found: C, 57.23; H, 9.44%. Calcd for $C_7H_{14}O_3$: C, 57.51; H, 9.65%.

Tri-O-acetyl-(1,3/2,4)-4-methyl-1,2,3-cyclohexanetriol (7). A solution of **1** (0.5 g) in ethyl acetate (10 ml) was hydrogenated in a Parr shaker apparatus in the presence of Raney nickel T-4[7] (5 ml) and Amberlite IR-45 (OH^-) (7 ml) under an initial hydrogen pressure of 3 kg cm^{-2} at ambient temperature overnight. The catalyst and resin were removed by filtration and the filtrate was evaporated to give a crystalline residue, which was recrystallized from ethanol to give **7** (0.29 g, 92%) as feathers: mp 92—93.5 °C; ^{1}H NMR (60 MHz) δ 0.92 (3H, d, $J=6$ Hz, methyl), 1.98 (6H, s) and 2.00 (3H, s) (OAc), 4.54—5.18 (3H, m, H-1, H-2, and H-3).

Found: C, 57.07; H, 7.22%. Calcd for $C_{13}H_{20}O_6$: C, 57.34; H, 7.40%.

(1,3/2,4)-4-Methyl-1,2,3-cyclohexanetriol (8). Compound **7** (0.1 g) was treated with methanolic sodium methoxide in the same way as in the preparation of **6**. The crude product was recrystallized from ethanol–ether to give **8** (53 mg, 99%) as colorless crystals: mp 120.5—121 °C. ^{1}H NMR (60 MHz in D_2O) δ 0.93 (3H, d, $J=5.5$ Hz, methyl), 1.09—2.04 (5H, m, two ring methylene and H-4), 2.64—3.66 (3H, m, H-1, H-2, and H-3).

Found: C, 57.27; H, 9.46%. Calcd for $C_7H_{14}O_3$: C, 57.51; H, 9.65%.

Tetra-O-acetyl-(1,3/2,4)-4-hydroxymethyl-1,2,3-cyclohexanetriol (10). A solution of tetra-*O*-acetyl-(1,3/2,4,6)-4-bromo-6-hydroxymethyl-1,2,3-cyclohexanetriol (**9**)[2] (0.5 g) in ethyl acetate (10 ml) was hydrogenolyzed as in the preparation of **7**. Crystallization of a crude product from ethanol gave **10** (0.39 g, 96%) as prisms: mp 99.5—100 °C; ^{1}H NMR (60 MHz) δ 2.00 (9H, s) and 2.03 (3H, s) (OAc), 1.2—2.3 (5H, m, ring methylene and H-4), 3.83—4.03 (2H, AB-quartet, H-7 and H-7'), 4.62—5.12 (3H, m, H-1, H-2, and H-3).

Found: C, 54.71; H, 6.68%. Calcd for $C_{15}H_{22}O_8$: C, 54.54; H, 6.71%.

(1,3/2,4)-4-Hydroxymethyl-1,2,3-cyclohexanetriol (11). Compound **10** (0.22 g) was *O*-deacetylated with methanolic sodium methoxide as in the preparation of **6**. The crude product was recrystallized from ethanol to give **11** (0.11 g, 97%) as prisms: mp 126.5—127 °C.

Found: C, 51.93; H, 8.56%. Calcd for $C_7H_{14}O_4$: C, 51.84; H, 8.70%.

(1,3,4/2)-4-Hydroxymethyl-1.2,3-cyclohexanetriol (Validatol) (14) and Its Tetraacetate (13). a) To a stirred solution of **2** (0.5 g) and sodium borohydride (0.24 g) in THF (15 ml) was added dropwise a solution of 47% boron trifluoride etherate (2.4 ml) in THF (4.8 ml) at ambient temperature over a period of 1 h. After the reaction mixture had been set aside at ambient temperature overnight, an excess of sodium borohydride was destroyed by addition of 50% aqueous THF (5 ml). The reaction mixture was then treated with a mixture of 3 M aqueous sodium hydroxide (6 ml) and 30% hydrogen peroxide (3 ml). The resulting mixture was evaporated and the residue was treated with acetic anhydride (10 ml) and pyridine (10 ml) at ambient temperature overnight. Insoluble substance was removed by filtration and the filtrate was evaporated to give a syrup, which was purified by fractionation on a silica-gel column (50 g) with butanone–toluene (1: 10, v/v). A major product was obtained as a homogeneous syrup, 0.17 g (30%), whose ^{1}H NMR (60 MHz) spectrum showed that the product consists of **9** and tetra-*O*-acetyl-(1,3,6/2,4)-4-bromo-6-hydroxymethyl-1,2,3-cyclohexanetriol (**12**) in a 1: 2 ratio. Without further fractionation, the mixture was hydrogenolyzed as in the preparation of **7** to give a syrup (0.12 g, 85%). The ^{1}H NMR (60 MHz) spectrum showed that the product consists of **10** and **13** in a 1: 2 ratio. Since **10** and **13** showed a similar mobility on TLC in various solvent systems, attempts were made to separate them by converting them into tetrols **11** and **14**. The mixture (0.29 g) was treated with 1 M methanolic sodium methoxide in methanol (20 ml) at ambient temperature overnight. After treatment with Amberlite IR-120 (H^+), the reaction mixture was evaporated to give a syrup (0.13 g, 90%), which was shown by TLC [benzene–ethanol (3: 2, v/v)] to contain two components (R_f 0.46 and 0.32). The product was fractionated on a silica-gel column (7 g) with ethanol–toluene (2: 3, v/v) as an eluent. Fractions showing a single spot at R_f 0.46 were combined and evaporated to give **14** (55 mg) as a homogeneous syrup.

Found: C, 51.93; H, 8.50%. Calcd for $C_7H_{14}O_4$: C, 51.84; H, 8.70%.

Compound **14** was acetylated in the usual way to give **13** as a homogeneous syrup, whose ^{1}H NMR (100 MHz) spectrum was superimposable on that of an authentic optically active sample.[4b]

Fractions showing a single spot at R_f 0.32 were combined and evaporated to give **11** (30 mg) as crystals: mp 126—127 °C, identical with the compound obtained by hydrogenolysis of **10** followed by *O*-deacetylation.

b) Compound **3** (0.5 g) was hydroborated and subsequently worked up as described above. The acetylated product was chromatographed on a silica-gel column (50 g) with butanone–toluene (1: 10, v/v) to give a homogeneous syrup (0.18 g, 29%), which was shown by ^{1}H NMR (60 MHz) spectrum to consist of **10** and **13** in a 1: 2.5 ratio.

This work was carried out with financial support from the Ministry of Education. Elemental analyses were performed by Mr. Saburo Nakada, to whom our thanks are due.

References

1) All the compounds described in this paper are racemic. All the formulas depict one enantiomer of the respective racemates. The nomenclature is based on the IUPAC-IUB Tentative Cyclitol Nomenclature Rule [*J. Biol. Chem.*, **22**, 5809 (1968)].

2) For the previous paper in this series, S. Ogawa, K. Nakamoto, M. Takahara, Y. Tanno, N. Chida, and T. Suami, *Bull. Chem. Soc. Jpn.*, **52**, 1174 (1979).

3) T. Suami, S. Ogawa, K. Nakamoto, and I. Kasahara, *Carbohydr. Res.*, **58**, 240 (1977).

4) a) S. Horii, T. Iwasa, and Y. Kameda, *J. Antibiot.*, **24**, 57 (1971); b) S. Horii, T. Iwasa, E. Mizuta, and Y. Kameda, *ibid.*, **24**, 59 (1971).

5) When **1** was treated with sodium acetate in aqueous 2-methoxyethanol followed by acetylation, **9** was mainly obtained in 72% yield, and **2** and **4** could be isolated in very low yields from the mother liquor of **9** by silica gel chromatography.

6) S. Horii and Y. Kameda, *J. Chem. Soc., Chem. Commun.*, **1972**, 747.

7) S. Nishimura, *Bull. Chem. Soc. Jpn.*, **32**, 61 (1959).

8) A. Rosenthal and M. Sprinzl, *Carbohydr. Res.*, **16**, 337 (1971).

Friedel-Crafts Reaction of Aromatics with Epoxides. Stereochemistry and Selectivities

Masashi INOUE, Keizo CHANO, Osamu ITOH, Toshio SUGITA, and Katsuhiko ICHIKAWA*

Department of Hydrocarbon Chemistry, Faculty of Engineering, Kyoto University, Yoshida, Kyoto 606

(Received May 25, 1979)

The Friedel-Crafts reaction of toluene and anisole with 2-methyloxirane and 2,3-dimethyloxiranes was examined. The inter- and intramolecular selectivities of 2-methyloxirane were between those of conventional methylation and isopropylation. It was also found that all the positional isomers formed by the aluminum chloride-catalyzed reaction of toluene and anisole had almost completely inverted configurations of the epoxide carbons. These results are explained by a mechanism of the S_N2 type. Diminished stereospecificities were observed in aluminum bromide-catalyzed reactions.

The Friedel-Crafts reaction is one of the most intensively studied organic reactions.[1] Concerning the stereochemical aspect, it had been accepted until ten years ago that the alkylation proceeds with almost complete racemization. For example, Price and Lund reported that the alkylation of benzene with 2-butanol and boron trifluoride gave 2-phenylbutane with 1% net inversion.[2] Such other catalysts as aluminum chloride, hydrogen fluoride, sulfuric acid, and phosphoric acid also gave the product with less than 0.7% net inversion. Streitwieser and Stang reexamined the stereochemistry of the reaction by the use of 2-propanol-1-d_3[3] and found that the alkylation proceeded with at least 93% net racemization and very little net inversion in the presence of BF_3.[4] They concluded that the reaction is much like an S_N1 solvolysis and has little of the character of a direct (S_N2 type) displacement.

About ten years ago, Nakajima, Suga, and two of the present authors found a stereospecific Friedel-Crafts reaction of benzene with 2-methyloxirane (PO).[5] The reaction gave 2-phenyl-1-propanol with complete inversion, and the mechanism was concluded to be of the S_N2 type. At almost the same time, Brauman *et al.* reported that the alkylation of benzene with γ-valerolactone gave 4-phenylvaleric acid with 40% net inversion.[6] Thereafter, several reports have appeared concerning the stereospecific alkylations. The alkylating agents and stereospecificities are as follows: 2-methyltetrahydrofuran, 35% net inversion;[7] 3-chloro-1-butanol, 20% net inversion;[8] 3-chlorobutyric acid, 43% net inversion;[8] 2-chloro-1-phenylpropane, 82% net retention.[9,10] All of these stereochemical investigations, however, have been restricted to the reaction of benzene, and no attention has been paid to any aromatic substrate other than benzene. Thus, a problem remains unsolved: are the stereospecificities of the alkylation of toluene at each of the three possible positions really the same as that on benzene?

On the other hand, many papers have dealt with the intramolecular selectivity, *i.e.*, the isomer distribution in the alkylation of toluene, and with the intermolecular selectivity, *i.e.*, the relative rate of reaction, $k_{toluene}/k_{benzene}$.[11,12] The reaction mechanisms are most often discussed on the basis of the sets of these two selectivities. Although the stereochemical consequence of the reaction is also an essential component of any discussion of the mechanism, no report has appeared discussing the relationship between the stereochemical behaviour and the reactivity of the alkylating agent.

This paper will report on the Friedel-Crafts reaction of toluene and anisole with PO and with *cis*- and *trans*-2,3-dimethyloxiranes (*cis*- and *trans*-BO), and will discuss the stereochemistry and the intra- and intermolecular selectivities of the reaction.

Results and Discussion

Inter- and Intramolecular Selectivities of Friedel-Crafts Reaction with 2-Methyloxirane. The reaction of toluene with PO yielded three isomeric 2-tolyl-1-propanols (**1**). Nakajima *et al.* reported that an aromatic component attacked the methyl-substituted epoxide carbon in PO.[13] Although the product distributions in the reaction of xylenes with PO have already been discussed, those in the reaction of toluene with PO have not yet been examined because of the difficulties in the

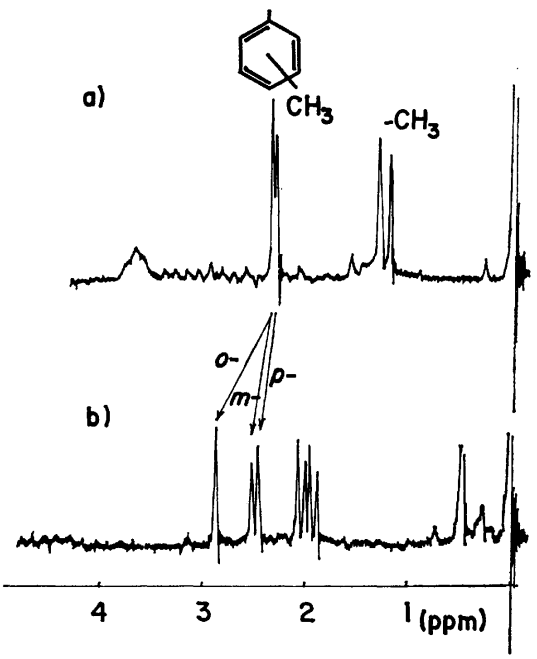

Fig. 1. NMR spectra of **1**; a) 7.0 mg of **1** in 581 mg of $CDCl_3$, b) sample a) plus 5.7 mg of tris(2,2-dimethyl-6,6,7,7,8,8,8-heptafluoro-3,5-octanedionato)europium-(III).

Table 1. Inter- and intramolecular selectivities in the hydroxypropylation with methyloxirane at 0 °C

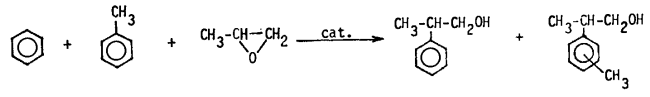

Catalyst	Yield[a] %	k_T/k_B	Isomer distribution/% o-	m-	p-	Stereospecificity[b] Inversion/%
$AlCl_3$	60	3.5	38	35	27	100
$AlBr_3$	28	3.3	36	31	33	48
$TiCl_4$	38	2.9	46	21	33	100
$FeCl_3$	12	2.9	36	29	35	—

a) Yields of isolated products from the reaction of toluene with PO. b) Stereospecificities in hydroxypropylation with (+)-PO. Ref. 5b.

separation of the three isomeric products on GLC.

Efforts were made to separate the three isomers on GLC. It was found that a Bentone-34 column can separate three peaks, but the separation was insufficient. Therefore, we turned our attention to the determination of the product distribution by NMR. Although the NMR spectra of the isomeric mixture could not be resolved into the three components, we found that an europium shift reagent can separate the signals of the methyl protons on the aromatic ring into three peaks, as is shown in Fig. 1. The product distributions determined by this method are given in Table 1, together with the previously reported stereospecificities of the reaction of benzene and the intermolecular selectivities (*vide infra*).

The intermolecular selectivities of the reaction were determined by the usual competitive method, using benzene and toluene in a fifty-fold excess to PO. To discuss the relative rate ratio, k_T/k_B, two conditions should be satisfied: that the reaction is not diffusion-controlled, and that no subsequent reaction occurs. The latter condition seems to be satisfied, since the yields of the high-boiling materials were 5% at the highest, 1—2% usually, and negligible in the case of $TiCl_4$ catalysis. Whether or not the former condition is satisfied in the heterogeneous $AlCl_3$-catalyzed reaction is uncertain, but the fact that there is no remarkable discrepancy in the results between the heterogeneous reaction and the $TiCl_4$-catalyzed homogeneous one appears to show that the data can be used for the estimation of k_T/k_B.

Whereas aluminum bromide catalysis has been reported to result in a remarkable decrease in stereospecificity,[5] there seems to be no remarkable difference between aluminum bromide and the other catalysts as far as the selectivities are concerned. The reason for the diminished stereospecificity in $AlBr_3$ catalysis is uncertain; it is now under investigation.

Table 2 shows some typical results of the selectivities of hydroxypropylation, that is, the alkylation with PO, together with those of the usual Friedel-Crafts reactions summarized by Brown *et al.*[11] Both the intra- and intermolecular selectivities of hydroxypropylation are between those of isopropylation and methylation. Brown *et al.*[14] emphasized that a Friedel-Crafts reaction with primary and probably secondary halides involves an S_N2-type displacement reaction by the aromatics on a polarized alkyl halide-metal halide addition complex. The situation of hydroxypropylation seems to be similar to those mentioned by Brown *et al.*, because the hydroxypropylation of benzene resulted in complete inversion[5] and because the formation of fully developed carbonium ions was confirmed in only a few acid-catalyzed nucleophilic substitutions of epoxides, such as 2,2-diphenyloxirane[15] and some steroid epoxides.[16,17] In an epoxide-Lewis acid complex, the cleavage of the C–O bond of epoxide is made difficult by the presence of another C–O bond. A large nucleophilic contribution by the attacking aromatics is required, because a large covalent character remains in the C–O bond as compared with that in secondary halides and alcohols. Thus, the k_T/k_B of hydroxypropylation is larger than that of isopropylation, but smaller than that of methylation, which seems to show that a larger covalent character remains in the methyl–halogen bond than in the secondary carbon–oxygen bond of PO.

*Stereospecificities of the Formation of Isomeric (*o-, m-, *and* p-*) Products from Toluene.* To explore the specificities of the reaction of toluene, we first examined the reaction with optically active PO. An isomeric mixture of the product was optically active, but, unfortunately, they could not be separated either by column chromatography or by preparative gas chromatography. Therefore, the reaction of toluene with BO was examined. This reaction afforded a mixture of 3-chloro-2-butanols and 3-tolyl-2-butanols (**2**). The stereochemistry of the formation of the former compounds was reported previously.[18] The yields and stereochemistry of **2** are given in Table 3.

Table 2. Summary of inter- and intramolecular selectivities in electrophilic substitution of benzene and toluene

Reaction	Reaction conditions	k_T/k_B	Isomer distribution/% o-	m-	p-	Ref.
Methylation	MeBr, $GaBr_3$, 25 °C	5.70	55.7	9.9	34.4	a)
Hydroxypropylation	$CH_3CH\text{–}CH_2$ (O), $TiCl_4$, 0 °C	2.9	46	21	33	b)
Ethylation	EtBr, $GaBr_3$, 25 °C	2.47	38.4	21.0	40.6	a)
Isopropylation	*i*-PrBr, $GaBr_3$, 25 °C	1.82	26.2	26.6	47.2	a)

a) Ref. 11. b) This work.

TABLE 3. STEREOCHEMISTRY OF ALKYLATION OF TOLUENE WITH 2,3-DIMETHYLOXIRANE

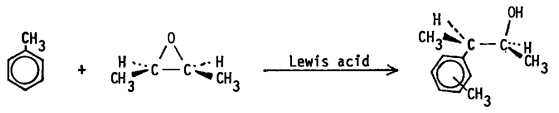

Epoxide	Catalyst	Yield %	Isomer distribution/%			Stereochemistry Inversion/%
			o-	*m*-	*p*-	
cis	$AlCl_3$	14.7	—	—	—	100
cis	$AlBr_3$	6.7	—	—	—	98
trans	$AlCl_3$	29.8	35.4	23.6	41.0	100
trans	$AlBr_3$	8.3	41.7	26.5	31.8	90

The yields of **2** in the reaction with BO were lower than those of **1** in the reaction with PO. The reaction of BO can be expected to proceed by the same S_N2 mechanism as in the case of PO. Since S_N2 reactions are sensitive to the steric factors, methyl substitution at the carbon which is in the β-position to the reacting carbon resulted in a decrease in the yield of the alkylation reaction. The fact that 2,2-dimethyloxirane gave only small amounts of a Friedel-Crafts reaction product under conditions similar to those in this paper[19] can be explained by the steric factors.

Although the retention times of the three isomers (*o*-, *m*-, and *p*-) of *erythro*-**2** on GLC were different from one another and were much larger than those of *threo*-isomers, the three isomers of *threo*-**2** could not be separated on GLC. As is shown in Table 3, only *threo*-**2** from *cis*-BO and only *erythro*-**2** from *trans*-BO were obtained in an aluminum chloride-catalyzed reaction. Therefore, all the three positional isomers of **2** were formed with complete inversion of configuration of the carbon attacked by toluene, showing that the reaction is of the S_N2 type. Aluminum bromide catalysis was found to decrease the stereospecificities, as in the reaction of benzene with PO.

Recent mechanistic works on Friedel-Crafts reactions have suggested that the transition state of the reaction of a reactive substrate resembles the nature of the π-complex[12] or the oriented π-complex,[20] which determines the substrate selectivity, the k_T/k_B value.[22] The second transition state, from the π-complex to the σ-complex, determines the positional (intramolecular) selectivity. However, the details of the structural change of the alkylating species accompanying π- and σ-complex formation have not been discussed.[21] The results reported in this paper show that the partial bond between the reacting carbon and the leaving group remains in the transition state, and that the reaction is of the S_N2 type. However, the above discussion does not answer the question whether the transition state of S_N2 alkylation involves a π-complex nature or a σ-complex one.[23]

Olah *et al.* examined the Friedel-Crafts benzylation and found that the reaction had high positional and low substrate selectivities.[28] They also found that aluminum chloride-catalyzed benzylation afforded a larger amount of the *meta* product than the other mild catalysis, they attributed this fact to the inter- and intramolecular rearrangement of the primary product. As the present hydroxypropylation has low substrate and low positional selectivities, the results might be explained by the subsequent isomerization processes, which are generally accepted as resulting in a substantial increase in the amount of the *meta* isomer. However, such an intramolecular-rearrangement mechanism that involves the cleavage of the bond between an aryl ring and an alkyl group, *e.g.*, ionization and subsequent internal return, cannot be applied to the hydroxyalkylation with epoxide, and intermolecular rearrangement or transalkylation can be excluded on the basis of the stereochemical results.

Reaction of Anisole with 2-Methyloxirane and 2,3-Dimethyloxiranes. A previous paper has described that the Friedel-Crafts reaction of anisole with epoxides proceeds by two different paths, *i.e.*, direct alkylation and the rearrangement of epoxides to carbonyl compounds, followed by condensation with anisole.[29] The products formed *via* the latter process in the reaction of anisole with PO were 1,1-bis(methoxyphenyl)propanes; the mechanisms of the reaction were discussed in some detail in the previous paper. The *o*-/*p*- isomer ratio of the 2-(methoxyphenyl)-1-propanols formed *via* direct alkylation of anisole with PO was 1.35. The reported *o*-/*p*- isomer ratio for the isopropylation of anisole with 2-propanol is 1.00—1.04, while that for methylation with methyl chloride is 1.75—1.91.[30] Thus, the present hydroxypropylation follows the general tendency of the usual primary and secondary alkylations.

The reaction of anisole with BO afforded a mixture composed of chlorohydrins,[18] 3-(methoxyphenyl)-2-butanols, and 1,1-bis(methoxyphenyl)-2-methylpropanes. The last-named compounds are formed *via* rearrangement, followed by condensation. The stereochemistries of the direct hydroxybutylation products are summarized in Table 4. As is the case of the reaction of toluene, the two isomers produced have a configuration with substantially complete inversion.

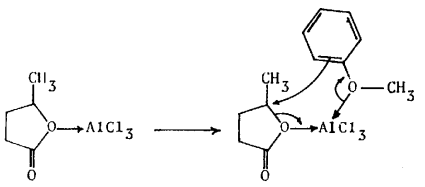

Scheme 1.

Kretchmer *et al.* proposed the mechanism depicted in Scheme 1 for the reaction of anisole with γ-valerolactone and several other alkylating agents on the basis of their finding that the proportions of the *ortho* products obtained from these reactions are higher than those from ordinary reactions.[31] This mechanism, however, cannot be applied to the reaction reported here, because the reaction mechanism expects the formation of an *ortho* product with retention of configuration.

It was demonstrated that the methylation of anisole proceeds concurrently by two paths: the direct alkylation of the aromatic nucleus and the alkylation of oxygen to form an oxonium ion, followed by inter-

TABLE 4. STEREOCHEMISTRY OF ALKYLATION OF ANISOLE WITH 2,3-DIMETHYLOXIRANE

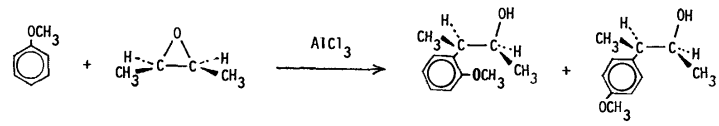

Epoxide	Isomer distribution	Stereochemistry	
		Inversion/%	Retention/%
cis	*o*- 47.8 %	100	0
	p- 52.2 %	99	1
trans	*o*- 25.7 %	92	8
	p- 74.3 %	100	0

molecular transalkylation.[32] If the latter path is assumed for the present hydroxyalkylation, the stereochemistry of the product should be retention (through double inversion) or racemization. Since the results given in Table 4 show almost complete inversion, the above oxonium ion-intermediate path would be only a minor one, even if it were to occur, in hydroxyalkylation with epoxides; the products seem to be formed by the direct alkylation of the aromatic nucleus of anisole.

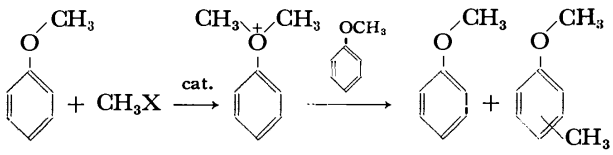

Scheme 2.

Experimental

Materials. *cis*- and *trans*-2,3-dimethyloxiranes (*cis*- and *trans*-BO's) were prepared by the method of Pasto and Cumbo.[34] Optically active 2-methyloxirane (PO), $[\alpha]_D^{26}$ 13.10 (neat) [lit,[37] $[\alpha]_D^{16}$ 12.72 (neat)], was prepared from chloroacetone.[35] Inactive PO was a commercially available material, and each epoxide was distilled over calcium hydride before use. Benzene and toluene were washed with sulfuric acid and were distilled before use. Anisole was dried over sodium hydroxide and distilled over calcium hydride before use. Aluminum chloride was purified by sublimation.

Authentic Samples. 2-(*m*-Tolyl)-1-propanol, bp 128—129 °C/18 mmHg, was prepared by the hydroboration-oxidation[38] of 2-(*m*-tolyl)propene, which has been prepared by the Grignard reaction of *m*-tolylmagnesium bromide with acetone, followed by dehydration with $KHSO_4$. 2-(*o*-Tolyl)-1-propanol was prepared in a similar fashion, bp 119—121 °C/13 mmHg. (*Z*)- and (*E*)-2-(*o*-, *m*-, and *p*-tolyl)-2-butenes were prepared by methods similar to those used for preparing all the isomers of 2-(methoxyphenyl)-2-butenes described by Sneeden and Zeiss.[39] The hydroboration-oxidation of (*E*)-2-(*o*-methoxyphenyl)-2-butene yielded *threo*-3-(*o*-methoxyphenyl)-2-butanol (54% yield), bp 122—123 °C/6 mmHg. *erythro*-3-(*o*-Methoxyphenyl)-2-butanol was obtained in a similar fashion from (*Z*)-2-(*o*-methoxyphenyl)-2-butene (55% yield), bp 122—123 °C/6 mmHg. Similarly, other analogs were synthesized from suitable 2-butenes except for the cases of *erythro*-3-(*o*- and *m*-tolyl)-2-butanols. In these cases, (*E*)-2-(*o*- and *m*-tolyl)-2-butenes could not be obtained in the desired purity.[40] *erythro*-3-(*m*-Tolyl)-2-butanol was prepared by the reaction of lithium bis(*m*-tolyl)cuprate with *trans*-BO (18% yield),[41] bp 126—130 °C/29 mmHg; ^{13}C NMR ($CDCl_3$), 16.1, 21.0, 21.4, 47.1, 72.4, 124.8, 127.1, 128.2, 128.5, 137.9, and 144.1 ppm from TMS. The ^{13}C NMR spectrum of the *threo*-isomer was 17.6, 20.4, 21.4, 47.8, 72.1, 124.9, 127.3, 128.3, 128.7, 137.9, and 143.6. *erythro*-*o*-Methyl and *p*-methoxyl substituted analogs were also prepared in a similar fashion. The NMR spectra of the authentic samples are given in Table 5.

Isomer Distribution. A Typical Procedure of Aluminum Chloride-catalyzed Reaction. To a stirred mixture of toluene (30 ml) and aluminum chloride (12 mmol), cooled in an ice bath, a solution of PO (10 mmol) in 20 ml of toluene was slowly added over a period of 2 h. The resulting mixture was stirred for an additional 30 min and then poured into ice water, extracted with diethyl ether, dried over $MgSO_4$, and concentrated; the crude product was distilled *in vacuo* to give a mixture of 2-tolyl-1-propanols, bp 117—129 °C/20 mmHg (60 % yield). The isomer distribution of this fraction was determined by NMR using an europium shift reagent; it is shown in Fig. 1.

Competitive Hydroxypropylation. A Typical Procedure of Aluminum Chloride-catalyzed Reaction. To a mixture of benzene (0.5 mol), toluene (0.5 mol), and aluminum chloride (12 mmol), cooled in an ice bath, a solution of PO (10 mmol) in 50 ml of 1,2-dichloroethane was added, drop by drop with vigorous stirring over a period of 2.5 h. The vigorous stirring was essential to prevent the formation of undesired oligomers of PO. After the reaction has been allowed to proceed further for 30 min, the reaction mixture was poured into ice water. After the usual work-up, the crude product was analyzed by GLC.

Hydroxypropylation of Toluene with Optically Active PO. Optically active PO (10 mmol) in toluene (20 ml) was added to toluene (30 ml) in the presence of aluminum chloride (12 mmol) at an ice-bath temperature over a period of 2 h, after which the reaction was continued for an additional 30 min. After the usual work-up, the distillation of the crude product gave a mixture of 2-tolyl-1-propanols (60% yield) which was optically active, $[\alpha]_D^{18}$ 8.02 (*c* 3.08, $CHCl_3$). Chromatography on neither silica gel nor alumina could spearate the mixture into three components.

Aluminum Chloride-catalyzed Reaction of Toluene with BO. Into a mixture of toluene (150 ml) and aluminum chloride (60 mmol), a mixture of *cis*-BO (50 mmol) and toluene (50 ml) was added over a period of 3 h with vigorous stirring in an ice bath. The stirring was then continued for an additional 30 min. After the usual work-up, the crude product was distilled giving 1.21 g (15%) of *threo*-3-tolyl-2-butanols, bp 91—94 °C/4 mmHg. GLC analysis showed that the product was not contaminated with the *erythro*-isomers.

TABLE 5. NMR SPECTRA OF 3-TOLYL-2-BUTANOLS (**2**) AND 3-(METHOXYPHENYL)-2-BUTANOLS (**3**)

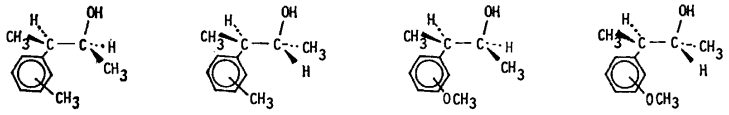

threo-**2** *erythro*-**2** *threo*-**3** *erythro*-**3**

Compd	Chemical shifts/ppm							Coupling constants/Hz[a]		
	H(1)	H(2)	H(3)	H(4)	OH	CH_3	Phenyl	$J_{1,2}$	$J_{2,3}$	$J_{3,4}$
threo-**2**-*o*	1.24	3.77	3.00	1.18	1.7	2.34	7.1	6.7	7.9	5.9
threo-**2**-*m*	1.14	3.77	2.60	1.20	2.0	2.31	7.0	6.0	7.0	7.0
threo-**2**-*p*	1.20	3.81	2.63	1.24	1.6	2.33	7.1	6.1	7.2	7.1
erythro-**2**-*o*	1.10	3.89	3.30	1.28	1.7	2.31	7.1	6.8	6.6	6.8
erythro-**2**-*m*	1.07	3.86	2.68	1.30	1.7	2.33	7.0	6.3	6.2	7.0
erythro-**2**-*p*	1.05	3.83	2.68	1.29	1.9	2.32	7.0	6.3	6.4	6.9
threo-**3**-*o*	1.16	3.93	3.21	1.21	1.9	3.79	7.0	6.0	6.9	6.9
threo-**3**-*p*	1.18	3.77	2.61	1.22	1.6	3.78	7.0	6.0	7.2	7.0
erythro-**3**-*o*	1.07	3.94	3.26	1.26	2.1	3.80	7.0	6.1	5.5	7.1
erythro-**3**-*p*	1.06	3.81	2.67	1.28	2.0	3.77	6.9	6.2	5.9	7.0

a) Limits of error: ± 0.2 for $J_{1,2}$ and $J_{3,4}$, ± 0.5 for $J_{2,3}$.

Reaction of Anisole with BO in the Presence of Aluminum Chloride. The reaction was carried out in a procedure similar to that described in a previous paper.[29] After the usual work-up, the crude product was chromatographed on silica gel. Benzene eluted a mixture of 1,1-bis(methoxyphenyl)-2-methylpropanes. Recrystallization from hexane gave a pure bis-*para* isomer; mp 62—63 °C; NMR ($CDCl_3$) $\delta = 1.8^6$ (d, 7.8 Hz, 6H), 2.37 (m, 1H), 3.30 (d, 10.9 Hz, 1H), 3.73 (s, 6H), 6.9 (phenyl, AA'BB' type coupling, 8H); Found: C, 79.76, H, 8.42%. Further elution with 5% ethyl acetate–benzene gave a mixture of the two isomers of 3-(methoxyphenyl)-2-butanols. The isomer distribution of this fraction was determined by GLC.

References

1) "Friedel-Crafts and Related Reactions," ed by G. A. Olah, Interscience, New York (1964).

2) C. C. Price and M. Lund, *J. Am. Chem. Soc.*, **62**, 3105 (1940); H. L. Burwell, Jr., and S. Archer, *ibid.*, **64**, 1032 (1942).

3) This compound was used to avoid the ambiguity that apparent racemization of *s*-butylation may result from the rapid equilibration of the cationic charge between the 2- and 3-positions in the 1-methylpropyl cation.

4) A. Streitwieser, Jr., and P. J. Stang, *J. Am. Chem. Soc.*, **87**, 4953 (1965).

5) a) T. Nakajima, S. Suga, T. Sugita, and K. Ichikawa, *Bull. Chem. Soc. Jpn.*, **40**, 2980 (1967); b) *Tetrahedron*, **25**, 1807 (1969).

6) J. I. Brauman and A. J. Pandell, *J. Am. Chem. Soc.*, **89**, 5421 (1967).

7) J. I. Brauman and A. Solladié-Cavallo, *Chem. Commun.*, **1968**, 1124.

8) S. Suga, T. Nakajima, Y. Nakamoto, and K. Matsumoto, *Tetrahedron Lett.*, **1969**, 3283.

9) S. Masuda, T. Nakajima, and S. Suga, *J. Chem. Soc., Chem. Commun.*, **1974**, 954.

10) See also T. Nakajima, Thesis, Kyoto University (1971); T. Nakajima, Y. Nakamoto, and S. Suga, *Bull. Chem. Soc. Jpn.*, **48**, 960 (1975).

11) L. M. Stock and H. C. Brown, *Adv. Phys. Org. Chem.*, **1**, 35 (1963).

12) G. A. Olah, *Acc. Chem. Res.*, **4**, 240 (1971).

13) S. Suga, T. Nakajima, A. Takagi, and T. Takahashi, *Kogyo Kagaku Zasshi*, **70**, 81 (1967).

14) H. C. Brown and H. Jungk, *J. Am. Chem. Soc.*, **78**, 2182 (1956).

15) J. Biggs, N. B. Chapman, A. F. Finch, and V. Wray, *J. Chem. Soc.*, **1971**, 55; J. Biggs, N. S. Chapman, and V. Wray, *ibid.*, **1971**, 63, 66, and 71.

16) B. N. Blackett, J. M. Coxon, M. P. Hartshorn, B. L. J. Jackson, and C. N. Muir, *Tetrahedron*, **25**, 1479 (1969).

17) For the reviews of the epoxide reaction, see P. E. Parker and N. S. Isaacs, *Chem. Rev.*, **59**, 737 (1959); J. G. Buchanan and H. Z. Sable, "Selective Organic Transformations," ed by B. S. Thyagarajan, Wiley-Interscience, New York, N. Y. (1972), Vol. 2, pp. 1—95; Y. Pocker and B. P. Ronald, *J. Am. Chem. Soc.*, **100**, 3122 (1978), and the references cited therein.

18) M. Inoue, T. Sugita, Y. Kiso, and K. Ichikawa, *Bull. Chem. Soc. Jpn.*, **49**, 1063 (1976).

19) Y. Nakamoto, T. Nakajima, and S. Suga, *Kogyo Kagaku Zasshi*, **72**, 2594 (1969).

20) R. Nakane, A. Natsubori, and O. Kurihara, *J. Am. Chem. Soc.*, **87**, 3597 (1965); R. Nakane, O. Kurihara, and A. Natsubori, *ibid.*, **91**, 4528 (1969); R. Nakane, O. Kurihara, and A. Takematsu, *J. Org. Chem.*, **36**, 2753 (1971).

21) Olah *et al.* found that the *o*-/*p*- isomer ratio of the ethylation of toluene with diethylhalonium ions (0.60—0.92) was significantly lower than those obtained in the ethylation of toluene with all the other conventional Friedel-Crafts ethylating agents (1.09—1.84); they explained the observation in terms of steric hindrance in an S_N2-like transition state.[22] As they mentioned that the positional selectivity was determined by the transition state from the π-complex to the σ-complex, their complex must involve a partial bond or some interaction between the alkyl cation and the leaving group, which is consistent with the finding reported in this paper.

22) G. A. Olah, J. R. Demember, Y. K. Mo, J. J. Svoboda, P. Schilling, and J. A. Olah, *J. Am. Chem. Soc.*, **96**, 884 (1974).

23) It was demonstrated that epoxides have specific interaction with aromatics.[24] It was also reported that an aromatic solvent have some effects in the acid-catalyzed ring-

opening reaction of epoxides.[25,26] We wish to point out the possibility that epoxide and aromatics form a weak complex which may resemble the π-complex, and that the equilibrium constant of the process determines the substrate selectivity. The complex is transformed to the σ-complex with a release of the leaving group through the transition state of highest energy, which process determines the positional selectivity. The overall processes may resemble the preequilibrium complex formation demonstrated in some S_N2 reactions.[27]

24) R. J. W. LeFenre, D. V. Radford, G. L. D. Ritchie, and P. J. Stiles, *J. Chem. Soc., B*, **1968**, 148.
25) A. Balsamo, P. Crotti, B. Macchia, and F. Macchia, *Tetrahedron*, **29**, 119 (1973).
26) M. Inoue, Y. Taguchi, T. Sugita, and K. Ichikawa, *Bull. Chem. Soc. Jpn.*, **51**, 2098 (1978).
27) J. Hayami, T. Koyanagi, N. Hihara, and A. Kaji, *Bull. Chem. Soc. Jpn.*, **51**, 891 (1978), and the references cited therein.
28) G. A. Olah, S. Kobayashi, and M. Tashiro, *J. Am. Chem. Soc.*, **94**, 7448 (1972).
29) M. Inoue, T. Sugita, and K. Ichikawa, *Bull. Chem. Soc. Jpn.*, **51**, 174 (1978).
30) P. Kovacic and J. J. Hiller, *J. Org. Chem.*, **30**, 1581 (1965).
31) R. A. Kretchmer and M. B. McCloskey, *J. Org. Chem.*, **37**, 1989 (1972).
32) P. Beak, J. T. Adams, P. D. Klein, P. A. Szczepanik, D. A. Simpson, and S. G. Smith, *J. Am. Chem. Soc.*, **95**, 6027 (1973).
33) G. A. Olah and E. G. Melby, *J. Am. Chem. Soc.*, **95**, 4971 (1975).
34) D. J. Pasto and C. C. Cumbo, *J. Org. Chem.*, **30**, 1271 (1965).
35) The authors wish to thank Dr. T. Tanaka, Mr. K. Tanaka and Mr. S. Kamimori of the Kyowa Peterochemicals Co., Ltd., for providing the pure chloroacetone. A reported method[36] for the preparation of chloroacetone gave a mixture of chloroacetone and 1,1-dichloroacetone.
36) K. Nakajima, S. Asahara, and T. Miyoshi, "Yuki-kagobutsu Goseiho," Gihodo, Tokyo (1966), Vol. 9, p. 11.
37) E. Abderhalden and E. Eichwald, *Ber. Deut. Chem. Gesell.*, **51**, 1312 (1918).
38) H. C. Brown and G. Zweifel, *J. Am. Chem. Soc.*, **83**, 2544 (1961).
39) R. P. A. Sneeden and H. H. Zeiss, *J. Organomet. Chem.*, **40**, 163 (1972).
40) H. C. Brown and C. J. Kim, *J. Am. Chem. Soc.*, **93**, 5765 (1971).
41) G. M. Whitesides, W. F. Fischer, Jr., J. S. Filippo, Jr., R. W. Bashe, and H. O. House, *J. Am. Chem. Soc.*, **91**, 4871 (1969).

The Modification of Tryptophyl Residues during the Acidolytic Cleavage of Boc-groups. I. Studies with Boc-Tryptophan[1)]

Yoshihiro MASUI,* Naoyoshi CHINO, and Shumpei SAKAKIBARA
Protein Research Foundation, Peptide Institute, 476 Ina, Minoh, Osaka 562

(Received June 16, 1979)

The formation of a component, X, was observed when a reaction mixture of *t*-butyloxycarbonyl-tryptophan (Boc-Trp), trifluoroacetic acid (TFA), and 1,2-ethanedithiol was analyzed by cellulose TLC. The side product was isolated and further separated into two components by column chromatography on silica gel. The subsequent analysis of the NMR spectra of these components confirmed that they were N^{in}-Bu^t-Trp and C^{in}-Bu^t-Trp.** The reaction of Boc-Trp with TFA and with anhydrous hydrogen fluoride (HF) was examined as model systems in order to determine conditions which would minimize the formation of the X component during the synthesis of peptides containing Trp. The addition of 10 molar equivalents of 1,2-ethanedithiol completely suppressed the formation of the X component in HF, but additives were less efficient in TFA. A combination of dimethyl sulfide and 1,2-ethanedithiol was the most effective method for suppressing the formation of the X component in TFA. The behavior of N^{in}- and C^{in}-Bu^t-Trp in acidic media was also investigated, and a possible pathway for the *t*-butylation of the tryptophyl residue will be proposed.

The acidolytic cleavage of protective groups from Trp-containing peptides is known to be accompanied by several side reactions. The first group of side reactions is the so-called oxidative destruction of the tryptophyl residue. This is a series of complicated reactions of the highly reactive indole ring characterized by coloration[2)] or by an increase in the fluorescence[3)] of the reaction mixture. These reactions can be effectively avoided by the addition of such antioxidants as 2-mercaptoethanol[4)] or 1,2-ethanedithiol[2)] to the acidic reagents. The second group of side reactions is the alkylation of the tryptophyl residue by fragments of the protective groups. The *t*-butylation of the indole ring during the deprotection of the Boc groups was first observed in 1970 by Alakhov *et al.*[5)] using mass spectrometry. Boc-Trp-Gly-OMe was treated with TFA to remove the Boc group. The newly formed amino group was acetylated, and the product was subjected to mass spectrometry. The spectrum indicated the presence of an ion at *m/e*(M+56) in addition to the original molecular ion. Alakhov *et al.* also observed that 95% TFA gave less butylated by-products, as did 2 M HCl in acetic acid or ethyl acetate. The formation of side products was still noticeable in all cases. In 1972, Wünsch *et al.*[6)] reported that a significant amount of side products was formed when a protected analog of human gastrin was treated with TFA to remove the Boc and Bu^t groups. They later isolated a side product and found that the tryptophyl residue was *t*-butylated at the NH group of the indole ring.[7,8)] Kisfaludy *et al.*[7)] observed a similar phenomenon during the synthesis of ACTH. They then examined the reaction of Trp with isobutylene under relatively drastic conditions and isolated a crystalline product, 2,5,7-tri-Bu^t-Trp. From these observations, Wünsch and Kisfaludy concluded that the tryptophyl residue is readily converted to mono-or multi-butylated Trp by isobutylene in acid or during the deprotection of Boc or Bu^t groups with TFA, and that N^{in}-Bu^t-Trp was a major product. They emphasized that HF caused more alkylation of the tryptophyl residue than did TFA and that the yield of alkylated products was as high as 50%.[7)]

We also observed that side products, detectable by TLC, were produced when Trp-containing peptides were treated with TFA to remove the Boc group, even though 1,2-ethanedithiol was added to the system. We examined the reaction of Boc-Trp with TFA and with HF as model systems. TFA and HF were chosen as acids since they are commonly used active reagents for the removal of protective groups and also since they are excellent solvents for almost all peptide derivatives.

This paper will deal with the isolation of *t*-butylated products from the reaction mixture and with the evaluation of additives in the deprotection reaction, with the goal of minimizing the formation of side products. We will also discuss the different characteristics of HF and TFA as deprotecting reagents.

Results

Isolation and Structure Determination of Side Products. The cellulose TLC of reaction mixtures of Boc-Trp with TFA containing 1,2-ethanedithiol always indicated the presence of one major side component (X component) and some minor ones, as is shown in Fig. 1(A). The isolation of the X component from the reaction mixture was achieved by column chromatography on Dia-ion HP-20. The reaction mixture was placed in the top of the column, and Trp was washed out with 20% aqueous methanol. The minor components were eluted by increasing the concentration of methanol to 30%, and then to 40%. X component was eluted with 50% aqueous methanol. The yield of the X component was about 10% of the starting material. Silica gel TLC [Fig. 1(B)] revealed that the X component consisted primarily of almost equal amounts of two sub-components, Xa and Xb, which were both ninhydrin- and Ehrlich-positive. Therefore, these two components were separated by column chromatography on silica gel.

Elemental analysis showed that both components, Xa

** C^{in}-Bu^t-Trp:

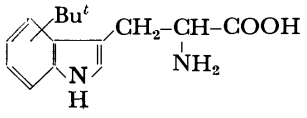

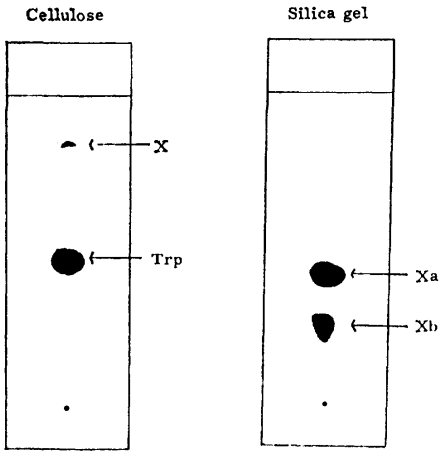

Fig. 1. TLC of products of Boc-Trp in TFA containing 1,2-ethanedithiol.

and Xb, had the same composition, mono-*t*-butylated Trp. The ^{1}H-NMR spectra of the Xa component in a mixture of C_5D_5N–D_2O (1 : 1) and in a mixture of DMSO-d_6–D_2O (1 : 1) (Fig. 2) clearly indicated that one Bu^t group was attached at the indole nitrogen of Trp. This conclusion was also confirmed by the analysis of the ^{13}C-NMR spectrum. However, the ^{1}H-NMR spectrum of the Xb component indicated 4H on the indole carbons and one Bu^t group at a carbon somewhere in the indole ring, but the location of the Bu^t group could not be determined. It was considered that the Xb component was a mixture of mono-*t*-butylated tryptophans substituted at various positions on the indole ring.

Determination of the X Component and Trp; Effect of Additives as Scavengers. The elution pattern of

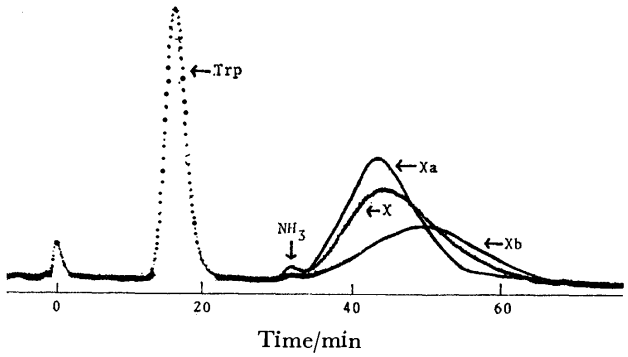

Fig. 3. Ion-exchange chromatogram of Trp, X, Xa, and Xb by amino-acid analyzer.

Xa, Xb, and Trp on an amino-acid analyzer is shown in Fig. 3. No efficient condition was found for determining Xa and Xb separately on the same chromatogram. Therefore, an isolated X component was used as a standard for measuring the total amount of mono-*t*-butylated Trp, Xa and Xb, on an amino-acid analyzer.

By using this procedure, we measured the *t*-butylated Trp and the intact Trp in reaction mixtures of Boc-Trp in TFA and in HF under various conditions (Tables 1 and 2). If no scavenger was added with the TFA, the reaction mixture turned brown, a large quantity of the X component was formed (14%), and the recovery of Trp was low (67%). The addition of 1,2-ethanedithiol effectively prevented coloration, but the addition of even 50% of this material to the TFA failed to reduce the formation of the X component to less than 4.2%. A combination of a large excess of dimethyl sulfide with 1,2-ethanedithiol was the best scavenger in TFA. This mixture gave the maximum recovery of intact Trp after deprotection, yet the formation of the X component was significant (see Table 1). The addition of anisole, which is frequently used as a scavenger during acidolysis, was ineffective in suppressing *t*-butylation.[9]

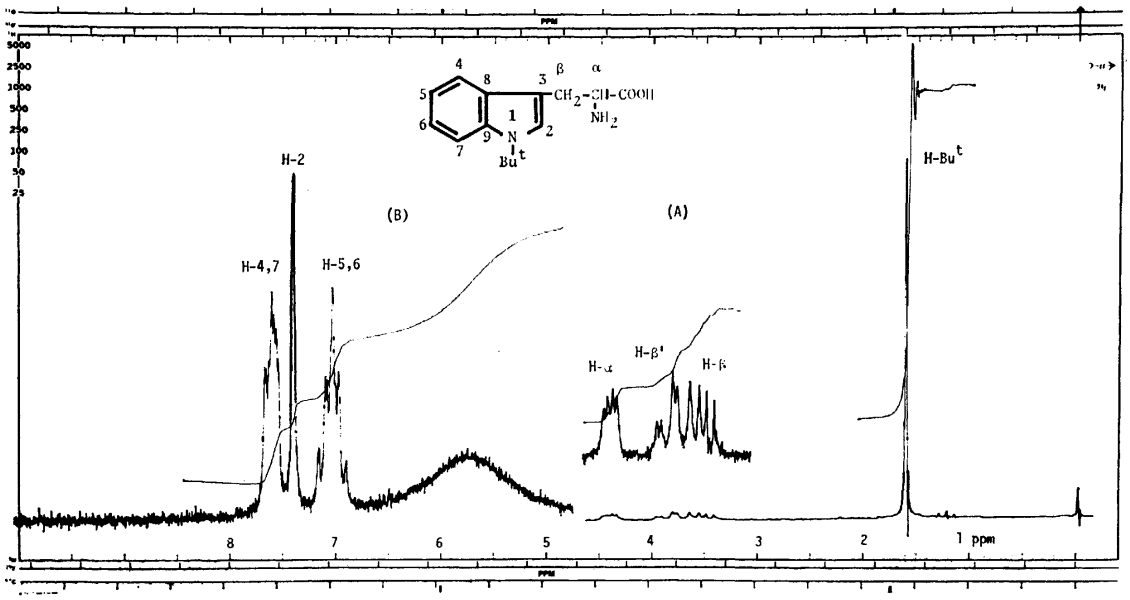

Fig. 2. NMR spectra of Xa in C_5D_5N–D_2O (1 : 1)(A) and in DMSO-d_6–D_2O (1 : 1)(B) at 100 MHz.

Table 1. Effect of additives on the formation of X component in TFA[a]

Additives			Recovery/%	
1,2-Ethanedithiol	Others		X	Trp
None			14.2	67
1.0 ml	None		4.2	93
0.3 ml			5.1	91
	Me–S–Me	1.0 ml[b]	1.1	99
0.1 ml		0.5 ml	2.6	97
		0.3 ml	4.3	96
	Me–S–Et	1.0 ml	2.6	97
	Me–S–Ph	1.0 ml	3.2	96
0.1 ml	Et–S–Pr^i	1.0 ml	4.9	94
	Pr^i–S–Pr^i	1.0 ml	6.4	92
	Anisole	1.0 ml	6.3	91

a) For the reaction conditions, see the Experimental section. b) 137 equiv against Boc-Trp.

Table 2. Effect of additives on the formation of X component in HF[a]

Additives	Amount (equiv)[b]	Recovery/%	
		X	Trp
None		15.6	57
1,2-Ethanedithiol	10	ND[c]	99
Anisole+E[d]	10+10	ND[c]	99
Me–S–Me+E[d]	10+10	ND[c]	99
Anisole	10	2.4	94

a) For the reaction conditions, see the Experimental section. b) Equiv against Boc-Trp. c) Not detectable. d) 1,2-Ethanedithiol.

On the other hand, the formation of the X component in HF was negligible when 10 equivalents of 1,2-ethanedithiol were added to the reaction mixture, even without the addition of anisole or dimethyl sulfide (Table 2). This result differs from that reported in the absence of scavengers by Wünsch *et al.*[7,10] Scavengers seem to be effective in HF, but not in TFA.

Behavior of Xa and Xb in Acidic Reagents. The chemical stability of Bu^t groups of Xa and Xb was examined in acidic reagents. The Xa and Xb were dissolved separately in TFA and in HF in the presence of additives, and the reaction mixtures were examined with an amino-acid analyzer and by TLC. As is shown in Table 3, over 90% of the Xa was converted to Trp in HF, which indicates that the N^{in}-Bu^t-group is quite unstable in HF. In TFA, however, only 50% of the N^{in}-Bu^t-group was removed, and about 10% of the starting Xa was converted to Xb during the treatment. No formation of N^{in},C^{in}-di-*t*-butylated Trp was observed. Although a small amount of Trp was detectable in a reaction mixture of Xb with HF, Xb seemed to be fairly stable in both reagents, as was to be expected. Interestingly, the C^{in}-Bu^t-group was removable under the conditions of the acid hydrolysis of peptides.

Table 3. Stability of Bu^t groups in N^{in}-Bu^t-Trp (Xa) and C^{in}-Bu^t-Trp (Xb) in acidic media

Conditions	Xa Recovery/%		Xb Recovery/%	
	Trp	Xa+Xb	Trp	Xb
HF/HS–CH_2–CH_2–SH/ Anisole 0 °C, 1 h	92	Trace	5	90
TFA/HS–CH_2–CH_2–SH 0 °C, 10 min and rt, 50 min	50	40+10[a]	None	100
6 M HCl/Mercaptoacetic Acid[11] 108 °C, 22 h	99	None	84	Trace

a) The ratio of Xa and Xb was estimated from the silica gel TLC.

Discussion

In discussing the modification of tryptophyl residues during deprotection procedures, the contribution of scavengers cannot be eliminated. Wünsch and others have shown that the modification of the tryptophyl residues is higher in HF than in TFA when no scavenger is added to the reaction mixture. Similar results were obtained in the reactions of Boc-Trp in this study; the recovery of intact Trp was 67% in TFA and 57% in HF under the conditions used for the removal of Boc groups (see Tables 1 and 2). In the presence of scavengers, however, the situation changed dramatically. The formation of *t*-butylated Trp was negligible in HF when 10 molar equivalents of 1,2-ethanedithiol were added, but a considerable amount of modified Trp was detectable in reaction mixtures with TFA, even when an excess of promising scavengers was added. This result may be explained by the reactivity with acidic reagents of Bu^t groups attached to the N or C atom of the indole group. As can be seen in Table 3, the N^{in}-Bu^t-group is reasonably stable in TFA, but quite unstable in HF. Therefore, in HF the scavengers must compete with the C^{in}-*t*-butylation reaction. The effectiveness of scavengers in HF can be clearly explained if the *S*-*t*-butylation is much faster at 0 °C than the *C*-*t*-butylation of the indole moiety. In TFA at room temperature, however, the scavenger must compete with the N^{in}-*t*-butylation reaction and the formation of N^{in}-Bu^t-Trp may be much faster than the formation of the *S*-Bu^t-derivatives of scavengers.

In the presence of 10% 1,2-ethanedithiol in TFA, the formation of C^{in}-Bu^t-Trp from N^{in}-Bu^t-Trp was 10%, and 50% of the N^{in}-Bu^t-Trp was converted to Trp. Under these conditions, the formation of C^{in}-Bu^t-Trp from Boc-Trp was only 5%. No *t*-butylation at the indole nucleus was observed when Boc-Trp(For)*** was treated with TFA (see Experimental section). The above facts suggest that N^{in}-Bu^t-Trp is more reactive with Bu^t cations than is an unsubstituted tryptophyl residue. We therefore propose the following scheme for the formation of these side products in TFA: (1) N^{in}-*t*-butylation is the first step in the side reaction, (2) once a Bu^t group is attached to the indole nitrogen, the carbon atoms of the indole moiety become more susceptible to attack by Bu^t cations, and (3) the N^{in}, C^{in}-

*** For: N^{in}-formyl.

di-Bu^t-Trp thus formed degrades to C^{in}-Bu^t-Trp.

It must be noted that the formation of *t*-butylated Trp cannot be detected after the acid hydrolysis of the peptide (see Table 3). Thus, *t*-butylation must be detected in the intact peptide or after the enzymatic digestion of the peptide.

Since the present study used Boc-Trp as a model compound, the above observations must be confirmed with peptides which are protected with Boc or Bu^t groups. These studies are now being carried out in our laboratory.

Experimental

All melting points are uncorrected. Amino-acid analysis was performed on a JEOL JLC-6AH Amino-Acid Analyzer. The UV spectra were obtained on a Hitachi 124 Spectrophotometer, and the IR spectra, on a Hitachi EPI-G2 Grating Infrared Spectrophotometer. The optical rotations were measured with a Perkin-Elmer 141 Polarimeter. The ^{1}H-NMR and ^{13}C-NMR measurements were performed with a Varian XL-100 Spectrometer, using tetramethylsilane as the internal reference. The solvent systems used for TLC on silica gel G (Merck Art 7731) or cellulose (Merck Art 5552) were (A) 1-butanol–acetic acid–water (4: 1: 5, upper phase) and (B) chloroform–methanol–acetic acid (85: 15: 2). For silica gel-column chromatography, silica gel 60 (Merck Art 7734) was used.

Isolation of By-products, Xa and Xb. A solution of Boc-Trp (10 g, 33 mmol) in TFA (30 ml) containing 1,2-ethanedithiol (3 ml) was allowed to react at 0 °C for 10 min and then at room temperature for 50 min. The TLC of this reaction mixture is shown in Fig. 1(A). The solution was concentrated under reduced pressure, and the residue was triturated with ether and hexane to obtain a powder. The product was collected by filtration and dried in a vacuum desiccator over sodium hydroxide pellets at room temperature for 24 h. The dried material was dissolved in a mixture of water (400 ml) and methanol (20 ml), and the solution was neutralized with 5% aq sodium hydrogencarbonate. This solution was then poured into the top of a column (4×20 cm) of Dia-ion HP-20, Mitsubishi Kasei Co., Ltd., which was then eluted with 2 l of water, 1-l portions each of 20%, 30%, and 40% aq methanol, and 2 l of 50% aq methanol successively. Each fraction was monitored by TLC, the X component was found to be eluted by 50% aq methanol. This fraction was then collected and condensed. The residue was purified by reprecipitation from methanol with ether and dried over P_2O_5 at 35 °C for 24 h; yield, 1.0 g (11%); R_f 0.85 on cellulose TLC using Solvent A. Found: C, 67.79; H, 8.09; N, 10.22%. Calcd for $C_{11}H_{11}O_2N_2 \cdot C(CH_3)_3 \cdot 1/3\ H_2O$: C, 67.64; H, 7.82; N, 10.52%.

This product, X component, gave two spots on silica gel TLC, as is shown in Fig. 1(B). It was applied to the top of a column (3×20 cm) of silica gel and was eluted with a mixture of chloroform–methanol–acetic acid (85: 15: 2).

The fraction containing Xa was collected and concentrated to a residue, which was then triturated with ether to obtain a powder. The product was purified by reprecipitation from methanol with ether and dried over P_2O_5 *in vacuo* at 45 °C for 120 h; yield, 421 mg (4.9%); mp 179 °C (dec). $[\alpha]_D^{29.5}$ −29.6° (c 0.5, 80% aq ethanol). UV (H_2O) max: 286 nm (ε 6000), 223 nm (ε 37000). ^{1}H-NMR [100 MHz, C_5D_5N–D_2O (1: 1)]: H-Bu^t: δ 1.61 (9H, s), H-β: 3.55 (1H, dd, J=9.0, 16.0 Hz), H-β': 3.91 (1H, dd, J=4.0, 16.0), H-α: 4.44 (1H, dd, J=4.0, 9.0), [100 MHz, DMSO-d_6–D_2O (1:1)]: H-5, 6: 7.03 (2H, m), H-2: 7.36 (1H, s), H-4, 7: 7.62 (2H, d, J=9.0), [100 MHz, DMSO-d_6]: Absence of indole NH signal. ^{13}C-NMR [25.2 MHz, DMSO-d_6]: C-β: δ 27.1, *C*-methyl (Bu^t): 29.2, C-α: 55.0, *C*-methine (Bu^t): 55.6, C-3: 107.9, C-7: 111.5, C-4: 118.2, C-6: 119.2, C-5: 120.7, C-2: 125.6, C-8: 129.6, C-9: 135.3, C-(C=O): 171.4. IR(KBr): 2955 cm^{-1} (ν_{C-H}, Bu^t), 1215 cm^{-1} (ν_{C-C}, Bu^t). Found: C, 69.50; H, 7.63; N, 10.78%. Calcd for $C_{11}H_{11}O_2N_2 \cdot C(CH_3)_3$: C, 69.20; H, 7.74; N, 10.76%. From the above data, the Xa component was identified as N^{in}-Bu^t-Trp.

The fraction containing Xb was collected and treated in the same manner as Xa; yield, 455 mg (5.3%). ^{1}H-NMR [100 MHz, DMSO-d_6]: H-Bu^t: δ 1.32, 1.34, 1.44 (9H, three singlet signals), H-indole ring: 6.90—7.54 (4H, unresolved signals). Found: C, 69.31; H, 7.69; N, 10.73%. Calcd for $C_{11}H_{11}O_2N_2 \cdot C(CH_3)_3$: C, 69.20; H, 7.74; N, 10.76%. From the above data, the Xb component was considered to be mono-*t*-butylated Trp, substituted at various positions on C atoms of the indole ring.

Determination of X Component and Trp on the Amino-acid Analyzer. A mixture of X component (0.35 μmol) and Trp (0.20 μmol) was analyzed on the amino-acid analyzer under the following conditions: length of column with LC-R-2 resin, ϕ 0.8×15 cm; solvent, 0.5 M sodium citrate buffer at pH 5.24 containing 1% benzyl alcohol; flow rate, 1.0 ml/min; jacket temperature, 52 °C. The pattern obtained is shown in Fig. 3.

Reaction of Boc-Trp with Cleavage Reagents for the Evaluation of Additives. (A) Reaction with TFA: Boc-Trp (30.4 mg, 0.1 mmol) was dissolved in TFA (1 ml) containing various additives, and the solution was stirred at 0 °C for 10 min and at room temperature for 50 min. The reaction mixture was then concentrated *in vacuo*, and the residue was diluted with 0.5 M sodium citrate buffer (pH 5.20) to 10 μmol/ml and to 0.2 μmol/ml. These solutions were then analyzed under the conditions described above for determining the recovery of X component and Trp respectively. The analytical data are shown in Table 1.

(B) Reaction with HF: Boc-Trp (30.4 mg, 0.1 mmol) was treated with HF (1 ml) in the presence of various additives at 0 °C for 1 h in the usual manner.[12] The reaction mixture was concentrated at reduced pressure, and the residue was redissolved in acetic acid (10 ml). The solvent was evaporated *in vacuo*, and the residue was diluted with 0.5 M sodium citrate buffer (pH 5.20). The recovery of X component and Trp was determined in the same manner as has been described previously in the case of TFA treatment. X component was not detected on the chromatogram of amino-acid analysis using only 10 equiv of 1,2-ethanedithiol as an additive. The analytical data are shown in Table 2.

Reaction of Xa or Xb with Acids. (A) Reaction of Xa or Xb with TFA: Xa (26.0 mg, 0.1 mmol) was treated with TFA (1 ml) in the presence of 1,2-ethanedithiol (0.1 ml) at 0 °C for 10 min, the solution was then maintained at room temperature for 50 min and worked up as has been described for the reaction of Boc-Trp with TFA. The recovery of Trp and X was determined on the amino-acid analyzer. A part of the reaction mixture was placed in the top of the column of Dia-ion HP-20 and eluted with 20% aq methanol, and then methanol. When each fraction was monitored by TLC, only Trp was detected in the 20% aq methanol fraction. X component was found in the methanol fraction. This fraction was collected, concentrated, and analyzed by TLC on a silica gel G plate using the B solvent system. The ratio of Xa and Xb was estimated to be 4: 1, and N^{in},C^{in}-di-Bu^t-Trp was not detected. The analytical data are shown in Table 3. Xb (26.0 mg, 0.1 mmol) was treated in the same manner as Xa.

(B) Reaction of Xa or Xb with HF: Xa (26.0 mg, 0.1 mmol) was treated with HF (1 ml) in the presence of 1,2-ethanedithiol (0.1 ml) and anisole (0.1 ml) at 0 °C for 1 h and then worked up as has been described for the reaction of Boc-Trp with HF. The recovery of Trp and X component was determined on the amino-acid analyzer. The treatment of Xb (26.0 mg, 0.1 mmol) was carried out in the same manner as Xa.

(C) Reaction of Xa or Xb with 6 M HCl: Xa (2.6 mg, 10 μmol) was treated with 6 M HCl in the presence of 2% mercaptoacetic acid[11] in an evacuated, sealed ampule at 108 °C for 22 h and then analyzed on the amino-acid analyzer. Xb (2.6 mg, 10 μmol) was treated in the same manner as Xa.

Reaction of Boc-Trp(For)[13] with TFA. Boc-Trp(For) (33.2 mg, 0.1 mmol) was treated with TFA (1 ml) containing 1,2-ethanedithiol (0.1 ml) at 0 °C for 10 min, and then the mixture was maintained at room temperature for 50 min. The reaction mixture was concentrated and the residue was treated with 0.1 M piperizine (1 ml) for 1 h at room temperature to remove the For group. The solution was then applied into the top of a column of Dia-ion HP-20 and eluted with water, 20% aq methanol, and methanol. Each fraction was collected and analyzed by TLC. Only Trp was eluted by 20% aq methanol. Although other by-products were present in the methanol fractions, Xa and Xb were not detected. Thus, no *t*-butylation occurred during this reaction.

References

1) A part of this work was presented at the 15th and 16th Symposia on Peptide Chemistry; N. Chino, Y. Masui, and S. Sakakibara, "Peptide Chemistry 1977," Proceedings of the 15th Symposium on Peptide Chemistry, ed by T. Shiba, Protein Research Foundation, Minoh, Osaka (1978), p. 27; Y. Masui, N. Chino, S. Sakakibara, T. Tanaka, and H. Kita, "Peptide Chemistry 1978," Proceedings of the 16th Symposium on Peptide Chemistry, ed by N. Izumiya, Protein Research Foundation, Minoh, Osaka (1979), p. 189.

2) J. J. Sharp, A. B. Robinson, and M. D. Kamen, *J. Am. Chem. Soc.*, **95**, 6097 (1973).

3) R. A. Uphaus, L. I. Grossweiner, J. J. Katz, and K. D. Kopple, *Science*, **129**, 641 (1959).

4) G. R. Marshall, "Pharmacology of Hormonal Polypeptides and Proteins," ed by N. Back, L. Martini, and R. Paoletti, Plenum Press, New York (1968), p. 48.

5) Yu. B. Alakhov, A. A. Kiryushkin, V. M. Lipkin, and G. W. A. Milne, *Chem. Commun.*, **1970**, 406.

6) E. Wünsch, E. Jaeger, M. Deffner, and R. Scharf, *Hoppe-Seyler's Z. Physiol. Chem.*, **353**, 1716 (1972).

7) E. Wünsch, E. Jaeger, L. Kisfaludy, and M. Löw, *Angew. Chem.*, **89**, 330 (1977).

8) E. Jaeger, P. Thamm, I. Schmidt, S. Knof, L. Moroder, and E. Wünsch, *Hoppe-Seyler's Z. Physiol. Chem.*, **359**, 155 (1978).

9) Recently, Lundt *et al.* also reported that anisole gave little protection against *t*-butylation in TFA, judging from the results of kinetic studies; B. F. Lundt, N. L. Johansen, A. Vølund, and J. Markussen, *Int. J. Peptide Protein Res.*, **12**, 258 (1978).

10) Just before this work was finished, Wünsch *et al.* reported a series of papers which followed the preliminary short report listed as Ref. 7. See E. Jaeger, P. Thamm, S. Knof, E. Wünsch, M. Löw, and L. Kisfaludy, *Hoppe-Seyler's Z. Physiol. Chem.*, **359**, 1617 (1978); E. Jaeger, P. Thamm, S. Knof, and E. Wünsch, *ibid.*, **359**, 1629 (1978); M. Löw, L. Kisfaludy, E. Jaeger, P. Thamm, S. Knof, and E. Wünsch, *ibid.*, **359**, 1637 (1978); M. Löw, L. Kisfaludy, and P. Sohár, *ibid.*, **359**, 1643 (1978). In these papers, the authors pointed out that the *t*-butylation of the indole ring during acidolysis occurred more extensively in Trp-containing peptide than in Trp. We are now studying the *t*-butylation in HF and in TFA using several model peptides in order to minimize the occurrence of this side reaction.

11) H. Matsubara and R. M. Sasaki, *Biochem. Biophys. Res. Commun.*, **35**, 175 (1969).

12) S. Sakakibara, "Chemistry and Biochemistry of Amino Acids, Peptides, and Proteins," ed by B. Weinstein, Marcel Dekker, Inc., New York (1971), Vol. 1, p. 51.

13) M. Ohno, S. Tsukamoto, S. Sato, and N. Izumiya, *Bull. Chem. Soc. Jpn.*, **46**, 3280 (1973).

The Acid-catalyzed Reaction of the 2-Oxabicyclo[4.1.0]hept-3-en-5-one System: Isomerization from Homo-4-pyrones into 2-Furylacetone Derivatives

Hiroshi YAMAOKA, Ikuhiro MISHIMA, Mitsuko MIYAMOTO, and Terukiyo HANAFUSA*

Department of Chemistry, Faculty of Science, Hiroshima University, Higashi-senda-machi, Hiroshima 730

(Received July 2, 1979)

The monocyclopropanation of 4-pyrones with dimethyloxosulfonium methylide, using a dimethyl sulfoxide–hexamethylphosphoric triamide medium in place of neat dimethyl sulfoxide, gave homo-4-pyrone derivatives, which were then rearranged into the 2-furylacetone derivatives, along with hydrated triketones or the dehydrated naphtho[2,1-*b*]furan derivative, by means of strong acid catalysis at room temperature.

In 1965 Corey *et al.* reported that dimethyloxosulfonium methylide is a convenient reagent for preparing cyclopropyl ketones starting from the corresponding α,β-unsaturated ketones.[1] Thus, the treatment of chromones (**1**), regarded as α,β-unsaturated carbonyl compounds, with the above ylide in dimethyl sulfoxide (DMSO), which has been preferentially used in cyclopropanation,[2] affords 3,4-benzo-2-oxabicyclo[4.1.0]-hept-3-en-5-one(homochromone) derivatives (**2**).[3,4] We have been investigating their mass spectra[5] and the solvolytic behavior of the corresponding secondary ester, **3**,[3] in connection with homoconjugation or homoaromaticity, two of the most interesting concepts in organic chemistry.[6]

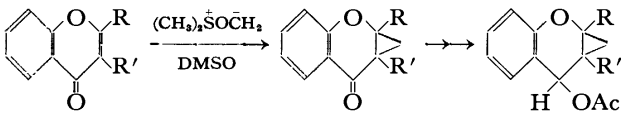

	R	R′		R	R′	
1a	CH_3	CH_3	**2a**	CH_3	CH_3	**3**
1b	$-(CH_2)_3-$		**2b**	$-(CH_2)_3-$		

The parent 2-oxabicyclo[4.1.0]hept-3-en-5-one (homo-4-pyrone) (**4**), free from a condensed benzene ring, may be one of the best substrates for use in order to procure further information about the structural characteristics of homochromones **2**. As homo-4-pyrones have not been mentioned to date, we now wish to report the preparation and the acid-catalyzed reactions of **4**.

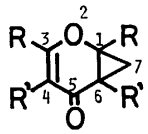

	R	R′
4a	CH_3	Ph
4b	CH_3	CH_3
4c	CH_3	H

Results and Discussion

Syntheses. Cyclopropanation of 4-Pyrones: According to the previously reported manner, 2,6-dimethyl-3,5-diphenyl- (**5a**), 2,3,5,6-tetramethyl- (**5b**), and 2,6-dimethyl-4-pyrone (**5c**) were prepared.[7] While the treatment of benzo-condensed 4-pyrones, **1**, with dimethyloxosulfonium methylide (**6**) for several hours gave cyclopropyl ketones (homochromones), **2**, in a fairly good yield,[3,4,8] the choice of solvent was found to be critical for the reaction when parent 4-pyrones, **5a**—**5c**, free from a condensed benzene ring, were subjected to cyclopropanation. As is shown in Table 1, tetramethyl-4-pyrone (**5b**), corresponding to the benzo-condensed compound **1a**, was intact after having been in contact with **6** in DMSO at 60 °C for many hours. When the reaction was carried out in mixtures of hexamethylphosphoric triamide (HMPA) and DMSO (1 : 1 by volume), time studies of aliquots by means of either NMR or TLC exhibited the formation of homo-4-pyrone, **4**. A change in the HMPA/DMSO ratios brought about no appreciable alterations in the yields of **4** within the region from 0.3 to 3.0, although DMSO was essential for the generation of **6** *in situ* because no evolution of hydrogen accompanied by the formation

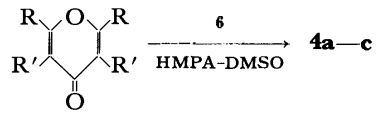

	R	R′
5a	CH_3	Ph
5b	CH_3	CH_3
5c	CH_3	H

Table 1. Entry for cyclopropanation from 4-pyrones with **6**

Run	Pyrone	Ylide **6** (mol)	Solvent[a]	Temperature (time)	Product (yield/%)	Ref.
1	**1a**	1.1	D	r. t. (0.5 h)	**2a** (28)	4
2	**1a**	1.1	D	r. t. (2 h)	**2a** (90)	8
3	**1b**	1.1	D	r. t. (2.5 h)	**2b** (70)	3
4	**5a**	2.5	H–D (1 : 1)	40 °C (6 h)	**4a** (53)[c]	b)
5	**5b**	Excess(>4)	D	60 °C (2 d)	No reaction	b)
6	**5b**	Excess[d]	H–D (1 : 1)	40 °C (4 d)	**4b** (40)	b)
7	**5c**	2.5	H–D (1 : 1)	40 °C (1 h)	**4c** (15)	b)
8	**4a**	2.5	H–D (1 : 1)	40 °C (1 d)	No reaction	b)

a) D: DMSO, H: HMPA. b) Present work. c) 15% Recovery of **5**. d) Additional **6** was necessary in order to promote the formation of **4b** at several-hour intervals.

of **6**[1] occurred when neat HMPA was chosen as the reaction medium.

The purification of the crude product was done by means of column chromatography on either deactivated neutral alumina or silica gel, using ether–light petroleum as the eluent. Thus, the diphenyl derivative **4a** was isolated as colorless prisms (mp 101—102 °C), while both **4b** and **4c** were less stable. Therefore, the structural assignments of the latter compounds may be elucidated by a comparison of the spectral data with those of **4a**.

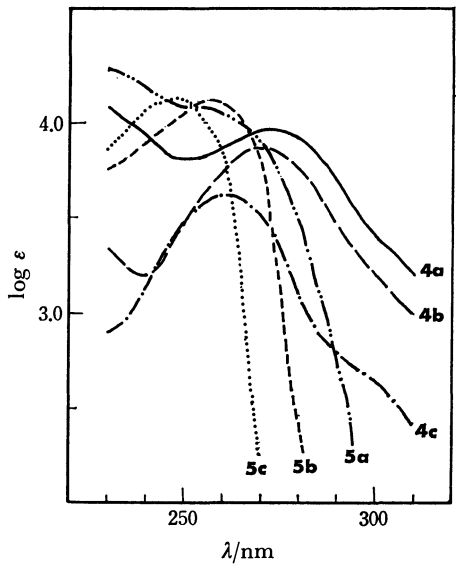

Fig. 1. UV spectra of **4a**—**c** and **5a**—**c** in methanol.

The UV spectra of **4a**—**4c** are shown in Fig. 1, along with those of the corresponding 4-pyrones, **5a**—**5c**. The change in the wave numbers for maximum absorption ($\nu_{C=O}$) according to the variation in the properties of the carbonyl function from **5** to **4** was not so remarkable as that in the benzo-condensed compounds, **2**.[3] Unlike the ambiguous information given concerning the production of cyclopropyl ketones, the mass spectra indicated an expulsion of the CHO radical from the molecular ion, M−29, which has been found to be a characteristic fragmentation in homochromones, **2**,[5] as well as in the parent ion (M^+) (see Table 2).

Table 2. Data of the mass spectra of homo-4-pyrones **4**

Compd	M^+(*m/e*)	M−15	M−28	M−29[b]	M−43
4a	290(100)[a]	275(28)	262(20)	261(15)	247(40)
4b	166(100)	151(73)	138(4)	137(18)	123(68)
4c	138(100)	123(13)	110(8)	109(19)	95(65)

a) Relative intensity. b) Expulsion of the CHO radical.

In the NMR spectrum of **4a**, protons belonging to the cyclopropane were not obvious because of the duplication with the signal of a methyl group (δ, 1.80), but a typical AB quartet (J=6 Hz) peculiar to cyclopropyl methylene protons (δ, 1.56 and 1.82) was revealed by the treatment of **4a** with alkaline 1,2-dimethoxyethane (DME)–D_2O, in analogy with that of 2,3-dimethylchromone (**1a**), which could be deuterated at the 2-methyl group, in the β-position to the α,β-unsaturated carbonyl group, to give **1a'** in our preliminary experiment. 4-Pyrone **5a** could be converted into 2,6-bis(trideuteriomethyl)-3,5-diphenyl-4-pyrone (**5a'**) under the same conditions. However, no deuterium exchange took place in the case of the homochromone **2a**. Taking these results into account, it seems that trideuteriomethylation on **4a** cannot proceed on the methyl group attached to cyclopropane (the C-1 position at δ, 1.28), while it can on the other methyl group (δ, 1.80 for the 3-methyl group adjacent to β-carbon for the α,β-unsaturated carbonyl function). The experimental results agreed exactly with this expectation, and the chemical shifts of all the aliphatic protons suggested a monocyclopropyl ketone, **4a'**, in comparison with those of related compounds, as is shown below.

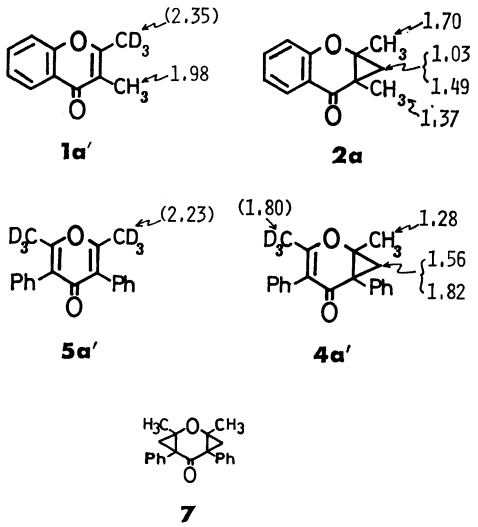

Fig. 2. ^1H NMR chemical shifts for aliphatic protons on 4-pyrones and homo-4-pyrones (δ, ppm).

Although deuterium exchange for either **4b** or **4c** failed to yield decomposition products, structural assignments could be made on the basis of their ^1H NMR spectra as well as the mass spectra. For example, the NMR spectrum of **4c** included two methyl signals, at δ=1.93 (3-methyl) and 1.63 ppm (attached to cyclopropane); a vinyl proton at δ=5.03 ppm for the singlet, and a methine proton at δ=*ca.* 1.8 ppm for the multiplet (C-6 position). Methylene protons of cyclopropane were observed at δ=1.43—1.03 ppm for the multiplet. Three different homo-4-pyrones were prepared; the most stable, **4a**, was employed for the further reactions.

An attempt to prepare the dicyclopropyl ketone (bishomo-4-pyrone), **7**, from **4a** with **6** in HMPA–DMSO was unsuccessful to be recovered so far.

Acid-catalyzed Reaction of Homo-4-pyrone ***4a*** *by Means of Trifluoroacetic Acid*: Since it has been reported that the cationic intermediate may be highly stabilized by the homoaromatic conjugation depicted in **8** in either the solvolysis of the secondary cyclopropylmethyl ester, **3**,[3] or the electrophilic addition of tetracyanoethylene to

the 4-methylene-4*H*-homochromene derivatives, **9**,[9] we attempted to isolate secondary alcohols or vinylcyclopropanes corresponding to **3** or **9** starting from **4**, but we could not do so because of the cleavage of cyclopropane.[8] Therefore, we studied the protonation to the carbonyl function of homo-4-pyrone, **4a**, by means of acid catalysis as another way for investigating the cationic intermediate from **4a**.

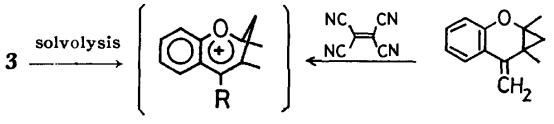

8 **9**

R=H (from **3**)
R=CH_2-C(CN)$_2$-$\bar{C}$(CN)$_2$ (from **9**)

When **4a** was dissolved in trifluoroacetic acid (TFA) at room temperature for 1 d, followed by the usual work-up process, the column chromatography of the crude product on silica gel afforded three products in 6, 32, and 30% yields; they are recognized as a dehydrated, an isomeric, and a hydrated compound of **4a** respectively on the basis of both microanalyses and mass spectrometry.

*Reaction of Homo-4-pyrone, **4a**, by Means of an Other Acid Catalysis*: The same products, a dehydrated, an isomeric, and a hydrated one, were isolated in trace, 12, and 34% amounts respectively by the treatment of **4a** with *p*-toluenesulfonic acid in benzene at room temperature for 1 d, although **4a** was fairly stable in acetic acid. An acid-catalyzed reaction by the use of three polychloroacetic acids, CH_2ClCO_2H, $CHCl_2CO_2H$, and CCl_3CO_2H, afforded the hydrated product in 16, 30, and 36% yields respectively; moreover, the **4a** was recovered, judging from the NMR spectra of the mixture. As an isomeric compound could not be detected in either case, the production of an isomeric compound seems to occur by means of strong acid catalysis.

Structural Assignment of the Dehydrated Product: The IR absorptions obviously demonstrated the existence of neither hydroxyl nor carbonyl group, so this compound may possess an ether linkage. The NMR spectrum included signals for two methyl protons (δ, 2.43 and 2.57), a vinyl proton (δ, 6.80), and nine aromatic protons (δ, 7.33 to 8.25), in which the existence of a solitary multiplet (δ, 7.92 to 8.25 for 2H) in a fairly low field may be conjectured upon *peri*-(5, 8) protons in the naphthalene ring, which is probably crowded with substituents upon at least the 1,4-positions, judging from the NMR data for related naphthalenes in the literature as is shown in Table 3.[10]

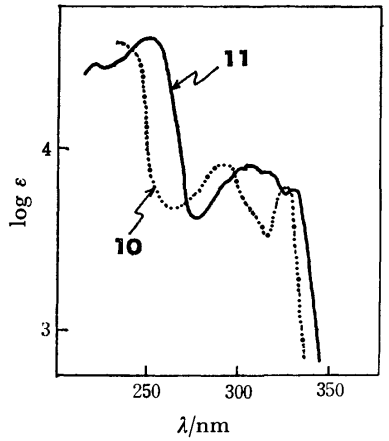

Fig. 3. UV spectra of naphtho[2,1-*b*]furans.

The ^{13}C NMR data at δ=154 and 102 ppm suggest the furan moiety,[11] although the other set of signals due to the furan ring cannot be found because of complicated signals between at δ=137 ppm and 122 ppm. Therefore, the structure of the ether may be speculated to be condensed furan, a so-called naphthofuran. On the basis of this speculation, the presence of α-methyl (δ_C, 14; δ_H, 2.43) and β-proton (δ_H, 6.80) on the furan moiety may be well interpreted; also the signal at 122 ppm for β-carbon shows a doublet under the off-resonance conditions in the ^{13}C NMR spectrum. The other methyl signal at δ=16 ppm was assigned to a substituent of the naphthalene; the *peri*-position is more plausible than the other positions, judging from the chemical shift of the ^1H NMR spectrum at δ=2.43 ppm (see Table 3).[10]

The UV spectrum showed maxima at 330, 304, and 249 nm (log ε 3.78, 3.94, and 4.63 respectively), nicely in accord with those of the parent naphtho[2,1-*b*]furan, **10**, reported in the literature,[12] as is illustrated in Fig. 3. On the basis of these data, the structure of the dehydrated product was identified as dimethylphenylnaphthofuran, **11**.

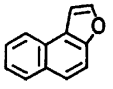

10

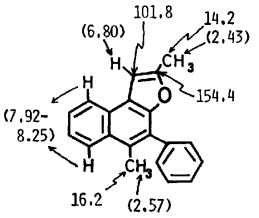

11

Chemical shifts; δ_C (δ_H)

Structural Problem of the Isomeric Product: Because of a monooxime formation as well as the IR absorption at 1720 cm^{-1}, and its freedom from a hydroxyl group, the other oxygen atom of the isomeric product probably performs an ether function. That a cleavage of the cyclopropane ring had occurred was indicated by the ^1H NMR spectrum of the product, which had signals at δ=4.92 and 6.05 ppm for each singlet instead of the AB quartet for cyclopropyl methylene (δ, 1.56 and 1.82) in **4a**. Methyl signals were transferred into somewhat lower fields (δ, 2.02 for the sharp singlet and 2.33 for the broad singlet) in comparison with those of **4a**. Then, $Eu(fod)_3$ was added in portions to the substrate dissolved in deuteriochloroform, and the ^1H NMR spectra were recorded under various molar ratios in order to ascertain structural information. If the substrate is a methyl ketone, a remarkable lanthanoid-induced downfield shift may be expected for the methyl group adjacent to the carbonyl group.[13] The experimental results of the downfield shifts are presented in Fig. 4.

The relative extents of the induced shifts for both the sharp singlet for the methyl group (δ, 2.02) and the

TABLE 3. CHEMICAL SHIFTS IN NAPHTHALENES AND RELATED COMPOUNDS

Compd	Chemical shifts (δ, ppm)[a]		
	Aromatic protons		Methyl protons
	peri-	Others	
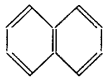	7.75—7.5	7.2—7.4	—
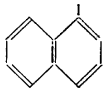	7.9—7.2		2.63[b]
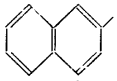	7.9—7.2		2.47
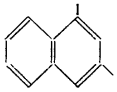	7.85—7.0		2.40, 2.57[b]
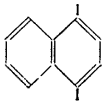	8.05—7.9	7.55—7.35, 7.14	2.67[b]
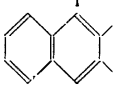	7.7—7.15		2.40
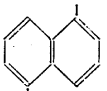	7.9—7.7	7.45—7.15	2.63[b]
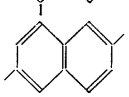	7.7—7.2		2.47
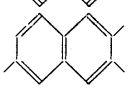	7.6—7.05		2.45, 2.38
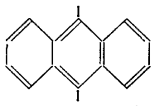	8.4—8.25	7.6—7.4	3.10[b]
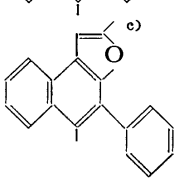	8.25—7.92	7.67—7.33, 6.80	2.43, 2.57[b]

a) $CDCl_3$ was used as the solvent unless otherwise noted.
b) Chemical shift assigned to α-methyl. c) In CCl_4.

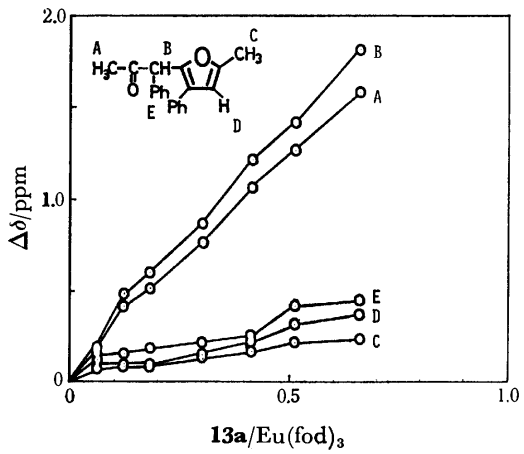

Fig. 4-1. $Eu(fod)_3$-induced shifts for **13a**.

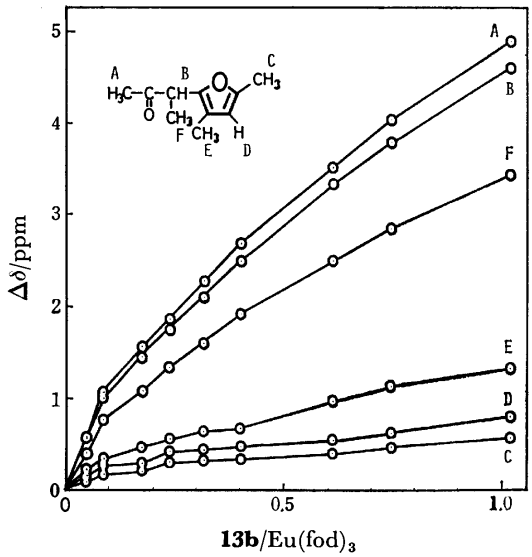

Fig. 4-2. $Eu(fod)_3$-induced shifts for **13b**.

singlet for the methine proton (δ, 4.92) were much larger than any other proton signals. Accordingly, the product may possess a CH_3–C(=O)–CH(Ph)– moiety, an idea which is also supported not only by the facile disappearance of the methine signal (δ, 4.92) adjacent to the carbonyl group in its ^1H NMR spectrum after hydrogen-deuterium exchange upon treatment with alkaline DME–D_2O, but also by an intense fragment at *m/e* 247 (M−43) which may be readily accounted for by an expulsion of the acetyl group in the mass spectrum.

The formation of a one-to-one adduct with *N*-phenylmaleimide may be proof of the furan skeleton of the product. The stractural assignment of the adduct was carried out by means of a comparison with the adduct, **12**, which had been prepared from 2-methylfuran with maleic anhydride as reported in the literature[14] and as is demonstrated in Fig. 5. In the ^1H NMR spectrum of the *N*-phenylmaleimide adduct, one methyl signal of the isomeric product of **4a** (δ, 2.33) underwent an extraordinary upfield shift to δ=1.73 ppm, so that the methyl group changed into the substituent at α-carbon in the furan which had been obtained by the acid catalysis of **4a**.

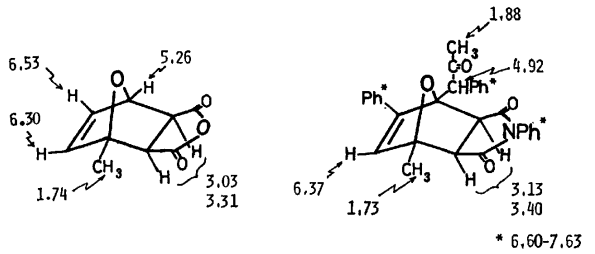

12 **adduct**

Fig. 5. ^{1}HNMR chemical shifts for Diels-Alder adducts (δ, ppm).

The conclusive information concerning the structural assignment of the isomeric product of **4a** was given by means of ^{13}C NMR measurement. In accordance with the data on the chemical shifts in the literature,[11] the singlets at both δ=152 and 145 ppm (α-carbons), and both the singlet at 125 ppm and the doublet at 108 ppm (β-carbons) under the off-resonance conditions, confirm the presence of the furan moiety. Although not all the signals could be assigned because of the duplication of signals in the region of the phenyl carbons (δ, 126 to 137), the signals at δ=203 ppm for the singlet and δ=29 ppm for the quartet (off-resonance spectrum) also showed CH_3–C(=O) function.

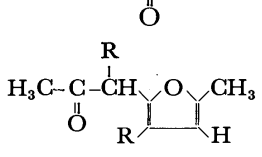

13

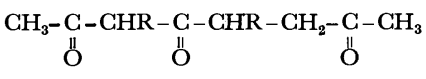

14

(**a**; R=Ph, **b**; R=CH_3, **c**; R=H)

As a long-range coupling of the allyl type was found between the signals of the methyl group (δ, 2.33) and the vinyl proton (δ, 6.05), the –CH=C(–)–CH_3 moiety should be included in the furan ring. After all, then, the structure of the isomeric product could be deduced to be that of the 2-furylacetone derivative, **13a**.

The Structure of the Hydrated Product: This was assigned by means of its spectroscopic data to **14a**; it was dissolved in TFA for several hours to give a dehydrated compound, **11**, in about a 10% yield, accompanied by the recovery of **14a**. For the purpose of obtaining further information about the reaction pathway, the exposure of either deuterium-labelled **4a′** or other homo-4-pyrones in TFA was carried out; also, the decisive structural assignment of the isomeric product, **13**, will be made.

Acid-catalyzed Reaction of Trideuteriomethyl-substituted 4a′ in TFA: By using the procedure mentioned above, three products were isolated analogously. The ^1H NMR spectrum of the dehydrated one showed only one methyl signal (δ, 2.43) which could be identified as α-methyl in the furan, while the signal for the naphthylmethyl group (δ, 2.57) scarcely appeared at all. Therefore, the CD_3 group on the C-3 position in homo-4-pyrone, **4a′**, can be said to have been specifically transferred into the *peri*-position on the naphthalene ring of **11**.

On the other hand, the signal for the methyl group at a lower field (δ, 2.02) identified as acetyl protons completely disappeared, and the signal for α-methyl in the furan ring (δ, 2.33) was observed exclusively in the ^1H NMR spectrum of the isomeric product. Consequently, the α-methyl group belonging to the furan ring seems to be derived from the bridgehead methyl group (C-1 position) in 2-oxabicyclo[4.1.0]hept-3-en-5-one derivatives, **4a**, in either **11** or **13a**. In the case of 2-furylacetone, **13a**, further evidence was provided by the mass spectrum of **13a′**. Thus, accompanying the parent peak at *m/e* 293 ($C_{20}H_{15}D_3O_2$), there was a peak at *m/e* 247 (M−46, base) corresponding to the loss of the CD_3CO moiety; this peak appeared entirely cut off from any surrounding peaks, so upon acid catalysis that the CD_3 group in **4a′** seems move into the acetyl group as the side chain of the furan ring in **13a′**.

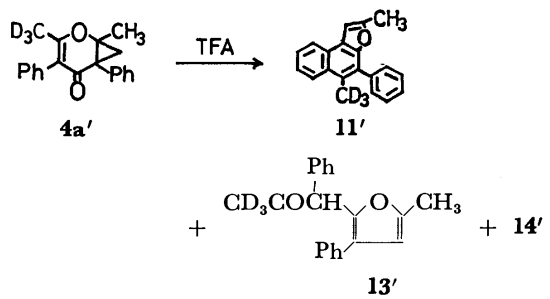

Mechanism: On the basis of the above experimental results, a plausible mode of formation that we favor for **11**, **13a**, and **14a** is illustrated below. Protonation onto the carbonyl group of **4a** occurs to give a cationic intermediate such as **15** by strong acid catalysis, *e.g.*, TFA,[15] followed by nucleophilic attack by a solvent

on the C-1 position adjacent to ether oxygen coexisting with a ring enlargement due to the cleavage of the cyclopropane. Then, the acetal **16** thus produced undergoes ketonization to yield 3,5-diphenyl-2,4,7-octanetrione (**14a**). Such a product was also obtained when the benzo-condensed compound **2a** was submitted to an acid-catalyzed reaction; in this case, one of the carbonyl groups was enolated to **17** as a phenol, as is depicted below.[4]

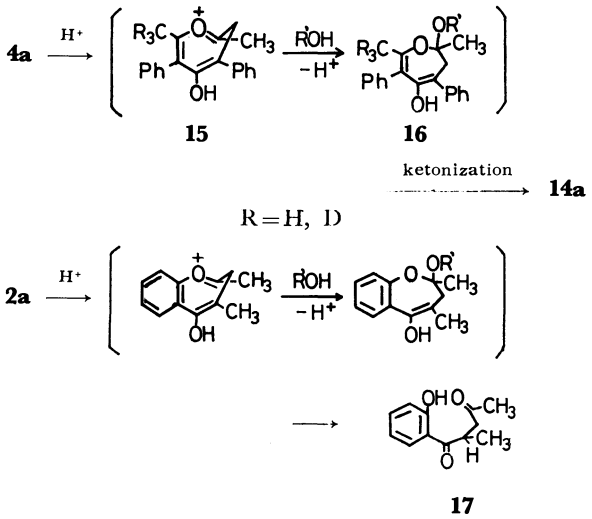

As it is a convenient route for furan synthesis for the dehydration of 1,4-diketones to take place under appropriate conditions, *e.g.*, in the presence of sulfuric acid (the so-called Paal-Knorr-type reaction),[16] the formation of the 2-furylacetone derivative, **13a**, may be expected in a similar manner. Support for this reaction mechanism was provided by the deuterium-labelled experiment. Thus, the 3-methyl group of **4a** was changed into acetonyl function in **13a**, while the other methyl group (the C-1 position of **4a**) was changed into the 2-furylmethyl function, as has been described above; therefore, it may be speculated that carbons belonging to the furan in **13a** originate as carbons at the 1, 5, 6, and 7 positions in **4a**.

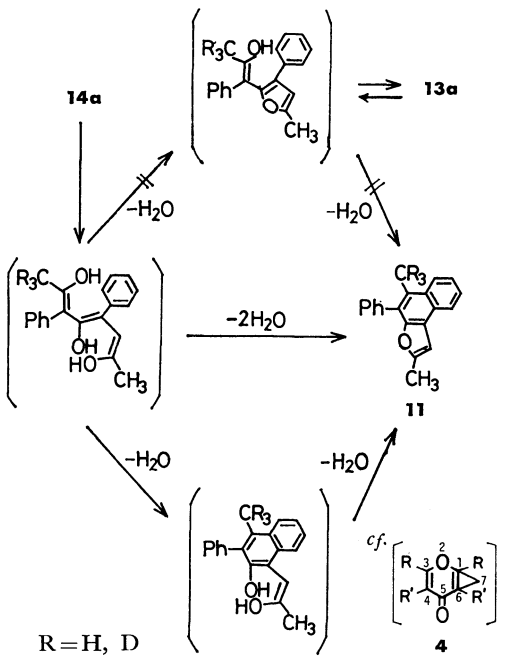

Taking this postulation into account, the conversion from triketone, **14a**, into naphthofuran, **11**, can be explained: (i) the furan moiety was made from the carbons of the C-1, 5, 6, 7 positions in **4a**; (ii) the carbons of the C-3, 4, 5, 6 positions in **4a** belong to the new benzene ring, which condenses with the phenyl group at the C-6 position in **4a** to give a naphthalene in which the CD_3 group may be assigned as a substituent at the *peri*-position in the case of the deuterium-labelled experiment, as is shown below.

Nevertheless, the correct mechanism of 2-furylacetone **13a** formation seems to be somewhat different from the above deduction, judging from the following experimental results:[19] (i) when the reaction of **14a** with TFA was followed by means of either ^1H NMR spectroscopy or TLC at intervals, the formation of **13a** was undetectable, and (ii) interconversion from **13a** into **11** did not occur in TFA at room temperature.

Accordingly, **13a** is not given from **14a** by means of a Paal-Knorr reaction in the present case, but was directly formed from the starting material, although it seems, on the basis of the above deuterium-labelled experiment, likely that the C-1, 6 bond fission of **4a** occurred during the production of **13a**.

Thus, the interconversions among **4a**, **11**, **13a**, and **14a** may be finally expressed as below. This scheme may be well interpreted by the fact that the product ratio, **13a**/(**11**+**14a**), for the treatment of **4a** with TFA was found to be inevitably constant for at least six entries:

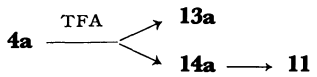

It is noteworthy that a similar mode of the cleavage of the cyclopropane ring has been deduced from the product studies of either the solvolysis of the secondary ester, **3**,[3] or the electrophilic addition of tetracyanoethylene to the *exo*-methylene compound, **9**,[9] and that the same characteristic cleavage of cyclopropane may also be involved in the acid-catalyzed reaction of homo-4-pyrone, **4a**.

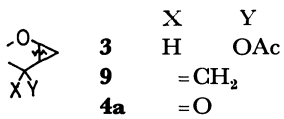

Mode of cleavage of the cyclopropane ring

Reaction of Other Homo-4-pyrones with TFA: An isomerization of both **4b** and **4c** by means of acid catalysis took place analogously with the case of **4a** to give **13b** and **13c** in 40 and 15% yields respectively, along with a triketone **14c** (20% yield, starting from **4c**), although TFA was diluted with an equal volume of carbon tetrachloride or chloroform for the purpose of relieving a vigorous reaction moderately. The structural assignments of the products were made by means of both their ^{13}C NMR spectra, in which a furan moiety was clearly indicated, as is shown in Table 4, and their other spectral characteristics in comparison with those

Table 4. The ^{13}C NMR chemical shifts for 2-furylacetones **13**

Compd	C=O					$-\overset{*}{C}-\overset{\|}{C}HR-$ (O)	$\overset{*}{C}H_3C-$ (O)		CH_3
13a	203	152	145	125	108 (d)	57 (d)	29 (q)	14 (q)	
13b	206	151	146	117	109 (d)	46 (d)	28 (q)	14 (q) 13 (q)	10 (q)
13c[a)]	205	152	147	109	107	43	29	14	

a) Only an off-resonance spectrum was obtained.

of **13a**. The proton NMR data of **13b** including $Eu(fod)_3$ were closely analogous with those of **13a**, as is shown in Fig. 4.

In connection with reports on the chemistry of flavors, 2-furylacetone **13c** has been identified as one of the components in molasses aroma, bread aroma, meat flavor, and so on,[17] and antibiotic nonactic acid, which has been noted to have structural characteristics[18] analogous to the carbon skeleton of **13**. The production of 2-furylacetone starting from homo-4-pyrone in our present study is interesting because of the versatile utility of the product as well as the finding that aromatization into five-membered heterocycle may be one of the most suitable pathways for the cleavage of the cyclopropane of homo-4-pyrones under strong acid catalysis.

Experimental

General. All the melting and boiling points are uncorrected. The IR spectra were measured using a Hitachi 215 spectrometer; the UV spectra, on a Hitachi 124 spectrometer; the mass spectra, on a Hitachi RMU-6L spectrometer, and the ^1H NMR spectra, on a Varian T-60 spectrometer. The chemical shifts on both ^1H and ^{13}C NMR spectra are given in δ, with tetramethylsilane as the internal standard.

Materials. The preparation of 2,6-dimethyl-3,5-diphenyl-4-pyrone (**5a**) was carried out according to the procedure reported by Letsinger *et al.*[7] Mp 208—211 °C (lit, 202—206 °C)[7] (40% yield; flaky crystals, from benzene–ligroin). Analogously 2,3,5,6-tetramethyl-4-pyrone (**5b**) was synthesized from 3-pentanone in a 13% yield. Bp 154 °C/25 mmHg, mp 90—91 °C (lit, 90 °C)[7] (colorless prisms, from light petroleum). Starting from commercially available dehydroacetic acid, 2,6-dimethyl-4-pyrone (**5c**) was obtained. Mp 132—134 °C (lit, 130 °C),[7] bp 155 °C/35 mmHg (65% yield, colorless needles, from chloroform–hexane). Dimethyloxosulfonium methylide (**6**) was generated *in situ* by the treatment of sodium hydride with trimethyloxosulfonium iodide in dimethyl sulfoxide which had been distilled on calcium hydride under reduced pressure. Hexamethylphosphoric triamide was also distilled *in vacuo* before use and dried on molecular sieves.

General Procedure for the Cyclopropanation of 4-Pyrones. Dimethyldiphenylhomo-4-pyrone(1,3-dimethyl-4,6-diphenyl-2-oxabicyclo[4.1.0]hept-3-en-5-one) (4a): To mineral oil-free sodium hydride, prepared from commercial NaH (5.5 g, 0.14 mol; 61% in mineral oil) by means of triple decantation with light petroleum, we added trimethyloxosulfonium iodide (30 g, 0.14 mol) in one portion, after which we stirred in freshly distilled dimethyl sulfoxide (DMSO) (60 ml) over a period of 15 min, at first very carefully, at 20 °C. After the cessation of the violent evolution of hydrogen, the milky-white solution was kept in a nitrogen atmosphere. Into the dimethyloxosulfonium methylide generated in DMSO we poured hexamethylphosphoric triamide (HMPA) (60 ml), after which we added **5a** (15 g, 0.054 mol) in several portions, because of the poor solubility of **5a** in the medium. The solution was then allowed to stand at room temperature for 3 h under nitrogen, warmed at 40 °C for 6 h, and then cooled in an ice-bath; anhydrous ether (100 ml) was then added to the solution. The mixture was then poured into ice water and separated; the aqueous layer was extracted thoroughly with ether, and at last it was extracted once with benzene. The combined organic layer was satisfactorily washed with water and then dried on anhydrous sodium sulfate. The solution was evaporated *in vacuo*; a brown syrup (16.3 g) thus obtained was chromatographed on neutral alumina (80 g, deactivated by the addition of 10% water (w/w)) using ether–light petroleum (1: 10 by volume) as the eluent, and the solvent was evaporated *in vacuo* to give 8.31 g (53%) of **4a**. Mp 101—102 °C (colorless prisms, from light petroleum). IR (Nujol): 1655, 1515 cm^{-1}. ^1H NMR (CCl_4): 7.3—7.0 (10H, m, aromatic), 1.80 (3H, s, methyl), 1.28 (3H, s, methyl), 1.82, 1.56 (2H, AB quartet, J=6 Hz, cyclopropane). Found: C, 82.69; H, 6.29%. Calcd for $C_{20}H_{18}O_2$: C, 82.73; H, 6.25%. MS and UV data (see Table 2 and Fig. 1). About 15% of the **5a** was recovered in the column chromatography as a more polar fraction than **4a**.

Tetramethylhomo-4-pyrone(1,3,4,6-tetramethyl-2-oxabicyclo[4.1.0]-hept-3-en-5-one) (4b): According to the general procedure, **4b** was obtained as a colorless oil (see Table 1). IR (neat): 1640, 1625, 1440, 1400, 1195, 1035, 805 cm^{-1}. ^1H NMR (CCl_4): 1.89 (3H, s, methyl), 1.65 (3H, s, methyl), 1.57 (3H, s, methyl), 1.22 (3H, s, methyl), 1.22, 0.78, (2H, AB quartet, J=7 Hz, cyclopropane). MS and UV data (see Table 2 and Fig. 1).

Dimethylhomo-4-pyrone(1,3-dimethyl-2-oxabicyclo[4.1.0]hept-3-en-5-one) (4c): The synthetic procedure was analogous to those used for the other homo-4-pyrones mentioned above. (see Table 1). IR (neat): 1650, 1610, 1400, 1170, 965, 840 cm^{-1}. ^1H NMR (CCl_4): 5.03 (1H, s, vinyl), *ca.* 1.8 (1H, m, methine), 1.93 (3H, s, methyl), 1.63 (3H, s, methyl), 1.4—1.0 (2H, m, cyclopropane). MS and UV data (see Table 2 and Fig. 1).

General Procedure for Deuterium Exchange: A solution of the substrate (**4a**; 0.10 g) in DME (3 ml) was added to a stirred solution of a catalytic amount of sodium hydroxide in DME–D_2O (1: 1 by volume, 6 ml). After having been stirred overnight at room temperature, the solvent was evaporated *in vacuo* without heating; then the residue was extracted twice with dry ether (20 ml). The extracts were combined, washed with water, and dried over anhydrous sodium sulfate. The solution was condensed *in vacuo* to give a residue (**4a'**; 0.09 g), whose spectroscopic data have been discussed above.

General Procedure on the Treatment of Homo-4-pyrones 4 with Trifluoroacetic Acid: A wine-red solution of homo-4-pyrone **4a** (0.50 g) in trifluoroacetic acid (TFA) (5 ml) was subjected to ^1H NMR measurement, but a complicated pattern was observed. The solution was stirred at room temperature for 1 d, diluted with dry ether (50 ml), poured into an ice-cold

aqueous sodium hydrogencarbonate solution, and extracted three times with ether (100 ml); the combined organic layer was washed thoroughly with cold aqueous sodium hydrogencarbonate and with water, and then dried over anhydrous sodium sulfate. A yellow syrup (0.49 g) obtained by the subsequent evaporation of the ether was chromatographed on silica gel (15 g), using ether–light petroleum (1:9) as the eluent, to give three crystalline products: **11**, 30 mg (6%), mp 115—117 °C (from light petroleum). IR (nujol): 1600, 1580, 1360, 1230, 1180, 1010 cm^{-1}. ^1H NMR (CCl_4): 8.25—7.92 (2H, m, aromatic), 7.67—7.33 (7H, m, aromatic), 6.80 (1H, broad s, vinyl), 2.57 (3H, sharp s, methyl), 2.43 (3H, broad s, methyl). ^{13}C NMR ($CDCl_3$): 154.4 (s), 136.7 (s), 130.7, 130.2, 128.2, 127.5, 127.2, 126.5, 125.6, 124.5, 123.9, 122.4, 101.8 (d), 16.2 (q), 14.2 (q) (see also text). MS (*m/e*): 272 (M^+, base), 229. UV data (see Fig. 1). Found: C, 87.65; H, 5.94%. Calcd for $C_{20}H_{16}O$: C, 88.20; H, 5.92%. **13a**, 160 mg (32%), mp 35—37 °C (from light petroleum). IR (neat): 1720, 1600, 1570, 1450, 1150, 760, 690 cm^{-1}. ^1H NMR (CCl_4): 7.20 (10H, aromatic), 6.05 (1H, broad s, vinyl), 4.92 (1H, s, methine, disappeared when alkaline DME–D_2O) was used, 2.33 (3H, broad s, methyl), 2.02 (3H, sharp s, methyl), ^{13}C NMR ($CDCl_3$): 203.7 (s), 151.9 (s), 144.6 (s), 137.2 (s), 133.8 (s), 130.8, 130.5, 130.2, 129.0, 128.7, 128.0, 127.4, 127.1, 125.5 (s), 108.1 (d), 57.7 (d), 28.5 (q), 13.5 (q) (see also Table 4). MS (*m/e*): 290 (M^+), 247 (base). Found: C, 82.44; H, 6.34%. Calcd for $C_{20}H_{18}O_2$: C, 82.73; H, 6.25%. Monooxime, mp 154—156 °C (from methanol). Found: C, 78.28; H, 6.25; N, 4.50%. Calcd for $C_{20}H_{19}NO_2$: C, 78.66; H, 6.27; N, 4.59%. **14a**, 160 mg (30%), mp 75—77 °C (from light petroleum). IR (Nujol): 1715, 1600, 1160, 760, 730, 690 cm^{-1}. ^1H NMR ($CDCl_3$): 7.7—6.7 (10H, m, aromatic), 4.3—3.3 (4H, m), 2.13 (3H, s, methyl), 1.78 (3H, s, methyl). MS (*m/e*): 308 (M^+), 290 (base), 247. Found: C, 78.09; H, 6.61%. Calcd for $C_{20}H_{20}O_3$: C, 77.90; H, 6.5%. In addition to these products, an almost one-to-one mixture of **13a** and **14a** was also isolated (130 mg; 25%).

*Reaction of **4a** by Means of* p-*Toluenesulfonic Acid*: Homo-4-pyrone, **4a** (0.50 g), and an equal amount of *p*-toluenesulfonic acid were dissolved in benzene (5 ml) at room temperature for 1 d. The mixture was then washed with aqueous sodium hydrogencarbonate and with water, and dried on anhydrous sodium sulfate. The solution was evaporated, and the residue was subjected to chromatography to yield **11** (trace), **13a** (60 mg, 12%), and **14a** (180 mg, 34%).

*Treatment of **4a** with Polychloroacetic Acids*: To each solution of **4a** (50 mg) in $CDCl_3$ (0.4 ml), equimolar polychloroacetic acid, CCl_3CO_2H (28 mg), $CHCl_2CO_2H$ (22 mg), or CH_2ClCO_2H (16 mg), was added, after which the mixture was kept at 40 °C for 1 d. Since **14a** was the sole isolable product in each case, the yields were estimated by ^1H NMR spectroscopy on the basis of the ratio for the characteristic signals identified as **14a** to the recovered **4a**. When the reaction was carried out in neat $CHCl_2CO_2H$, **14a** was the single isolable product in addition to the reactant. The yields have been shown above.

Preparation of N-*Phenylmaleimide Adduct*: a) Homo-4-pyrone **4a** (0.50 g, 1.72 mmol), *N*-phenylmaleimide (0.30 g, 1.72 mmol), and TFA (3 ml) was stirred at room temperature for 30 h, and then diluted with dry ether (100 ml), and poured into ice-cold sodium hydrogencarbonate; the mixture was extracted twice with ether (50 ml), and the combined organic layer was thoroughly washed with aqueous sodium hydrogencarbonate, washed with water, and dried over anhydrous sodium sulfate. The subsequent evaporation of the solution gave a syrup (0.80 g) which was subjected to preparative TLC on silica gel, using methyl acetate–light petroleum (1:6) as the eluent, to yield pale yellow needles. (290 mg, 45%, from ether). Mp 125 °C. IR (Nujol): 1710, 1500, 1200, 1180, 750, 715, 690 cm^{-1}. ^1H NMR data (see the text). Found C, 77.46; H, 5.48; N, 2.91%. Calcd for $C_{30}H_{25}NO_4$: C, 77.74; H, 5.44; N, 3.02%.

b) The same product was obtained by the reaction of **13a** with equimolar *N*-phenylmaleimide in $CDCl_3$ at room temperature for several days; it was confirmed on the basis of both ^1H NMR spectrometry and the TLC analysis of the standard sample as has been described in Method a.

*Isomerization from Homo-4-pyrone **4b** into 2-Furylacetone **13b** by Means of Trifluoroacetic Acid*: Trifluoroacetic acid was diluted with chloroform (1:1 by volume). Analogously with the procedure of the reaction starting from **4a**, **13b** was isolated in a 40% yield from **4b**, along with the recovery of **4b** in an 8% yield. Purification was accomplished by column chromatography (silica gel, with ether–light petroleum (1:4) as the eluent). **13b**; colorless oil. IR (neat): 1730, 1590, 1450, 1360 cm^{-1}. ^1H NMR ($CDCl_3$): 5.65 (1H, broad s, vinyl), 3.55 (1H, q, J=6 Hz, methine), 2.20 (3H, s, methyl), 1.92 (3H, s, methyl), 1.90 (3H, s, methyl), 1.30 (3H, d, J=6 Hz, methyl). MS (*m/e*): 166 (M^+), 123 (M−43, base). Monooxime, mp 48—49 °C. MS (*m/e*): 181 (M^+).

*Acid-catalyzed Reaction of Homo-4-pyrone **4c***: Trifluoroacetic acid–carbon tetrachloride (1:1 by volume) was used as the medium. After 1 d-reaction at room temperature, the mixture was worked up as has been described above; purification was carried out by column chromatography on silica gel, using ether–light petroleum (1:3) as the eluent. **13c**; colorless oil (15%). IR (neat): 1720, 1570, 1355, 1220, 1025, 780 cm^{-1}. ^1H NMR (CCl_4): 6.03 (1H, d, J=3 Hz, vinyl), 5.90 (1H, d, J=3 Hz, vinyl), 3.57 (2H, s, methylene), 2.30 (3H, broad s, methyl), 2.10 (3H, sharp s, methyl). MS (*m/e*): 138 (M^+), 111, 95 (M−43, base). ^{13}C NMR data (see Table 4). **14c**; colorless oil (20%). IR (neat): 1710, 1610, 1400, 1360 cm^{-1}. ^1H NMR (CCl_4): 5.50 (s), 3.63 (s), 2.93—2.20 (m, total 6H), 2.20 (3H, s, methyl), 2.02 (3H, s, methyl). MS (*m/e*): 156 (M^+), 138, 123, 113 (M−43), 99, 85, 71.

We are indebted to Dr. Masaaki Mishima, Kyushu Univ., Mr. Yoshinori Ikebe, Hitachi, Ltd., and Dr. Yasuhito Uchio, Hiroshima Univ., for obtaining the ^{13}C NMR spectra; we also wish to thank to Dr. Shizuko Eguchi, Hiroshima Univ., for her measurements of the mass spectra. We are indebted to the Ministry of Education for a Scientific Research Grant-in-Aid (374168).

References

1) E. J. Corey and M. Chaykovski, *J. Am. Chem. Soc.*, **87**, 1353 (1965).

2) B. M. Trost and L. S. Melvin, Jr., "Sulfur Ylides," Academic Press, New York (1975).

3) H. Yamaoka, K. Ohkata, and T. Hanafusa, *Bull. Chem. Soc. Jpn.*, **49**, 245 (1976).

4) G. A. Caplin, W. D. Ollis, and I. O. Sutherland, *J. Chem. Soc., C*, **1968**, 2302.

5) M. Nakayama, H. Yamaoka, S. Eguchi, T. Hanafusa, and S. Hayashi, *Org. Mass Spectrom.*, **12**, 416 (1977).

6) S. Winstein, *Quart. Revs.*, **23**, 141 (1969); H. Klein and W. Grimme, *Angew. Chem. Int. Ed. Engl.*, **13**, 672 (1974); P. Barraclough, S. Bilgic, J. B. Pedley, A. J. Rogers, and D. W. Young, *Tetrahedron*, **35**, 99 (1979).

7) T. L. Emmick and R. L. Letsinger, *Org. Synth.*, Coll. Vol. V, 450 (1973); R. L. Letsinger and J. D. Jamison, *J. Am. Chem. Soc.*, **83**, 193 (1961); M. Ohta and H. Kato, *Bull.*

Chem. Soc. Jpn., **32**, 707 (1959).

8) Unpublished results.

9) H. Yamaoka, Y. Yamada, S. Ono, and T. Hanafua, *Chem. Lett.*, **1979**, 523.

10) C. J. Pouchert and J. R. Campbell, "The Aldrich Library of NMR Spectra," Aldrich Chemical Company, Wisconsin (1974), Vol. 4, pp. 26, 27, 28, 30; F. F. Yew, R. J. Kurland, and B. J. Mair, *Anal. Chem.*, **36**, 843 (1964); B. A. Nagasampagi, R. C. Pandey, V. S. Pansare, J. R. Prahlad, and S. Dev, *Tetrahedron Lett.*, **1964**, 411.

11) T. F. Page, Jr., T. Alger, and D. M. Grant, *J. Am. Chem. Soc.*, **87**, 5333 (1965).

12) C. E. Loader and C. J. T. Timmons, *J. Chem. Soc., C*, **1967**, 1677.

13) "Nuclear Magnetic Resonance Shift Reagents," ed by R. E. Sievers, Academic Press, New York (1973).

14) S. Selzer, *J. Am. Chem. Soc.*, **87**, 1534 (1965).

15) The possibility of the intervention of the highly delocalized cationic species, the so-called homopyrylium ion, is now being studied. **4a** was found to be much more stable for TFA than *trans*-2-phenoxycyclopropyl phenyl ketone, whose synthetic route has been discussed previously (see Ref. 9). Protonation to cyclopropyl ketones by the use of a strong acid has afforded homoaromatically stabilized cationic intermediates; *e.g.*, H. A. Corver and R. F. Childs, *J. Am. Chem. Soc.*, **94**, 6201 (1972).

16) C. Paal, *Ber.*, **18**, 367 (1885); L. Knorr, *ibid.*, **18**, 299 (1885).

17) For example: M. Winter, F. Gutschi, I. Flament, and M. Stoll, U. S. Patent, 3952026 (1976) (*Chem. Abstr.*, **85**, p94216e); U. S. Patent, 3989713 (*Chem. Abstr.*, **86**, 43556d); U. S. Patent, 3924015 (1975) (*Chem. Abstr.*, 84, p164364g); K. Watanabe and Y. Sato, *J. Agric. Food Chem.*, **20**, 174 (1972); M. Yokota and I. S. Fagerson, *J. Food Sci.*, **36**, 1091 (1971); E. J. Mulders, M. C. de Brauw, and S. V. Straten, *Z. Lebensm. Unters. Forsch.*, **150**, 306 (1973) (*Chem. Abstr.*, **78**, 70418b).

18) H. Gerlach and H. Welter, *Helv. Chim. Acta*, **57**, 2306 (1974), and the references cited therein.

19) These additional experiments were done in the referee's recommendation, which seemed appropriate.

Asymmetric Benzoin Condensation Catalyzed by Optically Active Thiazolium Salts in Micellar Two-phase Media

Waichiro TAGAKI,* Yoshiharu TAMURA, and Yumihiko YANO

Department of Chemistry, Faculty of Engineering, Gunma University, Kiryu, Gunma 376

(Received July 9, 1979)

Three thiazolium salts, 3-[2-(*l*-3-*p*-menthyloxy)ethyl]thiazolium bromide (**1**), 3-(*l*-3-*p*-menthyl)thiazolium halides (**2**), and 3-(*l*-3-*p*-menthyl)-4-methylthiazolium perchlorate (**3**) have been examined for the catalysis of benzoin condensation in micellar two-phase media. The catalytic activities on the chemical yields of benzoin were observed to be high for **1** and **2** but low for **3**. On the contrary, for the asymmetric induction, **3** gave much higher optical purity of 35.3% than in the cases of **1** and **2** (0.8—3.5%). These results are discussed in terms of micellar and conformational effects.

Thiazolium salts are well known to catalyze the benzoin condensation (Scheme 1).[1] The catalytic activity, however, is generally not large in aqueous media. Therefore, the catalysts are commonly used in organic solvents such as in methanol for the purpose of synthesis.[2] Meanwhile, we have found that *N*-(long chain alkyl)thiazolium salts are highly active catalysts when used in aqueous two-phase system.[3] We consider that such enhanced activity was produced by combined effects of micellar[4] and phase transfer[5] catalyses. For the past decade, these catalytic systems have been extensively studied as the enzyme models, and some success appears to have been achieved in the simulation of enzymic rate enhancement. However, relatively little success has been achieved in the simulation of enzymic stereospecificity, although there have been some interesting examples of stereospecific micellar[6] and phase transfer[7] reactions.

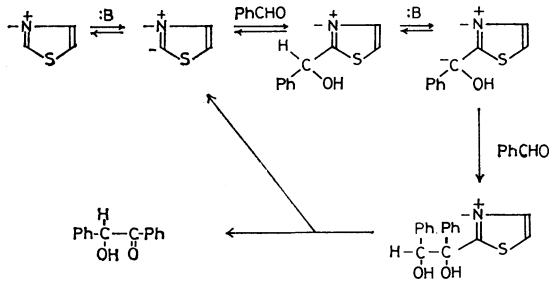

Scheme 1.

In the meantime, Sheehan and the coworkers have already studied the asymmetric benzoin condensation and obtained fairly high optical purity of 52% by using some optically active thiazolium salt of highly constrained structure.[8] Unfortunately, they examined the reactions only in methanol. Therefore, we have reexamined similar asymmetric benzoin condensation, but under micellar conditions in aqueous media.

Results and Discussion

Synthesis of the Catalysts. All catalysts were prepared starting from crystalline *l*-menthol, as outlined in Scheme 2. Synthetic procedures for **1** involve no disturbance of asymmetric center. Whereas in the syntheses of **2** and **3**, the chirality of the 3-position of *l*-menthol was once destroyed by the oxidation leading

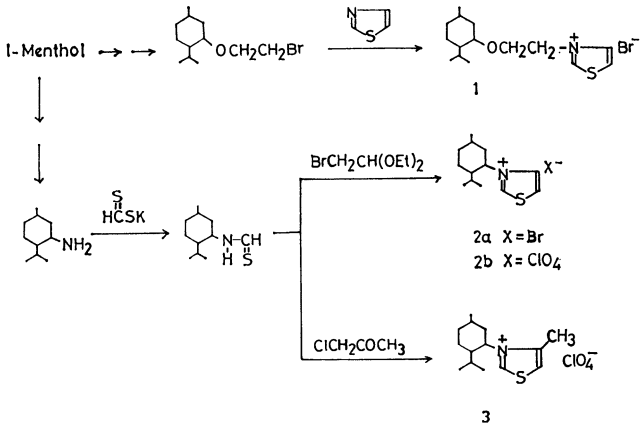

Scheme 2.

to *l*-menthone. However, this and the subsequent transformations to (*l*-3-*p*-menthyl)amine are well established procedures.[9] The conversions of (*l*-3-*p*-menthyl)-amine to **2** and **3** were carried out according to the method of Sheehan *et al.*[8]

Benzoin Condensation. The reactions were carried out in a Thunberg tube under the nitrogen atmosphere at room temperature. The reaction mixture was homogeneous when carried out in methanol containing triethylamine. While it was heterogeneous when carried out in aqueous phosphate buffer (pH 8) because of insolubility of benzaldehyde. Each catalyst was soluble in aqueous buffer, but when stirred in the presence of benzaldehyde it was extracted nearly completely from the aqueous phase to the liquid benzaldehyde phase. The benzoin thus formed was isolated by column chromatography on silica gel. The results are compiled in Table 1.

Table 1 indicates the following features: (a) In all the cases, the benzoin yield is higher in water (heterogeneous) than in methanol (homogeneous). The yield is also higher with bromide (**2a**) than with perchlorate (**2b**). (b) Racemization of the product benzoin occurs to some extent for a prolonged reaction duration. (c) The catalyst **2a** gave rotation of opposite sign to that given by **1** and **3**. (d) The 4-methyl substituent in **3** caused the highest optical purity, but the lowest benzoin yield.

The higher benzoin yield in water has already been observed for the catalyst (**4**).[3] The **4** forms micelle (CMC $=3.3\times10^{-3}$ M in H_2O) and its H-D exchange

Table 1. Thiazolium salt catalysis of benzoin condensation[a]

Catalyst	Solvent	Time h	Benzoin yield[b] %	$[\alpha]_D^{20}$ °	Optical purity[c] %
1	H_2O[d]	2	78	−5.43	3.3
	H_2O[d]	24	77	−3.00	1.8
	MeOH[e]	24	38	−5.67	3.5
2a	H_2O[d]	2	26	+5.34	3.2
	H_2O[d]	24	82	+1.27	0.8
	MeOH[e]	24	20	+3.00	1.8
2b	H_2O[d]	40	61	+2.85	1.8
3	H_2O[d]	41	20	−57.5	35.3
	MeOH[e]	41	trace		

a) PhCHO=2.8 mmol, cat=0.15 mmol, under N_2, at room temp. b) Isolated yields by column chromatography (silica gel, $CHCl_3$). c) (*R*)-Benzoin,[10] $[\alpha]_D^{20}$ −163.04° (*c* 1.0, MeOH) was used. d) 0.5 M Phosphate buffer (pH 8), 10 ml. e) MeOH (10 ml), Et_3N (0.16 mmol).

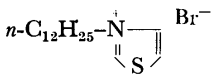

4

rate at the 2-position is 16 fold faster than that of non-micelle forming 3-methyl analogue.[3,11] The incorporation of **4** into benzaldehyde phase during the catalysis is also the same as observed for **1**, **2**, and **3**. Therefore, the micellar or phase transfer activation may be appropriate to account for the reactivities of these salts. The effect of counter anion (**2a** *vs.* **2b**) is also consistent with the micellar effects, since it is known that the perchlorate anion is bound more tightly to cationic micelle than bromide ion and a tighter binding causes a stronger inhibition of micellar reactivity.[4]

The 4-methyl group in **3** showed profound effects on both chemical and optical yields of benzoin. These effects may be understood in the following way. Namely, the conformations of **2** and **3** can be drawn as in the following formula **A** and **B**.[12] The CPK molecular model indicates that the isopropyl group enforces the plane of thiazolium ring to assume the conformations in such a way to bisect the plane of cyclohexane ring (C_1–C_3–C_5 and C_2–C_4–C_6). The interconversion between **A** and **B** is relatively easy when R=H (**2**), but severely restricted when R=Me (**3**) favoring **A** much more than **B**. On the other hand, the condensation should be easier through **B** than **A** since the reaction

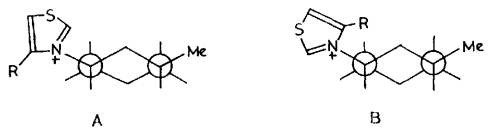

A B

R: H, Me

at 2-position of thiazolium ring is shielded by cyclohexane ring in **A**. Thus **2** should be more reactive (more in the reactive **B**) than **3** (more in the less reactive **A**). Meanwhile, the accounting for stereospecificity is not easy, since there are two addition steps to create two asymmetric carbons (see Scheme 1), both of which should be important, although the asymmetry of the first carbon (or carbanion) is lost after the condensation. Only we can suspect is that stereochemical confinement may be more stringent for more conformationally frozen **3** than **2**.

The above observation that the highest optical purity was obtained with the lowest yield is rather disappointing, since in the enzymic catalyses the rate enhancement and stereospecificity appear to be inseparable in the same catalytic mechanism.[13] For the present micellar two-phase system, the hydrophobic interaction between the catalyst and the substrate is considered to be important for the rate enhancement. However, some more special hydrophobic or multifunctional interactions are necessary for enzymic stereospecificity.

Experimental

3-[2-(l-3-p-menthyloxy)ethyl]thiazolium Bromide (1). The salt was synthesized starting from *l*-menthol *via* the following intermediates successively: (*l*-3-*p*-menthyloxy)acetic acid, ethyl(*l*-3-*p*-menthyloxy)acetate, 2-(*l*-3-*p*-menthyloxy)ethanol, and 2-(*l*-3-*p*-menthyloxy)ethyl bromide. The last bromide 1 g (3.8 mmol) and thiazole 0.35 g (4.1 mmol) was heated (100 °C) in a sealed tube for 44 h. Crystals formed were collected and recrystallized from ethanol–ether, yield 0.74 g (56%), mp 188—189 °C, $[\alpha]_D^{20}$ −54.3° (*c* 0.97, MeOH). Found: C, 51.46; H, 7.53; N, 4.05%. Calcd for $C_{15}H_{26}BrNOS$: C, 51.71; H, 7.54; N, 4.02%.

(l-3-p-Menthyl)amine Hydrochloride. *l*-Menthol was converted to *l*-menthone by chromium trioxide oxidation followed by further conversion to *l*-menthone oxime. This oxime was reduced by metallic sodium in ethanol according to the literature procedures to give (*l*-3-*p*-menthyl)amine which was isolated as the hydrochloride, mp 255 °C, $[\alpha]_D^{20}$ −35.5° (*c* 2.0, H_2O) [lit,[9] $[\alpha]_D^{20}$ −36.1° (*c* 2.0, H_2O)].

N-thioformyl-(l-3-p-menthyl)amine was prepared by the same procedures as reported by Sheehan *et al.*[8]

3-(l-3-p-menthyl)thiazolium Bromide (2a). To a stirred solution of *N*-thioformyl-(*l*-3-*p*-menthyl)amine (5 g, 25 mmol) in benzene (40 ml) was added α-bromoacetaldehyde diethyl acetal (5 g, 25 mmol) in benzene (10 ml). The mixture was stirred overnight at room temperature. After benzene was evaporated, ether (20 ml) was added and neutralized with $NaHCO_3$ and extracted with ether to remove unreacted materials. The aqueous layer was evaporated to dryness. The residue was recrystallized from acetone–ether, 4.2 g (52%), mp 201—203 °C, $[\alpha]_D^{20}$ −31.8° (*c* 1.0, MeOH). Found: C, 51.72; H, 7.53; N, 4.64; S, 10.10%. Calcd for $C_{13}H_{22}BrNS$: C, 51.30; H, 7.30; N, 4.60; S, 10.54%.

3-(l-3-p-menthyl)thiazolium Perchlorate (2b). To a stirred

solution of **2a** 0.5 g (1.64 mmol) in methanol (5 ml) was added silver perchlorate 0.34 g (1.64 mmol). Silver bromide precipitated was filtered off and methanol was evaporated. The residue was dissolved in acetone and the insoluble silver bromide was again removed. Acetone was removed and the crystalline residue was finally recrystallized from ethanol–ether, yield 0.45 g (84%), mp 113—115 °C, $[\alpha]_D^{20}$ −32.1° (*c* 0.62, MeOH). Found: C, 48.05; H, 6.71; N, 4.28; S, 9.86%. Calcd for $C_{13}H_{22}ClNO_4S$: C, 48.21; H, 6.86; N, 4.33; S, 9.90%.

3-(l-3-p-Menthyl)-4-methylthiazolium Perchlorate (3). To a stirred solution of *N*-thioformyl-(*l*-3-*p*-menthyl)amine (4.1 g, 20.5 mmol) in benzene (40 ml) was added chloroacetone (1.9 g, 20.5 mmol) in benzene (20 ml). The mixture was stirred for 24 h and finally refluxed for 15 min. Benzene was evaporated, water was added, and neutralized with sodium carbonate (pH 7—8). The aqueous layer was extracted with ether to remove the unreacted materials. The water was evaporated to dryness. The residue was dissolved in dichloromethane to remove sodium chloride. The dichloromethane layer was dried over sodium sulfate. The dichloromethane was removed to give pasty residue. This paste was dissolved in acetone and treated with silver perchlorate in acetone. Silver chloride precipitated was filtered off and ether was added to the filtrate to give crystalline precipitates. The crystalline precipitates were collected and recrystallized from ethanol–ether, yield 0.16 g (16%), mp 199—200 °C, $[\alpha]_D^{20}$ −57.0° (*c*, 1.00, MeOH). Found: C, 50.10; H, 7.35; N, 4.07; S, 9.50%. Calcd for $C_{14}H_{24}ClNO_4S$: C, 49.76; H, 7.17; N, 4.15; S, 9.49%.

Asymmetric Benzoin Condensation. In a Thunberg tube, the solvent (10 ml) containing a catalyst (0.15 mmol) was bubbled with nitrogen for 20 min. The reaction was initiated by mixing the solvent with benzaldehyde (2.8 mmol) which was placed with a stirring rod in the upper flask of Thunberg tube. Stirring was continued at room temperature for a given time. The reaction mixture was extracted with ether, and the ether layer was dried over anhydrous magnesium sulfate. The ether was evaporated to dryness and the residue was chromatographed on a silica gel column with chloroform. The fraction containing benzoin was collected and the solvent was removed. Further recrystallization was noted to be unnecessary.

Optical rotation was recorded with a JASCO-SL automatic polarimeter, the precision of reading to be within ±0.002°.

We thank Mr. T. Higashiyama, Toyo Hakka Co., Ltd., for generous gift of *l*-menthol. We also thank Drs. Oya and Katakai for allowing the use of above polarimeter. This research was supported in part by Grant-in-Aid for Scientific Research from the Ministry of Education, Japan.

References

1) a) R. Breslow, *J. Am. Chem. Soc.*, **79**, 1762 (1957); b) T. C. Bruice and S. J. Benkovic, "Bioorganic Mechanism," W. A. Benjamin, Inc., New York (1966), Vol. II, Chap. 8; c) W. P. Jencks, "Catalysis in Chemistry and Enzymology," McGraw-Hill, New York (1966), pp. 127—133.

2) a) H. Stetter and M. Schreckenberg, *Angew. Chem. Int. Ed. Engl.*, **12**, 81 (1973); *Tetrahedron Lett.*, **1973**, 1461; *Chem. Ber.*, **107**, 210 (1974); H. Stetter, M. Schreckenberg, and K. Wiemann, *Chem. Ber.*, **109**, 541 (1976); b) H. Stetter and H. Kuhlmann, *Tetrahedron Lett.*, **1974**, 4505; *Angew. Chem. Int. Ed. Engl.*, **13**, 539 (1974); c) H. Stetter and H. Kuhlmann, *Synthesis*, **1975**, 379.

3) W. Tagaki and H. Hara, *J. Chem. Soc., Chem. Commun.*, **1973**, 891.

4) a) J. H. Fendler and E. J. Fendler, "Catalysis in Micellar and Macromolecular System," Academic Press, New York (1975); b) C. A. Bunton in "Application of Biochemical Systems in Organic Chemistry," ed by J. B. Jones, C. J. Sih, and D. Perlman, John Willy and Sons, New York (1976), Part II, Chap. IV.

5) a) C. M. Starks, *J. Am. Chem. Soc.*, **93**, 195 (1971); **95**, 3613 (1973); b) A. M. Herriott and D. Picker, *ibid.*, **97**, 2345 (1975); c) J. Dockx, *Synthesis*, **1973**, 441; d) E. V. Dehmlow, *Angew. Chem. Int. Ed. Engl.*, **13**, 170 (1974); e) W. P. Weber and G. W. Gokel, "Phase Transfer Catalysis in Organic Synthesis," Springer Verlag KG (1977); f) C. M. Starks and C. Liotta, "Phase Transfer Catalysis," Academic Press, New York (1978).

6) a) J. M. Brown and C. A. Bunton, *J. Chem. Soc., Chem. Commun.*, **1974**, 969; b) Y. Ihara, *ibid.*, **1978**, 984; c) R. A. Moss, Y.-s. Lee, and T. J. Lukas, *J. Am. Chem. Soc.*, **101**, 2499 (1979).

7) a) S. Colonna, R. Fornasier, and U. Pfeiffer, *J. Chem. Soc., Perkin Trans. 1*, **1978**, 8; b) S. Colonna and R. Fornasier, *ibid.*, **1978**, 371; c) H. Wynberg and B. Greijdans, *J. Chem. Soc., Chem. Commun.*, **1978**, 427; d) S. Colonna, H. Hiemstra, and H. Wynberg, *ibid.*, **1978**, 239; e) J. C. Hummelen and H. Wynberg, *Tetrahedron Lett.*, **1978**, 1089.

8) J. C. Sheehan and T. Hara, *J. Org. Chem.*, **39**, 1196 (1974).

9) J. Read and R. A. Storey, *J. Chem. Soc.*, **1930**, 2761.

10) a) H. G. Rule and J. Crawford, *J. Chem. Soc.*, **1937**, 138; b) H. Wren, *ibid.*, **95**, 1583 (1909); A. McKenzie and H. Wren, *ibid.*, **93**, 309 (1908).

11) H. Hara, Thesis, Faculty of Engineering, Gunma University, (1974).

12) Other conformations of axial thiazolium ring are possible, but they should be more unstable than **A** and **B**.

13) a) K. R. Hanson and I. A. Rose, *Acc. Chem. Res.*, **8**, 1 (1975); b) I. A. Rose and K. R. Hanson in Ref. 4b, Part II, Chap. I.

The Synthesis and Cation-complexing Ability of Alkyl Crown Ethers

Tadashi MIZUNO, Yohji NAKATSUJI, Shozo YANAGIDA, and Mitsuo OKAHARA*

Department of Applied Chemistry, Faculty of Engineering, Osaka University, Yamadakami, Suita 565

(Received July 11, 1979)

Alkyl-15-crown-5 and alkyl-12-crown-4 were prepared *via* polyethylene glycol β-haloalkyl ethers in two steps from terminal olefins, and their complexing ability with cations of alkali and alkaline earth metals was measured by using ^{1}H NMR; it was found to be almost identified with that of the corresponding unsubstituted crown ether. A new type of alkyl crown ether with a chloro substituent could also be synthesized according to this method.

Synthetic macrocyclic polyethers have received attention in recent years, as phase-transfer catalysts in a variety of organic reactions because they possess the ability to form complexes with salts of the alkali and alkaline earth metals to raise the reactivity of the counter anion; they are also expected to be useful selective carriers for the transport of cations through a liquid membrane.[1,2]

Modifications of their solubilities in various organic solvents by introducing lipophilic groups into the macrocyclic ring seem to be desirable for these purposes. For substituted macrocyclic compounds, the balance between lipophilic and hydrophilic parts is supposed to be one of the important factors influencing their properties; this balance can easily be adjusted by changing the substituents and the ring size.

From this standpoint, alkyl-substituted crown ethers, cryptands, and cyclic tetraamines were synthesized *via* the multi-step reactions reported by Cinquini,[3,4] Lehn,[5] and Tundo[6] and found to show high catalytic activity in several two-phase reactions. On the other hand, alkyl-substituted cyclams were synthesized and successfully used as the extraction of heavy metal ions from an aqueous solution by Tabushi.[7]

In the course of our investigation, a convenient method of synthesizing these alkyl crown ethers *via* polyethylene glycol β-haloalkyl ethers was found and previously reported in a preliminary paper.[8]

In this paper, we will describe the preparation of alkyl-15-crown-5 and alkyl-12-crown-4 and their complexing ability with alkali and alkaline earth cations, as measured by means of the ^{1}H NMR method.

Experimental

The ^{1}H NMR spectra were taken at 100 MHz on a JEOL JNM-PS-100 spectrometer, using tetramethylsilane as the internal standard, except for the measurement of the complexing ability. The infrared spectra were obtained on a JASCO IR-E spectrometer. The mass spectra were measured with a Hitachi RMU-6E mass spectrometer at an ionization potential of 70 eV. The GLC analyses were done on a Shimadzu GC-3A using a 1 m×3 mm column packed with 10% Silicone SE-30 on 60—80 mesh Celite 545. The halogen contents of the polyethylene glycol β-haloalkyl ethers were measured according to the conventional method.[9]

*Preparation of Polyethylene Glycol β-Haloalkyl Ether (**1** or **2**).* To a stirred suspension of 136.0 g (0.7 mol) of tetraethylene glycol and 35.6 g (0.2 mol) of NBS we added, drop by drop, 18.5 g (0.22 mol) of 2-methyl-1-pentene over a 15-min period at 45—50 °C; the mixture was then stirred at that temperature for 2 h until the positive halogen had been consumed. The reaction mixture was cooled to room temperature and worked up adding water and then extracting with ether. The ether extracts were dried over anhydrous magnesium sulfate and concentrated to give 47.8 g (67%) of the crude product (**1h**). Some of the results are shown in Table 1.

*Preparation of Alkyl-15-crown-5 (**3**); 2-Methyl-2-propyl-15-crown-5 (**3h**).* To a stirred suspension of 4.7 g (0.11 mol) of sodium hydroxide in 174 ml of diglyme we added, drop by drop, 35.7 g (0.1 mol) of **1h** over a 3.5-h period at 120—125 °C; the mixture was then stirred at 110—140 °C for 7 h. The reaction was followed by GLC and continued until the starting material (**1h**) had been completely consumed. The resultant mixture was cooled to room temperature, and sodium bromide was removed by filtration. The filtrate was evaporated under reduced pressure to give 29.3 g of a brown viscous liquid. A portion of the crude product (9.6 g) was distilled to give 3.83 g (43%) of a colorless liquid. The product was further purified on a silica-gel column (hexane: acetone = 10: 1) to afford the following analytical sample (**3h**): n_D^{20}, 1.4636; IR max (neat) 2980, 2880, 1465, 1360, 1297, 1200, and 1125 cm^{-1}; mass: 276 (M) and 233 (M−R); NMR (CCl_4) δ 0.90 (t, 3H), 1.06 (s, 3H), 1.38 (m, 4H), and 3.28—3.68 (m, 18H). Found: C, 60.88; H, 10.27%. Calcd for $C_{14}H_{28}O_5$: C, 60.84; H, 10.21%.

*Preparation of Alkyl-12-crown-4 (**4**); 2-Methyl-2-propyl-12-crown-4 (**4d**).* A suspended mixture of 20.0 g (0.064 mol) of **2d** and 5.92 g (0.14 mol) of sodium hydroxide in 165 ml of diglyme was stirred at 130—145 °C for 19 h until the starting material (**2d**) had been completely consumed. A brown viscous liquid (14.2 g) was then obtained according to the procedure mentioned above. A portion of the crude product (9.0 g) was distilled to give 1.93 g (21%) of **4d** as a colorless liquid. All the spectroscopic analytical results shown in Table 4 support the expected structure.

*Preparation of Crown Ether Containing a Chloro Substituent; 2-Chloromethyl-2-methyl-15-crown-5 (**3i**).* To a stirred suspension of 3.0 g (0.07 mol) of sodium hydroxide in 100 ml of diglyme we added, drop by drop, 18.2 g (0.05 mol) of **1i** in 25 ml of diglyme over a 4.5-h period at 80—125 °C, and then the mixture was stirred for 6 h at 110—120 °C. A purification procedure similar to that described above afforded the following analytical sample (**3i**): IR max (neat) 2900, 2850, 1455, 1350, 1250, 1100, 930, 770, and 730 cm^{-1}; mass: 233 (M−R); NMR (CCl_4) δ 1.18 (s, 3H) and 3.40—3.76 (m, 20H). Found: C, 51.90; H, 8.44; Cl,[9] 12.1%. Calcd for $C_{12}H_{23}O_5Cl$: C, 50.97; H, 8.20; Cl, 12.5%.

Measurement of Complexing Ability Using ^{1}H NMR. The ^{1}H NMR were measured as a 1% solution of crown ether in acetone-d_6, with 8% dioxane in benzene used as an external standard. The chemical shift of ^{1}H NMR signals of the main oxyethylene protons in the crown ether was compared with that in a sample containing an equimolar amount of the metal salt (thiocyanate).[10] The difference in the chemical shifts of these two samples was regarded as the downfield shift, based on the formation of the complex. The results are summarized in Tables 5 and 6.

Results and Discussion

Preparation of Alkyl-substituted Crown Ethers via *Polyethylene Glycol β-Haloalkyl Ethers.* The overall reaction process is shown in Scheme 1.

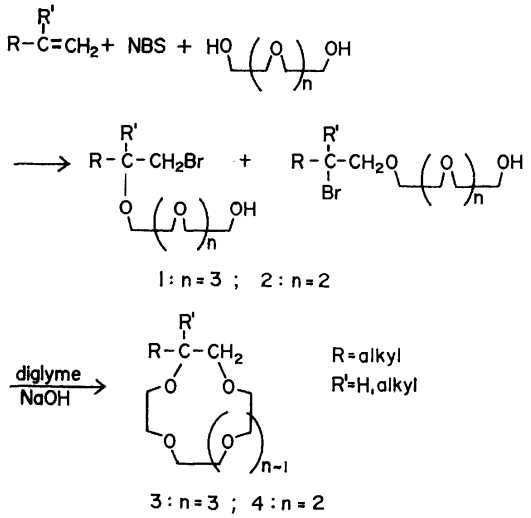

Scheme 1.

The polyethylene glycol β-haloalkyl ether was prepared by adding 1-alkene to a suspension of polyethylene glycol and a halogenating agent (NBS or NBA) and was then converted to the alkyl-substituted crown ether by heating with sodium hydroxide in diglyme. The β-haloalkyl ethers were obtained as a mixture of two isomers (Markownikoff and *anti*-Markownikoff adducts of the terminal olefins[11,12]). However the two isomers afford only one type of alkyl-substituted crown ether after a cyclization reaction.

Table 1 shows the halogenating agents used, the yields, and the halogen contents of the products in the preparation of polyethylene glycol β-haloalkyl ethers. Although the intermediate haloethers (**1** or **2**) were cyclized to crown ethers without further purification,[13] the halogen contents of the crude products coincided well with the calculated values.

The results of the cyclization to alkyl-15-crown-5 are shown in Table 2, while the analytical data are shown in Table 3. A reaction temperature above 100 °C was found to be optimal for the cyclization without any undesirable formation of olefins. The use of a high-dilution technique with a varied dropping rate of polyethylene glycol β-haloalkyl ether did not improve the yield appreciably. Dioxane had been used as the solvent in the preparation of alkyl-15-crown-5 in the previous paper,[8] but diglyme was preferable to dioxane from the viewpoint of making it possible to adopt higher reaction temperatures.

Table 1. Synthesis of polyethylene glycol β-haloalkyl ethers

Compd	R	R'	*n*	Halogenating agent	Yield %	Found (Calcd) Halogen(%)
1a	*n*-C_4H_9	H	3	NBA	62	22.3 (22.4)
1b	*n*-C_6H_{13}	H	3	NBS	85	21.0 (20.7)
1c	*n*-C_8H_{17}	H	3	NBS	77	21.6 (19.3)
1d	*n*-$C_{10}H_{21}$	H	3	NBA	74	22.7 (18.1)
1e	*n*-$C_{12}H_{25}$	H	3	NBS	84	17.5 (17.0)
1f	CH_3	CH_3	3	NBS	36	25.1 (24.3)
1g	C_2H_5	CH_3	3	NBS	76	22.4 (23.3)
1h	*n*-C_3H_7	CH_3	3	NBS	67	23.0 (22.4)
1i	CH_2Cl	CH_3	3	NBS	77	30.5 (31.7)
1j	C_2H_5	C_2H_5	3	NBS	74	22.7 (22.4)
2a	C_2H_5	H	2	NBS	24	25.6 (25.5)
2b	CH_3	CH_3	2	NBS	38	28.2 (28.0)
2c	C_2H_5	CH_3	2	NBS	76	24.9 (26.7)
2d	*n*-C_3H_7	CH_3	2	NBS	65	25.6 (25.5)
2e	CH_2Cl	CH_3	2	NBS	73	35.7 (36.3)

The yield of alkyl-12-crown-4 (**4**) was lower than that of the corresponding alkyl-15-crown-5 (**3**) in spite of the severer reaction conditions, as is shown in Tables 2 and 4; this finding suggests that the sodium cation did not function effectively as the template ion in the formation of the former.[14]

A new type of crown ether (**3i** and **4e**) with a chloro substituent, which is potentially useful for the preparation of variously functionalized crown ethers, could also be synthesized according to this method. Although the intermediate product (**1i** or **2e**) possesses two different halogen atoms, the results of the NMR and elementary analyses showed that the chlorine atom was preferentially conserved in the final product (**3i** or **4e**) after the cyclization reaction (Scheme 2).

Table 2. Synthesis of alkyl-15-crown-5 (**3**)

Compd	R	R'	Solvent	LiCl/**1**[a]	Reaction temp/°C	Time/h	Yield/%[b]
3a	*n*-C_4H_9	H	Dioxane	2.0	reflux	30	12
3b	*n*-C_6H_{13}	H	Diglyme	1.7	80—100	18	35
3c	*n*-C_8H_{17}	H	Dioxane	—	25—80	53	6
3d	*n*-$C_{10}H_{21}$	H	Diglyme	3.0	90—120	27	30
3e	*n*-$C_{12}H_{25}$	H	Diglyme	1.2	90—120	27	36
3f	CH_3	CH_3	Diglyme	—	80—125	6	38
3g	C_2H_5	CH_3	Diglyme	—	105—130	9	39
3h	C_3H_7	CH_3	Diglyme	—	110—140	7	43
3i	CH_2Cl	CH_3	Diglyme	—	110—120	6	25
3j	C_2H_5	C_2H_5	Diglyme	—	105—140	12	22

a) mol/mol. b) After purification.

Table 3. Analysis of alkyl-15-crown-5 (**3**)

Compd	MS	NMR (CCl_4, δ)	Bp (°C/Torr)
3a	276 (M) 219 (M−R)	0.90 (t, 3H), 1.34 (s, 6H) 3.22—3.72 (m, 19H)	—[a]
3b	304 (M) 219 (M−R)	0.90 (t, 3H), 1.32 (s, 10H) 3.16—3.76 (m, 19H)	—[a]
3c	332 (M) 219 (M−R)	0.88 (t, 3H), 1.26 (s, 14H) 3.24—3.70 (m, 19H)	—[a]
3d	360 (M) 219 (M−R)	0.88 (t, 3H), 1.26 (s, 18H) 3.26—3.70 (m, 19H)	—[a]
3e	388 (M) 219 (M−R)	0.88 (t, 3H), 1.26 (s, 22H) 3.30—3.70 (m, 19H)	—[a]
3f	248 (M) 233 (M−R)	1.12 (s, 6H) 3.28—3.68 (m, 18H)	89—91/0.05
3g	262 (M) 233 (M−R)	0.83 (t, 3H), 1.04 (s, 3H) 1.46 (m, 2H), 3.28—3.68 (m, 18H)	98—100/0.04
3h	276 (M) 233 (M−R)	0.90 (t, 3H), 1.06 (s, 3H) 1.38 (m, 4H), 3.28—3.68 (m, 18H)	103—105/0.10
3i	233 (M−R)	1.18 (s, 3H) 3.40—3.76 (m, 20H)	—[a]
3j	276 (M) 247 (M−R)	0.81 (t, 6H), 1.48 (q, 4H) 3.32—3.72 (m, 18H)	108—110/0.05

a) Purified on a silica-gel column.

Table 4. Synthesis and analysis of alkyl-12-crown-4 (**4**)

Compd	R	R′	Reaction temp/°C	Time/h	Yield/%[b]	MS	NMR (CCl_4, δ)	Bp (°C/Torr)
4a	C_2H_5	H	100—110	24	15	204 (M) 175 (M−R)	0.91 (t, 3H), 1.38 (m, 2H) 3.27—3.70 (m, 15 H)	—[a]
4b	CH_3	CH_3	120—140	11	12	204 (M) 189 (M−R)	1.06 (s, 6H) 3.20−3.72 (m, 14H)	64/0.09
4c	C_2H_5	CH_3	120—140	14	23	218 (M) 189 (M−R)	0.84 (t, 3H), 1.04 (s, 3H) 1.45 (m, 2H), 3.24—3.72 (m, 14H)	63/0.06
4d	*n*-C_3H_7	CH_3	130—145	19	21	232 (M) 189 (M−R)	0.90 (t, 3H), 1.04 (s, 3H) 1.38 (m, 4H), 3.20—3.80 (m, 14H)	71/0.09
4e	CH_2Cl	CH_3	100—110	7	14	189 (M−R)	1.16 (s, 3H) 3.32—3.76 (m, 16H)	—[a]

a) Purified on a silica-gel column. b) After purification.

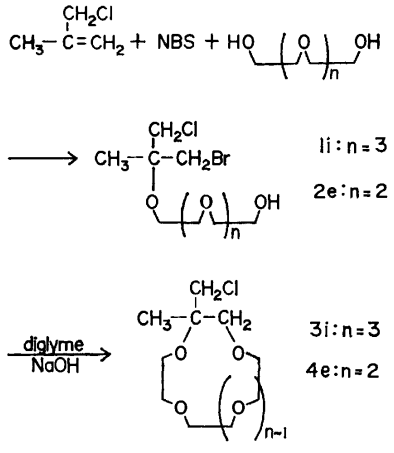

Scheme 2.

Complexing Ability of Alkyl-substituted Crown Ethers. The lipophilicity of crown ethers may be supposed to be important, together with their complexing properties, when they are used as phase-transfer catalysts, as is the case with quaternary ammonium salts, which were discussed recently.[15] The lipophilicity of alkyl crown ethers can be controlled by changing the number or the chain length of the alkyl group. However, the introduction of the alkyl group into the crown ether rings may cause a decrease in their complexing ability toward the metal cations because of the steric effect or the loss of symmetry.[16]

Therefore, we investigated the complexing ability of some of the alkyl crown ethers prepared in this study and compared it with that of the unsubstituted crown ethers. The ^1H NMR spectrum of each alkyl crown

Table 5. Downfield shift in 100 MHz NMR of alkyl-15-crown-5 caused by MSCN (Hz)

Cation	Compd									
	3[a]	**3a**	**3b**	**3c**	**3d**	**3e**	**3f**	**3g**	**3h**	**3f**
Na^+	13.9	13.1	13.7	14.7	13.5	13.9	10.6	13.9	13.8	12.6
K^+	11.2	12.3	12.3	12.8	13.0	12.1	10.1	11.1	11.9	10.9

a) Unsubstituted 15-crown-5.

ether as a 1% solution in acetone-d_6 was measured, with or without an equimolar amount of the metal salt. An 8% solution of dioxane in benzene was used as the external standard.

The influence of the change in the alkyl group in alkyl-15-crown-5 (Table 5) and alkyl-12-crown-4 (Table 6) on the complexing ability toward sodium and potassium cations was found to be almost the same as that of the corresponding unsubstituted crown ether. This finding suggests that it is possible to adjust the lipophilic/hydrophilic balance of crown ethers without changing the complexing ability toward alkali metal cations. In other words, there is possibility of designing a suitable crown compound for a specified purpose without imparing their complexing ability and selectivity.

TABLE 6. DOWNFIELD SHIFT IN 100 MHz NMR OF ALKYL-12-CROWN-4 CAUSED BY MSCN OR $M(SCN)_2$ (Hz)

Cation	Compd			
	4[a]	**4b**	**4c**	**4d**
Na^+	15.6	13.2	15.8	14.7
K^+	10.6	8.2	9.7	9.2
Mg^{2+}	2.2	0.8	2.2	3.3
Ca^{2+}	—[b]	20.2	24.5	20.1

a) Unsubstituted 12-crown-4. b) Precipitation of insoluble salts.

Table 6 also demonstrates the complexing ability of alkyl and unsubstituted 12-crown-4 for magnesium and calcium cations. The complexing ability of unsubstituted 12-crown-4 for the calcium cation could not be measured because of the formation of an insoluble complex in the acetone-d_6 solution.[17] About a 20 Hz downfield shift was observed in the combination of 12-crown-4 and the calcium cation, but in the case of the magnesium cation the shift was little. The selectivity of alkyl-12-crown-4 for magnesium and calcium cations was similar to that of unsubstituted 12-crown-4.

Consequently, the complexing ability and the selectivity of alkyl-15-crown-5 and alkyl-12-crown-4 for alkali and alkaline earth metal cations were found to be almost equal to those of the corresponding unsubstituted one, and the raise in the lipophilicity of crown ethers can be expected to bring about a favorable result when crown ether is used as a phase-transfer catalyst or a selective carrier for the transport of cations.

References

1) C. N. Starks and C. L. Liotta, "Phase-transfer Catalysts, Principles and Technique," Academic Press (1978).
2) M. Hiraoka, "Crown Compounds," Kodansha Scientific (1978).
3) M. Cinquini and P. Tundo, *Synthesis*, **1976**, 516.
4) M. Cinquini, F. Montanari, and P. Tundo, *J. Chem. Soc., Chem. Commun.*, **1975**, 516.
5) D. Clement, F. Damm, and J.-M. Lehn, *Heterocycles*, **5**, 477 (1976).
6) P. Tundo, *Tetrahedron Lett.*, **1978**, 4693.
7) I. Tabushi and M. Fujiyoshi, *Heterocycles*, **7**, 851 (1977).
8) M. Okahara, M. Miki, S. Yanagida, I. Ikeda, and K. Matsushima, *Synthesis*, **1977**, 854.
9) W. Kimura, *Kogyo Kagaku Zasshi*, **37**, 1310 (1934).
10) S. Yanagida, K. Takahashi, and M. Okahara, *Bull. Chem. Soc. Jpn.*, **51**, 1294 (1978).
11) A. Iovchev, H. Reinheckel, K. Haage, and R. Pomakova, *Monatsh. Chem.*, **97**, 1620 (1966).
12) I. Michev, N. Khristova, R. Pomakova, B. Ponaitova, and A. Iovchev, *Z. Chem.*, **15**, 191 (1975).
13) Decomposition was observed in most cases in the course of distillation.
14) N. Kawamura, M. Miki, I. Ikeda, and M. Okahara, *Tetrahedron Lett.*, **1979**, 535. A dependence of the template effect on the reaction temperature had been found in the synthesis of crown ethers.
15) D. Landini, A. Maia, and F. Montanari, *J. Chem. Soc., Chem. Commun.*, **1977**, 112.
16) C. J. Pedersen, *J. Am. Chem. Soc.*, **89**, 7017 (1967).
17) P. P. North, E. C. Steiner, F. P. van Remoortere, and F. P. Boer, *Acta Crystallogr., Sect. B*, **32**, 370 (1976), and the references cited therein. The crystal structure of the complex of unsubstituted 12-crown-4 with metal halides was determined by a single-crystal X-ray diffraction study.

Reactions of Trimethylsilyl Cyanide and *N*-(Trimethylsilyl)diphenylmethyleneamine with Nitrones and Thermal Decompositions of Their Adducts

Otohiko Tsuge,* Satoshi Urano, and Takahiko Iwasaki

Research Institute of Industrial Science, Kyushu University 86, Hakozaki, Higashi-ku, Fukuoka 812

(Received July 16, 1979)

Trimethylsilyl cyanide (**1**) and *N*-(trimethylsilyl)diphenylmethyleneamine (**2**) reacted with α-aryl-*N*-phenylnitrones to afford the corresponding 1:1 adducts **4** and **5** respectively. Thermal decomposition of **4** in refluxing xylene gave azoxybenzene, stereoisomers of 2,3-diarylsuccinonitriles, α-iminonitriles and/or benzanilides, whose yields depended on the nature of substituents on phenyl group of **4**. On heating in benzene **5** afforded a mixture of azoxybenzene and *meso*-*N*,*N*′-bis(diphenylmethylene)-1,2-diarylethylenediamines. On the other hand, reactions of **1** and **2** with *N*-(diphenylmethylene)aniline *N*-oxide or *N*-(9-fluorenylidene)aniline *N*-oxide did not give the corresponding 1:1 adducts, but instead compounds arising from thermal decomposition of initial 1:1 adducts were directly obtained. The reaction of **1** with *N*-(*p*-diethylaminophenyl)-α-phenylnitrone leading to the corresponding α-imino nitrile is also described.

It is known that trimethylsilyl cyanide (**1**) is a good reagent for introducing cyano group, acylation, protecting and activating carbonyl groups in organic syntheses.[1] Recently, Ojima and his coworkers have developed versatility of **1** for syntheses of heterocyclic compounds by the reaction with isocyanates[2] or isothiocyanate,[3] and of α-amino nitriles by the reaction with Schiff bases.[4,5] It has also been reported that *N*-(trimethylsilyl)diphenylmethyleneamine (**2**) reacted with isocyanates, isothiocyanates, and benzimidoyl chlorides to give useful products for syntheses of heterocyclic compounds.[6]

However, little attention has been drawn to the reactions of **1** and **2** with nitrones. In this paper we wish to report on the reactions of **1** and **2** with α-aryl-*N*-phenylnitrones (**3**) and thermal decomposition of the adducts. In this context, the reactions of **1** and **2** with aromatic nitrones other than **3** are also described.

Results and Discussion

Reactions of Trimethylsilyl Cyanide (1) and N-*(Trimethylsilyl)diphenylmethyleneamine (2) with α-Aryl*-N-*phenylnitrones (3).* Treatment of **1** with nitrones, **3a**—**3d**, afforded the corresponding 1:1 adducts, α-[*N*-(trimethylsilyloxy)phenylamino]arylacetonitriles, **4a**—**4d**, in excellent yields respectively. Also, **2** reacted with nitrones, **3a**—**3d**, to give the corresponding 1:1 adducts, α-[*N*-(trimethylsilyloxy)phenylamino]-*N*-(diphenylmethylene)benzylamines, **5a**—**5d**, in good yields (Scheme 1).

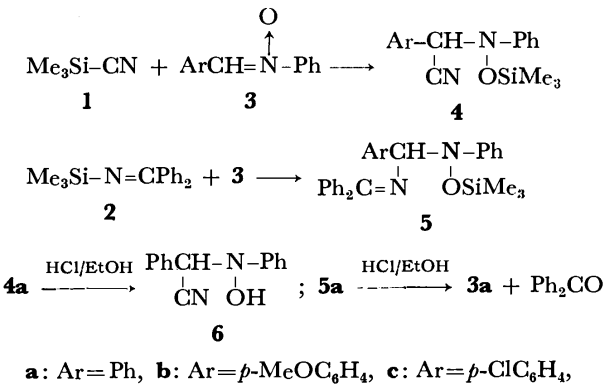

a: Ar=Ph, **b**: Ar=*p*-$MeOC_6H_4$, **c**: Ar=*p*-ClC_6H_4, **d**: Ar=*p*-$NO_2C_6H_4$

Scheme 1.

Structural elucidation of these adducts **4** and **5** was accomplished on the basis of elemental analysis and spectral data. Detrimethylsilylation of **4a** with hydrochloric acid in ethanol afforded α-(*N*-hydroxyphenylamino)phenylacetonitrile (**6**) in good yield, whereas **5a** was readily converted into nitrone **3a** and benzophenone under similar conditions.

The reaction conditions, yields, physical and analytical data for **4** and **5** are summarized in Tables 1 and 2.

Although **1** did not react with *N*-(diphenylmethylene)aniline *N*-oxide (**7**) or *N*-(9-fluorenylidene)aniline *N*-oxide (**8**) in refluxing benzene, on heating with **7** or **8** at 120 °C without solvent **1** afforded a mixture of tetraphenylsuccinonitrile (**9**) or 9,9′-dicyano-9,9′-bifluorenyl (**10**) and azoxybenzene (**11**) respectively.

Table 1. Reaction conditions, yields, melting points, and appearance for **4** and **5**

Compound	Reaction conditions	Yield/%	Mp/°C	Appearance
4a	C_6H_6, reflux, 4 h	95[a]	88—89	colorless prisms
4b	C_6H_6, reflux, 2.5 h	97	102—102.5	colorless prisms
4c	C_6H_6, reflux, 3 h	95	94—96	colorless needles
4d	C_6H_6, reflux, 5.5 h	97	118—119.5	colorless needles
5a	CH_2Cl_2, r.t., 12 h	84	105—106	colorless needles
5b	CH_2Cl_2, r.t., 14 h	73	102—104	colorless prisms
5c	CH_2Cl_2, r.t., 16 h	83	93—95	colorless prisms
5d	CH_2Cl_2, r.t., 13 h	74	125.5—127	colorless prisms

a) In the reaction at room temperature (r.t.) for 12 h **4a** was obtained in 50% yield.

Table 2. Spectral and analytical data of **4** and **5**

Compd	IR/cm^{-1} $\nu_{C\equiv N}$	IR/cm^{-1} $\nu_{C=N}$	^{1}H NMR ($CDCl_3$) $Si(CH_3)_3$ δ/ppm	^{1}H NMR ($CDCl_3$) $>CH$ δ/ppm	MS M^+ (*m/e*)	Found (%) C	Found (%) H	Found (%) N	Calcd (%) C	Calcd (%) H	Calcd (%) N
4a	2220	—	−0.22	5.12	296	68.72	6.75	9.37	68.91	6.75	9.45
4b	2230	—	−0.12	5.19	326	66.22	6.70	8.56	66.22	6.79	8.58
4c	2230	—	−0.14	5.14	330, 332	61.77	5.70	8.41	61.71	5.79	8.47
4d	2230	—	−0.12	5.32	341	59.72	5.54	12.37	59.80	5.61	12.31
5a[a]	—	1610	−0.15	5.50	450	77.42	6.79	6.26	77.29	6.71	6.21
5b	—	1610	−0.13	5.30	480	74.96	6.71	5.83	74.93	6.60	5.76
5c	—	1625	−0.12[b]	5.33[b]	470, 472[c]	71.90	5.99	5.75	71.80	6.03	5.77
5d	—	1620	−0.10	5.54	495	70.26	5.84	8.61	70.28	5.90	8.48

a) ^{13}C NMR ($CDCl_3$) δ 0.73 ($Si(CH_3)_3$, 86.4 (tert. **C**), 168.4 (**C**=N). b) Measured in CCl_4. c) No parent peaks were observed. These peaks correspond to the ions (M^+−Me).

On the other hand, **2** reacted with **7** or **8** in dichloromethane at room temperature to give a mixture of **11** and *N,N'*-bis(diphenylmethylene)tetraphenylethylenediamine (**12**) or 9,9'-bis(diphenylmethyleneamino)-9,9'-bifluorenyl (**13**) respectively (Scheme 2).

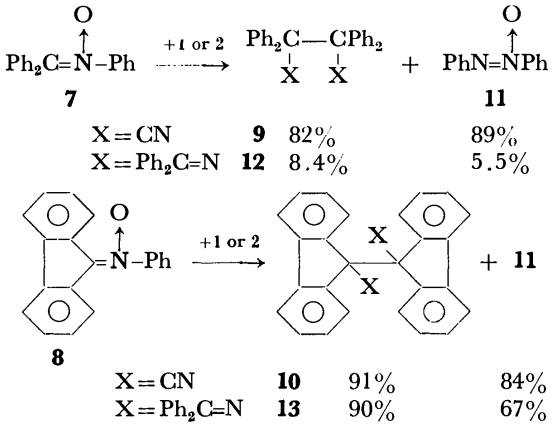

Scheme 2.

Compounds **9**, **10**, **12**, and **13** were prepared by other routes respectively, but the above reactions provide a one-pot syntheses for these compounds.

Thermal Decomposition of 1:1 Adducts. It is reasonable to assume that the reactions shown in Scheme 2 proceeded through the rupture of the C–N bonds of initial adducts of types **4** and **5**. Thus, we have investigated thermal decompositions of adducts **4** and **5**.

When a solution of **4a** or **4b** in xylene was refluxed, a mixture of **11** and stereoisomers of the corresponding 2,3-diarylsuccinonitriles (**14**) respectively. Under similar conditions **4c** afforded α-phenylimino-*p*-chlorophenylacetonitrile (**15c**) and *p*-chlorobenzanilide (**16c**) together with **11** and stereoisomers of 2,3-bis(*p*-chlorophenyl)-succinonitriles (**14c**). In the thermal decomposition of **4d**, however, α-phenylimino-*p*-nitrophenylacetonitrile (**15d**) was obtained as a major product, accompanied with a small amount of *p*-nitrobenzanilide (**16d**) as shown in Scheme 3.

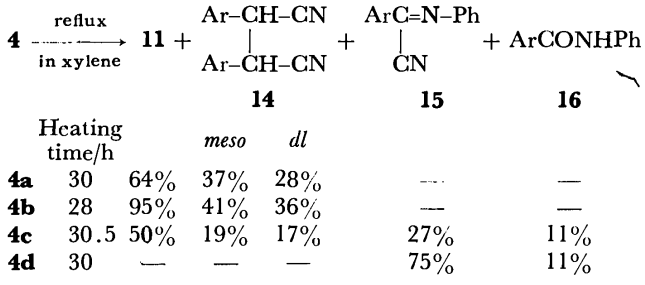

	Heating time/h		*meso*	*dl*		
4a	30	64%	37%	28%	—	—
4b	28	95%	41%	36%	—	—
4c	30.5	50%	19%	17%	27%	11%
4d	30	—	—	—	75%	11%

a: Ar=Ph, **b**: Ar=*p*-$MeOC_6H_4$, **c**: Ar=*p*-ClC_6H_4, **d**: Ar=*p*-$NO_2C_6H_4$

Scheme 3.

Structural elucidation of **14**, **15**, and **17** was accomplished on the basis of their spectral data and/or comparison with physical data of the compounds reported previously.[7]

As mentioned above, α-imino nitriles **15c** and **15d** were formed in thermal decomposition of **4c** and **4d**. It is reasonable to assume that these α-imino nitriles **15** are formed by the elimination of trimethylsilanol from the corresponding **4**, because *p*-chlorophenyl and *p*-nitrophenyl groups enhance the acidity of α-hydrogen atom of **4**. Thus, it is also expected that thermal decomposition of an adduct of type **4** possessing an electron-donating group on *N*-phenyl will give an α-imino-nitrile. In fact, α-(*p*-diethylaminophenylimino)phenylacetonitrile (**20**) was obtained directly even at room

On the other hand, thermal decomposition of **5a**—**5d** in refluxing benzene afforded a mixture of **11** and the corresponding *meso-N,N'*-bis(diphenylmethylene)-1,2-diarylethylenediamines, **17a**—**17d**, respectively (Scheme 4). Hydrolysis of **17a** gave a mixture of *meso*-1,2-diphenylethylenediamine (**18**) and benzophenone.

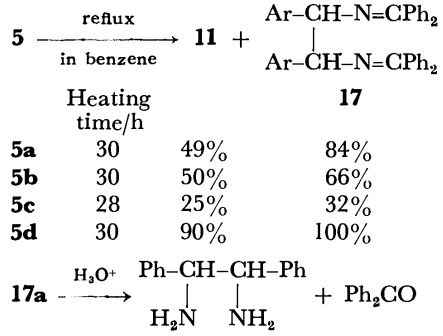

	Heating time/h		
5a	30	49%	84%
5b	30	50%	66%
5c	28	25%	32%
5d	30	90%	100%

a: Ar=Ph, **b**: Ar=*p*-$MeOC_6H_4$, **c**: Ar=*p*-ClC_6H_4, **d**: Ar=*p*-$NO_2C_6H_4$

Scheme 4.

temperature by the reaction of **1** with *N*-(*p*-diethylaminophenyl)-α-phenylnitrone (**19**).

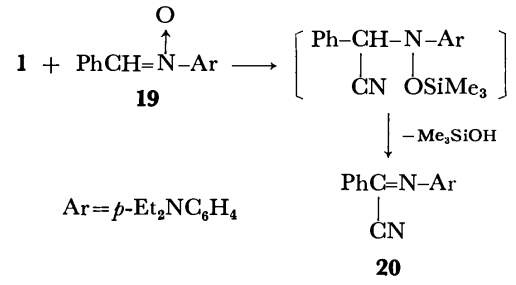

Although mechanistic considerations are still speculative, a plausible pathway for the formation of **11** and **14** or **17** from **4** or **5** is outlined in Scheme 5. The homolytic rupture of the C–N bond of **4** or **5** yields radical **A** and **B**. The radical **A** dimerizes to give **14** or **17**, and the dimerization of **B** with subsequent elimination of di(trimethyl)siloxane affords **11**.

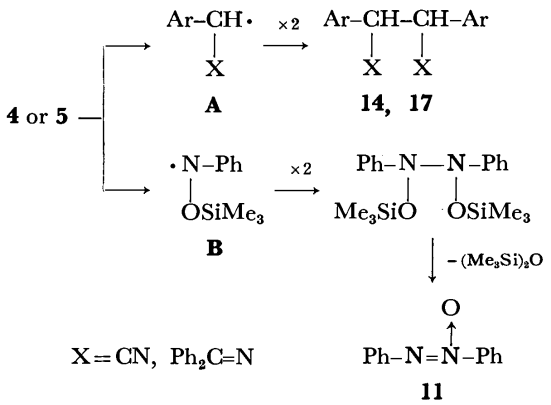

Scheme 5.

Experimental

Melting points are uncorrected. IR, NMR, and mass spectra were obtained on a JASCO IRA-1 spectrometer, Hitachi R-40, JEOL SX-100 spectrometers, and a Hitachi RMS-4 spectrometer, respectively. IR and NMR spectra were taken in KBr disks and $CDCl_3$ solutions respectively. Mass spectra were obtained at 70 eV.

Materials. Trimethylsilyl cyanide (**1**)[8] and *N*-(trimethylsilyl)diphenylmethyleneamine (**2**)[9] were prepared from trimethylsilyl chloride and silver cyanide or lithium diphenylmethanimine by the reported methods respectively. α-Aryl-*N*-phenylnitrones **3a**—**3d**,[10] *N*-(diphenylmethylene)aniline *N*-oxide (**7**),[11] *N*-(9-fluorenylidene)aniline *N*-oxide (**8**)[11] and *N*-(*p*-diethylaminophenyl)-α-phenylnitrone (**19**)[12] were prepared according to the reported methods respectively.

General Procedure for the Reaction of 1 with 3. A solution of **1** (0.01 mol) and **3** (0.005 mol) in benzene (5 ml) was refluxed. The reaction mixture was evaporated *in vacuo*, and recrystallization of the residue from hexane afforded the corresponding α-[*N*-(trimethylsilyloxy)phenylamino]arylacetonitrile **4**. Reaction conditions, yields, physical and analytical data for **4** are given in Tables 1 and 2.

General Procedure for the Reaction of 2 with 3. A solution of **2** (0.001 mol) and **3** (0.001 mol) in CH_2Cl_2 (20 ml) was stirred at room temperature. The reaction mixture was concentrated *in vacuo* to leave a residue. The residue was triturated with hexane to give crystals, which on recrystallization from hexane afforded the corresponding α-[*N*-(trimethylsilyloxy) phenylamino]-*N*-(diphenylmethylene) benzylamine **5**. Reaction conditions, yields, physical and analytical data for **5** are also shown in Tables 1 and 2.

Detrimethylsilylation of 4a. A solution of **4a** (1.0 g) in EtOH (25 ml) was stirred with concd HCl (20 ml) at room temperature for 1 h. The reaction mixture was poured into water (100 ml) to give solid, which on recrystallization from hexane–benzene afforded 0.69 g (91%) of α-(*N*-hydroxyphenylamino)phenylacetonitrile (**6**), mp 127.5—128.5 °C, as colorless needles. IR 3280 (OH), 2240 cm^{-1} (C≡N); ^1H NMR δ 5.37 (s, 1H, >C**H**), 5.50 (s, 1H, O**H**), 7.0—7.7 (m, 10H); MS *m/e* 224 (M^+). Found: C, 75.09; H, 5.32; N, 12.50%. Calcd for $C_{14}H_{12}N_2O$: C, 74.99; H, 5.38; N, 12.49%.

Treatment of 5a with Hydrochloric Acid in EtOH. A solution of **5a** (0.5 g) in EtOH (10 ml) was stirred with concd HCl (0.5 ml) at room temperature for 0.5 h. To the reaction mixture was added water (6 ml), and filtration gave 0.13 g (61%) of **3a**. The filtrate was extracted with $CHCl_3$, and the extract was concentrated *in vacuo* to leave 0.16 g (80%) of benzophenone.

Reaction of 1 with 7. A mixture of **1** (1.5 g, 0.15 mol) and **7** (0.5 g, 0.0018 mol) was heated at 120 °C for 2 h. The reaction mixture was concentrated *in vacuo* and the residue was triturated with hexane to give crystals, which on recrystallization from AcOEt afforded 0.28 g (82%) of tetraphenylsuccinonitrile (**9**), mp 206—208 °C (lit,[13] mp 213—215 °C), as colorless prisms. IR 2240 cm^{-1} (C≡N); ^1H NMR δ 7.2—7.4 (m); ^{13}C NMR δ 59.2 (quart. C), 121.0 (**C**≡N). Found: C, 87.52; H, 5.16; N, 7.33%. Calcd for $C_{28}H_{20}N_2$: C, 87.47; H, 5.24; N, 7.29%.

The hexane filtrate was chromatographed on silica gel using hexane as eluent to give 0.16 g (89%) of azoxybenzene (**11**).

Reaction of 1 with 8. A mixture of **1** (1.5 g, 0.015 mol) and **8** (0.5 g, 0.0018 mol) was heated at 120 °C for 2 h. A similar treatment of the reaction mixture to that described above afforded 0.31 g (91%) of 9,9′-dicyano-9,9′-bifluorenyl (**10**) as colorless leaves and 0.15 g (84%) of **11**.

10: Mp 284—286 °C (lit,[14] mp 253—255 °C); IR 2240 cm^{-1} (C≡N); ^1H NMR δ 7.0—7.5 (m); ^{13}C NMR δ 53.6 (quart. **C**), 118.5 (**C**≡N). Found: C, 88.36; H, 4.21; N, 7.36%. Calcd for $C_{28}H_{16}N_2$: C, 88.40; H, 4.24; N, 7.36%.

Reaction of 2 with 7. A solution of **2** (1.8 g, 0.0071 mol) and **7** (1.5 g, 0.0055 mol) in CH_2Cl_2 (20 ml) was stirred at room temperature for 21 h. The reaction mixture was concentrated *in vacuo*, and the residue was triturated with hexane to give 1.3 g (86%) of unreacted **7**. MeOH (10 ml) was added to the hexane solution to give crystals. Filtration and recrystallization of the crystals from hexane–benzene afforded 80 mg (8.4%) of *N*,*N*′-bis(diphenylmethylene)tetraphenylethylenediamine (**12**), mp 147—149 °C, as colorless prisms. IR 1620 cm^{-1} (C=N); ^1H NMR δ 6.4—7.6 (m); ^{13}C NMR δ 80.2 (quart. **C**), 168.1 (**C**=N). Found: C, 89.98; H, 5.73; N, 4.12%. Calcd for $C_{52}H_{40}N_2$: C, 90.17; H, 5.66; N, 4.05%.

The hexane–MeOH filtrate was concentrated *in vacuo*, and the residue was chromatographed on silica gel using hexane as eluent to give 30 mg (5.5%) of **11**.

Reaction of 2 with 8. A solution of **2** (0.5 g, 0.002 mol) and **8** (0.5 g, 0.0018 mol) in CH_2Cl_2 (10 ml) was stirred at room temperature for 24 h. The reaction mixture was concentrated *in vacuo*, and the residue was triturated with hexane to give crystals, which on recrystallization from AcOEt–$CHCl_3$ afforded 0.55 g (90%) of 9,9′-bis(diphenylmethyleneamino)-9,9′-bifluorenyl (**13**), mp 206—207.5 °C

(dec), as colorless plates. IR 1610 cm^{-1} (C=N); ^1H NMR δ 6.0—8.0 (m); ^{13}C NMR δ 79.9 (quart. **C**), 167.8 (**C**≡N); MS *m/e* 344 ($M^+/2$). Found: C, 90.61; H, 5.29; N, 4.00%. Calcd for $C_{52}H_{36}N_2$: C, 90.66; H, 5.27; N, 4.07%.

Thermal Decomposition of ***4a***. A solution of **4a** (1.4 g) in xylene (12 ml) was refluxed for 30 h. On cooling to room temperature, crystals separated from solution. Filtration and recrystallization of the crystals from benzene–EtOH afforded 0.2 g (37%) of *meso*-2,3-diphenylsuccinonitrile (*meso*-**14a**), mp 240—242 °C (lit,[15] mp 238—239 °C), as colorless needles. IR 2240 cm^{-1} (C≡N); ^1H NMR δ 4.23 (s, 2H), 7.1—7.5 (m, 10H). Found: C, 82.50; H, 5.12; N, 12.19%. Calcd for $C_{16}H_{12}N_2$: C, 82.73; H, 5.21; N, 12.06%.

The xylene filtrate was concentrated *in vacuo*, and the residue was triturated with hexane to give crystals. Recrystallization from EtOH afforded 0.15 g (28%) of *dl*-2,3-diphenylsuccinonitrile (*dl*-**14a**), mp 169—171 °C (lit,[16] mp 160 °C), as yellow prisms. IR 2250 cm^{-1} (C≡N); ^1H NMR δ 4.22 (s, 2H), 7.1—7.5 (m, 10H). Found: C, 82.54; H, 5.14; N, 12.00%. Calcd for $C_{16}H_{12}N_2$: C, 82.73; H, 5.21; N, 12.06%.

The hexane solution was chromatographed on silica gel using hexane as eluent to give 0.28 g (50%) of **11**.

A similar thermal decomposition of **4b** (1.6 g) in xylene (16 ml) afforded 0.29 g (41%) of *meso*-2,3-bis(*p*-methoxyphenyl)succinonitrile (*meso*-**14b**), 0.26 g (36%) of *dl*-2,3-bis(*p*-methoxyphenyl)succinonitrile (*dl*-**14b**), and 0.46 g (95%) of **11**.

meso-**14b**: Mp 239—241 °C; IR 2260 cm^{-1} (C≡N); ^1H NMR δ 3.80 (s, 6H), 4.15 (s, 2H), 6.8—7.4 (m, 8H); MS *m/e* 292 (M^+), 146 ($M^+/2$). Found: C, 74.05; H, 5.61; N, 9.69%. Calcd for $C_{18}H_{16}N_2O_2$: C, 73.95; H, 5.52; N, 9.58%.

dl-**14b**: Mp 189—190 °C; IR 2250 cm^{-1} (C≡N); ^1H NMR δ 3.84 (s, 6H), 4.12 (s, 2H), 6.8—7.4 (m, 8H); MS *m/e* 292 (M^+), 146 ($M^+/2$). Found: C, 73.89; H, 5.54; N, 9.55%. Calcd for $C_{18}H_{16}N_2O_2$: C, 73.95; H, 5.52; N, 9.58%.

Thermal Decomposition of ***4c***. A solution of **4c** (1.9 g) in xylene (19 ml) was refluxed for 30 h. After being cooled to room temperature, filtration gave crystals which on fractional recrystallization from MeOH–$CHCl_3$ afforded 0.16 g (19%) of *meso*-2,3-bis(*p*-chlorophenyl)succinonitrile (*meso*-**14c**), mp 229—230 °C (lit,[15] mp 234—236 °C), as colorless prisms and 0.1 g (11%) of *p*-chlorobenzanilide (**16c**).

The xylene filtrate was concentrated *in vacuo*, and MeOH (12 ml) was added to the residue to give crystals. Filtration and fractional recrystallization of the crystals from MeOH afforded 0.15 g (17%) of *dl*-2,3-bis(*p*-chlorophenyl)succinonitrile (*dl*-**14c**), mp 181—183 °C, as colorless prisms and 0.38 g (27%) of α-phenylimino-*p*-chlorophenylacetonitrile (**15c**), mp 107—108 °C (lit,[17] mp 108—108.5 °C), as yellow needles. The MeOH filtrate was concentrated *in vacuo*, and the residue was chromatographed on silica gel using hexane as eluent to give 0.28 g (50%) of **11**.

meso-**14c**: IR 2250 cm^{-1} (C≡N); ^1H NMR δ 4.20 (s, 2H), 7.0—7.4 (m, 8H). Found: C, 63.68; H, 3.33; N, 9.23%. Calcd for $C_{16}H_{10}N_2Cl_2$: C, 63.81; H, 3.35; N, 9.30%.

dl-**14c**: IR 2225 cm^{-1} (C≡N); ^1H NMR δ 4.28 (s, 2H), 7.1—7.5 (m, 8H). Found: C, 63.72; H, 3.41; N, 9.18%. Calcd for $C_{16}H_{10}N_2Cl_2$: C, 63.81; H, 3.35; N, 9.30%.

15c: IR 2220 cm^{-1} (C≡N). Found: C, 69.84; H, 3.72; N, 11.56%. Calcd for $C_{14}H_9N_2Cl$: C, 69.86; H, 3.77; N, 11.64%.

Thermal Decomposition of ***4d***. A solution of **4d** (1.5 g) in xylene (16 ml) was refluxed for 30 h. On cooling to room temperature, 0.12 g (11%) of *p*-nitrobenzanilide (**16d**) crystallized out of solution. The xylene filtrate was concentrated *in vacuo*, and recrystallization of the residue from EtOH afforded 0.82 g (75%) of α-phenylimino-*p*-nitrophenylacetonitrile (**15d**), mp 121—123 °C, as yellow prisms. IR 2180 cm^{-1} (C≡N); ^1H NMR δ 7.2—7.6 (m, 5H), 8.4 (m, 4H). Found: C, 67.13; H, 3.55; N, 16.81%. Calcd for $C_{14}H_9N_3O_2$: C, 66.92; H, 3.61; N, 16.73%.

Thermal Decomposition of ***5***. A typical run is shown for the thermal decomposition of **5a**. A solution of **5a** (0.74 g) in benzene (4 ml) was refluxed for 30 h. The reaction mixture was concentrated *in vacuo*, and the residue was triturated with hexane (3 ml) to give crystals, which on recrystallization from AcOEt afforded 0.37 g (84%) of *meso*-*N,N'*-bis(diphenylmethylene)-1,2-diphenylethylenediamine (**17-a**), mp 238—239 °C (lit,[18] mp 228 °C), as colorless prisms. IR 1615 cm^{-1} (C=N); ^1H NMR δ 4.88 (s, 2H), 6.4—7.5 (m, 30H); MS *m/e* 270 ($M^+/2$). Found: C, 88.73; H, 5.96; N, 5.23%. Calcd for $C_{40}H_{32}N_2$: C, 88.85; H, 5.96; N, 5.18%.

The hexane filtrate was chromatographed on silica gel using hexane as eluent to give 79 mg (49%) of **11**.

The results on the thermal decompositions of **5b**—**5d** are shown in Scheme 4.

meso-N,N'-*Bis(diphenylmethylene)-1,2-bis(*p-*methoxyphenyl)ethylenediamine (**17b**)*: Mp 229—230 °C as colorless prisms; IR 1625 cm^{-1} (C=N); ^1H NMR δ 3.72 (s, 6H), 4.78 (s, 2H), 6.4—7.4 (m, 28H); MS *m/e* 600 (M^+), 300 ($M^+/2$). Found: C, 83.91; H, 6.07; N, 4.76%. Calcd for $C_{42}H_{36}N_2O_2$: C, 83.97; H, 6.06; N, 4.66%.

meso-N,N'-*Bis(diphenylmethylene)-1,2-bis(*p-*chlorophenyl)ethylenediamine (**17c**)*: Mp 230—232 °C as colorless prisms; IR 1625 cm^{-1} (C=N); ^1H NMR δ 4.79 (s, 2H), 6.4—7.5 (m, 28H); MS *m/e* 608, 610, 612 (M^+), 304, 306 ($M^+/2$). Found: C, 78.81; H, 4.94; N, 4.50%. Calcd for $C_{40}H_{30}N_2Cl_2$: C, 78.81; H, 4.96; N, 4.60%.

meso-N,N'-*Bis(diphenylmethylene)-1,2-bis(*p-*nitrophenyl)ethylenediamine (**17d**)*: Mp 253—256 °C (dec) as colorless prisms; IR 1620 cm^{-1} (C=N); ^1H NMR δ 4.95 (s, 2H), 6.3—8.2 (m, 28H); MS *m/e* 315 ($M^+/2$). Found: C, 76.21; H, 4.75; N, 8.93%. Calcd for $C_{40}H_{30}N_4O_4$: C, 76.17; H, 4.79; N, 8.88%.

Hydrolysis of ***17a***. A solution of **17a** (0.48 g) in EtOH (20 ml) was stirred with 12% hydrochloric acid (3 ml) at room temperature for 25 h. The reaction mixture was poured into water and extracted with benzene. The benzene extract was concentrated *in vacuo* to give 0.11 g (34%) of benzophenone. The aqueous solution was made basic with aqueous NaOH, and then extracted with $CHCl_3$. The $CHCl_3$ extract was concentrated *in vacuo*, and recrystallization of the residue from cyclohexane afforded 0.1 g (53%) of *meso*-1,2-diphenylethylenediamine (**18**), mp 119—119.5 °C (lit,[18] mp 118 °C), as colorless plates. IR 3330, 3250 cm^{-1} (NH_2); ^1H NMR δ 1.35 (s, 4H, NH_2), 4.02 (s, 2H), 7.0—7.7 (m, 10H); MS *m/e* 212 (M^+). Found: C, 79.08; H, 7.67; N, 13.14%. Calcd for $C_{14}H_{16}N_2$: C, 79.21; H, 7.60; N, 13.20%.

Reaction of ***1*** *with* ***19***. A mixture of **1** (1.0 g, 0.01 mol) and **19** (1.0 g, 0.0037 mol) in benzene (20 ml) was stirred at room temperature for 6 h, during which time the mixture turned into a red solution. The reaction mixture was concentrated *in vacuo*, and the residue was chromatographed on silica gel using $CHCl_3$ as eluent to give 0.9 g (87%) of α-(*p*-diethylaminophenyl)iminophenylacetonitrile (**20**), mp 112—113 °C, as red prisms. IR 2210 (C≡N), 1610 cm^{-1} (C=N); ^1H NMR δ 1.20 (t, 6H), 3.42 (q, 4H), 7.5—8.2 (m, 9H); MS *m/e* 277 (M^+). Found: C, 77.87; H, 6.95; N, 15.15%. Calcd for $C_{18}H_{19}N_3$: C, 77.94; H, 6.91; N, 15.15%.

References

1) D. A. Evans and L. K. Truesdale, *Tetrahedron Lett.*, **1973**, 4929; D. A. Evans, L. K. Truesdale, and G. L. Carroll, *Chem. Commun.*, **1973**, 55; D. A. Evans, J. M. Hoffman, and L. K. Truesdale, *J. Am. Chem. Soc.*, **95**, 5822 (1973); W.

Lidy and W. Sundermeyer, *Tetrahedron Lett.*, **1973**, 1449; W. Lidy and W. Sundermeyer, *Chem. Ber.*, **106**, 587 (1973).

2) I. Ojima, S. Inaba, and Y. Nagai, *J. Chem. Soc., Chem. Commun.*, **1974**, 826.

3) I. Ojima and S. Inaba, *Tetrahedron Lett.*, **1979**, 817.

4) I. Ojima, S. Inaba, K. Nakatsugawa, and Y. Nagai, *Chem. Lett.*, **1975**, 331.

5) I. Ojima, S. Inaba, and Y. Nagai, *Chem. Lett.*, **1975**, 737.

6) I. Matsuda, K. Itoh, and Y. Ishii, *J. Chem. Soc., Perkin Trans. 1*, **1972**, 1678; I. Matsuda, S. Yamamoto, and Y. Ishii, *ibid.*, **1976**, 1523, 1528.

7) From the analogy to reported melting points of *meso*- and *dl*-**14a**, the compound having higher melting point was assigned to be the *meso* isomer in **14b** and **14c** respectively. Compounds **17a**—**17d** were assigned to be the *meso* isomer respectively, since the melting point of **18** which was obtained by hydrolysis of **17a** agreed with that of *meso*-1,2-diphenylethylenediamine.[18]

8) D. A. Evans, C. L. Carroll, and L. K. Truesdale, *J. Org. Chem.*, **39**, 914 (1974).

9) L. H. Chan and E. G. Rochow, *J. Organomet. Chem.*, **9**, 231 (1967).

10) O. H. Wheeler and P. H. Gore, *J. Am. Chem. Soc.*, **78**, 3363 (1956).

11) A. W. Johnson, *J. Org. Chem.*, **28**, 252 (1963).

12) F. Kröhnke, *Ber.*, **71**, 2583 (1938).

13) K. Auwers and V. Meyer, *Ber.*, **22**, 1227 (1889).

14) J. M. Birnie and N. Campbell, *Proc. R. Soc. Edinburgh, Sect. A*, **1969**, 68 (Pt. 2), 120; *Chem. Abstr.*, **71**, 101586s (1969).

15) R. B. Davis, *J. Am. Chem. Soc.*, **80**, 1752 (1958).

16) D. G. Coe, M. M. Gale, R. P. Linstead, and C. J. Timmons, *J. Chem. Soc.*, **1957**, 123.

17) J. G. Smith and D. C. Irwin, *Synthesis*, **1978**, 894.

18) H. A. Staab and F. Vögtle, *Chem. Ber.*, **98**, 2681 (1965).

^{13}C-NMR Study of the Solvent Effect of the *N*-Acetyl-L-alanine Methyl Ester

Tetsuo ASAKURA* and Atsuo NISHIOKA

Department of Polymer Chemistry, Tokyo Institute of Technology, Ookayama, Meguro-ku, Tokyo 152

(Received July 16, 1979)

The ^{13}C-NMR spectra of the *N*-acetyl-L-alanine methyl ester in solution were observed in order to clarify the solvent effect. The assignment of the two kinds of carbonyl groups was carried out on the basis of the difference in the long-range ^{1}H–^{13}C coupling patterns and the spectral change through the hydrolysis of the ester group in a D_2O solution. The internal rotational angle around the N–C$^{\alpha}$ bond was estimated as $-94°$ from the observed value of $^{3}J_{C'-N-C^{\alpha}-H}$, using Bystrov equation. In a trifluoroacetic acid solution, the formation of strong hydrogen bonds accompanying partial protonation between the *N*-acetyl-L-alanine methyl ester and the solvent was suggested. Moreover, the acetyl C=O group tends to interact with trifluoroacetic acid more strongly than the alanyl C=O group.

High resolution NMR spectroscopy has been extensively used to study the helix-coil transition of some synthetic polypeptides induced by such organic acids as trifluoroacetic acid.[1,2]

As the cause of the chemical shift change of the α-CH proton in the backbone chain through the helix-coil transition, two possibilities have been mainly considered. One possibility is a change in the intramolecular shielding effect which is intrinsic to the polypeptide conformation, and the other one is a solvent effect of the peptide residue by the organic acids in the coil state.[1]

On the basis of a theoretical chemical-shift calculation of poly(L-alanine), taking into account only the intramolecular shielding contribution, we have suggested that the latter is more probable, since the α-CH peak in the coil state was predicted to resonate upfield slightly (by 0.1 ppm) from the helical peak position; this is, however, contrary to the observed spectral behavior.[3,4]

In order to clarify such a polypeptide-solvent interaction in solution, it seems useful to investigate the solvent effect of the dipeptide model compounds, since the flexibility of the polypeptide backbone chain originates essentially from the rotation about the N–C$^{\alpha}$ and C$^{\alpha}$–C′ single bonds adjacent to the α-carbons; also, polypeptide-solvent interaction can be expected to occur in a relatively short range along the polypeptide chain.

In our previous paper,[5] we have studied the modes of the self-association of the *N*-acetyl-L-alanine methyl ester (Ac–Ala–OMe) and *N*-acetyl-L-alanine methylamide (Ac–Ala–NHMe) in deuteriochloroform, which is widely used as a helix-supporting solvent of polypeptides, using ^{1}H and ^{13}C-NMR spectroscopies.

In this paper, the ^{13}C-NMR spectra of Ac–Ala–OMe were measured in several kinds of solvents, including trifluoroacetic acid, which is used as a coil solvent of polypeptides, in order to study the solvent effect.

Especially, the ^{13}C-NMR resonances of the carbonyl groups give useful information on the peptide-solvent interaction. However, there is a considerable problem in assigning the carbonyl resonances, since the range of the chemical shifts is relatively small and since the resonance positions of the carbonyl groups depend strongly on the solvent. Thus, the ^{13}C assignment of the acetyl and alanyl carbonyl resonances in Ac–Ala–OMe was carried out on the basis of the difference in the long-range ^{1}H–^{13}C coupling patterns[6,7] and the spectral change through the hydrolysis of the ester group in deuterium oxide.

Experimental

The Ac–Ala–OMe sample was synthesized as has been described previously.[5] The carbon tetrachloride (CCl_4), sulfuric acid (H_2SO_4), and trifluoroacetic acid(CF_3COOH) were purchased from the Tokyo Kasei Company, Ltd. The benzene-d_6 (C_6D_6), dimethyl-d_6 sulfoxide (Me_2SO-d_6), deuteriochloroform ($CDCl_3$), and deuterium oxide (D_2O) were purchased from CEA, France.

The ^{1}H-decoupled ^{13}C-NMR spectra were mostly recorded at 25 °C with a JEOL PS-100 spectrometer equipped with PFT-100 Fourier transform units operating at 25.14 MHz. As for the measurement of the ^{1}H-coupled spectrum, a JEOL FX-60 spectrometer was used operating at 15.01 MHz at 40 °C. The chemical shifts were represented in ppm downfield from internal tetramethylsilane (Me_4Si) except for the D_2O solution. In the D_2O solution, only the partial spectra of the carbonyl region were observed.

Results and Discussion

Assignment of the Carbonyl Resonances in D_2O. Figures 1a) and b) show the ^{1}H-decoupled and -coupled ^{13}C-NMR spectra of the carbonyl carbons of Ac–Ala–OMe in D_2O respectively. The use of D_2O as a solvent leads to a simplification of the ^{1}H-coupled spectrum because the coupling between an exchangeable NH proton and every ^{13}C nucleus in this molecule disappears when the NH proton is exchanged with deuterium. On the basis of the difference in the long-range ^{1}H–^{13}C coupling patterns between the two kinds of carbonyl resonances, the higher-field resonance can easily be assigned to the acetyl C=O group, and the lower-field resonance, to the alanyl C=O group. The long-range ^{1}H–^{13}C coupling constants obtained from the first-order analysis of the spectrum are given as follows:

Acetyl C=O $^{2}J_{C'-C-H} = 5.9\pm0.1$ Hz

$^{3}J_{C'-N-C^{\alpha}-H} = 2.5\pm0.1$ Hz

Alanyl C=O $^{2}J_{C'-C^{\alpha}-H} = 8.1\pm0.2$ Hz

$^{3}J_{C'-C^{\alpha}-C-H} = 4.3\pm0.2$ Hz

$^{3}J_{C'-O-C-H} = 4.3\pm0.2$ Hz

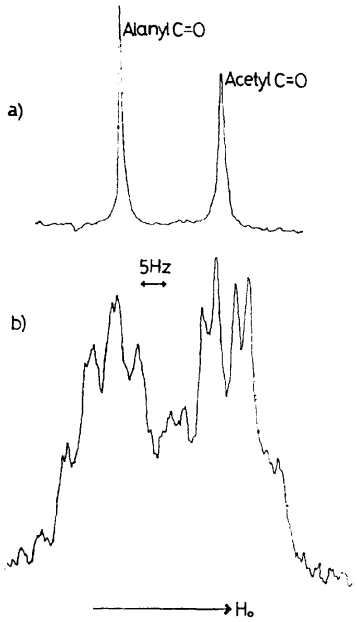

Fig. 1. ^{1}H-decoupled a) and -coupled b) ^{13}C-NMR spectra for the carbonyl region of *N*-acetyl-L-alanine methyl ester at 15.01 MHz (35 v/v % in D_2O at 40 °C). 500 and 2500 transients were collected to obtain the spectra a) and b), respectively. Pulse interval of 30 s was used.

The relative shielding order of these resonances is consistent with that in neat liquid, although the chemical-shift difference between the two peaks becomes small in D_2O (1.68 ppm in 50 v/v% D_2O, 2.16 ppm in neat liquid).[8]

It should be noticed that the acetyl C=O resonance is broader than the alanyl C=O resonance in the ^{1}H-decoupled spectrum (Fig. 1a)). This might come from the coupling between the ^{14}N nucleus and the *N*-linked acetyl C=O nucleus and also the coupling between the amide deuterium and the acetyl C=O nucleus.

Moreover, these carbonyl resonances were also assigned on the basis of the spectral change through the hydrolysis of the ester group in Ac-Ala-OMe. When a trace of NaOD is added to the D_2O solution, the following hydrolysis occurs:

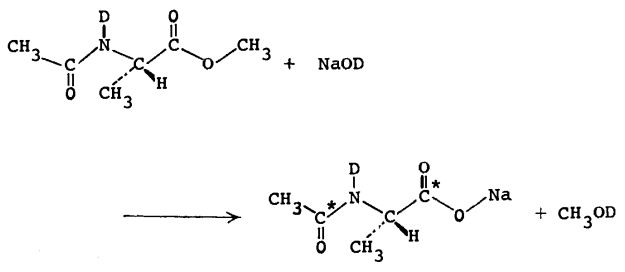

As is shown in Fig. 2, the C=O peaks of the expected hydrolysis product marked by an asterisk appear after the addition of a trace of NaOD to the solution. The peak shifted remarkably to a low field by the hydrolysis can be assigned to the alanyl C=O resonance. This assignment is in agreement with that carried out on

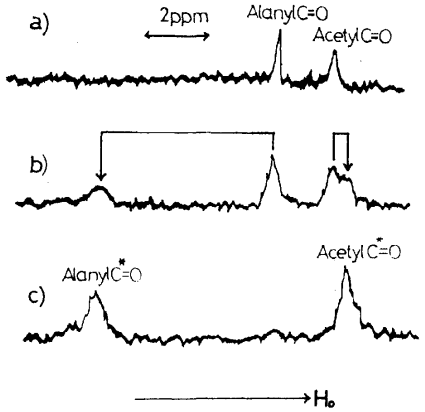

Fig. 2. ^{1}H-decoupled ^{13}C-NMR spectra for the carbonyl region of *N*-acetyl-L-alanine methyl ester at 25.14 MHz at 25 °C.
a) 50 v/v % in D_2O. b) After addition of a trace of NaOD to the solution a). c) Same as b) except for the increase of the amounts of NaOD in the solution.

the basis of the difference in the long-range ^{1}H–^{13}C coupling pattern in the ^{1}H-coupled spectrum.

Conformation of Ac-Ala-OMe in D_2O. Comparing the long-range ^{1}H–^{13}C coupling constants of acetyl C=O and alanyl C=O resonances in the Ac-Ala-OMe spectrum with the corresponding ^{1}H–^{13}C coupling constants of *N*-methylacetamide[7] and methyl acetate[9] respectively, it is found that the values of the corresponding coupling constants are almost the same except for the $^{2}J_{\underline{C}'-C-\underline{H}}$ of the alanyl C=O group. The value of the $^{2}J_{\underline{C}'-C-\underline{H}}$ of alanyl C=O in Ac-Ala-OMe is larger than that in methyl acetate[9] by about 1 Hz.

Especially, the $^{3}J_{\underline{C}'-N-C^{\alpha}-\underline{H}}$ constant is known to obey the general Karplus relation and can be used for determining the internal rotational angle around the N–C^{α} bond, ϕ.[10,11] This value of $^{3}J_{\underline{C}'-N-C^{\alpha}-\underline{H}}$, 2.5 Hz in Ac-Ala-OMe is coincident with the value of $^{3}J_{\underline{C}'-N-C^{\alpha}-\underline{H}}$, 2.5 Hz in Ac-Ala-NDMe in methanol-d_4[10] and corresponds to four angles, ϕ,[12] −94°, −146°, −6°, and 126°, using the Karplus-like equation reported by Bystrov.[10] However, Ingwall and Goodman[13] have reported a conformational energy map for Ac-Ala-OMe in which the low-energy areas enclosed by the 1 kcal mol^{-1} energy contours are spread over the range of $-50° < \phi < -180°$. Thus $\phi = -6°$ and 126° can clearly be eliminated. In our previous paper,[5] we have observed the vicinal coupling constant, $^{3}J_{\underline{H}-N-C^{\alpha}-\underline{H}}$, between the NH and C^{α}–H protons in the ^{1}H-NMR spectra of Ac-Ala-OMe as a function of its concentration in $CDCl_3$. $^{3}J_{\underline{H}-N-C^{\alpha}-\underline{H}}$ increased from 6.1 Hz in neat liquid to 6.9 Hz in 23 v/v% in a $CDCl_3$ solution with dilution. Using the Karplus-like equation reported by Ramachandran *et al.*,[14] the increase in $^{3}J_{\underline{H}-N-C^{\alpha}-\underline{H}}$ from 6.1 Hz to 6.9 Hz corresponds to the variation in ϕ from −75° to −81°. Since the value of $\phi = -94°$ is near to the value obtained from $^{3}J_{\underline{H}-N-C^{\alpha}-\underline{H}}$ in a 23 v/v% $CDCl_3$ solution, $\phi = -94°$ was chosen for the internal rotational angle around the N–C^{α} bond. Taking into account the energy map by Ingwall and

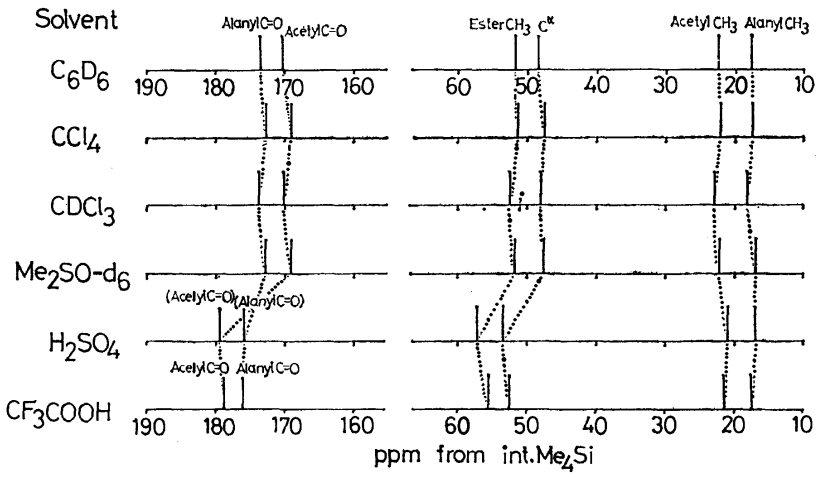

Fig. 3. ^{13}C-NMR stick spectra of *N*-acetyl-L-alanine methyl ester observed in several kinds of solvents (10 v/v %, at 25 °C). Chemical shifts were represented from internal Me_4Si.

Goodman, the value of $\phi = -94°$ may be regarded as ϕ averaged over the low-energy conformations.

Solvent Effect. The ^{13}C-NMR spectra of Ac-Ala-OMe observed in several kinds of solvents are shown in Fig. 3 as stick spectra.

In C_6D_6, CCl_4, and $CDCl_3$ solutions, the resonance positions of the ^{13}C nuclei are scarcely changed among these solvents. A similar spectrum of Ac-Ala-OMe was observed in Me_2SO-d_6. Thus, the amount of the shift induced by Me_2SO-d_6 is very small, although this solvent is well known as a good hydrogenbond-accepting solvent.[5,14-17]

On the other hand, two C=O resonances shift markedly to a low field in the H_2SO_4 solution. Since the peak positions of the acetyl and alanyl C=O groups are reversed in the CF_3COOH solution relative to those in the $CDCl_3$ solution, as will be discussed below, the relative shielding order of these peaks might be reversed in the H_2SO_4 solution compared with that in nonpolar solvents. In this solvent, protonation to the carbonyl groups of Ac-Ala-OMe would occur[18] and the ^{13}C chemical shifts of every ^{13}C nucleus in Ac-Ala-OMe would be influenced by the polarization of these carbonyl groups.[19-23] In truth, the ester CH_3 and C^α carbon resonances shift remarkably to a low field, whereas the acetyl CH_3 and alanyl CH_3 resonances shift slightly a high field.

A ^{13}C peak behavior similar to that of the H_2SO_4 solution was observed in the CF_3COOH solution. However, the amounts of the induced ^{13}C chemical shift are smaller in the CF_3COOH solution than in the H_2SO_4 solution. Thus, it is likely that strong hydrogen bonds with partial protonation[18,24-29] are formed between the solvent and the carbonyl groups of Ac-Ala-OMe in the CF_3COOH solution.

Moreover, the ^{13}C-NMR chemical shift of Ac-Ala-OMe is shown in Fig. 4 as a function of the CF_3COOH composition in the CF_3COOH-$CDCl_3$ solvent systems. With an increase in the CF_3COOH composition, the two carbonyl, ester CH_3 and C^α peaks shift gradually to a low field, while the acetyl CH_3 and alanyl CH_3 carbons shift to a high field in the region of 0—30

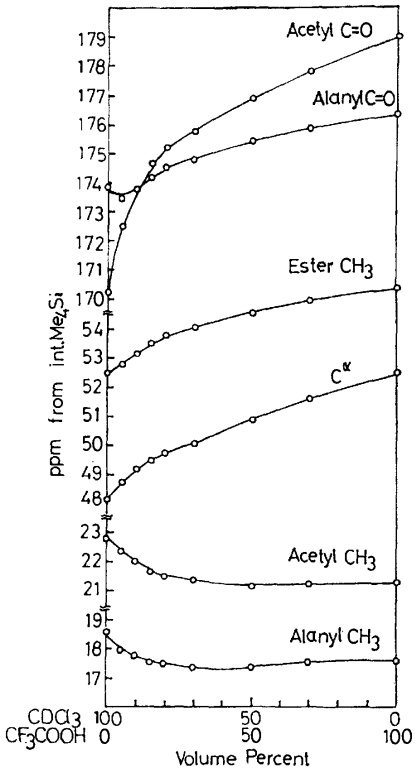

Fig. 4. ^{13}C-NMR chemical shift of *N*-acetyl-L-alanine methyl ester represented as a function of the CF_3COOH composition in $CDCl_3$-CF_3COOH solvent system (10 v/v %, at 25 °C). Chemical shifts were represented from internal Me_4Si.

v/v% CF_3COOH compositions, but do not shift upon a further increase in the CF_3COOH composition. In the two carbonyl resonances, the acetyl C=O peak shift is larger than that of the alanyl C=O peak with an increase in the CF_3COOH composition; as a result, the relative resonance position in the $CDCl_3$ solution is reversed in the CF_3COOH solution. The amount of the solvent-induced shift of the acetyl C=O carbon in Ac-Ala-OMe is comparable with that of the acetyl C=O carbon in

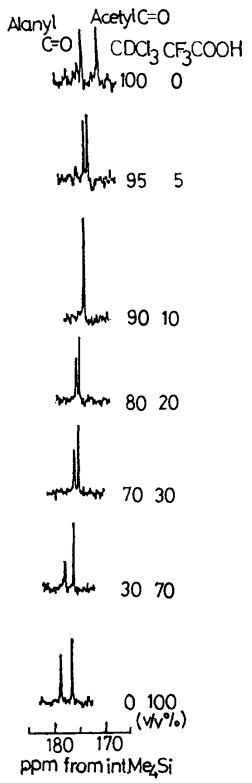

Fig. 5. ^{13}C-NMR spectra for the carbonyl region of *N*-acetyl-L-alanine methyl ester observed in $CDCl_3$–CF_3COOH solvent system (10 v/v %, at 25 °C). Chemical shifts were represented from internal Me_4Si.

N,N-diethylacetamide in the $CDCl_3$–CF_3COOH solvent system.[23] As is shown in Fig. 5, the acetyl C=O peak becomes broader in the region of 20—70 v/v% CF_3COOH composition and again becomes sharp in the 100% CF_3COOH solution, contrary to the alanyl C=O peak behavior. Thus, the acetyl C=O group tends to interact with the CF_3COOH molecule more strongly than the alanyl C=O group. A similar difference in the solvent effect by CF_3COOH is observed among the internal alanyl C=O groups and the *N*-terminal acetyl C=O group in the *N*-acetyl-L-alanyl-L-alanine methyl ester from the ^{13}C-NMR measurements.[30]

These results suggest that the interaction between trifluoroacetic acid and the internal peptide groups of poly(L-alanine) is weaker than that between the acid and simple amide molecules where protonation occurs.[23,26-28] That is, a hydrogen-bond interaction might take place.

The authors are greatly indebted to Dr. Kazuo Sato, of the Central Research Laboratory, Idemitsu Kosan Co., for the measurement of the ^{1}H-coupled NMR spectrum of Ac-Ala-OMe.

References

1) E. M. Bradbury, P. D. Cary, C. Crane-Robinsons, and P. G. Hartman, *Pure Appl. Chem.*, **36**, 53 (1973).
2) F. A. Bovey, *J. Polym. Sci., Macromol. Rev.*, **9**, 1 (1974).
3) T. Asakura, I. Ando, and A. Nishioka, *Makromol. Chem.*, **178**, 1111 (1977).
4) T. Asakura, I. Ando, and A. Nishioka, *Makromol. Chem.*, **178**, 1521 (1977).
5) T. Asakura, M. Kamio, and A. Nishioka, *Biopolymers*, **18**, 467 (1979).
6) J. Feeney, P. Partington, and G. C. Roberts, *J. Magn. Reson.*, **13**, 268 (1974).
7) D. E. Dorman and F. A. Bovey, *J. Org. Chem.*, **38**, 1719 (1973).
8) The assignment of these peaks made in our previous paper (Ref. 5) should be revised.
9) D. E. Dorman, D. Bauer, and J. D. Roberts, *J. Org. Chem.*, **40**, 3729 (1975).
10) V. F. Bystrov, *Prog. NMR Spectroscopy*, **10**, 41 (1976).
11) V. F. Bystrov, A. S. Arseniev, and Yu. D. Gavrilov, *J. Magn. Reson.*, **30**, 151 (1978).
12) IUPAC-IUB Commission on Biochemical Nomenclature, *Biochemistry*, **9**, 3471 (1970).
13) R. T. Ingwall and M. Goodman, *Macromolecules*, **7**, 598 (1974).
14) G. N. Ramachandran, R. Chandrasekaran, and K. D. Kopple, *Biopolymers*, **10**, 2113 (1971).
15) D. W. Urry, L. W. Mitchell, and T. Ohnishi, *Proc. Nat. Acad. Sci., U. S. A.*, **71**, 3265 (1974).
16) D. W. Urry, L. W. Mitchell, and T. Ohnishi, *J. Mol. Biol.*, **96**, 101 (1975).
17) M. Llinas and M. P. Klein, *J. Am. Chem. Soc.*, **97**, 4731 (1975).
18) F. A. Bovey, "High Resolution NMR of Macromolecules," Academic Press, New York (1972), p. 247.
19) W. J. Horsley and H. Sternlicht, *J. Am. Chem. Soc.*, **90**, 3738 (1968).
20) I. Morishima, K. Yoshikawa, K. Okada, T. Yonezawa, and K. Goto, *J. Am. Chem. Soc.*, **95**, 165 (1974).
21) A. R. Quirt, J. R. Lyerla, Jr., I. R. Peat, J. S. Cohen, W. F. Reynolds, and M. H. Freedman, *J. Am. Chem. Soc.*, **96**, 570 (1974).
22) J. G. Batchelor, J. Feeney, and G. C. K. Roberts, *J. Magn. Reson.*, **20**, 19 (1975).
23) Y. Suzuki, Y. Inoue, and R. Chujo, *Biopolymers*, **16**, 2521 (1977).
24) F. Quadrifoglio and D. W. Urry, *J. Phys. Chem.*, **71**, 2364 (1967).
25) F. A. Bovey, *Pure Appl. Chem.*, **16**, 417 (1968).
26) W. E. Stewart, L. Mandelkern, and R. E. Glick, *Biochemistry*, **6**, 150 (1967).
27) J. W. O. Tam and I. M. Klotz, *Spectrochim. Acta, Part A*, **29**, 633 (1973).
28) R. M. Stephens and E. M. Bradbury, *Polymer*, **17**, 563 (1976).
29) M. M. Exner and R. J. Kostelnik, *Biopolymers*, **16**, 1387 (1977).
30) T. Asakura, T. Hasegawa, and A. Nishioka, unpublished data.

Phenanthro[4,5-*bcd*]furan Derivatives. VI. Some Electrophilic Substitution Reactions and Hydrogenation of 4*H*-Cyclopenta-[*def*]phenanthrene, Phenanthro[4,5-*bcd*]furan, and 4*H*-Benzo[*def*]carbazole

Takaaki HORAGUCHI,* Reiko YAMAZAKI, and Teishiro ABE†

Department of Chemistry, Faculty of Science, Niigata University, Ikarashi, Niigata 950-21

†*Department of General Education, Niigata University, Ikarashi, Niigata 950-21*

(Received July 19, 1979)

Some electrophilic substitution reactions and hydrogenation of 4*H*-cyclopenta[*def*]phenanthrene (**1a**), phenanthro[4,5-*bcd*]furan (**1b**), and 4*H*-benzo[*def*]carbazole (**1c**) have been investigated. The bromination of **1a** and **1b** with bromine gave the corresponding 8-bromo derivatives. The bromination of **1c** however gave the 1,3,5,7-tetrabromo derivative as the sole product. The benzoylation of **1a** and **1b** afforded the corresponding 1-benzoyl derivatives, but in the case of **1c**, the 1,7-dibenzoyl derivative was obtained together with the 4-benzoyl derivative. It appears that ortho- and para-orientation of the nitrogen atom in **1c** is much stronger than that of the methylene group or the oxygen atom in **1a** or **1b**. Hydrogenation of **1a**, **1b**, and **1c** with palladium–charcoal catalyst afforded the corresponding 8,9-dihydro derivatives (**4a**, **4b**, and **4c**). The reduction of **1a** and **1c** with sodium–ethanol gave **4a** and **4c**. The reduction of **1b** however gave the 3,3a,8,9,9a,9b-hexahydro derivative. It appears that facile hydrogenation of the carbon-carbon double bonds at the 8,9-positions in **1a**, **1b**, and **1c** are due to strain in the fused ring system.

The unique structures of 4*H*-cyclopenta[*def*]phenanthrene (**1a**), phenanthro[4,5-*bcd*]furan (**1b**), and 4*H*-benzo[*def*]carbazole (**1c**) are represented by the formulae **1a**—**c** which consist of phenanthrene and methylene or hetero-atom bridge linkages. Therefore, it is expected that **1a** has both the character of phenanthrene (**6**) and fluorene, **1b** has those of **6** and dibenzofuran, and **1c** has those of **6** and carbazole.

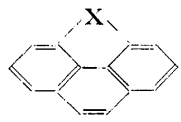

1a: X=CH_2
1b: X=O
1c: X=NH

The ultraviolet spectra of **1a**, **1b**, and **1c** are shown in Fig. 1 and those of **6** and pyrene are shown in Fig. 2. **1a** has an absorption spectrum similar to that of phenanthrene itself in the position of absorption bands and shapes suggesting that interaction (hyperconjugation) between the methylene bridge linkage and π-electrons on the phenanthrene ring is very weak. **1c** exhibits absorptions at much longer wavelengths than phenanthrene and the shapes are similar to those of pyrene which is isoelectronic with **1c** showing that interaction between non-bonding electrons on the nitrogen atom and π-electrons on the phenanthrene ring is strong. In addition the position of the absorption spectrum of **1b** lies between those of **1a** and **1c** and the shapes are similar to that of pyrene. It appears therefore that the interaction between non-bonding electrons on the oxygen atom and π-electrons on the phenanthrene ring is of medium intensity. Thus, all absorption regions of **1a**—**c** shift to longer wavelengths as X changes from the methylene group to the oxygen or the nitrogen atom. Consequently a difference in reactivity is expected upon electrophilic substitution. Additionaly it may be expected that the carbon-carbon double bonds at the 8,9-positions in **1a**, **1b**, and **1c** have abnormal character towards hydrogenation compared with the double bond at the 9,10-positions in the phenanthrene owing to the bridge linkage of X. The reactivity of phenanthro-

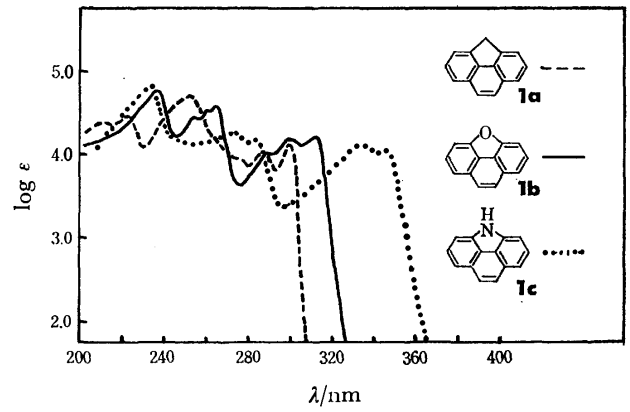

Fig. 1. The ultraviolet spectra of 4*H*-cyclopenta[*def*]-phenanthrene (**1a**), phenanthro[4,5-*bcd*]furan (**1b**), and 4*H*-benzo[*def*]carbazole (**1c**) in ethanol.

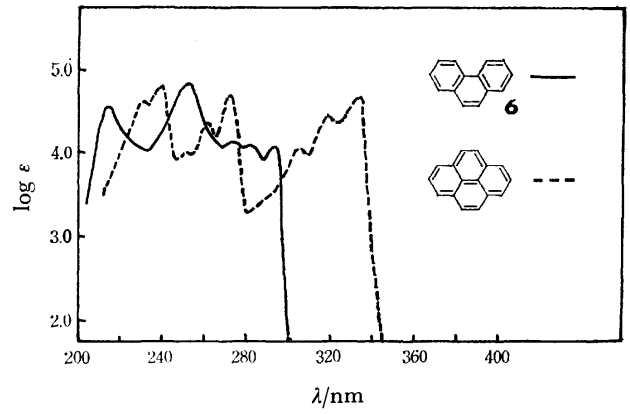

Fig. 2. The ultraviolet spectra of phenanthrene (**6**) and pyrene in ethanol.

[4,5-*bcd*]furan (**1b**) has been previously reported,[1] but there are few reports on the reactivity of **1a**[2] and **1c**.[3] Therefore, the electrophilic substitution reactions and hydrogenation of **1a** and **1c** have been examined and the reactivity of **1b** with that of **1a**, **1c**, and **6** compared.

Results and Discussion

1a was synthesized by the dehydrogenation of 1-hydroxy-1,2,3,3a-tetrahydro-4*H*-cyclopenta[*def*]phenanthrene with palladium–charcoal according to the method of Bachmann.[4] **1c** was prepared in a 53% yield by heating 4-phenanthrylamine at 560 °C using calcium oxide as the catalyst in a nitrogen atmosphere; Kruber *et al.*[3a] have obtained **1c** in a 20% yield at a reaction temperature of 400 °C.

The results of several electrophilic substitution reactions and hydrogenation of **1a**, **1b**, **1c**, and phenanthrene (**6**) are summarized in Table 1.

The bromination of **1a** with bromine gave two products, 8-bromo-4*H*-cyclopenta[*def*]phenanthrene (**2a**) and 4-bromo-4*H*-cyclopenta[*def*]phenanthrene (**2e**) in 42% and 30% yields, respectively. It appears that **2a** was produced by an addition-elimination mechanism and **2e** was formed by a radical reaction. In fact, the bromination of **1a** with *N*-bromosuccinimide gave only **2e** in a 73% yield. The bromination of **1b** and phenanthrene with bromine afforded the corresponding 8-bromophenanthro[4,5-*bcd*]furan (**2b**)[1] and 9-bromophenanthrene (**7**),[5] respectively suggesting that in the case of **1a** and **1b** bromination proceeds by an addition-elimination mechanism rather than by an aromatic substitution mechanism. The reason for this is that the electron density at the ortho- and para-positions to the methylene group or the oxygen atom in **1a** or **1b** is not sufficiently high or the double bonds at the 8,9-positions in **1a** and **1b** are more reactive than the double bond at the 9,10-positions in the phenanthrene owing to strain introduced by bridge linkages as discussed below. Though the former explanation may be reasonable for the bromination of **1a**, the latter is at least plausible for the bromination of **1b** as phenanthrene-4,5-diol afforded 1,3,6,8-tetrabromophenanthrene-4,5-diol[7] by an aromatic substitution mechanism. Therefore, **1a** and **1b** have the character of phenanthrene rather than that of fluorene[8] or dibenzofuran[9] under the bromination conditions. The bromination of **1c** gave a sole product of 1,3,5,7-tetrabromo-4*H*-benzo[*def*]carbozole (**2c**) suggesting that the ortho- and para-positions to the nitrogen atom of **1c** have high electron density by strong resonance between non-bonding electrons on the nitrogen atom and π-electrons on the phenathrene ring. Therefore, the bromination of **1c** proceeds by an aromatic substitution mechanism in preference to the addition-elimination mechanism. Thus, **1c** has the

Table 1. Electrophilic substitution reactions and hydrogenation of 4*H*-cyclopenta[*def*]phenanthrene (**1a**), phenanthro[4,5-*bcd*]furan (**1b**), 4*H*-benzo[*def*]carbazole (**1c**), and phenanthrene (**6**)

	Starting materials			
Reagents	**1a** 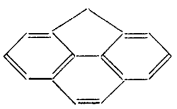	**1b** 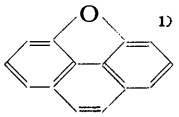	**1c** 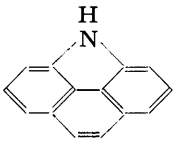	**6** 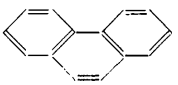
Br_2	**2a** 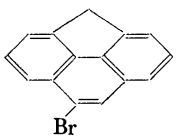	**2e** 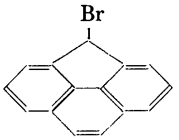	**2b** 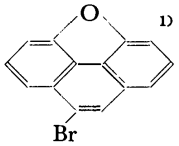	**2c** 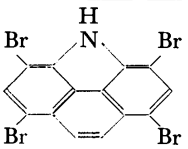	**7** 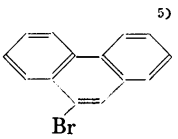
C_6H_5COCl $AlCl_3$	**3a** 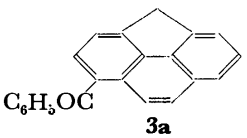	**3b** 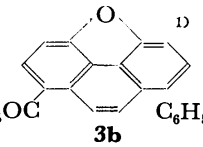	**3c** 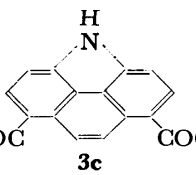	**3g** 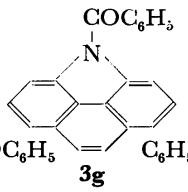	**8** 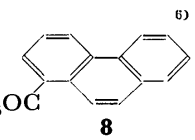
H_2/Pd–C	**4a** 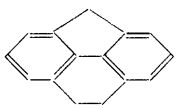	**4b** 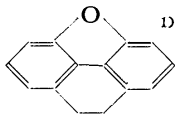	**4c** 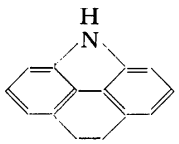	no reaction
Na–EtOH	**4a**	**5b** 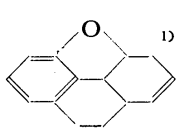	**4c**	**5c** 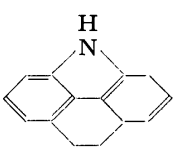	no reaction

character of carbazole rather than that of phenanthrene as carbazole[10] is most reactive at 3- and 6-positions under the bromination conditions. The experimental results of bromination are parallel to the shifts in the ultraviolet spectra of **1a**, **1b**, and **1c**.

The Friedel-Crafts reaction of **1a** and benzoyl chloride using aluminium chloride as the catalyst gave 1-benzoyl-4*H*-cyclopenta[*def*]phenanthrene (**3a**). The Friedel-Crafts reaction of **1b** and benzoyl chloride afforded 1-benzoylphenanthro[4,5-*bcd*]furan (**3b**).[1] The reaction of **1c** with benzoyl chloride however gave only 1,7-dibenzoyl-4*H*-benzo[*def*]carbazole (**3c**) together with 4-benzoyl-4*H*-benzo[*def*]carbazole (**3g**). The corresponding monobenzoyl derivative was not isolated. The results of the Friedel-Crafts reaction suggest that the para-position to the nitrogen atom in **1c** has higher electron density than those to the methylene group or the oxygen atom in **1a** and **1b**.

The hydrogenation of **1a**, **1b**, and **1c** in the presence of palladium–charcoal gave the corresponding 8,9-dihydro derivatives, **4a**, **4b**, and **4c**, respectively. The double bond at the 9,10-positions of phenanthrene were not hydrogenated under the reaction conditions. Gas chromatographic analysis showed that the rate of reduction from pyrene to 4,5-dihydropyrene was comparable to that of the double bond at the 8,9-positions in **1a** but the rate from 4,5-dihydropyrene to 4,5,9,10-tetrahydropyrene was very slow. This suggests that facile hydrogenation of **1a**, **1b**, and **1c** to the corresponding 8,9-dihydro derivatives (**4a**, **4b**, and **4c**) are due to strain in the fused ring system of **1a**—**c**. This explanation is supported by the fact that reduction of **1b** with lithium aluminium hydride afforded 4-phenanthrol.[1]

The reduction of **1a** with sodium–ethanol gave **4a**, and the reduction of **1b** afforded 3,3a,8,9,9a,9b-hexahydrophenanthro[4,5-*bcd*]furan (**5b**). In the case of **1c**, two products, **4c** and 3,8,9,9a-tetrahydro-4*H*-benzo[*def*]carbazole (**5c**), were obtained in 44% and 29% yields, respectively. Thus, not only the double bonds at the 8,9-positions but also the benzene rings which have hetero-atom substituents were readily reduced when the bridge linkage of X was a hetero-atom. The double bond at the 9,10-positions in phenanthrene was however not reduced under the reaction conditions. Thus, the double bonds at the 8,9-positions in **1a**, **1b**, and **1c** were readily reduced with sodium–ethanol and by catalytic hydrogenation.

Experimental

4H-Cyclopenta[def]*phenanthrene (**1a**).* Colorless plates from methanol; mp 113.5—114.5 °C (lit,[4] 114—115 °C). IR (KBr): ν_{max} 754, 817 cm^{-1} (Ar–H). ^{1}H NMR ($CDCl_3$): δ 4.22 (2H, s, $-CH_2-$), 7.45—7.78 (6H, m, Ar–H), 7.73 (2H, s, Ar–H). ^{13}C NMR ($CDCl_3$): δ 37.1 (C-4), 120.9 (C-3), 122.4, 125.1, 127.0, 127.9 (C-9), 138.2 (C-9b), 141.6 (C-3a). UV(EtOH): λ_{max} (ε) 210 (24300), 220^{sh} (26600), 222 (27800), 225 (24700), 249^{sh} (47500), 252 (50700), 261 (18400), 275 (8700), 287 (10600), 299 nm (12800).

4H-Benzo[def]*carbazole (**1c**).* Colorless plates from benzene–hexane; mp 172—173 °C (lit,[3a] 170—173 °C). IR (KBr): ν_{max} 750, 820 (Ar–H), 3445 cm^{-1} (NH). ^{1}H NMR ($CDCl_3$): δ 7.25 (2H, dd, J=3 and 6 Hz, Ar–H), 7.62—7.80 (5H, m, Ar–H+NH), 7.94 (2H, s, Ar–H). ^{13}C NMR ($CDCl_3$): δ 106.0 (C-3), 115.3, 122.3 (C-9b), 126.0, 126.8, 127.4 (C-9a), 138.8 (C-3a). UV(EtOH): λ_{max} (ε) 234 (63100), 273 (17600), 283 (13500), 332 (12200), 346 nm (10900).

1,3,5,7-Tetrabromo-4H-benzo[def]*carbazole (**2c**).* Bromine (1.1 g) in carbon tetrachloride (20 ml) was added to a carbon tetrachloride solution (30 ml) of **1c** (300 mg), and the mixture stirred for 1 h at room temperature. The precipitated crystals were collected by filtration to give 660 mg (83%) of **2c**. Recrystallization from tetrahydrofuran–benzene gave colorless needles; mp 294—295 °C (lit,[3b] mp 292—293 °C). IR (KBr): ν_{max} 808 (Ar–H), 3460 cm^{-1} (NH). UV(EtOH): λ_{max} (ε) 242 (45800), 248 (50000), 272 (18300), 288 (19000), 298 (13600), 353 (19100), 372 nm (21200). Found: C, 33.25; H, 1.14; N, 2.85%. Calcd for $C_{14}H_5NBr_4$: C, 33.18; H, 0.99; N, 2.76%.

8-Bromo-4H-cyclopenta[def]*phenanthrene (**2a**) and 4-Bromo-4H-cyclopenta*[def]*phenanthrene (**2e**).* Bromine (540 mg) in carbon tetrachloride (10 ml) was added to a carbon tetrachloride solution (30 ml) of **1a** (600 mg), and the solution stirred for 1 h at room temperature. After removal of the solvent, the resulting oil was chromatographed on silica gel and eluted with benzene–hexane (1:9). The first fraction gave 370 mg (42%) of **2a**. Recrystallization from methanol gave colorless needles; mp 91—92 °C. IR(KBr): ν_{max} 770, 780 cm^{-1} (Ar–H). NMR ($CDCl_3$): δ 4.13 (2H, s, Ar–CH_2–), 7.42—7.90 (6H, m, Ar–H), 7.96 (1H, s, Ar–H). UV (EtOH): λ_{max} (ε) 206 (26900), 223 (33900), 251 (48800), 257 (44400), 267 (22000), 283 (9600), 295 (14000), 308 nm (15500). Found: C, 66.73; H, 3.40%. Calcd for $C_{15}H_9Br$: C, 66.94; H, 3.37%.

The second fraction afforded 260 mg (30%) of **2e**. Recrystallization from methanol gave colorless needles; mp 131—132 °C. IR(KBr): ν_{max} 825 cm^{-1} (Ar–H). NMR ($CDCl_3$): δ 6.30 (1H, s, Ar–CHBr), 7.50—7.80 (8H, m, Ar–H). UV (EtOH): λ_{max} (ε) 227 (56700), 243 (21900), 257 (20700), 285 (13600), 298 nm (11700). Found: C, 66.89; H, 3.65%. Calcd for $C_{15}H_9Br$: C, 66.94; H, 3.37%.

*Bromination of **1a** with* N*-Bromosuccinimide.* *N*-Bromosuccinimide (600 mg) was added to a carbon tetrachloride solution (10 ml) of **1a** (300 mg) and the mixture refluxed for 2 h. After removal of insoluble materials by filtration the solvent was evaporated. The resulting crystals were chromatographed on silica gel and eluted with benzene–hexane (1:9) to give 320 mg (73%) of **2e**. The compound was identical with the product obtained by the bromination of **1a** with bromine.

1,7-Dibenzoyl-4H-benzo[def]*carbazole (**3c**) and 4-Benzoyl-4H-benzo*[def]*carbazole (**3g**).* Anhydrous aluminium chloride (840 mg) was added to a carbon disulfide solution (16 ml) of **1c** (400 mg) and benzoyl chloride (800 mg). The mixture was stirred for 6 h at room temperature, decomposed with dilute hydrochloric acid, and extracted with tetrahydrofuran. The solution was washed with water, dried, and evaporated. The resulting crystals were divided into a benzene-insoluble portion and a benzene-soluble portion. The benzene-insoluble portion (270 mg; 32%) was recrystallized from tetrahydrofuran–benzene to give **3c** as yellow needles; mp>300 °C. IR (KBr): ν_{max} 820 (Ar–H), 1630 (Ar–CO), 3240 cm^{-1} (NH). UV (EtOH): λ_{max} (ε) 210 (31200), 237 (41200), 258 (43500), 296 (23000), 397 nm (33500). Found: C, 84.36; H, 4.43; N, 3.55%. Calcd for $C_{28}H_{17}O_2N$: C, 84.19; H, 4.29; N, 3.51%.

The benzene-soluble portion was chromatographed on silica gel and eluted with benzene. The first fraction gave 100 mg (25%) of the starting material (**1c**), and the second fraction afforded 90 mg (15%) of **3g**. Recrystallization from ethanol

gave colorless needles; mp 141—142 °C (lit,[3a] 141—142 °C). IR (KBr): ν_{max} 825 (A–H), 1660 cm^{-1} (Ar–CON). NMR ($CDCl_3$): δ 7.36—7.77 (11H, m, Ar–H), 7.84 (2H, s, Ar–H). UV (EtOH): λ_{max} (ε) 213 (42800), 227 (43000), 256 (30600), 303 (15500), 315[sh] (13900), 338 (2800), 345 (1500), 354 nm (2000). Found: C, 85.50; H, 4.61; N, 4.60%. Calcd for $C_{21}H_{13}ON$: C, 85.40; H, 4.44; N, 4.74%.

1-Benzoyl-4H-cyclopenta[def]*phenanthrene (3a).* Anhydrous aluminium chloride (300 mg) was added to a carbon disulfide solution of **1a** (300 mg) and benzoyl chloride (330 mg). The mixture was stirred for 6 h at room temperature, decomposed with dilute hydrochloric acid, and extracted with ether. The ethereal layer was washed with water, dried, and evaporated. The resulting oil was chromatographed on silica gel and eluted with benzene–hexane (4: 1) to give 380 mg (82%) of **3a**. Recrystallization from methanol gave colorless needles; mp 129—130 °C. IR (KBr): ν_{max} 1640 cm^{-1} (Ar–CO). NMR ($CDCl_3$): δ 4.29 (2H, s, Ar–CH_2), 7.32—7.90 (7H, m, Ar–H), 8.23 (1H, d, J=9 Hz, Ar–H). UV (EtOH): λ_{max} (ε) 210 (34200), 225 (29200), 252 (51200), 321 nm (9600). Found: C, 89.54; H, 4.92%. Calcd for $C_{22}H_{14}O$: C, 89.77; H, 4.79%.

8,9-Dihydro-4H-benzo[def]*carbazole (4c).* A mixture of **1c** (400 mg), 8% palladium–charcoal (350 mg), and ethanol (30 ml) was shaken for 20 h at room temperature under a hydrogen atmosphere. After removal of the catalyst by filtration, the ethanol was evaporated under reduced pressure. The resulting crystals were chromatographed on silica gel and eluted with benzene–hexane (1: 1) to give 330 mg (82%) of **4c**. Recrystallization from benzene–hexane gave colorless plates; mp 124—125 °C (lit,[3b] 124—125 °C). IR (KBr): ν_{max} 773 (Ar–H), 3430 cm^{-1} (NH). NMR ($CDCl_3$): δ 3.27 (4H, s, $-CH_2-+-CH_2-$), 6.93 (2H, d, J=8 Hz, Ar–H), 7.01 (2H, d, J=8 Hz, Ar–H), 7.26 (2H, t, J=8 Hz, Ar–H), 7.39 (1H, broad s, NH). UV (EtOH): λ_{max} (ε) 216 (40300), 246 (34500), 255 (24000), 294 (12000), 316 (3600), 329 nm (3000). Found: C, 86.82; H, 5.83; N, 7.01%. Calcd for $C_{14}H_{11}N$: C, 87.01; H, 5.74; N, 7.25%.

8,9-Dihydro-4H-cyclopenta[def]*phenanthrene (4a).* Hydrogenation of **1a** to **4a** (89% yield) was conducted by the method employed for reduction of **1c**. Recrystallization from methanol gave colorless plates; mp 139—140 °C (lit,[3a] 138—140 °C). IR (KBr): ν_{max} 765 cm^{-1} (Ar–H). NMR ($CDCl_3$): δ 3.10 (4H, s, Ar–CH_2+Ar–CH_2), 3.83 (2H, s, Ar–CH_2), 6.99—7.34 (6H, m, Ar–H). UV (EtOH): λ_{max} (ε) 214 (37000), 228 (15100), 273 (18000), 282 nm (14000). Found: C, 93.47; H, 6.40%. Calcd for $C_{15}H_{12}$: C, 93.71; H, 6.29%.

Reduction of 1c with Sodium and Ethanol. An ethanolic solution (20 ml) of **1c** (200 mg) was heated under reflux. To the solution sodium (3.7 g) was added in limited amounts. When precipitates of sodium ethoxide were produced, additional ethanol (20 ml) was introduced into the solution and the residual sodium was added. After the sodium had disappeared (1 h), the mixture was poured into ice water, and extracted with ether. The ethereal layer was washed with water, dried, and evaporated. The resulting oil was chromatographed on silica gel and eluted with benzene–hexane (1: 1). The first fraction gave 90 mg (44%) of **4c**. The product was identical with the product obtained by the catalytic hydrogenation of **1c** in melting points and infrared spectra. The second fraction afforded 60 mg (29%) of **5c** as crystals. Recrystallization from benzene–hexane gave colorless needles; mp 127—128 °C (lit,[3a] 125—126 °C). IR (KBr): ν_{max} 3420 cm^{-1} (NH). NMR ($CDCl_3$): δ 1.13—1.53 (1H, m, $-CH_2-$), 2.12—2.35 (1H, m, $-CH_2-$), 2.70—3.32 (4H, m, $-CH_2-+-CH_2-$), 3.37—3.53 (1H, m, Ar–CH–), 5.72—6.01 (2H, m, –CH=CH–), 6.72—7.31 (4H, m, Ar–H+NH). UV (EtOH): λ_{max} (ε) 230 (31900), 283 nm (5800). Found: C, 86.25; H, 6.73; N, 7.41%. Calcd for $C_{11}H_{13}N$: C, 86.11; H, 6.71; N, 7.17%.

Reduction of 1a with Sodium and Ethanol. **1a** was reduced by a method similar to the hydrogenation of **1c** with sodium and ethanol. The resulting oil was chromatographed on silica gel and eluted with benzene–hexane (1: 9) to give 130 mg (65%) of **4a**. The product was identical with the sample obtained by the catalytic hydrogenation of **1a** with palladium–charcoal in melting points and infrared spectra.

The authors wish to express their thanks to Mr. Takao Oono for the NMR analyses.

References

1) T. Horaguchi, *Bull. Chem. Soc. Jpn.*, **50**, 3329 (1977).
2) (a) L. F. Fieser and J. Cason, *J. Am. Chem. Soc.*, **62**, 1293 (1940); (b) W. E. Bachmann and J. C. Sheehan, *ibid.*, **63**, 2598 (1941).
3) (a) O. Kruber and G. Grigoleit, *Chem. Ber.*, **87**, 1895 (1954); (b) M. Zander and W. H. Franke, *ibid.*, **99**, 1279 (1966).
4) W. E. Bachmann and J. C. Sheehan, *J. Am. Chem. Soc.*, **63**, 204 (1941).
5) H. Henstock, *J. Chem. Soc.*, **119**, 55 (1921); H. Henstock, *ibid.*, **123**, 3097 (1923).
6) W. E. Bachmann, *J. Am. Chem. Soc.*, **57**, 555 (1935).
7) M. S. Newmann and R. L. Childers, *J. Org. Chem.*, **32**, 64 (1967).
8) (a) A. I. Levchenko and V. V. Beloglazova, *Khim. Atsetilena*, **1968**, 211 [*Chem. Abstr.*, **71**, 30278e (1969)]; (b) R. C. Fuson and H. D. Porter, *J. Am. Chem. Soc.*, **70**, 895 (1948); (c) N. G. Sidrova, A. I. Bokova, and I. P. Tsukervanik, *Zh. Org. Khim.*, **4**, 1658 (1968) [*Chem. Abstr.*, **70**, 3621j (1969)].
9) H. Gilman and S. Abakian, *J. Am. Chem. Soc.*, **68**, 580 (1946).
10) (a) N. P. BuuHoĭ and R. Royer, *Recl. Trav. Chim. Pays-Bas*, **66**, 533 (1947) [*Chem. Abstr.*, **42**, 5014i (1948)]; (b) S. G. P. Plant, K. M. Rogers, and S. B. C. Williams, *J. Chem. Soc.*, **1935**, 741; (c) S. G. P. Plant and M. L. Tomlinosn, *ibid.*, **1932**, 2188.

An X-Ray Photoelectron Spectroscopic Study of Several Hydroxy Azo Compounds

Tooru YOSHIDA

Osaka Prefectural Industrial Research Institute, 2-1-53, Enokojima, Nishi-ku, Osaka 550

(Received July 23, 1979)

The tautomerism of several solid hydroxy azo compounds has been examined by X-ray photoelectron spectroscopy. It has been found that the proportion of enol and keto tautomers may be readily estimated from the relative intensities of the two peaks in the O(1s) electron spectrum which corresponds to the protonated and deprotonated oxygen atoms. The resonance structures of the sodium salt of 1-phenylazo-2-naphthol and 5-phenylazo-8-quinolinol have been discussed on the basis of the N(1s) and O(1s) electron binding energies.

Phenylazo derivatives of phenols and naphthols can exist either in the enol form (*e.g.* **1**) or in the keto form (*e.g.* **2**). Numerous investigations have been conducted to establish the structure in solution or solid by a variety of techniques *e.g.* visible and UV,[1] Raman,[2] IR,[3] NMR,[4] and X-ray diffraction analysis.[5] Phenylazo derivatives of phenol appear to exist in the enol form both in solution and the solid, whereas in the phenylazo derivatives of naphthols both forms coexist even in the solid state. There have been however few studies concerning a quantitative analysis of the tautomers in solid hydroxy azo compounds.[1e]

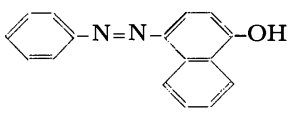

1

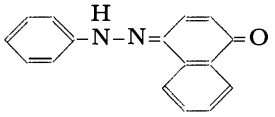

2

X-Ray photoelectron spectroscopy (XPS), which is sensitive to the charge distribution, is suitable for the detection of protonated atoms.[6] The purpose of the present XPS study is to determine the proportions of enol and keto form tautomers of several solid hydroxy azo compounds, and furthermore, to examine the chemical structures of two compounds; the sodium salt of 1-phenylazo-2-naphthol and 5-phenylazo-8-quinolinol. In the former compound a mobile hydrogen atom is absent in the molecule and in the latter a mobile hydrogen atom is considered fixed by an intramolecular hydrogen bond.

Experimental

The X-ray photoelectron spectra were measured on an AEI ES200 spectrometer. Mg $K\alpha$ (1253.6 eV) X-ray radiation was used as the excitation source. The samples were ground to a powder and dusted on to double-backed adhesive tape. The measurements were conducted at room temperature under a vacuum of about 10^{-7} Torr. The binding energy of the C(1s) electron peak was used as the energy standard throughout the present work and has been taken to be 285.0 eV. The reproducibilities of the values thus obtained were within ± 0.1 eV. Appreciable X-ray damage was not observed throughout the experiments. All the compounds used and their binding energies are given in Table 1. Phenylazo, naphthylazo, and quinolylazo derivatives of naphthols were prepared by the standard diazo-coupling reaction with the naphthols. 5-Phen-

TABLE 1. MEASURED BINDING ENERGIES AND PROPORTIONS OF KETO TAUTOMER

Compound	R	Binding energy/eV		R/%[a]	
		N(1s)	O(1s)	A[b]	B[c]
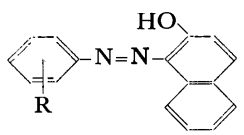	*o*-OCH_3	400.4	533.3; 530.9	69	
	p-OCH_3	400.2	533.2; 531.2	32	55
	o-CH_3	400.5	533.1; 531.1	62	
	p-CH_3	400.4	533.0; 531.0	59	65
	H	400.5	533.0; 531.1	64	70
	o-Cl	400.5	533.0; 531.0	64	
	p-Cl	400.4	532.9; 531.1	53	65
	m-Cl	400.5	533.2; 531.3	69	65
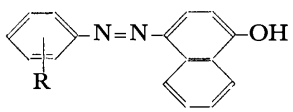	*p*-OCH_3	400.4	533.2; 530.9	60	65
	H	400.5	533.1; 531.0	73	80
5-Phenylazo-8-quinolinol		400.3; 399.4	532.9	≈0	
1-(2-Pyridylazo)-2-naphthol		400.5; 399.0	533.0; 530.9	76	
1-(8-Quinolylazo)-2-naphthol		400.3; 398.9	533.0; 530.8	68	
1-(1-Naphthylazo)-2-naphthol		400.5	533.0; 531.0	69	
4-(Phenylazo)phenol		400.3	533.1	≈0	
1-Phenylazo-2-naphthol sodium salt		400.5; 399.0	531.0		
1,1′-Azonaphthalene		400.2			

a) The proportion of keto tautomer. b) The values estimated in this study. c) The reported values[1e] estimated from electronic spectra.

ylazo-8-quinolinol was obtained by diazo-coupling with 8-quinolinol in acetic acid.[7] 4-(Phenylazo)phenol and 1-(2-pyridylazo)-2-naphthol were obtained commercially and used after recrystallization from ethanol. The sodium salt of 1-phenylazo-2-naphthol was obtained by treating the naphthol with NaOH in a mixture of ethanol and water: the black crystals separated out were subject to hydrolysis by water and ethanol. Therefore, the crystals collected by filtration were rapidly washed with a small amount of alkaline ethanol and diisopropyl ether, and dried *in vacuo* at 90 °C. The salt thus obtained was brownish black. Found: C, 71.69; H, 4.42; N, 10.47%. Calcd for $C_{16}H_{11}N_2ONa$: C, 71.11; H, 4.07; N, 10.37%. 1,1'-Azonaphthalene and two nickel complexes of phenylazo derivatives of 2-naphthol as reference compounds were prepared according to the literature.[8,9] All compounds were checked by elemental analysis, and all compounds except for the sodium salt and the two metal complexes were also checked by melting point measurement.

Results and Discussion

The Determination of the Equilibria of Tautomers. The O(1s) electron spectrum of 1-phenylazo-2-naphthol is shown in Fig. 1. E_b in the figure indicates the binding energy. The spectrum clearly showed two peaks, which suggested the presence of two types of oxygen atoms in the molecule. The peaks with full-width at half-maximum height (FWHM) of approx. 1.5 eV indicated by the broken lines in the figure were obtained by graphical resolution. P_1 and P_2 indicate their peak heights in Figs. 1 and 2. The binding energy difference between the two peaks was 1.9 eV. The reported values of the difference between the O(1s) binding energies of protonated and deprotonated oxygen atoms have been in the range of 1.4—1.9 eV.[10] Furthermore, the O(1s) electron spectrum of 4-(phenylazo)phenol, which is known to exist as the pure azo compound from the IR study,[3] showed a single peak with a FWHM of 1.5 eV. The binding energy was very similar to that of the peak with the higher binding energy of 1-phenylazo-2-naphthol. Therefore, it appears to be reasonable to assign the peaks with high and low binding energies in Fig. 1 to the protonated and deprotonated oxygen atoms respectively.

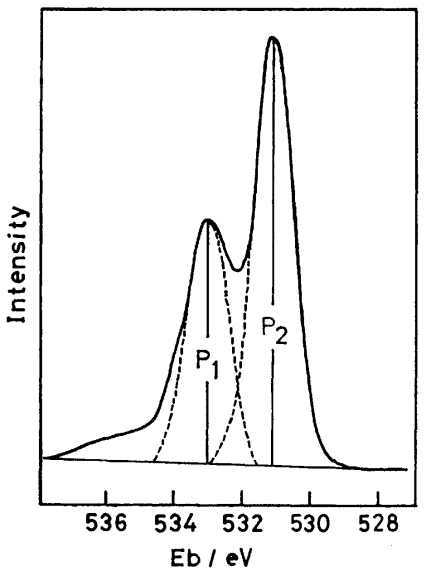

Fig. 1. O(1s) electron spectrum of 1-phenylazo-2-naphthol.

In XPS, the relative intensities of the peaks of a certain atom correspond to the relative amounts of the atom present in different states in the molecule. Therefore, it may be considered that the equation $100 \cdot P_2/(P_1+P_2)$ corresponds to the proportion(%) of the deprotonated oxygen atom and consequently, of the keto form tautomer in such a compound as 1-phenylazo-2-naphthol, which contains only two kinds of oxygen atoms in the molecule—protonated and deprotonated oxygens.

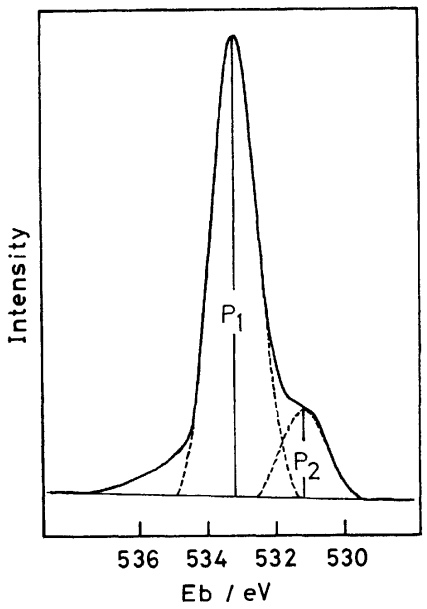

Fig. 2. O(1s) electron spectrum of 1-(*p*-methoxyphenylazo)-2-naphthol.

The O(1s) electron spectrum of 1-(*p*-methoxyphenylazo)-2-naphthol is shown in Fig. 2, as an example of a compound containing a methoxyl group in the molecule. It was found that the O(1s) binding energy of the oxygen atom of a methoxyl group was almost the same as that of a protonated oxygen atom in respect to the O(1s) electron spectra of the two nickel complexes. The O(1s) electron spectrum of bis[1-(*p*-methoxyphenylazo)-2-naphtholato]nickel(II) showed two peaks with nearly equal intensities, and that of bis(1-phenylazo-2-naphtholato)nickel(II) showed a single peak. The O(1s) electron binding energies of the former complex were 533.2 eV and 531.3 eV, and that of the latter was 531.3 eV.

Therefore, the single peak with the higher binding energy of the two in Fig. 2 can be assigned to the oxygen of the methoxyl group in addition to the protonated oxygen, and the other to the deprotonated oxygen. Consequently, in the case of a compound such as 1-(*p*-methoxyphenylazo)-2-naphthol, which contains a methoxyl group, it may be considered that the equation $100 \cdot P_2/(P_1'+P_2)$, where $P_1'=P_1-(P_1+P_2)/2$, corresponds to the proportion of the keto form tautomer.

The O(1s) electron spectra of all other naphthol derivatives showed two types of peak similarly to 1-phenylazo-2-naphthol.

The proportions of keto form tautomer estimated in the above ways are given in Table 1, together with the reported values derived from the electronic spectra by use of the potassium bromide disc.[1e] The values are comparable with the reported values. In this study, errors of approx. 5% were unavoidable due to the incompleteness of graphical resolution.

It appears that the XPS method is more suitable than the electronic spectra method for the determination of equilibria of tautomers in the solid state since the latter method involves considerable uncertainty in the values of the true energies and intensities of the bands of the individual tautomers. Furthermore, it has been said that the spectra obtained by the potassium bromide disc method are not free from the influence of the diluent.[1f]

The N(1s) electron spectra of all hydroxy azo compounds except for the three hydroxy azo compounds containing heterocyclic nitrogen atoms and the sodium salt of 1-phenylazo-2-naphthol showed a single peak with a FWHM (≈1.6 eV) and a binding energy similar to that of a reference compound 1,1'-azonaphthalene, which exists in the pure azo form. Therefore, it was impossible to examine the equilibria of the tautomers on the basis of the N(1s) spectra.

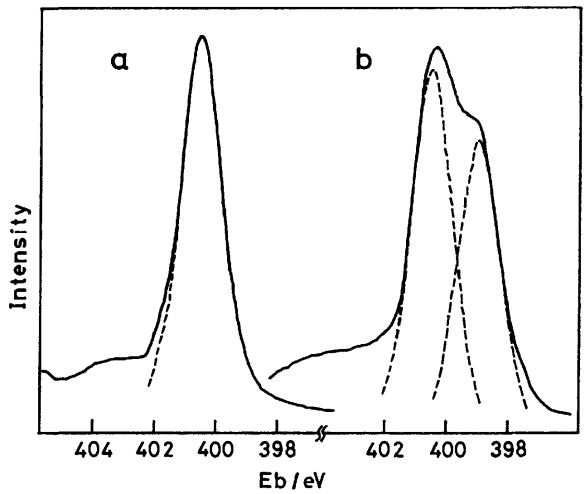

Fig. 3. N(1s) electron spectra of a: 1-phenylazo-2-naphthol and b: its sodium salt.

The Sodium Salt of 1-Phenylazo-2-naphthol. The N(1s) spectra of 1-phenylazo-2-naphthol and its sodium salt are shown in Fig. 3. The N(1s) spectrum of 1-phenylazo-2-naphthol showed a single peak, suggesting that the charge densities on the three types of nitrogen atoms, the nitrogen atoms of the azo group, the protonated and deprotonated nitrogen atoms of the hydrazono group, are almost equal. The spectrum of the salt showed two comparable peaks, which suggested the presence of two types of nitrogen atom. The peaks indicated by the broken lines in the figure were obtained by graphical resolution, as were those in Fig. 4. Furthermore, the O(1s) binding energy of the salt was very close to those of the keto form oxygen of hydroxy azo compounds. The results suggest the following resonance contribution:

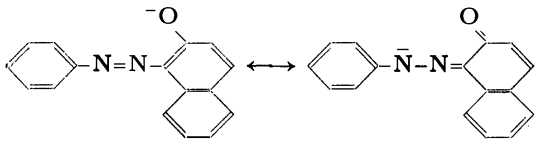

The inequality in intensities of the two peaks of the salt in Fig. 3(b) may be due to an impurity (probably, 1-phenylazo-2-naphthol produced by hydrolysis of the salt) in the sample. The O(1s) spectrum of the salt showed a peak with some intensity around the energy (533 eV) corresponding to a protonated oxygen atom.

5-Phenylazo-8-quinolinol. The O(1s) electron spectrum of 5-phenylazo-8-quinolinol showed a single peak with a FWHM of 1.6 eV. From its binding energy, the peak was assigned to the protonated oxygen atom. This is consistent with the results[11] from the electronic spectra that 5-phenylazo-8-quinolinol exists predominantly in the enol form in solution due to the presence of an intramolecular hydrogen bond between the heterocyclic nitrogen and the hydroxyl hydrogen.

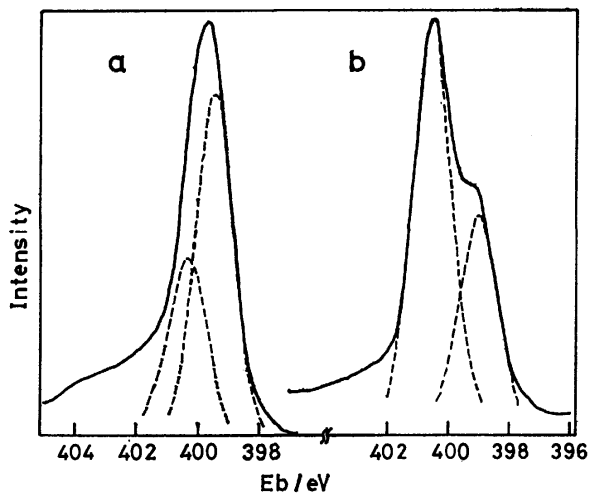

Fig. 4. N(1s) electron spectra of a: 5-phenylazo-8-quinolinol and b: 1-(2-pyridylazo)-2-naphthol.

The N(1s) spectra of 5-phenylazo-8-quinolinol and 1-(2-pyridylazo)-2-naphthol are shown in Fig. 4. Both spectra showed two peaks with an intensity ratio of approx. 2: 1. The N(1s) spectrum of 1-(8-quinolylazo)-2-naphthol was very similar to that of 1-(2-pyridylazo)-2-naphthol.

The peak with the lower binding energy of the two in 1-(2-pyridylazo)-2-naphthol and 1-(8-quinolylazo)-2-naphthol can be readily assigned to the heterocyclic nitrogen atom and the other to the nitrogen atoms of the azo group, by comparison with the N(1s) spectra of 1-phenylazo-2-naphthol and 1-(1-naphthylazo)-2-naphthol. That is, the N(1s) binding energy of the heterocyclic nitrogen atom is approximately 399.0 eV.

Therefore, it appears reasonable to assign the two peaks in 5-phenylazo-8-quinolinol with high and low binding energies to the nitrogen atom adjacent to the quinoline ring in the azo group and the remaining

nitrogen atom of the azo group in addition to the heterocyclic nitrogen atom respectively. The inequality of the two nitrogen atoms of the azo group may be caused by the following resonance:[3a)]

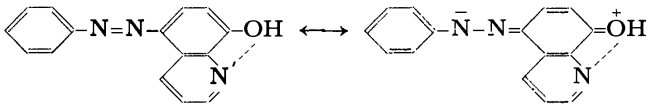

Here, the presence of an intramolecular hydrogen bond may stabilize the dipolar form, since the N(1s) spectra of all the hydroxy azo compounds having no such intramolecular hydrogen bond did not show any inequality for the two nitrogen atoms of the azo group.

The intramolecular hydrogen bond appears to be relatively strong, since the O(1s) binding energy of 5-phenylazo-8-quinolinol was not larger than those of the other hydroxy azo compounds. In fact, the N(1s) binding energy of the heterocyclic nitrogen atom was 0.4—0.5 eV higher than those of 1-(2-pyridylazo)-2-naphthol and 1-(8-quinolylazo)-2-naphthol.

In 5-phenylazo-8-quinolinol the contribution of the resonance structure with unit negative charge on the nitrogen atom of the azo group appears to be smaller than that in the sodium salt of 1-phenylazo-2-naphthol from the following result. The differences between the N(1s) binding energies of the two nitrogen atoms of the azo group are 0.9 eV for the former compound and 1.5 eV for the latter.

The author wishes to thank Drs. Kiyoshi Yamasaki and Shigemasa Sawada and Mr. Nobuhiro Kuramoto for their help in performing this experiment and Mr. Taichiro Hirohara for the elemental analysis.

References

1) a) J. N. Ospension, *Acta Chem. Scand.*, **4**, 1351 (1950); b) J. N. Ospension, *ibid.*, **5**, 491 (1951); c) A. Burawoy, A. G. Salem, and A. R. Thompson, *J. Chem. Soc.*, **1952**, 4793; d) A. Burawoy and A. R. Thompson, *ibid.*, **1953**, 1443; e) I. Saito, Y. Bansho, and A. Kakuta, *Kogyo Kagaku Zasshi*, **70**, 1715 (1967); f) C. Dehari, Y. Matsunaga, and K. Tani, *Bull. Chem. Soc. Jpn.*, **43**, 3404 (1970); g) Schreiber, J. Socha, and K. Rothschein, *Collect. Czech. Chem. Commun.*, **35**, 857 (1970).

2) a) A. R. Monahan, A. F. DeLuca, and A. T. Word, *J. Org. Chem.*, **36**, 3838 (1971); b) Y. Saito, B. K. Kim, K. Machida, and T. Uno, *Bull. Chem. Soc. Jpn.*, **47**, 2111 (1974); c) P. J. Trotter, *Appl. Spectrosc.*, **31**, 30 (1977).

3) a) D. Hadzi, *J. Chem. Soc.*, **1956**, 2143; b) K. J. Morgan, *J. Chem. Soc.*, **1961**, 2151.

4) a) A. H. Berrie, P. Hampson, S. W. Longworth, and A. Mathias, *J. Chem. Soc., B*, **1968**, 1308; b) V. Bekarek, J. Dobas, J. Socha, P. Vetesník, and M. Vecera, *Collect. Czech. Chem. Commun.*, **35**, 1406 (1970); c) F. D. Saeva, *J. Org. Chem.*, **36**, 3842 (1971).

5) A. Whitaker, *J. Soc. Dyers Colour.*, **1978**, 431.

6) a) K. Siegbahn, *et al.*, "ESCA Atomic, Molecular and Solid State Structure Studied by Means of Electron Spectroscopy," Almqvist and Wiksells AB, Uppsala (1967); b) K. Siegbahn, *et al.* "ESCA Applied to Free Molecules," North-Holland Publ. Co., Amsterdam (1969).

7) C. Matsumura, *J. Am. Chem. Soc.*, **52**, 4164 (1930).

8) A. Hantzsch and M. Schmiedel, *Berichte*, **30**, 81 (1897).

9) K. Ueno, *J. Am. Chem. Soc.*, **79**, 3066 (1957).

10) a) Ref. 6b, p. 127; b) T. Yoshida and S. Sawada, *Bull. Chem. Soc. Jpn.*, **49**, 3319 (1976); c) T. Yoshida, *ibid.*, **51**, 3257 (1978).

11) a) G. M. Badger and R. G. Buttery, *J. Chem. Soc.*, **1956**, 614; b) E. Sawicki, *J. Org. Chem.*, **22**, 743 (1957).

Photochemical Reactions of Aromatic Compounds. XXXIII.[1] Photoreactions of 1-Cyanonaphthalene with Indene in Various Solvents

Masahide YASUDA, Chyongjin PAC,* and Hiroshi SAKURAI
The Institute of Scientific and Industrial Research, Osaka University, Suita, Osaka 565
(Received July 25, 1979)

The stereospecific photocycloaddition of 1-cyanonaphthalene to indene occured in cyclohexane, benzene, diethyl ether, tetrahydrofuran, and ethyl acetate, giving the *endo* head-to-head cycloadduct as the sole 1 : 1-adduct. The mechanism was discussed in terms of the exciplex intermediacy. In methanol or in acetonitrile in the presence of water, the photoreaction gave the dihydrocycloadduct (**8**), accompanied by the formation of 2-methoxyindan and 2,2′-dimethoxy-1,1′-biindanyl or 2-indanol and 1-hydroxy-2,2′-biindanyl. In these solvents, the reactions were suggested to be initiated by photochemical electron transfer; the methoxylated or hydroxylated compounds are formed by the nucleophilic attack of methanol or water on the indene cation. Anionic species, including the 1-cyanonaphthalene anion, were suggested to play important roles in the formation of **8**.

Photocycloadditions of aromatic nitriles to furan and olefinic compounds have been extensively investigated with regard to the chemistry of exciplexes.[2,3] The photoreactions more or less depend on the solvent polarity[2a,b,e,f,i,3b,4] and, in a few cases, afford other products in polar solvents which arise from ion radicals.[2f,4] Solvent effects on the photophysics of typical exciplexes have been well documented,[5] and the dissociation into ion radicals has been confirmed to occur in polar solvents.[5,6] The irradiation of exciplex-formation systems in very polar solvents can thus provide a convenient method for the generation of ion radicals, and synthetic applications have been increasingly reported in recent years.[7-9] However, the formation of the final products must compass complex reaction pathways since there independently or concurrently participate such various reaction intermediates as exciplexes, ion-pairs, cation radicals, anion radicals, and free radicals. For example, the photochemical *anti*-Markownikoff addition of methanol to an aromatic olefin in the presence of an electron acceptor includes, at least, a photochemical electron transfer from the olefin to the electron acceptor, the nucleophilic attack of methanol on the cation radical of the olefin, and the reduction of the methoxylated radical by the anion radical of the electron acceptor.[9] Moreover, electron acceptors which are usually aromatic nitriles are more or less consumed by unreclaimed reactions, and the products have not been fully characterized. Thus, the features of the photoreactions of exciplex-formation systems in polar solvents would often vary from system to system. During the course of our investigation of the photoreactions of aromatic nitriles with furan and olefinic compounds, we have found that the photoreactions of 1-cyanonaphthalene (**1**) with indene (**2**) depends not only on the solvent polarity, but also on the nature of the solvent, as is shown in Scheme 1, and that a novel type of photocycloaddition occurs in polar protic media to give a reduced cycloadduct (**8**), which is formed *via* the anionic species of **1**.

Results

Photoreaction in Less Polar Solvents. The irradiation of **1** and **2** in benzene through Pyrex with a high-pressure mercury arc at an ambient temperature gave **3** as the exclusive 1 : 1-adduct, accompanied by small amounts of indene dimers, though over-irradiation resulted in the formation of complex mixtures. Similar results were obtained in the photoreactions of cyclohexane, diethyl ether, tetrahydrofuran, and ethyl acetate solutions. Isomers of **3** could neither be detected

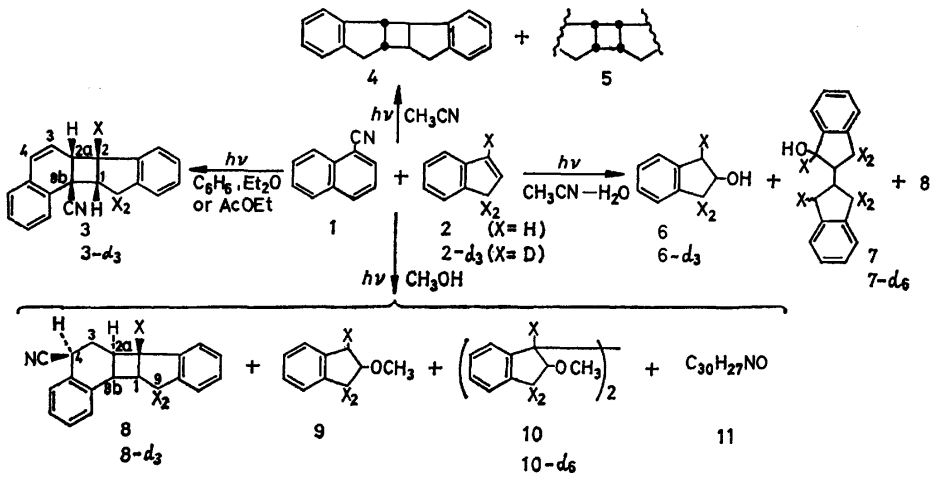

Scheme 1.

by the GLC of the photolysate nor by the NMR of a crude product which had been obtained by passing a photolysate through a short column of silica gel to remove indene dimers and polymeric materials.

The structure of **3** was indicated by its elemental composition and the spectral properties. The ^{1}H NMR spectrum consisted of two sets of double doublets for C_9-methylene protons, two sets of multiplets for H-1 and H-2a, a triplet for H-2, a doublet of doublets for H-3, a doublet for H-4, and multiplets for aromatic protons. Since the signal for H-2 appears as a triplet, **3** can be identified as a head-to-tail adduct. This assignment was further confirmed by the NMR spectrum of **3**-d_3; this compound was obtained by the photocycloaddition of **1** to indene-1,1,3-d_3 (**2**-d_3). It showed a broad singlet for H-1 and a broad doublet for H-2a at positions identical to those of the respective centers of the two sets of multiplets for **3**, while the olefinic and aromatic resonances were essentially identical to those for **3** in all respects.

The *endo*-configuration for **3** was suggested by the unusually high chemical shifts of the olefinic protons and an aromatic proton; the olefinic protons show upfield shifts of more than 0.34 and 0.27 ppm relative to the corresponding protons of similar compounds.[2b,h-j,3a,b,10] Similarly, the aromatic proton is considerably shielded (more than 0.2 ppm). The shielding effects on the protons can be reasonably understood by means of molecular models with the *endo*-configuration; the benzene ring of the indan moiety is located just over the olefinic protons and the aromatic proton of the indan moiety extends over the edge of the other benzene ring. On the other hand, the shielding effects can not be expected from the *exo*-configuration.

Photoreaction in Acetonitrile in the Presence of Water. The irradiation of an acetonitrile solution of **1** and **2** gave an *anti* head-to-head cyclobutane dimer, **4**, in a 50% yield, accompanied by only small amounts of **3** and the *syn* head-to-head cyclobutane dimer, **5**, whereas 70% of the **1** was recovered. Control experiments using 313 nm light, where **1** absorbed mostly the incident light, showed that **4** and **5** were formed in a 95: 5 ratio, while the head-to-tail dimers could not be detected.

The formation of the indene dimers was remarkably "quenched" by water. In the presence of 10 vol% of water we obtained 2-indanol, **6**, 1-hydroxy-2,2′-biindanyl, **7**, and a new cycloadduct, **8** in 58%, 23%, and 25% yields respectively, while the indene dimers were not formed. The structure of **6** was unambiguously determined by a direct comparison with an authentic sample prepared by the reduction of 2-indanone[11] with sodium borohydride.

The structure of **7** was deduced from the spectral properties. The NMR spectrum showed a broad triplet for H-1, a broad doublet for O–H, and complex signals for the other aliphatic protons and aromatic protons. On the addition of deuterium oxide, the broad doublet disappeared along with a collapse of the broad triplet into a sharp doublet. The NMR spectrum of **7**-d_6 showed a broad singlet for O–H at δ 1.7, a broad doublet for H-2 at δ 2.3, an asymmetrical broad triplet for H-2′ at δ 2.46, and two sets of doublets with small splittings for H-1′ at δ 2.86—3.24, clearly supporting the structure assigned. Probably, H-1′ is located in either a *cis* or *trans*-relationship with H-2′.

The mass spectrum of **8** which showed a very weak molecular ion peak at *m/e* 271 and strong fragment-ion peaks at *m/e* 116 and 155, indicates that **8** is a dihydro-adduct of **1** and **2**. The ^{1}H NMR spectrum consisted of signals for nine aliphatic protons and eight aromatic protons, but showed none for olefinic protons. Each signal for the aliphatic protons was resolved by means of extensive double-irradiation experiments, lanthanoid-induced shifts (LIS), and deuterium-labelling experiments. The data are listed in Table 1. For example, the doublet of doublets at δ 3.64 can easily be assigned to the signal for the proton (H-4) attached to cyanated carbon, since this signal showed the largest shift downfield on the addition of Eu(fod)$_3$ and since this signal was absent in the spectrum of **8**-*d*; this compound was obtained by refluxing a dioxane–methanol-*O*-*d* solution of **8** in the presence of sodium methoxide.

In the NMR spectrum of **8**-d_3, the signal for H-8b appeared as a broad triplet, demonstrating that **8** is a head-to-tail adduct. The *cis*-relationship between H-2a and H-4 was deduced from the vicinal couplings with H-3A (one of the C-3 methylene protons); the coupling constants are very similar to those of the axial-axial couplings for cyclohexane compounds.[12] When a solution of **8** in dioxane–methanol was refluxed in the presence of sodium methoxide, an equilibrium mixture

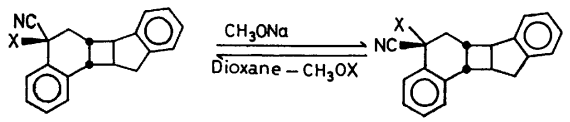

20% **8** (X=H) **8**-*d* (X=D)

80% **12** (X=H) **12**-*d* (X=D)

Table 1. ^{1}H NMR spectral data for **8** and **12**[a]

Compd	Chemical shifts (ppm in $CDCl_3$) (multiplicities)									Coupling constants/Hz
	H-1	H-2	H-2a	H-3A	H-3B	H-4	H-8b	H-9		
8	3.4—3.8	4.1	2.9—3.2	1.16	2.0	3.64	3.94	2.7	3.1	$J_{3A,2a}=J_{3A,3B}=J_{3A,4}=13.0$
	(m)	(t)	(m)	(q)	(d-d-d)	(d-d)	(t)	(d-d)	(d-d)	$J_{3B,2a}=7.0, J_{3B,4}=3.0$
LIS[b]	3.6—4.0	4.3	3.3—3.6	1.82	2.68	4.82	4.22	2.95	3.2	$J_{1,8b}=J_{2a,8b}=9.0$
12	3.2—3.8	4.1	3.2—3.4	1.3—2.0		3.0	4.0	2.44	2.9	$J_{3A,4}=7.5, J_{3B,4}=5.0$
	(m)	(t)	(m)	(m)		(d-d)	(t)	(d-d)	(d-d)	$J_{3A2a}=5.0, J_{3B,2a}=6.5$

a) Aromatic signals (δ 6.9—7.5) are omitted. b) 0.4 equiv of Eu(fod)$_3$ added.

of **8** and **12** was obtained in a 1 : 4 ratio, clearly demonstrating that **8** is thermodynamically less stable than **12**.

For **8**, the half-chair conformation (A) would be much more favorable than the negative half-chair conformation (B) because of the steric repulsion between the cyano group and the cyclobutane ring. In fact, the vicinal coupling constants of H-3A and H-3B are very similar to those of the axial-axial and axial-equatorial couplings for cyclohexane compounds respectively. Similarly, the B conformer or, more probably, an equilibrium mixture of A and B would be favorable for **12**. With the *endo*-structure, however, B is extremely unstable because of the nonbonding interaction between H-4 and the benzene ring of the indan moiety, since the closest separation between them is only 1.8—2.0 Å, as is shown by the molecular models. If **8** and **12** had this structure, **8** could be expected to be more stable than **12**. Therefore, this structure can not be accepted. On the other hand, **12** can exist in either A or B with the *exo*-configuration; it is thus more stable than **8**. Therefore, the *exo*-configuration can be assigned to **8** and **12**.

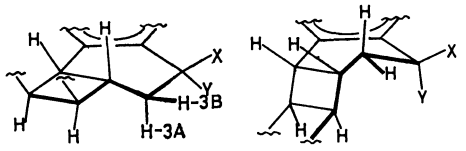

A B

8 (X=H; Y=CN) **12** (X=CN;Y=H)

Photoreaction in Methanol. The irradiation of a methanolic solution of **1** and **2** gave **8** in a 35% yield, along with several other products, including mainly 2-methoxyindan (**9**) and diastereoisomeric mixture of 2,2′-dimethoxy-1,1′-biindanyl (**10**). These compounds were confirmed to be the primary photoproducts, since their formation increased linearly with the irradiation time up to *ca.* a 10% conversion.

The structure of **9** was determined by a direct comparison of its spectral properties with those of an authentic sample which had been prepared by the methylation[13] of 2-indanol with diazomethane in the presence of boron trifluoride etherate.

The repeated chromatography of mixtures of **10** on silica gel gave three isomers (**10a**, **10b**, and **10c**) contaminated by small amounts of the others and a fourth isomer (**10d**) in a mixture with an equal amount of **10b**. In the mass spectra, only **10c** showed the molecular ion peak at *m/e* 296, whereas the main fragment-ion peaks at *m/e* 262 and 198 were commonly observed for **10a**—**c**. The NMR spectra of **10a**—**c** commonly consisted of the signals for aliphatic protons, methoxyl protons, and aromatic protons in the area ratio of *ca.* 4 : 3 : 4, showing that **10a**—**c** are dimeric compounds of **2** which possess two methoxyl groups.

The signals of aliphatic protons are too complex to be assigned. Therefore, the d_6-compounds of **10** were prepared by a photoreaction using **2**-d_3; the NMR spectra were then taken (Table 2). The aliphatic resonances should be the signals for H-2 and H-2′. Since the chemical shifts are relatively low, two methoxyl groups can be said to attach themselves to C-2 and C-2′. For structural elucidation, it should be noted that H-2 and H-2′ or the two methoxyl groups are magnetically equivalent for **10c** and **10d**, but not for **10a** and **10b**. Therefore, **10a** or **10b** appears to be either isomer of the *cis*, *trans*-structure. The *trans*, *trans*- or *cis*, *cis*-structure should be reserved for **10c** and **10d**.

TABLE 2. ^{1}H NMR SPECTRAL DATA FOR **10**(**a**—**d**)-d_6

	H-2 and H-2′		OCH_3	
10a	3.65	3.98	2.80	3.15
10b	3.65	4.20	3.24	3.38
10c	3.60		2.96	
10d	3.88		3.25	

From complex mixtures of oligomeric and polymeric materials, a 1 : 2 : 1-adduct of **1**, **2**, and methanol (**11**) was isolated by repeated chromatography. However, the isolation was poorly reproducible because of the low yields as well as difficulties in the isolation. The structure could not be determined.

Discussion

An excited-singlet mechanism is responsible for the formation of **3**, since the fluorescence of **1** was quenched by **2** at a diffusion-controlled rate ($k_q = 1.2 \times 10^{10}$ dm^3 mol^{-1} s^{-1} in benzene) and the triplet photosensitization using benzophenone or Michler's ketone did not give **3** at all. It is of mechanical interest to note that the *endo* cycloadduct (**3**) was exclusively formed. This stereoselectivity can be interpreted in terms of the intermediacy of the **1**—**2** exciplex possessing a sandwich-type configuration. The excited singlet **1** has been known to form exciplexes with a variety of alkenes,[14] and the ionization potential of **2** is low (8.14 eV)[15] enough for the formation of the **1**—**2** exciplex. Therefore, the exciplex mechanism is not unreasonable, though exciplex emission could not be detected. Moreover, it should be noted that the head-to-tail structure of **3** can not be expected from the most stable 1,4-biradical and 1,4-dipolar intermediates. This suggests that the photocycloaddition is stereospecific in nature, as has been reported in the photocycloaddition of **1** to *cis*- and *trans*-1-phenoxypropenes.[2h]

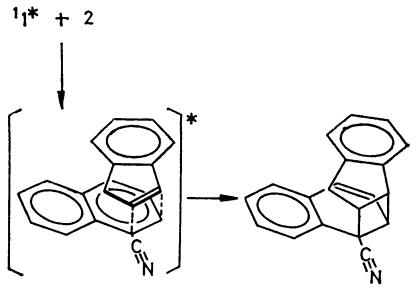

This photocycloaddition still occurs in such a moderately polar solvent as ethyl acetate, but it does not in acetonitrile and methanol; the exciplex formation is dominant in ethyl acetate and less polar solvents. In very polar solvents, however, a complete electron-transfer reaction predominantly occurs to give the

anion radical of **1** ($\mathbf{1}^{\cdot-}$) and the cation radical of **2** ($\mathbf{2}^{\cdot+}$), a conclusion supported by the free-energy change (ΔG) calculated using Eq. 1:[16]

$$\Delta G(\text{kcal/mol}) = 23.06[E_{1/2}(\mathbf{2}/\mathbf{2}^{+}) - E_{1/2}(\mathbf{1}/\mathbf{1}^{-}) - e_{o}^{2}/\varepsilon\alpha] - E_{0-0}(\mathbf{1}) \quad (1)$$

where $E_{1/2}(\mathbf{2}/\mathbf{2}^{+}) = 1.24$ V *vs.* Ag/Ag^{+} in acetonitrile, $E_{1/2}(\mathbf{1}/\mathbf{1}^{-}) = -2.33$ V *vs.* Ag/Ag^{+} in acetonitrile, and $E_{0-0}(\mathbf{1}) = 89.1$ kcal/mol.[17] If the Coulombic term ($e_{o}^{2}/\varepsilon\alpha$) is estimated to be small (*ca.* 1.5 kcal/mol), the value of ΔG can be calculated to be *ca.* -5 kcal/mol, indicating that the electron-transfer process is substantially exothermic, probably occuring at a diffusion-controlled rate.[16]

Table 3. Isomer ratios of indene cyclobutane dimers

Reaction type	Head-to-head		Head-to-tail	
	syn	*anti*	*syn*	*anti*
This work	5±2	95±2	0.0	0.0
Cation radical mechanism[a]	3	97	0.0	0.0
Direct irradiation[b,c]	14—18	69—72	5	7—9
Benzophenone-sensitization[c]	3	84	5	8

a) Ref. 18. b) In the presence of 1,3-cyclohexadiene. c) W. Metzner and D. Wendisch, *Ann.*, **730**, 111 (1969).

In fact, the photoreaction in acetonitrile gave the *syn* and *anti* indene dimers in a ratio very similar to that observed in the dimerization *via* $\mathbf{2}^{\cdot+}$,[18] as is shown in Table 3. This cation radical mechanism is further supported by the remarkable "quenching" of dimer formation on the addition of only a few vol% of methanol or water. This "quenching" appears to be caused by the nucleophilic attack of methanol or water on $\mathbf{2}^{\cdot+}$, which ultimately results in the formation of **9** and **10** or **6**, as is shown in Scheme 2.

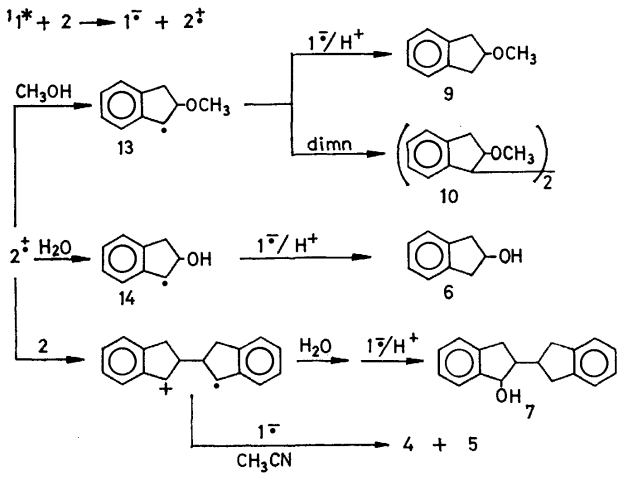

Scheme 2.

Table 4 lists the product distribution of the photoreactions in methanol and in acetonitrile in the presence of methanol and water. The most notable points are (1) the slow formation of the products in methanol, (2) the poor yields of **9** and the formation of considerable amounts of **10** in either methanol or acetonitrile–methanol, and (3) the relatively good yield of **6** and the lack of any formation of a compound corresponding to **10** (*i.e.* 2,2′-dihydroxy-1,1′-biindanyl) in acetonitrile–water.

Apparently, the **13** radical can undergo the dimerization reaction competitively with the reduction by $\mathbf{1}^{\cdot-}$, while the reduction of the **14** radical by $\mathbf{1}^{\cdot-}$ is much faster than the dimerization reaction. The reduction potential of **13** is not significantly different from that of **14**, as is to be expected from their similar π-electronic structures. Therefore, the efficient reduction of **14** must be caused by factors other than the reduction potential. For example, a hydrogen-bonding between $\mathbf{1}^{\cdot-}$ and **14** would necessitate their approaching within an effective distance for the reduction and/or would facilitate the electron flow from $\mathbf{1}^{\cdot-}$ to **14**. On the other hand, such a hydrogen-bonding can not occur with **13**.

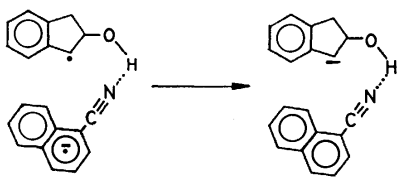

Compound **8** was confirmed to be formed *via* anionic species including $\mathbf{1}^{\cdot-}$, since the photoreaction in methanol-*O*-*d* gave **8**-3,4-d_2. In the NMR spectrum, the signals of H-4 and H-3B were completely absent, whereas that of H-3A at δ 1.16 appeared as a broad doublet ($J \simeq 13$ Hz). The NMR data demonstrate the stereospecific incorporation of the two deuterium atoms in the *cis*-relationship at C-3 and C-4. Scheme 3 delineates the possible mechanistic pathways which can interpret the stereochemistry in the formation of **8** and **8**-3,4-d_2. The anion radical of **1** would undergo a radical type of addition to **2**, giving the addend anion radical (**15**). The protonation of **15** probably occurs on the less hindered side at cyanated carbon, thus assuring the *cis*-relationship between the cyano group and the cyclobutane ring in **8**. Similarly, the deuterium incorporation at C-3 would stereospecifically occur on

Table 4. Product distribution of the photoreactions of **1** with **2** in protic media[a]

Solvent	Irradn time / h	Conversion/%		Product (yield/%)[b]	
		1	**2**		
CH_3CN–H_2O (9: 1)	15	42	≈100	**6** (55)	**7** (25)
CH_3CN–CH_3OH (9: 1)	19	42	≈100	**9** (37)	**10** (53)
CH_3OH	22	56	63	**9** (23)	**10** (23)

a) [**1**] = [**2**] = 0.1 mol dm^{-3}; irradiation at 313 nm using a merry-go-round apparatus. The yields of **8** were not determined. b) GLC yields based on the **2** consumed.

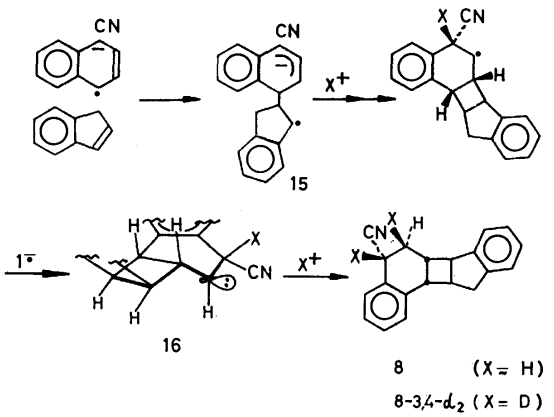

Scheme 3.

the *quasi*-equatorial position of the half-chair conformation A of the anion (**16**). On the other hand, the selective formation of **8** can not be reasonably interpreted by an alternative mechanism that includes the initial protonation at cyanated carbon of $\mathbf{1}^{\cdot-}$, followed by the addition of the protonated radical to **2**. According to this mechanism, the sterically favorable approach of **2** to the protonated radical seems to occur in the *trans*-relationship with the cyano group rather than in the *cis*-relationship, leading to the formation of **12**. Finally, it should be pointed out that this type of reductive photocycloaddition *via* the anion radical has not been reported previously, though photochemical cross-cycloadditions *via* cation radicals are known.[19]

Experimental

The following instruments were used for the spectral measurements: ^{1}H NMR, Hitachi R-24 (60 MHz) and JEOL JNM PS-100 (100 MHz); IR, Shimadzu IR-400; UV, Hitachi 124; MS, Hitachi RMU-6E; fluorescence spectra, Hitachi MPF-2A. The GLC was carried out on a Shimadzu GC-3BF apparatus using a column of SE-30 (5% on Celite 545, 0.75 m) at 195 °C for **3**, **7**, **8**, and **10** and at 180 °C for **4** and **5**, and a column of Ucon Oil LB-550X (5% on Celite 545, 0.75 m) at 170 °C for **6** and **9**. Irradiation was carried out in a Pyrex vessel with an Eikosha PIH-300 high-pressure mercury arc under cooling with water. All the solutions were bubbled with an N_2 stream for 30 min before irradiation. The melting points are uncorrected.

Materials. Commercial thiophene-free benzene was washed with sulfuric acid until no further coloration of the acid layer took place, and then washed with water and distilled from P_2O_5. Spectrograde cyclohexane (Nakarai Chemicals) was used without further purification. The dioxane was refluxed over sodium and then distilled. The tetrahydrofuran and diethyl ether were distilled from $LiAlH_4$. The acetonitrile was distilled three times from P_2O_5 and then from CaH_2. The methanol was refluxed over CaH_2 and then distilled. The indene was distilled from sodium under reduced pressure prior to use. The 1-cyanonaphthalene (Tokyo Kasei) was chromatographed on silica gel and then distilled *in vacuo*.

Preparation of Indene-1,1,3-d_3. A solution containing indene-d_0 (23 g, 0.2 mol), 1,8-diazabicyclo[5.4.0.]undec-7-ene (3 g, 20 mmol), and deuterium oxide (40 g, 2.0 mol) in dry dioxane (100 ml) was refluxed under an N_2 atmosphere for 20 h and then about one half of dioxane was distilled off. The remaining solution was poured into 1000 ml of ice-water. The oil layer was separated, washed with 1 mol dm^{-3} hydrochloric acid, with an aqueous solution of $NaHCO_3$, and three times with water, and then dried ($MgSO_4$). After filtration, the filtrate was distilled *in vacuo* to give deuterated indene. The above procedure was repeated for this indene. Finally, 12 g of indene-1,1,3-d_3 (50% yield) were obtained. The isotopic purity was confirmed to be over 95% by a study of the NMR and mass spectra.

Photoreaction in Less Polar Solvents. As a typical run, the photoreaction in diethyl ether will be described. A solution of **1** (0.47 g, 3 mmol) and **2** (7.5 g, 67 mmol) in 200 ml of diethyl ether was irradiated for 20 h. After the removal of the diethyl ether, 6.5 g of **2** was recovered by the vacuum distillation of the remaining oil. The residue was chromatographed on silica gel, using mixtures of hexane and benzene as the eluents. After **4** and **5** (*ca.* 0.1 g) had been eluted with hexane, 0.32 g of **1** was eluted with 30% benzene in hexane. Further elution by a 1: 1-mixture of hexane–benzene gave 0.1 g of **3** (38% yield based on the unrecovered **1**), which was then recrystallized from ethanol–benzene; mp 146—147 °C; IR (Nujol): 2220 (C≡N) and 1640 cm^{-1} (C=C); UV (CH_3CN): λ(log ε) = 302 (sh), 273 (3.89), and 265 nm (3.89); MS: 269 (M^+, vw), 153, and 116; NMR ($CDCl_3$): δ 2.8 and 3.2 (d-d each, 2H, $-CH_2-$), 3.9 (m, H-1), 4.1 (m, H-2a), 4.32 (t, J=8.0 Hz, H-2) 5.38 (d-d, J=4.5 and 10.0 Hz, H-3), 5.96 (d, J=10.0 Hz, H-4), 6.5 (d, 1×ArH), and 6.8—7.3 (m, 7×ArH); Found: C, 89.03; H, 5.58; N, 5.11%. Calcd for $C_{20}H_{15}N$: C, 89.18; H, 5.61; N, 5.20%.

Photoreaction in Acetonitrile. A solution of **1** (0.94 g, 6 mmol) and **2** (11 g, 100 mmol) in 250 ml of acetonitrile was irradiated for 100 h. After the removal of the acetonitrile, 9.3 g of **2** were recovered by vacuum distillation. The residue was chromatographed on silica gel; subsequent elution with hexane gave 0.85 g of the *anti* head-to-head indene dimer **4** (50% yield based on the unrecovered **2**), which was then recrystallized from ethanol; mp 109—110 °C (lit,[20] 110 °C). Further elution with 30% of benzene in hexane gave 0.7 g of **1**.

Photoreaction in Acetonitrile–Water. A solution of **1** (0.2 g, 1.3 mmol) and **2** (2.0 g, 18 mmol) in 55 ml of acetonitrile–water (10: 1) was irradiated for 50 h. GLC showed that the **1** had been completely consumed. The solids which had been precipitated during the irradiation were filtered out and then washed with 10 ml of cold methanol; 0.19 g of **7** was thus obtained. The filtrate was condensed, and then 10 ml of hot methanol were added. After cooling, the solids were again precipitated; filtration and washing with 10 ml of cold methanol gave another 0.18 g of **7**. The combined yield of **7** was 23%, based on the unrecovered **2**. The **7** was then recrystallized from ethanol; mp 182—183 °C; UV (CH_3CN): λ (log ε) = 272 (3.32), 265 (3.31), and 259 nm (sh); MS: 250 (M^+, vw), 232 ($M-H_2O$), and 116; NMR ($CDCl_3$): δ 1.8 (d, O–H), 2.14—3.46 (m, 8H), 4.96 (t, OCH), and 7.0—7.5 (m, 8H); Found: C, 86.14; H, 7.11%. Calcd for $C_{18}H_{18}O$: C, 86.36; H, 7.25%.

To the filtrate, a 20-ml portion of chloroform was added, and then the mixture was dried ($MgSO_4$). After filtration, vacuum distillation gave 0.5 g of **2** and 1.0 g of 2-indanol **6** (mp 68—69 °C, 58% yield). The residue was chromatographed on silica gel; elution with 40% benzene in hexane gave 90 mg of **8** (25% yield based on the **1** used), which were then recrystallized from ethanol–benzene; mp 207—208 °C; IR (KBr): 2220 cm^{-1} (C≡N); MS: 271 (M^+, vw), 155, and 116; UV (cyclohexane): λ (log ε) = 274 (3.11), 267 (3.11), and 262 nm (3.04); Found: C, 88.27; H, 6.28; N, 5.20%. Calcd for $C_{20}H_{17}N$: C, 88.52; H, 6.32; N, 5.16%.

Photoreaction in Methanol. A solution of **1** (1.0 g, 6.5 mmol) and **2** (6.0 g, 54 mmol) in 200 ml of methanol was

irradiated for 25 h. After the removal of the methanol, vacuum distillation gave 3.5 g of **2** and 0.4 g of 2-methoxyindan **9** (12.5% yield, based on the unrecovered **2**). The residue was chromatographed on silica gel; after a mixture of **4** and **5** (*ca.* 0.1 g, 4% yield) had been eluted with hexane, elution with 40% benzene in hexane gave a viscous oil, to which 10 ml of hot methanol were then added. Cooling while the solution was scratched gave white solids, which were then filtered and washed with 5 ml of cold methanol; 0.31 g of **8** (35% yield based on the unrecovered **1**) was thus obtained. The subsequent vacuum distillation of the filtrate gave 0.5 g of **1**. Further elution with benzene and acetone gave mixtures of **10** and polymeric materials. Vacuum distillation gave 0.6 g of **10** (160—163 °C/0.1 mmHg, 19% yield), which was chromatographed on silica gel, using benzene and 2—10% ethyl acetate in benzene as the eluents. Each fraction was further chromatographed. This procedure was repeated three times for each fraction to give 30—50 mg of **10a**, **10b**, a mixture of **10b** and **10d**, and **10c**. **10a**: mp 97—98 °C (from methanol); MS: 262 ($M-CH_3OH$) and 147 (M/2); NMR (CCl_4): δ 2.7—3.15 (m, 4H), 2.83 (s, OCH_3), 3.16 (s, OCH_3), 3.6—4.0 (m, 4H), and 7.0—7.4 (m, 8H); Found: C, 81.37; H, 7.44%. Calcd for $C_{20}H_{22}O_2$: C, 81.60; H, 7.53%. **10b**: mp 170—172 °C (from methanol); MS: 262 ($M-CH_3OH$) and 147 (M/2); NMR ($CDCl_3$): δ 2.7—3.1 (m, 4H), 3.24 (s, OCH_3), 3.38 (s, OCH_3), 3.55—3.75 (m, 2H), 4.13—4.35 (m, 2H), and 7.0—7.3 (m, 8H); Found: C, 81.41; H, 7.39%. Calcd for $C_{20}H_{22}O_2$: C, 81.60; H, 7.53%. **10c**: mp 70—73 °C (from methanol); MS: 294 (M^+, w), 262 ($M-CH_3OH$), and 147 (M/2); NMR (CCl_4): δ 2.7—3.1 (m, 4H), 2.96 (s, $2\times OCH_3$), 3.3—3.7 (m, 4H), and 6.9—7.3 (m, 8H).

In another run, a fraction which had been eluted with benzene was further chromatographed on silica gel. Subsequent elution with 30% hexane in benzene gave solids, which were then recrystallized from ethanol to give 50 mg of **11**; mp 229—231 °C; MS: 417 (M^+, vw), 301 ($M-C_9H_8$, w), 271 ($M-C_{10}H_{10}O$, w), 155, 154, 147 (100%), and 116 (24 %); NMR ($CDCl_3$): δ 1.5 (t, 1H), 2.27 (d-d, 1H), 3.02 (d-d, 1H), 3.38 (s, 3H, OCH_3), 3.3—3.8 (m, 3H), 4.0—4.4 (m, 3H), 5.68 (d, 1H), 6.7—7.6 (m, 13H); Found: C, 85.94; H, 6.44; N, 3.33%. Calcd for $C_{30}H_{27}NO$: C, 86.30; H, 6.52; N, 3.36%.

Sodium Methoxide-catalyzed Isomerization of **8**. A solution of **8** (100 mg, 0.6 mmol) and sodium methoxide (11 mg, 2 mmol) in dry dioxane–methanol (15 ml) was bubbled with an N_2 stream and then refluxed for 5 h. GLC showed that the solution contained an equilibrium mixture of **8** and **12** in a 1:4 ratio. After the evaporation of the solvent under reduced pressure, 50 ml of chloroform were added; the solution was washed three times with water and then dried ($MgSO_4$). Filtration and evaporation left a glassy material, to which 10 ml of hot methanol were added; the mixture was then allowed to stand overnight at room temperature. After the filtration of the **8** (10 mg) thus precipitated, the filtrate was condensed to *ca.* one half its original volume and allowed to stand overnight in a refrigerator; 60 mg of **12** were thus obtained; mp 79—80 °C; MS: 271 (M^+, vw), 155, and 116; IR (CCl_4): 2220 cm^{-1} (C≡N); Found: C, 88.35; H, 6.26; N, 5.22%. Calcd for $C_{20}H_{17}N$: C, 88.52; H, 6.32; N, 5.16%.

This work was supported by a Scientific Research Grant-in-Aid, No 447067, from the Ministry of Education. Chyongjin Pac is grateful to the Manyu Kim Foundation for its financial support.

References

1) Part XXXII: C. Pac, K. Mizuno, H. Okamoto, and H. Sakurai, *Synthesis*, **1978**, 589.

2) a) C. Pac, T. Sugioka, and H. Sakurai, *Chem. Lett.*, **1972**, 39; b) C. Pac, T. Sugioka, K. Mizuno, and H. Sakurai, *Bull. Chem. Soc. Jpn.*, **46**, 238 (1973); c) T. Sugioka, C. Pac, and H. Sakurai, *Chem. Lett.*, **1972**, 791 and 667; d) K. Mizuno, C. Pac, and H. Sakurai, *ibid.*, **1973**, 309; e) C. Pac, K. Mizuno, T. Sugioka, and H. Sakurai, *ibid.*, **1973**, 187; f) K. Mizuno, C. Pac, and H. Sakurai, *J. Am. Chem. Soc.*, **96**, 2993 (1974); g) K. Mizuno, C. Pac, and H. Sakurai, *J. Chem. Soc., Perkin Trans. 1*, **1974**, 2360; h) K. Mizuno, C. Pac, and H. Sakurai, *J. Chem. Soc., Chem. Commun.*, **1974**, 684; i) K. Mizuno, C. Pac, and H. Sakurai, *J. Chem. Soc., Perkin Trans. 1*, **1975**, 2221; j) K. Mizuno, C. Pac, and H. Sakurai, *J. Org. Chem.*, **42**, 3313 (1977); k) C. Pac and H. Sakurai, *Chem. Lett.*, **1976**, 1067; l) T. Majima, C. Pac, and H. Sakurai, *Bull. Chem. Soc. Jpn.*, **51**, 1811 (1978).

3) a) T. S. Cuntrell, *J. Am. Chem. Soc.*, **94**, 5929 (1972); b) J. J. McCullough, R. C. Miller, D. Fung, and W.-S. Wu, *ibid.*, **97**, 5942 and the references cited therein; c) N. C. Yang and K. Srinivasachar, *J. Chem. Soc., Chem. Commun.*, **1976**, 48 and the references cited therein; d) R. A. Caldwell and D. Creed, *J. Am. Chem. Soc.*, **100**, 2905 (1978) and the references cited therein.

4) J. J. McCullough and W.-S. Wu, *J. Chem. Soc., Chem. Commun.*, **1972**, 1136.

5) J. B. Birks, "Photophysics of Aromatic Molecules," Wiley-Interscience, New York, N. Y. (1970); P. Froehlich and E. L. Wehry, in "Modern Fluorescence Spectoroscopy," ed by E. L. Wehry, Plenum Press, New York, N. Y. (1976), Vol. 2, pp. 381—386.

6) A. Weller, *Pure Appl. Chem.*, **10**, 115 (1968); M. Ottolenghi, *Acc. Chem. Res.*, **6**, 153 (1973).

7) K. Mizuno, C. Pac, and H. Sakurai, *J. Chem. Soc., Chem. Commun.*, **1975**, 553 and 839.

8) J. A. Barltrop, *Pure Appl. Chem.*, **33**, 179 (1973).

9) R. A. Neuteufel and D. R. Arnold, *J. Am. Chem. Soc.*, **95**, 4080 (1973); Y. Shigemitsu and D. R. Arnold, *J. Chem. Soc., Chem. Commun.*, **1975**, 407; D. R. Arnold and A. J. Maroulis, *J. Am. Chem. Soc.*, **98**, 5931 (1976) and **99**, 7355 (1977).

10) N. C. Yang, J. Libman, and M. F. Savitzky, *J. Am. Chem. Soc.*, **94**, 9226 (1972); N. C. Yang and J. Libman, *ibid.*, **94**, 9228 (1972); R. M. Bowman, C. Carlo, J. J. McCullough, R. C. Miller, and I. Singh, *Can. J. Chem.*, **51**, 1060 (1973).

11) J. E. Horan and R. W. Schiessler, *Org. Synth.*, Coll. Vol. V, 647 (1973).

12) L. M. Jackman and S. Sternhell, "Applications of Nuclear Magnetic Resonance Spectroscopy in Organic Chemistry," 2nd ed, Pergamon Press, Oxford (1969), p. 288.

13) E. Müller and W. Runel, *Angew. Chem.*, **70**, 105 (1958).

14) G. N. Taylor, *Chem. Phys. Lett.*, **10**, 355 (1971).

15) M. J. S. Dewar, E. Haselbach, and S. D. Worley, *Proc. R. Soc. London, Ser. A*, **315**, 431 (1970).

16) D. Rehm and A. Weller, *Israel J. Chem.*, **8**, 259 (1970).

17) S. L. Murov, "Handbook of Photochemistry," Marcel Dekker, New York, N. Y. (1973).

18) S. Farid and S. E. Shealer, *J. Chem. Soc., Chem. Commun.*, **1973**, 677.

19) S. Farid, S. E. Hartman, and T. R. Evans, in "The Exciplex," ed by M. Gordon and W. R. Ware, Academic Press, New York, N. Y. (1975), p. 327; K. Mizuno, R. Kaji, and Y. Otsji, *Chem. Lett.*, **1977**, 1027.

20) G. O. Schenk *et al.*, *Chem. Ber.*, **95**, 1642 (1962).

Synthesis of L-Epicapreomycidine

Tadashi TESHIMA, Kunikazu KONISHI, and Tetsuo SHIBA*

Department of Chemistry, Faculty of Science, Osaka University, Toyonaka, Osaka 560

(Received August 17, 1979)

A cyclic guanidino amino acid, L-epicapreomycidine, isolated from hydrolyzates of protease inhibitors such as chymostatin and elastatinal was synthesized. This amino acid is a diastereomer of L-capreomycidine which is a component amino acid of tuberactinomycin N,O and capreomycin. A new synthetic route from β-hydroxy-DL-ornithine *via* an aziridine compound to DL-capreomycidine was applied to the synthesis of L-epicapreomycidine starting from *erythro*-β-hydroxy-L-ornithine. A convenient and one-step technique to obtain L-*erythro* form from a mixture of four diastereomers of β-hydroxyornithine by means of enzymatic reaction was newly exploited. The synthetic L-epicapreomycidine obtained was identical with natural one in all respects, thus confirming the proposed structure.

A cyclic guanidino amino acid, L-epicapreomycidine, was found as a component amino acid of peptides produced by microorganism, *i.e.*, chymostatin and elastatinal which are known as protease inhibitors.[1] This amino acid is a diastereomer of L-capreomycidine which is a constituent of antibiotics capreomycin[2] or tuberactinomycin N and O.[3] DL-Capreomycidine and DL-epicapreomycidine had been synthesized by Bycroft *et al.* by the method based on an oximation of methyl (2-amino-4-pyrimidinyl)acetate followed by hydrogenation.[4]

Owing to the disadvantage in this method by which one of the diastereomers can not be secured purposely and optically active isomers for each diastereomer are not easily obtained unless an efficient technique of an optical resolution for such peculiar guanidino amino acid is developed.

In our previous work, we exploited an entirely novel approach to synthesize DL-[5] and also L-capreomycidine[6] stereoselectively employing N^{δ}-benzyloxycarbonyl-*threo*-β-hydroxyornithine as a key intermediate. In the present study, where *erythro* isomer of optically pure β-hydroxyornithine was taken as an intermediate in a similar synthetic strategy, epicapreomycidine of the natural steric configuration was successfully obtained for the first time.

3-(Benzyloxycarbonylamino)propionaldehyde **3**[7] was condensed with bis(glycinato)copper(II) to give a mixture of *erythro* and *threo* N^{δ}-benzyloxycarbonyl-β-hydroxy-DL-ornithine in a ratio of 1:1. Since use of aqua[*N*-(1-carboxylatoethylidene)glycinato]copper(II) as in the preparation of L-capreomycidine[8] has been found to give a *threo*-rich mixture, the usual copper complex of glycine was used in this case where *erythro* isomer is a desirable isomer. After fractional recrystallization of the condensed product from water was repeated six times, a pure DL-*erythro* isomer **4a** was obtained. Acetyl derivative **5a** derived from **4a** was treated with the acylase to give L-*erythro* isomer. However, since the tedious fractional recrystallization caused a low yield of the desired product, the product of the coupling reaction was directly subjected to the enzymatic resolution without fractionations of the diastereomers. Interestingly, the deacetylation of *erythro* isomer was found to proceed much faster than that of *threo* one. Thus, when the reaction was stopped just before the *threo* isomer became susceptible to the enzyme, N^{δ}-benzyloxycarbonyl-*erythro*-β-hydroxy-L-ornithine was obtained in an optically pure form without any further purification through single reaction procedure. This new procedure is very advantageous in a sense that not only the optical resolution, but also the diastereomeric separation took place simultaneously in a one-step enzymatic reaction.

Erythro isomer of β-hydroxy-L-ornithine derivative **6a** was converted to L-epicapreomycidine according to a series of the reaction which is the same in principle to that for the synthesis of L-capreomycidine.[6] Thus, successive procedures of N^{α}-tosylation, methyl esterification, amidation and *O*-mesylation gave an intermediate **10**. The acid amide form is requisite for the purpose of *O*-mesylation followed by aziridine ring formation to prevent an elimination of β-hydroxyl function.

O-Mesyl amide **10** was treated with diethylamine to give an aziridine derivative **11**. The aziridine ring in **11** was then opened with ammonia, and benzyloxycarbonyl group was removed by hydrogenolysis to give triamino amide derivative **12**.

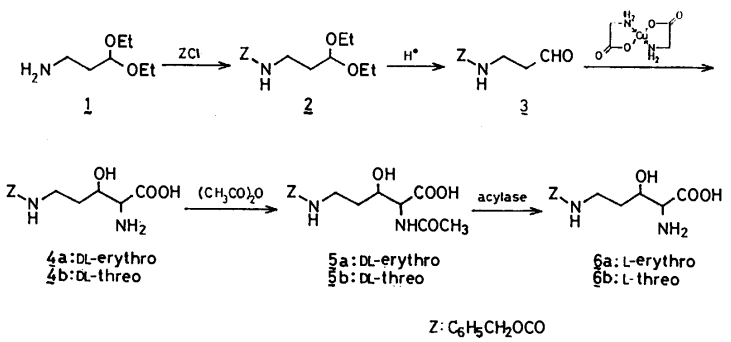

Fig. 1.

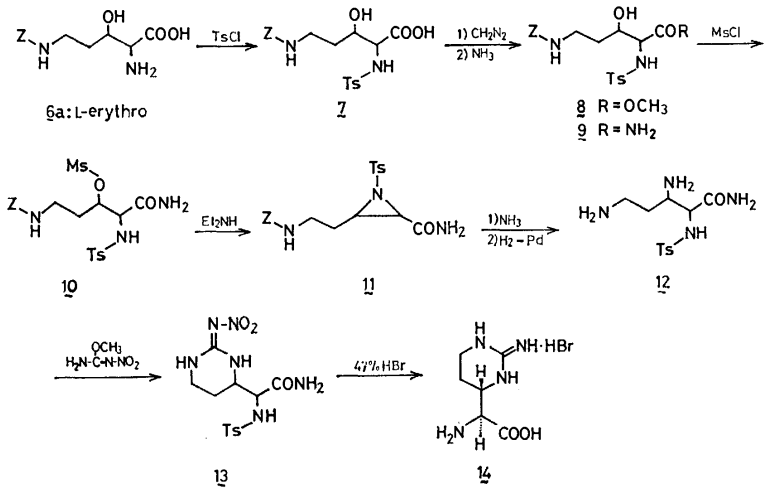

Fig. 2.

Concerning the stereoselectivity, the fact that *erythro* form of β-hydroxyornithine derivative **10** afforded *trans* aziridine **11** which turned to *erythro* form of triaminopentanamide derivative **12** was well understood by double S_N2 reaction mechanism as described in the synthesis of DL-capreomycidine.[5] The *trans* configuration of the aziridine compound **11** was supported by NMR data which showed a coupling constant of $J=$ 6 Hz for two protons at the aziridine ring.

Two free amino groups in **12** were coupled with *O*-methyl-*N*-nitroisourea in the presence of sodium hydroxide to give cyclic nitroguanidino derivative **13**. All the protecting groups of **13** were finally removed by hydrolysis with 47% hydrobromic acid to obtain epicapreomycidine hydrobromide **14**. Synthetic compound is identical with natural epicapreomycidine in all respects (mp, $[M]_D$, NMR, TLC, PC, amino acid analysis) (Table 1).

Table 1. Comparison of synthetic and natural epicapreomycidine hydrobromide

			Epicapreomycidine		Capreomycidine
			Synthetic	Natural	
Mp (dec) (°C)[a]			198—205	199—202	218—230
$[M]_D$ (*c* 1.19, 6 M HCl)			+21.0°	+18.4°	+44°
R_f	TLC[b]	a	0.11	0.11	0.11
		b	0.50	0.50	0.50
	PC[b]	c	0.34	0.34	0.34
		d	0.16	0.16	0.16
Amino acid analysis (min)[c]			215	215	205

a) Melting points were compared for diflavianates. b) Developing solvent: a) 1-butanol–acetic acid–water (4: 1: 2), b) phenol–water–28% ammonia (30: 10: 1), c) *t*-butyl alcohol–acetic acid–water (2: 1: 1), d) 1-butanol–ethyl methyl ketone–28% ammonia–water (5: 3: 3: 1). c) Following conditions were applied; 27 cm column, pH 5.28, 0.35 M sodium citrate buffer.

Experimental

All melting points are uncorrected. NMR spectra were measured with a Varian XL-100-15 spectrometer. The optical rotations were measured with a Perkin-Elmer 141 polarimeter. TLC was carried out by the ascending method on silica gel G using developing solvents, 1-butanol–acetic acid–water (4: 1: 2) (solvent A) and phenol–water–28% ammonia (30: 10: 1) (solvent B). Paper chromatography was carried out on Toyo Roshi No. 51 paper using developing solvents, *t*-butyl alcohol–acetic acid–water (2: 1: 1) (solvent C) and 1-butanol–ethyl methyl ketone–28% ammonia–water (5: 3: 3: 1) (solvent D). Amino acid analysis was carried out with a Hitachi KLA-5 Amino Acid Analyzer (55 cm column, 0.20 M sodium citrate buffer pH 3.25 (92 min) and 4.25, flow rate 60 ml/h). An acylase was gifted from Tanabe Seiyaku Co., Ltd.

3-(Benzyloxycarbonylamino)propionaldehyde Diethyl Acetal (2). To a solution of 3-aminopropionaldehyde diethyl acetal (**1**) (35.3 g, 0.240 mol) and triethylamine (49.9 ml, 0.360 mol) in 500 ml of chloroform, benzyloxycarbonyl chloride (44.7 g, 0.264 mol) was added dropwise for 1.5 h with stirring at 0 °C. The mixture was stirred at 0 °C for 1 h and then at room temperature overnight. Excess benzyloxycarbonyl chloride was decomposed by addition of *N*-(2-aminoethyl)piperazine (4.5 ml, 35 mmol). The reaction mixture was washed with 20% aqueous citric acid, 4% $NaHCO_3$, and brine. The organic layer was dried over anhydrous $MgSO_4$ and concentrated *in vacuo* to give a colorless oil; yield 64.5 g (95.7%).

For elemental analysis, a small amount of this oil was distilled.

Found: C, 63.56; H, 8.23; N, 4.84%. Calcd for $C_{15}H_{23}NO_4$: C, 64.03; H, 8.24; N, 4.98%.

3-(Benzyloxycarbonylamino)propionaldehyde (3). A mixture of **2** (27.8 g, 99.0 mmol) in 800 ml of acetone and 100 ml of 0.1 M† HCl was heated under reflux for 1 h, and concentrated *in vacuo* to one eighth volume. The mixture was extracted with ethyl acetate and organic layer was washed with brine. Organic layer was dried over anhydrous $MgSO_4$ and concentrated *in vacuo*. An oily residue was triturated with hexane to give crystals; yield 17.6 g (85.9%), mp 57—58 °C. For elemental analysis, the product was converted to a 2,4-dinitrophenylhydrazone derivative, mp 161 °C.

Found: C, 52.56; H, 4.48; N, 18.07%. Calcd for $C_{17}H_{17}N_5O_6$: C, 52.71; H, 4.42; N, 18.08%.

N^5-Benzyloxycarbonyl-β-hydroxy-DL-ornithine (4). To a suspension of bis(glycinato)copper(II) (208 g, 981 mmol) and Na_2CO_3 (104 g, 981 mmol) in 1.8 l of H_2O, a solution of **3**

† 1 M = 1 mol dm^{-3}.

(81.2 g, 392 mmol) in 400 ml of dichloromethane was added dropwise at 60 °C for 15 min. The reaction mixture was stirred at 60 °C for 1.5 h and neutralized with HCl on cooling in ice bath. H_2S was bubbled through the solution with stirring for 1.5 h. Copper sulfide was filtered off and washed with 4 l of 1 M HCl. The filtrate and washings were combined and aerated to remove H_2S. The solution was neutralized with ammonia to give crystals; yield 15.7 g (14.2%) (*erythro*: *threo* (1: 1)). From the mother liquor, a further crop was recovered; yield 4.8 g (4.3%) (*erythro*: *threo* (1: 1.3)). The ratio of *erythro* and *threo* isomers were obtained by amino acid analysis (retention time: *threo*, 186 min; *erythro*, 197 min).

N$^{\delta}$-Benzyloxycarbonyl-erythro-*β-hydroxy*-DL-*ornithine (4a)*. Crude product (*erythro*: *threo* (1: 1.3)) (13.9 g) of **4** was recrystallized six times from H_2O (250—300 ml per g of the crude crystals) to give a pure *erythro* isomer **4a**: yield 1.41 g (10.1%), mp 248—248.5 °C (dec).

Found: C, 55.29; H, 6.41; N, 9.86%. Calcd for $C_{13}H_{18}N_2O_5$: C, 55.31; H, 6.43; N, 9.92%.

N$^{\alpha}$-Acetyl-N$^{\delta}$-benzyloxycarbonyl-erythro-*β-hydroxy*-DL-*ornithine (5a)*. To a solution of **4a** (539 mg, 1.90 mmol) in 1 M NaOH (1.90 ml, 1.90 mmol), acetic anhydride (0.32 ml, 3.40 mmol) and 1 M NaOH (3.80 ml, 3.80 mmol) were added dropwise at the same time with stirring at 0 °C. Keeping the pH of the solution at 9 by addition of 1 M NaOH, the mixture was stirred at 0 °C for 2 h and then at room temperature overnight. The reaction mixture was acidified with HCl and extracted with ethyl acetate. The organic layer was washed with H_2O and dried over anhydrous $MgSO_4$. The oily residue after concentration *in vacuo* was triturated with ethyl acetate and ether to give crystals: yield, 413 mg (67.0%). They were recrystallized from ethyl acetate; yield, 312 mg (50.6%), mp 123—125 °C.

Found: C, 55.46; H, 6.21; N, 8.58%. Calcd for $C_{15}H_{20}N_2O_6$: C, 55.55; H, 6.22; N, 8.64%.

N$^{\delta}$-Benzyloxycarbonyl-erythro-*β-hydroxy*-L-*ornithine (6a)*. To **5a** (283 mg, 0.873 mmol) was added 0.1 M LiOH until a clear solution was obtained, and the solution was adjusted to pH 7.1 with 0.1 M LiOH. To the solution, 1.5 ml of 0.01 M cobalt chloride and the acylase (35 mg, 20 units/mg) were added, and the solution was incubated at 37 °C for 20 h. When crystals of free *erythro*-L-form were separated out, pH of the mixture decreased to 6.4. After the solution was adjusted again to pH 7.1, the incubation was continued for further 60 h. After cooling in ice bath, crystals deposited were collected by filtration; yield 95 mg (77%). They were recrystallized from H_2O; yield, 75 mg (61%), mp 237 °C (dec), $[\alpha]_D^{20}$ +6.2° (*c* 1.0, 2 M HCl).

Found: C, 55.40; H, 6.40; N, 9.88%. Calcd for $C_{13}H_{18}N_2O_5$: C, 55.31; H, 6.43; N, 9.92%.

Convenient Preparation of N$^{\delta}$-*Benzyloxycarbonyl*-erythro-*β-hydroxy*-L-*ornithine (6a) from a Mixture of Four Diastereomers*. *N$^{\delta}$*-Benzyloxycarbonyl-*β*-hydroxy-DL-ornithine (**4**) (*erythro*: *threo* (1: 1)) (21.0 g, 74.5 mmol) was acetylated in the manner similar to that in the preparation of **5a** to give a mixture of *erythro* and *threo* isomers of *N$^{\alpha}$*-acetyl-*N$^{\delta}$*-benzyloxycarbonyl-*β*-hydroxy-DL-ornithine (**5**) as a colorless oil. The enzymatic reaction of this mixture with the acylase was carried out in the manner similar to that in the reaction of **5a**. After the reaction mixture was cooled in an ice bath, crystals separated out were collected by filtration. They were found to be pure *erythro* isomers from the result of amino acid analysis; yield 2.08 g (39.6%).

N$^{\delta}$-Benzyloxycarbonyl-N$^{\alpha}$-p-*tolylsulfonyl*-erythro-*β-hydroxy*-L-*ornithine (7)*. To a suspension of **6a** (737 mg, 2.61 mmol) in 6.5 ml of THF–H_2O (1: 2) were added triethylamine (0.82 g, 8.1 mmol) and *p*-toluenesulfonyl chloride (763 mg, 4.00 mmol) portionwise during a period of 30 min with stirring at room temperature. After stirring for 2 h, the reaction mixture was concentrated *in vacuo* and an aqueous solution of the residue was extracted with ether. The ether layer was reextracted with aqueous $NaHCO_3$. Both aqueous layers were combined and acidified with HCl to give colorless needles; yield 939 mg (82.4%). Recrystallization from ethanol–ether–hexane, gave a pure sample for elemental analysis; mp 164.5—166.5 °C, $[\alpha]_D^{19}$ +19.4° (*c* 1.13, EtOH).

Found: C, 54.92; H, 5.54; N, 6.39; S, 7.25%. Calcd for $C_{20}H_{24}N_2O_7S$: C, 55.03; H, 5.54; N, 6.42; S, 7.32%.

N$^{\delta}$-Benzyloxycarbonyl-N$^{\alpha}$-p-*tolylsulfonyl*-erythro-*β-hydroxy*-L-*ornithine Methyl Ester (8)*. To a solution of **7** (2.41 g, 5.52 mmol) in 14 ml of THF–dioxane (1: 1), was added excess diazomethane in ether and allowed to react for 1 h. Excess diazomethane was decomposed with acetic acid and the solution was concentrated *in vacuo* to give needles; yield 2.49 g (100%). For elemental analysis, they were recrystallized from ethyl acetate–hexane; mp 108—112 °C, $[\alpha]_D^{19}$ −0.1° (*c* 1.03, MeOH), $[\alpha]_{365}^{19}$ +27.0° (*c* 1.03, MeOH).

Found: C, 55.89; H, 5.95; N, 5.91; S, 6.77%. Calcd for $C_{21}H_{26}N_2O_7S$: C, 55.99; H, 5.82; N, 6.22; S, 7.10%.

N$^{\delta}$-Benzyloxycarbonyl-N$^{\alpha}$-p-*tolylsulfonyl*-erythro-*β-hydroxy*-L-*ornithinamide (9)*. A solution of **8** (2.49 g, 5.53 mmol) in 120 ml of methanol, was saturated with ammonia in a pressure bottle and kept at room temperature for 4 d. Concentration *in vacuo* gave crystals; yield 1.58 g (65.5%). For elemetal analysis they were recrystallized from methanol–ether–hexane; mp 206—208 °C, $[\alpha]_D^{19}$ +15.9° (*c* 1.10, DMF).

Found: C, 55.31; H, 5.74; N, 9.58; S, 7.48%. Calcd for $C_{20}H_{25}N_3O_6S$: C, 55.16; H, 5.79; N, 9.65; S, 7.36%.

N$^{\delta}$-Benzyloxycarbonyl-N$^{\alpha}$-p-*tolylsulfonyl-O-methylsulfonyl*-erythro-*β-hydroxy*-L-*ornithinamide (10)*. To a solution of **9** (661 mg, 1.52 mmol) in 7 ml of pyridine, methanesulfonyl chloride (0.939 ml, 12.1 mmol) was added portionwise with stirring at −25 °C during a period of 2.5 h. After an additional stirring for 2 h, the reaction mixture was concentrated *in vacuo* and extracted with ethyl acetate after addition of 30 ml of H_2O. The organic layer was washed with 5% aqueous citric acid, $NaHCO_3$ and brine successively, dried over anhydrous $MgSO_4$ and concentrated *in vacuo*. The residue was triturated with hexane to give colorless needles; yield 691 mg (91.5%). Recrystallization from acetone–hexane gave a pure sample for elemental analysis; mp 159—162 °C, $[\alpha]_D^{19}$ +34.3° (*c* 1.00, acetone).

Found: C, 49.22; H, 5.28; N, 8.19; S, 12.37%. Calcd for $C_{21}H_{27}N_3O_8S_2$: C, 49.11; H, 5.30; N, 8.18; S, 12.49%.

(2S,3R)-5-Benzyloxycarbonylamino-trans-*2,3*-[N-*(*p-*tolylsulfonyl)epimino]pentanamide (11)*. A solution of **10** and diethylamine (0.54 ml, 5.2 mmol) in 7 ml of THF was kept at 38—42 °C for 3 h, and then concentrated *in vacuo*. An aqueous solution of the residue was extracted with chloroform. After the extract was dried over anhydrous $MgSO_4$, the solvent was evaporated *in vacuo* to an oil, which was triturated with benzene to give needles; yield 267 mg (56.4%). They were recrystallized from chloroform–hexane; yield 246 mg (52.0%), mp 136—137 °C, $[\alpha]_D^{20}$ +21.8° (*c* 1.06, DMF).

Found: C, 57.18; H, 5.53; N, 9.92; S, 7.53%. Calcd for $C_{20}H_{23}N_3O_3S$: C, 57.54; H, 5.55; N, 10.07; S, 7.68%.

(2S,3R)-erythro-*3,5-Diamino-2-(*p-*tolylsulfonylamino)pentanamide (12)*. A solution of **11** (283 mg, 0.678 mmol) in 100 ml of methanol was saturated with ammonia in a pressure bottle, and allowed to stand at 30 °C for 4 d. The residue obtained after concentration *in vacuo* was dissolved in methanol and hydrogenolyzed in the presence of Pd-black. After removal of catalyst, the reaction mixture was concentrated *in vacuo* to give crystals which were recrystallized from metha-

nol–ether; yield 136 mg (52.1%), mp 200—209 °C (dec), $[\alpha]_D^{15}$ +76.5° (*c* 1.06, MeOH).

Found: C, 37.87; H, 6.13; N, 14.58; S, 8.37; Cl, 18.24%. Calcd for $C_{12}H_{22}N_4O_3SCl_2 \cdot 1/2H_2O$: C, 37.70; H, 6.06; N, 14.65; S, 8.39; Cl, 18.55%.

L-*Epicapreomycidine Hydrobromide (**14**)*. To a solution of **12** (74 mg, 0.20 mmol) in 2 ml of methanol and a trace of H_2O, were added 1 M NaOH (0.40 ml, 0.40 mmol) and *O*-methyl-*N*-nitroisourea (47 mg, 0.40 mmol) portionwise with stirring at 0 °C during a period of 2 h. The reaction mixture was stirred at 0 °C for 1 h and then at room temperature overnight. More amount of *O*-methyl-*N*-nitroisourea (20 mg, 0.168 mmol) was added to the reaction mixture. After 3 h, the reaction mixture was acidified with 1 M HCl. The residue obtained after concentration *in vacuo* was triturated with a small amount of H_2O and ethyl acetate to give a nitroguanidino derivative **13** as crystals; yield 40 mg (55%). The product was heated with 8 ml of 47% HBr and 3 ml of anisole under reflux for 5 h. An aqueous layer was separated from anisole layer and concentrated *in vacuo*. A solution of the residue in methanol was neutralized with pyridine. Addition of ethanol to the solution gave colorless prisms of monohydrobromide **14**; yield 23 mg (45%). They were recrystallized from H_2O–ethanol; yield 14 mg (28%). $[\alpha]_D^{20}$ +8.31° (*c* 1:19, 6 M HCl). For elemental analysis, the hydrobromide was converted to diflavianate of yellow prisms; mp 198—205 °C (dec).

Found: C, 38.86; H, 3.19; N, 14.00; S, 7.55%. Calcd for $C_{26}H_{24}N_8O_{18}S_2 \cdot 1/2H_2O$: C, 38.57; H, 3.11; N, 13.84; S, 7.92%.

The authors are grateful to Prof. Hamao Umezawa, Institute of Microbial Chemistry, for his gift of the natural sample of L-epicapreomycidine.

References

1) a) K. Tatsuta, N. Mikami, K. Fujimoto, S. Umezawa, H. Umezawa, and T. Aoyagi, *J. Antibiot.*, **26**, 625 (1973). b) H. Umezawa, T. Aoyagi, A. Okura, H. Morishima, T. Takeuchi, and Y. Okami, *J. Antibiot.*, **26**, 787 (1973).

2) a) E. B. Herr, Jr., *Antimicrob. Agents Chemother.*, **1962**, 201; b) E. B. Herr, Jr., and M. O. Redstone, *Ann. New York Acad. Sci.*, **135**, 940 (1966).

3) H. Yoshioka, T. Aoki, H. Goko, K. Nakatsu, T. Noda, H. Sakakibara, T. Take, A. Nagata, J. Abe, T. Wakamiya, T. Shiba, and T. Kaneko, *Tetrahedron Lett.*, **1971**, 2043.

4) B. W. Bycroft, L. R. Croft, and A. W. Johnson, *J. Chem. Soc., C*, **1971**, 3040.

5) T. Wakamiya, K. Mizuno, T. Ukita, T. Teshima, and T. Shiba, *Bull. Chem. Soc. Jpn.*, **51**, 850 (1978).

6) T. Shiba, T. Ukita, K. Mizuno, T. Teshima, and T. Wakamiya, *Tetrahedron Lett.*, **1977**, 2681.

7) Badische Anilin- & Soda-Fabrik (I. G. Farbenindustrie Akt. Ges. "In Auflösung") (Friedrich Becke, inventor). Ger. Patent 845348, July 31, 1952 (Cl. 12q. 3201).

8) a) T. Ichikawa, S. Maeda, T. Okamoto, Y. Araki, and Y. Ishido, *Bull. Chem. Soc. Jpn.*, **44**, 2779 (1971); b) S. Ohdan, T. Okamoto, S. Maeda, T. Ichikawa, Y. Araki, and Y. Ishido, *Bull. Chem. Soc. Jpn.*, **46**, 981 (1973).

Layered Compounds. LXII.[1] Triple-layered [*m.m*][*n.n*]Paracyclophanes: Syntheses and Spectra

Tetsuo Otsubo,† Takashi Kohda, and Soichi Misumi*

The Institute of Scientific and Industrial Research, Osaka University, Suita, Osaka 565

(Received August 7, 1979)

A series of the title cyclophanes (*m*, *n*=2—4) were synthesized by the thermal- and photo-desulfurization methods from dithia intermediates. Their absorption and emission spectra were measured to examine the transannular electronic interaction. The absorption spectra of the title compounds and their TCNE complexes gave the same order of the interaction as seen in the case of double-layered system: [2.2]>[3.3]>[4.4] in neutral state and [3.3]>[2.2]>[4.4] in CT state. The emission spectra are discussed in terms of the existence of excited trimer.

In the previous papers of this series we reported the physical and chemical properties of multilayered [2.2]paracyclophanes to be strongly affected by the transannular π-electronic interactions among the stacked benzene rings. In addition to the electronic interaction, their severe molecular strain due to rigid [2.2]phane framework gave rise to intriguing behaviors such as catalytic skeletal rearrangement.[3] In order to pursue only transannular electronic interaction without strain effect, it is more instructive to study some series of multilayered [*m. n*]paracyclophanes with longer bridging chain.

For example, [3.3]paracyclophane is much more suitable for this purpose because of far less strained sandwich framework compared to [2.2]paracyclophane. It was already pointed out that double-layered [3.3]-paracyclophane **8** is a better system for both intermolecular and intramolecular charge-transfer interactions than [2.2]paracyclophane **7**.[4,5] So, multilayered [3.3]paracyclophanes are expected to reveal more unique behaviors with the increase of layer number. In addition, it is interesting to see if [4.4]phane system exerts such a multilayer effect although [4.4]paracyclophane **9** exhibits less transannular interaction.

For the above-stated purpose, we have intended to investigate a series of triple-layered [*m.m*][*n.n*]paracyclophanes **1**—**6** with combined numbers of the bridging methylene, *i.e.*, *m* and *n*=2—4.[6] This paper presents their syntheses and spectral properties.

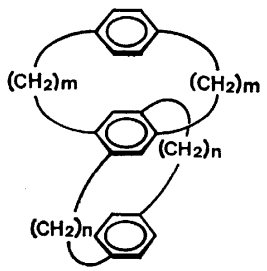

1, m = n = 2
2, m = 2, n = 3
3, m = n = 3
4, m = 2, n = 4
5, m = 3, n = 4
6, m = n = 4

Scheme 1.

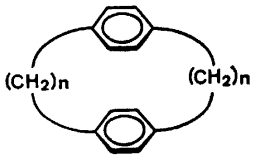

7, n = 2
8, n = 3
9, n = 4

Scheme 2.

Results and Discussion

Syntheses. Although the syntheses of [3.3]- and [4.4]paracyclophanes, **8** and **9**, were difficult before, new synthetic routes through sulfur extrusion of the corresponding dithia homologs have recently developed for the general use.[7] These methods are also useful to the syntheses of the present triple-layered [*m.m*][*n.n*]-paracyclophanes **2**—**6**, that is to say, by stepwise stacking of *para*-substituted benzenes. For example, in the case of [2.2][3.3]paracyclophane **2** the [2.2]-framework was at first constructed by the Hofmann elimination method as previously reported.[2] The resulting 4,7-bis(bromomethyl)paracyclophane **11**[8] was treated with 1,4-bis(2-mercaptoethyl)benzene **10**[7a] to give dithia[2.2][4.4]paracyclophane **12** in 25% yield. Irradiation of **12** in triethyl phosphite with a high pressure mercury lamp for 6 h led to the formation of the desired cyclophane **2** in 23% yield.

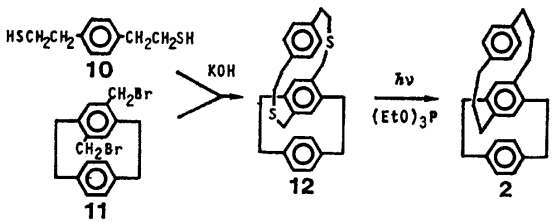

Scheme 3.

A similar route to derive [3.3][3.3]homolog **3** requires 5,8-bis(bromomethyl)[3.3]paracyclophane **20** as a key intermediate, which is not readily accessible.[9]

† Present address: Department of Applied Chemistry, Faculty of Engineering, Hiroshima University, Sendamachi, Hiroshima 730.

One successful but laborious approach has been developed. Treatment of 2,5-dibromo-*p*-xylene **13**[10] with NBS gave 2,5-dibromo-1,4-bis(bromomethyl)-benzene **14** in 34% yield. A coupling reaction between **10** and **14** led to 16,19-dibromo-2,13-dithia[4.4]paracyclophane **15** in 62% yield, which was treated with copper(I) cyanide in *N*-methylpyrrolidinone to afford dicyano derivative **16** in 68% yield. 5,8-Dicyano-[3.3]paracyclophane **18** was obtained in 40% yield by oxidation of **16** with hydrogen peroxide to give disulfone **17**, followed by pyrolysis. Although hydrolysis of **18** in basic conditions failed, it was hydrolyzed in a boiling solution of sulfuric acid–acetic acid, and treatment of the resulting acid with thionyl chloride and then with absolute ethanol produced 5,8-bis(ethoxycarbonyl)[3.3]paracyclophane **19** in 46% yield. Reduction of **19** with lithium aluminium hydride followed by bromination with phosphorus tribromide gave the desired bromide **20** in satisfactory yield. [3.3][3.3]Paracyclophane **3** was derived from **20** in quite similar manner as described for **2**.

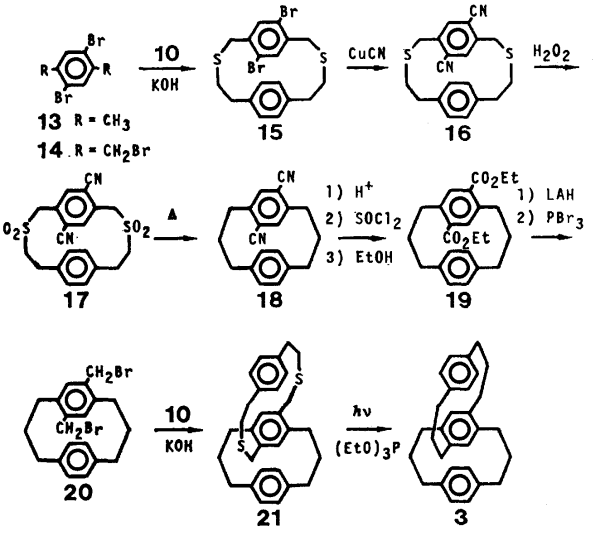

Scheme 4.

For [4.4]phane series, 6,9-bis(bromomethyl)[4.4]-paracyclophane **28** was prepared according to the same reaction sequence. Dithiacyclophanes **30**, **31**, and **33** were similarly obtained by reactions of bromide **28** with dithiols **29**, **10**, and **22**, respectively, in high yields. Photodesulfurization of **30** proceeded smoothly to afford [2.2][4.4]paracyclophane **4** in 55% yield. A similar reaction of **31** was ineffective with a high pressure mercury lamp because of the poor absorbance of **31**. This was improved by use of a low pressure mercury lamp, and [3.3][4.4]paracyclophane (**5**) was formed in 12% yield together with 6,9-dimethyl[4.4]-paracyclophane (**32**) as a by-product. On the other hand, the formation of [4.4][4.4]paracyclophane (**6**) was accomplished by the pyrolytic method (5% yield), for any photochemical attempt was unsuccessful.

Electronic Absorption Spectra. It is well known that the transannular electronic interaction in cyclophane results in the bathochromic and hyperchromic shifts

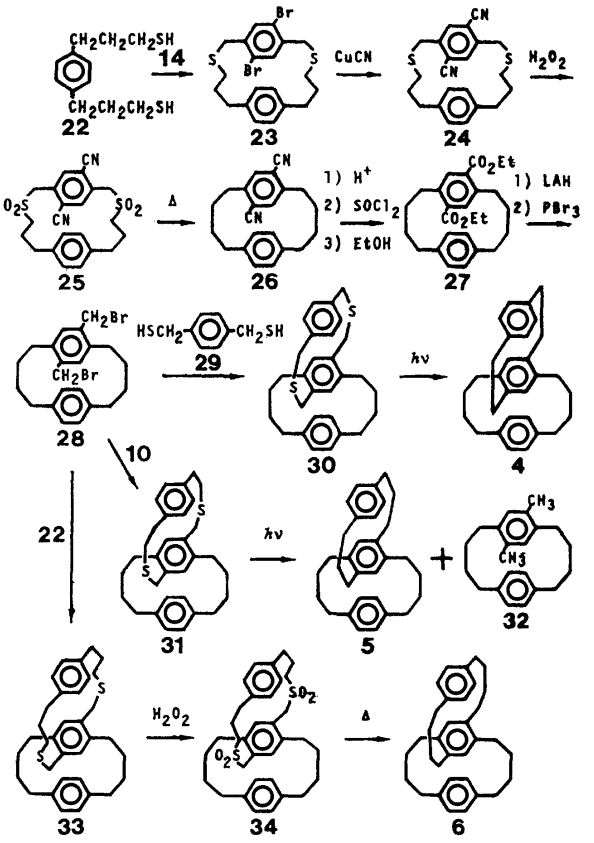

Scheme 5.

of the absorption bands in its electronic spectrum and the magnitude of these shifts is simply utilized as a measure of the interaction.[2] As shown in Fig. 1, the shifts of a series of triple-layered paracyclophanes are in an order of [4.4][4.4]PC **6**<[3.3][4.4]PC **5**<[2.2]-[4.4]PC **4**<[3.3][3.3]PC **3**<[2.2][3.3]PC **2**<[2.2][2.2]-PC **1** (PC: paracyclophane). It is evidently concluded

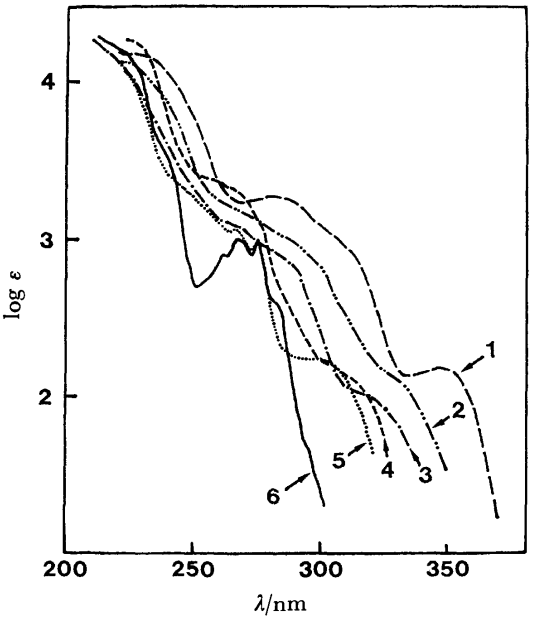

Fig. 1. Electronic absorption spectra of triple-layered [m.m][n.n]paracyclophanes **1**—**6** in tetrahydrofuran.

Table 1. Charge-transfer absorption maxima of cyclophane–TCNE complexes in dichloromethane

Compd		λ_{max}/nm	Compd		λ_{max}/nm
[2.2][2.2]PC[a]	**1**	530[b], 630	[4.4][4.4]PC[a]	**6**	423, 499
[2.2][3.3]PC	**2**	412, 640	[2.2]PC	**7**	521
[3.3][3.3]PC	**3**	421, 655	[3.3]PC	**8**	485, 600
[2.2][4.4]PC	**4**	425[b], 525,	[4.4]PC	**9**	475,
[3.3][4.4]PC	**5**	420, 546, 625[b]	*p*-xylene		420, 465[b]

a) PC: paracyclophane, b) Shoulder.

that the transannular interactions of triple-layered paracyclophanes depend mainly on a pair of the ring-to-ring distances in each molecule and [2.2]phane system with the shortest distance is most effective. [4.4]Phane system shows no interaction even when triply layered, that is, the $^1B_{2u}$ transition of **6** still retains fine structure, characteristic of alkylbenzenes. Also the spectral shapes of **4** and **5** are essentially same as those of [2.2]paracyclophane **7** and [3.3]paracyclophane **8**, respectively.[11]

Charge-transfer Complexes. The charge-transfer spectra of cyclophane–tetracyanoethylene complexes were measured to obtain further information concerning the transannular interaction. The π-donor character of the complexing benzene in cyclophane is enhanced by a transannular electron release from the remaining faced benzene ring. Cram *et al.* reported that double-layered [3.3]paracyclophane **8** was rather stronger π-donor than [2.2]paracyclophane **7**.[4] This indicates that [3.3]phane system is favored over [2.2]phane system for the transannular interaction in charge-transfer state. The CT spectra of a series of triple-layered paracyclophanes are shown in Fig. 2 and Table 1. The order of the shifts is the same as seen in double-layered case. Thus, [3.3][3.3]paracyclophane **3** is the strongest donor of all the triple-layered cyclophanes. The presence of the transannular interaction in CT complexes of [4.4]-phane system is supported by a red shift of the CT band of [4.4][4.4]paracyclophane **6** compared with *p*-xylene or [4.4]paracyclophane **9**.

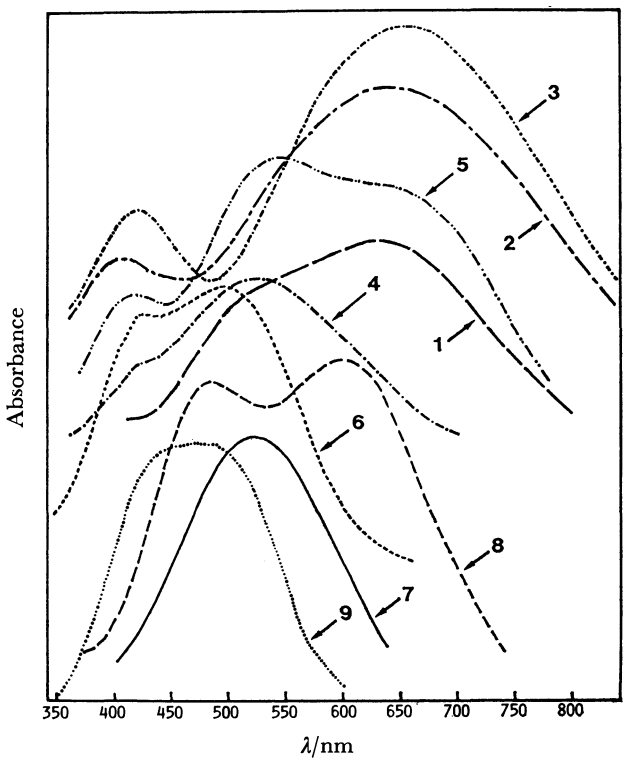

Fig. 2. Charge-transfer spectra of cyclophane–TCNE complexes in dichloromethane. Curves are all displaced on the vertical axis for separation.

Emission Spectra. Some of double-layered cyclophanes provide suitable models for the study of excimer which is well known to exist only in excited state and to show a fluorescence band in longer wavelength than the monomer fluorescence.[12] In the previous paper, we described on the basis of fluorescence spectra data that [2.2]- and [3.3]paracyclophanes, **7** and **8**, have structures resemble to the benzene excimer, whereas [4.4]paracyclophane **9** undergoes conformational change for the excimer formation.

An interesting question is whether any excited trimer exists or not. There has been found an example of termolecular exciplex composed of 2: 1 ratio of donor: acceptor.[13] The formation of neutral excited intramolecular trimer is also possible when considered a marked interaction in multilayered cyclophanes, although it is unfavorable on entropy to form intermolec-

Table 2. Emission data of triple-layered [*m.m*][*n.n*]-paracyclophanes and [*m.n*]paracyclophanes in EPA

Compd		Temp	Fluorescence λ_{max}/nm	Phosphorescence λ_{max}/nm
[2.2][2.2]PC[a]	**1**	77 K	380[c]	524, 542, 560
		RT[b]	384[c]	
[2.2][3.3]PC	**2**	77 K	381[c]	513
		RT	381[c]	
[3.3][3.3]PC	**3**	77 K	376[c]	474
		RT	377[c]	
[2.2][4.4]PC	**4**	77 K	358[c]	467
		RT	356[c]	
[3.3][4.4]PC	**5**	77 K	357[c]	457
		RT	356[c]	
[4.4][4.4]PC	**6**	77 K	285[d]	389
		RT	330[c], 395[c]	
[2.2]PC	**7**	77 K	354[c]	470
		RT	350[c]	
[3.3]PC	**8**	77 K	361[c]	463
		RT	358[c]	
[4.4]PC	**9**	77 K	281[d]	379
		RT	335[c]	

a) PC: paracyclophane. b) Room temperature. c) Excimer emission, broad. d) Monomer emission with fine structure.

ularly a termolecular aggregate. The present triple-layered paracyclophanes are expected to provide a helpful information about the excited trimer.

Their emission data are summarized in Table 2. The excimer fluorescences are characterized by broadening and large Stokes shift and are clearly distinguishable from ordinary monomer type of fluorescence. The excimer fluorescence bands of **1**, **2**, and **3** appear at much longer wavelength than those of double-layered paracyclophanes, **7** and **8**, indicating that the third stacked benzene obviously serves to stabilize the excited trimer state.

On the other hand, [4.4][4.4]paracyclophane **6** shows another type of excited trimer formation. It reveals monomer emission at low temperature but excimer emission at room temperature as seen for [4.4]paracyclophane **9**. However, the emission of **6** can be considered as superposition of two distinct excimer bands. Thus, the band at 330 nm is associated with excited dimer in analogy with the excimer band at 335 nm for **9** and another band at 395 nm is assigned to excited trimer emission.

Table 2 also shows large red shift of phosphorescence bands. There are rather correlated to absorption bands than fluorescence bands, indicating that the excimers are independent of triplet state.

Experimental

Melting points are uncorrected. All solvents are of reagent grade. NMR measurements were made with a Hitachi Perkin-Elmer R-20 spectrometer (60 MHz) or a JEOL JNM-FX 100 in deuteriochloroform using TMS as an internal standard. Mass spectra were determined on a Hitachi RMU-7 spectrometer at 70 eV using direct insertion technique. UV spectra were recorded on a Hitachi EPS-3T spectrophotometer. Emission spectra were taken on a Hitachi MPF-2A spectrophotometer attached with a HTV R-446F photomultiplier in EPA (diethyl ether–isopentane–ethanol of 5:5:2 volume ratio). A solution of about 1×10^{-3} M was prepared and degassed by freeze-pump-thaw method. Emission spectra were uncorrected.

Dithia[2.2][4.4]paracyclophane (12). A mixture of 1,4-bis(2-mercaptoethyl)benzene **10**[7a] (0.79 g, 4.0 mmol) and 4,7-bis(bromomethyl)[2.2]paracyclophane **11**[8] (1.73 g, 4.4 mmol) in benzene (200 ml) was slowly added into a refluxing ethanol solution (500 ml) of potassium hydroxide (0.71 g) under nitrogen. The addition took 6 h and the reflux was continued for further 6 h. The solvent was evaporated and the residue was chromatographed on silica gel with 1:1 benzene–hexane to give the desired cyclic compound **12** (0.44 g, 25%), colorless plates from benzene–hexane, mp 156.5—158 °C.

NMR ($CDCl_3$, 60 MHz) δ=6.67 (4H, s, ArH), 6.37 (4H, A_2B_2m, ArH), 5.80 (2H, s, ArH), 3.51 (2H, ABd, J=14 Hz, $ArCH_2S$), 3.07 (2H, ABd, J=14 Hz, $ArCH_2S$), 2.3—3.1 (16H, m, CH_2); MS *m/e* 430 (M^+). Found: C, 78.06; H, 7.22; S, 15.11%. Calcd for $C_{28}H_{30}S_2$: C, 78.09; H, 7.02; S, 14.89%.

Triple-layered [2.2][3.3]Paracyclophane (2). Dithiacyclophane **12** (70 mg) was dissolved in a mixture of benzene (5 ml) and triethyl phosphite (5 ml) in a quartz tube and irradiated with a high pressure mercury lamp for 6 h in a nitrogen atmosphere. After evaporation to dryness, the residue was chromatographed on silica gel with 1:9 benzene–hexane to give the desired product **2** from the first eluate, 13 mg (23%), colorless prisms from hexane, mp 161—162.5 °C.

NMR ($CDCl_3$, 60 MHz) δ=6.46 (4H, s, ArH), 6.35 (2H, A_2B_2dd, J=7 Hz, ArH), 6.14 (2H, A_2B_2dd, J=7 Hz, ArH), 5.57 (2H, s, ArH), 1.7—3.4 (20H, m, CH_2); MS *m/e* 366 (M^+). Found: C, 91.49; H, 8.29%. Calcd for $C_{28}H_{30}$: C, 91.75; H, 8.25%.

2,5-Dibromo-1,4-bis(bromomethyl)benzene (14). A mixture of 2,5-dibromo-*p*-xylene **13** (79 g, 0.3 mol) and NBS (111 g, 0.62 mol) in carbon tetrachloride (500 ml) was refluxed for 1 h using sunlight as a catalyst. The hot solution was filtered and the insoluble succinimide was washed with dichloromethane. The filtrate and the washings were combined, washed with water, and dried over anhyd magnesium sulfate. The solution was concentrated *in vacuo*, and the residue was recrystallized from benzene to give colorless columns, 43 g (34%), mp 160—161 °C.

NMR ($CDCl_3$, 60 MHz) δ=4.51 (4H, s, CH_2), 7.66 (2H, s, ArH). Found: C, 22.84; H, 1.35; Br, 75.50%. Calcd for $C_8H_6Br_4$: C, 22.78; H, 1.43; Br, 75.78%.

16,19-Dibromo-2,13-dithia[4.4]paracyclophane (15). A mixture of 1,4-bis(2-mercaptoethyl)benzene **10** (1.98 g, 0.01 mol) and 2,5-dibromo-1,4-bis(bromomethyl)benzene **14** (4.22 g, 0.01 mol) in benzene (300 ml) was slowly added into a refluxing ethanol (1 L) containing potassium hydroxide (1.78 g) under nitrogen. The addition took one day. After the addition was complete, the reflux was continued half a day. The mixture was concentrated, and the residue was chromatogphed on silica gel with 1:1 benzene–hexane. The first eluate gave the desired coupling compound **15** (8.54 g, 62%), colorless scales from benzene–hexane, mp 181.5—182.5 °C.

NMR ($CDCl_3$, 60 MHz) δ=7.00 (2H, s, ArH), 6.89 (4H, s, ArH), 3.68 and 3.26 (4H, ABq, J=14 Hz, $ArCH_2S$), 3.6—2.3 (8H, m, CH_2); MS *m/e* 458 (M^+). Found: C, 46.94; H, 3.75; S, 13.92; Br, 34.67%. Calcd for $C_{18}H_{18}S_2Br_2$: C, 47.17; H, 3.96; S, 13.99; Br, 34.88%.

16,19-Dicyano-2,13-dithia[4.4]paracyclophane (16). A suspension of dithia compound **15** (6.79 g, 14.8 mmol) in *N*-methyl-2-pyrrolidinone (28 ml) was heated at 180 °C with stirring in a nitrogen atmosphere for 1.5 d. The hot mixture was poured into 15% ammonia water (50 ml) and cooled in an ice bath. The resulting cake was filtered and dried in the air. The desired product **16** was extracted from the cake with dichloromethane by use of a Soxhlet extraction and purified by chromatography on silica gel with dichloromethane, 3.53 g (68%), colorless scales from benzene–hexane, mp 259.5—261.5 °C.

NMR ($CDCl_3$, 60 MHz) δ=7.26 (2H, s, ArH), 6.90 (4H, s, ArH), 3.80 and 3.45 (4H, ABq, J=15 Hz, $ArCH_2S$), 3.5—2.5 (8H, m, CH_2). Found: C, 68.38; H, 5.00; N, 7.96; S, 18.29%. Calcd for $C_{20}H_{18}N_2S_2$: C, 68.53; H, 5.18; N, 7.99; S, 18.30%.

5,8-Dicyano[3.3]paracyclophane (18). Dithia[4.4]paracyclophane **16** (3.19 g, 9 mmol) was mixed with acetic acid (24.3 ml) and 35% hydrogen peroxide (6.1 ml) and heated at 100 °C for 5 h. The mixture was cooled in an ice bath and resulting colorless solid of disulfone **17** was collected by filtration, washed with water, and dried, 3.09 g (82%).

Disulfone **17** (500 mg) was packed in a Pyrex tube sealed at one end. The open end was connected to a rotary pump and the system was maintained under 0.5 mmHg. The tube was placed in a furnace (15 cm in length, preheated at 650 °C) in such a way as the middle of the tube could be heated. The sample part was slidden smoothly inside the furnace. As soon as the pyrolysis started, an oily product condensed

near the opposite cool end. Column chromatography of the product on silica gel with benzene gave pure dicyano[3.3]-paracyclophane **18**, 176 mg (49%), colorless columns from benzene–hexane, mp 190.5—191.5 °C.

NMR ($CDCl_3$, 60 MHz) δ=7.11 (2H, s, ArH), 7.01 (2H, A_2B_2dd, J=8, 2 Hz, ArH), 6.79 (2H, A_2B_2dd, J=8, 2 Hz, ArH), 3.4—1.8 (12H, m, CH_2); MS *m/e* 286 (M^+). Found: C, 83.61; H, 6.05; N, 9.73%. Calcd for $C_{20}H_{18}N_2$: C, 83.88; H, 6.34; N, 9.78%.

5,8-Bis(ethoxycarbonyl)[3.3]paracyclophane (19). Dicyano compound **18** (185 mg, 0.65 mmol) was mixed with 1:1 concd H_2SO_4–H_2O (3 ml) and acetic acid (1 ml), and refluxed with stirring for one day in a nitrogen atmosphere. The mixture was diluted with 30 ml of water. The resulting precipitate of 5,8-dicarboxy[3.3]paracyclophane was collected by filtration, washed with water, and dried, 184 mg (88%).

The above dicarboxylic acid (100 mg, 0.31 mmol) was treated under reflux with thionyl chloride (2 ml) in dry benzene (10 ml) for 1.5 h. After complete removal of thionyl chloride by distillation, absolute ethanol (5 ml) was added. The mixture was refluxed for 1 h and diluted with benzene (50 ml). The solution was washed with sat. aq NaCl and dried over anhyd magnesium sulfate. After evaporation, the residue was chromatographed on silica gel with benzene to give the desired diester **19**, 61 mg (52%).

NMR ($CDCl_3$, 100 MHz) δ=1.46 (6H, t, J=7.1 Hz, CH_3), 2.05 (4H, m, CH_2), 2.70 (6H, m, CH_2), 3.65 (2H, m, CH_2), 4.42 (4H, q, OCH_2), 6.74 (4H, s, ArH), 7.34 (2H, s, ArH).

An analytical sample was purified by gel permeation liquid chromatography and recrystallized from pentane, colorless plates, mp 82.5—83 °C. Found: C, 75.81; H, 7.38%. Calcd for $C_{24}H_{28}O_4$: C, 75.76; H, 7.42%.

5,8-Bis(bromomethyl)[3.3]paracyclophane (20). Diester **19** (132 mg) was mixed with excess of lithium aluminium hydride in dry THF (20 ml) and refluxed for 30 min. After successive addition of ethyl acetate, water, dil hydrochloric acid, and NaCl, the mixture was extracted with ether. The extract was washed with sat. aq NaCl solution and dried over anyd magnesium sulfate. Evaporation of solvent gave a colorless solid of 5,8-bis(hydroxymethyl)[3.3]paracyclophane, 98 mg (96%).

NMR ($CDCl_3$, 100 MHz) δ=2.0—3.0 (12H, m, CH_2), 4.68 (4H, center of ABq, J=12.8 Hz, CH_2O), 6.72 (4H, center of ABq, J=8.0 Hz, ArH), 6.76 (2H, s, ArH).

This diol was used in the following bromination without purification.

The above diol (98 mg) was stirred with phosphorus tribromide (0.5 ml) in dry benzene (20 ml) for 1 h at room temperature. The mixture was washed with sat. aq NaCl, dried over anhyd magnesium sulfate, and evaporated. The residue was filtered through a short column of silica gel with benzene to give the pure compound **20**, 104 mg (74%), colorless plates from hexane, mp 136.5—137.5 °C.

NMR ($CDCl_3$, 100 MHz) δ=1.9—3.1 (12H, m, CH_2), 4.45 (4H, center of ABq, J=10.3 Hz, CH_2Br), 6.69 (2H, s, ArH), 6.77 (4H, center of ABq, J=8.6 Hz, ArH). Found: C, 56.74; H, 5.13; Br, 37.62%. Calcd for $C_{20}H_{22}Br_2$: C, 56.90; H, 5.25; Br, 37.85%.

Dithia[3.3][4.4]paracyclophane (21). Compound **21** was obtained in 63% yield from a coupling reaction of the above dibromide **20** and 1,4-bis(2-mercaptoethyl)benzene **10** in a similar manner as described for dithia[2.2][4.4]paracyclophane **12**, colorless prisms from benzene–hexane, mp 204—205 °C.

NMR ($CDCl_3$, 60 MHz) δ=6.63 (4H, s, ArH), 6.57 (4H, s, ArH), 6.06 (2H, s, ArH), 3.69 (2H, ABd, J=14 Hz, $ArCH_2S$), 3.11 (2H, ABd, J=14 Hz, $ArCH_2S$), 3.5—1.5 (20H, m, CH_2); MS *m/e* 458 (M^+). Found: C, 78.27; H, 7.19; S, 13.94%. Calcd for $C_{30}H_{34}S_2$: C, 78.55; H, 7.47; S, 13.98%.

Triple-layered [3.3][3.3]Paracyclophane (3). Photodesulfurization of dithia compound **21** was carried out in similar manner as described in the synthesis of [2.2][3.3]analogue **2**. [3.3][3.3]Paracyclophane **3** was obtained in 16% yield, colorless plates from hexane, mp 166—168 °C.

NMR ($CDCl_3$, 100 MHz) δ=6.54 (4H, A_2B_2dd, J=6.7, 0.7 Hz, ArH), 6.43 (4H, A_2B_2dd, J=6.7, 0.7 Hz, ArH), 5.89 (2H, s, ArH), 3.0—1.8 (24H, m, CH_2); MS *m/e* 394 (M^+). Found: C, 91.11; H, 8.68%. Calcd for $C_{30}H_{34}$: C, 91.31; H, 8.69%.

18,21-Dibromo-2,15-dithia[5.5]paracyclophane (23). Dithia compound **23** was prepared from 2,5-dibromo-1,4-bis-(bromomethyl)benzene **14** and 1,4-bis(3-mercaptopropyl)-benzene **22**[7a] in similar manner as for dithia[4.4]analogue **15**, yield 87%, colorless plates from hexane, mp 137—138 °C.

NMR ($CDCl_3$, 60 MHz) δ=7.45 (2H, s, ArH), 6.99 (4H, s, ArH), 4.03 (2H, ABd, J=14 Hz, $ArCH_2S$), 3.44 (2H, ABd, J=14 Hz, $ArCH_2S$), 2.63 (4H, m, $ArCH_2$), 1.96 (8H, m, CH_2); MS *m/e* 486 (M^+). Found: C, 49.11; H, 4.60; S, 13.27; Br, 32.69%. Calcd for $C_{20}H_{22}S_2Br_2$: C, 49.39; H, 4.56; S, 13.19; Br, 32.86%.

18,21-Dicyano-2,15-dithia[5.5]paracyclophane (24). Dithia compound **24** was derived from dibromo derivative **23** in similar manner as for dithia[4.4]analogue (**16**), yield 53%, colorless plates from benzene, mp 164—165 °C.

NMR ($CDCl_3$, 60 MHz) δ=7.60 (2H, s, ArH), 6.94 (4H, s, ArH), 4.02 (2H, ABd, J=14 Hz, $ArCH_2S$), 3.55 (2H, ABd, J=14 Hz, $ArCH_2S$), 2.65 (4H, m, $ArCH_2$), 1.92 (8H, m, CH_2); MS *m/e* 398 (M^+). Found: C, 70.05; H, 6.12; N, 7.47; S, 16.87%. Calcd for $C_{22}H_{22}N_2S_2$: C, 69.80; H, 5.86; N, 7.40; S, 16.94%.

6,9-Dicyano[4.4]paracyclophane (26). The above dicyano dithia compound **24** was oxidized to disulfone **25** in 96% yield. The pyrolysis as described in [3.3]analogue **18** gave the desired [4.4]paracyclophane **26** in 48% yield, colorless columns from benzene–hexane, mp 206.5—207.5 °C.

NMR ($CDCl_3$, 60 MHz) δ=7.12 (2H, s, ArH), 6.76 (4H, s, ArH), 3.1—0.9 (16H, m, CH_2); MS *m/e* 314 (M^+). Found: C, 84.34; H, 7.08; N, 8.78%. Calcd for $C_{22}H_{22}N_2$: C, 84.04; H, 7.05; N, 8.91%.

6,9-Bis(ethoxycarbonyl)[4.4]paracyclophane (27). Diester **27** was derived from dicyano compound **26** in similar manner as in the case of [3.3]analogue **19**, colorless plates from pentane, mp 59.5—61.5 °C, yield 77%.

NMR ($CDCl_3$, 100 MHz) δ=7.30 (2H, s, ArH), 6.66 (4H, s, ArH), 4.37 (4H, q, J=7.2 Hz, OCH_2), 1.42 (6H, t, J=7.2 Hz, CH_3). Found: C, 76.69; H, 7.95%. Calcd for $C_{26}H_{32}O_4$: C, 76.44; H, 7.90%.

6,9-Bis(bromomethyl)[4.4]paracyclophane (28). Bromomethyl derivative **28** was prepared *via* 6,9-bis(hydroxymethyl)[4.4]paracyclophane from the above diester **27** in overall yield 72%, colorless prisms from hexane, mp 129—130 °C.

NMR ($CDCl_3$, 100 MHz) δ=6.75 (2H, s, ArH), 6.67 (4H, s, ArH), 4.37 (4H, centered ABq, J=10.2 Hz, CH_2Br), 3.0—1.0 (8H, m, CH_2). Found: C, 58.97; H, 5.80; Br, 35.46%. Calcd for $C_{22}H_{28}Br_2$: C, 58.69; H, 5.82; Br, 35.49%.

Dithia[3.3][4.4]paracyclophane (30). The synthesis of **30** was accomplished by a reaction of dibromide **28** and 1,4-bis(mercaptomethyl)benzene **29** in similar manner as described in dithia[2.2][4.4]paracyclophane **12**, yield 88%, colorless columns from benzene–hexane, mp 206.5—208 °C.

NMR ($CDCl_3$, 100 MHz) δ=6.76 (4H, centered A_2B_2, ArH), 6.51 (4H, s, ArH), 6.20 (2H, s, ArH), 3.79 (2H, ABd,

J=15 Hz, $ArCH_2S$), 3.71 (4H, s, $ArCH_2S$), 3.42 (2H, ABd, J=15 Hz, $ArCH_2S$), 2.9—1.0 (16H, m, CH_2); MS *m/e* 458 (M^+). Found: C, 78.29; H, 7.43; S, 13.71%. Calcd for $C_{30}H_{34}S_2$: C, 78.55; H, 7.47; S, 13.98%.

Triple-layered [2.2][4.4]Paracyclophane (4). Triple-layered cyclophane **4** was obtained in 55% yield by photodesulfurization of dithia[3.3][4.4]paracyclophane **30** as described in the case of **2**, colorless plates from pentane, mp 129—130 °C.

NMR ($CDCl_3$, 100 MHz) δ=6.53 (4H, s, ArH), 6.35 (2H, A_2B_2dd, J=7.4, 1.0 Hz, ArH), 6.20 (2H, A_2B_2dd, J=7.4, 1.0 Hz, ArH), 5.64 (2H, s, ArH), 3.2—1.0 (24H, m, CH_2); MS *m/e* 394 (M^+). Found: C, 91.32; H, 8.58%. Calcd for $C_{30}H_{34}$: C, 91.31; H, 8.69%.

Dithia[4.4][4.4]paracyclophane (31). The synthesis of **31** was accomplished by a reaction of 6,9-bis(bromomethyl)[4.4]paracyclophane **28** and 1,4-bis(2-mercaptoethyl)benzene **10** in similar manner as described in dithia[2.2][4.4]paracyclophane **12**, yield 77%, colorless plates from benzene–hexane, mp 280—282 °C.

NMR ($CDCl_3$, 100 MHz) δ=6.66 (4H, s, ArH), 6.53 (4H, s, ArH), 6.03 (2H, s, ArH), 3.46 (2H, ABd, J=14 Hz, $ArCH_2S$), 3.03 (2H, ABd, J=14 Hz, $ArCH_2S$), 3.2—0.9 (16H, m, CH_2). Found: C, 78.70; H, 7.63; S, 13.39%. Calcd for $C_{32}H_{28}S_2$: C, 78.96; H, 7.87; S, 13.17%.

Triple-layered [3.3][4.4]Paracyclophane (5) and 6,9-Dimethyl-[4.4]paracyclophane (32). The above dithia compound **31** (49 mg), triethyl phosphite (10 ml), and benzene (20 ml) were mixed in a Vycor tube, and the mixture was irradiated with a low pressure mercury lamp for 12 h in a nitrogen atmosphere. After evaporation of the solvent, the residue was chromatographed on silica gel with hexane. From the first eluate, compound **32** was obtained, 2 mg (7%), colorless prisms from hexane, mp 113—114.5 °C.

NMR ($CDCl_3$, 100 MHz) δ=6.67 (4H, s, ArH), 6.47 (2H, s, ArH), 2.07 (6H, s, CH_3), 2.8—1.1 (16H, m, CH_2); MS *m/e* 292 (M^+). Found: C, 90.18; H, 9.16%. Calcd for $C_{22}H_{28}$: C, 90.35; H, 9.65%.

From the second eluate, the desired triple-layered compound **5** was obtained in 12% yield (5 mg), colorless columns from pentane, mp 170—171 °C.

NMR ($CDCl_3$, 100 MHz) δ=6.60 (2H, ABd, J=7.1 Hz, ArH), 6.53 (2H, ABd, J=7.1 Hz, ArH), 6.51 (4H, s, ArH), 5.96 (2H, s, ArH), 2.8—1.3 (28H, m, CH_2); MS *m/e* 422 (M^+). Found: C, 91.20; H, 8.80%. Calcd for $C_{32}H_{38}$: C, 90.94; H, 9.06%.

Dithia[4.4][5.5]paracyclophane (33). Dithia compound **33** was obtained in 67% yield by the reaction of 6,9-bis(bromomethyl)[4.4]paracyclophane **28** and 1,4-bis(3-mercaptopropyl)benzene **22** in similar manner as described in dithia[2.2][4.4]paracyclophane **12**, colorless prisms from pentane, mp 120—122 °C.

NMR ($CDCl_3$, 100 MHz) δ=6.80 (4H, s, ArH), 6.62 (4H, s, ArH), 6.44 (2H, s, ArH), 3.66 (2H, ABd, J=14.1 Hz, SCH_2), 3.28 (2H, ABd, J=14.1 Hz, SCH_2), 3.1—1.0 (28H, m, CH_2); MS *m/e* 514 (M^+). Found: C, 79.40; H, 8.32; S, 12.30%. Calcd for $C_{34}H_{42}S_2$: C, 79.32; H, 8.22; S, 12.46%.

Triple-layered [4.4][4.4]Paracyclophane (6). The above dithia compound **33** (290 mg) was mixed with acetic acid (2 ml) and 35% hydrogen peroxide (0.6 ml), and heated at 100 °C for 12 h to give colorless precipitate of disulfone **34** (190 mg, 58%).

The above disulfone **34** (50 mg) was pyrolyzed by the method described for 5,8-dicyano[3.3]paracyclophane **18**. The pyrolytic product was chromatographed on silica gel with benzene–hexane and recrystallized from benzene–hexane to give colorless columns of paracyclophane **6**, 2 mg (5%), mp 250 °C (dec).

NMR ($CDCl_3$, 100 MHz) δ=6.55 (8H, s, ArH), 5.99 (2H, s, ArH), 1.6—0.8 (32H, m, CH_2); MS *m/e* 450 (M^+). Found: C, 90.61; H, 9.39%.

The present work was partially supported by a Grant-in-Aid for Scientific Research No. 847019 from the Ministry of Education, Science and Culture.

References

1) Part LXI: T. Kaneda, T. Otsubo, H. Horita, and S. Misumi, *Bull. Chem. Soc. Jpn.* in press.

2) T. Otsubo, S. Mizogami, I. Otsubo, Z. Tozuka, A. Sakagami, Y. Sakata, and S. Misumi, *Bull. Chem. Soc. Jpn.*, **46**, 3519 (1973); S. Misumi and T. Otsubo, *Acc. Chem. Res.*, **11**, 251 (1978) and references cited therein.

3) H. Horita, N. Kannen, T. Otsubo, and S. Misumi, *Tetrahedron Lett.*, **1974**, 501; H. Horita, Y. Sakata, and S. Misumi, *ibid.*, **1976**, 1509; H. Horita, Y. Koizumi, T. Otsubo, Y. Sakata, and S. Misumi, *Bull. Chem. Soc. Jpn.*, **51**, 2668 (1978).

4) D. J. Cram and R. H. Bauer, *J. Am. Chem. Soc.*, **81**, 5971 (1959); M. Sheehan and D. J. Cram, *ibid.*, **91**, 3553 (1969).

5) T. Shinmyozu, T. Inazu, and T. Yoshino, *Chem. Lett.*, **1977**, 347; H. Horita, T. Otsubo, and S. Misumi, *ibid.*, **1978**, 807.

6) For a preliminary report see T. Otsubo, T. Kohda, and S. Misumi, *Tetrahedron Lett.*, **1978**, 2507.

7) a) T. Otsubo, M. Kitasawa, and S. Misumi, *Chem. Lett.*, **1977**, 977; *Bull. Chem. Soc. Jpn.*, **52**, 1515 (1979); b) M. W. Haenel, A. Flatow, V. Taglieber, and H. A. Staab, *Tetrahedron Lett.*, **1977**, 1733; c) D. T. Longone, S. H. Küsefoglu, and J. A. Gladysz, *J. Org. Chem.*, **42**, 2787 (1977); d) L. Rossa and F. Vögtle, *J. Chem. Res.* (s), **1977**, 264.

8) N. Kannen, T. Umemoto, T. Otsubo, and S. Misumi, *Tetrahedron Lett.*, **1973**, 4537; N. Kannen, T. Otsubo, Y. Sakata, and S. Misumi, *Bull. Chem. Soc. Jpn.*, **49**, 3307 (1976).

9) A short approach by means of bromination of 5,8-dimethyl[3.3]paracyclophane with NBS was unsuccessful.

10) P. Ruggli and F. Brandt, *Helv. Chim. Acta*, **27**, 274 (1944).

11) D. J. Cram, N. L. Allinger, and H. Steinberg, *J. Am. Chem. Soc.*, **76**, 6132 (1954).

12) Th. Förster, *Angew. Chem. Int. Ed. Engl.*, **8**, 333 (1969); M. T. Vala, J. Haebig, and S. A. Rice, *J. Chem. Phys.*, **43**, 886 (1965); T. Umemoto, S. Satani, Y. Sakata, and S. Misumi, *Tetrahedron Lett.*, **1975**, 3159; D. Schweitzer, K. H. Hausser, R. G. H. Kirrstetter, and H. A. Staab, *Z. Naturforsch., Teil A*, **31**, 1189 (1976); T. Hayashi, N. Mataga, Y. Sakata, S. Misumi, M. Morita, and J. Tanaka, *J. Am. Chem. Soc.*, **98**, 5910 (1976).

13) H. Beens and A. Weller, *Chem. Phys. Lett.*, **2**, 140 (1968); N. Tsujino, H. Masuhara, and N. Mataga, *ibid.*, **21**, 301 (1973); M. Yoshida, H. Tatemitsu, Y. Sakata, and S. Misumi, H. Masuhara, and N. Mataga, *J. Chem. Soc., Chem. Commun.*, **1976**, 587.

Photocyclization of 2′-Hydroxychalcones to 4-Flavanones

Ryoka MATSUSHIMA* and Ichiro HIRAO

Department of Industrial Chemistry, Faculty of Engineering, Shizuoka University, Hamamatsu 432

(Received September 3, 1979)

On irradiation with light of $\lambda \geqq 365$ nm, parent and methoxy-substituted 2′-hydroxychalcones undergo facile photocyclization to give corresponding 4-flavanones in high efficiencies in ethyl acetate or dioxane, whereas in low or nil efficiencies in benzene, chloroform, carbon tetrachloride, ether, acetonitrile, ethanol, or *t*-butyl alcohol. The low reactivity in benzene is, however, significantly increased by the addition of liquid paraffin to increase the solvent viscosity. 3′,4′-Benzo-2′-hydroxychalcone showed low reactivities in any solvents. The formation of 4-flavanones is neither quenched by triplet quenchers nor depressed by the addition of free radical scavengers. The reaction mechanism is discussed in terms of enolization.

It has previously been reported that the photolysis of substituted 4-flavanones undergo ring opening to give 2′-hydroxychalcones[1-3] or hydrogen atom abstraction to give dimeric products,[2,3] depending on the substituent and solvent.

The photocyclization of 2′-hydroxychalcone in benzene has been reported as a new method for flavanone synthesis (53% yield),[4] though the mechanism has little been studied. The photocyclization of 2′-hydroxychalcones is apparently the reverse process of the photochemical ring opening of 4-flavanones, and it appeared of interest to investigate further the scope of these reactions. The present investigation has emphasized on the solvent effects on the relative reactivity or yield for the photocyclization of parent and substituted 2′-hydroxychalcones.

Experimental

2′-Hydroxychalcones[5] and 4-flavanones[6] were prepared according to the literatures methods. Other reagents and solvents were of guaranteed grade (Wako Chemicals).

Each sample solution was degassed by bubbling with purified nitrogen and sealed in a 5 ml or 10 ml pyrex ampul prior to irradiation. The light source was a 400 W high pressure mercury lamp. A cut-off glass filter (Toshiba UV-35) or an aqueous copper(II) solution filter[7] was employed to eliminate short wavelength regions. The transmittance characteristics of the filters and the main emission from the light source, as well as the absorption spectra of **1a** and **1b**, are illustrated in Fig. 1. Irradiation was carried out by means of a merry-go-round apparatus in a thermostat controlled at 20±1 °C.

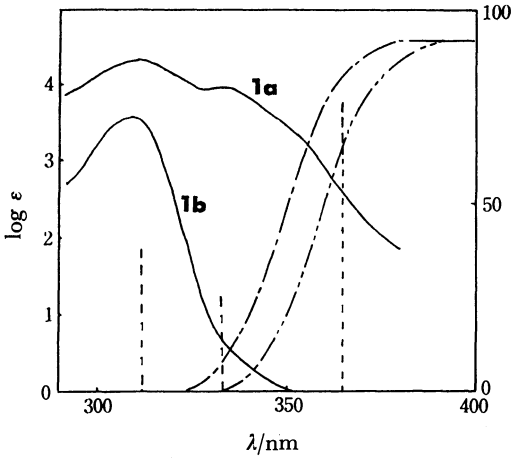

Fig. 1. Absorption spectra of **1a** and **1b** in benzene, and the transmittance characteristics of cut-off filters for selective excitation of **1a**. (— - —): Transmittance of a UV-35 glass filter, (— - - —): transmittance of aqueous copper(II) solution filter, (——): emission from a high pressure mercury lamp.

Photolyzed mixture solutions were condensed below 40 °C and separated by PLC on silica gel–benzene. The photoproducts from **1a** and **2a** were confirmed to be **1b** and **2b** respectively by comparing their NMR and IR spectra, while the photoproducts from **3a**—**5a** were assigned to be **3b**—**5b** respectively by comparing their UV spectra and TLC, with those of the authentic samples prepared independently. The amounts of the products and the reactants in the photolyzed mixtures were determined by colorimetric or gravimetric analysis after separation by PLC on silica gel–benzene. Quantum yields were measured with monochromatic 360—366 nm light from the light source by using a combination of filters (Toshiba UV-35 and UV-D2). For the estimation of the light quanta absorbed by the sample solutions, a mixture of 0.1 M benzophenone and 0.1 M benzhydrol in benzene[8] was used.

UV absorption spectra were measured by the use of a Hitachi 124 spectrophotometer. NMR and IR spectra were measured by means of a Hitachi R-24 NMR spectrometer and a Nihonbunko IRA-1 IR spectrometer, respectively.

Results

Photocyclization of 2′-Hydroxychalcones in Various Solvents. By selective excitation with light of $\lambda \geqq 365$ nm, a series of 2′-hydroxychalcones **1a**—**5a** in deoxygenated solutions underwent photocyclization to give corresponding 4-flavanones **1b**—**5b**, respectively (Scheme 1).

Photolyses of **1a**—**5a** were carried out in a variety of solvents, and the qualitative results are shown in Table 1. Both **1a** and **2a** undergo photocyclization in benzene, ether, ethyl acetate, 1,4-dioxane, acetonitrile, and ethanol, but not in chloroform and *t*-butyl alcohol. Both **3a** and **4a** photocyclize in benzene, ether, ethyl acetate, and 1,4-dioxane, but not in chloroform, carbon tetrachloride, acetonitrile, ethanol, and *t*-butyl alcohol. **5a** shows low reactivity in most solvents.

Effects of the Wavelength of Light. Irradiation of light involving shorter wavelength regions led to the complication of the reaction and the decrease in the rates. Figure 2 illustrates wavelength effects on the relative rates of **2a** and **4a** in benzene.

On irradiation with light of $\lambda \geqq 313$ nm, the consumption rate of **4a** is decreased to 2/5 of that with $\lambda \geqq 334$

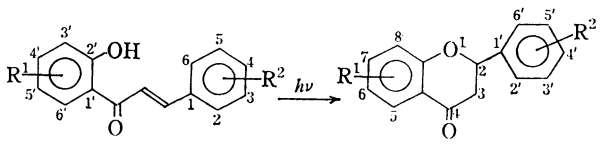

1a—5a			1b—5b		
2′-Hydroxychalcone	R^1	R^2	4-Flavanone	R^1	R^2
1a	H	H	**1b**	H	H
2a	H	2-OMe	**2b**	H	2′-OMe
3a	4′-OMe	H	**3b**	7-OMe	H
4a	6′-OMe	H	**4b**	5-OMe	H
5a	3′,4′-Benzo	H	**5b**	7,8-Benzo	H

Scheme 1.

Table 1. Formation of 4-flavanones **1b—5b** by the photolyses of 2′-hydroxychalcones **1a—5a**

2′-Hydroxy-chalcone	Benzene	Carbon tetrachloride	Chloro-form	Ethyl ether	Ethyl acetate	1,4-Dioxane	Aceto-nitrile	Ethanol	*t*-Butyl alcohol
1a	**1b**	**1b**	—	**1b**	**1b**	**1b**	**1b**	**1b**	—
2a	**2b**	—	—	**2b**	**2b**	**2b**	**2b**	**2b**	—
3a	**3b**	—	—	**3b**	**3b**	**3b**	—	—	—
4a	**4b**	—	—	**4b**	**4b**	**4b**	—	—	—
5a	**5b**	—	—	—	**5b**	**5b**	—	—	—

a) Irradiated with a 400 W high pressure mercury lamp through a UV-35 glass filter for 10 h at 20 °C. Initial concentrations of 2′-hydroxychalcones were 1 mM. 4-Flavanones formed were detected by TLC on silica gel–benzene.

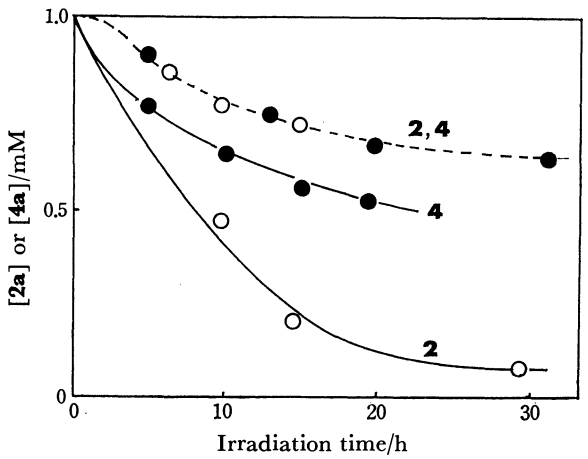

Fig. 2. Wavelength effects on the photoreaction rates of **2a** (○) and **4a** (●) in benzene. (—○—): Irradiation of **2a** with $\lambda \geqq 334$ nm, (--○--): Irradiation of **2a** with $\lambda \geqq 313$ nm, (—●—): irradiation of **4a** with $\lambda \geqq 365$ nm, (--●--): irradiation of **4a** with $\lambda \geqq 334$ nm.

nm. Similarily, the rate of **2a** on irradiation with $\lambda \geqq 334$ nm is 3/5 of that with $\lambda \geqq 365$ nm. A UV-35 (Toshiba) glass filter or an aqueous copper(II) solution filter appears to be suitable to cut shorter wavelength regions (see also Fig. 1).

Variation in the Photoreaction Rates. Relative rates of the reaction were measured in benzene, ethyl acetate, and 1,4-dioxane, since in these solvents all of the 2′-hydroxychalcones **1a—5a** undergo photocyclization (Table 1). Table 2 compares the consumption rates at a constant (5 h) irradiation time, while Figs. 3 and 4

Table 2. Variation in the relative rates with solvent and substituent[a)]

2′-Hydroxy-chalcone	Consumption of 2′-hydroxychalcone (%) in		
	Benzene	1,4-Dioxane	Ethyl acetate
1a	8.2	94	95
2a	10	97	91
3a	14	35	63
4a	30	30	84
5a	7.4	1.4	1.3

a) Initial concentration of each 2′-hydroxychalcone was 1 mM, irradiation time was 5 h.

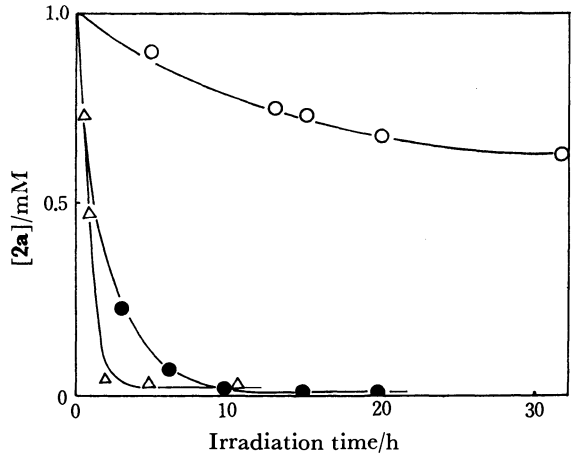

Fig. 3. Consumption of **2a** with irradiation time in benzene (○), 1,4-dioxane (△), and ethyl acetate (●). Similar plots were obtained for **1a**.

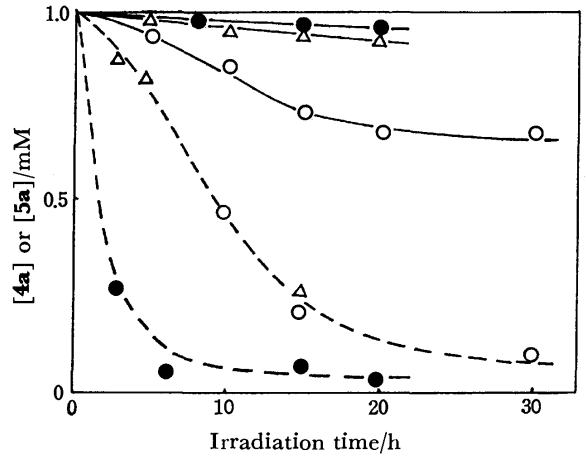

Fig. 4. Consumption of **4a** (broken line) and **5a** (solid line) with irradiation time in benzene (○), 1,4-dioxane (△), and ethyl acetate (●).

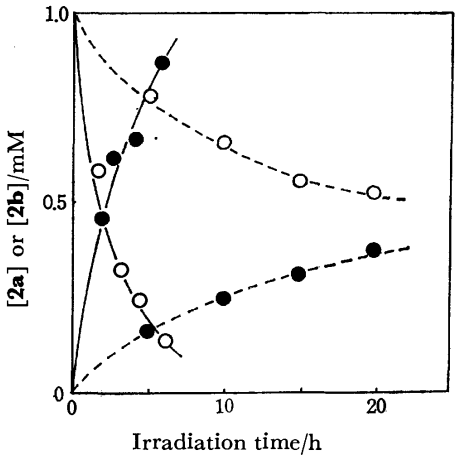

Fig. 5. Concentration changes in **2b** (●) and **2a** (○) with irradiation time in benzene (broken line) and ethyl acetate (solid line).

illustrate the concentration changes with irradiation time.

The results show that the rates are high in ethyl acetate or 1,4-dioxane, and low in benzene, though **5a** has the lowest reactivities in each solvent. It is notable that the rates of **1a** and **2a** are higher in ethyl acetate than in benzene by a factor of 20—40 (Fig. 3).

The quantum yields for the consumption of **1a** and **2a** (1 mM) excited at 365—366 nm were 0.3—0.4 in ethyl acetate and 0.01 in benzene, though they varied depending on the concentration of the reactants and on the extent of the reaction. The low reactivity of **2a** in benzene is significantly increased with the increase in the solvent viscosity (Table 3).

TABLE 3. EFFECTS OF SOLVENT VISCOSITY ON THE QUANTUM YIELD FOR THE CONSUMPTION OF **2a** IN BENZENE–LIQUID PARAFFIN

Liquid paraffin/vol%	Relative viscosity[a)]	Quantum yield × 100
0	1.0	1.0
20	1.4	1.1
40	2.3	1.7
60	4.8	2.7
80	18	3.8
100	150	11

a) Measured at 20±0.5 °C by means of an Ostwald viscositometer.

Variation in the Yields of 2b. The amounts of **2b** formed and **2a** recovered were determined at various irradiation time for the photoreaction of **2a**. Figure 5 illustrates the increasing curve of **2b** and the decreasing curve of **2a** in benzene and ethyl acetate.

The curves of **2a** and **2b** are symmetrical to each other, indicating that the reaction is *clean*. The yields of **2b** based on the consumed amounts of **2a** are listed in Table 4.

Though the values are somewhat scattered, the yields of **2b** are equal or close to unity in ethyl acetate. This implies that the quantum yield for the formation

TABLE 4. YIELDS OF **2b** AT VARIOUS IRRADIATION TIME IN BENZENE, 1,4-DIOXANE, AND ETHYL ACETATE[a)]

Solvent	Irradiation time/h	[2a]/mM Recovered	[2b]/mM Formed	Yield of 2b/%[b)]
Benzene	5	0.77	0.17	74
	10	0.66	0.24	71
	15	0.55	0.34	69
	20	0.52	0.40	83
Dioxane	1	0.79	0.17	82
	2	0.57	0.48	100
	3	0.31	0.55	79
	4	0.06	0.35	58
Ethyl acetate	2	0.57	0.45	100
	3	0.32	0.62	91
	4.5	0.23	0.65	84
	6	0.14	0.86	100

a) Initial concentration of **2a** was 1 mM. Cut-off filter was a 1.5 cm-depth solution of copper(II) sulfate (80 g) and copper(II) nitrate (80 g) in 400 ml water, which had been pre-irradiated for 10 h. The amounts of **2a** and **2b** in the photolyzed mixtures were determined colorimetrically after separation by PLC. b) The yield of **2b** based on the consumed amount of **2a**.

of **2b** is equal or close to the quantum yield value for the consumption of **2a**, or 0.3—0.4 in ethyl acetate. It should be noted that longer irradiation may lower the yield, thus the practical conversion yield of **2b** is 55% at best in 1,4-dioxane. In ethyl acetate the conversion yield of **2a** into **2b** is fairly high, *e.g.*, 86% at 6 h irradiation. The high conversion yield and the cleanness of the reaction (the high yield of **2b** based on the consumed amount of **2a**) in ethyl acetate may be of preparative use, if the wavelength and the time of irradiation *etc.* are suitablly controlled. Since the reaction can be achieved in neutral (mild) media, it may be useful for cyclization of 2'-hydroxychalcones having labile groups to acid or base.

Effects of Triplet Quenchers and Radical Scavengers. The formation of **2b** by the photolysis of **2a** in aerated benzene was not significantly quenched, though unknown side products were also formed. The formation

of **2b** was not quenched in the photolysis of **2a** (1 mM) in benzene in the presence of ferrocene (1 mM), *trans*-stilbene (1 mM), or acenaphthylene (2 mM). Selective excitation of **2a** in the presence of acenaphthylene gave isomeric dimers of acenaphthylene, though the formation of **2b** was not quenched. Further, the *anti*/*syn* ratio of dimers was higher than that by direct excitation of acenaphthylene. Thus, the formation of **2b** is not quenched, even when triplet energy is transferred from **2a** to the quenchers.

The addition of 2,6-di-*t*-butylphenol (1 mM) altered neither the rate nor the yield of the formation of **1b** in the photolysis of **1a** (1 mM) in ethyl acetate.

Discussion

The lack of quenching by triplet quenchers and the lack of inhibition by free radical scavengers (2,6-di-*t*-butylphenol and dissolved oxygen) may imply that a mechanism involving triplet states or free radicals is unlikely. The higher reactivities in polar solvents than in nonpolar solvent (Fig. 3 and Table 2) may support that the reaction takes place through ionic or polar processes.

Though the effects of solvent and substituent on the reactivities (Table 1) are far from explainable as yet, it seems that polar solvents, particularly aprotic polar solvents (basic solvents), are effective for the reaction, while nonpolar solvents are less effective. This may suggest some role of the interactions of solvent with the hydroxyl group of 2′-hydroxychalcones. One may assume, for example, that the intramolecular hydrogen bonding of the 2′-hydroxychalcones would be broken or loosened by solvation or proton transfer from the hydroxyl group to a basic or polar solvent, affecting the structures and reactivities in their ground state or excited states. The NMR signal of the phenolic proton of **1a** at $\delta \approx 12.5$ ppm was not changed at all with the change in the solvent from benzene to ethyl acetate, 1,4-dioxane, and 1,4-dioxane–water (3: 1), implying that the intramolecular hydrogen bonding in the ground state remains unchanged even in basic or polar solvents. Thus, the ground state structures of the 2′-hydroxychalcones may be represented by **10** regardless of solvent.

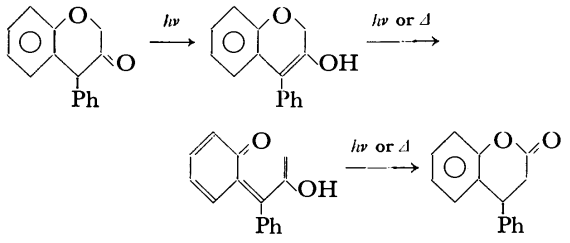

Scheme 2.

A. Padwa *et al.* have shown that the photochemical rearrangements of 3-chromanone derivatives take place *via* enolization (Scheme 2).[9] Similar mechanism has also been proposed for the photochemical ring opening reaction of the substituted 4-flavanones in benzene (Scheme 3).[3] It is noted that the photocyclization

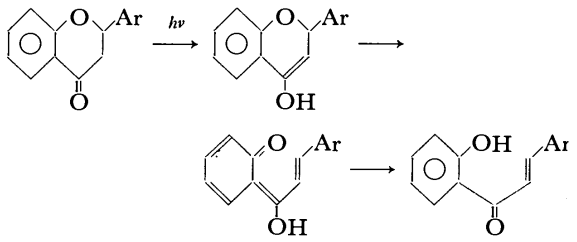

Scheme 3.

of the 2′-hydroxychalcones to the 4-flavanones is apparently the reverse reaction of the photochemical ring opening of the 4-flavanones and that the both reactions can indeed be reversible under suitable conditions.

It seems, therefore, reasonable to assume a similar mechanism (involving enolization) for the photocyclization (Scheme 4). Photochemical excitation of **10** would lead to enolization to give **11**, which needs, however, to undergo *cis-trans* isomerization to **12** for the subsequent cyclization to occur. The cyclization of **12** to **13** may be exothermic or less endothermic due to the recovery of aromatic stability, and proceed effectively *via* a thermal 6-π electrocyclic process.

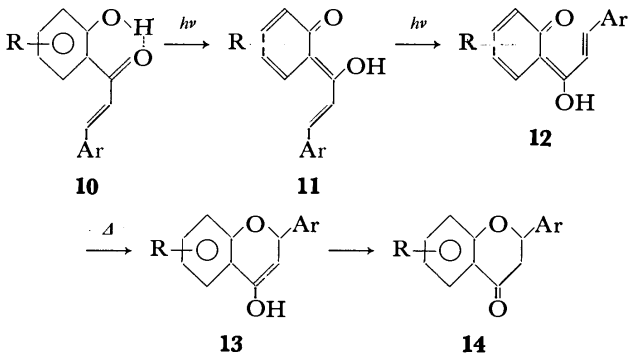

Scheme 4.

The two-photon mechanism in Scheme 4 requires that the upper limit of the quantum yield for the formation of 4-flavanone should be 0.5. The quantum yield estimated for the formation of **2b** in ethyl acetate ranges in 0.3—0.4, which is close to the upper limit. The estimated quantum yield is strikingly high despite the short lifetimes of the excited singlet states of aromatic ketones in solution. The reaction would proceed so rapidly and effectively that it dominates over rapid deactivation processes of excited singlet states, such as intersystem crossing and internal conversion *etc.* It is known that the acidities of phenols are greatly increased in the excited singlet states.[10] The increased acidity of **10** in the excited singlet state would allow facile acid-catalyzed enolization, and polar solvents may accelerate the reaction by stabilization of the enols.

In non polar solvents, such as benzene, the enols would be less stabilized and the reaction is less efficient so that deactivation processes may compete with or dominate over. The increase in the reaction efficiency with the solvent viscosity (Table 3) may imply that bimolecular deactivation processes, as well as unimolecular ones, compete well with the forward reaction in benzene.

The authors wish to thank Mr. H. Mizuno for his hospitality and considerable assistance in the preparation of the samples. They also wish to thank Dr. M. Suzuki, Mr. M. Morioka, and Miss S. Yamazaki for their comments and encouragement.

References

1) P. O. Mack and J. T. Pinkey, *J. Chem. Soc., Chem. Commun.*, **1972**, 451.
2) R. Matsushima, T. Kishimoto, and M. Suzuki, *Chem. Lett.*, **1976**, 579.
3) R. Nakashima, K. Okamoto, and T. Matsuura, *Bull. Chem. Soc. Jpn.*, **49**, 3355 (1976).
4) F. R. Stermitz, J. A. Adamovics, and J. Geigert, *Tetrahedron*, **31**, 1593 (1975).
5) T. A. Geissman and R. O. Clinton, *J. Am. Chem. Soc.*, **68**, 697 (1946).
6) A. Lowenbein, *Ber.*, **57**, 1515 (1924); J. Shinoda, *Yakugaku Zasshi*, **48**, 35 (1928); G. Woker, *Ber.*, **39**, 1649 (1906).
7) J. G. Calvert and J. N. Pitts, "Photochemistry," John Wiley and Sons. Inc., New York, N. Y. (1966), p. 736.
8) W. M. Moore and M. Ketchum, *J. Am. Chem. Soc.*, **84**, 1388 (1962).
9) A. Padwa, A. Au, G. A. Lee, and W. Owens, *J. Am. Chem. Soc.*, **98**, 3555 (1976); A. Padwa and W. Owens, *J. Org. Chem.*, **42**, 3076 (1977).
10) H. D. Becker, "The Chemistry of the Hydroxyl Group," ed by S. Patai, John Wiley and Sons, Inc., London (1971), Part II, pp. 894—920.

Aromatization of Ring-A in α-Bromocholestan-6-ones

SHAFIULLAH* and ISLAMUDDIN
Department of Chemistry, Aligarh Muslim University, Aligarh 202001, India
(Received May 8, 1978)

Pyridine promoted dehydrohalogenation of 3β-chloro-5-bromo-5α-cholestan-6-one resulting in ring-A aromatization with expulsion of C-10 angular methyl group to give 19-norcholesta-1,3,5(10)-trien-6-one along with 3α,5-cyclo-5α-cholest-7-en-6-one, cholesta-2,4-dien-6-one, and 5α-cholestane-3,6-dione. Similar treatment of 3β-chloro-5,7β-dibromo-5α-cholestan-6-one ends up with the aromatization of ring-A with migration of C-10 angular methyl group to give 1-methyl-19-norcholesta-1,3,5(10)-trien-6-one.

Our understanding of principles involved in selective ring-A aromatization of steroids[1] has acquired enormous attention in recent years as a result of brilliant investigations carried out by Hora,[2] Hanson,[3] and Mazur.[4] They have enlightened the mechanistic aspect of aromatization reactions. Moreover, aromatic steroids have proved their usefulness as important starting material in the synthesis of 19-norsteroids.[5] In addition to above, 10-nor-analog steroidal hormones[5] began to receive immense attention when it was realized that the presence of the angular methyl group at C-10 was not essential to biological activity and in fact, that the removal of this group, in many cases, results in great enhancement of this reactivity. This paper is the subject of outcome of the generalizations in the light of above historical background.

Results and Discussion

The compounds **2** ($C_{27}H_{44}OClBr$) and **7** ($C_{27}H_{43}OClBr_2$) were obtained from 3β-chloro-5α-cholestan-6-one (**1**)[6] by usual α-bromination. The identity of these products were based upon spectral and chemical evidences. In IR spectra the carbonyl frequencies at 1712 cm^{-1} was indicative for the axial (α) oriented bromine at C5 in **2** and 1725 cm^{-1} for equatorially substituted at C7 in **7**.[7,8] The NMR spectra (60 MHz, $CDCl_3$) exhibited signals at δ 4.5 ($W/2$ 21 Hz) and δ 4.39 ($W/2$ 20 Hz) for (C3-αH; axial) implying trans ring junction[9] in **2** and **7**. Interestingly, C3-protons of **2** and **7** display paramagnetic shifts, compared to parent ketone (**1**) where it appears at δ 3.8, ascribable to the field effect of axial bromine at C5.[10] In the spectrum of **7** a doublet at δ 5.35 (C7-αH) very decisively supported that the bromine at C7 is equatorially introduced and the axial hydrogen is split by C8-axial hydrogen (β) with J value of 8 Hz.[10] Singlets due to C10β-methyl and C13β-methyl appeared at δ 1.0 and 2.69 in **2** and at δ 1.1 and 0.72 in **7** respectively.

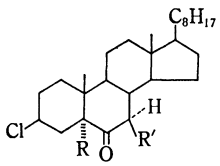

	R	R′
1	H	H
2	Br	H
7	Br	Br

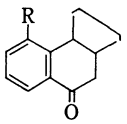

	R
3	H
8	CH_3

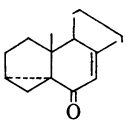

4

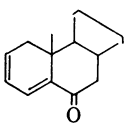

5

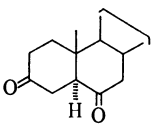

6

The halo ketone (**2**) on subjection to dehydrohalogenation provided **3** in about 38%, 3α,5-cyclo-5α-cholest-7-en-6-one (**4**), (9%) cholesta-2,4-dien-6-one (**5**)[11] (11%) and 5α-cholestane-3,6-dione (**6**)[12] (22%). The structures were established on spectral evidences and by comparison with authentic samples in known cases. The compound (**3**)[2] showed IR bands at 3060 (C=C–H), 1680 (C=O) and 1600 cm^{-1} (>C=C<).[10] The UV spectrum gave absorption maxima at 253 and 295 nm. Signals in the NMR spectrum were observed at δ 8.05 m (C4-H, J=8 Hz, o-coupled; J=2 Hz, m-coupled), 7.3m (C1-H, C2-H, C3-H). The multiplet at δ 8.05 strongly supported C4-H location β- to C6-oxo function. C13β-Methyl protons appeared as singlet at δ 0.76.

The mechanistic pathway through which **2** is converted into **3** is depicted in Scheme 1.

The product 4 in IR spectrum showed bands at 3080 (C=C–H), 1665 (C=C–C=O), 1605 cm^{-1} (>C=C<). The prominent bands at 1030 and 1010 cm^{-1} suggested the presence of cyclopropane moiety.[13] An α,β-unsaturated ketonic chromophore was also supported by absorption maximum at 253 nm (ε 8000). A signal in NMR spectrum (60 MHz) at δ 6.22s devoid of any vicinal proton, easily ascribable to a vinylic proton (C7-H). A multiplet at δ 2.55 was ascribable to protons at C9 and C14, allylic to C7-8 olefinic linkage. Signals due to C10β-methyl and C13β-methyl protons are at δ 1.22s and 0.76s. It is pertinent to mention that the

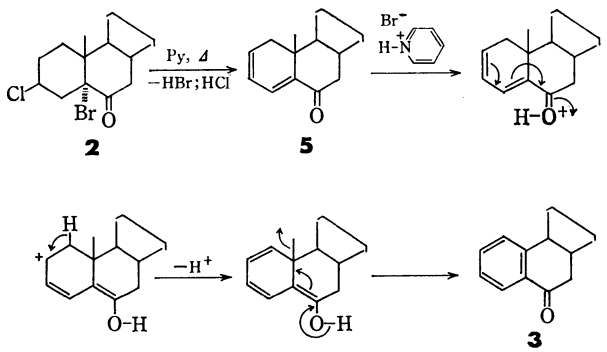

2 **5** **3**

Scheme 1.

nearby location of electron withdrawing C6-oxo function causes downfield shift of cyclopropane protons which merge with the methylene envelope.[14] The formation of **4** was, under the reaction conditions, rationalized on the basis of earlier report.[15]

On being refluxed with pyridine and after usual work up of the reaction mixture (**7**) provided exclusively **8** with 38% yield, a product of ring-A aromatization involving methyl migration from C10 to C1 owing to the presence of C6-oxo function.[3] The IR spectrum of **8** exhibited bands at 1685 (-C=O), 3010w (C=C-H) and 1600 cm^{-1} (>C=C<) and supported by UV absorption maxima at 255 and 300 nm. The NMR spectrum gave signals at δ 7.95d,d (C4-H; J=8 Hz; *o*-coupled, J=2 Hz; *m*-coupled; β to C6-oxo function), 7.35m (C2-H and C3-H). The C1-methyl and C13β-methyl protons appeared as singlet at δ 2.42 and 0.73 respectively.

Experimental

All melting points are uncorrected. IR spectra in Nujol were recorded with a Perkin-Elmer 237 spectrophotometer and UV spectra in 95% EtOH with a Beckmann DK2 spectrophotometer. NMR spectra were run in $CDCl_3$ with a Varian A60 instrument, chemical shifts (δ) being given in ppm relative to internal TMS and mass spectra were measured on an AEI MS-9 mass spectrometer. Light petroleum refers to fractions by 60—80 °C. TLC plates were coated with silica gel and sprayed with 20% perchloric acid solution.

3β-Chloro-5-bromo-5α-cholestan-6-one (2). The compound **1**[6] (4.0 g) in ether (50 ml) at 0 °C was treated with a solution of bromine in glacial acetic acid (40 ml, 5%); the addition of bromine solution was completed over a period of 1 h (catalysed with hydrobromic acid). Decolourization proceeded rapidly and crystalline material separated after the addition of approximately half of the bromine solution. The reaction mixture was further allowed to stand at 0 °C for 1/2 h to ensure complete crystallization. The solid was filtered under suction and recrystallized from light petroleum ether from which **2** (3.5 g) separated as white crystals, mp 124—125 °C, positive Beilstein halogen test (homogeneous by TLC, solvent petroleum ether–diethyl ether); Found: C, 65.54; H, 8.5%. Calcd for $C_{27}H_{44}OClBr$: C, 64.85; H, 8.8%; ν_{max} 765 (C-Cl), 740 cm^{-1} (C-Br).

3β-Chloro-5,7β-dibromo-5α-cholestan-6-one (7). To a solution of **1**[6] (4.0 g) in ether (20 ml) at room temperature was added bromine solution. The experimental technique was similar to that detailed under **2** except, the reaction mixture was allowed to stand at room temperature for three days. Recrystallization from petroleum ether afforded the halo ketone (**7**) (3.8 g), mp 174—175 °C, positive Beilstein halogen test (homogeneous TLC; solvent system petroleum ether–diethyl ether); Found: C, 55.85; H, 7.45%. Calcd for $C_{27}H_{43}OClBr_2$: C, 55.95; H, 7.59%; ν_{max} 768 (C-Cl), 736 and 655 cm^{-1} (C-Br).

Dehydrohalogenation of 2. The halo ketone **2** (10 g) in freshly distilled pyridine (70 ml) was heated under reflux for 10 h. Most of the solvent was removed by distillation under reduced pressure, the residue diluted with water and extracted with ether. The ethereal solution was washed successively with water, dilute hydrochloric acid, water, $NaHCO_3$ (5% aqueous solution) and water and dried over anhydrous sodium sulfate. Solid material (5.0 g) thus obtained was chromatographed over silica gel (100 g). Fractions of 10 ml were collected. Elutes from petroleum ether–benzene (20: 1) and (15: 1) gave cholesta-2,4-dien-6-one (**5**),[11] (1.1 g) mp and mixed mp 128—129 °C and 5α-cholestane-3,6-dione (**6**),[12] (2.2 g), mp and mixed mp 168 °C, respectively.

Further elution with petroleum ether–benzene (12: 1) gave 3α,5-cyclo-5α-cholest-7-en-6-one (**4**) which was crystallized from petroleum ether (0.9 g), mp 118—119 °C, negative Beilstein halogen test MS (10 eV) *m/e* 382 (80.3%) (M^+); Found: C, 84.6; H, 10.7%. Calcd for $C_{27}H_{42}O$: C, 84.8; H, 10.9%.

Elution with petroleum ether–ether (9: 1) gave 19-norcholesta-1,3,5(10)-trien-6-one (**3**) which was recrystallized from petroleum ether (3.76 g), mp 110 °C, negative Beilstein halogen test; MS (70 eV) *m/e* 366 (82.0%) (M^+); Found: C, 85.03; H, 10.5%. Calcd for $C_{27}H_{38}O$; C, 85.24; H, 10.38%.

Dehydrohalogenation of 7. The halo ketone **7** (5.0 g) in freshly distilled pyridine (35 ml) over KOH heated under reflux for 10 h. The reaction mixture worked up in the manner described under **2**. Removal of the solvent gave semi solid material (4.0 g) which was chromatographed over silica gel (80.0 g). Fractions of 10 ml were collected. Elutes from petroleum ether–benzene (6: 1) gave 1-methyl-19-norcholesta-1,3,5(10)-trien-6-one (**8**) which was recrystallized from petroleum ether (1.9 g), mp 140 °C, negative Beilstein halogen test; MS (70 eV) *m/e* 380 (100%) (M^+); Found: C, 85.06; H, 11.2%. Calcd for $C_{29}H_{40}O$: C, 85.26; H, 10.52%.

We thank Prof. W. Rahman, Head, Department of Chemistry for providing facilities and Prof. M. S. Ahmad for helpful discussion.

References

1) P. Morand and J. Lyall, *Chem. Rev.*, **68**, 85 (1968).
2) J. Hora, *Tetrahedron Lett.*, **1968**, 3605.
3) D. Baldwin and J. R. Hanson, *J. Chem. Soc. Perkin Trans. 1*, **1975**, 1107 and references cited therein.
4) J. Libman and Y. Mazur, *Chem. Commun.*, **1971**, 729.
5) C. Djerassi, M. Ehrenstein, and G. W. Barber, *Justus Liebigs Ann. Chem.*, **612**, 93 (1958).
6) A. Windaus and O. Dalmer, *Ber.*, **52**, 162 (1919).
7) L. J. Bellamy, "The Infrared Spectra of Complex Molecules," John Wiley and Sons (1958).
8) E. J. Corey, *J. Am. Chem. Soc.*, **76**, 175 (1954).
9) N. C. Bhacca and D. H. Williams, "Application of NMR Spectroscopy in Organic Chemistry," Holden-Day, San Francisco (1964).
10) M. S. Ahmad, N. Z. Khan, and Z. Farooq, *Indian J. Chem.*, **12**, 452 (1974).
11) H. Reich, F. E. Walker, and R. W. Collins, *J. Org. Chem.*, **16**, 1753 (1951).
12) I. M. Heilbrom, E. R. H. Jones, and F. S. Spring, *J. Chem. Soc.*, **1937**, 801.
13) A. R. H. Cole, *J. Chem. Soc.*, **1954**, 3807.
14) J. Tadanier and W. Cole, *J. Org. Chem.*, **27**, 4624 (1962).
15) I. M. Heilbron, J. Hodges, and F. S. Spring, *J. Chem. Soc.*, **1938**, 759.

 © 1980 The Chemical Society of Japan Bull. Chem. Soc. Jpn., 53, 525—532 (1980)

The Formation and Some Properties of Hydrous Manganese(IV) Oxide

Eiichi NARITA* and Taijiro OKABE

Department of Applied Chemistry, Faculty of Engineering, Tohoku University, Aramaki, Sendai 980

(Received January 22, 1979)

The properties of two kinds of hydrous manganese(IV) oxides (abbreviated as hydrous MnO_2) prepared by the reduction of $KMnO_4$ and by the disproportionation of K_2MnO_4 in alkaline solutions were investigated by means of chemical analysis, X-ray analysis, IR spectroscopy, wide-line NMR spectroscopy, thermal analysis, magnetic susceptibility measurement, *etc.* The chemical reactivity of the hydrous MnO_2 was also evaluated from the extent of oxidation to K_2MnO_4 by the reaction with an alkaline $KMnO_4$ solution at 80 °C. The properties and reactivity of the hydrous MnO_2 predominantly depended on the pH of the suspensions. At a pH 8 or higher, amorphous ternary compounds of manganese(IV) oxide with an approximate composition of $K_2O \cdot 4MnO_x \cdot 4H_2O$ ($x = 1.97$—2.00) were formed. The IR spectra and wide-line NMR spectra showed that the chemically bound water was in two different forms. The hydrous MnO_2 had the greater chemical reactivity, being easily soluble as manganate(VI) ions by the reaction described above. The contents of the chemically bound water and alkali in the hydrous MnO_2 decreased with a decrease in the pH of the suspensions and upon the acid-treatment of the precipitates. This variation in the chemical composition caused a decrease in the reactivity and a marked variation in the thermal behavior. The structure of the hydrous MnO_2 was discussed on the basis of findings regarding the magnetic susceptibility and its temperature dependence.

The synthetic manganese(IV) oxide prepared by the reduction of $KMnO_4$ in alkaline solutions is generally called "Hydrous MnO_2"[1] because of a large content of chemically bound water. It is also a giant molecule which is seldom stoichiometric. In the chemical industries, the hydrous MnO_2 is formed only in the production of saccharin as a by-product. Therefore, studies of its properties and chemical reactivity have been performed in comparison with those of various MnO_2 substances prepared by the pyrolysis of manganese(II) compounds or by the oxidation of manganese(II) ions in acid solutions. According to Regner *et al.*[2] and Sterr and Schmier,[3] the hydrous MnO_2 has the formula of $3MnO_2 \cdot MOH \cdot 2H_2O$ (M=K, Na) and the structure of δ-MnO_2, but there remains a lack of understanding the relationship between the various properties and the conditions of preparation. The present authors have now studied the reactivity of various kinds of hydrous MnO_2 in order to develop an alkaline $KMnO_4$ solution for use in air-pollution control, such as the removal of nitrogen oxides from waste gas,[4] and have found that the properties and reactivity are greatly influenced by the conditions of formation. The main purpose of this paper is to report on the factors influencing the chemical composition, the reactivity, and some properties of the hydrous MnO_2 prepared by the reduction of alkaline $KMnO_4$ solutions and by the disproportionation of alkaline K_2MnO_4 solutions.

Experimental

Materials. $KMnO_4$ and K_2MnO_4 were used as the starting materials. The $KMnO_4$ was a commercial extra pure reagent. The K_2MnO_4 was prepared by the decomposition of $KMnO_4$, boiling it in a 6 M (1 M=1 mol dm^{-3}) potassium hydroxide solution and then keeping it dry in a desiccator over phosphorus(V) oxide.

Preparation of Hydrous MnO_2. The hydrous MnO_2 substances were prepared by the following two reactions. (1) A four-necked flask was equipped with a reflux condenser, a dropping funnel, a glass electrode of a pH meter, and a thermometer. A definite quantity of an alkaline solution of 0.1—0.2 M $KMnO_4$ in the range from 300 to 500 cm^3 was introduced into the flask, and then heated to the desired temperatures (30, 56, 86 °C). A solution of the reducing agent, such as H_2O_2, K_2SO_3, and KNO_2, in the dropping funnel was then added, drop by drop (100 cm^3/h), to the $KMnO_4$ solution during violent agitation by means of a magnetic stirrer. Potassium hydroxide was used as an alkali component, while potassium hydrogencarbonate was suitably used as a pH controller. After the completion of the addition, the suspensions were stirred for a further 30 min. The products were then separated from the suspensions by filtration, washed with distilled water, and dried overnight at 110 °C. (2) A definite quantity of an alkaline solution of 0.6 M K_2MnO_4 in the range from 300 to 500 cm^3 was introduced into the flask, and then the mixture was heated to 50 °C. A 0.5—1.0 M H_2SO_4 solution in a dropping funnel was added, drop by drop (100 cm^3/h), to the K_2MnO_4 solution with violent agitation until the pH of the suspensions attained the desired value. The subsequent treatment of the precipitated hydrous MnO_2 was the same as has been described above (1).

Analysis of Chemical Composition of Hydrous MnO_2. The hydrous MnO_2 substances were dried overnight in an electric oven in air to eliminate the adsorbed water and subsequently analyzed for available oxygen, manganese, and potassium contents. The available oxygen was determined by the standard oxalic acid method.[5] Absorption spectroscopy was used for the determination of the manganese content. In this analysis, the manganese(II) ion obtained by the reduction of the sample with oxalic acid was oxidized to the permanganate ion by potassium periodate in the presence of a mixed acid (HNO_3: H_3PO_4: H_2O=1 : 1 : 1). The x-value in MnO_x was calculated from the resulting data. The potassium content was determined by atomic absorption spectroscopy. The balance was regarded as the chemically bound water.

Characterization of Hydrous MnO_2. The X-ray diffraction patterns were obtained using a Rigaku Denki Geigerflex D-2F with Mn filtered Fe $K\alpha$ radiation, with 25 kVP and 10 mA. The IR absorption spectra were obtained using a Shimadzu I-430 spectrometer with the KBr pellet technique. The wide-line NMR absorption spectra measurements were made at 40 MHz using a Nippon Denshi JNMW-40 spectrometer equipped with a 9000 variable-frequency oscillator. The samples were pressed to form tablets in order to increase

the proton number per unit volume. The surface area was measured by means of the BET nitrogen adsorption at 78 K, after outgassing at 373 K. The samples were prepared by the acetone drying of the hydrous MnO_2 suspensions after filtration in order to keep the original particle shape. The magnetic susceptibility was measured at temperatures from 77 to 298 K using a magnetic balance with a maximum magnetic field strength of 2 T. DTA and TG were performed using a Rigaku Denki Thermoflex over the range from room temperature to 1200 °C. The rate of temperature rise was 10 °C/min.

Evaluation of Chemical Reactivity of Hydrous MnO_2. The chemical reactivity of the hydrous MnO_2 with an alkaline $KMnO_4$ solution was measured as follows. The hydrous MnO_2** (5.00×10^{-3} mol Mn) was stirred in a 200 cm^3 Erlenmeyer flask with a 100 cm^3 portion of a 6.0 M potassium hydroxide solution. Subsequently, a 1.586 g portion of fine-ground $KMnO_4$ (1.000×10^{-2} mol) was added to the hydrous MnO_2 suspension, after which the reaction was continued under violent agitation for a period of 2 h at 80 °C† as

$$MnO_2 + 2KMnO_4 + 4KOH = 3K_2MnO_4 + 2H_2O. \quad (1)$$

After having been filtered, the amount of the residual hydrous MnO_2 was determined by the absorption spectroscopy previously described. The chemical reactivity was defined as the degree of the oxidation (abbreviated as D.O. hereafter), which is given by

$$\text{D.O. (\%)} = \frac{[MnO_2]_0 - [MnO_2]_t}{[MnO_2]_0} \times 100$$

$[\ ]_0$: Initial amount, $[\ ]_t$: amount after 2 h.

Results and Discussion

The chemical composition and reactivity of the hydrous MnO_2 prepared by the reduction of alkaline $KMnO_4$ solutions and by the disproportionation of

TABLE 1. REDUCTION CONDITIONS OF POTASSIUM PERMANGANATE SOLUTIONS, CHEMICAL COMPOSITION AND REACTIVITY, D.O., OF THE HYDROUS MnO_2 SUBSTANCES

No.	Conditions						Composition[a]				D.O.
	$KMnO_4$ M	KOH M	$KHCO_3$ M	pH	Temp °C	Reducing agent	MnO_2 wt%	x in MnO_x	K_2O wt%	H_2O wt%	%
1	0.1	0.2	—	13.3—12.5	86	0.6%-H_2O_2	66.3	1.93	17.2	16.5	54.8
2	0.1	0.2	1.0	9.2—9.3	86	0.6%-H_2O_2	66.3	1.93	17.0	16.7	57.1
3	0.1	0.2	—	13.3—12.8	30	3%-H_2O_2	67.7	1.97	18.1	14.2	81.9
4	0.1	0.2	—	13.3—12.8	86	3%-H_2O_2	67.4	1.90	16.1	16.5	66.0
5	0.1	0.2	—	13.3—12.6	50	0.1 M-K_2SO_3	68.2	1.98	18.4	13.4	79.6
6	0.1	—	0.1	8.5—9.6	50	0.1 M-K_2SO_3	67.1	1.99	17.6	15.3	69.3
7	0.1	0.2	—	13.1—11.7	86	0.1 M-K_2SO_3	67.4	1.98	17.1	15.5	56.6
8	0.2	0.1	—	12.8—12.1	50	0.3 M-KNO_2	67.9	2.00	16.4	15.7	80.8
9	0.2	—	0.5	8.1—9.1	50	0.3 M-KNO_2	70.0	1.99	16.8	13.2	74.6
10	0.2	0.1	0.5	9.3—9.5	50	0.3 M-KNO_2	68.3	1.98	16.9	14.8	93.9
11	0.2	0.1	0.5	9.3—9.6	30	0.3 M-KNO_2	67.2	1.98	15.1	17.7	91.1
12	0.2	0.1	0.5	9.3—9.5	86	0.3 M-KNO_2	73.1	1.98	14.9	15.1	61.9

a) The calculated chemical composition of the $K_2O\cdot4MnO_2\cdot4H_2O$ formula is as 18.3 K_2O, 67.7 MnO_2, and 14.0 H_2O (wt%).

TABLE 2. DISPROPORTIONATION CONDITIONS OF POTASSIUM MANGANATE(VI) SOLUTIONS, CHEMICAL COMPOSITION AND REACTIVITY, D.O., OF THE HYDROUS MnO_2 SUBSTANCES.

No.	Conditions					Composition[a]				D.O.
	K_2MnO_4 M	KOH M	pH	Temp °C	Acid	MnO_2 wt%	x in MnO_x	K_2O wt%	H_2O wt%	%
13	0.6	0.1	13.5—12.7	50	0.5 M-H_2SO_4	69.0	1.99	18.2	12.8	72.7
14	0.6	0.1	13.5—4.1	50	0.5 M-H_2SO_4	80.5	1.94	8.8	10.7	37.4
15	0.6	0.1	13.5—3.2	50	0.5 M-H_2SO_4	83.2	1.92	7.7	9.1	14.7
16	0.6	1.0	13.9—13.0	50	1 M-H_2SO_4	66.0	1.99	17.7	16.3	92.4
17	0.6	1.0	13.8—8.1	50	1 M-H_2SO_4	68.4	2.00	16.4	15.2	82.1
18	0.6	1.0	13.6—6.0	50	1 M-H_2SO_4	73.0	1.98	12.5	14.5	75.2
19	0.6	1.0	13.9—4.0	50	1 M-H_2SO_4	80.7	1.94	6.4	12.9	72.4
20	0.6	1.0	13.8—3.3	80	1 M-H_2SO_4	78.9	1.94	7.7	13.4	53.0
21	0.6	1.0	13.9—2.1	50	1 M-H_2SO_4	84.8	1.91	2.2	13.0	22.6
22	1 M H_2SO_4 treatment of Sample No. 16					93.4	1.88	1.1	5.5	15.1
23	10 M KOH treatment of Sample No. 14					81.7	1.94	8.5	9.8	36.9

a) The calculated chemical composition of the $K_2O\cdot4MnO_2\cdot4H_2O$ formula is as 18.3 K_2O, 67.7 MnO_2, and 14.0 H_2O (wt%).

** Because these was no difference in the reactivity between dried and undried samples, the later was used for this reaction.

† It has been found that the reaction is complete under these conditions.

alkaline K_2MnO_4 solutions are given in Tables 1 and 2 respectively.

Effects of pH. In the case of the reduction of a $KMnO_4$ solution, a low pH of the solution causes the reduction of $KMnO_4$ to the manganese(II) ion. The pH was, therefore, kept at about 8 or higher in the following reactions:

$$2KMnO_4 + H_2O_2 = 2MnO_2 + 2KOH + 2O_2 \quad (2)$$

$$2KMnO_4 + 3K_2SO_3 + H_2O = 2MnO_2 + 3K_2SO_4 + 2KOH \quad (3)$$

$$2KMnO_4 + 3KNO_2 + H_2O = 2MnO_2 + 3KMNO_3 + 2KOH \quad (4)$$

The hydrous MnO_2 obtained from the solution of pH$\gg$8 had an approximately constant composition, with the formula of $K_2O \cdot 4MnO_x \cdot 4H_2O$ (x=1.97—2.00), as is shown in Table 1. According to the X-ray diffraction patterns, they were all amorphous. The stoichiometry indicates that the hydrous MnO_2 substances shown in Table 1 are similar to the synthetic product studied by Sterr *et al.* and called δ-MnO_2, the formula of which is $KOH \cdot 3MnO_2 \cdot 2H_2O$, and to the active MnO_2 studied by Regner *et al.*, the K_2O content of which is 11.3—14.9 wt%. However, the hydrous MnO_2 obtained in this experiment had the chemically bound water and a little more K_2O than the synthetic MnO_2 in their earlier studies. These differences in the chemical composition appeared to be dependent on the conditions of the washing treatment of the hydrous MnO_2 after filtration. Especially, the K_2O are involved with the MnO_2 particles with quite small bond forces at the time of the formation of the hydrous MnO_2. Its content was, therefore, decreased by repeated washings with distilled water. The hydrous MnO_2 substances shown in Tables 1 and 2 have been washed with the minimum amount of distilled water possible to remove only physically adsorbed ions, that is, until the absorbed permanganate ion was not observed in the wash water. All of the hydrous MnO_2 substances obtained from the solutions of pH$\gg$8 at low temperatures (30, 50 °C) were chemically active in the reaction (Eq. 1), the D.O. values being high, as is shown in Table 1. The results show that the pH of the original suspensions is an important factor in getting the highly active hydrous MnO_2. In the process of removing NO_x from waste gas with an alkaline $KMnO_4$ solution,[4] the hydrous MnO_2 obtained as a by-product is regenerated to a soluble manganate(VI) by a reaction according to Eq. 1. It is easy to oxidize the manganate(VI) to permanganate by the electrolytic oxidation.

The disproportionation of K_2MnO_4 solutions was performed by the drop-by-drop addition of a H_2SO_4 solution until the pH of the suspensions attained the desired value. Although the pH successively varied during the drop-by-drop addition of the acid in the following reaction:

$$3K_2MnO_4 + 2H_2SO_4 = MnO_2 + 2KMnO_4 + 2K_2SO_4 + 2H_2O \quad (5)$$

the effect was kept negligible by keeping the hydrous MnO_2 in a mother liquor at the each last pH shown in Table 2. Figure 1 clearly indicates the chemical

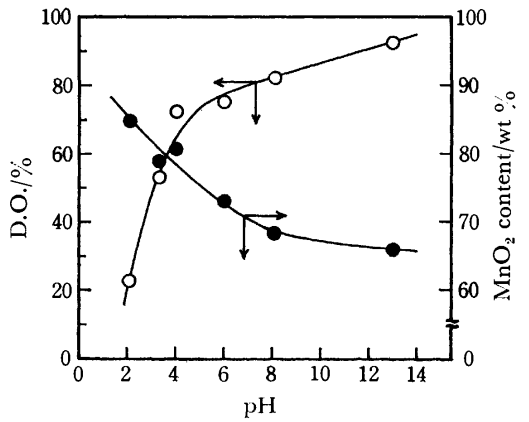

Fig. 1. The chemical reactivity, D.O. and MnO_2 content of the hydrous MnO_2 as a function of pH of suspensions obtained by disproportionation.

reactivity, D.O., and the MnO_2 content as functions of the pH of the suspensions obtained by the disproportionation. The chemical composition and reactivity of the hydrous MnO_2 were influenced by the pH, especially in the range from pH 6 down. As is shown in Table 2, the hydrous MnO_2 substances precipitated at high pHs had chemical compositions and reactivities similar to those prepared by the reduction of $KMnO_4$ solutions described above. The MnO_2 content increased with a decrease in the pH; the chemical reactivity and the x-value in MnO_x also decreased simultaneously. The same tendency was observed by the acid-treatment of the hydrous MnO_2. A typical hydrous MnO_2, Sample No. 16, was mixed with a 1 M H_2SO_4 solution for 2 h at 50 °C. The chemical composition, reactivity, and D.O. of the resulting acid-treated MnO_2, Sample No. 22, are shown in Table 2. The hydrous MnO_2 lost not only a considerable amount of the chemically bound water and alkali, but also its high chemical reactivity upon the acid treatment. The X-ray diffraction pattern suggests that Sample No. 22 was slightly crystallized as α-MnO_2. On the other hand, when a hydrous MnO_2 with a low reactivity, Sample No. 14, was mixed with a 10 M KOH solution for 3 h at 80 °C, there was no change in the chemical composition and reactivity, as is shown in Table 2. The surface state of the hydrous MnO_2 obtained from the high pH of the suspensions is thermodynamically unstable and active. However, it easily becomes stable upon the acid treatment, though it recovers its original surface state by the alkali treatments only with great difficulty.

In the reaction of the hydrous MnO_2 with an alkaline $KMnO_4$ solution for a period of 2 h at 80 °C, only the manganate(VI) was always obtained as a final soluble manganate species in spite of the differences in the chemical reactivities of the hydrous MnO_2. In addition to the dissolved manganese, the solution contained some unreacted hydrous MnO_2. The results show that the decomposition of the alkaline $KMnO_4$ solution simultaneously occurred as follows: an available oxygen of $KMnO_4$ is wastefully consumed by

$$4KMnO_4 + 4KOH = 4K_2MnO_4 + 2H_2O + O_2 \quad (6)$$

the decomposition, which is accelerated by the presence

of manganese(IV) oxides.[6,7] The hydrous MnO_2 substances with high D.O. values were, therefore, regarded as the active MnO_2 in reacting with permanganate ions. The reactivity of the hydrous MnO_2 substances with the alkaline $KMnO_4$ solution increased with increases in the chemically bound water and alkali contents. The results show that the chemically bound water and alkali play an important role in the oxidation of the hydrous MnO_2, (Eq. 1).

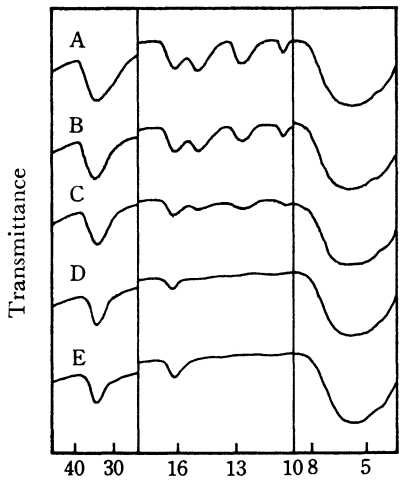

Fig. 2. IR spectra of the hydrous MnO_2 prepared at various pH of suspensions.
A: Sample No. 1—13, 16, 17 (pH>8.1), B: Sample No. 18 (pH 6.0), C: Sample No. 20 (pH 3.3), D: Sample No. 21 (pH 2.1), E: Sample No. 22 (pH<1).

IR and NMR Absorption Spectra. The IR spectra for the hydrous MnO_2 prepared at various pH values of the suspensions are given in Fig. 2. Sample No. 16, prepared at a high pH, has the typical composition of the hydrous MnO_2, and its spectrum displays five distinct bands at the frequencies of 440—620, 1050, 1280, 1510, 1630, and 3400 cm^{-1}. The bands at 1630 and 3400 cm^{-1} are the OH stretching band and the OH bending vibration band respectively. The broad band at 440—620 cm^{-1} is based on the Mn–O bond. The spectrum of the typical hydrous MnO_2 is characterized by additional three bands at 1050, 1280, and 1510 cm^{-1}. It seems likely that these three bands are based on the OH bending vibration combined with the Mn atom. However, it is possible that the bands are based on the bending vibration of the hydroxyl group containing alkali because of the correlation between the intensity of the absorbance and the K_2O content. No clear reversion could be made. Despite many studies[8] of the IR spectra of the natural MnO_2 ores and the synthetic MnO_2 obtained from the acid solutions by the use of various methods, these three bands shown in Fig. 2 have not yet been reported. The intensity of the absorbance of these three bands gradually becomes weaker with a decrease in the pH, until those for such hydrous MnO_2 substances as Sample No. 21, prepared at the lowest pH in this experiment, are ultimately not observed. A similar tendency was observed in the case of the acid-treated hydrous MnO_2, Sample No. 22. According to the chemical analysis, these hydrous MnO_2 substances still have a considerable amount of the chemically bound water, most of it in the form of the H_2O molecule. The evaluation of the chemical reactivity was possible by the measurement of the IR spectra because of the close correlation between the intensity of absorbance of the three bands and the chemical reactivity of the hydrous MnO_2.

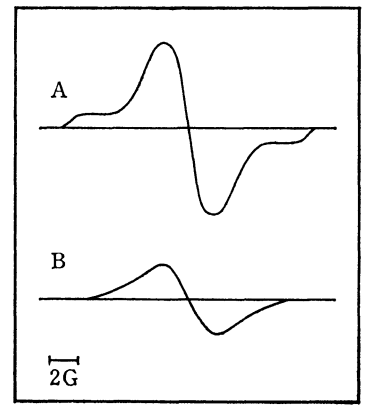

Fig. 3. Typical NMR spectra of the hydrous MnO_2.
A: Sample No. 3, B: Sample No. 22 (Acid-treated MnO_2).

A typical NMR spectrum of the hydrous MnO_2, Sample No. 3, is shown in Fig. 3(A). This spectrum consists of a narrow absorption line, ΔH 3.8 G, superimposed on a broad one, ΔH 15.5 G. The broad line and the narrow one appear to be dependent on the hydroxyl group combined with the MnO_2 polymeric structure and on the H_2O molecule with a comparatively weak interaction to the lattice atom respectively. Glemser[9] distinguished between adsorbed water and chemically bound water by NMR spectroscopy for δ-MnO_2 and γ-MnO_2. These MnO_2 substances showed a broad line, with a superimposed narrow line with a width of 2.1—2.2 G which is due to the physically adsorbed water. The proton causing the narrow line in Fig. 3(A) is not so free in the hydrous MnO_2 structure. Therefore, it appears to belong to the H_2O molecule combined with the lattice. The hydrous MnO_2 obtained from the alkaline solution is a kind of hydro-gel, for it is amorphous and contains a large amount of water and alkali. The water in such gels never has a definite form in the bond state such as the physically adsorbed water and the water of crystallization have. In the case of the hydrous MnO_2, the water may be contained in a porous structure of the MnO_2 polymer in various bond states, and the polymer chain is cleaved to form the hydroxyl group as follows:

$$\begin{array}{c} | \quad | \\ -Mn-O-Mn- \\ | \quad | \end{array} \xrightarrow{H_2O} \begin{array}{c} | \\ -Mn-OH \\ | \end{array} + \begin{array}{c} | \\ HO-Mn- \\ | \end{array}$$

The influence of the chemical composition on the reactivity of the hydrous MnO_2 indicates that the H_2O molecule in the hydrous MnO_2, which forms most of the chemically bound water, is not merely the physically adsorbed water. The NMR spectrum of the acid-

treated hydrous MnO_2 containing 5.5 wt% of chemically bound water, Sample No. 22, is shown in Fig. 3(B). While a broad absorption line vanished, a narrow one still remained with a weak intensity. These spectra indicate the same results as those of the IR spectra shown in Fig. 2.

Effects of Temperature. The chemical composition of the hydrous MnO_2 varied depending upon the temperature of the suspensions shown in Table 1, but this variation was not so remarkable as the effect of the pH. The contents of the chemically bound water and alkali in the hydrous MnO_2 slightly decreased with an increase in the temperature of the suspensions, and the chemical reactivity decreased because of the reduction of the active sites in the reaction (Eq. 1). The x-value in MnO_x of the hydrous MnO_2 prepared by reduction at a high temperature decreased to 1.90—1.93 when the H_2O_2 solution was used as a reducing agent. However, this tendency was not observed in the case of the hydrous MnO_2 prepared by the use of other kinds of reducing agents. The difference in the amount of available oxygen of the hydrous MnO_2 appeared to originate from the reducing force of the reducing agent used. The redox of the manganese ion and the replacement of O^{2-} by any other ions occur without any changes in the crystal lattice in manganese(IV) oxides, well known as typical homogeneous, solid redox systems.[10]

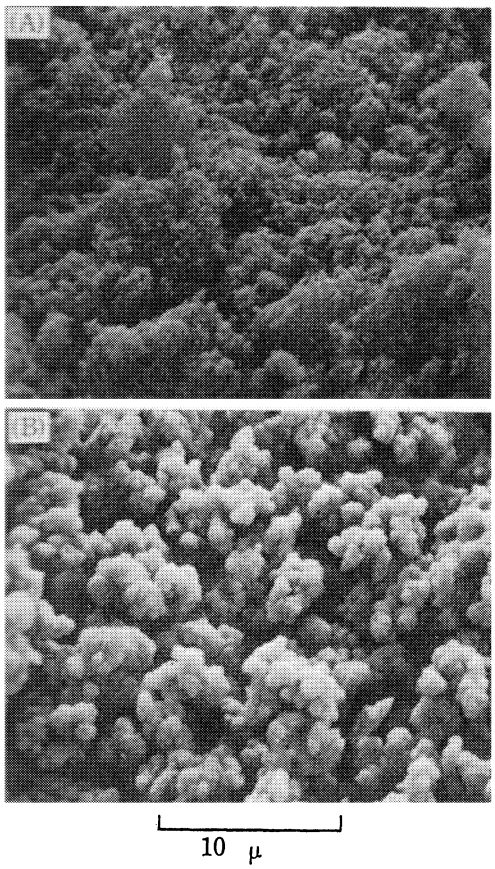

Fig. 4. Scanning electron micrographs of the hydrous MnO_2 prepared by reduction.
(A): Reduction by H_2O_2 (Sample No. 3), (B): Reduction by KNO_2 (Sample No. 8).

A H_2O_2 solution, therefore, reacts with the precipitated hydrous MnO_2 to produce the scarece oxygen hydrous MnO_2 at high temperatures because of the strong reducing force.

Effects of Reducing Agents. The particle shape of the hydrous MnO_2 varied with the kind of reducing agent in spite of the constant chemical composition and reactivity. Some typical SEM photographs of the hydrous MnO_2 are shown in Fig. 4. While the hydrous MnO_2 prepared by reduction with the H_2O_2 solution (**A**) was irregularly piled with fine amorphous particles, the one prepared with the KNO_2 solution (**B**) coagulated to quite a large spherical shape. The hydrous MnO_2 prepared with the K_2SO_3 solution also coagulated to a spherical shape, but the size of the second-order particle was smaller than that prepared with the KNO_2 solutions. A spherical-shape hydrous MnO_2 such as Sample No. 8 has been also produced as a by-product of the absorption of NO_x gas with a high alkaline solution of $KMnO_4$. The surface area of a representative hydrous MnO_2 is tabulated in Table 3. As would be from the particle shape shown in Fig. 4, the surface area varied with the conditions of preparation. The hydrous MnO_2 substances prepared both by the reduction of $KMnO_4$ with the H_2O_2 solution and by the disproportionation of the K_2MnO_4 solution have large surface areas. Figure 5 indicates the chemical reactivity, the D.O., and the MnO_2 content as functions of the surface area of the hydrous MnO_2 in Table 3. Although Samples Nos. 3, 5,

Table 3. Surface area of the hydrous MnO_2 measured by the BET method

No.	Surface area m^2/g
3[a)]	136.6
5[a)]	16.1
8[a)]	9.1
16[b)]	92.6
21[b)]	147.5

a) Prepared by reduction. b) Prepared by disproportionation.

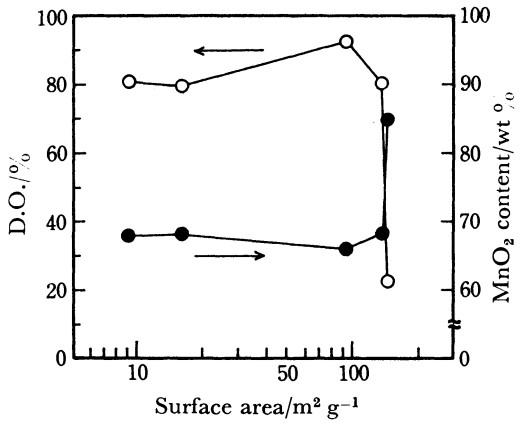

Fig. 5. The chemical reactivity, D.O. and MnO_2 content of the hydrous MnO_2 as a function of the surface area measured by the BET method.

TABLE 4. PHASE VARIATIONS OF THE HYDROUS MnO_2 WITH HEATING

K/Mn molar ratio	Temperature rising		
0.5	amor.[a] → amor. / $K_2Mn_4O_8$[b]	→ $K_2Mn_4O_8$	
0.125	amor. → KMn_8O_{16}[c]	→ $K_2Mn_4O_8$ / Mn_2O_3[d]	→ $K_2Mn_4O_8$ / Mn_3O_4[e]
0.05	amor. → Mn_2O_3 / amor.	→ Mn_2O_3 / $K_2Mn_4O_8$	→ Mn_3O_4 / K_2Mn_4O

a) Amorphous. b) Potassium permanganite. c) Cryptomelane. d) Bixbyte. e) Hausmannite.

and 8 were prepared under the same conditions except for the kind of reducing agent, there was no correlation between the chemical reactivity and the surface area. Sample No. 16, obtained from the suspension with a pH of 13.0, had the same chemical composition and reactivity as Samples Nos. 3, 5, and 8. On the other hand, the chemical reactivity of Sample No. 21, obtained from a suspension with a pH of 2.1, decreased very much in spite of its large surface area. The results show that the diffusion of the permanganate ion into the particles of the hydrous MnO_2 is fast, without any correlation to the apparent surface area, and that the chemical reactivity is only influenced by the chemical composition, that is, the number of active sites as has previously been described. The hydrous MnO_2 prepared by the disproportionation of K_3MnO_4, which if formed by the oxidation of pyrolusite with KOH–KNO_3 molten salts,[11] was similar to those obtained in this experiment.

Thermal Behavior. TG and DTA curves of the hydrous MnO_2 substances obtained from suspensions with various pHs were classified into the three types shown in Fig. 6. The DTA curves varied according to the pH of the suspensions. As has been described previously, the chemical composition, especially the K_2O content of the hydrous MnO_2, also varied according to the pH of the suspensions. Therefore, the K_2O content appeared to cause the varying thermal behavior of the hydrous MnO_2. The results of the X-ray analysis and chemical analysis of the heated samples obtained at different temperatures are shown in Table 4. Sample No. 16, the K/Mn molar ratio of the chemical composition of which was about 0.5, gradually crystallized to form potassium permanganite,[12] $K_2Mn_4O_8$, during the heating process and was completely transformed to $K_2Mn_4O_8$ above 900 °C. The continuous weight loss in the heating process to about 900 °C indicated on the TG curve, which was due to the release of a large amount of the chemically bound water, corresponded with the broad endothermic peak of the DTA curve. The chemically bound water still remained in the hydrous MnO_2 at a considerable high temperature, and the IR spectrum of the sample heated at about 700 °C had the absorption bands based on the chemically bound water. On the other hand, Sample No. 19, with a K/Mn molar ratio of 0.15, rapidly crystallized to form cryptomelane,[13] KMn_8O_{16}, with a sharp exothermic peak at 450 °C. This exothermic peak was generally shown on the DTA curves of the hydrous MnO_2 with a K/Mn molar ratio of about 0.1—0.3. The nearer the K/Mn molar ratio came to the theoretical value, 0.125, the larger and sharper the exothermic peak became. On further heating, this material was decomposed into $K_2Mn_4O_8$ and bixbyte,[14] Mn_2O_3, which was then further decomposed into hausmannite,[15] Mn_3O_4, with an increase in the temperature. In the case of Sample No. 21, the K/Mn molar ratio of which was still small, the exothermic peak due to the formation of KMn_8O_{16} was not seen on the DTA curve. The thermal behavior of the hydrous MnO_2 prepared by the reduction of the $KMnO_4$ solution was quite similar to that of such a hydrous MnO_2 as Sample No. 16. Table 4 shows that the DTA curves of the hydrous MnO_2 substances continuously varied according to the change in the K_2O content. The other kinds of manganese(IV) oxide with no K_2O content, such as synthetic β-MnO_2 and γ-MnO_2, indicated similar thermal behavior, as is shown in Fig. 6, upon the addition of potassium hydroxide to the samples. Therefore, the presence and amount of potassium must be checked in advance in the study of the thermal behavior of manganese(IV) oxides.

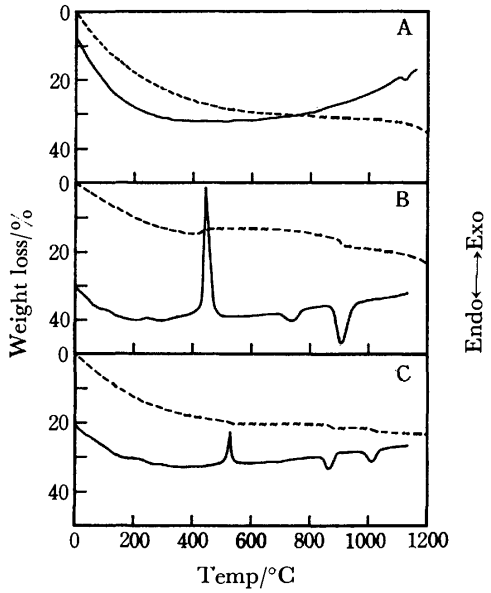

Fig. 6. TG and DTA curves of the hydrous MnO_2 prepared by disproportionation at various pH of suspensions.
A: Sample No. 16 (pH 13.0), B: Sample No. 19 (pH 4.0), C: Sample No. 21 (pH 2.1), amount of sample (mg)——A: 22.3, B: 21.9, C: 17.5, ——: TG, ——: DTA.

Table 5. Magnetic susceptibilities of the hydrous MnO_2 substances and the other kinds of MnO_2

No.	$\chi/10^{-6}$, (Temp/°C)
3[a]	65.1(26.5), 74.7(−25.0), 87.5(−75.3), 105.0(−112.7), 130.8(−159.7), 167.1(−195.8)
5[a]	62.2(26.5)
8[a]	66.2(26.5)
16[b]	46.9(23.0), 68.8(−64.8), 89.3(−126.0), 108.5(−155.2), 137.5(−195.8)
19[b]	53.1(23.5)
21[b]	55.4(18.8), 57.1(−7.8), 64.6(−62.0), 77.5(−107.0), 90.7(−144.6), 118.6(−195.8)
26 (α-MnO_2)	36.6(23.5)
27 (β-MnO_2)	27.2(21.9), 27.3(−17.2), 29.6(−75.0), 30.9 (−114.4), 33.4(−150.5), 34.3(−195.8)
28 (γ-MnO_2)	33.5(22.8)
29 (δ-MnO_2)	52.9(23.4)

a) Prepared by reduction. b) Prepared by disproportionation.

Two different DTA curves have been reported for the hydrous MnO_2 substances by Sterr *et al.* and by Regner *et al.* According to Sterr *et al.*, the DTA curve of the hydrous MnO_2 has an exothermic peak at 520 °C, but the DTA reported by Regner *et al.* has no exothermic peak. In view of our results, these different phenomena of the DTA curves appear to be dependent on the K_2O content of the hydrous MnO_2.

Magnetic Susceptibility. The structures and states of manganese(IV) oxides can be investigated by the measurement of their magnetic susceptibilities because of the paramagnetic property due to the unpaired electrons in the 3 d orbit. The magnetic susceptibilities of some typical hydrous MnO_2 substances are shown in Table 5 in contrast with those of the well-known α-, β-, γ-, and δ-MnO_2. The values in Table 5 are the magnetic susceptibilities per gram of MnO_2. The magnetic susceptibilities of the hydrous MnO_2 substances were all high, especially the values of those prepared by the reduction of the $KMnO_4$ solution by the H_2O_2 solution. Selwood *et al.*[16] have measured the magnetic susceptibilities of various kinds of manganese(IV) oxides, all confined within the range of $25—45\times10^{-6}$ (25 °C). The high magnetic susceptibility of the hydrous MnO_2 substances can be attributed to the free spin of the unpaired electrons of the paramagnetic ion (Mn^{4+}). In other words, the distribution of ions is disordered, and the mutual interference of ions is extremely weak in the MnO_2 lattice. According to the magnetic classification of oxides by Selwood *et al.*, the hydrous MnO_2 substances could all be classified as typical "Disperse Oxides." The magnitude of the magnetic susceptibilities of the other MnO_2 substances was of the order of: δ->α-$\geqslant\gamma$->β-MnO_2. There is a good agreement between our results and those of earlier workers. β-MnO_2 is the most stable crystal phase of all the MnO_2, and it has the highest degree of crystallization, according to the results of X-ray analysis. Therefore, β-MnO_2 had the lowest magnetic susceptibility, and its temperature dependence was not observed because of the interruption due to the free distribution of the spin of the unpaired electron. β-MnO_2 can be magnetically classified as a typical "Massive Oxide." The relationship between the magnetic susceptibilities of the hydrous MnO_2 substances and the pH's of the suspensions obtained by the disproportionation of K_2MnO_4 solution is shown in Fig. 7. The magnetic susceptibility increased

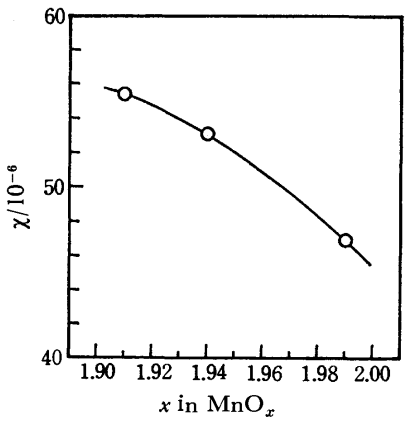

Fig. 7. Magnetic susceptibilities of the hydrous MnO_2 prepared by disproportionation as a function of x in MnO_x.

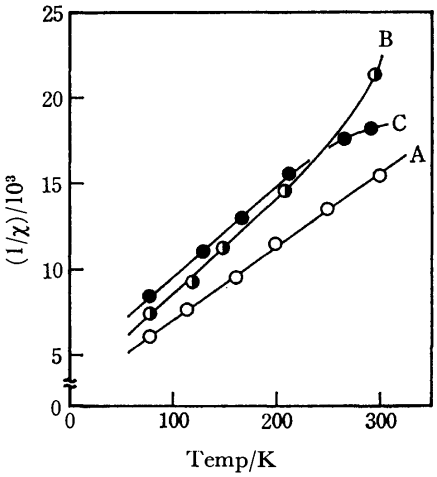

Fig. 8. Inverse magnetic susceptibilities of the hydrous MnO_2 prepared at various pH of suspensions as a function of temperature.
A: Sample No. 3 (pH 12.8), B: Sample No. 16 (pH 13.0), C: Sample No. 21 (pH 2.1).

with a decrease in the pH, which was itself due to the increase in the number of unpaired electrons in the hydrous MnO_2, namely, the decrease in the x-value of MnO_x. The temperature dependence of the magnetic susceptibility in the range from 77.4 K to room temperature is shown in Fig. 8. It was possible to calculate the

magnetic moment because any hydrous MnO_2, Sample No. 3, appeared to follow the Curie-Weiss law. The moment for the manganese in this hydrous MnO_2 was 4.00 Bohr magneton compared with a theoretical moment of 3.87 Bohr magneton, while the Weiss constant was 63°. Two other hydrous MnO_2 substances, Samples Nos. 16 and 21, also appeared to follow the Curie-Weiss law in the temperature range from 77.4 to 220 K. The magnetic susceptibility of Sample No. 21 was higher than that of Sample No. 16 because of the increase in the number of unpaired electrons, but its temperature dependence was conversely small. The moments for the manganese of Samples Nos. 16 and 21 were 3.6 and 3.7 Bohr magneton, and the Weiss constants were 54 and 89°, respectively. This tendency can be explained by the mechanism by which the distribution of the manganese ion in the MnO_2 lattice becomes more regular during the removal of the chemically bound water and alkali by means of the decrease in the pH's of the suspensions.

The authors would like to thank Mr. Takeshi Sakano of the Mitsubishi Metal Corp. for his discussion and encouragement, Dr. Masayoshi Ito of the Science University of Tokyo for his measurement of the wide-line NMR spectra, Professor Minoru Takahashi of the Department of Applied Physics, Tohoku University, for his guidance and support in the measurement of the magnetic susceptibility, and Mr. Keizo Hara for his experimental assistance.

References

1) Kirk-Othmer, "Encyclopedia of Chemical Technology," 2nd ed, Vol. 13, John Wiley and Sons, New York (1964), p. 9.
2) A. Regner, V. Ettel, and J. Vepřek-Šiška, *Collect. Czech. Chem. Commun.*, **28**, 2854 (1963).
3) G. Sterr and A. Schmier, *Z. Anorg. Allg. Chem.*, **368**, 225 (1969).
4) A. Obuchi, A. Okuwaki, and T. Okabe, *Nippon Kagaku Kaishi*, **1974**, 1425; A. Obuchi, T. Hanei, A. Okuwaki, and T. Okabe, *ibid.*, **1974**, 1461; T. Okabe, A. Okuwaki, and S. Nakabayashi, U. S. Patents 3929966 (1975); 4001372 (1977), *etc.*
5) JIS M 8233 (1969).
6) F. R. Duke, *J. Phys. Chem.*, **56**, 882 (1952).
7) J. Vepřek-Šiška and V. Ettel, *J. Inorg. Nucl. Chem.*, **31**, 789 (1969).
8) For example, O. Glemser, G. Gattow, and H. Meisiek, *Z. Anorg. Allg. Chem.*, **309**, 1 (1961); G. A. Kolta, F. M. Abdel Kerim, and A. A. Abdel Azim, *ibid.*, **384**, 260 (1971); W. B. White and R. Roy, *Am. Mineral.*, **49**, 1670 (1964), *etc.*
9) O. Glemser, *Nature*, **183**, 943 (1959).
10) A. Kozawa and R. A. Powers, *J. Electrochem. Soc.*, **113**, 870 (1966); *J. Chem. Educ.*, **49**, 587 (1972).
11) E. Narita, M. Mita, and T. Okabe, *Nippon Kagaku Kaishi*, **1975**, 281.
12) X-Ray powder data file (ASTM card 16-205).
13) X-Ray powder data file (ASTM card 12-706).
14) X-Ray powder data file (ASTM card 8-10).
15) X-Ray powder data file (ASTM card 16-154).
16) P. W. Selwood, R. P. Eischens, M. Ellis, and K. Wethington, *J. Am. Chem. Soc.*, **71**, 3039 (1949); P. W. Selwood, M. Ellis, and C. F. Davis, Jr., *ibid.*, **72**, 3549 (1950).

INDO Molecular Orbital Interpretation of Thermal Singlet Oxygen-complex Generation by Strained Acetylenes

Katsutoshi OHKUBO* and Hiroyuki SATO

Department of Synthetic Chemistry, Faculty of Engineering, Kumamoto University, Kumamoto 860

(Received February 16, 1979)

Synopsis. A three-center interaction between the $(\pi_u)_y$ of strained XC≡CX (X=H,F, or OCH_3) and the $(\pi_g)_y$ of $^3O_2$ separated the two half-occupied π_g MOs of $^3O_2$ on an energy scale of 428—494 kJ/mol causing spin inversion in $^3O_2$. A perepoxide-type $^1O_2$–XC≡CX intermediate once formed is transformed into a stable dioxetene-type $^1O_2$ complex from which the free generation of $^1O_2$ was found to be difficult.

The generation of $^1O_2$ has hitherto been realized by the reaction of sodium hypochlorite and hydrogen peroxide,[1-3] the decomposition of peroxides[4-8] and ozonides,[9-12] and the photosensitization[1,13,14] or microwave discharge[15,16] of $^3O_2$. The possibility of thermal $^1O_2$ formation from $^3O_2$ with 3,3,6,6-tetramethyl-1-thia-4-cycloheptyne **1** has recently been reported:[17]

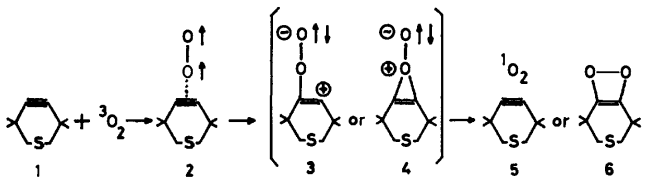

The above reaction mechanism, however, remains obscure. Consequently an INDO-MO[18] study of the above reaction process has been conducted using a simple model of the strained acetylene **1**, XC≡CX (X=H, F, or CH_3O), in order to shorten the computation time.

Results and Discussion

The strained acetylene molecule **1** is characterized by split π MOs, and the spectrophotometrically estimated energy difference between the π MOs is 30.5 kJ/mol at the strained angle (146°) of the acetylene **1** molecule.[17,19] In the case of XC≡CX, the energy difference between the π MOs has been estimated to be 170 kJ/mol (X=H), 89.5 kJ/mol (X=F), and 612 kJ/mol (X=CH_3O) at ∠XCC=146° using standard geometric parameters.[18] The destabilization of the $(\pi_u)_y$ MO expanding on the XC≡CX molecular plane ($(\pi_u)_y$ MO is energetically kept practically constant) is monotonically promoted by widening the strained angle thereby permitting overlap between the s or p AO of X and the p_y AO of C (overlap intergral=0.27 at 146° in HC≡CH). Therefore, the deviation of the C–X bond from the linear arrangement in XC≡CX makes the ionization energy of the highest doubly-occupied $(\pi_u)_y$ MO smaller and facilitates electron transfer from the strained acetylene molecule to $^3O_2$.

In view of the most reactive MOs of the strained acetylene and $^3O_2$, *i.e.*, the $(\pi_u)_y$ MO of the former and the π_g MOs of the latter, two distinctive interacting systems (three-center and four-center) may be considered as the mode of interaction between them (Fig. 1). The formation of a dioxetene-type intermediate from the strained acetylene and $^3O_2$ *via* the four-center interacting systems is however thermally forbidden since orbital symmetry in the σ-type orbital correlation such as $(\pi_g)_y-(\pi_g)_y$ or $(\pi_u)_y-(\pi_u)_y$ in the F-type interacting system should be inversely rearranged in the reaction process.[20] Therefore, the present thermal generation of $^1O_2$ from $^3O_2$ with the strained acetylene molecule must first pass through the three-center interacting system in which electron transfer from the $(\pi_u)_y$ MO in the acetylene to the $(\pi_g)_y$ (or $(\pi_g)_z$ in the B or C system) of $^3O_2$ would be expected together with back electron donation from the $(\pi_g)_x$ (and/or $(\pi_u)_x$) of the latter to the $(\pi_g)_y$ (or $(\pi_g)_z$ in the E system) of the former.

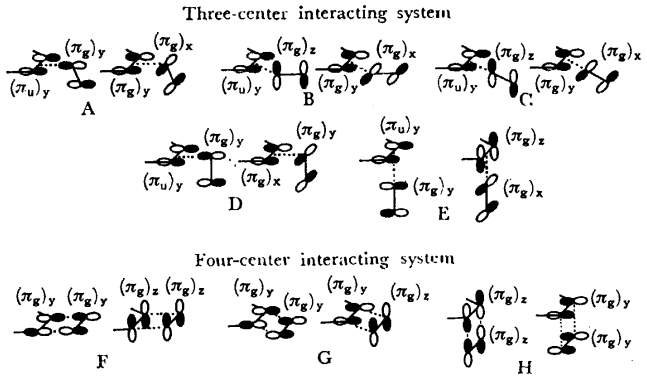

Fig. 1. Three-center and four-center interacting systems of the strained acetylene and $^3O_2$.

The three-center interacting systems of HC≡CH–$^3O_2$ were calculated utilising the geometric parameters in Table 1 and the relative stabilities of the interacting systems are given in the order: A>B>C>D>E. The one-electron attraction term (E_I) was large and negative in the order of D>A>E>B>C. The interelectronic and internuclear repulsions (E_{II} and E_N respectively) were larger and in the same order. The balance between the nuclear-electron attraction and the above repulsions results in the A-type interacting system being the most plausible mode of interaction.

The approach of the $^3O_2$ molecule to the strained acetylene in the A-type interacting system is an energy stabilization process and results in a quasi-stable perepoxide-type intermediate **2'**. For example, the potential curve for the HC≡CH–$^3O_2$ interacting system shown in Fig. 2, was obtained by optimizing the geometric parameters (see Table 1) by minimizing the total energies of the interacting systems with a repeated SCF-procedure.[21] As Fig. 2 illustrates, the change of electronic configuration from the triplet-state to the singlet-state interacting system could be expected

Table 1. Relative stabilities of the three-center interacting systems

	r_{CO}/Å[a]	r_{OO}/Å	θ/deg.	ϕ/deg.	E_I/a.u.	E_{II}/a.u.	E_N/a.u.	E_{total}/a.u.
A	2.00	1.15	0	120	−188.7708	84.2764	54.5565	−49.9379
B	2.00	1.15	30[a]	210[a]	−186.9356	83.3466	53.6561	−49.9329
C	2.00	1.14	30[a]	180[a]	−186.6873	83.1985	53.5591	−49.9297
D	2.00	1.15	0	90[a]	−192.5395	86.1563	56.4551	−49.9281
E	2.00	1.14	90	180[a]	−187.7066	83.7018	54.0780	−49.9268

a) Fixed values in the calculations.

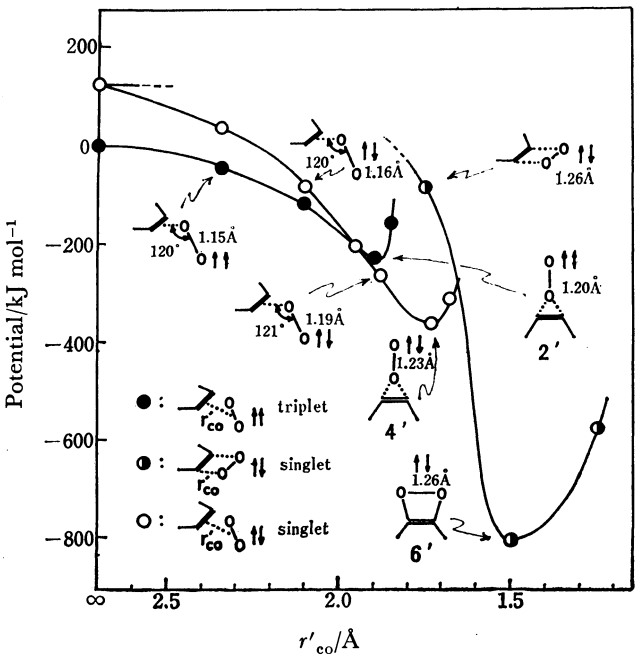

Fig. 2. Potential curves for the interacting system of the strained HC≡CH (∠HCC=146°) and $^3O_2$ or $^1O_2$. (The four-center interacting system of HC≡CH–$^1O_2$ at $r'_{CO}=\infty-1.8$ Å was not treated for shortening computation time.)

before the formation of the above-mentioned triplet-state intermediate **2'**. As the distance (r'_{CO}) between the two centers of C–C in HC≡CH and O–O in O_2 becomes smaller, the highest half-occupied MO formed by $(\pi_u)_y$ (HC≡CH)–$(\pi_g)_y(^3O_2)$ is destabilized with respect to the half-occupied MO of $(\pi_g)_y$(HC≡CH)–$(\pi_g)_x(^3O_2)$. The energy separation between the above two MOs are 194, 303, and 428 kJ/mol at r'_{CO}=2.3, 2.1, and 1.9 Å respectively. Such a remarkable energy separation between the two half-occupied MOs may result in an electronic rearrangement (*viz.*, electron migration from the $(\pi_g)_y$ MO to the $(\pi_g)_x$ MO in $^3O_2$ via spin inversion) by changing the triplet-state interacting system into the energetically more stable singlet-state system at the intersystem crossing point (r'_{CO}= 1.94 Å). In the A-type interacting system of $CH_3OC{\equiv}COCH_3$ (or FC≡C)–$^3O_2$ (∠OCC=∠FCC=146°), the electron-donative (or attractive) nature of CH_3O (or F) resulted in the intersystem crossing at a slightly longer range of r'_{CO}=1.96 Å (or at a slightly shorter range of r'_{CO}=1.91 Å) with an energy separation between the above-mentioned half-occupied MOs of 485 kJ/mol (or 494 kJ/mol). The strained acetylene-$^1O_2$ system once formed *via* spin inversion, then, moves to a quasi-stable perepoxide-type intermediate **4'** (see Fig. 2). The singlet oxygen complex of the intermediate **4'**, then, transforms into a stable dioxetene **6'** (456 kJ/mol lower in potential energy than **4'**) with an activation energy of 58 kJ/mol. The generation of free $^1O_2$ from the dioxetene-type intermediate **6'** however appears difficult because the isolation of free $^1O_2$ from **6'** requires 920 kJ/mol (Fig. 2). Therefore, the reaction between $^3O_2$ and strained acetylenes such as **1** generates a dioxetene-type $^1O_2$ complex which thermally transforms into a dione with chemiluminescence (fluorescence).[17]

References

1) C. S. Foots, *Acc. Chem. Res.*, **1**, 104 (1968).
2) C. S. Foots and S. Wexler, *J. Am. Chem. Soc.*, **86**, 3879 (1964).
3) E. Mckeon and W. A. Waters, *J. Chem. Soc., B*, 1966, 1040.
4) H. H. Wasserman and J. R. Scheffer, *J. Am. Chem. Soc.*, **90**, 3073 (1968).
5) H. H. Wasserman, J. R. Scheffer, and J. L. Cooper, *J. Am. Chem. Soc.*, **94**, 4991 (1972).
6) S. R. Abbott, S. Ness, and O. M. Hercules, *J. Am. Chem. Soc.*, **91**, 1128 (1970).
7) A. M. Trozzolo and S. R. Fahrenholtz, *Ann. N. Y. Acad. Sci.*, **171**, 61 (1970).
8) H. H. Wasserman and D. L. Larsen, *J. Chem. Soc., Chem. Commum.*, **1972**, 253.
9) R. M. Hurray and H. L. Kaplan, *J. Am. Chem. Soc.*, **90**, 537, 4161 (1968); **91**, 5358 (1969).
10) L. M. Stephenson and D. E. McClure, *J. Am. Chem. Soc.* **95**, 3074 (1973).
11) R. M. Murray, W. C. Luman, Jr., and J. W. -P. Lin, *J. Am. Chem. Soc.*, **92**, 3205 (1970).
12) A. P. Schaap, A. L. Thayer, G. R. Faler, K. Goda, and T. Kimura, *J. Am. Chem. Soc.*, **96**, 4025 (1974).
13) D. R. Kearns, A. U. Khan, C. K. Duncan, and A. H. Maki, *J. Am. Chem. Soc.*, **91**, 1039 (1969).
14) I. R. Politzer, G. W. GriHin, and J. L. Laseter, *Chem. -Biol. Interact.*, **3**, 73, (1971).
15) E. J. Corey and W. C. Taylor, *J. Am. Chem. Soc.*, **86**, 3881 (1964).
16) S. J. Arnold, M. Kubo, and E. A. Ogryzlc, *Adv. Chem. Ser.*, **77**, 133 (1968).
17) N. J. Turro, V. Ramamurthy, K. -C. Liu, A. Krebs, and R. Kemper, *J. Am. Chem. Soc.*, **98**, 6758 (1976).
18) J. A. Pople and D. L. Beveridge, "Approximate Molecular Orbital Theory," McGrow-Hill, New York (1970), p. 80.
19) H. Schmidt, A. Schweig, and A. Krebs, *Tetrahedron Lett.*, **1974**, 1471.
20) R. B. Woodward and R. Hoffmann, "The Conservation of Orbital Symmetry," Verlag Chemie, GmbH (1971).
21) For instance, see K. Ohkubo, T. Yoshida, and K. Tomiyoshi, *Bull. Chem. Soc. Jpn.*, **49**, 2397 (1976).

Acidity and Catalytic Activity of Iron(II) Sulfate Heat-treated at High Temperature

Kazushi ARATA* and Makoto HINO†

Hokkaido University of Education, Hachiman-cho, Hakodate 040

†*Hakodate Technical College, Tokura-cho, Hakodate 042*

(Received February 23, 1979)

Synopsis. Acidity and catalytic activity of $FeSO_4$ calcined at 500—900 °C were studied. The product obtained by calcination at 700 °C showed maximum acidity at $H_0 \leqq 1.5$ and activity for isomerization of *d*-limonene oxide, polymerization of isobutyl vinyl ether and dehydration of 2-propanol. When calcined at 750 °C the product showed no acidity or activity.

Studies were carried out on the Friedel-Crafts benzylation,[1] benzoylation[2] and isopropylation[3] of toluene with their corresponding halides and polycondensation of benzyl chloride[4] catalyzed by iron sulfates heat-treated in the air at 200—900 °C. Maximum activity was found for the catalyst calcined at 700 °C. The specific surface area of the calcined sulfates indicated no relationship with their catalytic activities. The acidic property of calcined iron sulfates has not been investigated as regards relationship with catalytic activity, though several workers observed the maximum acidity of iron sulfates calcined at 120—200 °C.[5,6] In this paper we report the acidity of $FeSO_4$ calcined over 500 °C and its correlation with catalytic activities for isomerization of *d*-limonene oxide, polymerization of isobutyl vinyl ether and dehydration of 2-propanol.

Experimental

Catalysts were prepared by heating $FeSO_4 \cdot 7H_2O$ at 200—300 °C for 1—1.5 h followed by powdering below 100 mesh. Calcination was then carried out in the air in Pyrex glass tubes (quartz tubes for temperatures over 600 °C) for 3 h. The catalysts were stored in sealed ampoules.

The acidic property of the catalysts was determined by titration with butylamine using 4-phenylazodiphenylamine as a Hammett indicator: 0.05—0.2 ml of 0.1 M butylamine benzene solution was added to 0.5 g of the powder (below 100 mesh) suspended in 30 ml of benzene at intervals of 5—6 h. Since the catalyst is colored, the end point of titration was taken when a color change was observed on SiO_2–Al_2O_3 plastered on a small slip of filter paper, acidic coloration being seen with an indicator. The slip consumed 0.02—0.03 ml of 0.1 M butylamine. As the amount of consumed amine, 0.03 ml was subtracted from the titre per slip after slips were added until the acidic color of the indicator on SiO_2–Al_2O_3 remained unchanged. It took 4—5 d for titration.

Isomerization of *d*-limonene oxide was carried out with a mixture of 0.5 ml of the epoxide, 2.5 ml of toluene and 0.3 g of the catalyst with stirring at 90 °C for 15 min.[7]

Polymerization of isobutyl vinyl ether was performed with a mixture of 5 ml of the ether, 45 ml of toluene and 80 mg of the catalyst with stirring at room temperature for 30 min. Conversion (%) on the polymerization reaction was obtained on the basis of the unreacted monomer by gas chromatography using a 1-m column of tricresyl phosphate on Celite 545 (95 °C, He: 1.0 kg/cm²) with benzene as an internal standard.

Dehydration of 2-propanol was carried out at 170 °C by using a microcatalytic pulse reactor (catalyst amount: 30 mg, carrier gas: He, flow rate: 30 ml/min, pulse size: 0.4 μl). The catalyst was heat-treated in a reactor at 500 °C for 1.5 h before the reaction. Effluent products were directly introduced into a gas chromatographic column for analysis (Porapak R-2 m, 128 °C). The percentage conversion is given as the average value from the 5 to 10 th pulse reaction.

Results and Discussion

Figure 1 shows the acid amount ($pK_a \leqq 1.5$) of $FeSO_4$ calcined at 500—800 °C. The substance obtained by calcination at 700 °C was found to be the most acidic. It is of interest that the acid amount was zero when calcined at 750 °C. The substance obtained by treatment at 900 °C also showed no acidity. The acidic amount of $FeSO_4$ treated at 700 °C was 0.052 mmol/g at $pK_a \leqq -3.0$.

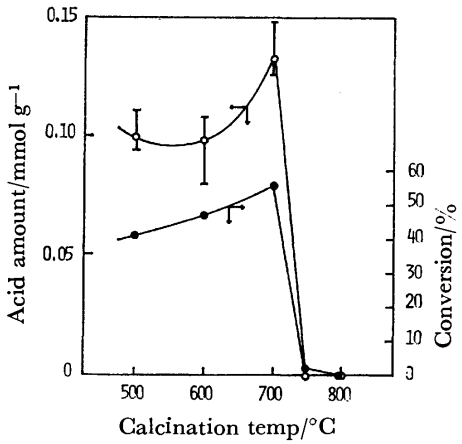

Fig. 1. Acidity of calcined $FeSO_4$ and its catalytic activity for isomerization of *d*-limonene oxide.
(○): Acid amount at $pK_a \leqq 1.5$,
(●): isomerization of *d*-limonene oxide.
Selectivity was 20% 1-methyl-3-isopropenylcyclopentyl-1-carboxaldehyde (I), 66% dihydrocarvone (II), 7% *exo*-carveol (III) and 7% *endo*-carveol (IV) in all runs.

Since the acidity could not be determined accurately because of the coloration of the substance, catalytic activities by several acid-catalyzed reactions were examined. The activity for isomerization of *d*-limonene oxide is shown in Fig. 1. We see that the activity is in line with acidity, the catalyst calcined at 750 °C being quite inactive in spite of the remarkable activity attained by heat treatment at 700 °C.[8]

The following two reactions were carried out (Fig. 2): (1) polymerization of isobutyl vinyl ether, which is known to be catalyzed by Lewis catalysts such as BF_3-

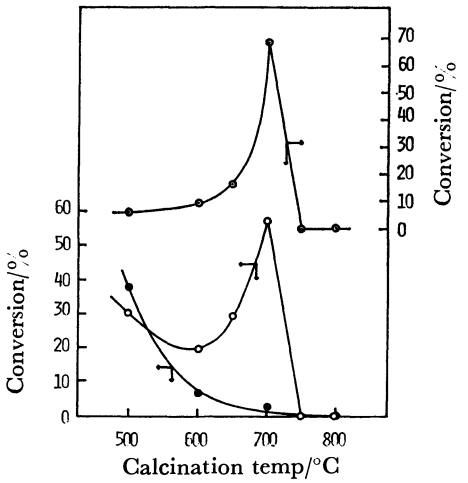

Fig. 2. Catalytic activities for polymerization of isobutyl vinyl ether (⊙) and for dehydration of 2-propanol (○). (●): dehydration of 2-propanol over $NiSO_4$ at 190 °C.

etherate and $TiCl_4$,[9] and (2) the dehydration of 2-propanol to propylene, which is generally catalyzed by acidic sites at $-3<H_0\leqq+1.5$.[10] Both reactions give maximum activity by calcination at 700 °C. Both activities are in line with the acidity (Fig. 1), the catalyst calcined at 750 °C being inactive.

In order to examine such a rapid decrease in catalytic activity for other metal sulfate, $NiSO_4$ was subjected to reaction with 2-propanol. The activity decreased rapidly by calcination above 500 °C. The catalysts calcined above 700 °C were almost inactive. The acidity of $NiSO_4$ increases initially with rise in temperature of heat-treatment, reaching a maximum at *ca.* 350 °C, and decreasing subsequently.[11] It seems that activity is related with acidity. The amount of diisopropyl ether formed by the dehydration of 2-propanol was almost negligible for all the catalysts of $FeSO_4$ and $NiSO_4$.

In the polymerization of isobutyl vinyl ether, $FeSO_4$ (700 °C) gave 91% conversion for 2 h. The yield insoluble in an excess amount of methanol was 74% with 0.96 dl/g of the reduced viscosity.[12]

ESCA studies of $FeSO_4$ showed that the sulfate completely decomposes to form α-Fe_2O_3 at 675—700 °C, recrystallization proceeding rapidly.[13] A small amount of sulfur (0.12—0.15 wt %), which remains in the catalyst after decomposition, exists as SO_4^{2-} on the surface treated at 700 and 750 °C.[14] $NiSO_4$ reveals its acidity on the sulfate configuration between the monohydrate and anhydrous forms.[15] Other metal sulfates, $Al_2(SO_4)_3$, $ZnSO_4$, $MgSO_4$, and $CdSO_4$, also show surface acidity on the sulfate salts, the maxima appearing at 180—400 °C.[11] The creation of acid sites on the Fe_2O_3 catalyst by decomposition of the sulfate at 700 °C is specific, and the inactivity caused by calcination at a slightly higher temperature, 750 °C, is noteworthy.

As regards the polymerization of isobutyl vinyl ether, solid acid catalysts such as $NiSO_4$ (calcined at 350 °C), SiO_2–Al_2O_3 (500 °C, Al_2O_3: 15 wt %, Nikki Chemical Co.), Al_2O_3 (500 °C, KAT6, Nishio Chemical Co.) and TiO_2 (hydrogel) were found to be almost inactive under the present reaction conditions.

References

1) K. Arata, K. Sato, and I. Toyoshima, *J. Catal.*, **42**, 221 (1976).
2) K. Arata, K. Yabe, and I. Toyoshima, *J. Catal.*, **44**, 385 (1976).
3) K. Arata and I. Toyoshima, *J. Catal.*, **47**, 109 (1977).
4) K. Arata, A. Fukui, and I. Toyoshima, *J. Chem. Soc., Chem. Commun.*, **1978**, 121.
5) S. Hasegawa and T. Kawaguchi, *Nippon Kagaku Kaishi*, **91**, 1038 (1970).
6) I. Toyoshima, K. Tanabe, T. Yoshioka, J. Koizuka, and H. Ikoma, 20 th National Meeting of the Chemical Society of Japan, Tokyo, April 1969, Abstr. No. 06405.
7) For details of experiment, *cf.* K. Arata, S. Akutagawa, and K. Tanabe, *J. Catal.*, **41**, 173 (1976).
8) High activity of $FeSO_4$ (700 °C) was also observed in the isomerization of carvomenthene oxide. The catalyst (0.27 g) in a mixture of 0.5 ml epoxide and 2.5 ml toluene gave 82% total conversion in 10 min at 80 °C, the selectivity being 30 and 55% for the products corresponding to I and II, respectively, in the case of *d*-limonene oxide.
9) S. Nakane, K. Iwasaki, and H. Fukutani, *J. Polym. Sci., Part A*, **1**, 3277 (1963).
10) K. Tanabe, "Solid Acids and Bases," Kodansha, Tokyo (1970), p. 125.
11) Ref. 10, pp. 82—83.
12) The viscosity was determined by 0.5 g of polymer in 100 ml of benzene at 25 °C. The catalysts calcined at 500, 600, and 650 °C gave 43, 59, and 61% conversions with the methanol-insoluble yields of 12, 32, and 46%, respectively, for 24 h.
13) K. Yabe, K. Arata, and I. Toyoshima, *J. Catal.*, **57**, 231 (1979).
14) K. Arata, K. Yabe, M. Hino, and I. Toyoshima, *Shokubai*, **19**, 246 (1977).
15) K. Tanabe and T. Takeshita, *Adv. Catal.*, **17**, 315 (1967).

The Mössbauer Effect of ^{119}Sn in the Dimethylbis(8-quinolinolato)-tin(IV) Single Crystal

Hisao NEGITA,* Ryukei BOKU, and Sumio ICHIBA
Department of Chemistry, Faculty of Science, Hiroshima University, Hiroshima 730
(Received June 8, 1979)

Synopsis. The Mössbauer absorption spectrum of ^{119}Sn in the single crystal of dimethylbis(8-quinolinolato)tin-(IV) was studied by an intensity-tensor method. The orientation of the principal axes of the electric-field gradient (EFG) was discussed from the point of view of point-charge formalism.

For the octahedral coordination, all the signs of V_{zz}, the principal component of EFG, are in good agreement with those to be expected from the point-charge formalism with the exception of the *cis* configuration.[1-4] From the magnetic perturbation study of a powder sample of dimethylbis(8-quinolinolato)tin(IV), $Sn(Me)_2(oxin)_2$, which has a distorted *cis*-octahedral configuration, Parison and Johnson[4] have proposed that this inconsistency comes from a deviation from a regular octahedral geometry. The sign of V_{zz} as well as the orientation of the EFG axes can be inferred from the single crystal absorption spectra.[5-10] The purpose of the present study is to examine their proposition in more detail by means of Mössbauer experiments on the single crystal of $Sn(Me)_2(oxin)_2$. The method employed here was first suggested by Zimmermann and applied by him to $FeCl_2 \cdot 4H_2O$,[11] and recently it has also been applied to $Fe(NH_4)_2(SO_4)_2 \cdot 6H_2O$.[12] It is based on the fact that the quadrupole line intensities can be characterized by means of an intensity tensor.

Crystal Structure and Experimental

$Sn(Me)_2(oxin)_2$ has monoclinic symmetry, and its space group is $P2_1/c$.[13] The dimensions of the unit cell are $a=9.44$, $b=13.28$, and $c=15.67$ Å, with $\beta=110.0°$. A unit cell consists of four $Sn(Me)_2(oxin)_2$ molecules, as is shown in Fig. 1. These four molecules can be grouped into two sites, I and II, with different orientations of the EFG relative to the crystal axes. The symmetry relation between Site I and Site II is a 180° rotation about the b axis.

A single crystal of the complex was cut parallel to the 001 plane, and a crystal plate of *ca.* 13×8 mm^2 was polished to a thin plate, the surface density of which was 27.5 mg of Sn per cm^2. The Mössbauer spectra were obtained in the manner described in our previous paper,[10] except that the absorber was kept at 110 K and the source was $Ca^{119m}SnO_3$.

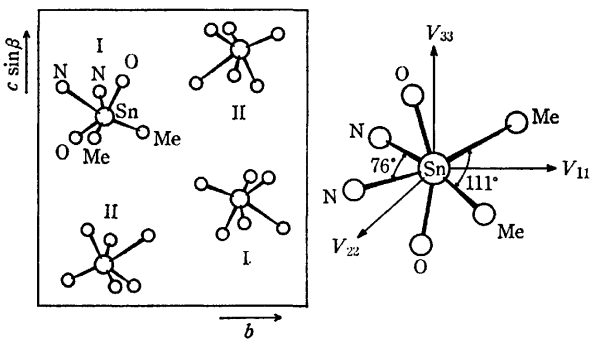

Fig. 1. The molecular geometry of the $SnMe_2N_2O_2$ unit in dimethybis(8-quinolinolato)tin(IV) and the orientations in the unit cell.

Results and Discussion

A typical Mössbauer spectrum with computer-fitting Lorenzian curves is shown in Fig. 2. The parameters obtained from these spectra are presented in Table 1. In the table, the values of A^h/A^{tot}, the intensity of the higher energy peak line divided by the total intensity, were obtained from the observed spectra, whereas those of I^h/I^{tot} were calculated from Eq. 1 using a recoilless fraction of $f'=0.11$, estimated from powder samples:

$$\frac{A^h}{A^{tot}}-\frac{1}{2}=F\left(\frac{I^h}{I^{tot}}-\frac{1}{2}\right) \quad (1)$$

where $F=[1+0.125T_a(1-4a^2)]^{-1}$, with $T_a=nf'\sigma_0$, the effective thickness of absorber, and $a=I^h/I^{tot}$.

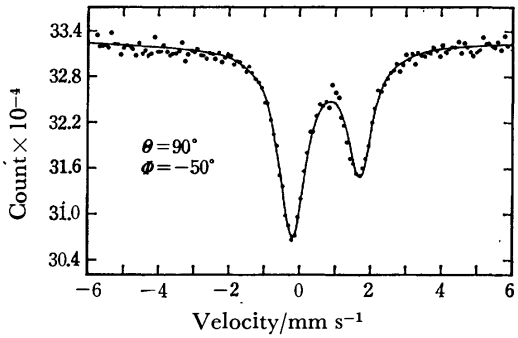

Fig. 2. Mössbauer absorption spectrum of dimethylbis-(8-quinolinolato)tin(IV) single crystal at 110 K. The γ-ray is in the pq plane and $-50°$ from the p axis.

Table 1. Experimental parameters for $Sn(Me)_2(oxin)_2$

$\Theta^{a)}$ deg.	$\Phi^{a)}$ deg.	A^h/A^{tot}	I^h/I^{tot}
90	−50	0.391±0.012	0.356±0.015
90	−40	0.390±0.011	0.360±0.014
90	−30	0.403±0.014	0.379±0.016
90	−20	0.426±0.015	0.409±0.018
90	−10	0.470±0.015	0.464±0.019
90	0	0.504±0.014	0.505±0.017
90	10	0.545±0.014	0.556±0.018
90	20	0.570±0.014	0.586±0.017
90	30	0.583±0.012	0.604±0.014
90	50	0.589±0.010	0.618±0.013

a) The polar angles of the γ-ray relative to O_{pqr}.

Since the crystal axes, a, b, and c, are not orthogonal with each other, a orthogonal system, O_{pqr}, is introduced. The base vectors, $\boldsymbol{p}$, $\boldsymbol{q}$, and $\boldsymbol{r}$, are parallel to $\boldsymbol{a}\times\boldsymbol{b}$, $\boldsymbol{a}$, and $\boldsymbol{b}$ respectively. The components of the

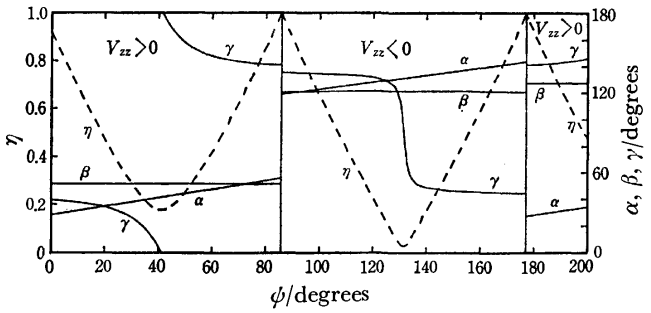

Fig. 3. Sign of V_{zz}, α, β, γ, and η as a function of the parameter ϕ.

macroscopic-intensity tensor obtained by a least-squares analysis from the data of Table 1 are $I^{m}_{pp}=0.005\pm0.002$, $I^{m}_{qq}=-0.029\pm0.006$, $I^{m}_{rr}=0.024\pm0.006$, $I^{m}_{pq}=0.133\pm0.002$, and $I^{m}_{pr}=I^{m}_{qr}=0$. The observable tensor thus has monoclinic symmetry, and two components of the local site tensor are not recorded. However, the introduction of an unknown parameter, ϕ (see Ref. 11 for the definition), makes it possible to represent the local intensity tensor. Figure 3 shows the values of the asymmetry parameter (η) and the Euler angles (α, β, γ), designating the orientation of the principal-axes system of EFG relative to O_{pqr}, as a function of the ϕ angle. Although the values of ϕ are restricted to $0°\leqslant\phi\leqslant200°$, the solutions for $\pi\leqslant\phi\leqslant2\pi$ are obtained by the following transformation from those for $0\leqslant\phi\leqslant\pi$:

$$\eta\rightarrow\eta,\ (\alpha,\beta,\gamma)\rightarrow(\alpha,\pi-\beta,\pi-\gamma)\ \text{for}\ \phi\rightarrow\pi+\phi.$$

From the point-charge model for *cis*-R_2SnX_4 structures, it is expected that, for bond angles of R–Sn–R greater than the tetrahedral angle (109.5°), V_{zz} lies on the R–Sn–R plane, and is normal for a bisector of the R–Sn–R, and has the sign opposite to that expected for a regular *cis* geometry, *i.e.*, a negative sign.[4]

Although the 2Me, 2N, and Sn of the complex are not on a common plane, the local symmetry about the tin in $Sn(Me)_2(oxin)_2$ is approximately C_{2v}. We take an unweighted least-squares plane through the four ligand atoms (2Me and 2N) for the Sn atom as the Me_2SnN_2 plane and define V_{11} as the field gradient in the direction of the bisector of projection which two Sn–Me bonds form on the plane, and V_{33}, as that in the normal direction of the plane (see Fig. 1). The direction of V_{22} is normal with regard to V_{11} and V_{33}. The Me–Sn–Me angle is opened out to 111°, so that V_{zz} can be expected to coincide with V_{22}. However, the uncertainty as to the directions of V_{xx} and V_{yy} remains.

We shall refer only to the I site in the following discussion. Two possible cases are considered:

$$V_{xx}//V_{11},\ V_{yy}//V_{33},\ \text{and}\ V_{zz}//V_{22} \quad \text{(i)}$$

$$V_{xx}//V_{33},\ V_{yy}//V_{11},\ \text{and}\ V_{zz}//V_{22} \quad \text{(ii)}$$

The Euler angles for (i) and (ii) are $\alpha=93°$, $\beta=128°$, and $\gamma=135°$ and $\alpha=93°$, $\beta=128°$, and $\gamma=45°$ respectively (the corresponding values for the II site are obtained by the transformation of $(\alpha,\beta,\gamma)\rightarrow(\alpha,\pi-\beta,\pi-\gamma)$ in each case). Though the point symmetry of the tin sites imposes no restrictions on η, the value of η is expected to be large judging from the point-charge model (*cf.* Fig. 3 in Ref. 4). This value is seen, along with the values of α, β, and γ, in the $V_{zz}<0$ range in Fig. 3. The solutions for $86°\leqslant\phi\leqslant132°$ correspond to (i), and those for $132°\leqslant\phi<177°$, to (ii). The α values in the range of the former are closer to 93° than those of the latter. This suggests that the direction of the principal axes of the EFG may be as in Case (i). If η is found by an additional investigation, as in the case of $FeCl_2\cdot4H_2O$,[11] the precise orientation of the EFG axes can be established.

References

1) B. W. Fitzsimmons, *J. Chem. Soc., A*, **1970**, 3235.
2) B. A. Goodman and N. N. Greenwood, *J. Chem. Soc., A*, **1971**, 1862.
3) B. A. Goodman, N. N. Greenwood, K. L. Jaura, and K. K. Sharma, *J. Chem. Soc., A*, **1971**, 1865.
4) R. V. Parish and C. E. Johnson, *J. Chem. Soc., A*, **1971**, 1906.
5) P. Zory, *Phys. Rev. A*, **140**, 1401 (1965).
6) K. Chandra and S. P. Puri, *Phys. Rev.*, **162**, 272 (1968).
7) R. W. Grant, R. M. Housley, and U. Gonsor, *Phys. Rev.*, **178**, 523 (1969).
8) T. C. Gibb, *J. Phys. C*, **7**, 1001 (1974).
9) T. C. Gibb, *J. Chem. Soc., Dalton Trans.*, **1976**, 1237.
10) H. Negita, R. Boku, M. Nakamura, and S. Ichiba, *Bull. Chem. Soc. Jpn.*, **50**, 584 (1977).
11) R. Zimmermann, *Nucl. Instrum. Methods*, **128**, 537 (1975).
12) T. C. Gibb, *J. Chem. Soc., Dalton Trans.*, **1978**, 743.
13) E. O. Schlemper, *Inorg. Chem.*, **6**, 2012 (1967).

The Isomerization of 1-Butene over the ReO_3 Catalyst

Tsutomu YAMAGUCHI, Nobuo TSUDA,** and Kozo TANABE*

Department of Chemistry, Faculty of Science, Hokkaido University, Sapporo 060

***National Institute for Research in Inorganic Materials, Namiki, Niihari-gun, Ibaraki 300-31*

(Received July 2, 1979)

Synopsis. The catalytic activity of the single crystals of ReO_3 was examined by using the isomerization of 1-butene as a test reaction. The results indicate that there are two types of surfaces: one is sensitive to the introduction of hydrogen, and the other is not.

The isomerization of butenes has been investigated extensively over various metal oxides, including both acidic and basic oxides, such as silica-alumina[1] and alkaline earth metal oxides.[2] In contrast with work with such oxides, little work has been done on single crystals of oxides. This report will deal with the catalytic properties of the single crystals of ReO_3, which have been prepared by different methods.

Experimental

Materials. Rhenium(VI) oxide (ReO_3) was prepared by the following methods. Rhenium(VII) oxide (Re_2O_7) was obtained by oxidizing Re metal (Hermann C. Starck, Berlin, 99.9%) in an oxygen stream.

Sample #1: Rhenium(VII) oxide was dissolved in methanol and heated in a CO atmosphere at 90 °C to yield ReO_3. The resulting oxide was washed with water, acetone, and methanol, and then dried under a vacuum at room temperature. An X-ray analysis revealed the oxide to be ReO_3, and an electron-micrographic analysis showed that the particles were in the form of a rectangle. An electron-diffraction pattern and a lattice image of a ReO_3 particle showed that the sample was a single crystal with {100} surfaces.

Sample #2: Rhenium(VII) oxide was reduced to yield ReO_3 as in the case of #1. The resulting oxide was annealed in air for 1 d at 230 °C, and then washed by acetone, water, and methanol and dried in air at 120 °C. An X-ray analysis revealed the oxide to be ReO_3.

Sample #3: Rhenium(VII) oxide was dissolved in water and reduced with H_2 at 300—320 °C. The resulting oxide was ennealed in air at 230 °C for 138 h, washed with water, and dried in air at 120 °C.

Sample #4: Rhenium(VII) oxide was dissolved in methanol and reduced with CO and H_2 at 280 °C. The resulting oxide was annealed in air at 230 °C for 1 d.

Sample #5: The impregnation of a Re_2O_7-methanol-water solution with silica gel and subsequent CO treatment at 280 °C yielded the oxide, which was washed with methanol and water, heated in air at 230 °C to remove the Re_2O_7, and annealed in air at 180 °C for one night. The atomic ratio of Re/Si was estimated to be 1/3.

Reaction. The isomerization of 1-butene was carried out in a closed recirculation system at 200 °C. The sample oxide was evacuated *in situ* at 300 °C for 3 h prior to use.

Results and Discussion

The results are summarized in Table 1. Samples #1 and #2 are characterized by intermediate activity, a large hydrogen effect, and no metathesis activity. Samples #3 and #4 have very low activity. Sample #5 shows high activity in the isomerization and the metathesis reaction.

TABLE 1. REACTION OF 1-BUTENE OVER ReO_3 CATALYSTS

Catalyst	Rate[a] / 10^{-5} mol min^{-1} g^{-1}	*cis*/*trans*	H_2 effect	Surface area / m^2 g^{-1}
#1	1.6	1.1	large	12
#2	3.9	1.2	large	—
#3	<0.3	—	—	1.7
#4	<0.3	—	no	—
#5	23[b]	1.1	—	136

a) Initial rate; estimated on the basis of the disappearance of 1-butene. b) *Ca.* 20% of the metathesis reaction is included.

A distinct Re line with 4±1G of a full width at half the maximum was obtained by NMR at 300 K for the samples prepared similarly as in Samples #3 and #4; this indicates that the structure of both samples is pure ReO_3, since this line was not observed in a defective structure of ReO_3, even when the oxide has been identified as ReO_3 by X-ray spectrometry.

A higher activity was obtained when Samples #1 and #2 were evacuated at a higher temperature (about 500 °C) for a short period during the standard pretreatment. A drastic change in the isomerization rate upon the addition of 100 Torr of hydrogen during the reaction was observed only when the catalyst was evacuated

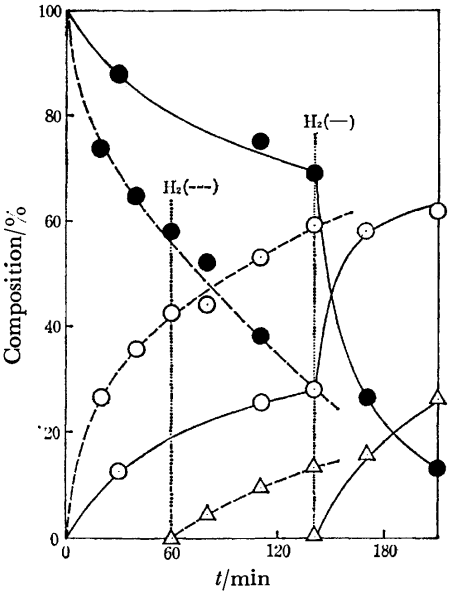

Fig. 1. Reaction of 1-butene over ReO_3 (#2) catalyst. ——: Evacuated at 300 °C for 3 h, ——: evacuated at 300 °C for 2.5 h and 500 °C for 0.5 h. ●: 1-Butene, ○: 2-butene. △: butane. H_2 (—), H_2 (——): addition of 100 Torr of H_2, corresponding to the lines — and ——, respectively.

under the standard pretreatment conditions (Fig. 1).

Those observations indicate that the isomerization takes place on two types of surfaces; one (Surface I) is sensitive to the nitroduction of hydrogen, while the other (Surface II) is not. The former surface is dominant when the catalyst is prepared by methanol reduction and treated by successive evacuation at 300 °C. The introduction of hydrogen onto Surface I during the reaction caused a large enhancement of the reaction rate, with the formation of butane. This suggests that the isomerization proceeds *via* an alkyl intermediate (probably secondary-alkyl). The addition of one hydrogen atom to the C–C double bond gives the alkyl intermediate, and the following removal of one hydrogen from the intermediate yields 2-butene, or the addition of another hydrogen results in the production of butane.

Surface II is not sensitive to the introduction of hydrogen, and so its proportion may increase upon evacuation at an elevated temperature. This type of surface can be obtained by removal of the oxygen atoms from the surface lattice or by the partial decomposition of ReO_3 to ReO_2; the resulting surface will be highly defective. The exposed Re atom may act as a Lewis acid center. An increase in the region of the Surface II may be accompanied by the destruction of the Surface I.

Catalysts #3 and #4 showed low activity. This could be attributed to their lower surface area. However, if we consider the observation that even the addition of hydrogen during the reaction did not bring about any increase in the reaction rate, it seems more likely to conclude that the pure single crystals of ReO_3 do not have the Surface I and are tolerant of such a reduction upon evacuation that will bring about catalytically active sites.

The highest activity was obtained in Catalyst #5. This catalyst was the only one that gave the metathesis products. The acidic centers, which were produced by the combination of two oxides, may be responsible for the isomerization reaction, since it is known that the combination of two oxides can produce a new acidic center,[3] which will then act as an active center for the isomerization.

References

1) J. W. Hightower and W. K. Hall, *Chem. Eng. Prog. Symposium Series*, **63**, 122 (1959).

2) K. Tanabe, N. Yoshii, and H. Hattori, *J. Chem. Soc., Chem. Commun.*, **1971**, 464; H. Hattori, N. Yoshii, and K. Tanabe, *Proc. 5th Intern. Congr. Catal.*, **10**, 233 (1972).

3) K. Tanabe, T. Sumiyoshi, K. Shibata, T. Kiyoura, and J. Kitagawa, *Bull. Chem. Soc. Jpn.*, **47**, 1064 (1974).

Kinetics of Dissociation of the Hydrogen Bond in the (n, π^*) Singlet State of 9,10-Diazaphenanthrene

Iwao YAMAZAKI,* Hiroyuki TAKEDA, and Hiroaki BABA

Division of Chemistry, Research Institute of Applied Electricity, Hokkaido University, Sapporo 060

(Received July 6, 1979)

Synopsis. Changes of fluorescence properties with temperature have been examined for 9,10-diazaphenanthrene (DAP) in proton-donating solvents. From a kinetic analysis, the rate constant for dissociation of the hydrogen bond in the (n, π^*) singlet state of DAP is evaluated to be 4.3×10^8 s^{-1} at 113 K, and the activation energy of the dissociation is 10.0 kJ/mol.

In proton-donating solvents the n→π^* absorption spectrum of 9,10-diazaphenanthrene (DAP) exhibits a large blue shift which is attributable to formation of a hydrogen bond between solute and solvent molecules.[1] On the contrary, the n←π^* fluorescence shows only a small shift, indicating that the hydrogen bond is broken in the (n, π^*) excited singlet state within its lifetime.[1]

Baba and Mugiya[2] reported that a large blue shift occurs in the fluorescence spectrum of DAP in an aprotic polar solvent at low temperature. They interpreted the blue shift as due to the fact that the relaxation process from the Franck-Condon excited to the equilibrium excited state, with respect to the orientation of solvent dipoles, is inhibited at such a low temperature that the solvent becomes rigid. For DAP in proton-donating solvents at low temperature, Rau and Bisle[3] suggested that the dissociation of the hydrogen bond in the excited state is more or less inhibited owing to an increase in solvent viscosity with lowering temperature.

In this study, the fluorescence spectrum and lifetime have been examined for DAP in a mixture of alcohols at temperatures ranging from 300 to 77 K with a view to obtaining quantitative information as to the kinetic behavior of the hydrogen bond in the ^{1}(n, π^*) state.

Experimental

A mixture of methanol and ethanol (volume ratio, 1: 1) and that of isopentane and methylcyclohexane (volume ratio, 4: 1) were used as a proton-donating solvent and a nonpolar reference solvent, respectively. These mixtures, hereafter referred to as ME and PM, respectively, give good rigid glasses at 77 K. A DAP concentration of less than 10^{-4} M was adopted to prevent the formation of a dimer of DAP in PM at low temperature.[4]

Fluorescence decay measurements were made with a single-photon counting apparatus using a time-to-amplitude converter.[5] The lifetime could be determined quantitatively down to 0.5 ns on the basis of the deconvolution method.

Results and Discussion

Table 1 gives the frequencies of n→π^*absorption and n←π^* fluorescence maxima, denoted by ν_a and ν_f respectively, and the fluorescence lifetimes τ_f for DAP in PM and proton-donating solvents at 300 and 77 K. The table gives also the frequency shifts, $\Delta\nu_a$ and $\Delta\nu_f$, relative to the frequencies in PM at 300 K. The values of ν_a in proton-donating solvents were estimated on the assumption that the shape and half-width of the n→π^* absorption curve are the same as those in PM. When the solvent is changed from PM to ME at 300 K, the absorption spectrum is greatly displaced to the blue, whereas the fluorescence shows only a small blue shift, *i.e.*, $\Delta\nu_a=1550$ cm^{-1} and $\Delta\nu_f=220$ cm^{-1}. On the contrary, at 77 K the fluorescence shift in ME is almost as large as the absorption shift, *i.e.*, $\Delta\nu_f=1330$ cm^{-1}. It should be emphasized that the absorption and fluorescence spectra in PM containing a small amount (0.5% by volume) of ethanol are essentially the same as those in ME. The fluorescence in PM has a constant lifetime of about 4 ns irrespective of temperature. In ME the fluorescence lifetime varies distinctly according to the temperature; the lifetime in ME at 300 K is comparable to the one in PM, whereas it is 1.2 ns at 77 K. All these results indicate that at 300 K the hydrogen-bonded complex between solute and solvent molecules dissociates in the ^{1}(n, π^*) state of DAP, but that at 77 K the breakage of the hydrogen bond is inhibited owing to the high viscosity of the solvent. Thus the fluorescence spectra in ME at 77 and 300 K originate from the hydrogen-bonded complex and the free DAP molecule, respectively.

Table 1. Frequencies of absorption and fluorescence maxima and fluorescence lifetimes of DAP in different solvents

Solvent	ν_a / cm^{-1}	ν_f / cm^{-1}	$\Delta\nu_a$ / cm^{-1}	$\Delta\nu_f$ / cm^{-1}	τ_f / ns
PM					
300 K	24630	19940	0	0	4.9
77 K[a]	24950	20280	320	340	3.6
PM+ethanol (0.5%)					
300 K	26050[b]	20120	1420	180	4.9
77 K	26110[b]	21280	1480	1340	1.2
ME					
300 K	26180[b]	20160	1550	220	3.5
77 K	26180[b]	21270	1550	1330	1.2

a) A small amount of ethyl ether (5% by volume) was added to prevent the formation of DAP dimer.
b) Estimated values (see text).

The changes of the fluorescence spectrum and lifetime in ME with temperature occur in the range 150—77 K. The spectrum shifts rapidly to the blue as the temperature is lowered from 150 K, as is seen in Fig. 1. Furthermore, at the intermediate temperatures, the fluorescence lifetimes were found to exhibit different values depending on the wavelength where the fluorescence was monitored. Therefore, each of the fluorescence spectra obtained at temperatures between 150 K and 77 K is regarded as a superposition of two kinds of spectra: one originating from the hydrogen-bonded complex and the other from the free DAP molecule. On the assumption that

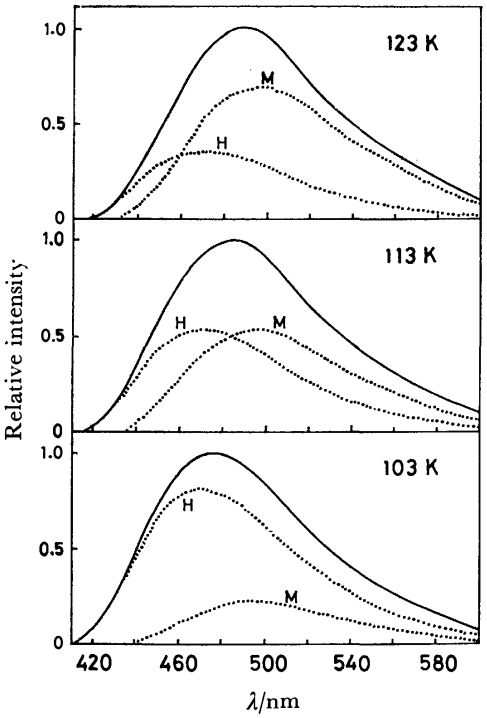

Fig. 1. Fluorescence spectra of DAP in ME at different temperatures (solid lines), and analysis of the individual spectra into the components (dotted lines) of the hydrogen-bonded complex (H) and the free DAP molecule (M). For each of the observed spectra the maximum fluorescence intensity is normalized to a unit relative intensity.

the spectral shape of each fluorescence component is independent of temperature in this temperature range, one can analyze the whole spectrum into separate components; the results are shown in Fig. 1 for three temperatures. It is seen that, as the temperature is lowered, the contribution from the fluorescence component of the hydrogen-bonded complex increases, while that from the component of the free DAP molecule decreases. This means that on lowering the temperature the solvent becomes rigid and the dissociation of the hydrogen bond is inhibited in varying degrees, depending upon the viscosity of the solvent.

The deactivation processes in the excited state involving the dissociation of the hydrogen bond are represented by the following kinetic scheme:

$$\begin{array}{ccc} \text{DAP*}\cdots\text{H} & \xrightarrow{k_d(T)} & \text{DAP*} \\ \downarrow k_{fH},\ k_{qH} & & \downarrow k_{fM},\ k_{qM} \end{array}$$

where DAP* and DAP*···H denote the excited singlet states of the free DAP molecule and hydrogen-bonded complex, respectively; k_{fH}, k_{qH}, k_{fM}, and k_{qM} are the radiative (f) and radiationless (q) decay constants for the hydrogen-bonded complex (H) and free molecule (M); $k_d(T)$ is the rate constant for the dissociation of the hydrogen bond as a function of temperature, T. The rate constants other than $k_d(T)$ are assumed to be independent of T in the range concerned here (150—77 K). Then the ratio of the fluorescence quantum yield of the free molecule to that of the hydrogen-bonded complex, $\Phi_M(T)/\Phi_H(T)$, is expressed as

$$\Phi_M(T)/\Phi_H(T) = (k_{fM}/k_{fH})k_d(T)/(k_{fM}+k_{qM}). \quad (1)$$

In this equation, $k_{fM}+k_{qM}\simeq 1/\tau_f(150\text{ K})=3\times10^8\text{ s}^{-1}$ and $k_{fM}/k_{fH}=0.69$; these values are obtained by using the ratio (0.5) of Φ_H(77 K) to Φ_M(150 K) and the lifetimes at 77 and 150 K (1.2 and 3.5 ns, respectively). The quantum yield ratio $\Phi_M(T)/\Phi_H(T)$ can be evaluated from the analysis of the spectrum as shown in Fig. 1. Thus, the rate of the hydrogen-bond dissociation, $k_d(T)$, can be calculated from Eq. 1. At 113 K where the two quantum yields Φ_M and Φ_H are nearly equal (Fig. 1), $k_d=4.3\times10^8\text{ s}^{-1}$, which value is comparable to $k_{fH}+k_{qH}\simeq 1/\tau_f(77\text{ K})=8.3\times10^8\text{ s}^{-1}$. The k_d value becomes smaller at lower temperatures and negligible at 77 K compared with $k_{fH}+k_{qH}$, while at higher temperatures k_d becomes larger and at 150 K it dominates over $k_{fH}+k_{qH}$. This means that, within the lifetime of the $^1(n, \pi^*)$ state, the dissociation of the hydrogen bond is completed at temperatures higher than 150 K, but that practically no dissociation occurs at 77 K.

In the previous study by Baba and Mugiya[2] concerning the Franck-Condon blue shift of the fluorescence of DAP in an aprotic solvent, it was noted that the reorientation of solvent dipoles occurs with the rate which follows an equation of the Arrhenius type, and that the activation energy for the reorientation process is about 17 kJ/mol. The rate constants at different temperatures obtained in the present study for the hydrogen-bond dissociation were found to be well described in terms of the Arrhenius equation with an activation energy of 10.0 kJ/mol. This somewhat small value of activation energy is consistent with the view that in the case of hydrogen-bonding interaction in the $^1(n, \pi^*)$ state a repulsive force is operative between the proton donor and acceptor. Furthermore, the smaller activation energy is favorable for the expectation that the hydrogen bonding interaction would be localized at a limited portion of the donor–acceptor system concerned.

References

1) C. Mugiya and H. Baba, *Bull. Chem. Soc. Jpn.*, **40**, 2201 (1967).

2) H. Baba and C. Mugiya, *Bull. Chem. Soc. Jpn.*, **43**, 13 (1970).

3) von H. Rau and H. Bisle, *Ber. Bunsenges. Phys. Chem.*, **77**, 281 (1973).

4) D. N. de Vries Reilingh, R. P. H. Rettschnick, and G. J. Hoytink, *J. Chem. Phys.*, **54**, 2722 (1971).

5) I. Yamazaki, M. Fujita, K. Uchida, Y. Shindo, and H. Baba, *Bull. Res. Inst. Appl. Elec., Hokkaido University*, **26**, 124 (1974).

Formation of Five-coordinate Ni(II) Complexes with 2,12-Dimethyl-3,7,11,17-tetraazabicyclo[11.3.1]heptadeca-1(17),2,11,13,15-pentaene Analogs and Halide Ions in Nitromethane

Katsura Mochizuki, Tasuku Ito,† and Masatoshi Fujimoto*
Department of Chemistry, Faculty of Science, Hokkaido University, Sapporo 060
†*Institute for Molecular Science, Okazaki 444*

(Received May 11, 1979)

Synopsis. Formation of 5-coordinate Ni(II) complexes of the title quadridentate ligands and halide ions (Cl^-, Br^-, and I^-) in nitromethane was investigated. Some of the formation constants were estimated by means of curve-fitting method.

Nickel(II) complexes of the title ligand, L, and its analogs, $[Ni(L+nH)](ClO_4)_2$ ($n=-2$ (**1**), 0 (**2**), 2 (**3**), and 4 (**4**)) form 5- and 6-coordinate complexes with halide ions in nitromethane solutions. In the absence of halide ions, these complexes exist as 4-coordinate, diamagnetic species in nitromethane, which were confirmed by means of the ^1H NMR and electronic spectra. The present note discusses the solution equilibria between the complexes **1**—**4** and halide ions (Cl^-, Br^-, and I^-) in nitromethane.

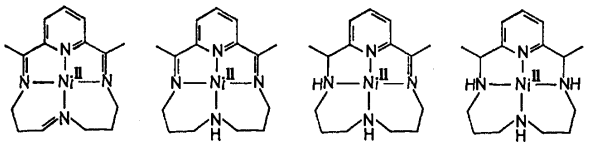

1 **2** **3** **4**

The electronic spectra of the complexes **1**—**4** in nitromethane solutions were measured in the presence of various amounts of tetraethylammonium halides. The equilibria attained rapidly under the experimental conditions.[1]

Figure 1 shows the typical spectra of $[Ni(L+2H)](ClO_4)_2$ in the absence and the presence of halide ions. The results of the molar-ratio methods are shown in Fig. 2(a). In the chloride system, a 6-coordinate 1 : 2 complex forms predominantly, a small amount of a 1 : 1 complex being also formed. The decrease in the spectral intensity of the chloride system as compared with that

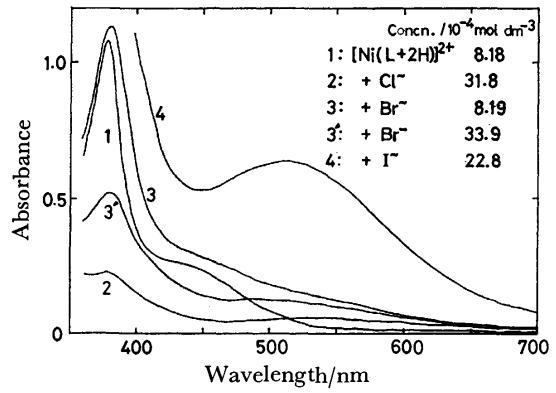

Fig. 1. Absorption spectra of the nitromethane solutions of $[Ni(L+2H)](ClO_4)_2$ (1) and in the presence of Et_4NX (2, 3, 3′, and 4) at 25±0.2 °C.

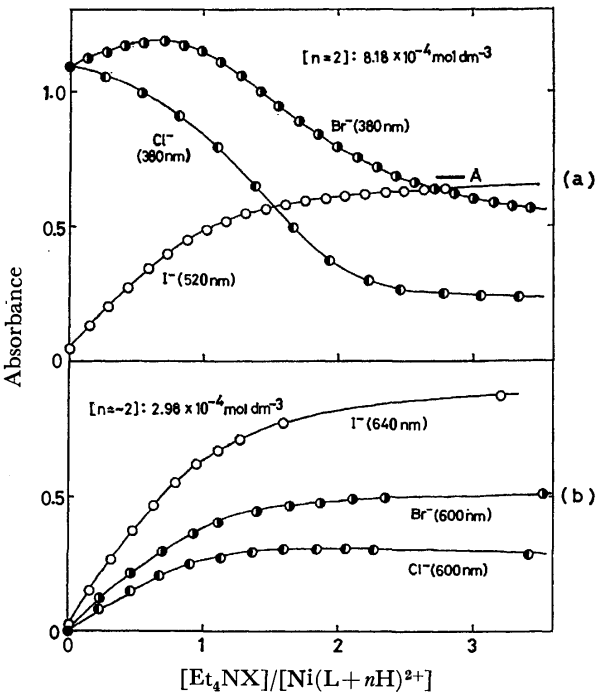

Fig. 2. The molar-ratio method applied to the systems, $[Ni(L+nH)](ClO_4)_2$ and Cl^-(◐), Br^-(◑), and I^-(○) for $n=2$ (a) and -2 (b). The horizontal line **A** indicates the calculated limiting value (see the text).

of the 4-coordinate species also supports the above result.[7] In the iodide system, the spectrum is quite different from both that of a 4-coordinate and of a 6-coordinate complex, *viz.*, a single broad absorption with much larger extinction coefficient is observed around 520 nm. This feature suggests the formation of a 5-coordinate complex with a square-pyramidal structure.[2] The formation of a 5-coordinate 1 : 1 iodo complex was confirmed by the molar-ratio method (Fig. 2(a)). The behavior of the bromide system was intermediate between those of the chloride and the iodide systems. The spectrum changed markedly, depending on the amount of the added Et_4NBr. As is clear from Fig. 2(a), the 5-coordinate complex and then the 6-coordinate complex form with an increase in the concentration of the added Et_4NBr.

In contrast to the $[Ni(L+2H)](ClO_4)_2$ system, the complexes in $[Ni(L-2H)](ClO_4)_2$–halide system exist predominantly as 5-coordinate species, regardless of the kind of halide ions (Fig. 2(b)). Incorporation of the double bonds in the macrocyclic skeleton causes an increase in the in-plane ligand field strength.[3] The tendency to form the 6-coordinate complex would be thereby decreased in the $[Ni(L-2H)]^{2+}$ system.

Table 1. Equilibrium constants at 25±0.2 °C for the reactions, $[Ni(L+nH)]^{2+}+X^- \rightleftharpoons [Ni(L+nH)X]^+$ (X=Cl⁻, Br⁻, and I⁻), and the molar extinction coefficients of $[Ni(L+nH)I]^+$

	$K_1(Cl^-)$ / 10^4 mol^{-1} dm^3	$K_1(Br^-)$ / 10^4 mol^{-1} dm^3	$K_1(I^-)$ / 10^3 mol^{-1} dm^3	ε_p / mol^{-1} dm^3 cm^{-1} (λ / nm)
Ni(L+4H)[a]	—	—	1—2	108—123 (550)
Ni(L+2H)	—	—	8.5	831 (520)[b]
Ni(L)	—	3.2	140	2500 (600)
Ni(L−2H)	3—4	2.6	19	3138 (640)

a) α-*C*-*meso* isomer (see Ref. 7). b) See the text and Fig. 2(a).

As a result of similar experiments for other systems, it was found that a relatively large amount of 5-coordinate complex forms in the systems, $[Ni(L-2H)]^{2+}$–I^-, $-Br^-$, $-Cl^-$; $[Ni(L)]^{2+}$–I^-, $-Br^-$; and $[Ni(L+2H)]^{2+}$–I^-.

For the equilibria of $[Ni(L+nH)]^{2+}$,

$$[Ni(L+nH)]^{2+} + X^- \overset{K_1}{\rightleftharpoons} [Ni(L+nH)X]^+, \quad (1)$$

the formation constant of the 5-coordinate complex, K_1, and the observed absorbance of the solution, A, are expressed as follows.[4]

$$K_1[X^-] = \frac{A-\varepsilon_s[Ni(L+nH)^{2+}]_t}{\varepsilon_p[Ni(L+nH)^{2+}]_t - A} = Y, \quad (2)$$

where [ ] and [ ]$_t$ denote the equilibrium and the total concentration, respectively, and ε_s and ε_p the molar extinction coefficient for the 4- and 5-coordinate species, respectively. The values of $[X^-]$ and Y can be calculated on the basis of the assumed ε_p. The values of K_1 and ε_p were determined by varying values of ε_p until a straight line was obtained for the plot of Y against $[X^-]$. The values of K_1 and ε_p thus obtained are listed in Table 1. For some of the systems, the linear plots were not obtained due to the predominant formation of the more stable 6-coordinate 1:2 complex.

For the $[Ni(L+2H)]^{2+}$–I^- system, the value of ε_p seemed to be reasonable judging from the position of the horizontal line **A** in Fig. 2(a), which indicates the limiting value of the absorbance for the 5-coordinate iodo complex as calculated from the evaluated ε_p. The values of $K_1(I^-)$ and $K_1(Br^-)$ lie in the range 10^3—10^5 mol^{-1} dm^3. These values are in the same order of magnitude as corresponding values of $K_1^{-1}=2.5\times10^{-4}$ mol dm^{-3} for the analogous reaction of 1,4,8,11-tetrathiacyclotetradecane, ttp, $[Ni(ttp)I]^+ \rightleftharpoons [Ni(ttp)]^{2+}+I^-$.[5] The values of the equilibrium constants in Table 1 indicate that the 5-coordinate complexes $[Ni(L)X]^+$ and $[Ni(L-2H)X]^+$ are more stable than $[Ni(L+4H)X]^+$ and $[Ni(L+2H)X]^+$. In fact, the isolation of crystalline $[Ni(L)Br]Br\cdot H_2O$ was reported.[6] The relative stabilities of the 5-coordinate complexes should be related also to the values of the equilibrium constants, $K_2(X^-)$, for the step $[Ni(L+nH)X]^+ + X^- \rightleftharpoons [Ni(L+nH)X_2]$. The value of $K_2(Br^-)$ for the formation of $[Ni(L)Br_2]$ was evaluated by an analogous method to be *ca.* 3×10^3 mol^{-1} dm^3. This value is nearly 1/10 of $K_1(Br^-)$, suggesting that the increased relative stability of 5-coordinate species compared with the 6-coordinate species in the solution containing comparable concentrations of $[Ni(L)]^{2+}$ and Br^-.

The tendency to form the 5-coordinate complexes depends on the nature of the axial as well as the in-plane ligands, and also on the easiness with which the 6-coordinate species form. For the present systems in the nitromethane solutions, 5-coordinate complexes form predominantly when the in-plane ligand field is strong and the axial ligand field is weak.

Experimental

Reagent grade nitromethane (Wako) was dried with calcium chloride and distilled. Reagent grade tetraethylammonium halides were dried over phosphorus pentaoxide and kept in the dark. The complexes **1**—**4** were prepared according to the literature.[7] The purity was confirmed by elemental analysis. The absorption spectra were measured at 25±0.2 °C with a Hitachi recording spectrophotometer model EPS-3T.

References

1) The stopped-flow measurements revealed that the formation of the 5-coordinate complexes proceeds too fast to be observed.

2) E. B. Fleischer and S. W. Hawkinson, *Inorg. Chem.*, **7**, 2312 (1968); E. K. Barefield and D. H. Busch, *ibid.*, **10**, 1216 (1971).

3) For the detailed discussion, see L. Y. Martin, C. R. Sperati, and D. H. Busch, *J. Am. Chem. Soc.*, **99**, 2968 (1977).

4) The contribution of the ion-pairs and/or the undissociated species could be regarded as negligible based on the linear relationship (Eq. 2).

5) W. Rosen and D. H. Busch, *J. Am. Chem. Soc.*, **91**, 4694 (1969).

6) J. L. Karn and D. H. Busch, *Nature*, **211**, 160 (1966). The 5-coordinate iodide species, $[Ni(L+nH)I]I$, $n=-2$ and 0, was also isolated in our laboratory. The details will be reporated elsewhere.

7) J. L. Karn, Ph.D. Dissertation, The Ohio State University, 1966; J. L. Karn and D. H. Busch, *Inorg. Chem.*, **8**, 1149 (1969); E. Ochiai and D. H. Busch, *ibid.*, **8**, 1798 (1969); E. K. Barefield, F. V. Lovecchio, N. E. Tokel, E. Ochiai, and D. H. Busch, *ibid.*, **11**, 283 (1972).

The Polarographic Reduction of Various Ammonium Cations in Hexamethylphosphoric Triamide**

Sachiko SAKURA,*,† Ryuji NAKATA, and Taitiro FUJINAGA

Department of Chemistry, Faculty of Science, University of Kyoto, Sakyo-ku, Kyoto 606

†*Department of Chemistry, Faculty of Medicine, Hamamatsu University School of Medicine, Hamamatsu 431-31*

(Received May 22, 1979)

Synopsis. The reductions of tetradecylammonium, tetradodecylammonium, benzyldimethyl(tetradecyl)ammonium, and ammonium ions were examined in hexamethylphosphoric triamide. The reduction behavior of these ions was found to be a function of the size and the charge of the cation of the supporting electrolytes.

The present authors have studied the polarographic reductions of various metal ions in hexamethylphosphoric triamide (HMPA) which is the most basic solvent in the aprotic solvents available thus far. The reduction behavior of certain kinds of metal ions is remarkably influenced by the cations of the supporting electrolyte. For example, in a 0.05 M (1 M = 1 mol dm^{-3}) tetraethylammonium perchlorate (Et_4NClO_4) solution, the sodium ion is not reduced until the reduction of the supporting electrolyte is observed. In contrast, in a lithium perchlorate ($LiClO_4$) solution, the reduction of sodium ion is diffusion-controlled.[1] From the measurements of the electrolytic conductivities, it was found that the solvated radius of the lithium ion is much larger than that of the tetraethylammonium ion, while that of the sodium ion is between them.[2] With the use of the larger cation as the supporting electrolyte, the reduction of the metal ion is promoted.

The above phenomena suggest that the relative difference in size between the supporting electrolyte cation and the depolarizing ion must control the electrode reaction. If various ammonium ions are used as the depolarizing ions, the situation is as follows; the chemical character and charge are the same, and there is only a difference in size. Therefore, it is expected that the relationship between the cation of the supporting electrolyte and that of the depolarizing ion could be made more clear.

The physical characters of various ammonium ions in HMPA have already been investigated.[3] Some of them are reduced at a very negative potential, while the others are reduced at a less negative potential. The latter were used as the depolarizing ions for the purposes of this research.

Experimental

The equipment used was a Yanagimoto polarograph, Type P8-DP. All the experiments were carried out at 25 °C±0.1 °C. All the potentials were referred to a freshly-prepared Ag/0.1 M $AgClO_4$(HMPA) electrode. The dropping mercury electrode used had the following characteristics in 0.05 M Et_4NClO_4–HMPA at h=62 cm: m=1.760 mg s^{-1} with an open circuit and t=1.450 s at −2.6 V *vs.* Ag/0.1 M Ag^+.

All the solutions were prepared from the perchlorate salts. The supporting electrolytes were 0.05 M Et_4NClO_4, tetrabutylammonium perchlorate (Bu_4NClO_4), and $LiClO_4$. As the depolarizing cation, the ammonium, benzyldimethyl(tetradecyl)ammonium (BDT^+), tetradecylammonium (Dec_4N^+), and tetradodecylammonium (Dod_4N^+) cations were used. The methods of preparing these reagents and the purification of HMPA have been described in previous papers.[1]

Results and Discussion

In Figs. 1 and 3, the polarograms of various ammonium ions in Et_4NClO_4, Bu_4NClO_4, and $LiClO_4$ solutions are shown.

Ammonium Ion: In the Et_4NClO_4 solution, the reduction of the ammonium ion was very irreversible, judging from the log-plot of the wave analysis, which was obtained by means of the plots of the values of $\log i/(i_l - i)$ and E (where i is the current at potential E and where i_l is the limiting current) (see Fig. 1 and Table 1).

When Bu_4NClO_4 was used as the supporting electrolyte, the reduction potential shifted in the positive direction. In the solution of $LiClO_4$, the potential of the reduction was shifted towards a more positive value. As the reduction wave showed a large maximum in this case, the measurement of the current heights was impossible (see also Table 1). The value of the I ($=i_l c^{-1} m^{-2/3} t^{-1/6}$; c is the concentration) of NH_4^+ in the Bu_4N^+ solution showed 0.67 $\mu A\ s^{1/2}\ mM^{-1}\ mg^{-2/3}$ (1 mM = 10^{-3} mol dm^{-3}). The caesium ion in Et_4NClO_4 has the I value of 0.74 $\mu A\ s^{1/2}\ mM^{-1}\ mg^{-2/3}$, as was shown in previous papers.[1] The reduction of the caesium ion is reversible and diffusion-controlled. From the value of the caesium ion, the diffusion coefficient should be assumed to be $1.486 \times 10^{-6}\ cm^2\ s^{-1}$. Using this, the value of n (the mol equivalent electron number) in the case of NH_4^+ reduction was obtained as 0.88 in Bu_4N^+. Therefore, the reduction, by one electron, to the neutral radical ($NH_4 \cdot Hg$) seems to have occurred, as has been reported in other aprotic solvents.[4]

Figure 2 shows the dependence of the limiting current of the ammonium ion on the square root of the height of the mercury column in the Et_4NClO_4 and Bu_4NClO_4 solutions. In the Bu_4NClO_4 solution, the height of the limiting current (i_l) was proportional to the square root of the mercury height. This means that, in this solution, the reduction process of the ammonium ion was diffusion-controlled. On the other hand, in the 0.05 M Et_4NClO_4 solution the value of i_l was proportional to $h^{1/2}$, but the line did not pass through the point of origin. In this case, therefore, the limiting current of the ammonium ion was not fully diffusion-controlled.

Benzyldimethyl(tetradecyl)ammonium (BDT^+) Ion: In the Et_4NClO_4 solution, the log-plot analysis of the

Electrochemical Studies in Hexamethylphosphoric Triamide, IX: For VIII: S. Sakura, *Bunseki Kagaku*, **28, 274 (1979).

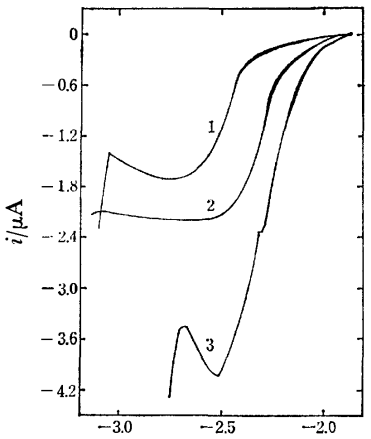

Fig. 1. Polarograms of 1.960 mM NH_4ClO_4 in HMPA solution.
Supporting electrolyte: Curve 1, Et_4N^+; Curve 2, Bu_4N^+; and Curve 3, Li^+. All are in 0.05 M.

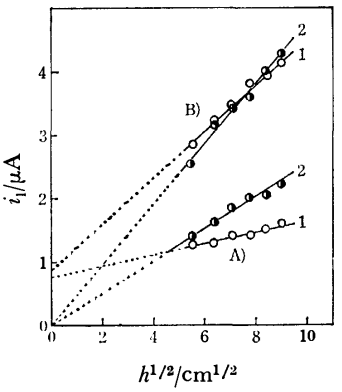

Fig. 2. Relationship between the limiting current (i_l) and square root of mercury height ($h^{1/2}$).
A) NH_4^+ and B) BDT^+.
Supporting electrolyte: Curve 1, Et_4N^+ and Curve 2, Bu_4N^+.

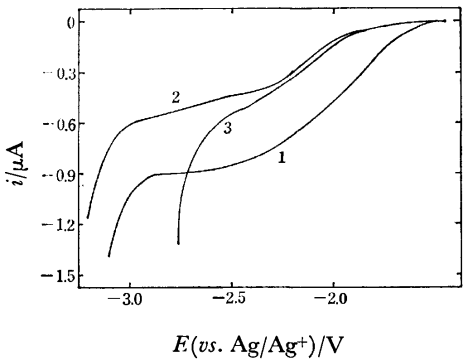

Fig. 3. Polarograms of 1.004 mM Dec_4NClO_4 in HMPA solution.
Supporting electrolyte: Curve 1, Et_4N^+; Curve 2, Bu_4N^+; and Curve 3, Li^+. All are in 0.05 M.

TABLE 1. POLAROGRAPHIC DATA OF VARIOUS AMMONIUM CATIONS IN HMPA (25.0 °C)

	Et_4N^+(4.0)		Bu_4N^+(4.9)		Li^+(5.1)	
	$E_{1/2}$/V vs. Ag/Ag+	log-plot mV	$E_{1/2}$/V vs. Ag/Ag+	log-plot mV	$E_{1/2}$/V vs. Ag/Ag+	log-plot mV
Dec_4N^+ (4.94)	−1.98	338	−2.24	330	*ca.* −2.25	280
Dod_4N^+ (4.34)	−2.03	280	−2.23	250	−2.10	180
BDT^+ (5.07)	−2.57	87	−2.45	77	*ca.* −2.50	—
NH_4^+ (4.86)	−2.48	106	−2.31	150	*ca.* −2.26	—

The values in parentheses show the solvated radii in HMPA (Ref. 3).

reduction wave of BDT^+ ion showed 87 mV. This means that the BDT^+ ion was reduced irreversibly. When Bu_4N^+ or Li^+ was used as the supporting electrolyte cation, the reduction potential of the BDT^+ ion was shifted toward a positive value. In the $LiClO_4$ solution, its reduction wave was accompanied by a large maximum, as is shown in the case of NH_4^+. The measurement of the limiting current was impossible. From the relationship between $h^{1/2}$ and i_l shown in Fig. 2, the reduction current of BDT^+ in the Et_4NClO_4 solution was found to be partly controlled by a kinetic process. On the other hand, in the Bu_4NClO_4 solution its reduction process was completely diffusion-controlled and the log-plot showed 77 mV.

Tetradecylammonium (Dec_4N^+) Ion: The polarographic reduction of Dec_4N^+ in HMPA is shown in Fig. 3. The slope of the reduction wave in any supporting electrolyte examined was very gentle, showing the process to be fairly irreversible. The values of the log-plot were 280 mV, 330 mV, and 338 mV in $LiClO_4$, Bu_4NClO_4, and Et_4NClO_4 respectively. The reduction process in $LiClO_4$ was most reversible among these three solutions, judging from the values of the log-plot. However, the values of the half-wave potential showed that Dec_4N^+ was reduced at a more positive potential in the Et_4N^+ than in the Bu_4N^+ and Li^+ solutions. In this sense, the effect of size of the supporting electrolyte cation was not the same as with ammonium or BDT^+ ion.

Tetradodecylammonium (Dod_4N^+) Ion: The polarographic behavior of Dod_4N^+ resembled that of the Dec_4N^+ ion. The reduction was most reversible in $LiClO_4$ among the three solutions, judging from the values of the log-plot of the wave analysis. The values of the half-wave potential showed that Dod_4N^+ was reduced at a more positive potential in the Et_4N^+ than in the Bu_4N^+ and Li^+ solutions. In this case, the effect of the size of the supporting electrolyte cation was the same as that for Dec_4N^+.

The relationship between the size of the supporting electrolyte cation and that of the depolarizing ion could be generally the same as in the case of the reductions of metal ions. Especially in the case of the ammonium and BDT^+ ions, the potentials of reduction shifted in the positive direction, and the process of the reduction was more reversible, when the larger cation of the supporting electrolyte was used. However, in the cases of Dod_4N^+ and Dec_4N^+, the effect of the supporting electrolyte cation was different: in Et_4N^+, the potential of $E_{1/2}$ was the most positive, though the reduction process was very irreversible. The reductions of these two cations occurred at around −2.0 V, though other normal tetraalkylammonium ions, such as the tetramethylammonium, Et_4N^+, tetrapropylammonium, Bu_4N^+, tetrahexylammonium, and tetraheptylammonium ions, were reduced at around −3.0 V.[3] Therefore, the reductions of the higher tetraalkylammonium ions, such as Dec_4N^+ and Dod_4N^+, seem to be different from those of ammonium, BDT^+, and metal ions.

References

1) K. Izutsu, S. Sakura, and T. Fujinaga, *Bull. Chem. Soc. Jpn.*, **45**, 445 (1972); *ibid.*, **46**, 493 (1973); S. Sakura, *J. Electroanal. Chem.*, **80**, 315, 325 (1977).

2) T. Fujinaga, K. Izutsu, and S. Sakura, *Nippon Kagaku Kaishi*, **1973**, 191.

3) S. Sakura, *Bunseki Kagaku*, **28**, 274 (1979).

4) C. K. Mann and K. K. Barnes, "Electrochemical Reactions in Nonaqueous Systems," Marcel Dekker, New York (1970), p. 292; J. E. Dubois, A. Monvernav, and P. C. Lacaze, *Electrochimica Acta*, **15**, 315 (1970).

Effect of Plasticizer on the Selectivity of Potassium-selective PVC Membrane Electrodes Based on Bis(crown ether)s

Hiroshi TAMURA, Keiichi KIMURA,* and Toshiyuki SHONO*

Department of Applied Chemistry, Faculty of Engineering, Osaka University, Yamada-kami, Suita, Osaka 565

(Received July 16, 1979)

Synopsis. Potassium-selective PVC membrane electrodes based on bis(crown ether)s containing benzo-15-crown-5 moiety were prepared, *o*-nitrophenyl octyl ether (NPOE) or dipentyl phthalate (DPP) being used as a plasticizer. Selectivity coefficients for various monovalent ions were measured. The preference of potassium over sodium in the bis(crown ether) (I; $n=5$)–NPOE electrode system is close to that in the valinomycin system.

Neutral carrier type ion-selective electrodes have been remarkably developed, attempts being made to prepare electrodes based on valinomycin and macrocyclic polyethers.[1,2] A report was given on the preparation of potassium-selective PVC membrane electrodes based on bis- and poly(benzo-15-crown-5)s.[3] However, the electrodes of poly(crown ether)s were impractical due to the poor response to activity change of potassium ion and the long response time, whereas the bis(crown ether)s were found to be high-selective active components.

In this note, we would like to report on the effect of plasticizers upon the selectivity of potassium-selective PVC membrane electrodes based on bis(benzo-15-crown-5)s.

Experimental

Chemicals. The syntheses of crown ether derivatives (I, II) were reported.[3] (Hexanoyloxymethyl)benzo-15-crown-5 (III) was synthesized from 4-hydroxymethyl-15-crown-5 and hexanoyl chloride in chloroform in the presence of triethylamine, and purified by recrystallization from petroleum ether. The plasticizers, NPOE and DPP were prepared according to reported methods.[4,5]

Electrode. The PVC membrane electrode was prepared as reported.[3] The electrochemical cell can be represented as follows: Ag, AgCl/0.001 M KCl/PVC membrane/measured solution/0.1 M NH_4NO_3/KCl (sat.)/Hg_2Cl_2 (s), Hg.

Measurements. All the measurements of e.m.f. were made at 25±0.1 °C using Corning pH meter 130. Standard potassium solutions for calibration plots were obtained by gradual dilution of 1 M potassium chloride solution. Selectivity coefficient k_{KM} was calculated by FIM (fixed interference method).[6] The constant concentrations of Na^+, Rb^+, Cs^+, and NH_4^+ are 1×10^{-1}, 1×10^{-3}, 1×10^{-3}, and 1×10^{-2} M, respectively.

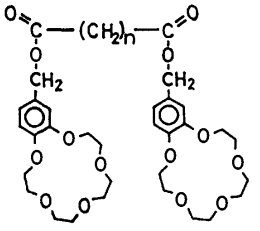

(I; n = 1,3,5,7)

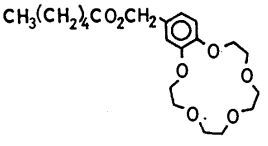

(III)

Results and Discussion

In order to elucidate the effect of plasticizer upon the electrode property, potassium-selective PVC membrane electrodes based on bis(crown ether)s (I; $n=1$, 3, 5, 7) were prepared with use of NPOE or DPP as the plasticizer. For comparison, benzo-15-crown-5 II, (hexanoyloxymethyl)benzo-15-crown-5 (III), and valinomycin (IV) were also employed as a neutral carrier. The electrode properties are sumarized in Table 1.

The electrodes of bis(crown ethers) (I; $n=1$, 3, 5, 7) showed a linear response to the activity of potassium chloride in the range 10^{-5}—10^{-1} M (1 M=1 mol dm^{-3}). The slopes of calibration plots were 55—59 mV per decade of activity change at 25 °C. These electrodes showed the same tendency in selectivity coefficients as reported.[3] The electrode of bis(crown ether) (I; $n=5$) showed the highest selectivity, which might be partly due to dependence of the chain length connecting two crown ether moieties upon the complex formation constant.[7]

The electrodes of monomeric analogs, II and III, also showed a linear response with a near-Nernstian slope in the activity range 10^{-5}—10^{-1} or -3×10^{-1} M KCl. However, the potassium-selectivity of the electrodes of I surpasses that of II about one to two order of magnitude, reflecting the high extractability of bis(benzo-15-crown-5) for potassium as compared to the monomeric analog.[8,9] Modification by a lipophilic chain such as III improves the potassium selectivity of benzo-15-crown-5.

It should be noted that the selectivity coefficients of the NPOE systems are generally much smaller than those of the DPP systems in the crown ether-based electrodes. The DPP systems are nearly equal in the selectivity coefficient to the dibutyl phthalate systems. NPOE was found to be the best plasticizer of the three in our PVC membrane electrode systems. Partition of cation to membrane should affect the selectivity of electrode, which depends on dielectric constant of plasticizer. NPOE which has a higher dielectric co sta t tha DPP is considered to increase the selectivity of electrode.

Thus, the selectivity coefficient of potassium over sodium (k_{KNa}) for the bis(crown ether) (I; $n=5$)–NPOE system is close to that for the valinomycin system. In the selectivity coefficients of potassium over other interfering ions, this system is also superior to the valinomycin system. Our potassium-selective electrodes can be compared favorably with the electrode based on valinomycin in the selectivity, electrode response, and response time (within 10 s). Moreover, they have an advantage over valinomycin-based electrodes since the

Table 1. Electrode properties of PVC membranes containing crown ether derivatives

Crown ether	Plasticizer	Maximal slope (mV/decade)	Range pK^+	k_{KM}			
				Na^+	Rb^+	Cs^+	NH_4^+
Bis(crown ether) (I; $n=1$)	NPOE[a)]	56	4.5—1	4×10^{-4}	1×10^{-1}	2×10^{-2}	1×10^{-2}
Bis(crown ether) (I; $n=3$)	NPOE	58	5—1	5×10^{-4}	1×10^{-1}	2×10^{-2}	1×10^{-2}
Bis(crown ether) (I; $n=5$)	NPOE	58	5—1	3×10^{-4}	2×10^{-1}	1×10^{-2}	1×10^{-2}
Bis(crown ether) (I; $n=7$)	NPOE	57	5—1	4×10^{-4}	1×10^{-1}	1×10^{-2}	1×10^{-2}
Monocyclic crown ether (II)	NPOE	57	5—0.5	2×10^{-3}	1	3×10^{-1}	8×10^{-2}
Monocyclic crown ether (III)	NPOE	58	5—1	1×10^{-3}	7×10^{-1}	1×10^{-1}	5×10^{-2}
Valinomycin (IV)	NPOE	59	4.5—1	2×10^{-4}	1.4	3×10^{-1}	1×10^{-1}
Bis(crown ether) (I; $n=1$)	DPP[b)]	59	5—1	5×10^{-4}	2×10^{-1}	2×10^{-2}	8×10^{-3}
Bis(crown ether) (I; $n=3$)	DPP	55	5—1	2×10^{-3}	2×10^{-1}	2×10^{-2}	1×10^{-2}
Bis(crown ether) (I; $n=5$)	DPP	56	5—1	7×10^{-4}	2×10^{-1}	1×10^{-2}	9×10^{-3}
Bis(crown ether) (I; $n=7$)	DPP	58	5—1	9×10^{-4}	2×10^{-1}	1×10^{-2}	1×10^{-2}
Monocyclic crown ether (II)	DPP	58	5—0.5	1×10^{-2}	5×10^{-1}	5×10^{-1}	1×10^{-1}
Monocyclic crown ether (III)	DPP	58	5—1	4×10^{-3}	9×10^{-1}	3×10^{-1}	8×10^{-2}
Valinomycin (IV)	DPP	59	5—1	9×10^{-5}	2.1	5×10^{-1}	2×10^{-2}

a) *o*-Nitrophenyl octyl ether. b) Dipentyl phthalate.

bis(crown ether)s can be synthesized more easily than valinomycin.

References

1) G. A. Rechnitz and E. Eyal, *Anal. Chem.*, **44**, 370 (1972).
2) M. M. Mascini and F. Pallozzi, *Anal. Chim. Acta*, **73**, 375 (1974).
3) K. Kimura, T. Maeda, H. Tamura, and T. Shono, *J. Electroanal. Chem. Interfacial Electrochem.*, **95**, 91 (1979).
4) O. Ryba and J. Petranek, *J. Electroanal. Chem. Interfacial Electrochem.*, **44**, 425 (1973).
5) *Org. Synth.*, Vol. III, 140 (1955).
6) G. J. Moody and J. D. R. Thomas, "Selective Ion-Sensitive Electrodes," Merrow, London (1971).
7) M. Bourgoin, K. H. Worg, J. Y. Hui, and J. Smid, *J. Am. Chem. Soc.*, **97**, 3462 (1975).
8) K. Kimura, T. Maeda, and T. Shono, *Anal. Lett.*, **All**, 821 (1978).
9) K. Kimura, T. Maeda, and T. Shono, *Talanta*, **26**, 945 (1979).

Synthesis and Magnetism of $M^{II}Cu^{II}_3$-type Tetranuclear Complexes, the Nickel(II) and the Cobalt(II) Complexes with *N,N'*-Bis(aminoalkyl)oxamidatocopper(II)

Hisashi Okawa,* Yukitaka Kawahara, Masahiro Mikuriya, and Sigeo Kida
Department of Chemistry, Faculty of Science, Kyushu University, Hakozaki, Higashiku, Fukuoka 812
(Received September 3, 1979)

Synopsis. Hetero-metal tetranuclear complexes, tris-[*N,N'*-bis(aminoalkyl)oxamidatocopper(II)]cobalt(II) and tris[*N,N'*-bis(aminoalkyl)oxamidatocopper(II)]nickel(II) perchlorate (or nitrate), were synthesized and characterized. Cryomagnetic investigation demonstrated that a considerably strong antiferromagnetic spin-exchange interaction is operating between copper(II) and cobalt(II) or nickel(II) ions.

Use of metal complexes as a ligand is one of the effective methods for synthesizing hetero-metal polynuclear complexes. *N,N'*-Bis(aminoalkyl)oxamidatocopper(II) acts as a bidentate ligand with its two carbonyl oxygens, and binuclear metal complexes bridged by the oxamide group were first prepared by Ojima and Nonoyama.[1] Subnormal magnetic moments of these complexes are indicative of antiferromagnetic spin-exchange interaction operating between the metal ions.[1] However, cryomagnetic investigation of the oxamide-bridged polynuclear complexes has not yet been reported.

We report here the synthesis and magnetic property of the $M^{II}Cu^{II}_3$-type tetranuclear complexes of *N,N'*-bis(aminoalkyl)oxamides, where copper(II) ions lie at the corners of a triangle with a M(II) ion at the center. *N,N'*-Bis(3-aminopropyl)oxamidatocopper(II) (abbreviated as Cu(apoxa)) and *N,N'*-bis(2-aminoethyl)-oxamidatocopper(II) (Cu(aeoxa)) were used as a ligand in this study.

Experimental

Syntheses. Cu(apoxa) and Cu(aeoxa)·$2H_2O$ were prepared by the method of Ojima and Yamada.[2] Syntheses of the tetranuclear complexes are exemplified by Co[Cu(apoxa)]$_3$(ClO_4)$_2$·$4H_2O$. Cu(aeoxa) (790 mg) and cobalt(II) perchlorate hexahydrate (366 mg) were dissolved in water (20 ml). The purple solution thus obtained was slowly concentrated at a temperature below 30 °C to give purple crystals. They were collected and dried under reduced pressure.

Elemental analyses of the complexes are given in Table 1.

Measurements. IR spectra were measured with a Hitachi IR spectrophotometer Model 215 on a KBr disk. Electronic spectra were measured with a Shimazu Multipurpose spectrophotometer Model MSP-5000 by a reflection on a powder sample. Magnetic susceptibilities were measured by the Faraday method in the temperature range 80—300 K. The apparatus was calibrated using $HgCo(NCS)_4$.[3] Magnetic moments were determined by the expression, $\mu_{eff} = 2.828\ (\chi_M \times T)^{1/2}$.

IR spectra of the tetranuclear complexes exhibit the C=O stretching band at 1590 cm^{-1}, which is practically the same in frequency as that of Cu(apoxa) and Cu(aeoxa)·$2H_2O$. On the other hand, the C=O deformation at 720 cm^{-1} of the ligand complexes[2] disappeared in the spectra of the tetranuclear complexes. This fact may be attributed to the coordination of the carbonyl oxygens to the nickel(II) and the cobalt(II) ions. The bands due to free perchlorate and nitrate ions were found around 1110 and 1380 cm^{-1} respectively.

Visible spectra of the tetranuclear complexes are characterized by a band at 18000 cm^{-1}, which is assigned to a d-d band of the copper(II) ion. The corresponding band of the mononuclear complexes is found near 20000 cm^{-1}. The shift of this band indicates that the ligand field of the [CuN_4]-chromophore is weakened when the carbonyl oxygens coordinate to the M(II) ion. The bands at 9000 and 13000 cm^{-1} for Co[Cu(apoxa)]$_3$(ClO_4)$_2$·$4H_2O$ are assigned to the $^4T_{2g} \leftarrow {}^4T_{1g}$ and the $^4A_{2g} \leftarrow {}^4T_{1g}$ transitions, respectively, of a cobalt(II) ion under O_h symmetry. The bands at 8500 and 13500 cm^{-1} for the $Ni^{II}Cu^{II}_3$-complexes are assigned to the $^3T_{2g} \leftarrow {}^3A_{2g}$ and the $^3T_{1g} \leftarrow {}^3A_{2g}$ transitions, respectively, of an octahedral nickel(II) ion. Based on the IR and visible spectral data, we assumed that the complexes possess the structure shown in Fig. 1.

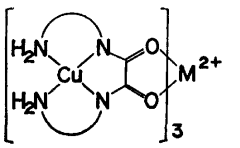

Fig. 1. Structure of complexes.

Magnetic moments of the complexes at room temperature are given in Table 1. Each moment is lower than the value expected for a magnetically non-interacting $Co^{II}Cu^{II}_3$-system (5.85 BM) and $Ni^{II}Cu^{II}_3$-system (4.53 BM), assuming the moments for copper(II), cobalt(II), and nickel(II) ions at 1.85, 4.90, and 3.20 BM, respectively. Furthermore, the moments decrease with lowering of temperature. These

Table 1. Elemental analyses and magnetic moments of complexes

	Found(%)					Calcd(%)					μ_{eff}[a] BM
	C	H	N	Cu	M	C	H	N	Cu	M	
Co[Cu(apoxa)]$_3$(ClO_4)$_2$·$4H_2O$	25.77	4.69	14.51	17.23	5.40	25.71	5.03	14.99	17.00	5.26	5.11
Ni[Cu(apoxa)]$_3$(ClO_4)$_2$·$5H_2O$	25.27	5.46	14.68	17.21	5.54	25.31	5.13	14.76	16.74	5.15	4.11
Ni[Cu(apoxa)]$_3$(NO_3)$_2$·$4H_2O$	27.73	5.01	18.40	18.70	5.54	27.56	5.40	18.74	18.22	5.61	4.21
Ni[Cu(aeoxa)]$_3$(ClO_4)$_2$·$6H_2O$	20.69	4.29	15.48	17.79	5.63	20.15	4.51	15.67	17.77	5.47	3.49

a) Moment per molecule at room temperature.

facts imply that an antiferromagnetic spin-exchange interaction is operating in the molecules.

The magnetic susceptibility expression for the $M^{II}Cu^{II}_3$-system with M(II) ion at the center and copper(II) ions at the corners of a triangle (Fig. 2) was derived by extension of Kambe's approach.[4] The Hamiltonian for this system is given by $\mathcal{H}=-J(S_T^2-S_{123}^2)$, where $S_T=S_0+S_1+S_2+S_3$ and $S_{123}=S_1+S_2+S_3$. J is the exchange integral between M(II) and copper(II) ions. The states, (S_T, S_{123}; E), formed by the spin-spin coupling for the $Co^{II}Cu^{II}_3$-system are as follows: (3, 3/2; $-6J$), $2\times$(2, 1/2; $-3J$), (2, 3/2; 0), $2\times$(1, 1/2; J), (1, 3/2; $4J$), and (0, 3/2; $6J$). By applying the Van Vleck equation,[5] the susceptibility expression for this system is given by

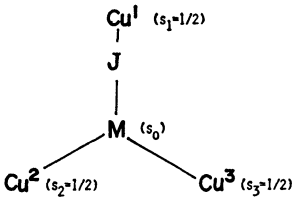

Fig. 2.

$$\chi_M = \frac{2Ng^2\beta^2}{kT} \times \frac{14\exp(6J/kT)+10\exp(3J/kT)+5+2\exp(-J/kT)+\exp(-4J/kT)}{7\exp(6J/kT)+10\exp(3J/kT)+5+6\exp(-J/kT)+3\exp(-4J/kT)+\exp(-6J/kT)} \quad (1)$$

where each symbol has its usual meaning. In the same way the states, (5/2, 3/2; $-5J$), $2\times$(3/2, 1/2; $-3J$), (3/2, 3/2; 0), $2\times$(1/2, 1/2; 0), and (1/2, 3/2; $3J$), are formed for the $Ni^{II}Cu^{II}_3$-system. The magnetic susceptibility expression for this system is given by

$$\chi_M = \frac{Ng^2\beta^2}{2kT} \times \frac{35\exp(5J/kT)+20\exp(3J/kT)+12+\exp(-3J/kT)}{6\exp(5J/kT)+8\exp(3J/kT)+8+2\exp(-3J/kT)} + N\alpha. \quad (2)$$

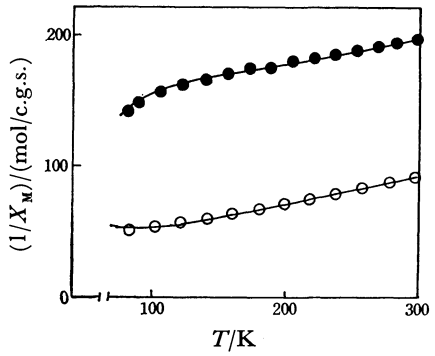

Fig. 3. Temperature variations of inverse magnetic susceptibilities of (○) $Co[Cu(apoxa)]_3(ClO_4)_2\cdot 4H_2O$ and (●) $Ni[Cu(aeoxa)]_3(ClO_4)_2\cdot 6H_2O$. Solid lines represent the theoretical values drawn on the basis of the expression (1) with $J=-23$, $g=2.29$ and $N\alpha=450\times 10^{-6}$ (top) and the expression (2) with $J=-75\ cm^{-1}$, $g=2.20$ and $N\alpha=400\times 10^{-6}$ c.g.s./mol (bottom).

Magnetic susceptibilities of $Co[Cu(apoxa)]_3(ClO_4)_2\cdot 4H_2O$ and $Ni[Cu(aeoxa)]_3(ClO_4)_2\cdot 6H_2O$ were well interpreted in terms of the expressions (1) and (2), respectively. The best fits between the experimental and the theoretical inverse susceptibilities are shown in Fig. 3. Magnetisms of $Ni[Cu(apoxa)]_3(ClO_4)_2\cdot 5H_2O$ and $Ni[Cu(apoxa)]_3(NO_3)_2\cdot 4H_2O$ also obeyed the expression (2). The magnetic parameters determined are as follows. $Ni[Cu(apoxa)]_3(ClO_4)_2\cdot 5H_2O$: $-J=42$, $g=2.49$, and $N\alpha=400\times 10^{-6}$; $Ni[Cu(apoxa)]_3(NO_3)_2\cdot 4H_2O$: $-J=49\ cm^{-1}$, $g=2.40$, and $N\alpha=400\times 10^{-6}$ c.g.s./mol. However, the g values of these complexes are large compared with 2.20 of $Ni[Cu(aeoxa)]_3(ClO_4)_2\cdot 6H_2O$. This would be indicative of the presence of paramagnetic impurity such as hexaaquanickel(II) ion. If this is taken into consideration, the $-J$ values for these complexes might exceed the values obtained above. Thus, we may conclude that a considerably strong antiferromagnetic spin-exchange interaction operates between the copper(II) and M(II) ions through the oxamidebridge.

References

1) H. Ojima and K. Nonoyama, *Z. Anorg. Allg. Chem.*, **429**, 282 (1977).
2) H. Ojima and K. Yamada, *Nippon Kagaku Kaishi*, **89**, 490 (1968).
3) B. N. Figgis and R. S. Nyholm, *J. Chem. Soc.*, **1959**, 331.
4) K. Kambe, *J. Phys. Soc. Jpn.*, **5**, 48 (1950).
5) J. H. Van Vleck, "Electric and Magnetic Susceptibilities," Oxford Univ. Press, London (1932).

Complexation of Arenediazonium Ions with a Macrocyclic Polyether. The Stability Constants for the Complexes

Yoji HASHIDA* and Kohji MATSUI

Department of Synthetic Chemistry, Faculty of Engineering, Gunma University, Kiryu, Gunma 376

(Received May 10, 1979)

Synopsis. The stability constants for 18-crown-6 complexes with arenediazonium salts have been determined spectrophotometrically. The Hammett plot for *m*- and *p*-substituted benzenediazonium salts showed good correlation with a reaction constant 0.98 in methanol. The solvent effect on the stability of the complexes has been discussed.

Complexation of arenediazonium ions with macrocyclic polyethers, *i.e.* crown ethers, have been elucidated by NMR[1,2] and IR[3] spectroscopy. Such complexation with the appropriate crown ether reduces the thermal[4] and photochemical[5] decomposition of arenediazonium ions. Several preparative uses for crown ethers which include halogen displacement[6] and effective arylation[7,8] of aromatic substrates have been explored. This note will deal with the stability constants (K_S) for the 18-crown-6 complexes with arenediazonium salts:

$$Ar\text{-}N_2^+BF_4^- + P \overset{K_s}{\rightleftharpoons} Ar\text{-}N_2^+,\ P,\ BF_4^- \qquad (1)$$

$$K_s = [Ar\text{-}N_2^+,\ P,\ BF_4^-]/[Ar\text{-}N_2^+BF_4^-][P]$$

where P denotes the crown ether. 18-Crown-6 was chosen as the host, since it has an appropriate cavity size for the diazonium ion,[2] and is transparent in the UV region.

It has been found that the absorption maxima of arenediazonium ions shift to shorter wavelengths on complexation with the crown ether. Figure 1 shows a typical spectral change for the *p*-methoxybenzenediazonium salt in chloroform with increasing addition of 18-crown-6. The difference in UV spectra was used as an analytical tool to determine the stability constant, by adding known amounts of diazonium salt and crown compound into the solvent (see Experimental).

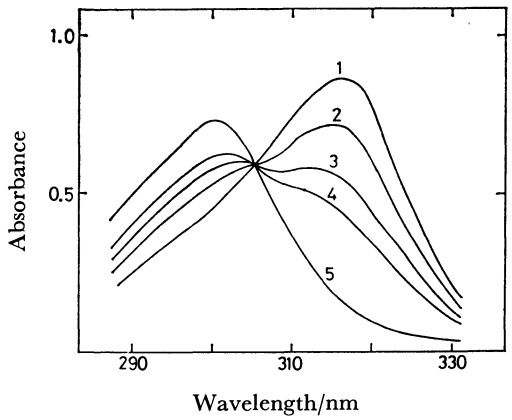

Fig. 1. UV spectrum of *p*-methoxybenzenediazonium tetrafluoroborate in chloroform in the absence and presence of 18-crown-6; $[Ar\text{-}N_2^+BF_4^-]_0 = 2.19 \times 10^{-5}$ M, (1), $[P]_0 = 0$, (2) $[P]_0 = 1.2 \times 10^{-4}$ M, (3), $[P]_0 = 2.3 \times 10^{-4}$ M, (4) $[P]_0 = 4.7 \times 10^{-4}$ M, (5) $[P]_0 = 5.2 \times 10^{-2}$ M (Further addition of the crown ether did not change the spectrum).

The stability constants measured in several organic solvents are given in Table 1, together with the spectral properties of diazonium ions and their complexes. The

Table 1. Stability constants (K_S) for the 18-crown-6 complexes with (X)-substituted benzenediazonium tetrafluoroborates at 15 °C

No.	Substituent (X)	Solvent	ε[a]	E_T[b]	pK_a[c]	log K_s[d]	λ_{max}^{Dz}/nm[e]	λ_{max}^{Cx}/nm[e]
1	*p*-NO_2	Methanol	32.7	55.5	−2.2	3.10	256	249
2	*p*-CN	Methanol				3.15	262	255
3	*m*-Cl	Methanol				2.71	261	251
4	*m*-OCH_3	Methanol				2.63	275	260
5	H	Methanol				2.46(2.37)[f]	259	247
6	*p*-CH_3	Methanol				2.39(2.26)[f]	275	266
7	*p*-OCH_3	Methanol				2.09	311	297
8	*p*-$N(CH_3)_2$	Methanol				1.56	380	362
9	*p*-OCH_3	Dioxane	2.2	36.0	−2.92	1.87	309	302
10	*p*-OCH_3	THF	7.6	37.4	−2.08	2.27	309	299
11	*p*-OCH_3	Acetone	20.7	42.2	−7.2	2.56	327	323
12	*p*-OCH_3	CH_2Cl_2	9.1	41.1		3.23	328	295
13	*p*-OCH_3	$CHCl_3$	4.8	39.1		3.45	317	301
14	*p*-OCH_3	$ClCH_2CH_2Cl$	10.4	41.9		4.67	321	298
15	*p*-CH_3	$ClCH_2CH_2Cl$				5.10	282	264
16	*o*-CH_3	$ClCH_2CH_2Cl$				3.97	270	250
17	2,6-$(CH_3)_2$	$ClCH_2CH_2Cl$				2.01	274	265

a) Dielectric constant of solvent (from Ref. 16). b) Ref. 13. c) Ionization constant of conjugate acid of solvent (from Ref. 16). d) K_S: M^{-1} e) Maximum wavelength for the free diazonium ion (λ_{max}^{Dz}) and its complex (λ_{max}^{Cx}). f) Ref. 9.

observed stability constants are in reasonable agreement with those determined by titration calorimetry (Nos. 5, 6).[9]

One interesting aspect in Table 1 is the structural effect of diazonium salts on the stability of the complexes. The stability constant depended on the nature of the substituent in the diazonium salt as expected, *i.e.* as the electrophilicity of the diazonio group increases, the stability of the complex increased. The Hammett plot for the *m*- and *p*-substituted compounds (Nos. 1—8) shows a good correlation; a least-squares treatment gives an equation, $\log K_s = 0.98\sigma + 2.43$ with a correlation coefficient (r) of 0.986. The ρ value found is relatively low compared with those in other diazo-equilibrium systems, such as arenediazocyanide-($\rho = 3.53$),[10] arenediazosulfone-($\rho = 3.76$),[11] arenediazosulfonate)-($\rho = 5.5$),[12] and arenediazotate-formation ($\rho = 6.58$).[10] Ortho-substitution on the diazonium ion considerably reduces complex stability; the introduction of the *o*-methyl (No. 16) and 2,6-dimethyl groups (No. 17) lowered the pK_s by *ca.* one and three units respectively. This behavior undoubtedly results from steric hindrance.[2]

It was shown that the solvent has a pronounced effect on the stability (Nos. 7, 9—14). As can be seen, there is no observable correlation between stability of the complex and the common solvent properties such as dielectric constant and E_T-value.[13] Rather, the stability of the complex appears to be influenced by the basicity of the solvent, *i.e.* relatively stable complexes were formed in less basic solvents such as acetone and chlorinated alkanes.[14] This is explainable since the free diazonium ion is more stabilized by significant solvation in a solvent of higher basicity.

Experimental

Materials. 18-Crown-6 was prepared as described in the literature[15] (mp 38—40 °C). Arenediazomiun fluoroborates were prepared using reagent grade aromatic amines and purified by dissolving them in the minimum amount of acetonitrile, followed by reprecipitation with the addition of diethyl ether. The solvents were purified by standard procedures.[16]

pK_s *Measurement.* A solution of the diazonium salt *ca.* 2×10^{-4} M (1 M = 1 mol dm^{-3}) was prepared. In a typical run, a sample (5 ml) of this solution was added to a mixture of MeOH–H_2O (1 : 1, in volume) containing the R-salt (2-naphthol-3,6-disulfonic acid) and sodium carbonate; the solution was subsequently diluted to a specified volume and the absorbance measured, in order to determine the original concentration of diazonium salt. The remaining diazonium solution was employed for pK_s measurements; known quantities of the solution were added to a solution containing specified amounts of crown ether and the optical spectrum recorded at 15 °C. The stability constant K_s based on the Eq. 1 was calculated using a spectrally determined [Ar–N_2^+, P, BF_4^-]/[Ar–$N_2^+BF_4^-$] ratio under a given condition, in conjuction with the following equations;

$$[\text{Ar–N}_2^+\text{BF}_4^-]_0 = [\text{Ar–N}_2^+\text{BF}_4^-] + [\text{Ar–N}_2^+, \text{P}, \text{BF}_4^-]$$

$$[\text{P}]_0 = [\text{P}] + [\text{Ar–N}_2^+, \text{P}, \text{BF}_4^-]$$

where [Ar–$N_2^+BF_4^-$]$_0$ and [P]$_0$ denote the original concentrations of diazonium salt and the crown ether, respectively.

References

1) G. W. Gokel and D. G. Cram, *J. Chem. Soc., Chem. Commun.*, **1973**, 481.
2) E. P. Kyba, R. C. Helgeson, K. Madan, G. W. Gokel, T. L. Tarnowski, S. S. Moore, and D. J. Cram, *J. Am. Chem. Soc.*, **99**, 2564 (1977).
3) B. L. Haymore, J. A. Ibers, and D. W. Meek, *Inorg. Chem.*, **14**, 541 (1975).
4) R. A. Bartsch, H. Chen, N. F. Haddock, and P. N. Juri, *J. Am. Chem. Soc.*, **98**, 6753 (1976).
5) R. A. Bartsch, N. F. Haddock, and D. W. McCann, *Tetrahedron Lett.*, **1977**, 3779.
6) G. W. Gokel, S. H. Korzeniowski, and L. Blum, *Tetrahedron Lett.*, **1977**, 3779.
7) S. H. Korzenioski and G. W. Gokel, *Tetrahedron Lett.*, **1977**, 1637.
8) H. K. Stephen, B. Lorna, and W. G. George, *Tetrahedron Lett.*, **1977**, 1871.
9) R. M. Izatt, J. D. Lamb, B. E. Rossister, N. E. Izatt, and *J. J. Christensen, J. Chem. Soc., Chem. Commun.*, **1978**, 386.
10) C. D. Ritchie and D. J. Wright, *J. Am. Chem. Soc.*, **93**, 6574 (1971). For a more detailed discussion of ρ values in diazotate formation, see Ref. 10.
11) C. D. Ritchie, J. D. Saltiel, and E. S. Lewis, *J. Am. Chem. Soc.*, **83**, 4601 (1961).
12) E. S. Lewis and H. Suhr, *Chem. Ber.*, **92**, 3031 (1959).
13) K. Dimroth, C. Reichardt, T. Siepmann, and F. Bohlmann, *Justus Liebigs Ann. Chem.*, **661**, 1 (1963).
14) The pK_a-value for chlorinated alkanes has not been reported. The lower basic properties, however, have been elucidated by infrared spectrophotometry: a) A. G. Burden, G. Collier, and J. Shorter, *J. Chem. Soc., Perkin Trans. 2*, **1976**, 1627; b) E. M. Arnett, "Progress in Physical Organic Chemistry," Interscience, New York (1963), Vol. 1, p. 223.
15) G. W. Gokel, D. J. Cram, C. L. Liotta, H. P. Harris, and F. L. Cook, *J. Org. Chem.*, **39**, 2445 (1974).
16) J. A. Riddick and E. E. Toops, Jr., "Organic Solvents," ed by A. Weissberger, Interscience Publishers, New York (1955).

Phenyl- and Tolylthallium(III) Bis(trichloroacetate)s; Preparation and Reactions

Sakae UEMURA,* Haruo MIYOSHI, Mikio WAKASUGI, Masaya OKANO, Osamu ITOH,** Takaaki IZUMI,** and Katsuhiko ICHIKAWA**

Institute for Chemical Research, Kyoto University, Uji, Kyoto 611

***Department of Hydrocarbon Chemistry, Faculty of Engineering, Kyoto University, Kyoto 606*

(Received May 28, 1979)

Synopsis. Phenyl- and tolylthallium(III) bis(trichloroacetate)s [$ArTl(OCOCCl_3)_2$, **1** (Ar=phenyl or tolyl)] were prepared from thallium(III) oxide, trichloroacetic acid, benzene, and toluene. The replacement of the thallium moiety in **1** with iodo, chloro, cyano, selenocyanato, and nitro groups and the aromatic coupling of **1** proceeded smoothly to give the corresponding aromatic derivatives in good yields. In the presence of $PdCl_2$–NaOAc, **1** (Ar=phenyl) reacted with acrylonitrile and methacrylonitrile to afford cinnamonitriles(*trans* and *cis*) and a mixture of α-benzylacrylonitrile and β-phenylmethacrylonitriles(*Z* and *E*) respectively.

Direct aromatic thallation by thallium(III) acetate–$HClO_4$ in acetic acid[1] or thallium(III) trifluoroacetate in trifluoroacetic acid[2] is an effective method for the preparation of arylthallium(III) compounds, which are useful in organic syntheses. However, trifluoroacetic acid is an expensive and hazardous reagent, and the method using $HClO_4$ is dangerous in some cases because of the danger of explosion.[3] We have now found a simple method for direct aromatic thallation using trichloroacetic acid, useful for large-scale syntheses in the cases of benzene and toluene. We wish to report the preparation of phenyl- and tolylthallium(III) bis(trichloroacetate)s [$ArTl(OCOCCl_3)_2$, **1** (Ar=phenyl or tolyl)] and their use in organic syntheses.

A mixture of benzene or toluene, thallium(III) oxide, and trichloroacetic acid was stirred at 65—70 °C for 1—5 h to give a white solid of **1** (Scheme 1). The reaction conditions, the yields of **1**, the melting points,

$$2ArH + Tl_2O_3 + 4CCl_3CO_2H \longrightarrow 2ArTl(OCOCCl_3)_2 \quad (1)$$

1

the isomer ratios, and the analytical and ^1H-NMR data are shown in Table 1. The scope of this aromatic thallation is, unfortunately, very limited; thus, **1** could not be obtained from anisole, thiophene, nitrobenzene, benzaldehyde, or methyl benzoate.[4] No aromatic thallation of benzene and toluene occurred when acetic, chloroacetic, or dichloroacetic acid was used under the conditions shown in Table 1.

The replacement of the thallium moiety in arylthallium(III) compounds with halogen,[5] pseudohalogen,[6] and a nitro group[7] and the aryl-coupling reaction[8] have been reported to give the corresponding aromatic derivatives. Although the yields of the products have depended on the kind of ligand on the thallium (*i.e.*, the yield of ArX is sometimes very low when the ligand is CN, Cl, OAc, or SCN), **1** where a ligand is CCl_3CO_2 was subjected quite successfully to all such reactions. Some typical results of the application of these reactions to **1** are summarized in Table 2. It has been known that arylthallium(III) compounds reacted with styrene and methyl acrylate in the presence of Li_2PdCl_4, the overall reaction being the replacement of an olefinic hydrogen by the aryl group.[9] When **1** (Ar=phenyl) was treated with styrene, ethyl acrylate, acrylonitrile, and methacrylonitrile in acetic acid or methanol in the presence of palladium(II) chloride or palladium metal and sodium acetate, *trans*-stilbene, ethyl cinnamate, cinnamonitriles(*trans*: *cis*=59: 41), and a mixture of α-benzylacrylonitrile (**2**) and (*Z*)- and (*E*)-β-phenylmethacrylonitriles (**3** and **4**) (**2**: **3**: **4**=55: 26: 19)

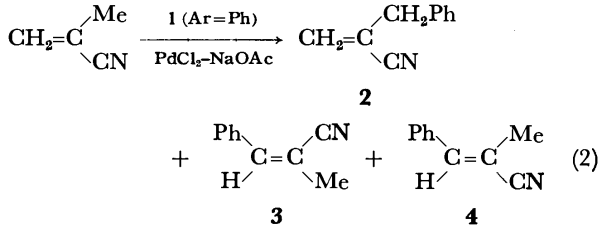

2

(Scheme 2) were produced respectively in good to excellent yields.[10] The product distributions in the latter two reactions were very close to those obtained in the reaction of phenylmercury(II) chloride under similar conditions, showing the presence of the same reactive species, probably the phenylpalladium(II) species. This is the first example of the arylation of α,β-unsaturated nitriles by the use of arylthallium(III) compounds and also of the arylation of olefins by arylthallium(III) compounds by the use of palladium metal as a catalyst. Some typical results are listed in Table 2.

TABLE 1. PREPARATION OF **1** AND THEIR CHARACTERIZATION

Aromatics (mol)		Tl_2O_3 (mol)	CCl_3CO_2H (mol)	Yield of **1** (%) Ar		Mp (dec) (°C)	Found (Calcd) (%) C	H	NMR (in CH_3OD) *o*-	*m*-	*p*-	J_{Tl-H}(Hz) *p*-CH_3
Toluene[a]	0.7	0.03	0.12	Tolyl[c]	64	182—184	21.62 (21.30)	1.44 (1.14)	974	358		58
Benzene[b]	0.8	0.03	0.12	Phenyl	66	220	19.74 (19.81)	1.02 (0.83)	915	345	115	

a) At 70 °C for 1 h. b) At 70 °C for 5 h. c) *o*: *m*: *p*=9: 5: 86, determined by analyzing the products obtained by nitrodethallation.[7]

Table 2. Results of the reactions of **1** with various reagents

1 (2 mmol) Ar	Reagent (mmol)		Solvent (ml)		Temp (°C)	Time (h)	Product and yield(%)[a]
Ph	KI	10	$THF+H_2O$	10+10	65	0.5	Iodobenzene 71
Tolyl	KI	10	$THF+H_2O$	10+10	65	0.5	Iodotoluene 94[b,c]
Ph	$CuCl_2 2H_2O$	2	Dioxane	20	101	5	Chlorobenzene 69
Ph	CuCN	8	Pyridine	20	115	4	Benzonitrile 64
Ph[c]	$Cu(SeCN)_2$	279	Dioxane	200	101	0.5	Selenocyanatobenzene 71
Tolyl	$NaNO_2$	6	CF_3CO_2H	15	25	3	Nitrotoluene 90[d]
Ph	$PdCl_2$	2	AcOH	20	117	1	Biphenyl 100
	NaOAc	4					
Ph	$PdCl_2$	2	AcOH	20	117	1	*trans*-Stilbene 86
	NaOAc	4					
	Styrene	10					
Ph	$PdCl_2$	2	AcOH	20	117	1	Ethyl cinnamate 91
	NaOAc	4					
	Ethyl acrylate	10					
Ph	Pd^0	2	MeOH	20	66	1	*trans*-Stilbene 100
	NaOAc	4					
	Styrene	10					
Ph	$PdCl_2$	2	AcOH	20	117	4	*trans*- and *cis*-Cinnamonitriles[e] 100
	NaOAc	4					
	Acrylonitrile	10					
Ph	$PdCl_2$	2	AcOH	20	117	4	**2**+**3**+**4**[f] 61
	NaOAc	4					
	Methacrylonitrile	10					

a) Determined by GLC. b) Isomer ratio not determined. c) Preparative scale experiment. **1** (Ar=Ph), 162 mmol. The yield is the isolated one (see Experimental). d) *o*: *m*: *p*=9: 5: 86. e) *trans*: *cis*=59: 41. Reaction with PhHgCl (for 1 h) afforded an 80% yield of a mixture of *trans*- and *cis*-cinnamonitriles (*t*: *c*=65: 35). f) **2**: **3**: **4**=55: 26: 19. Reaction with PhHgCl (for 1 h) gave a 57% yield of a mixture of **2**, **3**, and **4** (**2**: **3**: **4**=46: 31: 23).

Experimental

All the organic materials were commercial products and were distilled before use. Commercial inorganic materials were used without further purification. The organic product mixtures were analyzed by GLC by the use of a Shimadzu 4BMPF apparatus on EGSS-X-(15%)-Chromosorb-W (1 or 3 m) and Apiezon-L (1 m) columns (carrier gas, N_2). The NMR spectra were recorded on a Varian EM-360 spectrometer in CH_3OD, $CDCl_3$, or CCl_4, using tetramethylsilane as the internal standard.

Preparation of **1** *(Ar=phenyl).* A brown heterogeneous mixture of thallium(III) oxide (Tl_2O_3, 13.7 g, 30 mmol), trichloroacetic acid (19.6 g, 120 mmol), and benzene (70 ml) was stirred at 70 °C for 5 h to give a white, heterogeneous mixture. After the mixture had been cooled down to room temperature, the solid was filtered off, washed with benzene, and dried *in vacuo* over silica gel. Almost pure **1** (Ar=phenyl) was thus obtained; 24.0 g (39.6 mmol, 66% yield based on Scheme 1). This is soluble in alcohols, tetrahydrofuran, dimethyl sulfoxide, *N*,*N*-dimethylformamide, and pyridine and insoluble in chloroform, carbon tetrachloride, diethyl ether, and hexane.

The reaction of toluene was similarly carried out to give pure **1** (Ar=tolyl, *o*: *m*: *p*=9: 5: 86) in a 64% yield.

Preparation of Phenyl Selenocyanate from **1** *(Ar=phenyl).* The following is a typical example of the reactions of **1** with various reagents on a preparative scale. A black suspension of **1** (Ar=phenyl) (98.4 g, 162 mmol) and $Cu(SeCN)_2$ (76.2 g, 279 mmol) in dioxane (200 ml) was stirred at reflux for 0.5 h. After the mixture had then been cooled to room temperature, the precipitated dark grey solid was filtered off and washed with ether (*ca.* 50 ml). Water (200 ml) was added to the combined solution of the filtrate and the ether washing, and then it was extracted with ether (200 ml×3). The ether extract was washed with aqueous NaCl and dried over $MgSO_4$. Distillation afforded 21 g (115 mmol, 71% yield) of almost pure phenyl selenocyanate; bp 110—120 °C/4 mmHg (lit,[11] bp 134 °C/10 mmHg).

We wish to thank Dr. Takuzo Funabiki for kindly supplying *trans*- and *cis*-cinnamonitriles, **3**, and **4** for GLC analysis. This research is partly supported by a grant from the Ministry of Education.

References

1) K. Ichikawa, S. Uemura, T. Nakano, and E. Uegaki, *Bull. Chem. Soc. Jpn.*, **44**, 545 (1971).

2) A. McKillop, J. D. Hunt, M. J. Zelesko, J. S. Fowler, E. C. Taylor, G. McGillivray, and F. Kienzle, *J. Am. Chem. Soc.*, **93**, 4841 (1971).

3) S. Uemura, Y. Ikeda, O. Itoh, and K. Ichikawa, *Bull. Chem. Soc. Jpn.*, **44**, 2571 (1971).

4) From ethylbenzene at 70 °C for 24 h, a pure **1** (Ar=ethylphenyl) could not be obtained, the nitrodethallation of the crude product showing the formation of at least a 9% yield of **1** (*o*: *m*: *p*=10: 8: 82). In this case, 1-phenylethyl trichloroacetate was also formed: isolated yield, 14%; bp 110 °C/5 mmHg; NMR (δ, $CDCl_3$), 1.65 (d, 3H), 5.92 (q, 1H), 7.27 (s, 5H). From chlorobenzene at 65—70 °C for 20 h, **1** (Ar=chlorophenyl) was obtained in an 18% yield; mp 205 °C (dec) (*o*: *m*: *p*=24: ≈0: 76).

5) S. Uemura, Y. Ikeda, and K. Ichikawa, *Tetrahedron*, **28**, 5499 (1972).

6) S. Uemura, Y. Ikeda, and K. Ichikawa, *Tetrahedron*, **28**, 3025 (1972); S. Uemura, A. Toshimitsu, M. Okano, and K. Ichikawa, *Bull. Chem. Soc. Jpn.*, **48**, 1925 (1975).

7) S. Uemura, A. Toshimitsu, and M. Okano, *Bull. Chem. Soc. Jpn.*, **49**, 2582 (1976).

8) S. Uemura, Y. Ikeda, and K. Ichikawa, *Chem. Commun.*, **1971**, 390.

9) T. Spencer and F. G. Thorpe, *J. Organomet. Chem.*, **99**, C8 (1975).

10) A mixture of **2**, **3**, and **4** was isolated by distillation; bp 120—125 °C/20 mmHg; Found: C, 83.95; H, 6.25; N, 9.46%. Calcd for $C_{10}H_9N$: C, 83.88; H, 6.34; N, 9.78%. NMR (δ, CCl_4) for **2**, 3.58 ($PhC\underline{H}_2$), 5.72 and 5.96 ($=C\underline{H}_2$).

11) F. Challenger and A. T. Peters, *J. Chem. Soc.*, **1928**, 1364.

A New Catalytic System for the Preparation of Chromanols

Yoji TACHIBANA

Ueda Factory, Nisshin Chemical Co., Ltd., Kamishiodiri, Ueda, Nagano 386

(Received June 6, 1979)

Synopsis. In the presence of the cation exchange resin complexes of metal ions, hydroquinone, resorcinol, and catechol reacted with phytyl chloride to give chromanols in good yields. The enhanced activity of the catalysts compared with the corresponding metal halides has been ascribed to the participation of the sulfonyl group in the abstraction of the proton on the benzene ring or the hydroxyl group. The catalysts were recycled several times with little loss of activity.

The study of anchoring homogeneous catalysts to a solid support has been developed on account of the ease in separation of product, the ability to carry out sequential catalytic reaction and positional selectivity.[1-3] It has been reported that the cation exchange resin complexes of metal ions are useful catalysts for the preparation of vitamin E.[4] In the course of studying the uses of the metal resin catalysts, it was found that these catalysts showed enhanced selectivity in the preparation of other chromanols compared with the corresponding metal halides.

In the presence of metal resin catalysts, the reaction of phytyl chloride with hydroquinone, resorcinol and catechol afforded I, II, and III, IV in good yields, respectively. Each product was characterized by elemental analysis, IR, NMR, and mass spectroscopy, the results of which are given in Table 1. The catalysts were recycled for use several times with little loss of activity, the results of which are summarized in Table 2, together with the results using metal halides for comparison. In the preparation of vitamin E from trimethylhydroquinone, little difference in selectivity was observed between the metal resin catalyst and metal halide.[4] The use of hydroquinone, resorcinol, and catechol in place of trimethylhydroquinone gave chromanols in poor yields when catalyzed by metal halides. The low selectivity has been attributed to the lower electron density of the benzene rings of hydroquinone, resorcinol, and catechol compared to trimethylhydroquinone. Therefore, the degradation of phytyl chloride by metal halides is more likely to occur than with trimethylhydroquinone. The yield of chromanol decreased in the order; resorcinol> hydroquinone> catechol which agrees with the order of electron density on the ortho or para position for the hydroxyl group.

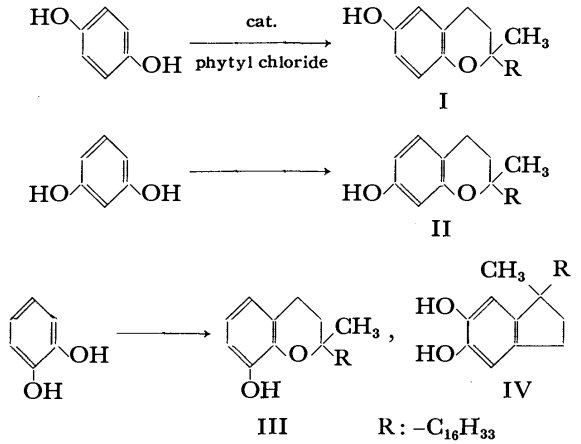

The metal resin catalysts appear to enhance the activity of the substrate, resulting in higher yields of chromanols. The enhanced selectivity in the reaction catalyzed by the metal resin catalysts has been explained by assuming the participation of the sulfonyl group of the resin in the abstraction of the proton on the benzene ring (Scheme 1) or the hydroxyl group[5] (Scheme 2),

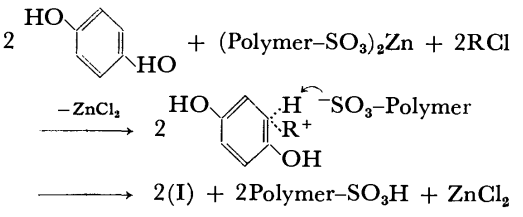

Scheme 1.

TABLE 1. SPECTRAL DATA AND ELEMENTAL ANALYSIS

	I	II	III	IV
NMR (CCl_4) δ/ppm	0.85 (12H, d, isoprenoid CH_3), 1.00—1.60 (24H, bs, CH_3, isoprenoid CH_2, CH), 1.70 (2H, t, CH_2), 2.60 (2H, t, CH_2), 5.23 (1H, s, OH), 6.00—6.83 (3H, m, aromatic)	0.86 (12H, d, isoprenoid CH_3), 1.00—1.56 (24H, bs, CH_3, isoprenoid CH_2, CH), 1.70 (2H, t, CH_2), 2.63 (2H, t, CH_2), 5.00 (1H, s, OH), 6.26—6.69 (3H, m, aromatic)	0.85 (12H, d, isoprenoid CH_3), 1.00—1.66 (24H, d, CH_3, isoprenoid CH_2, CH), 1.80 (2H, t, CH_2), 2.73 (2H, t, CH_2), 5.53 (1H, s, OH), 6.50—6.83 (3H, m, aromatic)	0.87 (12H, d, isoprenoid CH_3), 1.00—1.60 (24H, d, CH_3, isoprenoid CH_2, CH), 1.77 (2H, t, CH_2), 2.66 (2H, t, CH_2), 5.50 (2H, bs, OH), 6.47 (1H, s, aromatic), 6.57 (1H, s, aromatic)
Mass (*m/e*)	388 (M^+), 163 (M^+—R,) 123	388 (M^+), 163 (M^+—R), 123	388 (M^+), 163 (M^+—R), 123	388 (M^+), 163 (M^+—R), 123
IR $\bar{\nu}$/cm	3330, 2840, 1610, 1480, 1440, 1370, 1220, 1140	3400, 2920, 1630, 1600, 1520, 1470, 1390, 1150, 1000	3560, 2840, 1600, 1460, 1360, 1200,	3320, 2840, 1600, 1440, 1300, 1180
Found (Calcd) (%) C	80.12 (80.35)	80.08 (80.35)	80.21 (80.35)	80.07 (80.35)
Found (Calcd) (%) H	11.36 (11.41)	11.21 (11.41)	11.33 (11.41)	11.16 (11.41)

Table 2. Effect of recycling catalyst

Substrate	Metal ion	Run	Yield/%[a]
Hydroquinone	Zn	1	81
		2	77
		3	71
		4	70
	Sn	1	71
		2	74
		3	71
		4	70
	Al	1	63
		2	60
		3	58
		4	57
	$ZnCl_2$		38
	$SnCl_4$		52
	$AlCl_3$		18
Resorcinol	Zn	1	87
		2	84
		3	81
		4	77
	Al	1	73
		2	73
		3	70
		4	67
	$ZnCl_2$		25
	$AlCl_3$		38
Catechol	Zn	1	46 (49)[b]
		2	44 (45)
		3	45 (38)
		4	43 (35)
	Sn	1	40 (52)
		2	40 (50)
		3	39 (45)
		4	36 (41)
	$ZnCl_2$		30 (32)
	$SnCl_4$		15 (0)

Substrate: 90 mmol, phytyl chloride: 90 mmol, catalyst: 45 mmol (as metal ion), benzene: 100 ml, temp: reflux temp, and time 3 h. a) By GLC. b) Yield of IV.

thereby facilitating substitution of the cation derived from phytyl chloride. In Scheme 2, the interaction of the $Zn(SO_3)$-polymer with the oxygen atom of the hydroxyl group may be included to activate the substrate. The latter mechanism (Scheme 2) appears however to be more plausible considering the ease of proton abstraction. The formation of IV is thought to be due to chelation between the two hydroxyl groups of catechol rather than a steric factor. The chelation presumably prevents the participation of the hydroxyl group in the formation of III.

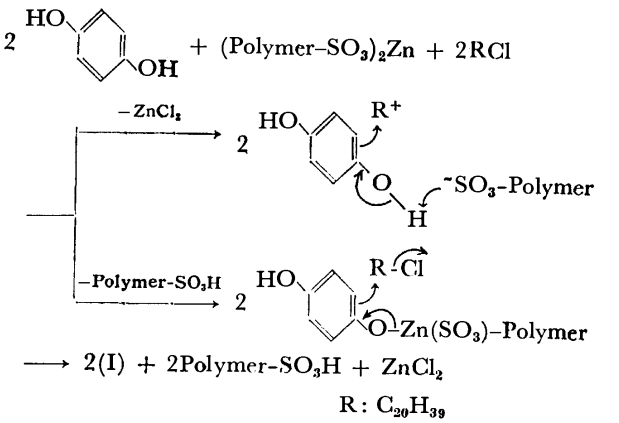

Scheme 2.

Further studies on the detailed mechanism of this system are now in progress.

Experimental

GLC and atomic absorption spectra were recorded on a Hitachi 023 gas chromatograph equipped with a flame ionizer detector and a Hitachi 208 atomic absorption spectrometer, respectively. Amberlyst 15 (Rohm and Haas, 4.8 meq/g dry resin, in $-SO_3H$ form) was employed as cation exchange resin. The metal resin catalysts were prepared in the same way as described in a previous paper.[4]

A typical procedure is described for the preparation of III and IV; A benzene solution (100 ml) containing catechol (9.9 g), phytyl chloride (28.5 g) and zinc resin catalyst (20 g, 2.25 mmol of zinc ion/g dry resin) was allowed to reflux for 3 h. After standing overnight, the catalyst was filtered off and washed with benzene and acetone. The filtrate was washed with 10% $NaHCO_3$ solution and water, dried over anhydrous Na_2SO_4 and concentrated under reduced pressure. The residue was purified by silica gel column chromatography using benzene/hexane solution (1/2) as eluent, to give 12.1 g of III and 7.9 g of IV, respectively. The catalyst was again applied for the subsequent reaction.

In a similar way, other chromanols (I, II) were isolated.

References

1) N. Takahashi, I. Okura, and T. Keii, *J. Mol. Catal.*, **4**, 65 (1978).
2) N. L. Holy, *J. Org. Chem.*, **43**, 4686 (1978).
3) K. Maruyama, H. Tsukube, and T. Araki, *Chem. Lett.*, **1979**, 499.
4) Y. Tachibana, *Bull. Chem. Soc. Jpn.*, **50**, 2477 (1977).
5) P. A. Wehrli, R. I. Fryer, and W. Metlesics, *J. Org. Chem.*, **36**, 2910 (1971).

Selective Decarboxylation of 1-Methyl-4,5-imidazoledicarboxylic Acid

Kazuyuki TAKAHASHI* and Keiryo MITSUHASHI

Department of Chemistry, College of Technology, Seikei University, Kichijoji, Musashino-shi, Tokyo 180

(Received June 22, 1979)

Synopsis. The selective decarboxylation of 1-methyl-4,5-imidazoledicarboxylic acid was carried out in various solvents. 1-Methyl-5-imidazolecarboxylic acid was obtained by heating in acetic or propionic anhydride, whereas 1-methyl-4-imidazolecarboxylic acid was obtained in *N,N*-dimethylformamide, *N,N*-dimethylacetamide, or *N*-methylpyrrolidone or by pyrolysis. The reaction mechanism is discussed.

The exhaustive decarboxylation of 4,5-imidazoledicarboxylic acids is well known, whereas the monodecarboxylation of the 1-substituted derivatives, which must lead to an isomeric product, has seldom appeared in the literature.

We have reported in a previous paper that the treatment of 1-methyl-4,5-imidazoledicarboxylic acid in an excess of boiling aniline at about 200 °C for 6—8 h gave 1-methyl-4-imidazolecarboxanilide in a yield of 56%.[1] On the other hand, Nematollahi reported the cyclic dimerization *via* the monodecarboxylation of 4,5-imidazoledicarboxylic acid in boiling acetic anhydride, yielding 5*H*,10*H*-diimidazo[3,4-*a*: 3′,4′-*d*]pyrazine-5,10-dione.[2]

The latter reaction conditions were then applied to 1-methyl-4,5-imidazoledicarboxylic acid in order to ascertain which isomer could be obtained by monodecarboxylation. The treatment in boiling acetic anhydride for only one hour gave 1-methyl-5-imidazolecarboxylic acid in a yield of 63.5%, while that at 100 °C for 4 h gave the same product in an almost quantitative yield. For the further investigation of the decarboxylation, acetic anhydride was replaced with various media; the results are summerized in Table 1.

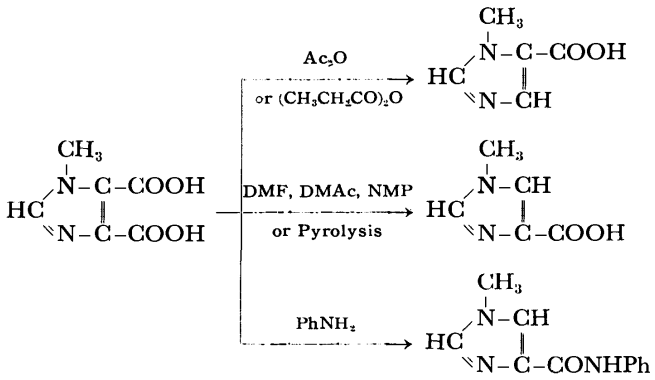

Fig. 1.

The successful effect of acetic anhydride on the selective decarboxylation seemed to suggest that the acylation of nitrogen at the 3-position is needed to promote the reaction. However, the use of anhydrides other than propionic anhydride, glacial acetic acid, acetyl chloride, and chloroacetyl chloride resulted in failure, probably because of the insolubility of the substrate in these acylating media.

On the other hand, the monodecarboxylation in such solvents as *N,N*-dimethylformamide, *N,N*-dimethylacetamide, *N*-methylpyrrolidone, and aniline, or by pyrolysis, where, in all cases, no electrophilic species was present, occurred at the 5-carboxyl group, giving the 4-carboxylic acid or its anilide. The reaction in *N,N*-dimethylaniline was hard to control.

TABLE 1. PRODUCTS AND CONDITIONS OF DECARBOXYLATION

Reaction media	Reaction temp/°C	Reaction time/h	Product	Yield/%
Acetic anhydride	reflux	1[a]	5-COOH	63.5
	100	4[a]	5-COOH	99
Propionic anhydride	130	4	5-COOH	23.8
	100	8	5-COOH	9.5
Octanoic anhydride	130	8	none[b]	—
Palmitic anhydride	130	8	none[b]	—
Benzoic anhydride	130	4	none[b]	—
Succinic anhydride	125	15	none[b]	—
Glacial acetic acid	reflux	24	none[b]	—
Acetyl chloride	reflux	24	none[b]	—
Chloroacetyl chloride	80	30	none[b]	—
	reflux	2	decomp.	—
Aniline	reflux	6—8	4-Anilide[b]	56[1]
	100	24	none[b]	—
N,N-Dimethylaniline	reflux	5	1-Methylimidazole	—
Triethylamine	reflux	50	none[b]	—
N,N-Dimethylformamide	reflux	3[a]	4-COOH	39.7
N,N-Dimethylacetamide	reflux	3[a]	4-COOH	64.3
N-Methylpyrrolidone	130	2	4-COOH	31.7
None(Pyrolysis)	250	1 min	4-COOH	30

a) Heated until the reaction mixture became homogeneous. b) Most of the substrate was recovered.

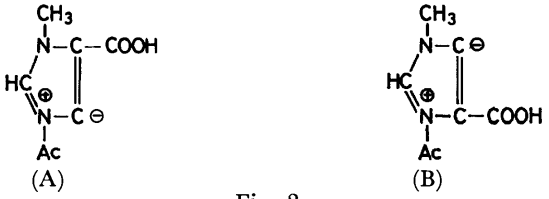

Fig. 2.

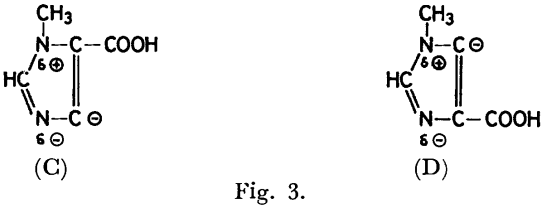

Fig. 3.

From the above results, the reaction mechanism can be thought to be as follows, on the basis of the adjacent charge effect: in the presence of such electrophilic species as acetic anhydride, the decarboxylated transition state (A) must be more stable than (B), consequently yielding the 5-carboxylic acid, while in the absence of electrophilic species, (D) must be preferable to (C), giving the 4-carboxylic acid or its derivative. Such a consideration on the basis of the electrostatic interaction has appeared in a paper by Cohen and his coworkers.[3] They studied the exchange reaction of ring hydrogens in 1-methylimidazole by NMR and concluded that the 5-carbanion was preferable to the 4-carbanion because of the electrostatic repulsion.

The present work provides a route to synthesize 1-methyl-4- and -5-imidazolecarboxylic acids and their derivatives which is more convenient than the known syntheses.[4]

Experimental

Decarboxylation in Acetic Anhydride. Into 100 ml of acetic anhydride, 3.4 g (0.02 mol) of 1-methyl-4,5-imidazoledicarboxylic acid was added, after which the suspension was heated at 100 °C for 4 h. After the reaction mixture became homogeneous, it was concentrated to dryness under reduced pressure. The resulting residue was washed with acetone and recrystallized from ethanol to give 1-methyl-5-imidazolecarboxylic acid in a yield of 2.5 g (99%); mp 256—257 °C (dec) (uncorr.) (lit,[4] 275—277 °C (dec)).

Decarboxylation in Propionic Anhydride. 1-Methyl-4,5-imidazoledicarboxylic acid (1.7 g, 0.01 mol) in 100 ml of propionic anhydride was heated, after which the reaction mixture was treated in the same way as that in acetic anhydride.

Decarboxylation in N,N-*Dimethylformamide.* Into 50 ml of *N,N*-dimethylformamide, a 1.7 g portion(0.01 mol) of 1-methyl-4,5-imidazoledicarboxylic acid was added, after which the suspension was heated under reflux for 3 h. The reaction mixture was then concentrated to dryness under reduced pressure. The resulting residue was washed with benzene and recrystallized from ethanol to give 1-methyl-4-imidazolecarboxylic acid in a yield of 0.5 g(39.7%); mp 246—247 °C (dec)(uncorr.)(lit,[2] 246—247 °C(dec)).

Decarboxylations in N,N-*Dimethylacetamide and* N-*Methylpyrrolidone.* The decarboxylations in *N,N*-dimethylacetamide and *N*-methylpyrrolidone were carried out in the same way as that in *N,N*-dimethylformamide.

Pyrolysis. In a test tube, 0.85 g (0.005 mol) of 1-methyl-4,5-imidazoledicarboxylic acid was placed and heated in a silicone oil bath at 250 °C for 1 min. The reaction mixture was then washed with benzene and recrystallized from ethanol to give 1-methyl-4-imidazolecarboxylic acid in a yield of 0.19 g (30%).

Isomeric Identification of the Monocarboxylic Acids. The carboxylic acids obtained were transformed to their methyl esters, which were then compared gas-chromatographically with authentic methyl 1-methyl-4- and -5-imidazolecarboxylates.

Methylation of 1-Methyl-4- and -5-imidazolecarboxylic Acids. Into 50 ml of thionyl chloride, a 2.5 g portion(0.02 mol) of 1-methyl-5-imidazolecarboxylic acid was added; the suspension was then heated under reflux for about 6 h till the mixture became clear. Immediately after the thionyl chloride has been distilled off, a 50 ml portion of methanol was added and the mixture was refluxed for 1 h. The reaction mixture was then cooled in an ice bath, and powdery sodium carbonate was added to make it alkaline. The solution was concentrated to dryness under reduced pressure, and the residue was extracted with chloroform. The chloroform layer was concentrated again, and the resulting residue was recrystallized from hexane to give methyl 1-methyl-5-imidazolecarboxylate in a yield of 1 g (35.7%); mp 54—56 °C (uncorr.) (lit,[4] 56—57 °C, 68—70 °C, 39—40 °C).

The methylation of the 4-carboxylic acid was carried out in a similar way. The methyl ester was obtained in a yield of 45%; mp 103—104 °C (lit,[1] 103—104 °C).

Preparation of Authentic Samples. Methyl 1-methyl-5-imidazolecarboxylate was prepared from methyl 4-imidazolecarboxylate with dimethyl sulfate according to Pyman's method,[4] while the 4-isomer was prepared from 1-methyl-4-imidazolecarboxanilide through hydrolysis, followed by esterification.[1] The isomeric structure of these authentic samples has previously been determined by a study of the Nuclear Overhauser Effect on NMR.[1]

Gas Chromatography. Gas chromatography was performed on a Shimadzu GC-6AMP instrument equipped with a 3 mm × 1000 mm glass column of OV-17 (5%) on DMCS. The column temperature was raised at a rate of 4 °C/min starting from 100 °C, and the flow rate was 30 ml of helium/min. The retention times of methyl 1-methyl-4- and -5-imidazolecarboxylates were 21 and 10 min, respectively.

References

1) K. Takahashi, T. Zaima, and K. Mitsuhashi, *Nippon Kagaku Kaishi*, **1974**, 385.

2) S. Kasina and J. Nematollahi, *Synthesis*, **1975**, 162.

3) Y. Takeuchi, H. J. C. Yeh, K. L. Kirk, and L. A. Cohen, *J. Org. Chem.*, **43**, 3565 (1978).

4) Syntheses of 1-methyl-4-imidazolecarboxylic acid and its derivatives: P. K. Martin, H. R. Matthews, H. Rapoport, and G. Thyagarajan, *J. Org. Chem.*, **33**, 3758 (1968) (Cyclization of 2-amino-3-(methylamino)propionic acid with triethyl orthoformate); E. P. Papadopoulos, *J. Org. Chem.*, **42**, 3925 (1977) (Methylation of 4-imidazolecarboxanilide with methyl iodide); Syntheses of 1-methyl-5-imidazolecarboxylic acid and its derivatives: W. Hubbull and F. L. Pyman, *J. Chem. Soc.*, **1928**, 21 (Methylation of methyl 4-imidazolecarboxylate with dimethyl sulfate); R. G. Jones, *J. Am. Chem. Soc.*, **71**, 644 (1949) (Cyclization of the *N*-methyl-*N*-acyl-α-formylglycine methyl ester with potassium thiocyanate, followed by the desulfurization of the resulting methyl 2-mercapto-1-methyl-5-imidazolecarboxylate); D. A. Shirley and P. W. Alley, *J. Am. Chem. Soc.*, **79**, 4922 (1957) (Reaction of lithium 1-methylimidazolium salt with solid carbon dioxide).

Infrared Spectra and Intramolecular Hydrogen Bonding of *p*-(Substituted phenoxy)-*α*-(dialkylamino)acetanilides

Kazuhisa ABE,* Minoru HIROTA, Michiharu SUGIURA,** and Yoshiki HAMADA**

Department of Applied Chemistry, Faculty of Engineering, Yokohama National University, Tokiwadai, Hodogaya-ku, Yokohama 240

***Faculty of Pharmacy, Meijo University, Tempaku-ku, Nagoya 468*

(Received June 28, 1979)

Synopsis. The title compounds were synthesized with pharmaceutical interests, and their infrared spectra in the NH and carbonyl stretching regions were measured. By comparing the spectra with those of *p*-phenoxyacetanilide, intramolecular hydrogen bonds are shown to exist between the amide NH and the α-dialkylamino groups.

The structures and the conformations of many amides and peptides have been discussed on the basis of their infrared spectra and several absorption bands are shown to be characteristic of amide functional group.[1] Among these characteristic absorptions, NH stretching bands and carbonyl stretching bands (amide I bands) are most extensively studied, and the former bands are proved to be very sensitive to the stereochemistry and to the participation in hydrogen bond formation.[2,3]

On pharmaceutical interests, a series of *p*-(substituted phenoxy)-*α*-(dialkylamino)acetanilides (**1**) were synthesized[4] and their hydrogen bonding behaviors were studied by measuring their infrared spectra in the NH and carbonyl stretching regions. Since the intra- and intermolecular hydrogen bonds often have remarkable effect on solubility, it can also affect on their biological activities.

Experimental

Syntheses of the *p*-(substituted phenoxy)-*α*-(dialkylamino)-acetanilides were reported previously.[4] Infrared spectra in solutions were measured with a Hitachi 225 recording spectrophotometer. Concentrations of the solutions were about 1×10^{-3} mol/l for the measurements in NH stretching region and about 5×10^{-4} mol/l for the measurement in C=O stretching region, at which concentrations the association of the solute is negligible. Measurement of ^{1}H-NMR spectra were carried out by a JOEL JNM C60-H spectrometer with solutions of which concentrations were about 0.5 mol/l. The chemical shifts (in ppm) of the NH proton siginals are rather insensitive to the changes in concentrations probably due to the formation of strong intramolecular hydrogen bonds.

Results and Discussion

Their infrared spectra were measured in a carbon tetrachloride solution enough dilute to avoid the effect of association in practice and were given in Tables 1 (NH stretching region) and 2 (C=O stretching region). The NH absorption bands of all amides in Table 1 are located at considerably lower frequencies and rather broad with half-widths ranging from 70 to 120 cm^{-1}. On the other hand, *p*-phenoxyacetanilide (**2**) has an NH band at 3448 cm^{-1} ($\varepsilon=188$), being by far a narrower band with a half-width of 10.3 cm^{-1}. In general, the amide group takes predominantly the trans conformation in which NH and C=O groups are anti to each other, and the NH band of trans conformer appears at a higher frequency than that of cis conformer. For example, the trans conformer of acetanilide absorbs at 3446 cm^{-1}, while the cis at 3402 cm^{-1}.[2,5] However the low frequency shifts observed with **1**'s are more than 100 cm^{-1} with reference to the NH frequency of **2**, being too large to attribute to the privileged cis con-

Table 1. NH stretching absorptions of $RC_6H_4OC_6H_4NHCOCH_2Y$ (**1**)[a] in CCl_4

R	Y: $-N(CH_3)_2$	$-N(C_2H_5)_2$	$-N$	$-N(CH_3)$	$-N$ O
H	3329 (109)	3311 (117)	3320 (93)	—	3337 (93)
2-CH_3	—	3310 (114)	3320 (83)	3309 (82)	3338 (107)
3-CH_3	—	3309 (111)	3320 (91)	3303 (95)	3336 (99)
4-CH_3	—	3307 (141)	3319 (116)	3300 (112)	3334 (121)
2-Cl	3330 (95)	3304 (94)	3310 (68)	3302 (86)	3337 (78)
3-Cl	3327 (130)	3309 (99)	3318 (100)	3302 (99)	3333 (99)
4-Cl	3328 (86)	3309 (122)	3314 (91)	3304 (101)	3333 (81)

a) Wave numbers (in cm^{-1}) of the absorption maxima are given together with their intensities ε_{max} (in l mol^{-1} cm^{-1}) in parentheses.

Table 2. C=O stretching absorptions of $RC_6H_4OC_6H_4NHCOCH_2Y$ (**1**)[a] in CCl_4

R	Y: $-N(CH_3)_2$	$-N(C_2H_5)_2$	$-N$	$-N(CH_3)$	$-N$ O
H	1695 (676)	1695 (769)	1697 (579)	—	1697 (532)
2-CH_3	—	1695 (637)	1699 (462)	1694 (496)	1698 (656)
3-CH_3	—	1695 (608)	1698 (569)	1695 (583)	1698 (561)
4-CH_3	—	1699 (754)	1703 (722)	1699 (669)	1703 (636)
2-Cl	1696 (700)	1696 (651)	1697 (392)	1696 (505)	1697 (615)
3-Cl	1697 (740)	1696 (577)	1700 (593)	1697 (562)	1700 (522)
4-Cl	1699 (499)	1699 (719)	1702 (672)	1698 (659)	1702 (550)

a) See footnote of Table 1.

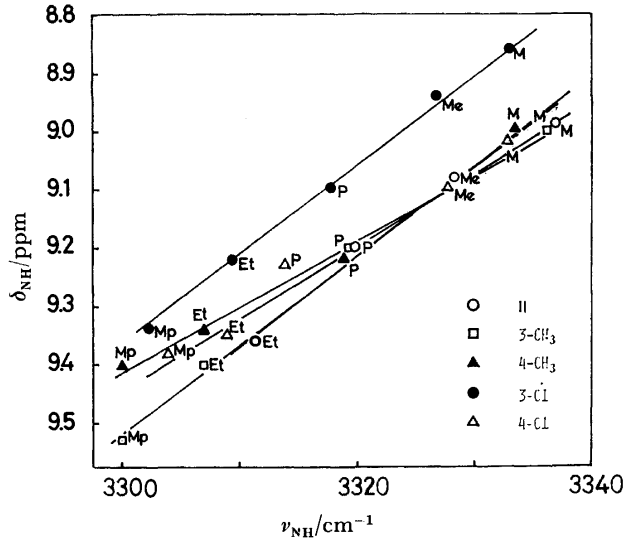

Fig. 1. The ν_{NH} *vs.* δ_{NH} plot.

former. Thus the NH group of **1** is suspected to be involved in a strong hydrogen bond. Since the NH absorptions of these amide are not concentration dependent and measured at very low concentrations, the hydrogen bond must be intramolecular (as illustrated by **3**).

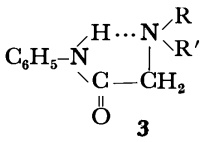

3

The NH stretching frequencies of **1**'s are mainly controlled by the nature of the α-dialkylamino groups. As shown in Table 1 and also in Fig. 1, the NH stretching frequencies generally decrease in the order: morpholino >dimethylamino>piperidino>diethylamino >2-methylpiperidino derivatives. The pK_a values of the parent amines are 8.33 for morpholine, 10.77 for dimethylamine, 11.22 for piperidine, and 10.93 for diethylamine.[6,7] Stronger base usually acts as stronger hydrogen acceptor and will cause larger low frequency shift of the stretching vibration of hydrogen donating NH group in hydrogen bond formation. The effect of the α-dialkylamino group is in line with this interpretation. The anomalously low frequency shifts observed with diethylamino derivatives, and presumably with 2-methylpiperidino derivatives, are explained that the bases are weakened by the so-called B strain probably operating when the ammonium ions are formed from these nitrogen bases. Hydrogen bonds are formed without considerable change in geometries of the acceptor molecules, the effect being negligible. The

Table 3. NH proton chemical shifts of $RC_6H_4OC_6H_4NHCOCH_2Y$ (1) in $CDCl_3$[a)]

R	Y: $-N(CH_3)_2$	$-N(C_2H_5)_2$	$-N$	$-N$	$-N$ O
				CH_3	
H	9.08	9.36	9.20	—	8.99
2-CH_3	9.02	9.28	9.18	9.32	8.98
3-CH_3	9.15	9.40	9.20	9.53	9.00
4-CH_3	9.05	9.34	9.22	9.40	9.00
2-Cl	9.08	9.38	9.24	9.36	9.04
3-Cl	8.94	9.22	9.10	9.34	8.86
4-Cl	9.10	9.35	9.23	9.38	9.02

a) Chemical shifts (in ppm downfields from internal TMS reference) are given.

pK_a's of diethylamine and 2-methylpiperidine are lower than expected from the electronic effect alone.

The hydrogen bond was also proved by ^{1}H-NMR spectra of **1**'s in chloroform-*d* (Table 3). The amide NH signals resonate in the range 8.9—9.5 ppm (downfield from TMS reference signal), which is obviously lower fields than the NH chemical shift of **2** (7.85 ppm) which is impossible to form intramolecular hydrogen bond. The NH stretching frequency (ν_{NH}) *vs.* NH chemical shift (δ_{NH}) plots in Fig. 1 are almost linear in all cases illustrated, and support evidently the fact that the low frequency shifts of ν_{NH} and the low field shifts of δ_{NH} are both due to the hydrogen bond formation, and the hydrogen bonds are formed with the α-dialkylamino group intramolecularly.

The NH stretching absorption bands of free amide group was not observed with any of **1**'s, and the α-dialkylamino-*p*-phenoxyacetanilides are supposed to exist solely as the intramolecularly hydrogen bonded conformers.

References

1) L. J. Bellamy, "The Infrared Spectra of Complex Molecules," pp. 175—198.
2) I. Suzuki, M. Tsuboi, T. Shimanouchi, and S. Mizushima, *Spectrochim. Acta*, **16**, 467 and 471 (1960).
3) Y. Senda and Y. Kudo, *Kagaku No Ryoiki, Suppl.* **68**, 115—138 (1965).
4) Y. Hamada, M. Sugiura, T. Nishina, K. Araki, K. Horigome, and Z. Henmi, *Yakugaku Zasshi*, **98**, 1597 (1978).
5) H. W. Russell and R. A. Thompson, *Spectrochim. Acta*, **8**, 138 (1956).
6) A. Albert and E. P. Serjeant, "The Determination of Ionization Constants," Chapman and Hall, London (1971).
7) H. K. Hall, Jr., *J. Am. Chem. Soc.*, **79**, 5441 (1957).

Asymmetric Synthesis of Aspartic Acid by Hydrogenation of Optically Active 1,4-Oxazine Derivative[1]

Minoru TAMURA and Kaoru HARADA*

Department of Chemistry, The University of Tsukuba, Niihari-gun, Ibaraki 305

(Received July 25, 1979)

Synopsis. The asymmetric hydrogenation of an optically active heterocyclic compound, (*R*)-3-methoxycarbonylmethylene-5-phenyl-3,4,5,6-tetrahydro-2*H*-1,4-oxazin-2-one(**2**), was studied. The compound **2** was hydrogenated with several catalysts, and was converted into optically active aspartic acid. The configuration of the resulting aspartic acid proved to be (*S*), and the optical yield was in the range 12—17%.

Recently we have reported[2] an asymmetric synthesis of alanine by hydrogenolytic transamination by the use of (*R*)-2-amino-2-phenylethanol (**1**) as a chiral reagent. The effects of the asymmetric moieties as well as the solvents on the optical yields were explained by the chelation hypothesis based on the interaction between the substrate and the catalyst.

In the present work, in order to study the effect of the structure of substrate on the optical yield, the optically active heterocyclic compound **2** was prepared from amino alcohol **1** and dimethyl acetylenedicarboxylate, and the asymmetric hydrogenation of **2** was carried out.

Kagan *et al.*[3,4] reported an efficient asymmetric synthesis by hydrogenation of the cyclic compound prepared from (1*S*,2*R*)-2-amino-1,2-diphenylethanol and dimethyl acetylenedicarboxylate. However, since asymmetric hydrogenation of **2** was not described in detail, we would like to report the results of the hydrogenation of **2** with aluminum amalgam, Raney nickel, and other catalysts.

TABLE 1. ASYMMETRIC SYNTHESIS OF ASPARTIC ACID BY HYDROGENATION OF **2**

Temp °C	Catalyst	Time h	Solvent	Route (A or B)	Yield[b]	$[\alpha]_D^{25}$ DNP-Asp[c]	Optical yield[d] (confign.)
5	Al–Hg	6	DME[a]	A	44	+14.1 (0.880)	15 (*S*)
0	Al–Hg	6	DME	A	61	+16.0 (0.702)	17 (*S*)
−20	Al–Hg	7	DME	A	62	+14.7 (1.35)	16 (*S*)
20	Raney Ni	48	EtOH	A	57	+13.0 (0.893)	14 (*S*)
20	Pd	48	MeOH	B	70	+14.7 (0.422)	16 (*S*)
20	Pd on C	48	MeOH	B	42	+14.8 (0.487)	16 (*S*)
20	Pd on C	48	Dioxane	B	48	+10.8 (0.573)	12 (*S*)

a) DME is 1,2-dimethoxyethane. b) The yields of **3** (route A) or **4** (route B). c) The specific rotations were measured in 1 mol dm^{-3} NaOH. d) Optical yield is defined as ($[\alpha]_D$ obsed/$[\alpha]_D$ lit) × 100, DNP-(*S*)-Asp, $[\alpha]_D^{25}$ +91.9° (1 mol dm^{-3} NaOH).

Cyclic compound **2** was prepared through the condensation of optically active amino alcohol **1** and dimethyl acetylenedicarboxylate at room temperature. The IR spectra of **2** indicated the presence of an intramolecular hydrogen bond.[5] In the NMR spectra of **2**, the chemical shift of the NH proton also suggested an intramolecular hydrogen bond.[6] From the results described above, it was concluded that compound **2** is of *Z*-configuration.

Compound **2** was hydrogenated with aluminum amalgam or Raney nickel (Scheme 1; route A). Product **3** was purified by the use of silica gel column chromatography without fractionation. The yield of **3** was

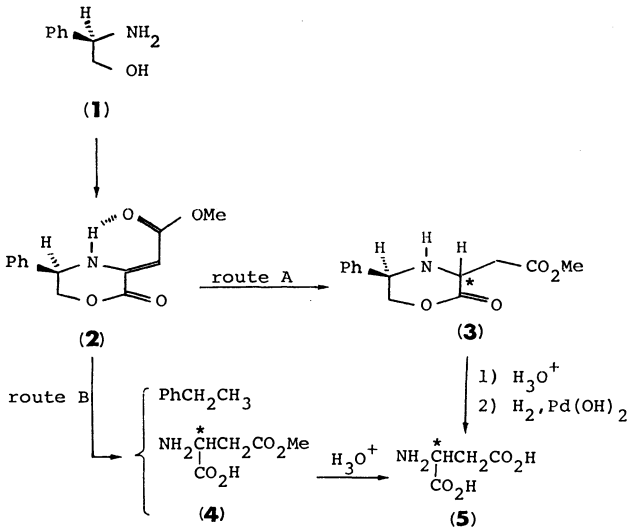

Scheme 1.

44—62%. Hydrolysis and subsequent hydrogenolysis of **3** gave optically active aspartic acid in 74—75% yields from **3**. The optical yields of the aspartic acid were determined as *N*-(2,4-dinitrophenyl)aspartic acid (DNP-Asp).[7] The configuration of aspartic acid was (*S*). The optical yields ranged from 14 to 17%. In the reaction with aluminum amalgam, the reaction temperature was lowered, however, no change of the optical yield was observed.

When palladium black or 5% palladium on charcoal was used as a catalyst, hydrogenation and hydrogenolysis took place simultaneously and β-methyl hydrogen aspartate (**4**) was obtained in 42—70% yields (route B). According to the time-course checked by TLC of the reaction mixture, it seems that hydrogenation takes place prior to hydrogenolysis.

It was found that the reductive cleavage of the benzylic C–N bond and also the homobenzylic C–O bond (Ph–CH_2–CH_2–O)[8] took place in route B. The existence of ethylbenzene in the reaction mixture, which was confirmed by gas-liquid chromatography, would support the hydrogenolytic cleavage of the homobenzylic C–O bond.

Compound **4**, which was obtained by the route B, was hydrolyzed to form optically active aspartic acid. The optical yield of DNP-aspartic acid ranged from 12 to 16%. And the configuration of aspartic acid was (*S*). The results are summerized in Table 1.

The examination of the conformation by the Dreiding model showed that the preferential formation of (*S*)-isomer was caused by the steric effect of the phenyl group on substrate **2**, and that the steric effect would be larger when the phenyl group is pseudo axial than pseudo equatorial. The optical yields obtained by

these reactions suggested that substrate **2** could largely take the conformation in which the phenyl group is pseudo equatorial.

Experimental

The NMR spectra were obtained by using a Hitachi H-60 and R-24 A spectrometers, and the IR spectra were measured with a Hitachi 215 type grating infrared spectrophotometer. The gas chromatography was carried out with a Hitachi 163 type gas chromatograph. The specific rotations were measured with a JASCO DIP-181 type digital polarimeter using a 50 mm cell. The amino acids were analyzed with a Yanagimoto LC-5 S instrument. The mass spectra were obtained by a Hitachi RMU-6 MG type high resolution mass spectrometer.

(R)-3-Methoxycarbonylmethylene-5-phenyl-3,4,5,6-tetrahydro-2H-1,4-oxazin-2-one (2). A solution of (*R*)-2-amino-2-phenyl-ethanol (**1**) ($[\alpha]_D^{25}$ −27.3° [c=1.08, methanol])[2] (0.5 g, 3.65 mmol) in 10 ml of MeOH was added dropwise to a solution of dimethyl acetylenedicarboxylate (0.518 g, 3.65 mmol) in 7 ml of MeOH with stirring for 20 min. After being stirred for additional 2.5 h, the mixture was evaporated and purified by silica gel column chromatography (30×210 mm, E. Merck No. 9385), eluted with benzene–AcOEt (9: 1 v/v) solvent. Compound **2** was obtained as colorless oil (0.791 g; 88%), which crystallized on cooling in a refrigerator. The recrystallization from ether–petroleum ether gave colorless needles. Mp 67—68 °C, $[\alpha]_D^{20}$ −259° (c=0.590, $CHCl_3$). Found: C, 63.11; H, 5.10; N, 5.83%. Calcd for $C_{13}H_{13}NO_4$: C, 63.15; H, 5.29; N, 5.66%. IR($CHCl_3$): 3300 (NH), 3000, 1740 (lactone), 1660 (ester), 1620 (C=C) cm^{-1}. δ($CDCl_3$): 3.65 (3H, s), 4.30—4.85 (3H, ABC m), 5.70 (1H, s, $-\underset{|}{C}=CH$), 7.30 (5H, s), 8.50 (1H, s, NH). The H–D exchange of the proton on NH was very slow (half life $T_{1/2}$: 2 d). Mass: M^+ (247), λ_{max}: 325 nm (ε=8330).

(R)-3-Methoxycarbonylmethyl-5-phenyl-3,4,5,6-tetrahydro-2H-1,4-oxazin-2-one (3) (Route A). An aluminum amalgam prepared from 500 mg of aluminum foil[9] was added to an ice-cooled magnetically stirred solution of **2** (500 mg, 2.02 mmol) in 30 ml of 1,2-dimethoxyethane. The mixture was treated with 4 ml of distilled water, and the stirring was continued for 6 h at 0 °C under nitrogen atmosphere. To the reaction mixture, Celite 545 (0.1 g) was added and filtered under suction, and the residue was washed with 1,2-dimethoxyethane (25 ml) and MeOH (25 ml). After evaporation of the solvent at 0—5 °C, the residue was dissolved in ethyl acetate and was dried (Na_2SO_4). After removal of the solvent at 0—5 °C, the residual oil was purified by silica gel column chromotography mentioned above. The combined fractions were evaporated at 0—5 °C to furnish colorless oli. Yield: 0.307 g (61%). IR (NaCl): 3300 (NH), 2950, 1750 (lactone), 1730 (ester) cm^{-1}. δ($CDCl_3$): 2.71 (1H, s, NH), 2.80—3.10 (2H, 6 peaks, $-C\underline{H}_2-CO_2CH_3$), 3.70 (3H, s), 4.00—4.45 (4H, m), 7.38 (5H, s). Mass: M^+ (249). In the case of Raney nickel, **2** (400 mg, 1.62 mmol) was dissolved in 20 ml of abs EtOH and Raney nickel (W-2 type, 600 mg) was added. Hydrogenation was carried out at room temperature for 48 h (initial pressure of hydrogen was 3 atm).

(S)-Aspartic Acid (Route A). The compound **3** was hydrolyzed with 6 mol dm^{-3} hydrochloric acid (10 ml) under reflux for 5 h. After evaporation, the hydrolyzate was dissolved in a small amount of distilled water and the pH was adjusted to about 4.5 with sodium hydrogen carbonate. Palladium hydroxide on charcoal (0.2 g) was added to the solution and the hydrogenolysis was carried out for 13 h. The catalyst was removed by filtration and the filtrate was evaporated to dryness. The residue was dissolved in a small amount of water and the solution was applied to a Dowex 50 column (H^+ form). The column was eluted with 3 mol dm^{-3} aqueous ammonia and the eluent was evaporated to dryness. A part of the solution was diluted appropriately and analyzed with an amino acid analyzer (yield: 74%). A part of aspartic acid was converted to DNP-Asp, which was purified by a Celite column (Hyflo-super-cel); $[\alpha]_D^{25}$ +16.0° (c=0.702, 1 mol dm^{-3} NaOH), optical purity 17%. The DNP-aspartic acid was further confirmed by TLC (MeOH: AcOEt=5: 1 v/v).

(S)-β-Methyl Hydrogen Aspartate (4) (Route B). To a solution of **2** (200 mg, 0.810 m mol) in 5 ml of abs. MeOH, palladium black (300 mg) was added, and the mixture was stirred for 48 h under hydrogen (1 atm). The catalyst was removed by filtration and a small part of the filtrate (1 μl) was applied on a gas-liquid chromatography, which showed the presence of ethylbenzene. The residual filtrate was evaporated to dryness and the residue crystallized by addition of a small amount of chloroform. Yield: 83.2 mg (70%); mp 199—200 °C; δ (D_2O): 2.80—3.35 (2H, ABX), 3.77 (3H, s), 4.35 (1H, dd); IR (KBr): 3400 (br), 3000 (br), 2070, 1720, 1650, 1600 cm^{-1}. Found: C, 40.80; H, 6.01; N, 9.22%, Calcd for $C_5H_9NO_4$: C, 40.81; H, 6.16; N, 9.52%.

(S)-Aspartic Acid (Route B). Crude **4** was refluxed with 6 mol dm^{-3} hydrochloric acid (10 ml) for 3 h. After evaporation, the residue was dissolved in a small amount of water and the solution was applied to a Dowex 50 column. The yield of aspartic acid was determined by an amino acid analyzer (91%), and the optical purity of the aspartic acid was determined as DNP-(*S*)-aspartic acid; $[\alpha]_D^{25}$ +14.7° (c 0.422, 1 mol dm^{-3} NaOH), optical purity 16%.

The authors wish to express their thanks to Dr Takenori Kusumi for his valuable discussions. We also would like to thank Dr. Shinya Nomoto for his discussion.

References

1) Sterically Controlled Synthesis of Optically Active Organic Compounds XXX; Part XXIX, Ref. 2.

2) K. Harada and M. Tamura, *Bull. Chem. Soc. Jpn.*, **52**, 1227 (1979).

3) J. P. Vigneron, H. Kagan, and A. Horeau, *Tetrahedron Lett.*, **1968**, 5681.

4) J. P. Vigneron, H. Kagan, and A. Horeau, *Bull. Soc. Chim. Fr.* **1972**, 3836.

5) The wave number of NH (3300 cm^{-1}) was independent of the concentration of the sample in $CHCl_3$.

6) N. F. Chamberlain, "The practice of NMR spectroscopy," Plenum Press, New York (1974), p. 189. The rate of H–D exchange of the NH proton of **2** was very slow.

7) K. Harada and K. Matsumoto, *J. Org. Chem.*, **31**, 2985 (1966).

8) E. W. Garbisch, Jr., *Chem. Commun.*, **1967**, 806.

9) E. J. Corey, R. McCaully, and H. S. Sachdev, *J. Am. Chem. Soc.*, **92**, 2485 (1970).

Stereochemical Control Exerted by Methoxyl Group on the Diiodomethane-Copper Methylenation of Cyclic Olefins Containing Methoxyl Group

Nariyoshi KAWABATA* and Naoki IKEDA

Department of Chemistry, Faculty of Polytechnic Science, Kyoto Institute of Technology, Matsugasaki, Sakyo-ku, Kyoto 606

(Received July 25, 1979)

Synopsis. In the diiodomethane-copper methylenation of 3- and 4-methoxycyclopentenes and 3-methoxycyclohexene, the cis isomers of the cyclopropane derivatives predominated over the corresponding trans isomers, the trans isomer of cyclopropane derivatives being predominantly obtained from 3-methoxycyclooctene.

Reports have been given on the synthesis of cyclopropane derivatives from olefins by the reaction with diiodomethane and copper.[1,2] The reaction gave

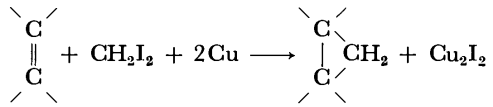

cyclopropane derivatives in good yields as in the corresponding Simmons-Smith reaction.[3] The reaction proceeded stereospecifically, *i.e.*, cis and trans olefins afforded cyclopropane derivatives whose configurations with respect to the olefin substituents were cis and trans, respectively. Moreover, the ether functions controlled the stereochemistry of the cycloaddition, *cis*-2-methoxybicyclo[4.1.0]heptane being exclusivel obtained from 3-methoxycyclohexene.[2] This type of

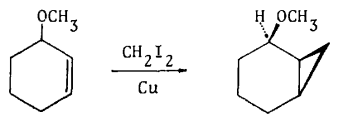

1 **2**

stereospecific synthesis of cyclopropane derivatives in the Simmons-Smith reaction has been widely used in synthesis.[4] The present work deals with an investigation of the stereochemistry of the diiodomethane-copper methylenation with olefins containing oriented ether functions.

Results and Discussion

Reaction of 3-methoxycyclopentene with diiodomethane and copper powder gave an 88: 12 mixture of *cis*- and *trans*-2-methoxybicyclo[3.1.0]hexane in 75% yield. Reaction of 4-methoxycyclopentene with diiodomethane and copper powder gave a 90: 10 mixture of

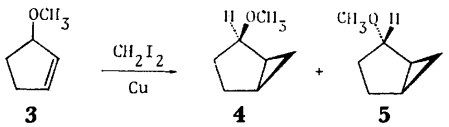

3 **4** **5**

88: 12

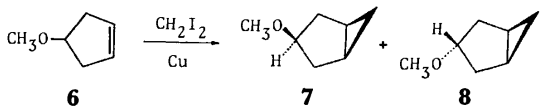

6 **7** **8**

90: 10

cis- and *trans*-3-methoxybicyclo[3.1.0]hexane in 70% yield. The structures of these cyclopropane derivatives were determined by comparison of their spectral data with those of authentic materials.[5]

Reaction of 3-methoxycycloheptene with diiodomethane and copper powder gave a 57: 43 mixture of *cis*- and *trans*-2-methoxybicyclo[5.1.0]octane in 77% yield. The relative configurations of these cyclopropane derivatives were assigned on the basis of their ^{1}H NMR spectra. The cis isomer **10** and the trans isomer **11** showed absorptions due to the protons geminal to the methoxyl group at δ 3.65 with a width at half-height of 13 Hz and δ 2.70 with a width at half-height of 17 Hz, respectively. This is in line with the cis and trans configurations of the cyclopropane ring to the methoxyl group, respectively. In the case of 2-hydroxybicyclo[5.1.0]octanes, the peak due to the hydrogen atom geminal to the hydroxyl group of the trans isomer appears at δ 3.3 with a width at half-height of 15 Hz, the corresponding peak of the cis isomer appearing at δ 4.2 with a width at half-height of 10 Hz.[6]

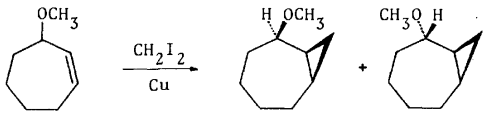

9 **10** **11**

57: 43

The reaction of 3-methoxycyclooctene with diiodomethane and copper powder gave an 18: 82 mixture of *cis*- and *trans*-2-methoxybicyclo[6.1.0]nonane in 83% yield. The relative configurations of these cyclopropane derivatives were also determined on the basis of their ^{1}H NMR spectra. The cis isomer **13** and the trans isomer **14** showed absorption due to the protons geminal to the methoxyl group at δ 3.78 with a width at half-height of 11 Hz, and δ 2.72 with a width at half-height of 18 Hz, respectively. This is in line with the cis and trans configurations of the cyclopropane ring to the methoxyl group, respectively.[6]

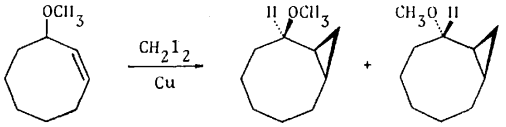

12 **13** **14**

18: 82

In brief, preferential cis-directive addition was observed in reactions with the methoxycyclopentenes and the methoxycyclohexene, and preferential trans-directive addition being observed in the reaction with the methoxycyclooctene. Stereochemical control of the

methoxyl group was weak in the reaction with the methoxycycloheptene.

The stereospecific synthesis in the Simmons-Smith reaction with cyclic allylic alcohols was explained in terms of the attack of organozinc reagent on the nearest face of the neighboring double bond after coordination to the oxygen atom of the substrate.[7] Models of the 3- and 4-methoxycyclopentenes and 3-methoxycyclohexene indicate that the methoxyl group can only function as a cis-director. The model of 3-methoxycyclooctene shows that addition in the trans-direction is favored. On the other hand, the model of 3-methoxycycloheptene is less useful for determining which face of the double bond is more accessible.

In the Simmons-Smith reaction with cyclic allylic alcohols,[7] the cis isomers of the corresponding cyclopropane derivatives were exclusively obtained from 2-cyclopenten-1-ol and 2-cyclohexen-1-ol, the trans isomers of the cyclopropane derivatives being exclusively obtained from 2-cycloocten-1-ol and 2-cyclononen-1-ol. A 90: 10 mixture of the cis and trans isomers of the cyclopropane derivatives was obtained from cyclohepten-1-ol.[7]

The methoxyl group shows a tendency in stereochemical control in the cycloaddition of copper carbenoid to cyclic olefins containing the methoxyl group similar to that in the Simmons-Smith reaction with cyclic allylic alcohols, although the control was weak in the diiodomethane–copper methylenation. This can be interpreted in terms of the weaker interaction of the methoxyl group with copper carbenoid in the transition state than that of the hydroxyl group with the organozinc intermediate in the Simmons-Smith reactions, since copper halides are weaker Lewis acids than zinc halides.

Experimental

Elemental analyses were performed at the Elementary Analyses Center of Kyoto University. ^{1}H NMR spectra were taken on a Varian T-60-A spectrometer in carbon tetrachloride using tetramethylsilane as an internal standard, IR spectra on a Hitachi 215 grating spectrophotometer, and mass spectra on a Hitachi Model RMU-6 mass spectrometer. VPC analyses were performed on a Shimadzu GC-4C gas chromatograph.

Materials. 3-Methoxycyclopentene was prepared according to the conventional procedure.[8] 4-Methoxycyclopentene, 3-methoxycycloheptene, and 3-methoxycyclooctene were prepared by the conventional method[9] from 3-cyclopenten-1-ol,[10] 2-cyclohepten-1-ol,[11] and 2-cycloocten-1-ol,[12] respectively. Commercial copper powder was used without further purification. Diiodomethane and benzene were purified by distillation. Other chemicals were used without further purification.

Procedure. Reactions of cyclic olefins containing methoxyl group with diiodomethane and copper powder were carried out as reported.[1,2] Yields were determined by VPC analysis of the reaction mixture on the basis of olefin. Products were isolated by collection from the reaction mixture by VPC, and analyzed.

2-Methoxybicyclo[3.1.0]hexane. Reaction of 3-methoxycyclopentene (0.20 g, 2.05 mmol), diiodomethane (1.05 g, 3.97 mmol), copper powder (0.58 g, 9.16 mmol), and iodine (0.015 g, 0.12 mmol) in 1.5 ml of benzene at 75 °C for 72 h gave an 88: 12 mixture of *cis*- (**4**) and *trans*-2-methoxybicyclo-[3.1.0]hexane (**5**) in 75% yield based on the olefin.

2-Methoxybicyclo[3.1.0]hexane. Reaction of 4-methoxycyclopentene (0.18 g, 1.85 mmol), diiodomethane (1.07 g, 4.00 mmol), copper powder (0.58 g, 9.13 mmol), and iodine (0.017 g, 0.14 mmol) in 1.5 ml of benzene at 75 °C for 72 h gave a 90: 10 mixture of *cis*- (**7**) and *trans*-3-methoxybicyclo-[3.1.0]hexane (**8**) in 70% yield based on the olefin.

2-Methoxybicyclo[5.1.0]octane. From 3-methoxycycloheptene (0.25 g, 1.95 mmol), diiodomethane (1.03 g, 3.86 mmol), copper powder (0.58 g, 9.16 mmol) and iodine (0.015 g, 0.12 mmol) in 1.5 ml of benzene at 75 °C for 96 h was obtained a 57: 43 mixture of *cis*- (**10**) and *trans*-2-methoxybicyclo[5.1.0]octane (**11**) in 77% yield based on the olefin. Found: C, 77.00; H, 11.62%. Calcd for $C_9H_{16}O$: C, 77.09; H, 11.50%. The cis isomer (**10**): ^{1}H NMR (CCl_4) δ 0.2—2.5 (m, 12H), 3.20 (s, 3H), 3.65 (m, 1H, width at half-height = 13 Hz). The trans isomer (**11**): ^{1}H NMR (CCl_4) δ 0.2—2.5 (m, 12H), 2.70 (m, width at half-height = 17 Hz), 3.35 (s, 3H).

2-Methoxybicyclo[6.1.0]nonane. From 3-methoxycyclooctene (0.25 g, 1.81 mmol), diiodomethane (1.04 g, 3.90 mmol), copper powder (0.61 g, 9.53 mmol), and iodine (0.015 g, 0.12 mmol) in 1.5 ml of benzene at 75 °C for 96 h was obtained an 18: 82 mixture of *cis*- (**13**) and *trans*-2-methoxybicyclo[6.1.0]nonane (**14**) in 83% yield based on the olefin. The cis isomer (**13**): $n_D^{30} = 1.4705$; ^{1}H NMR (CCl_4) δ 0.2—2.3 (m, 14H), 3.21 (s, 3H), 3.78 (m, 1H, width at half-height = 11 Hz); MS *m/e* (rel intensity) 154 (1.0, M^+), 93 (59), 81 (65), 80 (74), 79 (100). Found: C, 78.12; H, 11.83%. Calcd for $C_{10}H_{18}O$: C, 77.87; H, 11.76%. The trans isomer (**14**): $n_D^{30} = 1.4665$; ^{1}H NMR (CCl_4) δ 0.0—2.3 (m, 14H), 2.72 (m, 1H, width at half-height = 18 Hz), 3.29 (s, 3H); MS *m/e* (rel intensity) 154 (1.0, M^+), 93 (59), 81 (67), 80 (50), 79 (100); Found: C, 77.75; H, 11.79%. Calcd for $C_{10}H_{18}O$: C, 77.87; H, 11.76%.

References

1) N. Kawabata, M. Naka, and S. Yamashita, *J. Am. Chem. Soc.*, **98**, 2676 (1976).
2) N. Kawabata, I. Kamemura, and M. Naka, *J. Am. Chem. Soc.*, **101**, 2139 (1979).
3) H. E. Simmons, T. L. Cairns, S. A. Vladuchick, and C. M. Hoiness, *Org. React.*, **20**, 1 (1973).
4) See Ref. 3, p. 23.
5) P. K. Freeman, M. F. Grostic, and F. A. Raymond, *J. Org. Chem.*, **30**, 771 (1965).
6) A. C. Cope, S. Moon, and C. H. Park, *J. Am. Chem. Soc.*, **84**, 4843 (1962).
7) C. D. Poulter, E. C. Friedrich, and S. Winstein, *J. Am. Chem. Soc.*, **91**, 6892 (1969).
8) K. Alder and F. H. Flock, *Chem. Ber.*, **89**, 1732 (1956).
9) I. Fleming and E. J. Thomas, *Tetrahedron*, **28**, 4989 (1972).
10) (a) E. L. Allred, J. Sonnenberg, and S. Winstein, *J. Org. Chem.*, **25**, 26 (1960); (b) G. Zweifel and H. C. Brown, *Org. React.*, **13**, 30 (1963).
11) W. G. Dauben and G. H. Berezin, *J. Am. Chem. Soc.*, **85**, 468 (1963).
12) N. Heap and G. H. Whitham, *J. Chem. Soc., B*, **1966**, 164.

Quaternary Ammonium Periodate as a New Oxidizing Agent

Katsuhiko INOMATA,* Yukiharu NAKAYAMA, and Hiroshi KOTAKE
Department of Chemistry, Faculty of Science, Kanazawa University, Kanazawa 920
(Received July 28, 1979)

Synopsis. Quaternary ammonium periodate has been found to be a useful oxidizing agent to convert a 1,2-diol and an olefin to the corresponding carbonyl compound in anhydrous aprotic solvents. The resulting carbonyl compounds have been reacted with alkyllithium to prepare alcohols in one-pot from a 1,2-diol or an olefin.

Sodium and potassium periodate are useful oxidants to convert sulfides and 1,2-diols to the corresponding sulfoxides and carbonyl compounds. The necessity of employing water as a solvent or as a cosolvent mixed with an organic solvent such as methanol, however, places some restrictions on the use of periodates.[1]

In order to overcome the restrictions, the alkali salt has been converted to the quaternary ammonium salt. The quaternary ammonium periodate does not require water to oxidize a 1,2-diol and an olefin to the corresponding carbonyl compounds in aprotic solvents.

Three quaternary ammonium periodates (**2a**—**c**) were readily prepared from equimolar quantities of sodium periodate and the corresponding quaternary ammonium halides (**1a**—**c**) in aqueous solutions at 0 °C.

$$NaIO_4 + [R^1R^2R^3R^4N]^+X^- \xrightarrow{-NaX} [R^1R^2R^3R^4N]^+IO_4^-$$

1a; $R^1=CH_3(CH_2)_{15}$, $R^2=C_6H_5CH_2$, R^3, $R^4=CH_3$, $X=Cl$ — **2a**; 90%

1b; $R^1=C_6H_5CH_2$, R^2, R^3, $R^4=CH_3CH_2$, $X=Br$ — **2b**; 84%

1c; R^1, R^2, R^3, $R^4=CH_3(CH_2)_3$, $X=Br$ — **2c**; 94%

Each compound has similar oxidizing ability,[2] but benzylhexadecyldimethylammonium periodate (**2a**) was used in the following experiments since **2c** changed color yellow on storage at room temperature and **2b**, although readily soluble in dichloromethane, is sparingly soluble in ethereal solvents such as THF and dioxane.

2a was allowed to react with an equimolar amount of *dl*-1,2-diphenyl-1,2-ethanediol (**3dl**) in refluxing THF for 6 h, and almost all the **3dl** disappeared on TLC and a new spot of benzaldehyde appeared. The resulting benzaldehyde was isolated as a semicarbazone (81% yield).

$$C_6H_5CH(OH)\text{-}CH(OH)C_6H_5 + \mathbf{2a} \xrightarrow[-H_2O]{}$$

3dl

$$2C_6H_5CHO + [CH_3(CH_2)_{15}N(CH_3)_2CH_2C_6H_5]^+IO_3^-$$

81% (as semicarbazone) — **4**

The above reaction produces one equivalent of water, and so the oxidation was conducted in the presence of molecular sieves to remove the water. The resulting benzaldehyde (**5**) was subsequently allowed to react with an alkyllithium to give the corresponding alcohol in one-pot. For example, a mixed solution of **3dl** and **2a** in dioxane was refluxed in the presence of molecular sieves[3] for 2 h and the resulting benzaldehyde

$$\mathbf{3dl} + \mathbf{2a} \longrightarrow [C_6H_5CHO]$$

5

$$\xrightarrow{CH_3(CH_2)_3Li} C_6H_5CH(OH)(CH_2)_3CH_3$$

6, 71%

was treated with butyllithium without isolation to give 1-phenyl-1-pentanol (**6**) (71% yield).

Similarly the alcohol **8a**, **b**,[4] precursors of furan derivatives, were prepared from **3** and the corresponding alkyllithiums **7a**, **b**[5,6] in good yields.

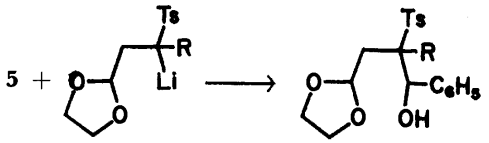

7a, R=H — **8a**, 82% from **3meso**

7b, R=CH_3 — **8b**, 87% from **3meso**, 84% from **3dl**

Pappo *et al.* have reported a procedure for the cleavage of olefinic bonds with sodium periodate and a catalytic amount of osmium tetraoxide. It was noted that water was required in all the reactions to effect hydrolysis of the intermediary osmate ester.[7] Consequently **2a** was used in the place of sodium periodate in this procedure in anhydrous aprotic solvents.

To a mixture of *trans*-stilbene and two molar quantities of **2a** in dioxane was added a catalytic amount of osmium tetraoxide at room temperature under nitrogen. The clear solution became green and then yellow and accompanied by the precipitation of **4**. After stirring for 3 h at room temperature and subsequent addition of THF, the reaction mixture was cooled to −78 °C and allowed to react with alkyllithium **7b** to give the expected alcohol **8b** (95% yield from stilbene).

$$C_6H_5CH{=}CHC_6H_5 + 2\,\mathbf{2a} \xrightarrow[r.t.,\ 3\,h]{cat.\ OsO_4}$$

$$[C_6H_5CHO] \xrightarrow[-78\,°C,\ 2\,h]{7b}$$

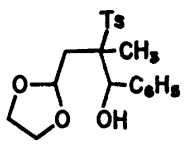

8b, 95%

This oxidation reaction was also conducted with equimolar quantities of *trans*-stilbene and **2a** and 36% of the stilbene was recovered and 51% of benzaldehyde (as semicarbazone) was obtained. The diol **3** was not detected on TLC.

From the above results, it is evident that water is not required in the oxidative cleavage of a diol or an olefin with quaternary ammonium periodate in aprotic solvents. Work is now in progress to determine the scope and limitation of this oxidation reaction.

Experimental

All melting points are uncorrected. The NMR and IR spectra were recorded on JEOL JNM/MH-60 and JASCO IRA-1 spectrometers, respectively.

Materials. All the solvents were distilled according to the standard methods and stored over a drying agent. Thin-layer chromatography (TLC) was performed on Merck's Kieselgel 60 PF_{254} (Art. 7749).

Benzylhexadecyldimethylammonium Periodate (2a). Benzylhexadecyldimethylammonium chloride (**1a**, 2.407 g, 6 mmol) and sodium periodate (1.070 g, 6 mmol) were dissolved in a minimal amount of water, respectively, and mixed at 0 °C. Whereby a white precipitate separated out immediately. After vigorous stirring for 30 min, the precipitated **2a** was filtered and dried under vacuum (3.168 g, 96%, mp 74—77 °C). Recrystallization from benzene–hexane gave pure **2a** (90% yield; 2.963 g). Mp 76—77 °C. Found: C, 54.15; H, 8.46; N, 2.54%. Calcd for $C_{25}H_{46}INO_4$: C, 54.44; H, 8.41; N, 2.54%.

In a similar manner, **2b** and **2c** were prepared from the corresponding quaternary ammonium halides and sodium periodate in excellent yields.

2b: Mp 149—150 °C. Found: C, 40.66; H, 5.79; N, 3.71%. Calcd for $C_{13}H_{22}INO_4$: C, 40.73, H, 5.74; N, 3.66%.

2c: Mp 193 °C (dec). Found: C, 44.18; H, 8.58; N, 3.30%. Calcd for $C_{16}H_{36}INO_4$: C, 44.34; H, 8.37; N, 3.23%.

Reaction of 2a with 3dl. A mixed solution of **3dl** (107 mg, 1/2 mmol) and **2a** (304 mg, 1.1/2 mmol) in THF (7 ml) was refluxed for 6 h under nitrogen. After evaporation of the solvent, the residue was partitioned between ether and water. To the ethereal layer was added a solution of semicarbazide hydrochloride (112 mg, 1 mmol) in water–methanol followed by the addition of several drops of pyridine and the mixture worked up in the usual way to give benzaldehyde semicarbazone (81% yield, 131 mg). Mp 223—224 °C (lit, 224—225 °C).

1-Phenyl-1-pentanol (6). A mixed solution of **3dl** (107 mg, 1/2 mmol) and **2a** (304 mg, 1.1/2 mmol) in dioxane (4 ml) was refluxed for 2 h in the presence of molecular sieves[3] under nitrogen. After the addition of THF (10 ml) at room temperature (the precipitated benzylhexadecyldimethylammonium iodate (**4**) was dissolved), the reaction mixture was cooled to −78 °C followed by the addition of butyllithium (1.1 mmol) and allowed to warm to room temperature and kept overnight. After the addition of buffer solution (pH 7) and filtration, the filtrate was evaporated to remove the organic solvent and saturated with sodium chloride followed by extraction with ether. The crude residue obtained by evaporation of the extract was subjected to preparative TLC (ethyl acetate/hexane=1/5) to give the expected alcohol **6** (116 mg, 71% yield). The compound exhibited IR and NMR spectral data in accordance with assigned structure.

Oxidative Cleavage of trans-*Stilbene with 2a.* To a mixed solution of *trans*-stilbene (90 mg, 1/2 mmol) and **2a** (606 mg, 2.2/2 mmol) in dioxane (2 ml) was added a catalytic amount of osmium tetraoxide (*ca.* 1.5 mg) dissolved in dioxane (2 ml) at room temperature under nitrogen. The clear solution became green and then yellow accompanied by the precipitation of **4**. After stirring for 3 h at room temperature followed by the addition of THF (10 ml), the reaction mixture was cooled to −78 °C and the lithium salt **7b** (1.1 mmol, THF solution) added. The pale yellow mixture was stirred for 2 h at −78 °C and treated with pH 7 buffer solution at −78 °C. After the similar work-up as described above, the expected alcohol **8b** (345 mg)[4] was obtained in a 95% yield from stilbene.

References

1) H. O. House, "Modern Synthetic Reactions," 2nd ed, W. A. Benjamin, Inc., Calfornia (1972), p. 353.

2) For example, when **2b** was reacted with an equimolar amount of **3** in dichloromethane at room temperature for 24 h under nitrogen, benzaldehyde was obtained in good yield (85% from **3dl** and 88% from **3meso** as semicarbazone, respectively).

3) Molecular Sieves 4A 1/16 from Wako Pure Chem. Ind. Ltd.

4) **8a** and **8b** consist of two diastereoisomers, respectively. The corresponding furan derivatives **9a** and **9b** were obtained by refluxing in dry benzene containing a trace of *p*-toluenesulfonic acid (see also Refs. 5 and 6). **9a** (R=H): 58% (from **8a**), oil, IR 1595, 1570, 1160, 1010, 900, 760 cm^{-1}; NMR (CCl_4) δ 6.51 (q, 1H), 6.69 (d, 1H), 7.2—7.9 (m, 6H). **9b** (R=CH_3): 63% (from **8b**), oil, IR 1600, 1590, 1160, 1060, 885, 760 cm^{-1}; NMR ($CDCl_3$) δ 2.20 (s, 3H), 6.20 (d, 1H, J=2 Hz), 7.05—7.70 (m, 6H).

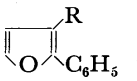

9a, b

5) K. Inomata, S. Aoyama, and H. Kotake, *Bull. Chem. Soc. Jpn.*, **51**, 930 (1978).

6) H. Kotake, K. Inomata, H. Kinoshita, S. Aoyama, and Y. Sakamoto, *Heterocycles*, **10**, 105 (1978).

7) R. Pappo, D. S. Allen, Jr., R. U. Lemieux, and W. S. Jonson, *J. Org. Chem.*, **21**, 478 (1956).

Photo-induced Reaction of 2-Bromo-3-methoxy-1,4-naphthoquinone with 1,1-Dicyclopropylethylenes

Kazuhiro MARUYAMA,* Masahiro TOJO, and Tetsuo OTSUKI
Department of Chemistry, Faculty of Science, Kyoto University, Kyoto 606
(Received August 22, 1979)

Synopsis. 2-(2,2-Dicyclopropylethenyl)-3-methoxy-1,4-naphthoquinone was isolated as a major product, accompanied by 2,2-dicyclopropyl-2,3-dihydronaphtho[2,3-*b*]furan-4,9-dione in the photochemical reaction of 2-bromo-3-methoxy-1,4-naphthoquinone with 1,1-dicyclopropylethylene. An ionic pathway to lead these products was suggested.

Photochemical reaction of 2-bromo-3-methoxy-1,4-naphthoquinone with a variety of 1,1-diarylethylenes was found to yield polycyclic aromatic *p*-quinones such as 5-arylbenz[*a*]anthracene-7,12-diones *via* 2-(2,2-diarylethenyl)-3-methoxy-1,4-naphthoquinone as their precursor (see an example in Scheme 1).[1]

To see a profound insight into the mechanistic aspects of the photochemical reaction —radical process or not— the photochemical reactivity of 1,1-dicyclopropylethylenes (**2**) with 2-bromo-3-methoxy-1,4-naphthoquinone (**1**) was examined here, because the radical generated at the α-position of cyclopropyl group was reported to cause the ring-opening reaction of cyclopropane, resulting in the isomerization to substituted 3-pentenyl radical in good yield (Scheme 2).[2]

When 2-bromo-3-methoxy-1,4-naphthoquinone (**1**) (1 mmol) and 1,1-dicyclopropylethylene (**2a**) (2 mmol) dissolved in benzene (25 ml) were irradiated by a high pressure Hg arc lamp (300 W), 2-(2,2-dicyclopropylethenyl)-3-methoxy-1,4-naphthoquinone (**3a**) (25%) and 2,2-dicyclopropyl-2,3-dihydronaphtho[2,3-*b*]furan-4,9-dione (**4a**) (5%) were isolated from the reaction mixture, accompanied by 4-cyclopropyl-3-pentenyl bromide (**5a**) (30% as a mixture of *E*- and *Z*-isomers) (Scheme 3). Moreover, 1,1-bis(2-methylcyclopropyl)-ethylene (**2b**) gave the similar mixture of products **3b** (25%) and **5b** (30%) in its reaction with **1**. **5** may be produced *via* the acid-catalyzed ring-opening reaction by hydrogen bromide liberated during the formation of **3** and/or **4**.

Although the present evidences are not conclusive because of the rather poor yield of the products isolated from the reaction mixture,[3] no products which are originated from the radical ring-opening reaction of 1,1-dicyclopropylethylenes can be identified so far. By analogy to the photochemical reaction of 1,1-diarylethylene with **1**, the charge transfer interaction between quinone **1** and 1,1-dicyclopropylethylene (**2**) may play a role in the initial stages of the reaction, leading to the formation of intermediate **6** *via* **7** by eliminating bromide ion.[4] **6** is a possible intermediate which could be stabilized finally as **3** or **4**. Thus, the ionic pathway including radical ions may be dominant at least in the photochemical reaction of 1,1-dicyclopropylethylenes (**2**) with 2-bromo-3-methoxy-1,4-naphthoquinone (**1**).

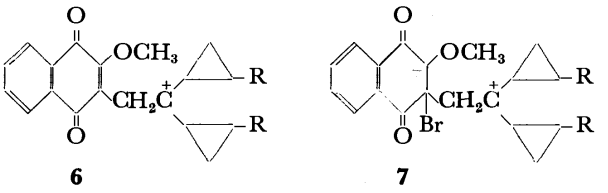

6 **7**

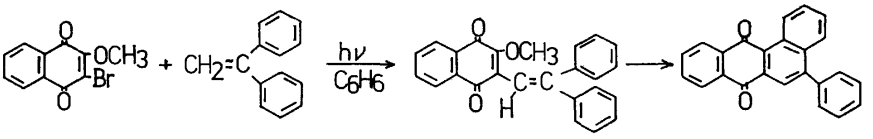

Scheme 1.

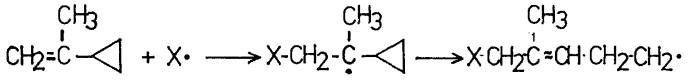

Scheme 2.

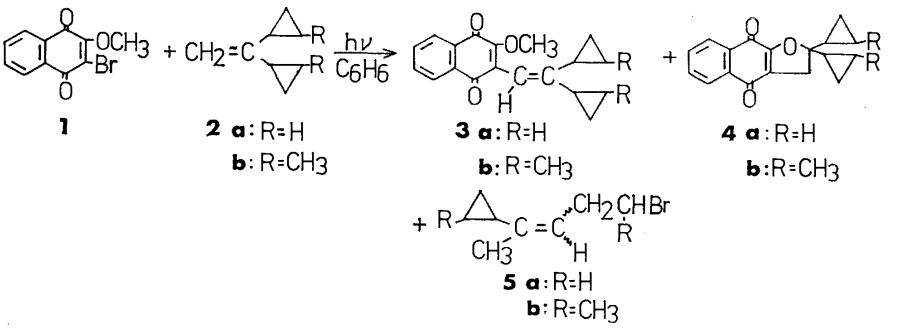

Scheme 3.

Experimental

Starting Materials. The synthesis of 2-bromo-3-methoxy-1,4-naphthoquinone (**1**) was described in the previous report.[1b] 1,1-Dicyclopropylethylene (**2a**) and 1,1-bis(2-methylcyclopropyl)ethylene (**2b**) were synthesized by the Wittig reaction[5] of the corresponding dicyclopropyl ketones.[6] 1,1-Dicyclopropylethylene (**2a**): colorless oil, bp 36—38 °C/22 mmHg. NMR (CCl_4): δ: 0.3—0.8 ppm (8H, m), 1.0—1.5 (2H, m), 4.41 (2H, s). IR (liq. film): 3100, 890 cm^{-1}. 1,1-Bis(2-methylcyclopropyl)ethylene (**2b**); colorless oil, bp 79—80 °C/62 mmHg. NMR (CCl_4): δ; 0.2—0.4 ppm (2H, m), 0.6—1.4 (4H, m), 1.10 (6H, d, J=5 Hz), 1.6—2.1 (2H, m), 4.36 (2H, s). IR (liq. film): 3100, 890 cm^{-1}.

Photochemical Reaction. A benzene solution (25 ml) of 2-bromo-3-methoxy-1,4-naphthoquinone (**1**) (1 mmol) and 1,1-dicylopropylethylene (**2**) (2 mmol) was irradiated by a high pressure Hg arc lamp (300 W). A half amount of quinone was consumed on irradiating the reaction mixture for 10 h at room temperature. After concentrated *in vacuo*, the reaction mixture was further purified by column chromatography on silica gel. The physical properties of the products were as follows. 2-(2,2-Dicyclopropylethenyl)-3-methoxy-1,4-naphthoquinone (**3a**): orange yellow needles, mp 84—86 °C. NMR ($CDCl_3$): δ; 0.6—0.8 ppm (8H, m), 1.2 (2H, m), 4.07 (3H, s), 5.97 (1H, s), 7.5—7.8 (2H, m), 7.9—8.2 (2H, m). IR (KBr): 3100, 1675 cm^{-1}. UV (C_2H_5OH): 424 nm (log ε: 3.15), 327 (3.34), 272 (4.11), 255 (sh) (4.06). MS: *m/e* (relative intensity); 294 (M^+, 36), 279 (M^+-15, 13), 266 (M^+-28, 57), 251 (M^+-43, 100). 2-[2,2-Bis(2-methylcyclopropyl)-ethenyl]-3-methoxy-1,4-naphthoquinone (**3b**): orange yellow needles, mp 98—100 °C. NMR ($CDCl_3$): δ; 0.4—1.4 ppm (14H, m), 3.92 (3H, s), 5.71 (1H, s), 7.3—7.6 (2H, m),7.7—8.0 (2H, m). IR (KBr): 3100, 1670 cm^{-1}. UV (C_2H_5OH): 427 nm (log ε: 3.18), 326 (3.32), 274 (4.13), 256 (sh) (4.04). MS: *m/e* (relative intensity): 322 (M^+, 14), 280 (M^+-42, 100), 266 (M^+-56, 53). 2,2-Dicyclopropyl-2,3-dihydronaphtho-[2,3-*b*]furan-4,9-dione (**4a**): yellow needles, mp 134—135 °C. NMR ($CDCl_3$): δ; 0.5—0.7 ppm (8H, m), 1.3 (2H, m), 2.85 (2H, s), 7.5—7.8 (2H, m), 7.9—8.2 (2H, m). IR (KBr): 3100, 1680 cm^{-1}. UV (C_2H_5OH): 397 nm (log ε: 2.94), 334 (3.30), 287 (3.95), 254 (4.23), 249 (sh) (4.21). MS *m/e*: (relative intensity); 280 (M^+, 26), 252 (M^+-28, 100), 224 (M^+-56, 28). 4-Cyclopropyl-3-pentenyl bromide (**5a**) as a mixture of *E*- and *Z*-isomers (the relative ratio of the two isomers, 40/60 (A/B),[7] was estimated on the basis of their NMR signals): colorless oil. NMR (CCl_4): δ; 0.5 ppm (4H, m), 1.46 (3H, s), 1.5 (1H, m), 2.6 (2H, m), 3.40 (2H, t, J=1.7 Hz), 5.2 (1H, m) for an isomer A. 0.5 ppm (4H, m), 1.56 (3H, s), 1.5 (1H, m), 2.6 (2H, m), 3.34 (2H, t, J=1.7 Hz), 5.2 (1H, m) for another isomer B. IR (liq. film): 3100 cm^{-1}. MS: *m/e* (relative intensity); 190 (M^+, 27), 188 (M^+, 27), 109 (M^+-Br, 100). 5-Bromo-2-(2-methylcyclopropyl)-2-hexene (**5b**) as a mixture of *E*- and *Z*-isomers (the relative ratio of the two isomers, 40/60 (A/B),[7] was estimated on the basis of their NMR signals): colorless oil. NMR (CCl_4): δ; 0.2—1.8 ppm (7H, m), 1.46 (3H, s), 1.72 (3H, d, J=4 Hz), 2.4—2.8 (2H, m), 3.8—4.2 (1H, m), 4.9—5.3 (1H, m) for an isomer A. 0.2—1.8 ppm (7H, m), 1.56 (3H, s), 1.66 (3H, d, J=4 Hz), 2.4—2.8 (2H, m), 3.8—4.2 (1H, m), 4.9—5.3 (1H, m) for another isomer B. IR (liq. film): 3100 cm^{-1}.

References

1) a) K. Maruyama and T. Otsuki, *Chem. Lett.*, **1975**, 87; b) K. Maruyama, T. Otsuki, and K. Mitsui, *Bull. Chem. Soc. Jpn.*, **49**, 3361 (1976); c) K. Maruyama, K. Mitsui, and T. Otsuki, *Chem. Lett.*, **1977**, 853; d) K. Maruyama, K. Mitsui, and K. Mitsui, *ibid.*, **1978**, 323; e) K. Maruyama, T. Otsuki, and K. Mitsui, *J. Org. Chem.* in press.; f) K. Maruyama, T. Otsuki, K. Mitsui, and M. Tojo, *J. Heterocyclic Chem.*, in press.

2) E. S. Heyser and T. D. Taliaferro, *J. Org. Chem.*, **28**, 3442 (1963).

3) The poor yields of the products could be partly due to the trivial reactions such as the demethylation of the starting quinone caused by hydrogen bromide liberated during the course of the reaction.

4) When 1,1-diarylethylene such as 1-(*p*-chlorophenyl)-1-phenylethylene, 1-phenyl-1-(2-thienyl)ethylene or 1-phenyl-1-(2-*N*-methylpyrrolyl)ethylene was submitted to the reaction (*cf.* Scheme 1), one of two aryl groups donating highly its π-electrons cyclizes preponderantly to give polycyclic aromatic *p*-quinone (see Refs. (1b), (1c), and (1d)). By inspection of molecular model it is clear that the isomeric distribution of the final products can be determined by the configuration of the intermediate, 2-(2,2-diarylethenyl)-3-methoxy-1,4-naphthoquinone. Therefore, these results indicate that the charge-transfer interactions between quinone and the aryl group of reacting ethylene in the initial stages are playing a role for determining the isomeric distribution of final products.

In addition, an important contribution of the similar charge-transfer interactions has been confirmed in the photosubstitution reaction of halogenated 1,4-naphthoquinones. (see K. Maruyama and T. Otsuki, *Chem. Lett.*, **1977**, 851, *Bull. Chem. Soc. Jpn.*, **50**, 3249 (1977)).

5) T. Teraji, I. Moritani, E. Tsuda, and S. Nishida, *J. Chem. Soc., C*, **1971**, 3252.

6) *Org. Synth.*, Coll. Vol. IV, 278 (1963).

7) The assignment of an isomeric mixture of A and B to that of *E*- and *Z*-isomers was not completed yet.

Coordinative Role of Alkali Cations in Organic Reactions. IV. Benzoylation, Phenacylation, and Benzylation of Kojic Acid

Narinder S. Poonia,* Ashok K. Arora, and Amritlal V. Bajaj
Department of Chemistry, University of Indore, Khandwa Road, Indore 452001, India
(Received April 21, 1979)

Synopsis. Using kojic acid (5-hydroxy-2-hydroxymethyl-4-pyrone) as a substrate, the title reactions were carried out with various alkali metal hydroxides. Whereas phenacylation (with KOH or NaOH) and benzylation (with KOH, NaOH, or LiOH) are possible only on the phenolic hydroxyl, benzoylation can be carried out selectively as well as collectively on both the hydroxyl group (in 80% aq EtOH). The results were discussed in terms of the interactive role of alkali cations with the substrate.

In earlier communications[1,2] we reported that an organic reaction involving the use of alkali hydroxide (MOH) is triggered by the alkali cation (M^+) and that the efficiency and the course of the reaction can be controlled by changing either M^+ or the conditions which influence the coordinative role of the latter. In this article we introduce, in addition, that during benzoylation (with benzoyl chloride), phenacylation (with phenacyl bromide), and benzylation (with benzyl chloride) of kojic acid (5-hydroxy-2-hydroxymethyl-4-pyrone, abbr. HO**k**CH_2OH, **1**), (i) MOH is not present just to neutralize the acid byproduct of the reaction but reacts with the substrate (**1**) (see **5**[3,4]) and determines the invitation to the electrophilic reagent, and (ii) the ion-association (insolubility) of the leaving alkali halide ion pair in the reaction medium determines the efficiency of the reaction.

The synthetic procedures for the derivatives of kojic acid, namely, 5-benzoyloxy-2-hydroxymethyl-4-pyrone (**2a**), 5-hydroxy-2-benzoyloxymethyl-4-pyrone (**2b**), 5-benzoyloxy-2-benzoyloxymethyl-4-pyrone (**2c**), 5-phenacyloxy-2-hydroxymethyl-4-pyrone (**3**) and 5-benzyloxy-2-hydroxymethyl-4-pyrone (**4**) have been standardized to maximize the product yields.

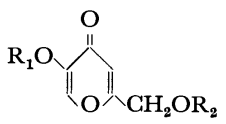

(R_1O**k**CH_2OR_2)

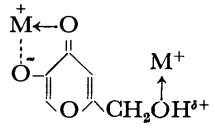

5

1, $R_1=R_2=H$
2a, $R_1=PhCO$; $R_2=H$
2b, $R_1=H$; $R_2=PhCO$
2c, $R_1=R_2=PhCO$
3, $R_1=PhCOCH_2$; $R_2=H$
4, $R_1=PhCH_2$; $R_2=H$

Results and Discussion

Benzoylation. As against the laborious procedures adopted earlier,[5] we provide herein one-step procedures involving the rather convenient use of MOH in EtOH–H_2O medium for obtaining **2a** (81%), **2b** (65%), and **2c** (79%) in higher yields (see Table 1).

Benzoylation reactions on **1** are possible on the phenolic or both the hydroxyl groups using appropriate amounts of PhCOCl and MOH; the reactions fail in the absence of MOH. The reactions are most favored when MOH of the lowest charge density M^+ (KOH) is used in an ionizing medium (EtOH–H_2O), *i.e.*, under the conditions favoring formation of the loose K^+–O**k**-$CH_2O^-K^+$ ion pairs which allow a facilitated M^+/-PhC^+O exchange at each negative site.

With an excess MOH of a high charge density M^+ (NaOH and especially LiOH), which can ensure an effective protection of the phenoxide through M^+, benzoylation of the $-CH_2OH$ group can be carried out using **1** and PhCOCl in equimolecular proportions. This reaction is novel. When the high charge density Li^+ is used, the reaction appears to involve Li^+–O**k**CH_2OH ($\downarrow Li^+$) coordinated species as an intermediate because **2b** can also be synthesized (in 32% yield) employing one mole each of **1**, LiOH, $LiClO_4$, and PhCOCl wherein whole LiOH is expected to be consumed by the phenolic hydroxyl while Li^+ ions of $LiClO_4$ carry out the reaction on the alcoholic hydroxyl. If $-CH_2O^-Li^+$ should have formed as an intermediate (alkoxide mechanism), the Li^+/PhC^+O exchange becomes rather difficult to visualize because such an exchange is not possible even at the comparatively delocalized phenoxide as evident from the lack of benzoylation of the phenolic hydroxyl under these conditions. Various sugars coordinate[6] with alkali and alkaline earth cations in water through the $-CH_2OH$ groups (NMR studies) and X-ray diffraction analysis reveals coordination of the cation with the $-CH_2OH$ group in the complexes $KI(3)_2$,[4a] $NaI(3)_2 \cdot 2H_2O$,[4b] and $NaClO_4$(1,4-anhydroerythritol).[7]

Phenacylation. As in methanol,[8] the direct product of the reaction in ethanol or acetone is the complex $MBr(3)_2$ instead of **3**; on decomposing the complex with water, **3** is recovered in a hydrated form (mp 90 °C and not 144—145 °C as reported earlier[9,10]) which can be dehydrated (mp 145 °C) by recrystallization from absolute ethanol. Using KOH in EtOH–H_2O (4: 1) the reaction efficiency is maximum with 77% yield of **3** (liberated from the complex).

In the presence of MOH only phenolic hydroxyl undergoes phenacylation as known earlier.[8] In the absence of MOH, **1** and $PhCOCH_2Br$ are recovered unreacted under all conditions. Condensation also fails when pyridine is used instead of MOH; the direct $PhCOCH_2Br$–pyridine reaction,[11] was avoided by mixing pyridine with **1** and adding $PhCOCH_2Br$ later. These observations indicate that MOH does not only function to neutralize HBr but reacts with the substrate to produce the reactive M^+–O**k**CH_2OH and that the nature of M^+ determines the reactivity of the phenoxide with $PhCOCH_2Br$.

The yield of **3** increases as media of increasing polarity and M^+ of decreasing charge density are used. This indicates that the C–Br bond is attacked in accordance with the "liberation" of the cation-controlled

Table 1. Reaction of **1** with $PhCOCl$, $PhCOCH_2Br$, and $PhCH_2Cl$ in the presence of different MOH[a)]

Reaction mixture (proportions)		Medium	Product (yield/%) KOH	NaOH	LiOH
		Benzoylation			
1-MOH-PhCOCl (↓)[b)]	(1:1:1)	EtOH–H_2O (4:1)	**2a**(81)[c)]	**2a**(75)	c_1 **2a**(54) c_2 **2c**(21)
		EtOH	c_1 **2a**(19) c_2 **2c**(25)	**2c**(37)	**2c**(23)
	(1:2:1)	EtOH–H_2O (4:1)	**2c**(66)	**2b**(41)	**2b**(65)[e)]
		EtOH	**2c**(15)	**2d**(82)[d)]	**2d**(58)
	(1:2:2)	EtOH–H_2O (4:1)	**2c**(79)[c)]	**2c**(69)	**2c**(31)
		Phenacylation[e)]			
1-MOH–$PhCOCH_2Br$ (↓)	(1:1:1)	Acetone–Water (4:1)	**3**(49)[c)]	**3**(43)[c)]	—
		EtOH	**3**(56)	**3**(46)	—
		EtOH–H_2O (4:1)	**3**(77)[c)]	**3**(60)	—
		EtOH–H_2O (3:2)	**3**(57)	**3**(48)	—
1-MOH (↓)–$PhCOCH_2Br$	(1:1:1)	EtOH–H_2O (4:1)	**3**(43)	**3**(34)	—
	(1:2:2)	EtOH–H_2O (3:2)	**3**(45)	**3**(38)	—
		Benzylation			
1-MOH–$PhCH_2Cl$ (↓)	(1:1:1)[b)]	EtOH–H_2O (4:1)	**4**(68)[c)]	**4**(61)	**4**(57)

— poor or no reaction. c_1 and c_2 stand for the first and the second crop; in case crops are not mentioned, product was the same in both. a) Each reaction has been investigated extensively under varied conditions but only those experiments are included here which either afforded the highest yield or threw light on the reaction mechanism. b) The reagent preceding the arrow was added to the mixture of the other two. c) Optimum conditions recommended for synthesis. d) **2d** represents M^+-**Ok**CH_2OH. e) Derivative recovered from the complex—$M^+(\mathbf{3})_2Br^-$. f) When 1:1:2 or 1:2:2 reaction mixture was employed or water was eliminated, yield of the product was decreased for each MOH; when both the changes were made at a time then particularly for NaOH and LiOH phenolic hydroxyl also failed to react and M^+-**Ok**CH_2OH was recovered.

phenoxide through loosening of the M^+-**Ok**CH_2OH ion pair; if the sequence of addition of the reactants is varied and **1**–MOH complexation is not allowed to occur prior to the addition of $PhCOCH_2Br$, the yield of the product is decreased.

Benzylation. Only phenolic hydroxyl can be benzylated (*cf.* phenacylation) and the **1**–$PhCH_2Cl$ reaction fails in the absence of MOH. Compound **4** is obtained in the highest yield (68%) when KOH is used and the reaction medium (EtOH) contains water. In a less ionizing medium (EtOH) the reaction is poor (KOH) or is completely stopped (NaOH or LiOH) especially in the presence of excess MOH due to the protection of phenoxide with the cation. This and that the reaction is favored in the order LiOH, NaOH, and KOH indicate that M^+/PhC^+H_2 exchange is facilitated as M^+-**Ok**CH_2OH ion pair loosens. The reaction on the phenolic hydroxyl in the presence of LiOH is possible with $PhCH_2Cl$ but not with $PhCOCH_2Br$ (see Table 1). The enhanced reactivity of $PhCH_2Cl$ with respect to that of $PhCOCH_2Br$ on a common substrate (Li^+-**Ok**CH_2OH) is interestingly significant because $PhCH_2Cl$ is expected to be a relatively inert reagent due to Ph^+ being a less electron withdrawing agent than PhC^+O and the C–Cl bond being a stronger bond than the C–Br one. The facilitated benzylation can only be because insolubility[14] and hence[15] solution stability of the leaving ion pair for $PhCH_2Cl$ (*i.e.*, LiCl) is higher than that for $PhCOCH_2Br$ (*i.e.*, LiBr) which forces an SN^1 contribution of $PhCH_2Cl$ to aid displacement of Li^+ from phenoxide.

Experimental

Recommended Procedure for Benzoylation, Phenacylation, and Benzylation. To a solution of **1** (1.42 g, 10 mmol) in EtOH–H_2O (4:1, v/v) (15 ml) was added the required amount of MOH. The clear reaction mixture was treated with the reagent concerned, and refluxed for 1 h on steam-bath. The product was crystallized by cooling, collected and authenticated. Specific conditions for the synthesis of compounds **2**—**4** are outlined below.

Synthesis of 2a. Compound **1** was taken in EtOH–H_2O (4:1) and treated with KOH (0.56 g, 10 mmol) followed by benzoyl chloride (1.41 g, 10 mmol). Yield 1.99 g (81%), mp 143 °C. *Synthesis of 2b.* Compound **1** was taken in EtOH–H_2O (4:1) and treated with excess LiOH (0.84 g, 20 mmol) followed by benzoyl chloride (1.41 g). Yield 1.59 g (65%), mp 174—175 °C. *Synthesis of 2c.* Compound **1** was taken in EtOH–H_2O (4:1) and treated with KOH (1.12 g, 20 mmol) followed by benzoyl chloride (2.81 g, 20 mmol). The isolated product was recrystallized from 10 ml acetone–water (1:1, v/v) to remove the traces of the by-product (benzoic acid). Yield 2.76 g (79%), mp 133—134 °C.

Synthesis of 3. Compound **1** was taken in EtOH–H_2O (4:1) and treated with KOH (0.56 g) followed by phenacyl bromide (1.99 g, 10 mmol). The isolated product was a crystalline complex $K^+(\mathbf{3})_2Br^-$ (mp 208 °C). The complex was decomposed with boiling water (20 ml) to get the hydrated form of **3** (mp 90 °C) which was recrystallized from ethanol to obtain anhydrous **3** (mp 145 °C). Yield 2.00 g (77%).

Synthesis of 4. Compound **1** was taken in EtOH–H_2O (4:1) and treated with KOH (0.56 g) followed by benzyl chloride (1.27 g, 10 mmol). Yield 1.57 g (68%), mp 133 °C.

Authentification of the Products. All the products are known compounds. They were authenticated with the help of elemental analysis, hot stage microscopic examination of melting points and IR spectroscopy. Absorption characteristics of >C=O in **2a**, **2b**, and **2c** deserve a mention in that the pyrone carbonyl of each compound absorbs at ≈1670 cm^{-1} whereas carbonyl of the benzoyl moieties absorbs at a higher position probably due to the presence of an oxygen in the vicinity. The benzoyl carbonyl near the phenolic oxygen absorbs at the highest —**2a** at 1755 cm^{-1}, **2b** at 1735 cm^{-1}, and **2c** at 1740 and 1667 cm^{-1}.

References

1) N. S. Poonia, B. P. Yadav, C. Kumar, and V. W. Bhagwat, *J. Org. Chem.*, **42**, 2030, 3311 (1977).

2) N. S. Poonia and B. P. Yadav, *J. Org. Chem.*, **43**, 2842 (1978).

3) J. A. Rendleman, Jr., *Adv. Carbohydr. Chem.*, **21**, 209 (1966).

4) a) D. L. Hughes, S. E. V. Phillips, and M. R. Truter, *J. Chem. Soc., Dalton Trans.*, **1974**, 907; b) S. E. V. Phillips and M. R. Truter, *J. Chem. Soc., Dalton Trans.*, **1975**, 1066.

5) A. Beelik and C. B. Purves, *Can. J. Chem.*, **33**, 1361 (1955).

6) S. J. Angyal, *Aust. J. Chem.*, **25**, 1957 (1972); S. J. Angyal, *Pure Appl. Chem.*, **35**, 131 (1973); J. Andrasko and S. Forsen, *Biochem. Biophys. Res. Commun.*, **52**, 233 (1973).

7) R. E. Ballard, A. H. Haines, E. K. Norris, and A. G. Wells, *Acta Crystallogr., Sect. B*, **30**, 1590 (1974).

8) C. D. Hurd and R. J. Sims, *J. Am. Chem. Soc.*, **71**, 2440 (1949).

9) S. E. V. Phillips and M. R. Truter, *J. Chem. Soc., Dalton Trans.*, **1975**, 1071, have carried out X-ray analysis of the hydrated **3** ($PhCOCH_2OkCH_2OH \cdot H_2O$); the water protons are found bonded with the carbonyl oxygens.

10) D. E. Fenton, *J. Chem. Soc., Dalton Trans.*, **1973**, 1380.

11) N. Campbell, "Chemistry of Carbon Compounds," ed by E. H. Rodd, Elsevier, Amsterdam (1957), Vol. IV A, p. 508; J. W. Baker, *J. Chem. Soc.*, **1938**, 445.

12) W. F. Linke, "Solubilities of Inorganic and Metal-Organic Compounds," 4th ed, American Chemical Society, Washington (1965), Vol. 2.

13) R. J. P. Williams, *Adv. Chem. Ser.*, **100**, 151 (1971).

Hydration Numbers of Sodium Chloride in Dioxane–Water Mixtures and the Volume Change Accompanying Hydration

Tsunemichi Okuwa

Institute of Scientific and Industrial Research, Osaka University, Yamadakami, Suita, Osaka 565

(Received February 5, 1979)

The density and the ultrasonic velocity were measured for dioxane–water solutions of sodium chloride at 25 °C. The hydration numbers of sodium chloride were estimated and were compared with those determined by electrical-conductivity measurements. The difference between them was discussed. The volume change caused by the dissociation of sodium chloride in a 60 wt % aqueous dioxane solution was determined from the data of the apparent molal volume. This value is in good agreement with that calculated from the excess ultrasonic absorption.

In a dioxane–water mixture with a lower dielectric constant than water, NaCl would dissociate incompletely and a dissociation equilibrium may be attained between the Na^+ ions, the Cl^- ions, and the undissociated NaCl molecules. If the water molecules bound to ions are considered to be incompressible, then a volume change attributable to ionization would be found. The volume change was estimated from density measurements of aqueous dioxane solutions of sodium chloride and was compared with that calculated from excess ultrasonic absorption, as reported in the previous paper.[1] The sound velocity increases with an increase in the concentration of NaCl in dioxane–water mixtures. This increase reflects a decrease in the compressibility of the solvent caused by hydration. The hydration numbers due to the ionization of NaCl were calculated using some assumptions.

Experimental

The densities were measured by a float method similar to that used by Desnoyers and Arel.[2] A float was suspended in the pan of a balance by means of a nylon thread 0.1 mm in diameter and was then placed in the solution in a thermostated cell. The volume of the float used was about 230 cm^3.

The difference between the density of a solution, d, and that of water, d_0, is related to the weights, W and W_0, of the float in the solution and in water respectively by

$$d - d_0 = (W_0 - W)/V, \quad (1)$$

where V is the volume of the float. Measurements were made at 25 °C.

The ultrasonic velocities were measured by the interference method of the pulse wave and the continuous wave at 5 MHz. The molalities of sodium chloride in mixed solvents containing 0 to 60 wt % dioxane were in the range of 0.1—1.0 m.

Results

The ultrasonic velocities in solutions of NaCl in dioxane–water mixtures are shown in Fig. 1.

The apparent molal volume, ϕ_v, and the apparent molal compressibility, ϕ_k, are given by

$$\phi_v = \frac{V - V_s}{n_2} = \frac{1000}{mdd_s}(d_s - d) + \frac{M}{d}, \quad (2)$$

and

$$\phi_k = -\left(\frac{\partial \phi_v}{\partial p}\right)_T = \frac{\beta V - \beta_s V_s}{n_2} = \frac{1000(\beta - \beta_s)}{md_s} + \beta\phi_v, \quad (3)$$

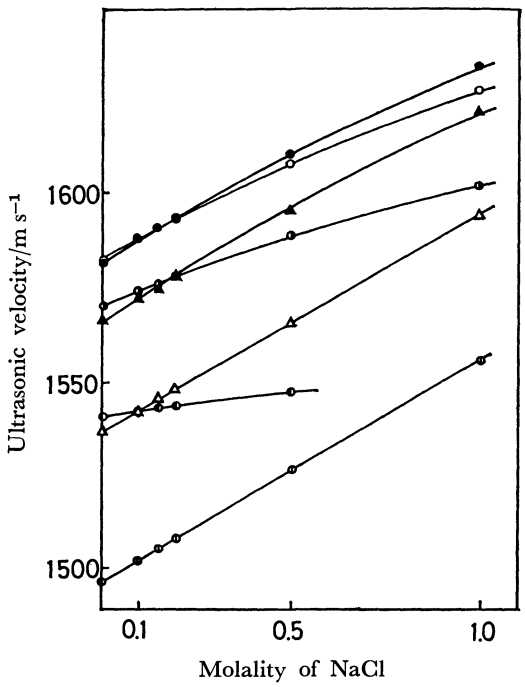

Fig. 1. Ultrasonic velocity in solutions of NaCl in dioxane-water mixtures at 25 °C.
Dioxane wt %: ⓘ 0, △ 10, ▲ 20, ● 30, ○ 40, ◑ 50, ◐ 60.

where n_2, m, and M are the number of moles, the molality (mole per 1000 g of solvent), and the molecular weight of NaCl respectively. V, d, and β are the volume, density, and compressibility of the solution respectively. The subscript s denotes the solvent. A typical example of the plot of ϕ_v *vs.* $(\text{molality})^{1/2}$ is shown in Fig. 2.

Discussion

Hydration Number of Sodium Chloride. In the solution of NaCl in a dioxane–water mixture, both water and dioxane molecules may participate in the formation of solvation shells around ions. As the dipole moment of a dioxane molecule is much smaller than that of water, the electrostrictive effect of the ions on dioxane molecules in the solvation shells might be negligible[3] in comparison with the electrostriction on water molecules. Therefore, the volume of dioxane molecules would be unchangeable in the solution. Assuming that the compressibilities of the ions and water molecules bound to the ions are equal to zero,

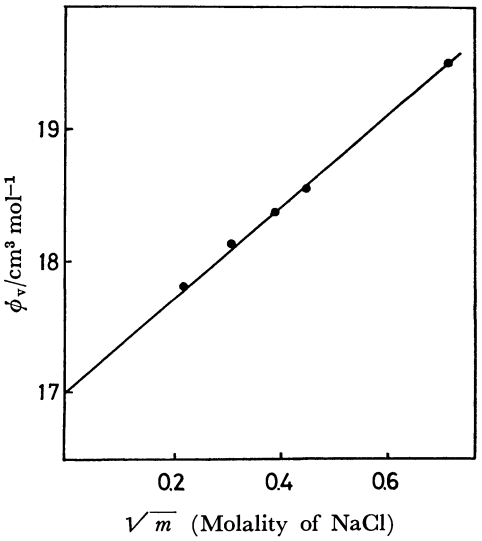

Fig. 2. Apparent molal volume of NaCl in 60 wt % aqueous dioxane solution at 25 °C.

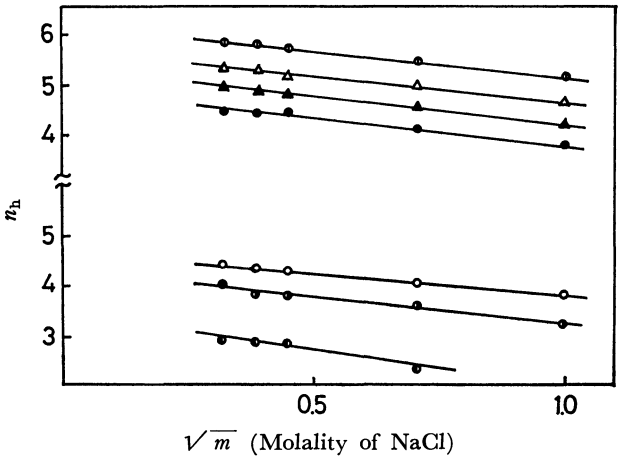

Fig. 3. Hydration numbers of NaCl in dioxane-water mixtures at 25 °C.
Dioxane wt %: ⦶ 0, △ 10, ▲ 20, ● 30, ○ 40, ◑ 50, ◐ 60.

the compressibility of the solution, β, is given by

$$\beta = -\frac{1}{V}\frac{\partial}{\partial p}\{V_0(n_1-n_i)+V_3n_3\}$$
$$= -\frac{1}{V}\{n_i\beta_0V_0-\beta_sV_s\}, \quad (4)$$

where n_1 is the total number of moles of water in the solution, n_i is the number of water molecules bound to the ions, V_0 is the molal volume of free water not bound to the ions, β_0 is the compressibility coefficient of pure water, and V_3 and n_3 are the molal volume and the number of moles of dioxane.

According to Eqs. 3 and 4, the hydration number, n_h, of sodium chloride in a dioxane–water mixture is expressed as

$$n_h = \frac{n_i}{\alpha n_2} = -\frac{\phi_k}{\alpha\beta_0V_0}, \quad (5)$$

where α is the degree of dissociation of NaCl. The values of n_h are shown in Fig. 3. In 0, 10, 20, and 30 wt % dioxane aqueous solutions, α is assumed to be approximately 1.

The dissociation equilibrium constants of NaCl in dioxane–water mixtures were obtained by electrical conductance measurements.[4–6] NaCl is considered to be in an equilibrium[6] such as

$$NaCl(aq) + kH_2O \overset{K^\circ}{\rightleftharpoons} Na(aq)^+ + Cl(aq)^-,$$
$$K^\circ = \frac{K}{C_{H_2O}^{k}}, \text{ and } K = \frac{C_{Na^+}\cdot C_{Cl^-}}{C_{NaCl}}, \quad (6)$$

where C_{H_2O} is the molar concentration of water and where k is the net change in the waters of solvation upon the dissociation of NaCl and corresponds to the hydration number. K° and k are found to be independent of C_{H_2O} and to vary only with the temperature:

$$\log K^\circ = -10.00, \quad k = 6.4 \ (25\,^\circ C)^{6}$$
$$\log K^\circ = -11.13, \quad k = 7.0 \ (50\,^\circ C)^{6} \quad (7)$$

As may be seen in Fig. 3, the hydration number, n_h, of NaCl in an aqueous solution is close to k (=6.4) at an infinite dilution, but n_h in dioxane–water mixtures decreases with an increase in the concentration of dioxane. The difference between n_h and k in a dioxane–water mixture might be caused by differences in the models used for the hydrated ion and the assumptions associated with these models. If the hydration number is constant and independent of the concentration of dioxane in dioxane–water mixtures, the compressibilities of hydrated ions must have definite values. The existence of dioxane molecules might influence the electrostriction of the ions in relation to the surrounding water molecules.

Volume Change Accompanying the Dissociation of Sodium Chloride. It is useful to estimate further the volume change which accompanies the ionization of NaCl in dioxane–water mixtures. The apparent molal volume of NaCl, ϕ_v, derived from Eq. 2, is related to the degree of dissociation, α, by

$$\phi_v = (1-\alpha)\phi_u + \alpha\phi_i, \quad (8)$$

where ϕ_i and ϕ_u are the apparent molal volumes of NaCl in the ionized and un-ionized states respectively.

The volume change caused by hydration, ΔV, is given by

$$\Delta V = \phi_i - \phi_u. \quad (9)$$

NaCl in dioxane–water mixture might be ionized completely at an infinite dilution; therefore, ϕ_i, can be approximately determined by the extrapolation of ϕ_v to zero concentration:

$$\phi_i \simeq \phi_v^\circ, \quad (10)$$

where ϕ_v° is the apparent molal volume at an infinite dilution.

As may be seen in Fig. 2., the value of ϕ_v° in a 60 wt% dioxane aqueous solution is 17.0 cm^3/mol. This value is a little larger than the ϕ_v° value of 16.628 cm^3/mol[7] in water. From Eqs. 8, 9, and 10, we obtain $\Delta V \approx -7$ cm^3/mol.

On the other hand, ΔV was estimated on the basis of ultrasonic absorption measurements.[1] In this paper, ΔV was calculated by considering the enthalpy change,

ΔH, for the reaction. The maximum excess ultrasonic absorption per wavelength at the relaxation frequency, μ_{max}, is given by[8,9]

$$\mu_{max} = \frac{\pi}{2\beta RTV}\left(\Delta V - \frac{l}{dC_p}\Delta H\right)^2 \frac{1}{\chi}$$

$$\chi = \left(\frac{1}{n_{Na^+}} + \frac{1}{n_{Cl^-}} + \frac{1}{n_{NaCl}}\right), \quad (11)$$

where l is the coefficient of thermal expansion, C_p is the heat capacity at a constant pressure, and n_{Na^+}, n_{Cl^-}, and n_{NaCl}, are the numbers of the moles of the sodium ion, the chloride ion, and undissociacted sodium chloride. The value of l/dC_p in a 60 wt % dioxane aqueous solution at 25 °C was estimated by interpolation of the literature values.[9]

The variation in the dissocication constant with the temperature is given by

$$\left(\frac{\partial \ln K}{\partial T}\right)_p = \frac{\Delta H}{RT^2}.$$

Taking the values derived from Eqs. 6 and 7, we find:

$$\Delta H \approx -6.6 \text{ kcal/mol}$$

Using these values in Eq. 11, we calculate $\Delta V \approx -8$ cm^3/mol. This value is in better agreement with the ΔV estimated from the density measurements than with $\Delta V \approx -5$ cm^3/mol, which was determined by neglecting ΔH in Ref. 1.

References

1) D. Tabuchi, T. Okuwa, and N. Inoue, *Nippon Kagaku Kaishi*, **9**, 1453 (1975).
2) J. E. Desnoyers and M. Arel, *Can. J. Chem.*, **45**, 359 (1967).
3) S. Ernst and B. Jezowska-Trzebiatowska, *J. Phys. Chem.*, **79**, 2113 (1975).
4) W. L. Marshall, *J. Phys. Chem.*, **74**, 346 (1970).
5) R. W. Kunze and R. M. Fouss, *J. Phys. Chem.*, **67**, 911 (1963).
6) T. H. Leong and L. A. Dunn, *J. Phys. Chem.*, **76**, 2294 (1972).
7) F. Vaslow, *J. Phys. Chem.*, **70**, 2286 (1966).
8) M. Eigen and L. De Maeyer, "Relaxation Methods," in "Technique of Organic Chemistry," John Wiley and Sons, New York (1963), Vol. VIII, Part II, pp. 895—1054.
9) G. G. Hammes and W. Knoche, *J. Chem. Phys.*, **45**, 4041 (1962).

Adsorption of *n*-Aliphatic Alcohols on Mercury Electrode and Their Effect on Electrode Kinetics

Katsumi NIKI* and Yumiko TAKIZAWA

Department of Electrochemistry, Yokohama National University, Tokiwadai, Hodogaya-ku, Yokohama 240

(Received May 11, 1979)

The adsorption parameters of butyl alcohol, amyl alcohol, and hexyl alcohol at mercury electrode were evaluated by means of the electrocapillary measurements and compared with those obtained by differential capacity measurements. A marked difference is observed both in the interaction parameters between adsorbed molecules and in the maximum surface excess, Γ_{max}. The inhibition effect by these alcohols on the electrode kinetics of the vanadium(III)/vanadium(II) couple in 0.5 M H_2SO_4 and of the europium(III)/europium(II) couple in 1.0 M HCl depends only on the surface coverage, $\theta=\Gamma/\Gamma_{max}$, of the electrode and is independent of the chain length of the adsorbed alcohol. The blocking effect is predominant in the inhibition of the electrode process by these alcohols.

The neutral surfactants adsorbed on the electrode surface often have a marked influence on electrode kinetics. The role of these surfactants can be interpreted by one of three classes of inhibition mechanisms. These involve: (a) a blocking effect, (b) an electrostatic effect, the change in the ϕ_2 potential, and (c) the effect on the activation energy for the charge transfer step. Lipkowski and Galus extensively discussed and compared the present theories with the available experimental data.[1] It has been shown that the interaction between the activated complex and the adsorbed surfactants may be described by the equation derived from Flory-Huggins, Frumkin or Blomgren-Bockris adsorption isotherms for the activated complex. It was found from the statistical analysis of the experimental data that the Flory-Huggins type equation[2,3] was better than the other two, namely:

$$k_\theta = k_0(1-\theta)^n \quad (1)$$

where k_θ is the apparent rate constant in the presence of adsorbed layer, k_0 the rate constant without surfactants, θ the surface coverage, and n is a constant.

In the present work, the effect of aliphatic alcohols on the electrode kinetics of the V(III)/V(II) and Eu(III)/Eu(II) couples has been studied in connection with the adsorption behavior of these alcohols on the dropping mercury electrode.

Experimental

Reagent grade butyl, amyl, and hexy alcohols (Tokyo Kasei) were used without further purification after their purity had been checked by gas chromatography. These alcohols were dissolved in either 0.5 M H_2SO_4 or 1.0 M HCl solutions. The base solutions were pre-treated with a purified activated charcoal. The electrocapillary curves for these solutions were obtained with a modified capillary electrometer and the radius of the capillary was determined by standardization against a solution of known surface tension as previously described.[4]

The V(III)/V(II) system in 0.5 M H_2SO_4 solution was prepared by reducing $VOSO_4$ *in situ* on a mercury pool cathode. The Eu(III)/Eu(II) system in 1.0 M HCl solution was prepared by dissolving Eu_2O_3 (electronic grade, 99.9%) and Eu(II) was generated cathodically *in situ*. The electrode kinetic parameters of the V(III)/V(II) and Eu(III)/Eu(II) systems were measured by conventional dc polarographic and pulse polarographic methods (Fuso Model 312 Polarograph). The detailed experimental procedure has been previously described.[5]

Measurements were made at (25±0.5) °C and, the electrode potential was referred to SCE.

Results and Discussion

Adsorption Isotherms. As shown in Table 1, the maximum surface excess of these alcohols is considerably smaller than that calculated from the projected area of the perpendicular orientation (7.90×10^{-10} mol cm^{-2}) and decreases linearly with the chain length of the alcohol. This is probably due to either the deviation of the alcohol dipole from vertical orientation at the electrode surface or the contamination of water molecules in the electrical double layer saturated by the alcohol. These results also suggest that the shift of the point of zero charge with respect to the surface excess of these alcohols at the electrode surface deviates from the curve predicted by the Frumkin model.[7]

The adsorption isotherms are well characterized by the Frumkin isotherm[5]

$$B_0c = \frac{\theta}{1-\theta}\exp(-2a_0\theta) \quad (2)$$

and

$$-\Delta G_A^\circ = RT\ln(55.5\,B_0) \quad (3)$$

where B_0 is the adsorption equilibrium constant, a_0 is the attraction constant between adsorbed molecules (a positive value of a_0 corresponds to the presence attraction between the adsorbed species, and *vice versa*), θ ($=\Gamma/\Gamma_{max}$) is the surface coverage of the mercury electrode, ΔG_A° is the standard free energy of adsorption of the alcohol, and c is the bulk concentration of the alcohol. The values of these parameters listed in Table 1 were obtained at the point of zero charge. The free energies of adsorption obtained by the present work agrees reasonably well with those obtained by Damaskin *et al.* from the differential capacity measurements.[8] However, both the maximum values of surface excess Γ_{max}, and the attraction constants a_0, in the present results differ markedly from their values.[8]

Figure 1 shows the dependence of θ on the relative concentration $c/c_{\theta=0.5}$ calculated from Eq. 2 in terms of the attraction constant. It is obvious from these plots that the higher the values of a_0 are, the lower the values of θ when $c<c_{\theta=0.5}$ and *vice versa* when

Table 1. Adsorption parameters of aliphatic alcohols on mercury electrode

	Γ_{max} / 10^{-10} mol cm^{-2}	$-\Delta G_A^\circ$ / kcal mol^{-1}	a_0
Butyl alcohol	6.67 (5.18)[a]	3.88 (3.83)[a]	0.39[3] (1.28)[a]
Amyl alcohol	5.9 (4.85)[a]	4.76 (4.58)[a]	0.42[6] (1.48)[a]
Hexyl alcohol	5.0 (4.64)[a]	5.68 (5.39)[a]	0.69[5] (1.68)[a]

a) The values in the parentheses are quoted from Ref. 8.

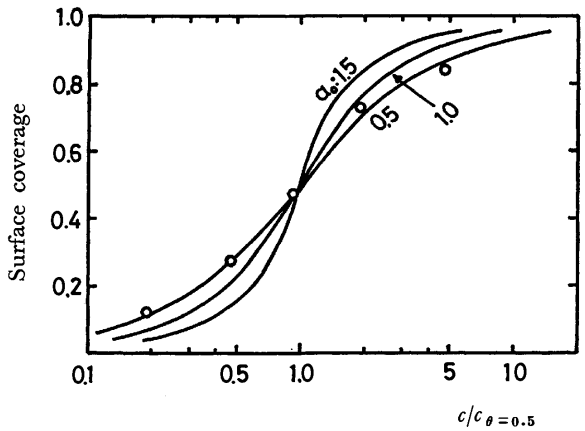

Fig. 1. Dependence of surface coverage of mercury electrode on the relative concentration, $c/c_{\theta=0.5}$, for butyl alcohol in 0.5 M H_2SO_4.

θ is greater than 0.5. The isotherms obtained by various investigators with the capillary electrometer generally agreed well[6] and the attraction constants calculated from these adsorption isotherms were always smaller than unity. On the other hand, the attraction constants evaluated from the differential capactiy measurements were much greater than unity. As was mentioned in the previous work,[6] the surface coverages evaluated from the differential capacity measurements are smaller than those evaluated from the electrocapillary measurements when the surface coverage of the electrode surface is less than 0.5 and *vice versa* when θ is greater than 0.5.

The concentration of the alcohol needed to give a certain coverage ($\theta=\Gamma/\Gamma_{max}$) at the point of zero charge decreases regularly with an increase in the chain length of the alcohols. This factor, Traube's factor, is about 5.1. On the other hand, the value reported by Kaganovich and Gerovich[9] and Damaskin *et al.*[8] were 3.0 and 3.7, respectively.

There are certain regularities in the solubility of n-aliphatic alcohols in water and in electrolyte solutions. The solubility of these alcohols decreases by the ratio of 3.9 in water[8] and 4.5 in 1 M KCl[9] for each additional CH_2 group. Therefore, the adsorption isotherms (the electrocapillary curves) are superimposable when the relative concentration, c/c_{satd} where c_{satd} is the solubility of the alcohol, of these alcohols is used as a measure of the concentration.

Electrode Kinetics. The standard rate constant of the V(III)/V(II) ($E^\circ=-0.505$ V, 0.5 M H_2SO_4) and Eu(III)/Eu(II) ($E^\circ=-0.612$ V, 1 M HCl) couples is not proportional to the uncovered electrode area, $1-\theta$, as stated in the previous work.[3] The inhibition

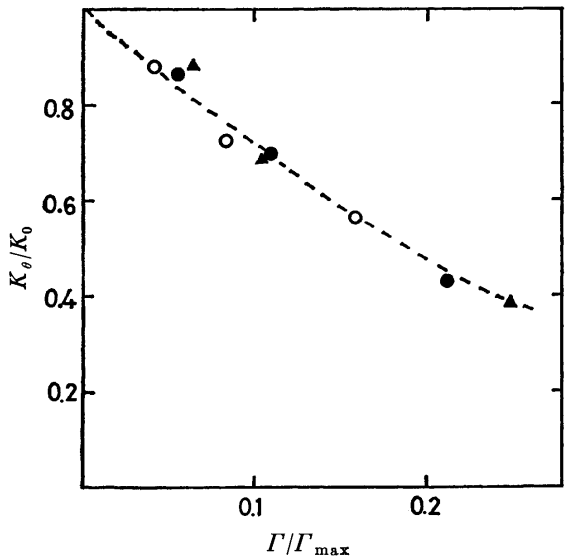

Fig. 2. Variation of the standard rate constants of V(III)+e=V(II) in 0.5 M H_2SO_4 with the surface coverage by alcohols.
○: Butyl alcohol, ●: amyl alcohol, ▲: hexyl alcohol.
----: $k_\theta=k_0(1-\theta)^{3.3}$.

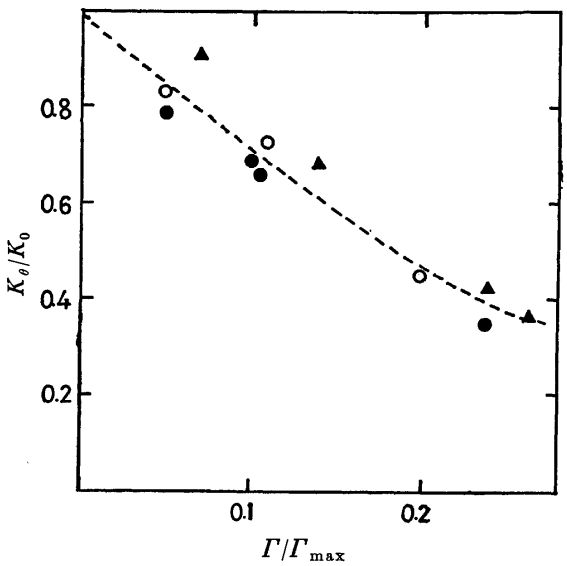

Fig. 3. Variation of the standard rate constants of Eu(III)+e=Eu(II) in 1.0 M HCl with the surface coverage by alcohols.
○: Butyl acohol, ●: amyl acohol, ▲: hexyl alcohol.
----: $k_\theta=k_0(1-\theta)^{3.3}$.

effect of butyl alcohol on the electrode kinetics is the least among these alcohols and that of hexyl

alcohol is the highest at a given surface excess. In the plot of the ratio of the standard rate constants, k_θ/k_0, against the surface coverage, θ, however, the variation of the rate constants of the V(III)/V(II) and Eu(III)/Eu(II) couples with respect to the surface coverage are superimposable regardless of the chain length of the alcohol as shown in Figs. 2 and 3. The standard rate constant of the uncovered electrode is denoted by k_0 and that at the electrode with the coverage of θ is denoted by k_θ. The plots of Figs. 2 and 3 are also superimposable. A similar electrode kinetic behavior of the vanadium couple to the europium couple is reasonable because the ionic charges of these couples are identical and the ionic sizes of these systems are roughly the same.

The transfer coefficient of the vanadium system and of the europium system does not depend on the nature of the alcohols and the extent of the coverage of the electrode surface. The transfer coefficient in the presence of the alcohols coincides with that without alcohols.

Andreev and his coworkers[13] noticed that the transfer coefficient decreases in the presence of the alcohols and is almost twice smaller than that in the solutions without alcohols in the reduction of cadmium ions in 0.5 M H_2SO_4. In the plot of $\log k_\theta$ against θ^2 in the range of $\theta=0.4$—0.9, the experimental data fit well on straight lines.[12] However, the linear plots with different alcohols were not superimposable. In the reduction of zinc ion in 0.1 M $NaClO_4$, on the other hand, amyl and hexyl alcohols have about equal inhibiting effect whereas the effect of butyl alcohol is somewhat weaker.[13]

The inhibition effect on the electrode kinetics depends only on the surface coverage, θ, of the electrode and is independent of the chain length of the adsorbed alcohol molecule. This evidence suggests that the "blocking effect" is predominant in the inhibition of the electrode process when aliphatic alcohols adsorbed on the electrode surface. The effect due to the interaction between the adsorbed alcohol molecules predicted by Biegler and Laitinen,[14] Sathyanarayana,[2] and Parsons[3] is negligible in the present experiments.

It is also interesting to note that the values of n in Eq. 1 calculated by Lipkowski and Galus[1] for various systems agree reasonably well when we employ the surface excess of the alcohols determined by the present work. The results are shown in Table 2. In the previous work,[5] on the other hand, the value of the closed packed coverage, $\Gamma_{max}=7.9\times10^{-10}$ mol cm^{-2} was used so that large values of n were obtained.

Table 2. The n value for the electrode reaction rate constant equation of $k_\theta=k_0(1-\theta)^n$

System	Alcohol	n	Ref.
V(III)/V(II)	amyl	4.2[a]	
		6.4	5
V(III)/V(II)	butyl, amyl, hexyl	3.3	present work
Eu(III)/Eu(II)	butyl, amyl, hexyl	3.3	present work
Cd(II)	butyl	4.0[a]	
		4.5	5
$HPbO_2^-$	butyl	4.8[a]	
		4.9	5
		2.8	1
$Fe(CN)_6^{3-}$	amyl	5.1[a]	
		3.0	1
Cu(II)	butyl	3.6[a]	
		2.1	1
$S_2O_8^{2-}$	amyl	6.0[a]	
		3.5	1

a) The n values were calculated by using the data in Ref. 6.

References

1) J. Lipkowski and Z. Galus, *J. Electroanal. Chem.*, **61**, 11 (1975).
2) S. Sathyanarayana, *J. Electroanal. Chem.*, **10**, 119 (1965).
3) R. Parsons, *J. Electroanal. Chem.*, **21**, 35 (1969).
4) C. A. Smolders and E. M. Duyvis, *Rec. Trav. Chim.*, **80**, 635 (1961).
5) K. Niki and N. Hackerman, *J. Phys. Chem.*, **73**, 1023 (1969); *J. Electroanal. Chem.*, **32**, 257 (1971).
6) K. Niki, *Bull. Chem. Soc. Jpn.*, **48**, 997 (1975).
7) A. N. Frumkin, *Z. Phys. Chem.*, **116**, 466 (1925).
8) B. B. Damaskin, A. A. Survila, and L. E. Rybalka, *Elektrokhimiya*, **3**, 146 (1967).
9) R. I. Kaganovich and V. M. Gerovich, *Elektrokhimiya*, **2**, 977 (1966).
10) A. Seidell, "Solubilities of Organic Compounds," D. Van Nostrand (1941).
11) J. W. Loveland and P. J. Elving, *J. Phys. Chem.*, **56**, 935 (1952).
12) L. A. Ternovskoi, B. N. Afanas'ev, and G. S. Ginzburg, *Elektrokhimiya*, **8**, 1119 (1972).
13) A. A. Adreev, I. A. Tikhomirova, and B. N. Afanas'ev, *Zh. Prikl. Khim.*, **43**, 2644 (1970).
14) T. Biegler and H. A. Laitinen, *J. Electrochem. Soc.*, **113**, 852 (1966).

 © 1980 The Chemical Society of Japan Bull. Chem. Soc. Jpn., 53, 577—582 (1980)

Polar Fluorescent State of 1- and 2-Acylanthracenes. II.[1] The Perturbation of Protic Solvents

Takashi TAMAKI

Research Institute for Polymers and Textiles, Yatabe-Higashi, Tsukuba, Ibaraki 305

(Received May 18, 1979)

The steady-state and time-resolved fluorescence spectra were measured for protic solutions of 1- and 2-acetyl- or 1- and 2-benzoylanthracenes at various temperatures. It has been demonstrated that the perturbation of protic solvents on the fluorescence spectra is caused by a combination of the orientational dipolar solvent-solute relaxation and the hydrogen bond interaction. Based on the time-dependent spectral shift and the temperature dependence of fluorescence polarization observed for 2-acylanthracene, the relaxation process of the excited solute has been supposed to involve the level inversion of dual fluorescent states, which respond differently to the solvation of the system.

The solvent perturbation on the solute emission has been subject of continuing interest in recent years.[2] The solvent dipole-solute dipole interaction is very important in the excited-state relaxation of a fluorescent solute which is electronically neutral in the ground state, but it led to a highly polar state upon photoexcitation. This solvent relaxation process occurs on the nanosecond time scale subsequent to a rapid ($>10^{-12}$ s) vibrational relaxation from the excited Franck-Condon (F.C.) state to the excited equilibrium (e.q.) state. In a fluid solution in which the solvent relaxation is much faster than the fluorescence decay, the excited e.q. state is eventually stabilized by the orientational relaxation of the surrounding solvent molecules. The fluorecsence spectrum becomes diffuse and red-shifted as a result of solvent reorientation, where as the absorption spectrum remains unchanged. The more polar the solvent, the greater the stabilization energy, leading to the larger red shift of the fluorescence maximum. As the solvent-relaxation time increases, *e.g.*, in a viscous solution at a low temperature, the time-dependent spectral shift of the fluorescence associated with the solvent relaxation becomes experimentally observable, for which time-resolved emission spectroscopy is promising.[3]

Some anthracene derivatives are known to reveal the related spectral shift in polar solvents.[4-7] Very recently, we have studied the solvent dependence of the fluorescence spectra of 1- (**1a**) and 2-acetyl- (**2a**) or 1- (**1b**) and 2-benzoylanthracene (**2b**) in aprotic solvents.[1] The structured spectra in nonpolar solvents have been found to become structureless and red-shifted in solvents with a higher polarity than ethyl ether. This solvent dependence was consistent with the well-established mechanism which involves orientational dipolar solvent-solute interaction. The dipole moment of the excited state has been estimated to be about 10 D for the compounds examined.

We wish now to report the perturbation of protic solvents on the fluorescence of these compounds. The steady-state and time-resolved fluorescence measurements indicate that the compounds are subjected to hydrogen bonding with the solvents in addition to the general orientational relaxation. Of particular interest is the observation concerning the time-dependent spectral shift for 2-acylanthracenes (**2a** and **2b**), because there is not only a peak shift, but also a significant change in the spectral shape. This finding is discussed in terms of the level inversion of the dual fluorescent states, which consist of the lowest excited state perturbed by the hydrogen bond and the excited CT state.

Experimental

The acylanthracenes (**1** and **2**) were the same as those used before.[1] The hexane, 1-propanol, and propylene glycol were spectro- or GR-grade reagents and were used without further purification. The ethanol was dried by refluxing over calcium hydride and distilled fractionally.

The steady-state fluorescence measurements were made using a Hitachi MPF 2A spectrofluorometer. The excitation wavelength was 390 nm. The time-resolved fluorescence and lifetime measurements were done using an Ortec SP-3X nanosecond spectrometer. The photoexcitation was done by means of the 337-nm light supplied by a 0.5-atm air-saturated flash lamp through a Corning 7-60 filter. The bandwidth of the monitoring wavelength was 2 nm for the time-resolved measurements and 5 nm for the lifetime measurements. The outputs from a multichannel analyser were displayed on an X-Y plotter (Hewlett-Packard). The fluorescence lifetime was determined from the slope of the decay curve drawn. The sample solutions were deoxygenated by the flushing of argon gas for 10 min prior to measurements. The sample absorbance in a 1-cm square quartz cell was made *ca.* 0.1 at the excitation wavelength, an optical density corresponding to the concentration of the order of 10^{-5} mol dm^{-3}. The measurements for the temperature dependence were carried out with sample cells placed in a cryostat (Oxford DN-704) combined with a temperature controller (Oxford DTC-2). The degree of fluorescence polarization (P) was measured by the ordinary method using the linearly polarized exciting radiation.[8] Since the instrument responded differently to the light quanta of the two polarized components, correction was done for the polarized fluorescence intensities ($I_{\parallel}$ and $I_{\perp}$) by measuring the corresponding fluorescence intensities ($I'_{\parallel}$ and $I'_{\perp}$) for a horizontally polarized exciting radiation, which can be expected to be the same. The value of P was calculated from this equation:

$$P = \frac{I_{\parallel} - I_{\perp}(I'_{\parallel}/I'_{\perp})}{I_{\parallel} + I_{\perp}(I'_{\parallel}/I'_{\perp})}$$

Results and Discussion

Hydrogen-bond Contribution. The fluorescence maxima of 1- and 2-acylanthracenes (**1** and **2**) in protic solvents move to lower frequencies than ex-

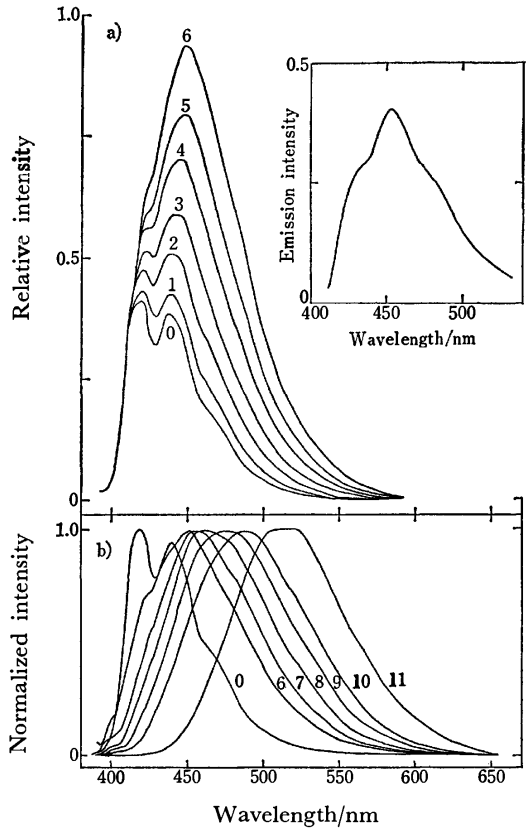

Fig. 1. Steady-state fluorescence spectra of 2-benzoylanthracene in hexane/1-propanol mixture. a) Normalized on the short wavelength side. Alcohol concentration: 0, pure hexane; 1, 0.013 mol dm^{-3}; 2, 0.027 mol dm^{-3}; 3, 0.04 mol dm^{-3}; 4, 0.054 mol dm^{-3}; 5, 0.067 mol dm^{-3}; 6, 0.081 mol dm^{-3}. Instert, hydrogen-bonded emission obtained by subtracting Spectrum 0 from Spectrum 4. b) Normalized at peak maxima. Alcohol concentration: 0, pure hexane; 6, 0.081 mol dm^{-3}; 7, 0.16 mol dm^{-3}; 8, 0.32 mol dm^{-3}; 9, 0.64 mol dm^{-3}; 10, 1.3 mol dm^{-3}; 11, pure 1-propanol.

pected from the properties of solvent polarity.[1] It appears probable that this extraordinary peak shift is attributable to hydrogen-bond formation, since these compounds have a carbonyl-type oxygen as a hydrogen-accepting site. Such protic solvent perturbation has been clearly demonstrated by the observation concerning the effect of very dilute concentrations of alcohols on the spectra of the compounds dissolved in a nonpolar solvent like hexane. As is shown in Fig. 1, the fluorescence spectra become structureless and red-shifted as the concentration of 1-propanol is increased. When perturbed by very small amounts of added alcohol (<0.01 M), which are insufficient to alter the absorption spectrum or the dielectric properties of the solvent, the spectrum does not only shift, but also broadens considerably (Fig. 1a). This suggests the appearance of new emission band(s). The emission spectra shown in Fig. 1a are normalized on the short-wavelength side, where the contribution of the new band is negligible. The subtraction of the unperturbed spectrum from the perturbed gives

Table 1. Peak positions of the fluorescence spectra of hydrogen-bonded 1- and 2-acylanthracenes

Compounds	λ_f/nm
1-Acetylanthracene (**1a**)	448
1-Benzoylanthracene (**1b**)	466
2-Acetylanthracene (**2a**)	420, 444
2-Benzoylanthracene (**2b**)	430, 454

rise to the emission band, presumably corresponding to a hydrogen-bonded species. The band peaks of all the compounds examined are listed in Table 1. On a further increase in the alcohol concentration, the fluorescence peak moves further to the red, the bandwidth remaining almost constant until the spectra coincide with that of the pure alcohol solution (Fig. 1b). This shift may be attributed to the general dipolar solvent-solute interaction. Thus, the protic solvent perturbation is due to a combination of the nonspecific dipolar and the specific hydrogen-bond interactions.

It can be noted that the hydrogen bond is facilitated in the excited state, because the photoexcitation leads to preferential electron migration from the anthryl group to the carbonyl group,[1] resulting in an increase in the carbonyl basity. Since the electron migration induces a resonance contribution to the π-electron conjugation of these two groups, a coplanar geometry of the molecular conformation is most likely to be attained, thus ensuring the delocalization of the π-electron.[9] The situation reported for methyl anthracenecarboxylate[6] is analogous to that in this study. It is of interest to mention the possibility of a change in geometry associated with photoexcitation, as was pointed out for methyl anthracenecarboxylate.[6] A difference in ground-state geometry appears among the three positional isomers of substituted anthracenes if the substituent lacks spherical or cylindrical symmetry.[10] Carbonyl-substituted anthracenes are just the same. It is known that the carbonyl group of the 9-isomer is perpendicularly torsional with respect to the plane of an anthryl ring because of the repulsive forces of two *peri*-hydrogen atoms.[10,11] Therefore, a significant geometry change is induced upon photoexcitation.[6a] On the other hand, the ground-state geometry of the 1- and 2-isomers stays rather coplanar because of these being less steric hindrance. This has been also confirmed for the compounds concerned by IR and UV absorption measurements. The carbonyl-stretching frequencies for **1a** and **2a** in $CHCl_3$ are 1675 cm^{-1} and 1678 cm^{-1} respectively, whereas the frequency for the 9-isomer is 1693 cm^{-1}. The lesser double-bond character of the carbonyl bond for the former compounds is consistent with a coplanar geometry.[10] The UV measurement indicates that all the acylanthracenes except the 9-isomer exhibit a fundamentally different spectrum from that of the parent substance, anthracene.[1] The observed spectral deformation can be explained as being due to an effective resonance contribution, which may lead to the same conclusion with respect to the ground-state geometry. In conclusion, the geometry change can be regarded as less

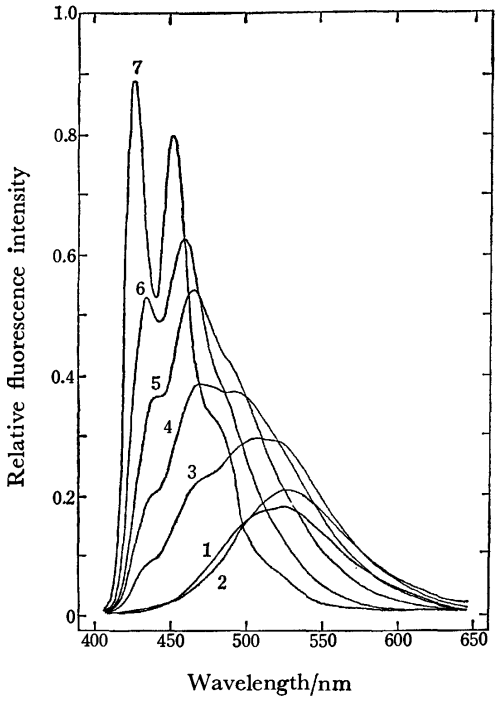

Fig. 2. Steady-state fluorescence spectra of 2-benzoylanthracene in ethanol. Temperature; 1, 20 °C; 2, −78 °C; 3, −117 °C; 4, −125 °C; 5, −135 °C; 6, −145 °C; 7, −175 °C.

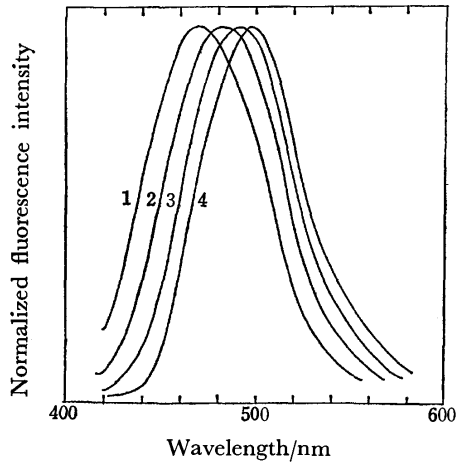

Fig. 3. Time-resolved fluorescence spectra of 1-benzoylanthracene in propylene glycol at −100 °C. 1, 5 ns; 2, 15 ns; 3, 20 ns; 4, 50 ns.

important in the cases we are studying than in the cases of methyl 1- and 2-anthracenecarboxylates.[6b]

Temperature and Time-dependent Spectral Shifts. The steady-state fluorescence spectra of **2b** in ethanol at various temperatures are shown in Fig. 2. At room temperature the spectrum is structureless and largely red-shifted, arising from a fully relaxed e.q. state. As the temperature is lowered, the spectra move to the blue and develop some structure, with a gradual increase in the emission intensity. At 77 K the spectrum is the same in both shape and peak position as that in a nonpolar solvent. No phosphorescence could be detected. The spectra of the other compounds (**1a**, **1b**, and **2a**) reveal a similar temperature dependence. In contrast with the emissive behavior, the absorption spectra show no corresponding change, except for the sharpening and slight intensifying of the bands at lower temperatures. The absence of the isoemissive point supports the view that the temperature-dependent spectral shift is due to solvent reorientation around the excited solute which is subjected to a hydrogen bond.

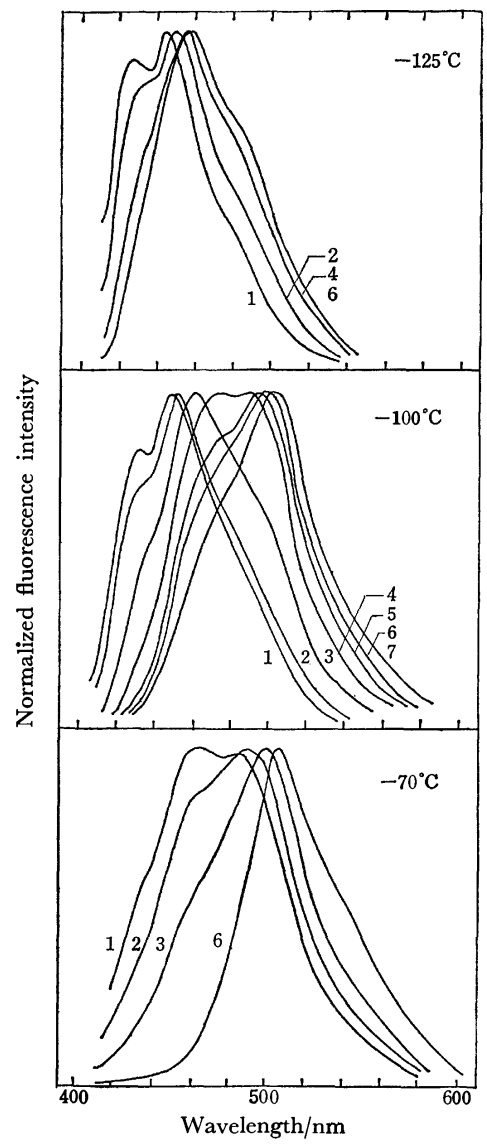

Fig. 4. Time-resolved fluorescence spectra of 2-benzoylanthracene in propylene glycol at the temperature indicated. 1, 5 ns; 2, 15 ns; 3, 20 ns; 4, 30 ns; 5, 40 ns; 6, 50 ns; 7, 70 ns.

The temperature-dependent spectral shift is, in fact, associated with the time-dependent spectral shift. The time dependence of the spectra is very intimate for each family of **1** or **2**. Some typical results for **1b** and **2b** in 1-propanol are shown in Figs. 3 and 4 respectively. Each spectrum is given at each delay time after the onset of a nanosecond flash lamp. The time-dependent spectral shifts amount to several tens of nanometers at −70 °C——100 °C. In this temperature range, the dielectric relaxation time of the solvent (τ_ρ=2.0—47×10^{-8} s[12]) is comparable in

order of magnitude to the fluorescence lifetime of $\tau_f \simeq 10^{-8}$ s. The wavelength span in which the spectra shift decreases on either further lowering or raising of the temperature, since the dielectric relaxation time becomes far from the fluorescence lifetime. At extreme temperatures, such as room temperature or 77 K, where the solvent relaxation is complete or totally inhibited, the spectrum is practically time-independent.

The wavelength region over which the spectral shift is observed moves to the blue with a decrease in the temperature. The extrapolation of the peak shift found at −125 °C to zero time provides the peak maxima of 450 nm for **1b** and 445 nm for **2b**. Although the dielectric relaxation at this temperature ($\tau_\rho \simeq 2 \times 10^{-5}$ s[12]) is much slower than the fluorescence decay, these peak positions lie about 20 nm to the red relative to the positions of the spectra at 77 K, which correspond nearly to the F.C. solvent configuration. This suggests that, even at −125 °C, the appreciable subnanosecond relaxation occurs. From the close resemblances of the zero-time spectra with the hydrogen perturbed spectra (Fig. 1a), it is clear that the hydrogen-bond interaction is responsible for this rapid relaxation.

The observed time-dependent spectral shifts are in many respects analogous for the systems of **1** and **2**. However, the difference between them is apparent at a glance in Figs. 3 and 4. While the spectra observed for **1b** retain, to a good approximation, their band width and shape during the progress of the peak shift (Fig. 3), it is striking that the spectra observed for **2b** exhibit a significant change in their structure (Fig. 4). In the latter case, there are at least two emissions with different solvent configurations. At −100 °C both emission spectra are observable: the one arises in the early stage of the delay time, and the other, in the later stage. The conversion of these two emissions occurs at an intermediate delay time of 30 ns. Each spectrum can be separately measured when the temperature is varied. At −125 °C only the early stage emission is predominant; it is attributed to the hydrogen bonded species. On the contrary, at −70 °C the later stage emission prevails, and it approaches the room-temperature spectrum. This temporal variation in the fluorescence spectra is very interesting, because it gives direct evidence of the solvent-induced change in the excited electronic structure.

At temperatures where there are time-dependent spectral shifts, the fluorescence lifetime is dependent on the excitation wavelength. For the system of 1-benzoylanthracene–propanol, which shows a continuous time-dependent spectral shift, the kinetics of the wavelength-dependent decay can be explained by the Bakhshiev formulation.[13] If the fluorescence quantum yield and the transition probability are time-independent, the decay law which describes the continuous orientational dipolar solvent-solute relaxation can be written as

$$I(\bar{\nu}, t) = \text{const} \cdot \exp(-t/\lambda) \cdot f(\bar{\nu}, t), \quad (1)$$

where $\exp(-t/\lambda)$ is a damping function which defines the electronic relaxation of the system and where $f(\bar{\nu}, t)$ represents the effects of the time-dependent spectral shifts on the observed fluorescence decay. $f(\bar{\nu}, t)$ can be estimated at a given wavelength from the normalized time-resolved spectra. The calculation of the decay time associated with $I(\bar{\nu}, t)$ can be made assuming an appropriate value for λ. The values calculated for **1b** at various wavelengths are listed in Table 2. The agreement between the measured and calculated values is gratifying.

Table 2. Observed and calculated fluorescence decay times for 1-benzoylanthracene in propylene glycol at −100 °C, taking $\lambda = 10$ ns

Wavelength/nm	$\tau_{f,\,obsd}$/ns	$\tau_{f,\,calcd}$/ns
440	4.4	4.6
460	7.5	7.1
480	9.9	9.6
500	11	10
520	11	11
540	12	11

Excited-state Level Inversion. The temporal variation in the fluorescence spectra found for the 2-benzoylanthracene-propanol system indicates that this system involves at least two fluorescent species which are chemically the same, but electronically different. The acylanthracenes may be viewed as forming an intramolecular donor–acceptor system in which the anthryl group is a donor, and the carbonyl group, an acceptor. A previous study of the solvent dependence of the fluorescence suggests that the excited state in highly polar solvents has a character of charge transfer.[1] Consequently, the appearance of the two emissions may be interpreted in terms of two excited states, $^1S_{HB}$ (the lowest excited state perturbed by the hydrogen bond) and $^1S_{CT}$ (the excited CT state), which respond differently to the solvent relaxation. The conversion of $^1S_{HB}$ to $^1S_{CT}$ is an intramolecular electron-transfer reaction.

These considerations are summarized in the following reaction scheme:

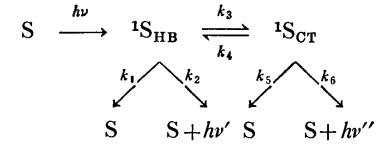

The transient populations of $^1S_{HB}$ and $^1S_{CT}$ are given by the following equations:[3]

$$[^1S_{HB}] = C_1 \exp(-t/\lambda_1) + C_2 \exp(-t/\lambda_2), \quad (2)$$

$$[^1S_{CT}] = C_3\{\exp(-t/\lambda_1) - \exp(-t/\lambda_2)\}, \quad (3)$$

where

$$1/\lambda_1,\ 1/\lambda_2 = (1/2)[k_1+k_2+k_3+k_4+k_5+k_6 \mp \{(k_1+k_2+k_3-k_4-k_5-k_6)^2+4k_3k_4\}^{1/2}].$$

It is of interest to examine whether or not this reaction scheme is consistent with the wavelength-dependent kinetic behavior measured for the 2-benzoylanthracene–propanol system. In this respect, it was confirmed that the decay law of Eq. 1 in itself was no longer applicable to the observed time-dependent spectral

Table 3. Observed and calculated fluorescence decay times for 2-benzoylanthracene in propylene glycol at −100 °C, taking $\lambda_1=15$ ns and $\lambda_2=12$ ns

Wavelength/nm	$\tau_{f,obsd}$/ns	$\tau_{f,calcd}$/ns	
		$^1S_{HB}$	$^1S_{CT}$
430	5.6	5.6	
440	7.4	7.5	
460	11	10	
480	13	11	16
500	16	13	17
520	18		19
540	20		21
560	22		23

change (Fig. 4), apparently indicating that the fluorescence lifetime and/or the transition probability is time-dependent. We have analyzed the experimental results in ways similar to those presented above, but on the assumption that the damping function in Eq. 1 is biexponential, as is presented in Eq. 2 or 3. Since it was difficult to measure the rise in the curve of the $^1S_{CT}$ fluorescence, the calculation for this fluorescence has been done only for the decay time. We have also assumed, for the sake of simplicity, that the conversion of the two excited states is irreversible, *i.e.*, $k_3 \gg k_4 \simeq 0$, and therefore, $[^1S_{HB}]$ is represented only by the second term of Eq. 2. Table 3 shows the values calculated at various wavelengths, taking $\lambda_1=15$ ns and $\lambda_2=12$ ns together with the measured values. While it is to be expected that the calculated value deviates from the measured value in the wavelength region where the two emission spectra are greatly overlapping, these two values agree to a good precision at the other wavelengths. This supports the validity of the reaction scheme postulated.

Since the level inversion involves a change in the dipole moment, the photoselection technique is helpful to characterize the phenomenon. On the basis of this technique, Suzuki and his coworkers have extensively investigated the fluorescence level inversion of the dual fluorescence for indole and such 1-naphthyl derivatives as hydroxyl, cyano, or amino.[14] Similarly, we have measured the degree of the fluorescence polarization (P) for the compounds of **1** and **2** at various temperatures. In Fig. 5, the excitation polarization spectra for **1a** and **2a** in an ethanol glass at 77 K are compared with those in glycerol at room temperature. In the case of **1a**, the general shapes of the polarization spectra for the two temperatures are substantially the same, though the absolute value of P in ethanol at 77 K is larger than that in glycerol at room temperature. The increase in P at low temperatures is due to the depletion of the rotational depolarization, as is to be expected from the solvent viscosity. On the other hand, the two polarization spectra for **2a** are significantly different. It is noted that, while the spectra in the long wavelength region (>340 nm) have the ordinary temperature effect, the effect occurs in the opposite direction at the shorter wavelengths.

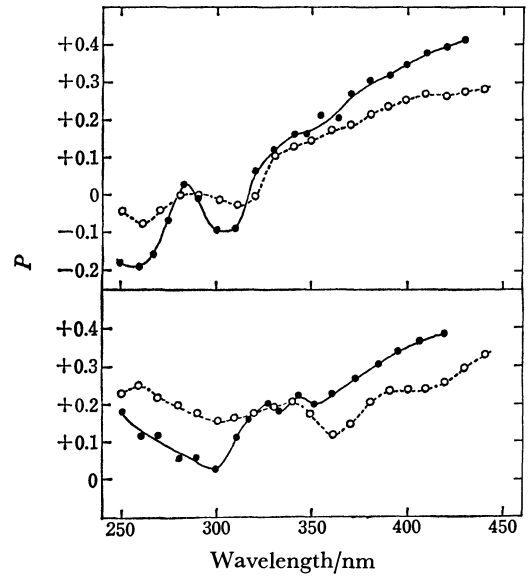

Fig. 5. Fluorescence excitation polarization spectra of 1-acetylanthracene (upper) and 2-acetlyanthracene (lower) in glycerol at 20 °C monitored at 510 nm (open circle) or in ethanol at 77 K monitored at 450 nm (closed circle).

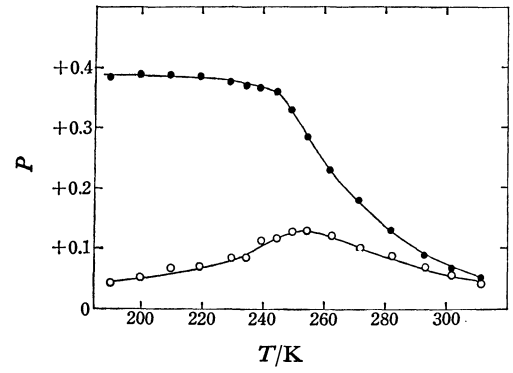

Fig. 6. Temperature dependence of the degree of fluorescence polarization of 2-acetylanthracene in propylene glycol monitored at 440 nm. The excitation wavelength was 400 nm (closed circle) and 300 nm (open circle).

The anomaly of the temperature effect is further evident from the measurement of P in propylene glycol by varying the temperature from 300 K to 200 K. As is shown in Fig. 6, when excited at 300 nm, the value of P first increases with a decrease in the temperature, reaching its maximum at about 250 K. On a further lowering in the temperature, though, it in turn decreases. This temperature dependence of P is in contrast with that for the excitation at a long wavelength, *e.g.*, 400 nm, which indicates a plateau in the values of P below 250 K. The decrease in P at low temperatures is characteristic of fluorescence-level inversion.[14]

There is an intense band near 300 nm in the absorption spectra of **2**. Since no corresponding band is present in the spectrum of the parent anthracene, this band may be identified as a CT transition band. However, it is reasonable that this CT band is too

high in energy to be ascribed to the emissive state in highly polar solvents at room temperature. An alternative band responsible for the polar fluorescence may subside in the longer-wavelength bands.

As has been demonstrated above, the temperature- and time-dependent spectral changes observed for **2** in protic solvents are partly due to the level inversion of dual fluorescence arising from the lowest excited singlet and excited CT states. Although the spectral shifts observed for **1** conform to a relaxation mechanism which involves the continuous orientational dipolar solvent-solute interaction, the possibility of a level inversion can not be excluded at this stage of the investigation. If the relevant energy levels are closely related, it appears unlikely that a drastic change in the fluorescence spectra is necessarily required.

References

1) Part 1: T. Tamaki, *Bull. Chem. Soc. Jpn.*, **51**, 2817 (1978).

2) a) N. Mataga and T. Kubota, "Molecular Interactions and Electronic Spectra," Marcel Dekker, New York (1970), Chap. 8; b) N. Mataga, *Kagaku*, **46**, 689 (1976).

3) W. R. Ware, "Creation and Detection of the Excited State," ed by A. A. Lamola, Marcel Dekker, New York (1971), Vol. 1, Part A. Chap. 5.

4) H. Baba and S. Suzuki, *Bull. Chem. Soc. Jpn.*, **35**, 683 (1962).

5) a) S. Suzuki and H. Baba, *Bull. Chem. Soc. Jpn.*, **37**, 519 (1964); b) K. Rotkiewicz and Z. R. Grabowski, *Trans. Faraday Soc.*, **65**, 3263 (1969).

6) a) T. C. Werner and R. M. Hoffman, *J. Phys. Chem.*, **77**, 1611 (1973); b) T. C. Werner, Th. Mattews, and B. Soller, *ibid.*, **80**, 533 (1976).

7) T. Okada, T. Fujita, and N. Mataga, *Z. Phys. Chem. N.F.*, **101**, 57 (1976).

8) G. Weber, "Fluorescence and Phosphorescence Analysis," ed by D. M. Hercules, John Wiley and Son (1966), Chap. 8.

9) R. N. Jones, *J. Am. Chem. Soc.*, **67**, 2127 (1945).

10) R. O. C. Normam and P. D. Ralph, *J. Chem. Soc.*, **1961**, 2221.

11) P. H. Gore, A. Hoskins, R. J. W. LeFevre, L. Radom, and G. L. D. Ritchi, *J. Chem. Soc., B*, **1969**, 227.

12) D. W. Davidson and R. H. Cole, *J. Chem. Phys.*, **19**, 1484 (1951).

13) N. G. Bakhshiev, Yu. T. Mazurenko, and I. V. Piterskaya, *Opt. Spektrosk.*, **21**, 307 (1966).

14) S. Suzuki, T. Fujii, A. Imai, and H. Akahori, *J. Phys. Chem.*, **81**, 1592 (1977).

 © 1980 The Chemical Society of Japan Bull. Chem. Soc. Jpn., 53, 583—589 (1980)

Microscopic Evaluation of Surfactant–Water Interaction in Apolar Media

Junzo SUNAMOTO,* Tomiko HAMADA, Takafumi SETO, and Shinji YAMAMOTO

Department of Industrial Chemistry, Faculty of Engineering, Nagasaki University, Nagasaki 852

(Received May 23, 1979)

Under the very limited conditions where the mole ratio of water to surfactant is about unity or so, the tightness of the interaction between various ionic surfactants and water solubilized in apolar media was evaluated using the O–H vibrational mode of water in the near infrared spectral region. Water solubilized in apolar solvents containing surfactant exhibited two absorption bands in the region. One of the two arises from water existing in bulk organic phase and appears around 1900—1910 nm. Another band arises from water bound to surfactant and appears over a range of 1920—2020 nm; it is affected primarily by the ionic head group of surfactant rather than by the counter ion. The cationic surfactants were thought to form more rigid micelles than the zwitterionic or anionic ones. The copper(II) ion cosolubilized in the system hardly altered the O–H vibrational energy of water. The dependence of the near infrared absorption band on water, the chemical shift and line width of water proton resonance in NMR, and the fluorescence intensity of terbium chloride all displayed an inflection at the point where the mole ratio of water to surfactant is about unity. This was interpreted in terms of the two step hydration mechanism.

The term "reversed micelles" describes aggregates of surfactants and polar solutes formed in aprotic media. Although reversed micelles have been investigated intensively, the structure of aggregates remains poorly understood even on the elementary level. Much of the interest in "the aggregates" or "reversed micelles" stems from their use as models of enzyme pockets or cell membranes.

Favorable substrate cosolubilization, orientation, and the unique properties of the system have been proposed to be responsible for the effects on reaction rates, paths, and equilibria occurring in the interior core.[1,2] Aggregates formed in apolar media certainly provide a specific and restricted field. The rigidity-flexibility or hardness-softness of the field is thought to be affected by the kind of surfactants and the amount of water added.[2] Depending on concentrations of surfactant and water added, the tightness of surfactant–water interaction,[2] the size of water pool,[3] the microscopic viscosity[4] and polarity of the interior[5] can be varied over a considerable range. However, the problem of rigidity and tightness of aggregates in conjunction with the structure of surfactants has been not investigated thoroughly thus far. Considering the correlation between the motion of reactants and reaction rates or pathways, we can not discard the problem of the "rigidity" of the reaction field. Certainly, several efforts to rationalize the correlation between the motional freedom and the amount of water added within interior cores have been made through NMR,[4] spin label,[6] and fluorescence studies.[3] However, one has scarecely paid attention to the state and nature of aggregates formed under the very limited condition where the mole ratio of water to surfactant is about unity or less.[7]

Very recently, we found that the configurational change between tetrahedral and octahedral species of cobalt(II) complexes takes place in reversed micelles formed by the several kinds of surfactants.[2] The phenomenon was interpreted in terms of solvochromism and thermochromism which were accompanied by the elimination-addition equilibrium of water between the metal ion and the surfactant.[2] Moreover, it seemed to be certainly connected with the rigidity (or flexibility) of the surfactant–water aggregates. In this work we would like to report the correlation between the structure of surfactants and the tightness of the surfactant-water interaction in apolar media as evaluated using the near infrared O–H vibrational mode of water bound to surfactants. We limited the amount of water to an extremely small extent so that the mole ratio of water to surfactant was about unity or so. It is sure that a portion of water is dispersed in the bulk phase of organic solvent. Of course, the surfactant molecule also may partly exist as the monomeric form in bulk solvent. We do not know, therefore, whether the 1:1 aggregate between water and surfactant in apolar media can be considered as a true reversed micelle.[7]

Experimental

Materials. Surfactants, hexadecyltrimethylammonium bromide (CTAB), dimethyldioctadecylammonium chloride (QD-Cl), egg phosphatidylcholine (EL), dodecylammonium propionate (DAP), and sodium 1,2-bis(2-ethylhexyloxycarbonyl)-1-ethanesulfonate (AOT), were the same as those used in previous studies.[2] 3-(Hexadecyldimethylammonio)-1-propanesulfonate (SB-16:3) was prepared by quarternizing *N,N*-dimethylhexadecylamine with propanesultone and purified according to the method described in literature.[8] Hexadecyltrimethylammonium chloride (CTACl) was a gift from Kao Soap Co., Ltd., Tokyo. Sodium dodecylbenzenesulfonate (DBS) was purchased from Wako Pure Chemicals Co., Ltd., Tokyo and purified by recrystallization from benzene prior to the use. Purity of all the surfactants adopted was inspected by TLC or HLC and elemental analysis.

Measurements. All the visible and near infrared spectra were measured on a Hitachi 323 recording spectrophotometer equipped with a thermoregulated cell compartment. NMR studies were run on a JEOL MH-100 spectrometer with TMS as an internal standard. Fluorescence measurements were carried out on a Hitachi 512 fluorospectrometer.

In all runs, the amount of water added was carefully determined every time after the spectroscopic measurements on a Karl-Fischer Moisture Automatic Titration Apparatus Model MK-A (Kyoto Electronics MFG Co., Ltd.) using Karl-Fischer reagent SS "Mitsubishi" ($f=0.3$ mg/mL) with standard water–methanol solution ($f=0.5$ mg/mL) for Karl-Fischer reagent, Mitsubishi Chemical Industries Ltd., Tokyo.

Results and Discussion

Near Infrared Spectra of O–H Vibrational Modes. In the near infrared region, water exhibits relatively strong absorption bands due to the ν_2 (scissoring) plus ν_3 (asymmetric stretching) combination mode of vibration.[9] The band observed in vacuum is 5332.0 cm^{-1} (1875 nm) arises from the B_1 species, which corresponds to the band at 5330.6 cm^{-1} (1876 nm) theoretically calculated.[9] This is completely freed from the hydrogen bonding itself. If the water molecule hydrogen-bonds or interacts with other polar molecules or ions, the band will shift toward the lower energy state or the longer wavelength. In pure bulk water the force constant of the O–H bond is compensated owing to the dual character of water as both proton donor and acceptor properties.[10] Bulk water shows, therefore, the band at 5181 cm^{-1} (1930 nm) in the near infrared region. In nonpolar solvents containing ionic surfactants, a part of cosolubilized water locates in the bulk organic phase, where the water molecules are mostly freed from hydrogen bonding themselves, and others interact with the ionic head of surfactant. In the near infrared region, the former exhibits absorption bands around 1900 nm and the latter over a range of 1920—2020 nm.[11,12] Figure 1 shows the near infrared spectra of water in chloroform containing different kinds of surfactant. In chloroform containing anionic surfactants such as AOT or DBS, the position of two bands is close to each other, and at larger amount of water both absorptions overlap to create a broad single band. Intensities of bands in the system containing anionic surfactants are usually stronger than those with zwitterionic and cationic surfactants.

Effect of Bulk Solvent. The near infrared spectra of water vary with the bulk solvents as well as the type of surfactants. In chloroform containing surfactants, the O–H vibrational mode in near infrared region separates into two distinct bands as described above. In less polar solvents such as hexane or carbon tetrachloride, only a single absorption band is observable in the corresponding region irrespective of the surfactants (Fig. 2). In hexane containing no surfactants, we could not obtain any reliable spectra because of the extremely low solubility of water in the solvent. Since the dipole moment of the O–H bond depends on the dielectric constant of the field,[13] the intensity of these bands should be affected by the polarity of bulk solvents. Seno and his coworkers also previously observed similar results on the absorption band arising from water dispersed in bulk solvents.[12] That the dipole moment of the O–H bond changes with solvents and/or surfactants means that the quantitative treatment in spectroscopic studies on the system is not feasible.[14] We can, therefore, interpret the data only in a qualitative manner.

Temperature Effect. There exists an equilibrium in the translocation between two different kinds of water existing in bulk solvents and bound to surfactants. Increasing temperature causes a decrease in intensity of the band arising from water bound to surfactants

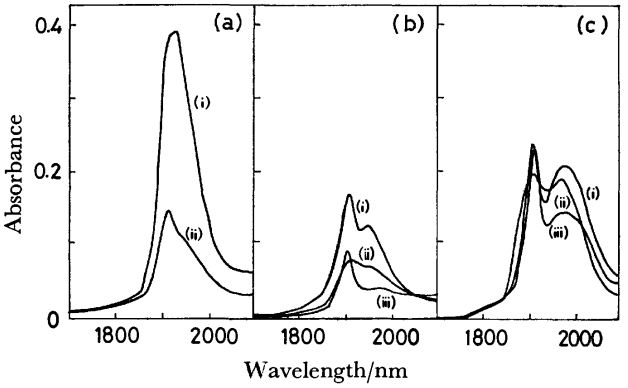

Fig. 1. Near infrared spectra of water solubilized in chloroform containing various kinds of surfactants at 25 °C: (a) anionic surfactants, (i) 0.20 M AOT/0.20 M H_2O and (ii) 0.10 M DBS/0.084 M H_2O; (b) zwitterionic surfactants, (i) 0.040 M SB-16:3/0.037 M H_2O, (ii) 0.045 M EL/0.055 M H_2O, and (iii) 0.20 M DAP/0.20 M H_2O; (c) cationic surfactants, (i) 0.20 M CTACl/0.20 M H_2O, (ii) 0.20 M CATB/0.22 M H_2O, and (iii) 0.20 M QD-Cl/0.18 M H_2O.

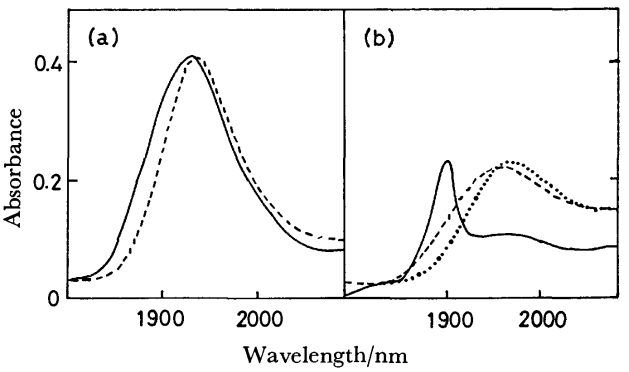

Fig. 2. Effect of bulk solvent on the distribution of water solubilized in apolar solvents containing surfactants at 25 °C: (a) 0.20 M AOT with 0.20 M water in chloroform (——) and 0.20 M AOT with 0.24 M water in carbon tetrachloride (----); (b) 0.20 M DAP with 0.20 M water in chloroform (——), 0.20 M DAP with 0.22 M water in carbon tetrachloride (----), and 0.20 M DAP with 0.22 M water in hexane (·····).

with a concomitant increase in the intensity of the absorption of water in the solvent phase (Fig. 3). A temperature increase enhances the mobility of water bound to surfactants, resulting in easier dispersion into the bulk organic phase. The result coincides with that previously observed on the thermochromism of the cobalt(II) complexes in the reversed micelles.[2]

Effect of Cosolubilized Metal Ion. The energy states of the O–H vibration in three different surfactant systems, AOT, DAP, and CTAB, with or without the copper(II) ion were determined as a function of added water (Fig. 4). The configuration of the copper(II) complexes in reversed micelles is drastically affected by the kind of surfactants and the amount of water present.[2,15] On the other hand, the O–H vibrational energy of water is not so significantly affected by cosolubilizing the copper(II) ion. In three sur-

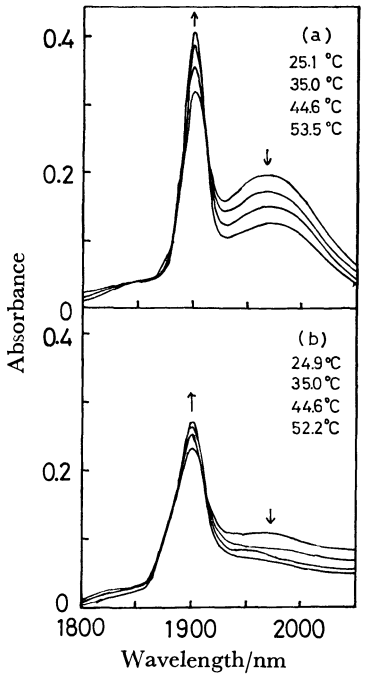

Fig. 3. The near infrared spectra of 0.20 M water solubilized in chloroform containing 0.20 M CTAB (a) and 0.20 M DAP (b) at different temperatures.

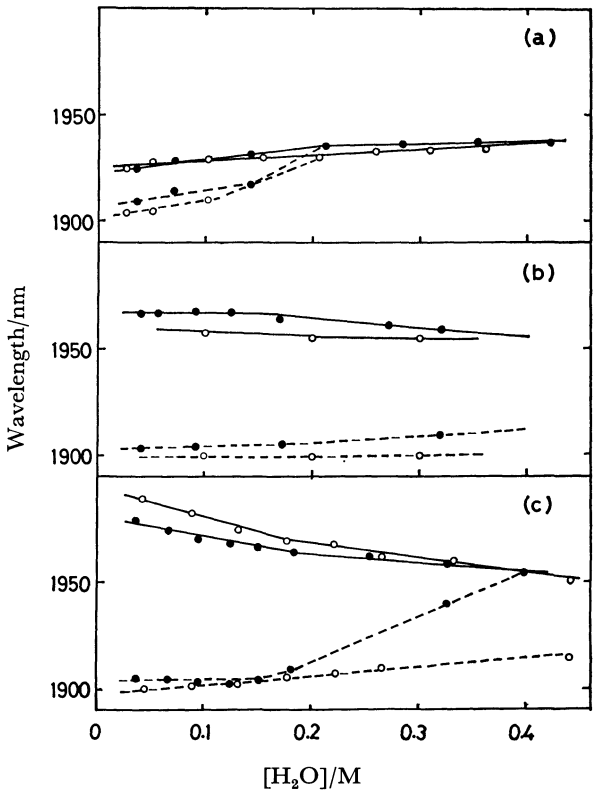

Fig. 4. Effect of the Cu(II)-ion on the near infrared absorption bands of water solubilized in three different surfactants/chloroform system as a function of water added at 25 °C: (a) 0.20 M AOT in chloroform without Cu(II) ion (○) and with 4.6×10^{-4} M Cu(II) ion (●); (b) 0.20M DAP in chloroform without Cu(II) ion (○) and with 2.7×10^{-3} M Cu(II) ion (●); (c) 0.20 M CTAB in chlorofrom without Cu(II) ion (○) and with 5.9×10^{-4} M Cu(II) ion (●). The copper-(II) ion was cosolubilized as the aqueous nitrate in all the systems. Solid lines are absorption bands of water bound to surfactant, while broken lines are those of water existing in bulk organic solvent.

factant systems, the energy state of the O–H bond of water changed as a function of water content, giving an inflection around the point where the mole ratio of water to surfactant is about unity. The addition of the metal(II) ion is expected to force water molecules into the interior core of reversed micelles from the bulk phase.[16] However, a concomitant increase of water bound to surfactants was not observed. Because of low solubility of the metal salt under the adopted conditions, it was impossible to cosolubilize more salts. Very recently, we reported solvochromisms of the cobalt(II)[2] and copper(II)[15] complexes in reversed micellar systems, where the configurational change between T_d and O_h takes place when water is added to the system. The present result coincides with those obtained for both the solvochromism of the metal(II) ions[2,15] and the hydrolysis of an amino acid ester as promoted by the copper(II) ion in the AOT/CCl_4 reversed micelles.[15,17]

Effect of Water Content and Tightness of Surfactant–Water Interaction. The interaction of water and various surfactants in apolar media was examined as a function of water amount added using the O–H vibrational modes in the near infrared region (Fig. 5). If water located in bulk solvents were completely free from any interactions with other polar or ionic molecules, the O–H vibrational mode of the water molecule would be identical irrespective of surfactants and/or bulk solvents. Since the band under consideration is affected a little by surfactants, however, the state and nature of water molecules in bulk phase seem to be altered by the solubility of surfactants in the bulk solvent and the polarity of the bulk phase (Fig. 5(b)). On the other hand, the vibrational energy of the O–H bond of water interacting with surfactants depends largely on the head group structure of surfactants (Figs. 1 and 5(a)). If the argument is limited to a series of surfactants under the same conditions, then it is reasonable to postulate that the shift in frequency of the O–H vibration reflects the relative strength of the interaction between water and surfactants.[18] Therefore, we can regard the difference ($\Delta\lambda$) between the theoretically calculated and observed wavelength as a semiquantitative parameter measuring the tightness of the interaction between water and other molecules under consideration:

$$\Delta\lambda = \lambda_0 - 1876\ (\mathrm{nm}), \qquad (1)$$

where λ_0 stands for the intrinsic absorption band which is graphically estimated, using data given in Fig. 5, by extrapolating the observed wavelength to the point where the mole ratio of water to surfactant is zero. Results are summarized in Table 1.

In dried apolar media, ionic surfactants will exist as intimate ion pairs. The interaction between water and surfactants, therefore, looks like a dipole-dipole interaction, especially under very limited conditions

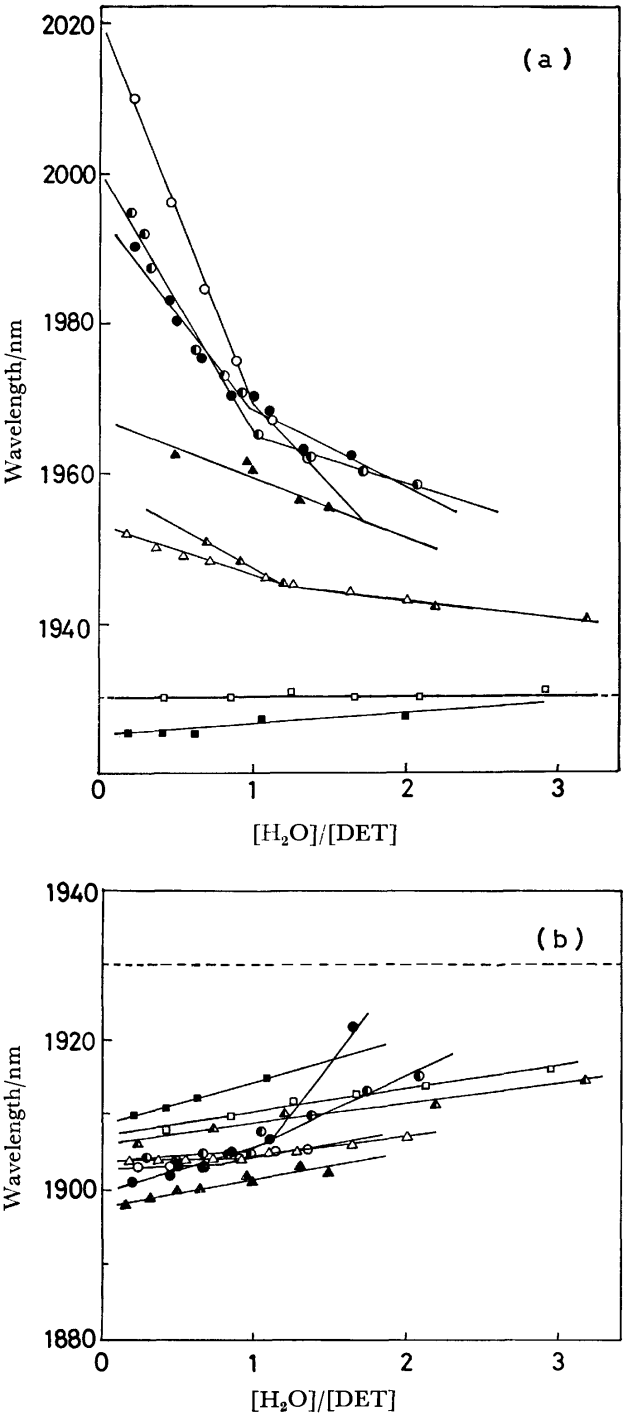

Fig. 5. Effect of water content on the near infrared spectra of water solubilized in chloroform containing various surfactants: (a) the absorption band of water bound to surfactants and (b) the absorption band of free water locating in bulk chloroform containing various surfactants; QD-Cl (○), CTACl (◐), CTAB (●), DAP (▲), EL (◭), SB-16:3 (△), DBS (□), and AOT (■). A broken line in (b) stands for the position of the absorption band of pure water (1930 nm).

where the mole ratio of water to surfactants is unity or less. It is of interest to clarify which ion species, the ion head group of surfactants or the counter ion, predominantly affects the interaction with water. Seno and his coworkers deduced that the carboxylato group in the DAP reversed micelles predominantly interacts with water from the shift of stretching frequency of carbonyl group as a function of water added.[12] If this is the case, water interacting with QD-Cl and CTACl must exhibit the absorption band at the same wavelength because both surfactants bear same counter anion, Cl^-. Furthermore, water interacting with AOT and DBS also will show the same absorption band since both surfactants bear the sulfonato group and sodium ion. Contrary to what would be expected, water interacting with CTACl in chloroform behaves similarly to that interacting with CTAB rather than QD-Cl. Water interacting with AOT exhibits different bands from those interacting with DBS. These results suggest that in apolar media the ion head of surfactant molecules, in spite of being more bulky, predominantly affects the force constant of the O–H bond of water. In order to secure more information of this point, we prepared hexadecylammonium chloride, sulfate, and perchlorate, sodium dihexadecyl phosphate, and potassium salts of anionic surfactants and tried to investigate the effect of small counter ions. Unfortunately, we were unable to utilize these surfactants owing to their diminished solubility in the usual apolar solvents.

Table 1. Intrinsic absorption bands of free water locating in bulk chloroform and water bound to various surfactants in the near infrared region at 25 °C[a]

Surfactant	Free water		Bound water		$\Delta\lambda_{0,(b-f)}$[b]
	$\lambda_{0,f}$	$\Delta\lambda_f$[c]	$\lambda_{0,b}$	$\Delta\lambda_b$[c]	
AOT	1908	32	1924	48	16
DBS	1907	31	1930	54	23
SB-16:3	1904	28	1953	77	49
EL	1906	30	1962	86	56
DAP	1897	21	1967	91	70
CTAB	1901	25	1996	120	95
CTACl	1903	27	2000	124	97
QD-Cl	1903	27	2020	144	117

a) Intrinsic absorption bands were graphically estimated using data given in Fig. 5 (see text). b) Difference between $\lambda_{0,f}$ and $\lambda_{0,b}$. Subscripts, f and b, refer to free water and water bound to surfactants, respectively. c) Calculated using Eq. 1.

Results given in Table 1 and Fig. 5 suggest to us that the tightness of interaction of water with surfactants in apolar media can be roughly classified into three categories depending on the head group structure of surfactants. CTAB, CTACl, and QD-Cl belong to the first category. Of surfactants adopted in this work, these cationic surfactants shift the O–H vibrational energy of the bound water most largely toward the lower energy state (longer wavelength). This means that these cationic surfactants interact tightly with water to reduce the force constant of the O–H bond of water and seem to form the most rigid reversed micelles. The second category includes DAP, EL, and SB-16:3. On the basis of the near infrared data,

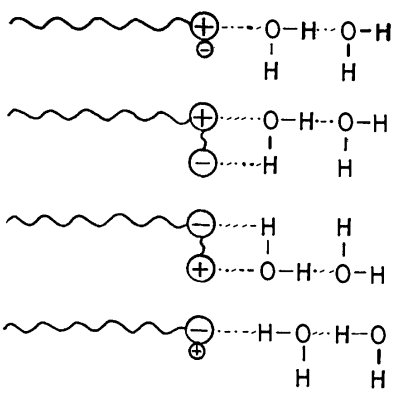

Fig. 6. Schematic representation of the mode of the interaction between water and surfactant in apolar media. From top to bottom, interactions of water with cationic surfactant, two different kinds of zwitterionic surfactants, and the anionic surfactant are shown, respectively.

DAP behaves as a zwitterionic surfactant rather than as cationic or anionic one. The anionic surfactants, AOT and DBS, belong to the different category from above two kinds of surfactants. The anionic surfactants seem to form the softest reversed micelles with water. These three distinct modes of the interaction between water and surfactants are represented schematically in Fig. 6. Assuming that in apolar media water predominantly interacts with the head group of surfactants, the interaction with the anionic surfactants is essentially hydrogen bonding,[19] while that with the cationic ones is the coordination type. In fact, water interacting with the anionic surfactants exhibits the band at the wavelength very close to that of pure bulk water. For the zwitterionic surfactants, two distinct types of interaction will compensate with each other. The difference in the absorption bands between the free water and water bound to surfactants, $\Delta\lambda_{b-f}$, decreases as one goes from cationic to zwitterionic and to anionic surfactant. The larger difference in the energy state between both state of water suggests a greater difficulty in the translocation of water between both states. This means that the surfactant-water aggregate under the circumstances may be relatively rigid. The hypothesis is not inconsistent with results obtained in previous studies on the solvochromism and the thermochromism of the cobalt(II) complexes in reversed micelles.[2] Both bands of free water and water bound to surfactants seem to approach the value of pure bulk water (1930 nm) as increasing the amount of water added (Fig. 5).[19] The state and nature of water in the cationic and the zwitterionic systems drastically change in the region where the mole ratio of water to surfactant is less than unity. The shift of absorption bands as a function of water content reveals an inflection point, where the $[H_2O]/[surfactant]$ ratio is about unity. The absorption bands of water bound to the cationic and the zwitterionic surfactants shift from the longer wavelength toward the shorter wavelength with increasing the amount of water, while the corresponding bands of the anionic surfactants move in the opposite direction. This reveals that between the cationic and anionic surfactant–water aggregates the nature of interaction of water with surfactants is different.

Evidences for the Two Step Hydration Mechanism. NMR of Water Interacting with Cationic Surfactant in Apolar Media: The chemical shift of the water proton in deuterochloroform containing CTAB was determined as a function of water amount added (Fig. 7 (b)). Over the range of water concentration examined, signals from methyl and methylene protons on the alkyl chain did not move, while *N*-methyl proton signal shifted a little toward the higher magnetic field with an inflection at the point of $[H_2O]/[CTAB] \fallingdotseq 1$. The proton signal of water moved substantially to the lower magnetic field with increasing water content, and again the inflection point appeared around the point where the mole ratio of water to CTAB is nearly unity. Increasing the water content in the system produces more hydrogen bonding between water molecules and causes the paramagnetic shift of the proton signal. The chemical shift of the water proton under consideration seems to finally reach the value of pure water (δ=4.66 ppm). Extrapolating the chemical shift to the point where the water content is zero gives 2.80 ppm. Water in deuterochloroform containing no surfactants shows a signal at 1.96 ppm. Interaction of the oxygen atom of water with the strongly electronegative cation-head of CTAB causes, therefore, a deshielding effect on the hydrogen atom of water molecule, resulting in the down-field shift of the proton signal. In contrast to the near infrared spectra, only one signal of water proton was observed by NMR. This means that the life time of both water protons, located in bulk phase and interacting with surfactant, is faster than the NMR time scale. In case of the phosphatidylcholine/diethyl ether micelles[20] and the AOT/heptane micelles,[4a] over a range where the mole ratio of water to surfactants is larger than 2, the line width of water proton resonance in NMR decreased as increasing the amount of water. Contrary to previous findings in the anionic and zwitterionic systems,[4a,20] in the present cationic system increasing water broadens the line width (Fig. 7 (a)). Again, we would like to note that the mode of interaction of water with cationic surfactants is different from that with anionic surfactants.

In the present system two possibilities must be considered to elucidate the broadening of the water proton signal: the viscosity of the medium and the proton exchange between free water and water bound to CTAB. Increased viscosity generally leads to line broadening by increasing the correlation time. In the reversed micellar system, in fact, adding a very little amount of water increases the macroscopic viscosity of the medium despite the decrease of the microscopic viscosity in the interior core.[21] Therefore, we can not eliminate the first possibility in interpreting our line broadening. Protons of water interacting with surfactants would have a shorter transversed relaxation time, T_2, than free water protons located in the bulk phase. When the rate of proton exchange between free water and the bound water is sufficiently

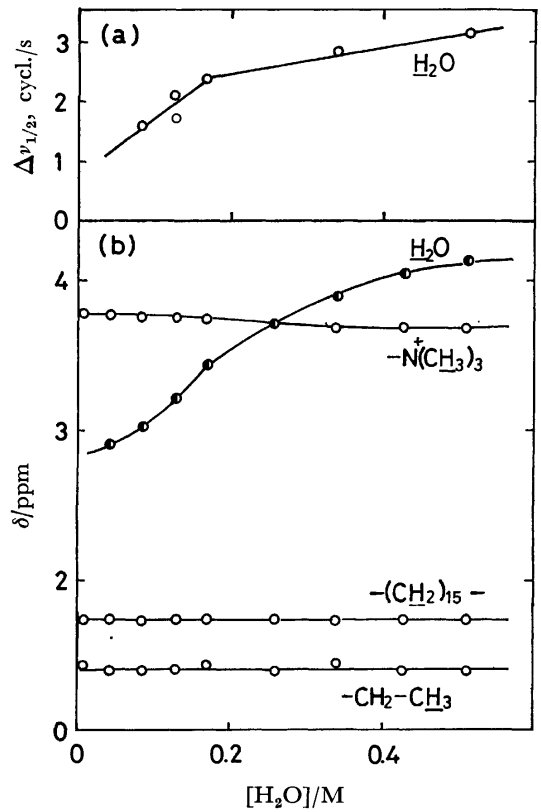

Fig. 7. NMR studies on the interaction of water with 0.20 M CTAB in deuterochloroform as a function of water content at 25 °C: (a) the line width of water proton signal at halfpeak height and (b) chemical shifts of proton signals of water, choline methyl, methylene, and terminal methyl, respectively.

great compared with the reciprocal of the relaxation time, the apparent line width ($\nu_{1/2}=1/T_2$) can be written as

$$1/T_2 = x_f(1/T_2)_f + x_b(1/T_2)_b, \quad (2)$$

where x is the mole fraction and the subscripts f and b refer to the free and bound water, respectively.[22] Since it is reasonable to assume that $(1/T_2)_b \ll (1/T_2)_f$, the line width will be affected mostly by water bound to surfactants. Increasing the hydrogen bonding of water very probably diminishes the mobility of water molecules and will cause the further line broadening of water proton signals. Anyway, the correlation between the mobility of water bound to surfactant and the strength of interaction of water and surfactant can be discussed only about the same ionic series of surfactants.

Fluorescence Intensity of Tb(III) in DAP Reversed Micelles: The fluorescence emission from the excited Tb^{3+} is strongly quenched in aqueous solution.[23] Removing some of water molecules from its hydration shell tends to enhance the fluorescence emission.[23] We found a significant enhancement of the fluorescence emission from the Tb^{3+}-ion when the concentrated aqueous solution of $TbCl_3$ was cosolubilized in hexane containing DAP. The relative fluorescence intensity decreased with increasing water content and an obvious inflection point was again observed where the mole ratio of water to DAP was about unity. Through the investigation of the state and nature of water interacting with surfactants in apolar media, we always observe an obvious inflection at the point where the mole ratio of water to surfactant is about unity. This is true for the O–H vibrational energy of water molecules in the near infrared spectra, the chemical shift and line width of water proton signal in the NMR, and the fluorescence intensity of terbium chloride. The most plausible explanation is a two step hydration mechanism.[2,15,17,20] When water is first introduced into the specific system, water tends to interact with surfactants irrespective of the presence of other polar or ionic solutes. Upon completion of the first hydration on the surfactants, water molecules start to interact with themselves by the hydrogen bonding or binding to other polar solutes cosolubilized in the interior core. Results obtained in this work coincide with those obtained in previous studies: the solvochromism of the metal(II) ion,[2,15] the hydrolysis of an amino acid ester as promoted by the copper(II) ion in the AOT/CCl_4 reversed micelles,[15,17] and the general acid-base catalysis of DAP on the hydrolysis of alkyl aryl carbonates in apolar media.[24]

We might conclude that in a very restricted field formed by reversed micelles or surfactant-water aggregates the situation closely resembles the hydrophobic pocket of enzymes or biomembranes. And also that the O–H vibrational modes of water in the near infrared region as well as the chemical shift and/or the line width of water proton resonance in NMR[4,20] can give an useful information on the tightness of the interaction of water with polar or ionic groups in the hydrophobic domain.

Professor Fredric M. Menger, Department of Chemistry, Emory University, is profoundly thanked for his reading through the manuscript and beneficial discussion. We are also grateful to Professor Syozaburo Takekiyo, Nagasaki University, for his comments.

References

1) (a) J. H. Fendler and E. J. Fendler, "Catalysis in Micellar and Macromolecular Systems," Academic Press, New York (1975); (b) J. H. Fendler, *Acc. Chem. Res.*, **9**, 153 (1976); (c) J. Sunamoto and H. Kondo, *Yukagaku*, **26**, 389 (1977).

2) J. Sunamoto and T. Hamada, *Bull. Chem. Soc. Jpn.*, **51**, 3130 (1978).

3) M. Wong, J. K. Thomas, and M. Grätzel, *J. Am. Chem. Soc.*, **98**, 2391 (1976).

4) (a) M. Wong, J. K. Thomas, and T. Nowak, *J. Am. Chem. Soc.*, **99**, 4730 (1977); (b) K. Tsujii, J. Sunamoto, and J. H. Fendler, presented a paper at the National Meeting of Chemical Society of Japan, Tokyo, April, 1977.

5) F. M. Menger and G. Saito, *J. Am. Chem. Soc.*, **100**, 4376 (1978).

6) F. M. Menger, G. Saito, G. V. Sanzero, and J. R. Dodd, *J. Am. Chem. Soc.*, **97**, 909 (1975).

7) H. F. Eicke and H. Christen, *Helv. Chim. Acta*, **61**, 2258 (1978).

8) E. J. Fendler, C. L. Day, and J. H. Fendler, *J. Phys. Chem.*, **76**, 1460 (1972).

9) G. Herzberg, "Molecular Spectra and Molecular Structure, II, Infrared and Raman Spectra of Polyatomic Molecules," Van Nostrand Reinhold Co., New York (1945), pp. 280—282.
10) S. Lewin, "Displacement of Water and Its Control of Biochemical Reaction," Academic Press, New York (1974).
11) O. D. Bonner and Y. S. Choi, *J. Phys. Chem.*, **78**, 1723 (1974).
12) M. Seno, K. Araki, and S. Shiraishi, *Bull. Chem. Soc. Jpn.*, **49**, 899 (1976).
13) A. B. F. Duncan, "Technique of Organic Chemistry, Vol. IX, Chemical Application of Spectroscopy," ed by A. Weissberger, Interscience Publisher, Inc., New York (1956), Chap. III, pp. 187—245.
14) It is difficult to obtain independently the correct molecular coefficients of both absorption bands arisen respectively from water locating in the bulk solvent phase and water bound to surfactants. Therefore, it seems impossible to discuss the equilibrium or the rate of translocation between both water species.
15) J. Sunamoto and T. Hamada, "Fundamental Research in Homogeneous Catalysis," ed by M. Tsutsui, Plenum Publishing Corporation, New York (1979), Vol. 3, p. 809.
16) S. G. Frank, Y. Shaw, and N. C. Li, *J. Phys. Chem.*, **77**, 238 (1973).
17) J. Sunamoto, H. Kondo, and K. Akimaru, *Chem. Lett.*, **1978**, 821.
18) E. D. Becker, *Spectrochim. Acta*, **17**, 436 (1961).
19) G. Zundel, "Hydration and Intermolecular Interaction," Academic Press, New York (1969).
20) M. A. Wells, *Biochemistry*, **13**, 4937 (1974).
21) ^{13}C-Spin lattice relaxation time, T_1, of glycine cosolubilized in the DAP/benzene reversed micelles increased as increasing the amount of water added, suggesting the decrease microscopic viscosity around the glycine molecule by increasing water content in the interior core: K. Tsujii, J. Sunamoto, and J. H. Fendler, unpublished results.[4b]
22) D. E. Gordon, B. Curnutte, Jr., and K. G. Lark, *J. Mol. Biol.*, **13**, 571 (1965).
23) H. F. Eicke, J. C. W. Shepherd, and A. Steinemann, *J. Colloid Interface Sci.*, **56**, 168 (1976).
24) H. Kondo, K. Fujiki, and J. Sunamoto, *J. Org. Chem.*, **43**, 3584 (1978).

Complex Formation and Ionization in 3,5-Dialkyl-4-hydroxybenzylidenemalononitrile in the Ground State, and Non-radiative Relaxation in the Excited State

Hiroko Mizukoshi and Michiya Itoh*

Faculty of Pharmaceutical Sciences, Kanazawa University, Takara-machi, Kanazawa 920

(Received May 28, 1979)

The interaction of 3,5-dialkyl-4-hydroxybenzylidenemalononitrile (HO-BMN) with ethanol, pyridine, and triethylamine in hexane gives rise to a hydrogen bonding complex formation in a low concentration of ethanol (pyridine and triethylamine) at room temperature. For ethanol concentration >5 mol dm^{-3}, the H-bonded complex exhibits further interaction with another ethanol (pyridine and triethylamine) molecule leading to the formation of anion form of this compound. However, no excited-state proton transfer was observed in several solvents. HO-BMN is fairly fluorescent in a solid solution of boric acid glass at room temperature, as well as in the rigid organic solution at 77 K, but almost non-fluorescent in fluid media at room temperature ($\phi \approx 10^{-4}$). The non-radiative process of HO-BMN in fluid media is discussed in terms of torsional relaxation of the excited state.

It was reported that 3,5-di-*t*-butyl-4-hydroxybenzylidenemalononitrile (*t*-Bu$_2$-HO-BMN) is the most potential uncoupler of oxidative phospholylation.[1,2] This is attributed to the properties of the proton transfer and conduction in phospholipid bilayer.[3] Yamaguchi *et al.* reported that the *t*-Bu$_2$-HO-BMN shows a ternary complex formation with valinomycin and potassium ion. On the other hand, this compound exhibits the dimer formation in 3-methylpentane at low temperature and the excited-state proton transfer in the dimer.[4] The unusual property of this compound seems to be attributable to the strong electron acceptor group (malononitrile) as a substituent of phenol.

This paper describes unusual spectroscopic properties of various 3,5-dialkyl-4-hydroxybenzylidenemalononitrile (HO-BMN) both in the ground and excited states. HO-BMN exhibits hydrogen bonded complex formation with ethanol (pyridine and triethylamine) in a dilute ethanol solution (*ca.* 1 mol dm^{-3}) in hexane. The ground-state ion-pair formation occurs by the further interaction between the H-bonded complex and another ethanol molecule in ethanol concentration greater than 5 mol dm^{-3}. However, no proton transfer was observed in the excited state of these compounds. Although HO-BMN shows fairly strong fluorescence in boric acid glass at room temperature and in several glassy or rigid solutions at low temperature, the compounds are almost non-fluorescent in the fluid solution at room temperature. Remarkable temperature dependence of fluorescence intensity and lifetime of the compounds dependent on rigidity of the solution was interpreted in terms of torsional relaxation of the excited state.

Experimental

The purification of materials and solvents was described.[4] Ethanol (Nakarai, 99.5%) was purified by distillation after refluxing over magnesium metal. Pyridine (Nakarai GR) and triethylamine (Nakarai GR) were distilled twice after refluxing over potassium metal for 3—5 h. Solid solution of boric acid glass was prepared as follows. Boric acid was heated and melted in a porcelain dish at 150—180 °C, transparent liquid being obtained. The samples were then dissolved into liquid glass at this temperature (the samples were stable in this process). Solid-glass solution was obtained after the temperature had fallen to room temperature.

Since materials are insoluble in aqueous solution, determination of pK_a was performed in aqueous ethanol solution (50, 40, and 30 w/v %). The pK_a in 100% aqueous solution (Table 1) was obtained by an extrapolation from values in the mixed solution.[5]

Measurement of fluorescence and absorption spectra was made as described previously.[4] Fluorescence quantum yield was determined using quinine sulfate (2.1×10^{-5} mol dm^{-3} in 0.5 mol dm^{-3} H_2SO_4) as a standard ($\phi = 0.546$ in the excitation at 365 nm).[6] Determination of fluorescence lifetimes was made by N_2 laser (Molectron UV-12) excitation and analysis of exponential decay curve. The data were analyzed by a convolution method.[4]

Results and Discussion

Complex and Ion-pair Formations in the Ground State. The absorption spectrum of 3,5-dialkyl-4-hydroxybenzylidenemalononitrile (HO-BMN) shows an absorption band at 350—370 nm in aprotic solvent and in an acidic ethanol–water mixed solution, and another band at 465 nm in basic ethanol–water. The former and the latter were attributed to the neutral form and to the anion form of the compound, respectively.[4] Absorption spectra of 3,5-dimethyl- and 3,5-di-*t*-butyl-4-hydroxybenzylidenemalononitrile (Me$_2$- and *t*-Bu$_2$-HO-BMN) were measured in hexane solution in the presence of various amounts of ethanol (Figs. 1 and 2). The spectral change of Me$_2$-HO-BMN exhibiting an isosbestic point at 345 nm indicates the complex formation between this compound and ethanol in concentration greater than 0.1 mol dm^{-3}, while the spectra exhibit a conspicuous red-shift owing to the change of solvent polarity (general solvent effect) by the addition of small amount of ethanol. In 3,5-diisopropyl-4-methoxybenzylidenemalononitrile (Pr$_2$-MO-BMN),[7] however, no significant ethanol concentration dependence of absorption spectra was detected, though a considerable red-shift of the absorption band owing to the general solvent effect was observed with increasing ethanol concentration. Thus, the electronic interaction of HO-BMN with ethanol can be attributed to the hydrogen bonding between the OH

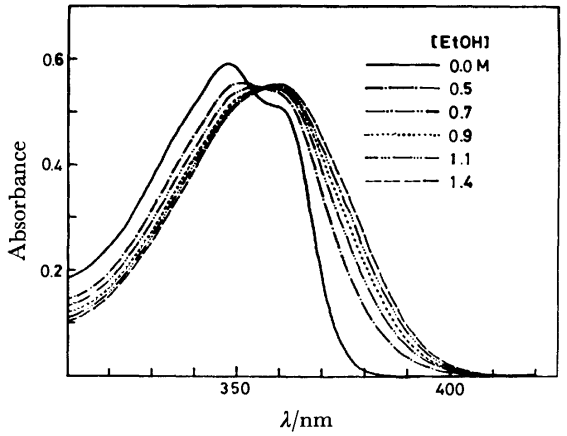

Fig. 1. Absorption spectra of t-Bu_2-HO-BMN (1.7×10^{-5} mol dm^{-3}) in hexane containing various amount of ethanol at room temperature (ethanol concentration <2 mol dm^{-3}) (1 M = 1 mol dm^{-3}).

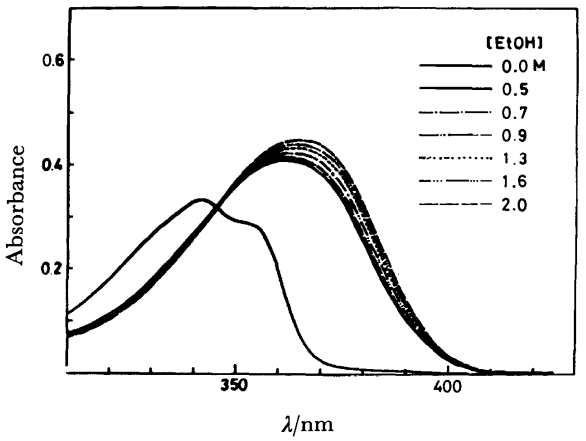

Fig. 2. Absorption spectra Me_2-HO-BMN (2.3×10^{-5} mol dm^{-3}) in hexane containing various amounts of ethanol (concentration $\simeq2$ mol dm^{-3}) (1 M = 1 mol dm^{-3}).

group in HO-BMN and ethanol molecule. With increase in ethanol concentration (>5 mol dm^{-3}), the absorption band of the H-bonded complex at 370 nm gradually decreased and another band at 465 nm appeared, increasing with an isosbestic point at 400 nm (Fig. 3). The second band corresponds to that of the anion form of the compound, mentioned above.

Here, the equilibria are expressed as follows:

$$\underset{C_f}{\text{HO-BMN}} + \underset{C_B}{\text{EtOH}} \overset{K_1}{\rightleftharpoons} \underset{C_b}{\text{H-bonded complex}}$$

$$\underset{C_b}{\text{H-bonded complex}} + \underset{C_B}{\text{EtOH}} \overset{K_2}{\rightleftharpoons} \underset{C}{\text{Anion form}}$$

$$\text{HO-BMN} + 2\,\text{EtOH} \overset{K_3}{\rightleftharpoons} \text{Anion form} \qquad (1)$$

where K_1, K_2, and K_3 are the corresponding equilibrium constants, and $K_1\times K_2=K_3$. The constants were obtained by the following equations:[8,9]

$$(\varepsilon-\varepsilon_f)/C_B = K_1\varepsilon_b - K_1\varepsilon \qquad (2)$$

$$1/C_B^2 = c/A - K_3,\ c=\text{const} \qquad (3)$$

where C_f, C_B, and C_b are the equilibrium concentrations

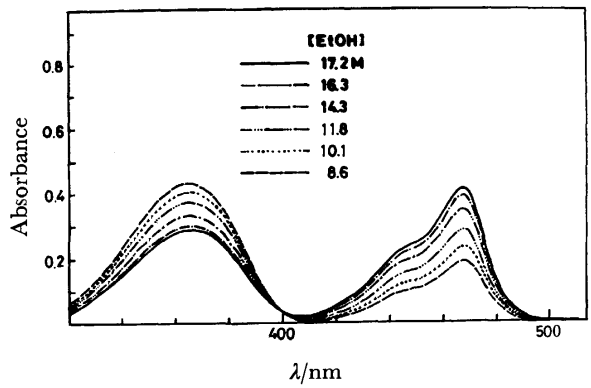

Fig. 3. Absorption spectra t-Bu_2-HO-BMN (1.7×10^{-5} mol dm^{-3}) in hexane containing various amounts of ethanol at room temperature (concentration >8 mol dm^{-3}) (1 M = 1 mol dm^{-3}).

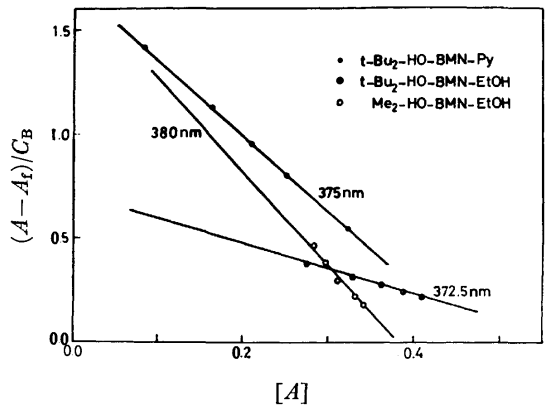

Fig. 4. Plots of $(A-A_f)/C_B$ *vs.* A, where ε and ε_f in Eq. 2 were replaced by the corresponding absorbance A and A_f, respectively (concentration of HO-BMN, 1—3 mol dm^{-3}).

of the free HO-BMN, ethanol and the H-bonded complex, respectively; and ε_f and ε_b are molar extinction coefficients of free HO-BMN and the complex, respectively; ε is apparent extinction coefficient. In Eq. 3, A is the absorbance of the anion form at 465 nm. A linear relationship of $(\varepsilon-\varepsilon_f)/C_B$ *vs.* A at 370 nm suggesting a 1:1 interaction of HO-BMN and ethanol is shown in Fig. 4. Plots of $1/C_B^2$ *vs.* $1/A$ suggesting also the reaction mechanism for the anion formation are shown in Fig. 5. The concentration dependence of the anion band at 465 nm shows remarkable deviation from Scot plots and Benesi Hildebrand plots of an ordinary 1:1 interaction between HO-BMN and ethanol molecule. Slopes of these linear plots (Figs. 4 and 5) afford equilibrium constants K_1 and K_3, respectively. The results are summarized in Table 1. Equilibrium constants K_1 and K_3 in the t-Bu_2-HO-BMN–ethanol system were determined at temperatures 5, 15, 20, and 30 °C. Conventional plots of ln K *vs.* $1/T$ showing a linear relation afford enthalpy changes of respective equilibrium ($\Delta H_1=-1.8$, $\Delta H_2=-1.0$, and $\Delta H_3=-2.8$ kcal mol^{-1}). The H-bonded complex formation of the other HO-BMN with ethanol was also observed (Table 1). Since the absorption band of the anion pair of the other HO-BMN was

Table 1. pK_a and equilibrium constants in hexane at room temperature, and fluorescence lifetimes in MTHF at 77 K

	pK_a[a]	K_1/mol^{-1}	K_2/mol^{-1}	K_3/mol^{-2}	τ/ns[b]
			[C_2H_5OH]		
Me_2-HO-BMN	4.8	4.5	—	—	2.3
Pr_2-HO-BMN	—	2.3	—	—	2.6
t-Bu_2-HO-BMN	4.9	1.1	4.1×10^{-3}	4.5×10^{-3}	1.5
Me_2-MO-BMN	—	—	—	—	2.3
			[pyridine]		
t-Bu_2-HO-BMN	—	4.3	2.3×10^{-3}	1.0×10^{-2}	—
			[TEA]		
t-Bu_2-HO-BMN	—	—	—	2×10^{-3}	—

a) pK_a (100% aqueous solution) extrapolated from values determined in the mixed systems (aqueous ethanol, 50, 40, and 30 w/v%). b) Fluorescence lifetimes in 2-methyltetrahydrofuran at 77 K.

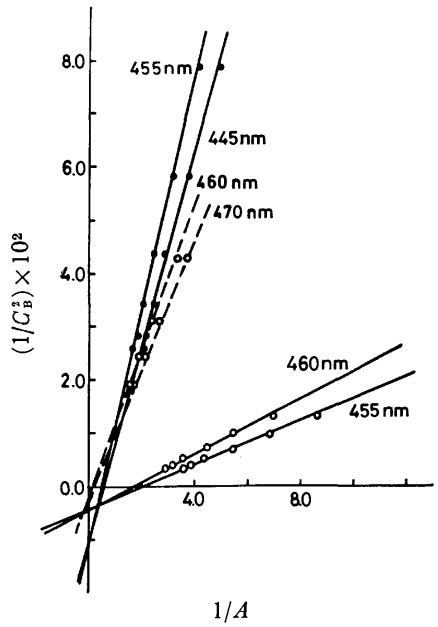

Fig. 5. Plots of $1/C_B^2$ *vs.* $1/A$; —○—, *t*-Bu_2-HO-BMN-ethanol system corresponding to spectra in Fig. 3; —●—, *t*-Bu_2-HO-BMN-pyridine system corresponding to spectra in Fig. 6; —○--, *t*-Bu_2-HO-BMN-TEA system corresponding to spectra of Fig. 8; concentrations of *t*-Bu_2-HO-BMN are $0.8—2.0\times10^{-5}$ mol dm^{-3} (1 M=1 mol dm^{-3}).

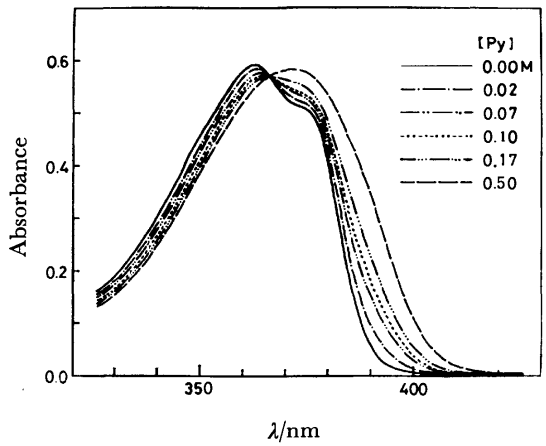

Fig. 6. Absorption spectra of *t*-Bu_2-HO-BMN (8.7×10^{-6} mol dm^{-3}) in hexane contaning various amounts of pyridine (1 M=1 mol dm^{-3}).

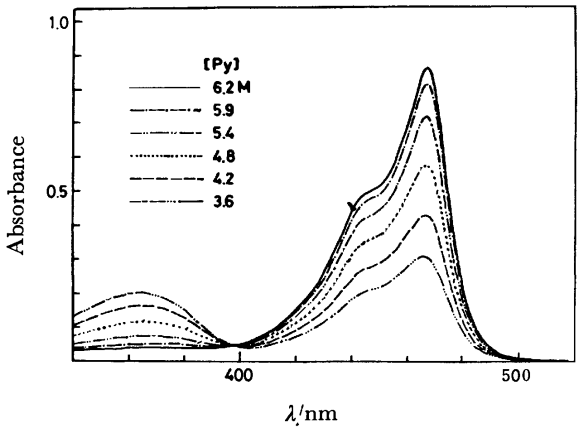

Fig. 7. Absorption spectra of *t*-Bu_2-HO-BMN (8.7×10^{-6} mol dm^{-3}) in hexane containing various amounts of pyridine (concentration >3 mol dm^{-3}) at room temperature (1 M=1 mol dm^{-3}).

small in intensity even in ethanol, the exact equilibrium constant K_3 was not obtained.

The H-bonding formation of *t*-Bu_2-HO-BMN and further anion pair formation were also observed in the interaction with pyridine and triethylamine (TEA). Figures 6 and 7 show the absorption spectra of *t*-Bu_2-HO-BMN in hexane with various concentrations of pyridine. Similarly, plots of $(\varepsilon-\varepsilon_f)/C_B$ *vs.* A, and of $1/C_B^2$ *vs.* $1/A$ afford K_1 and K_3, respectively. In the *t*-Bu_2-HO-BMN and TEA system, the concentration dependence of TEA upon the absorption band of the H-bonded complex in hexane exhibits no significant isosbestic points because of considerable red shift with increasing concentration of TEA (<2 mol dm^{-3}). Therefore, K_1 was not obtained in this system. Figure 8 shows absorption spectra of the anion band of *t*-Bu_2-HO-BMN in various concentrations of TEA (>4 mol dm^{-3}) in hexane. It is seen that the increase of the anion band follows Scheme 1 and not the ordinary 1:1 interaction. Plots of $1/C_B^2$ *vs.* $1/A$ (Fig. 5) afford K_3 (Table 1). The constants K_3 obtained in the three systems show almost similar values, though ethanol, pyridine and TEA differ considerably in dielectric property.

Baba *et al.*[8] reported the H-bonded complex formation between *p*-nitrophenol and TEA in several solvents, and subsequent proton transfer in the ground state. The proton transfer *i.e.*, anion pair formation of phenol in the H-bonded complex, takes place from nitrophenol to amine to yield a H-bonded ion pair, no further concentration dependence of amine upon the ion pair formation being detected. In these HO-BMN–ethanol, –pyridine, and –TEA systems, another ethanol (pyridine and TEA) molecule is involved in the ion pair formation from the H-bonded complex. The concentration dependence of the anion formation might be ascribed to the change of the dielectric property of the solvent system by the addition of ethanol (dielectric constant, ε=24.6),[10,11] pyridine (12.4) and TEA (2.42) in the hexane solution (1.88). However, the results of the anion pair formation in the interaction with three proton acceptors do not seem to be correlated with their dielectric constants. This shows that the ionization of the H-bonded complex can be attributed to a specific interaction between the complex and ethanol (pyridine and TEA) molecule.

Hoshino and Koizumi[12] reported a two-step interaction of ethanol molecule with *p*-amino- and *p*-dimethylaminobenzophenone in cyclohexane. They suggested the interactions of one ethanol molecule to the NH_2 group (or $N(CH_3)_2$) and one molecule to C=O of these compounds. The first specific interaction of ethanol with HO-BMN is ascribed to the hydrogen bonding with OH group, since ethanol, as well as TEA and pyridine, is a proton acceptor. In the interaction of the second ethanol molecule leading to the ion pair formation, there seem to be two possibilities: (a) a specific interaction of another ethanol molecule with malononitrile group, and (b) further interaction of the second ethanol molecule with an oxygen atom of the H-bonded OH group of HO-BMN or with a hydrogen atom of the first ethanol. However, since TEA and pyridine exhibit almost the same behavior as ethanol, (a) seems preferable.

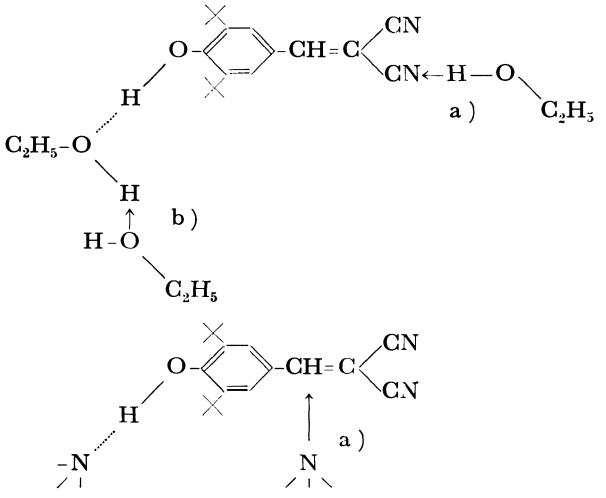

Fluorescence and Non-radiative Process. The neutral and anion forms of HO-BMN show very weak fluorescence spectra in 410—430 and 460—500 nm regions, respectively, at room temperature. The fluorescence intensity of the neutral form exhibits no

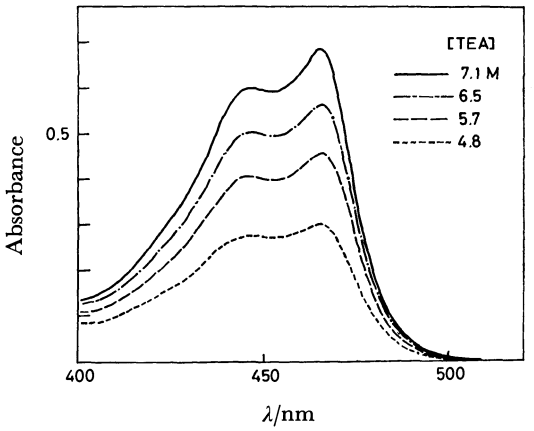

Fig. 8. Absorption spectra of *t*-Bu_2-HO-BMN in hexane containing various concentrations of TEA at room temperature (concentration of *t*-Bu_2-HO-BMN, 3.7×10^{-5} mol dm^{-3}) (1 M=1 mol dm^{-3}).

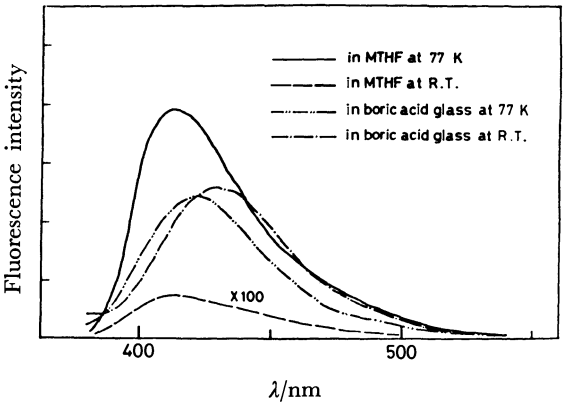

Fig. 9. Fluorescence spectra of *t*-Bu_2-HO-BMN in 2-methyl-tetrahydrofuran and in boric acid glass; Intensities are arbitrary unit.

significant difference between free (λ_{max} 410 nm in hexane) and H-bonded HO-BMN (λ_{max} 430 nm in ethanol). Fluorescence quantum yields of HO-BMN (neutral form) and MO-BMN in several solvents were determined approximately to be $1—5\times10^{-4}$ at room temperature. The fluorescence intensity of these compounds in various solvents remarkably increased with decreasing temperature at 150—77 K. Figure 9 shows fluorescence spectra of *t*-Bu_2-HO-BMN (neutral form) in MTHF, at 77 K and at room temperature. Figure 10 shows the temperature dependence of fluorescence intensity of *t*-Bu_2-HO-BMN in various solvents. Fluorescence intensity of *t*-Bu_2-HO-BMN increased in the temperature region below $\approx$100 K in MTHF and in methylcyclohexane (MCH). However, in 3-methylpentane–MCH mixed system (1:3), it increased markedly at temperatures below $\approx$90 K. A similar temperature dependence of fluorescence was also observed in MO-BMN. The temperature region in which fluorescence intensities increase seems to correspond to the increase of solvent rigidity (viscosity) from fluid to rigid glass. In order to confirm the influence of the rigidity of solution on fluorescence intensity, the fluorescence spectrum of HO-BMN in the solid solution of boric acid glass was determined at room temper-

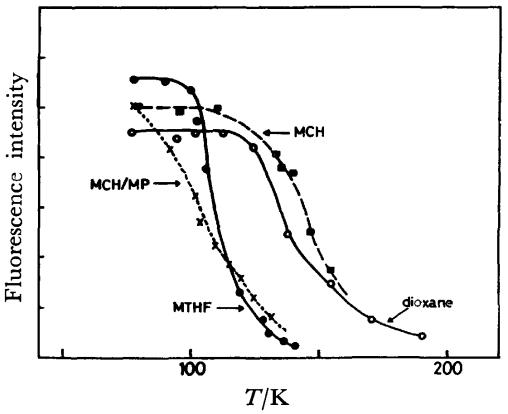

Fig. 10. Temperature dependence of fluorescence intensity (arbitrary unit) of t-Bu_2-HO-BMN in various solvents.

ature.[13] The spectrum shows fairly strong fluorescence at room temperature (Fig. 9), but no significant temperature dependence. Fluorescence lifetimes of these compounds in various solvents were determined to show also remarkable temperature dependence. The lifetimes in the rigid glass at 77 K are 1—3 ns (Table 1), while those decrease to within a duration of a laser pulse in fluid medium at 100—150 K. Fluorescence lifetimes of these compounds may be in the order of picosecond at room temperature.

Semi-empirical molecular orbital calculation (Pariser-Parr-Pople type) indicates that the first electronic transition of HO-BMN as well as MO-BMN is allowed, corresponding to an absorption band at 340—360 nm. Thus, natural radiative lifetimes τ_0 of these compounds were obtained as $1—3\times10^{-9}$ s (in ethanol, THF, and hexane) from absorption bands at 340—360 nm. The lifetimes of these compounds were estimated to be $10^{-12}—10^{-13}$ s from fluorescence quantum yield ($\approx10^{-4}$) and τ_0 ($\approx10^{-9}$ s). This suggests that the decay process of the compounds is mostly non-radiative. In the non-radiative process of HO-BMN in fluid medium, there are two possible mechanisms: (a) the excited-state proton transfer of OH group leading to the anion formation, *i.e.*, a photoionization, and (b) a torsional non-radiative relaxation process of the excited state.[14] (a) is ruled out from similar fluorescence behavior of MO-BMN to HO-BMN. Thus, (b) can be attributed to the non-radiative process, since the torsional non-radiative process seems to be frozen out in rigid solution at 77 K and in the boric acid glass at room temperature.

Hui and Rice reported a torsional non-radiative process in the excited state of styrene.[15] The non-radiative process of styrene consists of $S_1\rightarrow T_1$ and cis-trans isomerization, suggesting a plausible schematic potential energy surface for the torsional motion that leads to cis-trans isomerization. On the other hand, El-Bayoumi reported torsional relaxation of the excited state of 1,1,4,4-tetraphenylbutadiene (TPB).[16] In fluid media, TPB exhibits large Stokes shifts and their fluorescence spectra are diffuse, while the fluorescence maximum shifts to higher energy, and the vibrational structure being resolved by preventing this torsional relaxation in the rigid medium at low temperature. In HO-BMN, however, no longer-wavelength fluorescence corresponding to the large Stokes shift was observed in fluid medium. If the torsional equilibrium of S_1 state of this compound is in a low level and the intersystem crossing from S_1 to T_1 is predominant in the decay process, no fluorescence would be observed. According to this argument, HO-BMN dimer (or MO-BMN) as well as the double proton transfer species (or the excimer) should be fluorescent.[4] This is becuase the torsional relaxation in a component molecule of the dimer can be prevented by its sandwich-type structure. However, no exact potential energy curves concerned with C–C bond rotations of malononitrile double bond and of phenyl-malononitrile single bond were obtained at the present stage.

The authors wish to thank Dr. Kiyokazu Fuke for his valuable discussion on torsional non-radiative relaxation. The work was partly supported by a Grant-in Aid from the Ministry of Education.

References

1) S. Muraoka and H. Terada, *Biochim. Biophys. Acta*, **275**, 271 (1972).
2) H. Terada, *Biochim. Biophys. Acta*, **387**, 519 (1975).
3) A. Yamaguchi and Y. Anraku, *Biochim. Biophys. Acta*, **501**, 136 (1978); A. Yamaguchi, Y. Anraku, and S. Ikegami, *ibid.*, **501**, 150 (1978).
4) M. Itoh, K. Inoue, T. Kuzuhara, and T. Kusui, *Bull. Chem. Soc. Jpn.*, **52**, 1010 (1979).
5) A. Albert and E. P. Serjeant, "Determination of Ionization Constant," Chapman & Hall, New York (1971).
6) J. N. Demas and G. A. Grosby, *J. Phys. Chem.*, **75**, 991 (1971).
7) K. Inoue and M. Itoh, *Bull. Chem. Soc. Jpn.*, **52**, 45 (1979).
8) H. Bada, A. Matsuyama, and H. Kokubun, *Spectrochim. Acta, Part A*, **25**, 1709 (1969).
9) Y. Tanimoto and M. Itoh, *Chem. Phys. Lett.*, **57**, 179 (1978).
10) R. Fujishiro, K. Wada, and R. Tamamushi, "Property of Solution, II," Tokyo Kagakudojin, Tokyo (1968).
11) H. B. Robinson "Proton-Transfer Reactions," ed by E. F. Caldin and V. Gold, Chapman & Hall, London (1975).
12) M. Hoshino and M. Koizumi, *Bull. Chem. Soc. Jpn.*, **45**, 3075 (1972).
13) Determination in the solid solution of poly(methyl metacrylate) was attempted. However, no polymerization occurred, since HO-BMN (MO-BMN) seems to act as a radical quencher.
14) G. Oster and Y. Nishijima, *J. Am. Chem. Soc.*, **78**, 1581 (1956), and references therein.
15) M. H. Hui and S. A. Rice, *J. Chem. Phys.*, **61**, 833 (1974).
16) M. A. El-Bayoumi, *J. Phys. Chem.*, **80**, 2259 (1976).

 © 1980 The Chemical Society of Japan Bull. Chem. Soc. Jpn., 53, 595—598 (1980)

Topological Ligand Design. II. The Definition and Derivation of Extended and Complex Ligand Graphs*

Susumu TAKAMOTO

Department of Chemistry, Faculty of Sciences, Gakushuin University, Mejiro, Toshima-ku, Tokyo 171

(Received June 16, 1979)

An extended ligand graph is a set of several points corresponding to donor atoms, where each pair of points is connected by *n* lines when these atoms are able to form *n* chelate rings with a metal ion. These graphs can cover all the ligands, but they may not express the geometrical patterns of some complicated ligands clearely enough for them to be discriminated. A complex ligand graph is a set of some main points and sub-points connected by sub-lines, where the main points, sub-points, and sub-lines correspond to donor atoms, carbon atoms forming chelate bonds, and chemical bonds among them respectively. All the complex ligand graphs can then be systematically derived from donor-atomic graphs, which are composed of only main points and main lines and are equivalent to the simple ligand graphs previously designed. Another designing method of ligands is proposed for a certain coordination sturcture. A complex ligand graph to which no more sub-points or sub-lines can be added is called a parent ligand graph. Then all the complex ligand graphs for such a coordination are derived from the parent ligand graphs by neglecting some sub-points or by removing some sub-lines successively.

In the previous paper[1] a simple ligand graph was defined and all of the lower members were systematically derived. This is one of the most useful methods for designing and classifying ligands and can bring us various information about future ligands. However, it cannot cover some kinds of ligands containing special kinds of branched carbon atoms, where branches form their several chelate rings with a metal ion, since any branch point in a simple ligand graph should be not a carbon atom, but a donor atom. To cover these complicated ligands, the definition of the ligand graph must be further extended.

Theoretical

Extended Ligand Graph. An "extended ligand graph" is a set of several points corresponding to donor atoms, where each pair of points is connected by *n* lines when these atoms are able to form *n* chelate rings with a metal ion. For example, a complicated terdentate ligand (A) in Fig. 1 is expressed by the

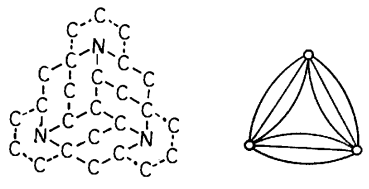

(A) (B)

Fig. 1. An example of the extended ligand graph. (A): Ligand, (B): its extended ligand graph.

extended ligand graph (B); some carbon chains connected by broken lines are neglected in this graph, because they cannot become the chelate ring. Therefore, branched carbon atoms may be commonly used for different chelate rings. These extended ligand graphs may contain some double or triple lines; the maximum degree of their points is nine, since every pair of points may have triple lines. They can represent all the chelate ligands and can be derived systematically

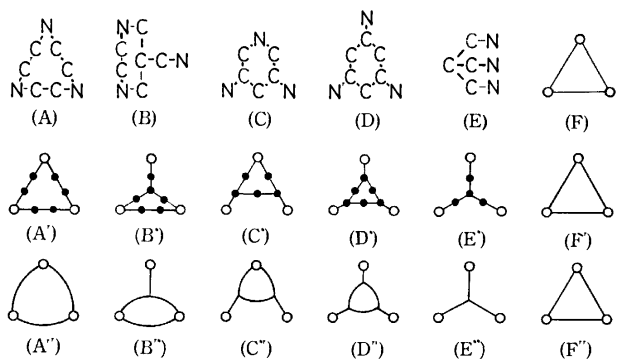

Fig. 2. Various graph expressions for some ligands. (A) to (E): ligands, (F): their extended ligand graph, (A′) to (E′): their several complex ligand graphs, (A″) to (E″): their several complex pattern graphs, (F′) and (F″): their composite pattern and donor-atomic graph.

from the simple ligand graphs by substituting some of their lines for double or triple lines. However, they do not express the geometrical patterns of complicated ligands well enough for them to be discriminated. For example, the ligands from (A) to (E) in Fig. 2 are expressed by the same extended ligand graph (F). In order to correct this defect, a complex graph should be applied which is a set of main points and main lines, with each main line also a graph composed of sub-points and sub-lines.

Complex Ligand Graph. A "complex ligand graph" is a set of several main points and sub-points connected by sub-lines, where the main points, sub-points, and sub-lines correspond to donor atoms, carbon atoms forming chelate bonds, and chemical bonds among these atoms respectively. Examples of the complex ligand graphs are shown as (A′) to (E′) in Fig. 2. The degree of the main points does not exceed three, while that of the sub-points is only two or three, since no carbon atom can be an end-point. The complex ligand graph contains neither multiple sub-lines nor self-loops, and is naturally a connected planar graph as well as a simple ligand graph.

On the complex ligand graph, a graph-theoretical path between two main points containing only two

* A preliminary report on this work was presented at the ACS/CSJ Chemical Congress, Honolulu, April 1979.

or three sub-points is called a "chelate path." For example, every N–C–C–N or N–C–C–C–N chain of the ligands in Fig. 1 or Fig. 2 is a chelate path. Accordingly, each line on an extended ligand graph corresponds to a chelate path. Every main point is a common terminal point of a maximum of nine chelate paths; this is obvious from the maximum degree of the points in the extended ligand graph. Every sub-point belongs to one, two, or three chelate paths.

When all the sub-points of degree two are neglected in a complex ligand graph, what is left is called a "complex pattern graph" and its lines are called a "series"; these definitions are equivalent to those in the simple ligand graph. Some examples are shown in Fig. 2, (A″) to (E″).

Then new terms are defined in order to derive these complex graphs from some simpler, non-complex graphs which have already been designed. When a pair of main points have at least one chelate path, they are connected by a "main line," while a set of several main points connected by several main lines is called a "donor-atomic graph," which is quite equivalent to the simple ligand graph, since it has neither sub-points, sub-line, multiple-line, nor self-loop. As the main line is not related to the number of the chelate paths or the branched carbon atoms contained in it, all the ligands in Figs. 1 and 2 can be represented by the same trigonal-shaped donor-atomic graph, as is shown in Fig. 2 (F″).

When several chelate paths between each pair of main points in a complex pattern graph are observed, there are four kinds of simple patterns (shown in Fig. 3) as far as ligands for five- or six-membered chelate rings are concerned; they are called "unit patterns." The (A), (B), (C), and (D) unit patterns contain one, two, two, and three chelate paths respectively.

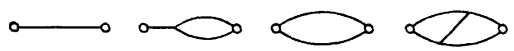

(A) (B) (C) (D)

Fig. 3. Unit patterns.

When each main line of a donor-atomic graph is displaced by one of the unit graphs, the complex graph thus produced is called a "composite pattern." As each main line in the complicate ligand in Fig. 1 contains three chelate paths, for example, the composite pattern for this ligand is obtained by displacing three main lines by the unit pattern (D) in Fig. 3. For the ligands from (A) to (E) in Fig. 2, their composite patterns are represented by the same trigonal graph (F′), which is identical to their donor-atomic graph (F″), since every main line contains only one chelate path; its unit pattern is the same as (A) in Fig. 3.

A composite pattern is not always identical to its complex pattern graph, for two adjacent unit patterns have some common sub-lines and sub-points. For example, all the ligands in Fig. 2 have the same composite pattern (F′); however, they are represented by several complex pattern graphs, (A″) to (E″), because they have different parts in common. In these complex pattern graphs in Fig. 2, the common parts of the unit patterns are expressed by straight lines, and the others, by curved lines.

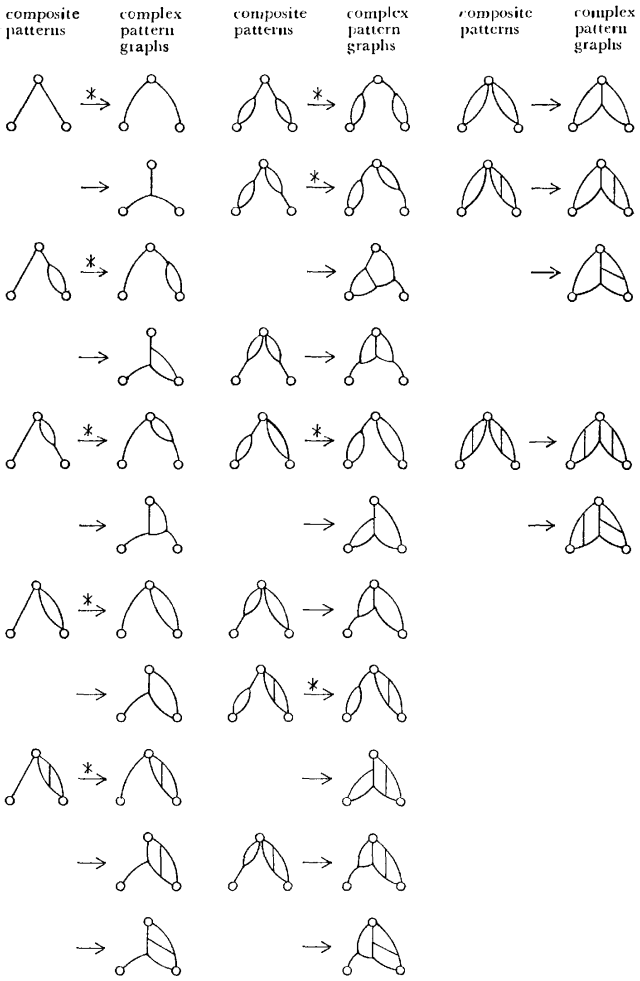

Fig. 4. Condensations between two unit patterns.
*: Without condensation.

Thus, a new concept of "condensation" should be introduced; it means a partial fusing of two patterns, as when the condensation of two benzene rings produces a naphthalene frame. All the condensations between a pair of adjacent unit patterns are summarized in Fig. 4. By various combinations of four kinds of unit patterns, many composite patterns are obtained from a donor-atomic graph, and by various condensations among the unit patterns, further, more complex pattern graphs are obtained. The condensation is not always necessary, but if the degree of a main point exceeds three in a composite pattern, the condensation must not be neglected.

Finally, the complex ligand graphs can be derived by allotting some sub-points of degree two to some series of a complex pattern graph, so that each chelate path may have two or three sub-points. Thus, all the complex ligand graphs can be obtained systematically from the donor-atomic graphs, which have already been designed.

On the contrary, any ligands can be reduced to their donor-atomic graphs. For example, a complicated quadridentate ligand (A) in Fig. 5 is represented

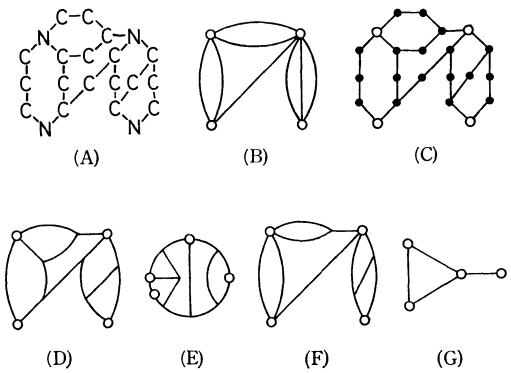

Fig. 5. Reduction of a ligand structure into its donor-atomic graph. (A): Ligand, (B): extended ligand graph, (C): complex ligand graph, (D): complex pattern graph, (E): its schematical illustration, (F): composite pattern, (G): donor-atomic graph.

by both the extended ligand graph (B) and the complex ligand graph (C). Then, (C) is reduced to the complex pattern graph (D) by neglecting all the sub-points of degree two. (E) is a schematical illustration of (D). When all the condensed chelate paths in (D) are separated into the unit patterns, its composite pattern (F) is obtained. Finally, (F) is reduced to its donor-atomic graph (G) by substituting each unit graph for a main line.

Ligand Design for a Certain Coordination Structure. The above derivation method for the complex ligand graphs is sufficiently systematic and can cover all of these graphs, but a ligand graph derived mechanically cannot always fit a special coordination structure, and in a computer manipulation it is not easy to select them. Furthermore, one often needs knowledge about all the ligands for a special coordination, such as octahedral, tetrahedral, or square planar.

When all the donor-atomic graphs which are fit for such special coordination are found, all the composite patterns, complex pattern graphs, and complex ligand graphs may be derived successively. The donor-atomic graphs for any planar coordinations are always only linear or circular graphs, while those for tetrahedral or octahedral coordination are equivalent to all the simple ligand graphs with $m=4$ or $m=6$, as was illustrated in Table 3 in the previous paper.[1] Therefore, all the ligands for such purposes may be designed by the above-described procedure, but they may still contain some useless ligands which cannot coordinate to a metal ion easily because of intricate carbon-chains. Therefore, an alternate designing method for these complex ligand graphs will be proposed.

In a certain coordination structure, a complex ligand graph to which no more sub-points or sub-lines can be added, *i.e.*, a high density complex graph, is called a "parent ligand graph." Several kinds of parent ligand graphs may exist in each coordination structure. If all of them are found, all the complex ligand graphs for such a coordination can be derived as their "daughter ligand graphs" by neglecting some sub-points or removing some sub-lines.

Planar Coordinations: The donor-atomic graph of the parent ligand graphs for an n-polygonal planar coordination is an n-polygonal graph. These parent ligand graphs are, then, obtained by displacing each edge of the n-polygon with one of the three "linear unit graphs" shown in Fig. 6. This procedure is similar to that used in deriving the composite patterns, but these unit graphs contain three sub-points of degree two or three on each chelate path. In this case, the condensation between two unit graphs would not occur, since two unit graphs surrounding a metal ion cannot approach each other so closely. For example, all the parent ligand graphs for the square planar coordination can be obtained by the combination of four unit graphs, so that every main point may have degree three as is shown in Fig. 7.

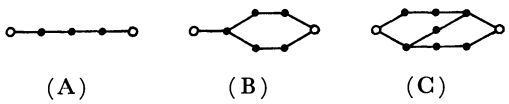

Fig. 6. Linear unit graphs.

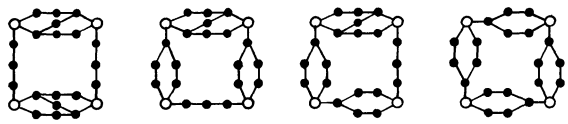

Fig. 7. Parent ligand graphs for the square planar coordination.

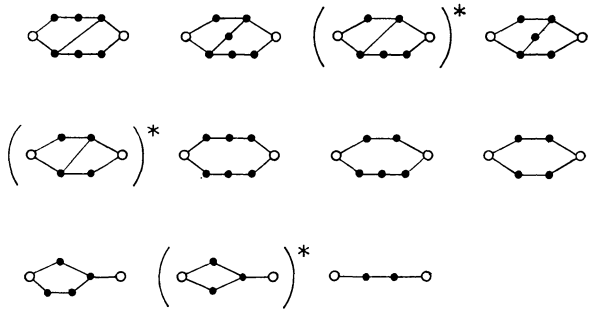

Fig. 8. Daughter unit graphs for the planar coordination. *: Omitted here because of containing less than five-membered ring.

In order to derive the daughter ligand graphs, all the "daughter unit graphs" of three unit graphs are found by neglecting sub-points or removing sub-lines from the unit graphs, as is shown in Fig. 8. Then a circular daughter ligand graph might be derived by substituting each edge of the n-polygon for one of those daughter unit graphs. All the linear daughter ligand graphs are derived by removing one unit graph or one daughter unit graph from those circular daughter ligand graphs and parent ligand graphs.

Polyhedral Coordinations: An m-polyhedron is covered with mn-polygons (sometimes different polygons). Then its parent ligand graphs are obtained when every surface is covered by n-polygonal unit graphs, with condensations on some edges. As a popular example, a tetrahedron or an octahedron is covered with four or eight equilateral triangles. The parent ligand graphs for such coordination are derived by covering all surfaces with five kinds of trigonal unit graphs, as is shown in Fig. 9.

The adjacency of two trigonal unit graphs is geo-

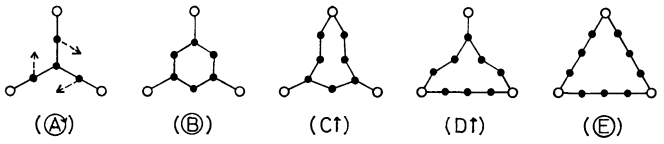

Fig. 9. Trigonal unit graphs.

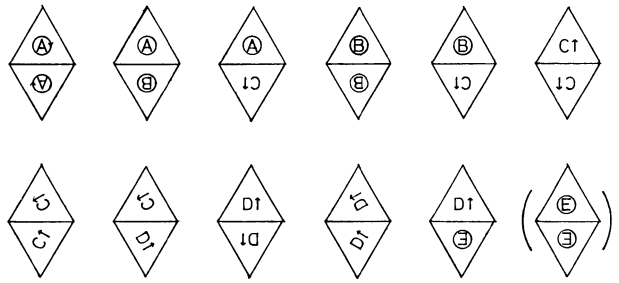

Fig. 10. Adjacency of two trigonal unit graphs.

metrically restricted. Every edge of the (A), (B), or (E) unit graph in Fig. 9 is equivalent by symmetry, but (C) or (D) has two kinds of edges. When two (A) graphs are adjacent, new sub-point and sub-lines are added along the arrow. The two rotational isomers of (A) were neglected here. All the possible geometries for a pair of adjacent unit graphs are shown in Fig. 10. As the unit graph (E) has less density, it can be used for the parent ligand graph only when it is surrounded with three unit graphs (D). Therefore, (E)-(E) adjacency is of no use, although possible geometrically.

Under these conditions, nine parent ligand graphs for the tetrahedral coordination are obtained, as is shown in the development diagrams in Fig. 11. They all have quite rigid cage structures in spite of being composed of three-membered carbon chains. If their metal chelates could ever be prepared, the cations would be spherical with a extreme stability and quite a hydrophobic nature.

Similar procedures can be applied to other polyhedral coordinations covered by any polygons other than a triangle when proper unit graphs for such polygon have been constructed. Furthermore, this method is also applicable to the polynuclear coordinations, since they are considered to be combined polyhedral coordinations.

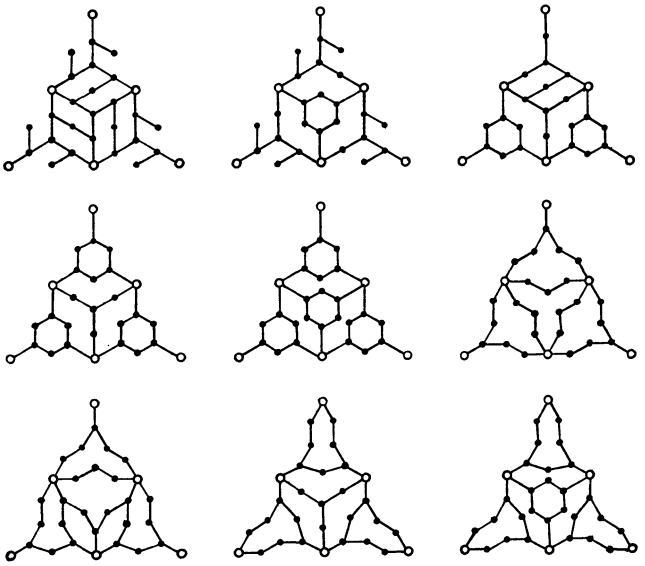

Fig. 11. Parent ligand graphs for the tetrahedral coordination.

The author wishes to express his thanks to professor Takeshi Iizuka of Gunma University and Mr. Nobuhide Tanaka of Gakushuin University for their valuable suggestions and discussions. The present work was partially supported by a Grant-in-Aid for Scientific Research from the Ministry of Education.

Reference

1) S. Takamoto, *Bull. Chem. Soc. Jpn.*, **52**, 2477 (1979).

Solution Properties of Phycocyanin. VI. The Characterization of the Phycocyanin Monomer†

Takahide Saito, Naomichi Iso,* Haruo Mizuno, Fumiaki Ozeki, and Yoshiyuki Matsui

Department of Food Science and Technology, Tokyo University of Fisheries, Konan, Minato-ku, Tokyo 108

(Received July 7, 1979)

The monomer molecular weight of phycocyanin was determined by sedimentation equilibrium measurements in 6 mol/l guanidine hydrochloride (GndCl) and by sodium dodecyl sulfate (SDS)–polyacrylamide gel electrophoresis. The former measurement gave the monomer molecular weight of 4.0×10^4. From the latter, the phycocyanin was found to be composed of two kinds of subunits, the molecular weights of which were 1.7×10^4 and 2.0×10^4. Assumimg that the phycocyanin monomer consists of two polypeptide chains, the molecular weight becomes 3.7×10^4. These values coincide with the value of 4.2×10^4 assumed in our previous works, which corresponds to one-sixth of the hexamer molecular weight. The sedimentation coefficient, s_{25w}, was 2.21 Svedberg unit, and the intrinsic viscosity in 6 mol/l GndCl was 19.5 ml/g, at 25.0 °C. From these values, it was clear that the phycocyanin monomer was unfolded in the solvent.

Phycocyanin, isolated from red- or blue-green algae, undergoes reversible self-associating reactions according to changes in the environment, such as in the pH, the ionic strength, the temperature, and the protein concentration of the solution.

In our previous papers,[1,2] we postulated, on the basis of the results of the sedimentation equilibrium measurements at various temperatures, that the dissociation-association behavior of phycocyanin could be explained by assuming a monomer⇌trimer⇌tetramer equilibrium system at pH 6.8 and the ionic strength (I) of 0.1. On the other hand, the dissociation-association of the same sample at pH 5.4 and I 0.1 was determined to follow a monomer⇌hexamer equilibrium system. The approach used in the estimation of the equilibrium constant from the centrifugal data requires the value of the monomer molecular weight, M_1. The molecular weight of the phycocyanin hexamer has been obtained as 2.56×10^5 from osmotic measurements at pH 5.4 and I 0.1.[3] However, the value of M_1 could not be determined in aqueous solutions because of the dissociation behavior in a lower-concentration region and because of the association behavior in a higher-concentration region. Thus, the value of 4.2×10^4 was assumed for M_1 in the previous works; this value corresponds to one-sixth of the value of 2.56×10^5 for hexamer.

This work was undertaken in order to decide the molecular weight of the phycocyanin monomer experimentally. For this purpose, two methods were employed; sedimentation equilibrium measurements in 6 mol/l guanidine hydrochloride (GndCl) and the sodium dodecyl sulfate (SDS)–polyacrylamide gel electrophoresis. Moreover, the sedimentation coefficient and the intrinsic viscosity were measured in 6 mol/l GndCl.

Experimental

Protein Preparation. The crystalline phycocyanin from *Porphyra tenera* used in this study was isolated and purified as has been described previously.[4] The proper amount of GndCl was dissolved in phycocyanin phosphate buffer solution, the pH of which was 6.8 and with I value of 0.1. The solution was dialysed against a GndCl–phosphate buffer (pH 5.4, I 0.1) at 5 °C for 72 h. The concentration of GndCl in the external solution was then adjusted to be the same as that of the phycocyanin solution. The external solution was used as a solvent in this work.

Sedimentation Equilibrium Measurements. The sedimentation equilibrium experiments were performed with a Hitachi Model UCA-1 ultracentrifuge using interference optics. The rotor speed was set at 19780 rpm, and the temperature was maintained at 25.0 °C. All the runs were made at that speed for approximately 24 h so as to ensure that an equilibrium was established in a liquid column of 1.5 mm. Since the solution has a blue color, it was difficult to decide the fringe numbers at the cell bottom exactly. Therefore, the Nazarian method[5] was used for the determination of the molecular weight from sedimentation interference patterns. According to the Nazarian method, the apparent molecular weight, M^a, is given by the following equation:

$$M^a = \frac{2RT}{(1-\bar{v}\rho)\omega^2}\frac{\mathrm{d}\ln \Delta_Q J}{\mathrm{d}(r^2)},$$

where R is the gas constant; T, the absolute temperature; $\bar{v}$, the partial specific volume of the solute; ρ, the density of the solvent; ω, the angular velocity of rotation, and r, the radial distance from the axis of rotation. $\Delta_Q J$ is the displacement of a fringe in the distance of the fixed Q and indicates the number of fringes crossed in traversing the interference pattern from r^2 to r^2+Q.

Sedimentation Velocity Measurements. The sedimentation velocity experiments were performed with the same ultracentrifuge as was used in the sedimentation equilibrium experiments, although Schlieren optics were used instead of the interference optics in those measurements. In all runs the rotor speed was set at 51200 rpm, and the temperature was maintained at 25.0 °C. The synthetic boundary cell was used, since the actual sedimentation rates of the solute were quite slow in 6 mol/l GndCl. The sedimentation coefficient, s, is represented by the following equation:

$$s = \frac{\ln(r_p/r_m)}{\omega^2(t-t_0)},$$

where r_p is the boundary position measured from the second moment of the refractive index gradient; r_m, the position of the meniscus; t, the time, t_0, the initial time correction.

Partial Specific Volume. The partial specific volume of phycocyanin in 6 mol/l GndCl was calculated by the

† Some of the experimental results in this paper were presented at the 28 th Annual Meeting of The Society of Polymer Science, Japan, Tokyo, May 1979.

usual method from the densities of the solvent and solutions at 25.0 °C; using the solvent density of 1.1426 g/ml, the value of 0.746 ml/g was thus obtained. The densities were measured with a Shibayama Densimeter, SS-D-200 Ext. Type.

SDS-Polyacrylamide Gel Electrophoresis. The SDS–polyacrylamide gel electrophoresis was done by the Weber-Osborn procedure.[6] The phycocyanin sample was incubated at 37 °C for 2 h in a 0.01 M sodium phosphate buffer, 1% in SDS, and 1% in 2-mercaptoethanol. The gel buffer was a 0.1 M sodium phosphate–1% SDS solution. Electrophoresis was performed at a constant current of 8 mA per gel. The proteins used as the references were obtained from Boehringer Marnheim: cytochrom C (molecular weight M=12500), chymotrypsinogen A (M=25000), ovalbumin (M=45000), and bovine serum albumin (M=67000).

Viscosity Measurements. The viscosity measurements were made with an Ubbelohde dilution-type viscometer. Kinetic energy corrections were not made. The intrinsic viscosity was obtained by using Huggins' equation.

Results and Discussion

Figure 1 shows the absorption spectra of phycocyanin at various concentration of GndCl. From Fig. 1, the denaturation of phycocyanin may be considered to be complete in a 1 mol/l GndCl solution. On the basis of these results, the concentration of GndCl of 6 mol/l was used in the sedimentation measurements and the viscosity measurements in this work.

Figures 2 and 3 show the results of the sedimentation equilibrium measurements. Plot of ΔJ (the displacement of a fringe) *versus* r^2 is shown in Fig. 2. The $\Delta_Q J$'s were estimated by selecting the Q value of 1 cm^2; they are plotted against r^2 in Fig. 3. As is shown, the plot is linear, and the apparent molecular weight, M^a can be estimated from the slope of the plot. As Ohta and Kawahara[7] have pointed out, the monodispersity of the solute cannot be decided even if the Nazarian plot is linear, and the molecular weight thus calculated is the z-average molecular weight in the case of a polydisperse solute. In this work, the sample was assumed to be monodiperse in the denaturated solvent. The reciprocals of M^a thus obtained are plotted against the protein concentration, c, in Fig. 4. The true molecular weight of the phycocyanin monomer could be estimated by the linear extrapolation of the plot to infinite dilution; the molecular weight of 4.0×10^4 was obtained. In previous studies, the monomer molecular weight was assumed to be 4.2×10^4, a value arrived at on the basis of the results of the osmotic measurements performed at pH 5.4 and I 0.1; this value was about one-sixth of the molecular weight of the phycocyanin hexamer. The assumed value coincides with the value of 4.0×10^4 obtained in this work.

The results of the SDS–polyacrylamide gel electrophoresis are shown in Fig. 5. The mobility, R_f, was calculated by using the following equation:

$$R_f = \frac{\text{distance of protein migration}}{\text{length after destaining}} \times \frac{\text{length before staining}}{\text{distance of dye migration}}$$

The electrophoresis pattern of the phycocyanin sample

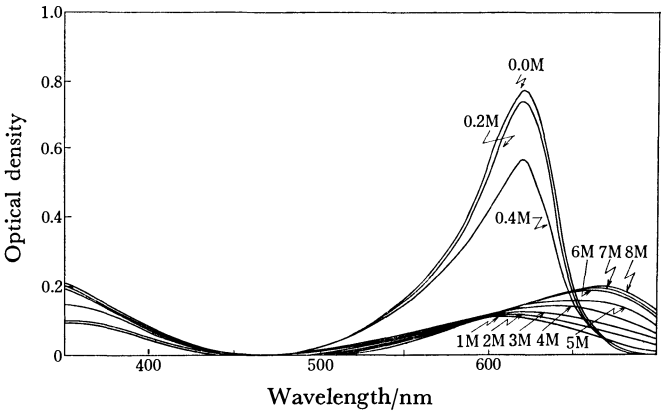

Fig. 1. The absorption spectra of phycocyanin at various concentrations of GndCl.

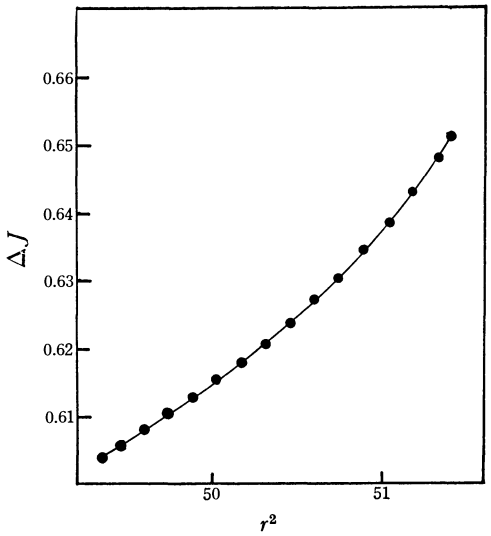

Fig. 2. A plot of ΔJ *versus* r^2, c=0.0654 g/dl.

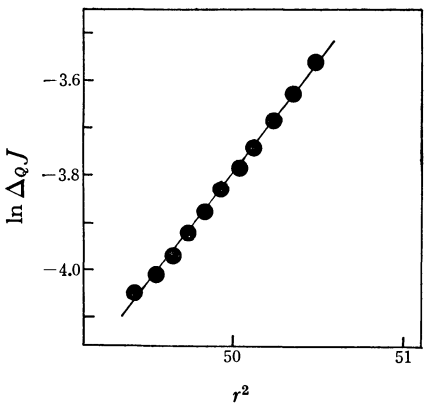

Fig. 3. A plot of log $\Delta_Q J$ *versus* r^2, c=0.0654 g/dl.

shows two bands, the quantities of which are nearly equivalent. Several investigators have reported that the phycocyanin monomer consisted of two kinds of subunits. For example, Glazer and Fang[8] reported that the phycocyanin from a blue-green alga (*Synechococcus sp.*) was composed of an α subunit (molecular weight, 1.77×10^4) and a β subunit (molecular weight, 1.9×10^4). The molecular weights of the two kinds of

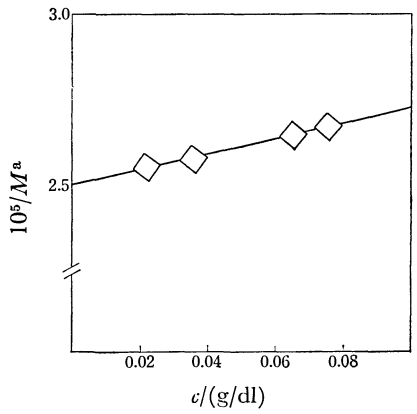

Fig. 4. A plot of $1/M^a$ *versus* c.

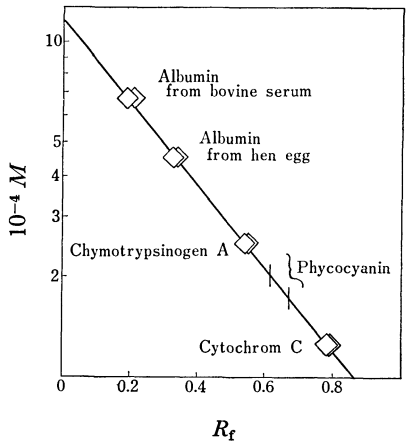

Fig. 5. A plot of M *versus* R_f.

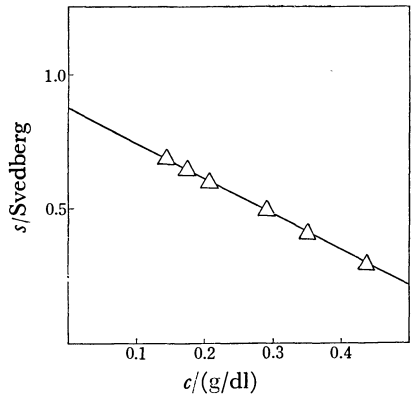

Fig. 6. A plot of s *versus* c.

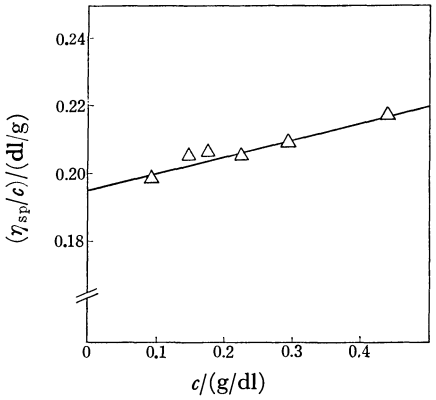

Fig. 7. A plot of η_{sp}/c *versus* c.

subunits in this work were calculated to be 1.7×10^4 and 2.0×10^4 on the basis of the data in Fig. 5. Assuming that the phycocyanin monomer is composed of two polypeptide chains, the molecular weights of which are 1.7×10^4 and 2.0×10^4, the molecular weight of the monomer becomes 3.7×10^4. The value of 3.7×10^4 corresponds to the value of 4.0×10^4 obtained by the sedimentation equilibrium measurements. The results show that the assumption that the phycocyanin monomer is composed of the two subunits is reasonable. In view of the fact that the sedimentation equilibrium measurements form an absolute method for the determination of the molecular weight, the monomer molecular weight of the phycocyanin should be 4.0×10^4.

The hydrodynamic measurements, sedimentation velocity measurements and viscosity measurements will be described below.

All of our sedimentation velocity patterns showed a single peak. Figure 6 shows the sedimentation coefficient of phycocyanin as a function of the protein concentration. From Fig. 6, the values of the sedimentation coefficient at an infinite dilution, s_0, and the concentration-dependence coefficient, k_s, were determined to be 0.88 S (Svedberg unit) and 1.53 respectively. The value of s_{25w}, the s-value in water at 25 °C, was calculated to be 2.21 S by the usual method.

The viscosity data for phycocyanin in 6 mol/l GndCl at 25.0 °C are shown in Fig. 7. The intrinsic viscosity, $[\eta]$, was determined by the linear extrapolation of the plot of η_{sp}/c, where η_{sp} is the specific viscosity and where c is the concentration of phycocyanin. From this extrapolation, the values of $[\eta]$ and of the Huggins' constant, k', for the phycocyanin monomer in 6 mol/l GndCl at 25.0 °C were found to be 19.5 ml/g and 1.29 respectively.

The Scheraga and Mandelkern parameter, β, was calculated by means of the following equation;

$$\beta = \frac{N_A s[\eta]^{1/3}\eta_0}{M^{2/3}(1-\bar{v}\rho)},$$

where N_A is the Avogadro number and η_0, the solvent viscosity (1.481×10^{-2} poise). The β-value of 2.6×10^6 was obtained for the phycocyanin monomer in 6 mol/l GndCl. Jennings[9] proposed a monomer model which was a prolate ellipsoid 35 Å in diameter and 105 Å in length. On the basis of this monomer model, the s- and $[\eta]$-values have been calculated to be 3.5 S and 4.2 ml/g respectively.[3] Using the s- and $[\eta]$-values, 2.0×10^6 is calculated for the β-value. The discrepancy of the β-values may be attributed to the fact that the conformation of the phycocyanin monomer in 6 mol/l GndCl was different from that of the monomer model proposed by Jennings; that is, the protein in 6 mol/l GndCl can be considered to be unfolded and to be expanded hydrodynamically.[10]

Rererences

1) N. Iso, H. Mizuno, T. Saito, N. Nitta, and K. Yoshizaki, *Bull. Chem. Soc. Jpn.*, **50**, 2892 (1977).

2) T. Saito, N. Iso, H. Mizuno, and I. Kitamura, *Bull. Chem. Soc. Jpn.*, **51**, 3471 (1978).
3) A. Kotera, T. Saito, N. Iso, H. Mizuno, and N, Taki, *Bull. Chem. Soc. Jpn.*, **48**, 1176 (1975).
4) T. Saito, N. Iso, and H. Mizuno, *Bull. Chem. Soc. Jpn.*, **47**, 1375 (1974).
5) G. M. Nazarian, *Anal. Chem.*, **40**, 1766 (1968).
6) K. Weber and M. Osborn, *J. Biol. Chem.*, **244**, 4406 (1969).
7) K. Ohta and K. Kawahara, *Tanpakushitsu Kakusan Koso*, **23**, 1002 (1978).
8) A. N. Glazer and S. Fang, *J. Biol. Chem.*, **248**, 659 (1973).
9) B. R. Jennings, *Biopolymers*, **6**, 1177 (1965).
10) C. Tanford, K. Kawahara, and S. Lapanje, *J. Am. Chem. Soc.*, **89**, 729 (1967).

Reflection Spectrum of the Single Crystal of Wurster's Blue Perchlorate

Yasushi Iyechika, Kyuya Yakushi, and Haruo Kuroda*

Department of Chemistry, Faculty of Science, The University of Tokyo, Hongo, Bunkyo-ku, Tokyo 113

(Received July 9, 1979)

The visible and near-infrared reflection spectrum of the single crystal of Wurster's blue perchlorate was measured at various temperatures over the range of 30—300 K, by using the microspectrophotometric method. The absorption spectra were derived by Kramers-Kronig transformation of the reflection spectra. The intensity ratio of the (0-0) and (0-1) vibronic bands of the local-excitation associated with the π-π^* ($^2B_{1u} \leftarrow {}^2B_{2g}$) transition of $TMPD^+$ was found to be anomalous when the spectrum was measured with the light polarized parallel to the b-axis, while not in the spectrum polarized parallel to the a-axis. The Davydov splitting between B_{3u} and B_{2u} components of this absorption band was found to be about 400 cm^{-1}. In the antiferromagnetic (low temperature) phase below 190 K, the charge-transfer band appeared in the a-axis spectrum, showing its absorption maximum at 11.6×10^3 cm^{-1}, and its intensity increased on lowering the temperature. At the same time, a marked temperature dependence was observed in the local-excitation band. These changes are interpreted in terms of the singlet-triplet model of the dimeric interaction of $TMPD^+$ ions in the low-temperature phase.

N,N,N',N'-Tetramethyl-*p*-phenylenediamine perchlorate (Wurster's blue perchlorate, WBP) is a well-known example of stable cation radical salts, of which magnetic behaviors have been extensively studied.[1-8] This salt exhibits a phase transition between the paramagnetic (high-temperature) phase and the antiferromagnetic (low-temperature) phase, the specific heat peak corresponding to this phase transition having been observed at 189.9 K.[9] The temperature dependence of the spin susceptibility in the low-temperature phase was interpreted in terms of the singlet-triplet model assuming a dimeric interaction of the cation radical of *N,N,N',N'*-tetramethyl-*p*-phenylenediamine (TMPD).[3] This model was also shown to be consistent with the change of the absorption spectrum of WBP powder at low temperatures.[8,10] The dimeric arrangement of $TMPD^+$ ions was confirmed later by de Boer and Vos from the crystal structure analysis of the low-temperature phase of WBP.[11]

The optical properties of WBP crystal have been previously studied by several authors.[8,10,12-15] The polarized absorption spectrum of WBP crystal at room temperature was observed some years ago by Sakata and Nagakura[8] and by Tanaka and Mizuno,[13] both by employing a microspectrophotometric method for the observation of transmission spectrum. The polarized absorption spectrum of the low-temperature phase and its temperature dependence were studied in our laboratory also by use of a microspectrophotometer for transmission spectroscopy of small single crystal.[15] Although several important aspects have been revealed by those studies, the absorption spectra which were reported in these works, are not very satisfactory in the following respects: First, the resolutions of the spectra were not high enough to reveal the details of absorption bands, and, second, there remained some ambiguities as regards the crystallographic characters of the crystal faces on which the observations were carried out. The reflection spectrum of a crystal offers informations complementary to those obtainable from the absorption spectrum observed by transmission method, and, furthermore, in the case of a strongly-absorbing crystal like WBP, the reflection spectroscopy has several experimental advantages over the observation of transmission spectrum. The preliminary study of the reflection spectrum of WBP at low temperatures was carried out earlier by Anderson,[14] who made the observation on a mosaic arrangement of needle crystals of WBP without making any attempt to identify the crystallographic characters of the observing crystal faces.

In the present study, we constructed an apparatus to measure the polarized reflection spectrum of a single crystal of microscopic size at low temperatures, incorporating a cryostat with a microspectrophotometer for reflection spectroscopy. Using this apparatus, we have studied the polarized reflection spectrum of WBP crystal and its temperature dependence over the temperature range of 30—300 K.

Experimental

Material. WBP was prepared according to the method reported by Michaelis and Granick.[16] Small single crystals of WBP were grown by slowly cooling a hot methanol solution of WBP. The crystals thus obtained were either a needle having (011) crystal face, or a plate with the developed face of (001).

Microspectrophotometer and Cryostat. The reflection microspectrophotometer used in the present study, is the same as the one which was previously constructed and used by us to study the reflection spectrum of benzidine-TCNQ complex. The details of this apparatus were described in our previous paper.[17] The optical system of Olympus MMSP is used as the reflection microscope optical system of this apparatus. In order to carry out the measurement at low temperatures, we took off the rotatable sample stage of the microspectrophotometer and installed a cryostat as shown in the photograph of Fig. 1.

The main body of the cryostat is a cryogenic refrigerator, CTi SPECTRIM^{tm}, made by Cryogenic Technology Inc. It is horizontally supported on a specially designed stage with a mechanism to adjust its position in three directions X, Y, and Z, with an accuracy of 10 μ. At the cold head of the refrigerator, we installed the sample-holding device which is illustrated in Fig. 2. The sample crystal is fixed on a miniature goniometer head, so that we can adjust the crystal orientation with respect to the optical axis. The crystal is cooled by means of the heat conduction through the goniometer head and the copper block on which the former is fixed. The temperature is controlled by adjusting the current of the electric heater installed at the cold head, and measured with a Au(Fe)–chromel thermo-couple fixed at the goniometer head. For the purpose of the radiation

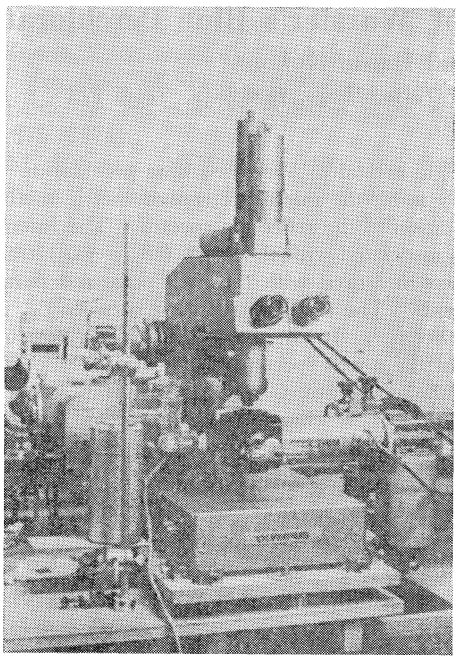

Fig. 1. Photograph of the microspectrophotometer with a low-temperature cryostat.

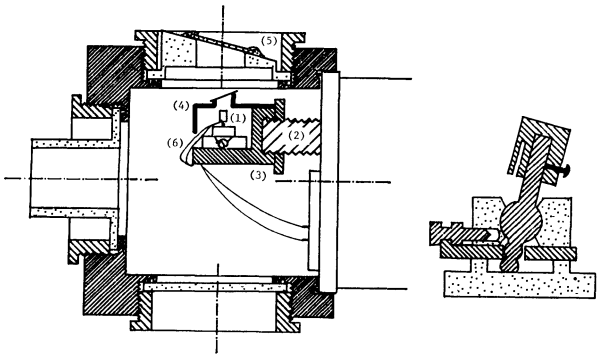

(a) (b)

Fig. 2. Schematic drawing of the sample-holding system: (a) Cross-section view of the sample chamber of the cryostat: (1) goniometer head, (2) cold head of the cryostat, (3) a copper block to support the goniometer, (4) a copper cup with a quartz window, (5) a quartz window, (6) thermo-couple.
(b) Structure of the miniature goniometer head.

shield and to avoid the water condensation on the crystal faces, we put a copper cup with a quartz window over the goniometer head. The face of the window is tilted from the horizontal plane by 30° to avoid the disturbance arising from the light reflection at the window. The system described above is covered with a vacuum-tight cover, and the inside of the above sample chamber was evacuated by the combined action of a rotary vacuum pump and a sorption pump. The pressure measured without the operation of the cryogenic refrigerator was about 5×10^{-5} Torr. Under the operation of the refrigerator, the pressure must be appreciably lower than the above value because of the cryogenic-pumping action of the cold head.

In the present study, we used an objective lens of the magnification of $\times5$. We had to use this lens of rather low magnification because of the requirement of a long working distance due to the geometry of our cryostat. The smallest size of the crystal face that can be used for the measurement of reflection spectrum, is 0.18 mmϕ under the condition adopted in the present study. The aperture angle of the used objective lens is 5.8°, so that we can safely treat the observed reflectance data as those obtained under the normal incidence condition.[18]

Analysis of Reflection Spectrum. Two different methods were employed in the present study to obtain optical constants from the measured reflectance data. The one was the dispersion analysis method (or curve-fitting method). In this case, we express the complex dielectric function as follows,

$$\varepsilon(\omega) = \varepsilon_c + \sum_j \frac{S_j\omega_j^2}{(\omega_j^2-\omega^2)-i\gamma_j\omega_j\omega} \tag{1}$$

and look for the parameter set, ε_c and (ω_j, γ_j, S_j), which gives the best agreement between the observed and calculated reflectance, using the following relation between the reflectance $R(\omega)$ and the complex dielectric function $\varepsilon(\omega)$.

$$R(\omega) = \frac{|\varepsilon(\omega)|+1-2\{|\varepsilon(\omega)|+\mathrm{Re}[\varepsilon(\omega)]\}^{1/2}}{|\varepsilon(\omega)|+1+2\{|\varepsilon(\omega)|+\mathrm{Re}[\varepsilon(\omega)]\}^{1/2}} \tag{2}$$

The optical constants, $n(\omega)$ and $k(\omega)$ of the crystal, can be obtained from $\varepsilon(\omega)$ by the following relations

$$\mathrm{Re}[\varepsilon(\omega)] = n(\omega)^2 - k(\omega)^2 \tag{3}$$

$$\mathrm{Im}[\varepsilon(\omega)] = 2n(\omega)k(\omega) \tag{4}$$

The details of the procedure of this analysis has been described in our previous paper.[17] The second method was the Kramers-Kronig analysis. To perform a direct Kramers-Kronig transformation, we need to know the reflectance over a very wide frequency range. However, our measurement of reflection spectrum was limited only in the near-infrared and visible region. Therefore, instead of carrying out a direct Kramers-Kronig transformation, we used the modified method which was proposed by Ahrenkiel.[21] This method was able to be successfully used in the present case. In order to see the spectrum corresponding to the absorption spectrum, we plotted the imaginary part of the complex dielectric constant, Im[$\varepsilon(\omega)$] against the frequency or wave number.

The method of obtaining the oscillator strength of an absorption band was as follows. In the case of dispersion analysis, we used one dispersion term.

$$\varepsilon_{[j]}(\omega) = S_j\omega_j^2/[(\omega_j^2-\omega^2) - i\gamma_j\omega_j\omega],$$

for each absorption bands.[19] Then the oscillator strength of the band (j) was calculated by the following equation.

$$f_{(j)} = \frac{m}{2\pi^2e^2N}\int_0^\infty \mathrm{Im}\,\varepsilon_{[j]}(\omega)\omega\,\mathrm{d}\omega,$$

where N is the number density of electrons concerned with the j-th transition, m is the electron mass, and e is the electron charge.

In the case of Kramers-Kronig analysis, the oscillator strength was calculated as follows,

$$f_{(j)} = \frac{m}{2\pi^2e^2N}\int_{\omega_a}^{\omega_b}\varepsilon_2(\omega)\omega\mathrm{d}\omega$$

where ω_a and ω_b are the low- and high-wave number limits of the concerned band. When absorption bands are overlapping on each other, there remains some arbitrariness as regards their decomposition. This gives a slight uncertainty of the oscillator-strengths of decomposed bands.

Results and Discussion

Spectrum at Room Temperature. The crystal of

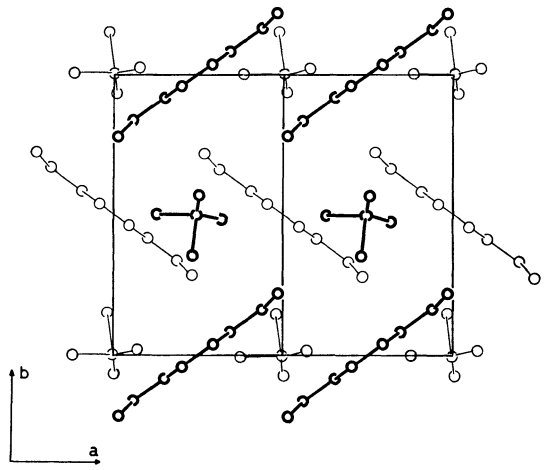

Fig. 3. Projection of the crystal structure of the high-temperature phase of WBP onto the (001) plane.

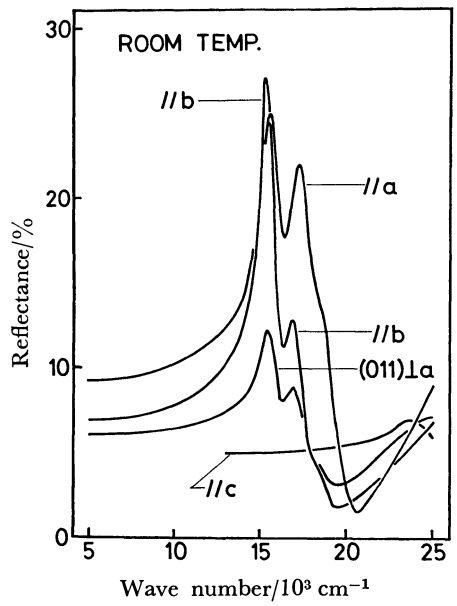

Fig. 4. Room-temperature reflection spectra observed on the (001), (011) and (010) crystal faces.

WBP is orthorhombic with the space group Pnnm, and the lattice constants, $a=5.956$ Å, $b=10.229$ Å, and $c=10.187$ Å.[11] Two molecular units of $TMPD^{+}\cdot ClO_4^{-}$, which are mutually related by the symmetry operation of a glide plane, are contained in the unit cell. The projection of the crystal structure, reported by de Boer and Vos,[11] is reproduced in Fig. 3.

Figure 4 shows the reflection spectra measured on the (001) face for the //a and //b polarizations and those measured on the (011) face for the //a and $\perp$a polarizations. A prominent dispersion of reflectance appears in the region of 13×10^3—20×10^3 cm^{-1}. This is the region where the absorption band due to the lowest π-π^* transition ($^2B_{1u}\leftarrow{}^2B_{2g}$) of $TMPD^{+}$ ion appears in the solution spectrum of WBP. The polarization direction which gives the strongest dispersion, agrees with the one that is expected for the local excitation band associated with the $^2B_{1u}\leftarrow{}^2B_{2g}$ transition which has its transition moment parallel to the long molecular axis. Below 14×10^3 cm^{-1}, the observed

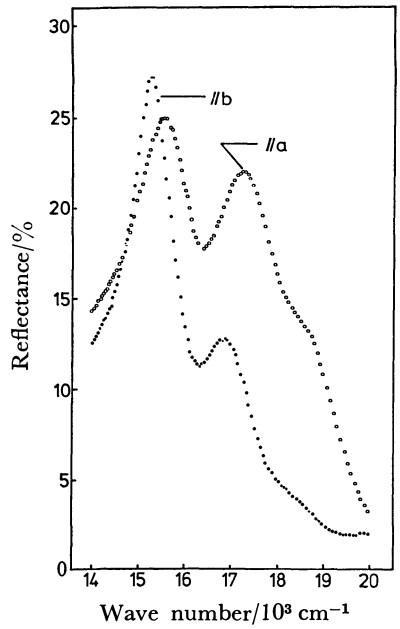

Fig. 5. Reflection spectra measured with 1.6 nm resolution at room temperature.

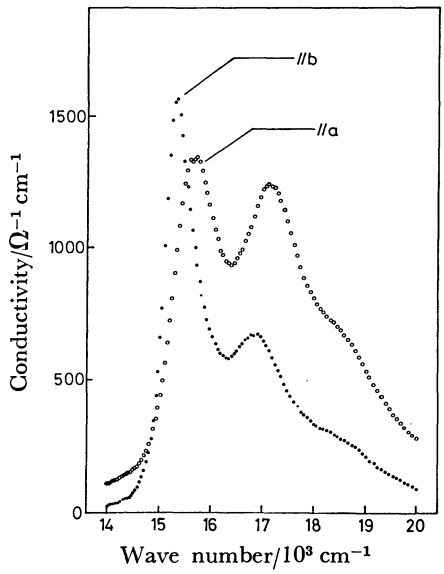

Fig. 6. Optical conductivity spectra obtained by the Kramers-Kronig transformation of the reflection spectra shown in Fig. 5.

reflection spectra show no distinct dispersion except a slight indication of the presence of a shoulder on the low-wave number tail of the //a spectrum of the (011) face, although a dispersion clearly appears around 11×10^3 cm^{-1} in the //a reflection spectrum observed at low temperatures as we will show later. The shape of the //a reflection spectrum which was reported by Anderson,[14] resembles to our //a spectrum of the (011) face, but the reflectance values reported by him, are significantly lower as compared with those obtained in the present study. This is naturally expected since his data were obtained on a mosaic arrangement of needle crystals, not on a good single crystal.

In order to reveal the details of the structure ap-

TABLE 1. OBSERVED WAVE NUMBERS AND OSCILLATOR STRENGTHS OF THE VIBRONIC BANDS IN THE LE BAND OF THE SPECTRUM OF WBP

Polarization direction	$\cos^2\theta$[a]	(0-0)band		(0-1)band		(0-2)band		f_t[b]
		$\bar{\nu}_{max}/cm^{-1}$	f	$\bar{\nu}_{max}/cm^{-1}$	f	$\bar{\nu}_{max}/cm^{-1}$	f	
// a	0.643	15800	0.24	17380	0.24	shoulder	≈0.1	0.61
// b	0.357	15430	0.19	16980	0.13	shoulder	≈0.05	0.38
// c	0.000	—	0.00	—	0.00	—	0.00	0.00
		($\Delta\bar{\nu}$[c]) = 370 cm^{-1}		400 cm^{-1}		—)		
Solution		16300	0.05	17700	0.06	shoulder	≈0.03	0.16

a) Squares of the direction cosines of the long axis of $TMPD^+$ ion to the crystallographic axes. b) Total oscillator strength. c) Splitting between the //a and //b bands ($\Delta\bar{\nu}=\bar{\nu}_{max}(//a)-\bar{\nu}_{max}(//b)$).

pearing in the reflection spectrum, we carried out the measurement with an increased resolution over the region from 14×10^3 cm^{-1} to 20×10^3 cm^{-1} [20]. The results are shown in Fig. 5. Figure 6 shows the optical conductivity spectra† which were obtained by the Kramers-Kronig transformation of the reflectance data given in Fig. 5. As we have already mentioned, the absorption band appearing here can be safely attributed to the local excitation (LE) associated with the $^2B_{1u}\leftarrow{}^2B_{2g}$ transition of $TMPD^+$. The obtained optical conductivity spectra resemble to the solution spectrum of $TMPD^+$ ion, having the vibrational progression of about 1530 cm^{-1} which can be attributed to an intramolecular vibration of $TMPD^+$. We decomposed the observed absorption band into vibronic bands, and estimated the oscillator strength of each vibronic band. The results are given in Table 1, together with the corresponding values of the solution spectrum. In Table 1, we give also the total oscillator strength f_t and the square of the direction cosines of the long molecular axis of $TMPD^+$ with respect to the a- and b-axes. The ratio of the observed oscillator strengths, $f_t(//b)/f_t(//a)=0.63$, is in good agreement with the value, 0.56, that is expected on the basis of the oriented-gas model. This is in accord with what one can expect for a LE band due to a strong, long-axis polarized transition of $TMPD^+$ ion. In the case of this absorption band, a deviation of the oscillator-strength ratio $f_t(//b)/f_t(//a)$ from the oriented-gas value, could arise either from the crystal-induced mixing of some intramolecular transition which are polarized perpendicular to the long molecular axis, or from the mixing of an intermolecular charge-transfer (CT) transition. However, in WBP crystal, the mixing of a short-axis polarized transition of $TMPD^+$ with a long-axis polarized transition is forbidden by the site symmetry of $TMPD^+$. Although the n-π^* transition of $TMPD^+$ and the intermolecular CT transition between $TMPD^+$ ions could mix with the long-axis polarized transition of $TMPD^+$, the mixings of these transitions can not significantly affect the polarization ratio of the above LE band, because the oscillator strengths of the n-π^* and CT transitions are quite small in the present case.[22] As for the absolute value of oscillator strength, we note that the values determined from the //a and //b spectra of WBP crystal are about twice the oriented-gas values calculated by use of the oscillator strength of the $^2B_{1u}\leftarrow{}^2B_{2g}$ band of the solution spectrum of $TMPD^+$ ion.[23] Seemingly, this fact indicates that the oscillator strength of the above LE band has been significantly enhanced in WBP crystal. This enhancement of oscillator strength is likely to be due to the crystal-induced mixing of higher-energy, long-axis polarized, strong transitions of $TMPD^+$.

The most interesting aspect that can be noted in Fig. 6 (or in Table 1), is that the intensity ratio of the (0-0) and (0-1) vibronic bands is significantly different between the //a and //b optical conductivity spectra. The band shape in the //b spectrum is very much different from that of the solution spectrum, while the band shape in the //a spectrum resembles to the solution spectrum. In the //b spectrum, the (0-0) vibronic band is appreciably sharper and its intensity relative to the (0-1) vibronic band is significantly higher as compared with the solution spectrum. This phenomenon is similar to the *J*-band of the helix polymer of the pseudo-isocyanine dye, where the (0-0) band becomes sharp and markedly strong as compared with other vibronic bands when the spectrum is observed with the light polarized parallel to the direction of the helix.[24] This characteristic feature of *J*-band has been explained in terms of the collective excitation along the chain. A possible explanation for the shape of the LE band of WBP can be given from the consideration of the exciton-phonon coupling and the exciton band width. The shape of an absorption band of a molecular crystal was theoretically discussed by Sumi,[25] who showed by the model calculation that the intensity of an absorption band will be more and more concentrated into its (0-0) band on increasing the strength of the intermolecular interaction. He introduced two parameters, S and B, which are determining the band shape, S being the parameter related to the coupling between the electronic transition and the intramolecular vibration, and B being the one corresponding to the half-width of the exciton band. For a free molecule, the oscillator strength of the (0-n) vibronic band can be approximately given by Eq. 5.

† For the purpose to compare with the theoretical band shapes predicted by Sumi, we plotted here optical conductivity, not $\mathrm{Im}[\varepsilon(\omega)]$, against wave number. The optical conductivity was calculated from $\mathrm{Im}[\varepsilon(\omega)]$ by the following relation;

$$\sigma(\omega)=8.854\times10^{12}\omega\cdot\mathrm{Im}[\varepsilon(\omega)] \qquad [\Omega^{-1}\,cm^{-1}]$$

where $\mathrm{Im}[\varepsilon(\omega)]$ is expressed in c.g.s. units.

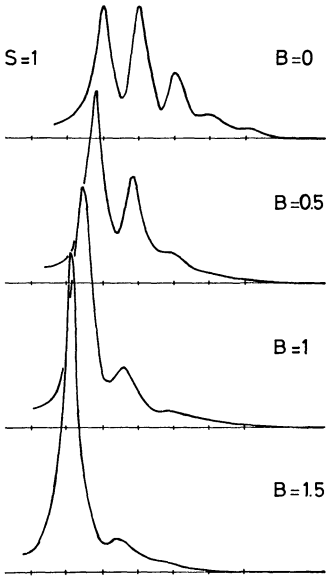

Fig. 7. Vibronic band shapes in optical conductivity spectra, theoretically predicted for various values of B, assuming that $S=1$. The spectra have been a little broadened than the original ones given in the paper by Sumi.[25]

$$f_{0-n} = A\frac{S^n}{n!}e^{-S} \tag{5}$$

When we apply the above relation to the $^2B_{1u}\leftarrow{}^2B_{2g}$ band of the solution spectrum of $TMPD^+$ ion, the S value is estimated to be 1.0 in the unit of a quantum of the intramolecular vibration.[26] Assuming that the same S value can be used for the corresponding LE band of WBP crystal, we compared the observed band shapes with the theoretical band shapes given by Sumi for different B values. The band shapes which are expected by Sumi's theory for the cases of $B=0$—1.5,[27] are illustrated in Fig. 7, where the width of each vibronic band has been a little broadened than the spectra given in Sumi's paper, for the purpose to compare with the observed spectra. When we compare the observed band shapes (Fig. 6) with the theoretical ones shown in Fig. 7, we can see that the observed band shape of the //b spectrum corresponds to the case of $B=0.5$—1.0 while that of the //a spectrum corresponds to the case of $B=0$—0.5.[27]

Since there are two sites of $TMPD^+$ in the unit cell, the exciton band associated with $^2B_{1u}$ molecular excited state splits into two bands, in which symmetries are B_{3u} and B_{2u}, respectively. The optical transition to B_{3u} exciton band is allowed for the a-axis polarized light, and that to B_{2u} exciton band is allowed for the b-axis polarized light. As shown in Table 1, the Davydov splitting of these two exciton states is about 400 cm^{-1}. The band shape analysis described above suggests that B_{2u} exciton band has a witdh of 1500—3000 cm^{-1} while B_{3u} exciton band has a considerably narrower band width, less than 1500 cm^{-1}.

Temperature Dependence of the Spectrum. WBP crystal undergoes a phase transition at about 190 K. The crystal of the low-temperature phase is monoclinic with the space group $B2_1/d$, the lattice constants being

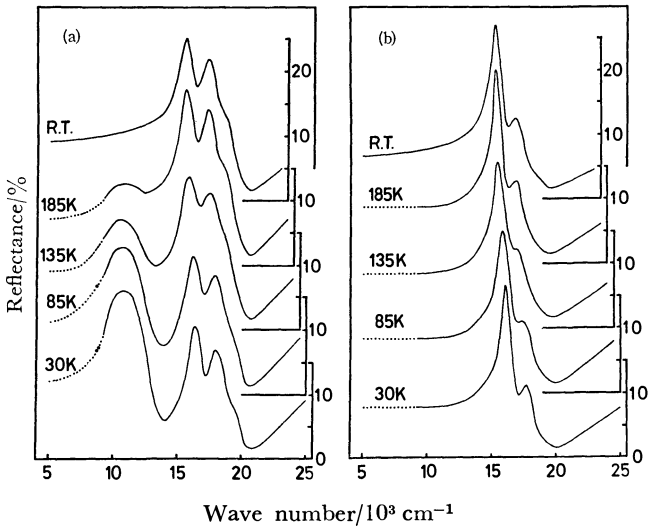

Fig. 8. Low-temperature reflection spectra of WBP. (a) //a spectra, (b) //b spectra.

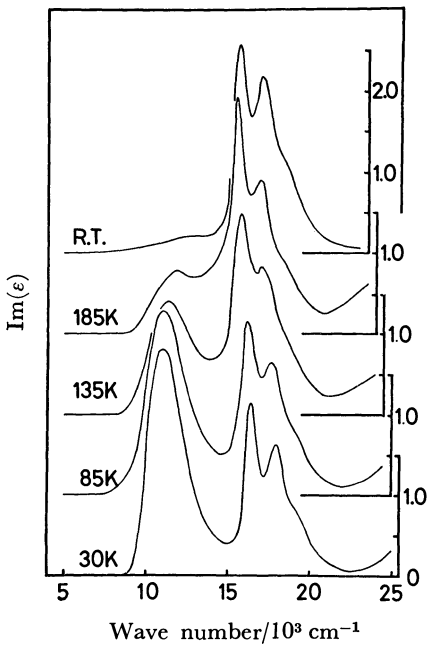

Fig. 9. $Im[\varepsilon(\omega)]$ spectra (//a) obtained by the Kramers-Kronig transformation of the reflection spectra shown in Fig. 8.

$a=11.655$ Å, $b=10.147$ Å, $c=20.130$ Å, and $\beta=92.57°$ at 110 K.[11] As compared with the high-temperature phase, the lengths of the a- and b-axes are doubled in the low-temperature phase, and the unit cell contains eight molecular units of $TMPD^+\cdot ClO_4^-$. The $TMPD^+$ ions are stacked along the a-axis as in the high-temperature phase, but with an alternation of intermolecular spacing showing definitely the character of a dimeric arrangement. The reflection spectra measured for the //a and //b polarizations at various temperatures are shown in Fig. 8. It should be noted that, in the low-temperature phase, a new broad dispersion of reflectance appears in the region of 9×10^3—15×10^3 cm^{-1}, and its amplitude increases on lowering the temperature. This dispersion can be observed most

TABLE 2. TEMPERATURE DEPENDENCE OF THE OSCILLATOR STRENGTH OF THE CHARGE-TRANSFER BAND AND THE TRIPLET POPULATION ESTIMATED BY VARIOUS METHOD

T/K	Oscillator strength		Triplet population/%			
			CT band		Paramagnetism[c]	Calcd by S-T model[d]
	K-K[a]	C-F[b]	K-K	C-F		
185	0.10	0.32	77	49	45	32
135	0.23	0.44	48	29	21	19
85	0.38	0.59	14	5	5	5
30	0.44	0.62	0	0	0	0

a) Kramers-Kronig transformation method. b) Curve-fitting (dispersion analysis) method. c) Estimated from the magnetic susceptibility data reported by Okumura.[2] d) Calculated by the singlet-triplet model, assuming the S-T separation as 235 cm^{-1}.[3]

strongly when the light is polarized parallel to the a-axis which is the direction of the $TMPD^+$ stack, and is not observable when the light is polarized perpendicular to it. This fact indicates that the dispersion mentioned above is associated with the charge transfer between $TMPD^+$ ions. Figure 9 shows the $Im[\varepsilon(\omega)]$ spectra obtained by Kramers-Kronig transformation of the //a reflection spectra. The general features of the obtained $Im[\varepsilon(\omega)]$ spectra are very similar to the low-temperature spectrum of WBP powder reported by Sakata and Nagakura.[10] The first absorption band is the charge-transfer band, which is very broad and structureless even at 30 K, having its absorption maximum at 11.6×10^3 cm^{-1}. Sakata and Nagakura pointed out that there is a close correlation between the decrease of the paramagnetic susceptibility and the increase of the intensity of the charge-transfer band.[8,10] Assuming the dimeric arrangement in $TMPD^+$ chain, they concluded that there is a thermally accessible triplet state (T_0) of $TMPD^+$ dimer above the ground singlet state (S_0), and since the optical transition to the charge-transfer (singlet) state of the dimer is allowed only from S_0, the decrease of the intensity of the CT band must be proportional to the increase of the triplet population, hence to the spin concentration. From the analysis of the temperature dependence of the CT band, they derived 230 ± 50 cm^{-1} for the singlet-triplet separation of the $TMPD^+$ dimer, which was in good agreement with the value (≈235 cm^{-1}) determined by Thomas *et al.*[3] from ESR data. We determined the oscillator strength of the CT band at each temperature from the observed spectrum, and estimated the fraction of $TMPD^+$ dimers which are in the triplet state, assuming that the transition moment of the CT transition does not vary with temperature. The results are given in Table 2. The triplet population $N_t(T)$ derived from the paramagnetic susceptibility χ_H by means of Eq. 6 and that calculated by the singlet-triplet model assuming the singlet-triplet separation of 235 cm^{-1}, are also given in the same table.

$$\chi_H = \frac{g^2\beta^2S(S+1)}{3kT}\cdot N_t(T) \qquad (6)$$

As shown in Table 2, the results by Kramers-Kronig analysis and curve-fitting analysis are a little different from each other. Seemingly this disagreement arised

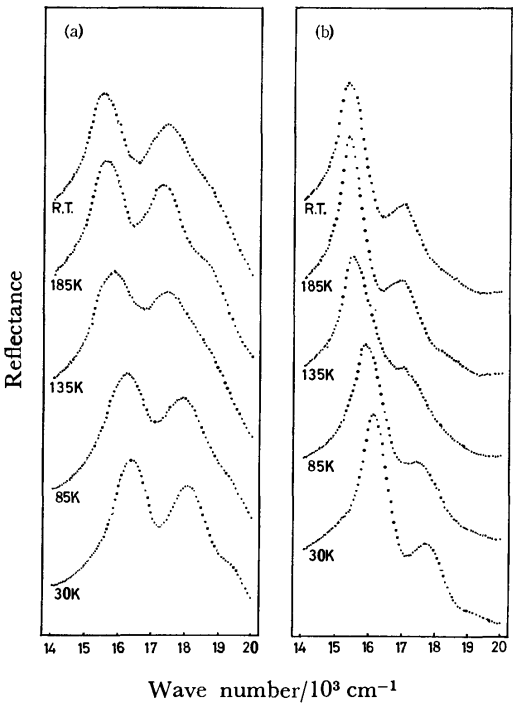

Fig. 10. Low-temperature reflection spectra, in the visible region, measured with 1.6 nm resolution.

from the inherent difficulty in determining the absolute value of oscillator strength from the reflectance data when an absorption band is very broad and weak as in the case of the CT band of WBP. No such discrepancy was found between the results of the two analysis methods in the case of the strong LE band of WBP crystal. The triplet population derived from the oscillator-strength values obtained by curve-fitting analysis, are in very good agreement with those derived from the paramagnetic susceptibility data. But this fact does not necessarily mean that the data by curve-fitting method are more reliable than those by Kramers-Kronig analysis, since the above agreement with the magnetic data looks too good if we take into account the situation that the transition moment of the CT excitation must vary to some extent with temperature accompanying the lattice contraction on lowering the temperature. Although there remains such a problem as regards the quantitative anaylsis of the

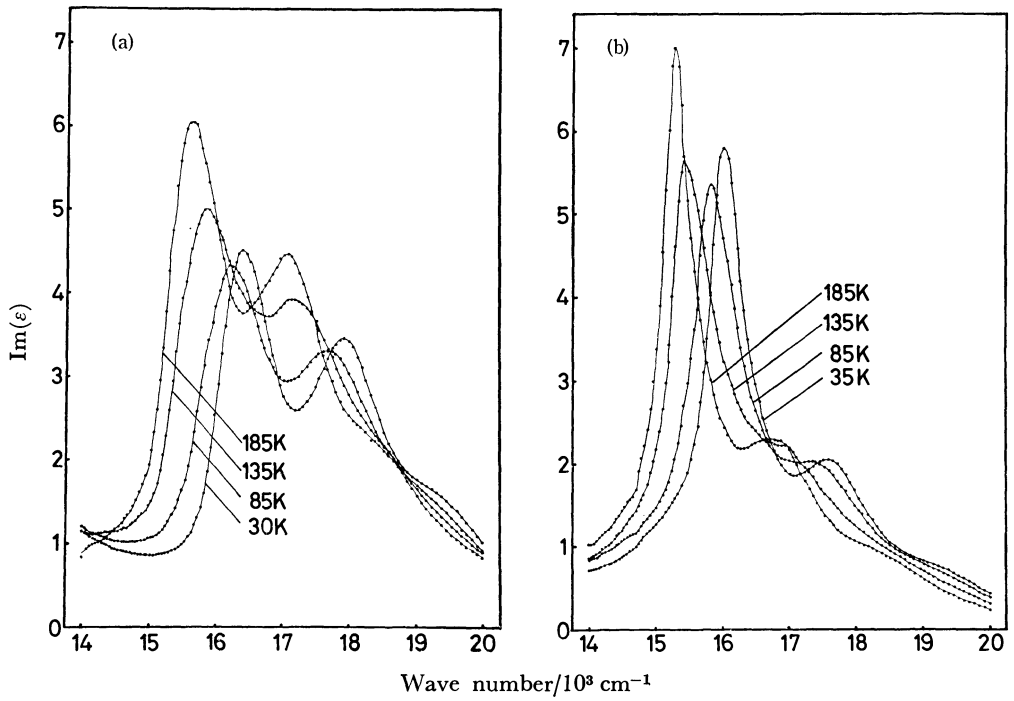

Fig. 11. Im[$\varepsilon(\omega)$] spectra obtained by the Kramers-Kronig transformation of the reflection spectra shown in Fig. 10: (a) //a spectra, (b) //b spectra.

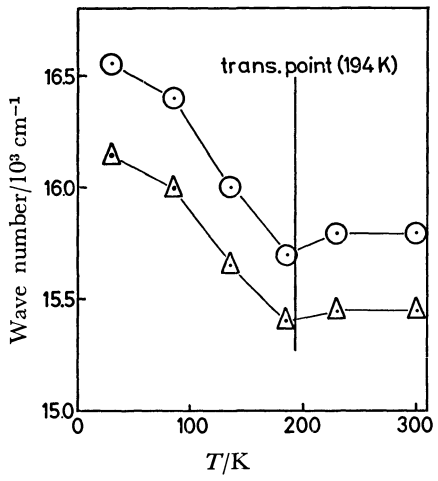

Fig. 12. Shift of the (0-0) band with temperature.

intensity change of the CT band, the results shown in Table 2 clearly indicate that the essential feature of the temperature dependence of the CT band can be well understood in terms of the singlet-triplet model as discussed by Sakata and Nagakura.[10] Incidentally, if we take up only the change, not the absolute value, of the oscillator strength with temperature, the results by the two analysis methods exactly agree with each other, and are also in good agreement with the data reported by Sakata and Nagakura for the spectrum of WBP powder.

The reflection spectrum in the region of 14×10^3—20×10^3 cm^{-1} was measured with an increased resolution, the resolution being 1.6 nm. The results are shown in Fig. 10. Figure 11 shows the Im[$\varepsilon(\omega)$] spectra obtained by Kramers-Kronig analysis of the above reflectance data. As we have mentioned in the case of the room-temperature spectrum, the absorption band appearing here is the LE band associated with the lowest π-π^* ($^2B_{1u}\leftarrow{}^2B_{2g}$) transition of TMPD$^+$. We can see three characteristic features of temperature dependence both in the //a spectrum and in the //b spectrum. The first is the shift of the absorption peaks with temperature. In Fig. 12, we plotted the wave number of the (0-0) band against temperature. One can clearly see that the position of the (0-0) band does not appreciably change with temperature in the high temperature phase, but is markedly blue-shifted on lowering the temperature in the low-temperature phase. The second is the change of the width of vibronic band. On lowering the temperature, the width gradually increases, shows the maximum broadness at 135 K, and then decreases at lower temperature. The third is the fact that the peak heights of the (0-0) and (0-1) bands gradually decrease on lowering the temperature from 185 K to 85 K and then increase at 30 K. In the case of a typical molecular crystal like anthracene, the (0-0) band shows a red-shift on lowering the temperature, the magnitude of this shift having been reported to be about 150 cm^{-1} between the room temperature and 4.2 K in the case of anthracene,[28] and usually the width of a vibronic band monotonously decreases on lowering the temperature. The temperature dependence observed for the LE band of WBP is very much different from the one mentioned above.

Examining the temperature dependence of the absorption spectrum of WBP powder, Sakata and Nagakura[10] reported that the spectra measured at different temperatures exhibited isosbestic points. They concluded that the singlet-singlet transition and the triplet-triplet transition of TMPD$^+$ dimer are overlapp-

ing on each other to give the observed LE band of the absorption spectrum of the powder, and the temperature dependence of its band shape can be understood by considering the thermal equilibrium between the singlet and triplet states of the dimer. The single-crystal spectra obtained in the present study show that the temperature dependence of the $\mathrm{Im}[\varepsilon(\omega)]$ spectrum of WBP crystal is, in reality, a little more complicated than described by the above authors. The observed spectra did not exhibit isosbestic points, so that it was not possible to carry out a simple quantitative analysis of the band shape in terms of the thermal equilibrium between the singlet and triplet states of $TMPD^+$ dimer. But the main feature of the observed temperature dependence can be understood, at least qualitatively, by the same model. As shown in Table 2, the triplet population becomes to be almost negligible at 30 K. Thus the band shape at 30 K can be regarded to be the one entirely due to the singlet-singlet transition, while, at higher temperatures, the band due to triplet-triplet transition is overlapping with the absorption band due to the singlet-singlet transition. Possibly, the band shape at just below the transition temperature is largely determined by the triplet-triplet absorption band. Seemingly this is the reason why the LE band is broader at intermediate temperatures. The shifts of absorption peaks and the change of the band shape suggest that the triplet-triplet absorption band is located at the wavenumber lower by 600—800 cm^{-1} than the singlet-singlet absorption band. We tried to reproduce the observed band shapes as the superposition of the singlet-singlet and triplet-triplet absorption bands, and found it necessary, in order to explain the observed band shapes, to consider that both the singlet-singlet and triplet-triplet absorption bands shift to higher wave number on lowering the temperature. This situation prevented us to carry out a further quantitative analysis of band shape, but we were able to conclude that the observed temperature dependence of the LE band is consistent with the change of the triplet population derived from the magnetic data or that from the intensity of the CT band.

The authors are grateful to Olympus Optical Co., Ltd. for their generous offer of the Olympus MMSP-RK system used in the present study. The authors wish to thank Dr. Koichi Ohno, Faculty of Education, The University of Tokyo, for helpful discussion.

References

1) W. Duffy, Jr., *J. Chem. Phys.*, **36**, 490 (1962).
2) K. Okumura, *J. Phys. Soc. Jpn.*, **18**, 69 (1963).
3) D. D. Thomas, H. Keller, and H. M. McConnell, *J. Chem. Phys.*, **39**, 2321 (1963).
4) H. J. Monkhorst and J. Kommandeur, *J. Chem. Phys.*, **47**, 391 (1967).
5) G. T. Pott and J. Kommandeur, *J. Chem. Phys.*, **47**, 395 (1967).
6) H. J. Monkhorst, G. T. Pott, and J. Kommandeur, *J. Chem. Phys.*, **47**, 401 (1967).
7) G. T. Pott, C. F. van Bruggen, and J. Kommandeur, *J. Chem. Phys.*, **47**, 408 (1967).
8) T. Sakata and S. Nagakura, *Bull. Chem. Soc. Jpn.*, **42**, 1499 (1969).
9) H. Chihara, M. Nakamura, and S. Seki, *Bull. Chem. Soc. Jpn.*, **38**, 1796 (1965).
10) T. Sakata and S. Nagakura, *Mol. Phys.*, **19**, 321 (1970).
11) J. L. de Boer and A. Vos, *Acta Crystallogr., Sect. B*, **28**, 835, 839 (1972).
12) Y. Iida, *Bull. Chem. Soc. Jpn.*, **41**, 2615 (1968).
13) J. Tanaka and M. Mizuno, *Bull. Chem. Soc. Jpn.*, **42**, 1841 (1969).
14) G. R. Anderson, *J. Chem. Phys.*, **47**, 3853 (1967).
15) K. Ishii, K. Kaneko, and H. Kuroda, *Bull. Chem. Soc. Jpn.*, **49**, 2077 (1976).
16) L. Michaelis and S. Granick, *J. Am. Chem. Soc.*, **65**, 1747 (1943).
17) K. Yakushi, M. Iguchi, and H. Kuroda, *Bull. Chem. Soc. Jpn.*, **52**, 3180 (1979).
18) The effect of aperture angle of objective lens was discussed in Ref. 17.
19) When the band exhibits a vibrational structure, we used one dispersion term for each vibronic band.
20) The resolution was 1.6 nm in these measurement.
21) R. K. Ahrenkiel, *J. Opt. Soc. Am.*, **61**, 1651 (1971).
22) Although the CT band appears with a considerable intensity the low-temperature spectrum of WBP crystal, it does not appear in the room-temperature spectrum.
23) In order to estimate those oriented-gas values of oscillator strength, we took three times of the observed oscillator sterngth of the corresponding absorption band of the solution spectrum.
24) J. S. Briggs and A. H. Herzenberg, *Mol. Phys.*, **21**, 865 (1971).
25) H. Sumi, *J. Phys. Soc. Jpn.*, **36**, 770 (1974); **38**, 825 (1975).
26) It is 1530 cm^{-1} in wave number.
27) The unit adopted here is the same as the one for the S value.
28) G. C. Morris and M. G. Sceats. *Chem. Phys.*, **3**, 164 (1974).

Electrophoresis and Diffusion Studies of the Solubilization of Polar and Nonpolar Oily Compounds with Sodium Dodecyl Sulfate. II

Keizo OGINO* and Nobuo TAKESHITA

Faculty of Science and Technology, Science University of Tokyo, 2641 Yamazaki, Noda, Chiba 278

(Received July 12, 1979)

The solubilization of polar and nonpolar oily materials into an aqueous sodium dodecyl sulfate (SDS) solution with and without sodium chloride was studied. Normal paraffins and their derivatives, with carbon numbers of C_7, C_8, and C_{10}, were used as solubilizates, the extents of solubilization, the relative viscosities of the solutions, the diffusion coefficients, and the electrophoretic mobilities of the micelles in the solutions were observed, and the effective specific volumes, the effective radii, the ζ-potentials, and the effective charge of the micelles were derived assuming that the micelles were spherical. The micelles of SDS showed increasing mobilities when they incorporated octanoic acid, 1-octanol, and decanoic acid, while the mobilities decreased when they incorporated heptane, octane and 1-decanol. On the basis of these results, we discussed the mechanism of the solubilization of polar and nonpolar oily compounds with SDS.

The behavior of the micelles of surfactants have been studied extensively by many investigators for SDS,[1] mixed ionic-nonionic surfactants,[2] polyether sulfate, and other surface-active agents,[3] but only a few investigations have been devoted to the micelles incorporating solubilizates in them.

In a previous paper[4] we observed the electrophoretic mobilities of micelles of SDS, $|U_M|$ in aqueous solutions, and showed that the $|U_M|$ increased with an increase in the concentration of octanoic acid and decreased with that of octane. We further studied the behavior of the micelles of SDS including polar or nonpolar oily materials in an aqueous medium in the presence or absence of electrolytes in order to elucidate the mechanisms of the solubilization of the oily materials. We suggest that strongly polar compounds are adsorbed on the outer surface, weakly polar compounds penetrate deeply into the palisade layers, and nonpolar compounds are occluded in the hydrocarbon cores of the micelles.

Experimental

Materials. *Surface-active Agent*: Sodium dodecyl sulfate (SDS) of a reagent grade was purchased and was purified by extraction with petroleum ether, followed by recrystallization from ethanol.

Solubilizates (Oily Materials): Octanoic acid, decanoic acid, 1-octanol, and 1-decanol were used as polar oily materials, and heptane and octane as nonpolar ones, all obtained in a purity of better than 99% from Wako Pure Chemical Industries.

Apparatus and Conditions. Sodium dodecyl sulfate was dissolved into a 0.2 M NaCl solution or into water at the concentrations of 0.3 and 1.5% (wt), which were higher than the critical micelle concentration (CMC) of SDS. The solubilization limits of the oily materials into the SDS solutions were determined as follows. Into 100-ml glass-stoppered Erlenmeyer flasks containing 50 ml of SDS solutions (0.3% and 1.5%), various amounts of one of the oily materials were added; the mixtures were stirred for 12 h at 25 °C and then left standing for 24 h until the solubilization equilibria were established. Then, the turbidities of the mixtures were measured with a spectrophotometer of the Hirama Type-2B at the wavelength of 655 nm. The turbidities of the solutions were plotted against the concentrations of the solubilizates, and the solubilization limits were determined from the break points of the relating curves. After that, the solubilizates were added until the solubilizing limit was reached and then submitted to dialysis by the use of cellulose tubing for 36 h at 25 °C.

The electrophoretic mobility and the diffusion coeffecient for the SDS solutions saturated with the oily materials were determined at 25 °C by a Schlieren method using a Hitachi Model HTB-2A Tiselius apparatus in combination with a Tsukasa Neurath cell, with the usual precautions.[2,3] The concentrations of both the upper and lower layers were chosen to be higher than the CMC in order to eliminate the contribution of the monomers to the diffusion coefficient; the initial concentration difference between layers was 1.2 g/dl. Then, a pair of 0.3 and 1.5% SDS solutions were set as the upper and the lower layers in the cell to minimize the boundary disturbance often encountered in electrophoresis and diffusion measurements. The electrophoretic measurements were performed under the following conditions: voltage the 50 V; current, 10 mA; migration time, 30—50 min. The calculation of diffusion coefficient was based on the maximum ordinate-area method.

The relative viscosities of the solutions containing the oily materials were measured at 25 °C with an Ubbelohde viscometer.

The specific gravity was determined using a pycnometer with a capacity of about 25 ml.

Results and Discussion

The Solubilized Amounts and the Susceptibilities to Solubilization. Figure 1 shows the solubilized amounts of the oily materials in the aqueous solutions of SDS with or without 0.2 M NaCl. The solubilized amounts widely changed according to the kinds of solubilizates in the aqueous solutions without NaCl, but it remained around a constant value in the presence of NaCl. The results also show that octanoic acid, 1-octanol, and decanoic acid are solubilized to greater extents, whereas 1-decanol, octane, and heptane are present to smaller extents in water than in 0.2 M NaCl solution. From the results presented in Fig. 1, the susceptibilities of the substances to the solubilization are determined as the moles solubilized by the mole of SDS in the solutions. The susceptibilities depend on the structures of the compounds much as they depend on the solubilized amounts. Klevens[5] found that the solubilized amounts of nonpolar compounds in aqueous surfactant solutions increased when electrolytes were added, and that some polar compounds

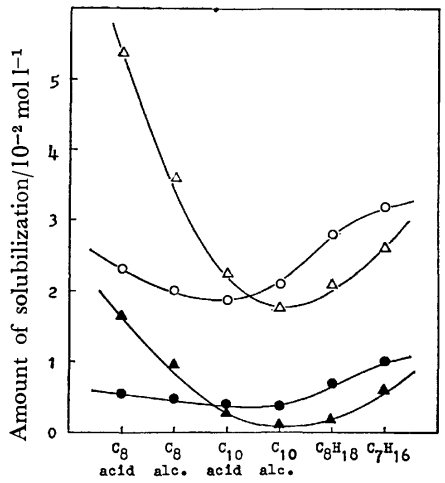

Fig. 1. Amount of solubilization in 0.2 M NaCl and pure water at 25 °C.
○: SDS 1.5% in 0.2 M NaCl, ●: SDS 0.3% in 0.2 M NaCl, △: SDS 1.5% in pure water, ▲: SDS 0.3% in pure water.

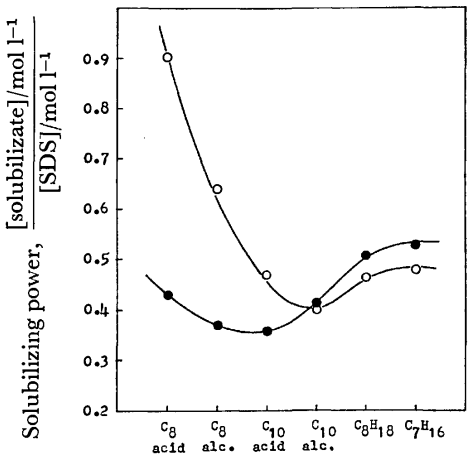

Fig. 2. The susceptibility to the solubilization of the solubilizates in 0.2 M NaCl and pure water at 25 °C.
○: In pure water, ●: 0.2 M NaCl.

with large alkyl groups and only weakly polar groups, such as 1-decanol, showed a solubilization similar to these of nonpolar compounds.

The plots in Figs. 1 and 2 indicate that carboxyl is a stronger solubilizing group than hydroxyl for the compounds of the same carbon number, probably because of its stronger depolarizing power. Furthermore, the electrolyte in the solution has effects not only on the solubilized amount, but also on the susceptibility to the solubilization of the materials in the SDS solution.

Relative Viscosities and Effective Specific Volume of the Micelles. The relative viscosities, η_r, of the solutions saturated with the solubilizates in 0.3 or 1.5% SDS solutions containing 0.2 M NaCl are plotted in Fig. 3. The relative viscosities of 0.3 and 1.5% SDS solutions both decreased in the following order of the dissolved compounds; octanoic acid>1-octanol>decanoic acid>1-decanol>octane>heptane. The viscosities changed over a wider range in the 1.5% SDS

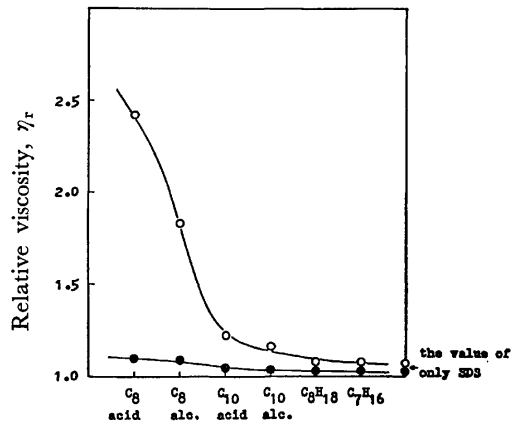

Fig. 3. Relative viscosty of the solubilized solution in 0.2 M NaCl at 25 °C.
○: SDS 1.5%, ●: SDS 0.3%.

solution than in the 0.3% solution. The relative viscosities of the solutions showed a larger change than the solubilized amounts of the components in the SDS solutions containing NaCl; the change seems to be related to the structures of the solubilizates. The solutions containing octanoic acid showed the largest viscosity. This large viscosity due to octanoic acid may be attributed to the adsorption of octanoic acid on the surface of the micelles of SDS, which would cause the increase in the mutual interaction of the micelles. On the other hand, nonpolar compounds are deeply occluded into the palisade layers and are occluded in the hydrocarbon cores of the micelles; consequently, the mutual interaction of the micelles is not influenced, and the relative viscosities of the solutions do not change because of the dissolution of the solubilizates.

Based on the Guth and Simha equation (Eq. 1),[6-9] which is an extension of Einstein's equation to the higher concentration range of the micelles in aqueous solution,

$$\eta_r = 1 + 2.5\,\phi + 14.1\,\phi^2, \quad (1)$$

the volume fraction of the spherical particles, ϕ, can be calculated from the relative viscosity, η_r. The effective specific volume, V, of SDS containing an oily material is given by[7,10]

$$V = \phi/C, \quad (2)$$

where C is the concentration of the solution presented in g/cm^3.

Figure 4 shows the effective specific volume, V, of the micelles of SDS containing solubilizates in 0.2 M NaCl solutions.

Nakagawa has suggested that the effective specific volume of micelles in various concentration ranges of the surfactant from 0.3 to 3.0% was nearly constant.[11,12] Our experimental results agreed approximately with this suggestion. For a solution of the surfactant alone, it can be said that, above the CMC, the number of micelles increases with an increase in the amount of the surfactant, whilst the size of the micelle remains almost unchanged (aggregates of 50—100).[13]

As is evident in Fig. 4, the effective specific volumes of the micelles containing octanoic acid and 1-octanol

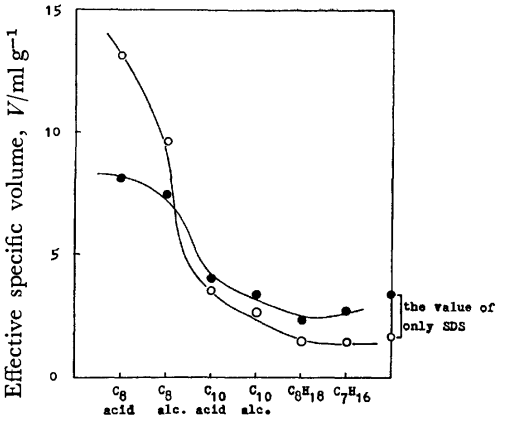

Fig. 4. Effective specific volume of the solubilized micelle in 0.2 M NaCl at 25 °C.
○: SDS 1.5%, ●: SDS 0.3%.

were larger than those of the micelles containing less polar or nonpolar compounds. Besides, the effective specific volumes of SDS micelles containing decanoic acid, 1-decanol, octane, and heptane were almost the same as that of SDS-single-component-micelles. The increase in the effective specific volume of the micelles upon the addition of polar solubilizates may be attributed to the adsorption of the solubilizate molecules on the surface of micelles, as if needles with bulky heads are inserted into a spherical needle pad.

Diffusion Coefficients and Effective Radii of the Micelles Containing Solubilizates. The diffusion coefficients, D, were calculated by means of the following equation, based on the maximum ordinate-area method,[14]

$$D = \frac{A^2}{4\pi t(H_m)^2} \cdot \frac{1}{G^2}, \tag{3}$$

where A is the area under the concentration gradient curve, H_m is maximum ordinate, t is the migration time, and G is the optical magnification (here $G=1$)

Figure 5 shows the diffusion coefficients, D, and effective radii of micelles, a, in 0.2 M NaCl solutions. Since a charged colloid interacts with an ionic medium, the diffusion of a hydrophilic-charged colloid is usually retardated in the presence of electrolytes in solutions, but this effect is suppressed in the concentration range of electrolytes higher than 0.2 M.[3,13]

The effective radii of micelles, a, can be calculated by means of the Stokes-Einstein's equation:[15,16]

$$a = kT/6\pi\eta D, \tag{4}$$

where k is the Boltzmann constant and η is the viscosity of the medium. The diffusion coefficient of the micelles of SDS containing solubilized octanoic acid was the smallest, while that of SDS containing heptane was the largest, though the incorporated amounts in the micelles were almost the same for the two solubilizates, as has been mentioned above. On the other hand, the effective radii of the micelles of SDS containing octanoic acid were the largest, and those containing heptane was the smallest. These results are in accordance with the results of the relative viscosities and the effective specific volumes of micelles of the systems.

Electrophoresis. From the measurements of the

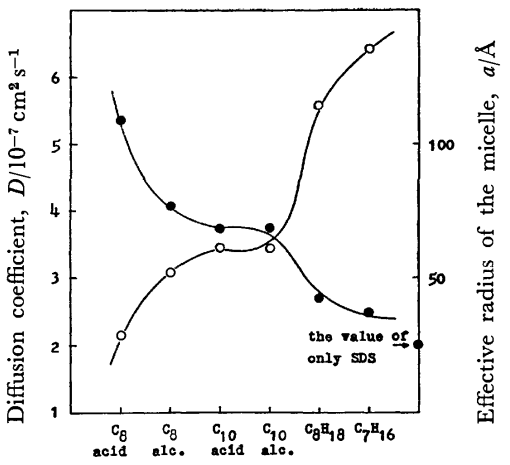

Fig. 5. Diffusion coefficient and effective radius of the solubilized micelle in 0.2 M NaCl at 25 °C.
○: Diffusion coefficient, ●: effective radius of the micelle.

migration velocities of micelles from the upper layer to the lower layer (V_a) or in the reverse direction (V_d) in a cell of the Tiselius apparatus, the electrophoretic mobility of micelles, $|U_M|$, was calculated by means of following equation:[2,17-19]

$$U_M = V_d\tau^\beta - \frac{V_a\tau^\alpha - V_d\tau^\beta}{(T_M{}^\beta/T_M{}^\alpha) - 1}, \tag{5}$$

where T_M is the transference number of micelles, and τ is the specific conductance of the solution, while the superscripts α and β refer to the upper and lower layers respectively.

$T_M{}^\beta/T_M{}^\alpha$ in Eq. 5 is expressed as

$$T_M{}^\beta/T_M{}^\alpha = \frac{C_M{}^\beta/\tau^\beta}{C_M{}^\alpha/\tau^\alpha}, \tag{6}$$

where $C_M{}^\alpha$ and $C_M{}^\beta$, which are the concentrations of the M^- ions in the α and β phases respectively, are given by

$$C_M{}^\alpha/C_M{}^\beta = \frac{(C-\mathrm{CMC})^\alpha}{(C-\mathrm{CMC})^\beta}, \tag{7}$$

where C is the concentration of the surfactant.

Figure 6 shows the electrophoretic mobilities of the micelles containing various solubilizates. The absolute value of the electrophoretic mobilities of the micelles solubilizing octanoic acid, 1-octanol, and decanoic acid were larger than that of SDS alone (presented by the dotted line), while those of the micelles containing 1-decanol, octane, and heptane were smaller. The $|U_M|$ of the micelles containing 1-decanol was smaller than that of SDS alone in the presence of NaCl; this is a result of the behavior of 1-decanol, like that of normal paraffins in a medium containing electrolytes.

The ζ-potential was calculated from U_M by the use of Henry's equation:[20]

$$\zeta = \frac{6\pi\eta}{\varepsilon f(\kappa a)} \cdot U_M, \tag{8}$$

where $f(\kappa a)$ is the Henry function, κ is the Debye-Hückel parameter, a is the radius of the micelle, and η and ε are the viscosity and dielectric constant of

Table 1. Electrophoretic and diffusion data for the solubilized micelles
(in a 0.2 M NaCl aq soln. at 25 °C)

	Solubilizates	$-U_M$ 10^{-4} cm^2 V^{-1} s^{-1}	D 10^{-7} cm^2 s^{-1}	a Å	$-\zeta$ mV	Q
Polar	C_8 acid	3.26	2.15	109.5	49.7	376
	C_8 alc.	2.97	3.07	76.7	46.9	180
	C_{10} acid	2.92	3.44	68.5	46.6	144
	C_{10} alc.	2.28	3.44	68.5	36.4	113
Nonpolar	n-C_8H_{18}	1.49	5.59	42.1	25.1	32
	n-C_7H_{16}	1.02	6.44	36.6	17.4	17
	SDS alone	2.56	9.33	25.2	45.3	23

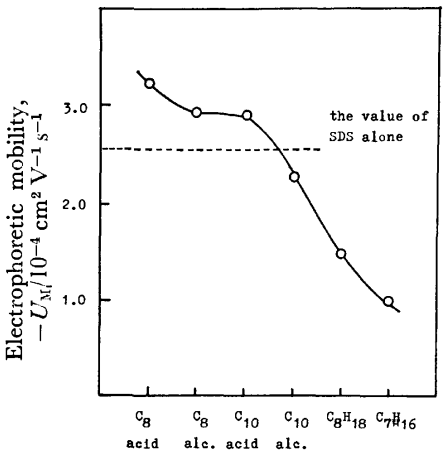

Fig. 6. Electrophoretic mobility of the solubilized micelles.
$|U_M|$ in 0.2 M NaCl at 25 °C.

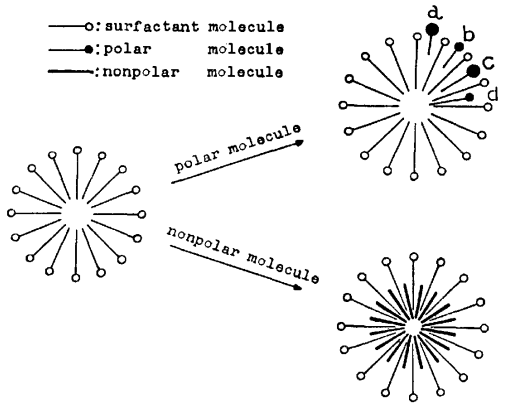

Fig. 7. Schematic solubilization model for the various solubilizates.

the medium respectively.

Furthermore, the number of the effective charge of micelles, Q, is estimated by means of the following equation:[20]

$$Q = \frac{1}{e} \cdot \frac{1+\kappa a+\kappa r_1}{1+\kappa r_1} \cdot \varepsilon a \zeta, \qquad (9)$$

where e is the elementary charge and r_1 is the radius of the counter ion, for which we adopted 0.22 nm in the present system.

Table 1 shows the results of electrophoretic and diffusion measurements for the micelles containing various solubilizates. The absolute value of the ζ-potential follows the order of $|U_M|$. As is evident from Table 1, the numbers of the effective charges of micelles containing polar solubilizates are larger than those of the micelles containing nonpolar solubilizates or no solubilizates, with that of the micelles of SDS containing octanoic acid being the largest. These results suggest that the micelles containing octanoic acid aggregate with each other to form the larger micelles, whereas the micelles containing nonpolar solubilizates seem not to aggregate, showing a charge similar to that of the micelles of SDS alone.

The large number of the charge of the octanoic acid-containing micelles may be attributed to the hydration of carboxyl groups. From the point of view of energy, the hydrated carboxyls would better remain on the surface of the micelles than be incorporated into the hydrocarbon cores of the micelles. The alkyl group of octanoic acid is considered to penetrate into the palisade layer of the micelles. This mechanism of the solubilization of polar oily compounds is shown schematically in Fig. 7. In this figure, **a** indicates octanoic acid; **b**, 1-octanol; **c**, decanoic acid, and **d**, 1-decanol. Since nonpolar compounds, such as octane and heptane, are not hydrated, all the molecules are thought to be incorporated into the hydrocarbon cores of the micelles, like needles buried in a spherical pad. The generally accepted model of the solubilization of oily materials by the micelles of a surfactant was proved to be consistently true in the present systems.[21,22]

References

1) J. N. Phillips and K. J. Mysels, *J. Phys. Chem.*, **59**, 325 (1955).
2) T. Nakagawa and H. Inoue, *Nippon Kagaku Zasshi*, **78**, 636 (1957).
3) F. Tokiwa and K. Ohki, *Bull. Chem. Soc. Jpn.*, **42**, 1216 (1969).
4) K. Ogino, M. Abe, and N. Takeshita, *Bull. Chem. Soc. Jpn.*, **51**, 1880 (1978).
5) H. B. Klevens, *Chem. Rev.*, **47**, 1 (1950).
6) E. Guth and R. Simha, *Kolloid-Z.*, **74**, 147 (1936).
7) D. C. Robins and I. L. Thomas, *J. Colloid Interface Sci.*, **26**, 415 (1968).
8) T. Ito and H. Mizutani, *Yakugaku*, **17**, 246 (1968).
9) K. Shinoda, T. Nakagawa, B. Tamamushi, and T. Isemura, "Colloidal Surfactants," Academic Press, New York (1963), p. 115.

10) Y. Iwadare and T. Suzawa, *Bull. Chem. Soc. Jpn.*, **43**, 2326 (1970).
11) G. S. Hartley, "Aqueous Solution of Paraffin Chain Salts," Harman, Paris (1936).
12) T. Nakagawa and H. Inoue, *Nippon Kagaku Zasshi*, **79**, 345 (1958).
13) H. R. Bruins, *Kolloid-Z.*, **57**, 152 (1931).
14) I. Watanabe, *Kagaku*, **18**, 421 (1948).
15) A. Einstein, *Ann. Physik.*, **17**, 549 (1905).
16) F. Tokiwa and K. Ohki, *J. Phys. Chem.*, **71**, 1343 (1967).
17) V. P. Dole, *J. Am. Chem. Soc.*, **67**, 1119 (1945).
18) F. Tokiwa and K. Ohki, *Bull. Chem. Soc. Jpn.*, **41**, 2828 (1968).
19) L. G. Longsworth, *J. Phys. Colloid Chem.*, **51**, 171 (1970).
20) D. C. Henry, *Proc. R. Soc. London, Ser. A*, **133**, 106 (1931).
21) C. B. Monk, "Electrolytic Dissociation," Academic Press, New York (1961), p. 271.
22) S. Riegelman, N. A. Allawalla, M. K. Hrenoff, and L. A. Strait, *J. Colloid Sci.*, **13**, 208 (1958).

Cotton Effect Induced in Optically Inactive Molecules and Molecular Complexes by Optically Active Environment. II. Acridine and Phenazine in Cellulose Diacetate Film

Yasumasa J. I'HAYA,* Taka-aki AOI, and Tatsuji SANO

Department of Materials Science and Laboratory for Magneto-Electron Physics, The University of Electro-Communications, Chofu-shi, Tokyo 182

(Received August 6, 1979)

Ultraviolet absorption spectra and induced circular dichroism (ICD) of acridine and phenazine were measured in cellulose diacetate film. The induced Cotton effect corresponding to each absorption maxima of these systems appeared. From the correspondence between the maxima of ICD and the peaks of the resolved absorption spectra, it was found that the sign of ICD is negative in the region where the molecular long-axis polarized transition plays a part in the CD induction and it is positive in the region where short-axis polarized transition does. A mechanism of CD induction tentatively proposed is that a dye molecule is imprisoned in a cage formed by an assembly of the folded chains of cellulose diacetate and the Cotton effect is induced by an electrostatic interaction between electronic transition dipole moments of the dye and of the chromophores involved in the cellulose diacetate cage.

The origin of the ICD (induced circular dichroism) spectra of optically inactive molecules dissolved in optically active medium is still controversial. The oldest explanation was a complex formation including hydrogen bonding between an achiral molecule and chiral solvent molecules,[1] but later on there have been discovered a variety of cases where the mechanism of ICD is not explained systematically. Among others, those which are worth notice are (a) due to the stereoregular arrangement of chiral host molecules such as cholesteric solvents[2] and helical biopolymers[3] along which achiral molecules are forced to line up in a regular way and (b) due to a formation of clathrates in which achiral species are imprisoned in an optically active cage.[4]

Part I of this series[5] has demonstrated that aromatic hydrocarbons and their molecular complexes embedded in acetylcellulose films exhibit the induced Cotton effect in their π-π^* absorption region and charge-transfer absorption region, respectively. The advantage of the experiment is that even very weak and/or closely overlapped vibrational bands and charge-transfer bands unresolved by the usual solution spectroscopy may be observed in such ICD spectra. We then tried to resolve vibrational bands in ICD spectra of several dye molecules in a film state and correlate them to the corresponding broad absorption spectra taken in solution. However, even when we used a high resolution spectropolarimeter together with a data processing computer, we found it difficult to resolve unambiguously each vibrational band in ICD spectra for filmed molecules which show rather broad absorption spectra in solution. Instead, we found an interesting correlation between the signs of ICD spectra and the direction of electronic transition moments of guest molecules. In the following, we report the ICD spectral feature of acridine and phenazine embedded in cellulose diacetate matrices, with specific emphasis on the correlation mentioned above.

Experimental

Acridine and phenazine, all commercial reagent grade, were purified by sublimation. Cellulose diacetate (Eastman Chemical, E-398-3, degree of polymerization 171) was used without further purification. An acetone solution of each dye was added to an acetone solution of cellulose diacetate, then the viscous solution was drawn onto a fused quartz plate and baked slowly in an oven to remove acetone. Original concentrations of the dyes and cellulose diacetate were held in the range $1—3\times10^{-4}$ mol dm^{-3}. The arrangement of the matrix, cellulose diacetate, was examined by the observation under a polarizing microscope. Films which were not opaque and showed no birefringence were selected. They were 5—15 μm in thickness with excellent transparency. The film thickness was roughly estimated from birefringence and retardation using a polarizing microscope. It was estimated that the dyes were doped at the ratio of 1:20—1:40 against the number of the sugar residues of cellulose diacetate.

Absorption spectra were taken on a JASCO UVIDEC-505 digital double-beam spectrophotometer. A JASCO model J-40S spectropolarimeter was used for the measurement of CD spectra of the sample films. In each measurement, the CD spectrum was calibrated with reference to the base line of the pure cellulose diacetate film whose thickness was identical with that of the sample film. An S/N ratio in a CD spectrum was improved by using a JASCO data processing machine DP-500 through repeated runs.

Results and Discussion

The UV and CD spectra of acridine embedded in a cellulose diacetate film are shown in Figs. 1 and 2 and those of phenazine in Figs. 3 and 4. The thickness of the sample film was 8 μm for acridine and 15 μm for phenazine when the spectra were taken in the longer wavelength region (280—500 nm), and it was 7 μm for acridine and 5 μm for phenazine when the spectra were taken in the shorter wavelength region (200—300 nm). The scales of the ordinate are the ellipticity (θ) for CD and the optical density (*O.D.*) for UV spectra. These quantities were not converted into the corresponding molecular characteristics, *i.e.*, molecular extinction coefficient and molecular ellipticity, since the thickness and concentration of each sample film could not be determined accurately. Incidentally, the same dyes dissolved in an acetone solution of cellulose diacetate did not show any induced Cotton effect.

The overall UV spectra of acridine and phenazine

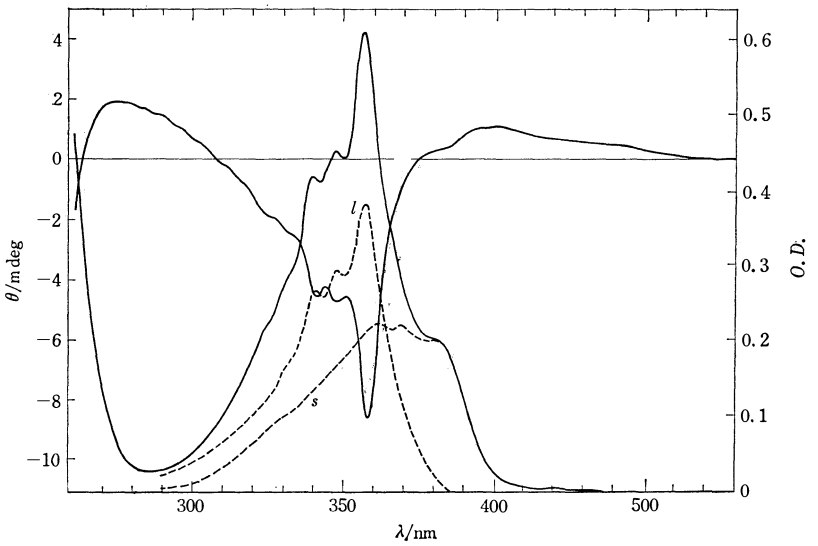

Fig. 1. UV and CD spectra of acridine in cellulose diacetate film in longer wavelength region. Film thickness: 8 μm. Dotted curves show the resolution of UV spectrum into the components of molecular long-axis polarized (*l*) and short-axis polarized (*s*) transitions.

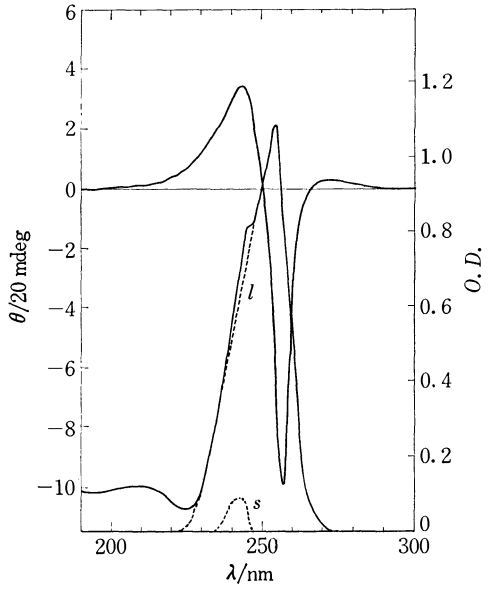

Fig. 2. UV and CD spectra of acridine in cellulose diacetate film in shorter wavelength region. Film thickness: 7 μm. Dotted curves are the same as in Fig. 1.

in film states shown in Figs. 1—4 are not very much different from those observed in CCl_4 and ethanol solutions; the overall spectral shifts to the red are 200 cm^{-1} at most. We also measured the infrared spectra of the sample films, which were not very much different (1—3 cm^{-1}) from those of the corresponding dyes in solution and in powder states. These suggest that the dye molecules embedded in cellulose diacetate films are the same and/or the like surroundings as those in solution. The calibration of CD curves with reference to the base line of the pure cellulose diacetate film is important, since cellulose diacetate itself has optical activity. The UV absorption and CD spectra of a typical cellulose diacetate film (thickness 10 μm) are shown in Fig. 5.

As seen in Figs. 1 and 2, the ICD spectrum of acridine is divided into five bands; a weak and trailing positive band peaked at around 400 nm (band I), an intense negative band whose vertex lies at 358 nm, being spread over 6000 cm^{-1} and rich in vibrational structures (band II), a weak positive band at 265—310 nm (band III), an intense and sharp negative band at 257 nm (band IV), and a positive band centered at 243 nm (band V). From Figs. 3 and 4, the ICD spectrum of phenazine is analyzed into the following; a weak and trailing positive band whose peak lies at around 405 nm (band I), an intense and broad negative band centered at 366 nm (band II), a medium positive band at 276 nm (band III), an intense and sharp negative band peaked at 255 nm (band IV), and a rather strong positive band whose maximum lies at 242 nm (band V).

It is well known that in these dye molecules the relatively weak ^1L_b bands (molecular long-axis polarized) overlap with the intense ^1L_a bands (short-axis polarized) in the wavelength region 300—400 nm, and the very weak ^1B_a bands (short-axis polarized) are hidden in the very intense ^1B_b bands (long-axis polarized) in the wavelength region 200—300 nm.[6] Furthermore, the longer wavelength region of these bands might be overlapped with very weak n→π* bands. Since there has been made no accurate experimental analysis so far, we tentatively try to resolve the overlapped bands into their components, consulting the dichroic spectral analyses of these dyes embedded in stretched poly (vinyl alcohol) sheets made by Inoue *et al.*[7] The divided spectra of acridine and phenazine are shown by the dotted lines in Figs. 1—4, where we have paid no regard for n→π* transitions.

From these band resolutions, we can safely say that in acridine and phenazine bands II and IV (negative) correspond to the long-axis polarized ^1L_b and ^1B_b bands, respectively. Band II of acridine has a detailed

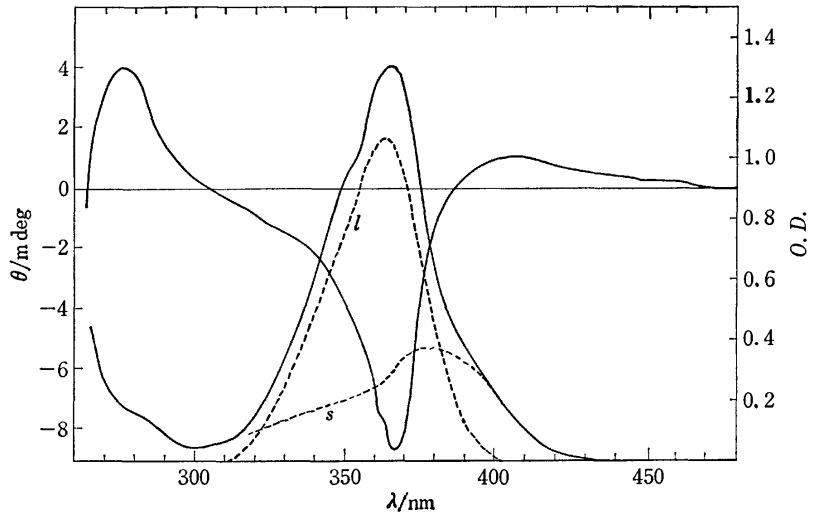

Fig. 3. UV and CD spectra of phenazine in cellulose diacetate film in longer wavelength region. Film thichness: 15 μm. Dotted curves are the same as in Fig. 1.

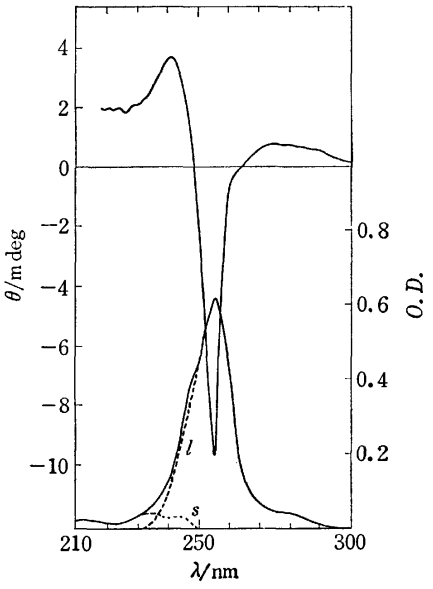

Fig. 4. UV and CD spectra of phenazine in cellulose diacetate film in shorter wavelength region. Film thickness: 5 μm. Dotted curves are the same as in Fig. 1.

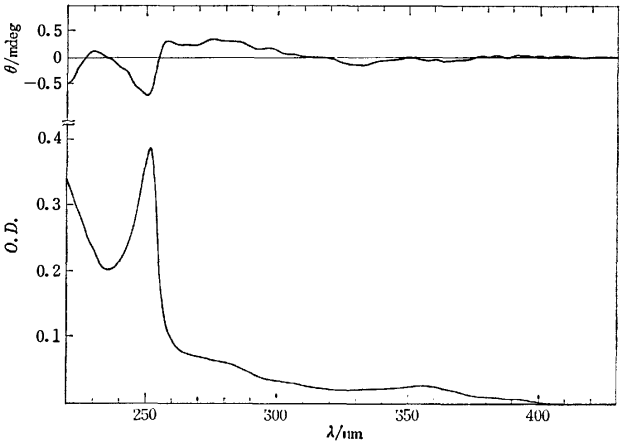

Fig. 5. UV and CD spectra of pure cellulose diacetate film.

structure, the ellipticity of each minimum being roughly proportional to the intensity of the corresponding vibrational absorption maximum in the UV spectrum. The peak of band I in the acridine film keeps at a distance from the maximum of the short-axis polarized ^1L_a transition, though the separation is not very large (*ca.* 2000 cm^{-1}), and its magnitude of ellipticity is too small if the origin of band I is assigned to be ^1L_a. This is probably because the originally rather intense positive band due to ^1L_a, which might be assumed to have a peak at around 370 nm, is partly cancelled out by very intense band II and then the resultant overlapped bandshape of Fig. 1 is observed. The same explanation applies to band I of the phenazine film (Fig. 3).

Band V of both acridine and phenazine is tentatively assigned to have an origin in the short-axis polarized ^1B_a transition. The question why the ellipticity of band V is so large while the resolved ^1B_a is very weak remains untouched. More inexplicable situation is the case of band IV. In the phenazine film, there appears a shoulder at about 280 nm in the absorption spectrum which roughly corresponds to the positive maximum of band III. Incidentally, such a shoulder is not observed in the solution spectrum of pure phenazine and phenazine+cellulose diacetate. On the contrary, even a shoulder does not appear in the 260—290 nm region of the absorption spectrum of the acridine film.

The whole spectral features mentioned above are summarized in Table 1. An obvious fact is that the long-axis polarized transition induces a *minus* CD and the short-axis polarized transition a *plus* CD. Furthermore, it may be safely said that the intensities of ICD bands I, II, and IV are proportional to those of the corresponding absorption spectra which have origins of CD induction.

We now discuss about a mechanism of the ICD in the present systems. A possibility of forming a charge-transfer complex between cellulose diacetate and the dye molecules is scarce, since we have not

Table 1. Correlation between the sign of induced circular dichroism (ICD) and the direction of polarization of allowed transitions

Band	$\frac{CD_{max}}{nm}$	CD sign	$\frac{\lambda_{max}}{nm}$	Direction of polarization	Tentative assignment
Acridine					
I	≈400 (w) [a]	+	370 (s)	short-axis	B_1
II	358 (s)	−	358 (s)	long-	A_1
III	275	+			
IV	257 (vs)	−	254 (vs)	long-	A_1
V	243 (s)	+	243 (vw)	short-	B_1
Phenazine					
I	≈405 (w)	+	380 (m)	short-	B_{2u}
II	366 (s)	−	365 (s)	long-	B_{1u}
III	265 (m)	+	(280) [b]		
IV	255 (vs)	−	255 (vs)	long-	B_{1u}
V	242 (m)	+	242 (vw)	short-	B_{2u}

a) Letters in parentheses are abbreviations for spectral intensities. b) A weak shoulder.

observed any absorption and CD spectra that are expected to be caused by a charge-transfer mechanism. Next, it is possible that the matrix partially forms a spatially regular helical structure along which the dye molecules are lined up just as mentioned in item (a) of the early paragraph. The entire cellulose diacetate matrix may be composed of a part where the cellulose chains line up regularly, probably in a helical structure in a certain spot, and a part where such chains are folded for some reason.[8] However, there were not enough dye molecules in our sample to induce CD through the dipole-dipole interaction between the helically stacked and/or intercalated dye molecules. Of course, it is still possible that the sparsely embedded dye monomer exhibits an ICD, being involved in a complicated interaction with the asymmetric environment of the matrix.[9] It will be mentioned later that even this will not be the case.

The remaining possibility is item (b) mentioned in the early paragraph. Our tentative model structure is that the dye molecule is imprisoned in a cage of a suitable spatial extent formed by an assembly of the folded chains of cellulose diacetate, and the Cotton effect is induced in the allowed transition region of the dye molecule due to the asymmetric perturbation of cellulose diacetate. It is hard to make proof of this model, but the following consideration might be of service to credit that the model is not an offhand one. First, the CD spectral shapes look closely like those induced in the β-cyclodextrin cage in which case we have succeeded in predicting the signs and magnitudes of ICD by making use of an approximate polarizability theory.[10] If a geometrical conformation of the cellulose diacetate cage were known, the very similar method could be applied to the present system in order to guess the ICD signs and intensities. Second, the relationship between the signs and intensities of the ICD spectra and the UV absorption spectral intensities in the present system can be compared with that observed for the DNA–dye and the RNA–dye systems.[9] In the latter systems we found two types of induced Cotton effect; one appearing at low P/D ratios (DNA phosphate residue/dye concentration) results from an interaction between dye dimers aggregated along the nucleic acid helices, which shows a quite different CD spectral feature from that of the present system, and the other appearing at high P/D ratios is probably due to an interaction between a dye monomer and an asymmetric perturber in DNA, which yields a CD spectral shape that closely resembles the present case. In the present study, we tried to find out whether the shape, sign, and intensity of the ICD are dependent on concentration, but we could not succeeded in getting a transparent film when the concentration of the dyes was increased. There is an evidence from polarized infrared measurements of a cellulose triacetate film that the folding of the cellulose chain occurs at a certain temperature in the vicinity of room temperature;[11] this fact suggests the existence of a spatial cavity in a cellulose film, either a perfect cage or mere vacant space.

At this stage of discussion, we must mention about our experimental detail, because there has often been asked the difficult problem of whether a strain effect remaning even in an unstretched film produces a spurious CD spectrum due to the linear dichroism of the sample;[12] the usual spectropolarimeter is unable to exclude a considerable amount of the linearly polarized beam passing through a sample. Strictly speaking, every film tested had an anisotropic portion which showed somewhat different absorption spectra when a linearly polarized light was illuminated and the film was rotated perpendicularly to the incident light. However, about two third of the whole surface of a good film selected under the inspection of a polarizing microscope were isotropic with regard to a linearly polarized light, and UV and CD spectra were obtained with reproducibility of 2%. These spectral data were not dependent on the film thickness (3—20 μm) and the dye and cellulose diacetate concentrations (1—8 $\times$ 10^{-4} mol dm^{-3} in acetone). We did not investigate the rate of vaporization of acetone, though it was considered to be important in order to prepare a film which is most suited for the study of this type. In-

cidentally, a sample made by immersion of the pure cellulose diacetate film in an acetone solution of the dyes did not show any CD spectrum. This way of preparing films are usally used in a linear dichroism observation for dyes embedded in stretched polymer films.[7,13] Therefore, the phenomenon demonstrated in the present article is not ascribable to a regular arrangement of the dye adhered to a distorted matrix as mentioned before.

Looking at a problem of CD induction in the present system from all angles just as mentioned hitherto, it admits of no doubt to believe that the circular dichroism to be induced in optically inactive molecules by optically active matrices is due to a complex formation between one molecule and one certain segment of the matrix. If this segment forms a cage in which the optically inactive molecule is imprisoned, the situation will be more favarable, though this is not a necessary condition. A direct mechanism of appearance of the ICD spectrum then is attributable to an electrostatic interaction between electronic transition dipole moments of the included molecule and of the chromophores involved in the segment cage. Unfortunately, a quantitative comparison between the signs and intensities of the observed ICD bands and those to be predicted along this line of theoretical consideration cannot be made unless a definite atomic arrangement of the cage in a film state is known. On the other hand, we will be able to do this with a clathrate compound whose three dimensional structure has been determined accurately and/or can be guessed without ambiguity. One of such systems is the clathrate between β-cyclodextrin and aromatic compounds, an analytical result of which will be presented soon.[10]

References

1) B. Bosnich, *J. Am. Chem. Soc.*, **89**, 6143 (1967).
2) E. Sackmann and J. Voss, *Chem. Phys. Lett.*, **14**, 528 (1972); S. F. Mason and R. D. Peacock, *J. Chem. Soc., Chem. Commun.*, **1973**, 712.
3) A. Blake and A. R. Peacocke, *Biopolymers*, **4**, 1091 (1966); K. Yamaoka and R. A. Resnick, *J. Phys. Chem.*, **70**, 405 (1966); B. J. Gardner and S. F. Mason, *Biopolymers*, **5**, 79 (1967).
4) M. Otagiri, K. Ikeda, K. Uekama, O. Ito, and M. Hatano, *Chem. Lett.*, **1974**, 679; S. Takenaka, N. Matsuura, and N. Tokura, *Tetrahedron Lett.*, **1974**, 2325.
5) Y. J. I'Haya and T. Yunoki, *Bull. Chem. Soc. Jpn.*, **45**, 3065 (1972).
6) For example, J. N. Murrell, "The Theory of the Electronic Spectra of Organic Molecules," Methuen, London (1963), Chap. 6.
7) H. Inoue, T. Hoshi, T. Masamoto, J. Shiraishi, and Y. Tanizaki, *Ber. Bunsenges. Phys. Chem.*, **75**, 441 (1971).
8) R. H. Till, *J. Polym. Sci.*, **24**, 301 (1957); A. Keller, *Philos. Mag.*, **2**, 1171 (1957); A. F. Klarman, A. V. Galanti, and L. H. Sperling, *J. Polym. Sci., Part A-2*, **7**, 1513 (1969).
9) Y. J. I'Haya and T. Nakamura, *Bull. Chem. Soc. Jpn.*, **44**, 951 (1971); T. Nakamura and Y. J. I'Haya, *Bull. Chem. Soc. Jpn.*, **45**, 2720 (1972).
10) Y. J. I'Haya and M. Miyake, to be published.
11) K. Ogura, Y. Miyachi, H. Sobue, and S. Nakamura, *Makromol. Chem.*, **176**, 1173 (1975).
12) A. Davidson and B. Norden, *Spectrochim. Acta, Part A*, **32**, 717 (1976).
13) A. Davidson and B. Norden, *Chem. Phys. Lett.*, **28**, 221 (1974).

The Crystal and Molecular Structure of Tetracyclo[6.4.3.0.0^{2,7}]-pentadec-4-en-13-one

Shigeru KOSHIBE,† Yasushi KAI, Noritake YASUOKA,†† and Nobutami KASAI*

Department of Applied Chemistry, Faculty of Engineering, Osaka University, Yamadakami, Suita, Osaka 565

(Received August 13, 1979)

The X-ray molecular structure of the photocycloadduct of bicyclo[4.3.0]non-1(6)-en-7-one with 1,4-cyclohexadiene has been determined. The crystals belong to the monoclinic system, space group $P2_1/c$, $Z=4$, $a=8.108(1)$, $b=8.836(1)$, $c=17.095(1)$ Å, and $\beta=95.38(1)°$ at 22 °C; $a=7.975(1)$, $b=8.760(1)$, $c=16.949(2)$ Å, and $\beta=94.85(1)°$ at −160 °C. The structure was solved by the direct method and refined by the least-squares procedure to $R=0.052$ (22 °C) and 0.053 (−160 °C) for 1777 and 2349 non-zero reflections respectively. The ring junction between the four- and six-membered rings is *trans*. The molecule has the *cis-anti-trans* structure. No essential difference is observed between the molecular structure at 22 °C and −160 °C except for the thermal motions.

Odaira and his coworkers[1] have found that a photoreaction between bicyclo[4.3.0]non-1(6)-en-7-one (**1**) and aliphatic cycloolefins (**2**) gave a single cycloaddition product (**3**) although four types of isomers were expected to be formed.

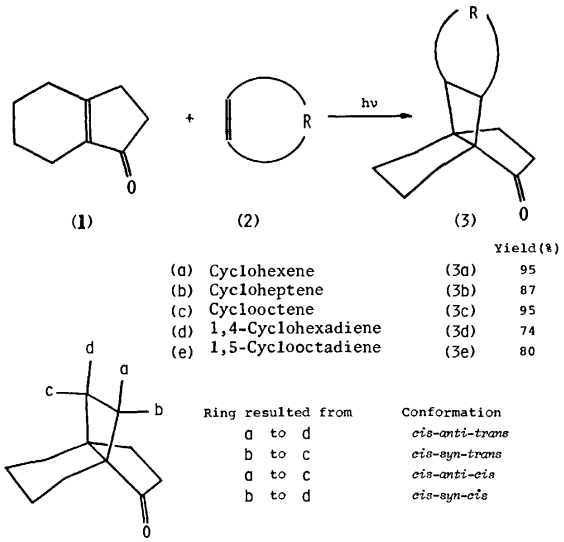

In order to determine the stereochemistry of the photocycloadducts, X-ray analyses of **3a**,[2] **3d**, and **3e**[3] have been carried out. This paper will deal with the molecular structure of **3d** at 22 °C and −160 °C. Interest in the effect of the ring size on the detailed structure of the photocycloadducts also prompted this study.

Experimental

Colorless, square-prismatic crystals were kindly supplied by Professor Y. Odaira and his coworkers of this University.

A Rigaku automated, four-circle diffractometer was used for the measurement of the unit-cell dimensions and the integrated intensities. Graphite-monochromatized Cu $K\alpha$ and Mo $K\alpha$ radiations were used at 22 °C and −160 °C respectively. The low temperature was attained by the gas-flow method of liquid nitrogen. Crystals with approximate dimensions of $0.25\times0.25\times0.3$ mm (22 °C) and $0.3\times0.3\times0.3$ mm (−160 °C) were used; they were coated with collodion to prevent sublimation. The crystal data are given in Table 1.

Table 1. Crystal data of **3d**

$C_{15}H_{20}O$, monoclinic	*F.W.* 216.3, mp 80—81 °C, space group $P2_1/c$	
	22 °C	−160 °C
a/Å	8.108(1)	7.975(1)
b/Å	8.836(1)	8.760(1)
c/Å	17.095(1)	16.949(2)
β/°	95.38(1)	94.85(1)
V/Å^3	1219.3(1)	1179.8(3)
D_m/g cm^{-3}	1.18	
Z	4	4
D_c/g cm^{-3}	1.18	1.218
μ/cm^{-1}	5.56 (for Cu $K\alpha$)	0.795 (for Mo $K\alpha$)

The unit-cell dimensions were determined by the least-squares fit of 2θ values of high-angle reflections.

The intensity data were collected by the θ-2θ scan technique at a 2θ rate of 2° min^{-1}. The scan widths were $\Delta2\theta=(2.0+0.28\tan\theta)°$ at 22 °C for Cu $K\alpha$ and $(2.0+0.70\tan\theta)°$ at −160 °C for Mo $K\alpha$. The backgrounds were counted for 10 s before and after the scan of each peak. Totals of 1808 ($\theta\leqq120°$ at 22 °C, Cu $K\alpha$) and 2730 ($\theta\leqq55°$ at −160 °C, Mo $K\alpha$) unique data were collected, of which 83 (22 °C) and 381 (−160 °C) less than $3\sigma(F)$ were classed as unobserved. Three standard reflections (400, 1,1,$\bar{1}\bar{0}$, and 040) were measured at every 60 reflections at both temperatures; no intensity decrease was observed during the data collection. Corrections for the usual Lp effect was carried out, but not for absorption [μ(Cu $K\alpha$)=5.56 and μ(Mo $K\alpha$)=0.795 cm^{-1}].

Structure Solution and Refinement

The structure was solved by the direct method with the *MULTAN* program,[4] using intensity data obtained at 22 °C. All the non-hydrogen atoms appeared clearly in the E map based on the set of signs with the highest figure of merit. All the hydrogen atoms were located by difference synthesis. The structure was refined

† Present address: Mukojima Research and Development Laboratory, Sumitomo Bakelite Co., Ltd., Sumida 1-4-54, Sumida-ku, Tokyo 131.

†† Present address: Institute for Protein Research, Osaka University, Yamadakami, Suita, Osaka 565,

TABLE 2. FINAL ATOMIC PARAMETERS, WITH e.s.d.'s IN PARENTHESES

(a) Non-hydrogen atoms ($\times 10^4$).

Anisotropic temperature factor ($\times 10^4$) of the form: $\exp[-\{\beta_{11}h^2+\beta_{22}k^2+\beta_{33}l^2+\beta_{12}hk+\beta_{13}hl+\beta_{23}kl\}]$.

Atom	x	y	z	β_{11}	β_{22}	β_{33}	β_{12}	β_{13}	β_{23}
22 °C									
O	5131(2)	2205(2)	2171.1(9)	326(4)	247(3)	409(6)	68(6)	−85(3)	−56(2)
C(1)	6915(2)	2498.8(19)	3374.6(9)	133(3)	100(2)	240(6)	1(4)	8(2)	−4.8(19)
C(2)	6823(2)	1185.9(19)	3992.7(10)	128(3)	97(2)	299(6)	−9(4)	4(2)	0.7(20)
C(3)	7734(2)	−307(2)	4060.6(12)	167(3)	101(3)	461(9)	18(5)	−10(3)	−2(2)
C(4)	7838(2)	−737(2)	4918.3(13)	149(3)	126(3)	544(10)	−27(5)	−26(3)	52(3)
C(5)	7511(2)	158(3)	5502.3(12)	166(4)	177(3)	393(8)	−94(6)	−19(3)	73(3)
C(6)	7043(3)	1816(3)	5432.4(11)	210(4)	170(3)	254(7)	−77(6)	12(3)	16(2)
C(7)	7450(2)	2303.9(20)	4623.9(10)	144(3)	112(3)	252(6)	−35(4)	11(2)	3.5(20)
C(8)	6754(2)	3602.2(19)	4082.8(9)	135(3)	92(2)	254(6)	−19(4)	12(2)	−6.5(19)
C(9)	7707(3)	5086(2)	4077.5(12)	216(4)	111(3)	385(8)	−80(5)	−10(3)	−5(2)
C(10)	9319(3)	4970(3)	3692.9(14)	206(4)	185(4)	523(10)	−180(7)	0(3)	49(3)
C(11)	9055(3)	4226(3)	2893.5(13)	196(4)	232(4)	456(9)	−62(7)	56(3)	60(3)
C(12)	8489(3)	2606(3)	2964.5(12)	180(4)	196(4)	316(7)	30(6)	52(3)	8(3)
C(13)	5345(3)	2667(2)	2840.8(11)	191(4)	116(3)	318(7)	−25(5)	−28(2)	−4(2)
C(14)	4088(2)	3523(2)	3253.9(13)	143(3)	152(3)	525(10)	38(5)	−21(3)	16(3)
C(15)	4862(2)	3857(2)	4077.7(12)	157(3)	126(3)	448(8)	46(5)	38(3)	−11(3)
−160 °C									
O	5136.8(17)	2247.6(15)	2148.8(7)	127(2)	95.1(19)	16.3(4)	20(3)	−32.2(15)	−17.3(15)
C(1)	6915.8(18)	2555.3(16)	3370.0(8)	53(2)	39.4(17)	9.5(5)	−0(3)	1.3(15)	−2.6(14)
C(2)	6819.4(18)	1218.1(17)	3985.8(9)	51(2)	41.1(18)	13.1(5)	−2(3)	1.1(16)	2.1(15)
C(3)	7768.7(19)	−282.6(18)	4043.4(10)	61(2)	42.4(18)	19.0(6)	4(3)	−5.3(18)	−3.4(17)
C(4)	7869.9(19)	−734.3(19)	4911.5(10)	51(2)	54.0(19)	22.8(6)	−14(3)	−13.7(19)	21.6(18)
C(5)	7495.5(20)	154(2)	5508.4(10)	63(2)	76(2)	15.5(5)	−40(4)	−9.0(18)	28.9(18)
C(6)	6985(2)	1820.6(19)	5441.3(9)	79(2)	67(2)	11.2(5)	−32(4)	3.7(17)	−0.7(17)
C(7)	7426.6(18)	2341.1(17)	4634.0(9)	56(2)	45.1(18)	11.2(5)	−11(3)	1.5(16)	1.3(15)
C(8)	6715.0(18)	3653.1(17)	4090.3(8)	54(2)	39.9(17)	10.4(5)	1(3)	5.2(15)	−0.6(15)
C(9)	7663(2)	5169.5(18)	4095.3(9)	83(2)	45.0(19)	14.6(5)	−22(4)	−5.0(18)	−3.4(16)
C(10)	9321(2)	5085.7(20)	3709.6(10)	76(2)	65(2)	20.4(6)	−54(4)	−1.4(20)	15.6(19)
C(11)	9074(2)	4348(2)	2893.0(10)	78(3)	82(2)	17.7(6)	−21(4)	19.7(20)	19.8(19)
C(12)	8532.7(20)	2684.8(19)	2962.7(9)	69(2)	70(2)	13.1(5)	13(4)	15.7(17)	3.8(17)
C(13)	5331.5(20)	2714.3(18)	2822.8(9)	72(2)	48.2(19)	14.1(5)	−16(3)	−9.7(17)	5.3(16)
C(14)	4026.1(19)	3584.3(19)	3243.2(10)	55(2)	60(2)	21.3(6)	4(4)	−10.9(18)	1.5(18)
C(15)	4781.6(19)	3879.1(18)	4088.7(10)	57(2)	52.2(19)	18.2(6)	16(3)	12.6(18)	−4.5(17)

(b) Hydrogen atoms ($\times 10^3$).

Atom	x	y	z	B/Å^2	Atom	x	y	z	B/Å^2
22 °C					−160 °C				
H(2)	560(2)	97.0(19)	405.0(9)	3.1(4)	H(2)	558.2(19)	98.4(18)	404.0(9)	0.6(3)
H(3A)	715(3)	−109(2)	372.7(12)	5.8(5)	H(3A)	719(2)	−112(2)	371.2(10)	1.5(3)
H(3B)	889(2)	−27(2)	391.1(12)	5.0(5)	H(3B)	894(2)	−18(2)	387.9(11)	2.1(4)
H(4)	823(3)	−183(3)	506.7(12)	6.2(5)	H(4)	826(2)	−180(2)	503.3(11)	2.1(4)
H(5)	762(3)	−22(3)	602.7(12)	5.9(5)	H(5)	758(2)	−25(2)	603.6(11)	2.0(4)
H(6A)	585(3)	191(3)	548.5(12)	6.0(5)	H(6A)	576(2)	192(2)	549.7(10)	1.5(4)
H(6B)	766(3)	240(3)	587.1(13)	6.5(6)	H(6B)	760(2)	238(2)	588.4(11)	1.6(4)
H(7)	873(2)	232(2)	463.6(10)	3.9(4)	H(7)	869(2)	238(2)	463.8(11)	1.5(4)
H(9A)	698(3)	591(2)	378.0(12)	5.8(5)	H(9A)	694(2)	596(2)	380.1(11)	2.3(4)
H(9B)	789(3)	544(2)	461.9(12)	5.7(5)	H(9B)	787(2)	552(2)	465.0(10)	1.5(4)
H(10A)	979(3)	600(3)	366.0(14)	7.0(6)	H(10A)	978(2)	614(2)	366.6(11)	2.3(4)
H(10B)	1021(3)	431(3)	403.1(13)	6.5(6)	H(10B)	1019(2)	447(2)	404.2(11)	2.0(4)
H(11A)	810(3)	483(2)	254.2(12)	5.7(5)	H(11A)	817(2)	493(2)	255.0(12)	2.4(4)
H(11B)	1011(3)	417(3)	261.4(14)	7.5(6)	H(11B)	1012(3)	438(2)	259.6(12)	2.5(4)
H(12A)	828(3)	212(2)	244.3(12)	5.3(5)	H(12A)	837(2)	218(2)	243.4(11)	2.1(4)
H(12B)	945(3)	198(3)	327.9(12)	5.6(5)	H(12B)	948(2)	210(2)	328.2(11)	1.8(4)
H(14A)	382(3)	441(3)	297.4(14)	7.2(6)	H(14A)	383(3)	452(3)	295.6(12)	3.0(5)
H(14B)	300(3)	292(3)	322.1(14)	7.4(6)	H(14B)	296(2)	302(2)	321.4(11)	2.1(4)
H(15A)	457(3)	488(2)	420.7(12)	5.2(5)	H(15A)	451(2)	490(2)	426.9(11)	1.7(4)
H(15B)	439(3)	320(2)	448.0(12)	5.3(5)	H(15B)	432(2)	316(2)	447.1(11)	1.8(4)

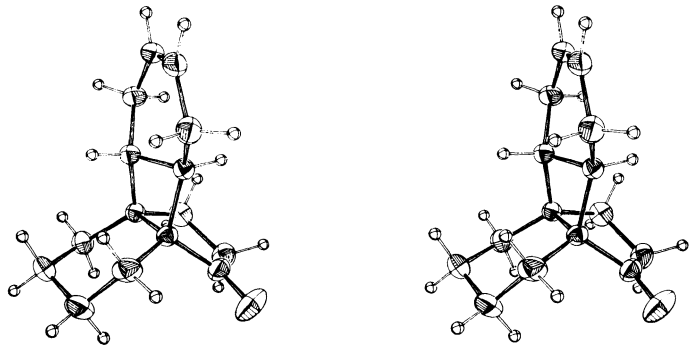

Fig. 1. An *ORTEP* drawing[9] of the molecule. Non-hydrogen atoms are represented by thermal ellipsoids at 20% probability level.

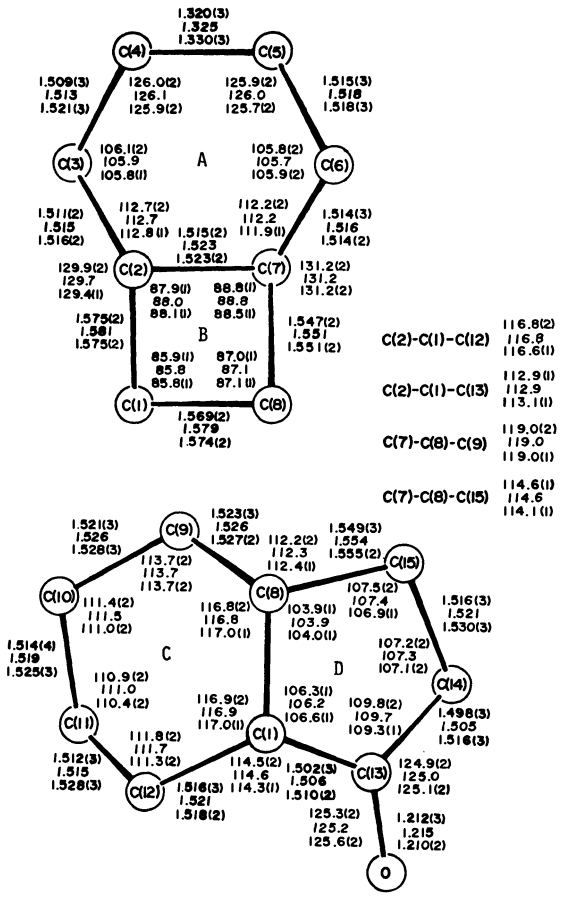

Fig. 2. Bond lengths and bond angles with e.s.d.'s in parentheses.
Upper figure: room temperature structure (22 °C). Middle figure: as above, corrected for the thermal motion by the rigid body approximation.[8] Lower figure: low temperature structure (−160 °C).

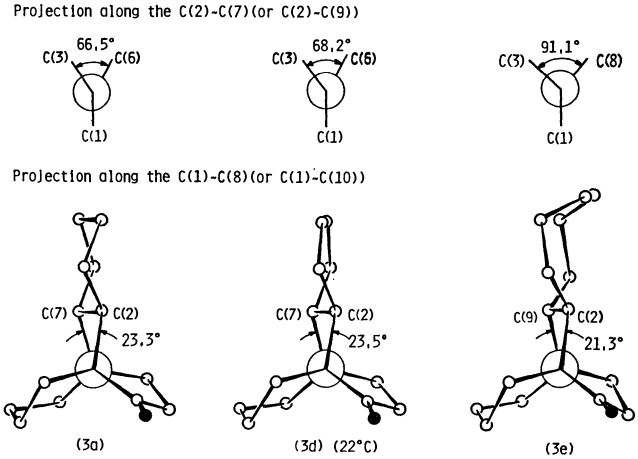

Fig. 3. A view of the three related molecules projected along the C(1)–C(8) or the corresponding C(1)–C(10) bond, and Newman projections along the C(2)–C(7) or the corresponding C(2)–C(9) bond. Oxygen atoms are expressed as dark circles.

with the weight unity by means of the block-diagonal least-squares procedure (*HBLS*-V program[5]). Anisotropic and isotropic thermal parameters were applied for non-hydrogen and hydrogen atoms respectively. The final R value was 0.052 for 1725 non-zero (0.055 for all 1808) reflections.

The anisotropic refinement of the low-temperature structure was started by using the atomic parameters obtained by the use of the room-temperature data. The locations of all the hydrogen atoms were confirmed by the difference systhesis, the parameters of which were refined isotropically. The final R value was 0.053 for 2349 non-zero (0.070 for all 2730) reflections. The weighting schemes used were $w=(\sigma^2(F_o)+a|F_o|+b|F_o|^2)^{-1}$ for $|F_o|>0$ and $w=c$ for $|F_o|=0$. In the case of $a|F_o|+b|F_o|^2<0$, $w=\sigma^{-2}(F_o)$ was used instead. The values of a, b, and c used at the final refinements were 0.026, −0.000, and 0.564. The computations were carried out on a NEAC 2200-700 computer at Osaka University.

The atomic scattering factors for non-hydrogen atoms were taken from Hanson *et al.*,[6] and for hydrogen, from Stewart *et al.*[7] The final atomic parameters are listed in Table 2.†††

Results and Discussion

Molecular Structure. A perspective view of the molecule is shown in Fig. 1, while the bond lengths and bond angles are given in Fig. 2.

No essential difference is observed between the molecular structures at 22 °C and −160 °C except for the

††† The tables of the structure factors (22 °C and −160 °C) are kept as Document No. 8005 at the Chemical Society of Japan.

TABLE 3. STRUCTURE OF THE CYCLOBUTANE RING MOIETIES IN THREE SIMILAR COMPOUNDS
(e.s.d.'s in parentheses) Lower figures are those corrected for thermal vibrations.

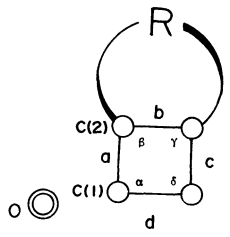

	$C_{15}H_{22}O$ (**3a**)	$C_{15}H_{20}O$ (**3d**, 22 °C) (Present study)	$C_{17}H_{24}O$ (**3e**)
Length [l/Å]			
a	1.571(2) *1.576*	1.575(2) *1.581*	1.581(3) *1.587*
b	1.524(2) *1.531*	1.547(2) *1.523*	1.550(3) *1.555*
c	1.552(2) *1.557*	1.547(2) *1.551*	1.550(3) *1.556*
d	1.573(2) *1.581*	1.569(2) *1.579*	1.549(3) *1.559*
Angle [ϕ/°]			
α	86.1(1) *86.2*	85.9(1) *85.8*	86.9(1) *87.0*
β	88.1(1) *88.1*	87.9(1) *88.0*	88.0(1) *87.9*
γ	88.5(1) *88.6*	88.8(1) *88.8*	88.2(1) *88.2*
δ	87.0(1) *87.0*	87.0(1) *87.1*	88.9(1) *88.9*
Dihedral angle [ϕ/°]	33.9	34.3	30.1

TABLE 4. STRUCTURE OF THE C AND D RING MOIETIES IN THREE SIMILAR COMPOUNDS
(e.s.d.'s in parentheses)

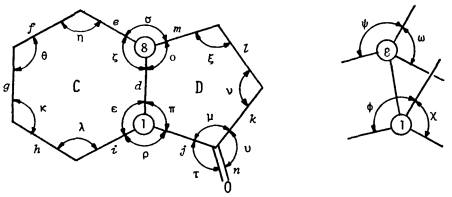

	$C_{15}H_{22}O$ (**3a**)	$C_{15}H_{20}O$ (**3d**, 22 °C) (Present study)	$C_{17}H_{24}O$ (**3e**)
Length [l/Å]			
e	1.522(2)	1.523(3)	1.523(3)
f	1.518(3)	1.521(3)	1.496(4)
g	1.523(3)	1.514(4)	1.506(4)
h	1.517(3)	1.512(3)	1.518(4)
i	1.522(2)	1.516(3)	1.515(3)
j	1.506(2)	1.502(3)	1.507(3)
k	1.511(2)	1.498(3)	1.487(3)
l	1.523(3)	1.516(3)	1.509(4)
m	1.553(2)	1.549(3)	1.557(3)
n	1.210(1)	1.212(3)	1.213(3)
Angle [ϕ/°]			
ε	117.1(1)	116.9(2)	116.2(2)
ζ	116.0(1)	116.8(2)	117.6(2)
η	113.4(2)	113.7(2)	113.8(2)
θ	110.9(2)	111.4(2)	111.1(2)
κ	110.7(2)	110.9(2)	110.6(2)
λ	111.6(1)	111.8(2)	112.1(2)
μ	109.2(1)	109.8(2)	109.0(2)
ν	106.9(1)	107.2(2)	106.5(2)
ξ	106.5(3)	107.5(2)	106.0(2)
o	103.6(1)	103.9(1)	103.1(2)
π	106.4(1)	106.3(1)	107.1(2)
ρ	114.7(1)	114.5(2)	114.3(2)
σ	112.5(2)	112.2(2)	111.7(2)
τ	125.7(1)	125.3(2)	125.9(2)
υ	126.1(2)	124.9(2)	125.1(2)
ϕ	115.2(1)	116.8(2)	116.0(2)
χ	113.8(1)	112.9(1)	113.2(2)
ψ	120.0(1)	119.0(2)	118.8(2)
ω	114.1(1)	114.6(1)	114.0(2)

thermal motions. The room-temperature structure shows a shortening of the bond lengths far from the center of the molecule due to the thermal motion of atoms. This shortening could be rather well corrected by the rigid body approximation of the molecule,[8] and the corrected values can be compared with those of the low-temperature structure (Fig. 2). However, some discrepancies are seen in the bond lenths of C(11)–C(12), C(13)–C(14), and C(14)–C(15). This may be due to the non-rigidity of the molecule.

The most distinctive feature of the molecular structure is that the A/B ring junction is *trans*, while the photocycloadduct has the *cis-anti-trans* structure (Scheme). The present compound has a structure very similar to those of **3a** and **3e** except for the local structure of the A ring. The similarity and difference in the room-temperature structures of the three related molecules may clearly be seen in Fig. 3. The torsional angle about the C(2)–C(7) bond in the present molecule [68.2°] is similar to that in **3a** [66.5°], but they are much smaller than that about the corresponding C(2)–C(9) bond in **3e** [91.1°]. This can be interpreted as being due to the size difference of the A ring. The torsional angle about the C(1)–C(8) bond [23.5°] is equal to that in **3a** [23.3°]; these values are slightly larger than that about the corresponding C(1)–C(10) bond in **3e** [21.3°].

The central cyclobutane ring (B Ring) is puckered, and such a puckering is also observed in the other two compounds; these structures are compared in Table 3. The longest C–C bond, a [1.575(2) Å], is much longer than the normal C–C single bond. The c bond [1.547(2) Å], the length of which is equal through the three compounds, is slightly longer than the usual length. No significant difference is observed between the corresponding bond lengths nor bond angles in **3a** and **3d**. However, some deviations from these are seen in **3e**; the b bond [1.544(3) Å] is longer, d [1.549(3) Å] is shorter, and the α [86.9(1)°] and γ

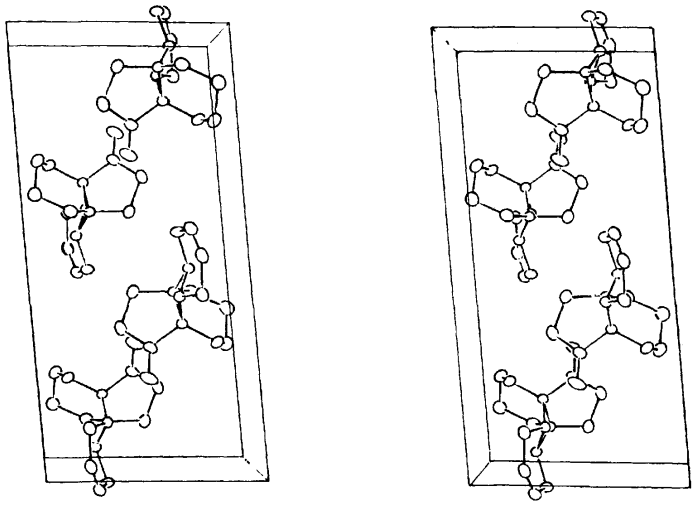

Fig. 4. A stereoscopic drawing of the crystal structure of **3d** (Present study).

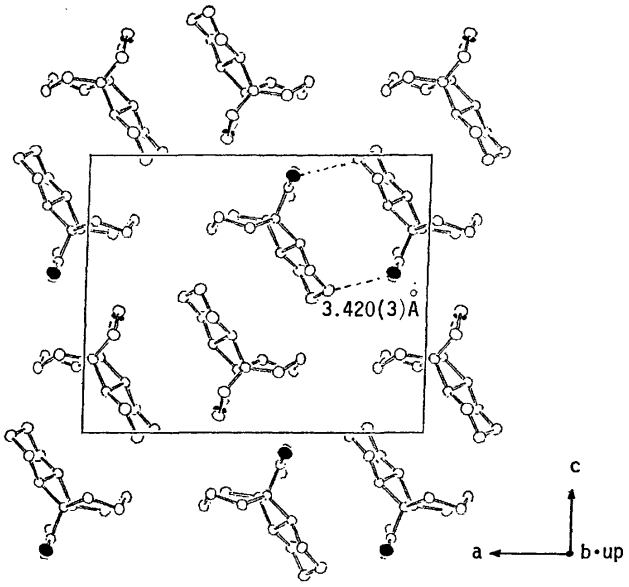

(a)

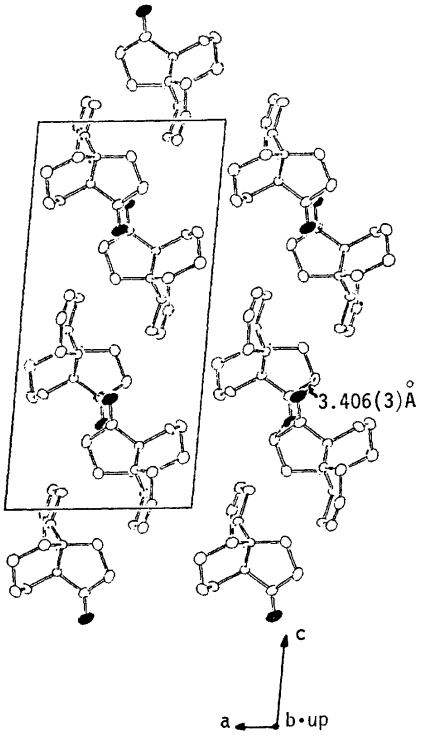

(b)

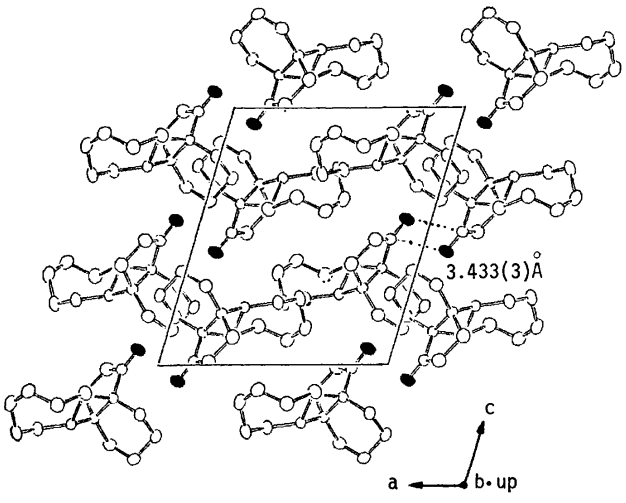

(c)

Fig. 5. Crystal structure of the three related molecules viewed down along the b axis.
(a) **3a**, (b) **3d**(Present study), (c) **3e**.
Oxygen atoms are expressed as dark ellipses.

[88.9(1)°] angles are larger than the corresponding bond lengths and angles in the other two compounds.

Almost all the bond lengths and bond angles in Rings C and D in the present compound (**3d**) are equal to the corresponding lengths and angles in **3a** and **3e**, within the limits of error, except for the bond lengths, f and k, and bond angles involving the bridgehead carbon atoms, ζ, ϕ, and χ (Table 4).

Crystal Structure. A stereoscopic drawing[9] of the molecular packing is given in Fig. 4. Some close atomic contacts are observed between molecules related

Table 5. Short intermolecular atomic contacts [*l*/Å] (less than 3.6 Å), with e.s.d.'s in parentheses

		22 °C		−160 °C
3d (Present study)				
C(6)···O[a)]		3.584(3)		3.455(2)
O···C(9)[b)]		3.526(3)		3.457(2)
O···C(14)[b)]		3.406(3)		3.356(2)
	key: a)	x,	$0.5-y$,	$0.5+z$
	b)	$1-x$,	$-0.5+y$,	$0.5-z$
3a				
O···C(4)[a)]		3.420(3)		
O···C(14)[b)]		3.535(3)		
	key: a)	$0.5-x$,	$-0.5+y$,	$1.5-z$
	b)	$1-x$,	$-y$,	$2-z$
3e				
O···C(16)[a)]		3.433(3)		
	key: a)	$-x$,	$-y$,	$1-z$

by a two-fold screw axis. The carbon atom next to the carbonyl group of the D ring, C(6), has the closest contact between the carbonyl oxygen atoms of the adjacent molecules along the 2_1 axis [3.406(3) Å at 22 °C]. The other close contacts are listed in Table 5.

The packings of the **3a** and **3d** molecules are compared with that of the present crystal in Fig. 5.[9] In the **3a** crystal, the carbonyl oxygen atoms have close atomic contacts between atoms in the adjacent molecules related by the 2_1 axis and the center of symmetry (Table 5). In the **3e** crystal, close intermolecular atomic distances are noticed between the two adjacent molecules related by the center of symmetry (Fig. 5(c) and Table 5). Throughout the three related compounds, it can be concluded that the carbonyl oxygen atoms of the D ring play an important role in the packing of molecules.

The authors wish to express their deep thanks to Professor Yoshinobu Odaira and his coworkers of this university for their kindness in supplying the crystals. The authors' thanks are also due to Miss Nobuko Kanehisa, who helped them with the *ORTEP* drawings.

References

1) a) Y. Tobe, H. Omura, A. Kunai, K. Kimura, and Y. Odaira, *Bull. Chem. Soc. Jpn.*, **50**, 319 (1977); b) Y. Tobe, A. Doi, A. Kunai, K. Kimura, and Y. Odaira, *J. Org. Chem.*, **42**, 2523 (1977).
2) M. Harada, Y. Kai, N. Yasuoka, and N. Kasai, *Acta Crystallogr., Sect. B*, **32**, 625 (1976).
3) S. Koshibe, Y. Kai, N. Yasuoka, and N. Kasai, *Acta Crystallogr., Sect. B*, **33**, 152 (1977).
4) G. German, P. Main, and M. M. Woolfson, *Acta Crystallogr., Sect. A*, **27**, 368 (1971).
5) T. Ashida, The Universal Crystallographic Computing System-Osaka, The Computation Center, Osaka University (1973), p. 55.
6) P. Hanson, F. Herman, J. D. Lea, and S. Skillman, *Acta Crystallogr.*, **17**, 1040 (1964).
7) R. F. Stewart, E. R. Davidson, and W. Simpson, *J. Chem. Phys.*, **42**, 3175 (1965).
8) D. W. J. Cruickshank, *Acta Crystallogr.*, **9**, 757 (1956).
9) C. K. Johnson, *ORTEP*-II, Report ORNL-5138, Oak Ridge National Laboratory, Tennessee, 1976.

Structural Studies of Asymmetric Hydrogenation. IV. The Crystal Structures of [(*R*)-1-Cyanoethyl][(*S*)(−)-α-methylbenzylamine]-bis(dimethylglyoximato)cobalt(III) at 293 K and 173 K

Yuji Ohashi,* Yoshio Sasada, Seiji Takeuchi,** and Yoshiaki Ohgo**

Laboratory of Chemistry for Natural Products, Tokyo Institute of Technology, Nagatsuta, Midori-ku, Yokohama 227

***Niigata College of Pharmacy, 5829 Kamishinei-cho, Niigata 950-21*

(Received August 20, 1979)

The structure of [(*R*)-1-cyanoethyl][(*S*)(−)-α-methylbenzylamine]bis(dimethylglyoximato)cobalt(III) has been determined by X-ray analysis at 293 K and 173 K. The crystal is monoclinic; the space group is $P2_1$; $Z=2$, with $a=8.665(2)$, $b=13.485(3)$, $c=9.584(3)$ Å and $\beta=96.95(3)°$ at 293 K, and $a=8.786(2)$, $b=13.500(2)$, $c=9.243(2)$ Å, and $\beta=98.09(3)°$ at 173 K. The structures were deduced by the heavy-atom method and refined by the block-diagonal least-squares technique to the final R values of 0.055 and 0.038 for 1940 and 1948 observed reflections at 293 K and 173 K respectively. The bis(dimethylglyoximato)cobalt moiety is twisted around its long axis because of the steric repulsion from the (*R*)-1-cyanoethyl group and the optically active amine. The degree of the twist is the same as that observed in the structure of [(*R*)-1-(methoxycarbonyl)ethyl][(*R*)(+)-α-methylbenzylamine]bis(dimethylglyoximato)cobalt(III). The conformation of the amine ligand was ascertained to be influenced by the substituted alkyl group through the bis(dimethylglyoximato)cobalt moiety.

The complexes of bis(dimethylglyoximato)cobalt (abbreviated to $Co(dmg)_2$ or cobaloxime) and optically active amine catalyze the asymmetric hydrogenation of olefins.[1-6] In order to clarify the mechanism of inducing the asymmetry, several crystal structures of related complexes have been determined by X-ray analysis.[7-9] In Part III of this series on the crystal structure of [(*R*)-1-(methoxycarbonyl)ethyl] [(*R*)(+)-α-methylbenzylamine] bis (dimethylglyoximato) cobalt-(III) (abbreviated to the R–R ester complex), it has been shown that the $Co(dmg)_2$ plane is twisted around its long axis because of the steric repulsion from the (*R*)-1-(methoxycarbonyl)ethyl group and the optically active amine, α-methylbenzylamine.[9] We proposed in that paper that the twist is one of the factors inducing asymmetry in the reaction step of σ-bond formation.

To examine whether or not the twist exists in other complexes, we have determined the crystal structure of the title complex, the R–S cyano complex, in which the methoxycarbonyl group is replaced by the cyano group. Preliminary experiments revealed that the crystal changes its unit-cell dimensions upon X-ray exposure without the degradation of a single-crystal form. The change was proved to reflect the racemization of the cyanoethyl group.[10] When the crystal was cooled, it contracted in an abnormally anisotropic manner and the gradual change of its unit-cell dimensions upon X-ray exposure was no longer detectable below 173 K.[11] The crystal structures at 293 K and 173 K were determined to confirm the mechanism of the racemization, which has already been reported.[11,12] This paper will present the twist of the $Co(dmg)_2$ plane caused by the short contacts with the cyanoethyl group and the conformation of the amine ligand.

Experimental

Dark red plate-like crystals of the R–S cyano complex, whose preparation will be reported elsewhere, were obtained from an aqueous methanol solution. The selection of the crystal was carefully made on a microscope because the preliminary photographic technique could not be used. A crystal $0.14\times0.20\times0.60$ mm in size was set up on a Rigaku four-circle diffractometer, Mo $K\alpha$ radiation monochromated by graphite being used ($\lambda=0.71069$ Å). The unit-cell dimensions were obtained by means of the least-squares technique with 15 reflections ($2\theta>20°$). Their values before and after the data collection are shown in Table 1. The average values in the last column were used in this work. The crystal data are summarized in Table 2. During the intensity-

Table 1. The change in the unit-cell dimensions

	Start 1[a]	Start 2[b]	End[c]	Average[d]
a/Å	8.665(2)	8.661(2)	8.657(2)	8.659
b/Å	13.485(3)	13.508(2)	13.540(2)	13.524
c/Å	9.584(3)	9.585(2)	9.581(2)	9.583
β/°	96.95(3)	97.07(3)	97.25(3)	97.16
V/Å^3	1111.6(5)	1112.8(4)	1114.0(4)	1113.4

a) Two h after the initiation of the X-ray irradiation. The data collection was unsuccessful because the change was so fast. b) After 4 h, at which the data collection was started. c) After 30 h, at which the data collection was over. d) The average values between 'Start 2' and 'End'. The structure factors and bond distances and angles are calculated using these values.

Table 2. Crystal data

Formula	$C_3H_4NC_8H_{11}N(C_4H_7N_2O_2)_2Co$			
$F.W.$	464.48			
a/Å	8.665(2)	(293K)	8.786(2)	(173K)
b/Å	13.485(3)		13.500(2)	
c/Å	9.584(3)		9.243(2)	
β/°	96.95(3)		98.09(3)	
V/Å^3	1111.6(5)		1085.5(4)	
Systematic absences	$0k0$; k odd			
Space group	$P2_1$			
Z	2			
D_m/g cm^{-3}	1.388			
D_c/g cm^{-3}	1.388			
μ(Mo $K\alpha$)/cm^{-1}	8.79			

Table 3. Fractional coordinates, with their standard deviations, multiplied by 10^4 for the non-hydrogen atoms and by 10^3 for the hydrogen atoms at 293 K

Atom	x	y	z	Atom	x	y	z
Co	25(1)	2500(0)	2646(1)	H(O1)	192(13)	186(10)	68(11)
N(1)	1627(5)	1533(4)	2845(5)	H(O2)	−162(10)	327(7)	468(9)
N(2)	112(6)	2259(4)	4590(5)	H(51)	370(9)	43(6)	519(8)
N(3)	−1602(6)	3423(4)	2465(5)	H(52)	418(10)	108(7)	439(9)
N(4)	−16(5)	2740(4)	687(4)	H(53)	337(9)	−8(6)	372(8)
O(1)	2383(5)	1252(3)	1759(4)	H(61)	20(9)	147(6)	705(8)
O(2)	−924(5)	2644(5)	5377(4)	H(62)	161(7)	66(5)	680(6)
O(3)	−2426(5)	3649(4)	3473(5)	H(63)	187(10)	186(7)	730(9)
O(4)	996(5)	2317(4)	−91(4)	H(71)	−412(8)	439(6)	135(7)
C(1)	2043(8)	1214(5)	4088(6)	H(72)	−295(6)	500(4)	64(5)
C(2)	1112(7)	1602(5)	5130(6)	H(73)	−379(9)	441(7)	14(8)
C(3)	−1980(7)	3797(5)	1180(7)	H(81)	−88(7)	443(5)	−137(6)
C(4)	−966(8)	3428(6)	152(7)	H(82)	−62(7)	349(5)	−173(6)
C(5)	3274(8)	435(6)	4446(8)	H(83)	−223(6)	363(4)	−175(5)
C(6)	1222(9)	1329(7)	6650(7)	H(N51)	−117(8)	109(5)	380(7)
C(7)	−3308(10)	4486(6)	829(9)	H(N52)	−281(8)	168(6)	287(7)
C(8)	−1190(9)	3743(6)	−1323(7)	H(9)	−81(6)	67(4)	91(5)
N(5)	−1629(6)	1373(4)	2343(5)	H(101)	−384(6)	0(4)	184(6)
C(9)	−1969(8)	792(5)	1069(7)	H(102)	−227(8)	−60(5)	198(7)
C(10)	−2770(10)	−195(6)	1390(9)	H(103)	−301(7)	−57(5)	50(6)
C(11)	−2971(7)	1352(5)	−92(7)	H(12)	−465(7)	189(4)	91(5)
C(12)	−4330(8)	1800(6)	111(7)	H(13)	−633(7)	271(5)	−82(6)
C(13)	−5271(8)	2255(6)	−983(8)	H(14)	−555(7)	275(6)	−299(6)
C(14)	−4823(10)	2211(7)	−2324(8)	H(15)	−334(7)	161(5)	−342(6)
C(15)	−3503(10)	1731(8)	−2547(8)	H(16)	−171(7)	110(4)	−167(6)
C(16)	−2595(8)	1296(7)	−1449(8)	H(17)	157(9)	408(6)	222(8)
C(17)	1569(9)	3635(5)	2999(7)	H(181)	376(10)	296(7)	372(8)
C(19)	1327(8)	4202(6)	4256(8)	H(182)	326(9)	260(8)	201(8)
N(6)	1106(9)	4677(6)	5153(8)	H(183)	390(8)	398(5)	291(7)
C(18)	3245(10)	3453(7)	2957(11)				

data collection, the orientation matrix was redetermined if the intensities of three monitor reflections were significantly deteriorated. The intensities of the independent reflections with $2\theta \leqq 50°$ were measured with an $\omega/2\theta$ scan, a scanning rate of $8°(2\theta)\ \mathrm{min}^{-1}$, and a scan range of $(1.0+0.35\tan\theta)°$. Stationary background counts were accumulated for 5 s before and after each scan. A total of 1940 independent reflections, $|F_o| \geqq 3\sigma(|F_o|)$, were obtained.

For the experiment at low temperatures, the nitrogen-gas-flow method was used. The experimental details were the same as those at room temperature, using a crystal $0.15 \times 0.25 \times 0.40$ mm in size. 1948 independent reflections, $|F_o| \geqq 3\sigma(|F_o|)$, were obtained. Corrections for the Lorentz and polarization factors were made, but no correction for absorption was applied.

Structure Determination

The structure at 293 K was deduced by the heavy-atom method and was refined by the block-diagonal least-squares technique. All the hydrogen atoms were found on the difference map. The final refinement was made with the anisotropic and isotropic temperature factors for non-hydrogen and hydrogen atoms respectively. The weighting scheme of $w=0.3$ if $|F_o| > 70.79$ and $|F_o| < 7.08$ and $w=(0.0023F_o^2-0.17906|F_o|+4.48559)^{-1}$ if $7.08 \leqq |F_o| \leqq 70.79$ was employed. The final R became 0.055 for 1940 reflections. No peaks higher than 0.25 e Å^{-3}, except a peak of 0.45 e Å^{-3} around the cobalt atom, were found on the final difference map.

The procedure of the structure determination at 173 K was the same as that at 293 K. The weighting scheme of $w=0.2$ if $|F_o| > 100.69$ and $|F_o| < 7.55$ and $w=(0.00185F_o^2-0.19964|F_o|+6.40248)^{-1}$ if $7.55 \leqq |F_o| \leqq 100.69$ was applied. The final R was 0.038 for 1948 reflections. No peaks higher than 0.23 e Å^{-3}, except the peaks of 0.58 e Å^{-3} around the cobalt atom, were found on the final difference map. The atomic-scattering factors were taken from the International Tables for X-Ray Crystallography.[13] The final atomic coordinates and their standard deviations at 293 K and 173 K are given in Tables 3 and 4 respectively. The lists of the thermal parameters and the observed and calculated structure factors are kept in the office of the Chemical Society of Japan (Document No. 8006). The computation was done on M-180 and M-160 computers at this Institute.

Description of the Structure

The equations of the mean planes of four nitrogen atoms and two dmg's are given in Table 5, together

Table 4. Fractional coordinates, with their standard deviations, multiplied by 10^4 for the non-hydrogen atoms and by 10^3 for the hydrogen atoms at 173 K

Atom	x	y	z	Atom	x	y	z
Co	22(1)	2500(0)	2613(1)	H(O1)	155(6)	215(4)	58(5)
N(1)	1665(4)	1569(3)	2760(4)	H(O2)	−172(7)	317(5)	470(6)
N(2)	122(4)	2174(3)	4604(4)	H(51)	385(6)	55(4)	526(6)
N(3)	−1637(4)	3407(3)	2461(4)	H(52)	369(5)	20(3)	342(5)
N(4)	−43(4)	2828(3)	630(4)	H(53)	325(6)	−3(4)	468(6)
O(1)	2376(4)	1337(3)	1605(4)	H(61)	109(7)	176(5)	730(6)
O(2)	−902(3)	2515(4)	5454(3)	H(62)	224(8)	98(5)	700(8)
O(3)	−2440(4)	3555(3)	3561(4)	H(63)	90(7)	40(5)	661(6)
O(4)	930(3)	2417(3)	−245(3)	H(71)	−392(4)	455(3)	165(4)
C(1)	2085(5)	1207(4)	4025(5)	H(72)	−300(6)	497(4)	43(6)
C(2)	1160(5)	1539(4)	5134(5)	H(73)	−421(6)	419(4)	5(5)
C(3)	−2019(5)	3823(4)	1174(5)	H(81)	−125(5)	450(3)	−161(4)
C(4)	−1047(5)	3489(4)	96(5)	H(82)	−59(5)	338(4)	−205(5)
C(5)	3392(6)	478(4)	4344(6)	H(83)	−215(5)	359(4)	−194(5)
C(6)	1342(6)	1178(4)	6673(5)	H(N51)	−102(5)	87(3)	287(5)
C(7)	−3358(6)	4492(4)	819(6)	H(N52)	−230(6)	166(4)	253(6)
C(8)	−1267(6)	3858(4)	−1442(5)	H(9)	−96(7)	68(5)	38(7)
N(5)	−1547(4)	1354(3)	2221(4)	H(101)	−347(6)	−11(4)	149(5)
C(9)	−1932(6)	847(4)	797(6)	H(102)	−213(6)	−53(4)	164(5)
C(10)	−2648(6)	−176(4)	992(7)	H(103)	−290(5)	−50(4)	9(5)
C(11)	−3030(5)	−1436(4)	−304(5)	H(12)	−449(5)	186(3)	109(4)
C(12)	−4370(5)	1866(4)	66(5)	H(13)	−620(5)	258(5)	−74(5)
C(13)	−5381(5)	2346(5)	−972(6)	H(14)	−584(5)	277(3)	−321(4)
C(14)	−5109(7)	2433(9)	−2395(6)	H(15)	−355(6)	195(4)	−368(5)
C(15)	−3782(7)	1980(5)	−2777(6)	H(16)	−212(7)	110(4)	−200(6)
C(16)	−2776(6)	1509(5)	−1744(6)	H(17)	183(7)	425(5)	221(6)
C(17)	1493(6)	3678(4)	3079(6)	H(181)	351(7)	308(5)	421(6)
C(19)	1204(6)	4177(4)	4417(6)	H(182)	328(6)	328(4)	205(5)
N(6)	992(6)	4587(4)	5427(5)	H(183)	395(6)	423(4)	319(5)
C(18)	3216(6)	3480(5)	3093(7)				

Table 5. Least-squares planes and deviations (l/Å) for equatorial ligands

X, Y, and Z in Å are referred to $\boldsymbol{a}$, $\boldsymbol{b}$, and $\boldsymbol{c}^*$ respectively.

(I) $Co(dmg)_2$ plane (293 K): $-0.6546X-0.7315Y-0.1909Z+2.7526=0$.
(I′) $Co(dmg)_2$ plane (173 K): $-0.6216X-0.7442Y-0.2445Z+2.8941=0$.
(II) dmg plane (293 K): $-0.6544X-0.7342Y-0.1807Z+2.7238=0$.
(II′) dmg plane (173 K): $-0.6160X-0.7548Y-0.2254Z+2.8549=0$.
(III) dmg plane (293 K): $-0.6536X-0.7170Y-0.2425Z+2.7704=0$.
(III′) dmg plane (173 K): $-0.6223X-0.7335Y-0.2733Z+2.8892=0$.

	(I)	(I′)	(II)	(II′)	(III)	(III′)
Co	0.008	0.003	0.021	0.034	0.072	0.041
N(1)	−0.020[a]	−0.014[a]	−0.014[a]	−0.007[a]		
N(2)	0.020[a]	0.014[a]	0.013[a]	0.007[a]		
N(3)	−0.020[a]	−0.014[a]			0.018[a]	0.005[a]
N(4)	0.020[a]	0.014[a]			−0.018[a]	−0.005[a]
O(1)	0.019	−0.024	0.035	−0.004		
O(2)	−0.105	−0.081	−0.118	−0.093		
O(3)	−0.160	−0.146			−0.076	−0.101
O(4)	0.095	0.007			0.026	−0.029
C(1)	0.029	0.033	0.023[a]	0.011[a]		
C(2)	−0.007	0.019	−0.022[a]	−0.011[a]		
C(3)	0.003	0.012			−0.030[a]	−0.009[a]
C(4)	0.107	0.053			0.030[a]	0.004[a]
C(5)	−0.007	0.060	−0.021	0.016		
C(6)	−0.058	−0.024	−0.089	−0.087		
C(7)	−0.104	−0.098			−0.166	−0.139
C(8)	0.139	0.084			−0.016	−0.005

a) Atoms included in the least-squares calculation.

with the deviations of the atoms from the planes. The projection of the structure at 293 K in the (I) plane is shown in Fig. 1, in which the short contacts between the non-bonded atoms are also given. The $Co(dmg)_2$ plane is twisted around its long axis, as is observed in the R–R ester complex. A fairly strong repulsion between N(1) and C(18) tilts the plane (II), whereas the contacts between N(4) and C(9) and between N(4) and C(11) tilt the plane (III) in the opposite sense. The deviations of the four nitrogen atoms at 293 K are the same as those of the R–R ester complex. However, the deviations of C(1), C(2), and C(3) are not so large. In the ester complex,

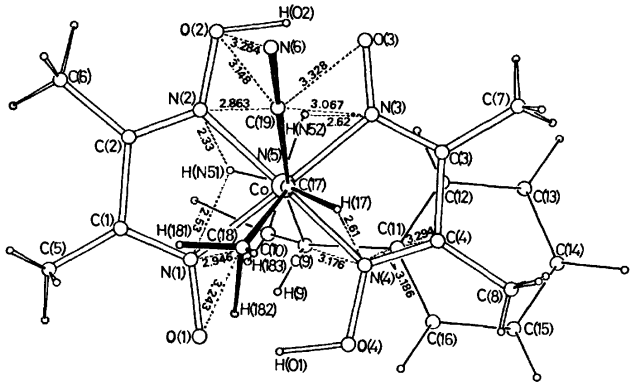

Fig. 1. Projection of the complex onto the mean plane of four nitrogen atoms of $Co(dmg)_2$ and the short contacts between non-bonded atoms (l/Å) at 293 K, their threshold values being 3.400 Å for distances between the non-bonded atoms and 2.70 Å for those including hydrogen atoms.

TABLE 6. SHORT CONTACTS BETWEEN THE NON-BONDED ATOMS (l/Å)

	293 K	173 K
N(1)···C(18)	2.946(12)	2.914(8)
N(1)···H(N51)	2.53(7)	2.56(5)
N(2)···C(19)	2.863(9)	2.880(7)
N(2)···H(N51)	2.33(7)	2.49(5)
N(3)···C(19)	3.067(11)	3.051(7)
N(3)···H(N52)	2.62(8)	2.44(6)
N(4)···C(9)	3.176(9)	3.163(7)
N(4)···C(11)	3.186(8)	3.245(6)
O(1)···C(18)	3.243(11)	3.244(8)
O(2)···C(19)	3.148(10)	3.142(7)
O(2)···N(6)	3·284(10)	3.257(8)
O(3)···C(19)	3.328(9)	3.296(6)
C(4)···C(11)	3.294(10)	3.266(7)

TABLE 7. BOND DISTANCES (l/Å) (e.d.s.'s are in parentheses)

	293 K	173 K		293 K	173 K
Co-N(1)	1.898(5)	1.904(4)	O(1)-H(O1)	1.34(13)	1.57(5)
Co-N(2)	1.883(5)	1.883(4)	O(2)-H(O2)	1.20(10)	1.28(7)
Co-N(3)	1.874(6)	1.893(4)	O(3)-H(O2)	1.37(10)	1.26(7)
Co-N(4)	1.901(5)	1.878(4)	O(4)-H(O1)	1.19(13)	0.94(5)
Co-N(5)	2.088(6)	2.070(6)	C(5)-H(51)	0.76(9)	0.89(6)
Co-C(17)	2.036(8)	2.056(6)	C(5)-H(52)	1.18(9)	1.00(5)
N(1)-O(1)	1.352(7)	1.348(5)	C(5)-H(53)	1.00(9)	0.77(6)
N(1)-C(1)	1.276(9)	1.273(7)	C(6)-H(61)	1.03(9)	1.01(6)
N(2)-O(2)	1.347(8)	1.355(7)	C(6)-H(62)	0.97(7)	0.85(7)
N(2)-C(2)	1.302(9)	1.296(7)	C(6)-H(63)	1.06(10)	1.12(7)
N(3)-O(3)	1.307(8)	1.331(6)	C(7)-H(71)	0.92(8)	0.97(4)
N(3)-C(3)	1.333(9)	1.316(6)	C(7)-H(72)	0.79(6)	0.82(6)
N(4)-O(4)	1.347(7)	1.374(6)	C(7)-H(73)	0.74(9)	1.04(6)
N(4)-C(4)	1.304(9)	1.302(6)	C(8)-H(81)	0.97(7)	0.88(5)
C(1)-C(2)	1.457(10)	1.466(7)	C(8)-H(82)	0.75(7)	1.09(5)
C(1)-C(5)	1.507(11)	1.510(8)	C(8)-H(83)	0.95(6)	0.92(5)
C(2)-C(6)	1.494(12)	1.491(8)	N(5)-H(N51)	0.86(7)	0.96(5)
C(3)-C(4)	1.485(10)	1.472(7)	N(5)-H(N52)	1.27(8)	0.86(6)
C(3)-C(7)	1.486(11)	1.482(7)	C(9)-H(9)	1.05(6)	1.00(7)
C(4)-C(8)	1.466(11)	1.493(7)	C(10)-H(101)	1.10(6)	0.92(5)
N(5)-C(9)	1.450(9)	1.480(7)	C(10)-H(102)	0.87(7)	0.85(6)
C(9)-C(10)	1.553(11)	1.539(8)	C(10)-H(103)	1.00(7)	0.94(6)
C(9)-C(11)	1.524(10)	1.524(7)	C(12)-H(12)	0.86(6)	0.96(4)
C(11)-C(12)	1.359(11)	1.398(7)	C(13)-H(13)	1.13(7)	0.84(7)
C(11)-C(16)	1.381(11)	1.384(8)	C(14)-H(14)	1.11(8)	1.03(5)
C(12)-C(13)	1.389(12)	1.375(8)	C(15)-H(15)	0.88(6)	0.89(5)
C(13)-C(14)	1.388(12)	1.374(14)	C(16)-H(16)	0.87(6)	0.85(6)
C(14)-C(15)	1.355(14)	1.405(14)	C(17)-H(17)	0.96(8)	1.18(6)
C(15)-C(16)	1.366(13)	1.364(10)	C(18)-H(181)	1.05(9)	1.17(6)
C(17)-C(18)	1.478(13)	1.536(9)	C(18)-H(182)	1.47(10)	1.01(6)
C(17)-C(19)	1.465(11)	1.461(8)	C(18)-H(183)	0.92(7)	0.96(10)
C(19)-N(6)	1.109(11)	1.123(8)			

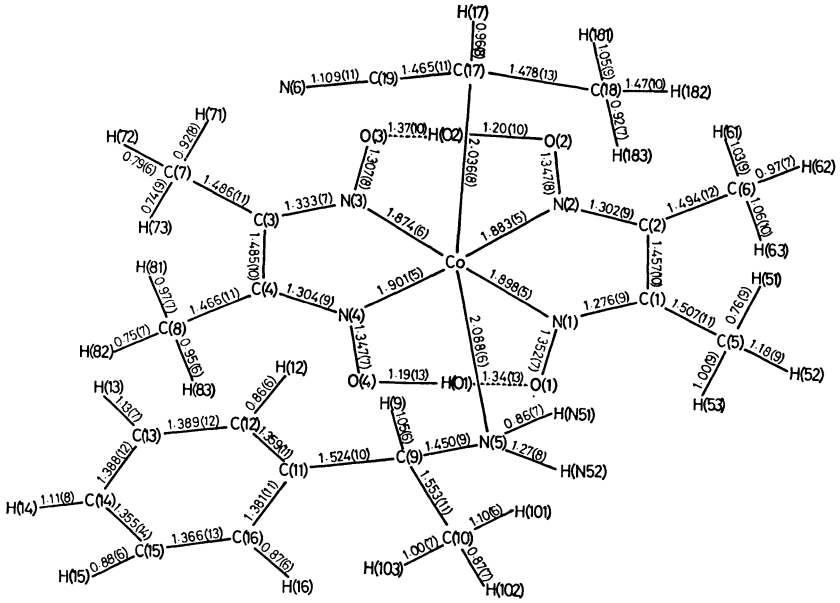

Fig. 2. Bond distances (l/Å) at 293 K. Their standard deviations are in the parentheses.

TABLE 8. BOND ANGLES (ϕ/°) (e.s.d.'s are in parentheses)

	293 K	173 K		293 K	173 K
N(1)-Co-N(2)	81.0(2)	81.1(2)	N(4)-C(4)-C(3)	112.0(6)	112.3(4)
N(1)-Co-N(3)	178.1(2)	179.0(2)	N(4)-C(4)-C(8)	126.0(7)	125.5(5)
N(1)-Co-N(4)	98.1(2)	98.3(2)	C(3)-C(4)-C(8)	121.6(7)	122.2(4)
N(1)-Co-N(5)	89.5(2)	89.9(2)	Co-N(5)-C(9)	125.2(4)	124.4(3)
N(1)-Co-C(17)	92.7(3)	92.8(2)	N(5)-C(9)-C(10)	110.3(6)	111.0(4)
N(2)-Co-N(3)	98.3(3)	98.8(2)	N(5)-C(9)-C(11)	112.5(6)	113.3(4)
N(2)-Co-N(4)	178.8(2)	179.1(2)	C(9)-C(11)-C(12)	122.7(7)	122.0(5)
N(2)-Co-N(5)	87.3(2)	86.2(2)	C(9)-C(11)-C(16)	118.7(7)	120.5(5)
N(2)-Co-C(17)	91.2(3)	92.0(2)	C(12)-C(11)-C(16)	118.0(7)	117.5(5)
N(3)-Co-N(4)	82.7(2)	81.8(2)	C(11)-C(12)-C(13)	121.7(8)	120.6(5)
N(3)-Co-N(5)	88.8(2)	89.1(2)	C(12)-C(13)-C(14)	118.3(8)	121.7(7)
N(3)-Co-C(17)	89.1(3)	88.3(2)	C(13)-C(14)-C(15)	120.4(9)	117.8(10)
N(4)-Co-N(5)	93.4(2)	94.4(2)	C(14)-C(15)-C(16)	120.0(9)	120.4(8)
N(4)-Co-C(17)	88.1(3)	87.4(2)	C(11)-C(16)-C(15)	121.4(8)	122.0(6)
N(5)-Co-C(17)	177.2(3)	176.5(2)	Co-C(17)-C(18)	119.8(6)	117.2(4)
Co-N(1)-O(1)	122.3(4)	121.9(3)	Co-C(17)-C(19)	111.9(5)	110.8(4)
Co-N(1)-C(1)	116.4(5)	116.0(4)	C(18)-C(17)-C(19)	110.6(7)	111.2(5)
O(1)-N(1)-C(1)	121.1(5)	122.1(4)	C(17)-C(19)-N(6)	175.6(9)	177.9(6)
Co-N(2)-O(2)	122.7(4)	122.9(3)			
Co-N(2)-C(2)	117.0(5)	117.2(4)	N(1)-O(1)-H(O1)	107(5)	95(2)
O(2)-N(2)-C(2)	119.9(6)	119.7(4)	N(2)-O(2)-H(O2)	107(5)	106(3)
Co-N(3)-O(3)	124.1(5)	121.7(3)	N(3)-O(3)-H(O2)	106(4)	108(3)
Co-N(3)-C(3)	115.7(5)	116.1(3)	N(4)-O(4)-H(O1)	108(6)	91(3)
O(3)-N(3)-C(3)	120.0(6)	122.0(4)	O(1)-H(O1)-O(4)	155(11)	157(5)
Co-N(4)-O(4)	122.8(4)	122.9(3)	O(2)-H(O2)-O(3)	154(4)	156(6)
Co-N(4)-C(4)	116.3(5)	117.3(3)	Co-N(5)-H(N51)	89(5)	99(3)
O(4)-N(4)-C(4)	120.5(5)	119.9(4)	Co-N(5)-H(N52)	106(3)	96(4)
N(1)-C(1)-C(2)	113.7(6)	114.0(5)	C(9)-N(5)-H(N51)	118(5)	106(3)
N(1)-C(1)-C(5)	124.0(7)	123.0(5)	C(9)-N(5)-H(N52)	115(3)	115(4)
C(2)-C(1)-C(5)	122.1(6)	123.0(5)	H(N51)-N(5)-H(N52)	97(6)	116(5)
N(2)-C(2)-C(1)	111.8(6)	111.6(5)	N(5)-C(9)-H(9)	96(3)	110(4)
N(2)-C(2)-C(6)	120.9(7)	123.5(5)	C(10)-C(9)-H(9)	111(3)	103(4)
C(1)-C(2)-C(6)	127.3(7)	124.9(5)	C(11)-C(9)-H(9)	116(3)	110(4)
N(3)-C(3)-C(4)	112.8(6)	112.5(4)	Co-C(17)-H(17)	114(5)	125(3)
N(3)-C(3)-C(7)	122.7(7)	123.6(5)	C(18)-C(17)-H(17)	89(5)	77(3)
C(4)-C(3)-C(7)	124.4(7)	123.7(4)	C(19)-C(17)-H(17)	109(5)	111(3)

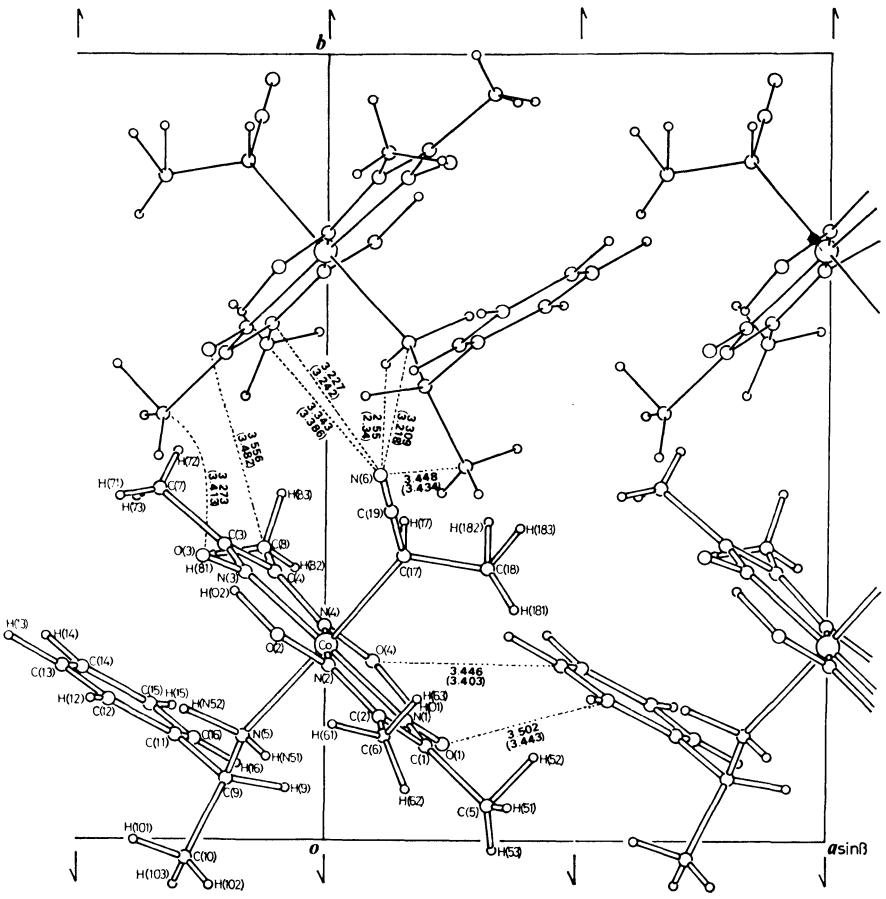

Fig. 3. Projection of the crystal structure along the c axis and short contacts bweteen complexes. The short contacts at 173 K are in the parentheses.

both of the methoxycarbonyl and methyl groups lie on the dmg planes. The carbon atoms of the dmg rings must deviate from the planes as a result of the steric repulsion from the methoxycarbonyl and methyl groups. The cyano and methyl groups in the present complex, on the other hand, are located over the gaps between the two dmg's. Therefore, only the nitrogen atoms should be affected by the steric repulsion from the cyanoethyl group.

The deviations of the atoms of the $Co(dmg)_2$ moiety from the plane (I') at low temperatures becomes smaller than those at room temperature. The short contacts between the non-bonded atoms at 173 K are compared with the corresponding ones at 293 K in Table 6. The distances at 173 K are rather smaller than those at 293 K.

The deviation of the cobalt atom from the mean plane of $Co(dmg)_2$ is small at both temperatures. The Co atom in the methyl complex is shifted by 0.04 Å from its mean plane of $Co(dmg)_2$ toward the amine ligand, whereas the Co atom in the ester complex deviates toward the ester group by 0.04 Å. This indicates that the deviation of the Co atom from the mean plane of $Co(dmg)_2$ is affected by the relative bulkiness of the axial ligands.

The bond distances at 293 K are shown in Fig. 2, and they are compared with the corresponding ones at 173 K in Table 7. The bond angles at both temperatures are listed in Table 8. The Co–C(17) and Co–N(5) bonds at 293 K are shorter by 0.02 Å and longer by 0.018 Å respectively than the corresponding ones at 173 K. The sums of the two bonds, however, are nearly equal at both temperatures. As the C(17) atom comes close to the cobalt atom at high temperatures, the angles of Co–C(17)–C(18) and Co–C(17)–C(19) become larger and the $Co(dmg)_2$ plane may be twisted more.

The three bonds around N(3), Co–N(3), N(3)–O(3), and N(3)–C(3), and the two bonds around N(4), Co–N(4), and N(4)–O(4) at 293 K have different distances from the corresponding ones at 173 K. The two angles around N(3), Co–N(3)–O(3), and O(3)–N(3)–C(3), have different values between the two temperatures. These differences may indicate that the resonance state of dmg is changed by the modified electronic state of Co, which is itself caused by the short Co–C distance at high temperatures.

The C(17)–C(18) distance at 293 K is significantly shorter then that at 173 K, probably because of the large thermal vibration of the C(18) atom. The other bond distances and angles are in fair agreement between the two temperatures.

The crystal structure viewed along the c axis is shown in Fig. 3, in which the short contacts are given. There is a short contact between N(5) and N(6) in the unit of $(-x, -0.5+y, 1-z)$. The N···N distances are 3.309 and 3.218 Å for 293 and 173 K respectively. The distanecs of H(N51)···N(6) and the angles of

Table 9. Characteristic dimensions of the amine in the various complexes

	Methyl	R-R ester	R-S(293 K)	R-S(173 K)	S-S(293 K)[a]	S-S(173 K)[a]	Average
Co-N(5)	2.087(9) Å	2.066(6)	2.088(6)	2.070(4)	2.054(5)	2.064(7)	2.072
N(5)-C(9)	1.463(15) Å	1.476(9)	1.450(9)	1.480(7)	1.487(9)	1.513(10)	1.479
C(9)-C(11)	1.541(16) Å	1.505(10)	1.524(10)	1.524(7)	1.508(10)	1.513(12)	1.519
N(4)-Co-N(5)	96.2(4)°	92.7(2)	93.4(2)	94.4(2)	94.3(2)	94.5(3)	94.3
Co-N(5)-C(9)	125.4(7)°	124.2(4)	125.2(4)	124.4(3)	125.4(4)	123.7(5)	124.8
N(4)···C(9)	3.252 Å	3.223(9)	3.176(9)	3.163(7)	3.132(9)	3.113(10)	3.177
N(4)-Co-N(5)-C(9)	17.6°	39.7	23.2	19.8	2.5	0.8	—
Co-N(5)-C(9)-C(11)	76.0°	89.9	77.4	78.3	79.7	80.2	78.3[b]
N(4)···C(11) or C(4)···C(11)	3.399 Å	3.340(9)	3.186(8)	3.245(6)	3.353(9)[c]	3.315(12)[c]	—
Bending of C(9)-C(11) from the phenyl ring	2.2°	4.0	4.0	2.9	3.3	4.8	3.5

a) Ref. 16. b) The value of the R-R ester is omitted. c) Distances of C(4)···C(11), the others being N(4)···C(11).

N(5)-H(N51)···N(6) are 2.55 Å and 149° for 293 K, and 2.34 Å and 152° for 173 K. This seems to be a weak hydrogen bond, judging from the previously reported N-H···N hydrogen bond.[14] The other contacts are not unusually short.

Discussion

In this serial study attempting to clarify the mechanism of inducing asymmetry, the distortion of the $Co(dmg)_2$ moiety has been examined for various substituted alkyl ligands. The optically acitve amine, α-methylbenzylamine, is kept unaltered except for its absolute configuration, because it seems necessary first to elucidate the effect of the substituted alkyl ligand on the $Co(dmg)_2$ moiety. For this purpose, it is assumed that the conformational change, if any, of the amine ligand is not seriously influenced by the intermolecular force or crystalline field, while it is influenced by the intramolecular force.

In Table 9, the characteristic dimensions and conformations of the amine in the crystal structures thus far determined are compared. As the crystals of the cyano complexes exhibit an abnormal thermal expansion, the values at 173 K are also listed. The Co–N(5) bond lengths range from 2.054 to 2.088 Å. Such variation seems to be brought about by the *trans* Co–C bond and will be discussed in detail in the following paper. The average length of N(5)–C(9) is in good agreement with the usual distance, 1.472± 0.005 Å.[15] The average distance of C(9)–C(11) is slightly longer than the usual one, 1.505±0.005 Å.[15] Bond distances, however, have relatively large variations. This may be due to the short contacts between the amine and the $Co(dmg)_2$ moiety.

The angles of N(4)–Co–N(5) and Co–N(5)–C(9) deviate from the right and tetrahedral angles respectively to avoid the short contact between N(4) and C(9). The average value of Co–N(5)–C(9)–C(11) is 78.3°. The torsion angle of the ester complex is significantly larger than the average value. This is due to the fact that the $Co(dmg)_2$ moiety is bent toward the amine. To avoid the short contacts between C(11)···N(4) and C(11)···C(4), the N(5)–C(9) bond rotates from the stable staggered form toward the eclipsed form.

The rotation around the Co–N(5) bond, that is, the torsion angle of N(4)–Co–N(5)–C(9), varies from 0.8° to 39.7°. In Part II of this series,[8] the most stable conformation was calculated to be 13°, and the potential energy curve against the torsion angle closely resembled a quadratic in the vicinity of 13°. For both cyano complexes, the deviations from the stable conformation are in the opposite direction, but are nearly equal. The energies should be practically the same for both complexes. The amine ligand in each cyano-complex crystal comes in contact with the cyanoethyl group of the neighbouring molecule. Such deviations in the opposite direction, therefore, should be brought about by the opposite configuration of the cyanoethyl group. The $Co(dmg)_2$ plane is bent toward the methyl group in the methyl complex, whereas it is bent toward the amine in the ester complex. The conformation around the Co–N(5) bond in the former complex is close to the stable one, whereas the bond in the latter rotates from the stable conformation to a considerable extent. These facts suggest that (i) the Co–N bond distance is apparently affected by the *trans* Co–C bond; (ii) although the conformation around the Co–N bond is affected by the crystalline field, the potential energy caused by such a conformation is nearly equal if the substituted alkyl group is the same except for its absolute configration, and (iii) the torsion angle of N(4)–Co–N(5)–C(9) depends on the bulkiness of the substituted alkyl group, showing 13+5° for the methyl group, 13±10° for the cyanoethyl group, and 13+27° for methoxycarbonyl group. The assumption mentioned above, therefore, holds good for the determined crystal structures. This seems to indicate that the difference in energy between the σ-complexes containing *R*- and *S*- substituted alkyl groups is attributable to the structure of the $Co(dmg)_2$ moiety or the Co–N and Co–C distances. These points will be discussed in detail in the following paper.

References

1) Y. Ohgo, S. Takeuchi, and J. Yoshimura, *Bull. Chem. Soc. Jpn.*, **44**, 283 (1971).

2) Y. Ohgo, S. Takeuchi, and J. Yoshimura, *Bull. Chem. Soc. Jpn.*, **44**, 583 (1971).
3) S. Takeuchi, Y. Ohgo, and J. Yoshimura, *Chem. Lett.*, **1973**, 265.
4) Y. Ohgo, S. Takeuchi, Y. Natori, and J. Yoshimura, *Chem. Lett.*, **1974**, 33.
5) Y. Ohgo, Y. Natori, S. Takeuchi, and J. Yoshimura, *Chem. Lett.*, **1974**, 709.
6) Y. Ohgo, Y. Natori, S. Takeuchi, and J. Yoshimura, *Chem. Lett.*, **1974**, 1327.
7) Y. Ohashi, Y. Sasada, Y. Tashiro, Y. Ohgo, S. Takeuchi, and J. Yoshimura, *Bull. Chem. Soc. Jpn.*, **46**, 2589 (1973).
8) Y. Ohashi and Y. Sasada, *Bull. Chem. Soc. Jpn.*, **50**, 1710 (1977).
9) Y. Ohashi and Y. Sasada, *Bull. Chem. Soc. Jpn.*, **50**, 2863 (1977).
10) Y. Ohashi and Y. Sasada, *Nature*, **267**, 142 (1977).
11) Y. Ohashi, Y. Sasada, and Y. Ohgo, *Chem. Lett.*, **1978**, 457.
12) Y. Ohashi, Y. Sasada, and Y. Ohgo, *Chem. Lett.*, **1978**, 743.
13) "International Tables for X-Ray Crystallography," Vol. IV, The Kynoch Press, Birmingham (1974), p. 72.
14) G. C. Pimentel and A. L. McClillan, "The Hydrogen Bond," W. H. Freeman and Company, San Francisco and London (1960) p. 288.
15) L. E. Sutton, "Tables of Interatomic Distances and Configuration in Molecules and Ions. Supplement," Special Publication No. 18, The Chemical Society, London (1965).
16) Y. Ohashi, Y. Sasada, S. Takeuchi, and Y. Ohgo, *Bull. Chem. Soc. Jpn.*, to be published.

The Deuteron Magnetic Resonance of Tin(II) Chloride Dihydrate Single Crystals in High- and Low-temperature Phases

Hideko KIRIYAMA* and Osamu NAKAMURA**

Department of Chemistry, Faculty of Science, Kobe University, Nada-ku, Kobe 657

***Government Industrial Research Institute, Osaka, Midorigaoka 1, Ikeda, Osaka 563*

(Received September 3, 1979)

The deuteron magnetic resonance spectra of $SnCl_2 \cdot 2D_2O$ single crystals have been measured from 208 to 300 K in order to elucidate the static and dynamic structures of water molecules in connection with the phase transition occuring at 234 K. The deuteron quadrupole coupling constants (asymmetry parameters) were determined at 208 K for four non-equivalent water deuterons. These values are 194.2±0.3 (0.066±0.004), 193.2±0.5 (0.112±0.003), 223.3±0.4 (0.206±0.003), and 244.0±0.4 kHz (0.058±0.003), depending largely on the hydrogen-bond strength or the D···O distance. The deuteron arrangements deduced from the EFG tensors agreed well with the ordered structure reported by an earlier ND study. The dynamical process of deuterons responsible for the high-temperature disordered structure was analyzed with the aid of the ND results and was ascribed to a combination of the flip motion of water molecules about each two-fold axis and their rotational motion around each pseudo-three-fold axis.

The phase transition in $SnCl_2 \cdot 2H_2O$ (abbreviated as SCD) was first found at 218 K (at 234 K for its deuterium analogue) from an anomaly in the dielectric constant measured by Kiriyama and Kiriyama.[1] An earlier X-ray work showed that two kinds of water molecules are arranged alternately to form a characteristic H-bonded layer in the crystal lattice, and also that the phase transition is accompanied by no distinct change in the structure of non-hydrogen atoms.[2] A subsequent neutron diffraction (ND) experiment determined the ordered and disordered arrangements of deuterons below and above the phase-transition temperature, T_t, respectively.[3,4] On the other hand, proton (PMR) and deuteron (DMR) magnetic resonance studies provided direct evidence that the phase transition is due to the ordering of hydrogen (or deuterium) atoms in the H-bonded network.[5] A closer X-ray examination of the structure has disclosed that, in the vicinity of T_t, the [100] and [001] axial lengths and, consequently, the three H-bonded O···O distances steeply change in association with the ordering of the hydrogen atoms.[4]

The ordering process of water hydrogens and the various critical phenomena upon the phase transition were investigated in detail by means of heat-capacity[6] and dielectric measurements[7] as well as by Raman spectroscopies.[8,9] A statistical theory developed for use with the two-dimensional H-bonded network by Salinas and Nagle is helpful in understanding the mechanism of the phase transition as well.[10]

In order to locate the hydrogen atoms in the low-temperature phase and to clarify their dynamic nature, involving the motion of the water molecules in the high-temperature phase, DMR and PMR experiments were carried out using single crystals. Some of these results have been reported previously.[1,5,11]

Experimental

Sample. A commercially available extra-pure reagent, SCD, was ground into a fine powder and then dehydrated in a vacuum desiccator for 12 d at room temperature. The anhydrous sample so obtained was identified by means of its X-ray powder patterns and IR spectra. For the present DMR work, large single crystals were needed to obtain suitable signals. About $20 \times 15 \times 40$ mm^3 in size, they were grown by very slow cooling from saturated aqueous (D_2O) solution of the anhydrate, $SnCl_2$, which had been acidified with DCl. The crystal shape was an elongated prism parallel to the [001] axis, with well-developed side planes, (100) and (110). All the interfacial angles of a deuterated crystal were identical to those of the non-deuterated one, within the limits of experimental error, in accord with the fact that the lattice constants of the two compounds are almost the same.[4] The single crystals were cut and shaped into cylindrical rods, typically 15 mm in diameter × 20 mm long. The axes of the three cylinders were chosen to be parallel to the crystallographic b and c axes, and the normal, to the (100) plane; the last direction will, hereinafter, be referred to as a* axis for convenience.

Measurements. The deuteron magnetic resonance spectra were measured at the Larmor frequency of 6.9 MHz with a frequency-variable, Pound-Watkins-type spectrometer and at 8 MHz with a bridge-type spectrometer (JNM-8, JEOL). The quadrupole effect on NMR or quadrupole splitting was measured at five-degree intervals of rotation angle about each of the mutually perpendicular axes, a*, b, and c. The temperature of a sample was measured by the use of a calibrated copper-constantan thermocouple and was controlled to ±0.3 K throughout the experiments.

Preliminary Remarks

Crystal Structure. The previous X-ray examination showed that no significant isotope effects on the lattice parameter and on the crystal structure are observed on deuterium substitution. Therefore, unless otherwise noted, the description of the structure will be concerned with ordinary $SnCl_2 \cdot 2H_2O$. The crystal is monoclinic, with the space group $P2_1/c$ and with $Z=4$. The lattice parameters are $a=9.158$, $b=7.156$, $c=8.942$ Å, and $\beta=114.50°$ at 88 K, and $a=9.320$, $b=7.277$, $c=8.970$ Å, and $\beta=114.91°$ at 293 K.[2,4] The unit cell contains two kinds of water molecules; the first, $H_2O(1)$, coordinates to a tin(II) atom to form a trigonal pyramid of the dichloroaquatin(II) complex, $SnCl_2 \cdot OH_2$, whereas the second, $H_2O(2)$, does not (Fig. 1). These two kinds of water molecules are alternately connected by three O–H···O-type H-bonds, and the resulting sheets run parallel to the (100) plane. On the assumption of a double-minimum

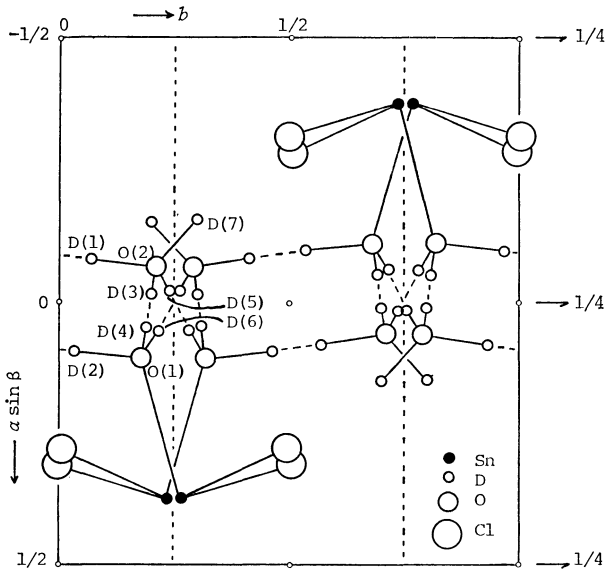

Fig. 1. The crystal sturcture projected on the (001) plane. The graphical symbols show the symmetry axes ($\bar{1}$ and 2_1) and the glide plane.

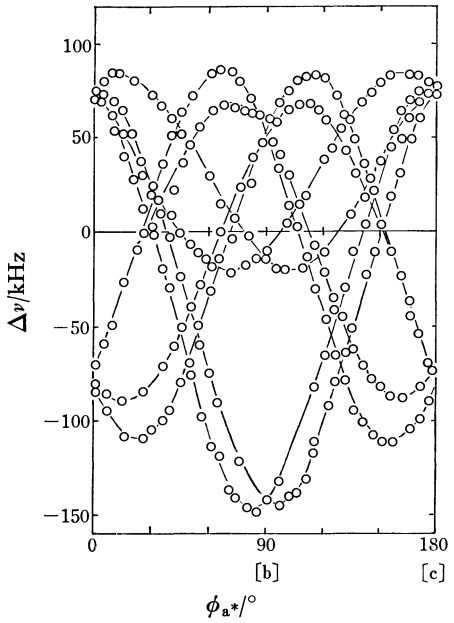

Fig. 2(a). The rotation pattern around the a* axis at 208 K.

potential for each H-bond, the seven sites shown in Fig. 1 are possible for four independent water–hydrogens.

Analytical Method. The quadrupole interaction in the present study can be treated as a first-order perturbation to the Zeeman energy, because the deuteron quadrupole coupling constant, e^2qQ/h, of about 200 kHz for a stationary water deuteron is much smaller than both Larmor frequencies of measurements. When a single crystal is turned about the z-axis, *i.e.*, for the z-axis rotation, the quadrupole splitting measured from the Larmor frequency, $\Delta\nu_z$, is expressed in the following convenient form:[12]

$$\Delta\nu_z = (3/8)(eQ/h)[V^1_{zz}-(V^1_{xx}-V^1_{yy})\cos 2\phi - 2V^1_{xy}\sin 2\phi] \quad (1)$$

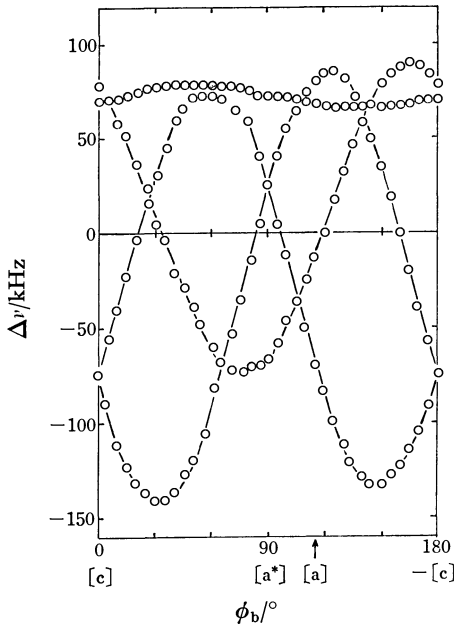

Fig. 2(b). The rotation pattern around the b axis at 208 K.

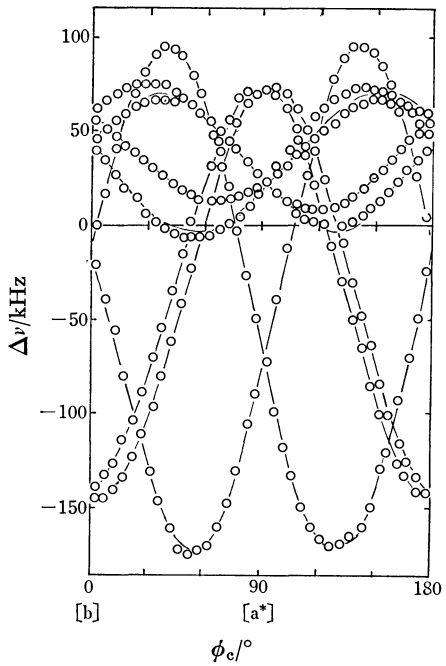

Fig. 2(c). The rotation pattern around the c axis at 208 K.

where V^1_{ij} is the electric-field gradient (EFG) tensor at a given deuteron site in the laboratory coordinate system (x, y, z) fixed to a probe head and where ϕ is the angle of the static magnetic field, H_0, measured from the reference axis (x-axis) on the rotation plane. The angular dependence or the rotation pattern of $\Delta\nu_z$ around the z-axis yields only the first three of the five independent EFG components, V^1_{xx}, V^1_{yy}, V^1_{xy}, V^1_{yz}, and V^1_{zx}. For this reason, the rotation patterns were measured around the three a*, b, and c axes, and then combined in the usual way. By diagonalizing the tensors thus obtained, the principal values and the direction cosines of the principal axes for every

Table 1. Quadrupole coupling constants(e^2qQ/h), asymmetry parameters(η), and direction cosines of the principal axes of the EFG tensors for Model I at 208 K, with the associated standard deviations in parentheses

	$\frac{e^2qQ/h}{\text{kHz}}$	η		Direction cosines a*	b	c
D (2)	194.2 (3)	0.066 (4)	q_{xx}	0.577 (24)	−0.141 (1)	−0.805 (17)
			q_{yy}	−0.815 (17)	−0.030 (4)	−0.579 (24)
			q_{zz}	−0.058 (1)	−0.990 (1)	0.132 (1)
D (4)	193.2 (5)	0.112 (3)	q_{xx}	−0.166 (13)	0.892 (6)	−0.420 (7)
			q_{yy}	0.843 (2)	0.349 (14)	0.409 (7)
			q_{zz}	−0.511 (1)	0.287 (1)	0.810 (1)
D (5)	223.3 (4)	0.206 (3)	q_{xx}	0.683 (4)	−0.721 (4)	−0.121 (3)
			q_{yy}	−0.552 (4)	−0.617 (4)	0.560 (1)
			q_{zz}	0.478 (1)	0.316 (1)	0.820 (1)
D (7)	244.0 (4)	0.058 (3)	q_{xx}	−0.205 (16)	−0.493 (17)	−0.846 (14)
			q_{yy}	−0.607 (6)	−0.614 (14)	0.505 (23)
			q_{zz}	−0.768 (1)	0.617 (1)	−0.173 (1)

Table 2. Quadrupole coupling constants, asymmetry parameters, and direction cosines of the principal axes of the EFG tensors for Model II at 208 K (standard deviations in parentheses)

	$\frac{e^2qQ/h}{\text{kHz}}$	η		Direction cosines a*	b	c
D (2)	194.2 (3)	0.066 (4)	q_{xx}	−0.577 (24)	−0.141 (1)	0.805 (17)
			q_{yy}	−0.815 (17)	0.030 (4)	−0.579 (24)
			q_{zz}	0.058 (1)	−0.990 (1)	−0.132 (1)
D (4)	195.0 (5)	0.066 (3)	q_{xx}	−0.455 (17)	−0.891 (1)	−0.005 (12)
			q_{yy}	−0.741 (10)	0.381 (20)	−0.553 (1)
			q_{zz}	−0.494 (1)	0.247 (1)	0.833 (1)
D (5)	223.0 (4)	0.117 (3)	q_{xx}	0.582 (7)	−0.813 (5)	−0.004 (6)
			q_{yy}	−0.647 (6)	−0.466 (9)	0.603 (1)
			q_{zz}	0.493 (1)	0.348 (1)	0.797 (1)
D (7)	244.0 (4)	0.058 (3)	q_{xx}	−0.205 (16)	−0.493 (17)	−0.846 (14)
			q_{yy}	−0.607 (6)	−0.614 (14)	0.505 (23)
			q_{zz}	−0.768 (1)	0.617 (1)	−0.173 (1)

EFG were determined in the crystallographic coordinate system.[13]

When a water molecule reorients rapidly at high temperatures, as in the present case, the EFG tensor for the moving deuteron should be averaged over the several sites spent by it. This averaging is actually performed by superposing the individual EFG's.

Results and Discussion

DMR Spectra in the Low-temperature Phase. Below the transition temperature (234 K), eight, four, and eight pairs of lines were observed about the a*, b, and c axes respectively, with a maximum splitting of about 180 kHz. These facts indicate that two nonequivalent water molecules are stationary in the low-temperature phase on the DMR scale. Every rotation pattern is consistent with the space group $P2_1/c$, which is the same as in the high-temperature phase. Thus, the present results provided no evidence in support of the antiferroelectric nature below T_t proposed by Mognaschi *et al.*,[7] in accord with the X-ray and ND results.

The rotation patterns measured at 208 K are presented in Fig. 2. As the figure shows, two independent pairs of sine curves cross at nearly the same point on each diagram when the magnetic field is along either the a*, b, or c axis. Therefore, the EFG tensors were calculated for 80 possible combinations of the sine curves. Such a large number of possibilities, however, was first reduced to one-half its initial number by assuming an e^2qQ/h value of about 200 kHz and an η value of nearly zero for a stationary water deuteron. Secondly, the number was further reduced to ten from the viewpoint of crystal symmetry involving the two-fold axis and the c-glide plane.

Then, we tried to assign the obtained EFG tensors to the individual deuterons on the basis of the following empirical rules:[12,14]

(1) the principal z axis of an EFG tensor is nearly

TABLE 3. RELATION BETWEEN THE DIRECTIONS OF THE PRINCIPAL AXES OF THE EFG TENSORS AT 208 K AND THE CONFIGURATION OF THE WATER MOLECULES IN SCD (standard deviations in parentheses)

		O(1)		O(2)	
		D(2)	D(4)	D(5)	D(7)
ϕ_z/°	Model I	6.9(16)	11.2(15)	3.0(39)	—
	Model II	14.0(22)	9.2(19)	3.0(38)	—
	ND	6.1(33)	8.0(29)	2.3(34)	—
ψ_z/°	Model I	10.9(22)	4.1(26)	1.1(42)	1.1(34)
	Model II	8.3(24)	2.3(25)	1.4(44)	1.1(34)
θ_{yy}/°	Model I	20.9(31)		4.7(76)	
	Model II	20.7(35)		10.5(107)	
θ_{zz}/°	Model I	98.5(1)		108.3(1)	
	Model II	112.5(1)		107.6(1)	
	ND	104.0(5)		106.4(5)	

parallel to the direction of an O–D bond, and

(2) the principal y axis is nearly perpendicular to the molecular plane of D_2O.

The assignment based on the empirical rules successfully reduced the combination number to only two. For these models, I and II, the values of e^2qQ/h and η are summarized in Tables 1 and 2, where the direction cosines of each EFG principal axis are also included. In practice, however, no significant difference is observed between them in regard to the deuteron arrangement, *viz.*, the configuration of the water molecules of interest.

Configuration of Water Molecules. As has been described previously, the crystal structure suggests three and four available deuteron sites in the neighborhoods of O(1) and O(2) respectively.[2] If the Bernal and Fowler rules hold for the H-bonded water layers in SCD, then three of deuteron arrangements or of H-bonding schemes may be anticipated for an ordered state below T_t. Of these, only one type of scheme could be judged by the assignment of EFG for either model. The results obtained were in good agreement with the ND results, in turn supporting our assignment (Fig. 3a).

In Table 3, the configurations of water molecules for Models I and II are compared with those from the ND work, by using four characteristic angles, ϕ_z, ψ_z, θ_{yy}, and θ_{zz}; ϕ_z is the angle between the principal z-axis and the assigned O(D)···O direction of a deuteron; ψ_z, the angle between the principal z-axis and the O–D direction determined by ND; θ_{yy}, the angle between the principal y axes at two deuteron sites of a water molecule, and θ_{zz}, the corresponding angle between the two principal z axes.

The ϕ_z angle is widely spread, from 3° to 14°, and its maximum was found at $D_2O(1)$, probably because of its small acceptor angles, O···O(1)···O, such as 90.2° at 88 K (88.2° at 297 K).[4] On the other hand, the values of ψ_z are nearly zero, within the limit of experimental error, except for D(2). These facts provide additional evidence for the validity of the empirical rule (1) which has been used for suggesting O–D directions on the basis of the DMR results. The θ_{yy} values of $D_2O(1)$ in both models are about 21°,

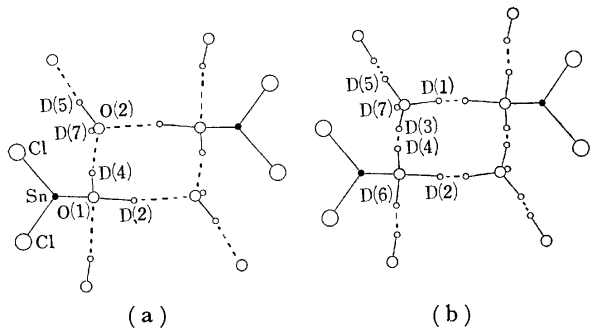

(a) (b)

Fig. 3. Configuration of water molecules in (a) low- and (b) high-temperature phases.

considerably larger than the experimental values in the literature. The θ_{zz}'s of $D_2O(2)$ for both models are very close to the average bond-angle (108°) for water molecules of crystallization, and also to the ND results. Concerning the θ_{zz}'s of $D_2O(1)$, a slight but significant difference was disclosed between the two models. That is, the θ_{zz} values are 98.5° for the configuration Model I and 112.5° for II, compared with the D–O–D angle of 104.0° at 88 K (102.7° at 297 K) obtained from the ND results. In addition to the fact that the bond angle of a water molecule may be affected by forming O–D···O hydrogen bonds only a little, the EFG at the deuteron site may be influenced to some extent by the H-bonded-acceptor oxygen. It is, therefore, probable that the θ_{zz} of $D_2O(1)$ is smaller than the D–O(1)–D bond angle determined by ND; for this reason, Model I has been chosen as the basis for further discussion.

As has been mentioned earlier, Salinas and Nagle proposed a statistical model of the two-dimensional H-bonded network in SCD. They succeeded in predicting the temperature dependence of hydrogen occupancy at individual sites as well as the deuteron arrangements in the ordered structure.[10] On the other hand, Wang *et al.* demonstrated that the intensity of the Raman spectra associated with H-bonded vibrations changes gradually and continuously near T_t. They discussed this feature on the basis of the occupation probabilities of hydrogens at the various sites.[9] Under these circumstances, it became necessary to confirm whether or not the present DMR data are of the completely ordered state, because the temperature of the measurements, 208 K, is lower than T_t by only 26 K. However, the experimental results regarding the two-fold b-axis showed that the resonance line assignable to D(5) has almost the same intensity as those of the remaining three lines and that no absorption due to D(6) can be detected. It is, therefore, certain that the ordered arrangements of deuterium atoms are well established, even at 208 K, at least on the DMR scale. Unfortunately, no spectra could be observed below 200 K, possibly because of the very long spin-lattice relaxation times.

H-bonds in the Ordered-phase below T_t. It has been recognized that the quadrupole coupling constant of a deuteron, e^2qQ/h, reflects the H-bond strength and, consequently, depends on the O···O distance or, more precisely, on the D···O distance. Soda and

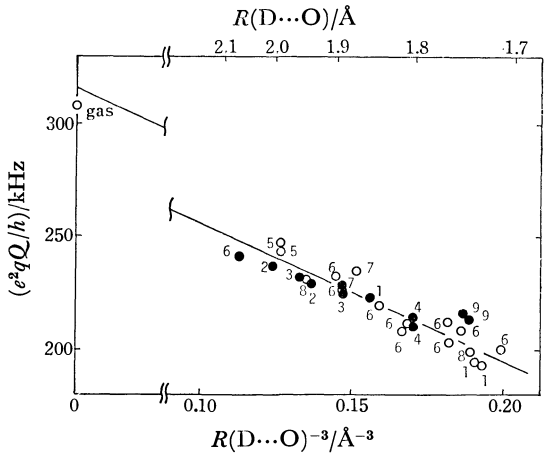

Fig. 4. Correlation between the observed quadrupole coupling constants and the reciprocal cube of hydrogen bond length R(D···O) in O-D···O type of hydrogen bonds. Black circles indicate the plot for non-coordinated water molecules. The plots correspond to 1: $SnCl_2 \cdot 2D_2O$ (this work and Ref. 4), 2: α-$(COOD)_2 \cdot 2D_2O$,[17,18] 3: β-$(COOD)_2 \cdot 2D_2O$,[17,18] 4: $(KCOO)_2 \cdot D_2O$,[19,20,21] 4: $Ba(ClO_3)_2 \cdot D_2O$,[12,22,23] 6: $CuSO_4 \cdot 5D_2O$,[15,24] 7: $NaHC_2O_4 \cdot D_2O$[25] 8: $LiHCOO \cdot D_2O$,[26,27] and 9: D_2O(Ice).[28,29]

Chiba first derived a useful relation based on the available DMR and ND results:[15]

$$e^2qQ/h = 310.0 - 3.0 \times \frac{190.6}{R(\mathrm{D}\cdots\mathrm{O})^3} \quad \text{(in kHz)}, \qquad (2)$$

where R(D···O) is the D···O distance in Å units. The coefficient, 190.6(kHz), is the e^2qQ/h value of a deuteron due to a unit charge placed apart from it by 1 Å. It is noteworthy that the constant, 310.0 kHz, is close to the e^2qQ/h value (307.95 kHz)[16] for a free water molecule in spite of the lesser reliablity of the early ND data. By using more reliable, three-dimensional ND results, including those in SCD, value of e^2qQ/h is plotted again as a function of R(D···O) in Fig. 4. The least-squares fitting on the 27 data points of nine hydrated crystals as well as of ice gave the following relation:

$$e^2qQ/h = 317.1 - 3.0 \times \frac{200.2}{R(\mathrm{D}\cdots\mathrm{O})^3} \quad \text{(in kHz)}, \qquad (3)$$

where, the coefficient, 200.2 kHz, is based on a recent, experimental value of eQ (2.875×10^{-27} cm^2).[30] As can be seen in Fig. 4, no discrimination between coordinated water molecules and non-coordinated ones is necessary at all for relating e^2qQ/h to R(D···O). The above relationship will be used below to estimate the unknown value of e^2qQ/h from a known R(D···O).

DMR Spectra in the High-temperature Phase. The pair separation, $2\Delta\nu$, and the width of each component line were almost unchanged up to T_t (234 K), above which the whole spectra disappeared. As the temperature was further raised up to about 280 K, the signal again became observable. Figure 5 represents a typical temperature dependence of the quadrupole splitting at a rotation angle of $\phi_b = 95°$ around the two-fold b axis where the ϕ_b angle is measured away from the positive c axis toward the positive a axis

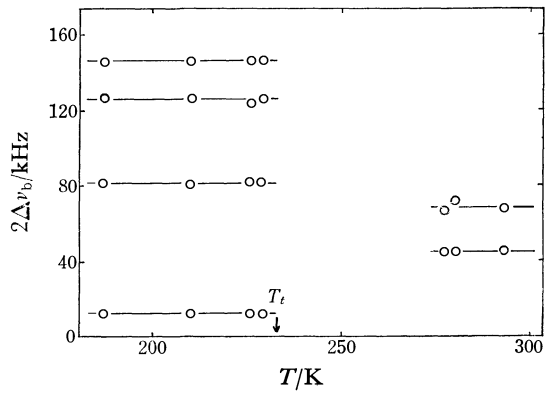

Fig. 5. The temperature dependence of quadrupole splittings around b-axis. $\phi_b = 95°$.

on the b plane (010). It should be noted that, in the high-temperature phase, the number of splitting is reduced by half and the pair separation, $2\Delta\nu$, decreases to less than half its low-temperature, rigid-lattice value. These facts indicate that all the deuterons are in some motional state above T_t and that their rate becomes fast enough to make the high-temperature spectra observable above 280 K. Since the S/N ratio of the signal was very poor, no motional parameter of deuterons could be estimated from the collapse of the splitting lines or line broadening. The above feature of the spectra, however, can be explained by assuming that the correlation time for deuterons is of the same order as for protons; the values determined from the pulsed PMR measurement are 2.3×10^{-5} and 2.3×10^{-7} s at 230 and 280 K respectively.[5]

Additionally, the high-temperature signal was observable only in a restricted angular region of less than 50° around the a* direction, which is perpendicular to the H-bonded water layer. The angular dependences of the experimental quadrupole splitting about the b and c axes are reproduced in Fig. 6.[5] The spectrum about the b axis clearly splitted into two pairs of lines. This finding, together with the symmetry relation, allowed us to expect the observation of four pairs of lines for the c-axis rotation. The outermost lines indeed showed the doublet structure at ϕ_c's of 105° and 110°, corroborating this expectation.

Deuteron Motion in the High-temperature Phase. The maximum splitting at room temperature is only about 40 kHz, much smaller than that expected for the two-fold reorientation, *i.e.*, the 180° flipping of water molecules. In the present case, however, the average EFG tensors for moving deuterons cannot be deduced because of the incomplete data above T_t. In order to clarify the dynamic process responsible for the deuteron disordered structure, we tried to simulate the rotation pattern for various types of motion suggested by the ND results (Fig. 3b). The average EFG for the moving deuteron in question was computed by using the method described previously. In this calculation, the empirical rules (1) and (2), and either the typical, found or expected values for e^2qQ/h and η in the stationary state were used. Then, the validity of each motional model was judged by the number of component lines about

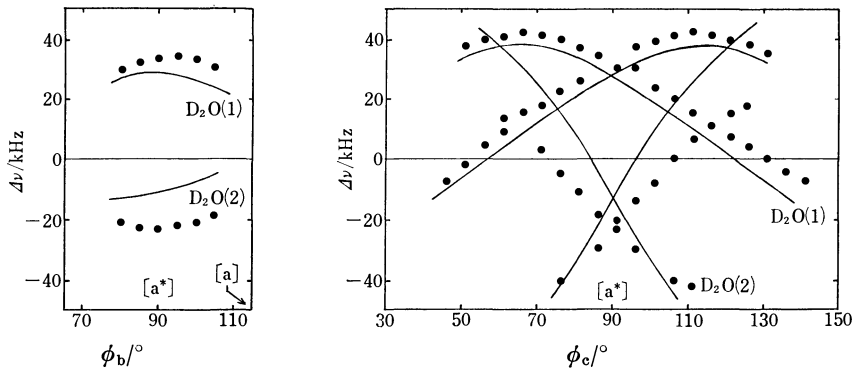

Fig. 6. Rotation patterns around (a) b-axis and (b) c-axis at room temperature. Soild curves indicate the calculated ones for Motion 5.

the unique b-axis, the width of quadrupole splitting, $\Delta\nu$, and its angular dependence.

First, the following three types of motion were checked:

Motion 1: *The 180°-flip of water molecules about each two-fold axis, as is found in many hydrated crystals.* The rotation pattern simulated about the b axis coincides with the observation in the number of splitting, but it differs greatly from the measurement in its magnitude and angular dependence.

Motion 2: *The jump motion of deuterons between two equilibrium positions in an O–D···O deuteriun bond, as is recognized in some H-bonded crystal like ferroelectric KH_2PO_4 substances.* This type of motion leads to four pairs of lines, which are assigned to the D(1)–D(2), D(3)–D(4), D(5)–D(6), and D(7) sites illustrated in Fig. 3b, in disagreement with the observation of only two pairs.

Motion 3: *The hindered rotation of both kinds of water molecules about their pseudo-three-fold axes, as proposed from the earlier ND results.*[5] In such a case, because one deuteron of $D_2O(2)$ is fixed at the D(7) site, three pairs of lines are expected; they are assigned to the D(7) and D(1)–D(3)–D(5) sites for $D_2O(2)$ and the D(2)–D(4)–D(6) sites for $D_2O(1)$, with an intensity-ratio of 1 : 1 : 2. This motion can also be excluded in view of the number of splitting.

Hence, it became necessary to combine either two or three of the above three types of motion in order to explain the experimental results. The following models were further examined:

Motion 4: *The combination of Motions 1 and 2.* This model gives rise to only a single spectral line, because all deuterons can move from one to another throughout all the seven deuteron sites, D(1)—D(7). Therefore, this can not be the case.

Motion 5: *The combination of Motions 1 and 3.* Two pairs of spectral lines are anticipated, because two deuterons of $D_2O(1)$ exchange their sites among the D(2), D(4), and D(6) sites, while those of $D_2O(2)$ do so among the D(1), D(3), D(5), and D(7) sites. The rotation pattern for this model was tentatively calculated by using the typical values of e^2qQ/h (=220 kHz) and $\eta(=0)$ for all the deuterons, regardless of the difference in H-bond strength discussed above. On averaging the EFG tensors, it must be taken into account that the molecular planes of both $D_2O(1)$ and $D_2O(2)$ change their orientations through Motion 5, with the probabilities depending on the occupancy factors of the individual deuteron sites, which are determined by the ND study. The occupancies of the D(2), D(4), and D(6) sites for $D_2O(1)$ were initially approximated by 2/3, while those of the D(1), D(3) and D(5) sites were approximated by 1/3 and that of D(7); by 1 for $D_2O(2)$.[3] Thus, the simulated rotation patterns around the b and c axes resemble to the experimental ones, especially in the magnitude of splitting and number (Fig. 3 in Ref. 5). This adequacy of the model led us to compute the rotation pattern based on the reasonable coupling constants derived from Eq. 3 and on the occupancies obtained from the ND study.[4] The results are shown in Fig. 6. The fit to the observation is not very good, but the agreement between them seems satisfactory enough in view of the oversimplified model and the uncertainty in both DMR and ND experiments at room temperature.

Motion 6: *The combination of Motions 2 and 3.* Two pairs of lines with the intensity ratio of 1 : 3 are to be expected for the b-axis rotation; the former is assigned to the D(7) site, and the latter, to all the other sites from D(1) to D(6). Since the observed intensity ratio was almost 1 : 1, this model is not adequate.

Motion 7: *The combination of Motions 1, 2, and 3.* Because all deuterons can travel to all the deuteron sites, from D(1) to D(7), the b-rotation pattern may be expected to consist of only one pair of lines, in conflict with the observation.

It is, therefore, concluded that the motion of deuterium atoms in the high-temperature, disordered phase of SCD is best described as a combination of the 180°-flip and the hindered rotation about the Sn–O(1) and D(7)–O(2) bonds for $D_2O(1)$ and $D_2O(2)$ respectively. The direction of Sn–O(1) makes an angle of 16° with the axis normal to the H-bonded water layer, *viz.*, the a* axis, while the corresponding angle for D(7)–O(2) amounts to 41°.

The proton dynamics associated with the phase transition, as has been mentioned previously, have been investigated by Mognaschi *et al.*[7] They explained the critical phenomena of the dielectric constant in terms of a "critical slowing down" of the electric polarization, which was ascribed to the proton

transfer along an H-bond in a double-minimum potential. We cannot discuss such critical behavior from the viewpoint of DMR, since our data are lacking in the vicinity of T_t. On the other hand, a logarithmic plot of the proton spin-lattice relaxation times *vs.* the reciprocal temperature showed a deep, cusp-shaped reduction around T_t, in contrast to the prediction by Mognaschi *et al.*[5,7] The structural information from X-ray results may be significant in this regard. On passing through the transition, the distances of the three non-equivalent H-bonds vary with the temperature in different ways. Consequently, the resulting change in the potential energy makes the critical dynamics too complex to discuss in the light of the present theories.

The present DMR study has shown that the dynamic process occuring in the high-temperature phase well above T_t is assignable to Motion 5, that is, the combination of the 180°-flip and pseudo-C_3 reorientation of water molecules, excluding the deuteron transfer. Therefore, even if the jump motion along an H-bond is involved in the disordered phase, its rate must be too slow to affect the DMR spectra. In the earlier paper we pointed out that the noticeable d.c. conductivity found in SCD is attributable to the proton mobility, as with ice.[1] Mognaschi *et al.* have recently provided strong evidence for the protonic conduction and proposed a combination of the translation of protons along H-bonds and the rotation of water molecules as the conduction mechanism.[31] Another striking feature of our model is that the deuteron at D(7), whcih is free from any deuterium-bond, is not stationary, but travels among the four allowed sites around D(2). The occupancy factor at D(7) is expected to be unity, the same as in the low-temperature, ordered state, this being consistent with the ND results.

The authors wish to express their thanks to Professor Emeritus Ryôiti Kiriyama of Osaka University for his continued interest and fruitful discussion.

References

1) H. Kiriyama and R. Kiriyama, *J. Phys. Soc. Jpn.*, **28**, S114 (1970).
2) H. Kiriyama, K. Kitahama, O. Nakamura, and R. Kiriyama, *Bull. Chem. Soc. Jpn.*, **46**, 1389 (1973).
3) R. Kiriyama, H. Kiriyama, K. Kitahama, and O. Nakamura, *Chem. Lett.*, **1973**, 1105.
4) K. Kitahama and H. Kiriyama, *Bull. Chem. Soc. Jpn.*, **50**, 3167 (1977).
5) H. Kiriyama, O. Nakamura, and R. Kiriyama, *Chem. Lett.*, **1976**, 689.
6) T. Matsuo, M. Tatsumi, H. Suga, and S. Seki, *Solid State Commun.*, **13**, 1829 (1973); T. Matsuo, M. Oguni, H. Suga, and S. Seki, *Bull. Chem. Soc. Jpn.*, **47**, 57 (1974).
7) E. R. Mognaschi, A. Rigamonti, and L. Menafra, *Phys. Rev. B*, **14**, 2005 (1976).
8) H. Morisaki, H. Kiriyama, and R. Kiriyama, *Chem. Lett.*, **1973**, 1061.
9) C. H. Wang, M. Tatsumi, T. Matsuo, and H. Suga, *J. Chem. Phys.*, **67**, 3097 (1977).
10) S. R. Salinas and J. F. Nagle, *Phys. Rev. B*, **9**, 4920 (1974). S. R. Salinas and J. F. Nagle, *J. Phys. Soc. Jpn.*, **41**, 1643 (1976).
11) H. Kiriyama, O. Nakamura, and R. Kiriyama, *Acta Crystallogr., Sect. A*, **28**, S240 (1972).
12) T. Chiba, *J. Chem. Phys.*, **39**, 947 (1963).
13) G. M. Volkoff, H. E. Petch, and D. W. L. Smellie, *Can. J. Phys.*, **30**, 270 (1952).
14) R. Bersohn, *J. Chem. Phys.*, **32**, 85 (1960).
15) G. Soda and T. Chiba, *J. Chem. Phys.*, **50**, 439 (1969).
16) J. Verhoeven, A. Dymanus, and H. Bluyssen, *J. Chem. Phys.*, **50**, 3330 (1969).
17) T. Chiba and G. Soda, *Bull. Chem. Soc. Jpn.*, **44**, 1703 (1971).
18) P. Coppens and T. M. Sabine, *Acta Crystallogr., Sect. B*, **25**, 2442 (1969).
19) B. Pedersen, *Acta Chem. Scand.*, **22**, 453 (1968).
20) J. W. McGrath and G. W. Ossman, *J. Chem. Phys.*, **46**, 1824 (1967).
21) A. Sequeira, S. Srikanta, and R. Chidambaram, *Acta Crystallogr., Sect. B*, **26**, 77 (1970).
22) K. Haland and B. Pedersen, Proc. Colloq. Amp. 15th, Amsterdam (1969), p. 409.
23) S. K. Sikka, S. N. Momin, H. Rajagopal, and R. Chidambaram, *J. Chem. Phys.*, **48**, 1883 (1968).
24) G. E. Bacon and D. H. Titterton, *Z. Krystallogr.*, **141**, 330 (1975).
25) B. Berglund and J. Tegenfeldt, *Mol. Phys.*, **26**, 633 (1973).
26) B. Berglund, J. Lindgren, and J. Tegenfeldt, *J. Mol. Struct.*, **21**, 135 (1974).
27) R. Tellgren, P. S. Ramanujam, and R. Liminga, *Ferroelectrics*, **6**, 191 (1974).
28) P. Waldstein, S. W. Rabideau, and J. A. Jackson, *J. Chem. Phys.*, **41**, 3407 (1964).
29) S. W. Peterson and H. A. Levy, *Acta Crystallogr.*, **10**, 70 (1957).
30) R. V. Reid, Jr., and M. L. Vaida, *Phys. Rev. Lett.*, **29**, 494 (1972).
31) E. R. Mognaschi, A. Chierico, and G. Parravicini, *J. Chem. Soc., Faraday Trans. 1*, **74**, 2333 (1978).

Dielectric Study of Aliphatic Esters in Cyclohexane Solutions at the Frequency of 100 GHz

Yoshikazu KANO, Ryuichi MINAMI, and Hiroaki TAKAHASHI*

Department of Chemistry, School of Science and Engineering, Waseda University, Shinjuku-ku, Tokyo 160

(Received August 29, 1979)

The dipole relaxation mechanism of carboxylic esters has been studied through the dielectric measurements of seventeen aliphatic esters in cyclohexane solution at 25 °C. The dielectric relaxation times obtained in this experiment are compared with those obtained for a number of rigid molecules under the same conditions. This result indicates that the dipole relaxation process of these esters RC*OOR′ is dominated by intramolecular rotation around the C–C bonds and/or the O–C bond rather than that around the C*–O bond.

This paper deals with the results of dielectric measurements of seventeen aliphatic esters in cyclohexane solution at 25 °C at the frequency of 100 GHz. The dielectric data obtained in this experiment and those by Crossley and Koizumi[1] obtained for the same esters under the same conditions using lower microwave frequencies were examined to explore the mechanism of the dielectric absorption of aliphatic esters RC*OOR′ (hereafter, C* means the carbon atom in a carbonyl group). All the results indicate that the dielectric

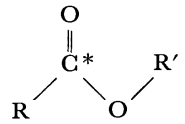

absorption of these esters is dominated by intramolecular relaxation. However, in contrast to Crossley and Koizumi[1] who considered that the dipole orientation of the methoxyl and ethoxyl groups around their C*–O bonds is very important especially for a few esters, the present authors reached the conclusion that rotations of groups around the C–C bonds and/or the O–C bond play the dominant role in the dielectric absorption of the aliphatic esters.

Experimental

The apparatus and procedure used to determine dielectric constants (ε') and losses (ε'') at 100 GHz have been described previously.[2] Static dielectric constants (ε_0) were measured at 1 MHz and refractive indices (n) were determined at the frequency of Na-D line. The slopes a_0, a', a'', and a_D were obtained from ε_0, ε', ε'', and n_D^2 of the solvent and solutions as in the previous papers.[2,3] The units of weight fraction were used to express the concentration of the solute in solution.

Results

The values of a_0, a', a'', and a_D obtained for the aliphatic esters in cyclohexane solution at 25 °C are listed in Table 1. Two relaxation times $\tau(1)$ and $\tau(2)$ given by

$$\tau(1) = \frac{1}{\omega}\frac{a''}{a'-a_D}; \quad \tau(2) = \frac{1}{\omega}\frac{a_0-a'}{a''}$$

are recorded in Table 1—ω denotes the angular frequency. The physical significance of $\tau(1)$ and $\tau(2)$ have been discussed in previous reports.[3,4] As a large error seems to arise from the bold assumption that a_D is equal to a_∞ (the slope at the extremely high frequency), we shall not place much reliance on values of $\tau(1)$.

For each of the esters Cole-Cole plots were made by use of a' and a'' of this experiment at 100 GHz together with those recalculated from Crossley and Koizumi's data obtained at *ca.* 35, 24, 16, 9, 6, 4, and 2 GHz. Crossley and Koizumi made the following remark concerning the highest frequency they employed. "In many cases the frequency of maximum loss is in the region of the highest experimental frequency, and thus the high frequency side of the dispersion is not well characterized." It may be added here that the high frequency side of the dispersion is examined first by the present experiment. The mean relaxation times (τ_0) and the distribution parameters (α) obtained in this way were compared with those given by Crossley and Koizumi using lower microwave frequency data alone (Table 2). We find our τ_0 values are slightly smaller than τ_0 obtained by Crossley and Koizumi in some esters but they compare well on the whole. Further we find values $\tau(2)$ to be sometimes smaller than our values for τ_0.

Discussion

If the Debye theory[5] of dielectric relaxation is correct, the relaxation times (τ_0) of all the rigid polar molecules measured in the same solvent at the same temperature should be proportional to the molecular volume of the solutes. This prediction is examined in Fig. 1 for a number of rigid molecules (code number 21—39; Table 3) in cyclohexane at 25 °C—the molecular volume is obtained by the ratio of the molecular weight (M) to the density (d). We find Debye's theory to be only qualitatively valid. The points for 21—39 scatter in a wide range and the fluctuation appears to be much larger than the error in estimating the molecular volume.[6] There exists a general tendency shown by curve A that the points for rigid molecules move upward with increasing molecular volume.

The relaxation times (τ_0) of seventeen aliphatic esters (code numbers 1—17) are also examined in a similar manner — as an exception, $\tau(2)$ is taken for methyl acetate since τ_0 is not available for this molecule. We can draw curve B through the points for esters. We notice that curve B is situated below curve A and is almost parallel to the abscissa for esters of large molecular volumes. This is a common feature of all flexible polar molecules.[7]

Two curves A and B intersect each other in the

Table 1. Slopes, relaxation times, and dipole moments for aliphatic esters in cyclohexane solution at 25 °C

Ester	a_0	a'	a''	a_D	$\tau(1)$/ps	$\tau(2)$/ps	μ/D
Methyl acetate	2.953	1.554	1.266	—	—	1.8	—
Methyl hexanoate	1.758	0.609	0.527	−0.092	1.2	3.6	1.68
Methyl octanoate	1.520	0.492	0.386	−0.059	1.1	4.4	1.71
Methyl decanoate	1.314	0.439	0.315	−0.034	1.1	4.5	1.71
Methyl hexadecanoate	0.875	0.337	0.209	0.016	1.1	4.2	1.64
Methyl octadecanoate	0.823	0.311	0.183	0.023	1.0	4.6	1.67
Methyl docosanoate	0.776	0.292	0.160	0.041	1.0	4.8	1.73
Methyl oleate	0.881	0.353	0.173	0.059	0.96	5.0	1.68
Ethyl acetate	3.086	1.058	0.985	−0.194	1.3	3.4	1.84
Ethyl hexanoate	1.742	0.452	0.414	−0.079	1.3	5.1	1.75
Ethyl octanoate	1.484	0.377	0.305	−0.049	1.2	5.9	1.75
Ethyl dodecanoate	1.155	0.310	0.221	−0.009	1.1	6.3	1.76
Ethyl octadecanoate	0.886	0.266	0.151	0.024	1.0	6.7	1.77
Ethyl linoleate	1.045	0.318	0.167	0.072	1.1	7.1	1.87
Ethyl lactate	5.020	1.001	0.782	−0.104	1.2	8.4	2.50
Pentyl acetate	2.211	0.621	0.512	−0.098	1.2	5.1	1.87
Diethyl tetradecanedioate	1.713	0.476	0.314	0.019	1.1	6.4	2.49

Table 2. Code numbers of the aliphatic esters and their Cole-Cole parameters τ_0 and α

Code	Ester	This study		Crossley and Koizumi[1]	
		τ_0/ps	α	τ_0/ps	α
1	Methyl acetate	—	—	—	—
2	Methyl hexanoate	3.9	0.13	4.1	0.08
3	Methyl octanoate	5.0	0.13	5.1	0.12
4	Methyl decanoate	5.0	0.17	6.0	0.11
5	Methyl hexadecanoate	6.5	0.20	6.3	0.19
6	Methyl octadecanoate	5.5	0.26	6.3	0.17
7	Methyl docosanoate	5.8	0.21	6.4	0.16
8	Methyl oleate	6.7	0.16	7.0	0.13
9	Ethyl acetate	2.7	0.12	2.8	0.09
10	Ethyl hexanoate	5.1	0.12	6.0	0.07
11	Ethyl octanoate	6.5	0.12	7.0	0.09
12	Ethyl dodecanoate	7.8	0.18	8.6	0.10
13	Ethyl octadecanoate	8.7	0.18	9.4	0.13
14	Ethyl linoleate	11.1	0.27	12.1	0.19
15	Ethyl lactate	13.2	0.16	13.7	0.16
16	Pentyl acetate	6.3	0.24	6.9	0.18
17	Diethyl tetradecanedioate	9.5	0.13	10.0	0.09

Table 3. Code numbers of the rigid molecules

Code	Molecule	Code	Molecule
21	Acetone[a]	22	Chloroform[a]
23	Furan[b]	24	Chlorobenzene[a]
25	Bromobenzene[a]	26	Nitrobenzene[c]
27	*p*-Chlorotoluene[d]	28	*m*-Chlorotoluene[d]
29	*p*-Bromotoluene[d]	30	1-Bromonaphthalene[e]
31	1-Chloronaphthalene[f]	32	9-Bromophenanthrene[c]
33	*N*-Methylaniline[f]	34	*N*,*N*-Dimethylaniline[f]
35	*N*,*N*-Diethylaniline	36	*o*-Dichlorobenzene[d]
37	Tetralin[g]	38	*N*-Methylpyrrole[h]
39	Nitrocyclohexane[i]		

a) J. Crossley, S. P. Tay, and S. Walker, *Adv. Mol. Relax. Proc.*, **6**, 69 (1974). b) Ref. 8. c) O. Kiyohara and K. Higasi, *Bull. Res. Inst. Appl. Elect.*, **18**, 123 (1966). d) S. W. Tucker and S. Walker, *Can. J. Chem.*, **47**, 681 (1969). e) G. D. Martin and S. Walker, *Can. J. Chem.*, **50**, 707 (1972). f) S. W. Tucker and S. Walker, *J. Chem. Phys.*, **52**, 2547 (1970). g) J. Crossley, W. F. Hassell, and S. Walker, *J. Chem. Phys.*, **48**, 1261 (1968). h) S. W. Tucker and S. Walker, *Trans. Faraday Soc.*, **62**, 2690 (1966). i) Ref. 6.

region of molecules with small molecular volumes. One finds that point 1 for methyl acetate is quite close to point 23 for furan.[8] Does this mean that methyl acetate should be considered to have a rigid planar configuration? We have strong evidence from microwave spectroscopy that methyl acetate[9] as well as methyl and ethyl formates[10,11] have plane configurations. Perhaps we can say that rotation of the methyl group around the C*–O bond is not completely free and that it does not dominate the dielectric relaxation. At least we cannot refute the view from our evidence that this C*–O bond is strongly hindered and hence the molecule has a planar configuration. On the other hand, point 9 (ethyl acetate) and 16 (amyl acetate) are on curve B. That is, their relaxation process is the intramolecular one. If the acetyl group cannot rotate around the C*–O bond, rotation of the acetoxy group around the O–C bond should occur instead. And the latter rotation is supposed to be the dominant mechanism for these molecules since the main dipole moment of the ester originates from the carbonyl group.

Lastly attention must be paid to the fact that point 15 for ethyl lactate is on the curve A between points

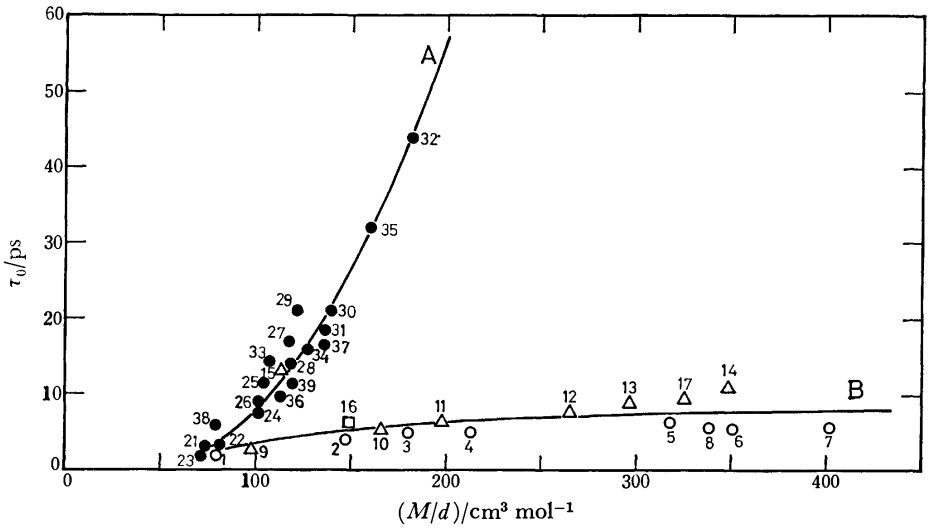

Fig. 1. Plot of relaxation time τ_0 in cyclohexane solution at 25 °C against the molecular volume: Code 1—17 aliphatic esters; 21—39 rigid molecules. M/d of esters 5, 7, and 17 are estimated values.
○: Methyl ester, △: ethyl ester, □: amyl ester, ●: rigid molecule.
Code: 1—17 see Table 2 and 21—39 Table 3.

25 (bromobenzene) and 28 (*m*-chlorotoluene) or between points 33 (*N*-methylaniline) and 39 (nitrocyclohexane). Planar configuration appears to be stabilized on account of formation of an intramolecular hydrogen bond in ethyl lactate.[12] Here, rotation of the groups around the central C–C* bond is hindered by the hydrogen-bond formation, and rotation of the ethoxyl group around the C*–O bond is also hindered on account of its partial double bond character. This phenomenon seems to be very important in understanding the nature of dielectric relaxation of flexible aliphatic esters.

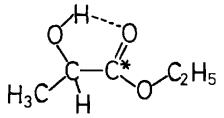

In conclusion, it should be pointed out that dielectric relaxation of aliphatic esters is largely dominated by intramolecular rotation around the C–C bonds and/or the O–C bond rather than that around the C*–O bond.

The authors would like to express their sincere thanks to Professor K. Higashi for his guidance throughout the course of this research, and to Professor N. Koizumi of Kyoto University for his very constructive critisism of the manuscript.

References

1) J. Crossley and N. Koizumi, *J. Chem. Phys.*, **60**, 4800 (1974).
2) K. Chitoku, K. Higasi, M. Nakamura, Y. Koga, and H. Takahashi, *Bull. Chem. Soc. Jpn.*, **44**, 992 (1971).
3) Y. Koga, H. Takahashi, and K. Higasi, *Bull. Chem. Soc. Jpn.*, **47**, 84 (1974).
4) K. Higasi, Y. Koga, and M, Nakamura, *Bull. Chem. Soc. Jpn.*, **44**, 988 (1971).
5) P. Debye, *Trans. Faraday Soc.*, Appendix 679 (1934).
6) See, in this connection, F. Hufnagel and H. Kilp, *Z. Naturforsch., Teil A*, **18**, 769 (1963).
7) J. Crossley, *Adv. Mol. Relax. Proc.*, **6**, 39 (1974).
8) J. Crossley, W. F. Hassell, and S. Walker, *Can. J. Chem.*, **46**, 2181 (1968).
9) G. Williams, N. L. Owen, and J. Sheridan, *Trans. Faraday Soc.*, **67**, 922 (1971).
10) R. F. Curl, *J. Chem. Phys.*, **30**, 1529 (1959).
11) J. M. Rivers and E. B. Wilson, Jr., *J. Chem. Phys.*, **46**, 4605 (1967).
12) N. Mori, Y. Asano, and Y. Tsuzuki, *Bull. Chem. Soc. Jpn.*, **41**, 1871 (1968).

Absorption Spectra of the Polyacetylene Films Doped with BF_3

Masashi TANAKA,* Atsushi WATANABE, and Jiro TANAKA
Department of Chemistry, Faculty of Science, Nagoya University, Chikusa, Nagoya 464
(Received September 13, 1979)

Optical absorption measurements are carried out on pure and BF_3 doped polyacetylene films over a wide wavelength region (200 cm^{-1}—54000 cm^{-1}). In the lightly doped polymer, the extra peak appears at 870 cm^{-1} and it is assigned to the transition from the valence band to the impurity level. This band becomes more intense at low temperature. For the heavily doped films, the dc conductivity of the $(CH)_x$ fibril is optically estimated to be $\sigma_0 = 10^4\ \Omega^{-1}\ cm^{-1}$. This value is in good agreement with the calculated value ($\sigma_0 = 0.8 \times 10^4\ \Omega^{-1}\ cm^{-1}$) due to the tight binding model.

Polyacetylene is one of the simplest linear conjugated polymers with a single chain structure. Accordingly, many theoretical and experimental studies[1] were reported upon the electronic structure of polyacetylene as a quasi one-dimensional conductor. Shirakawa and coworkers[2-4] succeeded in synthesizing high quality polycrystalline films of $(CH)_x$. The conductivity measured by the four point probe technique was about $10^{-9}\ \Omega^{-1}\ cm^{-1}$ for the *cis*-rich polyacetylene film. Recently, Shirakawa, Heeger, and MacDiarmid and coworkers[5-7] found out that, when flexible, crystalline silvery films of the *cis*-$(CH)_x$ or *trans*-$(CH)_x$ polymer were doped with controlled amounts of electron-attracting species such as chlorine, bromine, iodine, or AsF_5, their electrical conductivity could be systematically varied over a wide range from that of an insulator ($\sigma = 10^{-9}\ \Omega^{-1}\ cm^{-1}$) to a metal ($\sigma = 10^3\ \Omega^{-1}\ cm^{-1}$). Furthermore, the IR[8] and visible-UV[9-11] absorption spectra were measured upon exposure to vapors of chlorine, bromine, iodine, or AsF_5. Tanaka *et al.*[12] studied the infrared reflection spectra of oriented polyacetylene films, doped with varying concentrations of AsF_5 and iodine, and discussed about the relation between the reflectivity and the conductivity of doped $(CH)_x$ films.

In the present paper, we report the absorption spectra in the 200 cm^{-1}—54000 cm^{-1} region of *cis*-rich polyacetylene films doped with BF_3 and discuss about the electronic structure of the heavily doped $(CH)_x$ films.

Experimental

The *cis*-rich polyacetylene films were prepared from acetylene by treatment of the Ziegler catalyst in hexane at −80 °C as described by Shirakawa and coworkers.[2-4] The films were doped by exposure to the vapor of BF_3 at room temperature. The dopant concentration were determined by weight change of the sample.[17]

The IR transmission measurement of the thick films (*ca.* 5×10^{-3} cm) were taken with Hitachi EPI-L (200 cm^{-1}—700 cm^{-1}) and JASCO IRA-3 (330 cm^{-1}—5000 cm^{-1}) spectrophotometers at room temperature and with a JASCO DS-402G (600 cm^{-1}—4000 cm^{-1}) spectrophotometer at low temperature.

The visible and UV transmission data of the thin films (*ca.* 200 Å) polymerized on the inner surface of the 1 cm quartz cell were measured with JASCO IRA-3 (2500 cm^{-1}—5000 cm^{-1}) and Carl Zeiss M4Q (4000 cm^{-1}—54000 cm^{-1}) spectrophotometers.

Results and Discussion

Linear polyacetylene, $(CH)_x$, is the simplest conjugated organic polymer and the π-electrons on each carbon atom delocalize to form a band. The energy of the π-electrons is calculated by the MO theory,[1,11]

$$\varepsilon(k) = \pm\sqrt{t_1^2 + t_2^2 + 2t_1t_2\cos(ka)} \quad (1)$$

where t_1 and t_2 (>0) are the transfer integrals between successive sites, a the C–C bond length, and k the wave vector. In the absence of bond alternation ($t_1 = t_2$), the energy eigenvalues form a band of width $4t$ (Fig. 1-1) which is half-filled with the π-electrons. On the other hand, if one bond is longer than the

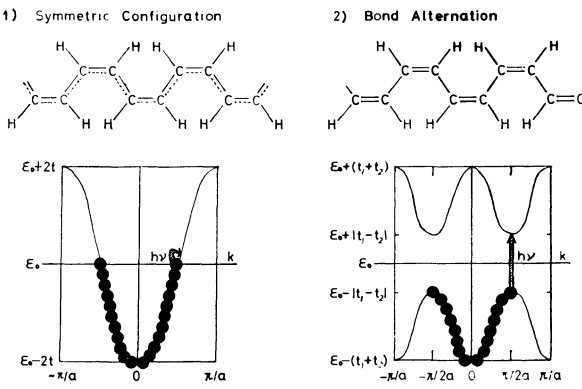

Fig. 1. Energy band diagram for the polyacetylene system.

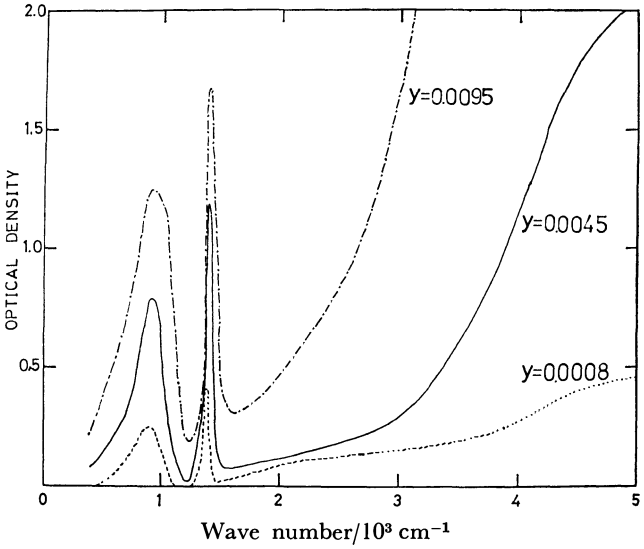

Fig. 2. IR absorption spectra of the thick films (*ca.* 5×10^{-3} cm) of $[CH(BF_3)_y]_x$.

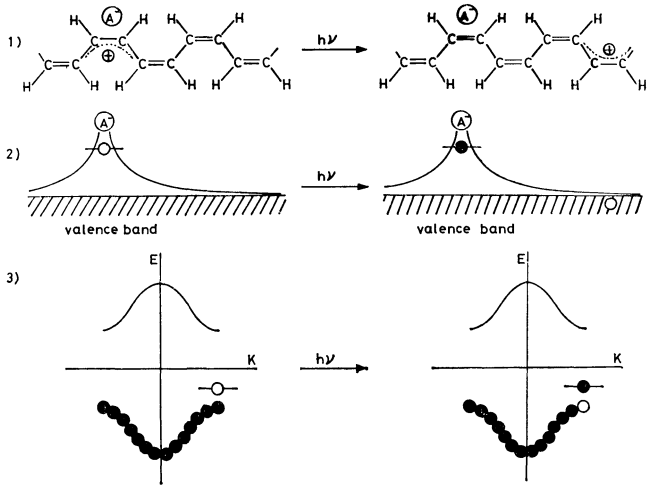

Fig. 3. Character of the 870 cm^{-1} band.
(1) Schematic diagram of acceptor ion (A^-) near a $(CH)_x$ chain. (2) The resulting hole on the polymer chain is bound by the Coulomb potential. (3) The resulting bound state is in the energy gap.

other ($t_1 \neq t_2$), a set of bonding (valence band) and antibonding (conduction band) orbitals is formed and the energy gap in the electronic spectrum is expected as shown in Figs. 1—2.

The absorption spectrum of the undoped polymer has the sharp absorption edge at 12000 cm^{-1} and the peak at 17000 cm^{-1} (Fig. 5, $y=0$). Accordingly, this absorption band can be assigned to the interband transition from the valence band to the conduction band, and shows that the bond alternation is present in the polymer.

In the lightly doped polymer, two infrared peaks of the additional absorption over the undoped sample are observed at 1370 cm^{-1} and 870 cm^{-1} (Fig. 2). The narrow mode at 1370 cm^{-1} was explained by Su, *et al.*[13] as the result of soliton formation in the long chain polyenes.

The broad band at 870 cm^{-1} can be assigned to the transition from the valence band to the hole level by applying the traditional approach in semiconductors. That is, the cation (hole) in the $(CH)_x$ chain is tightly bound to the charge center (A^-) by Coulomb force in a dielectric medium as shown in Fig. 3. Then, the binding energy E of the hole in the screened Coulomb field are given by the following equation,[8,16]

$$-\frac{\hbar^2}{2m^*}\frac{d^2}{dx^2}\psi_n - \frac{e^2}{\varepsilon|x|}\psi_n = E_n\psi_n \tag{2}$$

$$E_n = -\frac{m^*e^4}{2\hbar^2\varepsilon^2}\frac{1}{n^2}. \tag{3}$$

Taking the measured dielectric constant to be $\varepsilon=11$[8] and assuming $m^*/m=1$, the transition from the valence band to the impurity 1s level can be estimated to occur in the vicinity of 900 cm^{-1}. In the thermal equilibrium at room temperature, a few π-electrons can excite from the valence band to the impurity levels. This means that the optical absorption intensity increases at the low temperature. Figure 4 shows the temperature dependence of the 870 cm^{-1} band. The peak is observed at 870 cm^{-1} and located

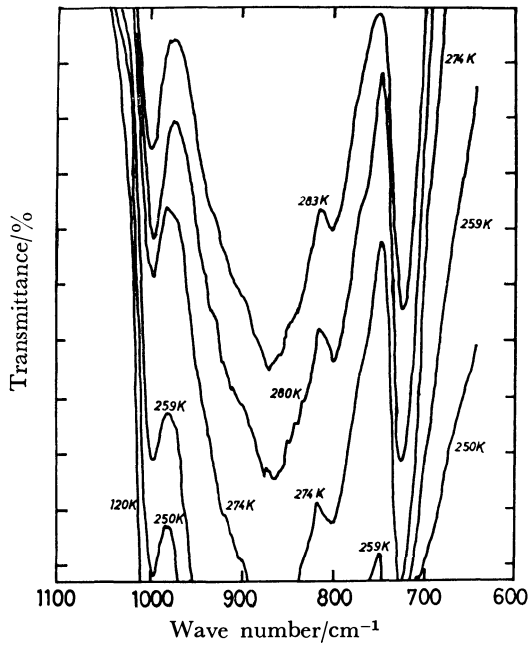

Fig. 4. IR transmission spectra of $[CH(BF_3)_{0.01}]_x$ at various temperature.

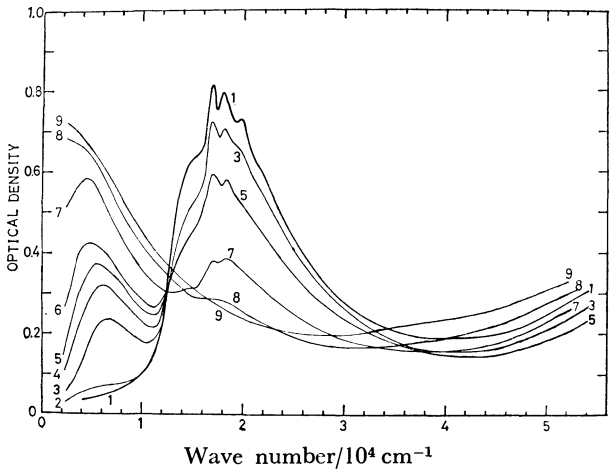

Fig. 5. Absorption spectra of the thin films of $[CH(BF_3)_y]_x$, (1) $y=0$, (2) $y=0.0045$, (3) $y=0.0095$, (4) $y=0.018$, (5) $y=0.025$, (6) $y=0.029$, (7) $y=0.038$, (8) $y=0.051$, (9) $y=0.077$.

between two C–H out of plane bending modes (1015 cm^{-1} in the *trans* isomer and 740 cm^{-1} in the *cis* isomer) and the transmittance of the 870 cm^{-1} band becomes smaller as the temperature decreases.

In addition to the 1370 cm^{-1} and 870 cm^{-1} bands, a broad band appears in the region of 8000 cm^{-1} and the absorption intensity of the interband transition at about 17000 cm^{-1} decreases (Fig. 5). The fact that there is an isosbestic point at 12000 cm^{-1} in the spectra clearly indicates that there is an equilibrium between two absorbing species. Furthermore, the red shift of the broad band suggests that doping removes the bond alternation leading to a uniform bond length as shown in Figs. 1 and 3. That is, the energy gap between the valence and conduction bands becomes small and the metallic state is formed in the heavily doped films. The maximum absorption coefficient of

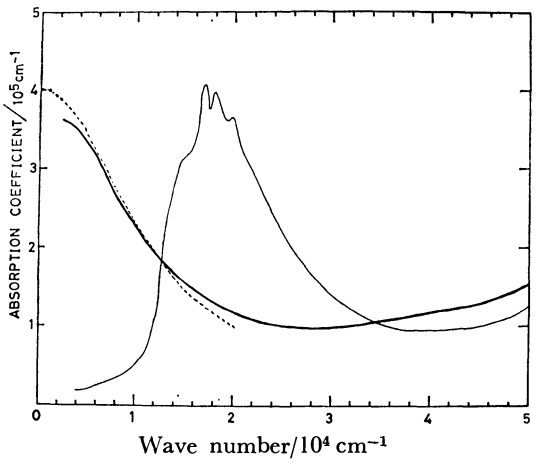

Fig. 6. Comparison between the calculated and observed absorption spectra of the intraband transition band of the metallic doped $(CH)_x$ film.
——: Pure $(CH)_x$, ——: $[CH(BF_3)_{0.077}]_x$, ----: calculated spectra.

the interband transition was determined to be 4×10^5 cm^{-1} near 17000 cm^{-1} by Fincher, *et al.*[11] Accordingly, the absorption coefficient of the intraband transition of the heavily doped films ($y=0.077$) can be estimated as shown in Fig. 6.

The relation between the absorption coefficient $\alpha(\omega)$ and the conductivity $\sigma_1(\omega)$ is given in the following equation,[14]

$$\alpha(\omega)=\frac{4\pi}{n(\omega)c}\sigma_1(\omega)=\frac{4\pi}{n(\omega)c}\frac{\sigma_0^{\text{film}}}{1+\omega^2\tau_0^2} \tag{4}$$

where $n(\omega)$ is the refractive index and c the velocity of light. σ_0^{film} and τ_0 are the dc conductivity of the $(CH)_x$ film and the relaxation time, respectively. These parameter were determined by the optimum fit of Eq. 4 to the experimental data where the refractive index $n(\omega)$ is taken to be unity. The fit was obtained with $\sigma_0^{\text{film}}=1070\ \Omega^{-1}$ cm^{-1} and $\tau_0=0.43\times 10^{-15}$ s. The calculated absorption spectrum based on these values is plotted for comparison with the experimental curves in Fig. 6.

Electron microscopy photographs of $(CH)_x$ films show a fibril structure with typical fibril diameter of about 200 Å. The individual fibrils are randomly oriented and the polymer has the volume filling factor of about $f=1/3$.[11] Then, the dc conductivity σ_0 of the fibrils is given by the next equation,

$$\sigma_0=\sigma_0^{\text{film}}/(f\delta)=10^4\ \Omega^{-1}\text{cm}^{-1} \tag{5}$$

where δ is the fractional alignment factor ($\delta=1/3$).

In the tight binding approximation, the effective mass m^* of the free carrier is calculated as follows,[15]

$$\frac{m}{m^*}=\frac{4ta^2m}{\pi\hbar^2}=1.1 \tag{6}$$

where t and a are taken to be 3.0 eV and 1.4 Å, respectively. From the measured density of $(CH)_x$ (0.4 g/cm^3) and the filling factor $f=1/3$, the number of π-electrons per unit volume of the fibril can be estimated to be $N=6\times 10^{22}$ cm^{-3}. Then, the plasma frequency ω_p and dc conductivity σ_0 for a metal are written in the conventional form,[15]

$$\omega_p^2=4\pi Ne^2/m^* \tag{7}$$

and

$$\sigma_0=\omega_p^2\tau_0/4\pi. \tag{8}$$

Using the above values for N, m^* and τ_0, ω_p is estimated to be 1.46×10^{16} s^{-1} ($\hbar\omega_p=9.1$ eV) and σ_0 to be $0.8\times 10^4\ \Omega^{-1}$ cm^{-1}. The calculated value of σ_0 is in good agreement with the optically determined value.

References

1) A. A. Ovchinnikov, *Sov. Phys. USP.*, **15**, 575 (1973).
2) H. Shirakawa and S. Ikeda, *Polym. J.*, **2**, 231 (1971).
3) H. Shirakawa, T. Ito, and S. Ikeda, *Polym. J.*, **4**, 460 (1973).
4) T. Ito, H. Shirakawa, and S. Ikeda, *J. Polym. Sci., Part A-1*, **12**, 11 (1974), **13**, 1943 (1975).
5) H. Shirakawa, E. J. Louis, A. G. MacDiarmid, C. K. Chiang, and A. J. Heeger, *J. Chem. Soc., Chem. Commun.*, **1977**, 578.
6) C. K. Chiang, C. R. Fincher, Jr., Y. W. Park, A. J. Heeger, H. Shirakawa, E. J. Louis, S. C. Gau, and A. G. MacDiarmid, *Phys. Rev. Lett.*, **39**, 1098 (1977).
7) C. K. Chiang, M. A. Druy, S. C. Gau, A. J. Heeger, E. J. Louis, A. G. MacDiarmid, Y. W. Park, and H. Shirakawa, *J. Am. Chem. Soc.*, **100**, 1013 (1978).
8) C. R. Fincher, Jr., M. Ozaki, A. J. Heeger, A. G. MacDiarmid, *Phys. Rev. B*, **19**, 4140 (1979).
9) H. Shirakawa, T. Sasaki, and S. Ikeda, *Chem. Lett.*, **1978** 1113.
10) C. R. Fincher, Jr., D. L. Peebles, A. J. Heeger, M. A. Druy, Y. Matsumura, A. G. MacDiarmid, H. Shirakawa, and S. Ikeda, *Solid State Commun.*, **27**, 489 (1978).
11) C. R. Fincher, Jr., M. Ozaki, M. Tanaka, D. Peebles, L. Lauchlan, A. J. Heeger, and A. G. MacDiarmid, *Phys. Rev. B*, **20**, 1589 (1979).
12) M. Tanaka, C. R. Fincher, Jr., A. J. Heeger, and A. G. MacDiarmid, to be published.
13) W. P. Su, J. R. Schrieffer, and A. J. Heeger, *Phys. Rev. Lett.*, **42**, 1698 (1979)
14) F. Wooten, "Optical Properties of Solids," Academic press, New York (1972), p. 81.
15) A. A. Bright, A. F. Garito, and A. J. Heeger, *Phys. Rev. B*, **10**, 1328 (1974).
16) C. Tric and O. Parodi, *Mol. Phys.*, **13**, 1 (1967).
17) A. G. MacDiarmid pointed out the presence of the H_3O^+ ion.

Catalytic Properties of Iron Oxide. III. Oxidative Dehydrogenation of Butenes over Iron Oxide Catalysts

Makoto Misono,* Kanji Sakata, Fumio Ueda, Yasuaki Nozawa, and Yukio Yoneda

Department of Synthetic Chemistry, Faculty of Engineering, The University of Tokyo, Hongo, Bunkyo-ku, Tokyo 113

(Received September 13, 1979)

Oxidative dehydrogenation of butenes was investigated by use of a flow reactor over three iron oxide catalysts having different structures, *i.e.*, α-Fe_2O_3, γ-Fe_2O_3, and Fe_3O_4, which were prepared *in situ* by controlled reduction and reoxidation with a pulse method. Under the working conditions of catalytic oxidation, the structures of α- and γ-Fe_2O_3 remained unchanged, while Fe_3O_4 was oxidized to γ-Fe_2O_3, the oxidation state of iron being Fe(III) in all of three iron oxide catalyst. These results are consistent with the kinetics that the reaction was of zeroth order in the partial pressure of oxygen and of nearly first order in the butene partial pressure. γ-Fe_2O_3, as well as γ-Fe_2O_3 formed from Fe_3O_4 under the catalytic conditions, was very active and selective for the reaction, as expected from the results obtained previously with a pulse reactor. It was concluded from the following facts that the oxygen species responsible for this reaction is lattice oxygen of γ-Fe_2O_3 and that the reaction proceeds by the redox cycles of γ-Fe_2O_3 $\rightleftharpoons$$\gamma$-$Fe_2O_{3-x}$. i) Reactivity of γ-iron oxide surface in the stoichiometric oxidation of butenes to butadiene did not change, when the surface oxygen was stepwisely removed by CO-pulses from γ-Fe_2O_3 to γ-$Fe_2O_{2.8}$. ii) Formation of butadiene from a butene pulse was little affected by whether butenes were pulsed with oxygen or not.

Iron oxide is widely used in oxidation reasctions a single or mixed oxides. However, as for allylic oxidation of olefin, it is not a selective catalyst.[2] Recently, we found by use of a pulse method that metastable γ-Fe_2O_3(maghemite) was very active and selective in oxidative dehydrogenation of butenes.[3] Reactivity and oxygen mobility of γ-Fe_2O_3 were already investigated in detail in relation to the oxidation of carbon monoxide.[1]

In the present study, we attempted to confirm the relationship between the structure and oxidation state of iron oxide and the catalytic activity for oxidative dehydrogenation. It was of prime interest whether or not the high activity and selectivity of γ-Fe_2O_3 observed by a pulse method can be reproduced in a flow reactor. Kinetic studies, structure determination of iron oxide under working conditions, and comparison of catalytic and stoichiometric oxidations were also carried out, in order to clarify the reaction mechanism and the nature of the active oxygen species.

Experimental

Apparatus and Procedure. Apparatus for the reaction was a combination of a pulse reactor and a flow reactor. The pulse reactor was the same that described previously,[3] in which carrier gas (He) was deoxygenated by a molecular-sieve trap kept at liquid nitrogen temperature. After the structure and oxidation state of iron oxide was controlled by its reduction and oxidation with the pulse method described previously,[3] the system was changed to a flow system by the operation of valves, and reaction gas mixtures (butene, oxygen, and helium) were introduced to pass over the catalysts. The reaction system was carefully designed, so that the catalyst was never exposed to any trace of oxygen during the valve operation. For example, a 6-way valve was covered by a metal jacket in which a stream of dry helium was continuously passed, to avoid oxygen diffusion from air into the flow of the feed gas. After 1 h of the flow experiment (usually reaction became almost stationary within 1 h), the system was changed again to the pulse system to examine the oxidation state and the structure of catalysts. Ordinary pulse-experiments were also carried out in some cases.

Reagents and Catalysts. α-Fe_2O_3, γ-Fe_2O_3, and Fe_3O_4 were the same as described in Part II.[1] $MgSO_4$–SiO_2 (abbreviated as Mg–S) and CaO were also the same as used before.[4,5] Butenes (Takachiho Shoji, >99.9%) and pentenes (Tokyo Kasei, >99%) were obtained commercially and used without further purification.

Results and Discussion

Comparison of α-Fe_2O_3, γ-Fe_2O_3, and Fe_3O_4 in Oxidative Dehydrogenation of 1-Butene (Flow Method). Reaction of 1-butene over iron oxides having different initial structures and oxidation states, which were prepared *in situ* as described in Experimental section was measured by the flow method at 300 °C. Typical results are given in Table 1. Reaction became nearly stationary within 1 h, the conversion becoming 1/2—2/3 of the initial value within this period. Deactivation was small when butene pressure was low and oxygen pressure was high. This deactivation was probably due to carbon deposit, since the initial activity was restored by burning off of the carbon deposit by oxygen pulses at 300 °C. The selectivity to butadiene was almost constant during the flow experiments.

After the flow experiments, the system was changed again to the pulse system by the procedure described in the Experimental section, carefully avoiding the contamination of the catalysts. Then the oxidation states of the catalysts were determined from the amounts of oxygen uptake by the catalysts from O_2-pulses. Although the structures of iron oxides were not determined by X-ray diffraction analysis, they were easily estimated from the oxidation state, color, and magnetic properties. These results are also given in Table 1. The oxidation states and structures of α-Fe_2O_3 and γ-Fe_2O_3 did not change during the flow experiments, when oxygen was present more than 0.5%. On the other hand, Fe_3O_4 was oxidized to γ-Fe_2O_3.

Table 1 clearly shows, in spite of the presence of deactivation, that the catalytic activity and selectivity

TABLE 1. OXIDATIVE DEHYDROGENATION OF 1-BUTENE OVER IRON OXIDE CATALYSTS BY A FLOW METHOD AT 300 °C

Starting iron oxide	Feed gas (% in He)		Stationary conversion	Selectivity to butadiene	Structure after run
	O_2	1-Butene	%	%	
α-Fe_2O_3	5.1	6.5	3	38	α-Fe_2O_3
γ-Fe_2O_3	5.4	5.5	12	89	γ-Fe_2O_3
γ-Fe_2O_3	0	4.8	0	—	mainly Fe_3O_4
Fe_3O_4	7.6	7.7	17	91	γ-Fe_2O_3

Total flow rate: 30 cm^3 min^{-1}, amount of catalyst: 150 mg.

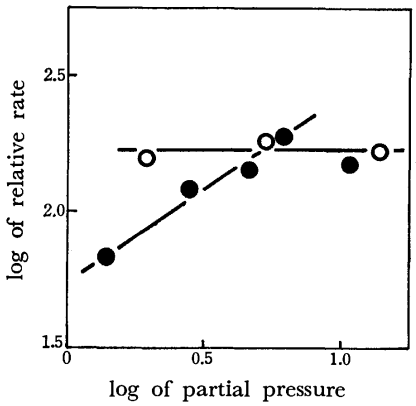

Fig. 1. Dependence of the rate on the partial pressure of 1-butene or oxygen.
Partial pressures are expressed by % in feed gas (1 atm). Reaction temperature: 300 °C, W/F: 5.0×10^{-2} g min cm^{-3}, ○: dependency on O_2 (butene: 4.5%), ●: dependency on butene (O_2: 4.5%).

were much higher with γ-Fe_2O_3 than with α-Fe_2O_3. Fe_3O_4 was little active at first, but it soon became comparable with γ-Fe_2O_3. This is natural, since Fe_3O_4 was oxidized to γ-Fe_2O_3 during the run. These results are in complete agreement with the results obtained by use of a pulse method.[3] Thus, it was confirmed also with a flow method that iron(III) oxide exhibits quite different behavior in allylic oxidation of olefin depending on its structure, γ-Fe_2O_3 (maghemite) being very active and selective.

Sazonova *et al.*[6] also studied the structural change of iron oxide during the oxidative dehydrogenation, and reported that iron oxide was in the states of α-Fe_2O_3 and Fe_3O_4 at high and low pressures of oxygen, respectively. However, the iron oxide they assigned to Fe_3O_4 could be γ-Fe_2O_3 in view of the present study. The X-ray powder diffraction patterns of Fe_3O_4 and γ-Fe_2O_3 are very close with each other. The selectivity they reported was not very high, probably because of the higher reaction temperature (365 °C).

Kinetics of Oxidative Dehydrogenation of 1-Butene over γ-Fe_2O_3 (Flow Method). Reaction mechanism was examined by a kinetic study. Figure 1 shows the dependency of the rate on the partial pressures of oxygen and 1-butene. As obvious from the figure, the reaction is of zeroth order with respect to oxygen. Selectivity of butadiene formation was nearly unchanged in this range of oxygen pressure. As for the rate dependency on the butene partial pressure, the rate data deviate from the straight line at high pressure. This was caused by significant deactivation of catalyst at this pressure region. At lower pressure-region, the reaction order was 0.7th. If the deactivation were properly taken into account, the reaction order would become closer to first order.

If the catalytic oxidation proceeds by a reduction-oxidation cycles of catalyst (redox mechanism), the result that kinetics was zeroth order in oxygen and first order in 1-butene means that the oxidation step of catalyst is much more rapid than the reduction step, and, therefore, the catalyst should be in a high oxidation state under the working conditions. This is in accord with the oxidation state actually found (Table 1). Furthermore, it was observed in the case of pulse experiments that the rate of reduction of γ-Fe_2O_3 by butene was slower than that of oxidation of γ-Fe_2O_{3-x} by oxygen. The reduction step was also slower than the oxidation step in the case of the oxidation of carbon monoxide over γ-Fe_2O_3.[1]

Comparison of the Rates of Catalytic and Stoichiometric Oxidation of 1-Butene (Pulse Method). In the redox mechanism, in which the reduction of catalyst is the slow step, the rate of stoichiometric oxidation of substrate by catalyst (oxidation of 1-butene by γ-Fe_2O_3 in the present system) is expected close to the rate of catalytic oxidation (1-butene+O_2 over γ-Fe_2O_3). This statement is valid when the oxidation states of the catalyst are the same in the stoichiometric and catalytic processes. Therefore, it is necessary that the rate of the former process is correctly measured for γ-Fe_2O_{3-x} having the same oxidation state as in the catalytic oxidation.

We measured the rate of the stoichiometric process by the reaction of a very small amount (usually 0.2 cm^3) of 1-butene pulsed over γ-Fe_2O_3 (50 mg), and measured the rate of catalytic process by a small pulse of a mixture of 1-butene and oxygen (usually, 1.0 cm^3 of 1 : 4 mixture). Under the working conditions, x of γ-Fe_2O_{3-x} was close to zero as described above, and the rate of butadiene formation in the stoichiometric oxidation was nearly independent of x in the range of x from 0 to 0.2 (*cf.* Fig. 3), so that the comparison by the present method is meaningful. We already reported the two rates were close enough to support the redox mechanism.[3] In the present study, the comparison was made in a little more accurate way.

Typical results are shown in Fig. 2, where % conversions to butadiene of 1-butene pulsed sequentially (with or without oxygen) are given, together with the extents of isomerization to 2-butenes. The trends seen in Fig. 2 were sufficiently reproducible. In runs

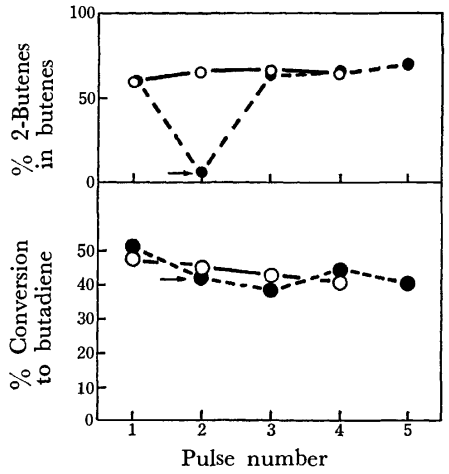

Fig. 2. Reactivity of 1-butene pulse with and without oxygen over γ-Fe_2O_3.
——: Run 1, ----: Run 2
Size of butene pulses was 0.2 cm^3. Data indicated by arrows are for the pulse of 1-butene (0.2 cm^3) pulsed with O_2 (0.8 cm^3).

1 and 2, the second pulses were 1-butene with oxygen and without oxygen, respectively, and all the other pulses contained only 1-butene. Conversion to butadiene decreased slightly by repeated pulses, due to carbon deposit. Results in Fig. 2 clearly show that the rates of two processes (stoichiometric and catalytic) were very close with each other (see the second pulse), supporting the redox mechanism.

The dependency on reaction temperature of butadiene formation in the stoichiometric process was small, apparent activation energies obtained from the conversions of first pulses being 15 kJ mol^{-1} (200—300 °C) and 25 kJ mol^{-1} (270—320 °C) for γ- and α-Fe_2O_3, respectively.

When the reaction temperature was raised to 350 °C, the rate of catalytic oxidation became significantly higher than the stoichiometric oxidation and the formation of carbon dioxide increased. At higher temperatures a mechanism which involves gaseous or adsorbed oxygen and favors complete oxidation is probably operative besides the redox mechanism.

As for the isomerization, two facts are noted: (i) the catalytic activity was much enhanced by the decrease in the oxidation state, butene composition from the second and subsequent pulses (without O_2) being in equilibrium, and (ii) the presence of gaseous oxygen greatly suppressed the isomerization rate. These two phenomena are probably both related to the number of iron sites exposed on the surface, which the reduction of catalyst may increase and (physical) adsorption of oxygen may decrease.

Reactivity of γ-Fe_2O_3 with 1-Butene as a Function of the Extent of Pre-reduction. Reaction of 1-butene pulse in the stoichiometric oxidation by iron oxide was measured over γ-Fe_2O_3, which was pre-reduced to various extents *in situ* by pulses of carbon monoxide. Reduction by CO-pulses minimized contamination of iron oxide during the reduction procedure. Figure 3 shows % conversions of 1-butene to butadiene plotted as a function of the extent of pre-reduction expressed by x of Fe_2O_{3-x}. The conversion remained unchanged in the range of x from 0 to 0.2 (Fe_2O_3 to $Fe_2O_{2.8}$). This is in contrast to the gradual decay of reactivity observed when γ-Fe_2O_3 was pre-reduced by butene itself (see Fig. 2). The decay in the latter case is, therefore, likely due to oxidation or polymerization products from butadiene. Further pre-reduction decreased the reactivity and finally to null at Fe_3O_4. Isomerization increased rapidly upon the pre-reduction as was before.

Reduction of Fe_2O_3 to $Fe_2O_{2.8}$ corresponds to the removal of several layers of oxygen from the surface of Fe_2O_3 (Fe ion going into inner bulk[1,8]). Therefore, the constant reactivity observed in the region between Fe_2O_3 and $Fe_2O_{2.8}$ was not the reactivity of adsorbed oxygen but that of lattice oxygen, since, if the adsorbed oxygen were responsible, the reactivity should have decreased much more rapidly when the oxygen was removed from the surface.

Reactivity and quantity of adsorbed oxygen on α-Fe_2O_3 were studied recently by Iwamoto *et al.* by means of thermal desorption.[7] They found several different adsorbed species, but the total oxygen atoms adsorbed was only about 2% of the surface layer (1.5×10^{19} O-atom m^{-2}).[1] Oxygen adsorbed reversibly on γ-Fe_2O_3 was about 20% of the surface layer at 12 kPa and 300 °C, as determined by a static measurement. But this was reversibly desorbed and not present when 1-butene was pulsed. Therefore, the amount of adsorbed oxygen present in the pulse experiments was probably much smaller than that utilized in butadiene formation from a butene pulse (without O_2). Then, also from this consideration, we can say that the contribution of adsorbed oxygen must be small in the stoichiometric pulse experiments. Actually, the % conversion to butadiene little changed when the pulse size was increased from 0.1 to 0.4 cm^3, indicating that the effect of small quantity of adsorbed oxygen is very low.

Oxygen Responsible for Selective Oxidation. Figure 2 demonstrated that the catalytic oxidation and the stoichiometric oxidation are governed by the same oxygen species, and the results in Fig. 3 indicate that the oxygen species responsible for the stoichiometric oxidation is lattice oxygen. If these two results are combined, it may be concluded that the oxygen species responsible for the catalytic oxidation of butenes over γ-Fe_2O_3 is the lattice oxygen. Possible reasons why γ-Fe_2O_3 was highly active and selective have been discussed previously.[1,3] It may be remarked that γ-Fe_2O_3 has an inverse spinel structure with cation deficiency and that reduction-oxidation between γ-Fe_2O_3 and Fe_3O_4 proceeds readily by the diffusion of Fe ion.[1,3,8] Spinels containing iron (ferrites) are already known as good catalysts for oxidative dehydrogenation of butenes.[9]

Here, the following may be worthy to remark as for the meaning of "lattice oxygen." (i) "Lattice oxygen" in the bulk cannot participate directly in the oxidation reaction. Of course, oxygen must be on the surface when it reacts with a substrate. (ii) "Lattice oxygen" on the surface is never in the same

TABLE 2. RELATIVE REACTIVITIES OF OLEFINS MEASURED BY A PULSE METHOD

Catalyst, reaction temp, and reaction.	C=C-C-C	C | C=C-C-C	C | C=C-C-C	C | C-C=C-C
α-Fe_2O_3, 270 °C				
oxid[a]	1.0	1.3	0.9	0.7
isom[b]	1.0	0.4	25	3.1
γ-Fe_2O_3, 180 °C				
oxid[a]	1.0	1.3	—	—
isom[b]	1.0	<0.1	—	—
$Fe_2O_{2.9}$,[c] 120 °C				
isom[b]	1.0	0.5	3.2	2.1
CaO, 100 °C				
isom[b]	1.0	1.0	2—3	—
Mg-S, 100 °C				
isom[b]	1.0	1.2	$>10^2$	—

a) Oxidative dehydrogenation to form diene. b) Double bond isomerization. c) α-Fe_2O_3 was reduced by CO pulses.

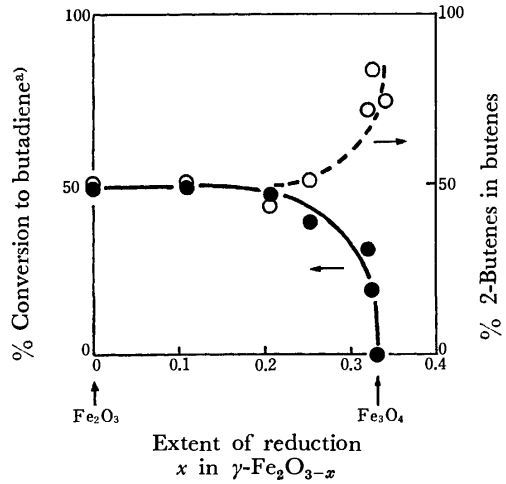

Fig. 3. Reactivity of 1-butene with γ-Fe_2O_{3-x} as a function of the extent of pre-reduction.
Reaction temperature: 200 °C, γ-Fe_2O_{3-x}: 50 mg, pulse size: 0.2 cm³, pre-reduction: by CO-pulses (1 cm³ each) at 300 °C.
a) No CO or CO_2 was formed.

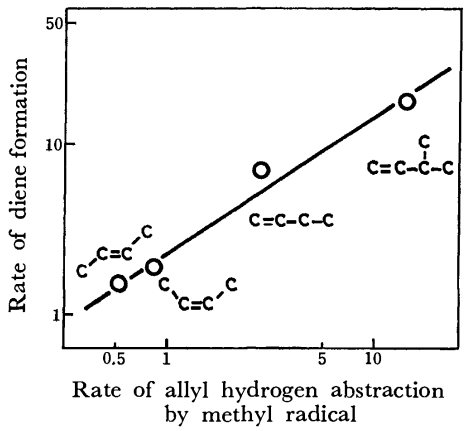

Fig. 4. Relative reactivity of olefins over γ-Fe_2O_3 (pulse method) plotted against the rate of allyl hydrogen abstraction by methyl radical.

electronic state as in the bulk. In some cases, surface "lattice oxygen" might be better described as O^- than as O^{2-}. Even in the bulk, it is not correct to regard oxide ion as having double negative charge, since electron is more or less delocalized to cation. Thus, it is not easy to determine in a general way whether the oxygen on the surface is lattice or adsorbed oxygen and whether the oxygen species responsible for catalytic oxidation is lattice or adsorbed oxygen. Sometimes, differentiation of lattice oxygen from adsorbed oxygen may not be meaningful. However, we may be able to state that the oxygen responsible for the catalytic oxidation is "lattice oxygen," when the rates of stoichiometric and catalytic processes agree and the oxygen used in the former process is not adsorbed oxygen from gas phase, as discussed in the preceding paragraph based on the results in Figs. 2 and 3.

Relative Reactivities of Olefins (δ_R-effect).[10] Effects of substituents on the reactivity provide useful information on the nature of reaction intermediate. In Fig. 4, reactivities of several olefins measured by the pulse method over α-Fe_2O_3 at 270 °C are plotted against the rate of hydrogen abstraction at allyl position at 65 °C, following Voge and Adams.[11] The data were obtained from the first pulses over freshly prepared iron oxides. According to the discussion of Voge and Adams,[11] the linear plot in Fig. 4 indicates that the formation of allylic intermediate is rate-determining. Relative reactivity normalized to one hydrogen atom at allylic positions was calculated from the reactivities of six olefins to be primary : secondary : tertiary = 1 : 4 : 12. However, the very rapid isomerization often observed over iron oxides is not consistent with the idea that the formation of allylic species is also the rate-determining step of isomerization.

We speculate on the basis of the discussion described below that the oxidation proceeds *via* an allyl radical (or cation) and the isomerization *via* an allyl anion.[12] Allylic species is likely the intermediate of oxidation

because of the results in Fig. 4 and because it seems difficult that butadiene is formed *via* an intermediate other than allylic species. Evidence which suggests a different intermediate for isomerization is also obtained from the δ_R-effects summarized in Table 2. Results obtained for typical solid acid (Mg–S) and base (CaO) are also given in this table. Since two reactions (oxidation and isomerization) proceeded over iron oxide simultaneously and could be competitive, the δ_R-effects observed might have been obscured to some extent. However, the following qualitative discussion may be made.

It is remarkable in Table 2 that in the case of iron oxides the methyl substitution at 3-position (3-methyl-1-butene) increased the rate of oxidation but decreased the isomerization. Suppressive effect of the 3-methyl group on isomerization was also observed over $Fe_2O_{2.9}$ at 120 °C, where the competitive oxidation was negligible. Therefore, the opposite behavior of oxidation and isomerization upon the methyl substitution is meaningful and suggests that two reactions proceed *via* different intermediates. Alkyl cations are not likely the intermediate for isomerization, because, if the alkyl cation were the intermediate, 2-methyl-1-butene should have been far the more reactive as in the case of Mg–S, due to the stability of tertiary cation.

The reactivity patterns of isomerization of iron oxides were more like that of CaO than that of Mg–S, so that allyl anions are presumably the intermediates as in the case of CaO.[5] The fact that the *cis*/*trans* ratio of 2-butene from the isomerization of 1-butene was about 1.5 at 150—200 °C is not in conflict with the allyl anion intermediate. If one assumes allyl radicals (or cations) for oxidation and allyl anions for isomerization, the opposite effects of 3-methyl group on oxidation and isomerization can reasonably be explained, since a methyl group destabilizes the anion but stabilizes the cation or radical.[13,14] Co-existence of two allylic intermediates, anionic and covalent, has been proposed for the isomerization of butene over chromia.[15] Change in the selectivity from acrolein to benzene in the allylic oxidation of propene over several oxide catalysts was also explained by the change in the charge of allylic intermediate.[2a]

References

1) Part II., K. Sakata, F. Ueda, M. Misono, and Y. Yoneda, *Bull. Chem. Soc. Jpn.*, **53**, 324 (1980).
2) a) T. Seiyama, N. Yamazoe, and M. Egashira, "Proc. 5 th Intern. Congr. Catal., Palm Beach, 1972," North-Holland (1973), p. 997; b) V. Fattore, C. A. Fuhrman, G. Manara, and B. Notari, *J. Catal.*, **37**, 215 (1975).
3) M. Misono, Y. Nozawa, and Y. Yoneda, "Proc. 6 th Intern. Congr. Catal., London, 1976," The Chemical Society (1977), p. 386.
4) M. Misono, N. Tani, and Y. Yoneda, *J. Catal.*, **55**, 314 (1978).
5) N. Tani, M. Misono, and Y. Yoneda, *Chem. Lett.*, **1973**, 591.
6) N. N. Sazonova, S. A. Ven'yaminov, and G. K. Boreskov, *Kinet. Katal.*, **14**, 1169 (1973).
7) M. Iwamoto, Y. Yoda, N. Yamazoe, and T. Seiyama, *Bull. Chem. Soc. Jpn.*, **51**, 2765 (1978).
8) K. Sakata, T. Nakamura, M. Misono, and Y. Yoneda, *Chem. Lett.*, **1979**, 273.
9) R. J. Rennard and W. L. Kehl, *J. Catal.*, **21**, 282 (1971); M. A. Gibson and J. W. Hightower, *ibid.*, **41**, 420 (1976).
10) Y. Yoneda, "Proc. 4 th Intern. Congr. Catal., Moscow, 1968," Akademiai Kiad, Budapest (1971) Vol. 2, p. 449.
11) H. H. Voge and C. R. Adams, *Adv. Catal.*, **17**, 151 (1967).
12) M. Misono, Y. Nozawa, and Y. Yoneda, *Shokubai*, **18**, 30 P (1976).
13) M. Misono, *Kagaku No Ryoiki*, **27**, 65 (1973).
14) Gy. Gaty and H. Knözinger, "Proc. 5th Intern. Congr. Catal., Palm Beach, 1972," North-Holland (1973), p. 819.
15) G. L. Haller and J. Saint-Just, "Proc. 6th Intern. Congr. Catal., London, 1976," The Chemical Society (1977), p. 235.

 © 1980 The Chemical Society of Japan Bull. Chem. Soc. Jpn., 53, 653—657 (1980)

Solvent Effect on the Adsorption of 1-Octadecanol at Oil/Water Interface

Takayuki IKENAGA, Norihiro MATUBAYASI, Makoto ARATONO,
Kinsi MOTOMURA, and Ryohei MATUURA*
Department of Chemistry, Faculty of Science, Kyushu University 33, Fukuoka 812
(Received December 11, 1978)

In order to study the effect of solvent on the adsorption at interfaces, interfacial tension was measured as a function of temperature and compositon for the systems of water and solutions of 1-octadecanol in cyclohexane, cyclohexene, mesitylene, toluene, and benzene. The interfacial density of 1-octadecanol and the entropy and energy of interface formation were calculated thermodynamically. It was found that cyclohexane causes a significant adsorption of 1-octadecanol and marked decreases in the entropy and energy changes, giving rise to phase transition from expanded to condensed film, while benzene, toluene, and mesitylene cause only a slight adsorption and small decrease in thermodynamic quantities. Cyclohexene was found to give rise to an intermediate adsorptive behavior of 1-octadecanol. The results were interpreted in terms of the mutual solubility between water and solvents and that of 1-octadecanol in the solvents.

The adsorption of various kinds of non-ionic surface active materials at oil/water and air/water interfaces has been investigated by many workers.[1-8] However, their thermodynamic treatment seems insufficient. Recently we have shown that the structure and property of the interface are clarified by applying rigorous thermodynamic treatment to the interfacial tension measured as a function of temperature, pressure, and concentration and evaluating the changes of the thermodynamic quantities associated with adsorption of long chain fatty alcohols at the hexane/water interface.[9-11]

It is evident that the adsorption of surface active substances to the interface is affected not only by temperature, pressure, and concentration but by properties of the solvent. However, the solvent effect on the behavior of the adsorbed film at oil/water interface has hardly been investigated systematically in spite of its importance.[12] The object of the present study is to obtain information on the solvent effect by use of the above treatment for systems consisting of water and the 1-octadecanol solutions in various organic solvents. The organic solvents employed in this work are hydrocarbons of six-membered ring structure differing in degree of saturation and in the side chain: cyclohexane, cyclohexene, benzene, toluene, and mesitylene.

The interfacial tension was measured as a function of temperature and mole fraction under atmospheric pressure. The entropy change, energy change, and the partial molar entropy change were estimated.

Experimental

Materials. 1-Octadecanol was purified by distillation under reduced pressure and triple recrystallization from hexane. Its purity was 99.9% as estimated by gas-liquid chromatography.

Benzene and toluene were purified by shaking with sulfuric acid and refluxing with metallic sodium for 8 h and by distillation under atmospheric pressure. Cyclohexane, cyclohexene, and mesitylene were purified by passing through a column of activated alumina (Woelm neutral activity grade I) and by distillation under atmospheric pressure.

Water was triply distilled, the second and third stages being done from dilute alkaline potassium permanganate solution. Water and each pure organic solvent were saturated mutually before measurements, but it was found to have little influence on the interfacial tension. The purity of water and each organic solvent was checked by the interfacial tension between them before use.

Interfacial Tension Measurements. The pendant drop technique[13,14] was used for the determination of equilibrium interfacial tension with an experimental error of *ca.* 0.05 mN m^{-1}. The values of interfacial tension were calculated by use of Fordham's correction table.[15] Measurements were carried out at fixed concentration and temperature under atmospheric pressure. The temperature was held constant within 0.05 K by circulating thermostated water around the pendant drop cell. The densities of water and pure organic solvents[16-18] were used for calculation of interfacial tension because of their small mutual solubility and low concentrations of solutions.

Results and Discussion

The interfacial tension γ of the system of cyclohexane solution of 1-octadecanol and water is plotted in Fig. 1 against temperature T at a constant mole fraction of 1-octadecanol x_1^0 in the cyclohexane solution, in which the solubility of water is neglected. At lower concentrations γ decreases linearly with increasing T, while at moderately high concentrations γ increases with increase in T. At higher concentrations there exists a point where the γ *vs.* T curve distinctly breaks at a lower temperature. The behavior of this system is very similar to that of hexane solution and water.[11] We conclude that the phase transition occurs from expanded to condensed film at the break point. It is seen that the slope of the γ *vs.* T curve, which is related to the entropy change, becomes larger from negative to positive with increase in concentration.

The interfacial tension, which is the interpolated value at constant temperature given in Fig. 1, is shown as a function of the mole fraction in Fig. 2. The γ *vs.* x_1^0 curve decrease monotonically at higher temperatures, the break point lying at 293.15 K.

Figure 3 shows the γ *vs.* T curves at constant x_1^0 for the system of cyclohexene solution and water. Cyclohexene gives rise to the phase transition of the adsorbed film of 1-octadecanol at very high concentrations and very low temperatures. Comparing cyclohexene and cyclohexane with hexane, we see that the temperature and concentration at which the condensed

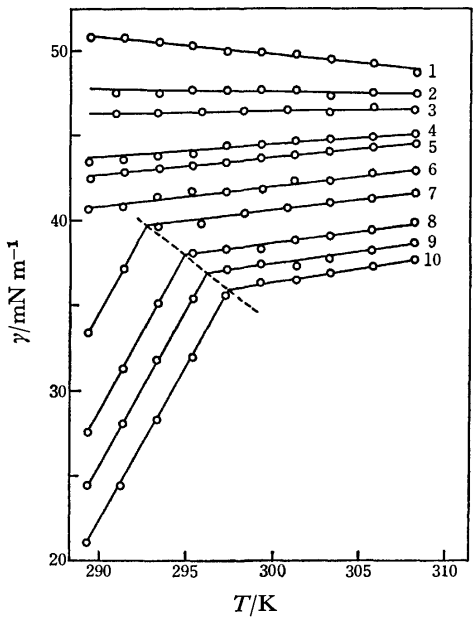

Fig. 1. Interfacial tension *vs.* temperature curves of 1-octadecanol at the cyclohexane/water interface at constant mole fraction: (1) $10^3 x_1^0=0$, (2) 0.138, (3) 0.241, (4) 0.522, (5) 0.734, (6) 1.012, (7) 1.556, (8) 2.065, (9) 2.542, (10) 3.049.

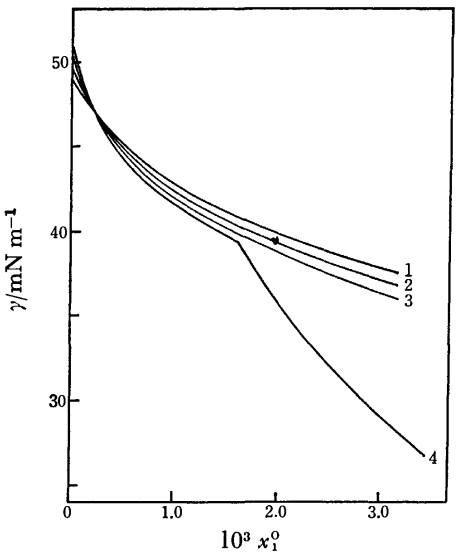

Fig. 2. Interfacial tension *vs.* mole fraction curves of 1-octadecanol at the cyclohexane/water interface at constant temperature: (1) 308.15 K, (2) 303.15 K, (3) 298.15 K, (4) 293.15 K.

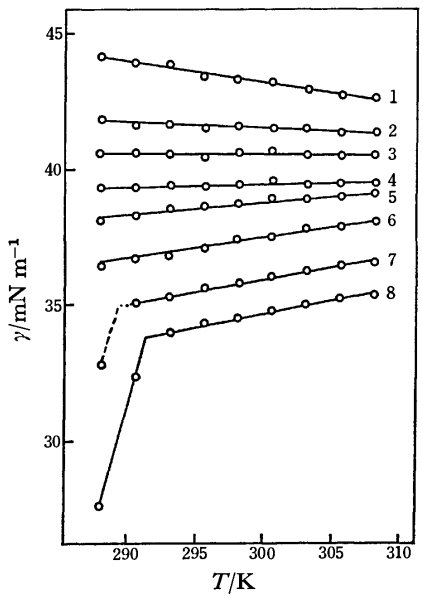

Fig. 3. Interfacial tension *vs.* temperature curves of 1-octadecanol at the cyclohexene/water interface at constant mole fraction: (1) $10^3 x_1^0=0$, (2) 0.165, (3) 0.546, (4) 0.886, (5) 1.240, (6) 2.117, (7) 3.454, (8) 4.733.

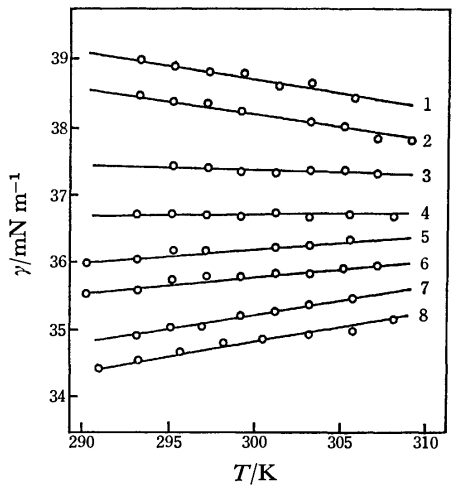

Fig. 4. Interfacial tension *vs.* temperature curves of 1-octadecanol at the mesitylene/water interface at constant mole fraction: (1) $10^3 x_1^0=0$, (2) 0.363, (3) 0.991, (4) 2.002, (5) 2.827, (6) 3.423, (7) 4.247, (8) 4.863.

film is formed becomes lower and higher, respectively, in the order of hexane, cyclohexane, and cyclohexene. It was also found that for the pure cyclohexene/water interface the slope of the γ *vs.* T curve is more gradual and the interfacial tension is smaller than for the pure cyclohexane/water and hexane/water interfaces.

In Fig. 4 γ *vs.* T curve is given for the system of mesitylene solution and water. Comparing Fig. 4 with Figs. 1 and 3 we see that the adsorptive behavior of 1-octadecanol from mesitylene seems similar to that from cyclohexane and cyclohexene at lower concentrations. However, no break point is observed over the whole range measured, the variation of γ with T being very small.

The γ *vs.* T curve for the system of toluene solution and water (Fig. 5) shows the system to behave virtually in the same manner as that of mesitylene, though the interfacial tension is smaller than that of mesitylene.

From the γ *vs.* T curve for the system of benzene solution and water (Fig. 6), we see that the variation of γ with T is steeper than that of toluene and the slope of γ *vs.* T curve is negative over the whole range measured, while the values of γ are smaller than those of toluene.

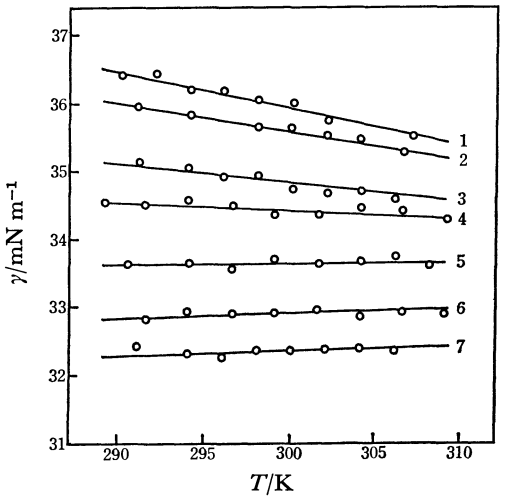

Fig. 5. Interfacial tension *vs.* temperature curves of 1-octadecanol at the toluene/water interface at constant mole fraction: (1) $10^3 x_1^0=0$, (2) 0.313, (3) 0.979, (4) 1.864, (5) 2.565, (6) 3.388, (7) 3.897.

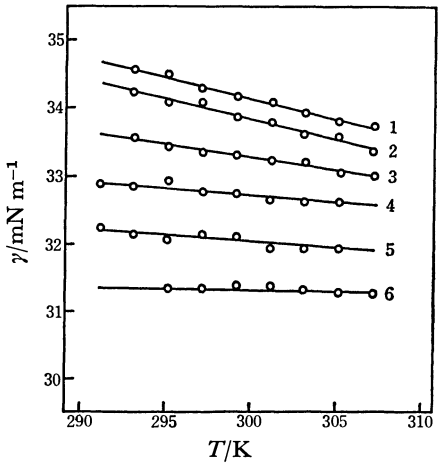

Fig. 6. Interfacial tension *vs.* temperature curves of 1-octadecanol at the benzene/water interface at constant mole fraction: (1) $10^3 x_1^0=0$, (2) 0.296, (3) 0.987, (4) 1.571, (5) 2.117, (6) 3.718.

In order to visualize the effect of solvent on the adsorption of 1-octadecanol at the interface, the γ *vs.* x_1^0 curves for the five solvents in the present study and hexane[11] at 293.15 K are compared in Fig. 7. Benzene, toluene, and mesitylene have a similar effect on the adsorption, but their effect differs a great deal from that of hexane and cyclohexane. The effect of cyclohexene seems to be intermediate between that of the two groups of solvents.

Let us now estimate the interfacial density of 1-octadecanol Γ_1^{H} which is calculated by applying the following equation to the γ *vs.* x_1^0 curve:

$$\Gamma_1^{\mathrm{H}} = -(x_1^0/RT)(\partial\gamma/\partial x_1^0)_{T,p}, \quad (1)$$

where the solution is assumed to be ideal.[10] The values of $\partial\gamma/\partial x_1^0$ are obtained by fitting the γ *vs.* x_1^0 data to the polynomial

$$\gamma = c_3 x_1^{03} + c_2 x_1^{02} + c_1 x_1^0 + c_0 \quad (2)$$

for cyclohexane and cyclohexene and to the function

$$\gamma = A\exp(Bx_1^0) + C \quad (3)$$

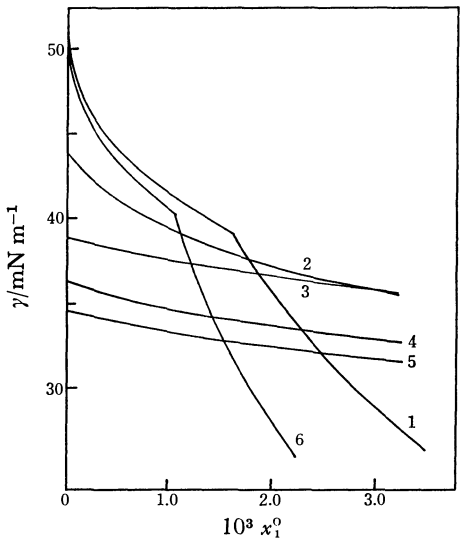

Fig. 7. Interfacial tension *vs.* mole fraction curves at 293.15 K: (1) cyclohexane, (2) cyclohexene, (3) mesitylene, (4) toluene, (5) benzene, (6) hexane.

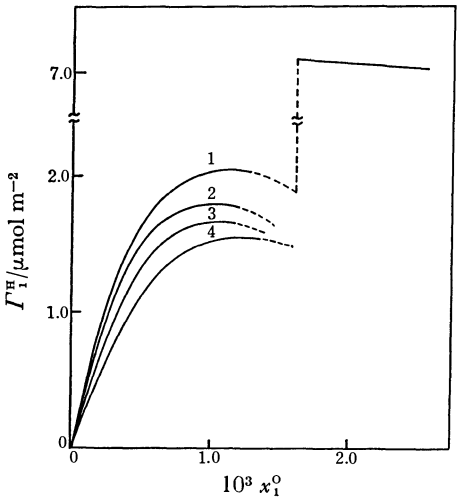

Fig. 8. Interfacial density *vs.* mole fraction curves of 1-octadecanol at the cyclohexane/water interface at constant temperature: (1) 293.15 K, (2) 298.15 K, (3) 303.15 K, (4) 308.15 K.

for benzene, toluene, and mesitylene by means of the least square method, where c_3, c_2, c_1, c_0, A, B, and C are constants.

The value of Γ_1^{H} calculated at constant temperature for the system of cyclohexane solution and water is plotted against x_1^0 in Fig. 8. Γ_1^{H} becomes smaller with rise in T. The Γ_1^{H} *vs.* x_1^0 curves seem to have maximums. The abnormal behavior may be due to the assumption of the ideal solution for Eq. 1. Practically alcohol molecules are known to undergo strong autoassociation in nonpolar solvents.[19] It is obvious that the discontinuity on the Γ_1^{H} *vs.* x_1^0 curve at 293.15 K corresponds to the first-order phase transition from expanded to condensed film.

In a similar manner we can calculate the values of Γ_1^{H} for the systems of cyclohexene, mesitylene, toluene, and benzene. For the sake of comparison the Γ_1^{H} *vs.* x_1^0 curves at 303.15 K are given for the five organic

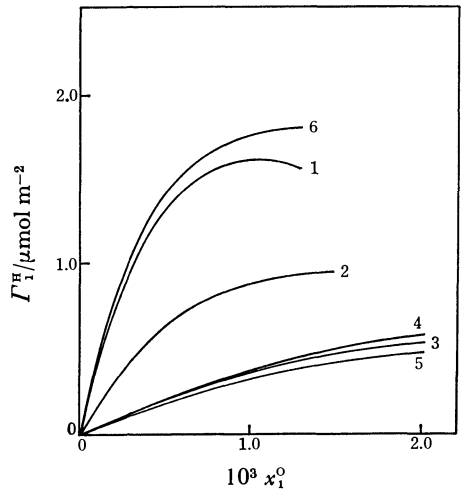

Fig. 9. Interfacial density *vs.* mole fraction curves at 303.15 K: (1) cyclohexane, (2) cyclohexene, (3) mesitylene, (4) toluene, (5) benzene, (6) hexane.

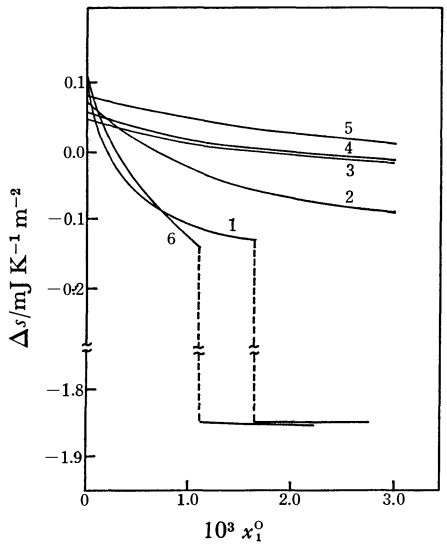

Fig. 10. Entropy of interface formation *vs.* mole fraction curves at 293.15 K: (1) cyclohexane, (2) cyclohexene, (3) mesitylene, (4) toluene, (5) benzene, (6) hexane.

solvents and hexane in Fig. 9. The value of Γ_1^H is remarkably large for cyclohexane and hexane while benzene and its derivatives give very small values. As expected, cyclohexene has an intermediate value. This suggests that the affinity of aromatic solvent molecules to water molecules is strong enough to reduce the adsorption of 1-octadecanol.

Next let us consider the entropy of interface formation, Δs. It is related to the slope of γ *vs.* T curve by[10]

$$\Delta s = -(\partial\gamma/\partial T)_{p,x_1^0}. \tag{4}$$

By estimating $\partial\gamma/\partial T$ graphically from the γ *vs.* T curve, the values of Δs are obtained which are given against x_1^0 at 293.15 K in Fig. 10. It is thought that the dependence of Δs on T is negligibly small since the γ *vs.* T curves are approximately linear. We find that in the cases of hexane and cyclohexane Δs

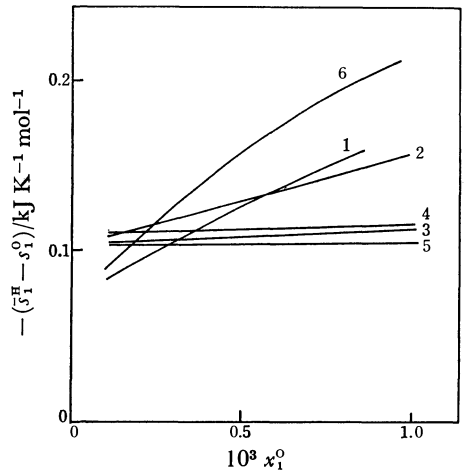

Fig. 11. Partial molar entropy change of 1-octadecanol *vs.* mole fraction curves at 303.15 K: (1) cyclohexane, (2) cyclohexene, (3) mesitylene, (4) toluene, (5) benzene, (6) hexane.

decreases rapidly with increasing x_1^0 from the positive value of pure interface to a negative value in a low concentration region. On the other hand, the extent of variation of Δs for mesitylene, toluene, and benzene is very small as compared with that for the above two solvents, the value of Δs becoming small in the order mesitylene, toluene, and benzene. It is clear that the formation of pure interface causes increase in the entropy of the whole system but the adsorption of 1-octadecanol diminishes it.

Comparing Figs. 9 and 10, we see that the value of Δs decreases as the value of Γ_1^H increases, indicating that the adsorption of 1-octadecanol to the interface is characterized by a negative change in entropy. The discontinuity in the Δs *vs.* x_1^0 curve for cyclohexane also indicates first-order phase transition from the expanded to the condensed film. The negative large value of entropy suggests that the freedom of motion of 1-octadecanol molecules is restrained a great deal in the condensed state.

The decrease in entropy leads us to expect a more regular conformation of 1-octadecanol in the interfacial region, which can be clarified by estimating the change in partial molar entropy of 1-octadecanol. The partial molar entropy change can be calculated from experimental data with the aid of

$$\bar{s}_1^H - s_1^0 = -[(\partial\gamma/\partial T)_{p,x_1^0} - (1-\Gamma_1^H\bar{a}_1)(\partial\gamma/\partial T)_{p,\Gamma_1^H}]/\Gamma_1^H, \tag{5}$$

where $\bar{a}_1$ is the partial molar area of 1-octadecanol.[10] In Fig. 11 the values of $\bar{s}_1^H - s_1^0$ are given against x_1^0 at 303.15 K for the low concentration region where the solutions are supposed to be ideal. It is of great significance that the value of the partial molar entropy change is definitely negative over the whole range of concentration and becomes more negative as the concentration increases. This indicates that the molecules of 1-octadecanol are compelled to take a more restricted conformation in the interface than in the bulk solution. The dependence of the partial molar entropy change on the bulk concentration seems to

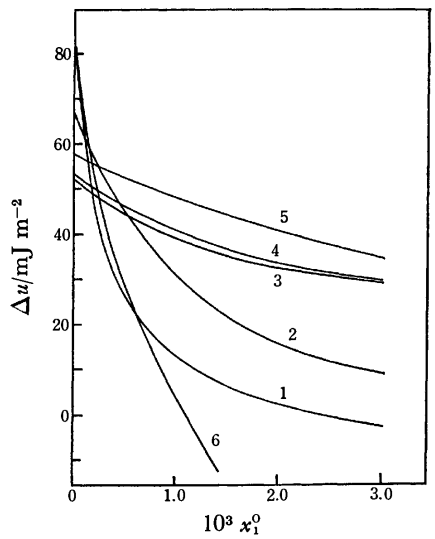

Fig. 12. Energy of interface formation *vs.* mole fraction curves at 303.15 K: (1) cyclohexane, (2) cyclohexene, (3) mesitylene, (4) toluene, (5) benzene, (6) hexane.

differ among the solvents. However, the difference is not so remarkable when the difference in the values of Γ_1^{II} shown in Fig. 9 is taken into consideration.

Let us calculate the energy of interface formation, Δu. We have the thermodynamic relation[9]

$$\Delta u = \gamma + T\Delta s - p\Delta v, \quad (6)$$

where Δv is the volume of interface formation. Since the term $p\Delta v$ is negligibly small as compared with the other terms on the right side of Eq. 6,[10] the value of Δu is determined by the values of γ and Δs. In Fig. 12 Δu is given against x_1^0 at 303.15 K for all the solvents. The values of Δu decrease steeply with x_1^0 for cyclohexane and hexane and decrease gradually for mesitylene, toluene, and benzene. Such a behavior is qualitatively similar to that of the Δs *vs.* x_1^0 curves (Fig. 10) except for the discontinuous changes of Δs attributable to the phase transition observed at 293.15 K. This indicates that the decrease in Δu by the adsorption of 1-octadecanol overcomes the disadvantage brought about by the decrease in Δs irrespective of the solvent.

The interfacial tension between organic liquid and water is related to their mutual solubility.[20] Thus, the small value of the interfacial tension between benzene and water is accounted for by the large affinity which the π electron system on the benzene ring possesses for water. When hydrophobic side chains are introduced in benzene molecule, interfacial tension increases and the entropy and energy of interface formation decrease. However, in spite of such a difference among benzene, toluene and mesitylene, the adsorptive behavior of 1-octadecanol at the interfaces between these solvents and water is very similar. The appreciable affinity of the aromaticity of the solvents for water plays a dominant role in the adsorption of 1-octadecanol.

On the other hand, the adsorption from the saturated hydrocarbons like cyclohexane and hexane is in striking contrast to that from the above aromatic solvents. It is characterized by the large value of Γ_1^{II}, the significant dependence of Δs and Δu on the concentration, and the phase transition from expanded to condensed film. Such a behavior is understandable on the basis of the low mutual solubility of saturated hydrocarbon and water, the high affinity of hydroxyl group of 1-octadecanol for water, and the strong lateral force between 1-octadecanol molecules. In terms of the solubilities of 1-octadecanol in cyclohexane and hexane, which are 1.81 and 0.47 in weight percent at 303.15 K, respectively, the slight difference in the adsorptive behavior between cyclohexane and hexane is also interpreted. For cyclohexene, we can expect an intermediate behavior between cyclohexane and benzene, which has been confirmed experimentally.

References

1) R. Aveyard, B. J. Briscoe, and J. Chapman, *J. Colloid Interface Sci.*, **44**, 282 (1973).
2) R. Aveyard and B. J. Briscoe, *Trans. Faraday Soc.*, **66**, 2911 (1970); *J. Chem. Soc., Faraday Trans. 1*, **68**, 478 (1972); *Can. J. Chem.*, **53**, 916 (1975).
3) J. J. Jasper and B. L. Houseman, *J. Phys. Chem.*, **67**, 1548 (1963); **69**, 310 (1965).
4) J. J. Jasper and R. D. Van Dell, *J. Phys. Chem.*, **69**, 481 (1965).
5) R. Vochten and G. Petre, *J. Colloid Interface Sci.*, **42**, 320 (1973); **51**, 360 (1975).
6) A. K. Chatterjee and D. K. Chattoraj, *J. Colloid Interface Sci.*, **26**, 1 (1968).
7) J. H. Clint, J. M. Corkill, J. F. Goodman, and J. R. Tate, *J. Colloid Interface Sci.*, **28**, 522 (1968).
8) E. S. Lutton, C. E. Stauffer, J. B. Martin, and A. J. Fehl, *J. Colloid Interface Sci.*, **30**, 283 (1969).
9) K. Motomura, *J. Colloid Interface Sci.*, **64**, 348 (1978).
10) K. Motomura, N. Matubayasi, M. Aratono, and R. Matuura, *J. Colloid Interface Sci.*, **64**, 356 (1978).
11) N. Matubayasi, K. Motomura, M. Aratono, and R. Matuura, *Bull. Chem. Soc. Jpn.*, **51**, 2800 (1978).
12) E. Hutchinson, *J. Colloid Sci.*, **3**, 235, 531 (1948).
13) J. M. Andreas, E. A. Hauser, and W. B. Tucker, *J. Phys. Chem.*, **42**, 1001 (1938).
14) N. Matubayasi, K. Motomura, S. Kaneshina, N. Nakamura, and R. Matuura, *Bull. Chem. Soc. Jpn.*, **50**, 523 (1977).
15) S. Fordham, *Proc. R. Soc. London, Ser. A*, **194**, 1 (1948).
16) "International Critical Tables," McGraw-Hill (1928), Vol. 3, p. 27.
17) F. K. Beilstein, "Handbuch der Organischen Chemie," Springer (1964), Vol. 3, p. 914.
18) W. F. Seyer and E. G. King, *J. Am. Chem. Soc.*, **55**, 3140 (1933).
19) A. N. Fretcher and C. A. Heller, *J. Phys. Chem.*, **71**, 3742 (1967).
20) D. J. Donahue and F. E. Bartell, *J. Phys. Chem.*, **56**, 480 (1952).

A Plot of the pH *vs.* the Logarithm of the Titrant Volume in Potentiometric Titration. The Determination of Phenol in Water

Katsuyoshi KAMAKURA

Department of Industrial Chemistry, Toyama Technical College, Hongo-cho, Toyama 930-11

(Received April 23, 1979)

The determination of phenol in water was successfully carried out by means of a new plot of the potentiometric titration data. The plot of the pH *vs.* the logarithm of the titrant volume gave a titration curve with an inflection between two linear portions, and the center of the inflection obtained by a graphical method was found to correspond to the equivalence point. In the titration of phenol, the data fitted well to the theoretical curve by taking into account the hydrolysis of the phenol ion. The mean of the results obtained from the apparent equivalence point in the concentration range of 1.0—7.7×10^{-3} mol dm^{-3} was 101.2% of the results obtained iodometrically after the bromination of phenol, and the precision of the results was ±2.7% (S.D.).

Nonaqueous solvents have been used for the titration of very weak acids,[1] but they are somewhat troublesome to use. This paper will discuss the titration data of aqueous phenol. In a plot of the pH *vs.* the titrant volume for the potentiometric titration of a very weak acid in water, the inflection at the equivalence point is not sharp, or even disappears. Gran's plot is well known as a special method for the determination of the equivalence point in potentiometric titration, but it can not apply to a solution containing a weak acid or a weak base. It was found that the plot of the pH *vs.* the logarithm of the titrant volume has an inflection between two linear portions, and that the center of the inflection obtained from a graphical method corresponds to the equivalence point. Measurements were made on the titrating solutions in the range from 1.0×10^{-3} to 7.7×10^{-3} mol dm^{-3} with the titrant of 1.1 mol dm^{-3} NaOH.

Theoretical

Titration Curve. We will first discuss the titration of aqueous phenol with aqueous sodium hydroxide, assuming that the volume change due to the addition of titrant is very small. The equilibrium for the ionization of phenol (AH) may be written as

$$AH \rightleftarrows A^- + H^+, \tag{1}$$

$$K_a = \frac{[A^-][H^+]}{[AH]}, \tag{2}$$

where K_a is the ionization constant of phenol. The hydrolysis reaction of sodium phenoxide during the titration is expressed as

$$A^- + H_2O \rightleftarrows AH + OH^-. \tag{3}$$

The equilibrium constant, K_h, in this case is

$$K_h = \frac{[AH][OH^-]}{[A^-]}. \tag{4}$$

Equation 2 may be written in logarithmic form as

$$\log [H^+] = \log \frac{[AH]}{[A^-]} + \log K_a. \tag{5}$$

The material balance for the dissociation of phenol is

$$[AH]_0 = [A^-] + [AH], \tag{6}$$

where $[AH]_0$ is the concentration of phenol in the solution before titration. Before the equivalence point, the material balance for hydrolysis is

$$[A^-] = [NaOH](1-h), \tag{7}$$

where [NaOH] is the concentration of titrant in the solution titrated and where h is the degree of hydrolysis. From Eqs. 5—7 we obtain

$$\log [H^+] = \log \left\{\frac{[AH]_0}{[NaOH](1-h)} - 1\right\} + \log K_a. \tag{8}$$

On substituting the numerical value,[2] $pK_a = 9.998 \approx 10$, into Eq. 8, pH is expressed as

$$pH = -\log \left\{\frac{[AH]_0}{[NaOH](1-h)} - 1\right\} + 10. \tag{9}$$

Beyond the equivalence point, the material balance for hydrolysis is

$$[A^-] = [AH]_0(1-h). \tag{10}$$

From Eqs. 5, 6, and 10, we obtain

$$\log [H^+] = \log \frac{h}{1-h} + \log K_a. \tag{11}$$

On substituting the same numerical value as Eq. 9, the pH is expressed as

$$pH = -\log \frac{h}{1-h} + 10. \tag{12}$$

Next, we will deal with the relation between h and [NaOH]. The concentration, $[OH^-]$, of the hydroxide ion before the equivalence point is expressed as follows:

$$[OH^-] = h[NaOH]. \tag{13}$$

The following equation was obtained by eliminating $[OH^-]$, $[A^-]$, and [AH] from Eqs. 4, 6, 7, and 13:

$$[NaOH]h^2 + ([AH]_0 - [NaOH] + K_h)h - K_h = 0. \tag{14}$$

Beyond the equivalence point, $[OH^-]$ is expressed as follows:

$$[OH^-] = h[AH]_0 + [NaOH] - [AH]_0. \tag{15}$$

Similarly, the following equation was obtained from Eqs. 4, 6, 10, and 15:

$$[AH]_0h^2 + ([NaOH] - [AH]_0 + K_h)h - K_h = 0. \tag{16}$$

When the numerical values of $[AH]_0$, [NaOH], and K_h ($=K_w/K_a$) are substituted into Eq. 14 or 16, we can estimate h. Then, the relation between pH and log [NaOH] is determined from Eq. 9 or 12. Assuming that the volume of the titrating solution is 100 cm^3 and that the volume change due to the addition of the titrant is very small, [NaOH] is expressed as follows;

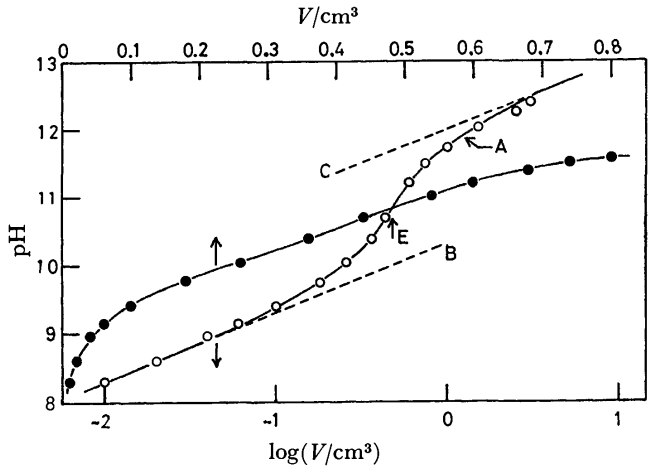

Fig. 1. Theoretical curve and experimental data.
○: Experimental data.
A: Theoretical curve, B and C: asymptotes obtained from Eqs. 18 and 21, respectively. E: Equivalence point, common to Figs. 1—5. Solution titrated: 5.2×10^{-3} mol dm^{-3} phenol, titrant: 1.1 mol dm^{-3} NaOH, temp: 25 °C.

$$[\mathrm{NaOH}] = [\mathrm{NaOH}]_t\frac{V}{100}. \tag{17}$$

Here, $[\mathrm{NaOH}]_t$ is the concentration of the titrant and V is the titrant volume. Therefore, we could obtain the relation of the pH *vs.* the logarithm of the titrant volume as is shown in Fig. 1 (A). The curve, quite consistent with the experimental data, consists of two linear portions.

The asymptotic equation for the linear portion at the beginning of titration is thus obtained for $h\rightarrow0$ in Eq. 9:

$$\mathrm{pH} \simeq \log[\mathrm{NaOH}] - \log[\mathrm{AH}]_0 + 10. \tag{18}$$

The asymptotic equation for the linear portion far beyond the equivalence point is thus obtained for $h\rightarrow0$ in Eq. 12:

$$\mathrm{pH} \simeq -\log h + 10. \tag{19}$$

Here, h is approximated for $[\mathrm{NaOH}]\gg[\mathrm{AH}]_0$ in Eq. 16 as follows:

$$h \approx \frac{K_h}{[\mathrm{NaOH}]}. \tag{20}$$

Consequently, the following asymptotic equation is obtained from Eqs. 19 and 20:

$$\mathrm{pH} \simeq \log[\mathrm{NaOH}] - \log K_h + 10. \tag{21}$$

The slopes of the two linear portions in the theoretical curve were proved identical from Eqs. 18 and 21.

Effect of pK_a *and Concentration of Acid on the Titration Curve.* The method presented above is based on the hydrolysis of the titrating agent, *i.e.*, phenol. Figures 2 and 3 show the relation between h and log V, while Figs. 4 and 5 show the relation between pH and log V. As the equivalence point corresponds to the peak in the curve of h *vs.* log V, the equivalence point is at the maximum of dpH/dlog V. When pK_a is large or the concentration of titrating agent is low, the curve of h *vs.* log V becomes unsymmetrical and the maximum of dpH/dlog V becomes obscure. If

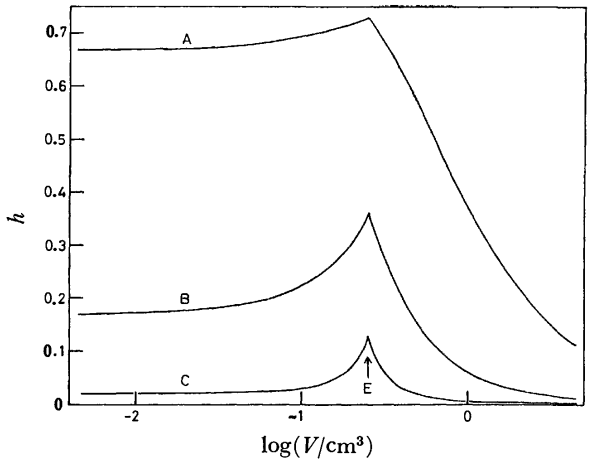

Fig. 2. Theoretical curves; the relation between h and log V.
$[\mathrm{AH}]_0$: 0.005 mol dm^{-3}, concn of titrant: 2 mol dm^{-3}.
pK_a; A: 12, B: 11, C: 10.

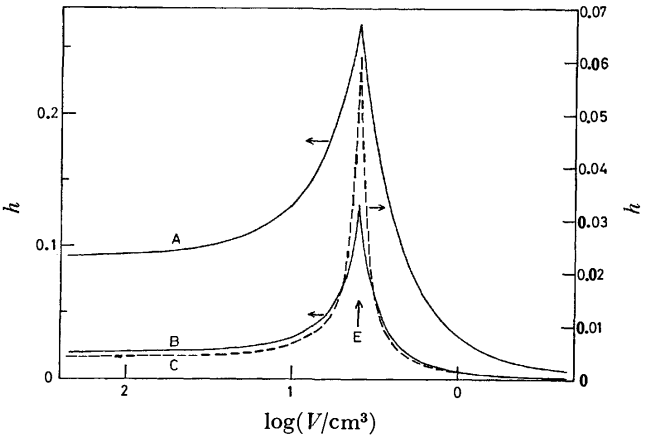

Fig. 3. Theoretical curves; the relation between h and log V.
pK_a: 10. $[\mathrm{AH}]_0$ and concn of titrant; A: 0.001 mol dm^{-3} and 0.4 mol dm^{-3}, B: 0.005 mol dm^{-3} and 2 mol dm^{-3}, C: 0.025 mol dm^{-3} and 10 mol dm^{-3}.

the curve of h *vs.* log V is symmetrical, the maximum of dpH/dlog V becomes much clearer and the equivalence point can be obtained by either the mathematical or the graphical method. We can designate the relation between the pK_a and the concentration of the titrating agent by drawing such curves as are shown in Figs. 2—5. Consequently, the concentration of the titrating agent must be higher than about 0.001 mol dm^{-3} for $pK_a=10$.

Experimental

Materials. All the chemicals were reagent grade and were used without further purification. The CO_2-free solution of NaOH was prepared from a saturated solution.

Titration Apparatus. A pH meter (Toa Electronics HM-5B) was used to obtain the titration curve. The buret was a pipet with a capacity of 0.2, 1, or 2 cm^3. The titration cell was a 120-cm^3 wide-mouthed bottle, in which the solution was stirred with a magnetic stirrer. All the titrations were carried out in a water bath at 25±0.1 °C. Nitrogen was passed slowly through the solution being titrated in order

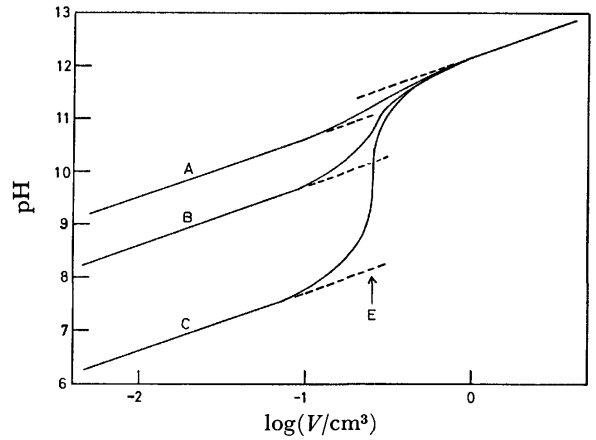

Fig. 4. Theoretical curves; the relation between pH and log V.
$[AH]_0$ and concn of titrant are the same as Fig. 2. pK_a; A: 11, B: 10, C: 8.

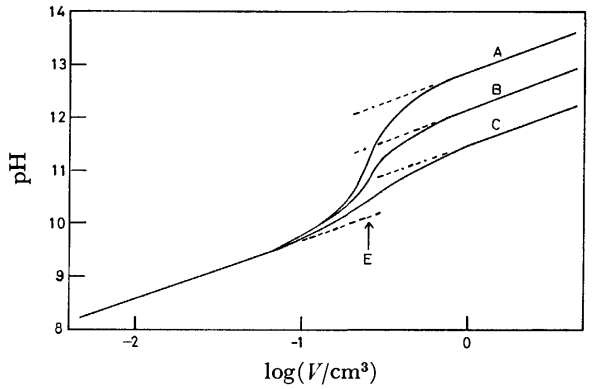

Fig. 5. Theoretical curves; the relation between pH and log V.
pK_a: 10. $[AH]_0$ and concn of titrant; A: 0.025 mol dm^{-3} and 10 mol dm^{-3}, B: 0.005 mol dm^{-3} and 2 mol dm^{-3}, C: 0.001 mol dm^{-3} and 0.4 mol dm^{-3}.

to avoid the absorption of CO_2. The electrodes, buret, and nitrogen inlet were inserted into the titration cell through a rubber stopper.

Titration Procedure. The pH meter was standarized with standard buffers of pH 4.01 and pH 6.86 at 25 °C. Distilled water (100 cm³) and concentrated phenol (0.2—1.5 cm³) were placed in the titration cell, and allowed to stand about ten minutes with stirring and while wet nitrogen gas was bubbled in for temperature equilibration at 25 °C. A correction for the volume change due to the addition of titrant has not been made.

Results and Discussion

Graphical Determination of the Equivalence Point. Figure 6 shows a typical potentiometric titration curve of phenol in water. The apparent equivalence point was determined graphically as follows: Line A was drawn at the initial part of the titration curve; Line B was then drawn parallel to A, tangent to the final portion of the titration curve; Line C was then drawn with a maximum slope tangent to the region of the equivalence point; Lines E and F were drawn vertically so as to pass through the intersections of Line C with

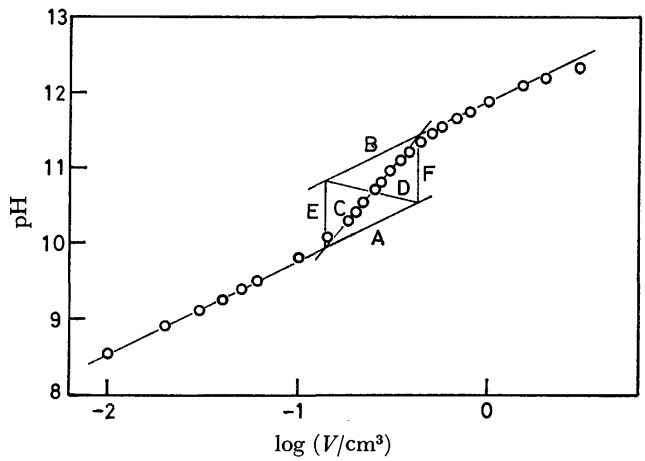

Fig. 6. Typical potentiometric titration curve of phenol in water and graphical determination of equivalence point. The solution titrated is 2.6×10^{-3} mol dm^{-3} phenol and other conditions are the same as those in Fig. 1.

Table 1. Determination of phenol in water

c_1[a] / 10^{-3} mol dm^{-3}	c_2[b] / 10^{-3} mol dm^{-3}	c_2/c_1 / %
1.04	1.08	103.8
1.04	1.10	105.8
2.60	2·68	103.1
2.60	2.62	100.8
5.17	5.12	99.0
5.17	5.00	96.7
7.72	7.76	100.5
7.72	7.69	99.6

a) c_1 is the concn of phenol obtained iodometrically after the bromination of phenol. b) c_2 is the concn determined by this method.

A and B; Line D was drawn from the intersection of Lines A and F to the intersection of Lines B and E. The intersection of Lines C and D was then taken to be the equivalence point.

Accuracy of the Method. Table 1 shows the results of the titration of phenol in water. The value of c_2/c_1 is the ratio of the amount of phenol obtained from this method to that obtained iodometrically after the bromination of phenol.[3] The average value of c_2/c_1 was 101.2% in the concentration range (1.0—7.7×10^{-3} mol dm^{-3}) of phenol, and the precision was ±2.7% (standard deviation).

References

1) J. S. Fritz and N. M. Lisicki, *Anal. Chem.*, **23**, 589 (1951).

2) "Kagakubinran (Handbook of Chemistry)," ed by The Chemical Society of Japan, Maruzen, Tokyo (1966), p. 1053.

3) M. Hojo, "Shin Zikken-Kagaku-Koza," ed by The Chemical Society of Japan, Maruzen, Tokyo (1977), Vol. 13 (I), p. 52; N. H. Furman, "Standard Methods of Chemical Analysis," 5 ed, D. Van Nostrand (1939), Vol. II, p. 2253.

Precise Complexometric Coulometric Titration of Disodium Dihydrogen Ethylenediaminetetraacetate Dihydrate and Aluminium†

Tatsuhiko TANAKA,* Kousei HOTTA, and Takayoshi YOSHIMORI
Faculty of Engineering, Science University of Tokyo, Kagurazaka, Shinjuku-ku, Tokyo 162
(Received June 11, 1979)

The purity of recrystallized disodium dihydrogen ethylenediaminetetraacetate dihydrate was determined accurately by titration with zinc ion coulometrically generated from an amalgamated zinc anode. The reagents used were of 99.446%±0.002% homogeneity when the sample was dehydrated and stored in a hygrostat (relative humidity, *ca.* 58% at 20 °C) over 1 year. Aluminium of high purity (99.99%) was coulometrically titrated with the purified reagent. Aluminium was allowed to react with a certain amount of the reagent, excess of the reagent being titrated with zinc ion anodically generated. The end point was determined potentiometrically using a mercury electrode. The purity was found to be 99.976% with a standard deviation of 0.010% for 6 degree of freedom. Cause of the lower result (0.01%) is discussed.

Marinenko reported on an accurate coulometric determination of gallium for the measurements of the stoichiometric composition of gallium arsenide and of the atomic weight of Ga.[1] The sample containing gallium was allowed to react with excess disodium dihydrogen ethylenediaminetetraacetate dihydrate (Na_2H_2edta) of known composition and the excess of the reagent was back-titrated with coulometrically generated zinc ion. The method requires standard Na_2H_2edta (as a solid) of sufficient purity and homogeneity. However, no mention was given on the quality of Na_2H_2edta.

H_4edta (free acid) of high purity (J. T. Baker Chemical Co., U.S.A.)[2] is insoluble in water and inadequate for the present investigation. Dihydrated disodium salt of the acid of high purity is not available owing to the uncertainty of the content of water of crystallization.

The purity of Na_2H_2edta has been determined by acidimetric[3] or complexometric[1,4–10] coulometry. Several electrogenerated metallic ions, zinc(II),[1,4] lanthanum(III),[5] bismuth(III),[6,7] lead(II),[8] mercury(II),[9] and copper(II)[10] ions, were used as complexometric titrants. The current efficiency for the generation of the titrants, except zinc(II), has not been measured accurately, some electrode materials of high purity not being available. On the other hand, metallic zinc of high purity is available and the current efficiency for the generation of zinc(II) ion has been measured accurately.[11] Moreover, zinc(II) ion is useful as a back-titrant for the determination of metallic ions which have a larger stability constant with edta than that of zinc–edta complex.

The Analytical Methods Committee in the U.K. reported recently the procedure for accurate standardization of Na_2H_2edta by spectrophotometric titration with the use of pure bismuth[12] or zinc[13] metal. However, it gives no satisfactory accuracy because of the difficulty in the detection of the end point.

Only the complexometric procedure can be applied to determine aluminium by coulometric titration. Several coulometric investigations with use of 8-quinolinol complex have been reported.[14–18] The precision attained was higher than 0.1%(as standard deviation), not being sufficient for determining the aluminium content in pure aluminium metal. On the other hand, Na_2H_2edta has high equivalent weight and its use is particularly advantageous for precise determination of metals of small atomic weight such as aluminium. So far, however, it has not been used for complexometric coulometric determination of aluminium.

In this investigation, Na_2H_2edta was purified by recrystallization from ethanolic solution,[19] and by storage in a hygrostat for a long time. Its purity was determined by coulometric titration, and the purity of metallic aluminium was coulometrically determined with the purified Na_2H_2edta.

Experimental

Apparatus and Reagents. Apparatus for coulometric generation of the titrant and for measurement of the time interval of the electrolysis as well as precautions in the weighing of sample were the same as reported.[20] As the Faraday constant, 96484.6 C mol^{-1} was used.

A tall lipless beaker (*ca.* 200 ml) made from quartz plugged with a silicone rubber stopper was used as the electrolytic cell. The generator anode was an amalgamated zinc rod (*ca.* 6 cm^2 in area), and the generator cathode a platinum plate (1×1 cm). The zinc rod was prepared from zinc metal (99.999%, guaranteed by the Industrial Inspection Institute of Japan as a standard reference material for titrimetric analysis). The diaphragm under the cathodic compartment was prepared as follows: the bottom of a polyethylene tube was closed with a polyethylene plate with many fine holes. An agar-agar gel saturated with potassium nitrate was plugged on the bottom, the thickness of the agar layer being about 2 cm.

The end point for titration of Na_2H_2edta was determined by an amperometric procedure using a mercury-plated platinum electrode[21] (applied voltage −1.25 V *vs.* SCE), and that for aluminium was determined potentiometrically with a mercury cup electrode[22] and an "Expandomatic" pH meter (Beckman Instruments, Inc.). A salt bridge of potassium nitrate–agar was used for connection of the electrolytic cell with a saturated calomel electrode in an outside compartment, since chloride ion interferes with the indication of the potential of mercury cup electrode.

All reagents were of analytical grade, and were used (except Na_2H_2edta) without further purification. A 0.5 mol dm^{-3} acetate buffer of pH 6.2 was used as the anolyte for the determination of purity of Na_2H_2edta. Small amounts

† Presented at the 37 th National Meeting of the Chemical Society of Japan, Yokohama, Japan, April 1978, the 27 th Annual Meeting of the Japan Society for Analytical Chemistry, Kanazawa, Japan, October 1978, and the ACS/CSJ Chemical Congress, Hawaii, U. S. A., April 1979.

of solid tungstic acid and 1 mol dm^{-3} potassium nitrate solution (*ca.* 15 ml) were placed in the cathodic compartment.

Procedure. *Coulometric Titration of Na_2H_2edta*: Residual oxygen in the anolyte specified above was removed by passing oxygen-free nitrogen gas for *ca.* 2 h under vigorous stirring. The gas was then allowed to flow over the anolyte throughout the titration.

As pretitration, *ca.* 50 mg of Na_2H_2edta was added to the cell and titrated with anodically generated zinc ion at a constant current of *ca.* 150 mA. Near the end point of titration, the generating current was cut off, the indicator current being measured with a microammeter (full-scale deflection: 10 μA). This was repeated after the end point had been determined. The end point was determined graphically. An Na_2H_2edta sample (*ca.* 400 mg accurately weighed) was then transferred to the cell. After dissolution, it was titrated with coulometrically generated zinc ion by the same procedure as above. The time interval of titration was measured from the two titration curves.

Preparation of Solution of Aluminium Sample: Small pieces of aluminium metal (99.99%) were dipped into hot 7% sulfuric acid for a few minutes, washed successively with water and ethanol, dried *in vacuo* and stored in a desiccator containing magnesium perchlorate. *Ca.* 150 mg of the sample was weighed into a decomposition flask (*ca.* 50 ml) fitted with a reflux condenser[23] to prevent loss by spitting, and dissolved in 10 ml of 6 mol dm^{-3} nitric acid in the presence of platinum wires as a catalyst. The solution was then transferred to the electrolytic cell and evaporated to a small volume (*ca.* 20 ml). A weighed amount of the Na_2H_2edta (solid, standardized) was added in slight excess and the pH of the solution was adjusted to 3.5 by gradual addition of solid sodium acetate trihydrate. The solution was heated nearly to boil for *ca.* 15 min on a hot plate to ensure the complete complexation reaction of aluminium ion with edta. After cooling, the pH of the solution was adjusted to 6.2 by the dropwise addition of 20% sodium hydroxide solution. The solution was finally diluted to *ca.* 150 ml with deaerated water.

Coulometric Titration of Aluminium: After deoxygenation of the solution of aluminium, the solution was cooled below 3 °C in an ice bath. Excess edta was back-titrated with electrogenerated zinc ion. Because of sluggish attainment of the equilibrium condition near the end point of the titration, the constant current was cut off near the end point, and the potential of the indicator electrode was measured after it became stable. This was repeated in order to obtain the titration curve. The end point was determined by means of the differential titration curve. A blank experiment was carried out throughout the procedure.

Results and Discussion

Standardization of Na_2H_2edta. The purity and pretreatment of commercial Na_2H_2edta were first investigated by the procedure described previously. Three different lots of analytical-grade Na_2H_2edta A, B, and C were analyzed (a) without any treatment and (b) after drying, the assay values being given in Table 1.

The results for both (a) and (b) indicate low purity and considerable inhomogeneity. Wendlandt pointed out that the composition of crystalline water among commercial Na_2H_2edta is not stoichiometric.[24] The results (Table 1) indicate similar phenomena. Duval found the evolution of water at 60 °C on heating Na_2H_2edta.[25] However, Blaedel and Knight recommended 80 °C as the optimum temperature for air-drying of the hydrated salt without decomposition.[19] The values of relative standard deviation seem to support 80 °C, since constant weight of Na_2H_2edta was obtainable by heating at the temperature for 4 d. JIS(Japanese Industrial Standard) recommends heating of the reagent at 80 °C for 5 h,[26] but the time is not sufficient to attain constant weight.

TABLE 1. ASSAYS OF ANALYTICAL-GRADE Na_2H_2edta

Sample	No. of detns.	Purity (%)	s_R / %
A	3	99.280	0.061
	3	99.653[a]	0.024
B	3	99.585	0.076
	3	99.961[a]	0.063
C	3	99.629	0.049
	3	99.728[a]	0.022
	10	99.697[b]	0.009[c]

a) Dried at 80 °C for 4 d. b) Stored in hygrostat (*ca.* 58% rel. humidity) for 6 months. c) $\sqrt{V}$ value.

TABLE 2. ASSAYS OF Na_2H_2edta RECRYSTD. FROM REAGENT B

Method of pretreatment	No. of detns.	Purity %	s_R %
Without drying	5	97.607	0.054
Dried at 80 °C for 4 d	6	98.981	0.080
Dried at 80 °C for 4 d[a]	4	99.211	0.017
Stored in hygrostat[b] for 6 months	4	99.268	0.010
Dehydrated *in vacuo* and stored in hygrostat[b]			
for 12 months	1	99.445	—
for 15 months	6	99.446	0.002

a) Ground prior to drying. b) About 58% rel. humidity.

The hydrated salt is stable over a wide range of humidity.[19] The weight of the reagent left under ordinary atmospheric conditions (35—60% relative humidity) changed from −0.017% to +0.025%. Thus, one of the reagents (Sample C, Table 1) was gently ground with an agate mortar, dried at 80 °C for 4 d, and stored in the hygrostat containing a saturated solution of sodium bromide at ordinary temperature (relative humidity *ca.* 58%) with frequent mixing. The results of assay of the Na_2H_2edta stored for 6 months in the hygrostat (Table 1) indicate that the reagent shows sufficient homogeneity.

Na_2H_2edta(Sample B, Table 1) of analytical grade was purified by recrystallization from ethanolic solution[19] in order to obtain pure Na_2H_2edta. The results obtained for the recrystallized reagent (Table 2) are somewhat lower than those of the original material. This may be mainly due to the contamination from glassware and distilled water. Since the recrystallized reagent may contain occluded water, it was dehydrated completely in a vacuum oven overnight at 120 °C,[19] and rehydrated by being kept in the hygrostat (relative humidity *ca.* 58%) until the purity became constant.

Table 3. Determination of high-purity aluminium (99.99%)[a]

Sample taken (mg)	Al found (mg)	Purity %
137.611	137.576	99.975
150.915	150.871	99.971
156.859	156.836	99.985
169.583	169.512	99.958
143.749	143.725	99.983
127.214	127.182	99.975
150.650	150.624	99.983
		Mean = 99.976±0.009%[b]
		R = 0.027%
		s_R = 0.010%

a) Value estimated by the manufacturer. b) The 95% confidence interval for the mean.

Excellent homogeneity could be attained by storing for more than 1 year.

In conclusion, the recrystallized reagent is suitable for use as a complexometric standard, when it is once dehydrated and then stored in a hygrostat, for example a desiccator containing a saturated solution of sodium bromide, for more than 1 year with frequent mixing.

Assay of Aluminium. The purity of the metallic aluminium (99.99%) was determined by the procedure described previously. When the electrolyte was not cooled, the aluminium content exceeded 100%. This may be caused by the displacement reaction of aluminium–edta complex to zinc–edta complex with the electrogenerated zinc ion, since the stability constant of aluminium–edta complex is similar to that of zinc–edta complex. The electrolyte was, therefore, cooled below 3 °C during the course of titration in order to prevent the displacement reaction. The results for the aluminium sample obtained by the proposed method are given in Table 3.

The purity was somewhat less than 99.99% (estimated by the manufacturer), though the standard deviation was small. The cause of this result was investigated.

Impurities in the sample were first examined. Semi-quantitative spectrographic analysis indicates that the sample contains in total *ca.* 30 ppm of metallic impurities, iron, copper, manganese, magnesium, silicon, and antimony. Oxygen was determined by bromine–methanol dissolution followed by spectrophotometric measurement (8-quinolinol extraction method),[27] the content being *ca.* 40 ppm. Thus, the purity of this sample can be evaluated as 99.99%.

Marinenko and Foley reported that the anodic oxidation of zinc proceeds at 100.000% current efficiency with current density between 10^{-2} and 10^3 mA cm^{-2}.[11] In the present investigation, the current density was *ca.* 25 mA cm^{-2}, no error due to the current efficiency being present. The error due to the location of end point was considered. Sharp potential breaks were usually obtained at the end point (*ca.* 12 mV per 1 μg of aluminium). The difference of 0.1 s in the duration of electrolysis corresponds to *ca.* 15 ppm of aluminium. Thus, the uncertainty of the graphical location of the end point is below several ppm. The standard deviation in the measurement of the generating current was not greater than 0.005%. Thus, the titration error can not be the cause of the lower result. Some displacement reaction between aluminium– and zinc–edta complexes might be the main source of *ca.* 0.01% error.

The authors express their thanks to Mr. Syuiti Ishiwari, Hitachi Co. Ltd., for the spectrographic analysis of the aluminium sample. The present work was partially supported by a Grant-in-Aid for Scientific Research from the Ministry of Education.

References

1) G. Marinenko, *J. Res. Natl. Bur. Stand., Sect. A*, **81**, 1 (1977).
2) A. J. Barnard, Jr., E. F. Joy, K. Little, and J. D. Brooks, *Talanta*, **17**, 785 (1970).
3) "Microchemical Analysis Section," National Bureau of Standards Technical Note 455, U. S. Government Printing Office, Washington, D. C. (1968), p. 74.
4) "Electrochemical Analysis Section," National Bureau of Standards Technical Note 543, U. S. Government Printing Office, Washington, D. C. (1970), p. 44.
5) D. J. Curran and K. S. Fletcher, *Anal. Chem.*, **40**, 1809 (1968).
6) Th. J. M. Pouw, G. den Boef, and U. Hannema, *Anal. Chim. Acta*, **67**, 427 (1973).
7) V. N. Basov, P. K. Agasyan, and T. N. Testoedova, *Zavod. Lab.*, **42**, 510 (1976); *Anal. Abstr.*, **31**, 5J126 (1976).
8) Th. J. M. Pouw, G. den Boef, and G. Hannema, *Anal. Chim. Acta*, **68**, 243 (1974).
9) J. L. Vandenbalck, C. A. Mairesse-Ducarmois, and G. J. Patriarche, *Analysis*, **3**, 473 (1975); *Anal. Abstr.*, **30**, 6C30 (1976).
10) A. A. Inkin and V. T. Kharlamov, *Zh. Anal. Khim.*, **31**, 2271 (1976); *Anal. Abstr.*, **32**, 5C27 (1977).
11) G. Marinenko and R. T. Foley, *J. Res. Natl. Bur. Stand.*, **79**, 747 (1975).
12) Analytical Methods Committee, *Analyst (London)*, **100**, 675 (1975).
13) Analytical Methods Committee, *Analyst (London)*, **103**, 93 (1978).
14) R. T. Iwamoto, *Anal. Chim. Acta*, **19**, 272 (1958).
15) G. Berraz and O. Delgado, *Rev. Fac. Ing. Quim., Argentina*, **28**, 39 (1959); *Anal. Abstr.*, **8**, 3150 (1961).
16) A. I. Kostromin and M. Kh. Akhmadeev, *Zavod. Lab.*, **29**, 402 (1963); *Anal. Abstr.*, **11**, 1228 (1964).
17) A. I. Kostromin and M. Kh. Akhmadeev, *Uch. Zap. Kazan. Gos. Univ.*, **124**, 166 (1964); *Anal. Abstr.*, **14**, 33 (1967).
18) A. I. Kostromin and A. I. Kruglov, *Uch. Zap. Kazan. Gos. Univ.*, **124**, 173 (1964); *Anal. Abstr.*, **13**, 6834 (1966).
19) W. J. Blaedel and H. T. Knight, *Anal. Chem.*, **26**, 741 (1954).
20) T. Yoshimori and T. Tanaka, *Anal. Chim. Acta*, **55**, 185 (1971).
21) T. Miwa, Dr. Thesis, Nagoya University, Nagoya, Japan, 1973, pp. 122—123.
22) C. N. Reilley, R. W. Schmid, and D. W. Lamson, *Anal. Chem.*, **30**, 953 (1958).
23) T. Yoshimori, I. Matsubara, T. Tanaka, K. Yoshida, K. Tanaka, and T. Tanabe, *Bull. Chem. Soc. Jpn.*, **44**, 734 (1971).
24) W. W. Wendlandt, *Anal. Chem.*, **32**, 848 (1960).
25) C. Duval, *Anal. Chim. Acta*, **16**, 545 (1957).
26) JIS K 8107 (1976).
27) "Methods of Chemical Analysis for Trace Elements in Aluminium." ed by the Chemical Analysis Committee, Japan Light Metal Association, Tokyo (1978), pp. 152—155 (in Japanese).

Kinetic Studies of the Acid Hydrolysis of Aquaoxo[*N*-(2-pyridylmethyl)-iminodiacetato]vanadium(IV) and Aqua(nitrilotriacetato)-oxovanadate(IV) in Aqueous Perchloric Acid Solution

Masato NISHIZAWA and Kazuo SAITO*

Chemistry Department, Faculty of Science, Tohoku University, Aoba, Aramaki, Sendai 980

(Received June 29, 1979)

Acid hydrolysis of aquaoxo[*N*-(2-pyridylmethyl)iminodiacetato]vandium(IV) [VO(pmida)H_2O], ([H^+]= 0.1—2.0 M, 1M= 1 mol dm^{-3}) and aqua(nitrilotriacetato)oxovanadate(IV) [VO(nta)H_2O]$^-$, ([H^+]=0.2—2.0 M) has been studied by the stopped-flow method in aqueous perchloric acid solution at an ionic strength 2.0 ($LiClO_4$). The pseudo first-order rate constant k_o is dependent on the proton concentration. The rate formula is expressed by $k_o=(k_1K_1[H^+]+k_2K_1K_2[H^+]^2)/(1+K_1[H^+]+K_1K_2[H^+]^2)$. A simulation curve fitting treatment gave the figures: k_1=0.02 and 0 s^{-1}, k_2=6 and 3000 s^{-1}, K_1=1.5 and 0.2 M^{-1}, and K_2=0.2 and 0.004 M^{-1} at 25 °C for [VO(pmida)-H_2O] and [VO(nta)H_2O]$^-$, respectively. These data indicate that the rate determining step corresponds to the dissociation of the second basal bond of the singly or doubly protonated oxovanadium(IV) complexes.

The ligand substitution reaction of oxovanadium(IV) complexes includes several kinds of mechanistically discriminated reaction on different coordination sites (Fig. 1).[1] We have determined the structure of a new complex aquaoxo[*N*-(2-pyridylmethyl)iminodiacetato]vanadium(IV) [VO(pmida)H_2O]·$2H_2O$ by X-ray crystallography to find that the tertiary amine occupies the trans site to oxo.[2] The anation reaction of this complex[1] with thiocyanate and azide proceeded much slower ($\simeq 10^{-1}$ s^{-1} at 25 °C) than the reported basal site substitutions[3] ($\simeq 10^3$ s^{-1} at 25 °C). We have thus considered that the hitherto known rates would not represent those of direct basal site substitution but involve the rearrangement from the apical to the basal site.

This new compound is stable toward acid hydrolysis above pH 3, but loses the quadridentate ligand in a more acid solution. Nitrilotriacetate(nta^{3-}) gives aqua(nitrilotriacetato)oxovanadate(IV) [VO(nta)-H_2O]$^-$ which was found also stable toward acid hydrolysis above pH 3.[4] Acid hydrolysis of these two complexes involve various steps but must include the dissociation of basal metal-ligand bond. This paper deals with the kinetic studies of aquation of [VO-(pmida)H_2O] and [VO(nta)H_2O]$^-$ in perchloric acid solutions containing 0.1 to 2.0 and 0.2 to 2.0 M (1 M= 1 mol dm^{-3}) acid, respectively, at an ionic strength 2.0 ($LiClO_4$). The overall reaction is expressed by Eq. 1 (L^{n-2} stands for the quadridentate ligand with n=0 or 1).

$$[VO(L)H_2O]^n + mH^+ \underset{k_f}{\overset{k_d}{\rightleftharpoons}} [VO_{aq}]^{2+} + H_mL^{m+n-2} \quad (1)$$

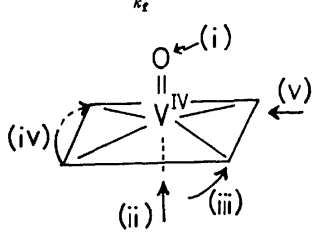

Fig. 1. Different substitution rates at various coordination sites of oxovanadium(IV) ion.
i) Very slow exchange of the oxo ligand, ii) very rapid substitution at the apical site, iii) fairly rapid intramolecular rearrangement from the apical to the basal site, iv) chelate formation at the basal site, v) rather slow direct basal substitution.

Experimental

Materials. The complex [VO(pmida)H_2O]·$2H_2O$[2] and K[VO(nta)H_2O]·H_2O[4] were prepared by the given methods, and the purity was checked by IR, UV, and visible absorption spectra and elemental analysis of carbon, hydrogen, and nitrogen. The ionic strength was adjusted with Special Grade sodium perchlorate and lithium perchlorate. The latter was prepared from the carbonate and perchloric acid and doubly recrystallized. Perchloric acid (Wako Chem. Co., Special Grade 60%) was used without further purification. The acid concentration was determined by the titration with sodium hydroxide.

Kinetic Runs. The UV absorption spectra at the initial and the final stage of the acid hydrolysis reaction are shown in Fig. 2. The rate was measured by monitoring the decrease of absorbance at 350 and 330 nm for the pmida and nta complexes, respectively, by the stopped-flow technique mainly at 25 °C and I=2.0 ($LiClO_4$). The difference in absorption at the given wave lengths before and after the acid hydrolysis coincided with those calculated from pure

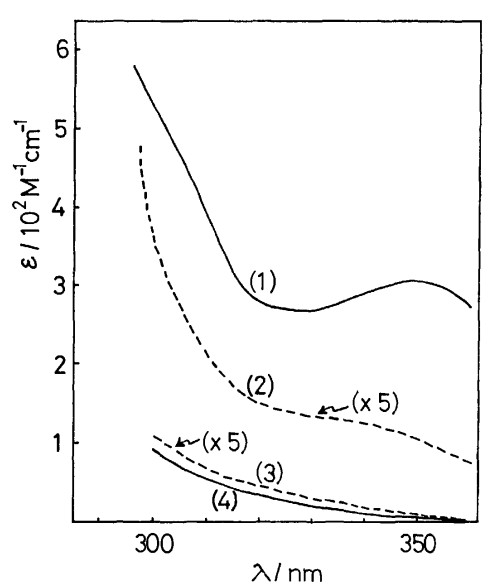

Fig. 2. UV absorption spectra in aqueous solution. 1) [VO(pmida)H_2O] at pH 4.7, 2) [VO(nta)H_2O]$^-$ at pH 4.7, 3) after equilibration of [VO(nta)H_2O]$^-$ containing 1 M acid, 4) after equilibration of [VO-(pmida)H_2O] containing 1 M acid.

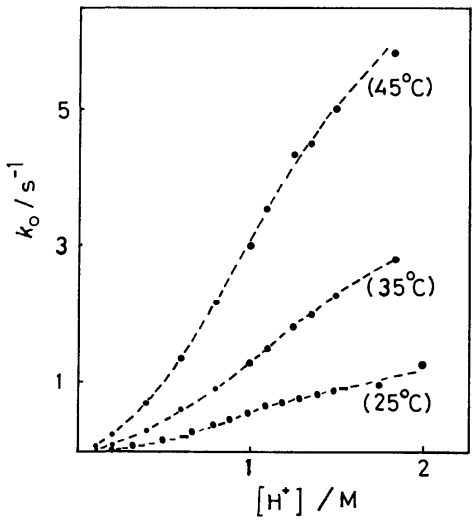

Fig. 3. Dependence of the first-order rate constant k_o upon the acid concentration for [VO(pmida)H$_2$O] (I=2.0, LiClO$_4$ at 25, 35, and 45 °C).
———; Simulation (see the text).

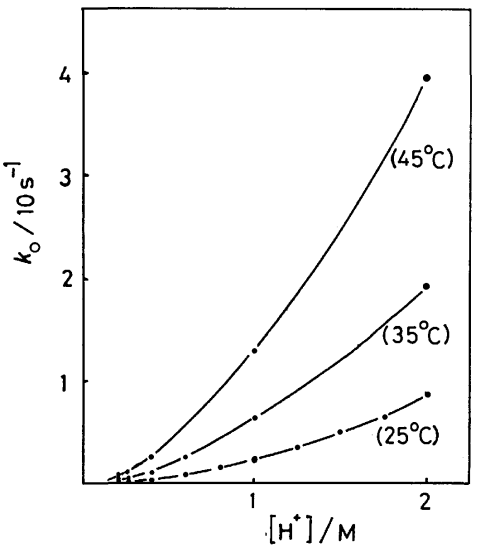

Fig. 4. Dependence of the first-order rate constant k_o upon the acid concentration for [VO(nta)H$_2$O]$^-$ (I= 2.0, LiClO$_4$ at 25, 35, and 45 °C).

solutions of [VO(L)H$_2$O]^n and [VO(H$_2$O)$_5$]$^{2+}$, and the free ligand. The absorption spectra of all the reaction mixtures 5 min after mixing were the same with those of the complexes in 5 M perchloric acid solutions. Plots of $\ln(A_t - A_\infty)$ against time were linear until the reaction reached 85% completion, where A_t and A_∞ stand for the absorptions at the given wave length at time t and infinity, respectively. The first-order rate constants k_o were obtained from the slopes by the least squares method. The apparatus (Union Giken, RA 601 stopped-flow spectrometer) was used on different time scales, and the reproducibility was satisfactory within an error ±3%.

Results

The Overall Rate. The observed rate constant, k_o is expressed by Eq. 2, where [VO] stands for the concentration of the original complex.

$$-\mathrm{d[VO]}/dt = k_o[\mathrm{VO}] \quad (2)$$

Since the acid hydrolysis proceeded to completion under the given conditions, only the k_d in Eq. 1 was observed. Addition of excessive H$_3$nta did not change the k_o values at [H$^+$]=0.2 M. Addition of H$_2$pmida to the [VO(pmida)H$_2$O] solution at [H$^+$]=0.1 M increased the observed first-order rate constant and the formula was expressed by Eq. 3. ([H$_x$pmida] stands for the sum of concentration of variously protonated species of free pmida^{2-})

$$k'_o = k_d + k_f[\mathrm{H}_x\mathrm{pmida}] \quad (3)$$

The observed k_d was 0.012 s^{-1}, coinciding with the k_o (0.012 s^{-1}) in the absence of excess of H$_2$pmida. Hence the formation reaction does not affect the rate of acid hydrolysis and no attention was paid to k_f.

Kinetic Formulae. The observed first-order rate constants for the two complexes showed rather complicated dependence on the acid concentration. (Figs. 3 and 4)

The pmida Complex: The curves in Fig. 3 suggests the participation of two routes involving one and two protons as shown by Eqs. 4, 5, and 6.

$$[\mathrm{VO(L)H_2O}]^n \overset{K_1(\mathrm{H^+})}{\rightleftarrows} [\mathrm{VO(HL)H_2O}]^{n+1} \overset{K_2(\mathrm{H^+})}{\rightleftarrows} [\mathrm{VO(H_2L)H_2O}]^{n+2} \quad (4)$$

$$[\mathrm{VO(HL)H_2O}]^{n+1} \xrightarrow{k_1} [\mathrm{VO_{aq}}]^{2+} + \mathrm{H}_x\mathrm{L} \quad (5)$$

$$[\mathrm{VO(H_2L)H_2O}]^{n+2} \xrightarrow{k_2} [\mathrm{VO_{aq}}]^{2+} + \mathrm{H}_x\mathrm{L} \quad (6)$$

On the basis of Eqs. 4 to 6, the rate formula is written by

$$k_o = (k_1K_1[\mathrm{H^+}] + k_2K_1K_2[\mathrm{H^+}]^2)/(1 + K_1[\mathrm{H^+}] + K_1K_2[\mathrm{H^+}]^2). \quad (7)$$

Individual values of k_1, k_2, K_1, and K_2 were obtained by the trial and error method from the experimental values and shown in Table 1. They may involve rather large errors. The broken lines in Fig. 3 drawn by use of these calculated values, however, fit the experimental plots well.

The nta Complex: When the same analysis was applied to the nta complex, the individual values of equilibrium and rate constants were calculated as shown in Table1. It seems as if there is no contribution of the route shown by Eq. 5. The usefulness of such an analysis was verified as follows. The simulated value of k_1 is almost zero, and the product $K_1K_2[\mathrm{H^+}]^2$ is very small

Table 1. Results of the simulation curve fitting

	pmida			nta	
Temp/°C	45	35	25	25	25[a]
K_1/M^{-1}	1.7	1.6	1.5	0.20	0.26
K_2/M^{-1}	0.1	0.1	0.2	0.004	$k_2 \cdot K_2$
k_1/s^{-1}	0.1	0.05	0.02	0.00	12±2
k_2/s^{-1}	40	20	6	3000	(M^{-1} s^{-1})

a) By use of Eq. 9; the apparent ΔH^* and ΔS^* calculated for the product k_2K_2 at 25, 35, and 45 °C are 38±17 kJ mol^{-1} and −96±50 J mol^{-1} K^{-1}, respectively.

TABLE 2. SALT EFFECTS ([H+]=0.2 M, 25 °C)

I	k_o/s^{-1}	
	pmida	nta
0.2	0.020	0.14
1.2	0.037	0.13
2.0	0.042	0.11

under the experimental conditions. Hence the first term of the numerator and the third term of the denominator of Eq. 7 can be ignored to give Eq. 8.

$$k_o = k_2K_1K_2[H^+]^2/(1+K_1[H^+]) \quad (8)$$

This is converted into Eq. 9.

$$[H^+]/k_o = 1/k_2K_1K_2[H^+] + 1/k_2K_2 \quad (9)$$

Plots of $[H^+]/k_o$ against $[H^+]^{-1}$ gave straight lines at the three temperatures, and the K_1 and the product k_2K_2 were obtained from the intercepts and gradients. The K_1 values obtained by such a plot and by the simulation method coincided with each other.

Medium Effects. The salt effect[5] was studied by changing the ionic strength, and the results are included in Table 2. A positive and a slightly negative effect were found for the pmida and the nta complex, respectively.

The chloride ion concentration did not affect the rate. The thiocyanate ion slightly accelerated the reactions of both complexes. The kinetic formula is too complicated to be analysed, but the anion seems to replace, at least partly, the coordinated water of the original complexes.[1,4]

Discussion

Whenever a substitution reaction of oxovanadium(IV) complexes is to be analysed, participation of mechanistically discriminated reactions should be considered (Fig. 1). They include i) very inert oxoanion exchange,[6] ii) extremely labile apical site substitution,[7,8] iii) basal ligand substitution involving intramolecular rearrangement of a ligand from apical to basal site,[3] iv) chelation at basal site,[9] and v) direct basal substitution.[1,4] For the present reactions, process iii and v should be considered.

Kinetic formulae for both the complexes indicate that proton catalysed bond breaks are the rate determining steps. Since coordinated nitrogen atoms have no lone pair of electrons, the protonation should take place on the oxygen of the acetate branch of the ligand.[10]

The pmida Complex. The X-ray structure has been determined and the bond lengths are known. The kinetic formula suggests the presence of two parallel paths, accompanied by single and double protonation. For the process iii to operate, break of at least two basal bonds should be needed. A plausible reaction mechanism is illustrated in Fig. 5.

The V–O bond lengths are 2.02 and 1.98 Å at the trans and cis site of the aqua ligand, respectively, in the crystalline state (Fig. 6). If the difference were preserved in the aqueous solution, the first protonation should take place at the trans site. The protonated acetate branch will leave the coordination sphere rapidly, so that the observed K_1 corresponds to the product of the equilibrium constant of the first protonation (I to II) and the break of the trans V–OH bond to the aqua (II to III).[11] The k_1 step can take place at either the V–O (cis to aqua) or the V–N (pyridine) bond. Their lengths are 1.98 and 2.11 Å respectively in the crystalline state. If a similar difference existed in the aqueous solution, the V–N bond would be broken at a rate k_1 [III]. The observed k_1 value is not very different from the ordinary rate constant of direct basal bond break (process v).[1]

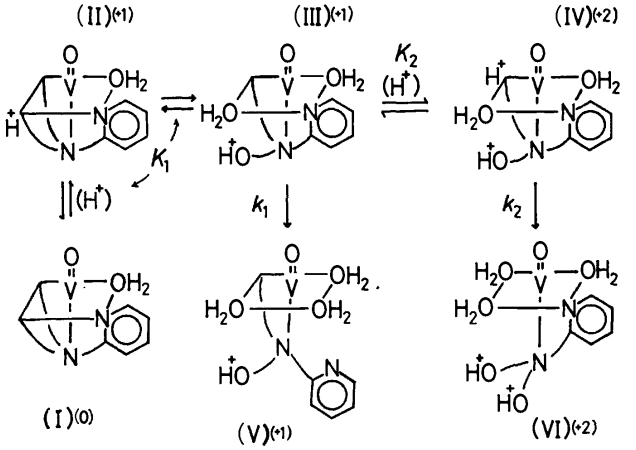

Fig. 5. Plausible reaction mechanism for [VO(pmida)-H_2O]. (The overall charges of the complex and the intermediates are in parentheses).

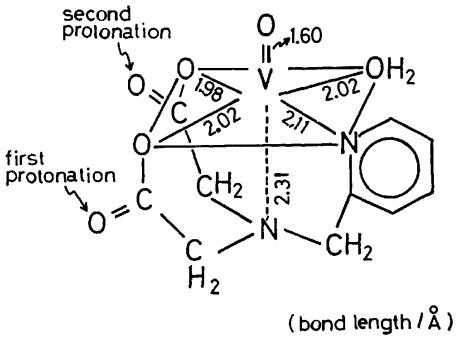

Fig. 6. X-Ray structure data of [VO(pmida)H_2O]·$2H_2O$ and plausible protonation site in solution.

The k_2 step involving the doubly protonated complex (IV) must be the break of the acetate arm cis to the aqua ligand. The larger k_2 than k_1 must be due to protonation. After the two basal bonds are broken, the tertiary nitrogen can dissociate very quickly (process ii) and the third basal bond (V–O and V–N(pyridine) for the intermediates V and VI, respectively) can move to the apical site (process iii) to result in complete dissociation of $H_x$pmida.

The contribution of the two paths depends on the acid concentration. The k_2 is much greater than k_1, but the small K_2 decreases its contribution, which however predominates at a high acid concentration.

The nta Complex. The X-ray structure of this complex is not known, but the tertiary amine was believed to occupy the apical position.[4] The simulated

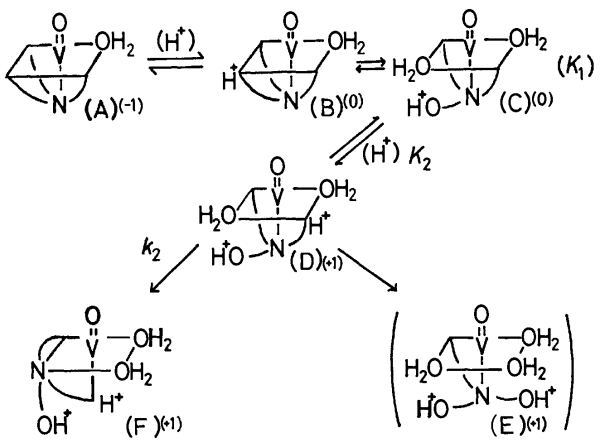

Fig. 7. Plausible reaction mechanisms for [VO(nta)-H_2O]$^-$ (see the text). (The overall charges of the complex and the intermediates are in parentheses).

small k_1 implies that the singly protonated species (C in Fig. 7) does not allow the dissociation of the complex. Whenever a similar process is assumed for this complex as for the pmida complex, the K_1 represents the overall equilibrium constant for the two processes, the protonation (form A to B) and the dissociation of a V–OH bond trans to aqua (B to C). The simulated K_1 is much smaller than that for the pmida complex. This fact may result from either the difficulty in first protonation or the ease of the backward reaction from C to B, suggesting in either case a stronger V–O bond than that for the pmida complex. The K_2 value indicating the ease of second protonation at the cis site to the aqua ligand is also smaller than that for the pmida complex. This fact also suggests a stronger V–O bond than that for the pmida complex. These observations are also reflected in the high acid concentration region, in which the acid hydrolysis can be measured. The simulated k_2 vaule ($\simeq 3000\ s^{-1}$) is, on the other hand, much greater than that of the pmida complex ($\simeq 6\ s^{-1}$). Although there can be complication from the difference in overall charge, it is unlikely that a stronger bond is more readily broken than a weaker bond under a similarly protonated circumstance. Hence the k_2 must reflect some other process than a mere break of V–OH bond (from D to E in Fig. 7). If the doubly protonated intermediate D underwent intramolecular rearrangement to give F, the protonated arm at the apical site would be readily broken (processes iii and ii). Such an intramolecular change is not generally feasible for a terdentate ligand. Molecular model studies, however, suggest that the nta complex is highly strained. The second protonation will elongate the V–O bond and can bring about the rearrangement of H_2nta^- to give F. The simulated k_2 is in the same region as those for the process iii.[12]

Comparison of the Two Complexes. The faster acid hydrolysis of the more stable nta complex than that of the pmida complex may be accounted for by considering different rate determining steps for both complexes as shown above. The reason why the pmida complex undergoes the intramolecular rearrangement to give F-type intermediate with difficulty may be attributed to the more highly oriented V–N (pyridine) bond brought about by the delocalization of electron between d_{xy} orbital of vanadium(IV) and the π-orbital of pyridine.

The influence of ionic strength upon k_o indicates the interactions between species with the same and opposite ionic sign for the pmida and the nta complex, respectively. Since interactions involving species without electric charge do not exhibit significant dependence on the ionic strength, the equilibrium constants K_2 and K_1 will be subject to the influence (see Figs. 5 and 7). The K_2 for the pmida complex will increase and the K_1 for the nta complex will decrease with increase in ionic strength. Since the second and third terms of the denominator of Eq. 7 are much less than unity, the influence of ionic strength will be predominating on the numerator. Hence the results of Table 2 are reasonably interpreted by the mechanisms shown in Figs. 5 and 7.

References

1) M. Nishizawa and K. Saito, *Inorg. Chem.*, **17**, 3676 (1978).

2) S. Ooi, M. Nishizawa, K. Matsumoto, H. Kuroya, and K. Saito, *Bull. Chem. Soc. Jpn.*, **52**, 452 (1979).

3) References cited in Ref. 1.

4) M. Nishizawa and K. Saito, *J. Chem. Soc., Chem. Commun.*, **1979**, 707.

5) A. D. Pethybridge and J. E. Prue, "Inorganic reaction mechanisms, II," ed by J. O. Edwards, Wiley-Interscience (1972).

6) R. K. Murmann, *Inorg. Chim. Acta*, **25**, L43 (1977).

7) F. A. Walker, R. L. Carlin, and P. H. Rieger, *J. Chem. Phys.*, **45**, 4181 (1966).

8) K. Wüthrich and R. E. Connick, *Inorg. Chem.*, **7**, 1377 (1968).

9) H. Tomiyasu and G. Gordon, *Inorg. Chem.*, **15**, 870 (1976).

10) Y. Sasaki and A. G. Sykes, *J. Chem. Soc., Dalton Trans.*, **1974**, 1468.

11) The absorption change corresponding to the step from species (II) to (III) seems too small to be detected. The rate of the bond break from II to III must be greater than those for the k_1 and k_2 paths but can be of similar order to that of the k_2 path.

12) This interpretation is based on the assumption that the first protonation takes place at the trans site to the aqua ligand as presumed for the pmida complex. If the first protonation occurred on the cis site, on the contrary, the intermediate product would involve a facially terdentated $Hnta^{2-}$ species. The nitrogen at the apical site would be labile, and the second protonated acetate arm can squeeze into the apical site while the nitrogen tentatively leaves the apical site. Such a mechanism is also in accord with the given kinetic formula and the simulated values of K_1, K_2, and k_2. So far as the bond lengths remain unknown the two possible reaction mechanisms cannot be discriminated.

Equilibrium Study of Iron Vanadium Sulfides in the Iron-rich Portion of the Composition Triangle of FeS–VS–S

Hiroaki WADA

National Institute for Researches in Inorganic Materials, Namiki, Sakura-mura, Niihari-gun, Ibaraki 305

(Received August 2, 1979)

An equilibrium study of a part of the Fe–V–S system at sections with atomic Fe:V ratios of 1:0, 9:1, and 4:1 was carried out by means of thermogravimetry. The thermochemical data which were obtained in the range of $\log(P_{S_2}/\text{atm}) = -4$ to -0.8 at temperatures between 520 and 814 °C are presented. The compositional limits of the univariant assemblage of $Fe_{1-\delta}S$-FeS_2-$(Fe,V)_3S_4$ were determined at 570 °C on the basis of X-ray analyses of the quenched specimens. The rate of FeS_2 formation under the experimental conditions employed was studied qualitatively from the point of view of the sulfidation kinetics of iron vanadium sulfides.

The results of equilibrium studies of the ternary compounds of Fe–V–S with the constant V/(Fe+V) ratio in the range of 0.29 to 1 were presented in earlier publications.[1-3] The author wishes to report in this paper the experimental results for a further series of samples with the V/(Fe+V) ratios of 0.20, 0.10, and 0. In this part of the Fe–V–S system, the following compounds are included: the hexagonal $(Fe,V)_{1-\delta}S$ solid solution, the monoclinic $(Fe,V)_3S_4$ solid solution, and the cubic FeS_2 (pyrite). With respect to the phase relations, it is known that the ternary univariant assemblage, which is composed of a three-phase mixture of FeS_2, the $(Fe,V)_3S_4$ solid solution, and $Fe_{1-\delta}S$, is stable over wide compositional ranges at 570 °C.[2] However, the compositional data on the phase boundary of the univariant assemblage have not yet been determined precisely in detail.

The primary aims of this study were to obtain the thermochemical data of iron vanadium sulfides under equilibrium conditions and to determine the phase relations and its compositional limits in detail. Considerable attention has been focussed on the determination of the univariant field of FeS_2–$Fe_{1-\delta}S$–$(Fe,V)_3S_4$ s.s.–vapor. In this connection, the sulfidation kinetics of iron vanadium sulfides was examined in order to obtain fundamental knowledge on the rate of FeS_2 formation under the experimental conditions employed.

The main thermochemical study was carried out with a gravimetric method by using a quartz spring balance at temperatures between 500 and 814 °C. The sulfur pressure in the N_2–sulfur vapor system was controlled by temperature regulation. The present paper is concerned with the P_{S_2} (equilibrium sulfur pressure)-T (temperature)-X (composition) relations, the phase relations, and the sulfidation rate of iron vanadium sulfides in the case of FeS_2 formation.

Experimental

Materials. Sulfide samples with atomic Fe : V ratios of 9 : 1 and 4 : 1 were synthesized by heating the mechanical mixtures of reagent-grade $VOSO_4 \cdot 3H_2O$ and $FeSO_4 \cdot (NH_4)_2SO_4 \cdot 6H_2O$ in an H_2S atmosphere at 1050 °C for 4 h. The iron sulfide samples were synthesized by means of a direct reaction from the elements. The iron powder (99.99%) and sulfur powder (99.9999%) were used for preparation. The mixture in desired quantities was sealed in an evacuated silica tube, heated at high temperatures, and quenched in water. Two samples with different compositions were used for the study of the Fe–S system. One was $FeS_{1.12}$, which had been synthesized at 800 °C for a week. The other was $FeS_{2.01}$, which had been heated at first at 450 °C for a week and then homogenized at 600 °C for a week. These artificial sulfides were used as the starting materials for the equilibrium study.

General Procedure. The equilibrium study of iron vanadium sulfide was carried out by both thermogravimetry and the rigid tube, quench-type, annealing experiment at temperatures between 520 and 814 °C. The general experimental procedures, the apparatus, and the methods of the chemical analyses and of the phase identification of quenched specimens are the same as those described in previous papers.[1-2]

Results and Discussion

Composition versus P_{S_2} Diagram in an Iron-rich Portion of the Composition Triangle of FeS–VS–S. The results of equilibrium studies of the Fe–V–S system at sections with atomic Fe:V ratios of 4:1, 9:1, and 1:0 are shown graphically in Figs. 1—3. The isothermal curves are drawn by a smooth fitting of data points which represent the relation of the equilibrium sulfur pressure, P_{S_2}, to the composition of the sulfides (X=S/(Fe+V)) at the selected temperature. Also, the phase relations which were revealed by the X-ray diffraction of the quenched specimens are given in Table 1 and Figs. 1—3. Below, a solid solution will be abbreviated as

Table 1. Results of X-ray identification of the specimens quenched from 570 °C

Composition Fe/(Fe+V)	Composition S/(Fe/V)	Time/h	Products
1.000	1.120	720	$Fe_{1-\delta}S$ (hexagonal:3c)
	1.150	90	$Fe_{1-\delta}S$
	1.170	90	$Fe_{1-\delta}S+FeS_2$
0.900	1.146	182	$(Fe_{0.90}V_{0.10})_{1-\delta}S$
	1.168	144	$(Fe,V)_{1-\delta}S+(Fe,V)_3S_4$
	1.220	109	$(Fe,V)_{1-\delta}S+(Fe,V)_3S_4$
	1.230	109	$Fe_{1-\delta}S+(Fe,V)_3S_4+FeS_2$
	1.750	111	$Fe_{1-\delta}S+FeS_2+(Fe,V)_3S_4$
	1.800	111	$FeS_2+(Fe,V)_3S_4$
0.800	1.146	182	$(Fe_{0.80}V_{0.20})_{1-\delta}S$
	1.160	95	$(Fe,V)_{1-\delta}S+(Fe,V)_3S_4$
	1.216	109	$(Fe,V)_{1-\delta}S+(Fe,V)_3S_4$
	1.500	1536	$(Fe,V)_3S_4+FeS_2+Fe_{1-\delta}S$
	1.550	127	$FeS_2+(Fe,V)_3S_4$

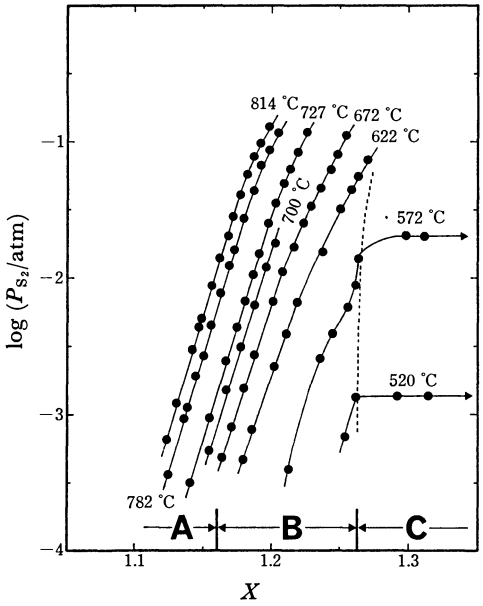

Fig. 1. P_{S_2}-composition (X=S/(Fe+V)) isotherm of $Fe_{0.80}V_{0.20}S_X$. Phase identifications of quenched specimens by X-ray powder diffraction method are shown in lower part of figure as follows A: $(Fe_{0.80}V_{0.20})_{1-\delta}S$. B: $(Fe,V)_{1-\delta}S+(Fe,V)_3S_4$ s.s. C: $Fe_{1-\delta}S+FeS_2+(Fe,V)_3S_4$ s.s. The dashed line indicates the phase boundary of the univariant field.

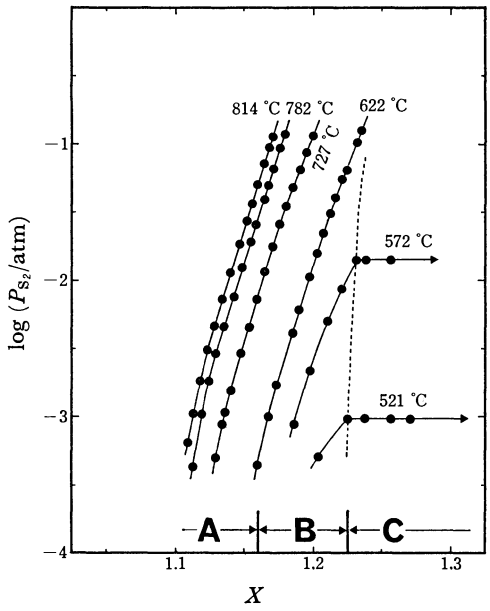

Fig. 2. P_{S_2}-composition isotherms of $Fe_{0.90}V_{0.10}S_X$. A: $(Fe_{0.90}V_{0.10})_{1-\delta}S$. B: $(Fe,V)_{1-\delta}S$ s.s.$+(Fe,V)_3S_4$ s.s.. C: $Fe_{1-\delta}S+FeS_2+(Fe,V)_3S_4$ s.s.

s.s. for convenience.

Figure 1 shows isotherms with the composition of $Fe_{0.80}V_{0.20}S_X$, where X ranges between 1.12 and 1.32. As listed in Table 1, the following phase relations are obtained at 570 °C: $(Fe_{0.80}V_{0.20})_{1-\delta}S$ phase, a two-phase mixture of $(Fe,V)_{1-\delta}S$ s.s. and $(Fe,V)_3S_4$ s.s., and a three-phase mixture of FeS_2, $Fe_{1-\delta}S$, and $(Fe,V)_3S_4$ s.s. in the compositional ranges of $X<1.16$, $1.16\leqq X<1.263$, and $1.263\leqq X<1.55$ respectively.

As is shown in Fig. 1, the isothermal curves for 814, 782, 727, and 700 °C exhibit continuous and gradual changes in the sulfur pressure with the composition. Although the sulfur-rich limit of the hexagonal $(Fe_{0.80}V_{0.20})_{1-\delta}S$ phase was determined to be about $X=1.16$ from the X-ray measurements of the quenched specimens, no characteristic curvature change in the isotherms is observed at $X=1.16$. This behavior of the isotherms seems to be indicative of the existence of a high-temperature phase, as has been reported previously.[2,3] There is the possibility that the homogeneity range of the $(Fe_{0.80}V_{0.20})_{1-\delta}S$ becomes broadened with an increase in the temperature and that its sulfur-rich limit has a composition with a value higher than $X=1.16$.

With respect to the isotherms for 572 and 520 °C, an abrupt change in the slope is observed at the composition of about $X=1.262$. In the compositional range of $X>1.262$, the isotherms become horizontal due to the formation of FeS_2, as has been discussed previously.[2] On the basis of the phase relations which were determined from the X-ray studies of the quenched specimens, it is suggested that the horizontal parts of the isotherms mean a univariant field of the Fe–V–S system, where $Fe_{1-\delta}S$, FeS_2, and $(Fe,V)_3S_4$ s.s. coexist at equilibrium.

Figure 2 shows the isothermal curves of the composition of $Fe_{0.90}V_{0.10}S_X$, where X ranges from 1.11 to 1.31. The phase relations obtained at 570 °C are as follows: $(Fe_{0.90}V_{0.10})_{1-\delta}S$ phase, a two-phase mixture of $(Fe,V)_{1-\delta}S$ and $(Fe,V)_3S_4$ s.s., and a three-phase mixture of $Fe_{1-\delta}S$, FeS_2, and $(Fe,V)_3S_4$ s.s., in the compositional ranges of $X<1.16$, $1.16\leqq X<1.23$, and $1.23\leqq X<1.75$ respectively.

The isothermal curves of $Fe_{0.90}V_{0.10}S_X$ are similar in shape to that of $Fe_{0.80}V_{0.20}S_X$ except that the entire curves are shifted to the sulfur-poor side with regard to the composition. As is evident in Fig. 2, no curvature changes are observed in the isotherms for 814, 782, and 727 °C at the sulfur-rich phase boundary of $(Fe_{0.90}V_{0.10})_{1-\delta}S$. It is noted that the isotherms for 521 and 572 °C become horizontal due to the FeS_2 formation at $X=1.225$ and $X=1.230$ respectively. However, no such change is observed in the isotherm for 622 °C in the present experimental compositional range. This suggests that the sulfur-poor limits of the three-phase field recedes toward the sulfur-rich side with an increase in the temperature.

Figure 3 shows the isotherms of the binary compound, FeS_X, where X lies in the range from 1.07 to 1.25. In this compositional range, only two phases were detected by the X-ray powder diffraction of the quenched specimens (Table 1). One is the hexagonal $Fe_{1-\delta}S$ (pyrrhotite), whose X-ray diffraction patterns exhibit 3c-type supper structure lines[4] in addition to the fundamental reflection lines of the NiAs type, while the other is the cubic FeS_2 (pyrite). The following phase relations were confirmed at 570 °C: the $Fe_{1-\delta}S$ phase, and a two-phase mixture of $Fe_{1-\delta}S$ and FeS_2, in the compositional ranges of $X<1.16$ and $X\geqq 1.16$ respectively.

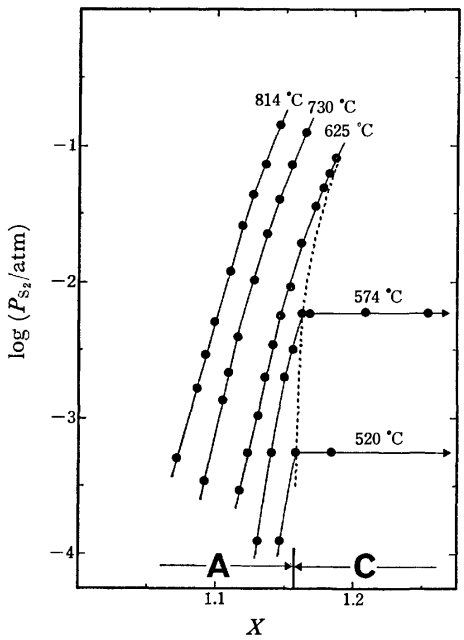

Fig. 3. P_{S_2}-Composition isotherms of FeS_X. A: $Fe_{1-\delta}S$. C: $Fe_{1-\delta}S+FeS_2$. The phase boundary of $Fe_{1-\delta}S$ is represented as the broken line.

With respect to the isotherm feature, it is noted that the horizontals associated with a two-phase equilibrium of $Fe_{1-\delta}S$ and FeS_2 appear at the compositions of $X=1.155$ and $X=1.160$ for 520 and 574 °C (Fig. 3). However, the isotherm for 625 °C does not show such horizontals in the range of $X<1.19$. Those results indicate that the homogeneity range of the $Fe_{1-\delta}S$ phase tends to be broadened to the sulfur-rich side with an increase in the temperature.

A few remarks should be made here regarding the equilibrium sulfur pressure of a two-phase mixture of $Fe_{1-\delta}S$ and FeS_2. For example, in the experiments for 574 and 520 °C, the sulfur pressure was controlled to bring the composition to a higher sulfur content than at the beginning of that series. The sulfidation of the specimens proceeded with an increase in the sulfur pressure, and isotherms became horizontal in a two-phase field due to the considerable increase in the sulfur content in the solids, associated with the FeS_2 formation. In this case, however, the values of the sulfur pressure at the horizontal parts of the isotherms are not regarded as truly resulting from a two-phase equilibrium of $Fe_{1-\delta}S$ and FeS_2, because a slightly higher sulfur potential than the equilibrium one is needed on the formation of FeS_2 in order to supply the activation energy of the reaction of $Fe_{1-\delta}S$ with sulfur vapor. Therefore, it is designated here as the upper limit of the equilibrium sulfur pressure.

The relation of the decomposition pressure of FeS_2 to temperature was examined in order to determine the lower limits of the equilibrium sulfur pressure of $Fe_{1-\delta}S$–FeS_2 mixtures. Experiments were carried out by thermogravimetry using $FeS_{2.01}$ as the starting material. When a significant weight loss of specimens was observed within the time interval of 30 min at the selected temperature and pressure, it was judged

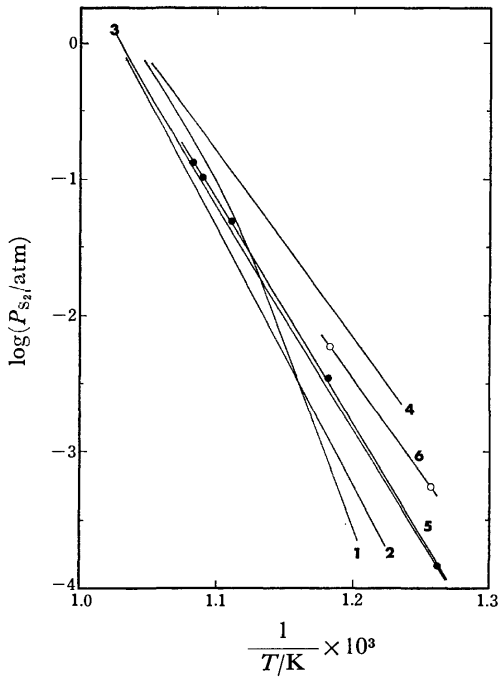

Fig. 4. The relation of decomposition pressure of FeS_2 with the inverse temperature. 1: Allen and Lombard (1917). 2: Rosenqvist (1954). 3: Toulmin and Barton (1964). 4: D'Or (1931). 5: Present work; ● decomposition pressure of FeS_2. 6: Present work; ○ sulfur pressure in the case of FeS_2 formation, as is seen in Fig. 3.

TABLE 2. RELATION OF THE DECOMPOSITION PRESSURE OF PYRITE TO THE TEMPERATURE

Temp / °C	$-\log(P_{S_2}/\text{atm})$
520	3.84
574	2.47
620	1.47
628	1.31
646	0.99
652	0.88

that FeS_2 begins to decompose to $Fe_{1-\delta}S$ and sulfur vapor. The experimental results are listed in Table 2 and shown in Fig. 4, together with the results reported by other investigators.[5-8] The data points obtained in this study are well represented by the following equation (least-squares treatment): $\log(P_{S_2}/\text{atm})=-16477/(T/\text{K})+16.96$, where 1 atm=101.325 kPa. This result is in good agreement with that of Toulmin and Barton,[5] as is shown in Fig. 4. The upper limit of the equilibrium sulfur pressure which was obtained on the sulfidizing specimens (Fig. 3) is given in Fig. 4 for comparison.

The true equilibrium value probably lies within the range between the upper and lower limits of sulfur pressure at a given temperature. The difference in the sulfur pressure between the formation and the reduction of FeS_2 is about $0.25=\log(P_{S_2}/\text{atm})$ at 574 °C. It may be considered that this discrepancy is derived from the sluggishness of the reaction rate of

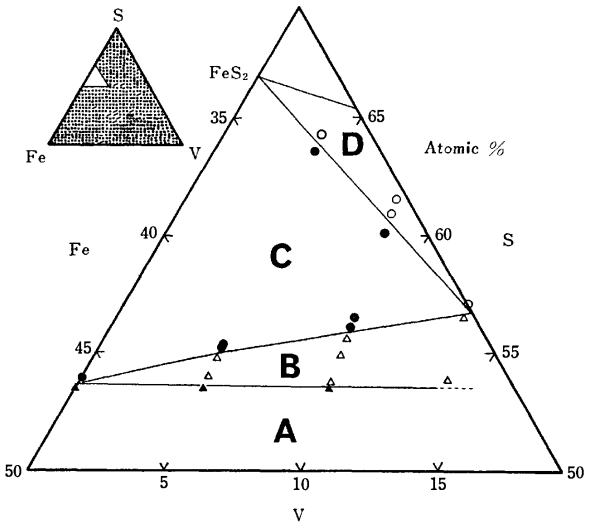

Fig. 5. Tentative phase diagram of the iron-rich portion of the composition triangle of FeS–VS–S at 570 °C. Phase relations are represented as follows. ▲: $(Fe,V)_{1-\delta}S$ s.s. △: $(Fe,V)_{1-\delta}S$ s.s.+$(Fe,V)_3S_4$ s.s. ●: $Fe_{1-\delta}S+FeS_2+(Fe,V)_3S_4$ s.s. ○: $FeS_2+(Fe,V)_3S_4$ s.s.

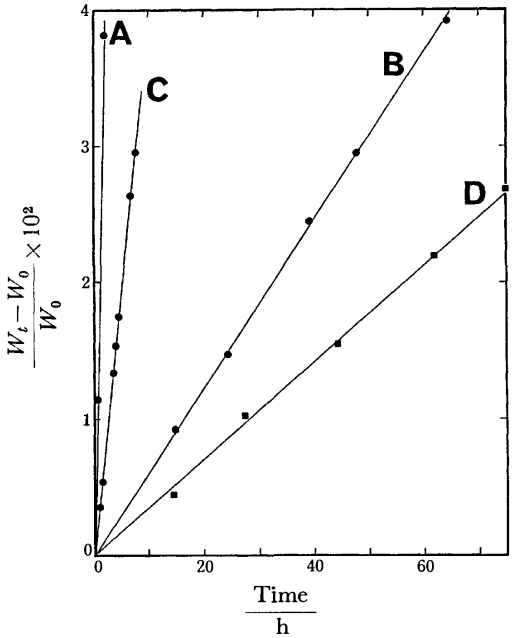

Fig. 6. The relation of the weight gain of the sample with time.

the formation or the reduction of FeS_2 under the present experimental conditions. On the assumption that the true equilibrium sulfur pressure of the $Fe_{1-\delta}S$–FeS_2 mixture is halfway between the upper and lower limits, the Gibbs free energy of the $[2/(1-2\delta)]Fe_{1-\delta}S+S_2=[2(1-\delta)/(1-2\delta)]FeS_2$ reaction was calculated in the temperature range of 520—580 °C: $\Delta G_r^\circ=-67100+68.5\,T$ cal_{th}, where 1 $cal_{th}=4.184$ J.

The Tentative Phase Diagram at 570 °C. The tentative isothermal phase diagram in the iron-rich portion of the composition triangle FeS–VS–S was constructed on the basis of the results of both thermogravimetry and rigid-tube, annealing, quench-type experiments. The phase relations and phase boundaries are shown in Fig. 5.

With respect to the Fe–S binary system, the sulfur-rich limit of $Fe_{1-\delta}S$ is determined to be 46.3 atom% Fe at 570 °C (Fig. 3). This value is in good agreement with the sulfur-rich limit of $Fe_{1-\delta}S$ (46.2 atom% Fe), which was reported by Arnold.[9] As is shown in Fig. 6, it is assumed that the $Fe_{1-\delta}S$ and $V_{1-\delta}S$ phases form a complete $(Fe,V)_{1-\delta}S$ solid solution (A region) at 570 °C. The sulfur-rich phase boundary of the $(Fe,V)_{1-\delta}S$ field is extended nearly parallel with the line joining FeS–VS from the Fe–S side to the V–S side in the $0\leqq V/(Fe+V)<0.3$ range.

The univariant field (C region) is determined by a smooth fitting of data points. The sulfur-poor boundary of the univariant field recedes progressively toward sulfur-poor compositions with an increase in the Fe content; its limits are 55.1 and 55.9 atom% S in the sections with atomic Fe:V ratios of 9:1 and 4:1 respectively. On the other hand, the sulfur-rich boundary of the univariant field is shifted progressively toward a sulfur-rich composition with an increase in the Fe content; its limits are about 63.9 and 60.6 atom% S in the sections with atomic Fe:V ratios of 9:1 and 4:1 respectively. It should be noted that the sulfur-rich boundary line intersects the line joining Fe–S at the composition of FeS_2.

The two-phase fields (B region) of $(Fe,V)_3S_4$ and $(Fe,V)_{1-\delta}S$ are present in the middle part between the A and C regions. However, the compositional relation of $(Fe,V)_{1-\delta}S$ to the coexisting $(Fe,V)_3S_4$ has not been determined in this study.

Sulfidation Kinetics of Iron Vanadium Sulfides. In a series of reports,[1-3] the phase relations and P_{S_2}-X-T relations of the Fe–V–S system have been presented without any particular regard for the reaction kinetics. In general, it is well known that the time required for equilibriation increases with the decrease in the temperature with respect to the phase equilibria. Therefore, it may be suggested that the thermochemical data reported in this series are perhaps somewhat less accurate at lower temperatures, such as 520 °C, because the establishment of the equilibrium could not be checked precisely. It is necessary to obtain experimental data on the sulfidation kinetics of iron vanadium sulfides in order to have a comprehensive understanding of the Fe–V–S system at lower temperatures.

In the course of the equilibrium study of the Fe–V–S system, the sulfidation rate was examined supplementally. Considerable attention has been focussed on the rate of FeS_2 formation in the univariant field (FeS_2–$Fe_{1-\delta}S$–$(Fe,V)_3S_4$ s.s.–vapor). The sulfidation kinetics of powder samples were determined by means of thermogravimetry.

The variation in the sample weight with time was examined along the horizontal parts of the isotherms (Figs. 1—3) in order to ascertain the sulfidation rate of the sulfide powder. The composition at the sulfur-poor limit of the horizontal line was selected as the starting composition in the sulfidation experiments. About 300 mesh and 1 g of powder samples were used.

The degree of the weight gain of the sample is shown in Fig. 6 for periods up to 80 h. The experimental results may be represented well as the following linear relation: $W_t=W_0(1+\alpha t)$, where α, t, W_t, and W_0 denote the gain in the sample weight per a unit of time, time/h, the sample weight at time $t=t$, and $t=0$ respectively. As a first approximation, it can be proposed that the slope of the linear equation, α, is related to the rate of FeS_2 formation. From Fig. 6, the following values are obtained for the slopes of Lines A, B, C, and D: for $FeS_{1.156}$, $\alpha_A=1.98\times10^{-2}$/h at 520 °C and $P_{S_2}=10^{-2.08}$, and $\alpha_B=0.06\times10^{-2}$/h at 520 °C and $P_{S_2}=10^{-3.26}$, for $FeS_{1.161}$, $\alpha_C=0.40\times10^{-2}$/h at 574 °C and $P_{S_2}=10^{-2.22}$, and for $Fe_{0.90}V_{0.10}S_{1.225}$, $\alpha_D=0.04\times10^{-2}$/h at 520 °C and $P_{S_2}=10^{-3.02}$. It should be noted that sulfidation rate of $Fe_{1-\delta}S$ (pyrrhotite) at 520 °C increases with an increase in the sulfur pressure in the P_{S_2} range from $10^{-3.26}$ to $10^{-2.08}$. On the basis of the assumption that the P_{S_2} values of Experiments B, C, D are very close to the equilibrium values at a given temperature, the following conclusions are obtained: (1) the sulfidation rate of $Fe_{1-\delta}S$ increases with an increase in the temperature, and (2) there is the tendency for the FeS_2 formation to be inhibited by the presence of vanadium in sulfides.

The over-all reaction rate of pyrrhotite for FeS_2 formation was calculated according to the $FeS_x+yS_2=FeS_2$ sulfidation reaction, where x and y are 1.156 and 0.422 respectively at 520 °C. In this case, the sulfidation rate was represented by the following equation; $-d[P]/dt=K_{obsd}[P]$ where [P] is the concentration of FeS_x with the composition at the sulfur-rich limit and where K_{obsd} is the apparent first-order rate constant. From the experimental results, the following K_{obsd} values were obtained from the slopes in the first-order plots in a region of low conversion ($0.87<P/P_0\leqq1$): $K_A=1.98\times10^{-5}$/s, $K_B=6.26\times10^{-7}$/s, and $K_C=4.13\times10^{-6}$/s. The activation energy of FeS_2 formation was calculated to be 191.6 kJ/mol by using values of K_B and K_C according to the Arrhenius equation. This value is much larger than that of the sulfidation of Fe metal (113.0 kJ/mol) under the sulfur pressure of 1 atm, which was reported by Narita and Nishida.[10] The reaction mechanism of iron vanadium sulfides on the sulfidation process could not be clarified in this study. Further detailed studies of the sulfidation kinetics will be necessary for a comprehensive understanding of the Fe–V–S system.

The author wishes to express his deep gratitude to Professor Mitsuoki Nakahira of Okayama College of Science for his encouragement and helpful discussions throughout this study.

References

1) H. Wada, *Bull. Chem. Soc. Jpn.*, **51**, 1368 (1978).
2) H. Wada, *Bull. Chem. Soc. Jpn.*, **52**, 2130 (1979).
3) H. Wada, *Bull. Chem. Soc. Jpn.*, **52**, 2918 (1979).
4) M. E. Fleet, *Acta Crystallogr.*, **27**, 1864 (1971).
5) P. Toulmin, III, and P. B. Barton, Jr., *Geochim. Cosmochim. Acta*, **28**, 641 (1964).
6) E. T. Allen and R. H. Lombard, *Am. J. Sci.*, **43**, 175 (1917).
7) L. D'Or, *J. Chim. Phys.*, **28**, 377 (1931).
8) T. Rosenqvist, *J. Iron Steel Inst.*, **176**, 37 (1954).
9) R. G. Arnold, *Economic Geology*, **75**, 72 (1962).
10) T. Narita and K. Nishida, Proc. 5th Int. Congr. Met. Corros., NACE, Houston, 719 (1974).

Transition Metal Alkoxides. Preparation and Properties of Bis(aryloxo)-iron(II) and Bis(alkoxo)iron(II) Complexes Having 2,2′-Bipyridine Ligands

Sanshiro KOMIYA, Shoshiro TANE-ICHI, Akio YAMAMOTO, and Takakazu YAMAMOTO*

Research Laboratory of Resources Utilization, Tokyo Institute of Technology, 4259 Nagatsuta, Midori-ku, Yokohama 227

(Received August 23, 1979)

A series of bis(aryloxo)iron(II), **2a**—**2g**, and bis(alkoxo)iron(II), **2h**—**2k**, complexes with 2,2′-bipyridine ligands ($Fe(OC_6H_4X)_2(bpy)_n$ and $Fe(OR)_2(bpy)_n$) have been prepared by the reactions of diethylbis(2,2′-bipyridine)-iron(II) (**1**) with corresponding *p*-substituted phenols and alcohols, respectively. (X=NO_2, CN, Cl, C_6H_5, H, and CH_3; R=CH_3, C_2H_5, *iso*-C_3H_7, and $CH_2C_6H_5$). These compounds were characterized by IR and NMR spectroscopies and elemental analyses as well as by chemical reactions. Kinetic investigation of the reactions of **1** with phenols by a visible spectroscopic method supports a mechanism involving partial dissociation of the 2,2′-bipyridine ligand, followed by coordination of phenol and activation of the Fe–C_2H_5 bonds giving the bis(phenoxo)iron(II) compound. Thermolysis of bis(alkoxo)iron(II) complexes gives not only disproportionation products of the alkoxo ligands (alcohols and aldehydes) but also organic products which are obtained as the result of C–O bond cleavage of the alkoxo groups. Interactions of **2** with acyl and alkyl halides lead to the formation of corresponding esters and ethers. Reactions of these iron(II) complexes with various organic acetates give corresponding acetates *via* an alkoxo exchange reaction. Bis(aryloxo)iron(II) complexes, **2**, are hydrolyzed with H_2O to yield phenols. Catalytic trans-esterification between ester and alcohol and Tishchenko type dimerization of benzaldehyde are effectively promoted under mild conditions by the bis(phenoxo)iron(II) and bis(benzyloxo)iron(II) complexes, respectively.

In contrast to non-transition metal alkoxides,[1] which are known to promote the catalytic reactions of carbonyl compounds such as Tishchenko reaction and Meerwein-Pondorf reaction, and to early transition metal alkoxides, which have been studied mainly from structural interest, the chemistry of Group VIII transition metal alkoxides has been much less explored. Formation of Group VIII transition metal alkoxides as intermediates has been implicitly postulated in reduction of transition metal halides on reactions with alcohols to low valent transition metal complexes,[2] or in oxidation of alcohols[3] as well as in trans-esterification reactions.[1a] The lack of well-characterized group VIII transition metal alkoxides has hindered our understanding of the mechanisms of these reactions. Although a growing number of Group VIII metal alkoxides have been synthesized and their properties studied,[4] more information is obviously needed concerning the chemistry of the Group VIII transition metal alkoxides to shed light on the mechanisms of transition metal promoted transformation of organic compounds.

We have found that diethylbis(2,2′-bipyridine)-iron(II), $Fe(C_2H_5)_2(bpy)_2$ (**1**) serves well as a starting material for preparing a variety of iron(II) aryloxides and alkoxides and studied their properties including catalytic activities. This paper also deals with the kinetic study of the reaction of **1** with alcohols and substituted phenols to form the alkoxides and aryloxides.

Results and Discussion

Preparation and Spectroscopic Properties of Bis(aryloxo)- and Bis(alkoxo)iron(II) Complexes. A variety of *p*-substituted phenols react with diethylbis(2,2′-bipyridine)iron(II), $Fe(C_2H_5)_2(bpy)_2$ (**1**)[5] to give bis-(phenoxo)iron(II) complexes having bpy ligands, $Fe(OC_6H_4X)_2(bpy)_n$ (**2**) (n=1 and 2) with evolution of two equivalents of ethane at ambient conditions. The bis(phenoxo)iron complexes are highly air sensitive, but thermally very stable.

$$Fe(C_2H_5)_2(bpy)_2 + 2HOC_6H_4X \longrightarrow Fe(OC_6H_4X)_2(bpy)_n + 2C_2H_6 \quad (1)$$

n=2; X=NO_2(**2a**), CN(**2b**)
n=1; X=CN(**2c**), Cl(**2d**), C_6H_5(**2e**), H(**2f**), CH_3(**2g**)

These complexes were characterized by elemental analyses, IR, and NMR spectroscopies, as well as by chemical reactions. The phenoxide complex **2f** was also prepared *via* an independent route by the reaction of $FeCl_2$ with $NaOC_6H_5$ in the presence of bpy, but the contamination of the product with salts prevented isolation of the pure material. Table 1 summarizes the elemental analyses and the yields of the complexes. The number of coordinating bpy ligand in the bis-(phenoxo)iron(II) complexes varies depending on the *p*-substituent in the phenoxo ligand. Electron-withdrawing substituents such as nitro and cyano groups favor the coordination of electron-donating two bpy ligands and less electron-withdrawing substituents give mono-bpy coordinated complexes. Bis(*p*-cyanophenoxo)iron(II) complex lies on the border between the two groups favoring mono- and bis-bpy complexes and both complexes **2b** and **2c** can be isolated under suitable conditions (see Experimental). Complexes **2a** and **2b** having two bpy ligands have considerable solubilities but the other complexes having one bpy ligand are much less soluble in organic solvents. Many metal alkoxides and phenoxides are known to be aggregated,[1a] and the coordinatively unsaturated complexes having only one bpy ligand per iron may well have polymeric structures accounting for the poor solubilities. In fact addition of excess bpy to a heterogeneous system of **2c** having one bpy ligand in acetone or toluene with heating caused dissolution of **2c** to give a homogeneous solution from which dark

TABLE 1. ANALYTICAL DATA OF $Fe(OC_6H_4X\text{-}p)(bpy)_n$ COMPLEXES

Complex		Yield/%	Found(Calcd) (%)			
			C	H	N	Cl
$Fe(OC_6H_4NO_2\text{-}p)_2(bpy)_2$	**2a**	63	59.0(59.6)	3.8(3.8)	13.3(13.0)	
$Fe(OC_6H_4CN\text{-}p)_2(bpy)_2$	**2b**	65	67.8(67.6)	4.0(4.0)	14.0(14.0)	
$Fe(OC_6H_4CN\text{-}p)_2(bpy)$	**2c**	96	64.5(64.3)	3.9(3.6)	12.1(12.5)	
$Fe(OC_6H_4Cl\text{-}p)_2(bpy)$	**2d**	66	56.2(56.6)	3.5(3.5)	5.9 (6.0)	15.0(15.1)
$Fe(OC_6H_4C_6H_5\text{-}p)_2(bpy)$	**2e**	84	72.5(74.2)	4.6(4.8)	4.9 (5.1)	
$Fe(OC_6H_5)_2(bpy)$	**2f**	51	65.7(66.3)	4.7(4.6)	6.9 (7.0)	
$Fe(OC_6H_4CH_3\text{-}p)_2(bpy)$	**2g**	86	66.6(67.6)	4.9(5.2)	6.4 (6.6)	

TABLE 2. ^1H NMR AND IR SPECTRA OF $Fe(OC_6H_4X\text{-}p)_2(bpy)_n$ COMPLEXES

Complex	^1H NMR (δ/ppm)			IR ν(C-O)/cm^{-1}
	Phenoxo	bpy	Other	
2a	6.2(d, 9 Hz), 7.8(d, 9 Hz)	7.4(m), 8.1(m), 8.6(m)		1290
2b	6.6(d, 8 Hz), 7.4(d, 8 Hz)	7.5(m), 8.2(m), 8.7(m)		1340
2c	6.4(m), 7.4(m)	7.4(m), 8.1(m), 8.6(m)		1310
2d	5.8—7.2(br)	7.3(m), 8.1(m), 8.6(m)		1280
2f	6.7(m), 7.2(m)	7.5(m), 8.2(m), 8.7(m)		1260
2g	6.5(m), 6.9(m)	7.4(m), 8.2(m), 8.8(m)	2.2(s)	1250

d, doublet; m, multiplet; br, broad; s, singlet.

red crystals of **2b** having two bpy ligands were obtained on cooling the solution to −78 °C. The bpy ligand may be acting to break the bridging phenoxo bonds.

IR spectra of these (*p*-substituted phenoxo)iron(II) complexes showed a strong characteristic ν(C-O) band at 1260—1340 cm^{-1} which is shifted to higher frequency by 10—15 cm^{-1} compared with ν(C-O) of free phenols (Table 2). Cyano and nitro groups in the present complexes do not seem to have an interaction with iron, since no frequency change of ν(CN) and $\nu(NO_2)$ from the starting phenols was observed.

^1H NMR spectra of these bis(*p*-substituted diphenoxo)iron(II) complexes (Table 2) showed two doublets assignable to ortho and meta hydrogens in the *p*-substituted phenoxo ligands and three groups of multiplets for the bpy ligand. Bis(phenoxo) complex **2f** showed two kinds of broad signals in a 2 to 3 ratio, one being attributable to ortho hydrogens and the other to meta and para hydrogens. These spectroscopic results suggest that the phenoxo ligand is normally bonded with iron through oxygen unlike the π-bonding between ruthenium and phenoxo ligand in $RuH(OC_6H_5)(PPh_3)_2$ as observed by Wilkinson *et al.*[6]

In the presence of free bpy ligand, ^1H NMR of **2f** in CD_3OD showed only averaged peaks of bpy ligands coordinated and uncoordinated at room temperature, indicating fast intermolecular exchange process between them in the solution. On the contrary, ^1H NMR of a mixture of **2a** and free bpy showed separated signals for free and coordinated bpy ligands, respectively. Ligand exchange rate of **2a** with free bpy is considered to be slow enough in NMR time scale to separate the peaks. The configuration of the six coordinated complex with two bpy ligands, **2a** and **2b**, is considered to be cis, because of the steric requirement. ^1H NMR of bpy ligand in the cis configuration has been reported to show two kinds of pyridyl rings giving complicated multiplets.[7] However, the observed ^1H NMR of the coordinated bpy in **2a** showed a relatively simple pattern. Fast intramolecular exchange of bpy ligands may account for this observation, while a trans structure for **2a** is not completely excluded.

The reactions of **1** with aliphatic alcohols (ROH) afforded bis(alkoxo)iron(II) complexes analogously to the reactions with phenols.

$$Fe(C_2H_5)_2(bpy)_2 + ROH \xrightarrow{-2C_2H_6} Fe(OR)_2(bpy)_n \quad (2)$$

$n=1$ for $R=CH_2C_6H_5$(**2h**), C_2H_5(**2i**), *iso*-C_3H_7(**2j**),
$n=0$ for $R=CH_3$(**2k**)

The alkoxoiron complexes are extremely sensitive to air to preclude the microanalysis and have been characterized mainly by chemical reactions (*vide infra*). IR spectra of **2h**—**2j** showed a characteristic strong ν(C-O) band at *ca.* 1000 cm^{-1} in addition to the bands attributable to the bpy ligand. On the other hand, the IR spectrum of **2k** showed only bands assignable to the methoxo ligands. The aliphatic alkoxoiron complexes, **2h**, **2i**, and **2j**, are all quite insoluble in organic solvents suggesting polymeric structures as are common among other metal alkoxides. Formation of polymeric iron(II) methoxide has been reported by Klein.[8]

Chemical Reactivities of Iron(II) Aryloxides and Alkoxides. The phenoxoiron complex **2f** smoothly reacted with alkyl and acyl halides to give corresponding ethers and esters, respectively (Table 3). The resulted solid product formed in the reaction of **2f** with CH_3COCl was identified as $FeCl_2(bpy)$ by comparing its IR spectrum with that of the sample prepared by the acidolysis of **1** with HCl.

Table 3. Reactions of aryloxo and alkoxoiron(II) complexes with alkyl and acyl halides at room temperature

Complex	Reagent (mol/Fe)	Solvent	Time/h	Product (mol/Fe)
2a	CH_3COCl(excess)	none	24	$CH_3CO_2C_6H_4NO_2$ (1.64)
2b	CH_3COCl(excess)	none	24	$CH_3CO_2C_6H_4CN$ (1.54)
2f	CH_3COCl (20)	THF	24	$CH_3CO_2C_6H_5$ (1.49)
	$C_6H_5CH_2Br$ (4)	toluene	5	$C_6H_5CH_2OC_6H_5$ (0.57)
	CH_3I(excess)	none	3	$C_6H_5OCH_3$ (0.16)
2h	CH_3COCl (6)	toluene	2	$CH_3CO_2CH_2C_6H_5$ (1.52)
2i	CH_3COCl (2)	THF	10	$CH_3CO_2C_2H_5$ (1.80)
2j	CH_3COCl (2)	THF	10	$CH_3CO_2C_3H_7{}^i$ (1.84)
2k	CH_3COCl (2)	THF	10	$CH_3CO_2CH_3$ (1.68)

Table 4. Reactions of aryloxo and alkoxoiron(II) complexes with esters[a)]

Complex	Ester(mol/Fe)	Product(mol/Fe)
2f	$CH_3CO_2C_6H_4NO_2$-*p* (4)	$CH_3CO_2C_6H_5$ (1.71)
	$CH_3CO_2C_6H_4CN$-*p* (4)	$CH_3CO_2C_6H_5$ (1.24)
	$CH_3CO_2C_6H_4$-*p*-CH_3 (4)	$CH_3CO_2C_6H_5$ (0.76)
	$CH_3CO_2CH_2C_6H_5$ (4)	$CH_3CO_2C_6H_5$ (0)
	$CH_3CO_2C_2H_5$ (4)	$CH_3CO_2C_6H_5$ (0)
2h	$CH_3CO_2C_6H_5$ (4)	$CH_3CO_2CH_2C_6H_5$ (1.82)
2j	$CH_3CO_2C_6H_5$ (4)	$CH_3CO_2C_3H_7{}^i$ (1.64)
2k	$CH_3CO_2C_6H_5$ (4)	$CH_3CO_2CH_3$ (1.52)

a) Reactions were carried out at 50 °C in THF for 5 h.

$$\mathbf{2f} \xrightarrow[CH_3COCl]{} CH_3COOPh + FeCl_2(bpy) \qquad (3)$$
$$\mathbf{2f} \xrightarrow[CH_3I]{} CH_3OPh + FeI_2(bpy)$$

Other bis(*p*-substituted phenoxo)- and bis(alkoxo)iron(II) analogs also gave corresponding organic acetates on reaction with acetyl chloride (Table 3).

Table 4 summarizes the results of the reactions of aryloxoiron(II) and alkoxoiron(II) complexes with various organic esters. *p*-Substituted phenyl acetates reacted with the phenoxoiron(II) complex, **2f**, to give phenyl acetate. Benzyl and ethyl acetates had no tendency to exchange with the phenoxo ligand under the same conditions. On the other hand, phenyl acetate underwent the exchange reaction with the benzyloxo, isopropoxo, and methoxoiron(II) complexes giving benzyl, isopropyl, and methyl acetates, respectively in good yields. The more electrophilic alkoxo ligand seems to have stronger affinity with iron(II). Hydrolysis of **2a**—**2g** with water gave corresponding *p*-substituted phenols.

A greenish grey bis(phenoxo)iron(II) complex, **2f**, is highly air sensitive and it turns red brown immediately on exposure to air at room temperature both in solution and in the solid state. Oxygen uptake by **2f** in solution was roughly half a mol per iron. The resultant red brown complex **2f′**, is almost insoluble in usual solvents and is paramagnetic with a μ_{eff} value of 4.3 B.M., suggesting a high spin Fe(III) species. IR spectrum of **2f′** is very close to that of **2f** indicating the existence of the intact phenoxo and bpy ligands in **2f′**. No absorption band attributable to ν(O–O) was detected, whereas most of the dioxygen complexes show the strong characteristic band at 800—900 cm^{-1}.[9] Therefore, the present complex **2f′** may be considered as a polymeric oxygen bridged complex having the bpy ligand. An oxygen bridged iron(II) complex has been reported by Teyssie *et al.*[10]

Although thermal decomposition of metal alkoxides usually affords exclusively disproportionation products of the alkoxo ligands,[1] alcohols and aldehydes, thermolysis of **2h**—**2k** in the solid state gave unusual products besides the disproportionation products as shown in Table 5.

$$\underset{\mathbf{2h}}{Fe(OCH_2C_6H_5)_2bpy} \longrightarrow C_6H_5CH_2CH_2C_6H_5 + C_6H_5CH_3 + C_6H_5CHO + C_6H_5CH_2OH + H_2 \qquad (4)$$

$$\underset{\mathbf{2j}}{Fe(OC_3H_7{}^i)_2(bpy)} \longrightarrow C_3H_6 + CH_3COCH_3 + iso\text{-}C_3H_7OH + H_2 \qquad (5)$$

$$\underset{\mathbf{2k}}{Fe(OCH_3)_2} \longrightarrow CH_4 + H_2 + etc. \qquad (6)$$

Formation of bibenzyl and toluene from **2h** indicates the involvement of the C–O bond cleavage on thermolysis, whereas benzaldehyde and benzyl alcohol were obtained by the usual disproportionation reaction of the alkoxo ligands. Thermolysis of **2j** gave propylene in addition to the disproportionation products, also suggesting a similar decomposition pathway. Compound **2k** mainly gave methane on thermolysis. The present unusual C–O bond fission may have arisen from the great affinity of iron metal with oxygen. Formation of an alkyl radical by the C–O bond cleavage probably accounts for the pyrolysis products. Analogous C–O bond breakage in a transition metal alkoxo compound is known.[11] On the other hand, thermolysis of **2i** and **2f** afforded ethanol and phenol as a major product respectively, although the hydrogen source is not clear.

Catalytic Reactions Promoted by Alkoxoiron(II) Complexes. The phenoxo complex **2f** was found to catalyze the trans-esterification. Isopropenyl acetate and benzyl alcohol were converted into benzyl acetate and acetone in a 73% yield in the presence of **2f** at room temperature.

$$CH_3CO_2C(CH_3)=CH_2 + C_6H_5CH_2OH \xrightarrow[\mathbf{2f}]{} CH_3CO_2CH_2C_6H_5 + (CH_3)_2CO \qquad (7)$$

In the trans-esterification reaction isopropene-2-ol may

Table 5. Thermal decomposition of alkoxoiron(II) complexes in solid state[a)]

Complex		Dp/°C	Product (mol/Fe)
$Fe(OCH_2C_6H_5)_2(bpy)$	**2h**	210—220	H_2(0.05), $C_6H_5CH_3$(0.30), C_6H_5CHO(0.52), $C_6H_5CH_2OH$(0.23), $C_6H_5CH_2CH_2C_6H_5$(0.20)
$Fe(OC_2H_5)_2(bpy)$	**2i**	170	H_2(0.03), C_2H_5OH(0.87)
$Fe(OC_3H_7^i)_2(bpy)$	**2j**	185	H_2(trace), C_3H_6(0.28), i-C_3H_7OH(0.24), $(CH_3)_2CO$(0.04)
$Fe(OCH_3)_2$	**2k**	200—220	H_2(0.10), CH_4(0.50), C_2H_6(trace)

a) The compounds were heated up to 220 °C.

be first formed and transformed to its tautomer, acetone. Methyl methacrylate and ethanol also gave ethyl methacrylate and methanol in a 38% yield in the presence of **2f**.

$$CH_2{=}C(CH_3)CO_2CH_3 + C_2H_5OH \xrightarrow[\mathbf{2f}]{} CH_2{=}C(CH_3)CO_2C_2H_5 + CH_3OH \quad (8)$$

The phenoxoiron(II) catalyst used was unchanged after the reaction as revealed by IR analysis, suggesting the phenoxo ligand in **2f** is not involved in the catalytic trans-esterification. A similar type of trans-esterification using Cu phenoxide[12] has been reported and a mechanism involving metal assisted nucleophilic replacement was postulated.

Non-transition metal alkoxides, especially aluminum isopropoxide, are known to catalyze Tishchenko reaction.[1] Among the iron alkoxides prepared in the present study dibenzyloxo(2,2'-bipyridine)iron complex **2h** was found to be most effective for the Tishchenko reaction, converting benzaldehyde into benzyl benzoate.

$$C_6H_5CHO \xrightarrow[80\,°C,\ 6\,h]{\mathbf{2h}} C_6H_5COOCH_2C_6H_5\ (63\,\%) \quad (9)$$

Recently a few transition metal complexes of Ru(II),[13] Fe(II),[14] and Mn(II)[15] have been reported to serve as catalysts for the dimerization of aldehyde, and formation of alkoxo-transition metal intermediates has been postulated.

Kinetic Study of the Formation of ***2f***. The rate of the formation of complex **2f** by the reaction of **1** with excess of phenol in THF was studied by following the change in the visible spectrum of the reaction mixture *in vacuo*. The decrease in the absorbance of a band at 590 nm which is known to be a CT band of **1**,[16] was used to estimate the rate of disappearance of **1**. Plot of $\log(A_t - A_\infty)$ against time gave a linear relationship indicating a first-order dependence of the rate on the concentration of **1**.

$$\frac{d}{dt}[\mathbf{2f}] = -\frac{d}{dt}[Fe(C_2H_5)_2(bpy)_2] = k[Fe(C_2H_5)_2(bpy)_2] \quad (10)$$

Figure 1 shows the dependence of the pseudo-first-order rate constant k on the phenol concentration. It is seen that the rate increase with the increase in the phenol concentration is leveled off at higher concentration of phenol and addition of the bpy ligand shows a marked effect to retard the rate of decomposition

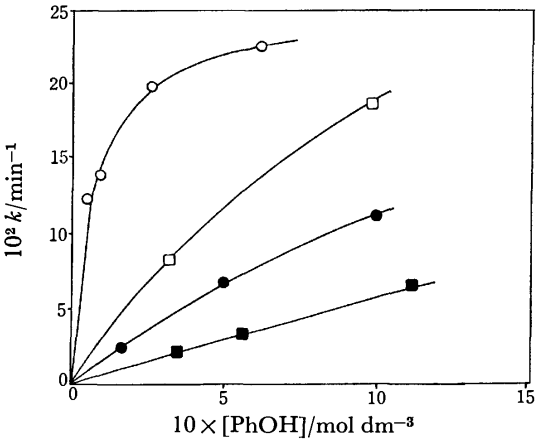

Fig. 1. Effect of [PhOH] on the first order rate constant k in various bpy concentrations for the reaction of **1** with phenol in THF at 23.2 °C. [bpy]=0 mol/dm³, ○; 0.90×10^{-3} mol/dm³, □; 2.71×10^{-3} mol/dm³, ●; 9.02×10^{-3} mol/dm³, ■.

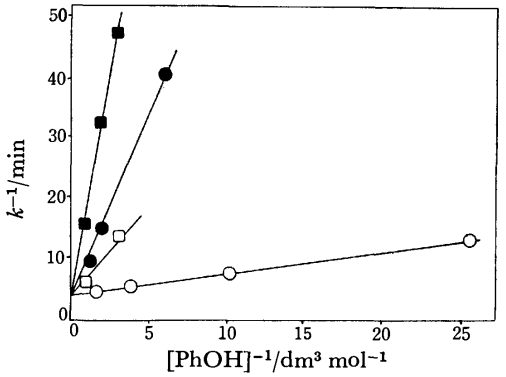

Fig. 2. Plot of the reciprocal of k *vs.* the reciprocal of [PhOH] in Fig. 1.

of **1**. The both reciprocal plots of k and phenol concentration at various bpy concentration shown in Fig. 2 gives straight lines. The effect of variation of the added bpy concentration on the slopes in Fig. 2 is shown in Fig. 3. These experimental results can be summarized by the following equation;

$$\frac{1}{k} = A + \frac{B + C[\mathrm{bpy}]}{[C_6H_5OH]} \quad (11)$$

where A, B, and C represent constants. A similar kinetic behavior has been previously observed by Yamamoto *et al.*[16] in the reaction of **1** with olefins. The present kinetic behavior can be explained by

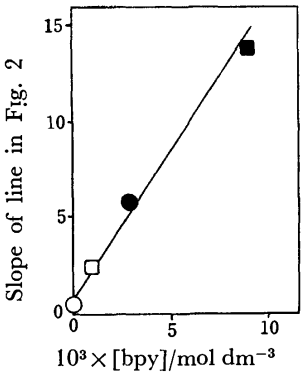

Fig. 3. Plot of the slope of line in Fig. 2 against [bpy].

assuming the following reaction mechanism.

$$\mathrm{Fe(C_2H_5)_2(bpy)_2} \underset{k_{-1}}{\overset{k_1}{\rightleftharpoons}} \underset{\mathbf{3}}{\mathrm{Fe(C_2H_5)_2(bpy)(bpy)^*}} \quad (12)$$
$$\mathbf{1}$$

$$\mathbf{3} + \mathrm{C_6H_5OH} \underset{k_{-2}}{\overset{k_2}{\rightleftharpoons}} \underset{\mathbf{4}}{\mathrm{Fe(C_2H_5)_2(bpy)(bpy)^*(C_6H_5OH)}} \quad (13)$$

$$\mathbf{4} \xrightarrow[-\mathrm{C_2H_6}]{k_3} \xrightarrow[+\mathrm{C_6H_5OH}\ -\mathrm{C_2H_6}]{\text{fast}} \underset{\mathbf{2f}}{\mathrm{Fe(OC_6H_5)_2(bpy)}} \quad (14)$$

$$\mathbf{3} + \mathrm{bpy} \underset{k_{-4}}{\overset{k_4}{\rightleftharpoons}} \underset{\mathbf{5}}{\mathrm{Fe(C_2H_5)_2(bpy)(bpy)_2^*}} \xrightarrow{k_5} \mathbf{1} \quad (15)$$

(bpy)*: partially dissociated bpy ligand

A partial dissociation of bpy from **1** takes place to give coordinatively unsaturated species **3** which presumably has a structure as shown below:

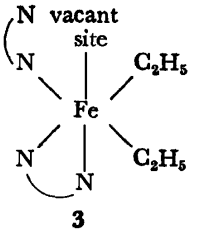

3

where $\widehat{\mathrm{N\ N}}$ represents the bpy ligand. Phenol then coordinates at the vacant site in **3** affording **4**. Activation of the Fe–Et bond by coordination of phenol leads to splitting of the ethyl group to give ethane as the rate-determining irreversible process. Further rapid reaction of phenol may follow to give **2f**. A competitive coordination of phenol and bpy toward **3** should be considered; Eq. 15 accounting for the inhibition effect of bpy on the reaction.

Since the starting material **1** and the final product **2f** are the only species observable during the reaction (actually 1:1 reaction mixture of **1** and phenol gave a 1:1 mixture of **1** and **2f**, indicating the absence of isolable reaction intermediates), the concentration of **3**, **4**, and **5** are considered to be negligible. Therefore by applying the steady state approximation for these species the following rate equation is derived.

$$\text{Rate} = -\frac{\mathrm{d}}{\mathrm{d}t}[\mathbf{1}] = k[\mathbf{1}]$$

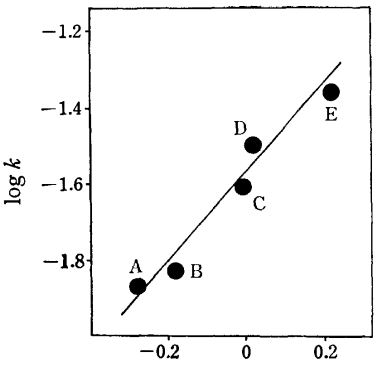

Fig. 4. Relation between log k in THF at 23.2 °C and Hammett substituent constant. $[\mathrm{XC_6H_4OH}] = 1.66 \times 10^{-1}$ mol/dm^3; A, X=CH_3O; B, X=CH_3; C, X=H; D, X=C_6H_5; E, X=Cl. $[\mathrm{bpy}] = 2.71 \times 10^{-3}$ mol/dm^3. Under these conditions, k increases with increasing the phenol concentration and does not level off.

$$k = \frac{k_1k_2k_3[\mathrm{C_6H_5OH}]}{k_{-1}(k_{-2}+k_3)+k_2k_3[\mathrm{C_6H_5OH}]+\dfrac{\bar{k}_4k_5(k_{-2}+k_3)[\mathrm{bpy}]}{k_{-4}+k_5}} \quad (16)$$

When k_{-2} is much greater than k_3, the observed pseudo-first-order rate constant k is given by

$$\frac{1}{k} = \frac{1}{k_1} + \frac{k_{-1}k_{-2}+\bar{k}[\mathrm{bpy}]}{k_1k_2k_3[\mathrm{C_6H_5OH}]} \quad (17)$$

$$\bar{k} = \frac{k_4k_5k_{-2}}{k_{-4}+k_5}$$

The experimental results expressed by Eq. 11 is in agreement with Eq. 17 supporting the validity of assumptions as expressed by Eqs. 12—15. Thus from constants A, B, and C in Eq. 11 rate constants and their ratios $1/k_1$, $k_{-1}k_{-2}/k_1k_2k_3$, and $\bar{k}/k_1k_2k_3$ may be obtained. The $1/k_1$ value of 4.0 min obtained from the intercept in Fig. 2 roughly agrees with the value observed in the reaction of **1** with olefins.[16] The agreement may be taken as additional support for that the similar reaction mechanism involving the partial dissociation of bpy ligand from **1** is operative in the reactions of **1** with phenols and with olefins.

The rates of the reactions of **1** with various *p*-substituted phenols were examined under the same conditions. The relation between log k and Hammett substituent constant σ[18] of X is demostrated in Fig. 4 ($\rho = +1.17$). More electron-withdrawing substituent facilitates the reaction, indicating electrophilic attack of phenols to **1**.

The pseudo-first-order rate constant k was estimated in various solvents such as acetone, THF, and toluene, having dielectric constants of 20.7, 7.6, and 2.4.[18] Figure 5 shows the results under various phenol concentrations. The fact that all the $1/k$ values lie on the same line as plotted *vs.* phenol concentration indicates the absence of solvent effect on the rate. This result suggests that non-polar active intermediate is involved in the rate determining step.[19]

Two types of interactions of iron(II) complex with phenol for **4** such as (A) and (B) are plausible.

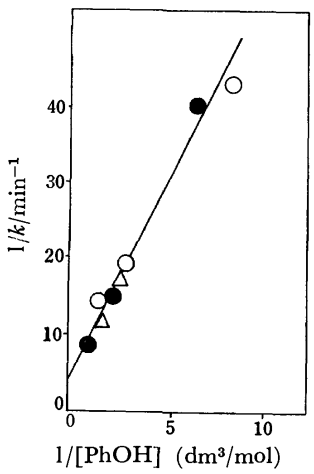

Fig. 5. Plot of the reciprocal of k *vs.* the reciprocal of [PhOH] at 23.2 °C in various solvents. Acetone, ○; THF, ●; toluene, △.

In the usual electrophilic cleavage of metal alkyls by acids, the three centered intermediate (B) has been suggested.[20] However, the intermediate (B) is not reasonable in the present reaction of **1** with phenols. The nucleophilic participation by $OC_6H_5^-$ to give four centered intermediate (A) is preferred by the following reasons, although the substituent effect of the phenols on the reaction rate suggests electrophilic attack of phenols at the ethyl ligand bonded to iron(II). Firstly, the absence of solvent effect agrees with the non-polar four centered intermediate rather than the ionic one (B). Secondly, the kinetic behavior of the present reaction is quite similar to that found in the reaction of **1** with olefin, in which facile Fe–C bond activation by the coordination of electron-defficient olefin to iron(II) has been reported.[17] On the other hand, however, the possibility of oxidative addition of phenol to Fe(II) giving Fe(IV) species in **4** followed by the reductive elimination of alkane can not be excluded.[21]

Experimental

All the procedures were carried out under nitrogen or *in vacuo*. The nitrogen gas used was deoxygenated by passing through a trap cooled to −196 °C in order to avoid the contamination by a trace of oxygen. Solvents were purified by usual manners under nitrogen and were stored under nitrogen or argon. $Fe(C_2H_5)_2(bpy)_2$ was prepared by the method previously reported.[5] Phenols and esters were commercial products and used without further purification. Alkyl and acyl halides were used after simple distillation of commercial products. IR and visible spectra were recorded on a Hitachi 295 infrared spectrometer and a Hitachi Type 200 spectrometer, respectively. ^1H NMR spectra were measured on a JEOL PS-100 spectrometer by Mr. Y. Nakamura. Micro analyses of C, H, N, and Cl were performed by using Yanagimoto CHN Corder Type MT-2 by Mr. T. Saito in our laboratory. Magnetic susceptibility was measured with Shimadzu Magnetic Balance Type MB-100. Gases were analysed by gas chromatography after collecting the gases evolved by a Toepler pump by which the gas volumes were measured. Amounts of the organic products were determined quantitatively by gas chromatography using suitable internal standards.

Preparation of the Bis(aryloxo)- and Bis(alkoxo)iron(II) Complexes and Their Reactions with H_2O and O_2. Phenol (497 mg, 5.3 mmol) was added to a THF (20 ml) solution of $Fe(C_2H_5)_2(bpy)_2$ (860 mg, 2.0 mmol) at −78 °C. After the evacuation of the reaction vessel, the mixtures was allowed to react at room temperature for 1 d. The color of the solution changed from deep purple to greenish grey and ethane (4.2 mmol) was detected in the gas phase. The solution was concentrated to *ca.* 10 ml and diethyl ether (30 ml) was added to give a greenish grey powder, which was washed with hexane and diethyl ether a few times and was dried *in vacuo*. (Yield 415 mg, 51%). The compounds **2a**, **2c**, **2d**, **2e**, **2g**, **2h**, **2i**, **2j**, and **2k** were prepared similarly. Elemental analyses, yields, and IR and ^1H NMR spectra of **2a**—**2g** are summarized in Tables 1 and 2, respectively. Micro analyses of **2h**—**2k** failed because of their extreme sensitivity toward oxygen. Results of thermolysis of **2h**—**2k** are listed in Table 5. Hydrolysis of **2f** (170 mg, 0.43 mmol) by distilled water (0.5 ml) in THF (6 ml) gave phenol (0.56 mmol) at 50 °C after 10 h. Hydrolysis of the other aryloxides, **2a**, **2b**, **2c**, **2d**, **2e**, and **2g** under similar conditions gave corresponding *p*-substituted phenols, the amount of respective phenols liberated being trace, 1.14, 0.85, 1.09, 1.18, 1.30, and 1.10 mol/complex. Dry air was introduced into the toluene suspension of complex **2e** (310 mg, 0.78 mmol) to give a brown heterogeneous solution. Oxygen absorbed (0.39 mmol) was measured by a gas burette. Resulted brown complex was filtered and dried *in vacuo* (100%). Found: C, 64.9; H, 4.6; N, 6.5%. Calcd for $C_{22}H_{18}N_2O_3Fe$: C, 63.8; H, 4.4; N, 6.8%. μ_{eff}=4.3 B.M. IR. ν(C–O)= 1260 cm^{-1}.

Preparation of $Fe(OC_6H_4CN\text{-}p)_2(bpy)_2$ (2b). The mixture of **2c** (440 mg) and bpy (320 mg) in dry toluene (10 ml) was heated to 100 °C to give a dark red homogeneous solution. After the filtration of this hot solution, it was kept in dry-ice temperature to deposit slowly dark red crystals. The resulted red crystals were filtered off, washed with diethyl ether containing free bpy and dried *in vacuo*.

Reactions of Bis(aryloxo)iron(II) Complexes with Organic Halides. Complex **2e** (41 mg, 0.10 mmol) in THF was treated with CH_3COCl (100 μl, 1.4 mmol) to cause immediate color change from greenish grey to dark red. After 1 d phenyl acetate (0.15 mmol) was detected in the solution. The red compound was obtained by removing all the volatile matter and was identified as $FeCl_2(bpy)$ by comparing its IR spectrum with that of an authentic sample which was prepared by **1** and HCl. (Yield 10 mg, 25%) Found: C, 42.5; H, 2.0; N, 10.0; Cl, 25.1%. Calcd: C, 43.2; H, 3.0; N, 10.1; Cl, 24.1%. Other reactions of various bis(aryloxo)iron(II) complexes with $PhCH_2Br$, CH_3I, and CH_3COCl were performed similarly and the results are summarized in Table 3.

Reaction of the Bis(aryloxo)iron(II) Complexes with p-Nitrophenyl Acetate. Complex **2f** (210 mg, 0.50 mmol) in THF (10 ml) was treated with *p*-nitrophenyl acetate (350 mg, 1.9 mmol) to give a dark red heterogeneous solution. After 5 h at room temperature phenyl acetate (0.83 mmol) was found in the solution by gas chromatography. The reactions of iron phenoxides and alkoxides with other organic acetates were carried out analogously and the results are shown in Table 4.

Catalytic Trans-esterification. Isopropenyl acetate (1 ml)

was mixed with benzyl alcohol (1 ml) in the presence of **2f** (90 mg, 0.23 mmol) to give immediately a red purple solution. After 2 d at room temperature acetone (6.6 mmol) and benzyl acetate (6.6 mmol) were detected in solution. (73% based on isopropenyl acetate). IR spectrum of the catalyst recovered was identical with that of **2f**. Transesterification of methyl methacrylate (3 ml) and ethanol (3 ml) in the presence of **2f** (110 mg, 0.28 mmol) also gave ethyl methacrylate (11.2 mmol) and methanol (11.2 mmol) in 1 d at room temperature (38% based on methyl methacrylate).

Tishchenko Type Reaction of Benzaldehyde Promoted by ***2h***. Benzaldehyde (5 ml, 50 mmol) was heated to 80 °C for 6 h in the presence of **2h** (120 mg) to afford a homogeneous blue solution. Benzyl benzoate (16 mmol, 63%) was found in the liquid phase by gas chromatography.

Kinetics. The rate of the formation of **2f** from **1** and phenol in THF was estimated by following the disappearence of the visible spectrum of **1** at 590 nm under vacuum. The pseudo-first order rate constants obtained by measuring the change at various wave lengths gave the same values. The solvent for spectroscopic measurements was dried over benzophenone ketyl and was introduced by a trap-to-trap distillation into the reaction mixture containing **1** and phenol.

References

1) (a) D. C. Bradley, R. C. Mehrotra, and D. P. Gaur, "Metal Alkoxides," Academic Press, London (1978) and references cited therein; (b) D. C. Bradley, "Progress in Inorganic Chemistry," Interscience Publishers Inc., New York (1960), Vol. 2, p. 303; (c) D. C. Bradley and K. J. Fisher, "MTP International Review of Science," (1972), Vol. 5, Part 1, pp. 65—91; (d) D. C. Bradley, "Adv. Inorg. Chem. Radiochem., 15," ed by H. J. Emeleus and A. G. Sharp, Academic Press, New York and London (1972), p. 259.

2) (a) B. N. Chaudret, P. J. Cole-Hamilton, R. S. Nohr, and G. Wilkinson, *J. Chem. Soc., Dalton Trans.*, **1977**, 1546; (b) J. Chatt and B. L. Shaw, *Chem. Ind.*, **1960**, 931; **1961**, 290; (c) J. Chatt and B. L. Shaw, *J. Chem. Soc.*, **1966**, 1437; (d) L. Vaska and J. W. DiLuzio, *J. Am. Chem. Soc.*, **83**, 1262, 2784 (1961); (e) L. Vaska, *ibid.*, **86**, 1943 (1964); (f) Y. Inoue, M. Hidai, and Y. Uchida, *Chem. Lett.*, **1972**, 1119; (g) J. Chatt, B. L. Shaw, and A. E. Field, *J. Chem. Soc.*, **1964**, 3466.

3) P. M. Maitlis, "The Organic Chemistry of Palladium," Academic Press, New York and London (1971), Vol. II, p. 119.

4) (a) M. A. Bennett, G. B. Robertson, P. O. Whimp, and T. Yoshida, *J. Am. Chem. Soc.*, **95**, 3028 (1973); (b) C. A. Reed and W. R. Roper, *J. Chem. Soc., Dalton Trans.*, **1973**, 1014, 1370; (c) T. Yoshida, T. Okano, and S. Otsuka, *ibid.*, **1976**, 993; (d) R. W. Adams, E. Bishop, R. L. Martin, and G. Winter, *Aust. J. Chem.*, **19**, 207 (1966); (e) R. Milburn, *J. Am. Chem. Soc.*, **89**, 54 (1967); **77**, 2064 (1955); (f) K. E. Jabalpurwala and R. M. Milburn, *J. Am. Chem. Soc.*, **88**, 3224 (1966).

5) A. Yamamoto, K. Morifuji, S. Ikeda, T. Saito, Y. Uchida, and A. Misono, *J. Am. Chem. Soc.*, **90**, 1878 (1968).

6) D. J. Cole-Hamilton, R. J. Young, and G. Wilkinson, *J. Chem. Soc., Dalton Trans.*, **1976**, 1995.

7) S. Komiya, M. Bundo, A. Yamamoto, and T. Yamamoto, *J. Organomet. Chem.*, **174**, 343 (1979).

8) H. F. Klein and H. H. Karsch, *Chem. Ber.*, **106**, 1433 (1973).

9) K. Nakamoto, "Infrared and Raman Spectra of Inorganic and Coordination Compounds," 3rd ed, John Wiley & Sons, New York (1977).

10) T. Ouhadi, J. Hubert, P. Teyssie, and E. G. Derouane, *J. Am. Chem. Soc.*, **95**, 6481 (1973).

11) (a) E. E. van Tamelen, B. Akermark, and K. B. Sharpless, *J. Am. Chem. Soc.*, **91**, 1552 (1969); (b) M. H. Chisholm, W. W. Reichert, and P. Thornton, *ibid.*, **100**, 2774 (1978).

12) M. Kubota and A. Yamamoto, *Bull. Chem. Soc. Jpn.*, **51**, 2909 (1978).

13) H. Horino, T. Ito, and A. Yamamoto, *Chem. Lett.*, **1978**, 17.

14) (a) M. Yamashita, Y. Watanabe, T. Mitsudo, and Y. Takegami, *Bull. Chem. Soc. Jpn.*, **49**, 3597 (1976); (b) S. Tane-ichi, S. Komiya, A. Yamamoto, and T. Yamamoto, unpublished results.

15) K. Maruyama, T. Ito, and A. Yamamoto, *Bull. Chem. Soc. Jpn.*, **52**, 849 (1979).

16) T. Yamamoto, A. Yamamoto, and S. Ikeda, *Bull. Chem. Soc. Jpn.*, **45**, 1104 (1972).

17) H. H. Jaffe, *Chem. Rev.*, **53**, 191 (1953).

18) "Handbook of Chemistry and Physics," 57th ed, ed by R. C. Weast, CRC Press (1976).

19) M. Szwarc, "Ion and Ion Pairs in Organic Reactions," Wiley-Interscience, New York (1972), Vol. I.

20) (a) R. Romeo, D. Minniti, S. Lanza, P. Uguagliati, and U. Belluco, *Inorg. Chem.*, **17**, 2813 (1978); (b) W. A. Nugent and J. K. Kochi, *J. Am. Chem. Soc.*, **98**, 5979 (1976); (c) S. Komiya and J. K. Kochi, *ibid.*, **98**, 7599 (1976).

21) U. Belluco, M. Giustiniani, and M. Graziani, *J. Am. Chem. Soc.*, **89**, 6494 (1967).

Reactions of CO_2 with Cu(I) Alkoxides and Amides to Give Alkylcarbonato-, μ-Carbonato-, Hydrogencarbonato-, and Carbamato-copper Complexes

Takakazu YAMAMOTO, Minoru KUBOTA, and Akio YAMAMOTO*

Research Laboratory of Resources Utilization, Tokyo Institute of Technology, 4259 Nagatsuta, Midori-ku, Yokohama 227

(Received September 13, 1979)

Carbon dioxide reacts with $ROCu(PPh_3)_2$ ($R=C_2H_5$, $C_6H_5CH_2$; PPh_3=triphenylphosphine) to produce $ROCO_2Cu(PPh_3)_2$. Hydrolysis or thermolysis of the alkylcarbonatocopper(I) complexes gives a binuclear carbonatocopper(I) complex $(PPh_3)_2CuOCO_2Cu(PPh_3)_2$, which is further converted into a hydrogencarbonatocopper(I) complex $[HOCO_2Cu(PPh_3)_2]_n$ by the reaction with CO_2 in moist solvents. The IR spectrum of $[HOCO_2Cu(PPh_3)_2]_n$ shows association of the $HOCO_2Cu(PPh_3)_2$ units through hydrogen bonds. The IR spectrum of $[HOCO_2Cu(PPh_3)_2]_n$ also reveals that the mode of the association depends on conditions of the crystallization of the complex. The reaction of $(PPh_3)_2CuOCO_2Cu(PPh_3)_2$ with CH_3I gives $(CH_3O)_2CO$ and the reaction of $[HOCO_2Cu(PPh_3)_2]_n$ with $C_6H_5NH_2$ affords $C_6H_5NHCO_2Cu(PPh_3)_2$ in high yields. Carbon dioxide reacts also with an amidocopper(I) complex $C_6H_5NHCu(PPh_3)_2$ to yield a carbamatocopper(I) complex $C_6H_5NHCO_2Cu(PPh_3)_2$. The reaction of $CH_3Cu(PPh_3)_2$(diethyl ether)$_{0.5}$ with CO_2 in the presence of $HN(C_2H_5)_2$ affords $(C_2H_5)_2NHCO_2Cu(PPh_3)_2$. The isocyanate group of phenyl isocyanate is inserted into the C_2H_5O–Cu bond of $C_2H_5OCu(PPh_3)_2$ to give a (ethyl *N*-phenylcarbamato)copper complex.

Considerable attention has been focused on the reactions of carbon dioxide with transition metal complexes from the interest of utilizing carbon dioxide for organic syntheses promoted by transition metal complexes.[1-6] Carbon dioxide has been reported to be inserted into metal–carbon,[1d,7-13] –hydride,[1d,14-16] –alkoxide,[17] –hydroxide,[18] and –amide[19] bonds to form carboxylato, alkylcarbonato, hydrogencarbonato, and carbamato complexes.

As a part of our program of studies on the reactivity of copper(I) complexes having Cu–C,[20] Cu–N,[21] Cu–O[22] or Cu–S[11] bonds we have studied[23] also the reaction of CO_2 with $ROCu(PPh_3)_2$ ($R=C_2H_5$, $CH_2C_6H_5$) and expanded the work to investigate the chemical properties of the produced alkylcarbonatocopper(I) complex. The result was compared with the reaction of CO_2 with copper(I) amides and with the reaction of phenyl isocyanate, an isoelectronic compound of CO_2, with a copper ethoxide.

Results and Discussion

Reactions of CO_2 with Alkoxocopper(I) Complexes. Reactions of carbon dioxide with alkoxocopper(I) complexes containing triphenylphosphine are summarized in Scheme 1.

Reactions of $C_2H_5OCu(PPh_3)_2$(**1a**)[22a] and $C_6H_5CH_2OCu(PPh_3)_2$(diethyl ether)(**1b**)[22a] with CO_2 at atmospheric pressure and at low temperatures afforded $C_2H_5OCO_2Cu(PPh_3)_2$(**2a**) and $C_6H_5CH_2OCO_2Cu(PPh_3)_2$ (**2b**) (Reaction 1). Very recently a similar reaction of CO_2 with copper(I) *t*-butoxide, *t*-C_4H_9OCu, in the presence of ligands was reported.[17a] Analytical data of **2a** and **2b** (Table 1) agree with the compositions for the alkylcarbonato copper having two PPh_3 ligands. The color and diamagnetism of **2a** and **2b** indicate that the oxidation state of copper is one. Table 2 summarizes the IR absorption bands of the alkylcarbonatocopper(I) and related complexes. Complexes **2a** and **2b** show strong ν(C=O) and ν(C–O) bands at 1660 cm^{-1} and in the region of 1380—1280 cm^{-1}, respectively, and $\pi(CO_3)$ near 800 cm^{-1}.[24] The IR pattern is consistent with the molecular formula and can be compared with those of alkylcarbonatomagnesiums, *t*-butylcarbonatocopper(I),[17a] bis(methylcarbonato)copper(II),[17b] and methyl(methylcarbonato)palladium[25] complexes. The appearance of the ν(C=O) band at a relatively high frequency suggests the coordination of the $ROCO_2$ ligand through one oxygen as represented by Form I.

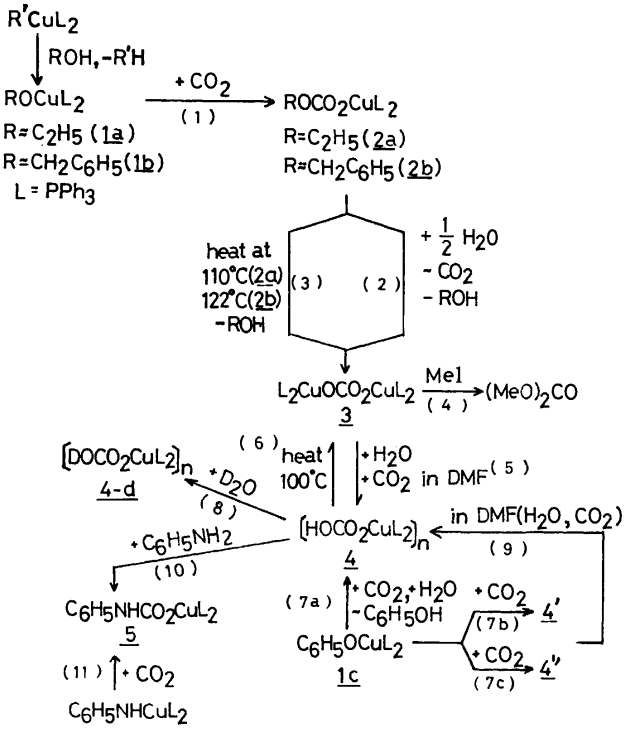

Scheme 1.

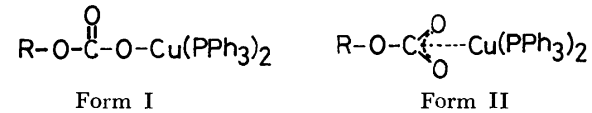

Form I Form II

Table 1. Analytical data of alkylcarbonato, carbonato, hydrogencarbonato, and related copper(I) complexes

Complex	Color	Dp[a] °C	C[b]	H[b]	N[b]	Cu[b]	CO_2/Cu	mol wt[b]
$C_2H_5OCO_2Cu(PPh_3)_2$	White	110[c]	69.2	5.2		9.2	0.41[c]	621
2a		(162)[d]	(69.2)	(5.2)		(9.4)	(0.92)[d]	(677)
$C_6H_5CH_2OCO_2Cu(PPh_3)_2$	White	120—122[c]	70.7	5.3		8.5	0.43[c]	685
2b		(162)[d]	(71.5)	(5.1)		(8.6)	(0.85)[d]	(739)
$(PPh_3)_2CuOCO_2(PPh_3)_2$	White	162	70.9	5.3		10.0	0.48	1140
3			(70.9)	(4.9)		(10.3)		(1240)
$[HOCO_2Cu(PPh_3)_2]_n$	White	*ca.* 100[c]	67.8	4.7		9.5	0.42[c]	
4		(153)[d]	(68.5)	(4.8)		(9.8)	(0.91)	
$[HOCO_2Cu(PPh_3)_2]_n$	White	(150)[d]	68.8	5.0		9.5		821
4′			(68.5)	(4.8)		(9.8)	(0.83)[d]	(650)[e]
$[HOCO_2Cu(PPh_3)_2]_n$	White	(159)[d]	68.1	4.7		9.6		793
4″			(68.5)	(4.8)		(9.8)	(0.77)[d]	(650)[e]
$C_6H_5NHCO_2Cu(PPh_3)_2$	White	205—207	70.5	5.2	2.0			
5			(71.3)	(5.0)	(1.9)			
$(C_2H_5)_2NCO_2Cu(PPh_3)_2\cdot\frac{1}{2}Et_2O$	White	134—135	66.4	5.7	1.7			
6			(67.3)	(5.8)	(1.8)			
$(C_6H_5NCOOC_2H_5)Cu(PPh_3)_2$	White	63—64	72.1	5.4	2.8			668
7			(71.9)	(5.3)	(1.9)			(751)

a) Decomposition point. b) Calculated values in the parentheses. c) Data for the conversion of the complexes into **3** on heating them. d) Data for the complete thermolysis of the complexes. e) Calcd value for $n=1$.

Table 2. IR and NMR spectral data of the complexes

Complex	Frequencies in cm^{-1}				NMR(δ, ppm)[a]
	ν(C=O)	ν(C-O)	$\pi(CO_3)$	ν(O-H)	
2a	1660 s	1380 m	800 m		1.12(3H, t, CH_3), 4.12(2H, q, CH_2),
		1285 m			7.0(18H, *o*-, *p*-phenyl), 7.6(12H, *m*-phenyl)
2b	1660 s	1380 m	805 m		5.20(2H, s, CH_2), 7.0(23H, *o*-, *p*-phenyl(PPh_3) +
		1280 s			$CH_2C_6\underline{H}_5$), 7.6(12H, *m*-phenyl(PPh_3))
2a′	1600 s	1390 m	810 m		
		1300 s			
3		1475 s	830 m		*ca.* 7.2(phenyl)
		1340 s			
4	1610 s	1400 m	820 m	2670 sh	
		1320 s		2600 m	
4′	1610 s	1400 m	820 m	2610 w	
	1640 s	1300 s			
	1595 s				
4″	1595 s	1445 sh	820 m	2600 w, br	
		1350 w			
5	1600 s	1420 s	815 sh		6.7—7.2(5H, N-$C_6\underline{H}_5$, *ca.* 7.3(phenyl(PPh_3)),
	1580 s	1350 s	795 m		8.1(1H, s, N$\underline{H}$)
6	1550 s	1400 s	795 m		1.08(9H, N-$CH_2C\underline{H}_3$ and O-$CH_2C\underline{H}_3$),
		1290 s			3.22(2H, O-CH_2), 3.56(4H, N-CH_2),
					7.0(18H, m, *p*-phenyl), 7.6(12H, *o*-phenyl)
7	1590 m				1.04(3H, t, CH_3), 4.48(2H, q, CH_2),
					7.0(23H, m, *p*-H of PPh_3 and N-$C_6\underline{H}_5$),
					7.6(12H, *o*-H of PPh_3)

a) Solvent: C_6D_6 for **2a**, **2b**, and **7**; CD_2Cl_2 for **3** and **5**; toluene-d_8 for **6**.

However, the coordinating mode of the alkylcarbonato ligand to Cu changes depending on delicate conditions of crystallization. For example, addition of hexane to a diethyl ether–ethyl alcohol (1:1) solution of **2a** gives complex **2a'** with the same composition as **2a** but with the different IR spectrum of **2a'** showing the ν(C=O) bands at considerably lower frequency, 1600 cm^{-1}. The lowering of ν(C=O) band suggests that the $C_2H_5OCO_2$ ligand in **2a'** coordinates to Cu through two oxygens as represented by Form II or the C–O oxygen has intermolecular interaction with Cu to form a polymeric compound in the solid state. Complex **2a'** can be reverted to **2a** by crystallization of **2a'** from toluene–ether. Cryoscopic molecular weight determination of **2a** and **2b** in dioxane (Table 2) reveals that they exist as monomers in the solutions. The somewhat lower observed values than the calculated molecular weights suggest partial dissociation of PPh_3 from the complexes. The reaction of ethyl bromide with **2a** affords diethyl carbonate in 10% yield. Although the formation of the alkylcarbonato complexes can be formally explained as insertion of CO_2 into the RO–Cu bond, the possibility of an indirect route as shown below promoted by intervention of a small amount of water cannot be ruled out.

$$ROCuL_2 + H_2O \rightarrow HOCuL_2 + ROH \quad (12)$$

$$ROH + CO_2 \rightleftharpoons ROCO_2H \quad (13)$$

$$ROCO_2H + HOCuL_2 \rightarrow ROCO_2CuL_2 + H_2O \quad (14)$$

Hydrolysis of **2a** or **2b** yields a μ-carbonatocopper(I) complex formulated as $(PPh_3)_2CuOCO_2Cu(PPh_3)_2$ (Reaction 2). Heating of **2a** and **2b** at 110 °C and 122 °C respectively also gives the carbonato complex, CO_2, and ROH (Reaction 3), but the source of hydrogen for ROH and stoichiometry of Reaction 3 have not been clarified. Recently similar dinuclear complexes having μ-carbonato ligand coordinated through one and two oxygens to two transition metals have been reported.[26,27] Similarlity of the IR spectrum of **3**, showing carbonato bands at 1480, 1370, and at 835 cm^{-1}, with those of $Pd_2Me_2(CO_3)(PPh_3)_3$[26] and $Rh_2(CO_3)(PPh_3)_5$,[27] for which the singly and doubly O-bonded structures have been established, suggests an unsymmetric structure as shown below.

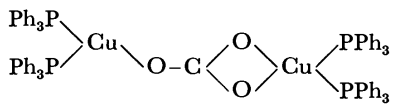

3

The IR spectrum of a symmetrical singly O-bonded μ-carbonatorhodium complex $Rh_2(CO)_2(CO_3)L_4$,[28] showing the carbonato bands at 1533, 1300, 1275, and 829 cm^{-1}, is somewhat different from those of the unsymmetrical carbonato complexes. The presence of two PPh_3 per Cu in **3** has been confirmed not only by elemental analysis but also by an NMR technique using acetone as a reference. Cryoscopic molecular weight determination in dioxane demonstrates that **3** remains binuclear in the solvent, although the somewhat low observed value for **3** suggests a partial dissociation of PPh_3 from **3** in the solution. The carbonato complex **3** has a higher thermal stability than **2a**, **2b**, and a hydrogencarbonatocopper(I) complex $HOCO_2Cu(PPh_3)_2$ **4** (*vide infra*) and thermolysis at 162 °C liberates *ca.* 1 mol of CO_2 per **3**.

Although the postulated structure for **3** indicates the presence of two different $Cu(PPh_3)_2$ moieties, ^{31}P-NMR shows only one sharp peak at 1.62 ppm (half width=7 Hz) downfield from external PPh_3 even at −83 °C in toluene. Rapid intramolecular exchange of the CO_3 group between two CuL_2 moieties or rapid exchange of the coordinated PPh_3 with free PPh_3 partly liberated from **3** accounts for the ^{31}P-NMR data. The rapid exchange between the coordinated PPh_3 and free PPh_3 certainly takes place in the presence of PPh_3 added as the ^{31}P-NMR spectrum of a mixture of **3** and PPh_3 (1:4 molar ratio) shows only one relatively broad signal at 1.16 ppm (half width=38 Hz) downfield from external PPh_3 at −63 °C. The reaction of **3** with CH_3I affords dimethyl carbonate in 82% yield (Reaction 4).

The reaction of **3** with H_2O in the presence of CO_2 in *N,N*-dimethylformamide (DMF) yields a hydrogencarbonatocopper(I) complex **4** (Reaction 5). Since **2a** and **2b** are converted into **3** (Eq. 2) by the hydrolysis and **3** is converted into **4** (Eq. 5) on standing them in solutions containing H_2O and CO_2, prolonged reaction of the alkoxocopper(I) complexes, **1a** and **1b**, with CO_2 in moist solvents is expected to yield directly the final product **4** through the serial Reactions 1, 2, and 5. This actually occurs in the reaction of **1a** with CO_2.

Similar reactions of a phenoxocopper(I) complex $PhOCu(PPh_3)_2$ **1c** with CO_2 in moist solvents also affords the hydrogencarbonatocopper(I) complex directly (Reaction 7a), but the IR spectrum of the complex varies depending on the preparative conditions and it was revealed that there are three types of complexes **4**, **4'**, and **4''** with the same composition $HOCO_2Cu(PPh_3)_2$.

$C_6H_5OCu(PPh_3)_2 + CO_2$ in moist THF

1c → **4** (7a) [−10—0 °C]

→ **4'** (7b)

→ **4''** (7c) [−10—0 °C, $+10C_6H_5OH$; −30 °C]

In the case of the reaction of **1c** attempts for the isolation of the complexes of type **2** and **3** were not successful even by using solvents dried over Na, presumably due to the high reactivities of **2** and **3** with water under the preparative conditions by using **1c** as the starting material and to the difficulty to remove a trace of water from the solvents and CO_2 gas employed.

The IR absorption bands in the region of 2600 cm^{-1} ascribable to the bridging ν(O–H···O) band observed in the three hydrogencarbonato complexes **4**, **4'**, and **4''** suggest the presence of associated species for these complexes. There are at least two ways of association as depicted below, which have been established by X-ray crystallography for $[PdR(OCO_2H)L_2]_2$[29,30] and $[RhH_2(OCO_2H)L_2]_2$.[28]

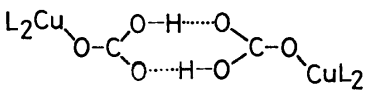

Form A[29]

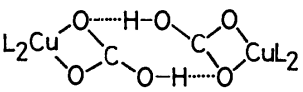

Form B[28]

Other modes of association as illustrated below may be also possible.

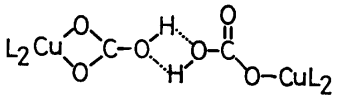

Form C

Assignment of the hydrogencarbonato complexes **4**, **4'**, and **4''** to the respective associated forms is not possible solely on the basis of the IR spectra, but the complex **4'** showing the high ν(C=O) band at 1640 cm^{-1} may be related to a species having non-interacting C=O group such as that represented by Form C. On deuteriation of **4** by treating with D_2O (Reaction 8), the ν(O–H···O) bands at 2670 and 2600 cm^{-1} are shifted to 2100 and 2040 cm^{-1}, while a δ(OHO) band hidden under absorption bands of PPh_3 in a region of 1400—1500 cm^{-1} appears at 1060 cm^{-1} and a coupled vibration ν(C–O)+ν(C=O)+δ-(OHO) at 1325 cm^{-1} is shifted up to 1365 cm^{-1}. These trends are consistent with those observed for $[Rh(CO)(O_2COH)L_2]_2$[28] and hydrogencarbonato dimer anion.[31]

Formation of the hydrogencarbonato complexes **4**, **4'**, and **4''** depends on slight differences in experimental conditions. Complex **4'** or **4''** in a moist DMF solution can be converted into **4** by addition of a 1:1 mixture of hexane and diethyl ether to crystallize out **4** (Reaction 9). The existence of the hydrogencarbonatocopper(I) complexes **4'** and **4''** predominantly as a monomer in solution is demonstrated by the cryoscopic molecular weight determination of **4'** and **4''** as well as by the IR spectrum of **4''** in $CHCl_3$. The ν(O–H···O) band of **4''** at 2600 cm^{-1} disappears whereas new bands at 3300 cm^{-1} (ν(O–H)) and 1660 cm^{-1} (ν(C=O)) emerge on dissolving in $CHCl_3$, indicating that the hydrogen bond is cleaved in the solution.

$$[HOCO_2Cu(PPh_3)_2]_n \xrightarrow{\text{organic solvent}} n\,H\text{-}O\text{-}\overset{\overset{O}{\|}}{C}\text{-}O\text{-}Cu(PPh_3)_2 \quad (15)$$

Complexes **4**, **4'**, and **4''** can be also obtained in the reactions of CO_2 with various organocopper(I) complexes such as cyanoethyl-,[32] nitroalkyl-,[32] and methylcopper(I)[20] complexes. Although it was previously reported that the reaction of the methylcopper-(I) complex $CH_3Cu(PPh_3)_2$(diethyl ether)$_{0.5}$ with CO_2 afforded $CH_3COOCu(CO_2)(PPh_3)_2$, whose characterization was based on the liberation of CH_3COOH and CO_2 upon acidolysis,[11] it has been later found that the product of the reaction was a mixture of $CH_3COOCu(PPh_3)_2$, **4'**, and **4''**. Heating of **4** at *ca.* 100 °C for 1.5 h yields the carbonato complex **3** (Reaction 6). The reaction of **4** with aniline affords a phenylcarbamatocopper(I) complex **5** in 79% yield (Reaction 10). The analytical data of **5** (Table 1) roughly agree with the formulation and the appearance of the ν(C=O) band at a relatively low frequency (Table 2) suggests the coordination of the carbamato ligand to copper through two oxygens. It is reported that the ν(C=O) absorption appears in a region of 1636—1680 cm^{-1} when a carbamato ligand coordinates to transition metal through one oxygen whereas the carbamato ligand coordinated through two oxygen gives rise to the ν(C=O) at lower frequencies.[19a]

Complex **5** may be formed through the condensation reaction between $C_6H_5NH_2$ and $HOCO_2$ ligand of **4** (Eq. 16) or through the formation of a phenylcarbamic acid by the reaction of $C_6H_5NH_2$ and CO_2 partly liberated from **4** (Eqs. 17a—17c).

$$C_6H_5\overset{H}{N}\text{-}H + HO\text{-}CO_2CuL_2 \longrightarrow C_6H_5NHCO_2CuL_2 + H_2O \quad (16)$$

4 **5**

$$\mathbf{4} \rightleftharpoons \underset{A}{HOCu(PPh_3)_2} + CO_2 \quad (17a)$$

$$\text{or} \quad \left.\begin{array}{l} C_6H_5NH_2 + CO_2 \rightleftharpoons C_6H_5NHCOOH, \\ 2C_6H_5NH_2 + CO_2 \rightleftharpoons C_6H_5NH_3{}^+C_6H_5NHCO_2{}^- \end{array}\right\} \quad (17b)$$

$$\text{or} \quad \left.\begin{array}{l} C_6H_5NHCOOH + A \rightleftharpoons \mathbf{5} + H_2O \\ C_6H_5NH_3{}^+C_6H_5NHCO_2{}^- + A \\ \qquad \rightarrow \mathbf{5} + C_6H_5NH_2 + H_2O \end{array}\right\} \quad (17c)$$

Equilibria of type 17b are known[33] and formation of carbamic acid has been proposed as the key step in an amine catalyzed exchange reaction between CO_2 and transition metal carbamates.[19b] Complex **5** affords a small amount (5 mol % per **5**) of ethyl phenylcarbamate by the reaction with C_2H_5I.

Reactions of Amidocopper(I) Complexes with CO_2. The reaction of phenylamidocopper(I) complex C_6H_5-$NHCu(PPh_3)_2$[21] with CO_2 gives the phenylcarbamatocopper(I) complex **5**. (Reaction 11). Reaction 11 may proceed through direct insertion of CO_2 into the Cu–N bond or an indirect route involving partial liberation of $C_6H_5NH_2$ from $C_6H_5NHCu(PPh_3)_2$ by the reaction with a trace of H_2O (Eq. 18) and formation of the carbamic acid (Eq. 17b).

$$C_6H_5NHCu(PPh_3)_2 + H_2O \rightleftharpoons HOCu(PPh_3)_2 + C_6H_5NH \quad (18)$$

$$C_6H_5NH_2 + CO_2 \rightleftharpoons C_6H_5NHCOOH \quad (17b)$$

$$HOCu(PPh_3)_2 + C_6H_5NHCOOH \rightarrow \mathbf{5} + H_2O \quad (19)$$

The formation of a carbamatocopper complex through the equilibrium of type 17b seems to occur in the reaction of $CH_3Cu(PPh_3)_2$(diethyl ether)$_{0.5}$ with diethylamine and CO_2.

$$CH_3Cu(PPh_3)_2(\text{diethyl ether})_{0.5} + (C_2H_5)_2NH + CO_2 \rightarrow \underset{\mathbf{6}}{(C_2H_5)_2NCOOCu(PPh_3)_2} \quad (20)$$

Although the interaction of the methylcopper complexes with N–H compounds generally affords amidocopper(I) complexes such as $C_6H_5NHCu(PPh_3)_2$ with

liberation of CH_4, the interaction of the methylcopper complex with diethylamine does not lead to the corresponding amidocopper(I) complex due to the too weak acidity of the hydrogen in $(C_2H_5)_2NH$.[21] Therefore the formation of **6** by Reaction 20 is considered to proceed most probably through the formation of diethylcarbamic acid which has acidic hydrogen. Similar behavior of methylpalladium complexes has been observed in the reactions with amines and CO_2.[26] The analytical data and IR and NMR spectral data of **6** agree with the formulation for **6**. Formation of methyl diethylcarbamate by the reaction of **6** with CH_3I in 58% yield also supports the formation of the carbamatocopper(I) complex.

Reactions of $CH_3Cu(PPh_3)_2$(diethyl ether)$_{0.5}$ with NH_3 and $C_6H_5NHNH_2$ under the bubbling of CO_2 also afford white copper complexes whose IR spectra show the formation of similar carbamatocopper(I) complexes. However, full characterization of the complexes were not successful due to the instability of complexes. The reaction of C_2H_5Br with the product of the reaction with NH_3 gives ethyl carbamate (20% based on copper).

$$CH_3Cu(PPh_3)_2(\text{diethyl ether})_{0.5} + NH_3 + CO_2 \rightarrow [NH_2COOCu(PPh_3)_2] \xrightarrow{C_2H_5Br} NH_2COOC_2H_5 \ (20\%) \quad (21)$$

It is reported that the reaction of $CuN(Si(CH_3)_3)_2$ with CO_2 affords copper(I) isocyanate.[34] However, no indication for the formation of copper(I) isocyanate complex was obtained in the reactions described above.

Insertion of Phenyl Isocyanate into the Cu–O Bond of ***1a***. Since phenyl isocyanate can be regarded as an isoelectronic compound of CO_2 and some examples of insertion of isocyanate into a metal–oxygen bond are known,[35] a reaction of phenyl isocyanate with the ethoxocopper(I) complex **1a** was examined to find out that **1a** undergoes a ready insertion of the isocyanate into the Cu–O at −10 to 0 °C to afford (ethyl phenylcarbamato-*N*-)copper(I) complex **7**.

$$\mathbf{1a} + C_6H_5\text{-}N{=}C{=}O \rightarrow C_6H_5\text{-}\underset{\displaystyle Cu(PPh_3)_2}{\underset{|}{N}}\text{-}COOC_2H_5 \quad (22)$$

7

As for the direction of the insertion of the isocyanate group into the C–O bond, a reverse type of insertion to afford $C_6H_5N(OC_2H_5)COCu(PPh_3)_2$ is possible, although it is less likely in view of the probable polarization of the Cu–O bond as $Cu^{\delta+}$–$O^{\delta-}$.

Experimental

General Procedure and Material. Preparation and recrystallization of copper complexes were carried out under deoxygenated nitrogen or argon or under vacuum. Solvents were dried by usual methods, distilled, and stored under argon or nitrogen. IR spectra were recorded on a Hitachi Model 295 spectrometer. ^{1}H-NMR spectra were recorded on a Japan Electron Optics Lab. JNM-PS-100 spectrometer. TMS was used as the internal standard. ^{31}P-NMR spectra were obtained in the pulsed Fourier transform mode at 40.50 MHz. Identification of the evolved gas was made with a Hitachi RMU 5B mass-spectrometer and a Shimadzu GC-5B gas chromatograph, and the amount of gas was measured with a Toepler pump. The microanalysis of carbon, hydrogen, and nitrogen was performed by Mr. T. Saito in our laboratory with a Yanagimoto CHN Autocorder Type MT-2. The alkoxo and phenoxo copper complexes **1a**, **1b**, and **1c** were prepared as previously reported.[22a] Carbon dioxide was dried by passing through a cold trap cooled to −78 °C.

*Preparation of Ethylcarbonatobis(triphenylphosphine)copper(I) (**2a** and **2a′**).* The ethoxocopper(I) complex **1a** (630 mg, 1.0 mmol) was dissolved in a mixture of diethyl ether (5 ml) and ethyl alcohol (5 ml). The atmosphere in the reaction vessel was replaced with CO_2 (50 ml) at −40 °C. The mixture was stirred at −40——30 °C for 1 h to yield a transparent colorless solution. Concentration of the solution to about 5 ml by evaporation and addition of excess hexane gave a white precipitate. Recrystallization from toluene–diethyl ether yielded white crystals of **2a** (550 mg, 81%). Drying the white precipitate obtained from diethyl ether–ethyl alcohol–hexane in vacuum gave **2a′**.

*Preparation of Benzylcarbonatobis(triphenylphosphine)copper(I) (**2b**).* The benzyloxocopper(I) complex **1b** (1.3 g, 2.0 mmol) was dissolved in a mixture of diethyl ether (3 ml) and benzyl alcohol (2 ml). The gas in the reaction vessel was evacuated and then CO_2 (50 ml) was introduced at −30 °C. Stirring the mixture for 1 h at −30——20 °C afforded a transparent solution. Condensing the solution and addition of hexane (15 ml) gave a white precipitate. Recrystallization from diethyl ether–toluene containing a small amount of PPh_3 yielded 530 mg (yield=36%) of **2b**.

*Preparation of Tetrakis(triphenylphosphine)(μ-carbonato)dicopper-(I) (**3**).* The ethylcarbonatocopper(I) complex **2a** (250 mg, 0.37 mmol) was dissolved in 20 ml of THF. Water (14 mg, 0.75 mmol) was added to the solution and the solution was stirred for 0.5 h at room temperature to yield a white precipitate with liberation of C_2H_5OH (0.34 mmol) and CO_2 (0.17 mmol). Recrystallization from CH_2Cl_2–hexane gave **3** (150 mg, yield=88%).

*Preparation of Hydrogencarbonatobis(triphenylphosphine)copper(I) (**4**).* Complex **3** (310 mg, 0.25 mmol) was dissolved in 15 ml of DMF containing 0.5 ml of H_2O. The gas in the reaction vessel was evacuated and CO_2 (50 ml) was introduced at −30 °C. After stirring the solution for 2 h at −30 °C, an excess amount of diethyl ether was added and the solution was cooled to −70 °C to obtain a white precipitate, which was washed with diethyl ether repeatedly and dried in vacuum to yield 160 mg (yield=49%) of **4**. Deuteriation of **4** was performed by stirring a suspension of **4** in excess D_2O at room temperature.

*Preparation of Complex **4′**.* Immediately after addition of 0.5 ml of water into a THF solution (5 ml) containing $C_6H_5OCu(PPh_3)_2$ **1c** (0.34 g, 0.5 mmol) and C_6H_5OH (5 mmol), CO_2 gas was bubbled into the solution at −10 to 0 °C for 5 min to produce a white precipitate. The precipitate was washed repeatedly with diethyl ether and dried under vacuum to give a white complex of **4′** (272 mg, yield 84%).

*Preparation of Complex **4″**.* CO_2 gas was bubbled into a THF solution (5 ml) of a mixture of **1c** (340 mg, 0.5 mmol) and 0.5 ml of water at −30 °C for 5 min to produce a white precipitate, which was washed repeatedly with diethyl ether and dried in vacuum to yield 280 mg (yield=91%) of **4″**. Complexes **4**—**4″** were also prepared through the pathways described in the text.

*Preparation of Phenylcarbamatobis(triphenylphosphine)copper(I) (**5**).* The hydrogencarbonato complex **4** was dissolved in 10 ml of DMF containing 0.5 ml (5.5 mmol) of aniline. The mixture was stirred at −30 °C in an atmosphere of

CO_2. After 10 h diethyl ether and hexane were added to the solution and the mixture was cooled to −78 °C to produce a white solid, which was collected by filtration and dried in vacuum to yield 190 mg (yield=79%) of **5**.

Preparation of Diethylcarbamatobis(triphenylphosphine)copper(I) (6). Diethylamine (71 μl, 0.69 mmol) was added to $CH_3Cu(PPh_3)_2$ (diethyl ether)$_{0.5}$[20] suspended in 10 ml of diethyl ether. After evacuation of the gas in the reaction vessel, 100 ml of CO_2 was introduced at −20 °C and the mixture was stirred for 30 min at the temperature. The color of the solution turned from light yellow to white. Addition of hexane to the solution yielded 420 mg (yield=89%) of **6**.

Preparation of (Ethyl Phenylcarbamato-N-)bis(triphenylphosphine)-copper(I) (7). Phenyl isocyanate (2 mmol) was added into a flask containing **1a** (630 mg, 1 mmol) and the white emulsion was stirred at −10—0 °C for 5 h to produce a white precipitate. Recrystallization from diethyl ether–toluene gave white crystals of **7** (600 mg, yield=80%).

Thermolysis of the Complexes. A Schlenk type tube containing 260 mg (0.39 mmol) of **2a** was immersed in an oil bath and the temperature was raised gradually. The color of the complex was slightly changed from white to brown at 110 °C and evolution of CO_2 started at the temperature. Heating of the complex at 110 °C afforded 0.16 mmol of CO_2 (41 mol%/**2a**), 0.36 mmol of C_2H_5OH (92 mol%/**2a**), and 210 mg of a brownish solid, whose IR spectrum essentially coincided with that of **3** prepared by the acidolysis of **2a**. Heating of **2a** at higher temperature, 162 °C, caused further liberation of CO_2 (0.92 mol%/**2a**) coordinated to Cu. The other thermolyses of the complexes were carried out in similar manners and the amount of CO_2 evolved is given in Table 1.

Reactions of the Complexes with Alkyl Halides. Methyl iodide (5 ml) was added to a flask containing 640 mg (0.52 mmol) of **3** and the mixture was stirred overnight at room temperature. Gas chromatographic analysis of the reaction mixture showed the formation of 0.43 mmol (82 mol%/**3**) of dimethyl carbonate. The other reaction of the complexes with alkyl halides were carried out in similar manners.

References

1) (a) M. E. Vol'pin, *Pure Appl. Chem.*, **30**, 607 (1972); (b) M. E. Vol'pin, *Z. Chem.*, **12**, 361 (1972); (c) M. E. Vol'pin and I. S. Kolomnikov, *Pure Appl. Chem.*, **33**, 567 (1972); *Organomet. React.*, **5**, 313 (1975).

2) Y. Iwashita, *Kagaku Kogyo*, **23**, 1596 (1972).

3) (a) M. Kobayashi and S. Inoue, *Kagaku*, **28**, 942 (1973); (b) S. Inoue, *Sekiyu Gakkai Shi*, **17**, 199 (1974); (c) S. Inoue, "Miriyo-Shigen to Gosei-Kagaku, Kagaku-Zokan 63," Kagaku-Dojin (1974), p. 29.

4) M. Hidai, T. Hikida, and Y. Uchida, *Sekiyu Gakkai Shi*, **17**, 193 (1974).

5) T. Saegusa and T. Tsuda, *Kagaku Kogyo*, **26**, 562 (1975).

6) (a) T. Ito and A. Yamamoto, *Yuki Gosei Kagaku Kyokai Shi*, **34**, 308 (1976); (b) T. Ito and A. Yamamoto, "Organic and Bio-organic Chemistry of Carbon Dioxide," ed by S. Inoue and N. Yamazaki, Kodansha Ltd. Tokyo, in press.

7) V. Zucchini, E. Albizzati, and V. Giannini, *J. Organomet. Chem.*, **26**, 357 (1971).

8) H. H. Karsch, *Chem. Ber.*, **110**, 2213 (1977).

9) G. N. Schrauzer and J. W. Sibert, *J. Am. Chem. Soc.*, **92**, 3509 (1970).

10) I. S. Kolomnikov, H. Stepovskaya, S. Tyrlik, and M. E. Vol'pin, *Zh. Obshch. Khim.*, **42**, 1652 (1972).

11) A. Miyashita and A. Yamamoto, *J. Organomet. Chem.*, **113**, 187 (1976).

12) (a) T. Tsuda, K. Ueda, and T. Saegusa, *J. Chem. Soc., Chem. Commun.*, **1974**, 380; (b) T. Tsuda, H. Habu, and T. Saegusa, *ibid.*, **1974**, 620; (c) T. Tsuda, Y. Chujo, and T. Saegusa, *ibid.*, **1975**, 963.

13) T. Yamamoto and A. Yamamoto, *Chem. Lett.*, **1978**, 615.

14) (a) L. S. Pu, A. Yamamoto, and S. Ikeda, *J. Am. Chem. Soc.*, **90**, 3896 (1968); (b) A. Yamamoto, S. Kitazume, L. S. Pu, and S. Ikeda, *ibid.*, **93**, 317 (1971); (c) S. Komiya and A. Yamamoto, *J. Organomet. Chem.*, **46**, C58 (1972).

15) A. Misono, Y. Uchida, M. Hidai, and T. Kuse, *J. Chem. Soc., Chem. Commun.*, **1968**, 981.

16) I. S. Kolomnikov, A. I. Gusev, G. G. Aleksandrov, T. S. Lobeeva, Yu. I. Struchkov, and M. E. Vol'pin, *J. Organomet. Chem.*, **59**, 349 (1973).

17) (a) T. Tsuda, Y. Chujo, and T. Saegusa, 38th National Meeting of the Chemical Society of Japan, Nagoya, October 1978, 4G09; (b) T. Tsuda and T. Saegusa, *Inorg. Chem.*, **11**, 2561 (1972).

18) B. R. Flynn and L. Vaska, *J. Am. Chem. Soc.*, **95**, 5081 (1973).

19) (a) M. H. Chisholm and M. W. Extine, *J. Am. Chem. Soc.*, **99**, 782 (1977); (b) M. H. Chisholm and M. W. Extine, *ibid.*, **99**, 792 (1977); (c) T. Tsuda, M. Miwa, and T. Saegusa, 37th National Meeting of the Chemical Society of Japan, Yokohama, April 1978, 4L41.

20) (a) A. Yamamoto, A. Miyashita, T. Yamamoto, and S. Ikeda, *Bull. Chem. Soc. Jpn.*, **45**, 1583 (1972); (b) T. Ikariya and A. Yamamoto, *J. Organomet. Chem.*, **72**, 145 (1975); (c) A. Miyashita and A. Yamamoto, *Bull. Chem. Soc. Jpn.*, **50**, 1102 (1977).

21) T. Yamamoto, Y. Ehara, M. Kubota, and A. Yamamoto, *Bull. Chem. Soc. Jpn.*, in press.

22) (a) M. Kubota and A. Yamamoto, *Bull. Chem. Soc. Jpn.*, **51**, 2909 (1978); (b) M. Kubota, T. Yamamoto, and A. Yamamoto, *ibid.*, **52**, 146 (1979).

23) A part of results described in this paper was reported in "3rd Symposium on the Utilization of Carbon Dioxide in Chemistry," Tokyo (1977), No. 19.

24) K. Nakamoto, "Infrared Spectra of Inorganic and Coordination Compounds", Wiley-Interscience, New York (1970), p. 169.

25) F. Ozawa, T. Ito, and A. Yamamoto, "4th Symposium on the Utilization of CO_2 in Chemistry," Kyoto (1978), No. 10.

26) F. Ozawa, T. Ito, and A. Yamamoto, *Chem. Lett.*, **1979**, 735.

27) S. Krogsrud, S. Komiya, T. Ito, J. A. Ibers, and A. Yamamoto, *Inorg. Chem.*, **15**, 2798 (1976).

28) T. Yoshida, D. L. Thorn, T. Okano, J. A. Ibers, and S. Otsuka, *J. Am. Chem. Soc.*, **101**, 4212 (1979).

29) R. J. Crutchley and J. Powell, *Inorg. Chim. Acta*, **24**, L15 (1977).

30) T. Ito, H. Tsuchiya, and A. Yamamoto, *Chem. Lett.*, **1976**, 851.

31) K. Nakamoto, Y. A. Sarma, and H. Ogoshi, *J. Chem. Phys.*, **43**, 1177 (1965).

32) T. Yamamoto, M. Kubota, and A. Yamamoto, *Bull. Chem. Soc. Jpn.*, **51**, 1835 (1978).

33) (a) A. Jensen, M. B. Jensen, and C. Faurhold, *Acta Chem. Scand.*, **8**, 1129 (1954); (b) F. Calderazzo, G. Dell'Amico, R. Netli, and M. Pasquali, *Inorg. Chem.*, **17**, 471 (1978).

34) T. Tsuda, H. Washita, and T. Saegusa, *J. Chem. Soc., Chem. Commun.*, **1977**, 468.

35) A. J. Bloodworth and A. G. Davies, *J. Chem. Soc.*, **1965**, 5238.

Effect of pH on Brdička Currents Produced by Cytochrome c

Tokuji IKEDA, Yoshiyuki YAMANE, Hideaki KINOSHITA,** and Mitsugi SENDA*
Department of Agricultural Chemistry, Kyoto University, Sakyo-ku, Kyoto 606
***Department of Chemistry, Kwassui Women's College, Higashi-yamate, Nagasaki 850*
(Received September 14, 1979)

Effect of pH and buffer concentrations on Brdička currents produced by horse heart cytochrome c was investigated in the presence of hexaamminecobalt(III) chloride in ammonia, tris(hydroxymethyl)aminomethane, *N,N*-dimethylglycine, borate, and carbonate buffer solutions at pH varying between 8.2 and 10.7. The Brdička current-activity of the protein varied with pH and the kind and concentration of buffers, but, if corrected for the effect of the buffer salts, showed a sigmoidal pH-dependence. The pH-dependence was interpreted as due to the protonic dissociation of Lys-79 of the protein. Brdička currents of the protein were observed also in unbuffered solutions containing no proton donor except water. The current intensity was explained by taking into account the change of pH at electrode surface. The results indicate that a main proton donor in the Brdička reaction is a water molecule.

Effect of the electrolyte pH and the kind and concentration of buffers on Brdička currents produced by SS- and/or SH-containing proteins has been studied extensively.[1-6] However, an understanding of the effect of these factors is far from complete. We have shown[7] that cytochrome c gives Brdička currents in ammoniacal buffers of pH 9.4 containing cobalt salts and that the heme group and its sixth ligand are important in determining the Brdička current-activity of the protein. Since the structure at heme moiety changes with pH,[8] it seems interesting to study the effect of pH on the Brdička current produced by cytochrome c. In this study we have investigated the pH effect on the Brdička current produced by horse heart cytochrome c in the presence of hexaamminecobalt(III) chloride in buffer solutions of various kinds at pH varying between 8.2 and 10.7 and shown that the pH-dependence of the Brdička current-activity can be interpreted as due to the protonic dissociation of Lys-79 of the protein. The results and discussion are presented in this paper. Importance of water molecule as a proton donor in the Brdička reaction is also described.

Experimental

Chemicals and Apparatus. Horse heart cytochrome c (cyt-c) was a product of Sigma Chemical Co. (Type IV, Lot No 78c-7040). The purity of the cyt-c was checked by SDS-disk electrophoresis. Stock solutions, usually 0.5% in cyt-c were stored at 5 °C. The concentrations were checked spectrophotometrically.[9] Other chemicals used were of a reagent grade quality. D.c. polarograms were recorded on a Yanagimoto P8 polarograph. The characteristics of the dropping mercury electrode (DME) were $m=1.60\ \mathrm{mg\ s^{-1}}$ and $\tau=6.3$ s at open circuit in ammoniacal buffer at 70 cm height of mercury reservoir.

Electrochemical Measurements. All measurements were made in an H-type cell immersed in a thermostat controlled at 25 °C. All potentials were measured against a saturated calomel electrode (SCE). Buffer solutions (0.06—0.30 M ammonium chloride–ammonia for pH 8.4—10.1, 0.06—0.25 M hydrogen chloride–tris(hydroxymethyl)aminomethane for pH 8.2—9.2, 0.06—0.24 M boric acid–potassium hydroxide for pH 9.1—9.4, 0.05—0.20 M *N,N*-dimethylglycine–potassium hydroxide for pH 9.7—10.7, and 0.025—0.10 M sodium hydrogencarbonate–disodium carbonate for pH 9.9) were used as the base solution. The ionic strength of the base solution was adjusted to 0.2 mol $\mathrm{dm^{-3}}$ with potassium chloride. Other details of the electrochemical measurements have been described previously.[7]

Results

Brdička Currents in Ammoniacal Buffers. Figure 1 shows polarograms of Brdička current of 0.34 μM cyt-c in the presence of 2×10^{-4} M hexaamminecobalt(III) chloride (Co(III)) in ammoniacal buffers at various pH-values. Two Brdička waves were observed in the pH range covered in Fig. 1, the first one exhibiting a peak. The peak potential of the first wave was shifted negatively with increasing pH, that is, from −1.31 V at pH 8.4 (Fig. 1a) to −1.38 V at pH 10.1 (Fig. 1g), whereas the potential of the second peak (or a shoulder) was almost independent of pH and appeared at −1.52 V. The height of the waves increased with increasing pH. Figure 2 shows the dependence of the Brdička current on the ammonia buffer concentration, $c_{amm}=(NH_4^+)+(NH_3)$, at pH 10.1. The height of the first wave increased greatly with increasing c_{amm} from 0.06 M (Fig. 2a) to 0.30 M (Fig. 2c), whereas the height of the second one was hardly influenced by c_{amm}. With decreasing pH the effect of c_{amm} on the Brdička current became smaller.

Brdička Currents in Tris(hydroxymethyl)aminomethane Buffers (Tris Buffers). Figure 3A shows a polaro-

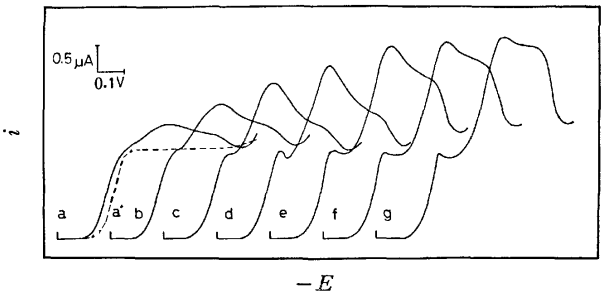

Fig. 1. Polarograms of Brdička current of 0.34 μM cyt-c in the presence of 2×10^{-4} M Co(III) in ammoniacal buffers; a) $c_{amm}=0.11$ M, pH 8.4, b) $c_{amm}=0.12$ M, pH 8.7, c) $c_{amm}=0.15$ M, pH 9.1, d) $c_{amm}=0.10$ M, pH 9.4, e) $c_{amm}=0.08$ M, pH 9.7, f) $c_{amm}=0.07$ M, pH 9.9, and g) $c_{amm}=0.06$ M, pH 10.1. Each curve starts from −0.9 V. (Broken line represents polarogram in the absence of cyt-c.)

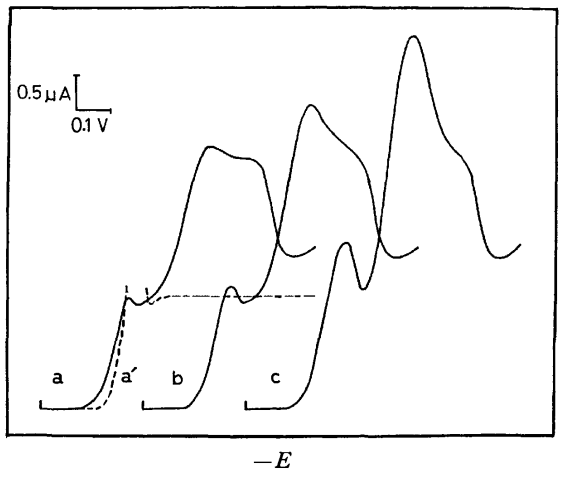

Fig. 2. Dependence of Brdička current of cyt-c on c_{amm} at pH 10.1; c_{amm}: a) 0.06 M, b) 0.12 M, and c) 0.30 M. Each curve starts from −0.9 V.

gram of Brdička current of cyt-c in the presence of Co(III) in 0.12 M tris buffer at pH 8.9. A rounded hump was observed at −1.34 V, followed by a shoulder at −1.52 V. The shape of the wave was similar at pH varying between 8.2 and 9.2, whereas the height of the wave increased with increasing pH. The shape and the height of the wave were hardly influenced by the concentration of tris buffer, c_{trls}, in the range 0.06—0.25 M at constant pH.

Brdička Currents in Borate Buffers. Figure 3B shows a polarogram of Brdička current of cyt-c in the presence of Co(III) in 0.24 M borate buffer at pH 9.1. Two waves of nearly equal wave height were observed at −1.32 and −1.52 V, respectively. At pH 9.4 the Brdička waves were similar in shape to but larger in height than those at pH 9.1. The shape and the height of the waves were hardly influenced by the concentration of borate buffer, c_{borate}, in the range 0.06—0.24 M at constant pH.

Brdička Currents in N,N-*Dimethylglycine Buffers.* Figure 3C shows a polarogram of Brdička current of cyt-c in 0.05 M *N,N*-dimethylglycine buffer at pH 10.0. Two waves observed at −1.36 and −1.52 V grew up to a certain limit with increasing pH from 9.7 to 10.7. With increasing concentration of *N,N*-dimethylglycine buffer, c_{dimet}, from 0.05 to 0.20 M at constant pH, the height of the two waves decreased slightly. In these buffer solutions the polarogram of Co(II) to Co(0) reduction step in the absence of cyt-c (Fig. 3C') appeared at the potential more negative by about 130 mV than that in ammoniacal buffer solutions (see Fig. 2a'). Similar negative shift of the reduction step of Co(II) to Co(0) has been reported[3] in glycine buffer solutions.

Brdička Currents in Carbonate Buffers. Figure 3D shows a polarogram of Brdička current of cyt-c in 0.025 M carbonate buffer at pH 9.9. Two waves were observed at −1.36 and −1.52 V, respectively. The height of the waves decreased with increasing concentration of carbonate buffer, c_{carb}, from 0.025 to 0.10 M. The polarogram of Co(II) to Co(0) reduction step in the absence of cyt-c (Fig. 3D') appeared at the

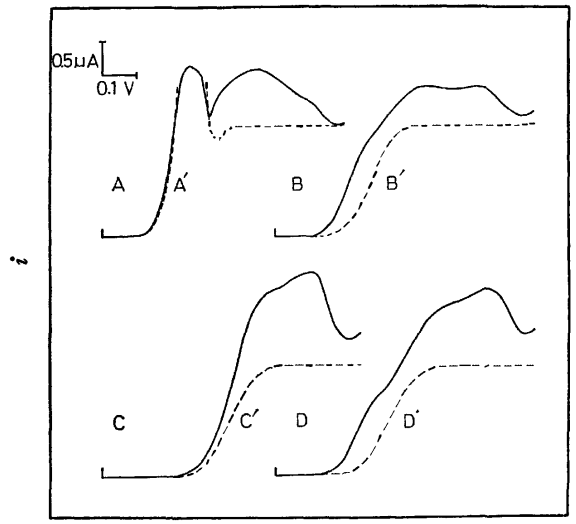

Fig. 3. Polarograms of Brdička current of 0.33 μM cyt-c in the presence of 2×10^{-4} M Co(III) in A) 0.12 M tris buffer, pH 8.9, B) 0.24 M borate buffer, pH 9.1, C) 0.05 M dimethylglycine buffer, pH 10.0, and D) 0.025 M carbonate buffer, pH 9.9. Each curve starts from −0.9 V. (Broken lines represent polarograms in the absence of cyt-c.)

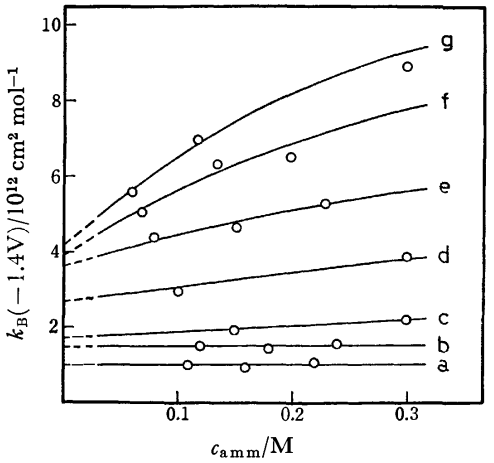

Fig. 4. Plots of k_B (−1.4 V) against c_{amm} at pH= a) 8.4, b) 8.7, c) 9.1, d) 9.4, e) 9.7, f) 9.9, and g) 10.1.

potential more negative by about 100 mV than that in ammoniacal buffer solutions.

$k_B(-1.4\,V)$-Value. It has previously been shown[7,10] that the Brdička current of cyt-c in ammoniacal buffers of pH 9.4 containing Co(III) at the concentration lower than 2×10^{-4} M can be expressed by

$$i_B = FAk_B\Gamma f_{Co}, \quad (1)$$

where F is Faraday, A the surface area of the DME, k_B a proportionality constant representing the Brdička current-activity of cyt-c, Γ the surface concentration of cyt-c adsorbed on the DME surface, and f_{Co} the flux of Co(III) ions at the electrode surface. Further it has been shown[7,10] that the adsorption of cyt-c on the DME surface at low bulk concentrations of cyt-c and at −1.4 V is cntrolled by diffusion and that

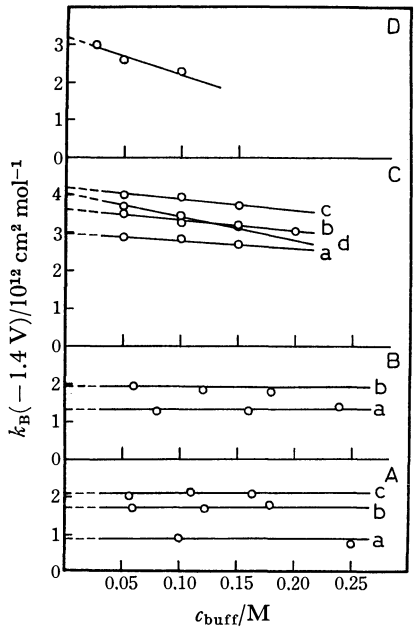

Fig. 5. Plots of k_B (−1.4 V) against A) c_{tris} at pH= a) 8.2, b) 8.9, and c) 9.2, B) c_{borate} at pH=a) 9.1 and b) 9.4, C) c_{dimet} at pH=a) 9.7, b) 10.0, c) 10.3, and d) 10.7, and D) c_{carb} at pH=9.9.

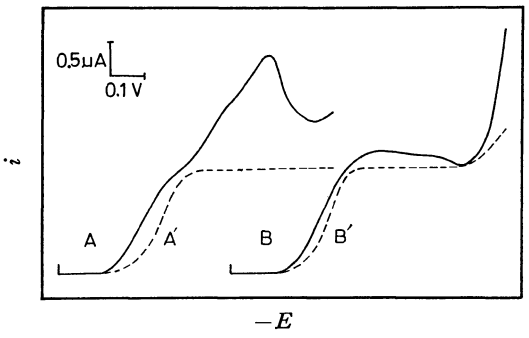

Fig. 6. Polarograms of Brdička current of 0.33 μM cyt-c in the presence of 2×10^{-4} M Co(III) in A) 0.2 M KCl solution and in B) 0.2 M NH_4Cl solution. Curves start from −0.9 V. (Broken lines represent polarograms in the absence of cyt-c.)

Γ can be estimated by Koryta's equation.[11] It was found that the Brdička currents of cyt-c measured under the present experimental conditions also obeyed Eq. 1 and that Γ at −1.4 V was able to be determined by Koryta's equation. The cobalt ion flux at the DME is given by the Ilković theory.[12] Thus, we determined the k_B-values of cyt-c in various buffer solutions by applying Eq. 1 to the Brdička currents at −1.4 V. The k_B(−1.4 V)-values are plotted against the buffer concentrations, c_{buff}, in Figs. 4 and 5.

Brdička Currents in Unbuffered Solutions. Figure 6 shows polarograms of Brdička current of 0.33 μM cyt-c in the presence of 2×10^{-4} Co(III) in 0.2 M KCl solution (Fig. 6A) and in 0.2 M NH_4Cl solution (Fig. 6B). Characteristic Brdička waves were observed in these solutions. The height of the waves in 0.2 M KCl solution was very much greater than that in 0.2 M NH_4Cl solution.

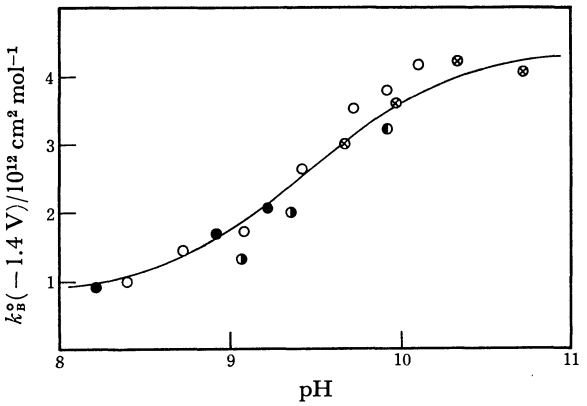

Fig. 7. Plots of k_B° (−1.4 V) against pH; data obtained in ○ ammonia buffer, ● tris buffer, ◑ borate buffer, ◐ carbonate buffer, and ⊗ dimethylglycine buffer. Solid line was calculated on the basis of equation and assumption in the texst.

Discussion

Experimental results show that the shape and the height of the Brdička waves of cyt-c vary with the electrolyte pH and the kind and concentration of buffers. Equation 1 predicts that the Brdička currents are controlled by two factors, k_B and Γ. As reported previously[7,10] at −1.4 V cyt-c is very strongly adsorbed on DME surface, so that at low bulk concentrations of cyt-c Γ can be estimated by Koryta's equation. With increasing negative potential, however, the protein becomes less strongly adsorbed on DME surface and Γ can no longer be evaluated by Koryta's equation. Accordingly, in the following we shall limit the quantitative analysis of the effects of pH and buffers on the Brdička currents to k_B-values at −1.4 V.

Figures 4 and 5 show the dependence of the k_B-(−1.4 V)-values on the buffer concentrations at various pH-values. In ammoniacal buffers, the k_B(−1.4 V) increases with increasing c_{amm} (Fig. 4). On the contrary, in *N,N*-dimethylglycine and carbonate buffers k_B(−1.4 V) decreases with their concentrations, whereas it is hardly affected in tris and borate buffers (Fig. 5). To eliminate these buffer effects, each k_B(−1.4 V) *vs.* c_{buff} plot was extrapolated to $c_{buff}=0$. Values of $k_B^\circ(-1.4\,V) \equiv \lim_{c_{buff}\to 0} k_B(-1.4\,V)$ thus estimated are plotted against pH in Fig. 7. They are on a single sigmoidal curve, independent of the kind of buffers.

In the pH range covered in Fig. 7 ferricytochrome c has two different conformational states depending on pH.[8] At the dme ferricytochrome c in the two states is adsorbed and reduced to ferrocytochrome c at the electrode surface.[7] Assuming that the ferrocytochrome c also has two states, state I and state II, and that the two states are in equilibrium as expressed by

$$\Gamma^{II}(H^+)/\Gamma^{I} = K_1, \qquad (2)$$

where Γ^{I} and Γ^{II} are the surface concentrations of state I and state II in the adsorption layer, respectively, and K_1 the protonic dissociation constant, we can get the following expression for the Brdička current;

$$i_B = FA(k_B^I \Gamma^I + k_B^{II} \Gamma^{II}) f_{Co}$$
$$= FA((k_B^I(H^+) + k_B^{II} K_1)/((H^+) + K_1)) \Gamma f_{Co}, \quad (3)$$

where k_B^I and k_B^{II} represent the Brdička current-activities of state I and state II, respectively. Thus, k_B in Eq. 1 is given by

$$k_B = (k_B^I(H^+) + k_B^{II} K_1)/((H^+) + K_1),$$

or

$$pH = pK_1 + \log((k_B - k_B^I)/(k_B^{II} - k_B)). \quad (4)$$

Solid line in Fig. 7 was calculated by Eq. 4 with $pK_1 = 9.45$, $k_B^I = 0.8 \times 10^{12}$ cm^2 mol^{-1}, and $k_B^{II} = 4.4 \times 10^{12}$ cm^2 mol^{-1}.

Previously we have shown that heme moiety is important in determining the Brdička current-activity of cyt-c.[7] Ferricytochrome c undergoes a transition with an apparent pK, pK_a, of 9.35, which corresponds to the heme-linked deprotonation of ε-amino group of Lys-79.[8] The value of pK_a has been reported to decline with the ionic strength, I, from 9.2 at $I=0.02$ to 8.9 at $I=0.3$.[13] In case of ferrocytochrome c the pK value for the deprotonation of Lys-79 has not been reported so far as we know, but it should have a higher value than the pK_a value of ferricytochrome c, since Lys-79 of ferrocytochrome c is free from bonding to the heme iron.[8] Accordingly, we may conclude that the equilibrium of Eq. 2 corresponds to the equilibrium for the deprotonation of Lys-79 in ferrocytochrome c adsorbed on the DME surface and that the lysine residue together with heme group contributes to the Brdička current-activity of cyt-c.

It has been supposed that the effect of buffer concentration on Brdička currents is due to an acidic component which works as a proton donor.[6,12] This implies that k_B increases with the concentration of an acidic component of buffer salt. However, as shown in Fig. 4 the $k_B(-1.4\text{ V})$-values of cyt-c are almost independent of c_{amm} at pH's lower than 9 at which the concentration of the acidic component, (NH_4^+), is in large excess over that of the basic component, (NH_3), indicating that the effect of (NH_4^+) is negligibly small. Tris and borate buffers also have negligible effect on the $k_B(-1.4\text{ V})$-values (Figs. 5 A and B). Even a decreasing effect is found in dimethylglycine and carbonate buffers (Figs. 5 C and D). As will be reported elsewhere,[14] Brdička current of a protein can be interpreted as due to the catalytic action of protein–Co(0) complex[12] which is transiently formed on electrode surface and the k_B-value depends on the catalytic activity constant, k_c, and the stability constant, k_f/k_d, k_f, and k_d being the formation and decomposition rate constants of the protein–Co(0) complex, respectively. The complicated effects of the buffers described above should be explained by taking into account the contribution of the buffers (probably the basic components) to the k_c and/or the k_f/k_d.

The results that $k_B^\circ(-1.4\text{ V})$ increases with increasing pH and that $k_B(-1.4\text{ V})$ is hardly influenced by the acidic components of the buffer salts indicate that a main proton donor in the Brdička reaction is a water molecule.

In order to get further evidence for the validity of this indication we measured polarograms of Brdička current of cyt-c in unbuffered solutions. As shown in Fig. 6A, in 0.2 M KCl solution containing only 2×10^{-4} M Co(III) cyt-c gave distinct Brdička waves of which $k_B(-1.4\text{ V})$-value was estimated as 3.0×10^{12} cm^2 mol^{-1} by Eq. 1. In 0.2 M NH_4Cl solution containing 2×10^{-4} M Co(III) the protein gave rather small Brdička waves (Fig. 6 B), of which $k_B(-1.4\text{ V})$-value was estimated as 0.8×10^{12} cm^2 mol^{-1}. In an unbuffered solution, pH of the solution in the vicinity of electrode surface must be different from that in the bulk of solution, since Brdička reaction (catalytic hydrogen evolution reaction) produces hydroxide ions, OH^-, and simultaneously the reduction of hexaamminecobalt(III) ions liberates NH_3 molecules. The OH^- and NH_3 molecules diffuse into the solution, so that their surface concentrations, $(OH^-)^\circ$ and $(NH_3)^\circ$, are related[15] to the Brdička current and the limiting current of Co(III), $i_{lim.Co}$, respectively, by the Ilković equations:

$$i_B = \kappa_{OH^-}(OH^-)^\circ \quad (5\text{-a})$$

and

$$i_{lim.Co} = \kappa_{Co}(Co(III))^* = \kappa_{NH_3}(NH_3)^\circ, \quad (5\text{-b})$$

where κ_{OH^-}, κ_{Co}, and κ_{NH_3} are the Ilković constants for OH^-, Co(III), and NH_3, respectively, depending on their respective diffusion coefficients, D_{OH^-}, D_{Co}, and D_{NH_3}, and $(Co(III))^*$ the bulk concentration of Co(III). By Eq. 5-a with $D_{OH^-} = 5.2 \times 10^{-5}$ cm^2 s^{-1} [12] and $i_B(-1.4\text{ V}) = 0.97$ μA (Fig. 6A), $(OH^-)^\circ$ is estimated as 9.5×10^{-5} M, which corresponds to pH 10.0. By Eq. 5-b $(NH_3)^\circ$ is estimated as 7.0×10^{-4} M at $(Co(III))^* = 2 \times 10^{-4}$ M, where $D_{Co} = 7.5 \times 10^{-6}$ cm^2 s^{-1} [10] is used; D_{NH_3} is assumed to be equal to the diffusion coefficient of NH_4^+: $D_{NH_4} = 1.9 \times 10^{-5}$ cm^2 s^{-1}.[12] The pH of 7.0×10^{-4} M NH_3 solution is calculated to be approximately 10. Accordingly, it will be safe to estimate the electrode surface pH as about 10, under the condition under which the Brdička current in Fig. 6 A is observed. In 0.2 M NH_4Cl solution OH^- ions produced by the Brdička reaction at the DME surface can react with NH_4^+ ions to form NH_3 molecules. The reduction of Co(III) ions also liberates NH_3 molecules. Thus, using Eqs. 5-a and 5-b, the ratio $(NH_4^+)/(NH_3)$ may be estimated as 2.5×10^2 at the electrode surface. This value of $(NH_4^+)/(NH_3)$ ratio corresponds approximately to pH 7. The results that $k_B(-1.4\text{ V}) = 3.0 \times 10^{12}$ cm^2 mol^{-1} in 0.2 M KCl (electrode surface pH$\approx$10) and $k_B(-1.4\text{ V}) = 0.8 \times 10^{12}$ cm^2 mol^{-1} in 0.2 M NH_4Cl (electrode surface pH$\approx$7) can reasonably be explained by the $k_B^\circ(-1.4\text{ V})$-pH curve in Fig. 7.

This work was supported by a Grant-in-Aid from the Ministry of Education.

References

1) R. Brdička, *Collect. Czech. Chem. Commun.*, **5**, 112 (1933).
2) G. J. Miller, *Biochem. J.*, **53**, 393 (1953).
3) V. Kalous, *Collect. Czech. Chem. Commun.*, **21**, 1227 (1956).
4) B. Alexander, M. Brezina, and V. Kalous, *Collect. Czech. Chem. Commun.*, **28**, 210 (1963).

5) M. Ito, *Mie Medical Journal*, **8**, 149 (1964).
6) a) I. M. Kolthoff, K. Yamashita, and Tan Boen Hie, *Proc. Natl. Acad. Sci. U. S. A.*, **71**, 2072 (1974); b) I. M. Kolthoff, K. Yamashita, Tan Boen Hie, and A. Kanbe, *J. Electroanal. Chem.*, **53**, 417 (1974); c) I. M. Kolthoff, K. Yamashita, Tan Boen Hie, and A. Kanbe, *J. Electroanal. Chem.*, **58**, 375 (1975).
7) T. Ikeda, H. Kinoshita, Y. Yamane, and M. Senda, *Bull. Chem. Soc. Jpn.*, **53**, 112 (1980).
8) R. E. Dickerson and R. Timkovich, "The Enzyme XI," ed by P. D. Boyer, Academic Press, New York (1975) p. 397.
9) W. D. Butt and D. Keillin, F. R. S., *Proc. R. Soc. London, Ser. B*, **156**, 429 (1962).
10) H. Kinoshita, Ph. D. Thesis, University of Kyoto, 1979.
11) J. Koryta, *Collect. Czech. Chem. Commun.*, **18**, 206 (1953).
12) J. Heyrovský and J. Kůta, "Principles of Polarography," Academic Press, New York and London (1966).
13) C. Greenwood and M. T. Wilson, *Eur. J. Biochem.*, **22**, 5 (1971).
14) M. Senda, T. Ikeda, and T. Kakutani, *Bioelectrochem. Bioenerg.*, in press.
15) T. Ikeda and M. Senda, *Bull. Chem. Soc. Jpn.*, **46**, 2107 (1973).

Asymmetric Transformation of α-Amino Acids Promoted by Optically Active Cobalt(III) Complexes. II.[1] *N*-Methylalaninatocobalt(III) Complexes with Tetramines

Motowo YAMAGUCHI, Shigenobu YANO, Masahiko SABURI, and Sadao YOSHIKAWA*

Department of Synthetic Chemistry, Faculty of Engineering, The University of Tokyo, Hongo, Bunkyo-ku, Tokyo 113

(Received September 17, 1979)

The preparation and structural assignments of *N*-methyl-(*S*)- and -(*R*)-alaninatocobalt(III) complexes with a few chiral derivatives of 2,3,2-tet (=3,7-diazanonane-1,9-diamine) and triethylenetetramine are described. The hydroxide ion-catalyzed epimerizations of these complexes are examined at pH 10. In the *N*-methylalaninato complexes the isomer ratio for *Λ*-*S*/*Λ*-*R* ranged from 76/24 to 90/10. In the most favorable case where tetramine is 2(*S*)10(*S*)-4,8-diazaundecane-2,10-diamine (abbreviated as 2(*S*)10(*S*)-Me_2-2,3,2-tet) the energy differences among the four possible diastereomers are discussed in relation to the prediction from strain energy minimization calculations.

In recent papers, bis(ethylenediamine)cobalt(III) complexes or triethylenetetraminecobalt(III) complexes of *N*-substituted amino acidate (sarcosinate,[2-5] *N*-methyl-(*S*)- and -(*R*)-alaninate,[3,6-9] and *N*-benzylglycinate[10]) have been investigated from stereochemical points of view. Buckingham and coworkers reported[2] the stereoselective coordination of the secondary nitrogen atom in the sarcosinatobis(ethylenediamine)cobalt(III) complex due to steric repulsions between the *N*-methyl group and the adjacent ethylenediamine chelate ring. The coordinated secondary N center of sarcosinate in the *Δ*-[Co(sar)$(en)_2$]$^{2+}$ ion was assumed to have the *S* configuration stereoselectively, which was confirmed later by an X-ray crystal structure analysis.[11] Though the presence of less stable isomer, *Δ*-[Co(*R*-sar)$(en)_2$]$^{2+}$ was predicted on the basis of strain energy minimization calculations, some earlier attempts to obtain the isomer failed.[3] Recently, the *Δ*-*R* isomer was isolated by Yamatera and coworkers,[4] so that the presence of all four isomers (*Δ*-*R*, *Δ*-*S*, *Λ*-*R*, and *Λ*-*S*) were proved.

In the case of the *N*-methyl-(*S*)- or -(*R*)-alaninato complex there are two chiral centers in the *N*-methylalaninate moiety: *N*-methyl and *C*-methyl groups. Consequently, nonbonded repulsive interactions possibly occur not only between the *N*-methyl group and the adjacent chelate ring but also between the *N*-methyl group and the *C*-methyl group in the *N*-methylalaninate. In the *Λ* configuration it was shown that the *N*-methyl-(*S*)-alaninato complex with the *N*-methyl group trans to the *C*-methyl group was obtained stereospecifically owing to these nonbonded interactions, while in the *N*-methyl-(*R*)-alaninato complexes (*Λ*-*R*) with trien[7] or trien derivatives[8,9] two diastereomers were found to coexist: the trans configuration involving considerable steric repulsion between the *N*-methyl group and the adjacent chelate ring, and the cis configuration having alternatively significant nonbonded repulsion between the two methyl groups.

Sargeson and coworkers showed[12] that the α-proton of chelated α-amino acidate moieties in chiral complex ions undergoes hydroxide ion-catalyzed exchange in basic aqueous solution, and gives rise to a diastereomeric mixture after the establishment of equilibrium. It was found that an equilibrated solution of the *Δ*-β_2-[Co(*N*-Me-ala)(trien)]$^{2+}$ (at pH 12) contains *Δ*-β_2-(*RRS*)-[Co(*N*-Me-(*R*)-ala)(trien)]$^{2+}$ (≈60%), *Δ*-β_2-(*RRS*)-[Co(*N*-Me-(*S*)-ala)(trien)]$^{2+}$ (≈20%), and *Δ*-β_2-(*RRR*)-[Co(*N*-Me-(*S*)-ala)(trien)]$^{2+}$ (≈20%).[7] From the viewpoint of asymmetric transformation at the C center, the isomer ratio for *Δ*-*R*/*Δ*-*S* was 60/40 in the *Δ*-β_2-[Co(*N*-Me-ala)(trien)]$^{2+}$ system. Further, the *Δ*-[Co(*N*-Me-ala)$(en)_2$]$^{2+}$ system gave an improved ratio *Δ*-*R*/*Δ*-*S*=80/20.[6] The strain energy minimization study on the *Δ*-[Co(*N*-Me-ala)$(en)_2$]$^{2+}$ and *Δ*-β_2-[Co(*N*-Me-ala)(trien)]$^{2+}$ isomers correctly predicted the stability order and the energy difference among the diastereomers.[3]

In order to obtain further information about the asymmetric transformation of *N*-methylalaninate, a few chiral derivatives of triethylenetetramine (=trien) and 3,7-diazanonane-1,9-diamine (=2,3,2-tet) were employed for quadridentate ligand (=N_4), and *Λ*-β_2-[Co(*N*-Me-(*S*)- and -(*R*)-ala)(N_4)]$^{2+}$ complexes were prepared. The structure and abbreviations for these tetramines are summarized in Table 1. The epimerization of the amino acidato complexes were accomplished in basic solution. Each equilibrated mixture contained three isomers *Λ*-β_2-(*R*)-*S*, *Λ*-β_2-(*R*)-*R*, and *Λ*-β_2-(*S*)-*R*, as shown in Fig. 1. The isomer ratios for *Λ*-*S*/*Λ*-*R* were obtained, and the results are discussed in relation to the prediction of strain energy minimization calculations.

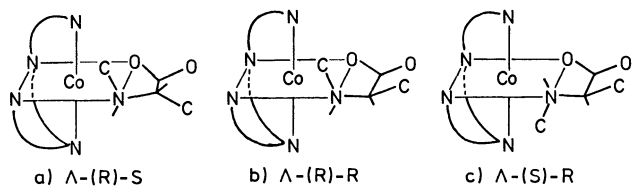

Fig. 1. Possible structures of the *Λ*-β_2-[Co(*N*-Me-ala)-(N_4)]$^{2+}$ cations; (a) *Λ*-(*R*)-*S*, (b) *Λ*-(*R*)-*R*, and (c) *Λ*-(*S*)-*R*.

Experimental

All material used were of reagent grade. The ligands 2(*S*),7(*S*)-dimethyl-3,6-diazaoctane-1,8-diamine (=3(*S*)8(*S*)-dimetrien),[13] 5(*R*)-methyl-1,4,7,10-tetraazadecane (=5(*R*)-metrien),[14] *N*,*N*′-bis(2-aminoethyl)-1(*R*),2(*R*)-cyclohexanedi-

TABLE 1. ABBREBIATION AND STRUCTURE OF QUADRIDENTATE LIGANDS

Structure	Abbreviation
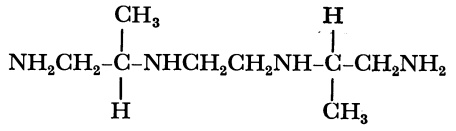	3(*S*)8(*S*)-dimetrien
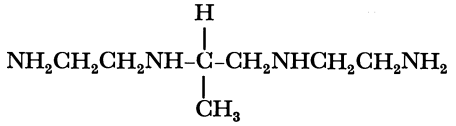	5(*R*)-metrien
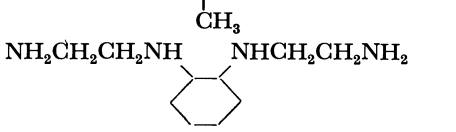	(*R*)-baetchxn
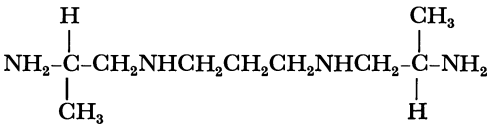	2(*S*)10(*S*)-Me_2-2,3,2-tet
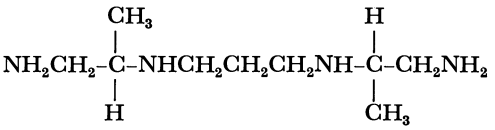	3(*S*)9(*S*)-Me_2-2,3,2-tet

amine (=(*R*)-baetchxn),[9] 2(*S*),10(*S*)-4,8-diazaundecane-2,10-diamine (=2(*S*)10(*S*)-Me_2-2,3,2-tet),[15] and 2(*S*),8(*S*)-dimethyl-3,7-diazanonane-1,9-diamine (=3(*S*)9(*S*)-Me_2-2,3,2-tet)[1] were prepared by the methods described previously. The dichlorocobalt(III) complexes (*trans*-[$CoCl_2$(3(*S*)8(*S*)-dimetrien)]ClO_4,[16] *Λ*-*β*-[$CoCl_2$(5(*R*)-metrien)]$Cl\cdot 0.5H_2O$,[14] *Λ*-*β*-[$CoCl_2$((*R*)-baetchxn)]$Cl\cdot 0.5H_2O$,[14] *trans*-[$CoCl_2$(2(*S*)-10(*S*)-Me_2-2,3,2-tet)]ClO_4,[1] and *trans*-[$CoCl_2$-(3(*S*)9(*S*)-Me_2-2,3,2-tet)]ClO_4[1]) were prepared according to the methods reported previously. *N*-Methyl-(*S*)-alanine and *N*-methyl-(*R*)-alanine were synthesized by the method of Quitt, *et al.*,[17] using (*S*)- and (*R*)-alanine, respectively.

Λ-*β*$_2$-[*Co*(N-*Me*-(S)- *or* -(R)-*ala*) (3(S)8(S)-*dimetrien*)]*Cl*·*ClO*$_4$·*0.5H*$_2$*O*. *N*-Methyl-(*S*)-alanine (or *N*-methyl-(*R*)-alanine) (0.26 g) was added to 5 ml of hot water, followed by $LiOH\cdot H_2O$ (0.088 g). The mixture was warmed to 70 °C until the compound dissolved. To the resulting solution was added *trans*-[$CoCl_2$(3(*S*)8(*S*)-dimetrien)]ClO_4 (0.80 g). The mixture was warmed for 15 min on a water bath at 70 °C. Solid $LiClO_4\cdot 3H_2O$ (0.48 g) was added to the solution, and the mixture was cooled in a refrigerator overnight. The orange-red crystals were collected, washed with methanol and acetone, successively, and air dried. The porduct was recrystallized from hot water. Calcd for [Co-($C_4H_8NO_2$)($C_8H_{22}N_4$)]$Cl\cdot ClO_4\cdot 0.5H_2O$: C, 30.07; H, 6.30; N, 14.61%. Found: for *N*-Me-(*S*)-ala complex, C, 30.33; H, 6.42; N, 14.81%, and for *N*-Me-(*R*)-ala compex, C 29.76; H, 6.45; N, 14.84%.

Λ-*β*$_2$-[*Co*(N-*Me*-(S)-*ala*)(5(R)-*metrien*)]$(ClO_4)_2$ was prepared by the method described previously.[8]

Λ-*β*$_2$-[*Co*(N-*Me*-(R)-*ala*)(5(R)-*metrien*)]$I_2\cdot 5H_2O$ was prepared by the method used for the preparation of *Δ*-*β*$_2$-[Co(*N*-Me-(*S*)-ala)(5(*S*)-metrien)]$I_2\cdot 2H_2O$ except that *Δ*-*β*-[$CoCl_2$-(5(*R*)-metrien)]$Cl\cdot 0.5H_2O$ and *N*-methyl-(*R*)-alanine were employed in place of the corresponding 5(*S*)-metrien complex and *N*-methyl-(*S*)-alanine, respectively.

Calcd for [$Co(C_4H_8NO_2)(C_7H_{20}N_4)$]$I_2\cdot 5H_2O$: C, 19.86; H, 5.76; N, 10.73%. Found: C, 19.83; H, 6.08; N, 10.46%.

Λ-*β*$_2$-[*Co*(N-*Me*-(S)-*ala*)((R)-*baetchxn*)]$(ClO_4)_2$ and *Λ*-*β*$_2$-[*Co*(N-*Me*-(R)-*ala*)((R)-*baetchxn*)]$ZnCl_4$ were prepared according to the method described previously.[9]

Λ-*β*$_2$-[*Co*(N-*Me*-(S)- *or* -(R)-*ala*)(2(S)10(S)-*Me*$_2$-2,3,2-*tet*)]$(ClO_4)_2\cdot H_2O$ and *Λ*-*β*$_2$-[*Co*(N-*Me*-(S)- *or* -(R)-*ala*)-(3(S)9(S)-*Me*$_2$-2,3,2-*tet*)]$(ClO_4)_2\cdot H_2O$ were prepared by the method used for the preparation of the *Λ*-*β*$_2$-[Co((*S*)-ala)(*SS*-pyht)]$(ClO_4)_2\cdot 2H_2O$.[1] Calcd for [$Co(C_4H_8NO_2)$-($C_9H_{24}N_4$)]$(ClO_4)_2\cdot H_2O$: C, 27.57; H, 6.05; N, 12.37%. Found: for *N*-methyl-(*S*)-ala complex with 2(*S*)10(*S*)-Me_2-2,3,2-tet, C, 27.14; H, 6.06; N, 12.02%; for *N*-methyl-(*R*)-ala complex with 2(*S*)10(*S*)-Me_2-2,3,2-tet, C, 27.53; H, 5.98; N, 12.13%; for *N*-methyl-(*S*)-ala complex with 3(*S*)9(*S*)-Me_2-2,3,2-tet, C, 27.31; H, 5.94; N, 12.13%; for *N*-methyl-(*R*)-ala complex with 3(*S*)9(*S*)-Me_2-2,3,2-tet, C, 27.65; H, 5.92; N, 12.37%.

Measurements. Visible absorption spectra were measured with a Shimadzu UV-210 spectrophotometer. Circular dichroism curves were obtained with a JASCO-J20 recording spectropolarimeter. Proton NMR (PMR) spectra (90 MHz) were obtained on a Hitachi R-40 spectrometer using sodium 2,2-dimethyl-2-silapentane-5-sulfonate (DSS) as an internal standard reference. FT carbon-13 NMR (CMR) spectra were obtained at 25.03 MHz with broad-band proton decoupling on a JEOL PS-99.5 MHz spectrometer employing the solvent deuterium signal as an internal lock. A pulse angle of 45 ° was employed with no pulse delay. The ambient temperature was 39 °C. Me_4Si sealed in a capillary was used as an external reference.

The perchlorate salts were suspended in the solvent (D_2O) and treated with twice the molar amount of tetraphenylarsonium chloride. The white precipitates were removed by filtration, and the filtrates were employed for NMR measurements.

Measurements of Isomer Ratios for Epimerization Reactions. (i) *N*-Methylalaninato complexes with the trien derivatives: Weighed samples (25 mg) of the *N*-methyl-(*S*)- or -(*R*)-alaninatocobalt(III) complexes with the trien derivatives were dissolved in 25 ml of 0.02 mol/dm^3 Na_2CO_3+0.02 mol/dm^3 $NaHCO_3$ buffer (pH 10.1), and the solution was warmed at 40 °C for 25 h. The solution was poured on a small column of SP-Sephadex C25 cation-exchange resin in the sodium form. The complex was eluted with 0.1 mol/dm^3 NaCl. Two bands were collected. The first

Table 2. Electronic and circular dichroism spectral data

Complex	Absorption maxima/nm (ε/M^{-1} cm^{-1})	Circular dichroism maxima/nm ($\Delta\varepsilon$/M^{-1} cm^{-1})
Λ-β_2-[Co(3(*S*)8(*S*)-dimetrien)-(*N*-Me-(*R*)-ala)]Cl·ClO_4·0.5H_2O	488(170) 354(182)	513(1.22), 357(−0.05)
Λ-β_2-[Co(3(*S*)8(*S*)-dimetrien)-(*N*-Me-(*S*)-ala)]Cl·ClO_4·0.5H_2O	485(163) 350(167)	506(1.55), 374(−0.23)
Λ-β_2-[Co(5(*R*)-metrien)-(*N*-Me-(*R*)-ala)]I_2·5H_2O	493(159) 355(167)	485(1.83), 358(−0.17)
Λ-β_2-[Co(5(*R*)-metrien)-(*N*-Me-(*S*)-ala)]$(ClO_4)_2$[a]	488(144) 351(147)	500(2.42), 356(−0.22)
Λ-β_2-[Co((*R*)-baetchxn)-(*N*-Me-(*R*)-ala)]$ZnCl_4$[b]	494(173) 357(172)	482(1.41), 362(−0.14)
Λ-β_2-[Co((*R*)-baetchxn)-(*N*-Me-(*S*)-ala)]$(ClO_4)_2$[b]	492(148) 354(154)	500(1.65), 360(−0.11), 328(0.06)
Λ-β_2-[Co(2(*S*)10(*S*)-Me_2-2,3,2-tet)-(*N*-Me-(*R*)-ala)]$(ClO_4)_2$·H_2O	503(166) 357(160)	540(2.16), 482(−1.25), 367(0.32), 351(0.33)
Λ-β_2-[Co(2(*S*)10(*S*)-Me_2-2,3,2-tet)-(*N*-Me-(*S*)-ala)]$(ClO_4)_2$·H_2O	501(154) 358(146)	529(1.32), 469(−0.56), 360(−0.26)
Λ-β_2-[Co(3(*S*)9(*S*)-Me_2-2,3,2-tet)-(*N*-Me-(*R*)-ala)]$(ClO_4)_2$·H_2O	502(160) 356(159)	536(1.70), 479(−0.99), 383(0.13), 342(0.17)
Λ-β_2-[Co(3(*S*)9(*S*)-Me_2-2,3,2-tet)-(*N*-Me-(*S*)-ala)]$(ClO_4)_2$·H_2O	502(152) 358(146)	530(1.22), 472(−0.58). 364(−0.30)

a) Ref. 8. b) Ref. 9.

pink band (bottom of the column) moved at a rate consistent with a univalent cation was assumed to be a hydrolysis product. The second orange-red 2+ band (top) which was a mixture of Λ-β_2-(*N*-Me-(*R*)-ala)Co(III) and Λ-β_2-(*N*-Me-(*S*)-ala)Co(III) complexes was concentrated to near dryness with a rotary evaporator, and excess NaCl was filtered off. After removing most of NaCl by addition of methanol, final desalting was carried out by gel permiation chromatography on a column (2.5×40 cm) of SP-Sephadex G15. The solution was passed down the column and collected. The resuting solution was evaporated to an appropriate concentration, then the CD curves was obtained. The best fitted curve with the observed CD curve of the equilibrated mixture was calculated by mixing the authentic CD curves of corresponding (*R*)- and (*S*)-amino acidato complex (in H_2O) between 560 nm and 400 nm using least-squares method, and the isomer ratio (Λ-*S*/Λ-*R*) was obtained. The agreement between the observed and calculated curves was satisfactory. Attempts to separate the diastereomeric isomers, (*R*)- and (*S*)-amino acidato complexes, failed.

(ii) *N*-Methylalaninato complexes with the 2,3,2-tet derivatives: Weighed samples (100 mg) of the *N*-methyl-(*S*)- or -(*R*)-alaninatocobalt(III) complex with the 2,3,2-tet derivatives were dissolved in 100 ml of 0.02 mol/dm^3 Na_2CO_3+0.02 mol/dm^3 $NaHCO_3$ buffer, and the compound was equilibrated and desalted by the above-mentioned procedure. The resulting solution was loaded on a SP-Sephadex C25 cation-exchange resin (2.5×40 cm), and eluted with 0.1 mol/dm^3 sodium L-tartratoantimonate(III). Since the length of the column was not sufficient for the complete separation, the eluate was recycled by a rotary pump. After 5—6 cycles the complexes separated cleanly into two bands. The bands were washed with 500 ml of water, eluted with 0.1 mol/dm^3 NaCl, and evaporated to near dryness. After desalting by a similar procedure as above their absorption spectra and CD curves were obtained. The first minor (bottom) and second major band (top) were assigned to the *N*-methyl-(*R*)-alaninato and *N*-methyl-(*S*)-alaninato complexes, respectively. The isomer ratio was estimated spectrophotometrically. Attempts to separate chromatographically the cis and trans isomers of the *N*-methyl-(*R*)-alaninato complexes failed.

In both methods the isomer ratios were reproducible to better than within ±2%.

Strain Energy Minimization Calculations. The minimized strain energies of the complexes Λ-β_2-[Co(*N*-Me-(*R*)- and -(*S*)-ala)(2(*S*)10(*S*)-Me_2-2,3,2-tet)]$^{2+}$ were calculated by the method reported previously.[1] The starting models were generated from the Λ-β_2-[Co(ala)(2(*S*)10(*S*)-Me_2-2,3,2-tet)]$^{2+}$ cations.[1] Calculations were carried out on a HITAC 8700/8800 computer at the Computer Center of this University.

Results and Discussion

β_2-[Co(*N*-Methyl-(*S*)- or -(*R*)-alaninato)(N_4)]$^{2+}$ complexes were prepared from *trans*-[$CoCl_2(N_4)$]$^+$ complexes or Λ-β-[$CoCl_2(N_4)$]$^+$ complexes by the methods described previously.[1,8,9]

The absolute configuration for the complexes was assigned to the Λ configuration based on their circular dichroism spectra. The complexes prepared by the present methods were expected to have the β_2 configuration.[1,18] The electronic and circular dichroism spectral data of Λ-β_2-[Co(*N*-Me-(*S*)- and -(*R*)-ala)(N_4)]$^{2+}$ complexes are listed in Table 2.

As described in the Introduction, only one isomer was anticipated for Λ-β_2-[Co(*N*-Me-(*S*)-ala)(N_4)]$^{2+}$ complexes, in which the *N*-methyl group was trans

TABLE 3. ASSIGNMENT OF PROTON RESONANCE SHIFTS[a] OF *N*-METHYLALANINATE MOIETIES

	C-CH_3	N-CH_3
Λ-β_2-[Co(*N*-Me-(*S*)-ala)-(3(*S*)8(*S*)-dimetrien)]$^{2+}$	1.54	2.54
Λ-β_2-[Co(*N*-Me-(*R*)-ala)-(3(*S*)8(*S*)-dimetrien)]$^{2+}$	1.41 unobsd.	2.36 2.58
Λ-β_2-[Co(*N*-Me-(*S*)-ala)-(5(*R*)-metrien)]$^{2+}$ [b]	1.53	2.61
Λ-β_2-[Co(*N*-Me-(*R*)-ala)-(5(*R*)-metrien)]$^{2+}$ [b]	1.42 1.50	2.38 2.58
Λ-β_2-[Co(*N*-Me-(*S*)-ala)-((*R*)-baetchxn)]$^{2+}$ [c]	1.50	2.58
Λ-β_2-[Co(*N*-Me-(*R*)-ala)-((*R*)-baetchxn)]$^{2+}$ [c]	1.43 1.51	2.40 2.57
Λ-β_2-[Co(*N*-Me-(*S*)-ala)-(2(*S*)10(*S*)-Me_2-2,3,2-tet)]$^{2+}$	1.47	2.42
Λ-β_2-[Co(*N*-Me-(*R*)-ala)-(2(*S*)10(*S*)-Me_2-2,3,2-tet)]$^{2+}$	1.45 1.52	2.45
Λ-β_2-[Co(*N*-Me-(*S*)-ala)-(3(*S*)9(*S*)-Me_2-2-3,2-tet)]$^{2+}$	1.46	2.37
Λ-β_2-[Co(*N*-Me-(*R*)-ala)-(2(*S*)9(*S*)-Me_2-2,3,2-tet)]$^{2+}$	1.43 1.48	2.39

a) ppm from DSS. b) Ref. 8. c) Ref. 9.

to the *C*-methyl group in the *N*-methylalaninate (=Λ-β_2-(*R*)-*S*). The PMR spectra of Λ-β_2-[Co(*N*-Me-(*S*)-ala)(N_4)]$^{2+}$ in D_2O exhibited a doublet at about 1.5 ppm and a singlet at 2.4—2.6 ppm arising from the *C*-methyl and *N*-methyl groups, respectively (Table 3 and Figs. 2b and 3a). These spectra are similar to those of other Λ-β_2 isomers of *N*-methyl-(*S*)-alaninato complexes with trien[7] and trien derivatives.[8,9] The ^{13}C-NMR spectrum of the Λ-β_2-[Co(*N*-Me-(*S*)-ala)-(3(*S*)9(*S*)-Me_2-2,3,2-tet)]$^{2+}$ complex exhibited twelve signals with one broad peak corresponding to two carbons, which was consistent with the number of the carbons expected for one kind of the isomer (Fig. 4b).

On the other hand, the presence of two isomers for Λ-β_2-[Co(*N*-Me-(*R*)-ala)(N_4)]$^{2+}$ has been reported.[3,7-9] The PMR spectrum of the *N*-methyl-(*R*)-alaninato complex with 3(*S*)8(*S*)-dimetrien showed two *N*-methyl resonances at 2.36 and 2.58 ppm, which were assigned to those of the *N*-methyl groups of the Λ-β_2-(*R*)-*R* and Λ-β_2-(*S*)-*R* complexes, respectively (Table 3 and Fig. 2a). The isomer ratio for Λ-β_2-(*R*)-*R*/Λ-β_2-(*S*)-*R* at equilibrium (pH 7) was estimated as about 3/1. This value is in contrast to those in the corresponding *N*-methyl-(*R*)-alaninato complexes with other tetramines, in which the isomer ratios for Λ-β_2-(*R*)-*R*/Λ-β_2-(*S*)-*R* were close to 1/1.[7-9] An X-ray structure analysis of the Λ-[$CoCO_3$(3(*S*)8(*S*)-dimetrien)]$^+$ ion[19] revealed that the apical five-membered chelate ring of the tetramine has the λ conformation with an axial *C*-methyl group in the crystal. If the apical chelate ring of the *N*-methylalaninato complex takes similarly the λ conformation, severe nonbonded repulsions will occur between the *N*-methyl group and the axial *C*-methyl group. Actually, the conformer

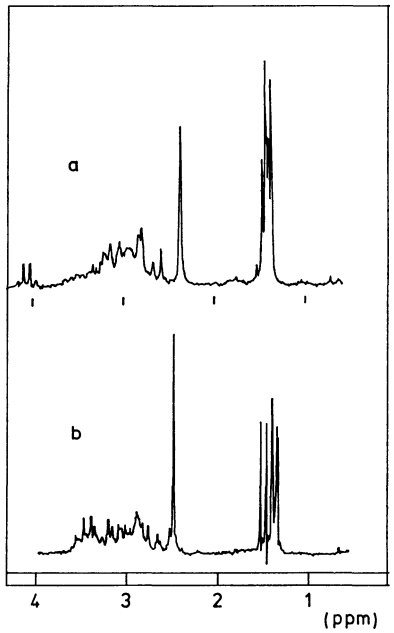

Fig. 2. PMR spectra of Λ-β_2-[Co(*N*-Me-ala)(3(*S*)8(*S*)-dimetrien)]$^{2+}$ ions in D_2O; (a) *N*-Me-(*R*)-ala and (b) *N*-Me-(*S*)-ala.

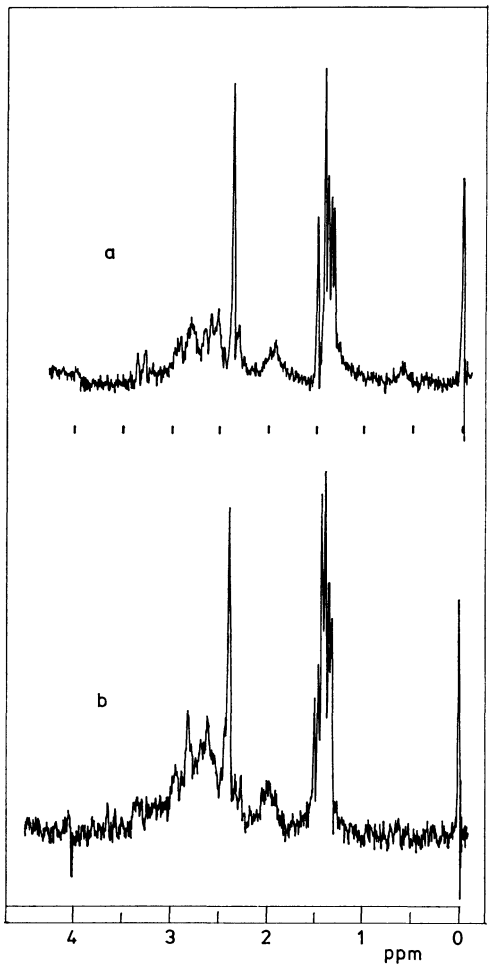

Fig. 3. PMR spectra of Λ-β_2-[Co(*N*-Me-ala)(3(*S*)9(*S*)-Me_2-2,3,2-tet)]$^{2+}$ ions in D_2O; (a) *N*-Me-(*S*)-ala and (b) *N*-Me-(*R*)-ala.

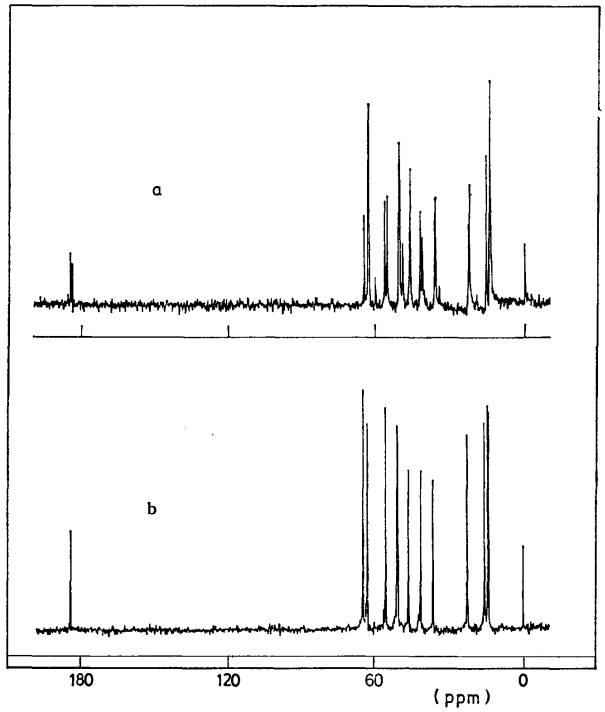

Fig. 4. CMR spectra of Λ-β_2-[Co(*N*-Me-ala)(3(*S*)9(*S*)-Me_2-2,3,2-tet)]$^{2+}$ ions in D_2O; (a) *N*-Me-(*R*)-ala and (b) *N*-Me-(*S*)-ala.

with the δ conformation with respect to the apical chelate ring will coexist in solution. It is probable that the steric repulsions between the *N*-methyl group and the axial *C*-methyl group in the apical chelate ring contribute properly to the destabilization of the Λ-β_2-(*S*)-*R* isomer in comparison with the Λ-β_2-(*R*)-*R* for the 3(*S*)8(*S*)-dimetrien complex.

In the PMR spectra of the *N*-methyl-(*R*)-alaninato complexes with the 2,3,2-tet derivatives the *N*-methyl resonance appeared as a singlet at about 2.4 ppm, while the PMR signals for the *C*-methyl group in the *N*-methyl-(*R*)-alaninate showed two kinds of doublets (Table 3 and Fig. 3b). This indicates that the chemical shift of the *N*-methyl signals of the Λ-(*R*)-*R* and Λ-(*S*)-*R* isomers are incidentally identical. The CMR spectrum of the Λ-β_2-[Co(*N*-Me-(*R*)-ala)(3(*S*)9(*S*)-Me_2-2,3,2-tet)]$^{2+}$ complex showed more complicated feature than that of the corresponding *N*-methyl-(*S*)-alaninato complex (Fig. 4a). Both signals at 184.4 and 185.0 ppm were assigned to the carboxyl carbon in the *N*-methyl-(*R*)-alaninate. It indicates the presence of the two species for the *N*-methyl-(*R*)-alaninato complex. The ratio of Λ-(*R*)-*R*/Λ-(*S*)-*R* at equilibrium (at pH 7) was estimated as about 1/1 from the CMR data.

It has been shown[6,7] that the epimerization at the C center of the *N*-methylalaninate ligand in the complexes occurs in basic aqueous solution. As Fig. 5 shows the PMR spectrum of the Λ-β_2-[Co(*N*-Me-(*R*)-ala)((*R*)-baetchxn)]$^{2+}$ at about pH 10 exhibited a new *C*-methyl doublet at 1.50 ppm and a new *N*-methyl singlet at 2.58 ppm. The equilibrated mixture should contain three isomers Λ-(*R*)-*S*, Λ-(*R*)-*R*, and Λ-(*S*)-*R*.[7-9] From the viewpoint of asymmetric transformation, the isomer ratios Λ-*S*/Λ-*R*, after the epimerization

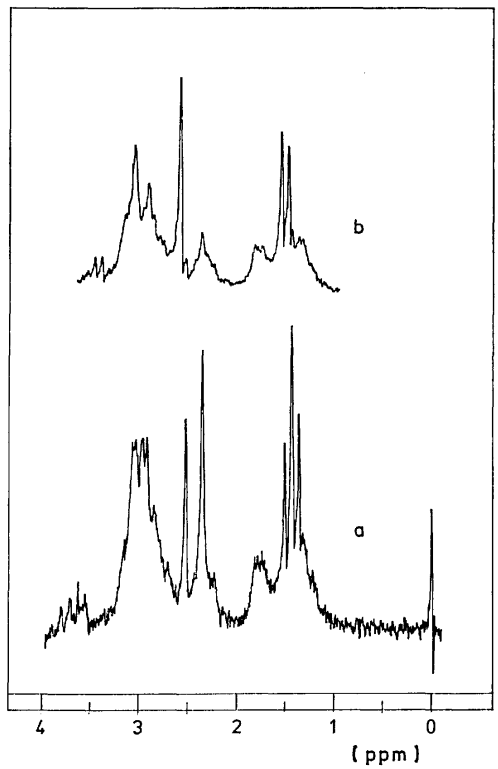

Fig. 5. PMR spectra of an equilibrated mixture of Λ-β_2-[Co(*N*-Me-(*R*)-ala)((*R*)-baetchxn)]$^{2+}$ ions; (a) equilibrated in D_2O (pD 7) and (b) equilibrated in H_2O (pH 10).

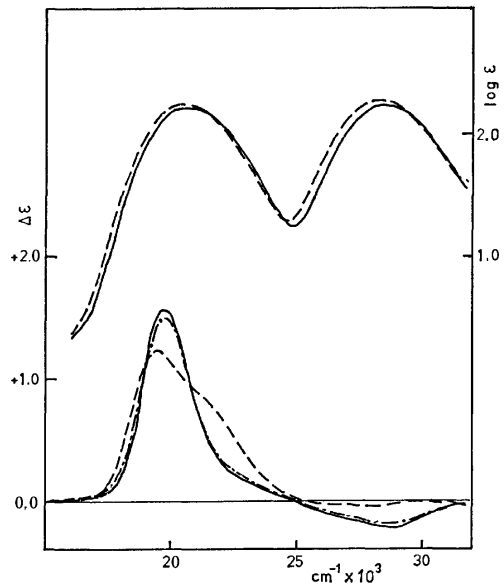

Fig. 6. Electronic absorption and CD spectra of Λ-β_2-[Co(*N*-Me-ala)(3(*S*)8(*S*)-dimetrien)]$^{2+}$ ions; (a) *N*-Me-(*S*)-ala (——), (b) *N*-Me-(*R*)-ala (— — —), (c) an equilibrated mixture (———).

equilibria had been established, were obtained by CD measurements or by means of chromatographic separation. The electronic and CD spectra of the *N*-methyl-(*S*)-alaninato and the *N*-methyl-(*R*)-alaninato complexes, and the equilibrated mixture with 3(*S*)8(*S*)-dimetrien are shown in Fig. 6.

TABLE 4. ISOMER RATIOS (*Λ*-*S*/*Λ*-*R*) OF *Λ*-β_2-[Co(amino acidato)(N_4)]$^{2+}$ a)

(N_4)	*N*-Me-ala	ala
	Λ-*S*/*Λ*-*R*	*Λ*-*S*/*Λ*-*R*
$(en)_2$	80/20 b)	50/50 d)
trien	60/40 c)	—
3(*S*)8(*S*)-dimetrien	85/15	50/50 e)
5(*R*)-metrien	76/24	—
(*R*)-baetchxn	88/12	—
2(*S*)10(*S*)-Me_2-2,3,2-tet	90/10	66/34 e)
3(*S*)9(*S*)-Me_2-2,3,2-tet	87/13	61/39 e)

a) At 40 °C, pH 10.1. b) Ref. 6. c) Ref. 7. d) Ref. 12. e) Ref. 1.

The isomer ratios for *Λ*-*S*/*Λ*-*R* are listed in Table 4. The isomer ratios for *Λ*-(*R*)-*R*/*Λ*-(*S*)-*R* at pH 10 were assumed to be the same as those at pH 7. The *Λ*-β_2-[Co(*N*-Me-ala)(N_4)]$^{2+}$ systems generally showed a considerable stereoselectivity on the epimerization. The degree of the stereoselectivity ranges from 85/15 to 90/10 ($\Delta G = -1.1 \sim -1.4$ kcal/mol) in this study except for the 5(*R*)-metrien complexes (76/24). These values are considerably larger than that for the [Co(*N*-Me-ala)(trien)]$^{2+}$ system (*Λ*-*S*/*Λ*-*R*=60/40),[7] and a little larger than for the [Co(*N*-Me-ala)$(en)_2$]$^{2+}$ system (80/20).[6]

As described in the Introduction, significant nonbonded repulsive interactions were anticipated in the *Λ*-*R* isomers between the *N*-methyl group and the adjacent chelate ring or alternatively between the *N*-methyl and the *C*-methyl groups in the *N*-methylalaninate. The effects of these two steric repulsions seem to be approximately equal, since the ratios for *Λ*-(*R*)-*R*/*Λ*-(*S*)-*R* are about 1/1 in all cases except for that of the 3(*S*)8(*S*)-dimetrien complexes. The observed thermodynamic preference of *Λ*-β_2-[Co(*N*-Me-(*S*)-ala)(N_4)]$^{2+}$ isomer over *Λ*-β_2-[Co(*N*-Me-(*R*)-ala)-(N_4)]$^{2+}$ isomer should be due to the absence of such steric disadvantage. The isomer ratio of the *Λ*-β_2-[Co(*N*-Me-ala)(5(*R*)-metrien)]$^{2+}$ complex is similar to that of the [Co(*N*-Me-ala)$(en)_2$]$^{2+}$ system, while those of the 3(*S*)8(*S*)-dimetrien or (*R*)-baetchxn complexes are considerably larger than that of the trien ones. Though the reason for these high selectivity with the substituted trien complexes is uncertain, it is probable that the relative stability is influenced by the *C*-methyl group substituted in the apical chelate ring of the 3(*S*)8(*S*)-dimetrien or by the increased rigidity due to the fused cyclohexane ring in the central chelate ring of the (*R*)-baetchxn.

The technique of strain energy minimization calculation was applied to the *Λ*-β_2-[Co(*N*-Me-(*R*)- and -(*S*)-ala)(2(*S*)10(*S*)-Me_2-2,3,2-tet)]$^{2+}$ complexes, the isomer ratio *Λ*-*S*/*Λ*-*R* in which was 90±2/10±2 ($\Delta G = -1.35 \pm 0.15$ kcal/mol). The 2,3,2-type tetramine ligands have the same geometrical structure in the cis configuration, while the *cis*-complexes with trien adopt two geometrical isomers.[20] Further, the conformation of 2,3,2-tet or its derivatives is assumed to be more rigid than that of trien series. Actually, a recent

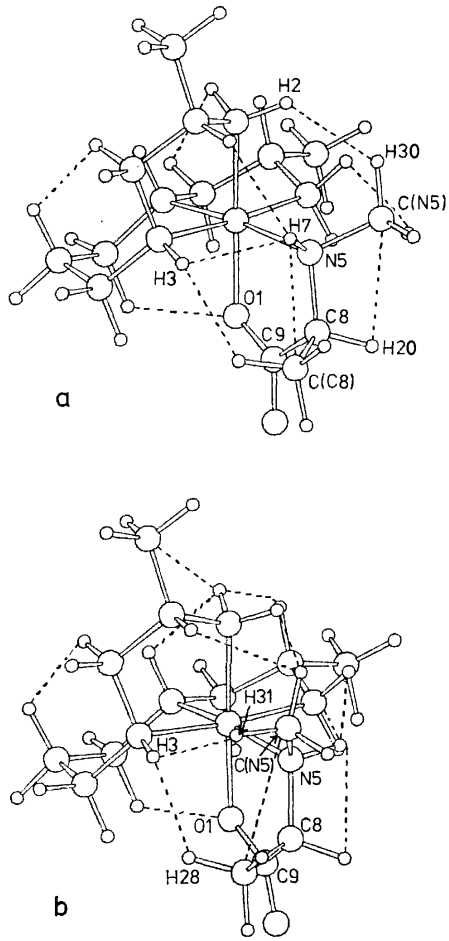

Fig. 7. Minimized structures for *Λ*-β_2-[Co(*N*-Me-(*S*)-ala)(2(*S*)10(*S*)-Me_2-2,3,2-tet)]$^{2+}$ ions; (a) *Λ*-(*R*)-*S* and (b) *Λ*-(*S*)-*S*. Dotted lines show interatomic repulsions greater than 0.3 kcal/mol.

X-ray analysis study revealed[21] that in the crystal of *cis*-β_2-[Co(gly)(trien)]$^{2+}$ two conformers coexist, the apical chelate rings of which have both the δ and λ conformations. On the other hand, the outer five-membered chelate rings of the methyl-substituted 2,3,2-tet employed in this study have the δ conformation due to the preference of the equatorial orientation of the *C*-methyl groups. Since the conformation and configuration of the 2,3,2-tet are thus fixed in the cis form, the stereoisomerism for the [Co(*N*-Me-ala)(2(*S*)10(*S*)-Me_2-2,3,2-tet)]$^{2+}$ system is simpler than the [Co(*N*-Me-ala)$(en)_2$]$^{2+}$ or the [Co(*N*-Me-ala)(trien)]$^{2+}$ systems.

The final minimized structures for the diastereomeric isomers are shown in Figs. 7 and 8, and the final energy terms are listed in Table 5. The most stable isomer is *Λ*-(*R*)-*S* with the *N*-methyl group trans to the *C*-methyl group, as shown in Fig. 7a. The calculated stability order, *Λ*-(*R*)-*S*, *Λ*-(*S*)-*R*, *Λ*-(*R*)-*R*, *Λ*-(*S*)-*S* is the same as that for the [Co(*N*-Me-ala)$(en)_2$]$^{2+}$ system. However, compared with the [Co(*N*-Me-ala)(trien)]$^{2+}$ system, the relative stabilities of the *Λ*-(*S*)-*R* with trans methyl groups and *Λ*-(*R*)-*R* with cis methyl groups are reversed (Table 6).

The starting models of the *N*-methylalaninate moiety was generated from both puckered and near-planar

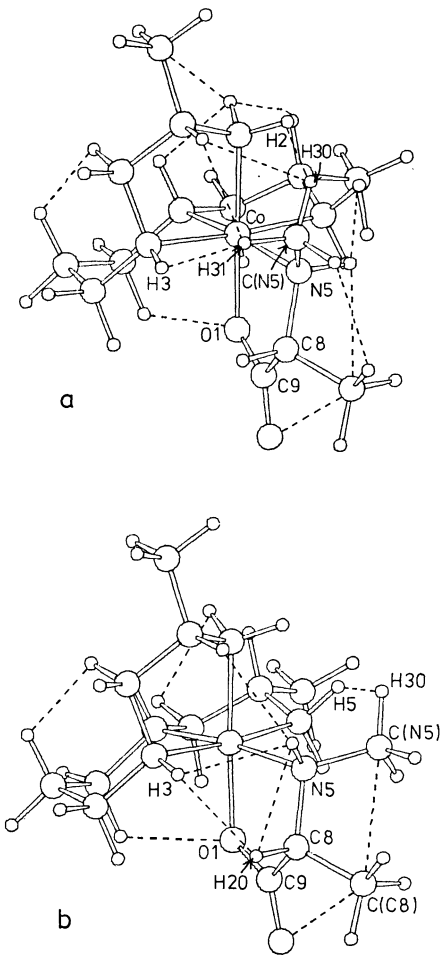

Fig. 8. Minimized structures for Λ-β_2-[Co(*N*-Me-(*R*)-ala)(2(*S*)10(*S*)-Me_2-2,3,2-tet)]$^{2+}$ ions; (a) Λ-(*S*)-*R* and (b) Λ-(*R*)-*R*. Dotted lines show interatomic repulsions greater than 0.3 kcal/mol.

conformation.[3] Except for the Λ-(*R*)-*S* isomer the planar conformation was unstable. In the case of the Λ-(*R*)-*S* ion the planar form was a little more stable than the puckered one (8.56 kcal/mol). Normally, the puckered conformation with a pseudo-equatorial *C*-methyl group was stable for the alaninate. However, in the Λ-(*S*)-*S* isomer the puckered form with a pseudo-axial *C*-methyl group was much more stable than the pseudo-equatorial form (13.1 kcal/mol). The dihedral angles, ϕ(Co–N5–C8–C9), were 6.7° Λ-(*R*)-*S*, 27.3° Λ-(*S*)-*R*, 30.1° Λ-(*R*)-*R*, 18.8° Λ-(*S*)-*S*, and ϕ(N5–C8–C9–O1) were 3.0° Λ-(*R*)-*S*, 22.6° Λ-(*S*)-*R*, 26.7° Λ-(*R*)-*R*, 18.7° Λ-(*S*)-*S*.

The introduction of the *N*-methyl group to the alaninate moiety produces significant strains in the complex. The calculated strain energies of the corresponding alaninato complexes were *ca.* 4 kcal/mol more stable than the most stable isomer of the *N*-methylalaninato complex.[1] Comparisons of the strain energy contributions among the isomers of the Λ-β_2-[Co(*N*-Me-ala)(2(*S*)10(*S*)-Me_2-2,3,2-tet)]$^{2+}$ ions show that the difference derives mainly from the bond-angle deformations, torsional strain, and nonbonded interactions. The Λ-(*R*)-*S* isomer has the smallest strain energy contributions in the bond-angle deformations

Table 5. Final energy terms[a] for the four isomers of the *N*-methylalaninato complexes

	trans-N(*R*)-C(*S*)	*trans*-N(*S*)-C(*R*)	*cis*-N(*R*)-C(*R*)	*cis*-N(*S*)-C(*S*)
Bond deformations	1.61	1.59	1.76	1.64
Angle deformations	6.22	7.30	7.52	8.98
Torsional strain	3.58	2.86	2.80	3.23
Nonbonded interactions	−2.93	−2.57	−2.19	−2.54
Out-of-plane	0.0	0.0	0.0	0.0
Total strain energy	8.49	9.18	9.89	11.31
Energy differences	0.0	0.69	1.40	2.82

a) For the Λ-β_2-[Co(*N*-Me-ala)(2(*S*)10(*S*)-Me_2-2,3,2-tet)]$^{2+}$, (kcal/mol).

Table 6. Strain energy differences[a] for [Co(*N*-Me-ala)(N_4)]$^{2+}$ systems

(N_4)	Λ-(*R*)-*S* (*trans*)	Λ-(*S*)-*R* (*trans*)	Λ-(*R*)-*R* (*cis*)	Λ-(*S*)-*S* (*cis*)
$(en)_2$[b]	0.0	1.0	1.3	3.8
trien[b]	0.0	1.9	0.6	4.0
2(*S*)10(*S*)-Me_2-2,3,2-tet	0.0	0.7	1.4	2.8

a) kcal/mol. b) Ref. 3.

and nonbonded interactions, though the *N*-methyl-(*S*)-alaninate ring adopts a strained, near-planar, conformation: Torsional strain for N5–C8 bond is 1.5 kcal/mol Λ-(*R*)-*S*, 0.6 Λ-(*S*)-*R*, 0.8 Λ-(*R*)-*R* and 0.8 Λ-(*S*)-*S*. The strain due to the *N*-methyl group extends the Co–N5 bond (2.02 Å, 0.6 kcal/mol) in all isomers, and distorts the Co–N5–C(N5) angle, Λ-(*R*)-*S* 118° (0.6 kcal/mol), Λ-(*S*)-*R* 120° (1.0), Λ-(*R*)-*R* 115° (0.3), and Λ-(*S*)-*S* 122° (1.3). The *N*-methyl group causes significant nonbonded interactions in all four isomers. In the case that the *N*-methyl group has the *S* configuration, nonbonded interactions between the *N*-methylalaninate and the adjacent chelate ring are considerably large: the H2···H30 (2.16 Å, 0.5 kcal/mol) and H3···H31 (2.14 Å, 0.6) in the *N*-methyl-(*R*)-alaninato complex, and H3···H28 (2.09 Å, 0.7) and H3···H31 (2.14 Å, 0.6) in the *N*-methyl-(*S*)-alaninato complex. In the complexes with *N*(*R*)-methyl group close contacts arise between the N–H proton and the *N*-methylalaninate ring: the C(C8)···H7 (2.45 Å, 0.5 kcal/mol), C(N5)···H20 (2.42 Å, 0.6), H2···H30 (2.11 Å, 0.7), and H3···H7 (2.09 Å, 0.7) in the *N*-methyl-(*S*)-alaninato complex, and the C(C8)···C(N5) (2.80 Å, 0.7), H3···H20 (2.13 Å, 0.6), and H5···H30 (2.12 Å, 0.6) in the *N*-methyl-(*R*)-alaninato complex.

The stability order and the calculated strain energy differences are in good agreement with the experimental results, though the strain energy of the Λ-(*S*)-*R* isomer was underestimated. This result suggested that the main source of the destabilization of the Λ-β_2-[Co(*N*-Me-(*R*)-ala)(N_4)]$^{2+}$ ions and the absence of the Λ-(*S*)-*S* isomer was due mostly to serious intramolecular strain energy. From the viewpoint of asymmetric transformation, *N*-substitution of the alaninate results in a striking improvement of the chiral selectivity in the *N*-methylalaninato complexes, in comparison with that for the

corresponding alaninato complexes.[1)]

This work was partially supported by a Grant-in-Aid for Scientific Research No. 911502 from the Ministry of Education, Science and Culture.

References

1) Part I. M. Yamaguchi, S. Yamamatsu, T. Furusawa, S. Yano, M. Saburi, and S. Yoshikawa, *Inorg. Chem.*, in press.
2) D. A. Buckingham, S. F. Mason, A. M. Sargeson, and K. R. Turnbull, *Inorg. Chem.*, **5**, 1649 (1966).
3) B. F. Anderson, D. A. Buckingham, G. J. Gainsford, G. B. Robinson, and A. M. Sargeson, *Inorg. Chem.*, **14**, 1658 (1975) and references cited therein.
4) M. Fujita, Y. Yoshikawa, and H. Yamatera, *Bull. Chem. Soc. Jpn.*, **50**, 3209 (1977).
5) L. G. Marzilli and D. A. Buckingham, *Inorg. Chem.*, **6**, 1042 (1967).
6) D. A. Buckingham, J. Dekkers, A. M. Sargeson, and M. Wein, *Inorg. Chem.*, **12**, 2019 (1973).
7) D. A. Buckingham, I. E. Maxwell, and A. M. Sargeson, *Inorg. Chem.*, **9**, 2663 (1970).
8) M. Saburi, M. Homma, and S. Yoshikawa, *Inorg. Chem.*, **12**, 1250 (1973).
9) M. Saburi and S. Yoshikawa, *Bull. Chem. Soc. Jpn.*, **47**, 1184 (1974).
10) B. T. Golding, G. J. Gainsford, A. J. Herlt, and A. M. Sargeson, *Tetrahedron*, **32**, 389 (1976).
11) J. F. Blount, H. C. Freeman, A. M. Sargeson, and K. R. Turnbull, *Chem. Commun.*, **1967** 324.
12) D. A. Buckingham, L. G. Marzilli, and A. M. Sargeson, *J. Am. Chem. Soc.*, **89**, 5133 (1967).
13) M. Saburi and S. Yoshikawa, *Bull. Chem. Soc. Jpn.*, **45**, 806 (1972).
14) M. Goto, M. Saburi, and S. Yoshikawa, *Inorg. Chem.*, **8**, 358 (1969).
15) (a) P. Harrington, S. Linke, and M. D. Alexander, *Inorg. Chem.*, **12**, 168 (1973); (b) M. Goto, T. Makino, M. Saburi, and S. Yoshikawa, *Bull. Chem. Soc. Jpn.*, **49**, 1879 (1976).
16) M. Goto, A. Okubo, T. Sawai, and S. Yoshikawa, *Inorg. Chem.*, **9**, 1488 (1970).
17) P. Quitt, J. Hellerbach, and K. Vogler, *Helv. Chim. Acta*, **46**, 327 (1963).
18) G. R. Brubaker and D. P. Schaefer, *Inorg. Chem.*, **10**, 2170 (1971).
19) K. Toriumi and Y. Saito, *Acta Crystallogr., Sect. B*, **31**, 1247 (1975).
20) S. Yoshikawa, M. Saburi, and M. Yamaguchi, *Pure Appl. Chem.*, **50**, 915 (1978).
21) D. A. Buckingham, M. Dwyer, G. J. Gainsford, V. J. Ho, L. G. Marzilli, W. T. Robinson, A. M. Sargeson, and K. R. Turnbull, *Inorg. Chem.*, **14**, 1739 (1975).

 © 1980 The Chemical Society of Japan Bull. Chem. Soc. Jpn., 53, 699—702 (1980)

Gas Chromatography under the Column Outlet Pressure Higher than Atmospheric

Koji Takeuchi, Kunio Ohzeki, and Tomihito Kambara*

Department of Chemistry, Faculty of Science, Hokkaido University, Sapporo 060

(Received September 18, 1979)

The effects of column outlet pressures on the HETP *vs.* carrier gas velocity curves are discussed on the basis of KOS theory. It is shown that when a column is operated at a constant outlet pressure higher than atmospheric the minimum of H-$\bar{u}$ curve shifts towards lower HETP and $\bar{u}$ values, and on the contrary the operation at reduced outlet pressure results in the shift of the minimum towards higher HETP and $\bar{u}$ values. The separation factor and number of theoretical plates obtained by a column operated at the outlet pressure of 4.0 atm are superior by *ca.* 10% to those obtained by normal gas chromatography.

Gas chromatographic columns are almost always operated under the constant outlet pressure of atmospheric. On the one hand, Haruki[1] investigated the gas chromatography under reduced pressure and concluded that the reduced pressure operation offered no advantage over normal atmospheric pressure operation. Recently, Hatch and Parrish[2] using capillary columns reported that at the optimum flow velocity, the reduced pressure operation produced efficiencies *ca.* 30% lower than those of normal gas chromatographic operation. On the other hand, Halasz *et al.*[3] and Novak and Bocek[4] reported that the column operation under the outlet pressure higher than atmospheric resulted in an improved column efficiencies. The problems were discussed theoretically on the basis of the van Deemter equation.[5,6] However, the equation being derived from the assumption of a uniform mobile phase velocity,[7] the application of the theory to gas chromatography requires an essential revision especially with respect to the pressure drop along the column.

In our previous papers,[8,9] a new equation for HETP was derived from the kinetic viewpoint, in which the pressure dependence of the diffusion coefficient in gas phase and the non-linear carrier gas velocity distribution along the column were dealt with mathematically. The validity of KOS theory[9] was confirmed experimentally in the study of the dependencies of HETP on carrier gas flow rate[9] and column length.[10] The present work aims at obtaining a clearer understanding of the effects of column outlet pressure higher than atmospheric on the HETP. The column efficiencies of the reduced pressure gas chromatography are also discussed theoretically.

Theoretical

According to KOS theory, the HETP is given by

$$H = \frac{l}{n} = \frac{9D^*l}{2w} \times \frac{(p_i^4 - p_o^4)}{(p_i^3 - p_o^3)^2} + \frac{3wF_s^2\beta^2}{2\alpha FK^2l} \times \frac{(p_i^2 - p_o^2)^2}{(p_i^3 - p_o^3)}, \quad (1)$$

where n the number of theoretical plates of a column of length l, D^* the diffusion constant under unit pressure, w permeability coefficient, p_i and p_o the inlet and outlet pressures, F and F_s the volume fractions occupied by the mobile and stationary phases, K the distribution coefficient (the ratio of concentration in the mobile phase to that in the stationary phase), α the rate constant of dissolution and β is given by

$$\frac{1}{\beta} = \frac{t_R}{t_0} = 1 + \frac{F_s}{KF}, \quad (2)$$

where t_R is the retention time of a given component and t_0 is that of air peak. The latter corresponds to the passing time of carrier gas through the whole column, and is the function of p_i and p_o,[11] namely,

$$t_0 = \frac{4l^2(p_i^3 - p_o^3)}{3w(p_i^2 - p_o^2)^2} \quad (3)$$

The average carrier gas velocity $\bar{u}$, is given by

$$\bar{u} = \frac{l}{t_0}. \quad (4)$$

The carrier gas flow-rate v, is given by the famous Darcy equation:

$$v = qu_op_oF = \frac{wqF(p_i^2 - p_o^2)}{2l}, \quad (5)$$

where q is the proportionality factor and u_o is the outlet linear velocity.

Equation 1 can be rearranged into

$$y = a + bx, \quad (6)$$

where

$$y = \frac{(p_i^3 - p_o^3)^2}{n(p_i^4 - p_o^4)} \quad (7)$$

$$x = \frac{(p_i^2 - p_o^2)(p_i^3 - p_o^3)}{(p_i^2 + p_o^2)} \quad (8)$$

$$a = \frac{9D^*}{2w} \quad (9)$$

and

$$b = \frac{3wF_s^2\beta^2}{2\alpha FK^2l^2}. \quad (10)$$

Experimental

The measurements were carried out with a Hitachi Model 063 gas chromatograph equipped with a Hitachi 056 recorder, thermal conductivity detertor being used. The sample cell outlet was connected to a pressure gauge and a needle valve, so that the column outlet pressure is controlled, the arrangement being almost the same as reported by Novak and Bocek.[4] Helium was used as carrier gas. The flow-rate was measured with a soap-film meter and corrected for the water vapor pressure. The stainless steel column of 1 m by 0.3 cm i.d. was packed with 25% dinonyl phthalate on 80—100 mesh Shimalite BT. The packed column was preconditioned for 10 h at 130 °C under an appropriate helium flow. The measurements of HETP were carried out at

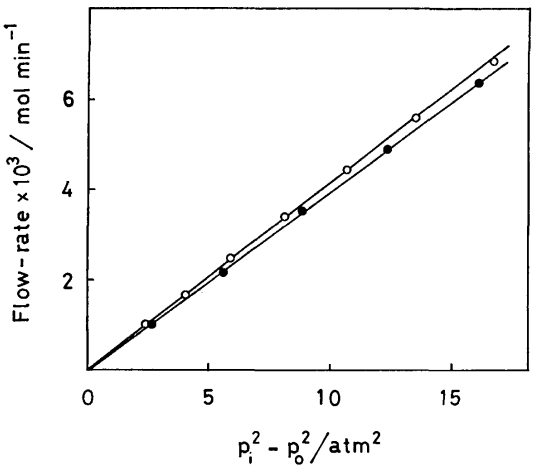

Fig. 1. Helium flow-rate plotted against $(p_i^2-p_o^2)$ at the constant outlet pressures: (○) p_o 1.0 atm, p_i 1.8—4.2 atm; (●) p_o 3.0 atm, p_i 3.4—5.0 atm. Column: 1 m by 0.3 cm i.d., 25% DNP on Shimalite BT, 74.0 °C.

the column temperature of 74.0 °C, employing benzene as a solute. The sample sizes of 0.8, 0.6, 0.4, and 0.2 μl were injected twice at each level. The numbers of theoretical plates were calculated from the formula[12]

$$n = 5.55(t_R/W_{1/2})^2, \quad (11)$$

where t_R and $W_{1/2}$ designate the peak maximum distance from the start line and the peak width at the half peak height, respectively, and extraporated to zero charge of sample amount. Peak asymmetry was estimated from the skewness which is defined as the ratio of the slopes of tangents at the inflection points of both sides of the peak.[13] The mean carrier gas velocity was evaluated from the retention time of air peak. The effect of column outlet pressure on the separation of adjacent peaks 1 and 2 was estimated from the value:[12]

$$R = \frac{2(t_{R-2}-t_{R-1})}{W_1+W_2} \quad (12)$$

Results and Discussion

In Fig. 1, the carrier gas flow-rate was plotted against $(p_i^2-p_o^2)$ for the column operations under atmospheric and increased outlet pressures. Both lines showed good linearity as expected from Eq. 5, only a slight difference in the slopes being found. The dependence of passing time of air peak on the pressure differences was shown in Fig. 2. The relationship between $\bar{u}$ and pressure drop given by Eqs. 3 and 4 can be now written as

$$\bar{u} = \frac{4.8(p_i^2-p_o^2)^2}{p_i^3-p_o^3}, \quad (13)$$

where $\bar{u}$ is expressed in cm s^{-1} and the coefficient 4.8 is evaluated from dividing the column length of 100 cm by the slope of plot in Fig. 2.

The effects of column outlet pressure on column efficiency were illustrated in Figs. 3 and 4. In Fig. 3, the validity of Eq. 6 was confirmed, the linear regression equation being determined as

$$y = 1.73\times10^{-3} + 2.29\times10^{-4}\,x$$

for atmospheric outlet pressure operation and

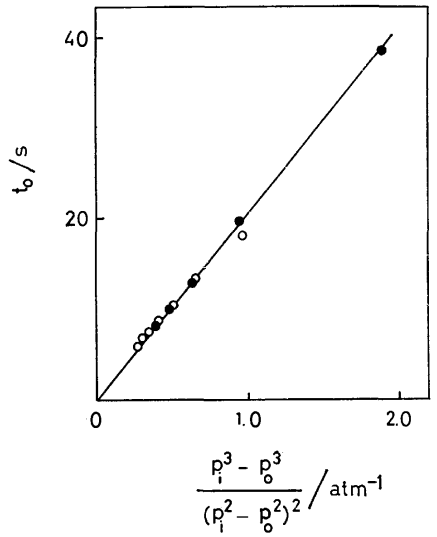

Fig. 2. Dependence of passing time of carrier gas on the inlet and outlet pressures. The open and closed circles have the same meanings as in Fig. 1.

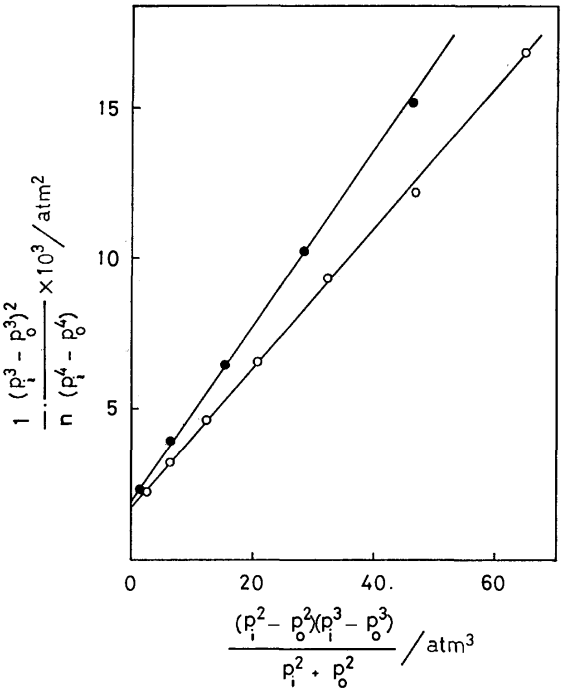

Fig. 3. Effect of column inlet and outlet pressures on HETP (*cf.* Eq. 6). The symbols on each line are the same as in Fig. 1.

$$y = 1.98\times10^{-3} + 2.88\times10^{-4}\,x$$

for the elevated outlet pressure of 3.0 atm. The 95% confidence limits of the expected value of y when $x=0$ were $(1.73\pm0.29)\times10^{-3}$ and $(1.98\pm0.22)\times10^{-3}$, respectively. No significant difference was found between the intercepts at the significance level of 5% (t-test). On the other hand, the regression coefficients with 95% confidence limits being $(2.29\pm0.08_6)\times10^{-4}$ and $(2.88\pm0.08_7)\times10^{-4}$, respectively, the difference between the slopes was highly significant. The β value and hence the K value being constant and independent of pressure drop as shown in Table 1, the variation in the slopes of lines may be due to the change

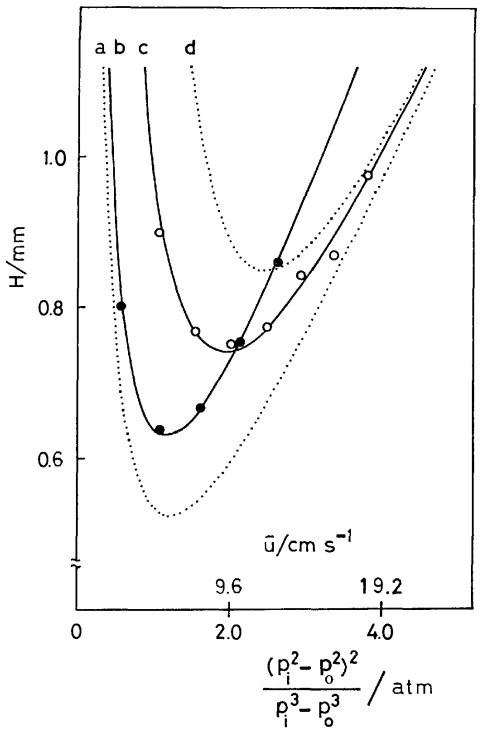

Fig. 4. Dependence of H-$\bar{u}$ curves on the column inlet and outlet pressures. Solid lines b and c are experimentally obtained H-$\bar{u}$ curves. The symbols have the same meanings as in Fig. 1. Dotted lines denote theoretically obtained H-$\bar{u}$ curves by the combination of Eqs. 13 and 14, inserting the values: (a) p_o 3.0 atm, p_i 3.3—6.6 atm; (d) p_o 0.1 atm, p_i 1.5—4.4 atm.

in the rate constant α of dissolution caused by the pressure change.

Inserting the numerical values obtained from the atmospheric outlet pressure operation into Eq. 1, the column length being 1000 mm, one derives

$$H/\text{mm} = \frac{1.73(p_i^4-p_o^4)}{(p_i^3-p_o^3)^2} + \frac{0.23(p_i^2-p_o^2)^2}{p_i^3-p_o^3}. \quad (14)$$

The so-called H-$\bar{u}$ curves were shown in Fig. 4, in which the solid lines on the plots were obtained from the regression equations. The dotted lines were illustrated by combining the calculated values of Eqs. 13 and 14. When Eq. 14 holds for the operation at column outlet pressure of 3 atm, curve a in Fig. 4 is given. The shift of the minimum towards lower $\bar{u}$ and H values is obviously found in the theoretically predicted H-$\bar{u}$ curve and experimentally obtained one, although the curves do not coincide completely each other as discussed previously. On the other hand, in the case of gas chromatography under the reduced column outlet pressure of 0.1 atm, the shift of the minimum towards higher $\bar{u}$ and H values is predicted as shown by curve d in Fig. 4. This tendency was already experimentally observed by Hatch and Parrish.[2]

The column operation under the increased pressure resulted in peaks with leading shape, the skewness decreasing with decreasing sample amount as shown in Fig. 5. It is interesting to compare the results

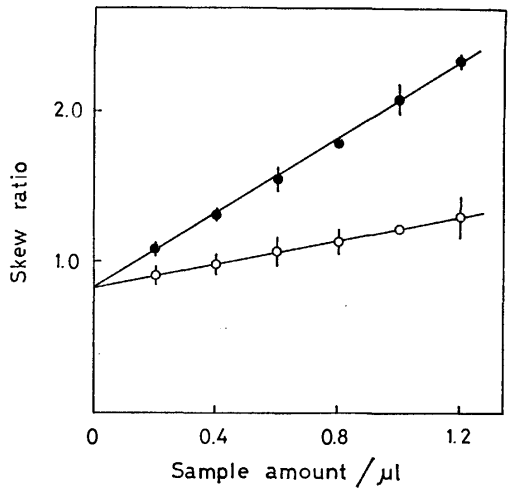

Fig. 5. Effects of pressure drop and sample amount on the skew ratio of benzene peak. The column inlet and outlet pressures are: (○) p_o 1.0 atm, p_i 2.4 atm; (●) p_o 4.0 atm, p_i 4.8 atm. Other conditions are the same as in Fig. 1. The vertical line on each plot denotes 95% confidence limits.

Table 1. Constancy of β value

Pressure/atm	$1/\beta = t_R/t_0 = 1+F_s/KF$
$p_o=1.0$	
$p_i=1.8-4.2$	$17.0_8 \pm 0.1_2$ $(n=7)$
$p_o=3.0$	
$p_i=3.4-5.0$	$16.9_7 \pm 0.3_8$ $(n=5)$

with that reported by Haruki,[1] who observed that the gas chromatography under the reduced pressure gave the peaks with trailing shape with decreasing inlet and outlet pressures.

An attempt was made to find the effect of the increased column pressure on the resolution. A 0.6 μl portion of a mixture containing 0.3 μl benzene, 0.1 μl ethylbenzene, 0.1 μl of *m*- and *o*-xylenes was chromatographed at 94.4 °C under the various outlet and inlet pressures, namely, one combination is $p_o=1.0$ and $p_i=1.8-3.6$ atm and the other is $p_o=4.0$ and $p_i=4.4-4.5$ atm. The resolution of ethylbenzene from *m*-xylene and the number of theoretical plates for *o*-xylene were calculated. At the optimum flow-rate, the elevated pressure operation resulting in the peaks with longer retention time produced both the column efficiency and the resolution *ca.* 10% higher than those of normal operation.

References

1) T. Haruki, *Bunseki Kagaku*, **9**, 865 (1960).
2) F. W. Hatch and M. E. Parrish, *Anal. Chem.*, **50**, 1164 (1978).
3) I. Halasz, G. Deninger, and H. -O. Gerlach, *J. Chromatogr.*, **35**, 1 (1968).
4) J. Novak and P. Bocek, *J. Chromatogr.*, **52**, 1 (1970).
5) J. J. Van Deemter, F. J. Zuiderweg, and A. Klinkenberg, *Chem. Eng. Sci.*, **5**, 271 (1956).
6) A. Klinkenberg and F. Sjenitzer, *Chem. Eng. Sci.*,

5, 258 (1956).
7) L. Lapidus and R. Amundson, *J. Phys. Chem.*, **56**, 984 (1952).
8) T. Kambara and K. Ohzeki, *J. Chromatogr.*, **21**, 383 (1966).
9) T. Kambara, K. Ohzeki, and K. Saitoh, *J. Chromatogr.*, **27**, 33 (1967).
10) K. Ohzeki, T. Kambara, and K. Kodama, *J. Chromatogr.*, **121**, 199 (1976).
11) T. Kambara, *J. Chromatogr.*, **19**, 478 (1965).
12) H. Purnell, "Gas Chromatography," John Wiley, New York, N. Y. (1962), pp. 104, 115.
13) A. J. B. Cruickshank and D. H. Everett, *J. Chromatogr.*, **11**, 289 (1963).

 © 1980 The Chemical Society of Japan Bull. Chem. Soc. Jpn., 53, 703—708 (1980)

The Coextraction of Water into Nitrobenzene with Alkali and Alkaline Earth Metal Salts of 2,2′,4,4′,6,6′-Hexanitrodiphenylamine in the Presence of Several Crown Ethers and Cryptands

Tadashi Iwachido,* Masayosi Minami,** Masaho Kimura,** Akira Sadakane,** Mikio Kawasaki,** and Kyoji Tôei**

College of Liberal Arts, Okayama University, Tsushima-naka, 2-1-1, Okayama 700

***Department of Chemistry, Faculty of Science, Okayama University, Tsushima-naka, 3-1-1, Okayama 700*

(Received September 20, 1979)

Alkali and alkaline earth metal salts of 2,2′,4,4′,6,6′-hexanitrodiphenylamine (HND) were extracted into nitrobenzene in the absence or presence of several crown ethers or cryptands which differ from one another in hole size. The quantity of water transferred to the nitrobenzene phase was determined by means of the Karl-Fischer method. The NMR and near-infrared spectra show that the coextraction of water is caused by the hydration of the cations. The number of water molecules attached to the cations increases upon going from Cs^+ (0.6) to Li^+ (5.6) and from Ba^{2+} (10.5) to Ca^{2+} (13.0). The complexation between these cations and the crown ethers causes a clear decrease in the hydration number; *e.g.*, in the 1:1 metal–crown ether complexes, more than half of the water molecules are removed, and in the 1:1 metal–cryptand complexes, less than one water molecule remains unremoved. The complexes of a 1:2 stoichiometry are also found; some are stable and carry virtually no water molecules. The number and type of donor atoms have no significant effect on the coextraction of water. The presence of fused benzo rings on the crown ether also has no influence on the number of water molecules.

Recently, interest in the coextraction of water into organic solvents with ion-pairs has been increasing.[1–5] In a previous paper,[6] it was shown that, when aqueous solutions containing alkali metal salts of 2,2′,4,4′,6,6′-hexanitrodiphenylamine (HND) are shaken with nitrobenzene, the water molecules strongly associated with the salts are transferred to the nitrobenzene phase.

It is well known that crown ethers and cryptands combine stoichiometrically with alkali and alkaline earth metal cations to form complexes, in which the cation is accommodated into the molecular hole of the ligand. Depending on the relative size of the hole and the metal ion, 1:1, 1:2, and 2:3 complexes are formed. In some complexes of small crown ethers, the cation lies in or slightly above the donor plane in the solid state;[7,8] a few of them are known to have the same structure in solution as well.[9] This 'metal in the hole' structure does not require a stripping of the entire hydration shell of the ion, since the contact of water molecules with the cation is still possible in the direction perpendicular to the plane of the donor ring. With regard to some solid cryptates, the cation has been found to be enclosed in the molecular cage of the ligand.[10] The cation, therefore, can be expected to exist as an unhydrated or only slightly hydrated state.

In the present study, the number of water molecules attached to alkali and alkaline earth metal complexes with several crown ethers and cryptands has been determined in order to make clear the effect of the ligands on the cation hydration. The number of the water of crystallization was also determined with the alkaline earth metal salts of HND and their complexes with dibenzo-18-crown-6 by means of thermogravimetric analysis.

Experimental

Materials. Commercial HND was purified by repeated recrystallizations from acetone. *N*-(2,4,6-trinitrophenyl)-2,4-dinitro-1-naphthylamine (TDN) was obtained by the reaction between 2-chloro-1,3,5-trinitrobenzene and 1-naphthylamine, followed by nitration.[11] 1,3,7,9-Tetranitrophenothiazine 5-oxide (TPO) was prepared by the nitration of phenothiazine.[12,13] The TDN and TPO thus obtained were recrystallized from acetic acid; their alkali and alkaline earth metal salts were prepared by treating these amines with the corresponding metal carbonate or hydroxide.

The crown ethers used were benzo-12-crown-4 (B12C4), 15-crown-5 (15C5), benzo-15-crown-5 (B15C5), 18-crown-6 (18C6), benzo-18-crown-6 (B18C6), dibenzo-18-crown-6 (DB18C6), dibenzo-24-crown-8 (DB24C8), and 5,6-benzo-4,7,13,16-tetraoxa-1,10-diaza-5-cyclooctadecene (2.2B). 15C5, 18C6, and DB24C8 were obtained from the Nisso Co., Ltd. The first two were used without further purification. DB24C8 was recrystallized from chloroform and then ethanol. B12C4, B15C5, B18C6, and DB18C6 were synthesized and purified by the method of Pedersen.[14] 2.2B was obtained from 3,6-dioxa-1,8-octanediamine and 1,2-bis(chloroformylmethoxy)benzene by the method of Dietrich *et al.*;[15] the product obtained was recrystallized from 4-methyl-2-pentanone. 2.2B was found to be a monohydrate by measuring the weight loss on heating.

The cryptands, 4,7,13,18-tetraoxa-1,10-diazabicyclo[8.5.5]-eicosane (2.1.1), 4,7,13,16,21-pentaoxa-1,10-diazabicyclo-[8.8.5]tricosane (2.2.1), 4,7,13,16,21,24-hexaoxa-1,10-diazabicyclo[8.8.8]hexacosane (2.2.2), and 5,6-benzo-4,7,13,16,21,24-hexaoxa-1,10-diazabicyclo[8.8.8]hexacos-5-ene (2.2.2B), were purchased from Merck and well used without further purification.

Some crown ether complexes were crystallized from methanol–water mixtures.

The nitrobenzene was treated with an aqueous sodium carbonate solution and washed with water several times prior to use.

Measurements. A nitrobenzene solution (20 cm^3 for crown ethers and 5 cm^3 for cryptands) containing the ligands (0—0.03 mol dm^{-3}) and HND or the other polynitro-substituted amines (0—0.01 mol dm^{-3}) was shaken with an equal volume of an aqueous alkali or alkaline earth metal chloride solution for 1 h at (25±0.01) °C in a thermostated water bath, the ionic strength being adjusted to 0.1 mol dm^{-3}, and the pH, to about 12, with the corresponding metal chloride (or sulfate) and hydroxide (or carbonate).

Table 1. The number of water molecules coextracted with M^{n+}, $h(M^{n+})$

Anion	M^{n+}							
	Cs 0.59[a]	Rb 0.66[a]	K 0.75[a]	Na 1.03[a]	Li 1.47[a]	Ba 2.49[a]	Sr 3.58[a]	Ca 4.04[a]
HND	0.6	0.9	1.3	3.5	5.6	10.5	12.1	13.0
TDN	0.1	0.8	1.4	3.8	5.5	8.6	10.4	13.8
TPO	—	—	—	2	5	13	14	13

a) z^2/r_c values.

The water-content in the nitrobenzene phase was determined by the use of a Mitsubishi Kasei CA-01 Karl-Fischer titrator. Nitrobenzene was treated with an aqueous solution under the same conditions, and the water-content increments, Δs, were obtained. The total metal concentration in the nitrobenzene phase, $[M(t)]_o$, was calculated from the difference between the total quantity of HND and the quantity of HND anions found in the aqueous phase by the use of Hitachi 124 spectrophotometer. The total concentration of the ligand, L, in the nitrobenzene phase, $[L(t)]_o$, was obtained by measuring the quantity of L left unextracted in the aqueous phase in the following manner: to the aqueous phase, a large excess of potassium chloride (sodium chloride for 15C5 and B15C5; lithium chloride for B12C4) and an excess of HND were added. L was then extracted as the potassium complex into benzene (1,2-dichlorobenzene for B12C4, 15C5, and B15C5). The concentration of the complex in the benzene phase was determined spectrophotometrically. From the total quantity of L and the concentration of the complex thus obtained, $[L(t)]_o$ was calculated.

The conductance measurements in nitrobenzene were carried out at (25±0.005) °C by the use of a universal bridge (Ando Electric Co., Ltd., LCR 10) equipped with platinized platinum electrodes.

The thermogravimetric curves were obtained on a Rigaku Denki TG unit under a nitrogen flow of about 30 cm³/min. The temperature rise was 0.625 °C/min.

Results and Discussion

Hydration of the Uncomplexed Cations. Nitrobenzene dissolves water at a concentration of 0.178 mol dm^{-3} at 25 °C, while a nitrobenzene solution containing the alkali or alkaline earth metals dissolves a slightly greater quantity of water. The quantity of water coextracted increases linearly with the increase in the metal concentration, as is shown in Fig. 1. From the slope of each line, the quantity of water coextracted, $h(M^{n+})$, is calculated.

Table 1 shows that the values of $h(M^{n+})$ increase linearly with the ratio of the charge to the ionic radii of the cations, z^2/r_c, except for those of the heavy alkali metals (K^+, Rb^+, and Cs^+). The $h(M^{n+})$ values are found not to be dependent on the anion species used. In general, bulky univalent anions are believed not to be hydrated in solution. These values, therefore, are assumed to be identical with the hydration numbers of the cations.

Stokes and Robinson, on the other hand, obtained the hydration numbers of the alkali and alkaline earth metal chlorides in an aqueous solution by means of activity measurements (Rb^+ 1.2, K^+ 1.9, Na^+ 3.5, Li^+ 7.1, Ba^{2+} 7.7, Sr^{2+} 10.7, and Ca^{2+} 12.0).[16] These

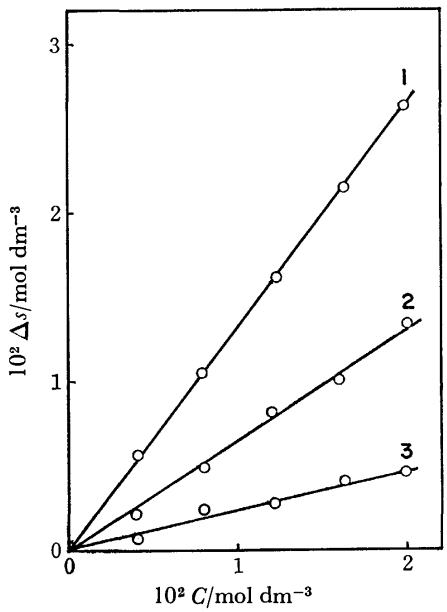

Fig. 1. Coextraction of water with DB18C6, the potassium salt of HND, and the complex.
1: Potassium salt of HND, 2: DB18C6, 3: complex.

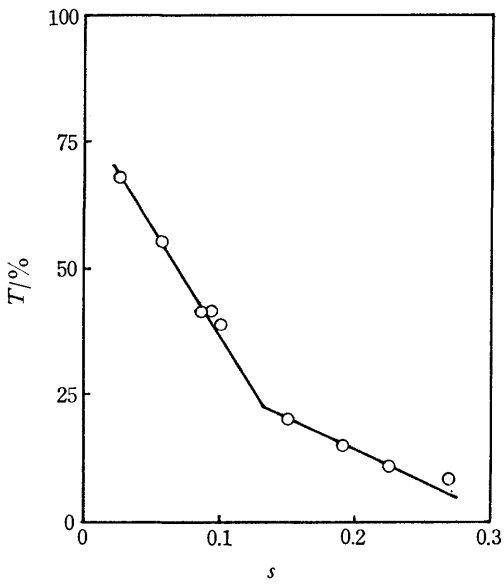

Fig. 2. Plot of T % *vs.* the water content, s, in the nitrobenzene phase.
$Ca(HND)_2$: 0.01 mol dm^{-3}.

values are similar in magnitude to the corresponding $h(M^{n+})$ values listed in Table 1. This fact suggests that the cations in the aqueous phase carry water into the nitrobenzene phase without being stripped

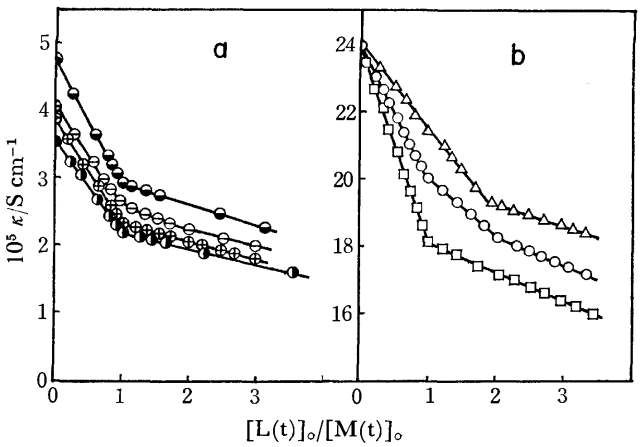

Fig. 3. Conductometric titration curves of the alkali metal and Ba^{2+} salts of HND.
a: DB18C6 complexes with Na^+ (⊕), K^+ (◒), Rb^+ (◑), and Cs^+ (⊖). Concentrations of the HND salts: Na^+ 0.01, K^+ 0.02, Rb^+ 0.01, and Cs^+ 0.012 mol dm^{-3}. b: Ba^{2+} complexes with 15C5 (△), 18C6 (○), and DB24C8 (□). The concentration of Ba(HND)$_2$: 0.005 mol dm^{-3}.

of the water molecules attached to them when they pass through the interface.

In a previous paper,[17] it was shown that the NMR and near-infrared spectra gave information concerning the behavior of water in a nitrobenzene solution containing the calcium salt of HND. The infrared spectra were also found to be useful for the investigation of water in the nitrobenzene solution. The transmittance, T %, of a 0.01 mol dm^{-3} solution of anhydrous Ca(HND)$_2$ in dry nitrobenzene was measured in the presence of varying amounts of water at 3660 cm^{-1}. The T % decreases with an increase in the water concentration, as is shown in Fig. 2. The curve obtained can be approximated by two line portions; the value of 13.3, which is obtained from the concentration ratio of water to Ca^{2+} at the intersection, agrees quite well with the $h(M^{n+})$ value for Ca^{2+}. It can thus be concluded that, when water is added to the nitrobenzene solution of Ca(HND)$_2$, the water binds exclusively to Ca^{2+}, and that the excess water then disperses into the solvent.

Complex Formation. The stoichiometries of the complexes in nitrobenzene were determined by means of conductometric titration. As an illustration, the conductometric titration curves for alkali metal–DB18C6 complexes and for some Ba^{2+}–crown ether complexes are shown in Fig. 3. The addition of ligands to the salts on HND in nitrobenzene results in a decrease in the specific conductance, κ. All the curves except for $Ba(15C5)^{2+}$ break at the first equivalence point, indicating the formation of stable complexes of a 1:1 stoichiometry. $Cs(DB18C6)^{2+}$ may be less stable than the others, because its titration curve shows no clear change at the equivalence point; this finding does not, however, necessarily mean the absence of the 1:2 complexes, as will be seen later.

The conductivity data of the alkali metal and ammonium–DB18C6 complexes in nitrobenzene were analyzed by means of the method of Schedlovsky.[18]

Table 2. Λ° and λ° values (S cm^2 mol^{-1}), together with the ion-pair formation constants, K

M^+	Λ°(M(L)HND)	$\lambda^\circ(ML^+)$	$\lambda^\circ(M^+)$	K/mol^{-1} dm^3 [a]
Na	21.4	9.6	16.3[b]	10
K	21.4	9.6	17.8[b]	7
Rb	21.5	9.7	—	8
NH_4	21.1	9.3	18.4[b]	5

a) $K=[M(L)HND]/[ML^+][HND^-]$. b) From Ref. 19.

The limiting equivalent conductivities, Λ°, were found to differ not all from one another. The limiting ionic equivalent conductivity for the anion of HND could be determined to be $\lambda^\circ(HND)=11.8$ S cm^2 mol^{-1}. The values of $\lambda^\circ(ML^+)$, therefore, were determined by using the $\lambda^\circ(M^+)$ values reported by Witschonke and Kraus.[19] Table 2 shows that the $\lambda^\circ(ML^+)$ values are not affected by the size of the central cation and are smaller than the λ° values for the uncomplexed cations. The K values in Table 2 show that virtually no ion-pairs are formed between ML^+ and the anion of HND. It is clear that ML^+ is much bulkier than M^+ and that the effective size of ML^+ is exclusively determined by the ligand size. These findings strongly support the view that ML^+ exists as a complex with the 'metal in the hole' structure, even in a dissolved state.

Hydration of the Free Ligands. As can be seen from Fig. 1, water is also coextracted with uncomplexed DB18C6. The Δs values for L were measured by means of the extraction method in the absence of HND. Under such conditions, the transfer of ligand as complexes was neglected. The number of water molecules attached to a molecule of a ligand, h(L), can be calculated from the slope of the plot. The data thus obtained, together with the hole diameters,[20,21] are summarized in Table 3.

Table 3 shows that the free ligands exist in a slightly hydrated form in the nitrobenzene phase. The benzo derivatives seem to be less hydrated. It should be noted that 2.2B exists as a monohydrate not only in the nitrobenzene phase, but also in the solid state. 18C6 and the uncomplexed potassium ion have 1.6 and 1.3 water molecules respectively, while the complex has only 0.3 water molecule. From these data, it is possible to assume that 1.6 water molecules are bound inside the ligand hole.

Hydration of the Complexed Cations, ML^{n+}. The number of water molecules attached to the complexed cations, $h(ML^{n+})$, is obtained from the slope of the Δs-$[M(t)]_0$ plot (Fig. 1) when 1:1 complexes alone are known to exist in the nitrobenzene phase. The $h(ML^{n+})$ values can also be obtained from an h-a plot, as is shown in Fig. 4, where $h=\Delta s/[M(t)]_0$ and $a=[L(t)]_0/[M(t)]_0$.

For a given metal cation, the h value at $a=0$ in Fig. 4, for example, is identical with the $h(M^{n+})$ value. Since ML^{n+} is less hydrated than M^{n+}, the h values decrease with the addition of L to a solution containing M^{n+} and HND anions ($a<1$). The intensity of the orange-red color of the aqueous phase, which shows the presence of HND anions, also decreases upon the addition of L. At the first equivalence point ($a=1$),

Table 3. The number of water molecules coextracted with the ligands, h(L)

L	B12C4	15C5	B15C5	18C6	B18C6	DB18C6	2.2B[a]	DB24C8	2.1.1	2.2.1	2.2.2	2.2.2B
Hole diameter (nm)	0.10—0.13	0.17 — 0.22			0.26 — 0.32			0.4	0.16	0.22	0.28	
h(L)	0.2	0.7	0.5	1.6	0.8	0.6	1.0	0.5	0.5	0.8	0.8	0.5

a) $pK_1=7.9$, $pK_2=8.7$.

Table 4. The number of water molecules coextracted with the 1:1 crown ether complexes, $h(ML^{n+})$

M^{n+}	Cation diameter (nm)	L								
		None	B12C4	15C5	B15C5	18C6	B18C6	DB18C6	2.2B	DB24C8
Li	0.136	5.6	2.9	2.0	1.4	2.5	2.6	2.9	2.5	2.4
Na	0.196	3.5	—	0.9	0.8	1.2	1.1	1.2	1.3	0.2
K	0.266	1.3	—	0.3	0.5	0.3	0.4	0.1	0.6	0.3
Rb	0.298	0.9	—	0.5	0.3	0.3	0.2	0.1	0.5	0.2
Cs	0.336	0.6	—	0.2	0.4	0.1	0.2	0.1	—	0.3
Ca	0.198	13.0	—	5.3	6.5	4.7	5.5	5.1	4.8	5.3
Sr	0.226	12.1	—	0.4[a]	0.5[a]	4.6	4.6	4.9	4.3	4.1
Ba	0.270	10.5	—	0.2[a]	0.2[a]	3.4	4.2	4.4	3.7	2.9

a) M:L=1:2.

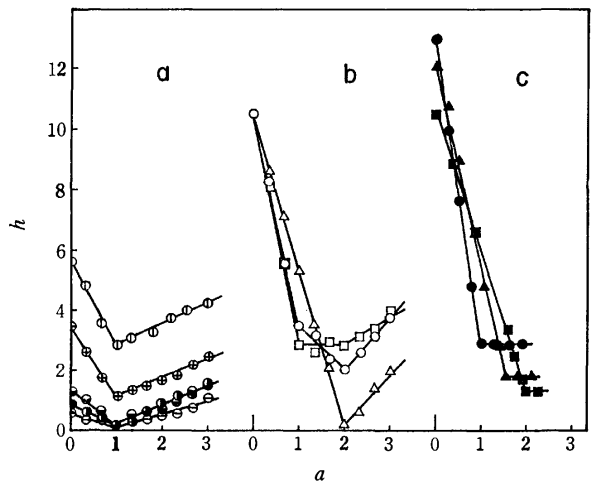

Fig. 4. Effect of the ligands on the coextraction of water.
a: Alkali metal complexes with DB18C6, Li^+ (◐), Na^+ (⊕), K^+ (◒), Rb^+ (◑), and Cs^+ (⊖). b: Ba^{2+} complexes with 15C5 (△), 18C6 (○), and DB24C8 (□) c: Alkaline earth metal complexes with 2.1.1, Ca^{2+} (●), Sr^{2+} (▲), and Ba^{2+} (■).

the aqueous phase becomes colorless, indicating the complete transfer of the HND anions as ion-pairs, M(L)HND or $M(L)HND_2$, from the aqueous to the nitrobenzene phases. As regards the Ba^{2+} complex with 15C5, the curve in Fig. 4(b) shows no change at $a=1$. This is also the case for the other 1:2 complexes listed in Table 4. The conductometric titration curves (Fig. 3) for these complexes also fall off smoothly until $a=2$, indicating that the 1:1 complexes do not exist or are not so stable as the 1:2 complexes. Figure 4(b) shows that the alkaline earth metals form 1:2 complexes with the crown ethers, whereas, in some instances, the formation of the 1:2 complexes is not clear from the conductometric titration curves. In the crown ether complexes, the h values calculated from the slopes of the third line portions ($a>2$) are identical with the h(L) values; this indicates that no 1:2 complexes undergo further complexation.

The cryptands used form stable 1:1 complexes with the alkali and alkaline earth metals. It must be noted that 2.1.1 forms the 1:2 complex with Ba^{2+} and the 2:3 complex with Sr^{2+} (Fig. 4(c)). The fact that these 1:1 complexes are not formed between these cations and the cryptand is evident from the observation of the color change in the aqueous phase.

The h values obtained with the 1:1 complexes, together with those for the 1:2 and 2:3 complexes, are listed in Table 4. If the 1:2 alkaline earth metal–crown ether complexes are sufficiently stable, the $h(ML_2^{2+})$ values can be determined from h values at $a=2$, but they are omitted from Table 4 because the stability data are lacking.

Table 4 shows that the number of water molecules attached to the metal cations decreases on complexation; roughly speaking, the $h(ML^{n+})$ values are reduced to less than one-half the $h(M^{n+})$ values. The number of water molecules released, for example, amounts roughly to as much as 6—8 for the alkaline earth metals. The heavy alkali metal complexes lose virtually all the water molecules on complexation. It is noteworthy that Sr^{2+} and Ba^{2+} complexes with 15C5 and B15C5 have no water molecules. B12C4 forms no stable complex with any of the cations tested except for Li^+, as can be expected from its small hole size (*cf.* Table 3). 2.2B also forms no complex with Cs^+, though the reason for this is not known.

The h values for the metal–cryptand complexes (cryptates) are listed in Table 5. It is clear that the cryptates are much less hydrated than the crown ether complexes. Two important features are that the cryptates always have about one water molecule and

Table 5. The number of water molecules coextracted with the 1:1 cryptands, $h(ML^{n+})$

M^{n+}	L			
	2.1.1	2.2.1	2.2.2	2.2.2B
Li	0.7	0.9	1.0	1.2
Na	0.4	0.8	0.5	0.5
Ca	2.9	0.6	1.0	1.3
Sr	1.8[a)]	0.7	1.2	1.2
Ba	1.3[b)]	0.8	1.2	1.0

a) M:L=2:3. b) M:L=1:2.

the h values are not affected by the cation size.

Complex Structures. For some crown ether complexes, the 'metal in the hole' structure is proved in the crystalline state and in solution. The complex formation, therefore, does not necessarily require a stripping of the entire hydration shell of the cation. The molecular holes of 15C5 and B15C5 are so small that Sr^{2+} and Ca^{2+} can not be well accommodated. Hence, these crown ethers form 1:2 complexes of a sandwich-type structure, in which the metal cation is located between the two parallel rings consisting of five donor atoms. In the complexes of this type, the number of donor atoms is twice as many as that in the 'metal in the hole' structure. It is, therefore, not likely that no binding sites of the metal cation are left for the further coordination of water molecules. In the alkaline earth metal–crown ether complexes, it can also be noted that the number of water molecules released by complexation is roughly equal to that of the donor atoms.

Table 5 shows that all the 1:1 cryptates except for $Ca(2.1.1)^{2+}$ are associated with only 0.4—1.3 water molecules; this finding is in striking contrast to the results obtained with the crown ether complexes. Such a marked decrease in the h values strongly supports the 'metal in the cage' structure. In solid complexes of 2.2.2 with $CaBr_2$[22] and $BaSCN_2$,[23] the cations are known to be coordinated by one water molecule in each case. It, therefore, likely seems that the 0.4—1.3 water molecules are attached to the central cation by coordination, even in the nitrobenzene phase.

As can be seen from Table 5, $Ca(2.1.1)^{2+}$ is highly hydrated; the fact may suggest that Ca^{2+} is surrounded by the ligand, as in typical crown ether complexes. Ba^{2+} is much larger than the hole size of 2.1.1 and forms 1:2 complexes with it. From analogy with potassium B15C5,[24] a sandwich structure is inferred for the cryptate. A 'club sandwich' structure is postulated for a 2:3 crown ether complex, in which three ligands are arranged as planes in three tires, each separated from the next by a metal cation.[20] With regard to the cryptate formed between Sr^{2+} and 2.1.1, however, such a structure is unlikely, because 2.1.1 is not a planar molecule like crown ethers.

Thermogravimetric Analysis. Li^+, Ca^{2+}, Sr^{2+}, and Ba^{2+} salts of HND were found to have 4, 11, 4, and 4 molecules of water of crystallization respectively. For the Ba^{2+} salt, a crystal with two molecules of water of crystallization was found. The stoichiometries of the crystalline solids of the alkaline earth metal–crown ether complexes were determined from the thermogravimetric curves by the help of the spectrophotometric method ($Ca(DB18C6)_2HND_2\cdot 6H_2O$, $Sr(DB18C6)_2HND_2\cdot 6H_2O$, and $Ba(DB18C6)_2HND_2\cdot 5.5H_2O$).

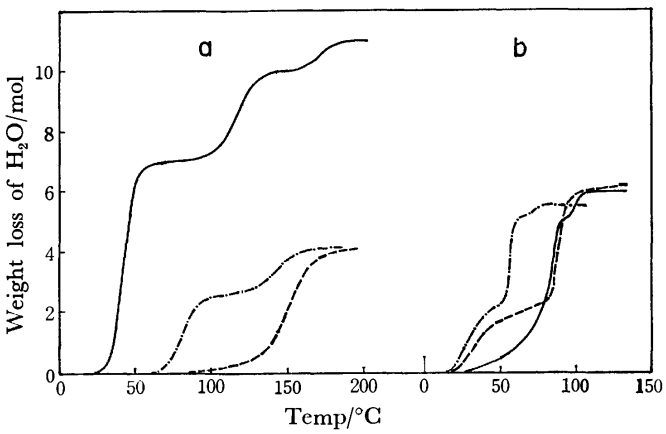

Fig. 5. Thermogravimetric analysis of water of crystallization.
a: $Ca(HND)_2\cdot 11H_2O$ (—), $Sr(HND)_2\cdot 4H_2O$ (----), and $Ba(HND)_2\cdot 4H_2O$ (——). b: $Ca(DB18C6)_2HND_2\cdot 6H_2O$ (——), $Sr(DB18C6)_2HND_2\cdot 6H_2O$ (— — —), $Ba(DB18C6)_2HND_2\cdot 5.5H_2O$ (——).

As an illustration, the thermogravimetric curves are shown in Fig. 5. In most cases, the thermal dehydration occurs in multistages in the range from about 30 to 180 °C. The DB18C6 complexes are found to lose their water of crystallization completely below about 100 °C; such is the case with 18C6. The uncomplexed salts still have some molecules of water of crystallization above 100 °C. It can be concluded that alkaline earth metal cation–water molecule bonds are much weaker in the complexes than in the uncomplexed salts. There are some instances in which h values are closely related to the number of water of crystallization. For example, Yamamoto *et al.* found that the ion-pairs formed between $Fe(phen)_3^{2+}$ (where phen refers to 1,10-phenanthroline) and ClO_4^-, SCN^-, I^-, and Br^- are accompanied by 1, 2, 2, and 6 water molecules respectively in the solid state and in the nitrobenzene phase as well.[25] In the present investigation, however, no such fine correlation was found. It can be recognized that large cations are at least less hydrated than smaller ones, both in the solid state and in the nitrobenzene phase.

The present work was partially supported by a Grant-in-Aid for Scientific Research from the Ministry of Education, Science, and Culture.

References

1) J. Rais, M. Kyrš, and M. Pivonkova, *J. Inorg. Nucl. Chem.*, **30**, 611 (1968).
2) M. Pivonkova and M. Kyrš, *J. Inorg. Nucl. Chem.*, **31**, 175 (1969).
3) W. E. Keder, E. C. Martin, and L. A. Bray, "Solvent Extraction of Metals," ed by H. A. C. McKay, T. V. Healy, I. L. Jenkins, and A. Naylor, Macmillan, London (1965),

p. 343.
4) L. M. Slater and M. Kukk, "Solvent Extraction Chemistry," ed by D. Dyrssen, J. O. Liljenzin, and J. Rydberg, North-Holland, Amsterdam (1967), p. 588.
5) R. Motley and C. E. Meloan, *Separ. Sci.*, **3**, 279 (1968).
6) S. Motomizu, K. Tôei, and T. Iwachido, *Bull. Chem. Soc. Jpn.*, **42**, 1006 (1969).
7) M. A. Bush and M. R. Truter, *J. Chem. Soc., Perkin Trans. 2*, **1972**, 341.
8) P. Seiler, M. Dobler, and J. D. Dunitz, *Acta Crystallogr., Sect. B*, **30**, 2744 (1974).
9) D. Live and S. L. Chan, *J. Am. Chem. Soc.*, **98**, 3769 (1976).
10) For example, B. Metz, D. Moras, and R. Weiss, *Chem. Commun.*, **1970**, 217.
11) K. Tôei, *Nippon Kagaku Zasshi*, **76**, 106 (1955).
12) A. Bernthsen and H. Sattler, *Ann.*, **230**, 116 (1885).
13) F. Kehrmann and F. Ringer, *Ber.*, **46**, 3018 (1913).
14) C. J. Pedersen, *J. Am. Chem. Soc.*, **89**, 7017 (1967).
15) B. Dietrich, J. M. Lehn, and P. J. Sauvage, *Tetrahedron Lett.*, **1969**, 2885.
16) R. H. Stokes and R. A. Robinson, *J. Am. Chem. Soc.*, **70**, 1870 (1948).
17) M. Kawasaki, K. Tôei, and T. Iwachido, *Chem. Lett.*, **1972**, 417.
18) T. Shedlovsky, *J. Franklin Inst.*, **225**, 739 (1938).
19) C. R. Witschonke and C. A. Kraus, *J. Am. Chem. Soc.*, **69**, 2472 (1947).
20) C. J. Pedersen, *J. Am. Chem. Soc.*, **92**, 386 (1970).
21) J. M. Lehn and J. P. Sauvage, *Chem. Commun.*, **1971**, 440.
22) B. Metz, D. Moras, and R. Weiss, *Acta Crystallogr., Sect. B*, **29**, 1377 (1973).
23) B. Metz, D. Moras, and R. Weiss, *Acta Crystallogr., Sect. B*, **29**, 1382 (1973).
24) P. R. Mallinson and M. R. Truter, *J. Chem. Soc., Perkin Trans. 2*, **1972**, 1818.
25) Y. Yamamoto, T. Tarumoto, and T. Tarui, *Chem. Lett.*, **1972**, 459.

The Thermal Cycloaddition of Dispiro[2.2.2.2]deca-4,9-diene to Isolated Carbon-Carbon Multiple Bonds

Tohru SHIBATA, Takashi TSUJI,* and Shinya NISHIDA

Department of Chemistry, Faculty of Science, Hokkaido University, Sapporo 060

(Received June 26, 1979)

The cycloadditions of dispiro[2.2.2.2]deca-4,9-diene (**1**) to isolated carbon-carbon multiple bonds have proceeded in two different modes, giving dispiro[2.2.4.2]dodeca-4,11-diene and tricyclo[6.4.0.0^{3,6}]dodeca-2,7-diene derivatives. Mono- and 1,2-disubstituted olefins and acetylenes gave the former adducts, whereas 1,1-disubstituted olefins gave the latter, as the major products. Evidence for the intermediacy of biradicals is provided. The observed difference in the mode of the cycloaddition is explained in terms of the stereoelectronic and/or steric effects in the transition state for the cyclization of the intermediate. The addition of **1** to tetracyanoethylene (TCNE) in wet acetone has proceeded *via* a zwitterionic intermediate(s), giving a 1:1:1 adduct of **1**, TCNE, and water.

We have previously reported the thermal cycloaddition reactions of dispiro[2.2.2.2]deca-4,9-diene (**1**) with some conjugated unsaturated compounds[1] which demonstrated the one-step production of [8]paracycloph-4-enes,[1] [4.2]paracyclophanes,[2] and 3-oxa[8]paracycloph-4-enes.[3] As a further inverstigation of the chemistry of **1**, we have now studied the reactions of **1** with compounds possessing an isolated carbon-carbon multiple bond. In the present paper, two novel types of the cycloadditions of **1**, giving dispiro[2.2.4.2]dodeca-4,11-diene and tricyclo[6.4.0.0^{3,6}]-dodeca-2,7-diene derivatives (**7** and **8**) will be described, and the evidence supporting the intermediacy of biradicals will be presented. We will also report the reaction of **1** with tetracyanoethylene (TCNE), which seems to proceed *via* dipolar intermediate(s).

Results

Addition Reactions Giving Dispiro[2.2.4.2]dodeca-4,11-diene Derivatives (7). As was reported briefly in the previous report,[1] **1** adds to dimethyl maleate (**10**) and dimethyl acetylenedicarboxylate (**11**) to give dispiro[2.2.4.2]dodecane derivatives, **7a** (42%) and **6a** (62%) respectively, under conditions (*ca.* 155 °C) giving rise to the homolytic scission of the cyclopropane ring in **1**. We have now further investigated the cycloaddition reactions of **1** to other unsaturated compounds possessing an isolated carbon-cabon multiple bond in order to examine the generality and the stereochemistry of the reactions.

The reactions were carried out as has previously been reported in *t*-butyl alcohol at 150 °C under a nitrogen atmosphere.[2] The reaction mixture of **1** with dimethyl fumarate (**12**) consisted of one major and five minor products and was quite similar in composition to that resulting from the reaction with **10**. Thus, the major product, isolated in an 11% yield, was found to be **7a**, identical with that produced in the reaction with **10**. On the other hand, the reaction with maleic anhydride (**13**) gave a single cycloadduct (**7c**) in a 29% yield. The successive treatment of **7c** with methanol and then with diazomethane afforded the dimethyl ester (**7b**) which was apparently different from **7a**, but which was identical with one of the minor products found in the product mixtures from both **10** and **12** in a proportion of six-hundredths of **7a**. The triethylamine-catalyzed epimerization at 155

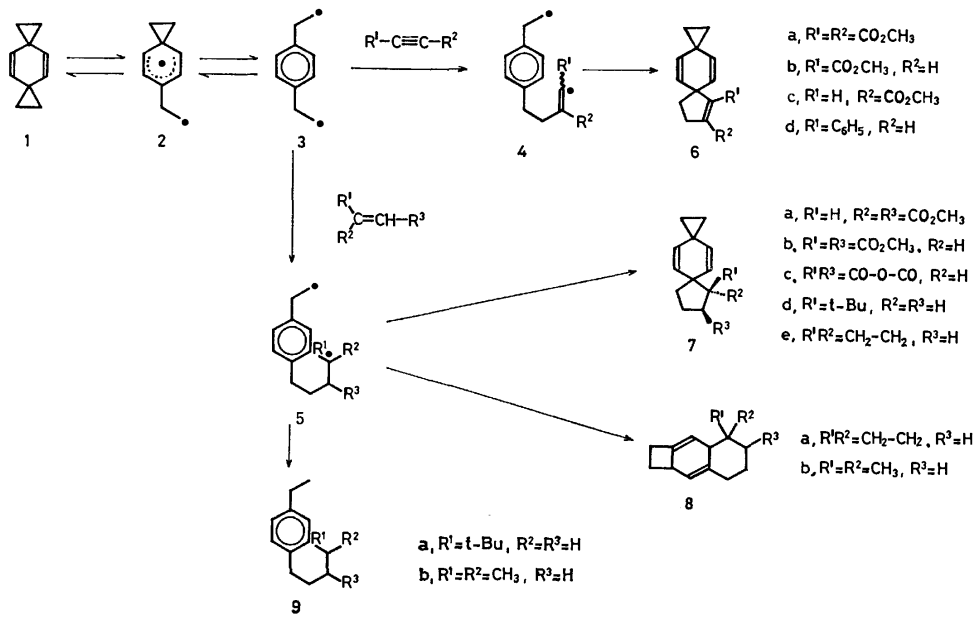

Scheme 1.

TABLE 1. REACTION PRODUCTS OF 1 AND UNSATURATED COMPOUNDS[a]

Reaction partner	[1]	[Reaction partner]	Solvent	Product (Yields/%)
10	0.025	0.10	*t*-butyl alcohol	**7a** (49)[b], **7b** (3)[b]
12	0.0031	0.013	*t*-butyl alcohol	**7a** (52)[b], **7b** (4)[b]
13	0.0062	0.025	hexane	**7c** (47)[b]
14	0.20	0.40	*t*-butyl alcohol	**7d** (2.4), **9a** (2.2)
15	0.10	0.46	*t*-butyl alcohol	**7e** (8)[b], **8a** (13)[b], **21** (4)[b], **22** (12)[b], **29** (8)[b,e]
18	0.20	1.0	*t*-butyl alcohol	**8b** (5), **9b** (1.6), **25** (15), **26** (2.3)
11	0.20	0.40	*t*-butyl alcohol	**6a** (62)
16	0.20	0.40	*t*-butyl alcohol	**6b** (21), **6c** (2.3), **27** (2.7)[c]
17	0.20	0.40	*t*-butyl alcohol	**6d** (13), **28** (2.3)[d]

a) The reactions were carried out at 155—160 °C for 9—13 h under nitrogen or argon. b) The yields were determined by GLC analysis. c) Methyl 3,4-dihydro-7-ethyl-1-naphthalenecarboxylate. d) [4.2]Paracycloph-1-ene. e) *p*-Diethylbenzene.

°C gave an equilibrium mixture composed of **7a** and **7b** in a 100:6 ratio starting from either compound. No epimerization, however, was observed in the absence of triethylamine.

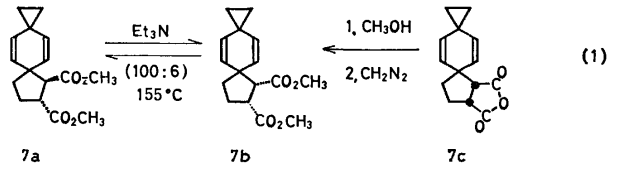

(1)

7a 7b 7c

These results show unequivocally that the substituents in **7b** and **7c** have a *cis* geometry with respect to the five-membered ring, whereas those in **7a** have a *trans* geometry.[4] Therefore, it may be concluded that the cycloadditions of **1** with **10** and with **12** are nonstereospecific and give mixtures of **7a** and **7b** in the same proportion as that in the equilibrium mixture.

In these reactions, it was noticed that the yields of the cycloadducts were remarkably dependent on the reactant concentrations and reached their maxima at 0.01—0.02 M (1 M=1 mol dm^{-3}) for **12**, at 0.1 M for **10** (**7a** in *ca.* 50% yields from both **10** and **12**), and at 0.03 M for **13** (**7c** in a 45% yield) when the reactions were carried out with the **1**/olefin molar ratio of 1/4. At concentrations lower or higher than the above optimums, the reactions resulted in lower yields. At a higher concentration, the addition of a second olefin molecule to the biradical intermediate, **5**, might become competitive with the ring closure of **5** to the product; hence the decreased yields might result. At a lower concentration, the interception of the biradical, **3**, (the interception of the biradical, **2**, would not be important; *vide infra*) by the solvent and/or the impurities prior to the addition of the olefin might reduce the product yield. According to Szwarc,[5] **12** is nearly five times as reactive as **10** toward alkyl radicals. The optimum concentration for **12** was, indeed nearly one-fifth of that for **10**.

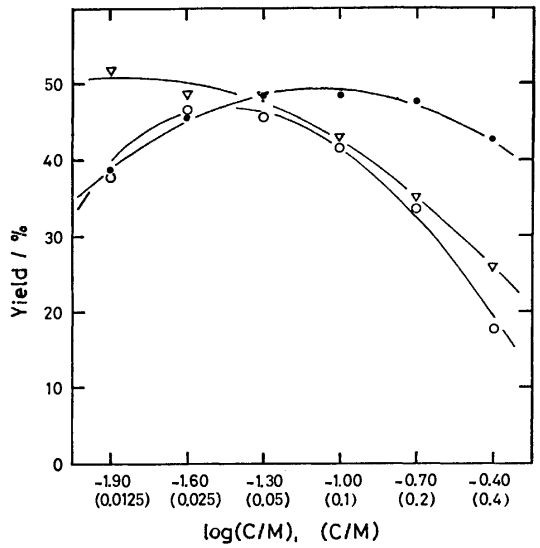

Fig. 1. Yields of the cycloadduct, **7a** or **7c**, *vs.* concentrations of the reactant, **10**, **12**, or **13**. The reactions were carried out maintaining the **1**/olefin molar ratio at a quarter.
●: Yields of **7a** from **1** and **10**, ▽: yields of **7a** from **1** and **12**, ○: yields of **7c** from **1** and **13**.

As is shown in Table 1, 3,3-dimethyl-1-butene (**14**) and methylenecyclopropane (**15**) underwent an analogous cycloaddition to give the dispiro products, **7d** and **7e**, though in lower yields. In addition to **11**, the acetylenic compounds, methyl propiolate (**16**) and ethynylbenzene (**17**),[2] also gave the dispiro adducts, **6b** and **6c**, and **6d**, respectively.

Addition Reactions Giving Tricyclo[6.4.0.0^{3,6}]dodeca-2,7-diene Derivatives (8). Two olefins, **15** and 2-methylpropene (**18**), gave tricyclic compounds as the major product. Kawamura *et al.* have reported the addition of methyl radical to **15** at the inner carbon atom and the subsequent rearrangement to the 3-methyl-3-butenyl radical (**19**).[6] If the addition of **1** to **15** proceeds analogously, the formation of 3-methylene-[7]paracyclophane (**20**) may be expected, as is de-

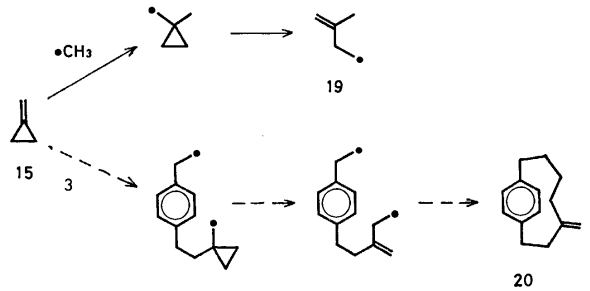

(2)

picted in Eq. 2. The reaction of **1** with **15**, however, gave a mixture of adducts which were isolated and assigned the structures represented by **7e**, **8a**, **21**, and **22**, but no cyclophane. The ozonolyiss of **7e** in methanol at −70——80 °C followed by an oxidative workup and subsequent treatment with diazomethane afforded the dimethyl dicarboxylate (**23**), in a 23% yield, this product was identical in all respects with the ester synthesized *via* an independent route, from **24** to **23**.

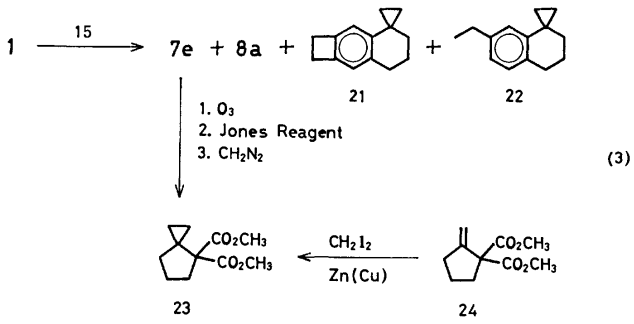

The product, **8a**, which showed two signals of olefinic protons at δ 4.88 and 5.29 in the NMR spectrum, could not be isolated in an analytically pure state because of its gradual conversion into **21** and a polymeric material during the purification. In the mass spectrum of **21**, the molecular ion peak appeared at *m/e* 184, indicating a loss of two hydrogens from a 1:1 adduct. The UV spectrum of **21** exhibited a characteristic fine structure which was very similar to those observed in the spectra of symmetrically substituted tetraalkylbenzenes,[7] but this structure was shifted considerably to a longer wave length (by 7 nm compared to 1,2,3,4,5,6,7,8-octahydroanthracene) and the NMR spectrum showed two singlets at δ 6.21 and 6.55, abnormally high field for aromatic proton. These observations are best accommodated by the structure identified as **21**, in which the spiro cyclopropane ring can give rise to the bathochromic shift in the UV spectrum and the high-field shifts of the aromatic proton signals in the NMR spectrum to the extents observed; hence, **8a**, a precursor of **21**, was assigned the 1,4-cyclohexadiene structure.[8] Compound **22**, as expected, also exhibited characteristic shifts in the UV and NMR spectra similar to those in the spectra of **21**.

The reaction of **1** with **18** afforded the tricyclic product, **8b**, in a 5% yield. The major product was *p*-(4-methyl-4-pentenyl)ethylbenzene (**25**) (15%), which was probably formed through the rapid intramolecular disproportionation. No dispiro adduct, however, was detected in the reaction mixture.

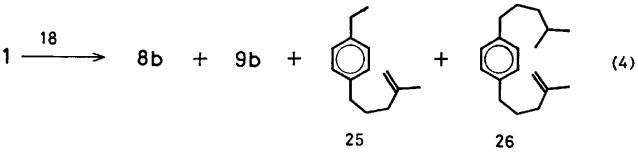

Reaction with TCNE. As has been reported previously, **1** reacts with tetracyanoquinodimethane to give [3.3]paracyclophanetetracarbonitrile *via* a zwitterionic intermediate.[1] TCNE is well known to add to electron-rich olefins,[9] and **1** is known to be an olefin possessing an unusually low ionization potential.[10] Therefore, it is of interest to investigate how **1** behaves toward TCNE. The reaction of **1** with TCNE proceeded rapidly in various solvents, such as acetonitrile, nitromethane, acetone, ethyl acetate, tetrahydrofuran, dichloromethane, and ether, accompanied by an apparent transient coloration of the mixtures in some of the solvents, and was completed in a few minutes at room temperature. In wet acetone, a 1:1:1 adduct of **1**, TCNE, and water, **31**, was obtained in a quantitative yield. In all other solvents, whether anhydrous or wet, however, the reactions gave only amorphous materials.

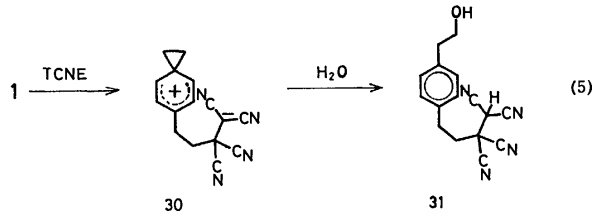

Discussion

Evidences for the Biradical Pathway for the Formation of Dispiro and Tricyclic Adducts. The cycloaddition of **1** to the olefins giving the dispiro[2.2.4.2]dodecane and tricyclo[6.4.0.0^{3,6}]dodecane derivatives, **6**, **7**, and **8**, can be reasonably explained by the pathway outlined in Scheme 1. Various observations support the above mechanism: 1) the occurrence of the reaction only above the temperature at which the homolytic cleavage of the cyclopropane ring in **1** commences; 2) the formation of the by-products characteristic to radical reactions, *i.e.*, a 1:2 adduct, **26**, hydrogen abstraction products, **9**,[11] and disproportionation products, **25** and **26**; 3) the inhibiting effect of the hydrogen donors, such as thiophenol, 2-propanol, and 2,2,4-trimethylpentane,[12] and 4) the nonstereospecificity of the reaction. The reactions of **1** with **10** and with **11** in methanol, as expected, did not show any notable differences in the product compositions.

Although the two biradicals, **2** and **3**, could react with the unsaturated compounds to produce the adducts, the major part, if not all, of the products would derive from **3**. The structure of **2** represents that **2** corresponds to the transition state (or the short-lived intermediate) for the 1,2-aryl shift in **3**.[13] Therefore, **2**, after its formation, would very rapidly rearrange to **3**[14] and have hardly any chance to react with the unsaturated compounds. The reaction of **1** with the styrene derivatives afforded only [4.2]paracyclophanes.[2] Neither dispiro[2.2.4.2]dodeca-4,11-diene nor tricyclo[6.4.0.0^{3,6}]dodeca-2,7-diene derivatives were detected. These results, in accord with the above reasoning, strongly support the ideas that the biradical reacting with the unsaturated compounds is **3** and that the cyclization of the resulting biradicals occurs in **5** (**32**).[15]

Two Modes of Ring Closure. The dispiro compound, **1**, underwent the cycloadditions in two different modes, depending on the unsaturated compounds.

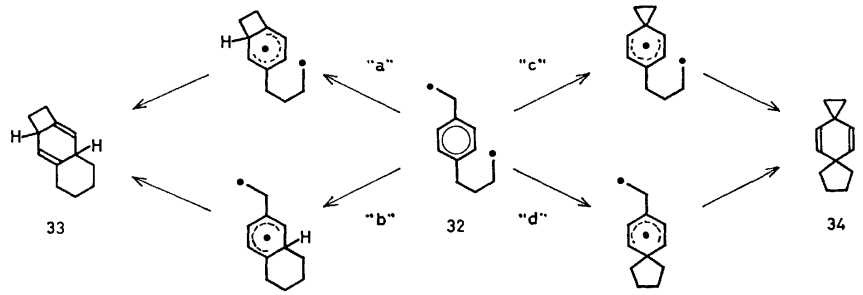

Fig. 2. Four possible cyclization routes for **32** to **33** and **34**. The substituents are omitted for clarity.

There could be four cyclization routes for the biradical intermediate, **32**, leading to two kinds of products, **33** and **34**, as is shown in Fig. 2. The (a) route, however, may be ruled out, since few, if any, instances of such a mode of cyclization of 2-arylethyl radicals have been established, whereas the other three cyclization modes are well documented.[13] In the reactions of the 1,2-disubstituted olefins and the acetylenes, **32** cyclized by the (c) and/or (d) pathways, which would be favored over the (b) pathway because of stereoelectronic[16] and/or steric[17a] effects. These cyclization pathways, (c) and (d), imply intramolecular trappings of the intermediates postulated for 1,2- and 1,4-aryl shifts in radical rearrangements, though the two possible pathways are not differentiated at present.

In the reaction with the 1,1-disubstituted olefins, however, the cyclization to the spiro compounds would be hindered by the repulsive interaction between the central six-membered ring and the two substituents, as is depicted in Fig. 3; hence, a less sterically hindered cyclization to the tricyclic products would result. The above explanation is supported by the finding that methylenecyclopropane, which seems to have less bulky substituents than 2-methylpropene,[18] afforded a mixture of the dispiro and tricyclic adducts. A similar substituent effect on the reaction mode has been known for the ring closure of 5-hexenyl radicals; that is, the less substituted **35** tend to rearrange to cyclopentylmethyl radicals, **36**, but increasing substitution results in an increasing **37**/**36** ratio.[16,17]

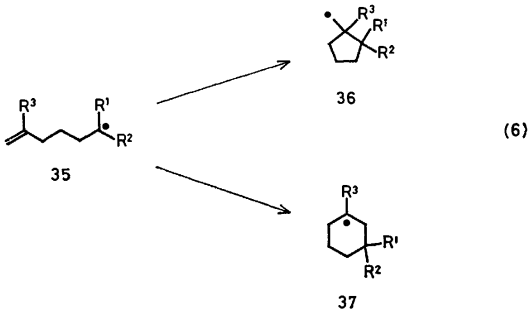

(6)

The cycloadditions leading to the dispiro products are formally insertions of the olefins into the cyclopropane ring. Although some analogous reactions producing five-membered rings from olefins and cyclopropane rings have been reported,[19] they are bimolecular or metal-catalyzed reactions. The present reactions are initiated by the unimolecular scission of the cyclopropane ring into the biradical, **3**, to which the unsaturated compounds then add. There is no precedent, to the best of our knowledge, for such an intermolecular cycloaddition of a biradical formed by the homolytic cleavage of a cyclopropane ring to a carbon-carbon multiple bond giving a five-membered ring, probably because 1,3-biradicals are generally too short-lived to be intercepted by unsaturated compounds.[20] In the present reactions, the biradical species reacting with the unsaturated compounds would be the 1,8-biradical, **3**, rather than the incipient 1,3-biradical, **2**; therefore, it would be sufficiently long-lived to add to the multiple bonds.[13]

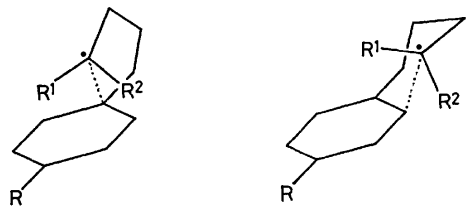

Fig. 3. Probable transition states for the two types of cyclization.

Reaction with TCNE. The rapid reaction of **1** with TCNE is clearly differentiated from the reactions initiated by the unimolecular ring scission in **1**. The formation of the water-incorporated product, **31**, is also incompatible with a radical mechanism and indicates the generation of the zwitterion, **30**. The ring-opening addition of TCNE to **1** rather than the usual addition to unsaturated bonds, and the low reactivity of **1** toward methylenemalononitrile, which adds no less rapidly than TCNE to such electron-rich olefins as vinyl ethers *via* zwitterions,[9b] coupled with the low ionization potential of **1**, suggest the electron transfer from **1** to TCNE prior to the formation of **30**.[9c]

The peculiar observations that **31** was produced only in wet acetone and that the reactions in many other kinds of solvents resulted in amorphous products are rather puzzling. De Meijere *et al.* have reported the reaction of TCNE with dispiro[2.0.2.4]deca-7,9-diene, **38**, a structural isomer of **1**, in tetrahydrofuran giving **39**,[21] but no related product was detected in the reaction of **1** with TCNE in tetrahydrofuran.

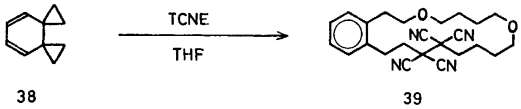

(7)

Experimental

General. The melting points are corrected. The NMR spectra were obtained with JEOL PS-100 and Hitachi R-24 spectrometers at 100 and 60 MHz respectively; the chemical shifts are given in ppm from $Si(CH_3)_4$. The IR spectra were taken on a Hitachi Model 215 grating spectrometer and are given in cm^{-1}. The mass spectra were recorded on a Hitachi Model RMU-6E spectrometer at an ionizing voltage of 80 eV, with the exception of that of **23**, which was recorded on a JEOL Model JMS-D300 spectrometer at an ionizing voltage of 70 eV; the ions of each spectrum were normalized to the spectrum's most intense ion, set equal to 100. The UV spectra were taken on a Cary Model 17 spectrophotometer and are given in nm. The GLC work was done on a Hitachi Type 063 gas chromatograph with a thermal conductivity detector, using helium as the carrier gas. The following glass columns were used: A, 20% Apiezon Grease L on Celite 545, 3 mm×1 m; B, 15% Apiezon Grease L on Celite 545, 3 mm×2 m; C, 20% PEG succinate on Celite 545, 4 mm×4 m; D, 15% Apiezon Grease L on Celite 545, 6 mm×1.5 m; E, 20% PEG 20M on Celite 545, 4 mm×1.8 m; F, 15% Apiezon Grease L on Celite 545, 3 mm×1 m; G, 5% Silicone Gum SE-30 on Chromosorb W, 3 mm×0.7 m; H, 20% Silicone DC-550 on Celite 545, 4 mm×1.5 m; I, 5% PEG phthalate on Celite 545, 4 mm×3 m; J, 20% Apiezon Grease L on Celite 545, 4 mm×2 m. The yields were calculated on the basis of the **1** used in the reaction.

Materials. The preparation of dispiro[2.2.2.2]deca-4,9-diene was carried out as has been described previously.[1] Methyl propiolate (**16**),[22] methylenecyclopropane (**15**),[23] 5-iodo-1-pentyne,[24] 3,3-dimethyl-1-butene,[25] TCNE,[26] and Zn–Cu couple[27] were prepared according to the procedures described in the literature. The other reagents were obtained from commercial sources and were purified by fractional distillation or by recrystallization except for 2-methylpropene (**18**), which was purchased from the Tokyo Kasei Co. and used without further purification.

*Reaction of **1** with Dimethyl Fumarate (**12**).* A solution of 132 mg of **1** (1.00 mmol) and 288 mg of **12** (2.00 mmol) in 50 ml of *t*-butyl alcohol was heated at 155 °C for 13.8 h under nitrogen. The solvent was then removed *in vacuo* and the residue was chromatographed on silica gel and eluted with chloroform. The first fraction contained 26 mg of **12**. From the second fraction, which weighed 100 mg, 66 mg of a crystalline mixture were separated by crystallization from petroleum ether. The removal of **12** by sublimation and the recrystallization of the residue from petroleum ether afforded **7a**; mp 68.2—68.7 °C (29 mg, 11%). The third fraction gave 231 mg of an intractable, viscous oil. The adduct obtained above showed no depression of its melting point in a mixed-melting-point measurement with that obtained from **1** and **10**.

*Reaction of **1** with Maleic Anhydride (**13**).* A solution of 132 mg of **1** (1.00 mmol) and 196 mg of **13** (2.00 mmol) in 50 ml of *t*-butyl alcohol was heated as above. After the solvent had been removed, the residue was distilled. The first fraction (bp 140 °C at 15 mmHg) (1 mmHg=133.322 Pa) was 24 mg of **13**. The second fraction (bp 170 °C at 0.02 mmHg) was 169 mg of a pale yellow liquid, from which 66 mg of crystalline **7c** were obtained (29%) by recrystallization from diethyl ether and preparative GLC separation (Column A, 200 °C). A mixture consisting of two components (15 mg) was separated by the preparative GLC, but the structures could not be determined. The residue of the distillation weighed 169 mg. **7c**, mp 79.0—80.5 °C; NMR (CCl_4, 100 MHz): 0.85 (m, 4H), 1.75 (m, 2H), 2.25 (m, 2H), 3.08 (d, J=9.5 Hz, 1H), 3.52 (m, 1H), 5.0—5.6 (m, 4H); mass: *m/e* 230 (M^+, 4), 130 (78), 129 (55), 118 (49), 117 (100), 115 (40), 91 (40); IR (KBr): 1862, 1773, 1222, 917. Found: C, 72.92; H, 6.25%. Calcd for $C_{14}H_{14}O_3$: C, 73.02; H, 6.13%.

Dimethyl cis-*Dispiro[2.2.4.2]dodeca-4,11-diene-7,8-dicarboxylate (**7b**).* A solution of 22 mg of **7c** (0.096 mmol) in 1.5 ml of methanol was heated at 100 °C for 10 h. After the solvent had been removed *in vacuo*, a solution of diazomethane in ether was added until the yellow color persisted. The subsequent distillation of the reaction mixture yielded 25 mg of **7b** (95%) (bp 150 °C at 0.02 mmHg), a colorless oil which differed from **7a** in GLC retention time and its spectral properties. **7b**, NMR (CCl_4, 100 MHz): 0.77 (s, 4H), 1.4—2.6 (complex m, 4H), 2.86 (d, J=8 Hz, 2H), 3.1 (m, 1H), 3,55 (s, 3H), 3.58 (s, 3H), 4.96 (d of m, J=10 Hz, 2H), 5.40 (m, 2H); mass: *m/e* 276 (M^+, 1), 216 (39), 158 (17), 157 (100), 156 (27), 129 (37), 117 (27); IR (liquid film): 1740, 1728. Found: C, 69.20; H, 7.26%. Calcd for $C_{16}H_{20}O_4$: C, 69.54; H, 7.30%.

*Epimerization between **7a** and **7b**.* A solution of **7b** in *t*-butyl alcohol (0.27 M) was heated at 155 °C for 22 h, but no epimerization was detected on GLC analysis (Column B, 200 °C). Similarly, a solution of **7a** in *t*-butyl alcohol (0.27 M) was stable at the above temperature. They, however, epimerized when they were heated at 155 °C in a 0.5 M methanolic solution of triethylamine. The ratio of **7b** to **7a** was found to be 0.06:1 after 10 h heating, regardless of the stereochemistry of the starting material; this ratio remained unchanged after 20 h heating. Reaction of **1** with **12** in methanol (155 °C, 12 h) gave the product mixture, in which the ratio of **7b** to **7a** was 0.05.

*Effect of the Reactant Concentration on the Yield of the Adducts, **7a** and **7c**.* To an aliquot (0.5 ml) of a solution of **1** in *t*-butyl alcohol in an accurately known concentration (*ca.* 0.1 M), were added 0.20 mmol of **10** or **12** and the following amount of the solvent; 0, 0.5, 1.5, 3.5, or 7.5 ml. These mixtures were heated in sealed ampoules at 151—153 °C for 14 h under nitrogen. After the reaction, the solvent was removed and the yields of the adducts were determined on GLC (Column B, 200 °C), using benzophenone as the internal standard. Similarly, hexane solutions of **1** and **13** were heated at 158 °C for 12 h under nitrogen and the product yields were determined. In the reactions of **1** with both **10** and **12**, the product ratio, **7b**/**7a**, was 0.06, regardless of the amount of the solvent added.

*Effect of Hydrogen Donors on the Reaction of **1** with **10**.* Five 200-μl aliquots were withdrawn from a solution of 35.5 mg of **1** (0.27 mmol) and 57.6 mg of **10** (0.40 mmol) in 1.00 ml of ether. From each aliquot, the solvent was removed and the following materials were added to the residue: (1) 2.00 ml of *t*-butyl alcohol, (2) 2.00 ml of *t*-butyl alcohol and 11 mg of thiophenol, (3) 2.00 ml of *t*-butyl alcohol and 55 mg of thiophenol, (4) 2.00 ml of 2-propanol, and (5) 2.00 ml of 2,2,4-trimethylpentane. These solutions were heated at 152—155 °C for 11 h under nitrogen, and then the relative yields of **7a** were determined on GLC, using benzophenone as the internal standard (Column B, 200 °C). The yield of **7a** in Run 1 was set equal to 100%. (1) 100%, (2) 38%, (3) 6.3%, (4) trace amount, and (5) 89%.

*Reaction of **1** with 3,3-Dimethyl-1-butene (**14**).* A solution of 132 mg of **1** (1.00 mmol) and 168 mg of **14** (2.00 mmol) in 5.0 ml of *t*-butyl alcohol was heated at 158 °C for 11.5 h under nitrogen. After the removal of the solvent, the residue was subjected to silica gel column chromato-

graphy and subsequently to preparative GLC (Column C, 170 °C), which yielded 4.7 mg of **9a** (2.2%), 5.3 mg of **7d** (2.5%), and 1.9 mg of an unidentified liquid. **7d**, NMR (CCl_4, 60 MHz): 0.65 (s, 4H), 0.86 (s, 9H), 1.2—1.8 (m, 7H), 4.75 (d, J=10 Hz, 2H), 5.26 (d, J=10 Hz, 1H), 5.54 (d, J=10 Hz, 1H). **9a**, NMR (CCl_4, 60 MHz): 0.80 (s, 9H), 1.0—1.8 (m containing t at 1.18, J=7 Hz, 9H), 2.45 (q, J=7 Hz, 4H), 6.83 (s, 4H).

*Reaction of **1** with Methyl Propiolate (**16**).* A solution of 132 mg of **1** (1.00 mmol) and 173 mg of **16** (2.06 mmol) in 5.00 ml of *t*-butyl alcohol was heated at 158 °C for 11.5 h under argon. After the reaction, 0.47 mmol of **16** remained. On GLC analysis (Column F, 170 °C), one major and six minor peaks were observed. The solvent was then removed, and the residue was chromatographed on silica gel. Elution with dichloromethane and then with a mixture of dichloromethane and ether (4:1) gave 53 and 164 mg of the product mixtures respectively. The preparative GLC (Column F, 170 °C) of the former mixture afforded 8.5 mg of **6b**, 4.9 mg of **6c** (2.3%), 5.9 mg of **27** (2.7%), and 1.6 mg of an unidentified product. That of the latter mixture gave 36.3 mg of **6b** (total 44.8 mg, 21%) and 5.9 mg of an unidentified product. An analytical sample of **6b** was obtained by recrystallization from petroleum ether, and those of others by preparative GLC (**6c**, with Column F and subsequently with Column I; **27**, with Column H and subsequently with Column I). Further elution with ether and with ethanol only produced an intractable, amorphous yellow solid. **6b**, mp 65.9—66.5 °C; NMR (CCl_4, 100 MHz): 0.76 (s, 4H), 1.97 (t, J=7.5 Hz, 2H), 2.46 (t of d, J=7.5 and 2.5 Hz, 2H), 3.61 (s, 3H), 4.96 (d, J=10 Hz, 2H), 5.34 (d, J=10 Hz, 2H), 6.67 (t, J=2.5 Hz, 1H); mass, *m/e* 216 (M^+, 8), 198 (25), 157 (21), 156 (24), 141 (27), 129 (100), 128 (36); IR (KBr): 1704, 1628. Found: C, 77.85; H, 7.48%. Calcd for $C_{14}H_{16}O_2$: C, 77.75; H, 7.46%. **6c**, NMR (CCl_4, 100 MHz): 0.76 (s, 4H), 1.93 (t, J=7.5 Hz, 2H), 2.59 (t of d, J=7.5 and 2.0 Hz, 2H), 3.68 (s, 3H), 4.96 (d, J=10 Hz, 2H), 5.38 (d, J=10 Hz, 2H), 6.29 (t, J=2 Hz, 1H); mass: *m/e* 217 (10), 216 (M^+, 75), 157 (100), 156 (24), 141 (42), 129 (93), 128 (42), 115 (29); IR (liquid film): 1713, 1626. **27**, NMR (CCl_4, 100 MHz): 1.24 (t, J=7.5 Hz, 3H), 2.40 (m, 2H), 2.5—2.9 (complex m, 4H), 3.79 (s, 3H), 6.89 (s, 2H), 7.03 (t, J=4.5 Hz, 1H), 7.58 (s, 1H).

*Reaction of **1** with Methylenecyclopropane (**15**).* A solution of 396 mg of **1** (3 mmol) and 400 mg of **15** (7.4 mmol) in 21 ml of *t*-butyl alcohol was heated at 152—155 °C for 8 h under nitrogen. The reaction mixture was found by GLC analysis to consist of four major and four minor products, besides *p*-diethylbenzene. Distillation (bath temp, 170 °C at 2 mmHg) and subsequent separation by preparative GLC (Column D, 180 °C) yielded 27.2 mg of **7e** (4.9%), 26.0 mg of **8a** (4.7%), 31.6 mg of **21** (5.7%), and 72.3 mg of **22** (13%). Analytical samples of **7e**, **21**, and **22** were obtained through further purification by GLC (**7e** and **21**, with Column E at 180 °C; **22**, with Column H at 200 °C). The NMR spectrum of **8a** was recorded, but other spectral and analytical data could not be obtained because of the decomposition, which gave **21** and a polymeric material. **7e**, NMR (CCl_4, 100 MHz): 0.34 (AA′ BB′ m, 4H), 0.68 (s, 4H), 1.6—1.9 (m, 6H), 4.91 (d, J=11 Hz, 2H), 5.37 (d, J=11 Hz, 2H); mass: *m/e* 186 (M^+, 4), 158 (35), 157 (40), 143 (25), 130 (100), 129 (80), 128 (34), 115 (34), 91 (30). Found: C, 90.33; H, 9.71%. Calcd for $C_{14}H_{18}$: C, 90.26; H, 9.74%. **8a**, NMR (CCl_4, 100 MHz); −0.1—0.7 (complex m, 4H), 0.8—1.2 (two m, 2H), 1.2—3.0 (complex m, 9H), 3.16 (m, 1H), 4.88 (m, 1H), 5.29 (m, 1H). **21**, NMR (CCl_4, 100 MHz): 0.76 (AA′ BB′ m, 4H), 1.48—1.72 (m, 2H), 1.72—2.00 (m, 2H), 2.81 (t, J=6.5 Hz, 2H), 3.04 (s, 4H), 6.20 (s, 1H), 6.54 (s, 1H); mass: *m/e* 185 (17), 184 (M^+, 100), 183 (46), 169 (55), 156 (38), 155 (70), 141 (41); IR (liquid film): 3075, 1478, 890, 857; UV (hexane), max: 277 (ε=2610), 282 (3360), 287 (3400), 292 (3450). Found: C, 91.13; H, 8.79%. Calcd for $C_{14}H_{16}$: C, 91.25; H, 8.75%. **22**, NMR (CCl_4, 100 MHz): 0.81 (AA′ BB′ m, 4H), 1.18 (t, J=7.7 Hz, 3H), 1.55—1.75 (m, 2H), 1.75—2.05 (m, 2H), 2.51 (q, J=7.7 Hz, 2H), 2.82 (t, J=6 Hz, 2H), 6.34 (s, 1H), 6.77 (AB q, J=8 Hz, 2H); mass: *m/e* 186 (M^+, 43), 158 (40), 157 (100), 129 (56), 128 (19), 115 (17), IR (liquid film): 3075, 1493, 1450, 810; UV (hexane), max: 268^{sh} (ε=670), 274 (1030). 283 (330). Found: C, 90.32; H, 9.78%. Calcd for $C_{14}H_{18}$: C, 90.26; H, 9.74%.

*Yields of the Adducts of **1** and **15**.* To 6.6 mg of **1** and 40 μl of a 50 vol % hexane solution of **15** was added a specified volume of *t*-butyl alcohol bubbled with argon, after which the mixture was heated at 155 °C for 9 h under argon. The yields of the adducts were determined by GLC (Column B, 180 °C), using benzophenone as the internal standard. In Run 2, the yield of *p*-diethylbenzene and the amount of **1** remaining were also determined to be 7.7 and 7.2% respectively, using tetralin as the internal standard.

Run	[1]/M	[15]/M	Yields of adducts/%			
			7e	**8a**	**21**	**22**
1	0.032	0.12	3	7	7	2
2	0.10	0.46	8	13	12	4
3	0.25	1.0	7	8	13	5

*Ozonolysis of **7e**.* Compound **7e** (8.0 mg) was dissolved in 5.0 ml of anhydrous methanol, after which ozone/oxygen was bubbled through the solution held at −70—−80 °C for 30 min. After bubbling nitrogen to displace the excess ozone, the methanol was removed *in vacuo* (2 mmHg). The residue was dissolved in 10 ml of acetone, cooled in an ice bath, and treated with 0.5 ml of a 2.67 M Jones reagent. After 20 min, 1.0 ml of methanol was slowly added to destroy the excess oxidizing reagent and the solvent was removed. The residue was dissolved in 5.0 ml of ether, treated with anhydrous magnesium sulfate, and decanted, and the precipitate was washed with another 5.0 ml of ether. The combined ethereal solutions were extracted with two 2-ml portions of aq potassium hydrogencarbonate (2.5 M). The combined extracts were acidified with dil sulfuric acid, saturated with sodium sulfate, and extracted with two 5-ml portions of ether. To the combined ethereal solutions dried with anhydrous magnesium sulfate, was added diazomethane in ether under ice cooling until the yellow color persisted. After standing for 15 min, the excess diazomethane was removed by bubbling nitrogen, and then the ether was evaporated. The isolation of the products by preparative GLC (Column G, 90—130 °C) yielded 2.2 mg of dimethyl 1,1-cyclopropanedicarboxylate, 2.1 mg of **23**, and 0.5 mg of an unidentified material. The Compound **23** thus obtained was identical to that synthesized *via* an independent route (*vide infra*) in all respects.

*Dimethyl 2-Methylene-1,1-cyclopentanedicarboxylate (**24**).* To 40 ml of anhydrous methanol was added 1.6 g of sodium (0.07 mol), and then 8.8 g of dimethyl malonate (0.066 mol) was slowly added to the stirred solution. After heating under reflux for 10 min, 9.7 g of 5-iodo-1-pentyne (0.05 mol) was added slowly and heating was continued for 4 h. Most of the methanol was removed under reduced pressure, the residue was dissolved in 200 ml of water, and the solution was extracted with ether three times. The ethereal extracts

were dried with anhydrous magnesium sulfate and distilled through a spinning-band column *in vacuo* to give 3.1 g of **24** (bp 34 °C at 0.02 mmHg), 2.2 g of dimethyl 4-pentyne-1,1-dicarboxylate (bp 46 °C at 0.02 mmHg), and 1.6 g of a mixture of the two compounds. **24**, NMR (CCl_4, 60 MHz): 1.65 (apparent quintet, J=7 Hz, 2H), 2.05—2.55 (complex m, 4H), 3.60 (s, 6H), 5.20 (m, 2H); IR (liquid film): 1665.

Dimethyl Spiro[2.4]heptane-4,4-dicarboxylate (23). A mixture of 645 mg of **24** (3.25 mmol), 2.7 g of diiodomethane (10 mmol), and 2.0 g of Zn(Cu) couple (30 mmol) in 17 ml of absolute ether was vigorously stirred under reflux. (A small amount of iodine was added at the start.) Two additional 2.7-g portions of diiodomethane were added after 21 and 45 h. After 78 h of reaction (then, the ratio of the product to the starting material was nearly 1, on the basis of GLC analysis), the ethereal solution was decanted, washed with saturated aq ammonium chloride four times, saturated aq potassium carbonate, and saturated aq sodium chloride, and dried with anhydrous magnesiun sulfate. After the removal of the solvent, distillation gave 611 mg of a liquid (bath temp, 140 °C at 3 mmHg), which was subjected to preparative GLC, affording 200 mg of the starting material (32%), 64 mg of an unidentified product, and 200 mg of **23** (30%). **23**, NMR (CCl_4, 100 MHz): 0.40—0.70 (AA′ BB′ m, 4H), 1.58—1.88 (m, 4H), 2.35 (s, 2H), 3.63 (s, 6H); mass: *m/e* 212 (M^+, 2), 153 (48), 152 (100), 121 (22), 120 (39), 93 (80); IR (liquid film): 3080, 1735, 1150. Found: C, 62.25; H, 7.70%. Calcd for $C_{11}H_{16}O_4$: C, 62.25; H, 7.60%.

Reaction of 1 with 2-Methylpropene (18). Into a solution of 133 mg of **1** (1.01 mmol) in 5.0 ml of *t*-butyl alcohol was bubbled **18** at 20 °C until the absorption of the gas became slow. (*Ca.* 5 mmol of **18** was dissolved, judging from the change in weight.) The mixture was heated at 156 °C for 12 h under argon. Then the solvent was removed, and the residue was divided by column chromatography on silica gel with petroleum ether into five fractions, which weighed 24, 12, 5, 31, and 92 mg respectively. They were subjected to preparative GLC (Column B, 170 °C). Thus, 9.5 mg of **8b** (5%) and a small amount of **9b** were obtained from the first fraction, a small amount of **9b** (total 3.0 mg, 1.6%) from the second, 2.7 mg of **25** and 5.8 mg of **26** (2.3%) from the fourth, and 25 mg of **25** (total 27.7 mg, 15%) from the fifth. Analytical samples of these compounds were obtained through further purification by GLC (Column B). **8b**, NMR (CCl_4, 100 MHz): 0.65 (s, 3H), 0.93 (s, 3H), 1.2—2.9 (complex m, 11H), 3.13 (m, 1H), 5.17 (m, 1H), 5.37 (broad s, 1H); mass: *m/e* 188 (M^+, 1), 145 (100), 118 (43), 117 (66), 91 (25); IR (liquid film): 1704, 1643; UV (hexane), max: 212^{sh} (ε=12000). Found: C, 89.41; H, 10.58%. Calcd for $C_{14}H_{20}$: C, 89.29; H, 10.71%. **9b**, NMR (CCl_4, 60 MHz): 0.82 (d, J=6 Hz, 6H), 1.0—1.8 (complex m containing t, J=7.5 Hz at 1.15, 8H), 2.42 (apparent quintet, J=7.5 Hz, 4H), 6.86 (s, 4H); mass: *m/e* 190 (M^+, 22), 120 (19), 119 (100), 105 (10), 91 (15). **25**, NMR (CCl_4, 100 MHz): 1.23 (t, J=7.7 Hz, 3H), 1.6—1.9 (m containing s at 1.71, 5H), 2.00 (t, J=7.5 Hz, 2H), 2.57 (q, J=7.7 Hz, 4H), 4.67 (s, 2H), 7.00 (s, 4H); mass: *m/e* 188 (M^+, 2), 133 (12), 132 (100), 119 (17), 117 (49), 91 (17); IR (liquid film): 1646; UV (hexane), max: 255^{sh} (ε=180), 260 (310), 266 (420), 268 (400), 274 (480). Found: C, 89.34; H, 10.70%. Calcd for $C_{14}H_{20}$: C, 89.29; H, 10.71%. **26**, NMR (CCl_4, 100 MHz): 0.88 (d, J=7 Hz, 6H), 1.0—1.4 (m, 2H), 1.4—1.9 (complex m containing s at 1.70, 8H), 2.00 (t, J=8 Hz, 2H), 2.52 (m, 4H), 4.64 (s, 2H), 6.92 (s, 4H); mass: *m/e* 244 (M^+, 3), 189 (17), 188 (99), 175 (18), 118 (20), 117 (100), 91 (19); IR (liquid film): 1646; UV (hexane), max: 255^{sh} (ε=245), 260 (370), 266 (490), 268 (400), 275 (540).

Reaction of 1 with TCNE. TCNE (33 mg, 0.26 mmol) and **1** (33 mg, 0.25 mmol) were each dissolved in 1 ml of simply distilled acetone, and nitrogen was bubbled through each solution for 5 min. When the two solutions were then mixed, a pale violet color appeared, but it then faded within a few min. After standing for 5 d, the reaction mixture was worked up. The crystallization of the product from chloroform yielded 69 mg of **31** (≈100%); mp 104.5—106.5 °C. Successive recystallization from ether and from a 5:1 mixture of ether and acetone gave an analytical sample melting at 107.8—109.0 °C. **31**, NMR (acetone-d_6, 100 MHz): 2.6—3.3 (complex m, 7H), 3.69 (t, J=7 Hz, 2H), 5.97 (broad s, 1H), 7.08—7.32 (m, 4H); mass: *m/e* 251 (M^+—HCN, 9), 221 (18), 135 (33), 105 (79), 104 (100), 103 (11), 91 (11); IR (KBr): 3550, 2120. Found: C, 69.25; H, 4.96; N, 20.06%. Calcd for $C_{14}H_{14}ON_4$: C, 69.05; H, 5.07; N, 20.13%. When the reaction of **1** with TCNE was repeated without bubbling nitrogen and for a shorter reaction time (15 min), **31** melting at 107.7—109.0 °C was obtained in an 85% yield after crystallization from ether. If the acetone distilled through a fractionation column and stored over a Linde 4A Molecular Sieve was used as the solvent, the product was an intractable yellow liquid.

References

1) T. Tsuji, T. Shibata, Y. Hienuki, and S. Nishida, *J. Am. Chem. Soc.*, **100**, 1806 (1978).

2) T. Shibata, T. Tsuji, and S. Nishida, *Bull. Chem. Soc. Jpn.*, **50**, 2039 (1977).

3) T. Shibata, T. Tsuji, and S. Nishida, unpublished.

4) G. J. Fonken and S. Shiengthong, *J. Org. Chem.*, **28**, 3435 (1963).

5) a) M. Szwarc and J. H. Binks, "Theoretical Organic Chemistry," Int. Union of Pure and Applied Chem., Paper presented to Kekule Symposium, Chem. Soc. (London), 1958, Butterworths, 1959; b) M. Szwarc and J. H. Binks, *J. Am. Chem. Soc.*, **79**, 5621 (1957).

6) K. Takeda, H. Yoshida, K. Hayashi, and S. Okamura, *Bull. Inst. Chem. Res., Kyoto Univ.*, **45**, 55 (1967).

7) a) I. Sheer, W. R. Nes, and P. B. Smeltzer, *J. Am. Chem. Soc.*, **77**, 3300 (1955); b) R. A. Friedel and M. Orchin, "Ultraviolet Spectra of Aromatic Compounds," John Wiley and Sons, New York, N. Y. (1951), Fig. 14; c) M, S. Norris and N. D. Coggeshall, *Anal. Chem.*, **25**, 83 (1953).

8) R. C. Hahn, P. H. Howard, S.-M. Kong, G. A. Lorenzo, and N. L. Miller, *J. Am. Chem. Soc.*, **91**, 3558 (1969).

9) a) R. Huisgen, *Acc. Chem. Res.*, **10**, 117 (1977); b) R. Huisgen and R. Shug, *J. Am. Chem. Soc.*, **98**, 7819 (1976); c) S. Nishida, I. Moritani, and T. Teraji, *Chem. Commun.*, **1971**, 36. See also F. Kataoka and S. Nishida, *ibid.*, **1978**, 864.

10) a) Y. Harada, K. Ohno, K. Seki, and H. Inokuchi, *Chem. Lett.*, **1974**, 1081; b) P. Asmus, M. Klessinger, L.-U. Meyer, and A. de Meijere, *Tetrahedron Lett.*, **1975**, 381.

11) The formation of the 7-ethyltetralin derivatives, **22** and **38**, along with that of the hydrogen abstraction product, **9**, can be explained as follows (the substituents are omitted for the sake of clarity):

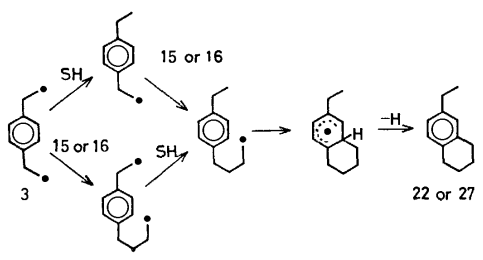

12) It is noteworthy that the extent of the inhibition by 2,2,4-trimethylpentane (*ca.* a 10% decrease in the yield of **7a** when it is used as the solvent) was nearly as large as that to be expected from the data of Szwarc *et al.*[6] assuming that the addition of **3** to **10** is in competition with the hydrogen abstraction.

13) a) J. W. Wilt, "Free Radicals," ed by J. K. Kochi, John Wiley and Sons, New York, N. Y. (1973), Vol. I, Chap. 8; b) A. L. J. Beckwith, "Essays on Free Radical Chemistry," Chem. Soc. Special Publ., No. 24 (1970), Chap. 9.

14) As expected, group-equivalent calculations indicate a higher energy content in **2** than in **3**.

15) For the intermolecular addition of radicals to aromatic rings giving cyclohexadiene derivatives, see M. J. Perkins, "Free Radicals," ed by J. K. Kochi, John Wiley and Sons, New York, N. Y. (1973), Vol. II, Chap. 16.

16) D. L. Struble, A. L. J. Beckwith, and G, M. Gream, *Tetrahedron Lett.*, **1968**, 3701. See also Ref. 13a, p. 442, adn Ref. 13b, p. 263.

17) a) M. Julia, *Pure Appl. Chem.*, **40**, 553 (1974); b) M. Julia, C. Descoins, M. Baillarge, M. Jacquet, D. Uguen, and F. A. Groeger, *Tetrahedron*, **31**, 1737 (1975); c) C. Walling and A. Cioffari, *J. Am. Chem. Soc.*, **94**, 6059 (1972).

18) S. Nishida and F. Kataoka, *J. Org. Chem.*, **43**, 1612 (1978).

19) a) Th. Martini and J. A. Kampmeier, *Angew. Chem. Int. Ed. Engl.*, **9**, 236 (1970); b) P. Gassman, *Acc. Chem. Res.*, **4**, 128 (1971); c) S. Nishida, I. Moritani, and T. Teraji, *Chem. Commun.*, **1971**, 36; d) A. A. P. Noodstrand, H. Steinberg, and Th. J. de Boer, *Tetrahedron Lett.*, **1975**, 2611; e) R. Noyori, Y. Kumagai, and H. Takaya, *J. Am. Chem. Soc.*, **96**, 634 (1974); f) R. Binger and J. McMeeking, *Angew. Chem. Int. Ed. Engl.*, **13**, 466 (1974); g) A. Baba, Y. Ohshiro, and T. Agawa, *J. Organomet. Chem.*, **110**, 121 (1976).

20) For example, L. B. Rodewald and C. H. De Puy, *Tetrahedron Lett.*, **1964**, 2951.

21) D. Kaufmann, A. de Meijere, B. Hingerty, and W. Saenger, *Angew. Chem. Int. Ed. Engl.*, **14**, 816 (1975).

22) E. H. Ingold, *J. Chem. Soc.*, **127**, 1203 (1925).

23) R. Koester, S. Arora, and P. Binger, *Synthesis*, **1971**, 322.

24) A. L. Henne and K. W. Greenlee, *J. Am. Chem. Soc.*, **67**, 484 (1945).

25) I. Schurman and C. E. Boord, *J. Am. Chem. Soc.*, **55**, 4931 (1933).

26) T. L. Cairns, R. A. Carboni, D. D. Coffman, V. A. Engelhardt., R. E. Heckett, E. L. Little, E. G. McGeer, W. J. Middleton R. M. Scribner, W. C. Theobald, and H. E. Winberg, *J. Am. Chem. Soc.*, **80**, 2775 (1958).

27) E. Le Goff, *J. Org. Chem.*, **29**, 2049 (1964).

28) As for the preparation of the corrsponding diethyl ester, see G. Eglinton and M. C. Whiting, *J. Chem. Soc.* **1953**, 3052.

Studies on the Tautomerism of 2-Anilinopyridine and Related Heterocycles. II. 2-Anilino-5-nitropyridine and 2-Anilinopyrimidine

Minoru HIROTA,* Toshiyuki SEKIYA, Akira HISHIKURA, Hiroko ENDO, Yoshiki HAMADA,** and Yoshio ITO**

Department of Applied Chemistry, Faculty of Engineering, Yokohama National University, Tokiwadai, Hodogaya-ku, Yokohama 240

***Faculty of Pharmacy, Meijo University, Tempaku-ku, Nagoya 468*

(Received June 28, 1979)

The tautomeric behavior of 5-nitro-2-anilinopyridine and 2-anilinopyrimidine was studied. 2-(*N*-Methylanilino) and 1-methyl-2-(phenylimino)-1,2-dihydro derivatives were prepared as models for the amino and imino tautomers, respectively, and their spectra were compared. The results and the assumed tautomeric equilibrium constants strongly suggest the equilibria to be favorable to the amino tautomers, the K_t values being considerably smaller than that of the parent 2-anilinopyridine.

Tautomeric equilibria of aminopyridines have been discussed by several investigators. From experimental evidences and theoretical consequences[1-5] it was concluded that the amino tautomers are considerably more stable than the imino tautomers. As regards 2-anilinopyridines, however, Bell *et al.*[6] and Rud'ko *et al.*[7] claimed the presence of a measurable amount of the imino tautomer on the basis of the splitting of their N–H stretching bands. Cook *et al.* discussed the tautomeric behavior from the ultraviolet spectra.[8] Studies were made on this problem and it was concluded that the tautomeric equilibria by far favor to the amino tautomer[9-10] and that the splitting of the N–H stretching bands is due to the presence of rotational isomers.[11] The tautomeric behavior of the title compounds was studied, since the introduction of the electron-withdrawing group, especially on the pyridine nucleus, might contribute to stabilize the imino tautomers.

Experimental

Preparation of Materials. 2-Anilino-5-nitropyridine (**1**) and 2-anilinopyrimidine (**4**) are known compounds and were prepared by condensing 2-chloropyrimidine and 2-chloro-5-nitropyridine with aniline. *N*-Methylanilino derivatives **2** and **5** were prepared similarly with use of *N*-methylaniline. 1-Methyl-5-nitro-2-(phenylimino)-1,2-dihydropyridine (**3**) and 1-methyl-2-(phenylimino)-1,2-dihydropyrimidine (**6**) are new compounds, and were prepared by the method previously reported.[10] **2**, mp 101 °C. Found: C, 62.80; H, 4.98; N, 18.15%, M^+, 229. Calcd for $C_{12}H_{11}N_3O_2$: C, 62.87; H, 4.84; N, 18.33%; M^+, 229. **3**, mp 119—120 °C. Found, C, 62.61; H, 5.10; N, 19.14%; M^+, 229 (an isomer of **2**). **5**, bp 125—126 °C/11 mmHg. Found C, 71.53; H, 6.16; N, 22.75%; M^+, 185. Calcd for $C_{11}H_{11}N_3$: C, 71.33; H, 5.99; N, 22.69% M^+, 185. **6**, mp 88—90 °C. Found: C, 71.80; H, 5.84; N, 22.51%; M^+, 185 (an isomer of **5**)

Measurement of Spectra. Ultraviolet and infrared spectra were measured with Hitachi EPS-3T and Hitachi 225 recording spectrophotometers, respectively. NMR spectra were obtained with a JEOL JNM C60-H spectrometer and, when necessary, $Eu(fod)_3$ was used to separate the overlapping signals. Details of the spectral measurement were imilar to those previously reported.[10]

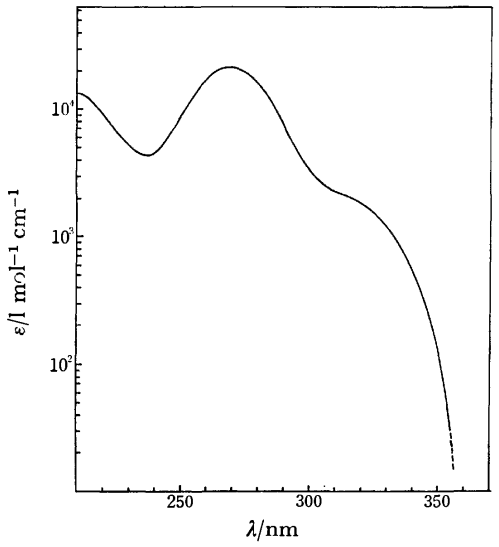

Fig. 1. Ultraviolet spectrum of **4** in aqueous ethanol (1:1).

Results and Discussion

Ultraviolet Spectra. The ultraviolet spectra of 2-anilino-5-nitropyridine (**1**), 2-anilinopyrimidine (**4**) and their *N*-methyl derivatives are given in Table 1. The spectra of **1** and **4** resemble considerably those of the corresponding *N*-methylanilino derivatives **2** and **5**, differing a great deal from those of the corresponding 1-methyl-2-(phenylimino)-1,2-dihydro derivatives **3** and **6**. Even when the measurements were carried out in highly polar solvents, **1** and **4** showed no absorption bands in the longer wavelength region in which the characteristic absorption bands of the pyridoneimine chromophores appear (Fig. 1). This suggests that **1** and **4** exist almost exclusively as the amino tautomer. Measurement in several other solvents also gave similar results.

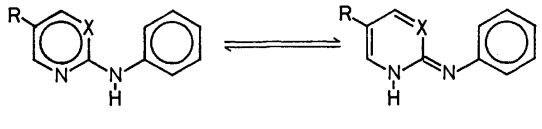

(I) (II)

In order to estimate the tautomeric equilibrium constants of **1** and **4**, the dissociation constants (K_a) of the amino (**2** and **5**) and the imino (**3** and **6**) model compounds were determined by means of the pH

Table 1. Ultraviolet spectra

Compound	λ_{max}/nm (ε_{max}/l·mol^{-1}·cm^{-1}) in C_6H_{12}		in CH_3CN		in C_2H_5OH	
1	247	(11500)	250	(15500)	215	(14700)
	348	(19400)	377	(21500)	378	(19300)
2 (amino)	220	(13600)	216—230	(12600)	218—233	(14400)
	350—353	(21500)	373	(19000)	365	(19300)
3 (imino)	217	(15900)	216	(15800)	215	(14300)
	350—354	(14500)	356—362	(13800)	350—356	(13000)
	376	(12000)*	375—392	(13000)*	394	(10300)*
4	270	(25800)	270	(28800)	273	(21300)
	300—310	(2500)*	310—315	(2500)*	308—310	(2300)*
5 (amino)	227	(13800)	234	(11500)	229	(12700)
	265	(12300)	254	(12300)	265	(14100)
	290—300	(2800)*	265—273	(11700)	300—320	(2400)*
			300—305	(3300)*		
6 (imino)	271	(7800)	280	(8900)	275	(7200)
	361	(1100)*	370	(1500)	367	(1400)

* shoulder

Table 2. The dissociation constants and tautomeric equilibrium constants

Compound	pK_a	K_t[a)]
1	0.59	8.0×10^3
2	0.76	
3	4.66	
4	5.20	5.5×10^2
5	5.26	
6	8.00	

a) K_t=[amino tautomer]/[imino tautomer].

Table 3. NMR spectra (in $CDCl_3$)

Compound	H(3)	H(4)	H(5)	H(6)	N-CH_3
1	6.92	8.22	—	9.03	—
2	6.25	7.87	—	8.95	3.55
3	6.30	7.48	—	8.42	3.61
4	—	8.34	6.65	8.34	—
5	—	8.28	6.53	8.28	3.51
6	—	8.07	5.80	8.07	3.47

Table 4. Infrared NH stretching absorptions (in CCl_4)

Compound	ν_{NH}/cm^{-1} (ε_{max}/l mol^{-1} cm^{-1})
2-Anilinopyridine	3417 (98)
	3444 (48)
1	3409 (84)
	3438 (39)
4	3432 (179)
3-Carboline	3476 (220)
Diphenylamine	3427

dependence of their ultraviolet spectra. The tautomeric equilibrium constants obtained from the K_a values by the equation $K_t=K_a$(amino)/K_a(imino) are given in Table 2. As expected, the K_t value of **1** and **4** is remarkably smaller than that of unsubstituted 2-anilinopyridine. The electron withdrawing nitro-group on the heterocyclic ring gives rise to the displacement of the unshared electrons on the exocyclic nitrogen atom towards the ring, favoring the imino tautomer. The effects is more pronounced when another carbon atom constituting the ring is substituted by a nitrogen atom. This is due to the electronegative nature of nitrogen atom. From the K_t value obtained, 2-anilinopyrimidine is expected to exist as a tautomeric mixture containing *ca.* 0.2% of the imino tautomer in aqueous ethanol solution. The amount of the imino tautomer corresponds to the apparent molar absorption coefficient of *ca.* 3 l mol^{-1} cm^{-1} in the longer wavelength region, being too low an intensity to be detected by the usual measurement of ultraviolet spectrum.

NMR Spectra. The NMR spectra of the heterocyclic ring protons of 2-anilino-5-nitropyridine, 2-anilinopyrimidine, and their *N*-methyl derivatives are given in Table 3.

The assignment of the signals was carried out by comparison with similar compounds, by using their lanthanoid induced shifts by Eu(fod)$_3$, and by the estimation from the electron densities. As has been shown from MO calculations,[10] the imino tautomer is expected to have considerable bond alternation in the heterocyclic part of its molecule. This causes a decrease in aromaticity of the heterocyclic ring, resulting in chemical shifts of the protons on the ring to displace towards higher fields. The effect is observed in the imino model compounds **3** and **6**, which is in line with the case of the imino models of 2-anilinopyridine and 2-anilino-4-methylquinoline. The spectra of **1** and **4** resemble as a whole the corresponding amino model compounds (**2** and **5**), there being no indication of the presence of the imino tautomers. Analogous to the case of unsubstituted 2-anilinopyridine, the hy-

drogen atom at the 3-position of the heterocyclic ring resonates at a higher field and is attributed to the anisotropy effect caused by the phenyl ring of anilino moiety, since the 3-H is located close on the phenyl ring in one (III) of the two possible rotational isomers. This is reasonable, since the effect is not predominant with **5** which is void of such steric hindrance and the molecule is supposed to be nearly planar.

Infrared Spectra and the Existence of Rotational Isomers. Existence of the tautomeric equilibrium is often presumed on the basis of the splitting in the N–H stretching bands of these and related aminopyridines. Surely it can be an indication of the tautomeric equilibria if other possibilities are excluded. However, the presence of rotational isomers (III and IV) has been suggested on several nitro-substituted 2-anilino-pyridines and -quinolines to explain the splitting of N–H absorptions.[11] As regards 2-anilinopyrimidine (**4**), the two rotational isomers are degenerate and the appearance of a single absorption band is predicted if the splitting is caused by rotational isomerism. In accord with this prediction, **4** has actually a single symmetrical absorption band at 3432 cm^{-1} in the N–H stretching region.

(III) (IV)

The imino compounds **3** and **6** exhibit very strong C=N stretching absorptions at 1649 and 1630 cm^{-1}, respectively. On the other hand, other compounds including **1** and **4** have no remarkable absorptions when the spectra were measured in carbon tetrachloride solutions.

From the results, the amino tautomers are found to be by far more favorable in the tautomeric equilibria of both **1** and **4**. As expected, the tautomeric equilibrium constants of these compounds are considerably lower than the tautomeric equilibrium constant ($K_t = 2 \times 10^{-5}$) of the parent 2-anilinopyridine.

This research was supported in part by a Grant-in-Aid for Special Project Research from the Ministry of Education, Science and Culture.

References

1) S. J. Angyal and G. L. Angyal, *J. Chem. Soc.*, **1952**, 1461.
2) M. J. Cook, A. R. Katritzky, P. Linda, and R. D. Tack, *Chem. Commun.*, **1971**, 510.
3) K. Undheim and T. Gronneberg, *Org. Mass Spectrom.*, **6**, 823 (1972).
4) K. Undheim and T. Gronneberg, *Tetrahedron Lett.*, **1972**, 3193.
5) N. Boder, M. J. S. Dewar, and A. J. Harget, *J. Am. Chem. Soc.*, **92**, 2929 (1970).
6) M. G. W. Bell, M. Day, and T. Peters, *J. Chem. Soc., C*, **1967**, 132.
7) A. P. Rud'ko, I. N. Chernyuk, and Yu. S. Rozum, *Ukr. Khim. Zh.*, **34**, 1275 (1968).
8) M. J. Cook, S. O. Chua, and A. R. Katritzky, *J. Chem. Soc., Perkin Trans. 2*, **1973**, 2111.
9) Y. Ito, Y. Hamada, and M. Hirota, *Chem. Pharm. Bull.*, **20**, 2678 and 2686 (1972).
10) Y. Takahashi, S. Otsuka, H. Masuda, M. Hirota, Y. Ito, and Y. Hamada, *Bull. Chem. Soc. Jpn.*, **49**, 2770 (1976).
11) T. Mizuno, M. Hirota, Y. Hamada, and Y. Ito, *Tetrahedron*, **27**, 6011 (1971).

An ESR Study of *N*-(Alkylthio)arylaminyls. Substituent Effects on ESR Parameters[1)]

Yozo MIURA,* Hidetsugu ASADA, and Masayoshi KINOSHITA

Department of Applied Chemistry, Faculty of Engineering, Osaka City University, Sumiyoshi-ku, Osaka 558

(Received June 28, 1979)

A series of *N*-(alkylthio)arylaminyls, ArNSR, were generated by hydrogen-abstraction from *N*-(alkylthio)-anilines or by the photolysis of *N*,*N*-bis(*t*-butylthio)anilines, and were studied by ESR spectroscopy. *N*-(*t*-Butylthio)aminyls were fairly long-lived, and their lifetimes were scarcely affected by oxygen. Substituent effects on the ESR parameters were also studied, and the results were compared with those for *N*-alkoxyarylaminyls.

A variety of *N*-alkoxyarylaminyls (**5**), ArNOR, were produced by hydrogen-abstraction from *N*-alkoxy-anilines,[2)] by addition of alkyl or metal radicals,[3)] and by the photolysis of peroxyoxalates,[4)] and they were studied in detail by means of ESR spectroscopy. Since the aminyls prossess an aromatic ring and an oxygen atom adjacent to the central nitrogen, they are significantly stabilized by such contributing resonance forms as $-\dot{N}-\ddot{O}\leftrightarrow\ddot{N}^{-}-\overset{+}{O}-$.

N-(Alkylthio)arylaminyls (**3**) are structurally very close to **5**; therefore, the comparison of their ESR parameters and stabilities with those for **5** is interesting. However, the aminyls **3** have never been reported on. In this paper we wish to report on the generation of **3** and their ESR spectroscopic investigation. In addition, the results will be compared with those for **5**.

Results and Discussion

The aminyls **3** were generated by hydrogen-abstraction from *N*-(alkylthio)anilines (**1**) by the *t*-butoxyl radical, which were produced by the thermal decomposition of di-*t*-butyl diperoxyoxalate (Method A) or by the photolysis of *N*,*N*-bis(*t*-butylthio)anilines (**2**) (Method B).

$$\mathrm{ArNHSR} \xrightarrow{-\mathrm{H}\cdot} \mathrm{ArNSR} \quad \text{(Method A)}$$

1 **3**

a: Ar = 4-$NO_2C_6H_4$, R = *t*-Bu
b: Ar = 3-$NO_2C_6H_4$, R = *t*-Bu
f: Ar = 3,5-*t*-$Bu_2C_6H_3$, R = *t*-Bu
n: Ar = 3,5-*t*-$Bu_2C_6H_3$, R = *i*-Pr
o: Ar = 3,5-*t*-$Bu_2C_6H_3$, R = *n*-Bu

$$\mathrm{ArN(SBu\text{-}}t)_2 \xrightarrow{h\nu} \mathbf{3} + t\text{-BuS}\cdot \quad \text{(Method B)}$$

2 (R = *t*-Bu)

c: Ar = C_6H_5
d: Ar = C_6D_5
e: Ar = 4-$CH_3C_6H_4$
f: Ar = 3,5-*t*-$Bu_2C_6H_3$
g: Ar = 4-ClC_6H_4
h: Ar = 3-ClC_6H_4
i: Ar = 4-BrC_6H_4
j: Ar = 4-$CH_3OC_6H_4$
k: Ar = 3-$CH_3OC_6H_4$
l: Ar = 4-$CH_3COC_6H_4$
m: Ar = 3-$CH_3COC_6H_4$

The precursors, **1**, were prepared by the reaction of the appropriate anilines with sulfenyl chlorides in the presence of triethylamine; **1a** and **1b** were obtained as yellow crystals, while **1f**, **1n**, and **1o** were each obtained as a viscous oil.[5)]

Hydrogen-abstraction from **1** was performed by the reaction with di-*t*-butyl diperoxyoxalate at room temperature; relatively strong ESR signals were thus obtained. The assignment of the signals were performed on the basis of their splitting patterns and also on the basis of their relatively large *g*-values (2.0061—2.0071). For example, the ESR spectrum of **3f** (Fig. 1) is split into 1 : 2 : 1 triplets (3.68 G), 1 : 1 doublets (4.20 G), and a 1 : 1 : 1 triplet (9.93 G). The 1 : 1 : 1 triplet is obviously due to the central nitrogen nucleus, while the 1 : 1 doublets and the 1 : 2 : 1 triplets are due to the para- and ortho-protons respectively. In the cases of **3n** and **3o**, splittings due to the γ protons were observed in addition to the splittings due to the nitrogen nucleus and the ring protons.

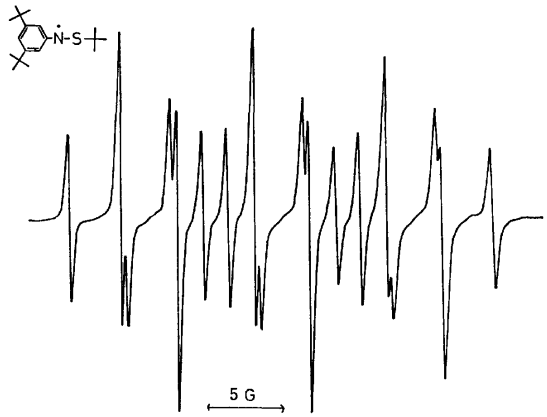

Fig. 1. ESR spectrum of **3f** recorded for the benzene solution containing **1f** and di-*t*-butyl diperoxyoxalate (17 °C).

The compounds **2** were prepared by the reaction of the appropriate anilines with more than two equivalents of sulfenyl chloride and were isolated as colorless crystals. The compounds **1** are relatively unstable because of the presence of the active hydrogen (NH). On the other hand, **2** are very stable and can be stored for a long time without any detectable decomposition.

The compounds **2** absorb light at 239—328 nm (ε: 2170—22500 in benzene) and, on irradiation with a high-pressure mercury lamp, undergo homolysis to give **3** in a moderate concentration. Therefore, this procedure (Method B) is excellent for the generation of **3**. However, when the irradiation was continued, secondary radicals often appeared and the analysis of the spectra was disturbed. For this reason, an appropriate period of irradiation, usually 0.5—3 min, is required in order to obtain clean ESR spectra of **3**. The aminyls, **3a**, **3b**, **3n**, and **3o**, were obtained by

Table 1. ESR parameters for *N*-(alkylthio)arylaminyls (**3**)[a]

	X	R	Coupling constant/G a_N	$a_{o\text{-H}}$	$a_{m\text{-H}}$	$a_{p\text{-H}}$	a_{other}	*g*-Value
3a[b]	4-NO_2	*t*-Bu	8.68	3.25	1.21	—	1.00 (NO_2)	2.0071
3b[b]	3-NO_2	*t*-Bu	9.64	3.56[c]	1.31	3.75		2.0068
3c[b]	H	*t*-Bu	9.92	3.79	1.27	4.10		2.0065
3d	D_5	*t*-Bu	9.92	—	—	—		2.0065
3e[b]	4-CH_3	*t*-Bu	9.83	3.83	1.27	—	4.71 (CH_3)	2.0062
3f[d]	3,5-*t*-Bu_2	*t*-Bu	9.93	3.68	—	4.20		2.0065
3g[b]	4-Cl	*t*-Bu	9.67	3.75	1.32	—		2.0068
3h[b]	3-Cl	*t*-Bu	9.76	3.64 and 3.79	1.29	4.09		2.0065
3i[b]	4-Br	*t*-Bu	9.58	3.79	1.29	—		2.0065
3j[b]	4-CH_3O	*t*-Bu	9.45	3.75	1.09	—	0.54 (OCH_3)	2.0061
3k[b]	3-CH_3O	*t*-Bu	9.88	3.54 and 4.08	1.29	4.29		2.0065
3l[b]	4-CH_3CO	*t*-Bu	9.32	3.52	1.23	—		2.0059
3m[b]	3-CH_3CO	*t*-Bu	9.78	3.70	1.22	3.97		2.0066
3n[b]	3,5-*t*-Bu_2	*i*-Pr	9.86	3.79	—	4.21	2.64 (γ-1H)	2.0065
3o[b]	3,5-*t*-Bu_2	*n*-Bu	9.75	3.73	—	4.21	2.59 (γ-2H)	2.0065

a) In benzene at 17 °C. b) The splitting constants were determined by computer simulation. c) The two ortho-protons seem to be magnetically unequivalent, but their a_H values were apparently equivalent because of the relatively broad hyperfine line. d) Absorbs at 556 nm (benzene).

Method A, while **3c**—**e** and **3g**—**m** were generated by method B and **3f** was obtained by both methods. The ESR parameters for the **3f** generated by Method A were identical with those for the **3f** obtained by Method B. The ESR parameters for **3** are summarized in Table 1.

In order to confirm that the present aminyls differ from the corresponding nitroxides **4**, **4a** was generated by the addition reaction of *t*-butylthiyl radical to nitrosobenzene and its ESR parameters were compared with those for **3c**. The ESR parameters for **4a** (in benzene) are 12.64 (a_N); 1.87 ($a_{o\text{-H}}$); 0.85 ($a_{m\text{-H}}$); 2.01 G ($a_{p\text{-H}}$); 2.0061 (*g*-value),[6] quite different from those for **3c**. Thus, the possibility that the present aminyls may be **4** was completely excluded.

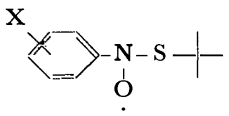

4 (**4a**: X=H)

The aminyl **3f** was also generated in some polar solvents (chloroform, THF, acetonitrile, and ethanol), and the ESR parameters were measured in order to examine the solvent effect on the splitting constants for **3**. The a_N values obtained for **3f** in these solvents are in the range of 9.89—9.93 G, indicating that the magnitudes of the a_N values are independent of the solvent polarity. From this result, it can be said that the spin distribution in **3** is scarcely influenced by the solvent polarity.

When R in **3** is *t*-butyl, the corresponding aminyls are fairly long-lived. The results of the decay kinetic studies are illustrated in Fig. 2. The aminyl, **3e**, decayed with clean second-order kinetics (k=1.7 l mol^{-1} s^{-1}), while **3c** and **3f** persisted for more than one day ($\tau_{1/2}$>half a day). The high persistence observed for

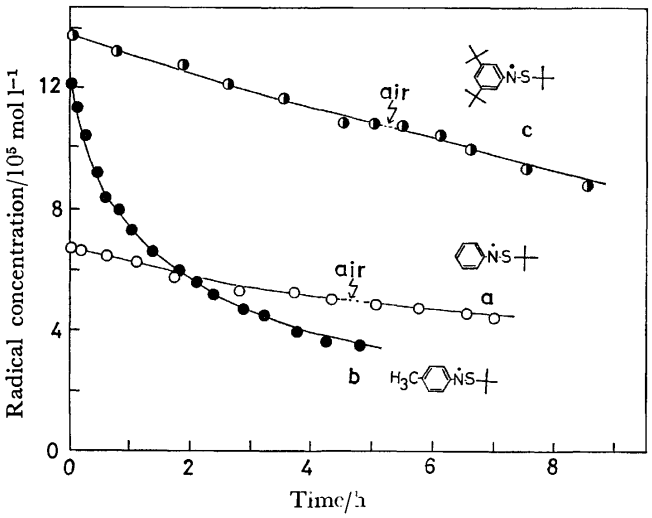

Fig. 2. Decay plots of **3c** (a), **3e** (b), and **3f** (c) in deoxygenated benzene and in benzene saturated with air (17 °C).

these aminyls is comparable to those of the oxygen analogs, **5**.[2-4]

The ESR signal intensity of **3f** in toluen, when the temperature was lowered to *ca.* −75 °C, became weaker, while when the temperature was raised to room temperature (20 °C), it was again restored, and this cycle was reversible. From this observation, it seems that **3** exist in equilibrium with a dimer.[2d]

In order to know whether **3** react with oxygen or not, the decay kinetics was also examined in the presence of oxygen. The results are shown in Fig. 2. After the measurement of the decay rate of **3** for 5 h under deoxygenated conditions, air was bubbled into the solution of **3** and the measurement was again carried out. As can be seen from the figure, the decay rates after

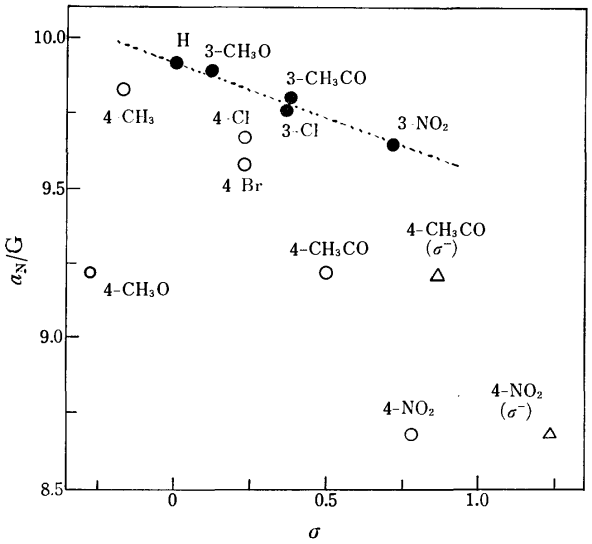

Fig. 3. Plots of a_N values *vs.* σ (○ and ●) and σ^- (△) for **3**.

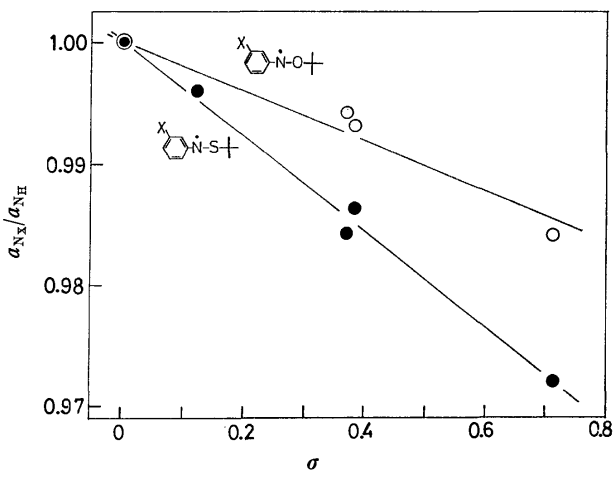

Fig. 4. Plots of a_{N_X}/a_{N_H} *vs.* σ for **3** (●) and **6** (○). a_{N_X}:a_N value for meta-substituted **3** and **6**; a_N:a_{N_H} value for unsubstituted **3** and **6**.

this point are almost identical with those observed under the deoxygenated conditions, suggesting that **3** do not react with oxygen much, if at all. Since **3** are typical nitrogen-centered free radicals, this result is of interest.

Substituent Effects. The a_N values for **3** lie in the range of 8.68—9.93 G, in the range of magnitude expected for nitrogen-centered free radicals in a π-electronic ground state.[7]

When we consider the substituent effects on ESR parameters, two limiting cases may be envisioned; that is, in terms of Walter's criteria, Class O and Class S.[8] Numerous ESR spectroscopic investigations of substituent effects have been reported, and aryl nitroxide radicals and nitrobenzene anion radicals have been classified as Class O,[9] while *N*-*t*-butylarylaminyls,[10] *N*-*t*-butoxyarylaminyls (**6**),[4] *N*-aryl-*N*-(arylthio)-aminyls (**7**),[11] *etc.* have been classified as Class S.

In Fig. 3, the a_N values for **3** are plotted against the Hammett σ and σ^- constants.[12] As can be seen from the figure, the a_N values do not correlate with these constants: both the electron-donating and electron-accepting substituents reduce the a_N values, and the unsubstituted aminyl, **3c**, exhibits the largest a_N value. Such a behavior of **3** in relation of the σ and σ^- constants indicates that **3** belong to Class S, where a_N values are determined predominantly by the extent of the delocalization of the unpaired electron onto the substituent. In the present aminyls, however, the substituents may also influence the relative importance of the resonance forms, A and B, just in the cases of **6**[4] and **7**.[11] That is, substituents not only delocalize the unpaired electron, but also influence the relative importance of the resonance forms, A and B, as has been pointed out by Danen *et al.*[4] When more powerful electron-accepting substituents are introduced, the polar form B becomes more important, resulting in a reduction of the spin density on the central nitrogen with an increase in the spin density on the sulfur. In the case of the para-substituted **3**, the two effects compete with each other in the determination of the magnitude of the a_N value. That is, when σ and σ^->0, both the effects reduce the a_N value. On the other hand, when σ<0, the former effect reduces the a_N value, while the latter effect (inductive effect) increases the a_N value. As can be seen from the figure, the a_N values are reduced in any case. From these results, it can be said that the magnitudes of the a_N values are determined predominantly by the extent of the delocalization of the unpaired electron onto the substituent, while the inductive effect is of secondary importance.

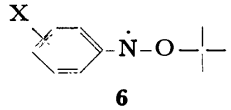

6

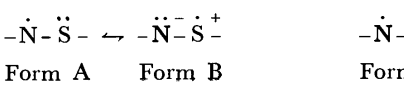

Form A Form B Form C Form D

On the other hand, in the case of the meta-substituted **3**, the extent of the delocalization of the unpaired electron onto the substituent is small. Therefore, the magnitudes of the a_N values are determined only by the inductive effect of the substituent; thus, the a_N values for the meta-substituted **3** are correlated with the σ constants (see Fig. 3). In conclusion, the magnitudes of the a_N values for **3** are determined predominantly by the extent of the delocalization of the unpaired electron onto the substituent; therefore, **3** belongs to Class S.

The aminyls **3** are structurally very close to **6**.[2d,4] The a_N values reported for **6** are in the range of 9.95—11.00 G, which are larger by *ca.* 1 G than those for **3**.[13] Similarly, the $a_{o\text{-H}}$ (4.34—4.80 G) and $a_{p\text{-H}}$ values (4.90—5.15 G) for **6** are also larger by *ca.* 1 G than those for **3**. This reduction in the magnitude of the splitting constants observed in going from **6** to **3** can be interpreted in terms of the greater ability of the sulfur to remove the spin from the central nitrogen compared with that of the oxygen.[14] In **3** and **6**, the spin is delocalized onto the sulfur or the oxygen by the contribution of the polar resonance form, B

TABLE 2. YIELDS, AND PHYSICAL AND ANALYTICAL DATA FOR *N*,*N*-BIS(*t*-BUTYLTHIO)ANILINES (**2**)

Compd	Yield[a] %	Mp °C	λ_{max}[b] nm	ε[b]	NMR[c] δ/ppm	Formula	Found (%) (Calcd) C	H	N
2c	18	47— 48	252	11000	1.20 (s, *t*-Bu, 18H), 6.75—7.72 (m, aromatic, 5H)	$C_{14}H_{23}NS_2$	62.55 (62.40	8.62 8.60	5.03 5.20)
2d	20	48— 49	252	11300	1.18 (s, *t*-Bu, 18H)	$C_{14}H_{18}ND_5S_2$	61.41 (61.25	8.40 8.45	4.80 5.10)
2e	26	96— 97	254	12600	1.16 (s, *t*-Bu, 18H), 2.24 (s, CH_3, 3H), 6.88 and 7.45 (d, J=9 Hz, aromatic, 4H)	$C_{15}H_{25}NS_2$	63.23 (63.55	8.95 8.89	4.58 4.94)
2f	56	87— 88	253	10400	1.22 (s, *t*-Bu, 18H), 1.33 (s, *t*-Bu, 18H), 6.92—7.65 (m, aromatic, 3H)	$C_{22}H_{39}NS_2$	69.04 (69.23	10.22 10.30	3.46 3.67)
2g	15	127—128	258	15000	1.20 (s, *t*-Bu, 18H), 6.98 and 7.46 (d, J=9 Hz, aromatic, 4H)	$C_{14}H_{22}NClS_2$	55.51 (55.33	7.46 7.30	4.56 4.61)
2h	14	68— 60	255	11500	1.21 (s, *t*-Bu, 18H), 6.62— 7.63 (m, aromatic, 4H)	$C_{14}H_{22}NClS_2$	55.40 (55.33	7.46 7.30	4.55 4.61)
2i	17	144—145	260	16400	1.19 (s, *t*-Bu, 18H), 7.16 and 7.50 (d, J=9 Hz, aromatic, 4H)	$C_{14}H_{22}NBrS_2$	48.38 (48.26	6.47 6.37	3.65 4.02)
2j	26	101—102	254 305	12200 2170	1.17 (s, *t*-Bu, 18H), 3.68 (s, CH_3, 3H), 6.59 and 7.40 (d, J=9 Hz, aromatic, 4H)	$C_{15}H_{25}NOS_2$	59.77 (60.15	8.62 8.41	4.43 4.68)
2k	18	66— 67	252 286 293	8870 3460 2990	1.20 (s, *t*-Bu, 18H), 3.71 (s, CH_3, 3H), 6.15—7.13 (m, aromatic, 4H)	$C_{15}H_{25}NOS_2$	60.00 (60.15	8.44 8.41	4.35 4.68)
2l[d]	13	132—133	308	22500	1.20 (s, *t*-Bu, 18H), 2.42 (s, CH_3 3H), 7.65 (s, aromatic, 4H)	$C_{16}H_{25}NOS_2$	61.46 (61.69	7.96 8.09	4.38 4.50)
2m[e]	16	100—101	239 328	24100 4330	1.20 (s, *t*-Bu, 18H), 2.46 s, CH_3, 3H), 7.15—8.19 (m, aromatic, 4H)	$C_{16}H_{25}NOS_2$	61.44 (61.69	8.04 8.09	4.40 4.50)

a) Yields are determined based on anilines. b) Solvent: hexane. c) Solvent: carbon tetrachloride. d) IR (KBr): 1670 cm^{-1} (CO). e) IR (KBr): 1680 cm^{-1} (CO).

or D.[15] When the relative importance of B in **3** is superior to that of D in **6**, the sulfur would remove the spin from the central nitrogen to a greater extent than the oxygen in **6**, and the central nitrogen in **3** would be charged more negatively than that in **6**. The greater ability of the sulfur to remove the spin compared with the oxygen can be explained from the results of the present study on the substituent effects. In Fig. 4, the ratio of a_{N_X}/a_{N_H} (a_{N_X} : a_N value for *meta*-substituted **3** and **6**; a_{N_H} : a_N value for unsubstituted **3** and **6**) are plotted against the σ constants. The slopes in the figure are determined by the amount of the negative charge on the central nitrogen in **3** or **6**. That is, the greater the negative charge on the central nitrogen, the larger becomes the slope. The slope obtained for **3** is −0.038, while it is −0.020 for **6**, indicating that the relative importance of B in **3** is superior to that of D in **6**. From this result, the greater ability of the sulfur to remove the spin from the central nitrogen can be explained by the greater contribution of B in **3** compared with that of D in **6**.

Experimental

All melting points are uncorrected. IR spectra were run on a JASCO Model IR-G spectrometer. UV and visible spectra were recorded with a Hitachi recording spectrometer, Model ESP-3T, and NMR spectra with a Hitachi Perkin Elmer R-20 spectrometer using TMS as an internal standard.

3,5-Di-*t*-butylaniline[16] and di-*t*-butyl diperoxyoxalate[17] were prepared by the reported methods. 2-Methyl-2-propanesulfenyl chloride was prepared as follows:[18] chlorine was bubbled into di-*t*-butyl disulfide (4.8 g, 0.027 mol) in hexane (50 ml) at 30±3 °C for 30—50 min, and then an excess of chloride dissolved in the reaction mixture was expelled by bubbling nitrogen. The hexane solution of the chloride thus obtained was used in the following reaction without any further purification. 1-Methylethanesulfenyl and butanesulfenyl chlorides were also prepared similarly. Other reagents were obtained commercially and were used without purification. Column chromatography was performed on alumina (E. Merck, Art 1097; column-size: 3×30 cm).

*N-(t-Buthylthio)-4-nitroaniline (**1a**).* A hexane solution of 2-methyl-2-propanesulfenyl chloride, prepared as has been described above, was added dropwise to a stirred solution

of 4-nitroaniline (7.0 g, 0.051 mol) and triethylamine (6.0 g, 0.059 mol) in dry THF (400 ml) at 0—5 °C. After the addition, the reaction mixture was stirred for 2 h at the same temperature and then filtered. The filtrate was concentrated under reduced pressure, and the resulting residue was chromatographed [eluent: benzene–hexane (10:1)]. Recrystallization from hexane gave yellow needles; mp 124—125 °C: yield, 1.3 g (11%). IR (KBr): 3310 cm^{-1} (NH). NMR (CCl_4): δ 1.31 (s, *t*-Bu, 9H), 6.08 (br s, NH, 1H), and 7.25 and 8.23 (d, J=10 Hz, aromatic, 4H). Found: C, 52.90; H, 6.04; N, 12.52%. Calcd for $C_{10}H_{14}N_2O_2S$: C, 53.07: H, 6.23; N, 12.38%.

N-*(t-Butylthio)-3-nitroaniline (**1b**)*. The aniline was obtained analogously to **1a**. Yellow plates; mp 100—102 °C; yield, 2.4 g (21%). IR (KBr): 3350 cm^{-1} (NH). NMR (CCl_4): δ 1.30 (s, *t*-Bu, 9H), 5.38 (br s, NH, 1H), and 7.35—8.01 (m, aromatic, 4H). Found: C, 52.98; H, 5.93; N, 12.56%. Calcd for $C_{10}H_{14}N_2O_2S$: C, 53.07; H, 6.23; N, 12.38%.

N-*(t-Butylthio)-3,5-di-t-butylaniline (**1f**)*.[5] A hexane solution of 2-methyl-2-propanesulfenyl chloride, prepared as has been described above, was added dropwise to a stirred solution of 3,5-di-*t*-butylaniline (10.4 g, 0.051 mol) and triethylamine (6.0 g, 0.059 mol) in dry ether (400 ml) at 0—5 °C. After the addition, the reaction mixture was stirred for 2 h at the same temperature and then filtered. The filtrate was concentrated under reduced pressure, and the resulting residue was chromatographed (eluent: hexane), giving a pale yellow oil of **1f** containing a slight amount of impurities. Yield, 2.4 g (15%). IR (neat): 3300 cm^{-1} (NH). NMR (CCl_4): δ 1.30 (s, *t*-Bu, 27H), 4.86 (br s, NH, 1H), and 6.92 (b, aromatic, 3H).

N-*(Isopropylthio)-3,5-di-t-buytlaniline (**1n**)*.[5] The aniline was prepared analogously to **1f** and was separated by column chromatography as a pale yellow oil containing a slight amount of impurities. Yield, 1.2 g (8%). IR (neat): 3320 cm^{-1} (NH). NMR (CCl_4): δ 1.20 (d, J=7 Hz, CH_3, 6H), 1.29 (s, *t*-Bu, 18H), 3.06 (sept. J=7 Hz, $CHMe_2$, 1H), 4.70 (br s, NH, 1H), and 6.75 (s, aromatic, 3H).

N-*(Butylthio)-3,5-di-t-butylaniline (**1o**)*.[5] The aniline was prepared analogously to **1f** and was separated by column chromatography as a pale yellow oil containing a slight amount of impurities. Yield, 1.8 g (12%). IR (neat): 3350 cm^{-1} (NH). NMR (CCl_4): δ 0.90—1.46 (br m, $CH_3CH_2CH_2$, 7H), 1.28 (s, *t*-Bu, 18H), 2.57 (*t*, J=8 Hz, SCH_2, 2H), 6.70 (s, aromatic, 3H).

General Procedure for the Preparation of N,N-*Bis(t-butylthio)-aniline (**2**)*. A hexane solution of 2-methyl-2-propanesulfenyl chloride, prepared as has been described above, was added dropwise to a stirred solution of aniline (0.015 mol) and triethylamine (0.069 mol) in dry ether (400 ml) at 0—5 °C. After the addition, the reaction mixture was stirred for 20 h at room temperature and then filtered. The filtrate was concentrated under reduced pressure, and the resulting oily residue was chromatographed on alumina [eluent: hexane for **2c—k** and benzene–hexane (1:2) for **2l** and **2m**]. Subsequent recrystallization from methanol afforded needles of **2**.[19] The yield, and physical and analytical data are summarized in Table 2.

*Generation of **3** from **1**.* Aniline **1** (20 mg), di-*t*-butyl diperoxyoxalate (20 mg), and benzene (0.20 ml) were placed in an ESR cell, degassed by three freeze-and-thaw cycles, and then sealed. The ESR spectra were recorded at 17 °C.

*Generation of **3** by Photolysis of **2**.* An aniline, **2** and a solvent (0.20 ml) were placed in an ESR cell, degassed as has been described above, and then sealed. After photolysis for 0.5—3 min in the cavity of an ESR instrument with a high-pressure mercury lamp (JES-UV-1, 100 W), the ESR signal was recorded.

*Generation of Nitroxide **4a**.* Nitrosobenzene (10 mg), 2-methyl-2-propanethiol (10 mg), di-*t*-butyl diperoxyoxalate (10 mg), and benzene (0.20 ml) were placed in an ESR cell, degassed as has been described above, and then sealed. The ESR signal was recorded at 20 °C.

Decay Kinetics. A degassed benzene solution (0.20 ml) of **2** in an ESR cell was irradiated for 0.5—3 min as has been described above. The decay rates of **3** were measured at 17 °C in the dark by monitoring the ESR signal intensities. The concentrations of **3** were determined as follows: integrated signals were recorded on the ESR instrument eqipped with a JES-ID-2 integrator. The areas under integrated curves were determined by means of their weights. The calibration curves were obtained using benzene solutions of 3,4-dihydro-2,4,6-triphenyl-2*H*-1,2,4,5-tetrazin-1-yl as a standard.[20] Integrated signals of the samples and the references were recorded with the same instrument settings. The concentrations are believed to be accurated to ±10%.

The ESR spectra were recorded on a JES-ME-3X spectrometer with an X-band microwave unit and 100 kHz field modulation. The splitting constants and the *g*-values for **3** were determined by comparison with the a_N value (13.09 G) and the *g*-value (2.0057) of Fremy's salt. The computer simulations of the ESR spectra were performed using a FACOM 230-60 computer equipped with a FACOM F-6201D plotter.

References

1) Part XI of this series, "ESR Studies of Nitrogen-centered Free Radicals," For Part X, see Y. Miura, Y. Katsura, and M. Kinoshita, *Bull. Chem. Soc. Jpn.*, **52**, 1121 (1979).

2) a) A. T. Balaban, P. T. Frangopol, M. Frangopol, and N. Negoita, *Tetrahedron*, **23**, 4661 (1967); b) N. Negoita, R. Baican, and A. T. Balaban, *Tetrahedron Lett.*, **1973**, 1877; c) F. Maria, P. T. Frangopol, and N. Negoita, *Rev. Roum. Chim.*, **19**, 1773 (1974); d) R. A. Kaba and K. U. Ingold, *J. Am. Chem. Soc.*, **98**, 7375 (1976).

3) a) S. Terabe and R. Konaka, *J. Chem. Soc., Perkin Trans. 2*, **1973**, 369; b) W. Ahrens and A. Berndt, *Tetrahedron Lett.*, **1973**, 4281; c) K. Reuter and W. P. Neumann, *Tetrahedron Lett.*, **1978**, 5235.

4) W. C. Danen, C. T. West, and T. T. Kensler, *J. Am. Chem. Soc.*, **95**, 5716 (1973).

5) Since the oily products **1** were found from their NMR spectra to be slightly contaminated with impurities, the distillation of **1** was carried out in order to purify them. However, this operation resulted in the decomposition of **1**. For this reason, the crude **1** were used in the reaction with di-*t*-butyl diperoxyoxalate without any further purification.

6) The coupling constants were fitted by computer simulation.

7) W. C. Danen and F. A. Neugebauer, *Angew. Chem.*, **87**, 823 (1975).

8) R. I. Walter, *J. Am. Chem. Soc.*, **88**, 1923 (1966).

9) E. G. Janzen, *Acc. Chem. Res.*, **2**, 279 (1969).

10) S. F. Nelsen, R. T. Landis, L. H. Kiehle, and T. H. Leung, *J. Am. Chem. Soc.*, **94**, 1610 (1972).

11) Y. Miura and M. Kinoshita, *Bull. Chem. Soc. Jpn.*, **50**, 1142 (1977).

12) For σ constants, see D. H. McDaniel and H. C. Brown, *J. Org. Chem.*, **23**, 420 (1958), and for σ^-, see A. I. Biggs and R. A. Robinson, *J. Chem. Soc.*, **1961**, 388.

13) For the equation $a_N = Q_N \rho_N$, the magnitude of Q_N for

3 seems to be similar to that for **6**. See Ref. 7 also.

14) a) A. Hudson and K. D. J. Root, *J. Chem. Soc., B*, **1970**, 656; b) A. Ohno, N, Kito, and Y. Ohnishi, *Bull. Chem. Soc. Jpn.*, **44**, 470 (1971); c) I. Biddles, A. Hudson, and J. T. Wiffen, *Tetrahedron*, **28**, 867 (1972); d) B. C. Gilbert, J. P. Larkin, and R. O. C. Norman, *J. Chem. Soc., Perkin Trans. 2*, **1973**, 272; e) G. Brunton, J. F. Taylor, and K. U. Ingold, *J. Am. Chem. Soc.*, **98**, 4879 (1976).

15) The participation of the d-orbital of the sulfur atom in **3** is not taken into consideration.

16) N. L. Allinger, H. M. Blatter, L. A. Freiberg, and F. M. Karkowski, *J. Am. Chem. Soc.*, **88**, 2999 (1966).

17) P. D. Bartlett, E. P. Benzing, and R. E. Pincock, *J. Am. Chem. Soc.*, **82**, 1762 (1960).

18) C. M. Himel, *Chem. Abstr.*, **52**, 14706a (1958). See also E. Kühle, *Synthetis*, **1970**, 561.

19) When **2** contained a significant amount of di-*t*-butyl disulfide, recrystallization was unsuccessful. In this case, the disulfide was removed by heating at 50 °C under a reduced pressure, and then the resulting residue was recrystallized.

20) R. Kuhn and H. Trischmann, *Monatsh. Chem.*, **95**, 457 (1964).

Reactions of Aryldiazomethanes with Chloranil

Takumi OSHIMA and Toshikazu NAGAI*

Institute of Chemistry, College of General Education, Osaka University, Toyonaka, Osaka 560

(Received July 3, 1979)

The reactions of several aryldiazomethanes (**1a**: *p*-tolyl; **1b**: phenyl; **1c**: *p*-chlorophenyl) with chloranil gave stilbenes (**3**) and spiro-oxetanes (**4**) at 20 °C in tetrahydrofuran or 1,2-dichloroethane. The isomer ratios of **3** were *ca.* 2 to 3:1 in favor of *cis*, depending on the solvents and on the substituents of **1**. In the case of **4**, however, stable *trans*-isomers were selectively formed. On the other hand, the presence of added CH_3OH suppressed the formations of **3** and **4** and, instead, induced redox reactions giving α,α-dimethoxyarylmethanes and tetrachlorohydroquinone (**6**). In these redox reactions, the acid decompositions of **1** with **6** were also found. However, the presence of CF_3CH_2OH allowed the formation of considerable amount of **3** and **4**, along with the redox products. The mechanism of these reactions will be discussed.

Diazoalkanes are useful synthetic intermediates in organic chemistry and are best represented as resonance hybrid structures with opposing dipoles.[1] These compounds, therefore, behave as 1,3-dipoles[2] or as nucleophiles[3] because of the high electron density on diazo carbon. On the other hand, quinones have conjugated two C=O and two C=C double bonds to be considered as dipolarophiles.[4] Moreover, halogen and/or cyano substituted quinones, such as chloranil and dichlorodicyano-*p*-benzoquinone, become strong electron acceptors.[5] Therefore, the reactions of diazoalkanes with quinones are interesting from the viewpoint of mechanistic study or synthetic application. For example, Pechmann[6] has reported the formation of a pyrazoline derivative through the 1,3-dipolar cycloaddition of diazomethane to the C=C bond of *p*-benzoquinone. In the case of tetrahalo-substituted quinones, epoxides were isolated in the reactions with diazomethane because the C=O bond is more reactive than the C=C bond in these quinones.[7] In this paper, we want to describe the reactions of some aryldiazomethanes(**1**) with chloranil(**2**) with or without added CH_3OH or CF_3CH_2OH.[8]

Results and Discussion

*The Reactions of Aryldiazomethanes (**1a**—**c**) with Chloranil (**2**) in THF or CH_2ClCH_2Cl.* The reactions of **1a**—**c** with **2** gave mainly *cis*- and *trans*-stilbenes(**3a**—**c**) and *trans*-spiro-oxetanes(**4a**—**c**), as is shown in Scheme 1. Besides **3** and **4**, small amounts of several products were isolated: benzaldehydes(**5′ a**—**c**), tetrachlorohydroquinone(**6**), tetrachloro-4-(benzyloxy)phenols(**7a**—**c**), tetrachloro-1,4-bis(benzyloxy)benzenes(**8a**—**c**), and tetrachloro-4-[4′-(benzyloxy)butoxy]phenols (**9a**—**c**). The **9** products were obtained only in the THF solution because these compounds incorporated the THF molecule. Since these by-products were afforded by the action of the residual water present in the solvent, a detailed mechanism will be presented later for the case of the reactions in the presence of CH_3OH or CF_3CH_2OH. The reaction conditions and the product distributions are summarized in Table 1.

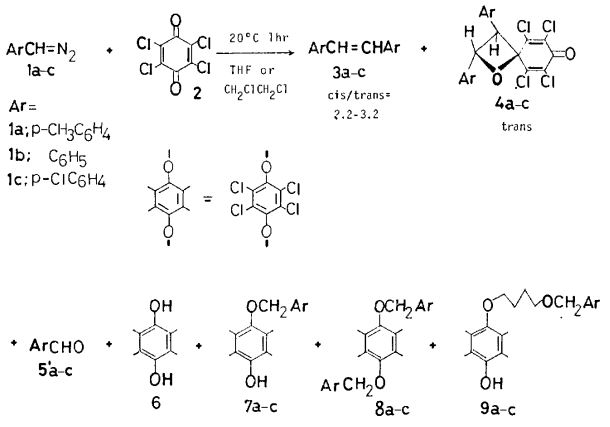

Scheme 1.

In both THF and 1,2-dichloroethane, **3** were major products. The yield of **4** was considerably greater in 1,2-dichloroethane than in THF. Here, particular attention should be paid to the stereochemistry of **3** because the thermodynamically less stable *cis*-isomers were about 2 to 3 times more numerous than the *trans*-isomers, depending on the solvents and on the substituents of **1**. On the other hand, **4** were shown to be the only stable *trans*-isomers by comparison with an authentic sample produced by the photoaddition of *trans*-**3b** and **2**, and also by the fact that the thermal decomposition of **4** at slightly over their melting points for several minutes gave *trans*-**3** and **2**. As is exemplified in the case of **1b** in THF, the ratio of **1** to **2** had no essential influence on the product distributions.

Mechanistically, the formation of **4** needs an intermediate because *cis*- or *trans*-**3** was quantitatively recovered after 5-hs' mixing with an equimolar amount of **2** in THF or 1,2-dichloroethane at room temperature. The most reasonable process is the occurrence of the diazonium betaine intermediate(II) which can produce **4** or **3** by way of Path(a) or Path(b), as is shown in Scheme 2.

Though II may be formed through the nucleophilic attack of **1** on the first diazonium betaine(I, or carbonium betaine given by the loss of N_2), the mechanism

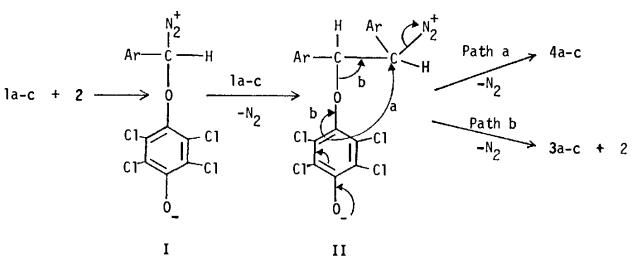

Scheme 2.

Table 1. Product distributions in the reactions of aryldiazomethanes (**1a—c**) with chloranil (**2**) in THF or CH_2ClCH_2Cl at 20 °C[a)]

1a—c and **2** (mmol)		Solv.	Yield/%[b)]						
			3(*cis*/*trans*)	**4**	**5′**	**6**	**7**	**8**	**9**
1a (7.35)	**2** (2.03)	THF	69.0 (2.4)	15.6	6	2	4	0.5	0.5
1b (8.47)	**2** (2.03)		75.5 (2.8)	8.1	6	1	2.5	0.5	2.5
1b (8.47)	**2** (4.06)		73.7 (2.8)	7.5	7	1.5	2.5	0.5	3
1c (6.58)	**2** (2.03)		72.3 (3.2)	6.2	10	1	4	1	3
1a (7.35)	**2** (3.25)	CH_2Cl | CH_2Cl	60.0 (2.2)	31.7	4	0.5	2	1	—
1b (8.31)	**2** (2.03)		59.7 (2.5)	26.4	6	2	3.5	1	—
1c (5.92)	**2** (2.03)		59.5 (2.9)	20.6	11	3	5	2	—

a) Reaction time 1 h. b) Yield as mole percentage based on **1**.

giving I remains unknown. However, three possible routes can be suggested. The first one is the radical-ion formation, followed by the simultaneous recombination presumed in our previous communication.[9)] Radical cations of diazoalkanes have already been postulated or actually detected in the electrochemical oxidation[10)] or in the reaction with copper(II) perchlorate.[11)] However, no direct evidence for the presence of the radical cation of **1** could be obtained in our system, though the radical anion of **2** was detected in the measurements of ESR and electronic absorption spectra.[9)] The second possible route is the formation of 2,5-dihydro-1,3,4-oxadiazole through 1,3-dipolar cycloaddition between **1** and **2**; the follow-up ring opening or the loss of N_2 gives I or carbonium betaine. In fact, 1,3,4-oxadiazole was isolated in the reaction of diazomethane with duroquinone.[12)] Other examples of the favoring of the 1,3,4-structure of oxadiazole were found in the reactions of diphenyldiazomethane with diphenylketene[13)] and of aryldiazomethanes with hexa- and pentafluoroacetones.[14)] The last possible route is the direct attack of the diazo carbon on the oxygen atom of **2**. Whichever route is adopted, it has to explain the observation that the qualitaitve N_2 evolution or disappearance of diazo-color was accelerated in the order of **1c**<**1b**<**1a**.

Stereochemistry in the Formations of ***3*** *and* ***4***. The high *cis*-to-*trans* ratio of stilbenes in the decomposition of **1a—c** with catalytic ammonium cerium(IV) nitrate has already reported by Trahanovsky and his coworkers.[15)] However, an unequivocal explanation of the high yield of the *cis*-isomer is lacking.

Why does the major path(b) preferentially yield *cis*-isomers rather than *trans*-ones, while the minor path(a) selectively yields *trans*-isomers? These stereochemical phenomena can be well interpreted by considering the transition state leading to II and the subsequent N_2 elimination process giving **3** and **4**. The nucleophilic attack of **1** on I should occur favorably through the transition state where the steric repulsion is as small as possible and where the opposite charges which appear attract each other.

As is pictured in Scheme 3, I contains a large chloranil moiety with a negative charge, a medium-sized aryl group, and a small H atom on the side remote from the N_2^+ group. Therefore, the approach of **1** to I from this side predominantly give such stable conformers as II-C

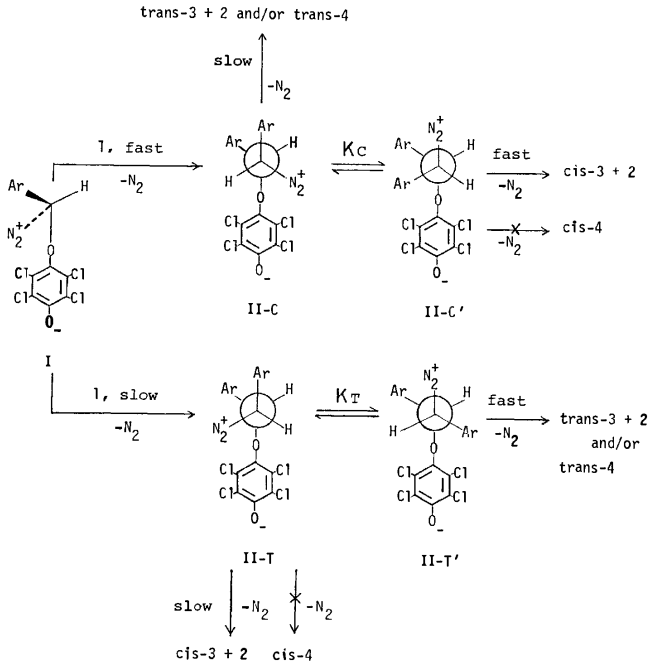

Scheme 3.

and II-T, avoiding the most striking steric repulsion between the chloranil moiety and the aryl group of **1**, and also satisfying the electronic requirement mentioned above. It should be noted here that the II-C has a lower free energy than II-T because the former can release some of the steric repulsion by placing the small H atom on the most hindered space between the chloranil moiety and the aryl group. Accordingly, the formation of II-C is more accelerated than II-T. However, in the conformational rotation to II-C′ and II-T′, the equilibrium constant, K_C, is apparently smaller than K_T because II-C′ has the highest free energy amoung these four isomers from the sterical point of view(Scheme 3). In view of the steric orientations of these isomers, it may be thought that the stereochemistry of the produtcs depends on how great extent the respective isomers contribute to the product formations. As is represented in Scheme 3, II-C and II-T may produce *trans*-**3** and *cis*-**3** respectively *via* a cis-type elimination; also, II-C may produce *trans*-**4** *via* an intramolecular S_N1-type reaction. On the other hand, II-C′ and II-T′ may produce *cis*-**3** and

Table 2. Product distributions in the reactions of **1a—c** with **2** in THF-CH_3OH or THF-CF_3CH_2OH and in the reaction of **1b** with **6** in THF at 20 °C[a]

1a—c, **2**, and **6** (mmol)		Additive[b]	Yield/%[c]						
			3(*cis*/*trans*)	**4**	**5′**	**6**	**7**	**8**	**9**
1a (7.35)	**2** (6.10)	CH_3OH	trace	ND[d]	53	23	22	2	7
1b (8.47)	**2** (8.50)	CH_3OH	trace	ND	52	13	19	3	18
1c (6.58)	**2** (6.10)	CH_3OH	trace	ND	46	12	15	2	17
1b (8.47)	**2** (8.50)	CF_3CH_2OH	58 (2.6)	6	24	11	3.5	1	3.5
1b (8.47)	**6** (8.47)	—	—	—	—	—	43	7	47

a) Reaction time 1 h. b) A four-fold excess was added with respect to **1**. c) Yield as mole percentage based on **1**. d) Not detected.

trans-**3** respectively *via* a trans elimination; also, II-T′ may produce *trans*-**4** *via* an intramolecular S_N2-type displacement. However, II-C′ or II-T can not give *cis*-**4**, probably because of the highly crowded model, which has the two aryl groups on the same side. In accordance with this idea, we obtained *trans*-**4b** alone in a 77.8 or 79.2% yield on the 3-h irradiation of a benzene solution of *trans*- or *cis*-stilbene containing an equimolar amount of **2**(50 mmol dm^{-3}), using a high-pressure mercury lamp at 20 °C: photochemical oxetane formation from olefins and C=O compounds is well known to proceed *via* a biradical intermediate,[16] such as III-C(from *cis*-stilbene) and III-T(from *trans*-stilbene); the former seems to afford no *cis*-**4** because of the highly crowded orientation as well as II-T and II-C′, but it does afford *trans*-**4** after pre-transformation into the stable III-T(Scheme 4).

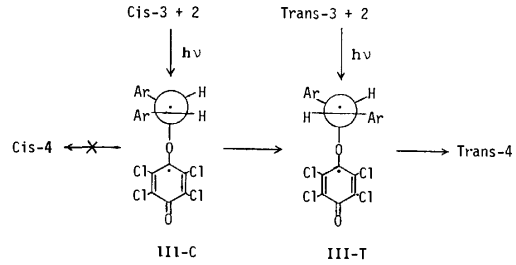

Scheme 4.

From these stereochemical considerations, the present high yield of *cis*-**3** can be reasonably explained as being responsible for the significant contribution of II-C′. Otherwise, the product distributions from the other conformers, II-C, II-T, and II-T′, would result in an excess formation of *trans*-**3** relative to *cis*-**3**, conflicting with the present results (Table 1). Therefore, it may be suggested that the rate of the product formation from II-C′ and II-T′ is much more rapid than that from II-C and II-T.

A further examination of Table 1 indicates the presence of the solvent and the substituent effects on the product distributions. The significant increase in *trans*-**4** in 1,2-dichloroethane compared with the amount in THF may be attributable to the lower solvating ability of the former medium, where the opposite charges of II should come close together, thus retarding the conformational rotation. This phenomenon results in the increase in path(a) and also in the increase of the product formation from II-C and II-T, giving more *trans*-**3** and *trans*-**4**. On the other hand, the substituents of **1** affect the relative ratio of II-C to II-T, since the stronger the nucleophilicity of **1**, the weaker the stereoselective attack of **1** on I becomes, as is supposed by the reactivity selectivity principle.[17] This assumption is in good agreement with the facts that the *cis*/*trans* ratio of **3** decreases, while *trans*-**4** increases, with the increase in the nucleophilic activity of **1**.

Reactions of ***1a—c*** *with* ***2*** *in THF-CH_3OH or THF-CF_3CH_2OH.* To establish the validity of the I intermediate, it is useful to attempt capturing it with suitable nucleophilic reagents. Indeed, marked changes in the product distributions were found on the addition of CH_3OH or CF_3CH_2OH, as is summarized in Table 2. The reactions in the presence of CH_3OH gave only a trace amount of **3**; instead, they afforded mainly acetals(**5**) and **6**, along with **7**, **8**, and **9**. **5** were isolated as benzaldehydes(**5′**) because of the easy degradation under the present acidic conditions as exhibited in the NMR measurement (see Experimental). These phenomena indicate that I undergoes a nucleophilic attack by CH_3OH rather than by **1** to turn into the redox products, as is formulated in Scheme 5. Furthermore, in this Scheme the forma-

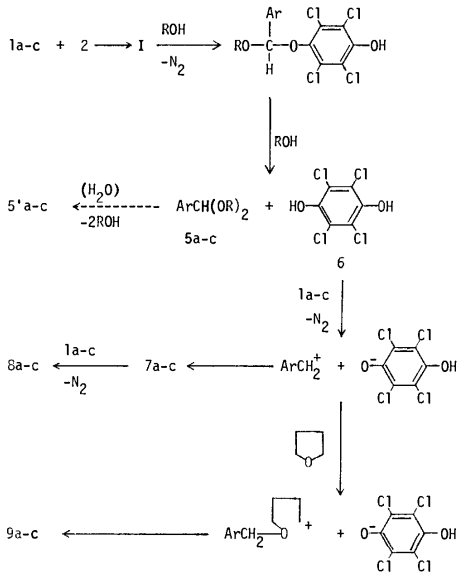

Scheme 5.

tion of **6** may be responsible for the products, **7**, **8**, and **9**, because this hydroquinone is so acidic as to decompose **1**, as was confirmed in a comparative experiment using **1b** and **6** (Table 2). Both **7** and **8** are simple mono- and dietherification products of **6** with **1**; however, **9** noticiably arises from the THF ring opening caused by the attack of the resulting benzyl cations.

On the contrary, the presence of CF_3CH_2OH allowed the substantial formation of **3b** and **4b** because of the lesser nucleophilic ability of this alcohol compared with CH_3OH. Keeping these results in mind, the appearance of small amounts of **5'**, **6**, **7**, **8**, and **9** in the absence of an additive may be attributed to the action of the residual water (ROH, R=H) present in the solvent in spite of careful drying; here unstable *gem*-diols seem to be produced instead of **5**.

In summary, aryldiazomethanes behave differently toward chloranil than in the epoxide formation in the case of diazomethane.[7] Stilbenes and spirooxetanes were formed from the intermediate, I, under the stereocontrolled conditions which furnished *cis*-rich for **3** and only the *trans*-isomer for **4**. However, the introduction of CH_3OH markedly changed these reaction features to the redox ones giving acetals and hydroquinone.

Experimental

The NMR spectra were obtained with a Varian EM-360 instrument. The IR and UV spectra were recorded with a Hitachi 215 infrared spectrometer and a 323 spectrophotometer respectively. The ESR spectra were observed with a JEOL JES-NE2X instrument.

Materials. The tetrahydrofuran(THF) was refluxed over lithium aluminum hydride and fractionated. The dichloroethane was dried over anhydrous calcium chloride for several days and fractionated. The methanol was treated with magnesium and fractionated. The 2,2,2-trifluoroethanol(Wako Pure Chemical Co., Ltd. >99%) was used without further purification. The chloranil was commercially obtained and was purified by recrystallization from dry THF; mp 290 °C. The oily aryldiazomethanes (**1a—c**) were prepared just before use by the method of Closs and Moss[18] and were used without further purification. Hence, small amounts of benzaldehyde azines given by the spontaneous decomposition of the diazo compounds were detected in the NMR purity check in the cases of **1a** and **1b**; therefore, these azines were discarded in calculating the reaction yields. The NMR signals of the aliphatic protons of these diazo compounds and the corresponding azines (in parentheses) are as follows: δ ($CDCl_3$) **1a**; 4.88 (8.26), **1b**; 4.90 (8.67), **1c**; 4.87.

*Reactions of Aryldiazomethanes (**1a—c**) with Chloranil (**2**).* These reactions were carried out in THF and 1,2-dichloroethane. The general procedures are exemplified in the case of **1a** in THF as follows. To a stirred solution of **2** (0.5 g, 2.03 mmol) in 20 ml of dry THF, we added, drop by drop, a THF solution (10 ml) containing **1a** (0.97 g, 7.35 mmol) over a 10-min period at 20 °C. The color of the solution was suddenly darkened by the addition of **1a**, and then it gradually faded with the vigorous evolution of N_2. After 1 h's standing, the removal of the solvent *in vacuo* gave a pasty reaction mixture. The washing of this mixture with 3×20 ml pentane and then with a small portion of ether left recovered **2** (130 mg) and **4a** (260 mg, 15.6%); the amount of **4a** was determined by the NMR measurement using an internal standard ($CHCl_2CHCl_2$, δ=5.8 (s)), while its analytical sample was obtained by fractional crystallization from benzene–petroleum ether. The evaporation of the solvent (pentane–ether) gave an oily residue (1.21 g), which was submitted to NMR measurement. The spectrum showed the formation of excess *cis*-**3a** compared with its *trans*-isomer, as was confirmed by subsequent chromatographic treatment (silica gel). Elution with pentane gave, successively, *cis*-**3a** (374 mg, 49%) and *trans*-**3a** (155 mg, 20%), while elution with a petroleum ether–benzene mixture gave **8a** (8 mg, 0.5%), **2** (55 mg), **5'a** (53 mg, 6%), **7a** (103 mg, 4%), and **9a** (16 mg, 0.5%), and subsequent elution with a benzene–ether mixture gave **6** (40 mg, 2%) and a small amount of an unidentified solid. The structures of **3a—c**, **4a—c**, **7a—c**, **8a—c**, and **9a—c** were determined by elemental analyses, and the IR and NMR spectra.

p,p'-Dimethylstilbene(*cis*-**3a**); colorless oil. NMR (δ, $CDCl_3$): 2.28 (6H, s, CH_3), 6.45 (2H, s, vinyl H), 6.88—7.20 (8H, q, aromatic H). Found: C, 92.13; H, 7.82%. Calcd for $C_{16}H_{16}$: C, 92.26; H, 7.74%.

p,p'-Dimethylstilbene(*trans*-**3a**); colorless leaflets (ether); mp 179—180 °C. NMR (δ, $CDCl_3$): 2.30 (6H, s, CH_3), 6.90 (2H, s, vinyl H), 6.95—7.40 (8H, q, aromatic H). Found: C, 92.24; H, 7.80%. Calcd for $C_{16}H_{16}$: C, 92.26; H, 7.74%.

Stilbene (*cis*-**3b**); colorless oil. NMR (δ, $CDCl_3$): 6.57 (2H, s, vinyl H), 7.22 (10H, s, aromatic H). Found: C, 92.94; H, 6.69%. Calcd for $C_{14}H_{12}$: C, 93.29; H, 6.71%.

Stilbene(*trans*-**3b**); colorless leaflets (ether); mp 123—124 °C. NMR (δ, $CDCl_3$): 7.07 (2H, s, vinyl H), 7.17—7.57 (10H, m, aromatic H). Found: C, 93.20; H, 6.70%. Calcd for $C_{14}H_{12}$: C, 93.29; H, 6.71%.

p,p'-Dichlorostilbene(*cis*-**3c**); colorless oil. NMR (δ, $CDCl_3$): 6.47 (2H, s, vinyl H), 7.07 (8H, s, aromatic H). Found: C, 67.38; H, 4.06%. Calcd for $C_{14}H_{10}Cl_2$: C, 67.50; H, 4.02%.

p,p'-Dichlorostilbene(*trans*-**3c**); colorless leaflets (ether); mp 178—181 °C. NMR (δ, $CDCl_3$): 7.0 (2H, s, vinyl H), 7.37 (8H, s, aromatic H). Found: C, 67.09; H, 4.11%. Calcd for $C_{14}H_{10}Cl_2$: C, 67.50; H, 4.02%.

*2,3,5,6-Tetrachloro-*trans-*3',4'-di-*p-*tolylspiro[2,5-cyclohexadiene-1,2'-oxetan]-4-one (**4a**).* Colorless prisms (benzene–petroleum ether); mp 154 °C (dec). IR (KBr): 1675, 1111, 953, 800, 718 cm^{-1}. NMR (δ, $CDCl_3$): 2.35 (3H, s, CH_3), 2.40 (3H, s, CH_3), 4.93 (1H, d, J=9.3 Hz), 6.67 (1H, d, J=9.3 Hz), 6.83—7.60 (8H, m, aromatic H). UV: λ_{max} (THF) 260, 306.5 nm (ε=12900, 6270). Found: C, 58.48; H, 3.56%. Calcd for $C_{22}H_{16}Cl_4O_2$: C, 58.18; H, 3.55%.

*2,3,5,6-Tetrachloro-*trans*-3',4'-diphenylspiro[2,5-cyclohexadiene-1,2'-oxetan]-4-one (**4b**).* Colorless prisms (benzene–petroleum ether); mp 150 °C (dec). IR (KBr): 1671, 1092, 955, 762 cm^{-1}. NMR (δ, $CDCl_3$): 4.98 (1H, d, J=9.1 Hz), 6.72 (1H, d, J=9.1 Hz), 6.90—7.83 (10H, m, aromatic H). UV: λ_{max} (THF) 259, 295 nm (ε=11400, 6995). Found: C, 56.62; H, 2.91%. Calcd for $C_{20}H_{12}Cl_4O_2$: C, 56.37; H, 2.84%.

*2,3,5,6-Tetrachloro-*trans*-3',4'-bis(*p*-chlorophenyl)spiro[2,5-cyclohexadiene-1,2'-oxetan]-4-one (**4c**).* Colorless prisms (benzene–petroleum ether); mp 172 °C (dec). IR (KBr): 1676, 1100, 952, 821, 726 cm^{-1}. NMR (δ, $CDCl_3$): 4.87 (1H, d, J=8.9 Hz), 6.60 (1H, d, J=8.9 Hz), 6.83—7.50 (8H, m, aromatic H). UV: λ_{max} (THF) 260.5, 296 nm (ε=13600, 7320). Found: C, 48.74; H, 2.13%. Calcd for $C_{20}H_{10}Cl_6O_2$: C, 48.52; H, 2.04%.

*2,3,5,6-Tetrachloro-4-(*p*-methylbenzyloxy)phenol (**7a**).* Colorless needles (benzene–petroleum ether); mp 134—135

°C. IR (KBr): 3390, 1437, 1391, 958, 708 cm^{-1}. NMR (δ, $CDCl_3$): 2.35 (3H, s), 4.92 (2H, s), 5.83 (1H, s, OH), 7.05—7.50 (4H, q, aromatic H). Found: C, 47.81; H, 2.88%. Calcd for $C_{14}H_{10}Cl_4O_2$: C, 47.76; H, 2.86%.

*2,3,5,6-Tetrachloro-4-(benzyloxy)phenol (**7b**).* Colorless prisms (benzene–petroleum ether); mp 142—143.5 °C. IR (KBr): 3390, 1436, 1386, 945, 708 cm^{-1}. NMR (δ, $CDCl_3$): 4.92 (2H, s), 5.85 (1H, s, OH), 7.13—7.50 (5H, m, aromatic H). Found: C, 46.09; H, 2.44%. Calcd for $C_{13}H_8Cl_4O_2$: C, 46.14; H, 2.37%.

*2,3,5,6-Tetrachloro-4-(p-chlorobenzyloxy)phenol (**7c**).* Colorless needles (benzene); mp 174—175 °C. IR (KBr): 3400, 1344, 1152, 1082, 808 cm^{-1}. NMR (δ, $CDCl_3$): 4.93 (2H, s), 5.95 (1H, s, OH), 7.40 (4H, s, aromatic H). Found: C, 41.88; H, 1.97%. Calcd for $C_{13}H_7Cl_5O_2$: C, 41.91; H, 1.89%.

*2,3,5,6-Tetrachloro-1,4-bis(p-methylbenzyloxy)benzene (**8a**).* Colorless needles (benzene); mp 211—212 °C. IR (KBr): 2911, 1424, 1352, 956, 799 cm^{-1}. NMR (δ, $CDCl_3$): 2.38 (6H, s), 5.00 (4H, s), 7.17—7.67 (8H, q, aromatic H). Found: C, 58.06; H, 4.02%. Calcd for $C_{22}H_{18}Cl_4O_2$: C, 57.92; H, 3.98%.

*2,3,5,6-Tetrachloro-1,4-bis(benzyloxy)benzene (**8b**).* Colorless needles (ether); mp 169—171 °C. IR (KBr): 1421, 1358, 959, 752, 694 cm^{-1}. NMR (δ, $CDCl_3$): 4.97 (4H, s) 7.1—7.35 (10H, m, aromatic H). Found: C, 56.04; H, 3.38%. Calcd for $C_{20}H_{14}Cl_4O_2$: C, 56.10; H, 3.30%.

*2,3,5,6-Tetrachloro-1,4-bis(p-chlorobenzyloxy)benzene (**8c**).* Colorless needles (benzene); mp 236—237 °C. IR (KBr): 1418, 1355, 959, 801 cm^{-1}. NMR (δ, $CDCl_3$): 4.96 (4H, s), 7.15 (8H, s, aromatic H). Found: C, 48.63; H, 2.46%. Calcd for $C_{20}H_{12}Cl_6O_2$: C, 48.33; H, 2.43%.

*2,3,5,6-Tetrachloro-4-[4'-(p-methylbenzyloxy)butoxy]phenol (**9a**).* Pale yellow prisms (benzene); mp 86—87 °C. IR (KBr): 3150, 1441, 1381, 1168, 1030, 709 cm^{-1}. NMR (δ, $CDCl_3$): 1.66—2.07 (4H, m, CH_2CH_2), 2.33 (3H, s, CH_3), 3.33—3.73 (2H, m, OCH_2), 3.76—4.17 (2H, m, OCH_2), 4.45 (2H, s, OCH_2Ar), 5.93 (1H, s, OH), 7.13 (4H, s, aromatic H). Found: C, 51.08; H, 4.31%. Calcd for $C_{18}H_{18}Cl_4O_3$: C, 50.97; H, 4.28%.

*2,3,5,6-Tetrachloro-4-[4'-(benzyloxy)butoxy]phenol (**9b**).* Pale yellow prisms (benzene); mp 84—85 °C. IR (KBr): 3240, 1445, 1384, 1171, 1041, 714 cm^{-1}. NMR (δ, $CDCl_3$): 1.70—2.10 (4H, m, CH_2CH_2), 3.40—3.8 (2H, m, OCH_2), 3.80—4.10 (2H, m, OCH_2), 4.43 (2H, s, OCH_2Ar), 5.83 (1H, s, OH), 7.18 (5H, s, aromatic H). Found: C, 49.78; H, 4.03%. Calcd for $C_{17}H_{16}Cl_4O_3$: C, 49.78; H, 3.93%.

*2,3,5,6-Tetrachloro-4-[4'-(p-chlorobenzyloxy)butoxy]phenol (**9c**).* Pale yellow prisms (benzene); mp 77—78 °C. IR (KBr): 3140, 1425, 1371, 1152, 1025, 699 cm^{-1}. NMR (δ, $CDCl_3$): 1.70—2.07 (4H, m, CH_2CH_2), 3.40—3.70 (2H, m, OCH_2), 3.80—4.10 (2H, m, OCH_2), 4.77 (2H, s, OCH_2Ar), 5.90 (1H, s, OH), 7.23 (4H, s, aromatic H). Found: C, 45.99; H, 3.36%. Calcd for $C_{17}H_{15}Cl_5O_3$: C, 45.92; H, 3.40%.

*Reactions of **1a—c** with **2** in THF–CH_3OH.* The reactions were carried out in THF containing CH_3OH. The general procedures may be illustrated by the case of **1a**. To a stirred solution of **2** (1.50 g, 6.10 mmol) in THF (50 ml) containing CH_3OH (1.0 g) we added a THF solution (10 ml) of **1a** (0.97 g, 7.35 mmol) over a 10-min period at 20 °C. After 1 h's standing, the removal of the solvent *in vacuo* gave a pasty reaction mixture. The washing of this mixture with 3×20 ml ether left only the recovered **2** (0.49 g); the subsequent evaporation of the ether solution gave oily products. The NMR spectrum of the oily products showed the presence of α,α-dimethoxy-*p*-tolylmethane (**5a**); (δ, $CDCl_3$), 3.28 (6H, s, OCH_3) and 5.30 (1H, s, $CH(OR)_2$). However, this acetal was easily degradated to *p*-tolualdehyde on work-up. Therefore, the acetal was identified as the aldehyde (**5'a**). The column chromatographic treatment of the oily products gave, successively, **3a** (trace), **8a** (35 mg, 2%), **2** (60 mg), **5'a** (470 mg, 53%), **7a** (565 mg, 22%), **9a** (220 mg, 7%), and **6** (420 mg, 23%).

*Reaction of **1b** with **2** in THF–CF_3CH_2OH.* To a stirred solution of **2** (2.09 g, 8.50 mmol) in THF (50 ml) containing CF_3CH_2OH (3.4 g) we added a THF solution (10 ml) of **1b** (1.0 g, 8.47 mmol) over a 10-min period at 20 °C. After 1 h's standing, the removal of the solvent *in vacuo* gave a pasty reaction mixture. The washing of the reaction mixture with 3×20 ml ether left **2** (1.2 g) and **4b** (110 mg, 6%). The ether was evaporated *in vacuo*, and the residue (1.7 g) was chromatographed. Contrary to the case of CH_3OH, a relatively large amount of **3b** (442 mg, 58%, *cis*/*trans*=2.6) was obtained, together with **5'b** (220 mg, 24%), **6** (230 mg, 11%), **7b** (100 mg, 3.5%), **8b** (20 mg, 1%), and **9b** (120 mg, 3.5%).

*Reaction of **1b** with **6** in THF.* An equimolar mixture of **1b** (1.0 g, 8.47 mmol) and **6** in THF (50 ml) gave **7b** (1.23 g, 43%), **8b** (0.13 g, 7%), and **9b** (1.63 g, 47%).

References

1) a) G. W. Cowell and A. Ledwith, *Quart. Rev. Chem. Soc.*, **24**, 119 (1970); b) S. Sorriso, "The Chemistry of Diazonium and Diazo Groups," ed by S. Patai, John Wiley & Sons (1978), Chap. 3.

2) a) R. Huisgen, *Angew. Chem. Int. Ed. Engl.*, **2**, 633 (1963); b) R. Huisgen, *J. Org. Chem.*, **33**, 2291 (1968); c) R. Huisgen, *J. Org. Chem.*, **41**, 403 (1976).

3) a) C. D. Gutsche, *Org. React.*, **8**, 364 (1954); b) F. Arndt, B. Eistert, and W. Ender, *Ber.*, **62**, 44 (1929); c) T. Oshima and T. Nagai, *Bull. Chem. Soc. Jpn.*, **50**, 1558 (1977).

4) a) K. T. Finley, "The Chemistry of the Quinonoid Compounds," ed by S. Patai, John Wiley & Sons (1974), Chap. 17; b) R. B. Woodward, F. Sondheimer, D. Taub, K. Heusler, and W. M. McLamore, *J. Am. Chem. Soc.*, **74**, 4223 (1952).

5) G. Briegleb, *Angew. Chem.*, **76**, 326 (1964).

6) H. Pechmann and E. Seel, *Ber.*, **28**, 860 (1895).

7) B. Eistert, H. Fink, and A. Müller, *Chem. Ber.*, **95**, 2403 (1962).

8) Part of this study was communicated in preliminary form in *Tetrahedron Lett.*, **1979**, 2789.

9) T. Oshima, A. Yoshioka, and T. Nagai, *Tetrahedron Lett.*, **1977**, 1789.

10) a) W. Jugelt and F. Pragst, *Angew. Chem.*, **80**, 280 (1968); b) W. Jugelt and F. Pragst, *Tetrahedron*, **24**, 5123 (1968); c) F. Pragst and W. Jugelt, *Electrochimica Acta*, **15**, 1543 (1970).

11) D. Bethell, K. L. Handoo, S. A. Fairhurst, and L. H. Sutcliffe, *J. Chem. Soc., Chem. Commun.*, **1977**, 326.

12) L. I. Smith and W. B. Pings, *J. Org. Chem.*, **2**, 95 (1937).

13) a) H. Staudinger and T. Reber, *Helv. Chim. Acta*, **4**, 1 (1921); b) W. Kirmse, *Chem. Ber.*, **93**, 2357 (1960).

14) N. Shimizu and P. D. Bartlett, *J. Am. Chem. Soc.*, **100**, 4260 (1978).

15) W. S. Trahanovsky, M. D. Robbins, and D. Smick, *J. Am. Chem. Soc.*, **93**, 2086 (1971).

16) a) D. R. Arnold, R. L. Hinman, and A. H. Glick, *Tetrahedron Lett.*, **1964**, 1425; b) J. F. Harris, Jr., and D. D. Coffman, *J. Am. Chem. Soc.*, **84**, 1553 (1962).

17) B. Giese, *Angew. Chem. Int. Ed. Engl.*, **16**, 125 (1977).

18) G. L. Closs and R. A. Moss, *J. Am. Chem. Soc.*, **86**, 4042 (1964).

 © 1980 The Chemical Society of Japan Bull. Chem. Soc. Jpn., 53, 731—735 (1980)

Bromination of 9-Allyltriptycenes: Bromoolefin Formation and Lifetime of an Intervening Bromonium Ion

Shiro HATAKEYAMA, Tsutomu MITSUHASHI, and Michinori ŌKI*

Department of Chemistry, Faculty of Science, The University of Tokyo, Tokyo 113

(Received July 7, 1979)

The bromination of 9-allyl-1,2,3,4-tetrachlorotriptycene affords a mixture of bromoolefins together with a minor quantity of the corresponding dibromide. By the examination of the reactions of model compounds, it is concluded that the first attack of bromine on the olefinic bond takes place in the *meso* rotamer and the resulted bromonium ion collapses either by attack of the tribromide ion to produce the dibromide or by internal rotation about the C_9–C_{allyl} bond followed by attack of the tribromide ion to produce the bromoolefin. Examination of the bromoolefin/dibromide ratios at various temperatures suggests that the activation energy for the attack of the tribromide ion on the bromonium ion is *ca.* 3 kcal/mol higher than the rotational barrier.

Since Roberts and Kimball postulated the intermediacy of a bridged ion in the bromination of alkenes,[1] there have been numerous studies on the behavior, of this ion[2] and its presence is now generally accepted. Curiously enough, however, no information about the lifetime of the bromonium ion has been available, although there has been a report that a bromonium ion formed during the bromination of a highly hindered alkene, adamantylideneadamantane, is stable.[3]

As a result of our work on restricted rotation,[4] we have been interested in reactivities of rotamers[5] and have extended the work to triptycene systems which show medium barriers to rotation. As has been briefly reported,[6] the bromination of 9-allyl-1,2,3,4-tetrachlorotriptycene (**2**) was found to afford substitution products together with a normal adduct. This is a striking fact since substitution is known to occur during the bromination if the olefin is conjugated[7] but no instance is reported for such substitution, to the best of our knowledge, in the case of unconjugated olefins. Thus the finding prompted us to investigate the driving force for the substitution reaction by carrying out similar reactions with related compounds.

We wish to furnish evidence in this paper for that the bromoolefin is produced because an intermediate bromonium ion formed from the *meso* rotamer of the compound in question undergoes internal rotation and the *dl*-rotamers subsequently formed are stabilized by the participation of the neighboring chloro group. As a by-product of the investigation, rough estimation of the lifetime of the bromonium ion becomes possible. The process of the estimation will be discussed in detail.

Experimental

Materials. 9-Allyltriptycenes were prepared by the Diels-Alder reactions of 9-allylanthracenes with benzynes, as illustrated in the scheme below. 9-Allylanthracenes were obtained, according to the procedure presented by Mosnaim *et al.*,[8] by the Grignard reaction of allylmagnesium chloride with substituted anthrone, followed by dehydration of the products. The purity of allylanthracenes was checked by ^{1}H NMR spectra and they were directly used for subsequent reactions.

9-Allyl-1,4-dimethylanthracene. 1,4-Dimethylanthrone[9] (5 g, 0.02 mol) was added in small portions to a stirred solution of allylmagnesium chloride (0.07 mol) in ether. After the addition was completed, 50 ml of dry tetrahydrofuran was added and the mixture was refluxed for another hour. The mixture was cooled and the Grignard complex was decomposed with dilute hydrochloric acid. Organic layer was separated, treated with concentrated hydrochloric acid for dehydration of the product, and washed with water. The dried solution was evaporated and the residue was chromatographed on silica gel, using hexane as an eluent. ^{1}H NMR ($CDCl_3$, δ): 2.76 (3H, s), 2.99 (3H, s), 4.3—5.4 (4H, m), 6.0—6.8 (1H, m), 7.15 (2H, s), 7.3—8.3 (4H, m), 8.49 (1H, s).

9-Allyl-2,3-dichloroanthracene was prepared similarly by using 2,3-dichloroanthrone.[10] ^{1}H NMR ($CDCl_3$, δ): 3.9—4.2 (2H, m), 4.5—5.2 (2H, m), 5.7—6.4 (1H, m), 7.1—8.2 (7H, m).

9-Allyl-1,2,3,4-tetrachloroanthracene was also prepared by using 1,2,3,4-tetrachloroanthrone.[11] In this case, phosphorus pentaoxide was used for dehydration in place of concentrated hydrochloric acid. ^{1}H NMR ($CDCl_3$, δ): 4.3—4.5 (2H, m), 4.7—5.4 (2H, m), 6.0—6.6 (1H, m), 7.3—8.3 (4H,

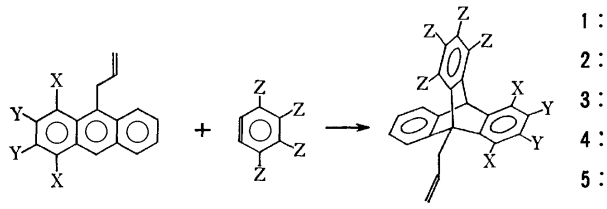

1 : X=Y=Z=H
2 : X=Y=H, Z=Cl
3 : X=CH_3, Y=Z=H
4 : X=Z=H, Y=Cl
5 : X=Y=Z=Cl

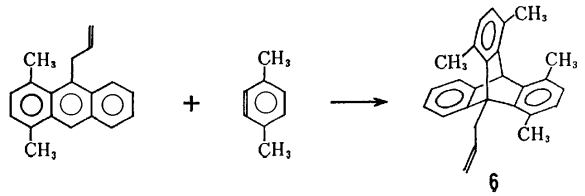

6

m), 8.60 (1H, s).

9-Allyltriptycene (1). To a refluxing solution of 3.5 g (0.03 mol) of isopentyl nitrite and 4.4 g (0.02 mol) of 9-allylanthracene in 30 ml of dichloromethane was added 4.1 g (0.03 mol) of anthranilic acid in 20 ml of acetone over a period of 2 h. The reaction mixture was heated for 1 h and cooled. The solvent was evaporated *in vacuo* and the residue was taken up in benzene. Chromatography on alumina, using hexane as an eluent, gave 4 g (68% yield) of **1**. The compound was recrystallized from hexane, mp 148—148.5 °C. Found: C, 93.65; H, 5.88%. Calcd for $C_{23}H_{18}$: C, 93.82; H, 6.18%. ^{1}H NMR ($CDCl_3$, δ): 3.6—3.9 (2H, m), 5.2—5.8 (2H, m), 5.36 (1H, s), 6.0—6.8 (1H, m), 6.8—7.6 (12H, m).

9-Allyl-1,4-dimethyltriptycene (3), mp 134—134.5 °C, was similarly prepared by using 9-allyl-1,4-dimethylanthracene. The yield was 65%. Found: C, 93.21; H, 6.60%. Calcd for $C_{25}H_{22}$: C, 93.12; H, 6.88%. ^{1}H NMR ($CDCl_3$, δ): 2.39 (3H, s), 2.54 (3H, s), 4.0—4.3 (2H, m), 5.0—5.7 (2H, m), 5.58 (1H, s), 5.8—6.7 (1H, m), 6.65 (2H, q, J_{AB}= 8.0 Hz, $\Delta\delta_{AB}$=4.1 Hz), 6.8—7.6 (8H, m).

9-Allyl-2,3-dichlorotriptycene (4), mp 234.5—235 °C, was similarly prepared in 65% yield and was recrystallized from dichloromethane–hexane. Found: C, 75.74; H, 4.30; Cl, 19.99%. Calcd for $C_{23}H_{16}Cl_2$: C, 76.04; H, 4.44; Cl, 19.52%. ^{1}H NMR ($CDCl_3$, δ): 3.6—3.9 (2H, m), 5.30 (1H, s), 5.2—5.8 (2H, m), 6.0—6.7 (1H, m), 6.9—7.6 (10H, m).

9-Allyl-1,2,3,4-tetrachlorotriptycene (2) was obtained by the reaction of 9-allylanthracene with tetrachlorobenzyne which was generated by the action of isopentyl nitrite on tetrachloroanthranilic acid.[12] The yield was 15%. It was recrystallized from chloroform–ether–hexane, mp 257.5—258 °C. Found: C, 64.17; H, 3.10; Cl, 32.61%. Calcd for $C_{23}H_{14}Cl_4$: C, 63.92; H, 3.27; Cl, 32.81%. ^{1}H NMR ($CDCl_3$, δ): 4.2—4.6 (2H, m), 5.1—5.7 (2H, m), 5.8—6.3 (1H, m), 6.02 (1H, s), 6.9—7.7 (8H, m). ^{13}C NMR ($CDCl_3$, ppm from TMS): 34.1, 52.6, 56.5, 59.8, 115.8, 123.0, 123.8, 123.9, 124.0, 124.4, 124.8, 126.7, 129.7, 135.7, 142.6, 142.8, 145.5.

9-Allyl-1,4,5,8-tetramethyltriptycene (6), mp 187.5—188.5 °C was prepared from 9-allyl-1,4-dimethylanthracene, isopentyl nitrite, and 3,6-dimethylanthranilic acid[13] in 60% yield. Found: C, 92.68; H, 7.56%. Calcd for $C_{27}H_{26}$: C, 92.52; H, 7.48%. ^{1}H NMR ($CDCl_3$, δ): 2.41 (3H, s), 2.50 (3H, s), 2.62 (6H, s), 4.0—4.7 (2H, m), 5.0—5.7 (2H, m), 5.7—6.3 (1H, m), 5.88 (1H, s), 6.5—7.7 (8H, m).

9-Allyl-1,2,3,4,5,6,7,8-octachlorotriptycene (5), mp 256.5—257.5 °C, was prepared from 9-allyl-1,2,3,4-tetrachloroanthracene, isopentyl nitrite, and tetrachloroanthranilic acid in 10% yield. It was recrystallized from dichloromethane–hexane and its purity was checked by the ^{1}H NMR spectrum. Mass spectrum showed widely distributed molecular ion peaks at 566, 568, 570, 572, 574, and 576 in accord with the natural abundance of ^{35}Cl and ^{37}Cl. The most intensive peak was 570. ^{1}H NMR ($CDCl_3$, δ): 4.0—4.3 (1H, m), 5.0—5.9 (4H, m), 6.70 (1H, s), 7.0—7.9 (4H, m).

Bromination. 9-Allyltriptycenes were brominated with a large excess of bromine in chloroform with stirring overnight. To the reaction mixture, an excess of pentenes was added and the solvent was evaporated *in vacuo*. In the cases of dimethyl and tetramethyl derivatives, the brominations were carried out by using equimolar amounts of bromine with stirring for 3 d since the substitution at the benzene nuclei occurred in the presence of excessive bromine. The ^{1}H NMR spectra of the resulting residue showed that the bromination was almost complete under the reaction conditions. A typical example follows.

To a solution of 0.15 g (0.94 mmol) of bromine in 20 ml of chloroform was added 10 ml of a chloroform solution containing 42.0 mg (0.095 mmol) of **2** and the mixture was stirred overnight at 0 °C. After treated with pentenes, the mixture was evaporated. The residue was chromatographed on alumina with hexane as an eluent. The first fraction contained *trans*- and *cis*-bromoolefins (**10**), and the second afforded dibromide (**9**). Careful chromatography and repeated recrystallization of the bromoolefin mixture from dichloromethane–hexane gave *trans*-**10** as a pure specimen.

trans-**10**, mp 239—239.5 °C. Found: C, 53.90; H, 2.38; Br, 15.50; Cl, 27.51%. Calcd for $C_{23}H_{13}BrCl_4$: C, 54.05; H, 2.57; Br, 15.63; Cl, 27.75%. ^{1}H NMR ($CDCl_3$, δ); 4.2—4.5 (2H, m), 6.04 (1H, s), 6.1—6.8 (2H, m), 6.9—7.7 (8H, m).

The following ^{1}H NMR data for the *cis* isomer were obtained by subtracting the signals due to the *trans* isomer from those of the *cis-trans* mixture: 4.2—4.5 (2H, m), 6.03 (1H, s), 6.4—6.6 (2H, m), 7.0—7.6 (8H, m).

9, mp 195—196.5 °C (from dichloromethane–hexane). Found: C, 46.69; H, 2.27; Br, 27.42; Cl, 24.33%. Calcd for $C_{23}H_{14}Br_2Cl_4$: C, 46.67; H, 2.38; Br, 27.00; Cl, 23.95%. ^{1}H NMR ($CDCl_3$, δ): 3.6—4.2 (2H, m), 4.2—4.6 (2H, m), 4.7—5.2 (1H, m), 6.01 (1H, s), 6.9—8.0 (8H, m).

Bromination of **1** gave 9-(2,3-dibromopropyl)triptycene only. It was recrystallized from chloroform–hexane, mp 201—202 °C. Found: C, 60.89; H, 3.82; Br, 35.48%. Calcd for $C_{23}H_{18}Br_2$: C, 60.82; H, 4.00; Br, 35.18%. ^{1}H NMR ($CDCl_3$, δ): 3.84 (2H, d, J=6.5 Hz), 4.0—4.6 (2H, m), 5.0—5.4 (1H, m), 5.32 (1H, s), 6.8—7.6 (12H, m).

Bromination of **5** gave a product which did not show any NMR signals ascribable to the corresponding dibromide but those consistent with the structure of bromoolefins. The mixture of bromoolefins resisted to separation. Mass spectrum showed widely distributed molecular ion peaks at 644, 646, 648, 650, 652, 654, 656, and 658 in accord with the olefinic structure and the natural abundance of ^{35}Cl, ^{37}Cl, ^{79}Br, and ^{81}Br. The most intensive peak was 648. ^{1}H NMR ($CDCl_3$, δ): 3.7—4.3 (1H, m), 4.9—5.5 (1H, m), 6.0—6.7 (2H, m), 6.69 (1H, s), 7.0—7.8 (4H, m).

Bromination of **4** gave 9-(2,3-dibromopropyl)-2,3-dichlorotriptycene only. It was recrystallized from dichloromethane–hexane, mp 103—104 °C. Found: C, 52.97; H, 3.18; Br, 31.01; Cl, 13.76%. Calcd for $C_{23}H_{16}Br_2Cl_2$: C, 52.81; H, 3.08; Br, 30.55; Cl, 13.56%. ^{1}H NMR ($CDCl_3$, δ): 3.7—4.3 (4H, m), 5.0—5.4 (1H, m), 5.27 (1H, s), 6.9—7.6 (10H, m).

Bromination of **3** afforded 9-(2,3-dibromopropyl)-1,4-dimethyltriptycene only. It was recrystallized from dichloromethane–hexane, mp 199—200 °C. Found: C, 62.23; H, 4.37; Br, 33.51%. Calcd for $C_{25}H_{22}Br_2$: C, 62.26; H, 4.60; Br, 33.14%. ^{1}H NMR ($CDCl_3$, δ): 2.33 (3H, s), 2.49 (3H, s), 3.5—4.3 (4H, m), 4.8—5.2 (1H, m), 5.55 (1H, s), 6.47 (2H, s), 6.8—7.9 (8H, m).

Kinetics. Competitive reactions were carried out as follows. An equimolar mixture of **1** and one of other 9-allyltriptycenes was added to a solution of an equimolar amount of bromine in chloroform which was pre-cooled to 0 °C. The mixture was stirred for 3 d at 0 °C. Relative reaction rate was calculated by measuring the amount of unreacted starting materials with a Waters M-6000 high pressure liquid chromatography apparatus, using hexachlorobenzene as the internal standard. The following equation was used to obtain relative rates.

$$k_N/k_1 = \log\frac{[N]}{[N]_0} \Big/ \log\frac{[\mathbf{1}]}{[\mathbf{1}]_0}$$

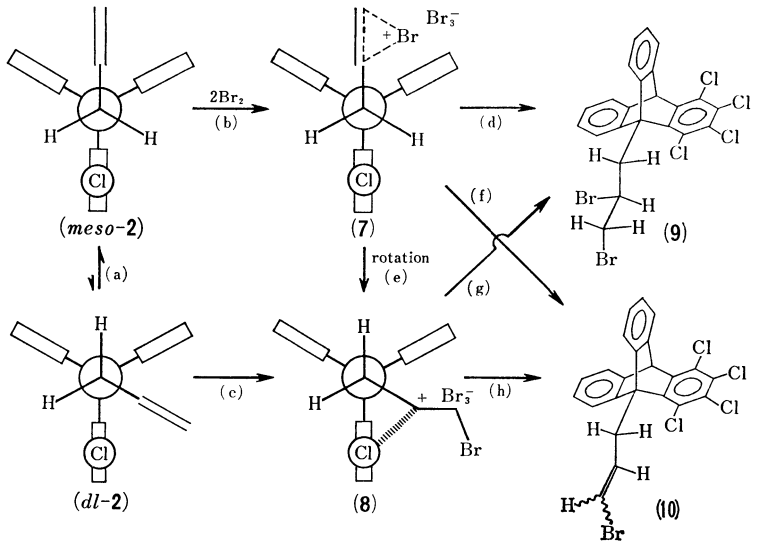

where N denotes the compound in question and subscript 0 the initial state.

The following is a typical procedure. A solution of 15.5 mg (5.3×10^{-5} mol) of **1**, 22.9 mg (5.3×10^{-5} mol) of **2**, 8.4 mg (5.3×10^{-5} mol) of bromine, and 10.7 mg of C_6Cl_6 in 7 ml of chloroform was stirred for 3 d at 0 °C. Then an excessive amount of pentenes was added and the solution was submitted for analysis. The relative rate of **2** to **1** was 0.47.

Temperature Dependence of the Product Ratio in the Bromination of 2. Bromination of **2** (8 mg of **2** and 27 mg of bromine in 6 ml of chloroform) was carried out at 40 °C, 20 °C, 0 °C, and −17 °C. After 1 h the unreacted bromine was removed by pentenes. Under these conditions, a considerable amount of **2** was recovered. The product ratio was determined by means of high pressure liquid chromatography.

Spectral Measurement. ^{1}H NMR spectra were recorded on a Hitachi R-20B spectrometer operating at 60 MHz. ^{13}C NMR spectra were obtained on a JEOL FX-60 spectrometer operating at 15.4 MHz.

Discussion

9-Allyl-1,2,3,4-tetrachlorotriptycene gave a mixture of *cis-trans* bromoolefins as a major product along with a normal adduct. This is anomalous in that the bromination of normal unconjugated olefins gives addition products and it is conjugated olefins that gives substitution products. The bromoolefin might be considered to be not a primary product: it may be formed as a result of dehydrobromination of a primary product, which is the normal product. Therefore, the dibromide was treated under the reaction conditions. No bromoolefin was found, however. Thus the bromoolefin must be a primaty product.

Possible pathways leading to the dibromide and the bromoolefin are shown in the above scheme. Advantages and disadvantages of these paths will be discussed by the experimental and available data.

As to the conformations of the molecule, the triptycene skeleton is rigid and thus there are two axes about which conformational changes are possible: C_9–C_{allyl} and C_{CH_2}–C_{vinyl} bonds. Although it is generally recognized that the most stable conformation of propene is that in which the C=C bond and one of the C–H's in the methyl eclipse with each other,[14] that kind of conformation is not stable in the present case because of the repulsion between the vinyl moiety and the peri-substituents. Rather it may be reasonable to assume that, as was the case in 9-benzyltriptycenes,[15] the vinyl group takes a conformation in which the π-system bisects the H–C–H angle of the allyl-methylene group. There are still two possible conformations after assuming the relation between the methylene and the vinyl groups: a =CH inside conformation and a C=C inside conformation. We are convinced that the C=C inside conformation is much less stable due to the steric effects.[16]

Since both the ^{1}H NMR spectra of 9-allyl-1,2,3,4-tetrachlorotriptycene (**2**) at ambient and low temperatures did not show any of the AB type signal but a rather sharp signal for the CH_2 group in the allyl, the compound may be assumed to exist as the *meso* form exclusively. The ^{13}C NMR spectrum of **2** supported the assumption: at −34 °C, where the internal rotation should be frozen,[17] the ^{13}C NMR spectrum gave lines in accordance with the molecular structure of C_{2v} symmetry. Thus the equilibrium shown as (a) in the scheme is lopsided in favor of the *meso* form.

However, these observations may not be taken as direct evidence for that the reaction takes place from the *meso* form, since the *dl* form, being more reactive due to the chloro participation, might react exclusively albeit their trace population. Therefore, another support is, at least, needed to exclude the reaction in the *dl*-conformation (path c).

We took advantage of reactions of model compounds to diagnose the presence or the absence of the reaction paths. As described in the Experimental section, brominations of 9-allyltriptycene (**1**) and its 2,3-dichloro (**4**) and 1,4-dimethyl (**3**) derivatives afforded only the corresponding addition products: formation of the substituted products is limited to the system carrying a peri-chloro group. The results indicate that the bromoolefin formation is not a result of the steric hindrance of the peri-substituent, since, if it were the case, the 1,4-dimethyl derivative should have given a bromoolefin. Neither the bromoolefin forma-

TABLE 1. RELATIVE BROMINATION RATES OF SUBSTITUTED 9-ALLYLTRIPTYCENES

Substrate	Substituent	Relative rate
1	none	1.00
2	1,2,3,4-Cl_4	0.47
3	1,4-$(CH_3)_2$	0.74
4	2,3-Cl_2	0.76
5	1,2,3,4,5,6,7,8-Cl_8	≈ 0
6	1,4,5,8-$(CH_3)_4$	<0.09

tion is attributed to the inductive effect, because the 2,3-dichloro derivative failed to give any of the corresponding bromoolefin. The formation of the bromoolefin from the *meso* bromonium ion (**7**) may thus be unlikely (path f). A logical intermediate will then be a chloronium ion (**8**) or a carbocation stabilized by a neighboring chloro group.

Neighboring chloro participation is present if the group is in the vicinity of a cationic center[18] and 5-membered cyclic chloronium ion have been postulated.[19] Since the cationic center and the chloro group are to form a 6-membered ring, this kind of stabilization is expected. Then a problem arises: is the stabilized cation directly formed from the *dl* form (path c) or is it formed by the attack of bromine on the *meso* form followed by the internal rotation (paths b and e)?

9-Allyl-1,2,3,4,5,6,7,8-octachlorotriptycene (**5**) was used as a model compound for the diagnosis. ^1H NMR spectra of this compound showed an AB pattern split by the adjacent protons but no signal ascribable to CH_2 protons of the *meso* form was observed. This is reasonable because the *meso* form, having the vinyl group inbetween the two tetrachlorobenzo bridges, is unstable relative to the *dl* form in this compound. The action of a large excess of bromine on **5** in chloroform at room temperature afforded the corresponding substituted product only in an almost quantitative yield after standing overnight. This observation suggests that the *dl* form of **2**, if reacted at all, affords only the substitution products and could in principle mean that the reaction occurs from the *dl* form of **5**.

We then ran competitive reactions to obtain further information about the reaction rates. The results are shown in Table 1. The relative rates, taken that of unsubstituted 9-allyl-triptycene (**1**) as a standard, suggest that substitution by chloro groups remote from the reaction site retards the reaction to a small extent (compare **1** and **4**). Therefore, the less reactivity of compound **2**, compared to **3**, must be derived by the electronic effect, because the steric effects in these compounds are almost the same. Another example of this sort is found in the defference in reactivities of **5** and **6**: **5** showed almost zero reactivity in the presence of **1**, whereas **6** reacted definitely, although a little, in spite of their similar steric environments. The low reactivities of **5** and **6** may now be taken as evidence for that the bromination of **2** does not take place in the *dl* form but in the *meso* form exclusively. Thus we rule out the path c: the bromination of **2** must proceed *via* path b.

As to the formation of two kinds of products, the dibromide and the bromoolefin, two pathways are still possible, although the intervention of the *dl* form of **2** is now excluded. A bridged bromonium ion (**7**) formed by the attack of bromine on the olefin in the *meso* form may react with the tribromide anion to afford the adduct (path d). Alternatively, **7** may undergo internal rotation to form the *dl* form which may quickly change to the chloronium ion (**8**) (path e). The chloronium ion may be attacked by the tribromide ion at the inside carbon to form the dibromide (path g) or at the proton of the outside carbon to form the bromoolefin (path h). The formation of the dibromide from the chloronium ion (path g), however, may be rejected for the following reasons. The octachloro compound (**5**) failed to give any of the corresponding dibromide. Since a bromonium ion formed from **5** may collapse to a chloronium ion easily, a dibromide should have been found in the bromination products, if the chloronium ion were to produce the dibromide. This is reasonable because the inside carbon in the chloronium ion (**8**) is sterically protected and more exposed protons of the bromomethyl group will be vulnerable to the attack.

Although it is not possible to rigorously exclude the possibility that the once-formed chloronium ion undergoes internal rotation to revert to the *meso* bromonium ion (**7**), we believe this will not occur because of the stability of the chloronium ion. The chloronium ion will be attacked to give the bromoolefins before the internal rotation.

Having established the paths of the reaction, we come to an interesting problem. It is most likely that both the internal rotation and the attack of the bromonium ion by the tribromide occur from the bromonium-tribromide ion pair.[20] The reasons are three fold: bromide salts are not added which would enhance the attack by the bromide ion, the bulkiness of the triptycyl group efficiently hinders the solvation of the charge center of the bromonium ion to disfavor the formation of free ions, and the low polarity of the solvent should be unfavorable for the formation of free ions. We may then approximate that both the internal rotation and the formation of the dibromide are unimolecular competitive reactions occurring from the same ion pair, although it can be argued, strictly saying, that the ion pair may have to dissociate for the rotation, the collapse of the solvent-separated ion pair is not purely unimolecular, *etc.* Then examination of the temperature dependence of the product ratio (**10**/**9**) will produce the ratio of rate constants and the difference in kinetic parameters of the two processes.

The results of the temperature dependence study of the ratios **10**/**9** are shown in Table 2. The ratio increases with the decreasing temperature. The Arrhenius polt of the data yields the difference in the activation energies as 3.0 kcal/mol and that in the entropies of activation as 8.0 e.u. The absolute value of the activation energy for rotation can not be obtained at the present time, but we tentatively assume that the size of the ion pair is roughly the same with that of a phenly group. Then the barrier to rotation

Table 2. Formation ratios of the bromoolefins *vs.* the adduct in the bromination of compound **2** at various temperatures

Temp/°C	Ratio (substitution/addition)
40.7	1.54
20.0	2.40
0.0	3.09
−17.0	7.36

(E_a 13.1 kcal/mol, ΔS^* −6.0 e.u.) is known for a model compound, 9-benzyl-1,2,3,4-tetrachlorotriptycene.[21] This indicates that the collapse of the ion pair requires thermal energy corresponding to these kinetic parameters: the energy of activation for rotation will be about 13 kcal/mol and that for the reaction of the ion pair about 16 kcal/mol. Using these values, we estimate the half life of the bridged bromonium ion as 0.1 s at 0 °C. This is by no means the general half life of bromonium ions but, we feel, is a special case where the lifetime of the intermediate is exceptionally long due to the steric conditions.

The change in entropies of activation, as observed from the ratio (**10**/**9**) is nearly equal to that for the rotation of 9-benzyl-1,2,3,4-tetrachlorotriptycene. If we rely upon the entropy of activation obtained by the DNMR method,[22] it follows that the activation entropy for the reaction of the bromonium ion with the tribromide ion is close to zero. This value seems to be plausible since the collapse of an ion pair is a unimolecular reaction and concurrent occurence of the bond formation (C–Br) and the bond cleavage (Br–Br_2) will compensate to result in a small entropy change.

The lack of the reactivity of the bromoolefins toward an excess of bromine is not limited under the conditions mentioned above. The isolated bromoolefins are also inert to bromine. Although the reason for this inertness is not well understood at the present time, we believe the steric effects must be playing an important role.

References

1) I. Roberts and G. E. Kimball, *J. Am. Chem. Soc.*, **59**, 947 (1937).
2) J. G. Traynham, *J. Chem. Educ.*, **40**, 392 (1963).
3) J. Strating, J. H. Wieringa, and H. Wynberg, *Chem. Commun.*, **1969**, 907.
4) M. Ōki, *Angew. Chem. Int. Ed. Engl.*, **15**, 87 (1976).
5) M. Nakamura, N. Nakamura, and M. Ōki, *Bull. Chem. Soc. Jpn.*, **50**, 1097 (1977).
6) S. Hatakeyama, T. Mitsuhashi, and M. Ōki, *Chem. Lett.*, **1978**, 559.
7) K. E. Koenig and Wm. P. Weber, *Tetrahedron Lett.*, **1973**, 2533.
8) D. Mosnaim, D. C. Nonhebel, and J. A. Russel, *Tetrahedron*, **25**, 3485 (1969).
9) F. Bell and D. H. Waring, *J. Chem. Soc.*, **1949**, 267.
10) E. de Barnett, M. A. Mathews, and J. L. Wiltshire, *Rec. Trav. Chim.*, **45**, 558 (1926).
11) P. Kniel, *Helv. Chim. Acta*, **46**, 492 (1963).
12) V. Villiger and L. Blangey, *Ber.*, **42**, 3549 (1909).
13) F. Mayer, W. Schäfer, and J. Rosenbach, *Arch Pharm.*, **267**, 571 (1929): S. Gronowitz and G. Hansen, *Ark. Kemi.*, **27**, 145 (1967).
14) D. R. Herschbach and L. C. Krisher, *J. Chem. Phys.*, **28**, 728 (1958).
15) F. Suzuki and M. Ōki, *Bull. Chem. Soc. Jpn.*, **48**, 596 (1975).
16) X-Ray data of 9-acetonyl-1,2,3,4-tetrachlorotriptycene suggest that the acetyl group assumes not a methyl-inside but an O-inside conformation. This is rationalized by the steric effects, a smaller group taking the inside position. N. Nogami, Ph. D. Thesis, The University of Tokyo, 1978.
17) We have numerous examples that show frozen rotation on the NMR time scale. The coalescence temperatures of the triptycenes which carry XCH_2-type substituent in the 9-position are generally around −10 °C. See also H. Nakanishi and O. Yamamoto, *Bull. Chem. Soc. Jpn.*, **51**, 1777 (1978).
18) P. E. Peterson and J. F. Coffey, *J. Am. Chem. Soc.*, **93**, 5208 (1971).
19) P. E. Peterson and E. V. P. Tao, *J. Am. Chem. Soc.*, **86**, 4503 (1964); G. A. Olah and P. E. Peterson, *J. Am. Chem. Soc.*, **90**, 4675 (1968).
20) R. E. Buckles, J. L. Miller, and R. J. Thurmaier, *J. Org. Chem.*, **32**, 888 (1967); R. J. Abraham and J. R. Monasterios, *J. Chem. Soc., Perkin Trans. 1*, **1973**, 1446.
21) M. Ōki, M. Kono, H. Kihara, and N. Nakamura, *Bull. Chem. Soc. Jpn.*, **52**, 1686 (1979).
22) Although entropies of activation obtained by the DNMR method must be treated carefully (R. R. Shoup, E. D. Becker, and M. L. McNiel, *J. Phys. Chem.*, **76**, 71 (1972)), it is also true that carefully derived ΔS^*'s are reliable at least in some instances (M. Nakamura, H. Kihara, N. Nakamura, and M. Ōki, *Org. Magn. Reson.*, **12**, 702 (1979)).

Base-catalyzed Autoxidation of Fluorene in the Presence of Phase Transfer Catalysts[1)]

Junzo YAMASHITA,* Shinji ISHIKAWA, and Harukichi HASHIMOTO

Department of Applied Chemistry, Faculty of Engineering, Tohoku University, Aramaki-Aoba, Sendai 980

(Received July 9, 1979)

Base-catalyzed autoxidation of fluorene to fluorenone has been carried out in an aqueous potassium hydroxide-benzene two-phase system in the presence of 18-crown-6 as a phase transfer catalyst. The initial rate of oxidation is proportional to the amount of fluorene. The addition of 18-crown-6 leads to the increased concentration of potassium hydroxide and water in the benzene phase, which is responsible for the increased rate of oxidation. Increasing the concentration of potassium hydroxide in the aqueous phase increases the concentration of 18-crown-6 and potassium hydroxide in benzene, resulting in a large increase in the rate of oxidation. The ease of oxidation with respect to the base is KOH>NaOH>LiOH>$Ba(OH)_2$. Less polar solvents such as cyclohexane used as an organic phase decrease the oxidation rate.

Fluorene, diarylmethanes, and other weak carbon acids that are unreactive toward oxygen in an aqueous or alcoholic solution can be oxidized in dimethyl sulfoxide or other dipolar aprotic solvents.[2)] For example, the oxidation of fluorene by molecular oxygen in the presence of potassium *t*-butoxide in *t*-butyl alcohol–dimethyl sulfoxide solution is known to proceed through fluorenide anion to yield fluorenone (Scheme 1).[2b)]

$$R_2CH_2 + B^- \longrightarrow R_2CH^- + BH$$
$$R_2CH^- + O_2 \longrightarrow R_2CH\cdot + O_2^{\cdot-}$$
$$R_2CH\cdot + O_2 \longrightarrow R_2CHOO\cdot$$
$$R_2CHOO\cdot + R_2CH^- \longrightarrow R_2CHOO^- + R_2CH\cdot$$
$$R_2CHOO\cdot + O_2^{\cdot-} \longrightarrow R_2CHOO^- + O_2$$
$$R_2CHOO^- \longrightarrow R_2CO + OH^-$$

R_2CH: 9-Fluorenyl

Scheme 1.

Recently the oxidation of fluorene, xanthene, 9,10-dihydroanthracene, and other aromatic weak carbon acids was successfully carried out in an aqueous sodium hydroxide–benzene or –tolune two-phase system in the presence of phase transfer catalysts.[3)]

In the present paper we describe the reaction as regards the function of 18-crown-6 as a phase transfer catalysts.

Results and Discussion

Benzene was chosen as an organic phase containing fluorene and 18-crown-6. An aqueous phase contained a large amount of potassium hydroxide as a base. The two-phase system of water(10 ml) and benzene (40 ml) in a 100 ml flask was vigorously shaken under oxygen pressure(1 atm) at 40.0 °C and the rate of oxygen absorption was measured by the usual constant pressure oxygen absorption apparatus.[2b)] Despite the complexities of the two-phase system, the oxidation rates were reproducible within ±5%. The shaking speed between 150 and 200 strokes/min did not affect the rate of oxidation; therefore, that of 170—180 strokes/min was used in determination of the kinetic effects.

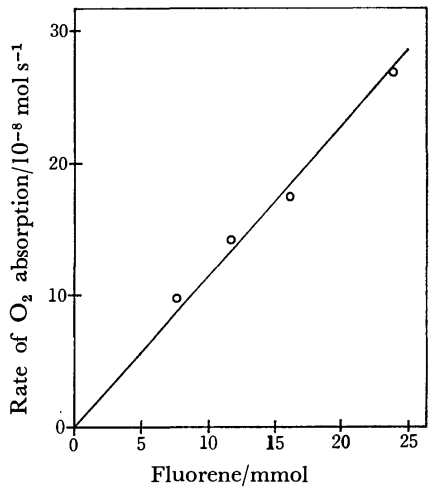

Fig. 1. Relation between fluorene used and the rate of O_2 absorption. Reaction conditions: benzene 40 ml, KOH 7.50 mol dm^{-3} in H_2O 10 ml, 18-crown-6 1.59 mmol, 40 °C.

TABLE 1. EFFECT OF TEMPERATURE[a)]

Temp °C	Fluorene mmol	KOH mol dm^{-3}	18-Crown-6 mmol	k[b)] 10^{-5} s^{-1}
30	16.2	7.50	1.56	1.04
40	16.3	7.50	1.59	1.07
50	16.2	7.50	1.57	1.31

a) Benzene 40 ml, H_2O 10 ml. See Fig. 1 for other reaction conditions. b) k=[rate of O_2 absorption (mol s^{-1})]/[fluorene (mol)].

The initial rate of oxidation is proportional to the amount of fluorene (Fig. 1), which agrees with other base-catalyzed autoxidation.[2)] The effect of temperature on the rate of oxidation is not very great since the partial pressure of oxygen in the reaction flask decreases with rise in temperature (Table 1).

Effects of various bases on the rate of oxidation are given in Table 2. As expected, potassium hydroxide is the most active, the order of activity being consistent with that of the stability of the corresponding metal complexes of 18-crown-6.[4)]

The solvent effects on the oxidation rate (Table 3)

Table 2. Effects of bases[a)]

	Base / mmol	Fluorene / mmol	k / s^{-1}
LiOH	34.4	3.06	5.1×10^{-6}
NaOH	59.9	3.04	7.8×10^{-4}
KOH	75.2	2.67	1.9×10^{-3}
$Ba(OH)_2$	46.5	3.01	small

a) Benzene 40 ml, 18-crown-6 5.0×10^{-5} mol. See Fig. 1 for other reaction conditions.

Table 3. Effects of solvents[a)]

Solvent	18-Crown-6 / mmol	k / 10^{-5} s^{-1}
Benzene	1.59	1.19
t-Butylbenzene	1.59	1.14
Cyclohexane	1.54	0.283

a) Fluorene 16.2 mmol, solvent 40 ml, KOH 7.50 mol dm^{-3} in H_2O 10 ml, 40 °C. See Fig. 1 for other reaction conditions.

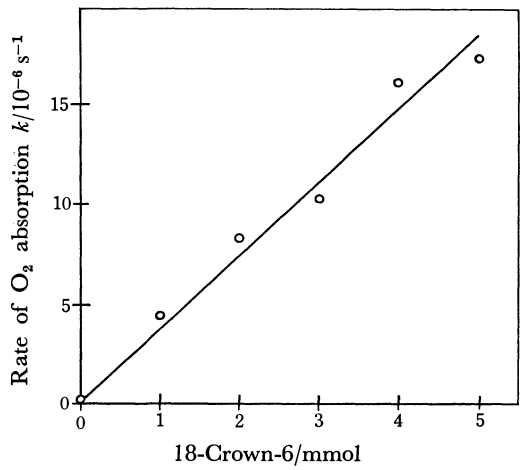

Fig. 2. Effect of 18-crown-6. Reaction conditions: fluorene 16.2 mmol, KOH 7.98 mol dm^{-3}, 40 °C. See Fig. 1 for other reaction conditions.

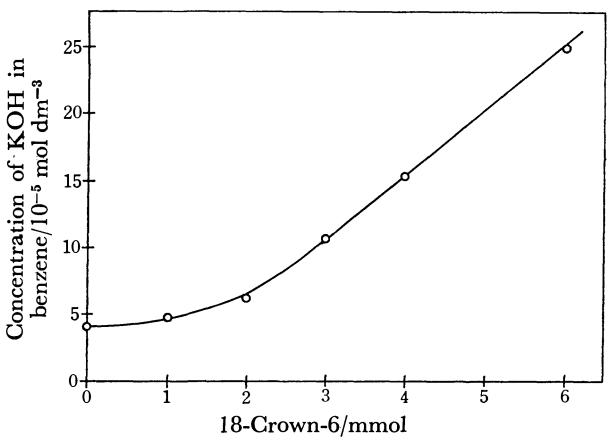

Fig. 3. The effect of 18-crown-6 on the concentration of KOH in benzene. Reaction conditions: See Fig. 1.

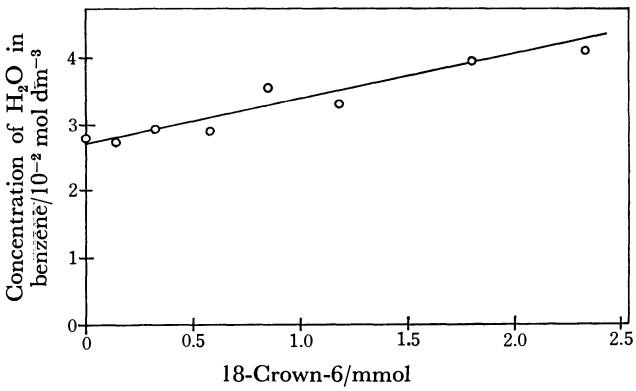

Fig. 4. The effect of 18-crown-6 on the concentration of H_2O in benzene. Reaction conditions: See Fig. 1.

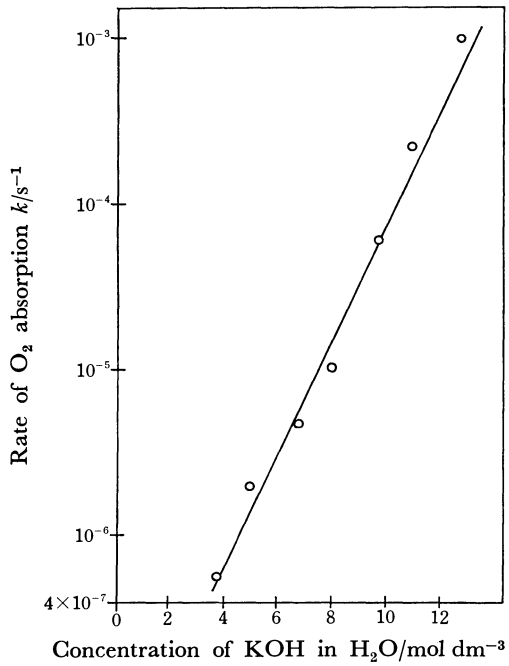

Fig. 5. Effect of the concentration of KOH. Fluorene 16.2 mmol, 18-crown-6 1.50 mmol, 40 °C. See Fig. 1 for other reaction conditions.

may be consistent with Scheme 1, since the less polar solvent or cyclohexane is presumed to involve the less amount of potassium hydroxide responsible for the formation of the fluorenide anion.

The Effect of Concentration of 18-Crown-6. The rate of oxidation is proportional to the amount of 18-crown-6 used, *ca.* 97% of which is distributed into the benzene phase (Fig. 2). The result can be predicted from Fig. 3 which shows the proportional relationship between the concentration of potassium hydroxide in benzene and that of 18-crown-6, since the rate of base-catalyzed autoxidation is known to be proportional to the concentration of bases.[2)] The extremely low concentration of potassium hydroxide in benzene as compared with that in the aqueous phase indicates that 18-crown-6 is not very effective in complexing and solubilizing potassium hydroxide into benzene.

The amount of water involved in benzene increases linearly with the concentration of 18-crown-6 (Fig. 4).

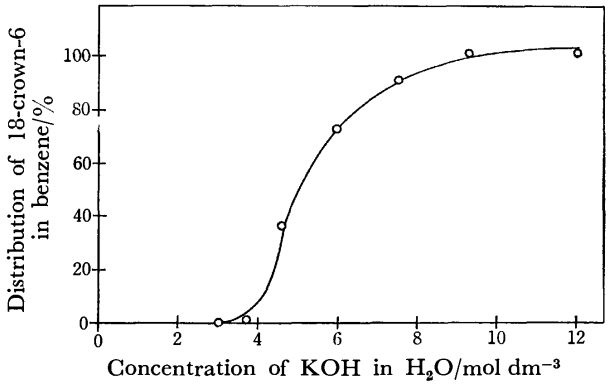

Fig. 6. Relation between the concentration of KOH in water and 18-crown-6 in benzene. Reaction conditions: See Fig. 5.

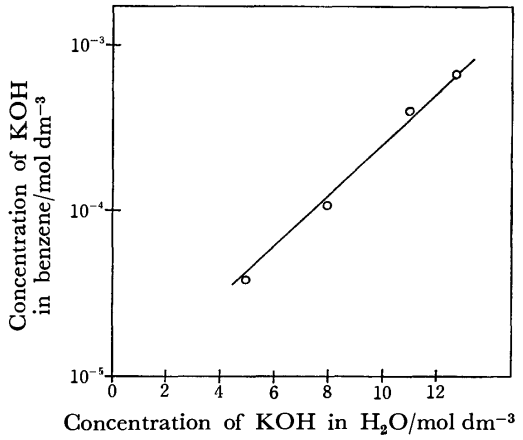

Fig. 7. Relation between the concentration of KOH in water and in benzene. Reaction conditions: See Fig. 5.

This might cause the decreased basicity of potassium hydroxide in benzene leading to a decrease in the rate of oxidation. The results shown in Figs. 2 and 4 indicate that the basicity of potassium hydroxide in benzene is almost constant at a high molar ratio of water to potassium hydroxide in benzene, calculated to be *ca.* 160—700 from Figs. 3 and 4.

Effect of the Concentration of Potassium Hydroxide in an Aqueous Phase. The concentration of potassium hydroxide in an aqueous phase has a large effect on the rate of oxidation (Fig. 5). The concentration of 18-crown-6 and potassium hydroxide in benzene increases rapidly with rise in that of potassium hydroxide in the aqueous phase. The large increase of the oxidation rate with the increasing concentration of potassium hydroxide in benzene (Fig. 9) suggests the increased basicity in the benzene phase. From Figs. 7 and 9, the molar ratios of water to potassium hydroxide in benzene are calculated to be *ca.* 1700 and 20, where the concentration of potassium hydroxide in the aqueous phase are 4.0 and 12.5 mol dm^{-3}, respectively. This indicates that the molar ratio decreases by a factor of 1/85 at the higher concentration of potassium hydroxide in the aqueous phase, which may be responsible for the increased basicity.[5] Thus, the increase of potassium hydroxide in the aqueous phase is doubly

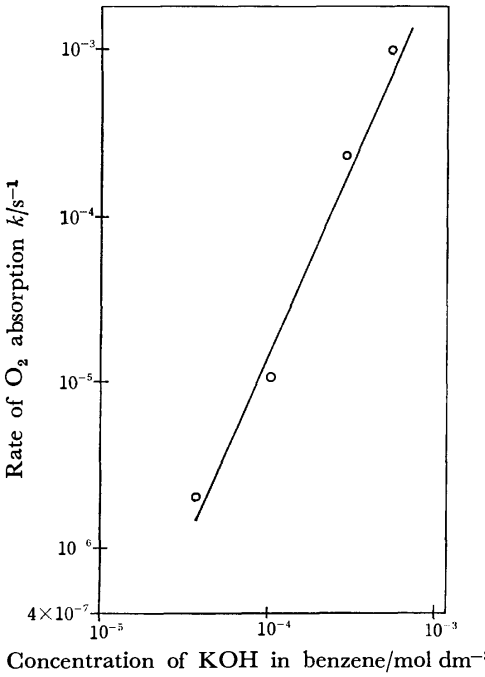

Fig. 8. Relation between KOH in benzene and the rate of oxidation. Reaction conditions: See Fig. 5.

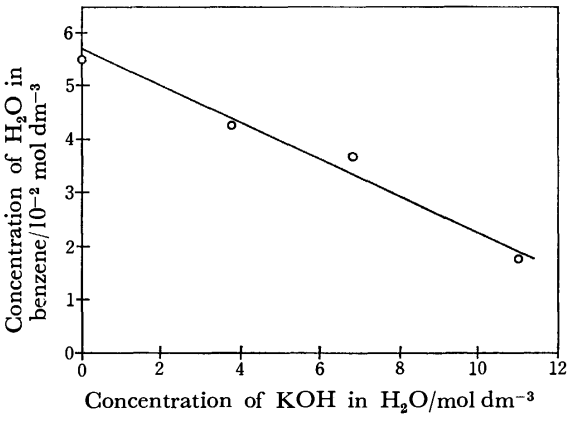

Fig. 9. Relation between the concentration of KOH in water and H_2O in benzene. Reaction conditions: See Fig. 5.

reflected on the rate of oxidation by increasing both the amount and base strength of potassium hydroxide in the benzene phase.

Experimental

Materials. Reagent grade fluorene was recrystallized twice from ethanol and dried *in vacuo*. 18-Crown-6 was prepared according to the reported procedure: mp 34.5—35.5 °C (lit, 36.5—38.0 °C).[6] Found: C, 54.61; H, 8.85; O, 36.54%. Calcd for $C_{12}H_{24}O_6$: C, 54.53; H, 9.15; O, 36.32%. Reagent grade benzene, *t*-butylbenzene and cyclohexane were shaken with sulfuric acid, washed, dried with sodium, and distilled. Hydroxides of lithium, sodium, potassium, and barium were of guaranteed grade.

Standard Oxidation Procedure. A 100 ml flask with a side arm containing 40.0 ml benzene solution of fluorene 2.71 g (16.3 mmol) and 18-crown-6 0.396 g (1.50 mmol) and 10.0 ml aqueous solution of potassium hydroxide (7.50 mol

dm^{-3}) was connected by rubber tubing to a gas buret, evacuated, and filled with oxygen a number of times. The flask was then shaken at a rate of 170—180 strokes/min with a movement of 10 cm in a thermostated water bath. The oxygen absorption was measured at 1 atm by the gas buret with an automatic pressure control apparatus.[2b] After 3 h, the reaction mixture was extracted with benzene and the extracts were used for analysis. The rate of oxygen absorption was not appreciable in the absence of fluorene or 18-crown-6.

Analysis. *Fluorenone*: The yield of fluorenone was determined on a Hitachi 163 type gas chromatograph using a 25 m Chemi-column coated with Silicone SF 96. The oxidation of 1 mol of fluorene to fluorenone under the reaction conditions mentioned above consumed *ca.* 1 mol of oxygen. No appreciable amount of other oxidation products of fluorene was detected.

Water in Benzene: The reaction mixture containing 40 ml of benzene phase and 10 ml of aqueous phase was shaken at 40.0 °C for 20 min and then left to stand for 10 min. A 10 ml sample pipetted from the benzene phase was used for the determination of water content by the Karl-Fischer method.

Potassium Hydroxide in Benzene: A 10 ml sample pipetted from the benzene phase was distilled off benzene *in vacuo* and then added with 10 ml of 0.035 mol dm^{-3} hydrochloric acid solution for measuring potassium ion on a Hitachi 207 type atomic absorption spectrometer.

18-Crown-6 in Benzene: A 5 ml sample pipetted from the benzene phase was diluted with 3 ml of benzene containing 1.44×10^{-2} g ml^{-1} of fluorenone and was determined at 180 °C on a Hitachi 163 type gas chromatograph using a 25 m Chemi-column coated with Silicone SF 96.

References

1) A part of this work was presented at The ACS/CSJ Chemical Congress: 1979, Honolulu, Hawaii, April 2, 1979.

2) a) T. J. Wallace, A. Schriesheim, and N. Jacobson, *J. Org. Chem.*, **29**, 2907 (1964); b) G. A. Russell, E. G. Janzen, A. G. Bemis, E. J. Geels, A. J. Moye, S. Mak, and E. T. Strom, "Selective Oxidation Processes, Advances in Chemistry Series, Vol. 51," American Chemical Society, Washington, D. C. (1965), p. 112; c) G. A. Russell and A. G. Bemis, *J. Am. Chem. Soc.*, **88**, 5491 (1966); d) G. A. Russell, A. J. Moye, E. G. Janzen, S. Mak, and E. R. Talaty, *J. Org. Chem.*, **32**, 137 (1967); e) G. A. Russell and E. G. Janzen, *J. Am. Chem. Soc.*, **89**, 300 (1967).

3) a) B. Dietrich and M. Lehn, *Tetrahedron Lett.*, **1973**, 1225; b) G. W. Gokel and H. D. Durst, *Synthesis*, **1976**, 168; c) E. Alneri, G. Bottaccio, and V. Carletti, *Tetrahedron Lett.*, **1977**, 2117; d) C. M. Starkes and C. Liotta, "Phase Transfer Catalysis," Academic Press, New York, N. Y. (1978), p. 298.

4) R. M. Izatt, D. E. Terry, D. P. Nelson, Y. Chan, D. J. Eatough, J. S. Bradshow, L. D. Hansen, and J. J. Christensen, *J. Am. Chem. Soc.*, **98**, 7626 (1976).

5) D. Clément, F. Damm, and J. M. Lehn, *Heterocycles*, **5**, 477 (1976).

6) G. W. Gokel, D. J. Cram, C. Liotta, H. P. Harris, and F. L. Cook, *J. Org. Chem.*, **39**, 2445 (1974).

Structural Aspects of Catalytic Activities of Thiazolium Salts in Benzoin Condensation Reaction in Methanol

Yumihiko YANO, Yoshiharu TAMURA, and Waichiro TAGAKI*

Department of Chemistry, Faculty of Engineering, Gunma University, Kiryu, Gunma 376

(Received July 20, 1979)

The rates of benzoin condensation catalyzed by thiazolium salts of varying structures have been determined in methanol containing triethylamine as the base by the method of gas chromatography. The condensation activity was observed not to be linearly correlated with the acidities of 2-position of catalyst thiazolium ring. The dimethylamino substituent was found not to act as an internal base for benzoin condensation, but rather exerted an inhibitory effect. In general, the effects of *N*-substituent on the rate of benzoin condensation were small. However, a large steric hindrance was observed for 3-methyl-4-menthylthiazolium perchlorate.

The mechanism of benzoin condensation catalyzed by a thiazolium salt is generally accepted as to involve multistep reaction pathways shown in Scheme 1.[1,2] In Scheme 1 are involved three ionization steps 1, 3, and 5, of which steps 1 and 5 were investigated and considered to be subject to lyate ion catalysis.[1c,3] However, the mechanism of base catalysis in step 3 has remained uncertain until recently as to whether it is subject to general base or lyate ion catalysis, although it has been demonstrated that the α-proton of 2-(1-hydroxyethyl)thiamine (analog of **c**) is exchangeable with solvent proton at pH 8.1.[4] Very recently, it has been shown that carbanion formation from 2-(1-hydroxyethyl)- and 2-(1-hydroxybenzyl)-thiazolium ions (analog of **c**) proceeds *via* a general base catalysis in aqueous buffer solutions.[5]

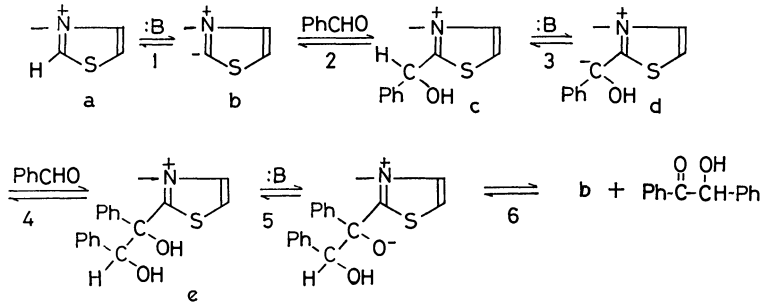

Scheme 1.

Meanwhile, we have observed general base catalysis in the H–D exchange reactions of 2,3,4-trimethylthiazolium iodide in methanol in the presence of amine.[6] This exchange reaction may also be the model of the above step 3 ionization process. Then one may expect an improved catalytic activity by attaching an appropriate basic group to the thiazolium ring which can act as an internal base. Another aspect of interests is the steric effect which we have also noted to be a determining factor for the asymmetric synthesis of benzoin.[7]

In this paper, we describe the kinetics of benzoin condensation in methanol containing triethylamine. The study was concerned with the structure-reactivity relationship of thiazolium salt catalysts such as mentioned above. It is surprising that there has been no report on the overall kinetics of benzoin formation from benzaldehyde catalyzed by thiazolium salt, although the kinetics of cyanide ion catalysis was studied in detail by Schowen and the coworkers.[8]

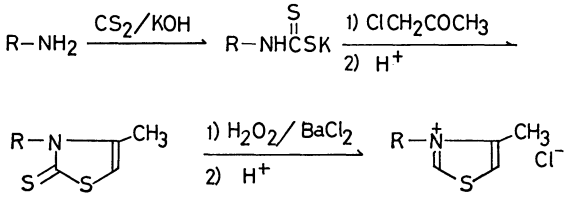

Scheme 2.

Results and Discussion

Synthesis of Thiazolium Salts. The thiazolium salts, **1**, **2**, **4**, **5**, and **6** were prepared by reacting the corresponding halides with thiazoles. 3-Phenyl (**3**), 3-[2-(dimethylamino)ethyl] (**9**), and 3-[3-(dimethylamino)propyl] (**10**) derivatives were synthesized from the corresponding amines, as shown in Scheme 2.[9] The preparation of menthyl derivatives, **7** and **8**, was described in a previous paper.[7]

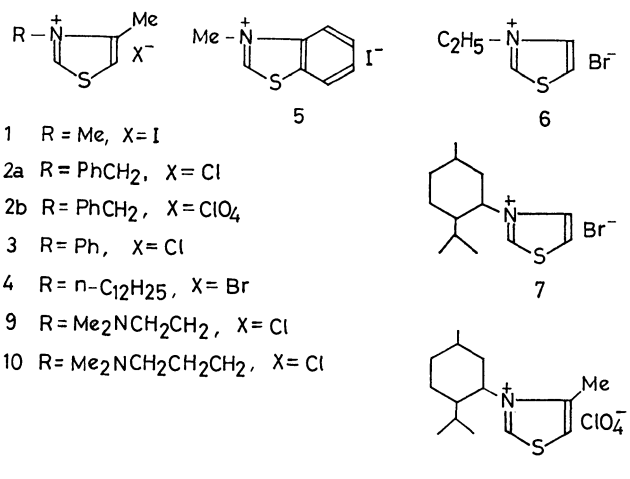

1 R = Me, X = I
2a R = $PhCH_2$, X = Cl
2b R = $PhCH_2$, X = ClO_4
3 R = Ph, X = Cl
4 R = n-$C_{12}H_{25}$, X = Br
9 R = $Me_2NCH_2CH_2$, X = Cl
10 R = $Me_2NCH_2CH_2CH_2$, X = Cl

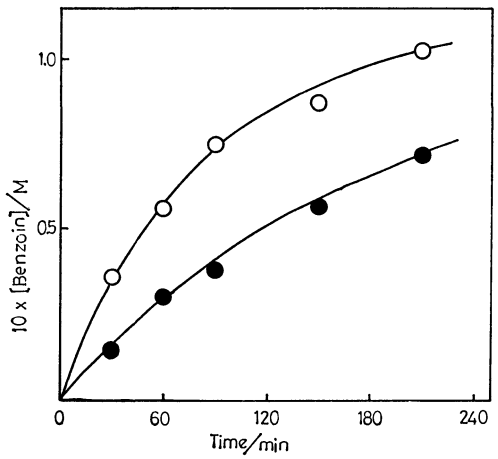

Fig. 1. Plots of benzoin yields *vs.* time, PhCHO= 0.31 M, catalyst=0.06 M, Et_3N=0.06 M, ●; **1**, ○; **2a**.

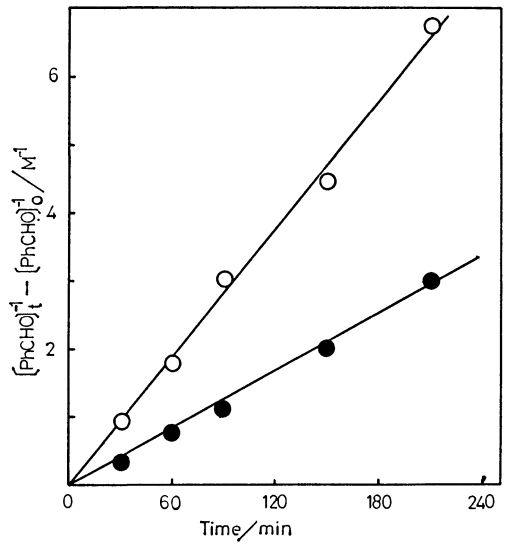

Fig. 2. Second order plots (see Fig. 1), ●; **1**, ○; **2a**.

Rates of Benzoin Condensation. In the cyanide ion-catalyzed benzoin condensation in methanol, Schowen *et al.* employed spectrophotometric method to follow the formation of benzoin at 320 nm.[8a] Unfortunately, however, in the thiazolium ion-catalyzed condensation in methanol containing triethylamine, the partial dimerization of thiazolium ion to form *N,N'*-disubstituted 2,2'-bithiazolinylidene[10] (**11**, Eq. 1) was encountered

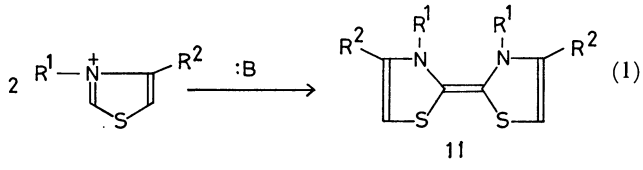

(1)

11

which disturbed the absorbance measurement at 320 nm. Therefore, we were forced to employ gas chromatography for the analysis of product benzoin by using 1,2-diphenylethane as an internal standard. The time courses of benzoin formation are illustrated in Fig. 1. The corresponding second order rate plots ($[PhCHO]_t^{-1} - [PhCHO]_0^{-1} = k_{obsd}t$) are shown in Fig. 2. Good linear plots were obtained up to more than 50% of the reaction for **1** and 70% for **2a**, although deviations were noted at the later half or one third of reaction due to the partial loss of catalytic activity by the dimerization of catalyst.

Table 1. The rate constants and benzoin yield after 20 h at 51 °C

Catalyst	$10^2 k_{obsd}$ / $l\,mol^{-1}\,min^{-1}$	k_{rel}	Benzoin yield / %
1	1.4[a]	1	66
2a	3.2[a]	2.3	79
2b	2.9[a]	2.0	67
3	1.3[a]	0.9	45
4	1.1[a]	0.8	67
5	≈0.03[a]	0.02	10
6	1.1[a]	0.8	61
	0.6[b]		—
	0.30[c]		46
7	0.94[a]	0.7	62
8	≈0.01[a]	0.01	3

a) PhCHO=0.31 M, catalyst=0.06 M, Et_3N=0.06 M. b) Et_3N=0.03 M. c) $Et_3N \cdot HCl$(0.06 M) was added.

The gas chromatographic method may be less accurate than the spectrophotometric method. Nevertheless, fairly reproducible second order rate constants were obtained. The results are listed in Table 1. In general, the rates are not very much sensitive to the *N*-substituent. Aliphatic methyl (**1**), ethyl (**6**), dodecyl (**4**), menthyl (**7**), and aromatic phenyl (**3**) substituents have almost the same effect. The effect of benzyl substituent is the largest one for the rate enhancement, but only 2—3 fold. The effect of the counter anion is also small as seen in **2a** and **2b**. The values for **5** are not accurate because of considerable decomposition of the catalyst . The activity of **8** is unusually low which is difficult to account for simply by the electronic effect, since the activity of **7** appears to be normal. As discussed in the previous paper,[7] CPK molecular model suggests that steric repulsion between 4-Me of thiazolium ring and isopropyl groups of *N*-menthyl part constrains the thiazolium ring to an unfavorable conformation for the catalysis.

Acidity of 2-Hydrogen. For several thiazolium salts, the rate constants of H–D exchange of 2-hydrogen were determined by NMR in D_2O buffered by 0.1 M acetate (mostly, pD=4.80) at 40 °C. The results are listed in Table 2.

The k_{OD^-}=5.84×10^5 $l\,mol^{-1}\,s^{-1}$ (40 °C) for **1** is reasonable in agreement with the value of 5.0×10^5 $l\,mol^{-1}\,s^{-1}$ (38 °C) reported by Haake *et al.*[3a] Such relative rates in Table 2 appear to be accounted for in terms of the electronic effects (inductive and resonance) except for that of **4**. An enhanced rate of **4** is apparently due to the micellar effect, as we had reported in a previous communication that **4** is highly active in water for benzoin condensation.[11] The salt **4** forms micelles at concentrations of the NMR measure-

TABLE 2. THE RATE CONSTANTS OF H-D EXCHANGE OF 2-HYDROGEN OF THIAZOLIUM SALT AT 40 °C

Thiazolium[a]	k_{OD^-}/l mol^{-1} s^{-1} [b]	k_{rel}
1	5.84×10^5	1
2a	2.30×10^6	3.9
3	7.94×10^6	13
4[c]	9.34×10^6	16
5	2.33×10^7	40

a) [salt]=0.4—0.5 M. b) pK_w(D_2O); 14.39 was used; A. K. Covington, R. A. Robinson and R. G. Bates, *J. Phys. Chem.*, **70**, 1820 (1966). c) Under micellar conditions.

TABLE 3. THE RATE CONSTANTS OF BENZOIN CONDENSATION CATALYZED BY **9** AND **10**[a]

[Et_3N]/[cat]	$10^2 k_{obsd}$/l mol^{-1} min^{-1}	
	9	**10**
1	— (trace)	— (5.6)
2	0.06 (12)[a]	0.14 (15)
3	0.14 (15)	0.20 (22)
4	0.24 (21)	0.29 (29)

a) PhCHO=0.31 M, catalyst=0.06 M. The number in parenthesis are the benzoin yields/% after 20 h.

ment which are much higher than the CMC of **4** (3.3×10^{-3} M in water). The micellar effect, of course, does not operate in methanol. Hence the rate constant for **4** in Table 1 is nearly the same as those of non micelle forming **1** and **6**, *etc.*

At any rate, Tables 1 and 2 indicate a poor correlation between the relative rates of H-D exchange of 2-hydrogen and those of benzoin condensation. Presumably, a ylide formed from **5** may be stabilized too much and lose activity for condensation.

Effect of Internal Base for Benzoin Condensation. We have suggested a possibility of general base catalysis by externally added base for the abstraction of α-hydrogen of the intermediate **c** (step 3 in Scheme 1).[5,6] Such general base catalysis would be much more favored when the reacting groups are arranged in appropriate intramolecular positions. Thus we have examined the catalytic activities of **9** and **10** for the benzoin condensation, where the dimethylamino group was expected to act as internal base as illustrated in the structure **12** for the addition intermediate. Meanwhile, Hine *et al.* demonstrated a remarkable bifunctional catalysis by 3-(dimethylamino)propylamine and 2-(dimethylaminomethyl)cyclopentylamine in dedeuteration of acetone-d_6.[12] These primary amines catalyze the reaction through the formation of iminium ion intermediate as illustrated in the structure **13** for the latter amine. Hine *et al.* proposed that the intramolecular general base catalysis by dimethylamino group occurs favorably when the reacting groups can be held in an eight-membered cyclic transition state, in which the carbon-deuterium bond being broken is in a plane nearly perpendicular to the plane of the iminium double bond as depicted in the structure **14**. The structural analogy between **12b** and **13** appears to be almost perfect if one ignores the difference of α-C–OH and α-C–D bond.

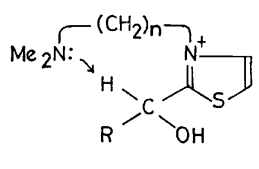

12a n=2
12b n=3

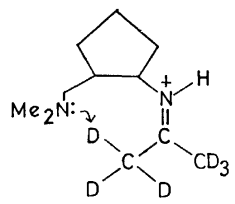

13

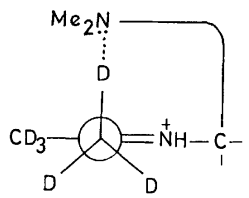

14

The pK_a values of the conjugated acids of dimethylamino group of **9** and **10** in water were determined to be 6.1 and 8.1 respectively by the NMR method.[13] They are very close to the pK_a values of the first ionization of 1,2-(dimethylamino)ethane (5.85[14]) and 1,3-(dimethylamino)propane (7.9[15]) in water. Thus it appears that the positive charge effect of thiazolium ring on the ionization of nearby protonated amino group is nearly the same as that of protonated dimethylamino group. At any rate, these pK_a values suggest the dimethylamino group, at least of **10**, to be basic enough for the ionization of α-CH bond.

Naturally, the hydrochlorides of **9** and **10** showed no activity of benzoin condensation in methanol. When an equimolar amount of triethylamine was added, the formation of benzoin was observed, but the yields of benzoin were trace for **9** and 5.6% for **10** after 20 h reaction. The increase of triethylamine concentration increased the rates and yields of benzoin formation as shown in Table 3. However, their values were unexpectedly low.

The pK_a of triethylamine is 10.78 in water[16] which is 3—5 units larger than the pK_a of **9** and **10**. These pK_a differences in water may also exist in methanol since a linear relationship is known between the pK_a values of amines in water and methanol.[17] Therefore, the dimethylamino group of **9** or **10** should be completely free in the presence of equimolar amounts of triethylamine, as verified qualitatively by NMR spectra. Yet the activity of both **9** and **10** was negligibly small. Meanwhile, as shown in Table 1, the rate constant for 3-ethyl analogue (**6**) was reduced from 1.1×10^{-2} to 0.3×10^{-2} l mol^{-1} min^{-1} in the presence of the equimolar amount of triethylamine hydrochloride (*i.e.*, $Et_3N=Et_3N\cdot HCl=0.06$ M). Thus the low activity of **9** and **10** appears partly due to this salt effect. For example, the addition of twice molar amount of free Et_3N over the catalyst hydrochloride should give a mixture of equimolar amounts of Et_3N, $Et_3N\cdot HCl$, and free dimethylamino group. However, with this salt effect alone, it seems difficult to account for such low activity. Namely, the rates of **9** and **10** are only about one fourth of that of **6** in spite of the same salt concentration. The use of **10** with partially free

amino group did not increase the rate appreciably. Electron-withdrawing inductive effect of free dimethylamino group should be small (σ_I=0.10). The CPK molecular model indicates no such steric hindrance for both **9** and **10** as noted for **8**. Both of **9** and **10** were quite stable under the present experimental conditions as far as the NMR spectra indicate. Thus we are unable to offer any reasonable explanation for the above low reactivity of **9** and **10**. However, it may be conceivable that the dimethylamino group in **9** and **10** can in fact act as internal general base as in **12b**, but the resulting carbanion loses reactivity for further condensation due to stabilization by charge delocalization which is favored to occur by ring formation involving hydrogen bonding (**12c** and **12d**).

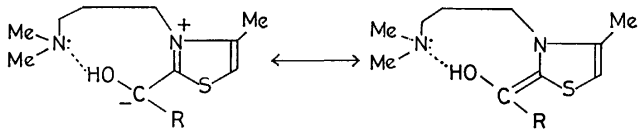

12c 12d

Experimental

NMR was recorded by a Varian A-60 spectrometer. Triethylamine was distilled on sodium hydroxide pellets, and methanol was refluxed with calcium oxide overnight and distilled. Benzaldehyde was distilled under N_2 prior to use.

Preparation of Thiazolium Salts. *3,4-Dimethylthiazolium iodide (**1**)* was prepared by reaction of 4-methylthiazole[18] with excess methyl iodide in ethanol, mp 119—121 °C (ethanol–ether) (lit,[19] mp 119—120 °C).

*3-Benzyl-4-methylthiazolium chloride (**2a**)* was prepared from benzyl chloride and 4-methylthiazole, mp 190 °C (lit,[3a] mp 191—192 °C).

*3-Benzyl-4-methylthiazolium perchlorate (**2b**)* was obtained by anion exchange of (**2a**) with silver perchlorate in ethanol. Recrystallized from ethanol–ether, mp 111—113 °C. Found: C, 45.50; H, 4.19; N, 4.84%. Calcd for $C_{11}H_{12}ClNO_4S$: C, 45.60; H, 4.18; N, 4.83%.

*3-Dodecyl-4-methylthiazolium bromide (**4**)* was prepared from 4-methylthiazole and dodecyl bromide in ethanol, mp 102—104 °C (ethanol–ether). Found: C, 55.00; H, 8.56; N, 3.98%. Calcd for $C_{16}H_{30}BrNS$: C, 55.15, H, 8.68; N, 4.02%.

*3-Methylbenzothiazolium iodide (**5**)* was prepared from benzothiazole and methyl iodide in ethanol, mp 210 °C, (lit,[10] mp 208—210 °C).

*3-Ethylthiazolium bromide (**6**)* was prepared from thiazole and ethyl bromide, mp 160—161 °C (ethanol–ether). Found: C, 30.81; H, 4.33; N, 7.10; S, 16.39%. Calcd for C_5H_8BrNs: C, 30.94, H, 4.15; N, 7.22; S, 16.52%.

3-Phenyl-4-methyl-4-thiazoline-2-thione. To a stirred solution of ammonium phenyldithiocarbamate[20] (10 g, 58 mmol) in methanol (100 ml) was added chloroacetone (5.4 g, 58 mmol) dropwise at room temperature and stirring was continued overnight. Then, 3—4 drops of concd hydrochloric acid was added and the solution refluxed for 30 min. Methanol was evaporated and water (100 ml) was added. After neutralization with $NaHCO_3$ solid, the solution was extracted with ether. The ether layer was dried over $MgSO_4$ and was evaporated to dryness. The crude crystals were recrystallized from methanol, yield 8.0 g (67%), mp 146—148 °C, NMR (CCl_4) δ 2.08 (3H, d, J=1.6 Hz) 6.50 (1H, d, J=1.6 Hz), 7.28—7.80 (5H, m).

*3-Phenyl-4-methylthiazolium Chloride (**3**).* A mixture of the above thione (2 g, 9.66 mmol), 30% hydrogen peroxide (4.4 g, 38.6 mmol) and one drop of concd hydrochloric acid in H_2O (20 ml) was stirred for 30 min at room temperature. $BaCl_2 \cdot 2H_2O$ (2.36 g, 9.66 mmol) was added and stirring was continued overnight. The precipitate ($BaSO_4$) was separated by centrifugation. The solution was evaporated to dryness. The crystals were recrystallized from ethanol–ether, yield 1.3 g (60%), mp 205—210 °C (dec). NMR (D_2O) δ 2.4 (3H, s), 7.55—7.88 (5H, m), 8.06 (1H, s), 10.10 (1H, s). Found: C, 56.70; H, 4.50; N, 6.45%. Calcd for $C_{10}H_{10}ClNS$: C, 56.73; H, 4.76; N, 6.62%.

3-[2-(Dimethylamino)ethyl]-4-methyl-4-thiazoline-2-thione. To a stirred solution of potassium 2-(dimethylamino)ethyldithiocarbamate (5.0 g, 25 mmol), which was prepared from the corresponding amine, potassium hydroxide and carbon disulfide in methanol (150 ml) was added chloroacetone (2.3 g, 25 mmol) at room temperature. Stirring was continued overnight and concd hydrochloric acid was added until the solution became acidic and stirred further for 30 min. Enough ether was added to give precipitates. The precipitates were filtered and recrystallized from ethanol–ether, yield 4.2 g (82% as HCl salt), mp 200—205 °C NMR (D_2O) δ 2.40 (3H, d, J=1.6 Hz), 3.09 (6H, s), 3.58 (2H, t, J=8.0 Hz), 4.72 (2H, t, J=8.0 Hz), 6.77 (1H, d, J=1.6 Hz).

*3-[2-(Dimethylamino)ethyl]-4-methylthiazolium Chloride (**9**).* The above thione (3.0 g, 13 mmol) and $BaCl_2 \cdot 2H_2O$ (3.1 g, 12.7 mmol) were dissolved in 10 ml of water with one drop of concd HCl and 30% hydrogen peroxide (4.9 g, 43 mmol) was added under ice-cooling. Stirring was continued overnight at room temperature. The precipitate was separated by centrifugation. The water layer was evaporated to dryness. The residue was dissolved in methanol (5 ml) and treated with charcoal and ether was added to give crystals. The crystals thus formed were recrystallized from methanol–ether, 2.6 g (84%), mp 200 °C (dec). NMR (CD_3OD) δ 2.75 (3H, s), 3.09 (6H, s), 3.84 (2H, t, J=8.0 Hz), 5.12 (2H, t, J=8.0 Hz), 8.07 (1H, m), 10.44 (1H, d, J=2.7 Hz). Found: C, 39.55; H, 6.60; N, 11.75%. Calcd for $C_8H_{16}Cl_2N_2S$: C, 39.51; H, 6.63; N, 11.52%.

3-[3-(Dimethylamino)propyl]-4-methyl-4-thiazoline-2-thione was prepared by the same procedures as described for the above 3-[2-(dimethylamino)ethyl]-4-methyl-4-thiazoline-2-thione. Yield 35%, mp 205 °C (as HCl salt). NMR (D_2O) δ 2.00—2.50 (2H, m), 2.42 (3H, d, J=1.6 Hz), 2.99 (6H, s), 3.37 (2H, t, J=7.5 Hz), 4.40 (2H, t, J=7.5 Hz), 6.80 (1H, d, J=1.6 Hz).

*3-[3-(Dimethylamino)propyl]-4-methylthiazolium Chloride (**10**).* was synthesized by the same manner as described for **9**. The yield was 61% from the corresponding thione, mp 200 °C (dec). NMR (CD_3OD) δ 2.30—2.80 (2H, m), 2.73 (3H, s), 3.00 (6H, s), 3.43 (2H, t, J=7.0 Hz), 4.70 (2H, t, J=7.5 Hz), 8.07 (1H, m), 10.50 (1H, d, J=3.0 Hz). Found: C, 42.00; H, 7.13; N, 10.88%. Calcd for $C_9H_{18}Cl_2N_2S$; C, 42.03; H, 7.05; N, 10.90%.

Kinetics of H-D Exchange of 2-Hydrogen. Deuterium oxide (99.75%, Merck) was used. The pH was measured on a Horiba (F-7DE) pH meter. The pD was then calculated by adding 0.40 to the observed pH.[21] The exchange was followed by the NMR method. The solutions for kinetics were prepared by weighing thiazolium salt (0.25 mol) in a NMR tube and by adding 0.5 ml of 0.1 M acetate buffer solution. The rate constants were calculated from the integrated areas of 2-hydrogen and those of non-exchangeable hydrogens (4-methyl, 5-hydrogen or phenyl).

pK_a *Determination.* The pK_a values of dimethylamino group of **9** and **10** in water were determined by NMR method described by Grunwald.[12] Namely, chemical shifts of dimethyl group from tetramethylammonium bromide (internal standard) were measured at seven pH's from pH 3 to 7.62 (0.2 M, citric acid–Na_2HPO_4 buffer). The pK_a values were calculated by the best fit of experimental points by using equation: $pH=pK_a+\log(\delta_{obsd}-\delta)/(\delta_{H^+}-\delta_{obsd})$, where δ_{H^+}, δ_{obsd}, δ are the chemical shifts from internal standard of fully protonated, partially dissociated at a given pH and free dimethylamino groups which were estimated because of instability of thiazolium ring at higher pH, respectively.

Kinetics of Benzoin Condensation. Into a 5 ml of septum-rubber capped flask were placed 2 ml of 0.62 M benzaldehyde, 0.5 ml of 0.48 M triethylamine and 1 ml of 0.30 M 1,2-diphenylethane (internal standard for GLC analysis). The flask was bubbled with N_2 saturated with methanol vapor for 10 min. After temperature equilibration at 51 °C for 10 min, 0.5 ml of 0.48 M solution of given catalyst was added under N_2 with appropriate time intervals, *ca.* 0.2 ml of reaction mixture was pipetted out by syringe and poured into a mixture of 2 ml of H_2O and 0.5 ml of benzene. After vigorous shaking, benzene layer was dried over $MgSO_4$. This layer was subjected to GLC analyses (column; 5% DMCS on Cromosorb WAW, 2 m, 200 °C). The amount of benzoin was determined by comparing the relative peak area of benzoin *vs.* internal standard with those of the calibration chart.

This research was supported in part by Grant-in-Aid for Scientific Research from the Ministry of Education, Japan.

References

1) a) R. Breslow, *J. Am. Chem. Soc.*, **79**, 1762 (1957); b) R. Breslow, *ibid.*, **80**, 3719 (1958); c) R. Breslow and E. McNelis, *ibid.*, **81**, 3080 (1959); d) R. Breslow, *Ann. New York Acad. Sci.*, **98**, 445 (1962).

2) a) L. O. Krampitz, *Ann. Rev. Biochem.*, **38**, 213 (1969); b) T. C. Bruice and S. J. Benkovic, "Bioorganic Mechanism," W. A. Benjamin, Inc., New York (1966), Vol. II, Chap. 8; c) W. P. Jencks, "Catalysis in Chemistry and Enzymology," McGraw-Hill, New York (1969), pp. 127—133.

3) a) P. Haake, L. P. Bauscher, and W. B. Miller, *J. Am. Chem. Soc.*, **91**, 1113 (1969); b) J. Ullrich and A. Mannschreck, *Biochim. Biophys. Acta*, **115**, 46 (1966); c) W. Hafferl, R. Lundin, and L. L. Ingraham, *Biochemistry*, **2**, 1298 (1963); d) P. S. Kemp and J. T. O'Brien, *J. Am. Chem. Soc.*, **92**, 2554 (1970); e) J. Crosby and G. E. Lienhard, *ibid.*, **92**, 5707 (1970).

4) J. J. Mieyal, R. G. Votaw, L. O. Krampitz, and H. Z. Sable, *Biochim. Biophys. Acta*, **141**, 205 (1967).

5) a) A. A. Gallo and H. Z. Sable, *J. Biol. Chem.*, **241**, 2564 (1976); b) J. A. Zoltewicz and S. Sridharan, *J. Org. Chem.*, **43**, 3785 (1978).

6) Y. Yano, Y. Tamura, and W. Tagaki, unpublished data.

7) W. Tagaki, Y. Tamura, and Y. Yano, *Bull. Chem. Soc. Jpn.*, **53**, 478 (1980).

8) a) J. P. Kuebrich, R. L. Schowen, M. S. Wang, and M. E. Lupes, *J. Am. Chem. Soc.*, **93**, 1214 (1971); b) J. P. Kuebrich and R. L. Schowen, *ibid.*, **93**, 1220 (1971).

9) For the preparation of thiamine, the method is briefly stated in the following patent, H. Nakao, Jpn. Patent 7027 981 (1970); *Chem. Abstr.*, **74**, 13176q (1971).

10) H. W. Wanzlick, H. J. Kleiner, I. Lasch, H. U. Fuldner, and H. Steinmaus, *Ann.*, **708**, 155 (1967).

11) W. Tagaki and H. Hara, *J. Chem. Soc., Chem. Commun.*, **1973**, 891.

12) a) J. Hine, M. S. Cholod, and J. H. Jensen, *J. Am. Chem. Soc.*, **93**, 2321 (1971); b) J. Hine, M. S. Cholod, and R. A. King, *ibid.*, **96**, 835 (1974).

13) E. Grunwald, A. Loewenstein, and S. Meiboom, *J. Chem. Phys.*, **27**, 641 (1957).

14) L. Spialter and R. W. Moshier, *J. Am. Chem. Soc.*, **79**, 5955 (1955).

15) R. Rometsch, A. Marxer, and K. Miescher, *Helv. Chim. Acta*, **34**, 1611 (1951).

16) W. S. Fyle, *J. Chem. Soc.*, **1955**, 1347.

17) a) R. P. Bell, "The Proton in Chemistry," Cornell University Press, New York, (1959), p. 44; b) M. Tanaka, "Acid and Base," Shoka-bo, Tokyo (1975), p. 46.

18) R. P. Kurky and E. V. Brown, *J. Am. Chem. Soc.*, **74**, 5778 (1952).

19) K. Daigo and L. J. Reed, *J. Am. Chem. Soc.*, **84**, 659 (1962).

20) F. B. Dains, R. Q. Brewster, and C. P. Olander, *Org. Synth.*, Coll. Vol. I, 447.

21) P. K. Glase and F. H. Long, *J. Phys. Chem.*, **64**, 188 (1960).

Cyclodehydrogenation of 3-Isopropenyl- and 3-(1-Phenylvinyl)-tropolones to 8*H*-Cyclohepta[*b*]furan-8-one Derivatives

Kimiaki IMAFUKU,* Kazuko YAMAGUCHI, and Hisashi MATSUMURA

Department of Chemistry, Faculty of Science, Kumamoto University, Kurokami, Kumamoto 860

(Received August 2, 1979)

3-(1-Phenylvinyl)tropolone (**3b**) was prepared by the hydrolysis of cycloadducts of 6-methyl-6-phenylfulvene with dichloroketene. 3-Isopropenyltropolone and **3b** were treated with 2,3-dichloro-5,6-dicyano-*p*-benzoquinone or performic acid to give 3-methyl- and 3-phenyl-8*H*-cyclohepta[*b*]furan-8-one, respectively. Reaction of **3b** with hydrazoic acid afforded an unexpected 3-acetyltropolone.

Several heterocycle-condensed troponoid skeletons have been found in natural products, but not troponoid condensed with furan ring. Kitahara and Funamizu[1] reported the formation of a furotropone, 2-methyl-8*H*-cyclohepta[*b*]furan-8-one, by peroxy acid oxidation of 3-propenyltropolone. Takase[2] also obtained the same compound by treatment of 3-acetonyltropolone with sulfuric acid. Papers have appeared concerning the synthesis of furotropone derivatives, prepared from tropone derivatives[3,4] and from furan derivatives.[5,6]

In this communication, we wish to report the synthesis of 3-methyl- and 3-phenyl-8*H*-cyclohepta[*b*]furan-8-one (**4a** and **4b**) by 2,3-dichloro-5,6-dicyano-*p*-benzoquinone (DDQ) or performic acid treatment of the corresponding 3-($\Delta^{\alpha,\beta}$-alkenyl)tropolones (**3a** and **3b**).

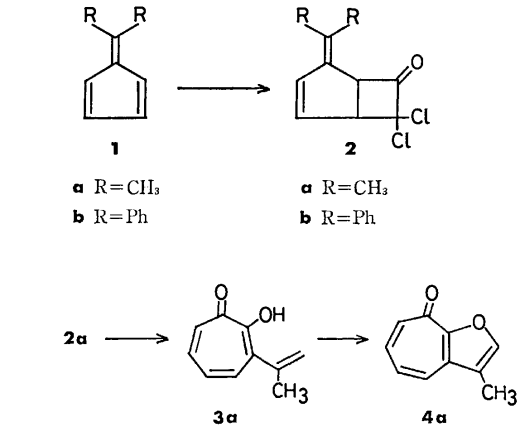

Scheme 1.

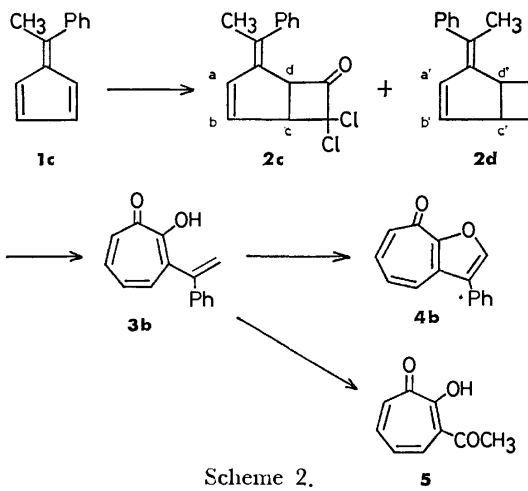

Scheme 2.

Results and Discussion

Synthesis of 3-(1-Phenylvinyl)tropolone (3b). Tropolones having an $\Delta^{\alpha,\beta}$-alkenyl group at C-3 position are of interest as synthetic precursors, being obtained by hydrolysis of cycloadducts of 6-alkyl-substituted fulvenes with dichloroketene,[7] which is an advantageous method of preparation.

Most cycloaddition reactions of fulvenes result in a 1,4-monoadduct. The formation of 1,2-monoadduct is little known except for the addition of benzonitrile oxide[8] and diazomethane[9] to 6,6-dimethylfulvene. 1,2-Cycloaddition reactions of dichloroketene to 6,6-dimethyl- (**1a**)[7] and 6,6-diphenylfulvene (**1b**)[10] were reported. The cycloadduct (**2a**) from dimethylfulvene was hydrolyzed to afford 3-isopropenyltropolone (**3a**),[7] a useful intermediate for the synthesis of 3-acetyltropolone.[11] The strucutre of the cycloadducts(**2b**) from diphenylfulvene was also established by detailed PMR spectral investigation.

We obtained the cycloadducts from the reaction of 6-methyl-6-phenylfulvene (**1c**)[12] with dichloroketene. The reaction of **1c** with dichloroketene (generated *in situ*) afforded an oily substance. The IR spectrum shows a strong carbonyl absorption at 1800 cm^{-1}, which is very similar to that of **2a** and **2b** and is reasonable for a saturated four-membered ring.[13] The PMR spectrum (Fig. 1) shows the oily substance to consist of two isomeric substances which may be produced by the presence of unequivalent methyl and phenyl groups at the C-6 position of the fulvene (**1c**). The two products were assigned to (*Z*)- and (*E*)-7,7-dichloro-4-(α-methylbenzylidene)bicyclo[3.2.0]hept-2-en-6-one (**2c** and **2d**), respectively, in comparison with the spectra of **2a** and **2b**. The assignments fit perfectly the structures (**2c**): δ/ppm: 2.21 (s, 3H, CH_3), 4.0—4.2 (m, 1H, H-c), 4.86 (d, 1H, J_{dc}=7.9 Hz, H-d), 5.8—6.1 (m, 1H, H-b), 6.47 (dd, 1H, J_{ab}=

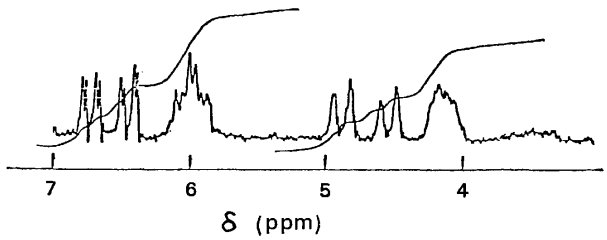

Fig. 1. PMR spectrum of mixture of cycloadducts (**2c** and **2d**).

6.0 Hz, J_{ac}=1.8 Hz H-a), 7.2—7.5 (m, 5H, Ph) and (**2d**): δ/ppm: 2.21 (s, 3H, CH_3), 4.0—4.2 (m, 1H, H-c'), 4.52 (d, 1H, $J_{d'c'}$=7.0 Hz, H-d'), 5.8—6.1 (m, 1H, H-b'), 6.72 (dd, 1H, $J_{a'b'}$=6.0 Hz, $J_{a'c'}$=1.8 Hz, H-a'), 7.2—7.5 (m, 6H, Ph). The spectrum (Fig. 1) also shows the formation of equimolar **2c** and **2d** isomers. However, the separation of the isomers was not achieved by distillation, column and TLC chromatography, and gas chromatography.

Hydrolysis of a mixture of the adducts (**2c** and **2d**) afforded 3-(1-phenylvinyl)tropolone (**3b**). The PMR spectrum of **3b** shows peaks at δ 5.34 (s, 1H), 5.81 (s, 1H), 6.70—7.65 (m, 4H), and 7.28 ppm (s, 5H), supporting the structure. The elemental analysis also gave a satisfactory result.

Cyclodehydrogenation with DDQ. Recently attempts have been made to synthesize 2*H*-chromenes by cyclodehydrogenation of 2-($\Delta^{\beta,\gamma}$-alkenyl)phenols with DDQ.[14] However, little is known about the cyclodehydrogenation of 2-($\Delta^{\alpha,\beta}$-alkenyl)phenols except for the reactions of 2-(3-methyl-1-butenyl)phenol and 2-(1-phenyl-1-propenyl)phenol.[15] The former gave 2,2-dimethyl-2*H*-chromene and the latter 2-methyl-3-phenylbenzofuran.

A solution of 3-isopropenyltropolone (**3a**) in dry benzene was refluxed for 20 h with DDQ to afford 3-methyl-8*H*-cyclohepta[*b*]furan-8-one (**4a**) in 22% yield. The UV spectrum [λ_{max}/nm (log ε): 227 (4.18), 273(4.27), 340 (3.57)] is very similar to that of 2-methyl isomer.[2] The IR spectrum of **4a** shows absorptions at 1639 (C=O) and 1090 cm^{-1} (C–O–C). These results indicate the formation of **4a**.

Reaction of 3-(1-phenylvinyl)tropolone (**3b**) with DDQ gave 3-phenyl-8*H*-cyclohepta[*b*]furan-8-one (**4b**) in 51% yield. The UV spectrum of **4b** is also very similar to that of **4a** and its 2-methyl isomer. The IR spectrum shows absorptions at 1638 (C=O) and 1102 cm^{-1} (C–O–C).

Oxidative Cyclization with Performic Acid. Nozoe and Hayashi[16] found that **3a** gives **4a** by peroxy acid oxidation, but their results have not been published.

We have carried out the same reaction of **3a** with performic acid and obtained **4a** (51%). 3-(1-Phenylvinyl)tropolone (**3b**) also reacted with performic acid to afford **4b** (62%). On the other hand, **3a** was not oxidized with alkaline hydrogen peroxide, **3a** being recovered (91%).

*Treatment of **3b** with Hydrazoic Acid.* In a previous paper,[11] it was reported that the reaction of **3a** with sodium azide in sulfuric acid gives 3-acetyltropolone (**5**). Phenyl derivatives (**3b**) was similarly treated with sodium azide in concentrated sulfuric acid to give 3-acetyltropolone (**5**) in 44% yield, the desired 3-benzoyltropolone not being obtained.

Experimental

The melting points were measured on a Yanagimoto MP-S2 melting point measuring apparatus and are uncorrected. The IR spectra were taken on a JASCO IRA-1 spectrophotometer, UV spectra on a Hitachi EPS-3T spectrophotometer, and PMR spectra on a Hitachi R-24 spectrometer (60 MHz).

*6-Methyl-6-phenylfulvene (**1c**).* 6-Methyl-6-phenylfulvene (**1c**) was prepared by the method of Thiele.[12] Bp 143.5 °C/18 Torr (lit,[12] 130.5 °C/10.5 Torr). PMR ($CDCl_3$) δ: 2.50 (s, 3H, CH_3), 6.05 (m, 1H), 6.35 (m, 1H), 6.48 (s, 2H), 7.30 ppm (s, 5H, Ph).

*Cycloaddition to 6-Methyl-6-phenylfulvene (**1c**).* A solution of triethylamine (18 ml) in anhydrous hexane (83 ml) was added dropwise to a solution of **1c** (10.2 g) and dichloroacetyl chloride (7 ml) in anhydrous hexane (83 ml) over a period of 3 h with stirring at room temperature. After additional stirring for 1 h, the mixture was allowed to stand overnight. The reaction mixture was filtered, the filtrate evaporated off and the residue distilled under reduced pressure to give a dark red oil. Yield 6.8 g (41%). Bp 169 °C/2 Torr. This oily substance was a mixture of (*Z*)- and (*E*)-7,7-dichloro-4-(α-methylbenzylidene)bicyclo[3.2.0]hept-2-en-6-one (**2c** and **2d**).

*3-(1-Phenylvinyl)tropolone (**3b**).* A mixture (16.7 g) of the cycloadducts (**2c** and **2d**) was refluxed for 16 h in acetic acid (71.5 ml)–water (7.2 ml) containing sodium hydroxide (13.2 g). The mixture was steam-distilled and the distillate was extracted with chloroform. The extract was washed with sodium hydrogencarbonate solution, water, and saturated sodium chloride solution. Evaporation of chloroform from the dried extract (over sodium sulfate) gave 3-(1-phenylvinyl)-tropolone (**3b**) as pale yellow scales (from hexane). Yield 1.8 g (14%). Mp 108—111 °C. IR ($CHCl_3$): 1620 cm^{-1} (C=O); PMR ($CDCl_3$) δ: 5.34 (s, 1H, =CH–H). 5.81 (s, 1H, =CH–H), 6.70—7.65 (m, 4H), 7.28 ppm (s, 5H, Ph). Found: C, 80.38; H, 5.40%. Calcd for $C_{15}H_{12}O_2$: C, 80.33; H, 5.40%.

Cyclodehydrogenation with DDQ. a): A mixture of 3-isopropenyltropolone (**3a**) (162 mg, 1 mmol) and DDQ (454 mg, 2 mmol) was refluxed for 6 h in dry benzene (20 ml). The reaction mixture was filtered, concentrated, chromatographed on a Wakogel B-10 plate (30×30 cm^2) with ethyl acetate, and recrystallized from hexane to afford 3-methyl-8*H*-cyclohepta[*b*]furan-8-one (**4a**) as pale orange prisms. Yield 15 mg (9.4%). Mp 95—96 °C. IR ($CHCl_3$): 1639, 1580, 1090 cm^{-1}; UV (MeOH) λ_{max}/nm (log ε): 227 (4.18), 273 (4.27), 340 (3.57); PMR ($CDCl_3$) δ: 2.24 (s, 3H, CH_3), 6.8—7.5 (m, 4H), 7.63 ppm (m, 1H, H-2). Found: C, 74.99; H, 5.01%. Calcd for $C_{10}H_8O_2$: C, 74.99; H, 5.03%.

b): Prolonged reaction (20 h) of **3a** (162 mg, 1 mmol) and DDQ (454 mg, 2 mmol) in dry benzene (20 ml) gave **4a** (35 mg, 22%) after the work-up mentioned above.

c): A mixture of 3-(1-phenylvinyl)tropolone (**3b**) (224 mg, 1 mmol) and DDQ (454 mg, 2 mmol) was refluxed for 20 h in dry benzene (20 ml). The reaction mixture was worked up in a similar way to that for *a)* and recrystallized from cyclohexane to give 3-phenyl-8*H*-cyclohepta[*b*]-furan-8-one (**4b**) as pale yellow needles. Yield 114 mg (51%). Mp 146—148 °C. IR ($CHCl_3$): 1638, 1580, 1102 cm^{-1}; UV (MeOH) λ_{max}/nm (log ε): 232 (4.35), 282 (4.20), 338^{sh} (3.67), 356^{sh} (3.45); PMR ($CDCl_3$) δ: 6.7—7.6 (m, 4H), 7.38 (s, 5H, Ph), 7.89 ppm (s, 1H, H-2). Found: C, 81.21; H, 4.47%. Calcd for $C_{15}H_{10}O_2$: C, 81.06; H, 4.54%.

Cyclization with Performic Acid. a): **3a** (420 mg, 2.6 mmol) was added to a performic acid solution, prepared from 85% formic acid (5 ml) and 30% hydrogen peroxide (1 ml), and heated on a water bath for 2 h. The reaction mixture was heated again with 6 M sodium hydroxide solution, neutralized with 3 M hydrochloric acid, and extracted with chloroform. The chloroform extract was dried over sodium sulfate and evaporated to dryness. The residue was recrystallized from hexane to afford **4a** (212 mg, 51%).

b): **3b** (448 mg, 2 mmol) was heated in performic acid, prepared in the same way as for *a)*, for 2 h and worked up as mentioned above. Crude product was recrystallized from cyclohexane to afford **4b** (227 mg, 62%).

*Treatment of **3b** with Hydrazoic Acid.* Sodium azide (200 mg) was added to a stirred mixture of **3b** (360 mg), concentrated sulfuric acid (1 ml), and chloroform (2 ml). The mixture was stirred at 50 °C for 3 h. After removal of chloroform layer, the acid layer was diluted with water (4 ml) and then left overnight. The crystals deposited were collected and recrystallized from methanol to afford 3-acetyltropolone (**5**)[11] as pale yellow needles. Yield 120 mg (44%). Mp 131—132 °C.

References

1) Y. Kitahara and M. Funamizu, presented at the Local Meeting of Tohoku Branch of the Chemical Society of Japan (1958). [See: T. Nozoe and K. Kikuchi, "Dai Yuki Kagaku," ed by M. Kotake, Asakura Publishing Co., Tokyo (1960), Vol. 13, p. 553.]

2) K. Takase, *Bull. Chem. Soc. Jpn.*, **28**, 301 (1965).

3) R. M. Harrison, J. D. Hobson, and A. W. Midgley, *J. Chem. Soc., Perkin Trans. 1*, **1976**, 2403.

4) H. Takeshita, K. Tajiri, and I. Kouno, *Heterocycles*, **6**, 1101 (1977); *Chem. Abstr.*, **87**, 201218x (1977).

5) C. Rivalle, J. Andre-Louisfert, and E. Bisagni, *Tetrahedron*, **32**, 89 (1976).

6) J. N. Chatterjiea, C. Bhakta, and S. Lal, *Indian J. Chem.*, **16B**, 567 (1978).

7) T. Asao, T. Machiguchi, T. Kitamura, and Y. Kitahara, *Chem. Commun.*, **1970**, 89.

8) A. Quilico, P. Grunager, and R. Mazzini, *Gazz. Chim. Ital.*, **82**, 349 (1952); *Chem. Abstr.*, **48**, 2039d (1952).

9) K. Alder, R. Braden, and F. H. Flock, *Chem. Ber.*, **94**, 456 (1961).

10) a) R. E. Harmon, W. D. Barta, and S. K. Gupta, *Chem. Commun.*, **1970**, 935; b) R. E. Harmon, W. D. Barta, S. K. Gupta, and G. Slomp, *J. Chem. Soc., C*, **1971**, 3645.

11) A. Yamane, M. Nagayoshi, K. Imafuku, and H. Matsumura, *Bull. Chem. Soc. Jpn.*, **52**, 1972 (1979).

12) J. Thiele, *Chem. Ber.*, **33**, 666 (1900).

13) J. M. Conia and J. L. Ripoll, *Bull. Soc. Chim. Fr.*, **1963**, 768.

14) a) H.-D. Becker, "The Chemistry of Quinoid Compounds," ed by S. Patai, John Wiley & Sons, Inc., New York (1974), p. 335; b) T. Kinoshita and T. Tokuyama, "Shin Jikken Kagaku Koza," Maruzen, Tokyo (1976), Vol. 15, p. 844; c) A. B. Turner, "Synthetic Reagents," ed by J. S. Pizey, Ellis Horwood Ltd., Sussex (1977), Vol. 3, p. 193.

15) G. Cardillo, R. Cricchio, and L. Merlini, *Tetrahedron*, **27**, 1875 (1971).

16) T. Nozoe and H. Hayashi, unpublished. [See: T. Nozoe, *Pure Appl. Chem.*, **28**, 239 (1971).]

Vinyl Polymerization. 393. Radical Polymerization of Vinyl Monomer Initiated by Aliphatic Aldehyde

Tatsuro OUCHI,* Noriyuki MURAYAMA, and Minoru IMOTO

Department of Applied Chemistry, Faculty of Engineering, Kansai University, Senriyama Suita, Osaka 564

(Received August 6, 1979)

The homogeneous polymerization of methyl methacrylate (MMA) initiated with butanal (PrCHO), pentanal (BuCHO), and hexanal ($C_5H_{11}CHO$) was carried out in dioxane. It was found that the rate of polymerization can be expressed by $R_p=k[MMA]^{1.5}[RCHO]^{0.5}$. The polymerization was confirmed to proceed through a radical mechanism. Overall activation energies, when PrCHO, BuCHO, and $C_5H_{11}CHO$ were used, were estimated to be 37.2, 36.3, and 36.0 kJ mol^{-1}, respectively. Instead of MMA, many kinds of vinyl monomer were applied. Various methacrylates and acrylates could be polymerized, but not styrene and acrylonitrile. The effect of solvent on the rate of polymerization was studied.

Imoto, Oishi, and Ouchi found that poly(acrylaldehyde-co-styrene)(AL/St)[1] and poly(methyl vinyl ketone-co-styrene)[2] can initiate the radical polymerization of methyl methacrylate (MMA). When the CHO group of AL/St was hydrogenated with $NaBH_4$ to CH_2OH group, the polymerization activity of AL/St was lost. It was thus concluded that the active center of AL/St is the pendent CHO group. Imoto, Maeda, and Ouchi reported that not only macromolecular aldehyde compounds, such as poly(formylstyrene)(*m*-: *p*-, 68:30)[3] and vanacryl,[4] but also low-molecular aldehydes of vanillin[4] or benzaldehyde (PhCHO)[5] can initiate the radical polymerization of MMA, the following mechanism of initiation being proposed.[4,5]

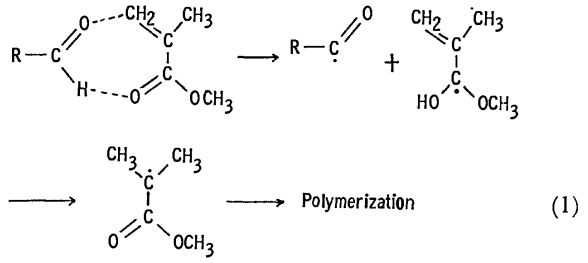

(1)

The present paper deals with the radical polymerization of vinyl monomers, particularly MMA, initiated by aliphatic aldehydes.

Experimental

Materials. Propanal (EtCHO, bp 49 °C), butanal (PrCHO, bp 74.8 °C), pentanal (BuCHO, bp 51.2 °C/121 mmHg), hexanal ($C_5H_{11}CHO$, bp 48 °C/40 mmHg) and benzaldehyde (PhCHO, bp 51 °C/5 mmHg), all of commercial special grade, were used. They were dried over anhydrous Na_2SO_4, distilled twice in a nitrogen atmosphere and furthermore distilled before use. No peroxyl group was found by the KI-method.

Vinyl monomers were purified by the usual methods. Dioxane was passed through a column filled with alumina and distilled, other solvents being purified by the usual methods.

Procedures. Vinyl monomer and aldehyde were dissolved in solvent and placed in a tube. The tube was thawed by nitrogen and sealed in a vacuum. The tube was shaken in a thermostat. After a certain time, the contents of the tube were poured into a large amount of methanol in order to precipitate the polymer produced. The conversion of the monomer was calculated from the weight of the polymer.

Number-average degree of polymerization, $\overline{P}_n$, of poly(MMA) was estimated by GPC-method (Type 501, ALC/GPC of Waters Ltd.).

ESR Measurement. The ESR spectrum was measured at room temperature by using a JES-FE 1X spectrometer with 100 kHz field modulation.

Results and Discussion

Effect of the Concentration of Aldehyde on the Polymerization of MMA. Polymerization of MMA was carried out by keeping the concentration of MMA constant at 2.79 mol dm^{-3} and varying the concentration of aldehyde (Fig. 1). The formyl group retards the radical polymerization by the following chain-transfer reaction:

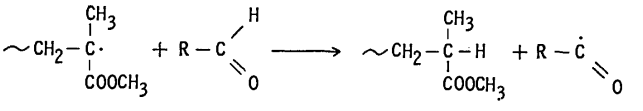

(2)

Thus with increase in the concentration of RCHO, the rate of chain-transfer reaction of MMA-radical to the aldehyde becomes greater, the conversion of MMA tending to decrease. The chain length of the alkyl group of RCHO remarkably affects conversion and rate of polymerization. The conversion increases, according to the order $C_2H_5<C_3H_7<C_4H_9$, but C_5H_{11} shows a lower activity than C_3H_7 or C_4H_9. EtCHO may have much higher activity for the chain-transfer reaction than the initiating reaction.

Figure 2 shows the decrease in $\overline{P}_n$ of poly(MMA)

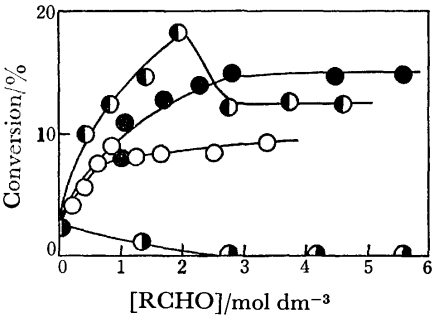

Fig. 1. Conversion of MMA *vs.* concentration of RCHO. [MMA]=2.79 mol dm^{-3}, in dioxane; 85 °C, 3 h. (◑) EtCHO, (●) PrCHO, (◐) BuCHO, (○) $C_5H_{11}CHO$.

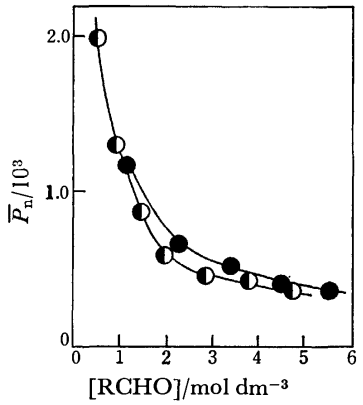

Fig. 2. Decrease of $\overline{P}_n$ of poly(MMA) with RCHO. [MMA]=2.79 mol dm^{-3}, in dioxane; 85 °C, 3 h. (●) PrCHO, (◐) BuCHO.

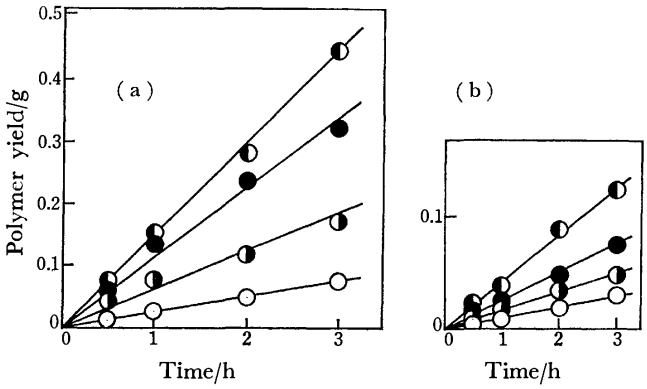

Fig. 3. Time-conversion curves.
(a) Overall conversion obtained in the presence of BuCHO *vs.* time. (b) Thermal conversion obtained in the absence of BuCHO *vs.* time. [BuCHO]= 0.94 mol dm^{-3}, in dioxane; 85 °C.
(○) [MMA]=0.93 mol dm^{-3}, (◑) [MMA]=1.86 mol dm^{-3}, (●) [MMA]=2.79 mol dm^{-3}, (◐) [MMA]= 3.72 mol dm^{-3}.

produced. This is due to the chain transfer reaction.

Reaction Orders with Respect to MMA and RCHO. Figures 3(a) and 3(b) show the time-conversion curves of MMA in the presence and absence, respectively, of BuCHO. From the straight lines in Fig. 3(a), the overall rate of polymerization, R_p(overall), can be calculated by dividing conversion by time. R_p-(thermal) is the rate of polymerization in the absence of BuCHO. Accordingly, the polymerization initiated with RCHO, R_p, was calculated by the equation.

$$R_p^2 = R_p^2(\text{overall}) - R_p^2(\text{thermal}) \quad (3)$$

The relationship between R_p and [MMA] or [RCHO] is shown in Figs. 4 and 5. From the slopes of the straight lines, the reaction orders with respect to MMA and RCHO were calculated (Table 1).

Table 1. Reaction order[a)]

RCHO	m	n
PrCHO	—	0.45
BuCHO	1.41	0.44
$C_5H_{11}CHO$	1.50	0.50

a) $R_p=k[\text{MMA}]^m[\text{RCHO}]^n$.

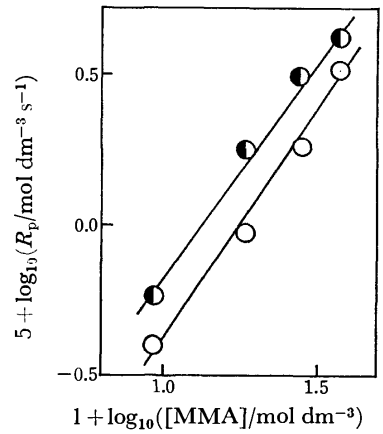

Fig. 4. Relationship between R_p and [MMA]. (◐) [BuCHO]=0.94 mol dm^{-3}, (○) [C_5H_{11}CHO]= 0.72 mol dm^{-3}, in dioxane; 85 °C.

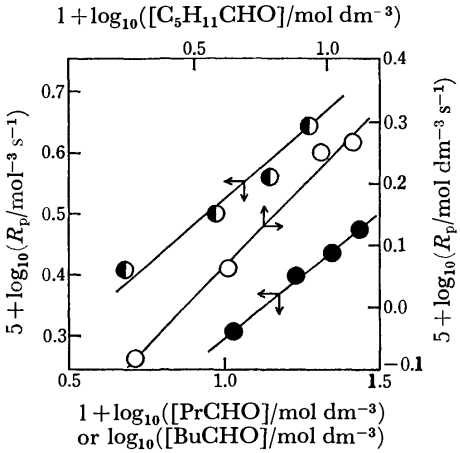

Fig. 5. Relationship between R_p and [RCHO]. [MMA]=2.79 mol dm^{-3}, in dioxane; 85 °C. (●) PrCHO, (◐) BuCHO, (○) $C_5H_{11}CHO$.

Table 2. Values of r_1 and r_2

RCHO	r_1	r_2
PrCHO	0.59	0.53
BuCHO	0.56	0.46
$C_5H_{11}CHO$	0.51	0.49

In the case of benzaldehyde, the rate equation was found to be $R_p=k[\text{MMA}]^{1.5}[\text{PhCHO}]^{0.5}$. Similarly in the present case of RCHO, the rate equation of the polymerization obeys the equation.

$$R_p = k[\text{MMA}]^{1.5}[\text{RCHO}]^{0.5} \quad (4)$$

Proofs of Radical Mechanism. That the polymerization of MMA initiated with RCHO proceeds through a radical mechanism was confirmed by two methods, (a) complete inhibition of the polymerization by 2,2-diphenyl-1-picrylhydrazyl (DPPH) (Fig. 6) and (b) copolymerization of MMA and St (Fig. 7). The calculated values of r_1 and r_2 are given in Table 2.

From these two experiments it was confirmed that the polymerization of MMA initiated with RCHO proceeds through a radical mechanism.

Selectivity of Vinyl Monomers. Instead of MMA, many kinds of methacrylate were used in the polymeri-

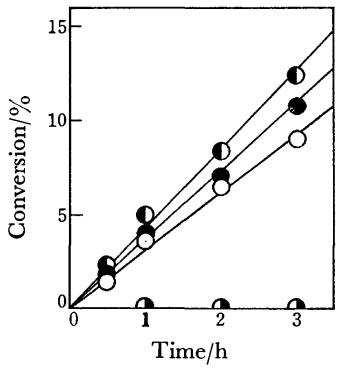

Fig. 6. Inhibition of the polymerization by DPPH. MMA 3 cm³, RCHO 1 cm³, in dioxane; 85 °C. (●) PrCHO, (◐) BuCHO, (○) $C_5H_{11}CHO$. The symbol ◑ includes the three results obtained by BuCHO, PrCHO or $C_5H_{11}CHO$.

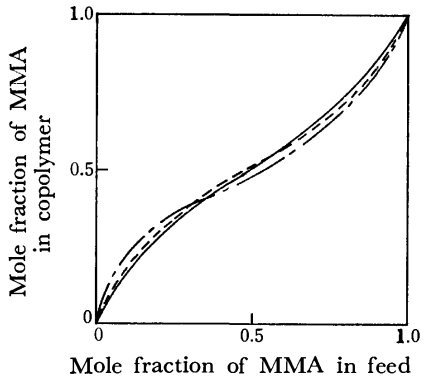

Fig. 7. Copolymerization of MMA(M_1) with St(M_2). (St+MMA) 3 cm³, RCHO 1 cm³, in dioxane; 85 °C, 3 h.
----: PrCHO, ——: BuCHO, ——: $C_5H_{11}CHO$.

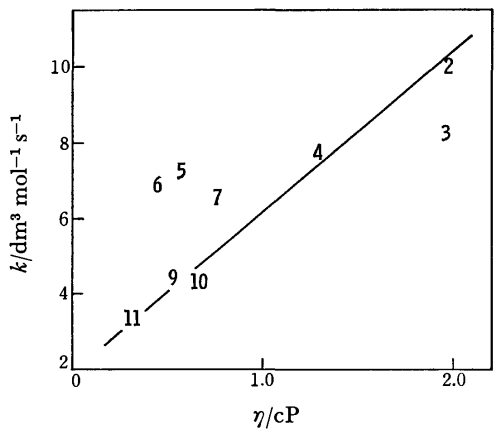

Fig. 8. *k vs.* η of solvent. The number refer to the experiments in Table 5.

zation initiated with BuCHO. Methacrylates were always easily polymerized (Table 3).

Vinyl monomers other than methacrylate were also examined (Table 4).

We see that acrylates and acrylamide can be more easily polymerized than methacrylates. Styrene, α-methylstyrene and acrylonitrile could not be polymerized. The results are in line with the proposed mechanism (1). Styrene and acrylonitrile form no adequate complex with RCHO.

Table 3. Polymerization of methacrylates initiated with BuCHO[a]

Monomer	Conversion/%	
	None[b]	BuCHO[c]
Methyl methacrylate	2.4	12.4
Ethyl methacrylate	1.9	10.3
Isopropyl methacrylate	3.0	7.4
Butyl methacrylate	2.6	12.0
Isobutyl methacrylate	8.9	16.1
t-Butyl methacrylate	5.8	11.2
Benzyl methacrylate	2.9	14.8
2-Hydroxyethyl methacrylate	11.2	17.9

a) Monomer 3 cm³, total volume 10 cm³, in dioxane; 85 °C, 3 h. b) None indicates the absence of BuCHO. c) BuCHO 1 cm³.

Table 4. Polymerization of vinyl monomers initiated with BuCHO[a]

Monomer	Conversion/%	
	None[b]	BuCHO[c]
Methyl acrylate	27.0	49.9
Ethyl acrylate	9.8	51.7
Styrene	1.4	2.4
α-Methylstyrene	0.0	0.0
Acrylonitrile	0.2	1.7
Methacrylonitrile	0.0	0.6
Acrylamide[d]	3.7	30.0
Methacrylamide[d]	1.8	8.3
Methacrylic acid	0.2	2.3

a) Monomer 3 cm³, total volume 10 cm³, in dioxane; 85 °C, 3 h. b) Absence of BuCHO. c) BuCHO 1 cm³. d) Monomer 3 g.

Table 5. Effect of solvent on R_p[a]

No.	Solvent	$k\times10^5$ / dm³ mol⁻¹ s⁻¹	ε[6]	η/cP[6]
1	Chloroform	10.10	4.9	0.563
2	DMSO	9.96	48.9	1.996
3	Ethyl benzoate	8.25	5.89	1.956
4	Dioxane	7.58	2.2	1.3
5	Benzene	7.16	2.28	0.6010
6	Ethyl acetate	6.94	6.02	0.449
7	DMF	6.46	36—71	0.802
8	H_2O[b]	4.98	80.10	1.0019
9	THF	4.35	7.58	0.55
10	Isobutyl acetate	4.26	5.29	0.697
11	Acetone	3.39	20.70	0.316
12	Methyl isobutyrate	3.00	—	—

a) MMA 3 cm³, BuCHO 1 cm³, solvent 6 cm³; 85 °C. b) H_2O 10 cm³; Heterogeneous polymerization.

Effect of Solvent on Polymerization. Twelve solvents were used in the polymerization of MMA initiated with BuCHO. The results obtained are given in Table 5, where *k* is calculated from the conversion of

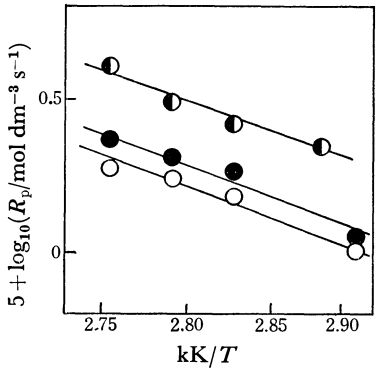

Fig. 9. Arrhenius plots.
[MMA]=2.79 mol dm^{-3}, (●) [PrCHO]=1.11 mol dm^{-3}, (◐) [BuCHO]=0.94 mol dm^{-3}, (○) [C_5H_{11}CHO]=0.72 mol dm^{-3}, in dioxane; 70—90 °C.

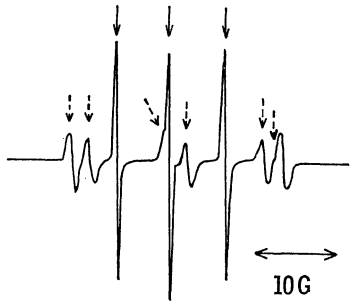

Fig. 10. ESR spectrum of the system of BuCHO/MA/BNO after reaction at 30 °C. [BuCHO]=9.4×10^{-1} mol dm^{-3}, [MA]=2.6 mol dm^{-3}, [BNO]=5.5×10^{-2} mol dm^{-3}, in benzene. ——→: (**3a**), ---→: (**4**).

MMA by the rate equation, $R_p=k[\text{BuCHO}]^{0.5}[\text{MMA}]^{1.5}$.

The effect of solvent on R_p could not be interpreted in terms of dielectric constants (ε). However, as Fig. 8 shows, R_p increased with the viscosity of the solvent, except in the cases of water (unhomogeneous polymerization) and chloroform (high chain transfer constant, 4.54×10^{-5}).

Estimation of Overall Activation Energy. The polymerization of MMA initiated with three kinds of RCHO was carried out in dioxane at 70—90 °C. The logarithms of the calculated R_p were correlated with the reciprocals of the polymerization temperature. The results obtained are shown in Fig. 9. The overall activation energy E_a was calculated from the slopes of the lines (Table 6).

Spin Trapping of Free Radicals with 2-Methyl-2-nitrosopropane (BNO). Attempts were made to detect the radicals produced in the polymerizing system of aldehyde and methyl acrylate (MA) by spin trapping technique.

Figure 10 shows the ESR spectrum observed from the system of BuCHO/MA/BNO in benzene at 30 °C. Two sets of ESR signals were observed; a triplet with A_N=8.0 G and a sextuplet with A_N=14.3 G, A_H^β=2.7 G. The former is considered to be due to (**3a**) and the latter to (**4**), which are derived from the reaction of BNO with acyl radical (**1a**) or 1-(methoxycarbonyl)ethyl radical (**2**), respectively.

When PhCHO was used instead of BuCHO, a similar spectrum was obtained; a triplet with A_N=8.2 G and a sextuplet with A_N=14.4 G, A_H^β=2.7 G.

Table 6. Overall activation energies

RCHO	Solvent	E_a/kJ mol^{-1}
PrCHO	Dioxane	37.2
BuCHO	Dioxane	36.3
C_5H_{11}CHO	Dioxane	36.0

Table 7. Reported values of coupling constant of spin adduct

Spin adduct	$\frac{A_N}{G}$	$\frac{A_H^\beta}{G}$	Ref.
5	8.1	—	7
3b	8.05	—	8
6	13.9	2.4	9
7	14.0	2.6	10

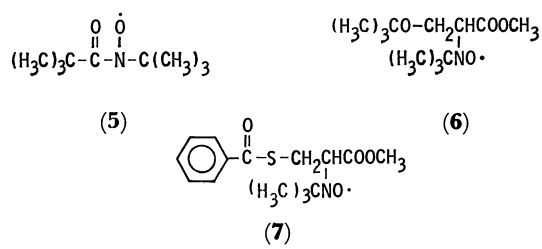

The coupling constants of nitroxyl radicals obtained by the addition of acyl radicals and 1-(methoxycarbonyl)ethyl derivative radicals to BNO are summarized in Table 7.

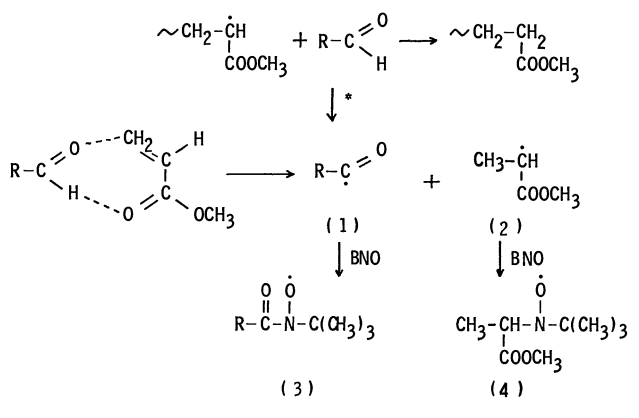

(5)

* Chain transfer reaction of propagating radical of MA onto aldehyde.

The values obtained above are close to those reported. Thus, our asignment for ESR signals is reasonable.

References

1) M. Imoto, M. Oishi, and T. Ouchi, *Makromol. Chem.*, **175**, 2219 (1974).
2) M. Imoto, M. Oishi, and T. Ouchi, *Makromol. Chem.*, **176**, 3287 (1975).
3) M. Imoto, T. Maeda, N. Murayama, and T. Ouchi, *Chem. Lett.*, **1979**, 719.
4) M. Imoto, T. Maeda, and T. Ouchi, *Chem. Lett.*,

1978, 153.
5) M. Imoto, T. Maeda, and T. Ouchi, *J. Polym. Sci. Polym. Chem. Ed.*, **17**, 385 (1979).
6) "Yozai Handbook," 1st ed, ed by S. Asahara *et al.* Kodansha, Tokyo (1976).
7) M. J. Perkins and B. P. Roberts, *J. Chem. Soc., Perkin Trans. 2*, **1974**, 297.
8) A. Ledwith, P. J. Russell, and L. H. Sutaliffe, *J. Chem. Soc., Perkin Trans. 2*, **1972**, 1925.
9) T. Sato and T. Otsu, *Makromol. Chem.*, **178**, 1941 (1977).
10) T. Sato, M. Abe, and T. Otsu, *Makromol. Chem.*, **178**, 1951 (1977).

 © 1980 The Chemical Society of Japan Bull. Chem. Soc. Jpn., 53, 753—756 (1980)

The Low-temperature Photolysis of Diazo Compounds. The Utility of Tertiary Alcohol in Matrix Studies of Carbene Chemistry

Hideo Tomioka,* Takaaki Miwa, Shinji Suzuki, and Yasuji Izawa

Department of Industrial Chemistry, Faculty of Engineering, Mie University, Tsu, Mie 514

(Received August 20, 1979)

Carbene processes within the *t*-BuOH matrix at −196 °C were investigated in order to show the utility of the matrix as a tool for the study of carbene chemistry. The photolysis of several aryldiazomethane derivatives in the *t*-BuOH matrix gave the olefinic dimer as the main product, probably arising from a combination of two triplet arylcarbenes in the aggregate of molecules. The similar photolysis of other diazo compounds (*e.g.*, N_2CHCOR, R=OR′, NEt_2, and Ph) resulted in no detection of the olefinic dimer. This was explained in terms of the structural effect on the ground-state multiplicity of carbene. The photolysis of Ph_2CN_2 in *t*-BuOH containing 5% EtOH at −196 °C gave almost exclusively O–H and C–H insertion products with the solute alcohol at the expense of the O–H insertion product with the host, *i.e.*, Ph_2CHOBu^t, which was the major product in the liquid-phase photolysis. This is ascribable to the co-aggregation of the carbene precursor with the solute alcohol because of the relatively large guest hole provided by the bulky tertiary alcohol matrix. A more general utility of this matrix was shown in the reaction of Ph_2C with Ph_2CO to give oxirane, in which the intervention of carbonyl ylide was demonstrated at low temperatures.

The low-temperature photolysis of organic compounds has attracted much attention from the standpoint of physical as well as organic chemistry because of its usefulness in detecting reaction intermediates which are suspected to be involved in processes carried out at much higher temperatures. It has been noted, however, that some of the photochemical processes at low temperatures are highly sensitive to matrix properties, *e.g.*, polarity. For example, Kolc has reported[1] that the photolysis of benzocyclobutene-1,2-dione in the EPA matrix at −196 °C underwent bisdecarbonylation to give benzyne, whereas a similar photolysis in the 3-methylpentane matrix gave no sign of benzyne being formed. A similar striking effect of matrix properties on the course of low-temperature photochemical reactions has been suggested[2] to account for some of the reported discrepancies between the results of different authors.[3,4]

In the course of our study of the low-temperature photolysis of diazo compounds, we also found[5] a striking host effect; arylcarbenes generated in the *t*-BuOH matrix at −196 °C give almost exclusively coupling products, *e.g.*, $Ph_2C{=}CPh_2$ and $Ph_2C{=}N{-}N{=}CPh_2$, despite the fact that they give mainly C–H and O–H insertion products with host molecules in other alcoholic matrices (*i.e.*, MeOH—*i*-PrOH). This striking effect of the host on the course of carbene reactions in the matrix is especially noteworthy from the viewpoint of recent growing interest in the behavior of carbene in a rigid matrix.[5-7] We wish now to report developments in the application of the method in synthetic and mechanistic studies of carbene chemistry and, more generally, in synthetic photochemistry at low temperatures.

Results and Discussion

In order to examine the general utility of the low-temperature synthesis of olefin *via* the dimerization of carbene within crystalline matrices, we have irradiated several diazo compounds in a *t*-BuOH matrix and found that olefinic dimer formation is extremely sensitive to the structure of the carbenes (Table 1). Thus,

Table 1. Detection of olefinic dimer in the photolysis of some diazo compounds in *t*-butyl alcohol matrix at −196 °C

R and R′ in $RR'C{=}N_2$	$RR'C{=}CR'R$ yield/%[a]
1a: R=R′=Ph	48.1
1b: R=Ph, R′=H	17.0
1c: R=Ph, R′=CO_2Me	25.1
2: R=R′=CO_2Me	13.2
3a: R=H, R′=CO_2Me	n.d.[b,c]
3b: R=H, R′=$CONEt_2$	n.d.[b,d]
3c: R=H, R′=COPh	n.d.[b,e]

a) Based on the $RR'C{=}N_2$ used. b) Not detected. c) The main products were O–H insertion and Wolff rearrangement products. d) The main products were *β*- and *γ*-lactam. See Ref. 10. e) The main product was a Wolff rearrangement product.

the formation of the olefinic dimer was observed in the low-temperature photolysis of the aryldiazomethane derivatives (**1a**—**c**), which are known[8] to yield carbenes with triplet ground states. A similar photolysis of **2** also gave ethylene tetracarboxylate. Markedly to the contrary, however, no trace of olefin was detected in the photolysis of **3a**—**c**, even after all the diazo compounds had been destroyed. The main products detected were Wolff rearrangement products[9] in the cases of **3a** and **b**, and intramolecular C–H insertion products[9,10] in the case of **3c**. It is very interesting

$PhCN_2R$	$N_2C(CO_2Me)_2$	N_2CHCOR
1	**2**	**3**
a, R=H		**a**, R=OMe
b, R=Ph		**b**, R=Ph
c, R=CO_2Me		**c**, R=NEt_2

to note that some of the carbenes derived from **3** have been frequently postulated[11] as having singlet ground states. One would not expect triplet carbene chemistry to occur in the low-temperature direct-photolytic method if one assumes that the carbene has a singlet ground state separated by somewhat more than 5 kcal mol^{-1} from an upper triplet state, and that the

Table 2. Product distributions[a] as a function of temperature. Photolysis of Ph_2CN_2 in *t*-BuOH containing EtOH

T °C	[EtOH] mol %	Ph_2CH_2	Ph_2CHOBu^t	Ph_2CHOEt	$Ph_2CHCHOH$ (CH$_3$)	$Ph_2CHCH_2CH_2OH$	Yield[b] %
24	1	0.7	96.7	2.6	0	0	98.2
	5	1.9	88.4	9.7	0	0	87.5
	10	3.0	78.9	18.1	0	0	84.9
−77	1	7.2	29.9	62.9	0	0	29.7
	5	6.3	22.5	71.2	0	0	54.7
	10	6.6	18.6	74.8	0	0	58.6
−196	1	4.0	16.5	45.0	34.5	trace	15.0
	5	2.6	8.2	44.6	44.6	trace	35.9
	10	3.2	5.8	42.0	45.4	3.6	68.5

a) Data are percentages of total products listed above normalized to 100%. The other products were benzophenone, the azine, and tetraphenylethylene. b) Total yields based on Ph_2CN_2 used.

Table 3. Product distribution as a function of temperature. Photolysis of Ph_2CN_2 in EtOH-*i*-PrOH mixture[a]

T °C	[EtOH] mol %	Ph_2CH_2	EtOH			*i*-PrOH			Yield[b] %
			O–H	α-CH	β-CH	O–H	α-CH	β-CH	
24	5	7.0	7.1	0	0	85.9	0	0	≈100
	95	2.3	95.0	0	0	2.7	0	0	≈100
−196	5	4.0	5.6	8.2	0	27.2	45.0	10.0	87.0
	95	3.1	32.2	63.1	0	0.4	1.2	0	89.7

a) See footnote a in Table 2. The O–H, α-CH, and β-CH terms refer to the OH, α-CH, and β-CH insertion products into alcohols respetively. b) Total yield.

intersystem crossing process of the diazo compound does not compete with the dissociation.[12] Furthermore, although it is highly improbable that a reactive carbene can meet with another carbene to form olefin in the liquid phase before it attacks the substrate, evidence has been accumulating which shows that olefin could be formed by the combination of two triplet carbenes in the case where the carbenes are highly stabilized by structural[13] and/or environmental[5] effects. Recently, the flash photolysis of **1b** in benzene at 25 °C has been shown[14] to give tetraphenylethylene as the major product; this substance has not been observed in the steady-state photolysis. The fact that there is no spectroscopic evidence for any significant concentration of another transient except the triplet diphenylmethylene indicates that tetraphenylethylene is formed *via* the dimerization of the triplet carbene. Theoretical consideration also shows[15] that the least-motion formation of ethylene from triplet methylenes is an allowed process. Thus, it is reasonable to assume that the dimerization of the carbenes within a crystalline matrix would be affected by the ground-state multiplicity. The present method may, then, be expected to give us important information on the reactivity and multiplicity of the ground-state carbene,[16] although, as with most negative results, there might be several possible explanations for the failure to observe the olefinic dimer. Quite recently, for example, Roth *et al.* have shown,[17] by EPR study, that **3a** has a ground-state triplet or a triplet state that lies a maximum of 10 cal above the singlet state. Interestingly, its EPR signals follow the Curie law in the temperature range of 10—40 K, but vanish at higher temperatures, presumably by means of the reaction of the triplet with a matrix or by the conversion of the triplet state to a more reactive state capable of undergoing intra- and intermolecular reactions.[9] This is in marked contrast with that phenomenon observed in arylcarbene systems, in which the triplet state has been shown[8] to be fairly stable even at 77 K. Our results for **3a** might indicate, then, that the 77 K matrix is not cool enough to populate the triplet **3a** by quenching the singlet reaction; hence, more extensive temperature experiments would be desirable to form a more widely applicable method.

The photolysis of Ph_2CN_2 in *t*-BuOH containing a small amount of EtOH (up to 10%) at 25 °C gave Ph_2CHOBu^t almost exclusively. Surprisingly, however, when photolysis was performed in the solid phase at −77 °C, O–H insertion with the solute alcohol increased dramatically at the expense of the product formed from the host alcohol (Table 2). *t*-Butyl ether was almost completely suppressed in −196 °C photolysis, with a concomitant formation of C–H and O–H insertion products of the solute alcohol. The coupling products were also greatly reduced with an increase in the concentration of EtOH in the −196 °C photolytic runs. Similar phenomena were also observed with other solute alcohols (*e.g.*, MeOH, *i*-PrOH) in other tertiary alcohols (*e.g.*, *t*-$C_5H_{11}OH$).

A parallel series of irradiations in the EtOH–*i*-PrOH mixed matrix (Table 3) showed, however, that no

selective reaction of carbene with the solute alcohol was observed in this system. This implies that tertiary alcohols provide a special environment for carbene reactions.

Several possible explanations may be offered for the selective reaction of carbene with solute alcohol in a *t*-BuOH matrix. First, it may be that the Ph_2C generated in a matrix at −196 °C migrates through the host matrix and reacts with the more reactive solute alcohol molecules, as has been proposed[18] in the tunnelling effect in the selective H-abstraction by an H atom in a crystalline alkane mixture at −196 °C. This is less likely, however, since it has been shown[19] that the cage about the precursor severely restricts the molecular motion of such large molecules. Further, phenyl migration has been shown to be highly unfavorable in a rigid matrix, even in intramolecular 1,2-shifts, while the 1,2-H shift was relatively easy under the same conditions.[20] Secondly, one may propose that most of the Ph_2C reacts when the matrix is thawed in the dark with the more reactive, and more rapidly melting, solute alcohol. There has been accumulating evidence,[6,7] however, which demonstrates that most of the reaction of the carbene in the matrix occurs while the reaction mixtures are still frozen (see below). A more probable explanation would be that the co-aggregation of the carbene precursor and the solute alcohol is occurring in the crystalline matrix. Similar striking effects of the host on the course of low-temperature photochemical reactions have been explained[1,2] in terms of such aggregation. Such co-aggregation might be attributable, at least in part, to the limited solubility of the solute molecules in the *t*-BuOH crystal at low temperatures. However, this is by no means unavoidable, since similar selective reactions between solute molecules has been noted in a 10% EtOH–*t*-$C_5H_{11}OH$ mixed matrix which does not crystallize, but which forms a glass at −196 °C. Also noteworthy is that all crystalline matrices were not unreactive to carbene at −196 °C. C–H insertion products were obtained[6b] in reasonable yields (40—50%) in the low-temperature photolysis of $PhCH{=}N_2$ in a crystalline matrix, *e.g.*, pentane, butane, and isobutane. The interpretation of these results we favor is that the guest cavity provided by bulky tertiary alcohol has enough space to bind a molecular aggregate inside it.

Finally, an example to show the more general utility of the *t*-BuOH matrix was obtained in the reaction of Ph_2C with Ph_2CO. The irradiation (>300 nm) of Ph_2CN_2 in a 5% Ph_2CO–*t*-BuOH mixture at −196 °C resulted in a rapid and splendid change in the original wine-red color of the reaction mixture to a

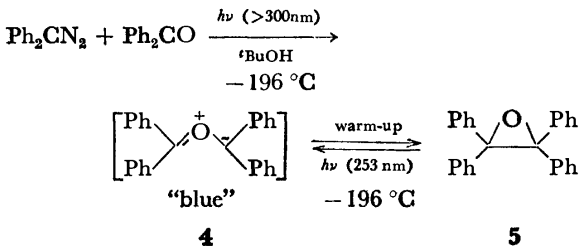

Table 4. Product distributions in the photolysis[a] of diphenyldiazomethane in the presence of benzophenone in *t*-butyl alcohol matrix at −196 °C

$[Ph_2CO]$ mol %	Yield/%			
	$Ph_2C{=}CPh_2$	Ph_2	$(Ph_2CH)_2$	$(Ph_2C{=}N)_2$
5	9.8	31.5	2.1	3.6
10	5.5	32.9	2.3	5.3

a) The yields were determined by GC and are based on the Ph_2CN_2 used.

deep blue, which rapidly faded to a light yellow solution when the matrix was then thawed in the dark. The GC analysis of the resulting mixture showed the presence of oxirane (**5**) as the main product (Table 4). The transient formation of a blue-colored species is very reminescent of the carbonyl ylide (**4**) which has been detected[21] in the low-temperature photolysis (253 nm) of the oxirane (**5**), although our attempt at the spectroscopic identification of **4** was not successful because of the extremely low transmission of the matrix. This strongly indicates the intervention of carbonyl ylide in the reaction of Ph_2C with the Ph_2CO, probably formed by the initial attack of carbene on carbonyl oxygen. Such an intermediate had been postulated[22] in the addition of carbene to a carbonyl compound, but it had not been detected before. It should be noted again that neither blue-colored species nor oxirane can be observed in similar photolyses within other alcoholic matrices, which form glass. The main products in this case are those formed from the host alcohol. The spin multiplicity of the attacking carbene poses a very interesting question. The attack by the triplet, followed by electron demotion, could explain the formation of ylide. However, the one-step formation of the electrophilic attack of the singlet could equally well be applied, since it has been shown that the presence of Ph_2CO as a sensitizer does not change the singlet/triplet ratio of carbene at −196 °C. This is ascribable to the rapid and reversible singlet-triplet equillibrium involved[9] in this carbene system. Note that the experimental[14] value for $E_S - E_T$ is ≤ 3 kcal/mol. Further studies to show the general usefulness of this matrix are in progress.

Experimental

The IR spectra were determined on a JASCO IR-G recording spectrometer. The H^1 NMR spectra were determined on a JEOL JNM-MH-100 NMR spectrometer. The GC-MS spectra were obtained on a Shimadzu GC-MS 1000 spectrometer using a column consisting OV-17 on Shimalite (5.0 mm×2.0 m). The GC analyses were performed on a Yanagimoto instrument, Model G-180, with a flame ionization detector. The following columns were used: A, 5.0 mm×2.0 m 10% OV-17 on 60—80 mesh Diasolid L; B, 5.0 mm×2.0 m 5% PEG 20 M on 60—80 mesh Diasolid L.

Materials. All the diazo compounds employed (**1a**,[23] **1b**,[23] **1c**,[24] **2**,[25] **3a**,[26] **3b**,[27] and **3c**,[28]) were prepared according to the literature procedures and were purified just prior to use. The *trans*-dibenzoylethylene was prepared

by means of the Friedel-Crafts reaction[29] with fumaryl chloride. The dimethyl α,β-diphenylmaleate was obtained by the reaction[30] of methyl α-bromophenylacetate with Na-NH_2. The *N,N,N',N'*-tetraethylfumaramide was prepared by the treatment of fumaryl chloride with diethylamine. The preparations of the other authentic specimens have been reported elsewhere.[6c] Satisfactory spectroscopic data have been obtained for all authentic compounds. The commercial alcohols were purified prior to use.

Photochemical Reactions and Analyses. All the irradiations were conducted using a Halos 300 W high-pressure mercury lamp with a water-cooled quartz jacket. In the general procedure, 0.06 mmol of Ph_2CN_2 was added to 2 ml of *t*-butyl alcohol with or without a second alcohol or Ph_2CO in a Pyrex tube with a capacity of 5 ml. The tube was suspended in a transparent Pyrex Dewar flask filled with coolant and irradiated until all of the precursor molecules had been destroyed. The coolants were water (24 °C), solid CO_2–EtOH (−77 °C), and liquid nitrogen (−196 °C). For solid-phase irradiations, the mixture was periodically warmed in the dark until the rigid glass or solid melted, so that mixing could occur. Control experiments ruled out the interconversion of the product during the irradiations and also showed that no reaction occurred in the absence of light in the range of temperatures studied.

The product identification and relative yields were easily determined by standard GC and/or GC-MS techniques.

The authors wish to express their thanks to Professor Gary W. Griffin, University of New Orleans, for the supply of tetraphenyloxirane.

References

1) J. Kolc, *Tetrahedron Lett.*, **1972**, 5321.
2) V. Dvorak, J. Kolc, and J. Michl, *Tetrahedron Lett.*, **1972**, 3443.
3) O. L. Chapman and C. L. McIntosh, *J. Am. Chem. Soc.*, **92**, 7001 (1970).
4) A. O. Pederson, S.-O. Lawesson, P. O. Klemmensen, and J. Kolc, *Tetrahedron*, **26**, 1157 (1970).
5) H. Tomioka and Y. Izawa, *J. Am. Chem. Soc.*, **99**, 6128 (1977).
6) (a) H. Tomioka, T. Inagaki, and Y. Izawa, *J. Chem. Soc., Chem. Commun.*, **1976**, 1023; *J. Chem. Soc., Perkin Trans. 1*, **1979**, 130; (b) H. Tomioka, *J. Am. Chem. Soc.*, **101**, 256 (1979); (c) H. Tomioka, G. W. Griffin, and K. Nishiyama, *ibid.*, **101**, 6009 (1979).
7) (a) R. A. Moss and U.-H. Dolling, *J. Am. Chem. Soc.*, **93**, 954 (1971); (b) R. A. Moss and M. A. Joyce, *ibid.*, **99**, 1262 (1977); (c) R. A. Moss and J. K. Huselton, *ibid.*, **100**, 1315 (1978); (d) R. A. Moss and M. A. Joyce, *ibid.*, **100**, 4475 (1078).
8) A. M. Trozzolo, *Acc. Chem. Res.*, **1**, 329 (1968), and references cited therein.
9) For reviews, see (a) W. Kirmse, "Carbene Chemistry," 2nd ed, Academic Press, New York, N. Y. (1971); (b) "Carbenes," ed by R. A. Moss and M. Jones, Jr., Wiley, New York (1974), Vol. 1.
10) (a) R. Rando, *J. Am. Chem. Soc.*, **92**, 6706 (1977); **94**, 1629 (1972); (b) H. Tomioka, H. Kitagawa, and Y. Izawa, *J. Org. Chem.*, **44**, 3072 (1979).
11) (a) J. Fenwick, G. Frater, K. Ogi, and O. P. Strausz, *J. Am. Chem. Soc.*, **95**, 124 (1973); (b) I. G. Csizmadia, H. E. Gunning, R. K. Gosavi, and P. O. Strausz, *ibid.*, **95**, 133 (1973); (c) M. Tanaka, T. Nagai, and N. Tokura, *J. Org. Chem.*, **37**, 4106 (1972); (d) M. Tanaka, T. Nagai, and N. Tokura, *ibid.*, **38**, 1602 (1973); (e) P. S. Skell, S. J. Valenty, and P. W. Humer, *J. Am. Chem. Soc.*, **95**, 5041 (1973).
12) For a discussion of this point, see P. P. Gasper and G. S. Hammond, "Carbenes," ed by M. Jones, Jr., and R. A. Moss, Wiley, New York (1975), Vol II, p. 327.
13) (a) H. E. Zimmerman and D. H. Paskovich, *J. Am. Chem. Soc.*, **86**, 2149 (1964); (b) P. A. S. Smith and E. M. Bruckman, *J. Org. Chem.*, **39**, 1047 (1974).
14) G. L. Closs and B. E. Rabinow, *J. Am. Chem. Soc.*, **98**, 8190 (1976).
15) R. Hoffman, R. Gleiter, and F. B. Mallory, *J. Am. Chem. Soc.*, **92**, 1460 (1970).
16) See, for example, (a) P. J. Stang and M. G. Mangum, *J. Am. Chem. Soc.*, **97**, 1459 (1975). (b) R. J. Norstrom, H. E. Gunning, and O. P. Strausz, *ibid.*, **98**, 1454 (1976).
17) R. S. Hutton and H. D. Roth, *J. Am. Chem. Soc.*, **100**, 4324 (1978).
18) (a) T. Wakayama, T. Miyazaki, K. Fueki, and Z. Kuri, *J. Phys. Chem.*, **77**, 2365 (1973); (b) T. Miyazaki and T. Hirayama, *ibid.*, **79**, 566 (1975); (c) T. Miyazaki, K. Kinugawa, M. Eguchi, and M. L. Guedes, *Bull. Chem. Soc. Jpn.*, **49**, 2970 (1976).
19) E. Wasserman and W. A. Yager, *J. Phys. Chem.*, **71**, 201 (1967).
20) H. Tomioka, H. Ueda, and Y. Izawa, submitted for publication.
21) (a) T. Do-Mihn, A. M. Trozzolo, and G. W. Griffin, *J. Am. Chem. Soc.*, **92**, 1402 (1970); (b) R. S. Becker, R. O. Bost, J. Kolc, N. R. Bertoniere, R. L. Smith, and G. W. Griffin, *ibid.*, **92**, 1302 (1970).
22) (a) R. H. Huisgen, *Angew. Chem. Int. Ed. Engl.*, **2**, 565 (1963); (b) Recently, it has been demonstrated that diazoalkanes add to penta- and hexafluoroacetone to give 2,5-dihydro-1,3,4-oxadiazoles, which subsequently decompose to oxidrane *via* carbonyl ylides; N. Shimidzu and P. D. Bartlett, *J. Am. Chem. Soc.*, **100**, 4260 (1978).
23) W. M. Jones, R. C. Joines, J. A. Myers, T. Mitsuhashi, K. E. Krajca, E. E. Waali, T. L. Davis, and A. B. Turner, *J. Am. Chem. Soc.*, **95**, 826 (1973).
24) M. Regitz and F. Menz, *Chem. Ber.*, **101**, 2622 (1968).
25) M. Regitz and A. Liedhegener, *Chem. Ber.*, **99**, 3128 (1966).
26) M. Regitz, J. Hocker, and A. Lichegener, *Org. Synth.*, Coll. Vol. V, 179 (1973).
27) R. A. Franich, G. Lowe, and J. Parker, *J. Chem. Soc., Perkin Trans. 1*, **1972**, 2034.
28) M. S. Newman and P. Beal, *J. Am. Chem. Soc.*, **71**, 1506 (1949).
29) R. E. Lutz, *Org. Synth.*, Coll Vol. III. 248 (1955).
30) M. Ramort-Lucas and M. J. Hoch, *Ann. Chim.*, **14**, 395 (1930).

Photocycloaddition Reaction of Alkyl-substituted 1,4-Naphthoquinones with Olefins. Substituent Effects on Controlling the Orientation of Cycloaddition Reaction

Kazuhiro MARUYAMA* and Noritsugu NARITA
Department of Chemistry, Faculty of Science, Kyoto University, Kitashirakawaoiwake-cho, Sakyo-ku, Kyoto 606
(Received August 23, 1979)

Photolysis of a benzene solution of 2-alkyl- or 2,3-dialkyl-substituted 1,4-naphthoquinone mixed with an aryl-substituted ethylene afforded 3,4-benzobicyclo[4.2.0]octene-2,5-dione derivatives (cyclobutane type adducts) in a good yield without any other types of products. The orientation of the cycloaddition was likely to control by the adverse van der Waals repulsion of the substituents of the quinone and olefin in addition to the electronic effects of the substituents. The predominant factor orientating the cycloaddition seems to play the van der Waals repulsion due to the substituents both of quinone and olefin.

Photochemical reaction of 1,4-naphthoquinones with olefins have been investigated by several workers[1-3]. Especially the photoaddition reactions are of versatile possibilities, for it consists from one-step C–C or C–O bond formation reaction. The photo-addition products of quinone and olefins can be classified into the following three structural types; cyclobutane type adduct **A**, spiro-oxetane type adduct **B** *via* $2\pi+2\pi$ cycloaddition processes, and cyclohexane type adduct **C** *via* $2\pi+2\pi+2\pi$ cycloaddition process.

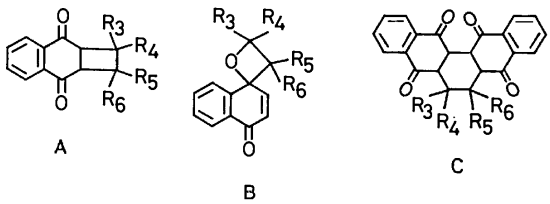

Fig. 1. The photo-addition products of 1,4-naphthoquinone and olefins.

The mechanism of the formation of type **C** products has been investigated in details by Maruyama, *et al.*[4]

Although photochemical reactions of substituted 1,4-naphthoquinones with some olefins have reported to yield cyclobutane type adducts **A**,[5,6] the systematic investigations in the fields have been sparse. In this paper, the present authors investigated the photochemical reactions of alkyl-substituted 1,4-naphthoquinones with aryl-substituted ethylenes and intended to clarify the substituent effects of quinones and olefins on the orientation of the photocycloaddition reaction.

Results and Discussion

Photocycloaddition Reaction of Alkyl-substituted 1,4-Naphthoquinones with Aryl-substituted Ethylenes. Irradiation of a solution of 2-methyl-1,4-naphthoquinone (**1a**) with styrene (**2a**) in benzene with the light through a Pyrex filter gave the mixture of three cycloaddition products in a high yield. The major product was isolated by thin layer chromatography (silica gel) and purified by recrystallization as white crystals. The structure was determined on the basis of spectroscopy (see Experimental) to be *anti*-1-methyl-8-phenyl-3,4-benzobicyclo[4.2.0]octene-2,5-dione(**3a**). The second

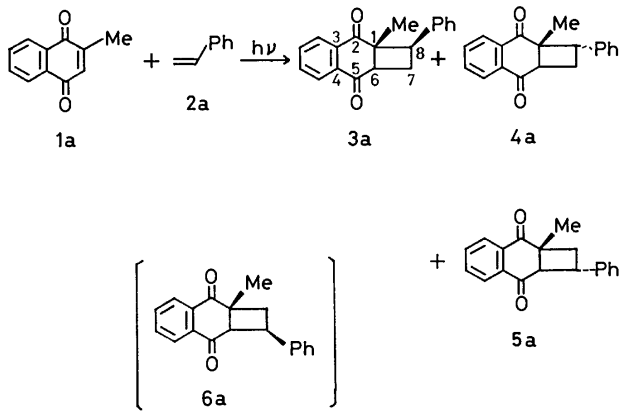

Fig. 2. Photochemical reaction of 2-methyl-1,4-naphthoquinone **1a** with styrene **2a**.

product was obtained as a mixture with **3a**. The structure was assigned to *syn*-1-methyl-8-phenyl-3,4-benzobicyclo[4.2.0]octene-2,5-dione(**4a**) on the basis of spectral data. The third product was obtained as pure crystals which structure was assigned to *syn*-1-methyl-7-phenyl-3,4-benzobicyclo[4.2.0]octene-2,5-dione(**5a**).

All of three products were cyclobutane type adducts *via* $2\pi+2\pi$ cycloaddition process. But, the corresponding *anti*-7-phenyl isomer expected(**6a**) was not detectable. These three products were unchanged by treatment with basic alumina, showing that the six-four ring fusion is cis.[8]

In a similar fashion, the photoreaction of 2-ethyl-1,4-naphthoquinone(**1b**) with styrene **2a** afforded three products **3b**, **4b**, and **5b**. No *anti*-7-phenyl isomer **6b** was obtained, too.

In these cases, the major products were the 8-phenyl isomers and the ratio of 7-phenyl isomer to 8-phenyl isomers was smaller for 2-methyl-1,4-naphthoquinone–styrene system, 1/6, than that for 2-ethyl-1,4-naphthoquinone–styrene system, 1/3.5.

The slow photo-induced isomerization between these two isomers (7-phenyl and 8-phenyl isomers) was realized, which was followed by means of NMR spectroscopy, but the rates of photo-isomerization were so slow that the distribution of the products was controlled kinetically.

The orientation of the addition could be affected

TABLE 1. RELATIVE YIELDS OF PHOTOPRODUCTS

Quinone	Olefin	Total yield %	7-Phenyl		8-Phenyl	
			Anti(%)	Syn(%)	Anti(%)	Syn(%)
1a	**2a**	80	(**6a**) 0	(**5a**) 15	(**3a**) 55	(**4a**) 30
1b	**2a**	73	(**6b**) 0	(**5b**) 24	(**3b**) 50	(**4b**) 26
1a	**2b**	95	(**6c**) 42	(**5c**) 10	(**3c**) 29	(**4c**) 19
1b	**2b**	95	(**6d**) 50	(**5d**) 14	(**3d**) 23	(**4d**) 13
1a	**2c**	73		(**5e**) 66	(**3e**) 34	
1b	**2c**	57		(**5f**) 80	(**3f**) 20	

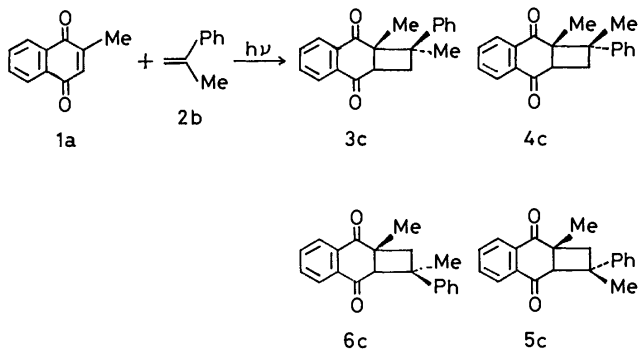

Fig. 3. Photochemical reaction of **1a** with 2-phenylpropene **2b**.

by both steric and electronic interactions between two substrates, 1,4-naphthoquinone and olefin. The results found in the 2-alkyl-1,4-naphthoquinone–styrene system indicate that the dipole-dipole interaction between the alkyl group on the quinone molecule and the phenyl group on styrene molecule presumably overcome the adverse van der Waals repulsion of these substituents.

The photocycloaddition of 2-methyl-1,4-naphthoquinone **1a** with 2-phenylpropene(**2b**) in bezene gave four cycloadducts. The major product (39%) was isolated as white crystals which structure was determined as *anti*-1,7-dimethyl-7-phenyl-3,4-benzobicyclo[4.2.0]-octene-2,5-dione(**6c**). The second product (28%) was *anti*-1,8-dimethyl-8-phenyl-3,5-benzobicyclo[4.2.0]-octene-2,5-dione(**3c**).

The *syn*-7-phenyl (**5c**) (9%) and *syn*-8-phenyl isomer (**4c**) (18%) were obtained as the mixture, and the yields were determined by means of NMR spectroscopy. The ratio of 7-phenyl isomers to 8-phenyl isomers was about 1.

The photochemical reaction of 2-ethyl-1,4-naphthoquinone **1b** with 2-phenylpropene **2b** gave similarly two 8-phenyl derivatives (**3d**) and (**4d**), and two 7-phenyl derivatives (**5d**) and (**6d**). The major product (48%) was *anti*-ethyl-7-methyl-7-phenyl-3,4-benzobicyclo[4.2.0]octene-2,5-dione (**6d**). The *anti*-8-phenyl isomer was obtained in a yield of 22%. The syn isomers were obtained as a mixture. The ratio of 7-phenyl derivatives to 8-phenyl ones was about 1.5, which was larger than that of isomers in the case of **1a** and **2b**.

When 2-phenylpropene was employed as olefin, the methyl group on C-2 carbon of olefin would cancel out the dipole-dipole interaction caused by the phenyl group, and the adverse van der Waals repulsion of the substituent groups on the quinone and olefin may force to reverse the orientation of addition. Thus the ratio of 7-phenyl/8-phenyl adducts increased in accordance with the bulkiness of substituent groups, *i.e.* from hydrogen to methyl group. To support this conclusion, the photocycloadditions of 2-methyl- and 2-ethyl-1,4-naphthoquinone with 1,1-diphenylethylene (**2c**) were investigated under the same conditions.

A benzene solution containing 2-methyl-1,4-naphthoquinone **1a** and 1,1-diphenylethylene **2c** was irradiated through a Pyrex filter. The products were 1-methyl-7,7-diphenyl-3,4-benzobicyclo[4.2.0]octene-2,5-dione (**5e**) (48%) and 1-methyl-8,8-diphenyl-3,4-benzobicyclo-[4.2.0]octene-2,5-dione (**3e**) (25%). Similarly, 2-ethyl-1,4-naphthoquinone **1b** reacted photochemically with 1,1-diphenylethylene **2c** to give 1-ethyl-7,7-diphenyl-3,4-benzobicyclo[4.2.0]octene-2,5-dione (**5f**) (45%) as the major product and 1-ethyl-8,8-diphenyl-3,4-benzobicyclo[4.2.0]octene-2,5-dione (**3f**) (12%).

In these cases, the major product was the 7,7-diphenyl derivative and the ratio of 7,7-diphenyl/8,8-diphenyl isomer was 2 for 2-methyl-1,4-naphthoquinone–1,1-diphenylethylene system, and 4 for 2-ethyl-1,4-naphthoquinone–1,1-diphenylethylene system.

The results were illustrated in Table 1.

These results given in Table 1 indicated that the adverse van der Waals repulsion among the substituent groups in transition state could overcome sometimes the electronic attractive interaction caused by the substituents of reactants.

In the photoadducts of the quinone and 1,1-diphenylethylene, one of the two phenyl groups was situated above the quinone moiety from molecular model examination. The π-π interaction between quinone moiety and one of the two phenyl groups could be expected, but not with the other.

To substantiate the fact, the photocycloaddition of 2-methyl-1,4-naphthoquinone **1a** and 1,1-bis(*p*-methylphenyl)ethylene was carried out under the same irradiation conditions. The major product (46%) was 1-methyl-7,7-bis(*p*-methylphenyl)-3,4-benzobicyclo-[4.2.0]octene-2,5-dione (**5g**). The minor product was assigned the structure as 1-methyl-8,8-bis(*p*-methylphenyl)-3,4-benzobicyclo[4.2.0]octene-2,5-dione (**3g**) (28%).

The NMR spectra of these products showed that the signals due to two methyl groups on the two phenyls appeared at δ 2.0 and 2.3 ppm in chloroform-*d*, respectively. The phenyl protons appeared in the region

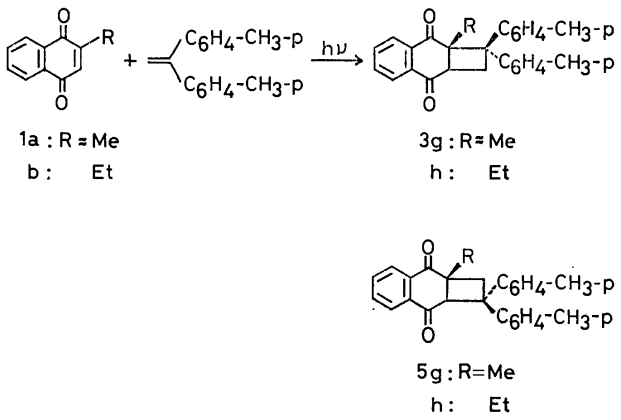

Fig. 4. Photochemical reaction of 2-alkyl-1,4-naphthoquinone with 1,1-bis(*p*-methylphenyl)ethylene.

of 6.9—7.1 and 7.2—7.3 ppm with two AB type quartets (see Experimental).

Analogous products, 1-ethyl-7,7-bis(*p*-methylphenyl)-3,4-benzobicyclo[4.2.0]octene-2,5-dione (**5h**) and 1-ethyl-8,8-bis(*p*-methylphenyl)-3,4-benzobicyclo[4.2.0]-octene-2,5-dione (**3h**) were obtained from the photoreaction of 2-ethyl-1,4-naphthoquinone **1b** with 1,1-bis(*p*-methylphenyl)ethylene.

The NMR spectra of both **3h** and **5h** also showed respectively two different *p*-methylphenyl signals. This fact clearly shows that between the one of two phenyl groups and quinone moiety the π-π interaction is operating.

The products ratio of two isomers, *i.e. anti* and *syn*, could reflect the steric or electronic courses of this type $2\pi+2\pi$ cycloaddition reaction. Further, the symmetrical 2,3-dialkyl-1,4-naphthoquinones were employed to investigate the substituent effects on the *anti*/*syn* isomers ratio of the products.

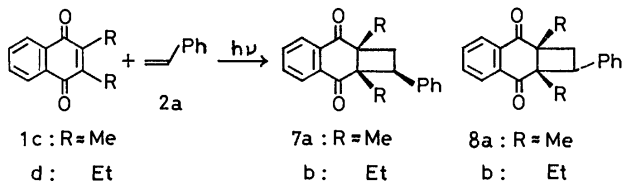

Fig. 5. Photochemical reaction of 2,3-dialkyl-1,4-naphthoquinone with styrene **2a**.

The photocycloaddition of 2,3-dimethyl-1,4-naphthoquinone (**1c**) with styrene **2a** gave *anti*-1,6-dimethyl-7-phenyl-3,4-benzobicyclo[4.2.0]octene-2,5-dione (**7a**) in a yield of 84%, and the corresponding *syn* isomer (**8a**) in a yield of 16%.

The photoreaction of 2,3-diethyl-1,4-naphthoquinone (**1d**) with styrene **2a** gave *anti*-1,6-diethyl-7-phenyl-3,4-benzobicyclo[4.2.0]octene-2,5-dione (**7b**) in a yield of 93% and the *syn* isomer (**8b**) in a yield of 7%.

The photoreaction of 2,3-dimethyl-1,4-naphthoquinone **1c** with 2-phenylpropene **2b** afforded two products, one of which was assigned as *anti*-1,6,7-trimethyl-7-phenyl-3,4-benzobicyclo[4.2.0]octene-2,5-dione (**7c**)(38%) and the other was its *syn* isomer (**8c**) (20%). Similarly, the photocycloaddition of 2,3-diethyl-1,4-naphthoquinone **1d** and 2-phenylpropene **2b** gave *anti*-1,6-diethyl-7-methyl-7-phenyl-3,4-benzobicyclo[4.2.0]octene-2,5-dione (**7d**) in a yield of 77% and the corresponding *syn* isomer (**8d**) in a yield of 13%.

Table 2. Anti/syn ratio of photoproducts

Quinone	Olefin	7-Phenyl adducts	8-Phenyl adducts
1a	**2a**	0	1.88
1a	**2b**	4.20	1.56
1b	**2a**	0	2.00
1b	**2b**	3.69	1.69
1c	**2a**	5.25	
1c	**2b**	1.52	
1d	**2a**	13.33	
1d	**2b**	6.00	

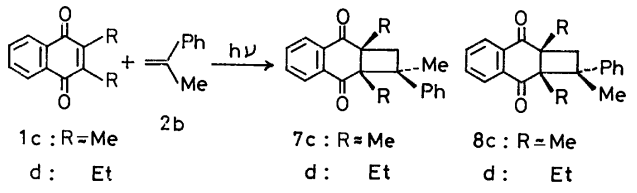

Fig. 6. Photochemical reaction of 2,3-dialkyl-1,4-naphthoquinone with 2-phenylpropene **2b**.

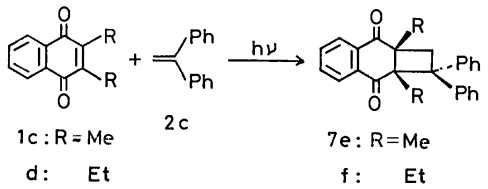

Fig. 7. Photochemical reaction of 2,3-dialkyl-1,4-naphthoquinone with 1,1-diphenylethylene **2c**.

The photocycloadditions of these symmetrical substituted 1,4-naphthoquinones(**1c** and **1d**) with 1,1-diphenylethylene **2c** gave 1,6-dialkyl-7,7-diphenyl-3,4-benzobicyclo[4.2.0]octene-2,5-dione (**7e** and **7f**) in high yields.

The results of the *anti*/*syn* ratio of photoproducts are given in Table 2.

The *anti*/*syn* ratio was larger than 1 with exception of the case of 7-phenyl derivatives obtained from 2-alkyl-1,4-naphthoquinone (**1a** and **1b**) and styrene **2a**. The ratio was reduced when the methyl group was introduced to C-1 carbon of styrene. The results found in these systems showed that the *anti* transition state was favored over the *syn* one, and that the adverse van der Waals repulsion of these substituents overcame the attractive force due to π-π overlap interaction between quinone moiety and phenyl group of olefin.

From the results it was shown that one of the major factors in determining the orientation of the photocycloaddition of alkyl-substituted 1,4-naphthoquinone and substituted styrene was the steric hinderance of the substituents of quinone and olefin.

Determination of Quantum Yields. The quantum yields were determined by using potassium tris(oxalato)-ferrate(III) as the chemical actinometer.[9] The light from a 300 W high pressure mercury-arc lamp was

TABLE 3. QUANTUM YIELDS FOR QUINONE DISAPPEARANCE (Φ_d) AND THE PRODUCT FORMATION (Φ_p)

Quinone	Olefin	Φ_d	Relative Φ_d	Φ_p			
				7-Phenyl		8-Phenyl	
				Anti	Syn	Anti	Syn
1a	**2a**	0.82	1.00	0	0.10	0.44	0.24
1a	**2b**	0.66	0.81	0.26	0.05[a]	0.18	0.12[a]
1a	**2c**	0.60	0.73	0.38		0.20	
1b	**2a**	0.80	0.98	0	0.17	0.35[a]	0.16[a]
1b	**2b**	0.64	0.78	0.30	0.09[a]	0.14	0.09[a]
1b	**2c**	0.57	0.69	0.45		0.12	
1c	**2a**	0.65	0.79	0.53	0.12		
1c	**2b**	0.46	0.56	0.24	b)		
1c	**2c**	0.25	0.31	0.25			

a) The values were estimated by means of NMR spectroscopy. b) The values could not be determined.

TABLE 4. YIELDS AND PHYSICAL DATA OF QUINONES

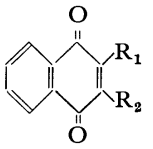

	R_1	R_2	Yield/%[a]	Mp/°C	$n\pi^*(\varepsilon)$	$\pi\pi^*(\varepsilon)$
1a	Me	H	28	105.0—107.0	440(50)	330(2840)
1b	Et	H	29	89.5— 90.5	440(70)	330(2570)
1c	Me	Me	30	130.0—131.0	440(60)	330(2770)
1d	Et	Et	27	69.0— 69.5	440(70)	330(2330)

a) The values are isolated yields based on the amount of quinone used.

filtered through a potassium chromate–sodium carbonate solution[10] (transmission: 300—330 nm).

Photochemical reactions for the determination were carried out holding the reaction at a low conversion to prevent an appreciable light absorption by the products. Quantum yields of the photochemical reactions measured in benzene solution were given in Table 3. Quantum yields for quinone disappearance were decreased in accordance with the larger steric repulsion of the substituent groups on quinone and olefin.

These results showed that the adverse van der Waals repulsion of substituent groups was playing an important role not only for controlling the orientation of the cycloaddition, but also for determining the rate of the reaction.

Reaction Mechanism. The absorption spectra of alkyl-substituted 1,4-naphthoquinones exhibited maxima (in chloroform) at 440 nm (ε: <100), 330 nm (ε: 2500—3000), and 245 nm(ε: *ca.* 15000). The lowest $\pi\pi^*$ absorption band of the quinones exhibited at 330 nm and $n\pi^*$ absorption was almost masked by the long wavelength tail of the $\pi\pi^*$ band, and was apparently observed as a shoulder. When the photoreaction of 2-alkyl- or 2,3-dialkyl-1,4-naphthoquinone with olefins was undertaken by using the longer wavelength light than 400 nm, then none of photoadduct could be detected by means of NMR spectroscopy, and the quinone was recovered almost quantitatively.

The photocycloaddition of 2-methyl- **1a** or 2,3-dimethyl-1,4-naphthoquinone **1c** with 1,1-diphenylethylene **2c** was not quenched by addition of fluoranthene as a triplet quencher[12-14] (E_T=54.2 kcal/mol) in the system. The present experimental results are likely to indicate the photocycloaddition between quinone and olefin proceeds *via* $\pi\pi^*$ singlet excited state of quinone, but to determine the true nature of the excited state responsible for the present cycloaddition reaction the further detailed mechanistic investigations should be done.

Experimental

The photolysis solution in a Pyrex test tube was irradiated externally with the light from a 300 W high pressure mercury-arc lamp (Eikosha, Halos PIH-300).

The melting points of photochemical products isolated were uncorrected.

The elemental analyses of photochemical products were performed at the Microanalysis Center of Kyoto University.

NMR spectra were observed with a JEOL PS-100 spectrometer at 100 MHz using TMS as the internal standard. Infrared spectra were observed with a JASCO IR-G spectrometer. Ultraviolet and visible spectra were observed with a Shimadzu UV-200 spectrometer,

The filter (Toshiba color glass filter VY-42) was employed for cutting the shorter wavelength light than 400 nm.

The 2-alkyl- and 2,3-dialkyl-1,4-naphthoquinones were prepared from 1,4-naphthoquinone and the corresponding carboxylic acid, acetic acid or propionic acid, according to the modification of Jacobsen and Torssell's method.[7]

A solution containing 20 mmol of 1,4-naphthoquinone, 80 mmol of carboxylic acid and 0.5 g of silver nitrate in 40 ml of acetonitrile–water (50% v/v) was allowed to stir

at 65 °C for the addition of 30 mmol of ammonium persulfate dissolved in 30 ml of water for 2 h. The mixture was allowed to stir for an additional 30 min. After neutralization with sodium carbonate, the solution was extracted with ether. The ethereal solution dried over magnesium sulfate was concentrated, and the crude residue was chromatographed through a silica-gel column using petroleum ether as the eluent. The yellow solid obtained was recrystallized from ethanol. The yields and physical data of alkyl-substituted 1,4-naphthoquinones were given in Table 4.

Styrene, 2-phenylpropene, and 1,1-diphenylethylene were purified by distillation under reduced pressure under nitrogen atomosphere. 1,1-Bis(*p*-methylphenyl)ethylene was prepared according to the method of Allen and Converese[15] from *p*-bromotoluene and *p*-methylacetophenone.

General procedure of photoreaction of alkyl-substituted 1,4-naphthoquinone with olefin was as follows. A solution containing 2 mmol of quinone and 4 mmol of olefin in 20 ml of benzene was irradiated in a Pyrex test tube for 12 to 24 h. After removal of the solvent under a reduced pressure, the residual yellow oil was separated by thin layer chromatography on silica gel.

Photolysis of 2-methyl-1,4-naphthoquinone **1a** with styrene **2a** afforded three products. The first product was *syn*-1-methyl-7-phenyl-3,4-benzobicyclo[4.2.0]octene-2,5-dione (**5a**) in a yield of 11%. **5a**; white crystals, mp 94.0—95.0 °C; IR (KBr disk) 1670 cm^{-1}; UV (chloroform) λ_{max} 340 (ε:210), 308 (1540), 299 (1660), 254 (12000), and 244 nm (11100); NMR ($CDCl_3$) δ 1.68 (s, 3), 2.44 (dd, 1, J=8 and 10 Hz), 2.86 (dd, 1, J=8 and 10 Hz), 3.62 (d, 1, J=10 Hz), 4.24 (q, 1, J=10 Hz), 6.8—7.2 (m, 5), 7.4—7.7 (m, 3), and 7.9—8.1 ppm (m, 1); MS *m/e* 276 (M^+) and 104.

The second product was assigned the structure of *anti*-1-methyl-8-phenyl-3,4-benzobicyclo[4.2.0]octene-2,5-dione (**3a**) (45%). **3a**; white crystals, mp 112.0—113.0 °C, IR (KBr disk) 1675 cm^{-1}; UV ($CHCl_3$) λ_{max} 335 (ε:250), 308 (2170), 298 (2300), and 255 nm (12900); NMR ($CDCl_3$) δ 1.14 (s, 3), 2.40—2.70 (m, 1), 2.90—3.25 (m, 2), 3.80—4.04 (m, 1), 7.0—7.4 (m, 5), 7.70—7.90 (m, 2), and 8.0—8.24 ppm (m, 2); MS *m/e* 276 (M^+) and 104; EA: Found; C, 82.52; H, 6.02%; Calcd for $C_{19}H_{15}O_2$; C, 82.58; H, 5.84%.

The third component was obtained as a mixture with **3a** and assigned as *syn*-1-methyl-8-phenyl-3,4-benzobicyclo-[4.2.0]octene-2,5-dione (**4a**) on the basis of the NMR spectroscopy. **4a**; NMR ($CDCl_3$) δ 1.36 (s, 3), 2.1—2.4 (m, 1), 2.8—2.95 (m, 1), 3.4—3.6 (m, 2), 7.0—7.2 (m, 5), 7.6—7.8 (m, 2), and 7.9—8.1 ppm (m, 2); MS *m/e* 276 (M^+) and 104.

The NMR signal of methyl proton of **3a** appeared at the higher field due to the shielding effect of *cis*-phenyl group than that of **4a**, of which phenyl group was *trans* to the methyl group.

The photoadduct **3a** (50 mg) was stirred with basic alumina (3.0 g) in ether (30 ml) for 40 h at room temperature. The alumina was removed by filteration, and the filtrate was concentrated to give a light yellow solid (48 mg). The NMR analysis showed that there was no change during this treatment, confirming the *cis* four-six ring fusion in **3a**.

The photoadduct **3a** (30 mg) in benzene-d_6 (0.5 ml) in NMR tube was irradiated with a high pressure mercury-arc lamp for 12 h. The NMR spectrum of the material showed that the isomerization of **3a** to **4a** occurred by 5% at most.

When 2-ethyl-1,4-naphthoquinone **1b** with styrene **2a** was irradiated in benzene, three products were obtained. The first component was the mixture of *anti*- and *syn*-1-ethyl-8-phenyl-3,4-benzobicyclo[4.2.0]octene-2,5-dione (**3b** and **4b**, respectively) (isomer ratio: 2:1) (total yield; 57%). The NMR spectrum of this component was very complex.[16]

The second component was obtained as white crystals. The structure was assigned *syn*-1-ethyl-7-phenyl-3,4-benzobicyclo[4.2.0]octene-2,5-dione (**5b**). **5b**; white crystals, mp 126.5—127.0 °C; IR (KBr disk) 1670 cm^{-1}; UV ($CHCl_3$) λ_{max} 335 (ε:270), 308 (2200), 300 (2360), 253 (16600), and 242 nm (15600); NMR ($CDCl_3$) δ 0.94 (t, 3, J=8 Hz), 1.6—2.44 (m, 2), 2.54 (dd, 1, J=12 and 8 Hz), 2.82 (dd, 1, J=12 and 8 Hz), 3.72 (d, 1, J=10 Hz), 3.9—4.4 (m, 1), 6.8—7.3 (m, 5), 7.4—7.8 (m, 3), and 7.9—8.2 ppm (m, 1).

Photoreaction of **1a** and 2-phenylpropene **2b** afforded four addition products. The first product was obtained as white crystals in a yield of 39%. The structure was assigned as *anti*-1,7-dimethyl-7-phenyl-3,4-benzobicyclo[4.2.0]octene-2,5-dione (**6c**). **6c**; white crystals, mp 109.0—110.0 °C; IR (KBr disk) 1685 and 1675 cm^{-1}; UV ($CHCl_3$) λ_{max} 335 (ε:200), 307 (1780), 298 (1880), and 256 nm (12900); NMR ($CDCl_3$) δ 1.12 (s, 3), 1.36 (s, 3), 2.69 (ABq, 2, J=26 and 16 Hz), 3.64 (s, 1), 7.0—7.44 (m, 5), 7.56—7.8 (m, 2), and 7.9—8.2 ppm (m, 2); EA; Found; C, 82.97; H, 6.17%; Calcd for $C_{0}H_{18}O_2$; C, 82.73; H, 6.25%.

The second product was assigned *anti*-1,8-dimethyl-8-phenyl-3,4-benzobicyclo[4.2.0]octene-2,5-dione (**3c**). **3c**; white crystals mp 143.0—144.0 °C; IR (KBr disk) 1670 cm^{-1}; UV ($CHCl_3$) λ_{max} 330 (ε:200), 307 (1710), 298 (1920), 254 (13000), and 242 nm (11200); NMR ($CDCl_3$) δ 1.20 (s, 6), 2.18 (d, 1, J=10 Hz), 2.88—3.24 (m, 2), 7.2—7.4 (m, 5), 7.6—7.8 (m, 2), and 7.96—8.2 ppm (m, 2); EA: Found; C, 82.88; H, 6.09%; Calcd for $C_{20}H_{18}O_2$; C, 82.73; H, 6.25%.

The third component was obtained as the mixture of two products. They were assigned *syn*-1,7-dimethyl-7-phenyl-3,4-benzobicyclo[4.2.0]octene-2,5-dione (**5c**) and *syn*-1,8-dimethyl-8-phenyl-3,4-benzobicyclo[4.2.0]octene-2,5-dione (**4c**) (9 and 18%, respectively) on the basis of the NMR spectra. **5c**; NMR ($CDCl_3$) δ 1.52 (s, 3), 1.74 (s, 3), 2.22 (d, 1, J=12 Hz), 3.50 (s, 1), 6.8—7.2 (m, 5), 7.4—7.7 (m, 3), and 7.7—8.0 ppm (m, 1). **4c**; NMR ($CDCl_3$) δ 1.18 (s, 3), 1.24 (s, 3), 2.6—3.1 (m, 3), 6.8—7.3 (m, 5), 7.4—7.8 (m, 3), and 7.8—8.0 ppm (m, 1).

Irradiation of **1b** and **2b** afforded four cycloaddition products. The major product (48%) was assigned the structure of *anti*-1-ethyl-7-methyl-7-phenyl-3,4-benzobicyclo-[4.2.0]octene-2,5-dione (**6d**). **6d**; NMR ($CDCl_3$) δ 0.72 (t, 3, J=8 Hz), 1.20 (s, 3), 1.40—2.10 (dq, 2, J=8 and 8 Hz), 2.72 (ABq, 2, J=18 and 14 Hz), 3.80 (s, 1), 7.2—7.6 (m, 5), 7.7—8.0 (m, 2), and 8.1—8.4 ppm (m, 2).

The second product (22%) was obtained as white crystals, of which structure was assigned *anti*-1-ethyl-8-methyl-8-phenyl-3,4-benzobicyclo[4.2.0]octene-2,5-dione (**4d**). **4d**; white crystals, mp 137.0—138.0 °C; IR (KBr disk) 1675 and 1665 cm^{-1}; UV ($CHCl_3$) λ_{max} 340 (ε:270), 308 (1770), 297 (2000), and 255 nm (13700); NMR ($CDCl_3$) δ 0.68 (t, 3, J=8 Hz), 0.8—1.4 (m, 1), 1.24 (s, 3), 1.8—2.2 (m, 1), 2.2—2.6 (m, 1), 3.0—3.4 (m, 2), 7.2—7.6 (m, 5), 7.7—8.0 (m, 2), and 8.1—8.4 ppm (m, 2); EA: Found; C, 82.98; H, 6.47%; Calcd for $C_{21}H_{20}O_2$; C, 82.86; H, 6.62%.

Photolysis of **1a** with 1,1-diphenylethylene **2c** gave two products. The first product (48%) was assigned the structure of 1-methyl-7,7-diphenyl-3,4-benzobicyclo[4.2.0]octene-2,5-dione (**5e**). **5e**; white crystals, mp 112.5—113.5 °C; IR (KBr disk) 1685 and 1670 cm^{-1}; UV ($CHCl_3$) λ_{max} 310 (ε:1980), 302 (2080), 252 (12800), and 242 nm (13300); NMR ($CDCl_3$) 1.40 (s, 3), 2.58 (d, 1, J=12 Hz), 3.80 (d, 1, J=12 Hz), 4.16 (s, 1), 6.6—7.6 (m, 12), and 7.6—8.0 ppm (m, 2), MS *m/e* 352 (M^+) and 180; EA: Found; C, 85.50; H, 5.86%; Calcd for $C_{25}H_{20}O_2$; C, 85.20; H, 5.72%.

The second product (25%) was obtained as white crystals, assigned the structure 1-methyl-8,8-diphenyl-3,4-benzobicyclo-

[4.2.0]octene-2,5-dione (**3e**). **3e**; white crystals, mp 141.0—142.0 °C; IR (KBr disk) 1670 cm^{-1}; UV ($CHCl_3$) λ_{max} 302 (ε:2050), 252 (13500), and 243 nm (13700); NMR ($CDCl_3$) δ 1.60 (s, 3), 3.14 (dd, 1, J=10 and 2 Hz), 3.42 (dd, 1, J=12 and 10 Hz), 3.74 (dd, 1, J=12 and 2Hz), 6.4—7.0 (m, 5), 7.0—7.6 (m, 7), and 7.7—8.0 ppm (m, 2), MS *m/e* 352 (M^+) and 180; EA: Found; C, 85.00; H, 5.59%; Calcd for $C_{25}H_{20}O_2$; C, 85.20; H, 5.72%.

Irradiation of **1b** with **2c** afforded two photoadducts. The first product (45%) was assigned the structure of 1-ethyl-7,7-diphenyl-3,4-benzobicyclo[4.2.0]octene-2,5-dione (**5f**). **5f**; white crystals, mp 135.0—136.0 °C; IR (KBr disk) 1665 cm^{-1}; UV ($CHCl_3$) λ_{max} 310 (ε:1800), 302 (1890), 250 (11900), and 242 nm (12700); NMR ($CDCl_3$) δ 0.72 (t, 3, J=8 Hz), 1.50—2.30 (m, 2), 2.64 (d, 1, J=12 Hz), 3.84 (d, 1, J=12 Hz), 4.30 (s, 1), 6.6—7.6 (m, 12), and 7.7—8.0 ppm (m, 2); MS *m/e* 366 (M^+) and 180; EA: Found; C, 84.94; H, 6.16%; Calcd for $C_{26}H_{22}O_2$; C, 85.21; H, 6.05%.

The second product was assigned the structure of 1-ethyl-8,8-diphenyl-3,4-benzobicyclo[4.2.0]octene-2,5-dione (**3f**). **3f**; white crystals, mp 105.0—106.0 °C; IR (KBr disk) 1675 cm^{-1}; UV ($CHCl_3$) λ_{max} 300 (ε:1800), 250 (13800), and 242 nm (14000); NMR ($CDCl_3$) δ 0.78 (t, 3, J=8 Hz), 1.38 (dq, 1, J=8 and 8 Hz), 2.76 (dq, 1, J=8 and 8 Hz), 3.1—3.7 (m, 3), 6.7—7.7 (m, 12), and 7.7—8.0 ppm (m, 2); MS *m/e* 366 (M^+) and 180; EA: Found; C, 85.10; H, 6.12%; Calcd for $C_{26}H_{22}O_2$; C, 85.21; H, 6.05%.

When **1a** was irradiated with 1,1-bis(*p*-methylphenyl)-ethylene, two products were obtained. The major product (46%) was assigned the structure of 1-methyl-7,7-bis(*p*-methylphenyl)-3,4-benzobicyclo[4.2.0]octene-2,5-dione (**5g**). **5g**; white crystals, mp 145.0—146.0 °C; NMR ($CDCl_3$) δ 1.44 (s, 3), 2.00 (s, 3), 2.32 (s, 3), 2.62 (d, 1, J=12 Hz), 3.84 (d, 1, J=12 Hz), 4.24 (s, 1), 6.82 (ABq, 4, J=18 and 8 Hz), 7.22 (ABq, 4, J=12 and 8 Hz), 7.4—7.6 (m, 2), and 7.7—8.0 ppm (m, 2); EA: Found; C, 85.35; H, 6.23%; Calcd for $C_{27}H_{24}O_2$; C, 85.23; H, 6.36%.

The minor product (28%) was obtained as white crystals, of which structure was assigned 1-methyl-8,8-bis(*p*-methylphenyl)-3,4-benzobicyclo[4.2.0]octene-2,5-dione (**3g**). **3g**; white crystals, mp 174.0—175.0 °C; NMR ($CDCl_3$) δ 1.60 (s, 3), 1.96 (s, 3), 2.28 (s, 3), 3.06 (dd, 1, J=10 and 2 Hz), 3.28 (t, 1, J=10 Hz), 3.62 (dd, 1, J=10 and 2 Hz), 6.66 (d, 2, J=8 Hz), 7.0—7.4 (m, 6), 7.4—7.6 (m, 2), and 7.8—8.0 ppm (m, 2); EA: Found; C, 85.01; H, 6.18%; Calcd for $C_{27}H_{24}O_2$; C, 85.23; H, 6.36%.

When **1b** and 1,1-bis(*p*-methylphenyl)ethylene were irradiated in benzene, two photoadducts were obtained. The major product (36%) was assigned the structure of 1-ethyl-7,7-bis(*p*-methylphenyl)-3,4-benzobicyclo[4.2.0]octene-2,5-dione (**5h**). **5h**; white crystals, mp 125.0—126.0 °C; IR (KBr disk) 1670 cm^{-1}; NMR ($CDCl_3$) δ 0.68 (t, 3, J=8 Hz), 1.76 (dq, 2, J=30 and 8 Hz), 1.90 (s, 3), 2.20 (s, 3), 2.42 (d, 1, J=12 Hz), 3.58 (d, 1, J=12 Hz), 3.98 (s, 1), 6.52 (ABq, 4, J=24 and 8 Hz), 6.92 (ABq, 4, J=20 and 8 Hz), 7.16—7.40 (m, 2), and 7.48—7.7 ppm (m, 2), MS *m/e* 394 (M^+) and 208; EA: Found; C, 85.38; H, 6.64%; Calcd for $C_{28}H_{26}O_2$; C, 85.24; H, 6.64%.

The minor product (25%) was obtained as a light yellow viscous oil. The structure was assigned 1-ethyl-8,8-bis(*p*-methylphenyl)-3,4-benzobicyclo[4.2.0]octene-2,5-dione (**3h**) on the basis of the NMR spectroscopy. **3h**; NMR ($CDCl_3$) δ 0.78 (t, 3, J=8 Hz), 1.10—1.50 (m, 1), 2.00 (s, 3), 2.30 (s, 3), 2.5—2.9 (m, 1), 3.1—3.7 (m, 3), 6.70 (d, 2, J=8 Hz), 7.0—7.4 (m, 6), and 7.5—7.6 ppm (m, 2), MS *m/e* 394 (M^+) and 208.

Photolysis of 2,3-dimethyl-1,4-naphthoquinone **1c** with styrene **2a** afforded two products. The major product (84%) was assigned the structure of *anti*-1,6-dimethyl-7-phenyl-3,4-benzobicyclo[4.2.0]octene-2,5-dione (**7a**). **7a**; white crystals, mp 107.0—108.0 °C; IR (KBr disk) 1655 cm^{-1}; UV ($CHCl_3$) λ_{max} 332 (ε:280), 306 (1900), 297 (2050), and 253 nm (13200); NMR ($CDCl_3$) δ 1.08 (s, 3), 1.12 (s, 3), 2.56 (d, 1, J=12 Hz), 2.58 (d, 1, J=12 Hz), 3.66 (dd, 1, J=12 and 8 Hz), 6.8—7.2 (m, 5), 7.6—7.8 (m, 2), and 8.0—8.2 ppm (m, 2); EA: Found; C, 82.86; H, 6.17%; Calcd for $C_{20}H_{18}O_2$; C, 82.73; H, 6.25%.

The minor product (16%) was assigned the structure of *syn*-1,6-dimethyl-7-phenyl-3,4-benzobicyclo[4.2.0]octene-2,5-dione (**8a**). **8a**; white crystals, mp 103.0—104.0 °C; IR (KBr disk) 1665 cm^{-1}; UV ($CHCl_3$) λ_{max} 337 (δ:200), 305 (1450), 295 (1600), and 250 nm (10900); NMR ($CDCl_3$) δ 1.54 (s, 3), 1.60 (s, 3), 2.22 (dd, 1, J=12 and 8 Hz), 2.74 (dd, 1, J=12 and 10 Hz), 3.72 (dd, 1, J=10 and 8 Hz), 6.76—7.2 (m, 5), 7.4—7.6 (m, 3), and 7.84—8.04 ppm (m, 1); EA: Found; C, 82.74; H, 6.54%; Calcd for $C_{20}H_{18}O_2$; C, 82.73; H, 6.25%.

Irradiation of 2,3-diethyl-1,4-naphthoquinone (**1d**) with styrene **2a** gave two photoadducts. The major product (93%) was obtained as a light yellow viscous oil. The structure was assigned *anti*-1,6-diethyl-7-phenyl-3,4-benzobicyclo[4.2.0]octene-2,5-dione (**7b**) on the basis of the NMR spectrum. **7b**; NMR ($CDCl_3$) δ 0.78 (t, 3, J=8 Hz), 0.82 (t, 3, J=8 Hz), 1.4—2.1 (m, 4), 2.48 (dd, 1, J=12 and 10 Hz), 2.68 (dd, 1, J=12 and 8 Hz), 3.54 (dd, 1, J=10 and 8 Hz), 7.0—7.4 (m, 5), 7.5—7.8 (m, 2), and 7.9—8.2 ppm (m, 2).

The minor product (7%) was obtained as a yellow oil, of which structure was assigned *syn*-1,6-diethyl-7-phenyl-3,4-benzobicyclo[4.2.0]octene-2,5-dione (**8b**) on the basis of the NMR spectroscopy. **8b**; NMR ($CDCl_3$) δ 0.56 (t, 3, J=8 Hz), 0.74 (t, 3, J=8 Hz), 1.2—2.8 (m, 5), 2.88 (dd, 1, J=12 and 8 Hz), 3.64 (dd, 1, J=10 and 8 Hz), 7.0—7.6 (m, 8), and 7.80 ppm (d, 1, 8 Hz).

Irradiation of **1c** with 2-phenylpropene **2b** afforded two products. The major product (38%) was obtained as white crystals. The structure was assigned *anti*-1,6,7-trimethyl-7-phenyl-3,4-benzobicyclo[4.2.0]octene-2,5-dione (**7c**). **7c**; white crystals, mp 125.0—126.0 °C; IR (KBr disk) 1660 cm^{-1}; UV ($CHCl_3$) λ_{max} 330 (ε:230), 296 (1880), and 254 nm (12900); NMR ($CDCl_3$) δ 1.12 (s, 3), 1.16 (s, 3), 1.26 (s, 3), 2.68 (s, 2), 7.0—7.4 (m, 5), 7.64—7.84 (m, 2), and 8.0—8.2 ppm (m, 2); EA: Found; C, 82.97; H, 6.53%; Calcd for $C_{21}H_{20}O_2$; C, 82.86; H, 6.62%.

The minor product (20%) was obtained as the mixture with **7c**. The former was assigned *syn*-1,6,7-trimethyl-7-phenyl-3,4-benzobicyclo[4.2.0]octene-2,5-dione (**8c**). **8c**; NMR ($CDCl_3$) δ 1.44 (s, 3), 1.52 (s, 3), 1.66 (s, 3), 2.16 (d, 1, J=14 Hz), 3.14 (d, 1, J=14 Hz), 6.8—7.2 (m, 5), 7.4—7.7 (m, 3), and 7.8—8.1 ppm (m, 1).

Photolysis of **1d** with **2b** gave two products. The major product (77%) was obtained as white crystals, of which structure was assigned *anti*-1,6-diethyl-7-methyl-7-phenyl-3,4-benzobicyclo[4.2.0]octene-2,5-dione (**7d**). **7d**; white crystals, mp 162.0—163.0 °C; IR (KBr disk) 1670 cm^{-1}; UV ($CHCl_3$) λ_{max} 330 (ε:240), 295 (1610), and 250 nm (11400); NMR ($CDCl_3$) δ 0.72 (t, 3, J=8 Hz), 0.88 (t, 3, J=8 Hz), 1.18 (s, 3), 1.1—2.1 (m, 4), 2.64 (s, 2), 7.1—7.5 (m, 5), 7.64—7.9 (m, 2), and 7.9—8.1 ppm (m, 2); EA: Found; C, 83.17; H, 7.23%; Calcd for $C_{23}H_{24}O_2$; C, 83.10; H, 7.28%.

The minor product (13%) was obtained as the mixture with **7d**. The structure of the former was assigned *syn*-1,6-diethyl-7-methyl-7-phenyl-3,4-benzobicyclo[4.2.0]octene-

2,5-dione (**8d**) on the basis of the NMR spectroscopy. **8d**; NMR ($CDCl_3$) δ 0.72 (t, 3, J=8 Hz), 0.96 (t, 3, J=8 Hz), 1.52 (s, 3), 1.6—2.2 (m, 3), 2.20 (d, 1, J=12 Hz), 2.4—2.8 (m, 1), 3.30 (d, 1, J=12 Hz), and 7.3—8.0 ppm (m, 9).

Photolysis of **1c** with 1,1-diphenylethylene **2c** afforded a white crystalline product. The sptructure was assigned as 1,6-dimethyl-7,7-diphenyl-3,4-benzobicyclo[4.2.0]octene-2,5-dione (**7e**) in a yield of 87%. **7e**; white crystals, mp 170.0—171.0 °C; IR (KBr disk) 1675 and 1665 cm^{-1}; UV ($CHCl_3$) λ_{max} 302 (ε:2200), 254 (14000), and 243 nm (13600); NMR ($CDCl_3$) δ 1.24 (s, 3), 1.52 (s, 3), 2.80 (d, 1, J=12 Hz), 3.90 (d, 1, J=12 Hz), 6.60—7.0 (m, 4), 7.0—7.6 (m, 6), 7.74—7.9 (m, 1), and 7.96—8.1 ppm (m, 1), EA: Found; C, 85.09; H, 6.17%; Calcd for $C_{26}H_{22}O_2$; C, 85.21; H, 6.05%.

When **1e** was irradiated with **2c** in benzene, white crystals were obtained after purification by thick layer chromatography. The strucutre was assigned 1,6-diethyl-7,7-diphenyl-3,4-benzobicyclo[4.2.0]octene-2,5-dione (**7f**) in a yield of 92%. **7f**; white crystals, mp 180.0—181.0 °C; IR (KBr disk) 1685 and 1670 cm^{-1}; UV ($CHCl_3$) λ_{max} 300 (ε:2240), 252 (14200), and 243 nm (14100); NMR ($CDCl_3$) δ 0.80 (t, 3, J=8 Hz), 0.88 (t, 3, J=8 Hz), 1.32—2.08 (m, 3), 2.4—2.9 (m, 1), 2.80 (d, 1, J=12 Hz), 3.82 (d, 1, J=12 Hz), 6.6—7.84 (m, 13), and 7.96—8.12 ppm (m, 1), EA: Found; C, 85.39; H, 6.65%; Calcd for $C_{28}H_{26}O_2$; C, 85.24; H, 6.64%.

All measurements of quantum yields were made on a rotating assembly with a central light source (internal water-cooler mercury-arc lamp, Eikosha, Halos PIH-300). Samples in 15 mm Pyrex ampoules were placed in holders on the assembly placed at approximately 5 cm apart from the immersion well. The light was filtered by circulation of a solution containing 0.27 g of potassium chromate and 1.0 g of sodium carbonate in 1000 ml of distilled water. All studies were made at room temperature. After the irradiation, the degree of reaction was determined by means of quantitative ultraviolet absorption spectroscopy. The conversions in quinone quantities were run at highest to 15% or less. The mass balance in these runs was generally better than 90%.

Solutions of the quinone and the olefin in benzene containing excess amount of fluoranthene as a triplet quencher were irradiated under the conditions where more than 95% of the light was absorbed by the quinone. The reaction was monitored by TLC and in no case was the amount of products formed affected by addition of fluoranthene.

References

1) C. H. Krauch and S. Farid, *Tetrahedron Lett.*, **1966**, 4783.
2) K. Maruyama, T. Otsuki, A. Takuwa, and S. Kako, *Bull. Inst. Res., Kyoto Univ.*, **50**, 344 (1972).
3) K. Maruyama, T. Otsuki, and Y. Naruta, *Chem. Lett.*, **1973**, 641.
4) K. Maruyama, Y. Naruta, and T. Otsuki, *Bull. Chem. Soc. Jpn.*, **48**, 1553 (1975).
5) S. P. Papas, B. C. Papas, and N. A. Portnoy, *J. Org. Chem.*, **34**, 520 (1969).
6) T. Otsuki, *Bull. Chem. Soc. Jpn.*, **47**, 3084 (1974); **49**, 2596 (1976).
7) N. Jacobsen and K. Torssell, *Liebigs Ann. Chem.*, **763**, 135 (1972).
8) J. J. McCullough, B. R. Ramachandran, F. F. Snyder, and G. N. Taylor, *J. Am. Chem. Soc.*, **84**, 2344 (1962) (see Footnote (17)).
9) C. G. Hatchard and C. A. Parker, *Proc. R. Soc. London, Ser. A*, **235**, 518 (1956).
10) M. Kasha, *J. Opt. Soc. Am.*, **38**, 929 (1948).
11) Toshiba color glass filter VY-42 was employed.
12) D. F. Evans, *J. Chem. Soc.*, **1957**, 1351.
13) A. Bylina, *Chem. Phys. Lett.*, **1**, 509 (1968).
14) S. Yamauchi and T. Azumi, *J. Am. Chem. Soc.*, **95**, 2709 (1973).
15) C. F. H. Allen and S. Converse, *Org. Synth.*, Coll. Vol. I, 226.
16) The NMR spectra of the photoadducts derived from 2-ethyl-1,4-naphthoquinone **1b** and 2,3-diethyl-1,4-naphthoquinone **1d** showed that the methylene protons of ethyl group appeared two double quartet signals according to assymmerty of C-1 or C-6 carbon of the photoadducts.

Photo-cycloaddition of Indene to Chlorofluoroethylenes and Some Reactions Concerning the Adducts

Hiroshi KIMOTO,* Kensuke TAKAHASHI,† and Hiroshige MURAMATSU

Government Industrial Research Institute, Nagoya, Hirate-machi, Kita-ku, Nagoya 462

† *Nagoya Institute of Technology, Gokiso-cho, Showa-ku, Nagoya 466*

(Received August 24, 1979)

Benzophenone photo-sensitized addition of indene to chlorofluoroethylenes [trichlorofluoroethylene, 1,2-dichloro-1,2-difluoroethylene, 1,1-dichloro-2,2-difluoroethylene, chlorotrifluoroethylene, tetrafluoroethylene] afforded 6,6,7,7-tetrahalogeno-2,3-benzobicyclo[3.2.0]hept-2-enes as corresponding cycloadducts. The structure of the cycloadducts obtained from unsymmetrical chlorofluoroethylenes shows that the addition reaction proceeds with good regioselectivity. Some reactions such as oxidation, reduction, dechlorination, and halogenation of the cycloadducts were also examined.

Fluoro olefins are known to undergo cycloaddition reaction upon heating.[1] In fact, most fluorine-containing cyclobutane derivatives have been synthesized by the thermal cycloaddition of fluoro olefins and by subsequent reactions of these cycloadducts. In contrast, only a few investigations on photo-cycloaddition of fluoro olefins have been reported.[2-4] Since the photo-cycloaddition reaction would be expected to give different results from the thermal reaction, we investigated the photo-sensitized addition of indene to chlorofluoroethylenes [trichlorofluoroethylene (TCFE), 1,2-dichloro-1,2-difluoroethylene (*sym*-DCDFE), 1,1-dichloro-2,2-difluoroethylene (*unsym*-DCDFE), chlorotrifluoroethylene (CTFE), tetrafluoroethylene (TFE)] as a part of our studies on syntheses of fluorine-containing fused polycyclic compounds.[5] It is known that the cycloadditions of *unsym*-DCDFE, CTFE, and TFE take place thermally but those of indene, *sym*-DCDFE and TCFE do not.[1] The effect of fluorine recently has become of considerable interest in photochemistry[4,6] in light of the fact that 5-fluorouracil has been reported to have superior regioselectivity compared with unsubstituted uracil in the photo-cycloaddition reaction with several olefins. Accordingly, we have investigated the regioselectivity and stereoselectivity in the photo-cycloaddition of indene to chlorofluoroethylenes by elucidating the structure of the cycloadducts by means of NMR spectroscopy.

Results and Discussion

Irradiation (>300 nm) of indene and an excess of chlorofluoroethylenes in the presence of benzophenone as a sensitizer gave 6,6,7,7-tetrahalogeno-2,3-benzobicyclo[3.2.0]hept-2-enes as the corresponding cycloadducts (**1**—**5**).

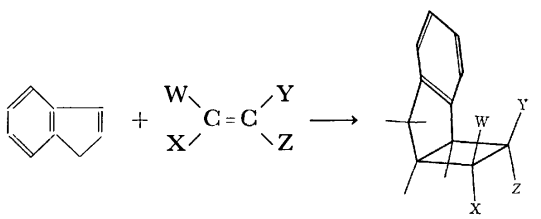

1a	W=F; X,Y,Z=Cl	**1b**	X=F; W,Y,Z=Cl
1c	Y=F; W,X,Z=Cl	**1d**	Z=F; W,X,Y=Cl
2a	W,Y=F; X,Z=Cl	**2b**	W,Z=F; X,Y=Cl
2c	X,Y=F; W,Z=Cl	**2d**	X,Z=F; W,Y=Cl
3a	W,X=F; Y,Z=Cl	**3b**	Y,Z=F; W,X=Cl
4a	W,X,Y=F; Z=Cl	**4b**	W,X,Z=F; Y=Cl
4c	W,Y,Z=F; X=Cl	**4d**	X,Y,Z=F; W=Cl
5	W,X,Y,Z=F		

Four different reaction conditions were employed (Methods A—D). In Methods A and B, irradiations were carried out in a Pyrex ampoule, while in Methods C and D, an immersion well photo-reactor was used. In order to study the effect of dilution with solvent, no solvent was used in Method B. Since TFE has a very low boiling point and polymerizes explosively, in Method D, TFE was bubbled into a solution of indene and benzophenone in 1,1,2-trichloro-1,2,2-trifluoroethane followed by irradiation in an immersion well reactor. In this procedure, the concentration of absorbed TFE was not determined. The reaction conditions and product yields are shown in Table 1.

As compared with Method A, Method B gave slightly higher conversion and slightly lower yield of cycloadduct. Hence, there are no marked differences in results from Methods A and B. When an immersion well photo-reactor was used (Method C), the conversions and yields were high even with shorter irradiation times.

Using Method A, the reaction of *unsym*-DCDFE gave high conversion (98.3%), while reactions of other chlorofluoroethylenes showed somewhat lower conversions (63—70%). In all cases, the yields of the cycloadducts **1**—**4** were similar (55—65%). Using Methods C and D, most of the indene (94%) was consumed and cycloadducts were obtained in good yields (84—85%) from TCFE and *unsym*-DCDFE. With TFE, the yield of cycloadduct (**5**) was very low and large amounts of high-boiling products were obtained.

The yields of the cycloadducts obtained from chlorofluoroethylenes are as following order: $CF_2{=}CCl_2 > CClF{=}CCl_2 > CClF{=}CClF \fallingdotseq CF_2{=}CClF > CF_2{=}CF_2$. This trend can be rationalized by considering the relative stability of the intermediate biradicals (see below) and steric factors. The indene dimer was a main by-product, obtained as a high-boiling residue. Tarry polymeric products were also generated, especially in the case of TFE, CTFE and *unsym*-DCDFE.

In thermal cycloadditions, it has been known[1] that a structual requirement for the fluoro olefins is the presence of a terminal difluoromethylene group. Fluoro olefins such as TFE, CTFE, and *unsym*-DCDFE undergo thermal cycloaddition to form cyclobutanes with themselves and other unsaturated compounds,

Table 1. Photo-sensitized addition reaction of indene to chlorofluoro olefins

	Chlorofluoro olefin	Indene	PhCOPh	$CF_2ClCFCl_2$	Method[a]	Irrad. time	Conversion of indene	Yield[b]	High-boiling product
	mol	mol	mol	mol		h	%	%	g
$CClF=CCl_2$	0.50	0.10	0.01	1.00	A	168	62.9	65.3	2.4
$CClF=CClF$	0.50	0.10	0.01	1.00	A	168	64.7	63.3	2.1
$CF_2=CCl_2$	0.50	0.10	0.01	1.00	A	168	98.3	57.6	3.8
$CF_2=CClF$	0.50	0.10	0.01	1.00	A	168	69.8	54.5	3.5
$CClF=CCl_2$	0.50	0.10	0.01	—	B	168	69.8	61.5	3.1
$CClF=CCl_2$	0.50	0.10	0.01	1.00	C	20	100	85.1	2.1
$CClF=CClF$	0.50	0.10	0.01	1.00	C	20	98.3	62.5	3.5
$CF_2=CCl_2$	0.50	0.10	0.01	1.00	C	8	97.4	84.1	2.1
$CF_2=CF_2$	0.50	0.10	0.01	1.50	D	20	94.0	4.9	12.8

a) Methods A and B: The reaction carried out in a Pyrex ampoule. Methods C and D: The reaction carried out by using an immersion well photo-reactor. b) The yields were calculated by the amounts of indene consumed.

but *sym*-DCDFE and TCFE do not cycloadd thermally. In contrast, there is no such a structural requirement in the photo-cycloaddition with indene. All chlorofluoroethylenes examined gave the corresponding cycloadducts. Thermal cycloaddition of indene has not been known.

The structures of the cycloadducts were elucidated by means of their elemental analyses, IR, NMR and mass spectra. In the mass spectra, the strongest peak of the cycloadducts corresponds to indene (*m/e*: 116, C_9H_8), which is formed by the cleavage of four-membered ring shown as follows:

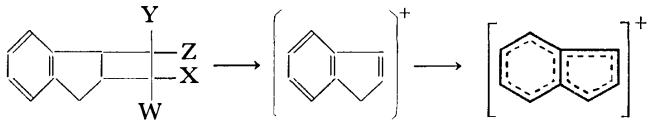

m/e : 116 *m/e* : 115

The presence of several stereoisomers of the cycloadducts was indicated in ^{19}F NMR spectra. The stereoisomers could not be separated by distillation or GLC. However, partial separation was achieved by fractional crystallization. The ratio of the isomers calculated from the intensity of ^{19}F NMR spectra are shown in Table 2 together with their ^{19}F chemical shifts.

The configurations of the stereoisomers were assigned by means of NMR spectra of their oxidized products. The cycloadducts (**1**—**5**) were oxidized by chromium trioxide to give the corresponding 6,6,7,7-tetrahalogeno-2,3-benzobicyclo[3.2.0]hept-2-en-4-ones (**6**—**10**).

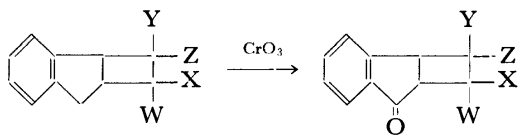

1—**5** **6**—**10**

In addition to the more easily interpreted NMR of these oxidized products, **6**—**10**, they are more easily crystallized due to the presence of the carbonyl group. The assignments of configuration of the stereoisomers, estimated from the values of chemical shifts, coupling constants and nuclear Overhauser effect (NOE) are shown in Table 3 together with ^{19}F chemical shifts.

Table 2. The isomer ratios and fluorine-19 chemical shifts of the cycloadducts

Compound	Isomer ratio	Fluorine-19 chemical shifts/ppm			
		W	X	Y	Z
1a	38	F 29.8	Cl	Cl	Cl
1b	46	Cl	F 5.3	Cl	Cl
1c	6	Cl	Cl	F 20.1	Cl
1d	10	Cl	Cl	Cl	F 11.8
2a	30	F 36.0	Cl	F 20.6	Cl
2b	12	F 45.0	Cl	Cl	F 36.2
2c	37	Cl	F 11.9	F 25.0	Cl
2d	21	Cl	F 30.9	Cl	F 25.6
3a	100	F 29.6	F 12.9	Cl	Cl
3b	0	Cl	Cl	F —	F —
4a	48	F 41.9	F 16.0	F 40.9	Cl
4b	52	F 33.1	F 27.4	Cl	F 37.9
4c	0	F —	Cl	F —	F —
4d	0	Cl	F —	F —	F —
5	100	F 44.6	F 30.1	F 35.4	F 35.4

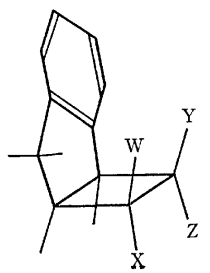

TABLE 3. FLUORINE-19 CHEMICAL SHIFTS AND MELTING POINTS OF THE OXIDIZED PRODUCTS OF THE CYCLOADDUCTS

Compound	Fluorine-19 chemical shifts/ppm				Mp
	W	X	Y	Z	°C
6a	F 20.3	Cl	Cl	Cl	132.1
6b	Cl	F 7.7	Cl	Cl	119.6
6c	Cl	Cl	F 16.6	Cl	not isol.
6d	Cl	Cl	Cl	F 11.3	not isol.
7a	F 26.7	Cl	F 19.8	Cl	113.4
7b	F 36.0	Cl	Cl	F 33.4	110.6
7c	Cl	F 14.4	F 21.7	Cl	114.3
7d	Cl	F 30.9	Cl	F 27.7	not isol.
8a	F 19.6	F 12.6	Cl	Cl	96.6
9a	F 31.8	F 15.6	F 37.7	Cl	94.8
9b	F 23.1	F 26.8	Cl	F 37.4	64.6
10	F 34.6	F 29.9	F 32.6	F 34.8	86.8

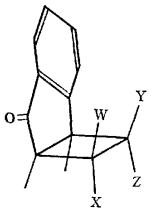

Thus, the resonance peak of fluorine of **6a** is shifted 9.5 ppm down-field from that of **1a**. The shift is due to the electric field effect of the neighboring carbonyl group. On the other hand, ^{19}F chemical shift of **6b** did not differ from that of **1b**. Similar shifts are observed only for the fluorines in the W position of other isomers. When the fluorine nucleus of **6b**

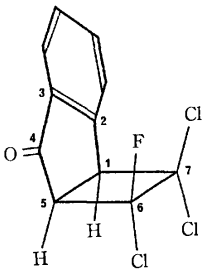

6a

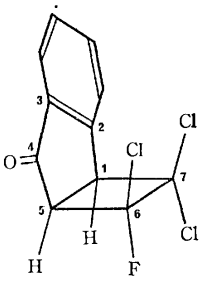

6b

was irradiated, the integral intensity of hydrogen on the 5 position increased (14%). However, no NOE was observed in the other isomer, **6a**. Similarly, for the other isomers, when the fluorine nucleus in the X position was irradiated, the integral intensity of hydrogen on the 5 position increased (more than 10%), and irradiation of fluorine in the Z position increased (10%) that of hydrogen on the 1 position. The NMR of the series of the compounds (**6**—**10**) will be reported elsewhere in more detail.[7]

As shown in Table 2, the distribution of the stereoisomers reflects good regioselectivity and poor stereoselectivity of the reaction. In the addition of TCFE, four cycloadducts, **1a**, **1b**, **1c**, and **1d**, were obtained in the ratio of 38:46:6:10. Two isomers (**1a** and **1b**) with a fluorine on the 6 position were obtained in higher yields than the other two isomers (**1c** and **1d**) with a fluorine on the 7 position. The reaction thus shows a minimum of 84% regioselectivity. In the case of *unsym*-DCDFE, only one isomer (**3a**) with two fluorines on the 6 position was formed, and the other isomer (**3b**) was not detected. From CTFE, two isomers (**4a** and **4b**) with a chlorine on the 7 position were obtained in the ratio of 52:48, but the other two isomers (**4c** and **4d**) were not detected. *unsym*-DCDFE and CTFE show complete regioselectivity in the reactions. *sym*-DCDFE gave four stereoisomers, **2a**, **2b**, **2c** and **2d**, in the ratio of 30:12:37:21.

The observed results for these photo-cycloadditions may be explained by a mechanism in which biradical intermediates are formed as shown below in the case of *unsym*-DCDFE.

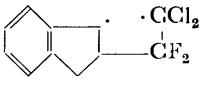

I

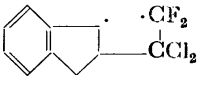

II

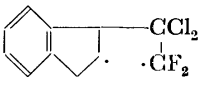

III

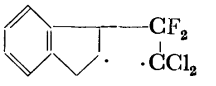

IV

A triplet state-excited indene would attack the *unsym*-DCDFE and four different biradicals might be generated as intermediates. These would lead to the cycloadducts by intramolecular coupling. Since the stabilities of halogenated carbon radicals follow the order: $\cdot CCl_2 > \cdot CClF \gg \cdot CF_2$, and the benzyl type radicals (I and II) are more stable than III and IV, the intermediate I would be formed preferentially to give **3a**. Presumably, the stereochemistry of this cycloaddition is mainly controlled by the stabilities of the intermediate biradicals. Other cofactors might be steric effects and fluorine hyperconjugation which has been proposed as an important factor in the increased amount of ring closure of the intermediate biradicals.[6]

The cycloadducts (**1a**, **b**, and **2a**—**d**) were dechlorinated with zinc powder and the corresponding cyclic olefins (**11a**, **b**) were obtained in high yields. Dechlorination of **2a**—**d** is more difficult than for **1a**,**b**

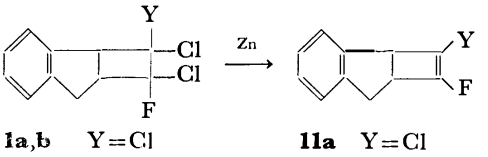

1a,**b** Y=Cl
2a—**d** Y=F

11a Y=Cl
11b Y=F

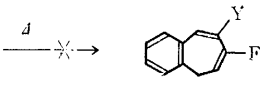

with only 15% of **2a—d** being dechlorinated under the conditions used for **1a,b**. Higher reaction temperature (140 °C) was required for complete dechlorination of **2a—d**.

The thermal ring expansion reaction of **11a** and **11b** did not occur at 200 °C. This is in accordance with the Woodward-Hoffmann's rule which predicts that the thermal cleavage of cyclobutenes will occur in a conrotatory fashion. In the case of **11a** and **11b**, which have the cyclobutene ring fused to the five membered ring, the conrotatory cleavage would lead to the sterically untenable *trans*-cycloheptatriene.

Similarly, the cyclic ketones (**6a,b** and **7a—d**) obtained from oxidation of the cycloadducts (**1a,b** and **2a—d**) gave the corresponding olefins (**12a,b**) by dechlorination with zinc. Longer reaction time was required for the dechlorination of **7a—d**. Upon heating **12a** and **12b** at 200 °C, thermal ring expansion to benzotropone again did not occur.

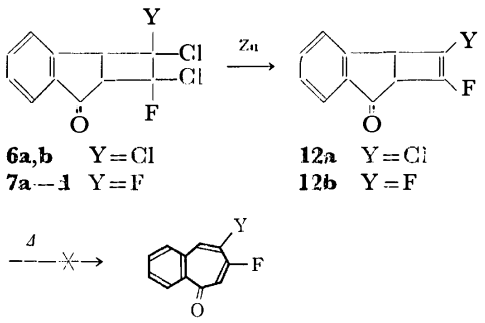

6a,b Y=Cl **12a** Y=Cl
7a—d Y=F **12b** Y=F

The cycloadduct (**3a**) was brominated with *N*-bromosuccinimide to give the monobromide (**13a**) almost quantitatively. The NMR signal of the hydrogen on the 4 position appears as a singlet at 5.51 ppm being shifted downfield by the geminal bromine. The singlet peak reflects a small H^4–H^5 coupling constant (less than 1 Hz). From the Karplus' relationship between vicinal H–H coupling constants and dihedral angles, H^4 is considered to be on the opposite side of the five membered ring plane from H^5. Hence, bromine substitution occurred on the sterically favorable position of the methylene group with high selectivity.

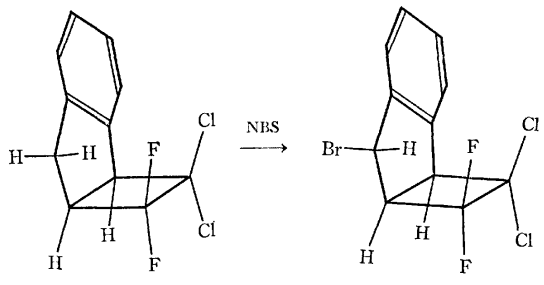

3a **13a**

Photo-chlorination of **3a** afforded the monochloride (**13b**) in 84.4% yield together with a small amount (6.3% yield) of the dichloride (**14**). Similar to bromination, the same hydrogen was replaced by chlorine in the first step with further chlorination taking place on the 1 position.

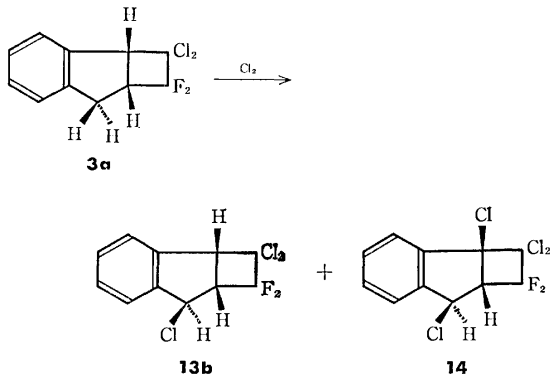

Reduction of **3a** with lithium aluminum hydride afforded **15**, **16** and **11a**, which presumably resulted from the elimination of hydrogen fluoride from **15**.

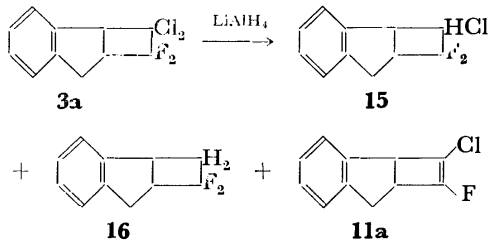

Experimental

The melting points were determined on a Mettler FPl with the elevating rate of 2 °C/min. The IR and mass spectra were measured using a Hitachi Model EPI-2 grating spectrometer and Model RMU-7 double-focusing mass spectrometer at 70 eV, respectively. The NMR spectra were obtained on a Hitachi Model R-22 apparatus (90 MHz) using TMS as an internal standard for ^1H, and on a Model R-20 B apparatus (56.45 MHz) using trifluoroacetic acid as an external standard for ^{19}F.

Materials. Commercially available indene was used after distillation under an argon atmosphere. The chlorofluoroethylenes were prepared by dechlorination from the corresponding chlorofluoroethanes.

Trichlorofluoroethylene (TCFE): Dechlorination of pentachlorofluoroethane by zinc powder in ethanol gave TCFE, which was distilled through 50 cm column packed with glass helices (bp 71—72 °C).

1,1-Dichloro-2,2-difluoroethylene (unsym-*DCDFE)*: 1,1,1,2-Tetrachloro-2,2-difluoroethane was prepared by the isomerization of 1,1,2,2-tetrachloro-1,2-difluoroethane using aluminum trichloride catalyst.[8] Dechlorination of 1,1,1,2-tetrachloro-2,2-difluoroethane gave *unsym*-DCDFE (bp 18—19 °C).

1,2-Dichloro-1,2-difluoroethylene (sym-*DCDFE) and Chlorotrifluoroethylene (CTFE)*: Dechlorination of 1,1,2,2-tetrachloro-1,2-difluoroethane and 1,1,2-trichloro-1,2,2-trifluoroethane gave *sym*-DCDFE (bp 19—20 °C) and CTFE (bp —26—27 °C), respectively.

Tetrafluoroethylene (TFE): TFE was prepared by debromination of 1,2-dibromotetrafluoroethane with zinc and introduced into a photo-reator immediately.

Photo-cycloaddition. Photo-cycloadditions were carried out using four different reaction conditions (Method A, B, C, and D). A typical procedure is described for each Method.

Method A; Reaction of Indene and Trichlorofluoroethylene (TCFE): A solution of indene (11.6 g, 0.100 mol), TCFE

TABLE 4. MELTING POINTS AND ANALYTICAL DATA OF THE CYCLOADDUCTS AND THEIR DERIVATIVES

Compound	Mp[a] °C	Formula	C%		H%	
			Found	Calcd	Found	Calcd
1a	101.3	$C_{11}H_8Cl_3F$	49.44	49.76	3.02	3.04
1b	81.1	$C_{11}H_8Cl_3F$	49.83	49.76	3.10	3.04
2a	111.9	$C_{11}H_8Cl_2F_2$	52.85	53.04	3.16	3 24
2b	86.3	$C_{11}H_8Cl_2F_2$	52.56	53.04	3.04	3.24
2c	65.3	$C_{11}H_8Cl_2F_2$	53.13	53.04	3.24	3.24
3a	74.3	$C_{11}H_8Cl_2F_2$	52.74	53.04	3.29	3.24
5	55.1	$C_{11}H_8F_4$	61.01	61.12	3.75	3.73
6a	132.1	$C_{11}H_6OCl_3F$	47.33	47.27	2.15	2.16
6b	119.6	$C_{11}H_6OCl_3F$	47.53	47.27	2.23	2.16
7a	113.4	$C_{11}H_6OCl_2F_2$	50.34	50.22	2.58	2.30
7b	100.6	$C_{11}H_6OCl_2F_2$	50.13	50.22	2.24	2.30
7c	114.3	$C_{11}H_6OCl_2F_2$	50.05	50.22	2.11	2.30
8a	96.6	$C_{11}H_6OCl_2F_2$	50.07	50.22	2.18	2.30
9a	94.8	$C_{11}H_6OClF_3$	53.38	53.57	2.37	2.45
9b	64.6	$C_{11}H_6OClF_3$	53.69	53.57	2.45	2.45
10	86.8	$C_{11}H_6OF_4$	57.06	57.40	2.65	2.63
11a	oil	$C_{11}H_8ClF$	67.91	67.88	4.13	4.14
11b	oil	$C_{11}H_8F_2$	74.05	74.15	4.23	4.53
12a	58.2	$C_{11}H_6OClF$	63.05	63.33	2.90	2.90
12b	oil	$C_{11}H_6OF_2$	67.81	68.75	3.23	3.15
13a	oil	$C_{11}H_7BrCl_2F_2$	40.42	40.28	2.32	2.15
13b	oil	$C_{11}H_7Cl_3F_2$	46.49	46.60	2.44	2.49
14	84.4	$C_{11}H_6Cl_4F_2$	41.45	41.55	1.91	1.90
15	136.2	$C_{11}H_9ClF_2$	61.41	61.55	4.14	4.23

a) Recrystallized from ethanol.

(74.7 g, 0.500 mol) and benzophenone (1.8 g, 0.010 mol) in 1,1,2-trichlorotrifluoroethane (187 g, 1.00 mol) was sealed under an argon atmosphere in a 300 ml Pyrex ampoule, and irradiated with a 100 W high pressure mercury lamp at room temperature for 168 h. After recovery of the solvent and TCFE by distillation, the residue was distilled *in vacuo* to give indene (4.3 g, 38.1% recovered), a cycloadduct (10.9 g, 65.3% yield) boiling at 131 °C/4 mmHg and a high-boiling residue, which contained benzophenone. The cycloadduct crystallized after standing overnight. The ^{19}F NMR spectrum of the cycloadduct indicated that it consisted of four isomers, **1a**, **1b**, **1c**, and **1d**, in the ratio of 38:46:6:10. Two of these, **1a** and **1b**, were isolated by fractional recrystallization. Indene dimer was also isolated from the high-boiling residue as colorless needles (mp 109.5 °C).

Method B; *Reaction of Indene and Trichlorofluoroethylene (TCFE)*: A mixture of indene (11.6 g, 0.100 mol), TCFE (74.7 g, 0.500 mol) and benzophenone (1.8 g, 0.010 mol) was irradiated in a 100 ml Pyrex ampoule with a 100 W high pressure mercury lamp for 168 h. The product was separated by distillation to give indene (3.5 g, 30.2% recovered), a cycloadduct (11.4 g, 61.5% yield, bp 120—122 °C/3 mmHg) and a high-boiling residue (4.9 g).

Method C; *Reaction of Indene and Trichlorofluoroethylene (TCFE)*: A solution of indene (11.6 g, 0.100 mol), TCFE (74.7 g, 0.500 mol) and benzophenone (1.8 g, 0.010 mol) in 1,1,2-trichlorotrifluoroethane (187 g, 1.00 mol) was irradiated for 20 h in an immersion well Pyrex photo-reactor (300 ml capacity with a water-cooled 100 W mercury lamp) under an argon atmosphere. All indene was consumed and a cycloadduct (22.6 g, 85.1% yield) and a high-boiling residue (3.0 g) were obtained.

Method D; *Reaction of Indene and Tetrafluoroethylene (TFE)*: A solution of indene (11.6 g, 0.100 mol) and benzophenone (1.8 g, 0.010 mol) in 1,1,2-trichlorotrifluoroethane (280 g) was placed in a 300 ml immersion well Pyrex photo-reactor, and cooled in an ice bath. TFE, which was generated from the debromination reaction of 1,2-dibromotetrafluoroethane (130 g, 0.500 mol) and zinc (100 g) in ethanol, was bubbled and absorbed into the solution. Then the solution was irradiated as in Method C for 20 h. Distillation gave indene (0.7 g, 6.0% recovered), a cycloadduct (1.0 g, 4.9% yield, bp 60—65 °C/3 mmHg) and a high-boiling residue (12.8 g).

Oxidation of the Adducts. The cycloadducts (**1**—**5**) were oxidized with chromium trioxide to the corresponding ketones (**6**—**10**). The oxidation of 6,6,7,7-tetrafluoro-2,3-benzobicyclo[3.2.0]hept-2-ene (**5**) is described as a typical experimental procedure.

*6,6,7,7-Tetrafluoro-2,3-benzobicyclo[3.2.0]hept-2-en-4-one (**10**)*: To a solution of chromium trioxide (2.4 g, 24 mmol) in water (5 ml) was added a solution of **5** (1.3 g, 6 mmol) in acetic acid (15 ml) and the mixture was heated at reflux for 8 h. After cooling, the solution was poured into an ice-cooled aqueous sodium hydrogensulfite solution and was extracted with two 30 ml portions of ether. The combined extracts were dried over sodium sulfate and evaporated. The residue crystallized after standing overnight. Recrystallization of the product from ethanol gave **10** (1.3 g, 94.1% yield) as colorless columns: mp 86.8 °C.

Dechlorination. The cycloadducts (**1a, b** and **2a—d**) and ketones (**6a, b** and **7a—d**) obtained by oxidation were dechlorinated with zinc powder to the corresponding olefins (**11a, b** and **12a, b**). The following procedures are illustrative.

*7-Chloro-6-fluoro-2,3-benzobicyclo[3.2.0]hepta-2,6-diene (**11a**)*: To a solution of the mixture of the isomers (**1a** and **1b**, 2.7 g,

10 mmol) in absolute ethanol (40 ml) was added zinc powder (6.4 g). The mixture was heated at reflux with stirring for 8 h. After removal of solid material by filtration, the filtrate was poured into diluted hydrochloric acid and was extracted with three 50 ml portions of dichloromethane. The combined extracts were dried over magnesium sulfate and evaporated to give an oily residue (2.6 g). Further purification was effected by preparative GLC (at 100 °C using an aluminum column, 6 m long × 10 mm diameter, packed with Silicone DC-QFl-Chromosorb W) to give **11a** (1.7 g, 87.3% yield) as colorless oil: n_D^{20} 1.5509, d_4^{20} 1.251, IR $\nu_{C=C}$ 1705 cm^{-1}.

*6,7-Difluoro-2,3-benzobicyclo[3.2.0]hepta-2,6-diene (**11b**)*: The synthesis of **11b** from the mixture of isomers (**2a—d**, 2.5 g, 10 mmol) followed the procedure used with **1a** and **1b**, except that a higher reaction temperature (140 °C) was adopted using ethylene glycol (25 ml) as a solvent. The product (**11b**, 1.3 g, 73.0% yield) was obtained as a colorless oil: n_D^{20} 1.5189, IR $\nu_{C=C}$ 1764 cm^{-1}.

*7-Chloro-6-fluoro-2,3-benzobicyclo[3.2.0]hepta-2,6-dien-4-one (**12a**)*: The synthesis of **12a** from the mixture of isomers (**6a** and **6b**, 2.8 g, 10 mmol) followed the procedure used with **1a** and **1b**. The product (1.7 g, 81.5% yield) was obtained as colorless prisms (from ethanol): mp 58.2 °C, IR $\nu_{C=C}$ 1705 cm^{-1}, $\nu_{C=O}$ 1721 cm^{-1}.

*6,7-Difluoro-2,3-benzobicyclo[3.2.0]hepta-2,6-dien-4-one (**12b**)*: The synthesis of **12b** from the mixture of isomers (**7a—d**) followed the procedure used with **1a** and **1b**, except that the reaction time was prolonged to 18 h. The product (**12b**, 83.3% yield) was obtained as a colorless oil: d_D^{20} 1.5410, IR $\nu_{C=C}$ 1773 cm^{-1}, $\nu_{C=O}$ 1724 cm^{-1}.

Halogenation of the Adduct. Bromination with *N*-bromosuccinimide and photo-chlorination of a cycloadduct (**3a**) gave corresponding 4-halides (**13a** and **13b**).

*4-Bromo-7,7-dichloro-6,6-difluoro-2,3-benzobicyclo[3.2.0]hept-2-ene (**13a**)*: To a solution of **3a** (2.5 g, 10 mmol) in tetrachloromethane (30 ml), were added *N*-bromosuccinimide (1.8 g, 10 mmol) and a small amount of benzoyl peroxide (*ca.* 3 mg). The mixture was heated at reflux under an argon atmosphere for 2 h. The white precipitate generated was filtered off and the filtrate was evaporated to give a yellow oil. Further purification was effected by liquid chromatography (silica gel, tetrachloromethane as an eluting solvent) to give **13a** (3.2 g, 97.6% yield) as a colorless oil: n_D^{20} 1.5612.

*4,7,7-Trichloro-6,6-difluoro-2,3-benzobicyclo[3.2.0]hept-2-ene (**13b**) and 1,4,7,7-Tetrachloro-6,6-difluoro-2,3-benzobicyclo[3.2.0]-hept-2-ene (**14**)*: Chlorine (1.5 g, 20 mmol) was absorbed by bubbling through a solution of **3a** (2.5 g, 10 mmol) in tetrachloromethane (200 ml). The solution was exposed to sun light for 10 min until the yellow color disappeared. After removal of the solvent by evaporation, the residue was distilled under reduced pressure to give **13b** (2.4 g, 84.4% yield) as a slightly yellow oil: bp 115—116 °C/2 mmHg, n_D^{20} 1.5523. Purification of the higher boiling products by using the preparative GLC gave **14** (0.2 g, 6.3% yield) as colorless prisms (from ethanol): mp 84.4 °C.

Reduction of the Adduct. The cycloadduct (**3a**) was reduced with lithium aluminum hydride.

*7-Chloro-6,6-difluoro-2,3-benzobicyclo[3.2.0]hept-2-ene (**15**)*: To a solution of **3a** (2.5 g, 10 mmol) in absolute ether (100 ml) was added lithium aluminum hydride (1.2 g, 30 mmol) and the mixture was heated at reflux for 20 h with stirring. The mixture was poured into ice-cooled diluted sulfuric acid. The organic layer separated was dried over magnesium sulfate and evaporated. The residue crystallized after standing overnight. The product was recrystallized from ethanol to give **15** (1.1 g, 51.2% yield)as colorless plates: mp 136.2 °C. Analysis of the mother liquid by a mass spectrometer coupled with GC showed the existence of by-products, 6,6-difluoro-2,3-benzobicyclo[3.2.0]hept-2-ene (**16**) and 7-chloro-6-fluoro-2,3-benzobicyclo[3.2.0]hepta-2,6-diene (**11a**).

References

1) W. H. Sharkey, "Fluorine Chemistry Reviews," Marcel Dekker Inc., New York (1968), Vol. II, p. 1.

2) N. J. Turro and P. D. Bartlett, *J. Org. Chem.*, **30**, 1849 (1965); P. D. Bartlett, B. M. Jacobson, and L. E. Walker, *J. Am. Chem. Soc.*, **95**, 146 (1973); P. D. Bartlett and J. J. B. Mallet, *J. Am. Chem. Soc.*, **98**, 143 (1976).

3) D. Bryce-Smith, A. Gilbert, and B. H. Orger, *Chem. Commun.*, **1969**, 800; B, Sket and M. Zupan, *J. Chem. Soc., Chem. Commun.*, **1976**, 1053; **1977**, 365; D, Bryce-Smith, A. Gilbert, B. H. Orger, and P. J. Twitchett, *J. Chem. Soc., Perkin Trans. 1*, **1978**, 243.

4) A. J. Wexler and J. S. Swenton, *J. Am. Chem. Soc.*, **98**, 1602 (1976); M. L. Greenlee, E. L. Fritzen, Jr., and J. S. Swenton, *J. Org. Chem.*, **43**, 4512 (1978).

5) H. Kimoto, H. Muramatsu, and K. Inukai, *J. Fluorine Chem.*, **9**, 417 (1977) and references cited therein.

6) P. J. Wagner and M. J. Thomas, *J. Am. Chem. Soc.*, **98**, 241 (1976).

7) K. Takahashi, H. Kimoto, and H. Muramatsu, manuscript in preparation.

8) K. Okuhara, *J. Org. Chem.*, **41**, 1487 (1976).

Carbon–Carbon Bond Formation by the Use of Chloroiodomethane as a C_1 Unit. II.[1] The Preparation and Synthetic Application of 1-Chloro-3-iodoheptane[2]

Sotaro Miyano,* Hiroshi Hokari, Yoshiharu Umeda, and Harukichi Hashimoto

Department of Applied Chemistry, Faculty of Engineering, Tohoku University, Aramaki-Aoba, Sendai 980

(Received August 24, 1979)

Terminal alkenes, R–CH=CH_2 (R=Et, *n*-Pr, *n*-Bu, *n*-Hex), were readily transformed into 1-chloro-3-iodoalkanes by the AIBN-induced free radical addition of chloroiodomethane. Thus, 1-chloro-3-iodoheptane was obtained from 1-hexene in an 88% yield; this in turn was allowed to react with dialkyl malonates in the presence of alkoxides in alcohols to give dialkyl 2-butylcyclobutane-1,1-dicarboxylates and dialkyl (*E*)-3-octene-1,1-dicarboxylates (**7**), either of which could be obtained preferentially by the choice of the experimental parameters. The olefinic product, **7**, was further utilized for the synthesis of (*E*)-5-decenyl acetate and/or 1,4-nonanolide.

The free radical-induced addition of polyhalogenated methanes to alkenes to give 1:1 products (Kharasch reaction) has been well known.[3] This reaction had, however, been practically restricted to those halides which contained no less than three halogen atoms unless they had other activating substituents, such as –CO– and –CN.[3a] In fact, only a few successful Kharasch reactions had been documented for dihalomethanes[4,5] before Walton *et al.* recently reported the peroxide- or photochemically initiated addition of chloroiodomethane and diiodomethane to ethylene and several fluoroalkenes from the mechanistic point of view.[6] Several other papers have claimed the formation of cyclopropanes *via* the reaction of diiodomethane with alkenes under the free radical reaction conditions.[7]

As part of a program directed toward a study of carbon–carbon bond formation by the use of chloroiodomethane as a C_1 unit,[1] we wish to report here a facile synthesis of 1-chloro-3-iodoalkanes (**1**) *via* the 2,2′-azobisisobutyronitrile (AIBN)-initiated addition of CH_2ClI to terminal alkenes. Also to be described is the utilization of 1-chloro-3-iodoheptane (**1c**) as an intermediate for several synthetic transformations, including a synthesis of (*E*)-5-decenyl acetate (**15**), a kind of insect pheromone.

Results and Discussion

AIBN-initiated Addition of Chloroiodomethane to Terminal Alkenes. A mixture of CH_2ClI and AIBN in 1-alkene was stirred and heated at 80 °C for 6 h in a stainless steel autoclave. Employing *ca.* a 1/10 molar amount of AIBN to CH_2ClI, almost all of the halide was consumed to give 1-chloro-3-iodoalkanes in *ca.* 80—90% yields (Eq. 1 and Table 1).

Part of the AIBN was consumed in the formation of tetramethylsuccinonitrile **2**. Thus, when the molar ratio of AIBN to CH_2ClI was 1/20 or 1/100, the yield of 1-chloro-3-iodoheptane **1c** from 1-hexene was reduced to 38% or 17% respectively, leaving unchanged CH_2ClI, while appreciable amounts of the adduct (**1c**) were also obtained (6.2% yield) in the absence of the initiator.

$$\mathrm{R{-}CH{=}CH_2 + CH_2ClI \xrightarrow{AIBN} R{-}\underset{\displaystyle I}{\underset{|}{CH}}{-}CH_2{-}\underset{\displaystyle Cl}{\underset{|}{CH_2}}} \quad (1)$$

1

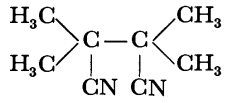

2

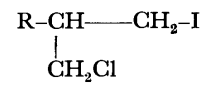

3

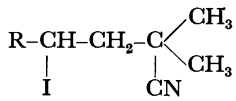

4

The structure of the 1:1 adduct **1** was confirmed on the basis of its NMR spectra, which showed two hydrogens of $-CH_2Cl$ comprised of four lines of a double doublet centered at *ca.* δ 3.6 (A_2 portion of an A_2MM' system, $J_{AM}\approx5.5$ Hz, $J_{AM'}\approx6.5$ Hz) and one hydrogen of –CHI– at δ 4.5—4.0 as a mulitplet. The dehydroiodination reaction of the 1:1 adduct by potassium hydroxide in aq methyl alcohol also supported the 1-chloro-3-iodoalkane structure; **1d** gave (*E*)-1-methoxy-2-nonene (**5a**) and (*E*)-1-chloro-3-nonene (**6a**) as the major products. Small amounts of a substance

Table 1. AIBN-induced addition of CH_2ClI to R–CH=CH_2[a]

	R–CH=CH_2 R	R–CH(I)–CH_2–CH_2(Cl) (1) Yield[b]/%	Bp °C/mmHg	Found (Calcd)% C	H
a	Et	81 (54)	74—76/9.5	25.91 (25.83)	4.26 (4.34)
b	*n*-Pr	76 (48)	88—90/8	29.47 (29.23)	4.80 (4.91)
c	*n*-Bu	88 (81)	96—97/7	32.59 (32.27)	5.57 (5.42)[c]
d	*n*-Hex	80 (67)	112—115/2	37.75 (37.46)	6.13 (6.29)

a) R–CH=CH_2, 15—20 ml; CH_2ClI, 3.0 ml (43 mmol); AIBN (mol)/CH_2ClI (mol)=1/10; 80 °C, 6 h. b) GLC yield based on CH_2ClI. Figures in parentheses show isolated yields. c) Halogen, 61.84%. Calcd for $C_7H_{14}ClI$: Cl, 13.61; I, 48.71%.

having a slightly longer GLC retention time than **1** were also detected (less than 4% of **1**). The substance was not isolated, but it seemed to have a branched chain structure, **3**, as was indicated by the reaction products from the dehydroiodination with potassium hydroxide in aq methyl alcohol (see Experimental). The isolation of the iodo nitrile **4** suggests that the initiation step of the radical chain involves mainly the attack of the isobutyronitrile radical from AIBN on the terminal carbon atom of the 1-alkenes.

Kaplan obtained cyclopropanes *via* a radical-induced methylene transfer from CH_2I_2 to alkenes using quite large amounts of peroxide initiators (more initiators than CH_2I_2 or alkenes).[7c] On the other hand, the AIBN-initiated addition of CH_2I_2 to 1-hexene gave 1,3-diiodoheptane in a 62% isolated yield under the reaction conditions of this work, while CH_2Br_2 was recovered unchanged.

An attempted addition to styrene resulted in the formation of a polymeric product, leaving CH_2ClI intact. Though little effort was made to optimize the reaction, extension to internal alkenes, including 2-heptenes, (*E*)-2-butene, (*E*)-stilbene, and cyclohexene, was not practical, either; large amounts of **2** were formed, and more than 80% of the CH_2ClI was recovered in these cases.

*Reaction of 1-Chloro-3-iodoheptane (**1c**) with Dialkyl Malonates/Alkoxides in Alcohols.* The treatment of **1c** with dimethyl malonate in the presence of sodium methoxide in methyl alcohol gave several products, as evidenced by GLC; among them we obtained dimethyl (*E*)-3-octene-1,1-dicarboxylate, **7a**, and dimethyl 2-butylcyclobutane-1,1-dicarboxylate, **8a**, as the major products in yields of 71% and 6.5% respectively (Eq. 2). Among other by-products were also identified (*E*)-1-methoxy-2-heptene, **5b**, and (*E*)-1-chloro-3-heptene, **6b**.

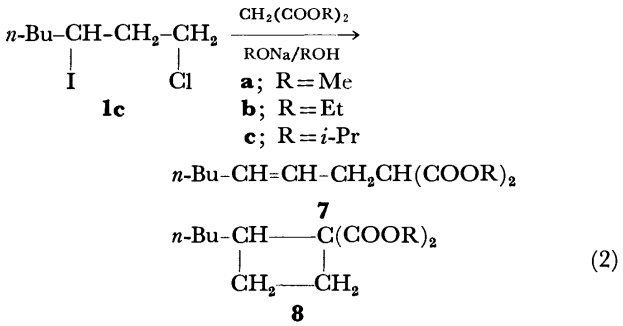

(2)

Tables 2 and 3 show the effects of the reaction variables on the relative yield of the olefinic products, **7**, to the ring-closure products, **8**. By the use of potassium *t*-butoxide or sodium isopropoxide, **1c** was preferentially transformed into the cyclobutanes, **8**, while dehydroiodination preceded when sodium methoxide or ethoxide was utilized, especially in lower concentrations. These results may be explained in terms of the base strength and steric bulkiness of the alkoxides used; these are both in the order of $MeO^- < EtO^- < i\text{-}PrO^- < t\text{-}BuO^-$. The E2-type dehydroiodination to **7** becomes unfavored as the base becomes bulkier, while the concentration of the malonate carbanion will increase with the basicity of the alkoxide. These

Table 2. Reaction of **1c** with $CH_2(COOR)_2$/RONa[a]

	$CH_2(COOR)_2$ R	Solvent ROH(50 ml)	Yield/% **7**+**8**	**7**/**8** Ratio
a	Me	MeOH	78	92/8
b	Et	EtOH	75	59/41
c	*i*-Pr	*i*-PrOH	57	11/89

a) **1c**, 19 mmol; $CH_2(COOR)_2$, 45 mmol; RONa, 44 mmol; Reflux, 3 h.

factors facilitate nucleophilic displacement at the iodine-bearing carbon atom in **1c** by the malonate anion. Subsequent intramolecular S_N2 attack on the terminal chlorine-carrying carbon atom leads to ring closure. On the other hand, where the carbanion concentration is not so much prevailing with the less strong bases of smaller bulk, dehydroiodination by alkoxides preceds to give allylic chloride, which is then displaced in a nucleophilic manner by the malonate anion to give **7**.

Synthesis of γ-Butyrolactones. The hydrolysis of **7a** with potassium hydroxide in boiling aq methyl alcohol gave the free dicarboxylic acid, **9a**, a pure sample of which was obtained as white crystals after recrystalization from petrol. ether. Heating at reflux in aq H_2SO_4 (2:1) changed **9a** into 1,4-nonanolide, **10a**; this is the so-called "coconut aldehyde," one of the most important lactones in perfumes and flavors, having a delicately fruity and coconutty odor of an excellent tenacity.[8] Starting from 1-octene, a similar treatment of **9b** gave 1,4-undecanolide, **10b**, the so-called "peach aldehyde," which has high quality, peach-like taste.

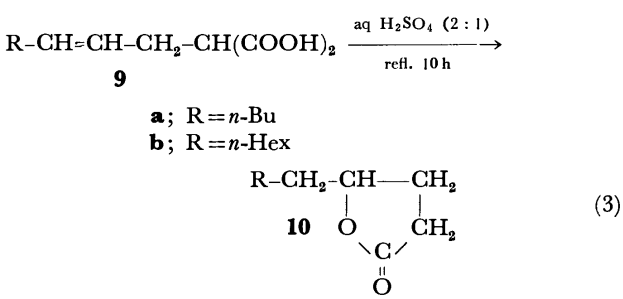

(3)

Utilization of the trans-*1,2-Disubstituted Olefinic Structure of 7 as a Synthetic Intermediate.* *trans*-1,2-Disubstituted olefinic bonds are common functional groups which are found in many synthetically useful intermediates and naturally occurring compounds.[9] Although the dehydroiodination-alkylation of **1c** with malonate/alkoxide should give rise several possible products in respect to stereo- and regiochemistry, the preferential formation of the *trans*-1,2-disubstituted alkene, **7a**, in a reasonable yield seemed to have some synthetic utility.

The thermolysis of **9a** at *ca.* 150 °C caused its decarboxylation to (*E*)-4-nonenoic acid, **11**.[10] The series of well-established transformations shown in Scheme 1 converted **11** to (*E*)-5-decen-1-ol, **14**, and its acetate, **15**, both of which are constituents of the sex pheromone for the male peach twig borer moth, *Anarsia lineatella Zeller*.[11] Another synthesis of **15** has been briefly reported, without any detailed physical or spectral data.[11] A synthesis of the (*Z*)-counterpart of **15** has appeared recently; (*Z*)-**15** is a sex attractant for the

Table 3. Reaction of **1c** with $CH_2(COOEt)_2$/EtONa

1c (mmol)	$CH_2(COOEt)_2$ (mmol)	EtONa (mmol)	EtOH (ml)	Reaction conditions[a)]	**7b/8b** Ratio
19	45	44	50	A, reflux, 3 h	59/41
5.1	9.6	11	30	A, reflux, 3 h	82/18
4.3	9.2	23	30	B, reflux, 3 h	65/35
9.7	19	40	30	B, reflux, 3 h	20/80
5.8	11	13	30	A, ambient, 24 h	91/9
		t-BuOK	*t*-BuOH		
4.0	9.2	39	30	A, reflux, 3 h	1/99

a) A, **1c** was added drop by drop; B, EtONa was added drop by drop.

male turnip moth *Agrotis segetum*.[12]

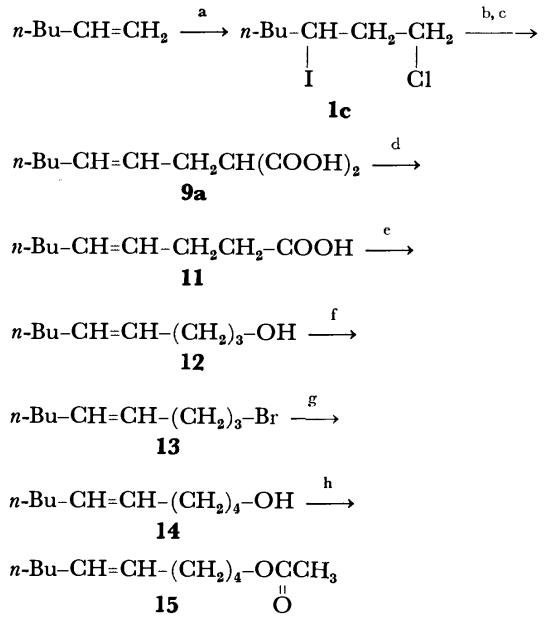

a; CH_2ClI, AIBN. b; $CH_2(COOCH_3)_2$/MeONa/MeOH. c; KOH/aq MeOH. d; 150 °C. e; $LiAlH_4/Et_2O$. f; Ph_3PBr_2/CH_3CN. g; Mg, CH_2O/Et_2O. h; CH_3COCl/Pyridine/PhH.

Scheme 1.

In conclusion, the net effect of the above transformations can be visualized as the displacement of the terminal *trans*-hydrogen atom with an alkyl moiety of more than two methylene units (Eq. 4).

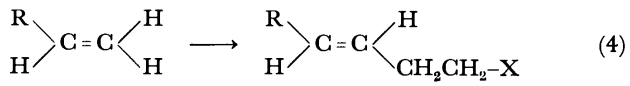

(4)

Experimental

The IR spectra were obtained using a Shimadzu IR 430 grating spectrophotometer. The NMR spectra were recorded on a Hitachi R-24A spectrometer (60 MHz), using carbon tetrachloride as the solvent (1—5% solution) unless otherwise noted. The absorption peaks were recorded in ppm units downfield from hexamethyldisiloxane as an internal standard. The analytical GLC was conducted on a Shimadzu GC 3AF and Hitachi 163 gas chromatograph equipped with flame-ionization detectors; a 300×0.3 cm stainless steel column packed with Silicone DC 550 (20%), Apiezon Grease L (20%), Silicone DC 410 (20%), or FFAP (10%) on Diasolid M (60—80 mesh), or a 20-m glass capillary column (0.25 mm i.d.) coated with silicone oil (OV-1 column), was used. The GLC yields of the reaction products were determined on the basis of the molar response, as determined from standard solutions of the products and appropriate internal standards. Preparative GLC separations were achieved with a Shimadzu GC 2C gas chromatograph using the appropriate column from among those noted above.

Materials. The chloroiodomethane was obtained by the procedure described before;[13] it was stored over a few tin pellets in the dark. The alkenes were distilled from sodium wire before use. The AIBN (dec 102 °C) and (*E*)-stilbene were used without further purification. The commercial dialkyl malonates were dried over $MgSO_4$ and distilled under reduced pressure. The solvents were purified as usual before use.

Addition of Chloroiodomethane to 1-Alkenes by Means of AIBN. A dry, 100-ml-inner-volume stainless steel autoclave equipped with a magnetic stirrer and a thermometer was charged with 4 mmol of AIBN, evacuated, and refilled with nitrogen. Then, 15—20 ml of 1-alkene and 3.0 ml (7.6 g, 43 mmol) of CH_2ClI were added by means of hypodermic syringe through a three-way cock under nitrogen. (1-Butene was distilled from a pressure bottle into the reaction vessel containing AIBN and CH_2ClI.) The mixture was stirred and heated in the course of 0.5 h to 80 ± 5 °C in an oil bath; that temperature was then maintained for 6 h. At the end of the reaction, the vessel was cooled in a water bath. The mixture was then subjected to distillation; after the excess alkene and tetramethylsuccinonitrile (**2**) had been removed *in vacuo*, the residue was fractionated through a short, packed column to give the corresponding 1-chloro-3-iodoalkane, **1**. Table 1 lists the results.

Diiodomethane was used in place of chloroiodomethane to give 1,3-diiodoheptane from 1-hexene: bp 105—107 °C/3.8 mmHg; yield, 62%. Found: C, 24.08; H, 3.91%. Calcd for $C_7H_{14}I_2$: C, 23.88; H, 4.01; I, 72.11%. NMR: δ 0.6—1.1 (3H, H_3C-), 1.1—2.0 (6H, H_3C-(CH_2)$_3$-), 2.0—2.5 (2H, -CH_2-CH_2I), 3.1—3.5 (2H, -CH_2I), 3.8—4.4 (1H, -CHI-).

Tetramethylsuccinontirile (2): An analytical sample was purified by sublimation: mp, 166—168 °C (lit,[14] 170.5—171.5 °C). The IR spectrum of the sample was superimposable upon that of the authentic one[14]; (KBr), 2220 cm^{-1} (νC≡N). NMR: δ 1.6 ($4\times H_3C$-).

2-Methyl-2-cyano-4-iodoheptane (4a): After 1-chloro-3-iodohexane had been recovered from the reaction mixture of 1-pentene, the distillation of the residue afforded a 0.6-g sample of **4a** boiling at 85—90 °C/1.5 mmHg. NMR: δ 0.7—1.1 (3H, H_3C-CH_2-), 1.3 and 1.4 (3H (s) and 3H (s), -C(CN)(CH_3)$_2$), 1.3—2.0 (4H, H_3C-(CH_2)$_2$-), 2.25 (2H, d, J=6.4 Hz, -CH_2-C(CN)(CH_3)$_2$), 3.9—4.4 (1H,

-CHI-). IR (neat): 2250 cm^{-1} (νC≡N).

A substantial rotational barrier, as judged by the PCK molecular model, may cause a magnetic non-equivalence between the two methyl groups of $-C(CN)(CH_3)_2$. The chemical shift of the C_3 methylene protons was assigned as above, because the irradiation of the sample at the -CHI- proton caused a collapse of the δ 2.25 doublet to a sharp singlet.

The **4a** was further transformed to (*E*)-2,2-dimethyl-3-heptenoic acid by heating at reflux for 5 h with KOH in ethylene glycol. NMR: δ 0.6—1.0 (3H, H_3C-CH_2-), 1.2 (6H, s, $-C(COOH)(CH_3)_2$), 1.1—1.7 (2H, H_3C-CH_2-), 1.7—2.4 (2H, $-CH_2-CH=CH-$), 5.3—5.6 (2H, -CH=CH-), 11.5 (1H, s, -COOH). IR (neat): 1700 (νC=O), 980 cm^{-1} (δ =CH_{trans}).

*Reaction of 1-Chloro-3-iodononane (**1d**) with Potassium Hydroxide in Aq Methyl Alcohol.* A heterogeneous mixture of **1d** (5.2 g) in a KOH (4 g) solution in MeOH (15 ml)-H_2O (4 ml) was stirred and then heated at reflux for 3 h. The cooled mixture was diluted with water and extracted with portions of ether. The ether extracts were then combined, washed successively with 2 M HCl and water, and dried over $MgSO_4$. The GLC analysis of the solution showed the presence of seven peaks (Apiezon Grease L column) (the following information is the compound, the percent of peak area on GLC, and the relative retention time); 1,3-nonadiene, 2.0%, 0.50; 3-methoxy-1-nonene, 0.4%, 0.72; 2-(methoxymethyl)-1-octene, 3.3%, 0.86; (*E*)-1-methoxy-3-nonene, 1.4%, 0.95; (*E*)-1-methoxy-2-nonene. 82.1%, 1.00; (*E*)-1-chloro-3-nonene, 10%, 1.15; unidentified, 0.8%, 1.33.

After the solvents had been removed by distillation, the residue was subjected to preparative GLC. A pure sample of (*E*)-1-methoxy-3-nonene was not isolated, but it was inferred from the fact that the treatment of (*E*)-1-chloro-3-nonene with KOH in aq MeOH increased the GLC peaks of the retention times of 0.50 (*i.e.*, 1,3-nonadiene) and of 0.95.

1,3-Nonadiene: NMR: δ 0.6—1.1 (3H, H_3C-), 1.1—1.7 (6H, $H_3C-(CH_2)_3-$), 1.7—2.4 (2H, $-CH_2-CH=CH-$), 4.6—6.8 (5H, $-CH=CH-CH=CH_2$). IR (neat): 1650 and 1605 ($\nu C=C_{diene}$), 1000 and 900 cm^{-1} (δ =CH_{vinyl}).

3-Methoxy-1-nonene: NMR: δ 0.6—1.0 (3H, H_3C-CH_2-), 1.0—1.8 (10H, $-(CH_2)_5-$), 3.0—3.5 (1H, $-CH(OCH_3)-$), 3.1 (3H, s, H_3CO-), 4.7—5.9 (3H, $-CH=CH_2$). IR (neat): 1640 (νC=C), 995 and 915 cm^{-1} (δ =CH_{vinyl}).

2-(Methoxymethyl)-1-octene: NMR: δ 0.7—1.1 (3H, H_3C-), 1.1—1.6 (8H, $H_3C-(CH_2)_4-$), 1.6—2.2 (2H, $-CH_2-CH_2-CH=$), 3.2 (3H, s, H_3CO-), 3.6—3.7 (2H, $-CH_2-OCH_3$), 4.6—4.9 (2H, $>C=CH_2$). IR (neat): 1650 (νC=C), 900 cm^{-1} (δ =$CH_{terminal\ methylene}$).

(E)-1-Methoxy-2-nonene: NMR: δ 0.7—1.1 (3H, H_3C-), 1.1—1.7 (8H, $H_3C-(CH_2)_4-$), 1.7—2.3 (2H, $-CH_2-CH_2-CH=$), 3.2 (3H, s, H_3CO-), 3.6—3.8 (2H, H_3CO-CH_2-), 5.3—5.7 (2H, -CH=CH-). IR (neat): 1670 (νC=C), 970 cm^{-1} (δ =CH_{trans}). Found: C, 76.61; H, 13.19%. Calcd for $C_{10}H_{20}O$: C, 76.86; H, 12.90%. The assignment of the *E* structure was based on the strong IR absorption at 970 cm^{-1}.

(E)-1-Chloro-3-nonene: NMR: δ 0.7—1.1 (3H, H_3C-), 1.1—1.7 (6H, $H_3C-(CH_2)_3-$), 1.7—2.2 (2H, $-CH_2-CH_2-CH=$), 2.2—2.7 (2H, $-CH_2-CH_2Cl$), 3.4 (2H, t, J=6.8 Hz, $-CH_2Cl$), 5.2—5.6 (2H, -CH=CH-). IR (neat): 970 cm^{-1} (δ =CH_{trans}).

Treatment of 1-Chloro-3-iodoheptane with Dimethyl Malonate/Sodium Methoxide in Methyl Alcohol. To a 200-ml, round-bottomed flask equipped with a condenser topped with a nitrogen inlet, a pressure-equalized dropping funnel, a thermometer, and a magnetic stirrer were added, under a nitrogen atmosphere, 50 ml of methyl alcohol and 1.0 g (43.5 mg-atom) of sodium metal. After the dissolution of the sodium, a 6.0 g (45 mmol) portion of dimethyl malonate was added. The mixture was heated to gentle reflux, and then a 5.0-g (19 mmol) portion of 1-chloro-3-iodoheptane **1c** was added dropwise. Stirring was continued for 3 h under gentle reflux. At the end of the reaction, the mixture was cooled, diluted with 30 ml of water, and extracted rapidly with portions of ether. The ether extracts were combined, washed successively with aq NH_4Cl and water, and dried over $MgSO_4$. An aliquot of the solution was used for the quantitative determination of the dimethyl (*E*)-3-octene-1,1-dicarboxylate, **7a**, and the dimethyl 2-butylcyclobutane-1,1-dicarboxylate, **8a**, by GLC. After the solvents and small amounts of the fore-run had been removed *in vacuo*, the residue was fractionated through a short, packed column. The yield of **7a** boiling at 100—104 °C/2 mmHg was 2.22 g, including small amounts of **8a** and trace amounts of an unidentified product; the retention time on GLC was in the order of **8a**, the unidentified, and **7a** (FFAP column). Pure sample of **7a** and **8a** were collected by preparative GLC.

The recovered solvent and the fore-run portion was concentrated to *ca.* a 1-ml volume, from which were detected and collected by preparative GLC 1-methoxy-2-heptene (**5b**) and 1-chloro-3-heptene (**6b**) among several other unidentified products.

*Dimethyl 2-Butylcyclobutane-1,1-dicarboxylate (**8a**)*: NMR: δ 0.6—1.0 (3H, H_3C-CH_2-), 1.0—1.5 (6H, $H_3C-(CH_2)_3-$), 1.5—2.1 (4H, ring-$(CH_2)_2-$), 2.1—2.6 (1H, -CH-), 3.6 (6H, $2\times H_3CO-$). IR (neat): 1730 cm^{-1} (νC=O).

*Dimethyl (E)-3-Octene-1,1-dicarboxylate (**7a**)*: Bp, 117 °C/2 mmHg; n_D^{15}, 1.4453. NMR: δ 0.6—1.0 (3H, H_3C-), 1.0—1.5 (4H, $H_3C-(CH_2)_2-$), 1.6—2.1 (2H, $-CH_2-CH_2-CH=$), 2.2—2.6 (2H, $=CH-CH_2-CH-$), 3.0—3.4 (1H, -CH-), 3.6 (6H, s, $2\times H_3CO-$), 5.0—5.5 (2H, -CH=CH-). IR (neat); 1740 (νC=O), 970 cm^{-1} (δ =CH_{trans}). Found: C, 63.01; H, 8.75%. Calcd for $C_{12}H_{20}O_4$: C, 63.13; H, 8.83%.

*(E)-3-Octene-1,1-dicarboxylic Acid (**9a**)*: The diester **7a** was hydrolyzed by refluxing it in aq MeOH in the presence of KOH. Mp, 65.5 °C (petr. ether) (lit,[10] 60—63 °C). Found: C, 60.28; H, 8.23%. Calcd for $C_{10}H_{16}O_4$: C, 59.98; H, 8.05%. NMR ($CDCl_3$): δ 0.6—1.0 (3H, H_3C-), 1.0—1.5 (4H, $H_3C-(CH_2)_2-$), 1.7—2.2 (2H, $-CH_2-CH_2-CH=$), 2.3—2.8 (2H, $=CH-CH_2-CH<$), 3.4 (1H, t-like, $-CH<$), 5.1—5.7 (2H, -CH=CH-), 11.8 (2H, s, $2\times$-COOH). IR (KBr): 1710 (δC=O), 965 cm^{-1} (δ =CH_{trans}).

*1-Methoxy-2-heptene (**5b**)*: NMR: δ 0.6—1.1 (3H, H_3C-), 1.1—1.7 (4H, $H_3C-(CH_2)_2-$), 1.7—2.4 (2H, $-CH_2-CH_2-CH=$), 3.2 (3H, s, H_3CO-), 3.6—4.0 (2H, H_3CO-CH_2-), 5.2—5.7 (2H, -CH=CH-). IR (neat): 1670 (νC=C), 970 cm^{-1} (δ =CH_{trans}).

*1-Chloro-3-heptene (**6b**)*: NMR: δ 0.7—1.1 (3H, H_3C-), 1.1—1.7 (2H, H_3C-CH_2-), 1.7—2.2 (2H, $Et-CH_2-$), 2.2—2.7 (2H, $ClCH_2-CH_2-$), 3.4 (2H, t, J=6.5 Hz, $ClCH_2-$), 5.1—5.6 (2H, -CH=CH-). IR (neat): 975 cm^{-1} (δ =CH_{trans}).

Similar treatment of **1c** with diethyl and diisopropyl malonate gave the corresponding alkene **7** and cyclobutane **8** (see Table 2); all the compounds exhibited satisfactory IR and NMR spectra.

*Diethyl (E)-3-Octene-1,1-dicarboxylate (**7b**)*: Bp, 117—120 °C/2 mmHg; n_D^{17}, 1.4405 (lit,[10] n_D^{25}, 1.4410). Found: C, 65.75; H, 9.62%. Calcd for $C_{14}H_{24}O_4$: C, 65.60: H, 9.44%.

*Diethyl 2-Butylcyclobutane-1,1-diacrboxylate (**8b**)*: Bp, 98—100 °C/2 mmHg; n_D^{17}, 1.4403. Found: C, 65.89; H, 9.52%. Calcd for $C_{14}H_{24}O_4$: C, 65.60; H, 9.44%.

*Diisopropyl 2-Butylcyclobutane-1,1-dicarboxylate (**8c**)*: Bp, 115—117 °C/2 mmHg; n_D^{15}, 1.4390. Found: C, 67.90; H, 9.59%. Calcd for $C_{16}H_{28}O_4$: C, 67.60; H, 9.89%.

*Reaction of (E)-3-Octene-1,1-dicarboxylic Acid (**9a**). (E)-4-Nonenoic Acid (**11**)*: A sample of the dicarboxylic acid **9a** (37.7 g, 0.19 mol) was heated to 150—160 °C. After gas evolution had ceased, the mixture was analyzed by GLC to show that it consisted of *ca.* 95% of (*E*)-4-nonenoic acid (**11**) and *ca.* 5% of 1,4-nonanolide (**10a**) (*vide infra*). The mixture was dissolved in 2 M Na_2CO_3 and extracted with portions of ether to remove the **10a**. The aqueous phase was acidified with 2 M HCl; the regenerated free acid was extracted with ether. The ether extracts were combined, washed with water, and dried over $MgSO_4$. Distillation gave (*E*)-4-nonenoic acid boiling at 98—102 °C/2.5—3 mmHg (lit,[10] bp, 112—113 °C/5 mmHg); 18.7 g (yield, 64%). NMR: δ 0.6—1.1 (3H, H_3C–), 1.1—1.6 (4H, H_3C–(CH_2)$_2$–), 1.6—2.1 (2H, *n*-Pr–CH_2–), 2.1—2.6 (4H, –(CH_2)$_2$–CO–), 5.1—5.5 (2H, –CH=CH–), 11.9 (1H, –COOH). IR (neat): 1710 (νC=O), 965 cm^{-1} (δ =CH_{trans}).

*1,4-Nonanolide (**10a**)*: The dicarboxylic acid **9a** (0.83 g) was refluxed in H_2O (40 ml)–H_2SO_4 (20 ml) for 10 h. After steam distillation, the distillate was worked up as usual. Bp, 105—107 °C/2 mmHg; 0.65 g; n_D^{13}, 1.4473 (lit,[15] n_D^{20}, 1.4462). Found: C, 69.15; H, 9.94%. Calcd for $C_9H_{16}O_2$: C, 69.19; H, 10.33%. NMR: δ 3.9—4.6 (1H, –CH–). IR (neat): 1770 cm^{-1} (νC=O).

*1,4-Undecanolide (**10b**)*: The method described above was applied to 1-chloro-3-iodononane (**1d**) to give **10b**. Bp, 132—135 °C/2 mmHg; n_D^{13}, 1.4512 (lit,[16] n_D^{20}, 1.4512). Found: C, 71.85; H, 11.33%. Calcd for $C_{11}H_{20}O_2$: C, 71.70; H, 10.94%. NMR: δ 3.9—4.6 (1H, –CH–). IR (neat): 1770 cm^{-1} (νC=O).

*Synthesis of (E)-5-Decenyl Acetate (**15**)*. To a stirred suspension of $LiAlH_4$ (0.6 g) in 300 ml of ether, we added a solution of (*E*)-4-nonenoic acid (**11**) (18.7 g, 0.12 mol) in ether (250 ml) over a 40-min period. The mixture was heated at reflux for another 3 h and then treated as usual. The subsequent evaporation of solvents left a 12.6 g sample of (*E*)-4-nonen-1-ol (**12**), the purity of which was *ca.* 97% as judged by GLC. NMR: δ 0.6—1.1 (3H, H_3C–), 1.1—1.7 (6H, 3×–CH_2–), 1.7—2.3 (4H, –CH_2–CH=CH–CH_2–), 2.5—2.8 (1H, –OH), 3.5 (2H, t, J=6.5 Hz, –CH_2–OH), 5.1—5.5 (2H, –CH=CH–). IR (neat): 970 cm^{-1} (δ =CH_{trans}).

Into an ice-chilled solution of triphenylphosphine (36 g) in 200 ml of acetonitrile was dropped 21.9 g of bromine (0.14 mol) to give triphenylphosphine dibromide, to which was then added the alcohol **12** (12.6 g). After the mixture had been stirred and heated at reflux for 1 h, the acetonitrile was evaporated *in vacuo*. The crude product (*E*)-1-bromo-4-nonene (**13**) was collected as a portion boiling at 50—55 °C/2—3 mmHg (*ca.* 85% yield); it was then filtered through a silica-gel column to give 5.03 g of a pure sample. NMR: δ 0.6—1.0 (3H, H_3C–), 1.0—1.5 (4H, –(CH_2)$_2$–CH_3), 1.5—2.5 (6H, 3×–CH_2–), 3.2 (2H, t, J=6.4 Hz, –CH_2Br), 5.1—5.5 (2H, –CH=CH–). IR (neat): 965 cm^{-1} (δ =CH_{trans}).

The bromide **13** (5.0 g) was treated with 1.5 g of magnesium turnings (62 mg-atom) in 80 ml of ether, to which was passed formaldehyde gas (prepared from 5 g of paraformaldehyde). A conventional work-up gave a 3.0-g portion distilling out at 78—84 °C/2—3 mmHg, which was finally purified by preparative GLC (FFAP column) to give **14** with a purity of 98% plus, as judged by the OV-1 capillary column GLC. Bp, 95—96 °C/2 mmHg; n_D^{15}, 1.4513. Found: C, 77.03; H, 12.66%. Calcd for $C_{10}H_{20}O$: C, 76.86; H, 12.90%. NMR: δ 0.6—1.0 (3H, H_3C–), 1.0—1.6 (8H, 4×–CH_2–), 1.5—1.7 (1H, –OH), 1.7—2.2 (4H, 2×–CH_2–), 3.3—3.6 (2H, t-like, –CH_2–OH), 5.1—5.3 (2H, –CH=CH–). IR (neat): 965 cm^{-1} (δ =CH_{trans}).

The treatment of the alcohol **14** with an excess amount of acetyl chloride in pyridine-benzene gave (*E*)-5-decenyl acetate, **15**: bp, 110—115 °C/16—17 mmHg; n_D^{19}, 1.4393. Found: C, 73.00; H, 11.22%. Calcd for $C_{12}H_{22}O_2$: C, 72.68; H, 11.18%. NMR: δ 0.6—1.0 (3H, H_3C–CH_2–), 1.0—1.6 (8H, 4×–CH_2–), 1.6—2.2 (7H, –OH+3×–CH_2–), 3.9 (2H, t, J=6.6 Hz, –CH_2–O–), 5.1—5.4 (2H, –CH=CH–). IR (neat): 1745 (νC=O), 970 cm^{-1} (δ =CH_{trans}).

Financial support of this work by a Grant-in-Aid (C-35536) from the Ministry of Education, Japan, is gratefully acknowledged (S.M.).

References

1) Part I: S. Miyano, Y. Izumi, K. Fujii, Y. Ohno, and H. Hashimoto, *Bull. Chem. Soc. Jpn.*, **52**, 1197 (1979).

2) Part of this work was presented at the 37 th National Meeting of the Chemical Society of Japan, Yokohama, April 1978. Some of the results reported at that meeting were, herein, reinvestigated and revised.

3) a) C. Walling, "Free Radicals in Solution," John Wiley & Sons, New York, N. Y. (1957), p. 247; b) C. Walling and E. S. Hyser, *Org. React.*, **13**, 91 (1963); c) J. M. Tedder and J. C. Walton, *Acc. Chem. Res.*, **1976**, 183.

4) J. Harmon, T. A. Ford, W. E. Hanford, and R. M. Joyce, *J. Am. Chem. Soc.*, **72**, 2213 (1950).

5) *Cf.* D. L. Decker, C. Moore, and W. F. Tousignant, U. S. Patent, 3862978; *Chem. Abstr.*, **82**, 125048w (1975).

6) a) N. McMurray, J. M. Tedder, L. L. T. Vertommen, and J. C. Walton, *J. Chem. Soc., Perkin Trans. 2*, **1976**, 63; b) I. Paterson, J. M. Tedder, and J. C. Walton, *J. Chem. Soc., Perkin Trans. 2*, **1978**, 884.

7) a) D. C. Blomstrom, K. Herbig, and H. E. Simmons, *J. Org. Chem.*, **30**, 959 (1965); b) L. Kaplan, *J. Am. Chem. Soc.*, **89**, 1753 (1967); c) L. Kaplan, *J. Am. Chem. Soc.*, **89**, 4566 (1967); d) L. Kaplan, *J. Chem. Soc., Chem. Commun.*, **1969**, 106; e) N. J. Pienta and P. J. Kropp, *J. Am. Chem. Soc.*, **100**, 655 (1978).

8) O. Okuda, "Koryo Kagaku Soran," 2nd ed, Hirokawa Publishing Co., Tokyo (1972).

9) See, for example, R. Rossi, *Synthesis*, **1977**, 817.

10) H. Nii, K. Furukawa, and M. Iwakiri, *Nippon Kagaku Zasshi*, **92**, 1214 (1974).

11) W. Roelofs, J. Kochansky, E. Anthon, R. Rice, and R. Cadrdé, *Environ. Entomol.*, **4**, 580 (1975).

12) H. J. Bestmann, O. Vostrowsky, K.-H. Koschatzky, H. Platz, T. Brosche, I. Kantardjiew, M. Rheinwald, and W. Knauf, *Angew. Chem. Int. Ed. Engl.*, **17**, 768 (1978).

13) S. Miyano and H. Hashimoto, *Bull. Chem. Soc. Jpn.*, **44**, 2864 (1971).

14) C. G. Overberger and M. B. Berenbaum, *Org. Synth.*, Coll. Vol. IV, 273 (1963).

15) Ref. 8, p. 1191.

16) Ref. 8, p. 1193.

 © 1980 The Chemical Society of Japan Bull. Chem. Soc. Jpn., 53, 775—784 (1980)

Physical Properties and Various Reactions of Thionitrites and Related Substances

Shigeru OAE,* Kōichi SHINHAMA, Ken FUJIMORI, and Yong Hae KIM

Department of Chemistry, University of Tsukuba, Niiharigun, Ibaraki 305

(Received August 27, 1979)

Several new sulfenyl or sulfonyl derivativives, thionitrates ($RSNO_2$), sulfonyl nitrites (RSO_2NO), were successfully isolated by treating corresponding thiols and sulfinic acids with dinitrogen tetraoxide (N_2O_4). Spectroscopic data of both stable and many rather unstable compounds were determined and compared with those of corresponding alkyl nitrites (RONO) or alkyl nitrates ($RONO_2$). Chemical reactivities of these uncommon, novel *S*-nitroso and *S*-nitro compounds were investigated.

Preparation of Thionitrites and Related Substances. We reported recently that various thionitrites (RSNO) (**2**) were prepared quantitatively by the reaction of thiols (**1**) with dinitrogen tetraoxide (N_2O_4)[1,2] (Eq. 1). Red colored thionitrites **2** were not so stable as to be isolated in pure form except *t*-alkyl or *s*-alkyl derivatives.

We found that stable *t*-alkyl thionitrates (**3a**—**c**) can be prepared in good yields by treating thiols with excess dinitrogen tetraoxide (Eq. 2). *t*-Pentyl thionitrate (**3b**) and 1,1-dimethylheptyl thionitrate (**3c**) are new additions in the literature. We also found that the novel aryl thionitrates (**3d**—**f**) can be isolated as unstable white crystals upon treating the corresponding thiols with excess dinitrogen tetraoxide in hexane at low temperatures (*ca.* −60 °C). However, these aryl thionitrates **3d**—**f** were found to decompose readily at room temperature. All the *t*-alkyl thionitrates **3a**—**c** were stable at room temperature and some aryl thionitrates **3d**—**e** were stable at low temperature, however, other thionitrates were found to be not stable enough to be isolated in pure form. Reaction

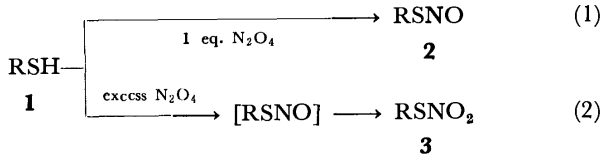

(1)

(2)

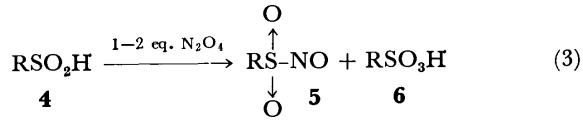

(3)

1a, **2a**, **3a**: R=*t*-Bu
1b, **3b**: R=*t*-C_5H_{11}
1c, **3c**: R=1,1-dimethylheptyl
4a, **5a**, **6a**: R=CH_3
1d, **3d**, **4b**, **5b**, **6b**: R=*p*-Tolyl
4c, **5c**, **6c**: R=Ph
1e, **3e**, **4d**, **5d**, **6d**: R=*p*-Cl-C_6H_4
1f, **3f**, **4e**, **5e**, **6e**: R=*p*-Br-C_6H_4
4f, **5f**, **6f**: R=*p*-CH_3O-C_6H_4

conditions and isolated yields of thionitrates **3a**—**f** are listed in Table 1.

Sulfonyl nitrites (**5**) were considered to be the reaction intermediates in the reaction of sulfinic acids with alkyl nitrites.[3] Nevertheless these compounds have not been isolated. We now have found that sulfonyl nitrites **5a**—**f**, new sulfonyl derivatives, can be isolated as brown unstable crystals upon treating sulfinic acids (**4a**—**f**) with dinitrogen tetraoxide. Corresponding sulfonic acids (**6a**—**f**) were also obtained nearly in the same yields (Eq. 3). Sulfonyl nitrites **5a**—**f** isolated had strong SO_2 absorption bands near 1840 cm^{-1}. Mass spectrum of sulfonyl nitrite **5b** showed the corresponding fragment ion peaks: *m/e* (rel intensity), 155 (9, *p*-Tol†SO_2^+), 91 (20, *p*-Tol^+), and 30 (100, NO^+). However, no molecular ion peak was observed due to the weak S–N bond of this compound.

Spectroscopic Data of Thionitrites and Related Substances. Spectroscopic data of *t*-butyl nitrite (**7**), *t*-butyl nitrate (**8**), *t*-butyl thionitrite (**2a**), *t*-butyl thionitrate (**3a**) and methanesulfonyl nitrite (**5a**) were obtained and compared with each other. Infrared absorption bands of these compounds are listed in Table 3. Thionitrite **2a** and thionitrate **3a** showed the infrared absorption bands at longer wavelengths than corresponding alkyl nitrite **7** and alkyl nitriate **8**. The same trend is known in C=O stretching of ester and thioester, and is explained in terms of the electronegativity difference between S and O.[4] This inductive effect may also play a major role in our case.[5] Thus the presence of a strongly electronegative sulfonyl group may be responsible for the shift of N=O stretching frequency of sulfonyl nitrite **5a** up to 1842 cm^{-1}. In this case lack of resonance between S and N may be partly responsible for the large wave number because

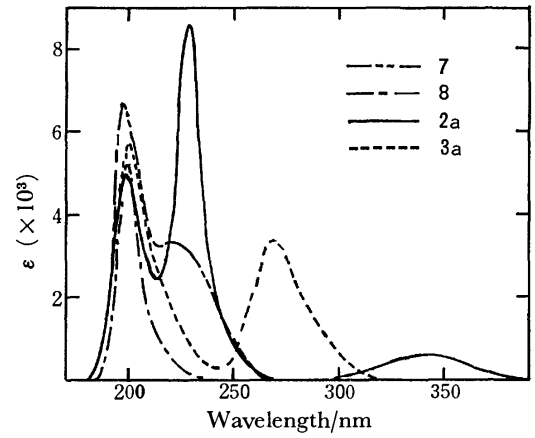

Fig. 1. UV spectra of *O*- and *S*-nitroso or nitro compounds.

† Tol=tolyl.

TABLE 1. REACTIONS OF THIOLS **1a—f** WITH EXCESS DINITROGEN TETRAOXIDE

Thiol	Solvent	$\frac{[N_2O_4]}{[RSH]}$[a]	Reaction temp/°C	Reaction time/min	Product	Isolated yield/%
1a	Ether	2.5	25	30	**3a**	84
1b	Ether	2.5	25	20	**3b**	55
1c	Ether	2.5	25	15	**3c**	48
1d	Hexane	1.5	−60	5	**3d**	86
1e	Hexane	1.5	−60	5	**3e**	65
1f	Hexane	1.5	−60	5	**3f**	73

a) Mole ratio.

TABLE 2. REACTIONS OF SULFINIC ACIDS **4a—f** WITH DINITROGEN TETRAOXIDE

Sulfinic acid	$\frac{[N_2O_4]}{[RSO_2H]}$[a]	Reaction temp/°C	Reaction time/min	Product	Isolated yield/%
4a	1.5	0	3[b]	**5a**	55
4b	2	0	10	**5b**	54
4c	2	−20	120	**5c**	38
4d	2	0	10	**5d**	47
4e	2	0	7	**5e**	38
4f	4	0	10	**5f**	44

a) Mole ratio. b) After stirring for 3 min at 0 °C sulfonyl nitrite **5a** precipitated out at −60 °C.

TABLE 3. IR ABSORPTION BANDS OF *O*- AND *S*-NITROSO OR NITRO COMPOUNDS

Compound	Absorption bands (cm^{-1})			
	NO	*asym* NO_2	*sym* NO_2	O-N or probably S-N
7	1620			800, 755
8		1608	1292	860
2a	1490			760
3a		1510	1300, 1257	820
5a	1842			a)

a) Several absorption bands were observed at 750—960 cm^{-1}.

the sulfur atom in sulfonyl nitrite **5a** has no lone pair to conjugate with nitroso group.

^{1}H-NMR of alkyl nitrite **7**, alkyl nitrate **8**, thionitrite **2a** and thionitrate **3a** were measured. Chemical shifts are listed in Table 4. Chemical shifts of *t*-butyl groups of thionitrite **2a** and thionitrate **3a** shifted toward the lower fields than corresponding alkyl nitrite **7** and alkyl nitrate **8** due to the effect of sulfur atom. UV spectra of these compounds were also recorded and shown in Fig. 1, while the numerical values of the UV spectra are listed in Table 5. Thionitrite **2a** showed a rather strong absorption at a visible wavelength region and had a greenish red color. Alkyl nitrite **7** showed a very weak absorption at a visible wavelength. All these compounds had N=O or NO_2 absorption bands at 250—180 nm.

Chemical Reactivities and Synthetic Applications of Thionitrites. Both aromatic and alkyl thiols (**1d**, **1j**, **1k**, **11**, **1e**, **1g**, **1h**, and **1i**) reacted readily with excess

TABLE 4. ^{1}H-NMR CHEMICAL SHIFTS OF *t*-BUTYL GROUPS IN *O*- AND *S*-NITROSO OR NITRO COMPOUNDS

Compound	Chemical shift of *t*-butyl group (CCl_4, ppm)
7	1.60
8	1.54
2a	1.85
3a	1.58

TABLE 5. UV SPECTROSCOPIC DATA OF *O*- AND *S*-NITROSO OR NITRO COMPOUNDS

Compound	Wavelength/nm (ε)
7	196 (6700), 219 (3300), 339 (28), 351 (48), 397 (57)
8	201 (5200), 380 (87), 397 (57)
2a	198 (5000), 228 (8600), 342 (630)
3a	201 (5700), 268 (3400)

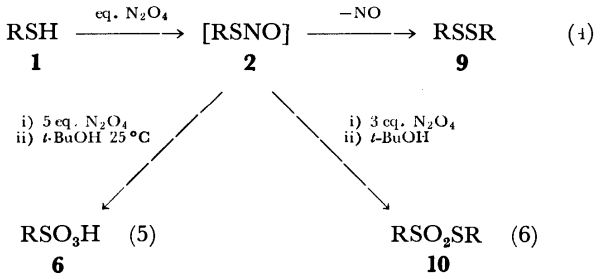

1a: R=*t*-Bu
1d, **6a**, **9b**, **10b**: R=*p*-Tolyl
1j, **2c**, **6b**, **9a**, **10c**: R=Ph
1k, **10d**: R=*m*-Tolyl
11, **10e**: R=*o*-Tolyl
1e, **10f**: R=*p*-Cl-C_6H_4
1g, **10g**: R=*p*-NO_2-C_6H_4
1h, **10h**: R=cyclohexyl
1i, **10i**: R=*n*-C_8H_{17}

dinitrogen tetroxide at a low temperature to afford the corresponding thiosulfonic *S*-esters (**10b—i**) in good yields (Eq. 6). Symmetrical thiosulfonic *S*-esters have generally been synthesized by the oxidation of disulfides[6] or by the reaction of sulfinic acids with sulfenyl chlorides.[7] These methods, however, involve two or more reaction steps and form such side products as thiosulfonic *S*-esters and sulfonic acids. Our new method is simple and involves only one pot reaction. When thiols **1d**, **1j**, **1k**, **11**, **1e**, **1g**, **1h**, and **1i** were mixed with excess dinitrogen tetraoxide at *ca.* −20—0 °C and then quenched with *t*-butyl alcohol, the corresponding thiosulfonic *S*-esters **10b—i** were obtained

Table 6. Reactions of thiols with dinitrogen tetraoxide

Thiol	Reaction time/min	Reaction temp/°C	$[N_2O_4]^{a)}/[RSH]$	Product	Isolated yield/%
1a	5	25	4	**3a**	87
1d	5	−20	4	**10b**	65
1j	5	−20	4	**10c**	88
1k	1	0	4	**10d**	65
1l	1	0	4	**10e**	77
1e	5	−20	4	**10f**	77
1g	1	0	4	**10g**	70
1h	5	−20	4	**10h**	62
1i	1	0	4	**10i**	60
1j	3	−70	1	**9a**	*ca.* 100
1j	120	25	6	**6a**	*ca.* 100
1d	120	25	6	**6b**	*ca.* 100

a) Mole ratio.

in good yields in such an inert solvent as ethyl ether. A solution of dinitrogen tetraoxide (in CCl_4) was added to a solution of a certain thiol in anhydrous ethyl ether at *ca.* −20 °C. Immediately, the mixture colored to bright red, characteristic of thionitrite **2**, which solution was stirred further for 1—5 min until the red color disappeared. The mixture was quenched with *t*-butyl alcohol. The *crude* product was purified by a preparative TLC. The results are summarized in Table 6. The yields of the thiosulfonic *S*-ester **10b**—**i** were markedly high when the reaction temperature was controlled at *ca.* −20 °C and quenched with excess *t*-butyl alcohol.

When the reaction mixture of thiol **1j** with dinitrogen tetraoxide was quenched with methanol or isopropyl alcohol instead of *t*-butyl alcohol, methyl benzenesulfinate (**13a**) (22% of yield) or isopropyl benzenesulfinate (**13b**) (10% of yield) was obtained at the expense of the intermediate such as benzenesulfinyl nitrite (**12**), which is probably in an equilibrium with phenyl thionitrate (**3g**), and methanol or isopropyl alcohol probably attacks the sulfinyl sulfur atom to form the corresponding sulfinate (Eq. 7). However,

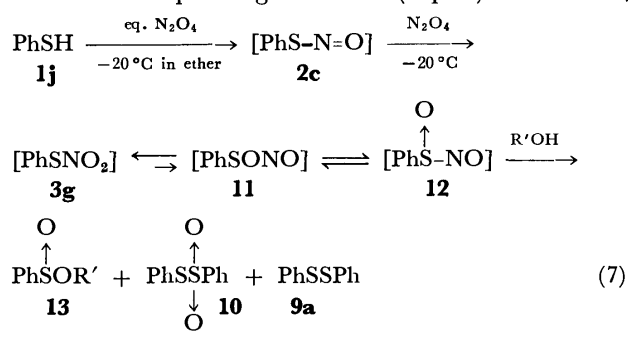

(7)

13a: R′=Me
13b: R′=Me_2CH

bulky *t*-butyl alcohol may not attack the sulfinyl sulfur atom due to the steric hindrance. When the reaction mixture was quenched with *t*-butyl alcohol, *t*-butyl benzenesulfinate could not be detected. Probably, homolytic scission of the unstable intermediate **12** may form the sulfinyl radical which is converted to the corresponding diphenyl α-disulfoxide (**14**), which then would be converted to the corresponding *S*-phenyl benzenethiosulfonate (**10c**)[8,9] (Eq. 8).

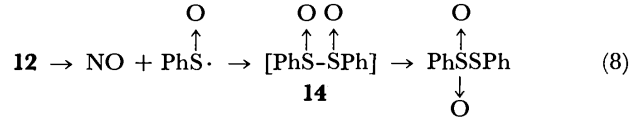

(8)

Meanwhile treatment of the thiol **1d**, and **1j** with 6 eq. dinitrogen tetraoxide at room temperature followed by quenching with excess *t*-BuOH gave the sulfonic acids (**6a**,**b**) quantitatively (Eq. 5), whereas treatment of thiol **1j** with 1 eq. with dinitrogen tetraoxide at −70 °C gave diphenyl disulfide (**9a**) quantitatively after decomposition of unstable phenyl thionitrite(**2c**) at room temperature (Eq. 4). Treatment of thiol **1a** with 3 eq. dinitrogen tetraoxide, however, gave thionitrate **3a** in an excellent yield. Therefore, the corresponding thiosulfonic *S*-ester **10b**—**i**, sulfonic acids **6a**,**b**, and disulfide **9a** can be prepared selectively by the simple and selective oxidation of the thiol **1** with dinitrogen tetraoxide when the reaction temperature, time and the concentration of dinitrogen tetraoxide are carefully controlled.

We reported in the previous paper that thionitrites reacted with thiols to afford the unsymmetrical disulfides nearly quantitatively.[2] When thionitrites **2a**,**b** were allowed to react with sodium benzenethiolate (**15**), the corresponding unsymmetrical disulfides (**16a**, **b**) were also obtained in good yields (Eq. 9).

(9)

2a, **16a**: R=*t*-Bu **2b**, **16b**: R=*p*-Tolyl

Chemical Reactivities and Synthetic Applications of Thionitrates. Thionitrate **3a**, one of the stable thionitrates, was also found to react with benzenthiolate **15** at room temperature to afford *t*-butyl phenyl disulfide (**16c**) in 69% isolated yield (Eq. 10).

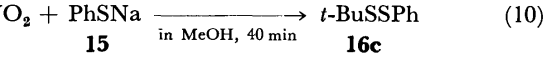

(10)

When thionitrate **3a** was heated in carbon tetrachloride for 1 h at 130 °C in a sealed tube, di-*t*-butyl disulfide (**9c**) was obtained as the major product, whereas decomposition of thionitrate **3d** at room temperature gave thiosulfonic *S*-ester **10b** as the main product together with a small amount of disulfide **9b** (Eq. 11). On the other hand, when thionitrates **3a**, **3d**, and **3e** were treated with a catalytic amount of pyridine, corresponding thiosulfonic *S*-esters **10j**, **10b**, and **10k** were obtained selectively in good yields (Eq. 12). Evolution of NO gas was confirmed by GC mass-spectroscopic analysis. When thionitrate **3d** was quenched with excess methanol, methyl *p*-toluenesulfinate **17** was obtained in 17% yiled (Eq. 13).

We also found that the reaction of isolated thionitrates **3a**—**e** with various *p*-aminophenols (**18a**—**i**) readily afforded the corresponding *N*-(*t*-alkylthio)-*p*-benzoquinone imines (**19a**—**i**) (Eqs. 14 and 15).

Only a few *N*-(alkylthio)-*p*-benzoquinone imines were prepared previously from *N*-chloro-*p*-benzoquinone imines and thiols.[10] Our new synthetic

method of quinone imines **19a**—**i** is simple and especially useful for the syntheses of *N*-*t*-alkylthio derivatives.

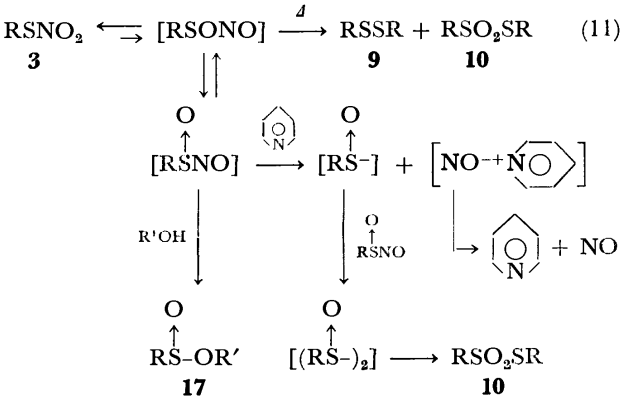

(11) (13) (12)

3a, **9c**, **10j**: R=*t*-Bu
3d, **9b**, **10b**: R=*p*-Tolyl
3e, **10k**: R=*t*-C_5H_{11}
17: R=*p*-Tolyl, R′=CH_3

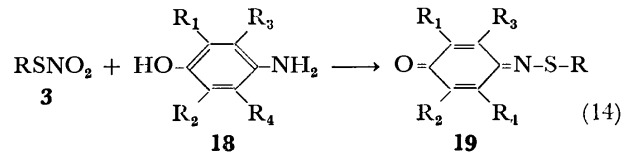

(14)

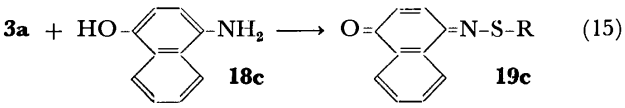

(15)

18a, **19a**: R=*t*-Bu, $R_1=R_2=R_3=R_4=H$
18b, **19b**: R=*t*-Bu, $R_3=CH_3$, $R_1=R_2=R_4=H$
18d, **19d**: R=*t*-Bu, $R_1=R_2=CH_3$, $R_3=R_4=H$
18e, **19e**: R=*t*-Bu, $R_1=R_2=Cl$, $R_3=R_4=H$
18f, **19f**: R=*t*-C_5H_{11}, $R_1=R_2=R_3=R_4=H$
18g, **19g**: R=1,1-dimethylheptyl, $R_1=R_2=R_3=R_4=H$
18h, **19h**: R=*p*-Cl-C_6H_4, $R_1=R_2=R_3=R_4=H$
18i, **19i**: R=*p*-Br-C_6H_4, $R_1=R_2=R_3=R_4=H$

Table 7. Reactions of thionitrates with aminophenols

Aminophenol	Thionitrate	Product	Isolated yield/%
18a	**3a**	**19a**	40
18b	**3a**	**19b**	45, 46[a]
18c	**3a**	**19c**	15, 16[b]
18d	**3a**	**19d**	47
18e	**3a**	**19e**	45
18f	**3b**	**19f**	40
18g	**3c**	**19g**	33
18h	**3e**	**19h**	18[d]
18i	**3f**	**19i**	11[d]
18j	**3h**	**19j**	10[c,d]
18k	**3d**	**19k**	6[c,d]

a) In this case $CuCl_2$ was not added. Chromatographic separation gave a poor result and the yield was determined by GLC. b) HCl salt was used as the starting material. c) An oxidative mixture of the thiol with 2 eq. N_2O_4 was used due to the instabilities of these thionitrates. d) $CuCl_2$ was not used in these cases for instabilities of these thionitrates in the presence of $CuCl_2$.

An oxidative mixture of *s*-BuSH (**1m**) or thiol **1d** with excess dinitrogen tetraoxide probably contains *s*-butyl thionitrate (**3h**) or thionitrate (**3d**), respectively, because of the formation of *N*-(*s*-butylthio)-*p*-benzoquinone imine (**19j**) or *N*-(*p*-tolylthio)-*p*-benzoquinone imine (**19k**) from the corresponding *p*-aminophenols (**18j**, **18k**) (Eq. 16). All these new compounds **19a**—**k** are quite stable and have vivid yellow colors due to the strong absorption band ($\varepsilon_{max}>10^4$) near 400 nm. Structures of the products **19a**—**k** were identified by IR, NMR, UV, and mass spectrocopies. Elemental analyses of these compounds **19a**—**k** all agree with these formulae. Isolated yields of compounds **19a**—**k** are listed in Table 7.

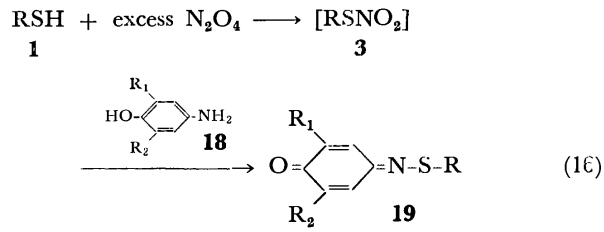

(16)

1m, **3h**: R=*s*-Bu
1d, **3d**: R=*p*-Tolyl
18j, **19j**: R=*s*-Bu, $R_1=R_2=Cl$
18k, **19k**: R=*p*-Tolyl, $R_1=R_2=H$

When compound **19a** was oxidized with an equivalent amount of *m*-chloroperbenzoic acid, a red colored unstable *N*-(*t*-butylsulfinyl)-*p*-benzoquinone imine **20** was obtained (70%) upon column chromatography (Eq. 17). This sulfinyl derivative **20** showed a strong absorption at 1080 cm^{-1} (SO) in IR spectrum, however, was found to decompose readily (*ca.* 1 h) at room temperature.

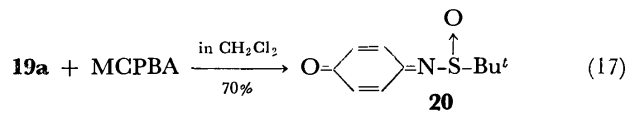

(17)

We also found that thionitrate **3a** reacted readily with octylamine (**21**) at room temperature for 10 min to give *N*-(*t*-butylthio)octylamine (**22**) in a good yield (Eq. 18).

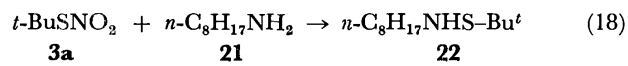

(18)

Chemical Reactivities of Sulfonyl Nitrites. When *p*-toluenesulfonyl nitrite (**5b**) was heated in dioxane or neat, vigorous evolution of gas was observed and white crystals were obtained. After recrystallization from acetic acid, elemental analysis of this crystalline compound showed the formula of $(p\text{-TolSO}_2)_3(NO)$ (**23**)[11] and IR spectroscopic data and melting point were identical with those of a known compound which was reported as tris(*p*-tolylsulfonyl)amine oxide by Kresze and Kort.[3] Other several sulfonyl nitrites **5a**, **5c**, **5d**, and **5e** were also found to undergo thermodecomposition to give white crystals described as formula $(RSO_2)_3(NO)$ (**23a**, **23c**—**e**) by elemental analyses (Eq. 19). However, since the compound **23a** gives two distinctly different peaks of metyl groups on both ^1H and ^{13}C-NMR spectra (integral ratio=2:1 on^1 H-NMR), the structure of these compounds **23a**—**e**

Table 8. Thermal decomposition of sulfonyl nitrites **5a—e**

Sulfonyl nitrite	Reaction time/min	Reaction temp/°C	Solvent	Product	Isolated yield/%
5a	5	70—80	None	**23a**	44
5b	10	90—100	None	**23b**	59
5b	3	60—80	Dioxane	**23b**	64
5c	15	60—90	None	**23c**	52
5d	10	90—100	None	**23d**	62
5e	10	90—100	None	**23e**	65

$$3\,RSO_2NO \longrightarrow (RSO_2)_3(NO) + 2\,NO \qquad (19)$$
5 **23**

5a, **23a**: R=CH_3 **5d**, **23d**: R=*p*-Cl-C_6H_4
5b, **23b**: R=*p*-Tolyl **5e**, **23e**: R=*p*-Br-C_6H_4
5c, **23c**: R=Ph

is belived to be represented by $(RSO_2)_2N$–O–SO_2R rather than $(RSO_2)_3NO$, and further detailed structure assignment is now underway. Meanwhile, the gas formed by thermal decomposition of sulfonyl nitrite **5b** showed a strong peak at *m/e* 30 (NO) in its mass spectrum. These results are listed in Table 8.

Sulfonyl nitrites **5a—e** were unstable compounds in protic solvents such as alcohols or thiols and decomposed in a few minutes (Eqs. 20 and 21). When sulfonyl nitrite **5b** was stirred in methanol, *N,N*-bis(*p*-tolylsulfonyl)hydroxylamine (**24**) was obtained in a good yield. Sulfonyl nitrite **5b** also reacted with thiol **1a** in dioxane to give hydroxylamine **24**. The reaction

$$2\,p\text{-}TolSO_2NO + MeOH \rightarrow (p\text{-}TolSO_2)_2NOH + MeONO \qquad (20)$$
5b **24**

$$2\,p\text{-}TolSO_2NO + t\text{-}BuSH \rightarrow \mathbf{24} + t\text{-}BuSNO \qquad (21)$$
5b **1a** **2a**

mixture of sulfonyl nitrite **5b** and thiol **1a** was found to turn to red in a few minutes due undoubtedly to the formation of thionitrite **2a**.

Sulfonyl nitrite **5b** also reacted with thionitrite **2a** in dioxane to give *S*-*t*-butyl *p*-toluenethiosulfonate (**25**) in 20% yield (Eq. 22). This reaction was slow and

$$p\text{-}TolSO_2NO + t\text{-}BuSNO \xrightarrow[1-3\,h]{25^\circ C} p\text{-}TolS(O)\text{-}S\text{-}Bu^t \qquad (22)$$
5b **2a** **25**

required for over 1 h at room temperature.

When sulfonyl nitrite **5b** was reduced with sodium borohydride, *N*-(*p*-tolylsulfonyl)hydroxylamine (**26**) was obtained in 16% yield (Eq. 23). Other major product was compound **23b**.

$$\mathbf{5b} + \text{excess } NaBH_4 \rightarrow p\text{-}TolS(O)NHOH + \mathbf{23b} \qquad (23)$$
26

Experimental

All the melting points and boiling points were uncorrected. Elemental analysis of sulfur was carried out by Sagami Chemical Research Center and the analyses of other elements were carried out by the Chemical Analysis Center at this University. Analytical determination by GLC were performed on a Hitachi 163 gas chromatograph fitted with the following column (3 mm o.d.×3 m): 10% SE-30 on Chromosorb W. ^{1}H-NMR spectra were taken at 60 MHz on a Hitachi R-24A apparatus. ^{13}C-NMR spectra were measured on a Bruker FXD 4-100 NMR spectrometer. Mass spectra were recorded with a Hitachi RMU-6M spectrometer.

The following compounds were obtained according to the known procedures which are described in the literature: Dinitrogen tetraoxide,[2] **8**,[12] **4a**,[13] **4d**,[14] **4e**,[15] **4f**.[16]

t-Butyl Thionitrite (2a). Dinitrogen tetraoxide[2] (0.1 mol) in carbon tetrachloride (11 ml) was added to a stirred solution of thiol **1a** (9.02 g, 0.1 mol) in dry ethyl ether (100 ml) for a few minutes at −70 °C. The solution was stirred further for several minutes and poured into the cold 5% $NaHCO_3$ aq solution and extracted with ethyl ether. The ethereal extract was dried ($MgSO_4$) in dark at 0 °C, and the solvent was evaporated *in vacuo* giving almost pure thionitrite **2a** (7.0 g, 59%), which was pure enough for the reaction over several months at −20 °C with molecular sieves: (lit,[17] bp 36 °C/48 mmHg). IR (neat): 1490 (NO), 1360, 1298, 1157, and 760 cm^{-1}. NMR (CCl_4): δ=1.85 (s). Thionitrite **2a** was usually used without distillation.

Other thionitrites were prepared similarly by the method already reported by Oae *et al.*[2] Generally thionitrites were not stable enough to be isolated in pure form, and they were usually used in ethereal solution after washing (5% aq $NaHCO_3$ solution) and drying ($MgSO_4$).

t-Butyl Thionitrate (3a). The following is a typical procedure to prepare stable *t*-alkyl thionitrates.

This reaction required a relatively large flask (2 l) fitted with a reflux condenser, which is open for air escape, since the reaction took place vigorously. Dinitrogen tetraoxide[2] (1.5 mol) in carbon tetrachloride (135 ml) was added dropwise to a stirred solution of thiol **1a** (55.3 g, 0.6 mol) in dry ethyl ether (500 ml) for over 30 min at the rate that ethyl ether slowly refluxed. After the addition was over, the solution was stirred further for *ca.* 30 min. The solution was washed with ice cold water and dried ($MgSO_4$), concentrated, and distilled (with molecular sieves) giving 67.5 g (84%) of thionitrate **3a** which had a stimulant odor.

Spectroscopic data, boiling points and elemental analytical data of stable thionitrates (**3a—c**) are listed in Tables 9 and 10.

p-Chlorophenyl Thionitrate (3e). The following is a typical procedure to prepare unstable aryl thionitrates.

Dinitrogen tetraoxide (0.15 mol) in carbon tetrachloride (13.5 ml) was added dropwise to a stirred suspension of thiol **1e** (15.7 g, 0.1 mol) in hexane (100 ml) for 5 min at −60 °C. Immediately the mixture colored to bright red, characteristic of the thionitrite. After the red color of thionitrite disappeared (*ca.* 2—3 min), the white crystalline thionitrate **3e** was collected by filtration in a cold room (*ca.* 0 °C) and recrystallized with ethyl ether at −70 °C to give 13.1 g (65%) of thionitrate **3e**. IR spectrum was measured in a cold room (maintained at *ca.* −20 °C) because of the instability of thionitrate **3e**. IR spectroscopic data and melting points of thionitrate **3d—f** were listed in Table 9.

Syntheses of Sulfonyl Nitrites (5a—f). A typical procedure is as follows. A solution of dinitrogen tetraoxide (0.1 mol) in carbon tetrachloride (11 ml) was added to a stirred suspension of sulfinic acid **4b** (15.6 g, 0.1 mol) and dry ethyl ether (50 ml) at 0 °C in a few minutes. The suspension soon turned to a pale brown color in a few minutes forming

Table 9. Spectroscopic data and melting points of thionitrates

Thionitrate	IR (neat, cm^{-1})	NMR (CCl_4, ppm)
3a	1510, 1300, 1263, 1155, 820	1.58 (s)
3b	1510, 1300, 1255, 1150, 821	1.00 (t, 3H, $-CH_2\underline{CH_3}$), 1.33 (s, 6H, $-C\underline{H_3}$), 1.70 (q, 2H, $-C\underline{H_2}-$)
3c	1510, 1297, 1250, 1130, 813	0.73—2.33 (m, 11H), 1.45 (t, 2H, $C\underline{H_2}CS$), 1.55 (s, 6H, $C\underline{H_3}$)
3d	1510, 1378, 1290, 800	Mp 32—33 °C (dec)
3e	1510, 1378, 1300, 1070, 1000, 810	Mp 44—45 °C (dec)
3f	1510, 1375, 1290, 1055, 1000, 812	Mp 49—50 °C (dec)

Table 10. Elemental analyses and boiling points of stable thionitrates

Thionitrate	Found (%)			Calcd (%)			Bp (°C/mmHg)
	C	H	N	C	H	N	
3a	——			——			40—41/6 (lit,[17] 55/13)
3b	40.05	7.29	9.01	40.24	7.43	9.38	36—38/3
3c	52.94	9.35	6.78	52.65	9.32	6.82	78—81/2

Table 11. Spectroscopic data of sulfonyl nitrites **5a**—**f**

Sulfonyl nitrite	IR (KBr, cm^{-1})		NMR ($CDCl_3$, ppm)	
	NO	SO_2	CH_3	Ring proton
5a	1842	1355, 1157	3.36 (br, s)	
5b	1850	1390, 1185	2.37 (s, 3H)	7.10 (d, J=8 Hz, 2H), 7.50 (d, J=8 Hz, 2H)
5c	1860, 1840	1390, 1190		7.21—7.85 (m, 4H)
5d	1859, 1835	1398, 1195		7.39 (d, J=10 Hz, 2H), 7.68 (d, J=10 Hz, 2H)
5e	1858, 1835	1390, 1191		7.65 (br, m)
5f	1880, 1860	1382, 1195	3.90 (s, 3H)	6.80—7.15 (m, 2H), 7.65—8.05 (m, 2H)

the precipitate of sulfonyl nitrite **5b**. The mixture was stirred further for 10 min at 0 °C. Then the brown precipitate was filtered, washed with dry ethyl ether and dried *in vacuo* giving 11.2 g (61%) of pure sulfonyl nitrite **5b**. IR and NMR spectra of sulfonyl nitrites **5a**—**f** are listed in Table 11, while elemental analyses of sulfonyl nitrites **5b**—**e** are listed in Table 12.

*Thiosulfonic S-Ester (**10b**—**i**).* A typical procedure is as follows. A solution of dinitrogen tetraoxide (20 mmol, in CCl_4) was added to a solution of thiol **1e** (723 mg, 5.0 mmol) in anhydrous ethyl ether (15 ml) with stirring at *ca.* 0 °C in the dark. Immediately, the mixture colored to bright red, characteristic of the thionitrite, which was stirred further for 1 min until the red color disappeared. The mixture was quenched with *t*-butyl alcohol (5 ml) for several minutes at 0—20 °C and then washed with 5% aq $NaHCO_3$ solution to remove nitric acid formed during the reaction. The *crude* product from the organic layer was purified by preparative TLC (silica gel, hexane:ether=20:1) to give 615 mg (77%) of thiosulfonic *S*-ester **10f**.

Table 12. Elemental analyses of sulfonyl nitrites **5b**—**e**[a]

Compound	Found (%)[b]				Calcd (%)			
	C	H	N	S	C	H	N	S
5b	45.43	3.76	7.37	17.16	45.39	3.80	7.56	17.31
5c	42.40	2.89	7.68	18.59	42.10	2.94	8.18	18.73
5d	35.43	1.97	6.36	15.73	35.04	1.96	6.81	15.59
5e	29.10	1.57	5.22	—	28.81	1.61	5.61	—

a) Compounds **5a** and **5f** were too unstable to be analyzed. b) Nitrogen contents of compounds **5b**—**e** were found to be in smaller values (0.19—0.50%) due to the gradual generation of NO gas at room temperature.

Table 13. Spectroscopic data and melting points of thiosulfonic *S*-ester **10b**—**i**

Compound	IR (cm^{-1}) *asym* SO_2	IR (cm^{-1}) *sym* SO_2	NMR (CCl_4, ppm)	Mp/°C
10b	1320	1137	2.33 (s, 6H), 6.9—7.5 (m, 8H)	76—78 (lit,[19] 78.5—79.5)
10c	1325	1143	7.0—7.7 (m)	44—45 (lit,[18] 45)
10d	1325	1138	2.26 (s, 3H), 2.27 (s, 3H), 6.9—7.5 (m, 8H)	Oil (lit,[20] Oil)
10e	1321	1143	2.16 (s, 3H), 2.63 (s, 3H), 6.9—7.5 (m, 8H)	52—54 (lit,[18] 55—56)
10f	1323	1139	7.2—7.5 (m)	135—136 (lit,[21] 138)
10g	1343	1142	7.3—8.5	176—178 (lit,[22] 180—180.5)
10h	1332	1135	0.7—2.5 (m, 20H), 2.9 (br, m, 1H), 3.3 (br, m, 1H)	Oil (lit,[23] 37—38)
10i	1325	1129	0.7—2.1 (m, 30H), 2.9—3.3 (m, 4H)	Oil (lit,[24] Oil)

Spectroscopic data of thiosulfonic *S*-esters **10b**—**i** are summarized in Table 13. Melting points or boiling points of thiosulfonic *S*-esters **10b**—**i** were identical with those of literatures.

*p-Toluenesulfonic Acid (**6a**).* A solution of dinitrogen tetraoxide (15 mmol, in CCl_4) was added to a solution of thiol **1d** (310 mg, 2.5 mmol) in anhydrous ethyl ether (7.5 ml) with stirring at *ca.* 0 °C. The solution was further stirred for 2.5 h at room temperature. After quenching the solution with *t*-butyl alcohol (5 ml) for 5 min, the volatile material was evaporated *in vacuo* giving 487 mg (quantitative) of sulfonic acid **6a**. IR and NMR spectra were identical with those of authentic samples.

*Diphenyl Disulfide (**9a**).* Dinitrogen tetraoxide (5

mmol, in CCl_4) was added to a stirred solution of thiol **1j** (550 mg, 5 mmol) in dry ethyl ether (10 ml) at −70 °C. After a few minutes the red colored solution was poured into the 5% $NaHCO_3$ aq solution. After the mixture was warmed to room temperature. After the red color of the thionitrite disappeared, the ethereal layer was separated, dried ($MgSO_4$) and evaporated giving 540 mg (quantitative) of disulfide **9a**. Spectroscopic data were identical with those of authentic sample.

*Methyl Benzenesulfinate (**13a**) and Isopropyl Benzenesulfinate (**13b**).* Dinitrogen tetraoxide (7.6 mmol, in CCl_4) was added to a solution of thiol **1j** (421 mg, 3.8 mmol) at −20 °C. After a few minutes, the solution was quenched with methanol (1.2 ml) and stirred further for 5 min at 0 °C. After evaporation of the solvent and TLC (hexane:ether=10:1) gave 65 mg (22%) of sulfinate **13a**: bp (bath temp) 90—100 °C/2 mmHg (lit,[25] 76—81 °C/0.45 mmHg). IR (neat): 1130 (SO), 965, 758, and 696 cm^{-1}. NMR (CCl_4): δ=3.33 (s, 3H, $-C\underline{H}_3$) and 7.54 (m, 5H, ring-protons). Other isolated products were disulfide **9a** (25%) and *S*-phenyl thiosulfonate (**10**) (43%), and spectroscopic data of these compounds were identical with those of authentic samples.

Sulfinate **13b** was also isolated by a similar procedure: bp (bath temp) 120—130 °C/2 mmHg (lit,[26] 110—117 °C/0.5 mmHg). IR (neat): 1143 (SO), 1102, 920, 845, and 735 cm^{-1}. NMR (CCl_4): δ=1.13 (d, J=6 Hz, 3H, $-C\underline{H}_3$), 1.34 (d, J=6 Hz, 3H, $-C\underline{H}_3$), 4.14 (m, 1H, $C\underline{H}$), and 7.47 (m, 5H, ring-protons). Other isolated products were disulfide **9a** (20%) and thiosulfonic *S*-ester **10c** (42%).

*Disulfides (**16a—c**).* Dinitrogen tetraoxide (5 mmol, in CCl_4) was added to a stirred solution of thiol **1d** (620 mg, 5 mmol) in 10 ml of ethyl ether at −70 °C. After a few minutes, 5% aq $NaHCO_3$ solution was added and extracted with 10 ml of ethyl ether. The ethereal solution was dried ($MgSO_4$) and filtered at 0 °C. Sodium benzenethiolate **15** (661 mg, 5 mmol) in methanol (6 ml) was added to the ethereal solution and the solution was stirred for 12 h at −10 °C. The solution was washed with $NaHCO_3$ aq solution and dried ($MgSO_4$). The solvent was evaporated and water was added. The mixture was extracted with ethyl ether. Ethereal extract was dried and evaporated to give 898 mg (77%) of disulfide **16a**.

A similar treatment of thionitrite **2a** or thionitrate **3a** with benzenethiolate **15**, gave disulfide **16b** (74%) and **16c** (69%), respectively. Stable thionitrite **2a** and stable thionitrate **3a** were used after purification, unlike unstable thionitrite **2b**.

IR and NMR spectroscopic data of disulfides **16a—c** were identical with those of authentic samples.

*Thermal Decomposition of t-Butyl Thionitrate (**3a**).* The solution of thionitrate **3a** (30 mg, 0.22 mmol) in carbon tetrachloride (0.25 ml) was heated in an oil bath at 130 °C in a sealed tube for NMR. After 1 h, NMR spectrum showed that nearly all the starting material was converted to di-*t*-butyl disulfide **9c**: NMR, IR, and mass spectroscopic data were identical with those of authentic sample.

*Reactions of Thionitrates (**3a**, **3c**, and **3d**) with Pyridine.* Thionitrate **3a** 1.89 g (14 mmol) was added dropwise to a stirred solution of pyridine (554 mg, 7 mmol) in carbon tetrachloride (20 ml) for 5 min. The solution was stirred further for 30 min. Distillation gave 1.03 g (70%) of thiosulfonic *S*-ester **10j**, 280 mg of pyridine, and 246 mg of solid which could not be characterized. Thiosulfonic *S*-ester **10j**: mp 22—24 °C, bp (bath temp) 80 °C/5 mmHg. IR (neat): 1445, 1360, 1290 (SO_2), 1140, and 1100 cm^{-1} (SO_2). NMR (CCl_4): δ=1.40 and 1.58. MS (70 eV), *m/e* (rel intensity), 210 (1, M^+), 89 (10, *t*-BuS^+), and 57 (100, *t*-Bu^+). Found: C, 45.59; H, 8.61; S, 30.29%. Calcd for $C_8H_{18}O_2S_2$: C, 45.68; H, 8.62; S, 30.48%.

Thiosulfonic *S*-ester **10b** (65%) and thiosulfonic *S*-ester **10k** (89%) were obtained from thionitrate **3d** and thionitrate **3c**, respectively. IR spectroscopic data of thiosulfonic *S*-ester **10b** were identical with those of authentic sample. Thiosulfonic *S*-ester **10k**: bp (bath temp) 80 °C/3 mmHg. IR (neat): 1455, 1295, and 1100 cm^{-1}. NMR (CCl_4): δ=1.00 (t, 6H, $CH_2-C\underline{H}_3$), 1.35 (s, 6H, $SC(C\underline{H}_3)_2$), and 1.88 (q, 4H, $C\underline{H}_2$). Found: C, 50.39; H, 9.43%. Calcd for $C_{10}H_{22}O_2S_2$: C, 50.38; H, 9.30%.

*Methyl p-Toluenesulfinate (**17**).* Methanol (5 ml) was added dropwise for a few minutes onto the crystals of thionitrate **3e** at −20 °C. After vigorous reaction, the *crude* material was purified by TLC to give 222 mg (17%) of sulfinate **17**: MS (70 eV) *m/e* (rel intensity), 170 (56, M^+), 139 (100, *p*-$TolSO_2^+$), and 91 (28, *p*-Tol^+). IR and NMR spectroscopic data were identical with those of literatures.[27] The other products were the corresponding thiosulfonic *S*-ester **10f** (36%) and di-(*p*-chlorophenyl) disulfide (**9d**) (12%).

*N-(t-Butylthio)-p-benzoquinone Imine (**19a**).* *p*-Aminophenol 546 mg (5 mmol) was added for 5 min into a stirred suspension of well-dried anhydrous copper(II) chloride (810 mg, 6 mmol) and thionitrate **3a** (1020 mg, 7.5 mmol) in anhydrous acetonitrile (15 ml). The mixture was stirred for 1 h at room temperature, and then hydrochloric acid solution (20%, 100 ml) was added to the suspension and the mixture was extracted with ethyl ether. The ethereal extract was dried ($MgSO_4$) and evaporated. After purifying the extract on silica gel TLC (hexane:ether=10:1) bright yellow crystals of benzoquinone imine **19a** were obtained (390 mg, 40%).

Compound **19a** was obtained nearly in the same yield, even without copper(II) chloride, however, separation of the products was quite difficult. When *p*-hydroxyaniline was treated with thionitrate **3a** without copper(II) chloride, excess thionitrate **3a** was not converted to corresponding disulfide **9c** but to the thiosulfonic *S*-ester **10j** by undesirable oxidation. Since the thiosulfonic *S*-ester formed was quite difficult to be removed completely unlike the disulfide by distillation or TLC from the benzoquinone imine **19a**, copper(II) chloride is a useful reagent especially in separating benzoquinone imine **19a** in pure form.

The ^{13}C-NMR spectrum (in $CDCl_3$, ppm) of compound **19a** is depicted in the following structure.

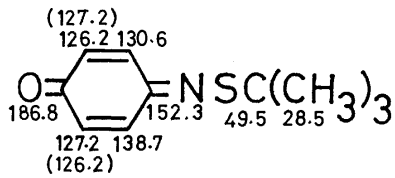

UV and IR spectra and elemental analytical data of compound **19a** and its derivatives are listed in Table 14. NMR and mass spectroscopic data of compound **19a** and its derivatives are listed in Tables 15 and 16, respectively.

*N-(s-Butylthio)-2,6-dichlorobenzoquinone Imine (**19j**).* Dinitrogen tetraoxide (30 mmol) in carbon tetrachloride (3 ml) was added to a stirred solution of *s*-BuSH (1.35 g, 15 mmol) at 0 °C. The solution turned immediately red, characteristic for *s*-butyl thionitrite and soon the red color disappeared, due undoubtedly to the formation of *s*-butyl thionitrite. Aminophenol **18j** (1.78 g, 10 mmol) was then added for a few minutes and the solution was stirred further for 1.5 h. The mixture was filtered[28] and the filtrate was diluted with ethyl ether, washed with aq $NaHCO_3$ solution, dried ($MgSO_4$), evaporated and the usual TLC separation

Table 14. Spectroscopic data (UV, IR) and elemental analyses of quinone imines **19a—k**

Compound	UV (hexane, λ_{max}, nm)	IR (νC=O, cm^{-1})	Found (%)				Calcd (%)			
			C	H	N	S	C	H	N	S
19a	401 ($\varepsilon=2.7\times10^4$)	1630	61.38	6.60	7.13	16.29	61.51	6.71	7.17	16.42
19b	399 ($\varepsilon=2.1\times10^4$)	1630	63.48	7.29	6.70	15.36	63.12	7.22	6.69	15.32
19c	418 ($\varepsilon=1.9\times10^4$)	1642	68.53	6.16	5.70	12.90	68.54	6.14	5.78	13.07
19d	405 ($\varepsilon=2.4\times10^4$)	1615	64.29	7.43	6.09	—	64.53	7.67	6.27	—
19e	424 ($\varepsilon=3.4\times10^4$)	1648	45.83	4.16	5.32	—	45.46	4.19	5.30	—
19f	402 ($\varepsilon=2.7\times10^4$)	1632	62.93	7.08	6.34	—	63.12	7.22	6.69	—
19g	405 ($\varepsilon=2.7\times10^4$)	1630	67.54	8.73	4.99	—	67.88	8.73	5.27	—
19h	447 ($\varepsilon=2.2\times10^4$)	1620	58.00	3.16	5.39	—	57.71	3.22	5.60	—
19i	448 ($\varepsilon=2.1\times10^4$)	1630	48.60	2.59	4.37	—	48.99	2.74	4.76	—
19j	425 ($\varepsilon=2.2\times10^4$)	1645	45.68	4.20	5.41	—	45.46	4.19	5.30	—
19k	438 ($\varepsilon=1.7\times10^4$)	1625	68.28	4.73	5.83	—	68.09	4.83	6.10	—

Table 15. ^{1}H-NMR spectroscopic data (CCl_4, ppm) of quinone imine **19a—k**

Compound	O=⟋—H	O=⟋=⟍H	Other proton
19a	6.13—6.50 (m, 2H)	6.75—7.35 (m, 2H)	1.45 (s, 9H, *t*-Bu)
19b	6.24 (s, 1H)	7.20 (d, $J=10$ Hz, 1H)	1.47 (s, 9H, *t*-Bu)
	6.34 (dd, $J=10$ Hz, $JJ=2$ Hz, 1 Hz)		2.40 (s, 3H, -C$\underline{H}_3$)
19c	6.57 (d, $J=10.5$ Hz, 1H)	7.32 (d, $J=10.5$ Hz, 1H)	1.52 (s, 9H, *t*-Bu)
			7.12—7.60 (m, 2H)
			7.89—8.20 (m, 2H)
19d		6.76 (br, s, 1H)	1.42 (s, 9H, *t*-Bu)
		7.00 (br, s, 1H)	1.97 (s, 6H, -C$\underline{H}_3$)
19e		7.32 (br, s, 1H)	1.50 (s, 9H, *t*-Bu)
		7.54 (br, s, 1H)	
19f	6.05—6.47 (m, 2H)	6.66—7.34 (m, 2H)	0.94 (t, 3H, $CH_2C\underline{H}_3$)
			1.37 (s, 6H, $-\overset{\displaystyle|}{\underset{\displaystyle|}{C}}-C\underline{H}_3$)
			1.76 (q, 2H, -C$\underline{H}_2$-)
19g	6.1—6.6 (m, 2H)	6.7—7.5 (m, 2H)	0.6—2.1 (m, 11H)
19h	6.4—6.7 (m, 2H)	6.75—7.63 (m, 6H)[a]	
19i	6.4—6.7 (m, 2H)	6.75—7.55 (m, 6H)[a]	
19j		7.28 (d, $J=3$ Hz, 1H)	1.07 (t, 3H, $CH_2C\underline{H}_3$)
		7.60 (d, $J=3$ Hz, 1H)	1.48 (d, $J=7$ Hz, 3H, -CHC$\underline{H}_3$)
			1.68—2.20 (m, 1H, S-C$\underline{H}$)
			3.10—4.10 (m, 2H, C$\underline{H}_2$)
19k	6.25—6.51 (m, 2H)	6.91—7.89 (m, 6H)[a]	2.42 (s, 3H, -C$\underline{H}_3$)

a) Contains ring proton.

Table 16. Mass spectroscopic data of quinone imines **19a—k**

Compound	MS (70 eV), *m/e* (rel intensity)
19a	195 (37, M$^+$), 138 (86), 57 (44)
19b	209 (28, M$^+$), 152 (44), 57 (100)
19c	245 (22, M$^+$), 188 (100), 57 (84)
19d	223 (44, M$^+$), 166 (100), 57 (61)
19e	263 (48, M$^+$), 206 (77), 57 (100)
19f	209 (31, M$^+$), 138 (100), 71 (50)
19g	265 (9, M$^+$), 138 (100), 127 (11)
19h	249 (100, M$^+$), 143 (73)
19i	294 (97, M$^+$), 188 (100)
19j	263 (41, M$^+$), 206 (69), 57 (100)
19k	229 (100, M$^+$), 123 (43), 91 (8)

(hexane:ether=7:1) gave 256 mg (10%) of benzoquinone imine **19j**. Spectroscopic data and elemental analytical data are listed in Tables 14, 15, and 16.

Oxidation of N-(t-*Butylthio*)-p-*benzoquinone Imine* (**19a**) *with* m-*Chloroperbenzoic Acid.* *m*-Chloroperbenzoic acid (360 mg, 1.88 mmol) was added to a stirred solution of benzoquinone imine **19a** in dichloromethane (15 ml) at 0 °C. The solution was further stirred for 30 min at 0 °C. The solvent was evaporated *in vacuo*. Column chromatography (hexane: chloroform=2:1—0:1) gave 276 mg (70%) of sulfinyl derivative **20**. IR (neat): 1080 cm^{-1} (SO). UV (hexane): λ_{max}= 415 nm. NMR (CCl_4): $\delta=1.32$ (s, 9H, *t*-Bu), 6.48 (d, $J=10$ Hz, 2H, O=C-CH), and 6.93 (d, $J=10$ Hz, 2H, O=C-C=CH). MS (70 eV), *m/e* (rel intensity), 211 (1, M$^+$), 154 (100, O=⟨=⟩=NSO$^+$), and 57 (17, *t*-Bu$^+$). Sulfinyl derivative **20** was unstable at room temperature, and soon

Table 17. Spectroscopic data of compound **23a—e**

Compound	IR (KBr, cm^{-1}) *asym* SO_2	IR (KBr, cm^{-1}) *sym* SO_2	Mp/°C
23a	1380	1175	139—140
23b	1390	1195	190—192
		1175	
23c	1395	1197	99—101
23d	1400	1190	168—170
23e	1395	1192	198—200

Table 18. Elemental analyses of compound **23a—e**

Compound	Found (%) C	Found (%) H	Found (%) N	Calcd (%) C	Calcd (%) H	Calcd (%) N
23a	13.57	3.23	5.14	13.48	3.39	5.24
23b	51.27	4.05	2.84	50.90	4.27	2.83
23c	47.49	3.24	2.76	47.67	3.33	3.09
23d	39.19	2.20	2.46	38.82	2.17	2.51
23e	31.44	1.60	2.00	31.32	1.75	2.02

decomposed (*ca.* 1 h) to give dark material.

N-*(t-Butylthio)octylamine (22).* Thionitrate **3a** (2.02 g, 15 mmol) in acetonitrile (10 ml) was added to a stirred solution of amine **21** in acetonitrile (20 ml) for 10 min at 0 °C. The solution was further stirred for 1 h. The solvent was evaporated. TLC (hexane:ether=10:1) gave 524 mg (24%) of sulfenamide **22**: bp (bath temp) 85—95 °C/4 mmHg. IR (neat): 1460, 1135, and 910 cm^{-1}. NMR (CCl_4): δ=0.6—2.0 (m, 15H, $CH_3(CH_2)_6$–), 1.17 (s, 9H, *t*-Bu), 2.36 (br, 1H, NH), and 2.86 (br, 2H, –$C\underline{H}_2$–NH). Found: C, 65.95; H, 12.41; N, 6.32%. Calcd for $C_{12}H_{17}NS$: C, 66.29; H, 12.52; N, 6.44%. The other main product was *t*-$BuSO_2S$-Bu^t (814 mg, 3.87 mmol). Di-*t*-butyl disulfide (180 mg, 1.01 mmol) was also obtained.

Thermal Decomposition of p-*Toluenesulfonyl Nitrite (5b).* Sulfonyl nitrite **5b** (1.85 g, 10 mmol) in dioxane (25 ml) was stirred for a few minutes at *ca.* 70 °C. Vigorous evolution of gas was observed and the brown color of the solution soon vanished. The solution was concentrated, and the product was recrystallized from acetic acid giving 1.06 g (64%) of compound **23b**. Spectroscopic data, melting points, and elemental analyses of compound **23b** and related compounds are listed in Tables 19 and 20.

N,N-*Bis(p-tolylsulfonyl)hydroxylamine (24).* *A)*: Sulfonyl nitrite **5b** (185 mg, 10 mmol) was stirred in methanol for 5 min. The solvent was evaporated *in vacuo* to give 170 mg (quantitative) of almost pure hydroxylamine **24**: mp 124—126 °C (from ether), (lit,[3] 126 °C). IR (KBr): 3260 (OH), 1380 (SO_2), 1190 (SO_2), 855, and 673 cm^{-1}. IR spectroscopic data were identical with those of authentic sample prepared by the method in the literature.[3]

B): Sulfonyl nitrite **5b** (185 mg, 10 mmol) was added to a stirred solution of thiol **1a** in dioxane (20 ml). The solution slowly turned red, characteristic for thionitrite **2a**, and the mixture was further stirred for 30 min. Then, volatile materials were evaporated to give 180 mg of hydroxylamine **24**.

S-t-*Butyl* p-*Toluenethiosulfonate (25).* Sulfonyl nitrite **5b** (725 mg, 5 mmol) was added to a stirred solution of thionitrite **2a** (595 mg, 5 mmol) in dioxane (20 ml) at 0 °C. The mixture was further stirred for 1 h. Then the mixture was concentrated and upon TLC (hexane:ether=5:1) gave 241 mg of thiosulfonic *S*-ester **25**: mp 68 °C (from ethanol), (lit,[29] 69 °C). IR (KBr): 1591, 1460, 1318, 1140, 811, and 702 cm^{-1}. NMR (CCl_4): δ=1.43 (s, 9H, *t*-Bu), 2.42 (s, 3H, $C\underline{H}_3$), 7.28 (d, J=8 Hz, 2H, ring proton), and 7.75 (d, J=8 Hz, 2H, ring proton). MS (70 eV), *m/e* (rel intensity), 244 (5, M^+), 187 (9, *p*-$TolSO_2S^+$), 155 (10, *p*-$TolSO_2^+$), 91 (27, *p*-Tol^+), 89 (5, *t*-BuS^+), and 57 (100, *t*-Bu^+).

N-*(p-Tolylsulfonyl)hydroxylamine (26).* Sodium borohydride 1.89 g (50 mmol) was added to a stirred solution of sulfonyl nitrite **5b** (1.85 g, 10 mmol) in dioxane (25 ml) at 0 °C. The mixture was stirred further for 40 min at *ca.* 5—10 °C, then excess borohydride was decomposed with acetone (10 ml) at 0 °C. After nearly all the volatile material was evaporated *in vacuo* saturated NaCl aq solution was added into the residue, which was extracted with ethyl ether. Etherial extract was dried ($MgSO_4$), evaporated and upon TLC (hexane:ether=2:1) 304 mg (16%) of hydroxylamine **26** was obtained: mp 129—130 °C (recrystallized from benzene and ether). IR (neat): 3360 (OH), 1345 (SO_2), 985, 815, and 730 cm^{-1}. NMR ($CDCl_3$): δ=2.45 (s, 3H, –$C\underline{H}_3$), 3.88 (br, 2H, N$\underline{H}$ and O$\underline{H}$), 7.32 (d, J=9 Hz, 2H, ring proton), and 7.82 (d, J=9 Hz, 2H, ring proton). Found: C, 44.76; H, 4.73; N, 7.11%. Calcd for $C_7H_9NO_3S$: C, 44.90; H, 4.84; N, 7.48%.

References

1) S. Oae, D. Fukushima, and Y. H. Kim, *J. Chem. Soc., Chem. Commun.*, **1977**, 407.
2) S. Oae, Y. H. Kim, D. Fukushima, and K. Shinhama, *J. Chem. Soc., Perkin Trans. 1*, **1968**, 913.
3) G. Kresze and W. Kort, *Chem. Ber.*, **24**, 2624 (1961).
4) a) R. C. Lord and F. A. Miller, *Appl. Spectroscopy*, **10**, 115 (1956); b) R. A. Nyquist and W. J. Potts, *Spectrochim. Acta*, **1959**, 514.
5) R. J. Philipe and H. Moore, *Spectrochim. Acta*, **1961**, 1004.
6) H. Nogami, J. Hasegawa, and K. Aoki, *Chem. Pharm. Bull.*, **19**, 2472 (1971).
7) I. B. Douglass and B. S. Farah, *J. Org. Chem.*, **24**, 973 (1959).
8) M. Chau and J. L. Kice, *J. Am. Chem. Soc.*, **98**, 7711 (1976).
9) S. Oae, Y. H. Kim, T. Takata, and D. Fukushima, *Tetrahedron Lett.*, **1977**, 1195.
10) D. N. Kramer and R. M. Gamson, *J. Org. Chem.*, **24**, 1154 (1959).
11) S. Oae, K. Shinhama, and Y. H. Kim, *Tetrahedron Lett.*, **1979**, 3307.
12) A. Michael and G. H. Carlson, *J. Am. Chem. Soc.*, **57**, 1268 (1935).
13) F. Wudl, D. A. Lightner, and D. J. Cram, *J. Am. Chem. Soc.*, **89**, 4099 (1967).
14) M. Kulka, *J. Am. Chem. Soc.*, **72**, 1214 (1950).
15) E. Bader and H. D. Hermann, *Chem. Ber.*, **88**, 46 (1955).
16) C. G. Overberger and J. J. Cadfrey, *J. Polymer Sci.*, **40**, 179 (1959).
17) G. Kresze and U. Uhlich, *Chem. Ber.*, **92**, 1048 (1959).
18) G. Leandri, A. Mangini, and A. Tundo, *J. Chem. Soc.*, **1597**, 52.
19) L. Field, *J. Am. Chem. Soc.*, **74**, 394 (1952).
20) G. Leandri and A. Tundo, *Boll. Sci. Fac. Chim. Ind. Univ. Bologna*, **11**, 51 (1953). *Chem. Abstr.*, **48**, 6392f (1954).
21) A. Wagner, H. Beck, and R. J. Klein, *Chem. Ber.*, **93**, 2736 (1960).
22) G. Bulmer and F. G. Mann, *J. Am. Chem. Soc.*, **71**,

3565 (1949).
23) B. Weibull, *Arkiv. Kemi*, **3**, 171 (1951). *Chem. Abstr.*, **46**, 3963g (1952).
24) J. P. Weidner and S. S. Block, *J. Med. Chem.*, **7**, 671 (1964). *Chem. Abstr.*, **61**, 13223h (1964).
25) I. B. Douglass, *J. Org. Chem.*, **30**, 633 (1965).
26) L. Field, C. B. Hoelzel, J. M. Locke, and J. E. Lawson, *J. Am. Chem. Soc.*, **83**, 1256 (1961).
27) J. W. Wilt, R. G. Stein, and W. J. Wagner, *J. Org. Chem.*, **32**, 2097 (1967).
28) Brown precipitate which had absorption of 2110 cm^{-1} (probably N≡N) in IR spectrum was filtered off.
29) T. F. Persons, J. D. Buckman, D. E. Person, and L. Field, *J. Org. Chem.*, **30**, 1923 (1965).

Structure of a Guaioxide-type Sesquiterpene from "San-shion"[1]

Hiroshi HIROTA, Yoshiaki TANAHASHI, and Takeyoshi TAKAHASHI*

Department of Chemistry, Faculty of Science, The University of Tokyo, Bunkyo-ku, Tokyo 113

(Received September 13, 1979)

The structure including absolute stereochemistry of "LB", one of the volatile constituents of "San-shion" (the roots of *Ligularia* species), was found to be (1*S*,4*R*,5*S*,7*R*,10*R*)-5,11-epoxyguaiane.

In connection with chemical investigations on plants of the genus *Ligularia* (Compositae),[2] we examined the constituents of a Chinese drug "San-shion," the roots of a *Ligularia* genus,[3,4] and isolated five volatile constituents named tentatively LA-LE,[4] along with furanoligularenone[3] and ligularenolide.[5] Four of the volatile constituents, LA, LC, LD, and LE, were found to be identical with cyperene, liguloxide, *p*-cymene, and limonene, respectively.[4a,b] The identity of LB with ogarukaya-ether A, isolated from *Cymbopogon Goeringii* (STEUD.) A. CAMUS, was confirmed by Fujita and Fujita,[6] structure **1** being proposed for ogarukaya-ether A based on biogenetic considerations.[6b] This paper deals with the structure determination leading to **2** for LB.

The molecular formula $C_{15}H_{26}O$ of LB was determined by elemental analysis and the appearance of a molecular ion peak at *m/e* 222 in the mass spectrum.[4a] The IR spectrum showed neither hydroxyl nor carbonyl absorption, the NMR spectrum suggesting the presence of two secondary and two tertiary methyl groups and the absence of olefinic proton (Experimental). The absence of unsaturated carbon–carbon linkage was revealed by treatment of LB with trifluoroperacetic acid which showed no consumption of the reagent. Thus, LB is a tricyclic saturated sesquiterpene containing an oxygen atom as a part of ether linkage. The absence of –O–CH– signal in the NMR spectrum suggests that both carbon atoms attached to the ether oxygen should be tertiary. Dehydrogenation of LB with palladium–charcoal gave *S*-guaiazulene as a major product and *Se*-guaiazulene as a minor one.[4a,b] Thus, two alternative structures (**A** and **B**; without stereochemical consideration) relating to a guaiane skeleton (**3**) can be suggested for LB.[4]

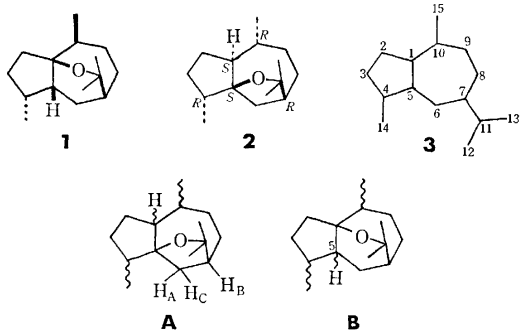

In the NMR spectrum of 1-epiguaioxide (**4**),[7,8] a double doublet signal due to $C_{(6\beta)}$–H (H_A; J=13 and J=6 Hz) appeared at δ 2.32 with small splittings (J=*ca.* 2 Hz). INDOR experiments[9] showed the presence of ABC-type spin-spin couplings for **4** (Fig. 1); the H_A proton couples with both the H_B proton (δ 1.87, dd, J=8 and J=6 Hz; $C_{(7\alpha)}$–H) and the H_C proton (δ 1.63, d, J=13 Hz; $C_{(6\alpha)}$–H). The small splittings are due to a W-letter long-range coupling between H_A and a proton on $C_{(8\beta)}$. The H_B proton couples further with the vicinal $C_{(8\beta)}$–proton (J=8 Hz). The presence of the same ABC-type spin-spin couplings was revealed for LB by INDOR experiments (Fig. 2). The H_A proton (δ 2.28, dd, J=13 and J=6.5 Hz; $C_{(6\beta)}$–H^{10}) was found to couple with both the H_B proton (δ 1.96, dd, J=9[11] and J=6.5 Hz; $C_{(7\alpha)}$–H^{10}) and the H_C proton (δ 1.69, d, J=13 Hz; $C_{(6\alpha)}$–H^{10}); the coupling constant between H_B and H_C was almost null. The structure **A** can only account for these results, excluding the structure **B** with a $C_{(5)}$–proton for LB.

Eight diastereomers (**2** and **4**—**10**) can be present for structure **A** without consideration of their enantiomers. Six of them, 1-epiguaioxide (**4**),[7,8] guaioxide (**5**),[12] bulnesoxide (**6**),[13] liguloxide (**7**),[8] 10-epiliguloxide (**8**),[8] and 1-epiliguloxide (**9**),[14] have so far been reported. None of the spectral data of the six known

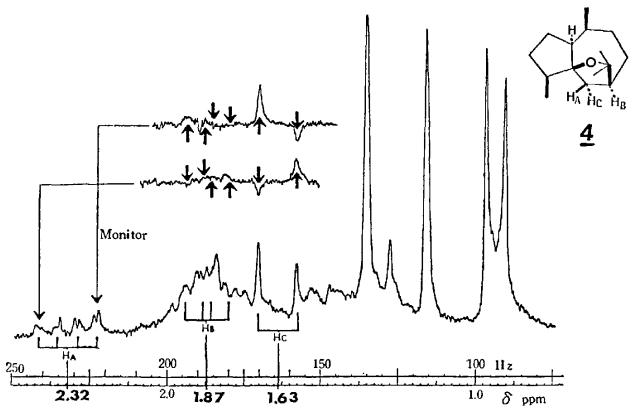

Fig. 1. INDOR experiments (100 MHz) for 1-epiguaioxide (**4**) in $CDCl_3$.

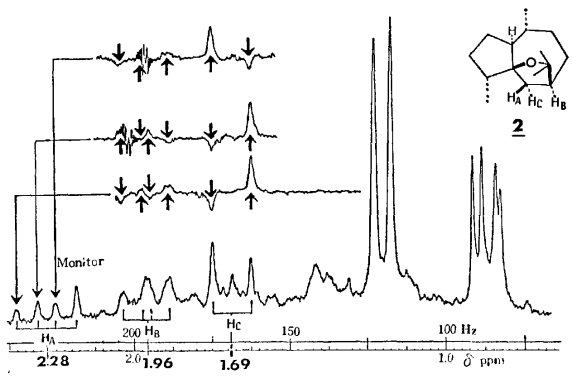

Fig. 2. INDOR experiments (100 MHz) for LB (**2**) in $CDCl_3$.

isomers are identical with those of LB. Thus, the structure of LB should be represented by either **2** or**10**, or by one of their enantiomers; the $C_{(1)}$-hydrogen atom and the $C_{(10)}$-methyl group are both oriented to the side opposite to the ether bridge for each of these structures.

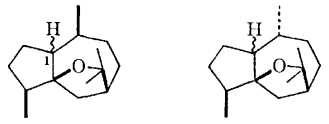

5 1β-H **6** 1β-H
4 1α-H **10** 1α-H

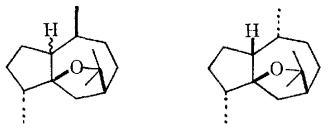

7 1β-H **8**
9 1α-H

Treatment of guaioxide (**5**) with *N*-bromosuccinimide (NBS) gave 4-bromoguaioxide which in turn afforded 3-dehydroguaioxide.[15] When LB was heated with 1.1—1.5 equivalent mol of NBS in carbon tetrachloride under reflux, a monobromide (**11**; $C_{15}H_{25}OBr$) and the unchanged LB were obtained in 8—17% and 67—83% yields, respectively. The NMR spectrum of **11** showed the presence of a secondary methyl and three tertiary methyl groups. One of the tertiary methyl signals appearing at δ 1.76 is due to $C\underline{H}_3$–$\underset{|}{C}$–Br. The bromide (**11**) was heated under reflux with potassium hydroxide in ethanol to give an olefin (**12**; $C_{15}H_{24}O$) in 76% yield. Hydroboration of **12** afforded an alcohol (**13**, $C_{15}H_{26}O_2$; 75% yield), which was oxidized with Jones reagent to give a ketone (**14**, $C_{15}H_{24}O_2$) in 81% yield. The IR spectrum ($\nu_{C=O}$ 1740 cm^{-1}) of **14** indicated the presence of five-membered ring ketone. This shows that the bromination of LB took place on $C_{(4)}$. The ketone (**14**) isomerized on a column of alumina into a hydroxy α,β-unsaturated ketone [**15**; λ_{max} 242 nm (ε 16700)] in 93% yield.[16] The NMR spectrum of **15** showed the presence of an olefinic methyl group (δ 1.70) and the absence of olefinic proton. The formation of the conjugated cyclopentenone derivative with an α-methyl group (**15**) from the ketone (**14**) provides further support for the location of an ether oxygen atom between $C_{(5)}$ and $C_{(11)}$ (structure **A**) rather than between $C_{(1)}$ and $C_{(11)}$ (structure **B**) for LB.

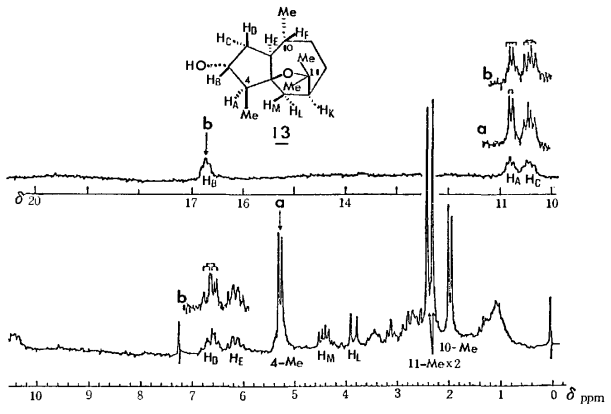

Fig. 3. NMR spectrum (100 MHz) of the alcohol (**13**) in $CDCl_3$ using $Eu(fod)_3$-d_{27} as a shift reagent [shift reagent/**13**=0.7 (M/M)]. NMDR experiments by irradiation of (a) $C_{(4)}$-CH_3 and (b) H_B are registered.

The hydroxy unsaturated ketone (**15**) was dehydrated to give an α,β: γ,δ-unsaturated ketone (**16**) quantitatively by refluxing with *p*-toluenesulfonic acid in benzene. The dienone (**16**) was found to be an enantiomer of known (1*R*,10*S*)-4,6-guaiadien-3-one (**17**)[15b] derived from guaioxide (**5**). This leads to a (1*S*,10*R*)-stereochemistry for LB and its derivatives (**11**—**16**).

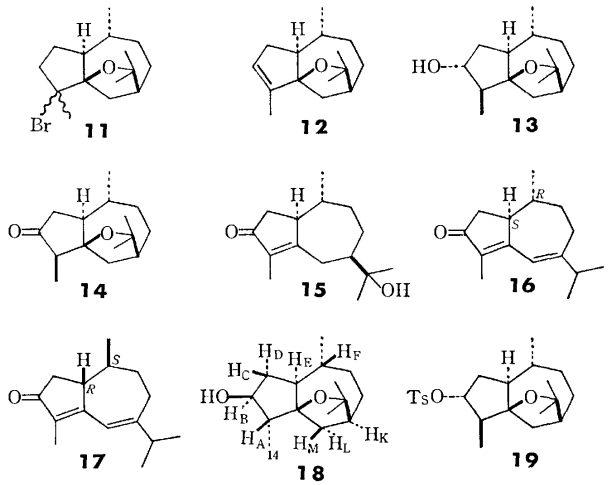

The stereochemistry of the 3-hydroxy derivative (**13**) was determined as follows. Since a *cis*-relationship between the hydroxyl group and a hydrogen atom on $C_{(4)}$ is required by the mode of formation, two alternative structures, **13** and **18**, can be suggested for the alcohol. The NMR measurements using $Eu(fod)_3$-d_{27} as a shift reagent coupled with NMDR experiments lead to the assignment of signals as shown in Fig. 3, when a $C_{(2)}$-hydrogen atom *cis* to the hydroxyl group is designated as H_C. The coupling constants in a first-order approximation were determined to be $J_{A,14}$=7, $J_{A,B}$=7, $J_{B,C}$=2, $J_{B,D}$=8.5, $J_{C,D}$=13.5, $J_{C,E}$=8, $J_{D,E}$=10.5, and $J_{E,F}$=10 Hz. The structure of **13** rather than **18** is shown for the alcohol, since $J_{D,E}$ was found to be greater than $J_{C,E}$ and a large lanthanoid induced shift was observed for H_E. The structure **14** fits the ketone which exhibited a negative Cotton effect ($[\theta]_{295}$ −12900), while 3-oxo-4-epiguaioxide (3-oxoliguloxide) showed a positive Cotton effect (a +273[12]).

Hydrogenation of 3-dehydro LB (**12**) over platinum catalyst gave a saturated ether (4-epi LB) as the sole product in 60% yield, which was found to be not identical with LB; no LB was formed. The alcohol (**13**) was converted into a tosylate (**19**) in 90% yield. Treatment of **19** with lithium aluminium hydride gave a saturated ether (**10**) and the hydroxy ether (**13**) in 18 and 67% yields, respectively. Compound (**10**)

was found to be identical with 4-epi LB mentioned above. Thus, the structure of 4-epi LB is shown by **10**, in which the $C_{(4)}$-methyl group should be in a $\beta(4S)$-configuration. This leads to the structure **2** with the $C_{(4)}$-methyl group in an $\alpha(4R)$-stereochemistry for LB.

In conclusion, the structures including absolute configuration of LB and 4-epi LB are found to be (1*S*,4*R*,5*S*,7*R*,10*R*)-5,11-epoxyguaiane (**2**) and (1*S*,4*S*,5*S*,7*R*,10*R*)-5,11-epoxyguaiane (**10**), respectively. Thus, all the diastereomers (**2** and **4**—**10**) represented by **A** (5,11-epoxyguaiane) have now been recorded.

Experimental

IR and UV spectra were measured with a Hitachi EPI-G2 spectrometer and a Hitachi 340 spectrophotometer, respectively, ^{1}H-NMR spectra with a JEOL PS-100 (100 MHz), a Varian HA-100 (100 MHz), or a Hitachi R-20B (60 MHz) spectrometer in deuteriochloroform solution containing tetramethylsilane as an internal standard, low resolution mass spectra with a Hitachi RMU-6-Tokugata mass spectrometer and high resolution mass spectra with a Hitachi RMH-2 or a JEOL D-300 mass spectrometer, with direct inlet system operating at 70 eV. CD spectra were carried out on a JASCO model J-20. For column chromatography Wakogel C-200 (Wako Pure Chemical Industries) was used. Thin-layer chromatography (TLC) was carried out on Kieselgel GF_{254} (E. Merck, Darmstadt) in 0.25 mm thickness, and vapor-phase chromatography (VPC) on a Shimadzu gas chromatograph model GC-2C.

Isolation of LB (2). LB (**2**; 340 mg) was isolated by the reported procedure[4a] from the benzene extract of the drug (7.7 kg) in a 0.0046% yield: a colorless oil, $[\alpha]_{578}$ −45° (*c* 2.0, $CHCl_3$); IR (film): 1380, 1365, 1160, 1150, 1100, 1020, 1010, 980, and 895 cm^{-1}; NMR: δ 0.87 (3H, d, J=5.5 Hz) and δ 0.89 (3H, d, J=7.5 Hz; $C_{(4)}$-CH_3 and $C_{(10)}$-CH_3), δ 1.18 and 1.24 [each 3H, s; $C_{(11)}$-$(CH_3)_2$].

Bromination of LB (2) with NBS. NBS (1.00 g; 5.62 mmol) was added to a solution of LB (**2**, 970 mg; 4.37 mmol) in carbon tetrachloride (15 ml), and the mixture was heated under reflux for 2.5 h with an infrared lamp. The reaction mixture was cooled and filtered. After removal of solvent under reduced pressure, the resulting residue was chromatographed on a column of silica gel. Elution with petroleum ether–benzene (*ca.* 4:1) gave a 4-bromo LB (**11**, 140 mg; 11% yield), an oil, IR (film): 1150, 1020, 1000, 895, and 805 cm^{-1}; NMR: δ 0.85—0.95 (3H, diffused d; $C_{(10)}$-CH_3), δ 1.20 and 1.22 [each 3H, s; $C_{(11)}$-$(CH_3)_2$], and δ 1.76 (3H, s; $C_{(4)}$-CH_3); MS: *m/e* 302 and 300 (relative abundance, each 15%; M^+), *m/e* 287 and 285 [each 100%; $(M-CH_3)^+$], and *m/e* 221 [40%; $(M-Br)^+$]. Found: *m/e* 302.1070. Calcd for $C_{15}H_{25}O^{81}Br$: M, 302.1069. Found: *m/e* 300.1115. Calcd for $C_{15}H_{25}O^{79}Br$: M, 300.1089. Successive elution with the same solvent mixture gave the starting compound (LB; **2**, 800 mg; 82.5%). Bromide (**11**), obtained in 8—17% yields, showed one spot on thin-layer chromatogram. The NMR spectrum showed methyl signals corresponding to one configurational isomer; the configuration at $C_{(4)}$ of **11** was left undetermined.

Dehydrobromination of the 4-Bromo LB (11). The bromide (**11**; 170 mg; 0.56 mmol) in an ethanolic potassium hydroxide (KOH 350 mg, EtOH 8 ml) was heated under reflux for 1.5 h and the reaction mixture was treated in the usual way to give a residue which was chromatographed on a column of silica gel. Elution with petroleum ether–benzene (1:1) gave an olefin (3-dehydro LB; **12**; 95 mg; 76% yield), an oil, IR (film): 1155, 1010, 995, 885, and 820 cm^{-1}; NMR: δ 0.88 (3H, d, J=6 Hz; $C_{(10)}$-CH_3), δ 1.20 and 1.27 [each 3H, s; $C_{(11)}$-$(CH_3)_2$], δ 1.74 (3H, br s; $C_{(4)}$-CH_3), and δ 5.65 (1H, m; $C_{(3)}$-H); MS: *m/e* 220 (52%; M^+), *m/e* 205 [77%; $(M-CH_3)^+$], *m/e* 202 [66%; $(M-H_2O)^+$], *m/e* 187 [63%; $(C_{14}H_{19})^+$], and *m/e* 159 [100%; $(C_{12}H_{15})^+$]. Found: *m/e* 220.1824. Calcd for $C_{15}H_{24}O$: M, 220.1827.

Hydroboration of the 3-Dehydro LB (12). A solution of diborane (3 mmol) in tetrahydrofuran (3 ml) was added dropwise to a solution of the olefin (**12**, 62 mg; 0.28 mmol) in tetrahydrofuran (4 ml) under a nitrogen atmosphere. After the mixture had been stirred at room temperature for 40 min, a small quantity of water, 2 ml of 3 M aqueous solution of sodium hydroxide, and 2 ml of 30% aqueous hydrogen peroxide solution were added in succession. The resulting mixture was stirred at 50 °C for 1.5 h, and then treated in the usual way to give a residue which was chromatographed on a column of silica gel. Elution with benzene–ether (4:1) gave a 3α-hydroxy 4-epi LB (**13**, 49 mg; 75% yield), white crystals, mp 84—85 °C (crystallized from benzene); IR (KBr disk): 3250 (br), 1150, 1100, 1065, 990, 980, 890, 800, and 770 cm^{-1}; NMR: δ 0.85 (3H, diffused d; $C_{(10)}$-CH_3), δ 1.04 (3H, d, J=7 Hz; $C_{(4)}$-CH_3), δ 1.17 and 1.26 [each 3H, s; $C_{(11)}$-$(CH_3)_2$], and δ 3.93 (1H, m; $C_{(3)}$-H); the NMR spectrum with addition of $Eu(fod)_3$-d_{27} (Fig. 3); MS: *m/e* 238 (73%; M^+), *m/e* 223 [100%; $(M-CH_3)^+$], *m/e* 220 [28%; $(M-H_2O)^+$], and *m/e* 205 [64%; $(C_{14}H_{21}O)^+$]. Found: *m/e* 238.1920. Calcd for $C_{15}H_{26}O_2$: M, 238.1932.

Oxidation of 3α-Hydroxy 4-Epi LB (13). A few drops of Jones reagent were added slowly to a stirred solution of the alcohol (**13**, 25 mg; 0.10 mmol) in acetone (1 ml) at 0—10 °C, and the mixture was further stirred for 10 min at the same temperature. The reaction mixture was treated in the usual way to give a residue which was chromatographed on a column of silica gel. Elution with benzene–ether (10:1) gave a ketone (3-oxo 4-epi LB; **14**; 20 mg; 81% yield), white crystals, mp 63—64 °C (crystallized from benzene); IR: (KBr disk): 1740, 1180, 1120, 1010, 995, 990, 890, 875, and 820 cm^{-1}; CD (*c* 1.17×10^{-3}, EtOH): $[\theta]_{330}$ ±0, $[\theta]_{295}$ −12900, $[\theta]_{250}$ ±0; NMR: δ 0.89 (3H, d, J=6 Hz; $C_{(10)}$-CH_3), δ 1.03 (3H, d, J=7 Hz; $C_{(4)}$-CH_3), δ 1.16 and 1.25 [each 3H, s; $C_{(11)}$-$(CH_3)_2$], and δ 2.20 (1H, q, J=7 Hz, $C_{(4\alpha)}$-H); MS: *m/e* 236 (90%; M^+), *m/e* 221 [100%; $(M-CH_3)^+$], *m/e* 218 [29%; $(M-H_2O)^+$], and *m/e* 203 [40%; $(C_{14}H_{19}O)^+$]. Found: *m/e* 236.1786. Calcd for $C_{15}H_{24}O_2$: M, 236.1776.

Isomerization of 3-Oxo 4-Epi LB (14) on Alumina. The ketone (**14**; 10 mg; 0.04 mmol) in a small amount of ether (*ca.* 3 ml) was placed on the top of a column of neutral alumina (5 g). After 4 h, elution with ether gave a hydroxy α,β-unsaturated ketone (**15**, 9.3 mg; 93% yield) as white crystals, mp 57—58.5 °C (crystallized from AcOEt); IR (KBr disk): 3450, 3250, 1675, 1610, 1140, and 970 cm^{-1}; UV (EtOH): λ_{max} 242 nm (ε 16700); NMR: δ 1.06 (3H, d, J=5 Hz; $C_{(10)}$-CH_3), δ 1.24 and 1.28 [each 3H, s; $C_{(11)}$-$(CH_3)_2$], and δ 1.70 (3H, s; $C_{(4)}$-CH_3); MS: *m/e* 236 (1%; M^+), *m/e* 221 [5%; $(M-CH_3)^+$], *m/e* 218 [100%; $(M-H_2O)^+$], and *m/e* 178 [18%; $(C_{12}H_{18}O)^+$]. Found: *m/e* 236.1783. Calcd for $C_{15}H_{24}O_2$: M, 236.1776.

Dehydration of the Hydroxy α,β-Unsaturated Ketone (15). *p*-Toluenesulfonic acid (18 mg; 0.10 mmol) was added to a solution of the hydroxy α,β-unsaturated ketone (**15**, 8.5 mg; 0.036 mmol) in benzene (5 ml) and the solution was heated under reflux for 1.5 h under a nitrogen atmosphere. The

reaction mixture was treated in the usual way to give a single product, (1*S*, 10*R*)-4,6-guaiadien-3-one (**16**; 7.6 mg; quantitative yield), an oil; IR (film): 1690, 1625, 1590, 1340, 1285, 1055, and 875 cm^{-1}; UV (EtOH): λ_{max} 293 nm (ε 20800); CD (c 3.50×10^{-4}, EtOH): $[\theta]_{365}$ ±0, $[\theta]_{295}$ −20300, $[\theta]_{240}$ ±0; NMR: δ 1.06 (3H, d, J=6 Hz; $C_{(10)}$-CH_3), δ 1.09 [6H, d, J=7 Hz; $C_{(11)}$-$(CH_3)_2$], δ 1.75 (3H, s; $C_{(4)}$-CH_3), and δ 6.35 (1H, br s; $C_{(6)}$-H); MS: *m/e* 218 (100%; M^+), *m/e* 203 [27%; $(M-CH_3)^+$], and *m/e* 175 [37%; $(M-C_3H_7)^+$]. Found: *m/e* 218.1682. Calcd for $C_{15}H_{22}O$: M, 218.1671.

The IR, UV, NMR, and mass spectra of **16** were found to be identical with those of known (1*R*, 10*S*)-4,6-guaiadien-3-one (**17**).[15b] The dienone (**16**) exhibits a negative Cotton effect and **17** a positive CD maximum ($[\theta]_{295}$ +18300).[15b]

Hydrogenation of 3-Dehydro LB (12). 3-Dehydro LB (**12**, 15 mg; 0.07 mmol) and platinum catalyst (prepared from platinum oxide; 10 mg) in a mixture of ethyl acetate (5 ml) and acetic acid (0.3 ml) were stirred under a hydrogen atmosphere at room temperature for 5 h. The catalyst was removed by filtration and the solvents evaporated to give a residue, which was purified by chromatography on a column of silica gel. Elution with petroleum ether–benzene (5:1) gave 4-epi LB (**10**, 9 mg; 60% yield). No LB (**2**) was obtained. On VPC examination (7% SE-30; 2.3 m; 125 °C; N_2 50 ml/min), the retention time of 4-epi LB (**10**) was found to be 12.3 min, and that of authentic LB (**2**) 11.1 min under the same conditions. 4-Epi LB (**10**), an oil; IR (film): 1150, 1140, 1020, 995, and 895 cm^{-1}; NMR: δ 0.85 (3H, diffused d) and δ 0.95 (3H, d, J=6 Hz; $C_{(4)}$-CH_3 and $C_{(10)}$-CH_3), δ 1.19 and 1.29 [each 3H, s; $C_{(11)}$-$(CH_3)_2$], and δ 2.15 (1H, dd, J=5 Hz and 12 Hz; $C_{(6\beta)}$-H); MS: *m/e* 222 (20%; M^+), *m/e* 207 [100%; $(M-CH_3)^+$], *m/e* 189 [40%; $(C_{14}H_{21})^+$], and *m/e* 164 [45%; $(C_{12}H_{20})^+$]. Found: *m/e* 222.1948. Calcd for $C_{15}H_{26}O$: M, 222.1983.

Tosylation of 3α-Hydroxy 4-Epi LB (13). A mixture of the alcohol (**13**, 49 mg; 0.21 mmol) and *p*-toluenesulfonyl chloride (100 mg; 0.53 mmol) in dry pyridine (1 ml) was left at 0 °C for 72 h under a nitrogen atmosphere. After the usual treatment, a tosylate (**19**, 75 mg; 90% yield) was obtained as white crystals. 3α-Tosyloxy 4-epi LB (**19**), mp 119—121 °C (dec.) (crystallized from MeOH–$CHCl_3$); IR (KBr disk): 1640 (w), 1335, 1175, 1100, 985, 955, and 865 cm^{-1}; NMR: δ 0.82 (3H, d, J=4 Hz) and δ 0.83 (3H, d, J=7 Hz; $C_{(4)}$-CH_3 and $C_{(10)}$-CH_3), δ 1.14 and 1.28 [each 3H, s; $C_{(11)}$-$(CH_3)_2$], δ 2.46 (3H, s; aromatic CH_3), δ *ca.* 4.5 (1H, m; $C_{(3\beta)}$-H), and δ 7.37 and 7.84 (each 2H, d, J=8.5 Hz; aromatic H's); MS: *m/e* 392 (1%; M^+), *m/e* 377 [2%; $(M-CH_3)^+$], *m/e* 237 [95%; $(C_{15}H_{25}O_2)^+$], *m/e* 220 [49%; $(C_{15}H_{24}O)^+$], and *m/e* 205 [100%; $(C_{14}H_{21}O)^+$]. Found: *m/e* 392.2021. Calcd for $C_{22}H_{32}O_4S$: M, 392.2021.

Reaction of the Tosylate (19) with Lithium Aluminium Hydride. A mixture of the tosylate (**19**, 20 mg; 0.05 mmol) and lithium aluminium hydride (50 mg; 1.3 mmol) in dry tetrahydrofuran (6 ml) was heated under reflux for 10 h under a nitrogen atmosphere. The reaction mixture was treated in the usual way to give a residue, which was chromatographed on a column of silica gel. Elution with benzene gave 4-epi LB (**10**, 2 mg; 18% yield), identical [TLC, VPC (SE-30), IR, and MS] with an authentic specimen. Successive elution with benzene–ether (2:1) gave 3α-hydroxy 4-epi LB (**13**, 8 mg; 67% yield).

The authors wish to thank Dr. Ken'ichi Takeda, Dr. Kazuo Tori, and Dr. Hiroshi Ishii, Shionogi Research Laboratory, Osaka, and the late Dr. Yasuji Fujita, Government Industrial Institute, Osaka, for their valuable discussions. Thanks are also due to Dr. Hiroshi Ishii for the supply of spectral data of the diastereomers (**4**, **6**, **8**, and **9**) of guaioxide.

References

1) A part of this work was reported in a preliminary form; H. Hirota, Y. Tanahashi, and T. Takahashi, *Tetrahedron Lett.*, **1975**, 4579.

2) T. Takahashi, The 21st Symposium on the Chemistry of Perfumes, Terpenes, and Essential Oils, Tokushima, November 4, 1977, Abstract Papers, p. 305, and references cited therein.

3) F. Patil, G. Ourisson, Y. Tanahashi, M. Wada, and T. Takahashi, *Bull. Soc. Chim. Fr.*, **1968**, 1047.

4) a) M. Okazaki, Y. Ishizaki, Y. Tanahashi, H. Hirota, and T. Takahashi, *Yakugaku Zasshi*, **94**, 881 (1974): the drug is probably the root of *Ligularia sibirica* CASS. or *Ligularia Hodgsoni* HOOK. *var. sutchuanensis* (FRANCH.) HENRY; b) Y. Ishizaki, M. Okazaki, M. Wada, Y. Tanahashi, and T. Takahashi, the 12th Symposium on the Chemistry of Perfumes, Terpenes, and Essential Oils, Hamamatsu, October 1, 1968, Abstract Papers, p. 53; *cf.* Y. Tanahashi, S. Tomoda, and T. Takahashi, *Bull. Chem. Soc. Jpn.*, **42**, 2076 (1969).

5) Y. Ishizaki, Y. Tanahashi, T. Takahashi, and K. Tori, *Tetrahedron*, **26**, 5387 (1970).

6) a) S. Fujita and Y. Fujita, *Yakugaku Zasshi*, **92**, 1285 (1972). b) S. Fujita and Y. Fujita, the 16th Symposium on the Chemistry of Perfumes, Terpenes, and Essential Oils, Hirosaki, October 6, 1972, Abstract Papers, p. 14.

7) C. Ehret and G. Ourisson, *Bull. Soc. Chim. Fr.*, **1968**, 2629.

8) H. Ishii, T. Tozyo, M. Nakamura, and H. Minato, *Tetrahedron*, **26**, 2911 (1970).

9) *E.g.* a) E. B. Baker, *J. Chem. Phys.*, **37**, 911 (1962); b) R. Kaiser, *ibid.*, **39**, 2435 (1963).

10) The assignment of the signal was given after the determination of the structure of LB (**2**).

11) This J-value seems to be due to the coupling between H_B and $C_{(8\alpha)}$-H.

12) H. Ishii, T. Tozyo, M. Nakamura, and H. Minato, *Tetrahedron*, **26**, 2751 (1970).

13) H. Ishii, T. Tozyo, and M. Nakamura, *Tetrahedron*, **27**, 4263 (1971).

14) H. Ishii, T. Tozyo, M. Nakamura, and E. Funke, *Chem. Pharm. Bull. (Tokyo)*, **20**, 203 (1972).

15) a) H. Hirota, S. Tomoda, Y. Tanahashi, and T. Takahashi, the 32nd National Meeting of the Chemical Society of Japan, Tokyo, April 4, 1975, Abstract Papers, p. 1883; b) H. Hirota, Y. Moriyama, H. Shirasaki, T. Tsuyuki, and T. Takahashi, *Bull. Chem. Soc. Jpn.*, **52**, 3755 (1979).

16) A similar isomerization has been reported on 3-oxo-guaioxide (Ref. 13), 3-oxo-4-epiguaioxide (Ref. 12), and 8-acetoxy-3-oxo-4-epiguaioxide (Ref. 12).

 © 1980 The Chemical Society of Japan Bull. Chem. Soc. Jpn., 53, 789—794 (1980)

Optical Resolutions and Configurations of Benzylmethylphenylsilylmethylamine and Its Derivatives

Daiyo Terunuma,* Katsutoshi Murakami, Masanori Kokubo, Kazuhisa Senda, and Hiroyuki Nohira

Department of Applied Chemistry, Faculty of Engineering, Saitama University, Urawa, Saitama 338

(Received September 10, 1979)

New optically active α-amino organosilanes, such as benzylmethylphenylsilylmethylamine, benzylmethyltolylsilylmethylamines, and anisylbenzylmethylsilylmethylamines, were obtained by the fractional crystallization of the salts of the amines and (+)-tartaric acid. Benzylmethylphenylsilylmethylamine was converted into benzylmethyl-1-naphthylphenylsilane, of which the configuration had been known. From these observations, it was found that benzylmethylphenylsilylmethylamine, benzylmethylphenylsilane, and benzylmethoxymethylphenylsilane had *S*(+), *S*(−), and *S*(+) configurations respectively.

The progress of the stereochemistry of organosilicon compounds owes much to the studies of L. H. Sommer and his co-workers of the reaction mechanism of the asymmetric silicon center using the optically active methyl-1-naphthylphenylsilyl systems.[1] However, only a few successful methods for obtaining optically active organosilanes in a high optical purity have been reported.[2] The difficulty of the resolution of organosilanes can be ascribed in part to the nature of their poor crystallizability. On the other hand, in the course of our studies of the synthesis of silacyclopentane derivatives, it was found that *trans*-3,3,5-trimethyl-3-silacyclopentylamine formed crystalline salts with (+)-tartaric acid.[3] In this paper, we wish to describe the resolution[4] of such α-amino silanes as benzylphenylmethylsilylmethylamine (**2a**), benzylmethyl-(*p*-, *m*-, *o*-)-tolysilylmethylamine(**2b**, **2c**, **2d**), (*p*-, *o*-)-anisylbenzylmethylsilylmethylamine(**2e**, **2f**), and benzylbutylmethylsilylmethylamine(**2g**) by using (+)-tartaric acid as a resolving reagent, and to describe the chemical interconversion of **2a** into benzyl-1-naphthylphenylmethylsilane.

Results and Discussion

Optical Resolution. The α-chlorosilanes (**1a**—**1g**) were synthesized by the step-by-step treatment of dichloromethylsilylmethyl chloride with the corresponding Grignard reagents. Then the chlorides were treated with excess ammonia in a stainless steel autoclave for 1.5 h at 100 °C.[4,6] The α-amino silanes (**2a**—**2g**) were obtained in 50—60% yields (Scheme 1 and Table 1).

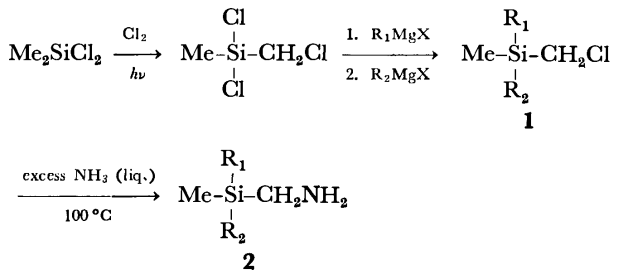

a R_1=Ph, R_2=$PhCH_2$–. **b** R_1=*p*-tolyl, R_2=$PhCH_2$–. **c** R_1=*m*-tolyl, R_2=$PhCH_2$–. **d** R_1=*o*-tolyl, R_2=$PhCH_2$–. **e** R_2=*p*-anisyl–, R_2=$PhCH_2$–. **f** R_1=*o*-anisyl, R_2=$PhCH_2$–. **g** R_1=Ph, R_2=*n*-Bu.

Scheme 1.

Table 1. Amination of **1**

	1 g(mol)	NH_3(liq.) g(mol)	**2** Bp(°C/Torr)	**2** Yield g(%)
a	26.8(0.10)	70(4.1)	160—163/4	16.5(66.5)
b	30.6(0.12)	74(4.3)	163—165/3	16.2(57.0)
c	70.0(0.26)	240(14.1)	155—158/2	34.6(52.7)
d	15.1(0.06)	36(2.2)	161—164/3	7.5(53.4)
e	37.5(0.13)	75(4.3)	170—174/2	20.6(58.8)
f	16.8(0.058)	36(2.2)	143—146/1	8.0(50.7)
g	54.7(0.24)	240(14.1)	143—145/18	24.3(48.9)

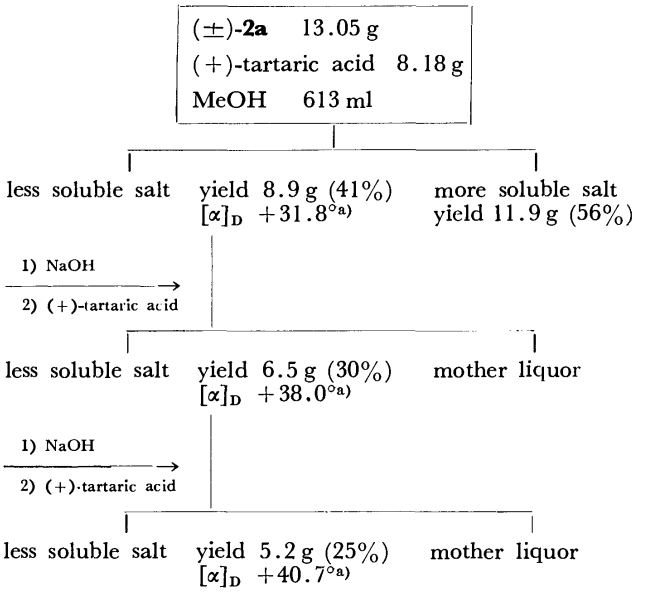

a) *c*=4 in DMF

Fig. 1. Fractional crystallization of **2a**.

The optical resolutions of the amine **2** were carried out by using (+)-tartaric acid as the resolving reagent (Table 2). Since the less soluble salts obtained by the method of fractional crystallization appeared to be unstable in methanol solution above 40 °C, further recrystallization of the salts was not undertaken. Instead, the partially resolved amines, which had been liberated from the less soluble salts by treating them with a caustic alkali solution, were treated with an equimolar amount of (+)-tartaric acid in methanol. Some typical results of the resolution of **2a** are shown in the flowing chart (Fig. 1). The optical resolutions

Table 2. Resolution of **2** using (+)-tartaric acid as the resolving reagent

	(±)-**2** (g)	A[a] (g)	MeOH (ml)	Less soluble salt		Optically active amine	
				Yield g(%)	$[\alpha]_D$(°)	Yield g(%)	$[\alpha]_D$(°)
2a	13.05	8.18	613	8.7(41)	+31.8[b]	4.6(35)	+9.5[e]
2b	10.12	6.02	602	6.3(39)	−25.5[c]	3.4(34)	−10.6[f]
2c	10.85	6.38	510	7.2(42)	+32.1[b]	3.8(35)	+9.9[g]
2d	4.00	2.19	220	2.8(45)	+20.7[b]	1.6(40)	+6.6[e]
2e	7.31	4.05	181	2.6(23)	−29.3[c]	1.3(18)	−9.6[e]
2f	9.44	5.22	260	4.3(30)	+37.8[c]	2.4(25)	+15.8[e]
2g	20.54	15.21	380[h]	17.1(56)	+20.6[d]	—	—

a) (+)-Tartaric acid. b) c=4 in DMF. c) c=1 in DMF. d) c=2 in MeOH. e) c=4 in Et_2O. f) c=3 in Et_2O. g) c=5 in Et_2O, h) c=4 in H_2O.

Table 3. The specific rotations of the salts and amines

	Salt			Amine	
	$[\alpha]_D$(°)[a]	(c)	Mp(°C)	$[\alpha]_D$(°)[b]	(c)
2a	+40.7	4	175	+12.7	2
2b	−40.0	1	165	−16.6	3
2c	+34.5	4	164	+10.7	5
2d	+25.5	4	163	+8.1	4
2e	−44.2	1	167	−14.5	4
2f	+45.2	4	170	+19.4	4
2g	+21.1	2[c]	147	−0.54[d]	—

a) DMF. b) Et_2O. c) MeOH. d) Neat.

Table 4. The dependence of the specific rotations of the salts on the concentration in DMF

	$[\alpha]_D$(°)		
	c=1	c=2	c=4
2a	+30.8	+38.0	+40.7
2b	−40.0	−41.5	—
2c	+23.0	+28.0	+34.5
2d	+10.6	+14.5	+25.5

were carried out in this manner until the specific rotations of the salts became constant (Table 3).

In the course of these experiments, it was noticed that the specific rotation of the salts changed remarkably in their dependence on the concentration of the salts in DMF (Table 4).

The partial discrepancy of the data in Table 3 with that of our preliminary communication[4] may result from the variability in the specific rotation of the salts. The optical purities of the **2a**—**2f** obtained from the first step of fractional crystallization (Table 2) were 75, 64, 93, 82, 66, and 81% respecitvely, based on the corresponding specific rotations in Table 3. These results indicate that the optically active organosilanes obtained from the first step of resolution are quite sufficient to be used for stereochemical studies.

Chemical Conversion of 2a. Recently, an interesting intramolecular rearrangement reaction which converts α-aminosilanes, such as *N*-benzyl- and *N*-cyclohexyltrimethylsilylmethylamine, into aminosilanes appeared in the literature.[7] We considered that

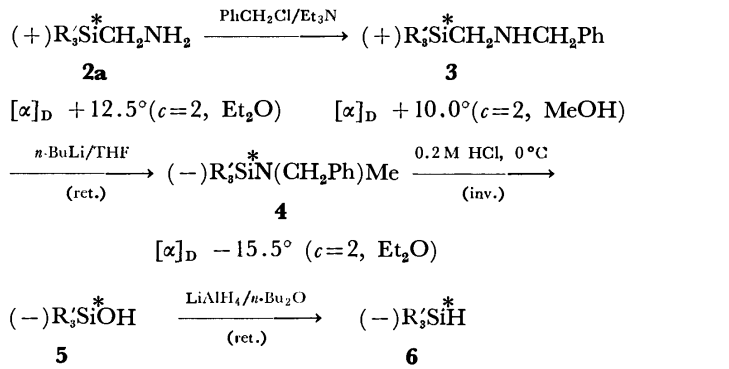

Scheme 2.

this reaction could be used to convert the optically active amine **2a** ($R'_3SiCH_2NH_2$) into siliconfunctional aminosilane. In this section, we wish to describe our attempt at the chemical interconversion of **2a** into benzylmethyl-1-naphthylphenylsilane (**9**), the absolute configuration of which is known.[5]

(+) - *N* - Benzylbenzylmethylphenylsilylmethylamine (**3**) was obtained by treating the (+)-**2a** with an equimolar amount of benzyl chloride in triethylamine. After the mixture of (+)-**3** and butyllithium in THF had been stirred 10 h at room temperature, (−)-*N*-benzyl-*N*-methylbenzylmethylphenylsilylamine (**4**) was obtained in a good yield. Although the steric course of this reaction has not yet been established, it may be assumed that this reaction proceeds with a retention of the configuration by considering to be an intramolecular rearrangement.[7] Then (−)-**4** was treated with 0.2 M (1 M=1 mol dm^{-3}) HCl at 0 °C to give (−)-benzylmethylphenylsilanol (**5**). It was observed that considerable racemization took place when the reaction was carried out at a temperature above 0 °C. The reduction of (−)-**5** with $LiAlH_4$ in dibutyl ether gave (−)-benzylmethylphenylsilane (**6**). The stereochemistry of these two reactions has been clarified by using methyl-1-naphthylphenylsilyl systems; *i.e.*, the former proceeds with inversion,[8] while the latter proceed with a retention of configuration[9] (Scheme 2).

Although optically active silane (**6**) had already been obtained by the partial reduction of (±)-benzylmethoxymethylphenylsilane (**8**) with asymmetric reduc-

tion reagents, *i.e.*, $LiAlH_4$–alkaloid systems, the specific rotation of **6** reported in the litrature is $-7.8°$,[10] which corresponds to the optical purity of 40% (e.e.) based on our sample $[\alpha]_D$ $-17.8°$ ($c=2$, Et_2O).

Some reactions of (−)-**6** were carried out in order to establish its configuration (Scheme 3). The chlorination of (−)-**6** in CCl_4 in the presence of a small amount of benzoyl peroxide[11] gave (−)-benzyl(chloro)methylphenylsilane (**7**). On the other hand, the methanolysis of (−)-**6** in the presence of Pd-C in pentane[12] at 0 °C afforded (+)-**8**. The reduction of (−)-**7** and (+)-**8** by $LiAlH_4$ in ether gave (+)-**6**. These results are in accordance with those of similar reactions of the methyl-1-naphthylphenylsilyl systems reported in the literature.[11,12]

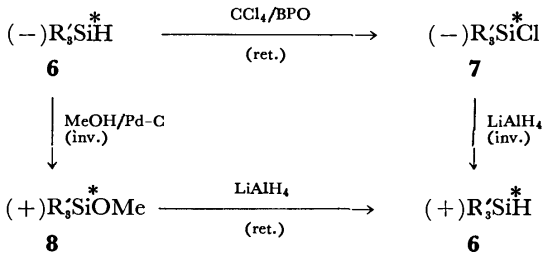

Scheme 3.

Further, the reactions of (−)-**7** and (+)-**8** with 1-naphthyllithium in ether were carried out; both reactions gave the same product, *i.e.*, (*S*)-(−)-benzylmethyl-1-naphthylphenylsilane (**9**)[5] (Scheme 4).

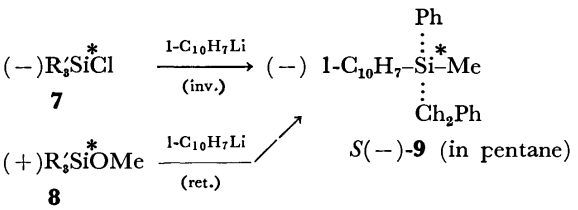

Scheme 4.

From these observations, it has become apparent that **7** and **8** have the *R*(−) and *S*(+) configurations respectively. Consequently, the configurations of the benzylmethylphenylsilyl systems treated in this paper are assigned as follows Scheme 5:

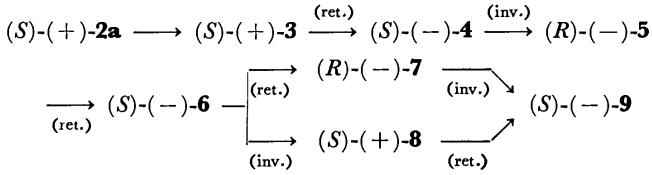

Scheme 5.

However, our results on the configuration of **6** and **8** are not in accordance with those of the previously reported assignments.[10,13] The configuration of **8** was previously determined based on the inversion reaction of **8** with the Grignard reagent of 1-bromonaphthalene in ether. Unfortunately, we could not succeed in following the reaction of **8** with 1-naphthylmagnesium bromide in ether. Therefore, some reactions of (−)-**7** and (+)-**8** with such organolithium reagents as butyllithium, (*p*-, *o*-)-tolyllithium, *p*-anisyllithium, and allyllithium were carried out in order to investigate the steric course of these reactions (Scheme 6).

From these observations, it is clear that the reactions of the alkyl- and the aryllithium with (+)-**8** proceed with a retention of the configuration, whereas that of allyllithium with (+)-**8** proceeds with an inversion of the configuration, if the reactions of the organolithium reagents with (−)-**7** are assumed to proceed with an inversion of the configuration. These results are in fair agreement with those for methyl-1-naphthylphenylsilyl systems.[14]

On the other hand, when the reaction of *p*-tolylmagnesium bromide with (+)-**8** was carried out, (−)-**12** was obtained as the product. Although it has been described in the literature[13] that the reactions

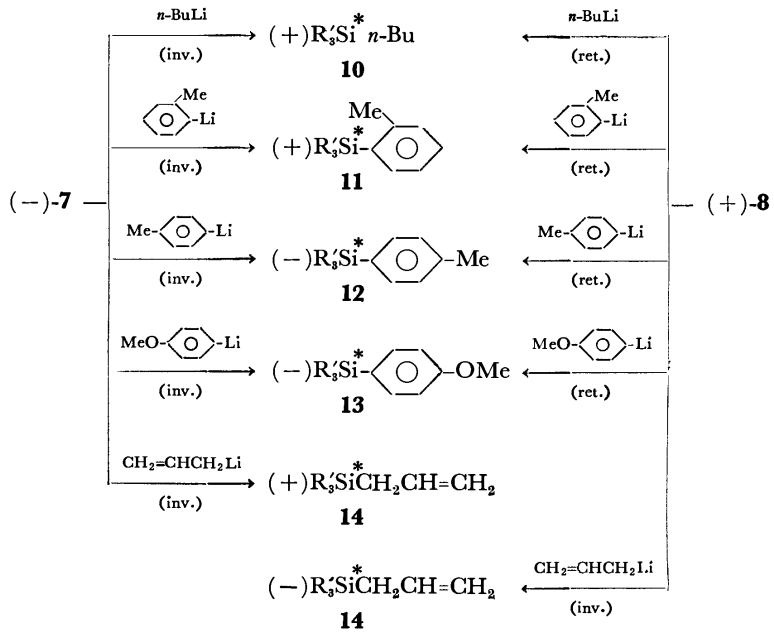

Scheme 6.

of such aryl Grignard reagents as mesityl-, and 1-naphthylmagnesium bromide with a methoxysilane proceed with an inversion of the configuration, our results indicate that the Grignard reaction with (+)-**8** proceeds with a retention of the configuration (Scheme 7). Many detailed studies of the Grignard reactions with (+)-**8** are in progress.

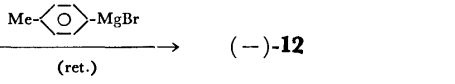

(+)-**8** → (−)-**12**

$[\alpha]_D$ +3.5°(c=2, pentane) $[\alpha]_D$ −3.7°(c=6, CH_2Cl_2)

Scheme 7.

The enantiomers, the configurations of which have been assigned on the basis of the evidence presented in this paper, are listed in Table 5.

TABLE 5. R'_3SiX ENANTIOMERS WITH THE (S)-(−)-R'^{*}_3SiH CONFIGURATION

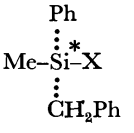

X	Sign of rotation	Solvent
H	$S(-)$	Et_2O
OH	$R(-)$	Et_2O
$N(CH_2Ph)Me$	$R(+)$	Et_2O
CH_2NH_2	$R(-)$	Et_2O
CH_2NHCH_2Ph	$R(-)$	MeOH
Cl	$R(-)$	CCl_4
OMe	$R(-)$	pentane
n-Bu	$R(-)$	CH_2Cl_2
p-Tolyl	$R(+)$	CH_2Cl_2
o-Tolyl	$R(-)$	CH_2Cl_2
p-Anisyl	$R(+)$	CH_2Cl_2
$CH_2=CHCH_2$	$R(-)$	CH_2Cl_2
1-$C_{10}H_7$	$R(+)$	pentane

Experimental

The melting points and boiling points are uncorrected. The IR spectra were determined with a JASCO IR-A2 spectrometer. The NMR spectra were determined at 60 MHz with a Varian A-60D spectrometer in CCl_4, using TMS as the internal standard. The optical rotations were measured with a JASCO DIP-181 polarimeter. All the reactions of the chlorosilanes and the methoxysilane with Grignard and organolithium reagents were carried out under a dry nitrogen atmosphere. The column chromatography was carried out using silica gel (200 mesh).

*Benzylmethylphenylsilylmethyl Chloride (**1a**).* In a three-necked flask, equipped with a magnetic stirrer and a reflux condenser, dichloromethylsilylmethyl chloride (114.5 g, 0.7 mol) and dry ether (150 ml) were placed. To the flask was added the Grignard reagent prepared from bromobenzene (121.2 g, 0.77 mol) and Mg (20 g, 0.82 mol) in ether (150 ml). The mixture was refluxed for 3 h with stirring. After the subsequent addition of THF (70 ml) to the mixture, the Grignard reagent prepared from benzyl chloride (96.6 g, 0.77 mol) and Mg (20 g, 0.82 mol) in ether (150 ml) was added, and the mixture was refluxed a further 5 h with stirring. Then the mixture was hydrolyzed with dil HCl. The organic layer was washed with water and dried ($CaCl_2$). Subsequent evaporation and distillation gave **1a** in 90% (164.6 g) yield. Bp 153—157 °C/3 Torr. NMR δ 0.30 (s, 3, Si-CH_3), 2.43 (s, 2, CH_2-Ph), 2.88 (s, 2, CH_2-Cl), 7.3—7.7 (m, 10, Ph).

The compounds (**1b**—**1g**) were obtained in manners similar to that described above. The yields and boiling points are as follows (yield (%), Bp (°C/Torr)): **1b** 74, 171—172/1, **1c** 78, 160—163/1, **1d** 64, 158—162/2, **1e** 78, 165—169/3, **1f** 77, 150—156/3, **1g** 87, 132/25.

*Benzylmethylphenylsilylmethylamine (**2a**).* In a stainless steel autoclave (200 ml), **1a** (26.8 g, 0.10 mol) and liquid ammonia (70 g, 4.1 mol) were added under a nitrogen atmosphere. The autoclave was then maintained for 1.5 h at 100 °C. The excess ammonia was liberated from the autoclave, and the contents were washed out with aqueous alkali (52 g, NaOH/ 300 ml H_2O) and benzene. The organic layer was separated, washed with aqueous alkali several times, and dried (Na_2SO_4). Subsequent evaporation and distillation gave **2a** in a 66% (16.5 g) yield. Bp 160—163 °C/4 Torr. IR (neat) 3400, 3300 cm^{-1} (w, -NH_2), 1250 cm^{-1} (s, Si-CH_3). NMR δ 0.32 (s, 3, Si-CH_3), 1.20 (s, 2, NH_2), 2.33 (s, 4, Si-CH_2-Ph, Si-CH_2-N), 6.7—7.5 (m, 10, Ph). Found: N, 5.74%. Calcd for $C_{15}H_{19}NSi$: N, 5.80%.

The amines (**2b**—**2g**) were obtained in manners similar to that described above. The boiling points and yields of the amines are listed in Table 1. **2b** NMR δ 0.14 (s, 3, Si-CH_3), 1.30 (s, 2, NH_2), 2.15—2.30 (7, CH_3-Ph, Si-CH_2Ph, Si-CH_2-N), 6.7—7.4 (m, 9, Si-C_6H_4-, Si-Ph). Found: N, 5.34%. Calcd for $C_{16}H_{21}NSi$: N, 5.48%. **2c** NMR δ 0.20 (s, 3, Si-CH_3), 0.57 (s, 2, NH_2), 2.10—2.25 (7, CH_3-Ph, Si-CH_2-Ph, Si-CH_2-N), 6.4—7.0 (m, 9, Si-C_6H_4-, Ph). Found: N, 5.54%. Calcd for $C_{16}H_{21}NSi$: 5.48%. **2d** NMR δ 0.26 (s, 3, Si-CH_3), 0.77 (s, 2, NH_2), 2.30—2.40 (7, CH_3-Ph, Si-CH_2-Ph, Si-CH_2-N), 6.6—7.4 (m, 9, Si-C_6H_4-, Ph). Found: N, 5.38%. Calcd for $C_{16}H_{21}NSi$: N, 5.48%. **2e** NMR δ 0.27 (s, 3, Si-CH_3), 1.63 (s, 2, NH_2) 2.4 (4, Si-CH_2-C, Si-CH_2-N), 3.80 (s, 3, O-CH_3), 6.8—7.5 (m, 9, Si-C_6H_4-, Ph). Found: N, 5.22%. Calcd for $C_{16}H_{21}NOSi$: N, 5.16%. **2f** NMR δ 0.20 (s, 3, Si-CH_3), 1.68 (s, 2, NH_2), 2.4 (4, Si-CH_2-C, Si-CH_2-N), 3.78 (s, 3, O-CH_3), 6.6—7.5 (m, 9, Si-C_6H_4-, Ph). Found: N, 5.21%. Calcd for $C_{16}H_{21}NOSi$: N, 5.16%. **2g** NMR δ 0.29 (s, 3, Si-CH_3), 0.62—1.67 (m, 11, Si-Bu, NH_2), 2.39 (s, 2, Si-CH_2-N), 7.3—7.5 (m, 5, Ph).

*Optical Resolution of **2a**.* To the solution of (+)-tartaric acid (8.18 g, 0.054 mol) in methanol (600 ml) in a 1 litre Erlenmeyer flask was added a solution of (+)-**2a** (13.05 g, 0.054 mol) in methanol (13 ml). A white crystalline precipitate started to separate almost immediately. The flask was then allowed to stand overnight at room temperature. The crystalline precipitate was filtered off, washed with a small amount of cold methanol, and then dried *in vacuo*. To the salt we added a 10% aqueous solution of NaOH at 0 °C. The liberated amine was extracted three times with 30 ml portions of ether. The extract was then dried (Na_2SO_4). Evaporation and distillation gave (+)-**2a** in a 35% (4.6 g) yield. $[\alpha]_D$ +9.5° (c=4, Et_2O).

The resolution of **2b**—**2g** were carried out in manners similar to that described above; the yields and specific rotations are shown in Table 2.

*(+)-N-Benzylbenzylmethylphenylsilylmethylamine (**3**).* A solution of **2a** (17.5 g, 0.0726 mol) $[\alpha]_D$ +12.5° (c=2, Et_2O), benzyl chloride (9.2 g, 0.0727 mol), and triethylamine (22.0 g,

0.257 mol) was stirred for 5 h at 100 °C. A large amount of a white solid was precipitated at the end of the reaction. Into the reaction mixture, water (20 ml) and hexane (100 ml) were then added. The organic layer was separated, washed with a 10% NaOH solution until the white precipitate could not be observed, and then dried (Na_2SO_4). Evaporation and distillation gave (+)-**3**. Bp 155—160 °C/0.07 Torr. Yield, 20.1 g (83.6%). $[\alpha]_D$ +10.0° (c=2, MeOH). NMR δ 0.25 (s, 3, Si-CH_3), 1.05 (broad s, 1, NH), 2.30 (s, 2, Si-CH_2-N), 2.40 (s, 2, Si-CH_2-Ph), 3.75 (s, 2, N-CH_2-Ph), 7.0—7.5 (m, 15, Ph). Found: N, 4.32%. Calcd for $C_{22}H_{25}NSi$: N, 4.22%.

(−)-N-Benzyl-N-methylbenzylmethylphenylsilylmethylamine (4). To a solution of (+)-**3** (20.1 g, 0.0606 mol) $[\alpha]_D$ +10.0 (c=2, MeOH), in THF (150 ml) we added *n*-BuLi (5 ml of a 10% wt/v hexane solution, *ca.* 8 mmol) by means of a syringe under a nitrogen atmosphere. The color of the solution changed to red immediately. After the solution had been stirred for 10 h at room temperature, water (50 ml) was added to the red solution. The organic layer was separated, washed with water, and then dried (K_2CO_3). Subsequent evaporation and distillation gave (−)-**4**. Bp 150 °C/0.04 Torr. Yield, 15.5 g (77.1%). $[\alpha]_D$ −15.5° (c=2, Et_2O). NMR δ 0.32 (s, 3, Si-CH_3), 2.36 (s, 3, N-CH_3), 2.52 (d, 2, Si-CH_2-Ph), 3.86 (s, 2, N-CH_2-Ph), 6.8—7.7 (m, 15, Ph). Found: N, 4.38%. Calcd for $C_{22}H_{25}NSi$: N, 4.22%.

(−)-Benzylmethylphenylsilanol (5). A solution of (−)-**4** (15.8 g, 0.0477 mol) $[\alpha]_D$ −15.5° (c=2, Et_2O) in ether (150 ml) was treated with 0.2 M HCl (150 ml) in a separating funnel at 0 °C. The organic layer was washed with water and then dried (K_2CO_3). Evaporation of the solvent gave (−)-**5**. The silanol, (−)-**5**, was used in the next reaction without further purification. $[\alpha]_D$ −13.2° (c=2, Et_2O). IR (neat) 3250 cm^{-1} (OH). NMR δ 0.25 (s, 3, Si-CH_3), 2.30 (s, 2, Si-CH_2-Ph), 2.7—3.0 (1, OH), 6.8—7.5 (m, 10, Ph).

(−)-Benzylmethylphenylsilane (6). A solution of (−)-**5**, obtained from the experiment described above, in dibutyl ether was added to a suspension of $LiAlH_4$ (6.0 g, 0.158 mol) in ether (150 ml). The mixture was kept at 90 °C for 30 min and then the solvent was removed. Then the mixture was stirred for 3 h at 140—145 °C. After satu. aqueous Na_2SO_4 had been carefully added to the mixture with ice cooling, the organic layer was separated, washed with dil HCl with water, and then dried ($CaCl_2$). Subsequent evaporation and distillation gave (−)-**6**. Bp 150—154 °C/20 Torr. Yield, 8.0 g (79.2% based on (−)-**4**). $[\alpha]_D$ −17.8° (c=2, Et_2O). IR (neat) 2100 cm^{-1} (Si-H). NMR δ 0.29 (d, J=3.5 Hz, 3, Si-CH_3), 2.34 (d, 2, Si-CH_2-Ph), 4.43 (sixted, 1, Si-H), 6.8—7.5 (m, 10, Ph).

(−)-Benzyl(chloro)methylphenylsilane (7). A solution of (−)-**6** (1.0 g, 0.0047 mol) and BPO (84 mg, 0.3 mmol) in CCl_4 (5 ml) was sealed in a sample tube under nitrogen atmosphere. The tube was then maintained for 11 h at 80 °C. The subsequent evaporation of the solvent gave (−)-**7**, $[\alpha]_D$ −25.0° (c=1, CCl_4). From the IR spectrum of the product, it was observed that the product contained about 10% of unreacted (−)-**6**. The chlorosilane (−)-**7** was extremely moisture-sensitive, and racemization occurred immediately in the presence of a trace of moisture. The product was used without further purification.

(+)-Benzylmethoxymethylphenylsilane (8). To a mixture of (−)-**6** (2.0 g, 0.0094 mol) $[\alpha]_D$ −17.8° (c=2, Et_2O), 5% Pd-C (0.2 g) in pentane (20 ml) we added methanol (1.0 g, 0.031 mol) at 0 °C. The evolution of hydrogen occurred over a period of 3 h. After bubbling had stopped, the reaction mixture was filtered to remove the catalyst. Subsequent evaporation and distillation gave (+)-**8**. Bp 158—160 °C/20 Torr. Yield, 1.8 g (78.9%). $[\alpha]_D$ +4.4° (c=2, pentane), $[\alpha]_D$ +5.3° (c=2, Et_2O). NMR δ 0.24 (s, 3, Si-CH_3), 2.32 (s, 2, Si-CH_2-Ph), 3.60 (s, 3, O-CH_3), 6.8—7.6 (m, 10, Ph).

When the reaction was carried out at a temperature above 0 °C, it was observed that racemization took place.

Reduction of (−)-7 with $LiAlH_4$. To a suspension of $LiAlH_4$ (1 g, 0.026 mol) in ether (15 ml) was added (−)-**7**, $[\alpha]_D$ −18.9° (c=2, CCl_4). The mixture was refluxed for 2 h with stirring and then hydrolyzed with satur. Na_2SO_4. The organic layer was separated, washed with dil HCl, water, and then dried ($CaCl_2$). Subsequent evaporation and distillation gave (+)-**6**. Bp 150 °C/20 Torr. Yield, 0.45 g (45%). $[\alpha]_D$ +8.3° (c=2, Et_2O). The IR spectrum of the product was identical with that of (−)-**6**.

Reduction of (+)-8 with $LiAlH_4$. A solution of (+)-**8** (2.0 g, 0.0083 mol) $[\alpha]_D$ +2.7° (c=2, Et_2O) in ether (20 ml) was added to a suspension of $LiAlH_4$ (1 g, 0.026 mol) in ether (15 ml). The mixture was then refluxed for 3 h, followed by hydrolysis with satur. Na_2SO_4. The organic layer was separated, washed, and then dried ($CaCl_2$). Subsequent evaporation and distillation gave (+)-**6**. Yield, 1.5 g (86%). $[\alpha]_D$ +7.6° (c=2, Et_2O). The IR spectrum of the product was identical with that of (−)-**6**.

Reaction of (−)-7 with 1-Naphthyllithium. To a solution of 1-bromonaphthalene (2 g, 0.0097 mol) in ether (100 ml) we added *n*-BuLi (4 ml of a 10% wt/v solution in hexane, *ca.* 0.0063 mol) by means of a syringe under a nitrogen atmosphere.[15] The mixture was then stirred for 30 min at room temperature. After a solution of (−)-**7** (1.0 g, 0.0047 mol) $[\alpha]_D$ −15.0° (c=1, CCl_4) in ether (5 ml) had been added to this mixture, it was stirred for 4 h at room temperature and then hydrolyzed. The organic layer was separated, washed with dil HCl, water, and then dried ($CaCl_2$). The subsequent evaporation of the solvent gave a pale yellow residue. Column chromatography of the residue was carried out (silica gel, hexane:benzene=4:1). The eluent was evaporated, and the viscous residue was distilled. Bp 182 °C/0.08 Torr. Yield, 0.8 g (54%). $[\alpha]_D$ −2.0° (c=3, pentane) (lit,[5] $[\alpha]_D$ −6.68° (c=2.8, pentane)). IR (neat) 1595, 1495, 1210, 985 cm^{-1}. NMR δ 0.57 (s, 3, Si-CH_3), 2.81 (s, 2, Si-CH_2-Ph), 6.7—8.1 (m, 18, Ph, 1-$C_{10}H_7$).

Reaction of (+)-8 with 1-Naphthyllithium. To a solution of 1-naphthyllithium prepared from 2 g (0.0097 mol) of 1-bromonaphthalene in ether (100 ml) and 4 ml of 10% wt/v *n*-BuLi in hexane as described above, we added (+)-**8** (1.0 g, 0.0041 mol) $[\alpha]_D$ +2.1° (c=2, pentane) in ether (5 ml). After the mixture had been stirred for 4 h at room temperature, it was hydrolyzed. The organic layer was separated, washed with dil HCl, water, and then dried ($CaCl_2$). The subsequent evaporation of the solvent gave an oily product. Chromatography (silica gel, hexane:benzene=4:1) and subsequent distillation gave (−)-**9**. Bp 191 °C/0.1 Torr. $[\alpha]_D$ −1.9° (c=2, pentane). The IR spectrum of the product was identical with that of (−)-**9**, obtained from the reaction of (−)-**7** with 1-naphthyllithium.

Reaction of (−)-7, and (+)-8 with n-BuLi. To a solution of (−)-**7**, $[\alpha]_D$ −19.0° (c=3, CCl_4), prepared from (−)-**6** (1 g, 0.0047 mol), $[\alpha]_D$ −13.5° (c=2, Et_2O) in ether (100 ml) we added 4 ml of a 10% wt/v solution of *n*-BuLi by means of a syringe at 0 °C. After having been stirred for 1 h at 0 °C, the mixture was hydrolyzed. The usual work-up of the mixture gave (+)-**10**. Bp 155—160 °C/14 Torr. Yield, 67.2%. $[\alpha]_D$ +5.0° (c=3, CH_2Cl_2). NMR

δ 0.20 (s, 3, Si-CH_3), 0.5—1.5 (m, 9, Bu), 2.28 (s, 2, Si-CH_2-Ph), 6.7—7.5 (m, 10, Ph). The reaction of (+)-**8** (1 g, 0.0041 mol) $[\alpha]_D$ +2.7° (c=2, Et_2O) with n-BuLi was carried out in the same manner. The compound (+)-**10** was thus obtained in a 72% (0.8 g) yield. $[\alpha]_D$ +5.8° (c=3, CH_2Cl_2). The IR and NMR spectra of the product were identical with those of (+)-**10**, obtained from the reaction of (−)-**7** with n-BuLi, as has been described above.

Reaction of (−)-7, and (+)-8 with o-*Tolyllithium.* To a solution of o-bromotoluene (1 g, 0.0058 mol) in ether (70 ml) we added 3 ml (*ca.* 0.0047 mol) of a 10% wt/v hexane solution of butyllithium by means of a syringe.[16] After the mixture has been stirred for 30 min at room temperature, (−)-**7** (1 g, 0.0041 mol) $[\alpha]_D$ −10.6° (c=2, CCl_4) in ether (5 ml) was added to the mixture at 0 °C. The usual work-up of the mixture gave (+)-**11** in a 75% (0.92 g) yield. Bp 155 °C/0.2 Torr. $[\alpha]_D$ +5.0° (c=4, CH_2Cl_2). NMR δ 0.43 (s, 3, Si-CH_3), 2.18 (s, 3, C-CH_3), 2.64 (s, 2, Si-CH_2-Ph), 6.7—7.5 (m, 10, Ph).

The reaction of (+)-**8** (1.0 g, 0.0041 mol) $[\alpha]_D$ +2.7° (c=2, Et_2O) with o-tolyllithium was carried out in a similar manner. The compound (+)-**11** was obtained in an 80% (0.99 g) yield. $[\alpha]_D$ +7.3° (c=2, CH_2Cl_2). The IR and NMR spectra of the product were identical with those of the product obtained by the reaction of (−)-**7** with o-tolyllithium.

Reaction of (−)-7, and (+)-8 with p-*Tolyllithium.* To a solution of p-bromotoluene (1.0 g, 0.0058 mol) in ether (100 ml) we added 3 ml (*ca.* 0.0047 mol) of a 10% wt/v hexane solution of butyllithium.[15] The mixture was stirred for 20 min at room temperature, and then (−)-**7** (1.0 g, 0.0041 mol) $[\alpha]_D$ −17.5° (c=1, CCl_4) was added to the mixture at 0 °C. The usual work-up of the mixture gave (−)-**12** in a 58% (0.7 g) yield. Bp 160 °C/0.2 Torr. $[\alpha]_D$ −4.5° (c=2, CH_2Cl_2). NMR δ 0.41 (s, 3, Si-CH_3) 2.33 (s, 3, C-CH_3), 2.55 (s, 2, Si-CH_2-Ph), 6.7—7.5 (m, 10, Ph).

The reaction of (+)-**8** (1.0 g, 0.0041 mol) $[\alpha]_D$ +4.4° (c=2, pentane) with p-tolyllithium was carried out in a similar manner. The compound (−)-**12** was thus obtained in a 48% (0.6 g) yield. $[\alpha]_D$ −5.5° (c=2, CH_2Cl_2).

Reaction of (−)-7, and (+)-8 with p-*Anisyllithium.* To a solution of p-anisyllithium prepared from p-bromoanisole (1.0 g, 0.0053 mol) in ether (100 ml) and 3 ml of 10% wt/v solution of butyllithium, we added (−)-**7** (1.0 g, 0.0041 mol) $[\alpha]_D$ −17.5° (c=1, CCl_4). After the mixture had been stirred for 2 h at room temperature, the usual work-up of the mixture gave (−)-**13** in a 50% (0.65 g) yield. Bp 175—180 °C/0.2 Torr. $[\alpha]_D$ −7.7° (c=2.5, CH_2Cl_2). NMR δ 0.40 (s, 3, Si-CH_3), 2.55 (s, 2, Si-CH_2-Ph), 3.75 (s, 3, O-CH_3), 6.7—7.5 (m, 10, Ph).

The reaction of (+)-**8** (1.0 g, 0.0041 mol) $[\alpha]_D$ +3.5° (c=2, pentane) with p-anisyllithium was carried out in a similar manner. The compound (−)-**13** was obtained in a 54% (0.7 g) yield. $[\alpha]_D$ −7.8° (c=3, CH_2Cl_2).

Reaction of (−)-7, and (+)-8 with Allyllithium. To a solution of allyllithium,[18] prepared from allyltriphenyltin (3.2 g, 0.0082 mol) and PhLi (0.0080 mol) in ether (70 ml), we added (−)-**7** (1.0 g, 0.0041 mol) $[\alpha]_D$ −11.0° (c=2, CCl_4) in ether (5 ml) with stirring at 0 °C. After the mixture had been stirred for 2 h at 0 °C, the precipitated tetraphenyltin was filtered off. The organic layer was washed with water and then dried ($CaCl_2$). Subsequent evaporation and distillation gave (+)-**14** in a 68% (0.7 g) yield. Bp 132—135 °C/0.2 Torr. $[\alpha]_D$ +0.82° (c=3.6, CH_2Cl_2). IR (neat) 1625 cm^{-1} (C=C). NMR δ 0.20 (s, 3, Si-CH_3) 1.75 (d, J=7.5 Hz, 2, Si-CH_2-C), 2.28 (s, 2, Si-CH_2-Ph), 4.5—5.0 (m, 2, =CH_2), 5.3—6.1 (m, 1, -CH=C), 6.7—7.5 (m, 10, Ph).

The reaction of (+)-**8** (1.0 g, 0.0041 mol) $[\alpha]_D$ +3.5° (c=2, pentane) with allyllithium was carried out in a similar manner. The compound (−)-**14** was thus obtained in a 59% (0.6 g) yield. $[\alpha]_D$ −1.0° (c=7, CH_2Cl_2).

Reaction of (+)-8 with p-*Tolylmagnesium Bromide.* To a solution of p-tolylmagnesium bromide, prepared from p-bromotoluene (5.0 g, 0.029 mol) and Mg (0.85 g, 0.035 mol) in ether (50 ml), we added a solution of (+)-**8** (1.0 g, 0.0041 mol) $[\alpha]_D$ +3.5° (c=2, pentane) in ether (5 ml). The mixture was refluxed for 30 h with stirring. The usual work-up of the mixture gave (−)-**12** in a 45% (0.46 g) yield. $[\alpha]_D$ −3.7° (c=6, CH_2Cl_2). The IR and NMR spectra of the product were identical with those of the product obtained by the reaction of (+)-**8** with p-tolyllithium.

The authors wish to thank the Shin-etsu Chemical Industry Co. for the gift of the organosilanes.

References

1) a) L. H. Sommer, "Stereochemistry, Mechanism and Silicon," McGraw-Hill, New York (1965); b) L. H. Sommer and M. A. Silverman, *J. Org. Chem.*, **38**, 656 (1973).

2) a) G. Eabon and C. G. Pitt, *J. Chem. Soc.*, **1966**, 1524; b) A. G. Brook, H. W. Kucera, and D. M. MacRae, *Can. J. Chem.*, **48**, 818 (1970); c) R. Corriu and G. Lanneau, *J. Organomet. Chem.*, **64**, 63 (1974); d) R. Corriu and G. Royo, *ibid.*, **14**, 291 (1968); e) R. Corriu and J. Masse, *Bull. Soc. Chim. Fr.*, **1968**, 3491; f) R. Corriu and J. Moreau, *ibid.*, **1975**, 901.

3) T. Araki, D. Terunuma, H. Nohira, H. Isomura, T. Nakamura, and K. Okayasu, *Kobunshi Ronbunshu*, **32**, 557 (1975).

4) D. Terunuma, T. Okada, T. Araki, and H. Nohira, *Chem. Lett.*, **1975**, 675.

5) L. H. Sommer, W. D. Korte, and P. G. Rodewald, *J. Am. Chem. Soc.*, **89**, 862 (1967).

6) J. E. Noll, J. L. Speier, and B. F. Daubert, *J. Am. Chem. Soc.*, **73**, 3867 (1967).

7) a) J. M. Duff and A. G. Brook, *Can. J. Chem.*, **55**, 2587 (1977); b) A. G. Brook, M. D. MacRae, and W. W. Limburg, *J. Am. Chem. Soc.*, **89**, 5493 (1967).

8) L. H. Sommer and J. D. Citron, *J. Am. Chem. Soc.*, **89**, 5797 (1967).

9) L. H. Sommer, C. L. Frye, and G. A. Parker, *J. Am. Chem. Soc.*, **86**, 3276 (1964).

10) A. Holt, A. W. Jarvie, and G. J. Jervis, *J. Chem. Soc., Perkin Trans. 2*, **1973**, 114.

11) H. Sakurai, *Nippon Kagaku Zasshi*, **91**, 885 (1970).

12) L. H. Sommer and H. Fujimoto, *J. Am. Chem. Soc.*, **90**, 982 (1968).

13) A. Holt and M. J. Smith, *J. Chem. Soc., Perkin Trans. 2*, **1976**, 952.

14) L. H. Sommer and W. D. Korte, *J. Am. Chem. Soc.*, **89**, 5802 (1967).

15) H. Gilman and F. W. Moore, *J. Am. Chem. Soc.*, **62**, 1845 (1940).

16) H. Gilman, W. Langharm, and F. W. Moore, *J. Am. Chem. Soc.*, **62**, 2327 (1940).

17) D. Seyferth and W. A. Weiner, *J. Org. Chem.*, **26**, 4797 (1961).

 © 1980 The Chemical Society of Japan Bull. Chem. Soc. Jpn., 53, 795—799 (1980)

The Study of Surfactant-Alcohol Mixed Micelles Using Conductance, Viscosity, and Electromotive Force Measurements

Toshihiro TOMINAGA,† Theodore B. STEM, Jr., and D. Fennell EVANS*

Department of Chemical Engineering, Carnegie-Mellon University, Pittsburgh, Pennsylvania 15213, U.S.A.

(Received April 28, 1979)

Conductance, viscosity, and EMF measurements were used to characterize solutions containing surfactant–alcohol micelles. The materials studied included sodium dodecyl sulfate (SDS), sodium octyl sulfate (SOS), decyltrimethylammonium bromide (DTAB), hexadecyltrimethylammonium bromide (CTAB) and the alcohols 1-pentanol through 1-octanol. The addition of alcohols caused the conductance of a 2% SDS solution to increase, and of a 3% solution of DTAB and of a 7% solution of SOS to decrease. CTAB showed both increases and decreases upon addition of alcohol. The EMF measurements permitted the concentration of free surfactant monomer and of unbound counterion in equilibrium with the micelle to be determined. When combined with the viscosity data, the change in conductance upon addition of alcohol can be interpreted in terms of changes in micellar shape and in the concentration of involved ions.

The aqueous solubility of many sparingly soluble organic compounds such as long-chain alcohols, lipids or hydrocarbons can be increased considerably by the addition of surfactant.[1] At surfactant concentrations above the critical level at which aggregation into micells occurs, such solubilization may have a profound influence on the physical properties of the solution. For example, the conductance of such mixed micellar solutions can decrease or increase by as much as 50% upon the addition of aliphatic alcohols. In spite of the importance of mixed micellar solutions in many industrial and biological processes such as detergency, polymeric synthesis and digestion, they have received far less attention than the simple binary surfactant–water systems. In order to study mixed micellar solutions in more detail we have carried out conductance, viscosity, and EMF measurements upon alkyltrimethylammonium bromide and sodium alkyl sulfate solutions as a function of added aliphatic alcohols.

Experimental

Apparatus and Technique. The conductance measurements were carried out in two cells: a Kraus-Erlenmeyer-type cell[2] with a cell constant equal to 2.383 for dilute solutions and a Mysels donut-type cell[3] with a cell constant equal to 47.87 for concentrated solutions. The electrodes were slightly platinized in order to minimize the frequency dependence of the measured resistance. The solution in the cell was stirred with a Teflon-coated magnetic stirring bar, to facilitate the dissolution of alcohol. The conductance cells were immersed in a constant temperature oil bath controlled to 25±0.005 °C. A 100 W light bulb was placed above the cell in order to prevent condensation of water in the top of the conductance cell. A shielded Shedlowsky conductance bridge was used to measure the solution resistance.

A conductance run was made by placing the surfactant solution in the cell and adding small increments of alcohol to the surfactant solution using a 10 ml Pyrex weight burette. After each addition the conductance was followed until a steady resistance reading was obtained. When the mole fraction of alcohol was small, approximately half an hour was required to dissolve the alcohol. As the alcohol concentration was increased, a considerably longer time was required.

The viscosity of the surfactant–alcohol solutions was measured using Cannon-Ubbelohde viscometers. The measurements were carried out in a constant temperature water bath at 25 °C±0.01 °C.

EMF measurements were carried out on the surfactant solution using surfactant and counterion electrodes.[4] The liquid membrane surfactant electrodes contained an ion exchanger, tributylhexadecylammonium ion for the anion surfactant and cholanate ion for cation surfactant. The ion exchanger was dissolved in a membrane solution consisting of a mixture of *o*-dichlorobenzene–hexachlorobenzene–bromoacetanilide. An Orion 92-00-00 electrode body with an Orion porous membrane support comprised the surfactant electrode. The EMF concentration cell for the dodecyl sulfate, an ion (Ds^-), is given by

$$\mathrm{Ag/AgCl}\,\Big|\,\begin{matrix}\mathrm{NaCl}\\ \mathrm{SDS}\end{matrix}\,\Big|\,\begin{matrix}\mathrm{Bu_3N(C_{16}H_{33})Ds}\\ \text{in}\\ \text{o-dichlorobenzene}\end{matrix}\,\Big|\,\begin{matrix}\mathrm{SDS}\\ \text{sample}\end{matrix}\,\Big|$$

$$\begin{matrix}\mathrm{NH_4NO_3}\\ (5\mathrm{M})\end{matrix}\,\Big|\,\begin{matrix}\text{Orion}\\ \#90\text{-}00\text{-}02\\ \text{inner filling solution}\end{matrix}\,\Big|\,\mathrm{Ag/AgCl}$$

The sodium, bromide and reference electrodes were Orion #94-11A, #94-35A, and #90-02-00 respectively.

The EMF's were measured with an Orion Research Meter (Model 801A). In pure surfactant solution and in SDS–alcohol solution steady and reproducible values of EMF were obtained with the surfactant electrodes. However, reproducible results for DTAB–alcohol solution could not be obtained with the surfactant electrode. The counterion electrodes, however, did give satisfactory results in all surfactant–alcohol combinations studied. Reproducibility was determined by repeatedly measuring the EMF in pure micellar and mixed micellar solutions. This was conveniently done with an Orion Research Manual Electrode Switch (Model 605) which permitted up to six ion electrodes to be used with one common reference electrode. Detailed procedures are given elsewhere.[4]

Results and Discussion

Conductance measurements were carried out on sodium dodecyl sulfate (SDS), sodium octyl sulfate (SOS), decyltrimethylammonium bromide (DTAB), and hexadecylmethylammonium bromide (CTAB) as a function of added alcohol. The results are given in

† Present address: Department of Fundamental Natural Science, Okayama University of Science, 1-1 Ridai-cho, Okayama 700.

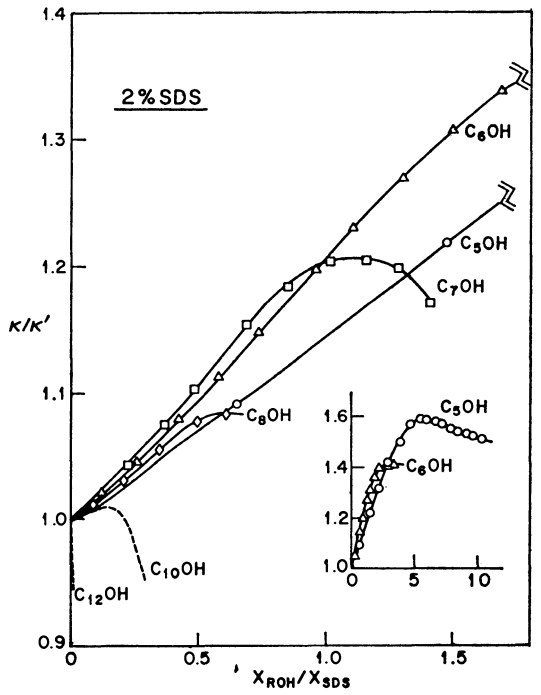

Fig. 1. The change in specific conductance of a 2% sodium dodecyl sulfate (SDS) solution upon addition of the aliphatic alcohols, pentanol through 1-octanol. The small insert shows the behavior upon addition of 1-pentanol and 1-hexanol up to the concentration at which the solution becomes cloudy.

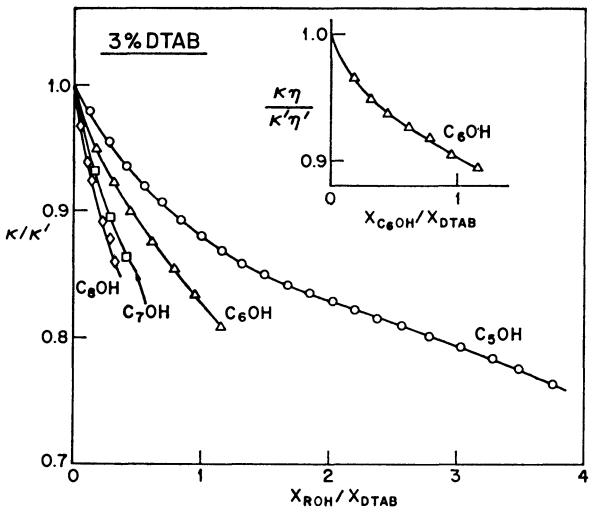

Fig. 2. The change in specific conductance of a 3% decyltrimethylammonium bromide (DTAB) solution upon addition of the aliphatic alcohols, 1-pentanol through 1-octanol. The small insert shows how the specific conductance-viscosity product for DTAB–1-hexanol solutions changes with composition.

Figs. 1—4. The initial concentration of surfactant was in all cases above the critical micelle concentration. The measurements extend up to the concentration of alcohol at which the solution becomes cloudy. Viscosity measurements were carried out on 21% SDS (0.069M), 3% DTAB (0.107M), and 2% (0.055M) and 5%

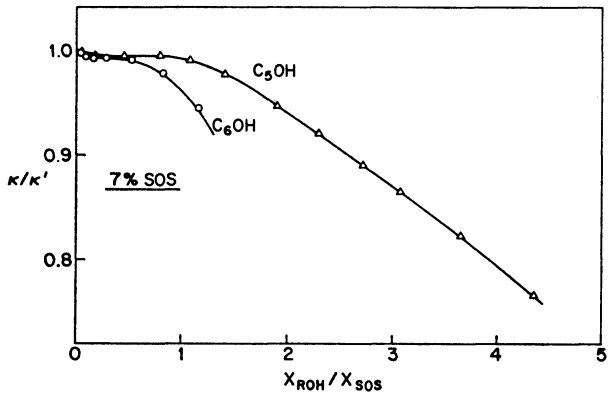

Fig. 3. The change in specific conductance of a 7% sodium octylsulfate (SOS) solution upon addition of 1-pentanol and 1-hexanol.

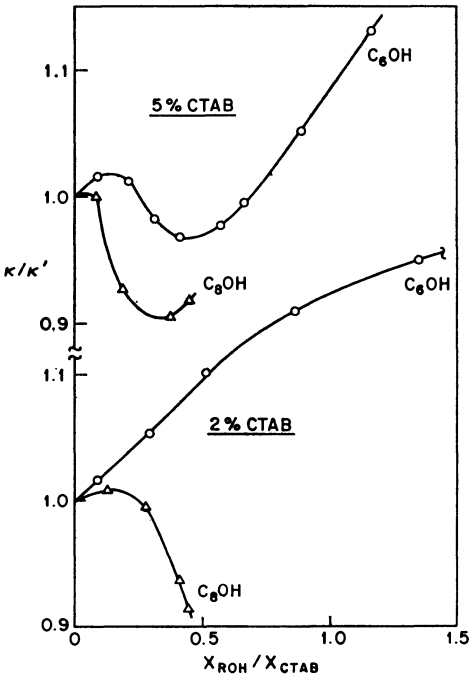

Fig. 4. The effect of surfactant concentration and alcohol chain length upon the specific conductance of hexadecyltrimethylammonium bromide (CTAB).

(0.137M) CTAB as a function of added 1-hexanol or 1-octanol and are shown in Fig. 5. EMF measurements were carried out on 2% SDS and 3% DTAB solutions as a function of added 1-hexanol and are given in Figs. 6 and 7 below.

In Figs. 1—4 the changes in specific conductance of the surfactants as a function of added alcohol are shown. The ratio of the specific conductance with and without added alcohol, κ/κ', is plotted *versus* the molar ratio of the alcohol to surfactant, x_{ROH}/x_S. If the change in surfactant concentration upon addition of alcohol is ignored, the value of κ/κ' can be replaced by the corresponding ratio of equivalent conductances. The figures show that the conductance curves are complex with initial slopes that increase in some cases, decrease in others and which may have maxima and minima.

Although it is unlikely that a single simple explanation will account for the variety of behavior, we will delineate the main factors that are responsible for the observed conductance.

In SDS solutions, while the conductance increases for all of the alcohols studied, the rate of increase and the maximum value attained depend upon the alcohol chain length. Our results for pentanol through heptanol are in agreement with the results given in graphical form by Lawrence and Pearson.[5] They measured the conductance of SDS upon addition of the alcohols, 1-ethanol through 1-heptanol. Their results show that the maximum conductance is observed for the SDS–1-pentanol solution at a mole ratio of 6 and that a 60% increase in conductance is observed. Our results show that the maximum initial slope is observed for 1-heptanol.

The conductance may be analyzed in more detail by taking into account the distribution of the alcohols between bulk water and micelles. From vapor pressure measurements of alcohols in equilibrium with a micellar solution, Hayase and Hayano[6] determined a distribution coefficient defined as

$$K = x_a/y_a = j/(S-\mathrm{CMC}(C_a)+C_a j/[(1-j)/55.5])$$

where y_a and x_a are the mole fractions in the aqueous phase and the micellar phase, respectively. The values of $1-j$ and j are the alcohol fractions in the aqueous and micellar phases, S is the total concentration of SDS, $\mathrm{CMC}(C_a)$ is the critical micelle concentration in the presence of alcohol, and C_a is the total concentration of the alcohol. Using the results for $\mathrm{CMC}(C_a)$ and K, the values of j shown in Table 3 can be calculated. For 1-pentanol most of the alcohol is in the aqueous phase while for 1-heptanol most is solubilized by the micelle. The partition coefficients in Table 1 permit the amount of alcohol solubilized at each value of x_{ROH}/x_{SDS} to be calculated. When these corrections are made, the values of the slope $d(\kappa/\kappa')/d(x_{ROH}/x_{DS})$ given in Table 1 are obtained. The corrected initial slopes for 1-pentanol, 1-hexanol, and 1-heptanol are very similar suggesting that these have identical effects upon the micelles. However, the initial slope is smaller for 1-octanol, and decreases further with increasing chain length.[7]

The initial increase in conductance of SDS upon the addition of alcohols can be attributed to the orientation of solubilized polar molecules with the polar head group remaining near the micellar surface and the hydrocarbon tails extending into the micellar interior. In pure SDS, the micelles are spherical and each surfactant molecule occupies approximately 60 Å^2 of surface.[8] The micelle exterior can thus be viewed as consisting of a number of surface sites. The incorporation of an alcohol molecule results in the surfactant molecules moving apart. This reduces the concentration of surfactant anions, lowers the surface charge density, and results in a release of bound counter ions.

Table 1. Effect of alcohols on the conductance of 2% SDS solution

Alcohols	K[a]	Uncorrected slope[b]	j[c]	Corrected slope[d]
C_5OH	722	0.14_4	0.50	0.25_5
C_6OH	2250	0.19_5	0.76	0.24_7
C_7OH	6020	0.21_0	0.90	0.23_7
C_8OH	16000	0.15_5	0.95	0.16_7

a) From Ref. 6. K for C_8OH was obtained by extrapolation of log K *vs.* alcohol-carbon-number curve. b) Initial slope of (κ/κ') *vs.* (x_{ROH}/x_{SDS}). c) (ROH, in micelle)/(ROH, total) at $x_{ROH}/x_{SDS}=0.3$. d) Initial slope of (κ/κ') *vs.* $(j\cdot x_{ROH}/x_{SDS})$.

Examination of the viscosity of the SDS–1-hexanol solutions supports this explanation. In Fig. 5, is shown the ratio η/η_{H_2O}, the relative viscosity for the micellar solution to that for water, *versus* the volume fraction of surfactant or surfactant plus alcohol. The surfactant volume was taken from the density data of Desnoyers.[9] For the alcohols, volumes were estimated using density data of pure substances.[10] The data for pure SDS fall on a straight line which extrapolates back to the intercept of η/η_{H_2O} close to unity. The data for SDS–1-hexanol fall on the same straight line indicating no change in micellar shape upon addition of alcohol.

In order to understand the behavior of these mixed micelles in more detail, we determined the activities of the sodium ions and dodecyl sulfate ions using ion electrodes. Since such electrodes give the activities of free ions, information about the sodium ions and dodecyl sulfate ions in equilibrium with the micelle can be determined.

We first measured the EMF of pure SDS solution and in Fig. 6 EMF *versus* log concentration of SDS is shown. In dilute solution, slopes close to the Nernst value of 59 mV per decade are obtained. At the CMC (8×10^{-3} M) a sharp break is observed. Above this concentration, the sodium activity continues to increase but with a smaller slope, reflecting the binding of counter ion to the micelle. The dodecyl sulfate activity decreases above the CMC. A positive slope corresponds to a decrease in activity for this ion. Assuming that activity coefficients can be ignored, the concentration

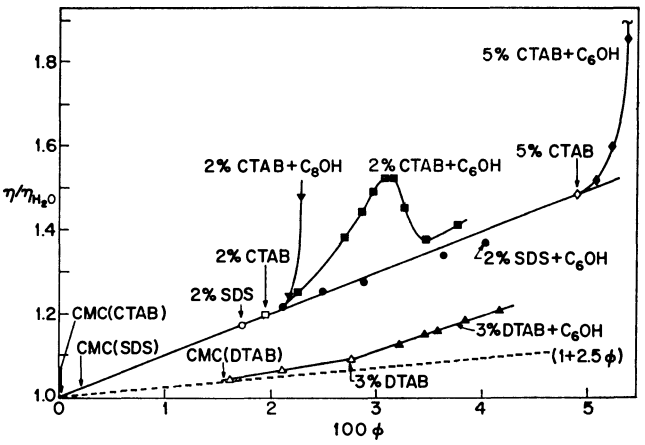

Fig. 5. The change in relative viscosity, η/η_{H_2O}, of SDS. DTAB and CTAB solutions upon addition of aliphatic alcohols as a function of volume fraction of added solute. The open points are for pure surfactant, the closed points are for surfactant plus alcohol; the dashed line represents $\eta=\eta_{H_2O}(1+2.5\,\varphi)$.

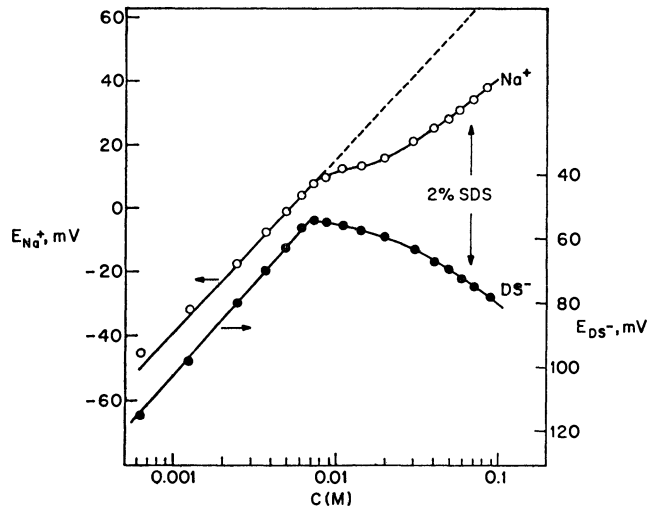

Fig. 6. The electromotive force (EMF) for sodium and dodecyl sulfate ions in 2% SDS solution. The break at 8×10^{-3} M corresponds to the CMC. Above this concentration the activities of Na^+ and Ds^- in equilibrium with the micelle can be determined.

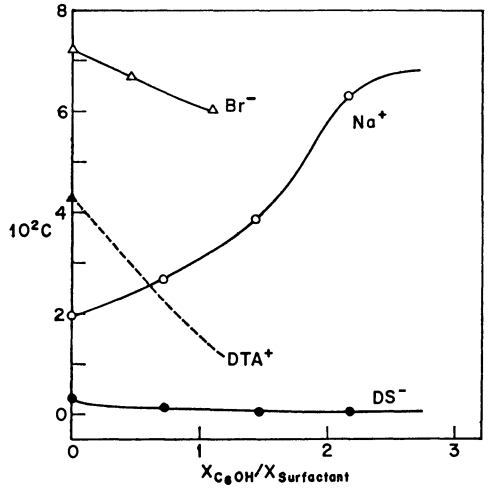

Fig. 7. The change in concentration of surfactant ions and counterions upon addition of 1-hexanol to 2% SDS and 3% DTAB as estimated from ionspecific electrodes.

of free monomer and unbound counter ion can be roughly estimated. In 2% SDS solution (0.068 M), the values of 0.02 M and 0.003 M are obtained for sodium ion and dodecyl sulfate ions respectively.

When 1-hexanol is added to 2% SDS, the ion activities change dramatically. The sodium ion concentration increases by a factor of 3 while the dodecyl sulfate concentration decreases by a factor of 10 as is seen in Fig. 7. Our results for the sodium ion activity are in substantial agreement with those of Lawrence and Pearson.[5] Since the initial concentration of free dodecyl sulfate ion is so small, even a major decrease has only a negligible effect on the conductance. However, the sodium electrode results show that the micelles release most of the bound counter ions, which results in a substantial increase in the conductance.

The conductance of DTAB–alcohol solutions is very different from that observed for SDS since it decreases upon addition of alcohol. One would expect that similarly to SDS, addition of polar compounds to DTAB should result in a release of counter ions. A decrease in the conductance of micellar solutions upon addition of non-polar solutes such as hydrocarbons is generally observed.[11] Such material appears to be solubilized entirely in the hydrocarbon interior of the micelle. The decrease in conductance arises from a corresponding increase in micellar size and perhaps by increases in counter ion binding.

One possible reason for the decrease in conductance of DTAB is that the addition of alcohol results in an increase in solution viscosity. However, the viscosity of DTAB increases by 10% up to a mole ratio, x_{ROH}/x_{DTAB}, of 1.1 while the conductance decreases by 20%. Alternatively, addition of alcohol could result in micellar reorganization such as a sphere to rod transition. This would cause the charged head groups to move closer together, increasing the micellar charge density and binding additional counter ions. That such a major reorganization does not occur can be seen from the relative viscosity shown in Fig. 5. There is a slight increase in the ratio, (η/η_{H_2O}), as 1-hexanol is added to 3% DTAB, however the increase is not as large as is usually observed for a major reorganization of micellar shape. Thus the viscosity measurements show that neither an increase in solution viscosity nor a change in micellar shape will account for the observed conductance behavior.

EMF measurements provide a clearer picture of what is happening. In a 3% (0.107M) DTAB solution the concentration of free Br^- is 0.072 M while that for DTA^+ is 0.043. Addition of 1-hexanol results in a small decrease in bromide concentration, when x_R/x_{DTAB} equals 1.1, the Br^- concentration drops to 0.060 M (see Fig. 7). Although we were not able to obtain reproducible EMF's with the DTA^+ ion electrode, the EMF decreased approximately 30 ± 10 mV suggesting a threefold decrease of monomer surfactant concentration. Since the initial concentration of free surfactant and counter ion are reasonably large, a substantial decrease in either species will have a pronounced effect on the conductance. Even in the case of 22% (0.33 M) DTAB solution the decrease in conductance is observed (Table 1) when 1-hexanol is added. This is mainly because surfactant monomer concentration is still reasonably high (0.032 M from EMF) even in such a concentrated solution.

A comparison of the SDS and DTAB results suggests that there may be major differences in the behavior of cationic and anionic surfactants upon the addition of aliphatic alcohols. However, when 1-pentanol and 1-hexanol are added to 7% (0.306 M) sodium octyl sulfate, the specific conductance decreases (Fig. 3). Similarly to DTAB, this suggests that the decrease in surfactant monomer concentration more than compensates for any change in sodium concentration. However, when the behavior for SDS and SOS are compared, the results suggest that the relative lengths of aliphatic chains in alcohol and surfactant may be an important factor in determining whether the conductance increases

or decreases. Inspection of Table 1 shows that when 1-octanol is added to SDS the increase in conductance is less than when 1-heptanol is added.

When the cationic surfactant chain becomes sufficiently long, addition of an alcohol can result in an initial increase in conductance as is shown in Fig. 4 for the addition of 1-hexanol to hexadecyltrimethylammonium bromide, CTAB. However, when 1-octanol is added the conductance increases slightly and then decreases rapidly. For 5% CTAB the addition of either 1-hexanol or 1-octanol results in both decreases and increases in the conductance. The viscosity of these solutions (Fig. 5) increases rapidly upon the addition of alcohol to either the 2% or 5% CTAB solution suggesting sphere to rod transitions.[12] In some cases the conductance rises even though the viscosity is also increasing. The behavior of 1-hexanol in 2% CTAB is pecular in this regard. Up to a mole ratio of 1.5 both the conductance and viscosity increase, above 1.5 they decrease. In general one would anticipate that an increase in viscosity would result in a decrease in conductance.

Conclusions

The results for SDS–alcohol and DTAB–alcohol micellar solutions show that when information from several experimental techniques is combined the main factors that determine the solution properties can be delineated. The two examples that we have considered in detail give reasonably simple behavior. The initial results in SOS and CTAB solution show that there are a number of complexities such as relative lengths of aliphatic chains in alcohol and surfactant, micellar reor anization and solution viscosity changes that are difficult to interpret unambiguously.

This work was supported by the National Science Foundation Grant ENG 77-02129.

References

1) a) T. Nakagawa and K. Shinudia, "Colloidal Surfactants," ed by E. M. Lobel, Academic Press, New York (1963), p. 139; b) P. H. Elworthy, A. T. Florence, and C. B. Macfarlane, "Solubilization by Surface-Active Agents and Its Application in Chemistry and the Biological Sciences," Chapman and Hall, London (1968).

2) H. M. Daggett, E. J. Blair, and C. A. Kraus, *J. Am. Chem. Soc.*, **73**, 799 (1951).

3) K. J. Mysels, *J. Phys. Chem.*, **65**, 1981 (1961).

4) a) T. J. Gilligan III., E. L. Cussler, and D. F. Evans, *Biochim. Biophys. Acta*, **497**, 627 (1977); b) K. Kale, E. L. Cussler, and D. F. Evans, *J. Phys. Chem.*, to be published.

5) A. S. C. Lawrence and J. T. Pearson, *Trans. Faraday Soc.*, **63**, 495 (1967).

6) K. Hayase and S. Hayano, *Bull. Chem. Soc. Jpn.*, **50**, 83 (1977).

7) Jung-Ja Lee, Ph. D. Thesis, Rutgers University (1966).

8) D. Stigter and K. J. Mysels, *J. Phys. Chem.*, **59**, 45 (1955).

9) G. M. Musbally, G. Perron, and J. E. Desnoyers, *J. Colloid Interface Sci.*, **48**, 494 (1974).

10) "Selected Values of Properties of Hydrocarbons and Related Compounds," American Petroleum Institute Research Project 44, Thermodynamics Research Center, Texas A & M University (1963).

11) A. J. Hyde and D. M. Stevenson, *Kolloid-Z. Z. Polym.*, **232**, 797 (1969).

12) The molar volume of CTAB is taken from P. Ekwall, L. Mandell, and P. Solyom, *J. Colloid Interface Sci.*, **35**, 519 (1971).

© 1980 The Chemical Society of Japan

NOTES

Bull. Chem. Soc. Jpn., 53, 800 (1980)

A Valence Structural Study of the Electronic Structure of S_2N_2

Hiroshi FUJIMOTO* and Takashi YOKOYAMA
Faculty of Engineering, Kyoto University, Kyoto 606

(Received December 6, 1978)

Synopsis. A valence structural analysis of S_2N_2 has been performed within the framework of the INDO approximation. The fractional double-bond character has been suggested to be the consequence of the interaction between nonionic and ionic structures, counterbalanced in part by the overlap repulsions in the ring.

The strength of pi-bonds in polar conjugated systems is a matter of great concern both experimentally and theoretically. For instance, the dimeric sulfur nitride, S_2N_2, decomposes very rapidly above −80 °C to give larger rings and polymeric materials.[1] In order to explain the weak pi-bond character of the four equivalent sulfur–nitrogen bonds, Patton and Raymond proposed that the ionic structures, II, III, IV, and V, shown in Fig. 1 should be dominant in the ground state of the S_2N_2 molecule.[2] In the course of our studies of the mechanisms of the formation and breaking of chemical bonds, we obtained a somewhat different view of the pi-bonds in S_2N_2. In this note, we wish to report the results of our qualitative calculation.

Results of Calculation

The S_2N_2 ring was assumed to be square-planar, with sulfur and nitrogen alternating at the bond distance of 1.619 Å.[3] The 3d atomic orbitals of the sulfur atoms were disregarded tentatively, since their participation has been reported to be insignificant.[4] The distribution of sigma electrons was determined by the INDO MO calculation without configuration interaction.[5] Then, this distribution was used to constitute the sigma core in the evaluation of the diagonal and off-diagonal matrix elements of the secular equation for the pi-electron configurations, I—X, in the valence-bond calculation. Table 1 gives the energies of these structures, as calculated within the framework of the INDO approximation. The nonionic structure, I, was found to lie lower than the other structures. Table 2 indicates clearly that the structures I and VI participate significantly in the ground state of S_2N_2. The linear combination of the structures II, III, IV, and V was found to be a poor representation, yielding an energy which was 7.7 eV higher than the ground state in the present calculation.

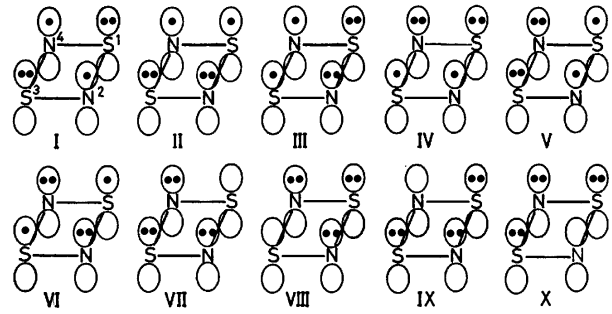

Fig. 1. Pi-electron configurations of S_2N_2.

The interactions of the valence structures I and VI with the structures II, III, IV, and V are obviously the major source of the pi character of the S–N bonds. The double-bond character is partially lifted because of the overlap repulsions which are inherent in the ring containing six pi-electrons on four centers.[6] In particular, the structures II—V themselves contribute to the weakening of the S–N bonds.

TABLE 1. THE RELATIVE ENERGIES OF VALENCE STRUCTURES

Structure	Energy/eV[a]
I	4.30
II, III, IV, V	9.33
VI	9.69
VII, VIII	16.93
IX, X	18.23

a) The ground state of S_2N_2 was taken as the standard.

TABLE 2. THE COEFFICIENTS OF VALENCE STRUCTURES IN THE GROUND-STATE WAVE FUNCTION OF S_2N_2

Structure	Coefficient
I	0.710
II, III, IV, V	0.305
VI	0.290
VII, VIII	0.103
IX, X	0.099

References

1) a) A. G. MacDiarmid, C. M. Mikulski, P. J. Russo, M. S. Saran, A. F. Garito, and A. J. Heeger, *J. Chem. Soc., Chem. Commun.*, **1975**, 476; b) C. M. Mikulski, P. J. Russo, M. S. Saran, A. G. MacDiarmid, A. F. Garito, and A. J. Heeger, *J. Am. Chem. Soc.*, **97**, 6358 (1975).

2) R. L. Patton and K. N. Raymond, *Inorg. Chem.*, **8**, 2426 (1969).

3) a) J. R. Warn and D. Chapman, *Spectrochim. Acta*, **22**, 1371 (1966); b) M. P. S. Collins and B. J. Duke, *J. Chem. Soc., Chem. Commun.*, **1976**, 701.

4) R. A. Adkins and A. G. Turner, *J. Am. Chem. Soc.*, **100**, 1383 (1978).

5) a) J. A. Pople and D. L. Beveridge, "Approximate Molecular Orbital Theory," McGraw-Hill, New York, N. Y. (1970); b) The standard parameters were used for nitrogen. As for sulfur, the standard CNDO parameters given by Pople (Ref. 5a) were incorporated with the one-center exchange-repulsion integrals taken from Stevenson and Burkey. See E. Stevenson and D. L. Burkey, *J. Am. Chem. Soc.*, **96**, 3061 (1974).

6) On the role of overlap repulsions, see, for instance, H. Fujimoto, Y. Osamura, and T. Minato, *J. Am. Chem. Soc.*, **100**, 2954 (1978), and the references cited therein.

The Crystal Structure of the β Form of *p*-Chlorobenzamide

Taiichi HAYASHI, Kazuaki NAKATA,* Yoshito TAKAKI, and Kiichi SAKURAI
Department of Physics, Osaka Kyoiku University, Tennoji-ku, Osaka 543

(Received August 20, 1979)

Synopsis. The crystal of the title compound is monoclinic, with space group $P2_1/a$, $a=9.11$, $b=9.54$, $c=8.18$ Å, $\beta=93.8°$, $Z=4$. The structure was solved by a packing analysis based on an ellipsoid-model and refined by block-diagonal least-squares calculations to $R=0.115$. The amide group makes a dihedral angle of 2.0° with the benzene ring.

p-Chlorobenzamide, C_7H_6ClNO, exhibits two polymorphs at room temperature.[1] They are triclinic with space group $P\bar{1}$ (α form) and monoclinic with $P2_1/a$ (β form). The structures of the α form at room temperature and −120 °C have been determined by Taniguchi *et al.*[2] Harada *et al.*[1] obtained crystals of the β form from an acetone solution, but they gave only crystal data. Therefore in this paper we deal with the structure determination of the β form.

Experimental

Many attempts were made to obtain crystals of the β form from acetone and other solutions, but they were all unsuccessful. Intensity data were then collected from Weissenberg photographs about the b axis ($k=0$—6) which have been prepared by Harada *et al.*,[1] although the quality of the photographs was rather poor. The intensities of 1067 reflections were measured visually and corrected for Lorentz and polarization factors. The cell dimensions were reconsidered on closer examination of the oscillation and Weissenberg photographs. The revised crystal data are: $a=9.11$ (10), $b=9.54$ (7), $c=8.18$ (15) Å, $\beta=93.8(5)°$, $Z=4$, space group $P2_1/a$.

A trial structure was successfully obtained from a packing analysis based on an ellipsoid-model[3] including a centrosymmetric dimer. The structure was refined by successive Fourier and by block-diagonal least-squares calculations[4] with a weighting scheme $w=1-\exp(-20\,s^2)$ with $s=\sin\theta/\lambda$. All the H atoms located from a difference Fourier map were included in the structure-factor calculations with an isotropic temperature factor of $B=4.0$ Å^2. The final R value was 0.115. The final atomic coordinates and thermal parameters are listed in Table 1.[5] All computations were made on an ACOS System 800 computer of the Computation Center of Osaka University.

Results and Discussion

Bond lengths and angles for the non-hydrogen atoms are shown in Fig. 1. The mean estimated standard deviations are 0.01 Å and 0.7°. The dihedral angle between the plane of the amide group and the mean plane of the benzene ring is 2.0°. This value is very close to that in *p*-nitrobenzamide[6] (2.3°), but unusually small as compared with those in the related amides, which vary from about 23°[7] to 29°.[8] The very small dihedral angle may give rise to a marked 'in-plane' bending of the C(1)–C(2) bond to reduce the interaction of the ortho-hydrogen with one of the NH_2 pro-

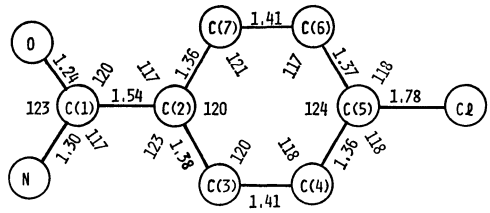

Fig. 1. A schematic diagram of the molecule showing the numbering of the atoms and the bond lengths (l/Å) and angles (ϕ/°).

TABLE 1. ATOMIC COORDINATES (×10³) AND THERMAL PARAMETERS (×10⁴) WITH THEIR ESTIMATED STANDARD DEVIATIONS

The anisotropic thermal parameters are of the form: $\exp\{-(B_{11}h^2+B_{22}k^2+B_{33}l^2+B_{12}hk+B_{13}hl+B_{23}kl)\}$.

	x	y	z	B_{11}	B_{22}	B_{33}	B_{12}	B_{13}	B_{23}
Cl	826(2)	9(3)	447(2)	76(2)	216(5)	269(4)	−33(4)	−101(4)	69(7)
C(1)	225(5)	6(7)	86(6)	77(6)	36(11)	179(10)	−22(11)	−9(12)	−19(15)
C(2)	377(5)	0(7)	181(6)	75(6)	60(11)	161(9)	8(11)	11(11)	19(15)
C(3)	462(6)	−120(8)	188(7)	93(7)	89(13)	186(13)	7(13)	1(13)	−11(17)
C(4)	601(6)	−119(9)	276(7)	86(7)	163(16)	197(12)	47(15)	−27(14)	−1(21)
C(5)	649(5)	4(8)	343(7)	63(6)	102(13)	188(11)	−8(12)	−19(12)	22(17)
C(6)	567(6)	125(9)	341(7)	99(7)	107(14)	189(11)	−49(14)	−27(14)	6(18)
C(7)	427(6)	120(8)	254(7)	87(6)	67(12)	213(12)	−14(13)	−17(13)	6(18)
N	177(5)	−108(7)	12(6)	81(6)	111(11)	222(11)	−13(12)	−54(12)	−24(16)
O	152(4)	116(6)	87(5)	86(5)	89(9)	259(10)	33(9)	−66(11)	−37(14)
H(3)	424	−210	136						
H(4)	675	−206	290						
H(6)	610	215	382						
H(7)	364	208	250						
H(N1)	92	−125	−50						
H(N2)	233	−201	−24						

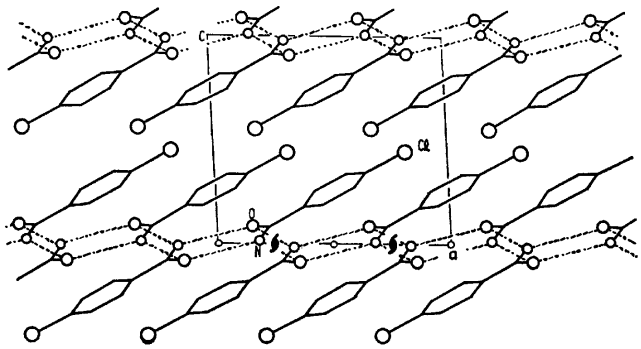

Fig. 2. The structure viewed along the b axis.

tons.[6] In fact, the difference between the C(1)–C(2)–C(3) and C(1)–C(2)–C(7) bond angles in the present compound and *p*-nitrobenzamide are remarkably large (6.0 and 6.7° respectively) as compared with those in the related amides.

The crystal structure viewed along the b axis is shown in Fig. 2. It consists of a stacking of hydrogen-bonded layers parallel to (001). Within a layer, two molecules are linked by NH···O hydrogen bonds of 3.06 Å to form a centrosymmetric dimer, and these dimers are linked by the other type of NH···O hydrogen bonds of 3.19 Å. This type of hydrogen-bond network (classified as 'screw-axis packing' by Leiserowitz and Schmidt[9]) is very rare in aromatic amides. The only case so far reported is that of *p*-chlorocinnamide.[10]

The Cl–Cl distance of 3.24 Å is appreciably shorter than those found in the α form of *p*-chlorobenzamide[2] at −120 °C (3.29 Å) and at room temperature (3.31 Å).

References

1) Y. Harada, T. Taniguchi, Y. Takaki, and K. Sakurai, *Mem. Osaka Kyoiku Univ.* **18**, Ser. III, 1 (1969).
2) T. Taniguchi, K. Nakata, Y. Takaki, and K. Sakurai, *Acta Crystallogr., Sect. B*, **34**, 2574 (1978).
3) Y. Takaki, *Mem. Osaka Gakugei Univ., Sect. B*, **14**, 39 (1965).
4) T. Ashida, HBLS-V, The Universal Crystallographic Computing System-Osaka, The Computation Center, Osaka University (1973), pp. 55—61.
5) The structure-factor table is kept at the Office of the Chemical Society of Japan (Document No. 8010).
6) F. D. Rienzo and A. Domenicano, *Acta Crystallogr., Sect. B*, **33**, 3854 (1977).
7) R. E. Cobbledick and R. W. H. Small, *Acta Crystallogr., Sect. B*, **28**, 2893 (1972).
8) S. Orii, T. Nakamura, Y. Takaki, Y. Sasada, and M. Kakudo, *Bull. Chem. Soc. Jpn.*, **36**, 788 (1963).
9) L. Leiserowitz and G. M. J. Schmidt, *J. Chem. Soc., A*, **1969**, 2372.
10) D. Rabinovich, *J. Chem. Soc., A*, **1969**, 2361.

The Crystal Structures of the α and β Forms of DL-Methionine

Tomohiko TANIGUCHI,* Yoshito TAKAKI, and Kiichi SAKURAI
Department of Physics, Osaka Kyoiku University, Tennoji-ku, Osaka 543

(Received September 10, 1979)

Synopsis. The crystal structures of the α and β forms of DL-methionine have been refined by block-diagonal least-squares calculations using three-dimensional X-ray data to $R=0.118$ and 0.088 respectively. The structures of both the forms are essentially the same as those previously reported by Mathieson (*Acta Crystallogr.*, **5**, 332 (1952)).

Mathieson[1] has determined the crystal structures of the α and β forms of DL-methionine, $C_5H_{11}NO_2S$, from two-dimensional X-ray data. Recently, Taniguchi *et al.*[2] found that crystals of the β form undergo a reversible solid phase transformation at about 326 K to the α form accompanied with characteristic diffuse scattering during the transformation. In the course of their X-ray study of the phase transformation, it seemed that the structures given by Mathieson[1] were too deficient in accuracy to interpret quantitatively the diffuse scattering patterns. Therefore, in this paper, we deal with a reexamination of the structures of the α and β forms.

Experimental

Plate-like crystals elongated along the b axis were obtained from aqueous solutions at room temperature. Weissenberg photographs showed that all the crystals examined were β form, but they gave diffraction patterns showing various degrees of streaking along the reciprocal-lattice rows parallel to c*. Therefore a crystal showing very weak streaks was selected for the data collection. A crystal of the α form with no streaking could be obtained from that of the β form by heating in a stream of hot air through the transition point, the crystal being kept at 333 K (±2 K) during X-ray exposure. Note that a few crystals of the α form obtained in this way did not transform to the β form even at room temperature but they were all poor in quality. Cell dimensions of the β form were determined from photographs taken with a Buerger back-reflection Weissenberg camera, and those of the α form were determined by examining double-exposure Weissenberg and oscillation photographs taken with the same crystal at room temperature (β form) and 333 K (α form). Crystal data obtained are: α form at 333 K, $a=9.89(2)$, $b=4.70(2)$, $c=16.74(3)$ Å, $\beta=102.3(7)°$, space group $P2_1/a$, $Z=4$; β form at 293 K, $a=9.912(5)$, $b=4.700(7)$, $c=33.13(2)$ Å, $\beta=106.3(3)°$, I2/a, $Z=8$.

Intensities of 1310 independent reflections for the α form at 333 K and 1494 reflections for the β form at 293 K were collected on equi-inclination Weissenberg photographs for $k=0$ to 3 (α form) and for $k=0$ to 4 (β form). The intensities were measured visually and corrected for Lorentz and polarization factors. No correction for absorption was made.

The structures of the α and β forms given by Mathieson[1] were refined by block-diagonal least-squares calculations[3] with unit weights. The H atoms for both forms were included in the least-squares calculations with fixed positional parameters deduced from the geometry of the molecules and fixed isotropic thermal parameters ($U=0.057$ and 0.044 Å^2 for the α and β forms respectively). At a later stage of refinement, the positions of the H atoms for both forms were confirmed from difference syntheses except those of terminal methyl groups. The final R values for the α and

TABLE 1. ATOMIC COORDINATES ($\times 10^4$) AND ANISOTROPIC THERMAL PARAMETERS ($\times 10^3$) FOR NON-HYDROGEN ATOMS WITH THEIR ESTIMATED STANDARD DEVIATIONS

The numbering of the atoms is the same as that given by Mathieson.[1] The anisotropic thermal parameters are of the form: $\exp\{-2\pi^2(h^2a^{*2}U_{11}+k^2b^{*2}U_{22}+l^2c^{*2}U_{33}+2hka^*b^*U_{12}+2hla^*c^*U_{13}+2klb^*c^*U_{23})\}$.

	x	y	z	U_{11}	U_{22}	U_{33}	U_{12}	U_{13}	U_{23}
α Form at 333 K									
O (1)	−57 (3)	−523 (10)	3756 (3)	18 (2)	26 (3)	68 (2)	5 (2)	10 (2)	2 (2)
O (2)	1722 (4)	−3212 (9)	4352 (2)	32 (2)	15 (3)	38 (2)	1 (2)	9 (1)	7 (2)
N	3586 (4)	571 (11)	4077 (2)	18 (2)	25 (4)	34 (2)	−5 (2)	5 (1)	−3 (2)
C (1)	1217 (4)	−1147 (13)	3934 (3)	21 (2)	8 (4)	38 (2)	1 (2)	9 (2)	−5 (2)
C (2)	2176 (4)	671 (13)	3553 (3)	17 (2)	26 (4)	31 (2)	0 (2)	4 (2)	−1 (2)
C (3)	2212 (6)	−574 (17)	2701 (3)	33 (3)	59 (6)	32 (2)	−5 (3)	8 (2)	5 (3)
C (4)	3158 (8)	1000 (21)	2262 (4)	64 (4)	92 (8)	49 (3)	−14 (5)	27 (3)	−5 (4)
S	3248 (3)	−573 (7)	1291 (1)	90 (1)	116 (2)	46 (1)	−2 (2)	34 (1)	−16 (1)
C (5)	1536 (11)	200 (39)	724 (6)	96 (7)	239 (18)	63 (5)	16 (10)	7 (5)	15 (9)
β Form at 293 K									
O (1)	−2687 (2)	2065 (6)	1867 (1)	14 (1)	26 (2)	49 (2)	3 (1)	14 (1)	3 (1)
O (2)	−874 (3)	−756 (6)	2165 (1)	25 (1)	21 (2)	26 (1)	2 (1)	12 (1)	7 (1)
N	995 (3)	2967 (7)	2025 (1)	11 (1)	24 (2)	20 (1)	−5 (1)	6 (1)	−2 (1)
C (1)	−1422 (3)	1327 (7)	1950 (1)	16 (2)	11 (2)	22 (1)	2 (1)	11 (1)	−3 (1)
C (2)	−483 (3)	3078 (7)	1749 (1)	15 (2)	10 (2)	22 (1)	2 (1)	7 (1)	0 (1)
C (3)	−576 (4)	1865 (9)	1315 (1)	26 (2)	27 (2)	20 (2)	−5 (2)	11 (1)	−3 (1)
C (4)	412 (5)	3219 (10)	1096 (1)	49 (3)	34 (3)	30 (2)	−10 (2)	23 (2)	−2 (2)
S	153 (2)	1575 (4)	587 (0)	76 (1)	69 (1)	27 (1)	−27 (1)	32 (1)	−18 (1)
C (5)	1526 (6)	3238 (17)	420 (2)	65 (4)	98 (5)	43 (3)	−10 (4)	34 (3)	−3 (3)

Table 2. Bond lengths and angles and torsion angles

	α Form	β Form
Bond lengths (l/Å)		
C (1)-O (1)	1.265 (7)	1.255 (5)
C (1)-O (2)	1.238 (7)	1.242 (4)
C (2)-N	1.481 (8)	1.492 (5)
C (1)-C (2)	1.514 (9)	1.528 (5)
C (2)-C (3)	1.549 (10)	1.525 (5)
C (3)-C (4)	1.503 (13)	1.514 (6)
C (4)-S	1.806 (11)	1.805 (5)
C (5)-S	1.792 (19)	1.788 (8)
Bond angles (ϕ/°)		
O (1)-C (1)-O (2)	125.2 (6)	126.3 (3)
O (1)-C (1)-C (2)	116.9 (5)	116.7 (3)
O (2)-C (1)-C (2)	117.8 (5)	116.9 (3)
C (1)-C (2)-N	109.2 (5)	109.1 (3)
C (3)-C (2)-N	109.2 (5)	110.6 (3)
C (1)-C (2)-C (3)	108.3 (5)	109.0 (3)
C (2)-C (3)-C (4)	113.8 (7)	114.8 (3)
C (3)-C (4)-S	113.2 (7)	109.1 (3)
C (4)-S-C (5)	99.8 (7)	100.5 (3)
Torsion angles (ϕ/°)		
O (2)-C (1)-C (2)-N	−29.3	−31.0
N-C (2)-C (3)-C (4)	300.2	305.6
C (1)-C (2)-C (3)-C (4)	181.4	185.6
C (2)-C (3)-C (4)-S	177.4	180.7
C (3)-C (4)-S-C (5)	68.9	185.6

β forms were 0.118 and 0.088 respectively. Positional and thermal parameters are given in Table 1.[4] Bond lengths and angles and torsion angles are given in Table 2. All computations were made on a NEAC 2200-700 computer of the Computation Center of Osaka University.

Discussion

The structures of both the α and β forms are essentially the same as those given by Mathieson.[1] No significant difference between the molecules of the α and β forms is observed in bond lengths and angles except for the torsion angles C(3)–C(4)–S–C(5) (68.9 and 185.6° for the α and β forms respectively), which define the conformation of the terminal C(5) atom to the C(3) atom as *gauche* in the α form and *trans* in the β form.

A fundamental difference between the crystal structures of the α and β forms lies in the arrangements of layers along the c axis. The α form consists of a single-layer unit, P, with a stacking sequence $PPP\ldots$, while the β form consists of a double-layer unit, $Q\overline{Q}$, with a sequence $Q\overline{Q}Q\overline{Q}\ldots$, where $\overline{Q}$ is related to Q by the translation $(\mathbf{a}+\mathbf{b})/2$. The structures of layers P and Q are very similar to each other except for the positions of the terminal methyl groups; both P and Q layers consist of molecules connected by three types of NH···O hydrogen bonds (2.83, 2.80, and 2.77 Å in layer P and 2.82, 2.80, and 2.79 Å in layer Q). The closest interlayer contacts are C(5)··· C(5) of 3.46 and 3.81 Å for the α and β forms respectively.

By comparing the structures of the two forms, the major change of the structure occurring on the phase transformation from the β to α forms may be explained in terms of the translation $(\mathbf{a}+\mathbf{b})/2$ of every second layer accompanied with the repositioning of the terminal methyl groups from *trans* to *gauche* to the C(3) atoms. A similar structural change can be seen on the phase transformation of DL-α-aminobutyric acid from the A to D forms.[5]

References

1) A. McL. Mathieson, *Acta Crystallogr.*, **5**, 332 (1952).
2) T. Taniguchi, Y. Takaki, and K. Sakurai, to be published.
3) T. Ashida, HBLS-V, The Universal Crystallographic Computing System-Osaka, The Computation Center, Osaka University (1973), pp. 55—61.
4) The structure factor tables are kept at the Office of the Chemical Society of Japan (Document No. 8011).
5) K. Nakata, Y. Takaki, and K. Sakurai, *Acta Crystallogr.*, in press.

A Cation-exchange Study of Cerium(III) and Thulium(III) Tartrate Complexes

Emiko OHYOSHI* and Akira OHYOSHI†
Yatsushiro College of Technology, Yatsushiro 866
†*Department of Industrial Chemistry, Kumamoto University, Kumamoto 860*
(Received May 18, 1979)

Synopsis. The tartrate complexes of Ce(III) and Tm(III) were studied by the cation-exchange method, where a series of solutions prepared so as to keep the [Htart$^-$] value nearly constant, while the [tart^{2-}] value was varied, was used for the estimation of the protonated complexes. Three kinds of complexes, M(Htart)$_2^+$, M(Htart)(tart), and M(tart)$_2^-$, were found in the lower pH region of the solutions.

When we use some dibasic or tribasic acids as complexing agents, there must be various kinds of protonated complexes equilibrated in a solution. However, most investigators seem to have neglected or underestimated these protonated complexes. Potentiometry can not be used for these studies since it is difficult to analyze various protonated complexes from a pH titration curve indicating a high degree of overlapping of the successive equilibria. In these cases, it is useful to estimate the amounts of free metal and ligand species equilibrated in a solution. As has previously been reported, it has been found that the citrate complexes of some lanthanoids[1] and actinoids[2,3] involving various types of protonated complexes could readily be analyzed by the cation-exchange method using a series of solutions prepared so as to keep the amount of one of the protonated ligands constant, while the other one was varied. In this note, we will discuss how we applied this method to the study of tartrate complexes of Ce(III) and Tm(III).

Experimental

Materials. The tracers, ^{144}Ce and ^{170}Tm in the chloride form, were obtained from the New England Nuclear Corporation. To a portion of each of the tracer solutions, a carrier was added to prepare stock solutions of 10^{-3} M (1 M= 1 mol dm^{-3}). A cation exchanger, Dowex 50W-X8 (100—200 mesh), in the sodium form was used. All the chemicals used were of a G. R. grade. Tartrate solutions were made in the following way: (1) To 0.1 M NaHtart solution, various amounts of H_2tart were added to prepare solutions containing a nearly constant amount of Htart$^-$ and various quantities of tart^{2-}. The ionic strength governed by the amount of the salt, NaHtart, was also maintained at 0.1 M. The compositions of the solutions are given in Table 1. The acid-dissociation constants used for the calculation of the respective ion concentrations were $pK_1=2.88\pm0.02$ and $pK_2=4.02\pm0.02$, which were determined by potentiometric titration at I=0.1 M and 25 °C. (2) Solutions containing various amounts of tartrate at the constant pHs of 2.74 and 3.90 were prepared by diluting a mixture of equal volumes of 0.1 M Na_2tart and 0.34 M H_2tart, and one of 0.1 M Na_2tart and 0.05 M H_2tart, with a 0.1 M $NaClO_4$ solution.

Table 1. The compositions of tartrate solutions prepared so as to maintain [Htart$^-$] nearly constant (0.1 mol dm^{-3})

pH	[H_2tart] mol dm^{-3}	[Htart$^-$] mol dm^{-3}	[tart^{2-}] 10^{-3} mol dm^{-3}
2.12	0.595	0.104	1.31
2.21	0.476	0.102	1.59
2.32	0.359	0.099	1.99
2.49	0.239	0.098	2.92
2.59	0.182	0.095	3.52
2.74	0.124	0.091	4.78

Procedure. The cation-exchange experiments were carried out in a manner similar to that described previously.[2] The distribution coefficient, K_d, was calculated as follows:

$$K_d = \frac{\text{Activity in the resin phase}}{\text{Activity in the solution phase}} \times \frac{\text{Volum of solution (ml)}}{\text{Mass of dry resin (g)}}. \quad (1)$$

Results and Discussion

Considering the formation of M(Htart)$^{2+}$ and M(tart)$^+$, the adsorption of these species on the cation exchanger was studied at I=0.1 and 0.2 mol dm^{-3} and was found to be negligible compared with that of the M^{3+} species.[4] Thus, the following equation is derived:

$$K_d^0/K_d - 1 = \sum K_{M(Htart)_i}[Htart^-]^i + \sum K_{M(Htart)_j(tart)_k}[Htart^-]^j[tart^{2-}]^k + \sum K_{M(tart)_l}[tart^{2-}]^l \quad (2)$$

where K_d^0 denotes K_d in the absence of the complexing agent, and where $K_{M(Htart)_i}$, $K_{M(Htart)_j(tart)_k}$, and $K_{M(tart)_l}$ are the formation constants of the M(Htart)$_i$, M(Htart)$_j$(tart)$_k$, and M(tart)$_l$ respectively. If we can set conditions so as to keep [Htart$^-$] nearly constant and to vary [tart^{2-}], Eq. 2 may be written as a function of [tart^{2-}] alone, thus:

$$K_d^0/K_d - 1 = A + B\sum K_{M(Htart)_j(tart)_k}[tart^{2-}]^k + \sum K_{M(tart)_l}[tart^{2-}]^l, \quad (3)$$

where A and B are constant. From a plot of $K_d^0/K_d - 1$ *vs.* [tart^{2-}], we can conclude which of the two species, Htart$^-$ and tart^{2-}, is the actual complexing ligand. It is difficult, however, to decide the type of complexes formed from only this plot. For example, if the plot shows a straight line with an intercept, we can not conclude whether $k=1$, $l=0$; $k=0$, $l=1$, or $k=l=1$. To make the difference clear, it is necessary to know the ratio of metal to ligand; this can be found by studying the relation between K_d^0/K_d-1 and $[\text{tartrate}]_{total}$ at a constant pH.

Figure 1 shows the plots of K_d^0/K_d-1 *vs.* [tart^{2-}], where [Htart$^-$] is kept constant (nearly 0.1 mol dm^{-3} for Ce(III) and Tm(III)). The fact that straight lines are obtained indicates the presence of two different type of complexes; one consists of only Htart$^-$, and while in the other the ratio of the metal to the ligand, tart^{2-}, is 1:1. As is shown in Fig. 2, the plots of $\log(K_d^0/K_d-1)$ *vs.* $\log[\text{tartrate}]_{total}$ at pH 2.74 give straight lines with the slope of 2, indicating that all

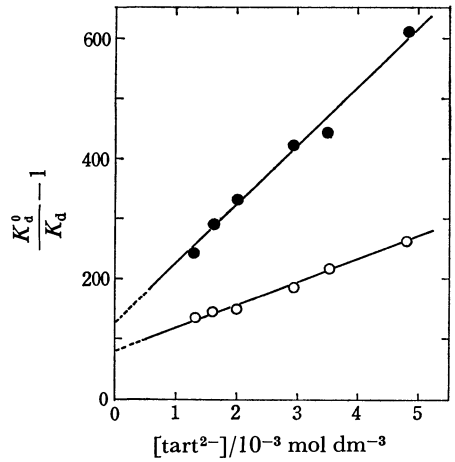

Fig. 1. Plots of (K_d^0/K_d-1) *vs.* [tart^{2-}] at [Htart$^-$]$\simeq$0.1 mol dm^{-3}.—○— Ce(III), —●— Tm(III).

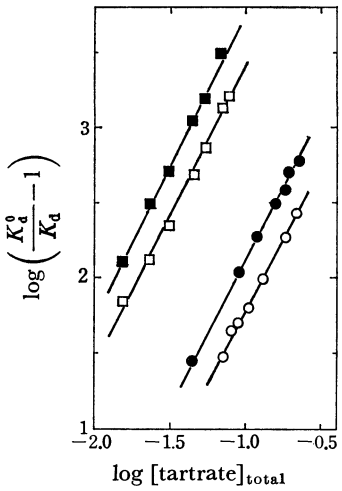

Fig. 2. Plots of log (K_d^0/K_d-1) *vs.* log[tartrate]$_{total}$ at constant pHs of 2.74 and 3.90.
—○— Ce(III), —●— Tm(III) at pH 2.74; —□— Ce(III), —■— Tm(III) at pH 3.90.

TABLE 2. FORMATION CONSTANTS OF Ce(III) AND Tm(III) TARTRATE COMPLEXES I=0.1 mol dm^{-3}, 25 °C

Metal ions	log $K_{M(Htart)}$	log $K_{M(Htart)_2}$	log $K_{M(tart)}$	log $K_{M(Htart)(tart)}$	log $K_{M(tart)_2}$
Ce(III)	2.54±0.03[a]	3.89±0.05	5.5±0.2[b]	5.60±0.05[e]	6.03±0.05
			3.84[c]	5.58±0.05[f]	8.4±0.2[b]
			3.09[d]		6.72[c]
Tm(III)		4.10±0.05	5.3[g]	5.99±0.05[e]	6.35±0.05
				5.97±0.05[f]	

a) Ref. 6. b) Ref. 7. c) Ref. 8, I; variable. d) Ref. 9, I=0.2 mol dm^{-3}. e) The values obtained from the plot in Fig. 1. f) The values obtained from the plot of log (K_d^0/K_d-1-A) *vs.* log [H$^+$]. g) Ref. 5. I=0 mol dm^{-3}.

the complexes formed in this pH region have a 1:2 metal-to-ligand ratio. On the basis of this, the two complexes, M(Htart)$_2^+$ and M(Htart)(tart), for Ce(III) and Tm(III) are considered. Their formation constants, $K_{M(Htart)_2}$ and $K_{M(Htart)(tart)}$, calculated from the intercepts and the slopes of the straight lines in Fig. 1, are listed in Table 2. Equation 3 can be simplified and reformed in this case:

$$K_d^0/K_d - 1 = A + BK_{M(Htart)(tart)}[tart^{2-}], \quad (3')$$

$$\log (K_d^0/K_d-1-A) = \log B^2k_2K_{M(Htart)(tart)} - \log [H^+], \quad (4)$$

where k_2=[H$^+$][tart^{2-}]/[Htart$^-$]. The $K_{M(Htart)(tart)}$ values are also obtained from the intercepts of the straight lines obtained from the plots of log(K_d^0/K_d-1-A) *vs.* log [H$^+$]. These values, also listed in Table 2, are found to be close to those presented above.

To examine another type of complexes, the experiments were carried out at a pH of 3.90. The plots of log (K_d^0/K_d-1) *vs.* log[tartrate]$_{total}$ given in Fig. 2 indicate the presence of 1:2 complexes, that is, M(Htart$^-$)(tart^{2-}) and M(tart^{2-})$_2$. The intercepts of the plots in Fig. 2 correspond to $\{K_{M(Htart)(tart)}k_1^2k_2\times[H^+]+K_{M(tart)_2}\times(k_1k_2)^2\}/([H^+]^2+k_1[H^+]+k_1k_2)^2$, where k_1=[H$^+$][Htart$^-$]/[H$_2$tart].

Since the $K_{M(Htart)(tart)}$ values are already known, the formation constants of Ce(tart)$_2^-$ and Tm(tart)$_2^-$ are determined to be as listed in Table 2. To confirm the reliability of these formation constants, we tried to obtain the relationships between log (K_d^0/K_d-1) and log[tartrate]$_{total}$ at pH 2.74, using these values for the calculation. The results are in good agreement with the solid lines shown in Fig. 2. The formation constants of other types of complexes reported in the literature are also listed in Table 2. It is of interest that, for both Ce(III) and Tm(III), the two complexes, M(Htart)(tart) and M(tart)$_2^-$, have stabilities of the same order. From this, M(Htart)(tart) is found to be the predominant species in solutions of the lower pH region.

The complex of the M(tart)$^+$ type, whose formation constants for Ce(III) and Tm(III) are listed in Table 2, was not found under these experimental conditions. There are no protonated couples other than Ce(Htart)$^{2+}$ in the literature. From our results, the type of M(Htart)(tart) is found to be appreciably stable. If this species is neglected in the estimations of other species, the resulting formation constants may involve a considerable error. This might be one of the reasons why there has been a remarkable disagreement among the values reported for the formation constants of Ce(tart)$^+$ and Ce(tart)$_2^-$.

References

1) A. Ohyoshi, E. Ohyoshi, H. Ono, and S. Yamakawa, *J. Inorg. Nucl. Chem.*, **34**, 1955 (1972).
2) E. Ohyoshi and A. Ohyoshi, *J. Inorg. Nucl. Chem.*, **33**, 4265 (1971).
3) E. Ohyoshi, J. Oda, and A. Ohyoshi, *Bull. Chem. Soc. Jpn.*, **48**, 227 (1975).
4) E. Ohyoshi, *Bull. Chem. Soc. Jpn.*, **46**, 2758 (1973).
5) S. S. Yun and J. L. Bear, *J. Inorg. Nucl. Chem.*, **37**, 1757 (1975).
6) F. Brezina, J. Rosicky, and R. Pastorek, *Monatsh.*, **96**, 533 (1965).
7) A. V. Stepanov, V. P. Shvedov, and A. P. Rozhnov, *Russ. J. Inorg. Chem.*, **10**, 750 (1965).
8) R. Pastorek and F. Brezina, *Monatsh.*, **97**, 1095 (1966).
9) N. K. Davidenko and V. F. Deribon, *Russ. J. Inorg. Chem.*, **11**, 53 (1966).

The Kinetics of the Thermal Deammonation of $[RhX(NH_3)_5]X_2$ in the Solid State

Susumu KOHATA,* Hitoshi KAWAGUCHI,** Noriko ITOH,** and Akira OHYOSHI**

Yatsushiro College of Technology, Hirayamashin-machi, Yatsushiro 866

***Department of Industrial Chemistry, Faculty of Engineering, Kumamoto University, Kurokami, Kumamoto 860*

(Received May 19, 1979)

Synopsis. The isothermal kinetics of the substitution reaction of an ammonia with an outer-sphere anion was studied in the solid state; $[RhX(NH_3)_5]X_2(s) \rightarrow [RhX_2(NH_3)_4]X(s) + NH_3(g)$ (X=Cl, Br, I). The kinetic parameters provided some evidence for a dissociative mechanism.

The metal ammine complexes, $[MX(NH_3)_5]X_2$ (M=Cr(III), Co(III), Ru(III), or Rh(III); X=Cl, Br, and I), are known to liberate ammonia molecules in the initial part of thermal degradation in the solid state.[1-3] We can classify their reactions into two types: in ammine cobalt(III) complexes, the release of the ammonia molecule is initiated by electron-transfer, while it is initiated by a replacement of an ammonia with an anion in the outer-sphere in the other metal complexes. It is of interest to compare the deammonation reactions among these transition-metal complexes with different electronic configurations. Unfortunately, there have been few reports on kinetic studies of deammonation considering the mechanism. In the present work, the kinetics of the deammonation reaction of $[RhX(NH_3)_5]X_2$ (X=Cl, Br, or I) has been investigated; the mechanism will be discussed.

Experimental

The pentaamminehalogenorhodium(III) complexes were prepared according to the method given in the literature.[4] They were identified by elemental analyses and by UV spectral measurements. The pyrolyses were made in a constant helium stream of 70 ml/min under the heating rate of 5 °C/min. About a 10-mg portion of the sample, which has been ground with a mortar into a fine, homogeneous powder, was used in each kinetic run. In the isothermal kinetic measurements, the complex was heated for 50—300 min at a temperature just below where the mass-loss begins to appear in the respective complexes. The temperatures were 296, 282, and 226 °C for the chloro, bromo, and iodo complexes respectively. The apparatus used for the pyrolyses or spectroscopic measurements are the same as those described in a previous paper.[2]

Results and Discussion

In our experiments, the temperatures at which the mass-loss begins to appear were 242 °C for $[RhI(NH_3)_5]I_2$, 281 °C for $[RhBr(NH_3)_5]Br_2$, and 300 °C for $[RhCl(NH_3)_5]Cl_2$. Wendlandt and Franke have reported the values of 290, 320, and 340 °C as the corresponding temperatures for the iodo, bromo, and chloro complexes respectively.[3] The difference may be attributable to differences in experimental conditions, such as in the apparatus and the atmosphere. Although the values of the temperature obtained by the present authors are different from the corresponding ones reported by Wendlandt and Franke, the orders of increasing thermal stability coincide with each other.

The analytical data of the reaction products, which are shown in Table 1, demonstrate that the thermal degradation can be expressed by Eq. 1:

$$[RhX(NH_3)_5]X_2(s) \rightarrow [RhX_2(NH_3)_4]X(s) + NH_3(g) \quad (X=Cl, Br, I) \qquad (1)$$

The plots of the first-order rate equation gave straight lines, with a good reproducibility, up to *ca.* 70% of Reaction 1. Reaction 1 can, therefore, be regarded as first-order with respect to the reactant. The rate constant obtained from the slopes and the activation parameters evaluated from the Arrhenius plots (Fig. 1) are given in Table 2.

The order of increasing rate constants is: $[RhCl(NH_3)_5]Cl_2 < [RhBr(NH_3)_5]Br_2 < [RhI(NH_3)_5]I_2$; the rate constants of the bromo and iodo complexes are, respectively, *ca.* 3 and 20 times greater than that of the chloro complex. If Reaction 1 proceeds through an associative mechanism, the rate constant should clearly increase along with the smaller size and the larger electronegativity of the entering group;[5] that is, the expected order of increasing rate constants is iodo-iodide<bromo-bromide<chloro-chloride. This assumption, however, is not consistent with the experimental results.

On the other hand, the values of the activation energies, (E^*/kJ mol^{-1}) for $[RhCl(NH_3)_5]Cl_2$ (196±1) and $[RhBr(NH_3)_5]Br_2$ (210±3), are close to each other; also, they are larger than that of $[RuCl(NH_3)_5]Cl_2$, for which an S_N1-type mechanism has been proposed.[2] These Rh(III) complexes also revealed a positive entropy change, ΔS^*, suggesting a five-coordinate complex in the activated state. In this case, therefore, the

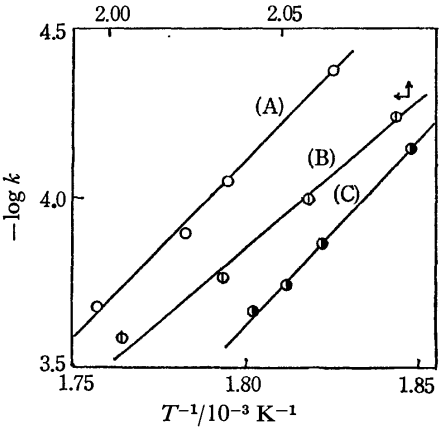

Fig. 1. Arrhenius plots for the deammonation-anation of $[RhX(NH_3)_5]X_2$. X=Cl(A), I(B), Br(C).

Table 1. Analytical data and electronic spectrum of reaction product

Complex	Temp °C	Time min	Product	Found, % (Calcd, %) H	N	Electronic spectrum (λ_{max}/nm) Obsd	Ref. a)	Ref. b)
$[RhCl(NH_3)_5Cl_2$	296	130	*trans*-$[RhCl_2(NH_3)_4]Cl$	4.76 (4.33	20.86 20.19)	412	412	298, 360
$[RhBr(NH_3)_5]Br_2$	282	100	$[RhBr_2(NH_3)_4]Br$	3.04 (2.92	14.08 13.63)	242, 350	235, 278, 438	—
$[RhI(NH_3)_5]I_2$	226	80	*trans*-$[RhI_2(NH_3)_4]I$	2.29 (2.18	10.52 10.15)	270, 340	222, 270, 340, 470	—

a) For *trans*-$[RhX_2(NH)_{34}]^+$ (X=Cl, Br, I); Ref. 9. b) For *cis*-$[RhCl_2(NH_3)_4]^+$; Ref. 10.

Table 2. Kinetic parameters for the deammonation-anation reaction

Complex	$k\times10^5$ s^{-1}	Temp °C	E^* kJ mol^{-1}	ΔS^* J K^{-1} mol^{-1}
$[RhCl(NH_3)_5]Cl_2$	4.15	(275)		
	8.92	(284)	196±1[a]	23±3
	12.9	(288)		
	20.7	(296)		
$[RhBr(NH_3)_5]Br_2$	7.17	(269)		
	13.7	(276)	210±3	58±2
	18.1	(279)		
	21.4	(282)		
$[RhI(NH_3)_5]I_2$	5.69	(207)		
	10.1	(213)	156±1	−5±2
	18.1	(219)		
	25.6	(226)		

a) Error recorded is e.s.d.

$Rh–NH_3$ bond-breaking is the rate determining step. It can, therefore, be considered that the deammonation-anation reactions of $[RhX(NH_3)_5]X_2$ (X=Cl and Br) proceed through a dissociative mechanism.

The remaining complex, $[RhI(NH_3)_5]I_2$, gives smaller values of E^* (156±1) and ΔS^* (−5±2/J K^{-1} mol^{-1}) than those of $[RhX(NH_3)_5]X_2$ (X=Cl and Br), though the former values are rather close to those of $[RuCl(NH_3)_5]Cl_2$. The deammonation of the iodo complex, then, proceeds *via* a partially associative mechanism. It may be explained by the strong basicity of the iodide ion, which causes the large value of the rate constant. In conclusion, the deammonation mechanism of $[RhX(NH_3)_5]X_2$ (X=Cl, Br, or I) seems, fundamentally, to belong to the category of dissociation mechanisms.

It is, then, of interest to shed light on the relation between the reaction mechanism and the product obtained from the solid-state reaction. By means of spectroscopic measurements, the main product was found to be *trans*-$[RhX_2(NH_3)_4]X$ (X=Cl and I), although the configuration of the corresponding bromo complex could not be determined. The reaction mechanism proposed in this work (dissociative mechanism) suggests the exertion of a "trans-effect" of halogen, although Evans *et al.*[7] have found no octahedral trans-effect of halogen in $[RhX(NH_3)_5]X_2$ (X=Cl or Br).

The mechanism in this sort of reaction shows a striking contrast among the Rh(III), Ru(III), and Co(III) ammine complexes. In $[CoX(NH_3)_5]X_2$ (X=Cl, Br, and I), an electron-transfer reaction takes place initially and is followed by a degradation reaction, while a replacement of ammonia with the outer-sphere anion initially takes place in $[RuX(NH_3)_5]X_2$ (X=Cl and Br) and $[RhX(NH_3)_5]X_2$ (X=Cl, Br, and I).

This difference might be explained by comparing the third-ionization potential of each metal ion, corrected with the CFSE based upon the optical data of each hexaammine complex.[8,9] The values are 32.0, 30.3, and 28.6 eV for Co, Ru, and Rh respectively; this suggests, then, that the $3d^6$ cobalt complex is more electron-acceptable than the other $4d^5$ and $4d^6$ metal complexes. This may, consequently, elucidate the difference in the thermal-degradation reactions of Co and Ru, Rh complexes described above.

References

1) N. Tanaka and K. Nagase, *Bull. Chem. Soc. Jpn.*, **41**, 1143 (1968); **40**, 546 (1967).
2) A. Ohyoshi, S. Kohata, M. Nishimori, Y. Shimura, and N. Iwasaki, *Bull. Chem. Soc. Jpn.*, **49**, 1284 (1976).
3) W. W. Wendlandt and P. H. Franke, Jr., *J. Inorg. Nucl. Chem.*, **26**, 1885 (1964).
4) S. A. Johnson and F. Basolo, *Inorg. Chem.*, **1**, 925 (1962).
5) F. Basolo and R. G. Pearson, "Mechanism of Inorganic Reactions," John Wiley & Sons, New York (1967), p. 137.
6) H. J. Peresie, J. A. Stanko, and D. N. Mulay, *Chem. Phys. Lett.*, **31**, 392 (1975).
7) R. S. Evans, E. A. Hopcus, J. Bordner, and A. F. Shreiner, *J. Cryst. Mol. Struct.*, **3**, 235 (1973).
8) M. Faraggi and A. Feder, *Inorg. Chem.*, **12**, 236 (1973).
9) C. K. Jørgensen, *Acta Chem. Scand.*, **10**, 500 (1956).
10) M. P. Hancock, *Acta Chem. Scand.*, **1975**, A29, 468.

Syntheses and Electronic Spectra of 4,4′-Diacetyl-2,2′-isopropylidenedi-8-quinolinol, Its Nickel(II), Copper(II), and Zinc(II) Chelates

Yoshinori YAMAMOTO,* Kunio SHIBAHARA, and Shinsuke TAKEI

Department of Industrial Chemistry, Faculty of Engineering, Ibaraki University, Nakanarusawa-cho, Hitachi 316

(Received July 2, 1979)

Synopsis. The title nickel chelate, which has a planar four-coordinated form, gave an intense new band, no corresponding band of which was observed with the other chelates, at the position between the first and second π-π^* bands. The spectra were compared with those of the corresponding compounds free from the acetyl group.

The crystalline compounds, Ni-, Cu-, and Zn(aipdq), have been obtained readily by the reaction of each of the metal ions with the ligand. The absorption data are given in Tables 1 and 2. The intra-ligand transition bands, termed the A-, B-, and C-bands, of each of the M(aipdq) can well be compared with those[1] of the corresponding chelates free from the acetyl group, M(ipdq), in the same solvents. Both Cu- and Zn(aipdq) in all the solvents and Ni(aipdq) in pyridine give similar spectral shapes (Table 1). When the solvents listed in Table 2 are used, the spectral shapes of the A- and C-bands of Ni(aipdq) are remarkably changed, together and an intense new band appears. A similar behavior was observed with the M(ipdq). The new band of Ni(aipdq) can be compared with an unassigned small shoulder band observed with planar four-coordinated Ni(ipdq).

On the basis of the d-d spectrum, Ni(aipdq) in pyridine is found to be coordinated by two pyridine molecules (Table 1). Both in the solid state and in *N*,*N*-dimethylformamide (DMF) (8×10^{-3} M, 1 cm cell), Ni(aipdq) gives no peak near 10000 cm^{-1}, suggesting[2] that the compound has a planar four-coordinated form (*cf.* Table 2). With the other solvents for Ni(aipdq), the measurement could not be performed because of their low solubilities, but a planar form can be expected because these solutions give intense bands similar to those in DMF (Table 2).

For the spectra of the planar nickel chelates, it is observed that, upon acetylation, both the C-band and the new band shift to the red, 1.3—1.6 and *ca.* 2×10^3 cm^{-1} respectively, in the same solvents. The C-bands of the M(ipdq) have been described in terms of the movement of the electronic charge from the phenol ring to the pyridine ring.[1] The decrease in the electron density in the pyridine ring upon the acetylation explains the movement of the C-bands to lower energies, though it should be noted that the quantity of the shift of the planar nickel chelate is less than those ($2.2—2.4\times10^3$ cm^{-1}) of the other chelates. The new band of planar Ni(aipdq) is not a part of the B- or C-band, since, when the solvent is changed to MeOH, the new band shifts strongly to the blue, despite the small shift of the B-band, while upon changing to the solid state the new band shows only a little change, despite a complex splitting of the C-band (Table 2). These observations suggest that the new band is to be described in terms of the charge transfer from metal to the ligand (MLCT). In the other chelates, the lack of the corresponding band near the B- or C-band is in contrast with the well-known MLCT of the Cu(II), Ni(II), *etc.* complexes with pyridine *N*-oxide and its derivatives, whose positions change slightly when the central metal is changed.[3] From the viewpoint of the development of *selective* colorimetric reagents for nickel analysis, it would be interesting to search for a modification of the ligand which would cause such a new band to appear in a lower energy range than the first π-π^* bands of the chelates.

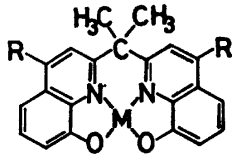

M(aipdq), R=$COCH_3$
M(ipdq), R=H
M=Ni(II), Cu(II), or Zn(II)

Experimental

The measurement and analyses were made by the same methods as in the previous paper.[1] Zn(ipdq) was prepared in a way similar to that[1] used for of Cu(ipdq); it was dried at 120 °C to give a deep yellow, crystalline powder. Found: Zn, 16.48%. Calcd: 16.60%.

4,4′-Diacetyl-2,2′-isopropylidenedi-8-quinolinol: This was prepared by a method similar to that developed by an Italian group.[4] To a solution of Ni(ipdq) (or ipdq) (10 mmol) in 40 cm^3 of EtOH and 8 cm^3 of concd H_2SO_4, $AgNO_3$ (0.4 g) in 80 cm^3 of water was added; the mixture was then heated at 40—50 °C and stirred for 2 h. During heating, pyruvic acid (8 cm^3) and $(NH_4)_2S_2O_8$ (10 g in 80 cm^3 of water) were added in two equal portions at hourly intervals. After cooling, the precipitate was collected, treated with 60 vol% aq EtOH (150 cm^3) containing AcOK (3.6 g), recollected, washed with water, and dried to give the crude product. Repeated recrystallization from toluene (45 cm^3 per 1.0 g), using activated characoal, gave yellow needles (1.3 g, 31%): mp 200.5—201.5 °C. Found: C, 72.17%; H, 5.20%. Calcd for $C_{25}H_{22}N_2O_4$: C, 72.45%; H, 5.35%. PMR ($CDCl_3$): δ=2.06 (6H, s, $>C(CH_3)_2$), 2.59 (6H, s, $-COCH_3$), 7.15—7.90 (8.8H, m, ring proton and a part of OH). IR (KBr): 3415 (OH), 1699, and 1678 cm^{-1} (C=O). UV_{max}: (Cyclohexane) 37.17×10^3 cm^{-1} (log ε 4.68) (A-band), 30.35 (3.67) and 29.33 (3.69) (B-band), 27.0 (sh 3.46) (C-band); (MeOH) 37.59 (4.67), 30.8 (sh 3.75) and 29.85 (3.76), 27.4 (sh 3.50); (0.1 M aq NaOH) 35.27 (4.59), 30.3 (sh 3.66) and 29.2 (sh 3.61), 25.2 (3.55); (6.0 M aq HCl) 36.36 (4.70), 30.8 (sh 3.86) and 29.67 (3.94), 25.3 (3.40).

(4,4′-Diacetyl-2,2′-isopropylidenedi-8-quinolinolato)nickel(II), Ni(aipdq): To a warmed solution of $Ni(OAc)_2\cdot4H_2O$ (1 mmol in 30 cm^3 of EtOH), a hot solution of the ligand (1 mmol in 20 cm^3 of acetone) was added. From the mixture shiny needles immediately separated out; they gradually

Table 1. The absorption data[a] of the metal chelates

Chelate	Solvent	A-band σ_{max}(log ε)	B-band σ_{max}(log ε)	B-band σ_{max}(log ε)	C-band σ_{max}(log ε)
Zn(ipdq)	MeOH	38.54(4.75)	31.10(3.31)	29.50(3.30)	25.6(3.51)
	DMF		30.3 (sh 3.46)	29.11(3.52)	24.5(3.52)
	Pyridine		30.0 (sh 3.51)	28.92(3.58)	24.1(3.52)
Zn(aipdq)	MeOH	36.83(4.58)	30.5 (sh 3.38)	29.4 (sh 3.28)	23.3(3.39)
	DMF	35.84(4.50)	30.0 (sh 3.46)	28.9 (sh 3.39)	22.1(3.39)
	Pyridine		29.9 (sh 3.51)	28.8 (sh 3.46)	21.8(3.39)
Cu(aipdq)	MeOH	37.11(4.60)	30.70(3.35)	29.6 (sh 3.32)	23.2(3.46)
	DMF	36.30(4.59)	29.79(3.43)	28.9 (sh 3.39)	21.8(3.46)
	DCE[b]	36.32(4.59)	30.08(3.37)	29.0 (sh 3.31)	21.7(3.45)
	Pyridine		29.37(3.52)	28.5 (sh 3.50)	21.2(3.48)
	$CHCl_3$[c]	36.17(4.63)	29.99(3.41)	28.9 (sh 3.34)	21.5(3.49)
Ni(aipdq)	Pyridine[d]		29.0 (sh 3.64)	27.93(3.70)	21.2(3.44)

a) The wave numbers are given in 10^3 cm^{-1} units, and sh means a shoulder band. b) 1,2-Dichloroethane. c) Containing 0.5 vol% EtOH. d) The d-d bands: 12.7(sh 1.40) and 11.4(1.49).

Table 2. The absorption data[a,d] of Ni(aipdq)

Solvent	A-band σ_{max}(log ε)	A-band σ_{max}(log ε)	B-band σ_{max}(log ε)	B-band σ_{max}(log ε)	New band σ_{max}(log ε)	C-band σ_{max}(log ε)
MeOH	42.64(4.56)	35.84(4.45)	29.9 (sh 3.58)	28.78(3.60)	27.2(sh 3.59)	22.3(3.67)
DMF[e]		34.60(4.36)	29.46(3.56)	28.6 (sh 3.55)	26.1(3.60)	21.1(3.68)
DCE[b]	41.41(4.63)	34.60(4.40)	29.28(3.58)	28.4 (sh 3.56)	25.8(3.61)	20.7(3.68)
$CHCl_3$[c]	41.41(4.61)	34.48(4.41)	29.28(3.58)	28.4 (sh 3.57)	25.8(3.60)	20.5(3.67)
solid[e,f]				28.8 (sh)	24.6	19.9[g]

a)—c) The footnotes are the same as those given in Table 1. d) The data of the pyridine solution are given in Table 1. e) The d-d band: 12.1 (ε: *ca.* 1) in DMF; 12.3 (weak sh) in the solid state, possibly a spin-forbidden band of a planar nickel chelate (Ref. 2). f) A mull method. A KBr disk technique gave a similar result. g) A very broad band accompanied by intense shoulder bands at 21.2, 18.1, and 16.9.

changed to plates. After cooling, the black-purple plates was collected, washed with EtOH, dried at 110 °C (a 94.5% yield), and recrystallized from DMF (20 cm^3 per 100 mg) by adding acetone (60 cm^3). Found: C, 63.82%; H, 4.44%; Ni, 12.47%. Calcd for $C_{25}H_{20}N_2O_4Ni$: C, 63.73%; H, 4.28%; Ni, 12.46%. IR (KBr): 1673 cm^{-1} (C=O).

Cu- and Zn(aipdq): These were prepared in ways similar to that used for of Ni(aipdq), using $Cu(OAc)_2 \cdot H_2O$ or $Zn(OAc)_2 \cdot 2H_2O$. The black needles of Cu(aipdq) were obtained in a 90.0% yield and were recrystallized from MeOH (120 cm^3 per 100 mg). Found: C, 63.19%; H, 4.47%; Cu, 13.37%. Calcd: C, 63.08%; H, 4.24%; Cu, 13.35%. IR (KBr): 1679 cm^{-1} (C=O). Zn(aipdq) (a 84.8% yield) was recrystallized from MeOH (80 cm^3 per 100 mg) to give deep maroon needles. Found: Zn, 13.40%. Calcd: Zn, 13.68%. IR: 1691 cm^{-1}.

The authors wish to thank Dr. Masahiko Takahashi for the elemental analyses.

References

1) Y. Yamamoto, A. Miura, A. Kawamata, M. Miura, and S. Takei, *Bull. Chem. Soc. Jpn.*, **51**, 3489 (1978).

2) M. D. Hobday and T. D. Smith, *Coord. Chem. Rev.*, **9**, 311 (1972—1973), and the references cited therein.

3) W. Byers, B. Fa-Chun Chou, A. B. P. Lever, and R. V. Parish, *J. Am. Chem. Soc.*, **91**, 1329 (1969); N. M. Karayannis, A. N. Speca, D. E. Chasan, and L. L. Pytlewski, *Coord. Chem. Rev.*, **20**, 37 (1976), and the references cited therein.

4) T. Caronna, G. Fronza, F. Minisci, and O. Porta, *J. Chem. Soc., Perkin Trans. 2*, **1972**, 2035.

Studies of the Hydrous Titanium Oxide Ion Exchanger. V. The Stability of the Hydrogen Form in Air

Yasushi INOUE* and Hiromichi YAMAZAKI

Department of Nuclear Engineering, Faculty of Engineering, Tohoku University, Aramaki, Sendai 980

(Received July 6, 1979)

Synopsis. After being allowed to stand in air at room temperature, the exchanger in the hydrogen form showed an abrupt decrease in its ion-exchange capacity between 3 and 6 months after the preparation. This is attributable to the preferential destruction of the most acidic hydroxyl groups by dehydrating condensation.

In the previous paper,[1] it was pointed out that the hydrous titanium oxide in the hydrogen form lost about a half of its ion-exchange capacity when it was allowed to stand for 1.5 years after the preparation. Despite the importance of this observation from the practical point of view, the decrease in the ion-exchange capacity has not yet been stuied in detail as a function of the lapse of time. The present paper will describe the results of our study of this subject.

Experimental

Materials. The hydrous titanium oxide ion exchanger prepared by the method reported previously[1] was used after having been conditioned by the following procedure. The exchanger, sieved to obtain a desired particle size (100—200 mesh), was poured into a glass column, 10 mm in inside diameter and 20 cm high, with glass wool for column support. Then at least thirty times the column volume of 0.1 M (1 M=1 mol dm^{-3}) HCl, 0.1 M NaOH, and 0.1 M HCl were passed through, in this order, at a rate of about 1.0 cm^3/min. After each step, the column was washed with water until the effluent became neutral. The exchanger in the hydrogen form thus prepared was air-dried and stored in a desiccator containing a saturated NH_4Cl solution. A part of the exchanger was heated to a constant weight at 80 °C and stored in the same desiccator. As the result of the above treatment, two kinds of exchangers were obtained:

Sample A: Hydrogen form dried at room temperature,

Sample B: Hydrogen form subjected to thermal treatment at 80 °C.

Their composition and ion-exchange capacities are shown in Table 1.

Titration Curves. In 50 cm^3 of a solution (ionic strength: 0.10 M), 0.5 g of the sample was immersed for 5 d at room temperature, with intermittent shaking. This was followed by the pH measurement of the solution and by the determination of the sodium ions in the solution. The sodium ions were converted to pure sodium chloride and indirectly determined by titrating the chloride ions by means of the Fajans' method. To obtain a titration curve, this procedure was repeated for various solutions which had been prepared using the desired combinations of 0.1 M NaOH and 0.1 M NaCl. The ion-exchange capacity was calculated from the amount of sodium ions taken up from the 0.1 M NaOH solution.

Results and Discussion

The dependence of the ion-exchange capacity of Sample A on the standing period is shown in Fig. 1. The capacity first decreased slightly with the lapse of time for about 95 d after the preparation, this decrease amounted to 0.25 meq/g in this period. Thereafter, it decreased abruptly until about 180 d, at which point about a half of its original value was lost. Thereafter, the capacity continued to decrease gradually with the lapse of time. This phenomenon may be understood by considering that such a gelatinous material as hydrous titanium oxide is in the metastable state, which tends to be stabilized on standing. If this argument is true, the material which has been forced to age by thermal treatment will behave differently. Therefore, the exchanger treated thermally at 80 °C (Sample B) was also examined in a similar way. The reason for selecting this temperature for the thermal treatment is that the release of water is accompanied by a certain degree of stabilization of

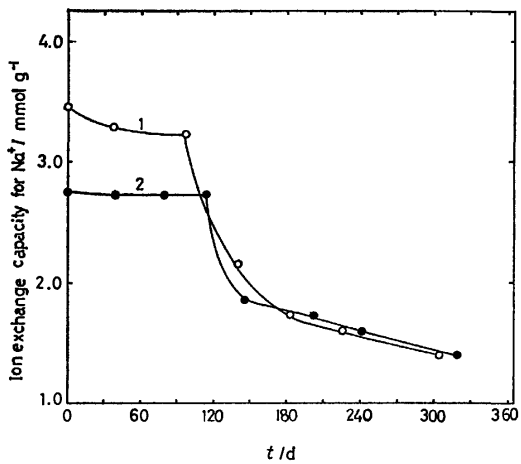

Fig. 1. Variation of ion-exchange capacity with time. ○: H^+ form, air-dried, ●: H^+ form, 80 °C heat-treatment.

TABLE 1. ION-EXCHANGE CAPACITY AND THE WATER CONTENT

Sample	Time of standing / d	Composition, molar ratio of H_2O/Ti	Ion-exchange capacity for Na^+ mmol Na^+/g	mmol Na^+/mmol Ti
A	0	2.08±0.10	3.47±0.05	0.407±0.007
	305	1.36±0.06	1.40±0.03	0.146±0.005
B	0	1.61±0.08	2.75±0.02	0.300±0.006
	310	1.09±0.07	1.38±0.03	0.138±0.004

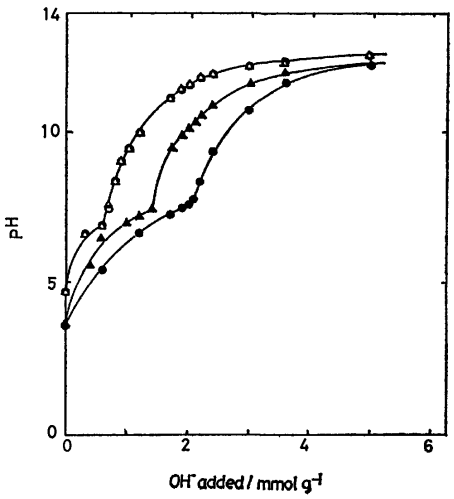

Fig. 2. Titration curve.
Exchanger of H^+ form and room temperature;
●: sample A, immediately after the preparation,
○: sample A, at 320 days after the preparation.
Exchanger of H^+ form and 80 °C heat-treatment;
▲: sample B, immediately after the preparation,
△: sample B, at 320 days after the preparation.

the network structure[1] and that the material does not suffer so much loss in capacity as to become useless as an ion exchanger. A comparison of Curves 1 and 2 indicates that the capacity of Sample B decreased in the same way as that of Sample A. Besides, the capacities of Samples A and B reached the same value after standing for 180 d in spite of the difference in the initial values between the two samples. These facts suggest that the stabilization of the network structure does not play an important role in the stability of the exchange sites. In order to examine the effect on the acid-base property brought about by aging, the titration curves were measured for the samples stored for 320 d after the preparation, as is shown in Fig. 2. The titration curves for these samples were almost all the same. The breaking points in the curves were, however, observed at smaller amounts of OH^- for the aged samples than for the original ones. The titration curves in the pH range higher than that point ran parallel with each other. These findings strongly suggest that the most acidic exchange sites are liable to be destroyed upon standing. The preferential destruction of the most acidic sites was also observed when the exchanger was thermally treated in air.[1] The change in the composition of the exchanger was then studied by estimating the content of water from the weight loss on ignition to TiO_2. Table 1 shows that an appreciable amount of water was lost from the exchanger which had been stored for a long time. Accordingly, in a study of this kind, the exchange capacity normalized per unit amount of titanium should be used instead of the capacity defined on the basis of the unit mass of the exchanger thus far used, because, when using the latter, we can not exactly compare the capacity based on the same amounts of the original materials. The normalized capacity is represented in the last column in Table 1. The results in Table 1 are compatible with the general relationship that an exchanger with a higher water content has a larger ion-exchange capacity.[2-4] A sample which had been allowed to stand for 320 d was subjected to conditioning once again in order to examine the possibility of recovering the ion-exchange capacity. The reconditioning, however, was found not to be effective for that purpose. These facts clearly indicate that the destruction of the exchange site proceeds by means of an irreversible dehydrating condensation of the hydroxyl group with the loss of water. This change, however, was not accompanied by crystallization, because X-ray analysis exhibited no such diffraction pattern as appeared when the exchanger was thermally treated at 324 °C.[1] From these considerations, we can conclude that the exchanger is subjected to a drastic change in its ion-exchange property when it is allowed to stand for three months in air and that this deterioration results basically from the same mechanism as that observed when the exchanger was thermally treated at a temperature below 159 °C.[1]

References

1) Y. Inoue and M. Tsuji, *Bull. Chem. Soc. Jpn.*, **51**, 794 (1978).
2) M. Abe and T. Ito, *Nippon Kagaku Zasshi*, **86**, 817 (1965).
3) M. Abe and T. Ito, *Nippon Kagaku Zasshi*, **86**, 1259 (1965).
4) N. J. Keen, *J. Brit. Nucl. Soc.*, **7**, 178 (1968).

Structure Determination of the Fluorescent Base from *Geotrichum candidum* Phenylalanine tRNA

Akihiko Mochizuki,* Yoshiaki Omata, and Yuji Miyazawa
Department of Chemistry, Science University of Tokyo, Shinjuku-ku, Tokyo 162
(Received February 7, 1979)

Synopsis. The chemical structure of the fluorescent base purified from *Geotrichum candidum* phenylalanine tRNA was determined as peroxywybutine by the use of MS, UV, and NMR measurements.

Modified nucleosides found in tRNA have been considered to play an important role in the functioning of tRNA. Hypermodified fluorescent bases, classified as "W," are located at the position adjacent to the 3′ side of the anticodon. The chemical structures of these fluorescent bases were determined as follows: α-(carboxyamino)-4,9-dihydro-4,6-dimethyl-9-oxo-1*H*-imidazo[1,2-*a*]purine-7-butyric acid dimethyl ester for wybutine obtained from yeast phenylalanine tRNA ($tRNA^{Phe}$),[1] 4,9-dihydro-4,6-dimethyl-9-oxo-1*H*-imidazo[1,2-*a*]purine for wye from *Torulopsis utilis* $tRNA^{Phe}$,[2] and α-(carboxyamino)-4,9-dihydro-β-hydroperoxy-4,6-dimethyl-9-oxo-1*H*-imidazo[1,2-*a*]purine-7-butyric acid dimethyl ester for peroxywybutine from rat liver $tRNA^{Phe}$.[3] Peroxywybutine was also found in wheat germ and bovine liver $tRNA^{Phe}$ by chromatographical[4] and spectrometrical[5] measurements respectively.

In this study, the hydrophobic and fluorescent base was purified from $tRNA^{Phe}$ of *G. candidum*[6,7] that is one of the simplest eukaryotic organisms and is classified as an aquatic fungus. The chemical structure of the base was determined to be peroxywybutine by the use of MS, UV, and NMR measurements.

Experimental

Preparation. Wet *G. candidum* cell[7] (10 kg) gave 4 g of crude tRNA by phenol extraction followed by the procedure of Miyazaki.[8] The crude tRNA was applied on a benzoylated DEAE-cellulose column and chromatographed as described by Gillam *et al.*[9] The rechromatography of the fraction eluted at 10% ethanol using the same column, as described by Litt,[10] showed a slight difference in the separation of $tRNA^{Phe}$ as compared with yeast $tRNA^{Phe}$. The specific activity of the $tRNA^{Phe}$ fractionated increased to 16 times that of the crude tRNA. The fraction containing 120 mg of $tRNA^{Phe}$ in 50 ml of water was incubated at 37 °C for 3.5 h at pH 2.9.[11,12] After neutralization, the fluorescent base liberated was extracted by ethyl acetate and purified by chromatography on Toyo No. 51A paper with a developing solvent prepared as the upper phase of a mixture of ethyl acetate : 1-propanol : water=4:1:2. The R_f value of the fluorescent base was 0.43. The base was extracted from the paper with water doubly distilled in a glass vessel. The base was then extracted again with the same volume of distilled chroloform six times and dried to an amorphous powder.

Measurements of Mass, UV, and NMR Spectra. The mass spectrum was measured with JMS-D300 on a lined JMA-2000 mass data system operated at 70 eV; PFK standard; $m/\Delta m=5000$; error, ±5 milli mass unit; 190 °C. The UV spectra were measured in water at pHs 2.42, 6.56, and 11.72 with the use of a Hitachi 200-20 spectrophotometer. The NMR spectrum was measured with JNM-PFT-100A in $CDCl_3$ containing 1% of C_2D_5OD, using TMS as the internal standard.

Results and Discussion

Table 1 shows the data of high-resolution MS of the base and elemental compositions. The ion peaks **1** and **c** are the parent and the base peaks respectively. The degradations of ions from the parent ion to the ion **2** and also from the ion **a** to the ion **b** correspond to a reduction of the mass unit equivalent to one oxygen atom. Fragmentations of the base can reasonably be presented by two pathways. The oxygen atom liberated would be originally found in the hydroperoxide group of the base, since hydroperoxides are known to lose an oxygen atom in mass spectrometry.[13] The results obtained by MS in this experiment show that the base contained the same fragment ion of $C_5H_8O_4N$ and the ion **c** as compared with those of wybutine previously reported,[1] though it contains two more oxygen atoms in the ion **a**. These results may be compared to the papers[3,5] reported for the chemical structure of peroxywybutine with quite a close agreement.

The UV spectra measured at each pH were very close to those of wybutine, and the absorption maxima were observed at 232 and 285 nm at an acidic pH, at 235, 262, and 311 nm at a neutral pH, and at 235, 265, and 303 nm at a basic pH. The comparison of the absorption maxima between the base measured in this experiment and the synthetic analogous compounds previously reported[1,14] suggests that the chromophore structure of this base is similar to that of wybutine.

In the NMR spectrum, the detection of four signals at 2.29, 3.71, 3.76, and 3.95 ppm was made possible by a scan repeated 17200 times. These peaks were close to those assigned to 6-C Me, methyl esters, and 4-N Me respectively, as reported for wybutine,[1,15] wye,[2] and peroxywybutine.[16]

As a result, discussions of the data obtained by MS, UV, and NMR lead to the conclusion that the fluorescent base purified from *G. candidum* $tRNA^{Phe}$ has the structure of the peroxide of wybutine.

Wye, wybutine, and peroxywybutine, all classified as "W," share the same 4,6-dimethylimidazopurine as a nucleus and have various side chains at the C-7 position of the nucleus. Wye and wybutine are found in simpler eukaryotic organisms, such as *Torulopsis utilis* and yeast $tRNA^{Phe}$'s respectively. On the other hand, peroxywybutine is found in such higher organisms as mammalian liver, *Lupinus luteus*, and wheat germ $tRNA^{Phe}$'s. It is interesting to find that $tRNA^{Phe}$ isolated from an aquatic fungus of *G. candidum* also gave the fluorescent base peroxywybu-

Table 1. Pertinent ions observed in the MS of the fluorescent base from *G. candidum* $tRNA^{Phe}$

Ion peaks	*m/e*	Elemental composition (mol wt)	Relative abundance/%
1	408.1358 (M^+)	$C_{16}H_{20}O_7N_6$ (408.1390)	3
2	392.1409	$C_{16}H_{20}O_6N_6$ (392.1441)	10
a	262.0989	$C_{11}H_{12}O_3N_5$ (262.0941)	14
b	246.1027	$C_{11}H_{12}O_2N_5$ (246.0992)	7
c	216.0886	$C_{10}H_{10}ON_5$ (216.0886)	100

tine, though recently Kasai *et al.*[17] reported a mass spectrum showing no peroxywybutine for rat liver $tRNA^{Phe}$.

The authors are grateful to Dr. Iiichi Ogahara, Department of Industrial Chemistry, Science University of Tokyo, for his advice on the mass spectrometry. They are also indebted to Mr. Eiji Kubota and Mr. Kenji Matsuura, JEOL, Ltd., for the measurement of the MS and to Mr. Shigeru Mita, Department of Chemistry, Science University of Tokyo, for the measurement of the NMR spectrum. They also thank the Kawaguchi Laboratory of Sapporo Breweries, Ltd., for their supply of the brewer's yeast used in this experiment.

References

1) K. Nakanishi, N. Furutachi, M. Funamizu, D. Grunberger, and I. B. Weinstein, *J. Am. Chem. Soc.*, **92**, 7617 (1970).
2) H. Kasai, M. Goto, S. Takemura, T. Goto, and S. Matsuura, *Tetrahedron Lett.*, **1971**, 2725.
3) K. Nakanishi, S. Blobstein, M. Funamizu, N. Furutachi, G. Van Lear, D. Grunberger, K. W. Lanks, and I. B. Weinstein, *Nature (London), New Biol.*, **234**, 107 (1971).
4) D. Yoshikami and E. B. Keller, *Biochemistry*, **10**, 2969 (1971).
5) S. H. Blobstein, D. Grunberger, I. B. Weinstein, and K. Nakanishi, *Biochemistry*, **12**, 188 (1973).
6) E. E. Butler and L. J. Petersen, *Mycologia*, **64**, 365 (1972).
7) K. Shimizu, J. Hosoi, M. Ueda, and Y. Miyazawa, *J. Electron Microsc.*, **26**, 41 (1977).
8) M. Miyazaki, "Kakusan Jikkenho," ed by A. Ishihama, R. Okazaki, Y. Kyogoku, and S. Nishimura, Kyoritsu Shuppan, Tokyo (1973), p. 60.
9) I. Gillam, S. Millward, D. Blew, M. von Tigerstrom, E. Wimmer, and G. M. Tener, *Biochemistry*, **6**, 3043 (1967).
10) M. Litt, *Biochem. Biophys. Res. Commun.*, **32**, 507 (1968).
11) R. Thiebe and H. G. Zachau, *Eur. J. Biochem.*, **5**, 546 (1968).
12) R. Thiebe and H. G. Zachau, "Methods in Enzymology," ed by K. Moldave and L. Grossman, Academic Press, New York (1969), Vol. 20, p. 179.
13) J. E. van Lear and L. L. Smith, *J. Org. Chem.*, **36**, 1007 (1971).
14) M. Funamizu, A. Terahara, A. M. Feinberg, and K. Nakanishi, *J. Am. Chem. Soc.*, **93**, 6706 (1971).
15) R. Thiebe, H. G. Zachau, L. Baczynskyj, K. Biemann, and J. Sonnenbichler, *Biochim. Biophys. Acta*, **240**, 163 (1971).
16) A. M. Feinberg, K. Nakanishi, J. Barciszewski, A. J. Rafalski, H. Augustyniak, and M. Wiewiorowski, *J. Am. Chem. Soc.*, **96**, 7797 (1974).
17) H. Kasai, Z. Yamaizumi, Y. Kuchino, and S. Nishimura, *Nucleic Acids Res.*, **6**, 993 (1979).

Structural Dependence in a One-electron Transfer Process: Naphthalene *peri* Ketones[1)]

Takeo SATO,* Masao KUBO, and Kenji NISHIGAKI

Department of Chemistry, Tokyo Metropolitan University, Setagaya-ku, Tokyo 158

(Received June 1, 1979)

Synopsis. The cyclic voltammetry of several naphthalene *peri* ketones was carried out in anhydrous DMF containing TBAP. The cathodic peak potential for carbonyl reduction was found to be shifted toward a more anodic potential when carbonyl, oxygen, and sulfur groups were present in the *peri* position. The controlled potential electrolysis of *peri* diketones gave an intramolecular coupling product *via* a bis-anion radical.

We have been exploring the relation between the oxidation-reduction potentials and the molecular geometry.[1,2)] It is particularly interesting to know how proximity effects influence an electron-transfer process. Since the *peri* positions in a naphthalene nucleus are only 2.4—2.5 Å apart,[3)] a series of those compounds with peri substituents will serve as good model substances for such studies. We examined the cyclic voltammetry (CV) of several naphthalene *peri* ketones in an aprotic solvent in order to elucidate the effect of the *peri* substituents on the carbonyl reduction.

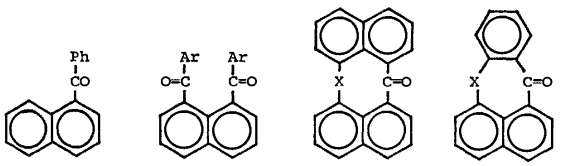

1 **2**, Ar=Ph **3**, Ar=α-naphthyl **4**, X=CO **5**, X=O **6**, X=S **7**, X=CH_2 **8**, X=CO

The *peri* ketones used in the present study are **1**—**8**. The CV measurements were carried out in anhydrous DMF, containing 0.1 mol dm^{-3} tetrabutylammonium perchlorate (TBAP) as a supporting electrolyte. The results are summarised in Table 1. For those compounds that gave a reversible voltammogram, such as **1** and **8**, the CV measurements were carried out at various scanning speeds. The results are shown in Table 2, together with several electrochemical parameters.

1-Benzoylnaphthalene (**1**) exhibited a quasi-reversible wave at $E^\circ=-1.71$ V *vs.* SCE. The peak-to-peak potential difference, $E_{pc}-E_{pa}$, was 220 mV at the scanning rate of 500 mV/s, but it became much smaller for lower scanning rates, which improve the reaction reversibility (Table 2). The current ratio, i_{pc}/i_{pa}, was nearly equal to unity. An interpretation that the reversible couple may correspond to a one-electron transfer process was derived by calculating n by using Randles-Cevcik equation[4)] (Table 2). When the scanning range was further extended to the cathodic side, another cathodic peak appeared at −2.5 V. For this second peak, however, no corresponding anodic peak was observed by reversed scanning. The addition of methanol caused E_{pc} to shift to the anodic side (Table 1). These results are considered to be specific for an aromatic ketone which has undergone succesive electron-transfer steps to give an anion radical and a dianion.[5)]

Compared with the monobenzoyl compound **1**, the *peri* diketones **2**, **3**, and especially **4** showed E_{pc}'s at an appreciably anodic potential. For example, the E_{pc} for **4** was −1.52 V compared with that of −1.8 V for **1**. These compounds also showed less reversible waves, as was assumed from the high i_{pc}/i_{pa} ratio of

Table 1. Cyclic voltammetry data for compounds **1**—**8**[a)]

Compound	E_{pc}/V	E_{pa}/V	E°/V	$(E_{pc}-E_{pa})$/mV	i_{pc}/i_{pa}	Additive
1[b)]	−1.82	−1.60	−1.71	220	1.1	
1[c)]	−1.78	−1.61	−1.70	170	1.8	
	−2.50	—	−2.42[f)]			
1[c)]	−1.80	−1.60	−1.70	200	1.7	MeOH
	—	—				
2	−1.67	−1.50[e)]	−1.59	170	2.5	
3	−1.60	−1.52[e)]	−1.56	80	3.2	
4	−1.52	−1.44	−1.48	80	2.3	
5	−1.40	−1.32	−1.36	80	2.0	
6[d)]	−1.46	−1.34	−1.40	120	1.5	
7	−1.54	−1.42	−1.48	120	1.2	
8	−1.30	−1.08	−1.19	220	1.1	
	−1.86	−1.62	−1.74	240	1.1	
8	−1.31	−1.10	−1.21	210	1.4	MeOH
	−1.86	−1.54	−1.70	320	1.5	

a) Determined in DMF–TBAP (0.1 M) at the scan rate of 500 mV/s using the method described in Ref. 2. Scanning potential range; 0—−2.0 V *vs.* SCE. $E^\circ=E_{pc}+(E_{pc}-E_{pa})/2$. b) Potential range; 0—−2.2 V. c) Potential range; −0.5—−2.7 V. d) Determined in DMSO–TBAP (0.1 mol dm^{-3}). e) Shoulder. f) The potential at which $i=0.85\ i_{pc}$.

TABLE 2. SLOW CYCLIC VOLTAMMETRY DATA AND ELECTROCHEMICAL PARAMETERS FOR COMPOUNDS **1** AND **8**[a)]

Compound	Scan rate mV/s	$(E_{pc}-E_{pa})$/mV	i_{pc}/i_{pa}	$i_{pc}/v^{1/2}$	n
1	10	100	1.0	24	0.93
	25	130	0.9	19	0.79
	50	160	1.0	19	0.81
	100	190	1.2	22	0.87
	250	250	1.2	19	0.81
8	25	120 140	1.3 1.3	24 24	0.90 0.90
	50	140 150	1.3 1.2	24 21	0.91 0.91
	100	180 190	1.2 1.3	23 22	0.88 0.84
	250	220 250	1.2 1.3	22 19	0.84 0.77

a) Determined in DMF-TBAP (0.1 mol dm^{-3}) at 25 °C. For the calculation of the n value, the Randles-Cevcik equation was used assuming $D=7.9\times10^{-7}$ cm^2/s (benzophenone); see Ref. 3.

2.3—3.2. The results can be well interpreted to indicate a two-electron reduction, giving the pinacolate dianion **9**, since the intramolecular radical coupling of the bis-anion radical is geometrically favored. In fact, an intramolecular coupling product, **10**, was obtained by the controlled potential electrolysis of **1** at −2.0 V in ethanol containing potassium hydroxide, using a lead cathode. Similar results using a mercury cathode in aq ethanol have been reported.[6)] The unique geometry of **4** is assumed to be responsible for the anodic shift of the E_{pc}. It is considered that the steric strain in **4** caused by the steric interaction between the two parallel carbonyl groups is relieved by its being reduced to a dianion analogous to **9**.

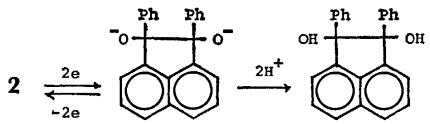

9 **10**

The presence of hetero atoms, such as oxygen or sulfur, at the peri position was found to cause a further anodic shift of the cathodic waves. Both **5** and **6** showed E° at −1.4 V, the ΔE° from **1** being 0.3 V, reflecting the intramolecular stabilization effect of the hetero atom toward the one-electron reduction of a nearby carbonyl group.

Unlike **2**, **3**, and **4**, 7,12-pleiadenedione (**8**) showed two reversible redox couples at −1.2 and −1.7 V, each corresponding to a one-electron transfer (Table 2). The controlled potential electrolysis of **8** gave a diol, **13**. In **8**, the intramolecular coupling of the bis-anion radical is sterically disfavored and results in a two-step reduction. It became evident that pleiadenone, **7**, was more readily reduced than benzoylnaphthalene, **1**.

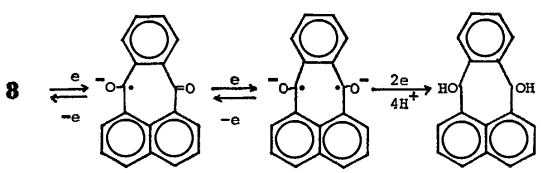

11 **12** **13**

Experimental

CV Measurements. The cyclic voltammetry was carried out in anhydrous DMF containing TBAP (0.1 mol dm^{-3}) using a two-compartment cell equipped with a nitrogen bubbler and SCE. A platinum inlay electrode (Beckman 32273) and a platinum wire were used as the working and counter electrodes respectively. The surface area of the working electrode was 0.204 cm^2. The electrochemical equipment used was the same as that described before.[2)]

Materials. The preparation of the *peri* ketones **1**—**8** has been reported elsewhere.[7)]

Controlled Potential Electrolysis of 2 and 8. A solution of 476 mg (0.96 mmol) of **2** in 200 ml of 2 mol dm^{-3} ethanolic potassium hydroxide was electrolyzed at −2.0 V using a lead cathode. The electrolysis was continued until 9 F/mol of electricity had been consumed. Compound **10** was then obtained in a 27.3% yield by chromatography on alumina eluted with hexane–benzene.

When compound **8** was similarly electrolyzed at −2.0 V, a 17% yield of the diol, **13**, was obtained; this was identical with the authentic sample (mp 197—200 °C), prepared by the sodium borohydride reduction of **8**.[8)] The electricity required was 4 F/mol.

References

1) Electron-organic Chemistry. V. Part IV: T. Sato, K. Torizuka, M. Shimizu, Y. Kurihara, and N. Yoda, *Bull. Chem. Soc. Jpn.*, **52**, 2420 (1979).

2) T. Sato and M. Kamada, *J. Chem. Soc., Perkin Trans. 2*, **1977**, 384; T. Sato and K. Torizuka, *ibid.*, **1978**, 1199; T. Sato, K. Torizuka, R. Komaki, and H. Atobe, *ibid.*, in press.

3) V. Balasubramaniyan, *Chem. Rev.*, **66**, 567 (1966).

4) I. L. Meites, "Polarographic Technique," 2nd ed, John Wiley, New York (1965), p. 671.

5) M. R. Rifi, "Technique of Electroorganic Synthesis," ed by N. L. Weinberg, Wiley-Interscience, New York (1974), Part II, Chap. VIII.

6) R. N. Gourley and J. Grimshaw, *J. Chem. Soc., C*, **1968**, 2388; T. Nonaka and M. Asai, *Bull. Chem. Soc. Jpn.*, **51**, 2976 (1978).

7) M. Kubo and T. Sato, *Bull. Chem. Soc. Jpn.*, in press.

8) P. T. Lansbury and F. D. Saeva, *J. Am. Chem. Soc.*, **89**, 1980 (1967).

A Convenient Synthesis of Telluronium Ylides

Seizo TAMAGAKI,* Ryuji AKATSUKA, and Seizi KOZUKA
Department of Applied Chemistry, Faculty of Engineering,
Osaka City University, Sugimoto-cho, Sumiyoshi-ku, Osaka 558
(Received June 15, 1979)

Synopsis. Several telluronium ylides were readily prepared by mixing the corresponding telluroxides and a variety of active methylene compounds in $CHCl_3$ at ambient temperature or under reflux. Arylselenonium ylides could also be obtained in a similar way.

We recentry reported a convenient procedure to prepare several alkyl and arylalkyl selenonium ylides by treating the corresponding selenoxides and active methylene compounds at room temperature.[1] Mean-

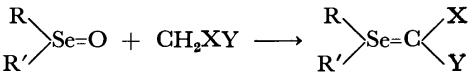

X, Y=CN or COOMe

while, only a few publications have been available on the general synthesis of telluronium ylides. Sadekov *et al.* reported that diaryl tellurium dichlorides gave the ylides when allowed to react with 5,5-dimethyl-1,3-cyclohexanedione (dimedone) in the presence of base in refluxing benzene.[2]

In this article it is described that the method previously developed by us for the synthesis of selenonium ylides can be applied successfully to the preparation of telluronium analogs starting from telluroxides which are easily available.

Results and Discussion

A typical reaction is as follows: phenyl methyl telluroxide was treated with a 3-fold excess of malononitrile and methyl cyanoacetate in $CHCl_3$ at ambient temperature. After 12 h, evaporation of the solvent afforded solids of phenylmethyltelluronium dicyanomethylide (I) and cyano(methoxycarbonyl)methylide (II), respectively.

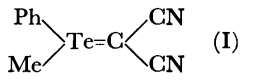

(I)

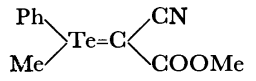

(II)

As was observed in the IR spectrum of the corresponding selenonium dicyanomethylide,[1,3] the cyano groups in the telluronium dicyanomethylide (I) also exhibited two absorption bands with comparable intensity at 2120 and 2160 cm^{-1}. The IR bands due to the cyano and carbonyl groups in II shift to lower wavelengths as compared to those of methyl cyanoacetate.

Meanwhile, when diphenyl telluroxide was utilized as a telluroxide, any reaction did not take place at room temperature. However, upon refluxing a chloroform solution of the oxide and an equimolar amount of methylene compounds for 10 h, the formation of

TABLE 1. PRODUCT YIELDS AND PHYSICAL PROPERTIES OF TELLURONIUM AND SELENONIUM YLIDES

Ylide	Yield %	Mp °C	IR(KBr) ν/cm^{-1}	NMR in $CDCl_3$ δ/ppm[b]
$PhMeTe{=}C(CN)_2$ (I)	82	148—149	2160, 2120	7.20—8.00(5H, m), 2.23(3H, s)
PhMeTe=C(CN)(COOMe) (II)	80	123—125	2150, 1620	7.28—8.00(5H, m), 3.79(3H, s), 2.30(3H, s)
PhMeTe=C(CN)(COOEt) (III)	75	131—132	2150, 1620	7.12—8.05(5H, m), 3.72—4.14(2H, q), 2.33(3H, s), 0.97—1.12(3H, t)
$Ph_2Te{=}C(CN)(COOMe)$ (IV)	78	a)	2130, 1610	7.1—7.6(10H, m), 3.65(3H, s)
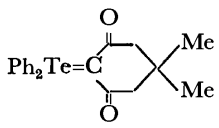 (V)	100	162—163	1524	7.40—7.80(10H, m), 2.37(4H, s), 1.10(6H, s)
$Ph_2Se{=}C(CN)(COOMe)$ (VI)	56	a)	2160, 1649	7.58(10H, s), 3.75(3H, s)
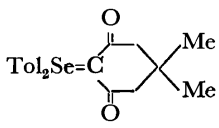 (VII)	100	128—129	1560	7.20—7.60(8H, m), 2.38(10H, s), 1.09(6H, s)

a) Oily and viscous materials. b) s: singlet; q: quartet; m: multiplet.

the ylides was attained in excellent yields. For instance, dimedone upon treatment with diphenyl telluroxide, afforded quantitatively the corresponding ylide (V).

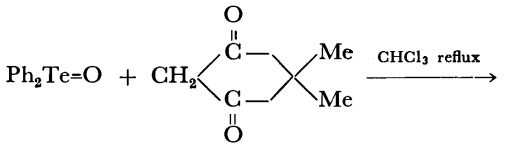

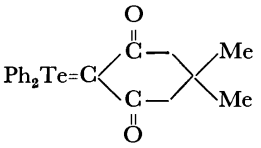

(V)

The yields and physical data of these ylides are summarized in Table 1.

In a similar way, the attempt to prepare diarylselenonium counterparts, which were not obtained previously by the reaction at room temperature, can be realized in good yields.

The method described here is a useful and convenient alternative for the preparation of telluronium ylides, since it involves merely mixing reagents under mild conditions and only simple work-up of the reaction mixture as compared with that of Sadekov *et al.*[2]

Experimental

Preparation of Ylides. A mixture of phenyl methyl telluroxide (1 mmol, 235 mg) and a 3-fold excess of malononitrile in 20 ml of $CHCl_3$ was kept standing at room temperature for 12 h. After evaporation of the solvent, the resulting solid was recrystallized from $CHCl_3$–ether, giving 82% of phenylmethyltellurium dicyanomethylide (I): Found: C, 41.86; H, 2.88; N, 9.68%. Calcd for $C_{10}H_8N_2Te$: C, 42.31, H, 2.82; N, 9.87%. Similarly, the corresponding cyano(methoxycarbonyl)methylide(II) was prepared: Found: C, 41.29; H, 3.80; N, 4.71%. Calcd for $C_{11}H_{11}NO_2Te$: C, 41.62; H, 3.51; N, 4.46%. III: Found: C, 43.44; H, 3.86, N, 4.29%. Calcd for $C_{12}H_{13}NO_2Te$: C, 43.56, H, 3.93; N, 4.23%.

Compounds (IV—VII) were prepared by refluxing a $CHCl_3$ solution of diaryl telluroxides (1 mmol) and one equivalent of methylene compounds for 15 h. After the solvent was stripped off, V and VII were purified by recrystallization from benzene–hexane and ether, respectively. V: Found: C, 57.05; H, 4.78%. Calcd for $C_{20}H_{20}O_2Te$: C, 57.18, H, 4.80%. VII: Found: C, 65.89; H, 5.91%. Calcd for $C_{22}H_{24}O_2Se$: C, 66.14; H, 6.06%. IV and VI were purified by precipitation with ether from their $CHCl_3$ solutions.

References

1) A. Tamagaki and K. Sakaki, *Chem. Lett.*, **1975**, 503.

2) I. D. Sadekov, A. A. Maksimenko, A. I. Usaches, and V. I. Minkin, *Zh. Obshch. Khim.* (*Leningrad*), **45**, 2563 (1975).

3) N. N. Magdesieva, R. A. Kandgetcyan, and A. A. Ibragimov, *J. Organomet. Chem.*, **42**, 399 (1972); B. H. Freeman and D. Lloyd, *Chem. Commun.*, **1970**, 924.

Electrolytic α-Bromination of Some α-Substituted Active Methylene Compounds

Sigeru Torii,* Kenji Uneyama, and Noritsugu Yamasaki
Department of Industrial Chemistry, School of Engineering, Okayama University, Okayama 700
(Received June 29, 1979)

Synopsis. Electrolytic α-bromination of methyl α-substituted malonates and methyl α-substituted acetoacetates was accomplished in 73—84% yields in dichloromethane containing tetraethylammonium bromide as an electrolyte and sodium methoxide as an enolizing reagent.

Electrolytic bromination and bromohydrination of olefins proceed *via* electrophilic attack by electrochemically generated bromonium ion or bromine.[1] Enolate **2** would be brominated in principle by electrolysis to give the corresponding bromo compounds **3**. Reports have appeared on the electrolytic α-halogenation of acetone,[2] cyclohexanone, acetophenone,[3] and acetic acid[4] in a strong acidic medium such as hydrochloric acid. However, α-bromonation of active methylene and methine of malonates and acetoacetates dose not seem to have been studied.[5,6] During the course of studies on the reaction by electrochemically generated halonium ion, we found a typical electrolytic condition which enables us to trap the electrochemically generated bromonium ion with active methylene compounds and also prevents oxidation of the enolate **2**, leading to dimerization. Although direct bromination with bromine gives the corresponding bromo compounds, active methylene compounds bearing an olefinic functional group may suffer bromination of the carbon-carbon double bond in the reaction. In this article we describe

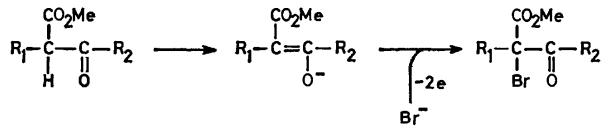

1a—f **2a—f** **3a—f**

a; R_1 = *n*-Bu, R_2 = MeO
b; $PhCH_2$, MeO
c; $(Me)_2C=CH-CH_2$, MeO
d; H, MeO
e; *n*-Bu, Me
f; $PhCH_2$, Me

Scheme 1.

an electrolytic α-bromination of **1** which is characterized by (1) bromination without use of molecular bromine or hydrobromic acid and (2) selective bromination at α-possition of olefinic active methylene compounds.

Compounds **1a—1f** were prepared by the alkylation of methyl malonate and methyl acetoacetate.[7] The reaction conditions and results of electrolysis of **1** are given in Table 1. The compounds gave α-brominated products **3** in 73—84% yields. Alkenylated substrate **1c** gave **3c** in 83% yield without modifying the carbon-carbon double bond. Dichloromethane was found to be a useful solvent for most of the substrates. Methanol and a mixed solvent of MeCN–H_2O were chosen for **1b** and **1d**, respectively, to attain the optimum yields of **3b** and **3d**. The quantity of sodium methoxide required for the electrolysis seems to be variable depending on the acidity of the substrate and polarity of the solvent.[8]

A characteristic feature of the electrolysis is that high current densities are required (87—133 mA/cm²) to terminate the reaction within a few minutes for the mili mole scale experiment. The yield of **3a** was unsatisfactory (42%) at lower current densities and several byproducts being obtained, one of which was the corresponding dimeric malonate (21%).[9] A soluble brominating reagent (electrolyte) was used. The behavior of **1d** in CH_2Cl_2 differed electrolysis with use of Et_4NBr (10—20 eq) affording *ca.* 50% of **3d** along with methyl α-chloromalonate (10—20%) as a byproduct. The yield of the chloro compound reached 50—60% at a lower concentration of Et_4NBr (1—2 eq). The use of sodium bromide in methanol resulted in a poor yield of **3d**. In contrast, electrolysis using Mg(II) or Cu(II) bromide in a mixed solvent of MeCN/H_2O (1/7 v/v) was successful.

Experimental

IR spectra were obtained with a JASCO IRA-1 spectrometer, and ^1H NMR spectra with a JNM FX-100 fourier

Table 1. Electrolytic bromination of **1a—f**

Substrate	Solvent	Supporting[a] electrolyte (eq)	MeONa[a] (eq)	Current mA	Electricity[b] F mol^{-1}	Temp °C	Yield of **3** %
1a	CH_2Cl_2	Et_4NBr (35)	5	260	3.5	0—5	84
1b	MeOH	NaBr (20)	5	400	30	20	78[c]
	CH_2Cl_2	Et_4NBr (35)	10	260	5	20	64
1c	CH_2Cl_2	Et_4NBr (35)	5	260	5	6—8	83
1d	MeCN/H_2O[d]	$MgBr_2$ (1.2)	1.8	400	3	2—3	77
		$CuBr_2$ (0.8)	1.8	400	4	2—3	72
1e	CH_2Cl_2	Et_4NBr (23)	2	260	6	−30	82
1f	CH_2Cl_2	Et_4NBr (28)	3	260	4	−30	73

a) Equivalent amount to substrate. b) Two Pt foils (2×1.5 cm²) were used for electrode. c) 12% of starting material **1b** was recovered. d) MeCN/H_2O = 1/7 (v/v).

transform spectrometer at 100 MHz in $CDCl_3$ using Me_4Si as an internal standard.

*Methyl α-(3-Methyl-2-butenyl)malonate (**1c**).* Compound **1c** was prepared by alkylation of methyl malonate with 1-chloro-3-methyl-2-butene: IR (neat) 2960, 1760, 1740, 1460, 1246, 1155 cm^{-1}; NMR δ 1.63 (3H, s, CH_3), 1.68 (3H, s, CH_3), 2.58 (2H, t, J=7.4 Hz, CH_2), 3.36 (1H, t, J=7.7 Hz, CH), 3.73 (6H, s, CH_3O), 5.03 (1H, t, J=7.3 Hz, CH=). Found: C, 59.70; H, 8.25%. Calcd for $C_{10}H_{16}O_4$: C, 59.98; H, 8.05%.

*Methyl α-Bromo-α-butylmalonate (**3a**) (Electrolysis of **1a**).* A mixture of **1a** (30 mg), Et_4NBr (850 mg), and MeONa (45 mg) dissolved in dry CH_2Cl_2 (7 ml) was electrolyzed using Pt foils (2×1.5 cm^2) at 6—8 °C with a constant current (260 mA) for 3.5 min. On passing electricity, the mixture turned yellow. After evaporating the solvent, the residue was mixed with water and acidified with 5% HCl. The organic substances were extracted with ether, treated with CH_2N_2, and chromatographed (SiO_2, benzene) to give **3a** (37 mg, 84%) as a colorless oil; IR (neat) 2966, 2880, 1743, 1435, 1254, 1130 cm^{-1}; NMR δ 0.92 (3H, t, J= 6.5 Hz, CH_3), 1.10—1.52 (4H, m, CH_2), 2.10—2.40 (2H, m, CH_2), 3.82 (6H, s, CH_3). Found: C, 40.34; H, 5.38%. Calcd for $C_9H_{15}O_4Br$: C, 40.47; H, 5.66%.

*Methyl α-Bromo-α-(3-methyl-2-butenyl)malonate (**3c**)*: IR (neat) 2945, 1747, 1434, 1243 cm^{-1}; NMR δ 1.64 (3H, s, CH_3), 1.73 (3H, d, J=1.2 Hz, CH_3), 3.01 (2H, d, J=7.3 Hz CH_2), 3.81 (6H, s, CH_3O), 5.10 (1H, t, J=7.3 Hz, CH=). Found: C, 42.83; H, 5.47%. Calcd for $C_{10}H_{15}O_4Br$: C, 43.03; H, 5.42%.

*Methyl 2-Acetyl-2-bromohexanoate (**3e**)*: IR (neat) 2960, 1730, 1439, 1250 cm^{-1}; NMR δ 0.92 (3H, t, J=6.5 Hz, CH_3), 1.10—1.50 (4H, m, CH_2), 2.08—2.32 (2H, m, CH_2), 2.40 (3H, s, CH_3), 3.82 (3H, s, CH_3O). Found: C, 43.25; H, 5.73%. Calcd for $C_9H_{15}O_3Br$: C, 43.05; H, 6.02%.

*Methyl 2-Benzyl-2-bromo-3-oxobutanoate (**3f**)*: IR (neat) 3040, 2965, 1730, 1440, 1255, 705 cm^{-1}; NMR δ 2.35 (3H, s, CH_3), 3.47 (1H, d, J=17.0 Hz, CH_2), 3.64 (1H, d, J=17.0 Hz, CH_2), 3.75 (3H, s, CH_3O), 7.24 (5H, m, ArH). Found: C, 50.70; H, 4.76%. Calcd for $C_{12}H_{13}O_3Br$: C, 50,55; H, 4.60%.

Bromo compound **3b** has been reported.[10]

References

1) a) J. A. M. Leduc, U. S. Patent 3288692 Nov. 29, 1966; b) M. T. Oakland and L. B. Ryland, U. S. Patent 2282682, May 12, 1942; c) M. M. Baizer, "Organic Electrochemistry," Marcel Dekker, Inc., New York (1973).

2) A. Richard, *C. R. Nebd. Seances Acad. Sci., Ser. C*, **133**, 878 (1901).

3) J. Szper, *Bull. Soc. Chim. Fr.*, **51**, 653 (1932).

4) a) A. A. Hering, Ger. Patent, 903451, Feb. 8, 1954; b) M. A. Youtz, *J. Am. Chem. Soc.*, **46**, 545 (1924); c) G. Durand and B. Tremillon, *Anal. Chim. Acta*, **49**, 135 (1970); d) F. Fichter and R. Ruegg, *Helv. Chim. Acta*, **20**, 1578 (1973).

5) a) T. Okubo and S. Tsutsumi, *Denkikagaku*, **33**, 637 (1965); b) D. A. White *J. Electrochem. Soc.*, **124**, 1177 (1977). The formation of α-iodomalonate was proposed as an intermediate for the dimerization of ethyl malonate.

6) S. Kato and G. Dryhurst, *J. Electroanal. Chem., Interfacial Electrochem.*, **62**, 415 (1975). Barbituric acid was electrochemically chlorinated.

7) **1a**: M. Jones, J., W. Ando, M. E. Hendrick, A. Kulczycki, Jr, P. M. Howley, K. F. Hummel, and D. S. Malament, *J. Am. Chem. Soc.*, **94**, 7469 (1972). **1b**; H, C. McBay, O. Tucker, and A. Milligan, *J. Org. Chem.*, **19**, 1003 (1954). **1e**; W. B. Renfrow, Jr. and G. B. Walker, *J. Am. Chem. Soc.*, **70**, 3957 (1948). **1f**; H, Paul, *J. Prakt. Chem.*, **21**, 186 (1963).

8) D. J. Cram, "Fundamental of Carbanion Chemistry," Academic Press, New York and London (1965).

9) Electrolysis was carried out under the same conditions as those employed for **1a** (Table 1) except for the current (30 mA). Electrolysis of ethyl α-butylmalonate in the presence of MeONa in MeCN gave 38% of the corresponding dimer. *Cf.* H. G. Thomas, M. Strenkens, and R. Peek, *Tetrahedron Lett.*, **1978**, 45.

10) W. Ando, H. Matsuyama, S. Nakaido, and T. Migita, *J. Chem. Soc., D*, **1970**, 1156.

New Effective Nickel(II) Catalysts for the Cross-coupling of an Aryl Grignard Reagent with Aryl Halide

Eiichi IBUKI, Shigeru OZASA, Yasuhiro FUJIOKA,* Motofumi OKADA, and Katsutoshi TERADA

Department of Organic Chemistry, Kyoto College of Pharmacy, Misasagi, Yamashina-ku, Kyoto 607

(Received July 9, 1979)

Synopsis. It has been found that seventeen nickel complexes of the Ni–O_4, Ni–S_4, Ni–O_2N_2, Ni–O_3N_3, Ni–N_4, Ni–N_6, and Ni–$(C_5)_2$ types exhibit a high catalytic activity for the selective cross-coupling reaction of an aryl Grignard reagent with aryl iodide, which make possible the synthesis of unsymmetrical aromatics of a high purity and in a high yield.

In connection with the search for an effective method of C_{ar}–C_{ar} bond formation, Corriu and Masse[1] have reported that bis(acetylacetonato)nickel(II) catalyzes the selective cross-coupling reaction between aromatic Grignard reagents and aryl or alkenyl halides. Tamao *et al.*[2] have independently found a high catalytic activity of nickel-phosphine complexes for similar cross-coupling reactions. The present study was undertaken in order to develop a new, efficient catalyst for the synthesis of unsymmetrical biaryls by means of a Kharasch-type reaction.

The catalytic activity of a variety of nickel complexes was examined using a cross-coupling reaction of phenylmagnesium bromide with 2-iodobiphenyl as a model under a standard set of conditions. The activities of seventeen complexes and those of the four known representative catalysts, determined as the yield of *o*-terphenyl[I], are given in Table 1. The seventeen complexes showed a fairly high activity (a 70—90% yield of I), eleven of them exhibiting an activity superior to that of the four known catalysts used for comparison (57—78%; **12**, **19**, **20**, and **21**). Although in all cases, I was accompanied by 16—43% of biphenyl[II] and no, or only a small amount of, *o*-quaterphenyl[III]. I could easily be separated from these contaminants. Thus, the seventeen complexes, particularly eleven of them, were found to be preferential catalysts for the synthetic production of unsymmetrical aromatics of a high purity and in a high yield.

The seventeen new catalysts are classified briefly into the following groups: i) the Ni–O_4 complexes of the β-diketones and aldehyde ligands (**2**, **10**, **14**, **16**, and **8**); ii) the Ni–S_4 complex of the β-dithioketone ligand (**11**); iii) the Ni–O_2N_2 complexes of the β-keto imines and Schiff-base ligands (**1**, **6**, and **4**); iv) the Ni–O_3N_3 complex of the amino acid ligand (**9**); v) the Ni–N_4 and Ni–N_6 complexes of substituted amides, dioxime, and the diamine ligands (**3** and **5**; **15**; **17**, **13**, and **18**), and vi) the Ni–$(C_5)_2$ complex of the carbanion ligand (**7**). Although most of the new catalysts are diamagnetic square-planar complexes of bis-bidentate or quadridentate ligands (**1**,[3] **2**,[4] **3**,[5] **4**,[6a] **5**,[5] **11**,[6b] and **15**), a few octahedral complexes of tris-bidentate ligands (**9**,[6c] **13**, and **18**) as well as strongly paramagnetic complexes (**7**[7] and **8**[8]) are also included in the new catalysts. In contrast to the trimeric octahedral structure of **12**[9a,b] and **14**[9c] in solution, **2** has been reported to exist as a monomeric structure, presumably because of the steric hindrance of the ligand.[4a] It seems of interest to note that the catalytic activity of coordinately saturated complexes (**9**, **13**, and **18**) is nearly comparable to that of unsaturated ones. Another result of considerable significance is the observation that the activities of a series of four closely related complexes (**10**, **12**, **14**, and **16**), the logarithms of their formation constants,[10] and the negative logarithms of the acid dissociation constants of the ligands[10] show a rather fair correlation, as is shown in Table 2.

The foregoing results suggest that the catalytic activity of the complexes has no remarkable relation with such factors as the kind and number of coordinate atoms, the size and number of chelate rings, the aggregation degree of complexes, and the steric effect of the ligands, or, consequently, with the configuration and magnetic susceptibility of the complexes. Ultimately, for the excellent catalytic activity of the complexes, the presence of Ni(II) as the central metal can be regarded

TABLE 1. CATALYTIC ACTIVITY OF VARIOUS NICKEL COMPLEXES FOR THE CROSS-COUPLING OF C_6H_5MgBr WITH 2-I·C_6H_4·C_6H_5 (Ar'I)[a]

Catalyst	x[b] %	[I][c] %	[III][c] %	[II][d] %
none	15	2	0	19
Ni(dpm)$_2$ (**2**)	100	90	0	16
Ni(tfa)$_2$ (**10**)	100	86	4	16
Ni(acac)$_2$ (**12**)	100	78	1	31
	100	80[e]	2[e]	27[e]
Ni(ba)$_2$·H_2O (**14**)	94	75	4	33
Ni(dbm)$_2$ (**16**)	99	71	1	34
Ni(sal)$_2$·$2H_2O$ (**8**)	100	86	2	24
Ni(SacSac)$_2$ (**11**)	100	83	3	26
Ni(acaen) (**1**)	100	90	0	22
Ni(acNH)$_2$ (**6**)	100	87	1	29
Ni(H-sal-fum)$_2$ (**4**)	100	89	2	43
K[Ni(L-pro)$_3$]·$3H_2O$ (**9**)	100	86	0	24
Ni($pc_{1,3}$-pn)·H_2O (**3**)	100	89	2	23
Ni($pc_{1,2}$-pn)·$3H_2O$ (**5**)	100	87	0	25
Ni(dgH)$_2$ (**15**)	92	72	4	27
Ni(en)$_2$Cl$_2$ (**17**)	100	70	4	37
Ni(en)$_3$Cl$_2$·$2H_2O$ (**13**)	100	79	3	32
Ni(bpy)$_3$Cl$_2$·$7H_2O$ (**18**)	100	70	17	35
Ni(C_5H_5)$_2$ (**7**)	100	87	4	26
Ni(dppp)Cl$_2$ (**19**)	88	63	14	40
Ni(Ph_3P)$_2$Cl$_2$ (**20**)	83	58	5	27
Ni(dppe)Cl$_2$ (**21**)	81	57	15	39

a) The mean value of the duplicate runs is presented. b) x: Conversion of Ar'I, 100% implies all the 2-I·C_6H_4·C_6H_5 is consumed. c) Based on the 2-I·C_6H_4·C_6H_5 used. d) Based on the C_6H_5MgBr used. e) Isolated yield.

Table 2. Correlation of the catalytic activity with the formation constant of the complexes and with the acid dissociation constant of the ligands

Complex	Activity yield of [I] %	log K_f(av)[a]	pK_D[a]
10	86	7.1	8.7
12	78	8.69	12.70
14	75	9.00	12.85
16	71	10.09	13.75

a) Ref. 10; 75 vol% dioxane-25 vol% water.

as essential,[11] and an appropriate range of stability may be attributable to one of the invaluable factors.

Experimental

Instruments. The melting points were determined with a Mettler FP-51 or FP-52 apparatus. The UV spectra were measured on a Shimadzu MPS-50L spectrophotometer in cyclohexane solutions. The ^{1}H NMR spectra were obtained with a Varian A-60A spectrometer in a $CDCl_3$ solution, using TMS as an internal standard. Quantitative GLPC was performed on a Shimadzu GC-5APTF gas chromatograph using a 1 m×3 mmϕ glass column 3% Dexsil 300GC or Silicone OV-17 on Chromosorb W AW-DMCS.

Materials. The following complexes used as catalysts, except those available commercially (**7**, **12**, and **15**), were prepared according to the references or by known methods, and all gave satisfactory physical data and acceptable results in elemental analyses.

N,N'-Bis(1-methyl-3-oxobutylidene) ethylenediaminatonickel(II)[3c] (**1**), bis(dipivaloylmethanato)nickel(II)[4b] (**2**), *N,N'*-dipicolinoyl-1,3-propanediaminatonickel(II) hydrate[5] (**3**), bis[*N*-(2-furylmethyl)salicylideneaminato]nickel(II)[6a] (**4**), *N,N'*-dipicolinoyl-1,2-propanediaminatonickel(II) trihydrate[5] (**5**), bis(4-imino-2-pentanonato)nickel(II)[12b] (**6**), bis(η-cyclopentadienyl)nickel(II) (**7**), bis(salicylaldehydato)-nickel(II) dihydrate[8] (**8**), potassium tris(L-prolinato)-niccolate(II) trihydrate[6c] (**9**), bis(trifluoroacetylacetonato)-nickel(II) (**10**), bis(dithioacetylacetonato)nickel(II)[6b] (**11**), bis(acetylacetonato)nickel(II) (**12**), tris(ethylenediamine)-nickel(II) chloride dihydrate[12a] (**13**), bis(benzoylacetonato)-nickel(II) hydrate[13] (**14**), bis(dimethylglyoximato)nickel(II) (**15**), bis(dibenzoylmethanato)nickel(II)[14] (**16**), dichloro-[bis(ethylenediamine)]nickel(II)[15] (**17**), tris(bipyridine)nickel-(II) chloride heptahydrate[16] (**18**), dichloro[1,3-bis(diphenylphosphino)propane]nickel(II)[17] (**19**), dichloro[bis(triphenylphosphine)]nickel(II)[18a] (**20**), dichloro[1,2-bis(diphenylphosphino)ethane]nickel(II)[17] (**21**).

Coupling Reactions. To an ethereal solution of phenylmagnesium bromide (20 mmol), prepared in the usual manner, we added, all at once, a mixture of 2-iodobiphenyl[18b] (10 mmol) and a catalyst **12** (0.5% of C_6H_5MgBr) in benzene at 0 °C under a nitrogen atmosphere. The mixture was stirred for 1 h, refluxed for 3 h, and hydrolyzed, and then the product was extracted with benzene. The organic layer was separated, washed with water, and then dried. Upon the withdrawal of a tenth part of the solution for analysis, the remainder was subjected to the isolation of the products. After the removal of the solvent, the resulting solid was separated into three fractions by chromatography on alumina, with cyclohexane as the eluent. Upon the evaporation of the solvent, the fractions afforded II, I, and III, which were identified by means of mixed-melting-point measurements and by means of a spectral comparison with each of the authentic samples.

o-*Terphenyl*[*I*]: Mp 56.7 °C (lit,[19] mp 56—57 °C); yield, 1.65 g (79.7%). NMR: δ 7.16 (10H, s, C_6H_5), 7.40 (4H, s, C_6H_4). UV: λ_{max} (ε) 197 (48300), 207 (46500), 233 (29100), 251 nm (sh) (13300).

Biphenyl[*II*]: Mp 69.4 °C; yield, 0.37 g (26.7%). NMR: δ 7.16—7.70 (10H, m, C_6H_5).

o-*Quaterphenyl*[*III*]: Mp 118 °C (lit,[18b] mp 118—119 °C); yield, 0.03 g (2.2%). UV: λ_{max} (ε) 201 (60600), 230 (34100), 245 nm (sh) (25600).

The yields of the coupling products were determined by quantitative GLPC, using *m*-terphenyl as an internal standard calibrated against the pure samples.

References

1) R. J. P. Corriu and J. P. Masse, *J. Chem. Soc., Chem. Commun.*, **1972**, 144.

2) a) K. Tamao, K. Sumitani, and M. Kumada, *J. Am. Chem. Soc.*, **94**, 4374 (1972); b) K. Tamao, K. Sumitani, Y. Kiso, M. Zembayashi, A. Fujioka, S. Kodama, I. Nakajima, A. Minato, and M. Kumada, *Bull. Chem. Soc. Jpn.*, **49**, 1958 (1976).

3) a) J. Willis and D. Mellor, *J. Am. Chem. Soc.*, **69**, 1237 (1947); b) N. Hall and B. Willeford, *ibid.*, **73**, 5419 (1951); c) P. J. McCarthy, R. J. Hovey, K. Ueno, and A. E. Martell, *ibid.*, **77**, 5820 (1955).

4) a) F. A. Cotton and J. P. Fackler, Jr., *J. Am. Chem. Soc.*, **83**, 2818 (1961); b) G. S. Hammond, D. C. Nonhebel, and C.-H. S. Wu, *Inorg. Chem.*, **2**, 73 (1963).

5) H. Ojima, *Nippon Kagaku Zasshi*, **88**, 333 (1967).

6) a) S. Yamada, K. Yamanouchi, W. Mori, and M. Kishita, *Bull. Chem. Soc. Jpn.*, **49**, 2111 (1976); b) A. Ouchi, M. Hyodo, and Y. Takahashi, *ibid.*, **40**, 2819 (1967); c) J. Hidaka and Y. Shimura, *ibid.*, **43**, 2999 (1970).

7) P. W. Jolly and G. Wilke, "The Organic Chemistry of Nickel," Academic Press, New York and London (1974), Vol. 1, p. 420.

8) G. N. Tyson, Jr., and S. C. Adams, *J. Am. Chem. Soc.*, **62**, 1228 (1940).

9) a) G. J. Bullen, R. Mason, and P. Pauling, *Nature*, **189**, 291 (1961); b) D. P. Graddon and E. C. Watton, *ibid.*, **190**, 906 (1961); c) D. P. Graddon, *ibid.*, **195**, 891 (1962).

10) L. G. Van Uitert, W. C. Fernelius, and B. E. Douglas, *J. Am. Chem. Soc.*, **75**, 457 (1953).

11) In the preliminary experiments of the present coupling reaction, five complexes of $M(acac)_n$ (where M=Co(II), Fe(III), Fe(II), Mn(III), and Cr(III)) showed only a slight activity (18, 25, 24, 20, and 18% yields of I respectively). In the cases of the other analogous complexes (M=Co(III), Li(I), Cu(II), Be(II), Mg(II), Zn(II), Al(III), Zr(IV), Th(IV), and Mn(II)), only a trace of I or none was observed.

12) a) H. M. State, *Inorg. Synth.*, **6**, 200 (1960); b) A. W. Struss and D. F. Martin, *ibid.*, **8**, 232 (1966).

13) R. Nast and H. Rückemann, *Chem. Ber.*, **93**, 2329 (1960).

14) L. Wolf and E. Butter, *Naturwissenschaften*, **48**, 378 (1961).

15) H. M. State and E. P. Dwyer, *Inorg. Synth.*, **6**, 198 (1960).

16) H. Ito, *Nippon Kagaku Zasshi*, **77**, 1399 (1956).

17) G. R. Van Hecke and W. D. Horrocks, Jr., *Inorg. Chem.*, **5**, 1968 (1966).

18) a) K. Yamamoto, *Bull. Chem. Soc. Jpn.*, **27**, 501 (1954); b) E. Ibuki, S. Ozasa, and K. Murai, *ibid.*, **48**, 1868 (1975).

19) D. F. DeTar and C.-C. Chu, *J. Am. Chem. Soc.*, **82**, 4969 (1960).

Synthesis of Cyclopentadecanone by Ring Contraction of Cyclohexadecanone

Tetsuya KATO,* Hisao KONDO, and Akihisa MIYAKE
Basic Research Laboratries, Toray Industries, Inc., Tebiro, Kamakura 248
(Received August 10, 1979)

Synopsis. Cyclopentadecanone has been synthesized from cyclohexadecanone. 2,2,15-Tribromocyclohexadecanone, upon treatment with sodium methoxide, underwent the Favorskii rearrangement *via* methyl 2-bromo-1-cyclopentadecene-1-carboxylate to produce a mixture of methyl 2-methoxy-1-cyclopentadecene-1-carboxylate, methyl 2-methoxy-2-cyclopentadecene-1-carboxylate, and methyl 2,2-dimethoxycyclopentadecane-1-carboxylate which was converted into cyclopentadecanone.

Cyclopentadecanone **1** occurs naturally as a secretion of the musk rat[1] and has attracted considerable interest due to its usefulness as a valuable perfume base. Many synthetic routes have been developed for the synthesis of cyclopentadecanone **1** from various starting materials.[2] In relation to our own interest in devising simplified approaches to the synthesis of cyclopentadecanone **1**, we have investigated the ring contraction of cyclohexadecanone **2** by applying the Favorskii rearrangement of trihalogenated ketones.[3] Our synthetic route is outlined in the following scheme.

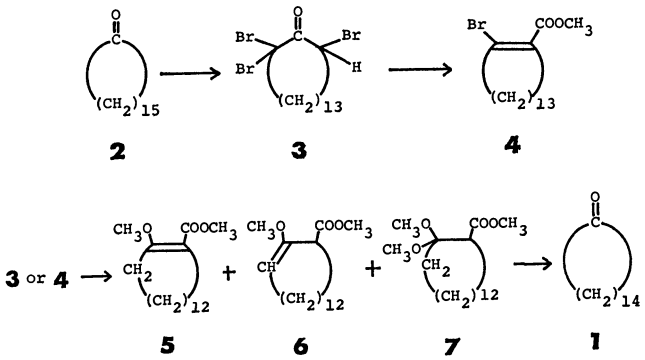

Cyclohexadecanone **2** was easily prepared according to the method developed by Nishino *et al.*[4] Bromination of the ketone **2** with 3.5 molar equiv of bromine in dichloromethane at 25—30 °C for 20 h gave 2,2,15-tribromocyclohexadecanone **3** as colorless crystals in 92% yield.

The Favorskii rearrangement of the tribromo ketone **3** was carried out by using 2.2 molar equiv of sodium methoxide in methanol at 20 °C to afford methyl 2-bromo-1-cyclopentadecene-1-carboxylate **4** as a mixture of *cis*- and *trans*-isomer in 83% yield. The distinction between the *cis*- and *trans*-isomer has been made on the basis of a comparison of the difference in the NMR chemical shifts of the allylic methylene protons.[5] The allylic methylene protons of the *cis*-isomer resonate at 2.16—2.60 ppm whereas those of the *trans*-isomer resonate at 2.20—3.30 ppm. Bases such as magnesium methoxide, triethylamine, or calcium hydroxide also gave satisfactory results.[6] Further treatment of the bromo ester **4** with 3.3 molar equiv of sodium methoxide in methanol afforded three major compounds **5**, **6**, and **7** in 88% yield (**5**+**6**, 71%; **7**, 17%). The reaction proceeded smoothly under reflux. In preparative runs the tribromo ketone **3** was directly converted into a mixture of the methoxy esters **5**, **6**, and **7**, without any separation of the bromo ester **4**, by using 5.2 molar equiv of sodium methoxide in methanol. Each methoxy ester was isolated by chromatographic purification on silica gel. The mixture of **5**, **6**, and **7** was then saponified with sodium hydroxide in refluxing aqueous methanol for 7 h to give the corresponding enol ether carboxylic acid and ketal carboxylic acid derivatives. Acid-catalyzed hydrolysis and subsequent decarboxylation of the resulting carboxylic acids with hydrochloric acid in methanol afforded cyclopentadecanone **1** in 80% yield.

Experimental

Melting and boiling points are uncorrected. Gas-liquid chromatography (GLPC) analyses were preformed on a Shimadzu 3BT instrument using 2% silicone SE-52 coated on Chromosorb GHP (80—100 mesh) packed in glass columns (3 mm×1.2 m). The following spectrometers were used: IR, Hitachi EPI-S-2; NMR, Varian XL-100 and HA-100 (TMS as internal standard); mass spectra, Hitachi RMU-7M and RMS-4. Silica gel (Merck, 70—230 mesh) was used for column chromatography.

*2,2,15-Tribromocyclohexadecanone (**3**).* Bromine (320 g 2.00 mol) was added dropwise over a period of 1.5 h to a cold (0—5 °C) stirred solution of cyclohexadecanone **2** (136 g. 0.571 mol) in dichloromethane (300 ml). After the addition was completed, stirring was continued at 25—30 °C for 20 h. The reaction mixture was poured into water and extracted with dichloromethane. The dichloromethane extracts were washed succesively with aqueous sodium hydrogensulfite solution and water and dried over anhydrous magnesium sulfate. Evaporation of the solvent under reduced pressure gave 273 g of yellow oil which was crystallized from methanol (−30 °C) to afford 250 g of tribromo ketone **3** (92%): mp 41—42 °C; IR (KBr) 1715 cm^{-1}; NMR ($CDCl_3$) δ 0.5—2.5 (m, 26H with a s at 0.77), 4.73 (dd, J=6 and 7.5 Hz, 1H). Found: C, 40.41; H, 5.50; Br, 50.68%. Calcd for $C_{16}H_{27}OBr_3$: C, 40.45; H, 5.73; Br, 50.48%.

*Methyl 2-Bromo-1-cyclopentadecene-1-carboxylate (**4**).* To a solution of tribromo ketone **3** (39.2 g, 82.5 mmol) in anhydrous methanol (220 ml) was added dropwise a solution of sodium methoxide in methanol (0.88 mol/l, 207 ml, 182 mmol) over a period of 1.5 h at 20 °C. After the addition was completed, stirring was continued at 20 °C for an additional 1 h. The reaction mixture was poured into cold water and extracted with hexane. The hexane extracts were washed with water and dried over anhydrous magnesium sulfate. After the solvent had been removed the residue was distilled (oil bath 180 °C/0.5 Torr) to give 26.3 g of yellow oil. GLPC analysis (165 °C) showed two major peaks due to *cis*- (50.1%) and *trans*-bromo ester **4** (39.8%). The yield was 83%. Each isomer was isolated by silica gel chromatography (benzene/hexane, 1/3—1/5).

4 (*trans*-isomer): bp 155—156 °C/0.8 Torr; $n_D^{20}=1.5120$; IR (neat) 1724, 1614 cm^{-1}; NMR ($CDCl_3$) δ 1.1—1.9 (s, 22H), 2.20—3.30 (m, 4H), 3.76 (s, 3H); *m/e* 346, 344 (M^+). Found: C, 59.14; H, 8.35; Br, 23.21%. Cacld for $C_{17}H_{29}O_2Br$: C, 59.13; H, 8.47; Br, 23.14%. **4** (*cis*-isomer): bp 159—160 °C/0.6 Torr; $n_D^{20}=1.5127$; IR (neat) 1727, 1641 cm^{-1}; NMR ($CDCl_3$) δ 1.1—1.8 (s, 22H) 2.16—2.60 (m, 4H), 3.77 (s, 3H); *m/e* 346, 344 (M^+). Found: C, 59.12; H, 8.24; Br, 23.23%. Calcd for $C_{17}H_{29}O_2Br$: C, 59.13; H, 8.47; Br, 23.14%.

*Methoxy Esters (**5**, **6**, and **7**).* A solution of sodium methoxide in methanol (3.0 mol/l, 50 ml, 150 mmol) was added to bromo ester **4** (17.25 g, purity 89.9%, 150 mmol) at 20 °C. The mixture was refluxed for 5 h, cooled, poured into cold water and dried over anhydrous sodium sulfate. After the solvent had been removed the residue was distilled (oil bath 180 °C/0.4 Torr) to give 12.25 g of oil. GLPC analysis showed that methoxy esters **5**, **6**, and **7** were obtained in 88% yield (**5**+**6**, 71%; **7**, 17%). Each ester was isolated by silica gel chromatography (benzene/hexane, 1/5—1/1). **5**: IR (neat) 1705, 1613 cm^{-1}; NMR ($CDCl_3$) δ 0.9—1.8 (s, 22H), 2.0—2.7 (m, 4H), 3.58 (s, 3H), 3.63 (s, 3H), *m/e* 296 (M^+). Found; C, 72.89; H, 10.63%. Calcd for $C_{18}H_{32}O_3$: C, 72.93; H, 10.88%. **6**: bp 142—143 °C/0.5 Torr; $n_D^{20}=1.4880$; IR (neat) 1737, 1655 cm^{-1}; NMR ($CDCl_3$) δ 1.1—2.3 (m, 24H with a s at 1.30), 3.38—3.60 (m, 1H), 3.46 (s, 3H), 3.64 (s, 3H), 4.48 (t, J=7 Hz, 1H); *m/e* 296 (M^+). Found: C, 72.94; H, 10.95%. Calcd for $C_{18}H_{32}O_3$: C, 72.93; H, 10.88%. **7**: IR (neat) 1739 cm^{-1}; NMR (CCl_4) δ 1.0—2.0 (m, 26H with a s at 1.38), 2.73 (dd, J=3 and 11 Hz, 1H), 3.12 (s, 3H), 3.19 (s, 3H), 3.62 (s, 3H); *m/e* 328 (M^+). Found: C, 69.69; H, 10.89%. Calcd for $C_{19}H_{36}O_4$: C, 69.47; H, 11.04%.

*Cyclopentadecanone (**1**).* A solution of sodium hydroxide (10.0 g, 250 mmol) in aqueous methanol (H_2O/MeOH, 1/3, 75 ml) was added to the ester mixture (14.8 g, **5**+**6** 90.9%, 45.4 mmol; **7** 6.7%, 3.0 mmol) and refluxed for 7 h. The reaction mixture was cooled and made acid to Bromophenol Blue by the addition of concentrated hydrochloric acid. After hydrochloric acid (35%, 30 ml) had been added, the reaction mixture was refluxed for 1 h, cooled, and extracted with benzene. The benzene extracts were washed with water and dried over anhydrous sodium sulfate. After the solvent had been removed the residue was distilled (oil bath 180 °C/0.4 Torr) to give 10.79 g of crude cyclopentadecanone. GLPC analysis showed one major peak due to cyclopentadecanone **1** (80% yield). Pure cyclopentadecanone was obtained by fractional distillation. The IR, NMR, and mass spectral data were identical with those of an authentic sample.

References

1) P. G. Stevens and J. L. E. Erickson, *J. Am. Chem. Soc.*, **64**, 144 (1942).
2) For recent syntheses see J. R. Sanderson, K. Paul, R. J. Winterdink, and J. Alford, *J. Org. Chem.*, **41**, 3767 (1976); M. Karpf and A. S. Dreiding, *Helv. Chim. Acta*, **58**, 2409 (1975); D, Felix, J. Schreiber, G. Ohloff, and A. A. Eschenmoser, *Helv. Chim. Acta*, **54**, 2896 (1971); B. D. Mookherjee, R. W. Trenkle, and R. P. Patel, *J. Org. Chem.*, **36**, 3266 (1971).
3) G. Hesse and F. Urbanek, *Chem. Ber.*, **91**, 2733 (1958).
4) M. Nishino, H. Kondo, and A. Miyake, *Chem. Lett.*, **1973**, 667.
5) H. B. Kagan, "Stereochemistry," Georg Thieme Publishers, Stuttgart (1977), Vol. 1, p. 50.
6) A. S. Kende, *Org. React.* **11**, 261 (1946).

Synthesis of 1-Substituted 3-(Dialkylaminoalkoxy)-4,5,6,7-tetrahydro-1*H*-indazoles

Takeo Soga,* Hirosuke Niwa, and Takanori Shiraishi

Oomiya Research Laboratory of Nikken Chemicals Co., Ltd., Kitabukuro-cho, Oomiya-shi, Saitama 330

(Received August 25, 1979)

Synopsis. 4,5,6,7-Tetrahydro-3-indazolone was prepared by catalytic hydrogenation of 3-indazolone, and its reaction with dialkylaminoalkyl chloride was studied. In addition, a number of 1-substituted 3-(dialkylaminoalkoxy)-4,5,6,7-tetrahydro-1*H*-indazoles were prepared.

Indazole[1] nucleus is of high therapeutic interest and benzydamine[2] represents an antiinflammatory drug with this heterocyclic nucleus. Barbaz *et al.*[3] reported the synthesis of 1-substituted 3-hydroxy-4,5,6,7-tetrahydro-1*H*-indazoles (**8**) by cyclization of *N*-substituted 2-chlorocyclohexene-1-carbohydrazides and the 3-*O*-alkylation of **8** to give 1-substituted 3-(dialkylaminoalkoxy)-4,5,6,7-tetrahydro-1*H*-indazoles (**7**). In this paper, we describe a new synthesis of a series of 3-(dialkylaminoalkoxy)-4,5,6,7-tetrahydro-1*H*-indazoles (**3**) and its 1-substituted derivatives (**7**). We have prepared 4,5,6,7-tetrahydro-3-indazolone (**2**) in good yield by catalytic hydrogenation of 3-indazolone (**1**) with palladium catalyst and identified it by comparison with an authentic specimen prepared by the procedure of Dieckmann.[4]

As to alkylation of **2**, Alt and Chupp[5] reported that the alkylation of **2** with alkyl halides in aqueous ethanolic sodium hydroxide gave 1-substituted derivatives (**8**). We have found that, when the reaction of **2** with 3-(dimethylamino)propyl chloride is carried out in a nonaqueous medium, a 3-*O*-monosubstituted derivative, namely, 3-[3-(dimethylamino)propoxy]-4,5,6,7-tetrahydro-1*H*-indazole (**3a**) is mainly produced in 57% yield. A minor product in this reaction was 1,3-*O*-disubstituted derivative, namely, 3-[3-(dimethylamino)propoxy]-1-[3-(dimethylamino)propyl]-4,5,6,7-tetrahydro-1*H*-indazole (**5**). Similar treatment of **2** with 2-(diethylamino)ethyl chloride in dioxane gave 3-[2-(diethylamino)ethoxy]-4,5,6,7-tetrahydro-1*H*-indazole (**3b**). The structures of **3a** and **3b** were deduced mainly from the NMR spectra, which exhibited signals at δ 4.10—4.12 (t, 3-O-C<u>H</u>$_2$-CH$_2$-), indicating the 3-*O*-substitution.

As an alternative possibility to the above mentioned synthesis of 3-*O*-substituted 4,5,6,7-tetrahydro-1*H*-indazolones (**3**), we studied the catalytic hydrogenation of 3-(dialkylaminoalkoxy)-1*H*-indazoles (**4**)[6] previously reported by us, and obtained **3a** from 3-[3-(dimethylamino)propoxy]-1*H*-indazole (**4a**) in 92% yield. Compound **3b** was further obtained by the similar catalytic hydrogenation of 3-[2-(diethylamino)ethoxy]-1*H*-indazole (**4b**).[6] The above mentioned compound **5** was also obtained by catalytic hydrogenation of 3-[3-(dimethylamino)propoxy]-1-[3-(dimethylamino)-propyl]-1*H*-indazole (**6**).[6]

Thus, the 3-*O*-substituted 4,5,6,7-tetrahydro-1*H*-indazolones (**3**) have been synthesized by the route (**1**)→(**2**)→(**3**) and another route (**4**)→(**3**). In addition, the 3-*O*-substituted compounds (**3**) were led to 1,3-*O*-disubstituted 4,5,6,7-tetrahydro-1*H*-indazolones (**7**) by reaction of the sodium salt of **3** with alkyl halides or other halides in liquid ammonia or hexamethylphosphoric triamide. The structures of **7** were confirmed by their NMR, IR, and UV spectra.

Experimental

4,5,6,7-Tetrahydro-3-indazolone (2). A solution of 3-indazolone (**1**,[7] 0.89 g) in acetic acid (30 ml) was hydrogenated in the presence of Pd–carbon (Pd 5%) (2.67 g) under hydrogen atmosphere at 50 °C for about 7 h. The catalyst was filtered off and the filtrate was evaporated *in vacuo* to give **2**, crystals, mp 289.5—291.5 °C (0.79 g, 86%). Recrystallization from methanol gave mp 293.5—295.0 °C. UV$_{max}$(C_2H_5OH): 250 nm (ε 6350). This material was identified by the determination of mixed melting point with an authentic specimen.[4]

3-[3-(Dimethylamino)propoxy]-4,5,6,7-tetrahydro-1H-indazole (3a). By Reaction of 2 with 3-(Dimethylamino)propyl Chloride: A sample of **2** (5.53 g) was dissolved in an aqueous 1 M sodium hydroxide (40 ml) with stirring. The solution was evaporated under reduced pressure to give a solid of sodium salt, which was further dried in an oven. The salt was powdered and suspended in dry dioxane (134 ml). A solution of 3-(dimethylamino)propyl chloride (5.11 g) in dry dioxane (66 ml) was added under stirring and refluxing over a 1.5 h period. Refluxing and stirring were further continued for 4.5 h. The reaction mixture was worked up in the usual way to give an oily product (6.65 g), which consisted of two components, **3a** and **5**, as judged by GLC

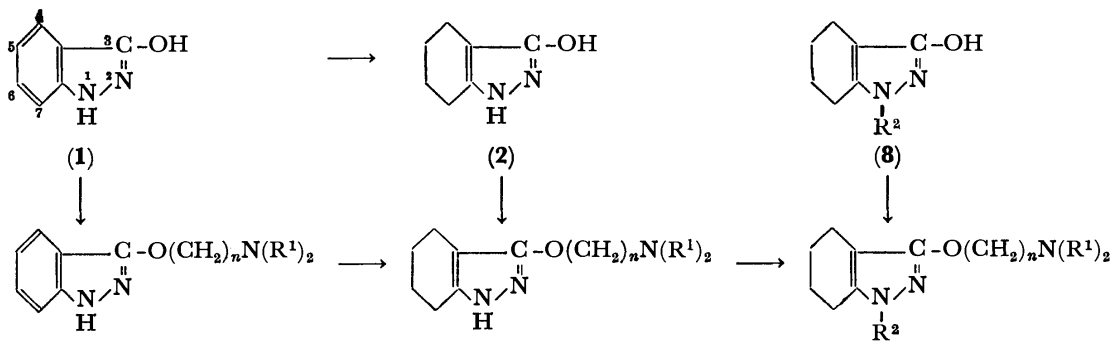

Table 1. 1-Substituted (R^2) 3-[3-(dimethylamino)-propoxy]-4,5,6,7-tetrahydro-1*H*-indazoles (**7c—i**)

No.	R^2	Yield[a] %	Formula[b]	Mp[b] °C	Found[b] (Calcd) (%) C	H	N	Cl
7c	CH_3	30	$C_{13}H_{24}ClN_3O$	158.0—160.0	56.79 (57.03)	8.78 (8.84)	15.40 (15.35)	12.76 (12.95)
7d	C_2H_5	92	$C_{14}H_{26}ClN_3O$	123.0—124.0	58.13 (58.42)	9.03 (9.10)	14.72 (14.60)	12.41 (12.32)
7e	o-$CH_3C_6H_4CO$-	65	$C_{20}H_{25}ClN_3O_2$	174.0—175.0	63.26 (63.56)	7.46 (7.47)	11.18 (11.12)	9.71 (9.38)
7f	m-$CH_3C_6H_4CO$-	51	$C_{20}H_{28}ClN_3O_2 \cdot H_2O$	90.0—91.5	60.97 (60.67	7.47 (7.64	10.73 (10.61	— 8.95)
7g	p-$CH_3C_6H_4CO$-	42	$C_{20}H_{26}ClN_3O_2$	170.0—170.5	63.86 (63.56)	7.43 (7.47)	11.00 (11.12)	9.22 (9.38)
7h	o,o-$(CH_3)_2C_6H_3CO$-	93	$C_{21}H_{30}ClN_3O_2$	179.0—180.0	64.04 (64.35)	7.82 (7.72)	10.63 (10.72)	9.35 (9.05)
7i	p-$CH_3C_6H_4SO_2$-	53	$C_{19}H_{28}ClN_3O_3S$	197.5—199.5	54.91 (55.13	6.93 (6.82	9.99 (10.15	— 8.56)

a) Free base. b) Hydrochloride. $UV_{max}(H_2O)$: **7c**,[b] 229 nm (ε 6820); **7d**,[b] 230 nm (ε 6650).

analysis. Chromatography on silica gel with benzene–diethylamine (9:1) afforded **3a**, an oil, 5.05 g (57%) as main product. $UV_{max}(C_2H_5OH)$: 226 nm (ε 5460). IR (neat): ν_{NH} 3150 and $\nu_{C=N}$ 1500 cm^{-1}. NMR (CCl_4): δ 2.19 (6H, s, $-N(C\underline{H}_3)_2$), 4.12 (2H, t, 3-O-$C\underline{H}_2$-CH_2-) and 10.1 (1H, broad, >N$\underline{H}$). Hydrochloride was recrystallized from methanol–ethyl acetate, mp 189.5—191.0 °C. Found: C, 55.53; H, 8.38; N, 16.21; Cl, 13.57%. Calcd for $C_{12}H_{22}ClN_3O$: C, 55.48; H, 8.54; N, 16.18; Cl, 13.63%.

A minor product, 3-[3-(dimethylamino)propoxy]-1-[3-(dimethylamino)propyl]-4,5,6,7-tetrahydro-1*H*-indazole (**5**), (an oil, 1.16 g, 9%) was obtained from the initial eluate with the same solvent. Hydrochloride was recrystallized from methanol–ethyl acetate, mp 194.0—195.0 °C.

*By Catalytic Hydrogenation of 3-[3-(Dimethylamino)propoxy]-1H-indazole (**4a**)*:[6] A solution of **4a** (6.22 g) in acetic acid (160 ml) was hydrogenated in the presence of Adams' catalyst (2.80 g) at room temperature for 12 h. The reaction mixture was worked up in the usual way to give **3a**, an oil, 5.80 g (92%). UV_{max} (C_2H_5OH): 226 nm (ε 5700). IR (neat): ν_{NH} 3160 and $\nu_{C=N}$ 1500 cm^{-1}. NMR (CCl_4): δ 4.10 (2H, t, 3-O-$C\underline{H}_2$-CH_2-). Hydrochloride: mp 188.0—189.0 °C.

*3-[3-(Dimethylamino)propoxy]-1-[3-(dimethylamino)propyl]-4,5,6,7-tetrahydro-1H-indazole (**5**).* Compound **6**[6] (1.00 g) was hydrogenated with Adams' catalyst (1.00 g) at 50 °C for 20 min in acetic acid (15 ml) to give **5** (0.94 g, 93%). UV_{max} (C_2H_5OH): 232 nm (ε 6800). IR (neat): ν_{CH} 2920—2750 and $\nu_{C=N}$ 1500 cm^{-1}. NMR (CCl_4): δ 2.12 (6H, s, 1-$(CH_2)_3N(C\underline{H}_3)_2$), 2.16 (6H, s, 3-O-$(CH_2)_3N(C\underline{H}_3)_2$), 3.75 (2H, t, 1-$C\underline{H}_2$-$CH_2$-) and 4.08 (2H, t, 3-O-$C\underline{H}_2$-$CH_2$-). Hydrochloride: mp 194.0—195.0 °C. Found: C, 52.23; H, 8.63; N, 14.02; Cl, 18.27%. Calcd for $C_{17}H_{34}Cl_2N_4O \cdot 1/2H_2O$: C, 52.30; H, 9.03; N, 14.35; Cl, 18.16%.

*3-[2-(Diethylamino)ethoxy]-4,5,6,7-tetrahydro-1H-indazole (**3b**). By Reaction of **2** with 2-(Diethylamino)ethyl Chloride*: A sample of **2** (2.76 g) was caused to react with 2-(diethylamino)-ethyl chloride (2.85 g) in dioxane (100 ml) as described for the preparation of **3a**. The oily product (3.97 g) was chromatographed on silica gel with cyclohexane–diethylamine (9:1) to afford **3b**, 3.10 g (65%). UV_{max} (C_2H_5OH): 225 nm (ε 6170). IR (neat): ν_{NH} 3180 and $\nu_{C=N}$ 1500 cm^{-1}. NMR (CCl_4): δ 1.00 (6H, t, J=7 Hz, $-N(CH_2C\underline{H}_3)_2$), 2.55 (4H, q, J=7 Hz, $-N(C\underline{H}_2CH_3)_2$), 2.73 (2H, t, J=6 Hz, 3-O-CH_2-$C\underline{H}_2$-N◇) and 4.12 (2H, t, J=6 Hz, 3-O-$C\underline{H}_2$-CH_2-N◇). Hydrochloride was recrystallized from methanol–ethyl acetate, mp 130.0—131.0 °C. Found: C, 56.85; H, 8.81; N, 15.34; Cl, 12.67%. Calcd for $C_{13}H_{24}ClN_3O$: C, 57.03; H, 8.84; N, 15.35; Cl, 12.95%.

*By Catalytic Hydrogenation of 3-[2-(Diethylamino)ethoxy]-1H-indazole (**4b**)*:[6] A sample of **4b** (1.17 g) was hydrogenated with Pd–carbon (Pd 5%) (2.00 g) at 60 °C for 10 h in propionic acid (30 ml) to give **3b**, 1.03 g (87%). IR (neat): ν_{NH} 3170 and $\nu_{C=N}$ 1500 cm^{-1}. NMR (CCl_4): δ 4.10 (2H, t, J=6 Hz, 3-O-$C\underline{H}_2$-CH_2-N◇). Hydrochloride: mp 130.0—131.0 °C.

*1-Benzyl-3-[3-(dimethylamino)propoxy]-4,5,6,7-tetrahydro-1H-indazole (**7a**).* A mixture of sodium metal (0.61 g) and iron(III) nitrate (20 mg) in liquid ammonia (60 ml) was shaken to precipitate sodium amide. A solution of **3a** (5.14 g) in liquid ammonia (40 ml) was added and kept at room temperature for 1h under shaking. Benzyl chloride (2.92 g) was added and, after shaking, the mixture was stood at room temperature overnight. After evaporation of ammonia, the residue was worked up in the usual way to give an oily product (6.24 g), which was chromatographed on silica gel with cyclohexane–diethylamine (9:1) to afford **7a**, 4.80 g (66%). UV_{max} (C_2H_5OH): 233 nm (ε 9050). IR (neat): $\nu_{C=N}$ 1500 cm^{-1}. NMR (CCl_4): δ 4.10 (2H, t, 3-O-$C\underline{H}_2$-CH_2-) and 4.90 (2H, s, 1-$C\underline{H}_2$-C_6H_5). Hydrochloride was recrystallized from 2-propanol–ethyl acetate, mp 149.0—150.0 °C (lit,[3] 143 °C). UV_{max} (H_2O): 232 nm (ε 8590) (lit,[3] 232 nm (ε 8900)). Found: C, 65.19; H, 7.88; N, 12.07; Cl, 10.13%. Calcd for $C_{19}H_{28}ClN_3O$: C, 65.22; H, 8.07; N, 12.00; Cl, 10.13%.

*1-Benzyl-3-[2-(diethylamino)ethoxy]-4,5,6,7-tetrahydro-1H-indazole (**7b**) and Others (**7c—i**).* To a solution of **3b** (1.60 g) in HMPT (4 ml), sodium hydride (50% in oil) (0.28 g) was added and the solution was heated at 100 °C with stirring for 30 min. After cooling, benzyl chloride (0.74 g) was added and stirred at room temperature for 1 h. The reaction mixture was worked up in the usual way to give **7b**, an oil, 2.04 g (93%). UV_{max} (C_2H_5OH): 232 nm (ε 8810). IR (neat): $\nu_{C=N}$ 1500 cm^{-1}. NMR (CCl_4): δ 4.11 (2H, t, J=6 Hz, 3-O-$C\underline{H}_2$-CH_2-N◇) and 4.90 (2H, s, 1-$C\underline{H}_2$-C_6H_5). Citrate was recrystallized from acetone, mp 77.5—81.5 °C. Found: C, 60.28; H, 7.38; N, 8.30%. Calcd for $C_{26}H_{37}N_3O_8$: C, 60.10; H, 7.18; N, 8.09%.

The other compounds (**7c—i**) shown in Table 1 were similarly prepared from **3a** and acid halides or alkyl halides.

The authors wish to thank Professor Sumio Umezawa, Director of the Institute of Bioorganic Chemistry, for his helpful guidance and Dr. Tsutomu Hatakeyama, Director of this Laboratory, for his support and encouragement.

References

1) L. Baiocchi, G. Corsi, and G. Palazzo, *Synthesis*, **1978**, 633.

2) G. Palazzo, G. Corsi, L. Baiocchi, and B. Silvestrini, *J. Med. Chem.*, **9**, 38 (1966).

3) B. S. Barbaz, H. I. Chernov, N. Finch, H. W. Gschwend, and A. Hamdan, *J. Med. Chem.*, **15**, 1027 (1972).

4) W. Dieckmann, *Ann.*, **317**, 102 (1901).

5) G. H. Alt and J. P. Chupp, *Tetrahedron Lett.*, **1970**, 3155.

6) T. Soga, H. Niwa, K. Okada, and S. Umezawa, *Yuki Gogei Kagaku Kyokai Shi*, **28**, 437 (1970).

7) E. F. M. Stephenson, *Org. Synth.*, Coll. Vol. III, 475 (1955).

Catalysis by Heteropolyacid. I. Polymerization Reaction of Benzyl Alcohols

Kenji NOMIYA, Tetsuo UENO, and Makoto MIWA*

Department of Industrial Chemistry, Faculty of Engineering, Seikei University, Musashino-shi, Tokyo 180

(Received September 3, 1979)

Synopsis. Benzyl alcohol and its derivatives catalyzed by heteropolymolybdic acids such as $H_3PMo_{12}O_{40}$ and $H_4SiMo_{12}O_{40}$ have been found to polymerize, leading to the formation of polyaromatics. The properties of the polymers obtained and the function of catalysts have been studied.

Heteropolyacid has high oxidation activity and strong acidic property.[1] From its structure it can be regarded as a polynuclear metal complex and also as a molecular model for solid catalyst.[2] Recently we found a new type of polymerization reaction of benzyl alcohol and its derivatives catalyzed by 12-heteropolymolybdic acids leading to aromatic polymers. The typical stoichiometry is as follows.

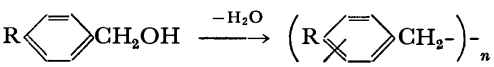

Heteropolyacids, $H_4SiM_{12}O_{40}$ and $H_3PM_{12}O_{40}$ (M= Mo, W), were examined as catalyst. These catalysts promote the reaction, but neither the tetraalkylammonium salts of their acids nor the mononuclear acids (H_2MoO_4 and H_2WO_4) show catalytic activity. In this paper the Mo system is discussed.

In all catalytic reactions, the catalyst undergoes the color change yellow→green→blue, corresponding to the various reduced states of molybdenum ions.[3] However, the reduction of catalyst, as indicated by the color change, would not be substantial in the coupling reaction since initial activity of catalyst, selectivity and yields of products were not influenced by the addition of an excess amount of reactants to the reduced blue acid obtained. Since the tetrabutylammonium salts of both the unreduced yellow anion and the reduced blue anion provide no catalytic activity, remarkably strong acidity of catalyst would be important. The reduction mechanism from yellow to blue has not been clarified as yet.

Characteristics of the reaction are as follows: (a) The amorphous polymer obtained has a low molecular weight. (b) No solvent is employed. (c) The reaction is carried out by merely passing a gas (oxygen, nitrogen *etc.*) through a benzyl alcohol solution of heteropolyacids at ambient temperature. (d) The reaction does not proceed in a sealed tube. (e) The temperature of the reaction depends on the flow rate of a passing gas, *e.g.*, under atmospheric oxygen the temperature is 195 °C, whereas with increase in flow rate it is lowered to 110 °C. (f) The reaction time for obtaining the polymer in 100% yield is a few minutes. (g) The catalyst is very stable, not being decomposed during the course of polymerization.

In (c) the role of the passing gas may be only to remove the water produced and keep the reaction mixture anhydrous; oxygen and inert gas fulfill this purpose. The refluxing of benzyl alcohol in the presence of a solvent such as benzene, toluene, or anisole also gives the same polybenzyl as that obtained in a solvent-free system. However, the yield is lowered because of the simultaneously promoted side-reaction such as alkylation and condensation-etherization.

In a typical experiment, 12.4 ml of benzyl alcohol (0.12 mol) and 73.0 mg of $H_4SiMo_{12}O_{40}$ (0.4 mmol) were added to a 100 ml wide-mounted Erlenmeryer flask equipped with a gas inlet tube and a thermometer on a hot-plate at 110 °C. The gas was passed (150 ml/min) through the vigorously stirred solution. The color of the reaction mixture changed from yellow to green, and finally to blue. While the reaction mixture turned green, it began to bubble slightly, the bubbling becoming drastic as soon as the color turned blue. Within a few seconds the vigorous bubbling ceased, the system becoming highly viscous. With fall of temperature the mixture began to solidify. On cooling, a resinous and brittle substance was obtained. It was found that the reduced blue catalyst is homogeneously dissolved in the system, above 40 °C, the polymer becoming stringy. The resionoid is soluble in chloroform and the catalyst contained can be readily removed by shaking the chloroform solution with water. The pure polymer was isolated by dissolving the reaction mixture in 50 ml DMF containing LiCl (1%) and adding the solution dropwise to 150 ml methanol. The precipitate was purified by reprecipitation. The almost colorless polymer obtained was dried *in vacuo* for *ca.* 30 h. The yield was 9.7 g (75%) of pure polymer having intrinsic viscosity $[\eta]=0.19$ dl/g (in *N,N*-dimethylacetamide containing 1% LiCl at 25 °C). Thermogravimetric analysis shows that the polymer is thermally stable up to 525 °C; in air it begins to lose weight at 375 °C.

The derivatives of benzyl alcohol as monomer reactant; 4-chlorobenzyl alcohol, 4-methylbenzyl alcohol, and 2,4,6-trimethylbenzyl alcohol gave the corresponding polyaromatics. However, no corresponding polymers were obtained from triphenylmethanol and 1- and 2-phenylethanols.

The IR spectra of polymers obtained show the disappearance of the original alcoholic OH group. ^{1}H-NMR intensities of benzene moieties, methyl substituents and benzyl methylenes in the polymers indicate that the polycondensation takes place on the elimination of one H of the benzene moiety of one reactant and one OH group of another reactant. Thus the highly branched species are not dominant. Analytical data, intrinsic viscosities, melting points and decomposition temperatures of the polymers are given in Table 1 and ^{1}H-NMR data in Table 2. Viscosities and melting points indicate that the polymers have low molecular

Table 1. Analytical data, intrinsic viscosities, melting points, and decomposition temperatures of polymers

Reactant	Polymer			Elemental analyses (%)				[η] dl/g	Mp °C	Dec temp °C
					C	H	Cl			
Benzyl alcohol	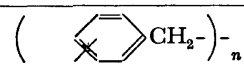	1	C_7H_6	Calcd	93.33	6.67		0.194	51—81	525
				Found	93.21	6.65				
4-Chlorobenzyl alcohol	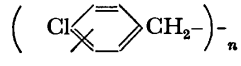	2	C_7H_5Cl	Calcd	67.47	4.02	28.51	0.055	86—119	478
				Found	67.61	4.05	28.51			
4-Methylbenzyl alcohol	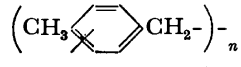	3	C_8H_8	Calcd	92.31	7.69		0.079	84—114	512
				Found	91.45	7.59				
2,4,6-Trimethylbenzyl alcohol	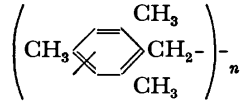	4	$C_{10}H_{12}$	Calcd	90.91	9.09		0.100	152—189	537
				Found	90.48	9.13				

Table 2. ^{1}H-NMR data for the polymers

Polymer	Chemical shift ppm from TMS			Observed intensity ratio
	Phenyl	Methylene	Methyl	
1	7.02	3.81		4 : 2
2	7.07 6.90	3.90		3 : 2
3	6.83	3.75	2.25 2.12	3 : 2 : 3
4	6.68	3.93	2.19 1.99 1.80	1 : 2 : 9

weight.

The electronic and MCD spectra in the 240—300 nm region of the polymer were measured in comparison with those of the corresponding monomer. The characteristic vibronic structure of the monomer is largely diminished, the whole spectral shape broadening. The maximum absorption of polymer shifted to the longer wavelength region by *ca.* 10 nm. This is also the case in the MCD spectra. In both the polymer and its monomer, the sign of MCD is negative, except in the case of poly(2,4,6-trimethyl-1,3-phenylenemethylene) and 2,4,6-trimethylbenzyl alcohol, in which the positive MCD of monomer turns to the negative MCD of polymer.

In the first run of the experiment, the reduced blue compound, converted from the initial yellow catalyst, is isolated as a tetraethylammonium salt having the formula $[Et_4N]_4[SiMo_{12}O_{40}H_n]$ (n=2—4). This was determined on the basis of the observed value of elemental analysis; C, 16.43; H, 3.30; N, 2.32%.

During the course of the reaction, no evidence was obtained of the direct coordination of arene ring of reactant to the molybdenum ion in the blue catalyst. The type of polymerization might be a carbonium ion mechanism brought about by the remarkably strong Brønsted acidity of catalyst.

The heteropolyacids also give the same polybenzyl from benzyl chloride by dehydrohalogenation as that obtained from benzyl alcohol in relatively high yields. Thus the acids appear to possess an analogous function to that of $Mo(CO)_6$ and arene-$Mo(CO)_3$ as "Friedel-Crafts" like catalyst.[4,5] However, particular advantages of the reduced blue heteropolyacid over $Mo(CO)_6$ and $ArMo(CO)_3$ have been observed in the undiminished activity for repeated use of the same catalyst with no decomposition. This remarkable stability of the reduced acid would be related to the fact that it does not dissociate into sexivalent molybdenum as in the case of unreduced form of the complex because of its resonant state in the molecule as a whole making each molybdenum have a mean valency less than +6.[3]

In this reaction, the heteroatoms Si and P of heteropolymolybdic acids would play no direct important role; rather they would contribute to the maintenance of Keggin-structure of catalyst and the complete valency saturation leading to the strong Brønsted acidity.

The authors wish to thank Dr. I. Ojima and Mr. T. Noguchi, Sagami Chemical Research Center, for their help in clarifying the structures of the products we obtained.

References

1) H. Tsuneki, H. Niiyama, and E. Echigoya, *Chem. Lett.*, **1978**, 645, 1183.

2) A. Kobayashi and Y. Sasaki, *Bull. Chem. Soc. Jpn.*, **48**, 885, 3146 (1975); M. Misono, Y. Konishi, M. Furuta, and Y. Yoneda, *Chem. Lett.*, **1978**, 709.

3) J. D. H. Strickland, *J. Am. Chem. Soc.*, **74**, 868 (1952).

4) M. F. Farona and J. F. White, *J. Am. Chem Soc.*, **93**, 2826 (1971).

5) J. F. White and M. F. Farona, *J. Organomet. Chem.*, **63**, 329 (1973).

Grignard Reaction of Peroxides Containing Neighboring Nitrogen Atom

Masao Ōkubo,* Takutomo Komatsu, Kyōko Tsuruta, and Yasuyo Sonoda
Department of Chemistry, Faculty of Science and Engineering, Saga University, Honjō-machi, Saga 840

(Received September 3, 1979)

Synopsis. The substituent effect on the reaction of bis(2-aryl-1,2,3,4-tetrahydro-1-isoquinolyl) peroxide with PhMgBr as well as the product obtained on the reaction of 2-*p*-tolyl-1,2,3,4-tetrahydro-1-isoquinolyl *t*-butyl peroxide with PhMgBr were interpreted in terms of the coordination of the neighboring nitrogen atom to Mg atom.

In the previous report on the Grignard reaction of neighboring oxygen- and/or nitrogen-containing peroxides,[1] the effect of coordination of the hetero atoms to the Mg atom was emphasized. However, it was doubted that the high reactivity of the previously studied *N*-methylanilinomethyl *t*-butyl peroxide (**1**) was due to its sterically unhindered and flexible molecular structure but not due to the effect of the neighboring nitrogen atom. This consideration led us to examine the Grignard reaction of peroxides having sterically crowded and rigid structures. The results of the study on the substituent effect of bis (2-aryl-1,2,3,4-tetrahydro-1-isoquinolyl) peroxides (**2**)[2] and the product obtained from 2-*p*-tolyl-1,2,3,4-tetrahydro-1-isoquinolyl *t*-butyl peroxide (**3**)[3] will be reported in this paper. These peroxides were selected from several nitrogen-containing ones reported by Rieche and his coworkers[4] on the basis of the molecular structure appropriate for the present purpose: the peroxides 1) having "neighboring" nitrogen atom and 2) having neither >NH nor –OOH groups were selected.

The reaction of **2a**, **2b**, and **2c** with one and a half molar equivalents of PhMgBr in THF at 10 °C under nitrogen was followed by iodometry. The results thus obtained are shown in Fig. 1 (a), which indicate that the higher electron-density on the nitrogen atom facilitates its coordination to the Mg atom and thus accelerates the decomposition.

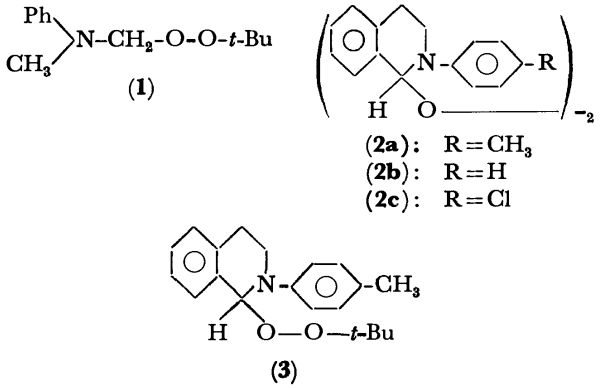

The similar plots obtained from the reaction of **3** are shown in Fig. 1 (b). When 1.30 molar equivalents of PhMgBr were used (Fig. 1 (b)-i), 36.4% of **3** remained even after stirring for 48 h at 15 °C. On the other hand, when 2.50 molar equivalents of the reagent were used (Fig. 1 (b)-ii), almost all (92.7%) of **3** was consumed after 24 h. As shown in Fig. 1 (b)-ii, the high decomposition velocity at the initial stage is clearly distinguished from the low velocity at the later stage. On the basis of the previous discussion given for the similar feature observed in the Grignard reaction of aroyl peroxides,[5] the low velocity at the later stage is ascribable to the aggregation of the unreacted peroxide with the reaction products: the aggregation could retard the attack of the Grignard species.[5]

The crude oily product obtained in a 91% yield after the treatment of **3** with three molar equivalents of PhMgBr for 24 h followed by the usual work-up, crystallizes on standing overnight. Purification by column chromatography (silica gel, petroleum benzine) and recrystallization from petroleum ether afforded colorless crystals, mp 76—77.5 °C. The product gave no ν_{OH} absorption band in its IR spectrum, and a large amount of phenol was detected by GLC after the treatment with dilute hydrochloric acid. The structure (**4**) can be given on the basis of NMR data (CCl_4): δ=6.58—7.15 (13H, m, aromatic), 5.20 (1H, s, >CH), 3.48 (2H, m, >N–CH_2–CH_2–), 2.82 (2H, t, –CH_2–Ar), and 2.09 (3H, s, CH_3–Ar). The chemical shift of the benzylic methine proton appeared in the remarkably lower field may be reasonable, because the methine carbon has both the neighboring oxygen and

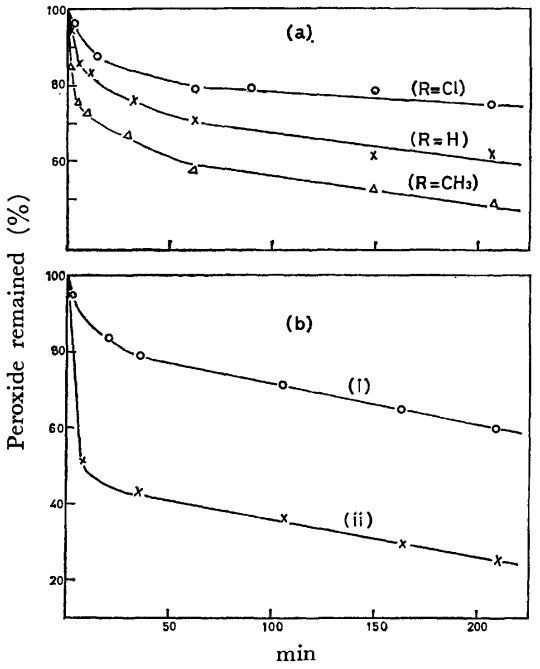

Fig. 1. Decomposition velocity of peroxides **2a**, **2b**, **2c**, and **3** on the reaction with PhMgBr.
(a) Peroxides **2a**, **2b**, **2c**: 0.0023 mol; PhMgBr: 0.0035 mol. At 10 °C; in 50 ml THF.
(b)-i) Peroxide **3**: 0.0064 mol; PhMgBr: 0.00835 mol.
ii) Peroxide **3**: 0.0096 mol; PhMgBr: 0.024 mol. At 15 °C; in 59 ml THF.

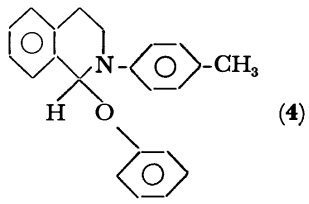

(4)

nitrogen atoms. If being stood for a few days, the product **4** decomposed gradually and gave pale yellow polymeric material insoluble in CCl_4 and benzene. Contrary to the products of the reaction of **1**,[1] the phenyl group of the Grignard reagent combines with the α-oxygen atom which is nearer to the nitrogen atom of **3**. This result is explicable if it is considered that the rigid structure of **3** requires the attack by the dimeric or trimeric aggregate of the reagent as illustrated in Fig. 2. The coordination of the nitrogen atom to Mg atom could induce some positive charge on the α-oxygen atom. This effect allows the exclusive attack of the anionic phenyl group of another Grignard molecule. This suggestion is compatible with the discussion given above for the substituent effect on the decomposition velocity.

Though the peroxides **2** and **3** are less reactive than the less crowded **1** which can be decomposed by the equimolar PhMgBr,[1] the results obtained are interpreted in terms of coordination of the neighboring nitrogen atom. In addition, the peroxides **2** and **3** were found to be titrated in the simplest manner by the use of KI and acetic acid.[6] The previously proposed correlation between the reactivity of peroxides toward alkali halides and that toward Grignard reagent[1] is thus confirmed.

Experimental

Materials. The peroxides **2**[2] and **3**[3] were prepared by the reported methods from the corresponding 2-aryl-3,4-dihydroisoquinolinium bromides[7] which were synthesized from isochroman. Tetrahydrofuran was dried over sodium wire, distilled, and stored on sodium wire.

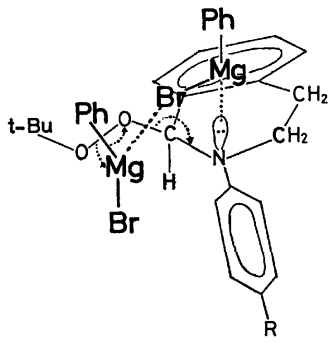

Fig. 2. Illustration of the reaction of peroxide **3** with the dimeric aggregate of PhMgBr.

Procedures. The THF solution (25 ml) of PhMgBr (0.0289 mol) was prepared under nitrogen. The peroxide **3** (0.00965 mol) dissolved in THF (40 ml) was added at once. The mixture was stirred for 24 h, and quenched by saturated aqueous NH_4Cl. The crude product obtained was purified in the manner described in the text.

The plots given in Fig. 1 were obtained by taking out the 1 ml portions of the respective reaction mixtures at definite time intervals followed by iodometric titration by the reported method.[6]

Elemental analysis of **4**: Found: C, 83.92; H, 6.72; N, 4.36; O, 5.02%. Calcd for $C_{22}H_{21}NO$: C, 83.80; H, 6.67; N, 4.44; O, 5.08%.

References

1) M. Ōkubo, H. Saitō, and T. Tomiyoshi, *Bull. Chem. Soc. Jpn.*, **47**, 1289 (1974).
2) A. Rieche, E. Hoeft, and H. Schultze, *Chem. Ber.*, **97**, 195 (1964).
3) E. Hoeft, and H. Schultze, *Z. Chem.*, **7**, 149 (1967).
4) R. Hiatt, "Alkyl Peroxides," in "Organic Peroxides," ed by D. Swern, Wiley-Interscience, New York (1978), Vol. 3, p. 1.
5) M. Ōkubo, K. Maruyama, and J. Ōsugi, *Bull. Chem. Soc. Jpn.*, **44**, 1365 (1971).
6) J. P. Wibaut, H. B. van Leewen, and B. van der Wal, *Rec. Trav. Chim. Pays-Bas*, **73**, 1033 (1954).
7) A. Rieche and E. Schmitz, *Chem. Ber.*, **89**, 1254 (1956).

Synthesis of 5,7-Dihydroxy-2′,4′,5′-trimethoxyisoflavone and Its 7-Methyl Ether (Robustigenin)

Mitsuru NAKAYAMA,* Susumu OHIRA, and Takanao MATSUI†

Department of Chemistry, Faculty of Science, Hiroshima University, Higashisenda-machi, Hiroshima 730

†*Department of Industrial Chemistry, Faculty of Engineering, Miyazaki University, Kirishima, Miyazaki 880*

(Received September 5, 1979)

Synopsis. The treatment of 2,4,6-trihydroxy-2′,4′,5′-trimethoxydeoxybenzoin with benzyl chloride gave a dibenzyl ether. The condensation of the ether with ethyl formate, followed by the debenzylation of the resulting isoflavone, afforded 5,7-dihydroxy-2′,4′,5′-trimethoxyisoflavone, which was then converted into a pentamethoxyisoflavone. The partial demethylation of the pentamethoxyisoflavone gave 5-hydroxy-2′,4′,5′,7-tetramethoxyisoflavone, which was identical with natural robustigenin.

Recently, robustigenin, $C_{19}H_{18}O_7$, was isolated from seed shells of *Derris robusta*. Its structure was identified as 5-hydroxy-2′,4′,5′,7-tetramethoxyisoflavone (**1**) on the basis of spectral evidence.[1] We attempted the synthesis of **1** in order to confirm the proposed structure. This paper will describe the synthesis of 5,7-dihydroxy-2′,4′,5′-trimethoxyisoflavone (**2**), which may be expected to occur in nature, and 7-methyl ether of **2** (**1**, robustigenin).

The treatment of 2,4,6-trihydroxy-2′,4′,5′-trimethoxydeoxybenzoin (**3**)[2,3] with benzyl chloride and anhydrous potassium carbonate in acetone gave a dibenzyl ether (**4**). The condensation of **4** with ethyl formate in the presence of sodium gave 5,7-bis(benzyloxy)-2′,4′,5′-trimethoxyisoflavone (**5**). The debenzylation of **5** by hydrogenolysis with palladium on charcoal afforded a dihydroxyisoflavone (**2**), which was then easily converted into a dimethyl ether (**6**). The isoflavone (**6**) was also prepared by the following procedure. The Hoesch reaction of phloroglucinol dimethyl ether and 2,4,5-trimethoxyphenylacetonitrile,[4] or the treatment of phloroglucinol dimethyl ether and homoasaronic acid (2,4,5-trimethoxyphenylacetic acid)[5] in the presence of boron trifluoride etherate, yielded 2-hydroxy-2′,4,4′,5′,6-pentamethoxydeoxybenzoin (**7**). The reaction of **7** and ethyl formate yielded the isoflavone (**6**).

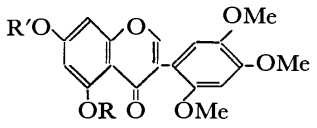

(**1**) R=H, R′=Me
(**2**) R=R′=H
(**5**) R=R′=$C_6H_5CH_2$
(**6**) R=R′=Me

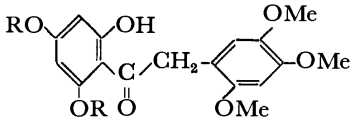

(**3**) R=H
(**4**) R=$C_6H_5CH_2$
(**7**) R=Me

The partial demethylation of **6** with anhydrous aluminium chloride in acetonitrile[6] gave the desired isoflavone (**1**). The spectral properties of the two synthetic samples **2** and **6** were superimposable upon those recorded for natural robustigenin and its methyl ether.[1]

Experimental

The melting points are uncorrected. The IR spectra were measured in nujol, while the UV spectra were measured in an ethanol, unless otherwise stated. The NMR spectra were recorded on either a Hitachi R-20 (60 MHz) or JEOL JNM MH-100 (100 MHz) spectrometer, and the chemical shifts are reported in δ values, with TMS as the internal standard.

4,6-Bis(benzyloxy)-2-hydroxy-2′,4′,5′-trimethoxydeoxybenzoin (4). A mixture of 2,4,6-trihydroxy-2′,4′,5′-trimethoxydeoxybenzoin (**3**)[2,3] (1.0 g), anhydrous potassium carbonate (6.0 g), and benzyl chloride (0.9 ml) in dry acetone (60 ml) was refluxed for 6 h. The reaction mixture was then filtered, and the filtrate was evaporated *in vacuo*. The residue was recrystallized from acetone to give colorless needles of **4** (1.1 g) (mp 198—199 °C), which showed a pale brown color with ethanolic $FeCl_3$. IR: 1633 cm^{-1}. Found: C, 72.07; H, 6.18%. Calcd for $C_{31}H_{30}O_7$: C, 72.36; H, 5.88%.

5,7-Bis(benzyloxy)-2′,4′,5′-trimethoxyisoflavone (5). A solution of **4** (500 mg) in anhydrous ethyl formate (35 ml) was added to powdered sodium (600 mg) at 0 °C, and then the mixture was left at room temperature for 12 h. The mixture was treated with ice water and acidified with 6 M HCl. After almost all the ethyl formate had been evaporated *in vacuo*, the resulting semi-solid was dried and heated with acetic anhydride (10 ml) for 0.5 h. The reaction mixture was diluted with cold water to give pale yellow precipitates. The precipitates were collected and recrystallized from methanol to give colorless needles of **5** (200 mg); mp 163—164 °C; IR: 1650 cm^{-1}; UV λ_{max} nm (log ε): 255 (4.46), 291 (4.20). Found: C, 72.98; H, 5.66%. Calcd for $C_{32}H_{28}O_7$: C, 73.27; H, 5.38%.

5,7-Dihydroxy-2′,4′,5′-trimethoxyisoflavone (2). A solution of **5** (180 mg) in ethyl acetate (30 ml) was submitted to catalytic hydrogenolysis in the presence of Pd–C (10%: 100 mg) at room temperature. After the catalyst had been filtered, the filtrate was evaporated *in vacuo*. The residue was recrystallized from methanol to give colorless needles of **2** (110 mg) (mp 243—244 °C), which showed a brown color with ethanolic $FeCl_3$. IR: 3350, 1655 cm^{-1}; UV λ_{max} nm (log ε): 260.5 (4.42), 296 (4.16). Found: C, 62.52; H, 4.77%. Calcd for $C_{18}H_{16}O_7$: C, 62.79; H, 4.68%.

Diacetate of 2: Hot acetic anhydride–pyridine method; mp 204—205 °C (colorless needles from methanol). IR: 1763, 1650 cm^{-1}; UV λ_{max} nm (log ε): 294.5 (4.11); NMR ($CDCl_3$): δ 2.38, 2.43 (each 3H, s, CH_3CO), 3.79, 3.88, 3.96 (each 3H, s, CH_3O), 6.67, 6.91 (each 1H, s, 3′-, 6′-H), 6.94, 7.29, (each 1H, d, J=2 Hz, 6-, 8-H), 7.93 (1H, s,

2-H). Found: C, 61.34; H, 4.90%. Calcd for $C_{22}H_{20}O_9$: C, 61.68; H, 4.71%.

2-Hydroxy-2',4,4',5',6-pentamethoxydeoxybenzoin (7). *Hoesch Reaction*: A mixture of phloroglucinol dimethyl ether (800 mg), 2,4,5-trimethoxyphenylacetonitrile[4] (1.0 g) and anhydrous zinc chloride (1.0 g) in dry ether (35 ml) was saturated with anhydrous hydrogen chloride at 0 °C for 3 h and then allowed to stand at room temperature for 12 h. The ethereal solution was decanted from the oily layer of ketimine hydrochloride which had separated. This oily layer was washed with dry ether and then heated with water on a steam bath for 1 h. After cooling and standing, the precipitates were collected and recrystallized from ethanol to give colorless needles of **7** (200 mg), mp 145—146.5 °C (lit, mp 143 °C,[2] mp 144—145 °C[3]), which showed a yellowish violet color with ethanolic $FeCl_3$. IR: 1645 cm^{-1}; UV λ_{max} nm (log ε); 289 (4.35). Found: C, 62.96; H, 6.09%. Calcd for $C_{19}H_{22}O_7$: C, 62.97; H, 6.12%.

BF_3 Method: A mixture of phloroglucinol dimethyl ether (1.0 g) and homoasaronic acid[5] (1.47 g) in dry ether (35 ml) was saturated with anhydrous boron trifluoride gas at 0 °C for 3 h and then heated on a steam bath for 0.5 h. After cooling and standing, the reaction mixture was diluted with water. The resulting precipitates were collected and recrystallized to give **7** (320 mg), mp 144—145 °C, whose IR spectrum was identical with those of the sample described above.

2',4',5,5',7-Pentamethoxyisoflavone (6). *From 2*: A mixture of **2** (100 mg), anhydrous potassium carbonate (500 mg), and methyl iodide (0.5 ml) in dry acetone (30 ml) was refluxed for 5 h. The reaction mixture was then filtered, and the filtrate was evaporated *in vacuo*. The residue was recrystallized from methanol to give colorless needles of **6** (90 mg), mp 190—191 °C (lit,[1] mp 192—193 °C); IR: 1658 cm^{-1}; UV λ_{max} nm (log ε): 255 (4.42), 291 (4.15); NMR ($CDCl_3$): δ 3.74, 3.83, 3.88, 3.92, 3.93 (each 3H, s, CH_3O), 6.39, 6.49 (each 1H, d, J=2 Hz, 6-, 8-H), 6.60, 6.98, 7.80 (each 1H, s, 3'- 6'-, 2-H), whose IR and NMR spectra were identical with those of the corresponding derivative from natural robustigenin.[1] Found: C, 64.21; H, 5.44%. Calcd for $C_{20}H_{20}O_7$: C, 64.51; H, 5.41%.

From 7: A solution of **7** (200 mg) in anhydrous ethyl formate (11 ml) was added to powdered sodium (300 mg) at 0 °C, and then the mixture was left at room temperature for 24 h. The reaction mixture was then worked up in the same manner as in the case of **5** to give **6** (180 mg), which was subsequently recrystallized from methanol as colorless needles; mp 189—191 °C. It was identical with the sample described above.

Robustigenin 5-Hydroxy-2',4',5',7-tetramethoxyisoflavone (1). A mixture of **6** (30 mg), anhydrous aluminium chloride (110 mg), and acetonitrile (7 ml) was stirred under gentle refluxing for 16 h. After the removal of the solvent, dilute hydrochloric acid was added to the residue. The resulting solid was collected, washed with water, dried, and then chromatographed on silica gel (10 g), using ether–benzene (5:95) as the eluent, to give colorless needles of **1** (10 mg), mp 177—178 °C (lit,[1] mp 174—175 °C), which showed a dark violet color with ethanolic $FeCl_3$. IR (KBr): 3090, 1660 cm^{-1}; UV λ_{max} nm (log ε): 260 (4.41); NMR ($CDCl_3$): δ 3.75 (3H, s, CH_3O), 3.83 (6H, s, CH_3O ×2), 3.89 (3H, s, CH_3O), 6.36 (2H, s, 6- and 8-H), 6.59, 6.86, 7.85 (each 1H, s, 3'-, 6'-, 2-H), 12.92 (1H, s, OH), whose IR, UV, and NMR spectra were identical with those of natural robustigenin.[1] Found: C, 63.82; H, 5.21%. Calcd for $C_{19}H_{18}O_7$: C, 63.68; H, 5.06%.

References

1) S. S. Chibber and R. P. Sharma, *Phytochemistry*, **18**, 1082 (1979).

2) W. J. Bowyer, A. Robertson, and W. B. Whalley, *J. Chem. Soc.*, **1957**, 542.

3) T. R. Govindachari, K. Nagarajan, and P. C. Parthasarathy, *J. Chem. Soc.*, **1957**, 548.

4) J. Harley-Mason and A. H. Jackson, *J. Chem. Soc.*, **1954**, 1165.

5) A. Robertson and G. L. Rusby, *J. Chem. Soc.*, **1935**, 1371.

6) M. Nakayama, S. Nishimura, T. Matsui, S. Hayashi, and K. Fukui, *Experientia*, **27**, 875 (1971).

Chemiluminescence of a *Cypridina* Luciferin Analogue, 2-Methyl-6-phenyl-3,7-dihydroimidazo[1,2-*a*]pyrazin-3-one, in the Presence of the Xanthine–Xanthine Oxidase System[1]

Toshio GOTO* and Tetsuyuki TAKAGI

Laboratory of Organic Chemistry, Faculty of Agriculture, Nagoya University, Chikusa-ku, Nagoya 464

(Received September 27, 1979)

Synopsis. The title compound chemiluminesces in aqueous solutions (pH 5—6.5) in the presence of xanthine–xanthine oxidase system; O_2^- and not $^1O_2$ was proven to be the active species. Quantitative determination of xanthine and xanthine oxidase as low as 5 nmol and 10^{-5} unit, respectively, is possible by measurement of the chemiluminescence light yield and the reaction rate.

In the case of the bioluminescence of *Cypridina* system, light is emitted during the oxidation of *Cypridina* luciferin (LH) with molecular oxygen by catalysis of an enzyme, *Cypridina* luciferase. It was suggested that the substrate reacts with molecular oxygen ($^3O_2$) when it is taken in a hydrophobic pocket of the enzyme,[2] since the luciferin reacts with molecular oxygen and emits light when it is dissolved in aprotic polar solvents such as dimethyl sulfoxide, diethylene glycol dimethyl ether, *etc.*, but in aqueous solutions no luminescence is observed without the enzyme. The chemiluminescence reaction in the aprotic solvents is second order with respect to the concentrations of the substrate (LH) and molecular oxygen;[3] a suggested mechanism involves a non-chain reaction between the luciferin anion and oxygen giving a hydroperoxide anion through a radical pair intermediate:[2]

$$LH \rightarrow L^- \xrightarrow{O_2} [L\cdot \cdot O_2^-] \rightarrow L\text{-}OO^- \rightarrow \text{products} + h\nu.$$

Similarly its analogue, 2-methyl-6-phenyl-3,7-dihydroimidazo[1,2-*a*]pyrazin-3-one (LA), chemiluminesces with molecular oxygen in the aprotic solvents but not in aqueous solutions.[2] It becomes chemiluminescent, however, even aqueous solutions when the reaction mixture contains some oxidants such as H_2O_2 and catalytic amounts of $K_3[Fe(CN)_6]$ or Fe^{3+}.[4] In these cases the active oxidant may be either superoxide (O_2^-) or singlet oxygen ($^1O_2$) produced by superoxide annihilation ($2\,HOO\cdot \rightarrow {}^1O_2 + H_2O_2$). To see if the superoxide can be the oxidant for the luminescence in aqueous solutions, we have examined the xanthine–xanthine oxidase (X–XOD) system since the system has been proven to produce superoxide ions.[5]

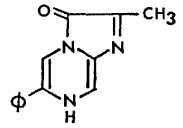

LA

Indeed, the luciferin analogue (LA) gives light in aqueous solutions in the presence of the X–XOD system (Fig. 1). The best pH range for the luminescence is between 5 and 6.5 (Fig. 2).[6] The light yield is decreased but rate of luminescence is increased as pH increases. Using 0.1 μmol of X in a 2.5 ml solution the linear relationship is obtained between the amount of LA and the total light yield up to 0.01 μmol of LA (Fig. 3). Thus, the maximum efficiency can be obtained when the molar ratio of X and LA is *ca.* 10:1.[7] When LA is present in more than 0.035 μmol, the total light yield is proportional to the amount of X ($X < 0.3$ μmol), whereas the rate of luminescence is independent of the concentration of X (Fig. 4).

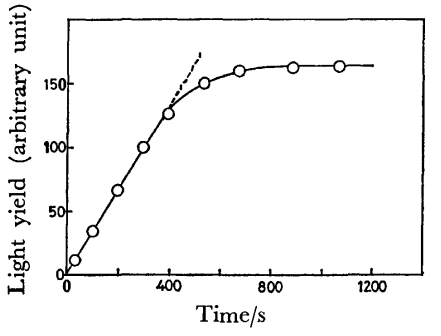

Fig. 1. Luminescence of LA in the presence of X–XOD system. X: 0.1 μmol; XOD: 0.05 unit; LA 0.01 μmol; pH 5.5.

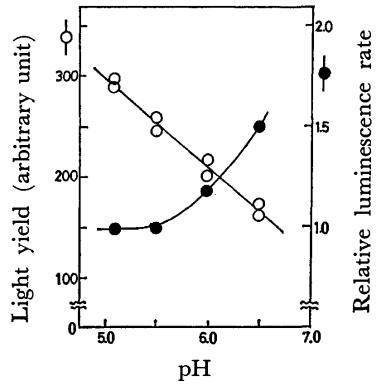

Fig. 2. pH dependence of light yield and luminescence rate. X: 0.4 μmol; XOD: 0.2 unit; LA: 0.04 μmol.

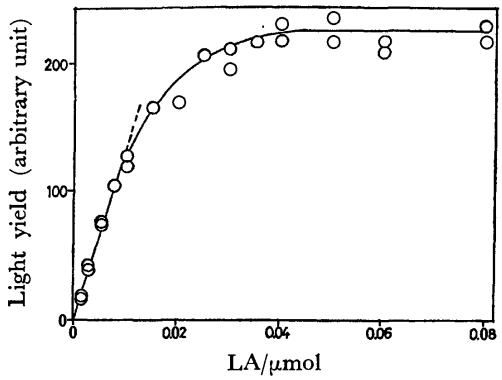

Fig. 3. Total light yield *vs.* quantity of LA. X: 0.1 μmol; XOD: 0.05 unit; pH 5.5.

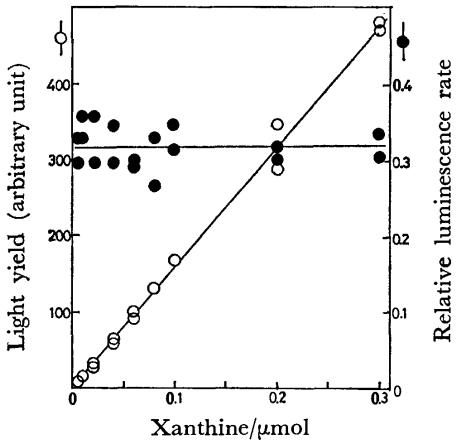

Fig. 4. Light yield and luminescence rate *vs.* quantity of xanthine. XOD: 0.05 unit; LA: 0.035 μmol; pH 5.5.

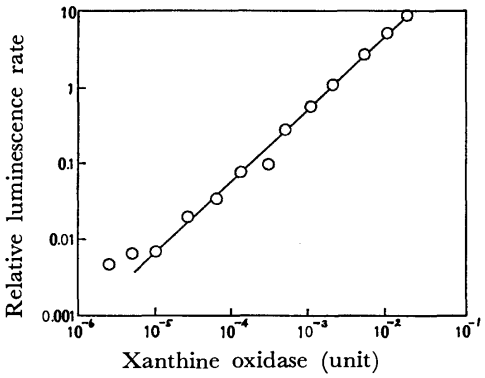

Fig. 5. Luminescence rate *vs.* quantity of xanthine oxidase. X: 0.01 μmol; LA: 0.001 μmol; pH 5.5.

Thus, the amount of X as low as 5 μmol in a 2.5 ml solution can be quantitatively determined by measuring the total light yield. On the other hand, by measurements of the initial rate of luminescence it is possible to determine the quantity of XOD as small as 10^{-5} unit (Fig. 5).

These results led to the conclusion that the reactive species of the luminescence is superoxide and not singlet oxygen;[8] if singlet oxygen were the reactive species the reaction rate must not be proportional to the amount of XOD. This was further supported by examination of the effect of sodium azide (a singlet oxygen quencher)[9] on the luminescence rate; additon of 1×10^{-3} M sodium azide did not affect the rate (4×10^{-5} M X and 0.05 unit XOD in 2.5 ml).

Involvement of superoxide was also demonstrated by addition of superoxide dismutase (SOD),[10] which is well known to decompose superoxide by the following equation: $2\cdot O_2^- + 2H^+ \xrightarrow{SOD} {}^3O_2 + H_2O_2$. SOD strongly inhibited the luminescence reaction, whereas little effect was observed with SOD preheated at 100 °C for 10 min.[11] Thus, the chemiluminescence of the luciferin analogue by the xanthine–xanthine oxidase system in aqueous solution involves superoxide as the reacting species.[12]

$$ {}^3O_2 \xrightarrow{\text{X-XOD}} \cdot O_2^- \xrightarrow{\text{LA}} h\nu $$

$$ v = k[\cdot O_2^- \text{ or } \cdot OOH] = k'[XOD] $$

The luciferin analogue may be widely applicable for detection of superoxide in physiological systems.

Experimental

Xanthine oxidase was purchased from the Boehringer Mannheim Co. The luciferin analogue (LA) was synthesized according to the literature.[13] The light yields and luminescence rates were measured with an automatic recording photomultiplier (Hamamatsu type R105)-amplifier system. Condition: 2.5 ml of 1/30 M phosphate buffer containing 10^{-4} M EDTA at 25 °C. No marked difference was observed when the buffer solution is changed from the phosphate to 0.1 M acetate.

We thank Dr. M. Nakano, Gumma University, for the generous gift of superoxide dismutase.

References

1) *Cypridina* Bioluminescence X. Preceding paper: *Tetrahedron*, **31**, 939 (1975).
2) T. Goto, *Pure Appl. Chem.*, **17**, 421 (1968).
3) T. Goto, S. Inoue, and S. Sugiura, *Tetrahedron. Lett.*, **1968**, 3873.
4) *Cypridina* luciferin does not chemiluminesce in aqueous solutions in the presence of these oxidants.[2] LA also gives chemiluminescence in aqueous solutions with KO_2+18-Crown-6 in diglyme, and with O_2+*N*,*N*′-disalicylideneethylenediaminatocobalt(II) in aqueous or methanol solutions (T. Goto, I. Kubota, N. Suzuki, Y. Kishi, and S. Inoue, "Chemiluminescence and Bioluminescence," ed by M. J. Cormier, D. M. Hercules, and J. Lee, Plenum Publ. Corp., New York (1973), p. 325).
5) I. Fridovich and P. J. Handler, *J. Biol. Chem.*, **233**, 1581 (1958); I. Fridovich, *J. Biol. Chem.*, **245**, 4053 (1970).
6) Totter *et al.* have reported that luminol and lucigenin give light in the presence of X–XOD system in strongly basic solutions (pH above 10): J. R. Totter, V. J. Medina, and J. L. Scoseria, *J. Biol. Chem.*, **235**, 238 (1960); J. R. Totter, E. C. de Dugros, and C. Riveiro, *J. Biol. Chem.*, **235**, 1839 (1960). Instead, LA gives light in physiological conditions suitable for its application to other enzyme systems.[12]
7) In the case of luminol the best results were obtained when the ratio of X and luminol is *ca.* 1:1 at pH 10.4, but the total light yield was less than one tenth of LA.
8) The X–XOD system gives extremely weak chemiluminescence; $^1O_2$ may be responsible for production of light: R. M. Arneson, *Arch. Biochem. Biophys.*, **136**, 352 (1970).
9) H. Hasty, P. B. Merkel, R. Radlich, and D. R. Kearns, *Tetrahedron Lett.*, **1972**, 49; I. Saito, K. Inoue, and T. Matsuura, *Photochem. Photobiol.*, **21**, 27 (1975).
10) J. M. McCord and I. Fridovich, *J. Biol. Chem.*, **244**, 6049 (1969); A. J. Bard, *J. Am. Chem. Soc.*, **96**, 4023 (1974); A. P. Schaap, *J. Am. Chem. Soc.*, **96**, 4026 (1974).
11) Inhibition of chemiluminescence with SOD in the luminol (or lucigenin) +X–XOD system has been reported: L. Greenlee, I. Fridovich, and P. Handler, *Biochem.*, **1**, 779 (1962); E. K. Hidgson and I. Fridovich, *Photochem. Photobiol.*, **18**, 451 (1973).
12) The luciferin analogue also gives chemiluminescence in the system of H_2O_2–peroxidase at pH 7.5 and the system of glucose oxidase–peroxidase–O_2 at pH 5.5.
13) S. Inoue, S. Sugiura, H. Kakoi, and T. Goto, *Tetrahedron Lett.*, **1969**, 1069.

On the Choice of Adsorptives for the Application of a Modified Dubinin-Radushkevich Equation

Fritz STOECKLI*, André PERRET, and Ueli HUBER†
Institute de Chimie de l'Université, CH-2000 Neuchâtel, Switzerland
†*GRD Laboratorium, CH-3752 Wimmis, Switzerland*
(Received June 9, 1979)

Synopsis. It is shown that great care has to be taken in the choice of the adsorptives for the assessment of microporosity and its heterogeneity. Methanol, for which selective interactions may occur, is not a suitable adsorptive to be used in the framework of the generalized Dubinin-Radushkevich equation proposed by Stoeckli.

A paper has been published recently in this Journal by Tsunoda,[1] on the application of a modified Dubinin-Radushkevich equation to adsorption on active carbons with heterogeneous micropore systems. It is based on a generalization of the Dubinin-Radushkevich equation, originally proposed by Stoeckli,[2] and fully investigated by Stoeckli *et al.* in a recent paper.[3]

On the basis of experimental evidence from the adsorption of simple gases on various active carbons, we showed that the following equation could be used

$$W = W_0 \exp\{-B_0 y\} \cdot \exp\{y^2 \Delta^2/2\} \cdot [1-\mathrm{erf}(x)]/2 \quad (1)$$

where

$$y=(T/\beta)^2 \log^2(p_0/p) \text{ and } x=(y-B_0/\Delta^2)\,\Delta/\sqrt{2}.$$

W_0 is the total volume of the micropores, and W represents the volume filled at (T, p).

Equation 1 is based on the idea of a Gaussian distribution of the micropore volume W with the structural constant B,

$$f(B)=[W_0/\Delta(2\pi)^{1/2}] \exp\{-(B-B_0)^2/2\Delta^2\} \quad (2)$$

combined with the original equation of Dubinin and Radushkevich,[4]

$$W = W_0 \exp\{-B(T/\beta)^2 \log^2(p_0/p)\}. \quad (3)$$

The quantity Δ, a measure of the spread of B around B_0, is related to the heterogeneity of the micropore system under investigation. This is a direct consequence of the empirical relation which exists between B and the gyration radius R_g of the micropores, derived from the scattering of X-rays at small angles.[5]

The so-called affinity coefficient, β, is a characteristic of the adsorptive. It is calculated[4] from the ratios of the parachores, benzene being the reference vapor with $\beta=1$. With the use of β, the isotherms of different gases on a given microporous carbon can be reduced to a single isotherm. As shown by Stoeckli *et al.*[3] this is also the case for the generalized equation (Eq. 1), when a number of non-specific adsorptives are used. (A representation of $\ln(W)$ *versus* y yields a single curve for heterogeneous carbons). Typical values of B_0 and Δ, obtained from our experimental data,[3] are shown in Table 1.

The smaller values of B_0 correspond to narrow systems of micropores, where the spread Δ is also reduced or equal to zero (molecular-sieves). The recent work of Tsunoda is essentially an extension of a generalized equation (Eq. 1), taking into account possibility of a non-negligeable fraction of the Gaussian distribution (Eq. 2) existing in the region of $B<0$, which is physically unrealistic.

Table 1. Parameters of Eq. 1 for various carbons

Carbon	Origin	W_0 / cm³ g⁻¹	B_0 / 10⁻⁶ K⁻²	Δ / 10⁻⁶ K⁻²
U-02	Mineral	0.43	0.92	0.21
F-02	Vegetable	0.64	1.03	0.29
F-85	Vegetable	0.75	0.98	0.35
Carbosieve	Polymer	0.51	0.57	—
AC-400 (7)	Mineral	0.42	0.73	0.21
AC-900 (7)	Mineral	0.43	0.72	0.28

Although this possibility is mathematically conceivable, our extended investigations have not revealed it so far. The typical values of B_0 and Δ given in the table correspond to negligeable contributions from the region $B<0$, since B_0 is close to 3Δ. Even for $B_0=2\Delta$, this contribution would only represent 2% of the total area of the normalized Gaussian (Eq. 2).

Relatively larger values were reported by Tsunoda[1] for the spread Δ, which may justify the use of his modification of Eq. 1. However, a closer examination reveals that his approach is based on the adsorption of methanol alone, and at a single temperature (30 °C). As found in our own investigation, methanol is not a suitable adsorptive. The main reason, as in the case of water, is the possibility of selective interactions with chemical groups on the surface of the carbon.

The isotherms may often be ill-defined, or of type III or V, not described by Eqs. 1 or 3. Therefore, they show a deviation from linearity in the classical Dubinin-Radushkevich plot of $\ln(W)$ *versus* $\log^2(p_0/p)$, reflecting specific differences in the mode of adsorption. This is fundamental difference with the usual collection of molecules without specific interactions, to which the theory of micropore filling essentially applies.

In the case of carbon U-02, well characterized by N_2, Xe, SF_6, N_2O, C_6H_6, and CCl_4, one finds the average values of Table 1.

The adsorption of methanol at 230 K, on the other hand, interpreted through Eq. 1, leads to $B_0=1.71\times10^{-6}$ K^{-2} and $\Delta=0.54\times10^{-6}$ K^{-2}, using the value $\beta(CH_3OH)=0.40$. The difference with the results from the other gases is evident, and it is also found that the ratio Δ/B_0 is larger for methanol. The results of a single gas like methanol, are therefore not necessarily representative for a range of adsorptives. This suggests that great care has to be taken in the choice of adsorptives for the assessment of microporosity.

We also would like to point out, that in the case of Tsunoda's modification of Eq. 1, the quantity B_0 is no longer comparable with ours, or with the structural constant B of the D-R equation (Eq. 3). This is due to the fact that the affinity coefficient β has been omitted, implying that methanol is now the reference vapor.

References

1) R. Tsunoda, *Bull. Chem. Soc. Jpn.*, **51**, 2261 (1978).
2) H. F. Stoeckli, *J. Colloid Interface Sci.*, **59**, 184 (1977).
3) U. Huber, H. F. Stoeckli, and J. Ph. Houriet, *J. Colloid Interface Sci.*, **67**, 195 (1978).
4) M. M. Dubinin, "Progress in Membrane and Surface Science," ed by D. A. Cadenhead, Academic Press, New York (1975) Vol. IX, pp. 1—70.
5) A. Janosi and H. F. Stoeckli, *Carbon*, **17**, 465 (1979); H. F. Stoeckli and J. Ph. Houriet, *Carbon*, **14**, 253 (1976); Yu. A. Kuzin, E. N. Syromolotov, G. M. Plavnik, and M. M. Dubinin, *Dokl. Akad. Nauk SSSR*, **182**, 1114 (1968); M. M. Dubinin and G. M. Plavnik, *Carbon*, **6**, 183 (1968).

Polyelectrolyte Complexes of Chitosan with Sodium Carboxymethylcellulose

Hiroshi FUKUDA

Faculty of Home Economics, Hiroshima Women's University, Uzina-machi, Hiroshima 734

(Received February 27, 1979)

A new water-insoluble precipitate was obtained by mixing chitosan with sodium carboxymethylcellulose, an anti-thrombogenic agent. The mole ratio of N/COO^- in the polyelectrolyte complexes was estimated to be 0.3935—0.9071. It was found that pH, mole ratio of N/Na in the reaction mixture and the order of mixing play an important role in determining the composition ratio of N/COO^-. In order to clarify the relationship between the molecular conformation of the polyelectrolyte complexes and their properties, IR spectroscopic studies, elementary analyses, color reaction with Toluidine Blue, studies on solubility and blood clotting test *in vitro* were performed. The polyelectrolyte complex, prepared at higher pH, differed from that prepared at lower pH, particularly in the density of -COOH group site. These results were interpreted in terms of the variation in the degree of electrolytic dissociation of the weak polyelectrolytes, caused by pH change. All the polyelectrolyte complexes revealed clot-inhibition *in vitro*. The clot-inhibiting behavior seems to be due to the clot-inhibiting surface of the polyelectrolyte complex, not to the elution of the activity from the surface.

A solution of charged polyelectrolyte reacts with one of oppositely charged polyelectrolyte to form a water-insoluble hydrous complex whose property is determined by various factor such as the degree of electrolytic dissociation of polyelectrolyte, composition of reaction mixture, order of mixing, pH and the polyion concentration. The polyion interaction or intermolecular reaction is remarkable not only as a model reaction *in vivo*, such as polyion interaction between charged polysaccharide and protein, but also as functional polymers or biomedical materials. Studies have been made on this subject.[1-3] However, the mechanism of polyion interaction and the probable structure of the polyelectrolyte complex (PEC) remains unclarified. Only a few papers[4,5] deal with the polyion interaction between polysaccharides or polysaccharide and synthetic macromolecule in spite of its importance as regards model reaction *in vivo* or biomedical applications.[6,7] The property of PEC can be made to satisfy the requirement.

Reports have appeared on novel reactions of sodium dextran sulfate with chitosan [poly(N-deacetylated chitin)],[8-11] sodium dextran sulfate with [2-(diethylamino)ethyl] dextran,[12] and sodium carboxymethyldextran with chitosan.[13] This paper describes a novel chemical interaction of sodium carboxymethylcellulose (CMC) with chitosan and studies on the PEC.

Experimental

Materials. CMC (Wako Pure Chemical Industries Co. Ltd., sodium content 7.79%, degree of substitution 0.753/A.G.U) and chitosan (Tokyo Kasei Co. Ltd., nitrogen content 7.95%) were used, the latter being purified by reprecipitation from its acidic solution with sodium hydroxide solution, but not CMC because of its high purity.

Preparation of PEC. When the pH of solution is below 2.0, no precipitates are formed by mixing chitosan with CMC, and when the pH of the chitosan solution is higher than 6.5, chitosan remain insoluble. When the pH of the chitosan solution is higher than 5.5, gelation of precipitate takes place. The reactions were thus carried out at pH 2.5 and 5.0, respectively. CMC was dissolved in water, and the pH of solution was adjusted to 2.5 and 5.0 with hydrochloric acid solution. Purified chitosan was dissolved in a 0.1 M hydrochloric acid solution, the pH of solution being adjusted to 2.5 and 5.0 with sodium hydroxide solution. These chitosan solutions were added dropwise to the corresponding CMC solutions, with stirring (rate of addition about 50 ml/30 min) under the conditions given in Table 1. Water-insoluble precipitates, the polyelectrolyte complexes PEC, were obtained. After standing for a half hour, the precipitates were washed with 0.01 M hydrochloric acid, water and methanol, and then separated by centrifugation, dried *in vacuo* for a week, until a constant weight was attained.

The elementary analyses of the PEC were performed at the Institute of Physical and Chemical Research, Wako-shi, Saitama, and the infrared spectra were taken by the KBr method. Nitrogen analysis was carried out by the Kjeldahl method.

Color Reaction of PEC with Toluidine Blue. The color change of PEC was examined in two ways: (a) addition of Toluidine Blue solution to PEC, (b) soaking of PEC in water for 1 day, and addition of Toluidine Blue solution to the filtrate. (a) was to confirm whether the surface of PEC is clot-promoting or clot-inhibiting, and (b) to see whether the clot-promoting or clot-inhibiting activities are transferred from the surface of PEC, since the reaction of anti-thrombogenic CMC with Toluidine Blue gives purple coloration.

Blood Clotting Test in Vitro. The blood clotting test was carried out according to the procedure of Imai and Nose[14] by gravimetrically measuring the amount of the clot formed at appropriate time intervals, after adding a calcium chloride solution (0.1 M, 0.02 ml) to ACD blood (0.2 ml), which had been in contact with a sample tablet: 200 mg PEC was pressed (8 t/4.5 cm^2) with poly(vinyl chloride) powder in a vacuum for 10 min. The ACD blood was prepared by adding blood (type A supplied by the Red Cross Hospital Blood Center) to an anti-coagulant citrate dextrose solution consisting of sodium citrate, citric acid and dextrose. The clotting tests were carried out concurrently under comparable conditions using the same method and the same ACD blood, after the blood had been stored for 3 days in a thermostat at 4—6 °C.

Solubility of PEC. Polyelectrolyte complexes are hardly soluble in most organic solvents. However, in order to clarify the property of PEC, it is necessary to find an appropriate solvent. Solubility tests were made on formic acid, dimethyl sulfoxide, *N,N*-dimethylformamide and two different ternary solvent mixtures (acetone/potassium bromide/water), (dioxane/water/hydrochloric acid).

Results and Discussion

Experimental conditions and yields in the preparation of PEC are given in Table 1, and, elementary analyses and compositions of PEC and pH of solutions after reaction in Table 2. Primarily, CMC is a salt of weak acid and chitosan is a salt of weak base, so that in a solution of lower pH the number of binding site $-OCH_2COO^-$ is smaller and that of binding site $-NH_3^+$ larger, as compared with a solution of higher pH.

$$-OCH_2COO^-Na^+ + H^+ \rightleftarrows -OCH_2COOH + Na^+$$

$$-NH_3OH + H^+ \rightleftarrows -NH_3^+ + H_2O$$

Thus, provided that $-COO^-$ groups in CMC participate just sufficiently to bind with $-NH_3^+$ in chitosan, in the lower pH condition (series A) the number of binding site $-NH_3^+$ is significantly larger than that of binding site $-OCH_2COO^-$. Consequently, the smaller the mole ratio of N/Na in the reaction mixture, the larger the yield for PEC. On the other hand, at pH 5.0 (series B) the number of binding site $-OCH_2COO^-$ in CMC increases and that of binding site $-NH_3^+$ decreases as compared with those at pH 2.5 (series A), so that the yield of PEC is not much affected by the mole ratio of N/Na. In general, the yield of PEC of series A is larger than that of series B. The tendency is similar to that in the PEC of chitosan with carboxymethyldextran[13] or chitosan with dextran sulfate.[10] The yield of PEC is influenced by the mixing order. When a polyelectrolyte of a large mole fraction in the reaction mixture is mixed with a polyelectrolyte solution, of a small mole fraction, the yield of PEC is larger than that obtained by reversing the order of mixing. In the case of polyelectrolyte, it seems that changes in the reaction mechanism, which affects the yield or molecular conformation of the PEC, are caused by the change in the order of mixing. The pH of reaction mixture tends to drop slightly after completion of PEC in both series. This indicates that the proton is liberated from the PEC on its formation.[6] In the pH range 2.5—5.0, the degree of electrolytic dissociation in polycation is significantly larger than

Table 1. Experimental conditions, yields in the preparation of polyelectrolyte complexes[a]

Sample code	Volume of chitosan solution ml	Volume of CMC solution ml	Mixing order	Mole ratio of N/Na in the reaction mixture	Yield g/100 ml chitosan solution
A-1[b]	200	110	CMC to chitosan	3/1	0.0531
A-2[b]	200	110	Chitosan to CMC	3/1	0.1006
A-3[b]	100	167.5	CMC to chitosan	1/1	0.2696
A-4[b]	100	167.5	Chitosan to CMC	1/1	0.3856
A-5[b]	50	251	CMC to chitosan	1/3	1.0434
A-6[b]	50	251	Chitosan to CMC	1/3	0.7712
B-1[c]	200	110	CMC to chitosan	3/1	0.0925
B-2[c]	200	110	Chitosan to CMC	3/1	0.1003
B-3[c]	100	167.5	CMC to chitosan	1/1	0.2131
B-4[c]	100	167.5	Chitosan to CMC	1/1	0.3830
B-5[c]	50	251	CMC to chitosan	1/3	0.2861
B-6[c]	50	251	Chitosan to CMC	1/3	0.2351

a) Concentrations of chitosan and sodium carboxymethylcellulose (CMC): 3.0 g/l. b) Both solutions adjusted to pH 2.5. c) Both solutions adjusted to pH 5.0.

Table 2. Elementary analyses, compositions of PEC and pH of solutions after reaction

Sample code	Nitrogen content[a] %	Sodium content[b] %	Chlorine content[b] %	Mole ratio of N/COO^- in the PEC	pH of mother liquor after completion of PEC
A-1	1.71	—	—	0.4595	2.40
A-2	1.77	—	—	0.4804	2.41—2.50
A-3	1.55	0.15	0.13	0.4062	2.40
A-4	1.51	0.00	0.11	0.3935	2.40
A-5	1.74	—	—	0.4701	2.40
A-6	1.79	—	—	0.4878	2.40
B-1	2.54	—	—	0.7877	4.78—5.00
B-2	2.57	—	—	0.8017	4.72
B-3	2.53	0.73	0.63	0.7833	4.80
B-4	2.69	0.35	0.32	0.8580	4.80
B-5	2.68	—	—	0.8579	4.90
B-6	2.79	—	—	0.9071	4.88—4.90

a) Nitrogen analysis carried out by the Kjeldahl method. b) Analyses performed at the Institute of Physical and Chemical Research.

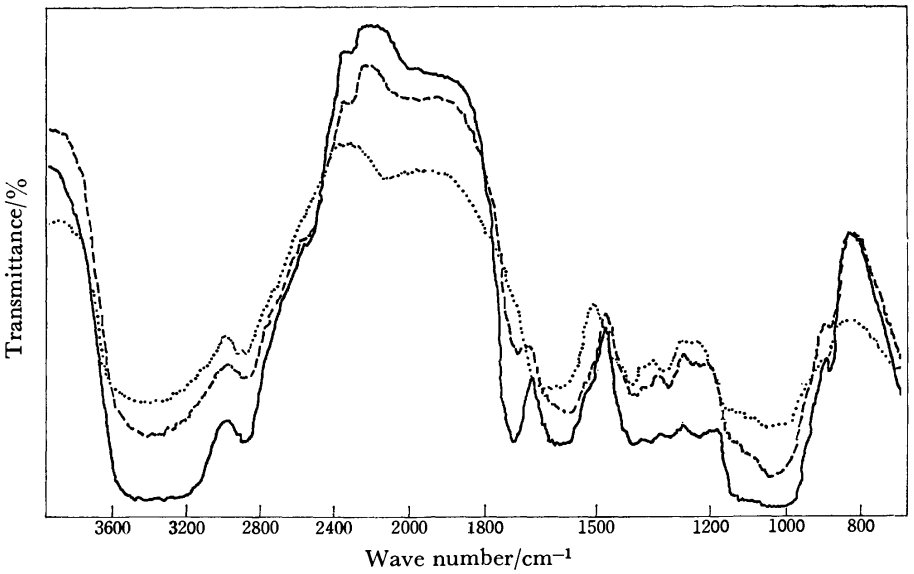

Fig. 1. IR spectra of polyelectrolyte complexes (PEC), series A and B, and of a blend polymer chitosan with sodium carboxymethyl cellulose (CMC).
——·: PEC of series A in Table 1, ——: PEC of series B in Table 1, ------: blend polymer chitosan with CMC, mole ratio of N/Na=1/3.

that in polyanion, all protons favoring release from the undissociated carboxyl groups. The nitrogen content in the PEC is not much influenced by the difference in the order of mixing or the mole ratio of N/Na. These results differ from those in the PEC, chitosan with carboxymethyldextran.[13] However, the nitrogen, sodium and chlorine contents in the PEC of B series are larger than those of series A, the results being similar to those in the PEC, chitosan with carboxymethyldextran[13] and chitosan with dextran sulfate.[10] However, the deviation of nitrogen content in the PEC, chitosan with carboxymethyldextran, with pH is larger than that in the PEC, chitosan with CMC. The results might be related to the fact that the difference in their viscous behavior,[15] or in effective molecular volume of polyelectrolyte in reaction solution, is caused by the pH change in carboxymethyldextran and CMC. The mole ratio of N/COO^- in the PEC, consequently, the nitrogen content in the PEC of series A should be smaller than that of series B. The results given in Table 2 (the mole ratios of N/COO^- in the PEC are calculated from the nitrogen contents in chitosan and PEC, and from the degree of substituent $-OCH_2COOH$ in CMC) are in line with the above consideration. This is also supported by IR spectra.

IR spectra of the PEC in series A are roughly similar to those of the PEC in series B and to those of blend polymer (blended chitosan with CMC in the same ratio as the complex composition), differing from each other in detail (Fig. 1). The absorption band around 1740 cm^{-1}, assigned to -COOH group, arises from the PEC, but not from the blend polymer. The absorption band around 1740 cm^{-1} in the PEC of series A is stronger than that of series B. This is in line with the electrolytic dissociation of $-OCH_2COO^-Na^+$ groups, the stronger the absorption band around 1740 cm^{-1}, the smaller the nitrogen content. The absorption band around 3500 cm^{-1}, attributable to -OH group in the blend polymer, seems to shift slightly towards lower wave number in the PEC. The absorption bands in the PEC of series A are assumed to become broader than those in the PEC of series B and in the blend polymer. The -OH groups in the PEC interact sparsely with other PEC molecules, probably through its -COOH groups. No such interaction was observed in the PEC of chitosan with carboxymethyldextran.[13] From the difference in absorption intensity of -COOH groups between the PEC of series A and series B, it seems that the intermolecular interactions in the PEC of series A through its -OH groups with other -COOH groups, are stronger than those of series B. This is supported by the results of solubility measurements. A weak absorption band around 1520 cm^{-1} assigned to $-NH_3^+$ groups is observed in the PEC, but none in the blend polymer. The sodium and chlorine contents in the PEC are distinctly smaller than those in CMC and chitosan, suggesting that the $-NH_3^+$ groups in chitosan participate in the binding with CMC

Table 3. Color reaction of PEC with Toluidine Blue

Sample code	Color of PEC itself	Color of solution in contact with PEC
A-1	blue	light blue
A-2	blue	light blue
A-3	blue	light blue
A-4	blue	light blue
A-5	blue	light blue
A-6	blue	light blue
B-1	light bluish purple	light blue
B-2	light bluish purple	light blue
B-3	light bluish purple	light blue
B-4	light bluish purple	light blue
B-5	bluish purple	light blue
B-6	bluish purple	light blue

probably through its $-COO^-$ groups, although the number of the ionic binding sites is small. The IR spectra of PEC are similar to those of CMC, being strongly affected by CMC rather than by chitosan. However, this might not be related to the fact that the mole ratio of N/COO^- in the PEC is small (Table 2).

Table 3 gives the results of color reactions of PEC with Toluidine Blue. No elution of CMC is observed in the solutions in contact with each PEC. The color reaction takes place not only on the surface but throughout the bulk of the complex, indicating a homogeneous dispersion of CMC into the PEC. The tint of the PEC differs with the conditions for the preparation of PEC. This seems to be closely related to the difference in the conformation in PEC.

TABLE 4. SOLUBILITIES OF PEC

Sample code	Formic acid			Dimethyl sulfoxide		
	R.T.	B	D.H.	R.T.	B	D.H.
A-1	×	△	▲	×	×	×
A-2	×	△	▲	×	×	×
A-3	×	△	▲	×	×	×
A-4	×	△	▲	×	×	×
A-5	×	△	▲	×	×	×
A-6	×	△	▲	×	×	×
B-1	△	▲	○	×	×	×
B-2	△	▲	○	×	×	×
B-3	△	▲	○	×	×	×
B-4	△	▲	○	×	×	×
B-5	△	▲	○	×	×	×
B-6	△	▲	○	×	×	×

All PEC are insoluble, even on direct heating, in N,N-dimethyl formamide and two sorts of ternary solvent mixture [acetone/potassium bromide/water (20: 20: 60 wt %)] [(dioxane/water/hydrochloric acid (50: 5: 45 wt %)], other than dimethyl sulfoxide. ○: almost soluble, ▲: considerably soluble, △: partially soluble, × : insoluble, R.T.: room temperature, B:heating on a water bath, D.H.: direct heating.

All PEC are insoluble in most organic solvents, even on heating, such as dimethyl sulfoxide, N,N-dimethylformamide and two different ternary solvent mixtures {[acetone/potassium bromide/water (20: 20: 60 wt%)] [dioxane/water/hydrochloric acid (50: 5: 45 wt%)]} (Table 4), but become partially soluble in formic acid on heating. There is an appreciable difference in solubility between the PEC of series A and series B. It seems that the number of intermolecular binding sites through -OH groups with -COOH groups in the PEC of series B is smaller than that of series A. This is in line with the IR spectra.

The PEC of series A and B show clot-inhibition *in vitro*; they suppress the coagulation of blood (Fig. 2). The amount of thrombus on the PEC is 10—20% of that on glass and 30—50% of that on poly(vinyl chloride) as a reinforcing agent. The difference in anti-thrombogenic behavior between the PEC of series A and that of series B can hardly be observed. The anti-thrombogenic property may be due to the clot-inhibiting surface of the PEC and not to the eluted

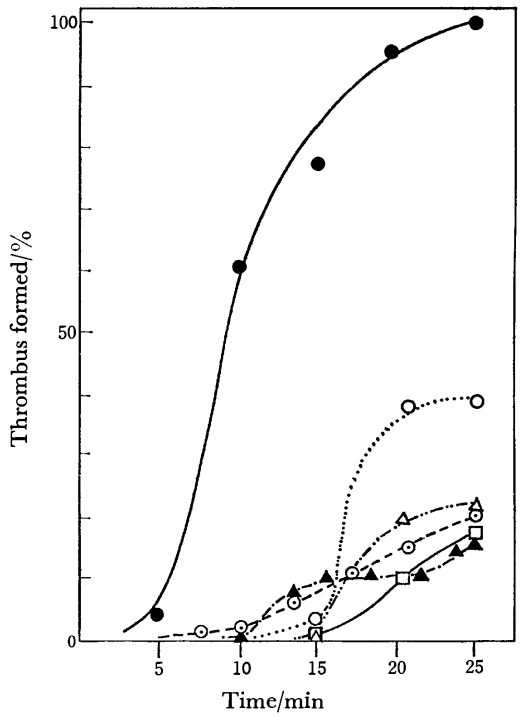

Fig. 2. Quantity of thrombus formed on polyelectrolyte complexes (PEC) compared with that on glass after a lapse of 25 min as a criterion.
●: Glass, □: A-3, △: A-4, ⊙: B-3, ▲: B-4, ○: poly(vinyl chloride) correspond to the PEC in Table 1.

activity from the surface as considered from the color reaction with Toluidine Blue. The clot-inhibiting factors of the PEC might be related to its molecular conformation or configuration.

References

1) E. Tsuchida and T. Osada, *Kobunshi Kagaku*, **22**, 384 (1973).
2) H. Noguchi, *Kobunshi Kagaku*, **22**, 402 (1973).
3) T. Tanaka, R. Tanaka, and T. Tsutsui, *Kobunshi Kagaku*, **26**, 804 (1977).
4) A. S. Michaels and N. S. Schneider, *J. Phys. Chem.*, **69**, 1477 (1965).
5) K. Shinoda and A. Nakajima, Summary of Papers in the 23th Polymer Symposium, Tokyo, Japan, (1974), p. 21.
6) A. Nakajima, *Kagaku To Kogyo*, **27**, 746 (1974).
7) Y. Mori and H. Tanzawa, *Kobunshi Kagaku*, **22**, 613 (1973).
8) Y. Kikuchi and H. Fukuda, *Makromol. Chem.*, **175**, 3593 (1974).
9) Y. Kikuchi and H. Fukuda, *Nippon Kagaku Kaishi*, **1976**, 1505.
10) H. Fukuda and Y. Kikuchi, *Makromol. Chem.*, **178**, 2895 (1977).
11) H. Fukuda and Y. Kikuchi, *J. Biomed. Mater. Res.*, **12**, 531 (1978).
12) Y. Kikuchi and H. Fukuda, *Nippon Kagaku Kaishi*, **1977**, 1051.
13) H. Fukuda and Y. Kikuchi, *Bull. Chem. Soc. Jpn.*, **51**, 1142 (1978).
14) Y. Imai and Y. Nose, *J. Biomed. Mater. Res.*, **6**, 165 (1972).
15) H. Fukuda, unpublished.

 © 1980 The Chemical Society of Japan Bull. Chem. Soc. Jpn., 53, 841—844 (1980)

An ESR Study of Hydrogen Atoms in Methane-Air Flame

Shoji NODA, Masazumi MIURA, and Hiroshi YOSHIDA*

Faculty of Engineering, Hokkaido University, Kita-ku, Sapporo 060

(Received June 7, 1979)

In order to give a basis for the utilization of ESR in combustion chemical studies, both diffusion flames and premixed flames of a methane–air mixture have been studied by the flame-in-cavity ESR method. A pair of spectral lines separated by 51.0 mT due to H atoms and a very weak single line due to unidentified reaction intermediates have been recorded from combusting gases in a modified Bunsen burner. The H atoms in the diffusion flame give the spectral linewidth of 0.15 mT and populate a confined region near the luminous cone. In the premixed flame, the H atom concentration is the highest at the outside of the luminous inner cone (reaction zone), but it is distributed as long as 4 cm along the gas stream. The profile of the local concentration has been obtained by the deconvolution method from the observed dependence of the spectral intensity on the location of the flame in the resonant cavity. The maximum concentration can be estimated to be 2.4×10^{15} atoms/cm^3, which is much higher than the equilibrium concentration calculated from the flame temperature, 1200 K, and the oxygen excess ratio, 0.67. The spectral linewidth (0.01—0.04 mT) and the microwave power saturation of the H atoms depend on the location in the flame. These results strongly suggest that the line broadening and the spin relaxation are principally determined by the collision between the H atoms and the molecular oxygen.

Combustion in high-temperature flames is a complex reaction system which comprises branched-chain reactions carried by free atoms and free radicals as essential reaction intermediates.[1-4] These reaction intermediates have been studied by the optical absorption and emission spectrometric methods and incorporated in elucidating the flame structure.[1,5] Electron spin resonance (ESR) is a powerful technique for studying atomic and free radical intermediates in gas-phase reactions,[6,7] and it has been utilized, though not very extensively, for the study of combustion chemistry. Systematic studies have been reported by Russian workers,[8-21] who have succeeded in detecting the ESR spectra of several free atoms and free radicals from rarefied flames. Westenberg and Fristrom[22] and Eberius *et al.*[23] have studied H and O atoms generated in low-pressure C_2-hydrocarbon and hydrogen–air flat-flames by using the point-by-point sampling of combustion gases. Bennett *et al.*[24] have briefly communicated the detection of H atoms from hydrogen, methane, and propane free-burning flames under ordinary pressure set in an ESR resonant cavity (by the flame-in-cavity method). Later, Samoilov *et al.*[25-28] applied the flame-in-cavity method to study the kinetic aspects of H atoms, mostly in hydrogen–air free-burning flames, though they have not focussed their attention on the nature of the H atoms in the ESR observations. These studies as a whole show that the ESR technique is promising, but must still be developed for studying the intermediates in combustion reactions.

The present investigation is an extention of those by Bennett *et al.* and Samoilov *et al.* It is aimed at fully elucidating the ESR-spectroscopic nature of H atoms in methane–air free-burning flames by the flame-in-cavity method and giving a basis for utilizing this method for combustion-chemical studies. The methane–air flames are the simplest model of hydrocarbon combustion. The present experimental conditions allow us to detect only H atoms, because neither non-S-state atoms nor free radicals in the gas phase can be detected by ESR unless the pressure is so low that the collision broadening is effectively removed.[7,29] However, the study of the H atom concentration and distribution in the flames by themselves are interesting from the combustion-chemical point of view, since H atoms are known to be one of the major reaction intermediates in the fuel-rich combustion of hydrocarbons.[30]

Experimental

The burner used is a modified Bunsen burner, made of thin quartz tubes, the inner and outer tubes of which are 0.4 and 0.9 cm in diameter respectively. It was directly inserted into the cylindrical TE_{011} resonant cavity and fixed by means of a specially designed adapter. Cooling air could flow through a hole in the adapter when required. The burner could be moved up and down along the axis of the resonant cavity.

Methane of a 99.9% purity (research grade) was used as a fuel gas. Air flowed in from a conventional air compressor. These gases were controlled with a glass capillary-flow meter combined with a precise needle valve. Premixed flames were obtained by supplying methane–air mixed gas into the inner tube and then stabilized by letting secondary air flow into the outer tube. Diffusion flames were obtained by letting methane flow into the inner tube, and air into the outer tube. A rough estimate of the flame temperature was made by using a fine Pt–Rh thermocouple covered with quartz.

The ESR measurements were carried out with an X-band straight-detection-type spectrometer with a 100 kHz magnetic-field modulation. The resonant cavity was water-cooled when

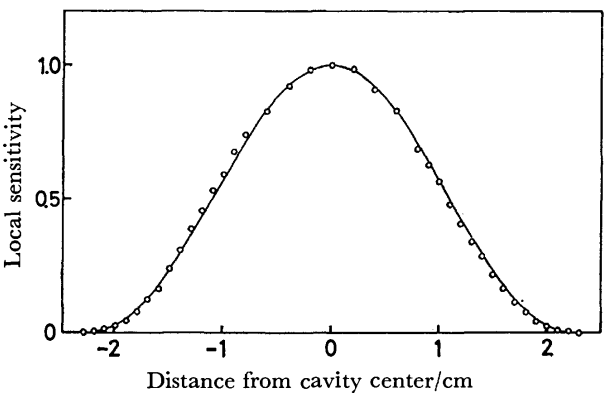

Fig. 1. Local sensitivity of ESR within the resonance cavity of TE_{011} mode.

the flame was set in it. The local sensitivity of the ESR within the resonant cavity was experimentally determined from the observed spectral intensity of a small piece of DPPH by moving it along the axis of the cavity. The sensitivity curve fit well with a sine-square function, as is shown in Fig. 1. The magnetic field inhomogeneity was checked by recording the sharp hyperfine lines of Fremy's salt in an aqueous solution; it was less than 0.002 mT within the effective volume in the cavity. The ESR saturation effect at a high microwave power level was studied at a 100 kHz magnetic-field modulation. The change in the power level was compensated for by an attenuator additionally set immediately before the crystal microwave detector, so that the crystal current was kept constant. This saturation measurement gives signals directly proportional to χ''.[31]

Results and Discussion

ESR Spectra from Diffusion Flames. A methane–air diffusion flame in a burner (with a flow rate of methane of 48 $cm^3\ min^{-1}$ and one of air of, 490 $cm^3\ min^{-1}$) formed a blue cone *ca.* 0.5 cm high and was stationary only for a limited methane/air ratio. The ESR signal recorded from this diffusion flame was composed of a pair of sharp lines with a separation of 51.0 mT around 330 mT, with a very sharp line at the center (g=2.005). The former is the spectrum due to H atoms. The latter spectrum was too weak for its nature to be studied, so that the entities responsible for this spectrum could not be identified. However, the inverted phase of the spectrum may be said to be due to the emission spectrum caused by the CIDEP effect of short-lived entities. Both the spectra were unquestionably due to unstable reaction intermediates in the flame, because they disappeared when the flame was extinguished.

The width (peak-to-peak of the derivative spectral curve) of the H atom spectrum was 0.15 mT; it remained unchanged when the burner was moved up and down along the cavity axis. In contrast, Bennett *et al.*[24] have reported the width of 0.08 mT for the H atoms in methane–air and propane–air diffusion flames. The difference in the width between the two observations is likely to result from the interaction of the H atoms with different concentrations of paramagnetic entities, such as carbons and soot compounds. The carbons and the soot compounds are the major products in the incomplete combustion of hydrocarbons, and they are generated in the reaction region of the diffusion flames.[32]

The intensity of the H-atom spectrum depended on the position of the burner in the cavity. The maximum intensity was obtained when the top of the luminous cone was situated at the center of the cavity. The variation in the intensity with the burner position almost completely followed the local sensitivity curve shown in Fig. 1. This indicates that the H atoms in the diffusion flame populate a limited region near the luminous cone, though the measurements were carried out for only a limited number of burner positions because of the poor signal-to-noise ratio.

ESR Spectra from Premixed Flames. The methane–air premixed flame, typically with a methane flow rate of 95 $cm^3\ min^{-1}$, a primary air flow rate of 600 $cm^3\ min^{-1}$, and a secondary air flow rate of 500 $cm^3\ min^{-1}$, in the burner was composed of a bell-shaped, luminous

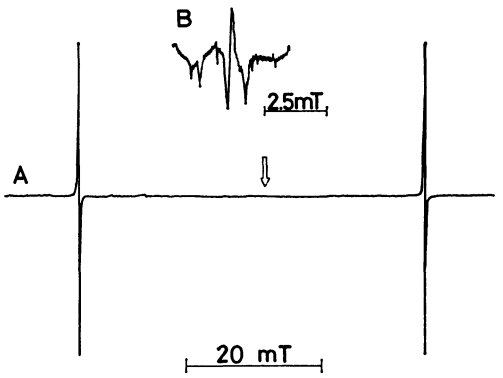

Fig. 2. ESR spectrum from a methane–air premixed flame (A) and the enlarged spectrum of the very weak signal whose resonance field is indicated by the arrow (B).

inner-cone flame *ca.* 1 cm high and of a faint-blue outer-cone flame. The outer-cone flame seemed to be partially quenched chemically and/or thermally on the wall of the outer quartz tube. The ESR signal from the premixed flame (Fig. 2) was qualitatively the same as that from the diffusion flame; it was composed of a pair of sharp lines due to H atoms and a very weak central, single line due to unidentified entities.

The linewidth and the intensity of the H atom spectrum varied depending on the position of the burner in the cavity. The microwave-power saturation behavior of the H-atom spectrum also depended on the burner position. These features of the premixed flame contrast with those of the diffusion flame.

The stationary premixed flame in the burner quartz tube could be obtained only within a limited methane/air composition range, that is, only for fuel-rich mixtures.

Concentration Profile of the H Atoms in the Premixed Flame. The intensity of the H-atom spectrum observed from the premixed flame is shown in Fig. 3 (open circles) as a function of the location of the burner in the cavity. The coordinate axis in the absolute concentration was

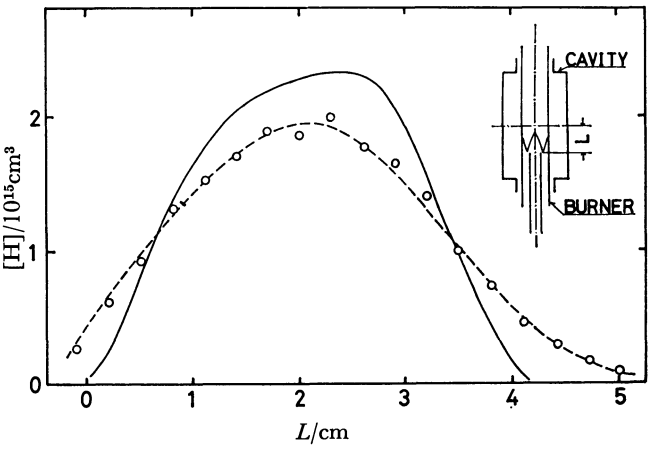

Fig. 3. The concentration profile of the hydrogen atom in a methane–air premixed flame: ○, observed signal intensities; solid line, true profile calculated by the deconvolution, dashed line, reconstructed apparent profile, where L is the distance between the cavity center and the top of the inner tube. (See Text for the details.).

calibrated with reference to the signal intensity of the molecular oxygen of the controlled concentration in the burner[7] by assuming that the H-atom concentration was uniform on a vertical cross-section plane of the burner. The maximum temperature was measured to be 1200 K, which was taken into account in the concentration calibration under the assumption that the temperature was uniform within the flame. The variation in the spectral intensity does not give the concentration profile of the H atom in the flame directly, because the local sensitivity curve of the resonant cavity (Fig. 1) causes the true concentration profile to deteriorate.

In order to get the true profile, the following deconvolution calculation was performed, using the Burger-Cittert method:[33]

$$g(L) = \int a(x)f(L-x)\mathrm{d}x, \qquad (1)$$

where $g(L)$ is the observed intensity variation, $a(x)$, the local sensitivity curve (Fig. 1), and $f(L)$, the true concentration profile. The $f(L)$ thus calculated is apparently narrower than $g(L)$, as is shown in Fig. 3 (solid curve). The convergence of the deconvolution treatment was checked by reconstructing $g(L)$, which agreed well with the original data (the reconstructed $g(L)$ is shown by the dashed curve in Fig. 3). The maximum local concentration of the H atoms shifts slightly compared with the maximum signal intensity; it is located 2.5 cm down-stream from the top of the inner tube. Comparing this with the 1 cm height of the luminous inner cone, one can see that the H atoms are located mostly in the down-stream region of the premixed flame.

The above concentration profile was obtained from a Bunsen flame confined in a narrow tube, not from a flat flame (a one-dimensional flame), for which the theoretical calculation of the flame structure is much easier. However, the present results obtained by the flame-in-cavity method are qualitatively consistent with the H atom concentration profile expected from the point-by-point sampling study for flat flames.[22,23]

In the present study, the flame was stationarily obtained for the oxygen excess ratio, α, in the narrow range of 0.63—0.75. The maximum H-atom concentration, *ca.* 2.4×10^{15} atoms/cm^2, was found for $\alpha=0.67$ in the fuel-rich region. This concentration amounts to only 0.4% of the total combustion products, in qualitative agreement with the previous results.[26,34] The equilibrium concentration of the H atoms for $\alpha=0.67$ and $T=1200$ K can be calculated to be 2×10^{-7} % of the total combustion products.[35] The observed H atom concentration is much higher than the equilibrium concentration, as has previously been reported for hydrogen-air flames.[28]

Linewidth of the H Atoms in the Premixed Flame. The spectral linewidth of the H atoms decreased monotonously, as is shown in Fig. 4; the width was 0.04 mT for the H atoms near the top of the inner tube, while it approached the instrumental resolution limit, 0.01 mT, in the down stream region of the flame. The spectral line was much narrower than that in the diffusion flame, anyway.

The H atoms possess an angular momentum of only

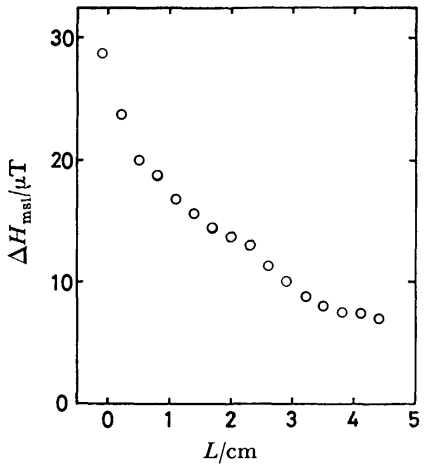

Fig. 4. The variation of the line width of the hydrogen atom in a methane–air premixed flame along the gas stream. L is the distance between the cavity center and the top of the inner tube.

spin. The collision with paramagnetic entities causes the relaxation of the spin states of the H atoms. The linewidth is determined by spin-exchange interaction between the H atoms themselves, magnetic interaction with other paramagnetic entities, magnetic-field inhomogeneity, and a broadening due to high-frequency magnetic-field modulation.[29] Among these factors, the spin-exchange interaction is unimportant, because the variation in the linewidth (Fig. 4) does not run parallel with the concentration profile of the H atoms shown in Fig. 3. There exist a variety of paramagnetic entities in hydrocarbon combustion, *i.e.*, stable molecular oxygen, reactive atomic oxygen, and several free radical intermediates. However, the H atoms are much more abundant than the atomic and free radical intermediates in fuel-rich combustion, so that the interaction between the H atoms and other paramagnetic reaction intermediates contributes little to the line broadening of the H-atom spectrum. On the other hand, the concentration of the molecular oxygen far exceeds that of the reaction intermediates. The interaction with the molecular oxygen will result in the spectral line-broadening of the H atoms. Although Westenberg and de Haas[29] have demonstrated that the molecular oxygen has little effect on the line-broadening when the oxygen concentration is comparable with the H-atom concentration, the linewidth variation observed from the present premixed flame can be attributed to the local concentration of the molecular oxygen, which is consumed mainly in the reaction zone of the premixed laminar flame and which gradually decays in concentration afterwards.[34] The reaction zone of the Bunsen flames is the luminous inner-cone flame.[32]

The variation in the linewidth along the gas stream in flames has been observed for the H atoms in hydrogen–air flames. This has been attributed to the variation in the molecular-oxygen concentration in the flames.[25] In the hydrogen–air flames, the linewidth changes drastically at the stoichiometric mixture ratios from 0.015 to 0.25 mT when the air/fuel ratio is increased. This also suggests the significant contribution of the

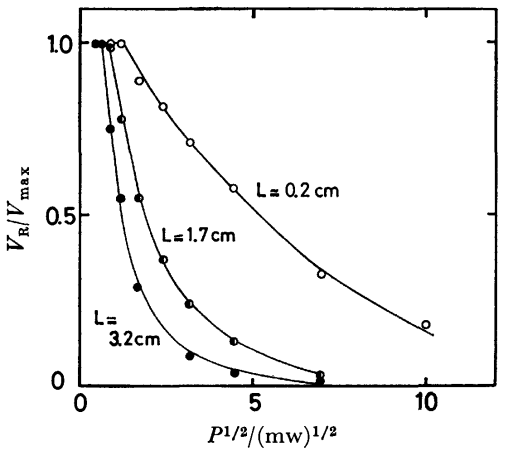

Fig. 5. Power saturation of the hydrogen atom in the different flame position of the methane–air premixed flame.

molecular oxygen to the line-broadening of the H atoms.[24]

Microwave-power Saturation of the H-atom Spectrum in the Premixed Flame. With an increase in the microwave power incident into the resonant cavity, the spectral lines of the H atoms became broader and the spectral intensity decreased simultaneously. The saturation of the spectral intensity is shown in Fig. 5 by simply plotting the peak-to-peak height of the spectrum as a function of the square-root of the microwave power. Although the analysis of the saturation curves is essentially complex because of the high-frequency field modulation (rapid passage condition), the plotted intensity is recorded so as to be parallel with χ'', as was mentioned in the Experimental section.

It is obvious from Fig. 5 that the H atoms in the luminous inner cone (reaction zone) are comparatively little saturated, while those in the down-stream region in the flame are readily saturated, with the increase in the microwave power. According to Westenberg and de Haas,[29] the spin-exchange collision between the H atoms and the molecular oxygen causes a remarkable reduction in the T_1 of the former. The observed dependence of the saturation behavior on the location in the flame is attributable to the local concentration of the molecular oxygen: the concentration initially decreases remarkably in the reaction zone, so that the T_1 of the H atoms becomes longer in down stream. This result is consistent with that of the linewidth variation.

This work was supported by the Toyota Foundation (77-1-174), to which the authors are very grateful.

References

1) G. J. Minkoff and C. F. H. Tipper, "Chemistry of Combustion Reactions," Butterworths, London (1962).
(2) "Comprehensive Chemical Kinetics," ed by C. H. Bamford and C. F. H. Tipper. Elsevier Scientific Publishing Co., Amsterdam, The Netherlands (1977), Vol. 17.
3) R. A. Strehlow, "Fundamentals of Combustion," International Textbook Co., Scranton, Pennsylvania (1968).
4) R. M. Fristrom and A. A. Westenberg, "Flame Structure," McGraw Hill, New York (1965).
5) A. G. Gaydon, "The Spectroscopy of Flames," 2nd ed, Chapman and Hall, London (1974).
6) R. S. Alger, "Electron Spin Resonance," John Wiley and Sons, New York (1968).
7) A. A. Westenberg, "Progress in Reaction Kinetics," Vol. 7, Pergamon Press, Oxford (1975).
8) V. N. Panfilov, Y. D. Tsuvetkov, and V. V. Voevodsky, *Kinet. Katal.*, **1**, 333 (1960).
9) V. P. Balakhin, Yu. M. Gershenzon, V. N. Kondrat'ev, and A. B. Nalbandyan, *Dokl. Akad. Nauk SSSR*, **154**, 883 (1964).
10) V. P. Balakhnin, Yu. M. Gershenzon, V. N. Kondrat'ev, and A. B. Nalbandyan, *Dokl. Akad. Nauk SSSR*, **154**, 1142 (1964).
11) V. P. Balakhnin, Yu. M. Gershenzon, and A. B. Nalbandyan, *Dokl. Akad. Nauk SSSR*, **172**, 375 (1967).
12) Z. G. Dzotsenidze, K. T. Oganesyan, G. A. Sachyan, and A. B. Nalbandyan, *Arm. Khim. Zh.*, **21**, 68 (1968).
13) V. V. Azatyan, L. A. Akopyan, and A. B. Nalbandyan, *Kinet. Katal.*, **2**, 940 (1961).
14) Yu. M. Gershenzon, O. N. Glebova, V. V. Azatyan, V. P. Balakhnin, and A. B. Nalbandyan, *Dokl. Akad. Nauk SSSR*, **168**, 851 (1966).
15) G. A. Sachyan and A. B. Nalbandyan, *Izv. Akad. Nauk SSSR, Ser. Khim.*, 1964, 1340.
16) Yu. M. Gershenzon, A. B. Nalbandyan, and G. A. Sachyan, *Dokl. Akad. Nauk SSSR*, **163**, 927 (1965).
17) G. A. Sachyan and A. B. Nalbandyan, *Arm. Khim. Zh.*, **19**, 135 (1966).
18) V. V. Azatyan, A. B. Nalbandyan, and E. N. Sarkisyan, *Dokl. Akad. Nauk SSSR*, **158**, 179 (1964).
19) E. N. Sarkisyan, V. V. Azatyan, and A. B. Nalbandyan, *Dokl. Akad. Nauk SSSR*, **168**, 1354 (1966).
20) V. V. Azatyan, Yu. M. Gershendyan, E. N. Sarkisyan, G. A. Sachyan, and A. B. Nalbandyan, 12th Int. Symp. Combust., Combust. Inst. (1969), p. 989.
21) V. Ya. Basevich, S. M. Kogarko, and G. A. Furman, *Izv. Adak. Nauk SSSR, Ser. Khim.*, 1971, 2191; 1972, 2139.
22) A. A. Westenberg and R. M. Fristrom, 10th Int. Symp. Combust., Combust. Inst. (1965), p. 473.
23) K. H. Eberius, K. Hoyerman, and H. GG. Wagner, 14th Int. Symp. Combust., Combust. Inst. (1973), p. 713.
24) J. E. Bennett, B. Mile, and R. Summers, *Nature*, **225**, 932 (1970).
25) I. B. Samoilov, O. B. Ryabikov, V. V. Zaichikov, Yu. M. Gershenzon, and L. A. Gussak, *Dokl. Akad. Nauk SSSR*, **205**, 1138 (1972).
26) L. A. Gussak, O. B. Ryabikov, I. B. Samoilov, Yu. M. Gershenzon, and A. P. Dement'ev, *Izv. Akad. Nauk SSSR, Ser, Khim.*, **2**, 298 (1972).
27) A. E. Vishnevskii, V. P. Bogoslavskii, and I. B. Samoilov, *Izv. Akad. Nauk SSSR, Ser. Khim.*, **4**, 749 (1976).
28) A. E. Vishnevskii, L. A. Gussak, and I. B. Samoilov, *Dokl. Akad. Nauk SSSR*, **232**, 363 (1977).
29) A. A. Westenberg and N. de Haas, *J. Chem. Phys.*, **51**, 5215 (1969).
30) R. M. Fristrom, *Chem. Eng. News*, 150, Oct. 14, (1963).
31) J. D. Goldsborough and M. Mandel, *Rev. Sci. Instr.*, **31**, 1044 (1961).
32) A. G. Gaydon, and H. G. Wolfhard, "Flames," 2nd ed, Chapman & Hall, London (1960).
33) H. C. Burger and P. H. Van Cittert, *Z. Phys.*, **79**, 722 (1932).
34) C. P. Lazzara, J. C. Biordi, and J. F. Papp, *Combust. Flame*, **21**, 371 (1973).
35) Y. Mizutani, "Nensho-Kogaku," Morikita Shutsupan, Tokyo (1977), pp. 61—67.

 © 1980 The Chemical Society of Japan Bull. Chem. Soc. Jpn., 53, 845—849 (1980)

An Ultrasonic Method for Determination of the Difference in Hard-Sphere Volume of Conformational Isomers

Masakatsu Aoi and Kiyoshi Arakawa*

Research Institute of Applied Electricity, Hokkaido University, Sapporo 060

(Received July 2, 1979)

An ultrasonic method for determining the difference in hard-sphere volume of conformational isomers from sound velocity has been worked out, its accuracy being improved by taking the temperature dependence of the effective hard-sphere diameter into account. The difference for 1,2-dibromoethane, 1,1,2-trichloroethane, methylcyclohexane, and 1,2-dichloroethane was determined. The fractions of volume differences $\Delta V/V$ in these liquids were found to be 4.5, 5, 11, and 19% for 1,2-dibromo-, 1,1,2-trichloroethane, methylcyclohexane, and 1,2-dichloroethane, respectively.

Determination of the effective hard-sphere volume of molecules in liquids is of interest from theoretical and practical points of view.[1] In most studies on conformational isomerism, *e.g.*, halogenated ethanes and cyclohexane derivatives,[2-6] the effect of difference in hard-sphere volume of conformers has been assumed to be negligibly small. Recently, questions with respect to this assumption have been raised.[1,7] The lack of a good experimental method is the main reason for the volume difference not being considered in these studies. Wyn-Jones *et al.*[7] adopted the ultrasonic absorption method, but its merit was restricted.

In the preceding paper,[1] we proposed for 1,2-dichloroethane (DCE) a method for determining the volume difference from sound velocity based on the recent development of the theory of solutions.[8] However, DCE is a special example: For the determination of ΔV it is necessary to know the magnitude of the hard-sphere volume for one of the two conformers from other sources. This is ascribed to the following property of the sample: The energy difference between the two isomers is zero in its liquid state,[2,4] the population ratio of the two conformers remaining unchanged with varying temperature. Further, the effect of relaxational processes was not taken into consideration.

We have improved the method and applied it to cases in which the energy difference between conformers is not zero, enhancing the accuracy by taking the temperature dependence of the effective hard-sphere diameter[9] into account. 1,2-dibromoethane (DBE), 1,1,2-trichloroethane (TCE), cyclohexane (CH), and methylcyclohexane (MeCH) were investigated. It was found that the method is useful for determining the difference in hard-sphere volume of conformers.

Method of Analysis

Formula for Isothermal Compressibility Derived from the Lebowitz Equation of Binary Mixtures.[1] An equilibrium mixture of conformational isomers is considered to be a hard-sphere mixture with two components. We obtained a formula for isothermal compressibility of the equilibrium mixture by means of the Lebowitz equation. The outline of the theoretical procedure is given here, the details being reported.[1] An analytical solution of the Percus-Yevick equation for binary hard-sphere mixtures[8] is

$$\frac{p}{kT}=\frac{1}{(1-\xi)^3}\left[(\rho_1+\rho_2)(1+\xi+\xi^2)-\frac{18}{\pi}\eta_1\eta_2(R_1-R_2)^2\times\{R_1+R_2+R_1R_2(\eta_1R_1^2+\eta_2R_2^2)\}\right],$$

$$\xi=\frac{\pi}{6}(\rho_1R_1^3+\rho_2R_2^3), \tag{1}$$

where p is pressure, k Boltzmann constant, T temperature, ξ packing fraction, $\rho_i=N_i/V$ number density, $\eta_i=\pi\rho_i/6$, and R_i hard-sphere diameter of the i-th component. Let us express R_i by

$$R_1=R_0,\quad R_2=R_0(1+\delta), \tag{2}$$

considering that δ is smaller than 0.1.[1]

The isothermal compressibility $\kappa_T=-(1/V)(\partial V/\partial p)_T$ is derived from Eq. 1 as

$$\kappa_{T,0}=\frac{V(1-\xi)^4}{RT(1+2\xi)^2}\left[1-\frac{\pi x_1x_2R_0^3\rho\delta^2}{2(1+2\xi)^2}\left\{4+2\xi+\frac{\pi}{2}R_0^3\rho+\delta(2+\xi+\frac{\pi}{2}R_0^3\rho(1+2x_2))+\delta^2\frac{3\pi}{2}R_0^3\rho x_2+\delta^3\frac{\pi}{2}R_0^3\rho x_2\right\}\right]^{-1}, \tag{3}$$

where suffix 0 indicates κ_T for fluids consisting of hard-sphere molecules, R gas constant, V molar volume, and x_i mole fraction of the i-th component. The second term in square brackets is smaller than 0.01.[1] Equation 3 can thus be approximated by

$$\kappa_{T,0}=\frac{V(1-\xi)^4}{RT(1+2\xi)^2}, \tag{4}$$

where ξ is the fraction of hard-sphere volumes of all molecules to molar volume of the liquid and is expressed by

$$\xi=\frac{\pi\rho(N_1R_1^3+N_2R_2^3)}{6N_A}=\frac{\rho(N_1v_1+N_2v_2)}{N_A}=\frac{\pi}{6}a^3\rho=\rho v_a,$$

$$\frac{N_1R_1^3+N_2R_2^3}{N_A}=a^3. \tag{5}$$

Here N_i is number of the i-th component, N_A Avogadro number, $\rho=N_A/V$, $v_i=\pi R_i^3/6$ hard-sphere volume of the i-th component, $v_a=\pi a^3/6$ average hard-sphere volume, and a the "average hard-sphere diameter."

For the usual fluids, it is necessary to take the effect of attractive forces into consideration. κ_T is expressed in this case by[1]

$$\kappa_T=\left[\frac{RT(1+2\xi)^2}{V(1-\xi)^4}-\frac{2}{V}(\Delta H_v-RT)\right]^{-1}, \tag{6}$$

where ΔH_v is enthalpy of vaporization.

Determination of Average Hard-Sphere Volume and Volume, Difference between Conformers. From adiabatic compressibility κ_S determined from sound velocity and density data, we obtain

$$\kappa_T = \kappa_S + \frac{TV\alpha^2}{C_p}, \quad \kappa_S = \frac{1}{dv^2}, \tag{7}$$

where α is thermal expansion coefficient of the liquid, C_p molar heat capacity at constant pressure, d density, and v sound velocity. When the values of T, V, κ_T, and ΔH_v are substituted into Eq. 6, the value of ξ and subsequently the average hard-sphere volume can be evaluated.

The values of V and N_i in Eq. 5 vary with temperature. The population ratio of two conformational isomers, N_2/N_1, is given by

$$\frac{N_2}{N_1} = \exp(-\Delta G/RT) = A\exp(-\Delta H/RT), \tag{8}$$

where ΔG is free energy difference between conformers, ΔH enthalpy difference, and A constant. Thus, if we know ξ from sound velocity data at various temperatures, we can estimate the hard-sphere volumes of each conformer, combining the temperature dependence of N_2/N_1 with that of ξ.

The total compressibility for an equilibrium system is given by

$$\kappa_T = \kappa_{T,\infty} + \kappa_{T,r}, \tag{9}$$

where $\kappa_{T,\infty}$ is an instantaneous part and $\kappa_{T,r}$ a relaxational one.[6,10] According to the magnitude of ultrasonic relaxation frequency f_r, the procedure for determination of average hard-sphere volumes can be classified into: (a) for CH and MeCH[6,11,12] in which f_r is much smaller than the frequency f used for the measurement of sound velocity, and (b) for DCE, DBE, and TCE.[6,7,13,14]

When $f \gg f_r$, the contribution of $\kappa_{T,r}$ to κ_T can be ignored and Eq. 9 is reduced to

$$\kappa_T = \kappa_{T,\infty}. \tag{10}$$

Substituting the value of κ_T into Eq. 6, we can determine the magnitude of ξ. In Eq. 5, the value of the average hard-sphere volume is related to hard-sphere volumes of components v_1 and v_2, and also to the population ratio of isomers. The temperature dependence of the average hard-sphere volume is chiefly ascribed to the temperature dependence of the population ratio, and the molar volume difference ΔV can be evaluated from Eqs. 5 and 8, where

$$\frac{\Delta V}{V} = \frac{N_A}{\xi V}(v_2 - v_1) = \frac{v_2 - v_1}{v_a}. \tag{11}$$

When $f \ll f_r$, the contribution of $\kappa_{T,r}$ to κ_T should be considered. According to Hall,[15] $\kappa_{T,r}$ is given by

$$\kappa_{T,r} = \frac{V(\Delta V/V)^2}{2RT\{1+\cosh(\Delta G/RT)\}}, \tag{12}$$

where ΔV is identical with that defined by Eq. 11.[16] Substituting the right hand sides of Eqs. 6 and 12 into Eq. 9, the following expression of κ_T is obtained.

$$\kappa_T = \left[\frac{RT(1+2\xi)^2}{V(1-\xi)^4} - \frac{2}{V}(\Delta H_v - RT)\right]^{-1} + \frac{V(\Delta V/V)^2}{2RT\{1+\cosh(\Delta G/RT)\}}. \tag{13}$$

The procedure for determining hard-sphere volumes of isomers starting from Eq. 13 is the same as in the preceding case.

Temperature Dependence of the Effective Hard-Sphere Volume. For the determination of hard-sphere volumes for conformers described above, the temperature dependence of the average hard-sphere volume is attributed to that of the population ratio only. However, we should consider also the contribution from the temperature dependence of the effective diameter of hard-sphere.[9,17-19]

According to the perturbation theory of fluid by Barker and Henderson, the "softness" of the hard core of a molecule is taken into consideration[9] and the effective hard-sphere diameter becomes

$$a_t = \int_0^\sigma [1-\exp\{-u(r)/kT\}]dr, \tag{14}$$

where $u(r)$ is an intermolecular pair potential and $u(\sigma)=0$. The temperature coefficient of a_t, l, becomes

$$l = \frac{1}{a_t}\frac{da_t}{dT} = -\frac{\int_0^\sigma \frac{u(r)}{kT^2}\exp\{-u(r)/kT\}dr}{\int_0^\sigma [1-\exp\{-u(r)/kT\}]dr}. \tag{15}$$

The Lennard-Jones (6—12) potential is chosen as $u(r)$, and $l(l<0)$ is computed numerically. Thus the effective hard-sphere volume at temperature T is expressed by

$$v_T = v_0(1+\alpha_t\Delta T) \text{ and } \alpha_t = 3l, \tag{16}$$

where v_0 is the value at T_0 as reference temperature and ΔT the deviation from T_0.

Experimental

Sound velocity was measured with an interferometer working at 3 MHz[20] and density with a pycnometer. Measurements were carried out at temperatures in the range 15—45 °C, the temperature being controlled within ±0.05 °C. Samples were carefully purified before measurements. The accuracy of v is ±0.3 m/s. Values of d and v compared with other data[21] at 20 °C are given in Table 1.

Results

Values of d, v, κ_S, and κ_T determined in the present experiment for DBE, TCE, CH, and MeCH are summarized in Table 2. Values of thermodynamic quantities required for the determination of κ_T and v_a, C_p, α, and ΔH_v are summarized in Table 3, together with energy difference ΔH between conformers for these liquids.

In the case of CH, only the chair form exists at room temperature since the energy difference is as large as 22 kJ/mol.[3] It can be regarded as one component system in the temperature range of the present study.

The temperature coefficient of the effective hard-sphere diameter was calculated by Eq. 15 and is plotted against ε/k at 25 °C in Fig. 1 (ε: an energy parameter in $u(r)=4\varepsilon[(\sigma/r)^{12}-(\sigma/r)^6]$). The curve is useful for

Table 1. Comparison of d and v with other data at 20 °C

	d / g cm^{-3}		v / m s^{-1}	
	This work	Ref.	This work	Ref.
DBE	2.1808_2	2.1804[a]	1006.8	1006.9[b]
		2.17988[b]		1007.9[c]
		2.18002[b]		
		2.18006[d]		
TCE	1.4409_8	1.4405[a]	1166.0	1176[e]
		1.4411[a]		
CH	0.7783_8	0.7783[a]	1279.9	1280.5[b]
		0.77853[a]		1279.1[c]
		0.77858[b]		
		0.77849[f]		
MeCH	0.7691_1	0.76944[a]	1237.0	1247[g]
		0.76936[a]		
		0.76925[a]		

a) Ref. 21. b) Ref. 26. c) R. Fischer, H. Posch, und F. Kohler, *Monatsh. Chem.*, **96**, 1865 (1965). d) A. Neckel und H. Volk, *Monatsh. Chem.*, **89**, 754 (1958). e) R.A. Padmanaban, *J. Sci. Industr. Res.*, **19B**, 336 (1960). f) H. Loiseleur, J-C. Merlin, et R.A. Paris, *J. Chim. Phys.*, **64**, 634 (1967). g) Ref. 11.

practical purposes. The variation of T from 0 to 100 °C shows a very slight difference in l, and l can be regarded as practically independent of the variation of T in the range 15—45 °C. The values of ε/k used for the estimation of l are 330, 430, 400, 330, and 330 K for DCE, DBE, TCE, CH, and MeCH,[22-24] respectively. When ε/k is larger than 300 K, the variation of l is small. The temperature dependence of the effective hard-sphere volume was estimated by using Eq. 16 (T_0: 25 °C) with the value of l given in Fig. 1.

The magnitudes of v_a, v_i, and $\Delta V/V$ for MeCH ($f \gg f_r \simeq 100$ kHz[6,11,12]) were determined by means of Eqs. 5, 6, 8, and 11. For DBE ($f \ll f_r$) and TCE ($f < f_r \simeq 16$ MHz at 25 °C[6,7]), those of v_a, v_i, and $\Delta V/V$ were determined by means of Eqs. 5, 8, 11, and 13. In the case of DCE[25] ($f \ll f_r$), the values of v_a and $\Delta V/V$ were calculated by means of Eqs. 5, 11, and 13 and the reported data.[1] For CH which is regarded as one component system, the average hard-sphere volume v_a was determined by the use of Eqs. 5 and 6. The results

Table 3. Thermodynamic parameters at 25 °C

	α[a] / 10^{-3} K^{-1}	C_p / J mol^{-1} K^{-1}	ΔH_v / kJ mol^{-1}	ΔH / kJ mol^{-1}
DBE	0.9665	134.9[b,c]	43.27[e,d]	3.10[e,f]
TCE	1.0851	148.0[g,h]	40.28[d]	1.05[e,f]
CH	1.2318	155.3[b]	33.22[c]	22.0[i]
MeCH	1.1403	184.5[c,j]	35.38[c,k]	7.11[i]

a) Observed values in this study. b) Ref. 26. c) Ref. 21. d) J. Laynez and I. Wadsö, *Acta Chem. Scand.*, **26**, 3148 (1972). e) Ref. 2. f) Ref. 4. g) R. W. Crowe and C. P. Smyth, *J. Am. Chem. Soc.*, **72**, 4009 (1950). h) R.J. L. Andon, J. F. Counsell, D. A. Lee, and J. F. Martin, *J. Chem. Soc., Faraday Trans. 1*, **69**, 1721 (1973). i) Ref. 3. j) Ref. 11. k) T. J. V. Findlay, *J. Chem. Eng. Data*, **14**, 229 (1969).

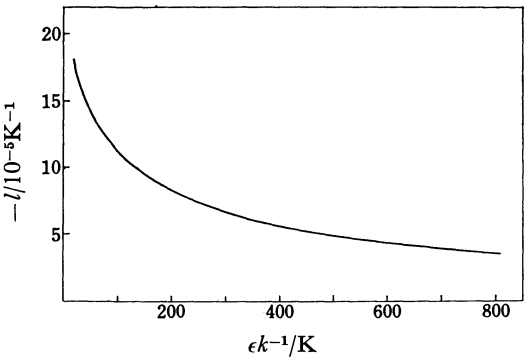

Fig. 1. The plot of l *vs.* ε/k at 25 °C.

Table 2. Values of d, v, κ_S and κ_T

		Temp/°C						
		15	20	25	30	35	40	45
d / g cm^{-3}	DBE	2.1912_0	2.1808_2	2.1703_7	2.1599_7	2.1493_8	2.1389_1	2.1287_2
	TCE	1.4487_3	1.4409_8	1.4332_8	1.4256_6	1.4178_1	1.4101_2	1.4022_9
	CH	0.7830_7	0.7783_8	0.7736_6	0.7689_9	0.7642_1	0.7594_7	0.7546_4
	MeCH	0.7734_3	0.7691_1	0.7647_7	0.7605_2	0.7561_3	0.7517_9	0.7473_9
v / m s^{-1}	DBE	1019.9	1006.8	993.9	981.2	968.4	955.5	942.7
	TCE	1183.6	1166.0	1149.2	1131.6	1114.4	1097.2	1080.1
	CH	1304.9	1279.9	1254.0	1229.1	1204.1	1181.4	1158.0
	MeCH	1259.5	1237.0	1214.9	1193.0	1171.2	1149.7	1128.9
κ_S / 10^{-11} Pa^{-1}	DBE	43.87	45.24	46.64	48.08	49.61	51.20	52.86
	TCE	49.28	51.04	52.83	54.77	56.80	58.91	61.12
	CH	75.00	78.42	82.20	86.08	90.26	94.34	98.82
	MeCH	81.51	84.97	88.59	92.39	96.41	100.64	104.99
κ_T / 10^{-11} Pa^{-1}	DBE	60.98	62.72	64.51	66.34	68.26	70.25	72.30
	TCE	70.38	72.63	74.90	77.34	79.86	82.48	85.20
	CH	105.97	109.75	113.90	118.15	122.69	127.14	132.00
	MeCH	107.88	111.65	115.56	119.65	123.96	128.46	133.09

Table 4. Average hard-sphere volumes and volume differences at 25 °C

	$\frac{v_a}{10^{-24}\,cm^3}$	$\Delta V/V$
DCE[a]	69.4_2	-0.19
DBE	76.4_0	-0.04_5
TCE	80.9_9	-0.05
MeCH	108.9_0	-0.11
CH	90.1_3	

a) Calculated by use of the previous data.

for v_a and $\Delta V/V$ thus obtained are summarized in Table 4.

Discussion

Examination of the Former Results Obtained by the Ultrasonic Absorption Method. In studies on conformational isomerism by means of the ultrasonic absorption method, it has been assumed so far that $(\Delta V/V)(C_p/\Delta H\alpha) \ll 1$,[6] and the effect of ΔV is negligible. However, we realized that there is no satisfactory evidence for the assumption, leading to an examination of the assumption. Wyn-Jones *et al.*[7] suggested that the assumption is not suitable when the value of $\Delta V/V$ is of the order of 0.1% or larger. For DBE, TCE, and MeCH, the magnitudes of $(\Delta V/V)(C_p/\Delta H\alpha)$ are estimated to be 2.0, 6.5, and 2.5, respectively, by using the data in Tables 3 and 4, indicating that the assumption is inadequate. For DCE, the value of ΔH in liquid state is zero;[2,4] the assumption does not hold.

According to Wyn-Jones *et al.*, the values of $\Delta V/V$ in conformational isomerism are *ca.* 1—3% for TCE in various solvents, and surmised to be 6% for pure liquid of TCE, the error of the estimation of ΔV being *ca.* 50%.[7] In the present study, the error might be small (<20%) as compared with that of the ultrasonic absorption method.

Consideration on the Magnitudes of v_1 *and* ΔV. All the values of $\Delta V/V$ are negative (Table 4). The value of v_1 for a stable isomer is larger than that of v_2 for another isomer. v_1 corresponds to the *anti*-form for DCE, DBE, and TCE, and to the equatorial form for MeCH.

The value of $\Delta V/V$ for DCE is found to be larger than that for DBE. This is reasonable, according to the suggestion by Findenegg *et al.*[26] based on the cell theory. For TCE, it is 5% in the present study, 6% by means of the ultrasonic absorption method of Wyn-Jones *et al.*,[7] and 4% from the pressure effect of infrared spectroscopy reported by Christian *et al.*[27]

For MeCH, the value of $\Delta V/V$ becomes 11% and the hard-sphere volume for the equatorial form is larger than that for the axial one. No data for MeCH directly correlated with our present result has been reported so far. It was suggested from density data[7,11] of similar substances that the volume of the equatorial form is larger than that of the axial one. For instance, *cis*-1,3-dimethylcyclohexane has two equatorial methyl groups in its chair form and *trans*-stereoisomer has an equatorial group together with an axial methyl group. The difference in density between the *trans*- and *cis*-stereoisomers is supposed to correspond to the volume difference between the axial and the equatorial form of conformational isomers for MeCH. The volume difference between stereoisomers for 1,3-dimethylcyclohexane is estimated to be 2.2%.[7] Though the volume difference between separable stereoisomers is not the same as that between conformational isomers, it is certain that the volume of the equatorial form is larger than that of the axial one. Our present result for MeCH confirms this.[27]

References

1) M. Aoi and K. Arakawa, *Bull. Chem. Soc. Jpn.*, **47**, 2639 (1974).
2) S. Mizushima, "Structure of Molecules and Internal Rotation," Academic Press, New York (1954), Chaps. 1—3; K. Kuratani and S. Mizushima, *J. Chem. Phys.*, **22**, 1403 (1954).
3) E. L. Eliel, N. L. Allinger, S. J. Angyal, and G. A. Morrison, "Conformational Analysis," Interscience Publ., New York (1967), Chaps. 1, 2.
4) N. Sheppard, *Adv. Spectrosc.*, **1**, 288 (1959).
5) R. J. Abraham and K. G. R. Pachler, *Mol. Phys.*, **7**, 165 (1964); R. J. Abraham, L. Cavalli, and K. G. R. Pachler, *ibid.*, **11**, 471 (1966).
6) J. Lamb, "Physical Acoustics," ed by W. P. Mason, Academic Press, New York (1965), Vol. 2A, Chaps. 4, 5.
7) E. Wyn-Jones and W. J. Orville-Thomas, "Molecular Relaxation Processes," Chem. Soc. Spec. Publ., No. 20 (1966), p. 209; K. R. Crook and E. Wyn-Jones, *J. Chem. Phys.*, **50**, 3445 (1969); K. R. Crook, E. Wyn-Jones, and W. J. Orville-Thomas, *Trans. Faraday Soc.*, **66**, 1597 (1970).
8) J. L. Lebowitz and J. S. Rowlinson, *J. Chem. Phys.*, **41**, 133 (1964); J. L. Lebowitz, *Phys. Rev. A*, **133**, 895 (1964).
9) J. A. Barker and D. Henderson, *J. Chem. Phys.*, **47**, 4714 (1967); K. Arakawa, "Kagaku Sosetsu, No. 11, Ions and Solvents," (1976), p. 13.
10) When the relaxation mechanism exists in the system studied, the compressibility determined in the frequency range higher than f_r is denoted by $\kappa_{T,\infty}$ and that in the reverse side by κ_T. The compressibility in the equilibrium state is written by $\kappa_T=\kappa_{T,\infty}+\kappa_{T,r}$, as in Eq. 9, where $\kappa_{T,\infty}$ is considered to be equal to Eq. 6.
11) J. E. Piercy, *J. Acoust. Soc. Am.*, **33**, 198 (1961); J. E. Piercy and S. V. Subrahmanyam, *J. Chem. Phys.*, **42**, 4011 (1965).
12) M. E. Pedinoff, *J. Chem. Phys.*, **36**, 777 (1962).
13) D. Sette, *J. Chem. Phys.*, **19**, 1337 (1951).
14) J. E. Piercy, *J. Chem. Phys.*, **43**, 4066 (1965).
15) L. Hall, *Phys. Rev.*, **73**, 775 (1948).
16) In the Hall theory, ΔV is the difference between the molar volumes of the two species and V is the molar volume of the total fluid. Here, the expression $\Delta V/V$ becomes identical with the ratio of the difference in hard-sphere volume of conformers to the average hard-sphere volume, giving Eq. 11.
17) S. W. Mayer, *J. Phys. Chem.*, **67**, 2160 (1963).
18) E. Wilhelm, *J. Chem. Phys.*, **58**, 3558 (1973).
19) P. R. Bienkowski and K-C. Chao, *J. Chem. Phys.*, **62**, 615 (1975).
20) O. Kiyohara and K. Arakawa, *Bull. Chem. Soc. Jpn.*, **43**, 975 (1970); *ibid.*, **43**, 3037 (1970).
21) J. Timmermans, "Physico-Chemical Constants of Pure Organic Compounds," Elsevier Publ., New York, Vol. 1, (1950); Vol. 2 (1965).
22) A. Neckel and H. Volk, *Z. Elektrochem.*, **62**, 1104 (1958).

23) J. O. Hirschfelder, C. F. Curtiss, and R. B. Bird, "Molecular Theory of Gases and Liquids," John Wiley and Sons, New York (1964), p. 1109.
24) E. Wilhelm and R. Battino, *J. Chem. Phys.*, **55**, 4012 (1971); *J. Chem. Thermodyn.*, **3**, 379 (1971).
25) In the previous method[1] for determination of volume difference for DCE, the procedure of analysis was carried out by using Eq. 6 instead of Eq. 13, which is inadequate according to the present analysis since $f \ll f_r$. We have calculated the values of v_a and $\Delta V/V$ for DCE by using Eq. 13, and the revised results are given in Table 4. The method of analysis in the present study is improved as shown in Eq. 13 including an additional term to Eq. 6, when $f \ll f_r$.
26) G. H. Findenegg and F. Kohler, *Trans. Faraday Soc.*, **63**, 870 (1967); E. Wilhelm, R. Schano, G. Becker, G. H. Findenegg, and F. Kohler, *ibid.*, **65**, 1443 (1969).
27) S. D. Christian, J. Grundnes, and P. Klaboe, *J. Chem. Phys.*, **65**, 496 (1976); *J. Am. Chem. Soc.*, **97**, 3864 (1975).

Polymerization of Silicic Acid Adsorbed on Iron(III) Hydroxide

Takushi YOKOYAMA, Tatsuo NAKAZATO,** and Toshikazu TARUTANI*

Department of Chemistry, Faculty of Science, Kyushu University 33, Hakozaki, Higashi-ku, Fukuoka 812

(Received July 9, 1979)

Adsorption of silicic acid on iron(III) hydroxide from aqueous solution and polymerization of adsorbed silicic acid were affected by pH, concentration of silicic acid before and after adsorption, or the relative amount of silicic acid and iron(III) hydroxide. The amount of adsorbed silicic acid and the rate of its polymerization were maximum at pH 9. The polymerization reaction of silicic acid on the surface of iron(III) hydroxide was found to consist of two steps: (1) polymerization of adsorbed monosilicic acid and (2) polymerization between monosilicic acid in the solution and silicic acid species already present on the surface of iron(III) hydroxide, giving a three-dimensional gel structure.

Iron(III) hydroxide removes silicic acid from a solution in a high amount by adsorption or coprecipitation reaction. Kato[1] reported that dissolved silica is controlled by the oxidation-reduction cycle of iron and manganese in lake water. Ferruginous sinters deposited from hot spring waters contain a large amount of silica. However, few reports have been published with respect to the behavior of silicic acid adsorbed on or coprecipitated with iron(III) hydroxide.

Harder and Flehmig[2] found the formation of quartz in iron(III) hydroxide-silica-precipitates. Kojima and Tarutani[3] reported that monosilicic acid adsorbed on iron(III) hydroxide polymerizes in a short period of time. Herbillon and Vinh An[4] studied precipitates formed by the addition of iron(III) and iron(II) chloride solutions to sodium silicate solutions. Their results indicate that Si is incorporated into the precipitate by two distinct processes. When SiO_2/Fe_2O_3 mole ratio (MR) was less than 0.1, Si was chemisorbed. In the range MR$>$0.1, silica polymerized as a separate phase.

In this work, factors controlling the amount of silicic acid adsorbed on iron(III) hydroxide and the polymerization of adsorbed silicic acid were studied. The term "monosilicic acid" refers to the total sum of monosilicic acid, H_4SiO_4, and its conjugate base, $H_3SiO_4^-$, the term "polysilicic acid" refers to dimer and larger polymer species.

Experimental

Samples and Reagents. All the reagents were of analytical reagent grade. A stock solution of monosilicic acid was prepared by dissolving silica gel (Mallinckrodt Chemical Works) in sodium hydroxide solution. Monosilicic acid solution of desired concentration was prepared by diluting stock solution.

Iron(III) hydroxide was precipitated by adding sodium hydroxide solution to iron(III) chloride solution and then washed with distilled water. Iron(III) hydroxide was prepared immediately before each experiment.

Procedure. Monosilicic acid solution (500 ml) of an appropriate concentration was adjusted to the desired pH with hydrochloric acid or sodium hydroxide solution. A known amount of iron(III) hydroxide was then introduced into the solution and the pH of the solution was readjusted. The suspension was stirred vigorously with a magnetic stirrer. The variation of pH of the suspension was maintained in the range of $\pm$0.1 pH by adding hydrochloric acid or sodium hydroxide solution. Adsorption experiments were carried out in a thermostated bath at 25 °C. After 5 h, an aliquot of suspension was pipetted and filtered through a membrane filter having pores of 0.1 μm. The concentration of monosilicic acid in the filtrate was determined by colorimetry. The iron(III) hydroxide on the membrane filter was dissolved with 1 mol dm^{-3} hydrochloric acid, the resulting solution being filtered and diluted to 50 ml with distilled water (solution A). After iron(III) ion in an aliquot of the solution A had been removed by treating with cation exchange resin, the amount of monosilicic acid was determined by colorimetry and the total silicic acid was determined after decomposition of polysilicic acid with alkali. Silica larger than 0.1 μm remaining on the filter was determined by colorimetry after the filter had been ashed and the silica was fused with sodium carbonate. Iron(III) ion concentration in solution A was determined by colorimetry.

The size distribution of polysilicic acids formed on the surface of iron(III) hydroxide was determined by gel chromatography. After iron(III) ion in solution A had been eliminated by treating with cation exchange resin, the pH of the solution was adjusted to 2 and silicic acid was chromatographed on an 1$\times$60 cm column of Sephadex G-25 according to the procedure of Shimada and Tarutani.[5] After the effluent had been collected with a fraction collector, the amounts of silicic acid in the fractions were measured by colorimetry after decomposition of polysilicic acid with alkali.

The following symbols are used. Si/Fe(MR): the mole ratio of monosilicic acid and iron(III) hydroxide in the initial solution, Si(M): the amount of monosilicic acid in solution A, Si($<$0.1): the total amount of silicic acid (smaller than 0.1 μm) in solution A, Si($>$0.1): the amount of silica larger than 0.1 μm remaining on the filter, Si(T): the sum of Si($<$0.1) and Si($>$0.1), Fe(A): the amount of iron(III) ion in solution A, Si(T)/Fe(A): the mole ratio of silicic acid adsorbed and iron(III) hydroxide, Si(M)/Si(T): the mole ratio of monosilicic acid and total silicic acid adsorbed on iron(III) hydroxide. This ratio indicates the degree of polymerization of adsorbed silicic acid.

Results

The Kinetics of Adsorption. The kinetic data for adsorption of silicic acid on iron(III) hydroxide at three Si/Fe(MR) ratios and at pH 9 are shown in Fig. 1. The initial concentration of monosilicic acid was 300 ppm (SiO_2). A rapid decrease in monosilicic acid concentration occurred in one hour, the rate of adsorption of silicic acid then becoming relatively slow with

** Present address: Hirata-machi, Naze-shi, Kagoshima 894.

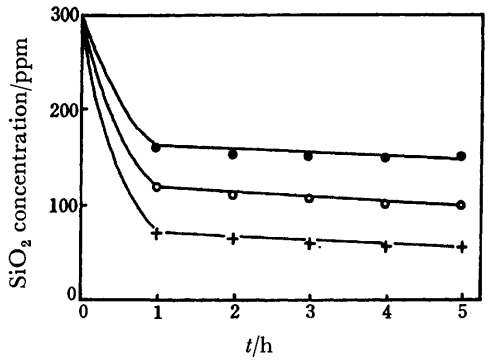

Fig. 1. The rate of adsorption of monosilicic acid by iron-(III) hydroxide at pH 9.
Initial monosilicic acid concentration: 300 ppm.
Si/Fe(MR): —●— 1.31, —○— 0.65, —+— 0.44.

time. Since monosilicic acid did not polymerize in the solution of 300 ppm within 5 h, only monosilicic acid was adsorbed by iron(III) hydroxide.

Effect of pH. Adsorption of silicic acid by iron(III) hydroxide and polymerization of adsorbed silicic acid were examined in the pH range 4—12. The results are shown in Figs. 2 and 3. Si(T)/Fe(A) ratio increased in the pH range 4—9, declining above pH 9. The maximum adsorption with respect to pH occurred at pH 9 (Fig. 2). Si(M)/Si(T) ratio decreased with increasing pH up to 9, increasing with further increase in pH. This indicates that the polymerization of silicic acid adsorbed on iron(III) hydroxide is most rapid at pH 9. In 300 ppm monosilicic acid solution, monosilicic acid adsorbed polymerized in the pH range 4—12. In 100 ppm monosilicic acid solution, the concentration being lower than the solubility of amorphous silica, monosilicic acid adsorbed polymerized in weakly alkaline solutions.

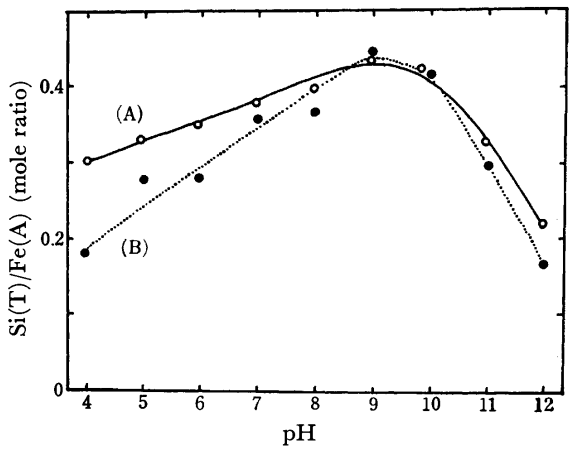

Fig. 2. The effect of pH on the amount of silicic acid adsorbed on iron(III) hydroxide after 5 h.
Initial monosilicic acid concentration: (A) 300 ppm, (B) 100 ppm.
Si/Fe(MR): (A) 0.63, (B) 1.31.

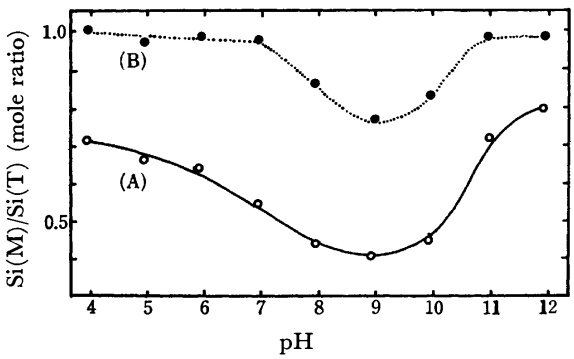

Fig. 3. The effect of pH on the degree of polymerization of silicic acid adsorbed on iron(III) hydroxide after 5 h.
The experimental conditions are the same as those of Fig. 2.

Distribution of Particle Size of Polysilicic Acids. As shown in Fig. 3, the amount of polysilicic acid formed on the surface of iron(III) hydroxide differs with pH. No information is available on the change in particle size of the polymers.

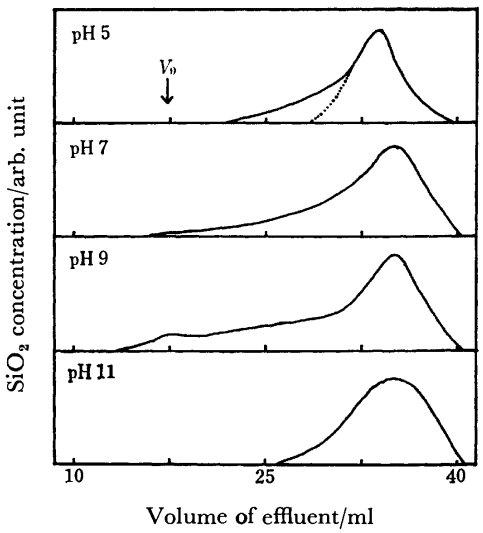

Fig. 4. Gel chromatograms for silicic acid adsorbed on iron(III) hydroxide at various pH after 5 h.
Initial monosilicic acid concentration: 300 ppm.
Si/Fe(MR): 0.63.

Silicic acid adsorbed on iron(III) hydroxide at various pH was chromatographed on Sephadex G-25 column. Elution curves for silicic acid are shown in Fig. 4. The dotted line is the elution curve for monosilicic acid, the position V_0 being the elution volume of Blue Dextran 2000, which does not seem diffusible in the gel phase. Polysilicic acid is eluted between the position V_0 and the elution position of monosilicic acid, the elution volume of polymer decreasing with increasing particle size. Polymers larger in size than those in the possible separation range for the gel are eluted together at V_0. From the elution curves we see that the growth of polymers is most rapid at pH 9.

Effect of Initial Concentration of Monosilicic Acid. Figure 5 shows the variation of Si(T)/Fe(A) and Si(M)/Si(T) ratios with initial concentration of monosilicic acid, the former increasing with an increase in the initial concentration of monosilicic acid and the latter decreasing. The amount of adsorbed silicic acid

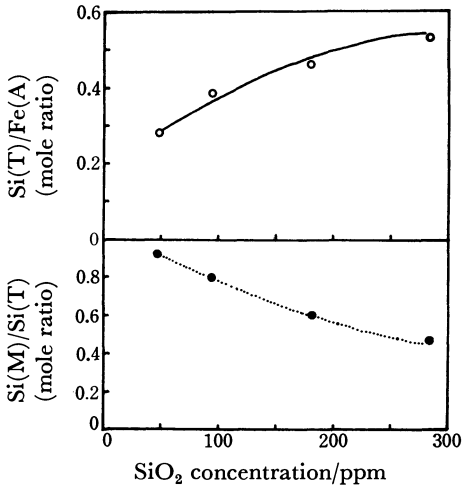

Fig. 5. The variation of Si(T)/Fe(A) and Si(M)/Si(T) ratios as a function of initial silicic acid concentration.
pH: 9. Reaction time: 5 h. Si/Fe(MR): 0.87.

and the degree of polymerization are greatly influenced by initial monosilicic acid concentration.

Effect of the Relative Amount of Silicic Acid and Iron(III) Hydroxide. Figure 6 shows the variation of Si(T)/Fe(A) and Si(M)/Si(T) ratios as a function of the Si/Fe(MR) ratio. Increase in the Si(T)/Fe(A) ratio and decrease in the Si(M)/Si(T) ratio were rapid with an increase in Si/Fe(MR) ratio in 300 ppm monosilicic acid solution. On the other hand, in 100 ppm monosilicic acid solution, at above Si/Fe(MR) ratio of unity, the Si(T)/Fe(A) ratio reached a limiting plateau region, indicating a *ca.* 0.38 Si(T)/Fe(A) ratio. The decrease in the Si(M)/Si(T) ratio became very slow at above a 2 Si/Fe(MR) ratio.

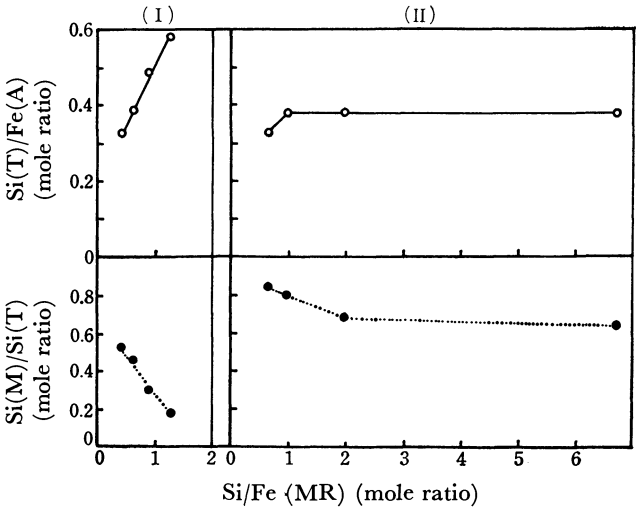

Fig. 6. The variation of Si(T)/Fe(A) and Si(M)/Si(T) ratios as a function of Si/Fe(MR) ratio.
Initial monosilicic acid concentration: (I) 300 ppm, (II) 100 ppm.
pH: 9. Reaction time: 5 h.

Effect of Standing Time. The variation of Si(T)/Fe(A) and Si(M)/Si(T) ratios with time in 300 ppm monosilicic acid solution is shown in Fig. 7. At a 0.65 Si/Fe(MR) ratio, both Si(T)/Fe(A) and Si(M)/Si(T) ratios reached limiting values after 10 h, indicating that adsorption and polymerization of silicic acid apparently do not proceed after 10 h.

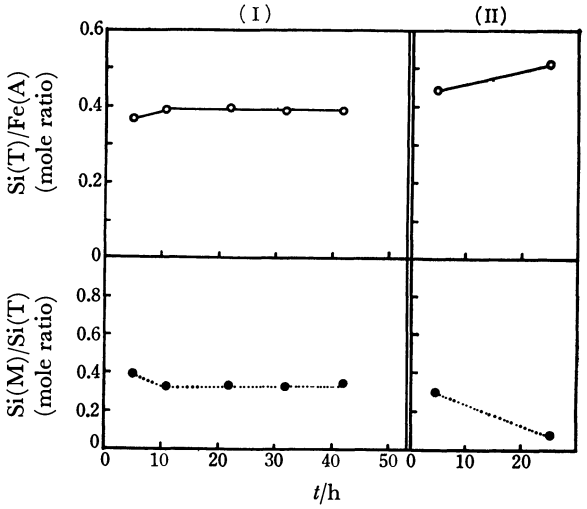

Fig. 7. The variation of Si(T)/Fe(A) and Si/(M)Si(T) ratios with time.
Initial monosilicic acid concentration: 300 ppm.
Si/Fe(MR): (I) 0.65, (II) 2.1. pH: 9.

At a 2.1 Si/Fe(MR) ratio, the Si(T)/Fe(A) ratio increased with time, the Si(M)/Si(T) ratio decreasing. Silica of size larger than 0.1 μm was obtained after 5 h, its amount increasing with time.

Discussion

Since the amount of silicic acid adsorbed on iron(III) hydroxide and the degree of polymerization of adsorbed

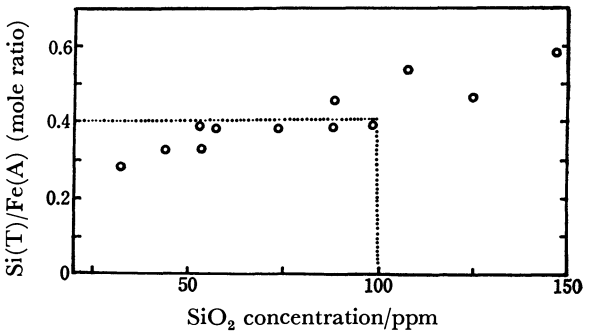

Fig. 8. Relationship between Si(T)/Fe(A) ratio and the concentration of monosilicic acid after 5 h at pH 9.

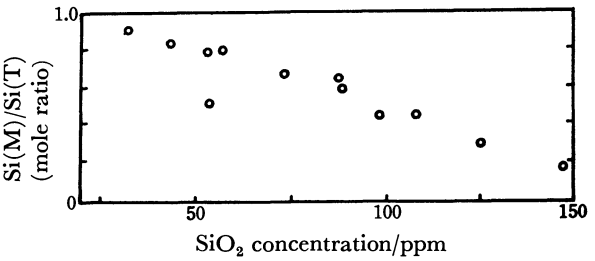

Fig. 9. Relationship between Si(M)/Si(T) ratio and the concentration of monosilicic acid after 5 h at pH 9.

silicic acid were largest at pH 9 (Figs. 2 and 3), the behavior of silicic acid was studied at pH 9.

The Si(T)/Fe(A) ratio increased with increasing initial concentration of silicic acid, the Si(M)/Si(T) ratio decreasing (Fig. 5). However, these ratios are expected to be affected also by silicic acid concentration after adsorption. On the basis of the experimental data (Figs. 5 and 6), Si(T)/Fe(A) and Si(M)/Si(T) ratios measured after 5 h were plotted against the concentration of silicic acid in the solutions. The results are shown in Figs. 8 and 9. The Si(T)/Fe(A) ratio is *ca.* 0.39 in the silicic acid solutions in the concentration range 50—100 ppm. Tarutani and Kato[6] reported that when 50 ppm monosilicic acid solution of pH 8 is continuously flowed through a flask containing iron(III) hydroxide, the Si(T)/Fe(A) ratio reaches the limiting value 0.39 after 10 d. It may be concluded that this value is the adsorption capacity of iron(III) hydroxide for silicic acid. When silicic acid concentration is higher than 100 ppm, the Si(T)/Fe(A) ratio increases with increasing silicic acid concentration. The Si(M)/Si(T) ratio decreased with increasing concentration of silicic acid (Fig. 9), suggesting that polymerization is affected by the concentration of silicic acid after adsorption as well as the initial silicic acid concentration.

The following conclusion was made. The polymerization reaction of silicic acid on the surface of iron(III) hydroxide consists of two steps: (1) the polymerization of adsorbed monosilicic acid and (2) the polymerization between monosilicic acid in the solution and silicic acid species already present on the surface of iron(III) hydroxide, giving rise to a three-dimensional gel structure.

In the solution of initial silicic acid concentration of 100 ppm, the amount of adsorbed silicic acid is nearly constant at above Si/Fe(MR) of unity, but the amount of polysilicic acid gradually increases with increasing Si/Fe(MR) ratio (Fig. 6). This suggests that polysilicic acid is mainly formed by Reaction 1. In silicic acid solutions in the concentration range 50—100 ppm, the Si(T)/Fe(A) ratio is almost constant (Fig. 8). When silicic acid concentration is higher than 100 ppm, the Si(T)/Fe(A) ratio increases with increasing silicic acid concentration. This seems to be caused by Reaction 2.

Amorphous silica of size larger than 0.1 μm is formed after 5 h on the surface of iron(III) hydroxide in the solution of initial silicic acid concentration of 300 ppm at a 2.1 Si/Fe(MR) ratio (Fig. 7). This suggests that polysilicic acid rapidly grows on the surface of iron(III) hydroxide in silicic acid solution which has a concentration higher than the solubility of amorphous silica.

References

1) K. Kato, *Geochem. J.*, **3**, 87 (1969).
2) H. Harder and W. Flehmig, *Geochim. Cosmochim. Acta*, **20**, 295 (1970).
3) T. Kojima and T. Tarutani, *Mem. Fac. Sci., Kyushu Univ., Ser. C*, **9**, 1 (1974).
4) A. Herbillon and J. Tran Vinh An, *J. Soil Sci.*, **20**, 223 (1969).
5) K. Shimada and T. Tarutani, *J. Chromatogr.*, **168**, 401 (1979).
6) T. Tarutani and H. Kato, *Mem. Fac. Sci., Kyushu Univ., Ser. C*, **11**, 197 (1978).

Kinetics of the Gas-phase Photochlorination of Dichloromethane in a Tubular Photoreactor†

Takuo SUGAWARA,* Makoto SUZUKI, and Hiroyasu OHASHI
Department of Fuel Chemistry, Mining College, Akita University, Akita 010
(Received July 23, 1979)

The gas-phase photochlorination of dichloromethane was conducted at a low extent of conversion from 9 °C to 100 °C in a tubular flow reactor irradiated by means of a circular array of low-pressure mercury lamps. The kinetics were studied with due consideration taken of the radial variation in light intensity across the reactor and with the proper selection of kinetic equations, including the recombination of dichloromethyl radicals as the dominant termination step. The dependence of the absorbed radiant energy on the chlorine concentration was well simulated by the use of the radial-light and line-source model. The predominance of the observed production rate of hydrogen chloride over that of chloroform was also reproduced well by the appropriately selected kinetic expressions, without any use of the long-chain approximation. The recombination rate constant of dichloromethyl radicals was determined to be $10^{13.5}$ cm^3 mol^{-1} s^{-1}; this is larger than the previously reported value by the factor of 12.6, and is in fair agreement with the theoretical value, $10^{13.3-13.4}$, calculated from the statistical factor, and with the collision rate constant based on the hard-sphere model.

Information has been accumulating for the past two decades on design procedures for photoreactors. The reaction characteristics were examined for a simple kinetic system, combined with the effects of the diffusion rates, the velocity distribution in a flow reactor, and the internal light filtered by a product or by an intermediate.[1,2] However, little work has been reported on photoreactor performance for a reaction system with a complex mechanism. Sugawara *et al.*[3] recently studied the photochlorination of chloroform in an annular reactor. They indicated the necessity for precise information on the kinetics as well as the incident light intensity, especially in the case of a high radiation intensity. Now that research on the angle characteristics of radiation from various types of light sources[4,5] has made possible kinetic studies by the use of a high-intensity lamp in an arbitrary position, it could be possible to examine the effect of a termination step on the overall rates of a reaction with a chain mechanism more precisely than with previous conventional approaches.[6,7]

The motivation of this study was mainly to investigate photoreactor performance in a flow system for series-parallel reactions. First of all, the authors studied the kinetics of the gas-phase photochlorination of dichloromethane in a tubular reactor within a circle of low-pressure mercury lamps. They then discussed the applicability of the long-chain approximation and determined the rate of the recombination of dichloromethyl radicals, one of the termination steps, using the radial-light and line-source model[4] to estimate the radial intensity distribution. The determined rate constant may also be used to estimate the behavior of such air pollutants as dichloromethane and chloroform in the atmosphere.

Stoichiometry and Reaction Mechanism

The stoichiometric equations for the gas-phase photochlorination of dichloromethane are given by Eqs. 1—4, while the proposed reaction mechanisms are given from Eq. 5 through Eq. 17:

$$Cl_2 + CH_2Cl_2 = CHCl_3 + HCl \quad (1)$$

$$Cl_2 + 2CH_2Cl_2 = C_2H_2Cl_4 + 2HCl \quad (2)$$

$$Cl_2 + CHCl_3 = CCl_4 + HCl \quad (3)$$

$$Cl_2 + 2CHCl_3 = C_2Cl_6 + 2HCl \quad (4)$$

Initiation: $Cl_2 \xrightarrow{\phi I_a} 2Cl\cdot$ (5)

Propagation: $Cl\cdot + CH_2Cl_2 \underset{k_3}{\overset{k_2}{\rightleftharpoons}} CHCl_2\cdot + HCl$ (6)

$$CHCl_2\cdot + Cl_2 \underset{k_5}{\overset{k_4}{\rightleftharpoons}} Cl\cdot + CHCl_3 \quad (7)$$

$$Cl\cdot + CHCl_3 \underset{k_7}{\overset{k_6}{\rightleftharpoons}} CCl_3\cdot + HCl \quad (8)$$

$$CCl_3\cdot + Cl_2 \underset{k_9}{\overset{k_8}{\rightleftharpoons}} Cl\cdot + CCl_4 \quad (9)$$

Termination: $CHCl_2\cdot + Cl\cdot \xrightarrow{k_{10}} CHCl_3$ (10)

$$CHCl_2\cdot + CHCl_2\cdot \xrightarrow{k_{11}} C_2H_2Cl_4 \quad (11)$$

$$CCl_3\cdot + Cl\cdot \xrightarrow{k_{12}} CCl_4 \quad (12)$$

$$CCl_3\cdot + CCl_3\cdot \xrightarrow{k_{13}} C_2Cl_6 \quad (13)$$

$$CHCl_2\cdot + CCl_3\cdot \xrightarrow{k_{14}} C_2HCl_5 \quad (14)$$

$$Cl\cdot + Cl_2 \underset{k_{16}}{\overset{k_{15}}{\rightleftharpoons}} Cl_3\cdot \quad (15)$$

$$Cl_3\cdot + Cl\cdot \xrightarrow{k_{17}} 2Cl_2 \quad (16)$$

$$Cl\cdot + \text{wall} \xrightarrow{k_{18}} \frac{1}{2}Cl_2 \quad (17)$$

The rate constants recommended in the literature are shown in Table 1.[7-11] The published value of k_{11}, $10^{12.4}$, may be open to question, since it is much lower than k_{13}; a simple kinetic model study[12] suggests that the recombination rate of dichloromethyl radicals should not deviate so much from that of trichloromethyl radicals.

† Presented at the Akita Meeting of the Society of Chemical Engineers, Japan, Akita, August, 1974.

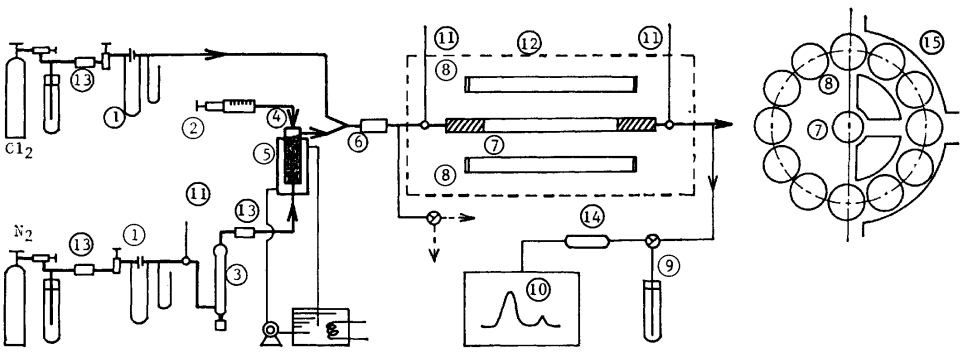

Fig. 1. Schematic diagram of experimental apparatus.
① Orifice meter, ② Microfeeder, ③ Soap-film flow meter, ④ Vaporizer, ⑤ Hot water jacket, ⑥ Mixer, ⑦ Quartz reactor, ⑧ Low pressure mercury lamp, ⑨ KI solution, ⑩ Gas chromatograph, ⑪ Thermometer, ⑫ Air bath, ⑬ Desiccating tube, ⑭ Cl_2 adsorber, ⑮ Bakelite holder.

Table 1. Rate constants in the literature for the elementary steps of the photochlorination of dichloromethane[a)]

k_2	$=10^{13.4}\exp(-3.10\times10^3/RT)$
k_3	$=10^{12.0}\exp(-11.2\times10^3/RT)$
k_4	$=10^{12.0}\exp(-4.00\times10^3/RT)$
k_5	$=10^{14.0}\exp(-21.0\times10^3/RT)$
k_6	$=10^{12.8}\exp(-3.35\times10^3/RT)$
k_7	$=10^{11.7}\exp(-11.3\times10^3/RT)$
k_8	$=10^{11.7}\exp(-5.00\times10^3/RT)$
k_9	$=10^{13.9}\exp(-20.0\times10^3/RT)$
k_{10}	$=10^{14.4}$
k_{11}	$=10^{12.4}$
k_{12}	$=10^{13.8}$
k_{13}	$=10^{13.0}$
k_{14}	$=10^{12.1}$
k_{15}	$=4.55\times10^7$
k_{16}	$=7.6\times10^5$
k_{17}	$=1.7\times10^{14}$
k_{18}	$=0.35$

a) R is 1.987 cal_{th} mol^{-1} K^{-1}, and T is the absolute temperature. k_{12}—k_{15} and k_{17} are in cm^3 mol^{-1} s^{-1}; k_{16} and k_{18} in s^{-1}.

Experimental

Reagents. *Dichloromethane*: The reagent on the market contains ca. 0.5% ethanol as a stabilizer. It produces acetyl chloride and hydrogen chloride by means of this stoichiometric equation (Eq. 18):

$$C_2H_5OH + 2Cl_2 = CH_3COCl + 3HCl \qquad (18)$$

Since the rate of the above reaction was observed in a preliminary study to be much faster than that of the photochlorination of dichloromethane, the ethanol was removed by shaking the mixture with a concentrated sulfuric acid solution and then with a dilute sodium hydroxide solution, followed by distilled water, and finally by drying it with calcium chloride. The remaining dichloromethane was further purified by distillation.

Chlorine and Nitrogen: The effect of the oxygen impurities in chlorine and nitrogen on the photochlorination of dichloromethane was considered negligible because of their extremely small amounts, *i.e.*, several ppm in each cylinder.

Experimental Apparatus and Procedure. A schematic diagram of the apparatus is shown in Fig. 1. Dichloromethane, fed in constantly with a microfeeder (2), was instantaneously vaporized in a vaporizer (4), diluted with nitrogen, and mixed with chlorine in the mixing chamber (6). The reactant gas mixture was then led to a quartz tube (7) through a connecting tube with an inside diameter of 8 mm and a length of 4.5 m. The reactants were irradiated in a test section located *ca.* 15—30 cm downstream from the inlet by means of 3, 6, or 12 low-pressure mercury lamps (Toshiba GL-30, 200 V-30 W; illuminating length, *ca.* 890 mm) arranged in a circle as is shown in the figure. The 100 Hz fluctuation of the light intensity, when the 50 Hz alternating

Table 2. Experimental conditions

Diameter of reactor, d or $2r_0$/cm	0.588, 0.690
Test-section length, l/cm	18.6, 24.0
Temperature, θ/°C[a)]	9, 58, 100
Total pressure, p/atm[b)]	*ca.* 1
Cl_2concentration, $[Cl_2]$/mol cm^{-3}	$(0.87—2.22)\times10^{-5}$
CH_2Cl_2concentration, $[CH_2Cl_2]$/mol cm^{-3}	$(2.26—4.00)\times10^{-6}$

a) θ/°C$=T$/K-273.15. b) 1 atm$=$101.325 kPa

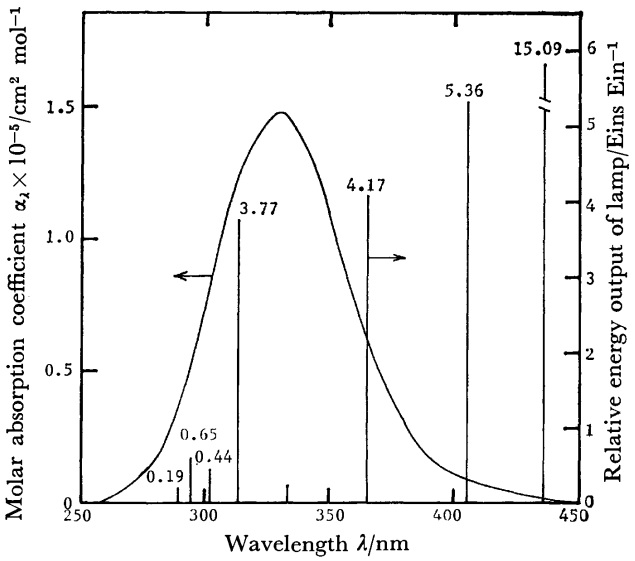

Fig. 2. Spectral distribution of molar absorption coefficient of chlorine and relative energy output of lamp.

current was applied, was minimized by setting one-third of the total number of lamps separately from the three-phase alternating current. The reactor dimensions are summarized in Table 2.

The spectral distribution of the molar absorption coefficient of chlorine,[13] α_λ, is shown in Fig. 2, along with the radiant emission spectra effective for the photochlorination.[14]

Quantitative Analysis. Gas sampled at the reactor inlet or outlet was led into a potassium iodide solution (9) which had been made slightly acidic with hydrochloric acid. The unreacted chlorine and the formed hydrogen chloride were determined with 0.1 mol dm^{-3} sodium thiosulfate and 0.01 mol dm^{-3} sodium hydroxide solutions respectively. Gas sampled through a packed column (14) to be described below was analyzed for dichloromethane, chloroform, and carbon tetrachloride by means of gas chromatography. The column (14) for the adsorption of chlorine was made of a glass tube with an inner diameter of 6 mm and a length of 300 mm, packed with small pellets containing calcium hydroxide, potassium iodide, and calcium chloride. It was ascertained beforehand that the adsorption of the other reactant and products was negligible within the limits of precision of the analysis. A gas chromatograph equipped with a copper column with an inner diameter of 3 mm and a length of 2.2 m, and packed with T.C.P. 30%/celite 545 (80—100 mesh), was operated at 88 °C and at a flow rate of 28.5 cm^3 (20 °C, with 1 atm) min^{-1} of hydrogen as the carrier gas.

Experimental Conditions. All the experiments were conducted under conditions in which a differential reactor could be assumed, where the extent of the conversion of chlorine and dichloromethane was low and where the production of carbon tetrachloride was negligible. The experimental conditions are shown in Table 2. The dark reactions were negligible under the conditions studied.

Results

Incident Light Intensity. It was previously reported that the incident light intensity got lower as time elapsed because of deposits on the reactor wall in the gas-phase photochlorination of hydrocarbons.[8,11,15] A study with a potassium trioxalatoferrate(III) actinometer[16] revealed a gradual drop in intensity, especially during the initial period of usage, but the rate of drop was so slow after about ten hours that the intensity in a run could be considered constant for several hours.

Production Rates of Hydrogen Chloride and Chloroform. Figures 3 and 4 show examples of the effect of the chlorine concentration, and Fig. 5 that of the dichloromethane concentration on the production rates of hydrogen chloride, ○, and chloroform, △. These figures indicate that the effect of chlorine is much greater than that of dichloromethane. The effect of the tempera-

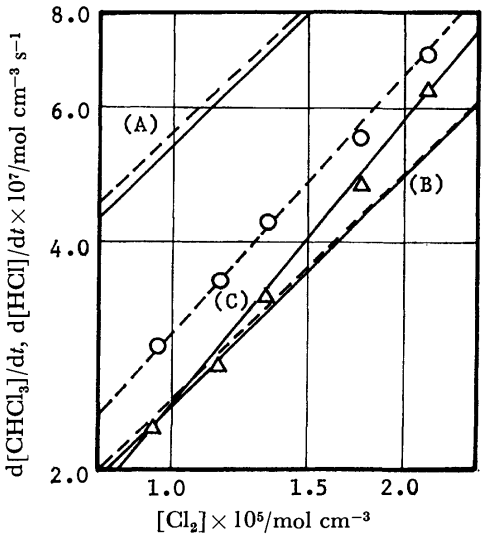

Fig. 3. Formation rates of $CHCl_3$ and HCl.
Exptl. values; △, $d[CHCl_3]/dt$ and ○, d[HCl]/dt. Exptl. conditions; θ/°C=9, d/cm=0.690, l/cm=24.0, $[CH_2Cl_2]$/mol $cm^{-3}=3.50\times10^{-6}$, and $(l/\bar{u})$/s=0.465. Calcd curves; ——, $d[CHCl_3]/dt$ and ——, d[HCl]/dt where $\phi\bar{I}_{a,6}\times10^8$/mol cm^{-3} s^{-1} and k_{11}/cm^3 mol^{-1} s^{-1} are 3.50 and $10^{12.4}$ for (A), 0.75 and $10^{12.4}$ for (B), and 3.50 and $10^{13.5}$ for (C), respectively.

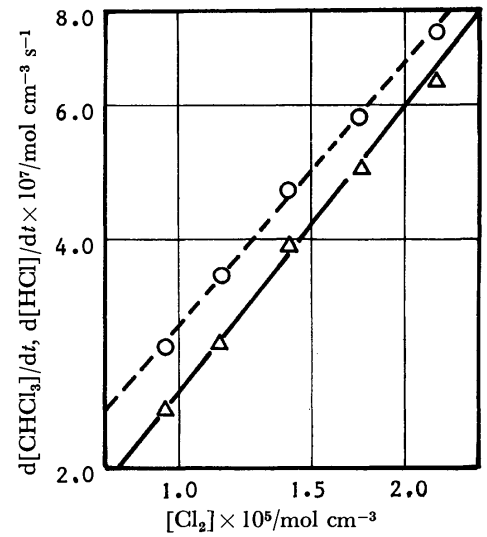

Fig. 4. Effect of chlorine concentration on the formation rates of $CHCl_3$ and HCl.
Exptl. values; △, $d[CHCl_3]/dt$ and ○, d[HCl]/dt. Exptl. conditions; θ/°C=9, d/cm=0.690, l/cm=24.0, $[CH_2Cl_2]$/mol $cm^{-3}=4.00\times10^{-6}$, and $(l/\bar{u})$/s=0.534. Calcd curves; ——, $d[CHCl_3]/dt$ and ——, d[HCl]/dt.

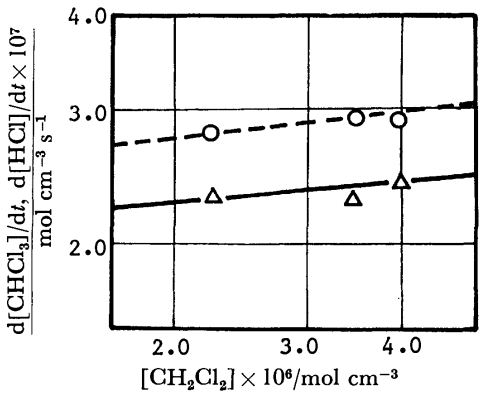

Fig. 5. Effect of dichloromethane concentration on the formation rates of $CHCl_3$ and HCl.
Exptl. values; △, $d[CHCl_3]/dt$ and ○, d[HCl]/dt. Exptl. conditions; θ/°C=9, d/cm=0.690, l/cm=24.0, $[Cl_2]$/mol $cm^{-3}=9.60\times10^{-6}$, and $(l/\bar{u})$/s=0.465—0.534. Calcd curves; ——, $d[CHCl_3]/dt$ and ——, d[HCl]/dt.

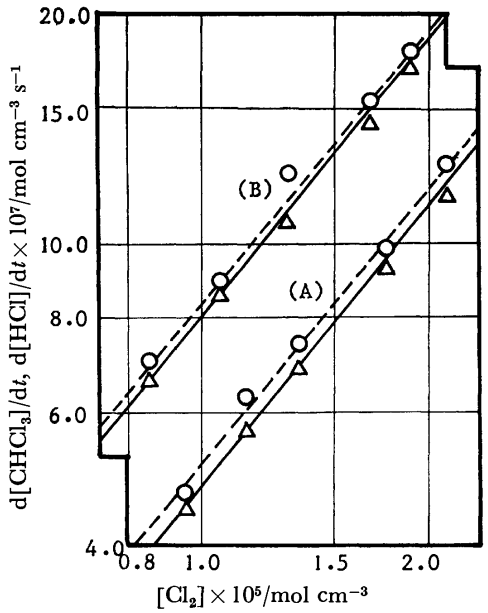

Fig. 6. Effect of temperature on the formation rates of $CHCl_3$ and HCl.
Exptl. values; △, $d[CHCl_3]/dt$ and ○, $d[HCl]dt$·/ Exptl. conditions; θ/°C=58(A) and 100(B), d/cm= 0.588, l/cm=18.6, $[CH_2Cl_2]\times10^6$/mol cm^{-3}=3.39(A) and 3.89(B), and $(l/\bar{u})$/s=0.254(A) and 0.225(B). Calcd curves; ——, $d[CHCl_3]/dt$ and ——, $d[HCl]/dt$.

ture is shown in Fig. 6. Figures 3—6 show that the production rates of hydrogen chloride are higher than that of chloroform, especially at low temperatures.

Discussion

Kinetics under the Conditions of a Low Extent of Conversion. Practical kinetic expressions should be derived to simulate the experimental results, since the proposed reaction mechanism is too complex. First, Eqs. 8, 9 and 12—14 may be neglected, because the chloroform produced was in a low concentration and no appreciable carbon tetrachloride was observed under the experimental conditions studied. Second, back reactions for Eqs. 6 and 7 are insignificant since k_3 and k_5 are much smaller than k_2 and k_4 respectively, as may be seen in Table 1. Third, the concentrations of the chlorine atom and the dichloromethyl radical, calculated by means of Eqs. 6, 7, and 10, and the observed formation rates of hydrogen chloride and chloroform revealed that the effect of Eqs. 15—17 on the total formation rate of chlorine atom is less important than that of Eqs. 6, 7, and 10, in which the trichloro-radical concentration could safely be estimated from the stationary-state hypothesis according to the method of Hutton and Wright.[10]

According to the above discussion, the following kinetic expressions may be considered to be reasonable under the experimental conditions studied:

$$\text{Initiation:}\quad Cl_2 \xrightarrow{\phi I_a} 2Cl\cdot \tag{5}$$

$$\text{Propagation:}\quad Cl\cdot + CH_2Cl_2 \xrightarrow{k_2} CHCl_2\cdot + HCl \tag{19}$$

$$CHCl_2\cdot + Cl_2 \xrightarrow{k_4} Cl\cdot + CHCl_3 \tag{20}$$

$$\text{Termination:}\quad CHCl_2\cdot + Cl\cdot \xrightarrow{k_{10}} CHCl_3 \tag{10}$$

$$CHCl_2\cdot + CHCl_2\cdot \xrightarrow{k_{11}} C_2H_2Cl_4 \tag{11}$$

The production rates of chloroform and hydrogen chloride are represented by Eqs. 21 and 22.

$$\frac{d[CHCl_3]}{dt} = k_4'[CHCl_2\cdot] + k_{10}[Cl\cdot][CHCl_2\cdot] \tag{21}$$

$$\frac{d[HCl]}{dt} = -\frac{d[CH_2Cl_2]}{dt} = k_2'[Cl\cdot] \tag{22}$$

where

$$k_2' = k_2[CH_2Cl_2] \simeq k_2[CH_2Cl_2]_o,$$
$$\text{and}\quad k_4' = k_4[Cl_2] \simeq k_4[Cl_2]_o, \tag{23}$$

and where the subscript o indicates the value at the reactor inlet.

$[Cl\cdot]$ and $[CHCl_2\cdot]$ are obtained by solving Eqs. 24 and 25:

$$\frac{d[Cl\cdot]}{dt} = 2\phi I_a - k_2'[Cl\cdot] + k_4'[CHCl_2\cdot] - k_{10}[Cl\cdot][CHCl_2\cdot] \tag{24}$$

$$\frac{d[CHCl_2\cdot]}{dt} = k_2'[Cl\cdot] - k_4'[CHCl_2\cdot] - k_{10}[Cl\cdot][CHCl_2\cdot] - 2k_{11}[CHCl_2\cdot]^2 \tag{25}$$

If the long-chain approximation is applicable, Eq. 26 is obtained for the prediction of the production rates of both chloroform and hydrogen chloride:

$$\frac{d[CHCl_3]}{dt} = \frac{d[HCl]}{dt} = \frac{(\phi I_a)^{1/2}k_4[Cl_2]}{\{(k_4k_{10}[Cl_2]/k_2[CH_2Cl_2]) + k_{11}\}^{1/2}} \tag{26}$$

Since some difference was observed in the production rates of chloroform and hydrogen chloride, simulation was conducted without the use of the long-chain approximation.

Radial Distribution of Light Intensity in the Reactor. It is necessary to know the relation of the radiant energy absorbed to the chlorine concentration if we are to determine the dependence of the rate of the initiation step on the chlorine concentration.

Now, it is assumed that the radial variation in the chlorine concentration and the effects of reflection and refraction are negligible, and that Beer's law is valid for the absorption of light at each wavelength. Then the light intensity at an arbitrary point P, $I_\lambda(r,\beta)$, and the total energy absorbed, I_a, are given by Eqs. 27 and 28 respectively when the radial-light and line-source model[4] is applied:

$$I_\lambda(r,\beta) \propto \sum_{j=1}^{n}\left\{\frac{1}{\overline{PO_j}}\exp\left(-\alpha_\lambda[Cl_2]\overline{PQ_j}\right)\right\} \tag{27}$$

$$I_a = \sum_\lambda I_{a,\lambda} \tag{28}$$

where

$$I_{a,\lambda} = \frac{\alpha_\lambda[Cl_2]}{\pi {r_o}^2}\int_0^{r_o}\int_0^{2\pi} rI_\lambda(r,\beta)d\beta dr \tag{29}$$

$$\overline{PO_j} = ({l_o}^2 + r^2 - 2l_o r\cos\beta_j)^{1/2} \tag{30}$$

$$\overline{PQ_j} = r\cos\alpha_j + (r_o^2 - r^2\sin^2\alpha_j)^{1/2} \quad (31)$$

$$\alpha_j = \sin^{-1}[\sin^2\beta_j/\{1+(r/l_o)^2-2(r/l_o)\cos\beta_j\}]^{1/2} \quad (32)$$

$$\beta_j = \beta - 2\pi(j-1)/n \quad (33)$$

Symbols refer to Fig. 7.

Figures 8 and 9 show examples of the computed results. The relative radiant energy absorbed, $I_a/I_{a,s}$,[††] as is shown in Fig. 9, was used for the estimation of I_a.

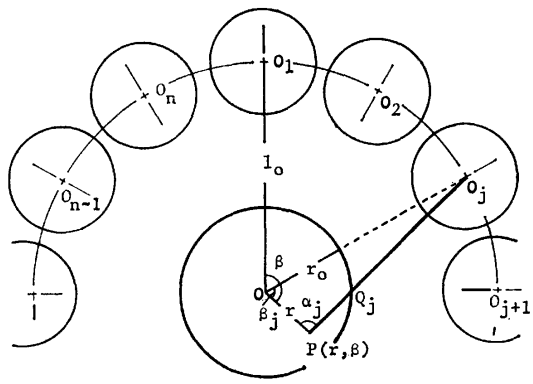

Fig. 7. Arrangement of a reactor and lamps.

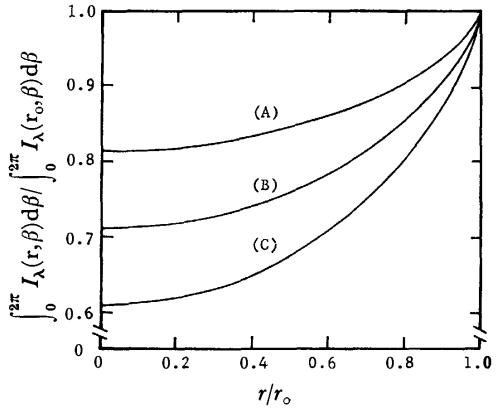

Fig. 8. Light intensity profiles in a reactor by radial light and line source model.
Conditions; $n=6$, λ/nm=313.2, l_o/cm=5.98, r_o/cm=0.345, and α_λ/cm^2 mol^{-1}=1.246×10^5. $[Cl_2]\times10^5$/mol cm^{-3}=1.0(A), 1.5(B), and 2.0(C).

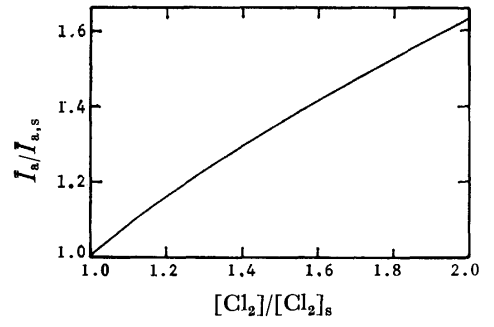

Fig. 9. Relative radiant energy absorbed *vs.* Cl_2 concentration by radial-light and line-source model.
Conditions; $n=6$, l_o/cm=5.98, r_o/cm=0.345, and $[Cl_2]_s$/mol cm^{-3}=1.0×10^{-5}.

†† The subscript s means the value at the reference concentration, $[Cl_2]$/mol cm^{-3}=1.0×10^{-5}.

The procedure will be described in the following section. Funayama *et al.*[5] showed that the radial-light and line-source model was applicable when the distance between a reactor and a low-pressure mercury lamp was less than one-fourth and more than one-eleventh of the lamp length. Thus, we may assume the radial light and line source for the geometric relation in this study.

Determination of the Rate Constant, k_{11}. Assuming no appreciable radial concentration gradient for any reactant, Eqs. 21 and 22 were used to simulate the experimental results. The steady-state chlorine-atom and dichloromethyl-radical concentrations were computed by means of Eqs. 24 and 25, and then applied to Eqs. 21 and 22. The RKG algorithm was used for the computation with the FACOM 270/20, throughout which the quantum efficiency, ϕ, was assumed to be constant. The preliminary study of the parametric sensitivity revealed that $\phi I_{a,s}$ and k_{11} affected the absolute and relative values of the production rates of chloroform and hydrogen chloride respectively when k_2 and k_4 were fixed so as to be correct. It should be noted that k_{10} was less effective than k_{11} for Eqs. 24 and 25, since the chlorine-atom concentration was calculated to be much lower than the dichloromethyl-radical concentration under the conditions studied. I_a for any chlorine concentration was estimated with the relative radiant energy absorbed, $I_a/I_{a,s}$, calculated in the above section, and with an appropriately selected value of $I_{a,s}$ so as to fit the experimental value of the production rate of *chloroform* at a chlorine concentration of 1.0×10^{-5} mol cm^{-3}. Then, the rate constant of the recombination of dichloromethyl radicals, k_{11}, was the parameter to be determined for the estimation of the experimental values of the production rate of *hydrogen chloride*. An example of the simulation is shown in Fig. 3. The solid and the broken lines represent the computed production rates of chloroform and hydrogen chloride respectively, with three sets of $\phi I_{a,s}$ and k_{11}. Although the dependence of ϕI_a on the chlorine concentration was fairly well simulated, the experimental results were not reproduced well for the cases of (A) and (B) in the figure where the previously reported value[8] of k_{11}, $10^{12.4}$, was adopted. Therefore, we sought to optimize k_{11} with an appropriately selected value of $\phi I_{a,s}$.

The experimental data were well simulated when $\phi I_{a,s}$ was assigned a value of 3.50×10^{-8} mol cm^{-3} s^{-1} and when the value of the rate constant, k_{11}, was chosen as $10^{13.5}$ cm^3 mol^{-1} s^{-1}, as is seen in the case of (C) in Fig. 3. The curves thus determined are shown in Figs. 4, 5, and 6, along with the specified values of $\phi I_{a,s}$ and k_{11} and the relative radiant energy absorbed, estimated by means of the radial-light and line-source model. The agreement between the computed and observed values is good, irrespective of changes in the chlorine and dichloromethane concentrations and in the reaction temperature from 9 °C to 100 °C. The good simulation while changing the reaction temperature indicates the reliability of the temperature dependence of the rate constants of the propagation steps and no appreciable activation energy for k_{11}. The determined value of k_{11},

$10^{13.5}$, is in fair agreement with the theoretical ones, $10^{13.3}$ at 9 °C and $10^{13.4}$ at 100 °C, calculated from the statistical factor and the collision-rate constant based on the hard-sphere model.[12] The radius of the dichloromethyl radical was assumed to be equal to that of dichloromethane[17] in the calculation of the collision-rate constant.

Conclusion

For basic information on flow-reactor performance for photoreactions with complex mechanisms, the gas-phase photochlorination of dichloromethane was kinetically studied at a low extent of conversion (from 9 °C to 100 °C) in a tubular quartz reactor irradiated by a circular array of low-pressure mercury lamps. The intense irradiation made it possible to examine the effect of the termination step, the recombination of dichloromethyl radicals, on the overall reaction rate more precisely than with conventional techniques.

The dependence of the absorbed radiant energy on the chlorine concentration was well simulated by the radial-light and line-source model, which takes the radial-intensity variation into consideration. The predominance of the observed production rate of hydrogen chloride over that of chloroform was also reproduced well by the appropriately selected kinetic equations without any use of the long-chain approximation.

The recombination-rate constant of the dichloromethyl radicals was determined to be $10^{13.5}$ cm^3 mol^{-1} s^{-1}. No appreciable activation energy was observed in the temperature range from 9 °C to 100 °C. The determined value is larger than the previously reported one by a factor of 12.6, and it is in fair agreement with the theoretical one, $10^{13.3-13.4}$, calculated from the statistical factor and the collision-rate constant based on the hard-sphere model.

This paper was prepared when one of the authors (T.S.) was at the University of Minnesota. Professor R. W. Carr's comments are appreciated. The authors also appreciate the experimental assistance of Mr. Hajime Muto. This work was supported by a Grant-in-Aid for Scientific Research from the Ministry of Education, Japan, in 1973 (No. 875485).

References

1) T. Sugawara, K. Omori, and H. Ohashi, *Kagaku Kogaku Ronbunshu*, **2**, 304 (1976).
2) T. Sugawara, K. Omori, and H. Ohashi, *J. Chem. Eng. Jpn.*, **12**, 143 (1979).
3) T. Sugawara, H. Ohashi, and T. Tadaki, *Kagaku Kogaku Ronbunshu*, **1**, 160 (1975).
4) T. Akehata and T. Shirai, *J. Chem. Eng. Jpn.*, **5**, 385 (1972).
5) H. Funayama, K. Ogiwara, T. Sugawara, and H. Ohashi, *Kagaku Kogaku Ronbunshu*, **3**, 354 (1977).
6) J. M. Tedder and J. C. Walton, *Trans. Faraday Soc.*, **63**, 2426 (1967).
7) G. R. De Maré and G. Huybrechts, *Trans. Faraday Soc.*, **64**, 1311 (1968).
8) G. Chiltz, P. Goldfinger, G. Huybrechts, G. Martens, and G. Verbeke, *Chem. Rev.*, **63**, 355 (1963).
9) R. Eckling, P. Goldfinger, G. Huybrechts, G. Martens, and G. Verbeke, *Chem. Ber.*, **93**, 3014 (1960).
10) E. Hutton and M. Wright, *Trans. Faraday Soc.*, **61**, 78 (1965).
11) T. Sugawara, T. Tadaki, and S. Maeda, *Kagaku Kogaku*, **37**, 614 (1973). The treatment is reviewed in "Hanno Sokudo no Kogaku," The Society of Chem. Eng. Jpn., Maruzen, Tokyo (1974), pp. 179—180.
12) R. E. Weston, Jr., and H. A. Schwarz, "Chemical Kinetics," Prentice-Hall, Englewood Cliffs (1972), pp. 89—90.
13) H. V. Halban and K. Seidentopf, *Z. Phys. Chem.*, **103**, 71 (1922).
14) "Toshiba Review," Toshiba, Tokyo (1956), Vol. 11, No. 9, p. 1019.
15) D. Ziolkowski, A. E. Cassano, and J. M. Smith, *AIChE J.*, **13**, 1025 (1967).
16) C. A. Parker, *Proc. R. Soc. London. Ser. A*, **220**, 104 (1953).
17) R. B. Bird, W. E. Stuart, and E. N. Lightfoot, "Transport Phenomena," John Wiley and Sons, New York (1960), p. 745.

Quenching of Excited Zinc(^3P_J) and Zinc($^1P_1$) Atoms by Several Gases

Shunzo YAMAMOTO,* Takashi TAKEI, Norio NISHIMURA, and Shigeo HASEGAWA
Department of Chemistry, Faculty of Science, Okayama University, Tsushima, Okayama 700
(Received July 23, 1979)

The intensities of the 307.6 nm and 213.9 nm resonance lines of zinc were measured at different pressures of several gases, and the quenching rate constants were determined on the basis of the Stern-Volmer plots. The quenching cross-sections obtained here were compared with those for mercury and cadmium. The simple charge-transfer curve-crossing theory proposed by Breckenridge and Renlund for the quenching of excited cadmium and mercury atoms by N_2, CO, CO_2, and so on was found to be useful for the quenching of excited zinc atoms, as well. Isotope effects on the quenching of Zn(^3P_J) and Zn($^1P_1$) by H_2 and D_2 were also discussed.

Recently, Breckenridge *et al.* have measured the quenching cross-sections of excited cadmium (^3P_J) and cadmium ($^1P_1$) atoms by several gases.[1] They have compared their values with those for the quenching of mercury ($^3P_1$ and $^3P_0$) atoms and other excited atoms, and have discussed several possible exit channels for the quenching of excited metal atoms.

In spite of several comprehensive studies of the quenching and chemical reactivity of excited mercury[2-4] and cadmium[5] atoms, there have been almost no studies of the excited states of zinc (valence isoelectronic atom with cadmium and mercury). Since the excitation energy of Zn($^3P_1$) lies between those of Cd($^3P_1$) and Hg($^3P_1$), we expected that a comparison of the reactions photosensitized by these three atoms would give further information about the detailed mechanism of the reactions.

In a previous short communication,[6] we reported the quenching cross sections of Zn(^3P_J) by H_2, D_2, and CH_4. The present paper will report the details of the quenching of Zn(^3P_J) and Zn($^1P_1$).

Experimental

The apparatus was the same as that previously described.[6] The reaction cell and the zinc lamp made of quartz were kept in a furnace at 305±2 °C. Two resonance lines (213.9 and 307.6 nm) are emitted from the lamp. These lines give rise to Zn($^1P_1$) and Zn($^3P_1$) atoms respectively. In the measurement of the quenching rate of the Zn(^3P_J) atoms, the 213.9 nm resonance line was filtered out by inserting a Pyrex plate between the cell and the lamp. The light intensities from the cell were measured by means of a Hitachi spectrophotometer, Model 139. The pressure of the gases was measured by means of a W & T model 62-075 pressure gauge (Nagano Keiki Co). The low pressures of the quenching gases were measured using calibrated expansion volumes.

The zinc metal used was high-purity zinc (99.9999%) manufactured by the Osaka Asahi Metal Co. Research-grade H_2(99.999%), D_2(99.5%), CH_4(99.95%), N_2(99.999%), CO(99.8%), and CO_2(99.99%) purchased from the Takachiho Shoji Co., were used without further purification. Pure-grade NH_3 (Takachiho Shoji Co. 99.5%) was freeze-pumped several times. Pure-grade Ar (Daido Sanso Co. 99.999%) was used without further purification.

Results

Pressure Dependence of the Emission Intensities at 213.9 and 307.6 nm. When a cell containing zinc vapor was illuminated by means of the exciting lamp, two resonance lines were observed, at 213.9 and 307.6 nm. The 213.9 nm resonance line disappeared when a Pyrex plate was inserted between the cell and the lamp. Upon the addition of argon, the intensities of the lines increased with the increase of the pressure, as is shown in Fig. 1.

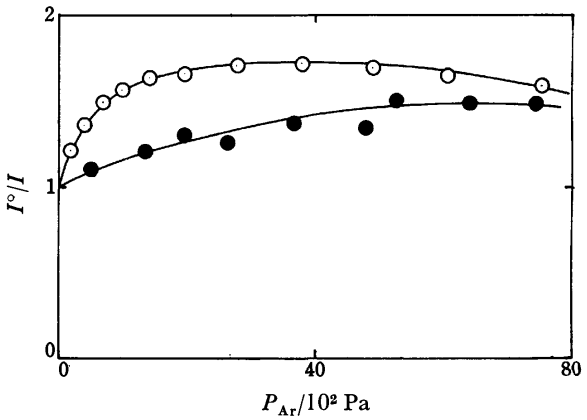

Fig. 1. Intensities of resonance lines at 213.9 (○) and 307.6 nm (●) as functions of argon pressures.

A similar increase of the intensity of the 326.1 nm resonance line of cadmium was previously observed; it was attributed to the increase in the light intensity absorbed by cadmium atoms because of the pressure broadening of the absorption line.[7] In order to minimize the pressure dependence of the absorption of the resonance line, quenchers were diluted with a large

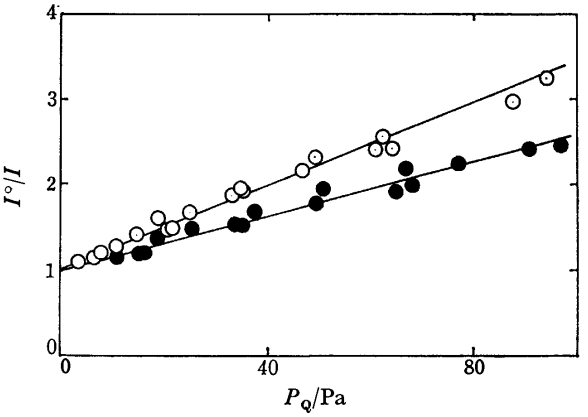

Fig. 2. Stern-Volmer plots for quenching of resonance line at 213.9 nm by H_2 (●) and D_2 (○). The total pressure is 4000 Pa.

amount of argon and the total pressure in the reaction cell was kept constant (4000 and 1300 Pa in the cases of the measurements at 213.9 and 307.6 nm respectively).

When quencher-argon mixtures were added, the intensities of the resonance lines decreased with the increase in the partial pressure of the quenchers. Representative Stern-Volmer plots for the quenching of the 213.9 and 307.6 nm resonance lines by several quenchers are shown in Figs. 2 and 3, where I° and I

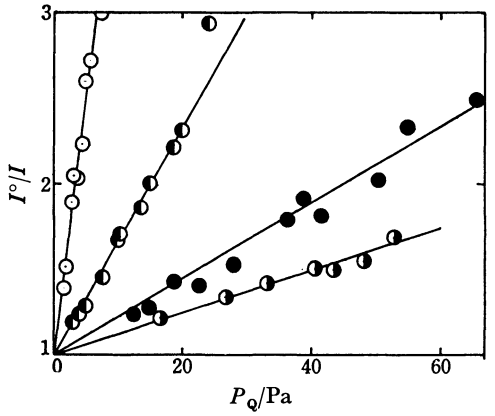

Fig. 3. Stern-Volmer plots for quenching of resonance line at 307.6 nm by CO_2 (○), CO (◐), N_2 (●), and CH_4 (◑). The total pressure is 1300 Pa.

are the intensities of the resonance lines in the absence and in the presence of quenchers respectively. All of the plots form straight lines, the intercepts of which are unity. Similar plots were obtained for other quenchers.

Quenching of the 307.6 nm Resonance Line. By analogy with the mechanism presented for the quenching of $Cd(^3P_J)$,[1a] the quenching of $Zn(^3P_J)$ can be discussed in terms of the following reactions:

$$Zn(^1S_0) + h\nu(307.6) \longrightarrow Zn(^3P_1) \quad I_a$$
$$Zn(^3P_1) \longrightarrow Zn(^1S_0) + h\nu(307.6) \quad k_0$$
$$Zn(^3P_1) + M \rightleftarrows Zn(^3P_0) + M \quad k_1, k_{-1}$$
$$Zn(^3P_1) + M \rightleftarrows Zn(^3P_2) + M \quad k_2, k_{-2}$$
$$Zn(^3P_0) + Q \longrightarrow \text{quenching} \quad k_3$$
$$Zn(^3P_1) + Q \longrightarrow \text{quenching} \quad k_4$$
$$Zn(^3P_2) + Q \longrightarrow \text{quenching} \quad k_5$$

Here, M denotes Ar and/or quenchers. As the energy differences between $Zn(^3P_0)$ and $Zn(^3P_1)$, and between $Zn(^3P_1)$ and $Zn(^3P_2)$ are very small (2.30 and 4.73 kJ/mol), equilibria must be attained fairly rapidly among these three states. By assuming the steady-state for $Zn(^3P_0)$, $Zn(^3P_1)$, and $Zn(^3P_2)$, the following equation can be derived:

$$\frac{[Zn(^3P_1)]_{Q=0}}{[Zn(^3P_1)]} = 1 + \frac{1}{k_0}\left(\frac{k_1}{k_{-1}}k_3 + k_4 + \frac{k_2}{k_{-2}}k_5\right)[Q] \quad (1)$$

As $I^\circ_{307.6} = k_0[Zn(^3P_1)]_{Q=0}$ and $I_{307.6} = k_0[Zn(^3P_1)]$, the above equation becomes:

$$\frac{I^\circ_{307.6}}{I_{307.6}} = 1 + \frac{1}{k_0}\left(\frac{k_1}{k_{-1}}k_3 + k_4 + \frac{k_2}{k_{-2}}k_5\right)[Q] \quad (2)$$

The linear Stern-Volmer plots in Fig. 3 are accounted for by Eq. 2. As the *f*-value of the zinc 307.6 nm line is about one-tenth of that of the cadmium 326.1 nm line,[8] the absorption of the 307.6 nm line by the zinc vapor at 0.36 Pa (305 °C) seems to be too small to cause any significant radiation trapping. If the lengthening of the effective radiation lifetime of $Zn(^3P_1)$ caused by radiation imprisonment is not negligible for the vapor pressure of zinc at 305 °C, the effective lifetime must be dependent on the total pressure. In Fig. 4, the values of $I^\circ_{307.6}/I_{307.6}$ obtained for H_2 and N_2

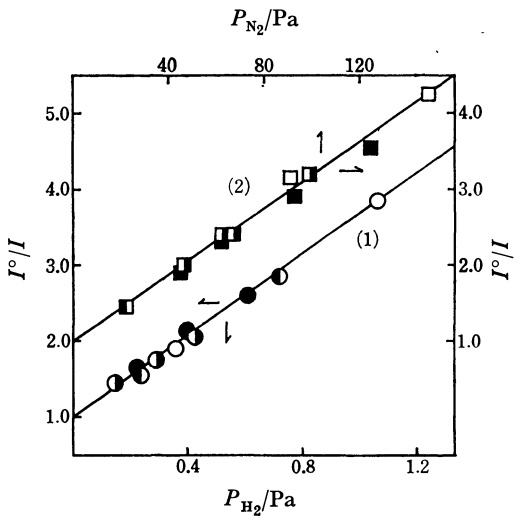

Fig. 4. Stern-Volmer plots for quenching of resonance line at 307.6 nm by H_2 and N_2.
1) H_2; total pressure are 7200 (○), 4900 (◐), 1300 (●), and 1000 (◑) in Pa. 2) N_2; 7200 (□), 4900 (◧), 1300 (□), and 1000 (◨).

at various total pressures are plotted as functions of the partial pressures of the quenchers. The points for each quencher lie on a straight line, and no dependence on the total pressure can be seen. This strongly suggests that the radiative lifetime of the $Zn(^3P_1)$ atoms in this system is independent of the pressure of the foreign gas. Therefore, k_0 can be taken as the reciprocal of the natural lifetime of $Zn(^3P_1)$ ($\tau = 2.0 \times 10^{-5}$ s[9]).

From the slopes of the straight lines in Fig. 3, the composite rate constants of the quenching, $(k_1/k_{-1})k_3 + k_4 + (k_2/k_{-2})k_5$, are estimated. Since the three triplet states are in equilibrium, $k_1/k_{-1} = (1/3)\exp(2300/RT)$ and $k_2/k_{-2} = (5/3)\exp(-4730/RT)$, and at 305 °C k_1/k_{-1} and k_2/k_{-2} are 0.54 and 0.62 respectively. The quenching rate constants, $k_q(=0.54k_3 + k_4 + 0.62k_5)$, are listed in Table 1. The corresponding quenching cross-sections

Table 1. Quenching of $Zn(^3P_J)$ by various gases

Gas	$10^{11}k_q$ / cm^3 molecule^{-1} s^{-1}	$10^{16}\sigma_q^2$ / cm^2
H_2	106.6±7.2	13.6±0.9
D_2	64.1±4.5	11.3±0.8
N_2	0.92±0.01	0.37±0.01
CO	2.58±0.18	1.04±0.07
CO_2	9.44±0.75	4.41±0.35
NH_3	9.54±0.93	3.20±0.31
CH_4	0.50±0.01	0.16±0.01

for equilibrated $Zn(^3P_{0,1,2})$ are calculated using the simple collision theory expression:

$$\sigma_q^2 = k_q\left(8\pi RT\frac{M_{Zn}+M_Q}{M_{Zn}M_Q}\right)^{-1/2} \quad (3)$$

where M_{Zn} and M_Q are the atomic and molecular weights of zinc and the quenchers respectively. The cross-sections are also listed in Table 1.

Quenching of the 213.9 nm Resonance Line. The quenching of $Zn(^1P_1)$ can be discussed in terms of the following reactions:

$$Zn(^1S_0) + h\nu(213.9) \longrightarrow Zn(^1P_1)$$
$$Zn(^1P_1) \longrightarrow Zn(^1S_0) + h\nu(213.9) \qquad k_r$$
$$Zn(^1P_1) + Q \longrightarrow \text{quenching} \qquad k_Q$$

The steady-state treatment gives the following relation:

$$\frac{I^\circ_{213.9}}{I_{213.9}} = 1 + \frac{k_Q}{k_r}[Q] \quad (4)$$

Here, $I^\circ_{213.9}$ and $I_{213.9}$ are the emission intensities at 213.9 nm in the absence and in the presence of quenchers respectively. From the slopes of the straight lines in Fig. 2, the values of k_Q/k_r can be obtained; they are listed in Table 2. k_r is the effective rate constant for the escape of 213.9 nm fluorescent photons from the reaction vessel. Contrary to the case of the 307.6 nm resonance line, k_r must be significantly different from the limiting rate of natural radiative decay at a very low vapor concentration, because radiation imprisonment can not be neglected because of the large absorption coefficient. Therefore, it is difficult to estimate the absolute k_Q values. Since the quenchers are diluted with a large amount of argon, it can be assumed that k_r is independent of the pressures of the quenchers and of the kind of quencher. The relative values of k_Q and relative quenching cross-sections are listed in Table 2.

TABLE 2. QUENCHING OF $Zn(^1P_1)$ BY VARIOUS GASES

Gas	$\frac{10^2 k_Q/k_r}{Pa^{-1}}$	k_Q(rel)	σ_Q^2 (rel)
H_2	2.42±0.02	1.00	1.00
D_2	1.56±0.01	0.64	0.90
N_2	0.83±0.01	0.34	1.08
CO	1.04±0.02	0.40	1.28
CO_2	1.10±0.01	0.46	1.70
NH_3	1.88±0.02	0.78	2.06
CH_4	1.37±0.01	0.56	1.44

Discussion

Breckenridge *et al.* discussed several factors which govern the quenching efficiencies of $Cd(^1P_1)$ and $Cd(^3P_J)$ by several gases.[1] They found that there is a correlation of the cross-sections for the quenching of excited metal atoms with a parameter, Δ, the energy difference between Me^*+Q and $Me^+ + Q^-$ at an infinite Me—Q distance, which is itself given by:

$$\Delta = I_p(Me^*) - E_a(Q)$$

They described[1b] that, in general, the cross-section increases with a decrease in Δ for the quenching of $Cd(^1P_1)$, $Cd(^3P_J)$, $Hg(^3P_0)$, and $Hg(^3P_1)$ by N_2, CO, CO_2, and so on, and that the charge-transfer curve-crossing theory is useful in explaining the magnitudes of the quenching cross-sections.

In Table 3, a comparison of the quenching cross-sections of $Zn(^3P_J)$, $Cd(^3P_J)$, $Hg(^3P_0)$, and $Hg(^3P_1)$ is shown. In this table, the values of Δ are also included. For mercury, the cross-section for the quenching processes, $^3P_1 \rightarrow {}^1S_0$ and $^3P_0 \rightarrow {}^1S_0$, have been determined separately.[4] However, for cadmium and zinc, only the composite cross-sections for the quenching of the ^3P_J states can be determined, for the equilibration reactions among these states are very rapid.

The quenching cross-sections of $Zn(^3P_J)$ by CH_4, N_2, CO, and CO_2 increase in this order. This order is almost the same as those for $Cd(^3P_J)$ and $Hg(^3P_1)$; it is also consistent with the order of the decrease in Δ. In the cases of $Cd(^3P_J)$ and $Hg(^3P_1)$, these orders have been successfully explained in terms of the charge-transfer curve-crossing mechanism.[1b] Therefore, it is reasonable to consider that the same mechanism may be valid for $Zn(^3P_J)$.

For a single quencher, the correlation between the cross-sections and Δ is not simple. For CO_2, the cross-sections increase with a decrease in Δ, but for the other quenchers they do not do so. Since the difference in Δ between the quenchers is comparatively large, the order of the quenching cross-sections for an excited atoms must be determined by only the magnitudes of Δ. However, since the difference in Δ between the metal

TABLE 3. COMPARISON OF QUENCHING CROSS-SECTIONS OF VARIOUS EXCITED METAL ATOMS

Gas	$Zn(^3P_J)$[a]		$Cd(^3P_J)$[a,b]		$Hg(^3P_0)$[c]		$Hg(^3P_1)$[c]	
	$\frac{10^{16}\sigma_q^2}{cm^2}$	$\frac{\Delta}{kJ}$	$\frac{10^{16}\sigma_q^2}{cm^2}$	$\frac{\Delta}{kJ}$	$\frac{10^{16}\sigma_q^2}{cm^2}$	$\frac{\Delta}{kJ}$	$\frac{10^{16}\sigma_q^2}{cm^2}$	$\frac{\Delta}{kJ}$
H_2	13.6	519	3.9		2.1		7.8	
D_2	11.3		2.0		2.9		7.2	
N_2	0.37	703	0.0076	686	2×10^{-4}	741	0.03	720
CO	1.04	644	1.7	628	0.69	682	3.0	661
CO_2	4.41	577	12.0	561	0.032	615	3.2	594
NH_3	3.20		0.044		0.016		2.75	
CH_4	0.16	812	0.0012	795	1.4×10^{-4}	849	0.07	828

a) The cross-sections are actually sums of population weighted cross-sections for equilibrated $Zn(^3P_{0,1,2})$ and $Cd(^3P_{0,1})$: $\sigma_q^2(Zn) = 0.54\sigma_0^2 + \sigma_1^2 + 0.62\sigma_2^2$; $\sigma_q^2(Cd) = 1.37\sigma_0^2 + \sigma_1^2$. b) Ref. 1. c) Ref. 4.

atoms is small, the order can not be determined by only the magnitudes of Δ; such other factors as the polarizability of the Me^+-Q^- complex must also be taken into account, as has been mentioned by Breckenridge and Renlund.[1b]

One major channel in the quenching of $Cd(^3P_J)$ and $Hg(^3P_{0,1})$ by NH_3 has been shown to involve the formation of Cd–NH_3* and Hg–NH_3* exciplexes, and the emission from these exciplexes has been observed.[10,11] In the $Zn(^3P_J)$–NH_3 system, however, the exciplex emission could not be observed. One of the following reasons may be responsible for this; (a) the exciplex does not form; or (b) even if the exciplex forms, it is completely quenched before emission, or (c) the exciplex emission is too weak to be observed by our detector. By analogy with the Cd–NH_3 and Hg–NH_3 systems, it does not seem reasonable to consider reason (a) and/or (b) to be responsible for the lack of luminescence in the Zn–NH_3 system.

If the quenching of $Zn(^3P_J)$ by ammonia occurs exclusively through the formation of the exciplex in a manner similar to that of $Cd(^3P_J)$, the emission intensity from the exciplex can be expressed as follows;

$$I_e = I^\circ[k_e/(k_e+k_n[Ar])] \quad (5)$$

where I° is the intensity of the resonance line and where k_e and k_n are the rate constants for the following reactions:

$$Zn\text{–}NH_3^* \longrightarrow Zn + NH_3 + h\nu_e \qquad k_e$$

$$Zn\text{–}NH_3^* + Ar \longrightarrow Zn + NH_3 + Ar \qquad k_n$$

In order to consider the emission intensity of the Zn–NH_3* exciplex by comparing the intensity with that for the Cd–NH_3* exciplex, we measured the cadmium-photosensitized luminescence of ammonia using our apparatus; we could thus observed an emission band consistent with that shown in the literature.[10] It was proved that, by our apparatus, we can not observe an emission whose intensity is smaller by a factor of 500 than that from the Cd–NH_3* exciplex. (The light intensity which can be detected by our spectrophotometer with the maximum sensitivity was estimated by means of potassium ferrioxalate actinometry to be about 5×10^{-14} Einsteins s^{-1} cm^{-2} at 400 nm at the incidence slit.) The intensity ratio of the resonance line of zinc to that of cadmium, corrected for the sensitivity of the spectrophotometer at 307.6 and 326.1 nm, was about 1/100 (the intensity of the zinc lamp was about 1/3 of that of the cadmium lamp; the other factor must be based on the difference in the absorption coefficients). Therefore, if the value of $k_e/(k_e+k_n[Ar])$ in the Zn–NH_3 system is smaller by a factor of 5 than that for the Cd–NH_3 system (0.67 for an argon pressure of 13300 Pa[10]), the emission from the Zn–NH_3* exciplex can not be detected by our apparatus. This seems the most reasonable explanation for our failure to observe the exciplex emission in the zinc-photosensitized reaction of ammonia.

In Table 4, the relative quenching cross-sections of $Zn(^1P_1)$ and the values of Δ are shown. For comparison, these values for $Cd(^1P_1)$ are also included. The quenching cross-sections of $Zn(^1P_1)$ and $Cd(^1P_1)$ by N_2, CO, and CO_2 again increase with a decrease in Δ. Thus,

Table 4. Comparison of relative quenching cross-sections of $Zn(^1P_1)$ and $Cd(^1P_1)$

Gas	$Zn(^1P_1)$		$Cd(^1P_1)$[a]	
	σ_Q^2 (rel)	$\frac{\Delta}{kJ}$	σ_Q^2 (rel)	$\frac{\Delta}{kJ}$
H_2	1.00		1.00	
D_2	0.90		1.25	
N_2	1.08	531	2.17	527
CO	1.28	473	2.33	469
CO_2	1.70	406	3.58	402
NH_3	2.06		2.00	
CH_4	1.44	640		

a) Ref. 1.

by analogy with the case of $Zn(^3P_J)$, it is reasonable to consider that the charge-transfer mechanism may be valid for $Zn(^1P_1)$.

As is shown in Table 3, $Zn(^3P_J)$ is quenched efficiently by the isotopic hydrogens. The difference between the quenching cross-sections of $Hg(^3P_0)$ and $Hg(^3P_1)$ by hydrogen has been explained simply by the difference in the energy content.[4] If the cross-sections are of a comparable magnitude for the quenching of the ^3P_J states of zinc and for those of cadmium by hydrogen, the cross-sections for $Hg(^3P_1)$ should be compared with half those for $Zn(^3P_J)$ and $Cd(^3P_J)$.[6] It can be said that the cross-sections of $Cd(^3P_1)$, $Zn(^3P_1)$, and $Hg(^3P_1)$ increase in this order; this order is consistent with the order of the excitation energy of metal atoms.

In a previous letter,[6] we discussed the isotope effects on the quenching of $Zn(^3P_1)$, $Cd(^3P_1)$, and $Hg(^3P_1)$ by hydrogen in terms of the following processes:

$$Me^* + Q \underset{k_b}{\overset{k_a}{\rightleftharpoons}} (Me-Q)^* \begin{cases} \xrightarrow{k_c} \text{decomposition of Q} \\ \xrightarrow{k_d} \text{vibrational excitation of Q} \end{cases}$$

Here, $(Me-Q)^*$ denotes a short-lived intermediate. The quenching rate constant, k, becomes:

$$k = k_a\frac{k_c+k_d}{k_b+k_c+k_d} \quad (6)$$

For the quenching of $Hg(^3P_1)$ by H_2 and D_2, it was pointed out that k is nearly equal to k_a, since $k_c \gg k_b$ and $k_c \gg k_d$, for the energy content of the complex is large enough to decompose H_2 and D_2; therefore, it does not show a large isotope effect.[4,12] On the other hand, in the cases of $Zn(^3P_1)$ and $Cd(^3P_1)$ the excitation energies are smaller than the bond energies of H–H and D–D, and perhaps k_c is not large enough for us to neglect k_b and k_d; therefore, the overall quenching-rate constants probably depend on the values of k_c+k_d. (1) If $k_c \gg k_d$, the quenching rate depends on the rates of the decomposition of H_2 and D_2, and the isotope effect based on the difference in the zero-point energies of H_2 and D_2 should be observed. (2) If $k_c \approx k_d$ or $k_c < k_d$, no conclusive explanation for the isotope effects can be deduced, since we have no information about the isotope effects on k_d. In this case, the observed isotope effects might indicate that $k_d(D_2) \approx k_d(H_2)$ or $k_d(D_2) < k_d(H_2)$. Actually, the quenching cross-sections of $Cd(^3P_1)$, $Zn(^3P_1)$, and $Hg(^3P_1)$ increase in this order,

while the isotope effects decrease in this order.

Recently, Breckenridge and Renlund measured the quenching cross-sections of $Cd(^3P_J)$ and $Cd(^1P_1)$ by means of isotopic hydrogens and compared these cross-sections with those of other excited metal atoms.[1c] They pointed out that the adiabatic pathways from Me^*+H_2 to MeH+H provide a reasonable explanation of the quenching of excited zinc, cadmium, and mercury atoms by hydrogen. In Table 5 the ratios of the quenching cross-sections of H_2 and D_2 for $Zn(^1P_1)$, $Zn(^3P_J)$, $Cd(^1P_1)$, $Cd(^3P_J)$, and $Hg(^3P_1)$ are shown.

TABLE 5. ISOTOPE EFFECT ON QUENCHING CROSS-SECTIONS

Reaction	$\frac{\Delta H}{\text{kJ mol}^{-1}}$	$\sigma_q^2[H_2]/\sigma_q^2[D_2]$
$Zn(^1P_1)+H_2\rightarrow ZnH+H$	−209	
$+D_2\rightarrow ZnD+D$	−204	1.11
$Zn(^3P_J)+H_2\rightarrow ZnH+H$	−39	
$+D_2\rightarrow ZnD+D$	−33	1.20
$Cd(^1P_1)+H_2\rightarrow CdH+H$	−158	
$+D_2\rightarrow CdD+D$	−151	0.80
$Cd(^3P_J)+H_2\rightarrow CdH+H$	0	
$+D_2\rightarrow CdD+D$	5	1.95
$Hg(^3P_0)+H_2\rightarrow HgH+H$	−53	
$+D_2\rightarrow HgD+D$	−47	0.72
$Hg(^3P_1)+H_2\rightarrow HgH+H$	−74	
$+D_2\rightarrow HgD+D$	−68	1.08

In Table 5 are also shown the ΔH values for the processes:

$$Me^* + H_2(D_2) \longrightarrow MeH(D) + H(D)$$

where Me^* is the $^1P_1$ state for $Zn(^1P_1)$ and $Cd(^1P_1)$ and is the $^3P_1$ state for $Zn(^3P_J)$, $Cd(^3P_J)$, and $Hg(^3P_1)$. For $Cd(^1P_1)$, $Zn(^3P_1)$, and $Hg(^3P_1)$, the $Me^*+H_2(D_2)\rightarrow MeH(D)+H(D)$ processes are both exothermic; therefore, the quenching cross-sections show very little isotope effect. However, in the case of $Cd(^3P_1)$, the $Cd^*+H_2\rightarrow CdH+H$ reaction is thermoneutral, while the $Cd^*+D_2\rightarrow CdD+D$ reaction is slightly endothermic. Therefore, for $Cd(^3P_1)$ a little larger isotope effect is observed. This explanation corresponds to the more detailed one for Case (2) of our explanation.

As is shown in Table 5, for $Zn(^1P_1)$ the reactions are largely exothermic and the isotope effect is very little. These findings are consistent with the above explanation of Breckenridge.

References

1) a) W. H. Breckenridge, T. W. Broadbent, and D. S. Moore, *J. Phys. Chem.*, **79**, 1233 (1975); b) W. H. Breckenridge and A. M. Renlund, *ibid.*, **82**, 1474 (1978); c) W. H. Breckenridge and A. M. Renlund, *ibid.*, **82**, 1484 (1978); d) W. H. Breckenridge and A. M. Renlund, *ibid.*, **83**, 303 (1979).

2) R. J. Cvetanovic, *Prog. React. Kinet.*, **2**, 39 (1964).

3) J. G. Calvert and J. N. Pitts, "Photochemistry," Wiley, New York, N. Y. (1966).

4) H. Horiguchi and S. Tsuchiya, *Bull. Chem. Soc. Jpn.*, **47**, 2768 (1974).

5) For example, S. Tsunashima, S. Satho, and S. Sato, *Bull. Chem. Soc. Jpn.*, **42**, 329 (1966); S. Yamamoto, S. Tsunashima, and S. Sato, *ibid.*, **48**, 1172 (1975).

6) S. Yamamoto, T. Takei, N. Nishimura, and S. Hasegawa, *Chem. Lett.*, **1976**, 1413.

7) S. Yamamoto, M. Takaoka, S. Tsunashima, and S. Sato, *Bull. Chem. Soc. Jpn.*, **48**, 130 (1975).

8) A. C. G. Mitchell and M. W. Zemansky, "Resonance Radiation and Excited Atoms," Cambridge University Press, Cambridge (1961).

9) F. W. Byron, M. N. McDermott, R. Novick, B. W. Perry, and E. Saloman. *Phys. Rev. A*, **134**, 47 (1964).

10) S. Tsunashima, T. Toyono, and S. Sato, *Bull. Chem. Soc. Jpn.*, **46**, 2654 (1973); S. Yamamoto, S. Tsunashima, and S. Sato, *Bull. Chem. Soc. Jpn.*, **48**, 1172 (1975).

11) C. G. Freeman, M. J. McEwan, R. F. C. Claridge, and L. E. Phillips, *Chem. Phys. Lett.*, **5**, 555 (1970); J. Koskikallio, A. B. Callear, and J. H. Connor, *Chem. Phys. Lett.*, **8**, 467 (1971).

12) Kang Yang, *J. Am. Chem. Soc.*, **87**, 5294 (1965).

 © 1980 The Chemical Society of Japan Bull. Chem. Soc. Jpn., 53, 865—868 (1980)

Dielectric Properties of the Hydrogen-bonded Liquids. Steric Effects on Dielectric Properties in Glycerol and Acetylated Glycerols

Eiji IKADA,* Kousaku YAMAMOTO, and Michio ASHIDA

Faculty of Engineering, Kobe University, Nada, Kobe 657

(Received August 7, 1979)

The dielectric constant and the dielectric loss of a monohydroxy molecule (glycerol diacetate) and a dihydroxy molecule (glycerol monoacetate) in the pure liquid state were measured over the frequency range from 23 Hz to 3 MHz in order to elucidate the relation between the steric effects of the acetoxyl group and the dielectric properties of alcohols. For a better understanding, the results of this work were discussed together with those of glycerol and glycerol triacetate. The static dielectric constants decrease in the order of glycerol, glycerol monoacetate, glycerol diacetate, and glycerol triacetate. This order agrees with the order of the decreasing number of hydroxyl groups per molecule. On the other hand, the four curves of a temperature variation of the relaxation times almost form one curve, although the molecular weights and interaction, which are important factors for the determination of relaxation times, differ greatly among the four molecules. Accordingly, it is concluded that the decrease in molecular weight due to the replacement of the acetyl group CH_3CO by a hydrogen atom counteracts the enhanced molecular interaction due to the increased OH···O hydrogen bonds. The experimental Cole-Cole arcs of the complex dielectric constants were well represented by the calculated curve of the Davidson-Cole empirical equation, for glycerol mono- and diacetate as well as for glycerol.

The dielectric properties of a hydrogen-bonded liquid are of interest because such a liquid generally shows abnormal dielectric behavior which is not observed in a non-hydrogen-bonded liquid. With some exceptions, such as acetic acid, the static dielectric constant of a hydrogen-bonded liquid is generally larger than that for a normal polar one, mainly because of the regular alignment of a dipolar molecule in the hydrogen-bonded cluster.[1] The static dielectric constants of alcohols,[2] *N*-methylamides,[3] and cyano compounds[4,5] are particularly large.

Another typical phenomenon with regard to the dielectric properties for a hydrogen-bonded liquid is seen in the distribution of relaxation times. For example, it is well known that a Debye-type semi-circular relaxation is generally observed for a liquid monohydroxy alcohol; on the other hand, a Davidson-Cole-type skewed arc relaxation is observed for liquid polyhydric alcohols, such as diol and triol.[6] As for the relaxation of liquid dielectrics, we have ourselves reported that a Havriliak-Negami-type relaxation, often observed in the α-relaxation of polymers,[7,8] is observed in the relaxation of a non-hydrogen-bonded liquid.[9] This relaxation is not, however, observed in a hydrogen-bonded liquid. A number of dielectric studies have made it clear that the distribution of the relaxation times of organic liquids is associated with both the liquid structure and the molecular structure. In this study we have compared the dielectric properties of glycerol[6] and its acetylated derivatives as follows:

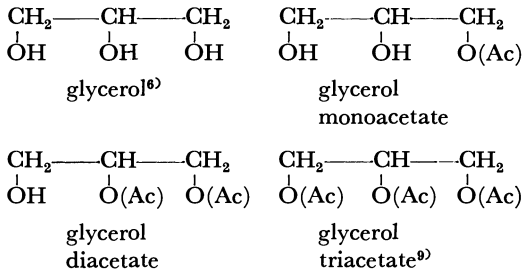

where Ac is the acetoxyl group.

Hitherto, there have been a number of studies of the dielectric properties of aliphatic mono- and polyhydric alcohols,[10] such as ethanol and pentanediol, however, little is known about the dielectric properties of the substituted alcohols.

Experimental

Purification of Glycerol Monoacetate and Diacetate. The glycerol monoacetate (Eastman Kodak Co.) and the glycerol diacetate (Merck Co.) are both commercial products, and both are mixtures composed of glycerol monoacetate, diacetate, and triacetate. Therefore, it is necessary to separate the mixtures into pure fractions. The fractional distillation under reduced pressures was, however, ineffective for this purpose. Next, a chromatographic column method was tested and adopted. Here, the packing gel was Wako Gel C-200 (Wako Chemical Co.), and the mobile phase used as the developer was a mixture of benzene and methanol, in a ratio which was continuously changed. The results of separation were examined by means of GLPC.

Dielectric Measurement. The dielectric constant and dielectric loss were measured with a ratio-arm transformer bridge (Ando Electric Co., TR-1BK type) over the frequency range from 23 Hz to 3 MHz. The dielectric cell for the liquid studied was a platinum concentric glass cell.

Results and Discussion

Static Dielectric Constant. The dielectric properties of glycerol and glycerol triacetate have been studied by Davidson and Cole[6] and by Ikada and Watanabe[9] respectively.** For comparison, the data have been cited from each reference. The temperature dependence of the static dielectric constant of all four molecules in the liquid state is represented by the linear relation shown in Fig. 1. We, however, recognize a marked variation in the values with the number of hydroxyl

Ras and Bordewijk also studied the dielectric properties of glycerol triacetate, tripropionate, and tributyrate (A. M. Ras and P. Bordewijk, *Recl. Trav. Chim. Pays-Bas*, **90, 1055 (1971)).

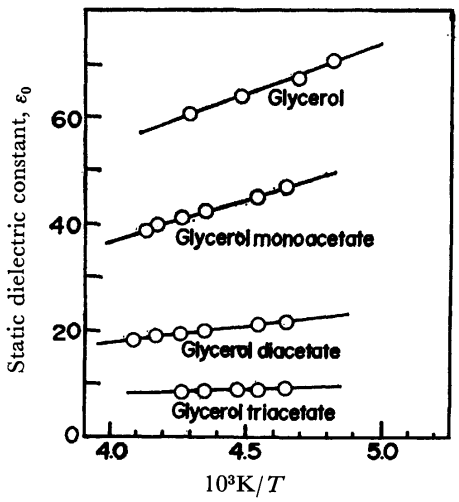

Fig. 1. Temperature dependence of the static dielectric constants of the four liquids. The data of glycerol and glycerol triacetate were cited from Ref. 6 and Ref. 9, respectively.

group per molecule, as the static dielectric constants for glycerol, *ca.* 60, are very large, while, on the other hand, those for glycerol triacetate are less than 10. Doubtless, this step-by-step variation in the static dielectric constant depends mainly on the number of intermolecular hydrogen bonds in each liquid structure, although the detailed conformation of the hydrogen-bonded cluster is not yet known. Strictly speaking, it is necessary to determine the dipole moment *in vacuo* of these molecules for a quantitative estimation of the local ordering due to hydrogen bonds in the liquid structure.[10] However, we can easily see a gradual decrease in the intermolecular hydrogen bonds with an increase in the replacement of a hydroxyl group by a non-hydrogen bonding acetoxyl group. For example, the static dielectric constants of glycerol diacetate are smaller than those for a monohydroxy aliphatic alcohol with the same main chainlength, such as 1-propanol. This decrease in the static dielectric constant of glycerol diacetate proves that the molecular association is destroyed by the hindrance of the large acetoxyl group on forming the hydrogen-bonded cluster.

Dielectric Relaxation. As for the relaxation mechanism of liquid normal alcohols, which has been discussed by many investigators and summarized in many books,[1,10] the explanation is explicit and seems to be well recognized. The proton jump along a hydrogen-bonded chain of monohydric alcohols clarifies the absence of any distribution of the relaxation times. On the other hand, the relaxation mechanism in such polyhydroxy compounds as glycerol appears to remain undetermined, partly because of difficulty in the structural analysis of liquid polyols. The contribution of the hydrogen bond to the dynamic properties of the polyhydric alcohol is apparent in the comparatively high viscosities of the liquids. In other words, the long relaxation times in polyols are due to the accompanying breaking and reforming of the hydrogen bonds on the molecular relaxation. Moreover, the fact that almost all the polyhydric aliphatic compounds show merely the Davidson-Cole-type relaxation in the liquid state makes us imagine a rather similar relaxation mechanism for the molecular motion in these molecules. However, the relaxation mechanism of polyol compounds has not yet been thoroughly clarified in detail. Almost all of the polyols show empirically the Davidson-Cole-type relaxation:[6]

$$\varepsilon^* - \varepsilon_\infty = \frac{\varepsilon_0 - \varepsilon_\infty}{(1+j\omega\tau_0)^\beta}$$

where ε^* is the complex dielectric constant, ε_0 and ε_∞ are the limiting low- and high-frequency dielectric constants respectively, ω is the angular frequency, τ_0 is the mean relaxation time, j is $\sqrt{-1}$, and β is the distribution parameter. As has been described above, Davidson and Cole reported that glycerol shows a Davidson-Cole-type relaxation.[6] On the other hand, glycerol triacetate, a completely acetylated glycerol, does not show this relaxation, but a Havriliak-Negami-type relaxation:[9]

$$\varepsilon^* - \varepsilon_\infty = \frac{\varepsilon_0 - \varepsilon_\infty}{[1+(j\omega\tau_0)^{1-\alpha}]^\beta}$$

where $1-\alpha$ is also the distribution parameter of the relaxation times. The distribution of the relaxation times of glycerol triacetate is wider than that for glycerol, as may be seen in Table 1. The broadening of the relaxation times results from the lack of a hydrogen bond in the liquid structure. The same broadening may be seen in a comparison of the dielectric properties of ethylenediamine and 2-aminoethanol.[12]

Table 1. Distribution parameters $(1-\alpha)$ and β in the Davidson-Cole and the Havriliak-Negami-type relaxations

	$\frac{T}{°C}$	$1-\alpha$	β	ε_∞	ε_0
Glycerol monoacetate[a]	−31.0		0.517	3.55	38.57
	−33.6		0.500	3.02	40.00
	−38.4		0.498	3.40	40.95
	−43.3		0.513	3.73	42.41
	−52.9		0.500	3.78	45.20
	−58.1		0.464	3.45	46.83
Glycerol diacetate[a]	−28.5		0.504	3.78	18.16
	−33.4		0.520	4.10	18.78
	−38.4		0.464	3.64	19.33
	−43.4		0.512	4.12	19.95
	−53.4		0.511	3.96	21.20
	−58.3		0.503	3.96	21.70
Glycerol triacetate[b,c]	−39.1	0.982	0.484	3.65	8.56
	−43.5	0.954	0.483	3.53	8.73
	−49.5	0.967	0.494	3.53	8.89
	−53.3	0.964	0.497	3.53	9.03
	−58.1	0.915	0.523	3.49	9.20
Glycerol[a,d]	−40.0		0.608	4.20	60.50
	−50.0		0.603	4.10	63.40
	−60.0		0.593	4.16	67.40

a) The distribution parameter of the Davidson-Cole-type relaxation. b) The distribution parameter of the Havriliak-Negami-type relaxation. c) The data from Ref. 9. d) The data from Ref. 6.

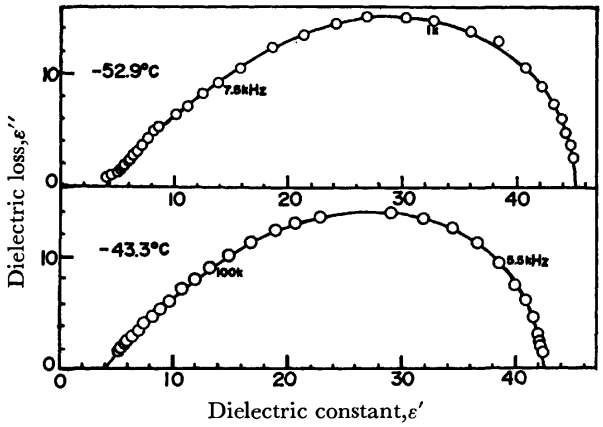

Fig. 2. Cole-Cole plots of glycerol monoacetate.

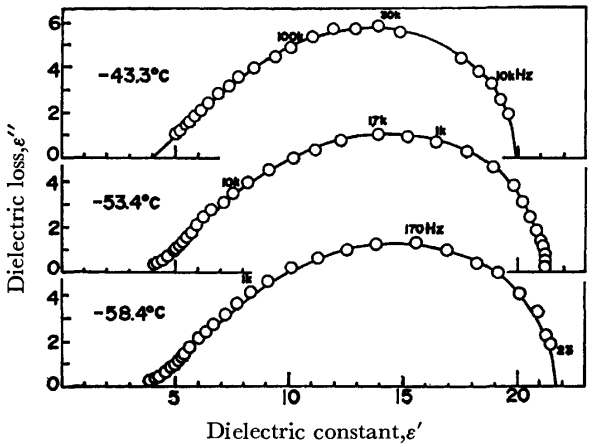

Fig. 3. Cole-Cole plots of glycerol diacetate.

Figure 2 shows the Cole-Cole plots of glycerol monoacetate. The experimental arcs agree well with the curves calculated according to the Davidson-Cole equation. It may, therefore, be concluded that the liquid structure of glycerol monoacetate is not so different from that of glycerol and that the steric hindrance of large CH_3CO–group in this molecule for hydrogen bonding is not so clearly seen. Figure 3 shows the Cole-Cole plots of glycerol diacetate. As may clearly be seen in this figure, these relaxations are expressed by the Davidson-Cole empirical equation. According to our expectations, glycerol diacetate, a monohydric alcohol, should show a Debye-type semicircular relaxation. The result fell short of our expectations, however. Judging from the small static dielectric constants, the hydrogen bonds in glycerol diacetate are much fewer in number than in normal alcohol. On the other hand, glycerol triacetate shows a Havriliak-Negami-type relaxation. The hydrogen bond in glycerol diacetate also contributes to the narrowing of the relaxation times.

Relaxation Times. Empirically, it is considered to be correct that the dielectric relaxation time of an organic molecule in the liquid state depends on the molecular size and weight. Figure 4 shows the relaxation times against the reciprocals of the absolute temperatures. The esterification of the hydroxy group by

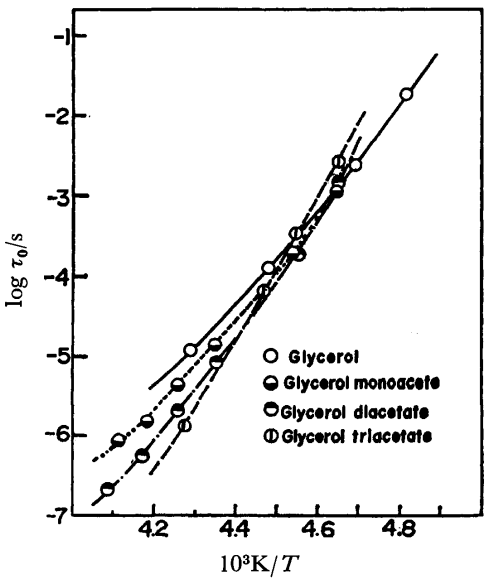

Fig. 4. Arrhenius plots of the relaxation times of the four glycerols. The unit of relaxation times is second.

acetic acid in glycerol leads to a large increase in the molecular size and weight. Nevertheless, the relaxation times do not increase, as is seen in Fig. 4, so much as would be expected from the molecular weight increase.

Another important factor determining a relaxation time is a molecular interaction such as an intermolecular hydrogen bond. The dielectric relaxation of a hydroxy compound in the liquid state generally appears at low frequencies because of this comparatively strong interaction. Thus, the esterification should also lead to a decrease in the intermolecular hydrogen bonds in the liquid structure, and consequently to a decrease in the relaxation times. Figure 4, however, does not show this anticipated tendency; Rather, it shows the four molecules to have almost the same values of relaxation times. The hidden effect due to the change in two important factors, *i.e.*, the molecular weight and the interaction, explains why the relaxation times of the four molecules do not change very much, although the two factors change markedly upon the replacement. The answer is thus given that the two effects counteract each other; therefore, apparently the relaxation times do not differ largely.

References

1) See, *e.g.*, A. H. Price, "Dielectric Properties and Molecular Behavior," ed by N. F. Hill, W. E. Vaughan, A. H. Price, and M. Davies, Van Nostrand, London (1969), Chap. 4.

2) F. X. Hassion and R. H. Cole, *J. Chem. Phys.*, **23**, 1756 (1955).

3) R. Lin and W. Dannhauser, *J. Phys. Chem.*, **67**, 1805 (1963).

4) R. H. Cole, *J. Phys. Chem.*, **59**, 2013 (1955).

5) Krishnaji and A. Mansingh, *J. Chem. Phys.*, **41**, 827 (1964).

6) D. W. Davidson and R. H. Cole, *J. Chem. Phys.*, **19**, 1484 (1951).

7) S. Havriliak and S. Negami, *Polymer*, **8**, 161 (1967).

8) E. Ikada and T. Watanabe, *J. Poly. Sci., Poly. Chem. Ed.*, **10**, 3457 (1972).
9) E. Ikada and T. Watanabe, *J. Phys. Chem.*, **78**, 1078 (1974).
10) C. P. Smyth, "Dielectric Behavior and Structure," McGraw-Hill, New York (1955), Chap. IV.
11) E. Ikada, *Bull. Inst. Chem. Res., Kyoto Univ.*, **45**, 352 (1967).
12) E. Ikada, Y. Hida, H. Okamoto, J. Hagino, and N. Koizumi, *Bull. Inst. Chem. Res., Kyoto Univ.*, **46**, 239 (1968).

Thermochemical Studies on Double- and Triple-layered [2.2]Paracyclophanes. Estimation of Molecular Strain Energies.

Keiichi Nishiyama, Ninoru Sakiyama,* Syûzô Seki** Hisanori Horita,†
Tetsuo Otsubo,†*** and Soichi Misumi†

Department of Chemistry, Faculty of Science, Osaka University, Toyonaka, Osaka, 560
†*The Institute of Scientific and Industrial Research, Osaka University, Suita, Osaka, 565*

(Received August 13, 1979)

The measurements of enthalpies of combustion by use of precision oxygen-bomb combustion calorimeter together with the measurement of carbon dioxide recovery were made for double- and triple-layered [2.2]paracyclophanes. The enthalpies of sublimation were also determined by the measurement of temperature dependence of the vapor pressures for the two compounds. The following values are reported for the standard enthalpy of combustion ΔH_c°(298.15 K)/kJ mol^{-1} and standard enthalpy of sublimation ΔH_s°(298.15 K)/kJ mol^{-1}, respectively: double-layered [2.2]paracyclophane, 8729.48$\pm$1.80, 99.6$\pm$1.8; triple-layered [2.2]paracyclophane, 14230.87 $\pm$3.59, 125.9$\pm$2.5. From analyses of the derived standard enthalpy of formation in gaseous state the following two values for total strain energy U_S/kJ mol^{-1} of a molecule of triple-layered [2.2]paracyclophane were obtained: 251.9$\pm$5.6 with group method and 245.6$\pm$9.8 with chemical similarity method, respectively. These values are approximately twice the magnitudes of the corresponding quantities for double-layered [2.2]paracyclophane. From the analysis of the total strain energy by use of the result of Boyd's molecular mechanical calculation, the contribution from the twisting of the inner benzene ring to the total strain energy of triple-layered [2.2]paracyclophane was estimated to be almost twice that from one outer bent benzene ring.

Molecular and crystal structures of double-layered [2.2]paracyclophane (**1**) have been studied by X-ray diffraction method first by Brown,[1] and later reinvestigated by Lonsdale *et al.*,[2] by Bekoe *et al.*[3] and by Hope *et al.*[4] The various striking features in the molecular structure of **1** are as follows: (i) bent aromatic rings, (ii) short contact between aromatic rings, (iii) out-of-plane deformation of methylene carbon and aromatic hydrogen atoms from the plane defined by the nearest and next-nearest three aromatic carbon atoms, and (iv) eclipsing of bridge methylene groups. These features are considered to be resulted, directly or indirectly, from trans-annular π-electron repulsion in the molecule. Hope *et al.*[4] have shown that in the ordinary temperature phase of the crystal each molecule is statistically disordered to simulate a dynamic disorder that occurs by a twist of the aromatic rings with the amplitude of 3° in opposite directions about their common normal. Additional support for the twist can be found in spectroscopic[43] and thermal[28] results.

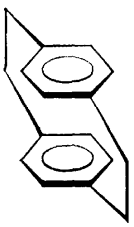

Compd. 1

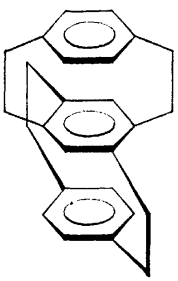

Compd. 2

Standard enthalpy of formation of **1** in the crystalline state has been reported by Boyd[5] and by Rodgers *et al.*[6] A significant difference of 9.4 kJ mol^{-1} has been found between these two values. Enthalpy of sublimation has been determined for this compound by Boyd[5] from the measurement of vapor pressure as a function of temperature. Strain energy has been estimated by Boyd[5] and by Rodgers *et al.*[6] from standard enthalpy of formation in gaseous state thus evaluated.

Boyd has also made calculation for this molecule based on a molecular mechanical method,[7] which enables simultaneous determination of molecular geometry, strain energy and thermodynamic quantities. Kao and Allinger[8] have applied a combined molecular orbital-molecular mechanics method to this molecule. They derived 199.2 kJ mol^{-1} for the standard enthalpy of formation in gaseous state which is significantly lower than both of the corresponding experimental values reported by Boyd[5] and by Rodgers *et al.*[6] and harboured a suspicion that the experimental results might be inaccurate. Lindner[9] also calculated standard enthalpy of formation for this compound in gaseous state by using a similar method.[10]

Molecular and crystal structures of triple-layered [2.2]paracyclophane (**2**) itself have not been reported. However, those for 1,4-bromo derivative of triple-layered [2.2]paracyclophane (**3**)[11] and for 4,4′,7,7′-tetramethyl-substituted centrosymmetric quadruple-layered [2.2]paracyclophane (**4**)[12] have been studied by X-ray diffraction method. While outer aromatic rings in these molecules are boat-shaped, inner aromatic

**Present address: Department of Chemistry, School of Science, Kwansei Gakuin University, Nishinomiya, Hyogo 662.
***Present address: Department of Applied Chemistry, Faculty of Engineering, Hiroshima University, Senda-machi, Hiroshima, 730.

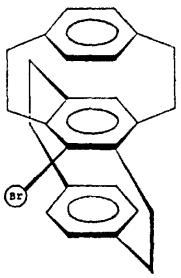

Compd. 3

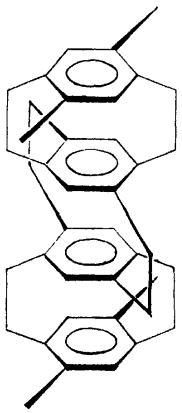

Compd. 4

rings are twisted by two upper and two lower methylene bridges. Most of the remaining anomalous features present in the molecule of **1** are found also in these molecules. It seems to be highly probable that the molecular geometry of **2** is similar to that of **3**. No thermodynamic study has been reported for this compound.

The present study has been carried out to examine the validity of the suspicion presented by Kao and Allinger[8] on the reported experimental results of **1** and to estimate the strain energy of **2**.[13] For this purpose, standard enthalpies of formation of **1** and **2** in the crystalline and gaseous states have been determined by bomb combustion calorimetry and by the measurement of temperature dependence of vapor pressure.

Experimental

Materials. Compound **1** was prepared by 1,6-Hofmann elimination method according to Winberg *et al.*[14] and purified by successive operations of gel-permeation liquid chromatography, recrystallization from chloroform (twice) and finally sublimation under vacuum (*ca.* 0.1 Pa).

Compound **2** was prepared as previously reported[15] and purified by gel-permeation liquid chromatography and then recrystallization from toluene solution (three times).

Combustion Calorimetry. An isoperibol precision rotating bomb calorimetric system described elsewhere[16] was used in this study without rotating the bomb. The following minor modifications were made on the calorimetric system after the publication of the previous paper: (1) The vacuum tube jacket temperature controller was replaced with a solid state device with proportional, integral and derivative actions. (2) The cooling device of the jacket water using ice was substituted with a refrigerator using semi-conductor Peltier elements which could supply cold water thermostatted within ± 30 mK. (3) The "Teflon" gasket for bomb-sealing was replaced with a rubber "O" ring. (4) The two unified connector-valves on the lid of the bomb using "Swagelok" fittings were replaced with the ones in which rubber "O" rings were used for sealing. (5) For connecting four lead wires to the calorimeter can, pin-connectors were used in place of soldering. (6) The oil-sealing of the calorimeter can were omitted to allow moderate vaporization of calorimeter water.

The calorimeter was calibrated by burning thermochemical standard benzoic acid (N.B.S. SRM-39i) under the standard bomb conditions.[17] The calibration experiments were interspersed between combustion experiments. Energy equivalents for the standard calorimetric system were derived from seven and eight calibration experiments for **1** and **2**, respectively. Mean and standard deviation of the mean were (15162.26 ± 1.08) J K^{-1} and (15164.06 ± 0.48) J K^{-1} for **1** and **2**, respectively.

Compound **1** was pressed into pellets by using a hand-press and an ordinary unevacuable die-set. The pellets exhibited a tendency to explode when partly burnt in the bomb. A deep crucible with a baffle described previously[18] was used for this compound.

Compound **2** was pressed into pellets by using a pellet press and a die-set usually used for making a KBr disk in infrared spectrometry. The pellets were burned in an ordinary platinum crucible. In two of experiments, a pellet of benzoic acid (thermochemical standard) weighing *ca.* 0.2 g was placed upon and under the pellet of the compound, respectively. In any experiments, a pellet of the compound did not explode when burned and significant amount of carbon monoxide was not detected from the bomb gas after combustion. However, the formation of a small amount of soot was observed in the crucible in every experiment.

In order to examine the completeness of combustion and/or the purity of a sample, carbon dioxide recovery was determined by the method developed by Rossini.[19] The absorption tube used in this study is shown in Fig. 1, which is similar in design to Pilcher's.[20] Ascarite (A.H. Thomas & Co., Ltd.) was used as an absorbent of carbon dioxide. In order to capture a small amount of water, which might be removed from the Ascarite layer, a small amount of Anhydrone

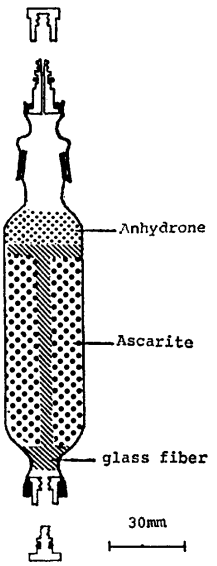

Fig. 1. Absorption tube for carbon dioxide analysis.

(Nakarai, S.P.R.) was placed next to the Ascarite layer. Heart of the absorption tube is the use of a small bundle of glass fiber placed from the inlet through the central portion of the Ascarite layer. The bundle of glass fiber exhibited a significant effect to secure the passage of bomb gas even after more than a half amount of Ascarite had lost its ability to absorb carbon dioxide. The ground glass joint was sealed with picein cement. The use of "O" ring along with metal connectors served to keep the absorption line leak-proof without loss of simplicity of experimental procedures. The flow rate of the gas liberated from the bomb was adjusted to *ca.* 2 $cm^3 s^{-1}$ with a needle valve. The gas was dried thoroughly by passage through the first absorption tube where Anhydrone was packed. The dried gas was then introduced into the second absorption tube, in which Ascarite was packed, and then examined for carbon monoxide by a detector tube (Kitagawa carbon monoxide detector type C, Kōmyo-Rikagaku Co., Ltd.) and finally released to air.

Before the analysis, the absorption train was flushed with oxygen. The carbon dioxide absorption tube was then disconnected, both the inlet and the outlet being closed, and the outer surface was cleaned with a piece of wiping paper wetted with ethyl ether, and then the tube was allowed to stand for 30 minutes. Just before weighing, pressure inside the tube was equalized with outside one by opening the gas inlet instantly. The tube was weighed and connected again to the train to start the absorption of carbon dioxide. After the pressure in the bomb decreased to atmospheric pressure, the bomb was flushed with oxygen (*ca.* 10 dm^3) at the average flow rate of 2 $cm^3 s^{-1}$. This flushing was performed to purge carbon dioxide in the gaseous and liquid phases completely. The absorption tube was then removed from the train and weighed in the same way as before.

From apparent increase in mass of the absorption tube Δm(tube), true mass of carbon dioxide captured, $m(CO_2$, obsd), was calculated by the following expression given by Rossini:[19]

$$m(CO_2, \text{obsd}) = 1.00045 \times \Delta m(\text{tube}).$$

In order to examine the validity of the results obtained by the procedure described above, combustion products of the calibration experiments were also analyzed. Carbon dioxide recovery defined as ratio of recovered to calculated masses of carbon dioxide $m(CO_2$, obsd$)/m(CO_2$, calcd) for successful seven analyses of the calibration experiments is as follows: 1.0000, 0.9997, 1.0002, 0.9999, 0.9999, 1.0001 and 1.0000. Mean and standard deviation of mean were 1.0000 ± 0.0001.

The CO detector is capable of detecting the concentration range of 0 to 3 ppm. Presence of carbon monoxide at the level of 3 ppm gives rise to an error of only 0.0015% in the standard energy of combustion.

Ordinary eight minutes flushing of the bomb prior to charging it with oxygen was sufficient to suppress the amount of nitric acid to a level less than 10^{-5} mol as the substances burned in this study contained no nitrogen. The nitric acid was determined spectrophotometrically using a UV absorption band at 202 nm.[21]

Determination of Sublimation Enthalpy. Enthalpies of sublimation were determined from temperature dependence of vapor pressure. Vapor pressures were measured by using a DuPont model 916 Thermal Evolution Analyzer which was a plug-in module of DuPont 990 Thermal Analysis System. The measurement is based on the gas saturation method in which a flame ionization detector (FID) is used to detect organic vapor present in carrier gas (usually nitrogen).[22]

A small amount (*ca.* 10 mg) of sample was placed in a cylindrical metallic cell with a small hole at the center of the lid together with silver granules used for improving heat conduction. The cell was inserted in a "Vycor" glass tube placed in a temperature-regulated furnace and the carrier gas was allowed to flow at a constant rate only outside the cell. FID current was then recorded. After thermal equilibrium was found to be established in the cell from the recorder trace, a small portion of the carrier gas was allowed to flow through the cell, while the total flow rate was kept constant. Organic vapor ran out through the hole into external carrier gas flow and the FID current increased. After saturation of the internal carrier gas flow with organic vapor was confirmed from the recorder trace, the carrier gas flow pattern was restored. Change in the FID current caused by changing the flow pattern was determined as a function of temperature. The change in the FID current was assumed to be proportional to saturated vapor pressure of the compound at that temperature and logarithm of it was plotted against reciprocal temperature. From the slope of the derived straight line, sublimation enthalpy at a mean temperature was obtained on the basis of the second law method.

The reliability of the method was examined by using naphthalene (Kishida Chemicals, SMA-SP-16) as a test substance in accordance with the recommendation of IUPAC.[23] The naphthalene sample is an organic micro-analytical standard sample certified by the Sub-committee of Organic Microanalysis of the Japan Society for Analytical Chemistry. Enthalpy of sublimation was derived from the vapor pressures in the range 301.8 to 347.2 K (fourteen measurements). The enthalpy of sublimation 70.7 kJ mol^{-1} at 324.5 K was reduced to the value at 298.15 K using heat capacities for gaseous[24] and solid[25] states. Enthalpy of sublimation at 298.15 K obtained in this way was 71.7 kJ mol^{-1}, while the value recommended by IUPAC[23] is 72.5 ± 0.25 kJ mol^{-1}. Accordingly, uncertainty of ± 1.5 kJ mol^{-1} was assigned tentatively to values obtained in this study.

Table 1. Auxiliary quantities

Compound	Formula	ρ / g cm^{-3}	c_p / J K^{-1} g^{-1}	$(\partial E/\partial p)_T$ / J MPa^{-1} g^{-1}
Compd. **1**	$C_{16}H_{16}$	1.229	1.21	−0.15[a]
Compd. **2**	$C_{26}H_{26}$	1.140	1.21[a]	−0.15[a]
Benzoic acid	$C_7H_6O_2$	1.320	1.21	−0.052

a) Estimated value.

Auxiliary Quantities. Experimental results in this paper are based on 1961 atomic weights. Auxiliary data adopted in the calculation of molar standard enthalpies of combustion ΔE_c°, *i.e.* the composition formula and the values (for 298.15 K) of density, ρ, of specific heat capacity, c_p, and of compression energy, $(\partial E/\partial p)_T$, for the combustible substances, are given in Table 1. The values for **1** were taken from Ref. 6. The density **2** was determined from the dimension of a pellet of known mass. Other auxiliary quantities are also collected in the table. Uncertainties are uncertainty intervals defined by Rossini,[26] unless otherwise stated.

Standard energies and enthalpies of combustion given in this paper refer to the following idealized combustion reaction at 298.15 K:

$$C_aH_b(c) + (a+b/4)O_2(g) = aCO_2(g) + (b/2)H_2O(l),$$

where $a=16$, $b=16$ for **1** and $a=26$, $b=26$ for **2**.

Results

Combustion Calorimetry. Results of typical combustion experiments for **1** and **2** are given in Table 2.

TABLE 2. TYPICAL COMBUSTION EXPERIMENTS

	Compd. **1**	Compd. **2**
m^i(compd.)/g	0.65238	0.61825
m^i(fuse)/g	0.00259	0.00250
$m^i(H_2O)$	1.0344	1.0229
p^i(gas)/MPa	3.040	3.040
θ_i/°C	23.139114	23.245857
θ_f/°C	24.971104	24.987338
$\Delta\theta_{corr}$/°C	0.029415	0.028176
$n^f(HNO_3)$/μmol	4	3
ΔE_{lgn}/J	7.6	2.7
ε^i(cont.)/JK^{-1}	19.62	16.87
ε^f(cont.)/JK^{-1}	20.98	18.15
ΔE_Σ/J	13.5	13.0
$\Delta E_{I.B.P}$/J	−27359.0	−26007.2
$\frac{\Delta E_c^\circ}{M}$/kJ g^{-1}	−41.8508	−41.9778

TABLE 3. SUMMARY OF COMBUSTION CALORIMETRIC RESULTS FOR DOUBLE-LAYERED [2.2]PARACYCLOPHANE

Exp. No.	$-\Delta E_c^\circ$(c)/kJ mol^{-1}	$\frac{m(CO_2, obsd)^{b)}}{m(CO_2, calcd)}$	$10^6 x$ (CO)	Soot on the bomb wall
3	8715.86	a)	1.5	None
4	8722.28	a)	1.4	None
5	8717.62	0.9994	2.4	None
6	8716.46	0.9993	0.9	None
7	8713.89	0.9985	2.4	Trace
8	8715.31	0.9986	3.0	Trace
11	8714.51	0.9987	0.9	None
13	8710.58	0.9976	0.9	None

a) CO_2 analysis was unsuccessful. b) $m(CO_2, obsd)$ and $m(CO_2, calcd)$ are observed and calculated masses of carbon dioxide for the total of combustible substances in the bomb, respectively.

Of thirteen combustion experiments on **1**, eight gave at least reasonably reliable calorimetric data. In Table 3, results of the successful experiments are summarized together with results of carbon dioxide and monoxide analyses and also with remarks on the presence of soot on the bomb wall after combustion. In no experiments in Table 3, soot was found in the crucible. Numerical values of ΔE_c° given in Table 3 are calculated on the basis of masses of samples.

In the previous letter,[13] the values of ΔE_c° for five experiments (No. 3, 4, 5, 6, and 11), in which no soot formation was observed and carbon dioxide recovery was not less than 99.85% (in the cases where the analysis was successful) have been used to calculate mean and standard deviation of the mean to obtain the following result: $\Delta E_c^\circ = -(8717.13 \pm 1.33)$ kJ mol^{-1} (Procedure I).

Discrepancy between the values of ΔE_c° reported by Boyd[5] and Rodgers *et al.*[6] amounted to only 9.4 kJ mol^{-1} (0.108% of the total) and carbon dioxide recovery higher than 99.90% was experienced only in two (No. 5 and 6) of the experiments given in Table 3. From these viewpoints, re-examination of the results of combustion calorimetry by different procedures seems to be desirable in order to estimate a correct value of ΔE_c° more confidently.

Use of results of experiments No. 5, 6, and 11, where no soot formation was observed and carbon dioxide analysis was successful, instead of the five results used in Procedure I, leads to the following result: $\Delta E_c^\circ = -(8716.20 \pm 0.29)$ kJ mol^{-1} and $m(CO_2, obsd)/m(CO_2, calcd) = 0.9991 \pm 0.0002$, where uncertainties are standard deviation of mean(Procedure I'). This Presult differs little from that of Procedure I. The carbon dioxide recovery is not satisfactorily high enough to allow for the precise estimation of a correct value for ΔE_c°. It appears to be reasonable to assume that the above-mentioned value gives a lower limit of possible ΔE_c° values.

One of possible procedures is to calculate the individual numerical values of ΔE_c° based on carbon dioxide recovery. Mean and standard deviation of the mean calculated in this way from the results of six experiments where the analysis was successful are as follows: $\Delta E_c^\circ = -(8726.21 \pm 1.33)$ kJ mol^{-1} (Procedure II). This procedure would be favorably applicable if a sample contaminated with incombustible impurities, such as water, was completely burnt or incompletely burnt in the sence that part of the sample remained unchanged after a combustion experiment. The same would hold if a pure sample was burnt incompletely in the same sence as described above. However, the present sample is not likely to be contaminated with incombustible impurities in view of the method of purification and possible impurities, if present, would be organic in nature. In addition to this, soot on the bomb wall is the product of the most significant side reaction. The numerical value of the mean given by Procedure II would therefore give an upper limit of possible ΔE_c° values.

Another possible procedure is to apply a least-squares analysis for the results of experiments to which Procedure II has been applied, to get ΔE_c° as a linear function of carbon dioxide recovery, $[m(CO_2, obsd)/m(CO_2, calcd)]$ (Procedure III). Derived linear function is as follows: ΔE_c°/kJ mol^{-1} $= -3669.00\,[m(CO_2, obsd)/m(CO_2, calcd)] - 5050.56$. Extrapolation of the function to $[m(CO_2, obsd)/m(CO_2, calcd)] = 1$ leads to the following result: $\Delta E_c^\circ = -(8719.56 \pm 0.56)$ kJ mol^{-1}, where uncertainty is standard deviation. In this procedure, results of, rigorously speaking, more or less incomplete combustion experiments for a sample of unknown purity are extrapolated practically to complete combustion of a pure sample. This procedure appears to the authors to be more reasonable than the other ones.

Consequently, the numerical value estimated by Procedure III was adopted as a correct ΔE_c° value for **1**.

Six of seven experiments on **2** were successful. The results are summarized in Table 4. The more complete combustion was achieved in general than for **1** possibly because of improvement in the preparation of the pellets, although a small amount of soot was found in the crucible after every experiment. The numerical values of ΔE_c° given in Table 4 are calculated on the basis of the masses of samples and corrected for soot formation by using ICSU-CODATA key value for

Table 4. Summary of combustion calorimetric results for triple-layered [2.2]paracyclophane

Exp. No.	$-\Delta E_c^\circ$(c)[a] / kJ mol^{-1}	$m(CO_2$, obsd)[b] / $m(CO_2$, calcd)	$10^6 x$ (CO)	m(soot) / mg
1	14210.33	1.0005(1.0008)	0.5	0.15
2	14208.94	0.9994(0.9997)	0.2	0.14
3	14217.38	———(———)[e]	0	0.14
4	14212.18	0.9990(0.9993)	0.6	0.17
6	14214.52[d]	0.9986(0.9991)	0.9	0.26
7	14210.88[d]	0.9984(0.9987)	0.1	0.16
mean and sdm[c]	14214.76±1.65	0.9992±0.0004 (0.9995±0.0003)		

a) Corrected for soot formation. b) Numerical values in parenthesis are corrected for soot. c) Standard deviation of mean. d) Benzoic acid was used as an auxiliary substance. e) CO_2 analysis was unsuccessful.

$\Delta H_f^\circ(CO_2, g)$.[27] The correction amounted to −8.52 kJ mol^{-1} (0.085% of the total) for an extreme case and to −5.57 kJ mol^{-1} in average. As an error was found in the calculation of the soot correction given in the previous letter,[13] ΔE_c° values are increased by 4.61 kJ mol^{-1} in comparison with the previous values. Corresponding revisions were made also on the numerical values of ΔH_c°(c) and ΔH_f°(c). As no significant difference was observed between the results of experiments with and without the use of benzoic acid as an auxiliary substance, all the values in Table 4 were used equally to calculate the mean value.

Enthalpy of Sublimation. Plots of log h against reciprocal temperature T^{-1} are given in Figs. 2 and 3 for **1** and **2**, respectively, where h is the increase in FID current caused by changing the flow pattern of the carrier gas so that part of the carrier gas flows through the sample cell while keeping the total flow rate constant. Analyses of the experimental data by means of the

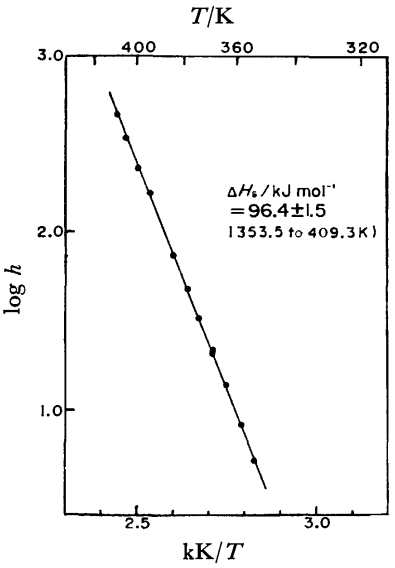

Fig. 2. Temperature dependence of vapor pressure of double-layered [2.2]paracyclophane in the crystalline state. Unit of FID current h, which is proportional to vapor pressure, is arbitrary.

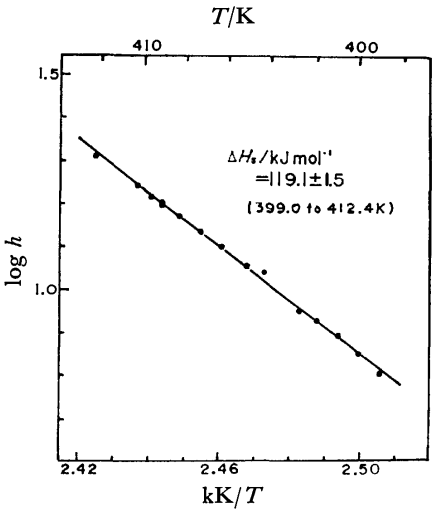

Fig. 3. Temperature dependence of vapor pressure of triple-layered [2.2]paracyclophane in the crystalline state. Unit of FID current h, which is proportional to vapor pressure, is arbitrary.

second law method gave the following enthalpies of sublimation at mean temperatures: 96.4±1.5 kJ mol^{-1} at 381.4 K and 119.1±1.5 kJ mol^{-1} at 405.7 K for **1** and **2**, respectively. Enthalpies of formation at 298.15 K were derived by use of the Kirchhoff's equation. For **1**, molar heat capacities of the gas calculated by Boyd[7] and those of the solid obtained by extrapolation of experimental heat capacities measured by Andrews and Westrum[28] were used in the calculation. For **2**, molar heat capacities of the gas and the solid were estimated from the corresponding values of **1** by assuming that specific heat capacity is of the same magnitude for both compounds. The corrections to 298.15 K amounted to 3.2±1.0 kJ mol^{-1} and 6.8±2.0 kJ mol^{-1} for **1** and **2**, respectively, where uncertainties were estimated arbitrarily.

Thermodynamic Quantities. Standard thermodynamic quantities at 298.15 K were calculated and summarized in Table 5. ICSU-CODATA key values[27] were used in the calculation of standard enthalpies of formation. Uncertainty for ΔE_c° of **2** was calculated as if all the combustion experiments were carried out by use of benzoic acid. So the result will be naturally overestimated.

Discussion

Comparison with Qiterature Values. The selected numerical value of ΔH_c° for **1** given in Table 5 is only by 2.21 kJ mol^{-1} more negative than the previously

Table 5. Thermodynamic quantities

	Double-layered [2.2]paracyclophane	Triple-layered [2.2]paracyclophane
$-\Delta E_c^\circ$(c)/kJ mol^{-1}	8719.56±1.80	14214.76±3.59
$-\Delta H_c^\circ$(c)/kJ mol^{-1}	8729.48±1.80	14230.87±3.59
ΔH_f°(c)/kJ mol^{-1}	146.69±2.77	283.82±4.96
ΔH_s°/kJ mol^{-1}	99.6± 1.8	125.9 ±2.5
ΔH_f°(g)/kJ mol^{-1}	246.3± 3.3	409.7 ±5.6

reported value of the authors[13] and lies between the values reported by Boyd[5] and by Rodgers *et al.*,[6] being closer to the latter. Both of the literature values are barely in the range of possible ΔH_c° values as estimated in the preceding section. It appears to be more reasonable and more consistent to employ the present value for the discussion in later sections, partly because the present value is substantiated by carbon dioxide analysis.

The present value for ΔH_s° at 298.15 K for **1** agrees with the Boyd's value 96.2 ± 4.2 kJ mol^{-1} [5] within the sum of assigned uncertainties. Re-examination of Boyd's experimental values of vapor pressure reveals that in the log p *vs.* T^{-1} plots one (at 373.10 K) deviates significantly from a straight line obtained by a least squares treatment of the remaining four values. Neglect of the deviated point leads to the following result (instead of reported 92.8 kJ mol^{-1}): $\Delta H_s^\circ = 94.2$ kJ mol^{-1} at 363 K. Furthermore, correction from 363 to 298.15 K was recalculated by using the (extrapolated) experimental molar heat capacities of Andrews and Westrum.[28] The correction amounted to $+2.5$ kJ mol^{-1}. Enthalpy of sublimation at 298.15 K thus calculated is (96.7 ± 4.2) kJ mol^{-1}, where uncertainty is unchanged from the original one. This value is close to Boyd's original value. Method and apparatus used in the present determination of ΔH_s° were examined as described in the preceding section, while no description is found in Boyd's papers.[5,29] Hence, the present value has been adopted to calculate the value of ΔH_f°(g).

Standard enthalpy of formation for gaseous **1** derived in this study is 246.3 ± 3.3 kJ mol^{-1}, which is 47.1 kJ mol^{-1} more positive than the value predicted by Kao and Allinger[8] based on the combined molecular orbital-molecular mechanics method. Even if scatter of experimental values of ΔH_c° and ΔH_s° described above and their uncertainties were taken into consideration, the predicted value is definitely away from the range of possible ΔH_f°(g) values. Generally speaking, the method of Kao and Allinger[8] were successful in reproducing precisely experimental enthalpies of formation of a number of gaseous conjugated hydrocarbons, but the above-mentioned fact seems to reveal that the method has been applied, in this case, to a too highly strained molecule beyond the applicability limit. On the other hand, ΔH_f°(g) value deduced from Lindner's[9] calculated enthalpy of atomization† is 257 kJ mol^{-1}, which is rather closer to the present experimental value.

No literature values are available for ΔH_c° and ΔH_s° of **2**.

Estimation of Strain Energy of Triple-Layered [2.2]-Paracyclophane. Strain energy brought about in a molecule of **2** by the formation of two larger ring systems composed of aromatic rings and methylene groups was estimated by the following two different methods.

(i) Group Method. In order to estimate the total strain energy U_s, standard enthalpy of formation in gaseous state for a "strain-free" reference structure ΔH_f°(g, ref.) was calculated by means of the group increments given by Cox and Pilcher,[30] which, together with terms for steric effect from *ortho* alkyl groups, had been proved to account for standard enthalpies of formation in gaseous state of nineteen simple alkyl-substituted benzenes within ± 4 kJ mol^{-1}, and it was compared with experimental standard enthalpy of formation in gaseous state ΔH_f°(g, exp.):

$$U_s = \Delta H_f^\circ(\text{g, exp.}) - \Delta H_f^\circ(\text{g, ref.}) - 2RT \qquad (1)$$

The final term in Eq. 1 is the (PV) correction,[31] which is needed in *a priori* estimation of ring strain energy. In this paper, standard enthalpy of formation in gaseous state for the reference structure was calculated without inclusion of steric effect from *ortho* methylene groups. The resultant value of ΔH_f°(g, ref.) is 152.8 kJ mol^{-1} for **2** and substitution of this value in Eq. 1 gives 251.9 ± 5.6 kJ mol^{-1} for the total strain energy. Total strain energy for **1** calculated similarly amounts to 126.0 ± 3.3 kJ mol^{-1}, which is of a half magnitude in comparison with the corresponding value for **2**.

(ii) Chemical Similarity Method. Another approach for estimating the total strain energy is to compare the reaction enthalpy for gas-phase homolytic hydrogenation-cleavage of four dimethylene bridges of **2** with four times the reaction enthalpy for the corresponding cleavage of the central C–C bond of 1,2-diphenylethane. The procedure, together with estimate of the total strain energy, is summarized in Table 6. Standard enthalpy of formation of gaseous toluene and xylene were taken from Ref. 32. The value of ΔH_f°(g) for 1,2-diphenylethane was calculated from standard enthalpy of formation in the crystalline state[32] and enthalpy of sublimation reported by Morawetz.[33] The value of ΔH_f°(g) for 1,2,4,5-tetramethylbenzene was calculated from standard enthalpy of formation for undercooled liquid at 298.15 K[34,35] and hypothetical enthalpy of vaporization at 298.15 K derived from Antoine equation analysis of liquid vapor pressures.[36] Derived strain energy 245.6 ± 9.8 kJ mol^{-1} is almost twice the value for **1**, 122.6 ± 5.4 kJ mol^{-1}, derived similarly. The strain energies calculated by this method agree with the corresponding values derived in the preceding section within the sum of uncertainties.

Analysis of the Total Strain Energy of Triple-Layered [2.2]paracyclophane. For **1**, Gantzel *et al.*[37] made an *a priori* estimation of total strain energy by using Brown's structure[1] and Whiffen's spectroscopic force constants.[38] Boyd[5] also made a similar analysis by using structure determined by Lonsdale[2] and force constants given by Kakiuti and Shimanouchi.[39] Later, Boyd[7] carried out a calculation based on molecular mechanics to determine molecular structure, strain energy and thermodynamic functions, simultaneously. The distribution of the total strain energy amounting to 147 kJ mol^{-1} among six parts thus determined is as follows: (i) out-of-plane deformation of aromatic rings, 43 kJ mol^{-1}; (ii) deformation of *para*-substituents, 35 kJ mol^{-1}; (iii) aliphatic bridge eclipsing, 29 kJ mol^{-1}; (iv) aliphatic bridge angle deformation, 3 kJ mol^{-1}; (v) aliphatic bridge bond stretching, 3 kJ mol^{-1}; and (vi) ring repulsion(non-bonded aromatic C···C), 34 kJ

† The quantity given if Ref. 9 as "Atomisierungenergie" is supposed to mean the enthalpy of atomization from the context of Refs. 9 and 10. The value 152.06 eV/molecule derived by the improved method II was employed in the calculation of the value in the text.

TABLE 6. SCHEME FOR ESTIMATING THE STRAIN ENERGY OF TRIPLE-LAYERED [2.2]PARACYCLOPHANE (2) BY CHEMICAL SIMILARITY METHOD

(i) Compd. **2** (g) + $4H_2$(g) = $2CH_3$- 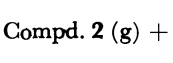 -CH_3(g) + 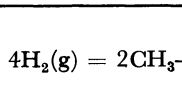 (g)

ΔH_f°(g)/kJ mol^{-1}:	409.7±5.6	0	18.0±0.9	−48.1±2.0[a]

ΔH_r°(i) = −421.8±6.2 kJ mol^{-1}

(ii) 4 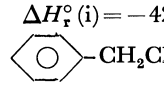 -CH_2CH_2- 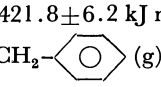 (g) + $4H_2$(g) = 8 CH_3- 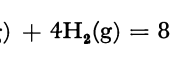 (g)

ΔH_f°(g)/kJ mol^{-1}:	143.0±1.8	0	50.1±0.3

ΔH_r°(ii) = −171.2±7.6 kJ mol^{-1}

Strain energy, $U_s = \Delta H_r^\circ(\text{ii}) - \Delta H_r^\circ(\text{i}) - 2RT$ = 245.6±9.8 kJ mol^{-1}

a) Assigned uncertainty

mol^{-1}. Rodgers *et al.*[6] suggested the necessity of downward revision for the value of item (iii), because two methylene groups eclipse completely in the final conformation determined by Boyd.[7] However, general agreement between the calculated and experimental structures and the calculated and experimental total strain energies is to be noted. Wynberg *et al.*[40] and Iwamura *et al.*[41] studied the stability of a bent benzene ring theoretically by molecular orbital methods.

In this paper, the total strain energy of **2** has been analyzed by dividing it into components in a similar way to that used in Boyd's molecular mechanical calculation.[7] The total strain energy of **2**, U_s, is expressed in a general form as follows:

$$U_s = 2U_1 + U_1^* + 2U_2 + 2U_2^* + 4U_3 + 4U_4 + 4U_5 + 2U_6 + 2U_7, \quad (1)$$

where U_1 is the contribution from the out-of-plane deformation of the outer aromatic ring, U_2, that from the deformation of the *para*-substituent on the outer aromatic ring, U_3, that from a pair of the eclipsing bridge methylenes, U_4, that from the deformation of the aliphatic bridge angle, U_5, that from the stretching of the aliphatic bridge bond, U_6, that from the repulsion between a pair of the aromatic rings, U_7, that from the repulsion between a pair of bridge methylenes bonded *ortho* with each other to the inner aromatic ring, U_1^*, that from the twisting of the inner aromatic ring, and U_2^*, that from the deformation of the substituent on the inner aromatic ring. Similarly, total strain energy of **1**, U_s', is expressed as follows:

$$U_s' = 2U_1' + 2U_2' + 2U_3' + 2U_4' + 2U_5' + 2U_6', \quad (2)$$

where U_i'(i=1∼6) are quantities corresponding to U_i(i=1∼6), respectively.

In Table 7, distances and angles which are relevant to the components of the total strain energies are compared among compounds **1**,[4] **3**[11] and **4**.[12] The symbols for distances and angles in Table 7 are schematically illustrated in Fig. 4. Similarity of the values for the parameters between **3** and **4** indicates that **3** can be a good model compound for **2** with respect to molecular structure. The values of parameters l_1, l_2, l_3, l_4, α, β, δ and ε for **1** are nearly equal to the corresponding values for **3**. This fact leads to an approximation that

$$U_i = U_i' \ (i=1\sim6) \quad (3)$$

In the preceding section, the following relation has been shown experimentally to hold:

$$U_s = 2U_s'. \quad (4)$$

From equations (1) to (4), the following expression is obtained:

$$U_1^* = 2U_1 + 2(U_2 - U_2^*) - 2U_7. \quad (5)$$

TABLE 7. COMPARISON OF MOLECULAR PARAMETERS RELEVANT TO STRAIN ENERGY COMPONENTS

Strain energy component[a]	Distance or angle[b]	Compound		
		Compd. **1**[4]	Compd. **3**[11]	Compd. **4**[12]
U_6, U_6'	l_1/nm	0.278	0.2744, 0.2753	0.2776, 0.2781
	l_2/nm	0.309	0.3061, 0.3047	0.3130, 0.3043
	l_3/nm	—	0.3184, 0.3192	0.3161, 0.3259
U_5, U_5'	l_4/nm	0.1562 (0.1593)[c]	0.1587, 0.1581	0.1581, 0.1597
U_1, U_1'	α/°	12.6	12.1, 12.3	12.5, 12.9
U_2, U_2'	β/°	11.2	10.9, 11.5	11.8, 10.8
U_2^*	β'/°	—	4.4, 6.7	6.5, 6.9
U_1^*	γ/°	—	13.6	13.4
U_4, U_4'	δ/°	113.7	111.6, 113.1	112.7, 112.0
	δ'/°	—	112.3, 111.8	111.5, 112.1
U_3, U_3'	ε/°	(6.4)[c]	6.8	8

a) For symbols, see the text. b) Symbols were defined as illustrated in Fig. 4. c) Distances and angles in compd. **1** have been determined less definitely due to the presence of molecular disorder in the crystal at room temperatures. Parenthesized values and the remaining values were calculated from parameters of Tables 7 and 1, respectively, of Ref. 4.

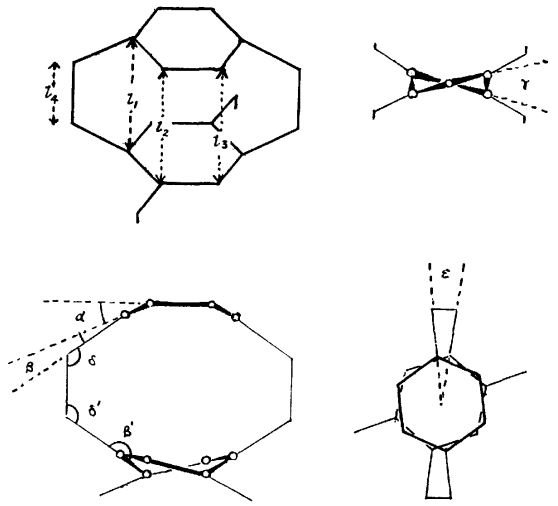

Fig. 4. Schematic illustration of interatomic distances and angles given in Table 7.

U_2* is estimated to be much smaller than U_2 on the basis of Boyd's definition of strain energy,[7] because a methylene carbon atom attached to the inner aromatic ring is significantly more coplanar with the adjacent three carbon atoms on one and the same aromatic ring than the one attached to the outer aromatic ring as shown in Table 7. The magnitude of U_7 is evaluated to be *ca.* 2 kJ mol^{-1} from extra contribution, assigned by Cox and Pilcher,[30] of a pair of *ortho* methyl and/or methylene groups to standard enthalpy of formation in gaseous state. Boyd's calculation[7] gave 21.5 and 17.5 kJ mol^{-1} for U_1' and U_2', respectively. From these considerations, the contribution from the twisted inner aromatic ring is estimated to be of more than two-fold magnitude as compared with that from the bent outer aromatic ring.

In the foregoing discussion, the contribution from transannular π-electron repulsion in **1** and **2** were assumed to be equal in magnitude. While this appears to be a sound approximation from the comparison of the values of l_1, l_2 and l_3 given in Table 7, there are evidences which indicate that the transannular repulsion is more enhanced in **2** than in **1**. Charge transfer bands in tricarbonylchromium,[42] tetracyanoethylene[15a] and 1,3,5-trinitrobenzene[15a] complexes of multilayered[2.2]-paracyclophanes show bathochromic shifts with the increase of the number of layers. Infrared bands for the tricarbonylchromium complexes associated with C=O stretching shift to lower frequencies with the increase of the number of layers. These facts show enhanced Lewis basicity of π-electrons with the increase of the number of layers, which reflects enhancement of the transannular π-electron repulsion. While there is little characteristic in the electronic spectra of multilayered [2.2]metacyclophanes in which transannular π-electron interaction is estimated to be much weaker than in [2.2]paracyclophanes due to small overlap of the aromatic rings, the electronic spectra of multilayered [2.2]paracyclophanes show marked bathochromic and hyperchromic shifts with the increase of the number of layers. This fact also suggests that the transannular π-electron repulsion is enhanced with the increase of the number of layers.

If this effect is taken into account, the contribution from the twisted inner aromatic ring is decreased correspondingly. While the magnitude of U_6' was evaluated to be 36 kJ mol^{-1} by Boyd, that of U_6 is still unknown at present. However, the difference between U_6 and U_6' is supposed to be small from the similarity of relevant nonbonding interatomic distances.

In conclusion, even if various approximations and suppositions made in the foregoing discussions were taken into consideration, it seems to be valid to argue that the twisted inner aromatic ring in triple-layered [2.2]paracyclophane molecule is at least more strained energetically than the bent outer ones, or that the contribution from the former ring to the total strain energy is approximately twice that from the latter ring. In other words, stabilization due to π-electron delocalization in the former ring is deteriorated at least more significantly than in the latter ring or possibly deteriorated by twice the magnitude as compared with that in the latter ring.

The authors are indebted to Dr. G. Pilcher of University of Manchester, England, and Dr. A. J. Head of National Physical Laboratory, England, for teaching the technique of carbon dioxide analysis to one of the authors (M. S.).

References

1) C. J. Brown, *J. Chem. Soc.*, **1953**, 3265.
2) K. Lonsdale, J. J. Milledge, and K. V. K. Rao, *Proc. Roy. Soc.* **A255**, 82 (1960).
3) A. D. Bekoe and K. N. Trueblood, Abstracts of the American Crystallographic Association, Bozeman, Montana, Paper J-12 p. 87 (1964).
4) H. Hope, J. Bernstein, and K. N. Trueblood, *Acta Crystallogr., Sect. B*, **28**, 1733 (1972).
5) R. H. Boyd, *Tetrahedron*, **22**, 119 (1966).
6) D. L. Rodgers, E. F. Westrum, Jr., and J. T. S. Andrews, *J. Chem. Thermodyn.*, **5**, 733 (1973).
7) R. H. Boyd, *J. Chem. Phys.*, **49**, 2574 (1968).
8) J. Kao and N. L. Allinger, *J. Am. Chem. Soc.*, **99**, 975 (1977).
9) H. J. Lindner, *Tetrahedron*, **32**, 753 (1976).
10) a) H. J. Lindner, *Tetrahedron*, **30**, 1127 (1974); b) H. J. Lindner, *Tetrahedron Lett.*, **1974**, 2479.
11) Y. Koizumi, T. Toyoda, H. Horita, and S. Misumi, 32nd National Meeting of the Chemical Society of Japan, Tokyo, April 1975, Abstr. I, p. 184.
12) H. Mizuno, K. Nishiguchi, T. Toyoda, T. Otsubo, S. Misumi, and N. Morimoto, *Actg Crystallogr., Sect. B*, **33**, 329 (1977).
13) Results of the present study has been reported briefly: K. Nishiyama, M. Sakiyama, S. Seki, H. Horita, T. Otsubo, and S. Misumi, *Tetrahedron Lett.*, **1977**, 3739.
14) H. E. Winberg, F. S. Fawcett, W. E. Mochel, and C. W. Theobald, *J. Am. Chem. Soc.*, **82**, 1428 (1960); H. E. Winberg and F. S. Fawcett, *Org. Synth.*, Coll. Vol. V, 883 (1973).
15) a) T. Otsubo, S. Mizogami, I. Otsubo, Z. Tozuka, A. Sakagami, Y. Sakata, and S. Misumi, *Bull. Chem. Soc. Jpn.*, **46**, 3519 (1973); b) T. Otsubo, H. Horita, and S. Misumi, *Synth. Commun.*, **6**, 591 (1976).
16) M. Sakiyama, T. Nakano, and S. Seki, *Bull. Chem. Soc. Jpn.* **48**, 1705 (1975).

17) F. D. Rossini, Ed., "Experimental Thermochemistry," Interscience Publishers, New York (1956), Vol. 1, p. 38.
18) A. Kamaguchi, T. Sato, M. Sakiyama, and S. Seki, *Bull. Chem. Soc. Jpn.*, **48**, 3749 (1975).
19) Ref. 17, p. 65.
20) G. Pilcher, private communication.
21) R. P. Buck, Singhadeja Samong, and L. B. Rogers, *Anal. Chem.*, **26**, 1240 (1954).
22) F. T. Eggertsen, E. E. Seibert, and F. H. Stross, *Anal. Chem.*, **41**, 1175 (1969).
23) E. F. G. Herington, Ed., and J. D. Cox, Collator, *Pure and Appl. Chem.*, **40**, 399 (1974).
24) D. R. Stull, E. F. Westrum, Jr., and G. C. Sinke, "The Chemical Thermodynamics of Organic Compounds," John Wiley and Sons, Inc., New York (1969), p. 389.
25) Extraporated values from the results of J. C. Southard and F. G. Brickwedde, *J. Am. Chem. Soc.*, **55**, 4378 (1933).
26) Ref. 17, p. 197.
27) ICSU-CODATA Task Group, Report on key values for thermodynamics, *J. Chem. Thermodyn.*, **4**, 331 (1972).
28) J. T. S. Andrews and E. F. Westrum, Jr., *J. Phys. Chem.*, **74**, 2170 (1970).
29) R. H. Boyd, R. L. Christensen, and R. Pua, *J. Am. Chem. Soc.*, **87**, 3554 (1965).
30) J. D. Cox and G. Pilcher, "Thermochemistry of Organic and Organometallic Compounds," Academic Press, New York (1970), p. 585.
31) B. Nelander and S. Sunner, *J. Chem. Phys.*, **44**, 2476 (1966).
32) J. B. Pedley and J. Rylance, "Sussex-N.P.L. Computer Analysed Thermochemical Data: Organic and Organometallic Compounds," University of Sussex, Brighton (1977).
33) E. Morawetz, *J. Chem. Thermodyn.*, **4**, 455 (1972).
34) W. D. Good, *J. Chem. Thermodyn.*, **7**, 49 (1975).
35) J. D. Ferry and S. B. Thomas, *J. Phys. Chem.*, **37**, 253 (1933).
36) R. C. Wilhoit and B. J. Zwolinski, "Handbook of Vapor Pressures and Heats of Vaporization of Hydrocarbons and Related Compounds," Thermodynamic Research Center, Texas A&M University, College Station (1971), p. 70.
37) P. K. Gantzel and K. N. Trueblood, *Acta Crystallogr.*, **18**, 958 (1965).
38) D. H. Whiffen, *Phil. Trans.*, A. **248**, 131 (1955).
39) Y. Kakiuti and T. Shimanouchi, *J. Chem. Phys.*, **25**, 1252 (1956).
40) H. Wynberg, W. C. Nieuwpoort, and H. T. Jonkman, *Tetrahedron Lett.*, **1973**, 4623.
41) H. Iwamura, H. Kihara, S. Misumi, Y. Sakata, and T. Umemoto, *Tetrahedron Lett.*, **1976**, 615; *Tetrahedron*, **34**, 3427 (1978).
42) H. Ohno, H. Horita, T. Otsubo, Y. Sakata, and S. Misumi, *Tetrahedron Lett.*, **1977**, 265.
43) A. Ron and O. Schnepp, *J. Chem. Phys.*, **37**, 2540 (1962).

Calculations of g Tensors and Hyperfine Splitting Tensors for Molecules in Their Triplet States

Tetsuo MORIKAWA, Yasumasa J. I'HAYA,*,† and Junji NAKANO

School of Pharmaceutical Science, Toho University, Funabashi-shi, Chiba 274

†*Department of Materials Science, The University of Electro-Communications, Chofu-shi, Tokyo 182*

(Received August 14, 1979)

The g tensors and hyperfine splitting (hfs) tensors of simple organic radicals in their triplet states have been calculated by using an all valence electron SCF MO method with a first order perturbation treatment. The molecular orbital spin density is partitioned into the σ- and π-electron spin delocalization (SD) terms and the rest terms of spin polarization (SP) which arise from the CI effect. The g tensors for CH_2 and several other carbenes which have triplet ground states and for formaldehyde in its $n\pi^*$ and $n\sigma^*$ excited triplet states are evaluated. The calculated α-proton hfs constants of CH_2 contributing from the π orbital well compare with the observed hfs constants of the triplet naphthalene and the doublet malonic acid radical. The anisotropic carbon-13 hfs constants of CH_2 are determined almost completely by the SD contribution and their absolute values are in good accord with those observed for CD_2. Contribution of the SP terms to the isotropic hfs constant is found to be fairly large. Prediction of the hfs constants in CF_2 and CHF is made.

Theoretical investigation and prediction of the g tensors and the hyperfine splitting (hfs) tensors of organic radicals give us valuable information on molecular geometry, identification of excited states, spin-orbit interactions, and so on in the radicals. Since measurements of the g tensors of molecules in their triplet states by means of electron paramagnetic resonance (EPR) spectroscopy were first reported,[1] rigorous theoretical prediction of the g tensors has rarely been found in the literature. The pioneering series of work done by McWeeny[2] are of course important and more recent efforts are made by Dalgaard and Linderberg[3] with a theory of electron propagator and by Nakatsuji and Hirao[4] with a symmetry-adapted cluster expansion. However, most of theoretical calculations carried out hitherto have been focused the zero-field splitting constants by using the π-electron approximation.

Quite recently, accurate principal g values have become available with the improvement of the EPR technique. For example, the observed deviation of the g values of triplet deutero methylene CD_2 from a free electron g_e is very large (0.0027—0.0285)[5,6] in comparison with those of organic (doublet) free radicals, for example 0.0003 in the CH_3 radical.[7] The present paper first intends to analyze the g tensors of CH_2 and other carbene radicals in their triplet states. The methylene radical has two unpaired electrons, one in a σ MO and the other in a π MO, so that the radical is supposed to have a dual characteristic of σ and π radicals. By partitioning an MO set, a total spin density operator is expressed as a sum of the MO spin density operators for the σ and π MO's in which an odd electron is placed and higher order terms arising from the CI effect. The former yields σ and π electron spin delocalization effect that extends over the entire system and the latter the spin polarization effect. We also report the results of our calculation on the α-proton and carbon 13 hyperfine splitting (hfs) tensors for CH_2 and the carbon 13 and fluorine 19 hfs tensors for CF_2 and CHF.

Spin Density Analysis

A method of spin density analysis which will be described below is a traditional one but we show that the method can be applied to any kinds of molecules in their triplet states, though a way of construction of MO's is restricted by the symmetry of a molecule to be considered. The spin density of paramagnetic radicals will be analyzed by a partitioning technique for the spin density operators and the spin density matrices. In this connection, we try to obtain some useful concepts and relationships which will be able to elucidate properties of the spin density. The method will explore the mechanisms of spin polarization and spin delocalization in triplet molecules.

According to McConnell,[8] a normalized spin density function $\rho(x, y, z)$ at a spatial point x, y, z whose origin is suitably taken in a molecule is defined as

$$\rho(x, y, z) = S_z^{-1}\sum_k{}'\langle \Psi, \hat{S}_{zk}\Psi\rangle_k. \quad (1)$$

Here, Ψ is the complete wave function of a paramagnetic molecule, which is an eigenfunction of the total z component of the electron spin angular momentum operator $\hat{S}_z=\sum_k\hat{S}_{zk}$ with eigenvalue S_z, $\hat{S}_{zk}$ being the z component of spin angular momentum for electron k. The quantity $\langle\Psi, \hat{S}_{zk}\Psi\rangle_k$ denotes a matrix element to be calculated by integrating over the spin and space coordinates of all the electrons except the space coordinates of electron k. The prime on the summation symbol indicates that after the sum has been carried out the indices k should be dropped. Equation 1 shows that a quantity $\rho(x, y, z)$ gives an expectation value of $\hat{S}_z$ at point x, y, z. The circumflex symbol denotes an operator quality hereafter.

If one expands Ψ, a single determinant and/or a linear combination of them, in terms of orthonormal functions ϕ_i, one can write $\rho(x, y, z)$ in terms of the density matrix referred to these discrete bases, $\rho=[\rho_{ij}]$;

$$\rho(x, y, z) = \sum_{i,j}\rho_{ij}\phi_j^*\phi_i. \quad (2)$$

The spin density function is associated with the one-particle density matrix $\gamma_1(x'; x)$;[2]

$$\rho(x, y, z) = S_z^{-1}\int \hat{S}_{z1}\gamma_1(x_1'; x_1)d\tau, \quad (3)$$

which shows that if the so-called natural spin-orbitals are used to constract Ψ then $\rho(x, y, z)$ is diagonalized, though we will not follow this procedure. We can define a normalized spin density operator $\hat{\rho}$ by the relation

$$\langle\phi_i, \hat{\rho}\phi_j\rangle = \rho_{ij}, \quad (4)$$

or using Dirac's bra-ket notation we write

$$\hat{\rho} = \sum_{i,j}|\phi_i\rangle\rho_{ij}\langle\phi_j| = \sum_{i,j}\hat{\rho}_{ij} = \sum_{i,j}\rho_{ij}\hat{P}_{ij}. \quad (5)$$

The last equation of Eq. 5 indicates that $\hat{\rho}$ can be expanded in terms of the projection (the transition-projection in the strict sense) operators $\hat{P}_{ij}\equiv|\phi_i\rangle\langle\phi_j|$.

When one introdues a row matrix $|\phi\rangle\equiv[|\phi_i\rangle]$, Eq. 5 is written compactly as

$$\hat{\rho} = |\phi\rangle\boldsymbol{\rho}\langle\phi|. \quad (6)$$

If molecular orbital functions are chosen as the basis $\{|\phi_i\rangle\}$, the matrix $\boldsymbol{\rho}$ may be called an MO spin density matrix and $\hat{\rho}_{ij}$ an MO spin density operator for orbitals ϕ_i and ϕ_j. The total MO spin density operator $\hat{\rho}$ is of course self-adjoint and normalized to unity; $\mathrm{tr}(\hat{\rho})=\sum_i\rho_{ij}=1$.

If one employs another set of $|\chi\rangle$ whose elements $|\chi_\mu\rangle$ are linearly independent but not necessarily orthonormal, first one constructs a set of orthonormalized vectors $|e\rangle=|\chi\rangle\boldsymbol{S}^{-1/2}$ with $\boldsymbol{S}\equiv\langle\chi|\chi\rangle$ (Löwdin's symmetric orthonormalization[9]), then one obtains instead of Eqs. 5 and 6

$$\hat{\rho} = \sum_{\mu,\nu}|e_\mu\rangle\bar{\rho}'_{\mu\nu}\langle e_\nu| = \sum_{\mu,\nu}\hat{\bar{\rho}}'_\nu = e\rangle\bar{\boldsymbol{\rho}}'\langle e|. \quad (7)$$

Further if one puts $\boldsymbol{S}^{-1/2}\bar{\boldsymbol{\rho}}'\boldsymbol{S}^{-1/2}\equiv\bar{\boldsymbol{\rho}}$, then one has

$$\hat{\rho} = |\chi\rangle\boldsymbol{S}^{-1/2}\bar{\boldsymbol{\rho}}'\boldsymbol{S}^{-1/2}\langle\chi| = \sum_{\mu,\nu}\bar{\boldsymbol{\rho}}_{\mu\nu} = |\chi\rangle\bar{\boldsymbol{\rho}}\langle\chi|. \quad (8)$$

The relationship $\bar{\rho}'=\boldsymbol{S}^{1/2}\bar{\rho}\boldsymbol{S}^{1/2}$ is important because it is useful in a general case which contains the overlap effect discussed by McConnell.[10] When $|\chi\rangle$ is chosen as a set of AO's, $\bar{\boldsymbol{\rho}}$ may be called the AO spin density matrix and $\hat{\bar{\rho}}_{\mu\nu}$ the AO spin density operator for AO's $|\chi_\mu\rangle$ and $|\chi_\nu\rangle$. Note that $\mathrm{tr}(\hat{\bar{\boldsymbol{\rho}}})=\mathrm{tr}(\bar{\boldsymbol{\rho}}')=\mathrm{tr}(\boldsymbol{S}^{-1/2}\bar{\boldsymbol{\rho}}\boldsymbol{S}^{-1/2})=\mathrm{tr}(\bar{\boldsymbol{\rho}}\boldsymbol{S})=1$. When $|\phi_i\rangle$ is expressed as a linear combination of $|\chi_u\rangle$'s

$$|\phi_i\rangle = |\chi\rangle\boldsymbol{C}_i \text{ or } |\phi\rangle = |\chi\rangle\boldsymbol{C}, \quad (9)$$

the matrices $\bar{\boldsymbol{\rho}}$ and $\boldsymbol{\rho}$ are related to one another in the way as[8]

$$\bar{\boldsymbol{\rho}} = \langle\eta|\hat{\rho}|\eta\rangle = \langle\eta|\phi\rangle\boldsymbol{\rho}\langle\phi|\eta\rangle = \boldsymbol{C}\boldsymbol{\rho}\boldsymbol{C}^\dagger, \quad (10)$$

where $|\eta\rangle=|\chi\rangle\boldsymbol{S}^{-1}$, that is $|\eta\rangle$ is the reciprocal vector with respect to $|\chi\rangle$. Note that Eq. 10 is valid in either case that $|\chi\rangle$ is orthonormal or not.

Now we mention the essence of the present method. First, we partition an MO set $|\phi\rangle$ into appropriate subsets, σ and π MO's *etc.*, and AO's $|\chi\rangle$ into those centered at atom A, B, $\cdots$:

$$|\phi\rangle \equiv (|\phi_\sigma\rangle|\phi_\pi\rangle\cdots),\ |\phi_\sigma\rangle \equiv (|\phi_{\sigma 1}\rangle|\phi_{\sigma 2}\rangle\cdots),$$
$$|\chi\rangle \equiv (|\chi_A\rangle|\chi_B\rangle\cdots),\ |\chi_A\rangle \equiv (|\chi_{A1}\rangle|\chi_{A2}\rangle\cdots). \quad (11)$$

Since the total MO spin density operator $\hat{\rho}$ may be considered to be totally symmetric only if those partitioned $|\phi_\sigma\rangle$ and $|\phi_\pi\rangle$ belong to irreducible representations of the σ and π symmetries (this is the case for Hartree-Fock MO's), the relationships $\langle\phi_\sigma|\hat{\rho}|\phi_\pi\rangle=0$ *etc.* hold and we obtain

$$\hat{\rho} = \hat{\rho}_{\sigma\sigma} + \hat{\rho}_{\pi\pi} + \cdots$$
$$= |\phi_\sigma\rangle\boldsymbol{\rho}_{\sigma\sigma}\langle\phi_\sigma| + |\phi_\pi\rangle\boldsymbol{\rho}_{\pi\pi}\langle\phi_\pi| + \cdots. \quad (12)$$

Here, the whole MO spin density matrix $\boldsymbol{\rho}$ is in general diagonalized in such a way that

$$\boldsymbol{\rho} = \begin{array}{c} \\ \sigma_1 \\ \sigma_2 \\ \vdots \\ \pi_1 \\ \pi_2 \\ \\ \end{array}\!\!\begin{array}{c} \begin{array}{cc} \sigma_1\sigma_1\cdots & \pi_1\pi_2\cdots \end{array} \\ \left[\begin{array}{c|c|c} \boldsymbol{\rho}_{\sigma\sigma} & 0 & \\ \hline 0 & \boldsymbol{\rho}_{\pi\pi} & \\ \hline & & \end{array}\right] \end{array}. \quad (13)$$

In short, the corresponding MO spin density operators $\hat{\rho}_{\sigma\sigma}$ and $\hat{\rho}_{\pi\pi}$ yield leading terms of the spin density for σ-type and π-type radicals, respectively. These terms actually manifest the so-called spin-delocalization (SD) effect.[11] The remaining higher order terms which are not shown in Eq. 12 come from the CI effect and contribute to spin-polarization.[11] Therefore, total $\hat{\rho}$ is a sum of operators which count out the spin density due to spin-delocalization and that which yields spin-polarization:

$$\hat{\rho} = \hat{\rho}^{SD} + \hat{\rho}^{SP}, \quad (14)$$

where one should note that $\mathrm{tr}(\hat{\rho}^{SD})=1$ and $\mathrm{tr}(\hat{\rho}^{SP})=0$.

What follows is an extention of the spin density formulation. Though we do not actually apply it to the present numerical analyses, it will be useful for more detailed exploration of the mechanism of spin polarization and spin delocalization. The degree of localization of the spin density of atom A is measured by

$$\bar{\rho}_A = \sum_{\mu\in A}\langle\eta_\mu|\hat{\bar{\rho}}|\eta_\mu\rangle = \bar{\rho}_A{}^{SD} + \bar{\rho}_A{}^{SP}, \quad (15)$$

where

$$\bar{\rho}_A{}^{SD} = \sum_{\mu\in A}\langle\eta_\mu|\hat{\bar{\rho}}^{SD}|\eta_\mu\rangle \quad (16)$$

and

$$\bar{\rho}_A{}^{SP} = \sum_{\mu\in A}\langle\eta_\mu|\hat{\bar{\rho}}^{SP}|\eta_\mu\rangle. \quad (17)$$

Then, one can say that the complete delocalization takes place on atom A when $\bar{\rho}_A=0$, and the complete localization occurs on atom A when $\bar{\rho}_A=1$. In the case that atom A is considered to be a radical center, the measure of delocalization of the spin density on the radical center is expressed as $1-\bar{\rho}_A$. On the other hand, a measure of localization of the spin density in bond A–B is given by

$$\bar{\rho}^{AB} = \sum_{\mu\in A,\ \nu\in B}\langle\eta_\mu|\hat{\bar{\rho}}|\eta_\nu\rangle, \quad (18)$$

which cannot be assigned to either of atom A and atom B.

Since the Hermitian matrix $\boldsymbol{\rho}_{\sigma\sigma}$ can be diagonalized such that $\boldsymbol{d}_\sigma=\boldsymbol{U}_\sigma^\dagger\boldsymbol{\rho}_{\sigma\sigma}\boldsymbol{U}_\sigma$ ($\boldsymbol{U}_\sigma$ is a unitary matrix), one obtains

$$\hat{\rho}_{\sigma\sigma} = |\phi_\sigma'\rangle\boldsymbol{d}_\sigma\langle\phi_\sigma'|, \quad (19)$$

with

$$|\phi_\sigma'\rangle = |\phi_\sigma\rangle\boldsymbol{U}_\sigma. \quad (20)$$

We may call $\boldsymbol{d}_\sigma$ an MO occupation spin density and $|\phi_\sigma'\rangle$ a spin density naturalized MO. A similar definition can be made for π MO's and higher symmetry MO's.

Using a unitary matrix $\boldsymbol{U}$ which diagonalizes $\boldsymbol{\rho}$, one can obtain a relationship which is similar to Eq. 10:

$$\vec{\boldsymbol{d}} = \boldsymbol{C}'\vec{\boldsymbol{d}}\boldsymbol{C}'^{\dagger}, \text{ with } \boldsymbol{C}' = \boldsymbol{U}^{\dagger}\boldsymbol{C}\boldsymbol{U}. \tag{21}$$

The quantity d^{A} defined by

$$d^{A} = \sum_{\mu\in A} d_{\mu\mu} = \sum_{\mu\in A}\langle\eta_{\mu}'|\hat{\rho}|\eta_{\mu}'\rangle \tag{22}$$

may be called an atomic occupation spin density on atom A, while $d_{\mu\mu}$ may be termed as an AO occupation spin density centered at atom A.

g Tensors of Triplet Molecules

First we describe the method of calculation of the 3×3 matrix elements $g^{ij}(i,j=\mathrm{x},\mathrm{y},\mathrm{z})$ of the g tensor. It is well known that in a π doublet radical certain negative spin density occurs on the proton in the molecular plane through the σ-π interaction.[8] This also will be the case for triplet radicals. Assuming such perturbation is small, we may construct a total wavefunction so as to mix the ground state function with excited functions by making use of a first-order perturbation theory.

Let $\Psi_{G}^{M}(M=-1, 0, 1)$ be the Slater determinant of the triplet ground state of a molecule, in which nondegenerate molecular orbitals ϕ_{m} and ϕ_{n} accomodate one unpaired electron each:

$$\Psi_{G}^{M} = |\phi_1\bar{\phi}_1\cdots\phi_i\bar{\phi}_i\cdots\phi_{m-1}\bar{\phi}_{m-1}\phi_m\phi_n|. \tag{23}$$

The one-electron excited state determinantal wave functions which are eigenfunctions of $\hat{S}_z$ and $\hat{S}^2$ are divided into the following four classes:

$$\left.\begin{aligned}\Psi_{i\to m}^{M} &= |\phi_1\bar{\phi}_1\cdots\phi_i\bar{\phi}_m\cdots\phi_m\phi_n|,\\ \Psi_{m\to k}^{M} &= |\phi_1\bar{\phi}_1\cdots\phi_i\bar{\phi}_i\cdots\phi_k\phi_n|,\end{aligned}\right\} \tag{24}$$

$$\left.\begin{aligned}\Psi_{i\to k}^{M}(A) &= (\Psi_1^{(m)}+\Psi_2^{(m)})/\sqrt{2},\\ \Psi_{i\to k}^{M}(B) &= (\Psi_1^{(m)}-\Psi_2^{(m)}-2\Psi_3^{(m)})/\sqrt{6},\\ \text{and/or } \Psi_{i\to k}^{M}(C) &= (\Psi_1^{(m)}-\Psi_2^{(m)}-2\Psi_3^{(n)})/\sqrt{6}\end{aligned}\right\} \tag{25}$$

with

$$\left.\begin{aligned}\Psi_1^{(m)} &= |\phi_1\bar{\phi}_1\cdots\phi_i\bar{\phi}_k\cdots\phi_m\phi_n|,\\ \Psi_2^{(m)} &= |\phi_1\bar{\phi}_1\cdots\phi_k\bar{\phi}_i\cdots\phi_m\phi_n|,\\ \Psi_3^{(m)} &= |\phi_1\bar{\phi}_1\cdots\phi_i\phi_k\cdots\bar{\phi}_m\phi_n|,\\ \Psi_3^{(n)} &= |\phi_1\bar{\phi}_1\cdots\phi_i\phi_k\cdots\phi_m\bar{\phi}_n|,\end{aligned}\right\} \tag{26}$$

where the suffices i and k refer to doubly occupied MO's and vacant MO's in Ψ_{G}^{M}, respectively. By direct calculation, we found that the former two (Eq. 24) contribute to the g tensor ffnd the latter two (Eq. 25) have an effect to the σ-π interaction in hfs tensor.

After mixing the former two functions, $\Psi_{i\to m}^{M}$ and $\Psi_{m\to k}^{M}$, with Ψ_{G}^{M} through the spin-orbit interaction $\hat{H}_{LS}=\sum_{t,j}\zeta_t\hat{L}_{jt}\cdot\hat{S}_j$ where $\hat{L}_{jt}$ is the orbital angular momentum operator for the jth electron with respect to the tth nucleus and ζ_t is the spin-orbit coupling constant, the total wave function Ψ_{T}^{M} to be used for the calculation of the g tensor is expressed as

$$\Psi_{T}^{M} = \Psi_{G}^{M} - \sum_{I,M'}\lambda_{I}^{M'}\Psi_{I}^{M'}, \quad (M'=-1, 0, 1) \tag{27}$$

where

$$\lambda_{I}^{M'} = \langle\Psi_{I}^{M'}|\hat{H}_{LS}|\Psi_{G}^{M}\rangle/[E(\Psi_{I}^{M'})-E(\Psi_{G}^{M})], \tag{28}$$

and I refers to $i\to m$ and $m\to k$.

As is well known, the anisotropic g tensor in the expression of the effective spin Hamiltonian $\hat{H}_{eff}=\mu_B H\cdot g\cdot\hat{S}'$, where μ_B is the electronic Bohr magneton, H the external magnetic field, and $\hat{S}'$ the ficititious spin, is estimated by the aid of the true Hamiltonian for the magnetic interaction $\hat{H}=\mu_B H\cdot(\hat{L}+g_e\hat{S})$, g_e being the gyromagnetic factor for a free electron ($g_e=2.00232$). That is, after calculating the 3×3 matrices for $\hat{H}_{eff}$ and $\hat{H}$ by using $\Psi_{T}^{M}(M=-1, 0, 1)$ as bases, and comparing the corresponding matrix elements term by term, one obtains the components of the g tensors as in the following:

$$g^{xy} = g_e\delta_{xy} + \Delta g^{xy}, \tag{29}$$

$$\Delta g^{xy} = \Delta g_m^{xy} + \Delta g_n^{xy}, \tag{30}$$

$$\Delta g_m^{xy} = \sum_i\Delta g_{mi}^{xy} - \sum_k\Delta g_{mk}^{xy}, \tag{31}$$

$$\Delta g_{mi}^{xy} = (2S)^{-1}(\Lambda_{mi}^{xy}+\Gamma_{mi}^{xy})/[E(\Psi_{i\to m}^{M'})-E(\Psi_{G}^{M})], \tag{32}$$

$$\Lambda_{mi}^{xy} = \langle\phi_m|\sum_{t,j}\hat{L}_{jt}^{x}|\phi_i\rangle\langle\phi_i|\sum_{t,j}\zeta_t\hat{L}_{jt}^{y}|\phi_m\rangle, \tag{33}$$

$$\Gamma_{mi}^{xy} = \langle\phi_m|\sum_{t,j}\hat{L}_{jt}^{y}|\phi_i\rangle\langle\phi_i|\sum_{t,j}\zeta_t\hat{L}_{jt}^{x}|\phi_m\rangle, \tag{34}$$

and so on. If the molecular axes coincide with principal axes of the g tensor, the two terms in the numerator of Eq. 32 reduce to one term. We can thus calculate the principal values of g by diagonalizing the matrix Δg^{xy} or g^{xy}.

Hyperfine Splitting Tensors

For triplet radicals having the ground state wave function Ψ_{G}^{M} of Eq. 23, the leading term of the total MO spin density operator $\hat{\rho}$, as given in Eq. 12, becomes

$$\hat{\rho}(\Psi_{G}^{M};\Psi_{G}^{M}) = \hat{\rho}_{mm}^{SD} + \hat{\rho}_{nn}^{SD}, \tag{35}$$

that is, corresponding to Eq. 13,

$$\rho(\Psi_{G}^{M};\Psi_{G}^{M}) = \begin{array}{c} \\ m \\ n \\ \\ \end{array}\begin{array}{c} \begin{array}{cccc} & & m & n \end{array} \\ \begin{bmatrix} 0 & \vdots & \vdots & \\ \cdots & 0.5 & \vdots & 0 \\ \cdots & \cdots & 0.5 & \\ & 0 & & 0 \end{bmatrix} \end{array}. \tag{36}$$

In the SCF framework, Ψ_{G}^{M} does not mix with $\Psi_{i\to m}^{M}$ and $\Psi_{m\to k}^{M}$ of Eq. 24 due to the Brillouin theorem. Also, $\hat{\rho}(\Psi_{G}^{M};\Psi_{i\to k}^{M}(A))=1/\sqrt{2}\,(-\hat{P}_{ik}+\hat{P}_{ik})=0$. Therefore, the ground state wave function Ψ_{T}^{M} can be improved by the mixing of only $\Psi_{i\to k}^{M}(B)$ and $\Psi_{i\to k}^{M}(C)$ of Eq. 25:

$$\Psi_{T}^{M} = \Psi_{G}^{M} + \sum_{i,k}\{\lambda_{ik}^{(m)}\Psi_{i\to k}^{M}(B)+\lambda_{ik}^{(n)}\Psi_{i\to k}^{M}(C)\}, \tag{37}$$

where

$$\left.\begin{aligned}\lambda_{ik}^{(m)} &= \frac{1}{\sqrt{6}}[3(mi|km)+(ni|kn)]/\Delta E^{(m)},\\ \lambda_{ik}^{(n)} &= \frac{1}{\sqrt{6}}[3(ni|kn)+(mi|km)]/\Delta E^{(n)},\end{aligned}\right\} \tag{38}$$

$$\left.\begin{aligned}\Delta E^{(m)} &= E(\Psi_{i\to k}^{M}(B)) - E(\Psi_{G}^{M}),\\ \Delta E^{(n)} &= E(\Psi_{i\to k}^{M}(C)) - E(\Psi_{G}^{M}),\end{aligned}\right\} \tag{39}$$

and

$$(pq|rs) = \iint\phi_p^*(1)\phi_q(1)(e^2/r_{12})\phi_r^*(2)\phi_s(2)dv(1)dv(2). \tag{40}$$

We thus finally obtain the total MO spin density

$$\rho(\Psi_{T}^{M};\Psi_{T}^{M}) = \rho_{mm}^{SD} + \rho_{nn}^{SD} + \rho^{SP}, \tag{41}$$

$$\rho^{SP} = \rho_{ik}^{(m)} + \rho_{ik}^{(n)} = -\frac{1}{\sqrt{6}}(\lambda_{ik}^{(m)} + \lambda_{ik}^{(n)}). \quad (42)$$

The AO spin density contribution due to spin polarization is obtained by means of Eq. 10:

$$(\bar{\rho}^{SP})_{\mu\nu} = \sum_i \sum_k (\rho^{SP})_{ik}(C_{\mu i}C_{\nu k}^* + C_{\mu k}C_{\nu i}^*). \quad (43)$$

The MO and AO spin density matrices necessary for the present calculation are listed in Appendix A.

The matrix elements of the anisotropic hfs tensor for nucleus N, A^{Nij}, are calculated by[12]

$$A^{Nij} = tr(\rho\Omega^{Nij}), \quad (i, j = x, y, z) \quad (44)$$

$$\Omega_{rs}^{Nij} = -g\mu_B\hbar\gamma_N t_{ij}(\chi_r\chi_s), \quad (45)$$

$$t_{ij}(\chi_r\chi_s) = \langle\chi_r(1)|r_{1N}^{-5}(r_{1N}^2\delta_{ij} - 3r_{1N}^i r_{1N}^j)|\chi_s(1)\rangle. \quad (46)$$

Here, $t_{ij}(\chi_r\chi_s)$ is the electron-nuclear dipolar interaction integral and γ_N the gyromagnetic ratio of nucleus N. By diagonalizing the matrix A^{Nij}, we obtain the principal values of the anisotropic hfs tensor and the direction cosines between the molecular and principal axes. The dipolar integrals $t_{ij}(\chi_r\chi_s)$ are evaluated by using the following approximations: (1) All the three-center integrals and all the two-center integrals involving the product $\chi_r\chi_s$ in which χ_r and χ_s belong to different atoms are neglected and the remaining one- and two-center integrals are analytically evaluated over the Slater-type orbitals; (2) the one-center dipolar integrals are improved by the use of Löwdin's SCF AO's.[13] Analytical formulas of the dipolar integrals are given in Appendix B.

The isotropic hfs constant for nucleus N is given by[12]

$$a^N = tr(\rho Q)^N, \quad (47)$$

$$(Q^N)_{rs} = (8\pi/3)g\mu_B\hbar\gamma_N\langle\chi_r(1)|\delta(r_{1N})|\chi_s(1)\rangle, \quad (48)$$

δ being the Dirac δ-function. The one-center integrals $\langle\chi_r(1)|\delta(r_{1N})|\chi_s(1)\rangle$ are evaluated over the Löwdin SCF AO's.[13]

Results and Discussion

First, we apply the above-mentioned calculation schemes to the g tensor of the methylene radical in its triplet state $^3B(n, \pi)$. The molecular geometry is as follows;[14] the C–H bond length 1.078 Å, the HCH bond angle 136°. The electron configuration is $(1a_1)^2(1b_1)^2(2a_1)^1(1b_2)^1(3a_1)^0(2b_1)^0$, the six valence electrons being taken into account. The molecular z axis is taken in the molecular plane so as to bisect the HCH angle and the y axis perpendicular to the molecular plane. The MO wave functions are obtained by using Roothaan's open-shell SCF operator[15] with the INDO approximation for integrals over AO's.[16] A pseudo-potential is added to Roothaan's operator in order to obtain fast and perfect convergence.[17] The exchange energy between the first excited singlet and the ground triplet states, $2K_{mn}$, is calculated to be 1.74 eV which is much larger than the electronic Zeeman energy. This gives convincing proofs of our assumption that the g tensor can be calculated by a perturbation treatment.

Methylene has the characteristics of both the double σ radical and the doublet π radical, since one of the two unpaired electrons occupy the σ orbital $2a_1$ and the other the π orbital $1b_2$. This situation is well expressed by Eq. 30 which can be written in this case as

$$\Delta g^{xy} = \Delta g^{xy}(2a_1) + \Delta g^{xy}(1b_2). \quad (49)$$

With Eqs. 30—34 and their analogues, the contribution of the one-electron excited wave functions of the type shown in Eq. 24 to the diagonal elements of Δg is calculated to be as in the following: (0, 12, 0) for $1b_1 \rightarrow 2a_1$, (0, −12, 0) for $2a_1 \rightarrow 2b_1$, (0, 0, 15) for $1b_1 \rightarrow 1b_2$, (−10, 0, 0) for $1b_2 \rightarrow 3a_1$, and (0, 0, −19) for $1b_2 \rightarrow 2b_1$, where the figures in parentheses denote the value of $(\Delta g^{xx}, \Delta g^{yy}, \Delta g^{zz}) \equiv \Delta g$ in units of 10^{-5}. The Δg values which come from other wave functions, $1a_1 \rightarrow 2a_1$, $1a_1 \rightarrow 1b_2$, and $2a_1 \rightarrow 3a_1$, are found to be very close to zero.

The principal values of the g tensor of methylene are then calculated to be (2.00222, 2.00232, 2.00228) which lie close to the free electron value g_e. We have confirmed that the structural dependence is rather small; *e.g.*, $\Delta g = (-12, 2, -4)$ when $\angle HCH = 111°$ and $(-8, -3, -5)$ when $\angle HCH = 150°$, all in units of 10^{-5}. The observed principal values of the g tensor for CD_2 in the xenon matrix at 4K are (1.9995, 1.9984, 1.9984),[5] which are 0.003—0.004 below our predicted values for an isolated CH_2. More recently, there have been reported much smaller g values; (1.9738, 1.9953, 1.9946) for CD_2 and (1.9742, 1.9955, 1.9942) for $^{13}CD_2$ both in xenon matrices.[18] These are not to be compared with our calculated values, since a solid solution matrix usually causes a large deviation from the g_e value due to intermolecular interactions with a host molecule and the effects of deuteration and molecular orientation.[19] The tendency that the deviation from g_e (and also anisotropy among the principal g values) is very small in the present prediction is in accord with experimental findings for organic doublet free radicals containing carbon and hydrogen only; 0.0003 for CH_3,[20] 0.0001 for $CH{=}CH_2$,[20] 0.0003 for $C{\equiv}CH$,[21] in their doublet ground states in solid solution matrices.

Table 1. Calculated principal g tensors of triplet molecules

	g^{xx}	g^{yy}	g^{zz}	g_{av}*)
CH_2	2.00222	2.00232	2.00228	2.00228
CF_2	2.00219	2.00348	2.00327	2.00298
$C(CN)_2$	2.00228	2.00233	2.00231	2.00231
CHF	2.00291	2.00210	2.00290	2.00264
H_2CO				
$^3A_2(n\pi^*)$	2.00286	2.00450	2.00685	2.00474
$^3B_1(n\sigma^*)$	2.00244	2.00425	2.00556	2.00408

*) $g_{av} = (1/3)(g^{xx} + g^{yy} + g^{zz})$

Table 1 lists the calculated principal values of the g tensor for other triplet molecules for which the very same calculation scheme has been used. Contrary to CH_2 in which the carbon atom mainly contributes to Δg because the spin-orbit interaction constant of hydrogen is negligibly small, anisotropy in CF_2 is rather large; our estimate made by the use of the partitioning method, $\Delta g = \Delta g_C + \Delta g_F + \Delta g_{F'}$ (geometry: $r(C\text{–}F) = 1.3$ Å, $\angle FCF' = 125°$), is $\Delta g_C = (-33, -1, -14)$ and $\Delta g_F = \Delta g_{F'} = (10, 58, 55)$ in units of 10^{-5}. The deviation

of the simple average value of g, $g_{av}=(1/3)(g^{xx}+g^{yy}+g^{zz})$, from the g_e value is larger in CF_2 and also in CHCHO.

At the bottom of Table 1, are shown the principal values of the g tensor calculated for the excited triplet states $^3A_2(n, \pi^*)$ and $^3B_1(n, \sigma^*)$ of formaldehyde. The molecular geometry corresponding to the minimum total energy is $r(C=O)=1.30$ Å, $r(C-H)=1.10$ Å, and $\angle HCH=121°$, the z axis being taken along the C=O bond and the y axis perpendicular to the molecular plane. We have assumed a planar structure for these excited triplet states of formaldehyde, though at least the $^3A_2(n\pi^*)$ state is known to have a bent structure (out of plane angle 35°).[23] This is simply because there are no experimental data available for the g tensors of these states and we try to compare the calculated results with the only available datum for the planar triplet benzophenone molecule.[22] The observed g tensor of the triplet benzophenone molecule is (1.9990, 1.9994, 2.0097),[22] the x and y axes here making angles of 60° and 30° respectively with the plane of the carbonyl group. Apart from these inclination of the x and y axes, the g^{xx} and g^{yy} values calculated for formaldehyde are larger than those observed for benzophenone, so is the case of the triplet ground state of methylene. On the contrary, the calculated g^{zz} value of formaldehyde is smaller than the experimental g^{zz} value of benzophenone, this being reversed in the case of methylene. Further investigation is needed as for whether these discrepancies are physically significant. From the experimental point of view, the two triplet excited states of formaldehyde are expected to be identified by an accurate measurement of the g tensor.

The effect of spin polarization in the MO spin density ρ of CH_2 calculated by using Eq. 42 is shown in Table 2. We should note that the non-vanishing off-diagonal elements are all negative and their values are within 6.4% of the diagonal element 0.5. Table 3 lists the AO spin density $\bar{\rho}=\bar{\rho}^{SP}+\bar{\rho}^{sp}$ of CH_2. The diagonal elements for the s orbitals are proportional to the corresponding isotropic hfs constants. The AO spin density of the carbon $2p_z$ orbital is 0.5 and the sum of the remaining diagonals is 0.5. Note that the negative spin density appears on the two protons.

TABLE 2. MOLECULAR ORBITAL SPIN DENSITY $\rho=\rho^{SD}+\rho^{SP}$ OF CH_2

MO	$1a_1$	$1b_1$	$2a_1$	$1b_2$	$3a_1$	$2b_1$
$1a_1$	0	0	0	0	−0.032	0.0
$1b_1$	0	0	0	0	0.0	−0.018
$2a_1$	0	0	0.500	0	0	0
$1b_2$	0	0	0	0.500	0	0
$3a_1$	−0.032	0.0	0	0	0	0
$2b_1$	0.0	−0.018	0	0	0	0

Table 4 shows the results on the analysis of the α-proton isotropic hfs constant, a^H, and the principal values of the α-proton anisotropic hfs tensor, A_{ii}^H(i=x, y, z), of the triplet CH_2 radical. Comparison of the third, fourth, fifth, and sixth columns shows that the anisotropic terms are determined almost completely by the spin delocalization contribution. Figures listed in the seventh column are the values per unit spin which come from the $1b_2$ π MO only, a simple double of a sum of the values in the fourth and the sixth columns since the spin density in the $1b_2$ π MO is 0.5. These values are well compared with the observed α-proton hfs constants per unit spin for triplet naphthalene[24] and the doublet malonic acid radical.[25] Going into details, the calculated isotropic constant is rather small; this is probably because the present perturbation treatment underestimates the contribution of spin polarization. Incidentally, a semi-quantitative estimate on a CH fragment ($S=1/2$) made by McConnell and Strathdee[26] is as follows: $a^H=-63$, $A_{xx}^H=-40$, $A_{yy}^H=42$, $A_{zz}^H=-6$ (all in MHz), the x axis being along the $2p\pi$ carbon

TABLE 3. ATOMIC ORBITAL SPIN DENSITY $\bar{\rho}=\bar{\rho}^{SD}+\bar{\rho}^{SP}$ OF CH_2[a]

	2s(C)	$2p_x$(C)	$2p_y$(C)	$2p_z$(C)	1s(H)	1s(H′)
2s(C)	0.114					
$2p_x$(C)	0	0.018				
$2p_y$(C)	0.171	0	0.384			
$2p_z$(C)	0	0	0	0.500		
1s(H)	−0.043	0.001	−0.080	0	−0.008	
1s(H′)	−0.043	−0.001	−0.080	0	0.010	−0.008

a) The z axis bisects the HCH angle in the molecular plane and the y axis is perpendicular to the plane.

TABLE 4. ANALYSIS OF α-PROTON hfs CONSTANTS OF TRIPLET CH_2(in MHz)

Term	Calculated contribution of spin densities						Observed	
	Total ρ	ρ_m^{SD} $(2a_1, \sigma)$	ρ_n^{SD} $(1b_2, \rho)$	ρ_m^{SP} $(2a_1, \sigma)$	ρ_n^{SP} $(1b_2, \pi)$	Contribution from π orbital only per unit spin[a]	Naphthalene ($S=1$) per unit spin Ref. 23	Malonic acid ($S=1/2$) per unit spin Ref. 24
a^H	−12	22	0	−14	−20	−40	−67	−60
A_{xx}^H	−27	−5	−20	−1	−1	−42	−31	−31
A_{yy}^H	47	20	23	2	2	50	36	31
A_{zz}^H	−21	−16	−3	−1	−1	−8	−5	−1

a) $2(\rho_n^{SD}+\rho_n^{SP})$

TABLE 5. ANALYSIS OF ^{13}C hfs CONSTANTS OF TRIPLET CH_2(in MHz)

Term	Calculated contribution of spin densities							Observed		
	Total ρ	ρ^{SD}	ρ^{SD}(H)	ρ_m^{SD} $(2a_1, \sigma)$	ρ_n^{SD} $(1b_2, \pi)$	ρ_m^{SP} $(2a_1, \sigma)$	ρ_n^{SP} $(1b_2, \pi)$	Wasserman *et al.* Ref. 5	Bernheim *et al.* Ref. 18	Ref. 6
a^C	+356	+281	—	+281	0	+26	+49	247	249	245
A_{xx}^C	−76	−78	+0.3	−33	−45	+1	+1	70	53	63
A_{yy}^C	+22	+22	−0.1	+67	−45	0	0	34	31	34
A_{zz}^C	+53	+55	−0.2	−34	+89	−1	−1	35	25	30

TABLE 6. PREDICTION OF THE HYPERFINE SPLITTING TENSORS OF CF_2 AND CHF (in MHz)

Term	CF_2						CHF								
	^{13}C			^{19}F			^{13}C			^{19}F			^{1}H		
	Total ρ	ρ^{SD}	ρ^{SP}	Total ρ	ρ^{SD}	ρ^{SP}	Total ρ	ρ^{SD}	ρ^{SP}	Total ρ	ρ^{SD}	ρ^{SP}	Total ρ	ρ^{SD}	ρ^{SP}
a	624	633	−9	113	105	8	475	462	13	84	49	35	60	66	−6
A_{xx}	−52	−51	−1	−146	−115	−31	−60	−61	1	−141	−109	−32	−23	−23	0
A_{yy}	−6	−7	1	136	106	30	4	4	0	92	70	22	37	36	1
A_{zz}	58	58	∼0	10	9	1	56	57	−1	50	39	11	−14	−14	0

orbitals and the z axis along the C–H bond.

The calculated carbon 13 hfs constants of CH_2 are listed in Table 5 together with the observed values for CD_2. Comparison of the second and the third columns shows that the anisotropic terms are determined almost completely by the spin delocalization contribution as in the case of the α-proton hfs constants, while the isotropic term receives a considerable effect of spin polarization. The fourth column shows the delocalization contribution from the spin densities on the hydrogen atoms to hfs constants; the effect of hydrogen is negligibly small. In the fifth and the sixth columns is divided the total contribution of ρ^{SD} into those from the $2a_1$ σ orbital and from the $1b_2$ π orbital. It is interesting to compare the algebraic signs and magnitudes of these contributions with those of ρ^{SD} (the third column). The spin polarization terms are also divided into those contributing from the σ and π orbitals in the seventh and the eighth columns. Their contribution to the isotropic hfs constant is large while those to the anisotropic hfs constants are small as mentioned before. The last three columns list the available experimental data for CD_2, though their algebraic signs are not determined by an EPR experiment. The magnitudes of our predicted hfs constants well compare with those observed.

We list in Table 6 our prediction of the hfs constants in CF_2 and CHF for which no experimental data are available. It is hoped that our predictions will serve as a guide in future experimental analyses for these radicals.

Appendix A. The MO and AO Spin Density Operators

The MO spin density operators over the states given in Eqs. 23—26 of the text are expressed in terms of the transition-operators $\hat{P}_{ij} \equiv |\phi_i\rangle\langle\phi_j|$ as follows:

$$\hat{\rho}(\Psi_G^M; \Psi_G^M) = \frac{1}{2}(\hat{P}_{mm} + \hat{P}_{nn}),$$

$$\hat{\rho}(\Psi_{i\to m}^M; \Psi_G^M) = -\frac{1}{2}\hat{P}_{im},$$

$$\hat{\rho}(\Psi_{m\to k}^M; \Psi_G^M) = \frac{1}{2}\hat{P}_{mk},$$

$$\hat{\rho}(\Psi_{i\to k}^M(A); \Psi_G^M) = 0,$$

$$\hat{\rho}(\Psi_{i\to k}^M(B); \Psi_G^M) = \hat{\rho}(\Psi_{i\to k}^M(C); \Psi_G^M) = -(1/\sqrt{6})\hat{P}_{ik},$$

$$\hat{\rho}(\Psi_1^{(m)}; \Psi_G^M) = -\hat{\rho}(\Psi_2^{(m)}; \Psi_G^M) = -\frac{1}{2}\hat{P}_{ik},$$

$$\hat{\rho}(\Psi_3^{(m)}; \Psi_G^M) = \hat{\rho}(\Psi_3^{(n)}; \Psi_G^M) = 0.$$

The AO spin density matrix $\bar{\rho}$ for the resultant state Ψ_T^M is easily obtained by making use of Eq. 10 of the text, whose element is

$$\bar{\rho}_{rs} = \frac{1}{2}(C_{rm}C_{sm}^* + C_{rn}C_{sn}^*) + \sum_i^{\text{doubly occupied}} \sum_k^{\text{vacant}} (1/\sqrt{6})(\lambda_{ik}^{(m)} + \lambda_{ik}^{(n)})(C_{ri}C_{sk}^* + C_{rk}C_{si}^*),$$

where λ_{ik}'s are given in Eq. 38 of the text.

Appendix B. Analytical Derivation of Dipolar Integrals

The formulas for the dipolar integrals over AO's which are needed in the evaluation of anisotropic hfs tensors are obtained by the use of the method of McConnell and Strathdee[26] with the corrections of Pitzer, Kern, and Lipscomb.[27]

In the case when the Slater-type AO's are centered at nucleus N, the evaluation of dipolar integrals is straightforward:

$$t_{ij}(2p_k, 2p_l) = (c/120)\{2\delta_{ij}\delta_{kl} - 3(\delta_{ik}\delta_{jl} + \delta_{il}\delta_{jk})\},$$

where $c = (Z/a_0)^3$, a_0 being the first Bohr radius, and all the dipolar integrals over spherically symmetric AO's vanish. Constant c in the above equation for the improved one-center dipolar integrals over the Löwdin SCF AO's is[13]

$$c = \frac{\sum_{k,k'} B_k B_{k'} (b_k + b_{k'})^{-2}}{\sum_{k,k'} B_k B_{k'} (b_k + b_{k'})^{-5} a_0^3},$$

Table A1. Formulas of dipolar integrals involving 1s, 2s, 2p STO's when nucleus N lies on the z axis

$\chi_r\chi_s$	t_{xx}	t_{yy}	t_{zz}	t_{xy}	t_{xz}	t_{yz}
1s1s	B_{1s}	B_{1s}	$-2B_{1s}$	0	0	0
2s2s	B_{2s}	B_{2s}	$-2B_{2s}$	0	0	0
2s2p$_x$	0	0	0	0	B_{sx}	0
2s2p$_y$	0	0	0	0	0	B_{sy}
2s2p$_z$	B_{sz}	B_{sz}	$-2B_{sz}$	0	0	0
2p$_x$2p$_y$	0	0	0	B_{xy}	0	0
2p$_x$2p$_z$	0	0	0	0	B_{xz}	0
2p$_y$2p$_z$	0	0	0	0	0	B_{yz}
2p$_x$2p$_x$	B^x_{xx}	B^y_{xx}	B^z_{xx}	0	0	0
2p$_y$2p$_y$	B^x_{yy}	B^y_{yy}	B^z_{yy}	0	0	0
2p$_z$2p$_z$	B_{zz}	B_{zz}	$-2B_{zz}$	0	0	0

$B_{1s}=(1-(4a^3/3+2a^2+2a+1)\exp(-2a))/R^3$

$B_{2s}=(1-(a^5/72+a^4/24+a^3/6+a^2/2+a+1)\exp(-a))/R^3$

$B_{sx}=(15/a-(a^4/8+5a^3/8+5a^2/2+15a/2+15/a)\exp(-a))R^3/\sqrt{3}$

$B_{sy}=B_{sx}$

$B_{sz}=(15/a-(a^5/24+a^4/8+5a^3/8+5a^2/2+15a/2+15+15/a)\exp(-a))/R^3/\sqrt{3}$

$B_{xy}=(-18/a^2+(a^3/8+3a^2/4+3a+9+18/a+18/a^2)\exp(-a))/R^3$

$B_{xz}=(72/a^2-(a^4/8+5a^3/8+3a^2+12a+36+72/a+72/a^2)\exp(-a))/R^3$

$B_{yz}=B_{xz}$

$B^x_{xx}=(1-54/a^2+(a^3/4+7a^2/4+8a+26+54/a+54/a^2)\exp(-a))/R^3$

$B^y_{xx}=(1-18/a^2+(a^2/4+2a+8+18/a+18/a^2)\exp(-a))/R^3$

$B^z_{xx}=-(B^x_{xx}+B^y_{xx})$

$B^x_{yy}=B^y_{xx}$

$B^y_{yy}=B^x_{xx}$

$B^z_{yy}=B^z_{xx}$

$B_{zz}=(1+72/a^2-(a^5/24+a^4/8+3a^3/4+7a^2/2+13a+37+72/a+72/a^2)\exp(-a))/R^3$

Table A2. Dipolar integrals when nucleus N lies at point (X, Y, Z)

$t_{ij}(1s1s)=(e_{ij}-2u_iu_j)B_{1s}$

$t_{ij}(2s2s)=(e_{ij}-2u_iu_j)B_{2s}$

$t_{ij}(2s2p_k)=(e_{ik}u_j+e_{jk}u_i)B_{sx}+(e_{ij}-2u_iu_j)u_kB_{sz}$

$t_{ij}(2p_k2p_l)=(e_{ik}e_{jl}+e_{il}e_{jk}-2e_{kl}u_iu_j)B^x_{xx}/2+\{e_{ij}e_{kl}-e_{kl}u_iu_j-(e_{ik}e_{jl}+e_{il}e_{jk})/2\}B^y_{xx}+(e_{ik}u_ju_l+e_{jl}u_iu_k+e_{il}u_ju_k+e_{jk}u_iu_l)B_{xz}+(e_{ij}-2u_iu_j)u_ku_lB_{zz}$

$u_x=X/R$, $u_y=Y/R$, $u_z=Z/R$, $e_{ij}=\delta_{ij}-u_iu_j$

where B_k and b_k are Löwdin's notation and which yields 268.73, 483.42, and 795.75 Å^{-3} for carbon, nitrogen, and oxygen, respectively.

When nucleus N lies on the z axis, the relevant two-center dipolar integrals over the Slater-type AO's, $t_{ij}(\chi_r\chi_s)$, are listed in Table A1, where R is the distance between nucleus N and the atom to which AO's χ_r and χ_s are centered and $a=ZR/a_0$.

The dipolar tensors for which nucleus N lies at point (X, Y, Z) can be obtained by the usual transformation. Table A2 is derived in this way in terms of the terms listed in Table A1.

References

1) C. A. Hutchison, Jr. and B. W. Mangum, *J. Chem. Phys.*, **34**, 908 (1961).
2) R. McWeeny, *J. Chem. Phys.*, **42**, 1717 (1965).
3) E. Dalgaard and J. Linderberg, *J. Chem. Phys.*, **65**, 692 (1976).
4) H. Nakatsuji and K. Hirao, *J. Chem. Phys.*, **68**, 4279 (1978).
5) E. Wasserman, V. J. Kuck, R. S. Hutton, E. D. Anderson, and W. A. Yager, *J. Chem. Phys.*, **54**, 4120 (1971).
6) R. A. Bernheim, T. Adl, H. W. Bernard, A. Songco, P. S. Wang, R. Wang, L. S. Wood, and P. S. Skell, *J. Chem. Phys.*, **64**, 2747 (1976).
7) R. W. Fessenden and R. H. Schuler, *J. Chem. Phys.*, **39**, 2147 (1963).
8) H. M. McConnell, *J. Chem. Phys.*, **28**, 1188 (1958).
9) P. O. Löwdin, *Adv. Quantum Chem.*, **5**, 185 (1970).
10) H. M. McConnell, *J. Chem. Phys.*, **24**, 764 (1956).
11) For example, D. Lazdins and M. Karplus, *J. Chem. Phys.*, **44**, 1600 (1966).
12) A. Carrington and A. D. McLachlan, "Introduction to Magnetic Resonance," Harper and Row, New York (1967), p. 14.
13) P. O. Löwdin, *Phys. Rev.*, **90**, 120 (1953).
14) G. Herzberg and J. W. C. Johns, *J. Chem. Phys.*, **54**, 2276 (1971).
15) C. C. J. Roothaan, *Rev. Mod. Phys.*, **32**, 179 (1960).
16) J. A. Pople, D. L. Beveridge, and P. A. Dobosh, *J. Chem. Phys.*, **47**, 2026 (1967).
17) S. Narita, K. Sazi, and Y. J. I'Haya, *Chem. Phys. Lett.*, **29**, 232 (1974).
18) R. A. Bernheim, H. W. Bernard, P. S. Wang, L. S. Wood, and P. S. Skell, *J. Chem. Phys.*, **54**, 3223 (1971).
19) B. R. Bicknell, W. R. M. Graham, and W. Weltner, Jr., *J. Chem. Phys.*, **64**, 3319 (1976).
20) B. H. J. Bielski and J. M. Gelicki, "Atlas of Electron Spin Resonance Spectroscopy," Academic Press, New York, (1967).
21) W. R. M. Graham, K. I. Dismuke, and W. Weltner, Jr., *J. Chem. Phys.*, **60**, 3817 (1974).
22) M. Sharnoff and E. B. Iturbe, *J. Chem. Phys.*, **62**, 145 (1975).
23) G. W. Robinson and V. E. Di Giorgio, *Can. J. Chem.*, **36**, 31 (1958).
24) N. Hirota, C. A. Hutchison, Jr., and P. Palmer, *J. Chem. Phys.*, **40**, 3717 (1964).
25) T. Cole, C. Heller, and H. M. McConnell, *Proc. Natl. Acad. Sci. U.S.A.*, **45**, 525 (1959); H. M. McConnell, C. Heller, T. Cole, and R. W. Fessenden, *J. Am. Chem. Soc.*, **82**, 766 (1960).
26) H. M. McConnell and J. Strathdee, *Mol. Phys.*, **2**, 129 (1959).
27) R. M. Pitzer, C. W. Kern, and W. N. Lipscomb, *J. Chem. Phys.*, **37**, 267 (1962).

Thermal Diffusion Measurements of Symmetric Tetraalkylammonium Bromides in Water

Zen'ei Yogi, Hiroshi Kitano, Izumi Tōma, Kazuhiro Kijima, and Toshio Ikeda*
Department of Chemistry, Faculty of Science, Shizuoka University, 836 Ohya, Shizuoka 422
(Received August 20, 1979)

The Soret coefficients for 0.01 M aqueous solutions of R_4NBr (R=H, Me, Et, *n*-Pr, *n*-Bu, *n*-Pen, *n*-Hex, and *n*-Hep) were measured by the Snowdon-Turner conductimetric method with accuracy within ±0.1%, and were found to be −0.13, −4.18, −7.16, −9.05, −9.61, −9.47, −8.65, and −7.34, respectively in 10^{-3} K^{-1}, at the mean temperature 25 °C. They show a maximum at the carbon number 4 or 5 in R, whereas the diffusion coefficients show a minimum at the same carbon number in an exactly inverse manner. The apparatus and procedure are described.

The peculiar property of tetraalkylammonium salts, *viz.* they are easily soluble in water despite the fact that they consist of ammonium type ions entirely substituted by hydrophobic alkyl chains, has attracted attention. Measurements on molar volumes,[1] activity coefficients,[2] specific conductivities,[3] viscosity *B*-coefficients,[4] NMR chemical shifts,[5] and apparent energies of activation[6] have been reported by many workers, the results being interpreted in terms of "hydrophobic bond,"[7] which emphasizes the water structure around the tetraalkylammonium ions. However, studies on the diffusion (ordinary and thermal) of tetraalkylammonium salts do not seem have been carried out. One of us (T. I.) predicted that tetraalkylammonium salts would show very large Soret coefficients in water,[8] and gave proper estimates which were found to be of the right order of magnitude by experiments using "combined thermocell" technique.[9,10] However, the technique provides essentially the Soret coefficients relative to an appropriately selectred reference, *e.g.*, LiCl, which shows a negligiblly small Soret effect. It is desirable to carry out direct, accurate determination of the Soret coefficients of tetraalkylammonium salts.

Experimental

Cell Assembly. Measurements were carried out according to the Snowdon-Turner conductimetric method[11,12] with minor revision. The cell (Fig. 1) consists of a rectangular cylindrical hole (10 mm ϕ, 10 mm height) drilled at a corner of 100×100 mm^2, 10 mm thick "Acrylite" (poly(methyl methacrylate)) plate, the remaining flat area being used as an apron on which a well calibrated level can be placed for levelling the cell. Platinized platinum disk electrodes, 20 mm ϕ, 0.5 mm thick (P_1 and P_2) are stuck watertight on either side of the top and bottom of the cell cylinder with a small amount of silicone paste ("Black Silicone" sealant, Tōre Chem. Ind. Co. Ltd.) which was drawn circularly along the peripheral region within 1 mm from the ends of the cylinder using a special applicator (Fig. 2) cut out from polyethylene plate, 1 mm thick. The silicone sealing is convenient and very effective for its adaptability and sufficient elasticity as well as for repelling water.

The cell cylinder is equipped with two capillaries, 2 mm ϕ, both at right angle to the cylindrical cell wall at the half level, extending horizontally through the cell and opening directly outside to the neighboring sides of the square cell at S_1 and S_2. The cell is filled through the 2 mm ϕ capillary *via* S_1 which is closed with a 5 mm ϕ teflon screw plug through which a pinhole (0.5 mm ϕ) is bored to allow for thermal expansion of the solution. The opening S_2 is closed by a 5 mm ϕ teflon screw plug through which a platinized platinum needle electrode P_3 (0.5 mm ϕ) is threaded, extending through the 2 mm ϕ hole to the point near the innermost, narrowed part of the capillary (0.2 mm ϕ) which communicates with the cell cylinder. The Acrylite cell cylinder, with the platinum disk electrode P_1 and P_2 stuck on either side, is sandwiched between two platinum plated copper plates (5 mm thick and 50×50 mm^2 area)

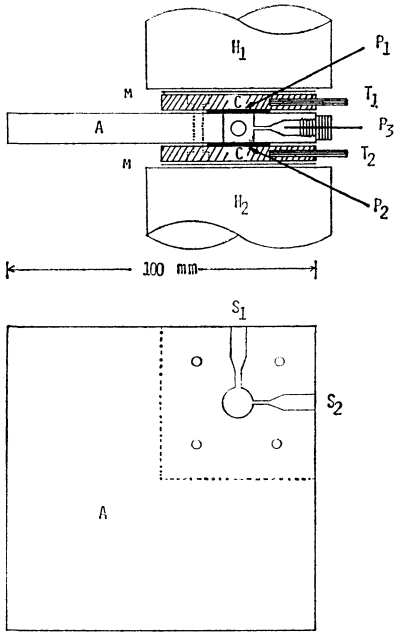

Fig. 1. Cell assemblies. A: Acrylite cylinder and apron. C: Heat conducting Cu-plate. M: Mica sheet. H_1 and H_2: Heat reservoirs. T_1 and T_2: Thermister probes. S_1 and S_2: Side holes. P_1 and P_2: Pt-disc electrodes. P_3: Pt-needle electrode.

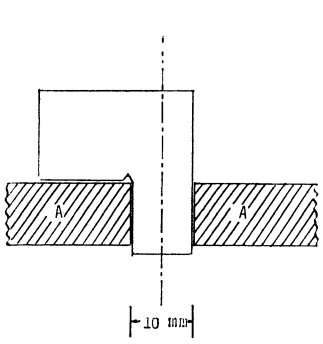

Fig. 2. Polyethylene applicator for pasting sealants.

which serve as a conductor for heat as well as electricity. They are fixed tightly together evenly with polycarbonate bolts and nuts at the four corners (Fig. 1). The cell assembly is further sandwiched between two heat reservoirs, H_1 and H_2, *via* mica sheet for electric insulation. The temperature of the heat reservoirs was maintained constant within ± 0.01 °C by circulation of thermostated water at 20 °C on the lower reservoir H_2 and at 30 °C on the upper H_1 to keep the mean temperature at 25 °C with thermo-circulators (CTE-2 and CTR-120,Komatsu Electronics Co. Ltd.).

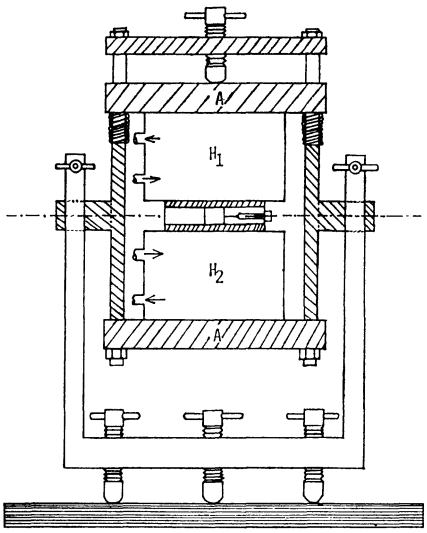

Fig. 3. Rotary cradle. H_1 and H_2: Heat reservoirs.

The entire system, including cell and heat reservoirs, was built in a stout rotary cradle supported on a massive iron rack provided with tripod screw for levelling (Fig. 3). This was placed in a large, foamy polystyrene box (30 mm thick wall) for thermal insulation from the exterior, empty space being stuffed loosely with cotton. Air conditioning of the laboratory around 25 °C (± 1 °C) is desirable.

The temperature of the platinum disk electrode was assumed to be the same as that of the central region of the heat conducting copper plate in contact with it, the latter being measured with a well-calibrated precision thermister thermometer (T-005A, Takara Instrument Co. Ltd.) to an accuracy ± 0.005 °C, where the thermister probe of 3.1 mm ϕ was mounted in a hole 3.2 mm ϕ and 25 mm deep reaching the center of the heat conducting plate.

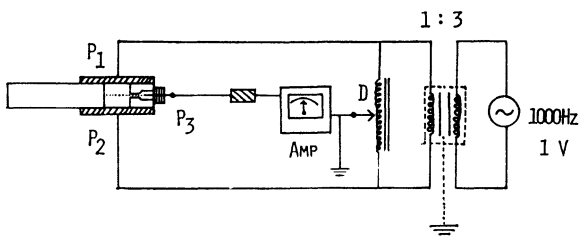

Fig. 4. Electric circuit. P_1, P_2, and P_3: Pt-electrodes. D: Decade ratio transformer. Amp: AC-amplifier as a detector.

Bridge Circuit. A block diagram of the bridge is shown in Fig. 4. Our aim was to find directly the ratio of resistances (impedances) Z_l and Z_u of the lower and upper halves of an electrolyte solution in the cell cylinder with respect to the central electrode P_3 by using a transformer bridge. A decade ratio transformer ("Decatran", DT-1145, Electroscientific Industries Ltd. U. S. A.) was used, with which we can read the resistance ratio, x, where $x=Z_u/(Z_l+Z_u)$, to the 5th figure below the decimal point, visually to the 6th. The sensitivity of this order is sufficient for the limited accuracy of the temperature control within ± 0.01 °C. Audiofrequency of 1 kHz and 1 V was supplied by an oscillator (VP-722, Matsushita Communication Ind. Co. Ltd.) driven by a battery source, but was dropped down to (1/3) V through a matching transformer before being applied across the top and bottom electrodes of the cell. By this arrangement the Joulean heat that evolves in the solution can be nearly swept away by the steady heat flow caused by the temperature gradient of 10 °C per cm between the two heat reservoirs. A highly sensitive AC amplifier 4402-AV-13C of Yokogawa-Hewlet-Packard (120 dB with sensitivity of 1 μV) was used as a zero indicator for the balancing of the bridge by means of an impedance matching preamplifier.

Sample Solutions. In the series of symmetric tetraalkylammonium bromides, R_4NBr (R=H, Me, Et, *n*-Pr, *n*-Bu, *n*-Pen, *n*-Hex, and *n*-Hep), the first six compounds were obtained from Wakō Pure Chem. Ind. Ltd., and the last two from Eastman Kodak Co. These chemicals were recrystallized from ethanol and used to make 0.01 M (1 M=1 mol dm^{-3}) solutions with conductance water, the concentration being determined by volumetric or potentiometric titration as regards bromide ions. Before use, all the solutions were subjected to partial deareation by boiling for about 10 s under reflux, followed by rapid cooling, thus avoiding the formation of minute bubbles on the surface of the platinum electrode on the hot side, which spoil the experiments, when temperature difference is imposed across the cell.

Conditioning of the Cell and Measurement. Thorough washing of the cell inside with running fresh water is essential. *Ca.* 10 L of partially deareated hot water (70—90 °C) was allowed to enter the cell cylinder by means of a siphon *via* the side hole S_1 and to run out of the second side hole S_2 over a period of *ca.* 10 h, while leaving both platinum electrodes at the short circuit. The cell cylinder was then rinsed several times with the sample solution with a syringe and left to stand overnight with the solution in it so that it might soak through all the corners inside the cell cylinder including the two side holes. The solution was renewed and the cell assembly was warmed up for measurement, fixed on the cradle, first in the reverse position, the top at 20 °C and the bottom at 30 °C (mean 25 °C) for 1 h to make the solution uniform throughout by the violent convective flow caused by an inverse temperature gradient. The cradle was then turned to the normal position, this instant being regarded as the time zero. The measurement was started after the levelling of the assembly had been roughly made within the first 10 s and completely within 5 min. Incomplete levelling causes a convective flow in the cell, spoiling the measurements. The bridge balance reading, x, read on the Dekatran were made every 5 min in the early stage and every hour in the latest stage. The duration of a run varied from 6 h for the fastest diffusing solute to 12 h for the slowest. Essential points for measurements are as follows: Thorough rinsing and soaking of the cell, strict control of temperature, correct levelling of the system, correct setting of the cell assembly, and deareation of solutions.

Analytical Method. General Description: Let R_l and R_u denote the resistance of the lower and upper, respectively, halves of the solution in the cell cylinder with respect to the center-tap electrode P_3 at time t after a temperature difference ΔT has been applied across the cell. With use of $Y(t)$, a function of time t, defined by

$$Y(t) = \frac{R_l - R_u}{R_l + R_u} \quad (1)$$

Agar and Turner[11] derived the following equation for the determination of the Soret coefficient σ:

$$Y(t) - Y(0) = \frac{8 b_{01} \sigma \Delta T}{\pi^3} F\left(\frac{t}{\theta}\right) \quad (2)$$

$$F\left(\frac{t}{\theta}\right) = \frac{\pi^3}{32} - \sum_{n=1}^{\infty} \frac{1}{n^3} \sin\left(\frac{n\pi}{2}\right) \exp\left(-\frac{n^2 t}{\theta}\right) \quad (3)$$

where $Y(0)$ is the Y value at time $t=0$. θ denotes the characteristic time constant defined by

$$\theta = \frac{a^2}{\pi^2 D} \quad (4)$$

where a is the cell height, D the diffusion coefficient at the mean temperature. σ is the Soret coefficient at the mean temperature defined by $\sigma = -(\partial \ln m / \partial T)_p$ in the steady state, where m is the molality. b_{01} is defined by

$$b_{01} = -\left(1 + \frac{\partial \ln \Lambda}{\partial \ln c}\right)_{T,P} \quad (5)$$

where Λ is the equivalent conductivity at concentration c at constant temperature T and pressure P.

When an appropriate value of θ is found, we can obtain σ readily from the slope of the $Y(t)$-F plot. However, it is difficult to find the exact value of θ from the values of a and D measured independently, since, owing to the elasticity of the silicone sealants, fluctuation in a values may result depending on the pressure put on the cell assembly when sandwiched between two heat reservoirs H_1 and H_2 and the value of D is scarcely known experimentally for tetraalkylammonium salts except n-Bu_4NBr.[13] Though D might be estimated from conductance data, it would be inaccurate. Consequently, we adopted an alternative method of finding a suitable, effective value of the characteristic time constant, θ_{eff}.

Determination of θ_{eff}: Since in the same run ΔT is kept constant (10 °C), we have

$$Y(t) - Y(0) = \alpha F\left(\frac{t}{\theta}\right) \quad (6)$$

where α is a constant. When Eq. 6 is satisfied, the following function which involves four observational points Y_1, Y_2, Y_3, and Y_4 at respective times t_1, t_2, t_3, and t_4,

$$G(\theta) = \frac{Y_1 - Y_2}{Y_3 - Y_4} - \frac{F\left(\frac{t_1}{\theta}\right) - F\left(\frac{t_2}{\theta}\right)}{F\left(\frac{t_3}{\theta}\right) - F\left(\frac{t_4}{\theta}\right)} = \frac{x_1 - x_2}{x_3 - x_4} - \frac{F\left(\frac{t_1}{\theta}\right) - F\left(\frac{t_2}{\theta}\right)}{F\left(\frac{t_3}{\theta}\right) - F\left(\frac{t_4}{\theta}\right)} \quad (7)$$

should be equal to zero (the Decatran reading x_i may be used instead of Y_i). Solving Eq. 7 we can find the value of θ that fits the experimental results, θ_{eff}. Calculation was performed by using a minicomputor TI-59 Texas Instrument. The results are given in Table 1. By means of this effective value θ_{eff}, we obtained a linear relation between $Y(t)$ and F with a correlation coefficient exceeding 0.9999, which is sufficient if we consider that the temperature control was accurate within ±0.01 °C.

In case of NH_4Br, however, θ_{eff} could not be obtained by this method, since NH_4Br shows a very slight Soret effect,[10] giving a small value of Y, and making $G(\theta)$ practically indefinite. The value of θ for NH_4Br was calculated from the diffusion coefficient D and the cell height a in a similar way as described below.

Results and Discussion

The results for aqueous 0.01 M solutions of R_4NBr are shown in Figs. 5-a and 5-b, where $Y(t)$ is plotted against t and F. The linearity of the Y-F relation is good. The Soret coefficients obtained from the slope in the $Y(t)$-F diagram and given in Table 1 are plotted in Fig. 6 against the carbon number of the alkyl chains of the tetraalkylammonium bromides in terms of the molar heats of transfer Q^* ($Q^* = -2RT^2B\sigma$ for uni-univalent electrolytes, where R is the gas constant and B is defined by $B = [1 + (\partial \ln \gamma_\pm / \partial \ln m)]_{T,P}$, $\gamma_\pm$ being the mean activity coefficient.). All the results for 0.01 M aqueous solutions, except for n-Hep_4NBr whose concentration was 0.000978 M owing to its limited solubility, are given at the mean temperature 25 °C, where a possible shift was within ±0.03 °C during 6—12 h of the measurements (Table 1). Q^* shows a maximum around the carbon number 4—5 of the alkyl chain of R_4NBr. The present Soret coefficients of 0.01 M tetraalkyl-

Table 1. Soret coefficients and heats of transfer for 0.01 M tetraalkylammonium bromides at the mean temperature 25 °C

Bromide	$-b_{01}$ [a]	B [b]	θ_{eff} / s	$10^9 D_{eff}$ [c] / $m^2\,s^{-1}$	$10^9 D_{calcd}$ [d] / $m^2\,s^{-1}$	$-10^3\sigma$ / K^{-1}	Q^* / kJ mol^{-1}	$-10^3\sigma_{calcd}$ [e] / K^{-1}
H_4NBr	0.966	0.955	—	—	1.926	0.13	0.18	−0.28
Me_4NBr	0.962	0.953	6400	1.37	1.438	4.18	5.89	5.78
Et_4NBr	0.956	0.945	8360	1.05	1.148	7.16	10.00	9.65
n-Pr_4NBr	0.950	0.941	10120	0.870	0.898	9.05	12.6	13.4
n-Bu_4NBr	0.945	0.934	11600	0.761[f]	0.761[f]	9.61	13.3	16.3
n-Pen_4wBr	0.939[g]	0.929[g]	11850	0.744	0.705	9.47	13.0	18.5
n-Hex_4NBr	0.934[g]	0.923[g]	10600	0.828	—	8.65	11.8	—
n-Hep_4NBr	0.928[g]	0.917[g]	7400	1.19	—	7.34[h]	9.95[h]	—

a) Ref. 3, graphical determination. b) Ref. 2, graphical determination. c) Values for 0.01 M R_4NBr families were obtained by means of Eq. 4 from θ_{eff} found by experiment for the respective bromide using the effective cell height, a_{eff}, determined from the best fit value of θ_{eff} for the cell of n-Bu_4NBr using the literature value of D for 0.01 M n-Bu_4NBr (Ref. 13). d) Calculated by the Nernst-Hartley equation. e) Theoretical prediction.[8] f) Ref. 13. g) Extrapolation of the bromide series. h) The value for 0.000978 M.

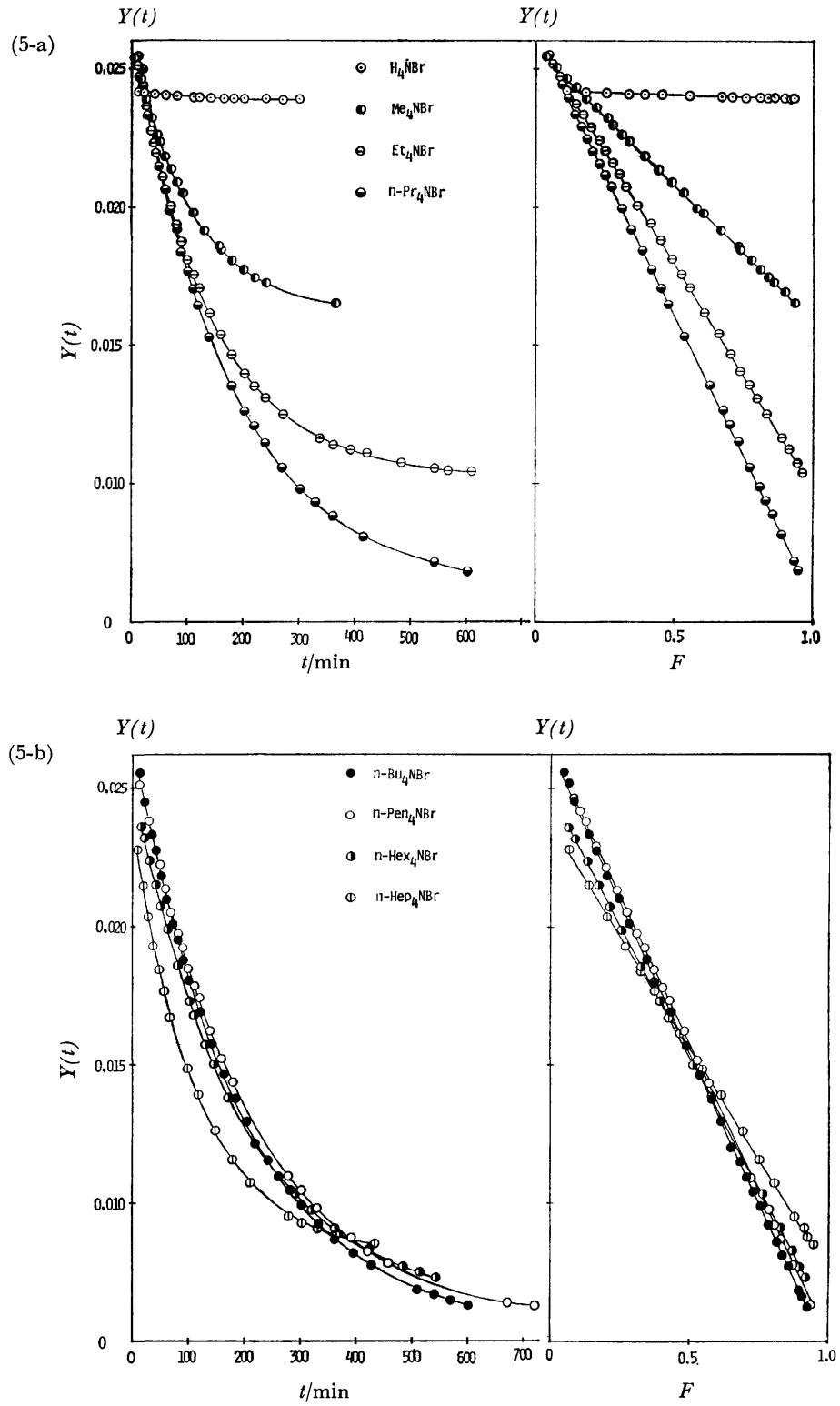

Fig. 5. (5-a and 5-b). $Y(t)$ plots *vs.* time and F.
⊙, H_4NBr; ◐, Me_4NBr; ⊖, Et_4NBr; ◒, *n*-Pr_4NBr; ●, *n*-Bu_4NBr;
○, *n*-Pen_4NBr; ◑, *n*-Hex_4NBr; ⊕, *n*-Hep_4NBr.

ammonium bromides are somewhat lower than those observed by Snowdon and Turner[12] by a similar method. One of us (T. I.) estimated theoretically the Soret coefficients of 0.01 M aqueous solutions of a series of R_4NBr, in the range R=H—R=*n*-C_5H_{11}, from the initial thermoelectric powers of thermocells of 0.01 M solutions of R_4NBr families by taking 144 JK^{-1} mol^{-1} for the molar transported entropy of the bromide ions.[8] The calculated values of the Soret coefficients σ (Table 1) are much greater than those observed, not showing any maximum but appearing to approach asymptotically a certain limit with increase in the carbon number of

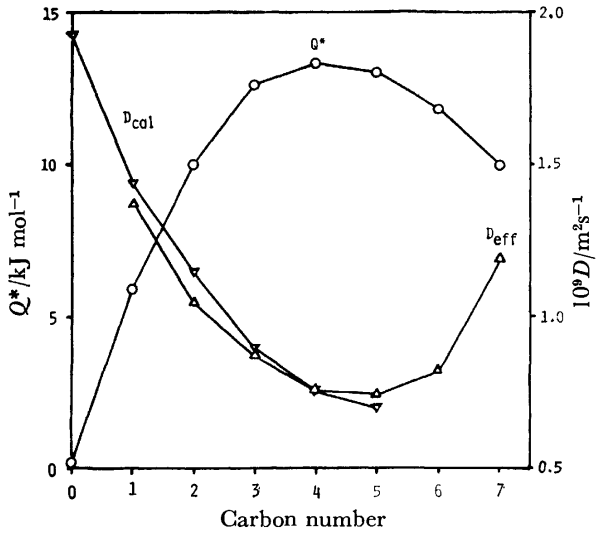

Fig. 6. Dependence of the heat of transfer or of the diffusion coefficient on the carbon number of the alkyl chain of R_4NBr.
○, Q^*; △, D_{eff}; ▽, D_{cal}.

the alkyl chain. This indicates that there is a limitation for calculation of the Soret coefficients from the initial thermoelectric power and the transported entropy, as in the case of the bromide ions where hydrophobic hydration becomes predominant, particularly in R_4NBr families with alkyl chain of higher carbon numbers beyond 4.

The diffusion coefficient, D, of the R_4NBr series has been determined experimentally only for n-Bu_4NBr.[13] For the other bromides, we could get rough estimates of D by (i) using θ_{eff} for the solution in question and the effective value of the cell height, a_{eff}, determined from the θ_{eff} for a reference solution such as Na_2SO_4 or n-Bu_4NBr, whose diffusion coefficient is known (D_{eff} in Table 1), and (ii) calculating the ionic equivalent conductance with use of the Nernst-Hartley equation,[14] (D_{calcd}). If we take into consideration the fact that D_{eff} and D_{calcd} were obtained from entirely different sources, the two diffusion coefficients are in fairly good agreement. We see that the D values pass minimum around the carbon number 4—5 of the alkyl chain, in an inverse tendency of Q^* showing maximum around the same carbon number (Fig. 6). This might be explained as a result of competition between two opposite tendencies: the enhancement of the water structure (hydrophobic bond formation) around the alkyl chain moieties of the tetraalkylammonium ion with increasing chain length, and the decrease in the number of completely dissociated free ions with increasing chain length owing to the reinforced ion-pairing effect[2,15] caused by the enhanced water structure around the ions.

The work was supported by Grant-in-Aid for Scientific Research Project No. (C)-754073 from the Ministry of Education.

References

1) R. Zana and E. Yeager, *J. Phys. Chem.*, **71**, 4241 (1967); L. H. Laliberte and B. E. Conway, *J. Phys. Chem.*, **74**, 4116 (1970); F. J. Millero, *Chem. Rev.*, **71**, 149 (1971).
2) S. Lindenbaum and G. E. Boyd, *J. Phys. Chem.*, **68**, 911 (1964).
3) D. F. Evans and R. L. Kay, *J. Phys. Chem.*, **70**, 366 (1966); R. L. Kay and D. F. Evans, *J. Phys. Chem.*, **70**, 2325 (1966); A. L. Surdo and H. E. Wirth, *J. Phys. Chem.*, **83**, 879 (1979).
4) R. L. Kay, T. Vituccio, C. Zawoyski, and D. F. Evans, *J. Phys. Chem.*, **70**, 2336 (1966); C. M. Criss and M. J. Mastroianni, *J. Phys. Chem.*, **75**, 2532 (1971).
5) B. Lindman, H, Wennerström, and S. Forsén, *J. Phys. Chem.*, **74**, 754 (1970).
6) T. Ikeda, *Rep. Fac. Sci. Shizuoka Univ.*, **8**, 25 (1973).
7) W. Kauzmann, *Adv. Protein Chem.*, **14**, 1 (1959).
8) T. Ikeda, *Rep. Liberal Arts Sci. Fac. Shizuoka Univ. (Nat Sci.)*, **2**(4), 153 (1959).
9) T. Ikeda and M. Matsumoto, *J. Phys. Chem.*, **69**, 3755 (1965).
10) T. Ikeda and H. Miyoshi, *J. Phys. Chem.*, **70**, 3361 (1966); T. Ikeda and Y. Yamamoto, *Bull. Chem. Soc Jpn.*, **47**, 838 (1974).
11) J. N. Agar and J. C. R. Turner, *Proc. R. Soc. London, Ser. A*, **255**, 307 (1960).
12) P. N. Snowdon and J. C. R. Turner, *Trans. Faraday Soc.*, **56**, 1409 (1960).
13) H. Kim, A. Revzin, and L. J. Gosting *J. Phys. Chem.*, **77**, 2567 (1973).
14) J. Koryta, J. Dvorak, and V. Bohackova, "Electrochemistry," Methuen & Co. Ltd., London (1970), p. 114.
15) R. M. Diamond, *J. Phys. Chem.*, **67**, 2513 (1963).

Electron Spin Resonance of 2,2′-Bipyridyl, Dimethyl-2,2′-Bipyridyls, and 2,2′-Biquinolyl in their Phosphorescent Triplet States

Jiro HIGUCHI,* Mikio YAGI, Takashi IWAKI, Makoto BUNDEN, Katsumi TANIGAKI, and Takeshi ITO**

Department of Chemistry, Faculty of Engineering, Yokohama National University, Hodogaya-ku, Yokohama 240

(Received September 28, 1979)

Electron spin resonance (ESR) of phosphorescent triplet states of 2,2′-bipyridyl, 3,3′-, 4,4′-, 5,5′-, and 6,6′-dimethyl-2,2′-bipyridyls, and 2,2′-biquinolyl has been studied in ethanol glasses. For 2,2′-bipyridyl, the ESR spectrum of both the *E* and *Z* conformers was observed in poly(vinyl alcohol) films and their assignment was examined by changing the direction of applied magnetic field. Using such a technique, the stretched polymer-film method has been developed for determining the molecular conformations which are difficult to be estimated from zero-field splitting (ZFS) parameters obtained in rigid glasses. As a result, the conformations in the phosphorescent triplet states of molecules studied here are confirmed to be all *E* in ethanol glasses, even for a case with a relatively small *E* value.

2,2′-Bipyridyl (BPY)† is one of typical bidentate ligands which are coordinated with many metal ions in the *Z* conformation. In the solutions or in the crystal, however, the ground state of the molecule is in the *E* conformation,[1,2] although the structure may not perfectly be planar. As a result, the *Z* conformer of free BPY has not conclusively been identified in any kind of experiments. Recently, we have succeeded in observing two sets of electron spin resonance (ESR) signals which are originated from the *Z* and *E* conformers in the phosphorescent triplet state when the molecules were dissolved in poly(vinyl alcohol) (PVA) films.[3,4] For the phosphorescent triplet states of symmetrically substituted dimethyl-2,2′-bipyridyls (DMBPY's)† and 2,2′-biquinolyl (BQL)†, the conformations are also expected to be *E* but any experimental evidence for it has not yet been reported. In the present work, therefore, a further ESR study of these molecules in ethanol glasses was carried out, in connection with their conformations. In this case, we have developed a new technique for determining the *Z* and *E* conformations of paramagnetic species by applying the stretched polymer-film method.

In the triplet state of molecules, the magnetic fine structure may well be explained by the following spin Hamiltonian:

$$\begin{aligned}\mathcal{H} &= g\mu_B \boldsymbol{B}\cdot\boldsymbol{S} + \boldsymbol{S}\cdot\boldsymbol{D}\cdot\boldsymbol{S} \\ &= g\mu_B \boldsymbol{B}\cdot\boldsymbol{S} - XS_x^2 - YS_y^2 - ZS_z^2 \\ &= g\mu_B \boldsymbol{B}\cdot\boldsymbol{S} + D[S_z^2 - (1/3)S(S+1)] + E[S_x^2 - S_y^2] \\ &\qquad (S=1).\end{aligned}$$

Here, $\boldsymbol{D}$ is the fine structure tensor with principal values of $-X$, $-Y$, and $-Z$, and D and E are the zero-field splitting (ZFS) parameters. The other symbols have their usual meaning and the anisotropy of g was disregarded. Assuming a planar structure of molecule in the phosphorescent triplet state, the coordinate axes were taken as follows: the principal magnetic axes, x and y, are in the molecular plane (the x axis is taken rather close to the long direction of molecule), while the z axis is perpendicular to the molecular plane.

In *Z* conformers of BPY's (or BQL), the x axis is taken to be parallel to the central C–C bond which connects the two pyridine (or quinoline) rings (hereafter, we will refer to such a direction as b), while that of *E* conformers should be separated to the b in direction by some angle of $\alpha_x (0 < |\alpha_x| < \pi/4)$. Such a difference on the direction of magnetic axis is certainly important for determining the conformation of molecules studied here.

Application of Stretched Polymer-Film Method for Determining Conformations

Only from the ESR spectrum observed in a rigid glass, the assignment of each peak is directly impossible and information about the conformation of the molecule studied is not easily obtainable. For symmetrically substituted biphenyls, bipyridyls, and related compounds, the molecular structures in the phosphorescent triplet state may in general be nearly planar, because of the increase of bond order in the central C–C bond which connects two of the same aromatic rings. For the *Z* conformers with symmetry C_{2v}, one of the principal axes of the $\boldsymbol{D}$ tensor, say x axis, should be parallel to this bond (x||b), while for the *E* conformers with symmetry C_{2h} the x axis is in a direction separated from b by α_x. When the magnetic induction $\boldsymbol{B}$ is applied parallel to one of the principal magnetic axes, the peak intensity at the corresponding resonance field is maximum in regularly oriented molecular assembly. These relations make possible to determine the conformation of these molecules by applying the stretched polymer-film method following the procedure described below.

When a PVA film containing appropriate amount of molecules to be studied is stretched more than 200% of stretch, we have already confirmed that these molecules are partially oriented with the following tendency: (1) the molecular plane is difficult to be oriented perpendicular to the stretched direction (s); (2) the long molecular axis has a tendency to align to the s direction; (3) the molecular plane is preferably oriented parallel to the film plane. From such a stretched film, we made several kinds of narrow oblong strips, the

** Present address: Department of Chemistry, Faculty of Education, Shinshu University, Nishinagano, Nagano 380.

† In the present paper, 2,2′-bipyridyl, dimethyl-2,2′-bipyridyl, and 2,2′-biquinolyl are abbreviated as BPY, DMBPY, and BQL, respectively.

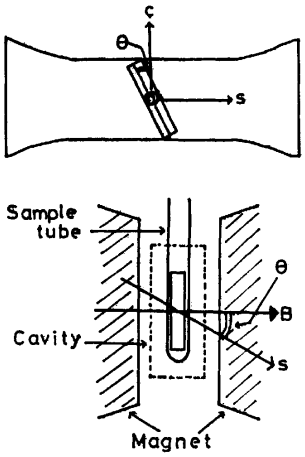

Fig. 1. Coordinate system in stretched PVA films, and the narrow oblong strips used in ESR measurements.

long sides of which were cut at various angles θ's with direction c which is perpendicular to s in the film plane, as shown in Fig. 1. When several sheets of such strips with the same θ are inserted and fixed in the same direction in the sample tube in the cavity, their s direction makes an angle of θ with $\boldsymbol{B}$ which is applied in the film plane. We will designate an angle between the principal magnetic x axis and the s direction as θ_X. Actually, the line shape of the ESR spectrum changes from the case with $\theta=\theta_X$ by using the strips with another angle of θ.

If the guest molecules are oriented in perfect ordering as in a single crystal, the intensities of the X peaks should be maximum when $\theta=\theta_X$ where the x axis is placed parallel to $\boldsymbol{B}$ (hereafter, we will refer to an angle giving the maximum intensity as θ_M). Although the molecules dissolved in stretched PVA films are partially oriented, the peak intensity decreases if the direction of $\boldsymbol{B}$ deviates from that of the principal magnetic axes. This means that the maximum intensity of each peak should be observed at $\theta_M \approx \theta_X$, even if the line shapes are generally broad in PVA films as compared with the case of a single crystal. As a result, we can reasonably distinguish the E conformer with $\theta_X \neq 0$ from the Z conformer with $\theta_X=0$, except the case when the θ_X of the E conformer is nearly zero. For E conformers in stretched polymer films, there are two types of orientations where the principal magnetic axes make angles $\pm\theta_X$ with the s direction even in an ideal alignment. Consequently, the X peak of the E conformer may be rather broad as compared with that of the Z conformer if the former θ_X is fairly small. Therefore, we may pertinently assign the conformation as follows: a peak with $\theta_X \neq 0$ and/or with relatively broad line shape generally arises from the E conformer, whereas that with $\theta_M=0$ and with relatively sharp line shape is attributed to the Z conformer.

Experimental

The ESR measurements were carried out for BPY, 3,3′-, 4,4′-, 5,5′-, and 6,6′-DMBPY's and BQL in ethanol glasses. A purified sample of 3,3′-DMBPY used was donated by Dr. H. M. Suzuki (Government Industrial Research Institute, Tohoku, Nigatake), and purified 4,4′- and 5,5′-DMBPY's were donated by Dr. Y. Kaizu (Tokyo Institute of Technology). All the other compounds were purchased from Tokyo Kasei Co.. BPY and BQL were purified by recrystallization, but DMBPY's were used without further purification.

In determining the conformation of some of these molecules, PVA films containing its appropriate amount were prepared by either the solution-evaporating method[3] or the diffusion-penetrating method.[4] In the case of BPY, the former method was used, that is, after mixing of an aqueous solution of PVA with an ethanol solution of BPY, a film with 2×10^{-2} cm thick was obtained by evaporating solutions on a glass plate. On the other hand, the latter method was used for 5,5′-DMBPY and BQL because of their insolubility in water, that is, a pure PVA film with 2×10^{-2} cm thick was made on a glass plate by evaporating water from the aqueous solution. After heat treatment for about an hour at 80 °C and swelling in water for about three hours at 30 °C, the film was soaked in methanol solution of a sample until its appropriate amount was penetrated into the film by diffusion. Then, the film thus prepared by either of the methods was stretched for about five minutes at about 60 °C. The obtained stretched films are about 7×10^{-3} cm thick, and with about 250% of stretch in the s direction and about 30% of contraction in the c direction.

For the ESR measurement, a sample tube containing ethanol solution with appropriate concentration of a compound was set in a quartz dewar with fingertip which was inserted in the cavity. The ESR spectra were observed at 77 K using JEOL JES-ME-3X spectrometer with 100 kHz modulation at microwave frequencies close to 9.2 GHz and the applied $\boldsymbol{B}$ between 0.1 and 0.5 T. The microwave field was perpendicular to $\boldsymbol{B}$ and the microwave frequency was measured with a cavity frequency meter. The magnetic induction was calibrated with a proton magnetic resonance technique. The exciting light was provided by a 500 W super-pressure mercury arc lamp filtered through 5 cm of distilled water and a Toshiba UV-31 or UV-D25 filter.

In the case of 3,3′-DMBPY, the observed ESR signals were considerably weak and accumulated by using a signal averager (1024 channel Kawasaki Electronica TM-1610S) for improving the signal to noise ratios in the following way: appropriate times of scans were accumulated with the exciting light on and the same times of scans were subtracted with the light off. In this way, we obtained a spectrum without perceptible baseline drifts which were due to signals of free radicals produced by UV irradiation and of magnetic contaminants in the cavity.

Results

In ethanol glasses, all the X, Y, and Z peaks for the $\Delta m=\pm1$ transitions of the phosphorescent molecules studied here were clearly observed as shown in Figs. 2 and 3, except the Y and Z signals of 3,3′-DMBPY and the high-field Y peak of BQL shown in Fig. 4. Accordingly, the Y and Z values of 3,3′-DMBPY were estimated from the resonance fields of X component and the trace-less relation of $\boldsymbol{D}$ tensor. The X, Y, and Z values of the other BPY's were directly obtained from the corresponding set of resonance fields. Since the observed resonance fields of DMBPY's did not significantly deviate from those of (E)-BPY, they were assigned to be in the same ordering of magnitude as those of (E)-BPY. For BQL, however, the assignment of the resonance fields has not yet been performed.[5] Therefore,

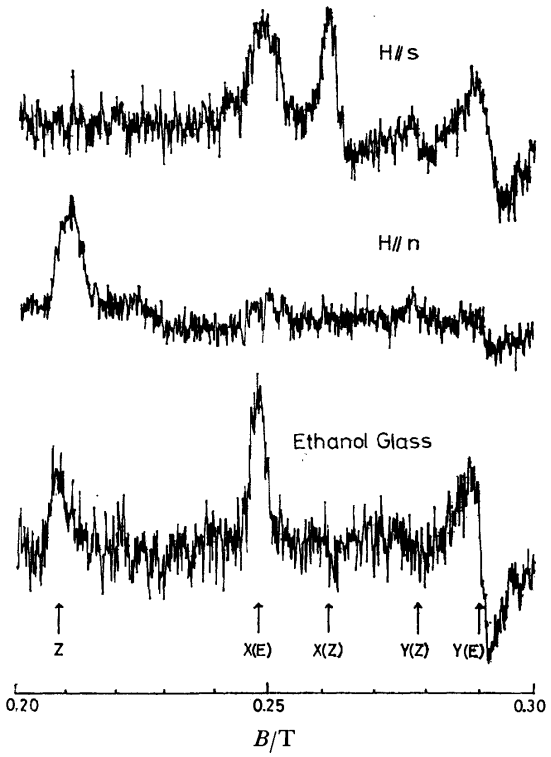

Fig. 2. ESR spectra of the low field $\Delta m=\pm 1$ transitions for the phosphorescent triplet state of (*Z*)- and (*E*)-2,2′-bipyridyl in a stretched PVA film and in ethanol glass at 77 K.

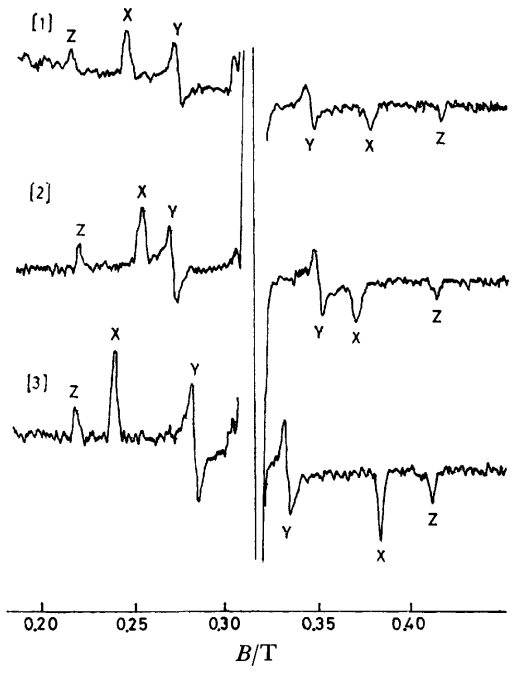

Fig. 3. ESR spectra of the $\Delta m=\pm 1$ transitions for the phosphorescent triplet states of 4,4′-dimethyl-2,2′-bipyridyl (1), 5,5′-dimethyl-2,2′-bipyridyl (2), and 6,6′-dimethyl-2,2′-bipyridyl (3) in ethanol glasses at 77 K.

we have carried out it by using the stretched polymer-film method[3,4] with reference to Fig. 4. The ZFS parameters thus obtained are listed in Table 1.

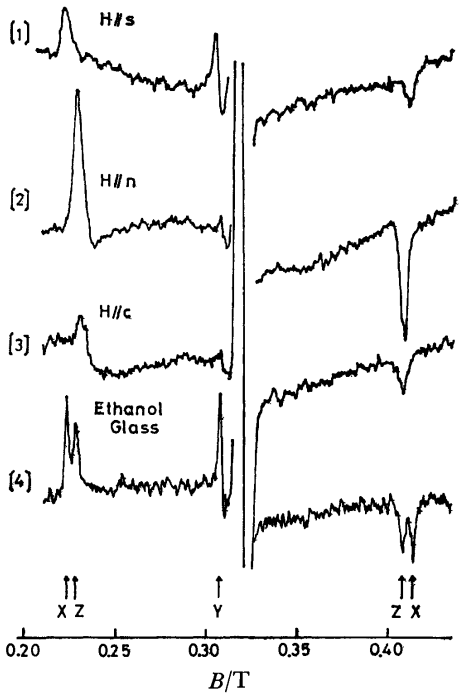

Fig. 4. ESR spectra of the $\Delta m=\pm 1$ transitions for the phosphorescent triplet state of 2,2′-biquinolyl in stretched PVA films (1—3), and in ethanol glass (4) at 77 K.

ESR measurements for the phosphorescent triplet state of BPY have already been carried out in rigid glasses[5,7] or in stretched PVA films.[3,4] Especially in the latter case, we observed two sets of X and Y peaks and one set of Z peaks for the $\Delta m=\pm 1$ transitions as shown in Fig. 2. When $\boldsymbol{B}||$s, the intensities of the X and Y peaks which can be observed in ethanol glasses are not much different from each other, but the other X peaks are relatively enhanced as compared with the other Y peaks. As a result, we have reasonably concluded that the former set of signals is pertinent to the *E* conformer and the latter to the *Z* conformer, since $\theta_X=0$ for the *Z* conformer while $\theta_X \neq 0$ for the *E* conformer.

Under these circumstances, we have tried to determine these conformation by applying the technique described previously. First, we prepared narrow oblong strips of the stretched BPY-containing PVA films with various θ. The ESR measurements were carried out for these samples under irradiation. In this case, the intensities of X peaks for the *Z* and *E* conformers, $I_X(Z)$ and $I_X(E)$, respectively, were actually changed by using a sample with different value of θ, while that of Z peaks, I_z, should not be varied if the strips prepared from the identical stretched film were used under the same condition of electromagnetic field in the cavity. Plotting the relative intensities of $I_X(Z)/I_z$ and $I_X(E)/I_z$, we found $\theta_M=0°$ and $\theta_M \approx 5°$ for the *Z* and the *E* conformer, respectively, although the variation of $I_X(E)/I_z$ is relatively gentle near θ_M as compared with that of $I_X(Z)/I_z$. This may apparently imply the facts that the previous conclusion is exactly correct and that the stretched polymer-film technique is actually available for determing the conformation of molecules even if only one set of peaks were observed. The ZFS para-

Table 1. Zero-field splitting parameters in the phosphorescent triplet states (cm^{-1})

Molecule	Host	$\|X\|/hc$	$\|Y\|/hc$	$\|Z\|/hc$	$\|D\|/hc$	$\|E\|/hc$	D^*/hc[a]	D^*/hc[b]
(*Z*)-2,2′-Bipyridyl	PVA film	0.0416	0.0327	0.0723	0.1094	0.0045	0.1097	0.1105
(*E*)-2,2′-Bipyridyl	EtOH glass	0.0487	0.0246	0.0737	0.1104	0.0121	0.1124	0.1121
	PVA film	0.0489	0.0242	0.0723	0.1089	0.0123	0.1110	0.1105
(*E*)-3,3′-Dimethyl-2,2′-bipyridyl	EtOH glass	0.0479	(0.019)	(0.067)	0.101	0.014	0.104	0.1052
(*E*)-4,4′-Dimethyl-2,2′-bipyridyl	EtOH glass	0.0475	0.0257	0.0732	0.1098	0.0109	0.1114	0.1109
(*E*)-5,5′-Dimethyl-2,2′-bipyridyl	EtOH glass	0.0418	0.0287	0.0705	0.1057	0.0066	0.1063	0.1070
	PVA film	0.0410	0.0291	0.0701	0.1051	0.0060	0.1056	0.1046
(*E*)-6,6′-Dimethyl-2,2′-bipyridyl	EtOH glass	0.0520	0.0178	0.0703	0.1052	0.0171	0.1093	0.1090
(*E*)-2,2′-Biquinolyl	EtOH glass	0.0699	(0.0037)	0.0662	0.0992	0.0368	0.1179	0.1178
	PVA film	0.0672	(0.0032)	0.0640	0.0960	0.0352	0.1137	0.1134

a) $D^*=(D^2+3E^2)^{1/2}$. b) Obtained from the observed resonance field of the $\Delta m=\pm 2$ transition with Kottis-Lefebvre's correction.[6]

meters obtained in the stretched PVA films are also given in Table 1.

For 3,3′-DMBPY, the *Z*-conformer should not be planar because of the steric hindrance between the two methyl groups. In such a case, the *D* value may be fairly large as compared with the planar (*Z*)-BPY by considering the result of phosphorescent 2,2′-dimethylbiphenyl by Scheve and Wagner.[8] Since the *D* value obtained is rather small as compared with that of BPY, one may reasonably infer that 3,3′-DMBPY observed in the present work is actually the *E* conformer.

4,4′- and 6,6′-DMBPY's are *meta*-methyl-substituents to the carbon 2 (and 2′) which is bonded to another pyridine ring. In these cases, the electronic structures may not be much different from that of BPY, and the *D* and *E* values of each conformer are expected to be relatively close to those by BPY with the same conformation. In the present result, the *D* and *E* values obtained for these molecules are rather close to those of (*E*)-BPY than those of (*Z*)-BPY. This may suggest the fact that the ZFS parameters of 4,4′- and 6,6′-DMBPY's listed in Table 1 are apparently those of the *E* conformers.

For 5,5′-DMBPY, the obtained *D* and *E* values appear to be close to those of (*Z*)-BPY rather than those of (*E*)-BPY. However, the molecule is a *para*-methyl-substituent to the carbon 2 (and 2′), and the influence of substitution to the electronic structure may not be very small. Further, all the other BPY's observed here are *E* conformers in ethanol glasses. Considering these facts, we have applied the stretched polymer-film technique for determining the conformation of the molecule. The experimental procedure adopted was quite the same as in the case of BPY. The resonance fields were scarcely changed from the case of ethanol glasses if the microwave frequency was kept nearly the same, and no new peak was detected. This is a quite different situation from the case of BPY where the peaks of both the *Z* and *E* conformers were observed. Then the relative intensity I_X/I_Z was plotted against θ and its maximum value was found at $\theta_M\approx 5°$. This may imply that 5,5′-DMBPY observed was the *E* conformer, inspite of its relatively small *E* value.

In the phosphorescent triplet state of BQL, the conformation has not conclusively been determined, although the possibility of *E* was discussed by Rabold and Piette.[5] For determining the conformation, therefore, experiments similar with those of 5,5′-DMBPY were carried out using the stretched BQL-containing PVA films. The resonance fields were almost unchanged from the case of ethanol glasses if the microwave frequency was kept nearly the same, and no new peak was observed. In this case, we have found a small peak for relative intensity of I_X/I_Z near $\theta_M\approx 15°$, although its variation is very gentle. This may possibly suggest the fact that the conformation of BQL detected here is also *E* as in its ground state.

Discussion

Applying the stretched polymer-film technique, we have succeeded in assigning the conformation of BPY's and BQL in the phosphorescent triplet state. As a further study, we leave some possibility to proceed for determining the direction of principal magnetic axes by improving the present procedure. In the present study, however, such a work was not undertaken, since the molecules studied here are rather reactive with the environments in the excited state and the ESR signals decrease rapidly during UV irradiation. For the purpose of such a determination, therefore, it may be desirable to choose a set of guest compound and host polymer which are stable with each other under irradiation. In this case, the analysis may actually become easier in the use of a stretched polymer film with better alignment of guest molecules, such as a stretched film without contraction in the c direction.[9] However, one should remember that there are two types of orientations with $\pm\theta_X$ for *E* conformers in stretched polymer films, even in an ideal alignment of guest molecules. Especially when the $|\theta_X|$ is small and/or when the *Z* conformers exist together with the *E* conformers with a small $|\theta_X|$, these ESR peaks may become overlapped with each other. As a result, one should analyze the ESR line shape by a satisfactory computer simulation using a distribution function with orthorhombic character.

In the present work, we have confirmed that the stable conformations of BPY, 3,3′-, 4,4′-, 5,5′-, and 6,6′-DMBPY's and BQL in the phosphorescent triplet

state are all E in ethanol glasses. This is a quite natural conclusion in consideration of the intramolecular steric interactions for the Z and E conformations, similar with those in the ground state. In these molecules, the D and E values have not hitherto been determined except for the case of BPY, although the D^* values of 4,4'- and 5,5'-DMBPY's[10] and BQL[5] have already been reported.

Among DMBPY's, the E values listed in Table 1 are fairly different from each other, whereas the change of the D values is relatively small. Such a difference of E values may be rather complicated because of the superposition of the change of spin distribution caused by the nitrogen heteroatom upon that by the substitution of another pyridine ring. As a result, the conformation of these molecules is generally difficult to determine merely from the magnitude of E value when only one of the conformers was detected.

In examining the trend of the ZFS parameter to the spin distribution, the E values of these molecules were simply evaluated from the lowest triplet configuration, in which one electron is excited from the highest occupied orbital ϕ^{ho} of the ground state to the lowest vacant orbital ϕ^{lv}. Using the simple LCAO-MO's with Streitwieser's parameters,[11] the spin densities at each atom, ρ^{ho} and ρ^{lv}, which originate from the singly occupied orbitals of ϕ^{ho} and ϕ^{lv}, respectively, were separately obtained within McLachlan's approximation.[12] Then the E values were roughly estimated from these spin densities by including only interactions between the neighboring atoms. In this calculation, the molecules were assumed to be planar, all the bond lengths and bond angles were taken the values of the ground state of benzene molecule,[13] and the electron spin dipoles were assumed to be located at each nucleus with the above spin distributions. In fact, such a treatment may be allowed to estimate in-plane components of the **D** tensor.

TABLE 2. E/hc VALUES OF 2,2'-BIPYRIDYLS CALCULATED FROM THE SPIN DENSITIES OF SINGLY OCCUPIED ORBITALS (cm^{-1})

	$E(Z)_{calcd}/hc$	$E(E)_{calcd}/hc$	$[E(E)_{obsd}-E(E)_{calcd}]/hc$[a]
2,2'-Bipyridyl	0.0089	0.0106	0.0015
3,3'-Dimethyl-2,2'-bipyridyl	0.0142	0.0161	−0.002
4,4'-Dimethyl-2,2'-bipyridyl	0.0059	0.0097	0.0012
5,5'-Dimethyl-2,2'-bipyridyl	0.0089	0.0089	−0.0023
6,6'-Dimethyl-2,2'-bipyridyl	0.0097	0.0158	0.0013

a) $E(E)_{obsd}$'s are the values observed in ethanol glasses.

As given in Table 2, the result thus obtained is in qualitative agreement with the experimental one except that the E value of 3,3'-DMBPY is slightly larger than that of 6,6'-DMBPY. Such a qualitative agreement may imply that the difference among the E values is mainly due to the change of spin distribution arising from the methyl position in each pyridine ring. As the overestimation of E value for 3,3'-DMBPY is actually small, this discrepancy may possibly be due to the formation of hydrogen-bond between the nitrogen atom and one of the methyl protons. It may be noted here that if the spin density of the triplet state at each atom $\rho_i=(\rho_i^{lv}+\rho_i^{ho})/2$ is used in such an evaluation only a qualitative trend for the E values cannot satisfactorily be obtained, since the ZFS originates from the interaction between two different electron spins. Actually, the present evaluation should be applicable to a comparison among molecules with similar structures because of its simplicity.

If the a axis is taken to be perpendicular to the b direction (parallel to the central C–C bond) in the molecular plane of BPY or symmetrically substituted BPY's, the off-diagonal component of the **D** tensor, $(3/4)g^2\mu_B^2\langle -2ba/r^5\rangle$, is non-zero for the E conformer, while it is zero for the Z conformer. So far as the simple LCAO-MO's are used for the evaluation of spin distribution, the other components of $(3/4)g^2\mu_B^2\langle(r^2-3z^2)/r^5\rangle$ and $(3/4)g^2\mu_B^2\langle(a^2-b^2)/r^5\rangle$ of the E conformer are unchanged from those of the corresponding Z conformer. As a result, one may roughly infer that the E value of the Z conformer is generally small as compared with that of the corresponding E conformer, while the D values in these conformations are nearly the same, as in the case of BPY. It may be noted here that such a relation should not be valid for cases where the higher order effects on the spin distribution are not very small and there are exceptions for some of the related molecules. For example, the E value of (Z)-dimethylbiphenyls is rather larger than that of the corresponding E conformer, although the difference between them is relatively small.[8]

Since the point-dipole approximation is less satisfactory to the out-of-plane component in the **D** tensor, the D values were not evaluated in the present work. A more detailed calculation of the ZFS parameters will be published in the forthcoming paper.

The authors wish to thank Professor M. Kinoshita, The University of Tokyo, and Professor K. Itoh, Osaka City University, for their kind advise. Also, they wish to thank Dr. Y. Kaizu, Tokyo Institute of Technology, for donating 4,4'- and 5,5'-DMBPY's, Dr. H. M. Suzuki, Government Industrial Research Institute, Tohoku, Nigatake, for donating 3,3'-DMBPY, and Professor T. Hoshi, Aoyama Gakuin University, for supplying BPY- and 5,5'-DMBPY-containing PVA films in the preliminary step of the present work. The present work was partially supported by a Grant-in-Aid for Scientific Research No. 347005 from the Ministry of Education, Science and Culture.

References

1) K. Nakamoto, *J. Phys. Chem.*, **64**, 1420 (1960); S. Castellano, H. Günther, and S. Ebersole, *ibid.*, **69**, 4166 (1965); T. McL. Spotswood and C. I. Tanzer, *Aust. J. Chem.*, **20**, 1227 (1967).

2) L. L. Merritt, Jr. and E. D. Schroeder, *Acta Crystallogr.*, **9**, 801 (1956).

3) T. Ito and J. Higuchi, *Chem. Lett.*, **1974**, 1519; T. Ito, J. Higuchi, and T. Hoshi, *Chem. Phys. Lett.*, **35**, 141 (1975).

4) J. Higuchi, T. Ito, M. Yagi, M. Minagawa, M. Bunden, and T. Hoshi, *Chem. Phys. Lett.*, **46**, 477 (1977).
5) G. P. Rabold and L. H. Piette, *Spectrosc. Lett.*, **1**, 211 (1968).
6) P. Kottis and R. Lefebvre, *J. Chem. Phys.*, **39**, 393 (1963).
7) Y. Gondo and A. H. Maki, *J. Phys. Chem.*, **72**, 3215 (1968).
8) B. J. Scheve and P. J. Wagner, *Chem. Phys. Lett.*, **25**, 324 (1974).
9) J. Higuchi, M. Yagi, and A. Shimizu, *Chem. Phys. Lett.*, **62**, 603 (1979).
10) R. Stösser, W.-H. Böhmer, D. Kohler, and K. Madeja, *Z. Chem.*, **18**, 187 (1978).
11) A. Streitwieser, Jr., "Molecular Orbital Theory for Organic Chemists," John Wiley & Sons, Inc., New York (1961), p. 135.
12) A. D. McLachlan, *Mol. Phys.*, **3**, 233 (1960).
13) B. P. Stoicheff, *Can. J. Phys.*, **32**, 339 (1954).

^{13}C Spin-lattice Relaxation and Molecular Motion in Liquid and Plastic 2,2-Dimethylpropanoic Acid

Tooru HASEBE*† Nobuo NAKAMURA, and Hideaki CHIHARA
Department of Chemistry, Faculty of Science, Osaka University, Toyonaka, Osaka 560
(Received October 4, 1979)

Individual ^{13}C spin-lattice relaxation times (T_1) of 2,2-dimethylpropanoic acid (DMPA) in plastic and liquid phases have been measured by a pulse Fourier transform NMR technique at 15.036 MHz. In the plastic phase (278.9 K to 308.5 K), the minimum in the T_1 was observed; 0.35 s at 289.0 K for methyl carbon and 2.67 s at 289.0 K for quaternary carbon. The temperature dependence of the T_1 was analyzed by extending Woessner's treatment to the case of three independent degrees of reorientational freedom; internal methyl reorientation, *t*-butyl reorientation about C–COOH bonding axis, and isotropic molecular reorientation. In the plastic phase the isotropic reorientation of molecular dimeric units formed through hydrogen bonds is responsible for the ^{13}C-relaxation. The activation parameters for this motion were obtained; $E_a=56.4\pm6.3$ kJ mol^{-1} and $\tau_0=(4.6\pm4.0)\times10^{-19}$ s. In the liquid phase from the melting point to 351 K, the T_1 showed a monotonous increase with increasing temperature. In this liquid phase the isotropic molecular reorientation of the dimer units of DMPA is also responsible for the ^{13}C-relaxation. The E_a of 23.4 ± 2.4 kJ mol^{-1} and the τ_0 of $(9.6\pm5.8)\times10^{-14}$ s for this motion were obtained.

2,2-Dimethylpropanoic acid ($C(CH_3)_3COOH$, hereafter abbreviated as DMPA) is a globular molecule and crystallizes in a face-centered cubic structure[1] which exists between 278.9 K and the melting point, 308.5 K. This phase is known as an orientationally disordered phase and its static and dynamic properties have been studied by various techniques.[2–11] A dielectric measurement by Kondo and Oda[2] reported relatively low dielectric constants both in the plastic and liquid phases in spite of the existence of the strongly polar carboxyl group in the molecule. They interpreted this phenomenon in terms of possible dimerization in these phases. They also observed that a small jump in the dielectric constant on passing the melting point is consistent with the change in the density accompanied with fusion, suggesting that the extent of the excitation of the molecular rotational motion in the plastic phase is comparable to that in the liquid. Measurements of the nuclear magnetic relaxation times provide information about the nature of the molecular translational diffusion in addition to the molecular rotational motion. Measurements of ^1H spin-lattice relaxation times T_1 in the laboratory-fixed coordinate system[6,8,10] as well as $T_{1\rho}$ in the rotating frame[6,10] on DMPA showed that the molecules undergo rapid isotropic reorientation in the plastic phase with the correlation time of about 10^{-9} s[10] at the melting point. The activation energy E_a in the plastic phase was reported to be 50.2 ± 8.4 kJ mol^{-1} (from $T_{1\rho}$)[10] and 63 ± 5 kJ mol^{-1} (from $T_{1\rho}$)[6] for the translational diffusion which are smaller than that found by a radio-active tracer experiment[4] by a factor of 0.55.

On the other hand, the correlation time at the infinite temperature, τ_0, determined by NMR[10] is larger than that by the tracer experiment[4] by a factor of 10^7. A similar discrepancy has been recognized in the case of cyclohexane.[12,13]

If it happens that the carboxyl proton can migrate independently of the molecular body, the proton relaxation time should be affected b its motion. It should be noted here that the relaxation measurement of ^{13}C instead of ^1H might provide information about the motion of the molecule as a whole: For it is reasonable to consider that the T_1 of ^{13}C nuclei located in the inner part of the molecule is determined dominantly *via* the dipolar interaction with the intramolecular protons and weakly depends on the motion of the other molecules. In order to examine the characteristics of the motion of the molecular body as a whole in more detail, we measured the spin-lattice relaxation time of ^{13}C in both the plastic and the liquid phases of DMPA. In the course of the present study preliminary experimental results of the T_1 measurements of ^{13}C in DMPA were published by Graham and Darby,[11] but no detailed analysis was made as to the modes of molecular motions nor the activation parameters were presented. This paper will present the results of the measurements of T_1 of ^{13}C and report the activation parameters deduced from these experiments. The microscopic modes of the molecular motions in the plastic and liquid phase will be discussed in relation to the previous works on ^1H-NMR and Rayleigh scattering.[9]

Experimental

DMPA (G.R.) was purchased from Tokyo Kasei Kogyo Co., LTD. The material was subjected to vacuum distillation and degassing *via* freeze-pump-thaw cycles and then sealed under vacuum in a Pyrex 8 mm tube in outside diameter. The ^{13}C spin-lattice relaxation time was measured at the frequency of 15.036 MHz by the $[\pi-t-\pi/2\ (\mathrm{FID})-t_0-]_n$ pulse sequences ($n=20$ and t_0—$10T_1$ in our experiment) using pulse Fourier transform NMR equipment JEOL-PFT-60, where FID stands for the free induction decay of magnetization. These measurements were performed between 278.9 K and 351 K. The proton decoupling technique was used at a power of 4 W of a noise modulated continuous rf wave at 59.80165 MHz; the noise band width was 2.5 kHz. A nuclear Overhauser effect (NOE) for the methyl carbon was determined by dividing the integrated intensity in the proton-decoupled ^{13}C-NMR spectra by the total integrated intensities in the proton-coupled ^{13}C-NMR spectra. The overall spec-

† Present address: Department of Chemistry, Faculty of Education, Fukushima University, Matsukawa-machi, Fukushima 960-12.

tral frequency range was 800 Hz and the number of accumulation was 500. The temperature was measured with a copper-constantan thermocouple and was controlled to within ± 1 K by means of a gas-flow crystat. The static magnetic field was controlled by the technique of NMR locking using an external deuteron standard.

Results and Discussion

Plastic Phase. Three resonance lines were observed in the ^{13}C-NMR of DMPA by the proton decoupling method. The most intense line at the highest frequency was assigned to the methyl carbon by means of the proton-coupling method. The lowest frequency line was due to the carboxyl carbon and the other one was due to the quaternary carbon. The temperature dependence of the line shapes of these signals are shown in Fig. 1. The chemical shift of the quaternary carbon

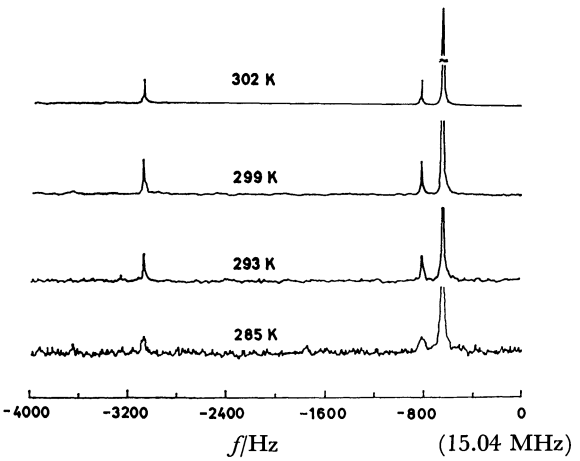

Fig. 1. Temperature dependence of line shape in plastic DMPA.

with respect to the methyl carbon is 11.44 ± 0.07 ppm and that of the carboxyl carbon is 158.62 ± 0.07 ppm. The magnitudes of these chemical shifts were almost temperature-independent. A coupling constant (J_{C-H}) between ^{13}C and ^{1}H nuclei in the methyl group is 127 ± 2 Hz at 302.2 K. Graham and Darby[11] pointed out that the J_{C-H} in the plastic phase differs by $\approx$20 Hz from that in the liquid phase, but such a difference was not observed in the present experiment within the experimental error. The line-width of each signal decreases gradually with increasing temperature in a way similar to the case of ^{1}H-NMR experiments,[3,5] suggesting the onset of the progressive excitation of self-diffusion. The temperature dependence of the T_1 for the methyl and the quaternary carbon is shown in Fig. 2, which shows the existence of a shallow minimum in T_1 of the methyl carbon at 289.0 K (0.35 s) and of the quaternary carbon at 289.0 K (2.67 s).

Jackson and Strange[6] observed a sudden jump of T_1 just below the melting point in their ^{1}H-NMR and attributed this phenomenon to some kinds of liquid-like behavior in the plastic phase. However, we did not find such a jump of T_1 up to the melting point in our ^{13}C-relaxation study. Kimtys[14] reported from his high

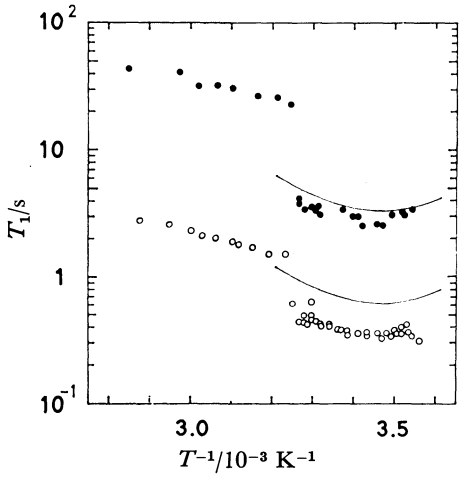

Fig. 2. Temperature dependence of spin-lattice relaxation times; ● for quaternary carbon and ○ for methyl carbon.
Two solid lines are calculated T_1 values.

resolution ^{1}H-NMR experiment that the carboxyl proton signal was accompanied with a satellite line on the low frequency side which he regarded as due to the hydrogen bonding effect; The intensity of that satellite line increased with decreasing temperature, whereas the intensity of the main carboxyl proton line decreased. In the case of the carboxyl ^{13}C signal in our experiment, however, such a phenomenon was not observed as is evident from Fig. 1. This fact suggests that the contribution of the motion of the carboxyl proton to the relaxation time of ^{13}C would be much smaller than that of the carboxyl proton to the ^{1}H-relaxation. Therefore, we can safely disregard the effect of the dynamics of the carboxyl proton in the analysis of the relaxation results of ^{13}C.

The basic expression for the ^{13}C nuclear spin-lattice relaxation rate due to dipole-dipole interaction under the proton-decoupled conditions is given by[15]

$$1/T_1 = \gamma_C^2\gamma_H^2\hbar^2 I(I+1)\sum\{J^{(0)}(\omega_C-\omega_H)/12 + 3J^{(1)}(\omega_C)/2 + 3J^{(2)}(\omega_C+\omega_H)/4\} \quad (1)$$

where γ_C and γ_H are the nuclear gyromagnetic ratios for ^{13}C and ^{1}H nuclei, respectively, $\hbar$ is Dirac's constant, I is the nuclear spin quantum number of the ^{1}H nucleus ($I=1/2$), and ω_C and ω_H are the Larmor frequencies of precession in the static magnetic field; In the present case these values are $\omega_C/2\pi=15.036$ MHz and $\omega_H/2\pi=59.802$ MHz, respectively. The sum in Eq. 1 is taken over all ^{13}C–^{1}H pairs. We assume that the following three types of molecular motions may occur in the plastic phase: (1) the internal reorientation of the methyl groups (C_3-reorientation), (2) the reorientation of the *t*-butyl group about the bonding axis between the quaternary carbon and the carboxyl carbon in the molecule (C_3'-reorientation), and (3) the isotropic molecular reorientation. These motions may be characterized by three different correlation times: τ_m (C_3-reorientation), τ_M (C_3'-reorientation), and τ_r (isotropic molecular reorientation). The self-diffusion is not taken into the consideration because it was found by our experiment[16] of the pressure dependence of the T_1

(^{1}H-NMR) that the self-diffusion was not responsible for the T_1 in the plastic phase of DMPA.

Woessner calculated T_1 for two identical spins ($I=1/2$) in the presence of anisotropic reorientation.[17] By extending his treatment to the case of three independent degrees of reorientational freedom mentioned above, we obtained the theoretical T_1 for the methyl carbon as follows:

$$1/T_1 = (3\gamma_C^2\gamma_H^2\hbar^2/10r^6)\{Wg(\omega_C, \omega_H, \tau_r) + Xg(\omega_C, \omega_H, \tau_1) + Yg(\omega_C, \omega_H, \tau_2) + Zg(\omega_C, \omega_H, \tau_3)\}, \quad (2)$$

where r is the ^{13}C–^{1}H internuclear distance in a methyl group and the function $g(\omega_C,\omega_H,\tau)$ has the form

$$g(\omega_C,\omega_H,\tau) = \tau/\{1+(\omega_C-\omega_H)^2\tau^2\} + 3\tau/\{1+\omega_C^2\tau^2\} + 6\tau/\{1+(\omega_C+\omega_H)^2\tau^2\}. \quad (3)$$

Here τ_i's are defined by

$$\tau_1 = 1/(1/\tau_r+1/\tau_M),$$
$$\tau_2 = 1/(1/\tau_r+1/\tau_m), \quad (4)$$
$$\tau_3 = 1/(1/\tau_r+1/\tau_M+1/\tau_m).$$

Coefficients W, X, Y, and Z were calculated to be

$$W = (3\cos^2\Delta-1)^2(3\cos^2\theta-1)^2/16,$$
$$X = 3(3\cos^2\Delta-1)^2(\sin^2 2\theta + \sin^4\theta)/16,$$
$$Y = 9(\sin^2 2\Delta \sin^2 2\theta+\sin^4\Delta \sin^4\theta)/32,$$
$$Z = 3\{4\sin^2 2\Delta(2-3\sin^2 2\theta/4) + \sin^4\Delta(3\sin^2 2\theta/4+3\cos^2\theta+5)\}/32, \quad (5)$$

where Δ is the angle between the ^{13}C–^{1}H internuclear vector and the C_3-axis, and θ is the angle between the C_3-axis and the molecular C_3'-axis. Here intermethyl interactions and cross-correlation effect have been ignored. In our model $\Delta=\theta=\cos^{-1}(1/3)$ and these coefficients become $W=1/81$, $X=8/81$, $Y=160/729$, $Z=488/729$; Here the bond angles of H–C–H in methyl group and C–C–H has been assumed to be tetrahedral. As the C_3- and the C_3'-reorientations are rapid enough in the plastic phase (*e.g.*, $\tau_m\approx10^{-11}$ s and $\tau_M\approx10^{-12}$ s just below the transition point[10]), all terms except the first in the braces of Eq. 2 are negligibly small compared with the first term. Hence Eq. 2 can be written as

$$1/T_1 = (3W\gamma_C^2\gamma_H^2\hbar^2/10r^6)g(\omega_C, \omega_H, \tau_r). \quad (6)$$

The activation parameters for the isotropic molecular reorientation were obtained by fitting the T_1 data of Fig. 2 to Eq. 6 assuming the Arrhenius type of activation process

$$\tau = \tau_0 \exp(E_a/RT). \quad (7)$$

The results for the methyl carbon are E_a(methyl)$=56.4\pm6.3$ kJ mol^{-1} and τ_0(methyl)$=(4.6\pm4.0)\times10^{-19}$ s, and tabulated in Table 1 together with the results reported previously. The theoretical T_1 calculated by use of Eq. 6 is given in Fig. 2 where $r=0.109$ nm was assumed; $T_{1\,min}$(calcd)$=0.64$ s at 287.2 K. If the same mechanism governs the T_1 of the quaternary carbon, we obtain the T_1 for this carbon as follows,

$$1/T_1 = (9W'\gamma_C^2\gamma_H^2\hbar^2/10l^6)g(\omega_C, \omega_H, \tau_r) \quad (8)$$

where $\Delta=28.2°$ and $\theta=\cos^{-1}(1/3)$ and the coefficient W' is 0.04911. l is the internulear distance between the quaternary carbon and a methyl proton. We obtained from the curve-fitting the activation parameters for the quaternary carbon as E_a(quat.)$=56\pm11$ kJ mol^{-1} and τ_0(quat.)$=(4.3\pm4.0)\times10^{-19}$ s. These activation parameters coincide with those for the methyl carbon. The calculated T_1 curve with $l=0.216$ nm is shown in Fig. 2; $T_{1\,min}$(calcd)$=3.23$ s at 287.2 K. The activation parameters obtained here do not agree with the results of the ^{1}H-NMR experiments; E_a is twice as large as E_a from ^{1}H-NMR (25.1—36.0 kJ mol^{-1})[6,10,16] and τ_0 is very short compared with that of ^{1}H-NMR (10^{-13}—10^{-15} s).[6,10,16] Our results agree well with the results ($E_a=60.0\pm4$ kJ mol^{-1} and $\tau_0=3.7\times10^{-19}$ s) of depolarized Rayleigh scattering experiment by Bird, *et al.*[9] but do not agree with the results ($E_a=30.9\pm3.9$ kJ mol^{-1} and $\tau_0=3.1\times10^{-14}$ s) obtained by Beysens, *et al.*[18] Although our activation parameters may involve some error which comes from the neglect of the contributions to the T_1 other than the molecular overall rotation, the discrepancy between our value and those obtained by the ^{1}H resonance exceeds the combined experimental uncertainty. This fact suggests that the migration of the acidic protons with some smaller activation energy[7] contributes to the relaxation times of the protons.

As shown in Fig. 2 the calculated T_1(methyl) is twice as large as the observed T_1(methyl), and the calculated T_1(quat.) is larger than the observed T_1 (quat.) by about 20 per cent. Such a discrepancy is probably due to the neglect of contributions of the C_3- and C_3'-reorientations to the T_1. It is interesting to see that the correlation time (10^{-8} to 10^{-9} s) for the isotropic molecular reorientation is much longer in DMPA than those in other undimerized plastic crystals. For example, the correlation time of 5.5×10^{-12} s (at 295 K) in plastic $C_6F_9H_3$ was obtained from the neutron scattering study[19] and that of 10^{-12}—10^{-13} s in plastic $C(CH_3)_4$ was obtained by the infrared,[20] the Raman scattering,[20] and the cold neutron scattering studies.[21] The very slow reorientational motion of DMPA may be attributed to the hydrogen bonding between neighbouring molecules which probably hinders the reorientation. This mechanism is supported by the

TABLE 1. THE ACTIVATION PARAMETERS IN THE PLASTIC PHASE OF DMPA

E_a/kJ mol^{-1}	τ_0/s	Experimental method	Ref.
36.0 ± 3	2.8×10^{-15}	broad line ^{1}H-NMR (T_1)	6
25.1 ± 2.5	$(1.69\pm0.2)\times10^{-13}$	broad line ^{1}H-NMR (T_1)	10
35.0 ± 0.8	$(4.9\pm1.6)\times10^{-15}$	broad line ^{1}H-NMR (T_1)	16
60.0 ± 4	3.7×10^{-19}	Rayleigh scattering	9
30.9 ± 3.9	3.1×10^{-14}	Rayleigh scattering	18
56.4 ± 6.3	$(4.6\pm4.0)\times10^{-19}$	high resolution ^{13}C-NMR (T_1)	this work

dielectric study[2] and also by the X-ray diffraction study[1] which reports that the crystal is made up of dimers orienting randomly. Recently we measured T_1 of DMPA as a function of pressure and obtained the activation volume of $\Delta V^* = (0.24—0.26) V_m$,[16] which is about twice as large as those in normal undimelized plastic crystals.[22] This fact also supports the formation of the dimers in the plastic phase of DMPA. Therefore, we conclude that the isotropic molecular reorientation of the dimer units is responsible for the ^{13}C spin-lattice relaxation in the plastic phase.

Liquid Phase The observed T_1 for the methyl and quaternary carbon in the liquid phase increase monotonously as shown in Fig. 2. The T_1 values of the quaternary carbon are larger than those of the methyl carbon by a factor of 16 but the slopes of the T_1 for these two kinds of carbons agree with each other within experimental error. No change has been observed on melting in the magnitude of the relative chemical shifts of the quaternary carbon as well as the carboxyl carbon with respect to the methyl carbon. The J_{C-H} values in a methyl group are 128.0±0.3 Hz at 319 K and 128.0± 0.3 Hz at 333 K, respectively, and depend little on temperature.

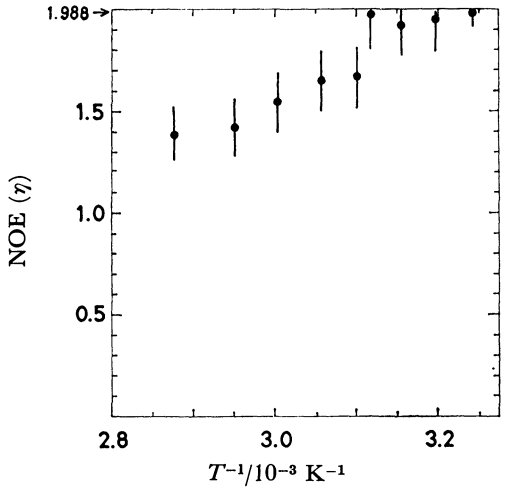

Fig. 3. Temperature dependence of NOE for methyl carbon.

The nuclear Overhauser effect (η) for the methyl carbon decreases from $\eta=1.988$ to 1.38 with increasing temperature as shown in Fig. 3. It shows that dipolar contribution to the relaxation becomes small with increasing temperature. When the ^{13}C–^{1}H dipole-dipole interaction is the dominant mechanism in the ^{13}C-relaxation, the theoretical maximum NOE (η) shoud be $\eta=1.988$.[23] In the present case, the dipole-dipole relaxation competes with other relaxation mechanisms, *e.g.* spin-rotational relaxation, chemical shift anisotropy relaxation, scalar relaxation, *etc.* The contribution of the dipole-dipole interaction to the spin-lattice relaxation time, T_1^{DD}, may be calculated by using the experimental NOE;[23,24]

$$T_1^{DD} = 1.988 T_1^{obsd}/\eta, \quad (9)$$

where T_1^{obsd} stands for the observed value. The temperature dependences of T_1^{obsd} and T_1^{DD} are shown

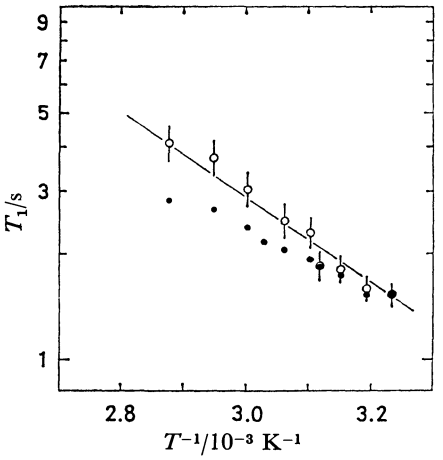

Fig. 4. Temperature dependence of T_1 for methyl carbon in the liquid phase; ● for T_1^{obsd} and ○ for T_1^{DD}.

in Fig. 4 by closed circles and open circles, respectively. Under the condition of the proton decoupling it may be assumed that the intermolecular dipole-dipole relaxation is insignificant, as has been mentioned by Kuhlmann *et al.*[23] We may also neglect the contribution of the C_3- and C_3'-reorientations to the T_1^{DD} in the liquid state. Therefore only one dominant relaxation mechanism is the isotropic reorientation of the molecules and, under the condition of the extreme narrowing limit, Eq. 6 leads to the expression of the T_1^{DD} as

$$1/T_1^{DD} = 3W\gamma_C^2\gamma_H^2\hbar^2\tau/r^6, \quad (10)$$

where τ is the correlation time for the isotropic molecular reorientation. The correlation time, which decreases slightly from 8.8×10^{-10} s at the melting point to 2.9×10^{-10} s at 351 K calculated from Eq. 10 with $r=$ 0.109 nm is longer by a factor of ten than the correlation time (6.5×10^{-11} s at the melting point decreasing to 3.1×10^{-11} s at 351 K) of the liquid DMPA obtained by depolarized Rayleigh scattering experiment by Beysens *et al.*[18] From the slope of the correlation time against the inverse of temperature, we obtained the activation parameters of $E_a=23.4\pm2.4$ kJ mol^{-1} and $\tau_0=(9.6\pm5.8)\times10^{-14}$ s. These parameters are to be compared with those obtained by Beysens *et al.*[18]—$E_a=$ 15.4±1.0 kJ mol^{-1} and $\tau_0=1.6\times10^{-13}$ s. It is interesting to see that the correlation time obtained here is longer than those in the non-associated globular compounds by a factor of 10^2 to 10^3, *e.g.*, liquid $C(CH_3)_4$ (10^{-12}—10^{-13} s),[20] and liquid norbornadiene ($\approx10^{-13}$ s).[25] This fact also suggests that the DMPA molecules behave as the self-associated dimeric units even in the liquid state.

References

1) Y. Namba and T. Oda, *Bull. Chem. Soc. Jpn.*, **25**, 225 (1952).
2) S. Kondo and T. Oda, *Bull. Chem. Soc. Jpn.*, **27**, 567 (1954).
3) H. Suga and S. Seki, *J. Phys. Chem. Solids.*, **24**, 330 (1963).
4) H. M. Hawthorne and J. N. Sherwood, *Trans. Faraday Soc.*, **66**, 1783 (1970).
5) P. Bladon, N. C. Lockhart, and J. N. Sherwood, *Mol.*

Phys., **20**, 577 (1971).
6) R. L. Jackson and J. H. Strange, *Mol. Phys.*, **22**, 313 (1971).
7) G. M. Hood, N. C. Lockhart, and J. N. Sherwood, *J. Chem. Soc., Faraday Trans. 1*, **68**, 736 (1972).
8) G. Soda and H. Chihara, *Chem. Lett.*, **1972**, 201.
9) M. J. Bird, D. A. Jackson, and J. G. Poles, *Mol. Phys.*, **25**, 1051 (1973).
10) S. Albert, H. S. Gutowsky, and J. A. Ripmeester, *J. Chem. Phys.*, **64**, 3277 (1976).
11) J. D. Graham and J. S. Darby, *J. Magn. Reson.*, **24**, 287 (1976).
12) S. B. W. Roeder and D. C. Douglass, *J. Chem. Phys.*, **52**, 5525 (1970).
13) A. V. Chadwick and J. N. Sherwood, *J. Chem. Soc., Faraday Trans. 1*, **68**, 47 (1972).
14) L. Kimtys, *Org. Magn. Reson.*, **7**, 179 (1975).
15) A. Abragam, "The Principle of Nuclear Magnetism," Oxford Univ. Press, London and New York (1961), Chap. 8.
16) T. Hasebe, G. Soda, and H. Chihara, to be published.
17) D. E. Woessner, *J. Chem. Phys.*, **36**, 1 (1962); **37**, 647 (1962).
18) D. Beysens, R. Vacher, G. M. Searby, L. Boyer, and M. Adam, *Rev. Phys. Appl.*, **9**, 465 (1974).
19) A. J. Leadbetter, A. Turnbull, and P. M. Smith, *J. Chem. Soc., Faraday Trans. 2*, **72**, 2205 (1976).
20) R. C. Livingston, W. G. Rothschild, and J. J. Ruch, *J. Chem. Phys.*, **59**, 2498 (1973).
21) T. Mansson, L. G. Olsson, and K. E. Larsson, *J. Chem. Phys.*, **66**, 5817 (1977).
22) R. Folland, S. M. Ross, and J. H. Strange, *Mol. Phys.*, **26**, 27 (1973).
23) K. F. Kuhlmann, D. M. Grant, and R. K. Harris, *J. Chem. Phys.*, **52**, 3439 (1970).
24) G. C. Levy, *Acc. Chem. Res.*, **6**, 161 (1973).
25) J. Grandjean and P. Laszelo, *Mol. Phys.*, **30**, 413 (1975).

Conformations of Acetanilide and Related Compounds Studied by Ultraviolet Photoelectron Spectroscopy

Ryoichi NAKAGAKI,# Tsunetoshi KOBAYASHI,† and Saburo NAGAKURA*

The Institute for Solid State Physics, The University of Tokyo, Roppongi, Minato-ku, Tokyo 106

† *The Institute of Physical and Chemical Research, Hirosawa, Wako, Saitama 351*

(Received October 19, 1979)

Conformations of acetanilides were studied by UPS in the vapour phase. The dihedral angle, θ, between the amide group and the phenyl group was evaluated from the difference in the vertical ionization energy, ΔE_{iv}, between the two MO's, the anti-bonding and bonding type combinations of the benzene ring $e_{1g}(S)$ orbital and the highest occupied π orbital of the amide group. The steric inhibition of conjugation due to *N*-methylation is larger than that due to ortho-methylation. For this series of compounds, ΔE_{iv} is directly proportional to $\cos\theta$ and this simple relationship is useful for the rough estimation of θ.

Ultraviolet photoelectron spectroscopy (UPS) is useful for the study of conformations of rather large molecules in the vapour phase. UPS has hitherto been used for the investigation of steric hindrance effects upon the conformations of various aromatic compounds such as nitrobenzenes, anilines, biphenyls, phenylethylenes, and so forth.[1-5] In this paper we report the conformations of some gaseous acetanilides studied by UPS, comparing the conformational data in the vapour phase with those in the crystalline state obtained by the X-ray diffraction method.

Experimental

The compounds studied are as follows: acetanilide (**1**), *o*-methylacetanilide (**2**), *N*-methylacetanilide (**3**), *N*,*o*-dimethylacetanilide (**4**), *N*,2′,6′-trimethylacetanilide (**5**), and oxindole (**6**).

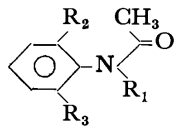

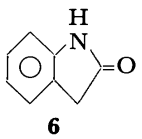

6

1: $R_1=R_2=R_3=H$
2: $R_1=R_2=H$, $R_3=CH_3$
3: $R_1=CH_3$, $R_2=R_3=H$
4: $R_1=R_2=CH_3$, $R_3=H$
5: $R_1=R_2=R_3=CH_3$

The photoelectron spectra of these compounds were measured with the photoelectron spectrometer described previously,[1] the 21.22 eV He I resonance line being used as the excitation source.

Results and Discussion

The photoelectron spectra of acetanilide and related compounds were measured with the results shown in Fig. 1. The vertical ionization energies, E_{iv}, derived from the spectra are listed in Table 1. In the region of 8—11 eV, the spectra of **1**, **2**, **3**, **4**, and **6** consist of four bands: two bands correspond to the two molecular orbitals, $\pi_-(S)$ and $\pi_+(S)$, which are interpreted approximately to be brought about by the antibonding and bonding type combinations of the benzene ring $e_{1g}(S)$ orbital and the highest occupied π orbital of the acetylamino group; the other two bands correspond to the a_2-like MO, $\pi(A)$, derived from the benzene ring $e_{1g}(A)$ orbital and to the non-bonding orbital of the carbonyl oxygen, n(O).

The assignments of $\pi_-(S)$, $\pi_+(S)$, $\pi(A)$, and n(O)

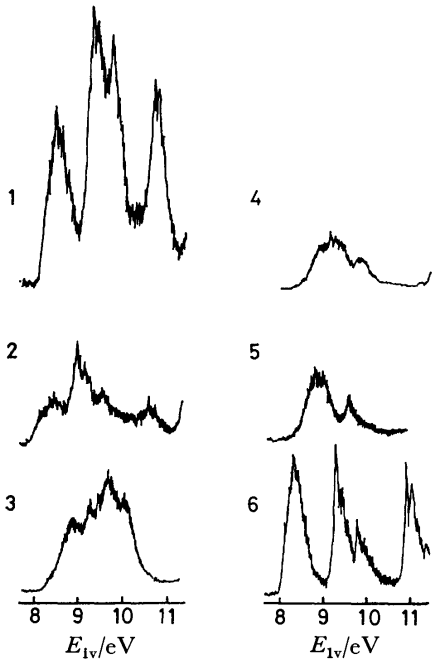

Fig. 1. Photoelectron spectra of acetanilide and related compounds.
1: Acetanilide, 2: *o*-methylacetanilide,
3: *N*-methylacetanilide, 4: *N*,*o*-dimethylacetanilide,
5: *N*,2′,6′-trimethylacetanilide, 6: oxindole.

Table 1. Vertical ionization energies

Compound	E_{iv}/eV			
	$\pi_-(S)$	$\pi(A)$	$\pi_+(S)$	$n(O)$
1	8.46	9.35	10.75	9.70
2	8.34	8.92	10.59	9.51
3	8.81	9.28	10.02	9.68
4	8.82	9.08	9.39	9.79
5	8.8		9.0	9.64
6	8.36	9.32	10.86	9.79

Present address: The Department of Chemistry, The University of British Columbia, Vancouver, B.C., Canada V6T 1W5.

bands of **1**, **2**, **3**, **4**, and **6** were made on the basis of the previous interpretation of the photoelectron spectra of anilines[1] and aliphatic amides.[6] The result is given in Table 1. The assignments of π(A) and n(O) bands were supported by the methyl substituent effect. Ortho-methylation is expected to decrease the ionization energy of π(A) MO, while *N*-methylation may have little effect on the value. The ionization energies of the n(O) MO's of **1**, **2**, **3**, **4**, and **6** are expected to vary only slightly by the alkylation on the ortho-position of the ring or on the nitrogen atom and to have the values similar to those of aliphatic amides, *i.e.*, 9.5—10 eV.[6] Comparative consideration of the E_{iv} values between **1** and **2** and between **1** and **3** leads us to the assignment given in Table 1. The UPS bands of the other compounds were assigned in a similar manner. In all cases except for **5** (see the later discussion) the first bands correspond to the ionization from the π_-(S) MOs.

The ionization energy difference between the π_+(S) and π_-(S) bands of acetanilides, $\Delta E_{iv}[\pi_+(S), \pi_-(S)]$, is approximately given by the following equation[2] (the two-orbital model):

$$\Delta E_{iv}[\pi_+(S), \pi_-(S)] = E_{iv}[\pi_+(S)] - E_{iv}[\pi_-(S)] = [(A_{Am} - A_{Ph})^2 + 4B_\theta^2]^{1/2}, \quad (1)$$

where $A_{Am} = \langle\psi_{Am}|H|\psi_{Am}\rangle$,

$A_{Ph} = \langle\psi_{Ph}|H|\psi_{Ph}\rangle$,

and $B_\theta = \langle\psi_{Am}|H|\psi_{Ph}\rangle$.

ψ_{Am} and ψ_{Ph} are the wave functions of the acetylamino (Am) and phenyl (Ph) moieties, respectively, and A_{Am} and A_{Ph} are set equal to the negative of the first E_{iv}'s of the corresponding *N*-methylated acetamides[6] and those of the benzenoid molecules,[1b] respectively. The off-diagonal element, B_θ, depends on the dihedral angle, θ, between both moieties and is assumed to be represented by the following relation: $B_\theta = B\cos\theta$ where B is the matrix element for the completely planar molecule, oxindole ($\theta = 0°$). The dihedral angles evaluated by putting the numerical values into Eq. 1 are listed in Table 2 together with the ΔE_{iv} values.

In the case of the trimethylated anilide, **5**, the assignment of the first UPS band around 9 eV was not unambiguous because of the considerable overlap of the π_-(S), π(A), and π_+(S) bands. If the first peak is of π(A) nature, as for *m*-xylene,[7] the dihedral angle should be very close to 90°, and if it is attributed to the π_-(S) MO, the dihedral angle is calculated to be 85°. In either case the dihedral angle is surely larger than that of the dimethylated anilide, **4**.

The enhancement of non-planarity by *N*-methylation was also found by means of the X-ray crystal analysis technique.[8] In the crystalline phase the dihedral angles of **1** and **3** were reported to be 17.6°[8a] and 90°,[8b] respectively. It is interesting to note that the twisting of the amide group in **3** is not so extreme in the vapour phase as in the solid state, while those of **1** in both phases are comparable to each other.

From Table 2, it is concluded that *N*-methylation causes more drastic steric inhibition of conjugation than ortho-substitution. By considering the conformational change induced by *N*-methylation, the conspicuous hypsochromic effect observed for the *N*-methylated anilides, **3** and **4**, can be explained in terms of reduced π conjugation.[9]

Table 2. Difference in ionization energies, ΔE_{iv}, and dihedral angles, θ

Compound	ΔE_{iv}/eV[a]	θ/° (gas)[b]	θ/° (crystal)[c]
Acetanilide (**1**)	2.29	23	17.6
o-Methylacetanilide (**2**)	2.25	27	
N-Methylacetanilide (**3**)	1.21	60	90
2′,6′-Dimethylacetanilide	1.10[d]	69	
N,*o*-Dimethylacetanilide (**4**)	0.57	77	
N,2′,6′-Trimethylacetanilide (**5**)	(0.2)	85—90	
Oxindole (**6**)	2.50	0	

a) Experimental error of ±0.05 eV. b) Uncertainty of ±3° is estimated for θ values from the error of ΔE_{iv}. Numerical values used in the calculation of the dihedral angles were as follows: $A_{Am} = -9.68$ eV for the secondary amides, **1**, **2**, and **6**, $A_{Am} = -9.09$ eV for the tertiary amides, **3**, **4**, and **5**,[6] $A_{Ph} = -9.23$ eV for the benzene derivatives, **1** and **3**, $A_{Ph} = -9.13$ eV for the toluene derivatives, **2**, **4**, and **6**, and $A_{Ph} = -9.03$ eV for the *m*-xylene derivative, **5**.[1b] A virtual MO for toluene which results in the formation of acetanilide derivatives is estimated to have an orbital energy of −9.13 eV, which is the negative of the average ionization energy of the corresponding MO's for benzene and *m*-xylene: the benzene e_{1g} π orbital with E_{iv} of 9.23 eV and the *m*-xylene b_1 π orbital with E_{iv} of 9.03 eV.[1b] This averaging procedure is based on the additive nature of the methyl substituent effect on the lower π ionization energies of benzenes (see, for example, Ref. 1b). c) Determined by means of the X-ray diffraction[8]. d) From Ref. 5.

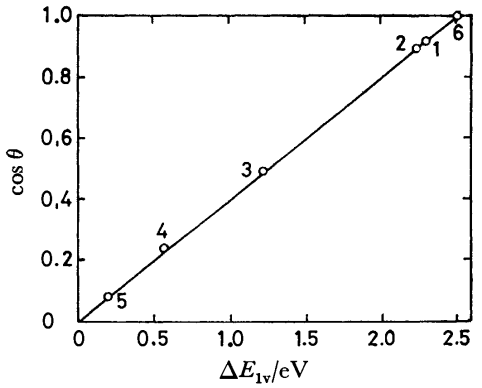

Fig. 2. Plot of cos θ against the difference in ionization energy, $\Delta E_{iv}[\pi_+(S), \pi_-(S)]$.

Finally, the cos θ's estimated for the vapour phase are plotted against $\Delta E_{iv}[\pi_+(S), \pi_-(S)]$'s in Fig. 2. The plotted points fall on a straight line passing through the origin. This is because the $(A_{Am} - A_{Ph})$ term values in Eq. 1 are small for the compounds studied here. The linear relation in Fig. 2 may be useful for the rough estimation of the dihedral angles in acetanilides.

We are indebted to Dr. Michio Kondo, Central Research Laboratories, Sankyo Co. Ltd., for his kindness in giving us *N*,2′,6′-trimethylacetanilide.

References

1) a) T. Kobayashi, K. Yokota, and S. Nagakura, *J. Electron Spectrosc. Relat. Phenom.*, **2**, 449 (1973); b) T. Kobayashi and S. Nagakura, *Bull. Chem. Soc. Jpn.*, **47**, 2563 (1974) and the references cited therein; c) T. Kobayashi, K. Yokota, and S. Nagakura, *ibid.*, **48**, 412 (1975).

2) a) J. P. Maier and D. W. Turner, *Faraday Discuss. Chem. Soc.*, **54**, 149 (1972); b) J. P. Maier and D. W. Turner, *J. Chem. Soc., Faraday Trans.* 2, **69**, 196, 521 (1973).

3) S. A. Cowling and A. W. Johnstone, *J. Electron Spectrosc. Relat. Phenom.*, **2**, 161 (1973).

4) P. S. Dewar, E. Ernstbrunner, J. R. Gilmore, M. Godfrey, and J. M. Mellor, *Tetrahedron*, **30**, 2455 (1974).

5) a) L. Szepes, G. Distefano, and S. Pignataro, *Ann. Chim. (Roma)*, **64**, 159 (1974); b) F. P. Colonna, G. Distefano, G. Reichenbach, and S. Santini, *Z. Naturforsch., Teil A*, **30**, 1213 (1975).

6) D. A. Sweigart and D. W. Turner, *J. Am. Chem. Soc.*, **94**, 5592 (1972).

7) M. Klessinger, *Angew. Chem.*, **84**, 544 (1972).

8) a) C. J. Brown and D. E. C. Corbridge, *Acta Crystallogr.*, **7**, 711 (1954); C. J. Brown, *ibid.*, **21**, 442 (1966); b) B. F. Pedersen, *Acta Chem. Scand.*, **21**, 1415 (1967).

9) a) P. Ramart-Lucas, *Bull. Soc. Chim. Fr.*, **17**, 317 (1950); b) V. Balliah and T. Rangarajan, *Naturwissenschaften*, **46**, 107 (1959).

Correlation NMR Spectroscopy with a Water Signal Subtracting System

Hideo AKUTSU, Yoshimasa KYOGOKU,* and Isao KAGAWA†
Institute for Protein Research, Osaka University, Suita, Osaka 565
†*JEOL Technical Service Co. Ltd., Nishinakajima 5-14-22, Yodogawa-ku, Osaka 532*
(Received October 23, 1979)

A modified correlation NMR method which includes the baseline correction systems in both hard- and softwares has been developed. By applying this method the proton signals of cytochrome b_5 and adenosine 5′-monophosphate at low concentration in H_2O solutions were obtained.

In the investigation of biological systems by proton magnetic resonance very strong signal of the solvent H_2O or HOD is troublesome. It is especially serious in the measurements of the imino and amino proton signals of proteins and nucleic acids. They are slowly exchangeable with water protons and their signals can only be detected in H_2O solutions. If a normal pulse Fourier transform (FT) NMR is applied for H_2O solutions, the signals of the sample at low concentration are hardly detected because the ratio of the sample signal to the solvent signal is too small that the finite dynamic ranges of the receiver and analog-digital (A/D) converter overlook the sample signal. Some groups have tried to eliminate or reduce the effect of the strong solvent signal by modifying the pulse FT NMR.[1-6] Another important device to solve the problem is correlation NMR, which has been introduced by Dadok and Sprecher,[7] and developed by other groups.[8-10] In this method the spectrum can be scanned only in the necessary frequency region and optimum conditions for observing the spectra are easily adjustable. We tried to develope the method taking its advantage into account. At the present work we will show a system of correlation NMR spectroscopy containing baseline correction systems in a sampling process, which is useful to eliminate the tail of the solvent signal. And also some applications to the biological substances in H_2O solutions will be presented. We are successful in getting the spectra at low concentrations.

Instrumentation

The principle for obtaining a correlation spectrum is based on the report of Gupta *et al.*[8] The method with a reference signal is employed instead of a theoretical function method to eliminate wiggles.

Figure 1 shows the block diagram of our system of the correlation NMR spectroscopy. A JEOL PS-100 NMR spectrometer was used together with a DP-1A pulse programmer and a EC-100 computer. The computer has 20 K words of memory (16 bits/word). We constructed a sweep generator where sawtooth waves are digitalized by the use of a D/A converter (12 bits). The digitalization of the sawtooth wave is essential to determine the chemical shift because we can know the exact sweep range from the frequency counter by holding the

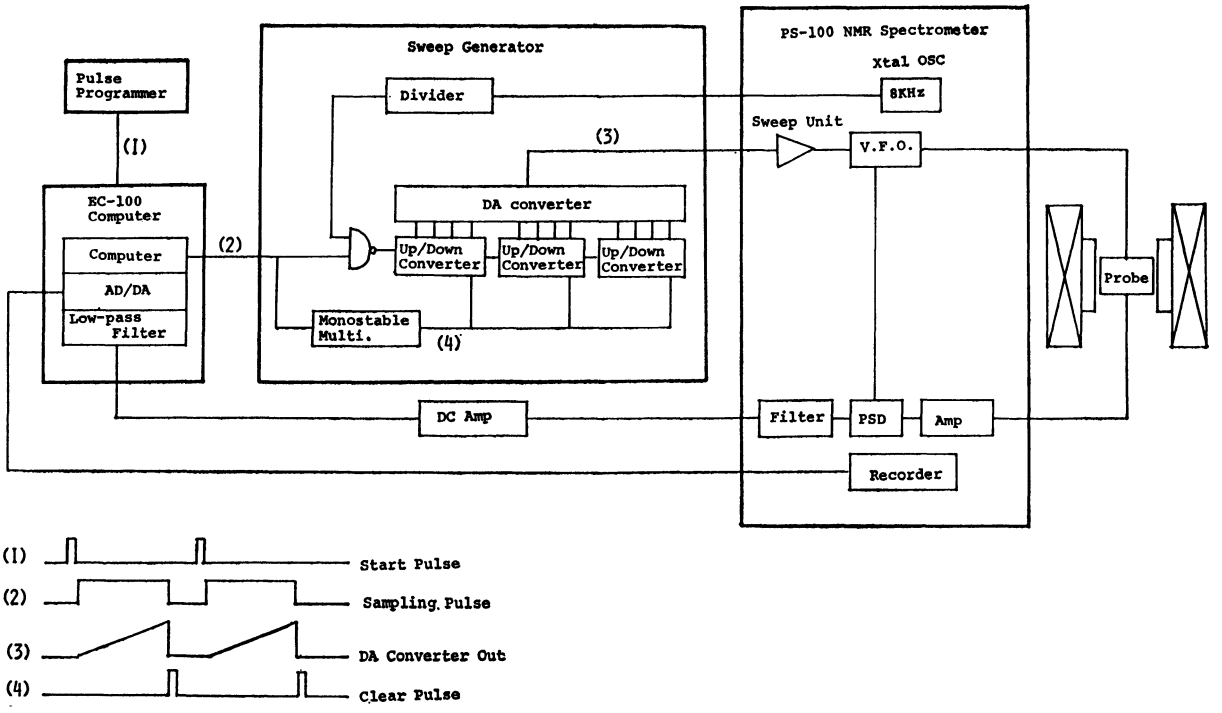

Fig. 1. A block diagram of a correlation spectrometer and a timing diagram for a computer control of a digitalized frequency sweep.

voltage of the sawtooth at the beginning and the end of the scan. The shapes of the control pulses and their relations with each other are also shown in Fig. 1. The transient response to the frequency sweep is passed through a low-pass filter and A/D converter (12 bits), then collected in the computer. The computer program for the system was written down by modifying the JEOL PFT-100 computer program. When we collect a transient response of a sample in a 4K words memory area and that of a reference signal in another 4K words memory area, we can get a final spectrum in a 8K words memory area (a 4K area for a real part and the other 4K area for an imaginary part). We confirmed the linearity of the frequency sweep and the accuracy of the chemical shift by measuring the mixture of chloroform, dichloromethane, dioxane, 1,1,1-trichloroethane, acetone, cyclohexane, and tetramethylsilane. The linearity was good enough so that the error of the chemical shift of every signal was less than 0.1%.

A hardware system for the baseline correction in the process of collecting the data was added to this correlation NMR spectrometer in order to reduce the effect of the tail of the H_2O signal. The flow chart of this system was illustrated in Fig. 2. Two kinds of baseline correction treatments were introduced into the hard and softwares. The process to eliminate the effect of a large tail of the solvent signal is as follows. At the first step, a function (a quadratic or exponential function) is subtracted from the transient response in an electronic circuit just before the phase sensitive detector (hardware subtraction). Beforehand the same treatment was done for the signal of pure solvent under the same conditions and stored in a certain memory area of the computer. This residual baseline of the solvent is further subtracted from the hardware treated sample spectrum in the computer (software subtraction). The transient response can be accumulated for certain times before this subtraction. The resultant spectrum was further accumulated in another memory area. It should be noted that the first baseline correction took away to some extent the saturation of the phase sensitive detector (PSD) by the strong solvent signal and improved the signal condition to pass through the dynamic range restriction of the A/D converter. The second step enchanced the efficiency of accumulation.

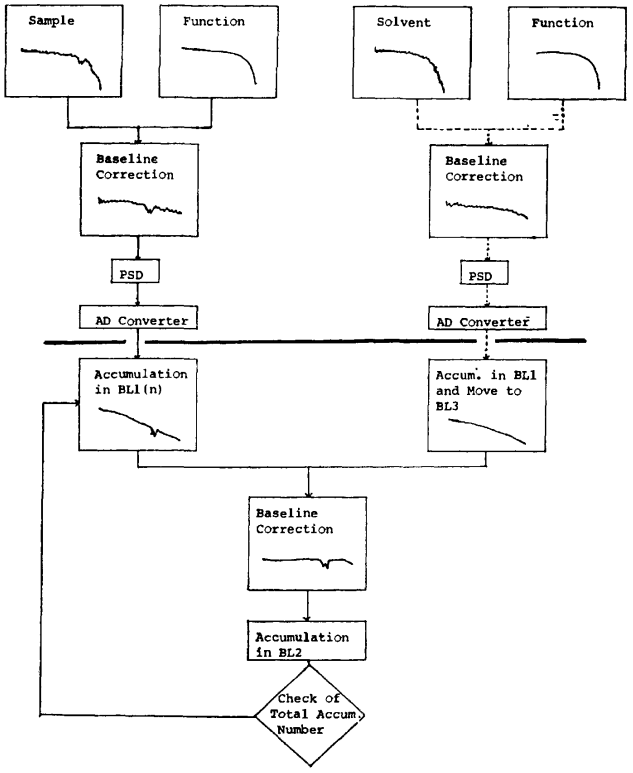

Fig. 2. A flow chart of a baseline correction system. Upper: in a hardware, lower: in a software. The part shown in broken lines indicates the one which should be operated before the treatment of the sample signal. BL1 (2 or 3): Block 1 (2 or 3) in the memory area.

Spectral Measurement

The above described correlation NMR spectroscopic method was applied to the aqueous solutions of some biological substances. Figure 3 is the 100 MHz proton magnetic resonance spectrum of the aromatic region of the oxidized cytochrome b_5 (solubilized with trypsin from rabbit liver microsomes) in D_2O solution (0.1 M phosphate buffer pD 7.0). The protein concentration is 7 mM (*MW=ca.* 12000). The chemical shift is expressed relative to the internal standard of sodium (2,2,3,3-tetradeuterio-3-trimethylsilyl)propionate (TMSP-d_4). The conditions of the measurement are given in the figure legend. All spectra hereafter were measured under the internal lock on H_2O (or HOD) signal. And their correlation was taken with a transient response

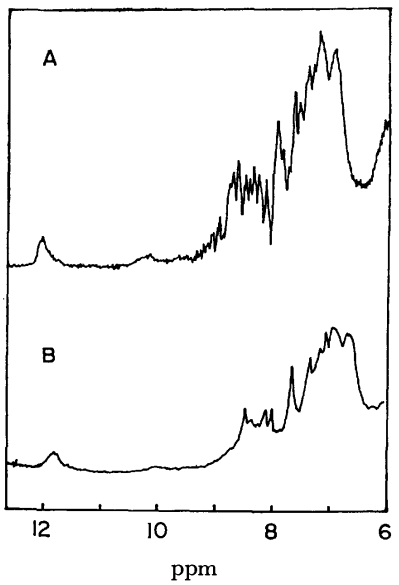

Fig. 3. (A) Transient response and (B) correlation spectrum of oxidized cytochrome b_5 from rabbit liver microsome in D_2O (0.1 M phosphate buffer pD 7.0). The concentration is 7 mM (*MW=ca.* 12000). The reference is TMS signal. Sweep direction: from higher to lower field, sampling point: 4096, sweep rate: 381.5 Hz/s, sampling time: 2.03 s, sweep repetition time: 2.10 s, filter: 250 Hz, number of accumulation: 3000. Chemical shifts are given relative to the signal of TMSP-d_4.

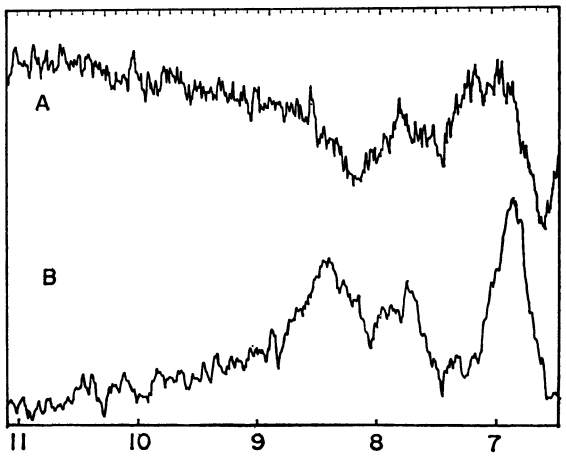

Fig. 4. (A) Transient response and (B) correlation spectrum of oxidized cytochrome b_5 in H_2O(0.1 M phosphate buffer pH 7.0). Concentration: 1 mM, reference: TMS, sweep direction: from lower to higher field, sampling point: 4096, sweep rate: 122.3 Hz/s, sampling time: 4.08 s, sweep repetition time: 5.00 s, filter: 20 Hz (sample), 125 Hz (reference), number of accumulation: 3000. Chemical shifts are given relative to the signal of TMSP-d_4.

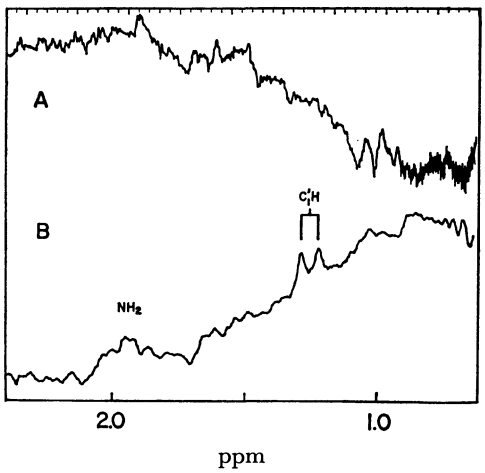

Fig. 5. (A) Transient response and (B) correlation spectrum of adenosine 5′-monophosphate sodium salt in H_2O.
Concentration: 2.5 mM, reference: TMS, sweep direction: from lower to higher field, sampling point: 4096, sweep rate: 51.3 Hz/s, sampling time: 4.09 s, sweep repetition time: 6.00 s, filter: 20 Hz, number of accumulation: for the second baseline correction(in BL 1) 10, and total 1000. A quadratic function was subtracted in the first baseline correction. Chemical shifts are given relative to the signal of H_2O.

of tetramethylsilane (TMS). Figure 3(A) is the transient spectrum and (B) is the obtained final spectrum. The spectrum shows good quality. As can be seen in Fig. 3(B) the effect from the linewidth of the reference signal (TMS) is negligible in the case of such macromolecules as proteins.

At the next step we tried to get the spectrum of the same sample in a dilute H_2O solution in the same frequency region. The spectra in Fig. 4 were obtained from the 1 mM H_2O solution of the oxidized cytochrome b_5 (0.1 M phosphate buffer at pH 7.0). Because of its severe conditions the spectrum in the higher field region than 7 ppm is not reliable. Comparing it with Fig. 3 we can see the contribution from NH_2 or NH group of this protein at 8.5 ppm. It is often required to take the spectra of proteins in H_2O at such a low concentration because of the low solubility and limitted amount of the sample.

Finally we tried to get a weak signal located closely to the solvent H_2O signal with the aid of our baseline correction system. Figure 5 shows the 100 MHz proton spectrum of the H_2O solution of adenosine 5′-monophosphate sodium salt (5′-AMP) at 2.5 mM. The observed doublet signal at about 1.2 ppm lower field from water signal comes from the C-1 proton of the ribose moiety and the broad signal at about 2 ppm is due to the amino protons of the adenine base. The long range noises arise from the subtracted baseline in a software. They obscure the broad signal to some extent. The important point of this system is to use a highly smoothed baseline at the second step of baseline correction. Otherwise, the noises are accumulated and disturb the spectrum. It should be noted, however, that a weak signal at about 1 ppm from water (6 ppm from TMSP-d_4) could be obtained, while it was impossible without the baseline correction system as shown in Fig. 4.

Discussion

Although a modified WETT method,[3] the water signal saturation method,[4] and Redfield pulse method[5] in FT NMR have shown their usefulness for aqueous solution systems, they have some disadvantages respectively. Those methods usually can eliminate only one strong signal. And it is necessary for the first method that the relaxation time of nuclei which give the signal to be eliminated is much longer than those of the other nuclei. The second method can not be applied to the exchangeable protons such as NH_2 and NH protons because of the saturation transfer from the irradiated solvent protons. The Redfield method is hard in setting the pulse condition and troublesome in baseline correction. The correlation method can avoid such disadvantages and Ozawa and Arata introduced an elegant wing processing method in correlation NMR to correct a titled baseline.[11] However correlation NMR had not yet been so far successful in getting weak signals within 1 ppm from water resonance, which was performed by the modified WEFT method.[3] It can be said that our method with a baseline correction system is promising in getting the proton signals of biological substances very close to the water resonance of solution. The system can also be applied to biomembranes or proteins in detergents where not only the solvent signal but the strong signals due to the CH_2 group of phospholipids and detergents also disturb the observation of the aimed resonance signals.

Authors wish to thank Mr. K. Nakagawa, JEOL Co. Ltd., for his kind help in the programming and also Mr. S. Tajima, Institute for Protein Research, Osaka University, for the gift of cytochrome b_5.

References

1) A. G. Redfield and R. K. Gupta, *J. Chem. Phys.*, **54**, 1418 (1971).
2) S. L. Patt and B. D. Sykes, *J. Chem. Phys.*, **56**, 3182 (1972).
3) E. S. Mooberry and T. R. Krugh, *J. Magn. Reson.*, **17**, 128 (1975).
4) H. E. Bleich and J. A. Glasel, *J. Magn. Reson.*, **18**, 401 (1975).
5) A. G. Redfield, S. D. Kunz, and E. K. Ralph, *J. Magn. Reson.*, **19**, 114 (1975).
6) N. R. Krishna, *J. Magn. Reson.*, **22**, 555 (1976).
7) J. Dadok and R. F. Sprecher, *J. Magn. Reson.*, **13**, 243 (1975).
8) R. K. Gupta, J. A. Ferretti, and E. D. Becker, *J. Magn. Reson.*, **13**, 275 (1974).
9) Y. Arata and H. Ozawa, *J. Magn. Reson.*, **21**, 67 (1976).
10) Y. Arata, H. Ozawa, T. Ogino, and S. Fujiwara, *Pure Appl. Chem.*, **50**, 1273 (1978).
11) H. Ozawa and Y. Arata, *Bull. Chem. Soc. Jpn.*, **49**, 1542 (1976).

The Crystal Structure of *N*-(*t*-Butoxycarbonyl)-L-methionylglycine Benzyl Ester

Takashi YAMANE,* Takashi UMEMURA, Tadao KOJIMA, Yasuyuki YAMADA, and Tamaichi ASHIDA

Department of Applied Chemistry, Faculty of Engineering, Nagoya University, Chikusa, Nagoya 464

(Received October 25, 1979)

The crystal structure of *N*-(*t*-butoxycarbonyl)-L-methionylglycine benzyl ester has been determined. The crystal data are: $P2_1$, $a=15.884(4)$, $b=5.083(2)$, $c=13.296(3)$ Å, $\beta=94.54(2)°$, $Z=2$. The final R is 0.055 for 1518 reflections. In the methionyl residue the C^{α}–C^{β} bond is longer than the C^{β}–C^{γ} bond. The tendency is consistent with that found in the other methionine compounds. The methionyl side chain has the most stable trans zig-zag conformation ($\chi^1=-73.2$, $\chi^2=175.3$, and $\chi^3=174.9°$). The peptide main chains are packed in a parallel β-sheet structure, the torsion angles (ϕ,ψ) of the methionyl residue being (−110.6, 108.3°).

The structure analyses of proteins have shown that the secondary structures, such as, α-helix,[1] β-structure,[2] and β-turn[3] play an important role in the folding of proteins. On the other hand, in the crystalline state many oligopeptides are also found to have either one of the secondary structures.[4] This fact suggests that the secondary structures are significant in the peptide structures of not only polymers but also oligomers. Thus, the precise parameters of the secondary structures obtained by the crystal analyses of oligopeptides are substantially important in the refinements and the model buildings of the protein structures or the structural analyses of fibrous proteins.

In this paper the structure of *N*-(*t*-butoxycarbonyl)-L-methionylglycine benzyl ester(Boc-L-Met-Gly-OBz)† having a parallel β-pleated sheet structure is reported.

Experimental

Boc-L-Met-Gly-OBz was prepared from dicyclohexylammonium *N*-(*t*-butoxycarbonyl)-L-methionate and glycine benzyl ester tosylate in a $CHCl_3$ solution. Needle crystals were obtained from an ethyl acetate–hexane solution. Crystal data are: $C_{19}H_{28}N_2O_5S$, $M.W.=396.50$, $P2_1$, $a=15.884(4)$,

TABLE 1. THE ATOMIC PARAMETERS AND THEIR ESTIMATED STANDARD DEVIATIONS($\times 10^4$)
Thermal parameters are in the form: $\exp(-\beta_{11}h^2-\beta_{22}k^2-\beta_{33}l^2-\beta_{12}hk-\beta_{13}hl-\beta_{23}kl)$.

	x	y	z	β_{11}	β_{22}	β_{33}	β_{12}	β_{13}	β_{23}
S	10888 (1)	2500 (4)	1079 (1)	50 (0)	489 (8)	102 (1)	10 (4)	18 (1)	−98 (5)
C (1)	7553 (4)	7975 (21)	5173 (6)	70 (3)	854 (56)	107 (5)	−155 (28)	45 (7)	−265 (32)
C (2)	8349 (14)	4433 (19)	6123 (6)	473 (44)	423 (44)	66 (5)	−20 (64)	150 (19)	1 (28)
C (3)	9127 (4)	8091 (18)	5404 (5)	63 (3)	694 (48)	112 (5)	123 (23)	−58 (7)	−290 (30)
C (4)	8360 (5)	6321 (15)	5281 (4)	120 (5)	414 (31)	43 (3)	27 (24)	18 (6)	−38 (18)
O (1)	8390 (3)	4611 (8)	4385 (2)	120 (3)	288 (17)	42 (2)	−9 (14)	23 (4)	−34 (11)
C (5)	8425 (3)	5667 (12)	3467 (3)	51 (2)	322 (24)	55 (3)	−34 (15)	4 (4)	−32 (16)
O (2)	8414 (3)	8036 (8)	3273 (3)	105 (3)	250 (18)	66 (2)	−20 (13)	13 (4)	8 (11)
N (1)	8451 (2)	3757 (10)	2766 (3)	51 (2)	308 (19)	52 (2)	0 (15)	−2 (3)	−19 (13)
C (6)	8453 (3)	4351 (11)	1074 (3)	42 (2)	293 (23)	42 (2)	−24 (13)	−4 (3)	−5 (14)
C (7)	9091 (3)	2970 (12)	1229 (3)	43 (2)	362 (25)	58 (3)	−52 (14)	8 (4)	−4 (16)
C (8)	10026 (3)	4287 (13)	1553 (4)	42 (2)	404 (29)	72 (3)	0 (15)	1 (4)	−58 (19)
C (9)	11746 (4)	4591 (15)	1460 (5)	48 (2)	526 (37)	101 (4)	−16 (19)	4 (6)	−19 (25)
C (10)	7616 (3)	3485 (12)	1173 (3)	46 (2)	345 (24)	49 (3)	0 (14)	10 (4)	30 (15)
O (3)	7418 (2)	1139 (8)	1047 (3)	49 (1)	246 (15)	94 (3)	−61 (9)	−10 (3)	−22 (12)
N (2)	7096 (2)	5492 (10)	863 (3)	41 (2)	321 (20)	77 (3)	8 (12)	−18 (4)	−11 (14)
C (11)	6266 (3)	4900 (15)	372 (4)	37 (2)	581 (36)	78 (3)	11 (16)	−6 (4)	−46 (22)
C (12)	6313 (3)	4046 (13)	−696 (4)	43 (2)	379 (28)	71 (3)	26 (16)	−4 (4)	−42 (19)
O (4)	6851 (2)	4530 (11)	−1239 (3)	56 (2)	738 (31)	84 (3)	−101 (14)	23 (3)	−62 (20)
O (5)	5625 (2)	2542 (11)	−978 (2)	52 (1)	620 (25)	69 (2)	−119 (14)	−5 (3)	−45 (15)
C (13)	5535 (4)	1712 (15)	−2032 (4)	71 (3)	505 (35)	62 (3)	−57 (20)	−11 (5)	−62 (20)
C (14)	5120 (4)	3886 (16)	−2684 (4)	60 (3)	533 (32)	53 (3)	−13 (20)	4 (5)	−97 (19)
C (15)	4271 (4)	4419 (20)	−2631 (5)	49 (2)	839 (53)	82 (4)	−88 (23)	17 (5)	−21 (28)
C (16)	3888 (4)	6401 (23)	−3225 (5)	51 (3)	1034 (68)	95 (5)	23 (27)	10 (6)	−108 (34)
C (17)	4339 (4)	7776 (18)	−3892 (5)	81 (4)	599 (40)	82 (4)	104 (25)	−28 (7)	−59 (26)
C (18)	5181 (5)	7172 (17)	−3691 (4)	89 (4)	529 (37)	73 (4)	−36 (26)	13 (6)	32 (23)
C (19)	5565 (4)	5279 (17)	−3360 (4)	59 (3)	625 (37)	67 (4)	0 (21)	24 (5)	−14 (22)

† The abbreviations used in this paper are: Boc-, *N*-(*t*-butoxycarbonyl); Ac-, *N*-acetyl; -OBz, benzyl ester; -OMe, methyl ester; -OEt, ethyl ester; -NMe, *N*-methylamide.

$b=5.083(2)$, $c=13.296(3)$Å, $\beta=94.54(2)°$, $D_m=1.235$, $D_x=1.242$ g cm^{-3}, $Z=2$, μ(Cu $K\alpha$)$=15.7$ cm^{-1}.

The intensity data were collected on a Hilger & Watts four-circle diffractometer, using Ni-filtered Cu Kα radiation. 1518 independent reflections with $2\theta \leq 110°$ were obtained, of which non-zero reflections were 1490. The ω-2θ step scan was adopted. The crystal used for the data collection had the dimensions of $0.09\times0.20\times0.43$ mm. The intensity data were corrected for Lorentz and polarization effects, but an absorption correction was not made.

Structure Determination

The structure was solved by the use of MULTAN.[5] The refinement was carried out by the block-diagonal least-squares method.[6] In the refinement, the function minimized was $\sum w(|F_o|-k|F_c|)^2$. The assignment of weight is; $w=(\sigma^2(F)+a|F_o|+b|F_o|^2)^{-1}$ for $|F_o|>0$ and $w=c$ for $|F_o|=0$, where $\sigma(F)$ is the standard deviation based on the counting statistics, and $a=-0.0479$, $b=0.0045$, and $c=0.3675$. The final R value is 0.055 for all reflections.

The atomic scattering factors were taken from "International Tables for X-Ray Crystallography," Vol. IV.[7] The calculations were carried out on a FACOM 230-75 computer at Nagoya University. The final atomic parameters are listed in Tables 1 and 2.[8]

Table 2. The parameters of hydrogen atoms ($\times 10^3$)
The standard deviations are given in parentheses.

	Bonded to	x	y	z
H(1)	C(1)	741(4)	894(18)	575(5)
H(2)	C(1)	706(4)	675(16)	498(5)
H(3)	C(1)	755(4)	911(17)	466(4)
H(4)	C(2)	826(4)	555(20)	673(5)
H(5)	C(2)	873(4)	356(19)	624(4)
H(6)	C(2)	789(4)	379(19)	598(5)
H(7)	C(3)	925(4)	886(18)	605(4)
H(8)	C(3)	905(4)	923(16)	487(5)
H(9)	C(3)	957(4)	668(16)	545(4)
H(10)	N(1)	861(4)	273(19)	292(5)
H(11)	C(6)	857(4)	652(17)	161(4)
H(12)	C(7)	910(4)	300(18)	39(5)
H(13)	C(7)	919(4)	118(18)	146(4)
H(14)	C(8)	1011(4)	457(19)	243(5)
H(15)	C(8)	1001(4)	626(18)	133(5)
H(16)	C(9)	1226(4)	422(17)	96(4)
H(17)	C(9)	1185(4)	443(19)	221(5)
H(18)	C(9)	1164(4)	610(18)	137(4)
H(19)	N(2)	729(4)	683(17)	85(4)
H(20)	C(11)	592(4)	631(17)	43(5)
H(21)	C(11)	597(4)	347(19)	75(5)
H(22)	C(13)	510(4)	−8(18)	−205(5)
H(23)	C(13)	619(4)	122(18)	−231(5)
H(24)	C(15)	396(4)	351(19)	−215(5)
H(25)	C(16)	332(4)	649(18)	−310(4)
H(26)	C(17)	404(4)	890(18)	−434(5)
H(27)	C(18)	542(4)	798(18)	−452(4)
H(28)	C(19)	630(4)	489(18)	−334(5)

Discussion

Bond lengths and angles of non-hydrogen atoms are listed in Table 3. The torsion angles of the peptide chain are shown in Fig. 1, together with the numbering of atoms. The definition of the torsion angles given by IUPAC-IUB Commission on Biochemical Nomenclature[9] is adopted. The stereoscopic view of the molecule drawn by ORTEP II[10] is shown in Fig. 2.

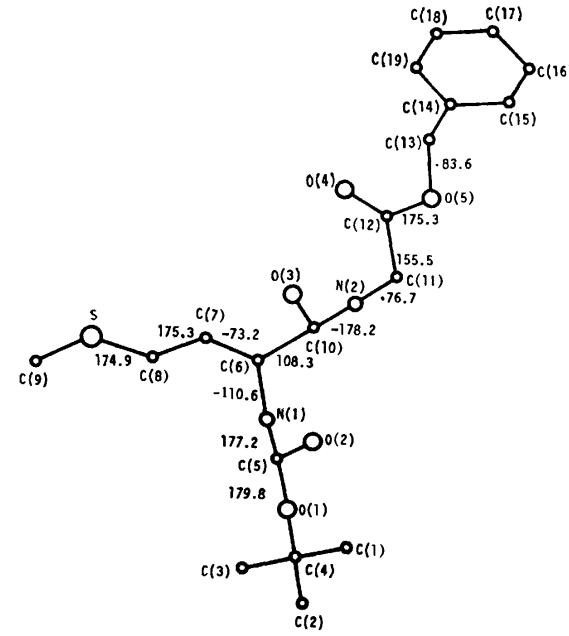

Fig. 1. Torsion angles of the peptide chain. Definitions for these angles are those given by IUPAC-IUB Commission on Biochemical Nomenclature (1970).

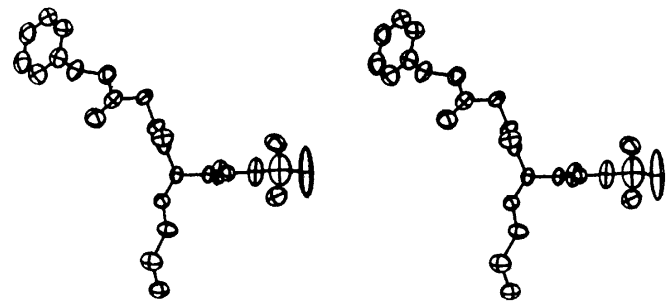

Fig. 2. Stereoscopic view with thermal ellipsoids drawn to enclose 50% probability.

The molecule is constructed with five planar groups, that is, ester I(Boc-L-Met), peptide, ester II(Gly-OBz), phenyl and methionyl side chain groups. The equations of the best planes and the related data are given in Table 4. Each pair of neighboring planes intersect roughly perpendicularly with each other, thus avoiding close contacts between the groups.

In the Boc group, the C(2)-C(4) bond length of 1.470(24) Å is significantly short. This may be attributed to the large thermal vibration of C(2), as shown in Fig. 2. The significant deformation of the bond angles

TABLE 3. THE BOND LENGTHS AND ANGLES FOR NON-HYDROGEN ATOMS

(a) Bond lengths (l/Å)

C(1)–C(4)	1.526(14)	C(2)–C(4)	1.470(24)	C(3)–C(4)	1.508(13)
C(4)–O(1)	1.473(10)	O(1)–C(5)	1.337(9)	C(5)–O(2)	1.221(8)
C(5)–N(1)	1.342(8)	N(1)–C(6)	1.445(8)	C(6)–C(7)	1.539(8)
C(7)–C(8)	1.515(9)	C(8)–S	1.795(7)	S–C(9)	1.765(8)
C(6)–C(10)	1.520(9)	C(10)–O(3)	1.231(8)	C(10)–N(2)	1.349(8)
N(2)–C(11)	1.456(10)	C(11)–C(12)	1.492(10)	C(12)–O(4)	1.186(9)
C(12)–O(5)	1.359(9)	O(5)–C(13)	1.459(10)	C(13)–C(14)	1.515(12)
C(14)–C(15)	1.382(13)	C(15)–C(16)	1.384(16)	C(16)–C(17)	1.371(15)
C(17)–C(18)	1.382(13)	C(18)–C(19)	1.357(13)	C(14)–C(19)	1.379(12)

(b) Bond angles (ϕ/°)

C(1)–C(4)–C(2)	111.3(11)	C(1)–C(4)–C(3)	110.6(8)
C(2)–C(4)–C(3)	111.0(11)	C(1)–C(4)–O(1)	108.9(7)
C(2)–C(4)–O(1)	103.9(11)	C(3)–C(4)–O(1)	110.9(7)
C(4)–O(1)–C(5)	120.8(6)	O(1)–C(5)–N(1)	110.7(6)
O(1)–C(5)–O(2)	125.6(6)	O(2)–C(5)–N(1)	123.7(6)
C(5)–N(1)–C(6)	122.2(5)	N(1)–C(6)–C(7)	111.6(5)
N(1)–C(6)–C(10)	108.9(5)	C(6)–C(7)–C(8)	111.3(5)
C(7)–C(8)–S	110.9(5)	C(8)–S–C(9)	101.1(4)
C(7)–C(6)–C(10)	110.2(5)	C(6)–C(10)–N(2)	114.7(6)
C(6)–C(10)–O(3)	122.9(6)	O(3)–C(10)–N(2)	122.3(6)
C(10)–N(2)–C(11)	119.6(6)	N(2)–C(11)–C(12)	112.0(6)
C(11)–C(12)–O(4)	127.9(7)	C(11)–C(12)–O(5)	108.8(6)
O(4)–C(12)–O(5)	123.3(7)	C(12)–O(5)–C(13)	116.1(6)
O(5)–C(13)–C(14)	110.3(6)	C(13)–C(14)–C(15)	119.6(8)
C(13)–C(14)–C(19)	121.2(8)	C(15)–C(14)–C(19)	119.1(8)
C(14)–C(15)–C(16)	119.8(10)	C(15)–C(16)–C(17)	120.4(10)
C(16)–C(17)–C(18)	119.3(9)	C(17)–C(18)–C(19)	120.5(9)
C(14)–C(19)–C(18)	120.8(8)		

TABLE 4. THE BEST PLANES

(a) Equation of the best planes

$X=ax+czcos\beta$, $Y=by$, $Z=czsin\beta$,

Plane I: O(1), C(5), O(2), N(1), C(6) $-0.9942X-0.0097Y-0.1067Z+13.450=0$

Plane II: C(6), C(10), O(3), N(2), C(11) $-0.4690X-0.0122Y+0.8831Z+4.255=0$

Plane III: C(11), C(12), O(4), O(5) $-0.4726X+0.8231Y-0.3147Z+2.809=0$

Plane IV: C(14), C(15), C(16), C(17), C(18), C(19) $-0.1932X-0.6808Y-0.7065Z+0.430=0$

Plane V: S, C(7), C(8), C(9), C(6) $-0.0582X+0.5285Y-0.8469Z+1.505=0$

(b) Dihedral angles (θ/°) between the planes

	I	II	III	IV
II	111.9			
III	119.7	93.8		
IV	105.9	121.7	104.3	
V	108.2	136.6	136.8	104.5

(c) Displacements($\times 10^3$d/Å) of atoms from the planes

The atoms with asterisks are not included in the best plane calculations.

O(1)	15	C(6)	10	C(11)	1	C(14)	−15	S	−42
C(5)	−12	C(10)	−9	C(12)	2	C(15)	15	C(6)	−21
O(2)	1	O(3)	0	O(4)	−1	C(16)	−3	C(7)	73
N(1)	−17	N(2)	−12	O(5)	−1	C(17)	−2	C(8)	−15
C(6)	15	C(11)	11	N(2)*	−559	C(18)	10	C(9)	10
C(2)*	17	H(19)*	−171	C(13)*	109	C(19)	−10		
C(4)*	20					C(13)*	7		
H(10)*	−284					H(24)*	−23		
						H(25)*	30		
						H(26)*	118		
						H(27)*	170		
						H(28)*	−115		

Table 5. The bond lengths (l/Å) and angles (ϕ/°) in the derivatives of methionine

	C^{α}–C^{β}	C^{β}–C^{γ}	C^{γ}–S^{δ}	S^{δ}–C^{ε}	C^{α}–C^{β}–C^{γ}	C^{β}–C^{γ}–S^{δ}	C^{γ}–S^{δ}–C^{ε}	Ref.
Ac-L-Met-OMe	1.538(6)	1.516(6)	1.800(5)	1.760(7)	113.0(3)	109.8(3)	102.0(3)	14
D,L-Ala-L,D-Met	1.526(4)	1.508(5)	1.811(4)	1.792(7)	113.9(3)	110.0(2)	99.1(2)	15
L-Met-L-Met(first)	1.531(4)	1.515(5)	1.816(3)	1.803(5)	112.7(3)	108.7(2)	99.8(2)	16
L-Met-L-Met(second)	1.543(4)	1.523(4)	1.813(3)	1.794(6)	112.2(2)	113.4(2)	99.9(2)	16
L-Met·HCl	1.532(7)	1.510(8)	1.818(8)	1.787(6)	113.8(8)	113.4(6)	101.3(6)	17
Boc-L-Met-Gly-OBz	1.539(8)	1.515(9)	1.795(7)	1.765(8)	111.3(5)	110.9(5)	101.1(4)	a
Average	1.535(6)	1.515(5)	1.809(9)	1.784(17)	112.8(10)	111.1(19)	100.4(12)	

a) This study.

Table 6. The torsion angles in the derivatives of methionine[a)]

	(χ^1/°)	(χ^2/°)	(χ^3/°)	Ref.
D,L-Met(α-form)	−60	177	81	12
D,L-Met(β-form)	−61	−176	−170	12
L-Met(molecule A)	−166.0	174.2	179.7	13
L-Met(molecule B)	−165.6	73.6	73.6	13
Ac-L-Met-OMe	−63.6	177.5	−178.6	14
D,L-Ala-L,D-Met	67.3	175.0	−173.8	15
L-Met-L-Met(first)	−167.2	−168.3	178.4	16
L-Met-L-Met(second)	68.0	−170.5	−57.6	16
L-Met·HCl	61	−178	69	17
Boc-L-Met-Gly-OBz	−73.2	175.3	174.9	b

a) All the torsion angles for the L-isomers are listed. b) This study.

around C(4), O(1), and C(5) are found, which are common in the Boc group.[11)]

The bond lengths and angles of the methionyl residue in several derivatives are compared in Table 5. The average bond lengths of C^{α}–C^{β} and C^{β}–C^{γ} of the methionyl residues are 1.535(6) and 1.515(5) Å, respectively. The corresponding bond lengths in the present peptide, 1.539(8) and 1.515(9) Å, are consistent to the average values. Thus in the side chain of the methionyl residue, the C^{α}–C^{β} bond is longer than the C^{β}–C^{γ} bond. As shown in Table 5, the C^{α}–C^{β}–C^{γ} angle is usually larger than the C^{β}–C^{γ}–S^{δ} angle, except for L-Met-L-Met (second).[16)] The C^{γ}–S^{δ}–C^{ε} angle of 101.1(4)° in the present peptide is close to the average of 100.4(1.2)°.

The torsion angles of the side chain of the methionyl residue are listed in Table 6, together with those of some methionine derivatives. The methionyl side chain, together with C′(=C(10)), has the most stable trans zig-zag conformation. The torsion angles of the side chain in the present peptide, χ^1=−73.2, χ^2=175.3, and χ^3=174.9°, coincide roughly with those of D,L-Met (β-form)[12)] and Ac-L-Met-OMe.[14)] In Table 6, the χ^1 values distribute uniformely in the values near −60, 180, and 60°. The present peptide takes χ^1 of −60°, which is favored as C^{γ} is between N and H. The χ^2 angle is around 180°, except for L-Met (molecule B),[13)] and it seems that the χ^3 angle tends to be predominantly near 180°.

The parallel β-sheet structure extended along the b axis is seen in the crystal, as shown in Fig. 3. The main chain torsion angles (ϕ,ψ) of the methionyl residue (−110.6, 108.3°) are close to those, (−119, 113°), of the parallel β-pleated sheet structure.[18)] The ten-membered

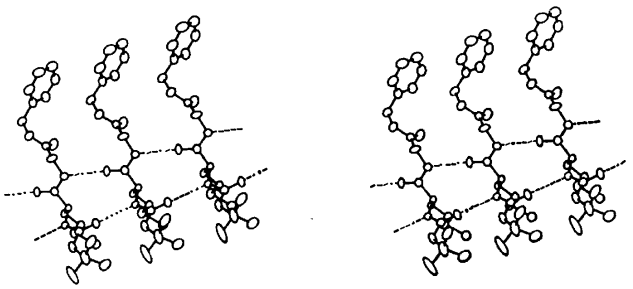

Fig. 3. Packing scheme viewed along the a axis (stereoscopic view). The parallel β-pleated sheet structure is formed. Hydrogen bonds are drawn as dotted lines.

ring hydrogen bonding pattern is formed from one molecule to the next molecule translated along the b axis. The geometries of the hydrogen bonds are: N(1)···O(2) 2.961 Å, H···O(2) 2.44 Å, ∠N(1)–H···O(2) 145°; N(2)···O(3) 2.897 Å, H···O(3) 2.19 Å, ∠N(2)–H···O(3) 159°.

The parallel β-structure is found in several other oligopeptides. Their torsion angles (ϕ,ψ) are; (−126, 132°) in Gly-L-Phe-Gly,[19)] (−102, 106°) in Br-Ac-L-Phe-L-Phe-OEt,[20)] (−100, 110°) in Cl-Ac-L-Phe-L-Phe-OEt,[20)] (−124, 103°) in Boc-(S-benzoyl)-L-Cys-Gly-OMe,[21)] (−106, 108°) in Ac-D,L-Phe-NMe,[22)] and (−107, 104°) in Ac-L-Phe-NMe.[23)]

The authors express their thanks to Professor Jiro Tanaka of Nagoya University, who kindly allowed them to use the diffractometer in his laboratory.

References

1) L. Pauling, R. B. Corey, and H. R. Branson, *Proc. Natl. Acad. Sci. U.S.A.*, **37**, 205 (1951).

2) L. Pauling and R. B. Corey, *Proc. Natl. Acad. Sci. U.S.A.*, **39**, 253 (1953).

3) C. M. Venkatachalam, *Biopolymers*, **6**, 1425 (1968).

4) T. Ashida, I. Tanaka, T. Yamane, and M. Kakudo, Int. Symp. on Biomolecular Structure, Conformation, Function and Evolution, Madras (1978).

5) G. Germain, P. Main, and M. M. Woolfson, *ta Crystallogr., Sect. A*, **27**, 368 (1971).

6) T. Ashida, "The Universal Crystallographic Computing System-Osaka," The Computation Center, Osaka University (1973), p. 55.

7) "International Tables for X-Ray Crystallography," The Kynoch Press, Birmingham (1974), Vol. IV, p. 72.

8) The F_o and F_c tables are available at the office of this Bulletin as Document No. 8012.

9) IUPAC-IUB Commission on Biochemical Nomenclature, *J. Mol. Biol.*, **52**, 1 (1970).
10) C. K. Johnson, "ORTEP II," Report ORNL-3794, Oak ridge National Laboratory, Tennessee (1971).
11) T. Ashida, I. Tanaka, Y. Shimonishi, and M. Kakudo, *Acta Crystallogr., Sect. B*, **33**, 3054 (1977).
12) A. Mathieson, *Acta Crystallogr.*, **5**, 332 (1952).
13) K. Torii and Y. Iitaka, *Acta Crystallogr., Sect. B*, **29**, 2799 (1973).
14) A. J. Geddes, S. Hamodrakas, and B. Sheldrick, *Cryst. Struct. Commun.*, **3**, 97 (1974).
15) R. E. Stenkamp and L. H. Jensen, *Acta Crystallogr., Sect. B*, **30**, 1541 (1974).
16) R. E. Stenkamp and L. H. Jensen, *Acta Crystallogr., Sect. B*, **31**, 857 (1975).
17) B. Di Blasio, V. Pavone, and C. Pedone, *Cryst. Struct. Commun.*, **6**, 845 (1977).
18) J. A. Schellman and C. Schellman, "The Proteins," ed by H. Neurath, Academic Press, New York (1964), Vol. 2, p. 1.
19) R. E. Marsh and J. P. Glusker, *Acta Crystallogr.*, **14**, 1110 (1961).
20) C. H. Wei, D. G. Doherty, and J. R. Einstein, *Acta Crystallogr., Sect. B*, **28**, 907 (1972).
21) S. Kashino, T. Ashida, and M. Kakudo, *Acta Crystallogr., Sect. B*, **30**, 2074 (1974).
22) Y. Harada and Y. Iitaka, *Acta Crystallogr., Sect.B*, **30**, 726 (1974).
23) Y. Harada and Y. Iitaka, *Acta Crystallogr., Sect.B*, **33**, 247 (1977).

Minimum-energy Conformation of Different Tropocollagen Models Calculated for Poly(Gly-Pro-Pro) by Considering Helical Constraints

Kenji Okuyama,* Haruaki Eto, Ikuo Nakaya, and Motowo Takayanagi
Department of Applied Chemistry, Faculty of Engineering, Kyushu University 36, Fukuoka 812
(Received November 27, 1979)

The minimum conformational energies for three helical models of tropocollagen were calculated by using energy functions and values of parameters obtained by Momany *et al.*. Three types of helical models containing 7/1, 10/1, and 12/1 helices were employed. Among the models with the 7/1 helix, only the conformation having the $N(Gly_1)\cdots O(Pro_2)$ type hydrogen bond was found to be energetically stable. Thus all the three helical models had the same type of hydrogen bond. The minimum-energy conformation of the 7/1 helix model was found to be more stable than those of the other two models by about 7 kcal/mol per tripeptide unit. This difference mainly came from the non-bonded energy terms of both intra- and inter-chains. Since the conformation of the 7/1 helix model was widely spread in the conformational space compared with those of the other models, it was concluded that the unit twist of the 7/1 helix model is well suited for peptide chains to conform a triplehelical structure. The above results strongly supported the 7/1 helix model for tropocollagen.

Collagen proteins form the connective tissues, such as bone, skin, tendon, cornea, and basement membrane, and are responsible for the structural integrity of the animal body. The collagen molecule (tropocollagen) is distinctive in containing the glycine residues in every third position, and has been designated as poly(Gly_1–R_2–R_3) in brief. Another feature of collagen is its high content of proline and hydroxyproline residues at the positions of R_2 and R_3. It is well known that the basic structure of tropocollagen has involved three stranded helices,[1] but its definite conformation has not been determined because of the meagre availability of the X-ray fiber patterns obtained from native collagen. So far, many researchers have proposed many structural models for tropocollagen. These models are basically divided into two types. One group contains 30 amino acid residues per turn in each chain of three strands,[2–5] and the other contains 36 residues per turn.[6] Recently two of us (K. O. and M. T.) and others[7] proposed the third type of collagen model having 21 amino acid residues per turn based on the structural analysis of single crystals of $(Pro\text{–}Pro\text{–}Gly)_{10}$ prepared.

On the other hand, some attempts have been made to determine the most stable conformation of tropocollagen by the method of conformational energy calculation. Tumanyan[8] minimized conformational energies of the triple-stranded helix of $(Gly\text{–}Pro\text{–}Pro)_n$ from many different combinations of the dihedral angles as starting points, using the Lennard-Jones pairwise potential function and the simple Morse-type potential function of hydrogen bonds. According to his calculations, the reasonable ranges for unit height and unit twist of the repeating unit Gly–Pro–Pro were 8.22—8.76 Å and 25—40°, respectively. Miller and Scheraga[9] calculated the conformational energies of $(Gly\text{–}Pro\text{–}Pro)_n$ for three different structures, that is, single-chain polymer, triple-stranded parallel-chain complexes and triple-stranded coiled-coils, and found that the last structure was the most stable. The unit heights and the unit twists of 10/1 and 12/1 helix models are within the corresponding ranges proposed by Tumanyan,[8] and the unit twist of the 7/1 helix model is far from this range. Miller and Scheraga,[9] however, showed that their lowest-energy structure was in good agreement with the 7/1 helix structure proposed for $(Pro\text{–}Pro\text{–}Gly)_{10}$.[10] The above calculations for $(Gly\text{–}Pro\text{–}Pro)_n$ were made without considering any constraints of helical structure. The present research is aimed to examine what type of helical model for tropocollagen is the most stable in terms of energetics by calculating the conformational energies under conditions with the helical constraints.

Method and Calculation

Three Helical Models for Tropocollagen. The polyproline II[11] type helix, the component of the triple-stranded coiled-coil structure of tropocollagen, has three amino acid residues in one turn (Fig. 1a), and it can be described as a 3/1 helix, since a chemical repeating unit contains one amino acid residue. If the helix axis of 3/1 helix further coils around the central axis, a coiled-coil structure is constructed (Fig. 1b). Here, the 3/1 helix is called the minor helix and the larger one with a longer period is called the major helix. If we consider the one turn of the minor helix (*i.e.*, three amino acid residues) as one repeating unit, the tropocollagen structure can be simply described as composed

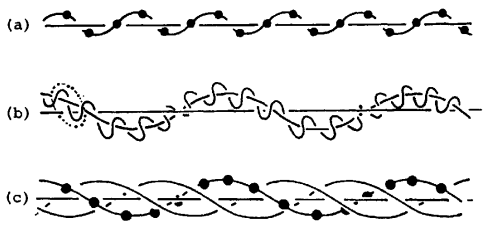

Fig. 1. Schematic representation of a triple-stranded helix of tropocollagen. (a) Simple 3/1 helical structure which contains three repeating units (filled circles) per turn. (b) Coiled-coil structure which is constructed by a further coiling of helix axis of (a). (c) Triple-stranded helix of tropocollagen. The filled circle represents one repeating unit, that is, one turn of the 3/1 helix which is shown by the dotted ellipse in (b).

TABLE 1. THREE HELICAL MODELS FOR TROPOCOLLAGEN

	Amino acid sequence $(Gly_1\text{–}R_2\text{–}R_3)_n$	Types of hydrogen bond	Helical parameters h	θ
7/1 helix model				
$(Pro\text{–}Pro\text{–}Gly)_{10}$[a),7)]	R_2 Pro	$N(Gly_1)\cdots O(R_2)$	8.61 Å	51.4°
	R_3 Pro	or $N(Gly_1)\cdots O(R_3)$		
10/1 helix model				
Collagen I[b),3)]	R_2 any residue	$N(Gly_1)\cdots O(Gly_1)$	8.58 Å	36.0°
	R_3 Gly only			
Collagen II[b),3)]	R_2 any residue	$N(Gly_1)\cdots O(R_2)$	8.58 Å	36.0°
	R_3 any residue			
$(Pro\text{–}Gly\text{–}Pro)_n$[c),4)]	R_2 Pro	$N(Gly_1)\cdots O(R_2)$	8.61 Å	36.0°
	R_3 Pro			
12/1 helix model				
"standard"	R_2 imino acid impossible	$N(Gly_1)\cdots O(R_3)$	8.73 Å	30.0°
structure[b),6)]	R_3 any residue	$N(R_2)\cdots O(R_2)$		
"one-bonded"	R_2 Pro	$N(Gly_1)\cdots O(R_2)$	8.73 Å	30.0°
structure[b),6)]	R_3 Hypro			

a) The structure is based on three dimensional X-ray diffraction patterns of single crystal of synthetic polypeptide $(Pro\text{–}Pro\text{–}Gly)_{10}$ whose distribution of molecular weight is monodispersed. b) These structures are based on X-ray fiber diagram of native collagen. c) The structure is based on X-ray fiber diagram of synthetic polypeptide $(Pro\text{–}Gly\text{–}Pro)_n$ whose molecular weight is about 15000. Throughout this paper 1Å= 0.1 nm, 1 cal=4.184 J.

of three identical helices with a common central axis (Fig. 1c). The helical models proposed so far can be divided into three types according to the number of the repeating units in the major helix (Table 1). The first type includes the structure of Collagen I and II proposed by Rich and Crick[3] and of $(Pro\text{–}Gly\text{–}Pro)_n$ proposed by Yonath and Traub,[4] which may be represented by a 10/1 helix model since they have 10 repeating units per one turn. The second type of models are Ramachandran's "standard" (or two-bonded) and one-bonded structures,[6] which may be represented by a 12/1 helix model. The third is our model[7] which may be described as a 7/1 helix model. In the case of last model, two possible types are proposed as has been described previously.[10] One type has the $N(Gly_1)\cdots O(Pro_3)$ type hydrogen bond (Model 1) and the other has the $N(Gly_1)\cdots O(Pro_2)$ type hydrogen bond (Model 2). The tropocollagen models are characterized by two helical parameters, h and θ. Here, h means the unit height, a vertical distance of one repeating unit along the helix axis. θ means the unit twist, a rotational angle of the unit around the helix axis. The h and θ values for the present models are listed in Table 1.

In this study, we assumed that the tropocollagen was constructed of three identical helices of poly(Gly–Pro–Pro) for the computational convenience, as had been adopted in energy calculations by Tumanyan[8] and by Miller and Scheraga.[9] Almost all conformations of poly(Gly–Pro–Pro) have been found to be those of a collagen-like triple-helix, since imino acid residues at the positions of R_2 and/or R_3 promote the construction of the triple-stranded helix. In fact, the single crystals of $(Pro\text{–}Pro\text{–}Gly)_{10}$ molecule were found to exhibit a 7/1 helix.[10] The fiber of $(Pro\text{–}Gly\text{–}Pro)_n$ gave an X-ray fiber pattern very similar to the native collagen and it was once proposed that the polypeptide chain formed a 10/1 helix.[4] These facts show that the above assumption may be reasonable.

Molecular Geometry. The backbone conformation in the three-residue repeating unit is defined not only by the coordinates of corresponding atoms, but also by bond lengths, bond angles, and dihedral angles of the backbone chain. Since bond lengths and bond angles are not so different among the homologous compounds, we can fix these at the known values of low molecular weight homologues. The latter method is advantageous for constructing conformations of fibrous large molecules. In the case of poly(Gly–Pro–Pro), there are 9 dihedral angles in a repeating unit. These are shown in Figure 2. The dihedral angles ϕ_2 and ϕ_3

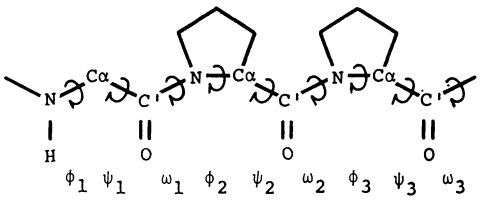

Fig. 2. Structural formula and the notation of dihedral angles in one repeating unit, Gly–Pro–Pro.

are restricted within narrow limits by pyroridine rings and they were fixed at −75° in the calculations. Further, if we confine the conformation to one of the above models, the two dihedral angles (in these calculations, ϕ_1 and ψ_1) will become dependent upon others. Then, the variable parameters were reduced to only five dihedral angles, ω_1, ψ_2, ω_2, ψ_3, and ω_3. The fixed values of bond lengths and bond angles, and the initial coordinates of pendant atoms (C_β, C_γ, and C_δ atoms in proline residues and all oxygen and hydrogen atoms) were according to Momany *et al.*[12] The definition of dihedral angles followed the recommendation of IUPAC IUB Commission.[13] Five dihedral angles were

changed systematically and the coordinates of all atoms in the unit were represented in the right-handed Cartesian coordinate system.[14] In this system, the origin coincided with a given atom of the back bone chain. One of the neighbouring atoms of the origin lay on the x-axis, and the other axes were chosen arbitrarily. Then the coordinate system was converted into the right-handed Cartesian coordinate system having the z-axis coinciding with the helix axis by the method of Sugeta and Miyazawa.[15] When the coordinates of the jth atom in the nth unit of the standard ($m=0$) chain are expressed in terms of $(x_j^{n,0}, y_j^{n,0}, z_j^{n,0})$, those of the corresponding atom in the next ($(n+1)$th) unit of the same chain $(x_j^{n+1,0}, y_j^{n+1,0}, z_j^{n+1,0})$ may be obtained by the following equations.

$$\boldsymbol{X}_j^{n+i,0} = \boldsymbol{R}_1 \boldsymbol{X}_j^{n,0} + i\boldsymbol{T},$$

where

$$\boldsymbol{X}_j^{n,0} = \begin{pmatrix} x_j^{n,0} \\ y_j^{n,0} \\ z_j^{n,0} \end{pmatrix}, \quad R_1 = \begin{pmatrix} \cos(i\theta) & -\sin(i\theta) & 0 \\ \sin(i\theta) & \cos(i\theta) & 0 \\ 0 & 0 & 1 \end{pmatrix},$$

and

$$\boldsymbol{T} = \begin{pmatrix} 0 \\ 0 \\ h \end{pmatrix}.$$

Similarly, the coordinates of the jth atom in the nth unit of the neighbouring chains $(x_j^{n,m}, y_j^{n,m}, z_j^{n,m})$ are obtained by the following equations.

$$\boldsymbol{X}_j^{n,m} = \boldsymbol{R}_2 \boldsymbol{X}_j^{n,0} + \frac{m}{3}\boldsymbol{T},$$

where

$$\boldsymbol{X}_j^{n,m} = \begin{pmatrix} x_j^{n,m} \\ y_j^{n,m} \\ z_j^{n,m} \end{pmatrix}, \quad R_2 = \begin{pmatrix} \cos(m\theta') & \sin(m\theta') & 0 \\ -\sin(m\theta') & \cos(m\theta') & 0 \\ 0 & 0 & 1 \end{pmatrix},$$

and $\theta' = 120° - \theta/3$.[10] m is the chain number (0, 1, or 2). When looking down the helical axis from the carbonyl- to the amino-terminus, the value m of the right-side chain is 2 and that of the left-side chain is 1 with respect to the standard chain (0).

Conformational Energies. Electrostatic energy (E_{es}), non-bonded energy (E_{nb}), and torsional energy (E_{ts}) were considered. The total conformational energy for one repeating unit (E_{tot}) was the sum of these energies. The hydrogen bond energy was included in non-bonded energy term. The energy functions and parameter values used were the same as those of Momany *et al.*[12] The torsional energy was calculated only about three peptide bonds in the unit. The same functions and values were used for both intra- and inter-chain energy calculations. The intramolecular energy for a unit was calculated for the region from this unit to the third one of the carbonylterminal side, since the interaction energy between a given unit and any of its three amino-terminal side neighbours was the same as that between the same unit and the corresponding carbonyl-terminal side neighbour. The intermolecular energy was calculated between a central unit of A-chain ($m=0$) and the nearest four unit both up and down along the B-chain ($m=1$) from the central unit of A. Since three chains are identical in each other, the energy between A- and C-chains ($m=2$) equals to the energy between B- and A-chains. In the case of 7/1 helix model, the units which were taken into account of calculations are shown in the radial projection of Fig. 3. The open circle in this figure represents one repeating unit. The solid lines denote the peptide chain direction and a down side of this line points to the amino terminal side. The letters A, B, and C correspond to the peptide chain number in the triple-stranded helix, 0, 1, and 2, respectively. The conformational energies of isolated triple-stranded helix were calculated by summing up the energy in the central unit (filled circle) and the interaction energies between the central unit and all the independent unit (half-filled circles) within about 30 Å from the central unit.

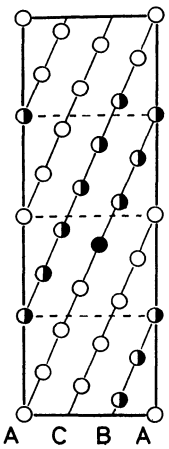

Fig. 3. The range of energy calculations of 7/1 helix model. The open circle denotes one repeating unit and the solid lines A, B, and C denote the peptide chains. The filled circle is the unit which conformational energy is calculated and the half-filled circle is the other unit responsible for the inter-unit conformational energy calculations.

It has been found that several water molecules per tripeptide unit are involved in the triple helices of tropocollagen[16] and model peptides of collagen[17] by way of hydrogen bonding. In addition to the stabilization by triple-helix itself, these hydrogen bonds may also contribute to the stabilization of the collagen-like triple-helix. However, Engel *et al.*[18] have shown that the peptides remain in a triple-helical conformation after dehydration, and concluded that water is not an essential component of forming the triple-helical structure. Therefore, in this study we did not take into account of water in order to simplify the problem, and calculated only the conformational energies of isolated triple-helix in a vaccum.

Computational Procedure. As described above, the

Table 2. Computational regions of dihedral angles

ω_1	175°—180°——175°
ϕ_2	−75° (fixed)
ψ_2	100°—180°——170°
ω_2	175°—180°——175°
ϕ_3	−75° (fixed)
ψ_3	100°—180°——170°
ω_3	175°—180°——175°

molecular conformation of poly(Gly–Pro–Pro) is defined by five dihedral angles (ω_1, ψ_2, ω_2, ψ_3, and ω_3) and helical parameters (h and θ). So the energy-minimum conformation of each model is included in the five

Table 4. Atomic distances used in the preliminary calculations

Atomic pair	Distance (Å)
C···C	2.50
C···N	2.59
C···O	2.30
N···N	2.67
N···O	2.38
O···O	2.09

Table 3. Number of conformations for which conformational energies are calculated

	Number of grid points[a)]	Number of conformations[b)]	Number of conformations after preliminary calculations
7/1 helix model	9747	4433	34 for Model 1 216 for Model 2
10/1 helix model	9747	4003	66
12/1 helix model	9747	2989	25

a) These were obtained by varing each dihedral angle at 5° intervals within its computational region. b) Number of conformations where the backbone conformation without pendant atoms can be constructed with each helical parameters.

Table 5. Low energy conformations at grid points of five-dimensional conformation space

No.	Dihedral angle/°							H-bond parameter		E_{tot}/[kcal/mol of (Gly–Pro–Pro)]
	ϕ_1[a)]	ψ_1[a)]	ω_1	ψ_2	ω_2	ψ_3	ω_3	r(N···O)/Å	∠HNO/°	
1) 7/1 helix model										
Model 1										
1	−59.9	168.6	180	170	−175	140	−175	4.41	32	−11.53
2	−58.7	165.2	180	175	−175	140	180	4.40	32	−9.99
3	−58.9	168.1	175	180	180	145	175	4.36	26	−3.13
4	−57.8	165.1	−175	175	−175	135	180	4.48	41	−1.51
Model 2										
1	−60.9	174.2	175	165	−175	145	−175	3.10	17	−25.76
2	−61.4	−177.7	180	170	175	140	180	3.45	21	−25.33
3	−62.7	−179.6	175	165	180	145	−175	3.35	22	−25.19
4	−61.9	−176.9	175	170	175	145	180	3.51	22	−25.07
5	−60.3	176.6	180	170	180	140	180	3.34	18	−25.02
6	−62.0	180.0	180	165	180	140	−175	3.22	23	−24.88
7	−60.5	−178.7	−175	170	175	135	180	3.28	22	−24.85
8	−61.1	177.4	175	170	180	145	180	3.45	17	−24.64
9	−64.5	−178.2	175	170	175	145	−175	3.49	23	−24.53
10	−64.1	−173.7	175	165	175	145	−175	3.48	27	−24.49
2) 10/1 helix model										
1	−51.1	162.0	−175	160	−175	125	−175	3.82	9	−17.88
2	−40.6	155.7	−175	165	−175	120	175	3.41	24	−17.61
3	−46.5	167.9	−175	165	175	120	180	4.02	14	−17.29
4	−49.2	157.1	−175	165	−175	125	180	4.11	18	−17.22
5	−51.0	160.6	180	160	−175	130	−175	4.25	29	−17.05
6	−43.2	160.7	180	160	−175	125	180	3.49	16	−16.98
7	−50.3	166.2	−175	155	−175	125	−175	4.14	45	−16.88
8	−42.1	160.7	−175	160	−175	120	180	3.18	35	−16.73
9	−44.5	166.8	−175	160	180	120	180	3.82	40	−16.69
10	−54.0	168.3	−175	160	180	125	−175	4.45	5	−16.63
3) 12/1 helix model										
1	−42.7	158.8	180	160	180	125	175	3.45	34	−18.69
2	−53.1	165.3	−175	155	180	125	−175	3.65	20	−18.57
3	−51.0	160.7	−175	160	180	125	180	3.90	11	−18.09
4	−48.4	158.3	180	155	−175	130	180	3.86	41	−17.78
5	−48.4	155.7	−175	165	180	125	175	4.05	14	−17.72
6	−45.3	163.6	175	155	180	130	180	3.56	32	−17.22
7	−44.5	164.9	180	160	175	125	175	4.16	47	−17.21
8	−51.5	160.2	180	160	180	130	180	4.44	17	−16.73
9	−53.7	164.8	180	155	180	130	−175	4.09	3	−16.64
10	−43.7	159.1	175	160	180	130	175	3.83	13	−16.49

a) ϕ_1 and ψ_1 were calculated numerically from other dihedral angles and helical parameters of the model.

dimensional space of conformation with the range shown in Table 2. All the dihedral angles of the peptide bond, ω_1, ω_2, and ω_3, were assumed to be *trans* conformation. Although it has been known that the peptide bond preceding proline residue is able to have a *cis* conformation (*e.g.*, the structures of poly-L-proline I[19] and of z-Gly-Pro-Leu[20]), these were taken to be *trans* in all the previous models of collagen. Then we considered only *trans* conformation in our calculations. The dihedral angles of C_α–C′ in the proline residue, ψ_2 and ψ_3, were assumed to lie in the ranges of 100°—180°—−170° based on the structural analyses of oligopeptides[21,22] and the energy calculations of prolyl oligomers.[23]

At first the above conformational space was divided into 9747 grid points which were obtained by varing each dihedral angle at 5° intervals, and remaining dihedral angles (ϕ_1 and ψ_1) at each grid point were calculated numerically by using the helical parameters.[24] The conformations which gave the ϕ_1 and ψ_1 values outside the ranges of −180°——30° and 20°—180°——150°, respectively, were rejected in the following calculations. These criteria for glycyl residue are based on the regions of left-handed polyproline II structure in the energy map of diglycine.[25] In the resulting conformations, the dihedral angle ϕ_1 for three models was in the range of −130°——30°, and the angle ψ_1 for the 7/1, 10/1, and 12/1 helix models was in the range of 145°—180°——165°, 140°—180°——175°, and 140°—175°, respectively. The number of solutions for each model was listed in Table 3. The number of grid points which satisfied the above criteria was assumed to be about one half of solutions, since the most grid points had two solutions.

In order to reduce the time of computation, the number of conformations was further decreased by the preliminary energy calculations and the examinations of inter-chain hydrogen bonds. That is, the conformations were removed, if they exhibit the non-bonded distance between pairs of atoms in different chains which was shorter than the corresponding distance listed in Table 4. The values shown in Table 4 were the distances which gave the non-bonded energies 100 times as large as those at the minimum positions ($<r_g^{kk}>$ or $<r_g^{kl}>$) of Ref. 26, and calculated from the Lennard-Jones 6-12 expression. It has been proposed that in the case of poly(Gly–Pro–Pro), the 10/1 and 12/1 helix models and one of the 7/1 helix models (Model 2) have the $N(Gly_1)\cdots O(Pro_2)$ type hydrogen bond.[3,6,10] Model 1 of the 7/1 helix model has the $N(Gly_1)\cdots O(Pro_3)$.[10] For each of these models the conformations which have the hydrogen bond distance $r(N\cdots O)$ longer than 4.5 Å or the hydrogen bond angle $\angle HNO$ larger than 60° were removed because these conformations would not have hydrogen bonds by only the small change of variable dihedral angles. The number of remaining conformations for each model are given in the last column of Table 3. The conformational energy was calculated for all of these conformations. The dihedral angles, total potential energies, and hydrogen bond parameters $r(N\cdots O)$ and $\angle HNO$, of only 10 low energy conformations of each model are given in Table 5. The conformations of Model 1 of the 7/1 helix model had rather high potential energies than all the other types of models. Of the conformations obtained only four with negative energies are listed. All of the conformations shown in Table 5 which had the $N(Gly_1)\cdots O(Pro_2)$ type hydrogen bond were taken as the starting points for energy minimization procedure according to Fletcher and Powell.[27] The helical parameters for each model were held constant during these procedures. When the energy did not change as much as 0.0001 kcal/mol per tripeptide unit within an iteration of the Fletcher-Powell algorism, or when all of the variable dihedral angles did not change as much as 0.01° within an iteration, it was regarded that the energy-minimum in the conformational space has been reached.

Results and Discussion

Comparison of Models 1 and 2 of the 7/1 Helix Model. According to the type of hydrogen bonding, the 7/1 helix models were divided into Models 1 and 2 (see above). The number of conformations of Model 1 after preliminary calculations was very few as seen in the last column of Table 3, and their total conformational energies were very high compared with those of Model 2 (Table 5). In the four conformations of Model 1 shown in Table 5, the hydrogen bond distances of $N(Gly_1)\cdots O(Pro_3)$ are about 4.4 Å, while those of $N(Gly_1)\cdots O(Pro_2)$ are 2.96, 3.17, 3.61, and 2.86 Å, in an increasing order of the conformational energy. It seems, therefore, that the hydrogen bond of $N(Gly_1)\cdots O(Pro_2)$ is stronger than that of $N(Gly_1)\cdots O(Pro_3)$. Further investigation showed that the 23 conformations out of 34 of Table 3 had the hydrogen bond of $N(Gly_1)\cdots O(Pro_2)$ with distance less than 4.5 Å. Therefore, they were also included in the 216 conformations of Model 2. The resulting conformation after minimization starting from No. 1 of Model 1 (Table 5) was in agreement with that of Model 2 (Table 6) with a deviation of each dihedral angle less than 1.5°. The above findings showed that the global minimum conformation in the conformational space of the 7/1 helix model was included in the region with the hydrogen bond of $N(Gly_1)\cdots O(Pro_2)$, and some conformations within this region had a rather short hydrogen bond of $N(Gly_1)\cdots O(Pro_3)$ and a high conformational energy compared with the global minimum one. Thus it was concluded that the structures of Model 1 were unstable and could not be present. Hereafter, the word "7/1 helix model" may indicate that the conformation has helical parameters of (8.61 Å, 51.4°) and a hydrogen bond of $N(Gly_1)\cdots O(Pro_2)$.

12/1 Helix Model. The 12/1 helix model, which was proposed by Ramachandran[6] as a modification of 10/1 helix model, is somewhat different from the 7/1 and 10/1 helix models. If the amino acid sequence of tropocollagen is represented by poly(Gly_1–R_2–R_3), the true repeating period in the 7/1 and 10/1 helix models is one-third the pitch length of the peptide chain, as we see in the radial projections (a) and (b) of Fig. 4. This period is 20.1 Å for the 7/1 helix model and 28.6 Å for the 10/1 helix model. In this figure the open circle denotes a tripeptide unit, Gly_1–R_2–R_3, and the solid

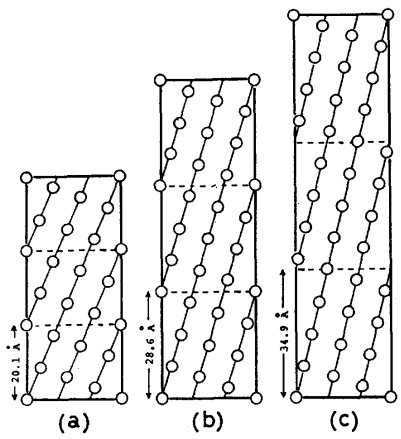

Fig. 4. Radial projections for three different kinds of tropocollagen models. The open circle denotes one repeating unit, Gly_1–R_2–R_3, and the solid line denotes the peptide chain direction. (a) 7/1 helix model, (b) 10/1 helix model, and (c) 12/1 helix model.

line denotes a direction of the peptide chain. Because of the finite molecular length of tropocollagen (about 3000 Å) and irregularities of occurrence of amino acids at the positions of R_2 and R_3 in the real sequence, these periods were usually called "pseudo-period."

On the other hand, the period obtained from X-ray fiber patterns of native collagen was taken to be 20.1 Å in the case of the 7/1 helix model or 28.6 Å in the case of 10/1 helix model. The above difference of the periods occurs from the ambiguity of indexing the layer lines which appear in the fiber patterns of native collagen. That is, if we take the meridional reflection of the spacing 2.86 Å as the 7th layer, the fiber period will be 20.1 (2.86×7) Å. And if we take that reflection as the 10th layer, the fiber period will be 28.6 (2.86×10) Å. In both 7/1 and 10/1 helix models, each pseudo-period of the models is naturally the same as that obtained from X-ray fiber patterns, because each model is constructed by using the periods obtained from the fiber pattern itself. In the case of 12/1 helix model, however, the one-third the pitch length is not a perfect repeating period as we see in Fig. 4(c), even though the amino acid sequence is represented by poly(Gly_1-R_2-R_3). Further, this value, 34.9 Å (2.91×12), does not agree with the period 29.1 Å obtained by Ramachandran.[6] Despite the apparent discrepancy, the conformational energy of the 12/1 helix model could be calculated in a similar manner as other models, since this did not affect the results obtained in the present study.

Comparison of Minimum-energy Conformations of the Three Models. The conformations with the minimum-energy for the three models are listed in Table 6 together with their energy terms and hydrogen bonding parameters. Tumanyan[8] carried out the minimization of conformational energies from many quadraplets of the dihedral angles (ϕ_1, ψ_1, ψ_2, and ψ_3) as starting points without constraints of helical parameters, and concluded that the minimum-energy conformation was obtained with helical parameters within the ranges of 8.22 Å$<h<$8.76 Å and $25°<\theta<40°$. It was also suggested by

Table 6. Minimum-energy conformations of three helical models

	7/1 helix	10/1 helix	12/1 helix
Dihedral angle/°[a]			
ϕ_1[b]	−62.3	−48.3	−53.0
ψ_1[b]	179.4	158.2	164.3
ω_1	−179.6	−172.2	−174.6
ψ_2	167.0	164.1	155.0
ω_2	180.0	−175.3	−179.2
ψ_3	139.6	121.6	125.0
ω_3	−175.0	−178.4	−175.0
H-bond parameter[c]			
r(N···O)/Å	3.17	3.54	3.50
∠HNO/°	16	18	20
Energy/[kcal/mol of (Gly–Pro–Pro)][d]			
E_{nb}(intra)	−0.30	3.59	3.53
E_{nb}(inter)	−9.18	−6.63	−6.62
E_{es}(intra)	−15.06	−15.28	−15.26
E_{es}(inter)	−1.70	−1.03	−1.11
E_{ts}	0.15	0.52	0.33
E_{tot}	−26.09	−18.83	−19.12

a) $\phi_2=\phi_3=-75.0°$. b) ϕ_1 and ψ_1 were calculated numerically from other dihedral angles and helical parameters of each model. c) These parameters are for N(Gly_1)···O(Pro_2) type of hydrogen bond. d) E_{nb} refers to the non-bonded energy term, E_{es} to the electrostatic energy term, E_{ts} to the torsional energy term: intra in the parenthese to intrachain, inter to interchain. $E_{tot}=E_{nb}$(intra)$+E_{nb}$(inter)$+E_{es}$(intra)$+E_{es}$(inter)$+E_{ts}$

Ramachandran[6] that the conformations whose unit twist is 50° or more cannot be stable because of short contacts between atoms in adjacent chains and worse situations about hydrogen bonds. According to our calculations as shown in Table 6, however, the conformations of the 7/1 helix model, whose unit twist is 51.4°, can exist stably and further, the minimum conformational energy of this model was the lowest among the three helical models. The energy difference of 7 kcal/mol per tripeptide unit between the 7/1 and the other two helix models is attributable to the non-bonded energy terms. With respect to the hydrogen bond, the distance of N(Gly_1)···O(Pro_2) of the 7/1 helix model is 3.17 Å and those of 10/1 and 12/1 helix models are somewhat longer (3.54 and 3.50 Å, respectively). Further, as seen in Table 5, the conformations in considerably wide regions of conformational space of the 7/1 helix model tend to have lower energies and more stable hydrogen bonds in comparison with those of the 10/1 and 12/1 helix models. It seems that these preponderance of the 7/1 helix model results from its large unit twist compared with those of the 10/1 and 12/1 helix models. (Unit heights are almost the same among these models (Table 1).) That is, in the case of 7/1 helix model, the number of conformations (4433), where the backbone conformation with no pendant atoms can be constructed, is much larger than those of the other models (4003 for 10/1 and 2989 for 12/1 helix model). And the last column shows the resulting numbers of conformation after preliminary calculations,

in which the conformations were removed if they have very short contacts between atoms or a hydrogen bonding distance longer than 4.5 Å. The differences between the numbers of conformation for the three models clearly showed that the conformational space of the 7/1 helix model at this stage is increasingly wider than those of the others, although the absolute space is narrower than that of the previous stage.

The difference of non-bonded energies between the 7/1 and the other two (10/1 and 12/1) helix models was the sum of the differences of inter- and intra-chain non-bonded energies, 2.5 and 4.0 kcal/mol per tripeptide unit, respectively (Table 6). As there were no short contact between atoms of different chains in each model structure, the stabilization of interchain non-bonded energy of the 7/1 helix model showed that the chain molecule with this conformation was suited to be packed into a collagen-like triple-stranded structure. On the other hand, the difference between intrachain non-bonded energies resulted from short contacts between atoms in the same chain. For example; for the 7/1 helix model, $H_\alpha(Pro_2)\cdots H_\delta(Pro_3)$, 2.09 Å; for the 10/1 helix model, $H_\alpha(Pro_2)\cdots H_\delta(Pro_3)$, 2.06; $O(Pro_3)\cdots C'(Gly_1)$, 2.74; $H_\alpha(Gly_1)\cdots C_\delta(Pro_2)$, 2.56; $H_\alpha(Gly_1)\cdots H_\delta(Pro_2)$, 2.02 Å; and for the 12/1 helix model, $H_\alpha(Pro_2)\cdots C_\delta(Pro_3)$, 2.45; $H_\alpha(Pro_2)\cdots H_\delta(Pro_3)$, 1.98; $H_\alpha(Gly_1)\cdots H_\delta(Pro_2)$, 2.08 Å. The atomic coordinates of the minimum-energy conformation of the 7/1 helix model are shown in Table 7.

The molecular structures with the minimum-energy conformations for the three models are illustrated in Fig. 5, in which the chains are projected along the direction perpendicular to the helix axis. As already mentioned, the periods along the helix axis for the 7/1 and 10/1 helix models are 20.1 and 28.6 Å, respectively. The period of the 12/1 helix model, however, is neither 29.1 nor 34.9 Å. In this case the true period is the pitch length itself, 2.91×36 Å.

Table 7. Atomic coordinates of the minimum-energy conformation with 7/1 helix

Residue	Atom	x/Å	y/Å	z/Å
Gly	N	1.61	0.00	0.00
	C_α	1.60	1.28	0.69
	C′	2.48	1.24	1.94
	O	3.09	0.22	2.24
Pro	N	2.58	2.36	2.65
	C_α	3.39	2.46	3.85
	C_β	3.58	3.95	4.07
	C_γ	2.49	4.64	3.27
	C_δ	1.90	3.62	2.31
	C′	2.71	1.75	5.03
	O	1.54	1.39	4.95
Pro	N	3.50	1.55	6.11
	C_α	2.99	0.89	7.30
	C_β	4.23	0.45	8.07
	C_γ	5.38	1.29	7.52
	C_δ	4.92	1.93	6.23
	C′	2.09	1.82	8.10
	O	2.37	3.01	8.22

The results obtained from above calculations showed that the minimum-energy of the 7/1 helix model is less than those of the other two models with 10/1 and 12/1 helices by about 7 kcal/mol per tripeptide unit. It is unknown that the present 7/1 helix model may represent the true conformation of the native tropocollagen.

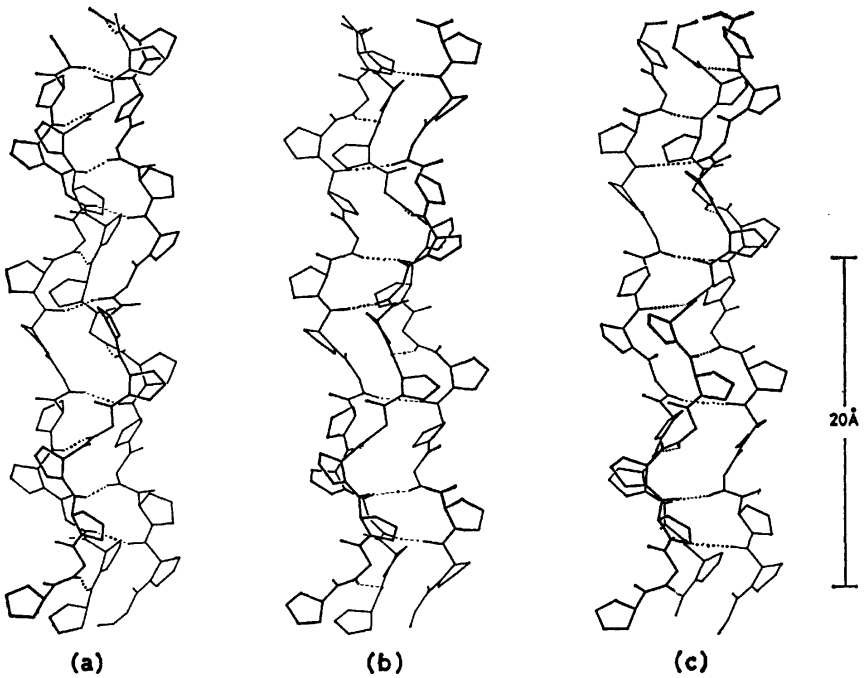

Fig. 5. Conformations with minimum-energy as projected along the direction perpendicular to helix axis. The dashed line denotes a hydrogen bond of $N(Gly_1)\cdots O(Pro_2)$. (a) 7/1 helix model, (b) 10/1 helix model, and (c) 12/1 helix model.

However, several lines of evidence suggest that this is the case. First, the synthesized molecule of $(Pro\text{–}Pro\text{–}Gly)_{10}$ as a collagen model can form a 7/1 helix in its single crystals.[10] Second, the hydrophobic interactions between tropocollagen molecules can form the stable microfibril structure only when the tropocollagen has a 7/1 helix model.[28] Third, the X-ray fiber diagram obtained from native collagen can be interpreted in terms of not only a 10/1 helix model but also a 7/1 helix model.[7] Taken these facts together with the present results, we may conclude that the 7/1 helix model is the best of the models so far presented for tropocollagen.

References

1) R. D. B. Fraser and T. P. MacRae, "Conformation in Fibrous Proteins," Academic, New York and London (1973), pp. 344—402.
2) G. N. Ramachandran and G. Kartha, *Nature*, **176**, 593 (1955).
3) A. Rich and F. H. C. Crick, *J. Mol. Biol.*, **3**, 483 (1961).
4) A. Yonath and W. Traub, *J. Mol. Biol.*, **43**, 461 (1969).
5) R. D. B. Fraser, T. P. MacRae, and E. Suzuki, *J. Mol. Biol.*, **129**, 463 (1979).
6) "Treatise on Collagen," ed by G. N. Ramachadran, Academic, New York (1967), Vol. 1, pp. 103—183.
7) K. Okuyama, M. Takayanagi, T. Ashida, and M. Kakudo, *Polymer J.*, **9**, 341 (1977).
8) V. G. Tumanyan, *Biopolymers*, **9**, 955 (1970).
9) M. H. Miller and H. A. Scheraga, *J. Polym. Sci., Symposium*, **54**, 171 (1976).
10) K. Okuyama, N. Tanaka, T. Ashida, and M. Kakudo, *Bull. Chem. Soc. Jpn.*, **49**, 1805 (1976).
11) V. Sasisekharan, *Acta. Crystallogr.*, **12**, 897 (1959.)
12) F. A. Momany, R. F. McGuire, A. W. Burgess, and H. A. Scheraga, *J. Phys. Chem.*, **79**, 2361 (1975).
13) IUPAC IUB Commision on Biochemical Nomenclature, *J. Mol. Biol.*, **52**, 1 (1970).
14) S. Arnott and A. J. Wonacott, *Polymer*, **7**, 157 (1966).
15) H. Sugeta and T. Miyazawa, *Biopolymers*, **5**, 673 (1967).
16) R. S. Bear, *Adv. Protein Chem.*, **7**, 69 (1952).
17) S. Sakakibara, K. Inouye, K. Shudo, Y. Kishida, Y. Kobayashi, and D. J. Prockop, *Biochem. Biophys. Acta.* **303**, 198 (1973).
18) J. Engel, H. Chen, D. J. Prockop, and H. Klump, *Biopolymers*, **16**, 601 (1977).
19) V. Sasisekharan, *J. Polym. Sci.*, **47**, 373 (1960).
20) T. Yamane, T. Ashida, K. Schimonishi, M. Kakudo, and Y. Sasada, *Acta Crystallogr., Sect. B*, **32**, 2071 (1976).
21) T. Ashida and M. Kakudo, *Bull. Chem. Soc. Jpn.*, **47**, 1129 (1974).
22) R. Balasubramanian, A. V. Lakshminarayanan, M. N. Sabesan, G. Tegoni, K. Venkatatesan, and G. N. Ramachandran, *Int. J. Protein Res.*, **3**, 25 (1971).
23) A. J. Hopfinger and A. G. Walton, *J. Macromol. Sci. Phys.*, **B3**, 171 (1969).
24) N. Go and K. Okuyama, *Macromolecules*, **9**, 867 (1976).
25) A. J. Hopfinger, Ph. D. Thesis, Case Western Reserve University, Cleveland, Ohio, 1970.
26) F. A. Momany, L. M. Carruthers, R. F. McGuire, and H. A. Scheraga, *J. Phys. Chem.*, **78**, 1595 (1974).
27) R. Fletcher and M. J. D. Powell, *Computer J.*, **6**, 163 (1963).
28) K. Okuyama, N. Go, and M. Takayanagi, *Chem. Lett.*, **1978**, 509.

Preparation and Solid-phase Thermal Reactions of Hexaamminechromium(III) Amino Polycarboxylates under Quasi-isothermal and -isobaric Conditions[1)]

Ryokichi Tsuchiya,* Akira Uehara, and Kazuhiko Kobayashi
Department of Chemistry, Faculty of Science, Kanazawa University, Kanazawa 920
(Received July 31, 1979)

The following hexaamminechromium(III) amino polycarboxylates were prepared: $[Cr(NH_3)_6]Naedta \cdot 3H_2O$, $[Cr(NH_3)_6]Napdta \cdot 6H_2O$, $[Cr(NH_3)_6]HK_3Cl(nta)_2 \cdot 2H_2O$ and $[Cr(NH_3)_6]KCl(nta) \cdot 2H_2O$, where edta, pdta and nta denote ethylenediaminetetraacetate, propylenediaminetetraacetate and nitrilotriacetate ions, respectively. Their thermal reactions in the solid-phase were examined by Q-derivatography (quasi-closed system; quasi-isothermal and -isobaric conditions) and D-derivatography (open system; dynamic conditions). The reactions in open system were too complicated to yield uniform intermediates. On the other hand, each reaction step in the quasi-closed system was definite and reproducible, the products obtained in each reaction step being remarkably pure.

Studies on the thermal reactions of metal complexes in the solid-phase have mostly been carried out in the open system.[2)] Two inherent problems have frequently been encountered, (a) difficulty of keeping the desired temperatures uniform over all parts of the sample, (b) change in the results caused by experimental conditions such as type of instrument, amount of sample, heating rate *etc.*

Recently, a new thermoanalytical instrument (Q-derivatograph) was developed, with which thermal reactions of samples can be followed under quasi-isothermal and -isobaric conditions.[3)] We studied the thermal reactions of hexaamminechromium(III) amino polycarboxylates under Q- and D-conditions[4)] and found that the results obtained under Q-conditions are reproducible and the intermediates in each reaction step can be obtained remarkably pure.

The present study was undertaken (1) to prepare the hexaamminechromium(III) amino polycarboxylates, (2) to observe the thermal reactions of the complexes under Q-conditions together with those under D-conditions, and (3) to test the possibility of synthesis of amino polycarboxylato-complexes by using the thermal reactions in the solid-phase.

Edta, pdta, and nta ions, which denote ethylenediaminetetraacetate, propylenediaminetetraacetate and nitrilotriacetate ions, respectively, were chosen mainly because of the expectation that the products obtained upon heating could be identified with certainty by referring to the well-known chromium(III) complexes containing these agents.

Experimental

Preparation of Complexes. Hexaamminechromium(III) Sodium Ethylenediaminetetraacetate Trihydrate, $[Cr(NH_3)_6]Naedta \cdot 3H_2O$. Fifteen grams (50 mmol) of H_4edta was dissolved in a solution of NaOH (8 g, 20 mmol) in 50 cm³ of water. The solution was then added to a solution of $[Cr(NH_3)_6]Cl_3$ (13 g, 50 mmol) in 50 cm³ of water. The resulting mixture was allowed to stand for a few days in a refrigerator, 18 g of yellow well-defined crystals being obtained and recrystallized from water.

Found: C, 22.82; H, 7.25; N, 21.21%. Calcd for $C_{10}H_{36}N_8O_{11}CrNa$: C, 23.12; H, 6.99; N, 21.57%.

Hexaamminechromium(III) Sodium Propylenediaminetetraacetate Hexahydrate, $[Cr(NH_3)_6]Napdta \cdot 6H_2O$. Sixteen grams (50 mmol) of H_4pdta was dissolved in a solution of NaOH (8 g, 20 mmol) in 70 cm³ of water. The solution was then added to a solution of $[Cr(NH_3)_6]Cl_3$ (13 g, 50 mmol) in 50 cm³ of water, to which *ca.* 10 cm³ of ethanol was gradually added. The resulting mixture was allowed to stand for several days in a refrigerator. 20 g of the products was thus obtained, which was recrystallized from water. The color of the samples containing $[Cr(NH_3)_6]$ cation was yellow irrespective of the anions involved.

Found: C, 22.39; H, 7.66; N, 19.11%. Calcd for $C_{11}H_{44}N_8O_{14}CrNa$: C, 22.49; H, 7.55; N, 19.07%.

Hexaamminechromium(III) Hydrogen Tripotassium Chloride Bis(nitrilotriacetate) Dihydrate, $[Cr(NH_3)_6]HK_3Cl(nta)_2 \cdot 2H_2O$. H_3nta (19 g, 100 mmol) was added to a solution of $[Cr(NH_3)_6]Cl_3$ (13 g, 50 mmol) in 150 cm³ of water. The slurry was continuously stirred under ice-cooling, aqueous KOH being added drop by drop in amounts enough to dissolve the H_3nta and to obtain a solution of pH 8. To this was added *ca.* 10 cm³ of ethanol, and the resulting solution was left to stand for a week in a refrigerator. 18 g of plate-like crystals was obtained. Recrystallization was carried out as follows. The crystals were dissolved in a small amount of water, a small amount of ethanol then being added and the resulting solution kept standing in a refrigerator for about a week. Purified triangular plate-like crystals were obtained.

Found: C, 20.36; H, 5.55; N, 15.36%. Calcd for $C_{12}H_{35}N_8O_{14}ClCrK_3$: C, 20.01; H, 4.90; N, 15.56%.

At first, the composition of the compound could not be determined, but the following nitrilotriacetate ($[Cr(NH_3)_6]KCl(nta) \cdot 2H_2O$) was obtained. This differs considerably in property from the former compound; for example the former was somewhat acidic in water (pH 4—5), whereas the latter was slightly alkaline (pH 8—9). A comparison of analytical data, IR spectra and thermal behavior between them revealed that the above composition is valid for the former complex.

Hexaamminechromium(III) Potassium Chloride Nitrilotriacetate Dihydrate, $[Cr(NH_3)_6]KCl(nta) \cdot 2H_2O$. Ten grams (50 mmol) of H_3nta was added to a solution of $[Cr(NH_3)_6]Cl_3$ (13 g, 50 mmol) in 150 cm³ of water. To the mixture was added aqueous KOH drop by drop with continuous stirring under ice-cooling, the final pH of the solution being adjusted to 10. *Ca.* 10 cm³ of ethanol was added to the resulting solution, which was kept standing in a refrigerator for a week, 12 g of the products being obtained. Recrystallization was carried out from water containing a small amount of ethanol. Octahedrally shaped crystals were obtained.

Found: C, 16.23; H, 6.12; N, 21.58%. Calcd for C_6H_{28}-

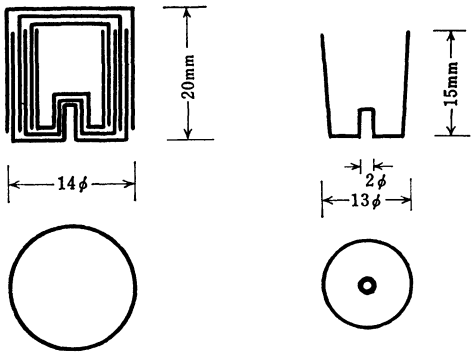

(a) Labyrinth crucible (b) Coverless crucible

Fig. 1. Pt crucibles employed in Q-derivatograph (a) and D-derivatograph (b).

N_7O_8ClCrK: C, 15.91; H, 6.23; N, 21.65%.

The presence of K^+ and Cl^- was quantitatively determined by the use of $[Co(NO_2)_6]^{3-}$ and Ag^+ ions.

Isolation of the Products Obtained in Each Thermal Reaction Step. Temperature and heating time were determined from the data obtained under Q- and/or D-conditions.

(1) $NH_4[Cr(edta)]\cdot 2H_2O$ from $[Cr(NH_3)_6]Naedta\cdot 3H_2O$: $[Cr(NH_3)_6]$Naedta·$3H_2O$ (1 g, 2 mmol) was put in a labyrinth crucible (Fig. 1-(a)), and heated at 150 °C for 5 h in an air-bath. A violet product (Na[Cr(edta)]) obtained was dissolved in a small amount of water. NH_4Cl (1 g, 16 mmol) was added and the solution was allowed to stand in a refrigerator for a few days, 0.5 g of violet crystals being obtained.

Found: C, 30.31; H, 5.25; N, 10.82%. Calcd for $C_{10}H_{20}N_3O_{10}Cr$: C, 30.47; H, 5.08; N, 10.66%.

Since the preparation of sodium salts was difficult, the products were purified as ammonium salts.

(2) $Na[Cr(pdta)]\cdot 3H_2O$ from $[Cr(NH_3)_6]Napdta\cdot 6H_2O$: One gram (2 mmol) of $[Cr(NH_3)_6]$Napdta·$6H_2O$ was charged in a labyrinth crucible and heated at 210 °C for one hour. Violet product (Na[Cr(pdta)]) thus obtained was dissolved in a small amount of water. Ethanol (one tenth of the whole volume) was added and the solution was allowed to stain in a refrigerator for about one week. 0.5 g of violet crystals were obtained.

Found: C, 30.42; H, 4.88; N, 6.45%. Calcd for $C_{11}H_{20}N_2O_{11}CrNa$: C, 30.64; H, 4.67; N, 6.50%.

(3) $Na_3[Cr(nta)_2]\cdot 5H_2O$ from $[Cr(NH_3)_6]HK_3Cl(nta)_2\cdot 2H_2O$: $[Cr(NH_3)_6]HK_3Cl(nta)_2\cdot 2H_2O$ (1.5 g, 2 mmol) was charged in a labyrinth crucible and heated at 135 °C for 3.5 h in an air-bath. A pink product ($K_3[Cr(nta)_2]$) was obtained, which was dissolved in water. The solution was passed through a column of Dowex 1-X8 (Cl-form) resin. The pink band was developed on the column, which was eluted with 0.4 mol cm^{-3} NaCl solution. The effluent was then concentrated to one-third of its volume at about 30 °C on a rotary evaporator, and kept standing in a refrigerator overnight. 0.2 g of pink powdered crystals were obtained.

Found: C, 24.35; H, 2.60; N, 4.68%. Calcd for $C_{12}H_{17}N_2O_{17}CrNa_3$: C, 24.75; H, 2.94; N, 4.81%.

(4) $[Cr(nta)(NH_3)_2]KCl$ from $[Cr(NH_3)_6]KCl(nta)\cdot 2H_2O$: $[Cr(NH_3)_6]$KCl(nta)·$2H_2O$ (1 g, 2 mmol) was put in a labyrinth crucible and heated at 130 °C for 6.5 h in an air-bath. 0.75 g of reddish brown products was obtained, which could not be purified because of the absence of suitable solvents. The products were highly soluble and readily hydrolyzed in water, so purification from water failed. The KCl contained in the products could not be removed. The results of elemental analyses indicate that the composition of the products is substantially uniform. This is a typical example showing that the thermal reaction of the samples proceeds uniformly under Q-conditions. It has not yet been clarified whether the KCl in the products is present in the crystals ($[Cr(nta)(NH_3)_2]KCl$) or as the contaminants ($[Cr(nta)(NH_3)_2]$+KCl).

Instruments. The TG curves of the complexes were measured under Q- and D-conditions by using a Q-derivatograph[3] and a D-derivatograph.[5] Figure 1 shows the Pt crucibles employed in this study. In the case of D-derivatography, all the measurements were caried out at a heating rate of 1 °C min^{-1}, 0.5 g of the samples being used in a coverless Pt crucible (Fig. 1-(b)). In Q-derivatography, 0.5 g of the samples were taken into a labyrinth Pt crucible (Fig. 1-(a)).[3] The crucible consists of three Pt cups and three Pt covers. They are joined alternately. The sample decomposes on heating, evolving gases. The gases first occupy the inside of the crucible. Excess gases go out from the crucible only when the inside pressure exceeds the outside pressure. Thus, the inside of the crucible fulfills the autogenerated quasi-isobaric condition. IR and UV spectra were measured with the same apparatus as employed previously.[6]

Results and Discussion

TG Curves of $CuSO_4\cdot 5H_2O$. $CuSO_4\cdot 5H_2O$ is used as a typical example to explain the difference in the results obtained under Q- and D-conditions. Figure 2 shows the TG curves measured under Q-conditions

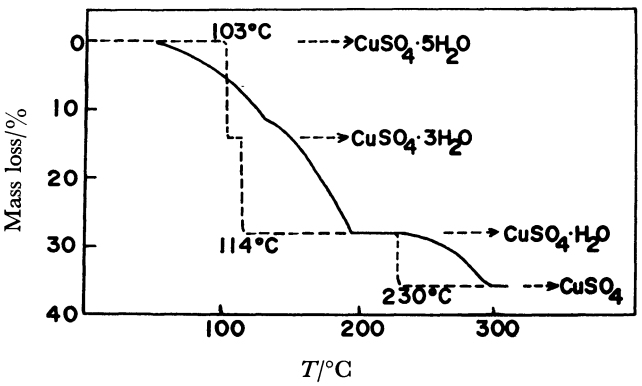

Fig. 2. TG curves of $CuSO_4\cdot 5H_2O$ measured under Q-(----) and D-conditions (——).

(broken line) and D-conditions (solid line). A general TG pattern measured under D-conditions, often influenced by experimental conditions such as instruments employed, sample amount and heating rate, is shown. Stepwise dehydration is distinctly detectable under Q-conditions. The TG pattern was not influenced by experimental conditions. Figure 3 shows the relationship between dissociation pressure (p) and temperature (T) in $CuSO_4\cdot 5H_2O$.[7] The first, second and third dehydration steps under one atmosphere are 102, 108 and 227 °C, respectively, close to the temperature (103, 114 and 230 °C) obtained under Q-conditions (Fig. 2). This indicates that under Q-conditions each dehydration step proceeds in a monovariant system and pure intermediates are obtainable in each plateau.

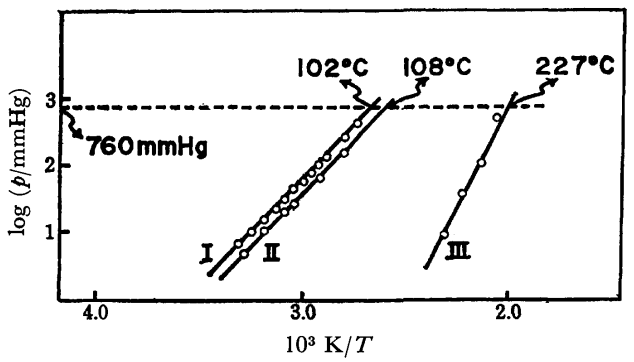

Fig. 3. Relationships between dissociation pressures (p) and temperatures (T) in $CuSO_4 \cdot 5H_2O$.
I. $CuSO_4 \cdot 5H_2O \rightleftharpoons CuSO_4 \cdot 3H_2O + 2H_2O$
II. $CuSO_4 \cdot 3H_2O \rightleftharpoons CuSO_4 \cdot H_2O + 2H_2O$
III. $CuSO_4 \cdot H_2O \rightleftharpoons CuSO_4 + H_2O$

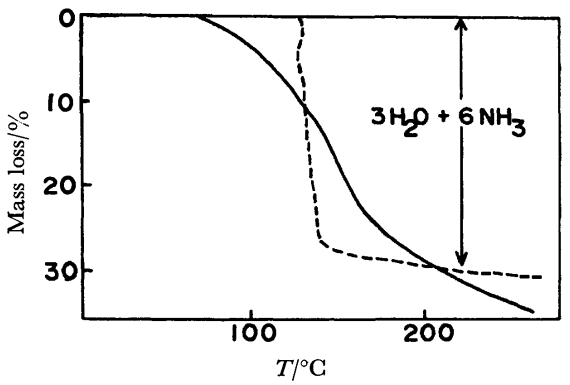

Fig. 4. TG curves of $[Cr(NH_3)_6]Naedta \cdot 3H_2O$ measured under Q-(——) and D-conditions (——).

TG Curves of the Complexes. *$[Cr(NH_3)_6]Naedta \cdot 3H_2O$*: Figure 4 shows the TG curves of $[Cr(NH_3)_6]$-Naedta·$3H_2O$. Under D-conditions (solid line), the complex begins to decompose at *ca.* 70 °C and gradually loses the weight of ($3H_2O+6NH_3$) up to about 200 °C; no plateau is detectable. Under Q-conditions (broken line), the complex suddenly loses weight at 130 °C and decomposes nearly isothermally, *viz.*, the complex evolves the gases ($3H_2O+6NH_3$) in a narrow temperature range (130—140 °C), after which a clear plateau is obtained in the TG curve. At this stage, the original yellow complex turned violet, indicating that the edta anion in outer-sphere is coordinated to Cr(III) ion upon heating. From the results, 150 °C for 5 h was selected as the optimal heating conditions for obtaining Na[Cr(edta)] from $[Cr(NH_3)_6]Naedta \cdot 3H_2O$.

$[Cr(NH_3)_6]Napdta \cdot 6H_2O$: The TG curve of the compound under D-conditions (Fig. 5) is essentially similar to that of the foregoing edta salt: the compound evolves the gases ($6H_2O+6NH_3$) at 50—200 °C and then decomposes gradually. Under Q-conditions, the complex begins to decompose at 80 °C, the weight loss up to 20 wt% taking place nearly isothermally and reaching a plateau at *ca.* 200 °C. The coloration turned from yellow to violet at this plateau, from which the optimal condition for obtaining Na[Cr(pdta)] from $[Cr(NH_3)_6]Napdta \cdot 6H_2O$ was selected as 200 °C for 1 h.

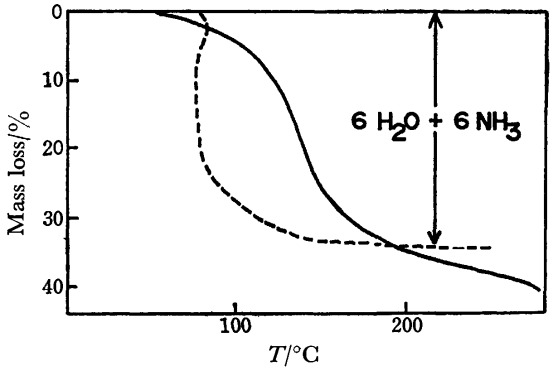

Fig. 5. TG curves of $[Cr(NH_3)_6]Napdta \cdot 6H_2O$ measured under Q- (——) and D-conditions (——).

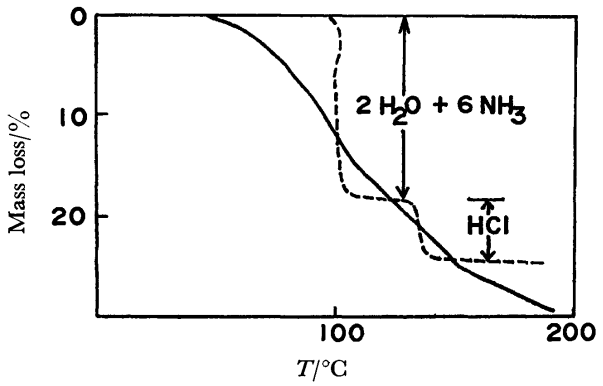

Fig. 6. TG curves of $[Cr(NH_3)_6]HK_3Cl(nta)_2 \cdot 2H_2O$ measured under Q- (——) and D-conditions (——).

It should be noted that the complex melts in its own crystalline water at the begining of the reaction under Q-conditions. A slight temperature drop appearing immediately after the weight loss begins is probably due to melting of the sample.

$[Cr(NH_3)_6]HK_3Cl(nta)_2 \cdot 2H_2O$: The TG curves of $[Cr(NH_3)_6]HK_3Cl(nta)_2 \cdot 2H_2O$ are shown in Fig. 6. The salt continues to decompose monotonously from 45 °C under D-conditions (solid line), no plateau being obtained in the TG curve. In contrast, two distinct plateaus are detectable under Q-conditions, one of which corresponds to the loss of the gases ($2H_2O+6NH_3$) at 100—105 °C and the other to the loss of one mole of hydrogen chloride at 130—135 °C. The inintial yellow complex turned pink at the first plaueau, the coloration remaining unchanged at the second plateau. The change in coloration indicates that the complex is in turn converted into $K_3[Cr(nta)_2]HCl$ and then $K_3[Cr(nta)_2]$. The condition (135 °C for 3.5 h) is suitable for preparing $K_3[Cr(nta)_2]$ from $[Cr(NH_3)_6]$-$HK_3Cl(nta)_2 \cdot 2H_2O$. $K_3[Cr(nta)_2]$ is readily hydrolyzed in water to yield $K[Cr(OH)(nta)(H_2O)]$,[8] but the situation is not so severe in the sodium salts and hence the thermal products were purified as sodium salts.

$[Cr(NH_3)_6]KCl(nta) \cdot 2H_2O$: The TG curve of the compound under D-conditions starts to fall at about 50 °C without reaching plateau (Fig. 7). Under Q-conditions, the complex evolves the gases ($2H_2O+4NH_3$) at 110—120 °C, a plateau being reached. The coloration turned from original yellow to reddish brown,

Table 1. IR data due to the C=O stretching vibrations

Complex	$\tilde{\nu}_{C=O}/cm^{-1}$ a)		
	-COOH	-COO-Cr(III)	-COO$^-$
$[Cr(NH_3)_6]Naedta \cdot 3H_2O$ (yellow)			1580(vs, br)
$NH_4[Cr(edta)] \cdot 2H_2O$ (violet)		1650(vs, br)	
$[Cr(NH_3)_6]Napdta \cdot 6H_2O$ (yellow)			1590(vs, br)
$Na[Cr(pdta)] \cdot 3H_2O$ (violet)		1650(vs, br)	
$[Cr(NH_3)_6]HK_3Cl(nta)_2 \cdot 2H_2O$ (yellow)	1715(s)		1590(vs, br)
$Na_3[Cr(nta)_2] \cdot 5H_2O$ (pink)		1640(vs, br)	1593(s)
$[Cr(NH_3)_6]KCl(nta) \cdot 2H_2O$ (yellow)			1580(vs, br)
$[Cr(nta)(NH_3)_2]KCl$ (reddish brown)		1650(vs, br)	

a) The terms s, vs and br denote strong, very strong and broad, respectively.

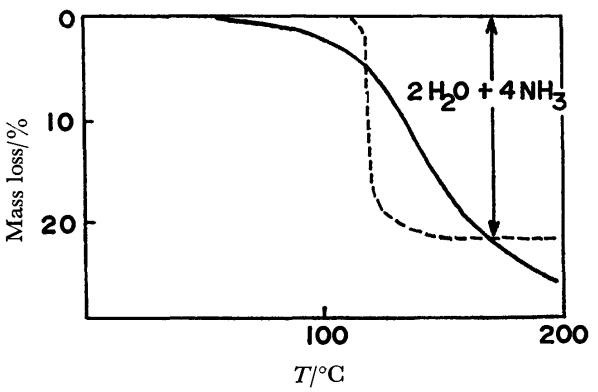

Fig. 7. TG curves of $[Cr(NH_3)_6]KCl(nta) \cdot 2H_2O$ measured under Q- (——) and D-conditions (——).

Table 2. Electronic spectral data due to d-d transition ($\tilde{\nu}/10^3$ cm^{-1})

Complex[a)]	$\tilde{\nu}_I$(log ε)	$\tilde{\nu}_{II}$(log ε)
$[Cr(NH_3)_6]Naedta \cdot 3H_2O$	21.55(1.59)	28.40(1.47)
$NH_4[Cr(edta)] \cdot 2H_2O$	18.40(2.33)	25.45(2.07)
$[Cr(NH_3)_6]Napdta \cdot 6H_2O$	21.55(1.57)	28.40(1.46)
$Na[Cr(pdta)] \cdot 3H_2O$	18.35(2.33)	25.45(2.04)
$[Cr(NH_3)_6]HK_3Cl(nta)_2 \cdot 2H_2O$	21.55(1.61)	28.40(1.49)
$Na_3[Cr(nta)_2] \cdot 5H_2O$	19.87(1.64)	27.84(1.47)
$[Cr(NH_3)_6]KCl(nta) \cdot 2H_2O$	21.55(1.59)	28.40(1.47)
$[Cr(nta)(NH_3)_2]KCl$[b)]	18.5	24.5

a) All the spectra were measured in water except for that of $[Cr(nta)(NH_3)_2]KCl$. b) The spectrum was measured by a diffuse reflectance method because the complex rapidly aquated in water.

indicating that the complex is converted into $[Cr(nta)(NH_3)_2]KCl$. Preliminary experiments showed that 130 °C for 6.5 h is the best condition for obtaining $[Cr(nta)(NH_3)_2]KCl$ from $[Cr(NH_3)_6]KCl(nta) \cdot 2H_2O$. The products were highly soluble and rapidly hydrolyzed in water, purification from water thus being always unsuccessful.

IR Data. The IR data obtained from the C=O stretching vibrations utilized for determining the coordination modes of carboxylato groups are summarized in Table 1. IR spectral studies on the metal complexes containing amino polycarboxylates reveal that the bands due to free carboxylic acid (-COOH), coordinated carboxylate (-COO-Metal) and ionic carboxylate (-COO$^-$) appear at 1700—1740, 1620—1690 and 1550—1600 cm^{-1}, respectively.[9] $[Cr(NH_3)_6]Naedta \cdot 3H_2O$ and $[Cr(NH_3)_6]Napdta \cdot 6H_2O$ give the band at 1580 and 1590 cm^{-1}, respectively, indicating that both the edta and pdta ions are present in ionic form in the salts. The presence of the bands (1650 cm^{-1}) in $NH_4[Cr(edta)] \cdot 2H_2O$ and $Na[Cr(pdta)] \cdot 3H_2O$ suggests that the carboxylato groups in both the complexes are coordinated to Cr(III) ions. The appearance of the bands (1715 and 1590 cm^{-1}) in $[Cr(NH_3)_6]HK_3Cl(nta)_2 \cdot 2H_2O$ indicates that the salt has free carboxylic acid and ionic carboxylato groups. The presence of both coordinated and ionic carboxylato groups in $Na_3[Cr(nta)_2] \cdot 5H_2O$ is supported by the bands at 1640 and 1593 cm^{-1}. The results also show that the nta ion in $[Cr(NH_3)_6]KCl(nta) \cdot 2H_2O$ is present in ionic form (1580 cm^{-1}), but that in $[Cr(nta)(NH_3)_2]KCl$ is in coordinated form (1650 cm^{-1}).

Electronic Spectral Data. Electronic spectral data due to d-d transition obtained in water are given in Table 2. The first and second bands of the hexaammine-chromium(III) complexes appear at 21.55 and 28.40×10^3 cm^{-1}, respectively, irrespective of anions. The bands at 18.40 and 25.45×10^3 cm^{-1} in $NH_4[Cr(edta)] \cdot 2H_2O$ and 18.35 and 25.45×10^3 cm^{-1} in $Na[Cr(pdta)] \cdot 3H_2O$ resemble those of $[Cr(edta)(H_2O)]^-$ ion (18.4 and 25.5×10^3 cm^{-1}).[10] This is due to the fact that both complexes are converted into $[Cr(edta \text{ or } pdta)(H_2O)]^-$ ion in water. $Na_3[Cr(nta)_2] \cdot 5H_2O$ has bands at 19.87 and 27.84×10^3 cm^{-1}, which are in the proximity of those of *trans*(N)-$(NH_4)_3[Cr(nta)_2] \cdot 4H_2O$ (20.0 and 27.8×10^3 cm^{-1}).[8] The spectrum of $[Cr(nta)(NH_3)_2]KCl$ was measured by a powder diffuse reflectance method since the complex is rapidly hydrolyzed in water. The bands at 18.5 and 24.5×10^3 cm^{-1} are substantially close to those of [Cr(nta)(bipy)] (18.6 and 24.6×10^3) where bipy denotes 2,2'-bipyridine.[11] It seems that the chromium(III) ion in the products is surrounded by a N_3O_3 chromophore.

Study on the thermal reactions of $[Cr(NH_3)_6]X_3$ (X is a simple monodentate anion such as Cl^-, Br^- and I^-) showed that the complexes undergo anation upon heating in open system and are successively converted into $[CrX(NH_3)_5]X_2$, $[CrX_2(NH_3)_4]$ and $[CrX_3(NH_3)_3]$.[12] It was found that under Q-conditions, even the complexes containing more complicated anions such as edta, pdta and nta ions undergo participation of these ions in the coordination sphere giving the corresponding

amino polycarboxylato-complexes. The use of thermal reactions in the quasi-closed system would lead to the production of other new metal complexes, which do not seem to have been prepared in solutions.

The authors wish to express their thanks to Hungarian Optical Works and Kubota Trading Co. for the use of Q-derivatograph.

References

1) Presented at the ACS/CSJ Chemical Congress: 1979, Hawaii, April 1979.

2) a) N. Tanaka and M. Nanjo, "Kagaku," Kagaku-dojin Pub. Co., Kyoto (1967), Extra Vol. 32, pp. 211—224; b) W. W. Wendlandt and J. P. Smith, "The Thermal Properties of Transition Metal Ammine Complexes," Elsevier Pub. Co., Amsterdam (1967); c) R. Tsuchiya, "Netsu-Ondo-Sokutei To Netsubunseki 1969," Kagakugijutsu-sha, Tokyo (1969), pp. 135—151; d) "Progress in Inorganic Chemistry," ed by J. O. Edwards, Interscience Publishers, New York (1972), Vol. 17, pp. 545—557; e) R. Tsuchiya, "Proceedings of Special Lectures in the 34th National Meeting of the Chemical Society of Japan," pp. 154—159 (1976).

3) a) F. Paulik and J. Paulik, *J. Therm. Anal.*, **5**, 253 (1973); b) R. Tsuchiya and A. Uehara, *Netsusokutei*, **6**, 16 (1979); c) O. T. Sørensen, *Thermochim. Acta*, **29**, 211 (1979).

4) Throughout this paper, the terms Q-conditions and D-conditions are used to denote Quasi-isothermal and -isobaric conditions and Dynamic-conditions, respectively. In the quasi-closed system measurements are made by means of a Q-derivatograph and in the open system by means of a D-derivatograph.

5) R. Tsuchiya, Y. Kaji, A. Uehara, and E. Kyuno, *Bull. Chem. Soc. Jpn.*, **42**, 1881 (1969).

6) M. Kimura, A. Uehara, E. Kyuno, and R. Tsuchiya, *Bull. Chem. Soc. Jpn.*, **51**, 466 (1978).

7) C. D. Carpenter and E. R. Jette, *J. Am. Chem. Soc.*, **45**, 578 (1923); A. W. C. Menzies, *ibid.*, **42**, 1951 (1920).

8) A. Uehara, E. Kyuno, and R. Tsuchiya, *Bull. Chem. Soc. Jpn.*, **40**, 2317 (1967).

9) a) D. T. Sawyer and J. M. McKinnie, *J. Am. Chem. Soc.*, **82**, 4191 (1960); b) D. T. Sawyer and P. J. Paulsen, *J. Am. Chem. Soc.*, **81**, 816 (1959); and c) D. H. Busch and J. C. Bailar, Jr., *J. Am. Chem. Soc.*, **75**, 4574 (1953).

10) H. Ogino, T. Watanabe, and N. Tanaka, *Inorg. Chem.* **14**, 2093 (1975).

11) A. Uehara, E. Kyuno, and R. Tsuchiya, *Bull. Chem. Soc. Jpn.*, **40**, 2322 (1967).

12) K. Nagase and N. Tanaka, *Bull. Chem. Soc. Jpn.*, **45**, 1097 (1972).

The Coprecipitation of Antimony(III or V) with Iron(III) Hydroxide

Yoshikazu INOUE and Makoto MUNEMORI*

Laboratory of Environmental Chemistry, College of Engineering, University of Osaka Prefecture, Mozu-Umemachi, Sakai 591

(Received August 2, 1979)

The coprecipitation of antimony(III or V) with iron(III) hydroxide as a function of the pH in the range from 4 to 12 was studied in the presence of the chloride ion. Antimony(III) is coprecipitated more easily at any given pH value than antimony(V). The coprecipitation of antimony(III) is quantitative in the pH range from 4 to 10 and is not affected by the chloride ion. On the other hand, the coprecipitation of antimony(V) is affected not only by the pH range, but also by the chloride-ion concentration.

Iron(III) and manganese(IV) oxides(or hydroxide) have been noted as substances which exert a major effect on the concentrations of other heavy metal ions in natural waters,[1-3] because these oxides associate with the heavy metal ions. For example, cadmium(II) and lead(II) are incorporated into the hydrous oxides of iron and manganese.[4,5] Arsenic(III),[6] chromium-(III),[7] and mercury(II)[8] are incorporated into iron-(III) hydroxide. This incorporation can be ascribable to adsorption, ion-exchange, or coprecipitation. Leckie and James[9] have suggested that the hydrolysis of the heavy metal ion plays an important role in these processes. The hydrolysis reaction differs depending on the oxidation state of the metal ion and is also affected by the presence of complexing agents.

In a previous paper,[10] we studied the coprecipitation of mercury(II) with iron(III) hydroxide in the absence and in the presence of halogenide ions and indicated that the coprecipitation behavior can be explained in terms of the hydrolysis of mercury, *i.e.*, the formation of $Hg(OH)_2$. The present investigation was undertaken in order to evaluate the coprecipitation of antimony-(III or V) with iron(III) hydroxide in the presence of the chloride ion. It has been reported that antimony-(III) is coprecipitated with iron(III) hydroxide and manganese(IV) oxide.[11,12] Fujinaga *et al.*[11] studied the coprecipitation of antimony(III) with iron(III) hydroxide in natural and artificial seawater and indicated that antimony(III) is quantitatively coprecipitated with iron(III) hydroxide in the vicinity of pH 7. For antimony(V), however, little has been published regarding coprecipitation with heavy metal hydroxides in natural waters.

This paper will describe a coprecipitation study of the antimony(III or V)-iron(III) system and will discuss the effect of the hydrolysis of antimony on its coprecipitation with iron(III) hydroxide and the antimony species which is responsible for coprecipitation from the viewpoint of chemical equilibrium.

Experimental

Reagents. The antimony(III) stock solution, 8.2×10^{-2} mol cm^{-3}, was prepared by dissolving antimony metal (99.999 %) in sulfuric acid with heating and by then diluting the mixture with dilute hydrochloric acid. The antimony(V) stock solution, 8.2×10^{-2} mol dm^{-3}, was prepared by dissolving potassium antimonate(V) in dilute hydrochloric acid(the antimonate is not appreciably soluble in sulfuric acid). The iron(III) stock solution was prepared by dissolving iron(III) sulfate in dilute sulfuric acid and was standardized by titration with potassium permanganate after reduction with zinc. The working solutions were prepared immediately before use by diluting the stock solutions. Sodium chloride was used as the source of the chloride ion. All the chemicals were of an analytical reagent grade.

Procedure. The hydrolysis study was carried out by employing a 500-ml portion of an 8.2×10^{-4} mol dm^{-3} antimony(III or V) solution. The solution was adjusted to pH 4, 10, or 12 with sodium hydroxide and was allowed to stand while it was being stirred at 25 °C. At fixed intervals of time, a 20-ml portion of the solution was filtered through a filter paper(Toyo filter paper No. 2). In the coprecipitation study, a 200-ml portion of a solution containing 8.2×10^{-4} mol dm^{-3} antimony(III or V) and 7×10^{-3} mol dm^{-3} iron(III) was used to obtain the data reported below unless otherwise indicated. The solution was adjusted to an appropriate pH value with sodium hydroxide and then allowed to stand while it was being stirred at 25 °C. After equilibrium had been reached(it required about 20 min), the solution was filtered through a filter paper(Toyo filter paper No. 2). All the pH values reported are equilibrium values. The antimony remaining in the filtrate was colorimetrically determined by the Rhodamine B method. Antimony(V) was reduced to antimony(III) with sodium sulfite by heating[13] and was then subjected to the Rhodamine B method immediately after the reoxidation of antimony(III) to antimony(V) with cerium.

Results and Disccusion

Hydrolysis of Antimony(III). The hydrolysis of antimony(III) was first studied at pH 4, 10, and 12 in

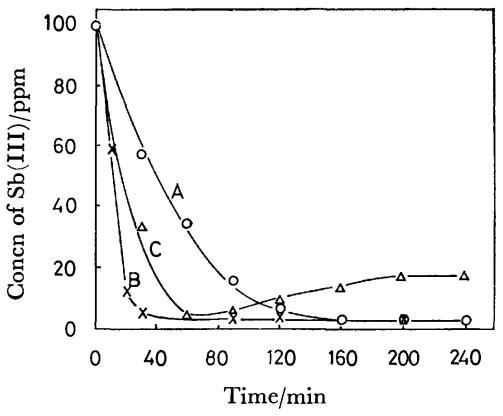

Fig. 1. Effect of pH on the hydrolysis of antimony(III) in the presence of 6×10^{-2} mol dm^{-3} chloride and 1.8×10^{-2} mol dm^{-3} sulfate (A) pH 4, (B) pH 10, and (C) pH 12.

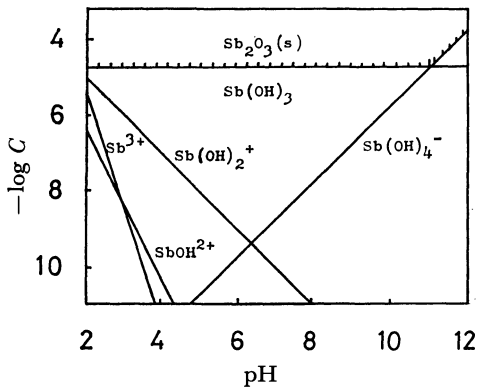

Reactions	Equilibrium constants
$Sb_2O_3(s)+3H_2O=2Sb^{3+}+6OH^-$	$10^{-4.14}$
$Sb_2O_3(s)+2H^++H_2O=2Sb(OH)_2^+$	$10^{-3.11}$
$Sb_2O_3(s)+3H_2O=2Sb(OH)_3$	$10^{-4.7}$
$Sb_2O_3(s)+2OH^-+3H_2O=2Sb(OH)_4^-$	$10^{-2.06}$
$SbOH^{2+}+H_2O=Sb(OH)_2^++H^+$	$10^{-1.4}$
$Sb(OH)_2^++H_2O=Sb(OH)_3+H^+$	$10^{-0.87}$
$Sb(OH)_3+H_2O=Sb(OH)_4^-+H^+$	$10^{-11.0}$

Fig. 2. Log concentration-pH solubility diagram for $Sb_2O_3(s)-H_2O$ system. The diagram was calculated using representative values[14,15] for equilibrium constants for solubility and hydrolysis.

the presence of chloride (6×10^{-2} mol dm^{-3}) and sulfate (1.8×10^{-2} mol dm^{-3}) ions. Figure 1 shows the results as a function of the time. At pH 4 and 10, the concentration of antimony(III) in the solution decreased continuously, depending on the pH, with the lapse of time until equilibrium was established. At pH 12, on the other hand, the concentration of antimony(III) once decreased to minimum and then increased until equilibrium was established. The equilibrium concentration at pH 4 and 10 was about 3 ppm (2.46×10^{-5} mol dm^{-3}), which agrees fairly well with the solubility of $Sb_2O_3(s)$ (2×10^{-5} mol dm^{-3}) as derived from Fig. 2. The equilibrium concentration at pH 12 was about 18 ppm (1.48×10^{-4} mol dm^{-3}), which corresponds with the solubility of $Sb_2O_3(s)$ at pH 12 (1.8×10^{-4} mol dm^{-3}) (Fig. 2). These results indicate that neither chloride nor sulfate ions affect the hydrolysis equilibrium for antimony(III); this is in accordance with the theoretical expectation based on the small formation constants of the antimony(III) chloride and sulfate complexes. Therefore, the hydrolysis of antimony can be expressed by the following chemical equations, even in the presence of chloride and sulfate ions:

$$Sb^{3+} + H_2O = SbOH^{2+} + H^+ \quad (1)$$

$$SbOH^{2+} + H_2O = Sb(OH)_2^+ + H^+ \quad (2)$$

$$Sb(OH)_2^+ + H_2O = Sb(OH)_3 + H^+ \quad (3)$$

$$2Sb(OH)_3 = Sb_2O_3(s) + 3H_2O \quad (4)$$

At pH 4 and 10, Reactions 1 to 4 take place and antimony(III) is precipitated as Sb_2O_3. Reactions 1 to 3 may be expected to be faster at higher pH values, while Reaction 4 is probably independent of the pH; therefore, the precipitation equilibrium is established faster at pH 10 than at pH 4.

At pH 12, however, Reaction 5 or 6 occurs in addition to the above reactions to produce the $Sb(OH)_4^-$ ion, while the formation of $Sb_2O_3(s)$ is retarded.

$$Sb(OH)_3 + OH^- = Sb(OH)_4^- \quad (5)$$

$$Sb_2O_3(s) + 2OH^- + 3H_2O = 2Sb(OH)_4^- \quad (6)$$

The appearance of the minimum solubility during the hydrolysis process clearly indicates that Reaction 6 is predominant.

Coprecipitation of Antimony(III) with Iron(III) Hydroxide. In the antimony(III)–iron(III) system, antimony(III) was precipitated within 20 min over a wide pH range. The concentration of antimony(III) remaining in the aqueous phase at pH 8 was less than 0.05 ppm (4.1×10^{-7} mol dm^{-3}), far less than that expected from the solubility of $Sb_2O_3(s)$ (2×10^{-5} mol dm^{-3}). These results indicate that antimony(III) is coprecipitated with iron(III) hydroxide. The concentration of the chloride ion in the range from 1×10^{-3} to 5.4×10^{-1} mol dm^{-3} did not affect the results, suggesting the absence of any effect of the ionic strength on the coprecipitation.

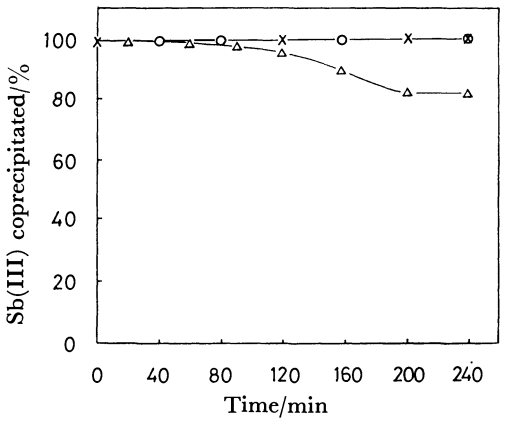

Fig. 3. Effect of hydrolysis of antimony(III) its coprecipitation with iron(III) hydroxide (○) pH 4, (×) pH 10, and (△) pH 12.

Effect of Hydrolysis of Antimony(III) on its Coprecipitation with Iron(III) Hydroxide. Figure 3 shows the effect of the hydrolysis of antimony(III) on its coprecipitation with iron(III) hydroxide. The experiment was performed in the following manner. Prior to the addition of iron(III), the antimony(III) solution was adjusted to pH 4, 10, or 12 with sodium hydroxide and then allowed to stand for a given time while it was being stirred at 25 °C. The time is taken as the abscissa in Fig. 3. The iron(III) solution was adjusted to pH 4, 10, or 12, and antimony and iron solutions with the same pH value were mixed. After the mixture has then been allowed to stand for 5 min while it being stirred at 25 °C, the suspension was filtered through a filter paper (Toyo filter paper No. 2). At pH 4 and 10, as is shown in Fig. 3, antimony(III) was quantitatively coprecipitated with iron(III) hydroxide, irrespective of the time needed for the hydrolysis of antimony. The concentration of antimony(III) remaining in the aqueous phase at both pH values was less than 0.05 ppm. At pH 12, the coprecipitation of antimony(III) was quantitative as long as the antimony(III) solution was allowed to stand for a period of less than 30 min

before mixing. After standing for a longer period, however, the extent of the coprecipitation of antimony(III) gradually decreased to a constant value, and then the concentration of antimony(III) remaining in the aqueous phase was 19 ppm (1.6×10^{-4} mol dm^{-3}), approximately equal to the solubility of Sb_2O_3(s) at pH 12. The coprecipitation behavior of antimony(III) described above can be explained by assuming that the $Sb(OH)_4^-$ ion is not coprecipitated with iron(III) hydroxide.

It can be concluded from the results presented above that the antimony(III) species except Sb_2O_3(s) are coprecipitated with iron(III) hydroxide, but there is no evidence to determine what species among Sb^{3+}, $SbOH^{2+}$, $Sb(OH)_2^+$, and $Sb(OH)_3$ is predominantly responsible for the coprecipitation process. Further investigation will be required for a more detailed elucidation of the coprecipitation mechanism.

Coprecipitation of Antimony(V) with Iron(III) Hydroxide. The effect of the pH on the formation of antimony(V) oxide was examined prior to the coprecipitation study of the antimony(V)–iron(III) system. Antimony(V) must be precipitated as Sb_2O_5 in an acid medium when its concentration is higher than 2×10^{-4} mol dm^{-3}.[16] In reality, however, no precipitate appeared when solutions containing 8.2×10^{-4} mol dm^{-3} antimony(V) and 6×10^{-2} mol dm^{-3} chloride were allowed to stand for about 200 min at 25 °C after the pH had been adjusted to 0, 4, 10, and 12. It seems, then, that antimony(V) is present in the solution as chloro complexes, *e.g.*, $Sb(OH)_xCl_{6-x}$ ions (x=2—6).

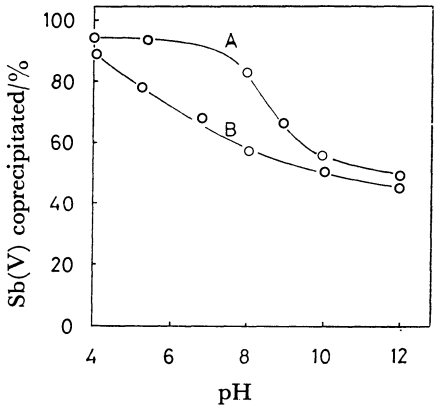

Fig. 4. Coprecipitation of antimony(V) with iron(III) hydroxide in the presence of chloride ion (A) 6×10^{-2} mol dm^{-3} and (B) 5.4×10^{-1} mol dm^{-3}.

In the antimony(V)–iron(III) system, however, antimony(V) was precipitated in the pH range shown in Fig. 4(A). These results indicate that antimony(V) is coprecipitated with iron(III) hydroxide. The coprecipitation of antimony(V) was affected by the concentration of the chloride ion, as is shown in Fig. 4 (A and B). With the increase in the chloride-ion concentration, the coprecipitation is prevented. The effect of the chloride ion may be attributed to the complex formation between antimony(V) and chloride ions, though the speciation of antimony is complicated at the present

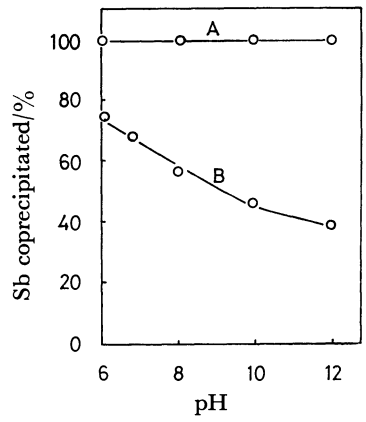

Fig. 5. Coprecipitation of antimony(III or V) with iron(III) hydroxide in artificial seawater (A) antimony(III) (B) antimony(V).

time[16,17] and further investigation will be required before we can infer the coprecipitation mechanism.

The Coprecipitation of Antimony(III or V) in Artificial Seawater. Coprecipitation behavior was studied in a mixture whose composition was similar to that of seawater with respect to inorganic anions, *i.e.*, 5.4×10^{-1} mol dm^{-3} chloride, 8.1×10^{-4} mol dm^{-3} bromide, 5.3×10^{-5} mol dm^{-3} fluoride, 3.2×10^{-7} mol dm^{-3} iodide, 2.8×10^{-2} mol dm^{-3} sulfate, 2.3×10^{-3} mol dm^{-3} carbonate, and 4.2×10^{-5} mol dm^{-3} borate ions. The results are shown as a function of the pH in Fig. 5. In the artificial seawater, antimony(III) was coprecipitated with iron(III) hydroxide more easily than antimony(V). At pH 8, for example, the concentration of antimony present in the solution was about 43 ppm (3.5×10^{-4} mol dm^{-3}) for antimony(V) and less than 0.05 ppm (4.1×10^{-7} mol dm^{-3}) for antimony(III). From these results, it may be said that, if the coprecipitation of antimony with iron(III) hydroxide occurs in seawater, antimony(III) will be coprecipitated more easily than antimony(V). The fact that antimony is mainly present in seawater as the quinquevalent state[18,19] is possibly ascribable to the difference in hydrolysis behavior between antimony(III) and antimony(V) described above.

Conclusion

The results described above indicate that the hydrolysis of antimony is a crucial step in the coprecipitation of antimony with iron(III) hydroxide. Antimony(III) is not coprecipitated with iron(III) hydroxide in the form of $Sb(OH)_4^-$ ion. The coprecipitation of antimony(V) is somewhat complicated when the chloride ion is present; therefore, further investigation will be required to elucidate the coprecipitation mechanism. The hydrolysis of antimony(III) is independent of the concentration of the chloride ion. The coprecipitation of antimony(III) is not affected by the chloride ion and takes place over a wide range of pH values. On the other hand, the coprecipitation of antimony(V) is affected not only by the pH, but also by the chloride-ion concentration. Accordingly, in seawater which contains

a large amount of chloride ion (*ca.* 5.4×10^{-1} mol dm^{-3}), antimony(III) may be coprecipitated with iron(III) hydroxide more easily than antimony(V).

The authors wish to acknowledge the assistance given by Mr. Yoshio Nishioka in the experimental work.

References

1) K. B. Krauskopf, *Geochim. Cosmochim. Acta.* **9**, 1 (1956).
2) E. G. Goldberg, "Oceanography," ACS, Washington, D. C. (1961), No. 67, p. 583.
3) R. C. Harris, *Nature*, **219**, 54 (1968).
4) R. R. Gadde and H. A. Laitinen, *Environ. Lett.*, **5**, 223 (1973).
5) R. R. Gadde and H. A. Laitinen, *Anal. Chem.*, **46**, 2022 (1974).
6) K. Sugawara, M. Tanaka, and S. Kanamori, *Bull. Chem. Soc. Jpn.*, **29**, 670 (1956).
7) R. Fukai and D. Vas, *J. Oceanog. Soc. Jpn.*, **23**, 298 (1967).
8) R. A. Lockwood and K. Y. Chen, *Environ. Lett.*, **6**, 151 (1974).
9) J. O. Leckie and R. O. James, "Aqueous-Environmental Chemistry of Metals," Ann Arbor Science Publishers, Ann Arbor, Mich. (1974), p. 1.
10) Y. Inoue and M. Munemori, *Environ. Sci. Technol.*, **13**, 443 (1979).
11) T. Fujinaga, M. Koyama, K. Izutsu, S. Himeno, and M. Kawashima, *Nippon Kagaku Kaishi*, **1974**, 1489.
12) J. E. Portman and J. P. Riley, *Anal. Chim. Acta*, **35**, 35 (1966).
13) Y. Inoue and M. Munemori, unpublished data.
14) L. G. Sillen and A. E. Martell, "Stability Constants of Metal Ion Complexes," Chem. Soc., London (1964), Spec. Publ. No. 17.
15) G. Charlot, "L'Analyse Qualitative et les Reaction en Solution," Masson et Cie, Paris (1963), p. 297.
16) C. F. Baes and R. E. Mesmer, "Hydrolysis of Cations," Interscience Publishers, New York (1976), p. 370.
17) H. M. Neumann, *J. Am. Chem. Soc.*, **76**, 2611 (1954).
18) S. Gohda, *Bull. Chem. Soc. Jpn.*, **48**, 1213 (1975).
19) P. G. Brewer, "Chemical Oceanography," 2nd ed, Academic Press, New York (1975), Vol. 1, p. 415.

An X-Ray Diffraction Study on the Structures of Bis- and Tris(ethylenediamine)cadmium(II) Complexes in Solution

Tadao FUJITA and Hitoshi OHTAKI*

Department of Electronic Chemistry, Tokyo Institute of Technology at Nagatsuta, Nagatsuta-cho, Midori-ku, Yokohama 227

(Received August 30, 1979)

The structures of cadmium(II) complexes with ethylenediamine(en) have been determined by means of X-ray diffraction. The measurements were performed at 25 °C for aqueous ethylenediamine solutions of cadmium nitrate, the mole ratios (en/Cd) in the solutions being 2.188 and 3.387. In the solution of the lower en/Cd mole ratio, the bis(ethylenediamine)cadmium(II) complex was predominant, whereas in the other solution the tris-(ethylenediamine)cadmium(II) complex was contained as the main species. From the analysis of the X-ray scattering data of the solutions, it was shown that in the bis-complex four nitrogen atoms within the two ethylenediamine molecules were tetrahedrally coordinated to the cadmium(II) ion at a distance of 2.339(4) Å. The nonbonding Cd···C distance within the bis-complex was also determined to be 3.04(1) Å. In the tris-complex the cadmium(II) ion was coordinated with six nitrogen atoms and the Cd–N and Cd···C distances were 2.371(5) and 3.19(1) Å, respectively. The strength of the Cd–N bond with changing coordination number of the complexes was discussed in terms of the frequencies of the Cd–N bond in the Raman spectra of these solutions and the bond lengths found from the X-ray scattering measurements.

In a previous paper,[1] the structures of the bis- and tris(ethylenediamine)zinc(II) complexes in solution have been investigated by the X-ray diffraction method. In the present study, we have attempted to determine the structures of the bis- and tris(ethylenediamine)-cadmium(II) complexes in aqueous nitrate solutions in a series of structural studies of chelate complexes of transition metals in solution. No crystallographic investigation of ethylenediamine complexes of cadmium-(II) has been reported so far.

Raman spectra of the test solutions were also studied for comparing the strength of the Cd–N bonds within the bis- and tris-complexes.

Experimental

Preparation and Analysis of Sample Solutions. Ethylenediamine was purified by the method previously described.[1] Cadmium(II) nitrate of reagent grade was purchased from Wako Pure Chemical Co., Osaka and was recrystallized twice from water. The sample solutions were prepared by dissolving cadmium(II) nitrate into aqueous ethylenediamine solution as in the similar way to that in the previous paper.[1]

Concentrations of cadmium(II) ions in the test solutions were determined by EDTA titration and electrogravimetry. The results of the two independent methods agreed each other within 0.2%. The concentration of the nitrate ion was determined from the stoichiometry of the cadmium nitrate. The density of the solutions was determined pychnometrically. The composition of the test solutions is given in Table 1.

TABLE 1. THE COMPOSITION (g-atom/dm³) AND THE STOICHIOMETRIC VOLUME V PER CADMIUM ATOM IN THE SOLUTIONS

	Solution	
	A	B
Cd	1.916	1.760
N	16.81	11.22
C	12.98	7.702
O	38.03	46.95
H	105.0	103.6
en/Cd	3.387	2.188
V/Å³	866.6	946.6
Density/g cm^{-3}	1.321	1.303

Method of Measurements and Treatment of X-Ray Scattering Data. The X-ray diffractometer used, the method of measurements and treatment of X-ray scattering data were the same as those described elsewhere.[1,2] Mo $K\alpha$ radiation (λ=0.7107 Å) was used for the measurements over the range $1°<\theta<70°$ (2θ is the scattering angle). The data were recorded twice over

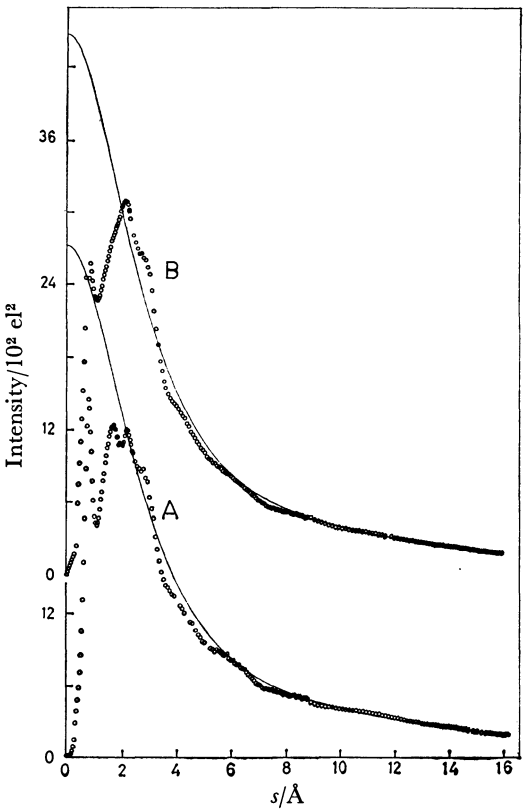

Fig. 1. Coherent scattering intensities of the sample solutions A and B. Experimentally obtained intensities I^{coh} are shown by circles and calculated independent scattering intensities by solid lines.

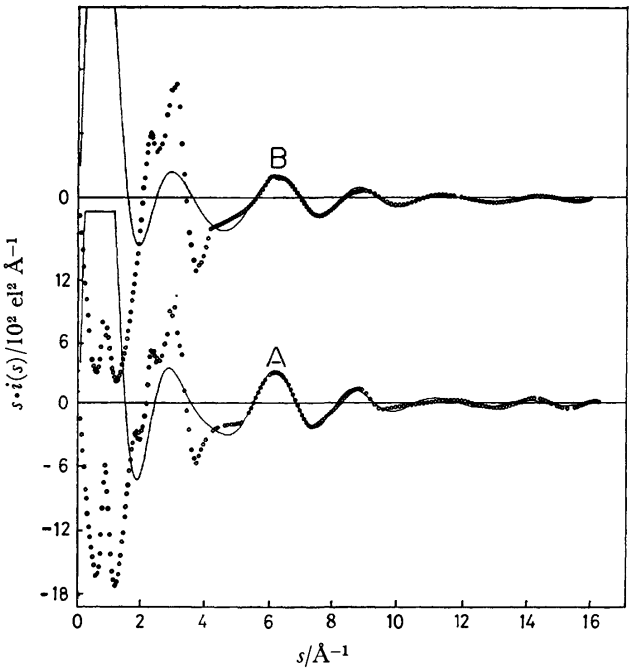

Fig. 2. The reduced intensities multiplied by s for solutions A and B. The observed $s \cdot i(s)$ curve is shown by circles and the calculated one by solid lines.

the whole angle range. The corrections and analysis of the scattering data were performed in the same ways as those in the previous papers.[1,2] Coherent intensities and reduced intensities multiplied by s of the test solutions are given in Figs. 1 and 2, respectively. The radial distribution function $D(r)$ was calculated by the usual method:

$$D(r) = 4\pi r^2\rho_0 + \frac{2r}{\pi}\int_0^{s_{max}} s \cdot i(s) \cdot M(s) \cdot \sin(sr)\mathrm{d}s, \quad (1)$$

where ρ_0 is the average scattering density in the stoichiometric volume V of the solution per cadmium atom, and s_{max} denotes the maximum s-value ($s = 4\pi\sin\theta/\lambda$) attained in the measurement ($s_{max} = 16.7$ Å^{-1}). $M(s)$ is the modification function, the function $[f_{Cd}(0)^2/f_{Cd}(s)^2] \cdot \exp(-0.01\, s^2)$ being chosen. The reduced intensities $i(s)$ are given by

$$i(s) = I^{coh}(s) - \sum_i n_i\{(f_i(s) + \Delta f_i')^2 + (\Delta f_i'')^2\}, \quad (2)$$

where n_i is the number of atom i and $f_i(s)$ denotes the scattering factor of atom i at s. $\Delta f_i'$ and $\Delta f_i''$ represent the real and imaginary parts of the anomalous dispersion, respectively. The radial distribution curve $D(r)$ of the solutions was drawn after the Fourier transform of the reduced intensity multiplied by s.

Results and Discussion

Solution A contains the tris(ethylenediamine)-cadmium(II) complex as the main species according to the formation constants so far reported.[3] In solution A, however, coexistence of the bis-complex may not be neglected. In solution B the bis(ethylenediamine)-cadmium(II) complex may be contained with a small amount of the tris-complex. Therefore, a successive approach of the analysis as described in the preceding paper[1] was employed in order to obtain the best fitted results for both radial distribution and reduced intensity curves of the test solutions.

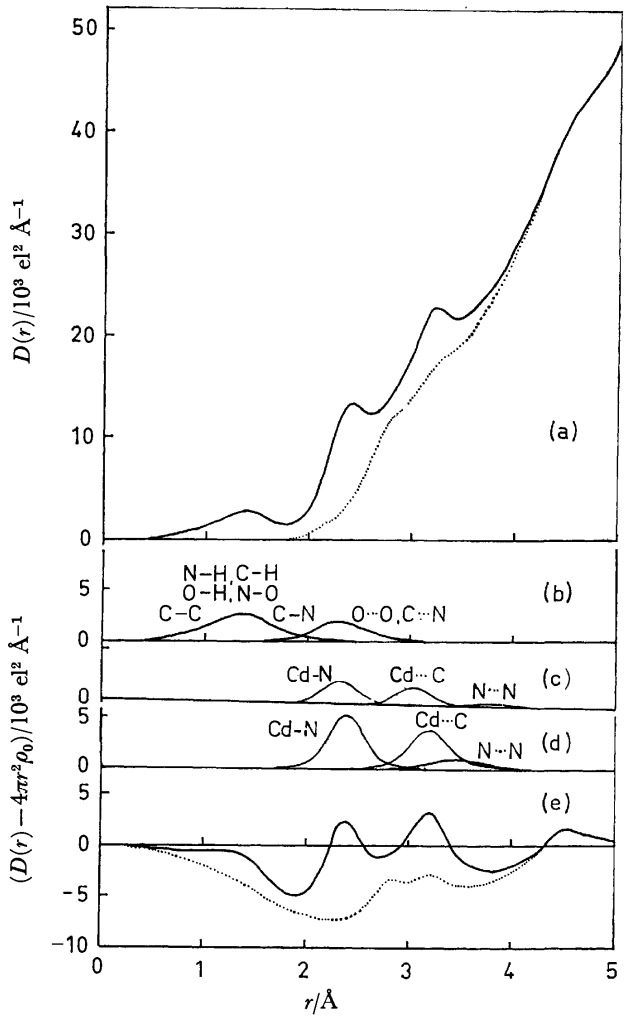

Fig. 3. (a) The radial distribution curve for solution A. (b) The theoretical peak shapes for the O–H bond within water, the N–H, C–H, C–C, C–N, and C···N pairs within an ethylenediamine molecule, and the N–O and O···O contacts within a nitrate ion. (c) The theoretical peak shapes for the Cd–N, Cd···C, and N···N pairs within the $Cd(en)_2^{2+}$ complex. (d) The theoretical peak shapes for the Cd–N, Cd···C and N···N interactions within the $Cd(en)_3^{2+}$ complex. (e) The corresponding $(D(r) - 4\pi r^2\rho_0)$ curve to the $D(r)$ in (a). The dotted lines in (a) and (e) show the residual radial and residual differential radial distribution curves, respectively, after subtraction of these theoretical peaks.

Solution A. The radial distribution curve of solution A showed four major peaks over the range 1—5 Å (Fig. 3a). A small peak at about 1.3 Å is composed of the peaks due to the O–H bond within water, the N–H, C–H, C–C and C–N bonds within an ethylenediamine molecule and the N–O bond within a nitrate ion (see Fig. 3b). The second peak appearing at 2.4 Å may be attributed to the interaction between a cadmium(II) ion and the nitrogen atoms of the ethylenediamine molecules coordinated to the central metal ion. The distances corresponding to the nonbonded C···N pairs within an ethylenediamine molecule and the O···O contacts within an NO_3^- ion may partly contribute to the peak. The third peak at 3.2 Å may be

ascribed to the nonbonded interactions between cadmium(II) ion and the carbon atoms within the ethylenediamine molecules coordinated. The broad peak at around 4—5 Å may include contributions from the relatively long range intermolecular interactions among the complexes, free ligands and solvent molecules, which we will not discuss in this paper. The temperature factors of atom pairs within water and ethylenediamine molecules and a nitrate ion used in this investigation were the same as those used in Ref. 1.

At a first approach, the Cd–N and Cd···C distances within the tris-complex were estimated from the radial distribution curve by assuming that the only tris-complex existed in the solution. The bond distances of 2.38 and 3.18 Å for the Cd–N and Cd···C interactions, respectively, were found, the temperature factor of the former bond being about 0.003 Å^2 and that of the latter 0.008—0.01 Å^2. The parameter values thus obtained for the tris-complex were inserted into the analytical procedure of determining the parameter values of the bis-complex in solution B. The procedure was continued until a smooth background of the radial distribution curve was obtained by assuming suitable concentrations of the bis- and tris-complexes in the solutions and parameter values of the former complex. The parameter values thus estimated for the both bis- and tris-complexes were again turned back to the calculation of the radial distribution curve of solution A in order to refine the values of the tris-complex at a fixed parameter values of the bis-complex and changing concentration ratio of the tris-complex to the bis-complex. The successive analyses were continued until no appreciable peak was left in the background of the radial distribution curves of the both solutions A and B. The values thus obtained were further refined by the least-squares method applied to the reduced intensities of the solutions.

Solution B. A successive approach for analyzing the radial distribution curve of solution B was employed as described in the previous section. The Cd–N and Cd···C distances within the bis-complex were estimated to be 2.35 and 3.05 Å, respectively (Fig. 4). The temperature factor of the former bond was about 0.003 Å^2, while that of the latter one was 0.006—0.008 Å^2.

A peak still remained at around 2.9—3.3 Å in the residual radial distribution curves of the both systems (dotted lines in Figs. 3 and 4) were attributed to the structures of bulk water and hydrated nitrate ions.[4]

Least-Squares Refinements. The parameter values (bond distance r, temperature factor b and frequency factor n) of the interactions in the models adopted were refined by comparing the observed $s \cdot i(s)$ curves with theoretical ones of solutions A and B at high angle regions. The refinements were carried out so as to obtain a minimum error-square sum $U=\sum s^2\{i_{obsd}(s)-i_{calcd}(s)\}^2$ by using the NLPLSQ program.[5] The s-region was varied in the calculations in order to avoid introduction of errors due to relatively long range intermolecular interactions, which mainly contribute to the intensity data at a low angle region, to the refined parameters.

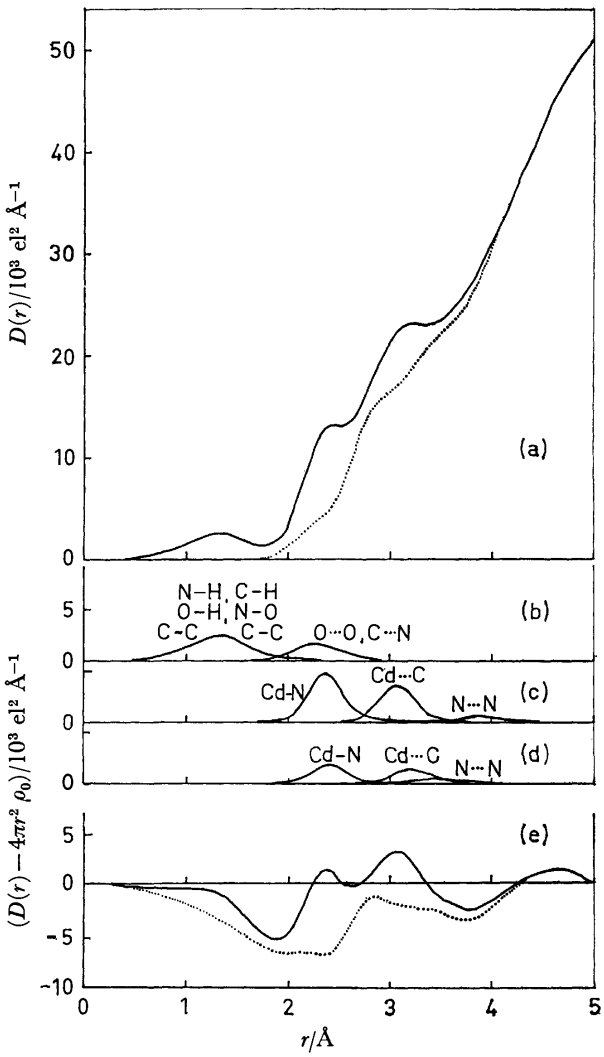

Fig. 4. (a) The radial distribution curve for solution B. (b) The theoretical peak shapes for the O–H bond within water, the N–H, C–H, C–C, C–N, and C···N pairs within an ethylenediamine molecule, and the N–O and O···O contacts within a nitrate ion. (c) The theoretical peak shapes for the Cd–N and Cd···C and N···N pairs within the $Cd(en)_2^{2+}$ complex. (d) The theoretical peak shapes for the Cd–N, Cd···C and N···N pairs within the $Cd(en)_3^{2+}$ complex. (e) The corresponding $(D(r)-4\pi r^2\rho_0)$ curve to the $D(r)$ in (a). The dotted lines in (a) and (e) show the residual radial and residual differential radial distribution curves, respectively, after subtraction of these theoretical peaks.

For the tris-complex the parameter values were refined with four ways (A-1, A-2, A-3, and A-4). In type A-1, fourteen parameter values (indicated by italic letters) listed in Table 2 were allowed to change simultaneously on the assumption of the tetrahedral structure of the bis-complex, which is confirmed as described later. In type A-2, an octahedral structure of the tris-complex was also assumed, that is, the frequency factor of the Cd–N and Cd···C interactions were fixed at 6 and the only bond distances and temperature factors of the models were refined. In both treatments, the frequency factors of the interactions within

TABLE 2. RESULTS OF THE LEAST-SQUARES REFINEMENTS OF SOLUTION A
The parameter values, r=distance (Å), b=temperature factor (Å^2) and n=number of distance per cadmium(II) atom were refined. Standard deviations are given in parentheses.

Interaction	Parameter	A-1	A-2	A-3	A-4
O···O(NO_3^-)	r	*2.19*(2)	*2.19*(2)	*2.20*(2)	*2.20*(2)
C···N(en)	r	*2.49*(5)	*2.48*(4)	*2.53*(4)	*2.53*(4)
Bis-complex					
Cd–N	r	*2.34*(1)	*2.33*(1)	*2.33*(1)	*2.33*(1)
	b	*0.0033*(6)	*0.0032*(5)	*0.0031*(5)	*0.0031*(5)
	n	4[a]	4[a]	4[a]	4[a]
N···N	r	*3.9*(4)	*3.8*(3)	3.80[a]	3.80[a]
	b	0.01[a,b]	0.01[a,b]	0.006[a]	0.006[a]
Cd···C	r	*3.03*(3)	*3.03*(3)	*3.02*(3)	*3.01*(3)
	b	*0.010*(2)	*0.012*(2)	*0.009*(1)	*0.009*(1)
	n	4[a]	4[a]	4[a]	4[a]
Tris-complex					
Cd–N	r	*2.378*(6)	*2.371*(4)	*2.371*(5)	*2.371*(5)
	b	*0.0032*(3)	*0.0033*(2)	*0.0031*(5)	*0.0031*(5)
	n	*5.94*(9)	6[a]	*6.0*(1)	6[a]
N···N	r	*3.32*(9)	*3.44*(9)	3.35[a]	3.35[a]
	b	0.01[a,b]	0.01[a,b]	0.006[a]	0.006[a]
Cd···C	r	*3.17*(2)	*3.18*(2)	*3.18*(1)	*3.19*(1)
	b	*0.0098*(7)	0.01[a]	*0.0074*(6)	*0.0075*(5)
	n	*6.0*(2)	6[a]	*5.6*(2)	6[a]

a) Fixed. b) Y. Yokozeki and K. Kuchitsu, *Bull. Chem. Soc. Jpn.*, **44**, 2926 (1971).

the bis-complex were fixed and the temperature factors of the N···N interactions within both bis- and tris-complexes were held constant at 0.01 Å^2, which was obtained in the gas phase. Beside A-2, various attempts were made for the sets of the parameters with descretely changing temperature factors of the N···N interactions of the complexes over the range $b_{N...N}$ from 0.01 to 0.006 Å^2 (twice of the $b_{Cd...N}$ value). However, no appreciable change for all parameter values was found, typical results being shown in A-3 and A-4 of Table 2. In these treatments $r_{N...N}$ and $b_{N...N}$ of the bis- and tris-complexes were fixed and $n_{Cd...C}$ of the tris-complex was varied in A-3, while $n_{Cd...C}$ of the tris-complex was fixed at 6 in A-4. Thus, it was found that the temperature factor of the N···N interactions within the complexes were insensitive to the parameter values given in Table 2. The parameter values were not practically influenced by changing s_{min} from 4.5 to 7.0 Å^{-1} (s_{max} was 16.7 Å^{-1}).

Similar treatments were examined for evaluating parameter values of the bis-complex. Thus, for solution B four types of the refinement (B-1, B-2, B-3, and B-4 in Table 3) were carried out. In types B-1 and B-3, the frequency factors of the Cd–N and nonbonding Cd···C interactions, as well as other parameter values indicated by italic, were refined. In types B-2 and B-4, on the other hand, a tetrahedral structure of the bis-complex was assumed. In B-1 and B-2, the temperature

TABLE 3. RESULTS OF THE LEAST-SQUARES REFINEMENTS OF SOLUTION B
The parameter values, r=distance (Å), b=temperature factor (Å^2) and n=number of distance per cadmium(II) atom were refined. Standard deviations are given in parentheses.

Interaction	Parameter	B-1	B-2	B-3	B-4
O···O(NO_3^-)	r	*2.17*(1)	*2.18*(2)	*2.17*(2)	*2.18*(2)
C···N(en)	r	*2.50*(4)	*2.54*(7)	*2.56*(5)	*2.57*(5)
Bis-complex					
Cd–N	r	*2.341*(3)	*2.341*(5)	*2.338*(4)	*2.339*(4)
	b	*0.0032*(1)	*0.0032*(3)	*0.0034*(2)	*0.0034*(2)
	n	*3.98*(4)	4[a]	*3.97*(5)	4[a]
N···N	r	*3.7*(1)	*3.6*(1)	3.82[a]	3.82[a]
	b	0.01[a,b]	0.01[a,b]	0.006[a]	0.006[a]
Cd···C	r	*3.05*(1)	*3.04*(1)	*3.04*(1)	*3.04*(1)
	b	*0.0067*(3)	*0.007*(1)	0.007[a]	0.007[a]
	n	*3.88*(7)	4[a]	*3.79*(9)	4[a]

a) Fixed. b) Y. Yokozeki and K. Kuchitsu, *Bull. Chem. Soc. Jpn.*, **44**, 2926 (1971).

factor of the N···N interaction within the bis-complex was assumed to be 0.01 Å^2, whereas the value was fixed at 0.006 Å^2 in the treatments of B-3 and B-4. In these four refinements, all of the parameter values of the tris-complex were fixed, because the concentration of the tris-complex was so low compared with that of the bis-complex that a reasonable refinement of the parameter values of the tris-complex could not be achieved by the least-squares method for the reduced intensities of the solution. Therefore, the parameter values of the tris-complex determined in the previous section were used in these calculations. In the refinement of the values of solution A, however, the parameter values of the bis-complex were also optimized, together with those of the tris-complex, since the concentration of the bis-complex was about 30 mol%.

The results obtained by these refinements obviously exclude the existence of the octahedral $Cd(OH_2)_2(en)_2^{2+}$ complex as the bis-species. If the $Cd(OH_2)_2(en)_2^{2+}$ complex would form, instead of $Cd(en)_2^{2+}$, the frequency factor for the Cd–N interaction within the bis-complex would be optimized to 6 in the treatments of B-1 and B-3, because the Cd–O bond would not be clearly distinguished from the Cd–N bond by the present measurements. When we fixed the n_{Cd-N} values of the bis-complex at 6, a fairly large error-square sum was resulted compared with that of B-4 in which n_{Cd-N} was fixed at 4. Moreover, the n_{Cd-N} value of the bis-complex tended to decrease and approached 4 in the course of the least-squares refinement of the $s \cdot i(s)$ values. Therefore, we concluded that the formation of the $Cd(en)_2^{2+}$ complex of a tetrahedral structure was confirmed and the existence of the $Cd(OH_2)_2(en)_2^{2+}$ was excluded. The parameter values listed in Table 3 were practically independent of varying s-regions from 5.0, 6.0, and 7.0 to 16.7 Å^{-1}. Since almost the same parameter values were obtained for the bis-complex regardless of the assumptions set for the calculations in the both solutions, the pre-assumption of $n_{Cd-N}=4$ for the bis-complex made in the treatment of solution A was confirmed as a reasonable one.

The observed intensities were compared with the calculated ones by using parameter values given in Tables 2 (A-2) and 3 (B-2) and Eq. 3:

$$i_{calcd}(s) = \sum\sum n_{ij}\{(f_i(s)+\Delta f_i')(f_j(s)+\Delta f_j') + (\Delta f_i'')(\Delta f_j'')\} \cdot \frac{\sin(r_{ij}s)}{(r_{ij}s)} \exp(-b_{ij}s^2). \quad (3)$$

A reasonable agreement was found for both curves A and B in Fig. 2 except at the low angle part of the intensity curves where long range intermolecular interactions significantly contribute to the curves.

In the bis- and tris(ethylenediamine)zinc(II) complexes,[1] the Zn–N bond of the former complex is shorter than that of the latter, as is expected from the smaller crystal ionic radius of zinc(II) ion within a complex of a tetrahedral structure than that of an octahedral one. In crystal the ionic radius of cadmium(II) ion having the coordination number 4 is also smaller than that of the coordination number 6.[6] However, in cadmium(II) iodide complexes in solution, we have found that the Cd–I bond distance within the distorted octahedral $CdI(H_2O)_5^+$ complex does not appreciably change by replacing the five water molecules to three iodide ions to form the tetrahedral CdI_4^{2-} complex.[2,7] In the case of cadmium ethylenediamine complexes, the change in the Cd–N bond distance with changing coordination number of the cadmium(II) ion was only a few hundredths ångstroms, which is much smaller than the difference of the bond length in the crystalline state.[6] The distance of the Cd–NH_3 bond within the $Cd(NH_3)_6^{2+}$ complex is also 2.37 Å.[8]

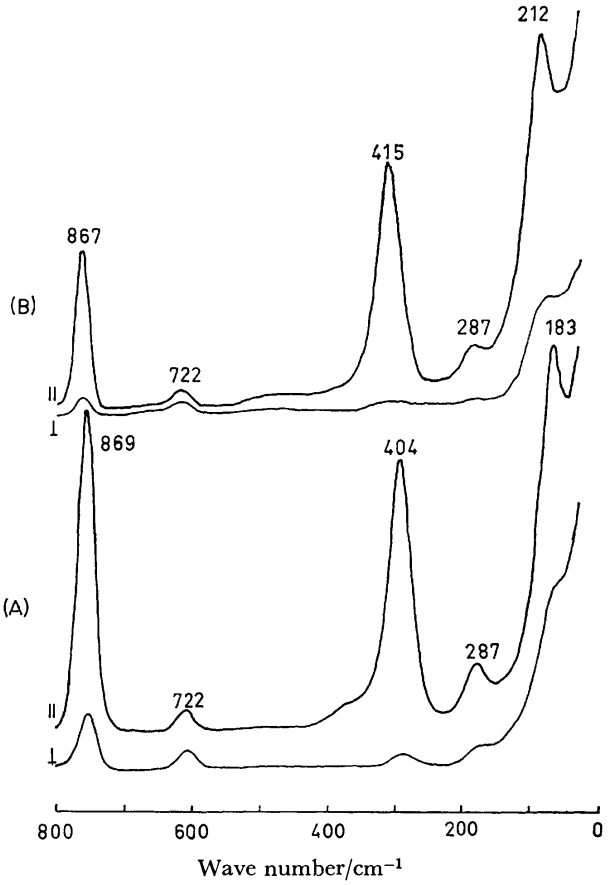

Fig. 5. Raman spectra of solutions A and B. The lines are the components parallel(∥) and perpendicular (⊥) to the direction of polarization of the incident light.

Raman Spectra of Solutions A and B. Krishnan and Plane[9] reported Raman spectra of the tris(ethylenediamine)cadmium(II) complex in an aqueous solution and assigned the line at 400 cm^{-1} to the totally symmetric Cd–N stretching vibration of the tris-complex. In solution A in this study we found a strongly polarized band at 404 cm^{-1} (Fig. 5). Another strong line observed at 869 cm^{-1} was ascribed to the CH_2 rocking vibration within ethylenediamine molecules.[10] A weak band at 722 cm^{-1} was assigned to the ν_4-vibration of nitrate ions. Some lines found in the region 170—300 cm^{-1} were not assignable. Krishnan and Plane[9] observed a line at 435 cm^{-1}, which was assigned to the totally symmetric Cd–N stretching for the bis(ethylenediamine)cadmium(II) complex. However, in solution B we found a strongly polarized band at 415 cm^{-1} which might be ascribed to the totally symmetric Cd–N stretching of the

bis-complex. The band of the bis-complex shifted by only 11 cm^{-1} to the higher frequency compared with that of the tris-complex. The bands appearing at 722 and 867 cm^{-1} were assignable to the nitrate ν_4 and CH_2 rocking vibrations, respectively.

The difference of the frequencies of the Cd–N stretching of the bis- and tris-complexes was small in contrast to the case of the zinc(II) ethylenediamine complexes.[1] The Cd–N bond distances within the bis-complex was almost the same as that of the tris-complex, whereas in the zinc(II) system the Zn–N bond length within the bis(ethylenediamine)zinc(II) complex was much shorter than that within the tris(ethylenediamine)zinc(II) complex, and the shorter Zn–N bond having a higher frequency within the bis-complex was concluded to be stronger than the longer Zn–N bond with lower frequency within the tris-complex, as described in the preceding paper.[1] In the case of cadmium ethylenediamine complexes, however, strength of the Cd–N bonds within the bis- and tris-complexes may not be appreciably different, because the lengths of the Cd–N bonds within the both complexes are practically the same and the shift of the frequency of the stretching vibration of the Cd–N bond within these complexes by changing their structures was small.

The Cd–N stretching vibration of the $Cd(NH_3)_6^{2+}$ complex appears at 341 cm^{-1},[8] which is lower than that of the tris-complex by about 63 cm^{-1}. The Cd–N bond distances within the hexaamminecadmium(II) and the tris-complexes are not significantly different, however. The higher frequency of the Cd–N stretching of the ethylenediamine complex may be due to coordination of a less freely movable amino group, which is attached to a CH_2 group, to the central metal ion, and the strength of the Cd–N bond within the $Cd(en)_3^{2+}$ and $Cd(NH_3)_6^{2+}$ complexes may be almost identical, because the enthalpy changes of the formation of the tris-complex ($\Delta H^\circ \simeq -84$ kJ mol^{-1}) is essentially the same as that of the hexaamminecadmium(II) complex ($\Delta H^\circ \simeq -88$ kJ mol^{-1}).[11]

The present work has been partially supported by a Grant-in-Aid for Scientific Research from the Ministry of Education.

References

1) T. Fujita, T. Yamaguchi, and H. Ohtaki, *Bull. Chem. Soc. Jpn.*, **52**, 3539 (1979).
2) H. Ohtaki, M. Maeda, and S. Ito, *Bull. Chem. Soc. Jpn.*, **47**, 2217 (1974).
3) L. G. Sillén and A. E. Martell, "Stability Constants," Spec. Publ. No. 17 and Supplement No. 1, Spec. Publ. No. 25, The Chemical Soc. London (1964) and (1971).
4) R. Caminiti, G. Licheri, G. Piccaluga, and G. Pinna, *J. Chem. Phys.*, **68**, 1967 (1978).
5) G. Johanson and M. Sandstöm, *Chem. Scripta*, **4**, 195 (1973); H. Ohtaki, T. Yamaguchi, and M. Maeda, *Bull. Chem. Soc. Jpn.*, **49**, 701 (1976).
6) R. D. Shannon, *Acta Crystallogr., Sect. A*, **1976**, 751.
7) M. Tsurumi, M. Maeda, and H. Ohtaki, *Denki Kagaku*, **45**, 367 (1977).
8) T. Yamaguchi and H. Ohtaki, *Bull. Chem. Soc. Jpn.*, **52**, 1223 (1979).
9) K. Krishnan and R. A. Plane, *Inorg. Chem.*, **5**, 852 (1966).
10) Y. Omura and T. Shimanouchi, *J. Mol. Spectrosc.*, **55**, 430; **57**, 480 (1975).
11) A. E. Martell and R. M. Smith, "Critical Stability Constants," Plenum (1974), Vol. 1; R. M. Smith and A. E. Martell, "Critical Stability Constants," Plenum (1975), Vol. 2.

ECE Mechanism as a Tool for the Investigation of Unstable Metal Complexes. II. Current-Potential Characteristics for the Reversible Deposition of an Insoluble Species: Case of Electrochemical Reduction of *trans*-Dibromobis-(ethylenediamine)cobalt(III) Complexes

Akifumi YAMADA,* Tadatsugu YOSHIKUNI, Yoshikiyo KATO, and Nobuyuki TANAKA
Department of Chemistry, Faculty of Science, Tohoku University, Sendai 980
(Received September 6, 1979)

Theoretical relations were derived for the ECE mechanism involving the reversible deposition of an insoluble species at constant potential (potentiostatic method). Assuming that the activity of deposit becomes equal to unity immediately after the beginning of electrolysis, current-potential relations were obtained for the case in which the first electron transfer step is irreversible and the second one, reversible. The method was used to study the acid hydrolysis of bivalent cobalt complex in the reduction of *trans*-dibromobis(ethylenediamine)cobalt(III) complex. The measurement made at 5 °C in 0.1 M acetate buffer solutions (pH 4.8) gave 0.4 s^{-1} for the acid hydrolysis of *trans*-dibromobis(ethylenediamine)cobalt(II) which was produced by the reduction of cobalt(III) complex.

The ECE electrode reaction mechanism[1] has attracted attention in recent years in both theoretical and experimental fields. Theoretical studies have been carried out for electrochemical methods such as chronopotentiometry, potential step chronoamperometry, cyclic voltammetry, a.c. polarography, and d.c. polarography.[2]

Although experimental studies were carried out for the ECE electrode reaction of organic substances, only a few examples have been reported in inorganic electrochemistry.[3–11] In previous chronopotentiometric[8,9] and polarographic[7,10] studies, the rate constant of the complex-forming reaction for ethylenediaminetetraacetate and chromium(II) (electrochemically produced from chromium(III) complex) was successfully determined. The results have confirmed that the concept of ECE mechanism is useful for the study of an unstable intermediate electrochemically generated.

A test of the electrode reaction of cobalt(III) complexes revealed that the ECE mechanism involving reversible deposition of an insoluble species proceeds with complexes having ligands such as Cl^-, Br^-, and I^-. This was also pointed out by Vlček.[4] For example, the mechanism can be observed by the reduction of *trans*-dibromobis(ethylenediamine)cobalt(III) complex at the mercury electrode. When the cobalt(III) complex is reduced to cobalt(II), the cobalt(II) complex liberates bromide ions because of its lability. The electrochemically generated bromide ions are easily oxidized at the electrode to form insoluble mercury(I) bromide as long as the potential is positive. This series of electrode reaction takes place through the following electrode process:[12]

$$\textit{trans}\text{-}[CoBr_2(en)_2]^+ + e^- \longrightarrow \textit{trans}\text{-}[CoBr_2(en)_2], \quad (1)$$

$$\textit{trans}\text{-}[CoBr_2(en)_2] + 6H_2O \longrightarrow [Co(H_2O)_6]^{2+} + 2Br^- + 2en, \quad (2)$$

$$2Br^- + 2Hg \longrightarrow Hg_2Br_2 + 2e^-. \quad (3)$$

In this process, electrolytic deposition of an insoluble species is encountered. In order to include the reversible deposition of an insoluble species, an extension of the theory of the potentiostatic method for ECE mechanism seems necessary. This paper presents such an extension.

Experimental data were obtained for the potentiostatic reduction of *trans*-dibromobis(ethylenediamine)cobalt-(III) complex. The current-potential curves were compared with simulated ones. Calculation was made on the rate constant of the acid hydrolysis reaction of *trans*-dibromobis(ethylenediamine)cobalt(II) produced by the first electron transfer step.

Theoretical

ECE electrode reaction mechanism for many soluble species have been widely studied in the past,[1–11] but few quantitative analyses can be found for the ECE mechanism involving the reversible deposition of an insoluble species. This is understandable because of the inherent difficulty: the activity of the deposit cannot usually be known before the electrode becomes completely covered with at least a monolayer of deposit. In view of this we have considered a case in which it can be assumed that the activity of the deposit becomes equal to unity immediately after the beginning of electrolysis. For the sake of convenience, we describe the case which the first electron transfer step is irreversible and the second one reversible. This is the case for *trans*-$[CoBr_2(en)_2]^+$, and appears to be fairly general for ECE mechanism of halogenocobalt(III) complexes.[12]

The chronoamperometric technique applied to the analysis of the ECE mechanism has been described in detail by Alberts and Shain.[13] The boundary value problem for the electrode reaction

$$A + n_1e \xrightarrow{k_c} B \quad (4)$$

$$B \xrightarrow{l} C \quad (5)$$

$$C + n_2e \overset{E_0}{\rightleftharpoons} D \text{ (insoluble)} \quad (6)$$

is similar to that used by them, although specific boundary conditions are somewhat different. Here, A, B, C, and D represent the species, k_c is the heterogeneous rate constant, l the homogeneous rate constant, E_0 the standard potential of Reaction 6, and $n_j (j=1, 2)$ the number of electrons involved in the j-th electro-

chemical reaction: $n_j<0$ and $n_j>0$ correspond to reduction and oxidation, respectively. A, B, and C are soluble, and D is insoluble.

Assuming a linear diffusion, Fick's second law gives

$$\frac{\partial c_A}{\partial t} = D_A\left(\frac{\partial^2 c_A}{\partial x^2}\right), \tag{7}$$

$$\frac{\partial c_B}{\partial t} = D_B\left(\frac{\partial^2 c_B}{\partial x^2}\right) - lc_B, \tag{8}$$

$$\frac{\partial c_C}{\partial t} = D_C\left(\frac{\partial^2 c_C}{\partial x^2}\right) + lc_B, \tag{9}$$

where c and D are the concentration and diffusion coefficients, respectively, of a species indicated by subscripts, x is the distance from the electrode, and t the time.

The initial and boundary conditions are:

$$t = 0,\ x \geq 0:\ c_A = c^\circ,\ c_B = c_C = 0 \tag{10}$$

$$t \geq 0,\ x \to \infty:\ c_A = c^\circ,\ c_B, c_C \to 0 \tag{11}$$

$$t > 0,\ x = 0:$$

$$D_A\left(\frac{\partial c_A}{\partial x}\right)_{x=0} + D_B\left(\frac{\partial c_B}{\partial x}\right)_{x=0} = 0, \tag{12}$$

$$D_A\left(\frac{\partial c_A}{\partial x}\right)_{x=0} = k_c(c_A)_{x=0}, \tag{13}$$

$$(c_C)_{x=0} = \exp\left[\frac{n_2 F}{RT}(E - E_0)\right] = \theta, \tag{14}$$

where c° is the bulk concentration of A. Equation 14 represents a reversible deposition of the insoluble species D whose activity is assumed to be unity.

The equation for the total current is given by

$$I = Fq\left[n_1 D_A\left(\frac{\partial c_A}{\partial x}\right)_{x=0} + n_2 D_C\left(\frac{\partial c_C}{\partial x}\right)_{x=0}\right], \tag{15}$$

where F is the Faraday constant and q the electrode area. In this equation, anodic current is positive and cathodic current negative. This boundary value problem can be solved by means of the Laplace transform. The result is

$$\frac{I}{I_d} = \lambda\sqrt{\pi t}\exp(\lambda^2 t)\operatorname{erfc}(\lambda\sqrt{t}) - \frac{n_2}{n_1}\left(\frac{\theta}{c^\circ\sqrt{D_A/D_C}}\right) + \frac{n_2}{n_1}\left(\frac{D_C l}{D_C - D_B}\right)\lambda\sqrt{\pi t}\left[\exp(\lambda^2 t)\operatorname{erfc}(\lambda\sqrt{t}) * \exp\left(-\frac{D_C l t}{D_C - D_B}\right)\right] - \frac{n_2}{n_1}\sqrt{\frac{D_B}{D_C}}\left(\frac{D_C l}{D_C - D_B}\right)\lambda\sqrt{\pi t} \times\left[\frac{\exp(-lt)}{\sqrt{\pi t}} * \left\{\frac{1}{\sqrt{\pi t}} - \lambda\exp(\lambda^2 t)\operatorname{erfc}(\lambda\sqrt{t})\right\} * \exp\left(-\frac{D_C l t}{D_C - D_B}\right)\right], \tag{16}$$

with

$$\lambda = \frac{k_c^\circ}{\sqrt{D_A}}\exp\left[-\frac{\alpha n F}{RT}E\right] = \frac{k_c}{\sqrt{D_A}}, \tag{17}$$

$$I_d = \frac{n_1 F q^\circ\sqrt{D_A c}}{\sqrt{\pi t}}, \tag{18}$$

where k_c° is the heterogeneous rate constant at $E=0$ and α the transfer coefficient. The symbol * represents the convolution.

It is evident from Eq. 16 that the current is stable when $D_C \geqq D_B$ but unstable or divergent when $D_C < D_B$. If $D_C < D_B$, peculiar phenomena might develop with time such as relaxational oscillations and jumps.

If Reaction 5 proceeds very rapidly and the condition $(D_C/D_B)\exp(lt) \gg 1$ is fulfilled, Eq. 16 is reduced to

$$\frac{I}{I_d} = \left(1 + \frac{n_2}{n_1}\right)\lambda\sqrt{\pi t}\exp(\lambda^2 t)\operatorname{erfc}(\lambda\sqrt{t}) - \frac{n_2}{n_1}\left(\frac{\theta}{c^\circ\sqrt{D_A/D_C}}\right) - \frac{n_2}{n_1}\sqrt{\frac{D_B}{D_C}}\lambda\sqrt{\pi t}\int_0^t \frac{\exp[-l(t-u)]}{\sqrt{\pi(t-u)}} \times\left(\frac{1}{\sqrt{\pi u}} - \lambda\exp(\lambda^2 u)\operatorname{erfc}(\lambda\sqrt{u})\right)du. \tag{19}$$

If $lt \gg 1$, Eq. 19 can be further simplified to

$$\frac{I}{I_d} = \left(1 + \frac{n_2}{n_1}\right)\lambda\sqrt{\pi t}\exp(\lambda^2 t)\operatorname{erfc}(\lambda\sqrt{t}) - \frac{n_2}{n_1}\left(\frac{\theta}{c^\circ\sqrt{D_A/D_C}}\right) - \frac{n_2}{n_1}\sqrt{\frac{D_B}{D_C}}\frac{\lambda}{\sqrt{l}} \times\left[\frac{1}{\sqrt{\pi t}} - \lambda\exp(\lambda^2 t)\operatorname{erfc}(\lambda\sqrt{t})\right]. \tag{20}$$

Equation 16 was solved numerically by the integral method of Gauss (Appendix). As expected, the computer results agree with the approximation given by Eq. 20 when the rate constant is large.

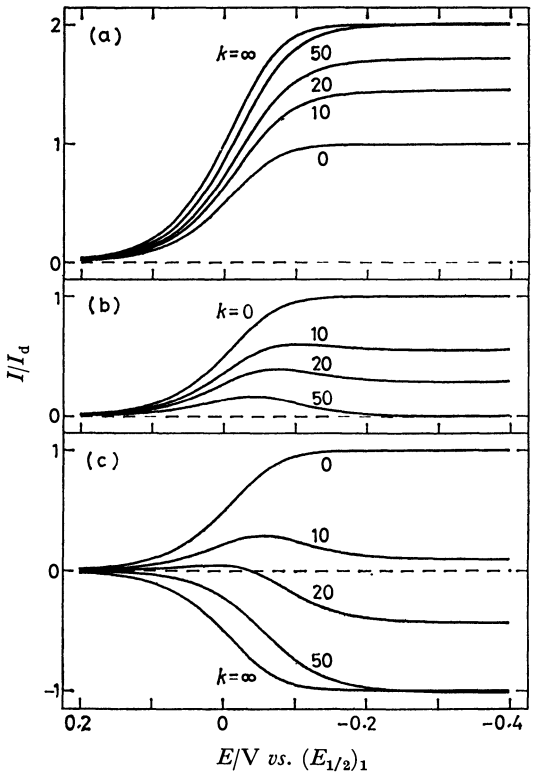

Fig. 1. Examples of predicted effects of homogeneous reaction rate on the current-potential curve for the consecutive ECE pathway (a) and the parallel ECE pathway (b, c).
Half-wave potential ($E_{1/2}$) and number of electrons (n) are: $(E_{1/2})_1 = 0$ V, $(E_{1/2})_2 = +0.5$ V, $n_1 = -1$, $n_2 = -1$ for curve (a); $(E_{1/2})_1 = 0$ V, $(E_{1/2})_2 = -0.5$ V, $n_1 = -1$, $n_2 = +1$ for curve (b); and $(E_{1/2})_1 = 0$ V, $(E_{1/2})_2 = -0.5$ V, $n_1 = -1$, $n_2 = +2$ for curve (c). Other parameter values are: $T = 25$ °C, $t = 0.05$ s, $\alpha = 0.5$, $D_A = B_B = 5 \times 10^{-6}$ cm^2 s^{-1}, $D_C = 10 \times 10^{-6}$ cm^2 s^{-1}. Homogeneous rate constants (in s^{-1}) are shown in figures.

According to Ruzic *et al.*[2] the ECE mechanism can be classified into a consecutive ECE pathway and a parallel one, the former dealing with the case where both heterogeneous steps are of the same type ($n_1n_2>0$), and the latter with heterogeneous electrode processes operating in the opposite direction ($n_1n_2<0$). Examples of the current-potential curve at various chemical reaction rates are shown in Fig. 1 for some interesting cases. Increase in current with increasing chemical reaction rate is seen for the consecutive ECE pathway (Fig. 1(a)), and decrease in current for the parallel ECE pathway (Fig. 1(b, c)). For a sufficiently fast chemical reaction the limiting current is diffusion-controlled for $n_1+n_2\neq 0$, but the net current is zero for $n_1+n_2=0$. This is a special case of parallel ECE pathway. Examples for $n_1+n_2=0$ are known for the electrode reaction of some chromium[6-10] and cobalt[3] complexes, though these are of soluble species.

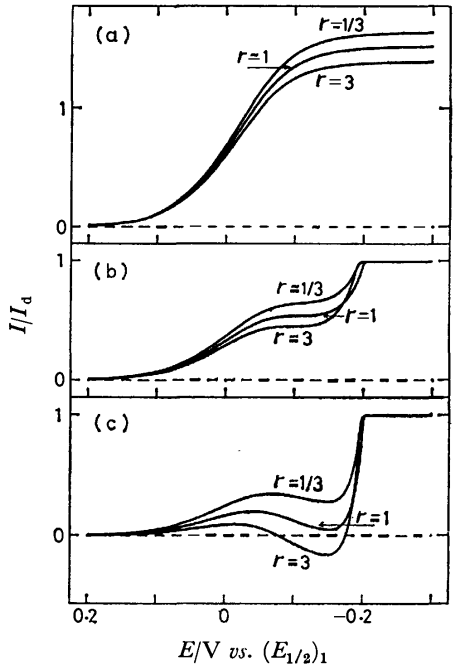

Fig. 2. Examples of predicted effects of the diffusion coefficient on current-potential curve for the consecutive ECE pathway (a) and the parallel ECE pathway (b, c). Ratios of diffusion coefficients of B and C (r) are shown in figures. Notation and parameter values are: $D_A=D_B=5\times10^{-6}$ cm^2 s^{-1}, $(E_{1/2})_1=0$ V, $l=15$ s^{-1}, $T=25$ °C, $t=0.05$ s, $\alpha=0.5$, $(E_{1/2})_2=+0.2$ V (a), -0.2 V (b, c). Number of electrons (n) are same as Fig. 1.

Figure 2 shows examples of the current-potential curve at different diffusion coefficients, calculated for the case of $D_B>D_C$, $D_B=D_C$, and $D_B<D_C$ when $D_A=D_B$. The effect of the diffusion coefficient on the current-potential curve dose not seem to be very small.

The current-potential curve should exhibit either one or two waves according to the difference in the half-wave potential of electrode reactions 1 and 3. This is shown clearly in Fig. 3, which depicts the current-potential curves with fast homogeneous chemical reactions.

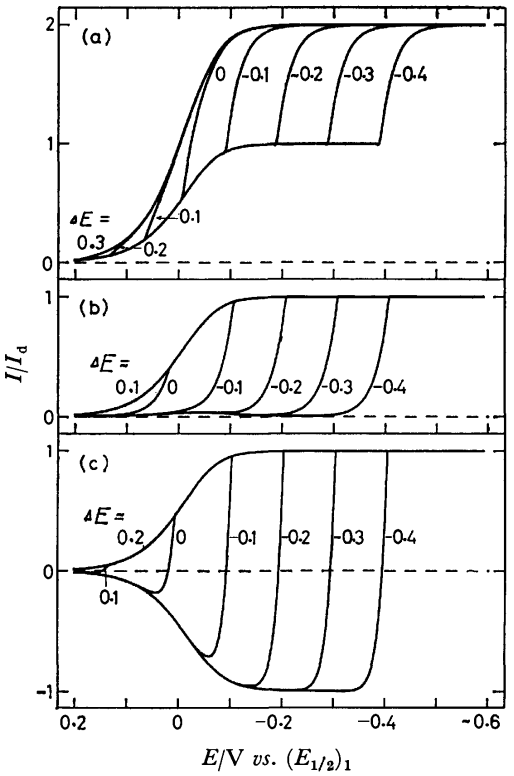

Fig. 3. Examples of predicted effects of the difference of half-wave potential corresponding to first and second electron-transfer steps on resolution of the current-potential curve for the consecutive ECE pathway (a) and the parallel ECE pathway (b, c). Potential differences ($\Delta E=(E_{1/2})_2-(E_{1/2})_1$) are shown in figures. Notation and parameter values are: $D_A=D_B=5\times10^{-6}$ cm^2 s^{-1}, $D_C=10\times10^{-6}$ cm^2 s^{-1}, $(E_{1/2})_1=0$ V, $l=100$ s^{-1}, $T=25$ °C, $t=0.05$ s, $\alpha=0.5$. Number of electrons (n) are same as Fig. 1.

When the two half-wave potentials are sufficiently separated with substance C which is more difficult to be reduced than A, the current-potential curve exhibits two waves (Fig. 3(a)). In this case, the current corresponding to the first wave represents the reduction of A only, depending on the kinetic parameters of the electrode reaction 1. The second wave is affected strongly by variation in the rate constant of chemical reaction 3. The current increases suddenly from the first wave, decreasing gradually after the diffusion current is reached.

When substance C is oxidized at a less positive potential than the reduction potential of substance A the cutoff of the first wave occurs: the decrease in current is pronounced with the increase in the rate of chemical reaction 2 (Fig. 3(b, c)). With $n_1+n_2=0$, the wave starts from the base line, increasing gradually. Theoretically, the slope of the current-potential curve should be infinite at the point where the current becomes diffusion-controlled. In the case $n_1+n_2>0$, the current starts from the anodic portion, increasing gradually. Then it decreases, crossing the zero current line. The final current is cathodic and controlled by Reaction 1. The shape of the current-potential curve is also angular at the beginning of the diffusion plateau.

Experimental

The current-potential curve were recorded with a Fuso Model 312 polarograph using a Watanabe Model WX441 x-y recorder. A three-electrode cell equipped with a saturated calomel reference electrode(SCE) and a platinum wire electrode(counter electrode) were employed. A junction of 0.1 M(1 M= 1 mol dm^{-3}) $NaNO_3$ was used between the SCE and the solution in order to avoid chloride contamination. A dropping mercury electrode (flow rate 1.17 mg s^{-1}, drop time 3.97 s in 0.1 M acetate buffer solutions) was used as a working electrode.

The complex used was prepared according to the procedure of Werner *et al.*[14] and identified by elemental analysis. A small amount of gelatin was added as a maximum suppressor.

Results and Discussion

Current-Potential Behavior. Figure 4 shows the current-potential curves of 0.5 mM *trans*-$[CoBr_2(en)_2]NO_3$ and 0.5 mM KBr obtained in 0.1 M acetate buffer solution at 25 °C. As expected from the electrode reaction of other cobalt(III) complexes,[15] *trans*-$[CoBr_2(en)_2]^+$ gave two polarographic waves, the first corresponding to the reduction of Co(III) to Co(II) and the second to the reduction of Co(II) to Co(0).

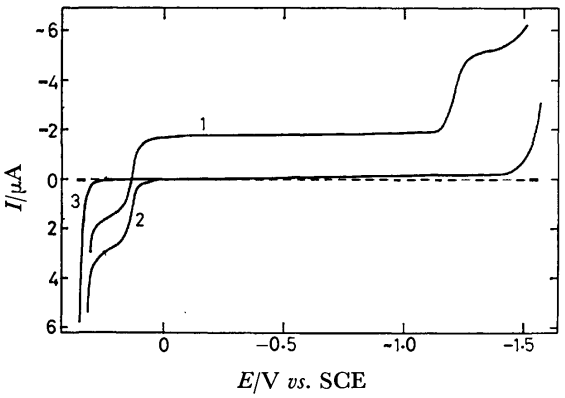

Fig. 4. Current-potential curves of (1) 0.5 mM *trans*-$[CoBr_2(en)_2]NO_3$ and (2) 0.5 mM KBr obtained in (3) 0.1 mM acetate buffer solutions containing 0.005% gelatin at 25 °C.

The first wave appears partly above and partly below the zero current line on the polarogram in Fig. 4. The cathodic limiting current of the first wave was diffusion-controlled and proportional to the concentration of the complex. The anodic limiting current of the first wave was also diffusion-controlled. The diffusion coefficients of the complex and Br^- ions were determined by means of the method reported.[16] The values are: 8.32×10^{-6} $cm^2\,s^{-1}$ for *trans*-$[CoBr_2(en)_2]^+$ and 25.1×10^{-6} $cm^2\,s^{-1}$ for Br^- at 25 °C and ionic strength 0.1.

The magnitude of the anodic current of the first wave was found to be identical with that of the cathodic one which corresponds to the reduction of Co(III) to Co(II). The first wave was very similar in shape to the dissolution wave of the mercury in the presence of Br^- ions (Fig. 4). This suggests that the mass transport toward the electrode is controlled not by the diffusion of Br^- ions but by that of *trans*-$[CoBr_2(en)_2]^+$. The shape of the first wave also indicates that the current-potential curve is characterized mainly by the anodic depolarization wave of Br^- ions. Thus, the overall electrode reaction in acid media might be expected to follows a mechanism given by Eqs. 1—3.

If we classify the ECE mechanism into the two types, consecutive and parallel ECE pathways,[2] the electrode reaction of *trans*-$[CoBr_2(en)_2]^+$ belongs to the parallel case. When the tervalent cobalt complex is reduced to the bivalent one, the substitution-labile bivalent complex liberates 2 mol of Br^- ions and dissolution wave of mercury by Br^- ions appears. This gives rise to the net current anodic. When the electrode potential becomes negative, dissolution ceases and a wave appears with a half-wave potential nearly equal to that of the anodic depolarization wave of Br^- ions.

The foregoing situation corresponds to the curve at $\Delta E=-0.3$ or -0.4 V (Fig. 3(c)) which depicts a global shape of the simulated parallel ECE pathway for $n_1=+2$. Strictly speaking, n_2 should be replaced by $2n_2$ for the electrode reaction of *trans*-$[CoBr_2(en)_2]^+$. Details are given below. In order to confirm the theory, a current-potential curve was simulated and the result compared with the measured one.

Simulation of Current-Potential Curve. Current-potential curves at more positive potential were obscured by the free dissolution wave of mercury.[17] However, both anodic and cathodic waves of *trans*-$[CoBr_2(en)_2]^+$ were resolved, each showing a limiting current plateau (Fig. 4). Thus, the half-wave potential of Reaction 1 would lie at least 0.3 V more positive than that of Reactions 3 as expected from Fig. 3(c). The current under these conditions does not depend on the heterogeneous rate constant of Reaction 1, but on the homogeneous rate constant of Reaction 2 as well as on the characteristics of electrode reaction 3.

The implicit solution of Eq. 16 is given in the Appendix. The current is given by Eq. A-2, where λ is made infinite and n_2 is replaced by $2n_2$ since 2 mol of Br^- ions are liberated from 1 mol of complex (Reaction 2). Thus, we have

$$\left(\frac{I}{I_d}\right)_{\lambda\to\infty} = 1-\frac{2n_2}{n_1}\left(\frac{\theta}{\sqrt[\circ]{D_A/D_C c}}\right)+\frac{2n_2}{n_1}\phi(a\sqrt{t}) - \frac{2n_2}{n_1}\sqrt{\frac{D_C}{D_B}}\exp(-lt)\phi\left(\sqrt{\frac{D_B}{D_C}}a\sqrt{t}\right), \quad (21)$$

with

$$\phi(x) = 2x\exp(-x^2)\int_0^x \exp(u^2)\mathrm{d}u, \quad (22)$$

where $a=\sqrt{D_C l/(D_C-D_B)}$.

For the sake of approximation, plane electrodes were assumed for derivation. This is because the corresponding derivation for an expanding plane electrode would be far more difficult and the activity of deposit during the course of expansion is not be known until the electrode is completely covered with deposit. Our data represent a preliminary study to demonstrate some phenomena predicted theoretically.

In the range of anodic current plateau, θ in Eq. 21 becomes zero. It follows that

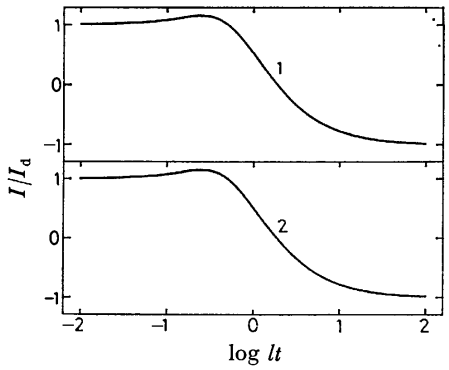

Fig. 5. Working curves for calculation of homogeneous rate constant. Diffusion coefficients are: (1) $D_A=D_B=8.32\times10^{-6}$ cm^2 s^{-1}, $D_C=25.1\times10^{-6}$ cm^2 s^{-1} and (2) $D_A=D_B=4.67\times10^{-6}$ cm^2 s^{-1}, $D_C=13.7\times10^{-6}$ cm^2 s^{-1}.

$$\frac{I}{I_d}=1+\frac{2n_2}{n_1}\left[\phi\left(\sqrt{\frac{D_C lt}{D_C-D_B}}\right)-\sqrt{\frac{D_C}{D_B}}\exp(-lt)\phi\left(\sqrt{\frac{D_B lt}{D_C-D_B}}\right)\right]. \quad (23)$$

In order to evaluate the rate constant, the value of I/I_d was calculated against lt and is plotted in Fig. 5 for two sets of diffusion coefficients. In this calculation, curve 1 corresponds to the case at 25 °C ($D_A=D_B=8.32\times10^{-6}$ cm^2 s^{-1}, $D_C=25.1\times10^{-6}$ cm^2 s^{-1}) and curve 2, to the case of 5 °C ($D_A=D_B=4.67\times10^{-6}$ cm^2 s^{-1}, $D_C=13.7\times10^{-6}$ cm^2 s^{-1}).

The value of I/I_d at +0.25 V *vs.* SCE was found to be 1 at 25 °C. This indicates that the acid hydrolysis reaction 2 proceeds very rapidly. The rate constant was obtained by varying temperature. The measurement made at 5 °C gave $l=0.4$ s^{-1} for the acid hydrolysis rate constant. The value was determined from the working curve 2 in Fig. 5. Reliability of the rate of Reaction 2 was tested by the following simulation of current-potential curves.

The preceding preliminary estimation indicates $(D_C/D_B)\exp(lt)\gg1$. Thus, Eq. 21 can be simplified to

$$\frac{I}{I_d}=1+\frac{2n_2}{n_1}\left(1-\frac{\theta}{c^\circ\sqrt{D_A/D_C}}\right)-\frac{2n_2}{n_1}\sqrt{\frac{D_B}{D_C}}\exp(-lt). \quad (24)$$

If $\theta=0$ and $D_B=D_C$, the relation agrees with the equation of Alberts and Shain.[13] In Eq. 24 the second term represents the depolarization term of Br$^-$ ions at mercury electrode, which can be calculated from the dissolution wave of mercury in the presence of Br$^-$ ions only. The anodic dissolution wave with Br$^-$ ions is given by[18]

$$I=(I_d)_C\left(1-\frac{\theta}{c^*}\right), \quad (25)$$

where $(I_d)_C=n_2Fqc^*\sqrt{D_C}/\sqrt{\pi t}$. Thus, $1-\theta/c^\circ\sqrt{D_A/D_C}$, which is required in the calculation of Eq. 24, can be obtained experimentally from the current-potential curve at $c^*=c^\circ\sqrt{D_A/D_C}$.

The simulated current-potential curves for the reduction of *trans*-$[CoBr_2(en)_2]^+$ at 25 °C and 5 °C are shown in Fig. 6 together with the experimental data. Curve 1 for $l>3$ s^{-1} and curve 2 for $l=0.4$ s^{-1}. In this

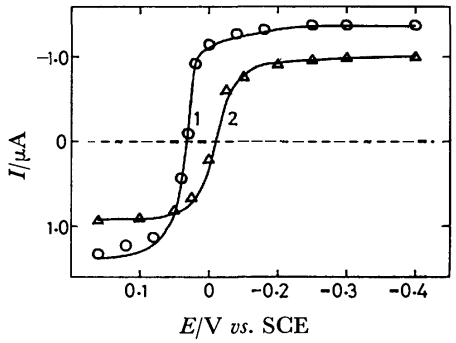

Fig. 6. Comparison of observed and simulated current-potential curves for the reduction of *trans*-$[CoBr_2(en)_2]NO_3$ at (1) 25 °C and (2) 5 °C. Circles and triangles, experimental; solid lines, theoretical.

calculation, when the current-potential curve of Br$^-$ ions was used for $c^*=c^\circ\sqrt{D_A/D_C}$, the zero-cross potential was *ca.* 25 mV more positive than the observed one. Good agreement was obtained by taking a value of $c^*=0.7$ mM for curve 1 and $c^*=0.6$ mM for curve 2. These values were used to construct the current-potential curves shown in Fig. 6. The discrepancy between theory and experiment is most likely due to the change in the activity of insoluble film.

The calculation given in Fig. 6 basically conforms to the concept of parallel ECE pathway. The current-potential behavior of *trans*-$[CoBr_2(en)_2]^+$ is thus in line with the overall mechanism given by Reactions 1—3 in which the parallel ECE pathway occurs.

Appendix

The boundary value problem stated by Eqs. 7—15 was solved by a straight-forward application of the laplace transformation. The following equation was obtained for the current:

$$I(s)=n_1Fc^\circ\sqrt{D_A\lambda}\frac{1}{\sqrt{s}(\sqrt{s}+\lambda)}+n_2F\sqrt{D_A}\left(\frac{D_C l}{D_C-D_B}\right)c^\circ\lambda\times\frac{1}{\sqrt{s}(\sqrt{s}+\lambda)\left(s+\frac{D_C}{D_C-D_B}l\right)}-n_2F\sqrt{D_C}\theta\frac{1}{\sqrt{s}}-n_2F\sqrt{D_A}\sqrt{\frac{D_B}{D_C}}\left(\frac{D_C l}{D_C-D_B}\right)c^\circ\lambda\times\frac{1}{\sqrt{s+1}(\sqrt{s}+\lambda)\left(s+\frac{D_C l}{D_C-D_B}\right)}. \quad (A\text{-}1)$$

The inverse transform of this expression can be found by using the convolution theorem[19] which is

$$L^{-1}[f_1(s)\cdot f_2(s)]=\int_0^t F_1(u)F_2(t-u)\mathrm{d}u=F_1(t)*F_2(t)$$

with $L[F_1(t)]=f_1(s)$ and $L[F_2(t)]=f_2(s)$.

Equation 16 is obtained from the table of Laplace transform pairs.[19]

For the numerical calculation, Eq. 16 can be rewritten as

$$\frac{I}{I_d}=\lambda\sqrt{\pi t}\exp(\lambda^2t)\operatorname{erfc}(\lambda\sqrt{t})-\frac{n_2}{n_1}\left(\frac{\theta}{c^\circ\sqrt{D_A/D_C}}\right)+\frac{n_2}{n_1}(\pm a^2)\lambda\sqrt{\pi t}\exp(\mp a^2t)$$

$$\times \int_0^t \exp\left[(\lambda^2 \pm a^2)u\right] \operatorname{erfc}\left(\lambda\sqrt{u}\right) du$$

$$-\frac{n_2}{n_1}\sqrt{\frac{D_B}{D_C}}\lambda\sqrt{\pi t}\left(\frac{\pm a^2}{\lambda^2 \pm a^2}\right)\int_0^t G(u)H(t-u)du \qquad \text{(A-2)}$$

with

$$G(u) = \exp\left(\mp a^2 u\right)\left[\lambda \pm a\frac{2}{\sqrt{\pi}}\int_0^{a\sqrt{u}} \exp\left(\pm r^2\right) dr\right]$$

$$-\lambda \exp\left(\lambda^2 u\right) \operatorname{erfc}\left(\lambda\sqrt{u}\right) \qquad \text{(A-3)}$$

$$H(u) = \frac{\exp\left(-lu\right)}{\sqrt{\pi u}} \qquad \text{(A-4)}$$

where $a=\sqrt{D_C l/(D_C - D_B)}$. The upper sign holds if $D_C > D_B$, the lower if $D_C < D_B$. Equation A-2 was computed numerically by the intergral method of Gauss.[20] The change of variable, $x=\sqrt{t-u}$, was employed in order to remove the singularity at $u=t$.

The function $\sqrt{\pi}x\exp(x^2)\operatorname{erfc}(x)$ in Eq. A-2 was calculated by a method described previously.[21]

The research was carried out by a Grant-in-Aid from the Ministry of Education. A part of the work was supported by Scientific Research Grant No. 364205.

References

1) A. C. Testa and W. H. Reinmuth, *Anal. Chem.*, **33**, 1320 (1961).

2) I. Ruzic, H. R. Sobel, and D. E. Smith, *J. Electroanal. Chem.*, **65**, 21 (1975) and the references cited therein.

3) H. A. Laitinen and P. Kivalo, *J. Am. Chem. Soc.*, **75**, 2198 (1953).

4) A. A. Vlček, "Polarographic Behavior of Coordination Compounds," in "Progress in Inorganic Chemistry," ed by F. A. Cotton, Interscience Publishers, New York (1963), Vol. 5, pp. 211—384.

5) K. Ebata, *Sci. Repts. Tohoku Univ., Ser. I*, **47**., 191 (1964).

6) N. Tanaka and K. Ebata, *J. Elecrtoanal. Chem.*, **8**, 120 (1964).

7) K. Ogino and N. Tanaka, *Bull. Chem. Soc. Jpn.*, **39**, 2672 (1966).

8) N. Tanaka and A. Yamada, International Congress of Polarography, Kyoto, September 1966, Abstr. p. 124.

9) N. Tanaka and A. Yamada, *Rev. Polarog. (Kyoto)*, **14**, 234 (1967).

10) E. Fisherova, O. Drăcka, and M. Meloun, *Collect. Czech. Chem. Commun.*, **33**, 473 (1968).

11) S. W. Feldberg and L. Jeftic, *J. Phys. Chem.*, **76**, 2439 (1972).

12) N. Tanaka, Y. Yoshikuni, Y. Kato, and A. Yamada, *J. Electroanal. Chem.*, **107**, 95 (1980).

13) G. S. Alberts and I. Shain, *Anal. Chem.*, **35**, 1859 (1963).

14) A. Werner, L. Gerb, S. Lorie, and J. Rapiport, *Ann.*, **386**, 111 (1912).

15) N. Maki and N. Tanaka, "Encyclopedia of Electrochemistry of the Elements," ed by A. J. Bard, Marcel Dekker Inc., New York (1975), Vol. 3, pp. 43—210.

16) A. Yamada, Y. Kato, T. Yoshikuni, Y. Tanaka, and N. Tanaka, *Anal. Chim. Acta*, **112**, 55 (1979).

17) I. M. Kolthoff and J. J. Lingane, "Polarography," Interscience Publishers, New York (1964), Vol. 2, pp. 577—581.

18) P. Delahay, "New Instrumental Methods in Electrochemistry," Interscience Publishers, New York (1954), p. 57.

19) R. V. Churchill, "Operational Mathematics," 2nd ed, McGraw-Hill Book Company, Inc., New York (1958).

20) H. Margenau and G. M. Murphy, "The Mathematics of Physics and Chemistry," D. Van Nostrand Company, Inc., Princeton, New Jersey (1943).

21) A. Yamada and N. Tanaka, *Anal. Chem.*, **45**, 167 (1973).

A Polarographic Rate Study on the Acid Hydrolysis of Several Halogeno Cobalt(III) Complexes

Akifumi YAMADA,* Tadatsugu YOSHIKUNI, Yoshikiyo KATO, and Nobuyuki TANAKA
Department of Chemistry, Faculty of Science, Tohoku University, Sendai 980
(Received September 10, 1979)

A polarographic rate study of the acid hydrolysis of $[CoX(NH_3)_5]^{2+}$- and *trans*-$[CoX_2(N)_4]^+$-type complexes (X=Cl^- and Br^-; $(N)_4=(NH_3)_4$, $(ethylenediamine)_2$, $(propylenediamine)_2$ and $(1,2\text{-cyclohexanediamine})_2$) has been carried out in 0.1 M acetate buffer solutions. These complexes gave two polarographic waves; the first wave corresponds to the reduction of Co(III) to Co(II) and the second one, to the reduction of Co(II) to Co(0). The relation between the current and the time of the first wave in a positive potential was dependent on the dissolution wave caused by halogenide ions produced by acid hydrolysis and also on the parallel ECE mechanism. The acid-hydrolysis rate of tervalent cobalt complexes was determined from the variation in the current of the first wave. The rates are: 1.31×10^{-6} s^{-1} for $[CoCl(NH_3)_5](NO_3)_2$, 6.25×10^{-4} s^{-1} for *trans*-$[CoCl_2(NH_3)_4]ClO_4$, 3.20×10^{-5} s^{-1} for *trans*-$[CoCl_2(en)_2]NO_3$, 4.28×10^{-5} s^{-1} for *trans*-$[CoCl_2(pn)_2]ClO_4$, 1.53×10^{-4} s^{-1} for *trans*-$[CoCl_2(chxn)_2]ClO_4\cdot H_2O$, 5.80×10^{-6} s^{-1} for $[CoBr(NH_3)_5](NO_3)_2$, 4.19×10^{-3} s^{-1} for *trans*-$[CoBr_2(NH_3)_4]ClO_4$, 1.51×10^{-4} s^{-1} for *trans*-$[CoBr_2(en)_2]NO_3$, 3.30×10^{-4} s^{-1} for *trans*-$[CoBr_2(pn)_2]ClO_4\cdot0.5H_2O$ and 5.10×10^{-4} s^{-1} for *trans*-$[CoBr_2(chxn)_2]NO_3$ at 25 °C and an ionic strength of 0.1.

The acid hydrolysis of several halogeno cobalt(III) complexes, such as $[CoX(NH_3)_5]^{2+}$ and $[CoX_2(N)_4]^+$, where X is Cl^- and Br^-, and where $(N)_4$ represents $(NH_3)_4$, $(en)_2$ and $(pn)_2$, has been studied by chemical and spectrophotometric methods.[1-6] There have, however, been only a few papers on the determination of the acid-hydrolysis rate constant under the same conditions. The accuracy is not yet satisfactory.

When the acid hydrolysis of a halogeno cobalt(III) complex proceeds, one mole or two moles of halogenide ions are liberated. It is well known that the halogenide ions, such as chloride and bromide ions, give a well-defined diffusion-controlled polarographic wave.[7] Therefore, by monitoring these liberated halogenide ions polarographically, the rate of the acid hydrolysis of such complexes can be obtained very accurately.

This paper will describe the polarographic determination of the acid-hydrolysis rate of halogeno cobalt(III) complexes, since we have obtained more satisfactory results.

Experimental

The electrolysis cell was of a conventional design, comprising a 50-ml cell, a platinum wire anode, and a saturated calomel electrode. The dropping mercury electrode (flow rate, 1.17 mg s^{-1} and drop time, 3.97 s in 0.1 M acetate buffer solutions (1M=1 mol dm^{-3})) served as a working electrode. The current-time curves during aquation were recorded by the use of a Fuso Model 312 polarograph with a Watanabe Model WX441 x-y recorder.

The complexes used were prepared according to the literature,[8-19] with partial modifications. The analytical data for all the complexes obtained are summarized in Table 1, together with the literature of the syntheses.

In a series of determinations of the acid-hydrolysis rates of various halogeno cobalt(III) complexes, the electrochemical procedure was as follows. After measurements of the residual current of a 40-ml portion of the supporting electrolyte solution, a solid sample of the cobalt complex being tested was added to the solutions. As soon as the complex had been dissolved by bubbling in nitrogen gas, the current attributable to the halogenide ions was measured against the time. All the measurements were carried out at 25 °C. A small amount of gelatin was added as a maximum suppressor.

TABLE 1. ANALYTICAL DATA FOR Co(III) COMPLEXES

Complex	C(%)		H(%)		N(%)	
	Found	Calcd	Found	Calcd	Found	Calcd
$[CoCl(NH_3)_5](NO_3)_2$[8]	—	—	5.04	4.98	32.84	32.30
trans-$[CoCl_2(en)_2]NO_3$[9]	15.25	15.40	5.21	5.17	22.36	22.44
trans-$[CoCl_2(pn)_2]ClO_4$[10]	19.12	19.09	5.49	5.34	14.91	14.84
trans-$[CoCl_2(chxn)_2]ClO_4\cdot H_2O$[11]	29.77	30.30	6.11	6.36	11.65	11.78
trans-$[CoCl_2(NH_3)_4]ClO_4$[12]	—	—	4.33	4.07	19.38	18.84
$[CoBr(NH_3)_5](NO_3)_2$[13]	—	—	4.59	4.34	28.02	28.17
trans-$[CoBr_2(en)_2]NO_3$[14]	11.90	11.98	4.15	4.02	17.66	17.47
trans-$[CoBr_2(pn)_2]ClO_4\cdot0.5H_2O$[15]	15.14	15.16	4.62	4.45	11.65	11.78
trans-$[CoBr_2(chxn)_2]NO_3$[11]	28.10	28.31	5.67	5.54	13.46	13.76
trans-$[CoBr_2(NH_3)_4]ClO_4$[16]	—	—	3.42	3.13	14.85	14.50
cis-$[Co(H_2O)_2(en)_2](ClO_4)_3$[17]	10.00	9.36	4.58	3.93	10.74	10.91
cis-$[Co(AcO)_2(en)_2]ClO_4$[18]	24.28	24.22	5.51	5.59	13.85	14.12
cis-$[Co(AcO)_2(pn)_2]ClO_4$[18]	28.43	28.28	6.41	6.17	12.44	13.19
cis-$[Co(H_2O)_2(NH_3)_4](ClO_4)_3$[19]	—	—	3.97	3.50	11.90	12.14

Results

The series of $[CoCl(NH_3)_5]^{2+}$, $[CoBr(NH_3)_5]^{2+}$, *trans*-$[CoCl_2(N)_4]^+$ and *trans*-$[CoBr_2(N)_4]^+$ complexes (where $(N)_4$ represents $(NH_3)_4$, $(en)_2$, $(pn)_2$ and $(chxn)_2$) gave two polarographic waves. Figure 1 shows examples of the current-potential curves of these halogeno cobalt(III) complexes obtained in 0.1 M acetate buffer solutions at 25 °C.

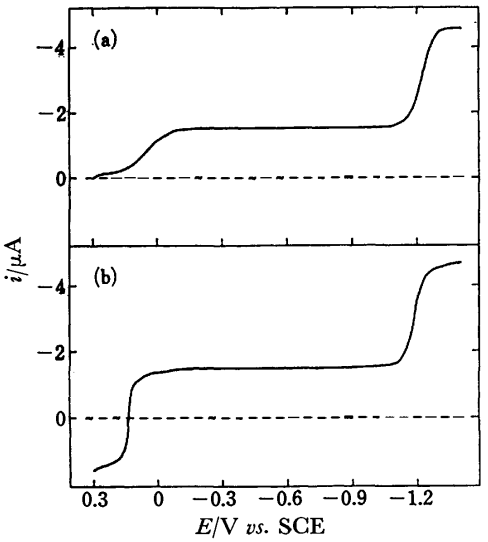

Fig. 1. Current-potential curves of 0.5 mM halogeno cobalt(III) complexes obtained in 0.1 M sodium acetate buffer solutions (pH 5.0) containing 0.005% gelatin at 25 °C. (a) $[CoCl(NH_3)_5](NO_3)_2$, (b) *trans*-$[CoBr_2(en)_2]NO_3$.

The first wave appeared in the field of the cathodic current for the monohalogeno cobalt(III) complex or in the field of the anodic and cathodic currents for the dihalogeno cobalt(III) complex. The first wave was considered to be a one-electron reduction of Co(III) to Co(II). Since the limiting current of the second wave was twice that of the first one, the second wave was considered to be a two-electron reduction, that is, Co(II)→Co(0), in analogy with the electrode reaction of other cobalt complexes.[20]

The cathodic limiting current of the first wave was diffusion-controlled and was proportional to the concentration of the complex. The anodic limiting current of the first wave was also diffusion-controlled, but increased gradually with the time elapsed corresponding to the acid hydrolysis of the tervalent cobalt complex, as is seen in Fig. 2. When the anodic current increased with the time, the cathodic current decreased slightly.

The polarographic characteristics, such as the diffusion current(i_d), the half-wave potential ($E_{1/2}$), and the reciplocal slope of the log-plot, are given in Table 2; they were obtained immediately after dissolving 0.5 mM of the complex in 0.1 M sodium acetate buffer solutions

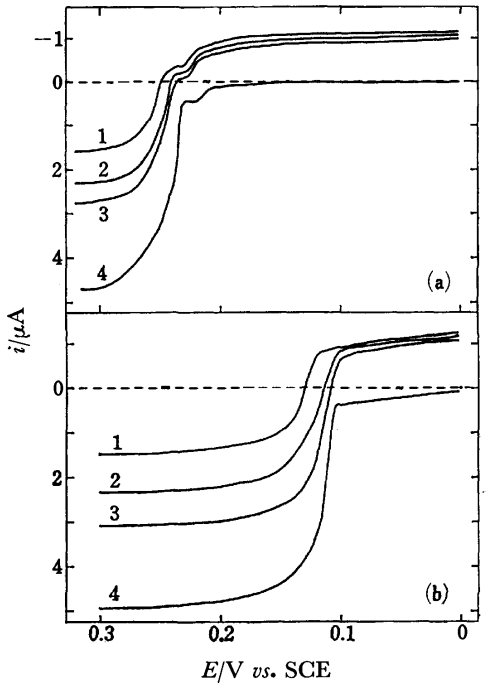

Fig. 2. Current-potential curves of (a) 0.5 mM *trans*-$[CoBr_2(chxn)_2]ClO_4 \cdot H_2O$ and (b) 0.5 mM *trans*-$[CoBr_2(pn)_2]ClO_4 \cdot 0.5H_2O$ obtained in 0.1 M sodium acetate buffer solutions (pH 5.0) containing 0.005% gelatin at 25 °C. Currents are measured (1) immediately after dissolving complex, (2) after 20 min and (3) after 40 min. Curves 4 are the current-potential curves of (a) 1 mM KCl and (b) 1 mM KBr, respectively.

Table 2. Polarographic characteristics of 0.5 mM halogenocobalt(III) complexes obtained in a 0.1 M sodium acetate buffer (pH 5.0) containing 0.005% gelatin at 25 °C

Complex	First wave		Second wave		
	i_d / μA	$E_{1/2}$ / V vs. SCE	i_d / μA	$E_{1/2}$ / V vs. SCE	slope / (mV)
$[CoCl(NH_3)_5](NO_3)_2$	1.51	0.05_6	3.04	−1.219	65
trans-$[CoCl_2(en)_2]NO_3$	1.49	0.24_1	3.04	−1.181	54
trans-$[CoCl_2(pn)_2]ClO_4$	1.43	0.23_8	2.96	−1.176	53
trans-$[CoCl_2(chxn)_2]ClO_4 \cdot H_2O$	1.20	0.22_5	2.69	−1.163	60
trans-$[CoCl_2(NH_3)_4]ClO_4$	1.59	0.22_9	3.10	−1.224	74
$[CoBr(NH_3)_5](NO_3)_2$	1.55	0.15_1	3.20	−1.221	72
trans-$[CoBr_2(en)_2]NO_3$	1.44	0.12_2	2.94	−1.183	56
trans-$[CoBr_2(pn)_2]ClO_4 \cdot 0.5H_2O$	1.37	0.12_2	2.88	−1.176	55
trans-$[CoBr_2(chxn)_2]NO_3$	1.31	0.06_6	2.92	−1.154	51
trans-$[CoBr_2(NH_3)_4]ClO_4$	1.50	0.10_5	2.99	−1.219	73

at 25 °C.

It has been reported that halogeno cobalt(III) complexes undergo acid hydrolysis with first-order kinetics and liberate halogenide ions:[1-4,6,21]

$$[Co^{III}X(NH_3)_5]^{2+} + H_2O \longrightarrow [Co^{III}(H_2O)(NH_3)_5]^{3+} + X^-, \quad (1)$$

$$trans\text{-}[Co^{III}X_2(N)_4]^+ + 2H_2O \longrightarrow [Co^{III}(H_2O)_2(N)_4]^{3+} + 2X^- \quad (2)$$

($X^- = Br^-$ and Cl^-;
$(N)_4 = (NH_3)_4$, $(en)_2$, $(pn)_2$ and $(chxn)_2$).

Thus, by monitoring the concentration of halogenide ions, the acid-hydrolysis rate can be measured.

Halogenide ions give a well-defined polarographic wave in the presence of gelatin:[7]

$$2Cl^- + 2Hg \longrightarrow Hg_2Cl_2 + 2e^-, \quad (3)$$

$$2Br^- + 2Hg \longrightarrow Hg_2Br_2 + 2e^-. \quad (4)$$

An example of the polarogram of the halogenide ions is also shown in Fig. 2. The anodic limiting current around *ca.* +0.25—+0.30 V *vs.* SCE is, therefore, given as the sum of the current attributable to the remaining halogeno cobalt(III) complex ($i_{complex}$) and the liberated halogenide ions ($i_{halogen}$). Assuming a first-order kinetics, the concentration of the liberated halogenide ions and that of remaining halogeno complex are represented[22] as $pc^\circ(1-\exp(-kt))$ and $c^\circ\exp(-kt)$, where c° is the initial concentration of the complex and where k is the first-order rate constant of acid hydrolysis given by Eq. 1 or 2. The anodic current can, therefore, be expressed as:

$$\begin{aligned} i_a &= i_{complex} + i_{halogen} \\ &= \alpha_1 c_{complex} + \alpha_2 c_{halogen} \\ &= \alpha_1 c^\circ \exp(-kt) + \alpha_2 pc^\circ(1-\exp(-kt)), \end{aligned} \quad (5)$$

where α_1 and α_2 are the proportional constant with respect to the concentration and where p is the number of halogenide ions liberated. In the present case, $p=1$ for the monohalogeno complex and $p=2$ for the dihalogeno complex.

The first-order rate constant of the acid hydrolysis of tervalent cobalt complex can be determined from the time variation of the current given by Eq. 5. The rearrangement of Eq. 5 yields:

$$\ln \frac{pc^\circ}{pc^\circ - c} = kt + \ln\left(1 - \frac{1}{p}\frac{\alpha_1}{\alpha_2}\right)^{-1}, \quad (6)$$

with:

$$c = \frac{i}{\alpha_2}. \quad (7)$$

Equation 6 shows that, if the values of α_1 and α_2 are constant with the time, the plot of $\ln[pc^\circ/(pc^\circ-c)]$ against the time should be a straight line. From the slope of this plot, the rate constant of acid-hydrolysis can be obtained.

The rate constant for the acid-hydrolysis of tervalent cobalt complexes was determined according to Eq. 5 with the concentrations obtained from the working curve prepared with the standard solutions of potassium chloride or potassium bromide. Examples of these plots are shown in Fig. 3, while the rate constants obtained are given in Table 3. The relation between $\ln[pc^\circ/(pc^\circ-c)]$ and the time gave a straight line with an intercept.

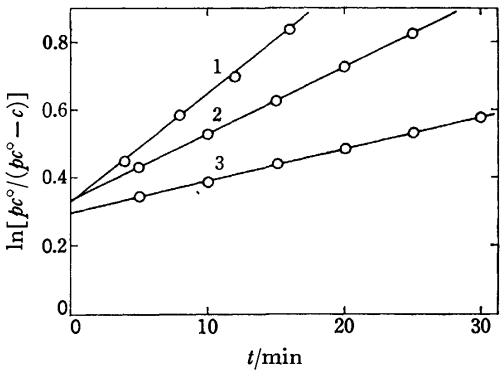

Fig. 3. Relations of $\ln[pc^\circ/(pc^\circ-c)]$ against time for (a) *trans*-$[CoBr_2(chxn)_2]NO_3$, (2) *trans*-$[CoBr_2(pn)_2]ClO_4 \cdot 0.5H_2O$ and (3) *trans*-$[CoCl_2(chxn)_2]ClO_4 \cdot H_2O$ obtained at ionic strength of 0.1 at 25 °C.

Discussion

For the series of $[CoX(NH_3)_5]^{2+}$ and *trans*-$[CoX_2(N)_4]^+$ complexes, all the rate data followed the first-order rate relation given by Eq. 6 with a satisfactory linearity. A good agreement between the data obtained in the present study and those in the literature was obtained except for *trans*-$[CoCl_2(NH_3)_4]^+$ and *trans*-$[CoBr_2(NH_3)_4]^+$ (Table 3). This suggests that the polarographic method based on the measurement of the dissolution wave can be applied for the determination of the acid hydrolysis of complexes by analogy with the chemical[2,3] and the spectrophotometric method.[2,3,6]

As for *trans*-$[CoCl_2(NH_3)_4]^+$, the value of 2.05×10^{-3} s^{-1} has been reported.[5] From our results, however, this value seems to be fast: if it is ture, aquation should proceed to an extent of 22% 2 min after the complex

Table 3. Rate data for the acid hydrolysis of Co(III) complexes obtained at 25 °C and an ionic strength of 0.1

Complex	$X^-=Cl^-$		$X^-=Br^-$	
	This study k/s^{-1}	Other studies k/s^{-1}	This study k/s^{-1}	Other studies k/s^{-1}
$[CoX(NH_3)_5]^{2+}$	1.31×10^{-6}	1.7×10^{-6} [1]	5.80×10^{-6}	6.3×10^{-6} [1]
trans-$[CoX_2(en)_2]^+$	3.20×10^{-5}	3.5×10^{-5} [6]	1.51×10^{-4}	1.4×10^{-4} [2-4]
trans-$[CoX_2(pn)_2]^+$	4.28×10^{-5}	6.2×10^{-5} [6]	3.30×10^{-4}	3.13×10^{-4} [6]
trans-$[CoX_2(chxn)_2]^+$	1.53×10^{-4}	2.16×10^{-4} [21]	5.10×10^{-4}	—
trans-$[CoX_2(NH_3)_4]^+$	6.25×10^{-4}	2.05×10^{-3} [5,6]	4.19×10^{-3}	*ca.* 7×10^{-3} [6]

is dissolved. Our results clearly indicate that this is not so. The literature values[6] for *trans*-$[CoBr_2(NH_3)_4]^+$ were estimated to be 3.5 times the rate constant for the dichloro analog; also the accuracy is not satisfactory. The acid-hydrolysis rate of *trans*-$[CoBr_2(chxn)_2]^+$ has not yet been reported, but the present value seems valid in comparison with the other halogeno analog.

The extinction coefficients of the halogeno complex are *ca.* 30—100 mol^{-1} cm^{-1}. Therefore, if a number of products with the same order of the extinction coefficient are produced, it seems difficult to determine the rate constant with any accuracy. On the other hand, in the polarographic method, only halogenide ions gave an anodic wave; furthermore, the diffusion coefficients of halogenide ions are about 3 times those of complexes. Therefore, the present polarographic method is very useful in the determination of the acid hydrolysis of such halogeno cobalt(III) complexes.

It is a well-known fact that the presence of excess mercuric ions accelerates the rate of the acid hydrolysis of several kinds of complexes.[23-25] In the case of the dropping mercury electrode, however, since mercurous and mercuric ions are in equilibrium, and since the mercuric ions amount to less than 1/120 of the mercury(I) ions,[26-28] the influence of the mercury(II) ions on the acid-hydrolysis of complex may be neglected compared with the large quantity of the bulk concentration of the complexes.

With the advance in acid hydrolysis, the cathodic limiting current decreased slightly. There are many factors to account for this: the effects of an ionic radius,[29] an increase or decrease in the charge,[30] a complex formation,[31] and an ion-pair formation.[32,33] However, those effects can not explain the present decrease in the current with the time. The decrease in the cathodic limiting current can be expected from the discussion given in connection with the change in the diffusion coefficient. The cathodic current of the first wave may be written as the sum of the current due to the remaining halogeno cobalt(III) and the aquated cobalt(III) complexes. Thus,

$$i_c = i_{complex} + i_{aquated} = \alpha_1 c_{complex} + \alpha_3 c_{aquated}, \quad (8)$$

where α_3 is the proportional factor of the aquated complex with respect to the concentration. If the current is diffusion controlled, α_1 and α_3 are related to the diffusion coefficient thus:[34]

$$\alpha_3 = An_1\sqrt{D_{Co(III)}}, \quad (9)$$

$$\alpha_3 = An_1\sqrt{D_{Co(III)aq}}, \quad (10)$$

where $D_{Co(III)aq}$ is the diffusion coefficient of the aquated cobalt(III) complex and where A is the constant including the flow rate of mercury and the drop time. Thus, the cathodic current is;

$$i_c = An_1\sqrt{D_{Co(III)}}c^\circ \exp(-kt) + An_1\sqrt{D_{Co(III)aq}}c^\circ(1-\exp(-kt)). \quad (11)$$

If the diffusion coefficient of the aquated complex is smaller than that of the original complex, the current will decrease with the time.

This speculation was confirmed by ascertaing the diffusion coefficients of the halogeno and aqua complexes. Some of the observed and reported values for the diffusion coefficient are listed in Table 4. The method for the precise determination of the diffusion coefficient has been described previously.[29] In this determination, the diffusion-controlled currents of the cobalt complex, Cl^- ions, and Br^- ions were measured at −0.70, +0.30 and +0.25 V *vs.* SCE respectively.

Table 4. Diffusion coefficient of Co(III) complexes and halogenide ions obtained in a 0.1 M sodium acetate buffer (pH 5.0) containing 0.005% gelatin at 25 °C

Complex	Diffusion coefficient ($D/10^{-6}$ cm^2 s^{-1})
$[CoCl(NH_3)_5]^{2+}$	9.13
trans-$[CoCl_2(en)_2]^+$	8.56
trans-$[CoCl_2(pn)_2]^+$	8.13
trans-$[CoCl_2(chxn)_2]^+$	6.79
trans-$[CoCl_2(NH_3)_4]^+$	9.37
$[CoBr(NH_3)_5]^{2+}$	9.11
trans-$[CoBr_2(en)_2]^+$	8.32
trans-$[CoBr_2(pn)_2]^+$	7.93
trans-$[CoBr_2(chxn)_2]^+$	6.56
trans-$[CoBr_2(NH_3)_4]^+$	9.18
cis-$[Co(H_2O)_2(en)_2]^{3+}$	6.18
cis-$[Co(AcO)_2(en)_2]^+$	6.15
cis-$[Co(AcO)_2(pn)_2]^+$	5.63
cis-$[Co(H_2O)_2(NH_3)_4]^{3+}$	7.11
Cl^-	22.31
Br^-	25.14

Although the aqua and acetato complexes are *cis*-type, the diffusion coefficients of the aqua and acetato complexes are smaller than those of the halogeno complexes. By using these diffusion coefficients, the cathodic limiting current at −0.7 V *vs.* SCE was calculated from Eq. 11 for various times elapsed. The calculated values agreed with the experimental ones within the limits of experimental error.

In the present study, the plot for first-order kinetics, $\ln[pc^\circ/(pc^\circ-c)]$ *vs.* t, has the intercept to be seen in Eq. 6, whereas the conventional plot has no intercept.[22] This arises from the parallel ECE pathway represented by the reaction:[35]

$$[Co^{III}X(NH_3)_5]^{2+} + e^- \longrightarrow [Co^{II}X(NH_3)_5]^+, \quad (12a)$$

$$[Co^{II}X(NH_3)_5]^+ + 6H_2O \longrightarrow [Co^{II}(H_2O)_6]^{2+} + X^- + 5NH_3, \quad (12b)$$

$$X^- + \frac{1}{2}Hg \longrightarrow \frac{1}{2}Hg_2X_2 + e^-, \quad (12c)$$

($X^- = Cl^-$ and Br^-)

or:

$$trans\text{-}[Co^{III}X_2(N)_4]^+ + e^- \longrightarrow trans\text{-}[Co^{II}X_2(N)_4], \quad (13a)$$

$$trans\text{-}[Co^{II}X_2(N)_4] + 6H_2O \longrightarrow [Co^{II}(H_2O)_6]^{2+} + 2X^- + (N)_4, \quad (13b)$$

$$2X^- + 2Hg \longrightarrow Hg_2X_2 + 2e^-. \quad (13c)$$

($X^- = Cl^-$ and Br^-;
$(N)_4 = (NH_3)_4$, $(en)_2$, $(pn)_2$, and $(chxn)_2$)

When the tervalent cobalt complex is reduced to the bivalent one, the bivalent complex, which is substitution-

labile, liberates one mole or two moles of halogenide ions and the dissolution wave of mercury attributable to halogenide ions appears. This results in a net current anodic for dihalogeno complexes and in a net current cathodic for monohalogeno complexes. As the potential becomes negative, dissolution ceases, and a wave with a half-wave potential nearly equal to that of the dissolution wave in the presence of bromide ions appears (Fig. 1).

At 25 °C, Reaction 13b for the acid hydrolysis of dibromo cobalt(II) may proceed very rapidly, and the net current for the parallel ECE pathway becomes diffusion-controlled. From the theory of parallel ECE pathway,[35,36]

$$\alpha_1 = A(n_1+n_2)\sqrt{D_{Co(III)}}, \quad (14)$$

and:

$$\alpha_2 = An_2\sqrt{D_{Br^-}}, \quad (15)$$

where n_1 and n_2 are the number of electrons involved in Reactions 12a and 13c respectively. The intercept (the second term on the right-hand side in Eq. 6) was calculated from the diffusion coefficients given in Table 3, and $n_1=-1$ and $n_2=+1$. The values are: 0.360 for *trans*-$[CoBr_2(NH_3)_4]^+$, 0.339 for *trans*-$[CoBr_2(en)_2]^+$, and 0.330 for *trans*-$[CoBr_2(pn)_2]^+$, while the observed values are 0.36, 0.34, and 0.33 respectively.

As for other complexes, α_1 was dependent on the electrode potential because the current-potential curve did not give a diffusion plateau. No kinetic parameters of the two electrode reactions 12a and 13a have been reported, and so no further calculation was made for these cases.

The authors wish to thank the Ministry of Education for the financial support granted for this research. A part of the work was supported by a Grant-in-Aid for Scientific Research, No. 364205.

References

1) F. Basolo and R. G. Pearson, "Mechanisms of Inorganic Reactions. A Study of Metal Complexes in Solution," John Wiley & Sons, New York (1967), pp. 158—177.
2) R. G. Pearson, R. M. Meeker, and F. Basolo, *J. Am. Chem. Soc.*, **78**, 709 (1956).
3) F. Basolo, W. R. Matoush, and R. G. Pearson, *J. Am. Chem. Soc.*, **78**, 4883 (1956).
4) S. C. Chan and M. L. Tobe, *J. Chem. Soc.*, **1963**, 5700.
5) R. G. Linck, *Inorg. Chem.*, **8**, 1016 (1969).
6) L. M. Eade, G. A. Rodley, and D. A. House, *J. Inorg. Nucl. Chem.*, **37**, 1049 (1975).
7) I. M. Kolthoff and J. J. Lingane, "Polarography," Interscience Publishers, New York (1964), Vol. 2, pp. 577—581.
8) G. G. Schlessinger, "Inorganic Syntheses," ed. by S. Y. Tyree, McGraw-Hill, New York (1939), Vol. 9, p. 160.
9) J. Springbørg and C. E. Schäffer, "Inorganic Syntheses," ed by A. Wold and J. K. Ruff, McGraw-Hill, New York (1973), Vol. 14, p. 68.
10) A. Werner and A. Fröhlich, *Ber.*, **40**, 2225 (1907).
11) R. S. Treptow, *Inorg. Chem.*, **5**, 1593 (1966).
12) S. M. Jørgensen, *Z. Anorg. Chem.*, **14**, 415 (1897).
13) H. Diehl, H. Clark, and H. H. Willard, "Inorganic Syntheses," ed by H. S. Booth, McGraw-Hill, New York (1939), Vol. 1, p. 186.
14) A. Werner, L. Gerb, S. Lorie, and J. Rapiport, *Ann.*, **386**, 111 (1912).
15) R. Tsuchiya, Y. Natsume, A. Uehara, and E. Kyuno, *Thermochim. Acta*, **12**, 147 (1975).
16) A. Werner and A. Wolberg, *Ber.*, **38**, 993 (1905).
17) A. Werner and G. Jantsch, *Ber.*, **40**, 265 (1907).
18) M. Linhard and M. Weigel, *Z. Anorg. Allg. Chem.*, **264**, 321 (1951).
19) R. G. Jørgensen, *Z. Anorg. Chem.*, **2**, 294 (1892).
20) N. Maki and N. Tanaka, "Encyclopedia of Electrochemistry of the Elements," ed by A. J. Bard, Mercel Dekker Inc., New York (1975), Vol. 3, pp. 43—210.
21) S. C. Chan and F. K. Chan, *Aust. J. Chem.*, **23**, 1477 (1970).
22) K. J. Laidler, "Chemical Kinetics," McGraw-Hill, New York (1965), Chap. 1.
23) J. N. Brønsted and R. Livingston, *J. Am. Chem. Soc.*, **49**, 435 (1927).
24) A. M. Sargeson, *Aust. J. Chem.*, **17**, 385 (1964).
25) J. H. Espenson and J. P. Birk, *Inorg. Chem.*, **4**, 527 (1965).
26) A. Ogg, *Z. Phys. Chem.*, **27**, 293 (1898).
27) E. Abel, *Z. Anorg. Chem.*, **26**, 375 (1901).
28) J. Revenda, *Collect. Czech. Chem. Commun.*, **6**, 453 (1934).
29) A. Yamada, Y. Kato, T. Yoshikuni, Y. Tanaka, and N. Tanaka, *Anal. Chim. Acta*, **112**, 55 (1979).
30) K. Asada, P. Delahay, and A. K. Sundarm, *J. Am. Chem. Soc.*, **83**, 3396 (1961).
31) J. J. Lingane, *Ind. Eng. Chem., Anal. Ed.*, **15**, 589 (1943).
32) N. Tanaka, K. Ogino, and G. Sato, *Bull. Chem. Soc. Jpn.*, **39**, 366 (1966).
33) N. Tanaka and A. Yamada, *Z. Anal. Chem.*, **224**, 117 (1967).
34) I. M. Kolthoff and J. J. Lingane, "Polarography," Interscience Publishers, New York (1964), Vol. 1. pp. 63—98.
35) N. Tanaka, T. Yoshikuni, Y. Kato, and A. Yamada, *J. Electroanal. Chem.*, **107**, 95 (1980).
36) A. Yamada, T. Yoshikuni, Y. Kato, and N. Tanaka, *Bull. Chem. Soc. Jpn.*, **53**, 936 (1980).

 © 1980 The Chemical Society of Japan Bull. Chem. Soc. Jpn., 53, 947—950 (1980)

Electrochemical Oxidation and Reduction of Ferredoxin Adsorbed on Mercury Electrode Surface. Phase-selective A. c. Polarography at DME†

Tadaaki KAKUTANI, Kazunobu TORIYAMA, Tokuji IKEDA, and Mitsugi SENDA*

Department of Agricultural Chemistry, Faculty of Agriculture, Kyoto University, Kyoto 606

(Received November 5, 1979)

The electrochemical behavior of *Clostridium pasteurianum* ferredoxin (Cl.Fd) was studied by a.c. polarography with the dropping mercury electrode. The a.c. polarograms observed in acidic media (pH<7) were assigned to RSH/RSHg redox reaction of the cysteine residues of apoferredoxin, whereas those observed in basic media (pH>8) were assigned to a two-step one-electron transfer (EE mechanism) to the iron-sulfur clusters of Cl.Fd adsorbed on the mercury electrode surface ($(Cl.Fd)_{ad}$). The a.c. polarographic behavior of $(Cl.Fd)_{ad}$ observed in basic media was interpreted by theory of a.c. polarography of a two-step surface redox reaction. The formal standard oxidation-reduction potential of $(Cl.Fd)_{ad}$ was determined to be −0.33 V *vs.* NHE at pH 7.0, and its pH dependence was −30 mV/pH between pH 8 and 10.

In a previous paper[1] we have shown that ferredoxin is adsorbed irreversibly on the surface of mercury electrode and decomposes gradually to apoferredoxin (cluster-free ferredoxin) in the adsorption layer. D.c. and a.c. polarographic studies on ferreoxins have been reported by several workers.[2-7] However, these authors did not fully consider the adsorption nature of ferredoxins on the electrode surface. Accordingly further examination is needed to find the exact relationship between the measured potentials being characteristic of the polarograms of ferredoxins and their oxidation-reduction potentials. In this study we have investigated the a.c. polarographic behavior of *Clostridium pasteurianum* ferredoxin (Cl.Fd) at the dropping mercury electrode (DME) with exact reference to the adsorption of ferredoxin on the electrode surface. The results show that the a.c. polarographic study of Cl.Fd with DME in basic media enables us to determine the electrochemical oxidation-reduction potential of the iron-sulfur clusters of the ferredoxin adsorbed on the electrode surface.

Experimental

Preparations of *Clostridium pasteurianum* ferredoxin and apoferredoxin as well as apparatus and methods of electrochemical measurements have been described previously.[1] The dropping mercury electrode was of a common type having a mercury flow rate of 1.01 mg s^{-1} and a drop time of 9.5 s at open circuit in distilled water at 45 cm height of mercury reservoir. Real and imaginary components of the alternating currents were recorded against d.c. potential applied to the DME. The a.c. current intensities were taken at the moment of the maximum growth of each mercury drop. Potentials were measured against a saturated calomel electrode (SCE). All measurements were carried out at 25 °C.

Results and Discussion

Figure 1 shows the real and imaginary components of the a.c. waves of 1.7 μM Cl.Fd at pH 4.4 (Fig. 1A) and at pH 9.2 (Fig. 1B). The wave heights grew up to a certain limit with increasing concentration of Cl.Fd, as seen in Fig. 2, where the peak heights of the imaginary a.c. wave, $\delta_1 I_p^{imag}$, are plotted against the Cl.Fd concentration, $C_{Cl.Fd}$, at pH 6.9. This indicates that Cl.Fd is accumulated on the DME surface and that the a.c. polarograms are due to the redox reaction of Cl.Fd adsorbed on the electrode surface. Upon assuming that the adsorption is a diffusion-controlled process,[1,8] $\delta_1 I_p^{imag}$ is given by $\delta_1 I_p^{imag} = kA\Gamma = kA(6/7)(7D_{Cl.Fd}\tau/3\pi)^{1/2} C_{Cl.Fd}$ at the initial linear portion of $\delta_1 I_p^{imag}$ *versus* $C_{Cl.Fd}$ plot in Fig. 2, where k is the proportionality constant, Γ the surface concentration in mole per cm^2

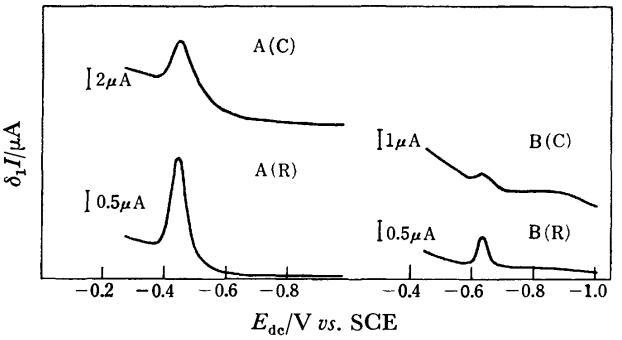

Fig. 1. A.c. polarograms of 1.7 μM Cl.Fd at 200 Hz. A(C) and A(R): Imaginary and real components at pH 4.4, B(C) and B(R): imaginary and real components at pH 9.2.

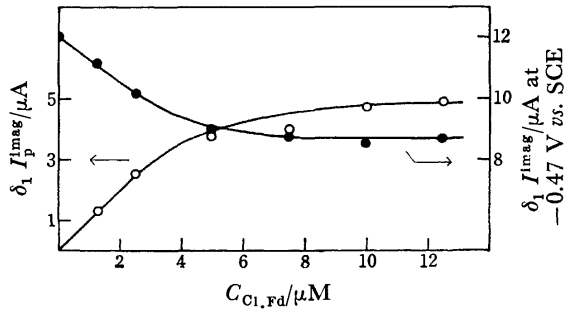

Fig. 2. Plots of $\delta_1 I_p^{imag}$ and $\delta_1 I^{imag}$ at −0.47 V against $C_{Cl.Fd}$ at pH 6.9 (frequency=200 Hz).
○: $\delta_1 I_p^{imag}$ (at −0.575 V *vs.* SCE), ●: $\delta_1 I^{imag}$ at −0.47 V *vs.* SCE.

† A main part of the experimental results of this work was presented at the 23rd Annual Meeting on Polarography, Nov. 4—5, 1977, Osaka: abstract; T. Ikeda, K. Toriyama, and M. Senda, *Rev. Polarogr. (Kyoto)*, **23**, 26 (1977).

of the adsorbed Cl.Fd, $D_{Cl.Fd}$ the diffusion coefficient of Cl.Fd, and A and τ are the surface area and the drop time of the DME, respectively. At high Cl.Fd concentrations a maximum current, $\delta_1 I_p^{max}$, is attained, which is given by $\delta_1 I_p^{max} = kA\Gamma^{max}$, where Γ^{max} is the maximum surface concentration of adsorbed Cl.Fd. Applying these two equations to the plot in Fig. 2, we estimated the Γ^{max} value as 1.4×10^{-11} mol/cm^2, $D_{Cl.Fd}=1.4\times10^{-6}$ cm^2 s^{-1} being assumed.[1] Adsorption of Cl.Fd also caused a decrease of the imaginary a.c. current in the potential region where the faradaic current does not appear, indicating that the differential double layer capacity of the mercury-solution interface decreases due to the adsorption of Cl.Fd on the electrode surface (see Fig. 2). Upon assuming that the relative decrease of the double layer capacitance, C_{dl}, is proportional to the surface coverage, θ, due to adsorption of Cl.Fd, that is, $\theta=\Gamma/\Gamma^{max}=(C_{dl}^{\circ}-C_{dl})/(C_{dl}^{\circ}-C_{dl}^{max})$, where C_{dl}° and C_{dl}^{max} are the double layer capacitances in the absence of Cl.Fd and at the maximum adsorption of Cl.Fd, respectively, Γ^{max} can be estimated by $\Gamma^{max}=(6/7)(7D_{Cl.Fd}/3\pi)^{1/2}C_{Cl.Fd}/((C_{dl}^{\circ}-C_{dl})/(C_{dl}^{\circ}-C_{dl}^{max}))$, where a diffusion-controlled adsorption of Cl.Fd is assumed. Application of this equation to the relative decrease of the imaginary a.c. current at -0.45 V at pH 6.9 leads to the Γ^{max} value of 1.3×10^{-11} mol/cm^2. These two Γ^{max} values agree well with each other and with the Γ^{max} value of 1.3×10^{-11} mol/cm^2 obtained for apoferredoxin (cluster-free ferredoxin) with the hanging mercury drop electrode (HMDE).[1]

In all a.c. polarograms of Cl.Fd recorded in this study, the peak potentials of the real and imaginary components, E_p^{real} and E_p^{imag}, coincided with each other and were independent of a.c. frequency between 50 and 500 Hz (see Table 1). As shown in Fig. 3 the peak potentials shifted by -60 mV/pH at pH lower than 7 and by -30 mV/pH at pH higher than 8. In the previous paper[1] we have shown that Cl.Fd adsorbed on the HMDE surface decomposes to the corresponding apoferredoxin and that the apoferredoxin gives d.c. and a.c. voltammograms due to the RSH/RSHg redox reaction of the cysteine residues of the apoferredoxin. At pH lower than 7 the peak potentials of the a.c. polarograms obtained with the DME agreed with the peak potentials of the RSH/RSHg redox couple observed with the HMDE.[1] Furthermore we found that at pH lower than 7 apo-Cl.Fd gives practically the same a.c. polarograms as Cl.Fd with the DME. These results indicate that at pH lower than 7 Cl.Fd adsorbed on the DME surface decomposes rapidly to apo-Cl.Fd and that the a.c. polarograms of Cl.Fd obtained here at pH lower than 7 should be assigned to the RSH/RSHg redox reaction of the cysteine residues of apo-Cl.Fd.

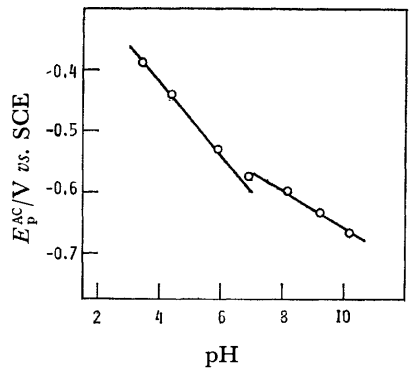

Fig. 3. Dependence of the peak potential, E_p^{AC}, on pH.

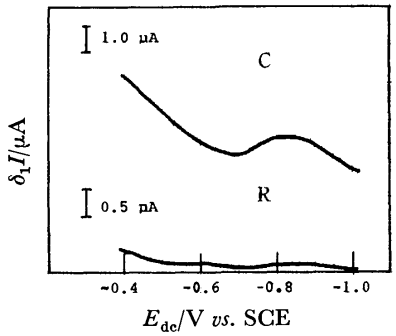

Fig. 4. A.c. polarograms of 1.5 μM apo-Cl.Fd at pH 9.2. R: Real component, C: imaginary component.

On the other hand at pH higher than 8 the a.c. polarograms of Cl.Fd with the DME (Fig. 1B) were obviously different from those of apo-Cl.Fd with the DME (Fig. 4). Furthermore the peak potentials of the a.c. polarograms of Cl.Fd with the DME in basic media (pH>8) were much more positive than the peak potentials of the steady-state cyclic a.c. or d.c. voltammograms at the HMDE which were assigned to the RSH/RSHg redox reaction of cysteine residues of apoferredoxin.[1] These results indicate that in basic media Cl.Fd adsorbed on the DME surface may remain undecomposed at least for a drop life of the DME, usually less than 9 s, and that the a.c. polarograms observed with DME in basic media should be assigned to the redox reaction of the iron-sulfur clusters of Cl.Fd adsorbed on the electrode surface. Figure 5 shows

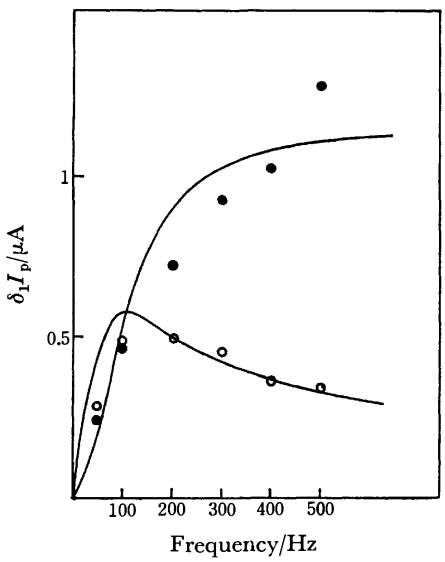

Fig. 5. Dependence of the peak heights of a.c. polarograms of 1.7 μM Cl.Fd on ac frequency at pH 9.2. ○: Real component, ●: imaginary component.

Table 1. Peak potential and half-peak width of a.c. polarograms of Cl.Fd adsorbed on DME surface at pH 9.2

Frequency/Hz	E_p^{real}/V *vs.* SCE	E_p^{imag}/V *vs.* SCE	$\Delta E_{p/2}^{real}$/mV Obsd	$\Delta E_{p/2}^{real}$/mV Calcd[a)]	$\Delta E_{p/2}^{imag}$/mV Obsd	$\Delta E_{p/2}^{imag}$/mV Calcd[a)]
50	−0.64	−0.64	25	24	35	35
100	−0.64	−0.64	30	29	40	45
200	−0.64	−0.64	35	37	—	64
300	−0.64	−0.64	40	43	—	77
400	−0.64	−0.64	45	48	—	87
500	−0.64	−0.64	50	51	—	96

a) Calculated by using $K=1$, $k_{sap}=3.9\cdot10^3\ s^{-1}$, and $G\theta_t=3.2$.

dependences of the peak heights of the two a.c. components on a.c. frequency at pH 9.2. The peak potentials, E_p^{real} and E_p^{imag}, and the half-peak widths, $\Delta E_{p/2}^{real}$ and $\Delta E_{p/2}^{imag}$ of the two components at pH 9.2 are gievn in Table 1.

The redox reaction of the iron-sulfur clusters of Cl.Fd in bulk solution has been studied by several authors using equilibrium techniques.[9–13] These studies have revealed that the stoichiometry of electron equivalents, n, is 2, whereas the potentiometric data fit the Nernst equation for which $n=1$.[10–13] Eisenstein and Wang[13] interpreted these results by assuming that Cl.Fd, which has two iron-sulfur clusters, is reduced in two reduction steps, each step involving a one-electron transfer to each cluster. More direct evidence was provided by Orme-Johnson and Beinert[14] and Mathews *et al.*,[15] who observed two different ESR signals arising sequentially during a reductive titration of Cl.Fd. Therefore, it is reasonable to suppose that the adsorbed Cl.Fd also is electrochemically reduced in two reduction steps at the mercury electrode surface.

According to theory of a.c. polarography[16] for a two-step surface redox reaction,

$$\begin{aligned} O_{ad} + n_1e &\rightleftharpoons S_{ad} \\ S_{ad} + n_2e &\rightleftharpoons R_{ad} \end{aligned} \qquad \text{(I)}$$

in which the interaction between the adsorbed reactants is taken into account, the real and imaginary components of the a.c. wave, $\delta_1 I_F^{real}$ and $\delta_1 I_F^{imag}$, for d.c. reversible process and $n_1=n_2=1$ may be, under appropriate simplifications,[17] expressed as

$$\delta_1 I_F^{real} = \frac{(r_1r_2-y_1y_2-x_1x_2)(r_1+r_2)+(r_1y_2+r_2y_1)(y_1+y_2+x_1-x_2)}{(r_1r_2-y_1y_2-x_1x_2)^2+(r_1y_2+r_2y_1)^2}\delta_1E \qquad \text{(1a)}$$

$$\delta_1 I_F^{imag} = \frac{(r_1y_1+r_2y_1)(r_1+r_2)-(r_1r_2-y_1y_2-x_1x_2)(y_1+y_2+x_1-x_2)}{(r_1r_2-y_1y_2-x_1x_2)^2+(r_1y_2+r_2y_1)^2}\delta_1E \qquad \text{(1b)}$$

with

$$r_1 = [(F^2/RT)\Gamma_t k_{sap}\bar{f}_1^{1/2}\bar{f}_2^{1/2}]^{-1}$$

$$r_2 = [(F^2/RT)\Gamma_t k_{sap}\bar{f}_2^{1/2}(1-\bar{f}_1-\bar{f}_2)^{1/2}]^{-1}$$

$$y_1 = [(F^2/RT)\Gamma_t\omega]^{-1}[(1/\bar{f}_1)+(1/\bar{f}_2)-G\theta_t]$$

$$y_2 = [(F^2/RT)\Gamma_t\omega]^{-1}[(1/\bar{f}_2)+(1/(1-\bar{f}_1-\bar{f}_2))-G\theta_t]$$

$$x_1 = -x_2 = [(F^2/RT)\Gamma_t\omega]^{-1}[(1/\bar{f}_2)-(1/2)G\theta_t]$$

In these equations δ_1E is the amplitude of applied ac voltage, ω the angular frequency, Γ_t the total surface concentration defined by $\Gamma_t=\Gamma_O+\Gamma_S+\Gamma_R$, Γ_i(i=O, S, or R) being the surface concentration of species i, θ_t the total surface coverage defined by $\theta_t=\Gamma_t/\Gamma^{max}$, Γ^{max} being the maximum value of Γ_t, $\bar{f}_1$ and $\bar{f}_2$ are the mean fractions of the surface coverages defined by $f_1=\overline{\Gamma}_O/\Gamma_t$ and $f_2=\overline{\Gamma}_S/\Gamma_t$, respectively, $\overline{\Gamma}_i$ is the mean or "d.c." value of Γ_i, k_{sap} the apparent rate constant of the charge transfer which depends on the adsorption parameters and on the total surface coverage θ_t, and G the parameter representing the interaction between the adsorbed reactants. The mean fractions $\bar{f}_1$ and $\bar{f}_2$ are related to the d.c. potential, E_{dc}, by

$$E_{dc} = E'_o + (RT/F)[\ln\sqrt{K}+\ln(\bar{f}_1/\bar{f}_2) - (1/2)(1-2\bar{f}_2)G\theta_t] \qquad \text{(2a)}$$

$$E_{dc} = E'_o + (RT/F)[-\ln\sqrt{K}+\ln(\bar{f}_2/(1-\bar{f}_1-\bar{f}_2)) + (1/2)(1-2\bar{f}_2)G\theta_t] \qquad \text{(2b)}$$

with

$$E'_o = (E'_{o1}+E'_{o2})/2 \qquad (3)$$

$$K = \exp[(F/RT)(E'_{o1}-E'_{o2})] \qquad (4)$$

where E'_{o1} and E'_{o2} are the formal standard potentials of the first and second surface redox steps, respectively. E'_o corresponds to the formal standard potential of the adsorbed redox couple O_{ad}/R_{ad}. The parameter K corresponds to the formation constant of the intermediate S_{ad}. These equations predict that both components of the a.c. wave are symmetrical with respect to the E'_o-axis and that within limited values of the parameters K, $G\theta_t$, and (ω/k_{sap}) the peak potentials of both components are independent of a.c. frequency and coincide with each other and with E'_o. These predictions are consistent with the present results. In Table 1 are also given values of the half-peak widths as calculated from these equations by assuming $K=1$, $G\theta_t=3.2$, and $k_{sap}=3.9\times10^3\ s^{-1}$. Solid lines in Fig. 5 are drawn by these equations using the same values of the parameters as above. Apparent agreement between the theory and experimental results seems reasonably good. However, it must be noted that the data can equally well fit the simplified equations (1) and (2) with other sets of k_{sap}, $G\theta_t$, and K for $0\leqq K\lesssim3$: for example, $k_{sap}=4.3\times10^3\ s^{-1}$, $G\theta_t=4$ and $K=3$, or $k_{sap}=5.8\times10^3\ s^{-1}$, $G\theta_t=2.5$ and $K=0.1$, or even $k_{sap}=5.0\times10^2\ s^{-1}$, $G\theta_t=0.95$ and $K=0$. The last set with $K=0$ corresponds to a single two-electron redox reaction, $O_{ad}+2e\rightleftarrows R_{ad}$[18] (II). In conclusion we may state that the a.c. polarographic behavior of Cl.Fd at DME in basic solution is explained by the redox reaction mechanism (I) with $0\leqq K\lesssim3$ (note that $K=0$ corresponds to the mechanism (II)).

As described above, the peak potentials of the a.c. polarograms, E_p^{AC}, in basic media should correspond to the formal standard redox potential of the iron-sulfur clusters of Cl.Fd adsorbed on the electrode surface. Table 2 summarizes our E_p^{AC} values and the values (extra- or interpolated to pH 7.0) of the standard redox potential, E'_o, of Cl.Fd determined by various equilibrium techniques.[9–13] The E'_o value cited from

TABLE 2. FORMAL STANDARD OXIDATION-REDUCTION POTENTIAL OF Cl.Fd

pH	E_o'/V *vs.* NHE	Method	Ref.
7.0	−0.33[a)]	A.c. polarography	This work
8.2	−0.355		
9.2	−0.390		
10.2	−0.420		
7.0	−0.33[a)]	Potentiometric titration in the presence of mediators.	9
7.0	−0.39[a)]	Equilibrium with H_2/H^+, hydrogenase.	10
7.0	−0.405		11
7.0	−0.403		12
7.4	−0.383	Equilibrium with methyl viologen (reduced)/(oxidized)	13

a) Value extra- or interpolated to pH 7.0.

Ref. 9 was determined by the direct potentiometric titration in the presence of mediators using a Pt electrode as an indicator electrode [direct method]. On the other hand, the E_o' values cited from Refs. 10 to 13 were measured by equilibrating a ferredoxin with another reducing redox couple such as H_2/H^+[10-12] or methyl viologen[13] using spectrophotometry [indirect method]. As seen from Table 2, our E_p^{AC} value extrapolated to pH 7 (= −0.33 V *versus* NHE) is *ca.* 60 to 70 mV more positive than the E_o' values determined by the "indirect" method.[10-13] This difference may be due to the difference in the free energy between the adsorbed redox couple and the redox couple in bulk of solution. On the contray the E_p^{AC} value agreed well with the E_o' value determined by the "direct" method (the value interpolated to pH 7.0 is −0.33 V *versus* NHE).[9] In addition the E_o' determined by the "direct" method shifted by −30 mV/pH, which is also in agreement with the pH dependence of the E_p^{AC} observed here in basic media. In the "direct" method a Pt electrode was used as an indicator electrode. Adsorption of plant ferredoxins on a Pt electrode was also reported.[5] Therefore it is likely that the E_o' determined by the "direct" method corresponds to the formal standard redox potential of the iron-sulfur clusters of Cl.Fd adsorbed on the Pt electrode surface.

This work was partially supported by a Grant-in-Aid for Scientific Research from the Ministry of Education.

References

1) T. Ikeda, K. Toriyama, and M. Senda, *Bull. Chem. Soc. Jpn.*, **52**, 1937 (1979).
2) P. D. J. Weitzman, I. R. Kennedy, and R. A. Caldwell, *FEBS Lett.*, **17**, 241 (1971).
3) H. Dalton and J. Zubieta, *Biochim. Biophys. Acta*, **322**, 133 (1973).
4) Y. W. Chien, *J. Pharm. Sci.*, **65**, 1471 (1976).
5) B. A. Kiselev, A. A. Kazakova, V. B. Evstigneev, V. K. Gins, and E. N. Mukhin, *Biofizika*, **21**, 35 (1976).
6) C. L. Hill, J. Renaud, R. H. Holms, and L. E. Mortenson, *J. Am. Chem. Soc.*, **99**, 2549 (1977).
7) P. Bianco and J. Haladjian, *Biochem. Biophys. Res Commun.*, **78**, 323 (1977).
8) J. Koryta, *Collect. Czech. Chem. Commun.*, **18**, 206 (1953).
9) B. Ke, W. A. Bulen, E. R. Shaw, and R. H. Breeze, *Arch. Biochem. Biophys.* **162**, 301 (1974).
10) K. Tagawa and D. I. Arnon, *Biochim. Biophys. Acta*, **153**, 602 (1968).
11) E. T. Lode, C. L. Murray, and J. C. Rabinowitz, *J. Biol. Chem.*, **251**, 1683 (1976).
12) N. A. Strombaugh, J. E. Sundquist, R. H. Burris, and W. H. Orme-Johnson, *Biochemistry*, **15**, 2633 (1976).
13) K. K. Eisenstein and J. H. Wang, *J. Biol. Chem.*, **244**, 1720 (1969).
14) W. H. Orme-Johnson and H. Beinert, *Biochem. Biophys. Res. Commun.*, **36**, 337 (1969).
15) R. Mathews, S. Charlton, R. H. Sands, and G. Palmer, *J. Biol. Chem.*, **249**, 4326 (1974).
16) T. Kakutani, K. Toriyama, T. Ikeda, and M. Senda, Paper presented at the 25th annual meeting on polarography, Oct. 5—6, 1979; abstract, *Rev. Polarogr. (Kyoto)*, **25**, 17 (1979).
17) These simplifications involve the following assumptions; $\alpha_1=\alpha_2=\beta_1=\beta_2=0.5$, $k_s(1)=k_s(2)$, $B_O(1)B_S(1)=B_S(2)B_R(2)$, $a_{OO}+a_{SO}=a_{OS}+a_{SS}=a_{OR}+a_{SR}=a_{SO}+a_{RO}=a_{SS}+a_{RS}=a_{SR}+a_{RR}$, $a_{1j}=a_{j1}$ (i, j=O, S, or R) where α_i and β_i are the cathodic and anodic transfer coefficients of the i-th charge transfer step, respectively, $k_s(i)$ is the standard rate constant of the i-th charge transfer step, $B_1(1)$ and $B_1(2)$ are the constants representing the adsorption free energy of species i on the electrode surface at $E=E_{o1}$ and $E=E_{o2}$, respectively, E_{o1} and E_{o2} the standard redox potentials of the redox couples O/S and S/R supposedly in the bulk of solution, respectively, and a_{1j} (i, j=O, S, or R) is the Frumkin's a-parameter of the interaction between the adsorbed reactions i and j.
18) T. Kakutani and M. Senda, *Bull. Chem. Soc. Jpn.*, **52**, 3236 (1979).

Pyrolytic Sulfurization Gas Chromatography. VI. The Continuous and Simultaneous Determination of the Atomic Ratio between C, H, O, and N in Various Compounds

Tadashi HARA,* Kaoru FUJINAGA, and Fujio OKUI

Department of Chemical Engineering, Faculty of Engineering, Doshisha University, Karasuma Imadegawa, Kamigyo-ku, Kyoto 602

(Received March 19, 1979)

The simultaneous determination of the atomic ratio between C, H, O, and N in various compounds including a metal organic chelate one has been presented in our previous papers.[1-3] With the objective of reducing the analysis time, an apparatus by which a continuous and simultaneous determination of the atomic ratio between C, H, O, and N can be carried out has been newly designed and constructed. Using this apparatus, many samples can be treated continuously at the rate of about 20 min for one sample, with satisfactory results.

It has been reported in the previous papers[1-3] that the simultaneous determination of the atomic ratio between C, H, O, and N in various compounds, including a metal organic chelate one, can be achieved with satisfactory results by pyrolytic sulfurization gas chromatography (PSGC). Since the analysis by the PSGC is, however, batch-by-batch, time-consuming, and laborious, an apparatus which made it possible to determine the atomic ratio between C, H, O, and N in a sample continuously and simultaneously was newly designed and constructed. An analysis can be carried out more rapidly and simply by this apparatus than by the previous one. In place of a Teflon-made gas sampler,[1] a new gas sampler consisting of three stainless steel crushing devices was constructed. The quartz ampule containing a sample was easily dashed to pieces in the present apparatus by driving the plunger of the crushing device in place of the jack used in the previous paper.[1] In the present gas sampler, the crushing device can be used for many analyses, unlike the more fragile Teflon tube in the previous paper. The analytical procedure using the crushing device consists of the following steps; 1) the introduction of an ampule, 2) the replacement of the air in the crushing device with helium(He) as a carrier gas, 3) analysis by gas chromatography, and 4) the recycling of these steps. Three crushing devices are set up in parallel with a gas chromatograph and operated separately in different steps. By this procedure the time necessary for an analysis was minimized; a sample could be analyzed within about 20 min, while it took about 30 min in the previous procedure. Using the present procedure, operating at the rate of 3 samples per hour, about three times as many samples as in the previous procedure could be treated; precision could also be improved by optimizing the reaction conditions.

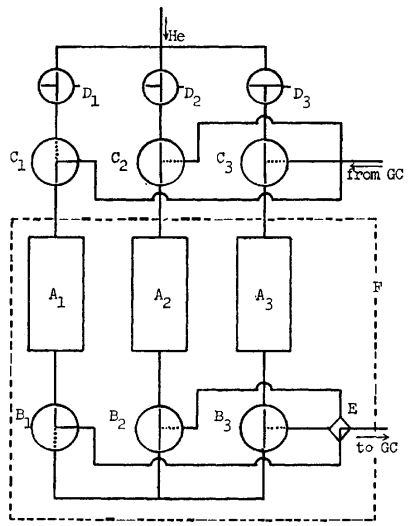

Fig. 1. Schematic flow diagram of the gas sampler. A_1, A_2, A_3: Crushing devices, B_1, B_2, B_3: electric valves-(heat-resistant), C_1, C_2, C_3: electric valves, D_1, D_2, D_3: three-way cocks, E: rotary cock, F: oven at 150 °C.

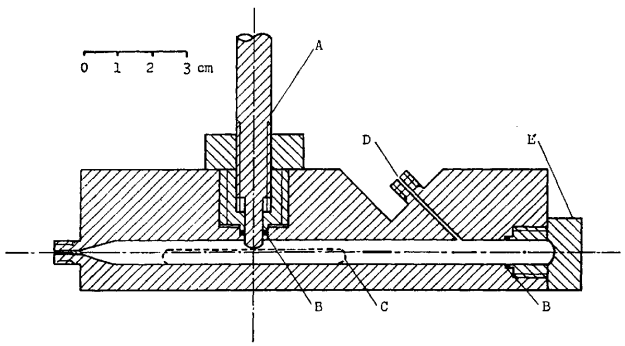

Fig. 2. Crushing device. A: Plunger for crushing an ampule, B: seals, C: an ampule containing a sample, D: carrier gas inlet, E: screwed cap for an ampule insertion.

Experimental

Apparatus. The new gas sampler is shown in Fig. 1. The gas sampler consists of three stainless steel crushing devices A(Fig. 2) and electric valves for the regulation of the gaseous flow. The inside of the crushing device was treated preliminarily by coating it with an aqueous solution of water glass, by drying it at room temperature under the reduced pressure, and by then elevating the temperature. The three crushing devices(A_1, A_2, and A_3) were laid out so as to connect them in parallel with a gas chromatograph by operating electric valves. The temperature of the gaseous flow between A and a gas chromatograph was held at 150 °C. The gas sampler was heated by connecting the crushing devices and electric valves with a hot brass plate into which cartridge heaters had been inserted. A Shimadzu GC-4B gas chromatograph was used for the analysis, while the other parts of the apparatus were the same as in the previous paper.

Reagents. The sulfur used as an oxidizing agent was obtained by purifying[4] commercially available sulfur (chemically pure). The organic compounds used as standard samples were of an analytical grade, while the metal organic chelate compounds were prepared carefully by the method found in the literature for their gravimetric analysis. The polymer samples were the same as in the previous paper.[5]

Procedure. The ampule containing a sample was prepared and the sample was made to react with sulfur as follows: Definite amounts of sulfur and a sample were placed in a quartz tube in which one end had been sealed, and the inside of the quartz tube was replaced with He, after which the other end of the quartz tube was sealed. The ampule thus obtained was held at 600 °C for 10 min and at 950 °C for 30 min. Thereafter, the ampule at 950 °C was slowly cooled in an electric furnace to room temperature by lefting it stand. Three ampules were at first inserted into the crushing devices, A_1, A_2, and A_3, and then the three flows including A_1, A_2, and A_3 were replaced with He, after which one of the three flows was connected with a gas chromatograph. Figure 1 shows that the flow-1 is in a state of an analyzing system, while the flows-2 and -3 are in a state of a replacing system. Here, A_2 is connected in series with A_3. Thus, the system replaced with He is shown by Scheme 1:

$$He \rightarrow D_2 — C_2 — A_2 — B_2 — B_3 — A_3 — C_3 — D_3 \rightarrow Exhaust$$

Scheme 1.

After the sample in the flow-1 has been completely analyzed, the flow-2 is connected with a gas chromatograph by turning the rotary cock, E, to the flow-2, while the flows-1 and -3 are in a state of a replacing system. Thus, the system replaced with He is shown by Scheme 2:

$$He \rightarrow D_3 — C_3 — A_3 — B_3 — B_1 — A_1 — C_1 — D_1 \rightarrow Exhaust$$

Scheme 2.

Here, the residual quartz pieces in A_1 are taken off and the next ampule is newly charged. After the 5 min necessary for the stabilization of the base line in a gas chromatogram, the column of the gas chromatograph is cooled for 5 min; then the ampule is broken with the plunger of A_2, followed by the gas-chromatographic analysis. In the present gas sampler, B and C in the same flow are designed so as to operate simultaneously. The analysis was carried out continuously by repeating the above-mentioned operation. The gas chromatogram was obtained under conditions similar to those used in a previous paper.[2]

Results and Discussion

Reaction Conditions. In the previous procedure the ampule at 950 °C was cooled to 90 °C immediately after the reaction, while it is cooled slowly to room temperature by being left standing in the electric furnace in the present procedure. The results obtained by the present procedure are superior to those obtained by the previous one in the following points; 1) the fluctuation of the individual peak area ratio on the chromatogram, 2) the evolution of carbon monoxide (CO) as an impurity, and 3) the fluctuation of the correction factors. The fluctuation of the ratio of the peak areas in the previous and the present procedures, which was obtained by analyzing 5 samples of glycine and by estimating the coefficient of variation in the ratio of the individual peak area, is shown in Table 1.

The amount of CO evolved in the present procedure was smaller than that in the previous procedure and was neglected much as before. As may be seen from the fact that the peak of CO overlaps with that of nitrogen(N_2) on the chromatogram, the present procedure may be expected to be more precise than the previous one. This is shown in Fig. 3 with regard to the compound consisting of C, H, and O, the relationship between the peak areas of carbonyl sulfide (COS) and of CO is plotted. It can easily be seen from Fig. 3 that the peak area of CO is approximately proportional to that of COS. No linear relationship was, however, obtained experimentally between CO and carbon dioxide or carbon disulfide. On the basis of these results, CO was considered to evolve by means of the equilibrium shown in Eq. 1:

$$CO(g) + \frac{1}{x}S_x(g) \rightleftharpoons COS(g). \quad (1)$$

By taking the complete decomposition of COS at high temperatures into consideration, and by supposing that the above equilibrium could not be established completely when the temperature was suddenly lowered to 90 °C from 950 °C, the evolution of a larger amount of CO in the previous procedure as compared with that in the present one was easily understood. The amount of CO evolved by dropping the ampule into water at 950 °C was found to be several times as great as the amount of CO evolved by the present procedure. This makes the above considerations reasonable.

TABLE 1. FLUCTUATION OF THE RATIO OF PEAK AREAS IN THE PREVIOUS AND THE PRESENT PROCEDURES

Procedure	Coefficient of variation (%)[a]				
	N_2	CO_2	H_2S	COS	CS_2
Present	0.2365	1.026	0.3895	0.1678	1.141
Previous	1.331	2.437	0.8553	1.406	1.940

a) Calculated from five runs for glycine.

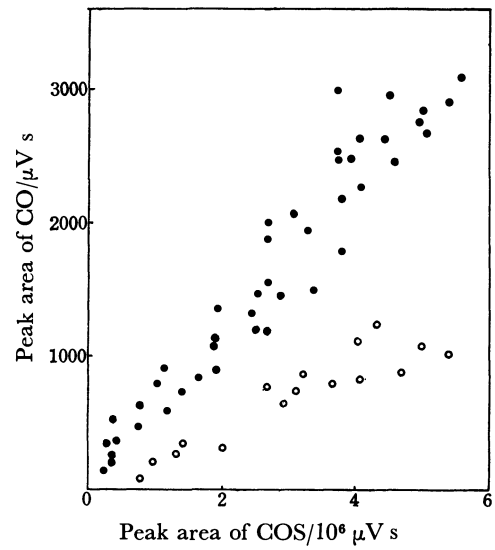

Fig. 3. Relationship between peak areas of COS and of CO in the compound consisting of C, H, and O.
○: Present procedure, ●: previous procedure.

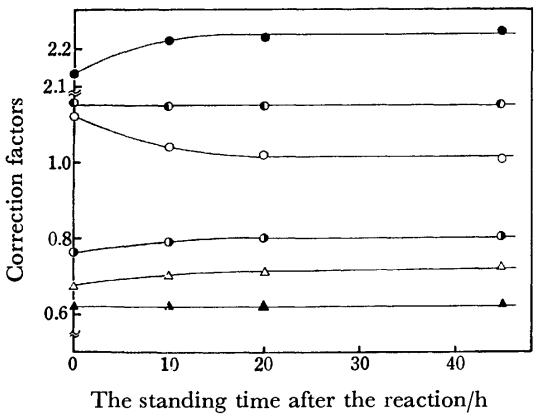

Fig. 4. Effect of the standing time on correction factors. ◐: $K(N_2)$, ○: $K(CO_2)$, △: K(COS), ●: $K(H_2O)$, ◑: $K(SO_2)$, ▲: $K(CS_2)$.

According to the experimental results, the correction factors changed with the standing time within several hours after the completion of the reaction (Fig. 4). It may also be seen from Fig. 4 that a definite period of standing for an ampule is indispensable for obtaining a good result. The correction factor of $N_2(K(N_2))$, which was defined by $K(N_2)=A(H_2S)/A(N_2)$, was obtained by the use of dicyandiamide.[2] Hydrogen sulfide was concluded to be stable, irrespective of the standing time of the ampule throughout the experiment, since N_2 was stable under the conditions of PSGC and since $K(N_2)$ was also constant experimentally. Though hydrogen (H_2) could not be detected under the conditions of PSGC, it was unnecessary, in the light of the above results, to pay much attention to H_2. Based on these results, the previous procedure was improved as in the present one, in which the ampule was analyzed for a definite period of standing after the reaction.

Pretreatment of a Crushing Device. The results obtained by the use of a crushing device without pretreating the internal surface fluctuated from sample to sample, and the peak of water (H_2O) was observed in spite of the fact that the H_2O should not evolve under the present experimental conditions. To avoid these phenomena, the internal surface of the crushing device was treated with an aqueous solution of disodium phosphate or water glass. The pretreatment with an aqueous solution of water glass was found to improve the analytical results markedly and to reduce the amount of evolved water to traces from $H_2O/N_2=0.0381$, which was obtained as the mean value of the peak-area ratio in 5 analyses of glycine. Therefore, the internal surfaces of all the crushing devices were coated with water glass for use.

Gas Sampler. The gas sampler used in the previous papers was made of Teflon and was occasionally broken with a piece of quartz. The previous procedure was also time-consuming, since such operations as 1) the removal of quartz pieces and the insertion of a sample, 2) the replacement of the air in the inside of a gas sampler with He, and 3) the analysis of the reaction products with a gas chromatograph were carried out with only one gas sampler. By setting up three crushing devices in parallel with a gas chromatograph, the gas sampler could be used for a long time and the time necessary for an analysis was minimized to about 20 min from the period of about 30 min needed in the previous procedure. According to the present procedure, the analysis could be carried out continuously at the rate of 3 samples per hour.

Analysis of Various Compounds. Various organic compounds, metal organic chelate compounds, and polymers were analyzed by the present procedure; the results are shown in Tables 2, 3, and 4, respectively. As may be seen from Tables 2—4, both precision and accuracy were superior to those by the previous procedure. After the sample in an ampule treated at 950 °C

Table 2. Analytical results of organic compounds

Sample	C wt%			H wt%			O wt%			N wt%		
	Theor.	Found	Error	Theor.	Found	Error	Theor.	Found	Error	Theor.	Found	Error
Glycine	32.00	31.93	−0.07	6.71	6.86	+0.15	42.63	42.30	−0.33	18.66	18.91	+0.25
L-Glutamine	41.09	41.04	−0.05	6.90	7.04	+0.14	32.84	32.78	−0.04	19.17	19.13	−0.04
Cholesterol	83.87	83.62	−0.25	11.99	12.03	+0.04	4.14	4.35	+0.21			
8-Quinolinol	74.47	74.40	−0.07	4.86	4.88	+0.02	11.02	10.94	−0.08	9.65	9.78	+0.13
Benzophenone	85.69	85.66	−0.03	5.53	5.51	−0.02	8.78	8.83	+0.05			
p-Dimethylamino-benzaldehyde	72.46	72.47	+0.01	7.43	7.53	+0.10	10.72	10.93	+0.21	9.39	9.08	−0.31
2,2′,3,3′,4,4′,5,5′,6-Nonamethyl-diphenylmethane	89.73	89.84	+0.11	10.27	10.16	−0.11						
Lauric acid	71.95	72.17	+0.22	12.08	12.07	−0.01	15.97	15.76	−0.21			
Myristic acid	73.63	73.76	+0.13	12.36	12.15	−0.21	14.01	14.09	+0.08			
Stearic acid	75.99	75.63	−0.36	12.76	12.75	−0.01	11.25	11.62	+0.37			
Palmitic acid	74.94	74.72	−0.22	12.58	12.51	−0.07	12.48	12.77	+0.29			
Suberic acid	55.16	55.01	−0.15	8.10	8.23	+0.13	36.74	36.77	+0.03			

TABLE 3. ANALYTICAL RESULTS OF METAL ORGANIC CHELATE COMPOUNDS

Sample[a]	C wt%			H wt%			O wt%			N wt%		
	Theor.[b]	Found	Error	Theor.[b]	Found	Error	Theor.[b]	Found	Error	Theor.[b]	Found	Error
Bis(8-quinolinolato)-magnesium(II) $Mg(C_9H_7ON)_2$	74.99	75.04	−0.05	4.20	4.19	−0.01	11.10	10.82	−0.28	9.72	9.93	+0.21
Tris(8-quinolinolato)-chromium(III) $Cr(C_9H_6ON)_3$	74.99	74.95	−0.04	4.20	4.18	−0.02	11.10	11.26	+0.16	9.72	9.61	−0.11
Bis(anthranilato)-manganese(II) $Mn(C_7H_6O_2N)_2$	61.76	62.15	+0.39	4.44	4.47	+0.03	23.51	23.44	−0.07	10.29	9.94	−0.35
Tris(8-quinolinolato)-iron(III) $Fe(C_9H_6ON)_3$	74.99	75.30	+0.31	4.20	4.04	−0.16	11.10	11.29	+0.19	9.72	9.36	−0.36
Bis(anthranilato)-cobalt(II) $Co(C_7H_6O_2N)_2$	61.76	62.01	+0.25	4.44	4.51	+0.07	23.51	23.23	−0.28	10.29	10.25	−0.04
Bis(8-quinolinolato)-nickel(II) $Ni(C_9H_6ON)_2$	74.99	75.23	+0.24	4.20	4.16	−0.04	11.10	11.12	+0.02	9.72	9. 6	−0.26
(Benzoin oximato)-copper(II) $Cu(C_{14}H_{11}O_2N)$	74.65	74.60	−0.05	4.92	4.65	−0.27	14.21	14.55	+0.34	6.23	6.20	−0.03
Bis(salicylaldehyde oximato)copper(II) $Cu(C_7H_6O_2N)_2$	61.76	61.61	−0.15	4.44	4.44	0	23.51	23.44	−0.07	10.29	10.50	+0.21
Bis(anthranilato)-copper(II) $Cu(C_7H_6O_2N)_2$	61.76	62.04	+0.28	4.44	4.55	+0.11	23.51	23.28	−0.23	10.29	10.11	−0.18
Bis(anthranilato)-zinc(II) $Zn(C_7H_6O_2N)_2$	61.76	61.96	+0.20	4.44	4.28	−0.16	23.51	23.66	+0.15	10.29	10.10	−0.19
Bis(8-quinolinolato)-cadmium(II) $Cd(C_9H_6ON)_2\cdot 2H_2O$	66.66	67.01	+0.35	4.94	4.88	−0.06	19.75	19.49	−0.26	8.65	8.62	−0.03
Tris(8-quinolinolato)-gallium(III) $Ga(C_9H_6ON)_3$	74.99	74.96	−0.03	4.20	4.15	−0.05	11.10	11.30	+0.20	9.72	9.59	−0.13
Tris(8-quinolinolato)-indium(III) $In(C_9H_6ON)_3$	74.99	75.39	+0.40	4.20	4.06	−0.14	11.10	11.14	+0.04	9.72	9.41	−0.31
Dioxobis(8-quinolinolato)molybdenum(VI) $MoO_2(C_9H_6ON)_2$	67.50	67.37	−0.13	3.78	3.70	−0.08	19.98	20.25	+0.27	8.75	8.68	−0.07
Dioxobis(8-quinolinolato)tungsten(VI) $WO_2(C_9H_6ON)_2$	67.50	67.35	−0.15	3.78	3.58	−0.20	19.98	20.19	+0.21	8.75	8.89	+0.14

a) Metal atoms were neglected in considering the composition of metal organic chelate compounds, since they couldn ot be determined. b) These values were also found to be correct by the C and H analysis carried out in the Elemental analysis Center of the Pharmaceutical Department of Kyoto University.

TABLE 4. ANALYTICAL RESULTS OF VARIOUS POLYMERS

Sample		C wt%		H wt%		O wt%	
		CH analysis[a]	PSGC	CH analysis[a]	PSGC	CH analysis[b]	PSGC
Phenol resin		82.49	82.75	10.76	10.38	6.78	6.87
Xylene resin		82.10	82.31	8.83	8.70	9.07	8.97
Terpene resin		85.37	85.31	11.42	11.31	3.21	3.37
Acrylonitrile/butadiene/stylene terpolymer	A	85.63	85.67	7.92	7.65	6.45	6.69
	B	85.52	85.86	7.81	7.76	6.67	6.39
Ethylene/vinyl acetate copolymer	A	81.36	81.19	13.71	13.41	4.93	5.39
	B	76.27	76.34	12.15	12.04	11.58	11.62
	C	72.99	73.36	11.27	11.18	15.74	15.48

a) The composition of the samples were confirmed by the C and H analysis carried out in the Elemental Analysis Center of the Pharmaceutical Department of Kyoto University. b) Determined by subtracting the sum of the C and H values from the total amount of a sample.

TABLE 5. ANALYTICAL RESULTS OF ORGANIC COMPOUNDS WHICH WERE LEFT STANDING FOR 3 WEEKS AFTER THE REACTION

Sample	C wt%			H wt%			O wt%			N wt%		
	Theor.	Found	Error	Theor.	Found	Error	Theor.	Found	Error	Theor.	Found	Error
Glycine	32.00	31.79	−0.14	6.71	6.62	−0.09	42.63	42.45	−0.18	18.66	19.14	+0.48
8-Quinolinol	74.47	74.41	−0.06	4.86	4.87	+0.01	11.02	10.93	−0.09	9.65	9.79	+0.14
Benzophenone	85.69	85.80	+0.11	5.53	5.48	−0.05	8.78	8.73	−0.05			
Suberic acid	55.16	55.47	+0.31	8.10	8.21	+0.11	36.74	36.31	−0.43			

was left standing for 3 weeks at room temperature, it was analyzed (Table 5). It may be seen from Table 5 that a good analytical value was obtained irrespective of the standing time after the temperature of a sample had been brought to room temperature in accordance with the present procedure.

The present gas sampler could also be used for the previous procedure so long as the correction factors obtained previously were used.

References

1) K. Tsuji, K. Fujinaga, and T. Hara, *Bull. Chem. Soc. Jpn.*, **50**, 2292 (1977).
2) T. Hara, K. Fujinaga, and K. Tsuji, *Bull. Chem. Soc. Jpn.*, **51**, 1110 (1978).
3) T. Hara, K. Fujinaga, and K. Tsuji, *Bull. Chem. Soc. Jpn.*, **51**, 2951 (1978).
4) T. Hara, K. Fujinaga, K. Tsuji, and F. Okui, *Bull. Chem. Soc. Jpn.*, **51**, 3079 (1978).
5) T. Hara, K. Fujinaga, and F. Okui, *Bull. Chem. Soc. Jpn.*, in press.

Metal Complexes of Amino Acids. XII.[1] The Deuteration of α-Hydrogen Atoms in Cobalt(III) Complexes Containing α-Amino Carboxylates

Tomoharu AMA,* Hiroshi KAWAGUCHI, Makoto KANEKIYO, and Takaji YASUI

Department of Chemistry, Faculty of Science, Kochi University, Akebono-cho, Kochi 780

(Received June 29, 1979)

The second-order rate constants (rate=$k_{D(base)}$[Complex][OD^-]) for the deuterium exchange of α-methylene or α-methine protons in the amino carboxylato complexes, *trans(O)*-, C_1-*cis(O)*-, and C_2-*cis(O)*-$[Co(gly)_2(en)]^+$ and -$[Co(gly)_2(tn)]^+$, $[Co(gly)(NH_3)_4]^{2+}$, $[Co(gly)(en)_2]^{2+}$, $[Co(gly)(tn)_2]^{2+}$, $[Co(sar)(en)_2]^{2+}$, and *Λ*- and *Δ*-$[Co(L\text{-ala})(en)_2]^{2+}$, were determined by the ^{1}H-NMR measurement. The major factors determining the deuteration rate of α-hydrogens in the amino carboxylate chelate are the geometry and charge of the complex, and the nature of the substituent bonded to the chelate ring to be deuterated; the minor factor is the chelate-ring size of the ligands other than amino carboxylate in a complex molecule.

It is well-known that the metal ions increase the reactivity of α-methylene protons in α-amino carboxylate. Since the magnitude and specificity of the effect were first shown by Williams and Busch[2] through a ^{1}H-NMR study of cobalt(III) complexes containing glycinate, alaninate, and ethylenediaminetetraacetate, a large number of studies involving the deuteration of the cobalt(III) complexes have been undertaken.[3-14] Many of these studies have treated polyamino carboxylato complexes. On the other hand, few studies have been made of the α-amino carboxylato complexes. It had been found that the deuteration rate of the glycinate methylene proton in the polyamino carboxylato complex is related to the chelate-ring strain; *i.e.*, the methylene protons of out-of-plane glycinate (less strained) in $[Co(edta)]^-$ are more rapidly deuterated than those of in-plane glycinate (strained).[2] However, factors (the charge and geometry of the complex and substituent in the ligand, and so on) other than the ring strain must also be related to the deuteration rate. In order to determine these factors, a study using α-amino carboxylato complexes is more profitable than one using polyamino carboxylato complexes because then we can exclude the effect of the chelate-ring strain.

In the present paper, we will evaluate the deuteration rates of α-protons in several types of cobalt(III) complexes containing the chelated glycinate, L-alaninate, and sarcosinate; we will also discuss the relation between the deuteration rate and the geometry of the complex, the charge of the complex ion, and the nature of the substituent in a ligand.

Experimental

Preparation of the Complexes. Synthesis and Separation of the Isomers of Bis(glycinato)(trimethylenediamine)cobalt(III) Chloride: A solution containing 10 g of cobalt(II) chloride hexahydrate in 10 ml of water was added to a solution containing 5 g of trimethylenediamine and 6.4 g of glycine in 30 ml of water. Lead dioxide (10 g) was then gradually added to the solution on a water bath, after which the solution was mechanically stirred at 55 °C for about 30 min. The precipitates were filtered off, and the filtrate was kept in a refrigerator overnight. The precipitates were filtered off again, and the filtrate was poured into a column containing a cation-exchange resin (Dowex 50W×8, 200—400 mesh, K^+ form). The column was flushed with water to sweep out any nonelectrolytic or anionic complexes, and then the adsorbed band was developed with a 0.2 M aqueous solution of potassium chloride. Two bands appeared: a violet one (lower) and a red-violet one (upper). It was confirmed from their absorption spectra that the early- and late-eluted solutions contain *trans(O)* and *cis(O)* (mixture of C_1-*cis(O)* and C_2-*cis(O)*) isomers respectively. Each eluted solution was evaporated to a small volume using a rotary evaporator, a small amount of ethanol was added to the concentrated solution, and the potassium chloride was filtered off. A crude product of the *trans(O)* isomer was obtained from the above solution (early eluate) on the addition of more ethanol. The C_1-*cis(O)* isomer was deposited as columnar crystals by the further addition of a small amount of ethanol to the above ethanolic solution (late eluate) and by then keeping the solution in a refrigerator overnight. After the C_1-*cis(O)* isomer had been removed by filtration, a large amount of ethanol was added to the filtrate. A crude product of the C_2-*cis(O)* isomer was obtained as fine needle crystals. Each isomer was recrystallized from water by the addition of ethanol. Found for the *trans(O)* isomer: C, 25.91; H, 6.14; N, 17.15%. Calcd for $[Co(gly)_2(tn)]Cl\cdot 0.5H_2O$: C, 25.81; H, 5.88; N, 17.20%. Found for the C_1-*cis(O)* isomer: C, 25.20; H, 6.13; N, 16.85%. Calcd for $[Co(gly)_2(tn)]Cl\cdot H_2O$: C, 25.12; H, 6.02; N, 16.74%. Found for the C_2-*cis(O)* isomer: C, 24.63; H, 6.29; N, 16.08%. Calcd for $[Co(gly)_2(tn)]Cl\cdot 1.5H_2O$: C, 24.46; H, 6.11; N, 16.30%.

The other cobalt(III) complexes examined here were prepared by the published methods[15-21] and were found to be analytically pure.

Measurements of Deuteration Rate. The deuteration runs were carried out under a flow of nitrogen in order to avoid a decrease in the pD by the absorption of CO_2 in air. Each complex (1 mmol) was dissolved in 9 ml of D_2O. The sample solution was kept at 30.0, 40.0, or 50.0 °C (±0.05 °C) in a thermostat, and then 20 μl of *t*-butyl alcohol and 1 ml of a 1 M Na_2CO_3–D_2O solution (or a 0.5 M Na_2CO_3–0.5 M $NaDCO_3$–D_2O solution) were added to the sample solution. The deuteration of the methylene protons of chelated glycinate began immediately after the Na_2CO_3–D_2O solution was added to the sample solution. At prescribed time intervals, 0.5-ml aliquot sample solutions were taken out from the container, kept in a thermostat. The exchange reaction was immediately stopped by adding the sample solution to 0.05 ml (or 0.038 ml) of 2 M DCl and by then cooling the mixture to 0 °C. The pD of the sample solution in the container was measured by the use of a pH meter (Beckman LABOMATE II) with a combination electrode. The pD=pH+0.4[22] and $[OD^-]=3.0\times 10^{-15}[D^+]^{-1}$ formulae were used to evaluate $[D^+]$ and $[OD^-]$ re-

spectively.

The ^{1}H-NMR spectra of the neutralized solutions were recorded at 100 MHz using a JEOL MH-100 NMR spectrometer at room temperature. The intensities of the ^{1}H-NMR signals of the methylene protons in the chelated glycinate were estimated by comparing them with that of *t*-butyl alcohol as a standard. The ^{1}H-NMR data are given with the chemical shifts *vs.* DSS.

Results and Discussion

trans(O), C_1-cis(O), and C_2-cis(O) Isomers of $[Co(gly)_2(en)]^+$. The ethylene proton signals arising from the chelated ethylenediamine were unchanged throughout the experiment. In addition, on developing the residual solution of each deuteration run in the cation-exchange column (SP-Sephadex), only one band was observed; no complexes resulting from decomposition or isomerization were detected. The neutralized solution used for the ^{1}H-NMR measurement did not show any change in its NMR intensity or spectral pattern for at least one day at room temperature.

The resonance peaks of the methylene protons of chelated glycinate appeared in the range of 3.4—3.7 ppm. The two glycinate methylenes in the C_2-*cis(O)* and *trans(O)* isomers are equivalent, but those in the C_1-*cis(O)* isomer are not. Figure 1 shows the resonance patterns which are to be expected from the symmetries of these isomers. Yoneda *et al.*[23] assigned the methylene signal at 3.60 ppm to the $H_a(H_a')$ of glycinate and that at 3.44 ppm to $H_b(H_b')$ (Fig. 1).

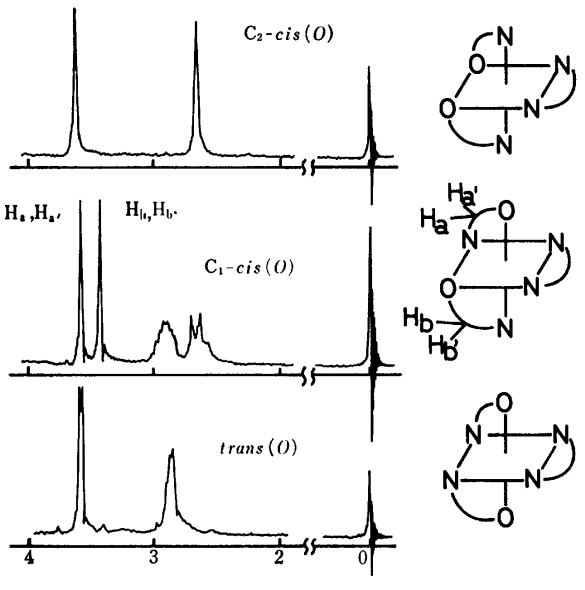

Fig. 1. ^{1}H-NMR spectra of C_2-*cis(O)*-, C_1-*cis(O)*-, and *trans(O)*-$[Co(gly)_2(en)]^+$ complex ions.

Plots of log *I vs.* the deuteration time at a constant pD yield straight lines, where *I* denotes the relative NMR intensities of the glycinate methylenes to the *t*-butyl alcohol methyls, the internal standard (Fig. 2). Accordingly, the deuteration rate at a constant pD

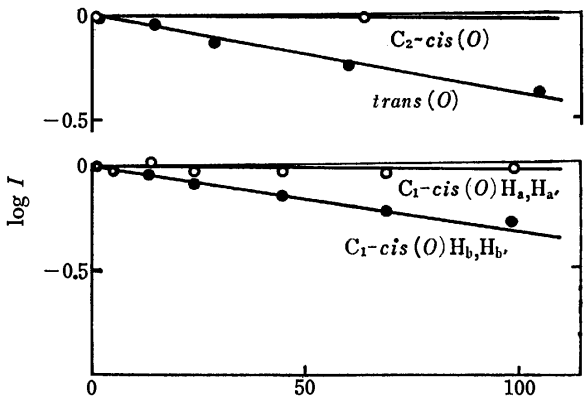

Fig. 2. Plots of log *I* (*I* denotes the relative NMR intensity of α-hydrogens) *vs.* deuteration time of three isomers in $[Co(gly)_2(en)]^+$ complex ion. pD=11.7; Temperature, 30.0 °C.

can be expressed as:

$$-\frac{d[complex]}{dt} = k'_{D(base)}[complex],$$

where $k'_{D(base)}$ is the apparent rate constant for the base-catalyzed deuteration at a constant pD. This result agrees with that obtained from the study of EDDA–Co(III) complexes by Sudmeier and Occupati.[5] The rate constants of the deuterium exchange of methylene protons in the chelated glycinate are given in Table 1. Sudmeier and Occupati showed, in their study of the base-catalyzed deuterium exchange of EDDA–Co(III) complexes, that the reaction was first-order in $[OD^-]$. Our present result coincides with their result; *i.e.*, the $k'_{D(base)}[OD^-]^{-1}$ values of the present complexes are constant at a given temperature.

The deuteration rates of the methylene protons in the chelated glycinate at 50 °C decrease in this order; *trans(O)*$\geq H_b(H_b')$ of C_1-*cis(O)*$>C_2$-*cis(O)*$\geq H_a(H_a')$ of C_1-*cis(O)*. Dabrowiak and Cooke[24] studied the reaction of acetaldehyde with cobalt(III) complexes containing chelated glycinate. They showed that the order of reactivity is: $[Co(gly)(en)_2]^{2+}$>*trans(O)*-$[Co(gly)_2(en)]^+$ >C_1-*cis(O)*-$[Co(gly)_2(en)]^+$>C_2-*cis(O)*-$[Co(gly)_2(en)]^+$. This order agrees with that of the deuteration rate determined in the present study. The fact that the rates are different among the geometrical isomers of the present complexes with the same 1+ charge suggests that the geometry of the complex is one of the most important factors affecting the deuteration rate.

It is obvious from Table 1 and Fig. 2 that the two non-equivalent glycinates in the bis(glycinato) complex differ in their deuteration rates; *i.e.*, the rate of the deuterium exchange of $H_b(H_b')$ in C_1-*cis(O)*-$[Co(gly)_2(en)]^+$ is larger than that of $H_a(H_a')$. It is known that the deuteration of the "out-of-plane" glycinate protons in $[Co(edta)]^-$ is far more rapid than those of any other CH_2 protons in the complex. Williams and Busch[2] suggested that such a difference between the two non-equivalent glycinates in $[Co(edta)]^-$ is a function of the ring strain. In the present complex, C_1-*cis(O)*-$[Co(gly)_2(en)]^+$, no such chelate-ring strain as in

TABLE 1. RATE CONSTANTS FOR THE DEUTERIUM-EXCHANGE REACTION OF GLYCINATE α-HYDROGENS IN *trans(O)*-, C_2-*cis(O)*-, AND C_1-*cis(O)*-$[Co(gly)_2(en)]^+$ COMPLEX IONS

Species	Temp °C	$k'_{D(base)}$ (10^{-4} s^{-1})	[OD^-] (mol/l)	$k_{D(base)}$ ($k'_{D(base)}/[OD^-]$)
trans(O)	20.0	0.29±0.01	0.19×10^{-2}	0.015±0.0006
	30.0	1.53±0.03	0.15×10^{-2}	0.100±0.0018
	50.0	1.26±0.13	0.61×10^{-4}	2.1 ±0.21
C_2-*cis(O)*	30.0	0.14±0.01	0.77×10^{-3}	0.018±0.0013
	40.0	0.66±0.03	0.74×10^{-3}	0.089±0.0036
	50.0	2.44±0.21	0.75×10^{-3}	0.325±0.0280
C_1-*cis(O)* H_b	30.0	1.12±0.03	0.17×10^{-2}	0.066±0.0016
	40.0	2.47±0.13	0.87×10^{-3}	0.29 ±0.015
	50.0	2.62±0.27	0.19×10^{-3}	1.4 ±0.14
	50.0	6.35±0.34	0.42×10^{-3}	1.5 ±0.08
C_1-*cis(O)* H_a	30.0	0.18±0.04	0.17×10^{-2}	0.011±0.0023
	40.0	0.46±0.04	0.87×10^{-3}	0.053±0.0049
	50.0	0.58±0.23	0.19×10^{-3}	0.31 ±0.12
	50.0	1.22±0.12	0.42×10^{-3}	0.29 ±0.028

TABLE 2. ACTIVATION PARAMETERS FOR THE BASE-CATALYZED DEUTERATION OF GLYCINATO α-HYDROGENS IN *trans(O)*-, C_2-*cis(O)*-, AND C_1-*cis(O)*-$[Co(gly)_2(en)]^+$ COMPLEX IONS

Species	$\Delta G^{\ddagger}$(50 °C) (kJ mol^{-1})	$\Delta H^{\ddagger}$ (kJ mol^{-1})	$\Delta S^{\ddagger}$ (JK^{-1} mol^{-1})
trans(O)	77±8	131±4	168±14
C_2-*cis(O)*	82±10	120±5	117±16
C_1-*cis(O)* $H_b(H_b')$	78±13	128±6	154±20
C_1-*cis(O)* $H_a(H_a')$	82±11	139±5	176±18

$[Co(edta)]^-$ can be expected between the two non-equivalent glycinates. Nevertheless, the rate constant of $H_b(H_b')$ is about five times as large as that of $H_a(H_a')$. This suggests that, in the bis(glycinato) complexes, there are factors other than the chelate-ring strain.

The activation parameters of these isomers are given in Table 2. Both the enthalpy and the entropy of activation for these isomers increase in this order: C_2-*cis(O)*< $H_b(H_b')$ of C_1-*cis(O)*<*trans(O)*<$H_a(H_a')$ of C_1-*cis(O)*. The order of $\Delta H^{\ddagger}$ and $\Delta S^{\ddagger}$ is different from the order of the deuteration rate.

trans*(O)*, C_1-cis*(O)*, *and* C_2-cis*(O) Isomers of* $[Co(gly)_2(tn)]^+$. The ^{1}H-NMR spectra of these complexes are shown in Fig. 3. The methylene resonances of the glycinates in the *trans(O)* and C_2-*cis(O)* isomers were observed at 3.57 and 3.58 ppm respectively. The methylene resonances of the C_1-*cis(O)* isomer appeared as singlet peaks at 3.57 ppm (assigned to H_a and H_a' on the basis of the theory proposed by Yoneda *et al.*)[23] and 3.35 ppm (assigned to H_b and H_b'). These isomers did not decompose or isomerize under the given conditions, and the neutralized solution used for the ^{1}H-NMR measurement did not indicate any change in NMR intensity and spectral shape for at least one day at room temperature.

The deuteration rates of the methylene protons of glycinates decrease in this order: $H_b(H_b')$ of C_1-*cis(O)*≳ *trans(O)*>C_2-*cis(O)*>$H_a(H_a')$ of C_1-*cis(O)* (at 50 °C; Table 3). This order is almost the same as that of the isomers of $[Co(gly)_2(en)]^+$. The difference in the deuteration rate between the two non-equivalent glycinates in the C_1-*cis(O)* isomer is obvious, as has been shown for the C_1-*cis(O)* isomer of the $[Co(gly)_2(en)]^+$ complex. The trimethylenediamine and ethylenediamine complexes indicated a nearly equal deuteration rate for each corresponding isomer.

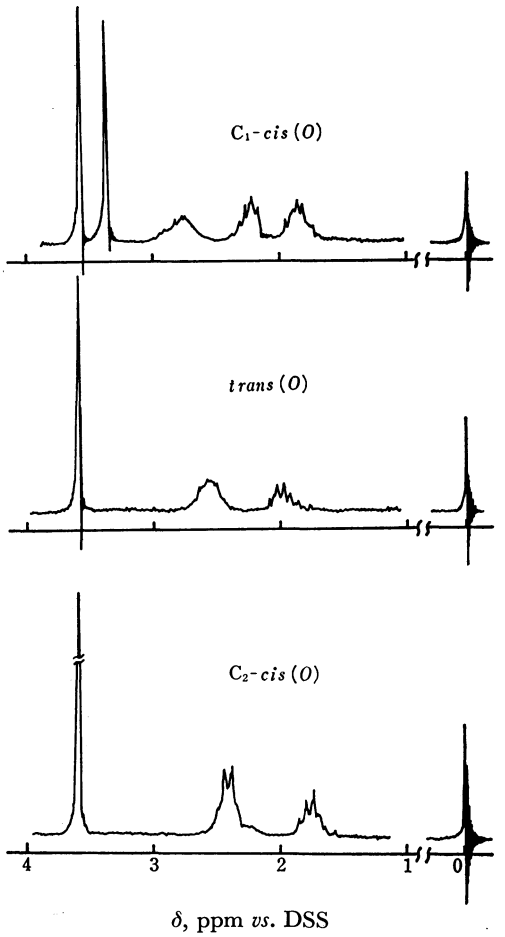

Fig. 3. ^{1}H-NMR spectra of C_1-*cis(O)*-, *trans(O)*-, and C_2-*cis(O)*-$[Co(gly)_2(tn)]^+$ complex ions.

$[Co(gly)(en)_2]^{2+}$, $[Co(gly)(tn)_2]^{2+}$, and $[Co(gly)$-

Table 3. Rate constants at 50 °C for the deuterium-exchange reaction of amino carboxylato α-hydrogens in various complex ions

Species	$k_{D}'_{(base)}$ (10^{-4} s^{-1})	[OD^-] (mol/l)	$k_{D(base)}$ ($k_{D}'_{(base)}$/[OD^-])
trans(*O*)-[$Co(gly)_2(tn)]^+$	8.7 ±0.2	0.48×10^{-3}	1.8 ±0.047
C_1-*cis*(*O*)-[$Co(gly)_2(tn)]^+$ $\{H_b(H_b')$	10.1 ±0.3	0.50×10^{-3}	2.0 ±0.067
$\quad\quad\quad

3) J. B. Terrill and C. N. Reilley, *Inorg. Chem.*, **5**, 1988 (1966).
4) D. A. Buckingham, L. G. Marzilli, and A. M. Sargeson, *J. Am. Chem. Soc.*, **89**, 5133 (1967).
5) J. L. Sudmeier and G. Occupati, *Inorg. Chem.*, **7**, 2524 (1968).
6) D. H. Williams, J. R. Angus, and J. Steele, *Inorg. Chem.*, **8**, 1374 (1969).
7) B. B. Smith and R. H. Betts. *Inorg. Chem.*, **9**, 2585 (1970).
8) P. F. Coleman, J. I. Legg, and J. Steele, *Inorg. Chem.*, **9**, 937 (1970).
9) J. L. Sudmeier, A. J. Senzel, and G. L. Blackmer, *Inorg. Chem.*, **10**, 90 (1971).
10) G. L. Blackmer and J. L. Sudmeier, *Inorg. Chem.*, **10**, 2019 (1971).
11) J. A. McClarin, L. A. Dressel, and J. I. Legg. *J. Am. Chem. Soc.*, **98**, 4150 (1976).
12) W. E. Keyes, R. E. Caputo, R. D. Willett, and J. I. Legg, *J. Am. Chem. Soc.*, **98**, 6939 (1976).
13) W. E. Keyes and J. I. Legg, *J. Am. Chem. Soc.*, **98**, 4970 (1976).
14) P. R. Norman and D. A. Phipps, *Inorg. Chim. Acta*, **28**, L161 (1978).
15) N. Matsuoka, J. Hidaka, and Y. Shimura, *Bull. Chem. Soc. Jpn.*, **40**, 1868 (1967).
16) S. H. Laurie, *Aust. J. Chem.*, **21**, 679 (1968).
17) Y. Fujii and T. Ejiri, *Bull. Chem. Soc. Jpn.*, **45**, 283 (1972).
18) M. B. Celap, T. J. Janjic, and D. J. Radanovic, *Inorg. Synth.*, Vol. IX, 173 (1967).
19) N. Matsuoka, J. Hidaka, and Y. Shimura, *Bull. Chem. Soc. Jpn.*, **48**, 458 (1975).
20) C. T. Liu and B. E. Douglas, *Inorg. Chem.*, **3**, 1356 (1964).
21) T. Ama and T. Yasui, *Bull. Chem. Soc. Jpn.*, **49**, 472 (1976).
22) P. K. Glasoe and F. A. Long, *J. Phys. Chem.*, **64**, 188 (1960).
23) H. Yoneda, U. Sakaguchi, and Y. Nakashima, *Bull. Chem. Soc. Jpn.*, **48**, 209 (1975).
24) J. C. Dabrowiak and D. W. Cooke, *Inorg. Chem.*, **14**, 1305 (1975).

Stereochemical Nonrigidity of {Poly(1-pyrazolyl)borato}palladium(II) Complexes Containing a Metal-1-Alkenyl or -Alkyl Bond†

Masayoshi ONISHI,* Katsuma HIRAKI,* Masaharu SHIRONITA, Yuzo YAMAGUCHI, and Shigeki NAKAGAWA

Department of Industrial Chemistry, Faculty of Engineering, Nagasaki University, Bunkyo-machi, Nagasaki 852

(Received July 30, 1979)

New{poly(1-pyrazolyl)borato}palladium(II) complexes, [Pd{CH=CCl-CMe$_2$(NMe$_2$)-1-*C,N*}(BPz$_4$)] (Pz= 1-pyrazolyl) **1**, [Pd{CH$_2$CMe(OMe)-CH$_2$S-*t*-Bu-1-*C,S*}(BPz$_3$Y)] (Y=Pz or H), and [Pd{CH$_2$CMe(OMe)-CH$_2$NMe$_2$-1-*C,N*}(BPz$_3$Y)] were prepared and characterized by means of elemental analysis and IR and ^{1}H-NMR spectroscopy. The stereochemical nonrigidity of these complexes was discussed on the basis of ^{1}H-NMR data. The fluxional behavior of the BPz$_4$ ligand in **1** was analyzed in detail by means of an approximate method based on the Bloch equation, and found to consist of three kinds of motions: inversion of the Pd-(N-N)$_2$-B boat-type six-membered ring, rotation of the BPz$_4$ ligand about the Pd-pyrazolyl nitrogen bond accompanying the inversion, and a tumbling process.

Stereochemical nonrigidity of a poly(1-pyrazolyl)-borate ligand of transition metal complexes has received considerable attention.[1-7] Fluxional motions of the tridentate poly(1-pyrazolyl)borate (BPz$_3$Y, Pz=1-pyrazolyl, Y=Pz or H) ligand in formally seven-coordinated molybdenum complexes, [Mo(1-3-η-CH$_2$CRCH$_2$)(BPz$_3$Y)(CO)$_2$][2] or in penta-coordinated platinum ones, [PtMe(BPz$_3$Y)L] (L=neutral ligand)[3] were analyzed by means of a simplified density matrix method. It is of interest to investigate the stereochemical nonrigidity of bidentate BPz$_3$Y ligands in square planar transition metal complexes, in comparison with that of the tridentate BPz$_3$Y ligands in molybdenum[1,2] or platinum complexes.[3]

Fluxional behavior has been reported for several {poly(1-pyrazolyl)borato}palladium(II) complexes which contain both metal-aryl and -nitrogen bonds.[6,7] ^{1}H-NMR spectra of these complexes involve fairly complicated aromatic protons, overlapping with some 1-pyrazolyl protons and it was difficult to analyze quantitatively the fluxional motion of the BPz$_3$Y ligands of the complexes.

We have prepared some {poly(1-pyrazolyl)borato}-palladium(II) complexes having a metal-1-alkenyl or -alkyl bond assisted by chelation with a nitrogen- or a sulfur donor site; the stereochemical nonrigidity of these complexes is discussed on the basis of ^{1}H-NMR spectra. The line shape analysis was carried out quantitatively as regards the fluxional motion of {2-chloro-3-(dimethylamino)-3-methyl-1-butenyl-1-*C,N*}{tetrakis(1-pyrazolyl)borato}palladium(II) [Pd(cdamb)(BPz$_4$)] {cdamb =CH=CCl-CMe$_2$(NMe$_2$)-1-*C,N*} (**1**).

Experimental

General Procedure. IR spectra were recorded and melting points determined according to the method given in the previous paper.[7] ^{1}H-NMR spectra at various temperatures were observed on a Japan Electron Optics Laboratory model MH-100 spectrometer (100 MHz), using CDCl$_3$, CD$_2$Cl$_2$, or CD$_3$CN as a solvent and tetramethylsilane as an internal standard. The temperature of the NMR samples was determined with methanol or 1,3-propanediol within an error of ±1 °C.

Sodium tetrakis(1-pyrazolyl)borate Na[BPz$_4$],[8] sodium hydrotris(1-pyrazolyl)borate Na[BPz$_3$H],[8] and starting dinuclear 1-alkenyl- or alkylpalladium(II) complexes, [{PdCl(cdamb)}$_2$],[9] di-μ-chloro-bis{3-(*t*-butylthio)-2-methoxy-2-methylpropyl-1-*C,S*}dipalladium(II) [{PdCl(btmmp)}$_2$] {btmmp=CH$_2$CMe(OMe)-CH$_2$S-*t*-Bu-1-*C,S*},[10] di-μ-chloro-bis{3-(dimethylamino)-2-methoxy-2-methylpropyl-1-*C,N*}dipalladium(II) [{PdCl(dammp)}$_2$] {dammp=CH$_2$-CMe(OMe)-CH$_2$NMe$_2$-1-*C,N*}[11] were prepared according to the reported methods.

Preparation of [Pd(cdamb)(BPz$_4$)]. A benzene suspension (25 ml) containing [{PdCl(cdamb)}$_2$] (0.61 mmol) and Na[BPz$_4$] (1.31 mmol) was stirred at room temperature for 16 h. The resulting solids were filtered off. The remaining solution was concentrated at a reduced pressure, followed by addition of hexane. On cooling, the mixture yielded pale yellow crystals, which were recrystallized from benzene–hexane to give [Pd(cdamb)(BPz$_4$)] (**1**).

Preparations of [Pd(btmmp)(BPz$_4$)] and [Pd(btmmp)(BPz$_3$H)]. A benzene suspension (20 ml) containing [{PdCl(btmmp)}$_2$] (0.63 mmol) and Na[BPz$_4$] (1.26 mmol) was stirred at room temperature for 2 h. The resulting supernatant solution was evaporated in a rotary evaporator to yield yellow oil. The oil was dissolved in diethyl ether, followed by addition of hexane at 5—8 °C. White needles precipitated, which were recrystallized from diethyl ether–hexane to afford [Pd(btmmp)(BPz$_4$)] (**2**).

Complex [Pd(btmmp)(BPz$_3$H)] (**3**) was prepared by a similar method, Na[BPz$_3$H] being used in place of Na[BPz$_4$].

Preparation of [Pd(dammp)(BPz$_4$)] and [Pd(dammp)(BPz$_3$H)]. A benzene suspension (20 ml) involving [{PdCl(dammp)}$_2$] (0.63 mmol) and Na[BPz$_4$] (1.26 mmol) was stirred at ambient temperature for 2 h. The resulting solid was filtered off and the remaining solution concentrated. On cooling, white solids precipitated gradually, which were collected and washed with diethyl ether and hexane to give [Pd(dammp](BPz$_4$)] (**4**).

A white complex [Pd(dammp)(BPz$_3$H)] (**5**) was synthesized in a similar manner to the preparation of **2**.

Line Shape Analysis

Method of Approximation. Fluxional motion of the BPz$_4$ ligand corresponds to the exchange of four protons at a given position on the four pyrazolyl groups. Line shape analysis of **1** was performed for a spin system of

† A preliminary report of this work was presented at the VIIIth International Conference on Organometallic Chemistry, Kyoto, September 1977. Abstract p. 161.

four pyrazolyl 3-H's of the BPz_4 ligand, since the 3-H's displayed well-resolved spectra of four doublets due to coupling to neighboring 4-H at low temperature, as shown in Fig. 2. In terms of spin notation, the process is an exchange of an ABCDXYZW spin system, since resonance frequencies of the 3-H's are far apart from those of the 4-H's. In a strict sense, complete line shape analysis of this spin system should be carried out by the density matrix method,[2,3,12,13] which is applicable to a spin-exchange system having spin-spin couplings. However, it needs too much computer-calculations to obtain theoretical spectra of the present exchanging system by this method. For a good approximation overcoming the difficulty, four doublets of the 3-H's were analyzed by means of the modified Bloch equation,[14] which should be applied to a spin system with no coupling, instead of the density matrix method, since the chemical shifts of the 4-H's are far apart from those of the 3-H's, and the mixing transition between spins of 3-H's and those of 4-H's might be small. A similar approximation has been reported on the NMR analysis of a restricted rotation of a tetrahedral carbon in 9-isopropyltriptycenes.[15]

Absorption intensity $I(\omega)$ at each frequency ω is derived from the modified Bloch equation:[14]

$$I(\omega) = \frac{1}{\pi}\mathrm{Re}[-P\cdot\{i(\Omega-\omega)+D\}^{-1}\cdot l]$$

where the notation of the matrices (P,Ω,ω,D,l) refer to the work of Johnson,[13] Re representing the real part of the matrix.

^{1}H-NMR spectra of three pyrazolyl 3-H's of the BPz_4 ligand showed remarkable temperature-dependency in the region 76——30 °C, while the doublet {at δ 7.49 (3 and 7) at −30 °C, in Fig. 2} corresponding to the fourth 3-H remained unchanged below 43 °C and showed temperature-dependent spectra only above 58 °C. The present analysis deals with the spin system of the four 3-H's appearing in the ^{1}H-NMR spectra in the range 43——30 °C. Concerning the former three pyrazolyl 3-H's, the exchange rate between two 3-H's {at δ 6.82 (1 and 5) and 7.25 (2 and 6) at −30 °C} differs from that between the former two 3-H's and the third one {at δ 7.59 (4 and 8) at −30 °C}. A parameter f was introduced in order to express these two different exchange rates. The terms fk and $(1-f)k$ denote the former and latter exchange rates, respectively.

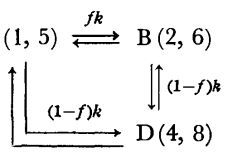

This treatment is based on the assumption that activation energies for these two exchange processes are virtually equal, since it is very difficult for the present exchange system to detect a fine difference between the two activation energies.

Moreover, as regards the exchange of the three 3-H's in the temperature range 43——30 °C, upper-field signals (1, 2, and 4 in Fig. 2) of the three doublets were assumed to undergo exchange with each other, as well as the lower-field ones (5, 6, and 8). It is unlikely that the lower-field level of one 3-H doublet exchanges with a higher-field level of another doublet. A similar assumption has been reported by Suzuki *et al.*[15]

Accordingly, the matrix D of the probability of the spin transfer is given as follows.

$$D = \begin{vmatrix}
-k-\frac{1}{T_1}, & fk, & 0, & (1-f)k, & 0, & 0, & 0, & 0, \\
fk, & -k-\frac{1}{T_2}, & 0, & (1-f)k, & 0, & 0, & 0, & 0, \\
0, & 0, & -\frac{1}{T_3}, & 0, & 0, & 0, & 0, & 0, \\
(1-f)k, & (1-f)k, & 0, & -2(1-f)k-\frac{1}{T_4}, & 0, & 0, & 0, & 0, \\
0, & 0, & 0, & 0, & -k-\frac{1}{T_5}, & fk, & 0, & (1-f)k, \\
0, & 0, & 0, & 0, & fk, & -k-\frac{1}{T_6}, & 0, & (1-f)k, \\
0, & 0, & 0, & 0, & 0, & 0, & -\frac{1}{T_7} & 0, \\
0, & 0, & 0, & 0, & (1-f)k, & (1-f)k, & 0, & -2(1-f)k-\frac{1}{T_8}
\end{vmatrix}$$

Full width in Hz at half height of the i-th peak is $(\pi T_i)^{-1}$ in the absence of exchanging broadening, and the parameter T_i is a transverse relaxation time modified by some effects, such as long-range coupling to 5-H, mechanical fluctuation of resolving power, and mixing transition. ^{1}H-NMR spectrum at −30 °C was actually a slow-exchange limiting one, and the parameters T_i's were obtained readily from line widths of respective peaks. Above this temperature, T_i's were estimated from the values at −30 °C, using observed line widths of signals of 1,1,2,2-tetrachloroethane as a reference.

Calculations. For the given parameter f and the rate constant k together with chemical shifts and line widths in the absence of the exchanging broadening, calculations of the theoretical spectra were carried out with a FACOM 270-20 computer. The spectra were accomodated in order to get the best visual fitting with

the observed spectra by varying both f and k. The theoretical spectra were checked up as regards 1/2, 3/4, 4/5, and 6/7 of f.

Results and Discussion

General Properties. The chloro-bridging dinuclear cyclopalladated complexes reacted fairly smoothly with $Na[BPz_3Y]$ in the suspension of a non-polar solvent, such as benzene, to afford the corresponding new {poly(1-pyrazolyl)borato}palladium(II) complexes **1**—**5**. Yields, analytical data, and some physical properties of the new palladium(II) complexes are summarized in Table 1. Complexes **1**—**5** are stable in a solid state in the air, and soluble in the usual organic solvents except saturated hydrocarbons. Complexes **2**—**5** are soluble even in diethyl ether, and can not easily be purified by recrystallization. The compositions of **1**—**5** were confirmed by elemental analysis (Table 1), IR data (Table 2), and ^{1}H-NMR evidence (Table 3). ^{1}H-NMR spectra of these five complexes showed considerable temperature-dependency in the region 85—−36 °C.

Two coordination types of the BPz_3Y ligands are possible for **1**—**5**. Possible structures for **1** are shown in Fig. 1, as a typical example. The definite structure in the solid phase should be determined by X-ray analysis. The BPz_3Y ligands of **1**—**5** in solution were assumed to serve as a bidentate chelate (structure **E**) for the following reasons.

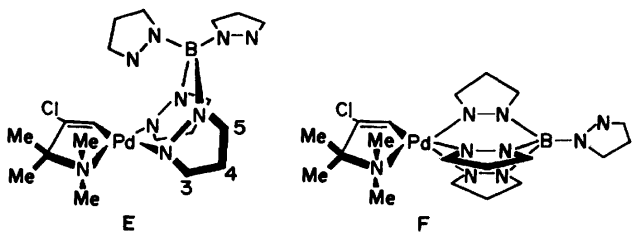

Fig. 1. Possible structures of **1**.

(1) The bidentate coordination of the BPz_3Y ligands was found in (acetophenone oximato-2-*C*,*N*){tetrakis(1-pyrazolyl)borato}platinum(II)[7] similar to **1**, **4**, and **5**, in $[Pd(1\text{-}3\text{-}\eta\text{-}C_3H_5)(BPz_4)]$,[1] and in $[PtMe(BPz_3H)(CO)]$ in the solid phase.[16]

(2) The relatively electron-rich palladium atom in **1**—**5** presumably prevents the third 1-pyrazolyl group of the BPz_3Y ligand from being coordinated to the palladium atom, in contrast with $[PtMe(BPz_4)(CO)]$ in solution[3] or $[PtMe(BPz_3H)(un)]$ {un=$F_3C\text{-}C{\equiv}C\text{-}CF_3$[17] or $F_2C{=}CF_2$[3]}, each of which possesses a considerably strong π-back-bonding ligand, CO or un.

(3) As regards the ^{1}H-NMR spectrum of **1** at −30 °C, both the chemical shift difference between two 3-methyl groups and that between two *N*-methyl ones are considerably large (Table 3). It seems unlikely that the conformation of the uncoordinated 1-pyrazolyl group in structure **F** would cause these large differences in **1**.

*^{1}H-NMR Spectra of $[Pd(cdamb)(BPz_4)]$ **1**.* At −30 °C, **1** exhibited the limiting slow exchange ^{1}H-NMR spectrum (Table 3). At this temperature, the four pyrazolyl groups are spectroscopically unequal, the BPz_4 ligand being coordinated to the central metal in a spectroscopically rigid state. In this state, it is expected that the differences in environments and chemical shifts among the four 3-H's are larger than those among the 5-H's, by considering the proposed

Table 1. Yields and elemental analyses of the new complexes

	Complex	Yield[a] %	Mp[b] °C	Found (Calcd) (%) C	H	N
1	$[Pd(cdamb)(BPz_4)]$	57	164—166	42.58 (42.88)	4.74 (4.73)	23.61 (23.69)
2	$[Pd(btmmp)(BPz_4)]$	17	130—138	45.13 (44.98)	5.63 (5.57)	20.08 (19.98)
3	$[Pd(btmmp)(BPz_3H)]$	16	108—126	43.69 (43.70)	6.00 (5.91)	17.13 (16.99)
4	$[Pd(dammp)(BPz_4)]$	23	155—170	43.98 (44.24)	5.46 (5.48)	24.56 (24.45)
5	$[Pd(dammp)(BPz_3H)]$	15	96—99	42.58 (42.73)	5.80 (5.84)	21.90 (21.81)

a) Based on the starting palladium(II) complexes. b) All complexes decomposed without melting.

Table 2. Characteristic IR bands of the complexes[a]

Complex	The BPz_3Y ligand ν(CH)	ν(BH)	The other ligand ν(C–O)	δ(Me)	δ(CH_2,Me)
1[b]	3085sh, 3110m	—	—	1380s	1470w
2	3090sh, 3130sh 3110w	—	1075s	1370m	1455m
3	3090sh, 3100m 3140w	2420m 2440w	1090s	1365m	1455m
4	3090sh, 3110sh 3130w	—	1075s	1385s	1462m
5	3080sh, 3100sh 3130sh	2440w 2480m	1070s	1380m	1462m

a) Measured in KBr disk, values in cm^{-1}. b) The other characteristic bands were observed at 660 cm^{-1} [ν(C–Cl), m] and 1580 cm^{-1} [ν(C=C), m].

TABLE 3. H-NMR DATA OF THE POLY(1-PYRAZOLYL)BORATE COMPLEXES[a)]

Complex	Temp °C	Pyrazolyl protons[b)]			The other chelate				
		3-H	4-H	5-H	1-CH_2 (1-CH)[d)]	2-Me[c)]	OMe[c)]	3-CH_2 (3-Me)[d)]	NMe[c)] (*t*-Bu)[e)]
1	−30	6.82(d), 7.25(d)	6.41(t), 6.44(t)	7.74(d), 7.76(d)	6.10[d)]	—	—	1.10[d)]	2.34
		7.49(d), 7.59(d)	6.47(t), 6.53(t)	7.95(d), 8.00(d)				1.41[d)]	2.83
2[f)]	−36	6.35(d), 6.77(d)	6.20(t, 3)	7.53(d), 7.56(d)	2.0[g)]	1.30,[h)]	3.32[h)]	2.78[i)]	0.96[e,h)]
		6.85(d), 7.33(d)	6.30(t)	7.68(d), 7.84(b)		1.57,[j)]	3.19[j)]	2.90[i)]	1.02[e,j)]
3[f)]	−36	7.6(b, 3)	6.24(b, 3)	7.7(b, 3)	2.1[g)]	1.36,[h)]	3.32[h)]	2.63[i)]	1.06[e,h)]
						1.58,[j)]	3.24[j)]	2.80[i)]	1.14[e,j)]
4[k)]	−31	6.6[l)], 6.7[l)], 7.0(b)	6.19(t), 6.34(b)	7.45(b), 7.56(b)	1.72[l)]	1.10	3.24	2.5[g)]	2.40
		7.12(d), 7.27(b)	6.24(t, 2)	7.68(b, 2)	1.86[l)]				2.95
5	−36	7.33(d), 7.40(b)	6.19(t)	7.56(d), 7.59(b)	1.90[c)]	1.13	3.17	2.5[g)]	2.4
		7.50(b)	6.24(t, 2)	7.73(b)					2.76

a) δ value (ppm) from TMS. In $CDCl_3$, unless stated otherwise. Abbreviations used: b=broad, d=doublet, t=triplet. b) An intensity for two or three protons is given in parentheses. See notes h), j), and l) about the isomers. c) Appearing as a singlet. d) For **1**. Appearing as a singlet. e) For **2** and **3**. f) In CD_3CN. g) Overlapping with solvent signal or the other signal. h) For the main isomer. i) Appearing as an AB type quartet. $^2J_{AB}$=10—12 Hz. j) For the minor isomer. See the text. k) In CD_2Cl_2.l) With an intensity of about 1/2.

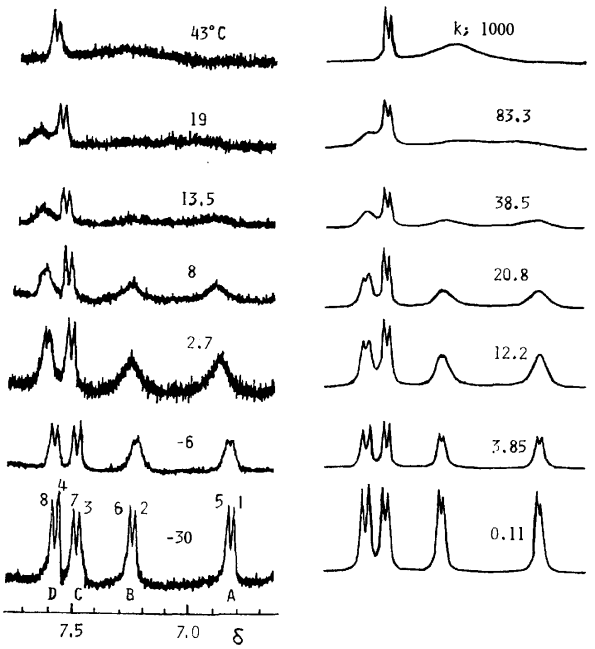

Fig. 2. ^{1}H-NMR spectra of 3-H's of the 1-pyrazolyl groups in **1** in $CDCl_3$. Left; Observed spectra. Right; Calculated spectra. See the text.

arrangement **E** shown in Fig. 1.

Two higher-field 3-H doublets (A and B at −30 °C, in Fig. 2)[18)] broadened at −6 °C, apparently disappearing at 19 °C. Above −6 °C, the third 3-H doublet at the lowest field (D in Fig. 2) broadened more gradually as compared with the former two. These three 3-H signals coalesced into a very broad hump at 43 °C, its height increasing slowly with rise in temperature. The fourth 3-H doublet (C in Fig. 2) remained actually unchanged below 43 °C, beginning to broaden only near 58 °C.

Two sharp 3-methyl singlets observed at −30 °C broadened near −6 °C, coalesced at 10 °C, turning into a sharp singlet at δ 1.29 at 43 °C. The 4-H's and 5-H's of the BPz_4 ligand and *N*-methyl signals of the cdamb moiety changed, corresponding to the 3-H's and the 3-methyl protons upon warming from −30 °C. Complex **1** in CD_3CN gave no limiting fast-exchange spectrum even at 79 °C.

There is a clear difference between the collapsing rates of the signals corresponding to the three pyrazolyl groups upon warming from −30 °C; the signals of the two pyrazolyl groups collapse more readily than that of the third pyrazolyl one. The former two pyrazolyl groups are reasonably associated with two uncoordinated ones at low temperature. Upon warming, an inversion of a Pd–$(N\text{–}N)_2$–B boat-type six-membered ring is expected to take place readily with no rupture of palladium-pyrazolyl nitrogen bond, accompanied by a simultaneous fluttering of two coordinated pyrazolyl groups. A similar inversion has been reported as for $[Mo(\eta^5\text{-}C_5H_5)(BPz_3Y)(CO)_2]$[4,5)] and $[Mo(\eta^5\text{-}C_5H_5)\text{-}(BPz_2Et_2)(CO)_2]$.[5)]

The third pyrazolyl group was assigned to the one coorrdinated at a *trans* position to a carbon-palladium σ-bond of the cdamb moiety, since comparatively strong *trans* influence of the 1-alkenyl group possibly gave rise to a moderately weak binding of the palladium-pyrazolyl nitrogen bond *trans* to the 1-alkenyl-palladium σ-bond. Above −6 °C, the third pyrazolyl group participated gradually in the fluxional motion, *viz.*, in a rotation of the three pyrazolyl groups around a palladium-nitrogen bond located at a *trans* position to a dimethylamino group, accompanied by a more rapid inversion of the Pd–$(N\text{–}N)_2$–B ring. Above 58 °C, the fourth pyrazolyl group began to participate in the fluxional motion of all pyrazolyl groups, *i.e.* in a "tumbling process."

As regards line shape analysis, agreement between the observed spectra and the theoretical ones was excellent, when the parameter f was 6/7, *viz.*, the inversion rate was six times greater than the exchange rate between the two pyrazolyl groups and the third one. Figure 3 shows the relationship between (log k) and $10^3/T$, obtained from the line shape analysis of **1**. From the results and Arrhenius' and Eyring's equations,

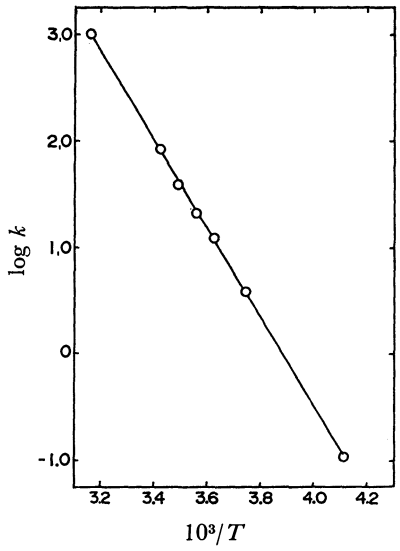

Fig. 3. The relationship between (log k) and $10^3/T$, obtained for **1**.

we find that $E_a=17.8\pm1.7$ kcal/mol, $\Delta G^{\ddagger}_{298}=14.5$ kcal/mol, $\Delta H^{\ddagger}_{298}=17.2$ kcal/mol, and $\Delta S^{\ddagger}=9.1$ cal/deg·mol for the fluxional motion of the three pyrazolyl groups. The value $\Delta G^{\ddagger}_{298}$ is considerably greater than $\Delta G^{\ddagger}_{198}$ for an internal rotation of the uncoordinated pyrazolyl ring and that for the exchange among the three coordinated pyrazolyl rings in $[PtMe(BPz_4)(CO)]$,[3] being comparable with $\Delta G^{\ddagger}_{298}$ for the exchange among the three coordinated pyrazolyl rings in $[PtMe(BPz_3H)(CO)]$.[3] The positive value of the $\Delta S^{\ddagger}$ for **1** is in contrast with the negative values of the $\Delta S^{\ddagger}$'s for $[PtMe(BPz_3Y)(CO)]$,[3] suggesting that the palladium-pyrazolyl nitrogen bonds are elongated, becoming loose in the transition states for the fluxional motion of **1**.

It is noteworthy that the fluxional motion of the BPz_4 ligand in **1** actually consists of three kinds of motion, *i.e.* inversion of the Pd–$(N–N)_2$–B ring, rotation of the three pyrazolyl rings accompanying a more rapid inversion, and the tumbling process, shifting from the former to the latter continuously upon warming from −30 °C. A similar behavior was observed also for **2** and **4**.

^{1}H-NMR Spectra of [Pd(btmmp)(BPz$_3$Y)] 2 and 3. As regards the BPz_3H ligand of **3** in CD_3CN, each of 3-H's and 5-H's gave a doublet at 28 °C, which turned into a broad signal at −36.5 °C. This indicates that the BPz_3H ligand is stereochemically non-rigid above −36.5 °C, the exchange rate decreasing moderately on cooling. The ^{1}H-NMR spectrum of the btmmp moiety at 28 °C contained three sharp singlets at δ 1.12 (9H, *t*-Bu), 1.40 (3H, 2-Me), and 3.32 (3H, OMe). Each of these singlets broadened near 8 °C and separated into a fairly sharp singlet and a small broad one with an intensity ratio *ca.* 8: 1 at −0.5 °C, Thus, the signals of the btmmp moiety separated into the two sets at this temperature, but not each of the pyrazolyl protons even at −36.5 °C. This indicates that an exchange of the two configurations of the *t*-butyl group takes place above −0.5 °C, independent of the stereochemically nonrigid motion of the BPz_3H ligand. Four conformational isomers were expected to be present owing to asymmetric 2-carbon and boron atoms, when the motion of the BPz_3H ligand was quenched at low temperature (Fig. 4), but could not be detected at −36.5 °C.

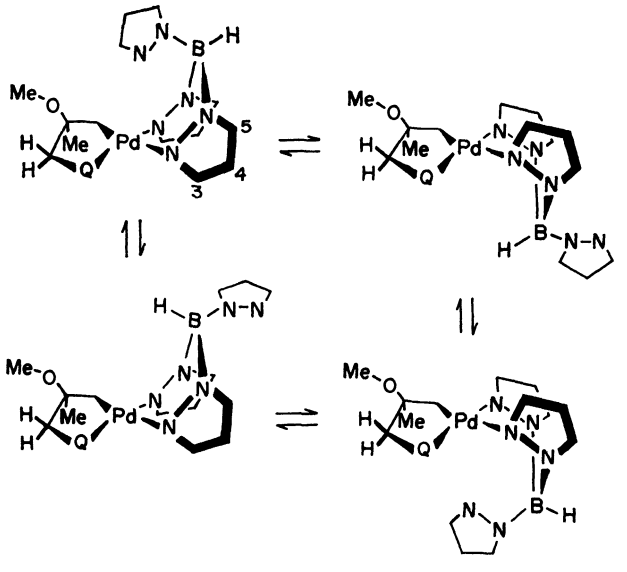

3 Q = S-^{t}Bu

5 Q = NMe$_2$

Fig. 4. Conformations of **3** and **5**.

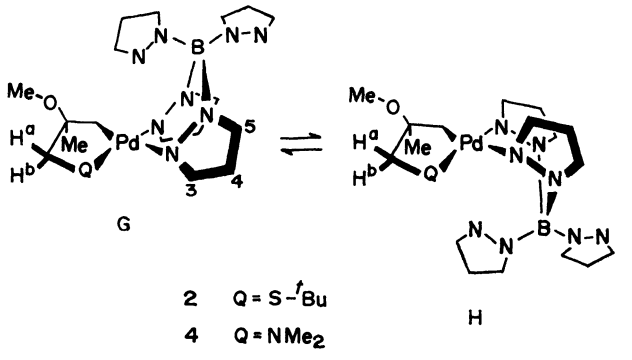

2 Q = S-^{t}Bu

4 Q = NMe$_2$

Fig. 5. Conformations of **2** and **4**.

At 85 °C, the ^{1}H-NMR spectrum of the btmmp moiety of **2** in CD_3CN showed three sharp singlets at δ 1.10 (9H, *t*-Bu), 1.44 (3H, 2-Me), and 3.38 (3H, OMe). Each of these singlets separated into a fairly sharp singlet and a small broad one with an intensity ratio *ca.* 6: 1 at −0.5 °C. In consideration of the very similar ^{1}H-NMR spectra of **2** to those of **3**, the two sets of the btmmp-signals are also associated with two configurations of the *t*-butyl group, which undergo exchange with each other rapidly at high temperature. Although two conformational isomers (**2G** and **2H** in Fig. 5) occur owing to an asymmetric 2-carbon atom when the stereochemically nonrigid motion of the BPz_4 ligand is quenched at low temperature, it seems unlikely that these isomers cause the two sets of the btmmp-signals.

The BPz_4 ligand of **2** exhibited a limiting slow exchange ^{1}H-NMR spectrum at −36 °C. It appears that the two configurational isomers due to the *t*-butyl group and the conformational isomers due to the quenching of the motion of the BPz_4 ligand show virtually identical signals as for the 3-H protons of the BPz_4 ligand. Three high-field 3-H doublets broadened at −21 °C and coalesced near −0.5 °C, whereas the fourth 3-H doublet remained unchanged below this temperature and began to collapse near 20 °C. These four 3-H signals united to a broad one near 47 °C and exhibited a slightly broad signal at 85 °C, while four pyrazolyl 5-H's resonated at δ 7.76 as a well-resolved doublet, indicating a fairly fast tumbling motion of the BPz_4 ligand on the NMR time scale. From the results it seems that the pyrazolyl groups in **2** move also in a similar mode to the case of **1** in the range −36—85 °C.

*^{1}H-NMR Spectra of [Pd(dammp)(BPz_3Y)] **4** and **5**.* At 85 °C, the ^{1}H-NMR spectrum of **4** in CD_3CN contained four sharp methyl singlets in the dammp moiety and three slightly broad pyrazolyl proton resonances at δ 6.4 (4H, 4-H's), 7.2 (4H, 3-H's), and 7.8 (4H, 5-H's). This spectrum did not correspond to a fast exchange limit, whereas the tumbling motion of the BPz_4 ligand was fairly fast on the NMR time scale.

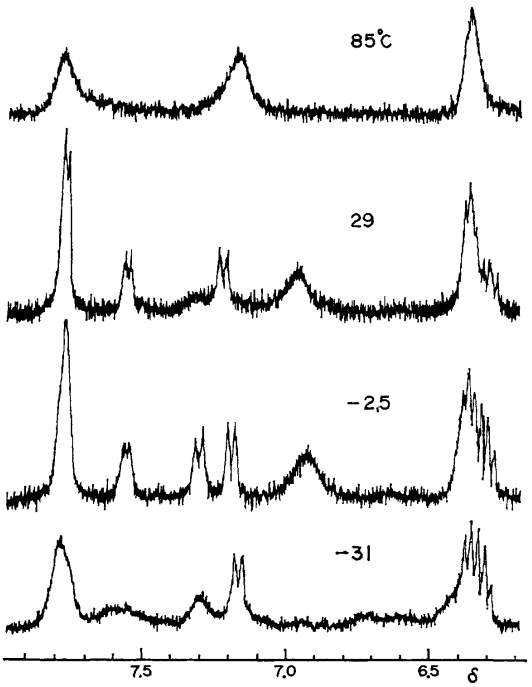

Fig. 6. ^{1}H-NMR spectra of the BPz_4 region of **4** in CD_3CN.

At 29 °C, the pyrazolyl 3-H resonance separated into a doublet at δ 7.18 (1H) and two broad signals at δ 6.9 (2H) and 7.3 (1H). The last broad signal turned into a doublet at −2.5 °C and broadened again at −31 °C. The larger broad signal at δ 6.9 separated into very broad humps near δ 6.6, 6.7, and 7.1 (overlapping with the doublet at δ 7.18) (Fig. 6). These broad humps were observed more obviously in CD_2Cl_2 (Table 3), and are tentatively ascribed to 3-H's of two conformational isomers (**4G** and **4H** in Fig. 5), which were distinguishable owing to the slowdown of the inversion of the Pd-$(N\text{-}N)_2$-B ring at low temperature. The broadening of the doublet at δ 7.3 at −31 °C might be due to the exchange between these two conformers. Each of the four methyl singlets also broadened considerably at this temperature, but did not separate into two signals expected for the two conformers. Complex **4** exhibited the three stages of the stereochemically non-rigid motion of the BPz_4 ligand, similar to **1**, no slow exchange limiting spectrum for **4** being obtained.

Concerning the BPz_3H group of **5** in $CDCl_3$ at 60.5 °C, each of 3-H's and 5-H's gave a doublet at δ 7.56 and 7.67, respectively, corresponding to a fast exchange limiting spectrum. The 3-H signal broadened at 25 °C, and separated into three broad ones of an equal intensity at −2.5 °C. The highest-field 3-H signal changed into a doublet at δ 7.33 at −36 °C, indicating that one of the three pyrazolyl groups is fixed and the others undergo exchange with each other at a slow rate. Above 25 °C, each of four methyl protons of the dammp moiety resonated as a sharp singlet, which broadened considerably with no separation at −36 °C, corresponding to the 3-H signals.

The BPz_3H ligand in **3** and **5** was more stereochemically non-rigid as compared with the BPz_4 ligand in **2** or **4**, analogous to the case of (acetophenone oximato-2-*C,N*){poly(1-pyrazolyl)borato}palladium(II) complexes.[7]

The authors are grateful to Miss Yumi Kojima and Mr. Yushichiro Ohama, Nagasaki University, for the ^{1}H-NMR measurements and technical assistance.

References

1) S. Trofimenko, *J. Am. Chem. Soc.*, **91**, 3183 (1969).
2) P. Meakin, S. Trofimenko, and J. P. Jessom, *J. Am. Chem. Soc.*, **94**, 5677 (1972).
3) L. E. Manzer and P. Z. Meakin, *Inorg. Chem.*, **15**, 3117 (1976).
4) J. L. Calderon, F. A. Cotton, and A. Shaver, *J. Organomet. Chem.*, **37**, 127 (1972).
5) J. L. Calderon, F. A. Cotton, and A. Shaver, *J. Organomet. Chem.*, **38**, 105 (1972).
6) M. Onishi, Y. Ohama, K. Sugimura, and K. Hiraki, *Chem. Lett.*, **1976**, 955.
7) M. Onishi, K. Sugimura, and K. Hiraki, *Bull. Chem. Soc. Jpn.*, **51**, 3209 (1978).
8) S. Trofimenko, *J. Am. Chem. Soc.*, **89**, 3170 (1967).
9) T. Yukawa, *Inorg. Chem.*, **7**, 1458 (1968).
10) Y. Takahashi, A. Tokuda, S. Sakai, and Y. Ishii, *J. Organomet. Chem.*, **35**, 415 (1972).
11) A. C. Cope, J. M. Kliegman, and E. C. Friedrich, *J. Am. Chem. Soc.*, **89**, 289 (1967).
12) J. L. Kaplan, *J. Chem. Phys.*, **28**, 278 (1958); **29**, 462 (1958).
13) C. S. Johnson, Jr., "Advances in Magnetic Resonance," Academic Press, New York (1965), Vol. 1, p. 33.
14) a) H. S. Gutowsky, D. W. McCall, and C. P. Slichter, *J. Chem. Phys.*, **21**, 279 (1953); b) H. M. McConnell, *ibid*, **28**, 430 (1958). c) H. Nakanishi, *Kagaku No Ryoiki*, **31**, 226 (1977).
15) F. Suzuki, M. Oki, and H. Nakanishi, *Bull. Chem. Soc.*

Jpn., **47**, 3114 (1974).
16) P. E. Rush and J. D. Oliver, *J. Chem. Soc., Chem. Commun.*, **1974**, 996.
17) B. W. Davies and N. C. Payne, *Inorg. Chem.*, **13**, 1848 (1974).
18) Coupling constants $^3J_{34}$ and $^3J_{45}$ of the BPz_3Y ligands are actually 1.6—2.5 Hz as for **1**—**5**.

An Application of the Extended Principal Component Analysis to Circular Dichroism and Optical Rotatory Dispersion. A Case of Poly(α-L-glutamic acid) in the Helix-Coil Transition Region

Kiwamu YAMAOKA,* Takumi MATSUDA, and Mineo TAKATSUKI
Faculty of Science, Hiroshima University, Higashisenda-machi, Hiroshima 730
(Received June 4, 1979)

The extended principal-component-analysis (PCA) method has been applied to circular dichroism (CD) and optical rotatory dispersion (ORD). The validity of this method has been examined with ideal binary and ternary equilibrium systems, for which the data CD spectra and ORD curves were computer-generated. Satisfactory results were obtained for these multicomponent optically active systems. As an example, the ultraviolet CD spectra of poly(α-L-glutamic acid) in the pH-induced helix-coil transition region were analyzed with the PCA procedure. By the extended PCA method, the pure CD spectra for both helix and random-coil conformations and the helix fractions in the transition region were determined from eight experimentally obtained CD spectra. By introducing an empirical parameter α into the Henderson-Hasselbalch equation, the helix-coil transition curve was reproduced reasonably well.

Many vectorial methods have been developed for the analysis of the optical spectra which result from either the light-absorbing species in chemical equilibria or the components in conformational equilibria.[1-18] The total number of species or conformers (both simply denoted as components) in such equilibria can be determined by means of rank analysis,[1-5] factor analysis,[6] and principal component analysis.[7-13] The principal component analysis (hereafter abbreviated as the PCA method) was extended by Kankare[10] and by the present authors[11-13] in order to resolve the observed optical spectra into the spectra of individual components involved in an equilibrium system.

The concentrations of individual components may be determined by factor analysis,[6] the least-square-curve-fitting method,[14-17] and the reciprocal function method.[18] Some of these methods have been applied to the circular dichroism (CD) spectra and optical rotatory dispersion (ORD) curves of optically active biopolymers in solution in order to interpret the observed optical data in terms of the various conformations.[5,6,14-18] In these methods, however, an appropriate reference spectrum must be assumed for each component. It is highly desirable to obtain the number of unknown polymer conformations (*i.e.*, components), the pure CD spectra or ORD curves of these components, and the fraction of each component, without assuming any reference spectra *a priori*. Therefore, the application of the PCA method to both CD and ORD is attempted in this work.

The extended PCA method has been utilized to analyze the absorption spectra of associative dyes in the monomer-dimer and acid-base equilibria[11] and in the binding with polyelectrolytes.[12,13] Two obvious physical conditions can be attached to the analysis of a given system: the absorbance and the concentration of each component are always non-negative. However, the CD and ORD are both signed quantities. The only remaining physical restriction is the non-negative concentration. Nevertheless, the extended PCA method is applicable to the CD and ORD data in a manner similar to the absorption, yielding the proper equilibrium scheme, the equilibrium constant, the number of optically active components, and the component CD spectra or ORD curves. As an illustration, the pH-induced change of the CD spectra of poly(α-L-glutamic acid) will be dealt with.

The Outline of the Extended PCA Method

Since the extended PCA method has previously been described in detail,[11,12] the procedure pertaining to the CD and ORD data will be given here. Suppose that m data CD spectra or ORD curves are experimentally available for a chemical system in equilibrium, which contains p optically active components, and that each data spectrum is a sum total of the p component spectra. The purpose of the extended PCA method is to determine the unknown number of components, p, and then the concentration and the pure spectrum of each component.

Over a certain wavelength region, m data CD spectra or ORD curves may be measured for m solutions, each of which contains a maximum of p components in equilibrium. If the Lambert-Beer-type additivity holds for the component CD spectra or ORD curves, as in the case of absorption spectra, the data matrix, $\boldsymbol{D}_\theta$ or $\boldsymbol{D}_\phi$, may be expressed as the product of the concentration matrix, $\boldsymbol{C}$, and the CD or ORD spectral matrix, $\boldsymbol{\theta}$ or $\boldsymbol{\phi}$, of the p components measured at n selected wavelengths:

$$\boldsymbol{D}_\theta = \boldsymbol{C}\boldsymbol{\theta} = \begin{bmatrix} C_{11} & \cdots & C_{1p} \\ \vdots & C_{ij} & \vdots \\ C_{m1} & \cdots & C_{mp} \end{bmatrix} \begin{bmatrix} \theta_{11} & \cdots & \theta_{1n} \\ \vdots & \theta_{jk} & \vdots \\ \theta_{p1} & \cdots & \theta_{pn} \end{bmatrix}, \quad (1)$$

or:

$$\boldsymbol{D}_\phi = \boldsymbol{C}\boldsymbol{\phi} = \begin{bmatrix} C_{11} & \cdots & C_{1p} \\ \vdots & C_{ij} & \vdots \\ C_{m1} & \cdots & C_{mp} \end{bmatrix} \begin{bmatrix} \phi_{11} & \cdots & \phi_{1n} \\ \vdots & \phi_{jk} & \vdots \\ \phi_{p1} & \cdots & \phi_{pn} \end{bmatrix}. \quad (2)$$

In these expressions, C_{ij} denotes the concentration of the jth component in the ith data spectrum, while

θ_{jk} and ϕ_{jk} are the θ and ϕ quantities of the jth component at the kth selected wavelength λ_k respectively.

A second-moment matrix, $\boldsymbol{A}$, is constructed from the data matrix as:

$$\boldsymbol{A} = {}^t\boldsymbol{D}_\theta\boldsymbol{D}_\theta \text{ or } \boldsymbol{A} = {}^t\boldsymbol{D}_\phi\boldsymbol{D}_\phi. \quad (3)$$

The eigenvalues $\Lambda_i (i=1, n)$ and the corresponding eigenvectors, $\boldsymbol{e}_i$, can be calculated from the $\boldsymbol{A}$ matrix by diagonalization. The relative magnitude of Λ_i permits us to determine the number of significant components.[11,12] Two new matrices, $\boldsymbol{f}$ and $\boldsymbol{t}$, are introduced as follows:

$$\boldsymbol{D}_\theta = \boldsymbol{f}_\theta\boldsymbol{e}_\theta \text{ or } \boldsymbol{D}_\phi = \boldsymbol{f}_\phi\boldsymbol{e}_\phi, \quad (4)$$

and:

$$\boldsymbol{\theta} = \boldsymbol{t}_\theta\boldsymbol{e}_\theta \text{ or } \boldsymbol{\phi} = \boldsymbol{t}_\phi\boldsymbol{e}_\phi. \quad (5)$$

The $\boldsymbol{e}$ matrix, consisting of p eigenvectors, is transformed to the $\boldsymbol{D}$ matrix by the $\boldsymbol{f}$ matrix, and also to the $\boldsymbol{\theta}$ and $\boldsymbol{\phi}$ matrices by the $\boldsymbol{t}$ matrix. The concentration matrix, $\boldsymbol{C}$, is given as:

$$\boldsymbol{C} = \boldsymbol{f}\boldsymbol{t}^{-1}. \quad (6)$$

Equations 4—6 indicate that the pure spectra of unknown components and their concentrations contributing to each data spectrum may be evaluated, once the elements of the $\boldsymbol{t}$ matrix are available.

In order to determine the $\boldsymbol{t}$ matrix, an appropriate equilibrium scheme must be selected.[11-13] The general expression for the scheme may be written as:

$$K = \prod_{i=1}^{q} [X_i]^{\nu_i}, \quad (7)$$

where K is the equilibrium constant, X_i is the ith component, which may be either optically active or inactive, and the ν is the stoichiometric coefficient. The brackets denote the molar concentration. It should be noted that the number of q is always larger than, or equal to, p. The coefficient of variation, S, is defined as:

$$S = \left[\frac{1}{m}\sum_{j=1}^{m}(K_j - \bar{K})^2\right]^{1/2} \Big/ \bar{K}, \quad (8)$$

where $\bar{K}$ is the mean equilibrium constant averaged over m equilibrium constants $K_j (j=1, m)$, by which an equilibrium (Eq. 7) is specified in m solutions (*i.e.*, m data spectra). Hence, the magnitude of the S value is the criterion for selecting the proper scheme for a given multicomponent equilibrium system.[11,12] It should be noted that, in any equilibrium system in which both L- and D-isomers of an optically active compound are involved, the $\boldsymbol{C}$ matrix (Eq. 6) describes only the difference in concentration between the two isomers. Thus, the number of components will be one instead of two in a racemization reaction (*e.g.*, L-isomer⇆D-isomer).

Results and Discussion

Ideal Binary System. Consider the following chemical equilibrium, in which an optically active chemical species, X_2, dissociates into an optically active species, X_1^-, and a proton:

$$X_2 \rightleftarrows X_1^- + H^+. \quad (9)$$

The quilibrium constant, K_a, is given by:

$$K_a = \frac{[X_1^-][H^+]}{[X_2]}. \quad (10)$$

When $K_a = 1 \times 10^{-6}$ M (=mol/dm^3) and when the pH of the system is varied from 7 to 5 by 0.25 pH units, a set of nine data CD spectra or ORD curves will be computer-generated, according to Eq. 10, by a linear combination of the hypothetical, component spectra of the X_1^- and X_2 species.

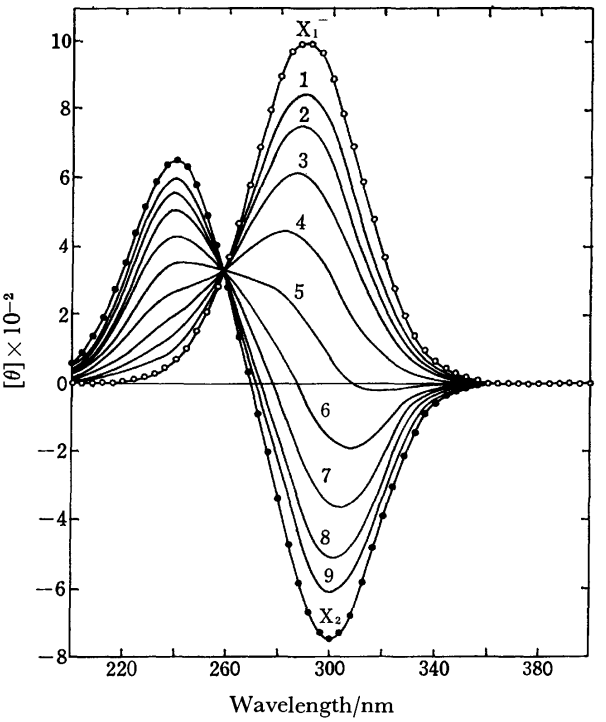

Fig. 1. The hypothetical component CD spectra (X_1^-, X_2) and the generated data CD spectra (1—9) for an ideal binary equilibrium system. The data spectra were computed according to Eq. 10 and expressed with the molar ellipticity [θ]. Symbols (○ and ●) indicate the estimated pure component spectra. The pH values of spectra 1 and 9 were set to be 5 and 7, respectively. For other details, see text.

The Case of CD. Figure 1 shows the component CD spectra of X_1^- and X_2. They were synthesized from a single Gaussian curve and a more complex Gaussian curve respectively. By using these component spectra, nine data CD spectra (Nos. 1—9) were computed at 4 nm intervals between 200 and 400 nm and at nine pH values. It is interesting to note that the data CD spectra (Nos. 1—9) all cross each other at a single wavelength near 260 nm, which may be termed the *isoelliptic* or *isodichroic* point by analogy with the isosbestic point of the absorption spectra. The presence of this point for a set of experimentally observed spectra should be taken as evidence for the two-optically-active-component system.

The supposedly unknown number of components in the equilibrium scheme (Eq. 9) is found from the eigenvalues of the second-moment matrix constructed from the nine data spectra. Figure 2(a) shows that a large gap exists between the second and third components. The gap

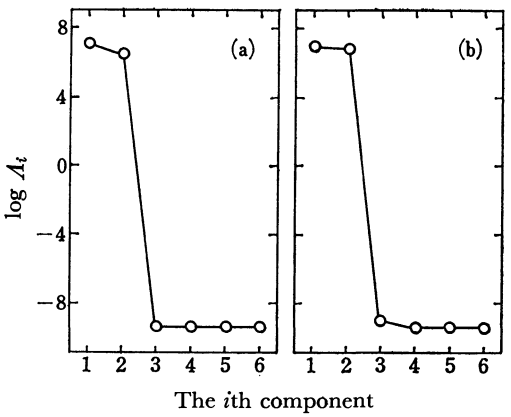

Fig. 2. The relation between eigenvalue Λ_i and the ith component for the ideal binary system. (a) the data CD spectra in Fig. 1 and (b) the data ORD curves in Fig. 3.

Table 1. The dependence of the S values on the parameter, α, in equilibrium expressions (Eqs. 12 and 16) for the ideal binary and ternary systems

α	Binary System (CD and ORD in 200—400 nm)[a)]	Ternary System (CD and ORD in 200—400 nm)[a)]
0.7	0.144	0.0012
0.8	0.082	0.0009
0.9	0.035	0.0005
1.0	0.000	0.0000
1.1	0.026	0.0009
1.2	0.040	0.0018
1.3	0.062	—
1.4	0.074	—

a) Identical results were obtained for both CD and ORD in the two narrower wavelength regions of 280—400 nm and 340—400 nm respectively.

indicates the correctness of the computing procedure for the assumed binary system. Analysis of the data spectra with Eq. 10 produced the values of 1×10^{-5} for S and 1×10^{-6} M for $\bar{K}_a$, the latter agreeing excellently with the preset value. The pure CD spectra of the X_1^- and X_2 components (open and filled circles) were reproduced quite well, as is shown in Fig. 1. The relative error between the computer-generated input data spectra and the iterated output component spectra was always less than 0.01% throughout the present work.

In actual CD measurements, experimental difficulties, such as the high absorbance and low CD signal of a solution, often limit the measurable wavelength region. Therefore, the 200—400 nm region was reduced to two narrower wavelength regions of 280—400 nm and 320—400 nm in this simulation, and the same PCA procedure as above was applied to each region. The values of $\bar{K}_a$ and S were all the same regardless of the wavelength region. This is conceivable because no experimental error was taken into account in the ideal system. Conversely, however, it is not necessary to cover the entire wavelength region where the complete CD features prevail if CD measurements are carried out with a sufficiently high accuracy.[11)]

In order to examine whether or not the given equilibrium scheme (Eq. 9) has been determined uniquely, a check is made with a general equilibrium scheme given as:

$$nX_2 \rightleftarrows nX_1^- + mH^+. \qquad (11)$$

The corresponding equilibrium constant, K_b, is written as:

$$K_b = \left(\frac{[X_1^-]}{[X_2]}\right)^{\alpha}[H^+], \qquad (12)$$

where $\alpha=n/m$. The data spectra in Fig. 1 were analyzed with the aid of the various values of α in Eq. 12 in order to compare the variation in S with the exponent α. The results are given in Table 1, which shows that the value of S increases as the α value deviates from unity. This trend is what should be expected for the present binary system, since the equilibrium scheme was generated with $\alpha=1$.

The Case of ORD. Experimental difficulties often forbid the CD spectra to be measured in the wavelength region where positive or negative bands are anticipated. In this case, the application of the PCA method is impracticable. The ORD is a dispersive quantity and displays the Cotton effect associated with a CD band. The peak or the trough of the Cotton effect, together with the sign and magnitude, can often be observed on the long-wavelength side removed from the CD band. In ORD measurements the optical path length of a sample solution may easily be increased outside the absorption peak. These facts lead to the usefulness of the highly accurate data ORD curves for the rigorous PCA treatment. The ORD data are thus valuable in complementing the shortcomings of the corresponding CD data. Therefore, the PCA procedure

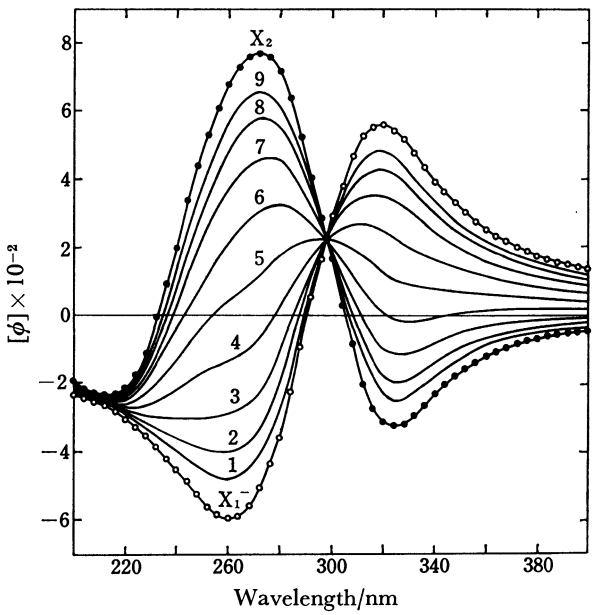

Fig. 3. The hypothetical component ORD curves (X_1^-, X_2) and the generated data ORD curves (1—9) expressed with the molar rotation $[\phi]$ for the same binary system as in Fig. 1. Symbols (○ and ●) indicate the estimated pure component curves.

is applied to the ORD data of the same ideal binary system as above.

Consider the same equilibrium scheme (Eq. 9) and the expression Eq. 10 with $K_a=1\times10^{-6}$ M. The hypothetical ORD curves for the X_1^- and X_2 components were computed from the corresponding CD spectra by the use of the Kronig-Kramers transform:[19,20]

$$[\phi(\lambda)] = \frac{2}{\pi}\int_{\lambda'_1}^{\lambda'_n}[\theta(\lambda')]\frac{\lambda'}{\lambda^2-\lambda'^2}d\lambda', \qquad (13)$$

where $[\theta]$ and $[\phi]$ are the molar ellipticity and the molar rotation respectively. The nine data ORD curves were similarly computed from the corresponding data CD spectra and are shown in Fig. 3. The *unknown* number of optically active components present in the equilibrium was determined from the eigenvalues using these curves. The result is shown in Fig. 2(b), in which a large gap again exists between the second and third components, indicating the system to be in a two-component equilibrium.

The PCA procedure was applied to this binary system using the general equilibrium scheme (Eq. 11). The results are given in Table 1. As in the CD treatment, the best simulation was obtained with $\alpha=1$ in Eq. 12, resulting in $S=1\times10^{-5}$ and $\bar{K}_b=1\times10^{-6}$ M, all of which are very close to the preset values. The pure ORD curves for X_1^- and X_2 (open and filled circles) resulting from the analysis of the nine data curves are in excellent agreement with the component ORD curves (X_1^- and X_2), as is shown in Fig. 3. As in the case of CD, the wavelength range was reduced to two narrower regions of 280—400 nm and 340—400 nm. The narrowing of the selected wavelength region did not affect the results. This indicates that even the *normal* ORD curves removed from the Cotton effect region are useful for extracting information on the equilibrium by the PCA method. Figure 3 suggests that the observed ORD curves should all cross each other at a wavelength which may be termed the *isodispersive point* if the concentration of one of the components is varied relative to the other in a two-component equilibrium system.

Ideal Ternary System. Consider a more complex equilibrium system which is composed of three optically active components, X_1, X_2, and X_3. The following equilibrium scheme is assumed:

$$X_1 + X_2 \rightleftarrows X_3, \qquad (14)$$

and:

$$K_c = \frac{[X_3]}{[X_1][X_2]} \qquad (15)$$

The CD spectrum and the corresponding ORD curve for each component were constructed in the same manner as in the binary system; they are shown in Figs. 4(a) and (b) respectively. Thirteen data CD spectra were generated (Nos. 1—13) from three pure component CD spectra with $K_c=5\times10^5$ M^{-1} in Eq. 15. In this case, the X_1 component was assumed to be titrated with X_2 to yield X_3 in such a way that the ratio of the concentration of the added X_2 to the initial concentration of X_1 was varied from 0.1 to 1.3. Since this series of data CD or ORD was synthesized from three components, the spectral features are very complicated, varying with the concentrations of the reactants, X_1 and X_2; *viz.*, no isoelliptic or isodispersive point exists.

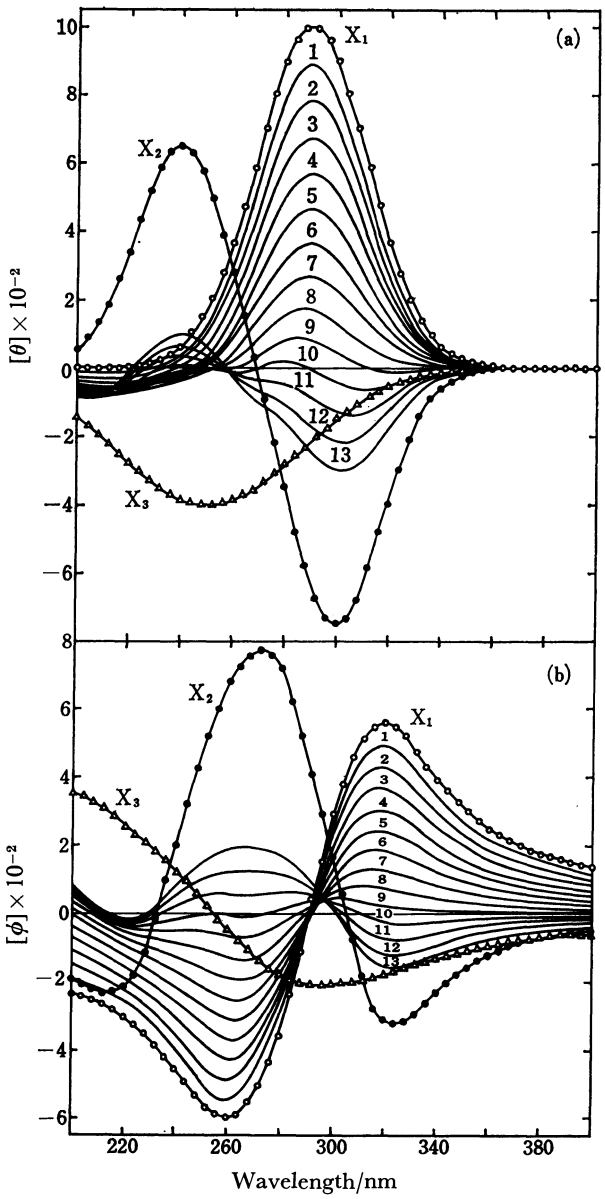

Fig. 4. The hypothetical component CD spectra and ORD curves (X_1, X_2, X_3) and the generated data (1—13) for an ideal ternary equilibrium system: (a) CD data were calculated from Eq. 15. (b) ORD data were computed from the corresponding CD spectra according to Eq. 13. Symbols (○, ●, and △) indicate the estimated pure component CD and ORD.

No visual inspection of these data CD spectra or ORD curves allows us to predict the number of optically active components involved in this equilibrium. The number was determined to be three by the PCA procedure, as is shown in Figs. 5(a) and (b). A large gap of eigenvalues exists between the third and fourth components, confirming the presence of three components. The most suitable expression for the chemical equilibrium has been searched for in the various equilibrium schemes by the use of the following general expression:

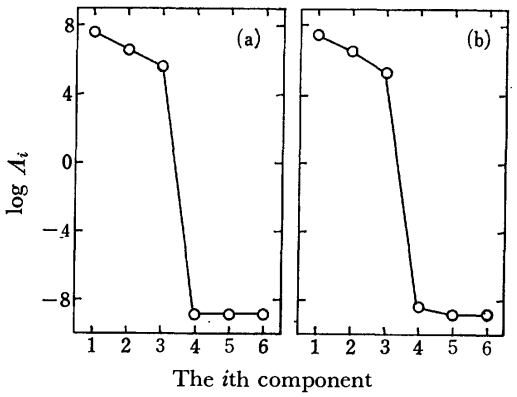

Fig. 5. The relation between eigenvalue Λ_i and the ith component for the ideal ternary system. (a) the CD data and (b) the ORD data in Fig. 4.

$$K_d = \left(\frac{[X_3]}{[X_1]}\right)^{\alpha}[X_2]^{-1}, \qquad (16)$$

in which the parameter, α, was varied from 0.7 to 1.2. The trial-and-error computer analysis produced the minimized S value of 1×10^{-5} at $\alpha=1$ and $\bar{K}_d=5\times10^5$ M^{-1}. These values all satisfy the originally assumed equilibrium conditions. A good agreement is seen between the component CD spectra or ORD curves originally set for the computer-generation and those determined from the thirteen data spectra by the PCA procedure, as is indicated by circles and triangles in Figs. 4(a) and (b). The S value increases as the α is varied from the preset value of unity. Thus, Eq. 15 is discriminated from the remainder as the most appropriate expression. No effect was observed on the final result when the wavelength region covered for the selected wavelengths was restricted, as in the case of the binary system.

A Real System of Poly(α-L-glutamic acid) in the Helix-Coil Transition Region. To the eight data CD spectra shown in Fig. 6, the PCA procedure was applied in order to determine the number of components (or conformations) present in poly(Glu) in the pH range of 5.13—7.49.[21] The eigenvalues are plotted against the components in Fig. 7, in which a considerable gap is observed between the second and third components. Since the difference in $\log\Lambda_i$ between the first and the third components is about 4, the poly(Glu) system can be concluded to consist of two components. This is the result that has been anticipated from the data CD spectra which all cross each other at 203.5 nm (the isoelliptic point).[21] These components may be assigned to the helical and random-coil conformations of poly(Glu).

Although the mechanism of the pH-induced helix-coil transition has not yet been fully resolved, the pH-induced transition may be formally written as:

$$\text{Helix} \rightleftarrows \text{Coil} + H^+ \qquad (17)$$

with an equilibrium constant, K. The equilibrium expression for scheme (17) is difficult to derive theoretically. Hence, the modified Henderson-Hasselbalch equation[22,23] is utilized under the assumption that it represents the experimental data by adjusting the parameter, α:

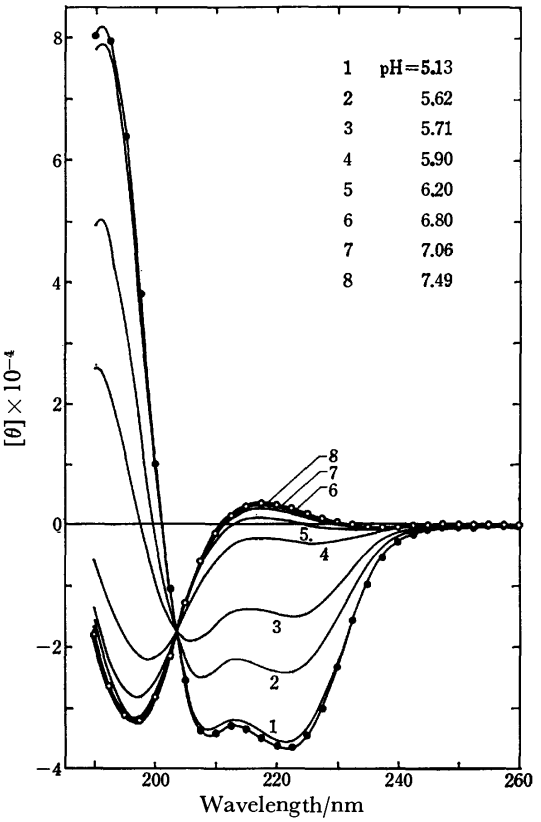

Fig. 6. The observed CD spectra of poly(α-L-glutamic acid) in the helix-coil transition region and the estimated pure helix (—●—) and pure coil (—○—) CD spectra. The data spectra are expressed with the molar ellipticity $[\theta]$ and taken from Ref. 21, to which the experimental details should be referred. The residue concentration was 8.0 mM in *ca.* 7.5 mM NaCl solutions throughout the pH range.

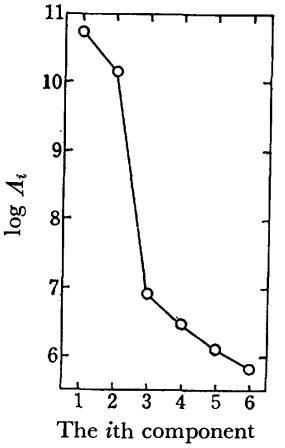

Fig. 7. The relation between the eigenvalue Λ_i and the ith component for the poly(Glu) system shown in Fig. 6.

$$\text{pH} = \text{p}K - \alpha\log\frac{[\text{Helix}]}{[\text{Coil}]}, \qquad (18)$$

where [Helix] and [Coil] denote the concentrations of the helix and coil conformations of poly(Glu). Equation 18 is quite suitable for the computer analysis, because it contains a single adjustable parameter, α, similar to the one that was determined uniquely in the ideal systems.

Table 2. The dependence of the S and $p\bar{K}$ values on the parameter, α, of the modified Henderson-Hasselbalch equation applied to the helix-coil transition of poly(Glu)

α	S	$p\bar{K}$
0.2	0.0262	5.75
0.3	0.0198	5.76
0.4	0.0150	5.74
0.5	0.0125	5.68
0.6	0.0132	5.60
0.7	0.0172	5.52
0.8	0.0229	5.41
0.9	0.0294	5.29
1.0	0.0368	5.18

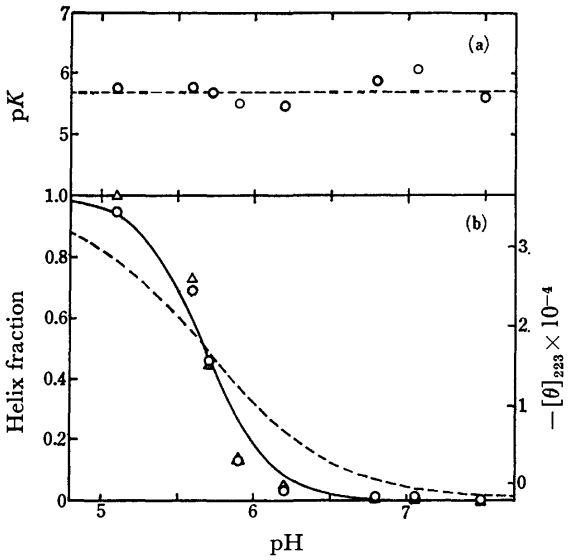

Fig. 8. (a) The pH dependence of pK values estimated from the PCA method and (b) the pH dependence of the helix fraction of poly(Glu). The helix fraction conventionally estimated from $[\theta]_{223}$ is indicated with triangles,[21] whereas the fraction obtained from the PCA procedure is denoted with circles. The solid curve was calculated by the use of the modified Henderson-Hasselbalch equation with $pK=5.68$ and $\alpha=0.5$. The dashed curve was calculated from the same equation with $\alpha=1$. For other details, see text.

The parameter should be considered to be only an empirical one which implicitly contains the effects on the conformational change of the ionic strength, the electrostatic surface potential, the shape factor, and other polyelectrolyte properties. The results of the PCA procedure are given in Table 2. Since the concentration of protons is measured in terms of pH, the S value is evaluated in terms of pK rather than K; it reaches its minimum at $\alpha=0.5$. The pK values for eight data CD spectra are plotted against pH in Fig. 8(a), where the average pK value, $p\bar{K}$, is 5.68 (dashed line). The pK values deviate from $p\bar{K}$ in a random fashion over the entire pH range, 5.1—7.5. This indicates that the PCA procedure is correctly applied to the appropriate equilibrium scheme.

The helix fraction at a given pH, which is defined as [Helix]/([Helix]+[Coil]), can be calculated from Eq. 18 with $p\bar{K}=5.68$ and $\alpha=0.5$. The results are plotted by the solid curve in Fig. 8(b). This curve is in good agreement with the helix fraction calculated from the $\boldsymbol{C}$ matrix by the PCA procedure (circles). Figure 8(b) also indicates that poly(Glu) is in the random-coil form almost completely at pH 7, but that nearly 95% of poly(Glu) is in the helix conformation at pH 5. The helix fraction has usually been calculated from the experimentally obtained molar ellipticity $[\theta]$ at a selected single wavelength, often at 222 or 223 nm, with the empirically chosen values of $[\theta]$ at two reference pH's which are assigned to the complete coil and helix conformations.[16,24] The results obtained from the PCA method make it clear that the conventional method (triangles) also yields a similar helix-coil transition curve.

It is worth emphasis that the modified Henderson-Hasselbalch equation with the single parameter, α, can describe the pH-induced helix-coil transition of poly(Glu) reasonably well over an entire pH range, permitting the evaluation of the helix fraction by the extended PCA method. The unmasked CD spectra for the complete helix and coil conformations are shown by filled and open circles respectively in Fig. 6. While the observed CD spectra at pH>7.1 may be considered as the pure CD spectrum for a coil, the pure CD spectrum for a helix is slightly higher than the highest observed CD spectrum at pH 5.13. Thus, the conventional estimation from $[\theta]_{223}$ would overestimate the helix fraction by approximately 5% in the low-pH region.

Finally, the results of the present work encourage the analysis of more complicated multicomponent systems, such as polylysine in alkaline solutions, in which three conformations (α-helix, β-structure, and random-coil) coexist, or natural proteins which undergo denaturation by environmental changes. For this purpose, our instrumental techniques must be improved so as to give highly accurate data worthy of the elaborate PCA procedure. The extended PCA method has so far been proved applicable to such optical spectra as the absorption, CD, and ORD. It may also be employed to analyze other spectral data like NMR, for which a Lambert-Beer-type linear combination rule holds.

Conclusion

The features of the extended PCA method as applied to both CD and ORD data of multicomponent equilibrium systems are: (1) the number of optically active components may be deduced from a set of data CD spectra or ORD curves (except for enantiomers), and (2) the unknown pure spectra of those components are determined by analyzing the data with appropriately chosen equilibrium expressions. Thus, the extended PCA method requires no presumption of the number of components (or conformations) or their characteristic spectra; these quantities must, by contrast, be assumed in other analytical methods. The application of the extended PCA method to the CD data of poly(Glu) has confirmed that the pH-induced helix-coil transition

can be described by a two-state equilibrium model over the pH range of 5.1—7.5.

References

1) R. M. Wallace, *J. Phys. Chem.*, **64**, 899 (1960).
2) R. M. Wallace and S. M. Katz, *J. Phys. Chem.*, **68**, 3890 (1964).
3) S. Ainsworth, *J. Phys. Chem.*, **65**, 1968 (1961).
4) D. Katakis, *Anal. Chem.*, **37**, 876 (1965).
5) C. March, C. Schneider, and L. Brehamet, *Biopolymers*, **17**, 1065 (1978).
6) R. W. Coombs, J. A. Verpoorte, and K. B. Easterbrook, *Biopolymers*, **15**, 2353 (1976).
7) T. W. Anderson, *Ann. Math. Statist.*, **34**, 122 (1963).
8) W. H. Lawton and E. A. Sylvestre, *Technometrics*, **13**, 617 (1971).
9) N. Ohta, *Anal. Chem.*, **45**, 553 (1973).
10) J. J. Kankare, *Anal. Chem.*, **42**, 1322 (1970).
11) M. Takatsuki and K. Yamaoka, *J. Sci. Hiroshima Univ. Ser. A*, **40**, 387 (1976).
12) K. Yamaoka and M. Takatsuki, *Bull. Chem. Soc. Jpn.*, **51**, 3182 (1978).
13) M. Takatsuki and K. Yamaoka, *Bull. Chem. Soc. Jpn.*, **52**, 1003 (1979).
14) N. Greenfield, B. Davidson, and G. D. Fasman, *Biochemistry*, **6**, 1630 (1967).
15) N. Greenfield and G. D. Fasman, *Biochemistry*, **8**, 4108 (1969).
16) Y. H. Chen, J. T. Yang, and H. M. Martinez, *Biochemistry*, **11**, 4120 (1972).
17) Y. H. Chen, J. T. Yang, and K. H. Chau, *Bicchemistry*, **13**, 3350 (1974).
18) C. C. Baker and I. Isenberg, *Biochemistry*, **15**, 629 (1976).
19) C. Djerassi, "Optical Rotatory Dispersion," McGraw-Hill Book Co., New York (1960), p. 160.
20) J. Y. Cassim and J. T. Yang, *Biopolymers*, **9**, 1475 (1970).
21) K. Yamaoka and T. Masujima, *Bull. Chem. Soc. Jpn.*, **52**, 1286 (1979).
22) A. Katchalsky and P. Spitnik, *J. Polymer Sci.*, **2**, 432 (1947).
23) H. P. Gregor and M. Frederick, *J. Polymer Sci.*, **23**, 451 (1957).
24) J. R. Parrish, Jr., and E. R. Blout, *Biopolymers*, **10**, 1491 (1971).

 © 1980 The Chemical Society of Japan Bull. Chem. Soc. Jpn., 53, 975—979 (1980)

Spin Exchange and Translational Diffusion of Nitroxide Radicals in Micelles. ESR Experiments and Spectra Simulation by Modified Bloch Equations

Masayuki AIZAWA,* Tsuyoshi KOMATSU, and Tsurutaro NAKAGAWA
Department of Polymer Science, Faculty of Science, Hokkaido University, Sapporo 060
(Received August 6, 1979)

The dependence of the ESR linewidth of hydrophobic radicals on their concentration in micelles is investigated in two solubilization systems at several temperatures. One system consists of 2,2,6,6-tetramethyl-4-benzoyloxy-1-piperidinyloxyl (BzONO) as a solubilizate and hexadecyltrimethylammonium bromide (CTAB) as a surfactant, and the other, of 2,2,6,6-tetramethyl-4-myristoyloxy-1-piperidinyloxyl (MyONO) and sodium dodecyl sulfate (SDS). The plot of the linewidth against the mole fraction of the radical is not represented by a straight line, as in the previous study. The propriety of the two kinds of models for the solubilization states of radicals which were proposed in the previous paper to explain the unusual shape of these plots is examined by spectra simulation with modified Bloch equations. As these models have proved to be inadequate, a new model taking account of the distribution of the radicals among the micelles is proposed. The simulation based on this model shows a good agreement with the experimental results. The translational diffusion coefficients of radicals in micelles are estimated on the basis of this model. Their values are in the range of $(1.5—2.9)\times10^{-11}$ m²/s.

In the previous study,[1] linewidth measurements of the ESR spectra of 2,2,6,6-tetramethyl-4-benzoyloxy-1-piperidinyloxyl (BzONO, Fig. 1(a)) in sodium dodecyl sulfate (SDS) micelles were carried out at various concentrations of BzONO. The plot of the linewidth, W, against the mole fraction, X, of the radical in micelles did not yield a straight line; rather, a break point seemingly appeared at a certain mole fraction, X_B. Except for one other workers' study,[2] no results like this have yet been reported.

Considering the electron spin-spin relaxation mechanism which causes the line broadening, it was inferred that the dipolar interaction predominates at $X<X_B$, whereas the spin-exchange interaction predominates at $X\geqq X_B$. This inference is based on the temperature dependence of the gradients of the lines in the two mole fraction ranges: at $X<X_B$, the gradient decreases with an increase in the temperature, but at $X\geqq X_B$, it behaves inversely.

In order to explain these unusual results, three kinds of models for a solubilization state of radicals were proposed. From the two of them, the translational diffusion coefficients of BzONO in SDS micelles at 31 °C were estimated to be 1.6×10^{-11} and 2.4×10^{-11} m²/s respectively.

Recently, studies of micellar solutions have been carried out with fluorescent probes.[3] The measurements of the fluorescence decay or quenching, the excimer formation, and so on have brought out several interesting pieces of information on micellar properties.

Some abnormal results, however, have been reported by these studies. For instance, Khuanga and his coworkers[4] have found that the concentration dependence of the intensity ratio ϕ'/ϕ of excimer/monomer fluorescence of pyrene in a 0.1 M aqueous SDS solution is not linear, but curves upwards at higher concentrations, and that when the quencher, oxygen, is added to the solution, the ϕ'/ϕ is increased. In homogeneous solutions, however, the addition of quenchers never increases ϕ'/ϕ. They have explained these results qualitatively on the basis of the distribution of the pyrene molecules among the micelles.

The unusual results obtained in our previous study may also be explained on the same basis.

Thus, the purposes of the present study are: a) to assure that other solubilization systems give a similar, unusual behavior of the W-X plots; b) to reexamine the propriety of the three models in the previous paper; c) to examine whether or not the behavior of the W-X plots can be explained by the distribution of the solubilizates among the micelles, and, finally, d) to estimate more reasonably the translational diffusion coefficients of the radicals in the surfactant micelles.

In order to achieve b) and c), the experimental spectra will be simulated by modified Bloch equations, including the terms for two exchange processes: spin exchange in the micelles and exchange of radicals between the bulk water and the micellar environment.

Experimental

The nitroxide radical, 2,2,6,6-tetramethyl-4-myristoyloxy-1-piperidinyloxyl (MyONO, Fig. 1(b)), was synthesized by the reaction of the corresponding acid chloride with the nitroxide alcohol in a way similar to that in the literature.[5] The crude MyONO was purified by Mr. Fujioka by column chromatography with silica gel (CH_2Cl_2 as the eluent), and then distilled at 122—124 °C under 1 mmHg. The results of the elemental analysis of MyONO was as follows: Found: C, 72.41; H, 11.71; N, 3.43%. Calcd for $C_{23}H_{44}NO_3$: C, 72.20; H, 11.59; N, 3.66%; mol wt 382.6.

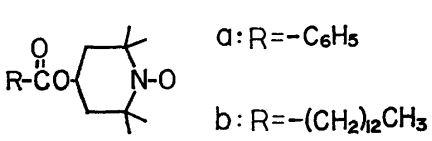

Fig. 1. (a) BzONO and (b) MyONO.

Hexadecyltrimethylammonium bromide (CTAB) of an extra pure grade was recrystallized several times from water solutions. Its CMC was 9.2×10^{-4} mol/dm³ at 25 °C.

In order to estimate the solubilization limits of radicals in surfactant solutions, the ESR spectra of radicals in the saturated solutions were recorded at 20, 30, and 40 °C.

The calculation of the spectra simulation was executed by means of the FACOM 230-60/75 computer in the Hokkaido University Computing Center.

The other experimental procedures and materials have been described in previous papers.[1,6]

Results and Discussion

As an example of the homogeneous solutions, the *W-X* plot of BzONO in ethanol is shown in Fig. 2. The linear relationship between W and X in the figure agrees with the theory of spin-spin interaction in homogeneous solutions.[7]

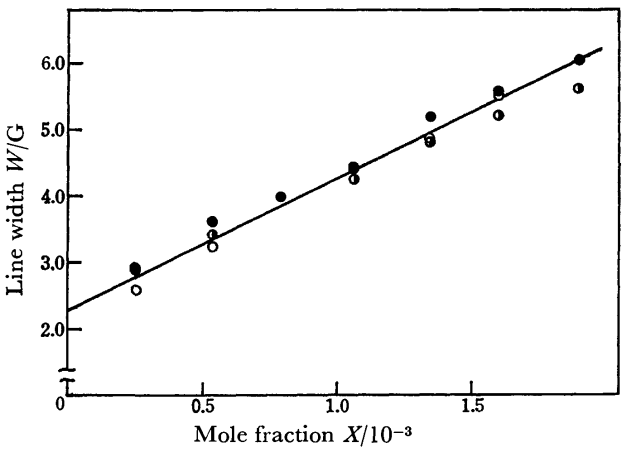

Fig. 2. Plot of W against X of BzONO in ethanol solution at 21 °C. ○: $M_I=+1$, ◑: $M_I=0$, and ●: $M_I=-1$ line width.

In SDS micelles in water, however, the same plot gives a straight line with a break point, as was reported in a previous paper.[1]

In the present study, two solubilization systems, BzONO/CTAB and MyONO/SDS, are investigated at several temperatures in a similar way.

Figures 3 and 4 show the *W-X* plots of MyONO/SDS at 30 °C and of BzONO/CTAB at 40 °C respectively. It may be observed that there is no simple linear relationship between W and X such as is seen in Fig. 2. The plots of the other results showed similar behavior.

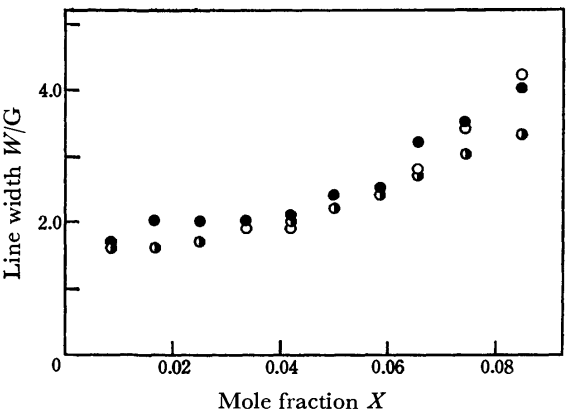

Fig. 3. Plot of W against X of MyONO in SDS micelles at 30 °C. ○: $M_I=+1$, ◑: $M_I=0$, and ●: $M_I=-1$ line width. [SDS]=5.30 wt%.

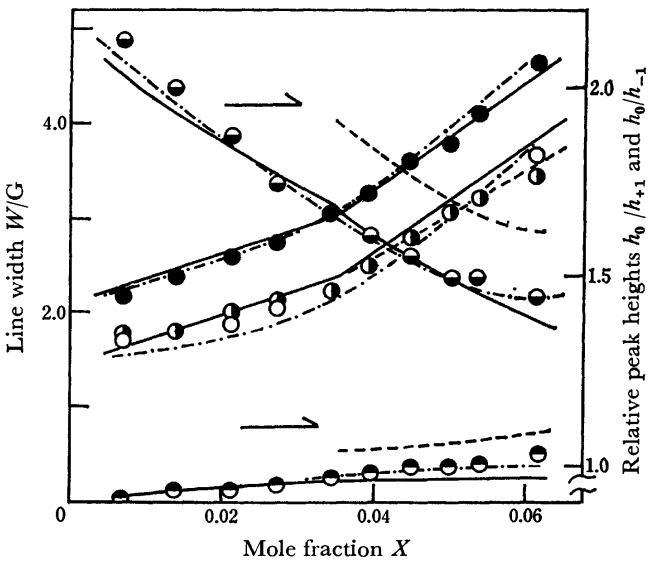

Fig. 4. Plots of W, h_0/h_{+1}, and h_0/h_{-1} against X of BzONO in CTAB micelles at 40 °C.
○: $M_I=+1$, ◑: $M_I=0$, and ●: $M_I=-1$ line width; ◓: h_0/h_{+1} and ◒: h_0/h_{-1}. [CTAB]=5.12%. Full, dotted and dot-dash lines represent the same plots obtained by the simulation with Model 1, Model 2, and the new model in which the distribution of solubilizates among micelles is considered, respectively.

If one considers that the plots can be represented by a straight line which breaks at a certain mole fraction, X_B, the value of X_B is estimated to be 0.035 for BzONO/CTAB and 0.045 for MyONO/SDS. The latter value coincides with that for BzONO/SDS.[1]

Thus, it may be concluded that, in the cases of radicals in ionic micelles in water, the concentration dependence of the linewidth is different from that in homogeneous solutions.

In the previous paper,[1] in seeking to explain this behavior of the *W-X* plots, three kinds of models for the solubilization states of the radicals in the micelles were proposed; they could account for, at least, the appearance of a break point. The propriety of the models, however, must also be examined by spectra simulation with modified Bloch equations.[8]

In the present solubilization systems, most of the nitroxide radicals are solubilized in a micellar environment, while a small amount of them is dissolved in the bulk water. In each of the two environments, the radicals exist in three energy states, which are split by the contact interaction between an electron spin ($S=1/2$) and a ^{14}N nuclear spin ($I=1$). Between the six energy states, there are two exchange processes: one is the exchange of a radical between the micellar environment and the bulk water,[9] and the other is a spin exchange in the micellar environment.[10] The spin exchange in the bulk water can be disregarded, since a molecular collision between radicals scarcely occurs in it at all.

Thus, the exchange scheme in the system is illustrated by Fig. 5. The symbols in the figure, W_{-1}, W_0, and W_{+1}, represent the three states in the bulk water, and M_{-1}, M_0, and M_{+1}, those in the micellar environment.

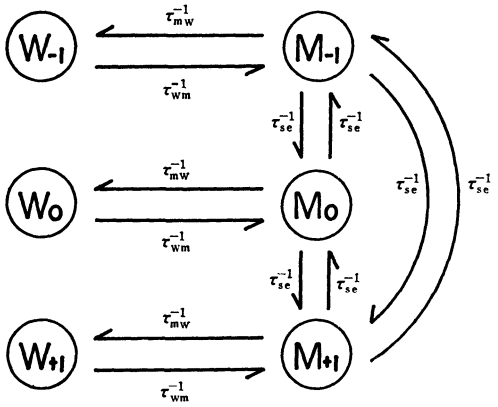

Fig. 5. Proposed scheme of radical exchange.

Their subscripts, -1, 0, and $+1$, correspond to the quantum numbers of a ^{14}N nuclear spin. τ_{mw}^{-1}, τ_{wm}^{-1}, and τ_{se}^{-1} are the exchange probabilities in the corresponding processes.

The modified Bloch equations including these exchange processes are formulated as follows:

$$\begin{cases} dG_{-1}^{w}/dt + \alpha_{-1}^{w}G_{-1}^{w} = Lp_{-1}^{w} - \tau_{wm}^{-1}G_{-1}^{w} + \tau_{mw}^{-1}G_{-1}^{m} \\ dG_{0}^{w}/dt + \alpha_{0}^{w}G_{0}^{w} = Lp_{0}^{w} - \tau_{wm}^{-1}G_{0}^{w} + \tau_{mw}^{-1}G_{0}^{m} \\ dG_{+1}^{w}/dt + \alpha_{+1}^{w}G_{+1}^{w} = Lp_{+1}^{w} - \tau_{wm}^{-1}G_{+1}^{w} + \tau_{mw}^{-1}G_{+1}^{m} \\ dG_{-1}^{m}/dt + \alpha_{-1}^{m}G_{-1}^{m} = Lp_{-1}^{m} + \tau_{wm}^{-1}G_{-1}^{w} - \tau_{mw}^{-1}G_{-1}^{m} \\ \qquad + \tau_{se}^{-1}(G_{+1}^{m}+G_{0}^{m}) - 2\tau_{se}^{-1}G_{-1}^{m} \\ dG_{0}^{m}/dt + \alpha_{0}^{m}G_{0}^{m} = Lp_{0}^{m} + \tau_{wm}^{-1}G_{0}^{w} - \tau_{mw}^{-1}G_{0}^{m} \\ \qquad + \tau_{se}^{-1}(G_{-1}^{m}+G_{+1}^{m}) - 2\tau_{se}^{-1}G_{0}^{m} \\ dG_{+1}^{m}/dt + \alpha_{+1}^{m}G_{+1}^{m} = Lp_{+1}^{m} + \tau_{wm}^{-1}G_{+1}^{w} - \tau_{mw}^{-1}G_{+1}^{m} \\ \qquad + \tau_{se}^{-1}(G_{0}^{m}+G_{-1}^{m}) - 2\tau_{se}^{-1}G_{+1}^{m} \end{cases} \quad (1)$$

where:

$$\alpha_{-1}^{w} = T_{2w}^{-1}(-1) + i(H-H_{-1}^{w}),$$
$$\alpha_{-1}^{m} = T_{2m}^{-1}(-1) + i(H-H_{-1}^{m}),$$
$$\alpha_{0}^{w} = T_{2w}^{-1}(0) + i(H-H_{0}^{w}),$$
$$\alpha_{0}^{m} = T_{2m}^{-1}(0) + i(H-H_{0}^{m}),$$
$$\alpha_{+1}^{w} = T_{2w}^{-1}(+1) + i(H-H_{+1}^{w}),$$
$$\alpha_{+1}^{m} = T_{2m}^{-1}(+1) + i(H-H_{+1}^{m}),$$

and $L=-2\pi i\nu M_0$=constant.

The notations in these equations have the following meanings.

G_{-1}^{w}, G_{0}^{w}, G_{+1}^{w}, and G_{-1}^{m}, G_{0}^{m}, G_{+1}^{m}: the complex magnetic moments at the energy states, with $M_I=-1$, 0, $+1$ in the bulk water, and with $M_I=-1$, 0, $+1$ in the micellar environment respectively.

$T_{2w}^{-1}(-1)$, $T_{2w}^{-1}(0)$, $T_{2w}^{-1}(+1)$, and $T_{2m}^{-1}(-1)$, $T_{2m}^{-1}(0)$, $T_{2m}^{-1}(+1)$: the spin-spin relaxation rates in the energy states, with $M_I=-1$, 0, $+1$ in the bulk water, and with $M_I=-1$, 0, $+1$ in the micellar environment respectively.

p_{-1}^{w}, p_{0}^{w}, p_{+1}^{w}, and p_{-1}^{m}, p_{0}^{m}, p_{+1}^{m}: the mole fractions of the radicals in the energy states, with $M_I=-1$, 0, $+1$ in the bulk water, and with $M_I=-1$, 0, $+1$ in the micellar environment respectively. $p_{-1}^{w}=p_{0}^{w}=p_{+1}^{w}=(1/3)p_w$, $p_{-1}^{m}=p_{0}^{m}=p_{+1}^{m}=(1/3)p_m$.

H_{-1}^{w}, H_{0}^{w}, H_{+1}^{w}, and H_{-1}^{m}, H_{0}^{m}, H_{+1}^{m}: the strength of the resonance magnetic fields in the energy states, with $M_I=-1$, 0, $+1$ in the bulk water, and with $M_I=-1$, 0, $+1$ in the micellar environment respectively. $H_{-1}^{w}-H_{0}^{w}=H_{0}^{w}-H_{+1}^{w}$, $H_{-1}^{m}-H_{0}^{m}=H_{0}^{m}-H_{+1}^{m}$.

ν: the frequency of the applied rotating rf field.

M_0: the z-component of the equilibrium magnetic moment.

i: the imaginary unit.

The sum of the solutions of these equations under the condition that $dG_{-1}^{w}/dt=\cdots=dG_{+1}^{m}/dt=0$ gives the total complex magnetic moment, G, in the stationary state. The real part of G corresponds to the dispersion line, and the imaginary part, to the absorption. Since the first derivative of the absorption line is recorded in the ESR experiment, the first derivative of G is obtained; its imaginary part, $f(H)$, is calculated for the sake of the spectra simulation as a function of the strength of the magnetic field, H—in practice, as a function of $(H-H_0^w)$.

Among the input values needed for the calculation of $f(H)$, τ_{mw}^{-1}, τ_{se}^{-1}, and the mole fraction, p_m, of the radicals in the micelles are fitting parameters, since $p_w=1-p_m$ and $\tau_{wm}^{-1}=\tau_{mw}^{-1}p_m/p_w$ hold. In the present systems, p_m is nearly equal to 1.0 and τ_{mw}^{-1} is negligibly small, as was reported in previous papers.[11,12]

Moreover, the spin-spin relaxation rate, T_{2D}^{-1}, by the dipolar interaction must be introduced as a parameter, since, in all three models, the dipolar interaction is considered to be an electron spin-spin interaction as well as a spin-exchange interaction. T_{2D}^{-1} is added to the spin-spin relaxation rates, T_{2m}^{-1}'s, in the micelles.

The other input values are obtained from the ESR spectra at a low radical concentration in water and from those in micelles. The values of T_{2m}^{-1}'s, however, are corrected to fit the experimental values of the relative peak heights of the three lines. This is because the linewidth, $W(=(2/\sqrt{3})T_2^{-1})$, in the present systems contains a contribution from the protons in the methyl groups adjacent to a nitroxide group in addition to that from a ^{14}N nuclear spin.[13] Equation 1 includes only the effect of a ^{14}N nuclear spin.

The concentration dependences of T_{2D}^{-1} and τ_{se}^{-1} as parameters will now be described on the basis of the respective models.

Model 1. According to this model, a micelle is constituted of several clusters of some surfactant molecules. Therefore, below the break point, X_B, which corresponds to the concentration at which each cluster solubilizes just one radical, only the dipolar interaction occurs.

On the other hand, above X_B, the spin-exchange interaction relaxes the electron spins as well as the dipolar interaction.

Thus, T_{2D}^{-1} and τ_{se}^{-1} can be written, at $X<X_B$, as:

$$\begin{cases} T_{2D}^{-1} = K_D X \\ \tau_{se}^{-1} = 0, \end{cases} \quad (2\text{-a})$$

and at $X\geqq X_B$, as:

$$\begin{cases} T_{2D}^{-1} = K_D X \\ \tau_{se}^{-1} = k_E'(X-X_B), \end{cases} \quad (2\text{-b})$$

where K_D and k_E' are the proportionality constants.

Model 2. In this model, X_B is regarded as the concentration at which a structural change in the micelles is induced by the solubilization. This structural

change quickly makes the dipolar interaction weaker near X_B.

T_{2D}^{-1} and τ_{se}^{-1} are given by the following expressions: At $X<X_B$;

$$\begin{cases} T_{2D}^{-1} = K_D X \\ \tau_{se}^{-1} = 0. \end{cases} \quad (3\text{-a})$$

At $X \geqq X_B$;

$$\begin{cases} T_{2D}^{-1} = 0 \\ \tau_{se}^{-1} = k'_E X. \end{cases} \quad (3\text{-b})$$

Model 3. This model, in which some association of the radicals in equilibrium with the monomeric one in a micelle is assumed, cannot be employed in the simulation, because it is impossible to separate the signal of the radical associates from that of monomeric ones. This fact indicates that this model is not applicable to the solubilization state of radicals.

Thus, on the first two models, the simulation was carried out by the calculation of $f(H)$ using the values of $p_m=1.0$ and $\tau_{mw}^{-1}=0$ and the parameters of τ_{se}^{-1} and T_{2D}^{-1}. The values of parameters which fit the experimental linewidth and the relative peak height were thus found.

The full lines and dotted lines in Fig. 4 represent the results of the simulations with Model 1 and Model 2 respectively. The relative peak heights, h_0/h_{+1} and h_0/h_{-1}, indicate the ratios of the peak height of the central line ($M_I=0$) to that of the low- ($M_I=+1$) and high-field ($M_I=-1$) lines respectively.

The full lines with $K_D=20.1$ G ($=2.01\times10^{-3}$ T) and $k'_E=15.6$ G and the dotted ones with $K_D=20.1$ G and $k'_E=25.7$ G agree with the experimental values so far as the linewidth is concerned. There is, however, a difference in the relative peak heights. The experimental values of h_0/h_{-1} decrease monotonously throughout the mole-fraction range, while the full line has a discontinuity of its gradient at X_B and does not agree with the experimental values at lower and higher mole fractions. The dotted line also has a discontinuity at X_B. (At $X<X_B$, the dotted lines coincide with the full ones).

Therefore, it can be said that each of the three models proposed in the previous study is improper as a basis for the calculation of the translational diffusion coefficients of the radicals in the micelles.

Another way to explain the unusual W-X plot is by taking account of the distribution of the radicals among the micelles. If one regards a micelle as a thermodynamical system which is surrounded by an aqueous phase and which is exchanging its components with the aqueous phase, there may be a certain distribution in the number of the radicals among the micelles.

The distribution function, $P_m(n)$, is described by the following equation, known as the binomial function:[14]

$$P_m(n) = {}_{N_m}C_n \chi^n/(1+\chi)^{N_m}, \quad (4)$$

$$\chi = \langle n\rangle/(N_m-\langle n\rangle), \quad (5)$$

where ${}_{N_m}C_n$ is the binomial coefficient; N_m, the maximum number of solubilizates in a micelle; χ, the quantity defined by Eq. 5 and related with the chemical potential of solubilizates in micelles, and $\langle n\rangle$, the mean number of solubilizates in a micelle.

$P_m(n)$ indicates the fraction of the number of micelles with n solubilizates in relation to the total micelles. This function is obtained on the assumptions that χ is independent of n and that all the micelles have the same N_m value. If $n \ll N_m$, the Poisson distribution function can be derived from Eq. 4.

Transforming $P_m(n)$ into the probability, $P_r(n)$, that a solubilizate belongs to a micelle with n solubilizates, one can write:

$$P_r(n) = nP_m(n)/\sum_{n=1}^{N_m} nP_m(n). \quad (6)$$

If the line-shape function, $f_n(H)$, of a radical in a micelle with n radicals is given, the apparent line-shape function, $F(H)$, is calculated as:

$$F(H) = \sum_{n=1}^{N_m} P_r(n) f_n(H). \quad (7)$$

Thus, the spectra simulation on this model is carried out as follows.

Firstly, $f_n(H)$ is calculated using four parameters, p_m, τ_{se}^{-1}, τ_{mw}^{-1}, and T_{2D}^{-1}, in the same way as in the previous case of $f(H)$. τ_{mw}^{-1}, however, can be neglected for the above-mentioned reason. T_{2D}^{-1} is also omitted, since the radicals in the micelles have enough mobility to make the dipolar interaction fade away, according to Scandella and his co-workers' results.[15]

The spin-exchange rate, τ_{se}^{-1} in a micelle with n radicals is described as:

$$\tau_{se}^{-1} = K_s(n-1)(N_s+1)/(N_s+n-1), \quad (8)$$

where K_s is constant and corresponds to τ_{se}^{-1} when $n=2$, and where N_s is the aggregation number of the surfactant molecules in a micelle. Here, as N_s, the mean aggregation number given in the literature[3] is used in the case of CTAB. However, in the SDS system, one is obliged to use a value lower than that in the literature, since the value in the literature produces the break point at a mole fraction lower than the experimental one. As p_m in Eq. 1, values near 1.0 are used.

TABLE 1. INPUT VALUES USED IN SPECTRA SIMULATION

	a_N^w/G	a_N^m/G	Δg_{mw}/G	N_s	N_m
BzONO/SDS	17.1	16.7	0.2	54	7
MyONO/SDS	17.1	16.6	0.2	54 (44)[a]	11 (9)[a]
BzONO/CTAB	17.1	16.3	0.4	60	6

a) The values at 40 °C.

These values and other input values are listed in Table 1. $a_N^w(=(H_{-1}^w-H_{+1}^w)/2)$ and $a_N^m(=(H_{-1}^m-H_{+1}^m)/2)$, respectively, mean the isotropic hyperfine splitting constants of the radicals in the bulk water and in the micellar environment. Δg_{mw} represents the difference in the resonance magnetic field of the central line between the two environments, $H_0^w-H_0^m$.

Secondly, using arbitrary values of $\langle n\rangle$ lower than N_m, $P_m(n)$ is calculated by means of Eqs. 4 and 5, and then $P_r(n)$ is derived from Eq. 6. Here, N_m is obtained from a mole fraction of a radical saturated in a micelle. The estimation of its mole fraction is performed by plotting the linewidth of the ESR spectra of the radicals

TABLE 2. K_s VALUES AND TRANSLATIONAL DIFFUSION COEFFICIENTS OF NITROXIDE RADICALS IN MICELLES

Temp °C	BzONO/SDS		MyONO/SDS		BzONO/CTAB	
	K_s/G	$D_{tr}/10^{-11}$ m^2 s^{-1}	K_s/G	$D_{tr}/10^{-11}$ m^2 s^{-1}	K_s/G	$D_{tr}/10^{-11}$ m^2 s^{-1}
20	0.40—0.45	1.8—2.0	0.33—0.35	1.5—1.6		
30	0.53—0.58[a)]	2.4—2.6[a)]	0.38—0.43	1.7—1.9	0.35—0.38	1.9—2.0
40	0.60—0.65	2.7—2.9	0.60—0.63	2.2—2.3	0.40—0.45	2.1—2.4
50					0.45—0.50	2.4—2.7

a) The values at 31°C.

saturated in the micellar solution on the W-X curves.

Finally, by substituting these $f_n(H)$ and $P_r(n)$ into Eq. 7, the apparent line-shape function, $F(H)$, at $<n>$ is obtained. If one executes a similar calculation of $F(H)$ with various values of $<n>$, the W-X plot can be represented by this relation: $<n>=Xp_mN_s/(1-X)$.

The dot-dash lines in Fig. 4 show the results of simulation on BzONO/CTAB at 40 °C by the calculation of $F(H)$. These lines were obtained by the simulation with $p_m=0.98$ and $K_s=0.45$ G. It may be observed that the dot-dash lines are in good agreement with the experimental values.

Therefore, it may be said that the appearance of an apparent break point in the W-X plot is caused by the distribution of the radicals among the micelles. The relation that the peak heights are inversely proportional to the square of their linewidths in the spectra of the Lorentzian lineshape contributes greatly to the phenomenon.

All the other systems are also simulated very well by this scheme. The values of K_s which give the best fits are listed in Table 2.

The translational diffusion coefficients, D_{tr}, of the nitroxide radicals in the micelles were calculated with the following equation, using these K_s values:

$$D_{tr} = \gamma_e K_s \lambda^2 (1+N_s)/4\pi \quad (9)$$

where $\gamma_e(=1.7608\times10^7$ s/rad·G) is the magnetogyric ratio of the electron and where λ^2 is the surface area of one polar head group. The values of λ^2 in the SDS micelles and the CTAB micelles are 5.8×10^{-15} and 6.2×10^{-15} cm^2 respectively.[16] Strictly speaking, the effects of the difference in the solubilization site of the solubilizates and of the deformation of the micellar shape induced by the solubilization of the radicals must also be taken into account in Eq. 9.

The values of D_{tr} obtained are listed in Table 2. These values are of the order of 10^{-11} m^2/s, the same as in the previous study.[1] They are taken to be reliable enough, because they are calculated on a reasonable model, as has been revealed in the above simulation.

It may be noticed in Table 2 that, at the same temperature, D_{tr} in BzONO/SDS is greater than in either MyONO/SDS or BzONO/CTAB. This fact may be related to the strength of the adhesion between the hydrophobic groups of the radicals and those of the surfactant molecules.

We would like to thank Professor Yoshio Matsunaga of the Department of Chemistry in Hokkaido University for his kind permission to use the ESR instruments.

References

1) M. Aizawa, T. Komatsu, and T. Nakagawa, *Bull. Chem. Soc. Jpn.*, **52**, 980 (1979).
2) M. D. Barrat, F. Franks, and P. N. Robinson, *J. Solution Chem.*, **6**, 625 (1977).
3) J. H. Fendler and E. J. Fendler, "Catalysis in Micellar and Macromolecular Systems," Academic Press, New York, N. Y. (1975), pp. 20, 293—301.
4) U Khuanga, B. K. Selinger, and R. McDonald, *Aust. J. Chem.*, **29**, 1 (1976).
5) E. G. Rozantsev and V. A. Golubev, *Izv. Akad. Nauk SSSR, Ser. Khim.*, **1968**, 1191.
6) M. Aizawa, T. Komatsu, and T. Nakagawa, *Bull. Chem. Soc. Jpn.*, **50**, 3107 (1977).
7) Y. Ayant, R. Besson, and A. Salvi, *J. Phys. (Paris)*, **36**, 571 (1975).
8) A. Carrington and A. D. McLachlan, "Introduction to Magnetic Resonance," Harper and Row, New York, N. Y. (1967), pp. 204—208.
9) T. Nakagawa and H. Jizomoto, *Kolloid Z.Z. Polym.*, **250**, 594 (1972).
10) E. Odgard, T. B. Melø, and T. Henriksen, *J. Magn. Reson.*, **18**, 436 (1975).
11) G. Aniasson, S. Wall, M. Almgren, H. Hoffman, I. Kielman, W. Ulbricht, R. Zana, J. Lang, and C. Tondre, *J. Phys. Chem.*, **80**, 905 (1976).
12) T. Nakagawa, *Colloid Polym. Sci.*, **252**, 56 (1974).
13) A. E. Stillman and R. N. Schwartz, *J. Magn. Reson.*, **22**, 269 (1976).
14) C. Kittel, "Thermal Physics," John Wiley and Sons, New York, N. Y. (1969), pp. 395—402.
15) C. J. Scandella, P. Devaux, and H. M. McConnell, *Proc. Natl. Acad. Sci. U. S. A.*, **69**, 2056 (1972).
16) H. V. Tartar, *J. Phys. Chem.*, **59**, 1195 (1955).

The Vibrational Fine Structure of the $^1T_{1g}\leftarrow{}^1A_{1g}$ Absorption Band of $[Co(NH_3)_6]^{3+}$

Yoshinori Komi and Akio Urushiyama*

Department of Chemistry, Faculty of Science, Rikkyo University, Nishiikebukuro, Toshima-ku, Tokyo 171

(Received August 17, 1979)

The crystal absorption spectra of $[Co(NH_3)_6][Ir(CN)_6]$ and $[Co(ND_3)_6][Ir(CN)_6]$ were studied at 4.2 K. The vibrational fine structure observed on the $^1T_{1g}\leftarrow{}^1A_{1g}$ absorption band of the hexaamminecobalt(III) complexes was interpreted in terms of a vibronic intensity scheme in comparison with the vibrational frequencies of the complexes. The deuteration shifts helped to confirm the assignments of the structure. It was found that, as well as the skeletal vibrations of the CoN_6 group, the NH_3 (and ND_3) rocking and the H–N–H symmetric deformation modes are effective in the vibronic intensity mechanism of the bands.

The vibrational fine structure of the $^1T_{1g}\leftarrow{}^1A_{1g}$ absorption band of $[Co(NH_3)_6]^{3+}$ was first studied by Wentworth.[1] He observed, in his low-temperature spectroscopic work, that at least twelve members of a progression with a spacing of about 420 cm^{-1} were superimposed on the band. Since then, several reports[2] have appeared concerning the temperature dependence of the band intensity and the vibronic interaction with the odd skeletal modes of the CoN_6 group. Recently, we examined the transmission spectra of $[Co(NH_3)_6][Co(CN)_6]$ at 4.2 K and resolved each progressional line into several components.[3] As a result of these transmission studies, it is thought that measurements with a higher resolution may give definite information as to the structure of the band.

It is our experience that the clarity of the fine structure observed on the $^1T_{1g}\leftarrow{}^1A_{1g}$ absorption band of the hexaamminecobalt(III) complexes is very dependent on particular crystal lattices. In the present paper, the low-temperature crystal-absorption spectra of $[Co(NH_3)_6][Ir(CN)_6]$ and $[Co(ND_3)_6][Ir(CN)_6]$ will be reported. These crystals showed the most extensive structure in our studies. The observed fine structure was interpreted on the basis of the infrared and Raman data of the complexes.

Experimental

Single-crystals of $[Co(NH_3)_6][Ir(CN)_6]$ were obtained when aqueous solutions of $[Co(NH_3)_6]Cl_3$ and $K_3[Ir(CN)_6]$ were mixed extremely slowly in a glass tube. The infrared and Raman spectra suggested that the skeletons of the complexes are retained through the procedure. Found: Co, 11.7%. Calcd for $[Co(NH_3)_6][Ir(CN)_6]$: Co, 11.6%. The deuterium-substituted compound was similarly obtained from D_2O solutions. The infrared and Raman bands of the hexaamminecobalt(III) complex shifted toward the low-wavenumber side (Table 1). Weissenberg photographs showed that the crystal of $[Co(NH_3)_6][Ir(CN)_6]$ belongs to the trigonal crystal system, $a=7.35(2)$ Å, $\alpha=97.9(1)°$, with the space group of R3 or $R\bar{3}$. The crystals of $[Co(ND_3)_6][Ir(CN)_6]$ are found to be very similar in appearance to those of $[Co(NH_3)_6][Ir(CN)_6]$ under a microscope. The low-temperature polarized absorption spectra of appropriate crystal samples were measured by the method previously reported.[3] All the spectra were taken with a spectral slit width of less than 160 μm, which corresponds to a resolution of 10 cm^{-1}. The fine structure observed on the band of $[Co(ND_3)_6]^{3+}$ was obscured after several days' exposure of the sample crystal in room air. The temperatures of an indium plate in which the samples were set with Apiezon N grease on a pinhole ($\phi=0.1$ mm) were monitored by means of a thermocouple (Au: Fe chromel). The sample dimensions were estimated by the use of a micrometer ocular. The infrared and Raman spectra were taken with a JASCO IR-F spectrometer and Narumi 750Z-1200 Raman spectrometer respectively.

Results and Discussion

Figures 1 and 2 show the crystal absorption spectra of $[Co(NH_3)_6][Ir(CN)_6]$ and $[Co(ND_3)_6][Ir(CN)_6]$ respectively in the $^1T_{1g}\leftarrow{}^1A_{1g}$ absorption region of the hexaamminecobalt(III) complexes. The counter complex anion, $[Ir(CN)_6]^{3-}$, can be expected to show no absorption in the visible region.[4] Some structure was detected also on the $^1T_{2g}\leftarrow{}^1A_{1g}$ absorption bands in the near-ultraviolet region. However, no detailed analysis was possible because of the low resolution. The absorption spectra taken with the polarized lights whose electric vectors are parallel and perpendicular to the crystal [111] axis were observed to be almost identical in the two samples.

It was found that the $^1T_{1g}\leftarrow{}^1A_{1g}$ band of $[Co(NH_3)_6]^{3+}$ consists of the progressional members of,

Table 1. Vibrational frequencies of hexaamminecobalt(III) complexes[a]

	$\delta_s(NH_3)$, (ND_3) / cm^{-1}	$\rho_r(HNH)$, (DND) / cm^{-1}	$\nu_1(a_{1g})$ / cm^{-1}	$\nu_2(e_g)$ / cm^{-1}	$\nu_3(t_{1u})$ / cm^{-1}	$\nu_4(t_{1u})$ / cm^{-1}	$\nu_6(t_{2u})$ / cm^{-1}
$[Co(NH_3)_6]^{3+}$	1329[b], 1324[b]	851[b]	480[b]	441[b]	480[b]	331[b]	252[e]
$[Co(ND_3)_6]^{3+}$	1020[c]	667[c]	452[d]		446[d]	294[c]	232[e]

a) Vibrations are denoted according to K. Nakamoto, "Infrared and Raman Spectra of Inorganic and Coordination Compounds," 3rd ed, John Wiley and Sons, New York (1978). b) T. V. Long, II, A. W. Herlinger, E. F. Epstein, and I. Bernal, *Inorg. Chem.*, **9**, 459 (1970). c) K. H. Schmidt and A. Muller, *J. Mol. Struct.*, **22**, 343 (1974). d) Present work on $[Co(ND_3)_6][Ir(CN)_6]$. e) W.A. Yeranos, *Inorg. Chem.*, **7**, 1259 (1968).

apparently, five structure components, (*na*), (*nb*), (*nc*), (*nd*), and (*nf*). The average spacing of the progression was estimated to be 401 cm^{-1}. In the case of $[Co(ND_3)_6]^{3+}$, the spacing of the progression was reduced to 370 cm^{-1}, and a new component, (*ne*), appeared distinctly in the lower-wavenumber vicinity of the $(n+1\,d)$ components. However, the energy differences between the components of (*na*), (*nb*), (*nc*), and (*nd*) exerted no significant change on the deuteration of the ligands.

Assuming a vibronic intensity scheme, the positions of the structure components can be expressed as $^1A_{1g}(O) \rightarrow {}^1T_{1g}(O') + \nu_i + n\nu_j$, where ν_i=the frequency of the odd vibration, ν_j=the frequency of the even vibration, and n=the integer. A large displacement of the potential surface of the electronic excited state from that of the ground state along the Q_j internal coordinate gives a long Frank-Condon progression with a spacing corresponding to that of ν_j on the band. An electronic excitation to the anti-bonding e_g orbital may relax the Co–N bonds and result in some frequency reductions in the electronic excited state.

The vibrational frequencies of the complexes studied are summarized in Table 1. The observed average spacings of 401 and 370 cm^{-1} may be correlated to the $\nu_1(a_{1g})$ vibrations of the CoN_6 skeletons of $[Co(NH_3)_6]^{3+}$ and $[Co(ND_3)_6]^{3+}$ respectively. However, as in the case of the $^4T_{2g} \leftarrow {}^4A_{2g}$ absorption band of $[Cr(NH_3)_6]^{3+}$ discussed by Wilson *et al.*,[5] there is, indeed, a possibility that the $\nu_2(e_g)$ mode is involved in the progression of the bands. In general, the $\nu_1(a_{1g})$ and the $\nu_2(e_g)$ M–N stretching modes of the hexacoordinated transition metal complexes are observed to have almost the same frequencies.[6] Therefore, further spectroscopic studies are necessary for more reliable assignments of the progression observed on the bands associated with the $t_{2g} \rightarrow e_g$ electronic transition of the complexes.

It is known[6] that the frequencies of the CoN_6 skeletal vibrations of the hexaamminecobalt(III) complex are lowered by about 10% on the deuteration of the ligands, whereas the NH_3 rocking, the H–N–H deformation, and the N–H stretching frequencies are reduced by as much as 20—28% on the deuteration. If the observed intervals between the components are compared with those of the infrared frequencies shown in the table, the following assignments seem reasonable:

(*na*) $\cdots {}^1A_{1g}(O) \longrightarrow {}^1T_{1g}(O') + \nu_{lattice} + n\nu_1(\nu_2)$
(*nb*) $\cdots + \nu_6 + n\nu_1(\nu_2)$
(*nc*) $\cdots + \nu_4 + n\nu_1(\nu_2)$
(*nd*) $\cdots + \nu_3 + n\nu_1(\nu_2)$
(*ne*) $\cdots + \nu(NH_3, ND_3 \text{ rocking}) + n\nu_1(\nu_2)$
(*nf*) $\cdots + \nu(\text{H–N–H sym. def.}) + n\nu_1(\nu_2)$.

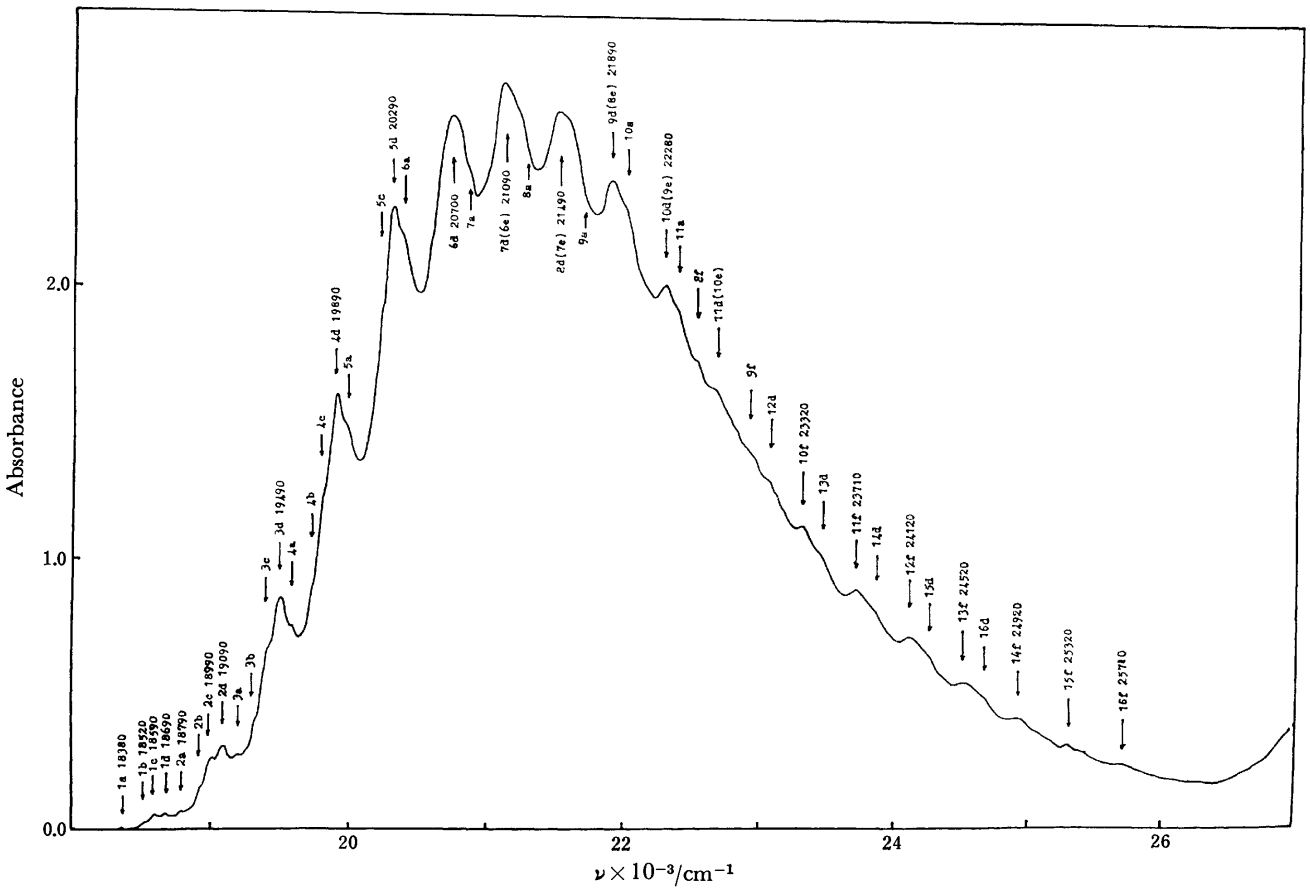

Fig. 1. Crystal absorption spectrum of $[Co(NH_3)_6][Ir(CN)_6]$ at 4.2 K with the polarized light whose electric vector parallel to the crystal [111] axis (crystal thickness is 0.14 mm).

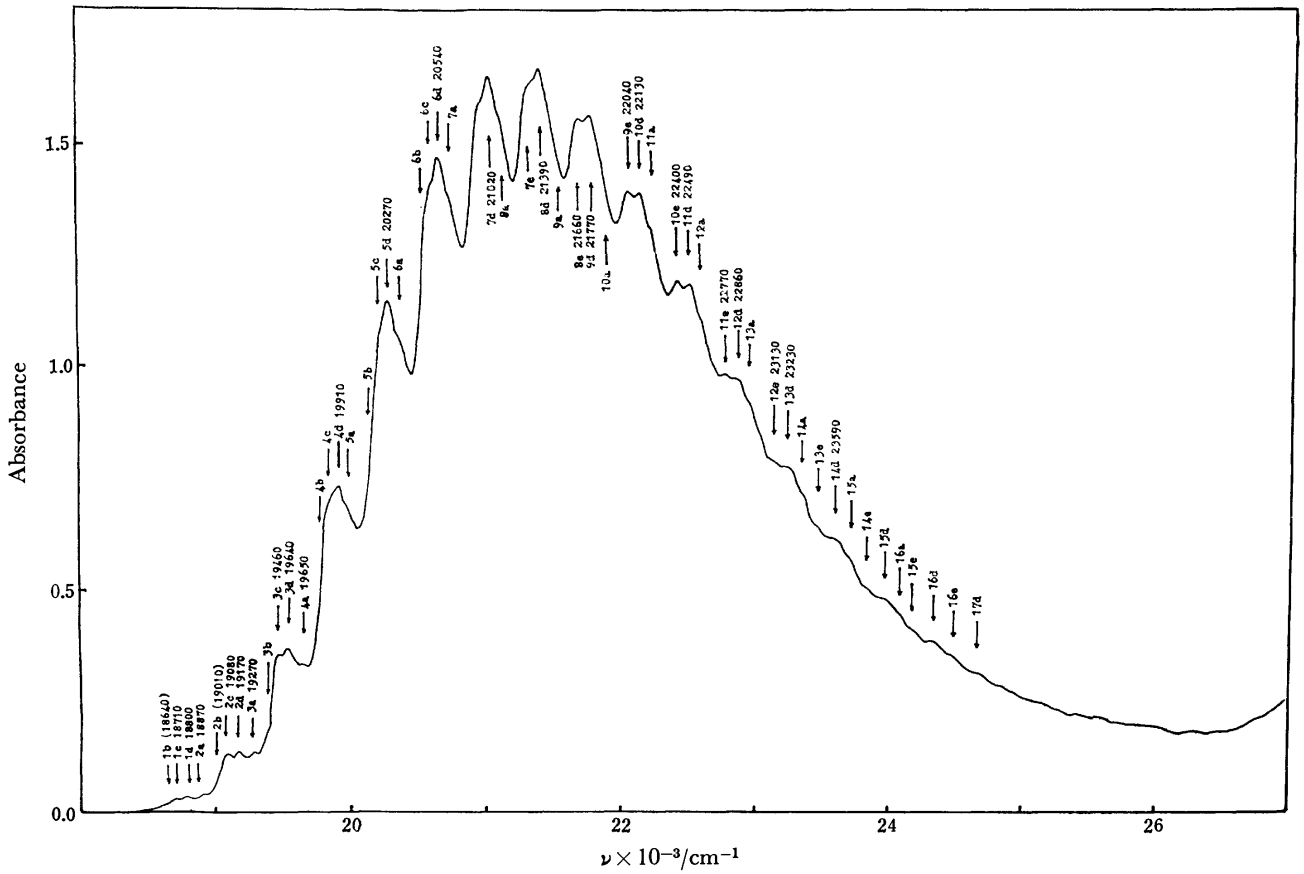

Fig. 2. Crystal absorption spectrum of $[Co(ND_3)_6][Ir(CN)_6]$ at 4.2 K with the polarized light whose electric vector parallel to the crystal [111] axis (crystal thickness is 0.08 mm).

The weak components, (*na*), were assigned to lattice vibrations of the crystals. In the case of $[Co(NH_3)_6]^{3+}$, the (*ne*) components are thought to be obscured due to their locations close to $(n+1\ d)$. The components of (*nf*) were also obscured on the band of $[Co(ND_3)_6]^{3+}$. A preliminary measurement of the $^4T_{2g}\leftarrow{}^4A_{2g}$ absorption band of $[Cr(NH_3)_6]^{3+}$ showed distinct structure components on the higher-wavenumber side of the band very similar to the (*ne*) and (*nf*) components in the present cases. As a matter of course, no structure components corresponding to (*ne*) and (*nf*) were reported in the fine structure of the $^1T_{1g}\leftarrow{}^1A_{1g}$ absorption band of $[PtF_6]^{2-}$ studied by Patterson *et al.*[7] In the present measurements, the O–O′ lines could not be detected even if the thickness of the samples was increased to 0.8 mm.

Flint *et al.*[8] have studied the structure of the $^4A_{2g}\leftarrow{}^2E_g$ emission of $[Cr(NH_3)_6]^{3+}$ and have detected the dominant vibronic components of the NH_3 rocking and the H–N–H sym. def. modes, as well as the skeletal modes of the CrN_6 group. They proposed that the spin-allowed absorption band of $^4T_{2g}\leftarrow{}^4A_{2g}$ should also involve the vibronic components attributable to the NH_3 rocking and the H–N–H sym. def. vibrations, since the mixing of the $^4T_{2g}$ state into the ^2E_g state is responsible for the intensity of the $^4A_{2g}\leftarrow{}^2E_g$ transition. The present experimental results are in line with their suggestion also in the case of the $^1T_{1g}\leftarrow{}^1A_{1g}$ absorption band of $[Co(NH_3)_6]^{3+}$ and $[Co(ND_3)_6]^{3+}$.

The authors wish to express their thanks to Professor Yukio Kondo, Rikkyo University, for his encouragement. We also would like to thank Dr. Hiroshi Saito for obtaining the Raman spectra and Miss Akiko Goto for her help in the analysis of some samples.

References

1) R. A. D. Wentworth, *Chem. Commun.*, **1965**, 532.

2) a) W. A. Yeranos, *Z. Naturforsch., Teil A*, **22**, 183 (1967); b) W. A. Yeranos, *ibid.*, **24**, 248 (1969); c) W. A. Yeranos, *Inorg. Chem.*, **7**, 1259 (1968).

3) K. Fukuda and A. Urushiyama, *Bull. Chem. Soc. Jpn.*, **51**, 1946 (1978).

4) H. H. Schmidtke, *Z. Phys. Chem. (Frankfurt am Main)*, **40**, 96 (1964).

5) R. B. Wilson and E. I. Solomon, *Inorg. Chem.*, **17**, 1729 (1978).

6) K. Nakamoto, "Infrared and Raman Spectra of Inorganic and Coordination Compounds," 3rd ed, John Wiley & Sons, New York (1978).

7) H. H. Patterson, W. J. DeBerry, J. E. Byrne, M. T. Hsu, and J. A. LoMenzo, *Inorg. Chem.*, **16**, 1968 (1977).

8) C. D. Flint and P. Greenough, *J. Chem. Soc., Faraday Trans. 2*, **68**, 897 (1972).

The X-Ray Study of Several Reaction Products of Substituted Benzodicyclobutene. I. 2,7-Di-*t*-butyl-11,11,12,12-tetracyano-4,5,9,10-tetraphenyltetracyclo[4.4.2.0^{1,8}.0^{3,6}]dodeca-2,4,7,9-tetraene

Harumichi Tsukada,* Hirotaka Shimanouchi, and Yoshio Sasada

Laboratory of Chemistry for Natural Products, Tokyo Institute of Technology, Ookayama, Meguro-ku, Tokyo 152

(Received August 22, 1979)

As a part of the studies of the reaction mechanism of a substituted benzodicyclobutene (**1**), the X-ray analysis of the title compound was carried out. The crystals are monoclinic; space group $P2_1/a$, $a=23.159(3)$, $b=20.369(3)$, $c=8.589(1)$ Å, $\beta=104.27(1)°$. The structure was solved by the direct method and was refined by the block-diagonal least-squares method to the final R factor of 0.070 for 5553 observed reflections. In the molecular structure, there is a bridge-bond formed by the "cross" addition of tetracyanoethylene (TCNE) to the C(1) and C(6) sites of **1**. The intermolecular interaction was calculated so as to make clear what kind of addition reaction is preferable for the molecule **1**. The result is consistent with the observation that, in addition to the linear adduct, a cross adduct is also obtained as a by-product.

There are several theoretical approaches to organic reactions based on electronic considerations. One of the most popular and useful theories is the Woodward-Hoffmann rule[1] for a Diels-Alder reaction between some planar conjugated molecules. In the reactions affected by steric hindrance, however, the rule sometimes fails to predict the observed reaction. For example, the Diels-Alder reaction of substituted heptafulvalene and tetracyanoethylene (TCNE) gives an unexpected adduct.[2] The calculation including all the valence electrons responsible for such a repulsion will require a great deal of time and effort. It may be better to deal with the non-bonded interaction using empirical parameters obtained in the investigation of the crystal packing.[3]

A series of the adducts of substituted benzodicyclobutene[4] (**1**) with some dienophiles are most profitable for such an energetic investigation of chemical reactions. This molecule undergoes many kinds of addition reactions, since there are many sites which dienophiles can attack. We can obtain "linear" adducts if dienophile adds to the C(4)–C(5) position of the molecule **1**. Addition to the C(3)–C(4) and C(1)–C(6) positions will produce "angular" and "cross" adducts respectively. TCNE reacts with **1** to give not only the linear adduct (**2**) as the main product, but also the cross adduct (**3**) as a by-product.[5,6] The structure determination of the former had been reported previously.[7] The present X-ray analysis of the latter has revealed the stereochemical difference between the main by-products, which will give some information regarding the steric effect of the bulky substituents on the reaction.

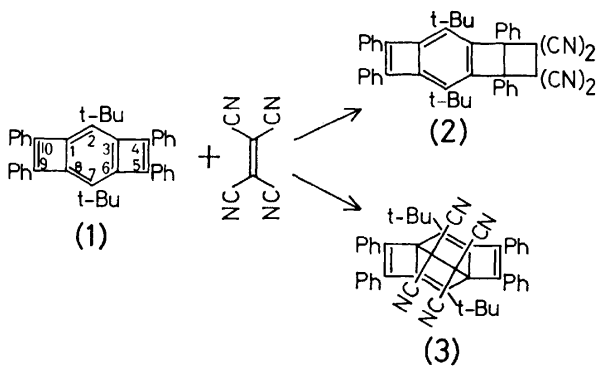

Experimental and Structure Determination

Crystals suitable for structure determination were provided by Professor Fumio Toda of Ehime University. The crystals were colorless needles. From the oscillation and Weissenberg photographs, the space group was uniquely assigned as $P2_1/a$. A Rigaku automated four-circle diffractometer with graphite-monochromated Mo $K\alpha$ radiation ($\lambda=0.71069$ Å) was used for the determination of the accurate unit-cell dimensions and for the measurement of the diffraction intensities. The crystal data are listed in Table 1. A total of 6901 independent reflections ($2\theta\leqq50°$) were obtained, of which 5553 had net intensities greater than the background. The intensities were corrected for the Lorentz and polarization effects, but not for the absorption and extinction.

Table 1. Crystal data of 2,7-di-*t*-butyl-11,11,12,12-tetracyano-4,5,9,10-tetraphenyltetracyclo-[4.4.2.0^{1,8}.0^{3,6}]dodeca-2,4,7,9-tetraene

$C_{48}H_{38}N_4$	
Molecular weight	670.9
Crystal system:	monoclinic
Space group:	$P2_1/a$
a	23.159(3) Å
b	20.369(3)
c	8.589(1)
β	104.27(1)°
U	3927(1) Å^3
Z	4
D_m	1.135 g cm^{-3}
D_x	1.135

The structure was solved by the direct method.[8] The E map, calculated from 450 normalized structure factors ($E\geqq1.7$) with determined signs, clearly revealed 52 non-hydrogen atoms. Fourier synthesis including all these atoms showed no other spurious peaks at all. The atomic parameters were refined by the block-diagonal least-squares method. After the convergence of the positional and isotropic thermal parameters, the contribution from hydrogen atoms located geometrically was included. At the subsequent stage of the refinement, with the introduction of anisotropic thermal parameters for the nonhydrogen atoms, the parameters of the

hydrogen atoms were not shifted, but their positions were recalculated at the last stage. The weighting scheme was; $w=0.8$ for $|F|=0$, $w=1.0$ for $0<|F|\leqq 30$, and $w=1/\{1+0.14(|F|-30)\}$ for $|F|>30$. The final R factor was 0.070 for 5553 observed reflections. In the final cycle of the least-squares, no shifts exceeded one tenth of their e.s.d's. The atomic scattering factors were taken from the "International Tables for X-Ray Crystallography.[9]" The final atomic parameters are listed in Table 2,[10] while the crystallographic numbering scheme is shown in Fig. 1.

Table 2. Atomic coordinates ($\times 10^4$)

	X	Y	Z
C(1)	1553(1)	2336(1)	7917(3)
C(2)	2123(1)	2357(1)	9309(3)
C(3)	2429(1)	1808(1)	9174(3)
C(4)	2952(1)	1382(1)	9712(3)
C(5)	2771(1)	947(1)	8485(3)
C(6)	2183(1)	1325(1)	7791(3)
C(7)	1548(1)	1113(1)	7831(3)
C(8)	1245(1)	1669(1)	7910(3)
C(9)	694(1)	2017(1)	7982(4)
C(10)	936(1)	2623(1)	7922(3)
C(11)	1753(1)	2377(1)	6275(3)
C(12)	2146(1)	1724(1)	6186(3)
C(13)	2251(1)	2864(1)	10656(3)
C(14)	2265(2)	3563(2)	10034(4)
C(15)	1757(2)	2812(2)	11566(4)
C(16)	2848(2)	2725(2)	11819(5)
C(17)	1349(2)	405(2)	7966(5)
C(18)	1708(3)	134(2)	9604(7)
C(19)	703(2)	376(2)	7923(11)
C(20)	1491(2)	-40(2)	6712(7)
C(21)	3503(1)	1424(1)	11028(3)
C(22)	3515(1)	1154(2)	12519(4)
C(23)	4029(2)	1205(2)	13762(4)
C(24)	4520(2)	1517(2)	13498(5)
C(25)	4513(2)	1784(2)	12017(5)
C(26)	4000(1)	1734(2)	10772(4)
C(27)	3078(1)	398(1)	7941(3)
C(28)	3533(1)	66(1)	9019(4)
C(29)	3857(1)	-423(2)	8506(4)
C(30)	3734(1)	-595(2)	6895(4)
C(31)	3286(2)	-271(2)	5813(4)
C(32)	2957(2)	221(2)	6316(4)
C(33)	89(1)	1809(2)	8056(5)
C(34)	-28(2)	1669(2)	9530(6)
C(35)	-606(2)	1488(3)	9584(9)
C(36)	-1043(2)	1443(3)	8217(10)
C(37)	-933(2)	1578(3)	6752(9)
C(38)	-363(2)	1771(2)	6669(6)
C(39)	678(1)	3281(1)	7767(3)
C(40)	152(1)	3404(2)	8249(4)
C(41)	-115(1)	4019(2)	8034(4)
C(42)	136(1)	4523(2)	7351(4)
C(43)	653(1)	4412(2)	6859(4)
C(44)	919(1)	3795(1)	7065(4)
C(45)	2108(1)	2967(1)	6181(3)
C(46)	1215(1)	2400(2)	4929(3)
C(47)	2755(1)	1901(2)	6091(4)
C(48)	1875(2)	1344(2)	4730(4)
N(1)	2392(1)	3419(1)	6118(4)
N(2)	795(1)	2422(2)	3904(4)
N(3)	3232(1)	2013(2)	6057(4)
N(4)	1668(2)	1058(2)	3591(4)

Standard deviations are given in parentheses.

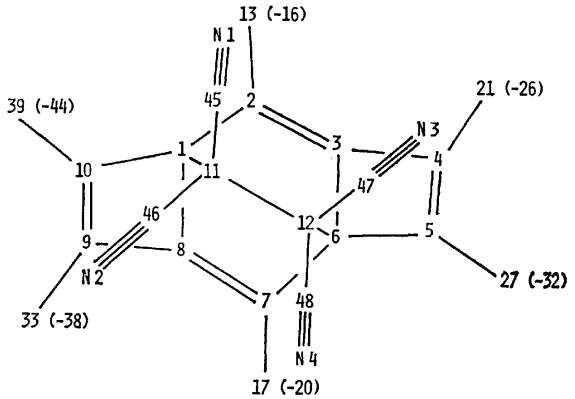

Fig. 1. Numbering scheme. Numbers in parentheses indicate the atoms of the substituents.

Description of the Structure

A stereoview of the crystal structure is shown in Fig. 2. The intermolecular contacts are normal, judging from the relevant van der Waals radii. Two perspective views of a single molecule are given in Fig. 3. This structure is consistent with that presumed by the spectroscopic study.[6] The molecular framework contains a bridge bond formed by the addition of TCNE at the bridge heads C(1) and C(6) for which the name "cross adduct" is suitable. It consists of three planar parts, which all include the C(1)–C(6) interatomic vector. The deviations of the atoms from the least-squares planes and the dihedral angles between these planes are given in Table 3. The chemically equivalent planes, I and II, make a dihedral angle of 125.0°, which is bisected by the plane, III, formed by the addition of TCNE.

Although these three planes have no significant distortion, the four-membered rings annelated to those parts are slightly but significantly folded, the C(4) atom approaching the cyano groups. On the other hand, the *t*-butyl groups are kept away from the cyano groups, the deviation of the tertiary carbon atoms from the planes, I and II, being 0.13 Å. These trends may be attributed to the steric effects of the bulky substituents, which may play an important role in the addition reaction.

The bond lengths and angles are listed in Tables 4 and 5 respectively. As this molecule has an approximate two-fold axis, average values are used in the following discussion. The lengths of two double bonds, C(2)=C(3)

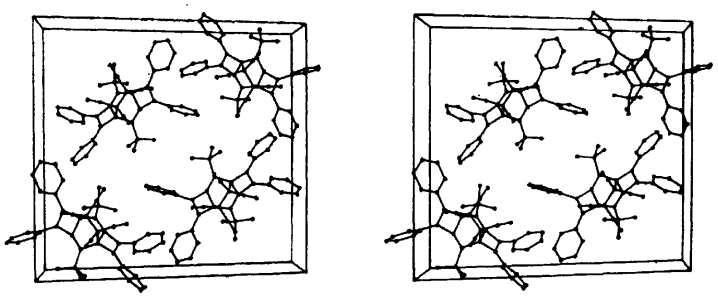

Fig. 2. Crystal structure viewed along the c axis.

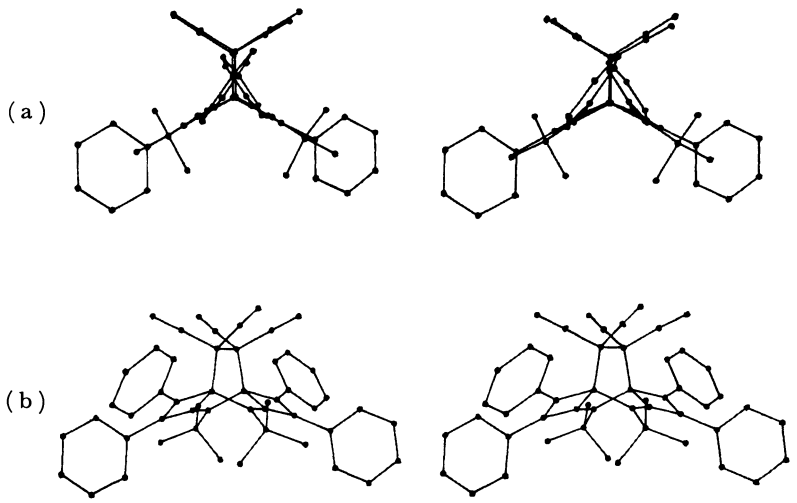

Fig. 3. Stereoscopic views. (a) viewed along the C(1)–C(6) direction. (b) viewed along the midpoints of C(1)–C(2) and C(6)–C(7).

Table 3. Deviations (l/Å) of the atoms from the least-squares planes and the dihedral angles (ϕ/°) between them

(Asterisks indicate the atoms defining the best plane.)

Plane I		Plane II		Plane III	
C(1)*	−0.002	C(1)*	0.002	C(1)*	−0.005
C(2)*	0.005	C(8)*	−0.005	C(11)*	0.009
C(3)*	−0.005	C(7)*	0.004	C(12)*	−0.009
C(6)*	0.003	C(6)*	−0.002	C(6)*	0.005
C(13)	−0.134	C(17)	−0.130		
C(4	0.014	C(9	0.001		
Plane IV		Plane V			
C(3)*	−0.012	C(1)*	0.014		
C(4)*	0.014	C(8)*	−0.014		
C(5)*	−0.013	C(9)*	0.016		
C(6)*	0.012	C(10)*	−0.015		
C(2)	−0.070	C(7)	−0.065		
C(21)	−0.023	C(33)	0.041		
C(27)	−0.209	C(39)	−0.155		

	II	III	IV	V
I	125.0	117.2	2.1	124.6
II		117.9	124.7	1.9
III			117.4	118.4
IV				124.1

Table 4. Bond length (l/Å)

C(1)	-C(2)	1.547(4)	C(17)	-C(20)	1.504(8)
C(1)	-C(8)	1.535(4)	C(21)	-C(22)	1.388(4)
C(1)	-C(10)	1.546(4)	C(21)	-C(26)	1.378(5)
C(1)	-C(11)	1.590(4)	C(22)	-C(23)	1.393(5)
C(2)	-C(3)	1.344(4)	C(23)	-C(24)	1.368(6)
C(2)	-C(13)	1.523(4)	C(24)	-C(25)	1.380(7)
C(3)	-C(4)	1.469(4)	C(25)	-C(26)	1.391(6)
C(3)	-C(6)	1.539(4)	C(27)	-C(28)	1.394(4)
C(4)	-C(5)	1.361(4)	C(27)	-C(32)	1.401(5)
C(4)	-C(21)	1.483(4)	C(28)	-C(29)	1.383(5)
C(5)	-C(6)	1.551(4)	C(29)	-C(30)	1.387(5)
C(5)	-C(27)	1.461(4)	C(30)	-C(31)	1.378(5)
C(6)	-C(7)	1.540(4)	C(31)	-C(32)	1.390(5)
C(6)	-C(12)	1.584(4)	C(33)	-C(34)	1.388(7)
C(7)	-C(8)	1.342(4)	C(33)	-C(38)	1.381(7)
C(7)	-C(17)	1.526(5)	C(34)	-C(35)	1.402(9)
C(8)	-C(9)	1.477(4)	C(35)	-C(36)	1.351(11)
C(9)	-C(10)	1.362(4)	C(36)	-C(37)	1.372(12)
C(9)	-C(33)	1.479(5)	C(37)	-C(38)	1.396(10)
C(10)	-C(39)	1.460(4)	C(39)	-C(40)	1.402(4)
C(11)	-C(12)	1.625(4)	C(39)	-C(44)	1.392(4)
C(11)	-C(45)	1.471(4)	C(40)	-C(41)	1.389(5)
C(11)	-C(46)	1.476(4)	C(41)	-C(42)	1.381(5)
C(12)	-C(47)	1.477(4)	C(42)	-C(43)	1.382(5)
C(12)	-C(48)	1.473(5)	C(43)	-C(44)	1.391(5)
C(13)	-C(14)	1.525(5)	C(45)	-N(1)	1.140(4)
C(13)	-C(15)	1.541(5)	C(46)	-N(2)	1.140(5)
C(13)	-C(16)	1.519(5)	C(47)	-N(3)	1.134(5)
C(17)	-C(18)	1.549(7)	C(48)	-N(4)	1.137(6)
C(17)	-C(19)	1.488(10)			

Standard deviations are given in parentheses.

and C(4)=C(5), are, though normal, somewhat different from each other. The atomic chain of C(2)=C(3)–C(4)=C(5) lies nearly on a plane and has almost the same bond lengths as those of *trans*-butadiene.[11] The two single bonds connecting the phenyl and the four-membered rings have significantly different lengths. This may be related to the dihedral angle between the four-membered and phenyl rings; one dihedral angle is 86.4°, and the other, 25.6°. The shorter single bond, C(5)–C(27), is accompanied by the smaller dihedral angle, indicating a conjugation effect between the π electron systems of the skeleton and the phenyl ring.

As for the other single bonds, it should be mentioned that they are stretched to some extent. In particular, C(11)–C(12) is 1.625 Å, about 0.09 Å longer than the normal C_{sp^3}–C_{sp^3} bond length.[12] These elongations may be partly the result of the electron-withdrawing effect of the cyano group; at the same time, the nearly eclipse conformation around this bond, the average torsion angle being 2.1°, may greatly affect the bond length. This is also the case with the compound **2** previously reported,[7] the corresponding values being 1.612 Å and 5.8° respectively.

Discussion

The theoretical approaches are quite difficult for the various chemical reactions of complicated organic molecules. We have treated interactions between the reacting molecules by dividing them into two parts: the electronic interaction between the active sites of both the pertinent molecules, and the non-bonded steric effect of the bulky substituents.

TABLE 5. BOND ANGLES (ϕ/°)

C(2)	-C(1)	-C(8)	109.5(2)	C(2)	-C(13)	-C(14)	112.6(3)
C(2)	-C(1)	-C(10)	126.9(2)	C(2)	-C(13)	-C(15)	108.0(3)
C(2)	-C(1)	-C(11)	107.8(2)	C(2)	-C(13)	-C(16)	110.4(3)
C(8)	-C(1)	-C(10)	84.6(2)	C(14)	-C(13)	-C(15)	108.9(3)
C(8)	-C(1)	-C(11)	106.2(2)	C(14)	-C(13)	-C(16)	108.0(3)
C(10)	-C(1)	-C(11)	117.0(2)	C(15)	-C(13)	-C(16)	108.9(3)
C(1)	-C(2)	-C(3)	106.2(2)	C(7)	-C(17)	-C(18)	107.6(4)
C(1)	-C(2)	-C(13)	125.0(2)	C(7)	-C(17)	-C(19)	110.9(5)
C(3)	-C(2)	-C(13)	128.4(2)	C(7)	-C(17)	-C(20)	113.0(4)
C(2)	-C(3)	-C(4)	151.2(3)	C(18)	-C(17)	-C(19)	108.5(5)
C(2)	-C(3)	-C(6)	119.7(2)	C(18)	-C(17)	-C(20)	105.8(4)
C(4)	-C(3)	-C(6)	89.1(2)	C(19)	-C(17)	-C(20)	110.7(5)
C(3)	-C(4)	-C(5)	94.0(2)	C(4)	-C(21)	-C(22)	119.9(3)
C(3)	-C(4)	-C(21)	133.8(2)	C(4)	-C(21)	-C(26)	120.0(3)
C(5)	-C(4)	-C(21)	132.1(3)	C(22)	-C(21)	-C(26)	120.1(3)
C(4)	-C(5)	-C(6)	92.7(2)	C(21)	-C(22)	-C(23)	119.8(3)
C(4)	-C(5)	-C(27)	131.6(3)	C(22)	-C(23)	-C(24)	119.7(4)
C(6)	-C(5)	-C(27)	135.1(2)	C(23)	-C(24)	-C(25)	120.9(4)
C(3)	-C(6)	-C(5)	84.2(2)	C(24)	-C(25)	-C(26)	119.6(4)
C(3)	-C(6)	-C(7)	109.6(2)	C(21)	-C(26)	-C(25)	119.9(4)
C(3)	-C(6)	-C(12)	105.9(2)	C(5)	-C(27)	-C(28)	120.5(3)
C(5)	-C(6)	-C(7)	127.2(2)	C(5)	-C(27)	-C(32)	121.4(3)
C(5)	-C(6)	-C(12)	116.3(2)	C(28)	-C(27)	-C(32)	117.9(3)
C(7)	-C(6)	-C(12)	108.5(2)	C(27)	-C(28)	-C(29)	121.3(3)
C(6)	-C(7)	-C(8)	106.1(2)	C(28)	-C(29)	-C(30)	120.3(3)
C(6)	-C(7)	-C(17)	125.1(3)	C(29)	-C(30)	-C(31)	119.1(3)
C(8)	-C(7)	-C(17)	128.4(3)	C(30)	-C(31)	-C(32)	121.0(3)
C(1)	-C(8)	-C(7)	120.0(3)	C(27)	-C(32)	-C(31)	120.3(3)
C(1)	-C(8)	-C(9)	88.8(2)	C(9)	-C(33)	-C(34)	119.9(4)
C(7)	-C(8)	-C(9)	151.2(3)	C(9)	-C(33)	-C(38)	120.2(4)
C(8)	-C(9)	-C(10)	93.8(2)	C(34)	-C(33)	-C(38)	119.9(4)
C(8)	-C(9)	-C(33)	134.6(3)	C(33)	-C(34)	-C(35)	119.2(5)
C(10)	-C(9)	-C(33)	131.6(3)	C(34)	-C(35)	-C(36)	120.4(7)
C(1)	-C(10)	-C(9)	92.7(2)	C(35)	-C(36)	-C(37)	120.9(8)
C(1)	-C(10)	-C(39)	134.8(2)	C(36)	-C(37)	-C(38)	119.7(7)
C(9)	-C(10)	-C(39)	132.3(3)	C(33)	-C(38)	-C(37)	119.8(5)
C(1)	-C(11)	-C(12)	106.8(2)	C(10)	-C(39)	-C(40)	120.1(3)
C(1)	-C(11)	-C(45)	112.4(2)	C(10)	-C(39)	-C(44)	122.1(3)
C(1)	-C(11)	-C(46)	108.8(2)	C(40)	-C(39)	-C(44)	117.7(3)
C(12)	-C(11)	-C(45)	109.8(2)	C(39)	-C(40)	-C(41)	120.9(3)
C(12)	-C(11)	-C(46)	111.4(2)	C(40)	-C(41)	-C(42)	120.4(3)
C(45)	-C(11)	-C(46)	107.8(2)	C(41)	-C(42)	-C(43)	119.7(3)
C(6)	-C(12)	-C(11)	106.8(2)	C(42)	-C(43)	-C(44)	119.9(3)
C(6)	-C(12)	-C(47)	109.1(2)	C(39)	-C(44)	-C(43)	121.4(3)
C(6)	-C(12)	-C(48)	112.9(2)	C(11)	-C(45)	-N(1)	178.9(3)
C(11)	-C(12)	-C(47)	110.9(2)	C(11)	-C(46)	-N(2)	179.0(4)
C(11)	-C(12)	-C(48)	110.1(2)	C(12)	-C(47)	-N(3)	176.9(4)
C(47)	-C(12)	-C(48)	107.1(3)	C(12)	-C(48)	-N(4)	178.9(4)

Standard deviations are given in parentheses.

Electronic Interaction in the Intermediate State. Benzodicyclobutene is a molecule with a conjugate planar skeleton. Therefore, the electronic interaction between this molecule, **R**, and a dienophile, **S**, can be calculated by using the equation presented by Fueno;[13]

$$\Delta E = 2(\sum_{i}^{occ}\sum_{j}^{un} - \sum_{i}^{un}\sum_{j}^{occ})(a_{ir}b_{js}\gamma_{rs} + a_{it}b_{ju}\gamma_{tu})^2/(E_i - E_j),$$

where E_i and E_j indicate the energy levels of the two molecules, where a_{ir} and b_{js} are the coefficients of the MO's and where γ is the resonance integral between the overlapping atoms. All these values were obtained by CNDO/2 calculation.[14] The distance between the two molecules is assumed to be 3.4 Å. The calculated energy corresponds to the stabilization of the intermediate state of the reacting molecules. The results are summarized in Table 6.

The sites of the molecule, **R**, (1,6), (3,4), and (4,5), indicate the "cross," "angular," and "linear" positions respectively. The stabilization is greatest in the cross addition. Although the electron-withdrawing effect of the cyano groups lowered the energy of the linear addition mode, it is less preferable than the cross addition mode. The result is not, however, consistent with the reactivity of the molecule **1** or the substituted **R**, with TCNE, since the main product is the linear adduct. Therefore, it is necessary to take account of the non-bonded interaction between the bulky substituents.

TABLE 6. ELECTRONIC INTERACTION ENERGY (eV)

R S

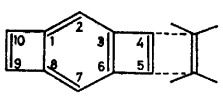

Site of **R**	Ethylene	TCNE
(1, 3)	−0.101	−0.106
(1, 6)	−0.144	−0.143
(1, 7)	−0.097	−0.099
(1, 8)	−0.035	−0.044
(2, 7)	−0.123	−0.121
(4, 5)	−0.003	−0.016

Non-bonded Interaction Energy. In the previous paper, we calculated the non-bonded interaction energy between the molecule **1** and the approaching TCNE. It was found that the energy is at its minimum when they have a slight torsion angle along the axis of the approaching direction and that the torsion angle is in qualitative agreement with that of the cyclobutane ring of **2**. Therefore, this kind of calculation, which has been used mainly for conformational or packing analysis, can be applied to the intermolecular interaction between the approaching reactants. In the present study, we shall extend this method to the discussion of what approaching mode is most to be preferred.

The potential function:

$$V(r) = Ae^{-Br}/r^D - C/r^6$$

and the parameters used were taken from Giglio.[3] Two parameters were used for the orientation of the approaching molecules, the distance, d, between the molecular planes, and the relative rotational angle, θ. (Fig. 4) The former was varied from 4.0 Å to 3.0 Å with 0.1 Å steps, and the latter, from 0° to 180° with 10° steps. In the two-dimensional energy map of d and θ (Fig. 5), there are three potential grooves along the former. The relative rotational angles for these approaches are 0°, 50°, and 130° (or −50°). The first one implies the addition of TCNE to the C(2)–C(7) of the molecule **1**, while the latter two will give the "cross" adduct. Since the two-dimensional energy map is inconvenient for a detailed comparison of the three approaching modes in the calculation or between the "linear" and "cross" addition, the cross section at the distance of 3.4 Å is shown in Fig. 6. The distance of 3.4 Å is chosen because it is the so-called van der Waals contact at which the π electron system of two molecules may, to some extent, interact with each other. Although the conformations of the substituents were varied in

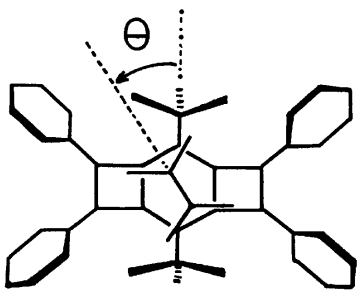

Fig. 4. Relative orientation θ in the cross approaching mode.

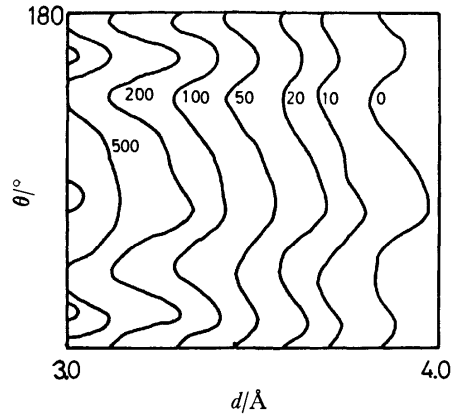

Fig. 5. Two-dimensional map of the non-bonded interaction energy (kcal mol^{-1}).

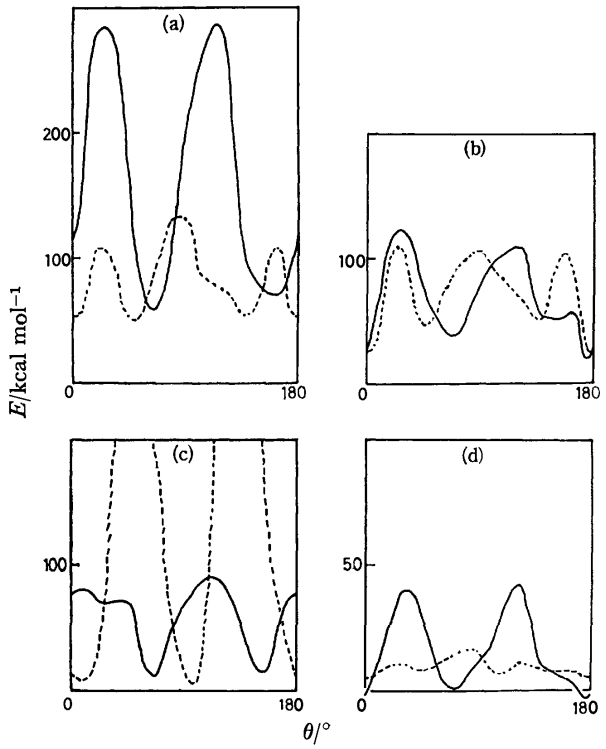

Fig. 6. Variations of the non-bonded interaction energy with the relative orientation θ at a constant distance (3.4 Å). (a) Dihedral angle of the phenyl ring from the four-membered ring being 60°, and (b) 50°. (c) The conformation of the *t*-butyl groups being fixed like Fig. 7. (d) All the substituents bent down 10° opposite to the approaching TCNE.

the subsequent calculation, the approaching direction was restricted as in Fig. 4 so as to reduce the number of total parameters. In all the energy maps hereafter, the value of the linear addition will be shown by a solid curve, and that of the cross addition, by a dashed curve.

In the conformer **a**, four phenyl groups are rotated by 60° from the four-membered ring in a propeller-like manner, and the *t*-butyl groups are fixed as in the figure. The conformer **b** has a relatively smaller rotational angle of the phenyl groups (50°), so as to make it possible to estimate the variation in the total

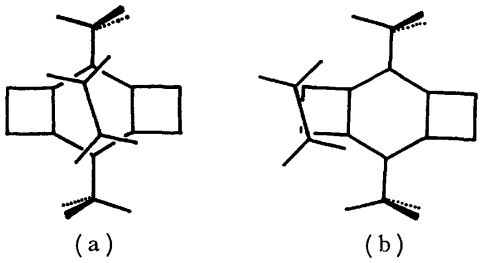

Fig. 7. Conformation model of the *t*-butyl groups.

energy with respect to the conformational change. The conformations of the *t*-butyl groups were varied for the same purpose; their conformations were assumed to be as in Fig. 7(a) and Fig. 7(b) in the linear and cross approaching modes respectively.

In the case of the 60° rotation of the phenyl groups (Fig. 6(a)), the potential groove of the cross approach is somewhat lower than that of the linear approach. Moreover, the width of the groove is narrower in the latter. Both these trends suggest that the cross addition is preferable. However, once the conformation of the terminal phenyl groups is varied in the calculation, the energy change in the linear addition is serious (Fig. 6(b)). This is attributable to the decrease in the repulsive contacts of TCNE with ortho hydrogen atoms of the phenyl groups. On the contrary, the energy of the cross approaching mode is not lowered so much as that of the linear one. In this energy map, the solid curve around 0° (or 180°) is lower by 30 kcal mol^{-1}† than the dashed curve around 60°. The former corresponds to the linear approach, and the latter, to the cross approach.

The results of the calculation in which the *t*-butyl groups are so arranged as to have the smallest repulsive contacts with the approaching TCNE indicate a more characteristic feature (Fig. 6 (c)). The minimum energy is greatly lowered in both of the approaching modes. The shape of the groove of the cross approach is, however, very narrow, whereas the shape of the solid curve shows no such drastic change. Although the difference between the minimum energies of the two modes is very small, the high energy potential barrier in the dashed curve prevents TCNE from approaching and so producing the cross adduct.

This discussion is based on the assumption that the substituent atoms directly attached to the skeleton of the molecule **1** are exactly on this plane. In order to check the effect of breaking this assumption, another calculation was carried out for the mode in which all the bonds connecting the substituents with the skeletal plane are bent by 10° from the plane toward the opposite side of the approaching TCNE. The results are shown in Fig. 6(d). The energy curves for both the cross and the linear addition are greatly lowered compared to those in Fig. 6(b), and the minimum around 0°(180°) suggests the linear addition; there is no substantial change as far as the preference of the reaction modes is concerned.

The results of calculation may be summarized as

† 1 kcal mol^{-1}=4.184 kJ mol^{-1}.

follows:

(1) The calculation of the stabilization energy of the reaction intermediates indicates that the skeletal molecule, without bulky substituents, would produce the "cross" adduct rather than the "linear" one. However, this is not the case in the observed reaction.

(2) Taking the non-bonded interaction energy into account, we can see that the linear approaching mode is preferable in terms of both the minimum value and the shape of the potential groove.

(3) The preference of the linear addition is, however, dependent on the conformation of the substituents of the molecule **1**. This is consistent with the fact that the cross adduct is obtained as a by-product.

Since any estimate of the relative weights of the electronic and steric energies must be quite ambiguous at present, it cannot be concluded which type of addition reaction will really take place. However, the qualitative agreement between our calculation and the observation indicates that the contribution of the non-bonded interaction energy should be included in any theoretical approaches to the chemical reaction.

Studies of related compounds are now in progress.

The authors are indebted to Professor Fumio Toda of Ehime University for supplying the sample and also for his valuable suggestions.

References

1) R. B. Woodward and R. Hoffmann, *J. Am. Chem. Soc.*, **87**, 395 (1965).
2) H. Prinzbach, *Pure Appl. Chem.*, **28**, 281 (1971).
3) E. Giglio, *Nature*, **222**, 339 (1969).
4) F. Toda and M. Ohi, *J. Chem. Soc., Chem. Commun.*, **1975**, 506.
5) F. Toda and N. Dan, *J. Chem. Soc., Chem. Commun.*, **1976**, 30.
6) F. Toda and T. Yoshioka, *J. Chem. Soc., Chem. Commun.*, **1977**, 561.
7) H. Tsukada, H. Shimanouchi, and Y. Sasada, *Bull. Chem. Soc. Jpn.*, **51**, 985 (1978).
8) J. Karle and I. L. Karle, *Acta Crystallogr.*, **21**, 849 (1966).
9) "International Tables for X-Ray Crystallography," Vol. IV, The Kynoch Press, Birmingham (1974), pp. 72—98.
10) The tables of the structure factors and the atomic parameters of the hydrogen atoms are kept as Document No. 8009 at the Chemical Society of Japan.
11) W. Haugen and M. Traetteberg, *Acta Chem. Scand.*, **20**, 1726 (1966).
12) "International Tables for X-Ray Crystallography," Vol. III, The Kynoch Press, Birmingham (1962), p. 276.
13) T. Fueno, *J. Syn. Org. Chem., Jpn.*, **29**, 1 (1971).
14) J. A. Pople and D. L. Beveridge, "Approximate Molecular Orbital Theory," McGraw-Hill, New York (1970).

Liquid Crystal Formation in Binary Systems. I. An Interpretation of the Phase Diagrams of the Azoxydianisole–Schiff Base Systems

Kotaro ARAYA and Yoshio MATSUNAGA*

Department of Chemistry, Faculty of Science, Hokkaido University, Sapporo 060

(Received August 25, 1979)

In order to confirm the presence of a transition at the temperature where the liquid crystal-isotropic liquid transition curve in the nematogen-rich region is met by the other transition curve, five binary systems comprising azoxydianisole (AA) and a Schiff base were examined by means of differential scanning calorimetry. A small but sharp endothermic peak due to a phase change is observable at the expected temperature upon heating, provided that it is well separated from the eutectic temperature. When the above-mentioned curve intersects the solid-liquid transition curve on the Schiff base-rich side, a liquid crystal coexisting with the solid base is transformed into an isotropic liquid coexisting with the same solid at this temperature. The presence of a nematic phase below this temperature could be demonstrated by measuring the separation of the outer hyperfine extrema in the ESR spectrum of bis(acetylacetonato)oxovanadium(IV) dissolved in the mixtures. The sequence of the transformation is entirely different when the intersection occurs on the AA-rich side. However, attempts to confirm the transition of the latter type by ESR were not successful.

Liquid crystal formation in binary systems, in which both, or one, or none of the component compounds give a mesomorphic phase, has been extensively studied by many workers. Nevertheless, the majority of reported phase diagrams are far from complete. For example, the system comprising azoxydianisole (AA), a mesomorphic compound, and *N*-(*p*-methoxybenzylidene)-*p*-anisidine, a non-mesomorphic compound, has been examined by Dave and Dewar employing the optical and thermal methods.[1] Although the nematic liquid crystal-isotropic liquid (N-L) transition curve on the AA-rich side is met well above the eutectic temperature by the solid-liquid (S-L) transition curve on the Schiff base-rich side, it is not clear whether or not the transition from the nematic liquid crystal (N) to the isotropic liquid (L) with the coexisting solid can be observed at the temperature of the intersection.

In the present series of papers, we are planning to report on the mesomorphic phases induced by some sort of molecular complexing in binary systems. In order to interpret our results, we felt that the subject mentioned above is of fundamental importance and should be clarified. For this purpose, we chose five representative systems of AA mixed with Schiff bases. As it is well known that an N phase can serve as an orienting solvent in magnetic resonance studies, measurements of the degree of alignment of the bis(acetylacetonato)oxovanadium(IV) molecules dissolved in the systems were attempted on the basis of the ESR spectrum. This particular chelate has been noted by Glarum and Marshall to be ordered to about the same extent as AA.[2] In this way, we hoped to establish the temperature ranges where an N phase exists with or without a solid-component compound.

Experimental

Materials. The AA was obtained from the Tokyo Chemical Industry Co. and was purified by recrystallization from ethanol. On the calorimetric curves, it melted at 117.5 °C and had an N-L transition point of 135 °C. These values are in good agreement with the literature values.[1] The Schiff bases were prepared by a condensation reaction between a *p*-X derivative of benzaldehyde and *p*-Y derivative of aniline; they were then recrystallized several times from ethanol and finally sublimed in a vacuum if necessary. Mixtures of AA and a Schiff base in known proportions were melted in small test tubes, shaken well to insure homogeneity, and then rapidly cooled.

Measurements. The calorimetric curves were recorded on a Rigaku Denki Thermoflex differential scanning calorimeter during the processes of heating and cooling. The heating rate in this work was 2.5 °C min^{-1}. The temperature was calibrated with the transition points of hexachloroethane (45 and 71 °C) and hexamethylbenzene (111 °C) and the melting points of naphthalene (80 °C), pyrene (150 °C), and indium (157 °C). The ESR spectra were recorded on a JEOL model JES-ME-3X (X band) spectrometer with 100 kHz modulation in the range between a temperature below the eutectic and a temperature above the S-L or N-L transition. The magnetic-field span was calibrated with Mn^{2+}-doped MgO powder.

Results and Discussion

*AA–*N-*(*p-*Methoxybenzylidene)*-p-*anisidine (X=Y=CH_3O) System.* The phase diagram has been reported by Dave and Dewar.[1] According to them, the N-L transition curve is met at 116.5 °C by the S-L transition curve on the Schiff base-rich side. They have drawn a horizontal dashed line at this temperature and marked four points observed in the cooling process above 40 mol% of AA. The eutectic point was located at 105 °C and about 72 mol% of AA. Our results are presented in Fig. 1. The open and shaded circles indicate the transitions found during the processes of heating and cooling respectively. The shaded circles are omitted when they coincide exactly with the open circles. The N-L transition above 60 mol% of AA is reversible, but the N phase is readily supercooled below the eutectic temperature and is suddenly solidified. When the AA content is less than 50 mol%, a sharp endothermic peak assignable to the N-L transition with the coexisting solid is observed at 117 °C on heating. This temperature is that of the intersection between the N-L transition curve and the S-L transition curve. Contrary to the observation reported by Dave and Dewar, the L phase in this composition range is super-

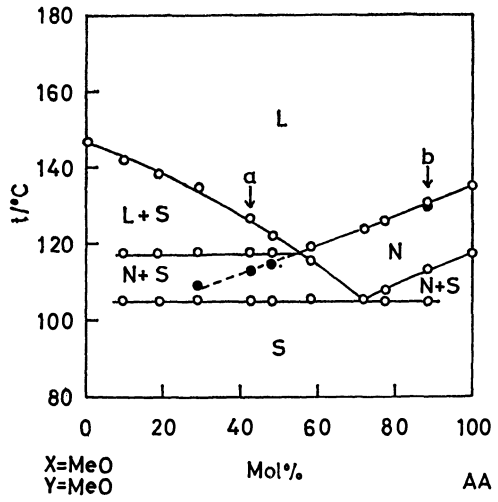

Fig. 1. The system azoxydianisole(AA)–*N*-(*p*-methoxybenzylidene)-*p*-anisidine.
The open and shaded circles are transitions observed in the processes of heating and cooling respectively.

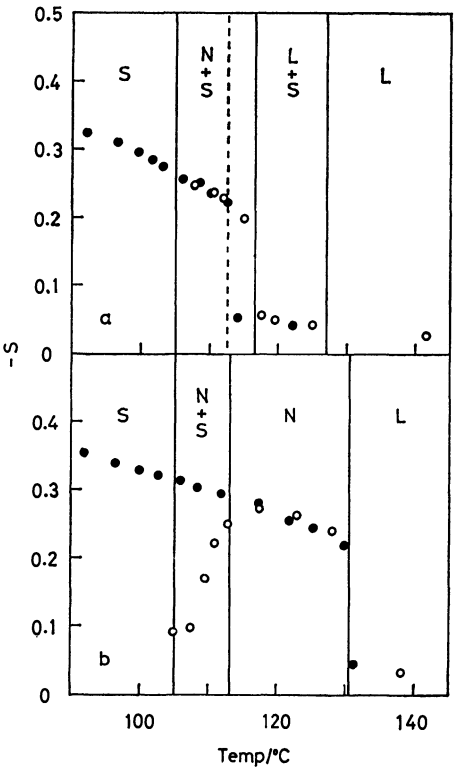

Fig. 2. Temperature dependence of the parameter S in AA–*N*-(*p*-methoxybenzylidene)-*p*-anisidine, (a) 42.5 and (b) 88.5 mol% of AA.
As to the open and shaded circles, see the caption of Fig. 1.

cooled and changes into the N phase. The transformation takes place at temperatures on a continuation of the reversible N-L transition curve, which is almost straight. Such a linear relationship has also been observed for a number of binary N systems when there is no significant difference in the molar volumes or densities of the components.[3-7] The value at 0 mol% of AA found by extrapolation may be considered to be the latent L-N transition temperature of the Schiff base. If the molten base could be cooled without solidification, the N phase would monotropically appear at about 97 °C.

In the N phase, the spin-probe molecules are not distributed uniformly in θ, the angle between the V=O bond direction of the chelate molecule and the magnetic field. The order parameter, S, defined by $<3\cos^2\theta-1>/2$, can be approximated by $(<A>-a)/2(a-A_\perp)$, where $A_\perp$ is the component perpendicular to the V=O bond direction of the nearly axial hyperfine tensor, a is the isotropic hyperfine constant, and $<A>$ is one-seventh of the separation of the outer hyperfine extrema. If the alignment of the probe is perfect, the parameter, S, is $-1/2$, because $<A>=A_\perp$. When the medium becomes isotropic, the probe molecules may rapidly tumble, and one may observe $S=0$. Thus, a marked difference in the S value can be expected below and above the N-L transition temperature. The ESR spectrum was measured at 42.5 and 88.5 mol% of AA (they are indicated by Arrows a and b in Fig. 1) as a function of the temperature. The parameter was calculated with the values of $A_\perp$ and a estimated from the ESR spectra in molten *o*-terphenyl, namely, 68 and 108 G (1 G=10^{-4} T). The results, shown in Figs. 2a and b, clearly support our interpretation of the phase diagram. Here again, the open circles were obtained in the process of heating, and the shaded ones, in the process of cooling. The vertical lines represent the transition temperatures taken from Fig. 1. In Fig. 2a, a sudden change in the order parameter is found at the N-L transition temperature, even in the presence of a solid Schiff base. Furthermore, the supercooling of the L phase is clearly demonstrated by a shaded circle located between the dashed line and the N-L transition line. In the other temperature ranges, the open and shaded circles are nearly on the same curve, indicating the reversibility. As the S value estimated using the above-mentioned $A_\perp$ and a is essentially zero in the L phase of pure AA, there must be some changes in $A_\perp$ and a upon mixing with the Schiff base. At 88.5 mol% of AA, a large hysteresis is seen in the heterogeneous region where the N phase coexists with solid AA (see Fig. 2b). The rapid change in the order parameter upon heating suggests that the coexisting solid AA strongly disturbs the alignment of the N phase. To avoid such a complication, the measurement at a lower content of AA seemed to be desirable. However, the temperature range where the N phase coexists with solid AA is too narrow to carry out the desired measurement, as the eutectic point is located at about 72 mol% of AA. Consequently, two more similar systems with eutectics at lower AA contents were examined.

*AA–*N-(p-*Nitrobenzylidene)*-p-*anisidine* (*X*=NO_2, *Y*=CH_3O) *System.* Dave and Dewar have reported the eutectic at 93 °C and 57 mol% of AA for this system.[5] The diagram reproduced by the S-L and L-N transition temperatures tabulated in their paper is in fair agreement with ours, shown in Fig. 3. Although the temperatures of the intersection of the L-S and N-L transition curves and of the eutectic agree well with

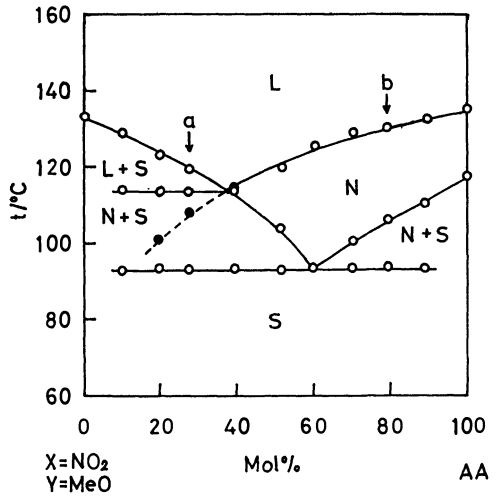

Fig. 3. The system AA–*N*-(*p*-nitrobenzylidene)-*p*-anisidine.

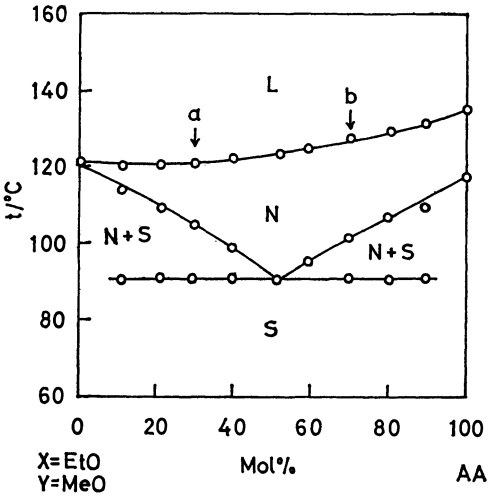

Fig. 4. The system AA–*N*-(*p*-ethoxybenzylidene)-*p*-anisidine.

those of Dave and Dewar, the compositions obtained by us are a little higher. It must be emphasized, however, that Dave and Dewar have reported neither the transitions at the horizontal N-L line of 113.5 °C on the Schiff base-rich side nor the transitions on the extrapolated part of the N-L curve on the AA-rich side. Contrary to the AA-*N*-(*p*-methoxybenzylidene)-*p*-anisidine system, the N-L curve on the AA-rich side is markedly convex upwards. The latent N-L transition temperature of about 80 °C is deduced by extrapolation to 0 mol% of AA.

The order parameter of the spin probe was measured at 27.6 and 79.3 mol% of AA (a and b in Fig. 3 respectively). At the former composition, the results are similar to those presented in Fig. 2a; however, the *S* values in the N+S region obtained during the process of heating are definitely higher than those in the supercooled N phase, possibly because of a larger difference between the two transition temperatures. As we hoped, the difference in the *S* value between the heating and cooling processes at the latter composition is much less than that found in Fig. 2b. The parameters measured on heating are about −0.23 throughout the N+S region and also in a part of the N phase.

AA-N-(p-*Ethoxybenzylidene*)-p-*anisidine* ($X=C_2H_5O$, $Y=CH_3O$) *System.* The Schiff base melts at 121.5 °C. When the melt is cooled, a monotropic transition to the N phase occurs at 121 °C. Therefore, the N-L transition curve looks as if it is met by the S-L transition curve at 0 mol% of AA. As is shown in Fig. 4, the N-L transition curve is slightly concave upwards; in other words, it shows a negative deviation from a linear relationship between the N-L transition temperatures of the two components. The eutectic is at 91 °C and about 51 mol% of AA. The order parameters of the spin probe examined at the compositions a and b are presented in Fig. 5. There is no supercooling of the L phase at either of the compositions. At 29.3 mol% of AA, the temperature variation in *S* is nearly reversible. On the other hand, a small but definite difference in the *S* value can be seen between the processes of heating

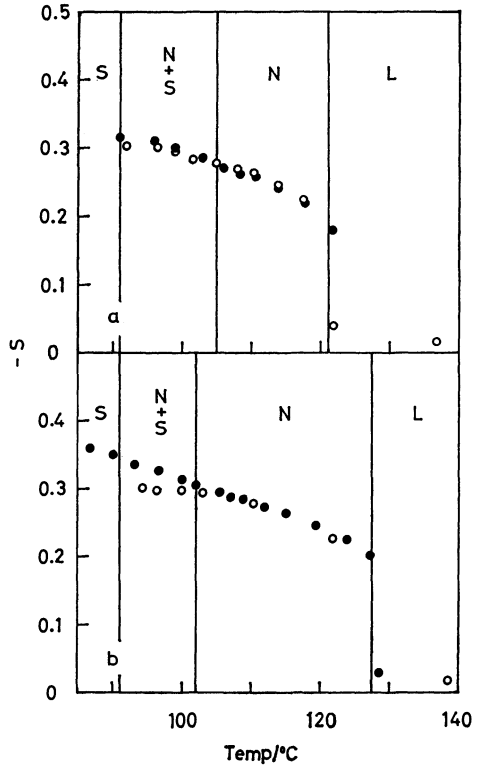

Fig. 5. Temperature dependence of the parameter *S* in AA–*N*-(*p*-ethoxybenzylidene)-*p*-anisidine, (a) 29.3 and (b) 70.5 mol% of AA.

and cooling in the N+S region at 70.5 mol% of AA. As the compositions a and b are selected almost symmetrically to the eutectic, the amount of the coexisting solid Schiff base at the composition a must be about the same as that of solid AA at the composition b. Therefore, the results in Fig. 5 indicate that the orientation of the AA-rich N phase by the magnetic field is more strongly disturbed by the coexisting solid AA than is the orientation of the Schiff base-rich N phase by the coexisting solid base.

The negative deviation of the N-L transition curve

from the ideal linear relationship may be due to the slightly repulsive interaction between the AA and Schiff-base molecules compared to the interaction between like molecules. On the other hand, the deviation found in the AA–*N*-(*p*-nitrobenzylidene)-*p*-anisidine system is in the direction opposite to the above-mentioned and is as much as 14 ° in the range of 40 to 50 mol% of AA, reflecting a strong attractive interaction between the AA and Schiff-base molecules in the N phase. A similar enhancement of the N-phase stability has been found by Park *et al.* in the binary system *N*-(*p*-methoxybenzylidene)-*p*-butylaniline and 4-cyano-4′-pentylbiphenyl and several other, closely related systems.[8] They have attributed the enhancement to molecular complexing by a weak charge-transfer interaction. This sort of intermolecular interaction may be more significant if one of the components carries a strong electron-donating substituent such as a dimethylamino group and the other, a strong electron-accepting substituent such as a nitro group. Work along this line will be reported in forthcoming papers of this series.

AA–N-(p-*Methylbenzylidene*)-p-*anisidine* (*X*=CH_3, *Y*=CH_3O) *System.* According to the work by Dave and Dewar, the eutectic is located at 72 °C and 25 mol% of AA, and the N-L transition curve is met by the transition curve on the AA-rich side at 100 °C and 62 mol% of AA.[5] In this case, the phase diagram is expected to be more complicated than those of the three systems described above. Below the temperature of the intersection, the isotropic L phase should coexist with solid AA, as is indicated by the endings of the isothermal tie-lines. Upon heating, this mixture is transformed into a mixture of the N phase and solid AA at the temperature of the intersection, then into the N phase only, and finally into the L phase. Thus, the sequence of the transformation at the temperature of the intersection is reversed compared with that we have found in the previous diagrams. Dave and Dewar reported neither the expected horizontal transition line nor the L-N transition to be shown by supercooled melts in the composition range below the intersection.

These missing transitions could, however, be detected by the present calorimetric measurements. The results are plotted in Fig. 6. The N-L transition curve observed with supercooled melts is slightly bent below 50 mol% of AA. The boundary between the N phase and the heterogeneous region where the N phase coexists with solid AA is straight. On the other hand, the S-L transition curve is really curved. The last two curves are of a different nature; that is, one of them represents the solubility of AA in the N phase, and the other, the solubility of AA in the L phase. Therefore, the discontinuity of the slope at the intersection is not unexpected, The eutectic was found at 72.5 °C and 27 mol% of AA, and the intersection, at 102 °C and 60 mol% of AA. The ESR measurements attempted at 68.2 and at 80.0 mol% of AA failed to prove the N phase to coexist with solid AA, probably because of the narrow temperature range and/or the disturbance from the relatively large amounts of solid AA. However, the L-N transition at 102 °C could be visually confirmed with the aid of a hot stage equipped with a polarizing microscope.

AA–N-(p-*Methoxybenzylidene*)-p-*chloroaniline* (*X*=CH_3O, *Y*=*Cl*) *System.* The binary system consisting of AA and *N*-(*p*-chlorobenzylidene)-*p*-anisidine gives a phase diagram of the same type. The intersection occurs at 98.5 °C and 60 mol% of AA, in good agreement with the results reported by Dave and Dewar.[5] This temperature is so close to the eutectic temperature, 92 °C, that the expected small endothermic peak is not detectable because of overlapping with a much larger peak due to the eutectic. The present system comprising AA and the isomeric Schiff base is, consequently, included as a further example. The eutectic has been located at 79.5 °C and 35 mol% of AA, and the intersection, at 99 °C and about 62 mol% of AA, by Dave and Dewar.[5] They made no mention of the horizontal transition line expected at the latter temperature and the L-N transition of supercooled melts. As is shown in Fig. 7, our measurements could indicate more complete relations for this system. The temperature of the intersection is firmly established at 100.5 °C by the transitions observed between 69.5 and 88.5 mol%

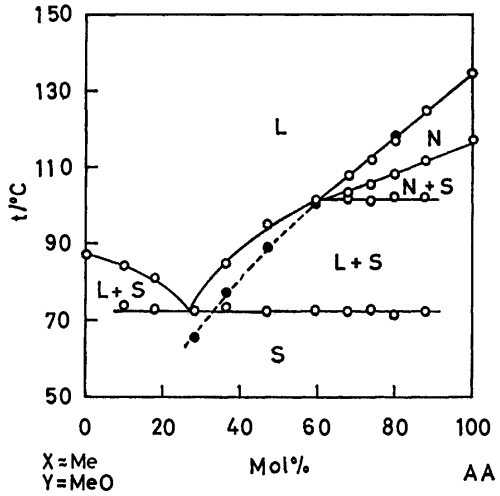

Fig. 6. The system AA–*N*-(*p*-methylbenzylidene)-*p*-anisidine.

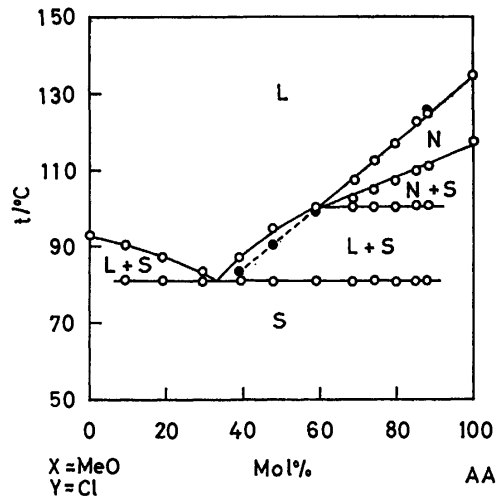

Fig. 7. The system AA–*N*-(*p*-methoxybenzylidene)-*p*-chloroaniline.

of AA. The N-L transition curve, now extended to 40 mol% of AA by the observations of the monotropic transformation of the supercooled melts, is essentially straight. If the curve is not bent below this composition, the latent L-N transition temperature of this Schiff base may be about 50 °C. The S-N transition curve is essentially straight, and its slope is considerably different from that of the S-L transition curve at the intersection. Attempts to confirm the N phase coexisting with solid AA by the ordering of the spin probe at 74.3, 79.8, and 85.6 mol% of AA did not meet with any success.

References

1) J. S. Dave and M. J. S. Dewar, *J Chem. Soc.*, **1954**, 4616.
2) S. H. Glarum and J. H. Marshall, *J. Chem. Phys.*, **46**, 55 (1967).
3) A. Bogojawlensky and N. Winogradow, *Z. Phys. Chem.*, **64**, 229 (1908).
4) R. Walter, *Ber.*, **58**, 2303 (1925).
5) J. S. Dave and M. J. S. Dewar, *J. Chem. Soc.*, **1955**, 4305.
6) J. S. Dave and J. M. Lohar, *J. Chem. Soc., A*, **1967**, 1473.
7) E. C. H. Hsu and J. F. Johnson, *Mol. Cryst. Liq. Cryst.*, **20**, 177 (1973).
8) J. W. Park, C. S. Bak, and M. M. Labes, *J. Am. Chem. Soc.*, **97**, 4398 (1975).

The Conformations and the Ring Inversions of Some 8- and 10-Methyl-substituted 8,9,10,11-Tetrahydro-7*H*-cycloocta[*de*]naphthalenes and Their 9-Oxo Derivatives

Toshihiro KAMADA* and Osamu YAMAMOTO
National Chemical Laboratory for Industry, Tsukuba Research Center, Ibaraki 305
(Received February 23, 1979)

The IR and NMR studies on the conformations of several 8- and 10-methyl-substituted 8,9,10,11-tetrahydro-7*H*-cycloocta[*de*]naphthalenes (*cis*-8,10-dimethyl (**3a**), *trans*-8,10-dimethyl (**4a**), 8,8-dimethyl (**5a**), 8,8,10-trimethyl (**6a**), and 8,8,10,10-tetramethyl (**7a**)) and their 9-oxo derivatives (**3b**—**7b**) have been described. It was found that compounds **3**—**7** exist exclusively in a boat conformation in the ground state, the peri ring of which is somewhat distorted (puckered) as a result of the steric repulsion between the interior benzyl protons; the molecules of **3a** and **3b** are rather strongly puckered, while those of **7a** and **7b** exist in a less puckered form than the conformations of the other methylated compounds. In the latter case, a novel type of the reflex effect was found arising from the 1,3-synaxial CH_3–CH_3 steric interaction and the interior benzyl H–H interaction. Moreover, it was revealed that free energy barriers ($\Delta G^{\ddagger}$) to boat inversion for compounds **5a**, **5b**, **7a**, and **7b** are markedly increased ($\Delta\Delta G^{\ddagger}$= 4.8—5.9 kcal/mol) as compared with the unmethylated compounds. These results were discussed in terms of the boat-to-boat interconversion process in which the pseudorotations of the peri bonds are involved. Some discussion was also made on the spectral and conformational features of the eight-membered pericyclized naphthalene ring system.

Previously, as parts of our studies on the chemistry of pericyclized naphthalene system, we have studied the conformations of 8,9,10,11-tetrahydro-7*H*-cycloocta-[*de*]naphthalene (**1a**)[1] and its 9-oxo compound **1b**.[2] Studies on the conformational equilibria of 8-monomethyl-substituted derivatives of this system **2a**[3] and **2b**[4] have also been reported. In these studies, it was found that the 8-membered peri rings in these compounds are rather strained due to the peri interaction inherent in the peri-substituted naphthalenes.[5] In the present paper, in order to determine the effects of the methyl substituent on the ring geometry and the ring inversion in these 8-membered pericyclized naphthalenic compounds, we have extended our study to more highly methylated compounds of this system, 8- and 10-methyl-substituted 8,9,10,11-tetrahydro-7*H*-cycloocta[*de*]naphthalenes (*cis*-8,10-dimethyl (**3a**), *trans*-8,10-dimethyl (**4a**), 8,8-dimethyl (**5a**), 8,8,10-trimethyl (**6a**), and 8,8,10,10-tetramethyl (**7a**)) and their 9-oxo derivatives (**3b**—**7b**).

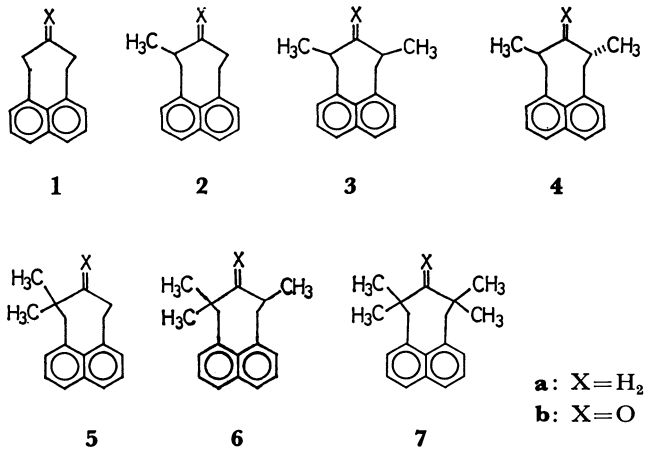

Here, we report the conformations of this series of methyl compounds based on the IR and NMR (^{1}H and ^{13}C) spectra, and discuss about the spectral and conformational features of these methylated compounds in comparison with the parent compounds **1a** and **1b** as well as the monomethyl derivatives **2a** and **2b**. Further we report the activation energies for ring inversions of some of the methylated compounds **3**—**7** by a study of the variable-temperature ^{1}H NMR spectra. Detailed discussion on these points will also be described.

Results and Discussion

The ^{1}H and ^{13}C NMR data of a series of the methylated compounds (**3a**—**7a**) and (**3b**—**7b**) are summarized in Tables 1 and 2. The assignment was made based on the data of the parent compounds **1a**[1] and **1b**[2] and the substituted derivatives **2a**[3] and **2b**,[4] as well as those of the deuterated compounds **3b**-8,10-d_2, **4b**-8,10-d_2, and **6b**-10-*d*. Also off-resonance technique was employed for the assignments of the ^{13}C spectra.

It is shown in the table that all the ^{1}H spectra of these compounds are relatively simple and the splitting patterns of the benzyl methylene protons in the hydrocarbons (**a**) are very similar to those in the corresponding 9-oxo compounds (**b**). This suggests that each methyl compound studied exists in one conformation in its ground state and both hydrocarbons (**a**) and ketones (**b**) assume the same geometry in each class of the methylated compounds.

It has previously been shown[1-4,6,7] that the interior benzyl protons (H_{in}) on C-7 and C-11 in the 8-membered pericyclized naphthalene system resonate at much lower field than the exterior protons (H_{ex}) due to the steric compression effect. In 8,8-dimethyl-8,9,10,11-tetrahydro-7*H*-cycloocta[*de*]naphthalene (**5a**) and its 9-oxo derivative **5b**, the interior proton on C-11 (H_{11in}) is coupled strongly with an adjacent C-10 proton (J=13.3 and 13.1 Hz). This indicates that the peri rings in these compounds exist in the boat form (**5B**) rather than in the chair (**5C**), since, as can

Table 1. ^{1}H NMR data of the methyl and benzyl protons of 8- and 10-methyl-substituted 8,9,10,11-tetrahydro-7*H*-cycloocta [*de*]naphthalenes (**3a**—**7a**) and their 9-oxo derivatives (**3b**—**7b**)[a-d]

Compound	H_{7in}[g]	H_{7ex}	H_{11in}	H_{11ex}	CH_3 8-ax	CH_3 8-eq	CH_3 10-ax	CH_3 10-eq
3a	4.28 J=14.4 6.5	2.63 J=14.4 i)	4.28 J=14.4 6.5	2.63 J=14.4 i)		0.84d J=6.8		0.84d J=6.8
4a[e]	4.17 J=14.5 6.5	2.64 J=14.5 1.4	3.71 J=14.1 12.8	2.90 J=14.1 6.7		0.80d J=6.7	1.22d J=7.0	
5a	3.98 J=14.3	2.51 J=14.3	3.92 J=14.5 13.3 6.3	2.88 J=14.5 6.9 1.6	1.16s (1.6)	0.80s (1.9)		
6a	4.00 J=14.3	2.50 J=14.3	4.21 J=14.3 6.4	2.59 J=14.3 1.5	1.16s	0.81s		0.80d J=6.8
7a	4.09 J=14.3 (2.8)[h]	2.53 J=14.3 (2.5)	4.09 J=14.3 (2.8)	2.53 J=14.3 (2.5)	1.29s (1.7)	0.74s (1.9)	1.29s (1.7)	0.74s (1.9)
3b	4.86 J=14.6 6.4	2.77 J=14.6 2.3	4.86 J=14.6 6.4	2.77 J=14.6 2.3		0.97d J=6.8		0.97d J=6.8
4b[f]	4.79 J=14.8 5.8	2.76 J=14.8 2.2	4.23 J=14.5 11.5	3.03 J=14.5 6.1		0.94d J=6.4	1.45d J=6.5	
5b	4.61 J=14.8 (3.6)	2.69 J=14.8 (3.0)	4.43 J=14.6 13.1 6.1	2.97 J=14.6 6.8 1.7	1.42s (1.8)	0.93s (2.2)		
6b	4.58 J=14.7	2.69 J=14.7	4.73 J=14.7 6.7	2.69 J=14.7 2.2	1.43s (1.4)	0.92s (1.8)		0.99d J=6.8
7b	4.69 J=14.5 (2.9)	2.72 J=14.5 (2.0)	4.69 J=14.5 (2.9)	2.72 J=14.5 (2.0)	1.48s (1.5)	0.92s (2.0)	1.48s (1.5)	0.92s (2.0)

a) All the samples except **4a** and **4b** were measured at 30 °C. b) The chemical shifts are expressed in ppm (δ) downfield from internal standard tetramethylsilane, and the coupling constants (J) are in Hz. c) The chemical shifts of the C-8 and C-10 protons are determined as follows; H_{8ax}: 2.16 (**3a**), 3.18 (**3b**), 3.39 ppm (**4b**), H_{10ax}: 2.15 (**5a**), 2.27 (**6a**), 3.35 (**5b**), 3.48 ppm (**6b**), H_{10eq}: 1.67 (**5a**), 2.82 (**4b**), 2.51 ppm (**5b**). d) The chemical shifts of the C-9 methylene protons are not determined because these signals are buried under the signals of methyl groups. e) Measured at −21.5°C. f) Measured at −65.9 °C. g) The numbers refer to the carbon position on the ring and the letters, in, ex, eq, and ax denote interior, exterior, equatorial, and axial protons, respectively. h) The figures in parentheses denote the line widths of the signals. i) This coupling ($J_{ex,ax}$) is small enough not to be resolved.

Table 2. ^{13}C chemical shifts of the methyl and the peri ring carbons of 8- and 10-methyl-substituted 8,9,10,11-tetrahydro-7*H*-cycloocta[*de*]naphthalenes (**3a**—**7a**) and their 9-oxo derivatives (**3b**—**7b**)[a,b]

Compound	C-7	C-8	C-9	C-10	C-11	CH_3 8-eq	CH_3 8-ax	CH_3 10-eq	CH_3 10-ax
3a	42.4	33.4	39.0	33.4	42.4	22.2		22.2	
4a[c]	42.1	27.1	35.4	34.3	43.8	21.8			20.4
5a	49.8	34.7	34.7	26.7	35.8	30.5	28.0		
6a	49.2	34.9	43.6	29.5	41.7	30.7	28.5	22.0	
7a	48.9	36.1	48.3	36.1	48.9	32.6	30.9	32.6	30.9
3b	41.7	45.7	213.2	45.7	41.7	15.0		15.0	
4b[d]	40.5	40.5	217.2	52.1	43.3	14.4			19.0
5b	49.0	48.5	214.8	42.9	34.6	23.5	28.1		
6b	49.6	48.7	215.3	41.0	41.4	23.8	28.1	15.5	
7b	48.7	50.2	218.3	50.2	48.7	27.0	30.1	27.0	30.1

a) All the samples except **4a** and **4b** were measured at room temperature. b) The chemical shifts are expressed in δ (ppm) from internal reference tetramethylsilane and are considered accurate to be ±0.1 ppm. c) Measured at −51.6 °C. d) Measured at −44.0 °C.

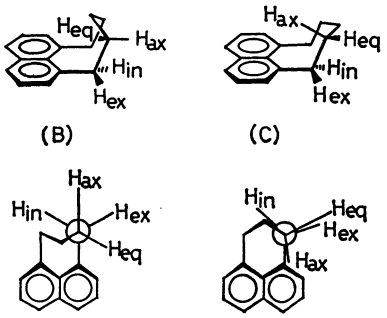

Fig. 1. The boat (**B**) and the chair (**C**) conformations for the 8,9,10,11-tetrahydro-7*H*-cycloocta[*de*]naphthalene ring and their Newman projections about the C_7–C_8 (C_{10}–C_{11}) bonds.

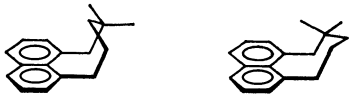

be seen in Fig. 1, the H_{in} proton in the boat conformation is situated in a position *trans* to an adjacent equatorial proton and thus a strong coupling is expected between these two protons. If the chair **5C** would be the predominant conformation for **5a** and **5b**, then the large J_{vic} value could be observed for the H_{ex} proton. Additionally, the splitting patterns of the C-11 interior protons observed in **5a** and **5b** are analogous to those of the parent compounds[1,2] and the monosubstituted derivatives,[3,4] which exist in the boat conformations alone. The **5B** conformation is also suggested from the line widths of the methyl and the benzyl protons. In both **5a** and **5b**, the equatorial methyl group shows somewhat broadened signal (half-width; 1.9 and 2.2 Hz) as compared to that of the axial methyl group (1.6 and 1.8 Hz), while the signal of the C-7 interior proton of **5b** is broader (3.6 Hz) than that of the corresponding exterior proton (3.0 Hz). This arises possibly from the long-range spin coupling of the interior proton with the equatorial methyl group because of their *trans* steric relationship,[7] and is a further evidence in favor of the boat conformation **5B** for **5a** and **5b**.

Similar type of long-range spin coupling is observed in the spectra of 8,8,10,10-tetramethyl compounds **7a** and **7b** (in both compounds, the signals of the interior benzyl proton and the equatorial methyl group are apparently broader than those of the exterior proton and the axial methyl group, respectively; see Table 1). Therefore, these compounds clearly assume a boat form (**7B**). This is strongly supported by the line widths

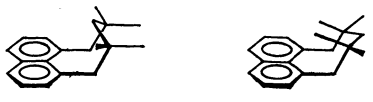

of the exterior benzyl protons; as can be seen in the table, the line widths of the interior benzyl protons are almost equal between the hydrocarbon **7a** (2.8 Hz) and the ketone **7b** (2.9 Hz), while the exterior proton of **7a** clearly shows a broadened signal (2.5 Hz) as compared to that of **7b** (2.0 Hz). This may be reasonably explained in terms of the W-type long-range spin coupling of the exterior proton with the C-9 equatorial proton, which is characteristic of the boat conformation as described before.[7]

In *trans*-8,10-dimethyl compounds **4a** and **4b**, the value of spin coupling constant between the C-7 interior proton and C-8 methine proton is small (J=6.5 and 5.8 Hz), while it is large between the C-11 interior proton and the C-10 methine proton (J=12.8 and 11.5 Hz). Thus it is clear that **4a** and **4b** exist in a boat (**4B**) in which the C-8 methyl is equatorial and that on C-10 is axial.

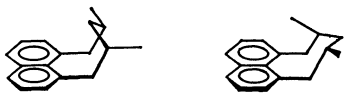

On the other hand, in the *cis*-dimethyl compounds **3a** and **3b**, the small J_{vic} values (6.5 and 6.4 Hz) observed between the interior benzyl proton and the vicinal methine proton suggest that **3a** and **3b** exist either in a boat form (**3B**) or in a chair form (**3C**) bearing equatorial methyl groups. However, in view of the fact that the equatorial isomers of the monomethyl compounds **2a** and **2b** exist exclusively in the boat conformation (**EB**) in their ground states (corresponding chair conformation **EC** is not obtained),[3,4] it seems reasonable to consider that the dimethyl compounds **3a** and **3b** exist in the boat (**3B**) rather than in the chair (**3C**). Actually, the chemical shifts and coupling

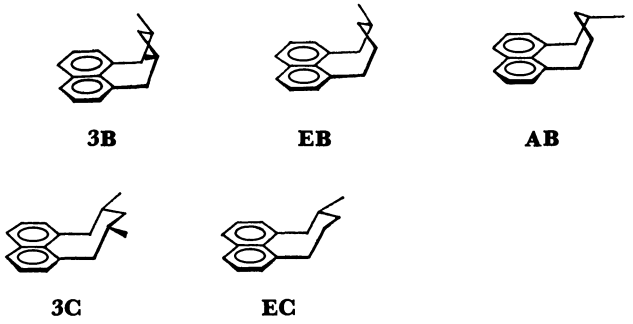

constants of the benzyl and the methyl protons observed in **3a** and **3b** are very similar to those found for the corresponding protons of the **EB** isomer. Moreover, the equilibration experiment revealed[8] that the *cis*-dimethyl ketone **3b** is much more stable than the *trans* isomer **4b** (**4B** conformation). Thus, considering the fact that the equatorial conformation (**EB**) is more stable than the axial conformation (**AB**),[3,4] it is apparent that the conformation of **3a** and **3b** is the boat form **3B**.

For the same reason, the small J_{vic} values (6.4 and 6.7 Hz) observed between the C-11 interior proton and the C-10 methine proton in the trimethyl compounds **6a** and **6b** suggest that these compounds exist in a boat (**6B**), in which the C-10 methyl group is equatorial. The somewhat broadened signal of the equatorial methyl group on C-8 (half-width; 1.8 Hz) in comparison

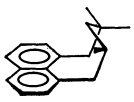

6B

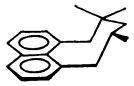

6C

with that of the corresponding axial methyl group (1.4 Hz) observed in **6b** results possibly from the long-range spin coupling of the equatorial methyl group with the C-7 interior proton as observed in **5B** and **7B** conformations.

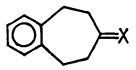

8a; X=H_2
8b; X=O

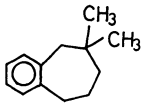

9

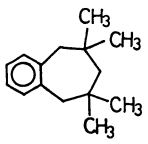

10

Consequently, it became clear that all the compounds (**3**—**7**) exist solely in the boat conformations (**3B**—**7B**) in their ground states. This result is in striking contrast to the case of structurally analogous benzocyclic compound, 6,7,8,9-tetrahydro-5*H*-benzocycloheptene system (**8**). It has been reported that 6,6-dimethyl- (**9**)[9] and 6,6,8,8-tetramethylbenzocycloheptene derivatives (**10**)[10] as well as the unsubstituted compounds **8a**[10,11] and **8b**[12] assume only the chair conformations in their ground states. The unusually greater stability of the boat conformation (**3B**—**7B**) over the chair (**3C**—**7C**) observed in **3**—**7** results chiefly from much lower torsional energy about the C_7—C_8 and C_{10}—C_{11} bonds of the boat conformation (staggered) than the chair (eclipsed), which is one of the unique features in the 8-membered pericyclized naphthalene system (Fig. 1). All compounds of this system studied so far, including the parent compounds[1,2,6] as well as the substituted derivatives,[3,4,7] exist solely in the energetically stable boat conformations. In addition, the closeness of the axial methyl group to the naphthalene ring in the chair[7] (**4C**—**7C**) makes this much less stable than the boat conformation (**4B**—**7B**).

The ^{13}C data of **3**—**7** shown in Table 2 fully agree with the boat conformations (**3B**—**7B**) described above. Thus a high-field shift of C-7 signal relative to that of C-11 ($\Delta\delta$=1.7 ppm) in the *trans*-dimethyl compound **4a** is caused by a gauche interaction[3,4] between the equatorial methyl group on C-8 and the peri bond. This interaction is also observed in the spectra of the *cis*-dimethyl (**3a**) and the trimethyl compounds (**6a**), the C-11 carbons of which show chemical shifts approximately equal to the value found in the C-7 carbon of **4a**. On the other hand, the C-8 carbon of **4a** is markedly shielded relative to the C-10 carbons of **3a** and **4a** ($\Delta\delta$=6.3 and 7.2 ppm, respectively) because of the so-called γ-effect.[3,4,13] By the same effect, the C-10 carbon of **6a** shifts to a 3.7 ppm higher field than that of **3a**, while the C-10 carbon of the *gem*-dimethyl compound **5a** is more shielded than the corresponding carbons of the parent compound **1a** and the monomethyl compound **2a** (**EB** conformer) by 3.0 (see footnote in Table 3) and 2.7 ppm,[3] respectively. Moreover, the C-9 carbons of **4a** and **5a** resonate at appreciably higher field than the C-9 carbon of **3a** ($\Delta\delta$=3.6 and 3.3 ppm, respectively) as a result of the γ-effect.

Thus, in compounds **3a**—**7a**, since the axial and the equatorial methyl carbons experience shieldings due to the γ-effect and the gauche interaction, respectively, the shift difference between the axial and the equatorial methyl groups in these compounds is considerably decreased ($\Delta\delta$=1.4—2.2 ppm) as compared with the cyclohexane ring (6.0 ppm).[13] This effect is also reflected in the chemical shifts of the methine carbons; the chemical shift difference between the methine carbon having an axial methyl group (C-10 of **4a**) and that having an equatorial methyl group (C-10 of **3a**) is only 0.9 ppm, much smaller than the value (4.5 ppm)[13] observed in the cyclohexane ring.

Similar spectral features are observed in the ketones (**3b**—**7b**) due to the gauche interaction and the γ-effect (see Table 2). In addition to this, in this series, also the methyl-carbonyl interaction[14,15] is observed as in the case of the monomethyl ketone **2b**.[3,4] Table 4 summarizes the effect of this interaction on the ^{13}C chemical shifts (Δ) of the methyl and the peri ring carbons in each class of the methyl compounds (**3**—**7**), which is obtained from the differences of the carbonyl substituent effects (δ^{ab}) (Table 3) between the methylated compounds (**3**—**7**) and the parent compound **1** ($\Delta=\delta^{ab}$ (**3**—**7**)$-\delta^{ab}$ (**1**); see Tables 3 and 4 and

Table 3. Effect of 9-keto function on the ^{13}C chemical shifts of some 8,9,10,11-tetrahydro-7*H*-cycloocta[*de*]naphthalenes (δ^{ab} in ppm)[a]

Compound	C-7	C-8	C-9	C-10	C-11	CH_3			
						8-eq	8-ax	10-eq	10-ax
1[b]	2.5	−16.3	−192.6	−16.3	2.5				
2-EB[c]	1.9	−12.0	−185.0	−16.4	1.4	7.4			
2-AB[c]	1.9	−17.9	−190.8	−17.4	2.4		0.9		
3	0.7	−12.3	−174.2	−12.3	0.7	7.2		7.2	
4	1.6	−13.4	−181.8	−17.8	0.5	7.4			1.4
5	0.8	−13.8	−180.1	−16.2	1.2	7.0	−0.1		
6	−0.4	−13.8	−171.7	−11.5	0.3	6.9	0.4	6.5	
7	0.2	−14.1	−170.0	−14.1	0.2	5.6	0.8	5.6	0.8

a) In each compound, $\delta^{ab}=\delta_{Hydrocarbon}-\delta_{Ketone}$; a minus sign indicates a low-field shift. b) Obtained from the chemical shift values; 36.6 (C-7,11), 29.7 (C-8, 10), and 21.3 ppm (C-9) (measured at −66.5 °C) for **1a** (Ref. 26) and from the data (**1b**) in Ref. 2. c) Refs. 3 and 4.

TABLE 4. EFFECT OF CARBONYL-METHYL INTERACTION ON ^{13}C CHEMICAL SHIFTS OF COMPOUNDS (**2**—**7**) (Δ in ppm)[a]

Compound	C-7	C-8	C-9	C-10	C-11	CH_3[b]			
						8-eq	8-ax	10-eq	10-ax
2-EB	−0.6	4.3	7.6	−0.1	−1.1	7.4			
2-AB	−0.6	−1.6	1.8	−1.1	−0.1		0.9		
3	−1.8	4.0	18.4	4.0	−1.8	7.2		7.2	
4	−0.9	2.9	10.8	−1.5	−2.0	7.4			1.4
5	−1.7	2.5	12.5	0.1	−1.3	7.0	−0.1		
6	−2.9	2.5	20.9	4.8	−2.2	6.9	0.4	6.5	
7	−2.3	2.2	22.6	2.2	−2.3	5.6	0.8	5.6	0.8

a) Obtained from the difference of the carbonyl substituent effect (δ^{ab}) (Table 3) between the methylated compounds (**2**—**7**) and the unsubstituted compound, $\Delta=\delta^{ab}_{(2-7)}-\delta^{ab}_{1}$; a minus sign indicates a low-field shift.
b) Data taken from Table 3.

footnotes therein). From this it is clear that, in all the methyl compounds, the axial methyl groups of the ketones (**b**) give chemical shifts almost comparable to the values found in the corresponding hydrocarbons (**a**), whereas the equatorial methyl groups of the ketones suffer marked shieldings (5.6—7.4 ppm) due to the eclipsed interaction between the carbonyl function and the equatorial methyl group. The carbonyl carbons of **3b**—**7b** ($\Delta\delta$=10.8—22.6 ppm) together with the C-8 (of **3b**—**7b**) and the C-10 (of **3b**, **6b**, and **7b**) carbons, which have the equatorial methyl groups on them ($\Delta\delta$=2.2—4.8 ppm), are also markedly shielded by the effect of this interaction.

The ^1H and ^{13}C data in the table show other spectral and conformational features characteristic of the boat conformation of the peri-eight membered ring. In both hydrocarbons (**a**) and the ketones (**b**), the proton chemical-shift differences between the axial and the equatorial methyl groups in **3**—**7** are greatly increased ($\Delta\delta$=0.35—0.55 ppm for **3a**—**7a** and 0.51—0.56 ppm for **3b**—**7b**) as compared with the cyclohexane system ($\Delta\delta$=0.07 ppm for methylcyclohexane[16] and 0.14 ppm for 2-methylcyclohexanone[17,18]) by the effect of the ring current of naphthalene.[3,7] The C-8 axial proton (H_{8ax}) of **3a** is greatly deshielded (*ca.* 0.8 ppm) relative to the corresponding proton (H_{1ax}) of *cis*-1,3-dimethylcyclohexane,[16] (see footnote in Table 1) since the H_{8ax} proton, which experiences the magnetic anisotropy effect of the adjacent C–C bondings smaller than that of the H_{1ax} proton (H_{8ax} is *trans* to the C_7–C_{6a} peri bond, see Fig. 1), is further deshielded by the ring-current effect of naphthalene ring (a calculation[7,19] reveals that the ring current of naphthalene deshields the axial and the equatorial protons on C-8 (and C-10) by *ca.* 0.52 and 0.37 ppm, respectively). Similar effect is observed for the H_{10ax} proton of **6a**, which is *ca.* 0.7 ppm deshielded relative to the corresponding proton of the cyclohexane ring.[16] On the other hand, marked deshieldings of the axial proton (H_{10ax}) (**3**, **5**, **6**; $\Delta\delta$= 1.02—1.21 ppm) relative to the equatorial proton (H_{10eq}) (**5**; $\Delta\delta$=0.84 ppm) by the effect of the carbonyl function might be caused chiefly by the σ-π bond overlap[20] as observed in the parent ketone **1b**.[2]

In all the compounds (**3**—**7**), whereas the chemical shifts of the exterior benzyl protons (δ=2.5—3.03 ppm) are almost comparable to the values (δ=2.219—2.875 ppm) found for the benzyl protons of the benzocyclic compounds **8**—**10**,[9-11] the interior protons of **3**—**7**, in contrast, are markedly deshielded (δ=3.71—4.86 ppm) due to the steric compression effect (the interatomic distance between the two interior protons has been calculated to be 0.652 Å for **1a**[1] and 0.632 Å for **1b**[3]). Thus it is expected that, as in the case of the parent compounds[1] and the monomethyl derivatives,[3] all the boat conformations (**3B**—**7B**) of compounds **3**—**7** exist in a somewhat distorted (puckered) form, in which the two interior protons are pushed apart mutually to relieve the steric repulsion between them.

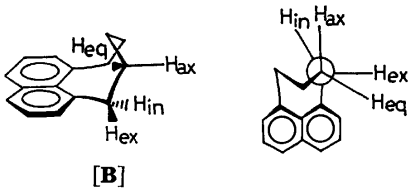

[B]

Fig. 2. The distorted (puckered) boat conformation [**B**] and its Newman projection about the C_7–C_8 (C_{10}–C_{11}) bonds.

Recently, the crystal structures of the non-cyclized 1,8-disubstituted naphthalenes have been studied based on the X-ray analyses. This shows that the peri bonds of 1,8-dimethylnaphthalene undergo in-plane bending to give a planar structure,[5,21] while, in the most of the other compounds including 1,8-di-tert-butylnaphthalene,[5,22] the molecules are seriously distorted from planarity due to the out-of-plane bending of the substituting groups. In the present case, since the molecules of **3** and **7** have a C_s symmetry as have been suggested from the NMR spectra, it is reasonable to consider that, as in the case of the parent compound **1**, the peri bonds of **3**—**7** undergo chiefly in-plane bending rather than out-of-plane bending in solution to result in a symmetric (C_s passing through the C-9 and the angular carbon atoms of naphthalene nucleus) peri ring conformation [**B**] (Fig. 2) or a conformation close near to it (the contribution of the out-of-plane deformation, even if it actually existed in **3**—**7**, seems very small, since it would give unsymmetrical conformations).

Actually, the spectra of **3**—**6** show features characteristic of the distorted conformation—*i.e.*, the axial proton (H_{ax}) always couples more strongly with the interior proton (H_{in}) (J_{vic}=5.8—6.7 Hz) than with

the exterior proton (H_{in}) (J_{vic}=0—2.3 Hz)—as observed in **1** and **2**. This result may be explained much better by the space arrangement of the distorted conformation [**B**] (the dihedral angle (θ) for the H_{in} and H_{ax} protons is smaller than 60°, while it is larger than 60° for the H_{ex} and H_{ax} protons) than by the space arrangement of the undistorted conformation (**B**) (θ is close to 60°) (see Figs. 1 and 2).

Furthermore, the distortion of peri ring is also indicated from the internal dihedral angles (Ψ) calculated from the vicinal coupling constants about the C_{10}—C_{11} bonds of the *gem*-dimethyl compounds **5a** and **5b** (the calculations were performed using *R*-value method[23] as reported previously[1]). The magnitudes of Ψ obtained for these compounds (Ψ=47° for **5a** (*R* value; 1.1) and 48° for **5b** (*R* value; 1.2)) are approximately equal to the value found in the parent compound **1a** (46°)[1] and much smaller than the value of cyclohexane (58°)[23] which has an almost staggered conformation. Consequently, it seems reasonable to consider that all compounds **3**—**7** exist in the puckered conformation [**B**] rather than in the normal boat conformation (**B**) as a result of the steric repulsion of the interior benzyl protons.

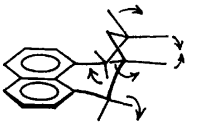

Fig. 3. Reflex effect in the 8,9,10,11-tetrahydro-7*H*-cycloocta[*de*]naphthalene ring.

Examination of molecular models reveals that the puckering of the boat conformation is accompanied by the following geometrical changes of the peri ring. Namely, as can be seen in Fig. 3, (i) the two axial methyl groups on C-8 and C-10 are compressed, (ii) the equatorial groups on these carbons come at a position more distant from the naphthalene nucleus, and (iii) the C–C–C bond angle at C-9 carbon becomes contracted.

Thus it is expected that molecules of the tetramethyl compounds **7a** and **7b** exist in a less distorted (thus more flattened) form than those of the other compounds (**1**—**6**) due to the steric repulsion between the 1,3-synaxial methyl groups (on the other hand, the presence of steric congestions around the C-9 carbon in **7a** and **7b** have been suggested from the difficulties in effecting reactions at this position[8]). This is clearly indicated from the observation that the axial methyl protons of **7a** are 0.13 ppm more deshielded than those of compounds **5a** and **6a** due to the steric compression,[24] while the equatorial methyl protons of **7a**, which come spatially closer to the naphthalene ring than the equatorial methyl protons of **3a**, are 0.10 ppm more shielded than the latter protons by the effect of the ring current of naphthalene (in the cyclohexane system in which the effect of the naphthalene ring is absent, the equatorial methyl protons of the 1,1,3,3-tetramethyl derivative give chemical shift value approximately equal to that (δ=0.88 ppm) found for the equatorial methyl protons of the *cis*-1,3-dimethyl derivative[24]).

Moreover, whereas, in compounds **5** and **6**, the axial methyl protons of the geminal methyl group are more greatly deshielded (0.26 and 0.27 ppm) than the corresponding equatorial methyl protons (0.11 and 0.13 ppm) by the effect of the carbonyl function, in contrast, in the case of the tetramethyl compound **7**, the magnitude of the carbonyl deshielding effect is almost comparable for the axial (0.19 ppm) and the equatorial methyl (0.18 ppm) protons probably due to the flattening of the boat conformation described above (Table 1).

The flattening of the boat in **7** is also suggested from the chemical shifts of the benzyl methylene protons. Table 5 summarizes the chemical shift values of the benzyl methylene protons of compounds **3**—**7** calculated from the chemical shifts of the parent compounds **1a** and **1b** and those of the axial and the equatorial isomers

Table 5. Calculated ^1H chemical shifts of the benzyl protons of compounds (**3**—**7**) (in ppm)[a,b]

Compound	H_{7in}	H_{7ex}	H_{11in}	H_{11ex}
3a	4.27(−0.01)	2.64(−0.01)	4.27(−0.01)	2.64(−0.01)
4a	4.15(0.02)	2.60(0.04)	3.69(0.02)	2.88(0.02)
5a	3.95(0.03)	2.60(−0.09)	3.89(0.03)	2.88(0.00)
6a	3.97(0.03)	2.58(0.08)	4.17(0.04)	2.58(0.01)
7a	3.87(0.22)	2.54(−0.01)	3.87(0.22)	2.54(−0.01)
3b	4.77(0.09)	2.70(0.07)	4.77(0.09)	2.70(0.07)
4b	4.77(0.02)	2.70(0.06)	4.19(0.04)	2.98(0.05)
5b	4.56(0.05)	2.75(−0.06)	4.40(0.03)	2.93(0.04)
6b	4.44(0.14)	2.67(0.02)	4.65(0.08)	2.62(0.07)
7b	4.32(0.37)	2.59(0.13)	4.32(0.37)	2.59(0.13)

a) The chemical shifts of compounds (**3a**—**7a**) were calculated from the chemical shifts of the parent compound **1a** (Ref. 1) and the values of the methyl substituent effects obtained from the chemical shifts of the axial (**AB**) and the equatorial isomers (**EB**) of the 8-monomethyl derivative **2a** (Ref. 3); **2a-AB**: −0.30 (H_{7in}), −0.04 (H_{7ex}), −0.10 (H_{11in}), −0.04 ppm (H_{11ex}), **2a-EB**: 0.28 (H_{7in}), −0.30 (H_{7ex}), 0.02 (H_{11in}), −0.02 ppm (H_{11ex}) (a minus sign indicates a high-field shift). Similarly, the chemical shifts of (**3b**—**7b**) were calculated from those of **1b** (Ref. 2) and the values of the methyl substituent effects, obtained from the chemical shifts of the **2b-AB** and **2b-EB** isomers (Ref. 4); **2b-AB**: −0.33 (H_{7in}), −0.03 (H_{7ex}), −0.12 (H_{11in}), −0.08 ppm (H_{11ex}), **2b-EB**: 0.25 (H_{7in}), −0.31 (H_{7ex}), −0.12 (H_{11in}), −0.08 ppm (H_{11ex}). b) Figures in parentheses denote the differences of the chemical shifts between the observed (Table 1) and the calculated values; $\Delta\delta=\delta_{obsd}-\delta_{calcd}$.

of the monomethyl derivatives **2a** and **2b** (see footnotes in Table 5). Comparison of these calculated values with those observed in the spectra of **3**—**7** (Table 1) reveals that the chemical shift values observed in the hydrocarbons (**3a**—**6a**) differ from the calculated values by only −0.09—0.08 ppm, while the value observed for the interior benzyl protons of the tetramethyl compound **7a** is greatly increased (0.22 ppm) relative to the value obtained by the calculation. Similar result is obtained for the ketones (**3b**—**7b**), in which the chemical shift value observed for the interior benzyl protons of the tetramethyl ketone **7b** is larger than the calculated value by 0.37 ppm. The pronounced deshielding of the interior benzyl protons in **7a** and **7b** results possibly from the less puckered conformation of **7** mentioned above, since the distance of the interior protons in such conformation is somewhat shortened relative to that of the other compounds due to the synaxial CH_3–CH_3 interaction and thus the interior protons of **7a** and **7b** are expected to be more greatly compressed than the interior protons of the latter compounds.

The above result is also reflected in the ^{13}C NMR spectra. The methyl carbons (both axial and equatorial) of **7a** are considerably deshielded (2—3 ppm) relative to those of **5a** and **6a** (Table 2), while the carbonyl shielding effect in **7** is rather decreased (equatorial methyl, 5.6 ppm) as compared with the latter compounds (6.9—7.0 ppm) (Table 3). The deshielding of methyl carbons due to the steric compression has also been observed in other ring systems.[25]

In Table 6 are shown the chemical shifts of the peri ring carbons of compounds (**3**—**7**) calculated from the chemical shifts of the parent compounds **1a**[26] and **1b**[2] and the monomethyl compounds **2a**[3] and **2b**[4] (see footnotes in the table). This indicates that, in the hydrocarbons (**3a**—**7a**), the calculated values well agree with the observed data in Table 2 (*ca.* ±1 ppm) for all the positions except the C-8 carbon of the tetramethyl compound **7a**, which resonates at appreciably lower field (4.4 ppm) than the calculated value (the rather large deviations of the observed values for the C-8 and C-10 carbons from those calculated in **5a** might be caused chiefly by the geminal effect as observed in the cyclohexane ring;[13] the observed data of **6a** and **7a** in Table 2 are in better agreement with the calculated values by use of the data of **5a** rather than by use of the data of **2a** alone (this effect is also observed in the ketone **5b**)). Similar result is obtained for the ketones (**3b**—**7b**), where the C-8 carbon of **7b** is markedly deshielded (*ca.* 5 ppm) relative to the value obtained by the calculation (although details are not known at present, the relatively large deviations of the observed data from those calculated for the carbonyl carbons might be attributed chiefly to the alterations in geometry around the carbonyl group, since the magnitude of the carbonyl–methyl shielding effect is highly dependent on the steric arrangement between the two interacting groups[3]).

Consequently, it can be considered that the molecules of **7a** and **7b** are more greatly destabilized than those of **1**—**6** in their ground states due to the steric repulsions arising from the interior benzyl protons as well as the 1,3-synaxial methyl groups. This is a novel type of the "reflex effect" inherent in the 8-membered pericyclized naphthalene system, though the analogous effect is reported for the cyclohexane system.[27] Here, it is interesting that, whereas the interior benzyl protons of **7a** and **7b** are more greatly deshielded relative to those of the other compounds (**1**—**6**) by virtue of the reflex effect (Table 5), the chemical shifts of the benzyl

TABLE 6. CALCULATED ^{13}C CHEMICAL SHIFTS OF THE PERI RING CARBONS OF COMPOUNDS (**3**—**7**) (in ppm)[a,b,c]

Compound	C-7	C-8	C-9	C-10	C-11
3a	41.9(0.5)	32.9(0.5)	37.9(1.1)	32.9(0.5)	41.9(0.5)
4a	42.3(−0.2)	27.9(−0.8)	35.2(0.2)	33.8(0.5)	43.9(−0.1)
5a	50.6(−0.8)	37.6(−2.9)	35.2(−0.5)	24.1(2.6)	35.6(0.2)
6a	49.9(−0.7)	37.3(−2.4)	43.5(0.1)	27.6(1.9)	41.6(0.1)
	[49.1(0.1)	34.4(0.5)	43.0(0.6)	30.2(−0.7)	41.8(−0.1)]
7a	49.6(−0.7)	32.0(4.1)	49.1(−0.8)	32.0(4.1)	49.6(−0.7)
	[49.0(−0.1)	31.7(4.4)	48.1(0.2)	31.7(4.4)	49.0(−0.1)]
3b	41.1(0.6)	45.0(0.7)	215.3(−2.1)	45.0(0.7)	41.1(0.6)
4b	40.5(0.0)	41.0(−0.5)	218.4(−1.2)	51.8(0.3)	43.1(0.2)
5b	49.3(−0.3)	51.2(−2.7)	218.4(−3.6)	41.6(1.3)	34.3(0.3)
6b	49.7(−0.1)	51.0(−2.3)	219.1(−3.8)	40.8(0.2)	40.9(0.5)
	[49.4(0.2)	48.3(0.4)	215.5(−0.2)	42.1(−1.1)	41.2(0.2)]
7b	49.5(−0.8)	46.8(3.4)	222.9(−4.6)	46.8(3.4)	49.5(−0.8)
	[49.5(−0.8)	45.4(4.8)	215.7(2.6)	45.4(4.8)	49.5(−0.8)]

a) The chemical shifts of compounds (**3a**—**7a**) were calculated from the chemical shifts of the parent compound **1a** (see footnote inTabe 3) and the values of the methyl substituent effects, obtained from the chemical shifts of the axial (**AB**) and the equatorial isomers (**EB**) of the 8-monomethyl derivative **2a** (Ref. 3); **2a-AB**: 8.0 (C-7), 4.4 (C-8), 5.6 (C-9), −5.3 (C-10), −0.3 ppm (C-11), **2a-EB**: 6.0 (C-7), 3.5 (C-8), 8.3 (C-9), −0.3 (C-10), −0.7 ppm (C-11) (a minus sign indicates a high-field shift). Similarly, the chemical shifts of **3b**—**7b** were calculated from those of **1b** (Ref. 2) and the values of the methyl substituent effects obtained from the chemical shifts of the **2b-AB** and **2b-EB** isomers (Ref. 4); **2b-AB**: 8.6 (C-7), 6.0 (C-8), 3.8 (C-9), −4.2 (C-10), −0.2 ppm (C-11), **2b-EB**: 6.6 (C-7), −0.8 (C-8), 0.7 (C-9), −0.2 (C-10), 0.4 ppm (C-11). b) Figures in brackets indicate the calculated shift values obtained by use of the observed data of **5a** or **5b** (Table 2). c) Figures in parentheses are the differences of the chemical shifts between the observed (Table 2) and the calculated values; $\Delta\delta=\delta_{obsd}-\delta_{calcd.}$

methylene carbons of **7a** and **7b**, in contrast, are little influenced by the steric compression effect (Table 6). On the other hand, the steric compression of the synaxial methyl groups in **7a** and **7b** is clearly reflected in both proton and carbon chemical shift values of the axial methyl group as described above.

Similar result is obtained from the spectra of the parent compound **1a**. Comparison of the ^{13}C data of **1a** (see footnote in Table 3)[26] with those of the structurally analogous benzocyclic compound **8a** (36.6 (C-5,9), 28.2 (C-6,8), 32.6 ppm (C-7))[28] reveals that, although the interior benzyl protons of **1a** are markedly deshielded ($\Delta\delta$=1.1—1.2 ppm)[1] relative to the benzyl protons of **8a** due to the steric compression, the chemical shift values of the benzyl methylene carbons are quite equal (δ=36.6 ppm) between these two compounds; however, it should be noted here that the C-9 carbon of **1a** which has the gauche steric arrangements with the peri bonds (C_7–C_{6a} and C_{11}–C_{11a} bonds) in the boat conformation (see Newman projection in Fig. 1) is greatly shielded ($\Delta\delta$=11.3 ppm) relative to the C-7 carbon of **8a** which exists in the chair conformation.

It is seen in Table 1 that in each class of methyl compounds, the interior benzyl protons of the ketones (**b**) are always greatly deshielded ($\Delta\delta$=0.51—0.63 ppm) relative to those of the corresponding hydrocarbons (**a**) (the values of shift difference are only 0.09—0.19 ppm for the corresponding exterior protons). Similar result was obtained for compounds **1** ($\Delta\delta$=*ca.* 0.67 ppm)[1,2] and **2** ($\Delta\delta$=0.5—0.7 ppm).[3,4] This result may be attributed chiefly to the difference in the interatomic distance of the interior benzyl protons. That is, the H_{in} protons of the ketone, the distance of which is shorter than that in the case of the hydrocarbon, are more greatly compressed and more greatly deshielded than the H_{in} protons of the hydrocarbon. However, in view of such large $\Delta\delta$ values found in the ketone, it is probable that the difference of the H_{in} distance between the ketone and the hydrocarbon is, in practice, somewhat larger than the value of 0.02 Å obtained from the calculation[1,3] (see above). Therefore it may be considered that the ketone exists somewhat in a less puckered form than the conformations of the hydrocarbon in each class of compound probably due to the rigid C-9 double (C=O) bond (see Fig. 3).

In the case of compounds **3a** and **3b** which have *cis*-diequatorial methyl groups, the molecules are expected to be more strongly puckered than the other compounds to relieve the steric interaction between the equatorial methyl groups and the naphthalene ring[3,4] (Fig. 3). The small $J_{ex,ax}$ value observed in **3a** (this coupling is small enough not to be resolved) probably reflects this (see Newman projection in Fig. 2).

The distortion of the peri ring is also reflected in the IR spectra. Table 7 shows the carbonyl stretching frequencies ν(C=O) of the methyl ketones (**2b**—**7b**) determined in the chloroform solution. The magnitudes of the ν(C=O) values obtained apparently depend on the orientations of the substituting methyl groups. This may be explained in terms of the inverse relationship between the stretching frequency and the carbonyl angle (>C=O)[27] as follows.

The carbonyl stretching frequency of the ketone **2b** (1706 cm^{-1}) having an equatorial methyl group (in **2b**, the methyl group prefers the equatorial conformation (**EB**) to the axials (**AB**) by 0.07 kcal/mol at room temperature)[4] is 3 cm^{-1} higher than the absorption (1703 cm^{-1})[29] of the unsubstituted ketone **1b**. This arises probably because the molecule of **2b** is more distorted (puckered) than that of **1b** to relieve the methyl-naphthalene interaction, which makes the carbonyl angle of **2b** somewhat smaller than that of **1b** (Fig. 3). This effect is more clearly shown in the spectrum of **3b** which has *cis*-diequatorial methyl groups. The carbonyl frequency of **3b** is increased by 8 cm^{-1} as compared with the parent ketone **1b**.

On the other hand, introduction of an axial methyl group at C-8 or at C-10 position of these compounds (**2b** and **3b**) results in a 5—8 cm^{-1} decrease in the carbonyl frequency (thus, 0—2 cm^{-1} decrease relative to **1b**) as observed in compounds (**4b**—**6b**), because the carbonyl angle in these compounds is, to some extent, expanded (thus the peri ring exists in a less puckered form) relative to that of the ketones **2b** and **3b** due to the 1,3-synaxial CH_3-H steric interactions (the existence of this interaction is also suggested from the observation that the C-8 or C-10 axial protons which have a synaxial steric relationship with a methyl group resonate at *ca.* 0.1—0.3 ppm lower field than the protons without such steric interactions; see footnote in Table 1). This effect is also observed in the axial isomer (**AB**) of 8-ethyl-8,9,10,11-tetrahydro-7*H*-cycloocta[*de*]naphthalen-9-one (**11**) (in this compound, the

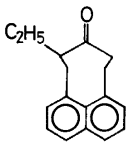

11

axial conformation is preferred to the equatorial conformation by 0.69 kcal/mol at room temperature),[4] where the carbonyl stretching frequency is lowered by 3 cm^{-1} as compared with the parent ketone **1b**.

The above result is in sharp contrast to the case of the α-methylcyclanones including the cyclohexane system previously reported. In 3-keto steroids,[30] introduction of one methyl group in the 2- or the 4-position causes a 4—7 cm^{-1} decrease in the carbonyl stretching frequencies, irrespective of whether the methyl group is in the axial or in the equatorial conformation; the carbonyl frequencies of the α-*gem*-dimethylated 3-keto steroids, therefore, are more greatly decreased (12—13 cm^{-1}) by the effect of the methyl groups[30] than in the case of the ketones (**4b**—**6b**) (0—2 cm^{-1}) which experience the puckering distortion due to the methyl(eq)–naphthalene steric interaction.

The carbonyl stretching frequency of the fully methylated ketone **7b** is greatly decreased (14 cm^{-1}) as compared with the parent ketone **1b**. Thus it is suggested that the carbonyl angle of **7b** is greatly expanded (thus the peri ring is flattened) relative to that of (**1**—**6**) in excellent agreement with the NMR spectra described above. Analogous effect was

TABLE 7. CARBONYL STRETCHING FREQUENCIES (νC=O) OF THE METHYL KETONES (**2b**—**7b**)[a]

Compound	Frequency ν(cm^{-1})	$\Delta\nu$[b]
Unsubstituted ketone (**1b**)[c]	1703	
8-Monomethyl ketone (**2b**)[d]	1706	+3
cis-8,10-Dimethyl ketone (**3b**)	1711	+8
trans-8,10-Dimethyl ketone (**4b**)	1701	−2
8,8-Dimethyl ketone (**5b**)	1701	−2
8,8,10-Trimethyl ketone (**6b**)	1703	0
8,8,10,10-Tetramethyl ketone (**7b**)	1689	−14
8-Ethyl ketone (**11**)[e]	1700	−3
Cyclooctanone	1694[f]	−9
Cyclohexanone	1708[g]	+5

a) The IR spectra were measured in chloroform (spectro grade) at room temperature, using a 0.1 mm-length KBr cell. The concentration of the samples was *ca.* 0.1 mol/l for all the ketones and the measurements were run twice for each sample. The positions of absorption maxima were obtained from the expanded spectra and calibrated with polystyrene ($\Delta\nu=\pm0.5$ cm^{-1}). b) Frequency shift from the parent ketone **1b**. c) Ref. 29. d) The equatorial isomer (**EB**) is more favored than the axials(**AB**) by 0.07 kcal/mol at 30 °C (Ref. 4). e) The axial conformation is preferred to the equatorial conformation by 0.69 kcal/mol at 30 °C (Ref. 4). f) Shifted to 1705 cm^{-1} in carbon tetrachloride (Lit. 1703 cm^{-1}; Ref. 31). g) Reported to be 1716 cm^{-1} in carbon tetrachloride (Ref. 31).

reported[30] for 2,2,4,4-tetramethylcholestan-3-one, in which the carbonyl frequency is lowered by *ca.* 17 cm^{-1} as compared with the unmethylated compound.

As can be seen in Table 7, the carbonyl frequency of **1b** (1703 cm^{-1})[29] is 9 cm^{-1} higher than that of cyclooctanone and 5 cm^{-1} lower than that of cyclohexanone. Therefore it may be considered that the carbonyl angle of **1b** is probably between that of these two cyclanones, if it could be assumed that the magnitude of the carbonyl frequency depend solely upon the carbonyl angle irrespective of the ring system to which the ketones belong. This is consistent with the NMR result that the internal bond angle at C-9 carbon of the peri-8-membered ring system is, to some extent, contracted as a result of the puckering of the boat conformation (Fig. 3).

Previously, we have studied the ring inversions in compounds **1a**[1] and **1b**.[2] In order to determine the effect of the C-8 and C-10 methyl substituent on the ring inversions in the 8-membered pericyclized naphthalene system, the free energy barriers to boat-to-boat interconversion process were investigated for several methylated compounds (8-methyl (**2a**), *trans*-8,10-dimethyl (**4a**), 8,8-dimethyl (**5a**), and 8,8,10,10-tetramethyl (**7a**)) and their 9-oxo derivatives (**2b**, **4b**, **5b**, and **7b**) by use of the variable-temperature ^{1}H NMR technique. In these conformational changes, three types of ring inversions are observed. In compounds **4** and **7**, a degenerate process occurs in which the conformer exchanges with itself. In compound **5**, the ring inversion process is enantiomeric, while **2** undergoes conformational inversion into its diastereomer. In all of these conformational processes, the methyl group in each compound is interchanged between the axial and the equatorial conformations of equal conformational energies (since the ($-\Delta G^\circ$) values for **2a**[3] and **2b**[4] are very small, the populations of the two isomers in these compounds were assumed to be equal at the temperatures studied).

We therefore examined the ^{1}H NMR spectra of the methyl groups of each compound as a function of the temperature (for **2a**, **2b**, and **4b**, the deuterated derivatives **2a**-8,10,10-d_3,[3] **2b**-8,10,10-d_3,[4] and **4b**-8,10-d_2 were employed, respectively). The methyl signals in all compounds show a change typical of the dynamic exchange processes on varying the temperature—*viz.*, the two separated methyl signals at low temperature broaden, coalesce, and then sharpen as the temperature is increased. From these spectral changes the free energy barrier (ΔG^*) to boat inversion for each methyl compound is calculated by means of the coalescence temperature (T_c) method (see footnotes in Table 8).[32] The results are summarized in Table 8 together with the data of the parent compounds **1a**[1] and **1b**[2] previously reported.

As can be seen in the table, the free energy barriers (ΔG^*) for 8-monomethyl derivative **2a** and *trans*-8,10-dimethyl compound **4a** are almost comparable to the value of the parent compound **1a** ($\Delta\Delta G^*=0.4$ and 0.6 kcal/mol, respectively), whereas barriers for the *gem*-dimethyl compound **5a** and the tetramethyl compound **7a** are markedly increased as compared with **1a** ($\Delta\Delta G^*=5.4$ and 5.9 kcal/mol, respectively). A similar trend is observed in the ΔG^* values of the ketones, where the ΔG^* for **5b** and **7b** is much higher than the value of **1b** ($\Delta\Delta G^*=4.8$ and 5.6 kcal/mol, respectively), whereas that of **2b** and **4b** is approximately equal to the value of **1b** ($\Delta\Delta G^*=-0.1$ and 0.2 kcal/mol, respectively). The observation of the same trend in ΔG^* for the hydrocarbons (**a**) and the ketones (**b**) strongly suggests that the boat conformation of both classes of methyl compounds interconverts through the same pathway. Therefore, it seems reasonable to assume[32] that ΔG^* differences in Table 8 ($\Delta\Delta G^*$) are fair approximations to $\Delta\Delta H^*$ for all the methylated compounds studied.

Recently, it has been shown that the boat-to-boat interconversion in the 8,9,10,11-tetrahydro-7*H*-cycloocta[*de*]naphthalene ring proceeds by pseudorotations of the peri bonds *via* the twist-boat conformation (**TB**) as an intermediate,[1,6] the transition state for this process being possibly a high-energy conformation (**TS**)[1,2] (see Fig. 4). The ΔG^* value of each methyl compound in Table 8 can be adequately explained in terms of the boat inversion mechanism described above.

In **2a** and **2b**, the methyl substituent could produce no serious steric interaction either in the (**TS**) or in the (**TB**) conformation during the ring inversion as is seen in Fig. 5. In these compounds, the transition state of boat inversion may somewhat be elevated as a result of the methyl substitution (which could cause some increase in the torsional barrier for rotation about the C_8–C_9 and C_9–C_{10} bonds in (**TS**)), but the ground state is also elevated due to the transannular synaxial CH_3–H interaction or to the eq-CH_3–naphthalene gauche

Table 8. Free energy barriers ($\Delta G^{\ddagger}$) to boat inversion for several 8- and 10-methyl-substituted 8,9,10,11-tetrahydro-7*H*-cycloocta[*de*]naphthalenes (**a**) and their 9-oxo compounds (**b**)[a,b]

Compound	Signal obsd	$\Delta\nu$/Hz[e]		T_c/°C		$\Delta G^{\ddagger}$/kcal·mol^{-1} [f]		Difference[g]
		(**a**)	(**b**)	(**a**)	(**b**)	(**a**)	(**b**)	
Unsubstituted (**1**)						14.5[c]	12.4[d]	2.1
8-Monomethyl (**2**)	CH_3	36	50	26.6	−21.3	14.9(0.4)	12.3(−0.1)	2.6
trans-8,10-Dimethyl (**4**)	CH_3	42	51	32.5	−15.0	15.1(0.6)	12.6(0.2)	2.5
8,8-Dimethyl (**5**)	CH_3	36	49	121.5	73.7	19.9(5.4)	17.2(4.8)	2.7
8,8,10,10-Tetramethyl (**7**)	CH_3	55	56	137.9	92.7	20.4(5.9)	18.0(5.6)	2.4

a) Variable-temperature ^{1}H NMR studies were carried out using deuteriochloroform solution for all compounds except **5a** and **7a**, which were measured in *o*-dichlorobenzene. The energy of activation ($\Delta G^{\ddagger}$) for the boat inversion was calculated from Eqs.; $\Delta G^{\ddagger}=4.57T_c(10.32-\log k_c+\log T_c)$ and $k_c=\pi\Delta\nu/\sqrt{2}$ (Ref. 32), using the coalescence temperature (T_c) of the methyl signal. b) In each compound, figures in the left column are due to the hydrocarbons (**a**), while those in the right are to the ketones (**b**). c) Obtained by means of the complete line-shape analysis method (Ref. 1); Nelsen and Gillespie reported this value to be 14.0 kcal/mol using the coalescence temperature method (Ref. 6). d) From Ref. 2. e) The chemical-shift difference of the methyl proton signals; data for compounds **4**, **5**, and **7** were taken from Table 1, while those for **2a** and **2b** were taken from Refs. 3 and 4, respectively. f) Figures in parentheses are the values of $\Delta G^{\ddagger}$ relative to the parent compounds **1a** and **1b**. g) The $\Delta G^{\ddagger}$ difference between the hydrocarbon (**a**) and the ketone (**b**).

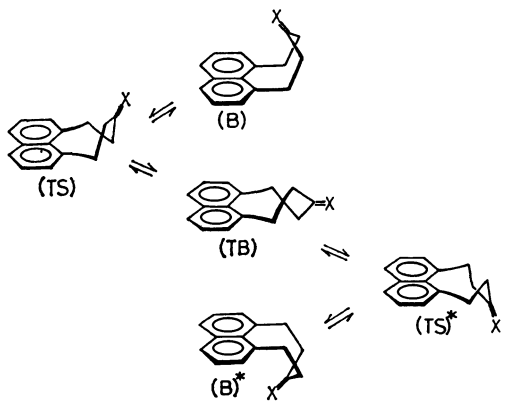

Fig. 4. Pathway for boat inversion of the 8,9,10,11-tetrahydro-7*H*-cycloocta[*de*]naphthalene ring (**a**; X=H_2, **b**; X=O, the signal marked with an asterisk indicates the inverted form).

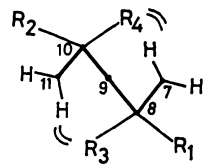

1; $R_1=R_2=R_3=R_4=H$
2; $R_1=CH_3$, $R_2=R_3=R_4=H$
3; $R_1=R_4=CH_3$, $R_2=R_3=H$
4; $R_1=R_2=CH_3$, $R_3=R_4=H$
5; $R_1=R_3=CH_3$, $R_2=R_4=H$
6; $R_1=R_2=R_3=CH_3$, $R_4=H$
7; $R_1=R_2=R_3=R_4=CH_3$

Fig. 5. Steric interaction in the twist-boat conformation (**TB**)(C_2) of compounds (**1**—**7**) viewed from in front of the C-9 carbon (naphthalene moiety is omitted).

interaction, as the result of which the effect of the methyl group on the barrier to ring inversion seems very small. Similar arguments are also valid for **4a** and **4b** (see Fig. 5). Therefore it is understandable to observe that the $\Delta G^{\ddagger}$ values for compounds **2a**, **2b**, **4a**, and **4b** are almost comparable to the values for the parent compounds or slightly higher than the values of the latter compounds.

On the other hand, in the case of compounds **5a** and **5b** which have one *gem*-dimethyl group in the C-8 position, the pseudorotations of the peri bonds give rise to a close approach of the methyl substituent to the peri hydrogen (at C-11) in the transition state as well as in the (**TB**) conformation (in compounds **2** and **4** without a *gem*-dimethyl group at C-8, this interaction is avoidable) (Fig. 5). Therefore, it is expected that the (**TS**) of **5a** and **5b** is more greatly elevated relative to **4a** and **4b** by the interaction of these two groups. In view of this together with that the energy of the ground state of **5a** and **5b** is close near to that of **4a** and **4b** (in both cases, the synaxial CH_3–H interaction and the (eq)CH_3–naphthalene interaction are the most important), it is understandable to observe that the $\Delta G^{\ddagger}$ values of **5a** and **5b** are unusually higher than the values of **4a** and **4b** as well as those of **2a** and **2b**.

For the same reason, the $\Delta G^{\ddagger}$ for the tetramethyl compounds **7a** and **7b** is also markedly increased as compared with the parent compounds (see Fig. 5). In this case, the $\Delta G^{\ddagger}$ value for **7a** and **7b** shows only a small increase ($\Delta\Delta G^{\ddagger}<1$ kcal/mol) relative to **5a** and **5b**, respectively, though the (**TS**) and (**TB**) of the former compounds are more greatly destabilized than those of the latter compounds (**7a** and **7b** involve twice a steric interaction as that present in **5a** and **5b**; Fig. 5). This arises probably because the ground state of **7** is greatly destabilized by virtue of the reflex effect arising from the the synaxial CH_3–CH_3 steric interaction coupled with the interior benzyl H–H interaction as described above.

The above result is in striking contrast to the case of other ring systems such as the cyclohexane and 6,7,8,9-tetrahydro-5*H*-benzocycloheptene (**8**). The $\Delta G^{\ddagger}$ value for the chair inversion of 6,6-dimethyl- (**9**) and 6,6,8,8-tetramethylbenzocycloheptene derivatives (**10**) is only slightly increased (**9**; 0.6 kcal/mol) or lowered (**10**; 0.3 kcal/mol) relative to the unmethylated com-

pound **8a**.[9] Similarly, the $\Delta G^{\ddagger}$ value for the 1,1-dimethyl- and 1,1,3,3-tetramethylcyclohexane derivatives is slightly higher (0.1 kcal/mol) or lower (0.9 kcal/mol), respectively, than the value for the parent cyclohexane.[33]

In each methyl compound, $\Delta G^{\ddagger}$ for the ketone (**b**) is always lower than the value for the corresponding hydrocarbon (**a**) by 2.4—2.7 kcal/mol. Similar trend has been observed for the parent compounds ($\Delta\Delta G^{\ddagger}$= 2.1 kcal/mol).[1,2] This result may be adequately explained in terms of the boat inversion mechanism described above. The pseudorotations of the peri bonds in the boat inversion are accompanied by rotations about the C_9–C_{10} and C_8–C_9 bonds in the conversions of (**B**)⇆(**TS**)⇆(**TB**) and (**TB**)⇆(**TS**)*⇆(**B**)*, respectively.[1] Thus, in view of the barriers to methyl rotation in propane (3.3 kcal/mol)[27] and acetone (0.8 kcal/mol),[33] it is expected that energies necessary for reaching the transition states in the ketone (**b**) are smaller than in the case of the hydrocarbon (**a**) by the value close to the difference in the barrier between propane and acetone.[33] Actually, the difference in $\Delta G^{\ddagger}$ observed between the ketone and the hydrocarbon in each methyl compound is almost comparable to the value observed in propane and acetone. Moreover, in each compound of (**2**—**7**), the effect of the methyl group on $\Delta G^{\ddagger}$ is always larger for the hydrocarbon than for the ketone by 0.3—0.6 kcal/mol. This might be taken chiefly as a reflection of the difference in the torsional barriers about the C_8–C_9 and/or C_9–C_{10} bonds between the hydrocarbon and the ketone caused by the steric interaction with the methyl group.

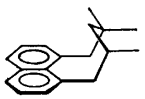

6B′

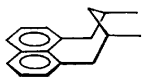

3B′

On the other hand, the ^{1}H NMR spectra of **3b** and **6b** reveals that conformations of **3B** and **6B** are also enough stable at room temperature (these spectra show no change below 90 °C), because another boat (**3B′** and **6B′**) involves steric repulsion due to the synaxial methyl groups and the (**TS**) and (**TB**) states involve the peri-H-CH_3 steric interaction as illustrated in Fig. 5.

All the results presented above provide a strong evidence that the boat inversion is caused by pseudorotations of the peri bonds in the 8-membered pericyclic naphthalene ring system. Consequently, this study reveals that the molecule of the 8-membered pericyclized naphthalenic compounds exists in a steric circumstance very different from that of the cycloalkanes and the benzocyclic compounds not only in the ground state but also in the transition state due to the peri strains involved.

Experimental

The synthesis of 8- and 10-methyl-substituted 8,9,10,11-tetrahydro-7*H*-cycloocta[*de*]naphthalenes (**3a**—**7a**) and their 9-oxo derivatives (**3b**—**7b**) have been reported previously.[8] The deuterated compounds, *cis*-8,10-dimethyl-8,9,10,11-tetrahydro-7*H*-cycloocta[*de*]naphthalen-9-one-8,10-d_2 (**3b**-d_2), *trans*-8,10-dimethyl-8,9,10,11-tetrahydro-7*H*-cycloocta[*de*]-naphthalen-9-one-8,10-d_2 (**4b**-d_2), and 8,8,10-trimethyl-8,9,10,-11-tetrahydro-7*H*-cycloocta[*de*]naphthalen-9-one-10-*d* (**6b**-*d*) were obtained from the ketones **3b** and **6b** using the deuterium exchange procedure previously described.[1] Deuteration of **3b** in a boiling mixture of potassium carbonate in dioxane and deuterium oxide gave an equilibration mixture from which **3b**-d_2 and **4b**-d_2 were isolated by recrystallization from ethanol. Similar result was obtained on reaction (boiling with a solution of sodium deuteroxide in dioxane and deuterium oxide) with diethyl 8,10-dimethyl-9-oxo-8,9,10,11-tetrahydro-7*H*-cycloocta[*de*]naphthalene-8,10-dicarboxylate.[8] The structures of the deuterated compounds were confirmed on the basis of the TLC, melting points (**3b**-d_2; 228—229 °C (**3b**; 230—231 °C),[8] **4b**-d_2; 125—126 °C (**4b**; 126—127 °C),[8] **6b**-*d*; 125—126 °C (**6b**; 124.5—125 °C)[8]), and their spectra (IR and NMR).

The ^{1}H NMR spectra were determined on a Varian HA-100D spectrometer at 100 MHz using a *ca.* 10% (w/v) solution of samples in deuteriochloroform (for compound **3b**, a *ca.* 3% solution was employed); the chemical shifts are expressed in ppm (δ) downfield from the internal standard, tetramethylsilane, and the coupling constants (J), in Hz with an accuracy of ±0.1 Hz. The variable-temperature ^{1}H NMR studies were carried out using a deuteriochloroform solution for all compounds except **5a** and **7a**, which were measured in *o*-dichlorobenzene. The sample temperature was controlled by passing precooled nitrogen through the sample cavity and measured by a calibrated copper–constantan thermocouple. The ^{13}C NMR spectra were determined on a Varian NV-14 FT NMR spectrometer operating at 15.087 MHz, using deuteriochloform as a solvent and tetramethylsilane as an internal standard (accuracy, ±0.1 ppm). The IR spectra were measured on a JASCO IR-G grating infrared spectrometer using a *ca.* 0.1 mol/l solution of samples in chloroform (spectro grade) with a 0.1 mm-length KBr cell. The measurements were run twice for each compound, and the positions of absorption maxima were calibrated with polystyrene ($\Delta\nu$= ±0.5 cm^{-1}).

References

1) T. Kamada and O. Yamamoto, *Bull. Chem. Soc. Jpn.*, **52**, 1159 (1979).
2) T. Kamada and O. Yamamoto, *Chem. Lett.*, **1976**, 843.
3) T. Kamada and O. Yamamoto, *Bull. Chem. Soc. Jpn.*, **52**, 2991 (1979).
4) T. Kamada and O. Yamamoto, *Tetrahedron Lett.*, **1977**, 691.
5) V. Balasubramaniyan, *Chem. Rev.*, **66**, 567 (1966).
6) S. F. Nelsen and J. P. Gillespie, *J. Am. Chem. Soc.*, **95**, 2940 (1973).
7) T. Kamada, N. Wasada and O. Yamamoto, *Bull. Chem. Soc. Jpn.*, **49**, 275 (1976).
8) T. Kamada, *Bull. Chem. Soc. Jpn.*, **52**, 170 (1979).
9) S. Kabuss, H. G. Schmid, H. Friebolin and W. Faisst, *Org. Mag. Res.*, **2**, 19 (1970).
10) S. Kabuss, H. G. Schmid, H. Friebolin and W. Faisst, *Org. Mag. Res.*, **1**, 451 (1969).
11) M. St-Jacques and C. Vaziri, *Org. Mag. Res.*, **4**, 77 (1972).
12) N. L. Allinger and W. Szkrybalo, *J. Org. Chem.*, **27**, 722 (1962); G. Bodennec and M. St-Jacques, *Can. J. Chem.*, **55**, 1199 (1977).
13) J. B. Stothers, "Carbon-13 NMR Spectroscopy," Academic Press, New York (1972).

14) F. Weigert and J. D. Roberts, *J. Am. Chem. Soc.*, **92**, 1347 (1970).
15) J. B. Grutzner, M. Jautelat, J. B. Dence, R. A. Smith and J. D. Roberts, *ibid.*, **92**, 7107 (1970).
16) D. Danneels and M. Anteunis, *Org. Mag. Res.*, **6**, 617 (1974).
17) F. Johnson, N. A. Starkovsky and W. D. Gurowitz, *J. Am. Chem. Soc.*, **87**, 3492 (1965).
18) F. Nerdel, D. Frank, and K. Rehse, *Chem. Ber.*, **100**, 2978 (1967).
19) R. E. Mayo and J. H. Goldstein, *Mol. Phys.*, **10**, 301 (1966).
20) K. M. Wellmann and F. G. Bordwell, *Tetrahedron Lett.*, **1963**, 1703.
21) D. Bright, I. E. Maxwell and J. de Boer, *J,. Chem. Soc., Perkin Trans.*, **2**, **1973**, 2101.
22) J. Handal, J. G. White, R. W. Franck, Y. H. Yuh, and N. L. Allinger, *J. Am. Chem. Soc.*, **99**, 3345 (1977).
23) J. B. Lambert, *Accounts Chem. Res.*, **4**, 87 (1971).
24) H. Werner, H. J. Kohler, M. Muhlstadt, A. Zschunke, and G. Mann, *Org. Mag. Res.*, **5**, 119 (1973).
25) S. H. Grover, J. P. Guthrie, J. B. Stothers, and C. T. Tan, *J. Mag. Res.*, **10**, 231 (1973).
26) T. Kamada and O. Yamamoto, Unpublished data.
27) E. L. Eliel, N. L. Allinger, S. Angyal, and G. A. Morrison, "Conformational Analysis," Interscience Publishers, New York (1965) and references therein.
28) H. Gunther, G. Jikeli, H. Schmickler, and J. Prestien, *Angew. Chem.*, **85**, 826 (1973).
29) T. Kamada and O. Yamamoto, *Tetrahedron Lett.*, **1977**, 1341.
30) Y. Mazur and F. Sondheimer, *J. Am. Chem. Soc.*, **80**, 5220 (1958), and references therein.
31) C. S. Foote, *ibid.*, **86**, 1853 (1964).
32) G. Binsch, "Topics in Stereochemistry," ed by E. L. Eliel and N. L. Allinger, Vol. 3, Interscience Publishers, New York, (1968), p. 97.
33) F. A. L. Anet and R. Anet, "Dynamic Nuclear Magnetic Resonance Spectroscopy," ed by L. M. Jackman and F. A. Cotton, Academic Press, New York (1975).

Synthetic Photochemistry. XIII.[1] Chiroptical Retention for the Reported "*antara-antara*"-3,3-Sigmatropy of Bicyclo-[3.2.0]hepta-3,6-dien-2-ones

Hitoshi TAKESHITA,* Masatoshi KUMAMOTO, and Isao KOUNO
Research Institute of Industrial Science, 86, Kyushu University, Hakozaki, Fukuoka 812
(Received March 26, 1979)

Troponoids were shown to form 2: 1-complexes with β-cyclodextrin and 1: 1-complexes with α-cyclodextrin. The photoisomerization of complexed tropolone and 2-methoxytropone gave optically active 1-hydroxy- and 1-methoxybicyclo[3.2.0]hepta-3,6-dien-2-ones in improved yields. The pyrolysis of the (+)-1-methoxybicyclo-[3.2.0]hepta-3,6-dien-2-one gave the (+)-3-methoxybicyclo[3.2.0]hepta-3,6-dien-2-one, ruling out the two-fold *supra-antara*-1,3-sigmatropy.

The utilizations of inclusion complexes for organic syntheses have been of interest,[2,3] but although there are many applications in various aspects including photolyses,[4] the photochemical valence-isomerization of guest molecules seems not to have been studied. We will herein describe the results of the photoisomerization of cyclodextrin (CDX)-complexed tropolone derivatives to give bicyclo[3.2.0]hepta-3,6-dien-2-ones, primary photoproducts, with improvements in the yields and in the rates of the reaction, For the large-scale preparation of bicyclo[3.2.0]heptadienones, the previous method, photoisomerization in solutions,[5,6] was inadequate.

When an aqueous solution of β-CDX was mixed with tropolone (**1**), colorless precipitates were formed immediately. According to the titrations, the precipitates, [**1**: β-CDX], were analyzed and found to contain 2 mol of **1** for a CDX unit. A similar type of 2: 1-complex was formed from 2-methoxytropone (**2**) and tropone (**3**). On the contrary, α-CDX was shown to form 1: 1-complexes with these troponoids.

The regeneration of troponoids from the complexes required a prolonged liquid-liquid extraction; a simple separatory extraction or solid-liquid (Soxlét) extraction was not effective.

By the external irradiation of [**1**: β-CDX] as a water dispersion, a known photoisomer of **1**, 1-hydroxybicyclo[3.2.0]hepta-3,6-dien-2-one (**4**),[6] was obtained in a 64% yield after the liquid-liquid extractions. As a minor product, 4-oxo-2-cyclopentenylacetic acid (**7**)[6] was also obtained. On the other hand, [**2**: β-CDX] and [**2**: α-CDX] were relatively soluble in water, and the photoreaction needed a prolonged time to give **5**, **6**, and **8**,[5] while in hexane the isomerization proceeded more efficiently. There is an apparent correlation between the solubility and the rate of the reaction; the less soluble the media, the greater the rate of the reaction. Figure 1 shows the comparative figures of this medium effect. It can also be noticed that, except for water, the rates of the reaction are not very different

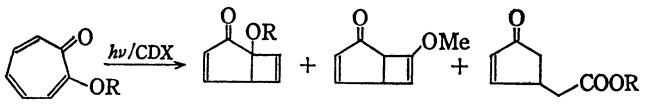

1: R=H **4**: R=H **6** **7**: R=H
2: R=CH_3 **5**: R= CH_3 **8**: R=CH_3

Chart 1.

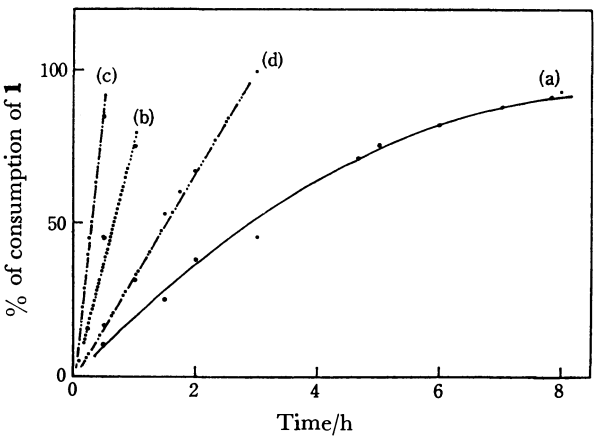

Fig. 1. Relative rates of photoreaction of **1** under various conditions. (a) in water without CDX, (b) in hexane without CDX, (c) as [**1**: α-CDX] in water, and (d) as [**1**: β-CDX] in water.

TABLE 1. THE PRODUCT DISTRIBUTIONS FOR THE PHOTOREACTION OF [**1**: CDX][a] IN VARIOUS SOLVENTS

Complexes	Media for dispersion	Isolated yields for **4**	Isolated yields for **7**
[**1**:α-CDX]	Water	68	21
	Methanol	65	15
	Acetone	58	10
	Hexane	66	20
[**1**:β-CDX]	Water	64	22
	Methanol	55	20
	Acetone	60	18
	Hexane	55	15

a) For each run, *ca.* 250 mg of **1** was used to prepare the complexes.

in various organic media, protic or aprotic; this is probably a reflection of a tight inclusion of troponoids in CDX. In the case of **2**, it is well known that the original product (**5**) was easily converted into the secondary photoproduct (**6**).[5]

These photoisomers were optically active; their ORD and CD curves are illustrated in Fig. 2, while some $[\alpha]_D^{20}$ values are shown in Table **2**.[7] The amplitudes of the optical rotation of the photoproducts obtained from [β-CDX] were larger than those obtained from

[α-CDX], and the amplitudes for the products of aprotic solvents were larger than those for protic solvents. Although we do not know the mechanism of this asymmetric reaction in detail, a host-guest interaction, *e.g.*, hydrogen bonding, may result in the geometrical fixation of troponoids in the asymmetric circumstance of the CDX molecules.[8] In this sense, it is interesting that the signs of the Cotton effect of **4** from **1** (proton-donor) and of **5** from **2** (proton-acceptor) are opposite. Furthermore, the opposite Cotton effects for **5** and **6** probably represents an inversion of asymmetric centers during the isomerization of **5** into **6**. This is in accord with the allowed 3*s*,3*s*-sigmatropy *via* the ketene intermediate (**B**), as has already been established.[9] The other path, the 1*s*,3*s*-process, retains the sign of the Cotton effect.

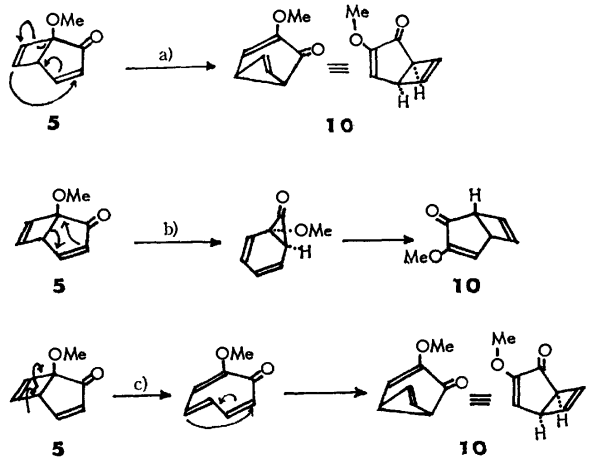

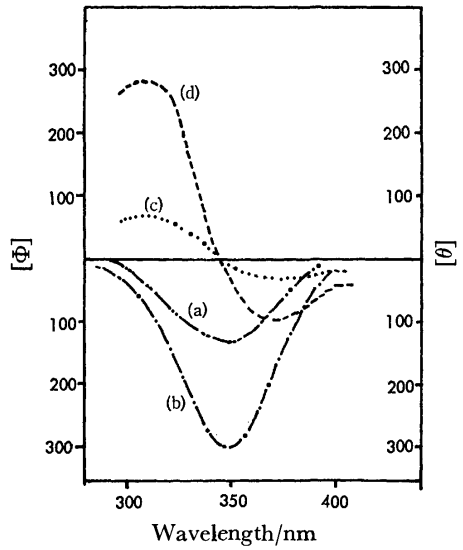

Fig. 2. The CD and ORD spectra of **4** obtained from [**1**: CDX]. (a) CD curve of **4** from [**1**: α-CDX] in water, (b) CD curve of **4** from [**1**: β-CDX] in water, (c) ORD curve of **4** from [**1**: α-CDX] in water, and ORD curve of **4** from [**1**: β-CDX] in water.

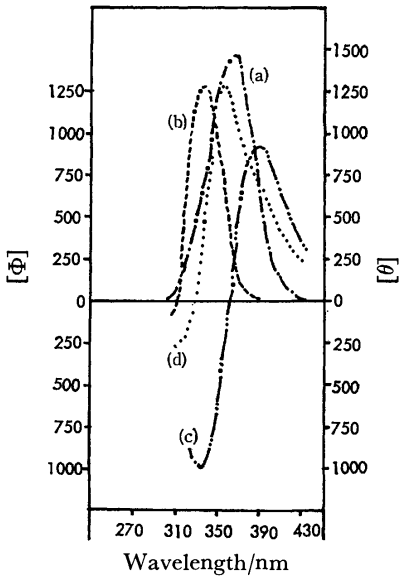

Fig. 3. The CD and ORD spectra of **5** and **10**. (a) CD curve of **5**, (b) CD curve of **10**, (c) ORD curve of **5**, and (d) ORD curve of **10**.

Table 2. The specific rotations of photoproducts

	$[\alpha]_D^{20}$(Concentration)	Irradiation conditions
4	−10.9°(*c*=1.15, MeOH)	(**1**: β-CDX) in H_2O
4	nil	(**1**: α-CDX) in H_2O
4	−9.8°(*c*=0.25, MeOH)	(**1**: α-CDX) in Hexane
5	+104°(*c*=0.24, MeOH)	(**2**: β-CDX) in H_2O
6	−22.7°(*c*=0.38, MeOH)	(**2**: α-CDX) in H_2O
6	−91.8°(*c*=0.24, MeOH)	(**2**: β-CDX) in H_2O

When a xylene solution of **4** was refluxed for 30 min, 3-hydroxybicyclo[3.2.0]hepta-3,6-dien-2-one (**9**) (25%) was obtained, together with **1** (25%). **9** has lost its optical activity. Even a brief heating at 110—115 °C for 5 min caused a complete racemization of the recovered **4** by means of a degenerated acyloin rearrangement.[10]

Then, an *o*-dichlorobenzene solution of **5** was refluxed for 3.5 h to give 3-methoxybicyclo[3.2.0]hepta-3,6-dien-2-one (**10**) (15%) as the sole isolable compound. **10** has retained its optical activity, with the same sign as the starting material, **5** (see Fig. 3).

This type of rearrangement, **5** to **10**, was originally found by Mukai *et al.*[11] during the pylolysis of the 6-isopropyl derivative of **5**; at the sametime, the arrangement of the carbon atoms in the products was proved by using deuterio derivatives. Since then, this has been referred to as a unique example of a 3*a*,3*a*-sigmatropy (Route a)) in the literature,[12-15] but the mechanism of the reaction is still a point in dispute. Routes b), a two-fold 1*s*,3*a*-sigmatropy,[16] and c), an intermediary formation of a *cis-trans-cis*-triene (a *trans*-tropone),[17] which then suffers a thermal conrotatory cyclization,[18] have been alternatively suggested as plausible mechanisms. The differentiation of a), a concerted process, and c), a step-by-step process, may come from the view of the intermediate *trans*-tropone, and the present results alone can not provide information on such a point. However, the retention of the sign of the optical rotation for **10**

TABLE 3. CHARACTERIZATIONS OF CDX-COMPLEXES OF TROPONOIDS

Complexes	Yields/%	Ratio of tropones/host by UV spectrometry
[**1**: α-CDX]	85	0.85
[**1**: β-CDX]	83	1.80
[**2**: α-CDX]	45	0.87
[**2**: β-CDX]	65	1.91
[**3**: α-CDX]	75	0.76
[**3**: β-CDX]	68	1.66

clearly rules out Route b), by which chiroptically inverted **10** should be produced, as is shown in Chart 2. At the same time, any route involving a radical process,[15,16] which has been discarded on kinetical grounds,[12] can be conclusively eliminated.

According to Day *et al.*,[6] the formation of **7** can be diminished also by irradiation in aprotic solvents; however, this does not mean an improvement of the yields. In fact, a satisfactory yield of **4** was obtained only by the reaction in a very diluted solution; otherwise, a tarry, intractible mass was formed.

Experimental

Preparation of Inclusion Complexes (General Method). To an aqueous solution of CDX, two molar equivalents (for β-CDX) or one molar equivalent (for α-CDX) of troponoids, **1**, **2**, and **3**, were added. The precipitates thus formed were collected by filtration. The subsequent evaporation of the filtrate and washings of the residue with hexane yielded an additional amount of complexes.

The UV Titrations of the Troponoids–CDX Complexes. A constant weight of the CDX complexes of troponoids was dissolved in water and then determined by UV spectrometry. The results are summarized in Table 3.

Titrations of [1: CDX]. Aqueous solutions of [**1**: CDX] were diluted with constant volumes of 0.01 M (1M=1 mol dm^{-3}) KOH solutions and titrated by 0.01 M HCl. The results showed **1**/α-CDX=0.97 and **1**/β-CDX=1.82.

Photochemical Reaction of 1 as the Inclusion Complex with CDX. a): (General Method). A powdered complex of **1**, [**1**: β or α-CDX], was dispersed in a solvent (water, ethanol, hexane, or acetone) and irradiated by means of a 400-W high-pressure mercury lamp for several hours. Water was then added to the mixture, and it was continuously extracted with diethyl ether. The extracts were purified by silica gel chromatography; fractions eluted with benzene: diethyl ether (10: 1) afforded **4**, while subsequent fractions eluted with benzene: diethyl ether (5: 1) afforded **7**.

b): [**1**: β-CDX] (820 mg) was spread over an aluminum foil and externally irradiated by means of a 100-W high-pressure mercury lamp for 5 h. Continuous liquid-liquid extraction (diethyl ether: water) and subsequent silica gel chromatography of the extracts afforded **4** (23 mg, 36%), **7** (10 mg, 16%), recovered **1** (45 mg, 42%), and an unidentified oil (3 mg).

Photochemical Reaction of 1 in Hexane (Without CDX). a): A hexane solution (45 cm^3) of **1** (20 mg) was externally irradiated by means of a 100-W high-pressure mercury lamp for 10 h. Subsequent silica gel column chromatography of the mixture afforded **4** (8.3 mg, 42%), **7** (3.9 mg, 17%), and an unidentified oil (3 mg).

b): A hexane solution (45 cm^3) of **1** (120 mg) was similarly irradiated. The separation of the mixture gave **4** (6.7 mg, 5.6%) and **7** (2.5 mg, 1.7%).

Photochemical Reaction of 2 as the Inclusion Complex with β-CDX. a): A water (45 cm^3) suspension of [**2**: β-CDX] (300 mg) was externally irradiated by means of a 100-W high-pressure mercury lamp for 72 h. The reaction mixture was then continuously extracted with diethyl ether and chromatographed on a silica-gel column; from benzene, **6**, 13 mg (45%), and **5**, 7 mg (24%), were obtained, while from benzene: diethyl ether (10: 1), **8**, 3 mg (9%), was obtained together with the recovered **2**, 5 mg.

b): [**2**: β-CDX] (480 mg) was dispersed in hexane (50 cm^3) and then irradiated by means of a high-pressure mercury lamp for 24 h. The subsequent separation of the reaction mixture yielded **5** (19 mg, 30%), **6** (20 mg, 32%), and **8** (9 mg, 13%), together with the unreacted **2** (12 mg).

Pyrolysis of 4. Optically active **4** (48 mg) was dissolved in dimethyl sulfoxide (0.5 cm^3) and heated at 130—135 °C for 2 h. The NMR spectrum of the mixture indicated the presence of **9** and **1** in a ratio of 3: 2, but every attempt to isolate **9** failed; only **1** (15 mg, 31%) was obtained by silica-gel chromatography. The $[\alpha]_D^{20}$ value of the pyrolysate mixture was determined to be $\pm 0°$.

A Brief Heating of 4. **4** (15 mg) was dissolved in dimethyl sulfoxide (0.5 cm^3) and heated at 110—115 °C for 5 min, after which, the mixture was fractionated to isolate the recovered **4** (8 mg, 53%). The $[\alpha]_D^{20}$ value of the recovered **4** was $\pm 0°$. The CD spectrum showed no Cotton effect.

Pyrolysis of 5. **5** (20 mg) was dissolved in *o*-dichlorobenzene (3 cm^3) and refluxed for 3.5 h. The mixture was heated *in vacuo* to remove the solvent; the residue was then chromatographed on a silica-gel column to give oily **10** (3 mg, 15%) as the sole product.

References

1) Part XII: H. Takeshita, T. Hatsui, R. Iwabuchi, and S. Itoh, *Bull. Chem. Soc. Jpn.*, **51**, 1257 (1978).
2) R. Breslow, *Chem. Soc. Rev.*, **1**, 553 (1972).
3) K. Yamada, *Kagaku To Kogyo*, **28**, 649 (1975).
4) K. Yamada, S. Kohmoto, and H. Iida, *Bull. Chem. Soc. Jpn.*, **49**, 1170 (1976).
5) W. G. Dauben, K. Koch, S. L. Smith, and O. L. Chapman, *J. Am. Chem. Soc.*, **85**, 2616 (1963).
6) A. C. Day and J. D. Ledlie, *J. Chem. Soc., Chem. Commun.*, **1970**, 1265.
7) The CD and ORD spectra were recorded on a Jasco (Nippon Bunko Co.) ORD UV 5 Model provided by the courtesy of the Pharmaceutical School, Kyushu University.
8) When 2-chlorotropone and 2,7-dichlorotropone complexes of β-CDX were exposed to the UV light, a diminishment in the tropone chromophore was observed by UV spectrometry, but no product could be liberated by extractions. Probably, a condensation of CDX with active species derived from the halotropones took place during the irradiations.
9) O. L. Chapman and J. D. Lassila, *J. Am. Chem. Soc.*, **90**, 2449 (1968).
10) A sort of thermal acyloin rearrangement of the 1-hydroxybicyclo[3.2.*n*]alkan-2-one system was encountered during the endo-exo isomerization of the Diels-Alder adducts of maleic anhydride and **1**. See S. Itô, H. Takeshita, Y. Shoji, Y. Toyooka, and T. Nozoe, *Tetrahedron Lett.*, **1968**, 3215.
11) T. Miyashi, M. Nitta, and T. Mukai, *Tetrahedron Lett.*, **1968**, 3433.
12) Although Mukai's original paper[11] contained an

illustration suggesting the Process a), more detailed discussions have been provided in later papers (a) T. Miyashi, M. Nitta, and T. Mukai, *J. Am. Chem. Soc.*, **93**, 3441 (1971); b) R. Miyamoto and T. Mukai, *Nippon Kagaku Kaishi*, **1974**, 1691, where they have expressed reluctance to accept the concerted mechanism.

13) H. J. Hansen and H. Schmid, *Chem. Brit.*, **1969**, 111.

14) R. B. Woodward and R. Hoffmann, "The Coservation of Orbital Symmetry," Verlag Chemie GmbH, Weinheim (1970), p. 126.

15) N.-T. Anh, "Les Regels des Woodward-Hoffmann," Ediscience S. A., Paries (1970), p. 72 (Japanese eddition, translated by T. Mita, Kagaku Dojin, Tokyo (1975), p. 88).

16) G. Frater, A. Habich, H.-J. Hansen, and H. Schmid, *Helv. Chim. Acta*, **52**, 335 (1969).

17) An occurrence of another *trans*-tropone (*trans-cis-cis*-tropone) was assumed in the photodimerization of **3**. See T. Tezuka, Y. Akasaki, and T. Mukai, *Tetrahedron Lett.*, **1967**, 5003.

18) J. H. Baldwin and M. S. Kaplan, *J. Chem. Soc., Chem. Commun.*, **1970**, 1560. Their main reason for proposing Process c) is based on the fact that the rearrangement requires a conjugated diene system in the molecules.

Cyclopentenone Synthesis from 1,1-Dichloroallyllithium–Ketone Adducts as Well as from Dichlorocarbene–Allyl Alcohol Adducts

Tamejiro HIYAMA,* Masaki SHINODA, Masao TSUKANAKA, and Hitosi NOZAKI
Department of Industrial Chemistry, Kyoto University, Yoshida, Kyoto 606
(Received July 3, 1979)

Treatment of (3,3-dialkyl-2,2-dichlorocyclopropyl)methanols with hydrobromic acid gives 2-cyclopentenones through postulated intermediates, 3-chlorocyclopentadienyl cations. Another method which should give the same cationic intermediates involves trifluoroacetic acid catalyzed reaction of 3,3-dichloro-1-alken-4-ols. This is found to be particularly useful for cyclopentenone annulation.

The construction of five-membered carbocyclic system is important in the synthesis of physiologically active natural products.[1] We wish to describe two new methods based on the thermal conrotatory ring-closure of 3-chloropentadienyl cation.[2]

During the course of the study of carbenoid chemistry,[3] it was found that dichlorocarbene generated by the phase-transfer technique[4] adds efficiently to allyl alcohols, in contrast to the previous observation by Seyferth and Mai.[5] For example, 4-methyl-3-penten-2-ol was converted into the dichlorocyclopropane **1** in 92% yield without appreciable deoxygenation[6] or chlorination.[7] When the adduct **1** was heated in 47% hydrobromic acid at 100 °C, 3,5-dimethyl-2-cyclopentenone (**2**)[8] was produced in 83% yield. Application of this procedure to various allyl alcohols **3** gave 2,3-disubstituted 2-cyclopentenones **5** (Table 1).

Table 1. Synthesis of 2-cyclopentenones from allyl alcohols

Allyl Alcohol	Dichlorocyclopropane[a] %yield	Cyclopentenone[b] % yield
3a	**4a**, 79	**5a**,[c] 44
3b	**4b**, 79	**5b**,[d] 56
3c	**4c**, 60	**5c**,[d] 59
3d	**4d**, 77[e]	**5d**,[f] 76

a) Dichlorocarbene was generated by the phase-transfer technique. b) The (dichlorocyclopropyl)methanol **4** was heated in hydrobromic acid at 100 °C for several hours unless otherwise specified. c) Ref. 28. d) Ref. 24. e) Alcohol was converted into α-ethoxyethyl ether before the dichlorocarbene addition and afterwards the protecting group was removed. f) Heating **4d** in trifluoroacetic acid under reflux for 90 h.

Although the dichlorocarbene addition generally proceeds well,[9] the yield of the particular adduct **4d** was very unsatisfactory, the overall yield of **5d** being only 37%.[2a] However, the yields were much improved by protecting the hydroxyl group with ethyl vinyl ether. Protection, dichlorocarbene addition and regeneration of the hydroxyl group[10] gave **4d** in 77% isolated yield. Subsequent acid treatment of **4d** was best performed with trifluoroacetic acid (TFA) which was found to be a less reactive reagent than hydrobromic acid but far more selective to give the desired enone **5d** in 76% yield.

The cyclopropylmethanol **7** obtained by selective $:CCl_2$ addition to the allyl alcohol **6**[4] was transformed into 2-methyl-3-(*trans*-1-propenyl)-2-cyclopentenone (**9**). Under these acidic conditions the anticipated cyclopentenone **8** isomerized to the conjugated dienone **9**.

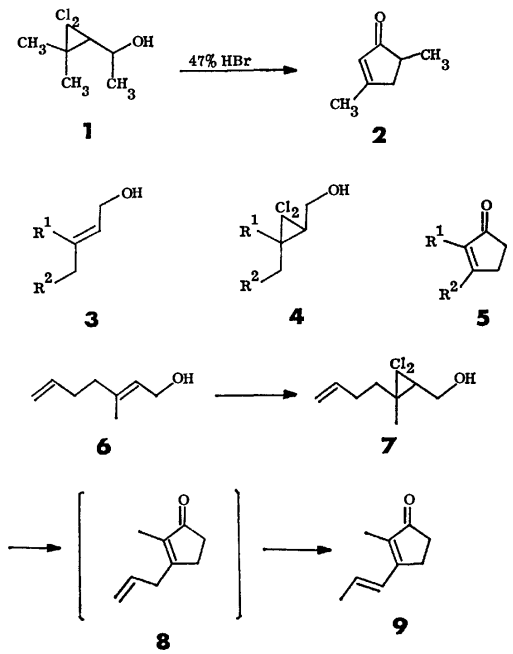

a, $R^1=CH_3$, $R^2=H$
b, $R^1=CH_3$, $R^2=n\text{-}C_4H_7$
c, $R^1=CH_3$, $R^2=n\text{-}C_5H_{11}$
d, R^1, $R^2=-(CH_2)_{10}-$

The mechanism of the cyclopentenone formation can be rationalized by Scheme 1. Conjugate dehydration of **4** gives a dichlorodiene **10**, which undergoes solvolysis to yield a chloropentadienyl cation **11**. Thermal conrotatory ring closure of **11** gives a chlorocyclopentenyl

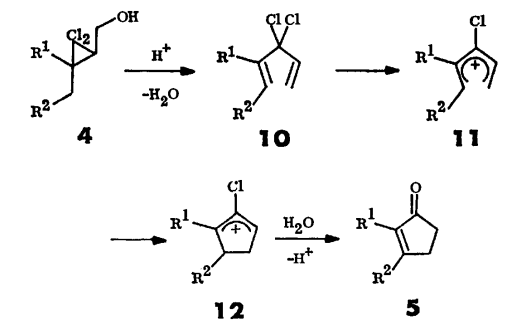

Scheme 1.

cation **12**, deprotonation followed by hydrolysis giving the cyclopentenone **5**. Noteworthy is the regiochemistry of the reaction. Heating **4b** in hydrobromic acid afforded 3-butyl-2-methyl-2-cyclopentenone (**5b**) exclusively, and none of the corresponding isomer, 2-pentyl-2-cyclopentenone was detected. It should be noted that the original methyl group is not incorporated into the five-membered ring and a long alkyl appendage resides at the C(3) position. The initial dehydration of **4** and the final deprotonation in **12** are controlled to give the more substituted olefins.[11]

In order to confirm the above mechanism we chose a dichlorohomoallyl alcohol (Scheme 2) as an alternative precursor of the intermediates **10**—**12**. The dichlorohomoallyl alcohol **14** was prepared according to the reported method.[12] Thus, 1,1-dichloroallyllithium was prepared *in situ* and directly allowed to react with ketone by adding lithium diisopropylamide to a mixture of a ketone and 3,3-dichloropropene. The adduct was successively subjected to acidic conditions. First we studied the conversion of **13d** into **5d** and found that various acids are effective. Acid, conditions, and % yield were: hydrobromic acid–acetic acid, reflux, 3 h, 55; titanium tetrachloride-dichloromethane, room temp, 3 h, 81; TFA, reflux, 1.5 h, 89; TFA, room temp, 1.5 h, 90. Thus, under the last condition **13c**—**g** were transformed into **5**. The results are summarized in Table 2.

Table 2. Cyclopentenone annulation

Ketone	Dichlorohomoallyl alcohol,[a] % yield	Cyclopentenone[b] % yield
13c	**14c**, 73	**5c**, 87
13d	**14d**, (66)[c]	**5d**,[d] 90
13e	**14e**, 68	**5e**,[d] 80
13f	**14f**, 63	**5f**,[e] 87
13g	**14g**,[f] 56	**5g**,[g] 71

a) The adducts were obtained by adding 1.5 equivalents of lithium diisopropyl amide to a mixture of **13** and 3,3-dichloropropene (1.5equiv) in tetrahydrofuran at −78°C. See Ref. 12a. b) Transformation of **14** to **5** was carried out in TFA at room temperature for a couple of hours. c) The yield was taken from Ref. 12a. d) Ref. 25. e) Ref. 26. f) This compound was synthesized by Seyferth *et al.* (Ref. 12b) using dichloroallyllithium generated by transmetallation. g) Ref. 27.

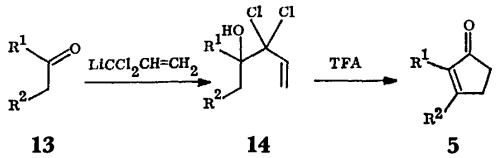

13 **14** **5**

c, $R^1=CH_3$, $R^2=n\text{-}C_5H_{11}$
d, R^1, $R^2=-(CH_2)_{10}-$
e, R^1, $R^2=-(CH_2)_6-$
f, R^1, $R^2=-(CH_2)_5-$
g, R^1, $R^2=-(CH_2)_4-$

Scheme 2.

Apparently the two step procedure is applicable to both cyclic and acyclic ketones and particularly efficient for cyclopentenone annulation. Although cationic intermediates are involved in the reaction sequence, transannular by-path[13] is negligible in the cyclization of the medium-ring compound **14e** which gives cyclopentenone **5e** in 54% overall yield. The two step process makes 5-substituted tetrahydroindanone derivatives more readily accessible as illustrated for the synthesis of **15** (55% overall yield) from 4-*t*-butylcyclohexanone.

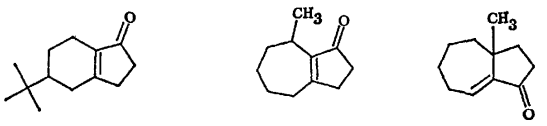

15 **16** **17**

Regioselectivity of the cyclopentenone formation depends on the structure of the substrate. 2-Octanone was converted into 2-methyl-3-pentyl-2-cyclopentenone (**5c**) exclusively. The selectivity may be explained in terms of the favored formation of the more substituted olefin at the dehydration step. On the other hand, when 2-methylcycloheptanone–dichloroallyllithium adduct was subjected to the annulation reaction, only **16** was produced with no trace of its isomer **17**.[14-16]

The key of the cyclopentenone annulation is the addition of 1,1-dichloroallyllithium at C(1) carbon. Although Seyferth *et al.*[12b] suggested that the regioselectivity of the addition of the lithium reagent to ketones or aldehydes is controlled by electronic rather than steric factor, 2-methylcyclohexanone gave only the adduct **18** in contrast to cyclohexanone or 2-methylcycloheptanone. Thus, steric hindrance as well as ring size[17] appear to determine the regiochemistry of the addition. TFA catalyzed reaction of **18** gave cyclopentenone **19**[18] in 47% yield.

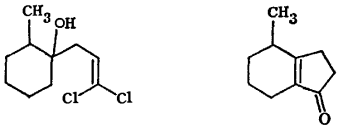

18 **19**

The two cyclopentenone forming reactions are summarized in Scheme 3. Both **3** and **14** give a common intermediate **11** and finally cyclopentenone **5** upon acid treatment. The carbonyl carbon of **5** originates from *gem*-dichloro carbon of **3** and **14**, which plays the role of a protected carbonyl. Particular attention should be paid to **14** whose dichloro carbon is introduced as a

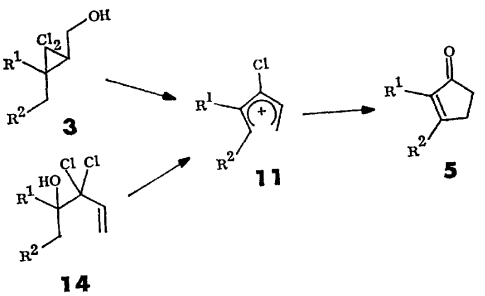

3 **11** **5** **14**

Scheme 3.

TABLE 3. PHYSICAL PROPERTIES OF (DICHLOROCYCLOPROPYL)METHANOLS AND CYCLOPENTENONES

Compound	Bp (°C/Torr)[a]	IR(cm^{-1})[b]	PMR(δ)[c]
4a[d]	110—120/35	3400, 1145, 1084, 1030, 850, 820, 805	1.20(s, 3H), 1.3—1.6 (t+s(δ 1.35), 4H), 3.05 (s, 1H), 3.55 (dd, J=7.5, 3 Hz, 2H)
4b[e]	90—100/2	3375, 1030, 830	0.5—2.5 (m+s (δ 1.17), 15H), 3.0 (br s, 1H), 3.56 (dd, J=7, 3 Hz, 2H)
4c[f]	120—125/5	3350, 1030, 850, 830	0.5—2.5 (m+s(δ 1.22), 17H), 2.8(br s, 1H), 3.60 (dd, J=7, 3 Hz, 2H)
4d[g]	140—150/0.08	3370, 1035, 855, 820	0.7—1.9 (m, 24H), 3.70 (dd, J=8, 1.5 Hz, 2H)
7[h]	140—150/7	3350, 3100, 1640, 1030, 998, 915, 854, 830, 807	1.0—2.4(m+s(δ 1.20), 8H), 2.6—3.2(br s, 1H), 3.70(d, 2H), 4.7—6.1 (m, 3H)
2[i]	120—140/140	1705, 1625, 1174	1.06 (d, J=6 Hz, 3H), 1.6—2.6 (m+s (δ 2.10), 6H), 5.80 (br s, 1H)
5b[j]	100—105/2	1702, 1649, 1345, 1300, 1073	0.7—2.0 (m+s (δ 1.63), 10H), 2.1—2.8 (m, 6H)
5c[j]	130—135/3	1698, 1650, 1384, 1340, 1302, 1072	0.6—1.9 (m+s (1.65), 12H) 2.0—2.7 (m, 6H)
9[k]	140—150/25[l]	3040, 1691, 1639, 1602, 1077, 962	1.73 (s, 3H), 1.95 (d, J=5.5 Hz, 3H), 2.1—2.9 (m, 8H), 6.3—6.9 (m, 2H)

a) Bath temperature. b) Neat liquid film. c) Measured in carbon tetrachloride solution. d) Found: C, 42.80; H, 6.13%. Calcd for $C_6H_{10}Cl_2O$: C, 42.63; H, 5.96%. e) Found: C, 53.24; H, 8.30%. Calcd for $C_{10}H_{18}Cl_2O$: C, 53.34; H, 8.06%. f) Found: C, 55.27; H, 8.69%. Calcd for $C_{11}H_{20}Cl_2O$: C, 55.24; H, 8.43%. g) Found:C, 61.43; H, 8.94%. Calcd for $C_{15}H_{26}Cl_2O$: C, 61.41; H, 8.92%. h) Found: C, 51.61; H, 6.93%. Calcd for $C_9H_{14}Cl_2O$: C, 51.69; H, 6.75%. i) Ref. 8. j) Ref. 24. k) MS *m/e*: 136 (M^+). Elemental analyses gave variable results due to the instability of this material. l) Distillation of the purified sample of **9** invariably gave resinous residue.

TABLE 4. PHYSICAL PROPERTIES OF DICHLOROHOMOALLYL ALCOHOLS

Compound	Bp (°C/Torr)[a]	IR(cm^{-1})[b]	PMR (δ)[c]
14c[d]	110—117/0.05	3450, 981, 936, 795	0.8—2.5 (m+s (δ 1.35), 17H), 5.34 (dd, J=10, 2 Hz, 1H), 5.70 (dd, J=16.5, 2 Hz, 1H), 6.38 (dd, J=16.5, 10 Hz, 1H)
14e[e]	99—106/0.05	3555, 3460, 1630, 984, 932, 790	1.1—2.2 (m, 15H), 5.24 (dd, J=10, 1 Hz, 1H), 5.65 (dd, J=16, 1 Hz, 1H), 6.25 (dd, J=16, 10 Hz, 1H)
14f[f]	110—115/0.09	3564, 3514, 1648, 980, 930	1.2—2.2 (m, 13H), 5.23 (dd, J=10, 1 Hz, 1H), 5.58 (dd, J=16, 1 Hz, 1H), 6.28 (dd, J=16, 10 Hz, 1H)

a) Bath temperature. b) Neat liquid film. c) Carbon tetrachloride solution. d) MS *m/e* (rel intensity): 155 (13), 153 (18), 129 ($M^+-Cl_2CH=CH_2$, 47), 69 (59), 43 (100). Found: C, 55.48; H, 8.52%. Calcd for $C_{11}H_{20}Cl_2O$: C, 55.24; H,8.43%. e) MS *m/e* (rel intensity): 201 (M^+-Cl, 2), 165 (11), 151 (15), 127 ($M^+-Cl_2CCH=CH_2$, 87), 109 (60), 81 (55), 67 (99), 55(100). Found: C,55.70; H, 7.54%. Calcd for $C_{11}H_{18}Cl_2O$: C, 55.71; H, 7.65%. f) MS *m/e*(rel intensity): 187 (M^+-Cl, 6), 113($M^+-Cl_2CCH=CH_2$, 100), 95 (93). Found: C, 53.75; H, 7.47%. Calcd for $C_{10}H_{16}Cl_2O$:C, 53.83; H, 7.22%.

nucleophile with Umpolung[19] of the carbonyl function. The latter methodology is highly effective for cyclopentenone annulation,[14,20] which involves addition of a three carbon chain followed by electrocyclic ring closure.[21-23]

Experimental

Distillation was carried out by use of Kugel-rohr (Buchi) and boiling points were determined by measuring the bath temperature. All the temperatures are uncorrected. PMR spectra (tetramethylsilane as an internal standard) were taken on a JEOL C-60H, Varian EM 360, or EM 390 spectrometer, chemical shifts being recorded in ppm unit. IR spectra were obtained on a Shimadzu IR-27G spectrometer in neat liquid film unless otherwise stated, MS on a Hitachi RMU-6L spectrometer, exact mass on a JEOL-JMS-D300 spectrometer. Tetrahydrofuran (THF) was freshly distilled before use over benzophenone ketyl. Commercially available hydrobromic acid (47%), chloroform, hexadecyltrimethylammonium bromide and butyllithium were used. Preparative TLC was prepared by use of Merck Kiesel-gel PF_{254}. Column chromatography was carried out with Wakogel C-100 (Wako Pure Chemical Co.).

Dichlorocarbene Addition to Allyl Alcohol. A Typical Procedure for ***1***. A mixture of 4-methyl-3-penten-2-ol (1.00 g, 10.0 mmol), chloroform (5.0 ml, 62 mmol) and hexadecyltrimethylammonium bromide (100 mg, 0.27 mmol) was heated at 50—55 °C, aqueous sodium hydroxide (0.60 g, 15 mmol, in 0.6 ml of water) being added drop by drop under vigorous stirring over a period of *ca.* 1 h. After addition was completed, the reaction mixture was maintained at the same temperature for 3 h and then cooled, neutralized with dil hydrochloric acid and extracted three times with dichloromethane. The organic phase was dried (Na_2SO_4), concentrated *in vacuo* and the residue distilled at 100 °C (bath temp)/45 Torr. The distillate (1.68 g, 92% yield) solidified and was recrystallized from hexane to give colorless needles (1.58 g) of **1**, mp 72—73 °C (Found: C, 45.76; H, 6.53%). Spectral data are in line with those recorded.[5] The characteristics of other adducts **4** are summarized in Table 3.

*Synthesis of 2-Methyl-3-pentyl-2-cyclopentenone (***5c***)*

Aqueous sodium hydroxide (1.5 g, in 1.5 ml of water) was added dropwise over a period of 15 min to a solution of 3-methyl-2-nonen-1-ol (**3c**) (880 mg, 5.64 mmol) and hexadecyltrimethylammonium bromide (50 mg) in chloroform (1 ml) under a nitrogen atmosphere at 55 °C. After being stirred for 3 h the mixture was neutralized with dilute hydrochloric acid and then worked up. Distillation at 120—125°C/5 Torr gave the adduct **4c** (806 mg, 60% yield). Spectral characteristics of **4c** are given in Table 3. The alcohol **4c** (476 mg, 2 mmol) was mixed with 47% hydrobromic acid (3 ml) and heated at 100 °C for 9 h. The reaction mixture was diluted with water and extracted with ether. The ethereal extract was washed with brine, aq sodium hydrogencarbonate solution, and finally with brine, dried (Na_2SO_4) and concentrated *in vacuo*. TLC purification of the crude product (silica gel, ether–hexane 3: 1, R_f 0.7) gave **5c** (196 mg, 59% yield, see Table 3).

*Synthesis of 2,3-Decamethylene-2-cyclopentenone (**5d**).* 2-(Cyclododecylidene)ethanol (342 mg, 1.62 mmol) was mixed with ethyl vinyl ether (1 ml) and dichloromethane (2 ml) containing pyridinium tosylate[10] (50 mg) and the mixture was stirred for 1 h. The usual work-up gave an oil which was dissolved in chloroform (2 ml) containing hexadecyltrimethylammonium bromide (30 mg). To the resulting mixture was added sodium hydroxide (0.6 g in 0.6 ml of water) over a period of 15 min with vigorous stirring at 50 °C under an argon atmosphere. Stirring was continued for 4h, and the reaction mixture was diluted with water, neutralized with 5% hydrochloric acid and extracted with dichloromethane. The organic phase was dried (Na_2SO_4) and concentrated. The crude product was dissolved in ethanol (5 ml) in the presence of pyridinium tosylate (50 mg) at room temperature for 1 h. The work-up followed by short column chromatography (silica gel, dichloromethane elution) gave the desired adduct **4d** (366 mg, 77% yield).

The adduct **4d** (170 mg, 0.58 mmol) dissolved in TFA (5 ml) was heated to reflux for 90 h under an argon atmosphere. Concentration and preparative TLC of the residue (silica gel, dichloromethane) gave **5d** (R_f 0.3—0.45) (88 mg, 76%) along with an oil tentatively assigned as a trifluoroacetate of **4d** (R_f 0.95—0.98) (*ca.* 35 mg); IR (neat): 1794, 1225, 1160 cm^{-1}.

*Synthesis of [3-(3-Butenyl)-3-methyl-2,2-dichlorocyclopropyl]-methanol (**7**).* Sodium hydroxide (1.0 g) dissolved in water (1 ml) was added dropwise over 15 min at 40—50 °C to a mixture of the (*E*)-3-methyl-2,6-heptadien-1-ol (**6**) (504 mg, 4.0 mmol), chloroform (2.8 ml, 34 mmol) and benzyl-(2-hydroxyethyl)dimethylammonium hydroxide (20 mg). After being stirred for 3 h at 50 °C, the reaction mixture was diluted with water (20 ml) and dichloromethane (20 ml). The aqueous phase was neutralized with dil hydrochloric acid and the organic phase was separated. The aqueous phase was extracted with dichloromethane (2×10 ml), organic phase being combined, washed with brine and concentrated *in vacuo*. Column chromatography on silica gel (benzene–ether 2: 1) gave the adduct **7** (450 mg, 57% yield, see Table 3).

Addition of 1,1-Dichloroallyllithium to Ketones. This reaction was carried out according to the reported conditions.[12a] Physical properties of simple ketone adducts are given in Table 4.

*Synthesis of Bicyclo[10.3.0]pentadec-1(12)-en-13-one (**5d**).* The dichlorohomoallyl alcohol **14d** (105 mg, 0.36 mmol) was dissolved in TFA (1.3 ml) at room temperature and the solution was vigorously stirred for 1.5 h, the color tunring from light red to dark red. The work-up was effected by adding ether (10 ml), neutralizing with aq sodium hydrogencarbonate solution and by extracting with ether (4×20 ml). The ethereal solution was dried (Na_2SO_4), and concentrated *in vacuo* to give an oil which was purified by preparative TLC (silica gel, dichloromethane–ether 10: 1, R_f 0.3—0.5), affording **5d** (71 mg, 90% yield). PMR: δ 0.9—1.9 (m, 16H), 1.9—2.6 (m, 8H); IR: 1690, 1634 cm^{-1}; MS *m/e* (rel intensity): 220 (M^+, 65), 177 (93), 163 (98), 149 (100), 110 (65).

*Synthesis of 3-t-Butylbicyclo[4.3.0]non-1(6)-en-7-one (**15**).* At −78 °C lithium diisopropylamide (15 mmol) in THF (10 ml) was added drop by drop over a period of 2 h to a THF (20 ml) solution of 4-*t*-butylcyclohexanone (1.54 g, 10.0 mmol) and 3,3-dichloropropene (1.33 g, 12.0 mmol) under an argon atmosphere. After the addition was completed the resulting dark purple solution was stirred for 80 min at −78 °C and then treated with methanol (2 ml) at −78 °C. The mixture was warmed to room temperature, treated with water (*ca.* 50 ml) and extracted with ether (4×20 ml). The organic phase was dried (Na_2SO_4) and concentrated under reduced pressure. The crude product was purified by column chromatography (silica gel, hexane–ether 50: 3) to give the desired adduct (1.42 g, mp 100.8—101.1 °C (hexane), 54% yield, 76% yield based on the consumed ketone) and the starting material (0.45 g). The adduct showed the following spectra. PMR: δ 0.83 (s, 9H, *t*-Bu), 1.0—2.1 (m, 10H), 5.32 (dd, J= 10, 1 Hz, 1H), 5.68 (dd, J=16, 1 Hz, 1H), 6.31 (dd, J=16, 10 Hz, 1H). IR: 3480, 981, 964, 933 cm^{-1}. Found: C, 59.02; H, 8.35%. Calcd for $C_{13}H_{22}Cl_2O$: C, 58.87; H, 8.36%.

The adduct (537 mg, 2.0 mmol) was mixed with THF (3 ml) at room temperature and the solution was stirred for 2.5 h. The work-up followed by preparative TLC (silica gel, hexane–ether 1: 1) gave the desired **15** (279 mg, 72% yield). Bp 102—110 °C (bath temp)/0.05 Torr. PMR: δ 0.93 (s, 9H, *t*-Bu), 1.1—2.6 (m, 11H); IR: 1692, 1658 cm^{-1}; MS *m/e* (rel intensity): 192 (M^+, 27), 164 (8), 136(74), 57 (100). Found: C, 80.91; H, 10.65%. Calcd for $C_{13}H_{20}O$: C, 81.20; H, 10.48%.

*Synthesis of 6-Methylbicyclo[5.3.0]dec-1(7)-en-8-one (**16**).* Under a nitrogen atmosphere at −78 °C, lithium diisopropylamide (15 mmol in THF 10 ml) was added drop by drop over 1.75 h to a THF (15 ml) solution of 2-methylcycloheptanone (1.26 g, 10.0 mmol) and 3,3-dichloropropene (1.33 g, 12.0 mmol), and the reaction mixture was stirred for 1.5 h at −78 °C and worked up. Column chromatography (silica gel, hexane–ether 20: 1) of the crude product gave the desired adduct (1.19 g, 50% yield). The adduct was apparently homogeneous as evidenced by PMR spectrum and TLC assay (silica gel, hexane–ether, 1: 1, R_f 0.63). Bp 118—124 °C (bath temp, partial decomposition)/0.05 Torr. PMR: δ 1.0—2.9 (m+d (δ 1.05, J=6.0 Hz), 15H), 5.25 (dd, J=10, 1 Hz, 1H), 5.68 (dd, J=16, 1Hz, 1H), 6.29 (dd, J=16, 10 Hz, 1H); IR: 3550, 3475, 982, 930 cm^{-1}; MS *m/e* (rel intensity): 236 (M^+, 1), 201 (11), 187 (29), 165 (28), 152 (28), 127 (47), 109 (74), 67 (89), 55 (100). Correct elemental analysis was not achieved due to partial decomposition on distillation.

The adduct (341 mg, 1.4 mmol) was dissolved in TFA (4 ml) at room temperature and the resulting solution was kept at room temperature for 6 h and at reflux temperature for 18 h. The work-up followed by preparative TLC (silica gel, hexane–ether, 2: 1, R_f 0.2—0.3) gave the desired product **16** (138 mg, 58% yield). Bp 122—128 °C (bath temp)/3 Torr. PMR: δ 0.96 (d, J=7.0 Hz, 3H), 1.1—2.1 (m, 6H), 2.1—3.2 (m, 7H); IR: 1689, 1638 cm^{-1}; MS *m/e* (rel intensity): 164 (M^+, 100), 149 (88), 136 (64), 122 (58), 107 (70), 93 (80). Found: C, 80.40; H, 10.08%. Calcd for $C_{11}H_{16}O$: C, 80.44; H, 9.82%.

Addition of 1,1-Dichloroallyllithium to 2-Methylcyclohexanone. Lithium diisopropylamide (23.0 mmol prepared from diisopropylamine (3.2 ml) and butyllithium (1.81 M hexane solution, 13.3 ml) in THF (15 ml) at 0 °C) was added drop

by drop at −78 °C under a nitrogen atmosphere to a THF (20 ml) solution of 2-methylcyclohexanone (1.67 g, 14.9 mmol) and 3,3-dichloropropene (2.00 g, 18.0 mmol) over a period of 2 h, and the resulting solution was stirred for another hour at −78 °C until quenching with methanol (1 ml) at −78 °C. The work-up followed by column chromatography (silica gel, hexane–ether 20: 1) gave the adduct **18** (0.94 g, 28% yield). Bp 126—131 °C (bath temp)/4 Torr. PMR: δ 0.75 (d, J=7.0 Hz, 3H), 0.9—2.7 (m, 10H), 4.12 (d, J=7.0 Hz, 2H), 6.15 (t, J=7.0 Hz, 1H); IR: 3480, 1642, 988, 850, 785 cm^{-1}; MS *m/e* (rel intensity): 226 (M^+ +4, 3), 224 (M^+ +2, 5), 222 (M^+, 19), 187 (54), 173 (86), 152 (75), 117 (69), 95 (72), 68 (100); Exact mass; 222.0561, 224.0533, 226.0514. Calcd for $C_{10}H_{16}Cl_2O$: 222.0577 (M^+), 224.0548 (M^+ +2), 226.0519 (M^+ +4). Elemental analysis gave an error of 0.46% for C probably due to partial decomposition on distillation.

The alcohol **18** (192 mg, 0.86 mmol) was dissolved in TFA (1.5 ml) and the solution was stirred at room temperature for 2.5 h. The work-up gave the hydroindanone **19**[18] (61 mg, 47%). PMR: δ 1.06 (d, J=6.0 Hz, 3H), 1.2—2.0 (m, 4H), 2.0—2.8 (m, 7H); IR: 1690, 1639 cm^{-1}; MS *m/e* (rel intensity): 150 (M^+, 83), 135 (39), 122 (48), 108 (96), 93 (100), 79 (65).

The work was carried out with Grant-in-aid for Scientific Research Nos 185188, 203014, 375462 from the Ministry of Education.

References

1) R. A. Ellison, *Synthesis*, **1973**, 397: T. L. Ho, *Synth. Commun.*, **4**, 465 (1974).

2) Preliminary reports: (a) T. Hiyama, M. Tsukanaka, and H. Nozaki, *J. Am. Chem. Soc.*, **96**, 3713 (1974); (b) T. Hiyama, M. Shinoda, and H. Nozaki, *Tetrahedron Lett.*, **1978**, 771.

3) (a) K. Kitatani, T. Hiyama, and H. Nozaki, *Bull. Chem. Soc. Jpn.*, **50**, 1600, 3288 (1977); (b) T. Hiyama, S. Takehara, K. Kitatani, and H. Nozaki, *Tetrahedron Lett.*, **1974**, 3295.

4) T. Hiyama, H. Sawada, M. Tsukanaka, and H. Nozaki, *Tetrahedron Lett.*, **1975**, 3013.

5) D. Seyferth and V. A. Mai, *J. Am. Chem. Soc.*, **92**, 7421 (1970).

6) W. Kirmse, "Carbene Chemistry," 2nd ed, Academic Press, New York, N.Y. (1971), p. 429.

7) I. Tabushi, Z. Yoshida, and N. Takahashi, *J. Am. Chem. Soc.*, **93**, 1820 (1971).

8) I. N. Nazarov and A. N. Elizarova, *Otd. Khim. Nauk*, **1951**, 295; *Chem. Abstr.*, **46**, 914h (1952).

9) K. Kleveland, L. Skattebøl, and L. K. Sydnes, *Acta Chem. Scand.*, **B 31**, 463 (1977).

10) M. Miyashita, A. Yoshikoshi, and P. A. Grieco, *J. Org. Chem.*, **42**, 3772 (1977).

11) One of the referees suggested the possibility of the stereoelectronic effect on the regioselectivity. However, starting with **3b** of various *E*/*Z* ratio, we always obtained **5b** only.

12) (a) H. Taguchi, H. Yamamoto, and H. Nozaki, *Bull. Chem. Soc. Jpn.*, **50**, 1588 (1977). (b) D. Seyferth, G. J. Murphy, and B. Mauzé, *J. Am. Chem. Soc.*, **99**, 5317 (1977).

13) A. C. Cope, M. M. Martin, and M. A. McKervey, *Quart. Rev. (London)*, **20**, 11 (1966).

14) T. Hiyama, M. Shinoda, and H. Nozaki, *J. Am. Chem. Soc.*, **101**, 1599 (1979).

15) A possible explanation of this selectivity is as follows. In the reaction of seven-membered ring compound the dehydration would be the rate-determining step, elimination of water to give dichloro diene **10** being kinetically controlled.

16) The adduct of dichloroallyllithium to 2-methylcycloheptanone was found to be stereochemically uniform, the methyl-dichloroallyl trans isomer probably being produced exclusively. The stereoelectronic effect suggested by a referee may be operative in the annulation, but we could not confirm it.

17) The reactivity of cyclic compounds often depends on the ring size and explained in terms of I-strain, See E. L. Eliel, "Stereochemistry of Carbon Compounds," Chap. 9, McGraw-Hill, New York, (1962).

18) J. W. Cook and R. Philip, *J. Chem. Soc.*, **1948**, 162.

19) B.-T. Gröbel and D. Seebach, *Synthesis*, **1977**, 357; D. Seebach, *Angew. Chem. Int. Ed. Engl.*, **18**, 239 (1979).

20) R. M. Jacobson and G. P. Lahm, *J. Org. Chem.*, **44**, 462 (1979).

21) P. Magnus, *Neuv. J. Chim.*, **2**, 555 (1978).

22) (a) F. Cooke, J. Schwindeman, and P. Magnus, *Tetrahedron Lett.*, **1979**, 1995; (b) W. E. Fristad, D. S. Dime, T. R. Bailey, and L. A. Paquette, *ibid.*, **1979**, 1999.

23) Y. Ganoni, *Tetrahedron Lett.*, **1976**, 2167, **1977**, 371, **1978**, 3277.

24) A. L. Voitsekhovskaya, N. A. Kosul'nikova, T. A. Rudol'fi, V. M. Dashunin, V. N. Belov, *Zh. Vses. Khim. O-va.*, **10**, 702 (1965); *Chem. Abstr.*, **64**, 9588a (1966); A. L. Voitsekhovskaya, N. A. Kosul'nikova, T. A. Rudol'fi, R. I. Sharapova, V. M. Dashunin, and V. N. Belov, *Zh. Org. Khim.*, **3**, 18 (1967); *Chem. Abstr.*, **66**, 94712w (1967).

25) S. Hirano, H. Hara, T. Hiyama, S. Fujita, and H. Nozaki, *Tetrahedron*, **31**, 2219 (1975).

26) Pl. A. Plattner and G. Büchi, *Helv. Chim. Acta*, **29**, 1608 (1946); C. D. Gutsche, I. Y. C. Tao, and J. Kozma, *J. Org. Chem.*, **32**, 1782 (1967).

27) W. S. Johnson, C. E. Davis, R. H. Hunt, and G. Stork, *J. Am. Chem. Soc.*, **70**, 3021 (1948).

28) H. N. Al-Jallo and E. S. Waight, *J. Chem. Soc., B*, **1966**, 73.

Layered Compounds. LXI.[1] Carbon-13 NMR Study of [*n*]-, [*n.n*]-, and Multilayered [2.2]Paracyclophanes

Takahiro KANEDA, Tetsuo OTSUBO,† Hisanori HORITA, and Soichi MISUMI*
The Institute of Scientific and Industrial Research, Osaka University, Suita, Osaka 565
(Received August 9, 1979)

The carbon resonances of several [*n*]paracyclophanes (*n*=8—12) were assigned with the aid of partially deuterated derivatives. The ^{13}C NMR spectra of the title paracyclophanes were examined from viewpoints of the steric compression effect and the ring-current effect. Although the compression effect is a dominant factor for carbon resonances of closely stacked paracyclophanes, the ring-current effect was evidently observed in the spectra of [10]paracyclophane–[10](9,10)anthracenophane pair, [3.3]paracyclophane, and multilayered [2.2]paracyclophanes.

It is well known that ^1H NMR spectra of a variety of cyclophanes are characterized by extraordinary upfield shifts due mainly to the ring-current effect of the benzenoid rings. Multilayered paracyclophanes composed of closely stacked benzenes were reported as suitable models for evaluating systematically such an effect.[2] On the other hand, it is difficult to evaluate the ring-current effect on ^{13}C NMR spectra because the range of carbon chemical shifts is much greater than that of proton chemical shifts and thereby carbon shieldings are often sensitive to other effects.[3] Especially in rigid or crowded systems there was observed the steric compression as a dominant effect which often obscured the ring-current effect. Recently, a small extent of the ring-current effect was reported on the resonances of the middle methylene carbons of [12]paracyclophane **5**.[4] The conclusion is, however, somewhat questionable because their assignment of methylene carbons remained equivocal. In order to investigate the anisotropic effect of a benzene ring on ^{13}C NMR in detail, we measured ^{13}C NMR spectra of [*n*]paracyclophanes **1**—**6**[5] and a dibenzo derivative, *viz.*, [10](9,10)anthracenophane **7**[6] as well as [*n.n*]-paracyclophanes **8**—**16**[7,8] and multilayered [2.2]-paracyclophanes **17**—**20**,[8] some of whose geometries are well confirmed by X-ray crystallography.

Experimental

All the samples were prepared as described in the previous papers.[5-8] The ^{13}C NMR measurements were made on deuteriochloroform solutions (concentration 0.2—0.5 M) using TMS as an internal standard. The spectra of most of the cyclophanes were recorded at 25.05 MHz on a JEOL FX-100 spectrometer equipped with a Fourier transform system, JEC-980B computer, ^2H field frequency lock, and noise-modulated proton-decoupling system. The observed free-induction decay after a 45° pulse width of 6 μs was sampled in 8192 data points with a spectrum width of 5000 Hz and a repetition time of 3 s (digital resolution 1.25 Hz). The spectra of [10](9,10)anthracenophane **7** and alkylbenzenes, **21** and **22**, were run on a Varian XL-100-15FT spectrometer (25.2 MHz), ^1H noise decoupling, 0.2 M $CDCl_3$, TMS as an internal standard, $\delta \pm 0.1$ ppm.

[11]Paracyclophane **4**. Catalytic hydrogenation of [11]-paracyclopha-3,5-diyne[19] (500 mg) by the usual method (5% Pd–C in MeOH) gave [11]paracyclophane **4** as a colorless liquid (427 mg, 82.4%), bp 168—178 °C (bath)/9 mmHg 1 mmHg=133.322Pa. Found: C, 88.40; H, 11.54%; M^+, 230. Calcd for $C_{17}H_{26}$: C, 88.62; H, 11.38%; MW 230.

Deuteration of [n]*Paracyclophadiynes*. Catalytic deuteration of [*n*]paracyclophadiynes[9] was performed by treatment of the substrate with 5% Pd–C and MeOD (Merck D-content >99%) at 40—60 °C for 1.5 h in an atmosphere of deuterium, which was evolved by addition of aluminium to *ca.* 2M D_2SO_4 prepared from concd D_2SO_4 (96—98%, Merck, D-content >99%) and D_2O (Merck, D-content>99.75%). Distillation of the crude product gave deuterated [*n*]paracyclophanes (*n*=10—12), **23**—**26**, in 84—93 wt% yield, bp 135—180 °C (bath)/4—5 mmHg. Deuterium-content and -distribution in these products were determined by mass spectrometry. Relative intensity ratios of the parent peaks due to isotopic species and of the base peaks due to *p*-xylene fragment showed that 79—85% of the products consisted of [*n*]paracyclophane-d_7—d_{11}, and isotopic species substituted by more than two deuterium atoms at the two benzyl methylenes were contained by 4—9% in the products.

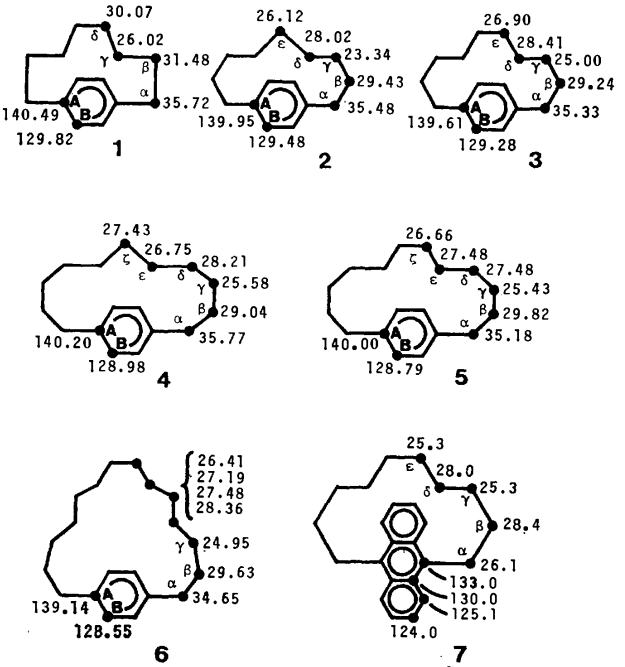

Fig. 1. ^{13}C NMR data of [*n*]paracyclophanes and [10]-(9,10)anthracenophane (δ value).

† Present address: Department of Applied Chemistry, Faculty of Engineering, Hiroshima University, Sendamachi, Hiroshima 730.

Results

All the ^{13}C NMR data are summarized in Figs. 1, 2, and 3. The ^{13}C signals were assigned by means of ^{1}H off-resonance and selective decoupling techniques. Comparisons of signal intensities and chemical shifts were also helpful to assign a group of similarly constructed compounds. The resonances of alkyl derivatives of the cyclophanes were assigned by considering the substituent effect on the data observed for non-substituted, parent cyclophanes. Additional shift parameters for dimethyl substitution can be evaluated by comparing the carbon resonances of **21** and **22** (Fig. 3).

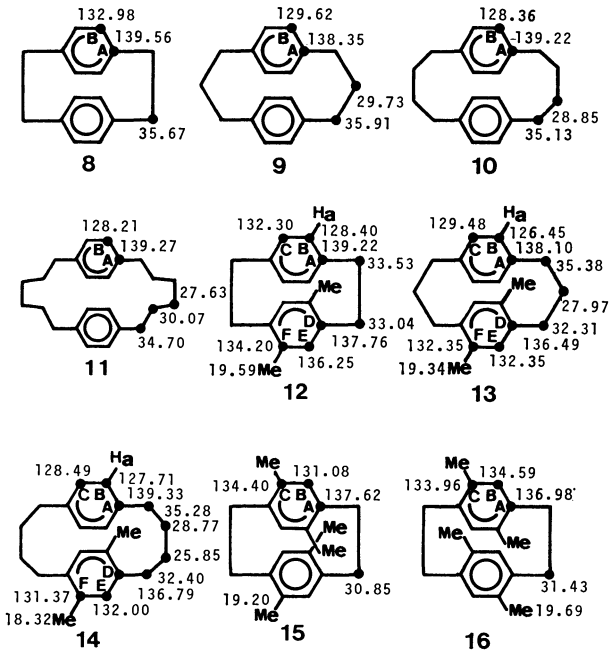

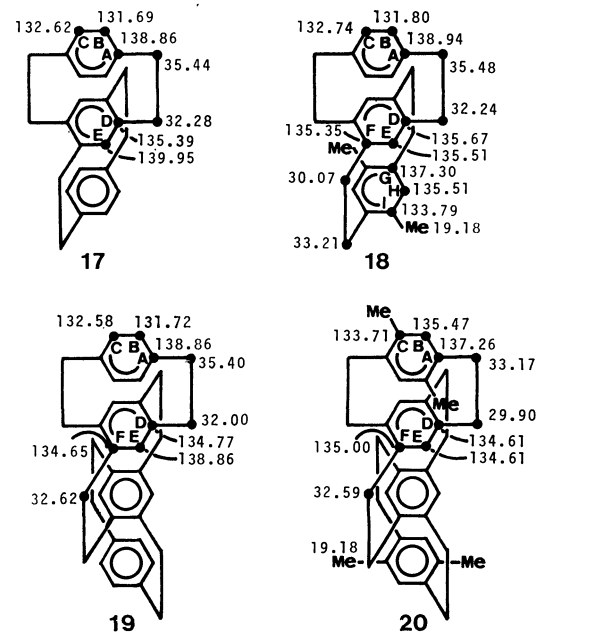

Fig. 2. ^{13}C NMR data of [*n.n*]paracyclophanes and multilayered paracyclophanes (δ value).

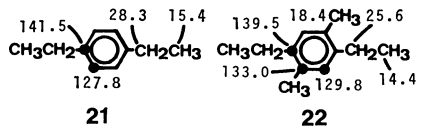

Fig. 3. ^{13}C NMR data of alkylbenzenes (δ value).

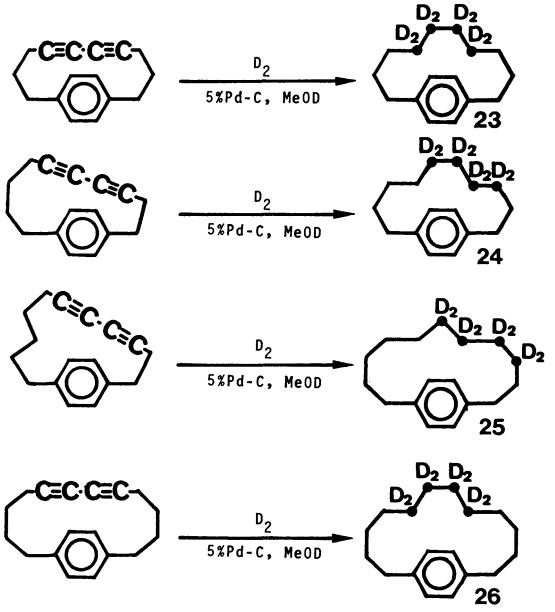

Fig. 4. Catalytic deuteration of [*n*]paracyclophadiynes.

The assignment for medium-sized [*n*]paracyclophanes has been not so easy because of closely positioned signals of the polymethylene carbons. This difficulty was overcome, for example, by deuterium substitution of the four middle methylene groups as seen in catalytic deuteration of a few [*n*]paracyclodiynes (Fig. 4).[9] [10]Paracyclophane **3** shows five signals of the methylene carbons, of which two signals at lower field, δ 35.33 and 29.24, are easily assigned to the α and β methylene carbons, respectively. Of the remaining three signals the two at δ 26.90 and 28.41 disappear in the spectrum of deuterated [10]paracyclophane **23**. For its isomeric deuterated [10]paracyclophane **24**, on the other hand, only one signal (δ 26.90) disappears and other two signals (δ 25.00 and 28.41) decrease to one-half of the initial intensities. Consequently, the three signals at δ 25.00, 28.41, and 26.90 are explicitly assigned to γ, δ, and ε methylene carbons, respectively.

TABLE 1. ^{1}H NMR DATA OF THE METHYLENE PROTONS OF [*n*]PARACYCLOPHANES (100 MHz, δ value)[b]

		α	β	γ	δ	ε	ζ
[8]PC[a]	**1**	2.64	1.43	0.87	0.19		
[9]PC	**2**	2.59	1.42	0.96	0.33	0.59	
[10]PC	**3**	2.60	1.54	1.07	0.48	0.69	
[11]PC	**4**	2.55	1.55	1.18	0.79		0.68
[12]PC	**5**	2.60	1.57	1.06	1.00		0.78

a) PC: paracyclophane. b) The spectra were recorded in $CDCl_3$ at ambient temperature on a JEOL FX-100 spectrometer equipped with a FT system and JEC-980B computer, using TMS as an internal standard.

The deuterium substitution of [*n*]paracyclophanes concomitantly enabled the signal assignment of methylene protons, which has not been clear so far. The data are given in Table 1. The middle methylene protons of the smallest cycle, [8]paracyclophane **1**, are situated just above the benzene ring according to X-ray analysis[10] and thereby resonate at a higher field than the other methylene protons owing to the magnetic anisotropy. On the other hand, the chemical shifts of the middle methylene protons are not the case for [9]- and [10]paracyclophanes **2** and **3**. As shown in Table 1, our assignment for **2** and **3** is the order of proton resonance: α, β, γ, ε, δ with the δ proton at highest field, which is distinct from the orders by Waugh and Fessenden:[11] α, β, δ, γ, ε and by Agarwal *et al.*:[12] α, β, γ, δ, ε. In addition, the present assignment emphasizes that the central methylene protons may not always appear at the highest field.

Discussion

[*n*]Paracyclophanes have a unique structure, in which a polymethylene chain is bridged at para-positions of the benzene ring and placed above the ring, and the benzene ring is bent into a boat shape as the length of the bridging chain shortens.[13] Therefore, the middle methylene groups are essentially shielded by the ring-current of the benzene and appear at higher fields as seen in Table 1. Levin and Roberts reported that in the ^{13}C NMR spectrum of [12]paracyclophane **5** the high-field resonances of the methylene carbons are attributed to the ring-current effect of the benzene ring.[4] However, noteworthy is that γ carbon signals appear in the highest fields for all the present [*n*]paracyclophanes. This upfield shift of γ carbons seems to be independent of the shielding effect of the benzene ring since the γ methylenes are presumably located in positions insusceptible to the effect, according to the ^{1}H NMR data in Table 1.

In the ^{13}C spectrum of [8]paracyclophane **1**, the methylene carbons reveal considerable deshieldings and no explicit dependence of the ring-current effect which is responsible for striking upfield shift of δ methylene protons in the ^{1}H spectrum. This can be explained by a direct carbon-carbon compression in the strained, small cyclic compound since the ring-current effect likely is concealed by the steric effect. For somewhat less strained compound or [9]paracyclophane **2**, however, the middle methylene carbon resonates at a relatively higher field, suggesting the ring-current effect.[18] Clear-cut evidence for the ring-current effect on ^{13}C shielding is given by comparison of two further less strained decamethylene compounds, [10]paracyclophane **3** and [10](9,10)anthracenophane **7**. In the latter compound, the two fused benzo groups do not affect steric environment of the middle methylene carbons. Accordingly, a marked upfield shift of the carbon resonances of **7** relative to **3** is ascribed to the larger ring-current effect of the anthracene ring than that of the benzene ring.[14]

[n.n]*Paracyclophanes and Methyl Derivatives.* The two benzenes of [*n.n*]paracyclophanes are, as $n<6$, stacked in parallel and brought close to each other with decreasing number of *n*. In [2.2]- and [3.3]paracyclophanes, the ring-to-ring distances are within the van der Waals contact, 3.4 Å, according to crystallographic analyses.[15] Therefore, the aryl carbons of both paracyclophanes are undoubtedly compressed by π-π repulsive interaction as described by Sato and coworker.[16] In order to pursue such a compression effect, the aryl carbon resonances of **8** were compared with those of strainless cyclophanes, [6.6]paracyclophane **11** and [14]paracyclophane **6**. A marked downfield shift was observed for the protonated carbon C_B, while no difference for the bridgehead carbon C_A. This downfield shift is comprehended with much easier polarization based on the π-π compression.

As one would expect, the protonated carbon C_B of [3.3]paracyclophane **9** exhibits a similar but smaller downfield shift reflecting its own less compression. On the other hand, the bridgehead C_A signal of **9** appears at a higher field by a little less than 1 ppm compared to those of **11** and **6**. This upfield shift is probably responsible for the ring-current effect of the faced benzene. In the case of [2.2]paracyclophane **8**, the chemical shifts of both aromatic carbons are explained by concealing the ring-current with strong compression effect.

The ^{13}C shifts of [4.4]- and [6.6]paracyclophanes **10** and **11** are almost the same as that of [14]paracyclophane **6**, indicating that the two benzenes in **10** and **11** are too apart from each other to interact sterically and magnetically.

Methyl substitution of [2.2]paracyclophane **12** gives a large perturbation on the shieldings not only for aryl carbons of the methyl-attached ring, but also for aryl carbons of the faced ring. The aryl carbon C_B pseudo-geminal to the methyl substituent is subjected to no deshielding effect compared to the corresponding carbon resonances of **6** and **11**, whereas the pseudo-ortho carbon C_C reveals a marked deshielding. This can be understood by depression of the polarization along the C_B–Ha bond due to strong compression of the methyl group on the proton Ha, since the compression was provided by ^{1}H chemical shifts.[2] Similar phenomena were observed for the pseudo-gem protonated carbons of other methyl derivatives, C_B of **15**, C_E of **18**, and C_E of **20**.

Dimethyl[3.3]paracyclophane **13** also shows the shielding of the protonated carbon C_B pseudo-geminal to the methyl group besides the bridgehead carbons C_A and C_D. Compared with the difference in C_B resonances of **8** and **12**, such a considerable upfield shift of C_B of less strained **13** indicates that the contribution of the ring-current effect on ^{13}C resonance becomes relatively larger in the [3.3]phane system than in the [2.2]phane system, while the compression effect becomes relatively lower. In the case of dimethyl[4.4]paracyclophane **14**, pseudo-gem C_B signal is shifted slightly upfield, although there are no longer steric and magnetic transannular effects in the parent cyclophane **10**. It is probably due to a weak compression effect of the bulky methyl group on the Ha proton.

Such a steric contribution by a methyl group is also

supported by progressive downfield shift of methyl carbon resonances as the methylene number of [*n.n*]-paracyclophanes decreases, that is, the ring-to-ring distance between two benzene rings shortens. A marked downfield shift of methyl carbon resonance due to the methyl-methyl compression is observed for centro-symmetric isomer **16** of tetramethyl[2.2]paracyclophane.

Triple- and Quadruple-layered [2.2]Paracyclophanes. The π-π compression also exerts pronounced effect on ^{13}C spectra of multilayered [2.2]paracyclophanes **17**—**20**. Thus, aryl carbons of all the outer benzene rings reveal the same extent of downfield shifts as those of double-layered series. The non-equivalence of protonated aromatic carbons C_B and C_C of **17**—**19** is caused by depressed C_B–H polarization due to the compression with the bridge methylene group, which is smaller than the compression with a methyl group.

It is noticeable that triple-layered [2.2]paracyclophane **17** provides a novel example of the double compression effect. The signal of aryl carbon C_E of **17** is shifted to a lower field by 7.95 ppm than the corresponding carbon resonance of a reference compound, **14**. This downfield shift is about twice as large as the difference value (4.25 ppm) between **12** and **14**, indicating an additivity of the steric compression contribution on carbon resonances.

Triple- and quadruple-layered [2.2]paracyclophanes may permit a straightforward evaluation of the anisotropic contribution arising from additional third and fourth benzene rings which are stacked on double-layered [2.2]paracyclophane, providing that the steric contribution can be eliminated from the total effect by choice of a suitable reference compound. The outer benzene rings of **17** and **19** have a geometry very similar to the double-layered homolog as revealed by the X-ray analyses.[17] Accordingly, a small upfield shift observed for the bridgehead carbon signal of the outer benzene of triple-layered cyclophanes **17** and **18** is considered to be due to the third benzene (C_A of **17** *vs.* C_A of **12**, −0.36 ppm; C_A of **18** *vs.* C_A of **12**, −0.28 ppm; C_G of **18** *vs.* C_A of **15**, −0.32 ppm), being close to an average shielding value (−0.22 ppm) seen in ^1H NMR data.[2] However, the shielding effect (*ca.* −0.05 ppm) of the fourth benzene was observed to be negligible by comparing the bridgehead carbon resonances of outer benzenes of both quadruple-layered cyclophanes, **19** and **20**, and triple-layered cyclophanes, **17** and **18**.

The authors are greatly indebted to Mr. Y. Takai and Dr. K. Lee for ^{13}C NMR measurements. The present work was partially supported by a Grant-in-Aid for Developmental Scientific Research No. 984015 from the Ministry of Education, Science and Culture.

References

1) Part LX: M. Yoshinaga, T. Otsubo, Y. Sakata, and S. Misumi, *Bull. Chem. Soc. Jpn.*, **52**, 3759 (1979).
2) T. Otsubo, S. Mizogami, Y. Sakata, and S. Misumi, *Bull. Chem. Soc. Jpn.*, **46**, 3831 (1973).
3) J. B. Stothers, "Carbon-13 NMR Spectroscopy," Academic Press, New York (1972).
4) R. H. Levin and J. D. Roberts, *Tetrahedron Lett.*, **1973**, 135.
5) D. J. Cram, C. S. Montgomery, and G. R. Knox, *J. Am. Chem. Soc.*, **88**, 515 (1966); N. L. Allinger, J. T. Sprague, and T. Liljefors, *ibid.*, **96**, 5100 (1974) and references cited therein; T. Otsubo and S. Misumi, *Synth. Commun.*, **8**, 285 (1978).
6) F. Vögtle and P. K. T. Mew, *Angew. Chem. Int. Ed. Engl.*, **17**, 60 (1978). We have independently obtained **7** by a catalytic hydrogenation of [10](9,10)anthracenopha-4,6-diyne; T. Inoue, T. Kaneda, and S. Misumi, *Tetrahedron Lett.*, **1974**, 2969.
7) D. J. Cram, *Rec. Chem. Progr.*, **20**, 71 (1959) and references cited therein; T. Otsubo, M. Kitasawa, and S. Misumi, *Bull. Chem. Soc. Jpn.*, **52**, 1515 (1979).
8) T. Otsubo, S. Mizogami, I. Otsubo, Z. Tozuka, A. Sakagami, Y. Sakata, and S. Misumi, *Bull. Chem. Soc. Jpn.*, **46**, 3519 (1973).
9) T. Matsuoka, T. Negi, and S. Misumi, *Synth. Commun.*, **2**, 87 (1972); T. Matsuoka, T. Negi, T. Otsubo, Y. Sakata, and S. Misumi, *Bull. Chem. Soc. Jpn.*, **45**, 1825 (1972).
10) M. G. Newton, T. J. Walter, and N. L. Allinger, *J. Am. Chem. Soc.*, **95**, 5652 (1973).
11) J. S. Waugh and R. W. Fessenden, *J. Am. Chem. Soc.*, **79**, 846 (1957); **80**, 6697 (1958).
12) A. Agarwal, J. A. Barnes, J. L. Fletcher, M. J. McGlindrey, and B. G. Sayer, *Can. J. Chem.*, **55**, 2575 (1977).
13) N. L. Allinger, T. J. Walter, and M. G. Newton, *J. Am. Chem. Soc.*, **96**, 4588 (1974) and references cited therein.
14) The ring-current effect was similarly observed for [*n*](9,10)anthracenophadiynes; T. Kaneda, T. Inoue, Y. Yasufuku, and S. Misumi, *Tetrahedron Lett.*, **1975**, 1543.
15) H. Hope, J. Bernstein, K. N. Trueblood, *Acta Crystallogr., Sect. B.*, **28**, 1733 (1972); P. K. Gantzel and K. N. Trueblood, *ibid.*, **18**, 958 (1965).
16) T. Sato, T. Takemura, and M. Kainosho, *Chem. Commun.*, **1974**, 97; T. Takemura and T. Sato, *Can. J. Chem.*, **54**, 3412 (1976).
17) H. Mizuno, K. Nishiguchi, T. Otsubo, S. Misumi, and N. Morimoto, *Tetrahedron Lett.*, **1972**, 4981; H. Mizuno, K. Nishiguchi, T. Toyoda, T. Otsubo, S. Misumi, and N. Morimoto, *Acta Crystallogr., Sect. B*, **33**, 329 (1977); Y. Koizumi, T. Toyoda, H. Horita, and S. Misumi, 32nd National Meeting of the Chemical Society of Japan, Tokyo, April 1975, Abstr. I, p. 184.
18) N. Mori and T. Takemura, *J. Chem. Soc., Perkin Trans. 2*, **1978**, 1259.
19) Synthesized by oxidative coupling of *p*-(3-butynyl)-(6-heptynyl)benzene, colorless columns from EtOH, mp 67—68 °C. T. Kaneda and S. Misumi, unpublished result.

The Enantioface-differentiating (Asymmetric) Hydrogenation of the C=O Double Bond with Modified Raney Nickel. XXXIV. The Adsorption Mode of 2-Hydroxy Acid on Raney Nickel

Tadao HARADA

Division of Organic Chemistry, Institute for Protein Research, Osaka University, Yamada-Kami, Suita, Osaka 565

(Received August 11, 1979)

The adsorbed species of the modifying reagent and the surface states of the catalyst caused by the modification of a Raney nickel with 2-hydroxy acid at various pH regions were investigated. The adsorption mode of 2-hydroxy acid was proposed in each modifying-pH region; that is, (1) in a pH region intrinsic to the solution of the free 2-hydroxy acid, nickel salt of 2-hydroxy acid was adsorbed on the catalyst surface corroded by the acid; (2) under weakly acidic conditions, nickel salt and sodium salt of 2-hydroxy acid were adsorbed on the catalyst surface partially corroded by the acid; (3) under neutral conditions, the sodium salt was adsorbed on the surface of the fresh Raney nickel, and (4) under strongly basic conditions, the sodium salt and NaOH were adsorbed on the surface of the fresh Raney nickel.

The modification of the metal surface to yield an enantioface-differentiating (asymmetric) hydrogenation catalyst has been intensively studied since 1962.[1] Among those substances examined, 2-hydroxy acids were found to be some of the most effective modifying reagents. In the course of the study, the enantioface-differentiating step was found to occur prior to the hydrogen addition to the adsorbed substrate.[2] That is, the interaction of the substrate with the modifying reagent adsorbed on the catalyst causes the substrate to face the catalyst surface predominantly with one of the enantiofaces. Therefore, the investigation of the adsorption mode of 2-hydroxy acid on Raney nickel (RNi) is essential to an understanding of the mechanism of the enantioface-differentiation.

Recently, the adsorptions of hydroxy acids on nickel were investigated by employing physicochemical techniques. Groenwegen *et al.* studied the adsorption of hydroxy acids from the vapor onto silica-supported nickel and inferred from their IR spectra that hydroxy acids were adsorbed as carboxylates.[3] Suetaka *et al.* studied the orientation of hydroxy acids on nickel plate and assumed, from their reflection IR spectra, that hydroxy acids were adsorbed as undissociated forms.[4]

Physicochemical techniques are not always relevant to studies of the modified Raney nickel catalyst (MRNi), because these techniques are mostly applied under conditions quite different from those of the modification or reaction processes. With this in view, some workers have studied the adsorption modes of hydroxy acids in connection with the enantioface-differentiating ability of MRNi. Tatsumi suggested that tartaric acid was adsorbed on the surface of RNi with two carboxyl groups under acidic conditions and with the 2-hydroxyl group and the 1-carboxyl group under neutral conditions.[5] Tanabe *et al.* studied the effect of the bases used for the pH adjustment of the modifying solution on the enantioface-differentiating ability of the catalyst, and concluded that, in the case of tartaric acid at pH 5, one of the carboxyl groups participated in the adsorption onto the catalyst, while the other was free from the catalyst surface.[6] Yasumori *et al.* investigated the effect of the modifying pH on the optical yield and the amount of tartrate adsorbed on a nickel powder catalyst, and inferred that, when the catalyst was modified with tartaric acid, tartrate dianion was the most effective species for the enantioface-differentiation, without reference to the counter-ion.[7] Harada proposed that the adsorption mode of 2-hydroxy acid was influenced by the pH value of the modifying solution and that the enantioface-differentiating ability of MRNi was directly governed by the adsorption mode of 2-hydroxy acid.[8]

This paper will describe our studies of the adsorbed species of 2-hydroxy acid at various pH regions of the modifying solution and on the change in the surface state of the catalyst caused by the modification.

Results and Discussion

Effect of the Modifying pH *on the Adsorbed Species and the Surface States.* When RNi was soaked in the modifying solution, some amounts of metallic nickel were corroded by the modifying reagent and were dissolved into the modifying solution as the nickel ion.

The amounts of the nickel ion produced during the

TABLE 1. AMOUNTS OF THE NICKEL ION IN THE RECOVERED MODIFYING SOLUTIONS (Ni(II)/mol)

Modifying reagent	Modifying pH			
	2.3	5.1	7.4	10.0
(*RS*)-Mandelic acid	2.9×10^{-4}	—	0.0×10^{-4}	0.0×10^{-4}
(*RS*)-Lactic acid	3.7×10^{-4}	—	0.2×10^{-4}	0.0
Glycolic acid	4.4×10^{-4}	1.1×10^{-4}	0.2×10^{-4}	0.0

Catalyst: 1.5 g as the alloy (Ni: Al=42: 58). Modifying solution: 100 ml of a 1% aqueous solution of the modifying reagent. The pH was adjusted with 1 M NaOH. Modification: at 0 °C for 90 min.

TABLE 2. AMOUNTS OF ADSORBED MODIFYING REAGENTS

No.	Reagent for acid treatment (g in 100 ml H_2O, pH)	Modifying reagent (g in 100 ml H_2O, pH)	Adsorbed glycolate (mol)
1	(*RS*)-Mandelic acid (1, pH 2.3)	Nickel glycolate[a)] (0.1, pH 6.8)	1.1×10^{-4} (Mandelate: 0.1×10^{-4})
2	—	Nickel glycolate[a)] (0.1, pH 6.8)	0.9×10^{-4}
3	Glycolic acid (1, pH 2.3)	Nickel glycolate[a)] (0.1, pH 6.8)	1.3×10^{-4}
4	—	Glycolic acid (1, pH 2.3)	1.3×10^{-4}

Catalyst: 1.5 g as the alloy (Ni: Al=42: 58). Acid-treatment and modification: at 0 °C for 90 min, using 100 ml of an acid-treating or modifying solution. a) The concentration (0.1%) of the nickel glycolate solution is comparable to that of the nickel glycolate found in the modifying solution after the modification with a 1% solution of glycolic acid at pH 2.3 (Table 1).

modification with 2-hydroxy acids at various modifying pH regions are listed in Table 1. Only trace amounts of nickel metal were corroded by the modification under neutral or basic conditions. Thus, no appreciable changes in the modifying reagent (*i.e.*, sodium salt to nickel salt of 2-hydroxy acid) or in the surface state of RNi were assumed during the modification under neutral or basic conditions.

The formation of the nickel ion in large amounts by soaking the catalyst in a 2-hydroxy acid solution suggested that the modifying reagent was no longer the free acid, but the nickel salt of the acid in the neighborhood of the catalyst surface, and also that the surface state of RNi was drastically changed by the corrosion. Thus, the MRNi prepared under acidic conditions was assumed to be quite different from those prepared under neutral or basic conditions with respect to the surface state of the catalyst and the species of the adsorbed modifying reagent.

In order to make clear the above-mentioned differences, modifications with nickel glycolate or glycolic acid were carried out using two types of RNi catalysts. One was prepared by a method reported before (fresh RNi),[9] while the other was prepared by the treatment of fresh RNi with 2-hydroxy acid (acid-treated RNi). The amounts of the glycolate adsorbed on the two types of catalysts are compared in Table 2. As is shown in Entry 1, most of the mandelate used for the preparation of the acid-treated RNi was replaced by glycolate on modification with nickel glycolate. By a comparison of the result shown in Entry 1 with that shown in Entry 2, it is apparent that the loading capacity of the catalyst for nickel glycolate was increased by prior treatment with 2-hydroxy acid.

As is shown in Entries 3 and 4, the modification of fresh RNi with a 1% solution of glycolic acid (pH 2.3) and the modification of an acid-treated RNi with a 0.1% solution of nickel glycolate (pH 6.8) gave the same results with respect to the amount of adsorbed glycolate. This fact strongly suggests that the modification of RNi with glycolic acid under acidic conditions consists of two processes; that is, the conditioning process of the RNi surface with the acid, and the following adsorption process of the nickel salt produced *in situ*.

After the modification of fresh RNi was performed with a solution of nickel glycolate, the molar ratio of the glycolate to the nickel ion adsorbed on the catalyst was found to be 1.8: 1 (Table 3). This value is close to that for $Ni(CH_2(OH)CO_2)_2$. Therefore, in this case

TABLE 3. AMOUNTS OF ADSORBED GLYCOLATE AND ADSORBED NICKEL ION ON MODIFICATION WITH NICKEL GLYCOLATE

	Modifying solution (solute/mol)		Adsorbed solute (mol)
	Initial	Final	
Ni(II)	4.9×10^{-4}	4.4×10^{-4}	0.5×10^{-4}[a)]
Glycolate	10.6×10^{-4}	—	0.9×10^{-4}

Catalyst: 1.5 g as the alloy (Ni: Al=42: 58). Modifying solution: 100 ml of an aqueous solution of nickel glycolate. Modification: at 0 °C for 90 min. a) Caculated value.

TABLE 4. AMOUNTS OF ADSORBED GLYCOLATE AND ADSORBED POTASSIUM ION ON MODFICATION WITH POTASSIUM GLYCOLATE

	Modifying solution (solute/mol)		Adsorbed solute (mol)
	Initial	Final	
K(I)	2.0×10^{-4}	1.8×10^{-4}	0.2×10^{-4}[a)]
Glycolate	2.0×10^{-4}	—	0.2×10^{-4}

Catalyst: 1.5g as the alloy (Ni: Al=42: 58). Modifying solution: 50 ml of an aqueous solution of potassium glycolate. Modification: at 0°C for 90 min. a) Calculated value.

the major adsorbed species is found to be $Ni(CH_2(OH)CO_2)_2$.

The adsorbed species on modification under neutral conditions were examined in the same way as in the modification with nickel glycolate. Table 4 shows the amounts of the adsorbed glycolate and the adsorbed potassium ion when the fresh RNi was modified with a solution of potassium glycolate (pH 6.8). The molar ratio of the glycolate to the potassium ion adsorbed on the catalyst was found to be exactly 1: 1. Therefore, the species adsorbed on modification with potassium glycolate is found to be potassium glycolate. Similarly, when sodium glycolate is used as the modifying reagent, sodium glycolate is assumed to be the adsorbed species.

Under weakly acidic modifying conditions, RNi was partially corroded by the acid to form a mixture of the catalyst with a fresh surface and with an acid-treated surface. The species adsorbed under this modifying conditions are expected to form a mixture of nickel glycolate and sodium glycolate.

Under strongly basic modifying conditions, the adsorbed species are considered to be the alkali salt

Table 5. Effects of acid treatment on the enantioface-differentiating ability of the catalysts

No.	Reagent for acid treatment (g in 100 ml H_2O)	Modifying reagent (g in 100 ml H_2O)	$[\alpha]_D^{20}$ of Methyl 3-hydroxybutyrate/°
1	(*S*)-3-Phenyllactic acid (1)	Nickel (*S*)-3-phenyllactate (0.1)	+0.58
2	(*RS*)-Lactic acid (1)	Nickel (*S*)-3-phenyllactate (0.1)	+0.62
3	—	Nickel (*S*)-3-phenyllactate (0.1)	+0.30
4	—	(*S*)-3-Phenyllactic acid (1)	+0.60
5	Sodium (*S*)-3-phenyllactate (1)	Nickel (*S*)-3-phenyllactate (0.1)	+0.36
6	—	Sodum (*S*)-3-phenyllactate (1)	+0.15
7	—	(*S*)-3-Phenyllactic acid (1)+NaOH (pH 5)	+0.30
8	—	(*S*)-3-Phenyllactic acid (1)+NaOH (pH 12)	−0.35

Catalyst: 1.5 g as the alloy (Ni: Al=42: 58). Acid-treatment and modification: at 0 °C for 90min. Substrate: 17.5 ml of methyl acetoacetate. Hydrogenating conditions: at 60 °C under an initial H_2 pressure of 90 kg/cm^2.

of 2-hydroxy acid and the alkali hydroxide. This consideration is supported by the fact that the amount of the adsorbed salt of 2-hydroxy acid was drastically decreased when the modifying pH was increased.[8]

The Effect of the Modifying pH *on the Enantioface-differentiating Ability of MRNi.* In the preceding section, MRNi was classified into four types on the basis of the adsorbed species and the surface states: that is, MRNi prepared in a pH region intrinsic to the solution of the free 2-hydroxy acid, under weakly acidic conditions, under neutral conditions, and under strongly basic conditions. Each type of MRNi was examined in order to elucidate the relationship between the enantioface-differentiating ability of MRNi and the adsorption mode of 2-hydroxy acid. (*S*)-3-Phenyllactic acid and its salts were used as the optically active modifying reagents. The ability of MRNi was evaluated by means of the optical yield of the hydrogenation of methyl acetoacetate to methyl 3-hydroxybutyrate. The results are summarized in Table 5.

As is shown in Entries 1 and 4, the same ability was obtained by MRNi prepared from an acid-treated RNi and a solution of nickel (*S*)-3-phenyllactate (pH 6.8), and MRNi prepared from fresh RNi and a solution of (*S*)-3-phenyllactic acid (pH 2.3). In addition, the difference in the acid used for the acid-treatment of fresh RNi did not influence the ability of MRNi (Entries 1 and 2). On the other hand, MRNi prepared from fresh RNi and a solution of nickel (*S*)-3-phenyllactate (pH 6.8) showed a lower ability (Entry 3).

The above results are well compatible with the results obtained in the adsorption studies. That is, MRNi prepared from fresh RNi and a solution of free 2-hydroxy acid is equivalent to that prepared from an acid-treated RNi and a solution of nickel salt of the acid. The difference in the ability between the nickel salt–MRNi prepared from the acid-treated RNi and that prepared from the fresh RNi indicates that the ability of MRNi depends not only on the adsorbed species of the modifying reagent, but also on the surface state of RNi.

The treatment of fresh RNi with a solution of sodium (*S*)-3-phenyllactate (pH 8.2) prior to the modification did not influence the ability of nickel (*S*)-3-phenyllactate–MRNi (Entries 3 and 5). This fact is in accordance with the result obtained in the preceding section; that is, the treatment of fresh RNi with sodium salt of 2-hydroxy acid resulted in no detectable change in the surface state of the catalyst.

Sodium (*S*)-3-phenyllactate–MRNi prepared from fresh RNi showed a different ability from that of nickel (*S*)-3-phenyllactate–MRNi prepared from fresh RNi (Entry 6). The difference can be explained in terms of the difference in the adsorbed species.

The ability of the catalyst modified with a solution containing both 2-hydroxy acid and its sodium salt (pH 5.1) was intermediate between that of 2-hydroxy acid–MRNi and that of its sodium salt–MRNi (Entry 7).

The ability of the catalyst modified under strongly basic conditions was quite different from that of the sodium salt–MRNi (Entry 8). In this case, the direction of the enantioface-differentiation was different from that of the sodium salt–MRNi. This fact indicates that the adsorbed sodium hydroxide drastically affects the adsorption mode of methyl acetoacetate on the catalyst.

As a whole, it can be concluded that the pH-dependence of the enantioface-differentiating ability can also be explained by common factors: the adsorbed species of the modifying reagent and the surface states of the catalyst.

Experimental

The preparation of the modified Raney nickel catalyst, the determination of the absorbed (*RS*)-mandelate and glycolate, the hydrogenation of methyl acetoacetate, and the measurement of the enantioface-differentiating ability of the catalyst were all carried out by the use of the procedures described in a previous paper.[9]

The Preparation of an Acid-treated RNi. A Raney-nickel catalyst obtained from 1.5 g of the alloy[9] was soaked in 100 ml of a 1% aqueous solution of the reagent for acid treatment at 0 °C for 90 min. The mixture was shaken every 15 min. After the acid treatment, the solution was removed by decantation and the catalyst was washed once with 10 ml of deionized water and then with three 50 ml portions of methanol. The resulting catalyst was used for the modification.

The Determination of Ni(II). The nickel ions in the modifying solution were determined by the EDTA titration method at pH 10—12, using murexide as the indicator and triethanolamine as the masking reagent for the aluminium ion.[10]

The Determination of K(I). The potassium ions in the modifying solution were determined by the gravimetric technique using sodium tetraphenylborate.[11]

The author wishes to thank Professors Yoshiharu Izumi and Akira Tai, Osaka University, for their many helpful discussions and suggestions in the course of this work.

References

1) Part XXXIII of this series: S. Murakami, T. Harada, A. Tai, and Y. Izumi, *Bull. Chem. Soc. Jpn.*, in press.
2) H. Ozaki, A. Tai, S. Kobatake, H. Watanabe, and Y. Izumi, *Bull. Chem. Soc. Jpn.*, **51**, 3559 (1978).
3) J. A. Groenewegen and W. M. H. Sachtler, *J. Catal.*, **33**, 176 (1974).
4) A. Hatta and W. Suetaka, *Bull. Chem. Soc. Jpn.*, **48**, 3441 (1975).
5) S. Tatsumi, *Bull. Chem. Soc. Jpn.*, **41**, 408 (1968).
6) T. Tanabe, K. Okuda, and Y. Izumi, *Bull. Chem. Soc. Jpn.*, **46**, 514 (1973).
7) I. Yasumori, Y. Inoue, and K. Okabe, "Int. Symp. on Relations between Heterogeneous and Homogeneous Catalytic Phenomena," 1974, p. 141.
8) T. Harada, *Bull. Chem. Soc. Jpn.*, **48**, 3236 (1975).
9) Y. Izumi, T. Harada, T. Tanabe, and K. Okuda, *Bull. Chem. Soc. Jpn.*, **44**, 1418 (1971).
10) K. Ueno, "Kireito-tekiteiho," 2nd ed, Nankodo, Tokyo (1976), p. 358.
11) E. R. Caley and H. D. Axilrod, *Ind. Eng. Chem. Anal. Ed.*, **14**, 242 (1942).

Thione S-Imides. The Reaction with Carbon-Hetero Atom Double Bond

Takao SAITO, Isao OIKAWA, and Shinichi MOTOKI*

Department of Chemistry, Faculty of Science, Science University of Tokyo, Kagurazaka, Shinjuku-ku, Tokyo 162

(Received August 14, 1979)

9-Fluorenethione *S*-*p*-toluenesulfonimide reacted as a 1,3-dipole with imines, oximes, and thiones to form (3+2)cycloadducts, while with symmetrical azines and aldehydes, unsymmetrical azines, *N*-(*p*-tolylsulfonyl) imines and fluorenone were obtained as a result of the decomposition of the cycloadducts.

Thione *S*-imides,[1] new thiocumulenes, have recently been synthesized by several workers.[2] However, there have been few reports on the cycloaddition reactions of the imides.[3]

Previously,[4] we reported the 1,3-dipolar, Diels-Alder-type cycloaddition, and ene reactions of 9-fluorenethione *S*-*p*-toluenesulfonimides (**1**) with compounds containing C=C bond(s). We have now attempted the reaction of **1** with compounds containing C=X bond(s) (X=NR, O, S) *i.e.*, imines (**2**), oximes (**6**), azines (**8**), aldehydes (**11**), and thiones (**14**).

Results and Discussion

The treatment of **1** with aldimines (**2**) in 1,2-dichloroethane at room temperature gave (3+2)cycloadducts, spiro[fluorene-9,5′-[1,2,4]thiadiazolidine] derivatives (**3**), regiospecifically. The results are shown in Tables 1 and 2. The adducts showed no characteristic νS=N absorption band in the IR spectra, and their mass-spectral fragmentation patterns exhibited *N*-(fluorenylidene)-*p*-toluenesulfonamide (Fl=NTs‡), *N*-(fluorenylidene)arylamine (Fl=NC$_6$H$_4$R^{2‡}), and aldimine (R^{1}C$_6$H$_4$CH=NC$_6$H$_4$R^{2‡}) ion peaks. Among these adducts, **3i** was a particularly unstable compound; it decomposed to form **5** in a solution. These observations are consistent with the proposed structure, **3**, rather than with the regioisomeric structure, **4**.

The reactions of **1** with *N*-alkylalkanimines or *N*-alkylarylmethanimines (*N*-cyclohexyl-2-butanimine, *N*-cyclohexyl-1-(2-methyl)propanimine, *N*-(2-butyl)-2-butanimine, *N*-cyclohexylphenylmethanimine, and *N*-(2-propyl)phenylmethanimine) resulted in complicated decomposition reactions, fluorenone and tar being formed. Reactions with ketimines such as *N*-phenyldiphenylmethanimine did not proceed under the same reaction conditions, whereas prolonged treatment at room temperature or by refluxing the 1,2-dichloroethane solution caused only decomposition reactions.

The reaction of **1** with oximes (**6**) proceeded rapidly to give (3+2)cycloadducts **7** (Tables 3 and 4). The IR spectra of **7** showed a distinct band at 3220—3320 cm^{-1} due to the hydroxyl group, but no νS=N band. The mass-spectral fragmentation pattern resembled that of **3**.

TABLE 1. 3′,4′-DIARYL-2′-*p*-TOLUENESULFONYLSPIRO[FLUORENE-9,5′-[1,2,4]THIADIAZOLIDINES] (**3**)

Compd	R^1	R^2	X	Reaction time/h	Yield %	Mp °C (dec)
3a	H	H	H	2	90	128—130
3b	H	CH_3	H	3	91	104—105
3c	H	Cl	H	4	80	117—119
3d	H	NO_2	H	16	91	126—128
3e	H	OCH_3	H	5	77	99—101
3f	OCH_3	H	H	0.5	86	88—90
3g	Cl	H	H	1.5	90	95—97
3h	Cl	Cl	H	4	87	113—114
3i	H	H	NO_2	2.5	53	119—120

TABLE 2a. IR AND NMR SPECTRAL DATA OF **3**

Compd	IR, cm^{-1} νSO_2		CH_3 (Ts)	NMR, δ in $CDCl_3$[a] Ar–H	Others
3a	1320	1160	2.42(s, 3H)	6.3—8.1(m, 22H)	
3b	1310	1165	2.44(s, 3H)	7.0—8.0(m, 17H), 6.31, 6.72 (dd, 4H)	2.07(s, 3H, CH_3–Ar)
3c	1305	1160	2.46(s, 3H)	7.0—8.0(m, 17H), 6.30, 6.80 (dd 4H)	
3d	1310	1165	2.47(s, 3H)	7.0—8.0(m, 17H), 6.24 (d, 2H)	
3e	1290	1165	b)	b)	b)
3f	1310	1165	2.39(s, 3H)	6.2—8.0(m, 21H)	3.77 (s, 3H, CH_3O)
3g	1310	1165	2.44(s, 3H)	6.3—8.0(m, 21H)	
3h	1315	1165	2.44(s, 3H)	7.0—8.0(m, 16H), 6.28, 6.80 (dd, 4H)	
3i	1315	1165	b)	b)	

a) s: singlet, d: doublet, m: multiplet. b) Clear spectral data could not be obtained because of their instability in solution.

Table 2b. Elemental analyses of **3**

Compd	Molecular formula (MW)	Calcd (%)			Found (%)		
		C	H	N	C	H	N
3a	$C_{33}H_{26}N_2O_2S_2$ (546.7)	72.50	4.79	5.12	72.30	4.79	4.98
3b	$C_{34}H_{28}N_2O_2S_2$ (560.7)	72.83	5.03	4.99	72.78	5.17	5.01
3c	$C_{33}H_{25}N_2O_2S_2Cl$ (581.1)	68.21	4.34	4.82	68.01	4.30	4.85
3d	$C_{33}H_{25}N_3O_4S_2$ (591.7)	66.99	4.26	7.10	66.65	4.39	7.12
3e	$C_{34}H_{28}N_2O_3S_2$ (576.7)	70.81	4.89	4.86	70.70	4.81	4.88
3f	$C_{34}H_{28}N_2O_3S_2$ (576.7)	70.81	4.89	4.86	70.61	4.91	4.74
3g	$C_{33}H_{25}N_2O_2S_2Cl$ (581.1)	68.21	4.34	4.82	68.50	4.68	4.81
3h	$C_{33}H_{24}N_2O_2S_2Cl_2$ (615.6)	64.39	3.93	4.55	64.10	4.18	4.60
3i	$C_{33}H_{25}N_3O_4S_2$ (591.7)	66.99	4.26	7.10	c)	c)	c)

c) An analytically pure sample could not be obtained because of the instability of **3i**.

Table 3. 4′-Hydroxy-3′,3′-disubstituted 2′-*p*-toluenesulfonylspiro[fluorene-9,5′-[1,2,4]thiadiazolidines] (**7**)

Compd	R^1	R^2	X	Reaction time/min	Yield %	Mp/°C (dec)
7a	CH_3	CH_3	H	5	92	127—129
7b	CH_3	C_2H_5	H	5	89	120—121
7c	$-(CH_2)_5-$		H	5	92	125—126
7d	CH_3	CH_3CO	H	30	83	142—143
7e	H	C_6H_5	H	60	84	oil[a]
7f	C_6H_5	C_6H_5	H	15	88	116—117
7g	C_6H_5	*p*-$CH_3C_6H_4$	H	10	87	106—107
7h	C_6H_5	*p*-$C_6H_5C_6H_4$	H	10	93	107—108
7i	C_6H_5	*p*-ClC_6H_4	H	15	95	168—170
7j	CH_3	CH_3	NO_2	5	89	161—162

a) Compound **7e** was purified by means of column chromatography on silica gel, with benzene as the eluent.

Table 4a. IR and NMR spectral data of **7**

Compd	IR, cm^{-1}			NMR, δ in $CDCl_3$			
	ν OH	ν SO_2		OH	CH_3(Ts)	Ar–H	Others
7a	3320	1320	1160	5.87(s, 1H)	2.35 (s, 3H)	7.0—7.9 (m, 12H)	1.93 (s, 6H, CH_3)
7b	3310 3230	1320	1160	5.87(s, 1H)	2.37 (s, 3H)	7.0—7.9 (m, 12H)	1.90 (s, 3H, CH_3) 1.67 (t, 3H, CH_3) 2.30 (q, 2H, CH_2)
7c	3220	1295	1165	5.82(s, 1H)	2.38 (s, 3H)	7.0—8.0 (m, 12H)	1.1—3.0 (m,10H, $(CH_2)_5$)
7d	3200 3300	1330	1165	6.07(s, 1H)	2.39 (s, 3H)	7.1—8.0 (m, 12H)	2.00 (s, 3H, CH_3) 2.43 (s, 3H, CH_3CO)
7e	3250	1295	1170	6.57(s, 1H)	2.28 (s, 3H)	7.0—8.1 (m, 17H)	
7f	3220	1320	1165	5.80(s, 1H)	2.33 (s, 3H)	7.0—8.0 (m, 22H)	
7g	3220	1320	1165	5.79(s, 1H)	2.38 (s, 3H)	7.0—7.9 (m, 21H)	2.35 (s, 3H, CH_3)
7h	3280	1295	1175	5.82(s, 1H)	2.30 (s, 3H)	7.0—8.0 (m, 26H)	
7i	3260	1305	1170	6.01(s, 1H)	2.33 (s, 3H)	7.0—8.0 (m, 21H)	
7j	3290	1320	1160	5.89(s, 1H)	2.36 (s, 3H)	7.0—7.9 (m, 9H) 8.12 (dd, 1H) 8.46 (d, 1H)	1.92 (s, 6H, CH_3)

The treatment of **1** with azines (**8**) afforded unsymmetrical azines (**9**) and *N*-(*p*-tolylsulfonyl) imines (**10**) (Tables 5 and 6). In this case, one of the arylmethylene moiety of **8** was replaced by the fluorenylidene group. This *trans*-imidation reaction can be explained by assuming a path involving a 1,3-dipolar cycloaddition reaction,[5] followed by ring fragmentation with an elimination of sulfur, as is shown in the scheme.

Aromatic aldehydes (**11**) reacted slowly with **1a** to afford *N*-(*p*-tolylsulfonyl)arylmethanimines (**12**) and fluorenone (**13**) (Table 7). The formation of these products also suggests the presence of an intermediary cycloadducts, as is shown in the scheme. No reaction was observed between **1a** and ketones, such as 2-propanone, 2-butanone, and benzophenone under the same conditions. On the contrary, diaryl thioketones (**14**) reacted with **1a** to form (3+2)cycloadducts, 1,4,2-dithiazolidines (**15**) (Tables 8 and 9). The mass-spectral fragmentations which involve $R_2C{=}NTs^+$, $Fl{=}S^+$, $Fl{=}NTs^+$, and $R_2C{=}S^+$ ion peaks are compatible

Table 4b. Elemental Analyses of **7**

Compd	Molecular formula (MW)	Calcd (%)			Found (%)		
		C	H	N	C	H	N
7a	$C_{23}H_{22}N_2O_3S_2$ (438.6)	62.99	5.06	6.38	62.79	5.17	6.42
7b	$C_{24}H_{24}N_2O_3S_2$ (452.6)	63.69	5.34	6.19	63.60	5.44	6.17
7c	$C_{26}H_{26}N_2O_3S_2$ (478.6)	65.25	5.48	5.85	65.20	5.46	5.52
7d	$C_{24}H_{22}N_2O_4S_2$ (466.6)	61.78	4.75	6.00	62.34	4.77	5.97
7e	$C_{27}H_{22}N_2O_3S_2$ (486.6)	66.65	4.56	5.75	66.81	4.62	5.66
7f	$C_{33}H_{26}N_2O_3S_2$ (562.7)	70.43	4.66	4.98	70.21	5.01	4.72
7g	$C_{34}H_{28}N_2O_3S_2$ (576.7)	70.81	4.89	4.86	70.90	4.88	4.91
7h	$C_{39}H_{30}N_2O_3S_2$ (638.8)	73.33	4.73	4.38	73.18	4.77	4.69
7i	$C_{33}H_{25}N_2O_3S_2Cl$(597.1)	66.38	4.22	4.69	66.78	4.31	4.79
7j	$C_{23}H_{21}N_3O_5S_2$ (483.5)	57.13	4.38	8.69	57.38	4.26	8.81

Table 5. Reaction of thione *S*-imide (**1a**) with azines (**8**)

	R^1	R^2	Yield/%		Mp/°C	
			9	**10**	**9**	**10**
a	Ph	H	47	76	87—88	108—109
b	*p*-CH_3Ph	H	46	59	132—133	114—116
c	*p*-CH_3OPh	H	61	a)	115—116	*
d	*p*-$(CH_3)_2N$Ph	H	36	a)	155—157	*
e	Ph	CH_3	12	a)	127—129	*

a) *p*-Toluenesulfonamide and the corresponding carbonyl compounds were obtained instead of **10**.

Table 6a. NMR and mass spectral data of **9**

Compd	NMR, δ in $CDCl_3$			MS, rel. intens.		
	Ar-H	R^2	Others	M^+	M^+-R^1	M^+-N_2
9a	7.0—8.0 (m, 1H) 8.0—8.7 (m, 12H)	8.53 (s, 1H)		100	82	49
9b	7.1—8.0 (m, 11H) 8.3—8.6 (m, 1H)	8.54 (s, 1H)	2.42 (s, 3H, *p*-CH_3)	100	74	38
9c	6.8—8.0 (m, 11H) 8.4—8.6 (m, 1H)	8.50 (s, 1H)	3.83 (s, 3H, *p*-CH_3O)	100	50	14
9d	7.0—8.5 (m, 10H) 6.75 (d, 2H)	8.53 (s, 1H)	3.05 (s, 6H, *p*-$(CH_3)_2N$)	100	29	26
9e	7.1—7.7 (m, 9H) 7.8—8.2 (m, 4H)	2.42 (s, 3H)		100	44	2

Table 6b. Elemental Analyses of **9**

Compd	Molecular formula (MW)	Calcd (%)			Found (%)		
		C	H	N	C	H	N
9a	$C_{20}H_{14}N_2$ (282.3)	85.04	5.00	9.92	84.91	5.01	9.71
9b	$C_{21}H_{16}N_2$(296.4)	85.11	5.44	9.45	84.76	5.47	9.31
9c	$C_{21}H_{16}N_2O$(312.4)	80.75	5.16	8.97	81.13	5.39	9.00
9d	$C_{22}H_{19}N_3$ (325.4)	81.21	5.89	12.91	80.94	6.07	13.05
9e	$C_{21}H_{16}N_2$ (296.4)	85.11	5.44	9.45	84.98	5.71	9.56

Table 7. Reaction of thione *S*-imide (**1a**) with aromatic aldehydes (**11**)

	Ar	Reaction time/d	Yield/%	
			12	**13**
a	Ph	6	23	98
b	*p*-CH_3Ph	6	24	65
c	*p*-CH_3OPh	7	a)	95
d	*p*-ClPh	12	a)	67

a) *p*-Toluenesulfonamide and the corresponding aldehydes were obtained instead of **12**.

with the proposed structure.

As has been described above, it has been found that **1** underwent 1,3-dipolar cycloaddition reactions with the dipolarophiles containing carbon-hetero atom double bond(s), such as **2**, **6**, **8**, **11**, and **14**, to afford the adducts as isolable products or unstable intermediates regiospecifically. However, the adducts, **3**, **7**, and **15**, are not quite stable and are gradually decomposed on long standing in a solid state or in a solution. When **3** or **7** adducts were dissolved in warm 1,2-dichloroethane, the solution turned orange-red immediately,[6] while the

Table 8. 1,4,2-Dithiazolidines (**15**)

Compd	R	Reaction time/h	Yield/%	Mp/°C(dec)	IR $\nu SO_2/cm^{-1}$
15a	Ph	1	73	142—144	1345 1170
15b	*p*-CH_3Ph	1	13	127—131	1340 1160
15c	*p*-CH_3OPh	0.5	88	140—142	1340 1170
15d	*p*-ClPh	19	57	152—154	1350 1170

Table 9. Elemental Analyses of **15**

Compd	Molecular formula (MW)	Calcd (%)		Found (%)	
		C	H	C	H
15a	$C_{33}H_{25}NO_2S_3$ (563.7)	70.31	4.47	69.93	4.57
15b	$C_{35}H_{29}NO_2S_3$ (591.7)	71.04	4.94	70.97	4.90
15c	$C_{35}H_{29}NO_4S_3$ (623.7)	67.40	4.68	67.51	4.63
15d	$C_{33}H_{23}NO_2S_3Cl_2$ (632.6)	62.65	3.66	62.87	3.81

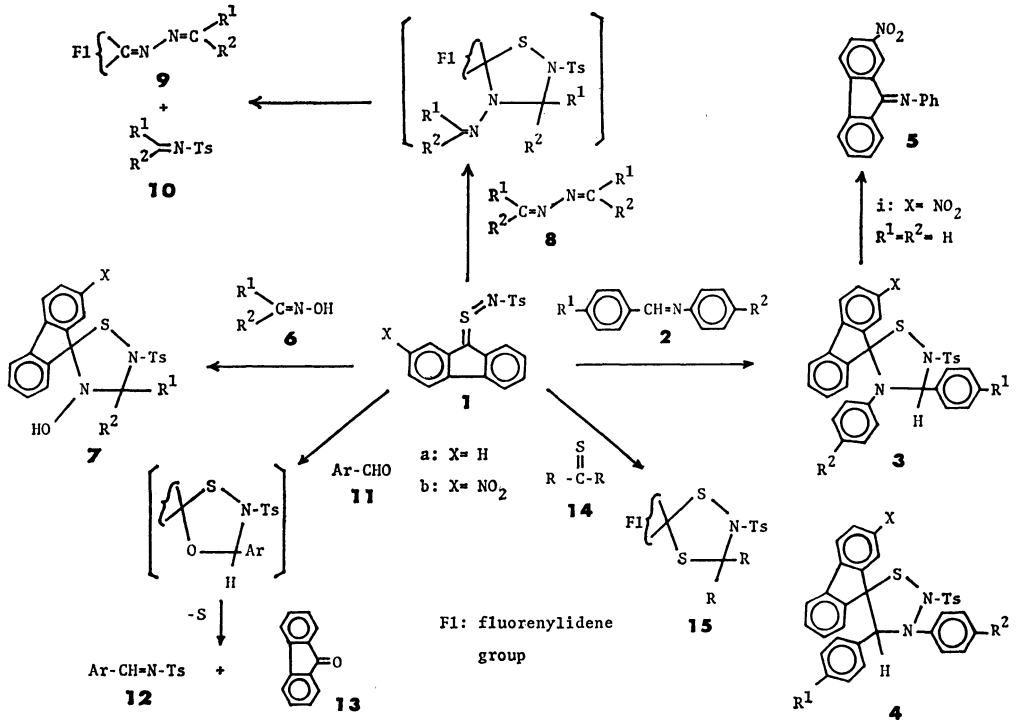

solution of **15** turned blue gradually. However, these adducts were recovered by cooling the solution or by evaporating the solvent. On the other hand, when the suspension of **3** in hexane was refluxed for several hours, **1** and **2** were recovered in good yields. These results suggest that the adducts can readily dissociate into their components reversibly in an appropriate solvent.

Experimental

All the melting points are uncorrected. The IR spectra were measured on a Hitachi Model 260-10 spectrometer. The NMR spectra were measured on a JEOL JNM-FX 100 or PMX-60 spectrometer. The mass spectra were recorded on a Hitachi double-focusing RMU-7M mass spectrometer. The elemental analyses were performed using a Shimadzu universal UM-3B organic micro analyzer and a Shimadzu NA-1 rapid-nitrogen analyzer.

Materials. The thione *S*-imides (**1**) were prepared by the reaction of triphenylphosphonium 9-fluorenylide with *N*-sulfinyl-*p*-toluenesulfonamide.[2f] The other reagents employed were commercial materials or were prepared by the usual methods.

Typical Procedures. Reaction of Thione S*-Imides (1) with Aldimines (2).* A mixture of **1a** (0.50 g, 1.37 mmol) and benzylideneaniline (**2a**) (0.37 g, 2.01 mmol) was stirred in dry 1,2-dichloroethane (10 cm^3) at room temperature for 2 h. The solvent was then evaporated *in vacuo*, and the residue was triturated by a good rubbing in cold diethyl ether–hexane (*ca.* 1 : 1). The resultant yellowish powder was collected and recrystallized from dichloromethane (3 cm^3)–hexane (6 cm^3) to give **3a** as colorless crystals in a 90% yield; mp 128—130 °C (dec), MS (15 eV) *m/e* 333 (1), 255 (10), 181 (100).

Decomposition of 3i. A solution of **3i** in 1,2-dichloroethane was allowed to stand overnight at room temperature. The solvent was then evaporated *in vacuo*, and the residue was subjected to column chromatography on silica gel, using

benzene as the eluent. *N*-(2-nitrofluorenylidene)aniline (**5**) was obtained as orange crystals in an 81% yield (recrystallized from benzene–hexane); mp 146—147 °C (lit,[7] mp 141 °C), IR (KBr) 1655 (C=N), 1520 and 1340 cm^{-1} (NO_2); NMR ($CDCl_3$) δ 6.6—8.0 (m, 10H), 8.28 (dt, 1H, J=2.0, 8.0 Hz), 8.72 (d, 1H, J=2.0 Hz); MS (70 eV) *m/e* 300 (100, M^+), 254 (43, $M^+ - NO_2$). Found: C, 76.01; H, 4.11; N, 9.51%. Calcd for $C_{19}H_{12}O_2N_2$ C, 75.99; H, 4.03; N, 9.33%.

Reaction of Thione S-*Imides (1) with Oximes (6).* A mixture of **1a** (1.00 g, 2.74 mmol) and acetone oxime (**6a**) (0.25 g, 3.42 mmol) was stirred in dry 1,2-dichloroethane (20 cm^3) at room temperature for 5 min. A work-up similar to that described for the preparation of **3** gave **7a** as colorless crystals in a 92% yield; mp 127—129 °C (dec); MS (70 eV) *m/e* 333 (14), 236 (19), 196 (10), 180 (50), 155 (34), 91 (85), 73 (10), 56 (100).

Reaction of Thione S-*Imide (1a) with Azines (8).* A mixture of **1a** (0.5 g, 1.37 mmol) and benzaldehyde azine (**8a**) (0.30 g, 1.44 mmol) was stirred in dry 1,2-dichloroethane at room temperature for 4 d. The solvent was then evaporated *in vacuo*, and the residue was column-chlomatographed on silica gel, using benzene as the eluent, to give **9a** as orange needles (recrystallized from benzene–hexane) in a 47% yield; mp 87—88 °C. Subsequent elution with the same solvent gave **10a** as colorless crystals in a 76% yield; mp 108—109 °C (lit,[8] mp 107 °C) (recrystallized from benzene–hexane).[9]

Reaction of Thione S-*Imide (1a) with Aromatic Aldehydes (11).* A mixture of **1a** (0.50 g, 1.37 mmol) and excess benzaldehyde (**11a**) was stirred in 1,2-dichloroethane at room temperature for 6 d. After the evaporation of the solvent, the residue was column-chromatographed on silica gel, using benzene as the eluent (followed by chloform), to give **12a** (mp 105—106 °C (lit,[8] mp 107 °C))[9] in a 23% yield and fluorenone (**13**) (mp 83—84 °C (lit,[10] mp 83.0—83.5 °C); IR 1720 cm^{-1} (C=O)) in a 98% yield (accompanied by the excess aldehyde). The yields of **13** and the recovered excess aldehyde were estimated by GLC.

Reaction of Thione S-*Imide (1a) with Thiones (14).* Into a suspension of **1a** (0.73 g, 2.0 mmol) in 1,2-dichloroethane (10 cm^3), a solution of 4,4-dimethoxythiobenzophenone (**14c**) (0.62 g, 2.4 mmol) in 1,2-dichloroethane (10 cm^3) was stirred, drop by drop, at room temperature. A colorless solid precipitated in a few min. After stirring for 30 min, the solid was collected and washed with ether–hexane to give **15c** in an 88% yield; mp 140—142 °C (dec); NMR ($CDCl_3$) δ 6.67—7.67 (m, 20H, arom), 3.85 (s, 6H, OCH_3), 2.38 (s, 3H, CH_3(Ts)), MS *m/e* 395 (11, *p*-$CH_3OC_6H_4C{=}NTst^+$), 333 (20, Fl=$NTst^+$) 269 (12, Fl=N–Tol-*p*·$^+$), 258 (25, *p*-$CH_3OC_6H_4)_2CS{\cdot}^+$), 240 (62, (*p*-$CH_3OC_6H_4)_2CN^+$), 196 (100, Fl=$S^+$). In the other cases, the reaction mixture was concentrated *in vacuo*, since no precipitation occurred. The residue was triturated in ether–hexane to afford the product.[11]

References

1) G. Bianchi, C. D. Micheli, and R. Gandolfi, "Supplement A, The Chemistry of Double-bonded Functional Groups," ed by S. Patai, Interscience, London (1977), Chap. 6, and the references cited therein.

2) a) S. Tamagaki and S. Oae, *Tetrahedron Lett.*, **1972**, 1159; b) E. M. Burgess and H. R. Penton, Jr., *J. Org. Chem.*, **39**, 2885 (1974); c) S. Holm, J. A. Boerma, N. H. Nilsson, and A. Senning, *Chem. Ber.*, **109**, 1069 (1976); d) I. Crossland, *Acta Chem. Scand., B*, **31**, 890 (1977); e) A. Tangerman and B. Zwanenburg, *Tetrahedron Lett.*, **1977**, 259; f) T. Saito and S. Motoki, *J. Org. Chem.*, **42**, 3922 (1977).

3) Burgess reported the reactions of *N*-benzoyl-*S*-(9-fluorenylidene)sulfilimine with enamines and a ynamine; Ref. 2b.

4) a) T. Saito and S. Motoki, *Chem. Lett.*, **1978**, 591; b) T. Saito and S. Motoki, *J. Org. Chem.*, **44**, 2493 (1979).

5) A few reactions of azines with 1,3-dipoles are known; for example, the reaction of benzaldehyde azine with *N*-phenylbenzonitrilimine; R. Huisgen, R. Grashey, E. Aufderhaar, and R. Kunz, *Chem. Ber.*, **98**, 642 (1965).

6) The IR spectra of the red solution showed the absorption due to the C=S=N bond at 980 cm^{-1}.

7) "Beilsteins Handbuch der Organischen Chemie," **12**, II, 118.

8) R. Albrecht, G. Kresze, and B. Mlakar, *Chem. Ber.*, **97**, 483 (1964).

9) The structures were identified by a comparison of their melting points and spectral data with those of the authentic samples reported by Kresze *et al.*[8]

10) E. H. Huntress, E. B. Hershberg, and I. S. Cliff, *J. Am. Chem. Soc.*, **53**, 2720 (1931).

11) No clear NMR spectra of **15a,b,d** could be obtained because of the instability and/or dissociation in a solution.

Liquid-phase Peptide Synthesis by Fragment Condensation on a Soluble Polymer Support. III.[1] The Influence of the Content and the Chain Length of a Peptide Anchored to a Soluble Polymer Support on the Reactivity of the Amino-free Terminal of the Peptide

Mitsuaki NARITA,* Shin-ichi ITSUNO, Masanori HIRATA, and Kazuya KUSANO

Department of Industrial Chemistry, Tokyo University of Agriculture and Technology, Nakamachi, Koganei, Tokyo 184

(Received August 18, 1979)

In order to investigate the influence of the content and the chain length of a peptide anchored to a soluble polymer support on the reactivity of the amino-free terminal of the peptide, chloromethylated polystyrene, which is a starting material for peptide synthesis on a matrix, was prepared by the copolymerization of (chloromethyl)-styrene with styrene. By the copolymerization, the chloromethyl content on the resin was easily controlled and obtained as reproducible. The repetitive peptide-chain elongations of a pentapeptide, $-(Ala_2-Leu_3)-$, and a decapeptide, $-(Ala_2-Leu_3-Pro_2-Leu_3)-$, were performed by the usual method, using soluble polymer supports with various contents of Ile–Ile, which was used as the internal reference to evaluate the coupling yields by means of amino-acid analyses of the resulting peptide resins. The solubility of the peptide resin, which depends on the content of the peptide and the solubility of the peptide fragment on the matrix, was found to be one of the important factors for an efficient coupling in liquid-phase fragment condensations on a soluble polymer support.

Solid-phase peptide synthesis by fragment condensation seems to be the most promising method for the synthesis of large, homogeneous proteins.[2,3] This strategy will alleviate the difficulty[3-5] in the purification of a peptide and sequence-dependent problems[6] in the coupling and deprotecting steps. These problems are serious in solid-phase peptide synthesis by step-by-step elongation. An annoying problem in the fragment condensation method is, however, of the lower yield in the coupling step, resulting mainly from the restriction of the permeability of an *N*-protected peptide fragment into a random cross-linked polymer support which carries the amino-free terminal of peptide.[2] The use of soluble polymer supports for peptide synthesis has several advantages in carrying out peptide synthesis under homogeneous conditions. In previous papers,[1,7] we have reported that the fragment condensation on a soluble polymer support can achieve an efficient coupling of an *N*-protected tetrapeptide acid to the amino-free terminal anchored to the soluble polymer support and that the peptide-chain length of the *N*-protected tetrapeptide acid has no influence on the reactivity of the *C*-terminal amino acid in the coupling reaction using DCC[8] plus HOBt and DEPC as the coupling reagents. In this paper, we wish to report on the influence of the content and the chain-length of the peptide anchored to the soluble polymer support on the coupling reaction of Boc-peptide acids with the amino-free terminal of the peptide on the matrix.

Results and Discussion

For the above purpose, it is desirable to obtain a chloromethylated polystyrene with a controlled chlorine content. Merrifield resins which have been used in peptide synthesis generally started from the chloromethylation of a copolymer of styrene with divinylbenzene.[9] The chloromethylation of polystyrene with chloromethyl methyl ether, which is a polymer reaction, is usually accompanied by concomitant cross-linking due to the intermolecular Friedel-Crafts reaction with a tin(IV) chloride catalyst; also, it is difficult to control the chlorine content.[10,11] One could expect the cross-linking to produce sterically unfavored reaction sites, which are chemically reactive but physically inaccessible.[12] A skillful technique is also required to get a reproducible chlorine value by the chloromethylation of polystyrene with chloromethyl methyl ether.[13] The use of tin(IV) chloride as a catalyst has been further claimed to be disadvantegeous in causing a clustering of the reaction sites.[14] The preparation of a soluble chloromethylated polystyrene by the copolymerization of styrene with (chloromethyl)styrene seems, though, to have several advantages. The copolymerizations of (chloromethyl)styrene (a mixture of *m*- and *p*-isomers, 63: 28, Tokyo Kasei Co.) with styrene, using AIBN as the initiator, were, therefore, carried out in benzene at 70 °C in molar ratios of (chloromethyl)-styrene as 1 mol%, 3 mol%, 10 mol%, and 30 mol% respectively. The results are summarized in Table 1. The chlorine contents of the chloromethylated polystyrenes were determined by the Volhard method after a reaction with pyridine; they were in fair agreement with those calculated from the feed-molar ratios. The molecular weights of the polymers were measured by vapor-pressure osmometric equilibrium (VPOE) method. The reactivity ratios of (chloromethyl)styrene with styrene were not determined, since the (chloromethyl)styrene used was a mixture of *m*- and *p*-isomers. The polymer was free from an insoluble material, homo-polystyrene. This was confirmed by the fact that the pyridinium chloride derived from the reaction of 10 mol% chloromethylated polystyrene with pyridine was soluble in methanol. It could, therefore, be estimated that the chloromethyl groups were distributed at random on the resin. In comparison with the chloromethylation of soluble polystyrene,[10] which is liable to cause a heterogeneous environment due to partial

Table 1. Results of the copolymerization of (chloromethyl)styrene with styrene[a)]

Monomers to be fed (mmol)		Mol% of (chloromethyl)-styrene (mmol/g)	Product		
Styrene	(Chloromethyl)styrene		Yield (%)	Cl content[c)] (mmol/g)	Mol. wt.[d)]
396	4	1 (0.096)	84	0.096	—
582	12	3 (0.28)	99	0.27	44000
540	60	10 (0.92)	61	0.89	17000
146	63	30 (2.53)[b)]	72	2.43	21000

a) The copolymerizations were carried out using AIBN (0.5 mol %) as the initiator in benzene at 70±0.5°C for 40 h. b) One mol % of AIBN was used as the initiator. c) Determined by the Volhard method. d) Determined by the VPOE method.

Table 2. Estimated secondary structures of Boc-peptide acids and peptides on polymer supports

Peptide	Estimated secondary structure
Boc–Ala_2–Leu_3–OH	β-Sheet
Boc–Ala_2–Leu_3–Pro_2–Leu_3–OH	Randam coil
H{Ala_2–Leu_3}$_n$$Ile_2$–$OCH_2$–resin	α-Helix ($n \geqq 2$)
H{Ala_2–Leu_3–Pro_2–Leu_3}$_n$$Ile_2$–$OCH_2$–resin	Randam coil ($n \geqq 1$)

cross-linking, the copolymerization of (chloromethyl)-styrene with styrene has several advantages; 1) easy control of the chloromethyl content on the resin; 2) the absence of any cross-linking reaction, affording polymers with a nearly homogeneous structure; 3) easy preparation of polymers with a reproducible chloromethyl content; 4) the exclusion of the use of carcinogenic chloromethyl methyl ether, and 5) the exclusion of the clustering of chloromethyl groups when tin(IV) chloride is used as the catalyst.

The efficient peptide-bond formation on the polymer support is put under the influence of several factors, such as the permeability of reagents, the steric micro-environment of reactive sites on the polymer support (peptide-peptide or peptide-resin steric interactions),[5] the secondary or tertiary structure of the *N*-protected peptide acid (reagent) and the peptide on the polymer support,[6] and the solvation of the matrix and the peptide chain.[5,6,15] In order to evaluate these difficulties, the repetitive elongation of a decapeptide or a pentapeptide on the polymer support was carried out using polymer supports with various Ile-Ile contents. Boc–Ala_2–Leu_3–OH and Boc–Ala_2–Leu_3–Pro_2–Leu_3–OH were used as the *N*-protected penta- and decapeptide acids respectively. The secondary structures of the sequential poly(penta- and decapeptide)s are estimated to be the α-helix and the random coil respectively by the methods of Chou and Fasman[16] and Katakai,[17] as is shown in Table 2.

All the peptides used here were synthesized using DCC and HOBt as coupling reagents. The deprotection of the Boc group was carried out in 3 M HCl–AcOEt, and the deprotection of Bzl group, by hydrogenolysis using 5% Pd/C as the catalyst. The amino group was liberated from the salt with NMM. The preparations of Boc–Ala_2–Leu_3–OH and H–Pro_2–Leu_3–OBzl·HCl are shown in Schemes 1 and 2. Boc–Ala_2–OBzl, Boc–Pro_2–OBzl, and Boc–Leu_2–OBzl were prepared in 93%, 76%, and 71% yields respectively by the coupling reactions of Boc-amino acids with benzyl esters. Boc–Leu_3–OBzl was prepared in a 67% yield by the step-by-step elongation, starting from H–Leu–OBzl·TosOH. Boc–Ala_2–Leu_3–OBzl and Boc–Pro_2–Leu_3–OBzl were obtained in 91% and 82% yields respectively by the coupling reactions of H–Leu_3–OBzl with Boc–Ala_2–OH and Boc–Pro_2–OH. The reaction between Boc–Ala_2–Leu_3–OH and H–Pro_2–Leu_3–OBzl gave Boc–Ala_2–Leu_3–Pro_2–Leu_3–OBzl in an 87% yield; this then provided the desired *N*-protected peptide acid, Boc–Ala_2–Leu_3–Pro_2–Leu_3–OH, in an 81% yield by hydrogenolysis.

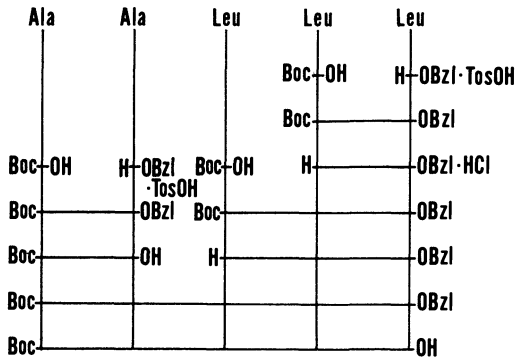

Scheme 1.

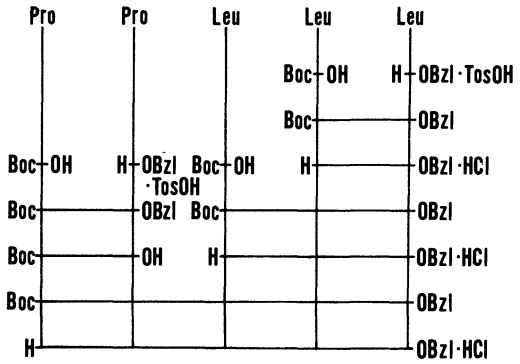

Scheme 2.

Ile–Ile was anchored to soluble polymer supports as the internal reference by the reaction of chloromethylated polystyrenes (1 mol%, 3 mol%, and 30 mol% chlorine content) with Boc–Ile_2–OH, using potassium carbonate in DMF, followed by deprotection and neutralization, to give Ile_2–OCH_2–resins (Resins A, B, and C respectively). Residual benzylic chlorine atoms, which cause unavoidable cross-linking, were removed by heating the Boc–Ile_2–OCH_2–resins with sodium acetate in DMF. The Ile contents in acid hydrolysates of Boc–Ile_2–OCH_2–resins (Resins A′, B′, and C′) are summarized in Table 3.

Table 3. Amino-acid analyses of Boc–Ile_2–OCH_2–resins (Resins A′, B′, and C′)

Cl content of the starting resin (mol %)	Product	Ile_2 content (mmol/g)	Conversion[b] (%)
1	Resin A′	0.088(0.093)[a]	95
3	Resin B′	0.25(0.261)[a]	96
30	Resin C′	1.24(1.39)[a]	89

a) Theoretical values calculated from each theoretical chlorine content. b) Conversion from the chloromethyl group to the Boc–Ile_2–OCH_2 group : calculated from each theoretical Ile content.

Boc–peptide acid + H–$(peptide)_{n-1}$–resin $\xrightarrow[\text{Step 1}]{\text{DCC, HOBt in DMF}}$

Boc–$(peptide)_n$–resin $\xrightarrow[\text{Step 3}]{CH_3COOH, \text{ DCC, HOBt in DMF}}$

$\xrightarrow[\text{Step 5}]{\text{5 M HCl–THF}}$ HCl·H–$(peptide)_n$–resin $\xrightarrow[\text{Step 7}]{Et_3N \text{ in DMF}}$

H–$(peptide)_n$–resin

Boc–peptide acid: Boc–Ala_2–Leu_3–OH and Boc–Ala_2–Leu_3–Pro_2–Leu_3–OH

resin: –Ile_2–OCH_2–resin (resin A, B, and C)

n: number of cycle (n=1, 2, and 3)

Scheme 3.

Each repetitive peptide-chain elongation of the penta- and the decapeptides was performed using the cycle summarized in Table 4. The reaction of each step is shown in Scheme 3. The fragment condensation on the soluble polymer support was carried out in DMF, using DCC and HOBt as coupling reagents (Step 1); this procedure had been shown to be effective for the fragment condensation.[7,18] The residual amino group was terminated by the treatment with acetic acid in DMF, using DCC and HOBt as coupling reagents (Step 3). The Boc group was removed with 5 M HCl–THF or 20% CF_3COOH–CH_2Cl_2 (v/v) (Step 5),[19] while the amino group was liberated from the salt, formed with the excess of the acid used for deprotection, by treatment with Et_3N in DMF (Step 7). In these processes, the inherent simplicity of peptide synthesis using the polymer support can be preserved for the separation and purification of intermediate resins (Steps 2, 4, 6, and 8). In these steps, the recovery of the resulting peptide resin by precipitation from the solution with a non-solvent was in a near-quantitative yield. After the termination reaction on each cycle, an aliquot of peptide resin was hydrolyzed with acid and analyzed for its amino-acid composition. The amino-acid ratios in the acid hydrolysates of the resulting peptide resins and the coupling yields in each cycle for the fragment condensations of Boc–Ala_2–Leu_3–OH and Boc–Ala_2–Leu_3–Pro_2–Leu_3–OH using the three resins, A, B, and C, are summarized in Tables 5 and 6. The yield of the coupling reaction on cycle n was calculated, by making correction by the use of the coupling yields of the n-2 and/or n-1 cycles, from the recovery of Leu in the acid hydrolysate, taking the recovery of Ile as the standard. The coupling reactions of the penta- and decapeptide acids with each resin kept a more than 90% yield in the first cycle. The yield on the reaction of the pentapeptide acid with the B and C resins in the second and third cycles decreased gradually in accordance with the decrease in the solubility of peptide resins in DMF. In the coupling reactions of the second cycles, in practice, gelation took place in the solutions of resins in which the peptide-bond formation was proceeding. Using Resin A, which bound peptides to the smallest degree, the peptide-bond formation on each cycle could proceed homogeneously and keep a high coupling yield. A tendency for the yield of the peptide-chain elongation to decrease was observed in the coupling reaction of the decapeptide acid with Resin C, which bound peptide to the highest degree. The solubility of Boc–Ala_2–Leu_3–Pro_2–Leu_3–OBzl in organic solvents is greater than that of Boc–Ala_2–Leu_3–Ala_2–Leu_3–OBzl, which is only slightly soluble in DMF, ethanol, and methanol. The solubility of the peptide fragment on the matrix directly affects that of the peptide resin.

In conclusion, the solubility of peptide resin, which is related to the solvation of the matrix and the peptide chain, the permeability of reagents, and the steric microenvironment of the reactive sites on the matrix,

Table 4. A cycle for the addition of one oligopeptide in each repetitive peptide elongation

Step	Function	Reagent, solvent, and/or nonsolvent
1	Coupling	Boc–peptide acid, DCC, and HOBt in DMF
2	Precipitation, wash, and dry	Ethanol, water, and methanol
3	Termination	Acetic anhydride and pyridine in DMF
4	Precipitation, wash, and dry	Ethanol, water, and methanol
5	Deprotection	5 M HCl–THF or 20% CF_3COOH–CH_2Cl_2
6	Precipitation, wash, and dry	Ethanol, water, and methanol
7	Neutralization	Et_3N in DMF
8	Precipitation, wash, and dry	Ethanol, water, and methanol

Table 5. The yields in each coupling step of the repetitive peptide-chain elongation of pentapeptide

Resin	Cycle 1			Cycle 2			Cycle 3		
	Amino-acid contents on resins (μmol/g)		Yield[a] (%)	Amino-acid contents on resins (μmol/g)		Yield[b] (%)	Amino-acid contents on resins (μmol/g)		Yield[c] (%)
	Ile	Leu		Ile	Leu		Ile	Leu	
A	80×2	73×3	91	75×2	63×6	87	72×2	60×9	90
B	221×2	210×3	95	207×2	178×6	81	185×2	124×9	34
C	709×2	700×3	99	512×2	423×6	67	529×2	337×9	39

a) Determined by means of the amino-acid ratios. b) Determined by means of the amino-acid ratios, making correction by the use of the coupling yields of Cycle 1. c) Determined by means of the amino-acid ratios, making correction by the use of the coupling yields of Cycles 1 and 2.

Table 6. The yields in each coupling step of the repetitive peptide-chain elongation of decapeptide

Resin	Cycle 1			Cycle 2			Cycle 3		
	Amino-acid contents on resins (μmol/g)		Yield[a] (%)	Amino-acid contents on resins (μmol/g)		Yields[b] (%)	Amino-acid contents on resins (μmol/g)		Yields[c] (%)
	Ile	Leu		Ile	Leu		Ile	Leu	
A	61×2	55×6	90	59×2	47×12	77	54×2	42×18	107
B	199×2	182×6	92	180×2	159×12	93	135×2	113×18	87
C	567×2	522×6	92	478×2	285×12	65	—	—	—

a) Determined by means of the amino-acid ratios. b) Determined by means of the amino-acid ratios, making correction by the use of the coupling yields of Cycle 1. c) Determined by means of the amino-acid ratios, making correction by the use of the coupling yields of Cycles 1 and 2.

is one of the most important factors in determining the efficient coupling yield in liquid-phase peptide synthesis on the soluble polymer support by means of fragment condensation. This technique has several advantages; 1) the reaction can easily be done in a homogeneous system and in a near-quantitative yield by controlling the peptide content on the matrix, 2) the intermediates can easily be handled for separation and purification, 3) the solubility of intermediates can easily be observed, and 4) there is a possibility of the optical analysis of the secondary structure of the peptide chain anchored to the matrix. There is, in fact, the prospect of the homogeneous synthesis of a large (50 amino acids or more) peptide or protein (100 amino acids or more).

Experimental

General. The uncorrected capillary melting points will be reported. The infrared spectra were recorded on a JASCO Model DS-403G. The molecular weights were determined by the VPOE method, using a Hitachi Model 117 molecular-weight-measurement instrument. The optical rotations were taken in a 1-dm cell on a JASCO Model ORD/UV-5 optical rotatory dispersion recorder. The elemental analyses were performed on a Perkin Elmer Model 240 elemental analyzer.[20] The amino-acid compositions of the acid hydrolysates were determined with a Hitachi Liquid Chromatograph, Model 034. The acid hydrolyses of the peptide resins were carried out on 20—40 mg samples of resins with propionic acid–12 M HCl (2: 1 v/v) for 35 h at 115 °C in sealed tubes. Ascending TLC was performed on silica gel plates (Wakogel Plate from Wako, Tokyo) using the following solvent system: chloroform–methanol–acetic acid (45: 4: 1 by vol).

Materials. The (chloromethyl)styrene (a mixture of *m*- and *p*-isomers, 63: 28) was purchased from the Tokyo Kasei Co., Tokyo, and was used without purification. The Boc-amino acids were prepared according to Nagasawa *et al.*[21] The amino acid benzyl ester tosylates[22a] and HOBt[22b] were prepared by the methods given in the literature. The DMF was purified as follows. To 1.5 l of DMF we added 75 g of phthalic anhydride, after which the mixture was kept overnight at room temperature and then distilled under reduced pressure. It was then redistilled under reduced pressure. The benzene, styrene, THF, and AcOEt were purified in the usual manners. All the other reagents were obtained from commercial sources and were used without further purification.

Soluble Chloromethylated Polystyrene. The copolymerizations of (chloromethyl)styrene with styrene, using AIBN as the initiator, were carried out in benzene for 40 h at 70 °C in molar ratios of (chloromethyl)styrene of 1 mol%, 3 mol%, 10 mol%, and 30 mol% under the conditions described previously.[7] The results are summarized in Table 1. The chlorine contents of the polymers were determined by the Volhard method after the reaction with pyridine. The 10 mol% polymer (0.5 g) was reacted in 3 ml of pyridine for 2 h at 100 °C, after which the solution was poured into water and a small amount of saturated aqueous sodium chloride was added. The precipitated polymer, pyridinium salt, was collected by filtration and dried *in vacuo*. It was soluble in methanol and free from insoluble material.

Boc–Ala$_2$–OBzl, Boc–Leu$_2$–OBzl, Boc–Pro$_2$–OBzl, and Boc–Ile$_2$–OBzl. Boc–Ala–OH (9.72 g, 51 mmol) and H–Ala–OBzl·TosOH (16.42 g, 47 mmol) were dissolved in 90 ml of THF, followed by the addition of NMM (4.72 g, 47 mmol) dissolved in 10 ml of THF and HOBt (7.20 g, 47 mmol). To the solution cooled at 0 °C we then added DCC (10.60 g, 51 mmol) dissolved in 30 ml of THF; the mixture was stirred for 2 h at 0 °C and then overnight at room temperature. After the solution had then been cooled for 30 min at 0 °C, the precipitates were filtered off and the filtrate was concentrated under reduced pressure. The residue was dissolved in 200 ml of AcOEt, and the solution was successively washed in the

usual way three times with 10% aqueous citric acid, twice with aqueous sodium chloride, three times with 4% aqueous sodium hydrogencarbonate, and twice with aqueous sodium chloride, and dried over sodium sulfate, using charcoal for decolorization. After the removal of the solvent *in vacuo*, the residue was dissolved in a mixture of AcOEt (90 ml) and petroleum ether (180 ml), and the solution was kept for 30 min at 0 °C. The precipitated *N,N'*-dicyclohexylurea was filtered off, and the filtrate was concentrated to give a crude peptide (15.3 g, 93% yield). Subsequent recrystallization from a mixture of AcOEt (20 ml) and hexane (120 ml) gave a substance, mp 69—71 °C (lit,[23] 68—70 °C); $[\alpha]_D^{22} = -60.2°$ ($c = 1.0$, CH_3OH); a single spot by TLC in the solvent system (R_f, 0.65). Boc-Leu_2-OBzl (mp 92—93 °C, lit,[24] 92—92.5 °C), Boc-Pro_2-OBzl (oil), and Boc-Ile_2-OBzl (mp 89.5—91.5 °C) were similarly prepared.

Boc-Leu_3-OBzl. The preparation was performed as has been described above using Boc-Leu-OH·H_2O (18.52 g, 74.3 mmol) and H-Leu_2-OBzl·HCl (27.55 g, 74.3 mmol), prepared by the treatment of Boc-Leu_2-OBzl with 3 M HCl-AcOEt in the usual way; 84% yield. Subsequent recrystallization from a mixture of AcOEt (20 ml) and hexane (200 ml) gave a substance, mp 127—128.5 °C; $[\alpha]_D^{25} = -64.9°$ ($c = 1.0$, CH_3OH); a single spot by TLC in the solvent system (R_f, 0.75). Found: C, 65.28; H, 9.06; N, 7.71%. Calcd for $C_{30}H_{49}N_3O_6$: C, 65.78; H, 9.02; N, 7.67%.

Boc-Ala_2-OH, Boc-Pro_2-OH, and Boc-Ile_2-OH. Boc-Ala_2-OBzl (14.0 g, 40 mmol) was hydrogenated at atmospheric pressure in a mixture of methanol (30 ml) and acetic acid (20 ml) in the presence of 5% Pd/C (1.0 g) as a catalyst. The reaction mixture was then stirred overnight at room temperature. After the removal of the Pd/C, the filtrate was concentrated under reduced pressure, followed by the repetition of the addition of water and its removal under reduced pressure to eliminate acetic acid, and drying *in vacuo*. The product was recrystallized from a mixture of AcOEt (80 ml) and hexane (120 ml) to give, in a near-quantitative yield, a material, mp 120—121 °C (lit, 85.5—87 °C,[25] 128—129 °C,[2d] 132—133 °C[26]); $[\alpha]_D^{22} = -39.1°$ ($c = 1.0$, CH_3OH); a single spot by TLC in the solvent system (R_f, 0.34). Boc-Pro_2-OH was purified as the dicyclohexylamine salt; mp 161—162 °C, $[\alpha]_D^{23} = -72.8°$ ($c = 1.0$, CH_3OH), R_f 0.40. Found: C, 65.86; H, 9.66; N, 8.67%. Calcd for $C_{27}H_{47}N_3O_5$: C, 65.69; H, 9.60; N, 8.51%.

Boc-Ala_2-Leu_3-OBzl and Boc-Pro_2-Leu_3-OBzl. The preparation of Boc-Ala_2-Leu_3-OBzl was carried out in THF in a manner similar to that described for the preparation of Boc-Ala_2-OBzl, using Boc-Ala_2-OH (11.5 g, 44 mmol) and H-Leu_3-OBzl·HCl (17.9 g, 37 mmol), prepared by the treatment of Boc-Leu_3-OBzl with 3 M HCl-AcOEt in the usual way; 91% yield. Subsequent recrystallization from a mixture of AcOEt and hexane (1: 3) gave a material, mp 230—235 °C (dec); $[\alpha]_D^{22} = -70.5°$ ($c = 1.0$, CH_3OH); a single spot by TLC in the solvent system (R_f, 0.53). Found: C, 62.40; H, 8.70; N, 9.93%. Calcd for $C_{36}H_{59}N_5O_8$: C, 62.68; H, 8.62; N, 10.15%.

Boc-Pro_2-Leu_3-OBzl was obtained by a similar method in an 82% yield. Subsequent recrystallization from a mixture of AcOEt and hexane (1: 3) gave a material, mp 91.5—93 °C; $[\alpha]_D^{26} = -119.2°$ ($c = 1.0$, CH_3OH); a single spot by TLC in the solvent system (R_f, 0.58). Found: C, 65.02; H, 8.56; N, 9.28%. Calcd for $C_{40}H_{63}N_5O_8$: C, 64.75; H, 8.56; N, 9.44%.

Boc-Ala_2-Leu_3-OH. The hydrogenolysis of Boc-Ala_2-Leu_3-OBzl in the manner described for the preparation of Boc-Ala_2-OH gave Boc-Ala_2-Leu_3-OH in an 87% yield. Subsequent recrystallization from a mixture of ethanol and AcOEt (1: 6) gave a substance, mp 265—270 °C (dec); $[\alpha]_D^{23} = -69.5°$ ($c = 1.0$, CH_3OH); a single spot by TLC in the solvent system (R_f, 0.46). Amino-acid ratios in acid hydrolysate: Ala 2.00, Leu 2.94. Found: C, 57.68; H, 8.73; N, 11.38%. Calcd for $C_{29}H_{53}N_5O_8$: C, 58.07; H, 8.91; N, 11.68%.

Boc-Ala_2-Leu_3-Pro_2-Leu_3-OBzl. Boc-Ala_2-Leu_3-OH (7.73 g, 12.9 mmol) and H-Pro_2-Leu_3-OBzl-HCl (7.95 g, 11.7 mmol), prepared from Boc-Pro_2-Leu_3-OBzl in the usual way, were dissolved in 100 ml of DMF, and then NMM (1.19 g, 11.7 mmol), dissolved in 20 ml of DMF and HOBt (1.98 g, 12.9 mmol), was added. To the solution cooled at 0 °C we then added DCC (2.66 g, 12.9 mmol), dissolved in 30 ml of DMF; the reaction mixture was stirred for 2 h at 0 °C and then overnight at room temperature. After the mixture had then been cooled for 1 h at 0 °C, the precipitates were filtered off and the filtrate was concentrated under reduced pressure. To the residue we added water to give a solid. On a glass filter, it was successively washed with 10% aqueous citric acid, water, 4% aqueous sodium hydrogencarbonate, and water, and dried *in vacuo*; yield, 87%. Recrystallization from AcOEt gave a material, mp 194—194.5 °C; $[\alpha]_D^{25} = -119.4°$ ($c = 1.0$, CH_3OH); a single spot by TLC in the solvent system (R_f, 0.54). Found: C, 62.45; H, 8.78; N, 11.33%. Calcd for $C_{64}H_{106}N_{10}O_{13}$: C, 62.82; H, 8.73; N, 11.45%.

Boc-Ala_2-Leu_3-Pro_2-Leu_3-OH. Boc-Ala_2-Leu_3-Pro_2-Leu_3-OBzl (9.0 g, 7.4 mmol) was hydrogenated at atmospheric pressure in a mixture of methanol (100 ml) and acetic acid (20 ml) in the presence of 5% Pd/C (1.0 g) as a catalyst; then it was subjected to the work-up procedures described in the preparation of Boc-Ala_2-OH. The product was recrystallized from a mixture of ethanol and AcOEt (1: 6) to give, in an 81% yield, a material, mp 187—188.5 °C; $[\alpha]_D^{25} = -134.2°$ ($c = 1.0$, CH_3OH); a single spot by TLC in the solvent system (R_f, 0.48). Amino-acid ratios in acid hydrolysate: Ala 2.00, Leu 5.95, Pro 2.09. Found: C, 60.31; H, 8.61; N, 11.89%. Calcd for $C_{57}H_{100}N_{10}O_{13}$: C, 60.40; H, 8.89; N, 12.36%.

H-Ile_2-resins (Resins A, B, and C). As a typical example, 1 mol% chloromethylated polystyrene (Cl content, 0.096 mmol/g; 10.0 g) and Boc-Ile_2-OH (0.99 g, 2.88 mmol) were dissolved in 100 ml of DMF. To the solution, maintained at 40 °C, we added potassium carbonate (0.20 g, 1.44 mmol), after which the reaction mixture was stirred for 100 h at 40 °C. The addition of this mixture to ethanol (1 l) caused the precipitation of a solid, which was collected, homogenized with water, filtered off again, washed with water and methanol, and dried *in vacuo*. A solution of the product in THF (200 ml) was poured into ethanol. For the precipitate we repeated the work-up procedures described above. The yield was 10.2 g (99%). Residual benzylic chlorides were removed by a reaction with sodium acetate in DMF at 105 °C for 24 h, as has been described in the literature.[10] The Resin A' obtained was negative to a Beilstein test, indicating it to be free from chlorine. The removal of the Boc-group with the saturated HCl-THF solution and the neutralization of the amine salt with Et_3N were performed by procedures similar to those described in the literature[10] to give Resin A. Resins B and C were obtained from 3 mol% and 30 mol% chloromethylated polystyrene respectively by the same work-up procedures. The Ile content of each resin is shown in Table 3.

A Cycle of Peptide-chain Elongation on the Matrix for the Addition of One Oligopeptide. Each repetitive peptide-chain elongation of the penta- and the decapeptides was performed using the cycle summarized in Table 4. The reaction conditions are shown in Table 7. As a typical example, Resin B (amino content, 0.25 mmol/g; 4.00 g), a two-fold equivalent of Boc-Ala_2-Leu_3-OH (1.20 g, 2.00 mmol), and HOBt (0.336 g, 2.20 mmol) were dissolved in DMF (60 ml). To the solution

Table 7. Reaction conditions for the addition of one oligopeptide in each repetitive peptide-chain elongation

Step	Reagents[a]	Solvent	Reaction conditions	
			Time/h	Temp/°C
1	Two-fold equivalent each of Boc-peptide acid and DCC, and a 2.2 times equivalent of HOBt	DMF 12—20 ml/g-resin	48 24[b]	0 r.t.
3	Two-fold equivalent each of acetic acid and DCC, and a 2.2 times equivalent of HOBt	DMF 12—20 ml/g-resin	20	r.t.
5[c]	5 M HCl–THF	THF 10—40 ml/g-resin	15	0
7	4—5 times equivalent of Et_3N	DMF or THF 20—40 ml/g-resin	10 min	r.t.

a) The amounts used were based on the amount of the Ile amino-free terminal of the starting resins, A, B, and C. b) On Cycles 2 and 3, 48 h. c) In the case of Cycle 2 using Resin C, the removal of the Boc group was performed in 20% CF_3COOH-CH_2Cl_2 (v/v), 20—30 ml/g resin, for 2 h at room temperature.

cooled at 0 °C we then added DCC (0.412 g, 2.00 mmol) dissolved in DMF (20 ml) and cooled at 0 °C; the mixture was stirred for 48 h at 0 °C and then for 24 h at room temperature. The reaction mixture was near-negative to a ninhydrin test. It was then poured into ethanol (1 l), and 10% aqueous sodium chloride (30 ml) was added. The precipitated resin was filtered off and washed successively with water and methanol to remove the soluble reactant. The resin was homogenized with ethanol (200 ml) overnight at room temperature under magnetic stirring, filtered off again, washed with water and methanol, and dried *in vacuo* at 50 °C. The yield was 4.45 g (recovery yield, 97%).

The termination reaction of the unreacted N-terminal amino group of the resin was carried out as follows. The resin (4.05 g) obtained above, acetic acid (0.12 g, 2.0 mmol), and HOBt (0.34 g, 2.2 mmol) were dissolved in DMF (120 ml). To the solution we then added DCC (0.41 g, 2.0 mmol) dissolved in DMF (30 ml), after which reaction mixture was stirred for 20 h at room temperature. The reaction mixture was negative to a ninhydrin test. The addition to ethanol (1 l) caused the precipitation of a solid, which was collected by filtration, washed with water and methanol, and dried *in vacuo* at 50 °C.

The removal of Boc-group with 6 M HCl–THF and the neutralization of the amine salt with Et_3N were performed in the usual ways under the conditions described in Table 7.

References

1) Part II of this series: M. Narita, *Bull. Chem. Soc. Jpn.*, **52**, 1229 (1979).

2) (a) H. Yajima, Y. Kiso, Y. Okada, and H. Watanabe, *J. Chem. Soc., Chem. Commun.*, **1974**, 106; (b) C. H. Wong, S. T. Chen, C. H. Ho, and K. T. Wang, *Biochim. Biophys. Acta*, **536**, 376 (1978); (c) R. Matsueda, H. Maruyama, E. Kitazawa, H. Takahagi, and T. Mukaiyama, *J. Am. Chem. Soc.*, **97**, 2573 (1975); (d) S. Takahashi, *Bull. Chem. Soc. Jpn.*, **50**, 3344 (1977).

3) N. Izumiya, T. Kato, M. Ohno, and H. Aoyagi, "Pepuchido Gosei," Maruzen, Tokyo (1975), p. 206.

4) S. Sakakibara, "Tanpakushitsu No Kagaku IV," ed by K. Narita and T. Murachi, Tokyo Kagaku Dojin, Tokyo (1977), Vol. I, p. 402.

5) J. M. Stewart, *J. Macromol. Sci., Chem.*, **A10**, 259 (1976).

6) (a) F. C. Westall and A. B. Robinson, *J. Org. Chem.*, **35**, 2842 (1970); (b) H. Hagenmaier, *Tetrahedron Lett.*, **1970**, 283; (c) W. S. Hancock, D. J. Prescott, P. R. Vagelos, and G. R. Marshall, *J. Org. Chem.*, **38**, 774 (1973); (d) E. Atherton, D. L. J. Clive, and R. C. Sheppard, *J. Am. Chem. Soc.*, **97**, 6584 (1975).

7) M. Narita, *Bull. Chem. Soc., Jpn.*, **51**, 1477 (1978).

8) The abbreviations for amino acids and protecting groups are those recommended by the IUPAC-IUB Commission on Biochemical Nomenclature, *J. Biol. Chem.*, **247**, 977 (1972). The amino-acid symbols denote the L-configuration. Additional abbreviations: DCC, *N,N'*-dicyclohexylcarbodiimide; HOBt, 1-hydroxyl-1*H*-benzotriazole; DEPC, diethoxyphosphoryl cyanide; AIBN, azobisisobutyronitrile; AcOEt, ethyl acetate; NMM, *N*-methylmorpholine; DMF, *N,N*-dimethylformamide; Et_3N, triethylamine; THF, tetrahydrofuran; TosOH, *p*-toluenesulfonic acid.

9) R. B. Merrifield, *J. Am. Chem. Soc.*, **85**, 2149 (1963).

10) B. Green and L. R. Garson, *J. Chem. Soc., C*, **1969**, 401.

11) J. H. Patterson, in "Biological Aspects of Reactions on Solid Supports," ed by G. Stark, Academic, New York (1973), p. 389.

12) M. A. Tilak, *Tetrahedron Lett.*, **1968**, 6323.

13) S. Sakakibara, "Tanpakushitsu No Kagaku IV," ed by K. Narita and T. Murachi, Tokyo Kagaku Dojin, Tokyo (1977), Vol. I, p. 405.

14) A. R. Mitchell, S. B. H. Kent, B. W. Erickson, and R. B. Merrifield, *Tetrahedron Lett.*, **1976**, 3795.

15) D. Yamashiro, J. Blake, and C. H. Li, *Tetrahedron Lett.*, **1976**, 1469.

16) (a) P. Y. Chou and G. D. Fasman, *Biochemistry*, **13**, 211 (1974); (b) *ibid.*, **13**, 222 (1974).

17) (a) R. Katakai, *J. Am. Chem. Soc.*, **99**, 232 (1977); (b) R. Katakai, *J. Chem. Soc., Perkin. Trans. 1*, **1979**, 905.

18) W. König and R. Geiger, *Chem. Ber.*, **103**, 788 (1970).

19) The Boc-protecting group on resin can be completely removed within 5 h by treatment with 6 M HCl–THF or within 1 h by treatment with 20% CF_3COOH-CH_2Cl_2 (v/v). The removal of the Boc-group was confirmed by the disappearance of IR absorption bands at 1720 and 1170 cm^{-1} due to the Boc-group.

20) We wish to thank Mrs. Asuke of this department for these analyses.

21) T. Nagasawa, K. Kuroiwa, K. Narita, and Y. Isowa, *Bull. Chem. Soc. Jpn.*, **46**, 1296 (1973).

22) (a) N. Izumiya, T. Kato, M. Ohno, and H. Aoyagi, "Pepuchido Gosei," Maruzen, Tokyo (1975), p. 72; (b) *ibid.*, p. 149.

23) F. Weygand and C. Di Bello, *Z. Naturforsch. B.*, **24**, 314 (1969).

24) M. D'Alagni, P. Berporad, and A. Garofolo, *Polymer*, **13**, 419 (1972).

25) B. B. Doyle, W. Traub, G. P. Lorenzi, F. R. Brown, III, and E. R. Blout, *J. Mol. Biol.*, **51**, 47 (1970).

26) V. A. Shibnev, L. I. Mar'yash, V. S. Grechishko, and K. T. Poroshin, *Izv. Nauk SSSR, Ser, Khim.*, **1970**, 2820.

Substituent Effects in Heterogeneous Catalysis. VI. Competitive Hydrogenation of Methylenecyclohexane and 2-Methylmethylenecyclohexane over Platinum Group Metals

Kazuo Taya, Shinya Morimoto, Chieko Abe, Kazumi Nomura, Okio Nomura,† and Kazunori Tanaka*,†

Tokyo Gakugei University, Koganei-shi, Tokyo 184

†*The Institute of Physical and Chemical Research, Wako-shi, Saitama 351*

(Received August 18, 1979)

Methylenecyclohexane and its 2-methyl derivative were hydrogenated competitively in cyclohexane at 30 °C over platinum group metals. The methyl derivative was less reactive than the unsubstituted olefin on all the metal catalysts used. The reactivity of the methyl derivative relative to the unsubstituted olefin was not much different in going from one catalyst to another. However, Pd was unique in its very high activity for double bond migration. MINDO/2 calculations have revealed that the olefinic double bonds of the substituted and unsubstituted olefins are essentially identical in bond order but somewhat different in charge density. The observed methyl substituent effect is compared with that observed previously in hydrogenation of cyclohexanone and its 2-methyl derivative.

In a previous work[1] of this series, we conducted competitive hydrogenation of cyclohexanone and its methyl derivatives (2-, 3-, and 4-methylcyclohexanone) using group VIII metals as catalysts in order to study the substituent effects. All of the methylcyclohexanones were less reactive than cyclohexanone. Interestingly, the reactivity of a methylcyclohexanone relative to cyclohexanone could be correlated with the atomic radius of the catalyst metal: among those catalysts on which the same type of reaction scheme operates, the greater the atomic radius the greater the relative reactivity.

A question may now be raised: is this correlation confined to ketone hydrogenation alone or does it extend to include hydrogenation of other types of organic compounds such as olefinic and acetylenic species? The purpose of the present study is to investigate this question by means of competitive hydrogenation of methylenecyclohexane and its 2-methyl derivative. Since this olefin pair is a structural analog of the earlier studied ketone pair, *i.e.*, cyclohexanone and its 2-methyl derivative, the present study will be compared with the earlier one to see how olefin hydrogenation is different from or similar to ketone hydrogenation.

Table 1 lists the abbreviated notations used subsequently for the starting olefins, isomerized olefins, and hydrogenation products.

Table 1. Nomenclature

Compound	In sentence	As subscript
(Starting olefins)		
Methylenecyclohexane	MeneC	A
2-Methylmethylenecyclohexane	2-MMeneC	B
(Isomerized olefins)		
1-Methylcyclohexene	1-MCene	
1,2-Dimethylcyclohexene	1,2-DMCene	
2,3-Dimethylcyclohexene	2,3-DMCene	
(Hydrogenation products)		
Methylcyclohexane	MC	P
cis-1,2-Dimethylcyclohexane	*c*-1,2-DMC	*c*-Q
trans-1,2-Dimethylcyclohexane	*t*-1,2-DMC	*t*-Q

Experimental

Catalysts. The Ru, Rh, Pd, and Os catalysts were prepared fresh from ruthenium trichloride, rhodium trichloride, palladium dichloride, and osmium tetraoxide, respectively, according to the procedure described in the previous paper.[1]

Two methods were used for preparation of the Ir catalyst. (a) It was prepared using iridium trichloride (Mitsuwa Kagaku Yakuhin, 99.9%) as the starting material according to the procedure described previously.[1] (b) A suspension of iridium tetrahydroxide (Mitsuwa Kagaku Yakuhin) in water was reduced at 100 °C for 20 min using an initial hydrogen pressure of 90 kg/cm^2 (1 kg/cm^2≈1 atm=1.013 $\times 10^5$ Pa). The resulting metal precipitate was washed repeatedly with water until the washings were neutral to Thymol Blue, dried under reduced pressure, and stored over silica gel.

The Pt catalyst was prepared by adding aqueous NaOH (10 wt%) in small portions to a stirred warm (60—70 °C) suspension of $PtCl_2$ (Koso Chemical) in water. The mixture was allowed to stand in that temperature range for half an hour. The resulting precipitate was filtered off, washed with water until the washings were neutral, and suspended in water. The reduction of this hydroxide suspension to a metal black was conducted in a glass reaction vessel at ambient temperature using hydrogen at atmospheric pressure. The resulting Pt black catalyst was washed and stored as described above for Ir catalyst (b).

Olefins. MeneC was either purchased from Aldrich Chemical Co. or prepared in our laboratory. The preparation of MeneC and 2-MMeneC was made using as the starting materials hexahydrobenzoic acid and its 2-methyl derivative, respectively. The procedure of Cope and Ciganek[2] was employed with slight modifications. One modification was the substitution of ether extraction for steam distillation in collecting *N,N*-dimethylcyclohexylmethylamine, one of the synthetic intermediates. Another important modification was made to the last stage of the synthetic procedure, *i. e.*, to the procedure for purifying the final product. In the original method, the crude MeneC was washed successively with diluted HCl, aqueous $NaHCO_3$, and with water. Because our preliminary experiment revealed that the alkali washing is prone to contaminate the final product with a trace of basic material (probably *N,N*-dimethylhydroxylamine), we

omitted this operation, and just repeated washing with water before and after HCl washing. The MeneC so prepared had a bp 101—102 °C with n_D^{25} 1.4472 (lit,[2] 102 °C, n_D^{25} 1.4474) and its yield was 18%. The 2-MMeneC obtained had a bp 126.5—128 °C with n_D^{25} 1.4510 (lit,[3] 124.5—124.8 °C/745 mmHg, n_D^{25} 1.4514) and its yield was 13%.

The 1,2- and 2,3-DMCene used as gas chromatography standards in identification of a few isomerized reaction intermediates were prepared from 2-methylcyclohexanone according to the method of Signaigo and Cramer.[4] In brief, 2-methylcyclohexanone was treated with the Grignard reagent CH_3MgI to form 1,2-dimethylcyclohexanol, and this alcohol was then dehydrated by distillation from anhydrous aluminum sulfate. The resulting olefin mixture of 1,2- and 2,3-DMCene and 2-MMeneC was fractionated between 110 and 140 °C. (lit,[3] bp 136.2 °C/745 mmHg for 1,2-DMCene and 130.3—130.7 °C/745 mmHg for 2,3-DMCene).

Procedures. Competitive hydrogenations were conducted according to a procedure similar to that used for the previous study[1] of competitive ketone hydrogenations. In brief, 10 ml of an equimolar solution of MeneC and 2-MMeneC (0.4 mol/l of each) in cyclohexane was placed, together with a weighed sample of metal catalyst (varying from 0.8 to 135 mg), in the glass reaction vessel — the one used in the previous study. The reaction vessel was further charged with an atmospheric pressure of hydrogen, and shaken at a reaction temperature of 30 °C. The reaction was followed volumetrically by measuring the hydrogen uptake and also gas chromatographically by analyzing aliquots of the reaction mixture at appropriate time intervals. The reaction temperature and hydrogen pressure were chosen to be identical with those in the earlier ketone study to permit direct comparison of both kinetic data.

Gas chromatography was carried out on a Yanako Model G 80 FID chromatograph using two columns in series (2.5 m ×3 mm i.d. 20 wt% trixylyl phosphate on Chromosorb W and 5 m×3 mm i.d. 30 wt% 3,3′-oxydipropionitrile on Chromosorb PAW at 65 °C). Base line resolution was obtained for all the peaks.

Two series of experiments were conducted using these procedures so as to measure R_B/R_A for all the catalyst metals in each series. In series I, both starting olefins MeneC and 2-MMeneC were prepared, stored in a refrigerator, and used without redistillation before use. In series II, commercial MeneC and prepared 2-MMeneC were used as the starting olefins. They were kept in the refrigerator and redistilled under nitrogen immediately before use. Ir catalyst (b) was employed in series I, and Ir catalyst (a) in series II.

Treatment of Kinetic Data

In this report we are dealing with competitive hydrogenation of the two olefins, *i.e.*, MeneC and 2-MMeneC. Let us assume that the reaction rate of each olefin is first order in the amount adsorbed, that the catalyst surface is bare in the presence of saturated hydrocarbons alone, and also that olefin adsorption obeys the Langmuir isotherm. These premises lead to the relative rate expression:

$$\frac{R_B}{R_A}\left(\equiv\frac{k_BK_B}{k_AK_A}\right)=\frac{d(C_{c\text{-}Q}+C_{t\text{-}Q})/C_B}{dC_P/C_A} \quad (1)$$

where R is the reaction rate per unit concentration of A or B, k is the rate constant, K is the adsorption coefficient and C is the concentration. The subscripts are listed in Table 1. Let $C_{A(i)}$ and $C_{B(i)}$ stand for the initial concentrations of C_A and C_B, respectively. Neglecting double bond migration and any other side reactions,

$$C_A = C_{A(i)} - C_P \quad (2)$$

and

$$C_B = C_{B(i)} - C_{c\text{-}Q} - C_{t\text{-}Q}. \quad (3)$$

Inserting Eqs. 2 and 3 into Eq. 1 and integrating between the limits $C_P=0$ and C_P and between $C_{c\text{-}Q}+C_{t\text{-}Q}=0$ and $C_{c\text{-}Q}+C_{t\text{-}Q}$ yields

$$\frac{R_B}{R_A}=\log\left(\frac{C_{B(i)}}{C_{B(i)}-C_{c\text{-}Q}-C_{t\text{-}Q}}\right)\Big/\log\left(\frac{C_{A(i)}}{C_{A(i)}-C_P}\right) \quad (4)$$

Results

Side Reactions. Over the $VIII_3$ metals (Os, Ir, Pt) little or no double bond migration occurred (always less than 1% of the conversion to the saturated products). Over Ru and Rh, double bond migration was appreciable but still less than 6% of the total MeneC conversion and less than 2% of the total 2-MMeneC conversion. In the case of Pd, double bond migration was even faster than hydrogenation at the initial stage. These results were not unexpected because group $VIII_2$ metals (Ru, Rh, Pd) were reported to be more active than group $VIII_3$ metals for double bond migration.[5-7] Especially in hydrogenation of 2-MMeneC with Pd, Mitsui *et al.*[8] observed, in accord with our experiments, isomerization/hydrogenation ratios of greater than unity.

Figure 1 shows a typical reaction profile on Pd. This result indicates that *endo*-olefins are much more slowly hydrogenated than *exo*-olefins.[9,10] The same tendency was observed with Ru and Rh.

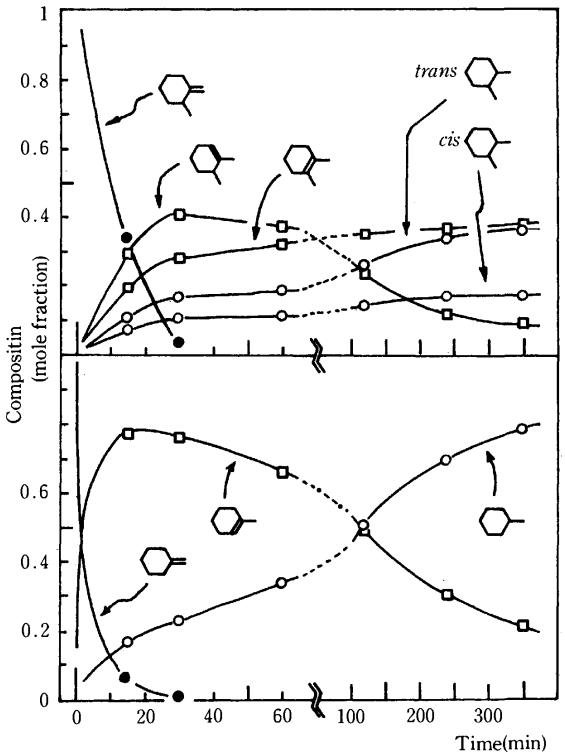

Fig. 1. Typical reaction profile on Pd.

Molar hydrogen uptake and molar olefin consumption were the same within experimental error for all the catalysts. This indicates that little or no hydrogenolysis occurred.

Substituent Effects. As in the earlier work on ketone hydrogenation, let us take the relative reactivity R_B/R_A as a measure of the methyl substituent effect. Except for Pd, the first-order log-log plots according to Eq. 4 were straight, and the R_B/R_A values were obtained from the slope of these plots. In an attempt to estimate the R_B/R_A values also for Pd, the sum $C_{c-Q}+C_{t-Q}$ was plotted against C_P and several slopes on that curve were inserted into Eq. 1 as the differential coefficient. The R_B/R_A values thus worked out, however, did not converge around a constant value.

Table 2. Substituent effect and stereoselectivity

Catalyst	R_B/R_A		*c*-1,2-DMC/*t*-1,2-DMC	
	Series I	II	Series I	II
Ru	0.19	0.14	1.7	3.6
Rh	0.26	0.21	1.1	3.2
Pd	—	—	0.6—0.7	0.5—0.7
Os	0.20	0.14	3.1	4.5
Ir	0.26	0.26	2.4	5.4
Pt	0.29	0.31	2.0	1.9

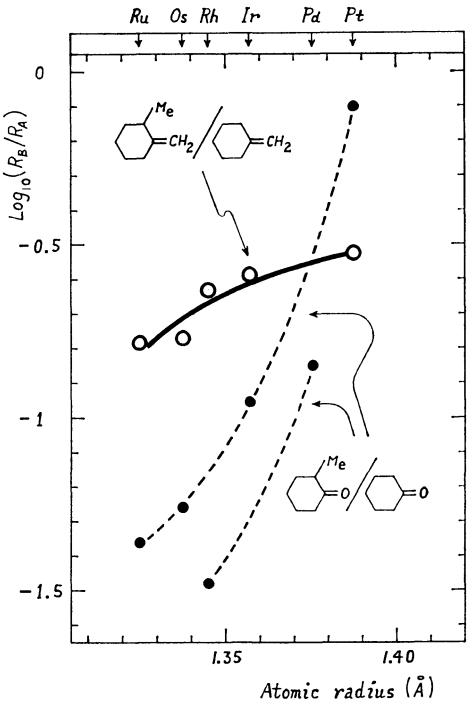

Fig. 2. Relative reactivity as a function of atomic radius of catalyst metal.

In series I, four or five competitive hydrogenation runs were carried out for each catalyst metal using different amounts of catalyst samples. In most cases, values of R_B/R_A for the same catalyst metal agreed within 8%, unless the catalyst amount was extremely small, say 2 mg or below. The experiments with such a small catalyst sample gave rise to either unusually high or low R_B/R_A values. In this case a sizable fraction of the catalyst surface may have been covered by some undetected impurities, and consequently the nature of the catalyst may have been altered so as to give such unusual results. Discarding the unusual R_B/R_A values, the others were averaged for each catalyst and are listed in Table 2. In series II, only one measurement of R_B/R_A was made for each metal catalyst using an appropriate amount of the catalyst. The values obtained are also listed in Table 2. For Ir and Pt, the agreement in R_B/R_A between series I and II is satisfactory. The cause of the small differences observed for the other metals is not clear.

In Fig. 2, the logarithm of R_B/R_A is plotted against the atomic radius of the catalyst metal,[11] where each of the R_B/R_A values is the average of the two values listed for each metal in Table 2. Figure 2 also includes for comparison the corresponding data for the earlier competitive hydrogenation of cyclohexanone and its 2-methyl derivative. It is seen that the $\log(R_B/R_A)$ values for the olefin system depends only slightly upon the atomic radius in contrast with a strong dependence of the ketone system. However, both olefin and ketone systems are alike in that the greater the atomic radius of the catalyst, the less negative is the value of $\log(R_B/R_A)$ or the less pronounced is the methyl substituent effect.

MINDO/2 Calculations. The charge densities and bond orders for MeneC and 2-MMeneC are basic to the understanding of the observed methyl substituent effect; they have been calculated using the MINDO/2 method on a Fujitsu computer Facom 230-75. It is very likely that MeneC is conformationally similar to cyclohexane, and that the chair form is its predominant ground-state conformation.[12] While definitive structural parameters for MeneC and 2-MMeneC are still lacking, a small difference from the cyclohexane skeleton would be expected because of the influence of the olefinic double bond. In particular, the bond angle C_2–$C_1(sp^2)$–C_6 in MeneC would be slightly larger than the cyclohexane C–C–C angle, 111.6°.[12,13] For our MINDO/2 calculations the following geometrical parameters were used for both MeneC and 2-MMeneC: angles 117° (C_2–$C_1(sp^2)$–C_6), 121.5° (C_2–$C_1(sp^2)$–$C_7(sp^2)$ and (C_6–$C_1(sp^2)$–$C_7(sp^2)$), 109.5° (for any other carbon set), 120° ($C_1(sp^2)$–$C_7(sp^2)$–H), 109.5° (H–C(sp^3)–H); distances 1.37 Å (C=C), 1.54 Å (C–C), 1.09 Å (C–H). The methyl substituent in 2-MMeneC was assumed to occupy the equatorial position. In order to define the rotational conformation of the methyl substituent, let us denote the three methyl hydrogens by H_α, H_β, and H_γ, with H_α representing the hydrogen that is taken as parallel to the axial C_3–H bond, and with H_γ representing the hydrogen that points away from the C_1=C_7 double bond. Were the six-membered ring of 2-MMeneC quite identical with that of cyclohexane, then the C_1–C_7–C_2 plane would bisect the H_α–C_8–H_β angle, and hence the distance H_α–C_7 would be equal to the distance H_β–C_7. However, owing to the widening of the C_2–C_1–C_6 angle and to the resulting structural deformation, C_7 should be closer to H_β than to H_α. The distances employed for MINDO/2 calculations

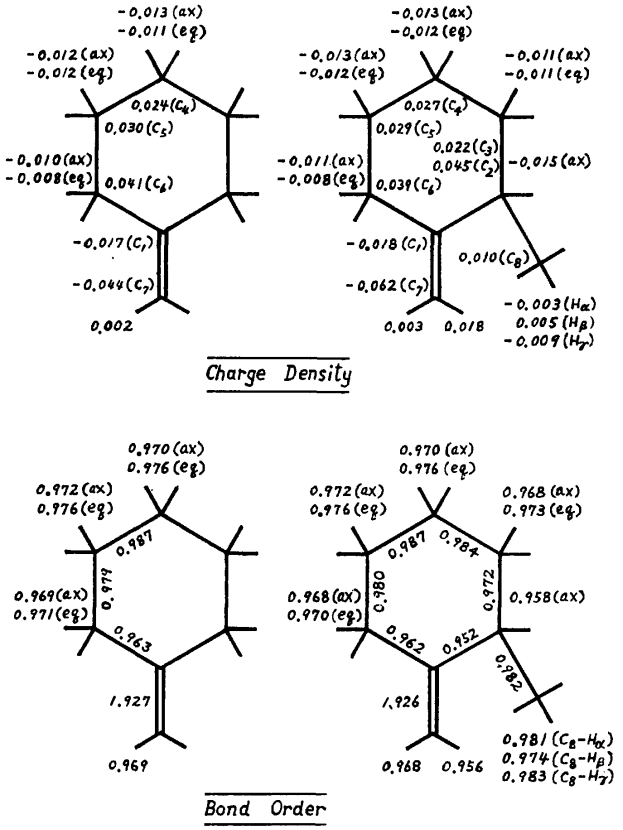

Fig. 3. Charge densities and bond orders for MeneC and 2-MMeneC.

were 2.26 Å for H_α–C_7 and 1.94 Å for H_β–C_7.

The results of the MINDO/2 calculations are shown in Fig. 3. Obviously, MeneC and 2-MMeneC are similar in bond order over the whole molecule, but dissimilar in charge density at and around the functional methylene group. The C=C double bond of 2-MMeneC is more negative and more polarized than that of MeneC. These results are reminiscent of a report of Libit and Hoffmann,[14] who made various molecular orbital calculations on propylene and toluene and showed that there is little net electron transfer from the methyl group to the ethylene or benzene but a significant polarization of the π electron system.

Other Data. Although not directly relevant to the substituent effect, the stereoselectivities measured in this study might be worth noting. Except for Pd, the observed isomeric ratios *c*-1,2-DMC/*t*-1,2-DMC were almost constant at conversions greater than 5%. The constant values are listed in Table 2. It is seen that except for Pd and Pt the absolute values for the isomeric ratio are considerably different between series I and II. However, the order of increasing *cis*/*trans* ratio in series I, Pd<Rh<Ru<Pt<Ir<Os, is not very much different from that in series II, Pd<Pt<Rh<Ru<Os<Ir, and these two sequences also resemble that observed by Nishimura and his associates, Pd≪Rh≈Ru=Pt<Os≈Ir.[15] Palladium is unique in that it produces more *trans* isomer than *cis*. Such *trans* selectivity on Pd was also reported earlier by others.[10,15]

Discussion

It might be worthwhile to make a few comments on Fig. 2 where a comparison is made of 2-methyl substituent effects between two structural analogs—MeneC and cyclohexanone. In the earlier ketone study, we could unambiguously rule out any polar factor because molecular orbital calculations have revealed that the carbonyl group of cyclohexanone and that of its methyl derivative are quite identical in charge densities and bond orders. In contrast, as seen in Figure 3, the olefinic double bond of MeneC is significantly different from that of 2-MMeneC in charge density. Thus, it is difficult to determine the main cause of the methyl substituent effect in the olefin system.

The present olefin system contrasts kinetically with the earlier ketone system in two respects; (i) with the exception of Pt, the olefin system is less negative in $\log(R_B/R_A)$ and (ii) the $\log(R_B/R_A)$ value depends only slightly upon the catalyst in the case of the olefin system, but very strongly in the case of the ketone system. Although more work is needed before these contrasts can be explained, the following matters may have some bearing. First, MeneC and its methyl derivatives are less flexible than their respective cyclohexanone counterparts.[16,17] Therefore, if the boat conformation play any role at all, this role would be more significant in ketone hydrogenation. Secondly, there can exist two distinct half-hydrogenated intermediates, *i.e.*, the C_1-metal- and C_7-metal-monoadsorbed species for olefins and the C_1-metal- and O-metal-monoadsorbed species for ketones. For either system, a larger substituent effect is expected when hydrogenation proceeds through the C_1-metal intermediate because the methyl substituent is closer to the catalyst surface on this intermediate. Thus, the substituent effect is probably influenced by the relative importance of these two intermediates. This relative importance may be quite different between olefin hydrogenation and ketone hydrogenation. Thirdly, the conformational equilibrium, *eq*-Methyl⇋*ax*-Methyl, is shifted further to the right in 2-MMeneC than in its ketone counterpart. Servies, *et al.*[18] experimentally determined the axial-methyl conformer content of 2-methylcyclohexanone to be 10.3% at 31.9 °C. On the other hand, Allinger *et al.*[13] calculated the enthalpy for the conformational equilibrium of 2-MMeneC (*eq*-Methyl⇌*ax*-Methyl) to be 0.50 kcal/mol. Assuming no entropy difference between the two conformers, this enthalpy value gives rise to an axial methyl content of 30.5% for 2-MMeneC at 31.9 °C. Finally, let us compare the C_1,C_7-diadsorbed olefin intermediate with its ketone counterpart, *i.e.*, the C_1,O-diadsorbed intermediate. Since the atomic radius of carbon is a little larger than that of oxygen, the C_7–metal bond in the adsorbed olefin must be a little longer than the O–metal bond in the adsorbed ketone.[19] Therefore, the 2-methyl substituent in the adsorbed olefin is expected to hang down a little further away from the catalyst surface compared with that in the adsorbed ketone. The further away the methyl substituent from the catalyst surface, the smaller

will be its hindrance to adsorption. This might be responsible in part for the less pronounced substituent effect in the olefin system compared with the ketone system on most of the catalyst metals.

Interestingly, Table 2 shows that the relative rate data are fairly reproducible on each catalyst despite large scatter in the *cis/trans* ratio data. This would mean that, compared to the relative rate, the *cis/trans* ratio is more profoundly affected by uncontrolled small variations of catalyst properties and environmental conditions, *e.g.*, change in surface structure due to aging and in minute traces of undetected impurities. The relative rate and the *cis/trans* ratio may be controlled by different steps of the overall hydrogenation pathway.

It is a pleasure to thank Dr. L. Breger (Inst. Phys. Chem. Res.) and Prof. F. S. Howell (Sophia Univ.) for their linguistic comments on the original manuscript.

References

1) K. Tanaka, Y. Takagi, O. Nomura, and I. Kobayashi, *J. Catal.*, **35**, 24 (1974). (Part I of this series).
2) C. Cope and E. Ciganek, *Org. Synth.*, Coll. Vol. 4, 339, 612 (1963).
3) G. S. Hammond and T. D. Nevitt, *J. Am. Chem. Soc.*, **76**, 4121 (1954).
4) F. K. Signaigo and P. L. Cramer, *J. Am. Chem. Soc.*, **55**, 3326 (1933).
5) G. C. Bond and P. B. Wells, "Advances in Catalysis," ed by D. D. Eley, H. Pines, and P. B. Weisz, Academic Press, New York (1964), Vol. 15, p. 206.
6) G. C. Bond and J. S. Rank, "Proceedings of the Third International Congress on Catalysis," ed by W. M. H. Sachtler, G. C. A. Schuit, and P. Zwietering, North-Holland, Amsterdam (1965), Vol. 2, p. 1225.
7) P. B. Wells and G. R. Wilson, *J. Catal.*, **9**, 70 (1967).
8) S. Mitsui, K. Gohke, H. Saito, A. Nanbu, and Y. Senda, *Tetrahedron*, **29**, 1523 (1973).
9) S. Siegel and G. V. Smith, *J. Am. Chem. Soc.*, **82**, 6082 (1960).
10) S. Siegel and G. V. Smith, *J. Am. Chem. Soc.*, **82**, 6087 (1960).
11) C. H. MacGillavry and G. D. Rieck, "International Tables for X-Ray Crystallography," ed by K. Lonsdale, The Kynoch Press, Birmingham (1962), Vol. 3, pp. 281—282.
12) J. T. Gerig and R. A. Rimerman, *J. Am. Chem. Soc.*, **92**, 1219 (1970).
13) N. L. Allinger, J. A. Hirsch, M. A. Miller, and I. J. Tyminski, *J. Am. Chem. Soc.*, **90**, 5773 (1968).
14) L. Libit and R. Hoffmann, *J. Am. Chem. Soc.*, **96**, 1370 (1974).
15) S. Nishimura, H. Sakamoto, and T. Ozawa, *Chem. Lett.*, **1973**, 855.
16) F. A. L. Anet, G. N. Chmurny, and J. Krane, *J. Am. Chem. Soc.*, **95**, 4423 (1973).
17) M. Bernard, L. Canuel, and M. St-Jacques, *J. Am. Chem. Soc.*, **96**, 2929 (1974).
18) K. L. Servis, D. J. Bowler, and C. Ishii, *J. Am. Chem. Soc.*, **97**, 73 (1975).
19) A. A. Balandin, "Advances in Catalysis," ed by D. D. Eley, H. Pines, and P. B. Weisz, Academic Press, New York (1969), Vol. 19, p. 31.

 © 1980 The Chemical Society of Japan Bull. Chem. Soc. Jpn., 53, 1039—1044 (1980)

The Total Synthesis of Hydroxyisochamaecynone and Its Stereochemical Assignment[1)]

Masayoshi Ando,* Toyonobu Asao,† and Kahei Takase

Department of Chemistry, Faculty of Science, Tohoku University, Aramaki-aza-Aoba, Sendai 980

(Received August 27, 1979)

The structure of an acetylenic nor-sesquiterpene, hydroxyisochamaecynone, was determined to be 4α-hydroxy-5β*H*-13-noreudesm-1-en-11-yn-3-one (Ib) by means of the stereoselective total syntheses of two possible stereoisomers, Ib and 4β-hydroxy-5β*H*-13-noreudesm-1-en-11-yn-3-one.

The acetylenic nor-sesquiterpene alcohol named "hydroxyisochamaecynone" has been isolated from the essential oil of the Benihi tree (*Chamaecyparis formosensis* Matsum., Cupressaceae) as an extremely minor component,[2)] together with the related acetylenic compounds.[2,3)] The structure of this compound has been inferred to be as is shown in I, except for the stereochemistry at C_4 by only the spectral evidence. This paper will give details of the total syntheses of 4β-hydroxy-5β*H*-13-noreudesm-1-en-11-yn-3-one (Ia) and its C_4-epimer, 4α-hydroxy-5β*H*-13-noreudesm-1-en-11-yn-3-one (Ib), in optically active forms in the regio- and stereo-selective manners, with the object of establishing the structure of "hydroxyisochamaecynone."

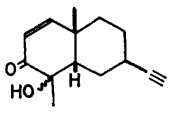

(I)

Fig. 1.

We chose an acetylenic ketone (**1**) as the starting material mainly for the following three reasons: 1) The ketone **1** can easily be obtained from *l*-α-santonin by means of the previously reported method,[4)] 2) the ketone **1** is conveniently functionalized as the starting material of both of Ia and Ib, and 3) although acetylenic ketone, **1**, and its related compounds are conformationally mobile and their reaction mode is rather complex, their stereochemical behavior has been well documented and their stereochemical reaction course is predictable.[4)]

The starting point of the synthesis is the enol acetylation of **1**. The treatment of **1** with isopropenyl acetate in the presence of *p*-TsOH gave mainly the thermodynamically more stable trisubstituted enol acetate (**2**). The amount of undesired $\Delta^{2,3}$-enol acetate (**16**) formed under these conditions was negligible, judging from the NMR spectrum of the crude product. In Compound **2** there are two possible conformers, the non-steroid conformation (**A**) and the steroid conformation (**B**), as is shown in Fig. 2. Judging from the results of the equilibrium reaction between **1** and its C_4-epimer (**17**),[5)] which was reported in the previous paper of this series,[4)] Compound **2** is presumed to exist as an equilibrium mixture of the **A** and **B** conformers in solution. Actually, the NMR spectrum of **2** showed

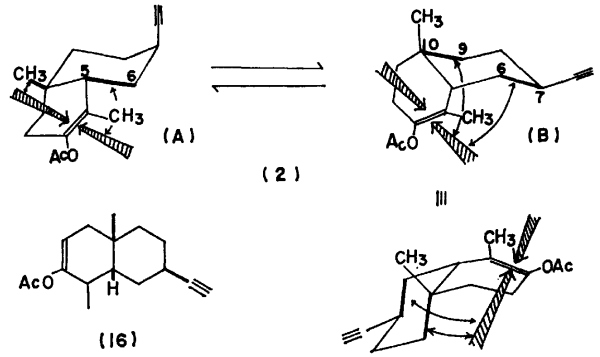

Fig. 2.

two pairs of methyl groups, possibly corresponding to **A** and **B**.

The treatment of **2** with monoperoxyphthalic acid gave an epoxide (**3**) as a single product. The high stereoselectivity of this reaction was explained as follows (Fig. 2). In the non-steroid conformation (**A**) the β-side approach of the incoming reagent is hindered by the angular methyl group, while its α-side approach is hindered by the C_5–C_6 bond. On the contrary, in the steroid conformation (**B**) there is no significant hindrance in the convexed β-side, although the α-side is strongly hindered by the C_6–C_7 and C_9–C_{10} bonds. Thus, in the epoxidation of the equilibrium mixture of the **A** and **B** conformers the reagent attacks the least hindered β-side of **B** to give β-epoxide (**3**) stereoselectively. This stereochemical assignment was confirmed by the epoxidation of the enol acetate (**12**) with a rigid conformation. A detailed discussion of this will appear below.

The hydrolysis of **3** gave a hydroxy ketone (**4**). The hydroxyl group of **4**, which was introduced newly at C_4, was assigned a β-configuration the same as that of the epoxide ring of **3**. Although we expected the preferential formation of α-bromo ketone (**6**) in the bromination of **4** in the presence of HBr,[4,6)] **4** gave a mixture of a tribromide (**5**) and the desired α-bromo ketone (**6**) under those reaction conditions. Probably the C_2 position of the enol form of **4** is sterically hindered, and the addition rate of Br_2 to the terminal triple bond and the enol double bond is comparable. In agreement with the **6** structure, IR ($CHCl_3$) showed carbonyl absorption at 1727 cm^{-1} and NMR (CCl_4) showed C_2–H at δ 5.05 (1H, q, J=7.0 and 13.0 Hz).

The dehydrobromination of **6** with LiBr–Li_2CO_3 in DMF produced 4β-hydroxy-5β*H*-13-noreudesm-1-en-11-yn-3-one (Ia), which exhibited completely different IR

† Present address: Department of Chemistry, College of General Education, Tohoku University, Kawauchi, Sendai 980.

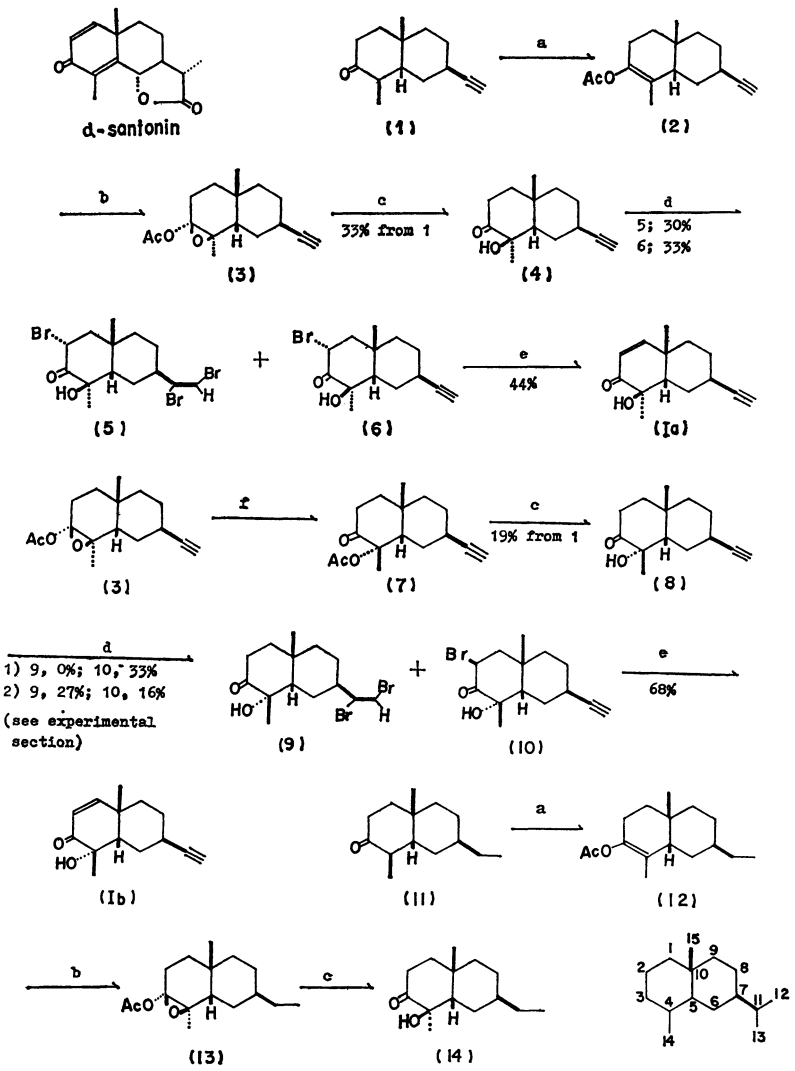

a: >-OAc, *p*-TsOH; b: monoperoxyphthalic acid, $CHCl_3$; c: 10% KOH aq soln, EtOH; d: 48% HBr, Br_2, AcOH; e: LiBr, Li_2CO_3, DMF; f: Δ (170—178 °C), 15 min.

Scheme 1.

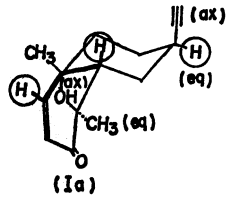

Fig. 3.

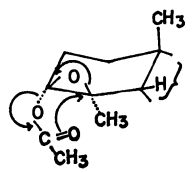

Fig. 4.

($CHCl_3$), NMR ($CDCl_3$), ORD (MeOH), and mass (70 eV) spectra from those of naturally occurring "hydroxyisochamaecynone." In accordance with the Ia structure with its non-steroid conformation, as is shown in Fig. 3, the NMR (CCl_4, 100 MHz) spectrum showed a long-range coupling (J=1.5 Hz) between C_1–H and C_5–H. The half-band width of C_7–H was *ca.* 14 Hz, which agreed with the expected value of α-(*eq*) C_7–H. The IR spectrum of Ia in CCl_4 showed absorption bands at 3580 (w) and 3500 (s) cm^{-1}, which suggested the existence of β(*ax*)-OH,[7,8] in accordance with the Ia structure with its non-steroid conformation.

Our next target was the synthesis of 4α-hydroxy-5β*H*-13-noreudesm-1-en-11-yn-3-one (Ib), the C_4-epimer of Ia. The thermal rearrangement of **3** gave a keto acetate (**7**). From the consideration of the reaction mechanism[9] depicted in Fig. 4, the stereochemistry of the newly introduced acetoxyl group was deduced to be the α-orientation. The hydrolysis of **7** gave a hydroxy ketone (**8**), which was the C_4-epimer of **4**. The bromination of **8** gave a mixture of an addition product (**9**) and the desired α-bromo ketone (**10**). The ratio of **9** to **10** depended upon the reaction conditions. Judging from the carbonyl absorption (1727 cm^{-1}) in IR (KBr) and the coupling pattern of C_2–H [δ 5.53 (q, J=7.0 and

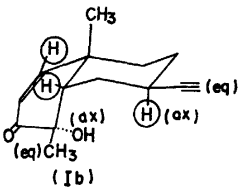

Fig. 5

13.0 Hz)] in NMR (CCl_4), the bromine atom at C_2 of **10** is situated in the $\beta(eq)$-configuration. The dehydrobromination of **10** with LiBr–Li_2CO_3 in DMF produced 4α-hydroxy-5β*H*-13-noreudesm-1-en-11-yn-3-one (Ib), which was identical with naturally occurring "hydroxyisochamaecynone" in its IR (KBr), NMR ($CDCl_3$), ORD (MeOH), and mass (70 eV) spectra and which showed no depression in its melting point when admixed with an authentic specimen. In accordance with the stereo-structure Ib with the steroid conformation, shown in Fig. 5, the NMR (100 MHz) did not show a long-range coupling between C_1–H and C_5–H. The half-band width of C_7–H was *ca.* 24 Hz, which agreed with the expected value of α(*ax*) C_7–H. The IR spectrum (CCl_4) of Ib showed two absorption bands, at 3590 (w) and 3500 (s) cm^{-1}, which agreed with the stereo-structure of a steroid conformation possessing an α(*ax*)–OH bond.[7,8] From the stereoselective syntheses mentioned above and the spectroscopic evidence concerning Ia and Ib, the structure of naturally occurring "hydroxyisochamaecynone" was concluded to be 4α-hydroxy-5β*H*-13-noreudesm-1-en-11-yn-3-one (Ib) with the steroid conformation, as is depicted in Fig. 5.

In the above-mentioned syntheses, we employed the epoxidation of a conformationally mobile enol acetate (**2**) as a key step and concluded by an examination of the Dreiding molecular models that the reagent should approach from the β-side. Since there is no similar example in the literature, we decided to confirm the above conclusion by the following chemical correlation. Hexahydroisochamaecynone (**11**) was employed as the starting material. The enol acetylation of **11** gave an enol acetate (**12**). Since this compound has a bulky ethyl group at C_7, the conformation was considered to be fixed in the steroid conformation, as is shown in Fig. 6. In this case, the epoxidation of **12** occurred, apparently from the convexed β-side,[10] giving a β-epoxide (**13**). The hydrolysis of **13** gave a hydroxy ketone (**14**), which was identical with the tetrahydro derivative obtained by the catalytic hydrogenation of **4**, in accordance with the above-mentioned conclusion.

The ORD Studies of the Synthetic Intermediates of Ia and Ib. In the *cis*-decalone derivatives with a mobile conformation, the studies of the ORD curves are a convenient method for predicting their conformations. For the application of this method to Ia, Ib, and their synthetic intermediates, we need to know the degree of the contribution of the axial hydroxyl group at the α-position of the carbonyl group. The ORD data of **4** and Ia and the corresponding deoxy derivatives (**17** and **18**) are summarized in Table 1. This table shows that the contribution of the β(*ax*)-hydroxyl group to the Cotton effect of **4** and Ia is negative, as predicted by the octant rule.

On the other hand, the ORD data of **15**, **8**, **10**, and Ib and the corresponding deoxy derivatives (**19**, **1**, **20**, and **21**), summarized in Table 2, show that the

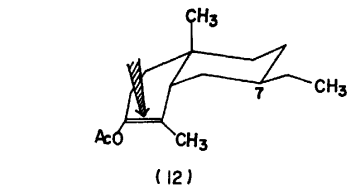

Fig. 6.

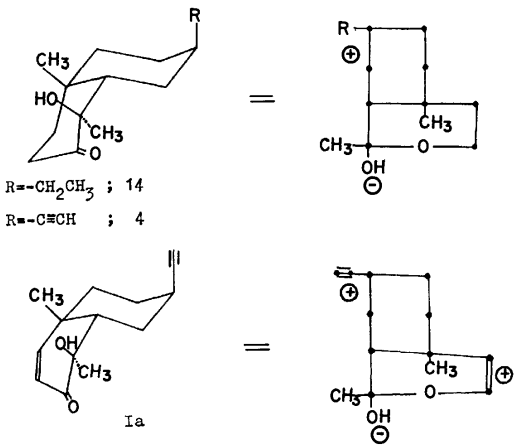

Fig. 7.

Table 1. The ORD spectral data of **14**, **4**, and Ia, and their reference deoxy derivatives, **17** and chamaecynone (**18**) in MeOH

Compound	ORD	Corresponding deoxy derivative	ORD	Contribution of OH (Δ*A*)
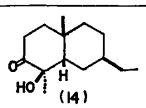 (14)	$[\phi]_{315}=-1100$ $[\phi]_{245}=+2610$ $A=-37$			
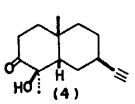 (4)	$[\phi]_{310}=-1490$ $[\phi]_{260}=+2000$ $A=-35$	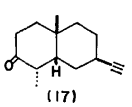 (17)	$[\phi]_{304}=+900$ $[\phi]_{205}=-1790$ $A=+27$	−62
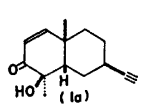 (Ia)	$[\phi]_{360}=-560$ $[\phi]_{310}=+220$ $A=-7.8$	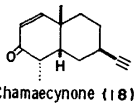 Chamaecynone (18)	$[\phi]_{352}=+600$ $[\phi]_{310}=-4000$ $A=+46$	−53.8

Table 2. The ORD spectral data of **15**, **8**, **10**, and Ib and their reference deoxy derivatives, **19**, **1**, **20**, and isochamaecynone (**21**) in MeOH

Compound	ORD	Corresponding deoxy derivative	ORD	Contribution of OH (ΔA)
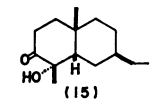 (15)	$[\phi]_{325}=+160$ $[\phi]_{260}=+1000$ $A=-8.4$	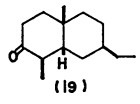 (19)	$[\phi]_{302}=-660$ $[\phi]_{260}=+1960$ $A=-26.2$	+17.8
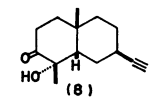 (8)	$[\phi]_{325}=-520$ $[\phi]_{300}=0$ $A=-5.2$	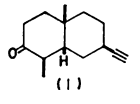 (1)	$[\phi]_{340}=-900$ $[\phi]_{265}=+1790$ $A=-26.9$	+21.7
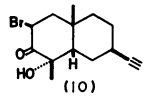 (10)	$[\phi]_{310}=-990$ $[\phi]_{270}=0$ $A=-9.9$	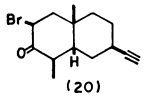 (20)	$[\phi]_{310}=-470$ $[\phi]_{260}=+600$ $A=-10.7$	+0.8
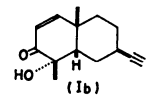 (Ib)	$[\phi]_{340}=-1010$ $[\phi]_{285}=+1450$ $A=-24.6$	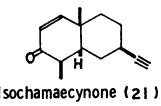 Isochamaecynone (21)	$[\phi]_{345}=-870$ $[\phi]_{270}=+2120$ $A=-29.9$	+5.3

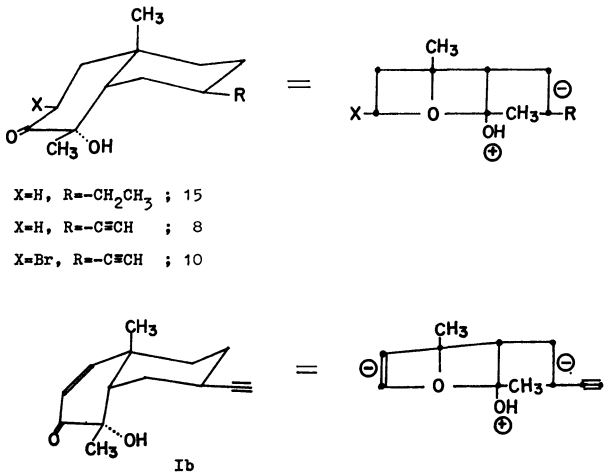

Fig. 8

contribution of the α(*ax*)-hydroxyl group of **15**, **8**, **10**, and Ib to the Cotton effect is positive, as predicted by the octant rule, though the magnitude of the ΔA value is irregular.

In conclusion, although the axial hydroxyl substituent at the α-position of the carbonyl group contributes to the Cotton effect, as predicted by the octant rule, it is difficult to estimate the conformation of the flexible hydroxy ketones on the basis of the ORD data only, because the magnitude of the contribution of the hydroxyl group to the Cotton effect is not constant.

Experimental

All the melting points are uncorected. The IR spectra were recorded on Shimadzu IR-27, Hitachi EPI-S2, and Hitachi EPI-G28 spectrophotometers. The NMR spectra were recorded on Varian A-60, Nichiden-Varian T-60, and Varian HA-100 spectrometers, employing tetramethylsilane as the internal reference. The ORD and CD spectra were recorded on a Nihonbunko ORD/UV-5 spectrophotometer.

3-Acetoxy-5βH-13-noreudesm-3-en-11-yne (2). A solution of 4α*H*,5β*H*-13-noreudesm-11-yn-3-one (**1**) (600 mg, 2.94 mmol) in isopropenyl acetate (6 ml) containing *p*-toluenesulfonic acid (60 mg) was heated under N_2 at the boiling point and then concentrated in 30 min to give a brown, oily residue, which was subsequently dissolved in ether (100 ml). The ether solution was washed with a saturated aq soln of NaCl (50 ml×2), dried ($MgSO_4$), and concentrated to give 600 mg of an oily material, which was a mixture of two conformers of **2**. IR (neat): 3300, 2160, and 1755 cm^{-1}. NMR (CCl_4): δ 1.02 (s, C_{10}–Me of the major component), 1.05 (s, C_{10}–Me of the minor component), 1.50 (m, C_4–Me of the major component), 1.56 (m, C_4–Me of the minor component), 1.90 (1H, d, J=3.0 Hz), and 2.03 (3H, s, –C(=O)–C<u>H</u>$_3$) ppm.

3α-Acetoxy-3β,4β-epoxy-5βH-13-noreudesm-11-yne (3). To a solution of **2** (600 mg, 2.44 mmol) in $CHCl_3$ (15 ml) we added a solution of monoperoxyphthalic acid (500 mg, 2.75 mmol) in ether (15 ml). The mixture was allowed to stand at room temperature for 7 days and then filtered to remove the phthalic acid. The filtrate was poured into an aq soln of KI and stirred for a few min. The organic layer was separated, and the aqueous layer was extracted with $CHCl_3$ (20 ml×2). The combined extracts were washed successively with a 0.2 M aq soln of $Na_2S_2O_3$, a saturated aq soln of $NaHCO_3$, and a saturated aq soln of NaCl, dried ($MgSO_4$), and concentrated to give 668 mg of an oily material, which was employed for the next reaction. This crude oil (445 mg) was chromatographed over silica gel (40 g, Merck, <230 mesh) and eluted with CCl_4–$CHCl_3$ (1:1) to give 103 mg of spectroscopically pure **3** (mp 48—50 °C), which was then recrystallized from pentane to give a crystalline material; mp 68—69 °C. IR ($CHCl_3$): 3289, 2123, and 1748 cm^{-1}. NMR (CCl_4): δ 1.13 (3H, s), 1.25 (3H, s), 2.02 (3H, s, –C(=O)–C<u>H</u>$_3$), 1.92 (1H, d, J=2.5 Hz, C_{12}–H), and 2.80 (1H, m, $W_{h/2}$=*ca.* 10 Hz, C_7–H) ppm. Found: C, 73.38; H, 8.45%. Calcd for $C_{16}H_{22}O_3$: C, 73.25; H, 8.45%.

4β-Hydroxy-5βH-13-noreudesm-11-yn-3-one (4). Into a solution of **3** (610 mg) [prepared from **1** (600 mg, 2.94 mmol) without any purification at any step] in ethanol (30 ml) we added a 10% aq soln of KOH (9 ml). The mixture was allowed to stand at room temperature overnight, poured into a saturated aq soln of NaCl (100 ml), and extracted with ether (30 ml×3). The combined ether layers were washed with a saturated aq soln of NaCl, dried ($MgSO_4$), and evaporated to give an oily material, which was then chromatographed over silica gel (25 g, Merck, <230 mesh) and eluted with CCl_4–$CHCl_3$ (1:1) to give spectroscopically pure **4** (214 mg, 33% overall yield from **1**); mp 89 °C. This was recrystallized from pentane to give the analytical sample;

mp 95 °C. IR (KBr): 3480, 3300, 2130, and 1712 cm^{-1}. NMR (CCl_4): δ 1.27 (3H, s), 1.45 (3H, s), and 1.90 (1H, d, J=2.5 Hz, C_{12}–H) ppm. ORD (MeOH): $[\phi]_{310}$=−1490, $[\phi]_{260}$=+2000; A=−35. Found: C, 76.51; H, 8.96%. Calcd for $C_{14}H_{20}O_2$: C, 76.32; H, 9.15%.

Bromination of ***4****. Formation of 2α,11,12-Tribromo-4β-hydroxy-5βH-13-noreudesm-11-en-3-one (****5****) and 2α-Bromo-4β-hydroxy-5βH-13-noreudesm-11-yn-3-one (****6****).* To a solution of **4** (170 mg, 0.77 mmol) in AcOH (5 ml) we added a 48% aq soln of HBr (0.1 ml) and Br_2 (140 mg, 0.88 mmol). The mixture was stirred for 1 h at room temperature, poured into a saturated aq soln of NaCl, and extracted with ether (20 ml ×3). The combined extracts were washed with a saturated aq soln of NaCl, dried ($MgSO_4$), and concentrated to give an oily product (250 mg), which was then chromatographed over silica gel (18 g, Merck, <230 mesh) and eluted with CCl_4–$CHCl_3$ (1: 1). The first fraction gave **5** (105 mg, 30%) as a crystalline material. IR (KBr): 3521, 3106, and 1730 cm^{-1}. NMR (CCl_4): δ 1.12 (3H, s), 1.47 (3H, s), 5.47 (1H, q, J=6.5 and 13.0 Hz, C_2–H), and 6.37 (1H, s, C_{12}–H) ppm. The second fraction gave **6** (77 mg, 33%) as a crystalline material. IR ($CHCl_3$): 3546, 3333, 2119, and 1727 cm^{-1}. NMR (CCl_4): δ 1.42 (3H, s), 1.59 (3H, s), 1.93 (1H, d, J=2.0 Hz, C_{12}–H), and 5.05 (1H, q, J=7.0 and 13.0 Hz, C_2–H) ppm.

4β-Hydroxy-5βH-13-noreudesm-1-en-11-yn-3-one (4β-Hydroxychamaecynone Ia). A mixture of **6** (22 mg, 0.10 mmol), Li_2CO_3 (22 mg, 0.30 mmol), and LiBr (22 mg, 0.25 mmol) in anhydrous DMF (4 ml) was stirred at 140—150 °C for 6.5 h under N_2, cooled, poured into a saturated aq soln of NaCl (30 ml), and extracted with ether (10 ml×3). The combined extracts were washed successively with 2 M HCl (10 ml) and a saturated aq soln of NaCl, dried ($MgSO_4$), and concentrated to give 17 mg of an oily material, which was then chromatographed over silica gel (2 g, Merck, <230 mesh) and eluted with CCl_4–$CHCl_3$ (1: 1) to give 7 mg (44%) of Ia as a crystalline material; mp 71 °C, IR ($CHCl_3$): 3521, 3322, 2114, and 1672 cm^{-1}. NMR (CCl_4, 100 MHz): δ 1.34 (3H, s), 1.44 (3H, s), 1.93 (1H, d, J=2.5 Hz, C_{12}–H), 2.83 (1H, m, $W_{h/2}$=*ca.* 14 Hz, C_{17}–H), 5.88 (1H, d, J=10.0 Hz, C_2–H), and 6.43 (1H, dd, J=1.5 and 10.0 Hz, C_1–H) ppm. UV (MeOH): λ_{max}=228 nm (ε=7400). ORD (MeOH): $[\phi]_{360}$=−560, $[\phi]_{310}$=+220, A=−7.8. CD (MeOH): $[\theta]_{340}$=−560.

*4α-Hydroxy-5βH-13-noreudesm-11-yn-3-one (****8****).* The crude epoxide (**3**, 860 mg) [prepared from **1** (800 mg, 3.92 mmol)] was heated at 170—178 °C under N_2 to give 4α-acetoxy-5β*H*-13-noreudesm-11-yn-3-one (**7**) as an oily material. IR (neat): 3279, 1730, and 1721 cm^{-1}. This crude material was dissolved in a mixture of EtOH (24 ml) and a 10% aq soln of KOH (8 ml). The mixture was allowed to stand at room temperature for 100 min, poured into a saturated aq soln of NaCl (100 ml), and extracted with petroleum ether (20 ml×4). The combined extracts were washed with a saturated aq soln of NaCl, dried ($MgSO_4$), and concentrated to give 463 mg of an oily material, which was then chromatographed over silica gel (25 g, Merck, <230 mesh) and eluted with a mixture of CCl_4–$CHCl_3$ (1: 1). The first fraction gave **4** (58 mg, 7% overall yield from **1**). The second fraction gave 163 mg (19% overall yield from **1**) of **8**, which was recrystallized from pentane to give colorless prisms; mp 103 °C. IR (KBr): 3436, 3268, 2119, and 1712 cm^{-1}. NMR (CCl_4): δ 1.22 (3H, s), 1.25 (3H, s), and 1.92 (1H, d, J=2.5 Hz, C_{12}–H) ppm. ORD (MeOH): $[\phi]_{325}$=−520, $[\phi]_{300}$=0, A=−5.2. CD (MeOH): $[\theta]_{312}$=−274. Found: C, 76.35; H, 9.09%. Calcd for $C_{14}H_{20}O_2$: C, 76.32; H, 9.15%.

Bromination of ***8****. Formation of 11,12-Dibromo-4α-hydroxy-5βH-13-noreudesm-3-one (****9****) and 2β-Bromo-4α-hydroxy-5βH-13-noreudesm-11-yn-3-one (****10****).* A solution of **8** (122 mg, 0.55 mmol) in AcOH (5 ml) was stirred in the presence of a 48% aq soln of HBr (0.1 ml) for 10 min at room temperature. Into the mixture we then added a solution of Br_2 (108 mg, 0.68 mmol) in AcOH (1 ml). The mixture was stirred for 40 min at room temperature, poured into a saturated aq soln of NaCl (50 ml), and extracted with petroleum ether (20 ml ×4). The combined extracts were washed successively with a 10% aq soln of Na_2CO_3 and a saturated aq soln of NaCl, dried ($MgSO_4$), and concentrated to give 172 mg of an oily material, which was then chromatographed over silica gel (10 g, Merck, <230 mesh) and eluted with $CHCl_3$–CCl_4 (1: 1) to give spectroscopically pure **10** (54 mg, 33%) as a semisolid compound. This was subsequently recrystallized from petroleum ether–ether to give prisms; mp 140.5 °C. IR (KBr): 3497, 3300, 2105, and 1727 cm^{-1}. NMR (CCl_4): δ 1.30 (3H, s), 1.50 (3H, s), 1.93 (1H, d, J=2.0 Hz), and 5.53 (1H, q, J=7.0 and 13.0 Hz, C_2–H) ppm. ORD (MeOH): $[\phi]_{310}$=−990, $[\phi]_{270}$=0, A=−9.9. Found: C, 57.34; H, 5.81%. Calcd for $C_{14}H_{19}O_2Br$: C, 56.23; H, 6.41%. In another experiment, to a solution of **8** (130 mg, 0.59 mmol) in AcOH (5 ml) we added a 48% aq soln of HBr (0.1 ml) and Br_2 (110 mg, 0.69 mmol) successively. The mixture was stirred for 40 min at room temperature, poured into a saturated aq soln of NaCl (50 ml), and extracted with petroleum ether (20 ml×4). The combined extracts were washed successively with a 10% aq soln of Na_2CO_3 and a saturated aq soln of NaCl, dried ($MgSO_4$), and concentrated to give 207 mg of an oily material, which was chromatographed over silica gel (10 g, Merck, <230 mesh) and eluted with CCl_4–$CHCl_3$ (1: 1). The first fraction gave spectroscopically pure **9** (61 mg, 27%) as a crystalline material; this was subsequently recrystallized from pentane to give microcrystals; mp 90 °C. IR (KBr): 3521, 3086, and 1706 cm^{-1}. NMR (CCl_4): δ 1.11 (3H, s), 1.46 (3H, s), and 6.35 (1H, s) ppm. Found: C, 44.25; H, 5.26%. Calcd for $C_{14}H_{20}O_2Br_2$: C, 44.21; H, 5.30%. The second fraction gave **10** (29 mg, 16%).

4α-Hydroxy-5βH-13-noreudesm-1-en-11-yn-3-one (4α-Hydroxyisochamaecynone, Ib). A mixture of **10** (83 mg, 0.28 mmol), LiBr (88 mg, 1.01 mmol), and Li_2CO_3 (88 mg, 1.19 mmol) in anhydrous DMF (10 ml) was stirred at 150—155 °C for 5 h under N_2, cooled, poured into a saturated aq soln of NaCl (50 ml), and extracted with ether (15 ml×3). The combined extracts were washed successively with 2 M HCl (15 ml) and a saturated aq soln of NaCl, dried ($MgSO_4$), and concentrated to give 75 mg of a crystalline material, which was subsequently chromatographed over silica gel (5 g, <230 mesh) and eluted with CCl_4–$CHCl_3$ (1: 1) to give spectroscopically pure Ib (41 mg, 68%) as a crystalline material, which was then recrystallized from pentane to give colorless prisms; mp 160 °C. This material showed no depression in its melting point when admixed with an authentic sample of natural "hydroxyisochamaecynone" and was identical in all respects with this specimen in IR (KBr), NMR ($CDCl_3$), ORD (MeOH), and MS (70 eV).

*Synthesis of 4β-Hydroxy-5βH-13-noreudesm-3-one (****14****) from 4αH,5βH-13-Noreudesman-3-one (Hexahydroisochamaecynone,* ***11****).* A solution of **11** (760 mg, 3.65 mmol) in isopropenylacetate (8 ml) containing *p*-toluenesulfonic acid (80 mg) was heated under N_2 at the boiling point and then concentrated for 30 min to give a brown, oily residue, which was subsequently dissolved in ether (100 ml). The ether solution was washed with a saturated aq soln of NaCl (50 ml×2), dried ($MgSO_4$), and concentrated to give 780 mg of crude 3-acetoxy-5β*H*-noreudesm-3-ene (**12**).

To a solution of this crude material (780 mg) in $CHCl_3$

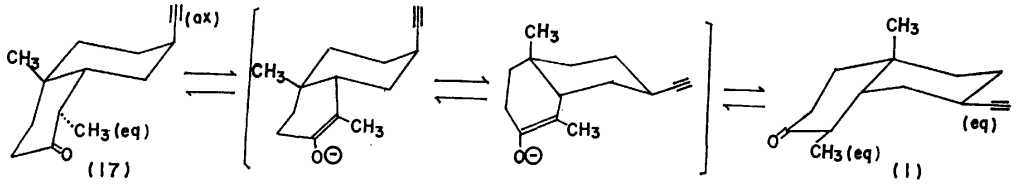

non-steroid conformation | non-steroid conformation | steroid conformation | steroid conformation

Fig. 9.

Table 3.

Compound	Absorptions of -OH (cm^{-1})		Absorptions of C=O (cm^{-1})
	Weak band	Strong band	
1			1716
Ia	3580	3500	1708 (sh), 1684
4	3590	3490	1715
14	3595	3475	1713
Ib	3590	3500	1710 (sh), 1685
8	3600	3490	1718
15	3597	3480	1716

These IR spectra were recorded by a Hitachi-EPI-G28 instrument in a 0.2 M CCl_4 solution.

(16 ml) we added a solution of monoperoxyphthalic acid (728 mg, 4.00 mmol) in ether (16 ml). The mixture was allowed to stand at room temperature for 5 days and then filtered to remove any phthalic acid. The filtrate was poured into an aq soln of KI and stirred for a few min. The organic layer was then separated, and the aqueous layer was extracted with $CHCl_3$ (30 ml×2). The combined extracts were washed successively with a 0.2 M aq soln of $Na_2S_2O_3$, a saturated aq soln of $NaHCO_3$, and a saturated aq soln of NaCl, dried ($MgSO_4$) and concentrated to give 850 mg of crude 3α-acetoxy-3β,4β-epoxy-5β*H*-13-noreudesmane (**13**). which was almost pure, judging from the TLC analysis and the spectroscopic evidence. IR (neat): 1739 cm^{-1}. NMR (CCl_4): δ 0.96 (3H, s), 1.38 (3H, s), and 2.03 (3H, s) ppm.

Into a solution of this crude material (850 mg) in EtOH (30 ml) we added a 10% aq soln of KOH (10 ml). The mixture was allowed to stand at room temperature for 2 h, poured into a saturated aq soln of NaCl (100 ml), and extracted with ether (30 ml×3). The combined ether layers were washed with a saturated aq soln of NaCl, dried ($MgSO_4$), and evaporated to give a crystalline material, which was subsequently chromatographed over silica gel (10 g, Merck, <230 mesh) and eluted with CCl_4–$CHCl_3$ (1: 1) to give spectroscopically pure **14** (143 mg, 17% overall yield from **11**). This was recrystallized from pentane to give needles; mp 91.5 °C. IR (KBr): 3484 and 1715 cm^{-1}. NMR (CCl_4): δ 1.12 (3H, s) and 1.35 (3H, s) ppm. ORD (MeOH): $[\phi]_{315}=-1100$, $[\phi]_{245}=+2610$, $A=-37$. Found: C, 75.08; H, 10.49%. Calcd for $C_{14}H_{24}O_2$: C, 74.95; H, 10.78%.

Catalytic Hydrogenation of **4**. *Formation of* **14**: A mixture of **4** (50 mg), EtOH (3 ml), and 5% Pd/C was shaken under an atmosphere of H_2 for 2 h and then filtered. The filtrate was concentrated to give **14** (50 mg) as a crystalline material.

Catalytic Hydrogenation of **8**. *Formation of 4α-Hydroxy-5β*H*-13-noreudesm-3-one (***15***)*: A mixture of **8** (40 mg), EtOH (3 ml), and 5% Pd/C was shaken under an atmosphere of H_2 for 2 h and then filtered. The filtrate was concentrated to give **15** (30 mg) as an oily material. IR (neat): 3472 and 1715 cm^{-1}. NMR (CCl_4): δ 1.05 (3H, s) and 1.32 (3H, s) ppm. ORD (MeOH): $[\phi]_{325}=+160$, $[\phi]_{260}=+1000$, $A=-8.4$. CD (MeOH): $[\theta]_{295}=-372$.

The authors wish to thank Dr. Takashi Toda of this Department for his helpful discussion.

References

1) Preliminary report of this work: M. Ando, T. Asao, and K. Takase, *Tetrahedron Lett.*, **1969**, 4689.

2) T. Nozoe, Y. S. Cheng, and T. Toda, *Tetrahedron Lett.*, **1966**, 3663.

3) T. Asao, S. Ibe, K. Takase, Y. S. Cheng, and T. Nozoe, *Tetrahedron Lett.*, **1968**, 3639; K. Takase, S. Ibe, T. Asao, T. Nozoe, H. Shimanouchi, and Y. Sasada, *Chem. Ind. (London)*, **1968**, 1638.

4) T. Nozoe, T. Asao, M. Ando, and K. Takase, *Tetrahedron Lett.*, **1967**, 2821; the full paper: *Bull. Chem. Soc. Jpn.*, in press.

5) In the equilibrium reaction between **17** and **1** in EtOH in the presence of KOH, **17** is the favorable isomer, but the energy difference is rather small ($\Delta H=+0.77$ kcal/mol). At 25 °C the ratio of **1**/**17**=0.63, which corresponds to $\Delta G=+0.27$ kcal/mol; see Fig. 9 and Ref. 4).

6) Generally, bromination on an enol double bond is faster than on a terminal triple bond; J. Hine, "Physical Organic Chemistry," 2nd ed, McGraw Hill Book Co., New York (1962), Chaps. 9 and 10.

7) N. L. Wendler, D. Taub, S. Dobriner, and D. K. Fukushima, *J. Am. Chem. Soc.*, **78**, 5027 (1956); R. B. Bates, G. Büchi, T. Matsuura, and R. R. Shaffer, *ibid.*, **82**, 2327 (1960).

8) The IR spectra summarized in Table 3 suggest that hydroxyl groups of Ia, Ib, and their derivatives (**4**, **14**, **8**, and **15**) are oriented in an axial arrangement.

9) K. L. Williamson and W. S. Jonson, *J. Org. Chem.*, **26**, 4563 (1961); K. L. Williamson, J. I. Coburm, and M. F. Herr, *ibid.*, **32**, 3934 (1967).

10) E. L. Eliel, N. L. Allinger, S. J. Angyal, and G. A. Morrison, "Conformational Analysis," John Wiley & Sons, New York (1965), Chapter 5.

 © 1980 The Chemical Society of Japan Bull. Chem. Soc. Jpn., 53, 1045—1048 (1980)

The Structure and Configuration of (+)-Glutionosone and (+)-Oxyglutinosone[1)]

Akio Murai, Hirofumi Taketsuru, Fujio Yagihashi, Nobukatsu Katsui, and Tadashi Masamune*

Department of Chemistry, Faculty of Science, Hokkaido University, Sapporo 060

(Received August 28, 1979)

The structure elucidation of (+)-glutinosone and (+)-oxyglutinosone, antifungal norsesquiterpenes qualified as phytoalexins in diseased tobacco leaves and in diseased potato tubers, respectively, is described.

In recent preliminary communications[2,3)] we reported the structure and configuration of (+)-glutinosone (**1**) and (+)-oxyglutinosone (**2**), antifungal norsesquiterpenes qualified as phytoalexins in diseased tobacco leaves and in diseased potato tubers, respectively. In the present paper we describe the details of the structure elucidation.

Glutinosone was isolated from leaves of *Nicotiana glutinosa* infected with tobacco mosaic virus and assigned formula **1'** by Burden and coworkers.[4)] However, the disposition of an isopropenyl group and the configuration of all asymmetric centers have not completely been determined yet. The following transformation of rishitin (**3**) into (+)-glutinosone[5)] has established that the relevant norsesquiterpene is represented correctly by formula **1**.

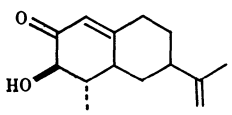

1'

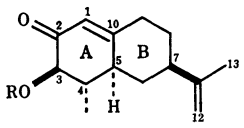

1 R=H
1a R=Ac

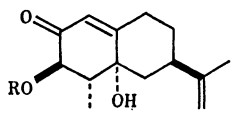

2 R=H
2a R=Ac

Treatment of (−)-rishitin[6)] (**3**) with acetic anhydride (2.3 equiv) in a 1: 20 mixture of pyridine and benzene (room temp, 5 h) followed by chromatography afforded the 2- and 3-monoacetates (**3a** and **3b**), mp 60.5—62.5 °C and 107—107.5 °C, in 34 and 23% yields, respectively, with the 2,3-diacetate[6)] (**3c**, 5%) and the starting glycol (**3**, 35%): **3a**, δ 3.31 (1H, t, J=8.5 Hz, 3-H) and 4.72 (3H, br, 2- and 12-H): **3b**, δ 3.62 (1H, do t, J= 6.5, 8.5, and 8.5 Hz, 2-H) and 4.60 (1H, t, J=8.5 Hz, 3-H). The 2- and 3-monoacetates (**3a** and **3b**), when oxidized with the Jones reagent in a heterogeneous mixture of ether and water (room temp, 16 and 21 h), were converted into the corresponding dehydro compounds, 3-oxo 2-acetate and 2-oxo 3-acetate (**4a** and **4b**), each oily, in 41 and 61% yields, respectively. In accordance with the assigned structures, the respective compounds (**4a** and **4b**) exhibited two strong absorption maxima at the carbonyl regions (**4a**, ν_{max} 1757 and 1737 cm^{-1}; **4b**, ν_{max} 1757 and 1744 cm^{-1}) and signals due to the protons at C-2 or C-3 [**4a**, δ 5.21 (1H, do d, J=11 and 8 Hz, 2-H); **4b**, δ 4.84 (1H, d, J=9 Hz, 3-H)] in the IR and NMR spectra.

Transformation of the oxo acetates (**4b** and **4a**) into glutinosone (**1**) was undertaken under various conditions. Treatment of **4b** with base (KOAc in ethanol or alumina in dry benzene, room temp, 24 h) gave a complex mixture containing at least five compounds, while acid treatment (dil HCl in diglyme, room temp, 16 h) led to recovery of the starting material (**4b**). On the other hand, attempted isomerization of **4a** with base [NaOAc or $(CH_3)_4NOAc$ in water–ether, room temp, 45 h] failed, **4a** being recovered unchanged. One-step conversion of **3b** into **1** or **1a** under conditions of a modification[7)] of the Oppenauer oxidation (aluminium isoproxide and *N*-methyl-4-piperidone, reflux, 5 h) also resulted only in hydrolysis of the acetoxyl group, giving **3**. The aimed transformation was achieved under most usual conditions; treatment of oxo acetate **4b** with base (KOH, 1.2 equiv) in methanol (room temp, 25 min) effected migration of the 5(10)-double bond with concomitant hydrolysis to give $\Delta^{1(10)}$-3-hydroxy 2-ketone (**1**), oily, in 46% yield, with the corresponding 3-acetate (**1a**, 41%), oily; **1**, λ_{max} 237 nm (ε 14500); ν_{max} 3470, 1676, 1645, and 1620 cm^{-1}; δ 3.79 (1H, d, J=12 Hz, 3-H) and 5.90 (1H, br s, W_H=4 Hz, 1-H). All these spectra were identical with those of natural glutinosone[4)] (**1**), establishing the

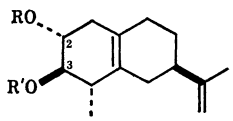

3 R=R'=H
3a R=Ac, R'=H
3b R=H, R'=Ac
3c R=R'=Ac

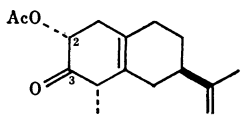

4a

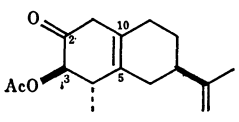

4b

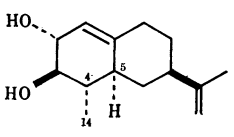

5

absolute configurations at C-3, C-4, and C-7 of (+)-glutinosone.[5]

Reduction of (+)-glutinosone (**1**) with sodium borohydride gave glycol[4] (**5**), mp 136—138 °C, in 44% yield. The NMR spectrum [δ 3.18 (1H, do d, J=10 and 8 Hz, 3-H) and 4.06 (1H, br d, J=8 Hz, 2-H)] indicated that the A ring existed in a half-chair conformation. Addition of 0.6 mol equiv of the shift reagent Eu(dpm)$_3$ effected complete separation of the NMR signals due to individual protons on the A ring, as shown in Fig. 1. Irradiation at δ 3.89 (14-H) collapsed a broad multiplet at 6.80 (4-H) into a slightly broad triplet (J=10 Hz), indicating the coupling constant

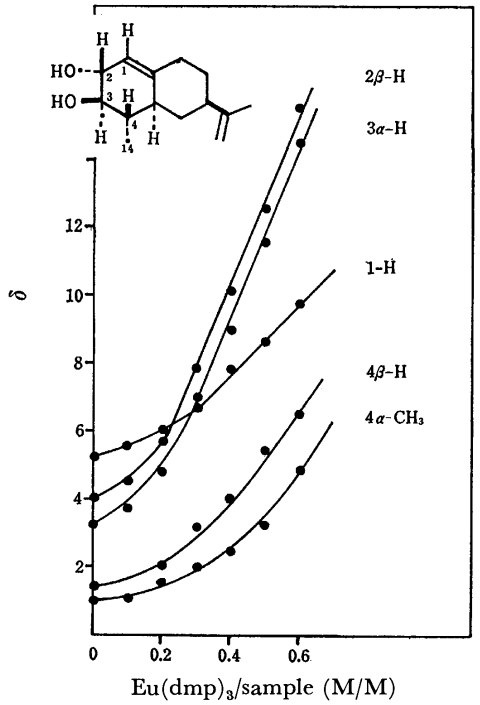

Fig. 1. Induced paramagnetic shifts for compound **5**.

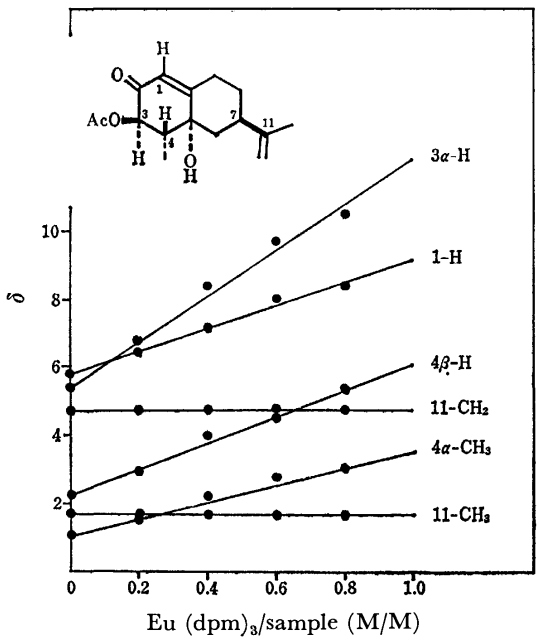

Fig. 2. Induced paramagnetic shifts for compound **2a**.

between two protons at C-4 and C-5 to be 10 Hz. It follows that the proton in question at C-5 must be oriented axial (α-configuration) and hence (+)-glutinosone is represented by formula **1**.

Oxyglutinosone (**2**) was isolated from tuber tissues of potatoes (*Solanum tuberosum*×*S. demissum*) infected by an incompatible race of *Phytophthora infestans* as follows. Neutral chloroform extracts (59 g), obtained from the diseased potato tubers (300 kg), were separated as described previously[6] to give "lubimin fraction" (Fraction E,[6] 4.7 g). This fraction was further purified by repeated chromatography to yield an oxyglutinosone and isolubimin-rich fraction (160 mg), with lubimin and epilubimin-rich fractions (174 and 110 mg), which on acetylation followed by preparative TLC over silica gel afforded oxyglutinosone (**2**) and isolubimin[3,8] (**6**) as the respective acetate (**2a**, 43 mg, and **6a**, 37 mg).

Oxyglutinosone acetate (**2a**), mp 99—101 °C and $[\alpha]_D$ +166°, was analyzed for $C_{16}H_{22}O_4$ [*m/e* 278 (M^+)] and hydrolyzed in a 1:1:2 mixture of trimethylamine, water and methanol (room temp, 3 h) to give oxyglutinosone (**2**), oily and $[\alpha]_D$ +130°, in 56% yield after purification by preparative TLC. The UV, IR, and ^{1}H-NMR spectra of these compounds indicated that oxyglutinosone (**2**) contained the following structural in units: a secondary methyl group [**2a**, δ 1.10 (3H, d, J=7 Hz)]: an isopropenyl [**2a**, ν_{max} 1642 (or 1638) and 897 cm^{-1}; δ 1.75 (3H, s) and 4.75 (2H, br s, W_H=6 Hz)]: an α,β-unsaturated carbonyl [**2a**, λ_{max} 230 nm (ε 12100); ν_{max} 1699 and 1638 (or 1642) cm^{-1}; δ 5.79 (1H, d, J=1.5 Hz, 1-H)]: two (secondary and tertiary) hydroxyl groups [**2**, δ 4.10 (1H, d, J=12 Hz, 3-H); **2a**, ν_{max} 3610, 3480, 1739, and 1240 cm^{-1}; δ 2.19 (3H, s) and 5.39 (1H, d, J=13 Hz, 3-H)]. These spectra, coupled with spin-decoupling studies on the spectra in the presence of the shift reagent [Eu(dpm)$_3$, 0.2—0.8 mol equiv] (Fig. 2), indicating the existence of the following partial formula; (*)-(CH_3)CH–CH-($OCOCH_3$)–C(=O)–CH=(*) in **2a**, in which (*) denotes a quaternary carbon, suggesting that oxyglutinosone (**2**) would be a 5-hydroxy derivative of glutinosone (**1**). This was supported by comparison of the ^{13}C-NMR spectra (Table 1) of both the 3-acetates

Table 1. The ^{13}C-NMR spectra of glutinosone acetate (**1a**) and oxyglutinosone acetate (**2a**)

Carbon No.	**1a** Chemical shift (δ, $CDCl_3$, 25 MHz)	**2a** Chemical shift (δ, $CDCl_3$, 25 MHz)
1	122.3	122.7
2	192.9	193.2
3	77.5	75.1
4	44.0	43.0
5	44.6	71.6
6	44.0	43.0
7	39.3	39.1
8	31.3	31.2
9	35.1	32.2
10	164.2	162.7
11	148.2	148.4
12	109.3	109.6
13	20.7	20.7
14	15.4	10.0

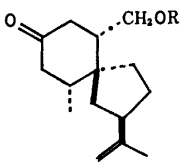

6 R=H
6a R=Ac

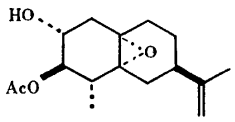

7

(**1a** and **2a**) and confirmed as follows.

Rishitin 3-acetate (**3b**) was oxidized with *t*-butyl hydroperoxide in the presence of bis(acetylacetonato)-oxovanadium(IV)[9] [VO(acac)$_2$] to the 5α,10α-epoxide (**7**), mp 142—143 °C, in 83% yield. The α-configurational assignment to the epoxy group was deduced from the IR and ^{1}H-NMR spectra; namely, (i) a broad absorption due to the hydrogen bond between the 2α-hydroxyl and epoxy groups was observed at 3480 cm^{-1} in highly dilute carbon tetrachloride solution (0.0012 M, cell length, 50 mm), and (ii) a ^{1}H-NMR signal due to the hydroxyl proton at δ 3.11 (1H, d, J=10 Hz) remained unchanged on dilution. The Collins oxidation of epoxide **7** followed by treatment with silica gel afforded hydroxy α,β-unsaturated ketone, mp 99—101 °C and $[\alpha]_D$ +153°, in 54% yield, whose spectra (MS, UV, IR, and ^{1}H-NMR) were identical with those of natural oxyglutinosone (**2a**). This transformation has established that oxyglutinosone (**2**) is 5α-hydroxy-glutinosone.

Experimental

All the melting points were uncorrected. The purity of each compound was always checked by TLC over silica gel (Wako-gel B-5 or Merck, Kieselgel GF-254) with various solvent systems, and the spots were developed with cerium(IV) sulfate in dil sulfuric acid, iodine, vaniline–sulfuric acid[6] and/or the Ehrlich reagent. The optical rotations, UV, IR, and NMR (100 MHz) spectra were measured in ethanol, ethanol, chloroform, and chloroform-*d*, unless otherwise stated. The abbreviations "s, d, t, q, m, br, and do" in the NMR spectra denote "singlet, doublet, triplet, quartet, multiplet, broad, and double," respectively. The preparative TLC was carried out over silica gel (Merck, Kieselgel GF-254) and the column chromatography over silica gel (Merck, Kieselgel 70—230 mesh).

Partial Acetylation of Rishitin (3). Compound **3** (3.09 g, $[\alpha]_D$ −35.1°) was treated with acetic anhydride (3.0 ml) in benzene (80 ml) and pyridine (4 ml) at room temperature for 5 h under stirring. After addition of water, the mixture was separated into organic (benzene) and aqueous layers, and the latter was extracted with ether. The benzene and ether solutions were combined, washed with 2 M hydrochloric acid (HCl), 5% aq sodium hydrogencarbonate ($NaHCO_3$) and water, dried over anhydrous sodium sulfate and evaporated to leave resinous material (3.68 g), which was separated by column chromatography over silica gel (400 g), benzene–ether mixtures being used as solvents. Fraction eluted with benzene–ether (5: 1) afforded reshitin diacetate[6] (**3c**, 0.22 g), mp 68—70 °C (from hexane), which was identical with an authentic sample. Early fractions eluted with benzene–ether (4: 1) gave rishitin 2-acetate (**3a**, 1.25 g), mp 60.5—62.5 °C and $[\alpha]_D$ −33.6°; MS, *m/e* 204 (base, M$^+$ −AcOH), 189, 186, 175, 171, and 161; IR, ν_{max} (Nujol) 3320, 3245, 3080, 1735, 1643, 1248, 1069, 1032, and 897 cm^{-1}; NMR, δ (CCl_4) 1.16 (3H, d, J=6.5 Hz, 14-H), 1.72 and 2.05 (each 3H, s, 13-H and $OCOCH_3$), 3.31 (1H, t, J=8.5 Hz, 3-H), and 4.72 (3H, br, 2-H and 12-H). Found: C, 72.82; H, 9.22%. Calcd for $C_{16}H_{24}O_3$: C, 72.69; H, 9.15%. Fractions eluted with benzene–ether (4: 1 and 3: 1) yielded rishitin 3-acetate (**3b**, 0.83 g), mp 107—107.5 °C (from hexane–diisopropyl ether) and $[\alpha]_D$ −38.9°; MS, *m/e* 204 (base, M$^+$ −AcOH), 189, 186, 175, 171, and 161; IR, ν_{max} (Nujol) 3440, 3400, 3080, 1736, 1644, 1239, 1075, 1032, 1021, 1009, and 883 cm^{-1}; NMR, δ (CCl_4) 1.03 (3H, d, J= 7 Hz, 14-H), 1.72 and 2.09 (each 3H, s, 13-H and $OCOCH_3$), 3.62 (1H, do t, J=6.5, 8.5, and 8.5, 2-H), 4.60 (1H, t, J= 8.5 Hz, 3-H), 4.60 and 4.68 (each 1H, br s, 12-H). Found: C, 68.37; H, 8.85%. Calcd for $C_{16}H_{24}O_3 \cdot H_2O$: C, 68.05; H, 9.28%. Fractions eluted with ethyl acetate gave rishitin (**3**, 1.07 g).

Oxidation of 3a and 3b. i) To a heterogeneous mixture of ether (5 ml) containing **3a** (52 mg) and water (2.5 ml) was added the Jones reagent (1 ml, 2.16 mmol) under stirring, and the mixture was further stirred vigorously at room temperature for 16 h. After dilution with ether, the mixture was separated into ether and aqueous layers, and the aqueous solution was extracted with ether. All the ether solutions were combined, washed with 5% aq sodium thiosulfate ($Na_2S_2O_3$), 5% aq $NaHCO_3$ and saturated brine, dried and evaporated to leave oil (44 mg), which was purified by chromatography over silica gel with benzene–ether (5: 1) to give 3-dehydrorishitin 2-acetate (**4a**, 24 mg), oily and $[\alpha]_D$ +9.6°; MS, *m/e* 262 (M$^+$), 202, 187, 172, 159 (base), 134, 105, and 60; IR, ν_{max} (neat) 3070, 1757, 1737, 1643, 1231, 1019, and 889 cm^{-1}; NMR δ (CCl_4), 1.19 (3H, d, J=7.5 Hz, 14-H), 1.75 and 2.10 (each 3H, s, 13-H and $OCOCH_3$), 2.92 (1H, q, J=7.5 Hz, 4-H), 4.67 and 4.73 (each 1H, br s, W_H=4.5 Hz, 12-H), and 5.21 (1H, do d, J=11 and 8 Hz, 2-H).

ii) Compound **3b** (159 mg) was oxidized with the Jones reagent (2.0 ml) in ether (16 ml) and water (7.5 ml) at room temperature for 21 h under stirring. The mixture was worked up as described above to leave an oily substance (159 mg), which was purified by chromatography over silica gel (8 g) with benzene–ether (5: 1) to give 2-dehydrorishitin 3-acetate (**4b**, 96 mg), oily and $[\alpha]_D$ +59.4°; MS, *m/e* 262 (M$^+$), 202, 187, 159, (base), 134, 91, and 60; IR, ν_{max} (neat) 3080, 1757, 1744, 1643, 1226, 1050, and 889 cm^{-1}; NMR, δ (CCl_4) 1.14 (3H, d, J=7 Hz, 14-H), 1.74 and 2.10 (each 3H, s, 13-H and $OCOCH_3$), 2.59 (1H, br, 4-H), 2.71 and 2.95 (each 1H, ABq, J=19 Hz, 1-H), 4.65 and 4.70 (each 1H, br s, W_H=4.5 Hz, 12-H), and 4.84 (1H, d, J=9Hz, 3-H). Fractions eluted with benzene–ether (3: 1) afforded the starting alcohol (**3b**, 29 mg).

Transformation of 4b into 1a and 1. To a methanol solution (2.0 ml) of **4b** (12.3 mg) was added 0.12 M potassium hydroxide in methanol (0.46 ml), and the whole solution was stirred at room temperature for 25 min under stirring. The solution was made acidic by addition of 3 M HCl and water, evaporated, and extracted with ethyl acetate (4×10 ml). The extracts were worked up as usual to leave oily residue (11.9 mg), which was separated into two fractions by preparative TLC over silica gel with benzene–ether (5: 1). A more mobile fraction gave an oily substance (5.0 mg), $[\alpha]_D$ +64.8°, showing a single spot on TLC and the following spectra: MS, *m/e* 262 (M$^+$), 234, 202, 173, 162, 159, 147, 134, 131, 121, 94 (base), and 91; UV, λ_{max} 236 nm (ε 15200); IR, ν_{max} 1748, 1692, 1643, 1627, 1228, and 895 cm^{-1}; NMR, δ 1.12 (3H, d, J=6 Hz, 14-H), 1.76 and 2.21 (each 3H, s, 13-H and $OCOCH_3$), 4.74 (2H, br s, W_H=5 Hz, 12-H), 5.11 (1H, d, J=12 Hz, 3-H), and 5.86 (1H, br s, W_H=5 Hz, 1-H). These spectral data were completely identical with the reported of glutinosone acetate.[4] A less mobile (more

polar) fraction afforded an oily substance (4.7 mg), $[\alpha]_D$ +57.2°, showing a single spot on TLC; MS, *m/e* 220 (M^+), 192, 191, 162, 147, 134, 121, and 94 (base); UV, λ_{max} 237 nm (ε 14500); IR, ν_{max} 3470, 1676, 1645, 1620, and 896 cm^{-1}; NMR, δ 1.23 (3H, d, J=6 Hz, 14-H), 1.73 (3H, s, 13-H), 3.72 (1H, s, OH), 3.79 (1H, d, J=12 Hz, 3-H), 4.72 (2H, br s, W_H=5 Hz, 12-H), and 5.90 (1H, br s, W_H=4 Hz, 1-H). These spectra were identical with the reported of glutinosone[4] (**1**). The latter (**1**, 3.6 mg), when treated with acetic anhydride (0.5 ml) and pyridine (1.0 ml) at room temperature for 14 h and then purified by chromatography over silica gel (1.0 g) with benzene–ether (1: 1), was converted into the acetate (4.0 mg), whose spectral data were identical with those of **1a**.

Hydride Reduction of 1. Compound **1** (20.5 mg) was treated with sodium borohydride (16.0 mg) in ethanol (3.0 ml) at room temperature for 2.5 h under stirring. After addition of acetic acid, the mixture was evaporated and shaken with water and ethyl acetate (4×10 ml). The acetate solution was worked up as usual to leave crystalline residue (13.3 mg), which was purified by preparative TLC with ether and recrystallized from ethyl acetate–hexane to yield dihydroglutinosone (**5**, 9.0 mg), mp 136—138 °C (lit,[4] 129—132 °C) and $[\alpha]_D$ −29.6°; MS, *m/e* 222 (M^+), 204, 189, 176, 161, 133, 123, 121, 107, 105, 96 (base), 93, and 91; IR, ν_{max} 3580, 3400, 3070, 1643, 1069, 1047, 1041, and 894 cm^{-1}; NMR, δ 1.11 (3H, d, J=6 Hz, 14-H), 1.73 (3H, s, 13-H), 3.18 (1H, do d, J=10 and 8 Hz, 3-H), 4.06 (1H, br d, J=8 Hz, 2-H), 4.70 (1H, br s, W_H=4 Hz, 12-H), and 5.28 (1H, br s, W_H=5 Hz, 1-H).

Isolation of Oxyglutinosone (2). The fraction E (4.7 g), described in the section of "Isolation of rishitin,"[6] was separated roughly into two fractions, less polar epilubimin and lubimin-rich (2.50 g) and more polar oxylubimin and isolubimin-rich fractions (2.14 g), by chromatography over silica gel (200 g) with a 5: 1 mixture of hexane and ethyl acetate mixture. The latter was further separated into less polar (158 mg), middle (688 mg) and polar fractions (773 mg) by chromatography over silica gel (100 g), hexane–ether mixtures (10: 1—3: 1) being used as solvents. The middle fraction was again submitted to chromatography over silica gel (50 g) with hexane and hexane–ethyl acetate mixtures to yield epilubimin-rich (110 mg), and oxyglutinosone and isolubimin-rich fractions (160 mg). The last fraction (160 mg) was treated lubimin-rich (174 mg) with acetic anhydride (1 ml) and pyridine (5 ml) at room temperature for 16 h. The reaction mixture was worked up as usual to give an oily substance (140 mg), showing two main spots on TLC, which was separated and purified by preparative TLC (3 plates) over silica gel. A less polar fraction gave isolubimin acetate[3,8] (**6a**, 37 mg) mp 49—51 °C (from diisopropyl ether) and $[\alpha]_D$ +34.4°, which a more polar fraction afforded oxyglutinosone acetate (**2a**, 43 mg), mp 101 °C (from diisopropyl ether) and $[\alpha]_D$ +166°; MS, *m/e* 278 (M^+), 260, 250, 218, 200, and 178 (base); UV, λ_{max} 230 nm (ε 12100); IR, ν_{max} 3610, 3480, 1739, 1699, 1642, 1638, 1240, and 897 cm^{-1}; NMR, δ 1.10 (3H, d, J=7 Hz, 14-H), 1.75 and 2.19 (each 3H, s, 13-H and OCOCH_3), 4.75 (2H, br s, W_H=6 Hz, 12-H), 5.39 (1H, d, J=13Hz, 3-H), and 5.79 (1H, d, J=1.5 Hz, 1-H).

The acetate (**2a**, 4 mg) was dissolved in a 1: 1: 2 mixture (2 ml) of triethylamine, water and methanol, and stirred at room temperature for 3 h. The solution was concentrated below 16 °C, and the residue was extracted with ether (20 ml). The ether solution was washed with saturated brine (10 ml), dried and evaporated to dryness to leave oily residue, showing two spots on TLC, which was separated by preparative TLC (1 plate) over silica gel to give the starting acetate (**2a**, 1.5 mg) and oxyglutinosone (**2**, 2.2 mg), oily and $[\alpha]_D$ +130°; MS, *m/e* 236 (M^+), 218, 200, and 178 (base); UV, λ_{max} 230 nm (ε 12100); IR, ν_{max} 3560, 3440, 1682, 1643, and 890 cm^{-1}; NMR, δ 1.25 (3H, d, J=6 Hz, 14-H), 1.74 (3H, s, 13-H); 4.10 (1H, d, J=12 Hz, 3-H), 4.73 (2H, br s, W_H=7 Hz, 12-H), and 5.89 (1H, d, J=1.5 Hz, 1-H).

Conversion of 3b into 2a. i) Compound **3b** (85 mg) was oxidized with *t*-butyl hydroperoxide (0.1 ml) in the presence of $VO(acac)_2$ (2 mg) in benzene (1.2 ml) under reflux for 10 min. After being cooled, the mixture was stirred with 5% aq sodium hydrogensulfite ($NaHSO_3$, 3 ml) at room temperature for 1 h. The benzene solution, after being separated from the aqueous solution, was washed with 5% aq $NaHSO_3$ (10 ml), 5% aq $NaHCO_3$ (10 ml) and saturated brine (10 ml), dried and evaporated to leave crystalline residue (75 mg), which was recrystallized from diisopropyl ether to give 5α,10α-epoxyrishitin 3-acetate (**7**, 75 mg), mp 140—143 °C and $[\alpha]_D$ −14°; IR, ν_{max} (Nujol) 3480, 1730, 1640, 1240, 1037, and 893 cm^{-1}; NMR, δ 1.27 (3H, d, J=6 Hz, 14-H), 1.71 and 2.07 (each 3H, s, 13-H and OCOCH_3), 3.11 (1H, d, J=10 Hz, OH), 3.69 (1H, do q, J=10, 5, 5, and 5 Hz, 2-H), and 4.70 (3H, br m, 3- and 12-H).

ii) To a suspended mixture of chromium(VI) oxide (70 mg) in dry pyridine (0.14 ml) and dichloromethane (2 ml) was added **7** (28 mg) in dichloromethane (0.4 ml) under stirring, and the whole mixture was stirred vigorously at room temperature for 15 min. The mixture was diluted with ether 30 ml) and filtered. The filtrate was washed with 5% aq $NaHCO_3$ and saturated brine, dried and evaporated to leave oily residue (21 mg), showing two spots on TLC. The residue was dissolved in chloroform (1 ml), put on front lines of silica gel plates (Merck, DC-Alufolien Kieselgel 60 F-254, 20×20 cm^2, 3 plates) for 20 min, and developed with a 1: 1 mixture of ethyl acetate and hexane. A fraction showing an UV spectrum was extracted with ethyl acetate to give **2a** (15 mg), mp 99—101 °C and $[\alpha]_D$ +153°, whose spectra (MS, UV, IR, and ^{1}H-NMR) were identical with the corresponding of natural oxyglutinosone acetate (**2a**).

References

1) a) Part XXIII of "Studies on the Phytoalexins," Part XXII, A. Murai, M. Ono, A. Abiko, and T. Masamune, *J. Am. Chem. Soc.*, **100**, 7751 (1978). The following paper is regarded as Part XXI of this series; K. Sato, N. Doke, K. Tomiyama, F. Yagihashi, A. Murai, N. Katsui, and T. Masamune, *Phytochemistry*, **17**, 1901 (1978).

2) A. Murai, H. Taketsuru, F. Yagihashi, N. Katsui, and T. Masamune, *Chem. Lett.*, **1977**, 663.

3) N. Katsui, F. Yagihashi, A. Murai, and T. Masamune, *Chem. Lett.*, **1978**, 1205.

4) R. S. Burden, J. A. Bailey, and G. G. Vincent, *Phytochemistry*, **14**, 221 (1975).

5) The optical rotation of glutinosone or any of its derivatives has so far been unknown; R. S. Burden (private communication, 1977).

6) T. Masamune, A. Murai, M. Takasugi, A. Matsunaga, N. Katsui, N. Sato, and K. Tomiyama, *Bull. Chem. Soc. Jpn.*, **50**, 1201 (1977).

7) M. L. Raggio and D. S. Watt, *J. Org. Chem.*, **41**, 1873 (1976).

8) A. Stoessl, J. B. Stothers, and E. W. B. Ward, *Can. J. Chem.*, **56**, 645 (1978); E. B. Kalan and S. F. Osman, *Phytochemistry*, **15**, 775 (1976).

9) M. N. Sheng and J. G. Zajacek, *J. Org. Chem.*, **35**, 1839 (1970); K. B. Sharpless and R. C. Michaelson, *J. Am. Chem. Soc.*, **95**, 6136 (1973).

The Synthesis of (±)-Glutinosone[1)]

Akio Murai, Hirofumi Taketsuru, and Tadashi Masamune*
Department of Chemistry, Faculty of Science, Hokkaido University, Sapporo 060
(Received August 28, 1979)

The synthesis of (±)-glutinosone, an antifungal norsesquiterpene from *Nicotiana glutinosa* infected with tobacco mosaic virus, is described. It has been completed by two processes, one being based on the Robinson annelation method and another on a modification of the Dastur procedure.

In the preceding paper[1b)] we reported the structure elucidation of (+)-glutinosone (**1**), a norsesquiterpene isolated from leaves of *Nicotiana glutinosa* infected with tobacco mosaic virus and qualified as a phytoalexin.[2)] The structure and configuration of **1** are characterized by a noreudesmane skeleton with a double bond at an angular position as well as three asymmetric centers in the A ring susceptible to facile aromatization. We now report that the synthesis of (±)-glutinosone [(±)-**1**] has been completed by two independent procedures.

The first synthesis[3)] of (±)-glutinosone was achieved by stereoselective functionalization of the A ring of a *trans*-decalin derivative and subsequent introduction of a double bond at the angular position, as in the case of that[4)] of rishitin (**2**). The Robinson annelation[5)] of dimethyl *trans*-2-oxocyclohexane-1,4-dicarboxylates[6)] (**3**) with 1-diethylamino-3-pentanone methiodide and sodium methoxide produced a 1: 1 mixture of C-7-epimers of dimethyl 4-methyl-3-oxooctahydronaphthalene-7,10-dicarboxylates[7)] (**4**) in a 52% yield. The octalone mixture (**4**), when hydrogenated over 10% alladium–charcoal in acetic acid, treated with acid ($HClO_4$ in acetic acid) and then with base ($NaOCH_3$ in methanol), and esterified with diazomethane,[5,8)] was converted into a *trans*-decalone (**5**), mp 105—106 °C, showing a single peak by GLPC and TLC, in a 66% yield. The spectral data [*m/e* 282 (M^+); ν_{max} 1735, 1720, and 1169 cm^{-1}; δ 1.08 (3H, d, J=7 Hz, $C\underline{H}_3$ at C-4), 3.06 (1H, do q, J=11, 7, 7, and 7 Hz, 4-$\underline{H}$), 3.71 and 3.79 (each 3H, s, $COOC\underline{H}_3$)] were in good accord with the structure (**5**).

Functionalization of the A ring of the *trans*-decalone was commenced by treatment of **5** with isopropenyl acetate and *p*-toluenesulfonic acid (*p*-TsOH) under reflux to give the corresponding enol acetate (**6**) in a 91% yield, in which the location of the double bond at C-2–C-3 was revealed by the NMR spectrum [δ 5.27 (1H, br d, J=6 Hz, 2-$\underline{H}$) and 1.04 (3H, d, J=7 Hz, $C\underline{H}_3$ at C-4)]. The compound (**6**), when oxidized with perbenzoic acid, was converted almost quantitatively into 2α,3α-epoxy 3-acetate (**7**), mp 138—139 °C. The α-configuration of the epoxy group was deduced tentatively from attack of the reagent from the less-hindered side (α) and confirmed by the following reactions. Treatment of the epoxy acetate (**7**) with acid (*p*-TsOH in acetic acid, room temp)[10)] effected rearrangement to give 3-oxo 2α-acetate (**8**), mp 142—143 °C, in a 90% yield. Further treatment of **8** with tetramethylammonium acetate in acetone[11)] led to formation of a 1: 1 equilibrium mixture of the starting 3-oxo 2α-acetate (**8**) and its isomeric 2-oxo 3β-acetate (**9**), mp 131—132 °C, from which the latter (**9**) could be isolated in a 46% yield. The structure and configuration of the two oxo acetates were determined on the basis of the NMR spectra: **8**, δ 1.68 (1H, t, J=13 Hz, 1α-$\underline{H}$), 2.59 (1H, do d, J=13 and 6 Hz, 1β-$\underline{H}$), and 5.05 (1H, do d, J=13 and 6 Hz, 2β-$\underline{H}$); **9**, δ 2.36 and 2.76 (each 1H, ABq, J=14 Hz, 1-$\underline{H}$) and 4.86 (1H, d, J=10.5 Hz, 3α-$\underline{H}$). The 2-oxo 3β-acetate (**9**) was then derived smoothly to the 3,3-ethylene acetal (**10**), mp 126—128 °C, in an 85% yield by a standard procedure.

Transformation of the methoxycarbonyl group at

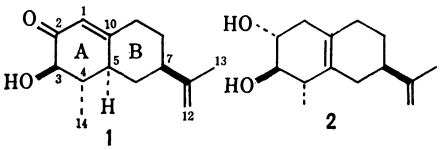

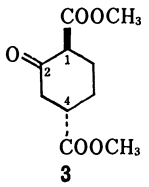

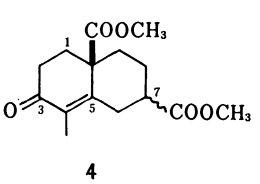

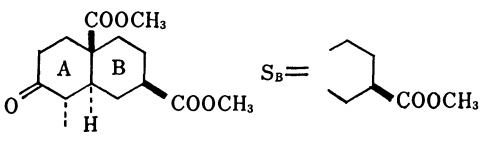

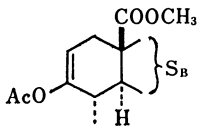

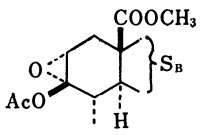

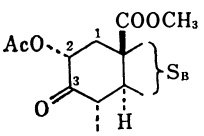

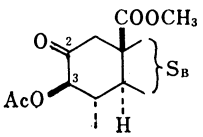

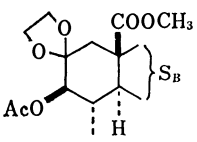

C-7 into an isopropenyl group was carried out by a modification[12] of the Wittig reaction; treatment of **10** with a *large excess* of methylenetriphenylphosphorane in dimethyl sulfoxide (DMSO) at 50 °C for 3 h produced a mixture of δ-lactones, which was separated roughly into two fractions by chromatography. One fraction eluted early afforded isopropenyl δ-lactone (**11**), mp 108—110 °C, in a 22% yield. On the other hand, another fraction eluted later, consisting mainly of acylated phosphorane (**11a**),[12] was hydrolyzed with base (10% KOH in methanol), treated with acetic anhydride and pyridine, and then purified by chromatography to give acetyl δ-lactone (**12**), mp 146—148 °C, in a 50% yield from **10**. The latter (**12**) was again submitted to the Wittig reaction under usual conditions [$(C_6H_5)_3P{=}CH_2$ (3 mol equiv) in DMSO], giving the afore-mentioned δ-lactone (**11**) in an 88% yield. In accordance with the assigned noreudesmane structure, compound **11** displayed following spectra: *m/e* 292 (M^+); ν_{max} 1757 (δ-lactone), 1642 and 895 cm^{-1} (terminal methylene); δ 1.24 (3H, d, J=7 Hz, 14-H), 1.68 (3H, s, 13-H), 1.85 and 2.08 (each 1H, ABq, J=14 Hz, 1-H), 3.97 (4H, br s, W_H=5 Hz, OC_2H_4O), 4.07 (1H, d, J=3 Hz, 3-H), and 4.68 (2H, br s, W_H=4 Hz, 12-H).

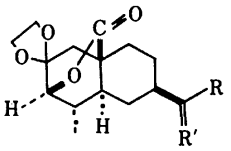

11 R=CH_3, R′=CH_2
11a R=CH=$P(C_6H_5)_3$, R′=O
12 R=CH_3, R′=O

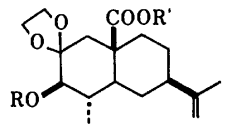

13 R=R′=H
13a R=Ac, R′=H
13b R=Ac, R′=CH_3

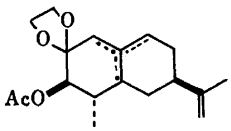

14

Hydrolysis of the δ-lactone (**11**) with base (10% KOH in methanol) produced hydroxy acid (**13**), mp 201—203 °C, in a 97% yield, which, on treatment with acetyl chloride and pyridine in ethyl acetate, was converted into the corresponding acetate (**13a**), mp 238—241 °C, in an 80% yield without regeneration into the δ-lactone (**11**). The acid was smoothly esterified with diazomethane into the methyl ester (**13b**), mp 139—140 °C. Treatment of the acid (**13a**) with lead(IV) acetate and pyridine in *N*,*N*-dimethylformamide (DMF) at room temperature[13] resulted in oxidative decarboxylation to give an olefin mixture (**14**) in a 78% yield. The olefins (**14**), when treated with base without further purification and then with triphenylmethyl fluoroborate in dichloromethane at room temperature,[14] were transformed into a mixture containing phenols, from which an α,β-unsaturated ketone, mp 63—65 °C, was obtained as a sole isolable product in a 30% yield. The ketone exhibited the following spectra: *m/e* 220 (M^+), 192, 191, 162, 147, 134, 121, and 94 (base); λ_{max} 234 nm (ε 13400); ν_{max} 3490, 1676, 1621, and 896 cm^{-1}; δ 1.22 (3H, d, J=6 Hz, 14-H), 1.73 (3H, s, 13-H), 3.72 (1H, s, OH), 3.77 (1H, d, J=12 Hz, 3-H), 4.72 (2H, br s, W_H=5 Hz, 12-H), and 5.89 (1H, br s, W_H=4.5 Hz, 1-H). All these spectra were identical with those reported for glutinosone[1b,2] (**1**), establishing a synthesis of (±)-glutinosone [(±)-**1**]. The overall yield amounted to 2.80% from compound **3**.

The second, improved synthesis of (±)-glutinosone was completed mostly according to a modification of the Dastur elegant procedure[15] for synthesis of (±)-nootkatone. The Diels-Alder reaction[16] of 3,6-dihydro-3,5-dimethylanisole, prepared by the Birch reduction of 3,5-dimethylanisole, with methyl acrylate at 150 °C in the *absence* of Lewis acids[16] afforded a 1 : 3 mixture of methyl 1-methoxy-5,8-dimethylbicyclo[2.2.2]oct-5-ene-2-carboxylates (**15a** and **15b**). While the mixture was used for subsequent transformations without further purification, it was separated by chromatography to yield each diastereoisomer (**15a** and **15b**). The spectral data of each isomer [**15a**, δ 0.81 (3H, d, J=6 Hz, CH_3 at C-8) and 2.66 (1H, do do d, J=11, 5, and 2.5 Hz, 2-H); **15b**, δ 0.83 (3H, d, J=6 Hz) and 2.78 (1H, do d, J=9 and 6 Hz)] and the following reaction indicated that (i) these isomers differed only in the configuration at C-2 and (ii) the methyl group at C-8 would probably be oriented *anti* to the secondary bridge and hence *cis* to the hydrogen atom at C-4; namely, each of these esters (**15a** and **15b**) was converted smoothly into the corresponding tertiary alcohols (**16a** and **16b**) in 90 and 90% yields. The respective alcohols, when treated with acid ($HClO_4$ in acetic acid), produced the same dienone (**17**), showing the following spectra: *m/e* 193 and 192 (M^+); ν_{max} 1670 and 1626 cm^{-1}; δ 1.02 (3H, d, J=6 Hz), 1.64, 1.73, and 1.97 (each 3H, s), 5.11 (1H, br t, J=6 Hz), and 5.76 (1H, br s, W_H=5 Hz).

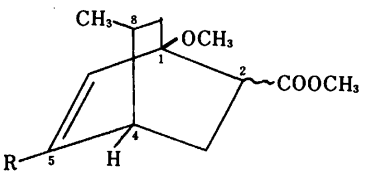

15a R=CH_3, *exo*-$COOCH_3$
15b R=CH_3, *endo*-$COOCH_3$
18 R=CHO
19 R=CH=CH_2

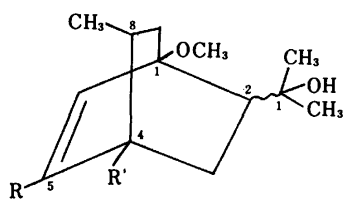

16a R=CH_3, R′=H, *exo*-$C(CH_3)_2OH$
16b R=CH_3, R′=H, *endo*-$C(CH_3)_2OH$
20 R=CH=CH_2, R′=H
22 R=CH=CH_2, R′=CH_3

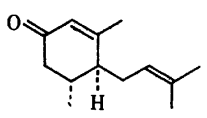

17

Treatment of the mixture (**15a** and **15b**) with selenium(IV) oxide in dioxane effected selective oxidation of the olefinic methyl group to give α,β-unsaturated

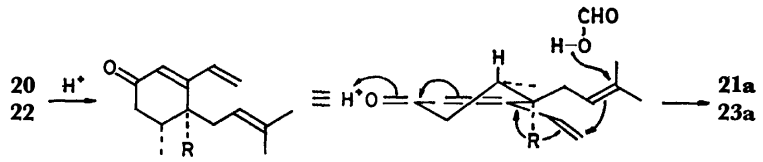

24 R=H
25 R=CH_3

Scheme 1.

aldehydes (**18**) [λ_{max} 233 nm (ε 8700); ν_{max} 2705 and 1680 cm^{-1}; δ 9.40 and 9.46 (total 1H, each s, CHO)] in a 77% yield. The Wittig reaction of aldehydes **18** under usual conditions [$(C_6H_5)_3P=CH_2$ (1.1 mol equiv) in DMSO at room temp] led to formation of dienes (**19**) in a 63% yield with recovery of the starting aldehydes (31%). The dienes (**19**) was then submitted to the Grignard reaction with an excess of methyllithium to yield the corresponding tertiary alcohols (**20**) almost quantitatively. The spectra were consistent with the assigned formulas (Experimental).

Treatment of the alcohols (**20**) with formic acid at room temperature followed by neutralization produced a mixture of bicyclic enones, which were isolated as the tertiary alcohol (**21**) and its formate (**21a**) in 45 and 41% yields, respectively. Naturally the formate (**21a**) was hydrolyzed easily to give the alcohol (**21**) in an 88% yield. This acid transformation of the bicyclooctenes (**20**) into the bicyclic enones (**21** and **21a**) would probably proceed *via* the same process (Scheme 1) as that proposed by Dastur for that of the corresponding 4-methyl derivatives (**22**), in which he emphasized the presence of the relevant methyl group as a factor controlling the configuration of C-7 in the resulting bicyclic enones (**23** and **23a**) (*cf.*, Schemes II and III in Ref. 15). However, the present high yield (86%) formation of the desired bicyclic enones (**21** and **21a**) indicates that, contrary to the Dastur rationalization,[15] the methyl group in question does not an important role in the cyclization of proposed intermediates (**24** and **25**). The structure of the alcohol (**21**) was supported completely by the spectral data: *m/e* 223 (M^++1) and 204; λ_{max} 237 nm (ε 14300); ν_{max} 3440, 1660, and 1624 cm^{-1}; δ 1.09 (3H, d, J=6 Hz, 14-H), 1.20 (6H, s, 12- and 13-H), and 5.81 (1H, br s, W_A=4 Hz, 1-H).

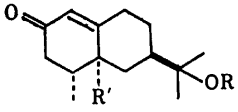

21 R=R'=H
21a R=CHO, R'=H
23 R=H, R'=CH_3
23a R=CHO,R'=CH_3

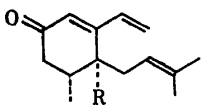

24 R=H
25 R=CH_3

Transformation of the intermediates (**21** and **21a**) into (±)-glutinosone was carried out in usual manners. Treatment of **21** with thionyl chloride in pyridine resulted in dehydration to yield an olefin mixture, which was separated by chromatography over silica gel containing 10% silver nitrate to give isopropenyl (**26**) and isopropylidene bicyclic enones (**27**) in 41 and 20% yields, respectively: **26**, ν_{max} 891 cm^{-1}; δ 1.75 and 4.73 (3H and 2H, each s, 13- and 12-H); **27**, δ 1.70 (6H, br s, 12- and 13-H). Likewise, the formate (**21a**), when treated with aluminium(III) oxide in collidine under reflux, produced a complex mixture, from which compounds **26** and **27** were isolated in 41 and 11% yields, respectively. Oxidation of the isopropenyl bicyclic enone (**26**) with lithium diisopropylamide (LDA) in tetrahydrofuran (THF) at −70 °C and then with the molybdenum peroxide complex MoO_5·Py·HMPA (MoOPH)[17] effected only hydroxylation at C-3 to afford a mixture of diastereoisomeric hydroxy ketones in a rather good yield (60%), with the starting ketone (**26**) (20%), from which equatorial and axial acetoxy ketones (**28a** and **29a**) were isolated in 33 and 59% yields, respectively, after acetylation and subsequent purification by preparative TLC: **28a**, ν_{max} 1753 cm^{-1}; δ 5.10 (1H, d, J=12 Hz, 3-H): **29a**, ν_{max} 1748 cm^{-1}; δ 5.47 (1H, d, J=5 Hz). These acetoxy ketones (**28a** and **29a**) were hydrolyzed with base (K_2CO_3 in ethanol) to give the corresponding hydroxy ketones (**28** and **29**) in 60 and 55% yields, respectively. The former (**28**), mp 64—66 °C, exhibited the same spectra as synthetic and natural samples of glutinosone, constituting an alternate, more efficient synthesis of (±)-glutinosone [(±)-**1**]. The synthesis involved only nine steps and the overall yield amounted to 3.64% from the bicyclooctanone mixture (**15a** and **15b**).

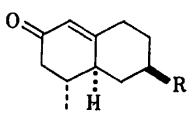

26 R=−C(=CH_2)CH_3
27 R=C(CH_3)$_2$

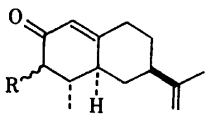

28 [=(±)-**1**] R=β-OH
28a R=β-OAc
29 R=α-OH
29a R=α-OAc

Experimental

All the melting points were uncorrected. The homogeneity of each compound was checked by TLC on silica gel (Wakogel B-5F) with various solvent systems, and the spots were developed with cerium(IV) sulfate in dil sulfuric acid. The UV, IR, and NMR (^{1}H-NMR) spectra were measured in ethanol, chloroform, and chloroform-*d*, respectively, unless otherwise stated. Abbreviations "s, d, t, q, m, br, and do" in the NMR spectra denote "singlet, doublet, triplet, quartet, multiplet,

broad, and double," respectively. The preparative TLC and column chromatography were carried out over silica gel (Wakogel B-5F, 20×20 cm²) and over silica gel (Merck, Kieselgel 60, 70—230 mesh), respectively.

The Robinson Annelation of Dimethyl trans-*2-Oxocyclohexane-1,4-dicarboxylate (3).* Compound **3** (1.08 g) was prepared by addition of an ether solution saturated with diazomethane into the corresponding diacid[6] (0.94 g) in ether (5 ml). The ester (**3**) had mp 99—100 °C (from methanol) (lit,[6] 75—77 °C) and showed the following spectra: MS, *m/e* 214 (M^+), 183, 182, 155, 154, and 123 (base); IR, ν_{max} (Nujol) 1732, 1704, 1201, 1162, and 1031 cm^{-1}; NMR δ 2.70 (1H, m, 4-H), 3.42 (1H, do d, J=9 and 5 Hz, 1-H), 3.74 and 3.78 (each 3H, s, $COOCH_3$). Found: C, 56.19; H, 6.78%. Calcd for $C_{10}H_{14}O_5$: 56.07; H, 6.59%.

To a methanol solution containing sodium methoxide, prepared from sodium (48 mg) and methanol (1 ml), were added **3** (264 mg) in methanol (9.0 ml) and then 1-diethylamino-3-pentanone methiodide in methanol, prepared from 1-diethylamino-3-pentanone (203 mg) and methyl iodide (267 mg) in methanol (1.0 ml). The whole mixture was stirred at room temperature for 17 h and then refluxed for 4.5 h. After being cooled, the mixture was evaporated and shaken with water and ether (6×20 ml). The ether solution was washed with 10% aq sodium carbonate (Na_2CO_3) and water, dried over anhydrous sodium sulfate, and evaporated to leave an oily substance, which was purified by preparative TLC over silica gel with chloroform to yield a 1:1 (by GLPC) mixture of 4-methyl-3-oxooctahydronaphthalene-7,10-dicarboxylates[7] (**4**, 181 mg): MS, *m/e* 280 (M^+), 248, 221, 220, and 161 (base); UV, λ_{max} 246 nm (ε 12400); IR, ν_{max} (neat) 1725, 1664, 1617, and 1175 cm^{-1}; NMR, δ 1.88 and 1.91 (each 1.5H, s, CH_3 at C-4), 3.67 and 3.71 (each 1.5H, s, $COOCH_3$ at C-7), and 3.75 (3H, s, $COOCH_3$ at C-10).

*Dimethyl (4*RS, *5*RS, *7*SR, *10*SR*)-4-Methyl-3-oxo-decahydronaphthalene-7,10-dicarboxylate (5).* Compounds **4** (494 mg) were hydrogenated over 10% palladium–charcoal in acetic acid at room temperature for 15 h. After removal of the catalyst by filtration and subsequent addition of 60% aq $HClO_4$ (one drop), the mixture was again stirred at room temperature for 15 h, diluted with water, and extracted with ether (3×20 ml). The ether extracts were worked up as usual to leave oily residue (480 mg), which was dissolved in methanol (4.0 ml). The methanol solution was added to methanol containing sodium methoxide, prepared from sodium (167 mg) and methanol (6.0 ml), and the whole mixture was refluxed under nitrogen for 40 min. After being cooled, the mixture was evaporated below 30 °C, diluted with water, made acidic with dil sulfuric acid, and extracted with ether (3×20 ml). The ether solution was washed with water, dried and mixed with an ether solution saturated with diazomethane, and evaporated to leave a crystalline substance (**5**, 327 mg), which was so pure as to be used for the next reactions. This was recrystallized from hexane-acetone for analysis and had mp 105—106 °C: MS, *m/e* 282 (M^+), 250, 223, 222, 163, 162, and 145 (base); IR (Nujol) and NMR, in the text. Found: C, 63.75; H, 7.80%. Calcd for $C_{15}H_{22}O_5$: C, 63.81; H, 7.85%.

*Dimethyl (4*RS, *5*RS, *7*SR, *10*SR*)-3-Acetoxy-4-methyl-1,4,5,-6,7,8,9,10-octahydronaphthalene-7,10-dicarboxylate (6) and Its 2α,-3α-Epoxide (7).* i) A solution of **5** (4.40 g) in isopropenyl acetate (23.0 ml) was evaporated slowly in the presence of *p*-TsOH (416 mg) for 13 h, the acetate (total 13 ml) being added dropwise during the time, when 16 ml of the acetate had been removed. After addition of water, the reaction mixture was mixed with water and extracted with ether (3×50 ml). The ether solution was washed with 5% aq sodium hydrogencarbonate ($NaHCO_3$) and water, dried and evaporated to leave an oily substance, which was purified by chromatography over silica gel. Fractions eluted with benzene–ether (19:1) afforded **6** (4.56 g), showing a single spot on TLC: MS, *m/e* 324 (M^+) and 282 (base); IR, ν_{max} (neat) 1762, 1742, 1734, 1683, 1210, 1180, 1151, and 1123 cm^{-1}; NMR, δ 1.04 (3H, d, J=7 Hz, CH_3 at C-4), 2.10 (3H, s, $OCOCH_3$), 2.64 (1H, do d, J=16 and 6 Hz, 1β-H), 3.69 (6H, s, $COOCH_3$), and 5.27 (1H, br d, J=6 Hz, 2-H). Found: C, 63.10; H, 7.55%. Calcd for $C_{17}H_{24}O_6$: C, 62.95; H, 7.41%.

ii) To a solution of **6** (5.54 g) in chloroform (30 ml) cooled with ice-water was added dropwise perbenzoic acid (purity 94%, 4.77 g) in chloroform (20 ml). The mixture was allowed to stand in a refrigerator for 15 h, and washed with 5% aq sodium hydrogensulfite ($NaHSO_3$), 5% aq $NaHCO_3$ and water, dried and evaporated to leave a crystalline substance (**7**, 5.80 g), mp 138—139 °C; NMR, δ 1.18 (3H, d, J=7 Hz, CH_3 at C-4), 2.05 (3H, s, $OCOCH_3$), 2.84 (1H, do d, J=15 and 6 Hz, 1β-H), 3.43 (1H, d, J=6 Hz, 2-H), 3.69 and 3.77 (each 3H, s, $COOCH_3$). This was used for the next reaction without purification.

*Dimethyl (2*SR,*4*SR,*5*RS,*7*SR,*10*SR*)-2-acetoxy-4-methyl-3-oxodecahydronaphthalene-7,10-dicarboxylate (8), Its 3-Acetoxy-2-oxo Isomer (9), and Its 3,3-Ethylene Acetal (10).* i) Compound **7** (2.5 g) was treated with *p*-TsOH (0.8 g) in acetic acid (100 ml) at room temperature for 14 h under stirring. The mixture, after being worked up as usual, afforded a crystalline substance (**8**, 2.3 g), which was so pure as to be used for the next rearrangement. The sample was recrystallized from hexane–acetone to give an analytical sample, mp 142—143 °C: MS, *m/e* 340 (M^+), 298, 281, 280, 266, 254, 238, and 226 (base); IR, ν_{max} (Nujol) 1762, 1735, 1730, 1237, and 1166 cm^{-1}; NMR, δ 1.09 (3H, d, J=7 Hz, CH_3 at C-4), 1.68 (1H, t, J=13 Hz, 1α-H), 2.14 (3H, s, $OCOCH_3$), 2.30 (1H, do d, J=10 and 2 Hz, 7-H), 2.59 (1H, do d, J=13 and 6 Hz, 1β-H), 3.18 (1H, do q, J=11, 7, 7, and 7 Hz, 4-H), 3.68 and 3.79 (each 3H, s, $COOCH_3$), and 5.05 (1H, do d, J=13 and 6 Hz, 2-H). Found: C, 59.98; H, 7.12%. Calcd for $C_{17}H_{24}O_7$: C, 59.99; H, 7.11%.

ii) An acetone solution (50 ml) containing **8** (1.16 g) was refluxed with tetramethylammonium acetate (0.72 g) for 16 h. The mixture was evaporated, mixed with water and extracted with ethyl acetate (3×50 ml). The acetate solution was washed with saturated brine, dried and evaporated to leave amorphous residue (1.18 g), which was separated by chromatography over silica gel (60 g) with a 4:3:2 mixture of hexane, ether and diisopropyl ether. Fractions eluted early afforded the starting material (**8**, 0.63 g), while those eluted later gave a crystalline substance (**9**, 0.53 g), which on recrystallization from hexane–acetone had mp 131—132 °C: MS, *m/e* 340 (M^+) and 298 (base); IR, ν_{max} (Nujol) 1735, 1242, 1212, and 1172 cm^{-1}; NMR, δ 1.10 (3H, d, J=7 Hz, CH_3 at C-4), 2.36 and 2.76 (each 1H, ABq, J=14 Hz, 1-H), 3.67 and 3.69 (each 3H, s, $COOCH_3$), and 4.86 (1H, d, J=10.5 Hz, 3-H). Found: C, 60.18; H, 7.12%. Calcd for $C_{17}H_{24}O_7$: C, 59.99; H, 7.11%.

iii) A solution of **9** (390 mg) in benzene (20 ml) was refluxed with ethylene glycol (0.4 ml) in the presence of *p*-TsOH (75 mg) for 20 h, water being removed by a Dean-Stark apparatus. The solution was cooled, evaporated, mixed with water and extracted with ethyl acetate (3×50 ml). The acetate solution was worked up as usual to leave amorphous residue (490 mg), which crystallized on trituration with hexane–acetone, and was collected by filtration and amounted to 130 mg. The filtrate was concentrated and then purified by chromatography over silica gel (9 g) with benzene–ether (6:1) to give an additional crystalline substance (250 mg). Both the crystal-

line substances (**10**, 380 mg) were recrystallized from hexane–acetone to give an analytical sample, mp 126—128 °C: MS, *m/e* 384 (M^+), 352, and 325 (base); IR, ν_{max} (Nujol) 1748, 1736, 1237, 1199, 1181, 1157, 1069, and 1032 cm^{-1}; NMR, δ 0.89 (3H, d, J=7 Hz, C$\underline{H}_3$ at C-4), 2.09 (3H, s, OCOC$\underline{H}_3$), 2.20 (1H, d, J=14 Hz, 1β-$\underline{H}$), 3.66 (6H, s, COOC$\underline{H}_3$), 3.90 (4H, br m, $C_2\underline{H}_4O_2$), and 4.72 (1H, d, J=11 Hz, 3-$\underline{H}$).

*(3*RS,*4*RS,*5*RS,*7*SR,*10*SR*)-7-Isopropenyl- (**11**) and (3*RS,-*4*RS,*5*RS,*7*SR,*10*SR*)-7-Acetyl-4-methyl-2-oxodecahydronaphthalene 10,3-Carbolactone 3,3-Ethylene Acetal (**12**).* i) To a solution of methyltriphenylphosphonium iodide (1.31 g) in DMSO (8.0 ml) was added a hexane solution (2.16 ml) containing 15% butylithium, and the whole solution was stirred at room temperature for 2 h. To a part (3.16 ml, 1.10 mmol equiv) of the ylide solution was added dropwise **10** (44 mg) in DMSO (1.5 ml). The mixture was stirred at room temperature for 1 h and then at 50 °C for 3 h, and the reaction was ceased by addition of water. The reaction mixture was ceased by addition of water. The reaction mixture was extracted with ethyl acetate (5×50 ml), and the acetate extracts were washed with saturated brine, dried and evaporated to leave resinous material (242 mg), which was submitted to chromatography over silica gel (7 g). Fractions eluted with benzene–ether (7: 1) afforded a crystalline substance (**11**, 7 mg), which was recrystallized from hexane–acetone to give an analytical sample, mp 108—110 °C; MS, *m/e* 292 (M^+, base), 207, 204, 165, 149, and 138; IR, ν_{max} 3100, 1757, 1642, 1192, 1097, and 895 cm^{-1}; NMR, δ 1.24 (3H, d, J=7 Hz, 14-$\underline{H}$), 1.68 (3H, s, 13-$\underline{H}$), 1.85 and 2.08 (each 1H, ABq, J=14 Hz, 1-$\underline{H}$), 3.97 (4H, br s, W_H=5 Hz, $C_2\underline{H}_4O_2$), 4.07 (1H, d, J=3 Hz, 3-$\underline{H}$), and 4.68 (2H, br s, W_H=4 Hz, 12-$\underline{H}$). Fractions eluted with methanol were combined and evaporated, and the residue (210 mg) was refluxed with 10% potassium hydroxide (KOH) in methanol (20 ml) for 2 d. The reaction mixture was evaporated, mixed with water, made acidic with 3M hydrochloric acid (HCl), and extracted with ethyl acetate (4× 50 ml). The acetate solution was worked up as usual to leave amorphous residue (540 mg), which was purified by chromatography over silica gel (24 g). Fractions eluted with benzene–ether (5: 1) afforded a crystalline substance (**12**, 17 mg), which was recrystallized from hexane–acetone to give an analytical sample, mp 146—148 °C; MS, *m/e* 294 (M^+), 251, 209, 208, 149, and 99 (base); IR, ν_{max} 1760, 1710, 1176, and 1099 cm^{-1}; NMR, δ 1.29 (3H, d, J=7 Hz, 14-$\underline{H}$), 1.89 and 2.15 (each 1H, ABq, J=15 Hz, 1-$\underline{H}$), 2.18 (3H, s, COC$\underline{H}_3$), 4.01 (4H, br s, W_H=4.5 Hz, $C_2\underline{H}_4O_2$), and 4.12 (1H, d, J=3 Hz, 3-$\underline{H}$).

ii) To a solution of methylenetripehnylphosphorane, prepared by addition of 15% butyllithium in hexane (0.22 ml) to methyltriphenylphosphonium iodide (164 mg) in DMSO (1 ml) and stirring at room temperature for 2.5 h, was added **12** (43 mg) in DMSO (1.5 ml). The solution was stirred at room temperature for 1.5 h and then at 50 °C for 5.5 h. The reaction mixture was worked up as described above to leave amorphous residue, which was purified by chromatography over silica gel (10 g) with benzene–ether (7: 1) to give **11** (37 mg), mp 107—110 °C, identical with an authentic sample (IR and NMR).

*(3*RS,*4*RS,*5*RS,*7*SR,*10*SR*)-3-Hydroxy-7-isopropenyl-4-methyl-3-oxodecahydronaphthalene-10-carboxylic Acid 3,3-Ethylene Acetal (**13**), Its 3-Acetate (**13a**), and Its Methyl Ester (**13b**).* Compound **11** (62 mg) was refluxed with 10% KOH in methanol (8 ml) for 3 h. After being cooled, the reaction mixture was evaporated, mixed with water, acidified with 3M HCl, and extracted with ethyl acetate (7×30 ml). The acetate extracts were worked up as usual to leave an amorphous substance (**13**, 72 mg), which on trituration with ether crystallized and had mp 201—203 °C: IR, ν_{max} (Nujol) 3325, 1715, 1642, 1180, 1165, 1074, 1039, and 890 cm^{-1}; NMR, δ 1.11 (3H, d, J=7 Hz, 14-$\underline{H}$), 1.73 (3H, s, 13-$\underline{H}$), 3.21 (1H, d, J=10.5 Hz, 3-$\underline{H}$), 4.04 (4H, br s, W_H=7 Hz, $C_2\underline{H}_4O_2$), and 4.72 (2H, br s, W_H=4 Hz, 12-$\underline{H}$).

The crude sample (72 mg) of **13** was stirred with acetyl chloride (0.1 ml) and pyridine (0.2 ml) in ethyl acetate (3 ml) at room temperature for 14 h. The reaction mixture was worked up as usual to leave amorphous residue (96 mg), which was purified by preparative TLC (2 plates) over silica gel, a 20: 1 mixture of benzene and acetic acid being used as a solvent, to give an amorphous substance (**13a**, 60 mg), which on trituration with ether crystallized and had mp 238—241 °C; IR, ν_{max} 2750—2580, 1739, 1711, 1644, 1237, 1036, and 893 cm^{-1}; NMR, δ 0.88 (3H, d, J=7 Hz, 14-$\underline{H}$), 1.71 and 2.11 (each 3H, s, 13-$\underline{H}$ and OCOC$\underline{H}_3$), 2.50 (1H, d, J=14 Hz, 1β-$\underline{H}$), 3.96 (4H, br m, W_H=18 Hz, $C_2\underline{H}_4O_2$), and 4.71 (2H, s, 12-$\underline{H}$), 4.76 (1H, d, J=11 Hz, 3-$\underline{H}$), and 6.60 (1H, br s, O$\underline{H}$).

The 3-acetate (**13a**) was converted quantitatively into the methyl ester (**13b**), mp 139—140 °C (from hexane–acetone) with diazomethane in ethyl by a standard procedure; MS, *m/e* 366 (M^+), 334, 307, 278, 239, 218, and 183 (base); IR, ν_{max} 1738, 1645, 1240, 1175, 1035, and 897 cm^{-1}; NMR, δ 0.86 (3H, d, J=6 Hz, 14-$\underline{H}$), 1.63, 2.07, and 3.63 (each 3H, 13-$\underline{H}$, OCOC$\underline{H}_3$, and COOC$\underline{H}_3$), 3.79 (4H, br m, W_H=30 Hz, $C_2\underline{H}_4O_2$), 4.65 (2H, s, 12-$\underline{H}$), and 4.70 (1H, d, J=11 Hz, 3-$\underline{H}$).

*Transformation of **13a** into (±)-Glutinosone [(±)-**1**].* A solution of **13a** (23.6 mg) in DMF (3 ml) containing pyridine (0.2 ml) was stirred with lead(IV) acetate (123.6 mg) in DMF (3 ml) at room temperature for 3 h. After addition of water, the mixture was made acidic with 3M aq HCl and extracted with ethyl acetate (5×20 ml). The acetate solution was worked up as usual to leave oily residue, which was separated by chromatography over silica gel (20 g). Fractions eluted with benzene–ether (5: 1) afforded an oily olefin mixture (**14**, 18.3 mg); ν_{max} 1737, 1644, 1374, 1244, 1043, and 895 cm^{-1}; NMR, δ 0.95 and 1.13 (total 3H, each d, J=7 Hz, 14-$\underline{H}$), 4.93, 4.99, and 5.13 (total 1H, each d, J=11, 10, and 13 Hz, 3-$\underline{H}$), 5.54 and 5.90 (total 2/3H, each br s, W_H=9 and 5 Hz, 1- and 9-$\underline{H}$).

The olefin mixture (**14**, 18.3 mg) was stirred with 5% KOH in methanol (1.5 ml) at room temperature for 70 min. The reaction mixture was worked up as described before to leave oily material (14.5 mg), which was stirred with triphenylmethyl fluoroborate (28.8 mg) in dichloromethane (2.1 ml) at room temperature for 1 h. The reaction mixture was then stirred with 5% aq $NaHCO_3$ (2 ml) at room temperature for 10 min. The aqueous layer was extracted with chloroform (2×10 ml). The dichloromethane and chloroform solutions were combined, washed with saturated brine, dried and evaporated to leave oily residue (35.8 mg), which was separated by preparative TLC (2 plates) over silica gel with benzene–ether (5: 1) to give an oily substance (3.3 mg, 23% from **13a**), whose spectra (in the text) were completely identical with the reported of natural glutinosone (**1**). The resulting (±)-glutinosone crystallized on standing and had mp 63—65 °C.

The Diels-Alder Reaction of 3,6-Dihydro-3,5-dimethylanisole and Methyl Acrylate. A mixture of the dihydroanisole[16] (47.6 g) and methyl acrylate (100.8 g) was heated at 150—155 °C (bath temp) for 40 h in an autoclave. After being cooled, the mixture was evaporated under reduced pressure, when most of excess of the acrylate and the dihydroanisole (10.6 g) were recovered at room temperature (8 Torr) and at 90—100 °C (8 Torr), respectively. The residue was then distilled to give a *crude* adduct (34.3 g) at 80—100 °C (0.3 Torr), which was used for the next reaction without further purification. A

part (3.9 g) of the crude adduct was separated by chromatography over silica gel, benzene and benzene–ether mixtures being used as solvents. Early fractions eluted with benzene and benzene–ether (50: 1) afforded an oily substance (1.26 g), which was assigned formula **30** [methyl 2-(3,5-dimethylphenyl)propionate] on the basis of the spectral data and the analogous examples:[18] MS, *m/e* 192 (M^+) and 133 ($M^+ - CO\text{-}OCH_3$); IR, ν_{max} (neat) 1743, 1605, 1198, 1175, and 1164 cm^{-1}; NMR, δ 1.46 (3H, d, J=7 Hz, 3-H), 2.27 (6H, s, CH_3 at C-3′ and C-5′), 3.64 (3H, s, $COOCH_3$), 3.66 (1H, q, J=7 Hz, 2-H), and 6.91 (3H, br s, W_H=4 Hz, 2′-, 4′-, and 6′-H). Middle fractions eluted with benzene–ether (20: 1) gave an exo-adduct, methyl 1-methoxy-5,8-dimethylbicyclo[2.2.2]oct-5-ene-2-carboxylate (**15a**, 0.21 g), showing a single spot on TLC: MS, *m/e* 224 (M^+), 193, 182, 138, 123 (base); IR, ν_{max} (neat) 1736, 1207, 1167, and 1098 cm^{-1}; NMR, δ 0.81 (3H, d, J=6 Hz, CH_3 at C-8), 1.81 (3H, br s, W_H=4 Hz, CH_3 at C-5), 2.66 (1H, do do d, J=11, 5, and 2.5 Hz, 2-H), 3.37 and 3.71 (each 3H, s, OCH_3 and $COOCH_3$), and 5.97 (1H, br s, W_H=7 Hz, 6-H). Next fractions eluted with benzene–ether (20: 1) afforded a 1: 1 (by NMR) mixture (0.72 g) of two adducts (**15a** and **15b**). Final fractions eluted with benzene–ether (20: 1) gave an isomeric endo-adduct (**15b**, 1.21 g), showing a single spot on TLC: MS, *m/e* 224 (M^+), 193, 182, 138, and 123 (base); IR, ν_{max} (neat) 1744, 1203, 1165, and 1103 cm^{-1}; NMR, δ 0.83 (3H, d, J=6 Hz, CH_3 at C-8), 1.86 (3H, br s, W_H=4 Hz, CH_3 at C-5), 2.78 (1H, do d, J=10 and 6 Hz, 2-H), 3.31 and 3.61 (each 3H, s, OCH_3 and $COOCH_3$), and 5.77 (1H, br s, W_H=6 Hz, 6-H).

*2-(1-Methoxy-5,8-dimethylbicyclo[2.2.2]oct-5-en-2-yl)-2-propanols (**16a** exo, and **16b** endo), and t-3-dimethyl-r-4-(3-methyl-2-butenyl)-2-cyclohexen-1-one (**17**).* i) A solution of **15a** (165 mg) in ether (3 ml) was stirred with methyllithium (3%) in ether (1 ml) at room temperature for 1 h. After addition of saturated brine under cooling, the mixture was extracted with ether (3×10 ml). The ether extracts were worked up as usual to give **16a** (160 mg), showing a single spot on TLC; MS, *m/e* 224 (M^+), 209, 207, 206, 149, 138, 124, and 123 (base); IR, ν_{max} (neat) 3490, 1391, 1377, 1165, and 1083 cm^{-1}; NMR, δ 0.82 (3H, d, J=6 Hz, CH_3 at C-8′), 1.10 and 1.33 (each 3H, s, $C(CH_3)_2OH$], 1.75 (3H, br s, W_H=4 Hz, CH_3 at C-3′), 3.34 (3H, s, OCH_3), and 5.98 (1H, br s, W_H=7 Hz, 2′-H).

Compound **16a** (127 mg) was stirred with 60% aq $HClO_4$ (one drop) in acetic acid (1 ml) at room temperature for 30 min. The mixture was diluted with water, basified with 6M aq ammonia, and extracted with ether (3×20 ml). The ether extracts were worked up as usual to give oily residue (118 mg), which was purified by chromatography over silica gel (5 g). Fractions eluted with benzene–ether (20: 1) gave an oily substance (**17**, 68 mg), showing a single spot: MS, *m/e* 193, 192 (M^+), 124 and 109 (base); IR, ν_{max} (neat) 1670, 1626, and 1244 cm^{-1}; NMR, δ 1.02 (3H, d, J=6 Hz, CH_3 at C-8), 1.64 and 1.73 [each 3H, s, $=C(CH_3)_2$], 1.97 (3H, s, CH_3 at C-3), 5.11 (1H, br t, J=6 Hz, 2′-H), and 5.76 (1H, br s, W_H=5 Hz, 2-H).

ii) Compound **15b** (251 mg) in ether (4 ml) was stirred with methyllithium (3%) in ether (3 ml) at room temperature for 1 h. The reaction mixture was worked up as described above to give **16b** (243 mg), showing a single spot: MS, *m/e* 224 (M^+), 209, 207, 206, 138, 124, and 123 (base); IR, ν_{max} (neat) 3490, 1391, 1377, 1167, and 1098 cm^{-1}; NMR, δ 0.84 (3H, d, J=6 Hz, CH_3 at C-8′), 1.04 [6H, s, $C(CH_3)_2OH$], 1.78 (3H, br s, W_H=4 Hz, CH_3 at C-3′), 3.37 (3H, s, OCH_3), and 5.82 (1H, br s, W_H=7 Hz, 2′-H).

Compound **16b** (193 mg) was stirred with 60% aq $HClO_4$ (0.06 ml) in acetic acid (1.5 ml) at room temperature for 30 min. The reaction mixture was worked up and purified as described above to give **17** (116 mg), whose spectral data were identical with the afore-mentioned.

*Methyl 5-Formyl-1-methoxy-8-methylbicyclo[2.2.2]oct-5-ene-2-carboxylates (**18**).* i) A solution of a mixture (247 mg) of the Diels-Alder reaction products (**15a** and **15b**), free from methyl phenylacetate (**30**), in dioxane (10 ml) was refluxed with selenium(IV) oxide (123 mg) for 16 h under nitrogen, when precipitates were removed by fitration. The precipitates were washed with ether. The dioxane (filtrate) and ether solutions were combined, dried and evaporated to leave oily residue, which was separated by chromatography over silica gel (10 g). Fractions eluted with benzene–ether (10: 1) gave a mixture (198 mg) of aldehydes (**18**), bp 105—120 °C (bath temp) (0.1 Torr): MS, 238 (M^+), 209, 152, 147, 123, and 99 (base); UV, λ_{max} 233 nm (ε 8700); IR, ν_{max} (neat) 2705, 1742, 1680, 1633, 1206, 1168, and 1106 cm^{-1}; NMR, δ 0.72 (3H, d, J=7 Hz, CH_3 at C-8), 3.33 (3H, s, $COOCH_3$), 3.57 and 3.68 (3H, each s, OCH_3), 7.00 and 7.06 (each, 1H, s, 6-H), 9.40 and 9.46 (1H, each s, CHO).

ii) The crude adduct mixture (**15a** and **15b**, 30.0 g) containing **30** (*cf.*, the Diels-Alder reaction described above) in dioxane (390 ml) was refluxed with selenium(IV) oxide (15.0 g) for 16 h under nitrogen. The reaction mixture was worked up as mentioned above to leave oily residue (42 g), which was separated by chromatography over silica gel (1 kg). Fractions eluted with benzene–ether afforded **30** (9.0 g) and those eluted with benzene–ether (10: 1) gave an aldehyde mixture (**18**, 17.0 g), whose spectra were practically the same as those described above.

*Methyl 1-Methoxy-8-methyl-5-vinylbicyclo[2.2.2]oct-5-ene-2-carboxylates (**19**).* A solution of methyltriphenylphosphonium iodide (46.7 g) in DMSO (240 ml) was treated with butyllithium (15%) in hexane (72 ml) at room temperature. A part (260 ml) of the resulting ylide solution was added to a solution of **18** (17.7 g) in DMSO (150 ml), and the whole mixture was stirred at room temperature for 30 min and then at 50 °C for 2 h. After addition of water, the reaction mixture was extracted with ethyl acetate (6×200 ml). The acetate solution was washed with saturated brine, dried and evaporated to leave oily residue (52 g), which was separated by chromatography over silica gel (450 g). Fractions eluted with benzene–ether (20: 1) afforded an oily substance (**19**, 12.9 g): MS, *m/e* 236 (M^+), 177, 161, 150, and 135 (base); UV, λ_{max} 235 nm (ε 18500); IR, ν_{max} (neat) 3090, 1742, 1630, 1593, 1203, 1165, 1107, 989, and 895 cm^{-1}; NMR, δ 0.78 and 0.81 (total 3H, each d, J=6 Hz, CH_3 at C-8), 3.38 and 3.44 (total 3H, each s, $COOCH_3$), 3.67 and 3.74 (total 3H, each s, OCH_3), 5.05 and 5.29 (each 1H, br d, J=10 and 18 Hz, $CH{=}CH_2$), and 6.08—6.63 (2H, m, $CH{=}CH_2$ and 6-H).

*2-(5-Methoxy-8-methyl-5-vinylbicyclo[2.2.2]oct-5-en-2-yl)-2-propanols (**20**).* To compounds **19** (10.0 g) in ether (30 ml) was added dropwise an ether solution (110 ml) containing methyllithium, prepared from methyl iodide (12.0 ml) and lithium (2.7 g), under cooling with an ice–water bath, and the whole mixture was stirred at room temperature for 2 h. After addition of 1M aq ammonium chloride, the mixture was extracted with ether (3×200 ml), and the ether extracts were worked up as usual to leave oily substance (**20**, 9.8 g), which was used for the next reaction: MS, *m/e* 236 (M^+), 221, 219, 218, 203, 150, and 135 (base); UV, λ_{max} 235 nm (18000); IR, ν_{max} (neat) 3495, 3045, 1631, 1591, 1390, 1377, 1208, 1166, 1100, 1077, 989, and 897 cm^{-1}; NMR, δ 0.76 (3H, d, J=7 Hz, CH_3 at C-8′), 0.95 and 0.97 [total 6H, each s, $C(CH_3)_2OH$], 3.39 (3H, s, OCH_3), 4.80 (1H, s, OH), 4.99 and 5.23 (each 1H, br s, J=11 and 17 Hz, $CH{=}CH_2$), 6.02—6.58 (2H, m, $CH{=}CH_2$ and 2′-H).

(4RS,5RS,7SR)-7-(1-Hydroxy-1-methylethyl)-4-methyl-2,3,4,-

5,6,7,8,9-octahydro-2-naphthalenone (21) and Its Formate (21a). Compounds **20** (5.6 g) were dissolved in formic acid (500 ml) and stirred at room temperature for 2 h under nitrogen. The solution was neutralized carefully by addition of 11.5 M aq sodium hydroxide (NaOH) under cooling and extracted with ether (4×500 ml). The ether solution was washed with saturated brine, dried and evaporated to leave oily residue (5.9 g), which was separated into two fractions by chromatography over silica gel (180 g). More mobile fractions eluted with benzene–ether (1: 1) afforded **21a** (2.40 g), showing a single spot on TLC: MS, 251 (M^++1), 234, 210, 204, and 162 (base); UV, λ_{max} 236 nm (ε 14500); IR, ν_{max} (neat) 1724, 1666, 1626, and 1197 cm^{-1}; NMR, δ 1.12 (3H, d, J=6 Hz, 14-H), 1.51 (6H, s, 12- and 13-H), 5.85 (1H, br s, W_H=5 Hz, 1-H), and 8.05 (1H, s, OCHO). Found: C, 71.79; H, 8.84%. Calcd for $C_{15}H_{22}O_3$: C, 71.97; H, 8.86%. Less mobile fractions eluted with ether–ethyl acetate (9: 1) gave **21** (2.4 g), showing a single spot on TLC: MS, *m/e* 223 (M^++1), 207, 205, 204, 164, 149, 107, and 59 (base); UV, IR, and NMR, in the text. Found: C, 75.48; H, 9.06%. Calcd for $C_{14}H_{22}O_2$: C, 75.63; H, 9.97%.

A solution of **21a** (102 mg) in *t*-butyl alcohol (3 ml) was stirred with 0.5 M aq NaOH at room temperature for 15 h. The mixture was evaporated to remove the alcohol, mixed with water and extracted with ethyl acetate (3×5 ml). The acetate solution was worked up as usual to leave oily residue (108 mg), which was purified by passing through a silica gel column (5.0 g) to yield **21** (78 mg), whose spectra were identical with those described above.

(4RS,5RS,7SR)-7-Isopropenyl-4-methyl-2,3,4,5,6,7,8,9-octahydro-2-naphthalenone (26) and the Corresponding 7-Isopropylidene Compound (27). i) A solution of **21** (3.56 g) in pyridine (51 ml) was stirred with thionyl chloride (1.5 ml) at 0 °C (bath temp) for 5 min. The reaction mixture was poured into ice–water under stirring, and extracted with ether (4×100 ml). The ether solution was washed with 2 M aq HCl and saturated brine, dried and evaporated to leave oily residue (2.48 g), which was separated by chromatography over a silica gel column (100 g) containing 10% silver nitrate, benzene–ether mixtures being used as solvents. Early fractions eluted with benzene–ether (7: 1) gave **27** (0.42 g), showing a single spot: MS, *m/e* 204 (M^+), 189, and 171 (base); UV, λ_{max} 232 nm (ε 13200); IR, ν_{max} (neat) 1667 and 1622 cm^{-1}; NMR, δ 1.11 (3H, d, J=6 Hz, 14-H), 1.70 (6H, br s, W_H=6 Hz, 12- and 13-H), and 5.84 (1H, br s, W_H=5 Hz, 1-H). Found: C, 82.24; H, 9.96%. Calcd for $C_{14}H_{20}O$: C, 82.30; H, 9.87%. Fractions eluted with benzene–ether (5: 1) afforded **26** (1.32 g), bp 95—105 °C (bath temp) (13 Torr), showing a single spot on TLC: MS, *m/e* 204 (M^+), 189, 176, 162, 147, 134, 121, and 94 (base); UV, λ_{max} 237 nm (ε 15100); IR, ν_{max} (neat) 3080, 1669, 1622, and 891 cm^{-1}; NMR, δ 1.09 (3H, d, J=6 Hz, 14-H), 1.75 and 4.73 (3H and 2H, each s, 13- and 12-H), and 5.82 (1H, br s, W_H=4 Hz, 1-H). Found: C, 82.21; H, 9.96%. Calcd for $C_{14}H_{20}O$: C, 82.30; H, 9.87%.

ii) A solution of **21a** (521 mg) in collidine (35 ml), distilled over calcium hydride, was heated with aluminium(III) oxide [Merck, Aluminiumoxide 90 (Aktivitätsstufe II—III) 70—230 mesh, 275 mg] under reflux for 16 h. The mixture was cooled, mixed with water, neutralized with 2 M aq HCl and extracted with ethyl acetate (4×50 ml). The acetate solution was washed with 2 M aq HCl, and saturated brine, dried and evaporated to leave oily residue (490 mg), which was separated by chromatography over silica gel (15 g). Fractions eluted with benzene–ether (49: 1, 40: 1, 19: 1, and 9: 1) afforded a 4: 1 (by NMR) mixture (281 mg) of **26** and **27**: MS, *m/e* 204 (M^+), 189, 161, 147, 133, 119, 93,, and 91 (base); IR, ν_{max} (neat) 3070, 1722, 1714, 1646, and 889 cm^{-1}; NMR, δ 1.01 and 1.06 (total 3H, each s, 14-H), 1.76 [3.6H, s, =C-(CH_3)$_2$ and -C(CH_3)=CH_2], and 4.74 [1.6H, br s, W_H=5 Hz, -C(CH_3)=CH_2]. Fraction eluted with benzene–ether (3: 1) and only with ether afforded **21a** (37 mg) and **21** (54 mg), respectively.

(±)-Glutinosone [(±)-1=28], Its 3-Epimer (29), and Their Acetates (28a and 29a). i) To a solution of LDA, prepared from diisopropylamine (0.35 ml) and butyllithium (15%) in hexane (1.5 ml) in THF (3 ml) cooled at −70 °C, was added **26** (125 mg) in THF (2 ml) under cooling at the temperature. To the mixture cooled at the temperature for 30 min was added rapidly MoOPH (814 mg), dried over diphosphorus pentaoxide in a desiccator, at −70 °C. The mixture was stirred at the temperature for 80 min, and the reaction was ceased by addition of water at room temperature. The heterogeneous mixture was shaken with ethyl acetate (3×30 ml). The acetate solution was washed with 2 M aq HCl, 5% aq $NaHCO_3$, and saturated brine, dried and evaporated to leave oily residue (189 mg), which was separated by preparative TLC (6 plates) over silica gel with benzene–ether (20: 1). A fraction with large R_f value gave the starting ketone (**26**, 26 mg), while that with small R_f value afforded a mixture (80 mg) of **28** and **29**, which resisted further purification. The mixture (37 mg) was then treated with acetic anhydride (1 ml) and pyridine (2 ml) at room temperature for 38 h under stirring. The reaction products were mixed with water and extracted with ethyl acetate (3×10 ml). The acetate extracts were worked up as usual to leave oily residue (46 mg), which was separated by preparative TLC (3 plates) over silica gel with benzene–ether (20: 1). A more mobile fraction gave a crystalline substance (**29a**, 25 mg), mp 80—85 °C, showing a single spot on TLC: MS, *m/e* 262 (M^+), 234, 220, 202, 201, 121, and 94 (base); IR, ν_{max} 3075, 1748, 1692, 1641, 1631, 1230, and 894 cm^{-1}; NMR, δ 1.04 (3H, d, J=6 Hz, 14-H), 1.73 and 2.17 (each 3H, s, 13-H and OCOCH_3), 4.74 (2H, br, s, 12-H), 5.47 (1H, d, J=5 Hz, 3-H), and 5.81 (1H, br s, W_H=4 Hz, 1-H). A less mobile fraction gave **28a** (16 mg), oily, showing a single spot; MS, *m/e* 262 (M^+), 234, 220, 202, 121, and 94 (base); IR, ν_{max} (neat) 3075, 1753, 1691, 1640, 1627, 1226, and 887 cm^{-1}; NMR, δ 1.08 (3H, d, J=6 Hz, 14-H), 1.72 and 2.19 (each 3H, s, 13-H and OCOCH_3), 4.72 (2H, s, 12-H), 5.10 (1H, d, J=12 Hz, 3-H), and 5.85 (1H, br s, W_H=4 Hz, 1-H).

ii) A solution of **29a** (8.5 ml) in ethanol (1 ml) was stirred with 0.27 M aq K_2CO_3 (0.15 ml) at room temperature for 12 h. After addition of water, the mixture was evaporated to remove ethanol and extracted with ethyl acetate (4×5 ml). The acetate solution was worked up as usual to leave an oily substance (5.8 mg), which was purified by passing through a silica gel column (3 g) with a 10: 1 mixture of benzene and ether to give **29** (3.6 mg), oily; MS, *m/e* 220 (M^+), 192, 177, 162, 147, 121, and 94 (base); UV, λ_{max} 237 nm (ε 12000); IR, ν_{max} 3380, 1677, 1646, 1631, 1090, and 893 cm^{-1}; NMR, δ 0.93 (3H, d, J=6 Hz, 14-H), 1.71 (3H, s, 13-H), 3.53 (1H, s, OH), 4.35 (1H, d, J=5 Hz, 3-H), 4.72 (2H, br s, W_H=7 Hz, 12-H), and 5.83 (1H, br s, W_H=3 Hz, 1-H).

A solution of **28a** (16.0 mg) in ethanol (1.5 ml) was stirred with 0.22 M aq K_2CO_3 (0.3 ml) at room temperature for 12 h under argon. The reaction mixture was worked up as described above to leave oily residue (16 mg), which was separated by preparative TLC (1 plate) over silica gel with benzene–ether (10: 1). While a more mobile fraction afforded the starting acetate (**28a**, 4.6 mg), a less mobile fraction gave **28** [(±)-**1**, 5.7 mg), which crystallized on standing and had mp 64—66 °C: MS, UV, IR, and NMR, in the text.

References

1) a) Part VIII of "Synthetic Studies of Rishitin and Related Compounds;" Part VII, A. Murai, M. Ono, A. Abiko, and T. Masamune, *J. Am. Chem. Soc.*, **100**, 7751 (1978). b) Part XXIV of "Studies on the Phytoalexins;" Part XXIII, A. Murai, H. Taketsuru, F. Yagihashi, N. Katsui, and T. Masamune, *Bull. Chem. Soc. Jpn.*, **53**, 1045 (1980).

2) R. S. Burden, J. A. Bailey, and G. G. Vincent, *Phytochemistry*, **14**, 221 (1975).

3) For a preliminary communication, see; A. Murai, H. Taketsuru, K. Fujisawa, Y. Nakahara, M. Takasugi, and T. Masamune, *Chem. Lett.*, **1977**, 665.

4) A. Murai, K. Nishizakura, N. Katsui, and T. Masamune, *Tetrahedron Lett.*, **1975**, 4399; Idem., *Bull. Chem. Soc. Jpn.*, **50**, 1206 (1977).

5) F. J. McQuillin and P. L. Simpson, *J. Chem. Soc.*, **1963**, 4726; P. S. Adamson, F. C. McQuillin, R. Robinson, and J. L. Simonsen, *J. Chem. Soc.*, **1937**, 1576.

6) The dimethyl ester (**3**), mp 99—100 °C (lit., 75—77 °C), was prepared quantitatively by treatment of the corresponding acid with diazometane; A. Baeyer and F. Tutein, *Chem. Ber.*, **22**, 2178 (1889). The *trans*-configuration of the two methoxycarbonyl groups was deduced from the spectral ground; δ 2.70 (1H, br, W_H=24 Hz, 4-H) and 3.42 (1H, do d, J=9 and 5 Hz, 1-H).

7) In this paper we regard most of new compounds (**4**—**14**, **21**, **21a**, and **23**—**29a**) as eudesmane derivatives and apply the numbering used for eudesmane to the compounds.

8) R. B. Turner, R. E. Lee, Jr., and E. G. Hildenbrand, *J. Org. Chem.*, **26**, 4800 (1961).

9) R. Villotti, H. J. Ringold, and C. Djerassi, *J. Am. Chem. Soc.*, **82**, 5693 (1960).

10) K. L. Williamson, J. I. Coburn, and M. F. Herr, *J. Org. Chem.*, **32**, 3934 (1967).

11) K. L. Williamson and W. S. Johnson, *J. Org. Chem.*, **26**, 4563 (1961).

12) A. P. Uijttewaal, F. L. Jonkers, and A. van der Gen, *Tetrahedron Lett.*, **1975**, 1439.

13) P. A. Sheldon and J. K. Kochi, *Org. React.*, **19**, 279 (1972).

14) D. H. R. Barton, P. D. Magnus, G. Smith, G. Streckert, and D. Zurr, *J. Chem. Soc., Perkin Trans. 1*, **1972**, 542.

15) K. P. Dastur, *J. Am. Chem. Soc.*, **95**, 6509 (1973); K. P. Dastur, *ibid.*, **96**, 2605 (1974).

16) A. J. Birch and K. P. Dastur, *J. Chem. Soc. Perkin Trans. 1*, **1973**, 1650.

17) E. Vedejs, *J. Am. Chem. Soc.*, **96**, 5944 (1974); E. Vedejs, D. A. Engler, and J. E. Telschow, *J. Org. Chem.*, **43**, 188 (1978).

18) I. Alfaro, W. Ashton, L. D. McManus, R. C. Newstead, K. L. Rabone, N. A. J. Rogers, and W. Kernick, *Tetrahedron*, **26**, 201 (1970).

The Synthesis of Benzofuroquinolines. II. Two Benzofuroquinolinones and Some Benzofuroquinoline Derivatives

Yoshiyuki KAWASE,* Seiji YAMAGUCHI, Mariko MORITA, and Taeko UESUGI
Department of Chemistry, Faculty of Science, Toyama University, Gofuku, Toyama 930
(Received September 3, 1979)

Two benzofuroquinolinones, 6,11-dihydrobenzofuro[2,3-*b*]quinolin-11-one and 5,6-dihydrobenzofuro[3,2-*c*]-quinolin-6-one, were obtained by the demethyl-cyclization of 4-hydroxy-3-(*o*-methoxyphenyl)-1,2-dihydroquinolin-2-one. The chlorination of these benzofuroquinolinones afforded the corresponding chlorobenzofuroquinolines which were then converted to the cyanobenzofuroquinolines. The linear chlorobenzofuroquinoline was converted to 11-methoxy- and 11-ethoxybenzofuro[2,3-*b*]quinolines, and the linear cyanobenzofuroquinoline to benzofuro-[2,3-*b*]quinoline-11-carboxylic acid and -11-carboxamide. The linear benzofuroquinolines thus obtained were oxidized to the corresponding *N*-oxides.

In the course of our studies of polycyclic heteroaromatics, we studied the synthesis of benzofuroquinolines in order to investigate their chemical reactivities and also to test their activities as mutagens, carcinogens, and also as anti-tumor substances. In a previous paper,[1] we reported the synthesis of benzofuro[2,3-*b*]quinoline, benzofuro[3,2-*c*]quinoline, and their methyl, styryl, and carboxy derivatives. Mohanty *et al.*[2] reported the synthesis of benzofuro[2,3-*b*]quinolin-11-ol (**1a**) by the condensation of anthranilic acid and 2(3*H*)-benzofuranone. However, they showed a very low melting point of 93—95 °C compared to those of our reported[1] benzofuroquinolines, and also had ambiguous elemental analysis data; Found: C, 75.95; H, 3.80%. Calcd for $C_{15}H_9NO_2$: C, 76.60; H, 3.83%. We checked this condensation reaction, but could not obtained the same compound. Therefore, in this paper, we will report the synthesis of two benzofuroquinolinones (corresponding to benzofuroquinolinols) and their conversion to chloro- and cyanobenzofuroquinolines.

4-Hydroxy-3-(*o*-methoxyphenyl)-1,2-dihydroquinolin-2-one (**5**) was prepared according to the reported procedure.[1] The amide (**4**), prepared from *o*-methoxyphenylacetyl chloride and methyl anthranilate, was cyclized to a hydroxyquinolinone (**5**) by the action of sodium hydroxide. The demethyl-cyclization of **5** by heating with pyridine hydrochloride furnished a mixture of two benzofuroquinolinones, an alkali-soluble benzofuroquinolinone (**6**) and an alkali-insoluble benzofuroquinolinone (**7**). These benzofuroquinolinones were converted to the corresponding chlorobenzofuroquinolines (**1b** and **2b**) by chlorination with phosphorus

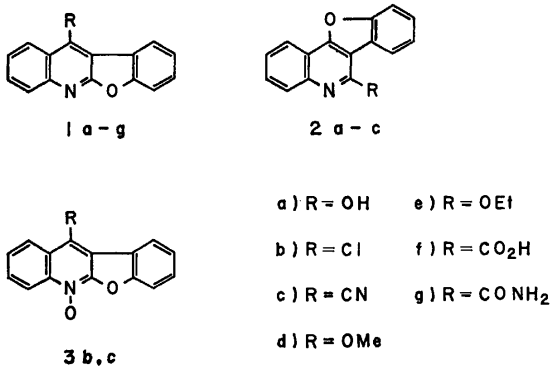

Chart 1.

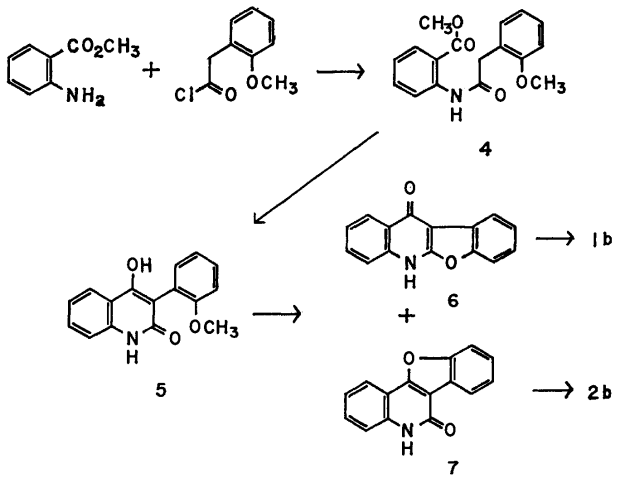

Chart 2.

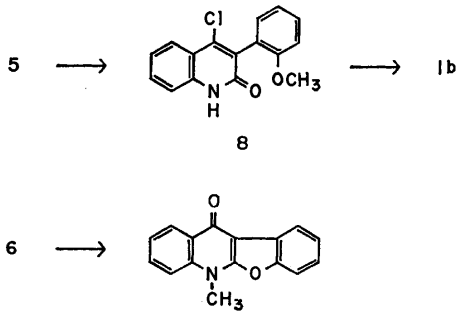

Chart 3.

pentachloride in phosphoryl chloride. In the UV spectra, 4,5-dihydrofuro[3,2-*c*]quinolin-4-one[3] corresponded to the benzofuroquinolinone (**7**) more than to the benzofuroquinolinone (**6**) (Fig. 1); the chlorobenzofuroquinoline (**1b**) derived from **6** was similar to linear benzofuro[2,3-*b*]quinoline,[1] and the chlorobenzofuroquinoline (**2b**) was similar to angular benzofuro[3,2-*c*]quinoline[1] (Fig. 2). These facts show that the benzofuroquinolinone (**6**) was linear 6,11-dihydrobenzofuro[2,3-*b*]quinolin-11-one with a quinolinol tautomerism, while the benzofuroquinolinone (**7**) was angular 5,6-dihydrobenzofuro[3,2-*c*]quinolin-6-one. The linear chlorobenzofuroquinoline (**1b**) was also obtained from **5** *via* 4-chloro-3-(*o*-methoxyphenyl)-1,2-dihydroquinolin-2-one (**8**) by monochlorination,

TABLE 1. ELEMENTAL ANALYSES OF NEW COMPOUNDS

Compound	Found			Formula	Calcd		
	C(%)	H(%)	N(%)		C(%)	H(%)	N(%)
1b	71.00	2.98	5.49	$C_{15}H_8ClNO$	71.02	3.18	5.52
1c	78.84	3.35	11.53	$C_{16}H_8N_2O$	78.69	3.28	11.48
1d	76.88	4.30	5.42	$C_{16}H_{11}NO_2$	77.09	4.45	5.62
1e	77.78	4.98	5.52	$C_{17}H_{13}NO_2$	77.55	4.98	5.32
1g	73.53	3.81	10.47	$C_{16}H_{10}N_2O_2$	73.27	3.84	10.68
2b	70.74	3.02	5.37	$C_{15}H_8ClNO$	71.02	3.18	5.52
2c	78.72	3.08	11.44	$C_{16}H_8N_2O$	78.69	3.28	11.48
3b	66.58	2.91	4.98	$C_{15}H_8ClNO_2$	66.85	2.99	5.20
3c	73.75	2.81	10.47	$C_{16}H_8N_2O_2$	73.84	3.10	10.77
4	68.05	5.75	4.69	$C_{17}H_{17}NO_4$	68.21	5.73	4.68
5	71.76	4.97	4.96	$C_{15}H_{13}NO_3$	71.90	4.90	5.24
6	76.55	3.75	5.69	$C_{15}H_9NO_2$	76.58	3.86	5.96
7	76.30	3.65	5.95	$C_{15}H_9NO_2$	76.58	3.86	5.96
8	67.50	4.02	4.78	$C_{16}H_{12}ClNO_2$	67.25	4.20	4.90
9	76.96	4.38	5.86	$C_{16}H_{11}NO_2$	77.09	4.45	5.62

TABLE 2. THE UV SPECTRAL DATA OF BENZOFUROQUINOLINE DERIVATIVES

Compound	λ_{max} (log ε) (nm)
1c	222(4.65) 262(4.64) 277sh(3.99) 349(4.33) 366(4.35)
1d	222(4.59) 250(4.69) 258(4.86) 274.5(3.87) 287sh(3.80) 304sh(4.18) 316(4.36) 330(4.18) 342sh(3.81)
1e	222(4.59) 250(4.70) 258(4.86) 274.5(3.93) 287sh(3.89) 305sh(4.17) 317(4.33) 330(4.15) 342sh(3.80)
1g	221(4.67) 250sh(4.57) 258(4.73) 325(4.34) 339sh(4.26)
2c	211(4.36) 229(4.32) 257sh(4.66) 265(4.70) 286(4.26) 298(4.14) 348(3.52) 360(3.50)
3b	224.5(4.42) 259(4.63) 267(4.65) 291sh(4.12) 325(4.11) 340(4.16)
3c	210.5(4.45) 233sh(4.27) 270(4.47) 362(4.16)
9	222(4.49) 258sh(4.49) 265(4.62) 288(4.00) 302(3.94) 326(4.03) 339(4.08) 356(3.81)

sh: shoulder

followed by demethyl-cyclization. The linear benzofuroquinolinone (**6**) gave 6-methyl-6,11-dihydrobenzofuro[2,3-*b*]quinolin-11-one (**9**) by *N*-methylation with methyl iodide. 11-Cyano-, 11-methoxy-, and 11-ethoxybenzofuro[2,3-*b*]quinolines (**1c**, **d**, **e**) were obtained from **1b** by means of nucleophilic substitution reactions with sodium cyanide, methanol–sodium hydroxide, and ethanol–sodium hydroxide, respectively. The acid hydrolysis of **1c** gave benzofuro[2,3-*b*]-quinoline-11-carboxylic acid (**1f**), and the alkaline hydrolysis of **1c** in ethanol gave benzofuro[2,3-*b*]-quinoline-11-carboxamide (**1g**). However, the alkaline hydrolysis of **1b** and **1c** in dimethyl sulfoxide gave a mixture of two benzofuroquinolinones (**6** and **7**). The cyanation of angular **2b** with sodium cyanide afforded linear **1c**, but this cyanation to angular 6-cyanobenzofuro[3,2-*c*]quinoline (**2c**) was effected with copper(I) cyanide. The benzofuroquinolines (**1b**, **c**) thus obtained were converted to the corresponding *N*-oxides (**3b**, **c**) by *N*-oxidation with trifluoroperacetic acid, but the

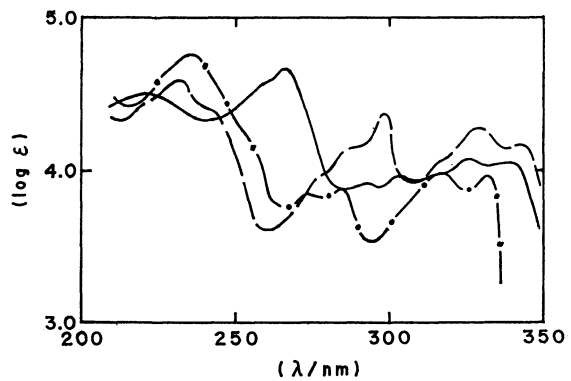

Fig. 1. The UV spectra of two benzofuroquinolones (**6** and **7**) and 4,5-dihydrofuro[3,2-*c*]quinolin-4-one.[3]
——: **6**, — —: **7**, —·—: 4,5-dihydrofuro[3,2-*c*]quinolin-4-one.

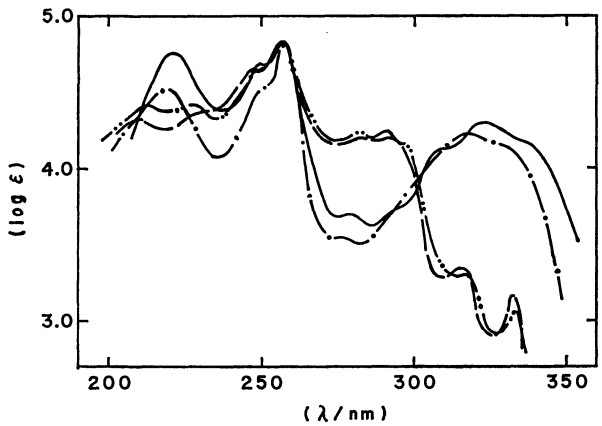

Fig. 2. The UV spectra of two chlorobenzofuroquinolines (**1b** and **2b**), linear benzofuro[2,3-*b*]quinoline,[1] and angular benzofuro[3,2-*c*]quinoline.[1]

N-oxidation of the angular benzofuroquinolines (**2b**, **c**) was unsuccessful under these conditions.

Compounds (**5**), (**7**), and (**8**) seem to possess 2-quinolone structures principally, since they have ν_{CO} bands around 1650 cm^{-1} in their IR spectra. In both the IR and UV spectra, compound (**6**) was similar to 6-methyl-6,11-dihydrobenzofuro[2,3-*b*]quinolin-11-one (**9**), not to 6-methoxybenzofuro[2,3-*b*]quinoline (**1d**). This evidence shows that compound (**6**) has mainly a benzofuroquinolinone, not a benzofuroquinolinol, structure.

Experimental

The melting points have not been corrected; the mass spectra were measured on a JEOL JMS-OISG-2 mass spectrometer, the IR spectra, on a Hitachi EPI-S2 spectrophotometer, and the UV spectra, on a Hitachi 124 spectrophotometer in an ethanol solution. The UV and elemental analyses data are summarized in the figures and the tables.

N-(o-*Methoxycarbonylphenyl*)-o-*methoxyphenylacetamide* (*4*). *o*-Methoxyphenylacetyl chloride (prepared from 25 g of *o*-methoxyphenylacetic acid and thionyl chloride) was added to a solution of methyl anthranilate (23 g) in pyridine (50 ml), after which, the mixture was refluxed for 1 h with stirring. The cooled reaction mixture was treated with water. The resulting precipitates were collected and recrystallized from ethyl acetate to give 34 g (75%) of **4** as colorless crystals; mp 116—117 °C; IR (KBr); 1710 and 1680 cm^{-1}.

*4-Hydroxy-3-(*o-*methoxyphenyl)-1,2-dihydroquinolin-2-one* (*5*). A mixture of **4** (34 g), sodium methylate (prepared from 10 g of sodium metal and absolute methanol), and dry benzene (210 ml) was refluxed for 6 h. The cooled reaction mixture was treated with water. The aqueous layer was acidified with dilute hydrochloric acid. The resulting precipitates were collected and recrystallized from *N,N*-dimethylformamide to give 31 g (80%) of **5** as colorless crystals; mp 311—312 °C; IR (KBr): 1645 cm^{-1}.

Demethyl-cyclization of 5. A mixture of **5** (2.6 g) and anhydrous pyridine hydrochloride (26 g) (bp 218 °C) was refluxed vigorously for 1.5 h. The cooled reaction mixture was treated with water, and the resulting precipitates were collected. Then the precipitates were treated with a 5% sodium hydroxide aqueous solution and filtered. The remaining precipitates were crystallized from ethanol to give 0.52 g (21%) of **7** as colorless crystals; mp 294—296 °C; MS (M^+): 235; IR (KBr): 1670 cm^{-1}. The filtrate was acidified with dilute hydrochloric acid, and the resulting precipitates were collected and recrystallized from ethanol to give 1.54 g (63%) of **6** as colorless needles; mp 342—344 °C (dec); MS (M^+): 235; IR (KBr): 1655 cm^{-1}.

11-Chlorobenzofuro[*2,3-*b]*quinoline* (*1b*). A mixture of **6** (3.9 g), phosphoryl chloride (23 ml), and phosphorus pentachloride (4.3 g) was refluxed for 2 h. The cooled reaction mixture was treated with water, and the resulting white precipitates were recrystallized from ethanol to give 3.6 g (85%) of **1b** as colorless crystals; mp 211—212 °C; MS (M^+): 253.

6-Chlorobenzofuro[*3,2-*c]*quinoline* (*2b*). By a method similar to that described for **1b**, a mixture of **7** (4.2 g), phosphorus pentachloride (4.6 g), and phosphoryl chloride (25 ml) afforded the crude chloride, which was recrystallized from ethanol to give 4.1 g (91%) of **2b** as colorless crystals; mp 157.5—158.5 °C; MS (M^+): 253.

11-Cyanobenzofuro[*2,3-*b]*quinoline* (*1c*). A mixture of **1b** (2.0 g), sodium cyanide (0.5 g), and *N,N*-dimethylformamide (30 ml) was refluxed for 6 h. The cooled reaction mixture was treated with water. The resulting precipitates were collected and recrystallized from ethanol to give 1.6 g (82%) of **1c** as colorless crystals; mp 242—243 °C; MS (M^+): 244; IR (KBr): 2230 cm^{-1}. Under these cyanation condition, 1c was also obtained from the angular chloride (**2b**) in a 72% yield.

6-Cyanobenzofuro[*3,2-*c]*quinoline* (*2c*). A mixture of **2b** (0.5 g), copper(I) cyanide (0.3 g), and *N,N*-dimethylformamide (5 ml) was refluxed for 6 h. The cooled reaction mixture was treated with ethylenediamine (10 ml) and water and extracted with diethyl ether. The ether layer was washed with a 10% sodium cyanide aqueous solution, filtered, washed with water, and dried over anhydrous sodium sulfate. The residue from the evaporation of the ether was crystallized from ethanol to give 0.1 g (21%) of **2c** as colorless crystals; mp 182—184 °C; MS (M^+): 244; IR (KBr): 2230 cm^{-1}.

Monochlorination of 6. A mixture of **6** (2.0 g), phosphorus pentachloride (2.0 g), and phosphoryl chloride (30 ml) was refluxed for 2 h. A treatment similar to that described for **1b** afforded white precipitates, which were recrystallized from methanol to give 0.95 g (44%) of **8** as colorless crystals; mp 101—103 °C; IR (KBr): 1640 cm^{-1}.

Demethyl-cyclization of 8. A mixture of **8** (0.55 g) and anhydrous pyridine hydrochloride (5.5 g) was refluxed for 1.5 h; this afforded 0.28 g (14%) of **1b** (mp 211—212 °C), which was identified with a sample obtained by the chlorination of **6**.

N-*Methylation of 6 to 9.* A mixture of **6** (0.5 g), sodium hydroxide (1.0 g), methyl iodide (1.3 g), and ethanol (30 ml) was refluxed for 3 h. After cooling, the reaction mixture was treated with dilute hydrochloric acid and filtered. The resulting precipitates were collected and recrystallized from ethanol to give 0.34 g (64%) of **9** as dark silky needles; mp 360—362 °C; MS (M^+): 249; IR (KBr): 1660 cm^{-1}.

11-Methoxy- and 11-Ethoxybenzofuro[*2,3-*b]*quinolines* (*1d,e*). A mixture of **1a** (0.53 g), potassium hydroxide (0.3 g), and methanol (15 ml) was refluxed for 2 h. The cooled reaction mixture was treated with water. The resulting precipitates were collected and recrystallized from cyclohexane to give 0.33 g (64%) of **1d** as a colorless powder; mp 165—165.5 °C; MS (M^+): 249. Similarly, **1b** afforded **1e** as a powder in a 23% yield; mp 72—73 °C; MS (M^+): 263.

Acid Hydrolysis of 1c. The linear cyano derivative (**1c**) (0.51 g) was suspended in 20 ml of 70% aqueous sulfuric acid. The mixture was refluxed for 3 h, and then treated with cold water. The resulting precipitates were collected and recrystallized from ethanol to give benzofuro[2,3-*b*]quinoline-11-carboxylic acid (**1f**); mp 326 °C (dec), as reported in the previous paper.[1]

Alkaline Hydrolysis of 1c. A mixture of **1c** (0.80 g), a 50% potassium hydroxide aqueous solution (1 ml), and ethanol (20 ml) was refluxed for 3 h. The resulting precipitates were collected and recrystallized from ethanol to give 0.32 g (38%) of benzofuro[2,3-*b*]quinoline-11-carboxamide (**1g**); mp 265—266 °C; MS (M^+): 262; IR (KBr): 1660 cm^{-1}. However, the similar hydrolysis in dimethyl sulfoxide converted **1c** to a mixture of **6** and **7** in 19 and 20% yields respectively.

Alkaline Hydrolysis of 1b. A mixture of **1b** (1.0 g), a 50% potassium hydroxide aqueous solution (20 ml), and dimethyl sulfoxide (10 ml) was refluxed for 3 h. After a treatment similar to that described for the demethyl-cyclization of **5**, 0.40 g (43%) of **6** and 0.17 g (19%) of **7** were obtained.

N-*Oxidation of 1b and 1c.* To a solution of **1b** (1.0 g) in trifluoroacetic acid (6 ml), a 30% hydrogen peroxide aqueous solution (0.7 ml) was added, after which the mixture was heated at 60—70 °C for 3 h. The heating was continued at

the same temperature for 6 additional hours with the addition of more of the 30% hydrogen peroxide aqueous solution (0.4 ml). The reaction mixture was then concentrated under reduced pressure and neutralized with a sodium carbonate aqueous solution. The resulting precipitates were collected and recrystallized from ethanol to give 0.63 g (59%) of **3b** as dark yellow needles; mp 257—259 °C; MS (M^+): 269. Similarly, **1c** (1.0 g) was oxidized to **3c** (0.52 g, 49%); mp 259.5—261 °C (from ethanol); MS (M^+): 260; IR (KBr): 2230 cm^{-1}.

References

1) Y. Kawase, S. Yamaguchi, O. Maeda, A. Hayashi, I. Hayashi, K. Tabata, and M. Kondo, *J. Heterocycl. Chem.*, **16**, 487 (1979).

2) N. Mohanty, P. C. Rath, and M. K. Rout, *J. Indian Chem. Soc.*, **44**, 1001 (1967).

3) M. F. Grundon, N. J. McCorkindale, and M. N. Rodger, *J. Chem. Soc.*, **1955**, 4284.

The Reaction of 2-(Trialkylsiloxy)furans with Lead(IV) Acetate. The Synthesis of *dl*-Pyrenophorin

Morio Asaoka, Noboru Yanagida, Naoyuki Sugimura, and Hisashi Takei*

Department of Life Chemistry, Tokyo Institute of Technology, Nagatsuta-cho, Midori-ku, Yokohama 227

(Received September 25, 1979)

The reaction of 2-(trimethylsiloxy)furans with lead(IV) acetate afforded the corresponding α,β-unsaturated γ-acetoxy-γ-lactones in good yields. The lactones were easily converted into the corresponding 3-acylacrylic acids. Utilizing this reaction, *dl*-pyrenophorin was synthesized.

Several macrolide antibiotics incorporate a γ-oxo α,β-unsaturated lactone moiety.[1] A variety of methods are available for the synthesis of 3-acylacrylic acids, but the methods applicable to the macrolide synthesis are not so simple and efficient.[2] Previously, we reported the synthesis of 2-(trialkylsiloxy)furans from unsaturated lactones and their reactions with dienophiles and some electrophiles.[3,4] In this paper we will describe the conversion of 2-(trialkylsiloxy)furans into 3-acylacrylic acids.

Results and Discussion

The treatment of 2-(trimethylsiloxy)furan (**1a**) and 5-methyl-2-(trimethylsiloxy)furan (**1b**) with lead(IV) acetate gave 4-acetoxy-2-buten-4-olide (**2a**) and 4-acetoxy-2-penten-4-olide (**2b**) in 87 and 76% yields respectively. The conversion of the latter product to 4-oxo-2-pentenoic acid (**3**) in an 86% yield was easily performed by acid hydrolysis.

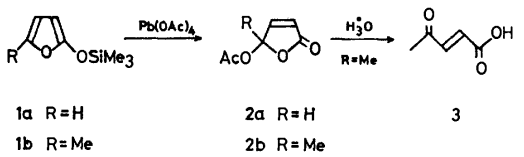

1a R=H 1b R=Me 2a R=H 2b R=Me 3

Scheme 1.

This three-step synthesis of 3-acylacrylic acid starting from unsaturated γ-lactones (formation of siloxyfurans, oxidation with Pb(IV) acetate, and acid hydrolysis) seems to be widely applicable, since a variety of methods of synthesizing unsaturated γ-lactones[5] are available and each step can be carried out in a high yield. Thus, the application of this strategy to the synthesis of pyrenophorin, a 16-membered dilactone isolated as a metabolite of plant pathogenic fungi,[1a] was examined. The starting material, 7-oxo-2-octen-4-olide (**4**), was easily obtained by the Michael addition of 2-buten-4-olide to 3-buten-2-one or the reaction of 2-(trimethylsiloxy)furan with 3-buten-2-one in the presence of Lewis acid. The silylation of **4** using triethylchlorosilane and triethylamine afforded the corresponding siloxyfuran derivative, **5**, in an 88% yield. First, the reduction of the carbonyl group, followed by the oxidation of siloxyfuran with lead(IV) acetate, was examined. The reduction of the carbonyl group proceeded smoothly by lithium aluminium hydride, but the oxidation of **6** (R=Li or Al) with lead(IV) acetate afforded the expected compound, **7**, in only a 16% yield, the major product was found to be the spiro compound (**8**, 51%; about a 1 : 1 mixture of the stereoisomers).[6] Though the yield of **7** was improved to 45% when **6** (R=H) was treated with lead(IV) acetate, the formation of **8** (35%) could not be avoided. When the siloxyfuran (**6**, R=Li or Al) was oxidized with copper(II) chloride, the spiro compound was obtained in a 60% yield. The 3-acylacryric acid derivative, **9**, was obtained in an almost quantitative yield by heating **7** in xylene in the presence of a small amount of 2-pyridinethiol. However, all attempts to prepare the hydroxy acid, **12**, from **9** or **7** failed. The hydrolysis of **9** as well as **7** under various reaction conditions afforded mainly the spiro compound, **8**.

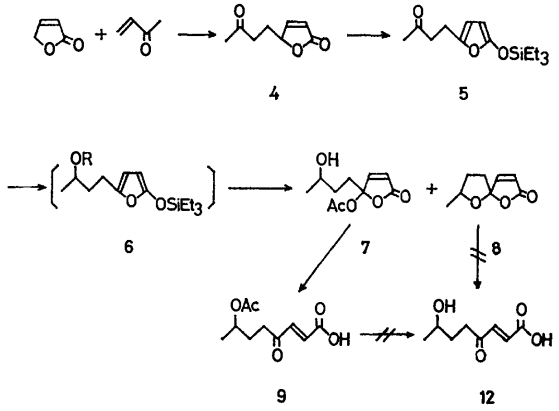

4 5 6 7 8 9 12

Scheme 2.

Then, the oxidation of **5** with lead(IV) acetate, followed by the reduction of carbonyl group, was examined. The oxidation of **5** with lead(IV) acetate gave 7-oxo-4-acetoxy-2-octen-4-olide (**10**) in an 83% yield. The acid hydrolysis of **10** yielded the desired 4,7-dioxo-2-octenoic acid (**11**) in a 75% yield. First, the selective reduction of **11**, followed by the dimerization cyclization, was examined. The selective reduction of **11** was achieved with sodium borohydride at −78 °C. However, the cyclization of the reduction product to pyrenophorin failed, probably because of the predominance of the hemiacetal structure, **13**. Then, the protection of the carbonyl groups of **11** was examined. The acetalization of two carbonyl groups was carried out using trimethyl orthoformate and methanol in the presence of an acid catalyst. The selective hydrolysis of **14** to **15** proceeded smoothly in THF–water. Sodium borohydride reduction of **15** at −30 °C afforded the hydroxy acid, **16**. All three of these compounds (**14**, **15**, and **16**) were relatively unstable oils and could not be

obtained in pure forms by silica-gel chromatography. However, the crude **16** was almost homogenious on TLC; thus, the crude **16** was used for the next lactonization step. The dimerization lactonization was carried out according to the method of Mitsunobu *et al.*,[7] using triphenylphosphine and diethyl azodicarboxylate; a mixture of *dl*- and *meso*-pyrenophorin bis(dimethyl acetal)s (**17**) was thus obtained in a 17% over-all yield from **11**. The acid hydrolysis of the diacetals with acetic acid–water proceeded quantitatively to give *dl*- and *meso*-pyrenophorin[8] (**18**), which could be separated by TLC. The structures of both were comfirmed by their elemental analyses and spectral data.

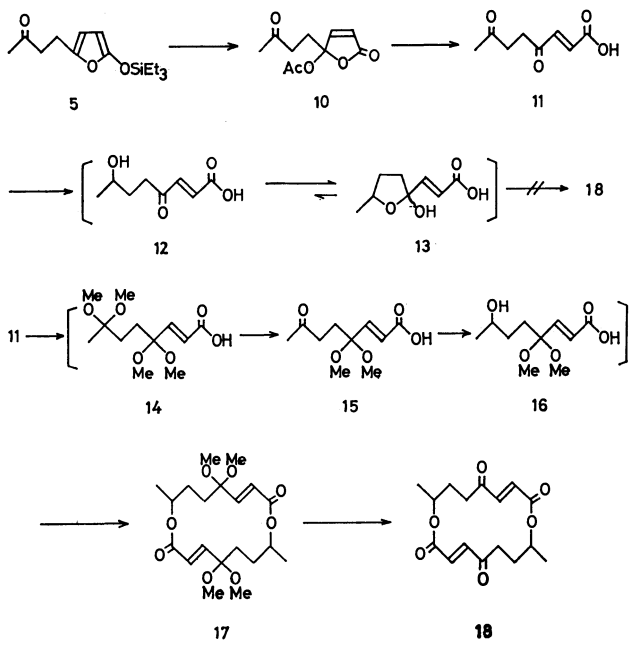

Scheme 3.

Experimental

4-Acetoxy-2-buten-4-olide (2a). To a suspension of lead(IV) acetate (1.17 g, 2.64 mmol) in dry dichloromethane (10 ml), 2-(trimethylsiloxy)furan (**1a**, 375 mg, 2.4 mmol)[3] was added, drop by drop, at −21 °C. The reaction temperature was gradually raised to room temperature over a period of 1 h. After the addition of ether (30 ml), the precipitate was filtered off. The filtrate was concentrated under reduced pressure, and the residue was purified by column chromatography on silica gel to give **2a** (297 mg, 87%), using hexane–ether as the eluent. IR(NaCl): 1820—1740 cm^{-1} (C=O), 1612 cm^{-1} (C=C), NMR ($CDCl_3$): δ 2.13 (3H, s), 6.26 (1H, d), 6.92 (1H, s), 7.35 (1H, d). Found: C, 50.57; H, 4.23%. Calcd for $C_6H_6O_4$: C, 50.71; H, 4.26%.

4-Acetoxy-2-penten-4-olide (2b). The reaction of 5-methyl-2-(trimethylsiloxy)furan (**1b**, 1.74 g, 10.2 mmol)[3] with lead(IV) acetate (6.6 g, 15 mmol) was carried out in dry benzene (40 ml) at 4 °C—room temperature for 3 h. Purification by short silica-gel column chromatography, followed by bulb-to-bulb distillation, afforded **2b** in a 76% yield (1.21 g); bp 150—155 °C/23—24 mmHg (bath temp.). NMR($CDCl_3$): δ=1.80 (3H, s), 2.05 (3H, s), 6.15 (1H, d), 7.59 (1H, d). IR(NaCl): 1770—1790, 1750 cm^{-1} (C=O), 1611 cm^{-1} (C=C). Found: C, 53.57; H, 5.14%. Calcd for $C_7H_8O_4$: C, 53.84; H, 5.16%.

4-Oxo-2-pentenoic Acid (3). A mixture of 4-acetoxy-2-penten-4-olide (**2b**, 1.21 g, 7.78 mmol) in 1 M hydrochloric acid (20 ml) was stirred for 3 d at room temperature. After the subsequent removal of the hydrochloric acid under reduced pressure, the residue was dissolved in benzene, which contained a catalytic amount (*ca.* 1 mg) of 2-pyridinethiol,[9] and heated to reflux. Upon cooling, **3** was precipitated as colorless crystals. After filtration, the filtrate was concentrated under reduced pressure. The residue was treated with 2-pyridinethiol in hot benzene as has been described above, and then these operations were repeated to give 760 mg (86%) of **3**; mp 126 °C. IR(KBr): 1670—1730 cm^{-1} (C=O), 1623 cm^{-1} (C=C). NMR($CDCl_3$): δ=2.36 (3H, s), 6.61 (1H, d), 7.06 (1H, d), 9.1—9.8 (1H, m). Found: C, 52.92; H, 5.36% Calcd for $C_5H_6O_3$: C, 52.63; H, 5.30%.

7-Oxo-2-octen-4-olide (4). A mixture of 2-buten-4-olide (176 mg, 2.1 mmol) and 3-buten-2-one (147 mg, 2.1 mmol) was cooled to −50 °C, and then 1 drop of 0.1 M potassium hydroxide was added to the mixture, After it had then been warmed to room temperature, the mixture was neutralized with Amberlite IRC-50. The crude product was purified by TLC to give **4** in a 75% yield; bp 144—146 °C/4.5 mmHg. IR(NaCl): 1720, 1760—1780 cm^{-1} (C=O), 1600 cm^{-1} (C=C), NMR ($CDCl_3$): δ=2.00 (2H, dt), 2.16 (3H, s), 2.68 (2H, t), 5.00—5.30 (1H, m), 6.12 (1H, dd), 7.52 (1H, dd). Found: C, 61.85; H, 6.57%. Calcd for $C_8H_{10}O_3$: C, 62.32; H, 6.54%. This compound was also synthesized according to the following procedure. 2-(Trimethylsiloxy)furan (**1a**, 37.5 g, 0.24 mol) and 3-buten-2-one (17.6 g, 0.25 mol) dissolved in dry dichloromethane (50 ml) were cooled to −78 °C. After the addition of tin(IV) chloride (500 mg), the reaction mixture was warmed to room temperature over a period of 12 h. After the addition of water, the product was extracted with dichloromethane. Purification by silica gel column chromatography (hexane–ether) afforded **4** (19 g, 52%).

5-(3-Oxobutyl)-2-(triethylsiloxy)furan (5). A mixture of triethylchlorosilane (4.98 g, 33 mmol) and triethylamine (3.34 g, 33 mmol) was added to 7-oxo-2-octen-4-olide (**4**, 4.62 g, 30 mmol) under an argon atmosphere. After three days, dry benzene was added and the precipitated ammonium salt was filtered off under an argon atmosphere. The subsequent distillation of the filtrate gave **5** in an 88% yield; bp 105—106 °C/0.06 mmHg. IR(NaCl): 1720 cm^{-1} (C=O). NMR($CDCl_3$): δ=0.43—1.22 (15H, m), 2.18 (3H, s), 2.78 (4H, s), 5.04 (1H, d), 5.86 (1H, d).

4-Acetoxy-7-hydroxy-2-octen-4-olide (7) and 7-Methyl-1,6-dioxaspiro[4,4]non-3-enone (8). After the addition of lithium aluminium hydride (280 mg) to a solution of **5** (2.58 g, 10 mmol) in dry tetrahydrofuran (20 ml), the mixture was stirred at room temperature for 0.5 h and then cooled to −10 °C. Lead (IV) acetate (5.0 g) was added in one portion, after which the reaction mixture was allowed to warm to room temperature over a period of 2 h. After the removal of metal salts by short silica gel column chromatography, the concentrated eluate was put on a silica-gel column and eluted with hexane–ether to give **7** (338 mg, 16%) and **8** (791 mg, 51%).

7: IR (NaCl): 3400 cm^{-1} (OH, broad), 1750—1800 cm^{-1} (C=O), 1615 cm^{-1} (C=C). NMR ($CDCl_3$): δ=1.22 (3H, d), 1.36—1.82 (2H, m), 2.10 (3H, s), 2.00—2.48 (2H, m), 3.60—4.10 (1H, m), 6.28 (1H, d), 7.68 (1H, d). Found: C, 56.05; H, 6.59%. Calcd for $C_{10}H_{14}O_5$: C, 56.07; H, 6.59%.

8: IR(NaCl): 1760—1770 cm^{-1} (C=O), 1615 cm^{-1} (C=C). NMR ($CDCl_3$): δ=1.28 (1.5H, d), 1.40 (1.5H, d), 2.04—2.48 (4H, m), 4.20—4.70 (1H, m), 6.10 (1H, d), 7.15 (1H, d). Found: C, 62.16; H, 6.54%. Calcd for $C_8H_{10}O_3$: C, 62.32; H, 6.54%.

A mixture of **5** (546 mg, 2.03 mmol) and lithium aluminium hydride (30 mg, 0.75 mmol) in tetrahydrofuran (10 ml) was stirred for 1 h at room temperature. The reaction mixture was then filtered through cellite and silica gel under an argon atmosphere and evaporated. The residue was dissolved in dry dichloromethane (5 ml) and added to a precooled suspension of lead(IV) acetate (910 mg, 2.04 mmol) in dry dichloromethane at −10 °C. The reaction mixture was then allowed to warm to room temperature for 2 h. The subsequent separation of the products by TLC gave **7** (45%) and **8** (35%).

The spiro compound, **8**, was also obtained by the following procedure. A mixture of **5** (536 mg, 2 mmol) and lithium aluminium hydride (38 mg, 1 mmol) dissolved in tetrahydrofuran (5 ml) was stirred at room temperature for 0.5 h. Anhydrous copper(II) chloride (540 mg, 4 mmol) was then added to the stirred solution at −40 °C, and the reaction mixture was warmed to room temperature. After the removal of the metal salts by short silica gel column chromatography, the purification of the product by TLC (hexane–ether) afforded **8** (186 mg, 60%).

*7-Acetoxy-4-oxo-2-octenoic Acid (**9**).* A solution of **7** (178 mg) and 2-pyridinethiol (1 mg) in xylene (3 ml) was refluxed for 1.5 h. The subsequent removal of the solvent under reduced pressure gave almost pure **9**; mp 66.0—66.5 °C (from cyclohexane–benzene). IR(KBr): 2350—3600 cm^{-1} (COOH, broad), 1675, 1695, 1735 cm^{-1} (C=O). NMR ($CDCl_3$): δ=1.26 (3H, d), 2.04 (3H, s), 2.02 (2H, t), 2.76 (2H, t), 6.64 (1H, d), 7.14 (1H, d), 9.56 (1H, s). Found: C, 56.28; H, 6.40%. Calcd for $C_{10}H_{14}O_5$: C, 56.07; H, 6.59%.

*4-Acetoxy-7-oxo-2-octen-4-olide (**10**).* To a suspension of lead(IV) acetate (980 mg, 2.2 mmol) in dry benzene, **5** (482 mg, 1.8 mmol) dissolved in dry benzene (4 ml), was added, drop by drop, at 4 °C. The mixture was put in a short silica gel column and eluted with ether. The eluate was evaporated under reduced pressure, and the residue was separated by TLC to give **10** in an 83% yield (316 mg). An analytical sample was obtained by bulb-to-bulb distillation; bp 115—120 °C/0.02 mmHg (bath temp). IR (NaCl): 1750—1805 cm^{-1} (C=O), 1720 cm^{-1} (C=C). NMR ($CDCl_3$): δ=2.05 (3H, s), 2.17 (3H, s), 2.2—2.5 (2H, m), 2.5—2.8 (2H, m), 6.17 (1H, d), 7.18 (1H, d). Found: C, 55.91; H, 5.66%. Calcd for $C_{10}H_{12}O_5$: C, 56.60; H, 5.70%.

*4,7-Dioxo-2-octenoic Acid (**11**).* Hydrochloric acid (1M, 40 ml) was added to **10** (2.8 g), and the heterogeneous mixture was stirred for 4 d. The resulting homogenious solution was extracted several times with ethyl acetate. After the removal of the ethyl acetate, the residue was treated with a catalytic amount of 2-pyridinethiol in benzene as described before (see the synthesis of **3**) to give **11** (1.69 g, 75%); mp 112—113.5 °C. IR (KBr): 1705, 1680 cm^{-1} (C=O), 1627 cm^{-1} (C=C). NMR ($CDCl_3$): δ=2.21 (3H, s), 2.86 (4H, s), 6.70 (1H, d), 7.10 (1H, d). Found: C, 56.47; H, 5.83%. Calcd for $C_8H_{10}O_4$: C, 56.46; H, 5.92%.

meso- *and* dl-*Pyrenophorin Bis(dimethyl acetal)s (**17**).* 4,7-Dioxo-2-octenoic acid (**11**, 200 mg, 1.18 mmol), trimethyl orthoformate (1 ml), amberlyst 15 (50 mg), and methanol (4 ml) were stirred for 1.5 h at room temperature. After filtration through the celite, the trimethyl orthoformate and the methanol were removed. Tetrahydrofuran (6 ml) and water (2 ml) were then added to the residue, and the mixture was stirred for 1 h at 45 °C and then cooled to room temperature. Sodium hydrogencarbonate (118 mg, 1.4 mmol) was then added, and most of the tetrahydrofuran was removed under reduced pressure. After the addition of methanol (8 ml), sodium borohydride (60 mg, 1.58 mmol) was added at −38 °C. One hour later, acetone (2 ml) was added, and the mixture was warmed to room temperature. The solution was passed through an acidic resin column, and the solvent was evaporated under reduced pressure. In order to remove the boric acid, the addition and evaporation of methanol was repeated. The residue was almost homogeneous on TLC. The crude 7-hydroxy-4,4-dimethoxy-2-octenoic acid (**16**) [IR (NaCl): 3400 cm^{-1} (OH, broad), 2820 cm^{-1} (OMe), 1700 cm^{-1} (COOH); NMR ($CDCl_3$): δ=1.2 (3H, d), 1.2—2.25 (4H, m), 3.15 (6H, s), 3.5—4.1 (1H, m), 6.2 (1H, d), 6.7 (1H, d)] was used for the next step without further purification. Dry toluene (200 ml) and triphenylphosphine (800 mg, 3.05 mmol) were added to **16**, and the resulting mixture was cooled to −25 °C. After the addition of diethyl azodicarboxylate (540 mg, 3.10 mmol) dissolved in dry toluene, the reaction temperature was gradually raised to room temperature for 3 d. A mixture of *meso* and *dl* pyrenophorin bis(dimethyl acetal)s (40 mg, 17%) was obtained by using TLC; mp 143—144 °C. IR (KBr): 1715 cm^{-1} (C=O), 1650 cm^{-1} (C=C). NMR ($CDCl_3$): δ=1.22 (6H, d), 1.3—2.1 (8H, m), 3.10 (6H, s), 3.19 (6H, s), 4.8—5.3 (2H, m), 6.09 (2H, dd), 6.45 (2H, d). MS: *m/e* 400 (M^+). Found: C, 60.17; H, 7.99%. Calcd for $C_{20}H_{32}O_8$: C, 59.98; H, 8.05%.

dl- *and* meso-*Pyrenophorin (**18**).* Pyrenophorin bis(dimethyl acetal)s (13 mg) was dissolved in tetrahydrofuran/acetic acid/water 1:3:1 (2 ml) and warmed for 2 h at 40 °C. After the removal of the solvent, isolation with TLC gave *dl*-pyrenophorin (4 mg) and *meso*-pyrenophorin (6 mg). *dl*-Pyrenophorin; mp 139—140 °C (lit,[8b] 139—140 °C). IR (KBr): 1717, 1694 cm^{-1} (C=O), 1631 cm^{-1} (C=C), NMR ($CDCl_3$): δ=1.30 (6H, d), 1.9—2.3 (4H, m), 2.4—2.8 (4H, m), 4.8—5.3 (2H, m), 6.60 (2H, d), 6.89 (2H, d). MS: *m/e* 308 (M^+). Found: C, 62.30; H, 6.37%. Calcd for $C_{16}H_{20}O_6$: C, 62.32; H, 6.54%. *meso*-Pyrenophorin: mp 128—128.5 °C; (lit,[8b] 126—127.5 °C). IR (KBr): 1717, 1694 cm^{-1} (C=O), 1631 cm^{-1} (C=C); NMR ($CDCl_3$): δ=1.31 (6H, d), 1.9—2.4 (4H, m), 2.4—2.7 (4H, m), 4.8—5.3 (2H, m), 6.51 (2H, d), 6.85 (2H, d), MS: *m/e* 308 (M^+). Found: C, 62.25; H, 6.37%. Calcd for $C_{16}H_{20}O_6$: C, 62.32; H, 6.54%.

References

1) a) Pyrenophorin: S. Nozoe, K. Hirai, K. Tsuda, K. Ishibashi, M. Shirasaka, and J. F. Grove, *Tetrahedron Lett.*, **1965**, 4675; b) Vermiculin: R. K. Boeckman, Jr., J. Fayos, and J. Clardy, *J. Am. Chem. Soc.*, **96**, 5955 (1974); c) Brefeldin A: H. P. Weber, D. Hauser, and H. P. Sigg, *Helv. Chim. Acta*, **54**, 2763 (1971); d) Colletoketol: J. Macmillan and T. J. Simpson, *J. Chem. Soc., Perkin Trans. 1*, **1973**, 1487; e) Cytochalasins A and B: C. Tamm, W. B. Turner, and H. Minato, *J. Chem. Soc., Perkin Trans. 1*, **1973**, 1146; f) Aspicilin: S. Huneck, K. Schreiber, and W. Steglich, *Tetrahedron*, **29**, 3687 (1973); g) A26771B: K. H. Michel, P. V. Demarco, and R. Nagarajan, *J. Antibiot.*, **30**, 571 (1977).

2) a) M. S. Newman, W. C. Sagar, and C. C. Cochrane, *J. Org. Chem.*, **23**, 1832 (1958); b) G. R. Pettit, B. Green, and G. L. Dunn, *ibid.*, **35**, 1367 (1970); c) H. Reinheckel and K. Haage, *Angew. Chem., Int. Ed. Engl.*, **5**, 511 (1960); d) H. J. Bestmann, F. Seng, and H. Schulz, *Chem. Ber.*, **96**, 465 (1963); e) H. J. Bestmann, G. Graf, and H. Hartung, *Justus Liebigs Ann. Chem.*, **706**, 68 (1967); f) M. Kucher, B. Kakac, and O. Nemecek, *Collect. Czech. Chem. Commun.*, **37**, 3950 (1972); g) P. A. Bartlett, *J. Am. Chem. Soc.*, **98**, 3305 (1976). See also Ref. 7.

3) M. Asaoka, K. Miyake, and H. Takei, *Chem. Lett.*,

1977, 167.

4) M. Asaoka, N. Sugimura, and H. Takei, *Bull. Chem. Soc. Jpn.*, **52**, 1953 (1979).

5) Y. S. Rao, *Chem. Rew.*, **76**, 625 (1976).

6) Compound **8** was recently synthesized by the photooxidation of 2(3-hydroxybutyl)furan; H. Fukuda, M. Takeda, Y. Sato, and O. Mitsunobu, *Synthesis*, **1979**, 368.

7) T. Kurihara, Y. Nakajima, and O. Mitsunobu, *Tetrahedron Lett.*, **1976**, 2455.

8) As for the synthesis of pyrenophorin, see: a) E. W. Colvin, T. A. Purcell, and R. A. Raphael, *J. Chem. Soc., Chem. Commun.*, **1972**, 1031; b) H. Gerlach, K. Oertle, and A. Thalmann, *Helv. Chim. Acta*, **60**, 2860 (1977); c) D. Seebach, B. Seuring, H. O. Kalinowski, W. Lubosch, and B. Renger, *Angew. Chem. Int. Ed. Engl.*, **16**, 264 (1977); B. Seuring and D. Seebach, *Justus Liebigs Ann. Chem.*, **1978**, 2044; d) P. Bakuzis, M. L. F. Bakuzis, and T. F. Weingartner, *Tetrahedron Lett.*, **1978**, 2371.

9) This compound was found to be effective for the isomerization of a contaminated *cis* isomer to a *trans* isomer.

 © 1980 The Chemical Society of Japan Bull. Chem. Soc. Jpn., 53, 1065—1069 (1980)

Direct Conversion of Arylamines to the Halides by Deamination with Thionitrite or Related Compounds and Anhydrous Copper(II) Halides

Shigeru OAE,* Kōichi SHINHAMA, and Yong Hae KIM

Department of Chemistry, University of Tsukuba, Niiharigun, Ibaraki 305

(Received September 25, 1979)

Reactions of various arylamines with either *t*-butyl thionitrite, *t*-butyl thionitrate, or *p*-toluenesulfonyl nitrite in the presence of anhydrous copper(II) halides under mild conditions gave corresponding aryl halides in good yields. This reaction in the presence of such olefins as acrylonitrile, styrene, and acrylic acid gave the corresponding 2-aryl-1-haloethanes as the main products. *t*-Butyl thionitrite, *t*-butyl thionitrate, and *p*-toluenesulfonyl nitrite were found to be better deaminative reagents than alkyl nitrites or alkyl nitrates due to their weak sulfur–nitrogen bonds.

We reported recently that various thionitrites can be prepared simply by treating thiols with one equivalent of dinitrogen tetraoxide,[1,2] whereas *t*-BuSH can be easily converted the corresponding thionitrate with excess (over 2 eq.) dinitrogen tetraoxide in a good yield.[3]

We now have found that various arylamines (**3**) reacted readily with either *t*-butyl thionitrite (**1**) or *t*-butyl thionitrate (**2**) in the presence of anhydrous copper(II) halides under mild conditions to afford the corresponding halides (**4**) in good yields (Eq. 1).

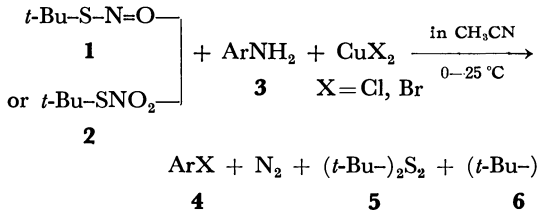

$$\left.\begin{matrix} t\text{-Bu–S–N=O} \\ \mathbf{1} \\ \text{or } t\text{-Bu–SNO}_2 \\ \mathbf{2} \end{matrix}\right\} + \mathrm{ArNH_2} + \mathrm{CuX_2} \xrightarrow[0\text{–}25\,^\circ\mathrm{C}]{\text{in } CH_3CN} \underset{\mathbf{3}}{\mathrm{X=Cl,\ Br}}$$

$$\mathrm{ArX} + \mathrm{N_2} + (t\text{-Bu–})_2\mathrm{S_2} + (t\text{-Bu–})_2\mathrm{S_3} \quad (1)$$
$$\mathbf{4} \qquad\qquad \mathbf{5} \qquad\quad \mathbf{6}$$

Both thionitrites and thionitrates are generally known to be unstable, however, *t*-butyl derivatives, *i.e.*, thionitrite **1** and thionitrate **2**, which can be readily synthesized quantitatively by mixing the thiol and dinitrogen tetraoxide, are stable enough to be used for these reactions. Although other nitrosyl compounds such as nitrosyl halide[4] and alkyl nitrite[5,6] have been successfully used for the same reaction, thionitrites or thionitrates are considered to be better reagents for deaminative halogenation of arylamines **3** due both to the relatively weaker S–N bond of thionitrite **1** or thionitrate **2** than the O–N bond of alkyl nitrites and also to the stronger complexation of thio-derivatives with copper salt than the oxygen and chloro analogs. Indeed, this was found to be the case. Starting with arylamines **3**, corresponding halides **4** were obtained in good yields at room temperature as shown in Table 1. Although alkyl nitrates did not give any deaminative product from arylamines even upon heating with copper(II) halides, thionitrate **2** was found to be an amazingly effective deaminative reagent. The nitroso or nitro group in thionitrite **1** or thionitrate **2** is used for the initial diazotization of arylamines **3**. The rest of the molecules was found to be converted to di-*t*-butyl disulfide (**5**) and di-*t*-butyl trisulfide (**6**), which was identified by elemental analysis, while N_2, quantitatively evolved and collected during the reaction, was identified by mass-spectroscopy. All the products were identified by comparing their IR and NMR spectra and melting or boiling points with those of authentic samples.

Treatment of arylamines **3** with thionitrite **1** and anhydrous copper(II) halides probably involves an initial formation of an intermediate diazonium salt (Eq. 2) like in the case with alkyl nitrites.[6] Trisulfide **6** was formed probably by the attack of *t*-butyldithio anion (**8**) or *t*-butyldithio radical (**9**) formed by heterolysis or homolysis of disulfide **5** on thionitrite **1** (Eq. 3).

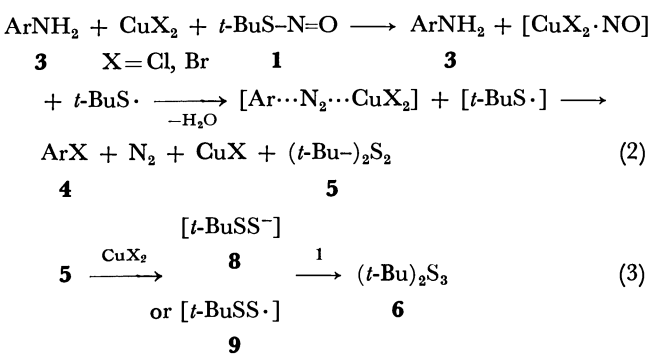

$$\underset{\mathbf{3}}{\mathrm{ArNH_2}} + \mathrm{CuX_2} + \underset{\mathbf{1}}{t\text{-BuS–N=O}} \longrightarrow \underset{\mathbf{3}}{\mathrm{ArNH_2}} + [\mathrm{CuX_2 \cdot NO}]$$

$$\mathrm{X=Cl,\ Br}$$

$$+\ t\text{-BuS}\cdot \xrightarrow[-H_2O]{} [\mathrm{Ar\cdots N_2\cdots CuX_2}] + [t\text{-BuS}\cdot] \longrightarrow$$

$$\underset{\mathbf{4}}{\mathrm{ArX}} + \mathrm{N_2} + \mathrm{CuX} + \underset{\mathbf{5}}{(t\text{-Bu–})_2\mathrm{S_2}} \quad (2)$$

$$\underset{\mathbf{5}}{} \xrightarrow{\mathrm{CuX_2}} \underset{\text{or } [t\text{-BuSS}\cdot]}{\underset{\mathbf{8}}{[t\text{-BuSS}^-]}} \xrightarrow{1} \underset{\mathbf{6}}{(t\text{-Bu})_2\mathrm{S_3}} \quad (3)$$
$$\mathbf{9}$$

The reaction of disulfide **5** with $CuCl_2$ under the same conditions afforded both the trisulfide **6** and the di-*t*-butyl tetrasulfide (**7**). Probably, in the presence of thionitrite **1** or thionitrate **2**, the anionic intermediate *t*-BuSS$^-$ or radical intermediate *t*-BuSS· reacts with the thionitrite **1** or the thionitrate **2** to give the trisulfide **6**. It is noteworthy that trisulfide **6** is formed as the major product along with a minor product *i.e.*, disulfide **5**.

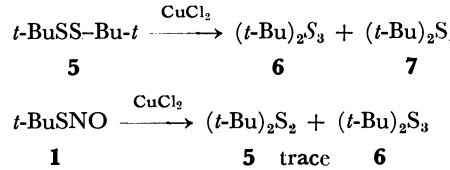

$$\underset{\mathbf{5}}{t\text{-BuSS–Bu-}t} \xrightarrow{CuCl_2} \underset{\mathbf{6}}{(t\text{-Bu})_2\mathrm{S_3}} + \underset{\mathbf{7}}{(t\text{-Bu})_2\mathrm{S_4}}$$

$$\underset{\mathbf{1}}{t\text{-BuSNO}} \xrightarrow{CuCl_2} \underset{\mathbf{5}}{(t\text{-Bu})_2\mathrm{S_2}} + \underset{\text{trace}}{} \underset{\mathbf{6}}{(t\text{-Bu})_2\mathrm{S_3}}$$

When thionitrate **2** was used instead of thionitrite **1**, nearly the same results were obtained (Table 2). If the reaction proceeds *via* a similar path as in the case of the thionitrite **1** either H_2O_2(instead of H_2O) or N_2O(instead of N_2) should be formed according to Eq. 4 or 5. However, the GC mass spectrum of gas trapped during the reaction showed only N_2 but not N_2O. A possibility of decomposition of N_2O to NO and N_2 in the mass process was ruled out by a control mass spectroscopic analysis of the authentic sample of N_2O, which showed a strong molecular peak (M^+, 44) of N_2O. Though H_2O_2 could not be confirmed, thiane and diphenyl sulfide in acetic acid was added for trapping H_2O_2

Table 1. Deamination of amines with thionitrite **1**, thionitrate **2**, or sulfonyl nitrite **14** and anhydrous copper(II) halides

Amine ($R-NH_2$)	Reagent	Reaction temp/°C	Reaction time/min	Yield of the product/% RCl	RBr	Other
p-NO_2-$C_6H_4NH_2$	**1**	25	2	98[a,c]	78[a]	
p-NO_2-$C_6H_4NH_2$	**1**	0	1	85[a]		
p-NO_2-$C_6H_4NH_2$	**1**	50	0.5	61[a]		
p-NO_2-$C_6H_4NH_2$	**2**	25	2	98[a,d]	74[a]	
p-NO_2-$C_6H_4NH_2$	**2**	0	1.5	87[b]		
p-NO_2-$C_6H_4NH_2$	**14**	25	1	89[a]		
o-NO_2-$C_6H_4NH_2$	**14**	25	1	87[a]	63[a]	
p-HO_2C-$C_6H_4NH_2$	**1**	25	2	97[a]	78[a]	
p-HO_2C-$C_6H_4NH_2$	**2**	25	1.5	86[a]		
p-HO_2C-$C_6H_4NH_2$	**2**	25	1		75[a]	
p-Cl-$C_6H_4NH_2$	**1**	25	2	78[b]	71[b]	
p-Cl-$C_6H_4NH_2$	**2**	25	2	71[b]	55[b]	
p-Cl-$C_6H_4NH_2$	**14**	25	1	76[a]	79[a]	
p-Br-$C_6H_4NH_2$	**14**	25	1	93[a]	78[a]	
$C_6H_5NH_2$	**1**	25	2	86[b]	58[b]	
$C_6H_5NH_2$	**2**	25	2	82[b]	83[b]	
p-MeO-$C_6H_4NH_2$	**1**	25	2	61[b]	36[b]	
p-MeO-$C_6H_4NH_2$	**2**	25	1.5	63[b]	57[b]	
p-MeO-$C_6H_4NH_2$	**14**	25	1	38[a]	60[a]	
p-HO-$C_6H_4NH_2$	**1**	25	2	57[a]	40[a]	
p-HO-$C_6H_4NH_2$	**2**	25	1	0		40[g]
p-HO-$C_6H_4NH_2$	**2**	25	4	0		43[h]
$C_6H_5CH_2NH_2$	**1**	25	2	18[a,e]		
$C_6H_5CH_2NH_2$	**2**	25	2	18[a,f]		
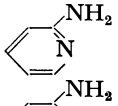	**1**	25	1.5	35[b]	7[a]	
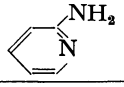	**2**	25	1.5	64[b]	13[b]	

a) Isolated yield. b) GC yield. c) Other side products originated from thionitrite **1** (7.5 mmol) were disulfide **5** (0.32 mmol) and trisulfide **6** (2.2 mmol). d) Other products originated from thionitrate **2** (7.5 mmol) were disulfide **5** (0.31 mmol) and trisulfide **6** (2.1 mmol). e) Benzaldehyde (13%) and benzyl alcohol (26%) were isolated. f) Benzaldehyde (32%) and benzyl alcohol (16%) were isolated. g) Compound **11** was isolated in 40% yield. h) Even in the reaction of p-aminophenol with thionitrate **2** without CuX_2, compound **11** was obtained in 43% of GC yield based on the amount of p-aminophenol.

into the reaction mixture both at the begining and after the completion of the reaction. However, both sulfides were recovered quantitatively and no sulfoxide was detected. H_2O_2 formed in the reaction may be readily consumed for further oxidation of copper complex. The reaction is presumed to proceed *via* a diazonium salt intermediate as shown by Eq. 4.

$$\underset{\mathbf{3}}{ArNH_2} + CuX_2 + \underset{\mathbf{2}}{t\text{-BuSNO}_2} \longrightarrow \underset{\mathbf{3}}{ArNH_2} + [CuX_2NO_2]$$

$$+\ t\text{-BuS}\cdot \begin{cases} \xrightarrow{-H_2O_2} [Ar\cdots N_2\cdots CuX_2] + t\text{-BuS}\cdot \longrightarrow ArX + N_2 + CuX + \mathbf{5} + \mathbf{6} \quad (4) \\ \qquad\qquad\qquad\qquad\qquad\qquad \mathbf{4} \\ \xrightarrow{-H_2O} [Ar\cdots N_2O\cdots CuX_2] + t\text{-BuS}\cdot \longrightarrow ArX + N_2O + CuX + \mathbf{5} + \mathbf{6} \quad (5) \\ \qquad\qquad\qquad\qquad\qquad\qquad \mathbf{4} \end{cases}$$

p-Aminophenol (**10**) did not give the corresponding halide with thionitrate **2** but gave N-(t-butylthio)-p-benzoquinone imine (**11**) in 40% yield. The reaction of p-hydroxyaniline **10** and thionitrate **2** without anhydrous copper(II) chloride also gave p-benzoquinone imine **11**, however, the corresponding S-t-butyl 2-methyl-2-propanethiosulfonate (**12**) was formed from thionitrate **2**, besides disulfide **5** and trisulfide **6**.

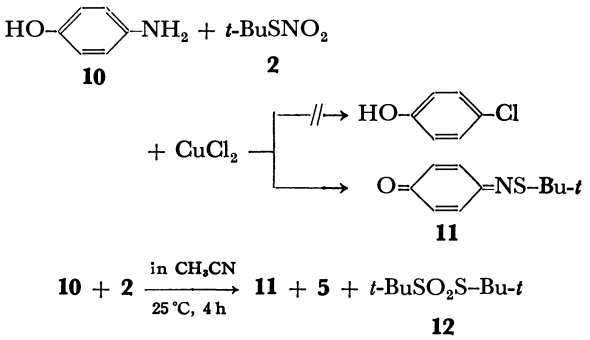

$$\mathbf{10} + \mathbf{2} \xrightarrow[25\,°C,\ 4\,h]{\text{in } CH_3CN} \mathbf{11} + \mathbf{5} + t\text{-BuSO}_2\text{S–Bu-}t$$

12

We have also found that the 2-aryl-1-haloethanes (**13**) were readily obtained in the Meerwein arylation when various arylamines **3** were stirred with thionitrite **1** or thionitrate **2** and anhydrous copper(II) halides in the presence of such olefins as acrylonitrile, styrene and acrylic acid as shown in Table 2. In this reaction,

Table 2. Deamination with thionitrite **1** or thionitrate **2** and anhydrous copper(II) halides in the presence of olefins

$ArNH_2$	(CuX_2) X	Reagent	$(CH_2=CHY)$ Y	Product and yield/% $ArCH_2CHR$ (X)	ArX
p-NO_2-$C_6H_4NH_2$	Cl	**1**	CN	48[a] (32[b])	32[a]
p-NO_2-$C_6H_4NH_2$	Cl	**2**	CN	78[a] (65[b])	11[a]
o-NO_2-$C_6H_4NH_2$	Cl	**1**	CN	29[a] (21[b])	25[a]
o-NO_2-$C_6H_4NH_2$	Cl	**2**	CN	64[a] (61[b])	36[a]
$C_6H_5NH_2$	Cl	**1**	CN	48[a] (31[b])	34[a]
$C_6H_5NH_2$	Cl	**2**	CN	50[a] (39[b])	46[a]
p-MeO-$C_6H_4NH_2$	Cl	**1**	CN	50[a] (40[b])	43[a]
p-MeO-$C_6H_4NH_2$	Cl	**2**	CN	28[a] (23[b])	19[a]
p-NO_2-$C_6H_4NH_2$	Cl	**2**	Ph	62[a] (58[b])	20[a]
p-NO_2-$C_6H_4NH_2$	Cl	**2**	CO_2Et	49[a] (35[b])	33[a]
$C_6H_5NH_2$	Cl	**2**	CO_2Et	56[a] (36[b])	22[a]
$C_6H_5NH_2$	Cl	**2**	c	40[a,d] (31[b,d])	20[a]
$C_6H_5NH_2$	Cl	**2**	CO_2H	31[a] (30[b])	20[a]
$C_6H_5NH_2$	Br	**2**	CO_2H	41[a] (38[b])	33[a]

a) GC yield. b) Isolated yield. c) Methyl methacrylate. d) $PhCH_2C(Me)(Cl)CO_2Me$.

$$\left.\begin{matrix}\mathbf{1}\\ \mathbf{2}\end{matrix}\right\rangle + ArNH_2 + CuX_2 + CH_2{=}CH{-}Y \xrightarrow[25\,^\circ C]{CH_3CN}$$

X=Cl, Br Y=CN, Ph, CO_2H, *et al.*

$$ArCH_2{-}\underset{X}{CH}{-}Y + ArX + N_2 + \mathbf{5} + \mathbf{6}$$

13 **4**

small amounts of corresponding aryl halides **4** were also formed. However, 2-aryl-1-haloethanes **13** were always the main products. Arylation of olefins proceeded more readily and gave the products in better yields with the thionitrate **2** than with the thionitrite **1**. The reaction of *p*-nitroaniline which has an electron-withdrawing nitro group proceeded readily giving the product nearly quantitatively, whereas, the reaction with *p*-methoxyaniline, which has an electron-donating methoxyl group, was somewhat anomalous and gave the adduct in a poor yield together with many uncharacterized substances. Thus thionitrite **1** and thionitrate **2** have now found to be excellent Meerwein type arylation reagents. Some of the compounds in Table 2 are quite useful compounds. For example, treatment of 2-bromo-3-phenylpropionic acid with aq. ammonia can give *dl*-phenylalanine,[7] while ethyl 2-chloro-3-(*p*-nitrophenyl)propionate could be used for the synthesis of chloramphenicol. Arylation of olefinic compounds is presumed to proceed *via* the Meerwein type arylation path which involves aryl radicals formed by the decomposition of diazonium salts as shown in Eq. 6.

$$Ar\cdot + CH_2{=}CHY \longrightarrow ArCH_2\dot{C}HY \xrightarrow{CuX_2} ArCH_2\underset{X}{CH}Y \quad (6)$$

p-Toluenesulfonyl nitrite (**14**), which is a new sulfonyl derivative prepared from the corresponding sulfinic acid with N_2O_4,[16] was also found to be an excellent deaminative reagent of arylamines. This reaction requires

$$\underset{\mathbf{14}}{p\text{-}TolSO_2NO} + \underset{\mathbf{3}}{ArNH_2} + CuX_2 \xrightarrow[25\,^\circ C,\,1\,h]{\text{in } CH_3CN}$$

X=Cl, Br

$$ArX + N_2 + \underset{\mathbf{15}}{(p\text{-}TolSO_2)_2NOH}$$

4

a larger amount of deaminative reagent **14** than thionitrite **1** or thionitrate **2** because of the formation of a nitrogen compound, *N,N'*-bis(*p*-tolylsulfonyl)hydroxylamine (**15**). When various arylamines **3** were treated with anhydrous copper(II) halides and excess sulfonyl nitrite **14** at room temperature, evolution of nitrogen gas was observed during the period of *ca.* 30 min and the corresponding aryl halides **4** were obtained in good yields. These results are listed in Table 1.

Experimental

All the melting points and boiling points were uncorrected. Elemental analysis of sulfur was carried out by Sagami Chemical Research Center and the analyses of other elements were carried out by the Chemical Analysis Center in our University. Analytical determinations by GLC were performed on a Hitachi 163 gas chromatograph fitted with the following column (3 mm o.d.×3 m): 10% SE-30 on Chromosorb W. ^{1}H-NMR spectra were taken at 60 MHz on a Hitachi R-24 A apparatus. IR spectra were recorded with a Hitachi 215 spectrometer. Mass spectra were recorded with a Hitachi RMU-6M spectrometer.

Synthesis of t*-Butyl Thionitrite (1).* Dinitrogen tetraoxide[1] (0.1 mol) in carbon tetrachloride (11 ml) was added to a stirred solution of *t*-BuSH 9.02 g (0.1 mol) in dry ether (100 ml) for a few minites at −70 °C. The solution was stirred further for several minutes and poured into the cold 5% $NaHCO_3$ aq. solution and extracted with ether. The ethereal extract was dried ($MgSO_4$) in dark at 0 °C, and the solvent was evaporated *in vacuo* giving almost pure thionitrite **1** 7.0 g (59%), which was pure enough for the reaction over several months at −20 °C with molecular sieves: bp 40—42 °C/55 mmHg (lit,[9] 36 °C/48 mmHg). IR (neat):

1490 (NO), 1360, 1298, and 1157 cm^{-1}. NMR (CCl_4): δ 1.85 (s).

Synthesis of t-*Butyl Thionitrate (2).* This reaction required a relatively large flask (2 l) fitted with a reflux condencer the end of which is open for air escape, since the reaction took place vigorously. Dinitrogen tetraoxide[1] (1.5 mol) in carbon tetrachloride (135 ml) was added dropwise to a stirred solution of *t*-BuSH 55.3 g (0.6 mol) in dry ether (500 ml) for over 30 min at the rate that ether slowly refluxed. After the addition was over, the solution was stirred further for *ca.* 30 min. The solution was washed with ice-cold water and dried ($MgSO_4$), concentrated, and distilled (with molecular sieves) giving 67.5 g (84%) of colorless oil which had a stimulating odor: bp 40—41 °C/6 mmHg (lit,[9] 55 °C/13 mmHg). IR (neat): 2950, 1520 (NO), 1300, 1263, 1155, and 825 cm^{-1}. NMR (CCl_4): δ 1.58 (s). Thionitrate **2** was pure enough for the reaction over several months at −20 °C with molecular sieves.

Reactions of t-*Butyl Thionitrite (1) and Primary Amines (3) with Anhydrous Copper(II) Halides.* The following is a typical run. After a solution of *t*-BuSNO 0.89 g (7.5 mmol) in dry acetonitrile (20 ml) was added onto well-dried anhydrous copper(II) chloride 0.85 g (6 mmol) under argon with vigorous stirring, *p*-nitroaniline 685 mg (5 mmol) was slowly added in a period of 5 min at 25 °C. The solution was stirred further for 2 h, and then hydrochloric acid solution (20%, 100 ml) was added. The solution, after saturated with NaCl, was extracted with ether. The extract was washed with water saturated with NaCl and dried ($MgSO_4$), concentrated. Recrystallization (from hexane) gave pure *p*-chloronitrobenzene 770 mg (quant.): mp 80—82 °C. IR and NMR spectra were identical with those of authentic samples. Other products were disulfide **5** (0.32 mmol) and trisulfide **6** (2.2 mmol). The amounts of these polysulfides were estimated by GLC and separated by distillation. Disulfide **5**: MS (70 eV), *m/e* 178 (M^+). IR spectrum was identical with that of authentic sample. Trisulfide **6**: mp 14—15 °C (lit,[10] 16.63 °C). IR (neat): 1450, 1360, and 1260 cm^{-1}; NMR (CCl_4): δ 1.36 (s) (lit.[11] δ 1.34). MS (70 eV), *m/e* 210 (M^+).

Reactions of t-*Butyl Thionitrate (2) and Primary Amines (3) with Copper(II) Halides.* The following is a typical run. Well-dried anhydrous copper(II) chloride 810 mg (6 mmol) and *p*-nitroaniline 682 mg (5 mmol) were treated with *t*-$BuSNO_2$, 1.02 g (7.5 mmol) under argon in a similar procedure to that of *t*-BuSNO, giving 780 mg (quant.) of *p*-chloronitrobenzene. Amounts of disulfide **5** (0.31 mmol) and trisulfide **6** (2.1 mmol) were also monitored by GLC and identified with IR, NMR, and MS spectral analyses after distillation.

Melting points, or boiling points, IR and NMR spectra of all halides in Table 1 were identical with those of authentic samples.

Reaction of t-*Butyl Thionitrate (2) and* p-*Aminophenol (10) with Copper(II) Chloride.* Anhydrous copper(II) chloride 810 mg (6 mmol) and *p*-aminophenol 546 mg (5 mmol) were treated with thionitrate **2** 1.02 g (7.5 mmol) for 1 h in a similar procedure to the former reaction. TLC (hexane: ether=10: 1) gave 390 mg (40%) of *N*-(*t*-butylthio)-*p*-benzoquinone imine as bright yellow crystals: mp 77—79 °C (recrystallized from hexane). Found: C, 61.38; H, 6.60; N, 7.13; S, 16.29%. Calcd for $C_{10}H_{13}NOS$: C, 61.51; H, 6.71; N, 7.17; S, 16.42%. IR (KBr): 1630 (C=O), 1475, 1450, 1360, 1143, 861, and 705 cm^{-1}. UV (hexane) max: 401 nm. NMR (CCl_4): δ 1.45 (s, 9H), 6.13—6.50 (m, 2H), and 6.75—7.35 (m, 2H). MS (70 eV), *m/e* (rel intensity): 195 (23, M^+), 138 (76, O= 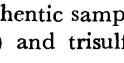 =NS$^+$), and 57 (100, *t*-Bu^+).

TABLE 3. SPECTRAL DATA OF 2-ARYL-1-HALOETHANES

Compound	IR (neat, cm^{-1})	^{1}H-NMR (CCl_4, δ)	MS (70 eV), *m/e*, M^+
p-NO_2-$C_6H_4CH_2CHCN$ (Cl)	1600, 1520, 1350, 857	a)	210, 213
o-NO_2-$C_6H_4CH_2CHCN$ (Cl)[b]	1520, 1343, 783, 722	3.53 (d, J=8 Hz, 2H), 4.87 (t, 1H), 7.14—8.15 (m, 4H)	210, 213
$PhCH_2CHCN$ (Cl)	2240, 1497, 725, 695	a)	165, 167
p-MeO-$C_6H_4CH_2CHCN$ (Cl)	1605, 1507, 1205, 835	a)	195, 197
p-NO_2-$C_6H_4CH_2CHPh$ (Cl)	1550, 1490, 1320, 1180	a)	261, 263
p-NO_2-$C_6H_4CH_2CHCO_2Et$ (Cl)	1720, 1507, 1335, 1166	a)	257, 259
$PhCH_2CHCO_2Et$[c] (Cl)	1730, 1260, 1160	1.28 (t, 3H), 3.14 (dd, J=7.5 Hz, JJ=4.5 Hz, 2H)4.12 (q, 2H), 4.24 (t, 1H), 7.14 (m, 5H)	212, 214
$PhCH_2C(Me)CO_2Me$[d] (Cl)	1730, 1435, 1260, 1207	1.62 (s, 3H), 3.10 (d, J=3 Hz, 2H), 4.20 (s, 3H),7.15 (m, 5H)	212, 214
$PhCH_2CHCO_2H$[e] (Cl)	3400—2500, 1710, 698	3.20 (d, J=8 Hz, 2H), 4.47 (t,1H), 7.17 (m, 5H), 11.30 (br, s, 1H)	184, 186
$PhCH_2CHCO_2H$[f] (Br)	3400—2500, 1710, 910	3.34 (m, 2H), 4.40 (m, 1H), 7.25 (m, 4H), 11.83 (br, s,1H)	228, 230

a) Spectral data were identical with those of literature.[8] b) Bp(bath temp) 160 °C/2 mmHg (lit,[14] 166—168 °C/4 mmHg). c) Bp (bath temp) 85—90 °C/20 mmHg (lit,[15] 85—89 °C/50 mmHg). d) Bp(bath temp) 100 °C/2 mmHg (lit,[12] 136—165 °C/15 mmHg). e) Bp (bath temp) 120 °C/2 mmHg (lit,[13] 176—177 °C/20 mmHg). f) Mp 45—47 °C (lit,[15] 48 °C).

Disulfide **5** (92 mg) and trisulfide **6** (250 mg) were also isolated by TLC and distillation.

Reaction of t-*Butyl Thionitrate (2) and* p-*Aminophenol (10) without Anhydrous Copper(II) Halide.* *p*-Aminophenol 109 mg (1 mmol) was added to a stirred solution of thionitrate **2** 202 mg (1.5 mmol) in dry acetonitrile (3 ml). The mixture was stirred further for 4 h. The amounts of the products were estimated by GLC: *p*-Benzoquinone imine **11** (0.43 mmol, 43%), disulfide **5** (0.19 mmol, 26%), thiosulfonic *S*-ester **12** (0.24 mmol, 33%). Thiosulfonic *S*-ester **12** was isolated by preparative GLC: mp 22—24 °C. IR (neat): 1290 and 1100 cm^{-1}. NMR (CCl_4): δ 1.40 (s) and 1.58 (s). MS (70 eV), *m/e* 210 (M^+). Found: C, 45.59; H, 8.61; S, 30.29%. Calcd for $C_8H_{18}O_2S_2$: C, 45.68; H, 8.62; S, 30.48%.

Reactions of t-*Butyl Thionitrite (1) or* t-*Butyl Thionitrate (2) and Arylamines (3) with Copper(II) Halides in the Presence of Olefins.* The following is a typical run. Thionitrate **2** 1.02 g (7.5 mmol) in acetonitrile (7 ml) and acrylonitrile (7 ml) were added to the well-dried anhydrous copper(II) chloride 810 mg (6 mmol). *p*-Nitroaniline 690 mg (5 mmol) in acetonitrile (5 ml) was added to the mixture in a period of 15 min with stirring. During this period, the flask was cooled by water. The mixture was kept stirring further for 30 min. Evolution of gas (110 ml) was observed during this period. Diluted aq. HCl solution (20%, 100 ml) was added to the mixture, which was then extracted with ethyl ether. The ethereal extract was dried ($MgSO_4$), and concentrated. TLC (hexane: ether=10: 1) gave 689 mg (65%) of 2-chloro-3-(*p*-nitrophenyl)propionitrile and 172 mg (22%) of *p*-chloronitrobenzene. Disulfide **5** 71 mg and trisulfide **6** 186 mg, were obtained directly by GLC.

Spectral data of the products were summarized in Table 3.

Reactions of p-*Toluenesulfonyl Nitrite (14) and Aryl Amines (3) with Copper(II) Halides.* The following is a typical run. Well-dried anhydrous copper(II) chloride 161 mg (1.2 mmol) and *p*-bromoaniline 191 mg (1.0 mmol) were treated with sulfonyl nitrite **14**[16] 444 mg (2.4 mmol) under argon in a similar procedure to that of thionitrite **1**, giving 177 mg (93% by GC) of *p*-bromochlorobenzene. Hydroxylamine **15** 340 mg (83%) was also isolated in this reaction: mp 124—125 °C (from ether), (lit,[17] 126 °C). IR spectrum of compound **15** was identical with that of an authentic sample prepared by the procedure described in the literature.[17]

References

1) S. Oae, D. Fukushima, and Y. H. Kim, *J. Chem. Soc., Chem. Commun.*, **1977**, 407.
2) S. Oae, Y. H. Kim, D. Fukushima, and K. Shinhama, *J. Chem. Soc., Perkin Trans. 1*, **1978**, 913.
3) Y. H. Kim, K. Shinhama, D. Fukushima, and S. Oae, *Tetrahedron Lett.*, **1978**, 1211.
4) M. P. Doyle, B. Siegfried, and J. J. Hammond, *J. Am. Chem. Soc.*, **98**, 1627 (1976).
5) M. P. Doyle and B. Siegfried, *J. Chem. Soc., Chem. Commun.*, **1976**, 433.
6) M. P. Doyle, B. Siegfried, and J. F. Dellaria, Jr., *J. Org. Chem.*, **42**, 2426 (1977).
7) J. C. Westfahl and T. L. Gresham, *J. Am. Chem. Soc.*, **77**, 2910 (1955).
8) M. P. Doyle, B. Siegfried, R. C. Elliott, and J. F. Dellaria, Jr., *J. Org. Chem.* **42**, 2431 (1977).
9) G. Kresze and U. Uhlich, *Chem. Ber.*, **92**, 1048 (1959).
10) T. V. Cullum and R. A. Dean, *J. Inst. Petroleum*, **39**, 206 (1953); *Chem. Abstr.*, **48**, 4429a (1954).
11) D. Grant and J. R. Van Wazer, *J. Am. Chem. Soc.*, **86**, 3012 (1964).
12) A. V. Dombrovskii, A. P. Terentév, and A. M. Yurkevich, *Zh. Obshch. Khim.* **27**, 419 (1957); *Chem. Abstr.*, **51**, 15454g (1957).
13) S. Kaneo, *J. Pharm. Soc. Jpn*, **58**, 256 (1938).
14) A. V. Dombroskii, A. M. Yurkevich, and A. P. Terentév, *Zh. Obsh. Khim.* **26**, 3214 (1956); *Chem. Abstr.*, **51**, 8038fg (1957).
15) A. V. Dombroskii, A. M. Yurkevich, and A. P. Terentév, *Zh. Obsh. Khim.* **27**, 3346 (1957); *Chem. Abstr.*, **52**, 9020a (1958).
16) S. Oae, K. Shinhama, and Y. H. Kim, *Tetrahedron Lett.*, **1979**, 3307.
17) G. Kreze and W. Kort, *Chem. Ber.*, **24**, 2624 (1961).

Synthesis of Linear Pyranocoumarins: Xanthoxyletin, 4-Methylxanthyletin, and 4-Phenylxanthyletin

Vindo Kumar Ahluwalia,* Mrs. Krishna Bhat, Chandra Prakash, and Shashi Bala
Department of Chemistry, University of Delhi, Delhi 110007, India

(Received June 6, 1979)

A convenient synthesis of linear pyranocoumarins (2*H*,8*H*-benzo[1,2-b: 5,4-b']dipyran-2-ones), *viz.*, xanthoxyletin, 4-methylxanthyletin and 4-phenylxanthyletin is described which uses blocking the 8-position of appropriate 7-hydroxycoumarin derivatives with iodine and 1,1-dimethyl-2-propynylation followed by cyclisation.

The occurrence of linear pyranocoumarins (2*H*,8*H*-benzo[1,2-b: 5,4-b']dipyran-2-one derivatives), *viz.*, xanthyletin,[1-3] xanthoxyletin,[3-5] luvangetin,[1] dentatin,[6] roubustic acid,[7-10] robustin,[10] their methyl ethers,[10] lonchocarpic acid[9,11-13] and lonchocarpen[13] prompted us to devise a convenient method for their synthesis. A few syntheses of these coumarins are known[14-17] but these involve a number of steps and the overall yield is poor.

It has been shown[16,18,19] that 7-hydroxycoumarin derivatives react with 3-chloro-3-methyl-1-butyne in acetone to yield the 7-(1,1-dimethyl-2-propynyl) ethers, which on heating with *N,N*-dimethylaniline resulted[17-19] in the formation of angular pyrano coumarins (2*H*,8*H*-benzo[1,2-b: 3,4-b']dipyran-2-one derivatives) *i.e.* cyclization takes place at more reactive 8-position due to fixation of double bond. But if 8-position is substituted,[15,16] the cyclization takes place at 6-position and the corresponding 8-substituted linear pyranocoumarins are obtained. Thus linear pyranocoumarins having 8-position free could not be prepared by this method. However these coumarins have been synthesized by very tedious methods.[14-17] A convenient method has now been developed for the synthesis of linear pyranocoumarins by blocking the 8-position with an easily introducable and removable group like iodine, which is knocked out on heating with *N,N*-dimethylaniline and cyclization takes place at 6-position. The required intermediate 7-(1,1-dimethyl-2-propynyloxy)-8-iodocoumarin derivatives were prepared by iodination of corresponding 7-hydroxycoumarin with iodine and periodic acid, followed by reaction with 3-chloro-3-methyl-1-butyne in acetone in presence of potassium carbonate.

Using the above method, the synthesis of 5-methoxy-8,8-dimethyl-2*H*,8*H*-benzo[1,2-b: 5,4-b']dipyran-2-one (xanthoxyletin) (**1**), 4,8,8-trimethyl-2*H*,8*H*-benzo[1,2-b: 5,4-b']dipyran-2-one (4-methylxanthyletin) (**2**) and 8,8-dimethyl-4-phenyl-2*H*,8*H*-benzo[1,2-b: 5,4-b']dipyran-2-one (4-phenylxanthyletin) (**3**) has been carried out. The synthesis of **1** was effected as follows. Iodination of 7-hydroxy-5-methoxycoumarin[20] with iodine/periodic acid gave 7-hydroxy-8-iodo-5-methoxycoumarin (**4**), the structure of which was confirmed by the ^{1}H NMR spectrum of its acetate. Etherification of **4** with 3-chloro-3-methyl-1-butyne in acetone/K_2CO_3 yielded 7-(1,1-dimethyl-2-propynyloxy)-8-iodo-5-methoxycoumarin (**5**), which on heating with *N,N*-dimethylaniline afforded **1**. That the cyclization takes place at 6-position and iodine was knocked out in above reaction was shown by its NMR spectral data, and its disagreement with angular isomer, *viz.*, 5-methoxy-8,8-dimethyl-2*H*,8*H*-benzo[1,2-b: 3,4-b']dipyran-2-one.[21]

Similarly, iodination of 7-hydroxy-4-methylcoumarin[22] with iodine/periodic acid gave 7-hydroxy-8-iodo-4-methylcoumarin (**6**). Its structure was confirmed by the NMR spectral data of its acetate, which showed the presence of two doublets (J=9.5 Hz) for ortho-coupled H5 and H6 protons. Etherification of **6** with 3-chloro-3-methyl-1-butyne in acetone/K_2CO_3 yielded 7-(1,1-dimethyl-2-propynyloxy)-8-iodo-4-methylcoumarin (**7**), which on heating with *N,N*-dimethylaniline afforded **2**. Its structure was in agreement with the NMR spectral data which showed the presence of two singlets for para-coupled H5 and H10 protons, along with other usual signals.

Using the above method, 4-phenylxanthyletin (**3**) has also been synthesized starting from 7-(1,1-dimethyl-2-propynyloxy)-8-iodo-4-phenylcoumarin (**8**), which was prepared by the iodination of 7-hydroxy-4-phenylcoumarin[23] with iodine and periodic acid to 7-hydroxy-8-iodo-4-phenylcoumarin (**9**), followed by etherification with 3-chloro-3-methyl-1-butyne in acetone in presence of potassium carbonate. Compound **8** on heating with *N,N*-dimethylaniline yielded **3**. Its structure was in agreement with its ^{1}H-NMR spectral data.

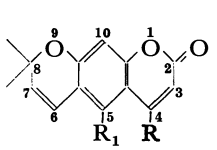

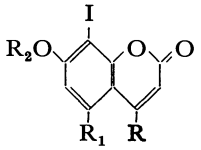

(**1**) R=H; R_1=OCH_3
(**2**) R=CH_3; R_1=H
(**3**) R=C_6H_5; R_1=H

(**4**) R=R_2=H; R_1=OCH_3
(**5**) R=H; R_1=OCH_3; R_2=$-C(CH_3)_2C{\equiv}CH$
(**6**) R=CH_3; R_1=R_2=H
(**7**) R=CH_3; R_1=H; R_2=$-C(CH_3)_2C{\equiv}CH$
(**8**) R=C_6H_5; R_1=H; R_2=$-C(CH_3)_2C{\equiv}CH$
(**9**) R=C_6H_5; R_1=R_2=H

Experimental

Melting points are uncorrected. Infrared spectra were recorded on a Perkin-Elmer Infra-cord spectrometer. The NMR spectra were recorded on Perkin Elmer R-32 instrument with TMS as internal standard.

*5-Methoxy-8,8-dimethyl-2*H*,8*H*-benzo[1,2-b: 5,4-b']dipyran-2-one (Xanthoxyletin) (1). (a) 7-Hydroxy-8-iodo-5-methoxycoumarin (4)*: 7-Hydroxy-5-methoxycoumarin[20] (2 g, 10.4 mmol) was dissolved in minimum amount of ethanol and to

this solution iodine (2.1 g) and periodic acid (0.5 g in water) were added. The mixture was stirred for 2 h at room temperature and then diluted with water to give the coumarin (**4**) (2.2 g, 6.91 mmol) (66.7%). It crystallized from ethanol as yellow needles mp 235—237 °C. Found: C, 37.6; H, 2.1%. Calcd for $C_{10}H_7O_4I$: C, 37.7; H, 2.2%. Its acetate (prepared by acetic anhydride–pyridine) melted at 205—207 °C. NMR (DMSO-d_6): δ 2.20 (s, 3H, 7-OAc); 3.75 (s, 3H, 5-OCH_3); 6.25 (d, 1H, J_0=9.5 Hz, H3); 6.85 (s, 1H, H6); 7.88 (d, 1H, J_0=9.5 Hz, H4).

(b) 7-(1,1-Dimethyl-2-propynyloxy)-8-iodo-5-methoxycoumarin (5): A solution of (**4**) (1 g, 3.14 mmol) in dry acetone (75 ml) was refluxed with 3-chloro-3-methyl-1-butyne (4 ml, 38.9 mmol) in presence of anhydrous potassium carbonate (3 g) and anhydrous potassium iodide (1.9 g) for 24 h. The solvent was distilled off and the residue was treated with ice. The separated solid was filtered, washed with a dilute solution of sodium carbonate and water and crystallized from benzene–petroleum ether to give (**5**) (0.62 g, 1.61 mmol) (51.7%) as yellow needles mp 178—179 °C. Found: C, 46.9; H, 3.5%. Calcd for $C_{15}H_{13}O_4I$: C, 46.8; H, 3.6%. NMR ($CDCl_3$) δ 1.62 (s, 6H, $-C(CH_3)_2$); 2.58 (s, 1H, $-C\equiv CH$); 3.82 (s, 3H, 5-OCH_3); 6.09 (d, 1H, J_0=9.5 Hz, H3); 6.88 (s, 1H, H6); 7.91 (d, 1H, J_0=9.5 Hz, H4).

(c) 5-Methoxy-8,8-dimethyl-2H,8H-benzo[1,2-b: 5,4-b']dipyran-2-one (Xanthoxyetin) (1): The above 1,1-dimethyl-2-propynyl ether (**5**) (0.1 g, 0.26 mmol), was refluxed with *N,N*-dimethylaniline (3 ml) for 12 h. The cooled reaction mixture was poured over ice-cold hydrochloric acid. The solution was extracted thrice with ethyl acetate (150 ml), washed with 5% HCl, 5% NaOH and finally with water and dried (Na_2SO_4). Distillation of ethyl acetate yielded **1** (50 mg, 0.19 mmol) (74.6%) which crystallized from benzene–petroleum ether as yellow needles, mp 132—133 °C (lit,[5] mp 132—133 °C). Found: C, 69.6; H, 5.5%. Calcd for $C_{15}H_{14}O_4$: C, 69.7; H, 5.4%. NMR ($CDCl_3$) δ 1.76 (s, 6H, $-C(CH_3)_2$); 4.16 (s, 3H, 5-OCH_3); 5.85 (d, 1H, J_0=9.5 Hz, H3); 6.32 (d, 1H, $J_{6,7}$=10 Hz, H6); 6.5 (s, 1H, H10); 7.08 (d, 1H, $J_{6,7}$=10 Hz, H7); 8.2 (d, 1H, J_0=9.5 Hz, H4). IR ν_{max} (KBr) (cm^{-1}) 1710 (C=O); 1610 and 1600 (C=C); 1350 and 1360 ($-C(CH_3)_2$).

4,8,8-Trimethyl-2H,8H-benzo[1,2-b: 5,4-b']dipyran-2-one (4-Methylxanthyletin) (2). (a) 7-Hydroxy-8-iodo-4-methylcoumarin (6): 7-Hydroxy-4-methylcoumarin[22] (2 g, 11.3 mmol) was dissolved in minimum amount of ethanol and to this solution iodine (2.31 g) and periodic acid (0.52 g in water) were added. The mixture was stirred for 2 h at room temperature and then diluted with water to give **6** (2.5 g, 8.27 mmol) (73.3%). It crystallized from ethanol as light yellow needles, mp 219—220 °C. Found: C, 39.6; H, 2.3%. Calcd for $C_{10}H_7O_3I$: C, 39.7; H, 2.3%. Its acetate (acetic anhydride-pyridine) melted at 180—181 °C. NMR ($CDCl_3$) δ 2.5 (bs, 6H, 4-CH_3 and 7-OAc); 6.48 (s, 1H, H3); 7.34 (d, 1H, J_0=9.5 Hz, H6); 7.85 (d, 1H, J_0=9.5 Hz, H5).

(b) 7-(1,1-Dimethyl-2-propynyloxy)-8-iodo-4-methylcoumarin (7): A solution of **6** (1 g, 3.31 mmol) in dry acetone (75 ml) was refluxed with 3-chloro-3-methyl-1-butyne (4 ml, 38.9 mmol) in presence of anhydrous potassium carbonate (3 g) and anhydrous potassium iodide (2.06 g) for 24 h. Working up of the reaction mixture yielded **7** (0.65 g, 1.76 mmol) (54.2%). It crystallized from benzene–petroleum ether as yellow needles, mp 185—186 °C. Found: C, 48.8; H, 3.4%. Calcd for $C_{15}H_{13}O_3I$: C, 48.9; H, 3.5%. NMR ($CDCl_3$) δ 1.81 (s, 6H, $-C(CH_3)_2$); 2.42 (s, 3H, 4-CH_3); 2.7 (s, 1H, $-C\equiv CH$); 6.15 (s, 1H, H3); 7.3 (d, 1H, J_0=9.5 Hz, H6); 7.55 (d, 1H, J_0=9.5 Hz, H5).

(c) 4,8,8-Trimethyl-2H,8H-benzo[1,2-b: 5,4-b']dipyran-2-one (4-Methylxanthyletin) (2): The above 1,1-dimethyl-2-propynyl ether (0.1 g, 0.27 mmol) was refluxed with *N,N*-dimethylaniline (3 ml) for 12 h. The cooled reaction mixture was poured over ice cold hydrochloric acid, worked up (as in the case of **1**) to yield **2** (50 mg, 0.20 mmol) (76.9%), which crystallized from benzene–petroleum ether as yellow needles, mp 237—238 °C. Found: C, 74.2; H, 5.8%. Calcd for $C_{15}H_{14}O_3$: C, 74.3; H, 5.7%. NMR ($CDCl_3$) δ 1.49 (s, 6H, $-C(CH_3)_2$); 2.35 (s, 3H, 4-CH_3); 5.65 (d, 1H, $J_{6,7}$=10 Hz, H6); 6.05 (s, 1H, H3); 6.26 (d, 1H, $J_{6,7}$=10 Hz, H7); 7.09 (s, 1H, H10); 7.22 (s, 1H, H5). IR ν_{max} (KBr) (cm^{-1}) 1710 (C=O); 1610 and 1600 (C=C); 1345 and 1360 ($-C(CH_3)_2$).

8,8-Dimethyl-4-phenyl-2H,8H-benzo[1,2-b: 5,4-b']dipyran-2-one (4-Phenylxanthyletin) (3). (a) 7-Hydroxy-8-iodo-4-phenylcoumarin (9): 7-Hydroxy-4-phenylcoumarin[23] (2 g, 8.40 mmol) was dissolved in minimum amount of ethanol and to this solution iodine (1.71 g) and periodic acid (0.39 g in water) were added. The mixture was stirred for 2 h at room temperature and then diluted with water to give coumarin (**9**) (2.5 g, 6.86 mmol) (80%). It crystallized from ethanol as light yellowish needles, mp 263—264 °C. Found: C, 49.3; H, 2.4%. Calcd for $C_{15}H_9O_3I$: C, 49.4; H, 2.5%. Its acetate (acetic anhydride–pyridine) melted at 178—179 °C. NMR ($CDCl_3$) δ 2.44 (s, 3H, 7-OAc); 6.38 (s, 1H, H3); 7.05 (d, 1H, J_0=9.5 Hz, H6); 7.32 (d, 1H, J_0=9.5 Hz, H5); 7.4 (bs, 5H, 4-Ph).

(b) 7-(1,1-Dimethyl-2-propynyloxy)-8-iodo-4-phenylcoumarin (8): A solution of **9** (1 g, 2.80 mmol) in dry acetone (75 ml) was refluxed with 3-chloro-3-methyl-1-butyne (4 ml, 38.9 mmol) in presence of anhydrous potassium carbonate (3 g) and anhydrous potassium iodide (1.5 g) for 24 h. Working up of the reaction mixture yielded (**8**) (0.7 g, 1.62 mmol) (63.6%) which crystallized from benzene–petroleum ether as brown needles mp 261—262 °C (Found: C, 55.7; H, 3.5%. Calcd for $C_{20}H_{15}O_3I$: C, 55.8; H, 3.4%). NMR ($CDCl_3$): δ 1.9 (s, 6H, $-C(CH_3)_2$); 2.76 (s, 1H, $-C\equiv CH$); 6.32 (s, 1H, H3); 7.32 (d, 1H, J_0=9.5 Hz, H6); 7.56 (s, 5H, 4-Ph); 7.66 (d, 1H, J_0=9.5 Hz, H5).

(c) 8,8-Dimethyl-4-phenyl-2H,8H-benzo[1,2-b: 5,4-b']dipyran-2-one (4-Phenylxanthyletin) (3). The above 1,1-dimethyl-2-propynyl ether (**8**) (0.1 g, 0.23 mmol) was refluxed with *N,N*-dimethylaniline (3 ml) for 6 h. The cooled reaction mixture was poured over ice cold hydrochloric acid and worked up (as in case of **1**) to yield **3** (45 mg, 0.14 mmol) (63.9%). It crystallized from benzene–petroleum ether as yellow needles, mp 181—182 °C. Found: C, 78.8; H, 5.3%. Calcd for $C_{20}H_{16}O_3$: C, 78.9; H, 5.2%. NMR ($CDCl_3$) δ 1.52 (s, 6H, $-C(CH_3)_2$); 5.62 (d, 1H, $J_{6,7}$=10 Hz, H6); 6.08 (s, 1H, H3); 6.18 (d, 1H, $J_{6,7}$=10 Hz, H7); 6.96 (s, 1H, H10); 7.3 (s, 5H, 4-Ph); 7.45 (s, 1H, H5). IR ν_{max} (KBr) (cm^{-1}) 1715 (C=O); 1615 and 1600 (C=C); 1345 and 1360 ($-C(CH_3)_2$).

Our thanks are due to UGC and CSIR, New Delhi for Research Grant.

References

1) P. K. Bose and A. Mookerjee, *J. Indian Chem. Soc.*, **21**, 181 (1944).
2) A. Mookerjee, *J. Indian Chem. Soc.*, **23**, 41 (1946).
3) F. E. King, J. R. Housley, and T. J. King, *J. Chem. Soc.*, **1954**, 1392.
4) Lindsey, H. Briggs, and R. H. Locker, *J. Chem. Soc.*, **1951**, 3131.
5) M. P. Hegarty and F. N. Lahey, *Aust. J. Chem.*, **9**, 120 (1956).

6) T. R. Govindachari, B. R. Pai, P. S. Subramaniam, and N. Muthukumarswamy, *Tetrahedron*, **24**, 753 (1968).
7) S. Krishna and T. P. Ghose, *Indian Forest Leaflet*, No. 2 (1942).
8) S. A. Harper, *J. Chem. Soc.*, **1942**, 181.
9) E. P. Clarke, *J. Org. Chem.*, **8**, 489 (1943).
10) W. D. Ollis, A. J. East, and R. E. Wheeler, *J. Chem. Soc., C*, **1969**, 365.
11) H. A. Jones, *J. Am. Chem. Soc.*, **56**, 1247 (1934).
12) H. A. Jones and H. L. Haller, *J. Org. Chem.*, **8**, 493 (1943).
13) C. P. Falshaw, R. A. Harmer, W. D. Ollis, R. E. Wheeler, V. R. Lalitha, and N. V. Subba Rao, *J. Chem. Soc., C*, **1969**, 374.
14) A. C. Jain and S. M. Jain, *Tetrahedron*, **29**, 2803 (1973).
15) D. Mowat and R. D. H. Murray, *Tetrahedron*, **29**, 2943 (1973).
16) J. Hlubuck, E. Ritchie, and W. C. Taylor, *Tetrahedron Lett.*, **1969**, 1369.
17) E. Spath and R. Hillal, *Ber.*, **72**, 2093 (1939).
18) P. S. Sampath Kumar, V. V. S. Murti, and T. R. Seshadri, *Indian J. Chem.*, **9**, 1319 (1971).
19) V. K. Ahluwalia, C. Prakash, and R. P. Singh, *Indian J. Chem.*, **15B**, 1033 (1979).
20) V. K. Ahluwalia, P. Venkateswarlu, and T. R. Seshadri, *Indian J. Chem.*, **7**, 115 (1969).
21) R. D. H. Murray, M. M. Ballantyne, and K. P. Mathi, *Tetrahedron*, **27**, 1247 (1971).
22) H. Pechman and G. Duisberg, *Ber.*, **16**, 2122 (1883).
23) F. W. Canten, F. H. Curd, and A. Robertson, *J. Chem. Soc.*, **1931**, 1262.

The Cyclodextrin-accelerated Cleavage of Thiocarboxylic *S*-Esters

Makoto KOMIYAMA† and Myron Lee BENDER*

Departments of Chemistry and Biochemistry, Northwestern University, Evanston, IL 60201, USA

(Received January 10, 1979)

The effect of α- and β-cyclodextrins on the cleavage of the thiocarboxylic *S*-esters, *S*-*p*-nitrophenyl thioacetate (**1**) and *S*-ethyl *p*-nitrothiobenzoate (**3**), was compared with their effect on the cleavage of the corresponding oxygen esters, *p*-nitrophenyl acetate (**2**) and ethyl *p*-nitrobenzoate (**4**). The rate constants of α- or β-cyclodextrin-accelerated cleavage of **1** (1.5×10^{-2} or 4.8×10^{-2} s^{-1} at pH 10.5, 25 °C) were almost identical with the values of **2** (1.6×10^{-2} or 4.2×10^{-2} s^{-1}), definitely showing the rate-determining formation of tetrahedral intermediates. The cleavage of **3** was accelerated by α- and β-cyclodextrins, whereas the cleavage of **4** was decelerated by β-cyclodextrin but was not affected by α-cyclodextrin. The contrast in the effect of cyclodextrins on **3** and **4** was ascribed to the difference of the rate of breakdown of the tetrahedral intermediates to products, caused by different pK's of the leaving groups of **3** (10.5) and **4** (16.0). The formation of tetrahedral intermediates confirmed in the cyclodextrin-accelerated hydrolyses of esters further strengthened the previous proposal that cyclodextrin is an excellent model of serine proteases, since these intermediates are also formed in enzymatic reactions.

It is well known that cyclodextrins (CDs) affect the rates of many kinds of chemical reactions. The most important feature of reactions involving CDs as accelerating (or retarding) reagents is the formation of inclusion complexes of substrates with CD, which is followed by chemical reaction. Thus, CD chemistry provides a good example of a "guest-host" relationship and CDs have been used as models of enzymes (especially of hydrolytic enzymes).[1,2]

Much work has been done on the CD-accelerated cleavage of oxygen esters,[1-6] showing clear-cut differences of the effect of CD depending on the leaving groups. Thus, cleavage of phenyl esters are accelerated by CD, whereas cleavage of alkyl esters are decelerated by CD, which was attributed to either the high pK_a of the leaving group (alcohol) or non-productive binding.[1,4] Cleavage of phenyl esters is a nucleophilic reaction by the secondary hydroxyl group of CD, resulting in acyl-CD and phenol.

In spite of the multitude of information on the cleavage of oxygen esters, however, no report has been made about the effect of CD on the cleavage thiocarboxylic *S*-esters. This report describes the rate effect of α-cyclodextrin (α-CD) and β-cyclodextrin (β-CD) on the cleavage of *S*-*p*-nitrophenyl thioacetate (**1**), an *S*-phenyl thioester, and *S*-ethyl *p*-nitrothiobenzoate (**3**), an *S*-alkyl thioester. For purposes of comparison, the rate effect of α-CD and β-CD on the cleavage of the corresponding oxygen esters, *p*-nitrophenyl acetate (**2**) and ethyl *p*-nitrobenzoate (**4**) was also determined.

The comparison between **1** and **2** can be a good test to check whether or not the cleavage of these substrates proceeds *via* tetrahedral intermediates. If the cleavage involves formation of tetrahedral intermediates, the rate constant of the CD-accelerated cleavage of **1** should be (approximately) equal to that of **2**. Alternatively, in an S_N2 type reaction, an –SR group of **1** should be displaced at least 250 times faster than an –OR group of **2**.[7,8]

Furthermore, the effect of CD on the cleavage of **3** (whether acceleration or deceleration) can probe whether the high pK_a of the leaving group or non-productive binding is the important factor in the deceleration of the cleavage of alkyl esters by CD, since ethanethiol has smaller pK_a (10.5)[9] than the nucleophilic hydroxyl group of CD (around 12).[4,6]

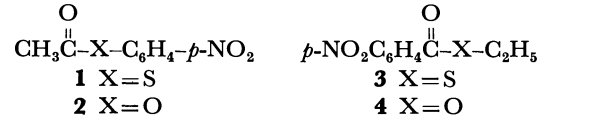

1 X=S **2** X=O **3** X=S **4** X=O

Experimental

Materials. **1** was synthesized from acetyl chloride and thiophenol, and recrystallized from cyclohexane; mp 82 °C (lit, 82 °C,[10] 82.3—82.6 °C[11]). **2** was recrystallized from chloroform–hexane; mp 79.5 °C (lit, 79.5—80 °C[11]).

3 was synthesized from *p*-nitrobenzoyl chloride and ethanethiol, and purified by recrystallization from acidified aqueous ethanol; mp 70.0—70.2 °C (lit, 69.5—70 °C,[7] 67—68 °C[12]). **4** was recrystallized from aqueous ethanol; mp 56.5—57 °C (lit, 56.5—57 °C). α-CD and β-CD were purified by recrystallization from water. All water used for kinetic studies was doubly distilled.

Kinetics. The cleavage of **1**—**4** was carried out at 25 °C and was followed at 410 nm (**1** and **2**) and 300 nm (**3** and **4**) by a Cary 14 spectrophotometer. Reactions were initiated by addition of stock solution of **1**—**4** in acetonitrile to a thermostatted buffer solution. In the reactions of **3**, buffer solution was flushed with nitrogen before the addition of the sample stock solution, since an accelerating effect by oxygen was reported.[7]

The kinetic data (k_{obsd}) were treated based on the following reaction scheme and the corresponding Lineweaver-Burk plots:[1]

$$\text{Ester} + \text{CD} \underset{K_d}{\rightleftharpoons} \text{Complex} \xrightarrow{k_c} \text{Products};\quad \text{Complex} \xrightarrow{k_{un}} \text{CD}$$

$$1/(k_{obsd} - k_{un}) = K_d/(k_c/k_{un})[\text{CD}]_0 + 1/(k_c - k_{un}).$$

Results

Both α-CD and β-CD showed acceleration of the cleavage of **1** and **2**. The rate constants of the cleavage of **1** and **2** in the presence of CD (in large excess),

† Current address: Department of Synthetic Chemistry, Faculty of Engineering, The University of Tokyo, Hongo, Tokyo 113.

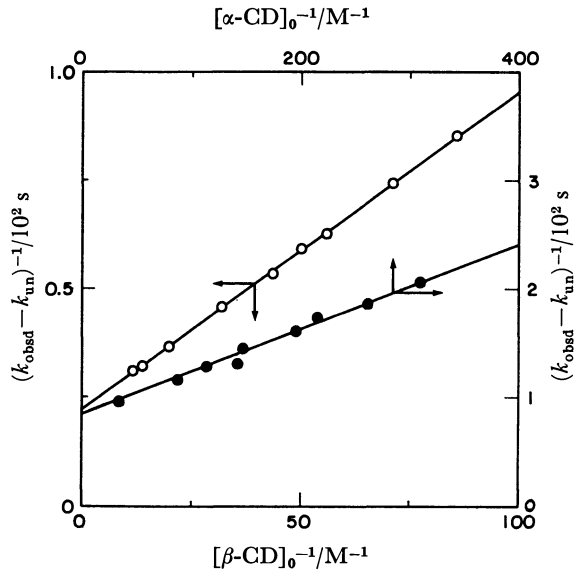

Fig. 1. Plot of $1/(k_{obsd}-k_{un})$ *versus* $1/[C]_0$ of the α-CD (●)- and β-CD (○)-accelerated cleavage of **1**. pH 10.5, I=0.2 M, 25 °C.

k_{obsd}, asymptotically approached a maximum value as $[CD]_0$ increased, showing the complex formation of CD with **1** and **2**. Thus, the rate constant of the cleavage of **1** and **2** complexed with CD, k_c, and the dissociation constant of the CD-**1** (or **2**) complex, K_d, were determined by plotting $1/(k_{obsd}-k_{un})$ *vs.* $1/[CD]_0$ as shown in Fig. 1. Here k_{un} is the rate constant in the absence of CD (see Experimental).

TABLE 1. VALUES OF k_c AND K_d FOR THE α-CD AND β-CD ACCELERATED CLEAVAGE OF **1** AND **2**[a,b]

Cyclodextrin	Substrate	k_c / 10^{-3} s^{-1}	K_d / 10^{-3} M
α-CD	**1**	15±1	4.8±0.3
	2	16±1	12±2
β-CD	**1**	48±3	3.0±0.4
	2	42±3	6.1±0.7

a) pH 10.5, I=0.2 M. b) k_{un}'s are 2.8×10^{-3} s^{-1} for **1** and 4.6×10^{-3} s^{-1} for **2**.

Table 1 lists the values of k_c and K_d for the CD-accelerated cleavage of **1** as well as those of **2**.

Significantly, k_c of **1** accelerated by α-CD is almost equal to that of **2** accelerated by α-CD. β-CD also gave almost identical values of k_c of **1** and **2**. Thus, *S*-phenyl thioester and phenyl ester are cleaved by CD at similar rates. This result shows that a rate-limiting step occurs before the hydroxyl or mercapto group partitions, since the cleavage of the *S*-phenyl thioester should be faster than that of the phenyl ester by at least 250 fold if breaking of the bond between the carbonyl atom and the sulfur atom (or oxygen atom) were rate-limiting.

The change of absorbance at 300 nm in the cleavage of **3** by CD did not follow first-order kinetics (Fig. 2). This result indicates a stepwise pathway (acylation of CD by **3**, followed by hydrolysis of acyl-CD, as shown

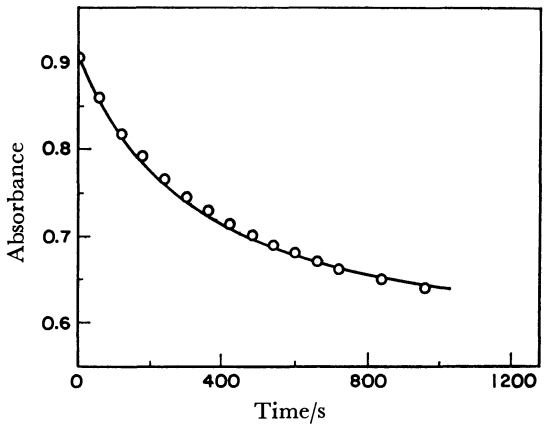

Fig. 2. Change of absorbance at 300 nm for the hydrolysis of **3** in the presence of 0.02 M α-CD at pH 10.5, 25 °C; blank circles are experimentally obtained, whereas the solid line is the theoretical line calculated by using $k_1=1.5\times10^{-3}$ s^{-1} and $k_2=7.5\times10^{-3}$ s^{-1} in Eq. 2.

by Eq. 1 which is consistent with CD-accelerated hydrolyses of phenyl esters.

$$\mathbf{3} + \mathrm{CD} \xrightarrow{k_1} p\text{-nitrobenzoyl-CD (}\mathbf{5}\text{)} + \text{ethanethiol}$$
$$\downarrow k_2 \qquad (1)$$
$$p\text{-nitrobenzoate (}\mathbf{6}\text{)} + \mathrm{CD} + \text{ethanethiol}$$

Of the species in Eq. 1, **3**, **5**, and **6** all absorb at 300 nm (molar absorption coefficients ε_3, ε_5,[13] and ε_6= 8.97×10^3, 2.04×10^3, and 5.84×10^3 M^{-1} cm^{-1}). When the rate constant of the hydrolysis of **5** (k_2) is comparable to that of the cleavage of **3** in the presence of CD (k_1) in magnitude, the intermediate **5** accumulates. Thus, k_1 was determined by fitting the observed absorbance at 300 nm (A) to the theoretical values calculated by Eq. 2.

$$A=\frac{A_0}{\varepsilon_3}\left[\varepsilon_3\exp(-k_1t)+\varepsilon_5\frac{k_1}{k_2-k_1}\{\exp(-k_1t)-\exp(-k_2t)\}\right.$$
$$\left.+\varepsilon_6\left\{1+\frac{k_2\exp(-k_1t)-k_1\exp(-k_2t)}{k_1-k_2}\right\}\right], \qquad (2)$$

where A_0 is the initial absorbance, and the first, second, and third terms of Eq. 2 correspond to the absorbance due to **3**, **5**, and **6**, respectively, in the reaction solution. k_2 was independently determined to be 7.5×10^{-3} s^{-1} at pH 10.5 using the change of absorbance at 260 nm in the hydrolysis of *m*-chlorophenyl *p*-nitrobenzoate in the presence of 0.02 M α-CD according to the previous paper.[4]

As shown in Fig. 2, the change of the absorbance at 300 nm in the hydrolysis of **3** in the presence of 0.02 M α-CD (blank circles) satisfactorily fits the theoretical line calculated from Eq. 2 by using $k_1=1.5\times10^{-3}$ s^{-1}.

Small deviations of the experimental results from the theoretical line are attributable to **3** alone not complexed with α-CD, being hydrolyzed by hydroxide ion without forming **5** as an intermediate. A rough estimate of the amount of complexed **3** was made by using the dependence of the initial slope of the absorbance change upon $[\alpha\text{-CD}]_0$, indicating that about 70% of **3** is complexed with α-CD when $[\alpha\text{-CD}]_0$ is 0.02 M. Similarly, k_1 of **3**

in the presence of 0.015 M β-CD, where about 80% of **3** is complexed with β-CD, was determined to be 5×10^{-4} s^{-1}.

On the other hand, the absorbance change at 300 nm in the hydrolysis of **4** in the presence of CD did not show any measurable deviation from first-order kinetics and the rate constant of its cleavage was determined by the usual first-order equation. This fact indicates that the cleavage of **4** does not follow Eq. 1 but rather proceeds by alkaline reaction, which is discussed later.

Table 2. Effects of α-CD and β-CD on the cleavage of **3** and **4**[a]

CD	Substrate	Observed rate constant (10^{-4} s^{-1})	Rate effect by CD[d]
α-CD[b]	**3**	15±2	6.5
	4	2.6±0.05	1.0
β-CD[c]	**3**	5±1	2.2
	4	1.5±0.03	0.57

a) pH 10.5, I=0.2 M, and 25 °C. b) 0.02 M. c) 0.015 M. d) The ratio of the rate of cleavage of **3** and **4** in the presence of CD to that in its absence.

Table 2 lists the rate constants of the cleavage of **3** and **4** in the presence of CD determined by the above method. It was found that 0.02 M α-CD and 0.015 M β-CD show 6.5 and 2.2 fold acceleration of the cleavage of **3**, an *S*-alkyl thioester. This is in contrast to (about 2 fold) deceleration by β-CD and virtually no effect by α-CD in the cleavage of **4**, an alkyl ester.

Discussion

The almost identical k_c's of **1** and **2** definitely showed the formation of tetrahedral intermediates in the CD-accelerated cleavage of esters. The change of leaving group from *p*-nitrophenol to *p*-nitrothiophenol does not produce a significant effect on k_c, since the formation of tetrahedral intermediates (rather than their breakdown to products) is rate-determining. This occurs because of the larger pK_a of the attacking secondary hydroxyl groups of the CD (around 12) than the pK_a's of the leaving groups (the pK_a's of *p*-nitrophenol and *p*-nitrothiophenol are 7.15[15] and 4.47[11]).

The formation of tetrahedral intermediates was also confirmed in the CD-accelerated cleavage of **3** by the deviation of the absorbance at 300 nm from first-order kinetics (Fig. 2). In the CD-accelerated cleavage of **1** and **2**, however, no deviation from first-order kinetics was observed in spite of the formation of tetrahedral intermediates, since spectroscopy directly followed the cleavage of **1** and **2** by release of *p*-nitrothiophenol and *p*-nitrophenol.

Now it is evident that formation of a tetrahedral intermediate is a common feature among serine protease-catalyzed[11,16] and CD-accelerated hydrolyses of esters (as well as alkaline hydrolyses of esters[17]).

The large difference of the effect of CD on the cleavage of **3** (acceleration by both α-CD and β-CD) from the effect on the cleavage of **4** (retardation by β-CD and no effect by α-CD) is mainly attributable to the difference of pK_a's of the leaving groups. Ethanethiol and ethanol have pK_a's of 10.5[9] and 16.0.[18] As the secondary hydroxyl group of CD has a pK_a around 12,[4,6] the formation of tetrahedral intermediate is rate-determining in the CD-accelerated cleavage of **3**, which can be facilitated by complexation. In the cleavage of **4**, however, reaction involving a tetrahedral intermediate produced by nucleophilic attack of CD is unlikely, since its breakdown to product is energetically unfavorable. Thus, the cleavage of **4** in the presence of CD proceeds largely *via* an alkaline reaction. Here, CD shows retardation because of steric hindrance (protection of the substrate by the wall of the CD) and electrostatic repulsion between two anions (the secondary hydroxide anion of CD and OH^-); with α-CD this effect is very small.

The above argument is consistent with the results of the aminolysis of **3** and **4**, showing no reaction of *n*-butylamine (pK_a 10.6[19]) with **4** as opposed to its considerable reaction with **3**.[7]

Non-productive binding can be partly responsible for the different effect of CD on **3** and **4**. Two structures of inclusion complexes are possible, *i.e.* structure A in which the *p*-nitrophenyl portion of **3** (or **4**) is included in the cavity of CD and the ethanol (or ethanethiol) portion protrudes from the secondary hydroxyl side of the cavity, and structure B in which the ethanol (or ethanethiol) portion is located inside the cavity and the rest is located outside. Of these two structures, only structure B is productive, whereas structure A is non-productive since cleavage the carbonyl carbon atom between and the ether oxygen (or sulfur) atom bond through nucleophilic attack by CD is sterically impossible as shown by CPK molecular models.

Since the sulfur atom is larger in size than the oxygen atom and is more apolar, thioester **3** assumes a structure (where the ethylthio portion is included in the apolar cavity of CD) more favorably than the oxygen ester **4** does (structure B). In other words, the proportion of structure B in the CD-**3** complex is larger than that in the CD-**4** complex. Since structure A is nonproductive and structure B is productive, as described above, the CD-**3** complex is more reactive than the CD-**4** complex.

In conclusion, it was found that CD accelerates the cleavage of *S*-phenyl thioester (**1**), *S*-alkyl thioester (**3**), and phenyl ester (**2**). However, the cleavage of the alkyl ester (**4**) was retarded by β-CD but was not affected by α-CD. The CD-accelerated cleavage of **1**—**3** proceeds *via* tetrahedral intermediates, which is consistent with serine protease-catalyzed reactions. Thus, the similarity between CD reactions and enzymatic reactions conforms to not only the overall pathway, as proposed before, but also the more detailed mechanism. The present finding shows that CD is an excellent model of serine proteases.

This work was supported by grants from National Science Foundation and the Hoffmann-LaRoche Co.

References

1) M. L. Bender and M. Komiyama, "Cyclodextrin

Chemistry," Springer-Verlag, Berlin (1978), and references therein.

2) M. L. Bender and M. Komiyama, "Bioorganic Chemistry Vol. 1," ed by E. E. Van Tamelen, Academic Press, New York (1977), Chap. 2.

3) R. L. Van Etten, J. F. Sebastian, G. A. Clowes, and M. L. Bender, *J. Am. Chem. Soc.*, **89**, 3242 (1967).

4) R. L. Van Etten, G. A. Clowes, J. F. Sebastian, and M. L. Bender, *J. Am. Chem. Soc.*, **89**, 3253 (1967).

5) J. L. Lach and T. F. Chin, *J. Pharm. Sci.*, **53**, 924 (1964).

6) T.-F. Chin, P.-H. Chung, and J. L. Lach, *J. Pharm. Sci.*, **57**, 44 (1968).

7) K. A. Connors and M. L. Bender, *J. Am. Chem. Soc.*, **26**, 2498 (1961).

8) R. B. Martin and R. I. Hedrick, *J. Org. Chem.*, **84**, 106 (1962).

9) J. P. Danehy and C. J. Noel, *J. Am. Chem. Soc.*, **82**, 2511 (1960).

10) M. Dessolin, M. Laloli-Diard, and M. Vilkas, *Bull. Soc. Chim. Fr.*, **1970**, 2573.

11) A. Frankfater and F. J. Kezdy, *J. Am. Chem. Soc.*, **93**, 4039 (1971).

12) H. L. Hansen and L. S. Fosdick, *J. Am. Chem. Soc.*, **55**, 2872 (1933).

13) Here ε_5 was taken as equal to the value of **4**, since the absorption spectrum of benzoyl-α-CD was practically superimposible on that of ethyl benzoate as shown in Ref. 4.

14) Similar treatment of data at 320 nm gave k_1 of 1.4×10^{-3} s^{-1}, which is identical with the result obtained at 300 nm within experimental error.

15) "Handbook of Chemistry and Physics, 49th ed" ed by R. C. Weast, Chemical Rubber Co., Cleveland, OH (1968—1969).

16) H. Hirohara, M. L. Bender, and R. S. Stark, *Proc. Natl. Acad. Sci. USA*, **71**, 1643 (1974).

17) M. L. Bender, *Chem. Rev.*, **60**, 53 (1960).

18) P. Ballinger and F. A. Long, *J. Am. Chem. Soc.*, **82**, 795 (1960).

19) A. G. Evans and S. D. Hamann, *Trans. Faraday Soc.*, **47**, 34 (1951).

Spectrophotometric Study on the Complex Formation of Hydroperoxide with Tetraphenylporphyrin Cobalt(II)

Teruaki YAMADA and Yoshio KAMIYA*

Department of Reaction Chemistry, Faculty of Engineering, The University of Tokyo, Hongo, Bunkyo-ku, Tokyo 113

(Received January 27, 1979)

The rate constants, activation energies, activation entropies and equilibrium constants for the coordination of 1,2,3,4-tetrahydro-1-naphthyl hydroperoxide (THP), 1-methyl-1-phenylethyl hydroperoxide (CHP) and *t*-butyl hydroperoxide (BHP) to para-substituted tetraphenylporphyrin Co(II), Co(*p*-X)TPP (X=OCH_3, H, Cl) were obtained by the visible spectral method at 235—245 K. The rate constants of coordination were k=0.097—2.03×10^2 M^{-1} s^{-1}, the equilibrium constants being K=0.692—2.5×10^{-6} M^{-1}. As a *para*-substituent effect on k and K, the constants were found to increase with increase in the electron donating property of the substituent group. They also depend on the kind of hydroperoxide, the rate constants decreasing in the order $k_{THP}>k_{CHP}>k_{BHP}$, and the equilibrium constants in the order $K_{CHP}>K_{BHP}>K_{THP}$. Activation energies were 7.0—7.8 kcal mol^{-1} and activation entropies −21——25 cal K^{-1}. No spectral change by the addition of hydroperoxide to CuTPP and NiTPP was observed.

The decomposition reaction of hydroperoxide catalyzed by transition-metal ion proceeds by the redox reaction[1] of transition-metal ion which has two valences. The reaction seems to consist of three steps, (a) coordination of hydroperoxide molecule to a metal ion, (b) migration of electron from metal ion to hydroperoxide followed by the cleavage of O–O bond of hydroperoxide, and (c) release of the fragmentation products from a metal ion.

Formation of the hydroperoxide–metal ion complex has been anticipated in many kinetic studies[2-8] since George[9] *et al.* proposed its formation. Richardson[10] reported evidence of the formation for the first time using NMR and visible spectral methods. Some qualitative studies using spectral method had been reported until 1971 when Bulgakova *et al.*[11] Svitych *et al.*[12,13] worked out quantitative studies.[11-13] They reported equilibrium constants and enthalpy of formation of hydroperoxide–metal ion complex using NMR method at low temperature.

In this report, tetraphenylporphyrin metal(II) complex was chosen because of its intense absorbance at the Soret band 410—420 nm, being sensitive to the change of coordination number. The coordination reaction was followed by the decrease of the Soret band using the visible spectra method at 235—245 K. The kinetic and thermodynamic data were calculated from experimental data and the results discussed in terms of the effects of *para*-substituent group, hydroperoxide, and central metal ion.

Experimental

Materials. The *para*-substituted tetraphenylporphyrin free bases H_2(*p*-X)TPP (X=OCH_3, H, Cl),[14] Co(*p*-X)TPP and CuTPP,[15] and NiTPP[16] were prepared according to reported methods. The products were chromatographed on silica gel four or five times using chloroform in each step. The visible spectra of Co(*p*-X)TPP, CuTPP, and NiTPP were very similar to those reported. 1,2,3,4-Tetrahydro-1-naphthyl hydroperoxide (THP) was prepared by the autoxidation of tetralin and crystallized from heptane.[17] Reagent grade 1-methyl-1-phenylethyl hydroperoxide (CHP) and *t*-butyl hydroperoxide (BHP) (Nippon Oils and Fats Co.) were purified and spectral grade dichloromethane was dried before use.

Measurements. Spectrophotometric measurements were carried out on a JASCO-UVIDEC-1 spectrophotometer equipped with a cryostat (type DN-704, Oxford Instrument Co.) in which a quartz cell was set at prescribed temperature within ±0.05 °C with a controller. Both the solution of M(II)TPP (2 ml) in cell and that of hydroperoxide (0.5 ml) in an injector set above the solution of M(II)TPP were cooled to the reaction temperature. Reaction was started when the solution of hydroperoxide was poured into the cell, and followed by measuring the decrease in the Soret band of M(II)TPP. The solution in the cell was stirred throughout the reaction with a magnetic stirrer set under the cryostat.

Results and Discussion

Spectral Chenges. A typical spectral change of Co(*p*-H)TPP with the addition of 1,2,3,4-tetrahydro-1-naphthyl hydroperoxide is shown in Fig. 1. There are three patterns in spectral changes according to the

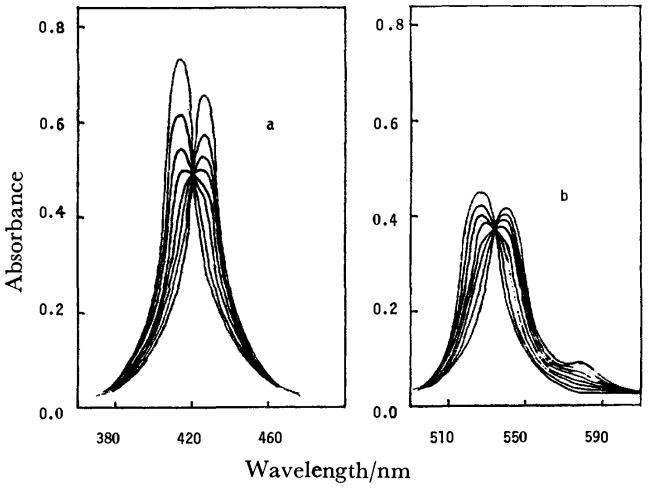

Fig. 1. Visible spectral change observed upon addition of THP to a solution of Co(*p*-H)TPP.
a) [Co(*p*-H)TPP]=2.1×10^{-6} M, [THP]=2.1×10^{-6} M, b) [Co(*p*-H)TPP]=5.0×10^{-5} M, [THP]=5.0×10^{-5} M in CH_2Cl_2 at 235 K.

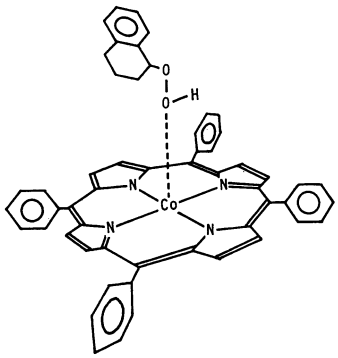

Fig. 2. Supposed structure of hydroperoxide–Co(*p*-H)-TPP complex.[24]

reaction temperatures. At 235 K, the Soret band (414 nm) of Co(*p*-H)TPP decreased with the addition of hydroperoxide, a new absorption band (427 nm) appearing. The isosbestic point at 417 nm is sharp, the decomposition reaction of hydroperoxide being negligible at this temperature. It can be assumed that the new absorption band (427 nm) results from the hydroperoxide–Co(*p*-H)TPP complex (Fig. 2). Similar spectral changes take place when pyridine or *t*-butyl alcohol is added to Co(*p*-H)TPP in line with the published data.[16,18] Absorption of the Q band (527 nm) also decreased, a new band (540 nm) appearing (Fig. 1). This spectrum is similar to that of Co(III)TPP.[21]

Rise in temperature from 250 K to 265 K gave rise to a new spectral change. A new absorption band (427 nm) decreased, accompanied by the temporary appearance of 414 nm band, giving a new absorption band (432 nm). Further rise in temperature from 265 K to 295 K made the absorption decrease and disappear.

Kinetic and Thermodynamic Data. Figure 3 shows the decay curve of the Soret band (414 nm) of

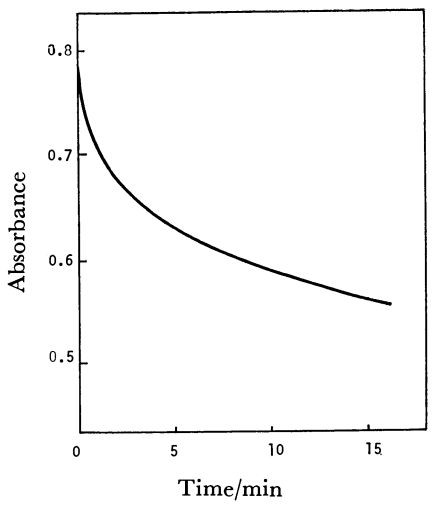

Fig. 3. Absorption decay curve of Co(*p*-H)TPP at 414 nm.
[Co(*p*-H)TPP]=2.1×10^{-6} M, [THP]=2.1×10^{-6} M, in CH_2Cl_2 at 235 K.

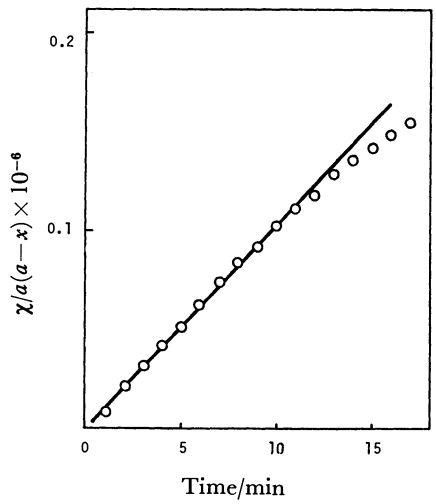

Fig. 4. Second-order plot for formation of Co(*p*-H)TPP–THP complex.
a=[Co(*p*-H)TPP]=2.1×10^{-6} M, [THP]=2.1×10^{-6} M in CH_2Cl_2 at 235 K.

Co(*p*-H)TPP caused by the addition of 1,2,3,4-tetrahydro-1-naphthyl hydroperoxide. The rate of decrease became slow, reaching an equilibrium state within 30 min after the reaction started. In the case of 1-methyl-1-phenylethyl hydroperoxide or *t*-butyl hydroperoxide, the initial rate was lower than that of 1,2,3,4-tetrahydro-1-naphthyl hydroperoxide, taking a long time to reach an equilibrium state. The results are plotted as a second-order reaction, the initial rate constant being calculated (Fig. 4). Activation energies were evaluated (Fig. 5) from the temperature dependance of the initial rate constant in the temperature range 235—245 K.

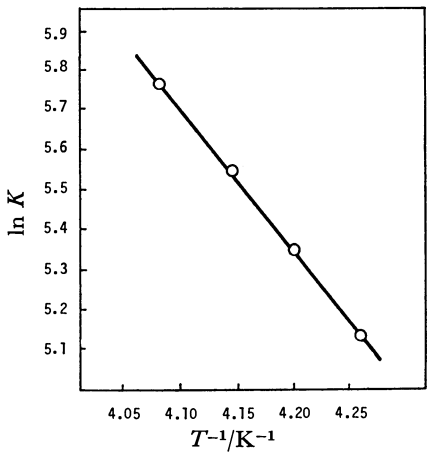

Fig. 5. Temperature dependence of rate constant for formation of Co(*p*-H)TPP–THP complex.
[Co(*p*-H)TPP]=2.1×10^{-6} M, [THP]=2.1×10^{-6} M.

The kinetic and thermodynamic data of the coordination of hydroperoxide to M(II)TPP are given in Table 1. The rate constants and equilibrium constants increased with the increase in electron donating property of substituent group of Co(*p*-X)TPP in all hydroperoxides.

Table 1. Rate constants, activation energies, activation entropies, and equilibrium constants for coordination of hydroperoxide to M(II)TPP

M(II)TPP	ROOH	k/M^{-1} s^{-1}	ΔE/kcal mol^{-1}	ΔS/cal K^{-1}	K/M^{-1}
Co(*p*-Cl)TPP	THP	1.32×10^{2}	7.2	−22	6.92×10^{5}
Co(*p*-H)TPP	THP	1.67×10^{2}	7.1	−22	8.31×10^{5}
Co(*p*-OCH_3)TPP	THP	2.03×10^{2}	7.3	−21	1.12×10^{6}
CuTPP	THP	0.00			
NiTPP	THP	0.00			
Co(*p*-Cl)TPP	CHP	2.53×10	7.5	−24	1.62×10^{6}
Co(*p*-H)TPP	CHP	3.20×10	7.3	−24	2.09×10^{6}
Co(*p*-OCH_3)TPP	CHP	4.05×10	7.0	−25	2.51×10^{6}
CuTPP	CHP	0.00			
NiTPP	CHP	0.00			
Co(*p*-Cl)TPP	BHP	0.97×10	7.8	−24	1.12×10^{6}
Co(*p*-H)TPP	BHP	1.27×10	7.5	−25	1.38×10^{6}
Co(*p*-OCH_3)TPP	BHP	1.56×10	7.6	−24	1.74×10^{6}
CuTPP	BHP	0.00			
NiTPP	BHP	0.00			

[M(II)TPP]$=2.1\times10^{-6}$ M, [ROOH]$=2.1\times10^{-6}$ M, 235 K, in CH_2Cl_2. THP=1,2,3,4-Tetrahydro-1-naphthyl hydroperoxide, CHP=1-methyl-1-phenylethyl hydroperoxide, BHP=*t*-butyl hydroperoxide.

Table 2. Comparison of oxidation potentials with rate constants and equilibrium constants for M(II)TPP

M(II)TPP	M(II)→M(III)/V	k[c]/M^{-1} s^{-1}	K[c]/M^{-1}
Co(*p*-Cl)TPP	0.75[a]	1.32×10^{2}	6.92×10^{5}
Co(*p*-H)TPP	0.58[a]	1.67×10^{2}	8.31×10^{5}
Co(*p*-OCH_3)TPP	0.62[a]	2.03×10^{2}	1.12×10^{6}
CuTPP	—[b]	0.00	
NiTPP	1.00[b]	0.00	

a) Ref. 19. b) Ref. 21. c) [M(II)TPP]: [THP]=1: 1, 235 K.

Fairly good correlations are observed between the oxidation potentials[19] and the rate constants or the equilibrium constants of Co(*p*-H)TPP (Table 2). The oxidation potential of metal ion seems to be an important factor affecting the two constants. This substituent effect is similar to that found in Co(*p*-H)TPP·py+O_2⇄Co(*p*-H)TPP·py(O_2) system studied in detail by Walker *et al.*[20] In the case of NiTPP, its too large oxidation potential[21] would prevent the coordination of hydroperoxide molecules. CuTPP showed no spectral change because of difficulty for it to take the five-coordination structure as judged from its stability constant. No activity in the decomposition of hydroperoxide on NiTPP and CuTPP can be attributed to the difficulty in coordination.

The rate constants and equilibrium constants change with the kind of hydroperoxide (Table 1). The order of rate constant k is $k_{THP}>k_{CHP}>k_{BHP}$, and the order of equilibrium constant K is $K_{CHP}>K_{BHP}>K_{THP}$ in hydroperoxide–Co(*p*-X)TPP (X=OCH_3, H, Cl) systems. A comparison of the half-wave potential[22] of hydroperoxide with the rate constant or equilibrium constant is given in Table 3. Except for the case of 1,2,3,4-tetrahydro-1-naphthyl hydroperoxide having a larger k and a smaller K than those expected from its half-wave potential, the orders $k_{CHP}>k_{BHP}$ and $K_{CHP}>K_{BHP}$ can be explained by the order of half-wave potential of hydroperoxide, $E_{1/2}$(CHP)$>E_{1/2}$(BHP). The higher half-wave potential which indicates the energy level of LUMO (Lowest Unoccupied Molecular Orbital) of O–O bond in hydroperoxide[23] would give a larger rate constant or larger equilibrium constant. The steric factor is attributable to the deviation in the case of 1,2,3,4-tetrahydro-1-naphthyl hydroperoxide. A configuration of 1,2,3,4-tetrahydro-1-naphthyl hydroperoxide more favorable to Co(II) ion than that of other two hydroperoxides might bring forth a larger constant k. This is in line with the smallest activation entropy of this system. The activation energies for coordination reaction of hydroperoxide to Co(*p*-X)TPP are 7.0—7.8 kcal mol^{-1}, which is reasonable in view of the activation energy 15—25 kcal mol^{-1} of the decomposition reaction of hydroperoxide. The activation entropies are −21——25 cal K^{-1}, in line with the formation reaction hydroperoxide–Co(*p*-X)TPP complex.

Table 3. Comparison of half-wave potentials with rate constants and equilibrium constants for ROOH

ROOH	$E^{a)}_{1/2}$/V	k[b]/M^{-1} s^{-1}	K[b]/M^{-1}
BHP	−0.96	1.27×10	1.38×10^{6}
THP	−0.73	1.67×10^{2}	8.31×10^{5}
CHP	−0.68	3.20×10	2.09×10^{6}

a) Ref. 22. b) [Co(*p*-H)TPP]: [ROOH]=1: 1, 235 K.

It is difficult to obtain the rate constant and the activation energy in the decomposition reaction of 1,2,3,4-tetrahydro-1-naphthyl hydroperoxide by Co(*p*-X)TPP at a temperature above 10 °C since the reaction proceeds too fast and the catalytic activity decreases within 30 s, the colored solution of Co(*p*-X)-TPP preventing accurate iodometry.

The authors thank Mr. H. Ogata for the synthesis of CoTPP complexes.

References

1) F. Haber and J. Wiess, *Proc. R. Soc. London, Ser. A*, **147**, 332 (1934).
2) J. Orr and H. L. Williams, *Can. J. Chem.*, **30**, 985 (1952).
3) A. J. Chalk and J. F. Smith, *Trans. Faraday Soc.*, **53**, 1214 (1957).
4) M. H. Dean and G. Skirrow, *Trans. Faraday Soc.*, **54**, 849 (1958).
5) Y. Kamiya, S. Beaton, A. Lafortune, and K. U. Ingold, *Can. J. Chem.*, **41**, 2034 (1963).
6) W. H. Richardson, *J. Am. Chem. Soc.*, **87**, 1096 (1965).
7) I. P. Skibida, M. S. Brodskii, M. Ya. Gervits, L. A. Goldina, and Z. K. Maizus, *Kinet. Katal.*, **14**, 885 (1973).
8) G. M. Bulgakova, I. P. Skibida, and Z. K. Maizus, *Kinet. Katal.*, **12**, 76 (1971).
9) P. George, E. K. Rideal, and A. Robertson, *Proc. R. Soc. London, Ser. A*, **185**, 288 (1946).
10) W. H. Richardson, *J. Am. Chem. Soc.*, **88**, 975 (1966).
11) G. M. Bulgakova, A. N. Shupik, I. P. Skibida, K. I. Zamaraev, and Z. K. Maizus, *Dokl. Akad. Nauk SSSR*, **119**, 376 (1971).
12) R. B. Svitych, A. L. Buchachenko, O. P. Yablonski, A. A. Petukhov, V. A. Belyaev, and A. K. Kobyakov, *Kinet. Katal.*, **15**, 1300 (1974).
13) R. B. Svitych, A. L. Buchachenko, O. P. Yablonski, N. N. Rzhevskaya, V. A. Belyaev, and A. A. Petukhov, *Kinet. Katal.*, **17**, 73 (1976).
14) A. D. Adler, F. R. Longo, J. D. Finarelli, J. Goldmacher, J. Assour, and L. Korsakoff, *J. Org. Chem.*, **32**, 476 (1967).
15) A. D. Adler, F. R. Longo, F. Kampas, and J. Kim, *J. Inog. Nucl. Chem.*, **32**, 2443 (1970).
16) F. A. Walker, E. Hui, and J. M. Walker, *J. Am. Chem. Soc.*, **97**, 2390 (1975).
17) N. Rabjohn, *Org. Synth.*, Coll. Vol. IV, 895 (1963).
18) F. A. Walker, Man-Wai Lo, and M. T. Ree, *J. Am. Chem. Soc.*, **98**, 5552 (1976).
19) M. Tezuka, Y. Ohkatsu, and T. Osa, *Bull. Chem. Soc. Jpn.*, **49**, 1435 (1976).
20) F. A. Walker, D. Beroiz, and K. M. Kadish, *J. Am. Chem. Soc.*, **98**, 3484 (1976).
21) A. Wolberg and J. Manassen, *J. Am. Chem. Soc.*, **92**, 2982 (1970).
22) C. O. Willits, C. Ricciuti, H. B. Knight, and D. Swern, *Anal. Chem.*, **24**, 785 (1952).
23) T. Yonezawa, H. Kato, and K. Fukui, *Nippon Kagaku Zasshi*, **87**, 24 (1966).
24) K. Ohkubo and H. Kanaeda, *Bull. Chem. Soc. Jpn.*, **45**, 2646 (1972).

 © 1980 The Chemical Society of Japan Bull. Chem. Soc. Jpn., 53, 1081—1084 (1980)

Photochemical Transformations of 1,2-Diketones and Benzhydrylamine

Kailash Nath MEHROTRA and Ganesh Prasad PANDEY

Department of Chemistry, Banaras Hindu University, Varanasi 221005, India

(Received April 28, 1979)

Photolysis of a mixture of substituted 1,2-diketones and benzhydrylamine (in 1:2 mole ratio) in benzene gave *N*-benzhydrylidenebenzhydrylamine, *N*-(diarylmethyl)benzamides, acyloins (**3**), *N*-(arylmethylene)benzhydrylamines, and benzophenone separated by fractional crystallization and column chromatography. The products have been characterised by analytical and spectral (IR, UV, and NMR) data and the structural assignments confirmed by the comparison (IR spectra and undepressed mixed mp) with authentic samples. Acyloins (**3**) are precursors for *N*-(diarylmethyl)benzamides and *N*-(arylmethylene)benzhydrylamines. A tentative mechanistic route for the formation of products has been suggested.

Irradiation of aromatic ketones and aliphatic amines (primary as well as secondary) in nonpolar media leads to a high yield of pinacols and substituted imines initiated by hydrogen abstraction from amine by the triplet-excited state of the ketone.[1] It has been observed that the presence of a hydrogen atom to the heteroatom in amine enhances its reactivity towards photoreduction of ketones.[2] Hydrogen abstraction by an excited state of benzil from 2-propanol and subsequent α-cleavage has been known to form benzoin, 2,3-dihydroxy-1,2,3,4-tetraphenyl-1,4-butanedione, small amount of benzoic acid, benzaldehyde, α-benzoylbenzylbenzoate, and 1,2-dibenzoyl-1,2-diphenylethylene dibenzoate.[3] Irradiation of benzil in butylamine has been reported to give *N*-butylbenzamide, deoxybenzoin, *dl* and *meso* forms of 1,2-dibenzyl-1,2-diphenyl-1,2-ethanediol and *N*-butylidine-2-butylamine.[4] In the present paper we describe the isolation of *N*-benzhydrylidenebenzhydrylamine, *N*-(diarylmethyl)benzamides, acyloins (**3**), *N*-(arylmethylene)benzhydrylamines, and benzophenone from the irradiation of 1,2-diketones and benzhydrylamine in benzene with UV light. The formation of *N*-(diarylmethyl)benzamides and *N*-(arylmethylene)-benzhydrylamines has been shown to occur through acyloins.

Results and Discussion

Irradiation of benzil (**1a**) and benzhydrylamine (**2**), in 1:2 mole ratio, in thiophene free benzene under nitrogen atmosphere by UV light for 32 h gave *N*-benzhydrylidenebenzhydrylamine, *N*-benzhydrylbenzamide, benzoin, *N*-benzylidenebenzhydrylamine, and benzophenone. These products were separated by fractional crystallization and column chromatography. The irradiated solution gave a positive Nessler's spot test for the presence of ammonia.[5] Similar results were obtained on irradiation (21—48 h) of a mixture of other diketones (**1b—d**) and benzhydrylamine. In each case the time of irradiation for complete disappearance of diketone (TLC) has been found to depend on the nature of substituents on the phenyl rings of the diketone (Table 1). It has been observed that the irradiation time increased and total yields of the products decreased as the diketone (**1**) was changed from **a** to **b** to **c**. The excited state reactivity of the diketones has been known to decrease with the presence of electron-donating groups on the *para* position of the phenyl rings of benzil,[6] the order of reactivity, H>CH_3>OCH_3, is in agreement with the observed behaviour of the diketones **1a—c** (Table 1). The reaction can be shown as

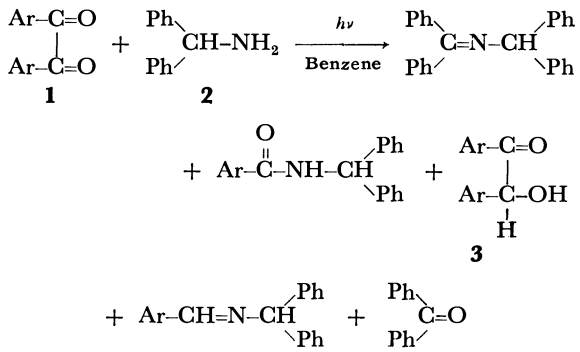

These products were not formed when a mixture of benzil and benzhydrylamine in benzene was heated to reflux for 24 h confirming the photochemical nature of the above reaction.

Irradiation of a mixture of benzoin and benzhydryl-

TABLE 1. PRODUCTS DISTRIBUTION OBTAINED ON IRRADIATION OF 1,2-DIKETONES AND BENZHYDRYLAMINE (in 1:2 mole ratio)

1,2-Diketones	Ar	Time of Irradiation / h	Ph(Ph)C=N-CH(Ph)Ph yield/%	Ar-C(=O)-NH-CH(Ph)Ph yield/%	Ph(Ph)C=O yield/%	Ar-CH=N-CH(Ph)Ph yield/%	Ar-CH(OH)-C(=O)-Ar yield/%
1a	C_6H_5	32	34	28	7	9	5
1b	C_6H_4·CH_3-*p*	36	30	19	10	9	4
1c	C_6H_4·OCH_3-*p*	48	21	15	8	11	6
1d		21	16	8	—	6	a)

a) Could not be isolated but its presence was detected by TLC.

amine (in 1 : 2 mole ratio) in benzene for 21 h in a similar manner as described above gave *N*-benzhydrylbenzamide and *N*-benzylidenebenzhydrylamine. This observation supports the view that acyloins (**3**) could be intermediates in the formation of *N*-(diarylmethyl)-benzamides and *N*-(arylmethylene)benzhydrylamines from the irradiation of diketones **1a—d**.

The photoreaction is initiated by an abstraction of a hydrogen α to the amino group in benzhydrylamine by an excited triplet state of the diketone leading to the α-aroyl-α-hydroxybenzyl radical (**a**) and α-aminobenzhydryl radical (**b**). This step is similar to the one given in the photoreduction of benzil in 2-propanol[3] and also in the photoreduction of benzophenone in primary amines[1,2] in which the initial step involves a hydrogen atom abstraction.

$$Ph_2C{=}O^{*3} + RR'CHNH_2 \longrightarrow Ph_2\dot{C}OH + RR\dot{C}NH_2$$

In deuterated amines, where electron release is more efficient, an electron transfer has been suggested to occur in the initial step.[2]

$$Ph_2C{=}O^{*3} + R_2CHND_2 \longrightarrow [Ph_2\dot{C}{-}O^- \quad R_2\overset{+}{C}H\dot{N}D_2]$$

Such electron transfer initiation has also been known to occur in photoreduction of aromatic ketones in tertiary amines.[7] Hydrogen abstraction by one of the carbonyl groups in 1,2-diketones[6] has been known to occur through an excited triplet state *via* a $^3(n\rightarrow\pi^*)$ excitation.[8] It has been observed that the presence of a hydrogen atom α to the amino group increases the hydrogen donating capability of amines in the photoreduction of ketones.[2] Rearrangement of **b** to **c** and subsequent hydrogen transfer to **a** may lead to the formation of acyloin (**3**) and diphenylmethanimine (**4**). The reaction between **4** and benzhydrylamine (**2**) may give rise to *N*-benzhydrylidenebenzhydrylamine and ammonia in a manner already reported.[9] The formation of *N*-benzhydrylidenebenzhydrylamine in each case, irrespective of the nature of the aryl group present in 1,2-diketones, strongly suggests that it must be arising from benzhydrylamine only which is in agreement with the step given in Scheme. The proposed Scheme also explains the requirement of two moles of benzhydrylamine per mole of the diketone in the reaction.

A photolytic carbon-carbon bond cleavage in acyloin (**3**) may give rise to radicals **d** and **e** in an analogous manner as proposed in the case of irradiation of benzoin ethers.[10] Recombination of the radicals **c** and **e** may form *N*-(diarylmethyl)benzamides and loss of hydrogen from radical **d** may lead to aldehydes which on reaction with benzhydrylamine form *N*-(arylmethylene)benzhydrylamines. Irradiation of benzoin with UV light has been known to give benzaldehyde.[11] Hydrolysis of diphenylmethanimine (**4**) may result in the formation of benzophenone and ammonia.

On the basis of the above observations a tentative mechanistic route can be shown as follows:

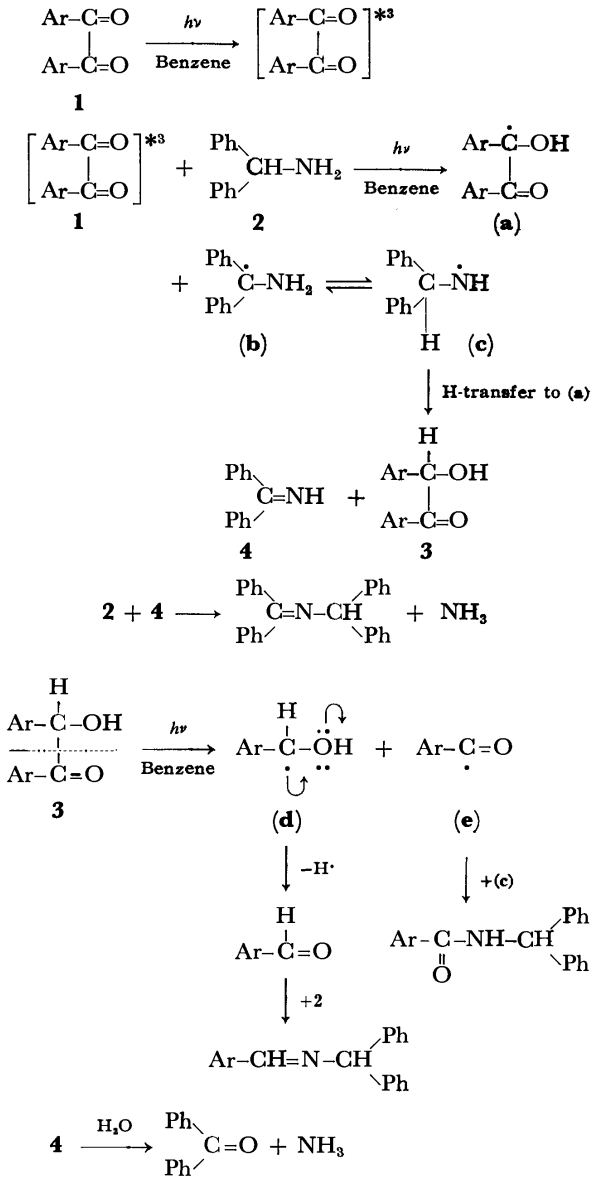

Experimental

General. Melting points have been determined in capillaries on Buchi melting point apparatus and are uncorrected. The IR spectra were measured in Nujol mull on a Perkin-Elmer 720 spectrophotometer and the UV in ethanol on a Cary-14 spectrophotometer. The NMR spectra were recorded on a Varian A-60 Hz spectrometer in $CDCl_3$ with TMS as the internal standard.

Materials. The 1,2-diketones were obtained from Ega Chemie, Germany and benzhydrylamine was prepared according to the reported method.[12]

General Irradiation Procedure. A solution containing 1,2-diketones (0.005 mol) and benzhydrylamine (0.010 mol) in 350 ml of benzene (thiophene free) was irradiated with UV light from a 200 W Hanovia lamp. Pre-purified nitrogen was bubbled into the solution prior to irradiation and a slow stream was continued during the course of photolysis. The progress of reaction was monitored by TLC. The irradiated solutions gave a positive Nessler's test for ammonia.[5] Irradiation was discontinued when the starting diketone had appreciably diminished. The solvent was evaporated under reduced pressure. The products were separated by fractional crystallization and column chromatography and were characterised on the basis of analytical and spectral (IR, UV, and NMR) data. The structural assignments were further confirmed by the comparison (IR spectrum and mixed mp) with authentic samples.

*Irradiation of Benzil (**1a**) and Benzhydrylamine.* Irradiation of a mixture of benzil and benzhydrylamine in benzene for 32 h and evaporation of the solvent gave a thick pasty mass which on treatment with ethanol afforded a white crystalline solid (34%), identified as *N*-benzhydrylidene benzhydrylamine, mp and mixed mp 149—151 °C (lit,[13] mp 152 °C); UV (EtOH, nm): 252; IR (Nujol, cm^{-1}): 1620 ($\nu_{C=N}$); NMR ($CDCl_3$, δ ppm): 5.60 (s, 1H, $CHPh_2$), 7.35 (m, 16H, arom.), and 7.90 (m, 4H, arom.). Found: C, 90.01; H, 6.20; N, 3.89%. Calcd for $C_{26}H_{21}N$: C, 89.91; H, 6.05; N, 4.03%.

Fractional crystallization of the mother liquor from benzene–hexane (1: 1) gave 28% of white needle shaped crystals which were shown to be *N*-benzhydrylbenzamide, mp and mixed mp 169—172 °C (lit,[14] mp 172—174 °C). UV (EtOH): end absorption; IR (Nujol, cm^{-1}): 3300 (ν_{NH}), 1640 ($\nu_{C=O}$); NMR ($CDCl_3$, δ ppm): 1.65 (bs, 1H, NH, exchangeable on deuteration), 6.39 and 6.53 (d, 1H, J=8.4 Hz, $CHPh_2$, doublet due to spin-spin coupling with NH[15]), 7.41 (m, 13H, arom.), and 7.75 (m, 2H, arom.). Found: C, 83.24; H, 5.51; N, 5.07%. Calcd for $C_{20}H_{17}NO$: C, 83.62; H, 5.92; N, 4.87%. The IR spectrum was superimposable with that of an authentic sample.[16]

The mother liquor was concentrated and subjected to column chromatography over neutral alumina (60 g, 2.5×45 cm) to give the following products by using hexane, hexane–benzene (7: 3), and hexane–benzene (1: 1) as eluants:

(*i*). Benzophenone (7%), identified as 2,4-dinitrophenylhydrazone derivative mp 229 °C.

(*ii*). *N*-Benzylidenebenzhydrylamine (9%), mp and mixed mp 98—99 °C (lit,[17] mp 98—100 °C). UV (EtOH, nm): 252; IR (Nujol, cm^{-1}): 1620 ($\nu_{C=N}$); NMR ($CDCl_3$, δ ppm): 5.58 (s, 1H, $CHPh_2$), 7.40 (m, 13H, arom.), 7.90 (m, 2H, arom.), and 8.34 (s, 1H, formyl). Found: C, 88.58; H, 6.35; N, 4.98%. Calcd for $C_{20}H_{17}N$: C, 88.56; H, 6.27; N, 5.17%.

(*iii*). Benzoin (5%), mp and mixed mp 136—138 °C. The IR spectrum was superimposable with that of an authentic sample.[18]

*Irradiation of 4,4′-Dimethylbenzil (**1b**) and Benzhydrylamine.* Irradiation of a mixture of 4,4′-dimethylbenzil (**1b**) and benzhydrylamine in benzene for 36 h and similar work up as described above gave the following products:

(*i*). *N*-Benzhydrylidenebenzhydrylamine (30%), mp and mixed mp 149—151 °C.

(*ii*). *N*-Benzhydryl-4-methylbenzamide (19%), mp and mixed mp 182—184 °C (lit,[14] mp 183—184 °C). UV (EtOH): end absorption; IR (Nujol, cm^{-1}): 3300 (ν_{NH}), 1640 ($\nu_{C=O}$); NMR ($CDCl_3$, δ ppm): 1.59 (bs, 1H, NH, exchangeable on deuteration), 2.30 (s, 3H, CH_3), 6.45 and 6.31 (d, 1H, J= 8.4 Hz, doublet due to spin-spin coupling with NH[15]), 7.26 (m, 12H, arom.), and 7.68 (m, 2H, arom.). Found: C, 83.78; H, 6.46; N, 4.72%. Calcd for $C_{21}H_{19}NO$: C, 83.85; H, 6.31; N, 4.65%. The IR spectrum was superimposable with that of an authentic sample.[16]

(*iii*). Benzophenone (10%), identified as 2,4-dinitrophenylhydrazone derivative, mp 229 °C.

(*iv*). *N*-(4-Methylbenzylidene)benzhydrylamine (9%), mp and mixed mp 103—105 °C. UV (EtOH, nm): 254; IR (Nujol, cm^{-1}): 1620 ($\nu_{C=N}$); NMR ($CDCl_3$, δ ppm): 2.40 (s, 3H, CH_3), 5.60 (s, 1H, $CHPh_2$), 7.38 (m, 12H, arom.), 7.80 (m, 2H, arom.), and 8.50 (s, 1H, formyl). Found: C, 88.52; H, 6.82; N, 5.01%. Calcd for $C_{21}H_{19}N$: C, 88.42; H, 6.66; N, 4.92%.

(*v*). 4,4′-Dimethylbenzoin (4%), mp and mixed mp 85—86 °C. The IR spectrum was superimposable with that of an authentic sample.[18]

*Irradiation of 4,4′-Dimethoxybenzil (**1c**) and Benzhydrylamine.* Irradiation of a mixture of 4,4′-dimethoxybenzil and benzhydrylamine in benzene for 48 h and separation of the components in a similar manner as described above gave the following products:

(*i*). *N*-Benzhydrylidenebenzhydrylamine (21%), mp and mixed mp 149—151 °C.

(*ii*). *N*-Benzhydryl-4-methoxybenzamide (15%), mp and mixed mp 198—199 °C (lit,[14] mp 198—200 °C). UV (EtOH, nm): 250; IR (Nujol, cm^{-1}): 3300 (ν_{NH}), 1640 ($\nu_{C=O}$); NMR ($CDCl_3$, δ ppm): 1.83 (bs, 1H, NH, exchangeable on deuteration), 3.76 (s, 3H, OCH_3), 6.53 and 6.39 (d, 1H, J= 8.4 Hz, $CHPh_2$, doublet due to spin-spin coupling with NH[15]), 6.83 (A_2B_2, 2H, J=9 Hz, arom.), 7.28 (m, 10H, arom.), and 7.75 (A_2B_2, 2H, J=9 Hz, arom.). Found: C, 79.43; H, 6.18; N, 4.51%. Calcd for $C_{21}H_{17}NO_2$: C, 79.49; H, 5.99; N, 4.41%. The IR spectrum was identical with that of an authentic sample.[16]

(*iii*). Benzophenone (8%), identified as 2,4-dinitrophenylhydrazone derivative mp 229 °C.

(*iv*). *N*-(4-Methoxybenzylidene)benzhydrylamine (11%), mp and mixed mp 108—110 °C (lit,[17] mp 110 °C). UV (EtOH, nm): 272; IR (Nujol, cm^{-1}): 1620 ($\nu_{C=N}$); NMR ($CDCl_3$, δ ppm): 3.70 (s, 3H, OCH_3), 5.43 (s, 1H, $CHPh_2$), 6.80 (A_2B_2, 2H, J=9 Hz, arom.), 7.23 (m, 10H, arom.), 7.70 (A_2B_2, 2H, J=9 Hz, arom.), and 8.27 (s, 1H, formyl). Found: C, 84.01; H, 6.52; N, 4.58%. Calcd for $C_{21}H_{19}NO$: C, 83.85; H, 6.30; N, 4.64%.

(*v*). 4,4′-Dimethoxybenzoin (6%), mp and mixed mp 115—117 °C. The IR spectrum was superimposable with that of an authentic sample.[18]

*Irradiation of 2,2′-Furil (**1d**) and Benzhydrylamine.* Irradiation of a solution containing 2,2′-furil and benzhydrylamine in benzene for 21 h and separation on a column packed with alumina gave the following products:

(*i*). *N*-Benzhydrylidenebenzhydrylamine (16%), mp and mixed mp 149—151 °C.

(*ii*). *N*-Benzhydryl-2-furamide (8%), mp and mixed mp 161—162 °C. UV (EtOH): end absorption; IR (Nujol, cm^{-1}): 3290 (ν_{NH}), 1650 ($\nu_{C=O}$); NMR ($CDCl_3$, δ ppm): 1.82 (bs, 1H, NH, exchangeable), 6.30 and 6.16 (d, 1H, J=8.4 Hz, $CHPh_2$[15]), and 6.25 (m, 13H, aromatic and 2-furoic). Found: C, 78.38; H, 5.32; N, 5.20%. Calcd for $C_{18}H_{15}NO_2$: C, 77.97; H, 5.41; N, 5.05%. The IR spectrum was superimposable with that of an authentic sample.[16]

(*iii*). *N*-(2-Furfurylidene)benzhydrylamine (6%), mp and mixed mp 104—106 °C. UV (EtOH, nm): 272; IR (Nujol, cm^{-1}): 1640 ($\nu_{C=O}$); NMR ($CDCl_3$, δ ppm): 5.58 (s, 1H, $CHPh_2$), 6.43 (m, 1H, furan CH_a), 6.46 (d, 1H, J=3 Hz, furan CH_b), 7.33 (m, 11H, 10 arom+1 furan CH_c), and 8.20 (s, 1H, formyl). Found: C, 83.03; H, 5.37; N, 5.45%. Calcd for $C_{18}H_{15}NO$: C, 82.75; H, 5.74; N, 5.36%. The IR spectrum was superimposable with that of an authentic sample prepared by following the method of Michaelis.[17]

In this case 2,2′-furoin could not be isolated although its presence was detected on TLC.

Irradiation of Benzoin and Benzhydrylamine. Irradiation of a mixture of benzoin and benzhydrylamine in a similar manner as described earlier gave *N*-benzhydrylbenzamide (28%) and *N*-benzylidenebenzhydrylamine (21%) identified on the basis of comparison (IR spectra and undepressed mixed mp) with authentic samples.

We are greatful to the University Grants Commission, New Delhi for financial support and to Professor O. P. Malhotra for encouragement and facilities.

References

1) S. G. Cohen and R. J. Baumgarten, *J. Am. Chem. Soc.*, **89**, 3471 (1967).
2) S. G. Cohen and H. M. Chao, *J. Am. Chem. Soc.*, **90**, 165 (1968).
3) D. L. Bunbury and T. T. Chuang, *Can. J. Chem.*, **47**, 2045 (1969).
4) G. E. Gream, J. C. Paice, and B. S. J. Uszynski, *Chem. Commun.*, **1970**, 895.
5) F. Feigel "Spot Tests," Elsevier Publishing Co., Amsterdam, (1954), Vol. I, p. 223.
6) Y. Ogata, K. Takagi, and Y. Fugi, *J. Org. Chem.*, **37**, 4026 (1972).
7) S. G. Cohen, N. Stein, and H. M. Chao, *J. Am. Chem. Soc.*, **90**, 521 (1968).
8) K. Maruyama, A. Osuka, and Y. Naruta, *Bull. Chem. Soc. Jpn.*, **51**, 3047 (1978).
9) E. S. Huyser, R. H. S. Wang, and W. T. Short, *J. Org. Chem.*, **33**, 4323 (1968); R. Cantarel, *C. R. Acad. Sci.*, **210**, 403 (1940); *Chem. Abstr.*, **34**, 3712 (1940).
10) P. J. Wagner, "Topics in Current Chemistry, Triplet State III," Springer-Verlag, Berlin, Heidelberg, New York (1976), p. 14.
11) G. Kornis and P. DeMayo, *Can. J. Chem.*, **42**, 2822 (1964).
12) J. C. Jochims, *Monatsh. Chem.*, **94**(4), 677—680 (1968); *Chem. Abstr.*, **59**, 13900 (1963).
13) A. Rahman and M. O. Farooq, *Ann.*, **585**, 200 (1954).
14) Busch and Leefhelm, *J. Prakt. Chem.*, **77**, 1 (1908).
15) L. Skulski, G. C. Palmer, and M. Calvin, *Tetrahedron Lett.*, **1963**, 1773.
16) *N*-Diarylmethylbenzamides were prepared by the reaction of acid chlorides and benzhydrylamine according to the method reported (*cf.* W. A. Dehn and A. A. Ball, *J. Am. Chem. Soc.*, **36**, 2091 (1914).
17) A. Michaelis, *Ber.*, **26**, 2169 (1893).
18) Acyloins were obtained from corresponding aldehydes in presence of cyanide ions as catalysts.

Fluorination with Xenon Difluoride. XXII. The Role of Catalyst and Temperature on the Fluorination of Norbornene and Norbornadiene

Ana GREGORČIČ and Marko ZUPAN*

Department of Chemistry and "Jožef Stefan" Institute, University of Ljubljana, Ljubljana, Yugoslavia

(Received June 20, 1979)

The reaction of norbornene was used as a mechanistic probe to elucidate the effect of catalyst (HF, HF–pyridine, BF_3, BF_3–etherate, and pentafluorothiophenol) and temperature (from −61 °C to 25 °C) on liquid phase fluorination with xenon difluoride, resulting in the formation of seven products, depending on the reaction conditions: fluoronortricyclane, 2-*endo*-3-*exo*-difluoronorbornane, 2-*exo*-7-*anti*-difluoronorbornane, 2-*endo*-5-*exo*-difluoronorbornane, 2-*exo*-5-*exo*-difluoronorbornane, 2-*exo*-3-*exo*-difluoronorbornane, and 2-*exo*-7-*syn*-difluoronorbornane. The catalyst has a significant effect on the reaction pathways, boron trifluoride etherate favouring the formation of 2-*endo*-5-*exo*- and 2-*exo*-5-*exo*-difluoronorbornane, while pentafluorothiophenol favoured the formation of fluoronortricyclane. The catalyst and temperature has much less effect on the reaction pathways in the case of norbornadiene, four products being formed: fluoronortricyclane, 3-*endo*-5-*exo*-difluoronortricyclane, 3-*exo*-5-*exo*-difluoronortricyclane, and 2-*exo*-7-*syn*-difluoro-5-norbornene. Pentafluorothiophenol as a catalyst, when used in a greater amount, favours the formation of fluoronortricyclane.

Xenon difluoride is a mild fluorinating agent for the fluorination of alkenes, acetylenes, aromatic and heteroaromatic compounds.[1] The mechanism of fluorine addition to olefins with xenon difluoride depends on structure of the olefin, the catalyst used, solvent polarity, and temperature. The formation of β-fluorocarbonium ions, free radical intermediates or ion radicals has been suggested (Scheme 1). The following substrates are convenient catalysts for the fluorination of olefins: hydrogen fluoride,[2] HF–pyridine,[3] trifluoroacetic acid,[4] bromine,[5] and boron trifluoride etherate.[6]

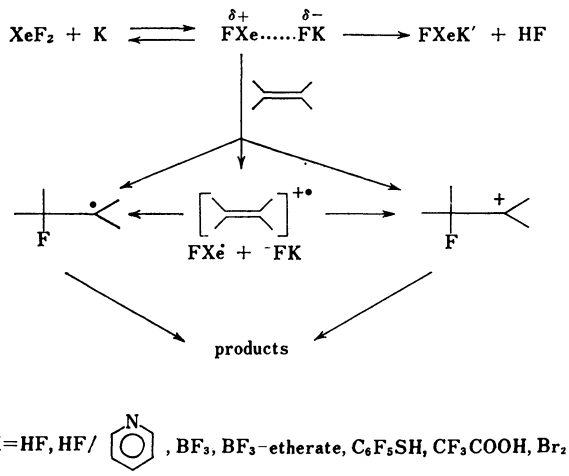

Scheme 1.

Recently it was found that boron trifluoride[7] is a convenient catalyst for the fluorination of less reactive organic compounds, while in the case of more sensitive organic compounds pentafluorothiophenol proved to be preferable to hydrogen fluoride, which causes acid catalyzed decomposition. The fluorination of norbornene with xenon difluoride in the presence of HF resulted in the formation of seven products. Besides the formation of carbonium ions free radical intermediates have also been observed.[8] Shackelford found that low temperature fluorination of norbornene, catalyzed by boron trifluoride etherate, gives only three products.[9] The reaction of norbornene has been used several times as a mechanistic device to elucidate the mechanism and stereochemistry of diverse reactions.[10] We have utilized the sensitivity of the reactions of norbornene to the reaction conditions for studying the effect of catalyst and temperature on the fluorination with xenon difluoride. The effect of catalyst and temperature on the fluorination of norbornadiene has also been studied.

Results and Discussion

The reaction of norbornene with xenon difluoride in dichloromethane at various temperatures and in the presence of various catalysts resulted in the formation of seven products (Scheme 2). Analysis of the reaction mixture by GLC gave the relative yields given in Table 1. The products of reaction were collected by preparative GLC. The structures of the compounds were determined on the basis of their mass, ^{19}F and ^{1}H NMR spectra and are in agreement with those reported.[8] The effect of catalysts, *i.e.* hydrogen fluoride, hydrogen fluoride–pyridine, boron trifluoride etherate, boron trifluoride, and pentafluorothiophenol, is most evident from the formation of fluoronortricyclane (**1**), 2-*endo*-3-*exo*-difluoronorbornane (**2**), 2-*exo*-3-*exo*-difluoronorbornane (**6**), and 2-*exo*-7-*syn*-difluoronorbornane (**7**).

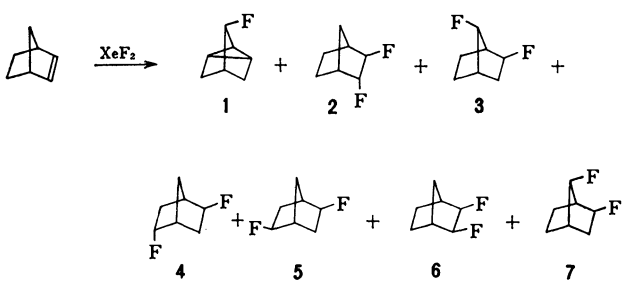

Scheme 2.

We have established that the formation of products **2** and **6** can partly be ascribed to free radical intermediates. The great selectivity in the formation of

TABLE 1. EFFECTS OF CATALYST AND TEMPERATURE ON THE ADDITION OF XeF_2 TO NORBORNENE

Catalyst	Temp/°C	Time/min	1	2	3	4	5	6	7	
HF	25	3	44	6	17	15.5	9	4	4.5	Ref. 8
	25	60	37.5	6	18	19	10	4	5.5	Ref. 8
HF–Pyridine	15	60	14	—	35	19	10	—	22	Ref. 3
BF_3/OEt_2	−61	10	4	—	38	33	18	—	7	
	−61→25	1275	2	—	3	33	61	—	1	
		1275	—	—	4.3	29.7	66	—	—	Ref. 9
	−46→−39	105	—	—	42.2	25.5	32.2	—	—	Ref. 9
	0	1	4	—	34	33	22	1	6	
	25	1	5	—	28	26	33	1	7	
	25	60	6	1	4	31	57	trace	1	
BF_3	25	60	11	3	29	27	20	3	7	
C_6H_5SH	25	10	64	—	13	12	7	—	4	
	25	60	63	—	14	12	7	—	4	

TABLE 2. EFFECT OF THE AMOUNT OF PENTAFLUOROTHIOPHENOL ON PRODUCT IN THE FLUORINATION OF NORBORNENE

C_6F_5SH/C_7H_{10} (mmol/mmol)	1	2	3	4	5	6	7
0.125	44	1	19	19	10	—	6
0.25	45	1	18	18	11	—	7
0.50	76	—	8	8	5	—	3
1.00	99	—	trace amount			—	—

2-*endo*-5-*exo*-difluoronorbornane (**4**), and 2-*exo*-5-*exo*-difluoronorbornane (**5**), pointed out by Shackelford,[9] arises from secondary isomerisation of 2-*exo*-7-*anti*-difluoronorbornane (**3**). In order to clarify the primary formed products in the BF_3–etherate catalyzed reaction, we made a 10 min experiment at −61 °C and confirmed that five products are formed. Besides difluoronorbornanes **3**, **4**, and **5**, fluoronortricyclane (**1**) and 2-*exo*-7-*syn*-difluoronorbornane (**7**) were formed as well. The experiment performed under the same conditions as reported[9] (temperature from −61 °C to +25 °C) resulted in a similar product distribution, while small amounts of fluoronortricyclane (**1**) and 2-*exo*-7-*syn*-difluoronorbornane (**7**) were also detected. The effect of temperature on the reaction pathways in BF_3–etherate catalyzed fluoronations is given in Table 1.

BF_3-catalyzed fluorination of norbornene at room temperature resulted in the formation of seven products. The formation of fluoronortricyclane as the major prodyct in pentafluorothiophenol catalyzed reactions (Table 1) stimulated us to study the effect of the amount of catalyst on product distribution (Table 2). The increase in the amount of pentafluorothiophenol is reflected in the increased formation of fluoronortricyclane (**1**), while the experiment with equimolar amounts of catalyst and norbornene resulted in only trace amounts of difluoronorbornanes **3**, **4**, and **5**.

The formation of seven products resulting from the fluorination of norbornene under various conditions (catalyst, temperature) can be mainly ascribed to the intermediately formed β-fluorocarbonium ion, which further undergoes Wagner-Meerwein rearrangements and hydride shifts (Scheme **3**). The mechanism involves the irreversibile hydride shifts 6,2-H and 1,2-H, based on the observation of isomerization of the products in dichloromethane in the presence of hydrogen fluoride, where similar carbonium ions are formed.[8] The formation of 2-*exo*-3-*endo*-difluoronorbornane (**2**) and 2-*exo*-3-*exo*-difluoronorbornane (**6**) formed in room temperature fluorination catalyzed by BF_3–etherate and BF_3, can be partly ascribed to the formation of free

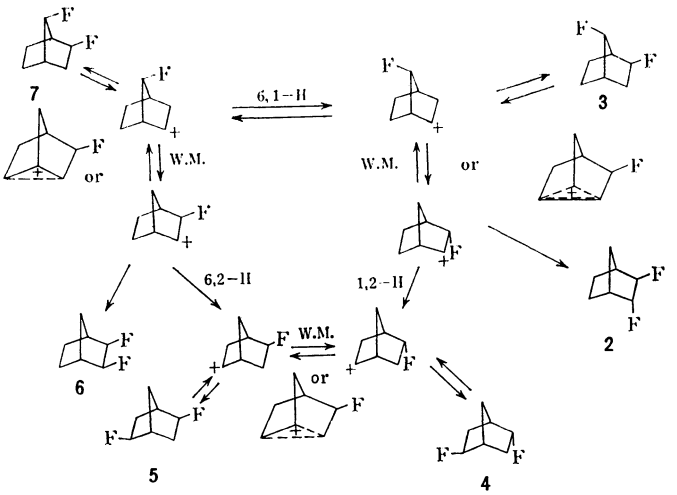

Scheme 3.

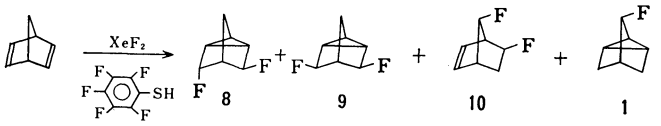

Scheme 4.

Table 3. Effects of catalyst and temperature on the addition of XeF_2 to norbornadiene

Catalyst	Temp °C	Time min	8	9	10	
HF	25	60	50	40	10	Ref. 8
HF–Pyridine	25	30	27	68	5	Ref. 11
BF_3	0	60	45	50	5	
	25	60	47.5	49	3.5	
BF_3/OEt_2	−61	10	36.5	58.5	5	
	0	1	38.5	55	6.5	
	25	1	39.5	53.5	7	
	25	60	41.5	50	8.5	

radical intermediates (Scheme 1). The effect of catalyst (HF, HF–pyridine, BF_3–etherate, BF_3, pentafluorothiophenol) on the reaction pathways is reflected most significantly in the amount of fluoronortricyclane formed.

The fluorination of norbornadiene resulted in the formation of four products, depending on the catalyst used (Scheme 4). It is evident that variation of catalyst, *i.e.* HF, HF–pyridine, BF_3–etherate, and temperature from −61 °C to 25 °C, has much less effect on the reaction pathways than in the case of norbornene (Table 3). However, in the pentafluorothiophenol catalyzed reaction, fluoronortricyclane (**1**) was formed besides[8] 3-*endo*-5-*exo*-difluoronortricyclane (**8**), 3-*exo*-5-*exo*-difluoronortricyclane (**9**), and 2-*exo*-7-*syn*-difluoronorbornene-5 (**10**). The effect of the amount of catalyst is shown diagramatically in Fig. 1. As in the case of norbornene, fluoronortricyclane became the main product when greater amounts of catalyst were used. An explanation for the formation of four products in the pentafluorothiophenol catalyzed reaction is given in Scheme 5. In the first step, polarization of XeF_2 by pentafluorothiophenol is suggested, which is then followed by the formation of two β-fluorocarbonium

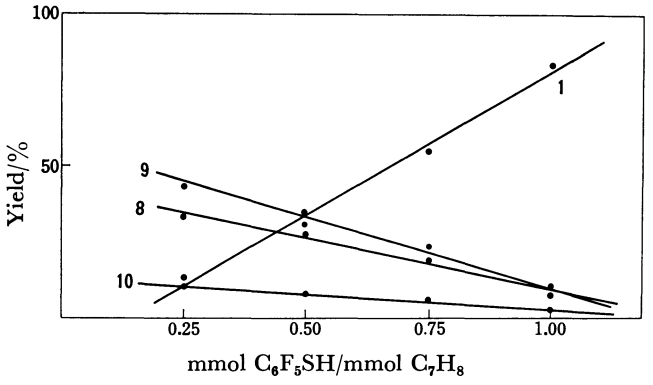

Fig. 1. Effect of the amount of pentafluorothiophenol on product distribution in fluorination of norbornadiene.

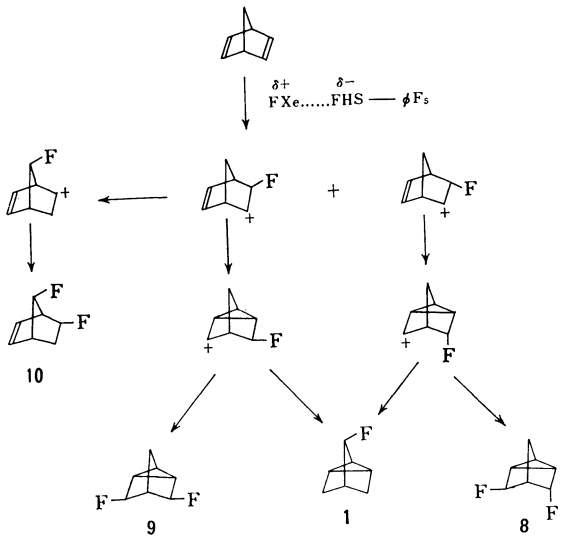

Scheme 5.

ions, giving two fluoronortricyclyl cations. The preferential *exo* attack[11] of the fluorine anion leads to the formation of difluoronortricyclane products (**8**, **9**), while reaction with pentafluorothiophenol results in the formation of fluoronortricyclane (**1**). In halofluorinations[11] of norbornadiene only the primary formed β-*exo*-fluorocarbonium ion undergoes Wagner-Meerwein rearrangement, leading to the formation of 2-*exo*-7-*syn*-5-norbornene (**10**).

Experimental

IR spectra were recorded with a Perkin Elmer 257 spectrometer and ^1H and ^{19}F NMR spectra with a JEOL JNM PS-100 from CCl_4 solution with Me_4Si and CCl_3F as internal references. Mass spectra were taken on a CEC 21-110 spectrometer. Gas-liquid partition chromatography was carried out on a Varian Aerograph Model 1800.

Materials. Norbornene, norbornadiene and pentafluorothiophenol were purified before use. Hydrogen fluoride and boron trifluoride of Fluka Purum quality were used without further purification. Dichloromethane and diethyl ether were purified and stored over molecular sieves.[12] Xenon difluoride was prepared by a photosynthetic method,[13] the purity being higher than 99.5%.

Addition and Isolation Procedures. To a solution of 1 mmol of olefin in dichloromethane (2 ml) in a Kel-F vessel was added 1 mmol of xenon difluoride at an appropriate temperature, the corresponding catalyst (HF, BF_3, BF_3–etherate, or pentafluorothiophenol) being introduced into the reaction mixture with stirring. The reactions were stopped by addition of dichloromethane (15 ml) and 10 ml of 5% $NaHCO_3$. The reaction mixture was washed with water, and dried over anhydrous sodium sulfate. The solvent was evaporated *in vacuo*. The crude reaction mixtures were analyzed by GLC, the products being isolated by preparative GLC. The

structures of the products were established by a comparison of their spectroscopic data with those published.[8] Each experiment was repeated several times, the average data being given in the tables; relative yields were determined by GLC (DDP-10%, Chromosorb Regular 100, 45—120 °C in the case of norbornene reaction, and Carbowax 20 M 25%, Varaport 30 70/80, 130 °C for norbornadiene). The maximum error between parallel experiments was ±1.5%.

We thank Prof. J. Slivnik for the xenon difluoride. Financial assistance of the Research Community of Slovenia is acknowledged.

References

1) R. Filler, *Israel J. Chem.*, **17**, 71 (1978).
2) M. Zupan and A. Pollak, *J. Chem. Soc., Chem. Commun.*, **1973**, 845.
3) A. Gregorčič and M. Zupan, *Collec. Czech. Chem. Commun.*, **42**, 3192 (1977).
4) M. Zupan and A. Pollak, *Tetrahedron Lett.*, **1974**, 1015.
5) S. Stavber and M. Zupan, *J. Fluorine Chem.*, **10**, 271 (1977).
6) S. A. Shackelford, R. R. McGuire, and J. L. Pflug, *Tetrahedron Lett.*, **1977**, 363.
7) S. Stavber and M. Zupan, *J. Chem. Soc., Chem. Commun.*, **1978**, 969.
8) M. Zupan, A. Gregorčič, and A. Pollak, *J. Org. Chem.*, **42**, 1562 (1977).
9) S. A. Shackelford, *Tetrahedron Lett.*, **1977**, 4265.
10) R. C. Fahey, *Top. Stereochem.*, **3**, 237 (1968); T. G. Traylor, *Acc. Chem. Res.*, **2**, 152 (1969); H. C. Brown, *Tetrahedron*, **32**, 179 (1976).
11) A. Gregorčič and M. Zupan, *Tetrahedron*, **33**, 3243 (1977).
12) "Technique of Organic Chemistry, Vol. VII, Organic Solvents," ed by A. Weissberger, Interscience, New York N. Y. (1955).
13) S. M. Williamson, *Inorg. Synth.*, **11**, 147 (1968).

 © 1980 The Chemical Society of Japan Bull. Chem. Soc. Jpn., 53, 1089—1100 (1980)

Chemistry of Dienyl Anions. II. Crystalline Bis(dienyl)magnesium. Selective Dienylation and Structure in Solution and in the Solid State

Hajime YASUDA, Michihide YAMAUCHI, Akira NAKAMURA,* Tsuyoshi SEI,†
Yasushi KAI,† Noritake YASUOKA,† and Nobutami KASAI†

Department of Macromolecular Science, Faculty of Science, Osaka University, Toyonaka, Osaka 560
†*Department of Applied Chemistry, Faculty of Engineering, Osaka University, Suita, Osaka 565*

(Received October 4, 1979)

Seven different crystalline bis(dienyl)magnesium·TMEDA complexes of open chain or cyclic structure were prepared by metal exchange reaction of corresponding potassium dienides. They are fluxional in solution due to the rapid 1,3-rearrangement. Terminally σ-bonded *trans* or (*E*) structure exists primarily in the open chain complexes while centrally σ-bonded *cis* structure in cyclic dienylmagnesium·TMEDA complexes. The former gave 1,3-dienes exclusively but the latter gave 1,4-dienes upon hydrolysis. Molecular structure of bis(2,4-dimethyl-2,4-pentadienyl)magnesium determined by X-ray crystallography showed that it has terminally σ-bonded structure. Addition of dienylmagnesium compounds to acetone followed by hydrolysis gave 1,4-diene derivatives regioselectively but that to diisopropyl ketone gave 1,3-diene derivatives selectively. Unsaturated alcohols with an elongated carbon chain were synthesized by thermal cracking of cyclic ether complexes. 1,3,7-Trienes can be obtained selectively by reaction of appropriate allyl halides in the presence of CuCl catalyst and regioselective dienylation occurred by using $TiCl_2(\eta^5\text{-}C_5H_5)_2$ as catalyst.

Allylic magnesium compounds have been utilized as an agent for introduction of olefin groups into various organic groups[1] or as a component of polymerization catalysts.[2] Stereoselective or regioselective introduction of the dienyl moiety into organic groups is also attractive especially for the synthesis of terpenoids or biologically active substances. Organic synthesis using dienylmetal compounds have been little developed due to the lack of suitable preparation methods though some diene syntheses catalyzed by transition metal compounds[3] and by Grignard type reaction[4] are recently reported. We present here a widely applicable novel route for the preparation of pure bis(dienyl)magnesium compounds, their structures, and some applications for organic synthesis. Bis(dienyl)magnesium compounds of five different linear dienes and of two cyclic dienes were prepared by transmetalation of dienyl anions with magnesium halides. All of these were isolated for the first time as crystals of *N,N,N',N'*-tetramethylethylenediamine (TMEDA) complexes. These dienylmagnesium compounds are fluxional in solution and their simple averaged ^{1}H-NMR spectra resemble well those of corresponding dienyl anions. Hence the fluxional structure is discussed in relation to the conformation[5] of the dienyl anions whose conformational stability was recently treated by extended Hückel MO calculations.[6]

Results and Discussion

Isolation of Crystalline Dienylmagnesium Compounds. Series of bis(dienyl)magnesium compounds and Grignard type dienylmagnesium halides were prepared by the metal exchange reaction. Bis(2,4-pentadienyl)-magnesium was synthesized by the 2:1 reaction of potassium pentadienide[7] with anhydrous magnesium halide in THF in 85—95% yield and was isolated as pure crystals of TMEDA complex **1**. Deuteriolysis of **1** gave two moles of pentadiene-1-*d* or -3-*d* and one mole of TMEDA as evidenced by GC of the resulting solution. Grignard type pentadienylmagnesium bromide can also be prepared by the 1:1 reaction of potassium

$$2\,C_5H_7K + MgX \xrightarrow{THF} (C_5H_7)_2Mg\cdot 2\,THF$$
$$\xrightarrow{TMEDA} (C_5H_7)_2Mg\cdot TMEDA$$
1

pentadienide with magnesium bromide. In the similar manner, TMEDA complexes of bis(2,4-hexadienyl)-magnesium **2** and hexadienylmagnesium bromide were prepared in 90% yield. The direct reaction of magnesium with 1-bromo-2,4-hexadiene in THF gave hexadienylmagnesium bromide in only 30% yield. The formation of homo coupling products, $C_{12}H_{18}$, (70% yield) was predominant in the latter case even when 1-bromo-2,4-hexadiene was added to an excess (10 equivalent)magnesium turnings very slowly. Thus, the present method is widely applicable and superior to the known method with regard to the yield and purity. This paper mainly deals with bis(dienyl)-magnesium compounds to avoid the complex problem arising from a Schlenk equilibrium observed for Grignard reagents. Other crystalline TMEDA complexes of bis(4-methyl-2,4-pentadien-1-yl)magnesium **3**, bis(3-methyl-2,4-pentadien-1-yl)magnesium **4**, bis(2,4-dimethyl-2,4-pentadien-1-yl)magnesium **5**, bis(2,6-cycloheptadien-1-yl)magnesium **6**, and bis(2,7-cyclooctadien-1-yl)magnesium **7** were prepared in essentially the same way as described for **1**. Their chemical characterization is given in Table 1. The molecular weights determined cryoscopically in benzene showed that they are all monomeric. Based on these facts, following formulae are given for **1**—**5** and **6**—**7**.

Population at Equilibria Existed in Bis(dienyl)magnesium. Monoalkyl substituted allylic Grignard reagents are known to be present in solution predominantly as γ-alkyl substituted species,[8] although it is equilibrating with the α-alkyl substituted one by rapid 1,3-rearrangement as evidenced by NMR spectroscopy and as deduced from structures of the products obtained by hydrolysis. The *cis*/*trans* ratio of the product decreased with an increase in bulkiness of the alkyl substituent,

Table 1. Characterization of bis(dienyl)magnesium-TMEDA complexes

Dienyl Compound	Mp (°C)[a]	Mg/% Found[b]	Mg/% Calcd	Diene/TMEDA[c] (mol/mol)	Mol wt[d] Found	Mol wt[d] Calcd
1	74.8	8.8	8.8	2.01	282	274
2	66.2	8.2	8.0	2.05	310	302
3	35.2	8.2	8.0	2.03	320	302
4	60.7	8.1	8.0	2.00	302	302
5	86.6	7.3	7.3	2.02	335	330
6	91.1	—	7.4	2.02	340	326
7	93.5	6.7	6.8	2.02	370	354

a) Measured with sealed capillary. b) Determined by 8-quinolinol method. c) Determined by ^{1}H-NMR from relative signal intensities. d) Determined cryoscopically in benzene.

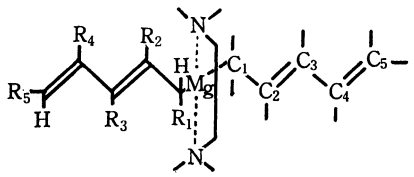

1: $R_1=R_2=R_3=R_4=R_5=H$
2: $R_5=CH_3$, $R_1=R_2=R_3=R_4=H$
3: $R_4=CH_3$, $R_1=R_2=R_3=R_5=H$
4: $R_3=CH_3$, $R_1=R_2=R_4=R_5=H$
5: $R_2=R_4=CH_3$, $R_1=R_3=R_5=H$

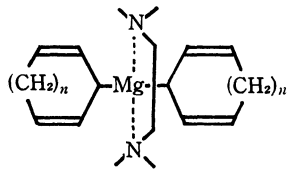

6: $n=2$
7: $n=3$

Equilibria for the dienylmagnesium compounds are rather complex because dienyl group has three reactive carbon atoms, C_1, C_3, and C_5. For example, following eight species are possible for the hexadienylmagnesium compounds (Scheme 1). To get the information on the configuration of the diene group and on the position at which the magnesium atom is bonded, hydrolysis of the bis(dienyl)magnesium compounds was carried out (Table 2). Compounds **1** and **4** gave 1,3-dienes primarily but the cyclic dienylmagnesium compounds **6** and **7** gave 1,4-dienes exclusively in line with hydrolysis

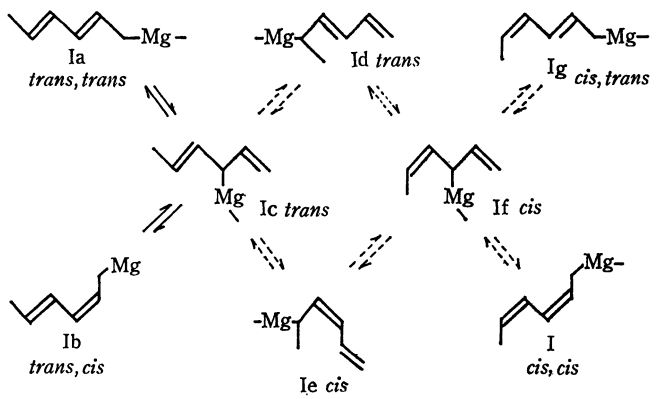

Scheme 1.

Table 2. Hydrolysis of bis(dienyl)magnesium-TMEDA complexes in benzene at 10 °C

Complexes	1,3-Dienes/% *trans*,(*E*)	1,3-Dienes/% *cis*,(*Z*)	1,4-Dienes/%
1	64.5	14.5	21.0
2	24.5[a]	21.6[b]	53.9[c]
3	29.5	2.0[d]	44.8
	23.7[e]		
4	62.5	3.4	34.1
5	41.2		58.8
6	0	7.9	92.1
7	0	6.5	93.5

a) *trans,trans*-2,4-Hexadiene. b) *trans, cis*-2,4-Hexadiene. c) *trans*-1,4-Hexadiene. d) 2-Methyl-1,3-pentadiene. e) 4-Methyl-1,3-pentadiene

data of the starting dienyl anions.[7] Other magnesium compounds **2**, **3**, and **5** gave nearly equal amounts of 1,3- and 1,4-dienes, although the corresponding dienyl anions gave only 1,3-dienes.[7] Thus dienylmagnesium compounds exist as an equilibrium mixture and the alkyl substitution on the pentadienyl group influences the ratio of resulting 1,3- to 1,4-dienes. Characteristic feature of the hydrolysis of **1**, **3**, and **4** is that *trans*(or *E*)-1,3-diene was produced in preference to *cis*(or *Z*)-1,3-diene. This result sharply contrasts to the hydrolysis of the corresponding potassium dienides which gave *cis*-1,3-diene selectively. In the case of **2**, nearly equal amounts of *trans,trans*- and *trans,cis*-2,4-hexadiene were produced upon hydrolysis. Two routes are possible for the production of *trans,cis*-2,4-hexadiene (from Ib and Ig in Scheme 1) but the route *via* Ib is more plausible. If Ig is equilibrating with Ia and the *trans,cis*-isomer is formed from Ig, other isomers (*i.e.*, 1,3-hexadiene derived from Id or Ie, *cis*-1,4-hexadiene from If and *cis,cis*-2,4-hexadiene from Ih) should be produced simultaneously but those yields were negligible. *Trans* configuration of 1,4-hexadiene obtained from **2** together with the configuration of above mentioned 2,4-hexadiene supports the postulate of equilibration between Ia and Ib. In contrast to the open chain dienylmagnesium compounds, cyclic dienylmagnesium compounds **6** and **7** gave *cis,cis*-1,4-dienes exclusively, indicating the negative charge being high on the C_3 atom.

The position of equilibrium was altered by change

Table 3. Effect of protonolysis agents on the distribution of the protonolysis products of $(C_5H_7)_2Mg \cdot 2THF$[a]

Agent	1,3-Pentadiene/%		1,4-Pentadiene/%
	trans	*cis*	
CH_3COOH	48	8	44
CH_3OH	52	6	42
H_2O	75	5	20
Pyrrolidine	95	5	0
Piperidine	96	4	0

a) Protonolysis was carried out in benzene at 10 °C.

of basicity of the protonolysis agents and of the ligands as shown in Table 3. The variation in distribution of the protonolysis products may be explained by considering both ionic species and covalent species which are equilibrating with each other as was described for magnesium–diene adducts;[9] *i.e.*, protonation with bases occurs at $C_1(C_5)$ position exclusively while that with acid occurs also at C_3 position. The former may be explained by the predominant cleavage of ionic Mg–C bond and the latter by the cleavage of covalent Mg–C bond presumably by a concerted mechanism. Based on this assumption, the effect of the ligand to the structure of the hydrolysis product was examined.

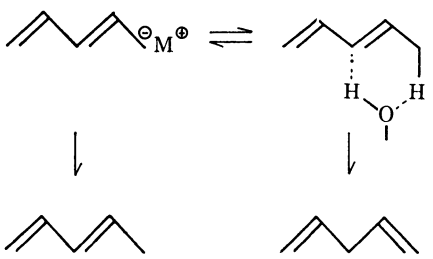

Coordination of strong donor such as 1,4,8,11-tetramethyl-1,4,8,11-tetraazatetradecane(tetramethylcyclam) and 1,4,7,10,13-pentaoxacyclopentadecane(15-crown-5) increases the ionic nature of the Mg–C bond and hence the dienyl group behaved similarly to the dienyl anion[7] giving 1,3-diene exclusively upon hydrolysis (Table 4). Linear polyethers bearing aromatic end groups are also being increasingly used for complexing the metal cations[10] but the polyethers shown in Table 4 have relatively little interaction with metal.

A typical example of the regioselective 1,4-diene formation is observed in hydrolysis of $K[(C_5H_7)_4Al]$ which was prepared by the 4: 1 reaction of potassium pentadienide with aluminium chloride (see experimental). It has terminaly-σ-bonded structure as evidenced by ^{1}H-NMR and it gave 1,4-pentadiene quantitatively (99%) upon hydrolysis. Thus, the complete conversion of a 1,3-diene to the thermally more unstable 1,4-diene was realized by the metalation of 1,3-diene with alkali metals, followed by the aluminium assisted reaction. Similar regioselectivity is found also for allylaluminium compounds and enediylaluminium compounds[11] obtained from endiylmagnesium compounds. The high regioselectivity should be ascribed to the larger covalent character of the Al–C bond compared to the Mg–C bond.

Table 4. Distribution of the hydrolysis products of $(C_5H_7)_2Mg$ coordinated with macromolecular ligands

Ligand		1,3-Pentadiene/%		1,4-Pentadiene/%
		trans	*cis*	
$CH_3O(CH_2CH_2O)_nCH_3$	$n=1$	37	8	55
	$n=2$	37	9	54
	$n=3$	35	11	54
	$n=4$	42	13	45
15-Crown-5		94	6	0
18-Crown-6		81	13	7
Tetramethylcyclam		95	5	0

Nuclear Magnetic Resonance Studies. ^{1}H-NMR spectra of TMEDA complexes **1**—**7** are collected to know the correlation between the population at equilibrium obtained by hydrolysis and the structure of the complexes in solution (Table 5). The values of chemical shifts of **1** clearly shows that the terminally σ-bonded structure (IIa and IIc) exists predominantly,

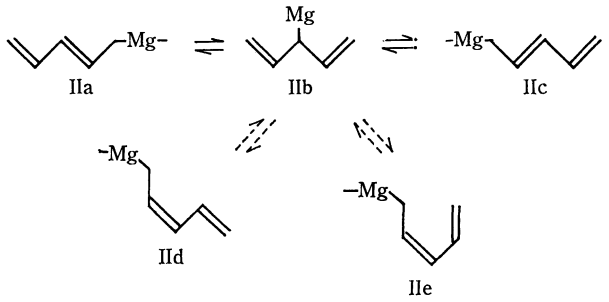

although it is equilibrating rapidly with IId or IIe *via* IIb the presence of which was not detected on the NMR time scale, a simple averaged A_2BX type spectrum being observed. Proton-proton coupling constant J_{23} (or J_{34}), of 11.7 Hz corresponds to the J_{23} of internal olefin protons of pentadienyl anions (11.5—13.5 Hz)[12] whose conformation is W-form (*trans* configuration). The coupling constant J_{23} for dienyl anions having *cis*-configuration is known to be 7—9 Hz.[13] The *cis*/*trans* ratio of **1** calculated from the magnitude of the coupling constant (assuming *trans* $J_{H,H}$ to be 12.5 Hz and *cis* $J_{H,H}$ to be 7.0 Hz) with a linear equation is 0.21 in line with the hydrolysis data (0.22). Thus **1** was concluded to be in equilibrium between IIa and IIc keeping *trans* configuration. The rapid equilibrating structure may be correlated to the W-form of the pentadienyl anion which also shows A_2BX spectrum. Based on the coupling constant, we may conclude that sickle(IId) and U(IIe) formed compounds which result by the rotation around the C_2–C_3 or C_3–C_4 bond have minor populations at equilibrium. Assignment of the signals of **2** was made in part from a decoupled spectrum and **2** was concluded to be terminally-σ-bonded structure. The value of proton-proton coupling of J_{45}, 13.1 Hz, indicates that C_4H=C_5H group assumes *trans* structure while that of J_{23} shows C_2H=C_3H group being in equilibrium between *trans* and *cis* structure (*cis*/*trans*=0.41). The higher field shift of C_1-proton

Table 5. Chemical shifts and coupling constants in ^{1}H-NMR spectra of complexes **1**—**7**[a)]

	C_1–H(J_{12}/Hz)	C_2–H	C_3–H(J_{23}/Hz)	Others
1	2.98 (d, 11.3)	6.55 (d of d)	5.58 (d of d, 11.7)	C_4–H=C_2–H, C_5–H=C_1–H
2	1.95 (d, 9.9)	6.51 (d of t)	5.76 (d of d, 10.9)	6.51 (d of d, 13.0, C_4–H) 5.24 (d of q C_5–H) 1.50 (d 9.9, CH_3)
3	2.88 (d, 11.5)	6.77 (d of t, 12.3)	5.72 (d)	3.21 (s, C_5–H) 1.91 (s, CH_3)
4	3.02 (d, 11.5)	6.54 (d of d)	—	1.91 (s, CH_3)
5	3.33 (s)	—	5.22 (s)	2.12 (s, CH_3)
6	4.68 (bd 9.7)	6.31 (d of d)	3.85 (d of d, 7.4)	2.77 (m, CH_2)
7	4.22 (d of d, 9.3)	6.40 (d of d)	3.34 (d of d, 6.5)	3.10 (d of t, 6.4, CH_2C=C) 1.62 (t of t, 6.3, CH_2CH_2)
1[b)]	1.49 (d, 8.9)	6.28 (m)	5.60 (d of d, 14.0)	6.18 (C_4–H, m) 4.91 (C_5–H, d of d, 15.8) 4.77 (C_5–H, d of d, 10.0)

a) Calibrated using benzene as internal standard (benzene peak, 7.20 ppm downfield from external TMS). Data were collected at 38 °C in C_6D_6. b) Bis(pentadienyl)magnesium-15-crown-5 complex at −60 °C in THF-d_8.

and lower field shift of C_5-proton compared to the values of **1**, suggest that the equilibrium in Scheme 1 are shifted to Ia and Ib in line with the hydrolysis data. The spectrum of **3** was composed of both A_2BX pattern signals and broad singlet assignable to the terminal CH_2 group. Magnitude of J_{23} corresponds to that of *trans* structure. Protons attached to C_1 and C_5 carbon atoms shifted to higher field by 1.9—2.1 ppm from C_1 and C_5-protons of the starting diene showing the presence of the equilibrium. Therefore, the following equilibria (A) and/or (B) which include *trans* configuration are considered for **3**. Equilibrium (C) including *cis* configuration may exist in only minor population, if any.

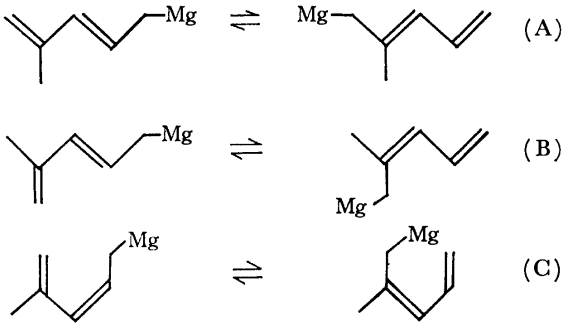

Although ^{1}H-NMR data of **4** gave no information about the configuration, it is possible to conclude based on chemical shift value that **4** has also terminally σ-bonded structure primarily. Hydrolysis data of **4** (exclusive production of (*E*)-3-methyl-1,3-pentadiene) strongly suggest that rapid 1,3-rearrangement occurs in solution keeping (*E*)-structure. If the conformation changes from (*E*) to (*Z*) during the rearrangement, (*Z*)-3-methyl-1,3-pentadiene should be produced in lager amounts.

In contrast to **1**—**4**, (*Z*)-configuration is most plausible for 2,4-dimethylpentadienylmagnesium **5** due to the steric repulsion between the two methyl groups. The double bonds in (*E*)-2,4-dimethylpentadienyl group can not be coplanar since the van der Waals radius of methyl group (*ca.* 2.0 Å) is much larger than the C_2–C_4 carbon distance (1.3 Å). The X-ray analysis of bis(2,4-dimethylpentadienyl)magnesium·TMEDA **5**, actually, showed that it has (*Z*)-configuration (details are given later in this paper). Chemical shift of **5** shows that it has terminally σ-bonded structure also in solution.

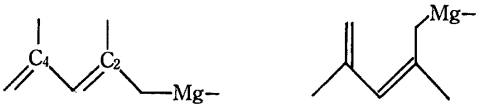

5 (*E*) **5** (*Z*)

Thus, (*E*)- and (*Z*)-pentadienylmagnesium compounds of open chain structure were realized. This finding prompted further interest in comparison of electron density distribution of **5** with that of (*Z*)-pentadienylmagnesium compounds of cyclic structure. Proton-proton coupling constants, J_{23} (7.4 Hz for **6** and 6.5 Hz for **7**) show that cyclic dienylmagnesium **6** and **7** have (*Z*)-structure as expected. The increased coupling constants of J_{12} (9.7 Hz for **6** and 9.3 Hz for **7**) may be explained by the torsion around the C_1–C_2 carbon bond derived from the nonplanar structure[14)] rather than the equilibrium between *cis* and *trans* structure because *cis,trans* (or *trans,trans*) conformation is much higher in energy than the *cis,cis* conformation in a ring system,[15)] especially for 1,3-cycloheptadiene.

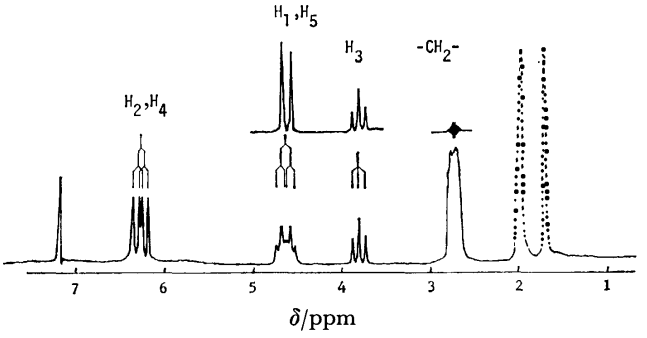

Fig. 1. ^{1}H-NMR spectrum of bis(cycloheptadienyl)-magnesium·TMEDA in benzene-d_6 at 38 °C.

Table 6. ^{13}C-NMR spectral data of the complexes **1**,**3**,**4**,**5**, and **7**[a,b]

	C_1 (C_5)	C_2 (C_4)	C_3	Others
1	63.1	143.9	112.0	
3	57.8 (C-1) (140)	140.8 (C_2) (145) 139.7 (C_2) (150)	112.1 (148) 111.3 (148)	147.9 (C_4) 69.1 (C_5) (141) 22.1 (CH_3) (128)
4	60.9	144.7	114.4	20.8 (CH_3)
5	67.8 (150)	143.9	109.3 (138)	28.4 (CH_3) (129)
7	98.5 (151)	139.7 (140)	66.5 (135)	26.3 (CH_2) (128) 19.1 (CH_2) (128)

a) In ppm downfield from external TMS (calibrated using benzene peak, assumed to be 128.0 ppm). b) Measured at 38 °C in C_6D_6.

The most striking feature in the spectra of **6** (Fig. 1) and **7** is that the signals of the proton attached to the central C_3-carbon atom appeared at higher field than that of C_1 and C_5 carbon stoms. This means that centrally bonded 1,4-diene type structure exists primarilly in **6** and **7** and the electron density on the C_3 carbon atom is higher than those on the C_1 and C_5 carbon atoms. Based on these facts, structure IIIa is considered for **6** as the abundant species although it is in equilibrium with the minor species IIIb of 1,3-dienyl type structure. For the structure IIIb, twisted structure is most plausible from view of the conformational stability.[16] Stereochemistry around the Mg–C bond in IIIa and IIIb could not be determined by spectral data. Since the

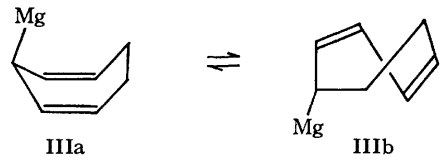

IIIa IIIb

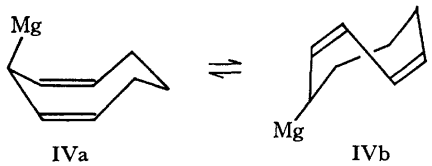

IVa IVb

boat-chair conformation[17] is known for 1,4-cyclooctadiene to be much more stable than the boat-boat conformation, structure IVa is reasonably considered as the predominant species for **7**. The minor species IVb which is equilibrating with IVa should have also nonplanar 1,3-diene structure because double bonds in 1,3-cyclooctadiene can not be coplanar.[18] Thus, a sharp contrast in electron density (or the position at which the metal bonds to a carbon atom) was observed between acyclic dienylmagnesium compound and cyclic dienylmagnesium compounds with (*Z*) structures. That is, the former has high electron density on the terminal carbon atoms while the latter on the central carbon atom.

^{13}C-NMR chemical shifts for dienyl anions have been reported[19] and provide the best measure of electron density distribution and the configuration of dienyl anions. ^{13}C-NMR spectral data of bis(dienyl)magnesium were collected in this view as shown in Table 6. Assignment of the spectrum was done with nondecoupled spectrum and by partial decoupling. The striking feature of these data is that signals of C_1 and C_5 atoms of linear dienylmagnesium compounds **1**—**5** appeared in higher field than that of C_3 atom, while those of cyclic compound **6** and **7** appeared in lower field than the signal of C_3 carbon atoms consistent to the ^{1}H-NMR data. The values of the carbon-proton coupling constant were useless for the determination of the configuration. Based on ^{13}C-NMR, ^{1}H-NMR, and hydrolysis data, it is reasonable to conclude that bis(dienyl)magnesium of open chain structure except **5** assume primarily the terminally σ-bonded (*E*) structure but those of cyclic dienyl structure assume the centrally σ-bended (*Z*) structure.

Although no appreciable change in chemical shift was observed for **1**—**7** over a 100 °C temperature (−80—50 °C) within 10 Hz and no limiting structure was realized even at −100 °C, freezing of the dynamic equilibrium was realized by coordination of a bulky ligand such as 15-crown-5 or 1,4,7,10,13,16-hexaoxacyclooctadecane (18-crown-6). ^{1}H-NMR spectrum of 1 : 1 complex of 15-crown-5 or 18-crown-6 showed A_2BX pattern at 0—30 °C but it showed the limiting structure (see Table 5) below −40 °C. Chemical shift and relative intensity of the signals observed at −60 °C are characteristic of the terminally σ-bonded structure and resemble well to that of bis(pentadienyl)zinc·TMEDA complex.[20] This is the first example of freezing out of the equilibrium of allylic type magnesium compound. The complete equilibrium shift may be attained by the steric repulsion between the crown ether and the pentadienyl group. Examination of models which permits the 1,3-rearrangement showed the following structure to be the most plausible for this complex.

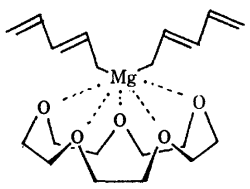

Solubility of the 1 : 1 crown ether complex in benzene becomes less than 1/5 of that of THF complex due to the increase in ionic character, being different from the behavior of the usual crown ether complexes.[21] Linear polyethers had no ability to freeze out the equilibrium even at −80 °C. Coordination of strong coordinating

TABLE 7. BOND LENGTHS [l/Å] AND BOND ANGLES [ϕ/°] IN $Mg(C_7H_{11})_2$·TMEDA
Estimated standard deviations are in parentheses.

Bond lengths			
Mg–N	2.202 (12)	C(2)–C(3)	1.402 (19)
Mg–C(1)	2.179 (15)	C(2)–C(6)	1.55 (3)
N–C(8)	1.49 (3)	C(3)–C(4)	1.466 (20)
N–C(9)	1.475 (20)	C(4)–C(5)	1.356 (22)
N–C(10)	1.49 (3)	C(4)–C(7)	1.54 (3)
C(1)–C(2)	1.467 (20)	C(8)–C(8′)	1.48 (5)
Bond angles			
N–Mg–N	84.2 (5)	C(3)-C(4)–C(7)	114.1 (13)
N–Mg–C(1′)	118.0 (6)	C(5)–C(4)–C(7)	119.7 (14)
N–Mg–C(1)	110.4 (6)	Mg–N–C(8)	104.4 (11)
C(1)–Mg–C(1′)	113.1 (6)	Mg–N–C(9)	112.5 (9)
C(1)–C(2)–C(3)	129.4 (13)	Mg–N–C(10)	111.8 (10)
C(1)–C(2)–C(6)	116.1 (13)	C(8)–N–C(9)	110.8 (13)
C(3)–C(2)–C(6)	114.5 (13)	C(8)–N–C(10)	106.4 (13)
C(2)–C(3)–C(4)	127.1 (13)	C(9)–N–C(10)	110.5 (12)
C(3)–C(4)–C(5)	126.3 (14)	C(8′)–C(8)–N	114.5 (18)

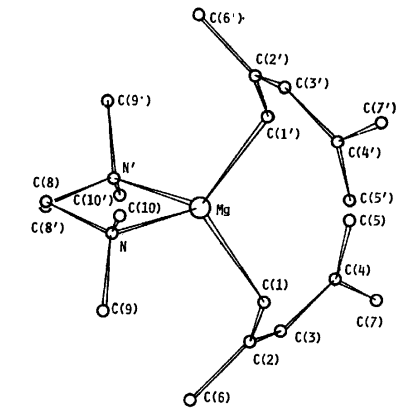

(a)

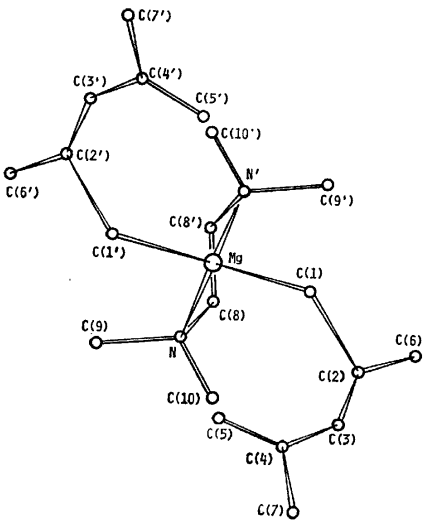

(b)

Fig. 2. Molecular structure of $Mg(C_7H_{11})_2$·TMEDA.
(a) Viewed down along the c axis.
(b) Viewed down along the two-fold axis.

ligand, trimethylamine oxide, was unable to shift the equilibrium and no significant changes in chemical shift were observed over a temperature range from 50 °C to −80 °C. Thus, steric factor rather than the donor property was considered to be dominant to bring about the complete shift of the equilibrium.

X-Ray Structural Studies of Bis(2,4-dimethyl-2,4-pentadienyl)magnesium·TMEDA. The molecular structure of **5** is given in Fig. 2. Bond lengths and bond angles are listed in Table 7. The molecules has a two-fold symmetry. The magnesium atom lies on a crystallographic two-fold axis parallel to the b axis, and is tetrahedrally coordinated by the two carbon atoms from two pentadienyl groups and two nitrogen atoms from the TMEDA. The dihedral angle between planes defined by Mg, C(1), and C(1′) and Mg, N, and N′ is 83.6°.

The remarkable feature of the structure is that the 2,4-dimethylpentadienyl group is terminally σ-bonded (1-η-C_7H_{11} structure) to the magnesium atom by the C(1) atom and has the (*Z*)-configuration (U-shape) but not the (*E*)-configuration (W-shape) like that observed for **1**—**4** in solutions by ^{1}H-NMR. The Mg–C(1) distance [2.179(15) Å] is the reasonable value. The Mg–C distances in $C_2H_5MgBr\cdot 2C_4H_{10}O$,[22] $[C_2H_5MgBr\cdot N(C_2H_5)_3]_2$,[23] $[C_2H_5Mg_2Cl_3\cdot(C_4H_8O)_3]_2$,[24] and $[(C_2H_5)_2Mg]_\infty$[25] are 2.15(2) Å, 2.18(2) Å, 2.19(3) Å, and 2.2$_6$ Å, respectively. Expected Mg–C covalent bond length for $C_6H_5MgBr\cdot 2C_4H_{10}O$[26] is 2.17 Å. Two double bonds in the dimethylpentadienyl group is not coplanar, the plane defined by the C(1), C(2), C(3), and C(6) atoms makes an angle of 22.6° with the plane made by C(3), C(4), C(5), and C(7). This is probably due to the steric repulsion between two methyl groups as mentioned before. In the pentadienyl moiety the bond alternation in bond length is observed, C(1)–C(2)=1.467(20), C(2)–C(3)=1.402(19), C(3)–C(4)=1.466(20), and C(4)–C(5)=1.356(22) Å. The C(2)–C(3) and C(4)–C(5) bond lengths are significantly smaller than the C–C bond(1.43 Å) of η^5-cyclopentadienyl group in $C_5H_5MgBr\cdot(C_2H_5)_2N(CH_2)_2N(C_2H_5)_2$.[27]

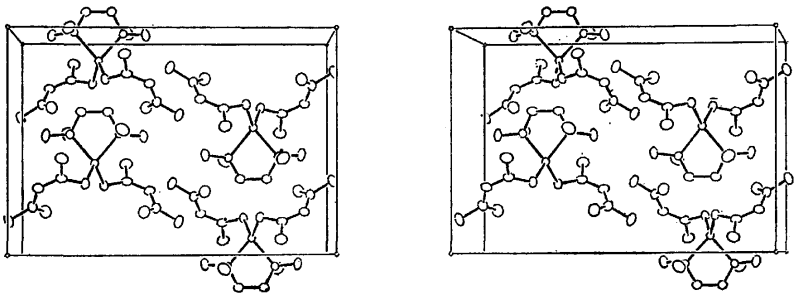

Fig. 3. A stereoscopic drawing of the crystal structure of $Mg(C_7H_{11})_2 \cdot TMEDA$.

The TMEDA coordinates to the magnesium atom by two nitrogen atom [Mg–N=2.202(12) Å]. The N–Mg–N′ angle[84.2(5) Å] largely deviates from tetrahedral angle and is comparable to that of $C_5H_5MgBr \cdot (C_2H_5)_2N(CH_2)_2N(C_2H_5)_2$ (82.5±0.5°) and that of $Li[(CH_3)_2N(CH_2)_2N(CH_3)_2]_2C_{10}H_8$(85.2°).[28] The Mg–N–C(8) angle[104.4(11)°] is also slightly smaller than the tetrahedral angle.

The crystal structure is shown in Fig. 3. No close intermolecular atomic contact less than the van der Waals distance(3.6 Å) was observed.

Regioselective Dienylation of Carbonyl Compounds. Addition of bis(dienyl)magnesium to carbonyl compounds was examined to check whether the abundancy of the solution species of **1**—**7** reflects the structure of the addition products. The result of the reaction with a simple ketone, acetone, is given in Table 8.

Table 8. Addition of ketones on the C_1 and C_3 carbon atoms of bis(dienyl)magnesium·TMEDA complexes[a]

Complex	Acetone		DIPK	
	C_1/%	C_3/%	C_1/%	C_3/%
1	2	98	100	0
2	2	98	100	0
3	5	95	65 35[b]	0
4	1	99	95	5
5	5	95	100	0
6	1	99	8	92
7	20	80	25	75

a) Reaction was carried out at 10 °C for 2 h in benzene. b) 2,5-Dimethyl-3-isopropyl-5,7-octadien-3-ol.

Regioselective addition occurred for **1**—**7**. The regioselectivity also depends on the ligand property. For example, compound **1** coordinated with THF, 1,2-dimethoxyethane, $CH_3O(CH_2CH_2O)_2CH_3$, $CH_3O(CH_2CH_2O)_3CH_3$, and $CH_3O(CH_2CH_2O)_4CH_3$ reacted with acetone on the C_3 carbon atom in 67, 81, 83, 78, and 77% conversion respectively in line with the hydrolysis data. The regioselectivity increased up to 99—100% by using 15-crown-5,18-crown-6, and tetramethylcyclam. The behavior to acetaldehyde was the same with that to acetone. In contrast to above, the reaction of **1**—**5** with a bulky ketone, diisopropyl ketone, gave 1,3-diene derivatives selectively presumably due to the steric repulsion between the isopropyl group and the diene moiety. The configuration of the dienyl group of the products obtained from **1**—**3** was trans. Similar behavior of the bulky ketone was found for the reaction with allylmagnesium compounds and is explained by S_E2' mechanism based on the kinetic studies.[29] Cyclic dienylmagnesium compounds also allow the selective reaction in this case.

Formation of Unsaturated Alcohols by Thermal Cracking of Bis(dienyl)magnesium·Cyclic Ether Complexes. Thermal cracking of bis(dienyl)magnesium·THF adduct followed by hydrolysis provided a novel route for the synthesis of unsaturated alcohols. Heating of THF complex of **1** in toluene at 120 °C for 3 h and hydrolysis of the reaction mixture gave 6,8-nonadien-1-ol (30%) and 5-vinyl-6-hepten-1-ol (70%) in 40—60% yield.

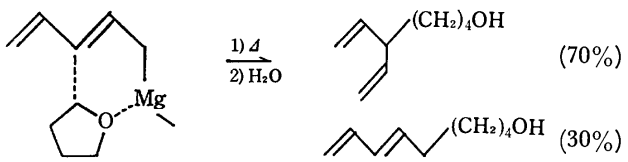

THF molecule was cleaved. By taking advantage of this reaction, synthesis of a precursor of an insect pheromone for *carpocapsa pomonella*[30] was attempted. Thermal cracking of oxepane complex of **2** gave 7-vinyl-8-decen-1-ol(63%) and its isomer, 8,10-dodecadien-1-ol in 6% yield. Thus, this reaction has an extensive utility in the synthesis of unsaturated alcohols with an elongated carbon chain. The order in reactivity of cyclic ethers followed that described for acid-catalyzed cleavage of cyclic ethers.[31]

Selective Synthesis of Trienes. Though transition

Table 9. Coupling reaction of allyl bromide with $(C_5H_7)_2$ Mg·2THF catalyzed by transition metal compounds[a]

Catalyst	Products/%	
	8	**9**
None	10	90
CuCl	1	99
$TiCl_2(\eta^5\text{-}C_5H_5)_2$	92	8
$ZrCl_2(\eta^5\text{-}C_5H_5)_2$	88	12
$NbCl_2(\eta^5\text{-}C_5H_5)_2$	60	40

a)Reaction conditions; 0 °C, 20 h in benzene, catalyst; 2 mol% for the magnesium compound. b) Reaction was carried out at 30 °C for 2 h.

metal-catalyzed triene synthesis are known for several conjugated dienes,[32] novel triene synthesis by the coupling reaction of dienylmagnesium compound with allyl halides is attractive since it has wider applicability. As a typical example, the reaction of pentadienylmagnesium bromide with allyl bromide catalyzed by transition metal compounds was examined (Table 9). The reaction catalyzed by $MX_2(\eta^5\text{-}C_5H_5)_2$(M=Zr,[33] Ti[34]) gave 3-vinyl-1,5-hexadiene **8** regioselectively while with copper(I) chloride catalyst it gave 1,3,7-octatriene **9** selectively. The poor selectivity by $NbCl_2(\eta^5\text{-}C_5H_5)_2$[35] may be due to its poor solubility. This type of reaction will be useful for obtaining desired trienes by an appropriate combination of dienylmegnesium compounds with allyl halides. The selectivity by Ni(II) chloride, Co(II) chloride, or $NiBr_2(PPh_3)_2$ catalyzed reaction was low while these were active for selective synthesis of linear tetraenes from dienyl anions.[7]

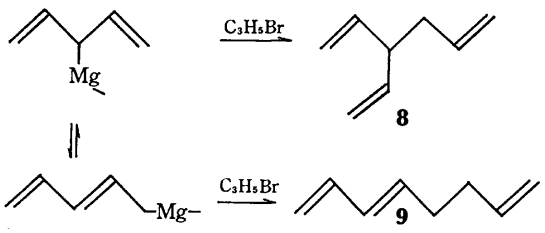

Experimental

Anhydrous magnesium bromide and magnesium chloride were prepared by the reaction of magnesium (1.0 mol) with 1,2-dibromoethane (1.0 mol) or 1,2-dichloroethane (1.0 mol) in ether at 0 °C and were stored in argon.[36] Commercial anhydrous magnesium halides were unsuitable for this examination because they include hydrates. All ethers were dried over Na/K alloy and distilled. Crown ethers (Nisso Chem. Corp.) were used without further purification or drying. TMEDA was dried over calcium hydride and distilled. Trimethylamine oxide was prepared according to the method of Meisenheimer[37] and was sublimed (140 °C/10^{-4} mmHg). Tetramethylcyclam was synthesized by the known method.[38] 1-Bromo-2,4-hexadiene was prepared from sorbic acid[39] in the usual manner. Potassium dienides were prepared by the procedure previously reported.[7] Melting points were measured in a sealed tube and were uncorrected. GC analysis and the separation of the reaction products were made with a Hitachi Model 163 gas chromatograph using a capillary column OV-1 or HB 2000 and a Varian-Aerograph Model 700 gas chromatograph using a column packed with Silicone DC-550. NMR spectra were recorded on a Varian XL-100 instrument with a VFT-100-620L Fourier transform accessory. IR spectra were recorded on a Hitachi EPI-2 spectrometer. All the procedures were conducted in an argon atomosphere by using flow system. Elemental analysis was carried out for the key substances with Yanagimoto Model MT-2 CHN-analyzer.

Preparation of Bis(pentadienyl)magnesium·TMEDA Complex **1**. A THF solution (40 ml) of anhydrous magnesium bromide (6.4 g, 35 mmol) was added over a 20 min period to potassium pentadienide (6.4 g, 60 mmol) dispersed in THF (100 ml) in a 300 ml Schlenk tube with stirring at 0—5 °C. The magnetic stirring continued for 3 h at 10 °C and the orange color of the solution changed to pale yellow. After the addition of pentane (100 ml), the resulting precipitate of magnesium bromide was separated by centrifugation with the use of a two-necked glass tube fitted with rubber stoppers. The supernatant liquid was evaporated to dryness and a mixture of diethyl ether (100 ml) and pentane (50 ml) was added to the residue for complete separation of the salt. Evaporation of the ether–pentane soluble fraction gave $(C_5H_7)_2Mg\cdot 2THF$ as pale yellow oil. Yield; 70—80% (6.3—7.2 g). Toluene solution of this complex gave pentadiene and THF in a 1:1 molar ratio upon hydrolysis as evidenced by GC. TMEDA complex was prepared by the addition of TMEDA (7.5 ml, 50 mmol) dissolved in pentane (40 ml) to the THF complex (6.0 g, 20 mmol) in THF (10 ml), stirring the mixture for 2 h at room temperature and then cooling to −20 °C to induce the crystallization. Yield; 85% (5.2 g). Concentration by evaporation and cooling of the supernatant solution further gave TMEDA complex (0.6 g). Recrystallization was made in 5:1 hexane–THF at −20 °C.

Preparation of Bis(pentadienyl)magnesium·diethyl ether Complex. Diethyl ether (150 ml) was added to the THF-free potassium pentadienide (5.3 g, 50 mmol) in 300 ml Schlenk tube cooled with ice–water (addition of potassium pentadienide to ether should be avoided since the THF-free potassium dienide is very explosive in the air). Anhydrous magnesium bromide (5.2 g, 28 mol) was added at once and magnetic stirring was continued for 10 h at 30 °C until the yellow solid changes to a white powder. The supernatant pale yellow solution was evaporated and the resulting oily ether complex was washed with two portions of pentane (30 ml) at −78 °C. Yield; 60% (4.7 g) based on potassium dienide. This ether complex can not be prepared from the THF complex **1** by ligand exchange reaction.

Preparation of Bis(pentadienyl)magnesium·15-crown-5 ether Complex. A solution of 15-crown-5 (2.2 g, 10 mmol) in benzene (10 ml) was added to bis(pentadienyl)magnesium·ethyl ether complex (3.2 g, 10 mmol) dissolved in benzene (20 ml) at room temperature with magnetic stirring, crystals of the complex being precipitated instantly. The precipitate was washed with two portions of pentane (20 ml) and recrystallized in toluene. Yield; 98%. The relative signal intensity ratio in ^{1}H-NMR spectrum showed the formation of 1:1 complex.

Preparation of Pentadienylmagnesium Bromide. In the same reaction conditions and the same procedures to the preparation of **1**, Grignard type dienylmagnesium bromide can be prepared by 1:1 reaction of a dienyl anion and magnesium bromide. For example, the reaction of potassium pentadienide (5.3 g, 50 mmol) with magnesium bromide (10.1 g, 55 mmol) in THF at 30 °C for 3 h gave pentadienylmagnesium bromide coordinated with two moles of THF as an oily substance. Yield; 90% (9.9 g). The reaction of the resulting THF complex (6.6 g, 30 mmol) with TMEDA (6 ml, 40 mmol) gave TMEDA complex having mp 122 °C quantitatively.

Preparation of Bis(dienyl)magnesium·TMEDA Complexes **2**—**7**. In essentially the same way to the preparation of **1**, crystals of TMEDA complexes of **2**—**7** were prepared. Recrystallization of **4** and **7** were done in a mixture of toluene and pentane (1:10) at 0 °C.

Crystal Data and Structure Determination of Bis(2,4-dimethylpentadienyl)magnesium·TMEDA. $C_{20}H_{38}N_2Mg$, *F.W.* 330.9, orthorhombic, space group Pbcn (No. 60), (20 °C) a=10.145(2), b=12.486(2), c=17.587(2) Å, V=2227.8(5) Å^3, D_C=0.987 g cm^{-3} for Z=4; (−60 °C) a=10.105(6), b=12.325(6), c=17.580(9) Å, V=2189.6(21) Å^3, D_C=1.004 g cm^{-3} for Z=4.

As the crystals are unstable in air, a crystal with suitable

size was selected and sealed in a thin-walled glass capillary tube. In spite of the repeated recrystallizations and the very careful sealing only a few crystals were found useful for the X-ray analysis. Preliminary X-ray photographic study determined the corresponding space group as Pbcn (systematic absence of reflections, $0kl$: $k=2n+1$, $h0l$: $l=2n+1$, $hk0$: $h+k=2n+1$).

Unit-cell dimensions and reflection intensities were measured on a Rigaku automated, four-circle diffractometer. Zirconium-filtered Mo $K\alpha$ radiation was used. The θ-2θ scan technique was applied. The scan rate was 4° min^{-1} and the scan range for each reflection was $\Delta 2\theta=(2.0+0.70\tan\theta)°$. Background of 5 s were measured before and after each scan. Intensity data were first collected at 20 °C, but the higher angle reflections were too weak to be observed and the structure determined was not sufficiently accurate. Intensity data were therefore collected again at −60 °C, a total of 1185 (714 non-zero) reflections being observed ($2\theta\leqq 42°$). But the number of unobserved reflections was still large. Low temperature was attained by the gas flow method of liquid nitrogen. However, as the crystal was sealed in the glass-capillaly tube, the deposition of the frost on the glass due to the moisture in air was much easier than the crystal without sealing in the glass capillary. The lowest temperature attained without the frost was only −60 °C. The intensity data were corrected for usual Lorentz and polarization effects but not for absorption [μ(Mo $K\alpha$)=0.88 cm^{-1}].

Since the space group is Pbcn and four molecules are contained per unit-cell, the molecule must lie on a special position, two-fold axis or center of symmetry.

The structure was solved by the heavy atom method, and refined isotropically by the block-diagonal least-squares procedure (*HBLS V*).[40] The room temperature structure was first determined, but the convergence of the refinement was insufficient (R=0.185 for 807 non-zero reflections). The structure was, therefore, refined using the intensity data obtained at −60 °C. After the R value decreased to 0.162, the refinement was carried out anisotropically with unit weight, and the final R value was rather high as 0.135 for 714 non-zero reflections. This limits the accuracy of the result. Atomic scattering factors were taken from the International Tables for X-Ray Crystallography, Vo. IV.[41] Calculations were done on an ACOS series 77 system 700 computer at Osaka University.[42] The final atomic positional and thermal parameters are listed in Table 10.[43]

Preparation of Pentadienylaluminium Compounds. Granules of anhydrous aluminium chloride (2.7 g, 20 mmol) was added to the potassium pentadienide (2.1 g, 20 mmol) dissolved in THF (60 ml) at 0 °C with stirring. After refluxing the solution for 30 min, the solution was reduced to *ca.* 30 ml by evaporation and then hexane (50 ml) was added to induce the precipitation of the salt. The supernatant liquid separated by centrifugation was evaporated to dryness and washed with hexane (50 ml) to give potassium tetrakis(pentadienyl) aluminium·THF complex as an oily material. Yield: 92% (7.4 g). ^{1}H-NMR (C_6D_6) δ=6.10, 6.30 (m, 8, CH=), 5.93 (d of t, 4, CH–), 4.90 (d of d, 4, J=14.0, *trans* CH_2=), 4.72 (d of d, 4, J=9.0, *cis* CH_2=), 3.65 (m, 4, CH_2O of THF), 1.40 (m, 4, CH_2 of THF), 0.16 (d, 8, CH_2).

In the similar manner, the 2:1 reaction of $(CH_3)_2AlCl$ with potassium pentadienide gave potassium dimethyldipentadienylaluminium in 70% yield. No tripentadienylaluminium corresponding to bis(pentadienyl)magnesium was obtained as evidenced by distillation of the whole reaction products in high vacuum. ^{1}H-NMR (C_6D_6) δ=6.14—6.33 (m, 4, CH), 5.60 (d of t, 2, J=14.0, CH–CH_2), 4.78, 4.72 (d of d, 8, CH_2=), 3.53 (m, 4, CH_2O of THF), 1.60 (m, 4, CH_2 of THF), 0.90 (d, 4, CH_2), −0.12 (s, 6, CH_3). Hydrolysis of $K[(C_5H_7)_4Al]$

Table 10. Atomic positional and thermal parameters of $Mg(C_7H_{11})_2$·TMEDA
Estimated standard deviations in parentheses.

Atom	X	Y	Z
Mg	0. (0)	0.0790(5)	0.2500(0)
N(1)	0.0508(11)	−0.0535(8)	0.3287(6)
C(1)	0.1745(14)	0.1764(11)	0.2249(7)
C(2)	0.2466(14)	0.1554(10)	0.1541(8)
C(3)	0.2275(14)	0.1999(11)	0.0815(8)
C(4)	0.1295(15)	0.2817(12)	0.0595(8)
C(5)	0.0135(15)	0.3025(14)	0.0955(9)
C(6)	0.3593(15)	0.0707(12)	0.1588(10)
C(7)	0.1657(18)	0.3452(14)	−0.0125(9)
C(8)	−0.004(3)	−0.1527(11)	0.2919(8)
C(9)	0.1948(14)	−0.0640(14)	0.3405(10)
C(10)	−0.0187(19)	−0.0422(13)	0.4029(8)

Atom	B(11)	B(22)	B(33)	B(12)	B(13)	B(23)
Mg	0.0116(7)	0.0061(5)	0.0029(3)	0. (0)	0.0004(8)	0. (0)
N(1)	0.0146(15)	0.0070(9)	0.0032(4)	0.0002(19)	−0.0003(14)	−0.0007(11)
C(1)	0.0154(19)	0.0103(13)	0.0033(6)	−0.011(3)	0.0034(18)	−0.0012(15)
C(2)	0.0111(16)	0.0066(11)	0.0061(7)	−0.005(3)	0.001(2)	−0.0001(15)
C(3)	0.0113(18)	0.0075(11)	0.0056(7)	−0.003(3)	−0.0012(19)	0.0007(16)
C(4)	0.017(3)	0.0101(14)	0.0040(7)	−0.009(3)	−0.006(2)	0.0005(16)
C(5)	0.0113(19)	0.0157(17)	0.0064(8)	0.001(4)	0.003(3)	0.002(3)
C(6)	0.014(2)	0.0107(15)	0.0075(9)	0.012(3)	−0.001(3)	0.002(3)
C(7)	0.024(3)	0.0151(19)	0.0040(7)	0.002(4)	−0.000(3)	0.0048(19)
C(8)	0.035(4)	0.0075(12)	0.0048(7)	0.000(4)	−0.012(4)	0.0001(15)
C(9)	0.0115(19)	0.0144(17)	0.0083(9)	0.002(4)	−0.008(3)	0.005(3)
C(10)	0.027(3)	0.0142(17)	0.0033(6)	0.010(4)	0.008(3)	0.0021(17)

and $K[(C_5H_7)_2(CH_3)_2Al]$ in toluene produced 1,4-pentadiene exclusively (99%) in 98% GC yield. Reaction of acetaldehyde and acetone, followed by hydrolysis gave 1,4-diene derivatives (purity, 99%) in 90% yield in both cases (spectral data of the products are given later in this section).

Dienylation of Carbonyl Compounds with **1**—**7**. To the benzene solution (60 ml) of bis(dienyl)magnesium **1**—**7** (20 mmol) was added acetone (2.9 ml, 40 mmol) dropwise at 5 °C. The reaction mixture was stirred for 2 h at 30 °C and hydrolyzed with 2 mol dm^{-3} HCl at 5 °C. After filtration, benzene fraction was distilled under reduced pressure. The reaction of bis(dienyl)magnesium with acetaldehyde was carried out in the same manner but with diisopropyl ketone at 50 °C for 3 h.

Dienylation of Acetone. *2-Methyl-3-vinyl-4-penten-2-ol from* **1**: IR (neat) 3440 (OH), 1638 (C=C), 1015, 915 cm^{-1} (CH=CH_2); ^{1}H-NMR ($CDCl_3$) δ=5.94 (d of d of d, 2, CH=), 5.15 (d of d, 2, J=16.5, *trans* CH_2=), 5.02 (d of d, 2, J=10.2, *cis* CH_2=), 2.75 (t, 1, J=8.0, CH), 1.98 (s, 1, OH), 1.18 (s, 6, CH_3); Found: C, 76.07; H, 11.4%; M^+-1, 125. Calcd for $C_8H_{14}O$: C, 76.19; H, 11.1%; M, 126.

trans-*2-Methyl-3-vinyl-4-hexen-2-ol from* **2**: IR (neat) 3450, 1635, 990, 912 cm^{-1}; ^{1}H-NMR ($CDCl_3$) δ=5.71 (d of d of d, 1, CH), 5.53 (d of d, 1, J=13.7 *trans* CH=CHCH$_3$), 5.53 (d of q, 1, CH), 5.12 (d of d, 1, J=10.3 *cis* CH_2), 5.07 (d of d, 1, J=16.5 *trans* CH_2), 3.14 (d of d, J=8.1, CH), 2.09 (s, 1, OH), 1.75 (d, 3, CH_3), 1.15 (s, 6, CH_3).

cis-*2-Methyl-3-vinyl-4-hexen-2-ol from* **2**: IR (neat) 3450, 1635, 990, 719 cm^{-1}; ^{1}H-NMR ($CDCl_3$) δ=5.71 (d of d of d, 1, CH), 5.53 (d of d, 1, J=9.2, *cis* CH=CHCH$_3$), 5.53 (d of q, 1, CH=), 5.08, 5.16 (m, 2, CH_2), 2.72 (d of d, J=8.0, CH), 2.09 (s, 1, OH), 1.87 (d, 3, CH_3), 1.15 (s, 6, CH_3).

2,4-Dimethyl-3-vinyl-4-penten-2-ol from **3**: IR (neat) 3490, 1635, 1000, 915 cm^{-1}; ^{1}H-NMR ($CDCl_3$) δ=6.10 (d of d of d, 1, CH), 5.15 (d of d, 1, J=10.4, for *cis* CH_2=), 5.02 (d, 2, J=2.2, CH_2), 5.00 (d of d, 1, CH_2), 2.75 (d, 1, CH), 1.87 (s, 3, CH_3), 1.73 (s, 1, OH), 1.25 (s, 6, CH_3).

2,3-Dimethyl-3-vinyl-4-penten-2-ol from **4**: ^{1}H-NMR ($CDCl_3$) δ=5.82 (d of d, 2, CH), 5.14 (d of d, 2, J=10.4 for *cis* CH_2, J=2.8 for gem H), 4.99 (d of d, 2, J=16.5, *trans* CH_2), 1.73 (s, 1, OH), 1.25 (s, 3, CH_3), 1.24 (s, 6, CH_3); MS, Found: M^+-1, 139.

2,4-Dimethyl-3-isopropenyl-4-penten-2-ol from **5**: IR (neat) 3500, 1643, 1020, 890 cm^{-1}; ^{1}H-NMR ($CDCl_3$) δ=4.91 (d, 4, J=2.9, CH_2), 2.54 (s, 1, CH), 2.24 (s, 1, OH), 1.72 (s, 6, CH_3), 1.16 (s, 6, CH_3); Found: C, 77.9; H, 11.5%; M^+-1, 153. Calcd for $C_{10}H_{18}O$; C, 77.86; H, 11.76%; M, 154.

2-(2,6-Cycloheptadienyl)-2-propanol from **6**: ^{1}H-NMR ($CDCl_3$) δ=5.81 (d of t, 2, J=12.2, CH_2CH=), 5.68 (d of d, 2, CH), 3.20 (d of d, 1, CH), 2.27 (m, 4, CH_2), 1.52 (s, 1, OH), 1.27 (s, 6, CH_3).

2-(2,7-Cyclooctadienyl)-2-propanol from **7**: IR (neat) 3510, 1638, 1075 cm^{-1}; ^{1}H-NMR ($CDCl_3$) δ=5.90 (d of d, 2, J=12.2, CH), 5.49 (d of t, 2, CH), 3.30 (d of d, 1, J=6.6, CH), 2.18 (m, 4, CH_2), 2.00 (s, 1, OH), 1.35 (m, 2, CH_2), 1.16 (s, 6, CH_3); Found: C, 79.46; H, 10.92%; M^+-1, 165. Calcd for $C_{11}H_{18}O$: C, 79.47; H, 10.91%; M, 166.

Dienylation of Acetaldehyde. *3-Vinyl-4-penten-2-ol from* **1**: IR (neat) 3380, 1637, 999, 915 cm^{-1}; ^{1}H-NMR ($CDCl_3$) δ=5.89 (d of d of d, 2, CH), 5.15 (d of d, 2, J=10.0, CH_2), 5.03 (d of d, 2, J=16.2, CH_2), 3.76 (d of d, 1, J=6.0, C<u>H</u>–CH_3), 2.82 (bt, 1, CH), 1.98 (s, 1, OH), 1.20 (d, 3, J=6.2, CH_3); MS, Found: M^+-1, 111.

1-(2,7-Cyclooctadienyl)ethanol from **7**: IR (neat) 3420, 1635, 1070 cm^{-1}; ^{1}H-NMR ($CDCl_3$) δ=5.65 (d of t, 2, CH), 5.62 (d of d, 2, J=11.8, CH), 3.82 (d of q, 1, CH), 3.25 (bt, J=6.5, CH), 2.30 (m, 4, CH_2), 1.98 (s, 1, OH), 1.47 (m, 2, CH_2), 1.20 (d, 3, J=6.8, CH_3); MS, Found: M^+-1, 151.

Dienylation of Diisopropyl Ketone. *2-Methyl-3-isopropyl-5,7-octadien-3-ol from* **1**: IR (neat) 3500, 1640, 1605, 988, 830, 784 cm^{-1}; ^{1}H-NMR ($CDCl_3$) δ=6.35 (d of d of d, 1, CH), 5.95 (d of t, 1, J=15.5, CH), 5.92 (d of d, 1, J=9.5, CH), 5.12 (d of d, 1, J=16.5, *trans* CH_2=CH), 5.02 (d of d, 1, J=10.2, *cis* CH_2=CH), 2.38 (d, 2, J=7.0, CH_2), 1.88 [m, 2, C<u>H</u>(CH_3)$_2$], 1.30 (s, 1, OH), 0.98 (d, 12, J=7.3, CH_3); Found: C, 78.85; H, 12.25%; M^+-1, 181. Calcd for $C_{12}H_{22}O$: C, 79.06; H, 12.16%; M, 182.

2-Methyl-3-isopropyl-5,7-nonadien-3-ol from **2**: IR (neat) 3500, 988, 950 cm^{-1}; ^{1}H-NMR ($CDCl_3$) δ=6.12 (d of d, 1, J=15.5, CH), 5.90 (d of d, 1, J=15.6, C<u>H</u>=CHCH$_2$), 5.52 (d of q, 1, CH), 5.48 (d of t, 1, CH), 2.30 (d, 2, J=7.5, CH_2), 1.92 [m, 2, C<u>H</u>(CH_3)$_2$], 1.73 (d, 3, J=6.5, CH_3), 1.40 (s, 1, OH), 0.95 (d, 12, J=7.5, CH_3).

2,5-Dimethyl-3-isopropyl-5,7-octadien-3-ol from **3**: IR (neat) 3510, 1644, 1610, 995, 898 cm^{-1}; ^{1}H-NMR ($CDCl_3$) δ=6.45 (d of d of d, 1, CH), 6.01 (d, 1, J=10.2, CH), 5.12 (d of d, 1, J=16.7, CH_2=), 5.00 (d of d, 1, J=10.2, CH_2=CH), 2.28 (s, 2, CH_2), 1.89 (m, 2, C<u>H</u>–CH_3), 1.59 (s, 1, OH), 0.98 (d, 12, CH_3).

*2,7-Dimethyl-3-isopropyl-5,7-octadien-3-ol from***3** : IR (neat) 3510, 1640, 905 cm^{-1}; ^{1}H-NMR ($CDCl_3$) δ=6.20 (d, 1, J=15.2, CH), 5.74 (d of t, 1, CH), 4.88 (d, 2, CH_2=), 2.34 (d, 2, J=8.4, CH_2), 1.89 (m, 2, C<u>H</u>–CH_3), 1.59 (s, 1, OH), 0.98 (d of d, 12, J=7.0 and 2.8, CH_3).

2,6-Dimethyl-3-isopropyl-5,7-octadien-3-ol from **4**: IR (neat) 3500, 1640, 1608, 990, 894 cm^{-1}; ^{1}H-NMR ($CDCl_3$) δ=6.43 (d of d, 1, CH), 5.64 (t, 1, CH), 5.13 (d of d, 1, J=17.0, CH_2=CH), 4.99 (d of d, 1, J=10.8, CH_2=CH), 2.42 (d, 2, J=7.8, CH_2), 1.89 (m, 2, C<u>H</u>CH_3), 1.78 (s, 3, CH_3), 1.28 (s, 1, OH), 0.97 (d, 12, J=7.5 and 2.8, CH_3); MS, Found: M^+-1, 195.

2,5,7-Trimethyl-3-isopropyl-5,7-octadien-3-ol from **5**: IR (neat) 3570, 1635, 894 cm^{-1}; ^{1}H-NMR ($CDCl_3$) δ=5.81 (s, 1, CH), 5.01, 4.85 (d, 2, J=2.5, CH_2=), 2.33 (s, 2, CH_2), 1.98, 1.85 (two s, 6, CH_3), 1.93 (m, 2, C<u>H</u>–CH_3), 1.35 (s, 1, OH), 0.98 (d, 12, CH_3); Found: C, 79.95; H, 12.25%; M^+-1, 209. Calcd for $C_{14}H_{26}O$: C, 79.93; H, 12.46%; M, 210.

3-(2,6-Cycloheptadienyl)-2,4-dimethyl-3-pentanol from **6**: IR (neat) 3510, 1665, 1641 cm^{-1}; ^{1}H-NMR ($CDCl_3$) δ=6.10 (d of d, 2, J=11.5, CH), 5.56 (d of t, 2, CH), 3.20 (bt, 1, CH), 2.30 (m, 4, CH_2), 1.90 (m, 2, CH), 1.60 (s, 1, OH), 1.00 (d, 12, CH_3); Found: C, 80.71; H, 11.60%; M^+-1, 207. Calcd for $C_{14}H_{24}O$: C, 80.70; H, 11.62%; M, 208.

3-(2,7-Cyclooctadienyl)-2,4-dimethyl-3-pentanol from **7**: IR (neat) 3370, 1658, 1080 cm^{-1}; PMR ($CDCl_3$) δ=5.3—5.8 (m, 4, CH), 3.58 (t, 1, CH), 2.38 (m, 4, CH_2), 2.30 (s, 1, OH), 1.90 (m, 2, CH), 1.40 (m, 2, CH_2), 1.00 (d, 12, CH_3).

Thermal Cracking of Pentadienylmagnesium·THF Complexes. Bis(pentadienyl)magnesium·THF complex (4.0 g) dissolved in toluene (50 ml) which contains 5 mol equivalent of THF was heated to 120 °C for 3 h in a sealed tube, gray precipitates of degradation products being formed. Resulting mixture was hydrolyzed with 2 mol dm^{-3} HCl and the toluene soluble fraction was distilled. The ratio of 6,8-nonadien-1-ol to 5-vinyl-6-hepten-1-ol was 3:7. Yield, 40%. In the same way, thermal cracking of pentadienylmagnesium bromide·THF complex was carried out at 130 °C for 4 h, the same products being obtained in a 7:3 ratio in 60% yield.

6,8-Nonadien-1-ol: IR (neat) 3450, 1642, 1605, 987, 905 cm^{-1}; ^{1}H-NMR ($CDCl_3$) δ=6.5—6.6 (m, 2, CH), 5.62 (d of t, 1, J=15.5, CH), 5.00, 5.12 (m, 2, CH_2=), 3.68 (t, 2, CH_2), 2.16 (d of t, 2, CH_2), 2.20 (s, 1, OH), 1.45 (m, 6, CH_2); M^+, 140. Calcd for $C_9H_{16}O$: M, 140.

5-Vinyl-6-hepten-1-ol: IR (neat) 3500, 1635, 995, 912 cm^{-1}; ^1H-NMR ($CDCl_3$) δ=5.78 (m, 2, CH), 5.00 (d of d, 2, J=10.2, *cis* CH_2=CH), 4.95 (d of d, 2, J=17.2, *trans* CH_2=CH), 3.62 (bt, 2, J=6.9, CH_2), 2.69 (m, 1, J=9.2, CH), 2.35 (s, 1, OH), 1.44 (m, 6, CH_2); Found: C, 77.85; H, 10.91%; M^+-1, 139. Calcd for $C_9H_{15}O$: C, 77.66; H, 10.85%; M, 140.

Thermal Cracking of Bis(hexadienyl)magnesium·oxepane Compound. Oxepane complex of bis(hexadienyl)magnesium was prepared by 2:1 reaction of THF free potassium hexadienide (2.4 g, 20 mmol) with magnesium bromide (1.8 g, 10 mmol) in oxepane (30 ml). After evaporation of oxepane in vacuum, oxepane complex was extracted from the residue with diethyl ether (100 ml). Bis(hexadienyl)magnesium·oxepane complex was obtained as an oily substance by evaporation of diethyl ether. Thermal craking was carried out in toluene at 120 °C for 5 h after the addition of 10 mol equivalent of oxepane. Yield, 40%.

8,10-Dodecadien-1-ol: IR (neat) 3510, 1640, 1602, 987, 910 cm^{-1}; ^1H-NMR ($CDCl_3$) δ=6.4—6.5 (m, 2, CH), 5.50 (d of t, 1, J=16.0, CH), 5.40 (d of q, 1, J=15.5, CH), 3.68 (bt, 2, J=6.9, CH_2), 2.10 (d of t, 2, CH_2), 2.20 (s, 1, OH), 1.68 (d, 3, CH_3), 1.49 (m, 10, CH_2), M^+-1, 181. Calcd for $C_{12}H_{22}O$: M, 182.

7-Vinyl-8-decen-1-ol: IR (neat) 3505, 1636, 995, 911 cm^{-1}; ^1H-MNR ($CDCl_3$) δ=5.81 (m, 1, CH), 5.62 (d of d, 1, J=15.2, CH), 5.50 (d of q, 1, CH), 5.00 (m, 2, CH_2), 3.65 (bt, 2, CH_2), 2.75 (m, 1, CH), 1.65 (d, 2, CH_3), 1.49—1.52 (m, 10, CH_2); Found: C, 79.53; H, 12.05%; M^+-1, 181. Calcd for $C_{12}H_{22}O$: C, 79.04; H, 12.18%; M, 182.

Preparation of Trienes: Catalysts, MCl_2 (η^5-C_5H_5)$_2$ (M=Ti, Zr, Nb, 2 mol%) or CuCl (0.12 g, 5 mol% to magnesium compounds), was added to the diethyl ether solution (100 ml) of pentadienylmagnesium bromide·2THF (7.9 g, 25 mmol) cooled to 0 °C and then 3-bromopropene (3.5 ml, 40 mmol) was added dropwise with vigorous stirring. The mixture was stirred for 20 h at 0 °C, then warmed to 30 °C for 1 h and quenched with 2 mol dm^{-3} HCl. Diethyl ether fraction was distilled. Typical yield: 90% based on 3-bromopropene.

3-Vinyl-1,5-hexadiene: IR (neat) 1650, 1635 cm^{-1}; ^1H-NMR ($CDCl_3$) δ=5.84 (d of d of d, 2, CH), 5.80 (d of d of d, 1, CH), 5.02 (d of d, 2, J=10.2, CH_2=CH), 4.98 (d of d, 2, J=16.0, CH_2=CH), 5.01, 4.98 (m, 2, CH_2=), 2.83 (m, 1, J=6.2, C<u>H</u>CH_2), 2.21 (d of d, 2, J=6.4, C<u>H</u>$_2$CH=); M^+, 108. Calcd for C_8H_{12}: M, 108.

1,3,7-Octatriene: IR (neat) 1645, 1604, 1004, 900 cm^{-1}; PMR ($CDCl_3$) δ=6.4—6.5 (m, 2, CH), 5.80 (m, 1, CH), 5.69 (d of t, 1, J=16.0, CH), 5.10, 4.98 (d of d, 2, CH_2), 5.05, 4.98 (d of d, 2, CH_2), 2.19 (m, 4, CH_2); MS, Found: M^+, 108.

References

1) a) L. Miginiac, *Tetrahedron Lett.*, **1976**, 3083; b) F. Barbot and Ph. Miginiac, *J. Organomet. Chem.*, **145**, 269 (1978); c) F. Derguini-Boumechal, R. Lorne, and G. Linstrumelle, *Tetrahedron Lett.*, **1977**, 1181; d) H. Lehmkuhl and D. Reiner, *J. Organomet. Chem.*, **57**, 29 (1973); e) H. Lehmkuhl, D. Reiner, D. Henneberg, and G. Schrith, *J. Organomet. Chem.*, **57**, 49 (1973); f) H. Lehmkuhl, D. Reiner, J. Brandt, and G. S. Schroth, *J. Organomet. Chem.*, **57**, 39 (1903).

2) a) M. Tomoi and H. Kakiuchi, *Polym. J.*, **5**, 195 (1973); b) E. W. Duck, D. Grant, A. V. Butcher, and D. G. Timms, *Eur. Polym. J.*, **10**, 77 (1974); c) B. Dobbs, R. Jackson, J. N. Gaitskell, R. F. Gray, G. Lynch, D. T. Thompson, and R. Whyman, *J. Polym. Sci., Polym. Chem. Ed.*, **14**, 1429 (1976).

3) a) T. Cohen and I. Cristea, *J. Am. Chem. Soc.*, **98**, 748 (1976); b) L. Farady, L. Bencze, and L. Marko, *J. Organomet. Chem.*, **10**, 505 (1967); c) S. Akutagawa and S. Otsuka, *J. Am. Chem. Soc.*, **97**, 6870 (1975).

4) a) C. W. Spangler, *Tetrahedron*, **32**, 2681 (1976); b) F. Gerard and Ph. Miginiac, *J. Organomet. Chem.*, **155**, 271 (1978); c) F. Gerard and Ph. Miginiac, *C. R. Acad. Sci., Ser. B*, **273**, 674 (1971).

5) R. Hoffmann and R. A. Olofson, *J. Am. Chem. Soc.*, **88**, 943 (1966).

6) R. J. Bushby and A. S. Patterson, *J. Organomet. Chem.*, **132**, 163 (1977).

7) a) H. Yasuda, Y. Ohnuma, and A. Nakamura, *Bull. Chem. Soc. Jpn.*, **52**, 2036 (1979); b) H. Yasuda, T. Narita, and H. Tani, *Tetrahedron Lett.*, **1973**, 2443.

8) D. A. Hutchison, K. R. Beck, R. A. Benkeser, and J. B. Grutzner, *J. Am. Chem. Soc.*, **95**, 7075 (1973).

9) a) K. Fujita, Y. Ohnuma, H. Yasuda, and H. Tani, *J. Organomet. Chem.*, **113**, 201 (1976); b) H. Yasuda, Y. Nakano, K. Natsukawa, and H. Tani, *Macromolecules*, **11**, 586 (1978).

10) G. Weber, W. Saenger, F. Vogtle, and H. Sieger, *Angew. Chem., Int. Ed.*, **18**, 226 (1979).

11) a) Y. Nakano, K. Natsukawa, H. Yasuda, and H. Tani, *Tetrahedron Lett.*, **1972**, 2833; b) K. Fujita, Ph. D. Thesis, Osaka University, 1974.

12) a) R. B. Bates, D. W. Gosselink, and J. A. Kaczynski, *Tetrahedron Lett.*, **1967**, 205; b) R. B. Bates, S. Brenner, C. M. Cole, E. W. Davidson. G. D. Forsythe, D. A. Mc Combs, and A. S. Roth, *J. Am. Chem. Soc.*, **95**, 926 (1973); c) G. J. Heiszwolf, J. A. A. Van Drunen, and H. Kloosterziel, *Recl. Trav. Chim. Pays-Bas*, **88**, 1377 (1969).

13) H. Kloosterziel and E. Zwanenburg, *Recl. Trav. Chim. Pays-Bas*, **88**, 1373 (1969).

14) E. A. Baude, *Chem. Ind. (London)*, **1974**, 1557.

15) N. L. Allinger and J. T. Sprauge, *Tetrahedron*, **29**, 3811 (1973).

16) F. Zuccarello, G. Buenmi, and G. Favini, *J. Mol. Struct.*, **18**, 295 (1973).

17) N. L. Allinger, J.F. Viskocil, Jr., U. Burkert, and Y. Yuh, *Tetrahedron*, **32**, 33 (1976).

18) F. A. L. Anet and I. Yavari, *Tetrahedron Lett.*, **1975**, 1567.

19) W. T. Ford and M. Newcombs, *J. Am. Chem. Soc.*, **96**, 309 (1976).

20) H. Yasuda and H. Tani, *Tetrahedron Lett.*, **1975**, 11.

21) a) C. L. Liotta and H. D. Harris, *J. Am. Chem. Soc.*, **96**, 2250 (1974); b) G. W. Gokel, *Synthesis*, **1976**, 168.

22) L. J. Guggenberger and R. E. Rundle, *J. Am. Chem. Soc.*, **86**, 5344 (1964).

23) J. Toney and G. Stucky, *Chem. Commun.*, **1967**, 1168.

24) J. Toney and G. Stucky, *J. Organomet. Chem.*, **28**, 5 (1971).

25) E. Weiss, *J. Organomet. Chem.*, **4**, 101 (1965).

26) G. D. Stucky and R. E. Rundle, *J. Am. Chem. Soc.*, **86**, 5825 (1964).

27) C. Johnson, J. Toney, and G. D. Stucky, *J. Organomet. Chem.*, **40**, C11 (1972).

28) J. D. Brooks, W. Rhine, and G. D. Stucky, *J. Am. Chem. Soc.*, **94**, 7346 (1972).

29) T. Holm, *Acta Chem. Scand., ser B*, **30**, 985 (1976).

30) a) W. Roelofs, A. Comeaw, A. Hill, and G. Milicevic, *Science*, **174**, 297 (1971); b) C. Descoins and C. A. Henrick, *Tetrahedron Lett.*, **1972**, 2999.

31) M. Sumitani, K. Kanemitsuya, H. Yasuda, and H. Tani, *Bull. Chem. Soc. Jpn.*, **51**, 1511 (1978).

32) a) H. J. Kablitz and G. Wilke, *J. Organomet. Chem.*, **51**, 241 (1973); b) S. Takahashi, T. Shibano, and N. Hagihara, *Bull. Chem. Soc. Jpn.*, **41**, 454 (1968); c) K. Takahashi, G. Hata, and A. Miyake, *Bull. Chem. Soc. Jpn.*, **46**, 600 (1973).

33) A. F. Reid, P. C. Wailes, *Aust. J. Chem.*, **19**, 309 (1966).
34) J. X. McDermott, M. E. Wilson, and G. M. Whitesides, *J. Am. Chem. Soc.*, **98**, 6529 (1976).
35) F. W. Siegert and H. J. L. Meijer, *J. Organomet. Chem.*, **23**, 177 (1970).
36) J. Meisenheimer, *Chem. Ber.*, **61**, 720 (1928).
37) J. Meisenheimer, *Justus Liebigs Ann. Chem.*, **397**, 286 (1913).
38) F. Wagner, M. T. Mocella, M. J. Daniello, Jr., A. H. J. Wang, and E. K. Barefield, *J. Am. Chem. Soc.*, **96**, 2625 (1974).
39) R. F. Nystrom and W. G. Brown, *J. Am. Chem. Soc.*, **69**, 1197 (1947).
40) T. Ashida, The University Crystallographic Computing System-Osaka, The Computation Center, Osaka University, 1973, pp. 55–61.
42) "International Table for X-Ray Crystallography," Kynoch Press, Birmingham, (1974), Vol. IV, pp. 71—98.
43) A list of observed and calculated structure factors are kept as Document No. 8016 at the Chemical Society of Japan.

Chemistry of Dienyl Anions. III. Crystalline Bis(2,4-pentadienyl)metal Compounds of Be and Zn. Terminally σ-Bonded Structure and Fluxional 1,5-Rearrangement

Hajime YASUDA, Yasuo OHNUMA, Akira NAKAMURA,* Yasushi KAI,†
Noritake YASUOKA,† and Nobutami KASAI†

Department of Macromolecular Science, Faculty of Science, Osaka Universiiy, Toyonaka, Osaka 560
†*Department of Applied Chemistry, Faculty of Engineering, Osaka University, Suita, Osaka 565*

(Received October 4, 1979)

A series of bis(dienyl)beryllium and bis(dienyl)zinc compounds were prepared by metal exchange reaction from seven different dienyl anions and were isolated as crystals of TMEDA complexes. Bis(dienyl)beryllium compounds of open chain structure obtained from pentadienyl, 2-methylpentadienyl, and 3-methylpentadienyl anions assume the terminally σ-bonded (*E*)-2,4-pentadienyl structure in solution as evidenced by ^{1}H-NMR and ^{13}C-NMR spectroscopies. Hydrolysis of these compounds gave 1,4-dienes regioselectively. The corresponding bis(dienyl)zinc compounds exist as a (*Z*), (*E*) mixture of teminally σ-bonded structures. An X-ray analysis of pentadienylzinc chloride·TMEDA complex showed that it had terminally σ-bonded (*E*)-2,4-pentadienyl structure with *s-trans* conformation. Steric effect of two methyl substituents in bis(2,4-dimethylpentadienyl)zinc induces the (*Z*) configuration which leads to the fluxional behavior by rapid 1,5-rearrangement above −80 °C.

In the previous paper, synthesis and chemical reaction of seven different bis(dienyl)magnesium compounds having fluxional structures in solution were reported.[1] A rapid 1,3-rearrangement (1,3-shift) between the magnesium-terminal C-1 (or C-5) and magnesium-central C-3 carbon bonds explains the fluxional behavior assisted by the ionic character of the Mg–C bonds. Substitution of the magnesium atom with more electro-negative metals, beryllium or zinc, may freeze the rapid equilibrium since the covalency of the M–C bonds does not favor suprafacial 1,3-sigmatropic shift which is thermally forbidden when covalency of the bond is complete. The position of the metal-carbon bond may be fixed to either C-1, C-3, or C-5 carbon atoms of the dienyl group reflecting the radius and the electronegativity of the metals. The position of the metal-carbon bond should also be influenced by a change in bulkiness of the substituents on the pentadienyl group because no remarkable difference in electron density was observed by CNDO-II calculations[2] among C-1, C-3, and C-5 of lithium pentadienide. Since the ionic radius of Zn (0.74 Å) is significantly larger than that of Be (0.41 Å), comparative studies on the structure of bis(dienyl)beryllium and bis(dienyl)zinc compounds will provide informations on the steric effect of the metal on the configuration or conformation of the dienyl group. Unique chemical behaviors of beryllium compounds resulting from its small ionic radius[3] are of interest but no compounds related to this work are reported.

Understanding the difference in the position of the metal-carbon bond, configuration of dienyl group, process for the rearrangement and chemical reactivity between dienylmetal compounds of Be, Mg, and Zn will be essential for selective dienylation of organic groups using these reagents. Like some organozinc compounds used for addition to olefins,[4] dienylzinc compounds reported here will be useful as the selective reagents for introducing a dienyl group to carbonyl compounds and olefins.

Results and Discussion

Preparation and Properties of Bis(dienyl)beryllium and -zinc Compounds. Bis(pentadienyl)beryllium and bis(pentadienyl)zinc compounds were prepared by the 2:1 reaction of potassium pentadienide[5] with anhydrous beryllium chloride and zinc chloride, respectively, in THF. Zinc chloride readily reacts with dienyl anions at 0 °C while beryllium chloride requires higher temperatures (>40 °C). The resulting dienylmetal compounds are coordinated by two moles of THF as evidenced by NMR and by GC of the hydrolyzate. The 1:1 reaction of pentadienyl potassium with zinc chloride gave $C_5H_7ZnCl\cdot 2THF$ similar to $C_5H_7MgBr\cdot 2THF$ but that with beryllium chloride gave

$$KC_5H_7 + MX_2 \xrightarrow{THF} C_5H_7MX\cdot 2THF \xrightarrow{KC_5H_7} (C_5H_7)_2M\cdot 2THF$$
$$M=Be,\ Zn$$

mainly $(C_5H_7)_2Be\cdot 2THF$ presumably due to the instability of RMX type structure.[6] Dienylzinc compounds are thermally the least stable among the Be, Zn, and Mg compounds. For example, bis(pentadienyl)zinc·2THF or bis(pentadienyl)zinc·$2N(C_2H_5)_3$ began to decompose at 10 °C giving metallic zinc and coupling dimers, $C_{10}H_{14}$.[7] The corresponding magnesium compound, $(C_5H_7)_2Mg\cdot 2THF$, decomposed at 80—90 °C and the ring cleavage of the coordinated THF occurred to afford unsaturated alcohols with an elongated carbon chain[1] while $(C_5H_7)_2Be\cdot 2THF$ was stable up to 100 °C in toluene. Remarkable difference in thermal stability was observed also for bis(cyclooctadienyl)metal compounds. The zinc compound was decomposed even at −20 °C but the magnesium and the beryllium compounds were stable at 50—60 °C. ^{1}H-NMR spectra of all the pentadienylmetal–THF complexes showed simple averaged AB_2X pattern signals (Table 1) due to the rapid 1,3-rearrangement as was observed for dienylmagnesium, allylmagnesium,[8] and allylaluminium[9] compounds. The chemical shifts (δ-values) of the protons at C-1 and C-3 increased with increasing covalent character of the M–C bond in the order Zn–C>Be–C>Mg–C.

The fluxionality can be frozen at room temperature by addition of bifunctional chelating ligands, *N,N,N',N'*-tetramethylethylenediamine (TMEDA) or *N,N,N',*

TABLE 1. CHEMICAL SHIFTS(δ-VALUES) AND COUPLING CONSTANTS OF FLUXIONAL PENTADIENYLMETAL COMPOUNDS[a)]

	C_1-H(C_5-H)	C_2-H(C_4-H)	C_3-H
$(C_5H_7)_2Be\cdot 2THF$	3.05 (11.1 Hz)	6.64	5.89 (12.2 Hz)
$(C_5H_7)_2Zn\cdot 2THF$	3.26 (11.1 Hz)	6.37	5.93 (11.5 Hz)
$C_5H_7ZnCl\cdot 2THF$	3.25 (11.1 Hz)	6.39	5.87 (11.5 Hz)
$(C_5H_7)_2Mg\cdot 2THF$	2.98 (11.3 Hz)	6.55	5.58 (12.0 Hz)

a) Data were collected at 38 °C in C_6D_6 and chemical shifts were calibrated using internal C_6H_6 signal assumed to be 7.20 ppm.

TABLE 2. CHARACTERIZATION OF BIS(DIENYL)BERYLLIUM·TMEDA COMPLEXES AND DISTRIBUTION OF THE HYDROLYSIS PRODUCTS

Complex	Mp/°C	Mol wt[a)] Found(Calcd)	Hydrolysis products 1,3-Diene/% (*E*)	(*Z*)	1,4-Diene/%
1	80	250(259)	13.7	1.2	85.1
2	78	280(287)	41.0	4.5	54.5
3	64	—(287)	22.0	1.1 2.6[b)]	74.3
4	78	270(287)	5.8[c)]	0.3[d)]	93.8
5	61	335(316)	8.1		91.9
6	88	320(311)	0.0	4.5	95.5[e)]
7	83	335(340)	0.0	3.5	96.5[f)]

a) Determined cryoscopically in benzene. b) 4-Methyl-1,3-pentadiene. c) (*E*,*E*)-2,4-Hexadiene. d) (*E*,*Z*)-2,4-Hexadiene. e) 1,4-Cycloheptadiene. f) 1,4-Cyclooctadiene.

TABLE 3. CHARACTERIZATION OF BIS(DIENYL)ZINC·TMEDA COMPLEXES AND DISTRIBUTION OF THE HYDROLYSIS PRODUCTS

Complex	Mp/°C	Mol wt Found(Calcd)	Hydrolysis products 1,3-Diene/% (*E*)	(*Z*)	1,4-Diene/%
8	59	310(316)	59.9	8.3	31.8
9	32	350(344)	67.1	1.4	31.5
10	17	—(344)	13.2	3.9 30.0[a)]	52.9
11	73	—(344)	12.2[b)]	12.3[c)] 1.5[d)]	74.0
12	44	395(372)	31.1		68.9

a) 4-Methyl-1,3-pentadiene. b) (*E*,*E*)-2,4-Hexadiene. c) (*E*,*Z*)-2,4-Hexadiene. d) 1,3-Hexadiene.

N'-tetramethyl-1,3-propanediamine (TMPDA) and a series of bis(dienyl)beryllium and bis(dienyl)zinc complexes which show the limiting structure in solution were isolated as crystals. They exist in monomeric form in benzene and the following formula are given for these complexes. Hydrolysis data are given in

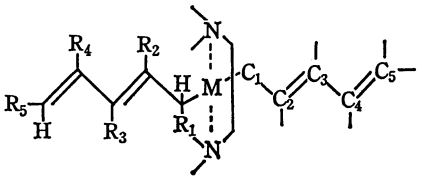

M; Be Zn

1	**8**	$R_1=R_2=R_3=R_4=R_5=H$
2	**9**	$R_3=CH_3$, $R_1=R_2=R_4=R_5=H$
3	**10**	$R_4=CH_3$, $R_1=R_2=R_3=R_5=H$
4	**11**	$R_5=CH_3$, $R_1=R_2=R_3=R_4=H$
5	**12**	$R_2=R_4=CH_3$, $R_1=R_3=R_5=H$

Tables 2 and 3. Formation of 1,4-dienes is remarkable as compared with that of 1,3-dienes especially for the beryllium compound. With respect to the 1,3-dienes, (*E*) structure predominated over (*Z*) structure for **1**—**4** and **8**—**10**. No information on the configuration of **5** and **12** was obtained by hydrolysis. If hydrolysis undergoes mainly through cyclic transition state[10] and partially by direct cleavage just as found for hydrolysis mechanism of allylic magnesium compounds,[1] terminally σ-bonded (*E*) structure is most plausible for **1**—**4** and **8**—**10**.

Nuclear Magnetic Resonance Studies on Bis(dienyl)beryllium Compounds. ^{1}H-NMR spectral data of seven different bis(dienyl)beryllium were measured and collected in Table 4. The assignment was done based on the values of chemical shift, relative intensities of the proton signals and the decoupling from the neighboring protons. It is clear that bis(pentadienyl)-beryllium·TMEDA complex **1** obtained from potassium pentadienide assumes terminally σ-bonded structure **1a** with (*E*) configuration ($J_{2,3}$=14.6 Hz). However, the TMEDA complex obtained from the reaction of $(C_5H_7)_2Mg\cdot 2THF$ with $BeCl_2$ comprises two species, (*E*) (**1a**) and (*Z*) (**1b**) isomers in an 8:1 ratio. The signals of major species are concordant in chemical shift with those of **1a** obtained from pentadienyl anion. Proton-proton coupling constant of $J_{2,3}$, 9.5 Hz, of minor signals corresponds to that of (*Z*) configuration.[11] Any signals derived from the

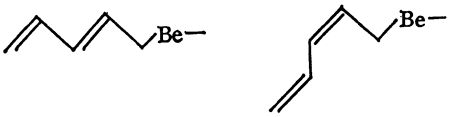

1a (*E*) **1b** (*Z*)

Be–C_3 carbon bond was not detected in the spectrum, although simple Hückel MO calculation suggests that the electron density of the pentadienyl anion is the highest on the C-3.[12] Therefore, the regioselective 1,4-diene formation is rationalized by concerted mechanism as described for allylic magnesium compounds[1] and the formation of 1,3-diene by direct cleavage of solvent-separated ionic species.[13] Proton signals attached to C-2 and C-4 unfortunately overlap with each other. Therefore, the correct assignment was made from the decoupled spectra with reference to the spectrum of bis(2,4-pentadienyl-1,1,5,5-d_4)-beryllium·TMEDA complex (Fig. 1) which was prepared by the reaction of beryllium chloride with potassium penta-

Table 4. ^{1}H-NMR chemical shifts(δ-values) and coupling constants of bis(dienyl)beryllium·TMEDA complexes[a]

Complex	C_1-H ($J_{1,2}$/Hz)	C_2-H	C_3-H ($J_{2,3}$/Hz)	C_4-H ($J_{3,4}$/Hz)	C_5-H ($J_{4,5}$/Hz)
1(*E*)	1.03 (d, 9.5)	6.69 (d of t)	5.89 (d of d, 15.3)	6.66 (d of q, 10.7)	4.92(d of d, 16.5) 4.72(d of d, 9.6)
1(*Z*)	1.16 (d, 9.5)	6.65 (d of d)	5.84 (d of d, 9.3)	6.66 (d of d)	5.04(d of d, 16.5) 4.85(d of d, 9.8)
2	1.01 (d, 9.3)	6.50 (t)	—	6.67 (d of d)	4.89(d of d, 16.5) 4.73(d of d, 10.0)
3	1.03 (d, 9.2)	6.70 (d of t)	6.05 (d, 15.0)	—	4.89 (d, 3.0)
4(*E*,*E*)	1.00 (d, 9.3)	6.53 (d of t)	5.89 (d of d, 14.9)	6.31 (d of d, 9.9)	5.37 (d of q, 13.5)
5	1.09(s) 1.38(s)	—	5.61(s) 5.40(s)	—	4.98(d, 3.6) 4.88(d, 3.6)
6[b]	2.77 (m, 9.6)	6.61 (d of d)	5.56 (d of d, 6.8)	6.16 (d of d, 10.8)	5.91 (d of t, 6.8)
7[c]	4.40 (m, 11.0)	5.92 (d of d)	5.32 (d of d, 9.7)	5.92	4.40

a) Measured in benzene-d_6 at 38 °C and calibrated using C_6H_6 peak, assumed to be 7.20 ppm. Assignments were made from the decoupled spectra. b) Bis(cycloheptadienyl)Be·TMEDA. c) Bis(cyclooctadienyl)Be·TMEDA.

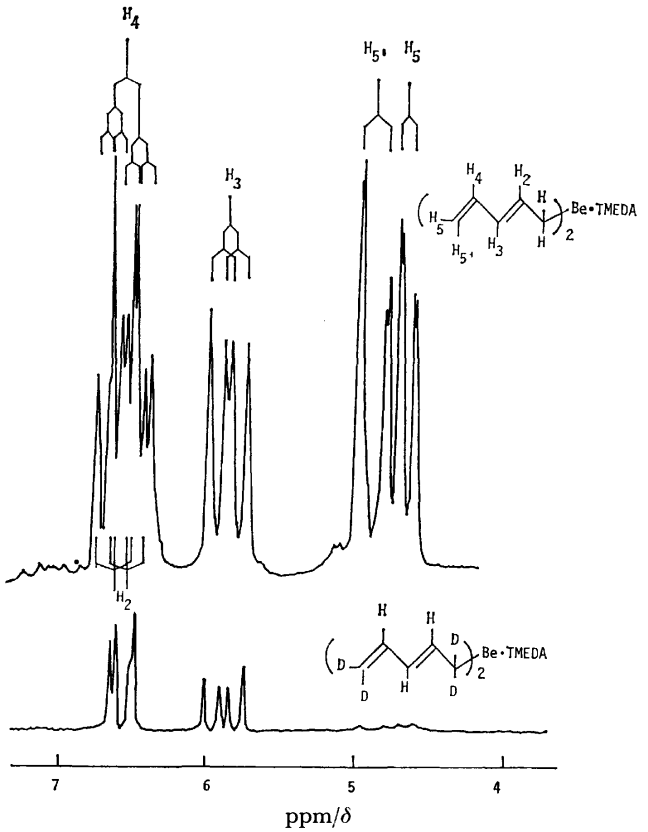

Fig. 1. ^{1}H-NMR spectra of $(C_5H_7)_2$Be·TMEDA and $(C_5H_3D_4)_2$Be·TMEDA in benzene-d_6 at 38 °C.

dienide-1,1,5,5-d_4. In a ^{13}C-NMR spectrum of **1** prepared from bis(pentadienyl)magnesium, two sets of five signals assignable to respective C_1—C_5 atoms of (*Z*) and (*E*) species were observed in an 8:1 ratio (Table 5) while **1** obtained from potassium pentadienide

Table 5. ^{13}C-NMR chemical shifts(δ-values) and coupling constants(Hz) for complexes **1**, **2**, **3**, **5**, **6**, and **8**[a]

Complex	C-1	C-2	C-3	C-4	C-5
1(*E*)	25.7 (t, 115)	150.0 (t, 149)	119.2 (d, 153)	140.7 (d, 137)	103.3 (t, 158)
1(*Z*)	22.2 (t, 115)	146.6 (t, 147)	115.2 (d, 151)	135.3 (d, 137)	107.2 (t. 154)
2	24.6	149.9	122.3	147.0	103.2
3	25.4 (t, 115)	145.0 144.7 (d, 142)	121.1	137.0	105.1
5(*E*)	25.7	152.2	127.8	144.5	108.9
5(*Z*)	22.9	150.1	127.7	140.3	116.1
6	49.6 (d, 139)	151.0 (d, 139)	113.3 (d, 150)	150.0 (d, 138)	112.2 (d, 150)
8	20.5	147.1	118.2	141.0	105.0

a) Calibrated using internal benzene peak, assumed to be 128.0 ppm downfield from external TMS. Data were collected at 38 °C in C_6D_6 and assignment was made by the partial decoupling method.

showed only five signals of (*E*) species consistent with the ^{1}H-NMR spectral data. Carbon-proton coupling constants obtained from non-decoupled spectra show no significant difference between (*Z*) and (*E*) structure.

The TMEDA complex of bis(3-methylpentadienyl)-beryllium **2** had simple ^{1}H-NMR pattern which was readily attributed to the terminally σ-bonded structure and the ^{13}C-NMR spectrum showed expected six signals derived from either (*E*) or (*Z*) isomer. With reference to the exclusive production of (*E*)-3-methyl-1,3-pentadiene[5] and 3-methyl-1,4-pentadiene upon hydrolysis

of **2**, one can conclude that **2** assumes solely terminally σ-bonded structure with (*E*)-configuration.

Two different structures, bis(2-methyl-2,4-pentadienyl)beryllium and bis(4-methyl-2,4-pentadienyl)beryllium, are possible for the compound obtained from potassium 2-methylpentadienide. In the case of the corresponding magnesium compound hydrolysis gave nearly equal amounts of 2-methyl-1,3-pentadiene and 4-methyl-1,3-pentadiene. However, the relative intensities of the signals of ^{1}H-NMR spectrum and the chemical shift values clearly show that bis[(*E*)-2-methyl-1,3-pentadienyl]beryllium **3** exists predominantly (95%) in the solution. It gave a 1,4-diene regioselectively by hydrolysis. Although a small amount of 4-methyl-1,3-pentadiene (2.6%) was formed by hydrolysis, their ^{1}H-NMR signals were too weak for making the correct assignment. All the expected six signals were observed also in the ^{13}C-NMR spectrum and their assignment was done by the partial decoupling method. Among the six signals, only that of C-2 splits into two peaks with a 1:1 intensity. Difference in chemical shift between the two signals (0.3 ppm) is too small to attribute them to (*E*) and (*Z*) isomers. Chemical shift difference between (*Z*) and (*E*) species observed for **1** is 3.4 ppm. Such predominance of (*Z*) isomer is ruled out in the present case by the hydrolysis data and the ^{1}H-NMR spectrum. Most plausible explanation is that those signals have arisen from the following two conformations (*s-cis* and *s-trans*). Free rotation around the C_3–C_4 bond would be hindered by the steric effect of the methyl group toward the TMEDA ligand. Thus. beryllium compounds **1**. **2**, and **3** assume *trans*-

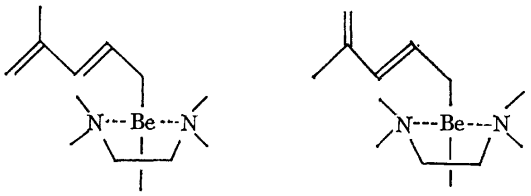

3 (*s-trans*) **3** (*s-cis*)

or (*E*)-structure. For the compounds obtained by reaction of potassium 2,4-hexadienide with beryllium chloride, many isomers are to be considered but the abundant species (80%) was found to be bis-[(*E*,*E*)-2,4-hexadienyl]beryllium·TMEDA complex **4** and minor species (20%) to be bis[(*E*.*Z*)-2,4-hexadienyl]beryllium. The results of hydrolysis of **4** [exclusive production of (*E*)-1,4-hexadiene and (*E*,*E*)-2,4-hexadiene] are concordant to the ^{1}H-NMR spectral data. Decoupled spectrum of **4** showed that the proton-proton coupling constants of $J_{2,3}$ and $J_{4,5}$ for (*E*,*E*)-isomer are 13.9 and 14.0 Hz and those for (*E*,*Z*)-isomer are 13.9 and 9.8 Hz, respectively. These coupling constants are in accord with the known values.[11,14] No methylene signals (CH_2=C) ascribable to C-3 or C-5 metalated species was detected.

NMR Studies on Crystalline Bis(dienyl)zinc Compounds of Open Chain Structure. For comparison with magnesium and beryllium compounds, the corresponding bis(dienyl)zinc·TMEDA complexes were prepared by the same method. The striking feature of the zinc compounds is that those are thermally unstable. For example, half-lives of bis(pentadienyl)zinc·2THF and bis(pentadienyl)zinc·2N(C_2H_5)$_3$ complexes at 30 °C were 10 and 15 min respectively in benzene as evidenced by ^{1}H-NMR and by gas chromatographic analysis of the hydrolyzate. These gave a 1:1 mixture of 1,3,7,9-dodecatetraene and 5-vinyl-1,3,7-octatriene quantitatively precipitating metallic zinc by raising the temperature to 80 °C. Radical coupling mechanism is most probable for this reaction. Indeed, CIDNP (chemically induced dynamic nuclear polarization) was detected on the ^{1}H-NMR spectrum at 38 °C. The two sets of resonances at 6.58, 5.12, 3.67 ppm and 6.02, 5.12, 2.78 ppm show A/E multiple polarizations[15] and are assigned to the pair of 1,4-pentadiene radicals and the pair of 1,4- and 1,3-pentadiene radicals respectively. Similar CIDNP has been reported for some organometallic compounds[16] and was recently detected for an allylzinc system[17] at higher temperatures (153 °C). By coordination with two moles of a strong donor, trimethylamine oxide, the thermal stability of bis(pentadienyl)zinc increased up to 100 °C but the rapid 1,3-rearrangement cannot be frozen even at −70 °C. The use of a chelating ligand such as TMEDA or TMPDA was essential to get the limiting structure. Another characteristic of bis(dienyl)zinc·TMEDA complex is that they comprise two or more isomeric species. The low mp of zinc compounds compared to beryllium compounds might be due to the contamination of the isomers.

Assignments of proton signals of the isomers were done by reference to the spectra of beryllium compounds (Table 6). Bis(pentadienyl)zinc·TMEDA **8** exists as a mixture of (*E*) and (*Z*) isomers in a 4:1 ratio, but C_5H_7ZnCl·TMEDA **8'** has solely (*E*) structure in solution below 80 °C. The importance of this finding prompted the determination of the crystal structure of C_5H_7ZnCl·TMEDA as the typical example of the pentadienyl metal compounds for the present work. While complex **8** decomposed at 70 °C, C_5H_7ZnCl·TMEDA was thermally more stable and it displayed fluxional behavior at 90—120 °C (*i.e.*, simple averaged spectrum was obtained) and finally decomposed at 125 °C.

Bis(3-methylpentadienyl)zinc·TMEDA **9** obtained from potassium 3-methylpentadienide also comprises (*E*) and (*Z*) isomers in a 4:1 ratio.

In sharp contrast with **3**, zinc complex **10** prepared from potassium 2-methylpentadienide are composed of three isomeric species, (*E*)-4-methyl-2,4-pentadienyl-(45%), (*Z*)-4-methyl-2,4-pentadienyl-(5%), and 2-methyl-2,4-pentadienylzinc (50%) species. Their assignments shown in Table 6 could be made with a decoupled spectrum by reference to the spectrum of beryllium compound **3**. It could not be determined

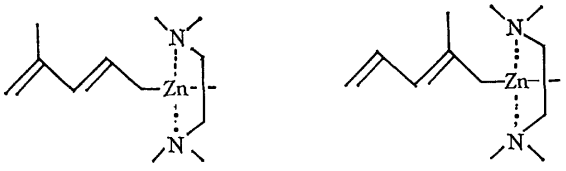

10a **10b**

Table 6. ^{1}H-NMR spectral data of bis(dienyl)zinc·TMEDA complexes(δ-values)[a]

Complex	C_1-H ($J_{1,2}$/Hz)	C_2-H	C_3-H ($J_{2,3}$/Hz)	C_4-H ($J_{3,4}$/Hz)	C_5-H ($J_{4,5}$/Hz)
8(*E*)	1.47 (d, 9.3)	6.57 (d of t)	6.02 (d of d, 14.6)	6.61 (d of q, 10.8)	4.99(d of d, 16.5) 4.74(d of d, 10.1)
8(*Z*)	1.50 (d, 9.3)	6.60 (d of t)	5.78 (d of d, 9.5)	6.58 (d of q, 10.6)	4.94(d of d, 16.0) 4.70(d of d, 10.3)
8′(*E*)	1.59 (d, 9.3)	6.53 (d of t)	6.02 (d of d, 14.1)	6.60 (d of q, 10.0)	4.96(d of d, 16.1) 4.74(d of d, 9.6)
9(*E*)[b]	1.56 (d, 9.5)	6.31 (t)	—	6.72 (d of d)	4.94(d of d, 16.3) 4.78(d of d, 10.3)
9(*Z*)	1.36 (d, 9.6)	6.27 (t)	—	6.58 (d of d)	4.94(d of d, 16.3) 4.79(d of d, 10.2)
10a	1.47 (d, 8.9)	6.34 (d of t)	5.94 (d, 15.6)	—	4.63(d, 7.0)
10b	1.49 (s)	—	5.46 (d)	6.83 (d of q, 10.8)	4.82(d of d, 14.2) 4.70(d of d, 11.0)
11(2*E*, 4*E*)	1.48 (d, 8.7)	6.09 (d of t)	5.64 (d of d, 9.8)	6.18 (d of d, 11.1)	5.29 (d of q, 14.0)
11(2*Z*, 4*E*)	1.57 (d, 8.7)	6.18 (d of t)	5.15 (d of d, 14.0)	6.17 (d of d, 11.1)	5.29 (d of q, 13.8)
12a	5.01(bs)	—	5.76(s)	—	1.48(bs)
12c	3.45(bs)	—	5.37(s)	—	3.45(s)

a) Data were collected at 38 °C in C_6D_6 and assignments were made from decoupled spectra by reference to the spectrum of the corresponding beryllium compound. b) Major signals were tentatively assigned to 9(*E*) based on the hydrolysis data.

from NMR data at hand whether **10** was composed of an asymmetric species of the type RZnR′,[18] 2-methylpentadienyl-4-methylpentadienylzinc, or a mixture of equal amounts of symmetric bis(4-methylpentadienyl)zinc (**10a**) and bis(2-methylpentadienyl)-zinc complex (**10b**)

Decoupled spectrum of bis(hexadienyl)zinc·TMEDA complex **11** showed that bis[(*E*,*E*)-2,4-hexadienyl]zinc (50%), bis[(*Z*,*E*)-2,4-hexadienyl]zinc (40%) and the other dienyl compound of unknown structure [10%, presumably (*E*,*Z*)-isomer] existed in the system. Thus, selective formation of the dienylmetal compound was not observed in cases of **10** and **11**. The poor selectivity should be ascribed to the large ionic radius of zinc atom compared to beryllium. Similar size effect of metal is known for the alkali-metal-catalyzed stereospecific polymerization of isoprene, Li favoring over Na or K for stereoregulation.[19] Thus, the use of beryllium is suitable for selective formation of one particular isomer of the dienylmetal compound.

The predominant formation of the (*E*) species observed for dienylberyllium compounds **1**—**4** and dienylzinc compounds **8**—**9** may be ascribed to the covalency in the M–C bonding. Similar behavior is also known for allylic metal compounds; *i.e.*, 2-butenylaluminium compounds assumes (*E*) structure[9] while more ionic allylic magnesium compounds[20] prefer the (*Z*) structure.

X-Ray Structural Study of Pentadienylzinc Chloride·TMEDA. TMEDA complexes of bis(pentadienyl)beryllium, bis(pentadienyl)zinc, and pentadienylzinc chloride have (*E*)-structure in solution as evidenced by ^{1}H-NMR spectroscopy. ^{1}H-NMR spectrum of the fluxional bis(pentadienyl)magnesium indicated that the rapid 1,3-shift occurs keeping *s-trans*-(*E*) conformation.[1] To determine whether they assume *s-trans*-(*E*) or *s-cis*-(*E*)-conformation (which corresponds to W-shaped or sickle-shaped structure for the pentadienyl anion[5]), X-ray analysis of C_5H_7ZnCl·TMEDA was done since it showed much more reflections compared to $(C_5H_7)_2$-Zn·TMEDA and $(C_5H_7)_2$Be·TMEDA. The molecular structure is given in Fig. 2. Bond lengths and bond angles are listed in Table 7. The coordination geometry around the zinc atom is essentially tetrahedral and the C(1)–Zn–Cl angle is slightly deviated [118.8(4)°] from the standard tetrahedral angle.

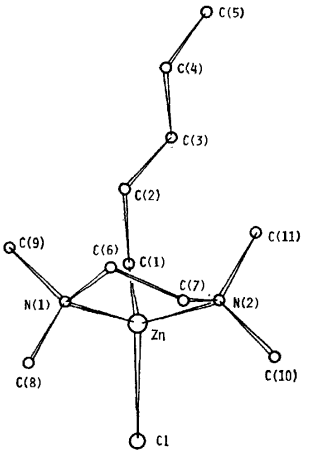

Fig. 2. Molecular structure of $ZnCl(C_5H_7)$·TMEDA.

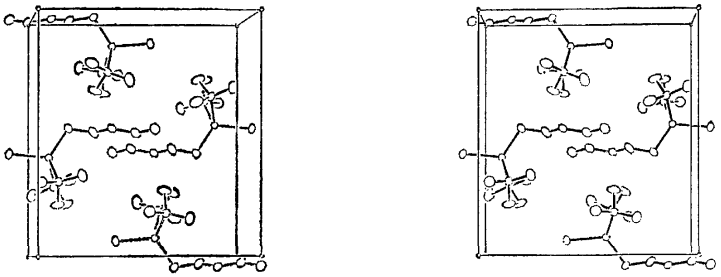

Fig. 3. A stereoscopic drawing[36] of the crystal strcuture of $ZnCl(C_5H_7)\cdot TMEDA$.

Table 7. Bond lengths [l/Å] and bond angles [ϕ/°] in $ZnCl(C_5H_7)\cdot TMEDA$
Estimated standard deviations in parentheses

Bond lengths			
Zn-Cl	2.263(3)	N(1)-C(6)	1.480(12)
Zn-N(1)	2.161(6)	N(1)-C(8)	1.482(13)
Zn-N(2)	2.151(6)	N(1)-C(9)	1.506(13)
Zn-C(1)	2.03(12)	N(2)-C(7)	1.460(12)
C(1)-C(2)	1.460(17)	N(2)-C(10)	1.509(11)
C(2)-C(3)	1.293(15)	N(2)-C(11)	1.482(12)
C(3)-C(4)	1.399(13)	C(6)-C(7)	1.498(15)
C(4)-C(5)	1.273(15)		
Bond angles			
Cl-Zn-C(1)	118.8(4)	Zn-N(1)-C(6)	104.7(6)
Cl-Zn-N(1)	105.04(17)	Zn-N(1)-C(8)	112.9(6)
Cl-Zn-N(2)	104.59(17)	Zn-N(1)-C(9)	111.6(6)
N(1)-Zn-N(2)	84.5(3)	C(6)-N(1)-C(8)	111.4(8)
N(1)-Zn-C(1)	118.2(4)	C(6)-N(1)-C(9)	107.6(8)
N(2)-Zn-C(1)	120.0(4)	C(8)-N(1)-C(9)	108.4(8)
Zn-C(1)-C(2)	114.9(9)	Zn-N(2)-C(7)	105.6(6)
C(1)-C(2)-C(3)	132.8(9)	Zn-N(2)-C(10)	113.3(5)
C(2)-C(3)-C(4)	132.3(10)	Zn-N(2)-C(11)	111.1(5)
C(3)-C(4)-C(5)	137.2(11)	C(7)-N(2)-C(10)	107.0(7)
N(1)-C(6)-C(7)	112.8(9)	C(7)-N(2)-C(11)	113.9(7)
N(2)-C(7)-C(6)	112.8(9)	C(10)-N(2)-C(11)	106.0(7)

The N(1)–Zn–N(2) angle [84.5(3)°] which is equal to the corresponding angle in $(C_7H_{11})_2Mg\cdot TMEDA$ [84.2(5)°][1] is largely deviated from the tetrahedral angle. The N–Zn–N angle in $ZnCl_2\cdot TMEDA$ is 87.9°.[21]

The remarkable feature of the molecular structure is that the pentadienyl group is σ-bonded to the zinc atom by the terminal C(1) [Zn–C(1)=2.031(12) Å] similar to the dimethylpentadienyl group in $(C_7H_{11})_2$-Mg·TMEDA, but the pentadienyl group in the present complex has the *s-trans*-(*E*) conformation (W-shaped structure). The Zn–C bond length is nearly equal to those of EtZnI(1.95 Å),[22] $(MeZnOMe)_4$ (1.94 Å),[23] $LiZn(CH_3)_4$(2.07 Å),[24] but shorter than the bond length of Zn–C(Cp) in $(C_5H_5)ZnCH_3$(2.28 Å).[25] The bond lengths in the pentadienyl group show the bond alternation, C(1)–C(2)=1.460(17), C(2)–C(3)=1.293 (15), C(3)–C(4)=1.399(13) and C(4)–C(5)=1.273(15) Å. Thus, C(2)–C(3) and C(4)–C(5) double bond and C(3)–C(4) single bond lengths are slightly shorter than the ordinary C–C bond (1.33 Å for C–C double bond and 1.5 Å for single bond). All the bond angles are more than 10° larger than that of the C(sp^2) bond angle. The pentadienyl group is planar within ±0.02 Å and the dihedral angle between this plane and the plane defined by the Zn, Cl, and C(1) is 71.2°. The bond length of Zn–Cl [2.263(3) Å] is reasonable value. The Zn–Cl bond length for $ZnCl_2(CH_3CN)_2$[26] and $ZnCl_2\cdot TMEDA$[21] are 2.17 and 2.208(4)Å, respectively.

The TMEDA coordinates to the zinc atom by two nitrogen atoms. The two Zn–N lengths are almost equal [Zn–N (1)=2.161 (6) and Zn–N (2)=2.151 (6) Å]. The TMEDA moiety has the similar structure as that in $(C_7H_{11})_2Mg\cdot TMEDA$ except the two-fold symmetry.

The crystal structure is shown in Fig. 3. No close intermolecular atomic contacts less than the van der Waals distance is observed.

1,5-Metallotropic Rearrangement Induced by σ-π Conjugation. The pathway of the metallotropic rearrangement of η^1-cyclopentadienylmetal compounds has been described as 1,2-shift,[27] although the equivalent pathway, 1,5-shift is prefered on the ground of orbital symmetry rules (*i.e.*, suprafacial 1,5-sigmatropic rearrangement).[28] If the stereochemistry required for the 1,5-shift is realized using dienylmetal compound of open chain structure (see Scheme 1), the 1,5-shift should be observable at a reasonable rate. Taking advantage of steric effect of two methyl substituents on C-2 and C-4 positions, we could realize the required geometry in bis(2,4-dimethyl-2,4-pentadienyl)zinc·TMEDA **12** as described below.

1,2- or 1,5-Metallotropic rearrangement in η^1-cyclopentadienyl compd.

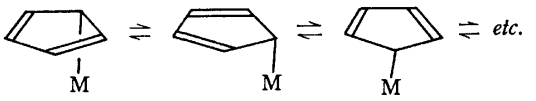

1,5-Metallotropic rearrangement in (*Z*)-2,4-dimethylpentadienylmetal compd.

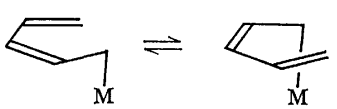

Scheme 1.

In the spectrum of **12**, two sets of signals (10:9 ratio) were observed. The similar ratio (10:7) was also observed for monodienyl substituted zinc compound, $C_7H_{11}ZnCl\cdot TMEDA$. One is very close in shape and in chemical shift values to bis(2,4-dimethylpentadienyl)magnesium compound of fluxional

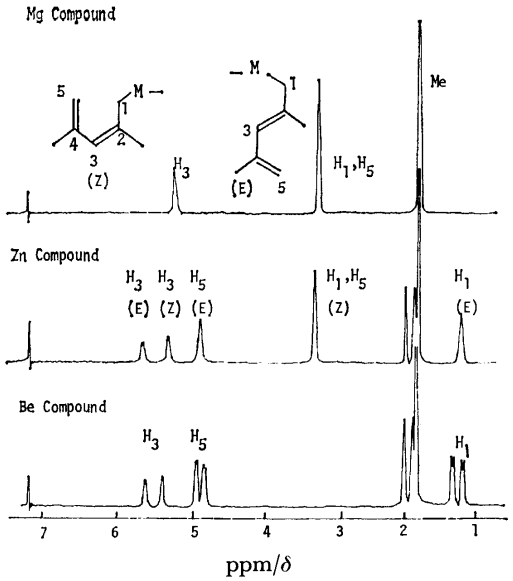

Fig. 4. ^{1}H-NMR spectra of bis(2,4-dimethylpentadienyl)metal·TMEDA complexes of Mg, Zn, and Be in benzene-d_6 at 10 °C (proton signals of TMEDA were neglected).

structure and the other corresponds to the terminally σ-bonded structure observed for bis(2,4-dimethylpentadienyl)beryllium·TMEDA (Fig. 4). Chemical shift values and the relative proton signal intensity ratio were independent of the concentration and temperature (−70—50 °C). Possibility of the equilibrium mixture is thus excluded. The effect of aggregation is negligible because **12** is monomeric in benzene independent of the concentration of the solution. Therefore, above two sets of signals can reasonably be assinged to independent (*Z*) and (*E*) species. Based on these facts, fluxional proton signals can be assigned to the (*Z*) species of **12** and are explained by rapid 1,5-rearrangement between **12a** and **12b**.

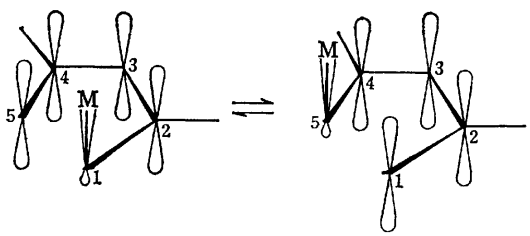

12a **12b**

The U-shaped geometry is also found for bis(2,4-dimethylpentadienyl)magnesium in solid state.[1] The polarized σ-bond M–C_1 or M–C_5 is in σ-π conjugation[29] with the p-orbital of C-2 or C-4 atom and hence the metal attached to the C-1 in **12a** can easily move to C-5 by least motion. In contrast, the stereochemistry of the (*E*) species **12c** does not allow such a facile rearrangement since the metal is far apart from C-5. The (*E*) structure is limited to the following sickle-shaped structure due to the steric repulsion between two methyl groups.

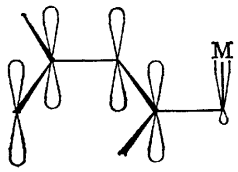

12c

If rapid 1,3-rearrangement occurs, the species **12c** should be in equilibrium also with **12a** to give a simple averaged spectrum as was found for dienylmagnesium compounds.

Bis(2,4-dimethylpentadienyl)beryllium·TMEDA **5** is not fluxional and two sets of resonances (7:5 ratio) attributable to (*Z*) and (*E*) terminally σ-bonded species were observed. Chemical shift values of ^{13}C-NMR spectrum support this explanation. Resonances appearing at lower field may be assigned to those of (*E*) species of **5** by reference to the chemical shift of **12**. The relatively small ionic radius of beryllium atom may be inadequate for 1,5-rearrangement at room temperature. At 80 °C, **5** displays the fluxional behavior similar to **12**.

This guide line appears to be generally applicable and unexpected simple ^{1}H-NMR spectral pattern of bis(cycloheptadienyl)beryllium·TMEDA **6** and bis(cyclooctadienyl)beryllium·TMEDA **7** complexes may be explained by the predominant occurrence of the 1,5-pathway. As previously noted, electron density of cycloheptadienyl and cyclooctadienyl metal compound of Mg[1] and alkali metals[5] is highest on the central C-3. Considering the distribution of the electron density, the centrally σ-bonded structure **6a** may be preferred for **6**. However, chemical shifts of **6** (Fig. 5)

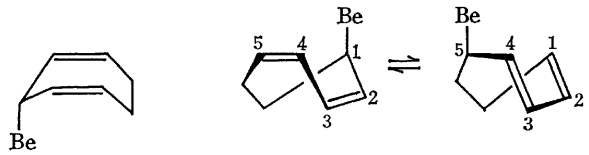

6a **6b**

indicate that it assumes (*Z*)-2,4-dienylmetal type structure **6b** at room temperature contrary to the prediction. Since 1,3-cycloheptadiene[30] and 1,3-cyclooctadiene are known to have twisted structure[31], C-1 atom is close to C-5 to allow the direct 1,5-shift by transannular interaction rather than sequential 1,2- or 1,3-shift observed for η^1-cyclopentadienylmetal compounds or dienylmagnesium compounds.

If this consideration is correct, the negative charge density on C-1 and C-5 should increase by the effect of metal in sharp contrast with the negative charge distribution of the magnesium compound. Thus, simple averaged spectra of **6** (at 90 °C) and that of bis(cycloheptadienyl)beryllium·2THF are measured. Indeed, a remarkable difference in chemical shifts between proton signals of the beryllim compound and magnesium compound (Table 8) was observed. Proton at C_1 and C_5 of beryllium compound appeared at 3.9 ppm and C_3-H at 5.1 ppm while the C_1-H

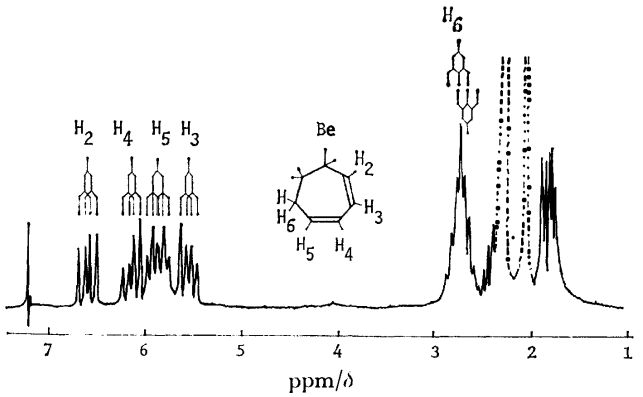

Fig. 5. ^{1}H-NMR spectrum of bis(cycloheptadienyl)-beryllium·TMEDA complex in benzene-d_6 at 38 °C.

and C_5-H signals of the magnesium compound appeared at 4.6 ppm and C_3–H signal at 3.5—3.9 ppm. Negative charge density is thus highest on the C-1 and C-5 for the beryllium compound **6** but highest on the C-3 for the magnesium compound. Bis(cyclooctadienyl)beryllium·TMEDA **7** also has the highest negative charge density on C-1 and C-5 atoms and is fluxional at room temperatures (see Table 4). Conformation of **7** will be more suited for the rapid rearrangement than that of **6**. Thus, the remarkably high chemical shift values of C_1- and C_5-protons of cyclic dienylberyllium compounds and their fluxionality can be explained by the rapid transannular 1,5-rearrangement induced by σ-π conjugation. Rearrangement observed for the magnesium compound should occur by the 1,3-pathway induced by dπ-pπ conjugation[32] due to the higher ionicity of the Mg–C bond. Bis(cycloheptadienyl)zinc·2THF also showed similar chemical shift values at −20 °C to that of the beryllium compound. The information on the conformation of the crystalline TMEDA complexes of bis(cycloheptadienyl)zinc **13** and bis(cyclooctadienyl)zinc **14** cannot be obtained at present due to their thermal instability. However, the location of the metal on the cyclooctadienyl group can be inferred by the reaction with carbonyl compounds. That is, reaction of **14** with acetone or acetaldehyde gave regioselectively 2-(2,7-cyclooctadienyl)-2-propanol or 1-(2,7-cyclooctadienyl)ethanol respectively at −30 °C (regioselectivity, 98% in both cases). Since six-membered cyclic transition state is generally assumed for this type of reaction, the above result indicates that the metal–C_1 bond is involved in the compound **14**. Corresponding beryllium compound **7** also reacted with acetone regioselectively. Regioselectivity of bis(dienyl)metal compounds of open chain structure **1**—**5**, **8**—**12** toward acetone is as high as that of cyclic dienylmetal compounds (Table 9). It is noteworthy that regioselectivity of **10** is high since **10a** and **10b** gave the same products. Chemical characterization of these addition compounds were reported in Ref. 1.

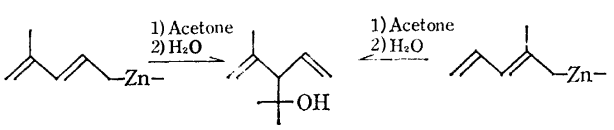

Table 8. Chemical shifts(δ-values) and coupling constants(Hz) of fluxional bis(cycloheptadienyl)metal compounds[a]

Compound	C_1-H(C_5-H) ($J_{1,2}$)	C_2-H(C_4-H)	C_3-H ($J_{2,3}$)
$(C_7H_9)_2$Be·2THF	3.85	6.26	5.12
	(8.9)		(8.5)
$(C_7H_9)_2$Be·TMEDA[b]	3.75	6.35	5.10
	(8.8)		(8.4)
$(C_7H_9)_2$Zn·2THF	3.80	6.15	5.12
	(bs)		(8.2)
$(C_7H_9)_2$Mg·2THF	4.55	6.15	3.45
	(10.0)		(7.8)
$(C_7H_9)_2$Mg·TMEDA	4.68	6.31	3.85
	(9.7)		(7.4)

a) Measured in toluene-d_8 at −20 °C (in ppm downfield from external TMS). b) Measured at 90 °C. Assignment was done from decoupled spectra and relative signal intensity ratios.

Table 9. Regioselective addition of dienyl group in bis(dienyl)metal compounds to acetone giving 1,4-diene derivatives[a]

Be compd	Regioselectivity %	Zn compd	Regioselectivity %
1	99	**8**	98
2	98	**9**	97
3	98	**10**	97
4	98	**11**	98
5	98	**12**	97
6	98	**13**	98
7	99	**14**	98

a) In benzene at 5 °C.

In summary, unambiguous evidence for symmetry-allowed 1,5-shift was obtained for covalently-bonded linear dienylmetal compounds. The absence of the corresponding 1,3-shift also indicated the unimportance of ionic character and d-orbital participation in the zinc-dienyl bonding. The covalency in the bonding in dienylberyllium or dienylzinc compounds thus dictates terminally bonded structure which in turn induces regioselective reaction of the dienyl group.

Experimental

Anhydrous zinc chloride and zinc bromide (Wako Pure Chem.) were used after drying at 140—150 °C for 20 h *in vacuo*. Anhydrous beryllium chloride was purified by dissolution of the commercial sample (needle crystals, Kishida Chem. Co.) in diethyl ether and then evaporation of the ether soluble fraction. Hydrates of beryllium chloride was thus removed. Benzene-d_6 (99.5%, Merck Co.) and toluene-d_8 (99%, Merck Co.) were dried over sodium/potassium alloy and distilled. All the procedures were done in an argon atmosphere with the high vacuum technique. ^{1}H-NMR spectra were recorded at 100 MHz and ^{13}C-NMR spectra at 25.2 MHz on a Varian XL-100 instrument with a VFT-100-620L Fourier transform accessory. All the other in-

strumental analyses were done as previously reported.[1] Melting points were measured in a sealed tube and were uncorrected.

Preparation of Bis(2,4-pentadienyl)beryllium·TMEDA **1**. To a chilled solution of beryllium chloride·diethyl ether complex (2.3 g, 10 mmol) in THF (30 ml) was added a THF solution (40 ml) of potassium pentadienide (2.2 g, 20 mmol) using a syringe over a 20 min period at 5—10 °C with vigorous stirring. The mixture was allowed to react at 50 °C for 1 h and pentane (100 ml) was added at 10 °C to induce the precipitation of the salt. The supernatant liquid was separated from the salt by centrifugation using a two-necked glass tube protected with plastic cover and equipped with two small rubber stoppers and then it was evaporated *in vacuo*. Extraction of the residue with a mixture of diethyl ether (100 ml) and pentane (30 ml) followed by evaporation gave bis(pentadienyl)beryllium·2 THF as a pale yellow oil. Typical yield: 80% (2.3 g). TMEDA complex **1** was prepared by the addition of TMEDA (2.2 ml, 15 mmol) to the THF complex (2.8 g, 10 mmol) in diethyl ether (10 ml) at 20 °C. After the addition of pentane (30 ml), the mixture was cooled to −20 °C to induce the precipitation of colorless needle crystals. Yield: 92% (2.2 g) based on the THF complex. Recrystallization was carried out in 1:3 ether–pentane solution. Found: pentadiene, 53.0%; TMEDA, 43.2% (by GC); Be, 3.10% by beryllium oxide method. Calcd for $BeC_{16}H_{22}N_2$, pentadiene, 53.39%; TMEDA, 43.03%; Be, 3.58%.

Preparation of Bis(2,4-pentadienyl-1,1,5,5-d_4)beryllium·TMEDA. In essentially the same way as **1**, bis(pentadienyl-1,1,5,5-d_4)beryllium·TMEDA was prepared by reaction of potassium pentadienide-1,1,5,5-d_4($KC_5H_3D_4$) with beryllium chloride. Preparation of $KC_5H_3D_4$ is as follows. A solution of dimethyl glutarate (32 g, 0.2 mol) in diethyl ether (50 ml) was added dropwise to the suspension of $LiAlD_4$ (10 g, 0.24 mol, Merck Co.) in ether (300 ml) at 0 °C. After stirring for 5 h at 0 °C, the mixture was hydrolyzed with 2M HCl and distilled to give 1,5-pentanediol-1,1,5,5-d_4 (110 °C/1 mmHg, 20.5 g, 95% yield). Resulting pentanediol was esterified with acetic anhydride by the known method and then pyrolysis of the 1,5-pentanediyl diacetate was carried out by passing it through a Pyrex tube heated to 575± 5 °C to produce 1,4-pentadiene-1,1,5,5-d_4. Yield: 57% based on diol (8 g). After purification by distillation and drying over calcium hydride, resulting deuterated 1,4-diene (4 g, 6 mmol) was allowed to react with metallic potassium (1.2 g, 3 mmol) in THF (7 ml) in the presence of triethylamine (5 ml) at 10 °C to give $KC_5H_3D_4$.

Preparation of Bis(dienyl)beryllium·TMEDA Complex **2**—**7**. In essentially the same way as described above, a series of bis(dienyl)beryllium·TMEDA complexes were prepared from the corresponding potassium dienide. Yield: 75—85%.

Preparation of Bis(2,4-pentadienyl)zinc·TMEDA **8**. To a solution of potassium pentadienide (2.2 g, 20 mmol) in THF (40 ml) cooled by ice–water was added powdered zinc chloride (1.4 g, 10 mmol) over a 30 min period with stirring. The mixture was stirred at 5 °C for 1 h and then the volume of the solution was reduced to 1/5 by evaporation. Pentane (80 ml) was added to the residue for complete precipitation of the salt, which was then separated by quick filtration with a glass filter or by centrifugation at 5—15 °C for 10 min. All the procedures were done below 15 °C to prevent thermal decomposition. The supernatant liquid was evaporated and washed with a small portion of pentane (10 ml) at −70 °C to give bis(pentadienyl)zinc·2THF as oily substance. Yield: 84% (2.9 g). Bis(pentadienyl)zinc·TMEDA **8** was prepared by the addition of TMEDA (2.2 ml, 15 mmol) to bis(pentadienyl)zinc·2THF (2.7 g, 8 mmol) in ether (8 ml) at 0 °C. After stirring for 30 min at 30 °C, pentane (15 ml) was added and the solution was allowed to stand at −20 °C to induce the precipitation of the crystals. Yield: 98% based on the THF complex (2.3 g). Recrystallization was carried out at −20 °C from THF–pentane (1:10 vol ratio).

The other complexes of triethylamine, TMPDA, and trimethylamine oxide were prepared in the same procedure as that for the THF complex and were recrystallized from pentane at −40 °C, ether–pentane at −20 °C, and toluene at 0 °C, respectively.

Preparation of Bis(dienyl)zinc·TMEDA **9**—**12**. A series of bis(dienyl)zinc·TMEDA complexes were prepared in the same procedure described for **8** from corresponding potassium dienides. The reaction of potassium 2,4-dimethylpentadienide with zinc chloride gave THF free bis(2,4-dimethylpentadienyl)zinc as evidenced by ^{1}H-NMR while the reaction of potassium 2-methylpentadienide, 3-methylpentadienide, and hexadienide gave the complexes coordinated with 2 moles of THF.

Preparation of Pentadienylzinc Chloride·TMEDA Complex. The sample for X-ray structural analysis was prepared as follows. A solution of potassium pentadienide (2.2 g, 20 mmol) in THF (40 ml) was added with a syringe over a 30 min period to a stirred solution of anhydrous zinc chloride (2.88 g, 20 mmol) in THF (30 ml) at 5 °C. The mixture was stirred for additional 1 h at 30 °C and then the salt was separated by centrifugation. THF fraction was evaporated to give $C_5H_7ZnCl·2THF$ as semi-solid, which was then extracted with two portions of toluene (20 ml). Addition of a mixture of TMEDA (3.3 ml, 22 mmol) and pentane (80 ml) to the toluene solution followed by cooling to −20 °C produced $C_5H_7ZnCl·TMEDA$ quantitatively as needle crystals; mp, 77 °C. Yield: 85% based on zinc chloride (4.6 g).

Dienylation of Acetaldehyde and Acetone. To the solution of **1**—**12** (5 mmol) in benzene (8 ml) was added a solution of acetaldehyde (0.6 ml, 12 mmol) or acetone (0.8 ml, 12 mmol) in benzene (3 ml) at 5 °C. Resulting mixture was hydrolyzed at 0 °C and distilled *in vacuo*. In cases of **13** and **14**, corresponding reaction was carried out in THF at −30 °C without isolating the complex. After the mixture was allowed to stand at 0 °C for 1 h it was quenched with 2 M HCl. Resulting alcohols were analyzed by GC using authentic samples (chemical characterization was previously reported. see Ref. 1). Yield by GC: 98%. Both acetaldehyde and acetone attacked the C-3 atom of dienyl group regioselectively in all cases.

Crystal Data and Structure Determination of Pentadienylzinc Chloride·TMEDA. $C_{11}H_{19}N_2ClZn$, *F. W.* 280.1, monoclinic, space group $P2_1/c$, a=8.935(2), b=13.587(2), c=12.096(2) Å, β=95.50(2)°. V=1461.7(5) Å^3, D_c=1.272 g cm^{-3} for Z=4.

Unit-cell dimensions and reflection intensities were measured on a Rigaku automated, four-circle diffractometer using graphite monochromatized Mo $K\alpha$ radiation. The θ-2θ scan technique was applied at a 2θ scan rate of 4°min^{-1}. The scan width was $\Delta 2\theta=(2.0+0.7\tan\theta)°$. Backgrounds were counted for 5 s before and after the scan of each peak. Intensities of three standard reflections were measured after every 60 reflections. A total of 2296 (1852 non-zero) reflections was collected up to $\Delta 2\theta$=48°. Usual Lorentz and polarization corrections were applied but no absorption correction was made [μ(Mo $K\alpha$)=17.1 cm^{-1}].

The structure was established by the heavy atom method and refined isotropically by the block-diagonal least-squares procedure (HBLS V).[33] After the R value decreased to 0.15, anisotropic refinements were carried out. Final R

TABLE 10. ATOMIC POSITIONAL AND THERMAL PARAMETERS OF $ZnCl(C_5H_7)\cdot TMEDA$
Estimated standard deviations in parentheses

Atom	X	Y	Z			
Zn	0.23418(10)	0.07752(6)	0.41436(6)			
Cl	0.2632(3)	0.06375(15)	0.60165(15)			
N(1)	0.0773(7)	0.1974(5)	0.3810(5)			
N(2)	0.4004(7)	0.1838(5)	0.3768(5)			
C(1)	0.2038(14)	−0.0467(6)	0.3216(7)			
C(2)	0.1782(15)	−0.0303(7)	0.2020(8)			
C(3)	0.2607(11)	−0.0439(6)	0.1211(7)			
C(4)	0.2353(12)	−0.0266(7)	0.0069(7)			
C(5)	0.3044(14)	−0.0412(8)	−0.0789(8)			
C(6)	0.1642(10)	0.2742(7)	0.3285(10)			
C(7)	0.3249(10)	0.2791(6)	0.3765(9)			
C(8)	0.0156(14)	0.2347(9)	0.4823(9)			
C(9)	−0.0521(12)	0.1682(8)	0.2985(10)			
C(10)	0.5329(11)	0.1889(7)	0.4638(8)			
C(11)	0.4630(11)	0.1598(8)	0.2710(8)			
Atom	$B(11)$	$B(22)$	$B(33)$	$B(12)$	$B(13)$	$B(23)$
Zn	0.01822(13)	0.00426(5)	0.00563(6)	0.00064(12)	0.00506(13)	0.00021(8)
Cl	0.0306(5)	0.00687(13)	0.00580(13)	0.0045(4)	0.0054(4)	0.00201(19)
N(1)	0.0143(9)	0.0066(4)	0.0078(5)	0.0013(10)	0.0038(10)	0.0037(7)
N(2)	0.0155(9)	0.0059(4)	0.0075(5)	0.0009(9)	0.0045(10)	−0.0001(7)
C(1)	0.041(3)	0.0058(5)	0.0071(7)	−0.0063(18)	0.0053(19)	−0.0029(9)
C(2)	0.044(3)	0.0079(7)	0.0110(9)	−0.019(3)	0.019(3)	−0.0084(12)
C(3)	0.0266(16)	0.0046(4)	0.0083(6)	−0.0018(13)	0.0005(16)	−0.0029(9)
C(4)	0.031(2)	0.0066(6)	0.0107(8)	−0.0069(16)	0.010(2)	−0.0042(10)
C(5)	0.034(3)	0.0083(7)	0.0104(9)	−0.009(2)	0.008(3)	−0.0031(12)
C(6)	0.0167(13)	0.0063(6)	0.0193(12)	−0.0026(14)	0.0000(19)	0.0088(13)
C(7)	0.0190(14)	0.0047(5)	0.0185(11)	0.0026(13)	0.004(2)	0.0037(12)
C(8)	0.040(3)	0.0139(10)	0.0120(10)	0.027(3)	0.024(3)	0.0063(16)
C(9)	0.0216(17)	0.0094(8)	0.0197(13)	−0.0075(18)	−0.015(3)	0.0062(16)
C(10)	0.0196(15)	0.0097(7)	0.0132(10)	−0.0025(16)	−0.0075(19)	0.0002(13)
C(11)	0.0274(19)	0.0115(8)	0.0098(8)	−0.007(2)	0.0186(19)	−0.0039(13)

value was 0.068 for non-zero reflections. Atomic scattering factors were taken from International Tables for X-Ray Crystallography, Vol. IV.[34] The weighting schemes used in the final refinement were $w=[\sigma^2(F_o)+a|F_o|+b|F_o|^2]^{-1}$ for $|F_o|>0$ and $w=c$ for $|F_o|=0$, where, $a=0.0067$, $b=0.002$, and $c=0.111$. The final atomic positional and thermal parameters are listed in Table 10. Calculations were done on an ACOS series 77 NEAC system 700 computer at Osaka University.[35]

References

1) H. Yasuda, M. Yamauchi, A. Nakamura, T. Sei, Y. Kai, N. Yasuoka, and N. Kasai, *Bull. Chem. Soc. Jpn.*, to be published.

2) R. J. Bushby and A. S. Patterson, *J. Organomet. Chem.*, **132**, 163 (1977).

3) a) E. Weiss, *J. Organomet. Chem.*, **4**, 101 (1965); b) K. Ziegler, R. Köster, H. Lehmkuhl, and K. Reinert, *Justus Liebigs Ann. Chem.*, **629**, 33 (1960); c) W. Strohmeier, W. Haecker, and G. Popp, *Chem. Ber.*, **100**, 405 (1967).

4) a) H. Lehmkuhl and H. Nehl, *J. Organomet. Chem.*, **60**, 1 (1973); b) H. Lehmkuhl, O. Olbrysch, D. Reinehr, G. Schomburg, and H. Hennberg, *Justus Liebigs Ann. Chem.*, **1975**, 145; c) H. Lehmkuhl and O. Obrysch, *ibid.*, **1975**, 1162.

5) a) H. Yasuda, Y. Ohnuma, M. Yamauchi, and H. Tani, *Bull. Chem. Soc. Jpn.*, **52**, 2036 (1979); b) H. Yasuda, T. Narita, and H. Tani, *Tetrahedron Lett.*, **1973**, 2443.

6) a) J. R. Sanders, Jr., E. C. Ashby, and J. H. Carter, II, *J. Am. Chem. Soc.*, **90**, 6385 (1968); b) H. Gilman and F. Schulze, *J. Chem. Soc.*, **1927**, 2663.

7) H. Yasuda and H. Tani, *Tetrahedron Lett.*, **1975**, 11.

8) D. A. Hutchison, K. R. Beck, R. A. Benkeser, and J. B. Grutzner, *J. Am. Chem. Soc.*, **95**, 7075 (1973).

9) H. Lehmkuhl and D. Reiner. *J. Organomet. Chem.*, **23**, C25 (1970).

10) a) R. A. Benkeser, *Synthesis*, **1971**, 347; b) D. O. Courtais and L. Miginiac, *J. Organomet. Chem.*, **69**, 1 (1974); c) E. A. Hill, *ibid.*, **91**, 123 (1975).

11) a) W. H. Glaze, J. E. Hanicak, M. L. Moore, and J. Chaudhuri, *J. Organomet. Chem.*, **44**, 39 (1972); b) H. Kloosterziel and J. A. A. van Drunen, *Recl. Trav. Chim. Pays-Bas*, **89**, 32 (1970); c) H. Kloosterziel and J. A. A. van Drunen, *ibid*, **89**, 37 (1970); c) R. B. Bates, D. W. Gosselink, and J. A. Kazynski, *Tetrahedron Lett.*, **1967**, 205.

12) R. Hoffmann and R. A. Olofson, *J. Am. Chem. Soc.*, **88**, 943 (1966).

13) a) H. Hostalka, R. V. Figini, and G. V. Schulz, *Makromol. Chem.*, **71**, 198 (1964); b) D. N. Bhattacharyya, J. Smid, and M. Szwarc, *J. Phys. Chem.*, **69**, 624 (1965).

14) K. H. Thiele, G. Engelhardt, J. Köhler, and M.

Arnstedt, *J. Organomet. Chem.*, **9**, 385 (1967).
15) R. Kaptein, *J. Am. Chem. Soc.*, **94**, 6251 (1972).
16) a) R. Benn, *Chem. Phys.*, **15**, 369 (1976); b) J. F. Garst. R. H. Cox, J. T. Barbas, R. D. Roberts, J. Morris, and R. C. Morrison, *J. Am. Chem. Soc.*, **92**, 5761 (1970); c) M. Lehnig, *Chem. Phys.*, **8**, 419 (1975); d) P. W. N. M. van Leeuwen, R. Kaptein, R. Huis, and W. T. Kalisvaart, *J. Organomet. Chem.*, **93**, C5 (1975).
17) R. Benn, E. G. Hoffmann, H. Lehmkuhl, and H. Nehl, *J. Organomet. Chem.*, **146**, 103 (1978).
18) a) W. Strohmeier and H. Landsfeld, *Z. Naturforsch.*, **15b**, 332 (1960); b) I. E. Paleeva, N. I. Sheverdina, and K. A. Kocheshkov, *Dokl. Akad. Nauk SSSR.*, **157**, 626 (1964).
19) A. V. Tobolsky and C. E. Rogers, *J. Polym. Sci.*, **40**, 73 (1959).
20) a) K. Fujita, Y. Ohnuma, H. Yasuda, and H. Tani, *J. Organomet. Chem.*, **113**, 201 (1976); b) H. Yasuda, Y. Nakano, K. Natsukawa, and H. Tani, *Macromolecules*, **11**, 586 (1978).
21) S. Htoon and M. F. C. Ladd, *J. Cryst. Mol. Struct.*, **3**, 95 (1973).
22) P. T. Moseley and H. M. M. Shearer, *J. Chem. Soc., Dalton Trans.*, **1973**, 64.
23) H. M. M. Shearer and C. B. Spenser, *J. Chem. Soc., Chem. Commun.*, **1966**, 194.
24) E. Weiss and R. Wolfrum, *Chem. Ber.*, **101**, 35 (1968).
25) A. Haaland, S. Samdal, and R. Seip, *J. Organomet. Chem.*, **153**, 187 (1978).
26) I. V. Isakov and Z. V. Zvankova, *Proc. Acad. Sci. USSR.*, **145**, 663 (1962).
27) a) L. M. Jackman and F. A. Cotton, "Dynamic Nuclear Magnetic Resonance," Academic Press, New York (1975); b) J. W. Faller, *Adv. Organomet. Chem.*, **16**, 211 (1977).
28) R. B. Woodward and R. Hoffmann, "The Conservation of Orbital Symmetry," Academic Press. New York (1970).
29) a) T. G. Traylor, W. Hanstein, H. J. Berwin, Nye A. Clinton, and R. S. Brown, *J. Am. Chem. Soc.*, **93**, 5715 (1971); b) W. Hanstein, H. J. Berwin, and T. G. Traylor, *ibid.*, **92**, 7476 (1970).
30) F. Zuccarello, G. Buenmi, and G. Favini, *J. Mol. Struct.*, **18**, 295 (1973).
31) a) F. A. L. Anet and I. Yavari, *Tetrahedron Lett.*, **1975**, 1567; b) N. L. Allinger, J. F. Viskocil, Jr., U. Burkert, and Y. Yuh, *Tetrahedron*, **32**, 33 (1976).
32) a) G. E. Coates, M. L. H. Green, and K. Wade, "Organometallic Compounds," Methuen, London (1968), Vol I, pp. 211 and references; b) H. Bock and H. Alt, *J. Am. Chem. Soc.*, **92**, 1569 (1970).
33) T. Ashida, "The University Crystallographic Computing System-Osaka," The Computation Center, Osaka University (1973), pp. 55—61.
34) "International Table for X-Ray Crystallography," Kynoch Press, Birmingham (1974), Vol. IV, pp. 71—98.
35) A list of observed and calculated structure factors is kept as Document No. 8017 at the Chemical Society of Japan.
36) C. K. Johnson, "ORTEP-II, Report ORNL-5138," Oak Ridge National Laboratory, Tennessee (1976).

Vinyl Polymerization. 394.[1] Radical Polymerization of Methyl Methacrylate Initiated with *Saccharomyces Cerevisiae*

Minoru Imoto,* Tatsuro Ouchi, Eijiro Morita, Minoru Yamada, Tai Tokuyama,†† and Hitoshi Obata

Laboratry of Synthetic High Polymers, Faculty of Engineering, Kansai University, Suita, Osaka 564

†† *Laboratory of Applied Biochemistry, Faculty of Engineering, Kansai University, Suita, Osaka 564*

(Received October 4, 1979)

The polymerization of methyl methacrylate with *Saccharomyces cerevisiae* was carried out in water, the reaction being found to proceed through a radical mechanism. The effect of the mass of reagent on the rate of polymerization and selectivity of vinyl monomer were studied. The isolated cell wall showed remarkable activity for polymerization. The change of surface of the polymerization system was observed with a scanning electron microscope.

Recently, it was reported[2] that the cell of yeast, *Saccharomyces cerevisiae*, can initiate the polymerization of methyl methacrylate (MMA) in the presence of Cu(II) ion. The polymerization was found to proceed on the exterior and interior of the cell, particularly on the cell wall. The present paper deals with a precise study of the polymerization. The radical mechanism is confirmed, effects of the mass of reactant on the conversion of MMA, selectivity of the vinyl monomer and polymerization by the cell wall isolated from the cells being given.

Experimental

Materials. Dry yeast *Saccharomyces cerevisiae* (SC-1, Oriental Yeast Co.) was used. MMA and other monomers were purified by the usual methods. Copper(II) chloride (special grade) was used without further purification. The water was ion-exchanged and distilled.

Procedures. MMA, water, and other reagents were placed in a tube which was then sealed in a vacuum after thawing with nitrogen and incubated at 30 or 85 °C with shaking or by being left to stand. After a certain time, the contents of the tube were poured into a large amount of methanol in order to precipitate the polymer formed. After filtration, the product was thoroughly washed with methanol, dried in a vacuum, and then weighed. The conversion of MMA was calculated by the following equation:

$$\text{Conversion}(\%) = \frac{\text{Wt. of products(g)} - \text{Initial wt. of cells(g)}}{\text{Wt. of MMA in the feed(g)}} \times 100$$

It was confirmed by turbidimetry that no multiplication of cell was observed during the course of polymerization at 30 °C for 10 d. The mode of the polymerization system was observed with a scanning electron microscope (SEM).[2] The number-average degree of polymerization (P_n) of poly(MMA) produced was estimated from the viscosity determined in benzene at 30 °C, using Welch's equation.[3]

Results and Discussion

Confirmation of Radical Mechanism. Copolymerization of MMA with Styrene (St) was carried out (Fig. 1), a radical mechanism being confirmed.

Selectivity of Vinyl Monomer. Polymerization of various monomers was carried out with the system SC-1, Cu(II) ion, and water. The results are given in Table 1.

The conversion of St and acrylonitrile (AN) was in the range of thermal polymerization or experimental errors. Thus, no initiating ability of the present initiator system for St and AN was observed. On the other hand, MMA, ethyl methacrylate (EMA), and methacrylic acid (MAA) were found to be polymerized.

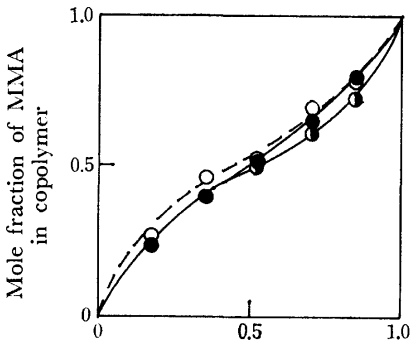

Fig. 1. Copolymerization of MMA and St. (MMA+St) 3 cm³, H_2O 10 cm³, SC-1 0.1 g, $CuCl_2 \cdot 2H_2O$ 1×10^{-3} g. ●(A), Copolymer produced at 85 °C after 3 h with shaking, including both copolymers produced in the water phase and monomer layer. ◗(B), Copolymer produced in the water layer at 30 °C after 10 d on standing. ○(C), Copolymer produced in the monomer layer at 30 °C after 10 d on standing.

Table 1. Polymerization of vinyl monomers[a]

SC-1/g	$CuCl_2 \cdot 2H_2O$/g	Conversion/%				
		MMA	St	AN	MAA	EMA
0	0	0	1.14	0	0	3.08
0.1	0	0	0.89	0	1.99	0.39
0	1×10^{-3}	0	1.43	0	0	0
0.1	1×10^{-3}	8.63	2.15	0.66	7.25	5.90

a) Monomer 3 cm³, H_2O 10 cm³; 30 °C, 10 d, with shaking.

AN: acrylonitrile, MAA: methacrylic acid, EMA: ethyl methacrylate, St: styrene, MMA: methyl methacrylate.

Effect of the Mass of Cu(II) Ion on the Polymerization of MMA. The effect of the mass of Cu(II) ion on the conversion of MMA was obtained for polymerization at 85 °C with shaking (Fig. 2) and on standing

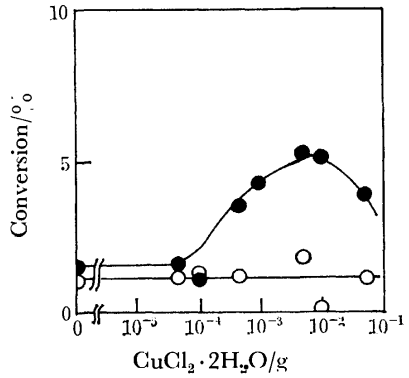

Fig. 2. Conversion of MMA with shaking *vs.* mass of $CuCl_2 \cdot 2H_2O$. MMA 3 cm³, ● SC-1 0.1 g, ○ SC-1 0 g, H_2O 10 cm³; 85 °C, 5 h.

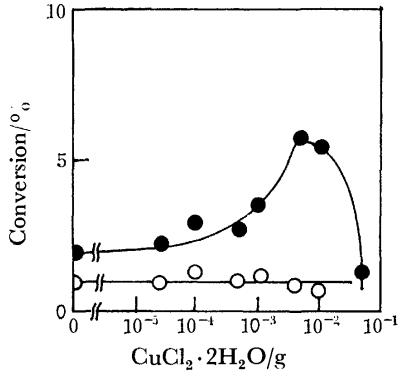

Fig. 3. Conversion of MMA on standing *vs.* mass of $CuCl_2 \cdot 2H_2O$. MMA 3 cm³, ● SC-1 0.1 g, ○ SC-1 0 g, H_2O 10 cm³; 85 °C, 5 h.

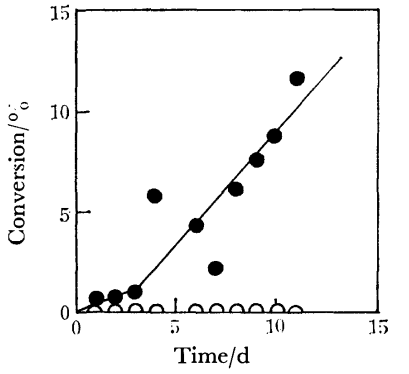

Fig. 4. Time-conversion curve.
MMA 3 cm³, ● SC-1 0.1 g, ○ SC-1 0 g, H_2O 10 cm³, $CuCl_2 \cdot 2H_2O$ 1×10^{-3}g; 30 °C, with shaking.

(Fig. 3). In both cases, the maximum conversion was observed at 5×10^{-2} g of $CuCl_2 \cdot 2H_2O$. The decrease in the conversion of MMA by excess Cu(II) ion was due to the following inhibition reaction of the propagating radical with Cu(II) ion:

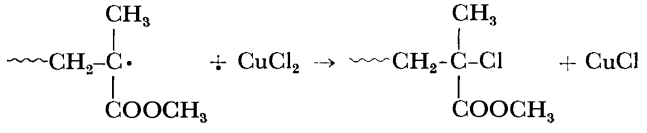

It should be noted that both conversion curves are similar to each other. The time-conversion curve of the polymerization of MMA is shown in Fig. 4. The white and black circles indicate the conversion of MMA in the absence and presence, respectively, of SC-1. There is an induction period of about 2 d.

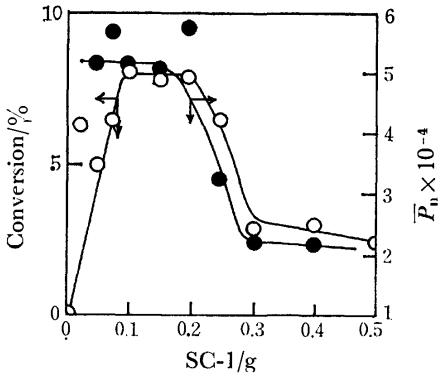

Fig. 5. Conversion of MMA or $\bar{P}_n$ of poly-(MMA) *vs.* mass of SC-1. MMA 3 cm³, H_2O 10 cm³, $CuCl_2 \cdot 2H_2O$ 1×10^{-3}g; 30 °C, 10 d, with shaking, ○ conversion. ● $\bar{P}_n$.

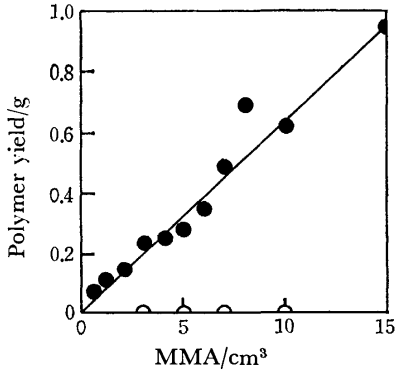

Fig. 6. Polymer yield *vs.* mass of MMA.
● SC-1 0.1 g, ○ SC-1 0 g, H_2O 10 cm³, $CuCl_2 \cdot 2H_2O$ 1×10^{-3}g; 30 °C, 10 d, with shaking.

Effect of the Mass of SC-1 on the Polymerization of MMA. Varying the mass of SC-1 and keeping that of Cu(II)-ion, MMA, and water constant, we carried out polymerization at 30 °C for 10 d with shaking. The results on the conversion of MMA and $\bar{P}_n$ of poly-(MMA) are shown in Fig. 5.

The conversion increased with the mass of SC-1, reaching maximum immediately and then decreasing. This was confirmed by repeated experiments. $\bar{P}_n$ also decreased with the mass of SC-1.

The only assumption to explain the behavior is as follows: the contents of some unknown free-radical other than the propagating poly-(MMA) radicals increase with the mass of SC-1 in the feed. The free-radicals could be produced by the chain transfer reactions of the propagating poly-(MMA) radicals with the vital macromolecules in the cell, and could scavenge the propagating poly-(MMA) radicals. Thus, above a certain amount of SC-1, the conversion of MMA and $\bar{P}_n$ of poly-(MMA) decreases. This was supported by the results of experimental studies on the chain-transfer reaction of poly-(MMA) radicals with nucleic acid bases and nucleosides.[4]

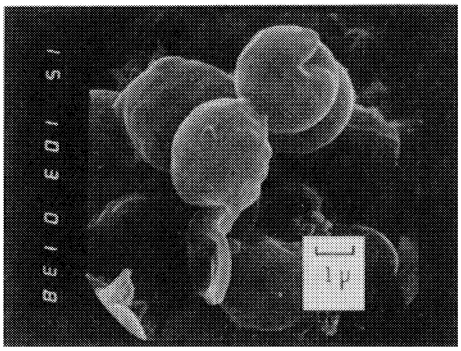

Fig. 7(a). Surface view of the SC-1.

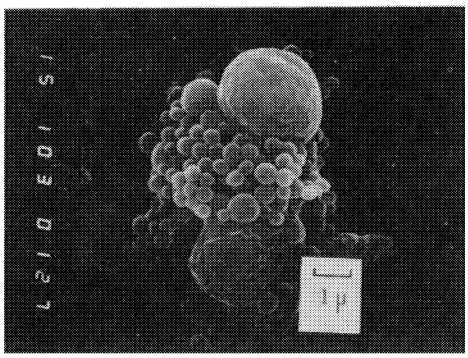

Fig. 7(b). Surface view of the polymerized system (SC-1, 0.1 g; MMA, 3 cm³; $CuCl_2 \cdot 2H_2O$, 1×10^{-3}g; H_2O, 10 cm³; 30 °C, 10 d, on standing; Conversion of MMA, 8.8%).

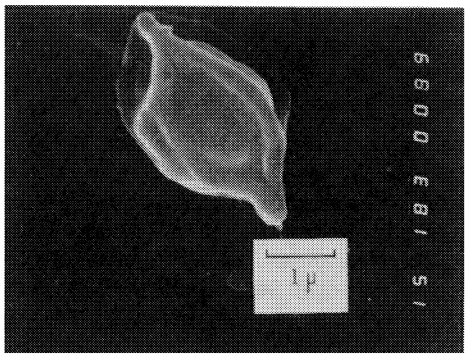

Fig. 7(c). Surface view of the polymerized system. After the polymerization, the product was washed under reflux with benzene for 50 h.

Effects of the Mass of MMA on Polymerization. The masses of SC-1, Cu(II) ion, and H_2O were kept constant. The polymerization was carried out at 30 °C for 10 d with shaking. The results are shown in Fig. 6. The polymer yield in g increased linearly with the amount of MMA.

Scanning Electron Microscopy (SEM). It was observed by transmission electron microscopy that the cell wall is disintegrated at a 3.1% conversion of MMA.[1] This is due to the particular easiness of the polymerization of MMA in the cell wall. When the conversion of MMA was only 2.1%, the cell wall became somewhat larger. We have treated the case in which the conversion of MMA reached 8.8%. The results of SEM are shown in Figs. 7(a), (b), and (c). Since the conversion was 8.8%, it seems that the wall was already disintegrated, thus becoming the active center for the polymerization of MMA. The propagating chain radicals were brought into the water phase. A similar polymerization to suspension polymerization takes place. Figure 7(b) is in line with the consideration. The small round particles near the cell are poly-(MMA) produced formed in the water phase. After washing with benzene for 50 h (Fig. 7(c)), the particles of poly-(MMA) produced in the water phase disappeared, only the cell containing poly-(MMA) produced in the interior being observed.

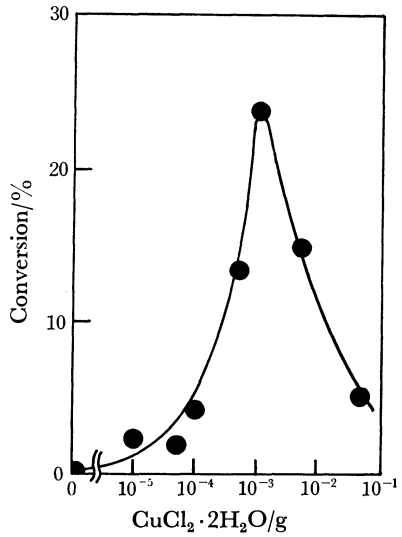

Fig. 8. The polymerization of MMA initiated by the cell wall of SC-1. MMA 3 cm³, cell wall 0.1 g, H_2O 10 cm³; 30 °C, 10 d, with shaking.

Polymerization of MMA Initiated with Cell Wall. The cell wall which is particularly active was isolated as follows. SC-1 was disrupted by means of an X-press. The cell wall was separated by centrifugation at 12000 rpm for 60 min, washed twice with cold distilled water and lyophilized, polymerization of MMA then being carried out. The results are shown in Fig. 8. The activity for polymerization of the cell wall became *ca.* 3 times higher than the original SC-1.

References

1) T. Ouchi, N. Murayama, and M. Imoto, *Bull. Chem. Soc. Jpn.* (Part 393), **53**, 748 (1980).
2) M. Imoto, T. Ouchi, Y. Nakamura, E. Morita, M. Yamada, T. Tokuyama, H. Obata, and T. Iwamoto, *J. Polym. Sci., Polym. Chem. Ed.*, **17**, 347 (1979).
3) F. J. Welch, *J. Polym. Sci.*, **61**, 243 (1962).
4) M. Imoto, A. Kuriyama, and T. Ouchi, *Chem. Lett.*, **1979**, 1145.

Preparation of New Nitrogen-bridged Heterocycles. A Facile Synthetic Method of Pyrano[2,3-*b*]indolizinone Derivatives

Akikazu KAKEHI,* Suketaka ITO, Kazunori NAKANISHI, Kozo WATANABE, and Masahiko KITAGAWA

Department of Industrial Chemistry, Faculty of Engineering, Shinshu University, Wakasato, Nagano 380

(Received October 5, 1979)

Pyrano[2,3-*b*]indolizinone derivatives were formed in 18—98% yields by the reactions of 3-[bis(alkylthio)-methylene]-2,3-dihydroindolizin-2-ones with various acetates in the presence of alkali. Dihydroindolizinones were readily obtained by the alkaline treatment of 1-[2,2-bis(alkylthio)-1-ethoxycarbonylvinyl]-2-ethylpyridinium iodides and -2-methylpyridinium iodides or by the *S*-alkylation of 3-[(alkylthio)mercaptomethylene]-1-phenyl-2,3-dihydroindolizin-2-ones with alkyliodides.

In a previous paper a report was given on the unexpected formation of 3-[bis(ethylthio)methylene]-1-methyl-2,3-dihydroindolizin-2-one in the reaction of 1-[1-ethoxycarbonyl-2,2-bis(ethylthio)vinyl]-2-ethylpyridinium iodide with alkali.[1] The compound is a quite new indolizine with an interesting structure: a) dihydroaromatic: b) enone and ketene dithioacetal: c) 2-methylene-1,2-dihydropyridine. We thus assumed that, if the structural contribution such as (C) (Fig. 1) for this 3-methylene-2,3-dihydroindolizin-2-one is present, the reaction of this molecule with a bifunctional reagent may lead to the condensed indolizine derivative. This was found to be the case, pyrano[2,3-*b*]indolizinone derivative being formed by the reaction with ethyl cyanoacetate under basic conditions. In this paper we wish to report the synthesis of some 3-methylene-2,3-dihydroindolizin-2-ones and their facile transformations into pyrano[2,3-*b*]indolizinone derivatives.

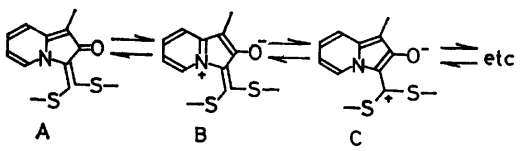

Fig. 1.

Results and Discussion

Preparation of 3-Methylene-2,3-dihydroindolizin-2-ones. The reactions of 1-[2,2-bis(alkylthio)-1-ethoxycarbonylvinyl]-2-ethylpyridinium iodides (**8** and **9**) and -2-methylpyridinium iodides (**10** and **11**), readily obtained from 1-(ethoxycarbonylmethyl)-2-ethylpyridinium bromide (**1**) and -2-methylpyridinium chloride (**2**) *via* the corresponding pyridinium ylides (**4**—**7**) (Scheme 1),[2] with alkali gave 3-[bis(alkylthio)methylene]-2,3-dihydroindolizin-2-one derivatives (**15**—**18**) as dark green prisms or oils in over 90% yields. In contrast with **10** and **11**,[3] alkaline treatment of 2-ethylpyridinium salts (**8** and **9**) in the presence of an activated ethoxymethylene compound such as ethyl (ethoxymethylene)cyanoacetate (**12**) afforded only 3-methylene-2,3-dihydroindolizin-2-ones (**15** and **16**) in comparable yields, and not the expected 2-allylidene-1,2-dihydropyridines (**13** and **14**). On the other hand, treatment of 2-benzyl-1-(ethoxycarbonylmethyl)pyridinium bromide (**3**) with carbon disulfide and then dialkyl sulfate in the presence of potassium hydroxide afforded 3-[(alkylthio)mercaptomethylene]-1-phenyl-2,3-dihydroindolizin-2-ones (**21** and **22**) as orange needles in 88 and 79% yields, respectively. *S*-Alkylation of the mercapto derivatives (**21** and **22**) with methyl and ethyl iodide in the presence of potassium carbonate in chloroform gave 3-[bis(alkylthio)methylene]-1-phenyl-2,3-dihydroindolizin-2-ones (**19** and **20**) in 96 and 91% yields, respectively.

The 3-methylene-2,3-dihydroindolizin-2-one derivatives (**15**, **16**, and **19**—**22**) were very stable under the usual conditions (below 80 °C), while the 1-unsubstituted derivatives (**17** and **18**) were considerably unstable even at room temperature and, in particular, very sensitive to column separation (alumina).

The structural assignment of the 2,3-dihydroindolizin-2-one derivatives (**15**—**22**) was accomplished mainly from physical and spectral data. For example, elementary analyses of the crystalline compounds (**15**, **19**, **21**, and **22**) were in good accord with the proposed structures. The IR spectra of **15**—**22** showed a strongly lowered carbonyl absorption near 1600 cm^{-1}, indicating the presence of the contribution of the polarized structure as observed in 2-methylene-1,2-dihydropyridine derivative,[4] and those of **21** and **22** exhibited also a weak mercapto absorption near 2500 cm^{-1} but no hydroxyl absorption over 3000 cm^{-1}. The IR spectra of **21** and **22** excluded the possibility of the 2-hydroxyindolizine structure. The NMR spectra (Table 1) of compounds **15**—**20**, and **21** and **22** are similar to each other, and the considerable low values of the skeletal protons in **15**—**20** in comparison with those of aromatic indolizines[5] strongly supported their dihydroindolizine structure. Furthermore, signals appearing at near δ 13 ppm in the NMR spectra of **21** and **22** should be due to the mercapto group hydrogen-bonding to the 2-carbonyl oxygen. The considerably high values of the chemical shifts of **21** and **22** as compared with those of **15**—**20** can be explained by the promoted aromatic character owing to the hydrogen-bonding.

Reactions of 3-Methylene-2,3-dihydroindolizin-2-ones with Various Acetates in the Presence of Alkali. In order to achieve transformation of these dihydroaromatic compounds (**15**—**20**) into condensed aromatic indolizine derivatives, we carried out their reactions with bifunctional reagents in the light of ketene dithioacetal chemistry.[6] We chose activated acetate derivatives, which can easily generate the nucleophilic carbanion under basic conditions and also have an electrophilic carbonyl carbon. When 3-methylene-2,3-dihydroindo-

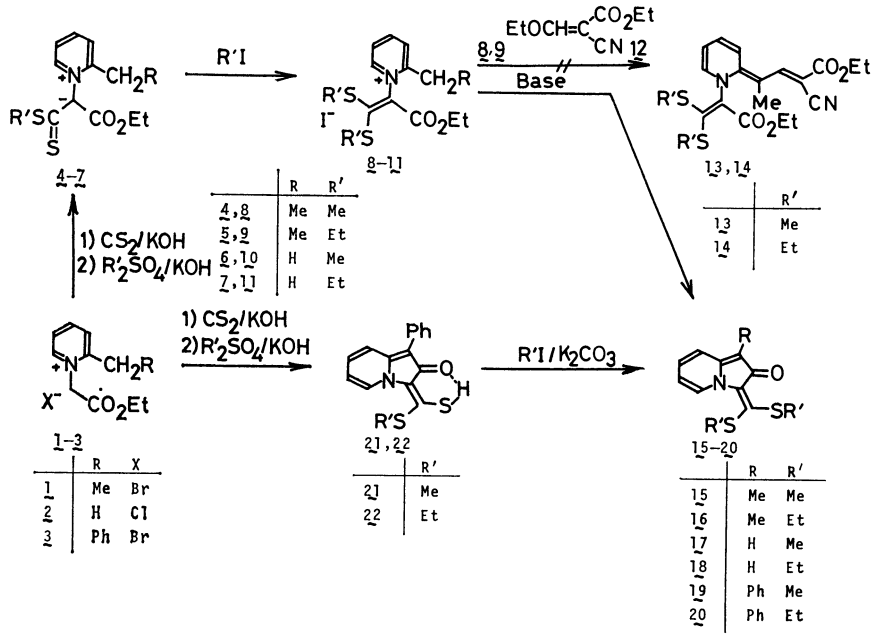

Scheme 1.

TABLE 1. NMR DATA OF 3-METHYLENE-2,3-DIHYDROINDOLIZIN-2-ONES

Compd no.	C-5	C-6	C-7	C-8	R	R′	R′(H)	Coupling constants
15	8.43 d	6.00 br t	6.5—7.0 m		1.79 s	2.37 s	2.63 s	$J_{5,6}=7.0$, $J_{6,7}=6.5$, $J_{6,8}=2.0$ Hz
16	8.59 d	5.93 dt	6.76 br t	6.53 br d	1.73 s	2.82 q 1.19 t	3.11 q 1.24 t	$J_{5,6}=J_{6,7}=7.0$, $J_{7,8}=9.0$, $J_{6,8}=2.0$ Hz
17	8.55 d	6.13 br t	6.6—7.0 m		5.21 s	2.39 s	2.64 s	$J_{5,6}=7.0$, $J_{6,7}=6.5$, $J_{6,8}=2.0$ Hz
18	8.73 d	6.08 br t	6.6—7.1 m		5.17 s	2.90 q 1.24 t	3.20 q 1.27 t	$J_{5,6}=7.0$, $J_{6,7}=6.5$, $J_{6,8}=2.0$ Hz
19	8.60 d	6.15 dt	a)	a)	6.7—7.9 m	2.37 s	2.65 s	$J_{5,6}=J_{6,7}=7.0$, $J_{6,8}=1.5$ Hz
20	8.76 d	6.10 dt	b)	b)	6.7—7.8 m	2.91 q 1.24 t	3.23 q 1.28 t	$J_{5,6}=J_{6,7}=7.0$, $J_{6,8}=1.5$ Hz
21	9.40 d	6.82 dt	c)	c)	7.0—7.9 m	2.84 s	12.92[d] s	$J_{5,6}=J_{6,7}=7.0$, $J_{6,8}=1.5$ Hz
22	9.42 d	6.79 dt	c)	c)	7.0—7.9 m	3.51 q 1.44 t	12.93[d] s	$J_{5,6}=J_{6,7}=7.0$, $J_{6,8}=1.5$ Hz

a) Overlapped with phenyl signals appearing at δ 6.7—7.9. b) Overlapped with phenyl signals appearing at δ 6.7—7.8. c) Overlapped with phenyl signals appearing at δ 7.0—7.9. d) Proton of mercapto group.

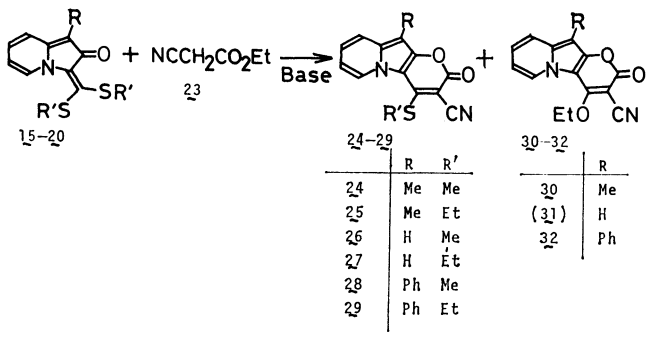

Scheme 2.

lizin-2-ones (**15**—**20**) were allowed to react with ethyl cyanoacetate (**23**) in benzene in the presence of triethylamine under reflux, smooth evolution of methanethiol or ethanethiol was observed, separation of the reaction solutions giving crystalline 4-alkylthio-3-cyano-2*H*-pyrano[2,3-*b*]indolizin-2-one derivatives (**24**—**29**). 4-Ethoxy derivatives **30** and **32** were also obtained in the reactions of **15** and **20** (Scheme 2). Furthermore, the respective replacement of the solvent and the base, benzene by ethanol and triethylamine by potassium *t*-butoxide, in the reactions of **15**, **16**, and **19** with **23** gave rise to increased formation of 4-ethoxypyranoindolizinones (**30** and **32**).

On the other hand, similar reactions of **15**—**20** with ethyl benzoylacetate (**33**), diethyl malonate (**34**), ethyl acetoacetate (**35**), and ethyl phenylacetate (**36**) in the presence of potassium *t*-butoxide gave only 4-alkylthio-2*H*-pyrano[2,3-*b*]indolizin-2-one derivatives (**37**—**60**) in 18—98% yields with the evolution of methanethiol or ethanethiol (Scheme 3). The use of triethylamine as a base in the above reactions did

Table 2. NMR data of pyrano[2,3-*b*]indolizinones

Compd no.[a]	C-6	C-7	C-8	C-9	C-10	C-3	C-4
24	9.45 d	——6.7—7.7m——			2.32 s	—	2.99 s
25	9.47 d	6.93 br t	7.33 br t	7.51 br d	2.27 s	—	3.50 q 1.41 t
26	9.46 d	——6.4—7.7m——			6.47 s	—	3.02 s
27	9.46 d	6.95 dt	7.32 br t	7.55 br d	6.39 s	—	3.53 q 1.41 t
28	9.43 d	6.99 dt	b)	b)	7.8—8.0m	—	3.01 s
29	9.59 d	6.97 dt	b)	b)	7.0—8.0m	—	3.53 q 1.46 t
30	8.78 d	c)	c)	c)	2.32 s	—	5.08 q 1.66 t
32	8.78 d	c)	c)	c)	7.2—8.0m	—	5.07 q 1.66 t
37	9.23 d	6.75 dt	7.08 br t	b)	2.30 s [d]	7.3—8.1m	2.33 s [e]
38	9.25 d	6.74 dt	7.09 br t	7.45 br d	2.28 s	4.40 q 1.39 t	2.52 s
39	9.28 d	6.82 dt	7.34 br t	7.49 br d	2.30 s	2.65 s	2.46 s
40	9.33 d	6.67 dt	6.97 br t	b)	2.32 s	7.1—7.6m	1.98 s
41	9.37 d	6.74 dt	7.08 br t	b)	2.34 s	7.3—8.1m	2.88 q 1.21 t
42	9.30 d	6.74 dt	7.08 br t	7.42 br d	2.28 s	4.41 q 1.40 t	2.97 q 1.31 t
43	9.36 d	6.78 dt	7.11 br t	7.45 br d	2.31 s	2.62 s	2.91 q 1.27 t
44	9.43 d	6.66 dt	6.98 br t	b)	2.35 s	7.2—7.6m	2.41 q 1.04 t
45	9.31 d	6.80 dt	7.10 br t	b)	6.38 s	7.3—8.1m	2.39 s
46	9.27 d	6.79 dt	7.10 bt t	7.47 br d	6.31 s	4.40 q 1.40 t	2.54 s
47	9.29 d	6.83 dt	7.15 br t	7.50 br d	6.36 s	2.66 s	2.49 s
48	9.41 d	6.70 dt	7.02 br t	b)	6.37 s	7.0—7.6m	2.03 s
49	9.43 d	6.88 dt	7.11 br t	b)	6.40 s	7.3—8.1m	2.89 q 1.21 t
50	9.51 d	6.88 dt	7.20 br t	7.58 br d	6.43 s	4.47 q 1.42 t	3.03 q 1.35 t
51	9.39 d	6.81 dt	7.13 br t	7.48 br d	6.32 s	2.61 s	2.92 q 1.29 t
52	9.50 d	6.70 dt	7.00 br t	b)	6.36 s	7.2—7.6m	2.42 q 1.05 t
53	9.38 d	6.80 dt	7.16 br t	b)	7.1—8.1m	7.1—8.1m	2.39 s
54	9.37 d	6.82 dt	7.13 br t	b)	7.2—7.9m	4.40 q 1.40 t	2.54 s
55	9.37 d	6.86 dt	b)	b)	7.0—8.0m	2.63 s	2.50 s
56	9.48 d	6.74 dt	7.04 br t	b)	7.2—7.9m	7.2—7.9m	2.03 s
57	9.55 d	6.85 dt	7.14 br t	b)	7.2—8.1m	7.2—8.1m	2.93 q 1.23 t
58	9.57 d	6.84 dt	b)	b)	7.0—8.0m	4.42 q 1.43 t	3.04 q 1.38 t
59	9.51 d	8.85 dt	b)	b)	7.0—8.0m	2.62 s	2.96 q 1.31 t
60	9.59 d	6.73 dt	7.05 br t	b)	7.1—8.0m	7.1—8.0m	2.43 q 1.07 t

a) The coupling constants are as follows: $J_{6,7}=J_{7,8}=7.0$ Hz, $J_{8,9}=8.0$ Hz, $J_{7,9}=2.0$ Hz, and $J_{Et}=7.0$ Hz. b) Overlapped with phenyl proton signals. c) Overlapped with the C_7-, C_8-, and C_9-proton signals of the 4-alkylthiopyranoindolizinones (**24**, **25**, **28**, and **29**). d) Or 2.33. e) Or 2.30.

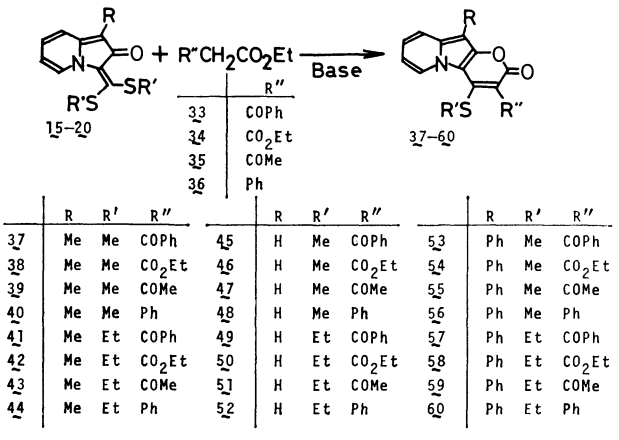

Scheme 3.

not give satisfactory results because of their diminished yields of pyranoindolizinones.

All the pyrano[2,3-*b*]indolizinones (**24**—**30**, **32**, and **37**—**60**) were very stable crystalline compounds with strong fluorescence. Elementary analyses of compounds **25**—**29** and **37**—**60** were in good accord with the postulated structures, the IR spectra always showing a strong absorption at 1670—1700 cm^{-1} due to the 2-pyrone carbonyl group (Table 4). As compared with 3-methylene-2,3-dihydroindolizin-2-ones (**15**—**22**), the NMR spectra of the pyranoindolizinones (**24**—**30**, **32**, and **37**—**60**) (Table 2) exhibited signals at a fairly low field attributable to the skeletal protons, whose values coincided with those of known aromatic indolizine derivatives.[5] For example, the NMR spectrum of **39** showed skeletal proton signals at δ 6.82 (1H, dt, J=7.0, 7.0, and 2.0 Hz, C_7–H), 7.34 (1H, br t, J=8.0 and 7.0 Hz, C_8–H), 7.49 (1H, br d, J=8.0 Hz, C_9–H), and 9.28 (1H, d, J=7.0 Hz, C_6–H), and methyl signals at δ 2.30 (3H, s, C_{10}–Me), 2.46 (3H, s, SMe), and 2.65 (3H, s, COMe), and the chemical shifts of the skeletal protons (δ 6.82—9.28) and of the C_{10}–Me protons (δ 2.30) were in line with those of 3-acylindolizines (δ 6.50—9.40)[3] and 1-methylindolizine (δ 2.27).[7] On the other hand, the NMR spectra of **30** and **32** were almost the same as those of 4-alkylthiopyrano[2,3-*b*]indolizin-2-ones (**24**—**29** and **37**—**60**)

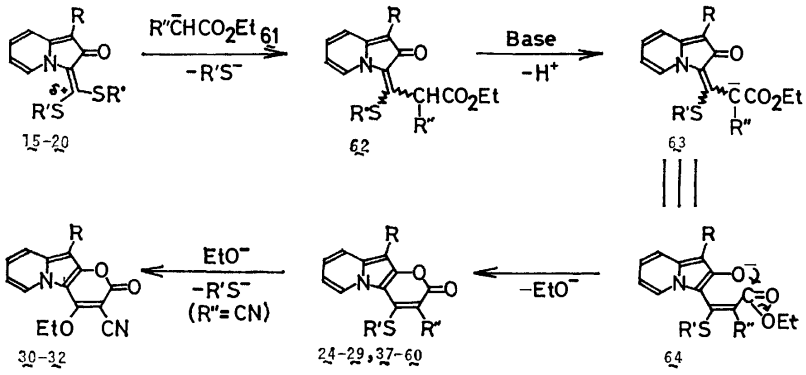

Scheme 4.

TABLE 3. DATA OF 3-METHYLENE-2,3-DIHYDROINDOLIZIN-2-ONES

Compd no.	Precursor	Yield %	Mp/°C	ν_{CO}^{KBr}	ν_{SH}^{KBr}	Formula	Calcd (%) C	H	N	Found (%) C	H	N
15[a]	**8**	95	86—88	1600	—	$C_{12}H_{13}NOS_2$	57.34	5.21	5.57	57.37	5.21	5.54
16[b]	**9**	92	Oil	1600[c]	—							
17[b]	**10**	100[d]	Oil	1600[c]	—							
18[b]	**11**	100[d]	Oil	1600[c]	—							
19[a]	**21**	96	131—133	1595	—	$C_{17}H_{15}NOS_2$	65.14	4.82	4.47	65.36	4.85	4.50
20[b]	**22**	91	Oil	1600[c]	—							
21[e]	**3**	88	121—122	1572	2550	$C_{16}H_{13}NOS_2$	64.18	4.38	4.68	64.00	4.41	4.63
22[e]	**3**	79	119—121	1570	2510	$C_{17}H_{15}NOS_2$	65.14	4.82	4.47	65.02	4.83	4.46

a) Dark green prisms. b) Dark green oil. c) Neat. d) Crude yield. e) Orange needles.

except for the absence of the alkylthio signals and the presence of an ethoxyl signals (δ near 1.7 (3H, t, J=7.0 Hz) and near 5.1 (2H, q, J=7.0 Hz)). From the results and mechanistic consideration, the products **24**—**29** and **37**—**60**, and **30** and **32** were concluded to be 4-alkylthio-2*H*-pyrano[2,3-*b*]indolizin-2-one derivatives and the 4-ethoxy isomers, respectively.

Reaction Mechanism. The formation of pyranoindolizinones (**24**—**29** and **37**—**60**) is explained by the nucleophilic substitution with the carbanion (**61**), generated *in situ* by the treatment of acetates with base, at the 3-methylene position of 2,3-dihydroindolizin-2-ones (**15**—**20**), followed by the hydrogen abstraction from the resulting product (**62**) by a base catalyst and then the intramolecular nucleophilic cyclization of the anion (**64**) (*via* the primary carbanion (**63**)) with the elimination of an ethoxide ion. The fact that the primary substitution compound (**62**) was not isolated at all suggests a very fast progress of steps **62**→**63**→**64**→**24**—**29** and **37**—**60**. On the other hand, 4-ethoxypyranoindolizinones such as **30**—**32** should be formed *via* the nucleophilic substitution of 4-alkylthio-3-cyanopyranoindolizinones by the ethoxide ion generated *in situ* in these reaction systems, since, if similar substitution for 3-methylene-2,3-dihydroindolizin-2-ones (**15**—**20**) could occour initially, other 4-ethoxypyranoindolizinone derivatives should be formed together with **30** and **32**. In these reactions the reason for only the formation of 4-ethoxy-3-cyano-2*H*-pyrano[2,3-*b*]indolizin-2-ones (**30** and **32**) is not clear, but it may be related to the strong electron-withdrawing effect and the smaller hindrance of the cyano group. The mechanisms are summarized in Scheme 4.

Experimental

Melting points were measured with a Yanagimoto micro-melting point appratus and are uncorrected. Microanalyses were carried out on a Perkin-Elmer 240 Elemental Analyzer. The NMR spectra were determined with a Varian EM360A NMR Spectrometer in deuteriochloroform with tetramethylsilane as an internal standard. The chemical shifts are expressed in δ values. The IR spectra were taken with a Hitachi 260-10 Infrared Spectrophotometer.

*Preparation of Pyridinium Salts (**8**—**11**).* All the 1-[2,2-bis(alkylthio)-1-ethoxycarbonylvinyl]-2-ethylpyridinium iodides (**8** and **9**) and -2-methylpyridinium iodides (**10** and **11**)[2,3] were prepared from 1-(ethoxycarbonylmethyl)-2-ethylpyridinium bromide (**1**) and -2-methylpyridinium chloride (**2**) according to the procedure of Tominaga *et al.*[2] The results and some properties of new compounds (**4**, **5**, **8**, and **9**) are as follows: (**4**), 56%, yellow needles, mp 146—149 °C, Found: C, 54.86; H, 6.05; N, 4.90%. Calcd for $C_{13}H_{17}NO_2S_2$: C, 55.09; H, 6.05; N, 4.92%. (**5**), 38%, yellow needles, mp 103—106 °C, Found: C, 39.48; H, 4.78; N, 3.30%. Calcd for $C_{14}H_{20}NO_2S_2I$: C, 39.52; H, 4.74; N, 3.29%. (**8**), 91%, pale yellow prisms, mp 109—112 °C, Found: C, 56.61; H, 6.42; N, 4.63%. Calcd for $C_{14}H_{19}NO_2S_2$: C, 56.53; H, 6.44; N, 4.71%. (**9**), 86%, pale yellow prisms, mp 117—120 °C, Found: C, 42.36; H, 5.31; N, 3.22%. Calcd for $C_{16}H_{24}NO_2S_2I$: C, 42.38; H, 5.34; N, 3.09%.

*Preparation of 3-Methylene-2,3-dihydroindolizin-2-ones (**15**—**18**). General Method*: A chloroform solution (50 ml) of pyridinium salt (1 or 2 mmol) was treated with potassium carbonate (5 or 10 g) at room temperature until the TLC spot of the

Table 4. Data of pyrano[2,3-*b*]indolizinones

Compd no.	React.[a]		Base[b]	Yield %	Mp/°C	ν_{CO}^{KBr}		ν_{CN}^{KBr}	Formula	Calcd (%)			Found (%)		
										C	H	N	C	H	N
24	**15**	CA	TA	*ca* 75[c]					Mixture (**24**+**30**)						
25	**16**	CA	TA	73	266—268	1689		2200	$C_{15}H_{12}N_2O_2S$	63.36	4.25	9.85	63.49	4.18	9.75
26	**17**	CA	TA	37	265—267	1700		2215	$C_{13}H_8N_2O_2S$	60.92	3.15	10.93	61.08	3.31	10.62
27	**18**	CA	TA	71	211—214	1692		2200	$C_{14}H_{10}N_2O_2S$	62.20	3.73	10.36	62.33	3.68	10.33
28	**19**	CA	TA	*ca* 31[d]	164—167	1690		2200	$C_{19}H_{12}N_2O_2S$	68.66	3.64	8.43	68.81	3.63	8.14
29	**20**	CA	TA	74	223—226	1700		2200	$C_{20}H_{14}N_2O_2S$	69.34	4.07	8.09	69.14	4.25	8.11
37	**15**	BA	KB	98	175—177	1685			$C_{20}H_{15}NO_3S$	68.75	4.33	4.01	68.64	4.33	4.11
38	**15**	ML	KB	36	112—114	1688			$C_{16}H_{15}NO_4S$	60.55	4.76	4.41	60.59	4.73	4.69
39	**15**	AA	KB	54	158—160	1685			$C_{15}H_{13}NO_3S$	62.70	4.56	4.88	62.52	4.57	4.90
40	**15**	PA	KB	48	206—207	1684			$C_{19}H_{15}NO_2S$	71.00	4.70	4.36	71.05	4.66	4.35
41	**16**	BA	KB	91	159—162	1685	1674		$C_{21}H_{17}NO_3S$	69.40	4.72	3.85	69.06	4.72	3.83
42	**16**	ML	KB	62	140—143	1694	1725		$C_{17}H_{17}NO_4S$	61.61	5.17	4.23	61.33	5.18	4.27
43	**16**	AA	KB	60	122—125	1674	1700		$C_{16}H_{15}NO_3S$	63.76	5.02	4.65	63.49	5.05	4.59
44	**16**	PA	KB	46	156—159	1687			$C_{20}H_{17}NO_2S$	71.61	5.11	4.18	71.36	5.10	4.24
45	**17**	BA	KB	52	197—199	1670			$C_{19}H_{13}NO_3S$	68.04	3.91	4.18	68.02	3.94	4.15
46	**17**	ML	KB	41	123—125	1680	1700		$C_{15}H_{13}NO_4S$	59.39	4.32	4.62	59.67	4.32	4.68
47	**17**	AA	KB	45	103—105	1680	1668		$C_{14}H_{11}NO_3S$	61.52	4.06	5.13	61.23	4.02	5.10
48	**17**	PA	KB	18	160—161	1679			$C_{18}H_{13}NO_2S$	70.33	4.26	4.56	70.32	4.33	4.50
49	**18**	BA	KB	82	115—117	1691			$C_{20}H_{15}NO_3S$	68.75	4.33	4.01	68.75	4.34	3.99
50	**18**	ML	KB	56	121—124	1699	1730		$C_{16}H_{15}NO_4S$	60.55	4.76	4.41	60.34	4.71	4.26
51	**18**	AA	KB	60	114—116	1687	1704		$C_{15}H_{13}NO_3S$	62.70	4.56	4.88	62.55	4.64	4.87
52	**18**	PA	KB	38	136—138	1685			$C_{19}H_{15}NO_2S$	71.00	4.70	4.36	70.63	4.67	4.31
53	**19**	BA	KB	67	197—199	1680			$C_{25}H_{17}NO_3S$	72.97	4.16	3.40	72.85	4.14	3.13
54	**19**	ML	KB	50	123—125	1685	1715		$C_{21}H_{17}NO_4S$	66.47	4.52	3.69	66.76	4.53	3.48
55	**19**	AA	KB	47	124—127	1699			$C_{20}H_{15}NO_3S$	68.75	4.33	4.01	68.73	4.35	4.01
56	**19**	PA	KB	29	218—221	1682			$C_{24}H_{17}NO_2S$	75.17	4.47	3.65	74.89	4.51	3.56
57	**20**	BA	KB	61	186—188	1695			$C_{26}H_{19}NO_3S$	73.39	4.50	3.29	73.37	4.50	3.31
58	**20**	ML	KB	85	149—151	1692	1731		$C_{22}H_{19}NO_4S$	67.15	4.87	3.56	67.07	4.92	3.59
59	**20**	AA	KB	84	180—181	1689			$C_{21}H_{17}NO_3S$	69.40	4.72	3.85	69.27	4.67	4.03
60	**20**	PA	KB	80	188—191	1691			$C_{25}H_{19}NO_2S$	75.54	4.82	3.52	75.51	4.86	3.51

a) Abbreviations are as follows: CA; ethyl cyanoacetate. BA; ethyl benzoylacetate. ML; diethyl malonate. AA; ethyl acetoacetate. PA; ethyl phenylacetate. b) Abbreviations are as follows: TA; triethylamine. KB; potassium *t*-butoxide. c) Combined yield of compounds **24** and **30**. d) Combined yield with small amount of 4-ethoxypyranoindolizinone (**32**).

salt disappeared (*ca.* 10—15 h). Insoluble inorganic substances were removed from the reaction solution by filtration and the filtrate was concentrated at reduced pressure. The residues were separated by column chromatography (alumina) using ether-chloroform as an eluent in the cases of 1-methyl-3-methylene-2,3-dihydroindolizin-2-ones (**15** and **16**). However, the column separation of 1-unsubstituted 3-methylene-2,3-dihydroindolizin-2-ones (**17** and **18**) was unsuccessful because of their instability. The results and properties are given in Table 3.

*Preparation of 3-[(alkylthio)mercaptomethylene]-1-phenyl-2,3-dihydroindolizin-2-ones (**21** and **22**).* To an ethanol solution (100 ml) of 2-benzyl-1-(ethoxycarbonylmethyl)pyridinium bromide (**3**, 10 mmol) and carbon disulfide (1.1 g, 15 mmol) aq potassium hydroxide (KOH (2.8 g, 50 mmol) in 5 ml water) was added dropwise at room temperature. After the reaction mixture had been stirred for 1 h, ice water (200 ml) and then dialkyl sulfate (12 mmol) were added. The crude 3-[(alkylthio)mercaptomethylene]-1-phenyl-2,3-dihydroindolizin-2-one (**21** or **22**) precipitated was collected by filtration, dried, and recrystallized from chloroform. The results are summarized in Table 3.

*Preparation of 3-Methylene-2,3-dihydroindolizin-2-ones (**19** and **20**).* *General Method*: A chloroform solution (50 ml) of mercapto derivative (3 mmol) was treated with potassium carbonate (10 g) and methyl or ethyl iodide (4 mmol) at room temperature for 1—2 d, and the reaction mixture was filtered in order to remove insoluble substances. The filtrate was concentrated, and the residual oil was separated by column chromatography (alumina) using ether–chloroform as an eluent. The data are given in Table 3.

*Preparations of Pyrano[2,3-b]indolizinones (**24—30**, **32**, and **37—60**).* *Method A*: A benzene solution (30 ml) of 3-methylene-2,3-dihydroindolizin-2-one (1 mmol), ethyl cyanoacetate (**23**, 0.34 g, 3 mmol), and triethylamine (2 g) was allowed to react under reflux for 6—12 h. The reaction mixture was concentrated at reduced pressure, and the residual oil was separated by column chromatography (alumina). Recrystallization from chloroform–ether gave the corresponding 4-alkylthio-3-cyano-2*H*-pyrano[2,3-*b*]indolizin-2-ones (**24—29**) and the 4-ethoxy derivatives (**30** and **32**).

Method B: A benzene solution (30 ml) of 3-methylene-2,3-dihydroindolizin-2-one (1 mmol), the acetate (3—5 mmol), and potassium *t*-butoxide (1.5—2 mmol) was allowed to react under reflux until the TLC spot of 3-methylene-2,3-dihydroindolizin-2-one disappeared (3 h—3 d). The reaction mixture was then filtered in order to remove insoluble inorganic substances and the filtrate was concentrated at reduced pressure. The usual separation of the residual oils gave the corresponding 4-alkylthio-2*H*-pyrano[2,3-*b*]indolizin-2-one derivatives (**37—60**).

In the reactions of **15**, **16**, and **19** with **23**, the replacement of the solvent and base, benzene by ethanol and triethylamine by potassium *t*-butoxide, gave rise to increased formation of 4-ethoxypyranoindolizinones (**30** and **32**).

In the reactions with various acetates (**23** and **33—36**), 1-unsubstituted 3-methylene-2,3-dihydroindolizin-2-ones (**17** and **18**) were used without purification, the yields of pyranoindolizinones (**26**, **27**, and **45—52**) being estimated from the corresponding pyridinium salts (**10** and **11**).

The results and properties are summarized in Table 4.

References

1) A. Kakehi, S. Ito, K. Nakanishi, and M. Kitagawa, *Chem. Lett.*, **1979**, 297.

2) Y. Tominaga, Y. Miyake, H. Fujito, Y. Matsuda, and G. Kobayashi, *Yakugaku Zasshi*, **97**, 927 (1977).

3) A. Kakehi, S. Ito, T. Maeda, R. Takeda, M. Nishimura, M. Tamashima, and T. Yamaguchi, *J. Org. Chem.*, **43**, 4837 (1978).

4) T. Melton and D. G. Wibberley, *J. Chem. Soc., C*, **1967**, 983.

5) (a) T. Sasaki, K. Kanematsu, A. Kakehi, and G. Ito, *Tetrahedron*, **28**, 4947 (1972); (b) Y. Tamura, Y. Sumida, and M. Ikeda, *J. Chem. Soc., Perkin Trans. 1*, **1973**, 2091; (c) T. Sasaki, K. Kanematsu, A. Kakehi, and G. Ito, *ibid.*, **1973**, 2089; (d) A. Kakehi and S. Ito, *Bull. Chem. Soc. Jpn.*, **47**, 938 (1974); (e) Y. Tamura, Y. Sumida, S. Haruki, and M. Ikeda, *J. Chem. Soc., Perkin Trans. 1*, **1975**, 575.

6) (a) T. Hatada, M. Sone, Y. Tominaga, R. Natsuki, Y. Matsuda, and G. Kobayashi, *Yakugaku Zasshi*, **95**, 623 (1975); (b) Y. Tominaga, H. Fujito, K. Mizuyama, Y. Matsuda, and G. Kobayashi, *Chem. Pharm. Bull.*, **25**, 1519 (1977); (c) Y. Tominaga, Y. Miyake, H. Fujito, K. Kurata, H. Awaya, Y. Matsuda, and G. Kobayashi, *Chem. Pharm. Bull.*, **25**, 1528 (1977).

7) Unpublished data.

Pseudo-sugars. VI. Synthesis of Six Isomers of 5-Hydroxymethyl-1,2,3,4-cyclohexanetetrol (Pseudo-hexopyranose) and Their Derivatives[1]

Seiichiro Ogawa,* Masayasu Ara, Takashi Kondoh, Michio Saitoh, Reiko Masuda, Tatsushi Toyokuni, and Tetsuo Suami

Department of Applied Chemistry, Faculty of Engineering, Keio University, Hiyoshi, Yokohama 223

(Received October 15, 1979)

Six isomers of 5-hydroxymethyl-1,2,3,4-cyclohexanetetrol, including naturally occurring (1,2/3,4,5)-isomer, and their several derivatives were synthesized from the *exo*-2-substituted *endo*-3-acetoxy-*endo*-5-acetoxymethyl-7-oxabicyclo[2.2.1]heptane compounds.

The isolation of an antibacterial substance, (+)-(1,2/3,4,5)-5-hydroxymethyl-1,2,3,4-cyclohexanetetrol (pseudo-α-D-galactopyranose) (**1**)[2] in fermentation broth of *actinomyces Streptomyces* sp. MA-4145[3] prompted us to investigate a structure-activity relationship of stereoisomers of (hydroxymethyl)cyclohexanetetrol (pseudo-hexopyranose) and its related substances. In the present paper, we wish to report a synthesis of two isomeric pseudo-hexopyranoses (**1**, racemate, and **14**) and their derivatives by acetolysis of *exo*-2-substituted *endo*-3-acetoxy-*endo*-5-acetoxymethyl-7-oxabicyclo[2.2.1]heptane compounds (**2**—**5**). In addition, nucleophilic substitution reaction of bromo(hydroxymethyl)cyclohexanetriols (**8** and **16**) thus obtained from **4** led to the other four isomers (**20**, **24**, **28**, and **32**) and their amino deoxy derivatives.

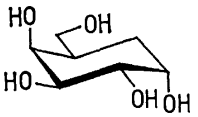

(+)-(1,2/3,4,5)-5-Hydroxymethyl-1,2,3,4-cyclohexanetetrol (**1**)

Treatment of *exo*-2, *endo*-3-diacetoxy-*endo*-5-acetoxymethyl-7-oxabicyclo[2.2.1]heptane (**2**)[4] with a mixture of acetic acid and acetic anhydride containing sulfuric acid in a sealed tube at 80 °C overnight resulted in cleavage of the anhydro ring giving rise to a mixture of products, from which on fractional crystallization penta-*O*-acetyl-5-hydroxymethyl-1,2,3,4-cyclohexanetetrols (**6**, 19%) and (**13**, 18%) were isolated. As expected, **6** and **13** were shown to be identical with authentic samples with (1,2/3,4,5)-[5] and (1,3,5/2,4)-configurations,[4] respectively. Compounds **6** and **13** were converted into the corresponding pentols (**1**, racemate) and (**14**) by treatment with methanolic sodium methoxide.

A similar procedure was used for the acetolysis of **3**,[6] **4**,[7] and **5**.[7] Compound **3** gave 2-*O*-methyl-(1,2/3,4,5)- (**7**) and 2-*O*-methyl-(1,3,5/2,4)-5-hydroxymethyl-1,2,3,4-cyclohexanetetrol tetraacetates (**15**) in 28 and 12% yields, respectively. In the ^{1}H NMR spectra of **7** and **15**, signals due to the protons on the carbon atoms attached to methoxyl groups appeared as a one-proton doublet of doublets with 3 and 11-Hz splittings at δ 4.30 and a one-proton triplet with 11-Hz splitting at δ 3.90, respectively, confirming the assigned structures. Similarly, the structures of tetra-*O*-acetyl-2-bromo-5-hydroxymethyl-1,3,4-cyclohexanetriols (**8**, 31%) and (**16**, 13%) obtained by acetolysis of **4** were assigned to possess (1,2/3,4,5)- and (1,3,5/2,4)-configurations, respectively, by the ^{1}H NMR signal due to the proton on the carbon atom attached to the bromo group.

On the other hand, acetolysis of **5** gave a sole crystalline tetra-*O*-acetyl(hydroxymethyl)cyclohexanetriol (**17**) in 58% yield. In order to establish the structure, **8** and **16** were subjected to hydrogenolysis with Raney nickel T-4[8] in the presence of Amberlite IR-45 (OH^-) to give the corresponding debromo compounds (**9**, 62%) and (**17**, 36%),[9] respectively. Compounds **9** and **17** were therefore assigned to tetraacetates of (1/3,4,5)- and (1,3,5/4)-5-hydroxymethyl-1,3,4-cyclohexanetriols, respectively. In the case of **5**, the anhydro ring was opened preferentially at C-1 by an acetate ion.

To prepare the other isomers of pseudo-hexopyranose and their derivatives, nucleophilic substitution reaction of **8** and **16** with an acetate or azide ion was studied. Treatment of **8** with an excess of sodium acetate in 90% aqueous 2-methoxyethanol at boiling temperature for 2 days gave, after acetylation, **6** (10%) and the hitherto unknown isomer (**19**, 31%). Since formation

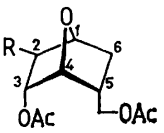

	R
2	OAc
3	OMe
4	Br
5	H

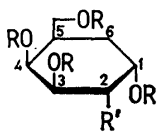

	R	R′
6	Ac	OAc
7	Ac	OMe
8	Ac	Br
9	Ac	H
10	H	H
11	Ac	N_3
12	Ac	NHAc

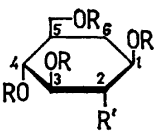

	R	R′
13	Ac	OAc
14	H	OH
15	Ac	OMe
16	Ac	Br
17	Ac	H
18	H	H

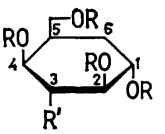

	R	R′
19	Ac	OAc
20	H	OH
21	Ac	N_3
22	Ac	NHAc

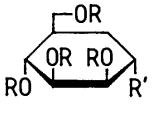

	R	R′
23	Ac	OAc
24	H	OH
25	Ac	N_3
26	Ac	NHAc

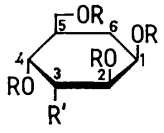

	R	R′
27	Ac	OAc
28	H	OH
29	Ac	N_3
30	Ac	NHAc

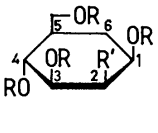

	R	R′
31	Ac	OBz
32	H	OH
33	Ac	OAc
34	Ac	N_3
35	Ac	NHAc

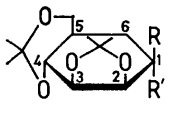

	R	R′
36	H	OH
37	-O	
38	OH	H

of **6** suggested that the reaction involved the intermediary 2,3-cyclic acetoxonium ion *via* an anchimeric assistance of the C-3 acetoxyl group, **19** was tentatively assigned to have (1,3/2,4,5)-configuration, resulting from the back side attack of an acetate ion at C-3.

The similar treatment of **16** with an acetate ion gave new isomers (**23**, 29%) and (**27**, 27%). When **16** was treated with sodium benzoate in dimethyl sulfoxide at 120 °C for 2 days, direct S_N2 reaction occurred to give 2-*O*-benzoyl-(1,2,3,5/4)-5-hydroxymethyl-1,2,3,4-cyclohexanetetrol tetraacetate (**31**) in 49% yield. The assigned structure was supported by appearance of a one-proton triplet (J=2.5 Hz, H-2) at δ 5.78 together with a one-proton triplet (J=10 Hz, H-4) at δ 5.40 and a one-proton doublet of doublets (J=2.5 and 10 Hz, H-3) at δ 5.04 in the ^{1}H-NMR spectrum.

O-Deacylation of **19**, **23**, **27**, and **31** in the usual way gave the corresponding pentols (**20**), (**24**), (**28**), and (**32**), respectively. Compound **32** was further characterized as the pentaacetate (**33**), which was found not to be identical with either **23** or **27**.

In order to determine the structures of **23** and **27**, the following sequence of the reactions was carried out. Treatment of **24** with 2,2-dimethoxypropane in *N*,*N*-dimethylformamide in the presence of *p*-toluenesulfonic acid gave a sole crystalline di-*O*-isopropylidene derivative (**36**) in 71% yield. Oxidation with ruthenium tetraoxide in a mixture of chloroform–water in the presence of sodium metaperiodate gave a ketone (**37**) in 61% yield, the structure of which was supported by ^{1}H NMR spectroscopy. Hydrogenation with platinum oxide in ethyl acetate gave a syrupy di-*O*-isopropylidene derivative (**38**) of pentol different from **36**. Compound **38** was then converted into a pentol identical with **32** in all respects. Three isomers with (1,3,5/2,4)-, (1,4/2,3,5)-, and (1,2,5/3,4)-configurations were considered to be formed from **16** by the anchimeric reaction involving the cyclic acetoxonium ions between C-1 and C-2, and/or C-2 and C-3. Therefore, these results showed that **23** was C-1 epimer of **32**, possessing (1,4/2,3,5)-configuration, and then **27** was tentatively assigned to the (1,2,5/3,4)-isomer.

Treatment of **8** with an excess of sodium azide in aqueous 2-methoxyethanol at boiling temperature for 2 days, followed by acetylation, gave two azides (**11**, 15%) and (**21**, *ca.* 80%). By analogy to the reaction with an acetate ion, two compounds were presumed to be tetra-*O*-acetyl-(1,2/3,4,5)-2-azido-5-hydroxymethyl-1,3,4- and tetra-*O*-acetyl-(1,3/2,4,5)-3-azido-5-hydroxymethyl-1,2,4-cyclohexanetriols. The ^{1}H NMR spectrum of **11** was fully interpreted by first-order method, being consistent with the former structure. In the spectrum of **21**, appearance of a one-proton triplet (J=10 Hz) due to the proton on a carbon atom attaching to the azido group showed that **21** had the latter structure, all the substituent except for the acetoxymethyl group locating in equatorial positions in the favored conformation. Hydrogenation of **11** and **21** with Raney nickel T-4 in methanol containing acetic anhydride gave the corresponding tetra-*O*-acetyl-(acetamido)(hydroxymethyl)cyclohexanetriols (**12**) and (**22**), respectively.

The similar azidolysis of **16** followed by acetylation gave, after fractionation by a silica gel column, two syrupy azides (**25**, 48%) and (**29**, 54%).[10] On hydrogenation and acetylation in the usual way, **25** and **29** were converted into the corresponding amino alcohol pentaacetates (**26**) and (**30**). Their structures were deduced by analogy to those of **23** and **27** obtained by the similar reaction with an acetate ion, and finally confirmed by ^{1}H NMR spectroscopy. Judging from the patterns of the signals due to C-7 methylene protons, the structures of **25** and **29** might be able to correlate with those of **23** and **27**, respectively. Further evidence was obtained by the spectrum of **26**, which showed after deuteration a one-proton narrow quartet (J= 3.5 Hz, H-4) at δ 4.18. Therefore, **26** and **30** were assigned to possess (1,4*N*/2,3,6)- and (1,2,5/3*N*,4)-configurations, respectively, as shown in the Scheme.

When dimethyl sulfoxide was used as the reaction solvent in the azidolysis of **16**, direct S_N2 reaction occurred to give an azide (**34**) with the inversion of the configuration at C-2. In the ^{1}H NMR spectrum, a narrow triplet (J=2.5 Hz, H-2) at δ 4.20 clearly supported the axial-equatorial-axial conformation for H-1, H-2, and H-3. Hydrogenation of **34** followed by acetylation gave tetra-*O*-acetyl-(1,2,3,5/4)-2-acetamido-5-hydroxymethyl-1,3,4-cyclohexanetriol (**35**).

Compounds **12** and **35** are considered to be carbocyclic analogs of 2-amino-2-deoxy-α-DL-galactopyranose and β-DL-mannopyranose. Biochemical and biological studies of pseudo-hexopyranoses and their amino deoxy derivatives obtained in this work are on the way.

Experimental

Unless otherwise stated, melting points were determined on a Büchi 510 capillary melting point apparatus and are uncorrected. Solutions were evaporated under reduced pressure at 40—50 °C. IR spectra were recorded on a Hitachi

225 spectrometer in potassium bromide pellets. ^{1}H NMR spectra were taken on a Varian EM-360A (60 MHz) in deuteriochloroform with reference to tetramethylsilane as an internal standard and the peak positions are given in terms of δ-values. Values given for coupling constants are of first-order. TLC was performed on precoated silica gel 60 F-254 plaques (Merck, Darmstadt; 0.25 mm thickness). The silica gel used for a column chromatography was Wakogel C-300 (Wako Pure Chemical Industries, Ltd.).

Acetolysis of exo-*2*, endo-*3-Diacetoxy*-endo-*5-acetoxymethyl-7-oxabicyclo[2.2.1]heptane (**2**).*[4] A mixture of **2** (4 g), acetic acid (12 ml), acetic anhydride (7 ml), and concentrated sulfuric acid (0.7 ml) was sealed in a glass tube and heated at 80—85 °C for 20 h in an oil bath. The brown reaction mixture was poured into ice–water (200 ml), and the solution was neutralized with sodium hydrogencarbonate and extracted with ethyl acetate (3×30 ml). The extracts were washed with water thoroughly, dried over anhydrous sodium sulfate, filtered through a short column of alumina and concentrated. The syrupy residue was crystallized from a small amount of ethanol to give penta-*O*-acetyl-(1,2/3,4,5)-5-hydroxymethyl-1,2,3,4-cyclohexanetetrol (**6**, 1.2 g, 19%) as crystals: mp 137—138 °C, 144.5—145 °C (hot-stage) [lit,[5] 147—148 °C (hot-stage)]. The ^{1}H NMR spectrum ($CDCl_3$) was superimposable on that of an authentic sample reported.[5] (Found: C, 52.57; H, 6.22%).

The mother liquor from **6** was concentrated to a small volume and kept in a refrigerator for a week to give penta-*O*-acetyl-(1,3,5/2,4)-5-hydroxymethyl-1,2,3,4-cyclohexanetetrol (**13**, 1.15 g, 18%) as practically pure crystals: mp 109.5—111 °C. Recrystallization from ethanol gave a pure sample: mp 111.5—112.5 °C (lit,[4] 111—112 °C), which was identified with an authentic sample by comparison with IR and ^{1}H NMR spectra.

Compound **6** (1 g) was treated with 1 M methanolic sodium methoxide (1.1 ml) in methanol (50 ml) at reflux temperature for 0.5 h. After cooling, the solution was neutralized with Amberlite IR-120 (H^+) and concentrated to give a crystalline residue, which was crystallized from ethanol to give racemic (1,2/3,4,5)-5-hydroxymethyl-1,2,3,4-cyclohexanetetrol (**1**, 0.44 g, 96%) as crystals: mp 167—168 °C [lit,[5] 173—174 °C (hot-stage)] (Found: C, 47.04; H, 7.92%).

Compound **13** was *O*-deacetylated as described above to give (1,3,5/2,4)-5-hydroxymethyl-1,2,3,4-cyclohexanetetrol (**14**) as a homogeneous syrup, identical with an authentic sample[4] in all respects.

Acetolysis of 3-endo-*Acetoxy-5*-endo-*acetoxymethyl-2*-exo-*methoxy-7-oxabicyclo[2.2.1]heptane (**3**).*[6] A mixture of **3** (3 g), acetic acid (9 ml), acetic anhydride (4 ml), and concentrated sulfuric acid (0.4 ml) was heated in a glass sealed tube at 90—95 °C overnight. The mixture was poured into ice–water (150 ml) and the solution was extracted with chloroform (3×30 ml). The extracts were washed thoroughly with aqueous sodium hydrogencarbonate and water, successively, dried, and filtered through a short column of alumina. Evaporation of the solvent gave a crystalline mixture of products (2.45 g, 59%), which was fractionally crystallized from ethanol to give first 1,3,4,7-tetra-*O*-acetyl-2-*O*-methyl-(1,2/3,4,5)-5-hydroxymethyl-1,2,3,4-cyclohexanetetrol (**7**, 0.49 g, 12%) as plates: mp 144.5—145 °C. ^{1}H NMR ($CDCl_3$) δ=2.04 (6H, s) and 2.10 (6H, s) (OAc), 3.36 (3H, s, OMe), 3.48 (1H, dd, J=3 and 10 Hz, H-2), 3.8—4.0 (2H, m, C<u>H</u>$_2$OAc), 5.06 (1H, dd, J=3 and 10 Hz, H-3), 5.50 (2H, m, H-1 and H-4).

From the mother liquor of **7**, 1,3,4,7-tetra-*O*-acetyl-2-*O*-methyl-(1,3,5/2,4)-5-hydroxymethyl-1,2,3,4-cyclohexanetetrol (**15**, 1.15 g, 28%) was obtained as prisms: mp 80—81.5 °C. ^{1}H NMR ($CDCl_3$) δ=2.05 (6H, s), 2.07 (3H, s) and 2.10 (3H, s), 3.30 (1H, t, J=10 Hz, H-2), 3.44 (3H, s, OMe), 3.9—4.2 (2H, m, C<u>H</u>$_2$OAc), 4.6—5.1 (3H, m, H-1, H-3, and H-4).

Found for **7**: C, 53.47; H, 6.67%; and for **15**: C, 53.27; H, 6.72%. Calcd for $C_{16}H_{24}O_9$: C, 53.33; H, 6.71%.

Acetolysis of endo-*3-Acetoxy*-endo-*5-acetoxymethyl*-exo-*2-bromo-7-oxabicyclo[2.2.1]heptane (**4**).* A mixture of **4** (4 g), acetic acid (12 ml), acetic anhydride (8 ml), and concentrated sulfuric acid (0.5 ml) was heated in a sealed tube at 90—95 °C overnight. The brown mixture was poured into ice–water (200 ml) and the resulting crystals were collected by filtration and washed with water. The product was dissolved in hot ethanol, treated with active carbon, and crystallized to give a mixture of crystals (3.7 g, 64%). Fractional crystallization from ethanol first gave tetra-*O*-acetyl-(1,2/3,4,5)-2-bromo-5-hydroxymethyl-1,3,4-cyclohexanetriol (**8**, 1.6 g, 31%) as prisms or plates: mp 161.5—162.5 °C. ^{1}H NMR ($CDCl_3$) δ=2.03 (3H, s), 2.06 (3H, s), 2.12 (3H, s), and 2.17 (3H, s) (OAc), 3.85—4.0 (2H, m, C<u>H</u>$_2$OAc), 4.30 (1H, dd, J=3 and 11 Hz, H-2), 5.27 (1H, dd, J=3 and 11 Hz, H-3), 5.38 (1H, t, J=3 Hz, H-4), 5.52 (1H, q, J=3 Hz, H-1).

From the mother liquor of **8**, tetra-*O*-acetyl-(1,3,5/2,4)-2-bromo-5-hydroxymethyl-1,3,4-cyclohexanetriol (**16**, 0.7 g, 13%) was obtained as thin plates: mp 145—146 °C. ^{1}H NMR ($CDCl_3$) δ=2.03 (6H, s), 2.07 (3H, s), and 2.10 (3H, s) (OAc), 3.9—4.1 (2H, m, C<u>H</u>$_2$OAc), 3.90 (1H, t, J=11 Hz, H-2), 4.88 (1H, t, J=11 Hz, H-3), 4.92 (1H, m, H-1), 5.23 (1H, t, J=11 Hz, H-4).

Found for **8**: C, 44.25; H, 5.11; Br, 19.20%; and for **14**: C, 44.06; H, 5.08; Br, 19.50%. Calcd for $C_{15}H_{21}O_8Br$: C, 44.02; H, 5.17; Br, 19.53%.

Acetolysis of 2-endo-*Acetoxy-6*-endo-*acetoxymethyl-7-oxabicyclo-[2.2.1]heptane (**5**).*[6] a) A mixture of **5** (4 g), acetic acid (12 ml), acetic anhydride (8 ml), and concentrated sulfuric acid (0.5 ml) was heated in a sealed tube at 90—95 °C overnight. The reaction mixture was poured into ice–water (100 ml) and the resulting precipitates were collected by filtration. The aqueous filtrate was extracted with chloroform and the extracts were worked up in the usual manner to give an additional crop of crystals. Recrystallization of the combined crude crystals from ethanol gave tetra-*O*-acetyl-(1,3,5/2)-3-hydroxymethyl-1,2,5-cyclohexanetriol (**17**, 3.42 g, 58.4%) as needles: mp 104—105 °C. ^{1}H NMR ($CDCl_3$) δ=1.97 (3H, s), 2.01 (3H, s), and 2.04 (6H, s) (OAc).

Found: C, 54.39; H, 6.55%. Calcd for $C_{15}H_{22}O_8$: C, 54.53; H, 6.73%.

b) A solution of **16** (0.88 g) in ethyl acetate (10 ml) was hydrogenated (Parr shaker apparatus) in the presence of Raney nickel T-4[8] (3 ml) and Amberlite IR-45 (OH^-) in the initial hydrogen pressure of 3.4 kg cm^{-2} at ambient temperature overnight. The catalyst and resin were filtered off and the filtrate was concentrated. The residue was recrystallized from ethanol to give **17** (0.24 g, 36%) as needles, which was identical with the compound obtained from **5** in all respects.

*(1,3,5/2,4)-3-hydroxymethyl-1,2,5-cyclohexanetriol (**18**).* To a solution of **17** (4 g) in methanol (200 ml) was added 1 M methanolic sodium methoxide (12 ml) and the mixture was refluxed for 1.5 h. The mixture was processed in the usual manner to give a product, which was crystallized from ethanol to give **18** (1.9 g, 96%) as needles: mp 125—127 °C.

Found: C, 51.68; H, 8.60%. Calcd for $C_7H_{14}O_5$: C, 51.84; H, 8.70%.

*Tetra-O-acetyl-(1,2,3/5)-3-hydroxymethyl-1,2,5-cyclohexanetriol (**9**).* A solution of **8** (3 g) in ethyl acetate (20 ml) was hydrogenated similarly as described in the preparation of **17**. The crude product was recrystallized from ethanol to give **9** (1.5 g, 62%) as needles: mp 98—99 °C. ^{1}H NMR ($CDCl_3$) δ=1.99 (3H, s), 2.05 (3H, s), 2.09 (3H, s), and 2.11 (3H, s) (OAc), 3.8—4.1 (2H, m, C$\underline{H}_2$OAc). 5.01 (1H, dd, J=2.5 and 9 Hz. H-1), 5.24 (1H, t, J=2.5 Hz, H-5), 5.46 (1H, t, J=2.5 Hz, H-2).

Found: C, 54.52; H, 6.70%. Calcd for $C_{15}H_{22}O_8$: C, 54.53; H, 6.73%.

*(1,2,3/5)-3-Hydroxymethyl-1,2,5-cyclohexanetriol (**10**).* Compound **9** (0.3 g) was *O*-deacetylated in methanol (20 ml) containing 1 M methanolic sodium methoxide (0.5 ml) similarly as described in the preparation of **1**. The crude product was purified by a silica gel column with methanol to give a homogeneous syrup (0.15 g, 98%).

Found: C, 52.12; H, 8.42%. Calcd for $C_7H_{14}O_4$: C, 51.84; H, 8.70%.

*Reaction of **8** with Sodium Acetate.* A mixture of **8** (2.9 g), anhydrous sodium acetate (3 g), and 90% aqueous 2-methoxyethanol (70 ml) was refluxed for three days and concentrated under reduced pressure. The solid residue was dried by coevaporation with toluene and then treated with acetic anhydride (10 ml) and pyridine (15 ml) at ambient temperature overnight. An insoluble material was removed by filtration and the filtrate was concentrated. The syrup was dissolved in chloroform and filtered through a short column of alumina. Removal of the solvent and crystallization from ethanol gave **6** (0.26 g, 10%) as prisms: mp 136—137 °C, identical with the compound obtained from **2**. The mother liquor of **6** was kept in a refrigerator for a week to give penta-*O*-acetyl-(1,3/2,4,5)-5-hydroxymethyl-1,2,3,4-cyclohexanetetrol (**19**, 0.8 g, 31%) as plates: mp 106—107 °C. ^{1}H NMR ($CDCl_3$) δ=2.00 (12H, s) and 2.12 (3H, s) (OAc), 4.18 (2H, d, J=6 Hz, C$\underline{H}_2$OAc).

Found: C, 52.81; H, 6.22%. Calcd for $C_{17}H_{24}O_{10}$: C, 52.57; H, 6.23%.

O-Deacetylation of **19** (0.5 g) with methanolic sodium methoxide in the usual manner to give a crystalline pentol (**20**, 0.17 g, 75%), which was recrystallized from ethanol to give an analytical sample: mp 154.5—156 °C.

Found: C, 46.95; H. 7.75%. Calcd for $C_7H_{14}O_5$: C, 47.18; H, 7.92%.

*Reaction of **16** with Sodium Acetate.* A mixture of **16** (2 g), anhydrous sodium acetate (2.9 g), and 90% aqueous 2-methoxyethanol was refluxed for 43 h and concentrated under reduced pressure. The reaction mixture was processed similarly as described in the reaction of **6**. A crystalline mixture of products (1.5 g) was fractionally crystallized from ethanol. The first crop of crystals (0.6 g) was recrystallized twice to give penta-*O*-acetyl-(1,4/2,3,5)-5-hydroxymethyl-1,2,3,4-cyclohexanetetrol (**23**, 0.27 g, 14%) as prisms: mp 99.5—100 °C. ^{1}H NMR ($CDCl_3$) δ=1.99 (3H, s), 2.04 (3H, s), 2.06 (3H, s), 2.12 (3H, s), and 2.13 (3H, s) (OAc), 3.98—4.15 (2H, m, C$\underline{H}_2$OAc), 4.98 (1H, q, J=3 Hz, H-1), 5.0—5.5 (3H, m, H-2, H-3, and H-4).

The second crop of crystals (0.9 g) was fractionally crystallized from ethanol to give practically pure **23** (0.3 g, total yield 29%) and penta-*O*-acetyl-(1,2,5/3,4)-5-hydroxymethyl-1,2,3,4-cyclohexanetetrol (**27**, 0.51 g, 27%) as prisms: mp 106—107 °C. ^{1}H NMR ($CDCl_3$) δ=2.01 (6H, s), 2.06 (3H, s), 2.10 (3H, s), and 2.13 (3H, s) (OAc), 4.05 (2H, d, J=5 Hz, C$\underline{H}_2$OAc), 4.9—5.35 (4H, m, H-1, H-2, H-3, and H-4).

Found for **23**: C, 52.71; H, 6.21%, and for **27**: C, 52.32; H, 6.11%. Calcd for $C_{17}H_{24}O_{10}$: C, 52.57; H, 6.23%.

O-Deacetylation of **23** (0.25 g) in the usual manner gave the pentol (**24**, 0.10 g, 84%) as a homogenous syrup.

O-Deacetylation of **27** (0.25 g) in the usual manner gave a crystalline pentol (**28**, 0.075 g, 65%), which was recrystallized from ethanol to give prisms: mp 143.5—144.5 °C.

Found for **24**: C, 47.34; H, 7.74%, and for **28**: C, 46.96; H, 7.74%. Calcd for $C_7H_{14}O_5$: C, 47.18; H, 7.92%.

*1,3,4,7-Tetra-O-acetyl-2-O-benzoyl-(1,2,3,5/4)-5-hydroxymethyl-1,2,3,4-cyclohexanetetrol (**31**).* A stirred mixture of **16** (1.24 g), sodium benzoate (1.2 g), 18-crown-6 (0.4 g) in dimethyl sulfoxide (30 ml) was heated at 115—120 °C for 2 d. After cooling, the reaction mixture was diluted with ethyl acetate (100 ml) and the solution was washed well with water. The organic layer was dried and filtered through a short column of alumina. The filtrate was concentrated and the residue was crystallized from ethanol to give **31** (0.67 g, 49%) as prisms: mp 134—135 °C. ^{1}H NMR ($CDCl_3$) δ=1.94 (3H, s), 1.96 (3H, s), 2.03 (3H, s), and 2.10 (3H, s) (OAc), 4.06 (2H, broad s, C$\underline{H}_2$OAc), 5.05 (1H, dd, J=2.5 and 10 Hz, H-3), 5.40 (1H, t, J=10 Hz, H-4), 5.79 (1H, t, J=2.5 Hz, H-2), 7.45 (3H, m) and 8.05 (2H, m) (phenyl).

Found: C, 58.79; H, 5.91%. Calcd for $C_{22}H_{26}O_{10}$: C, 58.66; H, 5.82%.

O-Deacylation of **31** (0.23 g) in the usual manner gave a crystalline pentol (**32**), which was recrystallized from ethanol–water to give needles: mp 198—199 °C.

Found: C, 47.16; H, 7.76%. Calcd for $C_7H_{14}O_5$: C, 47.18; H, 7.92%.

Acetylation of **32** (0.05 g) with acetic anhydride and pyridine in the usual manner gave, after crystallization from ethanol, a pentaacetate (**33**, 0.1 g, 90%) as prisms: mp 123—125 °C. ^{1}H NMR ($CDCl_3$) δ=1.98 (3H, s), 2.02 (3H, s), 2.06 (3H, s), and 2.20 (3H, s) (OAc), 4.01 (2H, broad d, J=4 Hz, C$\underline{H}_2$OAc), 4.91 (1H, dd, J=2.5 and 10 Hz, H-3), 5.23 (1H, t, J=10 Hz, H-4), 5.56 (1H, t, J=2.5 Hz, H-2).

Found: C, 52.69; H, 6.33%. Calcd for $C_{17}H_{24}O_{10}$: C, 52.57; H, 6.23%.

*2,3:4,7-Di-O-isopropylidene-(1,4/2,3,5)-5-hydroxymethyl-1,2,3,4-cyclohexanetetrol (**36**).* The crude **24** obtained from **23** (0.8 g) in the usual manner was heated with 2,2-dimethoxypropane (4 ml) in *N,N*-dimethylformamide (10 ml) in the presence of *p*-toluenesulfonic acid (15 mg) at 60 °C for 1 h. After cooling, the mixture was treated with Amberlite IRA-400 (OH^-) and concentrated. The residue was crystallized from ethanol to give **36** (0.36 g, 71%) as crystals: mp 147.5—148.5 °C. ^{1}H NMR ($CDCl_3$) δ=1.35 (3H, s), 1.41 (3H, s), 1.50 (3H, s), and 1.52 (3H, s) (isopropylidene), 3.61 (1H, d) and 3.80 (1H, broad d) (J=5 Hz, H-7 and H-7'), 4.10 (3H, broad s, H-2, H-3, and, H-4).

Found: C, 60.50; H, 8.60%. Calcd for $C_{13}H_{22}O_5$: C, 60.43; H, 8.60%.

The acetate was prepared in the conventional way. The crude product was recrystallized from ethanol to give prisms: mp 140.5—141 °C. ^{1}H NMR ($CDCl_3$) δ=1.37 (3H, s), 1.45 (3H, s), 1.49 (3H, s), and 1.51 (3H, s) (isopropylidene), 3.69 (2H, AB-quartet, H-7 and H-7'), 3.9—4.2 (2H, m, H-2 and H-3), 5.25 (1H, broad q, J=3 Hz, H-1).

Found: C, 59.72; H, 7.70%. Calcd for $C_{15}H_{24}O_6$: C, 59.98; H, 8.05%.

The tosylate was prepared by treatment with *p*-toluenesulfonyl chloride in pyridine. The crude product was crystallized from 2-propanol to give crystals: mp 137—138 °C.

Found: C, 58.46; H, 6.77; S, 7.52%. Calcd for $C_{20}H_{28}O_7S$: C, 58.22; H, 6.86; S, 7.77%.

2,3:4,7-Di-O-isopropylidene-(2,3,5/4)-2,3,4-trihydroxy-5-(hy-

*droxymethyl)cyclohexanone (**37**).* Compound **36** (0.5 g) was dissolved in ethanol-free chloroform (10 ml), and a catalytic amount of ruthenium dioxide and aqueous sodium hydrogencarbonate were added. A 5% aqueous sodium metaperiodate (10 ml) was added to the mixture during 20 min under ice cooling with vigorous agitation. After 2.5 h, an excess of periodate and ruthenium tetraoxide were destroyed with 2-propanol, and black precipitates were removed by filtration. The organic layer was separated, washed with water thoroughly, and dried. Removal of the solvent gave a crystalline residue which was recrystallized from ethanol to give **37** (0.3 g, 61%) as crystals: mp 124 °C (after sintering at 119 °C). ^{1}H NMR ($CDCl_3$) δ=1.40 (3H, s), 1.48 (3H, s), and 1.50 (6H, s) (isopropylidene), 1.8—2.6 (3H, m, H-5, H-6, and H-6'), 3.3—4.0 (3H, m, H-4, H-7, and H-7'), 4.4—4.6 (2H, m, H-2 and H-3).

Found: C, 61.01; H, 7.77%. Calcd for $C_{13}H_{20}O_5$: C, 60.92; H, 7.87%.

Compound **37** (0.13 g) was hydrogenated in ethyl acetate (5 ml) in the presence of platinum oxide in the usual manner to give a homogeneous syrup of 2,3:4,7-di-*O*-isopropylidene-(1,2,3,5/4)-5-hydroxymethyl-1,2,3,4-cyclohexanetetrol (**38**, 0.12 g), which was not identical with **36** in all respects. Crude **38** was directly treated with 80% aqueous acetic acid (5 ml) at 80 °C for 1 h. The reaction mixture was concentrated and the residue was recrystallized from ethanol–water to give **32** (83 mg, 92%): mp 196—197 °C, identical with the compound obtained from **31**.

*Reaction of **8** with Sodium Azide.* A mixture of **8** (5.7 g), sodium azide (6 g), and 90% aqueous 2-methoxyethanol (120 ml) was refluxed for 44 h and concentrated under reduced pressure. The residue was dried by coevaporation with toluene several times and then treated with acetic anhydride (20 ml) and pyridine (30 ml) at ambient temperature overnight. An insoluble material was removed by filtration and the filtrate was concentrated. The residue was dissolved in ethyl acetate (50 ml) and filtered through a short column of alumina (20 g). The filtrate was concentrated and the syrupy residue was crystallized from ethanol to give tetra-*O*-acetyl-(1,2/3,4,5)-2-azido-5-hydroxymethyl-1,3,4-cyclohexanetriol (**11**, 0.79 g, 15%) as prisms: mp 145—147 °C. ^{1}H NMR ($CDCl_3$) δ=2.03 (3H, s), 2.07 (3H, s), and 2.13 (6H, s) (OAc), 3.6—4.0 (2H, m, C<u>H</u>$_2$OAc), 3.75 (1H, dd, J=3 and 11 Hz, H-2), 5.17 (1H, dd, J=3 and 11 Hz, H-3), 5.40 (1H, q, J=3 Hz, H-1), 5.53 (1H, t, J=3 Hz, H-4).

Found: C, 48.67; H, 5.72; N, 11.11%. Calcd for $C_{15}H_{21}N_3O_8$: C, 48.52; H, 5.70; N, 11.32%.

The mother liquor of **11** was concentrated to give a syrup which consisted mainly of tetra-*O*-acetyl-(1,3/2,4,5)-3-azido-5-hydroxymethyl-1,2,4-cyclohexanetriol (**21**, 5.1 g). ^{1}H NMR ($CDCl_3$) δ=2.02 (3H, s), 2.09 (3H, s), 2.11 (3H, s), and 2.13 (3H, s) (OAc), 3.79 (1H, t, J=10 Hz, H-3), 4.8—5.2 (3H, m, H-1, H-2, and H-4). Purification of **21** was not attempted because its mobility on TLC was similar to that of **11** in various solvent systems.

*Tetra-O-acetyl-(1,2/3,4,5)-2-acetamido-5-hydroxymethyl-1,3,4-cyclohexanetriol (**12**).* A solution of **11** (0.6 g) in ethanol (35 ml), acetic anhydride (0.8 ml), and Raney nickel T-4 (one-spoonful) was hydrogenated with 3.4 kg cm^{-2} starting pressure of hydrogen gas at ambient temperature overnight in a Parr hydrogenation apparatus. The catalyst was removed by filtration and the filtrate was concentrated. Recrystallization of the crude product from ethanol gave **12** (0.48 g, 82%) as needles: mp 184—185.5 °C. ^{1}H NMR ($CDCl_3$) δ=1.83 (3H, s, NAc), 1.95 (3H, s), 2.02 (3H, s), and 2.13 (3H, s) (OAc), 3.85—4.0 (2H, m, C<u>H</u>$_2$OAc), 4.52 (1H, ddd, J=3, 9, and 11 Hz, H-2), 5.12 (1H, dd, J=3 and 11 Hz, H-3), 5.25 (1H, t, J=3 Hz, H-4), 5.53 (1H, q, J=3 Hz, H-1), 5.70 (1H, d, J=9 Hz, N<u>H</u>).

Found: C, 52.54; H, 6.41; N, 3.70%. Calcd for $C_{17}H_{25}NO_9$: C, 52.71; H, 6.51; N, 3.62%.

*Tetra-O-acetyl-(1,3/2,4,5)-3-acetamido-5-hydroxymethyl-1,2,4-cyclohexanetriol (**22**).* The crude **21** (5 g) was hydrogenated similarly as described in the preparation of **12**. The crude product was recrystallized from ethanol–ether to give **22** (2.7 g, 51% yield based on **8** used) as needles: mp 159—160 °C. ^{1}H NMR ($CDCl_3$) δ=1.91 (3H, s, NAc), 2.03 (6H, s), 2.07 (3H, s), and 2.13 (3H, s) (OAc), 4.2—4.3 (2H, m, C<u>H</u>$_2$OAc), 5.71 (1H, d, J=9 Hz, N<u>H</u>).

Found: C, 52.64; H, 6.45; N, 3.76%. Calcd for $C_{17}H_{25}NO_9$: C, 52.71; H, 6.51; N, 3.62%.

*Reaction of **16** with Sodium Azide.* A mixture of **16** (3 g), sodium azide (3.4 g), and 90% aqueous 2-methoxyethanol (70 ml) was refluxed for 40 h. The reaction mixture was processed and acetylated similarly as described in the reaction of **8**. The syrupy mixture (3.2 g) of azides obtained was chromatographed on a silica-gel column (70 g) with butanone–toluene (1:6, v/v) as an eluent to give tetra-*O*-acetyl-(1,4/2,3,6)-4-azido-6-hydroxymethyl-1,2,3-cyclohexanetriol (**25**, 1.3 g, 48%) as a homogeneous syrup, which crystallized on standing in a refrigerator for two months: mp 84—84.5 °C, and tetra-*O*-acetyl-(1,2,5/3,4)-3-azido-5-hydroxymethyl-1,2,4-cyclohexanetriol (**29**, 1.5 g, 54%) as a homogeneous syrup, which also crystallized on standing in a refrigerator for two months: mp 66—67 °C. ^{1}H NMR ($CDCl_3$) data for **25**: δ=1.99 (3H, s), 2.02 (3H, s), 2.05 (3H, s), and 2.12 (3H, s) (OAc), 3.8—4.1 (3H, m, H-4 and C<u>H</u>$_2$OAc), 5.0—5.3 (3H, m, H-1, H-2, and H-3), and for **29**: 2.00 (3H, s), 2.07 (3H, s), 2.12 (3H, s), and 2.14 (3H, s) (OAc), 4.0—4.1 (3H, m, H-3 and C<u>H</u>$_2$OAc), 4.9—5.3 (3H, m, H-1, H-2, and H-4).

Found for **25**: C, 48.31; H, 5.62; N, 11.11%, and for **29**: C, 48.51; H, 5.67; N, 11.17%. Calcd for $C_{15}H_{21}N_3O_8$: C, 48.52; H, 5.70; N, 11.32%.

*Tetra-O-acetyl-(1,4/2,3,6)-4-acetamido-6-hydroxymethyl-1,2,3-cyclohexanetriol (**26**).* The crude syrupy **25** (0.35 g) was hydrogenated similarly as described in the preparation of **12**. The crude crystalline product was recrystallized from ethanol–ether to give **26** (0.16 g, 44%) as prisms: mp 181—182 °C. The overall yield from **16** was 24%. ^{1}H NMR ($CDCl_3$) δ=1.99 (6H, s), 2.03 (3H, s), 2.06 (3H, s), and 2.10 (3H, s) (NAc and four OAc), 4.05 (2H, broad d, C<u>H</u>$_2$OAc), 4.18 (1H, m, H-4, the signal changes to a quartet with 3.5 Hz splitting on deuteration), 5.1—5.3 (3H, m, H-1. H-2, and H-3), 6.70 (1H, J=8 Hz, N<u>H</u>).

Found: C, 52.99; H, 6.57; N, 3.64%. Calcd for $C_{17}H_{25}NO_9$: C, 52.71; H, 6.51; N, 3.62%.

A mixture of **25** and **29** obtained from **16** (2.7 g) was without separation directly hydrogenated followed by acetylation to give **26** (0.12 g, 24%): mp 179—180 °C, cleanly crystallized out of the mixture of products.

*Tetra-O-acetyl-(1,2,5/3,4)-3-acetamido-5-hydroxymethyl-1,2,4-cyclohexanetriol (**30**).* The crude syrupy **29** (0.47 g) was hydrogenated and acetylated similarly as described in the preparation of **12**. The syrupy product (0.41 g, 84%) was purified by a silica gel column with chloroform–ethyl acetate (5:1, v/v) as an eluent to give **30** as a homogeneous syrup. ^{1}H NMR ($CDCl_3$) δ=1.96 (3H, s) and 2.05 (12H, s) (NAc and four OAc), 4.41 (2H, d, J=6 Hz, C<u>H</u>$_2$OAc), 4.62 (1H, broad td, J=4 Hz, H-3), 5.0—5.25 (3H, m, H-1, H-2, and H-4), 6.60 (1H, d, J=9 Hz, N<u>H</u>).

Found: C, 52.47; H, 6.38; N, 3.53%. Calcd for $C_{17}H_{25}NO_9$: C, 52.71; H, 6.51; N, 3.62%.

Tetra-O-acetyl-(1,2,3,5/4)-2-acetamido-5-hydroxymethyl-1,3,4-

*cyclohexanetriol (**35**).* A stirred mixture of **16** (2 g), sodium azide (2 g), and dimethyl sulfoxide (35 ml) was heated at 110 °C for 10 h. The reaction mixture was diluted with water (100 ml) and the solution was extracted with ethyl acetate (3×50 ml). The extracts were washed with water, dried, and filtered through a short column of alumina (10 g). The filtrate was concentrated to give tetra-*O*-acetyl-(1,2,3,5/4)-2-azido-5-hydroxymethyl-1,3,4-cyclohexanetriol (**34**, 1 g, 51%) as a chromatographically homogeneous syrup: ^{1}H NMR ($CDCl_3$) δ=2.07 (3H, s), 2.09 (3H, s), 2.11 (3H, s), and 2.13 (3H, s) (OAc), 3.93 (2H, broad s, C$\underline{H}_2$OAc), 4.20 (1H, t, J=2.5 Hz, H-2), 4.75—5.2 (3H, m, H-1, H-3, and H-4).

The crude syrup was directly hydrogenated and acetylated similarly as described in the preparation of **12**. The crude product was recrystallized from chloroform–ether to give **35** (0.6 g, 31% yield based on **16** used) as needles: mp 177—179 °C. ^{1}H NMR ($CDCl_3$) δ=1.97 (3H, s), 2.00 (3H, s), and 2.05 (9H, s) (NAc and four OAc), 4.02 (2H, AB quartet, C$\underline{H}_2$OAc), 4.8—5.2 (3H, m, H-1, H-3, and H-4), 6.10 (1H, J=8 Hz, N$\underline{H}$).

Found: C, 52.47; H, 6.45; N, 3.55%. Calcd for $C_{17}H_{25}NO_9$: C, 52.71; H, 6.51; N, 3.62%.

The present work was partially supported by a Grand-in-Aid for Scientific Research No. 355376 from the Ministry of Education, Science and Culture. The authors wish to express their thanks to Mr. Saburo Nakada for elemental analyses.

References

1) Presented in part at the 37th National Meeting of the Chemical Society of Japan, Yokohama, April 1978, Abstr. No. 3R04. For paper V of this series, see S. Ogawa, T. Toyokuni, M. Omata, N. Chida, and T. Suami, *Bull. Chem. Soc. Jpn.*, **53**, 455 (1980). All the compounds described in this paper are racemic. Unless otherwise stated, all the formulas depict one enantiomer of the respective racemates.

2) The nomenclature is based on the IUPAC-IUB Tentative Cyclitol Nomenclature Rule [*J. Biol. Chem.*, **22**, 5809 (1968)]. Alternatively, according to the proposal of G. E. McCasland [G. E. McCasland and S. Furuta, *J. Org. Chem.*, **31**, 1516 (1966)], 5-hydroxymethyl-1,2,3,4-cyclohexanetetrols are named as pseudo-hexopyranoses.

3) T. W. Miller, B. H. Arison, and G. Albers-Schönberg, *Biotechnol. Bioeng.*, **15**, 1075 (1973).

4) T. Suami, S. Ogawa, K. Nakamoto, and I. Kasahara, *Carbohydr. Res.*, **58**, 240 (1977).

5) G. E. McCasland, S. Furuta, and L. J. Durham, *J. Org. Chem.*, **33**, 2841 (1968).

6) S. Ogawa, K. Nakamoto, M. Takahara, Y. Tanno, N. Chida, and T. Suami, *Bull. Chem. Soc. Jpn.*, **52**, 1174 (1979).

7) S. Ogawa, I. Kasahara, and T. Suami, *Bull. Chem. Soc. Jpn.*, **52**, 118 (1979).

8) S. Nishimura, *Bull. Chem. Soc. Jpn.*, **32**, 61 (1959).

9) Formation of anhydro compounds during hydrogenolysis of **16** in the presence of the basic resin decreased the yield of **17**.

10) These azides crystallized spontaneously on standing in a refrigerator for two months. Analytical samples were obtained by recrystallization from ethanol.

 © 1980 The Chemical Society of Japan Bull. Chem. Soc. Jpn., 53, 1127—1131 (1980)

The Benzannelated Annulenes. Dibenzo[*d,j*]-6,8-bisdehydrothia[13]-, [15]-, and Dibenzo[*f,l*]-8,10-bisdehydrothia[17]annulene

Jūro Ojima,* Kiyomi Kusaki, Kazuyo Wada, and Yukiko Nakagawa
Department of Chemistry, Faculty of Science, Toyama University, Gofuku, Toyama 930
(Received October 18, 1979)

The title compounds have been synthesized by the double Wittig reaction of bis[(triphenylphosphonio)-methyl] sulfide dibromide with *o*-ethynylbenzaldehyde and/or *o*-ethynylcinnamaldehyde, followed by the oxidative coupling. The ^{1}H-NMR spectra of these compounds gave no evidence for a ring current.

Replacement of one of the double bonds of $(4n+2)$ or $(4n)\pi$ electron annulene with a sulfur atom which possesses a lone pair of electrons will lead to the potentially diatropic or paratropic system, respectively.

In connection with the studies to confirm the prediction Sondheimer *et al.* have synthesized dimethylbis-dehydrothia[13]- **1**,[1a] [15]- **2**,[1b] and [17]annulene **3**[1c] as well as their bis(cyclohexene)-annelated ones[1a,b,d] in which the sulfur atom is flanked by ethylenic bond on both sides.

The method consists in employing a double Wittig condensation of bis[(triphenylphosphonio)methyl] sulfide dibromide **4**[2] with an appropriate aldehyde containing terminal acetylene group, followed an intramolecular oxidative coupling of the resulting acyclic compound.

As an extension of our works on benzannelated annulenes,[3] we have now applied with advantage the method to the synthesis of benzannelated bisdehydrothiaannulenes by using *o*-ethynylbenzaldehyde **5**[3a] and/or *o*-ethynylcinnamaldehyde **10**[4] as the starting material and by the essentially same approach as that of Sondheimer *et al.*[1] We now describe the syntheses of the title compounds, *i.e.*, dibenzo[*d,j*]-6,8-bisdehydrothia[13]- **9**, -[15]annulene **14**, and dibenzo[*f,l*]-8,10-bisdehydrothia[17]annulene **12**.

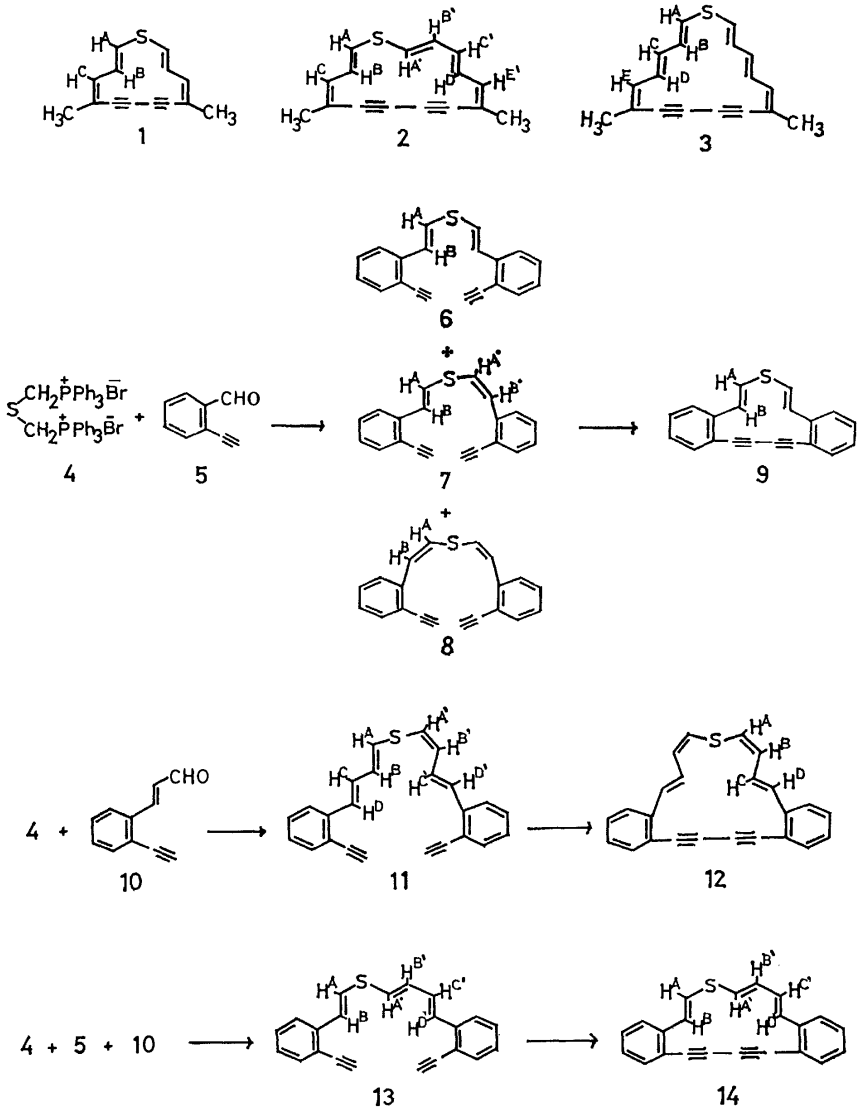

Table 1. The ^{1}H-NMR data of thiaannulenes **1**—**3** at 100 MHz and

	H^A	$H^{A'}$	H^B	$H^{B'}$	H^C	$H^{C'}$
1	4.49		5.40		2.80	
	d (15)		dd (15, 9)		d (9)	
9	3.43		3.20			
	d (16)		d (16)			
2	(3.55—4.2)	1.09	0.79	←———	3.55—4.2	———→
		d (14)	dd (15, 11)			
14	3.12[a]	(2.5—3.0)[a]	2.28	3.35[b]		(2.5—3.0)[b]
	d (16)		d (16)	dd (16, 9)		
3	4.42		4.85		3.09	
	d (15)		dd (15, 9)		dd (15, 9)	
12	3.40		3.62		(2.3—2.8)	
	d (9)		dd (9, 9)			

a, b) These assignments may be reversed in each group.

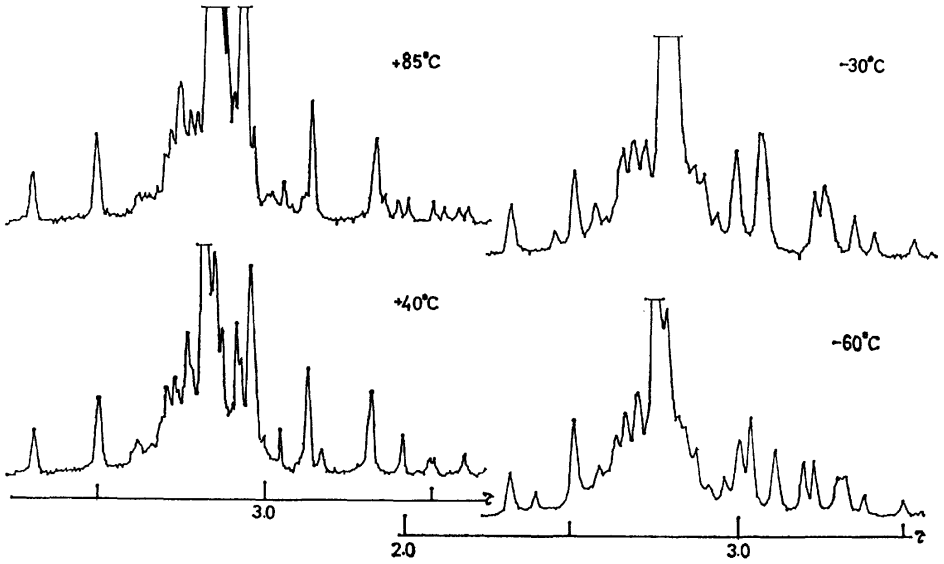

Fig. 1. ^{1}H-NMR FT spectra of **14** in $CDCl_3$ at 80 MHz (Internal Standard, TMS).

The double Wittig reaction of 2 molar equivalents of *o*-ethynylbenzaldehyde **5**[3a] and 1 molar equivalent of bis[(triphenylphosphonio)methyl] sulfide dibromide **4**[2] in *N,N*-dimethylformamide with ethanolic lithium ethoxide at 80 °C yielded an acyclic stereoisomeric mixture in a good yield, from which *trans-trans* isomer **6** (1%), *cis-trans* isomer **7** (21%), and *cis-cis* isomer **8** (25%) were isolated; only **8** was obtained as crystals. Configuration of each isomer was confirmed by IR and NMR spectra. Oxidative coupling of the mixture of **6**—**8** was carried out with anhydrous copper(II) acetate in pyridine and dry ether at 50 °C as reported by Darby *et al.*[5] Column chromatography of the product on alumina gave the cyclic compounds, from which we could isolate *trans-trans* isomer **9** as crystals in a 17% yield. Similarly, the reaction of the salt **4** with *o*-ethynylcinnamaldehyde **10**[4] gave a very unstable stereoisomeric mixture in a 35% yield, from which only mono-*cis* isomer **11** was isolated as bright yellow crystals. Coupling of the unstable mixture as before gave only di-*cis* isomer **12** in a 20% yield, although several isomers were obtained for both dimethyl-[1e] and bis(cyclohexene)-annelated [17]annulene.[1d] The double Wittig reaction between the salt **4** and each 1 molar equivalent of **5** and **10** was carried out at 70 °C in *N,N*-dimethylformamide. Column chromatography of the product afforded the desired acyclic compound of [15]annulene in an 18% yield along with analogues of [13]- and [17]annulenes. We isolated all-*trans* isomer **13** as yellow crystals by further purification. Oxidative coupling of the acyclic mixture containing **13** gave the mixture of the cyclic compounds, from which we could isolate all-*trans* isomer **14** in a 15% yield. The assignment of the structure of these compounds was made on the basis of their spectral properties as well as elemental analyses for the crystalline compounds, and the assigned conformations were given to these compounds in analogy with the dimethylthiaannulenes **1**—**3**, which were shown to have the conformations based on ^{1}H-NMR spectroscopy of the corresponding dideuterio compounds.[1] The dibenzo[*d,j*]-6,8-bisdehydrothia[13]annulene **9**, -[15]annulene **14**, and dibenzo[*f,l*]-8,10-bisdehydrothia-[17]annulene **12** formed light yellow needles (164 °C (dec)), yellow needles (141 °C (dec)), yellow needles (196 °C (dec)), respectively; all these compounds ap-

9, **12**, **14** AT 90 MHz IN $CDCl_3$ (τ-Values, TMS as an internal standard)

H^D	$H^{D'}$	H^E	$H^{E'}$	CH_3	Benzenoid H
				7.71	
				s	
					2.4—2.8
					m
	1.07		(3.55—4.2)	8.39, 8.43	
	dd(14, 14)			s s	
	(2.5—3.0)[a]				2.5—3.0
					m
5.63		2.81		7.78	
dd(15, 12)		d (12)		s	
3.22					2.3—2.8
d (16)					m

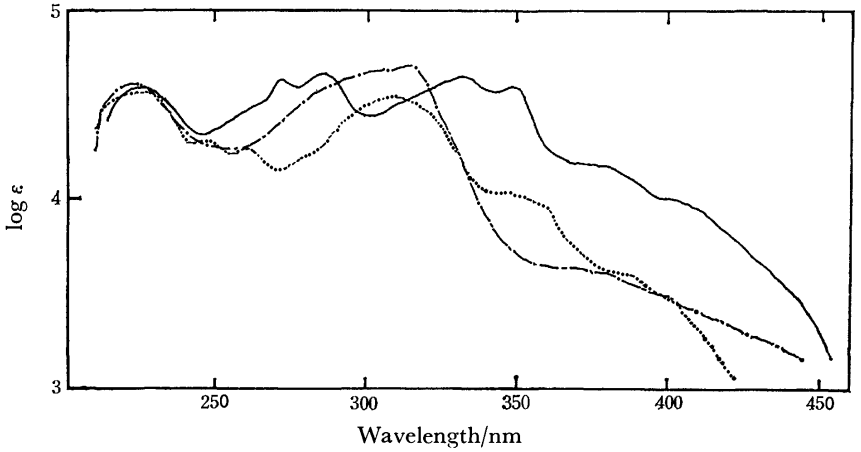

Fig. 2. Electronic spectra of dibenzothiaannulenes **9** (--------), **12**(———), and **14** (—·—·—) in THF.

pear to be considerably stable.

The ^{1}H-NMR spectral data of the protons of **9**, **12**, and **14**, altogether with those of **1**—**3** reported by Sondheimer *et al.*[1] are summarized in Table 1. The individual assignments were made on the basis of the multiplicity, coupling constants, and the data of the closely related compounds.[1] The signals of all olefinic protons could not be located precisely, because the signals due to benzenoid protons were also observed in almost the same region as those of olefinic protons. Comparison of the chemical shifts of the olefinic protons of the dibenzannelated annulene with those of the corresponding dimethylthiaannulene **1**—**3** shows that the dibenzothiaannulenes **9**, **12**, **14** are atropic, reflecting that annelation of two benzene rings eliminate the ring current observed for **1**—**3**. The NMR spectra of [13]- **9** and [17]annulene **12** proved to be temperature-independent in the range of −60 to 60 °C, in contrast to the cases for dimethylthia-[13]- **1** and [17]annulene **3**.[1a,c] On the other hand, the spectra of [15]annulene **14** which are illustrated in Fig. 1, are temperature-dependent, though the dimethylthia[15]annulene **2** being a rigid molecule. As seen from Fig. 1, the signals become more complex from +85 °C to −60 °C, especially in the τ 3.0—3.5 region. The change of the band is not understandable by taking for a rotation about a *trans* double bond. Thus, although this behavior is not understood, similar type of NMR temperature dependence has been observed in the case of the spectra of monodehydro-[14]annulene.[6] However, a possible explanation is the increase of the anisotropic effect of the fused benzene rings on cooling, reflecting that the macrocyclic ring becomes more planar.[7]

The electronic spectra of **9**, **12**, **14** are illustrated in Fig. 2. It is recognized that the electronic spectra of carbocyclic annulenes and dehydroannulenes have been shown to alternate, the main maxima of $(4n+2)\pi$-electron systems being at higher wavelength than those of $4n$ systems.[8] However, this trend is not exhibited for the electronic spectra of these benzothiaannulene series, reflecting that the compounds **9**, **12**, **14** are atropic.

Experimental

All melting points are uncorrected. Brockmann Alumina (Act. II—III) wasused for column chromatography. The IR spectra were measured on a Hitachi EPI-S2 spectrophotometer. The UV spectra were taken on a Hitachi 124 spectrophotometer and refer to tetrahydrofuran solution. Shoulders in UV spectra are indicated by sh. The NMR

measurements were made with a Varian EM-390, a Hitachi R-900 at 90 MHz or a Varian FT-80A spectrometer at 80 MHz in $CDCl_3$ using tetramethylsilane as an internal standard and recorded in τ-values. The mass spectra were obtained on a JEOL JMS-OI-SG-2 or JEOL JMS-D 100 spectrometer at 75 eV using direct insertion technique. Evaporation of solvents was carried out at water aspirator pressure.

Bis[2-(o-ethynylphenyl)vinyl] Sulfides **6**, **7**, *and* **8**. Lithium ethoxide prepared from lithium (0.33 g, 0.047 gatm) in ethanol (112 ml) was added dropwise with stirring under nitrogen atmosphere at 80—86 °C over a period of 1.5 h to a mixture of *o*-ethynylbenzaldehyde **5**[3a] (5.8 g, 0.045 mol) and bis[(triphenylphosphonio)methyl] sulfide dibromide **4**[2] (13.2 g, 0.0177 mol) in *N,N*-dimethylformamide (446 ml). After further 2 h of stirring at the same temperature, the mixture was then poured into water (500 ml) and extracted thoroughly with benzene. The extracts were washed with dilute hydrochloric acid, aq sodium hydrogencarbonate and saturated sodium chloride solution successively, dried over sodium sulfate, and evaporated to give a dark brown semisolid. Chromatography over a column of alumina (160 g) with hexane-ether (95:5—85:15) as eluent gave a mixture of acyclic compound. The mixture was again taken up in ether and absorbed on alumina (120 g). Careful elution with hexane-ether (98:2) resulted in separation of three isomers. Early eluents gave *trans-trans* isomer **6** (0.05 g, 1.0%) as a light yellow liquid, MS: *m/e* 286 (M^+, 100); mol wt, 286.3; IR (neat): 3300 (-C≡CH), 2100 (-C≡C-), 1585 (C=C), 960, 950 cm^{-1} (*trans* C=C); UV: λ_{max}225 (35100), 252 (25400), 337 nm (27300); NMR: *ca.* 2.4—2.9 (m, 10H, H^B and benzenoid H), 3.00 (d, J=16, 2H, H^A), 6.65 (s, 2H, -C≡CH). The following eluents gave *cis-trans* isomer **7** (1.05 g, 21%) as a light yellow liquid, MS: *m/e* 286 (M^+, 100); mol wt, 286.3; IR (neat): 3300 (-C≡CH), 2100 (-C≡C-), 1597 (C=C), 960, 945 (*trans* C=C), 712, 704 cm^{-1} (*cis* C=C); UV: λ_{max} 226 (37200), 250 (26200), 332 nm (31700); NMR: *ca.* 2.2—3.0 (m, 10H, H^B, $H^{B'}$, and benzenoid H), 3.10 (d, J=16, 1H, H^A), 3.42 (d, J=11, 1H, $H^{A'}$), 6.66 (s, 1H, -C≡CH), 6.67 (s, 1H, -C≡CH). The last eluents gave *cis-cis* isomer **8** (1.27 g, 25%) as solid, which was recrystallized from hexane-benzene to give colorless needles, mp 86—88 °C, MS: *m/e* 286 (M^+, 100); mol wt, 286.3; IR (KBr): 3300 (-C≡CH), 2100 (-C≡C-), 1590 (C=C), 706 cm^{-1} (*cis* C=C); UV: λ_{max}227 (27500), 248 sh (19600), 326 nm (21300); NMR: 2.2—2.9 (m, 8H, benzenoid H), 2.93 (d, J=11, 2H, H^B), 3.47 (d, J=11, 2H, H^A), 6.65 (s, 2H, -C≡CH).

Found: C, 84.01; H, 4.95%. Calcd for $C_{20}H_{14}S$: C, 83.88; H, 4.93%.

Dibenzo[d,j]-*6,8-bisdehydrothia*[*13*]*annulene* **9**. A solution of a mixture of **6**, **7**, and **8** (2.37 g, 8.3 mmol) in pyridine (141 ml) and dry ether (47 ml) was added dropwise to a stirred solution of anhydrous copper(II) acetate (10.6 g) in pyridine (303 ml) and dry ether (101 ml) during 2 h at 45—50 °C and the reaction mixture was stirred for further 1.5 h at the same temperature. After cooling, the mixture was diluted with benzene (500 ml) and filtered through Hyflo Super-Cel. The precipitates formed were washed with benzene (50 ml×2). The filtrate was then poured into 7% hydrochloric acid (1000 ml), and the aq layer was further extracted with benzene. The combined organic layer was washed with 7% hydrochloric acid, water, aq sodium hydrogencarbonate, saturated sodium chloride solution successively, and dried over sodium sulfate. A dark brown liquid obtained by solvent removal was chromatographed on alumina (120 g) with hexane as eluent. Early fractions gave a very unstable liquid which was turned to brownish amorphous on dryness and exposed to air. The following fractions gave *trans-trans* isomer **9** (0.045 g, 17%) as relatively stable crystals. Recrystallization from hexane–benzene afforded light yellow needles, mp 164 °C (dec); MS: *m/e* 284 (M^+, 100); mol wt, 284.3; IR (KBr): 2200 (-C≡C-), 1595 (C=C), 940 cm^{-1} (*trans* C=C); UV: λ_{max} 218 (40900), 227 sh (38300), 247 (19400), 261 (17900), 308 (34500), 346 (10600), 360 sh (8700), 388 sh nm (3100); NMR: see Table 1.

Found: C, 84.60; H, 4.26%. Calcd for $C_{20}H_{12}S$: C, 84.47; H, 4.25%.

Bis[4-(o-ethynylphenyl)-1,3-butadienyl] Sulfide **11**. Lithium ethoxide prepared from lithium (0.32 g, 0.046 gatm) in ethanol (106 ml) was added dropwise with stirring under nitrogen atmosphere at 70—75 °C during 2 h to a mixture of *o*-ethynylcinnamaldehyde **10**[4] (6.3 g, 0.040 mol) and the salt **4** (13.5 g, 0.018 mol) in *N,N*-dimethylformamide (422 ml). The reaction mixture was stirred for further 1.5 h under an atmosphere of nitrogen at the same temperature. After work up as described for the isolation of **8**, a dark red semisolid obtained was chromatographed on alumina (160 g). The fractions eluted with hexane–ether (98:2—96:4) gave the stereoisomeric mixture of acyclic compound as very unstable liquid (2.14 g, 35%). After the liquid was passed through a short column of alumina (30 g) with hexane–ether, the crystals (1.50 g, 25%) obtained was recrystallized from hexane–ether, giving mono-*cis* isomer **11** as light yellow needles, mp 134—136 °C, MS: *m/e* 338 (M^+, 100); mol wt, 338.4; IR (KBr): 3280 (-C≡CH), 2150 (-C≡C-), 1680, 1623 (C=C), 970 (*trans* C=C), 710, 700 cm^{-1} (*cis* C=C); UV: λ_{max} 233 (27500), 258 sh (20200), 267 (21500), 283 (19400), 365 nm (31100); NMR: 2.2—2.8 (m, 12H, H^C, $H^{C'}$, H^D, $H^{D'}$, and benzenoid H), 3.40—3.78 (m, 4H, H^A, $H^{A'}$, H^B, and $H^{B'}$), 6.60 (s, 2H, -C≡CH).

Found: C, 85.39; H, 5.08%. Calcd for $C_{24}H_{18}S$: C, 85.17; H, 5.36%.

Dibenzo[f,l]-*8,10-bisdehydrothia*[*17*]*annulene* **12**. A solution of the isomeric mixture containing **11** (0.57 g, 16.8 mmol) in pyridine (30 ml) and dry ether (10 ml) was added dropwise to a stirred solution of anhydrous copper(II) acetate (2.17 g) in pyridine (64 ml) and dry ether (21 ml) for 1.5 h at 50—55 °C and the reaction mixture was stirred for further 1 h at the same temperature. After work up as described for the isolation of **9**, a dark red brown liquid obtained was chromatographed on alumina (130 g). The fractions eluted with hexane-ether (97:3) gave di-*cis* isomer **12** (111 mg, 20%) as solid. Recrystallization from hexane-ether afforded pure **12** as yellow needles, mp 196 °C (dec), MS: *m/e* 336 (M^+, 100); mol wt, 336.4; IR (KBr): 2235, 2185 (-C≡C-), 1620 (C=C), 965 (*trans* C=C), 700, 680 cm^{-1} (*cis* C=C); UV: λ_{max} 226 (38300), 272 (41200), 286 (46300), 332 (44200), 348 (39400), 375 sh (16100), 404 sh nm (9720); NMR: see Table 1.

Found: C, 85.50; H, 4.51%. Calcd for $C_{24}H_{16}S$: C, 85.68; H, 4.79%.

2-(o-Ethynylphenyl)vinyl 4-(o-Ethynylphenyl)-1,3-butadienyl Sulfide **13**. Lithium ethoxide prepared from lithium (0.19 g, 0.027 gatm) in ethanol (46 ml) was added dropwise with stirring under nitrogen atmosphere at 69—71 °C over a period of 1 h to a mixture of *o*-ethynylbenzaldehyde **5** (1.39 g, 0.011 mol), *o*-ethynylcinnamaldehyde **10** (1.67 g, 0.011 mol), and the salt **4** (7.93 g, 0.011 mol) in *N,N*-dimethylformamide (249 ml). After further 2 h of stirring at the same temperature under nitrogen atmosphere, the mixture was poured into water (500 ml). After work up as described for the isolation of **8**, a dark brown semisolid was passed through a short column of alumina (40 g) with hexane–

ether to remove polymeric products. A dark red liquid obtained by evaporation of solvents was cautiously chromatographed on alumina (140 g) with hexane-ether (96:4). The early eluents gave a mixture of acyclic compound of [13]annulene (0.941 g). The following eluents afforded an unstable red liquid of a mixture of acyclic compound of the desired [15]annulene (0.609 g, 18%). The last fractions gave a mixture of acyclic compound of [17]annulene (0.171 g). The unstable red liquid of the acyclic mixture of [15]-annulene was passed through a short column of alumina (30 g). The eluents with hexane gave solid (0.203 g, 6.0%) which was recrystallized from hexane–ether to afford all-*trans* isomer **13** as light yellow needles, mp 117—118 °C, MS: *m/e* 312 (M^+, 100); mol wt, 312.4; IR (KBr): 3300 (-C≡CH), 2180 (-C≡C-), 1620, 1590, 1585 (C=C), 965 cm^{-1} (*trans* C=C); UV: λ_{max} 227 (33900), 237 sh (29300), 255 (25300), 290 (14100), 349 nm (33100); NMR: 2.17—3.03 (m, 11H, H^B, $H^{B'}$ or $H^{C'}$, $H^{D'}$, and benzenoid H), 3.49 (d, J=14, 1H, H^A or $H^{A'}$), 3.60 (d, J=14, H^A or $H^{A'}$), 3.65 (dd, J=14, 10, 1H, $H^{B'}$ or $H^{C'}$), 6.65 (s, 2H, -C≡CH).

Found: C, 84.31; H, 4.92%. Calcd for $C_{22}H_{16}S$: C, 84.57; H, 5.16%.

Dibenzo[d, j]-*6,8-bisdehydrothia*[*15*]*annulene* ***14***. A solution of the acyclic mixture containing **13** (1.92 g, 6.15 mmol) in pyridine (106 ml) and dry ether (35 ml) was added dropwise to a stirred solution of anhydrous copper(II) acetate (7.84 g) in pyridine (231 ml) and dry ether (77 ml) during 2 h at 46—50 °C. The mixture was stirred at the same temperature for further 2 h. After work up as in the isolation of **9**, the red liquid obtained was chromatographed on alumina (100 g). The all-*trans* isomer **14** (0.41 g, 21%) was obtained from fractions eluted with hexane–ether (98:2) as solid. Recrystallization from hexane–ether gave pure **14** as yellow needles, mp 141 °C (dec); MS: *m/e* 310 (M^+, 64%), 309 (100); mol wt, 310.4, IR (KBr): 2180 (-C≡C-), 1630, 1600, 1590 (C=C), 985 cm^{-1} (*trans* C=C); UV: λ_{max} 222 (40400), 283 sh (37000), 300 sh (46100), 313 (49800), 375 sh (4020); NMR: see Table 1.

Found: C, 84.83; H, 4.34%. Calcd for $C_{22}H_{14}S$: C, 85.12; H, 4.55%.

The authors wish to thank Professor F. Sondheimer and Dr. J. E. Anderson, University College London, for helpful suggestions and Dr. Akio Yasuhara, National Institute for Environmental Studies, for measurement of the mass spectra. One of the authors (J. O.) is grateful to the Ministry of Education for financial support of this investigation through a Grant-in-Aid (054103, 1975) for Scientific Research.

References

1) a) R. L. Wife and F. Sondheimer, *J. Am. Chem. Soc.*, **97**, 640 (1975); b) R. L. Wife, P. J. Beeby, and F. Sondheimer, *ibid.*, **97**, 641 (1975); c) R. L. Wife and F. Sondheimer, *Tetrahedron Lett.*, **1975**, 195; d) R. H. McGirk and F. Sondheimer, *Angew. Chem.*, **84**, 897 (1972).

2) K. Dimroth, H. Follmann, and G. Pohl, *Chem. Ber.*, **99**, 642 (1966).

3) a) J. Ojima, T. Yokomachi, and A. Kimura, *Bull. Chem. Soc. Jpn.*, **49**, 2840 (1976); b) J. Ojima, A. Kimura, and M. Ikeguchi, *ibid.*, **49**, 3709 (1976); c) J. Ojima, M. Enkaku, and C. Uwai, *ibid.*, **50**, 933 (1977).

4) J. Ojima, A. Kimura, Y. Yokoyama, and T. Yokoyama, *Bull. Chem. Soc. Jpn.*, **48**, 367 (1975).

5) a) N. Darby, T. M. Cresp, and F. Sondheimer, *J. Org. Chem.*, **42**, 1960 (1977); b) J. Ojima, Y. Shiroishi, and M. Fujiyoshi, *Bull. Chem. Soc. Jpn.*, **51**, 2112 (1978).

6) F. Sondheimer *et al.*, Special Publications No. 21, The Chemical Society, **1967**, p. 83.

7) The authors are deeply indebted to Prof. Sondheimer for this suggestions and pointing out Ref. 6.

8) P. J. Garratt and K. Grohmann, "Houben-Weyl, Methoden der Organischen Chemie," Geog Thieme Verlag, Stuttgart (1972), Vol. V, Part 1d, p. 533.

Modification of (*S*)-*N*,*N*-Dimethyl-1-[(*R*)-1′,2-bis(diphenylphosphino)-ferrocenyl]ethylamine (BPPFA) as a Ligand for Asymmetric Hydrogenation of Olefins Catalyzed by a Chiral Rhodium(I) Complex†

Keiji YAMAMOTO,* Junya WAKATSUKI, and Ryuichi SUGIMOTO
Department of Chemical Engineering, Tokyo Institute of Technology, Meguro, Tokyo 152

(Received October 6, 1979)

Asymmetric homogeneous hydrogenation of prochiral olefins catalyzed by chiral rhodium(I) complexes was carried out by using several ferrocenylphosphines as ligands which play a key role of the chiral recognition. Modifications of BPPFA were made in order to examine a steric effect of the given substutient at the asymmetric center on the efficiency of the chiral ligands, indicating the parent BPPFA to be superior to the others examined for the asymmetric hydrogenation of highly functionalized olefins.

Rapid development in asymmetric homogeneous hydrogenation of olefins catalyzed by chiral rhodium(I) complexes has encouraged significant efforts in the preparation of chiral phosphines for some years.

Although the choice of the chiral ligand for this purpose is still empirical at the present time, there are several efficient bisphosphine ligands which enable the catalyst for hydrogenation of certain functionalized prochiral olefins, *e.g.* α-(acylamino)acrylic acid, to attain 80—100% in enantioselectivity.[1] Among such ligands, (2*R*, 3*R*)-2,3-*O*-isopropylidene-2,3-dihydroxy-1,4-bis(diphenylphosphino)butane(DIOP),[2] (1*R*,2*R*)-bis[(*o*-methoxyphenyl)phenylphosphino]ethane (DIPAMP),[3] and (2*S*,3*S*)-2,3-bis(diphenylphosphino)-butane (CHIRAPHOS)[4] have equivalent diarylphosphino groups in the molecule, forming more or less rigid chelates with the metal atom. (2*R*)-1,2-Bis(diphenylphosphino)propane(PROPHOS)[5] and (1*S*)-1,2-bis(diphenylphosphino)-1-phenylethane[6] may also be included in this class of ligands.

The most convincing explanation for the existing effective chiral recognition by these chelate ligands is that the four phenyl (aryl) groups on the phosphorus atoms are arranged around the rhodium metal in an alternating 'edge-face' manner, which is dictated by the chiral centers present in the ligand molecule.[3,4]

On the other hand, (2*S*,4*S*)-*N*-*t*-butoxycarbonyl-2-[(diphenylphosphino)methyl]-4-(diphenylphosphino)-pyrrolidine (BPPM),[7] and (*S*)-*N*,*N*-dimethyl-1-[(*R*)-1′,2-bis(diphenylphosphino)ferrocenyl]ethylamine (BPPFA)[8] contain sterically non-equivalent phsophorus atoms and clear modelling of the 'edge-face' conformation is rather difficult. However, (*S*)-(*R*)-BPPFA is unique in that it has planar element of chirality which arises from introducing the phosphino groups into the optically pure *N*,*N*-dimethyl-1-ferrocenylethylamine.[9]

We describe here some modifications of BPPFA by changing a methyl group bound to the asymmetric carbon atom with an isopropyl or a phenyl group in order to examine a steric effect of the asymmetric center on the conformation of the chelate and thus the efficiency of the chiral ligands: They were used for the rhodium(I) complex-catalyzed hydrogenation of a variety of olefinic substrates.

† Presented in part at the 37th National Meeting of the Chemical Society of Japan, Tokyo, April 1978, Abstr. 4L12.

There has been another approach to the modification of BPPFA, which involves retentive substitution of a dimethylamino group with higher dialkylamino groups or a hydroxyl group, indicating a remarkable participation of these functional groups to the asymmetrically catalyzed reactions.[10,11]

Results and Discussion

Preparation of Analogs of BPPFA. *N*,*N*-Dimethyl-1-ferrocenyl-2-methylpropylamine (**1b**) was obtained by a similar procedure to the preparation of *N*,*N*-dimethyl-1-ferrocenylethylamine (**1a**)[9] (Eq. 1), and was resolved by crystallization of the tartrates from aqueous acetone.

$$\underset{\text{(Fc = ferrocenyl)}}{\text{Fc-CH(CN)NMe}_2} + \text{RMgX} \rightarrow \underset{\begin{array}{l}\textbf{1a},\ \text{R=Me}\\ \textbf{1b},\ \text{R=}i\text{-Pr}\end{array}}{\text{Fc-CHRNMe}_2} \qquad (1)$$

It was noted that the reaction with isopropylmagnesium chloride gave not only **1b**, but a ketone which came from an attack of the Grignard reagent on the nitrile group. Ugi *et al.*[12] have recently reported the preparation of optically active **1b**.

Optically pure *N*,*N*-dimethyl-α-ferrocenylbenzylamine (**1c**) (absolute configuration unknown) was prepared according to Scheme 1. Resolution of the

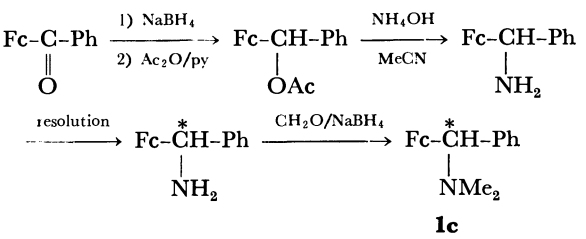

Scheme 1.

primary amine[13] was carried out by crystallization of the hydrogen dibenzoyltartrate from ethanol by a reported procedure.[14] The absolute configuration of (−)-**1c** was most likely estimated to be *S* by correlating CD spectra of BPPFA analogs (*vide infra*).

Chiral ferrocenylphosphines were prepared by way of stereoselective lithiation[9] of optically active ferrocenyl-substituted amines (**1a**—**c**). Thus, stepwise lithiation of **1a**—**c** with butyllithium in ether and with butyllithium / *N*, *N*, *N*′, *N*′ - tetramethylethylenediamine

Table 1. Physical and analytical data of BPPFA (2) and PPFA (3) analogs

		Mp/°C	$[\alpha]_D^{25}$ (deg) (*c*, $CHCl_3$)	Found (Calcd)(%)		
				C	H	N
(*S*)-(*R*)-BPPFA	(**2a**)	136	+349 (0.604)[a]		——	
(*R*)-(*S*)-BPPFA-IP	(**2b**)	85	−350 (0.496)	73.83(73.50)	6.41(6.34)	2.13(2.14)
(*S*)-(*R*)-BPPFA-Ph	(**2c**)	70	+260 (0.520)	74.36(75.11)	5.87(5.72)	2.11(2.04)
(*S*)-(*R*)-PPFA	(**3a**)	139	+343 (0.600)[b]		——	
(*R*)-(*S*)-PPFA-IP	(**3b**)	116	−396 (0.208)	70.82(71.65)	6.75(6.87)	2.70(2.98)
(*S*)-(*R*)-PPFA-Ph	(**3c**)	96	+238 (0.246)[c]	73.68(73.96)	6.07(6.01)	2.71(2.78)

a) Lit,[11] (*R*)-(*S*)-**2a**, $[\alpha]_D^{25}$ −349° (*c* 0.5, $CHCl_3$). b) Lit,[8a] (*S*)-(*R*)-**3a**, $[\alpha]_D^{25}$ +361° (*c* 0.6, EtOH). $[\alpha]_D^{25}$ +361° (*c* 0.50, EtOH) was observed. c) Optical purity 95%.

Table 2. IR and NMR spectral data of BPPFA (2) and PPFA (3) analogs

	IR (KBr) $\tilde{\nu}$/cm^{-1}	NMR ($CDCl_3$, TMS) (δ/ppm)
2b	2920, 1485, 1435, 745, and 700	1.03 and 1.39 (dd, J=6.8 Hz, CMe_2), 1.84 (s, NMe_2), 1.9—2.5 (m, $CHMe_2$), 3.25—4.49 (m, Cyclopentadienyl ring protons, Fc-CH[a]), and 7.05—7.75 (m, phenyls).
2c	1435, 740, and 700	1.74 (s, NMe_2), 3.04—3.40, 3.56—3.82 (m, C_5H_4, Fc-CH) 4.00—4.58 (m, C_5H_3), and 6.86—7.80 (m, phenyls).
3b	2920, 1475, 1435, 1025, 820,[b] 740, and 700	1.04 and 1.35 (dd, J=6.8 Hz, CMe_2), 1.86 (s, NMe_2), 1.9—2.65 (m, $CHMe_2$), 3.91 (s, C_5H_5), 3.65—4.03 and 4.42—4.47 (m, FcCH, C_5H_3), and 7.02—7.82 (m, phenyls).
3c	1435, 1110, 820,[b] 750, and 700	1.79 (s, NMe_2), 3.42 (s, C_5H_5), 3.99 (bm, Fc-CH), 4.23—4.27 (m, C_5H_3), and 7.10—7.85 (m, phenyls).

a) Fc=Ferrocenyl. b) Characteristic 9, 10 μ rule.

(TMEDA)[8a] led to the introduction of two diphenylphosphino groups into each of the cyclopentadienyl rings to give the corresponding BPPFA (**2a**) and its analogs (**2b** and **c**) in moderate yields (Eq. 2).

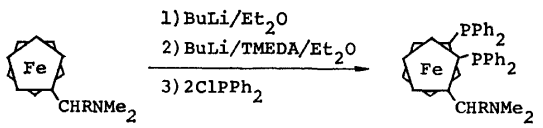

(2)

1a, R=Me
b, R=*i*-Pr
c, R=Ph

2a, BPPFA
b, BPPFA-IP (antipode)
c, BPPFA-Ph

Analogs of (*S*)-*N*,*N*-dimethyl-1-[(*R*)-2-(diphenylphosphino)ferrocenyl]ethylamine (PPFA) (**3a**) were also prepared from **1a—c** by single lithiation, followed by treatment with diphenylphosphinous chloride[8a] (Eq. 3).

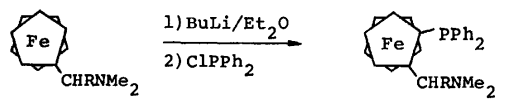

(3)

1a—c

3a, PPFA
b, PPFA-IP (antipode)
c, PPFA-Ph

Physical properties of ferrocenylphosphines (**2** and **3**) were given in Table 1 and NMR and IR spectral data of **2** and **3** were summarized in Table 2. The circular dichroism (CD) spectra of **2a—c** were shown in Fig. 1. Since the enantiomeric property of (*R*)-(*S*)-**2b** as compared with (*S*)-(*R*)-**2a** is obvious from the CD spectra, it is most probable that the absolute configuration of (−)-**2c** with a positive Cotton effect is (*S*)-(*R*), and in turn that of (−)-**1c** is *S*.

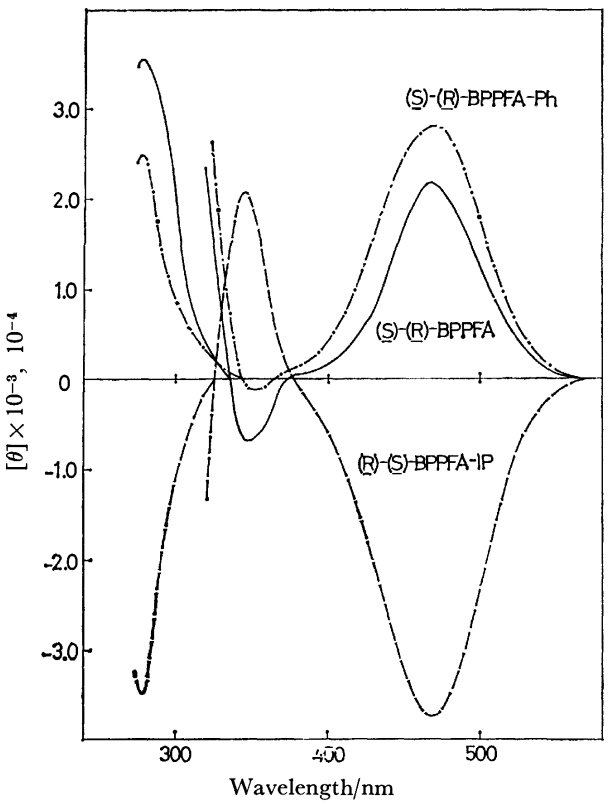

Fig. 1. Circular dichroism (CD) spectra of BPPFA (**2a—c**).

Asymmetric Hydrogenation of α-(Acylamino)acrylic Acids Using BPPFA Rhodium(I) Catalyst. We are primarily concerned with the modification of (*S*)-(*R*)-BPPFA (**2a**) which has been found to exert an effective chiral influence in the rhodium(I) complex-catalyzed hydrogenation of α-acetamidocinnamic acid.[8b] Kagan, *et al.*[15] have previously reported that the geometry of the olefinic acids and esters has a marked effect on the optical yield of phenylalanine derivatives obtained by asymmetric hydrogenation catalyzed by Rh(I)–DIOP system. Therefore, we have also carried out the hydrogenation of (*Z*)-α-acetamido- and (*Z*)- and (*E*)- α-benzamidocinnamic acid and their methyl esters using Rh(I)–BPPFA as catalyst under the standard conditions where complete hydrogenation of each substrate is confirmed. (details in Experimental)

TABLE 3. DEPENDENCE OF THE OPTICAL YIELDS ON THE GEOMETRY OF SUBSTRATES IN THE ASYMMETRIC HYDROGENATION CATALYZED BY Rh(I)-BPPFA

Substrate	Optical yield (% e.e.)[a]	
	(*S*)-(*R*)-BPPFA	(+)-DIOP[b]
Ph, H, NHAc, CO_2H	86	82
Ph, H, NHAc, CO_2Me	69	74
Ph, H, NHBz, CO_2H	37	70
Ph, H, NHBz, CO_2Me	35	38
Ph, H, CO_2H, NHBz	4	25
Ph, H, CO_2Me, NHBz	*nil*	5

a) (*S*)-Phenylalanine derivatives obtained. Optical yields are calculated with respect to the following values of the optically pure compounds: *N*-Acetylphenylalanine, $[\alpha]_D^{25}$ +46.8° (*c* 1.06, 95% EtOH).[15] Methyl ester, $[\alpha]_D^{25}$ +15.9° (*c* 2.0, MeOH): R. Glazer, *J. Organomet. Chem.*, **121**, 249 (1976). *N*-Benzoylphenylalanine, $[\alpha]_D^{25}$ −19.8° (*c* 8.8, 0.4 M NaOH).[2] Methyl ester, $[\alpha]_D^{25}$ −45.3° (*c* 1.325, 95% EtOH).[15] b) Lit.[15]

Table 3 shows the results together with the corresponding data reported by Kagan *et al.*[15] Dependence of the optical yield on the geometry of substrates is evident, deficiency of the optical yields starting from (*E*)-α-benzamidocinnamic acid and its ester being stronger in BPPFA than in DIOP. The results show that the same basis of the chiral recognition as mentioned above can be applied for these chelate ligands. Intrinsic low enantioselectivity with (*E*)-α-benzamidocinnamic acid has recently been discussed in terms of an inferior matching of the substrate with the catalyst in addition to a partial isomerization into the (*Z*)-isomer.[16,17]

BPPFA (**2a**—**c**) were examined as ligands in Rh(I) complex-catalyzed hydrogenation of (*Z*)-α-acetamidocinnamic acid and α-acetamidoacrylic acid, respectively. Results obtained were given in Table 4.

As is seen in Table 4, the parent BPPFA (**2a**) is much superior in asymmetric hydrogenation of these two amino acid precursors to the analogs **2b** and **2c**. Also PPFA–Ph (**3c**) is not effective as compared with **3a**, preferred configuration being inverted from *S* with bisphosphines **2** to *R* with monophosphines **3**. The fact that inverse enantioselectivity was observed between **2c** and **3c** as well as **2a** and **3a** despite the identical absolute configuration of these chiral ligands may well be explained by the different conformation of bisphosphine chelate of **2c** and **2a** from that of P–N chelate of **3c** and **3a**, respectively.

Although change in the structure at asymmetric carbon atom of BPPFA (**2a**) or PPFA (**3a**) so far deteriorated the enantioselective hydrogenation of the amino acid precursors, it does not appear to be true that the parent BPPFA (**2a**) is of sole choice of these chiral ferrocenylphosphines for the catalyzed asymmetric hydrogenation of various olefin substrates.

Asymmetric Hydrogenation of Itaconic Acid, Atropic Acid, and α-Ethylstyrene. These substrate were chosen

TABLE 4. ASYMMETRIC HYDROGENATION OF (*Z*)-α-ACETAMIDOCINNAMIC ACID AND α-ACETAMIDOACRYLIC ACID CATALYZED BY Rh(I)-BPPFAs

Substrate	Ligand	Optical yield %	Configuration
Ph, H, NHAc, CO_2H	(*S*)-(*R*)-BPPFA (**2a**)	86[a]	*S*
	(*R*)-(*S*)-BPPFA-IP (**2b**)	52	*R*
	(*S*)-(*R*)-BPPFA-Ph (**2c**)	52	*S*
	(*S*)-(*R*)-PPFA (**3a**)	67[b]	*R*
	(*S*)-(*R*)-PPFA-Ph (**3c**)	34	*R*
H_2C, NHAc, CO_2H	**2a**	55[c,d]	*S*
	2b	42	*R*
	2c	45	*S*

a) In ethanol, 93% e.e.[8b] b) W. R. Cullen and E. S. Yeh, *J. Organomet. Chem.*, **139**, C 13 (1977), 73—84% e.e. c) In ethanol, 69% e.e.[18] d) Based on the values of the optically pure compound: *N*-Acetyl-(*R*)-alanine, $[\alpha]_D$ +66.5° (*c* 2, H_2O): S. M. Birbaum, L. Levintov, R. B. Kingsley, and J. P. Greenstein, *J. Biol. Chem.*, **194**, 455 (1952).

Table 5. Asymmetric hydrogenation of itaconic acid, atropic acid, and α-ethylstyrene catalyzed by Rh(I)-BPPFAs

Substrate	Ligand	Optical yield[a] %	Configuration
CH_2=C-CO_2H CH_2CO_2H	BPPFA (**2a**)	32	*R*
	BPPFA-IP (**2b**)	21	*S*
	BPPFA-Ph (**2c**)	34	*R*
CH_2=C-CO_2H Ph	**2a**	8	*S*
	2b	3	*S*
	2c	9	*R*
CH_2=C-Et Ph	**2a**	6	*R*
	2b	3	*S*
	2c	34	*R*

a) Optical yields are calculated with respect to the following maximum rotations: (*R*)-α-Methylsuccinic acid, $[\alpha]_D^{20}$ +17.09° (*c* 4.41, abs. EtOH): R. Rossi, P. Diversi, and G. Ingrosso, *Gazz. Chim. Ital.* **38**, 1391 (1968). (*S*)-Hydratropic acid, $[\alpha]_D^{25}$ +76.3° (*c* 1.6, $CHCl_3$): S. P. Bakshi and E. E. Turner, *J. Chem. Soc.*, 171 (1961). (*R*)-2-Phenylbutane, $[\alpha]_D^{25}$ −27.3° (neat): W. A. Bonner and T. W. Greenlee, *J. Am. Chem. Soc.*, **81**, 3336 (1959).

because they lack any attractive interaction as is expected for α-(acylamino)acrylic acids which coordinate with both the olefin bond and the amido carbonyl group to the rhodium. We have reported the preparation of (*S*)-*N*,*N*-dimethyl-1-[2-(diphenylphosphino)-1-naphthyl]ethylamine (1,2-DPNEA),[19] which was used as ligand in the rhodium complex-catalyzed asymmetric hydrogenation of itaconic acid. The optical yield of α-methylsuccinic acid obtained was up to 54% e.e. with added triethylamine. Lately, rhodium(I)–BPPM system has been found to give rise to an exceedingly high optical yield in the hydrogenation of itaconic acid.[20,20a]

As simple olefinic acids, itaconic acid and atropic acid were readily hydrogenated under standard conditions employed with Rh(I)–BPPFA catalyst system, but only moderate to low optical yields for these substrates were observed (Table 5).

It is of interest, however, to note that three BPPFAs exert no significant difference in the extent of enantioselective hydrogenation of itaconic acid, whereas a marked dependence on these ligands was observed for α-acetamidocinnamic acid. Furthermore, atropic acid undergoes hydrogenation with no coincidence between the observed configuration of product and absolute configuration of BPPFAs used.

Finally, asymmetric hydrogenation of α-ethylstyrene, one of the simplest hydrocarbon prochiral olefins, was examined using Rh(I)–BPPFAs as catalyst. Results are given in Table 5. Although the low enantioselection by Rh(I)–BPPFAs is again due to the simple structure of nonfunctionalized olefin substrate, BPPFA–Ph (**2c**) gave much higher optical yield of *s*-butylbenzene than the other two. Thus, it is encouraging to find that the simpler the structure of substrate olefin is, the more efficient would be the steric effect at the asymmetric carbon in BPPFAs. On the other hand, the uniformyl low ability of BPPFA–IP (**2b**) in the present asymmetric hydrogenation is presumably explained by the fact that an isopropyl group is of the same steric bulk as the dimethylamino group, and rather interferes in the proper conformation of the chelate present in the parent BPPFA (**2a**).

Experimental

Preparation of N,N-*Dimethyl-1-ferrocenyl-2-methylpropylamine (**1b**).* To an ether solution of isopropylmagnesium chloride, prepared from isopropyl chloride (14.5 g, 0.185 mol) and magnesium turnings (4.5 g) in anhydrous ether (80 ml), was added α-ferrocenyl-α-dimethylaminoacetonitrile[9] (24.8 g, 0.092 mol) dissolved in ether (150 ml) at room temperature. The mixture was stirred for 4.5 h, and hydrolyzed with 10% aqueous ammonium chloride solution. The organic layer was separated and the aqueous layer was extracted with three 50 ml portions of ether. The combined organic layer and extracts were washed with brine and the solvent was removed by evaporation to give 28.8 g of crude product. This was taken up in benzene, extracted with aqueous phosphoric acid (30 g in 400 ml water). The extract was washed with benzene and neutralized with 10% sodium carbonate solution. The organic layer separated was extracted with benzene, and the benzene solution was dried ($MgSO_4$) and evaporated to give 21.1 g, of a mixture of **1b** and a ketone which was separated by distillation.

1b (17.5 g, 65% yield): bp 106—109 °C/0.05 Torr; mp 20—21 °C; NMR ($CDCl_3$, TMS): δ 1.10, 1.24 (dd, *J*= 6.8 Hz, CHMe), 1.81—2.48 (m, CHMe), 2.11 (s, NMe_2), 3.20 (d, *J*=6.0 Hz, Fc-CH), and 4.14 ppm (s, $C_5H_5FcC_5H_4$); IR: 3050 (m), 2900(s), 2800(m), 1448(m), 1100(s), 1020 (m), 1009(s), 1000(m), 810(s), and 730(m) cm^{-1}. The ketone (4.3 g, 15% yield, mp 81—82 °C) was found by its NMR and IR spectrum to be 1-ferrocenyl-1-dimethylamino-3-methyl-2-butanone. NMR ($CDCl_3$): δ 1.17 (d, *J*=7.2 Hz, $CHMe_2$), 2.10 (s, NMe_2), 3.15 (m, *J*=3.3 Hz, CHMe), 4.06 (s, C_5H_5), 4.15 (C_5H_4), and 4.45 ppm (m, CHN); IR (KBr): 1705 cm^{-1} (C=O).

*Resolution of **1b**.* Crude **1b** (23.75 g, 83 mmol) dissolved in acetone (30 ml) was added to a solution of (*R*,*R*)-tartaric acid (12.4 g, 83 mmol) in 85% aqueous acetone (35 ml). Crystals of the hydrogen tartrate formed (28.3 g, 65 mmol) were extracted with hot acetone to leave yellow crystals (11.4 g), while the acetone extract gave orange crystals (10.7 g) after evaporation. From these salts (+)-**1b** (7.79 g, 27.3 mmol, 42%), $[\alpha]_D^{20}$ +135.8° ($CHCl_3$), and (−)-**1b** (7.44 g, 26.0 mmol, 40%), $[\alpha]_D^{20}$ −125.3° ($CHCl_3$), were recovered, respectively. The procedure was repeated five times for further resolution to the highest and constant rotation:

(*S*)-**1b** (4.30 g, 24%), $[\alpha]_D^{20}$ +158.9° (*c* 1.00, $CHCl_3$)
$[\alpha]_D^{20}$ +190.0° (*c* 1.00, benzene)

(*R*)-**1b** (4.00 g, 21%), $[\alpha]_D^{20}$ −160.6° (*c* 1.00, $CHCl_3$)
$[\alpha]_D^{20}$ −192.0° (*c* 1.00, benzene)

The reported maximum rotation is $[\alpha]_D^{20}$ +192.8° (*c* 1, benzene).[12] It should be noted that (−)-**1b**-tartrate as orange crystals is more soluble in hot acetone than the (+)-**1b** salt, though the rate of formation of the latter is faster than that of the former. In addition, (−)-**1b**-tartrate was better purified at the later stage of resolution by washing with diethyl ether.

Preparation of N,N-*Dimethyl-α-ferrocenylbenzylamine (**1c**).*
α-Ferrocenylbenzylamine. To a stirred solution of α-fer-

TABLE 6. THE MOLECULAR ELLIPTICITY [θ] OF FERROCENYLPHOSPHINES

	[θ] (nm)
(*R*)-(*S*)-BPPFA-IP (**2b**)	-3.77×10^3 (469), 2.09×10^3 (345), -3.52×10^4 (279).
(*S*)-(*R*)-BPPFA-Ph (**2c**)	2.82×10^3 (469), -1.47×10^2 (351), 2.53×10^4 (279).
(*S*)-(*R*)-PPFA (**3a**)	2.07×10^3 (459), -1.42×10^3 (342), ——
(*S*)-(*R*)-PPFA-IP (**3b**)	1.30×10^3 (470), 14.0 (365), 5.52×10^3 (280).
(*S*)-*N*,*N*-Dimethyl-1-ferrocenylethylamine (**1a**)	3.91×10^2 (455), -72.0 (338), 3.86×10^3 (257)

rocenylbenzyl acetate[21] (8.0 g, 24 mmol) in acetonitrile (150 ml) was added 38% ammonia solution (35 ml), and the mixture was allowed to stand overnight at room temperature. (Methanol cannot be used as a solvent contrary to the reaction of 1-ferrocenylethyl acetate.[13])

The reaction mixture was evaporated to the minimum volume, and the residue was dissolved in ether (50 ml). The resulting solution was extracted with 8.5% phosphoric acid. The extract was washed with ether and an amine was set free by adding excess 20% sodium hydroxide solution. After usual work up, there obtained α-ferrocenylbenzylamine (4.35 g, 62%): mp 47—49 °C; NMR ($CDCl_3$): δ 1.87 (br.s, $-NH_2$), 4.00—4.32 (m, C_5H_4); 4.12 (s, C_5H_5), 4.81 (s, Fc–CH), and 7.10—7.40 ppm (m, C_6H_5); IR (KBr): 3080, 1600, 1490, 1100, 1000, 810, 720, 700 cm^{-1}.

Resolution of α-Ferrocenylbenzylamine. According to the procedure by Allenmark,[14] a hot solution of (*R*,*R*)-*O*,*O*′-dibenzoyltartaric acid monohydrate (6.48 g, 17.2 mmol) in ethanol (69.5 ml) was added to a hot solution of the racemic amine (5.01 g, 17.2 mmol). After the solution was cooled, an yellow salt precipitated was collected (6.88 g, 59.9%), $[\alpha]_D^{25}$ −87.6° (*c*, 0.502, MeOH). The mother liquor was evaporated to dryness to leave another salt (4.31 g, 37.5%), $[\alpha]_D^{25}$ −41.2° (*c* 0.712, MeOH). Further resolution of the yellow salt was carried out by successive extraction with hot ethanol (180 ml and 85 ml) to give 3.25 g (29.1%) of the purified salt, $[\alpha]_D^{20}$ −107.6° (*c* 0.392, MeOH) (lit,[14] $[\alpha]_D^{25}$ −107°). From this salt the pure (−)-amine was obtained (1.40 g, 96% recovery), mp 80—83 °C, $[\alpha]^{25}$ −27.3° (*c* 0.504, MeOH) (lit,[14] $[\alpha]_D^{25}$ −26.1°).

*(−)-N,N-Dimethyl-α-ferrocenylbenzylamine (**1c**).* To a solution of (−)-amine (1.87 g, 6.42 mmol, 94% optical purity) in methanol (80 ml) was added 37% aqueous formaldehyde (21 ml) in an ice–water bath. To the cooled solution was added sodium borohydride (4.01 g) portionwise, and the mixture was stirred at room temperature overnight. After usual work up and purification, there obtained pure dimethylated amine (1.51 g, 74%), mp 62—64 °C, $[\alpha]_D^{25}$ −106.9° (*c*, 0.350, MeOH). (lit,[14] $[\alpha]_D^{25}$ −109°).

NMR ($CDCl_3$): δ 2.03 (s, NMe_2), 3.68 (s, C_5H_5), 3.73 (s, Fc–CH), 3.98—4.20 (m, C_5H_4), and 7.13—7.50 ppm (m, C_6H_5). IR (KBr): 1450, 1110, 1005, 820, 740, 705 cm^{-1}. In the same procedure as above, optically pure (−)-amine was dimethylated, $[\alpha]_D^{25}$ −112° (MeOH).

*Preparation of BPPFA-IP (**2b**), PPFA-IP (**3b**), BPPFA-Ph (**2c**), and PPFA-Ph (**3c**).* The procedures were the same as those reported by Kumada and coworkers,[8] the following is typical: To a stirred solution of (*R*)-**1b** (2.02 g, 7.1 mmol), $[\alpha]_D^{20}$ −192° (benzene), in anhydrous ether (2 ml) cooled in an ice–water bath was added dropwise butyllithium (2.32 M in hexane, 3.3 ml, 7.7 mmol) under a nitrogen atmosphere. Stirring was continued for 1.5 h at room temperature. To the mixture was added dropwise a mixture of butyllithium (3.3 ml) and TMEDA (0.945 g, 8.1 mmol) with cooling. The resulting mixture was stirred for 4.5 h at room temperature, followed by addition of diphenylphosphinous chloride (4.65 g, 21.0 mmol) in ether. After the reaction mixture was stirred overnight, 5% sodium hydrogencarbonate solution (50 ml) was added. Usual work up and column chromatographic purification (silica gel, hexane–benzene–ethyl acetate) to give (*R*)-(*S*)-**2b** (1.53 g, 33% yield): mp 80—82 °C (ethanol). Similarly, using (−)-**1c** (0.874 g, 2.65 mmol) was obtained (*S*)-(*R*)-**2c** (0.564 g, 30%).

In the same manner as above but with single lithiation, (*R*)-(*S*)-**3b** (38%) and (*S*)-(*R*)-**3c** (35%; 95% optical purity) were prepared. Physical, analytical, and spectral data for these ferrocenylphosphines are given in Tables 1 and 2, respectively. CD spectra of BPPFAs (**2a—c**) were shown in Fig. 1. The molecular ellipticity [θ] of ferrocenylphosphines newly prepared were given in Table 6.

Assymmetric Hydrogenation of Olefins Using BPPFAs-Rh(I) Catalyst. Materials: (*Z*)-α-Acetamidocinnamic acid, its methyl ester,[15] (*E*)- and (*Z*)-α-benzamidocinnamic acid,[22] and their methyl esters were prepared by the known procedures. Atropic acid and α-ethylstyrene were also prepared from hydrolysis of ethyl atropate[23] and thermolysis of 2-phenylbutyl acetate,[24] respectively. Commercially available itaconic acid was used as received.

All solvents used were dried and distilled.

General Procedure of Hydrogenation. The following is chosen as standard conditions.

In a 50 ml microautoclave fitted with a glass tube were placed $[RhCl(C_6H_{10})]_2$ (5.5 mg, 1.25×10^{-2} mmol), BPPFA (**2**) (2.50×10^{-2} mmol), and a substrate olefin (5.00 mmol) under a nitrogen atmosphere. Benzene–methanol (10 ml, 1:3 v/v) previously deoxygenated was added to the mixture and hydrogen was then introduced after three successive substitution of nitrogen with hydrogen (20 atm). Reactions were carried out at 20 atm of initial hydrogen pressure and at room temperature with magnetical stirring for an appropriate period of time to ensure 100% conversion. The extent of reaction was monitored by approximately 3 atm of hydrogen uptake and was checked by NMR spectrum of the final products which were purified by a known procedure.

When a cationic rhodium(I) catalyst, $[Rh(COD)BPPFA]^+ClO_4^-$ or $[Rh(COD)PPFA]^+ClO_4^-$, was used, the concentration of the catalyst was also 2.5 mM and that of the substrate 0.50 M.

Tables 3—5 show all results obtained for the catalyzed asymmetric hydrogenation of a variety of olefins examined.

The authors are grateful to Prof. J. Tsuji for valuable suggestions. We thank Mr. T. Takakuwa of JASCO for the measurments of ORD and CD spectra. We owe to Dr. N. Morita for the preparation and resolution of **1b**. The present work was supported by a Grant-in-Aid for Scientific Research (155328) from the Ministry of Education.

References

1) For a review, see H. B. Kagan and J. C. Fiaud, "Topics in Stereochemistry," ed by E. L. Eliel and N. L.

Allinger, Interscience (1978), Vol. 10, p. 175.
2) H. B. Kagan and T. P. Dang, *J. Am. Chem. Soc.*, **94**, 6429 (1972).
3) W. S. Knowles, M. J. Sabacky, B. D. Vineyard, and D. J. Weinkauff, *J. Am. Chem. Soc.*, **97**, 2567 (1975).
4) M. D. Fryzuk and B. Bosnich, *J. Am. Chem. Soc.*, **99**, 6262 (1977).
5) M. D. Fryzuk and B. Bosnich, *J. Am. Chem. Soc.*, **100**, 5491 (1978).
6) R. B. King, J. Bakos, C. D. Hoff, and L. Markó, *J. Org. Chem.*, **44**, 1729 (1979).
7) K. Achiwa, *J. Am. Chem. Soc.*, **98**, 8265 (1976).
8) a) T. Hayashi, K. Yamamoto, and M. Kumada, *Tetrahedron Lett.*, **1974**, 4405; b) T. Hayashi, T. Mise, S. Mitachi, K. Yamamoto, and M. Kumada, *ibid.*, **1976**, 1133.
9) D. Marquarding, H. Klusacek, G. Gokel, P. Hoffmann, and I. Ugi, *J. Am. Chem. Soc.*, **92**, 5389 (1970).
10) T. Hayashi, M. Tajika, K. Tamao, and M. Kumada, *J. Am. Chem. Soc.*, **78**, 3718 (1976).
11) T. Hayashi, T. Mise, and M. Kumada, *Tetrahedron Lett.*, **1976**, 4351.
12) a) D. Marquarding, H. Burghard, I. Ugi, R. Urban, and H. Klusacek, *J. Chem. Res. (M)*, **1977**, 915; b) G. Eberle, I. Lagerlund, I. Ugi, and R. Urban, *Tetrahedron*, **34**, 977 (1978). We are indebted to Prof. Ugi for informing us of their results prior to publication.
13) G. W. Gokel, D. Marquarding, and I. Ugi, *J. Org. Chem.*, **37**, 3052 (1972).
14) S. Allenmark, K. Kalen, and A. Sandblom, *Chem. Scr.*, **7**, 97 (1975).
15) G. Gelbard, H. B. Kagan, and R. Stern, *Tetrahedron*, **32**, 233 (1976).
16) C. Detellin, G. Gelbard, and H. B. Kagan, *J. Am. Chem. Soc.*, **100**, 7556 (1978).
17) K. E. Koenig and W. S. Knowles, *J. Am. Chem. Soc.*, **100**, 7561 (1978).
18) T. Hayashi and M. Kumada, "Fundamental Research in Homogeneous Catalysis," ed by Y. Ishii and M. Tsutsui, Plenum (1978), Vol. 2, p. 159.
19) K. Yamamoto, A. Tomita, and J. Tsuji, *Chem. Lett.*, **1978**, 3.
20) I. Ojima, T. Kogure, and K. Achiwa, *Chem. Lett.*, **1978**, 567.
20a) Note added. It is recently reported that an intramolecular hydrogen bonding of itaconic acid remarkably interferes with the enantioselectivity. W. C. Christopfel and B. D. Vineyard, *J. Am. Chem. Soc.*, **101**, 4406 (1979).
21) M. D. Rausch, M. Vogel, and H. Rosenberg, *J. Org. Chem.*, **22**, 903 (1957).
22) Y. S. Rao and R. Filler, *Synthesis*, **1975**, 749.
23) G. R. Ames and W. Davey, *J. Chem. Soc.*, **1958**, 1794.
24) C. G. Overberger and D. Tanner, *J. Org. Chem.*, **20**, 369 (1955).

Asymmetric Synthesis Catalyzed by Chiral Ferrocenylphosphine-Transition Metal Complexes. I. Preparation of Chiral Ferrocenylphosphines

Tamio HAYASHI, Takaya MISE, Motoo FUKUSHIMA, Masahiro KAGOTANI, Nobuo NAGASHIMA, Yuji HAMADA, Akira MATSUMOTO, Sota KAWAKAMI, Mitsuo KONISHI, Keiji YAMAMOTO,† and Makoto KUMADA*

Department of Synthetic Chemistry, Faculty of Engineering, Kyoto University, Yoshida, Kyoto 606

(Received October 22, 1979)

As chiral ligands for transition metal complex catalyzed asymmetric reactions, various kinds of chiral ferrocenylphosphines, which have planar chirality due to 1,2-unsymmetrically substituted ferrocene structure and also have a functional group on the side chain of the ferrocene nucleus, were prepared. (*S*)-*N*,*N*-dimethyl-1-[(*R*)-2-(diphenylphosphino)ferrocenyl]ethylamine [(*S*)-(*R*)-PPFA], (*S*)-*N*,*N*-dimethyl-1-[(*R*)-1′,2-bis(diphenylphosphino)ferrocenyl]ethylamine [(*S*)-(*R*)-BPPFA], and their dimethylphosphino derivatives were prepared by way of lithiation of optically resolved *N*,*N*-dimethyl-1-ferrocenylethylamine. The 1-(dimethylamino)ethyl group on the ferrocenylphosphines was converted stereospecifically by nucleophilic substitution reactions into 1-methoxy-, 1-hydroxy-, 1-diphenylphosphino-, and several 1-(dialkylamino)ethyl groups. 1-Diphenylphosphino-2-(dimethylaminomethyl)ferrocene (FcPN) was optically resolved *via* its phosphine sulfide dibenzoyltartaric acid salt. The relationship between CD spectra of the chrial ferrocenylphosphines and the configuration of their planar chirality is discussed.

There has been intense interest and activity recently in asymmetric synthesis catalyzed by transition metal complexes with chiral ligands.[1,2] This has resulted in so great a success in asymmetric homogeneous hydrogenation by chiral phosphine rhodium complexes as to produce α-amino acids with over 90% optical purity.[3] One of the most significant problems in studies on the catalytic asymmetric synthesis is how to develop a chiral ligand which will enable the catalyst for a given reaction to be as efficient in stereoselectivity as possible, and considerable efforts have been devoted to searching for new chiral phosphine ligands. These chiral phosphines may be classified into two classes: (A) phosphines bearing an asymmetric center at the phosphorus atom and (B) phosphines whose chirality is due to asymmetric carbons in groups bonded to phosphorus.

Methylphenylpropylphosphine[4] was used by Horner *et al.*[5] and Knowles *et al.*[6] in their early studies on catalytic asymmetric hydrogenation. Many optically active tertiary phosphines have been prepared since Mislow *et al.* developed a new synthetic method for the chiral phosphines in 1967,[7] and some of them have been reported to be effective ligands for catalytic asymmetric reactions. (*o*-Methoxyphenyl)cyclohexylmethylphosphine (CAMP)[8] and 1,2-bis[(*o*-methoxyphenyl)phenylphosphino]ethane (diPAMP)[9] by Knowles *et al.* gave, when complexed with rhodium, optical yields of over 90% in the hydrogenation of α-(acylamino)acrylic acids.

Phosphines containing asymmetric alkyl groups were usually derived from optically active natural compounds. Kagan *et al.* have achieved a great success with 2,3-*O*-isopropylidene-1,4-bis(diphenylphosphino)-2,3-butanediol (DIOP),[10] prepared relatively easily from tartaric acid. The DIOP has been successfully applied in various kinds of catalytic asymmetric synthesis, *e.g.*, hydrogenation of olefins[11-15] and ketones,[16,17] hydrosilylation of ketones[18-21] and imines,[11a] hydroformylation,[22-24] Grignard cross-coupling,[25,26] and allylic alkylation.[27] Neomenthyldiphenylphosphine (NMDPP)[28,29] and its diastereomeric isomer (MDPP),[29] prepared by Morrison *et al.*, have been used for the hydrogenation of acrylic acids to give up to 62% optical yield.[3,28] They have also studied a bisphosphine ligand (CAMPHOS) derived from camphoric acid.[3] Dimenthylphosphines have been synthesized and used as chiral ligands for a nickel catalyzed cooligomerization of olefins.[30] Optically active amino acids, proline and hydroxyproline, have been employed as chiral sources of phosphine ligands. They are (*S*)-2-(diphenylphosphinomethyl)pyrrolidines[31] and (2*S*, 4*S*)-4-diphenylphosphino-2-(diphenylphosphinomethyl)pyrrolidines,[32] respectively, the latter affording enantiomeric excess of 83—91% in the hydrogenation of α-(acylamino)cinnamic acids. Mono- and diphosphines derived from sugars have been reported to be effective for the asymmetric hydrogenation.[33] (*S*,*S*)-2,3-bis(diphenylphosphino)butane (chiraphos) and (*R*)-1,2-bis(diphenylphosphino)propane (prophos) developed by Fryzuk and Bosnich[34] are among the best ligands for the synthesis of optically active amino acids by the rhodium complex catalyzed hydrogenation. 2,2′-Bis(diphenylphosphinomethyl)-1,1′-binaphthyl (NAPHOS),[35] whose chirality is due to binaphthyl axial chirality, has been prepared and used as a ligand in several catalytic asymmetric reactions.

Chiral ferrocenylphosphines, which have planar chirality due to 1,2-unsymmetrically substituted ferrocene structure[36] and also have various functional groups such as an amino or a hydroxyl group, have been found to give rise to a high asymmetric induction in several transition metal catalyzed asymmetric reactions, *viz.*, hydrogenation of olefins,[37,38] ketones,[39] and imines[40] catalyzed by rhodium complexes, hydrosilylation of ketones by rhodium complexes[41] and of olefins by palladium complexes,[42] Grignard cross-coupling by nickel[43] and palladium[44] complexes, and isomerization of allylamines to enamines by cobalt complexes.[45] In this paper, we wish to describe in detail the preparation of the chiral ferrocenylphosphines.

† Present address: Department of Chemical Engineering, Tokyo Institute of Technology, Meguro-ku, Tokyo 152.

Results and Discussion

Introduction of Phosphino Groups into N,N-*Dimethyl-1-ferrocenylethylamine.* Chiral ferrocenylphosphines are readily prepared by way of lithiation of optically resolved *N,N*-dimethyl-1-ferrocenylethylamine (**1**). The lithiation of (*R*)-**1** with butyllithium was previously reported by Ugi and coworkers[36] to proceed with high stereoselectivity to give preferentially (*R*)-*N,N*-dimethyl-1-[(*R*)-2-lithioferrocenyl]ethylamine[(*R*)-(*R*)-**2**] (Eq. 1).

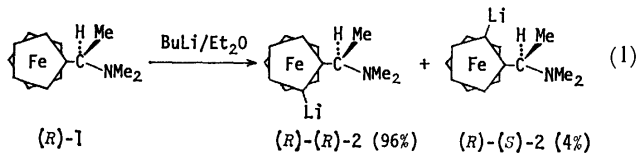

(1)

In our studies, (*R*)-**1** was lithiated, after the Ugi's procedures, with a slight excess of butyllithium in ether, and the lithiated ferrocene was then treated with chlorodiphenylphosphine. (*R*)-*N,N*-dimethyl-1-[(*S*)-2-(diphenylphosphino)ferrocenyl]ethylamine [(*R*)-(*S*)-PPFA] (**3a**), formed *via* (*R*)-(*R*)-**2**, was obtained in 55% isolated yield (Eq. 2). A small amount of

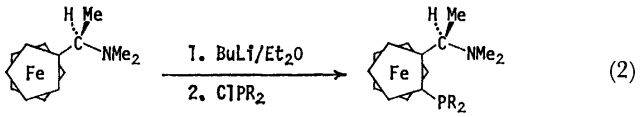

(2)

diastereomeric by-product (*R*)-(*R*)-PPFA (**3a**), formed *via* (*R*)-(*S*)-**2**, was readily removed by recrystallization. (*S*)-(*R*)-PPFA, which is an enantiomer of (*R*)-(*S*)-PPFA, was also prepared from (*S*)-**1** (Eq. 3). Simi-

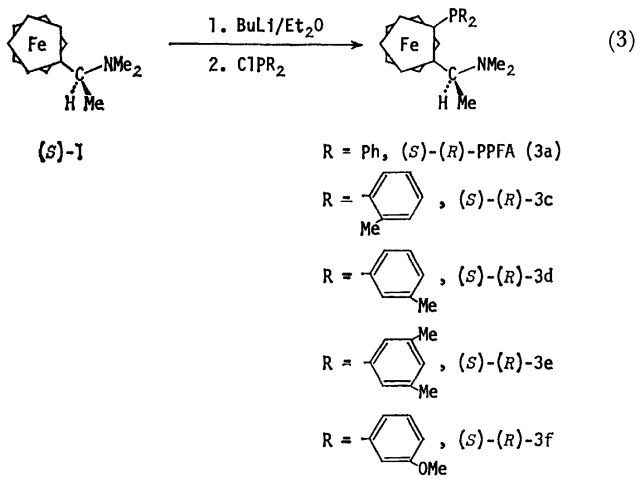

(3)

larly, (*R*)-*N,N*-dimethyl-1-[(*S*)-2-(dimethylphosphino)-ferrocenyl]ethylamine [(*R*)-(*S*)-MPFA] (**3b**) was prepared in 31% yield starting with (*R*)-**1** and with chlorodimethylphosphine. Several bis(substituted phenyl)phosphino groups, such as bis(2-methylphenyl)phosphino, bis(3-methylphenyl)phosphino, bis(3,5-dimethylphenyl)phosphino, and bis(3-methoxyphenyl)phosphino groups, were introduced into (*S*)-**1** in a similar manner using the corresponding chlorodiarylphosphines (Eq. 3).

Lithiation of ferrocene in the presence of *N,N,N',N'*-tetramethylethylenediamine (TMEDA) is known[46] to produce 1,1'-dilithioferrocene, and it was expected that chiral ferrocenylphosphines bearing two phosphino groups could be prepared by the dilithiation of **1**; indeed, the stepwise lithiation of (*S*)-**1** with butyllithium in ether and then with butyllithium/TMEDA in the same solvent followed by diphenylphosphination with chlorodiphenylphosphine led to the introduction of two diphenylphosphino groups, one onto each of the cyclopentadienyl rings to give (*S*)-*N,N*-dimethyl-1-[(*R*)-1',2-bis(diphenylphosphino)ferrocenyl]ethylamine [(*S*)-(*R*)-BPPFA] (**4a**) in 58% yield (Eq. 4). The analogous bis(dimethylphosphino) derivative [(*S*)-(*R*)-BMPFA] (**4b**) was also prepared. The lithiation of PPFA (**3a**) with butyllithium followed by phosphination with chlorodiphenylphosphine resulted in the formation of *N,N*-dimethyl-1-[2,5-bis(diphenylphosphino)ferrocenyl]ethylamine, and BPPFA (**4a**) was not formed in any noticeable amounts.

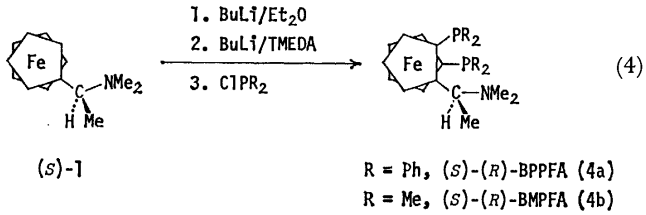

(4)

Although the ferrocenylphosphines with (*S*)-(*R*) or (*R*)-(*S*) configuration were readily obtained in good yields as shown in Eqs. 2—4, it was difficult to obtain pure (*R*)-(*R*) or (*S*)-(*S*) isomers in quantity by the lithiation-phosphination of **1**, since the lithioferrocene **2** which leads to (*R*)-(*R*) or (*S*)-(*S*) ferrocenylphosphine is produced only in small quantities from the highly stereoselective lithiation of **1** (see Eq. 1). This difficulty was solved by first protecting the ring hydrogen liable to lithiation with a trimethylsilyl group, then metalating the other lower reactive hydrogen, vicinal to the 1-(dimethylamino)ethyl group, followed by treating with chlorodiphenylphosphine, and finally desilylating. Thus, (*R*)-*N,N*-dimethyl-1-[(*S*)-2-(trimethylsilyl)ferrocenyl]ethylamine (**5**)[36] obtained by trimethylsilylation of (*R*)-**1** with butyllithium and chlorotrimethylsilane, was diphenylphosphinated with butyllithium and chlorodiphenylphosphine to give regioselectively (*R*)-*N,N*-dimethyl-[2-trimethylsilyl-5-(diphenylphosphino)ferrocenyl]ethylamine (**6**). Desilylation of **6** to (*R*)-(*R*)-PPFA was effected by treatment with potassium *t*-butoxide in dimethyl sulfoxide after Price's techniques.[47] Usual protodesilylation methods were not successful in this special case. Desilylation after introduction of the second diphenylphosphino group into **6** gave (*R*)-(*R*)-BPPFA.

Attempts to prepare bis[2-[1-(dimethylamino)ethyl]-ferrocenyl]phenylphosphine (**8**) by the lithiation of **1** with butyllithium and then addition of dichlorophenylphosphine failed, probably due to the low conversion (≈60%) of **1** into the lithioferrocene **2**. Main products were dibutylphenylphosphine and a phenyl-

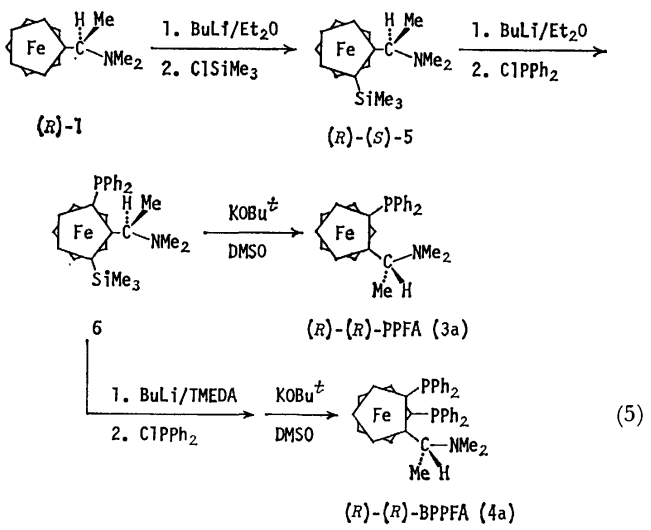

(5)

butylphosphinoferrocene derivative, formed by the reaction of chlorophosphines with unreacted butyllithium. The preparation of (*S*)-(*R*)-**8** was achieved *via* transmetalation of (*S*)-*N*,*N*-dimethyl-1-[(*R*)-2-(trimethylstannyl)ferrocenyl]ethylamine (**7**) which had been once isolated as a precursor of lithioferrocene (*S*)-(*S*)-**2** (Eq. 6).[48]

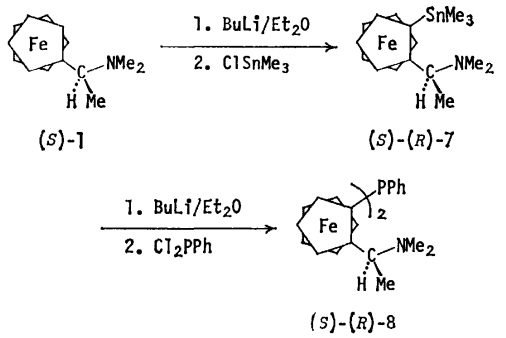

(6)

Modification of the Side Chain of Chiral Ferrocenylphosphines. Ferrocenylethane derivatives with a suitable leaving group such as trimethylammonium or acetate in the α-position have been reported[36,49] to undergo nucleophilic substitutions generally with complete retention of configuration.

Attempts to replace the dimethylamino group in (*S*)-(*R*)-PPFA (**3a**) by other dialkylamino groups by treating **3a** with methyl iodide and then with dialkylamines were not successful. The reaction of **3a** with methyl iodide formed preferentially the phosphonium salt rather than the desired ammonium salt. Protection of the diphenylphosphino group against the formation of phosphonium salt enabled the nucleophilic substitution to occur on the side chain. Thus, the preparation of several (*R*)-[(*S*)-1-(diaklylamino)-ethyl]ferrocenylphosphines (**11**) could be achieved first by converting (*S*)-(*R*)-**3a** into the phosphine oxide (**9**), then quaternization of the dimethylamino group, treatment with a dialkylamine and finally by reduction with lithium aluminum hydride or alane (Eq. 7). The diisopropylamino (**11a**), diisobutylamino (**11b**), 1-pyrrolidinyl (**11c**), piperidino (**11d**), 4-methyl-1-piperazinyl (**11e**), and morpholino (**11f**) derivatives were obtained in 30–60% overall yields. The phosphine oxide (*S*)-(*R*)-**9** could also be obtained by the reaction of lithioferrocene **2** with diphenylphosphinyl chloride in a similar way to the preparation of (*S*)-(*R*)-**3a**.

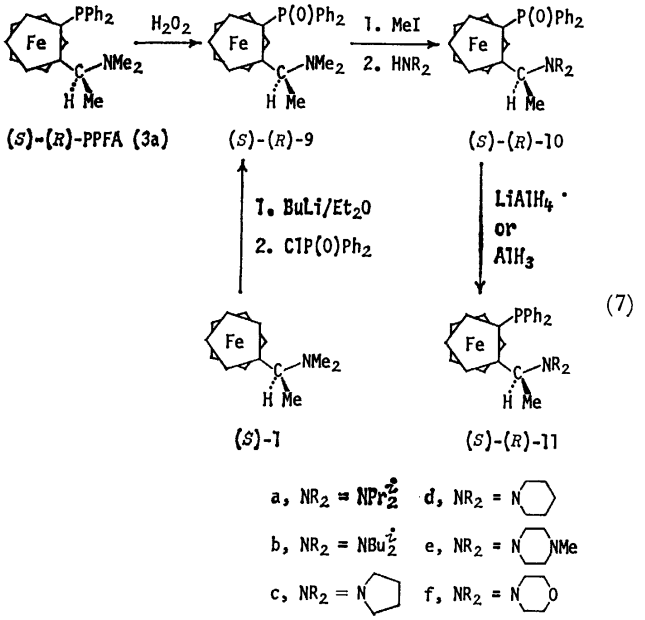

(7)

The dimethylamino group in (*S*)-(*R*)-PPFA (**3a**) was found to be substituted by other amino groups more conveniently by way of (*S*)-1-[(*R*)-2-(diphenylphosphino)ferrocenyl]ethyl acetate (**12**) (Eq. 8). (*S*)-(*R*)-PPFA (**3a**) was treated with an excess of acetic anhydride at 100 °C employing a modification of Nesmeyanov's procedure[50] to give the acetate (*S*)-(*R*)-**12** in the epimeric pure form in almost quantitative yield. The configuration *S* of the carbon central chirality of **12** was inferred from the result that the same substitution reaction on [1-(dimethylamino)-ethyl]ferrocene proceeded with nearly complete retention of configuration. (*S*)-(*R*)-**12** was then allowed to react with a dialkylamine in refluxing methanol to give (*S*)-(*R*)-**11f—k** in a high yield.

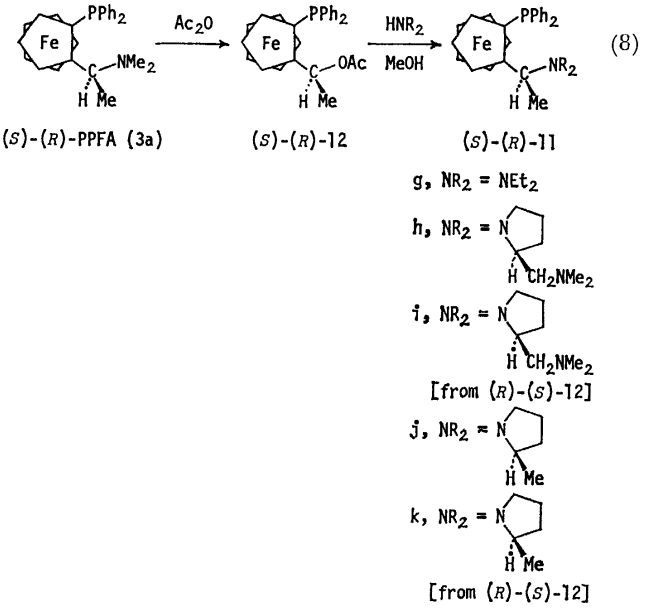

(8)

Replacement of the dimethylamino group in (*R*)-(*S*)-

BPPFA (**4a**) by other amino groups was also carried out *via* its acetate derivative (**13**) in a similar manner to the preparation of **11** (Eq. 9).

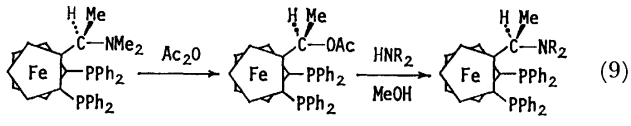

(9)

a, $NR_2 = NH_2$ f, $NR_2 = NMeCH_2CH{=}CH_2$
b, $NR_2 = NEt_2$ g, $NR_2 = NMeCH_2CH_2NMe_2$
c, NR_2 = N⬠ h, $NR_2 = NMeCH_2CH_2NHMe$
d, NR_2 = N⬡ i, $NR_2 = NMeCH_2CH_2OH$
e, NR_2 = N⬡NMe j, $NR_2 = N(CH_2CH_2OH)_2$

A methoxyl group also was introduced into the side chain of the chiral ferrocenylphosphines by treatment of the acetate (*R*)-(*S*)-**12** or (*R*)-(*S*)-**13** with refluxing methanol in the presence of 3-aminopropylated silica gel[51] (Eq. 10). (*R*)-(*S*)-**16** was also found to be formed by the reaction of (*R*)-(*S*)-**13** with sodium methoxide in methanol.

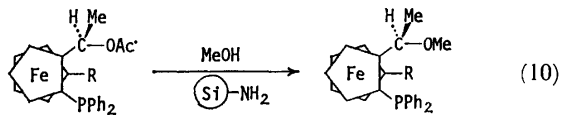

(10)

R = H, (*R*)-(*S*)-12 (*R*)-(*S*)-15
R = PPh_2, (*R*)-(*S*)-13 (*R*)-(*S*)-16

The acetate (*R*)-(*S*)-**13** was converted quantitatively into a ferrocenylphosphine with the hydroxyl group, (*R*)-1-[(*S*)-1′,2-bis(diphenylphosphino)ferrocenyl]ethanol (BPPFOH) (**18**) by treatment with an excess of butyllithium in ether followed by hydrolysis (Eq. 11). Direct acid or base hydrolysis of the acetate in the usual way gave only lower yields.

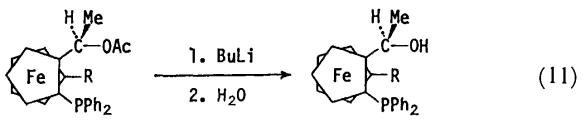

(11)

R = H, (*R*)-(*S*)-12 (*R*)-(*S*)-PPFOH (17)
R = PPh_2, (*R*)-(*S*)-13 (*R*)-(*S*)-BPPFOH (18)

The chiral ferrocenylphosphines mentioned above all contain both planar and central elements of chirality and also a functional group such as the amino, hydroxyl, or methoxyl. Ferrocenylphosphines, (*R*)-1-diphenylphosphino-2-ethylferrocene (PPEF) (**21**) and (*S*)-1′,2-bis(diphenylphosphino)-2-ethylferrocene (BPPEF) (**23**), having only a planar element of chirality, were prepared by a sequence of reactions as shown in Eqs. 12 and 13. (*S*)-(*R*)-**9** was subjected to Hofmann elimination to give a vinylferrocene (*R*)-**19**. Hydrogenation of (*R*)-**19** in the presence of chlorotris(triphenylphosphine)rhodium(I) to (*R*)-**20** followed by reduction with lithium aluminum hydride gave (*R*)-PPEF (**21**).

Treatment of (*R*)-(*S*)-**13** with potassium hydroxide in methanol gave elimination product (*S*)-**22** in 34% yield together with substitution product (*R*)-(*S*)-**18** (39%). (*S*)-**22** was then converted into (*S*)-BPPEF (**23**) by the rhodium catalyzed hydrogenation.

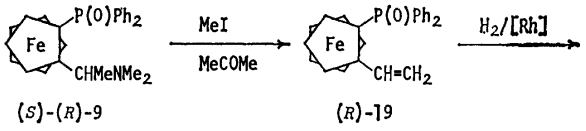

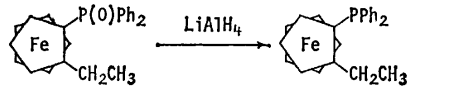

(12)

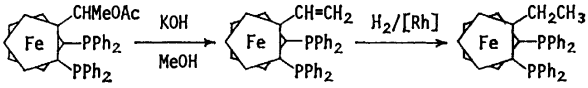

(13)

Finally, a new type of bisphosphine [(*R*)-1-[(*S*)-2-(diphenylphosphino)ferrocenyl]ethyl]diphenylphosphine (**24**) was prepared from (*R*)-(*S*)-**12** by substitution reaction with diphenylphosphine in methanol (Eq. 14).

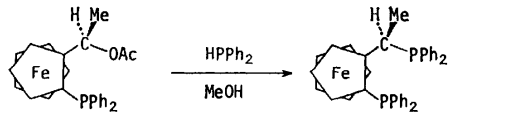

(14)

Preparation of Optically Active 1-Dimethylaminomethyl-2-(diphenylphosphino)ferrocene (FcPN). 1-Dimethylaminomethyl-2-(diphenylphosphino)ferrocene (FcPN)[52] (**25**), which is analogous to **3a** but lacks carbon central chirality, was optically resolved *via* its phosphine sulfide dibenzoyltartaric acid salt (Eq. 15). Attempted resolution of *dl*-**25** directly *via* its ammonium salts with optically active acids, such as tartaric acid, dibenzoyltartaric acid, or camphor-10-sulfonic acid, was not successful. Alkaline hydrolysis of one of the diastereoisomers, which were separated as crystals in the fractional recrystallization of the ammonium salts consisting of the *dl*-phosphine sulfide **26** and dibenzoyl-*d*-tartaric acid in methanol, gave (+)-isomer of **26**,

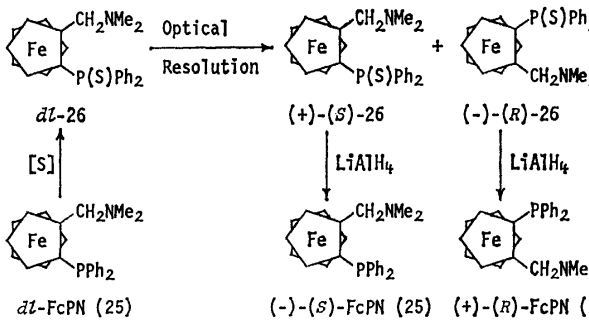

(15)

which was converted into (−)-**25** by reduction with lithium aluminum hydride in dioxane. The configuration of (−)-**25** was inferred to be *S* by comparison of its CD spectrum with that of other ferrocenylphosphines of definite configuration (*vide infra*). The phosphine sulfide **26** was converted into the hydroxy derivative **28** (Eq. 16), and the enantiomeric purity

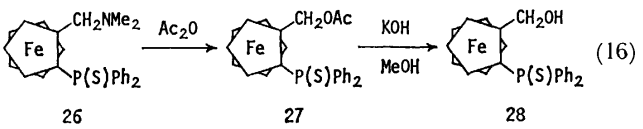

(16)

26 27 28

was determined by NMR spectroscopy using a chiral lanthanoid shift reagent,[53] tris(3-trifluoroacetyl-*d*-camphorato)europium(III) [Eu(facam)$_3$]. **26** of $[\alpha]_{545}^{25}$ ±50.5° (chloroform) turned out to be optically pure.

The bisphosphine (*S*)-**30** analogous to FcPN (**25**) was also prepared from the optically active **25** using the protecting method with the trimethylsilyl group (Eq. 17).

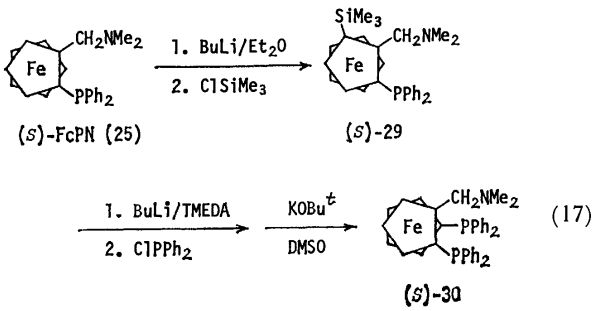

(17)

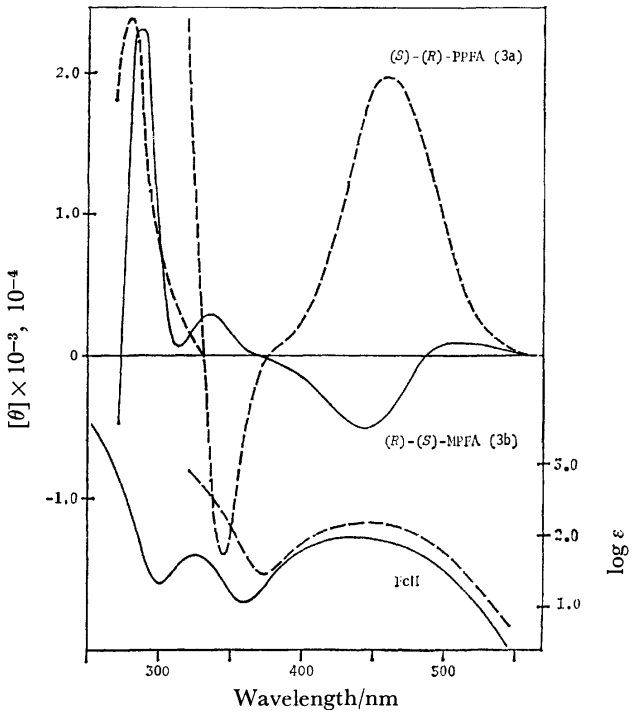

Fig. 1. CD and UV spectra of (*S*)-(*R*)-PPFA (**3a**) and (*R*)-(*S*)-MPFA (**3b**) in chloroform.

Physical Properties of Chiral Ferrocenylphosphines. Melting points, specific rotations, and analytical data for the chiral ferrocenylphosphines are summarized in Table 1. The absorption and CD spectra of PPFA (**3a**), MPFA (**3b**), BPPFA (**4a**), PPEF (**21**), and FcPN (**25**) are shown in Figs. 1, 2, and 3. The absorption spectrum of ferrocene has two long wavelength bands at 440 and 325 nm assignable to d-d type transition.[54] The CD spectra of chiral ferrocenylphosphines reveal optical activity arising from

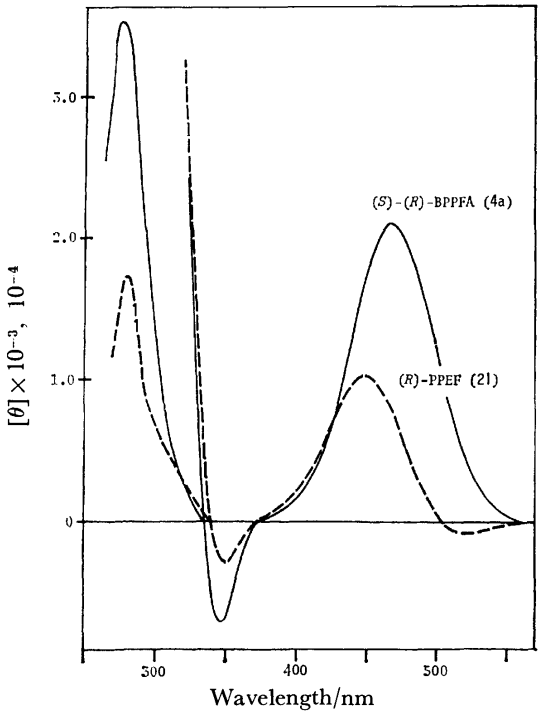

Fig. 2. CD spectra of (*S*)-(*R*)-BPPFA (**4a**) and (*R*)-PPEF (**21**) in chloroform.

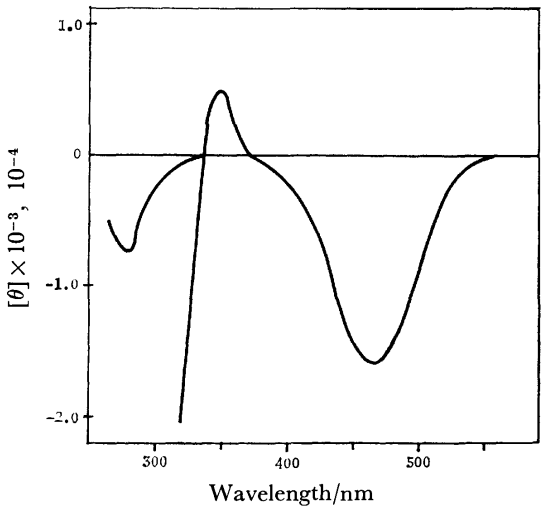

Fig. 3. CD spectrum of (*S*)-FcPN (**25**) in chloroform.

the planar chirality around these two absorption bands. The ferrocenylphosphines with planar chirality of *R* configuration, (*S*)-(*R*)-PPFA (**3a**), (*S*)-(*R*)-BPPFA (**4a**), and (*R*)-PPEF (**21**), all have positive Cotton effects around 450—470 and negative ones around 340—350 nm, whereas opposite Cotton effects are observed in the case of (*R*)-(*S*)-MPFA (**3b**) whose planar chirality is *S*. The negative and positive Cotton effects around 450—470 and 340—350 nm respectively observed in the CD spectrum of (—)-FcPN (**25**) shows that the absolute configuration of (—)-FcPN is *S*.

Conclusions. In conclusion we summarize some unique and significant features of the chiral ferrocenylphosphine ligands. (1) They all contain planar element of chirality due to 1,2-unsymmetrically substituted ferrocene structure, which must be highly asym-

metric enough to bring about high stereoselectivity in the catalytic asymmetric reactions. (2) Phosphines having either of the two configurations (*R* and *S*) of the carbon central chirality on the side chain of ferrocene and also those lacking this central chirality can be prepared: examples are (*S*)-(*R*)-**3a**, (*R*)-(*R*)-**3a**, and (*R*)-**25**. (3) Various kinds of functional groups such as an amino, alkoxyl, or hydroxyl can be introduced into the ferrocene side chain by nucleophilic substitution reactions, which proceed stereospecifically without any racemization or epimerization. (4) Both mono- and bisphosphines can be prepared from the same chiral source. They will coordinate with a transition metal as monodentate and bidentate ligands, respectively. The monophosphines with an amino group may possibly be a new type of chiral ligands that are capable of coordinating at both the phosphorus and nitrogen atoms.

The chiral ferrocenylphosphines have aforementioned advantages over other chiral phosphines, and they indeed gave rise to a high asymmetric induction in several transition metal complex catalyzed asymmetric reactions.[37-44] The high ability of the chiral ferrocenylphosphines is ascribed mainly to the attractive interactions between functional groups on a substrate and on the chiral ligand coordinated to a transition metal catalyst. The catalytic asymmetric reactions will be fully described elsewhere.

Experimental

All melting points are uncorrected. ^{1}H NMR spectra were recorded with a JEOL MH-100 or Varian EM-360 spectrometer, using tetramethylsilane as an internal standard in chloroform-*d*. The notations s, d, t, q, m, dd, and cm indicate singlet, doublet, triplet, quartet, multiplet, doublet of doublets, and complex multiplet, respectively. A letter b before these letters indicates broad. Infrared spectra were recorded with a Hitachi EPI-G3 grating spectrophotometer, UV spectra with a Hitachi EPS-3T spectrophotometer, and optical rotations were measured with a Yanagimoto OR-50 automatic polarimeter. ORD and CD spectra were obtained on a JASCO J-20 automatic recording spectropolarimeter. Wakogel (Silica gel) C-200 and Alumina Activated 200 (Nakarai) for column chromatography, and Alumina PF_{254} (Merck) and Silica gel 60 PF_{254} (Merck) for preparative TLC were used for the isolation and purification of the products.

dl-*N*,*N*-dimethyl-1-ferrocenylethylamine (**1**) was prepared by literature methods,[55,56] and optically resolved according to the reported procedure.[36]

Preparation of Chiral Ferrocenylphosphines. All manipulations for preparing phosphines were carried out in an oxygen-free dry nitrogen atmosphere. Melting points, optical rotations, and analytical data for the phosphines are summarized in Table 1.

*(S)-N,N-Dimethyl-1-[(R)-2-(diphenylphosphino)ferrocenyl]ethylamine [(S)-(R)-PPFA (**3a**)].* According to the procedure reported by Ugi *et al.*[36] for stereoselective lithiation of resolved *N*,*N*-dimethyl-1-ferrocenylethylamine (**1**), 12.4 ml of 1.4 M butyllithium in hexane was added to a solution of 3.60 g (14 mmol) of (*S*)-**1** ($[\alpha]_D^{24}$ −13.8° (*c* 1.5, ethanol)) in 20 ml of dry ether at 25—27 °C over a period of 20 min. The mixture was stirred at room temperature for 1.5 h and then 6.2 g (28 mmol) of chlorodiphenylphosphine in 10 ml of ether was added with heating under gentle reflux in the course of 45 min. After 4 h reflux aqueous sodium hydrogencarbonate was slowly added with cooling in an ice-bath. The resulting organic layer and benzene extracts from the aqueous layer were combined, washed with water, dried over anhydrous sodium sulfate, and concentrated *in vacuo* to afford a red oil. The oil was chromatographed on alumina (eluent: hexane/benzene, 3/1), and evaporated to give a crude product as orange crystals. The product was purified by recrystallization from ethanol to give 3.11 g (50% yield) of (*S*)-(*R*)-PPFA (**3a**), UV: λ_{max} ($CHCl_3$) 447 nm (ε 150), NMR: δ 1.19 (d, 3H, *J*=7 Hz, $CHC\underline{H}_3$), 1.77 (s, 6H, $NC\underline{H}_3$), 3.90 (s, 5H, $FeC_5\underline{H}_5$), 3.56—4.39 (m, 4H, $FeC_5\underline{H}_3C\underline{H}$), and 6.88—7.71 (cm 10H, $C_6\underline{H}_5$). The IR spectrum indicated the presence of the unsubstituted cyclopentadienyl ring (1105 and 1001 cm^{-1}) and phenyl groups (745 and 698 cm^{-1}). ORD (*c* 0.11 and 0.004, chloroform): $[\Phi]_{589}$ +1520°, $[\Phi]_{495}$ +3140° (pk), $[\Phi]_{434}$ +1590° (tr), and $[\Phi]_{294}$ +21900° (pk). The CD spectrum is shown in Fig. 1.

(*R*)-(*S*)-PPFA (**3a**) was prepared from (*R*)-**1** in a similar manner.

*(R)-N,N-Dimethyl-1-[(S)-2-(dimethylphosphino)ferrocenyl]ethylamine [(R)-(S)-MPFA (**3b**)].* At 27 °C, 3.14 g (12.2 mmol) of (*R*)-**1** ($[\alpha]_D^{24}$ +14.1° (*c* 1.6, ethanol)) was lithiated as described above. To the solution, 1.59 g (15.5 mmol) of chlorodimethylphosphine was added dropwise with stirring. A vigorous reaction occurred and the chlorodimethylphosphine was added at such a rate as to maintain boiling. The resulting mixture was heated under reflux for 3 h. Benzene/ether (1/1) (50 ml) and dilute sodium hydroxide solution (20 ml) were then added to the cooled reaction mixture. The organic layer was separated, dried over anhydrous sodium sulfate, and concentrated *in vacuo*. The residue was chromatographed on alumina (benzene) to give 1.10 g (31% yield) of (*R*)-(*S*)-MPFA (**3b**) as a red oil, UV: λ_{max} ($CHCl_3$) 446 nm (ε 131); NMR: δ 1.08 and 1.31 (a pair of d, 6H, *J*=2.6 Hz, $P(C\underline{H}_3)_2$), 1.34 (d, 3H, *J*=5.6 Hz, $CHC\underline{H}_3$), 2.14 (s, 6H, $NC\underline{H}_3$), 4.09 (s, 5H, $FeC_5\underline{H}_5$), 3.8—4.4 (cm, 3H, $FeC_5\underline{H}_3$). Methine proton resonances may lie under the cyclopentadienyl proton resonances. The IR spectrum indicated the presence of the unsubstituted cyclopentadienyl ring (1106 and 1000 cm^{-1}) and dimethylphosphino group (928 cm^{-1}). ORD (*c* 0.11 and 0.01, chloroform): $[\Phi]_{589}$ −425°, $[\Phi]_{473}$ −1120° (tr), $[\Phi]_{415}$ −615° (pk), $[\Phi]_{328}$ −1580° (tr), $[\Phi]_{304}$ −990° (pk), and $[\Phi]_{273}$ −8290° (tr). The CD spectrum is shown in Fig. 1.

*(S)-N,N-Dimethyl-1-[(R)-2-[bis(2-methylphenyl)phosphino]ferrocenyl]ethylamine [(S)-(R)-**3c**].* (*S*)-(*R*)-**3c** was prepared in a similar manner to that for the preparation of (*S*)-(*R*)-**3a** starting with (*S*)-**1** and with chlorobis(2-methylphenyl)phosphine;[57a] recrystallized from methanol, 30% yield; NMR: δ 1.35 (d, 3H, *J*=7.5 Hz, $CHC\underline{H}_3$), 1.82 (s, 6H, $NC\underline{H}_3$) 2.15 and 2.96 (a pair of s, 6H, $C_6H_4C\underline{H}_3$), 3.88 (s, 5H, $FeC_5\underline{H}_5$), 3.75—4.48 (m, 4H, $C_5\underline{H}_3C\underline{H}$), 6.9—7.3 (cm, 8H, $PC_6\underline{H}_4$).

*(R)-N,N-Dimethyl-1-[(S)-2-[bis(3-methylphenyl)phosphino]ferrocenyl]ethylamine [(R)-(S)-**3d**].* Prepared from (*R*)-**1** and chlorobis(3-methylphenyl)phosphine,[57b] 35% yield; NMR: δ 1.28 (d, 3H, *J*=7.5 Hz, $CHC\underline{H}_3$), 1.80 (s, 6H, $NC\underline{H}_3$), 2.25 and 2.40 (a pair of s, 6H, $C_6H_4C\underline{H}_3$), 3.96 (s, 5H, $FeC_5\underline{H}_5$), 3.84—4.42 (m, 4H, $FeC_5\underline{H}_3C\underline{H}$), 6.90—7.63 (cm, 8H, $PC_6\underline{H}_4$).

*(S)-N,N-Dimethyl-1-[(R)-2-[bis(3,5-dimethylphenyl)phosphino]ferrocenyl]ethylamine [(S)-(R)-**3e**].* Prepared from (*S*)-**1** and c lorobis(3,5-dimethylphenyl)phosphine (115—135 °C/0.015 mmHg, prepared by Yudina's method[57b]), 28% yield; NMR: δ 1.26 (d, 3H, *J*=7 Hz, $CHC\underline{H}_3$), 1.84 (s,

Table 1. Melting points, optical rotations, analytical data for chiral ferrocenylphosphines

Compound	Mp/°C	$[\alpha]_D^{25}$ (c, $CHCl_3$)	Found(Calcd) (%)		
			C	H	N
(*R*)-(*S*)-PPFA (**3a**)	139	−361° (0.6) [a]	70.74(70.76)	6.23(6.39)	2.95(3.17)
(*S*)-(*R*)-PPFA (**3a**)	139	+361° (0.6) [a]			
(*R*)-(*R*)-PPFA (**3a**)	oil	+364° (0.4)	70.46(70.76)	6.19(6.39)	3.05(3.17)
(*R*)-(*S*)-MPFA (**3b**)	oil	−134° (0.3)	60.61(60.59)	7.71(7.63)	4.51(4.42)
(*S*)-(*R*)-**3c**	123	+155° (0.4)	71.65(71.64)	6.81(6.87)	2.96(2.98)
(*R*)-(*S*)-**3d**	82.5—83	−349° (0.4)	71.58(71.64)	6.91(6.87)	3.03(2.98)
(*S*)-(*R*)-**3e**	oil	+280° (0.4)	72.67(72.44)	7.44(7.29)	2.91(2.82)
(*S*)-(*R*)-**3f**	111—112	+376° (0.4)	66.98(67.08)	6.39(6.43)	2.87(2.79)
(*S*)-(*R*)-BPPFA (**4a**)	139—140	+349° (0.5)	72.72(72.97)	6.00(5.96)	2.49(2.24)
(*R*)-(*S*)-BPPFA (**4a**)		−349° (0.5)			
(*R*)-(*R*)-BPPFA (**4a**)	oil	+335° (0.3)	72.68(72.97)	6.09(5.96)	2.32(2.24)
(*S*)-(*R*)-BMPFA (**4b**)	oil [b]	+14.8° (0.6)	57.47(57.31)	8.01(7.75)	3.62(3.71)
(*R*)-(*R*)-**6**	oil	+323° (0.5)			
(*S*)-(*R*)-**7**	oil	+5.95° (0.5)	48.75(48.62)	6.60(6.48)	3.32(3.34)
(*S*)-(*R*)-**8**	193.5—194	+477° (0.3)	65.83(65.83)	6.68(6.60)	4.54(4.52)
(*S*)-(*R*)-**9**	239—242 [c]	+161° (0.4)	68.54(68.28)	6.05(6.17)	2.92(3.06)
(*S*)-(*R*)-**10a**	175—178 [c]	+172° (0.4)	69.95(70.18)	6.93(7.07)	2.69(2.73)
(*S*)-(*R*)-**10b**	oil	+217° (0.4)	70.88(70.98)	7.46(7.45)	2.51(2.59)
(*S*)-(*R*)-**10c**	192—195 [c]	+140° (0.4)	69.28(69.58)	6.27(6.23)	2.60(2.90)
(*S*)-(*R*)-**10d**	200—210 [c]	+137° (0.4)	70.01(70.03)	6.61(6.48)	2.76(2.82)
(*S*)-(*R*)-**10e**	170	+192° (0.4)	68.05(67.98)	6.52(6.49)	5.36(5.47)
(*S*)-(*R*)-**10f**	217	+147° (0.4)	67.25(67.35)	5.90(6.06)	2.74(2.81)
(*S*)-(*R*)-**11a**	145.5—146	+359° (0.4)	72.16(72.43)	7.28(7.30)	2.78(2.82)
(*S*)-(*R*)-**11b**	oil	+389° (0.4)	72.79(73.14)	7.90(7.67)	2.50(2.67)
(*S*)-(*R*)-**11c**	102—103	+331° (0.3)	71.84(71.96)	6.67(6.47)	2.93(3.00)
(*S*)-(*R*)-**11d**	144—145	+331° (0.5)	72.32(72.36)	6.89(6.70)	2.97(2.91)
(*S*)-(*R*)-**11e**	101—102	+381° (0.4)	70.33(70.17)	6.72(6.70)	5·66(5.64)
(*S*)-(*R*)-**11f**	153	+343° (0.5)	69.86(69.58)	6.31(6.26)	3.07(2.90)
(*S*)-(*R*)-**11g**	124.5—125	+360° (0.4)	71.41(71.65)	6.80(6.87)	2.90(2.98)
(*S*)-(*R*)-**11h**	oil	+300° (0.4)	70.70(70.99)	7.25(7.11)	5.18(5.34)
(*R*)-(*S*)-**11i**	90—91	−275° (0.4)	70.98(70.99)	7.34(7.11)	5.23(5.34)
(*S*)-(*R*)-**11j**	128—129	+374° (0.5)	72.28(72.35)	6.91(6.70)	2.80(2.91)
(*S*)-(*R*)-**12**	117.5—118.5	+337° (0.9)	68.16(68.44)	5.68(5.96)	
(*R*)-(*S*)-**12**		−333° (0.4)			
(*R*)-(*S*)-**13**	153.5—155	−311° (0.5)	70.96(71.26)	5.05(5.35)	
(*R*)-(*S*)-**14a**	140—141	−302° (0.5)	72.35(72.37)	5.61(5.57)	2.30(2.34)
(*S*)-(*R*)-**14b**	190.5—191	+346° (0.4)	73.80(73.51)	6.38(6.32)	1.96(2.14)
(*S*)-(*R*)-**14c**	178	+344° (0.4)	73.54(73.74)	6.29(6.03)	2.06(2.15)
(*S*)-(*R*)-**14d**	150	+347° (0.4)	74.01(73.99)	6.19(6.21)	2.06(2.10)
(*S*)-(*R*)-**14e**	oil	+313° (0.2)	72.63(72.35)	6.33(6.22)	3.94(4.12)
(*R*)-(*S*)-**14f**	98—99	−327° (0.3)	73.73(73.74)	5.95(6.03)	2.06(2.15)
(*S*)-(*R*)-**14g**	oil	+313° (0.4)	71.83(72.14)	6.46(6.50)	3.77(4.10)
(*R*)-(*S*)-**14h**	137.5—138.5	−361° (0.4)	71.81(71.86)	6.25(6.33)	4.06(4.19)
(*R*)-(*S*)-**14i**	173—174.5	−368° (0.5)	71.47(71.46)	6.07(6.00)	1.98(2.14)
(*R*)-(*S*)-**14j**	163—164	−441° (0.5)	69.83(70.08)	6.12(6.03)	1.97(2.04)
(*R*)-(*S*)-**15**	120—121.5	−320° (0.2)	69.73(70.11)	5.84(5.88)	
(*R*)-(*S*)-**16**	164.5—165.5	−252° (0.7)	72.62(72.56)	5.55(5.60)	
(*R*)-(*S*)-PPFOH (**17**)	104.5—106	−271° (0.7)	69.32(69.58)	5.63(5.60)	
(*R*)-(*S*)-BPPFOH (**18**)	154—155	−285° (0.5)	72.31(72.25)	5.43(5.39)	
(*R*)-**20**	151.5—152	+118° (0.6)	69.75(69.58)	5.61(5.60)	
(*R*)-PPEF (**21**)	95.5	+273° (0.3)	72.36(72.38)	5.86(5.82)	
(*S*)-**22**	178.5—182	+83.3° (0.3)	74.37(74.50)	5.51(5.21)	
(*S*)-BPPEF (**23**)	166—167	−147° (0.3)	74.48(74.24)	5.58(5.54)	
(*R*)-(*S*)-**24**	oil	−330° (0.3)	74.53(74.24)	5.73(5.54)	
(*S*)-FcPN (**25**)	91.5	−325° (0.5)			
(*R*)-FcPN (**25**)	92	+324° (0.5)			
(*S*)-**26**	168—169.5	+50.2° (0.5) [d]	65.66(65.37)	5.94(5.70)	3.31(3.05)
(*R*)-**26**	169—171	−50.5° (0.5) [d]			
(*S*)-**27**	190—193 [c]		63.49(63.30)	4.87(4.89)	
(*S*)-**28**	192—194 [c]		63.51(13.90)	5.21(4.90)	
(*S*)-**29**	oil	−192° (0.4)			
(*S*)-**30**	135—136	−269° (0.3)	72.65(72.68)	5.74(5.77)	2.50(2.29)

a) Specific rotation in ethanol. b) Bp 157 °C/0.03 mmHg. c) Decomposition. d) $[\alpha]_{545}^{25}$ ($CHCl_3$).

6H, NC$\underline{H}_3$), 2.18 and 2.32 (a pair of s, 12H, $C_6H_3(C\underline{H}_3)_2$), 3.94 (s, 5H, $C_5\underline{H}_5$), 3.8—4.4 (m, 4H, $FeC_5\underline{H}_3C\underline{H}$), 6.7—7.3 (m, 6H, $PC_6\underline{H}_3$).

(S)-N,N-Dimethyl-1-[(R)-2-[bis(3-methoxyphenyl)phosphino]-ferrocenyl]ethylamine [*(S)-(R)-**3f***]. Prepared from (*S*)-**1** and chlorobis(3-methoxyphenyl)phosphine,[57b] 34% yield, recrystallized from hexane; NMR: δ 1.25 (d, 3H, J=7 Hz, C$H\underline{C}\underline{H}_3$), 1.78 (s, 6H, NC$\underline{H}_3$), 3.66 and 3.76 (a pair of s, 6H, OC$\underline{H}_3$), 3.95 (s, 5H, $FeC_5\underline{H}_5$), 3.8—4.4 (m, 4H, $FeC_5\underline{H}_3C\underline{H}$), 6.6—7.3 (cm, 8H, $PC_6\underline{H}_4$).

(S)-N,N-Dimethyl-1-[(R)-1',2-bis(diphenylphosphino)ferrocenyl]-ethylamine [*(S)-(R)-BPPFA (**4a**)*]. To a solution of 3.6 g (14 mmol) of (*S*)-**1** in 22 ml of dry ether, 12.0 ml of 1.4 M butyllithium in hexane was added at 27 °C over a period of 20 min. The mixture was stirred at room temperature for 1 h and then a mixture of 1.9 g (16 mmol) of freshly distilled TMEDA and 13.0 ml of 1.4 M butyllithium in hexane was added in 15 min. After 5 h stirring at room temperature, 9.3 g (42 mmol) of chlorodiphenylphosphine was added to the cooled reaction mixture. After standing overnight it was hydrolyzed with aqueous sodium hydrogencarbonate. The resulting organic layer and extracts (benzene 50 ml) from the aqueous layer were combined, dried over anhydrous sodium sulfate, and concentrated *in vacuo*. The residue was chromatographed on alumina (hexane/benzene 2/1) to give the crude product, which was recrystallized from ethanol to give 5.08 g (58% yield) of pure (*S*)-(*R*)-**4a**; UV: λ_{max} ($CHCl_3$) 443 nm (ε 194); NMR: δ 1.12 (d, 3H, J=7 Hz, C$H\underline{C}\underline{H}_3$), 1.75 (s, 6H, NC$\underline{H}_3$), 3.41—4.42 (m, 8H, $C_5\underline{H}_4FeC_5\underline{H}_3C\underline{H}$), 6.87—7.66 (cm, 20H, $PC_6\underline{H}_5$). The IR spectrum did not exhibit absorptions near 1100 and 1000 cm^{-1}, indicating the absence of the unsubstituted cyclopentadienyl ring. ORD (*c* 0.10 and 0.004, chloroform): $[\Phi]_{589}$ +2160°, $[\Phi]_{499}$ +3890° (pk), $[\Phi]_{446}$ +2680° (tr), and $[\Phi]_{299}$ +30,300° (pk). The CD spectrum is shown in Fig. 2.

(S)-N,N-Dimethyl-1-[(R)-1',2-bis(dimethylphosphino)ferrocenyl]-ethylamine [*(S)-(R)-BMPFA (**4b**)*]. (*S*)-**1** (14.0 g. 54.6 mmol) was lithiated first with 48 ml of 1.4 M butyllithium and then with 62 ml of 1.4 M butyllithium and 10.0 ml (66.8 mmol) of TMEDA as described in the preparation of (*S*)-(*R*)-BPPFA (**4a**). To the solution was added 16.0 ml (187 mmol) of chlorodimethylphosphine at 0 °C. After stirring at room temperature overnight, the reaction mixture was hydrolyzed with 100 ml of 2 M sodium hydroxide. The resulting solution was extracted with benzene (2 × 100 ml). Evaporation of the solvent gave a red oil, which was distilled to give 19.5 g of a mixture of (*S*)-(*R*)-MPFA (**3b**) and (*S*)-(*R*)-BMPFA (**4b**) (1:2 mixture, 120—157 °C/0.03 mmHg) and 2.5 g (12% isolated yield) of pure (*S*)-(*R*)-BMPFA (**4b**) (157 °C/0.03 mmHg); NMR: δ 1.00—1.43 (cm, 12H, PC$\underline{H}_3$), 1.50 (d, 3H, J=7 Hz, C$H\underline{C}\underline{H}_3$), 2.04 (s, 6H, NC$\underline{H}_3$), 3.58 (q, 1H, C$\underline{H}C\underline{H}_3$), 3.8—4.4 (cm, 7H, $C_5\underline{H}_4FeC_5\underline{H}_3$).

(R)-N,N-dimethyl-1-[(R)-2-(diphenylphosphino)ferrocenyl]ethylamine [*(R)-(R)-PPFA (**3a**)*]. To a solution of 1.47 g (4.47 mmol) of (*R*)-α-[(*S*)-2-trimethylsilylferrocenyl]ethyldimethylamine[36] [(*R*)-(*S*)-**5**] in 15 ml of dry ether was added 5.3 ml of 1.27 M butyllithium in hexane at room temperature. After stirring at 30 °C for 2 h, 2.0 g (9.0 mmol) of chlorodiphenylphosphine was added. The reaction mixture was refluxed for 2 h, and then hydrolyzed with 30% sodium hydroxide at 0 °C. The resulting mixture was extracted with benzene (2 × 50 ml). The benzene solution was washed with brine, dried over anhydrous sodium sulfate, and the solvent was removed under reduced pressure. The NMR spectrum of the residue indicated that about 50% of **5** was phosphinated. Preparative TLC (alumina, hexane/benzene 2/1) gave 0.65 g of recovered (*R*)-(*S*)-**5** (R_f 0.4) and 1.03 g (45% yield) of (*R*)-*N*,*N*-dimethyl-1-[2-trimethylsilyl-5-(diphenylphosphino)ferrocenyl]ethylamine (**6**) (R_f 0.6). NMR of (*R*)-**6**: δ 0.27 (s, 9H, SiC$\underline{H}_3$), 1.68 (s, 6H, NC$\underline{H}_3$), 1.83 (d, 3H, J=7 Hz, C$H\underline{C}\underline{H}_3$), 3.27 (q, 1H, C$\underline{H}C\underline{H}_3$), 3.92 (s. 6H, $C_5\underline{H}_5FeC_5\underline{H}$), 4.18 (d. 1H, J=3.2 Hz. $FeC_5\underline{H}$), 7.08—7.72 (m, 10H. $PC_6\underline{H}_5$).

A solution of 0.296 g (0.58 mmol) of (*R*)-**6** and 0.067 g (0.63 mmol) of potassium *t*-butoxide in 10 ml of dry dimethyl sulfoxide was warmed at 43 °C for 20 min. Benzene (20 ml) was added and the benzene solution was washed with brine, dried over anhydrous sodium sulfate. and evaporated. Column chromatography (alumina, ether) gave 0.111 g (44%) of crude (*R*)-(*R*)-**3a** containing 10% of epimerized ferrocenylphosphine, (*S*)-(*R*)-**3a**. The latter was removed as follows: The crude (*R*)-(*R*)-**3a** was dissolved in pentane. and the pentane was evaporated slowly until small amounts of crystals appeared. The crystals which consisted of *ca.* 1:1 mixture of (*S*)-(*R*)-**3a** and (*R*)-(*R*)-**3a** were removed by filtration, and the filtrate was evaporated to give almost pure (*R*)-(*R*)-**3a** (0.093 g, 37% yield) as a red oil; NMR: δ 1.35 (d, 3H, J=7.5 Hz, C$H\underline{C}\underline{H}_3$), 2.14 (s, 6H. NC$\underline{H}_3$), 3.60 (q, 1H, C$\underline{H}C\underline{H}_3$), 3.98 (s, 5H. $FeC_5\underline{H}_5$), 3.71, 4.24, 4.35 (m, 3H, $FeC_5\underline{H}_3$), 7.15—7.65 (cm, 10H, $PC_6\underline{H}_5$).

(R)-N,N-Dimethyl-1-[(R)-1',2-bis(diphenylphosphino)ferrocenyl]-ethylamine [*(R)-(R)-BPPFA (**4a**)*]. To a solution of 0.738 g (1.45 mmol) of (*R*)-**6** in 25 ml of dry ether was added dropwise with stirring 2.1 ml (13.5 mmol) of TMEDA and 11.5 ml (13.5 mmol) of 1.25 M butyllithium in hexane succesively at 0 °C. After stirring at room temperature, a solution of 2.9 ml (15 mmol) of chlorodiphenylphosphine in 10 ml of ether was added at 0 °C. The mixture was refluxed for 1 h, and then hydrolyzed with 30% sodium hydroxide (50 ml). The mixture was extracted with benzene. The organic phase was washed with water, dried over anhydrous sodium sulfate, and evaporated. The residue was chromatographed on alumina (benzene/ether 1/1). An orange band was collected. The NMR spectrum showed that *ca.* 20% of (*R*)-**6** was converted to the bisphosphine derivative. This mixture was used for the desilylation without further purification.

To the mixture thus obtained was added 0.15 g (1.35 mmol) of potassium *t*-butoxide and 10 ml of dry dimethyl sulfoxide. The mixture was warmed with stirring at 40 °C for 20 min. After usual work up. preparative TLC (silica gel, benzene/ether 1/1) gave (*R*)-(*R*)-PPFA (**3a**) (R_f 0.3) and 0.080 g (9% yield) of (*R*)-(*R*)-BPPFA (**4a**) (R_f 0.6). For (*R*)-(*R*)-**4a**, NMR: δ 1.35 (d, 3H, J=7 Hz, C$H\underline{C}\underline{H}_3$), 2.07 (s, 6H, NC$\underline{H}_3$), 3.32—4.48 (m, 8H, $C_5\underline{H}_4FeC_5\underline{H}_3C\underline{H}$), 7.00—7.55 (cm, 20H, $PC_6\underline{H}_5$).

(S)-N,N-Dimethyl-1-[(R)-2-(trimethylstannyl)ferrocenyl]ethylamine [*(S)-(R)-**7***]. (*S*)-**1** (5.0 g. 19.5 mmol) was lithiated as described above. To the solution was added a solution of 5.84 g (29.3 mmol) of trimethyltin chloride in 10 ml of dry ether over a period of 8 min. After refluxing for 2 h. the reaction mixture was hydrolyzed with aqueous sodium hydrogencarbonate at 0 °C. The organic layer was separated and extracted with dilute phosphoric acid. The aqueous solution was made alkaline with sodium carbonate and extracted with ether. The ether solution was washed with brine, dried over anhydrous magnesium sulfate, and evaporated under reduced pressure. The residue was chromatographed on alumina (benzene) to give 3.48 g (43% yield) of (*S*)-(*R*)-**7** as a red oil; NMR: δ 0.21 (s and d, 9H, J_{H-Sn}=37.7 Hz, SnC$\underline{H}_3$), 1.18 (d, 3H, J=6 Hz. C$H\underline{C}\underline{H}_3$). 1.99 (s, 6H, NC$\underline{H}_3$), 3.82 (q, 1H, C$\underline{H}C\underline{H}_3$), 4.00 (s, 5H,

$FeC_5\underline{H}_5$), 4.00 and 4.23 (m, 1H and 2H, $FeC_5\underline{H}_3$).

*Bis[(R)-2-[(S)-1-(dimethylamino)ethyl]ferrocenyl]phenylphosphine [(S)-(R)-**8**].* To a solution of 0.88 g (2.1 mmol) of (*S*)-(*R*)-**7** in 5 ml of dry ether was added 1.47 ml (2.2 mmol) of butyllithium in hexane (1.5 M) over a period of 10 min at 0 °C. After stirring at 0 °C for 30 min, 0.19 g (1.1 mmol) of dichlorophenylphosphine was slowly added (5 min). The reaction mixture was refluxed for 1 h and then hydrolyzed with aqueous sodium hydrogencarbonate at 0 °C. The resulting organic layer and ether extracts from the aqueous layer were combined and extracted with 10% phosphoric acid. The aqueous layer was made alkaline with sodium carbonate, and extracted with ether. The ether solution was washed with brine, dried over anhydrous sodium sulfate, evaporated under reduced pressure to give a red oil. The oil was chromatographed on alumina (benzene/ether 1/1) to give 0.157 g (21% yield) of (*S*)-(*R*)-**8**. A pure sample was obtained by recrystallization from pentane; NMR: δ 1.24 and 1.48 (a pair of d, 6H, J=6.3 Hz, $CHC\underline{H}_3$), 1.64 and 2.30 (a pair of s, 12H, $NC\underline{H}_3$), 3.57 and 3.96 (a pair of s, 10H, $FeC_5\underline{H}_5$), 3.9—4.6 (m, 8H, $FeC_5\underline{H}_3C\underline{H}$), 7.13—7.76 (m, 5H, $PC_6\underline{H}_5$).

*(S)-N,N-Dimethyl-1-[(R)-2-(diphenylphosphinyl)ferrocenyl]ethylamine [(S)-(R)-**9**].* (a) A solution of 8.8 g (37 mmol) of diphenylphosphinic chloride in 30 ml of ether was added in 15 min to the refluxing solution of 5.08 g (19.8 mmol) of (*S*)-**1** which had been lithiated as described in the preparation of (*S*)-(*R*)-**3a**. The mixture was refluxed for 9 h, and then hydrolyzed with aqueous sodium hydroxide. The resulting organic layer and benzene extracts from the aqueous layer were combined, dried over anhydrous sodium sulfate, and concentrated *in vacuo* to a minimum volume. The residue was chromatographed on alumina. Elution with benzene gave 2.5 g of starting amine (*S*)-**1**. Elution with benzene/ethyl acetate (1/1) gave the crude product. The product was purified by recrystallization from dichloromethane/light petroleum ether (1/4) to give 2.74 g (30% yield) of (*S*)-(*R*)-**9** which gave brown crystals; UV: λ_{max} ($CHCl_3$) 446 nm (ε 145); NMR: δ 1.12 (d, 3H, J=6 Hz, $CHC\underline{H}_3$), 1.61 (s, 6H, $NC\underline{H}_3$), 4.13 (s, 5H, $FeC_5\underline{H}_5$), 3.76—4.51 (m, 4H, $FeC_5\underline{H}_3C\underline{H}$), 7.13—8.02 (m, 10H, $PC_6\underline{H}_5$); IR (KBr): 1192 (P→O) and 1107, 1010 cm^{-1} (FeC_5H_5).

(b) To a solution of 3.29 g (7.44 mmol) of (*S*)-(*R*)-**3a** in 60 ml of acetone was added dropwise 3 ml of 30% hydrogen peroxide. After 30 min at room temperature, aqueous sodium thiosulfate was added to decompose an excess of the hydrogen peroxide. The reaction mixture was extracted with dichloromethane. The extract was washed with water, dried over anhydrous sodium sulfate, and then evaporated. Purification of the residue by short-column chromatography (alumina. ethyl acetate) gave 3.31 g (97% yield) of (*S*)-(*R*)-**9**.

*(S)-1-[(R)-2-(Diphenylphosphinyl)ferrocenyl]ethylamines [(S)-(R)-**10**].* The following procedure for the preparation of (*S*)-(*R*)-**10a** is typical. To a solution of 0.50 g (1.1 mmol) of (*S*)-(*R*)-**9** in 6 ml of acetonitrile was added 4 ml (64 mmol) of methyl iodide, and the mixture was stirred at room temperature for 1 h, then evaporated to *ca.* 2 ml. To the residue, 4 ml of acetonitrile and 4 ml (29 mmol) of diisopropylamine were added. The reaction mixture was kept stirring overnight, and the solvent was removed under reduced pressure. The product was extracted with dichloromethane, and the extract was washed with brine, dried over anhydrous magnesium sulfate, and evaporated. The residue was purified by column chromatography (alumina, ethyl acetate) to give 0.47 g (82% yield) of (*S*)-(*R*)-**10a**, which was recrystallized from ethanol; NMR: δ 0.60 and 0.94 (a pair of d, 12H, J=7 Hz, $N(CH(C\underline{H}_3)_2)_2$), 1.50 (d, 3H, J=7.5 Hz, C_5H_3-$CHC\underline{H}_3$), 3.05 (7, 2H, $NC\underline{H}$), 4.12 (s, 5H, $FeC_5\underline{H}_5$), 3.87—4.62 (m, 4H, $FeC_5\underline{H}_3C\underline{H}$), 7.20—7.92 (m, 10H, $PC_6\underline{H}_5$).

*(S)-(R)-**10b**.* Prepared from (*S*)-(*R*)-**9** and diisobutylamine in 60% yield; NMR: δ 0.50 and 0.67 (a pair of d, 12H, J=7 Hz, $N(CH_2CH(C\underline{H}_3)_2)_2$), 1.49 (d, 3H, J=7.5 Hz, $C_5H_3CHC\underline{H}_3$), 1.20—1.60 (m, 2H, $N(CH_2C\underline{H}$-$Me_2)_2$), 1.85—2.16 (m, 4H, $NC\underline{H}_2$), 4.02 (s, 5H, $FeC_5\underline{H}_5$), 4.00—4.59 (m, 4H, $FeC_5\underline{H}_3C\underline{H}$), 7.20—7.92 (cm, 10H, $PC_6\underline{H}_5$).

*(S)-(R)-**10c**.* Prepared from (*S*)-(*R*)-**9** and pyrrolidine in 55% yield, and recrystallized from hexane; NMR: δ 0.96—1.15 and 1.96—2.41 (bm, 4H and 4H, 1-pyrrolidinyl), 1.32 (d, 3H, J=7.5 Hz, $C\underline{H}_3$), 4.18 (s, 5H, $FeC_5\underline{H}_5$), 3.88—4.56 (m, 4H, $FeC_5\underline{H}_3C\underline{H}$), 7.25—7.93 (m, 10H, $PC_6\underline{H}_5$).

*(S)-(R)-**10d**.* Prepared from (*S*)-(*R*)-**9** and piperidine in 86% yield; NMR: δ 0.65—1.18 and 2.20 (b and deformed t, 6H and 4H, respectively, piperidino), 1.22 (d, 3H, J=7 Hz, $C\underline{H}_3$), 4.12 (s, 5H, $FeC_5\underline{H}_5$), 3.90—4.48 (m, 4H, $FeC_5\underline{H}_3C\underline{H}$), 7.12—7.93 (cm, 10H, $PC_6\underline{H}_5$).

*(S)-(R)-**10e**.* Prepared from (*S*)-(*R*)-**9** and *N*-methylpiperazine in 81% yield; NMR: δ 1.24 (d, 3H, J=7 Hz, $CHC\underline{H}_3$), 1.45—1.80 (bm, 4H, $MeNC\underline{H}_2$), 1.89 (s, 3H, $NC\underline{H}_3$), 2.24—2.44 (m, 4H, $CHNC\underline{H}_2$), 4.12 (s, 5H, $FeC_5\underline{H}_5$), 3.93—4.58 (m, 4H, $FeC_5\underline{H}_3C\underline{H}$), 7.30—7.89 (m, 10H, $PC_6\underline{H}_5$).

*(S)-(R)-**10f**.* Prepared from (*S*)-(*R*)-**9** and morpholine in 92% yield; NMR: δ 1.25 (d, 3H, J=7 Hz, $C\underline{H}_3$), 2.12—2.48 (m, 4H, $NC\underline{H}_2$), 2.68—3.04 (m, 4H, $OC\underline{H}_2$), 4.13 (s, 5H, $FeC_5\underline{H}_5$), 3.93—4.60 (m, 4H, $FeC_5\underline{H}_3C\underline{H}$), 7.25—7.92 (m, 10H, $PC_6\underline{H}_5$).

*(S)-1-[(R)-2-(Diphenylphosphino)ferrocenyl]ethyl Acetate [(S)-(R)-**12**].* In a degassed sealed glass tube, a mixture of 701 mg (1.59 mmol) of (*S*)-(*R*)-PPFA (**3a**) and 1.0 ml of acetic anhydride was heated at 100 °C for 2 h. It was then cooled in a refrigerator overnight and orange crystals formed were collected on a glass filter, washed with cold methanol, and dried *in vacuo* to give 646 mg (89% yield) of (*S*)-(*R*)-**12**; NMR: δ 1.20 (s, 3H, $COC\underline{H}_3$), 1.64 (d, 3H, J=7 Hz, $CHC\underline{H}_3$), 4.04 (s, 5H, $FeC_5\underline{H}_5$), 3.80, 4.35, 4.56 (bm, 3H, $FeC_5\underline{H}_3$), 6.18 (dq, 1H, J_{H-P}=3 Hz, $C\underline{H}CH_3$), 7.05—7.65 (m, 10H, $PC_6\underline{H}_5$).

(*R*)-(*S*)-**12** was also prepared starting with (*R*)-(*S*)-**3a** in a similar manner.

*(S)-1-[(R)-2-(Diphenylphosphino)ferrocenyl]ethylamines [(S)-(R)-**11**].*

*(S)-(R)-**11a**.* To a solution of 0.175 g (4.6 mmol) of lithium aluminum hydride in 15 ml of dry dibutyl ether and 10 ml of dry benzene, was added with stirring 0.121 g (0.236 mmol) of (*S*)-(*R*)-**10a**. The mixture was kept at 75 °C for 6 h, and then hydrolyzed by successive addition of water and 10% aqueous sodium hydroxide. The product was extracted with benzene, and the benzene solution was washed with brine and water, dried over anhydrous sodium sulfate, and evaporated to give a red oil. It was chromatographed (alumina, benzene) to give 83 mg (71% yield) of (*S*)-(*R*)-**11a**, which was purified by recrystallization from ethanol; NMR: δ 0.74 and 1.01 (a pair of d, 12H, J=7 Hz, $CH(C\underline{H}_3)_2$), 1.59 (d, 3H, J=7.5 Hz, $C_5H_5CHC\underline{H}_3$), 3.10 (7, 2H, $C\underline{H}Me_2$), 3.87 (s, 5H, $FeC_5\underline{H}_5$), 4.00—4.55 (m, 4H, $FeC_5\underline{H}_3C\underline{H}$), 7.08—7.68 (m, 10H, $PC_6\underline{H}_5$).

(*S*)-(*R*)-**11b**, **11c**, **11d**, and **11f** were prepared in a similar manner to that for the preparation of (*S*)-(*R*)-**11a**, starting with (*S*)-(*R*)-**10b**, **10c**, **10d**, and **10f**, respectively.

*(S)-(R)-**11b**:* 66% yield; NMR: δ 0.55 and 0.73 (a pair of d, 12H, J=7 Hz, $CH(C\underline{H}_3)_2$), 1.50 (d, 3H, J=7.5 Hz, $C_5H_3CHC\underline{H}_3$), 1.26—1.66 (m, 2H, $CH_2C\underline{H}(CH_3)_2$), 1.92 (d, 4H, $C\underline{H}_2CH(CH_3)_2$), 3.77 (s, 5H, $FeC_5\underline{H}_5$), 4.03—

4.40 (m, 4H, $FeC_5\underline{H}_3C\underline{H}$), 7.03—7.70 (m, 10H, $PC_6\underline{H}_5$).

*(S)-(R)-**11c***: 87% yield; NMR: δ 1.04—1.25 and 2.03—2.43 (m and m, 4H and 4H, respectively, 1-pyrrolidinyl), 1.40 (d, 3H, J=7.5 Hz, $C\underline{H}_3$), 3.90 (s, 5H, $FeC_5\underline{H}_5$), 3.82—4.42 (m, 4H, $FeC_5\underline{H}_3C\underline{H}$), 7.11—7.66 (m, 10H, $PC_6\underline{H}_5$).

*(S)-(R)-**11d***: 69% yield; NMR: δ 0.6—1.2 and 2.24 (bm and deformed t, 6H and 4H, respectively, piperidino), 1.27 (d, 3H, J=7 Hz, $C\underline{H}_3$), 3.89 (s, 5H, $FeC_5\underline{H}_5$), 3.85—4.41 (m, 4H, $FeC_5\underline{H}_3C\underline{H}$), 7.1—7.7 (m, 10H, $PC_6\underline{H}_5$).

*(S)-(R)-**11f***: 29% yield; NMR: δ 1.30 (d, 3H, J= 7 Hz, $C\underline{H}_3$), 2.10—2.46 (m, 4H, $NC\underline{H}_2$), 2.67—3.13 (m, 4H, $OC\underline{H}_2$), 3.92 (s, 5H, $FeC_5\underline{H}_5$), 3.86—4.42 (m, 4H, $FeC_5\underline{H}_3C\underline{H}$), 7.14—7.66 (m, 10H, $PC_6\underline{H}_5$).

*(S)-(R)-**11f*** was also prepared from *(S)-(R)-**12*** (*vide infra*).

*(S)-(R)-**11e***. To a solution of 0.57 g (1.11 mmol) of *(S)-(R)-**10e*** in 5 ml of benzene and 10 ml of dibutyl ether, a large excess of aluminum hydride, prepared from lithium aluminum hydride and aluminum chloride in ether, was added. The mixture was refluxed for 4 h, and then hydrolyzed with 20% aqueous sodium hydroxide at 0 °C. The organic layer was separated and the water layer was extracted with ether. The combined organic layer was washed with brine, dried over anhydrous sodium sulfate, and evaporated. The residue was purified by column chromatography (alumina, ether) to give 0.31 g (57% yield) of *(S)-(R)-**11e***; NMR: δ 1.25 (d, 3H, J=7 Hz, $CHC\underline{H}_3$), 1.4—1.9 (bm, 4H, $CH_3NC\underline{H}_2$), 1.88 (s, 3H, $NC\underline{H}_3$), 2.18—2.50 (m, 4H, $CHNC\underline{H}_2$), 3.90 (s, 5H, $FeC_5\underline{H}_5$), 3.84—4.42 (m, 4H, $FeC_5\underline{H}_3C\underline{H}$), 7.12—7.71 (m, 10H, $PC_6\underline{H}_5$).

*(S)-(R)-**11f***. A solution of 60 mg (0.13 mmol) of *(S)-(R)-**12*** and 0.6 ml of morpholine in 2.0 ml of methanol was refluxed for 5 h. Then the solvent was removed under reduced pressure, and 5 ml of benzene was added. The solution was washed with brine, dried over anhydrous sodium sulfate, and evaporated. The resulting red oil was column chromatographed (alumina, ether) to give 61.5 mg (98% yield) of *(S)-(R)-**11f***.

*(S)-(R)-**11g***. Prepared from *(S)-(R)-**12*** and diethylamine in 95% yield, recrystallized from dichloromethane/methanol; NMR: δ 0.65 (t, 6H, J=7 Hz, $NCH_2C\underline{H}_3$), 1.30 (d, 3H, J=7 Hz, $CHC\underline{H}_3$), 2.07—2.48 (cm, 4H, $NC\underline{H}_2$), 3.92 (s, 5H, $FeC_5\underline{H}_5$), 3.85—3.93, 4.19—4.52 (m, 4H, $FeC_5\underline{H}_3C\underline{H}$), 7.10—7.73 (m, 10H, $PC_6\underline{H}_5$).

*(S)-(R)-**11h***. Prepared from *(S)-(R)-**12*** and *(S)*-2-(dimethylaminomethyl)pyrrolidine[58] in 70% yield; NMR: δ 1.26 (m, 4H, $CH_2C\underline{H}_2C\underline{H}_2CH$), 1.49 (d, 3H, J=7 Hz, $CHC\underline{H}_3$), 1.6—1.7 (m, 2H, $C\underline{H}_2NMe_2$), 2.06 (s, 6H, $NC\underline{H}_3$), 2.2—2.9 (m, 3H, $C\underline{H}_2NC\underline{H}$), 3.91 (s, 5H, $FeC_5\underline{H}_5$), 3.96—4.45 (m, 4H, $FeC_5\underline{H}_3C\underline{H}$), 7.10—7.75 (m, 10H, $PC_6\underline{H}_5$).

*(R)-(S)-**11i***. Prepared from *(R)-(S)-**12*** and *(S)*-2-(dimethylaminomethyl)pyrrolidine[58] in 88% yield, recrystallized from ethanol; NMR: δ 1.30 (d, 3H, J=7 Hz, $CHC\underline{H}_3$), 2.18 (s, 6H, $NC\underline{H}_3$), 0.5—2.9 (m, 9H), 3.96 (s, 5H, $FeC_5\underline{H}_5$), 3.75, 4.22, 4.37 (m, 3H, $FeC_5\underline{H}_3$), 4.50 (m, 1H, $FeC_5H_3C\underline{H}$), 7.10—7.70 (m, 10H, $PC_6\underline{H}_5$).

*(S)-(R)-**11j***. Prepared from *(S)-(R)-**12*** and *(R)*-2-methylpyrrolidine[59] (contaminated with 30% of piperidine), purified by preparative TLC (alumina, benzene R_f 0.5), 36% yield, recrystallized from ethanol; NMR: δ 0.17 (d, 3H, J=6 Hz, $CH_2CHC\underline{H}_3$), 1.1—1.4 (m, 4H, $CH_2C\underline{H}_2C\underline{H}_2CH$), 1.55 (d, 3H, J=7 Hz, $C_5H_3CHC\underline{H}_3$), 2.1—2.7 (m, 2H, $NC\underline{H}_2$), 2.70—2.95 (m, 1H, $NC\underline{H}CH_2$), 3.88 (s, 5H, $FeC_5\underline{H}_5$), 4.00, 4.2—4.5 (m, 4H, $FeC_5\underline{H}_3C\underline{H}$), 7.1—7.7 (m, 10H, $PC_6\underline{H}_5$).

*(R)-(S)-**11k***. Prepared from *(R)-(S)-**12*** and *(R)*-2-methylpyrrolidine[59] (contaminated with 30% of piperidine) in 50% yield. The *(R)-(S)-**11k*** contained 25% of *(R)-(S)-**11d***, which could not be removed. NMR: δ 0.98 (d, 3H, J=6 Hz, $CH_2CHC\underline{H}_3$), 1.24 (d, 3H, J=7 Hz, $C_5H_3CHC\underline{H}_3$), 0.4—1.6 (m, 4H, $CH_2C\underline{H}_2C\underline{H}_2CH$), 1.9—2.3 (m, 2H, $NC\underline{H}_2$), 2.49 (6, 1H, $NC\underline{H}CH_2$), 3.96 (s, 5H, $FeC_5\underline{H}_5$). 3.75, 4.20, 4.35 (m, 3H, $FeC_5\underline{H}_3$), 4.49 (double q, 1H, J_{H-P}= 3 Hz, $C_5H_3C\underline{H}$), 7.05—7.65 (m, 10H, $PC_6\underline{H}_5$).

(R)-1-[(S)-1',2-Bis(diphenylphosphino)ferrocenyl]ethyl acetate [*(R)-(S)-**13***]. A mixture of 0.626 g (1.0 mmol) of *(R)-(S)*-BPPFA (**4a**) and 3 ml of acetic anhydride was heated at 100 °C for 1 h in a degassed sealed glass tube. After cooling the reaction mixture to room temperature, orange crystals formed were collected on a glass filter. and dried *in vacuo*. The crystals (0.576 g, 90% yield) were pure *(R)-(S)-**13***; NMR: δ 1.16 (s, 3H, $COC\underline{H}_3$), 1.49 (d, 3H. J= 6.5 Hz, $CHC\underline{H}_3$), 3.60—4.56 (m, 7H, $C_5\underline{H}_4FeC_5\underline{H}_3$), 6.12 (double q, J=6.4 Hz and 2.4 Hz, 1H, $C\underline{H}CH_3$), 7.00—7.56 (m, 20H, $PC_6\underline{H}_5$). IR (KBr): 1734, 1372, and 1240 cm^{-1} (CH_3COO).

(R)-1-[(S)-1',2-Bis(diphenylphosphino)ferrocenyl]ethylamine [*(R)-(S)-**14a***]. A mixture of 0.71 g (1.11 mmol) of *(R)-(S)-**13*** in 5 ml of saturated ammonia–methanol was heated at 100 °C for 7 h in a microautoclave. Benzene (20 ml) was added, and the solution was washed with dilute aqueous sodium hydroxide, dried over anhydrous sodium sulfate, and evaporated. The residue was chromatographed on alumina (ether/ethyl acetate 2/1) to give 0.57 g (86% yield) of *(R)-(S)-**14a***, which was recrystallized from hexane/dichloromethane; NMR: δ 1.30 (d, J=7 Hz, $C\underline{H}_3$), 1.27—1.41 (bs, 2H, $N\underline{H}_2$), 3.63, 4.10, 4.39 (m, 8H, $C_5\underline{H}_4FeC_5\underline{H}_3C\underline{H}$), 7.14—7.63 (m, 20H, $PC_6\underline{H}_5$).

*(S)-(R)-**14b***—**e** and *(R)-(S)-**14f***—**j** were prepared by the reaction of **13** with the corresponding dialkylamine in methanol. The following procedure for the preparation of *(S)-(R)-**14c*** is typical.

*(S)-(R)-**14c***. A solution of 0.450 g (0.70 mmol) of *(S)-(R)-**13*** and 4 ml of pyrrolidine in 15 ml of methanol was refluxed for 8 h. The solvent was removed under reduced pressure, and benzene was added. The solution was washed with brine, dried over anhydrous sodium sulfate, and evaporated. The residue was purified by column chromatography (alumina, ether) to give 0.368 g (81% yield) of *(S)-(R)-**14c***, which was recrystallized from ethanol; NMR: δ 0.86—1.24 and 1.98—2.44 (bm, 4H and 4H, pyrrolidino), 1.26 (d, 3H, J=7 Hz, $C\underline{H}_3$), 3.46—4.46 (m, 8H, $C_5\underline{H}_4FeC_5\underline{H}_3C\underline{H}$), 7.03—7.61 (m, 20H, $PC_6\underline{H}_5$).

*(S)-(R)-**14b***. Prepared from *(S)-(R)-**13*** and diethylamine in 62% yield, recrystallized from benzene/hexane; NMR: δ 0.63 (t, 6H, J=7.5 Hz, $NCH_2C\underline{H}_3$), 1.20 (d, 3H, J=7.5 Hz, $CHC\underline{H}_3$), 2.22 (m, 4H, $NC\underline{H}_2$), 3.40—4.60 (m, 8H, $C_5\underline{H}_4FeC_5\underline{H}_3C\underline{H}$), 7.00—7.70 (m, 20H, $PC_6\underline{H}_5$).

*(S)-(R)-**14d***. Prepared from *(S)-(R)-**13*** and piperidine in 88% yield, recrystallized from benzene/hexane; NMR: δ 0.66—1.20 and 2.03—2.40 (bm, 6H and 4H, respectively, piperidino), 1.19 (d, 3H, J=7.5 Hz, $C\underline{H}_3$), 3.40—4.40 (m, 8H, $C_5\underline{H}_4FeC_5\underline{H}_3C\underline{H}$), 6.98—7.60 (m, 20H, $PC_6\underline{H}_5$).

*(S)-(R)-**14e***. Prepared from *(S)-(R)-**13*** and *N*-methylpiperazine in 62% yield; NMR: δ 1.12 (d, 3H, J=7.5 Hz, $CHC\underline{H}_3$), 1.23—1.90 (bs, 4H, $C\underline{H}_2NMeC\underline{H}_2$), 1.78 (s, 3H, $NC\underline{H}_3$), 2.02—2.46 (bs, 4H, $C\underline{H}_2N(CH)C\underline{H}_2$), 3.36—4.38 (m, 8H, $C_5\underline{H}_4FeC_5\underline{H}_3C\underline{H}$), 6.95—7.50 (m, 20H, $PC_6\underline{H}_5$).

*(R)-(S)-**14f***. Prepared from *(R)-(S)-**13*** and *N*-methylallylamine, recrystallized from hexane, 81% yield; NMR: δ 1.15 (d, 3H, J=7.5 Hz, $CHC\underline{H}_3$), 1.66 (s, 3H, $NC\underline{H}_3$), 2.60—3.05 (m, 2H, $NC\underline{H}_2$), 3.52, 3.67, 3.97, 4.08, and 4.36 (m, 1H, 1H, 1H, 2H, and 2H, $C_5\underline{H}_4FeC_5\underline{H}_3$), 4.23 (m, 1H, $C\underline{H}CH_3$), 4.62—5.15 (m, 3H, $C\underline{H}$ $C\underline{H}_2$),

7.07—7.37 (m, 20H, $PC_6\underline{H}_5$).

*(R)-(S)-**14g***. Prepared from (*R*)-(*S*)-**13** and *N,N,N'*-trimethylethylenediamine in 74% yield; NMR: δ 1.07 (3H, J=7 Hz, $CHC\underline{H}_3$), 1.60 (s, 3H, $CHNC\underline{H}_3$), 1.45—1.70 and 2.07—2.41 (m, 4H, $NC\underline{H}_2C\underline{H}_2N$), 1.90 (s, 6H, $N(C\underline{H}_3)_2$), 3.37—4.30 (m, 8H, $C_5\underline{H}_4FeC_5\underline{H}_3C\underline{H}$), 6.80—7.50 (m, 20H, $PC_6\underline{H}_5$).

*(R)-(S)-**14h***. Prepared from (*R*)-(*S*)-**13** and *N,N'*-dimethylethylenediamine, recrystallized from hexane, 91% yield; NMR: δ 1.18 (d, 3H, J=7.5 Hz, $CHC\underline{H}_3$), 1.68 and 1.96 (s and s, 3H and 3H, $NC\underline{H}_3$), 2.12—2.86 (m, 5H, $NC\underline{H}_2C\underline{H}_2N\underline{H}$), 3.75, 3.86, 4.09, 4.34, and 4.42 (m, 1H, 1H, 1H, 2H, and 2H, respectively, $C_5\underline{H}_4FeC_5\underline{H}_3$), 4.22 (m, 1H, $C\underline{H}CH_3$), 7.10—7.40 (m, 20H, $PC_6\underline{H}_5$).

*(R)-(S)-**14i***. Prepared from (*R*)-(*S*)-**13** and 2-(methylamino)ethanol, recrystallized from ethanol, 88% yield; NMR: δ 1.18 (d, 3H, J=7.5 Hz, $CHC\underline{H}_3$), 1.62 (s, 3H, $NC\underline{H}_3$), 2.18—2.74 (m, 3H, $NC\underline{H}_2$ and $O\underline{H}$), 3.06—3.40 (m, 2H, $OC\underline{H}_2$), 3.47, 3.76, 3.90, 4.02—4.19, 4.34, and 4.43 (m, 1H, 1H, 1H, 2H, 1H, and 1H, respectively, $C_5\underline{H}_4FeC_5\underline{H}_3$), 4.26 (m, 1H, $C\underline{H}CH_3$), 7.10—7.38 (m, 20H, $PC_6\underline{H}_5$).

*(R)-(S)-**14j***. Prepared from (*R*)-(*S*)-**13** and di(2-hydroxyethyl)amine in 82% yield, recrystallized from hexane/methanol; NMR: δ 1.33 (d, 3H, J=7.5 Hz, $C\underline{H}_3$), 2.47 (t, 4H, J=5.5 Hz, $NC\underline{H}_2$), 3.16—3.38 (m, 4H, $OC\underline{H}_2$), 3.43, 3.71, 4.02, 4.05, and 4.18—5.03 (m, 1H, 1H, 1H, 1H, and 4H, $C_5\underline{H}_4FeC_5\underline{H}_3C\underline{H}$), 7.10—7.40 (m, 20H, $PC_6\underline{H}_5$).

(R)-1-[(S)-2-(Diphenylphosphino)ferrocenyl]ethyl methyl ether [*(R)-(S)-**15***]. A mixture of 92 mg (0.20 mmol) of (*R*)-(*S*)-**12** and 1.60 g of 3-aminopropylated silica gel[51] (0.236 meq/g nitrogen) in 10 ml of dry methanol was refluxed for 10 h. Methanol was evaporated, and 10 ml of ether was added. The silica gel was removed by short alumina column. Evaporation of the solvent gave crude (*R*)-(*S*)-**15**, which was recrystallized from methanol, 58% yield; NMR: δ 1.57 (d, 3H, J=7 Hz, $CHC\underline{H}_3$), 2.90 (s, 3H, $OC\underline{H}_3$), 3.98 (s, 5H, $FeC_5\underline{H}_5$), 3.83, 4.29, and 4.50 (bm, 3H, $FeC_5\underline{H}_3$), 4.45—4.75 (m, 1H, $C\underline{H}CH_3$), 7.1—7.7 (m, 10H, $PC_6\underline{H}_5$).

(R)-1-[(S)-1',2-Bis(diphenylphosphino)ferrocenyl]ethyl methyl ether [*(R)-(S)-**16***]. (a) A mixture of 72 mg (0.112 mmol) of (*R*)-(*S*)-**13** and 95 mg of 3-aminopropylated silica gel[51] (0.236 meq/g nitrogen), prepared from (3-aminopropyl)-triethoxysilane and activated silica gel, in 5 ml of methanol was refluxed for 29 h. The silica gel was filtered off. The filtrate was evaporated to give a quantitative yield of crude (*R*)-(*S*)-**16**, which was recrystallized from ethanol, 58 mg (85% yield).

(b) A solution of 81 mg (0.126 mmol) of (*R*)-(*S*)-**13** and 6.9 mg (0.128 mmol) of sodium methoxide in 10 ml of methanol was refluxed for 3 h, and then evaporated. The residue was passed through a short alumina column (ether/benzene) to give 67 mg (87% yield) of (*R*)-(*S*)-**16**; NMR: δ 1.45 (d, 3H, J=7.5 Hz, $CHC\underline{H}_3$), 2.88 (s, 3H, $OC\underline{H}_3$), 3.65, 3.95—4.20, 4.38, and 4.45 (m, 2H, 3H, 1H, and 1H, respectively, $C_5\underline{H}_3FeC_5\underline{H}_4$), 4.55 (m, 1H, $C\underline{H}CH_3$), 7.10—7.38 (m, 20H, $PC_6\underline{H}_5$).

(R)-1-[(S)-2-(Diphenylphosphino)ferrocenyl]ethanol [*(R)-(S)-**PPFOH (17)***]. To a solution of 60 mg (0.13 mmol) of (*R*)-(*S*)-**12** in 5 ml of dry ether was added 1.0 ml (1.25 mmol) of 1.25 M butyllithium in hexane. The mixture was kept stirring at room temperature for 1 h, and then hydrolyzed with water at 0 °C. Usual work up and column chromatography (alumina, ethyl acetate) gave 50 mg (92% yield) of (*R*)-(*S*)-**17**; NMR: δ 1.42 (d, 3H, J=7 Hz, $CHC\underline{H}_3$), 1.65 (bs, 1H, $O\underline{H}$), 3.95 (s, 5H, $FeC_5\underline{H}_5$), 3.71, 4.21, and 4.42 (m, 3H, $FeC_5\underline{H}_3$), 4.90 (dq, 1H, J_{H-P}=3 Hz, $C\underline{H}CH_3$), 7.05—7.55 (m, 10H, $PC_6\underline{H}_5$).

(R)-1-[(S)-1',2-Bis(diphenylphosphino)ferrocenyl]ethanol [*(R)-(S)-**BPPFOH (18)***]. To a suspension of 0.576 g (0.90 mmol) of (*R*)-(*S*)-**13** in 20 ml of dry ether, 1.7 ml of 1.27 M butyllithium in hexane was added at 0 °C. The resulting red solution was kept stirring at room temperature for 2 h, and hydrolyzed with water at 0 °C. The product was extracted with ether, and the ether solution was washed with water, dried over anhydrous sodium sulfate, and evaporated. The residue was chromatographed (alumina, ethyl acetate) to give 0.512 g (95% yield) of (*R*)-(*S*)-**18**. An analytically pure sample was obtained by recrystallization from ethanol; NMR: δ 1.38 (d, 3H, J=6.5 Hz, $CHC\underline{H}_3$), 1.78—1.98 (bs, 1H, $O\underline{H}$), 3.58—4.54 (m, 7H, $C_5\underline{H}_4FeC_5\underline{H}_3$), 4.88 (q, 1H, $C\underline{H}CH_3$), 6.94—7.70 (m, 20H, $PC_6\underline{H}_5$). IR (CCl_4): 3570 cm^{-1} (OH).

(R)-1-Diphenylphosphinyl-2-ethylferrocene [*(R)-**20***]. To a solution of 0.93 g (2.03 mmol) of (*S*)-(*R*)-**9** in 45 ml of acetone, 5.0 ml of methyl iodide was added at room temperature. The solution was refluxed for 15 min and concentrated *in vacuo* to *ca.* 15 ml. The residue was diluted with 30 ml of benzene, washed with 50 ml of 8.5% aqueous phosphoric acid and 50 ml of 10% aqueous sodium hydroxide, and dried over anhydrous sodium sulfate. After evaporation of the solvents, the residue was chromatographed on silica gel (benzene/ethyl acetate, 3/1) to give 0.61 g (73%) of crude (*R*)-1-diphenylphosphinyl-2-vinylferrocene (**19**) as a reddish-brown viscous oil; NMR: δ 4.12 (s, 3H, $FeC_5\underline{H}_3$), 4.22 (s, 5H, $FeC_5\underline{H}_5$), 4.7—5.5 (m, 2H, $CH{=}C\underline{H}_2$), 5.9—6.7 (m, 1H, $C\underline{H}{=}CH_2$), 7.1—7.9 (m, 10H, $PC_6\underline{H}_5$). IR: 1625 (vinyl), 1193 (P=O), and 1108 and 1002 cm^{-1} (FeC_5H_5).

The crude vinylferrocene (*R*)-**19** (0.57 g) in 5 ml of benzene solution was hydrogenated in a 50-ml steel autoclave at 130 kg/cm^2 of hydrogen in the presence of 10 mg of chlorotris(triphenylphosphine)rhodium to give, after chromatography on alumina (benzene/ethyl acetate 2/1), 0.29 g of (*R*)-**20**; NMR: δ 0.95 (t, 3H, J=7 Hz, $C\underline{H}_3$), 2.26—2.77 (cm, 2H, $C\underline{H}_2$), 4.25 (s, 5H, $FeC_5\underline{H}_5$), 3.72, 4.17, and 4.32 (m, 3H, $FeC_5\underline{H}_3$), 7.22—7.96 (m, 10H, $PC_6\underline{H}_5$).

(R)-1-Diphenylphosphino-2-ethylferrocene [*(R)-**PPEF (21)***]. A solution of 0.23 g (0.55 mmol) of (*R*)-**20** in 5 ml of benzene was added at room temperature to a solution of 0.1 g of lithium aluminum hydride in 4 ml of dry dibutyl ether over a period of 10 min. The reaction mixture was heated at 80—85 °C for 4.5 h. After work up in the usual way, chromatography on alumina using benzene as an eluent gave 0.17 g (78% yield) of (*R*)-**21**; UV: λ_{max} ($CHCl_3$) 446 nm (ε 155); NMR: δ 1.01 (t, 3H, J=7 Hz, $C\underline{H}_3$), 2.19—2.71 (m, 2H, $C\underline{H}_2$), 3.94 (s, 5H, $FeC_5\underline{H}_5$), 3.56, 4.10, and 4.27 (m, 3H, $FeC_5\underline{H}_3$), 6.76—7.62 (m, 10H, $PC_6\underline{H}_5$). ORD (*c* 0.12 and 0.005, chloroform): $[\Phi]_{589}$ +1080°, $[\Phi]_{474}$ +2450° (pk), $[\Phi]_{428}$ +1880° (tr), and $[\Phi]_{294}$ +14400° (pk). The CD spectrum is shown in Fig. 2.

(S)-1,1'-Bis(diphenylphosphino)-2-vinylferrocene [*(S)-**22***]. A solution of 1.17 g (1.83 mmol) of (*R*)-(*S*)-**13** in 10 ml of 10% potassium hydroxide in methanol was refluxed for 1 h. After usual work up, column chromatography (alumina) gave 0.360 g (34% yield) of (*S*)-**22** (benzene elution) and 0.431 g (39% yield) of (*R*)-(*S*)-**18** (ethyl acetate elution). (*S*)-**22**; NMR: δ 3.57, 3.68, 4.12, 4.23, 4.33, and 4.68 (m, 1H, 1H, 1H, 2H, 1H, 1H, respectively, $C_5\underline{H}_4FeC_5\underline{H}_3$), 4.95—5.40 (m, 2H, $CH{=}C\underline{H}_2$), 6.48—6.94 (m, 1H, $C\underline{H}{=}CH_2$), 7.0—7.6 (m, 20H, $PC_6\underline{H}_5$).

(S)-1,1'-Bis(diphenylphosphino)-2-ethylferrocene [*(S)-**BPPEF (23)***]. A solution of 85 mg (0.15 mmol) of (*S*)-**22** and 7 mg (0.015 mmol) of chlorotris(triphenylphosphine)-rhodium in 5 ml of benzene was placed in a microautoclave, and magnetically stirred with hydrogen at 50 atm for 18 h.

Column chromatography (alumina, benzene) gave 50 mg (57% yield) of (*S*)-**23**; NMR: δ 0.93 (t, 3H, J=7.5 Hz, $CH_2C\underline{H}_3$), 2.37 (q, 2H, $C\underline{H}_2CH_3$), 3.30—3.55, 3.55—3.75, 3.85—4.17, and 4.20—4.40 (bm, 1H, 1H, 3H, and 2H, respectively, $C_5\underline{H}_4FeC_5\underline{H}_3$), 6.8—7.6 (m, 20H, $PC_6\underline{H}_5$).

[(R)-1-[(S)-2-(Diphenylphosphino)ferrocenyl]ethyl]diphenylphosphine [(R)-(S)-**24**]. A solution of 69.2 mg (0.15 mmol) of (*R*)-(*S*)-**12** and 280 mg (1.5 mmol) of diphenylphosphine in 4.5 ml of methanol was refluxed under argon for 7 h. The solvent was removed under reduced pressure, and the residue was chromatographed on alumina (benzene) to give 74 mg (85% yield) of (*R*)-(*S*)-**24** as a red oil; NMR: δ 1.51 (dd, 3H, J_{H-H}=7.2 Hz, J_{H-P}=5.8 Hz, $PCHC\underline{H}_3$), 3.97 (s, 5H, $FeC_5\underline{H}_5$), 3.75—4.44 (m, 4H, $FeC_5\underline{H}_3C\underline{H}$), 7.31—7.95 (m, 20H, $PC_6\underline{H}_5$).

dl-1-Diphenylphosphino-2-(dimethylaminomethyl)ferrocene [dl-*FcPN* (**25**)]. *dl*-**25** was prepared according to the reported procedure,[52] mp 101.5—102 °C; NMR: δ 2.01 (s, 6H, $NC\underline{H}_3$), 3.48 (deformed AB, 2H, J=14 Hz, $\Delta\nu$=17 Hz, $C\underline{H}_2$), 3.94 (s, 5H, $FeC_5\underline{H}_5$), 3.87, 4.29, and 4.52 (m, 3H, $FeC_5\underline{H}_3$), 7.15—7.71 (m, 10H, $PC_6\underline{H}_5$).

dl-1-Diphenylthiophosphinyl-2-(dimethylaminomethyl)ferrocene [dl-**26**]. A solution of 26.9 g (62.9 mmol) of *dl*-**25** and 2.22 g (69.2 mmol) of sulfur in 60 ml of benzene was refluxed for 1 h. The solvent was removed under reduced pressure and the residue was purified by short-column chromatography (alumina) to give 25.8 g (89% yield) of *dl*-**26**, mp 166 °C; NMR: δ 1.92 (s, 6H, $NC\underline{H}_3$), 3.52 (AB, 2H, J=13 Hz, $\Delta\nu$=67 Hz, $C\underline{H}_2$), 4.27 (s, 6H, $FeC_5\underline{H}_5$ and one of $FeC_5\underline{H}_3$), 3.82 and 4.60 (m, 2H, $FeC_5\underline{H}_3$), 7.25—7.96 (m, 10H, $PC_6\underline{H}_5$).

(S)- and (R)-26. *dl*-**26** (5.72 g, 12.4 mmol) dissolved in 20 ml of hot benzene was added to a hot benzene (20 ml) solution of 4.68 g (12.4 mmol) of dibenzoyl-*d*-tartaric acid.[60] The benzene was removed by evaporation under reduced pressure to give ammonium salts as an orange powder. The ammonium salts were dissolved in 100 ml of warm (40 °C) ethanol. Very soon orange crystals started to separate out. After 8 h the crystals were collected and set free with aqueous sodium carbonate. The partially optically active **26** (2.05 g) obtained and 1.58 g of dibenzoyl-*d*-tartaric acid were mixed in 7 ml of dichloromethane. Ethanol (50 ml) was added, and the solution was kept at 50 °C. As dichloromethane was evaporated, orange needle crystals were formed. After 8 h 2.90 g of the crystals ($[\alpha]_D^{25}$ +12° (*c* 0.4, chloroform)) were obtained; this was converted with aqueous sodium carbonate to **26**, which was purified by a short alumina column (ether) to give 1.63 g (57% yield) of optically pure (*S*)-**26**; $[\alpha]_{545}^{25}$ +50.2° (*c* 0.5, chloroform). From the mother liquor of the first crystallization, was recovered 3.15 g of *R*-rich **26**, which was fractionally recrystallized using dibenzoyl-*l*-tartaric acid to give 1.50 g (52% yield) of (*R*)-**26**; $[\alpha]_{545}^{25}$ −50.5° (*c* 0.5, chloroform).

(S)-FcPN (**25**). To a solution of 1.38 g (3.0 mmol) of (*S*)-**26** in 20 ml of dry dioxane was added 0.6 g of lithium aluminum hydride, and the mixture was refluxed for 22 h. It was hydrolyzed with 10% aqueous sodium hydroxide, and then extracted with benzene. Column chromatography (alumina, ether) gave 1.06 g (83% yield) of crude (*S*)-**25**. Recrystallization from pentane (4 ml) gave 0.77 g of pure (*S*)-**25** as red cubic crystals. The CD spectrum is shown in Fig. 3.

In the same manner, (*R*)-**25** was obtained from (*R*)-**26** in 80% yield.

(S)-1-Diphenylthiophosphinyl-2-(acetoxymethyl)ferrocene [(S)-**27**]. In a degassed sealed glass tube, a mixture of 0.23 g (0.50 mmol) of (*S*)-**26** and 2.0 ml of acetic anhydride was heated at 100 °C for 20 h. Benzene (5 ml) was added and the benzene solution was washed with aqueous sodium hydroxide and water, dried over anhydrous sodium sulfate, and evaporated. Column chromatography (alumina, ethyl acetate) gave 0.20 g (84% yield) of (*S*)-**27**, $[\alpha]_{545}^{25}$ +59° (*c* 0.5, chloroform), mp 190—193° (decomp); NMR: δ 1.56 (s, 3H, $COC\underline{H}_3$), 4.35 (s, 6H, $FeC_5\underline{H}_5$ and one of $FeC_5\underline{H}_3$), 3.81 and 4.59 (m, 2H, $FeC_5\underline{H}_3$), 5.24 (AB, 2H, J=12 Hz, $\Delta\nu$=45 Hz, $C\underline{H}_2$), 7.22—7.90 (m, 10H, $PC_6\underline{H}_5$).

(S)-1-Diphenylthiophosphinyl-2-(hydroxymethyl)ferrocene [(S)-**28**]. A solution of 0.20 g (0.42 mmol) of (*S*)-**27** in 8 ml of 3 M aqueous potassium hydroxide and 18 ml of methanol was refluxed for 1 h. The solvent was removed, and 10 ml of benzene was added. The benzene solution was washed with water, dried over anhydrous sodium sulfate, and evaporated. The product was purified by column chromatography (alumina, chloroform/methanol 15/1) to give 0.16 g (88% yield) of (*S*)-**28**, mp 192—194 °C (decomp); NMR: δ 3.34 (dd, 1H, J=6 and 8 Hz, $O\underline{H}$), 4.31 (s, 5H, $FeC_5\underline{H}_5$), 3.70—4.78 (m, 5H, $FeC_5\underline{H}_3C\underline{H}_2$), 7.21—7.95 (m, 10H, $PC_6\underline{H}_5$).

dl-**28** was also prepared from *dl*-**26**; NMR of *dl*-**28** in the presence of 30 mol% of $Eu(facam)_3$: δ 5.30 and 5.88 (a pair of s, $FeC_5\underline{H}_5$).

(S)-1,1'-Bis(diphenylphosphino)-2-(dimethylaminomethyl)ferrocene [(S)-**30**]. To a solution of 1.02 g (2.4 mmol) of (*S*)-**25** in 25 ml of dry ether was added a solution of butyllithium in hexane (4.0 ml of a 1.25 M solution). After stirring at room temperature for 1.5 h, 1.5 ml (12 mmol) of chlorotrimethylsilane was added with heating under gentle reflux. The reaction mixture was refluxed for 2 h, hydrolyzed with 10 ml of water and 10 ml of 30% aqueous sodium hydroxide, and then extracted with benzene (2×40 ml). The combined benzene extracts were washed with brine and dried over anhydrous sodium sulfate. Evaporation of the solvent followed by column chromatography (alumina, benzene/ether 1/1) gave 1.02 g (85% yield) of 1-diphenylphosphino-2-dimethylaminomethyl-3-(trimethylsilyl)ferrocene [(*S*)-**29**]. Elution with ethyl acetate gave 0.15 g of recovered (*S*)-**25**. NMR of (*S*)-**29**: δ 0.28 (s, 9H, $SiC\underline{H}_3$), 1.78 (s, 6H, $NC\underline{H}_3$), 3.47 (ABX, 2H, $J_{H_A-H_B}$=13 Hz, J_{H_A-P}=3 Hz, J_{H_B-P}=0 Hz, $\Delta\nu$=16 Hz, $C\underline{H}_2$), 3.90 (s, 5H, $FeC_5\underline{H}_5$), 3.97 (d, 1H, J=3 Hz, one of $FeC_5\underline{H}_2$), 4.20 (d, 1H, one of $FeC_5\underline{H}_2$), 7.12—7.72 (m, 10H, $PC_6\underline{H}_5$).

(*S*)-**29** (1.02 g, 2.04 mmol) was lithiated with butyllithium (4.9 ml of 1.25 M hexane solution) and TMEDA (0.92 ml, 6.13 mmol). To the solution was added with stirring 1.5 ml (7.96 mmol) of chlorodiphenylphosphine at 0 °C. The reaction mixture was refluxed for 1.5 h, hydrolyzed with 30% aqueous sodium hydroxide at 0 °C, and extracted with benzene (2×30 ml). The benzene extracts were washed with brine, dried over anhydrous sodium sulfate, and evaporated. Column chromatography (alumina, hexane/benzene 1/1) gave 0.747 g of recovered (*S*)-**29** and 0.393 g of a mixture of recovered (*S*)-**29** and the desired phosphinated product (3:7).

The above-obtained mixture (0.318 g) was desilylated by treatment with 0.052 g (0.46 mmol) of potassium *t*-butoxide in 10 ml of dimethyl sulfoxide. Usual work up and preparative TLC (silica gel, benzene/acetone 1/1) gave 0.160 g of (*S*)-**30** (R_f 0.65); NMR: δ 1.94 (s, 6H, $NC\underline{H}_3$), 3.11, 3.14, 3.47, 3.57, 3.71, 3.99, 4.09, 4.16, 4.27, and 4.52 (m, 9H, $C_5\underline{H}_4FeC_5\underline{H}_3C\underline{H}_2$), 7.0—7.7 (m, 20H, $PC_6\underline{H}_5$).

The reaction of (R)-1 with Acetic Anhydride. A solution of 0.186 g (0.726 mmol) of (*R*)-(+)-**1** ($[\alpha]_D^{25}$ +14.1° (*c* 1.7, ethanol)) in 0.3 ml of acetic anhydride was heated at 100 °C for 2 h. Saturated aqueous sodium hydrogencarbonate was added at room temperature, and the product

was extracted with ether. The ether solution was washed with brine, dried over anhydrous sodium sulfate, and evaporated *in vacuo* to give 0.192 g (97% yield) of 1-ferrocenylethyl acetate, $[\alpha]_D^{25}$ −26.6° (*c* 1.0, ethanol), (lit,[49] (*R*)-1-ferrocenylethyl acetate, $[\alpha]_D^{25}$ −28.5° (*c* 1.4, ethanol)).

We thank the Ministry of Education for Grant-in-Aid (No. 235053, 303523, 311709, 355370) and the Asahi Glass Foundation for the Contribution to Industrial Technology for financial support of this work. We are indebted to Professor Y. Imanishi, Department of Polymer Chemistry, Kyoto University, for CD measurements.

References

1) a) J. D. Morrison and H. S. Mosher, "Asymmetric Organic Reactions," Prentice-Hall Englewood Cliffs, New Jersey (1971); b) H. B. Kagan and J. C. Fiaud, "Topics in Stereochemistry," ed by E. L. Eliel and N. L. Allinger, Wiley-Interscience, New York (1978), Vol. 10, p. 175.
2) a) J. W. Scott and D. Valentine, Jr., *Science*, **184**, 943 (1974); b) D. Valentine, Jr. and J. W. Scott, *Synthesis*, **1978**, 329.
3) For a review: J. D. Morrison, W. F. Masler, and M. K. Neuberg, *Adv. Catal.*, **25**, 81 (1976).
4) L. Horner, H. Winkler, A. Rapp, A. Mentrup, H. Hoffman, and P. Beck, *Tetrahedron Lett.*, **1961**, 161.
5) L. Horner, H. Siegel, and H. Büthe, *Angew. Chem.*, **80**, 1034 (1968).
6) W. S. Knowles and M. J. Sabacky, *Chem. Commun.*, **1968**, 1445.
7) a) O. Korpiun and K. Mislow, *J. Am. Chem. Soc.*, **89**, 4784 (1967); b) K. Naumann, G. Zon, and K. Mislow, *ibid.*, **91**, 7012 (1969).
8) a) W. S. Knowles, M. J. Sabacky, and B. D. Vineyard, *J. Chem. Soc., Chem. Commun.*, **1972**; 10, b) W. S. Knowles, M. J. Sabacky, and B. D. Vineyard, *Chem. Tech.*, **1972**, 591; c) W. S. Knowles, M. J. Sabacky, and B. D. Vineyard, *Ann. N. Y. Acad. Sci.*, **214**, 119 (1973).
9) a) W. S. Knowles, M. J. Sabacky, B. D. Vineyard, and D. J. Weinkauff, *J. Am. Chem. Soc.*, **97**, 2567 (1975); b) B. D. Vineyard, W. S. Knowles, M. J. Sabacky, G. L. Bachman, and D. J. Weinkauff, *ibid.*, **99**, 5946 (1977).
10) a) T. P. Dang and H. B. Kagan, *Chem. Commun.*, **1971**, 481; b) H. B. Kagan and T. P. Dang, *J. Am. Chem. Soc.*, **94**, 6429 (1972).
11) a) H. B. Kagan, N. Langlois, and T. P. Dang, *J. Organomet. Chem.*, **90**, 353 (1975); b) G. Gelbard, H. B. Kagan, and S. Stern, *Tetrahedron*, **32**, 233 (1976) and references cited therein.
12) R. Glaser and B. Vainas, *J. Organomet. Chem.*, **121**, 249 (1976) and their previous papers cited therein.
13) M. Tanaka, Y. Watanabe, T. Mitsudo, Y. Yasunori, and Y. Takegami, *Chem. Lett.*, **1974**, 137.
14) A. P. Stoll and R. Süess, *Helv. Chim. Acta*, **57**, 2487 (1974).
15) B. R. James, D. K. W. Wang, and R. F. Voigt, *J. Chem. Soc., Chem. Commun.*, **1975**, 574.
16) A. Levi, G. Modena, and G. Scorrano, *J. Chem. Soc., Chem. Commun.*, **1975**, 6.
17) a) B. Heil, S. Törös, S. Vastag, and L. Marko, *J. Organomet. Chem.*, **94**, C47 (1975); b) S. Törös B. Heil, and L. Marko, *ibid.*, **159**, 401 (1978).
18) a) I. Ojima, T. Kogure, M. Kumagai, S. Horiuchi, and T. Sato, *J. Organomet. Chem.*, **122**, 83 (1976); b) I. Ojima, T. Kogure, and M. Kumagai, *J. Org. Chem.*, **42**, 1671 (1977) and their previous papers cited therein.
19) T. Hayashi, Dissertation, Kyoto University, 1975.
20) W. Dumont, J. C. Poulin, T. P. Dang, and H. B. Kagan, *J. Am. Chem. Soc.*, **95**, 8295 (1973).
21) R. J. P. Corriu and J. J. E. Moreau, *J. Organomet. Chem.*, **85**, 19 (1975).
22) a) G. Consiglio, C. Botteghi, C. Salomon, and P. Pino, *Angew. Chem.*, **85**, 663 (1973); b) G. Consiglio, C. Botteghi, C. Solomon, and P. Pino, *Chimia*, **27**, 215 (1973); c) G. Consiglio and P. Pino, *Helv. Chim. Acta*, **59**, 642 (1976).
23) R. Stern, A. Hirshauer, and L. Sajus, *Tetrahedron Lett.*, **1973**, 3247.
24) a) M. Tanaka, Y. Ikeda, and I. Ogata, *Chem. Lett.*, **1975**, 1115; b) Y. Kawabata, T. M. Suzuki, and I. Ogata, *ibid.*, **1978**, 361.
25) G. Consiglio and C. Botteghi, *Helv. Chim. Acta*, **56**, 460 (1973).
26) Y. Kiso, K. Tamao, N. Miyake, K. Yamamoto, and M. Kumada, *Tetrahedron Lett.*, **1974**, 3.
27) a) B. M. Trost and P. E. Strege, *J. Am. Chem. Soc.*, **99**, 1649 (1977); b) J. C. Fiaud, A. Hibon de Gournay, M. Larcheveque, and H. B. Kagan, *J. Organomet. Chem.*, **154**, 175 (1978).
28) J. D. Morrison, R. E. Burnett, A. M. Aguiar, C. J. Morrow, and C. Phillips, *J. Am. Chem. Soc.*, **93**, 1301 (1971).
29) a) J. D. Morrison and W. F. Masler, *J. Org. Chem.*, **39**, 270 (1974); b) A. M. Aguiar, C. J. Morrow, J. D. Morrison, R. E. Burnett, W. F. Masler, and N. S. Bhacca, *J. Org. Chem.*, **41**, 1545 (1976). See also: M. Tanaka and I. Ogata, *Bull. Chem. Soc. Jpn.*, **48**, 1094 (1975). Y. Kiso, K. Yamamoto, K. Tamao, and M. Kumada, *J. Am. Chem. Soc.*, **94**, 4373 (1972).
30) B. Bogdanović, B. Henc, A. Lösler, B. Meister, H. Pauling, and G. Wilke, *Angew. Chem.*, **85**, 1013 (1973).
31) I. Ogata, F. Mizukami, Y. Ikeda, and M. Tanaka, Japan. Kokai, 76-43754; *Chem. Abstr.*, **85**, 124144z (1976); Japan Kokai, 76-39662; *Chem. Abstr.*, **85**, 124143y (1976).
32) a) K. Achiwa, *J. Am. Chem. Soc.*, **98**, 8265 (1976); b) K. Achiwa, Y. Ohga, Y. Iitaka, and H. Saito, *Tetrahedron Lett.*, **1978**, 4683, and their previous papers cited therein.
33) a) G. Descotes, D. Lafont, and D. Sinou, *J. Organomet. Chem.*, **150**, C14 (1978); b) D. Lafont, D. Sinou, and G. Descotes, *ibid.*, **169**, 87 (1979).
34) a) M. D. Fryzuk and B. Bosnich, *J. Am. Chem. Soc.*, **99**, 6262 (1977); b) M. D. Fryzuk and B. Bosnich, *ibid.*, **100**, 5491 (1978).
35) K. Tamao, H. Yamamoto, H. Matsumoto, N. Miyake, T. Hayashi, and M. Kumada, *Tetrahedron Lett.*, **1977**, 1389.
36) D. Marquarding, H. Klusacek, G. Gokel, P. Hoffmann, and I. Ugi, *J. Am. Chem. Soc.*, **92**, 5389 (1970).
37) T. Hayashi, T. Mise, S. Mitachi, K. Yamamoto, and M. Kumada, *Tetrahedron Lett.*, **1976**, 1133.
38) W. R. Cullen and E-S. Yeh, *J. Organomet. Chem.*, **139**, C13 (1977).
39) a) T. Hayashi, T. Mise, and M. Kumada, *Tetrahedron Lett.*, **1976**, 4351; b) T. Hayashi, A. Katsumura, M. Konishi, and M. Kumada, *ibid.*, **1979**, 425.
40) T. Hayashi, M. Nakatsuka, A. Katsumura, and M. Kumada, unpublished results.
41) T. Hayashi, K. Yamamoto, and M. Kumada, *Tetrahedron Lett.*, **1974**, 4405.
42) T. Hayashi, K. Tamao, Y. Katsuro, I. Nakae, and M. Kumada, *Tetrahedron Lett.*, in press.
43) a) T. Hayashi, M. Tajika, K. Tamao, and M. Kumada,

J. Am. Chem. Soc., **98**, 3718 (1976); b) K. Tamao, T. Hayashi, H. Matsumoto, H. Yamamoto, and M. Kumada, *Tetrahedron Lett.*, **1979**, 2155.
44) T. Hayashi, M. Konishi, S. Kawakami, and M. Kumada, unpublished results.
45) H. Kumobayashi, S. Akutagawa, and S. Otsuka, *J. Am. Chem. Soc.*, **100**, 3949 (1978).
46) M. D. Rausch and D. J. Ciappenelli, *J. Organomet. Chem.*, **10**, 127 (1967).
47) C. C. Price and J. R. Sowa, *J. Org. Chem.*, **32**, 4126 (1967).
48) B. J. Wakefield, "The Chemistry of Organolithium Compounds," Pergamon Press, New York (1974), p. 66.
49) G. W. Gokel, D. Marquarding, and I. Ugi, *J. Org. Chem.*, **37**, 3052 (1972).
50) A. N. Nesmeyanov, E. G. Perevalova, L. S. Shilovtseva, and V. D. Tyurin, *Izv. Akad. Nauk. SSSR, Otd. Khim. Nauk*, **1962**, 1997; *Chem. Abstr.*, **58**, 9132 (1963).
51) J. S. Fritz and J. N. King, *Anal. Chem.*, **48**, 570 (1976).
52) G. Marr and T. Hunt, *J. Chem. Soc., C*, **1969**, 1070.
53) G. R. Sullivan, "Topics in Stereochemistry," ed by E. L. Eliel and N. L. Allinger, Wiley-Interscience, New York, (1978), Vol. 10, p. 287.
54) M. Rosenblum, "Chemistry of the Iron Group Metallocenes," Wiley-Interscience, New York (1965), p. 40.
55) M. Rosenblum, A. K. Banerjee, N. Danieli, R. W. Fish, and V. Schlatter, *J. Am. Chem. Soc.*, **85**, 316 (1963).
56) C. R. Hauser and J. K. Lindsay, *J. Org. Chem.*, **22**, 906 (1957).
57) a) T. P. Dang, J.-C. Poulin, and H. B. Kagan, *J. Organomet. Chem.*, **91**, 105 (1975); b) K. S. Yudina, T. Ya. Medved, and M. I. Kabachnik, *Izv. Akad. Nauk. SSSR, Ser. Khim.*, **1966**, 1954; *Chem. Abstr.*, **66**, 76096u (1967).
58) T. Sone, K. Hiroi, and S. Yamada, *Chem. Pharm. Bull.*, **21**, 2331 (1973).
59) L. A. Paquette, J. P. Freeman, and S. Maiorana, *Tetrahedron*, **27**, 2599 (1971).
60) C. L. Butler and L. H. Cretcher, *J. Am. Chem. Soc.*, **55**, 2605 (1933).

Cyclotrimerization of Phenylacetylene Catalyzed by Halides of Niobium and Tantalum

Toshio MASUDA,* Taizo MOURI, and Toshinobu HIGASHIMURA
Department of Polymer Chemistry, Faculty of Engineering, Kyoto University, Kyoto 606
(Received November 8, 1979)

Halides of niobium and tantalum (NbX_5, TaX_5; X=Cl, Br, F) catalyzed the cyclotrimerization of phenylacetylene in hydrocarbon and chlorinated hydrocarbon solvents at 0—90 °C. When $NbCl_5$ and $TaCl_5$ were used as catalysts, two cyclic trimers, 1,2,4- and 1,3,5-triphenylbenzenes were exclusively formed, and their ratio varied from 17:83 to 94:6 depending on reaction conditions. The cyclotrimerization was more selective than those by other known catalysts. The cyclotrimerization by $NbBr_5$ and $TaBr_5$ occurred in a similar manner, but the reaction was less selective than that catalyzed by $NbCl_5$ and $TaCl_5$. Not only cyclotrimerization but also linear oligomerization proceeded by NbF_5 and TaF_5 as catalysts. The results obtained were discussed together with the linear polymerization of phenylacetylene catalyzed by $MoCl_5$ and WCl_6.

The cyclotrimerization of acetylenes is catalyzed by various transition-metal complexes to give benzene derivatives.[1] The best known catalysts for this reaction are Ziegler-type catalysts and Ni(0) complexes. The catalysts for the cyclotrimerization of acetylenes are usually either mixtures of a transition-metal compound and a reducing agent, or organo-transition metal complexes in which the metals are in a reduced state.

The cyclotrimerization of phenylacetylene by Ziegler-type catalysts gives a mixture of comparable amounts of 1,2,4- and 1,3,5-triphenylbenzene (1,2,4- and 1,3,5-TPB's).[2] The reaction catalyzed by Ni(0) complexes mainly provides a mixture of 1,2,4-TPB and linear oligomers.[3] A cobalt complex is reported to afford mainly 1,2,4-TPB in high yield.[4] In general, most catalysts so far reported for the cyclotrimerization of phenylacetylene show no high selectivity with respect to both cyclization and substituent position. Pure 1,3,5-TPB has been obtained by the acid-catalyzed condensation of acetophenone,[5] and pure 1,2,4-TPB by the reaction of 2,5-diphenylthiophene 1,1-dioxide with phenylacetylene.[6]

There has been a patent on the cyclotrimerization of acetylene and 1-alkyne by use of $NbCl_5$ and $TaCl_5$. The selectivity, however, has not been examined in detail.[7]

We have found that phenylacetylene is polymerized by the chlorides of molybdenum and tungsten to give selectively a linear high polymer (*MW* 5000—15000).[8] From this point of view, it is of great interest what reactions of phenylacetylene take place in the presence of the halides of niobium and tantalum.

The present paper describes the cyclotrimerization and linear oligomerization of phenylacetylene catalyzed by halides of niobium and tantalum (NbX_5, TaX_5; X=Cl, Br, F).

Experimental

Reagents. Phenylacetylene was prepared by the bromination of styrene and the subsequent dehydrobromination, according to the literature method.[9] The halides of niobium and tantalum (Alfa-Ventron, purity >99%) were used without further purification. Solvents were purified by the usual methods.

Procedures. Cyclotrimerization was carried out under a dry nitrogen atmosphere in a 30 ml Erlenmeyer flask equipped with a three-way stopcock, at $[PA]_0=1.0$ mol dm^{-3} and [Cat]=10 mmol dm^{-3} (PA: phenylacetylene, Cat: catalyst). The reaction was started by adding the monomer solution to the catalyst solution at a given temperature, and terminated by adding ammoniacal methanol. The consumption of monomer was determined by gas chromatography. The catalyst residue was removed by washing the reaction mixture with aqueous hydrochloric acid and water, and volatile materials were evaporated. The product obtained was dried under vacuum.

The number-average molecular weight of the products was measured on a Hitachi 117 molecular weight apparatus. The gel permeation chromatograms of the products were observed on a JASCO FLC-A700 chromatograph (column JSP 101, polystyrene gel, xl; eluent $CHCl_3$). The IR spectra of the produts were measured on a Shimadzu IR 27G spectrophotometer in KBr disks. The ratio of 1,2,4-TPB to 1,3,5-TPB in the products was determined from the ratios of D_{1600}/D_{1070}, D_{1495}/D_{1070}; and D_{1475}/D_{1070} in the IR spectra. Here, the absorption at 1070 cm^{-1} appears commonly in both 1,2,4- and 1,3,5-TPB's, while the absorptions at 1600, 1495, and 1475 cm^{-1} are characteristic of either 1,2,4- or 1,3,5-TPB. The ^{1}H NMR spectra were recorded on a JEOL JNM-MH 60 spectrometer.

Results and Discussion

Cyclotrimerization of Phenylacetylene Catalyzed by $NbCl_5$ and $TaCl_5$. The cyclotrimerization of phenylacetylene was performed with $NbCl_5$ and $TaCl_5$ in hydrocarbon and halogenated hydrocarbon solvents at 60 °C for 1 h ($[PA]_0=1.0$ mol dm^{-3}, [Cat]=10 mmol dm^{-3}). The reaction was fast and exothermic, and usually proceeded quantitatively. No reaction took place in such solvents as 2-butanone, acetonitrile, ethyl acetate, 1,4-dioxane and nitrobenzene.

The gel permeation chromatogram of the product showed only a peak at the position corresponding to the cyclic trimers. The number-average molecular weight of the product obtained agreed to the value for the trimers (306.4) within an error of 2%. These results indicate that no product other than the trimers was formed. Further, the IR, UV, and ^{1}H NMR spectra of the product were compared with those of authentic 1,2,4- and 1,3,5-TPB's, which revealed that the product was exclusively a mixture of 1,2,4- and 1,3,5-TPB's.

Table 1. 1,2,4-TPB content (%) of product in the cyclotrimerization of phenylacetylene catalyzed by $NbCl_5$ and $TaCl_5$[a)]

	C_6H_6	$C_6H_5CH_3$	n-C_6H_{14}	$\overline{-(CH_2)_6-}$	CCl_4	$CHCl_3$	$(CH_2Cl)_2$	C_6H_5Cl	o-$C_6H_4Cl_2$
$NbCl_5$	90	85	81	80	79	77	86	89	90
$TaCl_5$	70	51	42	45	40	40	48	68	54

a) $[PA]_0 = 1.0$ mol dm^{-3}, $[Cat] = 10$ mmol dm^{-3}, 60 °C (50 °C for $CHCl_3$), 1 h.

Table 2. 1,2,4-TPB content (%) of product in the cyclotrimerization of phenylacetylene catalyzed by $NbBr_5$ and $TaBr_5$[a)]

	C_6H_6	$C_6H_5CH_3$	n-C_6H_{14}	$\overline{-(CH_2)_6-}$	CCl_4	$CHCl_3$	$(CH_2Cl)_2$	C_6H_5Cl	o-$C_6H_4Cl_2$
$NbBr_5$	71	60	62	70	66	65	62	69	71
$TaBr_5$	61	58	50	51	49	60	54	57	69

a) $[PA]_0 = 1.0$ mol dm^{-3}, $[Cat] = 10$ mmol dm^{-3}, 60 °C (50 °C for $CHCl_3$), 1 h.

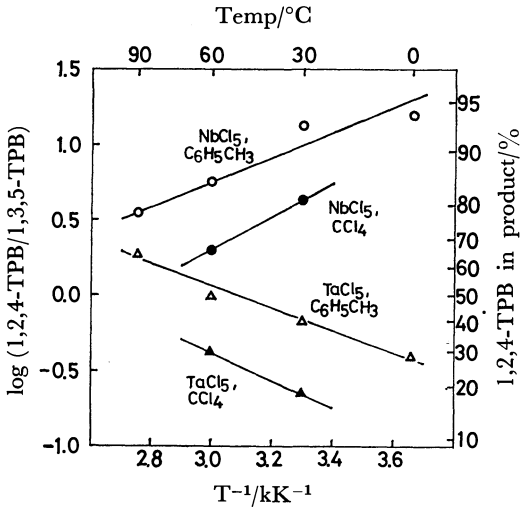

Fig. 1. Arrhenius plots of the ratio of 1,2,4-TPB to 1,3,5-TPB in the cyclotrimerization of phenylacetylene catalyzed by $NbCl_5$ and $TaCl_5$.
$[PA]_0 = 1.0$ mol dm^{-3}, $[Cat] = 10$ mmol dm^{-3}.

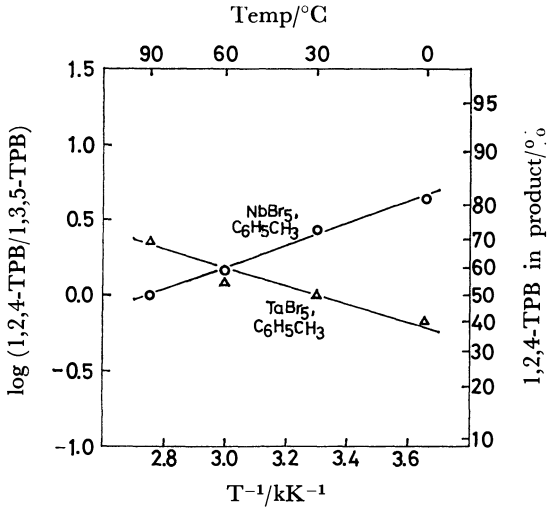

Fig. 2. Arrhenius plots of the ratio of 1,2,4-TPB to 1,3,5-TPB in the cyclotrimerization of phenylacetylene catalyzed by $NbBr_5$ and $TaBr_5$.
$[PA]_0 = 1.0$ mol dm^{-3}, $[Cat] = 10$ mmol dm^{-3}.

Table 1 shows the 1,2,4-TPB content of product expressed in %. In general, $NbCl_5$ gave a product containing more 1,2,4-TPB than $TaCl_5$ did. With regard to solvent, benzene gave a product having the highest 1,2,4-TPB content with both catalyst. On the other hand, 1,2,4-TPB was the least in carbon tetrachloride and in chloroform as solvents. This solvent effect on the product composition is not simply explained, for example in terms of solvent polarity. As seen in Table 1, the 1,2,4-TPB content varied in a range of 40—90% depending on the types of catalyst and solvent.

The dependence of the product composition on reaction temperature was investigated. Toluene and carbon tetrachloride were employed as two different types of solvents. As seen in Fig. 1, good linear relationships were observed in the Arrhenius plots. When $NbCl_5$ was used as a catalyst, the 1,2,4-TPB content of product increased with decreasing reaction temperature. For instance, it was 94% at 0 °C in toluene. $NbCl_5$ is thus an excellent catalyst for the synthesis of 1,2,4-TPB, especially when used at low temperature. On the other hand, the lower the temperature, the less the 1,2,4-TPB content when the $TaCl_5$ catalyst was used. For example, 1,2,4-TPB was 17% at 30 °C in carbon tetrachloride. Thus, the present cyclotrimerizations at low temperature are much more selective than those so far reported. Especially, the cyclotrimerization by $NbCl_5$ at low temperature seems to be a useful method of synthesizing 1,2,4-TPB, though 1,3,5-TPB can be easily prepared by the acid-catalyzed condensation of acetophenone.[5)]

It was confirmed by the following two ways that the product composition in the present cyclotrimerization is kinetically controlled: i) The product composition did not depend on the conversion with both $NbCl_5$ and $TaCl_5$ as catalysts, and ii) 1,2,4-TPB did not isomerize to 1,3,5-TPB in the presence of $TaCl_5$ under the same conditions as those of cyclotrimerization, and *vice versa* with $NbCl_5$.

Cyclotrimerization of Phenylacetylene Catalyzed by $NbBr_5$ and $TaBr_5$. Cyclotrimerization of phenylacetylene was performed with $NbBr_5$ and $TaBr_5$ as catalysts in hydrocarbons and halogenated hydrocarbons. The reaction was usually quantitative within 1 h; the reac-

tion rate was similar to or a little slower than that catalyzed by $NbCl_5$ and $TaCl_5$. It was confirmed in the same way as in the case of the chloride catalysts that the product comprised only the two cyclic trimers.

The 1,2,4-TPB content of product is listed in Table 2. Usually $NbBr_5$ produced more 1,2,4-TPB than $TaBr_5$ did. This is the same tendency as observed in the reaction by the chloride catalysts, but the difference in the compositions with $NbBr_5$ and $TaBr_5$ was smaller. The 1,2,4-TPB content only varied in a range of 49—71% in various solvents examined, when $NbBr_5$ and $TaBr_5$ were used.

Figure 2 shows the dependence of the product composition on temperature. As in the chloride-catalyzed reaction, good linear relationships held in the Arrhenius plots. The 1,2,4-TPB content of product obtained with $NbBr_5$ increased with decreasing temperature, whereas the opposite trend was observed with $TaBr_5$. This tendency is also the same as that found in the chloride catalyst systems.

Thus the bromide catalysts behave in a similar manner to the chloride catalysts. The effects of catalyst metal and solvent on the product composition, however, are smaller in the bromide-catalyzed reaction.

Cyclotrimerization and Linear Oligomerization of Phenylacetylene Catalyzed by NbF_5 and TaF_5. The gel permeation chromatogram of the product obtained with NbF_5 and TaF_5 showed many peaks due to oligomers as well as a peak due to the cyclic trimers. Since the molecular weights of these oligomers ranged from 204 (dimer) to several thousands and they are colored dark red, their structure seems to be linear. The ^1H NMR and IR spectra also indicated the formation of not only the cyclic trimers but also of compounds whose structure was similar to that of the linear polymer produced with WCl_6. Consequently, it is concluded that NbF_5 and TaF_5 catalyze not only cyclotrimerization but also linear oligomerization.

The ratio of the linear oligomers to the cyclic trimers in the product was tentatively determined from peak areas in the gel permeation chromatogram measured with a refractive index detector. As shown in Table 3, the linear oligomer content of product was higher in halogenated hydrocarbons than in paraffinic hydrocarbons. TaF_5 gave a product containing more linear oligomers than NbF_5 did. The conversion ranged from 45 to 100% under the reaction conditions shown in Table 3.

The product obtained with TaF_5 in ethylene dichloride virtually consisted of the linear oligomers. The ^1H NMR and IR spectra of the linear oligomers resembled those of a linear high polymer obtained with

TABLE 3. LINEAR OLIGOMER CONTENT (%) OF PRODUCT IN THE REACTION OF PHENYLACETYLENE CATALYZED BY NbF_5 AND TaF_5[a)]

	n-C_6H_{14}	-$(CH_2)_6$-	CCl_4	$CHCl_3$	$(CH_2Cl)_2$
NbF_5	30	26	55	41	79
TaF_5	59	51	100	91	100

a) $[PA]_0$ 1.0 mol dm^{-3}, [Cat] 10 mmol dm^{-3}, 60 °C (50 °C for $CHCl_3$), 24 h.

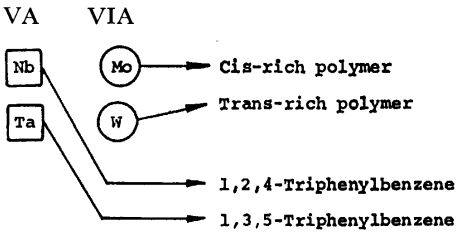

Scheme 1.

WCl_6. The number-average molecular weight was 1400.

When benzene and toluene were used as solvents, the yield of product did not agree with the consumption of reactant, but the former exceeded the latter. The product from a toluene solution proved to have tolyl group according to its ^1H NMR spectrum. These findings indicate that solvent-incorporated linear oligomers were formed. These oligomers seem to have been produced by the Friedel-Crafts alkylation, which suggests that the linear oligomerization proceeds *via* a cationic species. This is expected because the fluorides of niobium and tantalum are stronger Lewis acids than their chlorides and bromides are.

Characteristics of the Present Cyclotrimerization. Two characteristics are pointed out for the present cyclotrimerization.

One is that no reducing agent has to be added though the metals of NbX_5 and TaX_5 are in their highest oxidation state. This contrasts with the case of Ziegler-type catalysts, in which a reducing agent such as triethylaluminum is required for an active species to be formed. The metals of some metal halides such as $NbCl_5$, $MoCl_5$, and WCl_6 can be reduced by olefins and acetylenes.[10)] This reduction occurs through the halogenation of olefins and acetylenes. Thus, it is assumed that NbX_5 and TaX_5 are at first reduced by phenylacetylene in the present reaction.

The second characteristic is the striking contrast to the linear polymerization of phenylacetylene catalyzed by $MoCl_5$ and WCl_6. The relationships between catalyst metals and products (exclusive or principal) are shown in Scheme 1: The chlorides of niobium and tantalum brought about only cyclotrimerization. Further, there was a tendency for $NbCl_5$ to give 1,2,4-TPB as the major product and for $TaCl_5$ to give 1,3,5-TPB. On the other hand, $MoCl_5$ and WCl_6 polymerize phenylacetylene very effectively to give linear high polymers.[8)] The $MoCl_5$ catalyst provides a *cis*-rich polymer, while WCl_6 gives a *trans*-rich polymer. No cyclic trimer is formed in this polymerization at all. It is of great interest that the kind and structure of the product critically depend on the group and period of the metal in these reactions. On the other hand, Ziegler-type catalysts and Ni(0) complexes can catalyze both cyclotrimerization and linear polymerization, and it is often difficult to selectively bring about either of the two reactions with these catalysts.

It has been clarified that the cobalt-catalyzed cyclotrimerization of acetylenes proceeds *via* a metallo-

cyclopentadiene (metallole).[11,12] Since the present cyclotrimerization is also a coordination reaction and behaves in some respects similarly to the cobalt-catalyzed reaction, the present reaction might proceed by a similar mechanism. A further study on reaction behavior, mechanism, and intermediates is in progress.

References

1) See, for reviews, a) C. W. Bird, "Transition Metal Intermediates in Organic Synthesis," Academic Press, New York (1967), Chap. 1; b) C. Hoogzand and W. Huebel, "Organic Shntyeses *via* Metal Carbonyls," ed by I. Wender and P. Pino, Interscience, New York (1968), Vol. I, pp. 343—371; c) T. F. Rutledge, "Acetylenes and Allenes," Reinhold Book Corp., New York (1969), Chap. 4; d) M. M. Taqui Khan and A. E. Martell, "Homogeneous Catalysis by Metal Complexes," Academic Press, New York (1974), Vol. II.

2) a) A. Furlani, E. Cervone, and M. A. Biancifiori, *Rec. Trav. Chim.*, **81**, 585 (1962); b) A. Furlani, G. Moretti, and A. Guerrieri, *J. Polym. Sci., Part B*, **5**, 523 (1967); c) V. A. Sergeev, Yu. A. Chernomordik, V. S. Kolesov, V. V. Gavrilenko, and V. V. Korshak, *Zh. Org. Khim.*, **11**, 777 (1975).

3) a) L. S. Meriwether, E. C. Colthup, G. W. Kennerly, and R. N. Reusch, *J. Org. Chem.*, **26**, 5155 (1961); b) L. B. Luttinger, *ibid.*, **27**, 1591 (1962); c) A. Furlani Donda and G. Moretti, *ibid.*, **31**, 985 (1966).

4) W. Huebel and C. Hoogzand, *Chem. Ber.*, **93**, 103 (1960).

5) H. O. Wirth, W. Kern, and E. Schmitz, *Makromol. Chem.*, **68**, 69 (1963).

6) C. G. Overberger and J. M. Whelan, *J. Org. Chem.*, **24**, 1155 (1959).

7) Ciba, Ltd., British Patent 973934 (1964); *Chem. Abstr.*, **62**, 11734 (1965).

8) a) T. Masuda, K. Hasegawa, and T. Higashimura, *Macromolecules*, **7**, 728 (1974); b) T. Masuda, N. Sasaki, and T. Higashimura, *ibid.*, **8**, 717 (1975); c) T. Masuda, H. Kawai, T. Ohtori, and T. Higashimura, *Polym. J.*, **11**, 813 (1979).

9) Y. Hori, S. Nishimura, Y. Nagano, and H. Taniguchi, *Yuki Gosei Kagaku Kyokai Shi*, **9**, 777 (1973).

10) a) J. S. Filippo, Jr., A. F. Sowinski, and L. J. Romano, *J. Am. Chem. Soc.*, **97**, 1599 (1975); b) S. Uemura, A. Onoe, and M. Okano, *Bull. Chem. Soc. Jpn.*, **47**, 3121 (1974); c) S. Uemura, Kyoto University, personal communication, 1979.

11) D. R. McAlister, J. E. Bercaw, and R. G. Bergman, *J. Am. Chem. Soc.*, **99**, 1666 (1977).

12) a) H. Yamazaki and Y. Wakatsuki, *J. Organomet. Chem.*, **139**, 157 (1977); b) Y. Wakatsuki and H. Yamazaki, *ibid.*, **139**, 169 (1977).

Potentiometric Determination of the Concentration of Aggressive Anions That Can Be Tolerated by a Certain Passivator

Salah Mohamed Abd El Haleem and Ali Abd El Aal
Faculty of Science, Zagazig University, Zagazig, Egypt
(Received January 18, 1979)

The effect of various additives of Cl^-, Br^-, and I^- on the potential of a passivated steel electrode was established. In solutions of Na_2CrO_4, Na_2HPO_4, and Na_2WO_4, S-shaped relations were obtained between the steady-state potential and the quantity of the aggressive salt added. The resulting active potentials were established after an induction period which decreases with increase in the concentration of the attacking ions and/or decrease in that of the inhibiting anions. The concentration, C_{agg}, that can be tolerated by a certain concentration of the inhibiting anion, C_{inh}, is given by $\log C_{inh}=K+n \log C_{agg}$, where K and n are constants. The equation was derived theoretically on the basis of the changes produced in the structure of the double layer caused by specific adsorption of both aggressive and passivating ions. In solutions of $KMnO_4$, $NaNO_2$, and $K_3[(Fe(CN)_6)]$, the passivating film could not withstand the corroding action of the halide ions.

The minimum concentration of a certain passivator that can withstand the corroding action of a particular aggressive ion is of importance from theoretical as well as practical points of view.[1-9] The concentration was determined under certain conditions.[2-5,10-14] Only a few fundamental studies being carried out.[6-9,15] Some of the studies are based on time consuming measurements, such as weight loss or visual methods,[6-9,15-17] or on accelerated polarization techniques not in line with natural corrosion conditions.[18-20] It is desirable to establish a simple method to determine such a concentration, in a relatively short time and under natural corrosion conditions.

We have studied the variation of potential of a steel electrode under open circuit conditions, in order to establish the mode which the potential of an electrode, previously equilibrated in a certain passivator, would follow when increasing amounts of a corroding anion such as Cl^-, Br^-, and I^- were added to the solution, and to find a relation between the concentrations of the two counteracting anions. The type of corrosion that occurs always under these conditions is the localized type of attack, the extreme of which is pitting corrosion.[1,9]

Experimental Method and Materials

The steel electrodes (Delta steel Mill company, Cairo) have the same chemical composition as those used:[21,22]

C	Mn	S	P	Si
0.40	0.78	0.045	0.06	0.23%

The metal was machined in the form of short rods; length 2,4 cm, dia. 1 cm. This was fixed to Pyrex glass tubings with neutral wax. Electrical contact was achieved through thick copper wires soldered to the ends of the rods, not exposed to the solution. The electrodes were polished and abraded with the finest grade emery paper. They were then degreased with acetone and washed with triple-distilled water.

Two procedures were followed to achieve the variation of potential of the steel electrode.

Procedure A. The electrode was first equilibrated in a definite volume of the passivating (inhibiting) agent until a constant potential was established. Enough corrosive agent was then introduced into the solution to attain a definite concentration, and the change in potential was again followed with time. The effect of other quantities of the aggressive anions was examined in the same manner, starting always with a fresh solution of the inhibitor and with a newly polished electrode.

Procedure B. Increasing amounts of the aggressive salts were added to the same solution, allowing sufficient time for the establishment of constant potential.

Passivation (inhibition) of the steel electrode was carried out in solutions of different concentrations of Na_2CrO_4, Na_2HPO_4, Na_2WO_4, $KMnO_4$, $NaNO_2$, and $K_3[(Fe(CN)_6)]$. The concentration of the test solution was chosen to induce passivity rather than cause corrosion.[7,8,23,24] NaCl, NaBr and NaI (analytical grade) were used to introduce aggressive anion.

The potential of the steel electrode was measured, to the nearest mV, on Electronic Potentiometer (Metrohm pH meter type 512) relative to a saturated calomel electrode (SCE). This was separated from the main electrolyte by two salt bridges filled with the same passivating solution in order to prevent contamination with Cl^- ion. The steady-state potentials were considered valid when values were obtained, not changing more than 1 mV in 5 min. The electrolyte was stirred, a stream of oxygen, (2—3) bubbles/s) being passed during the course of experiment. Measurements were carried out at 25 ± 1 °C.

Results and Discussion

The curves with black circles in Fig. 1 represent the variation of the potential of the steel electrode with time in solutions of 0.1 M and 0.2 M Na_2CrO_4. The potential shifted towards positive values showing the occurrance of passivity,[23,24] and attained constancy after 160—180 min, following the immersion of the electrode in solution.

When a very small amount of Cl^- ion is introduced into the solution following passivation, the steady state potential remains more or less constant. Low Cl^- ion concentrations have no effect on the dissolution kinetics of the passive film already formed on the electrode surface.[22,25,26]

When the concentration of the Cl^- ion in solution is further increased, a state is soon reached where the Cl^- ion concentration is sufficent to undermine the protective film on the metal surface, causing the potentials of the electrode to change in the negative direction.

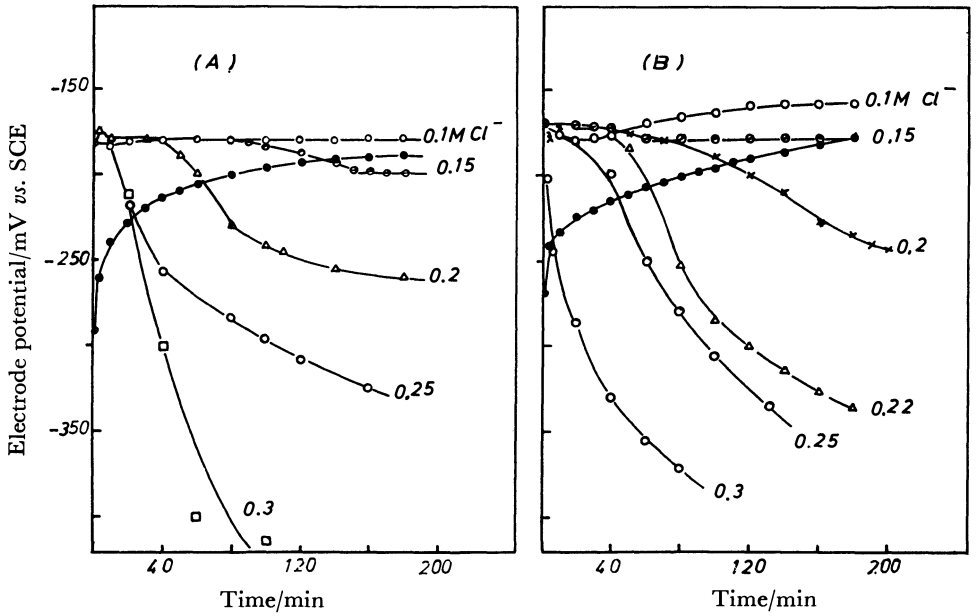

Fig. 1. Variation of the steel electrode potential with time in (A) 0.1 M and (B) 0.2 M Na_2CrO_4 in the presence of different NaCl additions.

Cl^- ions do not attack the passive electrode directly (cuves A and B, Fig. 1). A certain length of time elapses before the potential of the steel electrode changes from that measured in the Cl^--free solution. This is identified as the induction period[18,27] for pitting corrosion to occur. It decreases with the increase of the concentration of the aggressive anion.[18,27] In relatively concentrated Cl^- media, the induction period is too short to be recorded.

In the presence of Cl^- ions, the steel electrode acquires new steady state potentials. For a certain chromate concentration, these potentials become more negative the higher the Cl^- ion content. On the other hand, the potentials developed in equimolar solutions of Cl^- ion depend on the concentration of the passivating ion, being more positive the higher the chromate content.

The curves in Fig. 2 show the variation of the steady state potential of the passive steel electrode with the amount of NaCl, NaBr, and NaI in solutions of Na_2CrO_4 in the range 0.05—0.5 M using procedure (B) for measurements. Figures 3 and 4 represent the same behavior in Na_2HPO_4 and Na_2WO_4 solutions of different concentrations. They are sigmoid, showing normal mode of potentiometric titration, which may be used

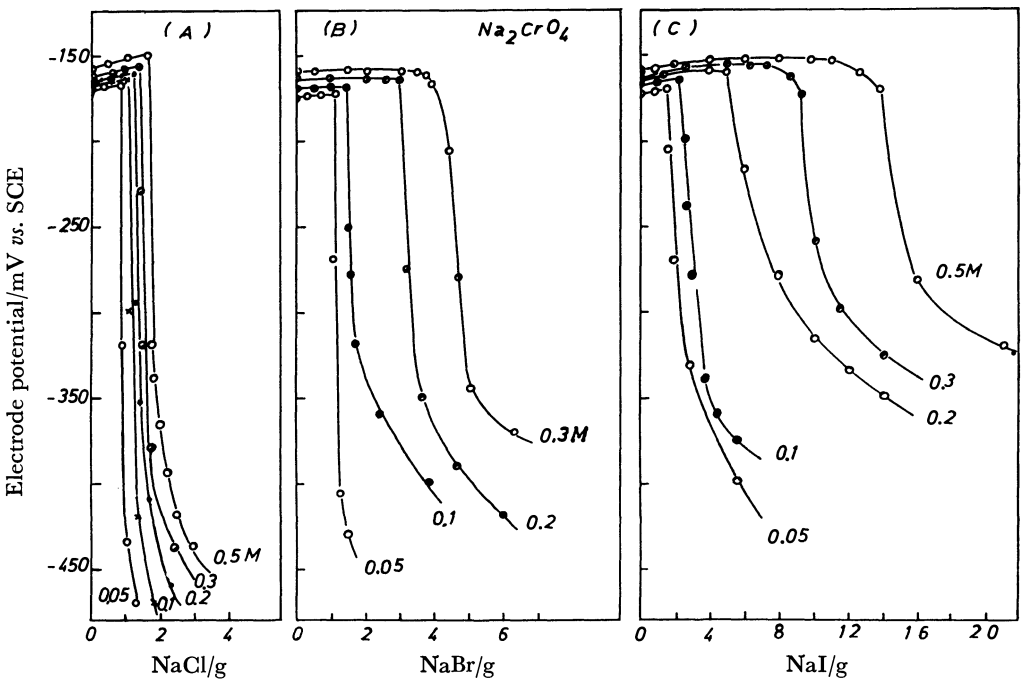

Fig. 2. Variation of the potential of the steel electrode previously passivated in different concentrations of Na_2CrO_4, with additions of NaCl, NaBr, and NaI.

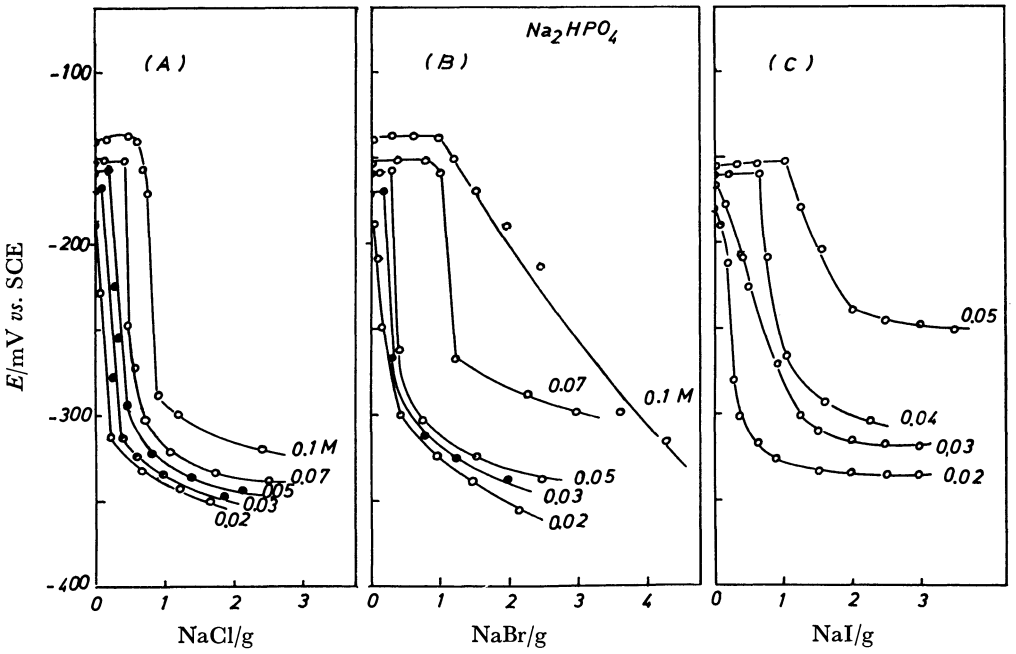

Fig. 3. Variation of the potential of the steel electrode previously passivated in different concentrations of Na_2HPO_4 with additions of NaCl, NaBr, and NaI.

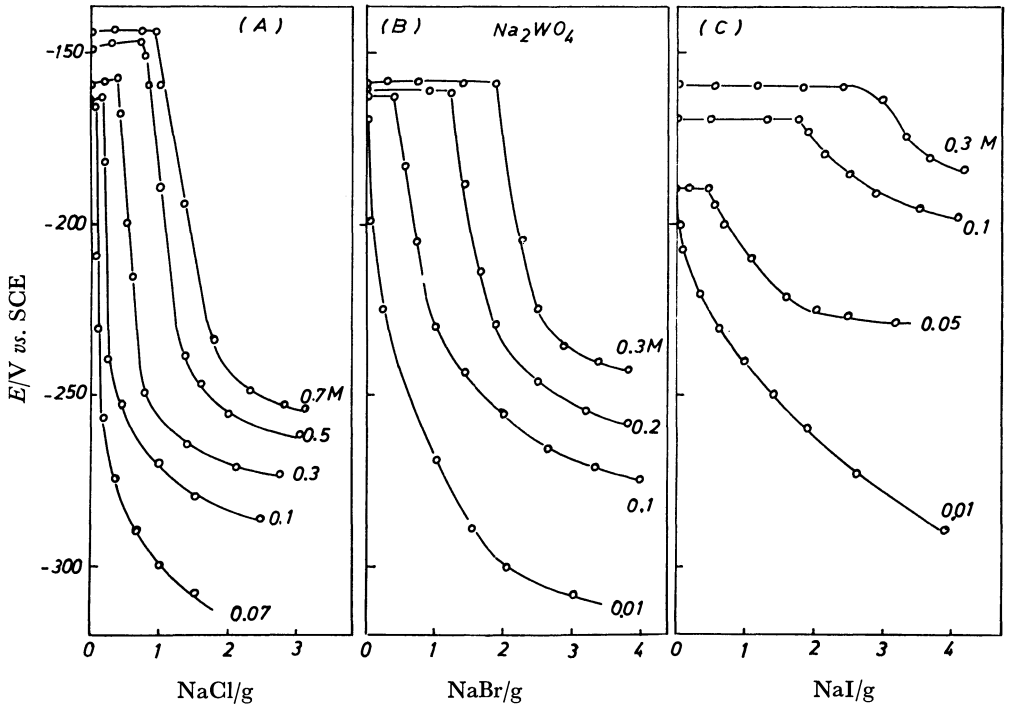

Fig. 4. Variation of the potential of the steel electrode previously passivated in different concentrations of Na_2WO_4 with additions of NaCl, NaBr, and NaI.

to determine the concentration of an inhibitor that can withstand a certain concentration of the aggressive ions. The starting potentials, measured in aggressive-free media, become more positive the higher the concentration of the inhibitor in solution. The rate of potential change at the inflexion point of the curves is inversely proportional to the same parameter. This is to be expected since it is easier to initiate pitting corrosion, which is the type of attack occurring under these conditions, in dilute passivating solutions than in concentrated ones. It appears that as the concentration of the inhibiting agent in solution is raised, more aggressive anion is needed to destroy the protective film on the metal surface and induce pitting corrosion.

The curves in Fig. 5 (A, B, and C) represent the effect of adding Cl^- ions of increasing concentrations

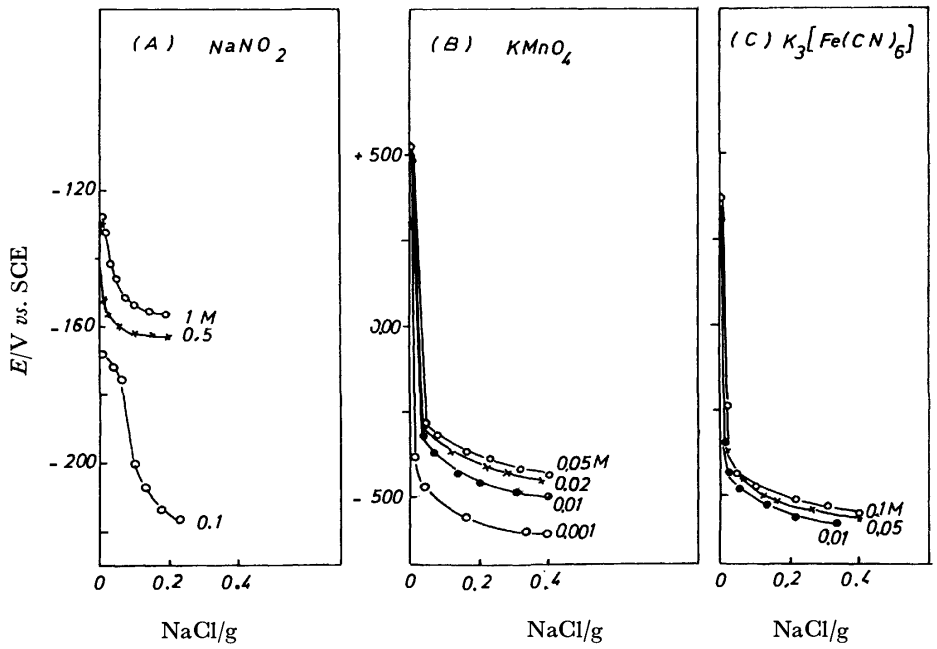

Fig. 5. Variation of the potential of the steel electrode previously passivated in different concentrations of (A) $NaNO_2$, (B) $KMnO_4$, and (C) $K_3Fe(CN)_6$, with the additions of NaCl.

to solutions of $NaNO_2$, $KMnO_4$, and $K_3[(Fe(CN)_6)]$, respectively. Despite the fact that the initial steady state potentials of the steel electrode in these media are equal to or higher than those measured in chromate, phosphate or tungestate solutions of the same concentration, the addition of Cl^- ions to the former solutions causes the potential to shift directly towards more negative values. Apparently treatment of the steel electrode in solutions of these oxidizing agents produces no permenant state of passivity.[1] This shows that the function of a certain passivator does not depend primarily on its redox-potential as much as on its ability to form an adhering and stable film on the metal surface. This is not the case with NO_2^-, MnO_4^-, and $[Fe(CN)_6]^{3-}$ anions, the reduction of which at the cathodic sites produces soluble corrosion products. Similar results were obtained in the case of zinc.[1]

Inflexion occurs in the potential of the steel electrode when enough aggressive salt is added to the inhibitive solution (Figs. 2—4). The inflexion indicates that the inhibiting film is being destroyed by the aggressive anions. Concentrated solutions of the passivator consume more attacking agent before the potential tends towards more negative values. The relation between the two variables is not linear.[1] There is no definite potential,[19,27] above which the metal withstands attack, and below which it undergoes corrosion. The choice of such a potential, to be taken as a basis for comparison, is thus arbitrary. Since the initial potential of the steel electrode in aggressive-free media depends on the ambient concentration of the passivator, choice of one and the same potential for all the solutions will not be free from error. It is more plausible, however, to relate this potential to that of the initial value in such a manner that it is common to all curves. Shams El Din and Abd El Haleem[1] assumed that the localized type of attack (pitting) is operative to the same extent in all solutions when enough of the aggressive anion is present to displace the initial potential to the negative direction by a constant value. The relation between C_{agg} and C_{inh} is considered at the point of inflexion (0 mV displacement), as well as at some other potentials (more negative to the starting potentials). The plot of the two variables on a double logarithmic scale for chromate solutions is given in Fig. 6. Similar results were obtained with phosphate and tungestate solutions. Parallel straight lines are obtained satisfying the relationship:

$$\log C_{inh} = K + n \log C_{agg}, \qquad (1)$$

where K and n are constants.

The values of the exponent n for solutions of Na_2CrO_4, Na_2HPO_4, and Na_2WO_4 containing the aggressive anion Cl^-, Br^-, and I^- are given in Table 1.

Table 1. Values of the exponent n in Eq. 1 for different inhibiting-aggressive pairs

Inhibitor	Na_2CrO_4			Na_2HPO_4			Na_2WO_4		
Aggressive	Cl^-	Br^-	I^-	Cl^-	Br^-	I^-	Cl^-	Br^-	I^-
n	3.25	1.2	0.93	0.72	0.6	0.45	1.0	0.97	0.33

It appears that (Fig. 1 and Table 1)
(1) n is independent of the potential at which it is determined, (2) n depends primarily on the type of the inhibitor, decreasing in the order $Cl^- > Br^- > I^-$, (3) the values of n in Na_2CrO_4 solution is significantly greater than that of the other two inhibitors.

Equation 1 was also obtained by other workers,[6-9,15,20] Matsuda and Uhlig[15] derived it by assuming the occurrence of competitive adsorption between the aggressive and the inhibiting anions. Brasher *et al.*,[9] on the other hand derived it by conferring

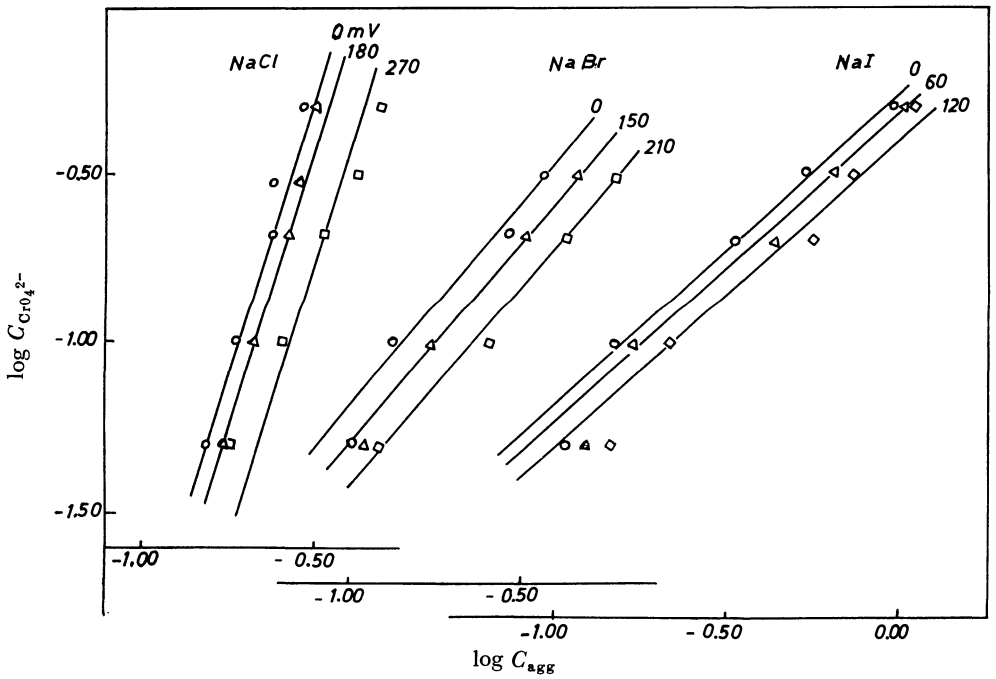

Fig. 6. log $C_{CrO_4^{2-}}$ – log C_{agg} plots at different potentials.

anion exchange properties to the oxide film formed on the metal surface. Selectivity for one or the other of two anions present in solutions was considered to depend on its nature as well as on its concentration. Anderson and Hocking[20] expressed a similar view.

In the present study, Eq. 1 is derived on the basis of the effect produced by both the inhibiting and corrosive anions, when specifically adsorbed on the metal surface, on the structure of the double layer at the metal/solution interface. The derivation is based on the following considerations: (a) In neutral solutions, the corrosive anions attack the passivating oxide film on the metal surface through specific adsorption of the anion,[28-30] their peptizing action on the metal oxide[31] and/or the creation of electrostatic fields through the oxide between opposite charges.[32] One or more of these processes is associated with decrease in the free energy of the system. (b) Inhibiting anions, on the other hand, play their role either by film repair as in the case of CrO_4^{2-} and NO_2^-,[6,7] or by blocking the active sites on the metal surface (benzoate).[8] Both effects involve a decrease in free energy at the metal/solution interface. (c) In solutions containing both the inhibiting and the corrosive anions, the process occurring depends primarily upon which of the two reactions is associated with a larger decrease in free energy. This, in turn, involves a number of associated features such as the concentration and charge of the ions, as well as their adsorbability on the oxide film. (d) The aggressive or the inhibiting anions should be adsorbed on the surface before reacting with the metal. Such adsorption affects both the structure of the double layer at the metal/solution interface, as well as the effective potential necessary for the electrochemical reaction. Figure 7 is a schematic presentation of the structure of the double layer, in which the specifically adsorbed anions occupy the inner Helmholtz plane (IHP), causing a potantial

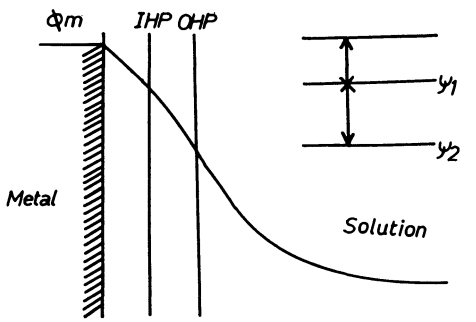

Fig. 7. Schematic presentation of the structure of the double layer at the metal/solution interface.

drop ϕ'. Anions bound only by electrostatic forces occupy the outer plane of the double layer (OHP) with a potential ϕ''. The diffuse double layer consisting of ions is dispersed in the direction of solution.

The relation between the surface concentration, C_s, and the bulk concentration, C_b, of a certain ionic species is given by[1]

$$C_s = C_b \exp(-\Delta G^\circ/RT), \quad (2)$$

where ΔG° is the standard electrochemical free energy change of adsorption, its value depending on the nature of interaction between the ions and the surface as well as their ionic charge, Z. In absence of specific adsorption, we have

$$\Delta \bar{G}^\circ = \pm ZF\phi''. \quad (3)$$

The positive and negative signs in Eq. 3 refer to whether adsorption of anions takes place on the negative or the positive side of the potential of the zero charge of the metal. On the other hand, for anions that are specifically adsorbed we have

$$\Delta \bar{G}^\circ = \Delta G^\circ \pm ZF\phi', \quad (4)$$

where ΔG° represents the standard chemical free energy of adsorption. The surface coverage, θ, with specifically adsorbed anions is given by

$$\theta = X \exp(-\Delta\bar{G}^\circ/RT), \quad (5)$$

where X is the mole fraction of the anion in the bulk of solution. However, in solutions of fixed concentration (x), θ is constant and ψ' is given by

$$\psi' = \pm\frac{RT}{ZF}\ln x + \text{constant}. \quad (6)$$

For a metal like iron immersed in a solution of an inhibiting anion (Z_1, X_1), until the establishment of the steady-state potential, a definite fraction of the metal surface is covered by specifically adsorbed anions, adsorbed either on the bare metal surface or on the oxide covering the metal. In this case, ψ_1' at the (IHP) is given by

$$\psi_1' = \pm\frac{RT}{Z_1F}\ln x_1 + \text{const}_1. \quad (7)$$

When an aggressive anion (Z_2) is added in a small amount after the establishment of the steady-state potential in an inhibiting solution, it will first be adsorbed on the free fraction of the surface. On gradual increase in the concentration of the aggressive ion, it will compete with the inhibiting anions for the sites occupied by the latter. Displacement of the inhibiting anions occurs by virtue of the smaller size of the aggressive ions (large charge density) and/or a large drop in the free energy of adsorption. When the concentration of the aggressive anions becomes equal to (X_2), *i.e.* at the end of the horizontal segments (curves, Figs. 2—4), it will represent the maximum amount of the aggressive anion that can be tolerated by the concentration X_1 of the inhibitor. The magnitude of ψ_2' corresponding to the aggressive anion at the (IHP) is given by

$$\psi_2' = \pm\frac{RT}{Z_2F}\ln x_2 + \text{const}_2. \quad (8)$$

Since $\psi_1'=\psi_2'$ apparently at the point of inflexion (Figs. 2—4), we have

$$\frac{RT}{Z_1F}\ln x_1 + \text{const}_1 = \frac{RT}{Z_2F}\ln x_2 + \text{const}_2 \quad (9)$$

or

$$\log X_1 = \frac{Z_1}{Z_2}\log X_2 + \text{constant}. \quad (10)$$

Equation 10 has the same form as that obtained experimentally or derived theoretically.[9,15] From the equation as well as the values of the exponent n (Table 1), we can draw the following conclusions:

1. Equation 10 is based on the idea of competitive adsorption, but unlike the treatment of Matsuda and Uhlig[15] and Brasher *et al.*,[9] it presumes no particular type of adsorption isotherms.

2. The potential of the working electrode remains practically constant until the ψ-potential for the electrode in the inhibiting medium starts to decrease as a result of excessive adsorption of the aggressive anion. The curves (Figs. 2—4) reveal that this is actually the case.

3. The exponent n of Eq. 1 is given here as the ratio of the electrical charges of the inhibiting/aggressive anions. Similar findings were suggested by Brasher *et al.*[9] The values (Table 1) show that this state of affairs is nearly fulfilled when HPO_4^{2-} and WO_4^{2-} are used as inhibitors. An exception is the WO_4^{2-}/I^- system, in which inhibition involves the reduction of the inhibitor with the probable formation of the iodocomplexes of the lower valent W. Concerning the CrO_4^{2-} ions, however, the value of n is almost twice that determined for the other two inhibitors. This is explained on the basis that CrO_4^{2-} reacts preferentially either in the $HCrO_4^-$ or the $Cr_2O_7^{2-}$ forms.[7]

4. Equation 1 holds not only at the inflexion points but also at other more active (negative) potentials, as long as they are referred to the starting potential measured in the aggressive-free media.

5. From the curves (Figs. 2—4) and Eq. 1, we can determine the concentration of the aggressive anion that can be tolerated by a certain concentration of the inhibiting anion, using a simple potentiometric method.

References

1) A. M. Shams El Din and S. M. Abd El Haleem, *Workstoffe Korros.*, **25**, 571 (1974).
2) E. Hoyn and O. Bener, *Mitt. K. Pruf. Amt. Berlin-Dahlem*, **26**, 74 (1908).
3) J. N. Friend and J. H. Brown, *J. Iron. Stell Inst.*, **83**, 125 (1911).
4) H. Endo, *Sci, Rep. Tokyo Univ.*, 1111 (1928).
5) T. P. Hoar and U. R. Evans, *J. Chem. Soc.*, **1932**, 2476.
6) D. M. Brasher and A. D. Mercer, *Br. Corros. J.*, **3**, 120 (1968).
7) A. D. Mercer and I. R. Jenkins, *Br. Corros. J.*, **3**, 130 (1968).
8) A. B. Morcer, I. R. Jenkins, and J. E. R. Brown, *Br. Corros. J.*, **3**, 136 (1968).
9) D. M. Brasher, D. Rachenberg, and D. Mercer, *Br. Corros. J.*, **3**, 144 (1968).
10) W. D. Robertson, *J. Electrochem. Soc.*, **98**, 94 (1951).
11) M. J. Pryora and M. Cohen, *J. Electrochem. Soc.*, **100**, 203 (1953).
12) R. Power and N. Hackerman, *J. Electrochem. Soc.*, **100**, 214 (1953).
13) B. E. Reetheli and G. L. Cox, *Ind. Eng. Chem.*, **23**, 1084 (1931).
14) M. Darrin, *Ind. Eng. Chem.*, **38**, 368 (1946).
15) S. Matsuda and H. H. Uhlig, *J. Electrochem. Soc.*, **111**, 156 (1958).
16) E. V. Bogatyreva and Balezin, *Zh. Prikl. Khim.*, **32**, 1071 (1959).
17) E. V. Bogatyreva and Balezin, *Izvest. Vyssh. Ucheb. Zaved., Khim. Khim. Tekh.*, **25**, 1 (1959).
18) M. P. Leckie and H. H. Uhlig, *J. Electrochem. Soc.*, **113**, 1262 (1966).
19) H. H. Uhilig and J. R. Gilman, *Corrosion*, **20**, 289t (1964).
20) P. J. Anderson and M. E. Hocking, *J. Appl. Chem.*, **8**, 352 (1945).
21) S. M. Abd El Haleem, S. S. Abd El Raheem, M. Sh. Shalaby, and A. M. Azzam, 4th Arabic Seminar, Cairo, 26—29, April (1975).
22) S. M. Abd El Haleem, S. S. Abd El Reheem, M. Sh.

Shalaby, and A. M. Azzam, *Werkstoffe, Korros.*, **27**, 630 (1976).
23) W. Robertson, *J. Electrochem. Soc.*, **98**, 49 (1951).
24) H. J. Engell and N. D. Stolica, *Z. Phys. Chem.*, **20**, 113 (1959).
25) S. M. Abd El Haleem, *Br. Corros. J.*, **11**, 215 (1976).
26) H. H. Uhlig, "The Corrosion Handbook," John Wiley and Sons, N. Y. (1948), p. 165.
27) W. Schwenk, *Corrosion*, **20**, 129t (1964).
28) A. Hickling, *Trans. Faraday Soc.*, **41**, 333 (1945).
29) B. Ershler, *Discuss. Faraday Soc.*, **1**, 269 (1947).
30) B. Kabanov, R. Burnstein, and A. Frumkin, *Discuss. Faraday Soc*, **1**, 259 (1947).
31) U. R. Evans, *Trans. Faraday, Soc.*, **18**, 1 (1922).
32) T. P. Hoar, D. Mears, and G. Rothwell, *Corros., Sci.*, **5**, 279 (1965).

Exact Relationship between Resonance Energies and Ring Currents of Aromatic Annulenes

Jun-ichi AIHARA

Department of Chemistry, Faculty of Science, Hokkaido University, Sapporo 060

(Received June 4, 1979)

Synopsis. Haddon's analytical relationship between the resonance energies and the ring currents of $(4n+2)\pi$-electron annulenes was decidedly improved by means of the graph theory of aromaticity.

An NMR criterion of aromaticity has widely been accepted according to which diamagnetic ring currents indicate aromaticity while paramagnetic ring currents indicate antiaromaticity.[1-2] However, it had not been clear that this magnetic criterion is equivalent to the energetic definition of aromaticity[3] until we previously proved that the diamagnetic susceptibility of a cyclic conjugated system[4,5] strongly reflects its conjugative stabilization.[6] In the case of annulenes, the sign of the susceptibility exactly accords with that of the resonance energy due to aromaticity.[7-10]

Recently, Haddon reported an analytical relationship between the resonance energies (*RE*s) and the reduced ring currents (*RC*s) of $(4n+2)\pi$-electron annulenes.[11] He adopted my former method (denoted by A-I)[7,8] to estimate the resonance energies, and found that the relationship takes the form

$$RE = \frac{\pi^2}{3S}RC, \tag{1}$$

where S is the area of the annulene ring, and RC the reduced ring current related linearly to the ring current intensity, I, in this manner:

$$I = \left[8\pi^2 c\left(\frac{e}{hc}\right)^2 H\right]RC. \tag{2}$$

Here, H is the applied magnetic field (taken perpendicular to the molecular plane), and the other symbols have their usual meaning.

The A-I method is one of the analytical methods for estimating the resonance energy of a cyclic conjugated system.[7,8] The π-bond energy of an infinitely large cyclic polyene is therein utilized in the definition of an olefinic reference structure. However, I have not been using this method since another method (denoted by A-II) was devised by means of graph theory.[8] At present, the A-II method appears to be physically much more sound and meaningful.[6,8-10] Accordingly, Haddon's treatment of ring currents[11] can naturally be improved on the basis of the A-II method. This is shown below.

Theory and Discussion

According to the A-II method,[8-10] a characteristic polynomial for an olefinic reference structure of a conjugated hydrocarbon can be written as

$$R(X) = X^N + \sum_{k=1}^{[N/2]} (-1)^k p(k) X^{N-2k}, \tag{3}$$

where N is the number of sp^2-carbon atoms in a conjugated system, $p(k)$ the number of ways of choosing k disjoint π bonds from the conjugated system,[12] and $[N/2]$ the maximum integer not larger than $N/2$. The resonance energy can be defined as the difference between the total π-electron energy of a conjugated system and that of its reference structure given by Eq. 3, and this is termed the A-II resonance energy.[8]

There are five kinds of $(4n+2)\pi$-electron annulenes; [4n+2]annulenes, $[4n]^{2+,2-}$annulenes, $[4n+1]^-$annulenes, and $[4n+3]^+$annulenes. These are all aromatic.[8-10] Fortunately, A-II resonance energies (*RE**) of these annulenes can be expressed analytically in the form[10]

$$RE^* = \frac{4(1-\cos\theta)\beta}{\sin 2\theta} \quad ([4n+2]\text{annulenes}) \tag{4a}$$

$$= \frac{4(1-\cos\theta)\beta}{\tan 2\theta} \quad ([4n]^{2+,2-}\text{annulenes}) \tag{4b}$$

$$= \frac{2(1-\cos\theta)\beta}{\sin\theta} \quad \begin{matrix}([4n+1]^-\text{annulenes and}\\ [4n+3]^+\text{annulenes}).\end{matrix} \tag{4c}$$

Here, $\theta=\pi/2N$. On the other hand, the reduced ring currents are given by[11,13]

$$RC = \frac{2S\beta}{N^2 \sin 2\theta} \quad ([4n+2]\text{annulenes}) \tag{5a}$$

$$= \frac{2S\beta}{N^2 \tan 2\theta} \quad ([4n]^{2+,2-}\text{annulenes}) \tag{5b}$$

$$= \frac{S\beta}{N^2 \sin\theta} \quad \begin{matrix}([4n+1]^-\text{annulenes and}\\ [4n+3]^+\text{annulenes}).\end{matrix} \tag{5c}$$

Combining Eq. 4 with Eq. 5, we obtain

$$RE^* = \frac{2N^2 RC}{S}(1-\cos\theta), \tag{6}$$

for all kinds of $(4n+2)\pi$-electron annulenes. It should be stressed that this is a single exact relationship found between the A-II resonance energies and the ring currents of aromatic annulenes.

In order to visualize the physical image of this relationship, let us expand the cosine in it into a corresponding power series as follows:

$$RE^* = \frac{\pi^2}{4S}RC\left(1-\frac{\pi^2}{48N^2}+\frac{\pi^4}{5760N^4}-\cdots\right). \tag{7}$$

Cleraly for large N it is possible to truncate Eq. 7 at the first term. Even for benzene ($N=6$), the error due to such truncation is less than one percent. Adopting this simplification, we obtain for the A-II resonance energy

$$RE^* = \frac{\pi^2}{4S}RC. \tag{8}$$

This expression is quite similar to Haddon's one (Eq. 1), but the proportionality constant is reduced to three-fourths. This is due to the fact that the A-I resonance energy is about 33 percent larger than the

A-II resonance energy for all aromatic annulenes, both neutral and ionic.[8] However, this difference is never a triviality. Considering that the A-II resonance energy only is closely related to the magnetic property of a cyclic conjugated system,[6] it will be evident that Eq. 8 is much more preferable to Eq. 1. In other words, Eq. 8 represents a more realistic relationship between the resonance energies and the ring currents of $(4n+2)\pi$-electron annulenes.

By the way, the diamagnetic susceptibility(χ_π) of an annulene conjugated system[5] is given by

$$\chi_\pi = \frac{SI}{cH}. \tag{9}$$

The following relationship then holds for aromatic annulenes:

$$\chi_\pi = 32\left(\frac{e}{hc}\right)^2 S^2 RE^*. \tag{10}$$

This expression indicates that the susceptibility is proportional both to the resonance energy and to the area of the annulene ring squared.

Concluding Remarks

The behavior of the ring current in relation to the A-II resonance energy has been considered above in the hypothetically bond-equalized case. The entire analysis has been simple and exact. As pointed out by Haddon,[11] encouraging evidence for Eqs. 1 and 8 has already been published in the case of aromatic bisdehydroannulenes,[14] for which proton chemical shifts nicely correlate with Hess-Schaad resonance energies.[15] However, any analytical relationship between resonance energies and ring currents cannot be obtained for antiaromatic annulenes, because bond alternation plays a crucial role in these compounds.[16]

Finally, it must be noted that Eq. 8 does not imply that a theoretical relationship must exist between the resonance energies and the ring currents of $(4n+2)\pi$-electron annulenes. It simply indicates the A-II resonance energy evaluated relative to the magnitude of the ring current. The close relationship found between these two quantities might have been regarded as superficial if a theoretical relationship between aromaticity and diamagnetism has not been established.[6]

Addendum. The realness of the roots of the same polynomial as Eq. 3 has already been proved by Heilmann and Lieb.[17] This proof warrants the realness of the A-II resonance energy. Professor L. J. Schaad kindly brought my attention to the Heilmann-Lieb paper.

References

1) See, *e.g.*, R. C. Haddon, V. R. Haddon, and L. M. Jackman, *Top. Curr. Chem.*, **16**, 103 (1971).
2) F. Sondheimer, *Acc. Chem. Res.*, **5**, 81 (1972).
3) J.-F. Labarre and F. Crasnier, *Top. Curr. Chem.*, **24**, 33 (1971); R. Breslow, *Acc. Chem. Res.*, **6**, 393 (1973).
4) B. Pullman and A. Pullman, "Les Théories Electroniques de la Chimie Organique," Masson et Cie, Paris (1952), Chap. IX.
5) L. Salem, "The Molecular Orbital Theory of Conjugated Systems," Benjamin, New York, N. Y. (1966), Chap. 4.
6) J. Aihara, *J. Am. Chem. Soc.*, **101**, 558 (1979).
7) J. Aihara, *Bull. Chem. Soc, Jpn.*, **48**, 517, 1501 (1975); **49**, 1427 (1976).
8) J. Aihara, *J. Am. Chem. Soc.*, **98**, 2750 (1976).
9) J. Aihara, *J. Am. Chem. Soc.*, **98**, 6840 (1976); **99**, 2048 (1977); **100**, 3339 (1978); *J. Org. Chem.*, **41**, 2488 (1976); *Bull. Chem. Soc. Jpn.*, **50**, 3057 (1977); **51**, 1788, 3540 (1978); **52**, 1529 (1979); I. Gutman, M. Milun, and N. Trinajstić, *J. Am. Chem. Soc.*, **99**, 1692 (1977).
10) I. Gutman, M. Milun, and N. Trinajstić, *Croat. Chem. Acta*, **49**, 441 (1977).
11) R. C. Haddon, *J. Am. Chem. Soc.*, **101**, 1722 (1979).
12) H. Hosoya, *Bull. Chem. Soc. Jpn.*, **44**, 2332 (1971); *Theor. Chim. Acta*, **25**, 215 (1972).
13) F. London, *J. Phys. Radium*, **8**, 397 (1937); R. McWeeny, *Mol. Phys.*, **1**, 311 (1958).
14) B. A. Hess, Jr., L. J. Schaad, and M. Nakagawa, *J. Org. Chem.*, **42**, 1669 (1977).
15) B. A. Hess, Jr., and L. J. Schaad, *J. Am. Chem. Soc.*, **93**, 305, 2413 (1971); **94**, 3068 (1972).
16) T. Nakajima and S. Kohda, *Bull. Chem. Soc. Jpn.*, **39**, 804 (1966); J. A. Pople and K. G. Untch, *J. Am. Chem. Soc.*, **88**, 4811 (1966).
17) O. J. Heilmann and E. H. Lieb, *Commun. Math. Phys.*, **25**, 190 (1972).

Thermodynamic Relation of Interfacial Tensions in Three Fluid Phases

Kazuo TAJIMA,* Takao TSUTSUI, and Hiroshi MURATA

Department of Chemistry, Faculty of Science, Tokyo Metropolitan University, Setagaya, Tokyo 158

(Received June 4, 1979)

Synopsis. The thermodynamic relation was derived for the interfacial tensions at the three interfaces of two immiscible solutions and their vapor phase at a constant temperature. The relation obtained was experimentally tested by measuring each interfacial tension of systems which consisted of organic (alcohols(C_4—C_{10}), triolein, and hexadecane) and aqueous phases. The relation of the interfacial tensions was valid for the polar oil–water systems. but not for the hexadecane–water system unless a surfactant was added.

It is well known as the so-called Antonoff rule that the interfacial tension at two liquid phases can be expressed by the difference in each surface tension at the vapor–solution interfaces. The validity of Antonoff rule, introduced without any theoretical proof,[1] has been tested by many investigators. The crucial conclusion, however, has not yet been drawn.[2–6]

The present work attempts to establish the thermodynamic relation between each surface tension at the three interfaces (*e.g.*, vapor–water, vapor–oil, and oil–water) of the vapor and the two liquid phases, which are mutually saturated. The relation derived will be verified by experiments.

Theoretical

The system taken is that in which the two liquid phases, which are mutually saturated, are equilibrated with the vapor phase at a constant temperature and pressure. Let us consider what relation is established in these interfacial tensions when the system is altered in an isothermal and reversible change, as is shown in Fig. 1, at a constant total volume and mass. We assume that the internal energy for the whole system, U, is completely defined by the variables of the following function:

$$U = U(T,\ V,\ \sum_{\theta} A^{\theta},\ N) \tag{1}$$

where T is the absolute temperature; V, the total volume of the system; A^{θ}, the interfacial area at the interface, θ, and N, the total number of moles of the species in the system. The interfacial total excess volume, V^e, is defined and assumed by the Gibbs convention as follows:

$$V^e = V - \sum_{j} V^j = 0 \tag{2}$$

Therefore, N is related to:

$$N = \sum_{ij} n_i^j + \sum_{i\theta} \Gamma_i^{\theta} A^{\theta} \tag{3}$$

where n_i^j is the mole numbers of the component i in the homogeneous bulk phase, j; Γ_i^{θ}, the mole numbers of the component i per unit area at the interface, θ; the summations of j and θ are taken over the three bulk (k, l, and m) and interfacial (α, β, and γ) phases, and i is taken for the binary components (1 and 2). The total excess internal energy of the interface, U^e,

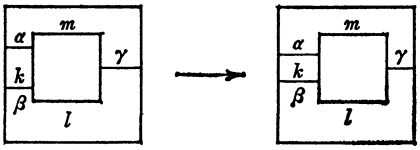

Fig. 1. Isothermal changes in interfacial area at constant total volume and mass. The phases, k, l, m show two immiscible solutions and their vapor, and α, β, γ three interfaces.

is defined as:

$$U^e = U - \sum_{j} U^j = \sum_{\theta} U^{\theta} \tag{4}$$

where U^j and U^{θ} denote the internal energies of the bulk phases, j, and the interfacial phase, θ, defined as follows:

$$\left.\begin{aligned} U^j &= U^j(T,\ V^j,\ \sum_i n_i^j) \\ \text{and:}\quad U^{\theta} &= U^{\theta}(T,\ A^{\theta},\ \sum_i \Gamma_i^{\theta}) \end{aligned}\right\} \tag{5}$$

Since, from the definition of Eq. 2, Γ_1^{θ} is equal to zero, for the infinitesimal changes of U^e we obtain:[7]

$$dU^e = \sum_{\theta}\left[\left(\frac{\partial U^{\theta}}{\partial T}\right)_{A,\Gamma} dT + \left(\frac{\partial U^{\theta}}{\partial A^{\theta}}\right)_{T,\Gamma} dA^{\theta} + \left(\frac{\partial U^{\theta}}{\partial \Gamma_2^{\theta}}\right)_{T,A} d\Gamma_2^{\theta}\right] \tag{6}$$

and:

$$\left(\frac{\partial U^{\theta}}{\partial A^{\theta}}\right)_{T,\Gamma} = \sigma^{\theta} + b^{\theta}$$

where σ^{θ} is the interfacial tension at the interface, θ, and b^{θ} is the heat of expansion of the interface, θ. Usually this term can not be neglected in the adiabatic expansion for the thin film surfaces, but it is customarily considered to be approximately zero for the adsorbed films. If the variation in the surface area does not affect any thermodynamic stabilities of the system under the conditions considered, we obtain:

$$dU^e = \sum_{\theta} (\sigma^{\theta} + b^{\theta}) dA \tag{7}$$

Furthermore, the changes in the surface area at each interface, according to the process shown in Fig. 1, are related to:

$$dA^{\alpha} = dA^{\beta} = -dA^{\gamma} = dA \neq 0 \tag{8}$$

This equiarea change at a constant total area establishes the trivial nature of the contribution of the b^{θ} term to the internal energy change of the system as a whole, because the dissipation of the surface at the γ interface and the creation of new surfaces at the α and β interfaces occur simultaneously. Thus, if the total b^{θ} terms are compensated for, the interfacial systems can be changed isothermally. Therefore, substituting Eq. 8 into 7, we obtain finally:

$$\sigma^{\alpha} + \sigma^{\beta} = \sigma^{\gamma} \tag{9}$$

Consequently, Eq. 9, the so-called Antonoff relation,

Table 1. Interfacial tensions in the vapor-oil-water interfaces

Substance	Temp °C	$\sigma^{v/w}$ mN m^{-1}	$\sigma^{v/o}$ mN m^{-1}	$\sigma^{o/w}$ mN m^{-1}	$\sigma^{o/w}_{cal}$ mN m^{-1} from Eq. 9[a]
1-Butanol	25	26.7	24.8	2.0	1.9
1-Hexanol	25	30.0	25.5	4.8	4.5
1-Octanol	25	33.5	27.0	6.7	6.5
1-Decanol	25	36.5	28.0	9.0	8.5
Triolein	30	50.3	31.2	19.0	19.1
Hexadecane	30	71.0	27.5	51.4	43.5
Hexadecane+surfactant[b]	30	65.8	27.0	38.2	38.8

a) α=v/o, β=o/w, γ=v/w. b) *N*-Dodecyl-β-alanine was added as a surfactant.

is derived thermodynamically for a system which is composed of the vapor and two liquid phases, which are mutually saturated at a constant temperature and pressure. The validity of Eq. 9 can be tested experimentally.

Experimental

Normal alcohols with carbon atoms of 4, 6, 8, and 10, triolein and hexadecane were used as one liquid phase, while the other was water. The organic and aqueous phases were mutually saturated by letting stand them for 10 days with occasional shaking. The surface tensions of the three interfaces were measured by the Wilhelmy plate method. When the tension of the oil–water interface was measured, particular attention was paid to the wetting and the correction of buoyancy for the plate.[8] The interfacial tension was measured within an experimental error of $\pm$0.3 mN m^{-1}. The temperature of the system was controlled by circulating the thermostatic water.

Results and Discussion

The results are shown in Table 1. It may be seen that Eq. 9 was valid for the alcohol–water and triolein–water systems, but not for the hexadecane–water system. The inconsistency of Eq. 9 with the experimental results for the hexadecane–water system was mainly considered to be the result of the incompleteness of the mutual solubilities.[9] The hexadecane–water system, however, to which a surfactant soluble in both liquid phases was added, obeyed the relation of Eq. 9. The use of such a surfactant is considered to promote the increasing mutual solubilities of the system and to favor the formation of stable films at each interface, as in the polar oil–water system.

In conclusion, if the system is allowed to reach the thermodynamic equilibrium, and if the equilibrium interfacial tensions are measured, Eq. 9 can be used to explain the correlation between the interfacial tensions of the three fluid phases, especially for the systems composed of the two polar liquid phases with high mutual solubilities.

References

1) N. K. Adam, "The Physics and Chemistry of Surfaces," Dover, New York (1968), pp. 179 and 215.
2) G. L. Gaines, Jr., and G. L. Gaines, III, *J. Colloid Interface Sci.*, **63**, 394 (1978); **66**, 593 (1978).
3) J. C. Lang, Jr., P. K. Lim, and B. Widom, *J. Phys. Chem.*, **80**, 1719 (1976).
4) L. A. Girifalco and R. L. Good, *J. Phys. Chem.*, **61**, 904 (1957).
5) R. L. Good and E. Elbing, "Chemistry and Physics of Interfaces," Am. Chem. Soc., Washington (1971), Vol. 2, p. 78.
6) F. M. Fowkes, "Chemistry and Physics of Interfaces," Am. Chem. Soc., Washington (1971), Vol. 2, p. 154.
7) R. Defay, I. Prigogine, A. Bellemans, and D. H. Everett, "Surface Tension and Adsorption," Longmans, London (1966), p. 34.
8) J. A. G. Taylor and J. Mingins, *J. Chem. Soc., Faraday Trans. 1*, **71**, 1161 (1975).
9) F. Franks, *Nature*, **210**, 87 (1966); F. P. Krause and W. Lange, *J. Phys. Chem.*, **69**, 3171 (1965).

The Solvent Extraction Study of a Dibenzo-18-crown-6 Complex with Silver Picrate

Yasuyuki TAKEDA* and Fujio TAKAHASHI

Department of Chemistry, Faculty of Science, Chiba University, Yayoi-chō, Chiba 260

(Received September 5, 1979)

Synopsis. The extraction constant of the silver ion–dibenzo-18-crown-6 (DB18C6) complex between benzene and water and the complex-formation constant of DB18C6 with silver picrate in benzene were determined at 25 °C. The Ag^+–DB18C6 complex is much more extractable than the Ag^+–18-crown-6 one. The Ag^+–DB18C6 complex is much more stable for benzene than for aqueous solutions.

The solvent extractions of uni- and bivalent metal ions with crown ethers to date have been investigated; these data show that the crown ethers form stoichiometrically stable complexes with the metal ions.[1] In some of these studies, the overall extraction equilibria have been analyzed by means of the constituent equilibria, and the extractability of the metal cation–crown ether complex as well as that of the metal cation have been discussed in detail.[1a–1d]

In the present study, the extraction constant values of the silver picrate and the silver picrate–dibenzo-18-crown-6 (DB18C6) systems have been determined between benzene and water, the overall extraction equilibrium of the latter system has been analyzed by means of the constituent equilibria, and the complex-formation constant values of DB18C6, 15-crown-5 (15C5), 18-crown-6 (18C6), and dibenzo-24-crown-8 (DB24C8) with the silver picrates in a benzene solution have been calculated using the extraction constant value of the silver picrate.

Experimental

The DB18C6 was obtained from the Aldrich Chemical Co., Inc. The $AgNO_3$ and picric acid were of an analytical grade and were from the Koso Chemical Co., Ltd. The method of the purification of DB18C6[2] and the determinations of the concentrations of $AgNO_3$ and the picric acid solutions[1d] have been described in the literature. Analytical-grade benzene (Wako-Pure Chemicals, Ltd.) was washed twice with distilled water. The benzene or the benzene solution of DB18C6 (4.0×10^{-4}—4.1×10^{-3} M; 1M=1 mol dm^{-3}) and the aqueous solution of $AgNO_3$ (3.0×10^{-3}—6.0×10^{-3} M) and the picric acid (1.9×10^{-3}—8.0×10^{-3} M) in stoppered 30-ml glass tubes were shaken in a thermostated water bath for approx. 30 min at 25±0.2 °C and then centrifuged. The initial volume of each phase was 10 ml in all cases. All the extractions were conducted in the pH range of 2.2—2.5. The Ag in the organic phase was back-extracted into a 1M nitric acid aqueous solution (8 ml), and the Ag concentration in the aqueous phase was determined by the use of a Seiko SAS-725 atomic absorption spectrophotometer.

Results

In an equilibrium between an aqueous solution of a univalent metal ion, M^+, a picrate ion, A^-, and benzene, and its solution of a crown ether, L, the equilibrium constants may be defined by the following equations:

$$K_{ex}(1) = [MA]_o[H^+]/[M^+][HA]_o \quad (1)$$

$$K_{ex}(2) = [MLA]_o[H^+]/[M^+][L]_o[HA]_o \quad (2)$$

$$K_{D,L} = [L]_o/[L] (K_{D,L} = 800 \text{ for DB18C6}^{1a)}) \quad (3)$$

$$K_{ex}(HA) = [HA]_o/[H^+][A^-] \quad (4)$$

$$K_{ML} = [ML^+]/[M^+][L] \quad (5)$$

$$K_{ex}(3) = [MLA]_o/[ML^+][A^-] \quad (6)$$

where the subscript "o" and the lack of subscript designate the organic phase and the aqueous phase respectively; square brackets indicate the molar concentrations. Thus, $K_{ex}(2)$ can be written as follows:

$$K_{ex}(2) = K_{D,L}^{-1}K_{ex}(HA)^{-1}K_{ML}K_{ex}(3) \quad (7)$$

In the absence of crown ether, the distribution ratio of the metal may be represented by:

$$D_M = [MA]_o/[M^+] \quad (8)$$

The substitution of Eqs. 1 and 4 into Eq. 8 gives:

$$D_M = K_{ex}(1)K_{ex}(HA)[A^-] \quad (9)$$

The $\log D_M$ *vs.* $\log[A^-]$ plot for Ag^+ in Fig. 1 shows a linear relationship with a slope of 1, indicating that the $K_{ex}(1)$ in the present study can be described by Eq. 1. The value of $[A^-]$ in Eq. 9 was calculated from Eq. 10:

$$[A^-] = ([HA]_t - [MA]_o)/\{1+(K_{HA}+K_{ex}(HA))[H^+]\} \quad (10)$$

where the subscript "t" denotes the total concentration. The value of $K_{ex}(HA)$ was spectrophotometrically determined to be 247 by using the association constant of picric acid ($K_{HA}=1.9_5$[3]). When a crown ether exists in the extraction system, D_M may be represented by:

$$D_M = [MLA]_o/([M^+]+[ML^+]) \quad (11)$$

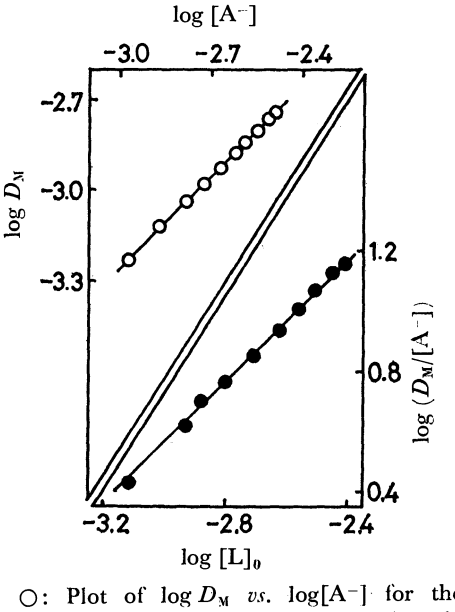

Fig. 1. ○: Plot of $\log D_M$ *vs.* $\log[A^-]$ for the Ag^+ system at 25 °C. ●: Plot of $\log(D_M/[A^-])$ *vs.* $\log[L]_o$ for the Ag^+–DB18C6 system at 25 °C.

Table 1. $\log K_{ML}$ and $\log\{K_{ex}(2)/K_{ex}(1)\}$ values for Ag^+-crown ether systems at 25 °C

Crown ether	$\log K_{ML}$	$\log\{K_{ex}(2)/K_{ex}(1)\}$
15C5	0.94[4]	4.71[a]
18C6	1.50[4]	4.70[a]
DB18C6	1.41[5]	3.82
DB24C8	—	3.35[b]

a) The $\log K_{ex}(2)$ values for 15C5 and 18C6 are 2.06 and 2.05 respectively.[1d] b) $\log K_{ex}(2) = 0.70$.[1e]

In the case of $[M^+] \gg [ML^+]$, Eq. 11 becomes:

$$D_M = K_{ex}(2)K_{ex}(HA)[A^-][L]_o \quad (12)$$

The $\log(D_M/[A^-])$ *vs.* $\log[L]_o$ curve in Fig. 1 is linear, with a slope of 1, indicating that DB18C6 forms a 1:1 complex with the Ag^+ ion. The values of $[A^-]$ and $[L]_o$ in Eq. 12 were calculated from Eqs. 13 and 14 respectively:

$$[A^-] = ([HA]_t - [MLA]_o)/\{1 + (K_{HA} + K_{ex}(HA))[H^+]\} \quad (13)$$

$$[L]_o = [L]_t - [MLA]_o \quad (14)$$

The values of $\log K_{ex}(1)$ and $\log K_{ex}(2)$ for the Ag^+ and the Ag^+–DB18C6 systems, as calculated from the data of Fig. 1, are −2.65 and 1.17 respectively.

Discussion

$K_{ex}(2)/K_{ex}(1)$ in Table 1 represents the formation constant for the 1:1:1 complex of the crown ether with the silver picrate in a benzene solution. Table 1 shows that the complex-formation constants are very much larger for benzene than for aqueous solutions. The stability of the 15C5 complex is the highest of all the crown ether complexes in a benzene solution; on the contrary, it is the lowest in an aqueous solution. The difference in the complex-formation constant values between 18C6 and DB18C6 considerably increases in going from water to benzene. The $\log\{K_{ex}(2)/K_{ex}(1)\}$ value of DB24C8 is the smallest, although it has the most donor oxygen atoms (eight) of all these crown ethers. The picrate anion was used as the only counter ion in this work. However, the anion effect on the complex-formation reaction in a low polar solvent may be very important, since an ion-pair complex-formation reaction, *e.g.*, $AgA + L \rightleftharpoons AgLA$ in the present study, occurs in a solvent with a low dielectric constant.

As may be seen from Table 2, in the cases of both 18C6 and DB18C6, the $\log K_{ex}(3)$ values of K^+ and Tl^+, which have very much smaller $-\Delta G_h^\circ$ values and much more optimum sizes for the 18C6 and DB18C6 cavities (radius: 1.3—1.6 Å[1c]) than does Ag^+, are larger than that of Ag^+; the $\log K_{ex}(3)$ values of Rb^+ and Cs^+, which have very much smaller $-\Delta G_h^\circ$ values than Ag^+ and no more optimum sizes for the 18C6 and DB18C6 cavities than Ag^+ has, are larger than that of Ag^+; the $\log K_{ex}(3)$ value of Ag^+, which fits more closely into the 18C6 and DB18C6 cavities than Na^+, is larger than that of Na^+, although the $-\Delta G_h^\circ$ value of Ag^+ is much greater than that of Na^+. It has been found that the structure of the crown ether complex with the cation in the center of the crown ether ring does not require the stripping of the entire solvation shell of the ion, since solvent contacts are still possible in the direction perpendicular to the plane of the ring.[8] It thus appears that the extractability of the univalent metal ion complex with the same crown ether in this work is determined primarily by both the ratio of the ionic size to the cavity size of 18C6 and the interaction of the metal ion trapped in the cavity with water molecules. The remarkable substituent effect of the two benzo groups attached to 18C6 on the extractability of the Ag^+ complex can be seen in Table 2; *i.e.*, the difference in the $\log K_{ex}(3)$ values of Ag^+ and Na^+ markedly increases from 18C6 to DB18C6, while, on the contrary, that of Ag^+ and each of the others decreases and the Ag^+–DB18C6 complex, whose molar volume is much larger than that of the Ag^+–18C6 complex, is much more extractable than the Ag^+–18C6 one.

References

1) a) T. Iwachido, A. Sadakane, and K. Tōei, *Bull. Chem. Soc. Jpn.*, **51**, 629 (1978); b) T. Sekine, H. Wakabayashi, and Y. Hasegawa, *ibid.*, **51**, 645 (1978); c) Y. Takeda and H. Katō, *ibid.*, **52**, 1027 (1979); d) Y. Takeda and H. Gotō, *ibid.*, **52**, 1920 (1979); e) Y. Takeda, *ibid.*, **52**, 2501 (1979).

2) N. Matsuura, K. Umemoto, Y. Takeda, and A. Sasaki, *Bull. Chem. Soc. Jpn.*, **49**, 1246 (1976).

3) "Dissociation Constants of Organic Acids in an Aqueous Solution," ed by G. Kortün, W. Vogel, and K. Andrussov, Butterworths, London (1961).

4) R. M. Izatt, R. E. Terry, B. L. Haymore, L. D. Hansen, N. K. Dalley, A. G. Avondet, and J. J. Christensen, *J. Am. Chem. Soc.*, **98**, 7620 (1976).

5) E. Shchori, N. Nae, and J. Jagur-Grodzinski, *J. Chem. Soc., Dalton Trans.*, **1975**, 2381.

6) H. L. Friedman and C. V. Krishnan, "Water," ed by F. Franks, Plenum, New York (1973), Vol. 3, p. 55.

7) L. Pauling, "The Nature of the Chemical Bond," 3rd ed, Cornell Univ. Press (1960).

8) D. Bright and M. R. Truter, *Nature (London)*, **225**, 176 (1970).

Table 2. $\log K_{ex}(3)$ values and free energies of hydration, ΔG_h°, at 25 °C and crystal ionic radii of metal ions

	Na^+	K^+	Rb^+	Cs^+	Ag^+	Tl^+
18C6[1d]	1.39	2.74	2.67	2.19	1.74	2.83
DB18C6	3.9[1a]	5.9[1a]	5.6[1a]	5.2[1a]	5.1	5.9[1b]
$-\Delta G_h^\circ$/kJ mol^{-1} [6]	411	338	320	297	479	343
Crystal ionic radius/Å[7]	0.95	1.33	1.48	1.69	1.26	1.40

Spin-trapping Reactions in γ-Irradiated Benzene Solutions. Generation of Authentic Spin-adduct Radicals

Tsuneki ICHIKAWA* and Hiroshi YOSHIDA
Faculty of Engineering, Hokkaido University, Kita-ku, Sapporo 060
(Received September 12, 1979)

Synopsis. Spin-trapping in γ-irradiated solutions of chlorinated hydrocarbons in benzene by using 2,4,6-tri-*t*-butylnitrosobenzene revealed that transient free radicals are generated almost exclusively by the dissociative electron attachment to the solutes. This provides a simple, useful method for preparing the authentic spin-adducts of hydrocarbon radicals.

The spin-trapping technique has been utilized for the detection of short-lived free radicals involved in chemical reactions. The technique comprises the conversion of the short-lived radicals into the stable nitroxide radicals (spin-adducts) by the reaction with nitroso or nitrone compounds (spin-traps) and the observation of the latter radicals by means of the conventional ESR method. The ESR spectra of authentic spin-adducts are essential for the identification of the spin-trapped short-lived radicals. The authentic spin-adducts have been generated by several methods.[1-4] We wish to report a simple radiation-chemical method which is applicable in spin-trapping studies.

The free radicals were generated by the dissociative electron attachment, $RCl+e^- \rightarrow R\cdot + Cl^-$, to chlorinated hydrocarbons in γ-irradiated benzene solutions. Benzene was chosen as solvent because the radiation-chemical yield of the free radicals from neat benzene (per 100 eV radiation energy absorbed, *G*-value) is as low as 0.4.[5] In contrast, the yield is generally as high as 3 in saturated hydrocarbons, so that the spin-adducts of the solvent radicals sometimes prevent detection of free radicals from solutes in saturated hydrocarbon solvents by the spin-trapping technique.

Experimental

Benzene of spectrograde was used. Reagent grade chlorinated hydrocarbons were used as solutes without further purification. The spin-trap, 2,4,6-tri-*t*-butylnitrosobenzene,[6] was supplied by Dr. Masahiro Tabata, Hokkaido University. The sample solutions were degassed by freeze-pump-thaw cycles, sealed in ESR tubes at 10^{-3} Pa irradiated with ^{60}Co γ-rays, and subjected to measurements with an ESR spectrometer (JEOL, JES-ME-2X). The yield of the spin-adducts was determined by using the DPPH solution in benzene as a standard. All the experimental procedures were carried out at ambient temperture (20±2 °C).

Results and Discussion

The ESR spectrum recorded from benzene containing only the spin-trap is predominantly due to the spin-adduct of phenyl radical[2] (Fig. 1A). The spectral lines indicated by arrows show a minor contribution from unidentified free radicals. The generation of phenyl radical from benzene is necessarily accompanied by the formation of hydrogen atoms. However, they cannot be observed by the spin-trapping technique.

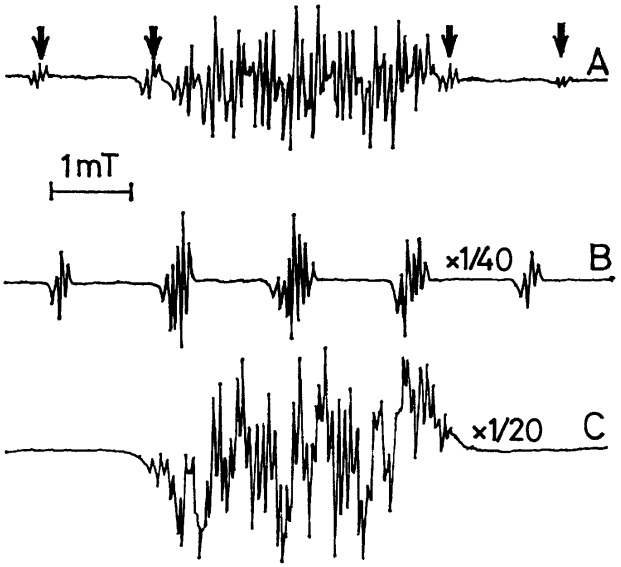

Fig. 1. ESR spectra of spin-adducts generated in benzene containing the 0.01 mol/dm³ spin-trap (A) with no other solute, (B) with benzyl chloride and (C) with *o*-chlorotoluene, γ-irradiated to the dose of 1×10^{19} eV/g.
The concentration of the chlorinated hydrocarbons is 0.2 mol/dm³ for all the samples. Arrows indicate the spectrum due to an unidentified spin-adduct. Relative sensitivity in the ESR measurements is shown in the figure.

Probably they readily react with benzene to form cyclohexadienyl radicals, which are too stable due to the π-conjugation to react with the spin-trap. The *G*-value of the spin-adduct of the phenyl radical is only 0.01 at 0.01 mol/dm³ of the spin-trap.

Effects of the addition of solutes to the solution are summarized as follows. No change observed in the spectrum on addition of 0.2 mol/dm³ toluene. The yield of the spin-adduct of phenyl radical increases by four times on addition of 0.2 mol/dm³ chlorobenzene. A spectrum almost exclusively due to the spin-adduct of benzyl radical (Fig. 1B) was observed on addition of 0.2 mol/dm³ benzyl chloride. In contrast, the spin-adduct of a phenyl-type radical (very probably *o*-methylphenyl radical) was observed on addition of *o*-chlorotoluene, but no formation of the benzyl-type radical.

The results indicate that short-lived free radicals are generated by the dissociative attachment of the electrons released by γ-rays to the chlorinated compounds and converted into the stable nitroxide radicals by the spin-trap. An alternative mechanism in which the free radicals are generated by the dissociation of the excited solutes resulting from the energy transfer from the solvent is excluded by the formation of the

phenyl-type radical from *o*-chlorotoluene. The bond energy for the benzyl–hydrogen bond (3.7 eV) is smaller than that for the phenyl–chlorine bond (4.1 eV),[7] so that the benzyl-type radical should be generated from the excited *o*-chlorotoluene.

The total energy for the dissociative electron attachment reaction is given by

$$E = BE(\text{R-Cl}) - EA(\text{Cl}) - E_s(\text{Cl}^-) - E(\text{e}^-), \quad (1)$$

where BE(R–Cl) denotes the C–Cl bond energy, and EA(Cl) the electron affinity of the chlorine atom, 3.6 eV.[7] The solvation energy of the chloride ion, $E_s(\text{Cl}^-)$, can be estimated to be 2.2 eV by the Born formula and from the ionic radius, 1.81 A,[7] and the dielectric constant of benzene, 2.28.[7] The energy of electron in benzene, $E(\text{e}^-)$, is −0.5 eV.[8] Thus eq. 1 is reduced to $E=BE(\text{R-Cl})-5.3$ eV. Since the C–Cl bond energy is generally smaller than 5.3 eV, the reaction is exothermic. Thus, the dissociative electron attachment readily occurs to give free radicals from chlorinated hydrocarbon solutes.

Propyl, butyl, α-methylbenzyl, and phenylethyl radicals can actually be generated by the dissociative electron attachment to the corresponding chlorides, and are detected by means of the spin-trapping technique. The hyperfine couplings of spin-adducts thus formed are in good agreement with those reported. The coupling constants for the spin-adduct of benzyl radical, 1.32 mT (two protons), 0.08 mT (two protons), and 1.48 mT (a nitrogen nucleus), differ slightly from the coupling constants observed in toluene solution, 1.362 mT, 0.083 mT, and 1.475 mT.[2] The solvent effect on the coupling constants is appreciable even between benzene and toluene.

Figure 2 shows the relation between radiation dose and the yield of the spin-adduct of butyl radical generated from butyl chloride. No influence of the dose rate indicates that the bimolecular recombination of butyl radicals is practically absent. The gradual decrease in the rate of formation of the spin-adduct with the radiation dose indicates that butyl radicals react competitively with the spin-traps and the spin-adducts. The latter reaction is generally found in spin-trapping studies and is important in the kinetic analysis of the spin-trapping reactions.[3,9]

The yield of the butyl radical spin-adduct is proportional to the concentration of the added butyl chloride: [spin-adduct]$=1.8\times10^{-5}$ [butyl chloride] has been obtained for the spin-trap concentration of 0.01 mol/dm^3, the butyl chloride concentration lower than 0.4 mol/dm^3, and the radiation dose of 1×10^{19} eV g^{-1}.

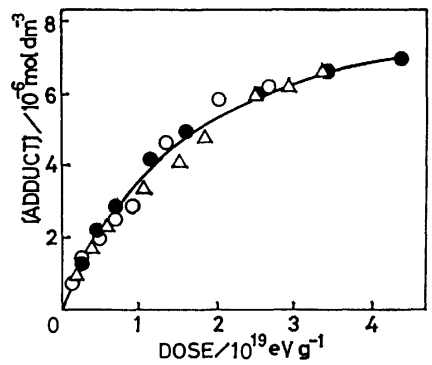

Fig. 2. Effect of dose and dose rate on the yield of the spin-adduct of butyl radical generated in the benzene solution containing the 0.01 mol/dm^3 spin-trap and 0.2 mol/dm^3 butyl chloride.
Key to the dose rate; ○, 3.6×10^{15} eV/g·s; ●, 7.6×10^{15} eV/g·s; △, 15.8×10^{15} eV/g·s.

The linear dependence suggests that the electrons disappear mostly in recombining with cations and only a small fraction of them react with butyl chloride. This is in line with a low *G*-value of the spin-adduct, 0.04, determined from the initial slope of the curve.

In conclusion, the spin-adducts of various free radicals can be authentically generated by the γ-irradiation of the benzene solutions, when the corresponding chlorinated compounds are available. The advantage of the present method lies in the fact that the ESR spectra of the spin-adducts can be recorded without interference of the spectra due to the by-product spin-adducts.

References

1) S. Terabe and R. Konaka, *J. Chem. Soc., Perkin Trans. 2*, **1972**, 2136.
2) S. Terabe and R. Konaka, *J. Chem. Soc., Perkin Trans. 2*, **1973**, 369.
3) T. Doba, T. Ichikawa, and H. Yoshida, *Bull. Chem. Soc. Jpn.*, **50**, 3124 (1977).
4) S. Noda, Y. Ohta, and H. Yoshida, *Bull. Chem. Soc. Jpn.*, **52**, 1916 (1979).
5) A. MacLachlan and R. L. McCarthy, *J. Am. Chem. Soc.*, **85**, 2519 (1962).
6) R. Okazaki, T. Hosogai, E. Iwadate, M. Hashimoto, and N. Inomoto, *Bull. Chem. Soc. Jpn.*, **42**, 3611 (1969).
7) "Handbook of Chemistry and Physics," 56th ed, Chemical Rubber Co. (1975—1976).
8) Y. Nakato, M. Ozaki, and H. Tsubomura, *J. Phys. Chem.*, **76**, 2105 (1972).
9) T. Doba, T. Ichikawa, and H. Yoshida, *Bull. Chem. Soc. Jpn.*, **50**, 3158 (1977).

Reactions of Imidoyl-palladium(II) Complexes with Electrophiles

Katsuma HIRAKI,* Yoshio FUCHITA,* and Toyohiko MASUMOTO

Department of Industrial Chemistry, Faculty of Engineering, Nagasaki University, Bunkyo-machi, Nagasaki 852

(Received September 4, 1979)

Synopsis. Imidoyl-palladium(II) complexes, derived from the reactions between imidoyl chlorides and tetrakis(triphenylphosphine)palladium(0), react with perchloric acid or triethyloxonium tetrafluoroborate to give new aminocarbene-palladium(II) complexes.

Tanaka and Alper[1] prepared several (*N*-arylimidoyl)chlorobis(triphenylphosphine)palladium(II) complexes with an oxidative addition of the corresponding imidoyl chlorides to tetrakis(triphenylphosphine)palladium(0). It has been reported that *N*-alkylbenzimidoyl chloride reacts with tetrakis(triphenylphosphine)platinum(0) and gives a few products, which are very difficult to be isolated.[2] This note deals with the preparation of chloro[*N*-(*p*-nitrobenzyl)-*p*-methylbenzimidoyl]bis(triphenylphosphine)palladium(II) (**1a**) and the corresponding *N*-(*p*-nitrophenyl)-*p*-methylbenzimidoyl complex (**1b**) and with the reactions of these imidoyl-palladium(II) complexes toward a few electrophiles. Crociani *et al.*[3] obtained a neutral and a cationic carbene complexes from reactions of chloro(*N*-phenylbenzimidoyl)bis(triphenylphosphine)palladium(II) with HCl and $HClO_4$, respectively.

Experimental

General Procedures. Tetrakis(triphenylphosphine)palladium(0)[4] and chloro[*N*-(*p*-tolyl)benzimidoyl]bis(triphenylphosphine)palladium(II) (**1c**)[1] were prepared according to the published methods. Imidoyl chlorides[5,6] and triethyloxonium tetrafluoroborate[7] were also synthesized according to the reported procedures. IR and ^{1}H-NMR spectra, conductivities and melting points were measured according to the previous paper.[8]

*Preparations of the Imidoyl-palladium(II) Complexes, **1a** and **1b**.* Slight excess imidoyl chloride (0.48 mmol) in benzene solution (10 ml) was added to a benzene solution (20 ml) of [Pd(pph$_3$)$_4$] (0.43 mmol), and the reaction mixture was stirred for 1 d at room temperature and concentrated. Addition of hexane to the concentrated reaction mixture gave yellow precipitates. Recrystallization from benzene and hexane yielded the imidoyl-palladium(II) complexes, **1a** and **1b**.

*Reaction of **1a**, **1b**, or **1c** with Perchloric Acid.* To a benzene solution (35 ml) of the imidoyl complex (0.22 mmol) was added perchloric acid (0.24 mmol) in 10 ml of diethyl ether. Off white precipitates formed immediately, which was filtered after stirring for 3 h at room temperature. Recrystallization from dichloromethane and hexane gave the aminocarbene-palladium(II) complex, **2a**, **2b**, or **2c**.

*Reaction of **1a** or **1c** with Triethyloxonium Tetrafluoroborate.* The mixture of **1a** or **1c** (0.29 mmol) and triethyloxonium tetrafluoroborate (0.32 mmol) in dichloromethane (25 ml) was stirred for 1 d at room temperature. Addition of diethyl ether to the concentrated reaction mixture gave the aminocarbene-palladium(II) complex, **3a** or **3c**.

Results and Discussion

N-(*p*-Nitrobenzyl)-*p*-methylbenzimidoyl chloride reacted with equimolar amount of tetrakis(triphenylphosphine)palladium(0) in benzene at room temperature to afford *trans*-chloro[*N*-(*p*-nitrobenzyl)-*p*-methylbenzimidoyl]bis(triphenylphosphine)palladium(II) (**1a**) in good yield, similar to the case of *N*-(*p*-nitrophenyl)-*p*-methylbenzimidoyl chloride and other *N*-arylimidoyl chlorides.[1] Although Tanaka and Alper[1] used two equivalents of the imidoyl chloride, a slightly excess amount of the imidoyl chloride was enough to obtain the imidoyl-palladium(II) complexes in good yield.

Reactions of **1a**, **1b**, and **1c** with perchloric acid gave stable off white crystals **2a**, **2b**, and **2c**, respectively, which contained a half mole of dichloromethane as solvent of crystallization. Complex **1a** and **1c** also reacted with triethyloxonium tetrafluoroborate in dichloromethane to produce **3a** and **3c**, respectively. Elemental analyses, IR and ^{1}H-NMR spectra together with some properties of the complexes prepared in this study are summarized in Tables 1 and 2.

N-(*p*-Nitrobenzyl)imidoyl complex **1a** is fairly unstable and turns pink within a week even under dry nitrogen atmosphere, whereas *N*-arylimidoyl complexes **1b** and **1c** are considerably stable in the same conditions. Trans configurations of **1a** and **1b** were inferred by the similarity of the structures to the complexes of Tanaka and Alper,[1] and ν(Pd–Cl) frequencies of **1a** and **1b** are reasonable (see Table 2).

On the basis of molar conductivities, elemental analyses, IR and ^{1}H-NMR spectra, complexes **2a**—**2c**, **3a**, and **3c** were assigned to new cationic aminocarbene-palladium(II) complexes, which were formed by an addition of a proton or an ethyl group to the secondary

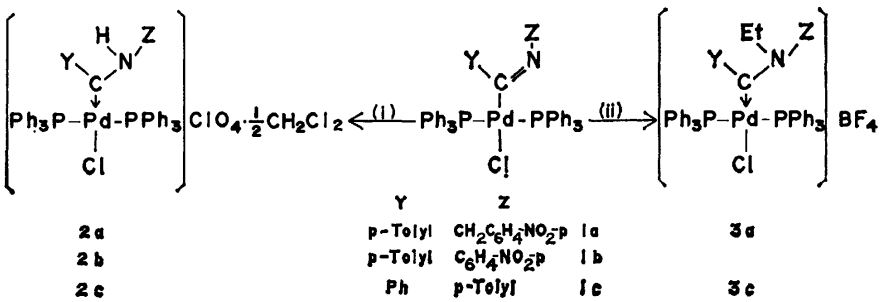

Scheme 1. Reactions of the imidoyl-palladium(II) complexes. Reagents: (i) $HClO_4$, (ii) [Et_3O] [BF_4].

Table 1. Yield and properties of the palladium(II) complexes

	Yield %	Mp[a] °C	Color	Found(Calcd), (%) C	H	N	^{1}H-NMR data (δ-value from TMS)[b] -CH_3	Others	Λ_M[c]
1a	81	186—198	Off white	65.57	4.55	2.96	2.20 s	4.88 s (CH_2)	—
				(66.60	4.71	3.05)			
1b	85	165—175	Yellow	67.16	4.59	2.88	2.25 s	—	—
				(66.31	4.56	3.09)			
2a	70	186—198	Off white	58.78	4.36	2.58	2.26 s	5.15 d (CH_2)[d], 10.40 b (NH)	120
				(58.21	4.27	2.64)		5.29 s ($\frac{1}{2}CH_2Cl_2$)	
2b	65	215—220	Off white	58.22	4.18	2.79	2.36 s	5.33 ($\frac{1}{2}CH_2Cl_2$)[e]	114
				(57.84	4.13	2.67)			
2c	95	180—185	Off white	60.71	4.24	1.27	2.43 s[f]	—[e]	136
				(60.44	4.42	1.40)	2.47 s[f]		
3a	60	190—195	Pale yellow	60.71	4.66	2.71	2.26 s	1.16 t ($NCH_2\underline{CH_3}$)[g], 4.99 s (CH_2)[f]	128
				(61.47	4.67	2.71)		3.48 q ($NC\underline{H_2}CH_3$)[g], 5.04 s (CH_2)[f]	
3c	65	215—220	White	62.56	4.66	1.48	—[h]	—[h]	138
				(63.96	4.85	1.43)			

a) With decomposition. b) In $CDCl_3$, except for **2c** and **3a**(CD_2Cl_2). The aromatic protons are omitted. c) Molar conductivity, Ω^{-1} cm^2 mol^{-1}, in 10^{-3} M acetonitrile solution at 25 °C. d) Coupled with NH proton. ^3J= 6 Hz. e) NH proton is not observed. f) See the text. g) ^3J=7 Hz. h) Not detected owing to its high insolubility.

nitrogen atom on the imidoyl ligand. The ^{1}H-NMR spectrum of **2c** showed two singlets at δ 2.43 and 2.47, assignable to two magnetically nonequivalent methyl protons in two isomers as shown in Fig. 1. Complex **3a** also exhibited nonequivalent two methylene resonances of *N*-(*p*-nitrobenzyl) group at δ 4.99 and 5.04. These isomers were caused by the restricted rotation around the C–N bond. Analogous isomerism probably exists in other aminocarbene complexes, in consideration of two ν(Pd–Cl) frequencies in their Far-IR spectra.

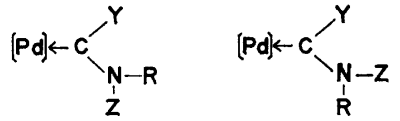

Fig. 1. Isomers for **2**(R=H) and **3**(R=Et).

The ν(Pd–Cl) frequency of the aminocarbene complexes is shifted to a higher wave number relative to that of the corresponding imidoyl complexes. These results indicate that the aminocarbene ligand has a weaker trans influence than the imidoyl one has.[9] On the other hand, the ν(C–N) frequency of the former complexes is lower than the ν(C=N) of the corresponding latter complexes. This is attributable to a decreased carbon–nitrogen bond order in the aminocarbene moiety.

Dimethyl sulfate reacted with **1c**, but gave no isolatable pure product. Other alkylating reagents such as methyl iodide and allyl iodide did not react with the imidoyl complex, and only the starting materials were recovered. This paper presents the first example of ethylation onto the nitrogen atom of an imidoyl ligand.

Table 2. IR spectra[a] of the palladium(II) complexes

	ν(NH)	ν(C–N) {ν(C=N)}[b]	ν(NO_2)	ν(ClO_4) {ν(BF_4)}[c]	ν(Pd–Cl)
1a	—	1590[b]	1350, 1519	—	272
1b	—	1560[b]	1322, 1500	—	273
2a	3152	1561	1340, 1510	1082	301, 309
2b	3149	1544	1337, 1512	1086	300, 310
	3206				
2c	3202	1556	—	1104	300, 308
3a	—	1565	1340, 1515	1080[c]	301, 311
3c	—	1540	—	1080[c]	305, 312

a) Values in cm^{-1}, in KBr disk. b) ν(C=N) for **1a** and **1b**. c) ν(BF_4) for **3a** and **3c**.

We are grateful to Mr. Makoto Noshiro, Asahi Glass Co. Ltd. in Yokohama City, for his help with the elemental analyses.

References

1) M. Tanaka and H. Alper, *J. Organomet. Chem.*, **168**, 97 (1979).
2) M. J. Doyle, M. F. Lappert, G. M. McLaughlin, and J. McMeaking, *J. Chem. Soc., Dalton Trans.*, **1974**, 1494.
3) B. Crociani, M. Nicolini, and T. Boschi, *J. Organomet. Chem.*, **33** C81 (1971).
4) D. R. Coulson, *Inorg. Synth.*, **13**, 121 (1972).
5) I. Ugi, F. Beck, und U. Fetzer, *Chem. Ber.*, **95**, 126 (1962).
6) K. Hiraki and Y. Fuchita, *Chem. Lett.*, **1978**, 841.
7) H. Meerwein, *Org. Synth.*, Coll. Vol. V, 1080 (1973).
8) K. Hiraki, M. Onishi, K. Sewaki, and K. Sugino, *Bull. Chem. Soc. Jpn.*, **51**, 2548 (1978).
9) B. Crociani and M. Nicolini, *J. Organomet. Chem.*, **104**. 259 (1976).

The Partial Molar Quantity of the Sulfur of the Compounds in the Fe–V–S System

Hiroaki WADA

National Institute for Researches in Inorganic Materials, Namiki 1-1, Sakura-Mura, Niihari-Gun, Ibaraki 305

(Received September 25, 1979)

Synopsis. An equilibrium study of the Fe–V–S system was carried out under controlled sulfur-pressure conditions. Partial molar enthalpies of the sulfur of the compounds in the Fe–V–S system were calculated on the basis of the P_{S_2}–T–X relations, which were established at temperatures between 520 and 814 °C.

The phase relations in the portion of the FeS–VS–S composition triangle have recently been clarified.[1-4] It has been found that the Fe–V–S system has extensive solid-solution phases, such as $(Fe,V)_{1-x}S$ and $(Fe,V)_3S_4$, which have a lattice intermediate between the NiAs-type and the $Cd(OH)_2$ lattice. However, no thermodynamic data on the ternary compounds of Fe–V–S have yet been reported. This note will be concerned with the partial molar enthalpy of sulfur, $\Delta\bar{H}_s$, which can be derived from the thermochemical data of compounds in the Fe–V–S system.

Experimental

The sulfide samples with the desired atomic Fe:V ratios were synthesized by heating mechanical mixtures of reagent-grade $VOSO_4 \cdot 3H_2O$ and $FeSO_4 \cdot (NH_4)_2SO_4 \cdot 6H_2O$ in an H_2S atmosphere at 1050 °C for 4 h; they were then used as the starting materials. The equilibrium study was carried out by means of thermogravimetry, using a quartz spring balance. The general experimental procedures, the apparatus, and the chemical analyses are the same as those described in the previous paper.[1]

Results and Discussion

The experimentally determined P_{S_2} (equilibrium sulfur pressure)–T(temperature)–X(composition) relations, which had been reported in three preceding publications,[1,3,4] were used in the computation of the activities and the partial molar enthalpies.

Under the experimental conditions employed, the vapor phase in equilibrium with iron vanadium sulfides contains various molecular species of sulfur from S_2 to S_8. In such a case, according to Geffken *et al.*,[5] the activity of sulfur, a_s, can be given by

$$a_s = \left(\frac{P_{S_n}}{P_{S_n}^{\circ}}\right)^{1/n}, \quad (1)$$

where the subscript, n, indicates the number of atoms in a molecule. If the reference state of sulfur is chosen as 0.5 S_2 (g), where the S_2 (g) is considered to be an ideal gas at a pressure of 1 atm at the given temper-

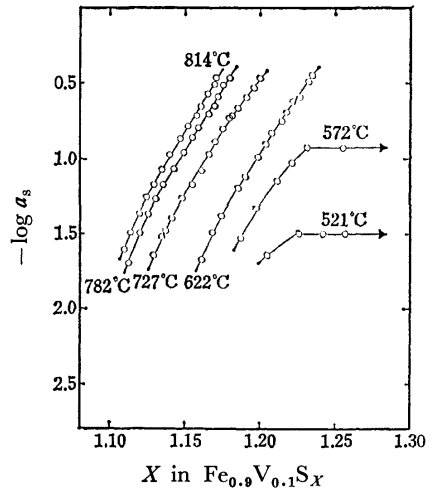

Fig. 1. The relation of log a_s with composition, X in $Fe_{0.90}V_{0.10}S_X$.

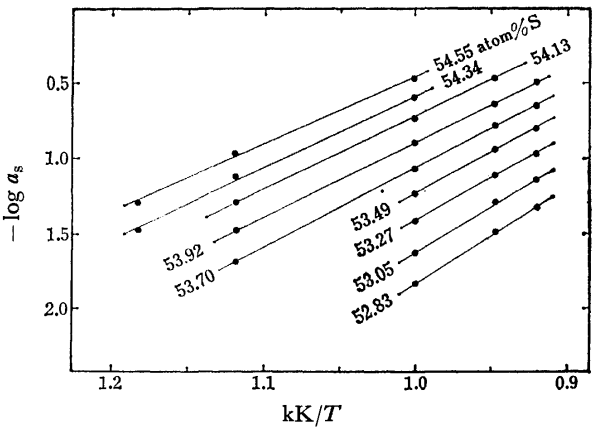

Fig. 2. The relation of log a_s with $1/(T/\mathrm{K})$.

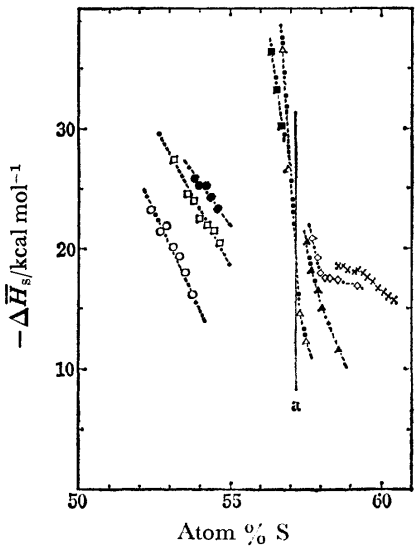

Fig. 3. $\Delta\bar{H}_s$ of compounds in the Fe–V–S system as function of composition. The stoichiometric Fe+V:S=3:4 composition is designated as the symbol a. ○: Fe:V=1:0, □: Fe:V=9:1, ●: Fe:V=4:1, ■: Fe:V=3:2, △: Fe:V=1:1, ▲: Fe:V=7:13, ◇: Fe:V=13:37, ×: Fe:V=1:19.

ature,[6] the activity of sulfur is expressed by:

$$\log a_s = 0.5 \log P_{s_2}. \quad (2)$$

The partial molar enthalpies can be computed from the Gibbs-Helmholtz equation[7] by using the activity data as follows:

$$\Delta\overline{H}_s = -4.574\, T^2 \frac{d \log a_s}{dT}. \quad (3)$$

Figure 1 shows a typical example of the isotherms of $Fe_{0.90}V_{0.10}S_x$, where the activity of sulfur is calculated according to Eq. 1. Figure 2 represents the log a_s versus the reciprocal temperature relations, which are derived from the experimental data shown in Fig. 1. It is found that the data points lie on a straight line for a given composition in the range from 52.8 to 54.5 atom% S. This suggests that the Gibbs-Helmholtz equation holds in the relation of log a_s with $1/T$ under the experimental temperature conditions. From the slopes of these straight lines, the partial molar enthalpies of the sulfur of $Fe_{0.90}V_{0.10}S_x$ were calculated by the least-squares method. The calculated partial molar enthalpies are plotted in Fig. 3 as a function of the composition, together with those of other samples. The $\Delta\overline{H}_s$ of $Fe_{0.90}V_{0.10}S_x$ increases linearly from -27.5 to -20.5 kcal/mol (1 cal=4.184 J) in the compositional range from 53.1 to 54.6 atom% S.

As is evident in Fig. 3, $\Delta\overline{H}_s$ varies with the composition of the iron vanadium sulfides. It can be concluded that (1) $\Delta\overline{H}_s$ decreases with an increase in the V/Fe ratio when the sulfur content is held constant and (2) $\Delta\overline{H}_s$ increases with an increase in the sulfur content when the V/Fe ratio is held constant.

References

1) H. Wada, *Bull. Chem. Soc. Jpn.*, **51**, 1368 (1978).
2) H. Wada, *Bull. Chem. Soc. Jpn.*, **52**, 2130 (1979).
3) H. Wada, *Bull. Chem. Soc. Jpn.*, **52**, 2918 (1979).
4) H. Wada, *Bull. Chem. Soc. Jpn.*, **53**, 668 (1980).
5) R. M. Geffken, K. L. Komarex, and E. M. Miller, *J. Solid State Chem.*, **4**, 153 (1972).
6) K. C. Mills, "Thermodynamic Data for Inorganic Sulphides, Selenides and Tellurides," Butterworths, London (1974), p. 25.
7) O. Kubaschewski, E. Ll. Evans, and C. B. Alcock, "Metallurgical Thermochemistry," 4th ed, Pergamon Press, London (1967), p. 42.

Studies on Bromites. III. Isolation and Characterization of Quaternary Ammonium Bromites

Toshifumi KAGEYAMA* and Tamotsu YAMAMOTO
Industrial Chemistry, Faculty of Engineering, Kanto Gakuin University, Mutsuura, Kanazawa-ku, Yokohama 236
(Received October 12, 1979)

Synopsis. Bromite, BrO_2^-, could be easily stabilized and isolated as quaternary ammonium salts by the reaction of sodium bromite with the corresponding ammonium halides. The bromites are more stable and non-hygroscopic in comparison to sodium bromite. The stability of the ammonium bromites depends a great deal on the structure of the ammonium groups.

Sodium bromite (**1**) (in aqueous solution) has been used as an oxidative desizing agent for textiles because of its mild oxidizing property.[1] The aqueous solution of **1** (*ca.* 4%) can be easily prepared by the reaction of sodium hydroxide with bromine, followed by dispropotionation.[2,3] However, troublesome operations such as concentration and purification at low temperature are necessary for the isolation of pure **1** from dilute solution.[4,5] Sodium bromite thus obtained contains small amounts of impurities, NaBr, $NaBrO_3$, and NaOH, even the most purified product being hygroscopic and unstable.

For studies on physical and chemical properties of BrO_2^-, stability of the compound is required. We could isolate an extremely stable bromite, tetrabutylammonium bromite (**3a**), during the course of the oxidation reaction using **1** in the presence of phase transfer catalyst, tetrabutylammonium chloride (**2**). In the present paper, we wish to describe the isolation and characterization of the quaternary ammonium bromites containing **3a**.

Isolation of the bromites **3** is very simple as shown in the following. An equimolar amount of **1** in water

$$\underset{\mathbf{1}}{NaBrO_2} + \underset{\mathbf{2}}{R^1{}_3R^2N^+\,Cl^-} \longrightarrow \underset{\mathbf{3}}{R^1{}_3R^2N^+\,BrO_2^-}$$

and tetrabutylammonium chloride **2** were mixed in water. The pH of the resulting solution was so adjusted with acetic acid that an orange crystal of **3a** almost insoluble in water was precipitated. The structure of **3a** was confirmed by means of IR and NMR spectra (in the presence of tetrabutylammonium) and analytical data of Br (total) and BrO_2^- obtained by titration with sodium arsenite[6] after dissolution in alkaline solution.

$$R^1{}_3R^2N^+\,BrO_2^- + NaOH \xrightarrow[\text{in } H_2O]{} NaBrO_2 + R^1{}_3R^2N^+\,OH^-$$

Other quaternary ammonium bromites, tetraethylammonium (**3c**), dodecyltrimethylammonium (**3d**), octadecyltrimethylammonium (**3e**) and benzyltrimethylammonium bromite (**3f**), were prepared in a similar way. However, tetramethylammonium bromite (**3b**) was not isolated because of decomposition with time. The results are given in Tables 1 and 2.

Most of the bromites **3** obtained have definite melting points and are stable and non-hygroscopic enough to be kept at room temperature for over half a year.

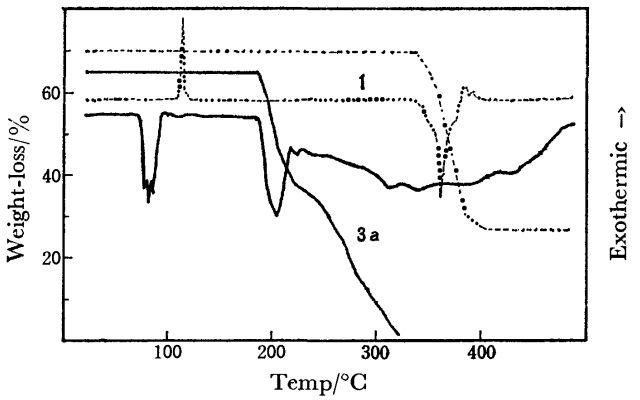

Fig. 1. DTA and TG curves of **1** and **3a**.

The instability seems to depend remarkably on the structure of the cation. The bromites having large and bulky groups on nitrogen are more stable than those containing no such groups, the order of stability being **3a**>**3c**≫**3b** in bulkiness and **3e**>**3d**≫**3b** in size of group.

The same tendency was observed quantitatively by means of thermal analysis. In the DTA curve of **3a** (Fig. 1) two peaks were observed at 74 and 188 °C. The former might correspond to melting point and the latter to decomposition temperature on the basis of thermogravimetry. The DTA curves of the other bromites showed the same pattern. The decomposition temperatures obtained from their curves are 115 (**3c**), 110 (**3d**), 167 (**3e**), and 115 °C (**3f**) and can be arranged in the order mentioned above.

The DTA curve of sodium bromite (dotted line, Fig. 1) has two peaks at 109 °C (exothermic, on the basis of dispropotionation) and at 359 °C (endothermic, on the basis of decomposition of sodium bromate).[5a] There is a remarkable difference between the curves of the bromites **3** and **1**, which seems to be due to the difference in their decomposition patterns.

The isolation of the quaternary ammonium bromites **3** is of importance not only as regards the stabilization of BrO_2^- but also because of their use in oxidation reactions in an organic medium, since **3** is soluble in benzene, dichloromethane, and chloroform.

Experimental

The IR spectra were recorded on a Hitachi 285 spectrophotometer and NMR spectra on a JNM-C-100 spectrometer (Japan Electron Optics Lab.), the thermal analysis being carried out on a DTA-TG apparatus 8055-EI, Rigaku Denki Co. Ltd.

Determination of BrO_2^- was carried out after dissolution in alkaline solution containing two fold amount of NaOH (in mol) to sample **3**.

Materials. Sodium bromite was prepared by the method described in a previous paper.[5a] Quaternary am-

Table 1. Preparation of quaternary ammonium bromites **3**

	$R^1_3R^2N^+$ BrO_2^-	Mp/°C	Yield/%	Found (%)		Calcd (%)	
				Br	BrO_2^-	Br	BrO_2^-
a	$R^1=R^2=C_4H_9$	74.0—74.5	≈100	22.4	31.6	22.5	31.6
b	$R^1=R^2=CH_3$	—	0				
c	$R^1=R^2=C_2H_5$	82.5—84.0	≈100	33.1	46.0	33.0	46.2
d	$R^1=CH_3$, $R^2=C_{12}H_{25}$	81.0—83.5	≈100	23.4	32.6	23.5	32.9
e	$R^1=CH_3$, $R^2=C_{18}H_{37}$	88.5—91.0	≈100	17.0	26.3	17.1	26.4
f	$R^1=CH_3$, $R^2=C_6H_5CH_2$	92.0—94.0	96	23.9	42.4	23.9	42.7

Table 2. IR and NMR spectra

	IR(KBr) $\tilde{\nu}$/cm^{-1}	NMR($CDCl_3$) δ/ppm
3a	2920, 2870, 1450, 1375, 990, 920, 880, 790, 730	1.11(t, 12H), 1.2—2.0(m, 16H), 3.26(t, 8H)
3c	2920, 1445, 1180, 1000, 790	decompn. during measurement
3d	2920, 2850, 1460, 965, 920, 725	0.89(t, 3H), 1.0—2.1(m, 20H), 3.36(s, 9H), 3.2—3.7(m, 2H)
3e	2920, 1470, 970, 900, 760	0.91(t, 3H), 1.1—2.0(m, 32H), 3.49(s, 9H), 3.3—3.8(m, 2H)
3f	3020, 2960, 1470, 1400, 975, 920, 890, 780, 730, 700, 620	decompn. during measurement

monium bromides and chlorides of reagent grade were used.

Isolative Preparation of Quaternary Ammonium Bromites **3**. *General Procedure*: To an aqueous solution (18%) of 10 mmol of sodium bromite was added 10 mmol of quaternary ammonium halide. After stirring for 30 min, the pH of the resulting solution was adjusted to 8—9 by the addition of acetic acid, stirring being continued for 60 min. An orange crystal of quaternary ammonium bromite **3** deposited. The crystal was dissolved in CH_2Cl_2 without filtration and the solution was extracted with CH_2Cl_2 (15 cm^3×3). The combined extracts were dried over anhydrous sodium sulfate and evaporated to dryness *in vacuo* to give an orange crystal of **3** which was purified by reprecipitation from CH_2Cl_2–Et_2O. The results are given in Tables 1 and 2.

We wish to thank Prof. M. Okawara, for advice and Mr. Y. Nakamura, for measuring NMR spectra (Tokyo Institute of Technology).

References

1) Société d'Études Chimiques pour l'Industrie et Agriculture, Brit. Patent 843 558 (1960).
2) J. Clarens, *C. R. Acad. Sci.*, **157**, 216 (1913).
3) R. M. Chapin, *J. Am. Chem. Soc.*, **56**, 2211 (1934).
4) About 18% solution of **1** was obtained by the modified method.[5a)]
5) a) T. Kageyama, *Nippon Kagaku Kaishi*, **1972**, 1964; b) Société d'Études Chimiques pour l'Industrie et Agriculture, Brit. Patent 843 559 (1960).
6) M. H. Hashmi and A. A. Ayaz, *Anal. Chem.*, **35**, 908 (1963).

A New Reaction of a 7,7-Diethoxybicyclo[4.2.0]octan-2-one Derivative. The Formation of the Bicyclo[3.2.1]octane Skeleton

Mitsutoshi YANAGIYA, Takamasa TOMITA, and Takeshi MATSUMOTO*
Department of Chemistry, Faculty of Science, Hokkaido University, Sapporo 060

(Received June 7, 1979)

Synopsis. 2,2-Diethoxytricyclo[6.4.0.0^{1,4}]dodecan-5-one was rearranged to 11-ethoxytricyclo[7.2.1.0^{1,6}]dodec-10-en-12-one under GLC conditions (Thermol-3 on Shimalite, 200 °C) in an 87% yield.

A bicyclo[3.2.1]oct-7-en-8-one derivative (**8**) was obtained in one step by an acid-catalyzed rearrangement of a 7,7-diethoxybicyclo[4.2.0]octane derivative (**1**) under GLC conditions. Since compounds of type **1** are readily obtainable through photocycloaddition, and since compounds with the bicyclo[3.2.1]octane skeleton are frequently found among natural products, the present reaction may be of some interest for the synthesis of such compounds as terpenoid.

The irradiation of a solution of 4,4a,5,6,7,8-hexahydro-2(3*H*)-naphthalenone in an excess of 1,1-diethoxyethylene afforded three stereoisomers: 2,2-diethoxytricyclo[6.4.0.0^{1,4}]dodecan-5-one **1** (60%), (**2**) (the C-1, C-4 epimer of **1**, 4.8%), and (**3**) (the C-4 epimer of **1**, 13.6%). The stereostructure of these compounds were determined as follows. On treatment with basic alumina, **3** was completely converted to **1**. The treatment of **1** with a catalytic amount of *p*-toluensulfonic acid afforded an enol ether (**4**) in a quantitative yield, this ether was then ozonized to give ethyl *trans*-decahydro-4-hydroxymethylene-3-oxo-4a-naphthalenecarboxylate (**5**) and *trans*-decahydro-4a-ethoxycarbonyl-3-oxo-4-naphthalenecarboxylic acid (**6**) in 22% and 66% yields respectively. Both **5** and **6** were treated with a refluxing aq alkaline solution to give *trans*-decahydro-3-oxo-4a-naphthalenecarboxylic acid (**7**).[1,2] The stereochemistry of **2** was confirmed by leading it to the *cis*-keto acid[2] in an analogous manner.

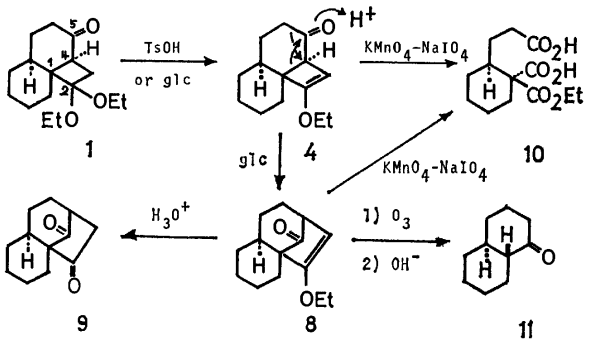

Passing the acetal ketone **1** through a column (Thermol-3 on Shimalite[3]) in a stream of helium gave 11-ethoxytricyclo[7.2.1.0^{1,6}]dodec-10-en-12-one (**8**) in an 87% yield. Compound **8** exhibited an IR absorption at 1759 cm^{-1}, and an olefinic structure was evidenced in its IR (1630 cm^{-1}) and NMR (1H, d, δ=4.75) spectra. The hydrolysis of **8** with dil acid afforded a bridged 1,3-diketone (**9**). The degradation of **8** with ozone, followed by an alkaline treatment, gave *trans*-1-decalone (**11**) (86% yield). On the other hand, the oxidation of **8** (and **4**) by the method of Lemieux-von Rudloff[4] afforded a dicarboxylic acid (**10**). Therefore, the structure of the new enol ether is represented by Formula **8**.

The rearrangement **1**→**8** probably proceeds through the bicyclo[4.2.0]oct-7-en-2-one intermediate **4**, since the treatment of **4** under similar GLC conditions afforded **8** in an almost quantitative yield. An analogous skeletal transformation of bicyclo[4.2.0]oct-7-en-2-one using acid washed alumina has been described by Cargill and Crawford.[5]

Experimental

Photocycloaddition of 4,4a,5,6,7,8-Hexahydro-2-(3H)-naphthalenone with 1,1-Diethoxyethylene. A solution of 4,4a,5,6,7,8-hexahydro-2(3*H*)-naphthalenone (1.48 g, 9.3 mmol) and 1,1-diethoxyethylene (16.8 g. 144 mmol) in 60 ml of hexane was irradiated using a 75 W high-pressure Hg lamp (Pyrex filter, −78 °C, 5 h, N_2 bubbling). The subsequent distillation of the product yielded a pale yellow oil (2.54 g, bp 103—122 °C/2 mmHg, 1 mmHg≃133.3 Pa). Three products, **1** (t_R=2.50, relative to the starting enone), **2** (t_R=3.26), and **3** (t_R=4.19), were separated by GLC (DGSP. 200 °C). Adduct **1** solidified on standing and was recrystallized from hexane at −78 °C. Adduct **3** (31 mg) was passed through basic alumina (2 g, benzene) to give **1** (29 mg). Adduct **1** (1.57 g, 60% yield): bp 110—112 °C/3 mmHg: mp 61—63 °C; IR (nujol) 1705, 1058 cm^{-1}; NMR (CCl_4) δ=3.55 (2H, q, J=8 Hz), 3.40 (2H, q. J=8 Hz), 2.62—2.30 (3H, m), 1.20 (3H, t, J=8 Hz), 1.15 (3H, t, J=8 Hz), 2.2—1.0 (13H, m). Found: C, 71.99: H, 9.78%. Calcd for $C_{16}H_{26}O_3$: C, 72.14; H, 9.84%. Adduct **2** (0.125 g, 4.8%): bp 110—112 °C/3 mmHg; IR (neat) 1705, 1055 cm^{-1}; NMR (CCl_4) δ=3.54 (2H, q, J=8 Hz), 3.49 (2H, q. J=8 Hz), 2.25 (3H, m), 1.20 (6H, t, J=8 Hz), 2.2—1.1 (13H, m). Found: C, 72.07; H, 9.75%. Adduct **3** (0.365 g, 13.6%): bp 120—122 °C/3 mmHg; IR (neat) 1730, 1055 cm^{-1}; NMR (CCl_4) δ=3.35 (2H, q, J=8 Hz), 3.40 (2H, q, J=8 Hz), 2.25 (3H, m), 1.12 (6H, t, J=8 Hz), 2.2—1.0 (13H, m). Found: C, 72.22; H, 9.80%.

Formation of the Enol Ether 4 from 1. A mixture of **1** (0.246 g, 0.923 mmol) and anhyd *p*-TsOH (1 mg) was heated to 120 °C (15 mmHg, 10 min), when the evolution of gas subsided. The subsequent distillation of the residue gave 0.199 g (98%) of **4**: bp 100—102 °C/2 mmHg; IR (neat) 1692, 1630 cm^{-1}; NMR (CCl_4) δ=4.44 (1H, s), 3.90 (2H, q, J=8 Hz), 2.60 (1H, S), 2.42 (1H, S), 2.7—2.2 (2H, b), 1.39 (3H, t, J=8 Hz), 2.2—1.0 (11H, m). Found: C, 76.36; H, 9.15%. Calcd for $C_{14}H_{20}O_2$: C, 76.32; H, 9.15%.

Oxidative Cleavage of 4 to 7. A solution of **4** (199 mg, 0.905 mmol) in hexane (10 ml) was treated with ozone (−78 °C, 0.5 h). After the excess ozone has been expelled, the solution was diluted with a mixture of MeOH–H_2O (1:1, 20 ml) and stirred for 24 h at r.t. Work up of the product gave an oil (253 mg), which was then chromatographed on silica gel (5 g, benzene) to give 52 mg (22%) of **5**: oil; IR (neat) 1730, 1630, 1590 cm^{-1}; NMR (CCl_4) δ=15.58 (1H, d, J=3 Hz), 9.15 (1H, d, J=3 Hz), 4.17

(2H, q, J=8 Hz), 2.45 (2H, m), 1.27 (3H, t, J=8 Hz), 2.1—1.0 (11H, m), and 163 mg (66%) of **6**: oil; IR (neat) 1730, 1710 cm^{-1}; NMR ($CDCl_3$) δ=12.8 (1H, b), 6.20 and 6.15 (1:4, 2H, each q, J=7 Hz), 3.74 and 3.60 (1:4, 1H, s), 2.48 (2H, m), 2.3—0.8 (11H, m). A solution of **5** (37 mg) in 10% aq KOH was refluxed for 2 h. The solution was acidified with HCl, and the product was taken up into ether. Evaporation of the ether yielded 25.5 mg (89.5%) of the keto acid **7**,[2] mp 116—118 °C, after recrystallization from $CHCl_3$–hexane. Similarly, the keto acid **6** (54 mg) was treated with the KOH solution (reflux, 2 h) to give the same *trans*-keto acid **7** (34 mg, 86%). The *cis*-adduct **2** was converted to the *cis*-keto acid, which was found to be identical (IR, NMR, TLC) with an authentic sample derived from *cis*-9-cyano-2-decalone.[2]

*Rearrangement of **1** (and **4**) to the Keto Enol Ether **8**.* This rearrangement was carried out at 180—220 °C using a Varian A-700 gas chromatograph equipped with a column packed with 15% Thermol-3 coated on Shimalite (3/8″×6 ft). Helium was used as the carrier gas (100 ml/min). In a typical run, an ethereal solution of **1** (330 mg in 1 ml) was used. After the elution of the solvent, the eliminated ethanol was eluted slowly (t_R=2 min) and **4** was eluted as pale yellow oil (t_R=10.5, 237 mg, 87% yield). The products were collected on granular anhyd Na_2SO_4 placed in a short glass tube fitted to the outlet. An analytical sample was obtained by distillation. Bp 100—105 °C/3 mmHg; IR (neat) 1759, 1613 cm^{-1}; NMR (CCl_4) δ=4.75 (1H, d, J=4 Hz, =C–**H**), 3.94 (2H, q, J=8 Hz), 2.77 (1H, m, =C–C–**H**), 1.40 (3H, t, J=8 Hz), 2.3—0.9 (13H, m); MS *m/e* 220 (M^+). Found: C, 76.34; H, 9.16%. Calcd for $C_{14}H_{20}O_2$: C, 76.32; H, 9.15%.

*Hydrolysis of **8**, Formation of the Diketone **9**.* To a solution of **8** (70 mg) in dioxane–H_2O (2:1, 3 ml), was added 0.1 ml of conc HCl with stirring. White crystals (60 mg, 97%) were immediately precipitated. Recrystallization from ether gave pure **9**: mp 117—118 °C, IR (nujol) 1760, 1720 cm^{-1}; NMR ($CDCl_3$) δ=3.1—2.45 (3H, m), 2.4—1.9 (2H, m), 1.9—0.9 (11H, m). Found: C, 75.12; H, 8.36%. Calcd for $C_{12}H_{16}O_2$: C, 74.97; H, 8.39%.

*Oxidation of **8** (and **4**) to Dicarboxylic Acid, **10**.* Following the method of Lemieux-von Rudloff,[4] **8** (51 mg, 0.23 mmol) was oxidized with 220 mg (0.125 mmol) of $KMnO_4$ and 486 mg (2.2 mmol) of $NaIO_4$ in *t*-BuOH–H_2O (3:1, 4 ml) to give **10**: mp 161—163 °C; IR (nujol) 1742, 1710 cm^{-1}. Found: C, 57.01; H, 7.40%. Calcd for $C_{13}H_{20}O_6$: C, 57.34; H, 7.40%.

Methyl Ester: Bp 135 °C (bath temp)/2 mmHg; IR (neat) 1735 cm^{-1}; NMR (CCl_4) δ=4.20 (2H, q, J=7 Hz), 3.72 (3H, s), 3.65 (3H, s), 2.28 (2H, t, J=6 Hz), 1.29 (3H, t, J=7 Hz), 2.5—1.0 (11H, m); MS *m/e* 300 (M^+). A similar treatment of **4** (141 mg) with $KMnO_4$ (60 mg)–$NaIO_4$ (1.2 g) gave a dicarboxylic acid which was completely identical with the **10** obtained from **8**.

*Degradation of **8** to **11**.* A solution of **8** (110 mg) in AcOEt (5 ml) was treated successively with an excess of ozone (−78 °C), KI (0.5 g) in MeOH–H_2O (1:1, 5 ml, 2 h), and $Na_2S_2O_3$. The product, obtained in the usual way, was heated in a mixture of aq 10% NaOH (2 ml) and EtOH (2 ml) for 6 h. The ethereal extract boiling at 105 °C/14 mmHg (66 mg) was identical with the authentic **11**.

References

1) The sequence of reactions may be useful for the hydrocarboxylation of α,β-cyclenones.

2) Authentic *trans*- and *cis*-keto acids were prepared from *trans*- and *cis*-9-cyano-2-decalones respectively; W. Nagata, M. Yoshioka, and S. Hirai, *Tetrahedron Lett.*, **1962**, 461.

3) Acidic character of Shimalite (a pink-colored support of the stationary phases, equivalent to Chromosorb P) was demonstrated. a) T. Matsuura, H. Komae, T. Araya, and S. Hayashi, *Kogyo Kagaku Zasshi*, **64**, 795 (1961); b) M. Verzele, J. Bouche, A. de Bruyne, and M. Verstappe, *J. Chromatogr.*, **18**, 253 (1965).

4) R. U. Lemieux and E. von Rudloff, *Can. J. Chem.*, **33**, 1701, 1710 (1955).

5) R. L. Cargill and J. W. Crawford, *J. Org. Chem.*, **35**, 356 (1970).

Some Reactions on 4*H*-Cyclopenta[*def*]phenanthrene-8,9-dione

Masaaki Yoshida, Atsushi Kadokura,† Masahiro Minabe,* and Kazuo Suzuki

Department of Industrial Chemistry, Faculty of Engineering, Utsunomiya University, Ishiicho, Utsunomiya 321-31

(Received June 18, 1979)

Synopsis. The oxidation of 8,9-dihydro-4*H*-cyclopenta[*def*]phenanthrene gave the 4-ketone by treatment with Triton B-oxygen, and afforded 8,9-diketone by the action of chromium (III) salt. The reduction of the quinone yielded the corresponding *meso*- and *dl*-diols.

The oxidation of 4*H*-cyclopenta[*def*]phenanthrene (**1**) has already been reported to give cyclopenta[*def*]phenanthren-4-one (**2**), 4*H*-cyclopenta[*def*]phenanthrene-8,9-dione (**3**), and other substances.[1,2] *meso*-8,9-Dihydro-4*H*-cyclopenta[*def*]phenanthrene-8,9-diol (**4a**) was obtained from **1** by treatment with osmium tetraoxide.[3] The quinone, **3**, has been prepared by the oxidation of **1** with iodic acid.[4]

The present paper will deal with another route to form **3** and some related reactions.

The air-oxidation of 8,9-dihydro-4*H*-cyclopenta[*def*]-phenanthrene (**5**)[5] gave the expected 8,9-dihydrocyclopenta[*def*]phenanthren-4-one (**6**) in a moderate yield, accompanied by the formation of 8,8′,9,9′-tetrahydro-4,4′-bi(4*H*-cyclopenta[*def*]phenanthren)-4-ol (**7**). This reaction may be initiated by the dissociation of more acidic protons on the active 4-methylene[6] than the 8,9-protons.

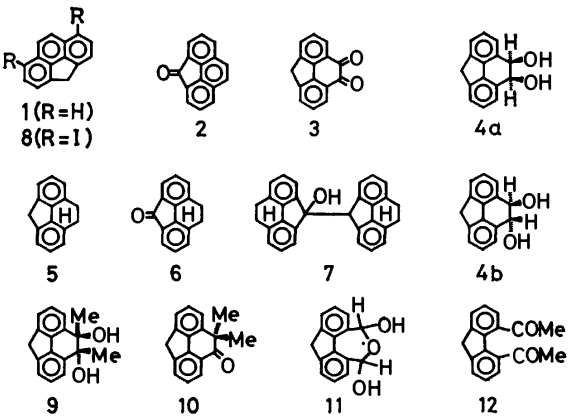

Scheme 1.

The reexamination of the oxidation of **1** using iodic acid resulted in **2**, **3**, and 1,7-diiodo-4*H*-cyclopenta-[*def*]phenanthrene (**8**).[4] Pure **3** was also isolated easily by the reaction of **5** with sodium dichromate, in spite of the dominant formation of **2**, which can be converted into **5**.

The reduction of **3** with lithium aluminium hydride afforded two isomeric diols, **4a**[3] and *dl*-8,9-dihydro-4*H*-cyclopenta[*def*]phenanthrene-8,9-diol (**4b**). The treatment of **3** with a large excess of methylmagnesium iodide gave only a single isomer, 8,9-dimethyl-4*H*-cyclopenta[*def*]phenanthrene-8,9-diol (**9**), of the expected diastereomeric diols. An inspection of the molecular model suggests that the attack of the second molecule of the Grignard reagent from the same side as in the first attack would be sterically hindered; hence, a *dl*-structure is tentatively assigned to **9**.

The pinacol-pinacolone rearrangement of **9** gave the expected 9,9-dimethyl-4*H*-cyclopenta[*def*]phenanthren-8-one (**10**). A similar transformation of **4a** and **4b** yielded only **3**. The oxidative cleavage of **4a** and **4b** afforded 6,10-dihydro-4*H*-fluoreno[4,5-*cde*]oxepin-4,6-diol (**11**),[7] and **9** was also converted into 4,5-diacetylfluorene (**12**). The UV absorbance at the characteristic maximum of **4a** (307 nm) is greater than those of **4b** (308 nm) and **9** (305 nm). This may result from the steric factor of the 8,9-substituents.

The reactivities of **4a** and **4b** towards periodic acid were compared to each other at 50 °C by measurements of the disappearance of the maximum at *ca.* 307 nm caused by the diol and the appearance of the peak at 298 nm of **11**. The reaction time of **4b** was twice that of **4a**. This difference in the reactivity is consistent with the assignments of the *meso*- and *dl*-configurations to **4a** and **4b** respectively.[8]

Experimental

All the melting points are uncorrected. The instruments used in this experiment were the same with those described elsewhere.[7]

Air-oxidation of 8,9-Dihydro-4H-cyclopenta[def]*phenanthrene (5).* Air was introduced into a solution of **5** (960 mg, 5 mmol) in pyridine (25 ml) containing Triton B (40%, 0.25 ml) at 17—19 °C for 20 h. After PhH (50 ml) has then been added, the reaction mixture was extracted with HCl (2 mol/l, 90 ml), and the PhH solution was washed with aqueous NaCl, dried over Na_2SO_4, and chromatographed on an alumina column, with PhH as the eluent. The first eluate was evaporated to dryness, and the residue was recrystallized from hexane to give 125 mg (13%) of **5**: mp 141—142 °C.

The second orange eluate afforded 714 mg (69%) of **6**: mp 141—143 °C (from HOEt); IR 1700 cm^{-1} (C=O); NMR ($CDCl_3$) δ 3.03 (4H, s) and 6.91—7.39 (6H, m); MS, *m/e*, 206 (M^+). Found: C, 87.29: H, 4.82%. Calcd for $C_{15}H_{10}O$: C, 87.35; H, 4.89%.

The colorless portion of the alumina yielded 39 mg (4%) of **7**: mp 219—221 °C (dec) (from cyclohexane); IR 3335 cm^{-1} (OH); NMR ($CDCl_3$) δ 2.01 (1H, s, OH), 2.93 (4H, s), 2.97 (4H, s), 4.88 (1H, s), and 6.71—7.03 (12H, m); MS, *m/e*, 398 (M^+), 207, and 191. Found: C, 90.50; H, 5.31%. Calcd for $C_{30}H_{22}O$: C, 90.42; H, 5.57%.

Oxidation of 4H-Cyclopenta[def]*phenanthrene (1) with HIO_3.* The hydrocarbon **1** (1.0 g, 5.3 mmol) was treated with HIO_3 (4.3 g), H_2O (25 ml), and HOAc (30 ml) in dioxane (270 ml) by a method similar to that described elsewhere:[4] 407 mg (41%) of **1** was recovered by sublimation *in vacuo*: mp 114—115 °C. Upon separation by column chromatography, 62 mg (6%) of **2** (mp 169.5—170.0 °C; lit,[1] mp 170 °C) and 272 mg (24%) of **3** (mp 256 °C, dec: lit,[4] mp 260 °C, dec)

† Present address: Tama Kagaku Kogyo, Ltd., Shinmachi, Yashio 340.

were obtained.

In addition, a 50-mg portion (2%) of **8** was isolated: mp 216—217 °C (from cyclohexane); NMR (CS_2) δ 4.20 (2H, s, H_4), 7.39 (2H, d, J=7.8 Hz, H_3, H_5), 7.75 (2H, s, H_8, H_9), and 8.00 (2H, d, H_2, H_6); MS, *m/e*, 442 (M^+), 315, and 188. Found: C, 40.98; H, 2.15%. Calcd for $C_{15}H_8I_2$: C, 40.76; H, 1.82%.

4H-Cyclopenta[def]*phenanthrene-8,9-dione (**3**).* A solution of **5** (2.40 g, 12.5 mmol) in HOAc (200 ml) was refluxed with $Na_2Cr_2O_7 \cdot 2H_2O$ (5.0 g) for 45 min. Upon treatment with PhH and H_2O, the PhH solution of the resulting precipitate was chromatographed on a silica-gel column, with PhH as the eluent; the first eluate gave 0.43 g (18%) of **1**. The lower yellow band on the column was extracted with HOEt, giving 1.43 g (56%) of **2**.

The upper orange-red band was extracted with EtOAc to give 0.54 g (20%) of **3**.

meso- *(**4a**) and* dl-*8,9-Dihydro-4H-cyclopenta*[def]*phenanthrene-8,9-diols (**4b**).* Quinone, **3** (440 mg, 2 mmol), in ether (80 ml) was added to a suspension of $LiAlH_4$ (304 mg, 8 mmol) in ether (20 ml) at 0 °C, after which the mixture was stirred for 10 h at room temperature. Upon decomposition with aqueous NaCl and the evaporation of the ether, the residue was purified by fractional recrystallization from CH_2Cl_2 to give 244 mg (55%) of **4b**: mp 200.0—200.5 °C (dec); IR 3240 cm^{-1} (OH); UV_{max} (HOEt) 270 (log ε 4.10), 296 (3.45), and 308 nm (3.30); NMR ($CDCl_3$) δ 1.76 (2H, s, OH), 3.94 (2H, s), 5.18 (2H, s), and 7.17—7.49 (6H, m); MS, *m/e*, 224 (M^+), 206, and 178. Found: C, 80.40; H, 5.31%. Calcd for $C_{15}H_{12}O_2$: C, 80.33; H, 5.39%.

In addition, 20 mg (5%) of **4a** was isolated; it was identical in all respects with the specimen obtained by the oxidation of **1** with OsO_4;[3] mp 183.5—184.5 °C (dec) (lit,[3] mp 180 °C, dec); IR 3395 and 3305 cm^{-1} (OH); UV_{max} (HOEt) 268 (log ε 4.14), 295 (3.40), and 307 nm (3.41); NMR ($CDCl_3$) δ 2.15 (2H, s, OH), 3.93 (2H, s), 5.08 (2H, s), and 7.28—7.62 (6H, m); MS, *m/e*, 224 (M^+), 206, and 178.

8,9-Dimethyl-4H-cyclopenta[def]*phenanthrene-8,9-diol (**9**).* A solution of **3** (550 mg, 2.5 mmol) in PhH (100 ml) was added to a mixture of MeMgI (prepared from MeI (1.2 ml, 20 mmol) and Mg) in ether at 15—20 °C, after which the new mixture was refluxed for an additional 5 h. Upon treatment with aqueous NH_4Cl, the resulting mixture was separated by means of a silica-gel column with PhH–EtOAc (95/5). The orange-red band on the column gave 72 mg (13%) of **3**. The upper light yellow band afforded 361 mg (57%) of **9**: mp 167.5—168.5 °C; IR 3470 cm^{-1} (OH); UV_{max} (HOEt) 273 (log ε 4.06), 294 (3.80), and 305 nm (3.16); NMR ($CDCl_3$) δ 1.50 (6H, s), 2.28 (2H, s, OH), 3.92 (2H, s), and 7.25—7.50 (6H, m); MS, *m/e*, 252 (M^+), 234, 189, and 165. Found: C, 80.55; H, 6.77%. Calcd for $C_{17}H_{16}O_2$: C, 80.92; H, 6.39%.

Pinacol-Pinacolone Rearrangement of Diols. a) 9,9-Dimethyl-4H-cyclopenta[def]*phenanthren-8-one (**10**):* A mixture of **9** (252 mg, 1 mmol) in HOAc (50 ml) containing H_2SO_4 (0.35 ml) was refluxed for 3 h to afford 132 mg (56%) of **10**: mp 99—100 °C (from aqueous DMF); IR 1662 cm^{-1} (C=O); NMR ($CDCl_3$) δ 1.57 (6H, s), 4.02 (2H, s), and 7.28—7.93 (6H, m); MS, *m/e*, 234 (M^+) and 219. Found: C, 87.20; H, 6.16%. Calcd for $C_{17}H_{14}O$: C, 87.15; H, 6.02%.

b): A solution of **4a** (112 mg, 0.5 mmol) in HOAc (10 ml) was refluxed with H_2SO_4 (0.1 ml) for 10 min, giving 37 mg (34%) of **3**. Similarly, **4b** (112 mg, 0.5 mmol) gave 48 mg (43%) of **3**.

*4,5-Diacetylfluorene (**12**).* The diol **9** (252 mg, 1 mmol) was treated with $Pb(OAc)_4$ (0.5 g) in PhH (50 ml) at room temperature for 5 h to yield 148 mg (59%) of **12**: mp 167—168 °C; IR 1670 cm^{-1} (C=O); UV_{max} (HOEt) 246 (log ε 4.36), 275 (3,52), and 322 nm (3.86); NMR ($CDCl_3$) δ 2.67 (6H, s), 3.90 (2H, s), and 7.13—7.64 (6H, m); MS, *m/e*, 250 (M^+), 235, 207, 193, and 165. Found: C, 81.28; H, 5.84%. Calcd for $C_{17}H_{14}O_2$: C, 81.58; H, 5.64%.

In addition, 30 mg (12%) of **9** were recovered.

Glycol Scission of Diols. A solution of **4a** (1.34×10^{-4} mol/l HOEt, 4.00 ml) was mixed with an aqueous solution of H_5IO_6 (5.07×10^{-3} mol/l, 0.11 ml) in a quartz cell, which was maintained at 50±1 °C. After the prescribed times, the UV spectra were measured in the range from 290 to 340 nm. The spectrum after 120 min was identical with that of **11**:[7] UV_{max} (HOEt) 265 (log ε 4.16), 287 (3.66), and 298 (3.74).

Two solutions of **4b** and H_5IO_6 were treated as a manner similar to that described above; the end point of the reaction was observed after 240 min.

The similar treatment of **9** showed no significant change after 24 h.

References

1) O. Kruber, *Ber.*, **67**, 1000 (1934).
2) H. Medenwald, *Chem. Ber.*, **86**. 287 (1953).
3) D. H. Reid, W. H. Stafford, and J. P. Ward, *J. Chem. Soc.*, **1955**, 1193.
4) B. M. Trost and P. L. Kinson, *J. Am. Chem. Soc.*, **97**, 2438 (1975).
5) L. F. Fieser and J. Cason, *J. Am. Chem. Soc.*, **62**, 1293 (1940).
6) Y. Sprinzak, *J. Am. Chem. Soc.*, **80**, 5449 (1958).
7) M. Yoshida, A. Kadokura, M. Minabe, and K. Suzuki, *Tetrahedron*, **35**, 2237 (1979).
8) G. J. Buist, C. A. Bunton, and J. H. Miles, *J. Chem. Soc.*, **1959**, 743.

A Convenient Method for the Preparation of Highly Pure *t*-Alkyl Bromides and Iodides

Hiromitsu MASADA* and Yoshiharu MUROTANI

Department of Industrial Chemistry, Faculty of Engineering, Kanazawa University, Kanazawa 920

(Received June 25, 1979)

Synopsis. Highly pure (99—100%) *t*-butyl and *t*-pentyl bromides and iodides, and 3-bromo-3-ethylpentane were readily prepared in 83—95% yields by the reactions of the corresponding alcohols with hydrobromic or hydroiodic acid, using lithium or calcium halide. The metal halides remarkably increased the yield and the purity of the products.

t-Alkyl bromides have been commonly prepared by the addition of hydrogen bromide to olefins[1] and by the reactions of *t*-alkyl alcohols with phosphorus(III) bromide,[2] hydrobromic acid,[3,4] or bromine and triphenylphosphine.[5] *t*-Alkyl iodides have been prepared by the reactions of the corresponding alcohols with potassium iodide and phosphoric acid,[6] or with trimethylsilyl iodide,[7] and by the iodination of *t*-alkyl chlorides.[8] However, the above preparations are not always satisfactory with regard to the purity and the yield of the product and the reaction conditions. The commercially available *t*-butyl bromide and iodide are contaminated by impurities (4—5%) which can not be readily removed.

We wish now to report a convenient and selective method of preparing highly pure *t*-alkyl bromides and iodides under very mild conditions, using lithium and calcium halides.

Results and Discussion

Table 1 shows the brominations of *t*-alkyl alcohols. The reactions of *t*-butyl alcohol with two and five molar equivalents of hydrobromic acid were carried out in the absence of the metal bromides at 0 °C to give *t*-butyl bromide in yields of only 9 and 43% respectively. By contrast, the yield of the bromide was increased up to 85% in the reaction of *t*-butyl alcohol with hydrobromic acid and metal bromide (molar ratio 1:2:1.5). A further excess of hydrobromic acid or metal bromide did not, though, improve the yield significantly. The product after simply being washed with ethylene glycol was 99.7—99.8% pure, with the only impurity being 0.2—0.3% of 2-methylpropene. Sodium and magnesium bromides were not effective for use in the preparation because of their poor solubility in hydrobromic acid. Similar brominations of *t*-pentyl alcohol and 3-ethyl-3-pentanol using metal bromides were also carried out to give the corresponding bromides of a high purity in 91 and 93% yields respectively.

Table 2 shows the iodinations of *t*-alkyl alcohols. The iodinations of *t*-butyl and *t*-pentyl alcohols with two equivalents of hydroiodic acid gave the corresponding iodides in only 21 and 35% yields respectively. The addition of 1—1.5 molar equivalents of lithium or calcium iodide to the system afforded highly pure *t*-butyl and *t*-pentyl iodides in 80—84% yields. Furthermore, the pure iodides could be readily obtained by the vacuum distillation of these highly pure products at room temperature.

On the whole, the metal halides in the reaction system remarkably increased the yield and the purity of the product. The hindered *t*-pentyl halides and 3-bromo-3-ethylpentane were more readily prepared than *t*-butyl halides. The hydrolysis of *t*-alkyl halides was much retarded by the addition of metal halides. Therefore, the halogenation of *t*-alkyl alcohols is in equilibrium with the hydrolysis, and the equilibrium is shifted very far to the right by these metal halides:

$$t\text{-ROH} + \text{HX(aq)} \underset{}{\overset{\text{MX}_n}{\rightleftharpoons}} t\text{-RX} + \text{H}_2\text{O}$$

TABLE 1. BROMINATIONS OF *t*-ALKYL ALCOHOLS WITH HYDROBROMIC ACID AND METAL BROMIDES

Alcohol[a]	HBr mol	Additive (mol)	Temp °C	Time h	Yield/% of product[b]	Purity/% of product GLPC	Purity/% of product Titrn.[c]
t-BuOH	0.2	None	0	4	9	99.3	99.4
t-BuOH	0.5	None	0	2	43	99.6	—
t-BuOH	0.2	LiBr (0.1)	0	2	77	99.6	99.7
t-BuOH	0.2	LiBr (0.15)	0	2	85	99.8	99.7
t-BuOH	0.2	LiBr (0.2)	0	2	87	99.8	99.8
t-BuOH	0.3	LiBr (0.15)	0	2	84	99.7	99.6
t-BuOH	0.3	$CaBr_2$ (0.15)	0	2	85	99.7	99.8
t-$C_5H_{11}OH$	0.2	None	−10	2	33	93.6	—
t-$C_5H_{11}OH$	0.2	LiBr (0.15)	−10	2	91	99.3	99.2
t-$C_5H_{11}OH$	0.3	$CaBr_2$ (0.15)	−10	2	86	98.9	98.8
Et_3COH	0.2	None	−15	3	51	85.4	—
Et_3COH	0.2	LiBr (0.15)	−15	3	93	99.2	99.6
Et_3COH	0.2	LiBr (0.2)	−15	3	95	99.2	99.6

a) A 0.1-mol quantity of *t*-alkyl alcohol was used. b) Isolated yield of *t*-alkyl bromide based on *t*-alkyl alcohol. c) Determined by titration with 0.1 M aqueous sodium hydroxide.

Table 2. Iodinations of *t*-alkyl alcohols with hydroiodic acid and metal iodides

Alcohol[a]	HI mol	Additive (mol)	Temp °C	Time h	Yield/% of product[b]	Purity/% of product GLPC	Purity/% of product Titrn.[c]
t-BuOH	0.2	None	0	1.5	21	99.2	—
t-BuOH	0.1	LiI (0.1)	0	1.5	74	99.7	99.7
t-BuOH	0.2	LiI (0.1)	0	1	80	99.7	99.7
t-BuOH	0.2	LiI (0.15)	0	0.5	83	99.8	99.8
t-BuOH	0.2	CaI_2 (0.1)	0	1	82	99.8	99.8
t-$C_5H_{11}OH$	0.2	None	−10	2	35	92.8	—
t-$C_5H_{11}OH$	0.2	LiI (0.15)	−10	2	84	99.1	99.4
t-$C_5H_{11}OH$	0.2	CaI_2 (0.1)	−10	2	82	99.1	99.4

a) A 0.1-mol quantity of *t*-alkyl alcohol was used. b) Isolated yield of *t*-alkyl iodide based on *t*-alkyl alcohol. c) Determined by titration with 0.1 M aqueous sodium hydroxide.

Experimental

The purity of the *t*-alkyl bromides and iodides was confirmed by GLPC and by titration with 0.1 M aqueous sodium hydroxide.[9] GLPC analyses were performed on a 3 m×3 mm column packed with 5% Silicone DC 550 or 5% Didecyl phthalate, at 50—60 °C and at the carrier gas (helium) flow rate of 60—80 cm^3/min. NMR spectra were recorded on a Hitachi NMR R-24B spectrometer operating at 60 MHz. Chemical shifts are reported in δ units, with tetramethylsilane as an internal standard.

Materials and Preparation. Lithium and calcium halides were of a commercial grade and were used without further purification. Hydrobromic acid (47%) and hydroiodic acid (55%) were GR grade reagents obtained from Nakarai Chemicals Co. *t*-Butyl and *t*-pentyl alcohols were distilled from sodium. 3-Ethyl-3-pentanol was prepared from diethyl ketone and ethylmagnesium bromide.

t-*Butyl Bromide*: Hydrobromic acid (23.2 cm^3, 0.2 mol) was added, drop by drop, to a mixture of lithium bromide (13.03 g, 0.15 mol) and *t*-butyl alcohol (7.412 g, 0.1 mol) at 0 °C in a 100-cm^3 Erlenmeyer flask. The mixture was then stirred magnetically for 2 h. The upper organic layer was separated and washed with ethylene glycol (10 cm^3×3) to remove the hydrobromic acid and the remaining *t*-butyl alcohol, and was then dried over anhydrous sodium sulfate, giving 11.72 g (85%) of 99.8% pure *t*-butyl bromide; this was later distilled *in vacuo* to give the pure bromide as a colorless liquid: bp 73.1 °C; NMR ($CDCl_3$) δ=1.78 (9H, s, *t*-Bu).

t-*Pentyl Bromide*: Yield, 91%; bp 107.4 °C; NMR ($CDCl_3$) δ=1.09 (3H, t, J=7.2 Hz, CH_2CH_3), 1.78 (6H, s, *gem*-CH_3), and 1.82 (2H, q, J=7.2 Hz, CH_2).

3-Bromo-3-ethylpentane: Yield, 93%; bp 55 °C/15 Torr;† NMR ($CDCl_3$) δ=0.99 (9H, t, J=7.2 Hz, CH_3) and 1.90 (6H, q, J=7.2 Hz, CH_2).

t-*Butyl Iodide*: Yield, 83%; bp 26 °C/50 Torr; NMR ($CDCl_3$) δ=1.95 (9H, s, *t*-Bu).

t-*Pentyl Iodide*: Yield, 84% bp 25 °C/15 Torr; NMR ($CDCl_3$) δ=1.06 (3H, t, J=6 Hz, CH_2CH_3), 1.66 (2H, q, J=7 Hz, CH_2), and 1.91 (6H, s, *gem*-CH_3).

References

1) M. S. Kharasch and J. A. Hinckley, Jr., *J. Am. Chem. Soc.*, **56**, 1243 (1934).
2) R. H. Goshorn, T. Boyd, and E. F. Degering, *Org. Synth.*, Coll. Vol. I, 38 (1956).
3) D. Bryce-Smith and K. E. Howlett, *J. Chem. Soc.*, **1951**, 1141.
4) J. F. Norris, M. Watt, and R. Thomas, *J. Am. Chem. Soc.*, **38**, 1078 (1916).
5) R. L. Hershkowitz, B. M. Rein, and B. C. Chung, *J. Am. Chem. Soc.*, **86**, 964 (1964).
6) H. Stone and H. Shechter, *Org. Synth.*, Coll. Vol. IV, 324 (1963).
7) M. E. Jung and P. L. Ornstein, *Tetrahedron Lett.*, **1977**, 2659.
8) M. J. Allen and N. M. John, *J. Chem. Soc., Perkin Trans. 1*, **1976**, 416.
9) H. C. Brown and N. H. Rei, *J. Org. Chem.*, **31**, 1090 (1966).

† 1 Torr=(101325/760) Pa.

Reactions of Enamino Ketones. VII. The Photochemical Reaction of 4-Methylamino-3-penten-2-one and 2,4-Pentanedione with Benzophenone

Takao Tokumitsu* and Takayuki Hayashi

Department of Chemistry, Faculty of Science, Yamaguchi University, Yoshida, Yamaguchi 753

(Received July 4, 1979)

Synopsis. The photochemical reaction of 4-methylamino-3-penten-2-one with benzophenone gave *N*-(2,2-dipenyl-2-hydroxyethyl)-4-amino-3-penten-2-one. The reaction of 2,4-pentanedione gave oxetane, resulting from the cycloaddition of benzophenone to the double bond of the enol form.

The photochemical reactions of enamines,[1] ketenimines,[2] and *N*-acyl enamines[3] with benzophenone (**2**) have been widely investigated. In general, the reactions of their compounds with **2** give diphenylmethylation products and/or oxetanes by the photocycloaddition of **2** to the carbon-carbon double bond. We have now investigated the photochemical reaction of **2** with secondary enamino ketones and β-diketones containing an analogous chelated structure.

The irradiation of a benzene solution containing an equimolar mixture of 4-methylamino-3-penten-2-one (**1**) and **2** for 48 h afforded *N*-(2,2-diphenyl-2-hydroxyethyl)-4-amino-3-penten-2-one (**3**) in a 17% yield, accompanied by benzopinacol (**4**). The structure of **3** was confirmed by the spectral data, and the regeneration, by the condensation of 2,4-pentanedione (**6**) with 2-amino-1,1-diphenylethanol (**5**),[4] which had been obtained by the acid hydrolysis of **3**. In this reaction, the light energy was absorbed exclusively by **2**. However, no oxetane, benzhydrol, and dimer of **1** was obtained. The reaction was also completely inhibited in the presence of 1,3-pentadiene, an efficient triplet quencher of **2**.[5] The hydrogen-source for the formation of **4** is presumed to be the amine part of **1** and the resinous by-products, which are produced in quantity in the reaction.[1]

The photochemical reaction of **2** with 4-anilino-3-penten-2-one (**11**) and 3-methylamino-1-phenyl-2-buten-1-one (**12**) containing the intramolecular hydrogen bonding did not give any photoadduct, the starting materials being recovered. This may be attributed to the circumstance that 95%< of the light energy was absorbed by **11** (at 365 nm ε *ca.* 2000) or **12** (at 365 nm ε *ca.* 8600) under the present reaction conditions. In contrast, 4-dimethylamino-3-penten-2-one (**13**), which can not form a chelate ring, gave, under similar conditions and in addition to **4**, *N*-(2,2-diphenyl-2-hydroxyethyl)-*N*-methylacetamide (**14**) in a 6% yield. The structure of **14** was also assigned on the basis of the spectral data and by elemental analysis. The formation of the amide **14** can be explained by assuming the formation of diphenylhydroxymethylation of **13**, which is oxidative-decomposed to yield the amide during the chromatographic treatment.

In the photochemical reaction of **2** with enamino ketones with a hydrogen atom at the α-position to the nitrogen, the diphenylhydroxymethylation exclusively occurs at this position, since its proton is easily abstracted by excited **2**.[1,3,6,7] Consequently, it appears that the intramolecular hydrogen bonding contributes only to the stability of the substrates and the products.

The irradiation of 2,4-pentanedione (**6**) with **2** for 72 h afforded 1:1 adducts, 2-acetyl-3-hydroxy-3-methyl-2,2-diphenyloxetane (**7**) in a 43.5% yield and acetonyl α,α-diphenylacetonyl ether (**8**) in a 44% yield. The structure of an adduct, **7**, was assigned to the oxetane on the basis of the spectral data and the elemental analysis. The IR absorptions at 3400 and 1704 cm^{-1} of **7** show the presence of an intramolecular hydrogen-bonded hydroxyl and carbonyl group. Furthermore, **7** reacts with 2,4-dinitrophenylhydrazine to give a single 2,4-dinitrophenylhydrazone. These results suggest that the methyl and acetyl groups on the oxetane ring have a *trans*-configuration. The oxetane, **7**, was cleaved to an ether, **8**, by boiling it with a solvent, such as benzene or ethanol, or by column chromatography. These conditions define the stability of the β-hydroxy ketone, since the dealdolization may involve a thermal process.[8] Consequently, it is considered that the ether, **8**, was produced by the cleavage of the oxetane, **7**, during the separation, by analogy with the photoadducts of cycloalkene and β-diketones.[8,9] **7** and **8** also afforded 1,1-diphenyl-2-propanone (**9**)[10] and methylglyoxal (**10**)[11] respectively by thermal cleavage under a nitrogen atmosphere. In this photoreaction, the light energy was absorbed exclusively by **2**; the reaction was also inhibited com-

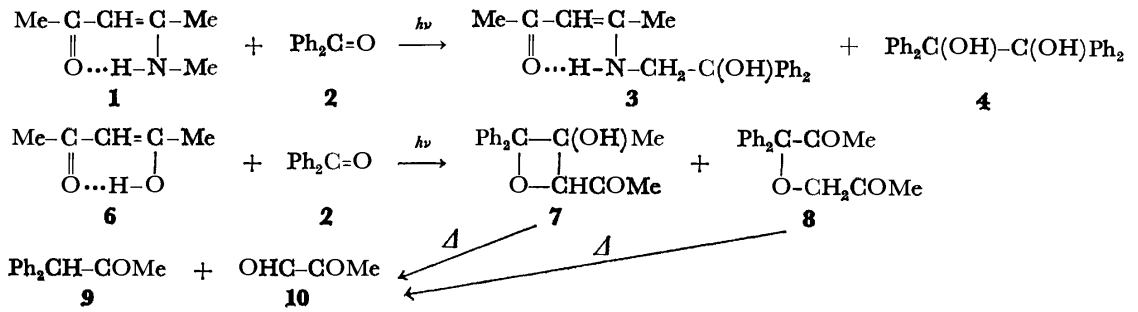

pletely in the presence of 1,3-pentadiene.[5] The photodimerization of enones is sensitized by **2**,[12] but no cross-coupling reaction of these compounds has been known. The formation of the oxetane, **7**, can easily be interpreted by assuming the attack of **2** in the triplet state on the double bond of the enolated **6**. An electron-deficient oxygen of the excited **2** can attack the more negative center at the 3-position of **6** to give the more stable intermediate diradical, followed by cyclization to form an oxetane. This consideration clearly explains the orientation mode in the formation of the oxetane, **7**.

The photochemical reaction of **2** with ethyl acetoacetate (**15**) and benzoylacetone (**16**) did not give a photoadduct such as oxetane. This may be attributed to the facts that the former has a low enol content and that the latter absorbs most of the light energy under the present reaction conditions.

The difference in the photochemical reactivity of **1** and enolated **6** with **2** may be attributed to the presence or absence of an α-hydrogen atom, which is easily abstracted by excited **2**.

Experimental

The enamino ketones were prepared from the corresponding β-diketones and amines. The **2**, benzene, and the other materials were purified in the usual way. The IR, NMR, and UV spectra were recorded with JASCO IRG, Hitachi R24B, and Hitachi 124 spectrometers respectively. The MS spectra were determined with a CEC21-110B mass spectrometer.

The irradiations were performed under a nitrogen atmosphere with a 100-W high pressure mercury lamp which had been lowered into a water-cooled Pyrex immersion well. The yields are based on the consumed **2**. All the melting points are uncorrected.

*Photochemical Reaction of **1** with **2***: A solution containing 7.9 g (70 mmol) of **1** and 12.7 g (70 mmol) of **2** in 400 ml of benzene was irradiated for 48 h. The reaction mixture was then concentrated *in vacuo* to *ca.* 30 ml, the residual solid was removed by filtration, and the filtrate was chromatographed on silica gel. Elution with benzene gave **4** (5.9 g, 75%) and **2** (4.9 g, 39% recovery). Elution with benzene–acetone (10:1) gave **1** (1.3 g, 17% recovery). Further elution with acetone gave a resinous substance. The collected solid was recrystallized with chloroform to give 2.1 g (17%) of **3** as colorless prisms; mp 223—224 °C. MS *m/e*: 295 (M^+). IR($CHCl_3$): 3570, 1610, and 1570 cm^{-1}. NMR (DMSO-d_6) δ=1.85 (3H, s), 1.89 (3H, s), 4.23 (2H, d, J=6 Hz), 5.02 (1H, s), 6.26 (1H, s), 7.5—7.9 (10H, m), and 11.12 (1H, s). UVmax (EtOH): 312.5 (ε 18000) and 318^{sh} nm (17000). Found: C, 76.98; H, 6.99; N, 4.72%. Calcd for $C_{19}H_{21}NO_2$: C, 77.25: H, 7.13; N, 4.74%. Hydrolysis of **3** by dil-HCl yielded **5** and **6**.

*Photochemical Reaction of **13** with **2***: A solution containing 8.9 g (70 mmol) of **13** and 12.8 g (70 mmol) of **2** in bezene (400 ml) was irradiated for 72 h. The solution was then removed, and the residue was chromatographed on silica gel. From the benzene eluents, 3.0 g (35%) of **4** were isolated; 4.2 g (33%) of **2** were also recovered. Further elution with benzene-methanol (5:1) gave a brown viscous oil, which was separated by carbon tetrachloride-hexane (1:1) to give 0.7 g of **14**; mp 138—139 °C. MS *m/e* 269 (M^+). IR ($CHCl_3$): 3280 (O–H), and 1620 cm^{-1} (C=O). NMR ($CDCl_3$) δ=2.03 (3H, s), 2.47 (3H, s), 4.22 (2H, s), 5.38 (1H, s), and 7.1—7.6 (10H, m). Found: C, 75.57; H, 7.06; N, 5.11%. Calcd for $C_{17}H_{19}NO_2$: C, 75.74; H, 7.11; N, 5.20%.

*Photochemical Reaction of **6** with **2***: A solution containing 8.0 g (80 mmol) of **6** and 14.5 g (80 mmol) of **2** in 400 ml of benzene was irradiated for 72 h. The reaction mixture was then concentrated *in vacuo* to *ca.* 30 ml, the crystals of the oxetane, **7**, were removed by filtration, and the filtrate was chromatographed on silica gel. From the benzene eluent, 0.5 g (12%) of **4** was isolated, while 10.5 g (72%) of **2** and 5 g (62%) of **6** were recovered. From the benzene–acetone (10:1) eluent we obtained 2.7 g (44%) of **8** as a viscous liquid; IR ($CHCl_3$): 1714, 1598, 1354, and 1098 cm^{-1}. NMR ($CDCl_3$) δ=2.11 (3H, s), 2.21 (3H, s), 3.35 (2H, s), and 7.3 (10H, s). Found: C, 76.40; H, 6.50%. Calcd for $C_{18}H_{18}O_3$: C, 76.57; H, 6.45%. The product, **8**, gave a mixture of 2,4-dinitrophenylhydrazones of **9** and **10** in ethanol. The former had a mp of 141—142 °C (from EtOH), undepressed on admixture with an independently synthesized authentic specimen with the same melting point.[10] The latter had a mp of 299—300 °C (from DMF) (Lit,[11] mp 299—300 °C). The oxetane, **7**, was washed with benzene; 2.7 g (43.5%); mp 141—142 °C (dec). IR ($CHCl_3$): 3550, 3400, 1721, 1704, 995, and 977 cm^{-1}. NMR ($CDCl_3$) δ=1.35 (3H, s), 2.13 (3H, s), 2.63 (1H, s), 4.90 (1H, s), and 7.3—7.7 (10H. m). UVmax (EtOH): 224 (ε 20000), 259 (3500), and 290^{sh} nm (1300). Found: C, 76.62; H, 6.48%. Calcd for $C_{18}H_{18}O_3$: C, 76.57; H, 6.45%. 2,4-Dinitrophenylhydrazone of **7** had mp 161—162 °C (from EtOH); IR (Nujol): 3550 (O–H), 3300 (N–H), and 995 cm^{-1} (C–O–C). Found: C, 62.41; H, 4.71; N, 12.14%.

Other Photochemical Reactions: The irradiation of a benzene solution containing 1,3-pentadiene, **1** or **6**, and **2** caused the unreacted starting materials to be recovered. The reaction of **15** with **2** in benzene for 48 h gave **4** (92%) and a resinous substance, while **2** (47%) and **15** (46%) were recovered. The irradiations of **11**, **12**, and **16** with **2**, a benzene solution containing only **1** and/or **6**, and a cyclohexene solution of **1** caused the unreacted starting materials to be recovered quantitatively.

References

1) M. Kawanisi, K. Kamogawa, T. Okada, and H. Nozaki, *Tetrahedron*, **24**, 6557 (1968).

2) L. A. Singer and G. A. Daivs, *J. Am. Chem. Soc.*, **89**, 598 (1967); L. A. Singer, G. A. Davis, and R. L. Knutsen, *ibid.*, **94**, 1188 (1972).

3) M. Ogata, H. Matsumoto, and H. Kanō, *Kogyokagaku Zasshi*, **72**, 195 (1969).

4) P. Weidenkaff, *Ber.*, **38**, 1689 (1905).

5) G. S. Hammond and P. A. Leermakers, *J. Phys. Chem.*, **66**, 1148 (1962).

6) S. G. Cohen and R. J. Baumgarten, *J. Am. Chem. Soc.*, **89**, 3471 (1967).

7) S. G. Cohen and H. M. Chao, *J. Am. Chem. Soc.*, **90**, 165 (1968).

8) P. de Mayo and H. Takeshita, *Can. J. Chem.*, **41**, 440 (1963).

9) M. Tada, H. Harada, and K. Miura, *Bull. Chem. Soc. Jpn.*, **51**, 839 (1978).

10) E. M. Schultz and S. Mickey, *Org. Synth.*, Coll. Vol. III, 343 (1955).

11) E. S. Waight, "Rodd's Chemistry of Carbon Compounds," ed by S. Coffey, Elsevier Publishing Co., Amsterdam (1965), Vol. I, Part D, Chap. 13, p. 65.

12) E. Y. Y. Lam, D. Valentine, and G. S. Hammond, *J. Am. Chem. Soc.*, **89**, 3482 (1967); J. L. Ruhlen and P. A. Leermakers, *ibid.*, **89**, 4944 (1967).

The Synthesis of 2-Imino-2,3-dihydro-1,3,4-selenadiazole Derivatives

Masahiko TAKAHASHI* and Michiyoshi KUROSAWA

Department of Industrial Chemistry, Faculty of Engineering, Ibaraki University, Hitachi, Ibaraki 316

(Received August 1, 1979)

Synopsis. The reaction of phenacyl selenocyanate with arenediazonium chlorides afforded 3-aryl-5-benzoyl-2-imino-2,3-dihydro-1,3,4-selenadiazoles, which were then acetylated and nitrosated to give the corresponding 2-acetylimino and 2-nitrosoimino derivatives respectively.

As compared with the chemistry of 1,3,4-thiadiazole,[1] that of 1,3,4-selenadiazole is less known, it has been studied intensively for only the last 10 years.[2] A few 1,3,4-selenadiazole derivatives have been shown to have significant antibacterial activity.[3] Recently it has been reported by Shawali *et al.*[4] that the diazonium coupling reaction of phenacyl thiocyanate (**1**) is a convenient route to 2-imino-2,3-dihydro-1,3,4-thiadiazoles (**2**). Similarly, the reaction of 3-thiocyanatopentane-2,4-dione (**3**) led to the one-step synthesis of **2**.[5] Accordingly, it appears possible to obtain 2-imino-2,3-dihydro-1,3,4-selenodiazoles by reacting phenacyl selenocyanate (**4**) with arenediazonium chlorides. We thus obtained the expected compound from readily-available starting material, **4**, in one step, although the yields were rather low. The direct synthesis of 2,3-dihydro-1,3,4-selenadiazoles has so far been known in only one case, *i.e.*, the reaction of hydrazonyl halides with potassium selenocyanate,[6] while several derivatives have been prepared indirectly from 2-amino-1,3,4-selenadiazoles.[7]

The treatment of **4** with arenediazonium chlorides at 0—5 °C gave precipitates. These precipitates contained a significant amount of tars; attempts to obtain analytical pure samples by recrystallization were unsuccesful. Crude products which showed only one spot on a thin-layer chromatogram were, however, obtained by repeating the precipitation with ether from a hot solution of acetic acid. In the IR spectra of these crude products, the selenocyanato absorption (2160 cm^{-1}) presented in **4** disappeared, and new imino absorptions were observed in the region of 2950—2860 cm^{-1} (Table 1). Although these IR spectra suggested the cyclization to the expected 3-aryl-5-benzoyl-2-imino-2,3-dihydro-1,3,4-selenadiazoles (**5**), the structure of **5** were not confirmed ultimately until their acetylation and nitrosation, since the elemental analyses of **5** were unsatisfactory because of the difficulties in purification.

The reflux of **5** in acetic anhydride afforded the acetate (**6**) in good yields (Table 2). The IR spectra of **6** showed no NH absorption, but exhibited two carbonyl absorptions in the regions of 1650—1621 cm^{-1} and 1636—1615 cm^{-1}, which were assigned to benzoyl carbonyls and acetyl carbonyls respectively. The meth-

Table 1. Physical properties of **5**

5	Yield/%	Mp/°C	IR (KBr) ν_{max}/cm^{-1}		
a	26	199—203	2880	1637	1620
			1592	1573	1530
b	53	204—210	2950	1633	1610
			1594	1575	1530
c	28	174—178	2860	1640	1610
			1593	1574	1523
d	28	205—211	2920	1637	1615
			1595	1574	1532
e	15	204—208	2900	1640	1594
			1576	1536	1477

Table 2. Physical properties and analytical data of **6** and **7**

Compound	Yield %	Mp °C	IR (KBr) ν_{max}/cm^{-1}			NMR ($CDCl_3$) δ/ppm ArH	ArMe	COMe	C% Found (Calcd)	H% Found (Calcd)
6a	89	169—171 (DMF-MeOH)	1645	1615	1594				55.04 (55.15)	3.70 (3.54)
			1578	1509	1490					
6b	89	153—155 (MeOH)	1632	1620	1592	7.23—8.37(m)	2.44(s)	2.37(s)	56.38 (56.26)	4.17 (3.93)
			1572	1502	1454					
6c	72	165—167 (DMF-MeOH)	1621	1594	1574	7.28—8.41(m)	2.45(s)	2.38(s)	56.14 (56.26)	3.95 (3.93)
			1510	1485	1464					
6d	61	148—150 (DMF-MeOH)	1650	1636	1595	7.40—8.37(m)		2.39(s)	50.47 (50.45)	2.98 (2.99)
			1575	1532	1479					
6e	65	198—201 (DMF-MeOH)	1640	1633	1600	7.43—8.39(m)		2.30(s)	50.37 (50.45)	3.00 (2.99)
			1578	1519	1481					
7a	80	128—129 (MeOH)	1635	1590	1573	7.40—8.40(m)			50.46 (50.43)	2.86 (2.82)
			1510	1486	1458					
7b	87	126—128 (MeOH)	1632	1595	1575	7.26—8.34(m)	2.45(s)		52.00 (51.76)	3.56 (3.26)
			1520	1504	1431					
7c	80	129—131 (DMF-MeOH)	1640	1612	1597	7.36—8.44(m)	2.47(s)		51.94 (51.76)	3.25 (3.26)
			1580	1525	1492					
7d	85	129—130 (MeOH)	1645	1592	1574	7.43—8.40(m)			46.10 (46.00)	2.33 (2.32)
			1512	1484	1447					
7e	81	125—127 (DMF-MeOH)	1645	1596	1577	7.47—8.43(m)			46.03 (46.00)	2.13 (2.32)
			1521	1479	1448					

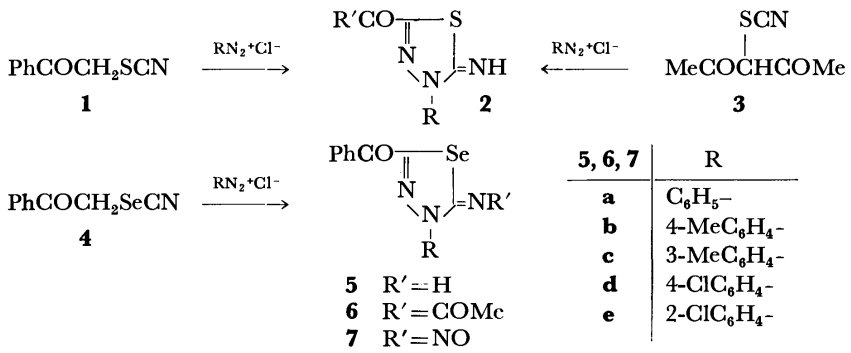

5, 6, 7	R
a	C_6H_5-
b	4-MeC_6H_4-
c	3-MeC_6H_4-
d	4-ClC_6H_4-
e	2-ClC_6H_4-

yl proton resonances were observed at δ 2.30—2.39 ppm in the NMR spectra. These spectral data and the satisfactory elemental analyses were consistent with the 2-acetylimino-3-aryl-5-benzoyl-2,3-dihydro-1,3,4-selenadiazole structures (**6**).

The treatment of **5** with sodium nitrite in acetic acid at room temperature gave the nitrosoimino derivatives (**7**), red to orange, in good yields (Table 2). The IR spectra of **7** showed no NH absorption, but did display carbonyl absorptions in the region of 1645—1632 cm^{-1}. The structures of 3-aryl-5-benzoyl-2-nitrosoimino-2,3-dihydro-1,3,4-selenadiazoles (**7**) were also supported by the NMR and analytical data.

Experimental

The IR and NMR spectra were taken on a JASCO IRA-2 spectrometer and a JEOL-PMX 60 spectrometer respectively. The elemental analyses were performed on a Shimadzu UM-3B apparatus.

*Reaction of **4** with Arenediazonium Chlorides.* To a stirred and ice-cooled solution of **4**[8] (2.2 g, 10 mmol) and sodium acetate (2.5 g) in MeOH (50 ml), an aqueous arenediazonium chloride solution (19 ml) prepared from arylamine (15 mmol) in the usual manner was added, drop by drop, below 5 °C. After stirring below 5 °C for 5 h, the separated solids were collected by filtration and rinsed with ether. They were dissolved into hot acetic acid, and then the solution was poured into ether. The collection of the resulting precipitates gave, as the crude products, **5a—e**.

*Acetylation of **5**.* A solution of **5** (1.0 mmol) in acetic anhydride (5 ml) was refluxed for 1 h. The subsequent evaporation of the solvent, rinsing of the residue with ether, and recrystallization gave the pure acetates (**6a—e**).

*Nitrosation of **5**.* To a stirred solution of **5** (1.0 mmol) in acetic acid (5 ml), an aqueous solution (2 ml) of sodium nitrite (140 mg, 2.0 mmol) was added, drop by drop, at room temperature. After 1 h, a small amount of water was added to the red solution, and the precipitates thus formed were collected by filtration. The subsequent rinsing of the precipitates with water, followed by recrystallization, afforded the pure nitroso derivatives (**7a—e**).

References

1) J. Sandström, "Advances in Heterocyclic Compounds," ed by A. R. Katritzky and A. J. Boulton, Academic Press, New York (1968), Vol. 9, p. 165.

2) D. L. Klayman and W. H. H. Günther, "Organic Selenium Compounds: Their Chemistry and Biology," Wiley-Interscience, New York (1973).

3) A. Shafiee, I. Lalezari, S. Yazdany, and A. Pournorouz, *J. Pharm. Sci.*, **62**, 839 (1973).

4) a) A. S. Shawali and A. O. Abdelhamid, *Tetrahedron Lett.*, **1975**, 163; b) A. S. Shawali and A. O. Abdelhamid, *J. Heterocycl. Chem.*, **13**, 45 (1976).

5) N. F. Eweiss and A. Osmen, *Tetrahedron Lett.*, **1979**, 1169.

6) R. Fusco and C. Munsante, *Gazz. Chim. Ital.*, **68**, 665 (1938).

7) a) I. Lalezari and A. Schafiee, *J. Heterocycl. Chem.*, **8**, 835 (1971); b) E. Bulka, D. Ehlers, and H. Storm, *J. Prakt. Chem.*, **315**, 164 (1973); c) E. Bulka and D. Ehlers, *J. Prakt. Chem.*, **315**, 510 (1973).

8) G. Hofmann, *Justus Liebigs Ann. Chem.*, **250**, 298 (1889); Beilsteins Handbuch der Organischen Chemie, **8**, 95 (1925).

Facile Synthesis of 2,5-Diacylthiophenes. II. The Reaction of Diketo Sulfides with 1,2-Diketones

Yuji MIYAHARA,* Takahiko INAZU, and Tamotsu YOSHINO

Department of Chemistry, Faculty of Science, Kyushu University 33, *Hakozaki, Higashi-ku, Fukuoka 812*

(Received August 7, 1979)

Synopsis. The base-catalyzed reaction of diketo sulfides $(RCOCH_2)_2S$ (R=phenyl, *p*-tolyl) with biacetyl or benzil have provided high yields of 2,5-diacyltetrahydrothiophene-3,4-diol derivatives rather than the expected 2,5-diacylthiophenes. The diols have been transformed cleanly into the corresponding 2,5-diacylthiophenes by treatment with thionyl chloride–pyridine. In contrast, the reaction of the diketo sulfide (R=*p*-tolyl) with phenylglyoxal afforded a 2,5-diacylthiophene directly in good yield.

We have recently demonstrated that the extension of the Hinsberg thiophene synthesis to the diketo sulfides of the type $(RCOCH_2)_2S$, affording 2,5-diacylthiophenes, is very successful when glyoxal is used as the 1,2-dicarbonyl compound and when the reaction is conducted under mild conditions.[1] An obvious extension of the thiophene synthesis is the condensation with 1,2-diketones such as biacetyl and benzil, which have been frequently used in the Hinsberg reaction.[2] When the reaction of α,α′-thiodiacetophenone (**1a**) with biacetyl was conducted under the usual Hinsberg conditions (a rather high concentration of sodium alkoxide), only an intractable tar was obtained. On addition of a dilute methanolic solution of sodium methoxide to a solution of **1a** and biacetyl in methanol at room temperature, a white crystalline precipitate started to separate in a few minutes, in a manner similar to the condensation with glyoxal yielding 2,5-diacylthiophenes. The product isolated at this stage was, however, not the expected thiophene derivative **4a** but an intermediate adduct 2,5-dibenzoyl-3,4-dimethyltetrahydrothiophene-3,4-diol (**2a**). Further addition of the base solution gradually dissolved the precipitate. The resultant dark homogeneous solution gave no crystalline substance. Similar results were obtained for the reactions of **1a** with benzil and **1b** with biacetyl or benzil. On the other hand, the reactions of aliphatic diketo sulfides (R=*t*-butyl, nonyl) gave dark tars with recovery of the starting materials. The yields of the diols **2a**, **2b**, **3a**, and **3b** were very variable, maybe because of the reversibility of the reaction and the complex condensation reactions of the regenerated diketo sulfides. In fact, reproducible high yields could be realized under conditions in which the less soluble diols crystallized out almost completely. The yields and the properties of the diols are summarized in Table 1. The diols thus obtained were pure, judging from their sharp melting points (with decomposition), IR and NMR spectral data, and TLC behavior. Each of them must, therefore,

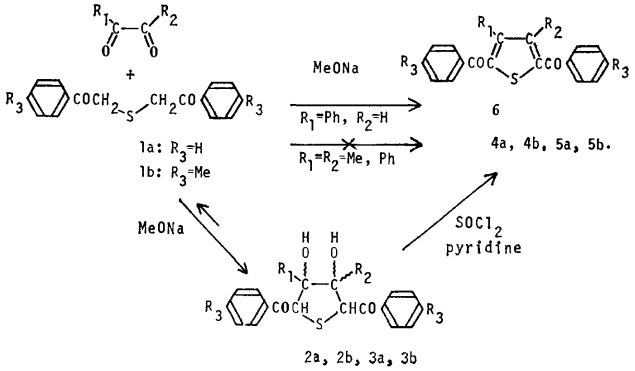

Scheme 1.

TABLE 1. THE YIELDS AND PROPERTIES OF THE PRODUCTS

Compound No.	R_1	R_2	R_3	Yield/%	Mp/°C	Molecular Formula	Found(Calcd) (%) C	Found(Calcd) (%) H	IR(KBr) cm^{-1}	NMR($CDCl_3$), δ/ppm R_1, R_2	CHCO	OH
2a	Me	Me	H	91.6	201—202 (dec)	$C_{20}H_{20}O_4S$	67.23 (67.40)	5.66 (5.66)	3500 (ν_{OH}) 1673 (ν_{CO})	1.45	5.21	5.3 (br)
2b	Me	Me	Me	89.7	207.5—208 (dec)	$C_{22}H_{24}O_4S$	68.44 (68.73)	6.25 (6.29)	3450 (ν_{OH}) 1653 (ν_{CO})	1.43	5.20	5.45
3a	Ph	Ph	H	83.8	161.5—162.5 (dec)	$C_{30}H_{24}O_4S$	74.92 (74.98)	5.01 (5.03)	3500 (ν_{OH}) 1665 (ν_{CO})	7.18	6.32	6.00
3b	Ph	Ph	Me	81.1	196—196.5 (dec)	$C_{32}H_{28}O_4S$	75.82 (75.57)	5.53 (5.55)	3390 (ν_{OH}) 1659 (ν_{CO})	7.18	6.31	6.13
4a	Me	Me	H	84.9	101.5—102.5 (lit.[6] 103—104)	$C_{20}H_{16}O_2S$	75.14 (74.97)	5.03 (5.03)	1641 (ν_{CO})	2.37		
4b	Me	Me	Me	95.4	71.5—72.5	$C_{22}H_{20}O_2S$	75.70 (75.83)	5.79 (5.78)	1641 (ν_{CO})	2.37		
5a	Ph	Ph	H	92.6	141—142 (lit.[7] 131.5—132)	$C_{30}H_{20}O_2S$	80.87 (81.06)	4.50 (4.53)	1640 (ν_{CO}) 1625 (ν_{CO})	6.96		
5b	Ph	Ph	Me	88.6	172.5—173	$C_{32}H_{24}O_2S$	81.15 (81.33)	5.04 (5.12)	1654 (ν_{CO})	6.99		
6	Ph	H	Me	67.8	129—130	$C_{26}H_{20}O_2S$	78.64 (78.76)	5.07 (5.08)	1655 (ν_{CO}) 1631 (ν_{CO})	7.22 (Ph) 7.74 (H)		

be one of the seven possible isomers, but the configurations could not be determined on the basis of the available data.[3] The most striking feature of the diols is the sterically hindered nature of the hydroxyl groups, which is evidenced by the unusually slow deuterium exchange of the hydroxyl protons in the diols, especially the bulky phenyl-substituted **3a** and **3b**, and the unexpectedly high Rf values on TLC (silica gel, benzene; 0.29 and 0.71 for **2a** and **3a**, respectively, compared with 0.27 for **1a**).

Although all the attempted dehydrations of the diols under basic (sodium alkoxide/alcohol) or acidic conditions (*p*-toluenesulfonic acid/benzene, phosphorus pentaoxide/benzene, acetic anhydride[3]) gave complex mixtures of products containing the original diketo sulfides and diketones, treatment with thionyl chloride–pyridine at room temperature readily effected the desired conversion to 2,5-diacylthiophenes in high yields, as shown in Table 1. Thus, the condensation of the diketo sulfides with 1,2-diketones was realized in two steps in good overall yields.

The marked difference in reactivity between glyoxal and 1,2-diketones in the reaction with the diketo sulfides led us to investigate the reaction of phenylglyoxal as an intermediate case. The reaction of **1b** with phenylglyoxal under conditions similar to those used for the reaction with 1,2-diketones provided 2,5-di-*p*-toluoyl-3-phenylthiophene (**6**), directly but less efficiently than that with glyoxal.[1]

The resistance of the diols to dehydration, therefore, may be associated with the steric crowding in the diols and the corresponding 2,5-diacylthiophenes. The successful Hinsberg condensation of thiodiacetate esters with 1,2-diketones, in contrast to the present reaction of diketo sulfides, must be ascribed to the neighboring-group assistance by the formation of a δ-lactone intermediate (a Stobbe-type condensation).[4]

Experimental

All the melting points were determined in capillary tubes and are uncorrected. The NMR spectra were recorded on a Hitachi R-20B spectrometer at 60 MHz in deuteriochloroform, with tetramethylsilane as an internal standard. The IR spectra were obtained on a Hitachi 215 spectrophotometer in KBr disks and were calibrated carefully with a polystyrene film.

Reaction of Diketo Sulfides with 1,2-Diketones. The reaction of **1a** with biacetyl yielding **2a** was best carried out as follows. To a stirred solution of **1a** (2.70 g, 10 mmol) and biacetyl (freshly opened, 1.00 g, 11.6 mmol) in 40 ml of methanol was added 0.5 ml of a solution of sodium methoxide (0.5 g of sodium dissolved in 100 ml of methanol) at *ca.* 40 °C. The precipitation of crystals occurred immediately with evolution of heat. After stirring for 1 h, the product was collected by filtration and washed with methanol. To the filtrate, biacetyl (0.5 g) and the base solution (0.5 ml) were added to give, after standing overnight, a small additional amount of the product. The yield of the colorless needles of **2a** amounted to 3.26 g (91.6%); mp 201—202 °C (decomposed with evolution of a gas), recrystallized from chloroform.

Other diols **2b**, **3a**, and **3b** were obtained similarly by the reaction of the diketo sulfides **1a** and **1b** with biacetyl or benzil as shown in Table 1. To be noted is the very slow deuterium exchange of the hydroxyl protons. The hydroxyl and the methine protons appeared close together as singlets in the NMR spectra. In order to make assignments the sample solutions were shaken with a drop of deuterium oxide. The procedure resulted in a slight decrease in the intensities of the hydroxyl peaks of **2a** and **2b** and almost no change in the case of **3a** and **3b**. In order to reduce the intensities of the hydroxyl peaks of **3a** and **3b** appreciably, it was necessary to heat and shake repeatedly.

*Dehydration of the Diols **2a**, **2b**, **3a**, and **3b**.* To a suspension of the diol (4.0 mmol) in 30 ml of chloroform and 4.0 ml of pyridine cooled in an ice bath, was added 4.0 ml of thionyl chloride. The resultant clear yellow solution was stirred at room temperature for 1 h. Then, the solution was poured into ice and water containing hydrochloric acid, and extracted with chloroform. After washing with water, the extracts were dried over magnesium sulfate and filtered through a short column of silica gel. After solvent evaporation, the residue was crystallized from methanol.

*Condensation of **1b** with Phenylglyoxal.* To a stirred, warm solution of **1b** (1.492 g, 5.0 mmol) and phenylglyoxal (freshly prepared,[5] 740 mg, 5.5 mmol) in 10 ml of methanol was added a solution of sodium methoxide (0.5 g of sodium dissolved in 100 ml of methanol, 10 ml) over a 10-min period. Crystals started to separate slowly. After it had been stirred for 30 min, the solution was allowed to stand for 2 d. The product was collected by filtration and washed well with methanol. **6** was obtained as pale yellow granules in 67.8% yield (1.345 g); recrystallized from benzene–methanol; mp 129—130 °C.

References

1) Y. Miyahara, T. Inazu, and T. Yoshino, *Chem. Lett.*, **1978**, 563; Y, Miyahara, *J. Heterocycl. Chem.*, **16**, 1147 (1979).

2) For a recent application of the Hinsberg condensation, see D. J. Chadwick, J. Chambers, G. D. Meakins, and R. L. Snowden, *J. Chem. Soc., Perkin Trans. 1*, **1972**, 2079.

3) For the isolation of diol products in the Hinsberg condensation and thier dehydration, see A. Birch and D. A. Crombie, *Chem. Ind. (London)*, **1971**, 177.

4) H. Wynberg and H. J. Kooreman, *J. Am. Chem. Soc.*, **87**, 1739 (1965).

5) H. A. Riley and A. R. Gray, *Org. Synth.*, Coll. Vol. II, 509 (1943).

6) J. L. Melles and J. Backer, *Recl. Trav. Chim. Pays-Bas*, **72**, 314 (1953).

7) A. Mangini and A. Tundo, *Z. Elektrochem.*, **64**, 694 (1960).

Reaction of Ethyl Azidoformate with Morpholines

Teruko Tsuchida,* Kikuhiko Koyama, Michiharu Mitani, and Hiroshi Takeuchi

Department of Synthetic Chemistry, Faculty of Engineering, Shinshu University, Wakasato, Nagano 380

(Received August 11, 1979)

Synopsis. Ethyl azidoformate (**1**) reacts rapidly with morpholine to give morpholinium azide and 4-(ethoxycarbonyl)morpholine in good yields. With 4-methylmorpholine (**3**), however, the azide **1** reacts at 115 °C with evolution of nitrogen to give formal nitrene-insertion products, 4-methyl-3-(ethoxycarbonylamino)morpholine and 4-(ethoxycarbonylaminomethyl)morpholine. There has not been found any product which might arise from the nitrene-insertion into C–H bond adjacent ot oxygen of **3**. These results can be accounted for on the basis of the n-donor abilities of heteroatoms, O and N.

Ethoxycarbonylnitrene generated photochemically or thermally from ethyl azidoformate inserts exclusively into C–H bonds adjacent to oxygen of cyclic and open-chain ethers.[1-3] The nitrene also exclusively reacts with CH_3 groups of *N,N*-dimethylaniline to give formal insertion product.[4]

The exclusive reactions at these activated C–H bonds have been considered to proceed with the initial formation of O–N or N–N ylids by coordinative attack of the electron-deficient nitrene on the heteroatoms with nonbonded electron pair, followed by the rearrangement to give formal insertion products.

Morpholine and its *N*-substituted derivatives are, therefore, particularly interesting in connection with the possibility of intervention of such ylid intermediates, because of bearing two kinds of C–H bonds activated by the adjacent oxygen and nitrogen atoms, respectively.

Results and Discussion

The reaction of ethyl azidoformate (**1**) with morpholine (**2**) was conducted by adding the azide **1** to **2** at room temperature and heating the solution to 120 °C for 2 h with stirring. A white solid formed immediately at the stage of the addition was separated by filtration, and proved to be morpholinium azide (**4**, 86% yield) on the basis of its spectral data. In addition, 4-(ethoxycarbonyl)morpholine (**5**) was obtained in 57% yield from the filtrate by the vacuum distillation. The structure of **5** was characterized by comparison with the authentic sample.

The result described above clearly indicates that the products **4** and **5** were formed by a simple displacement of azide ion[5] from **1** with **2**, which is a strong nucleophile[6] with mobile hydrogen atom on nitrogen, but via neither nitrene nor ylid intermediate, as shown in Scheme 1.

The thermolysis of the azide **1**, however, smoothly proceeded in 4-methylmorpholine (**3**) with evolution of nitrogen at 115 °C. After usual workup involving removal of unchanged **3**, three major products isolated by preparative VPC from a residual oil were identified as ethyl carbamate (**6**), 4-(ethoxycarbonylaminomethyl)morpholine (**7**) and 4-methyl-3-(ethoxycarbonylamino)morpholine (**8**), respectively. The structural assignment of these products, **6**, **7** and **8**, was based on their ^1H NMR and mass spectral data. The product distribution in the oily residue has tentatively been determined as 61.1% of **6**, 13.4% of **7**, 2.5% of **8** and 23% (total) of three unidentified products, instead of their exact yields, on the basis of their VPC peak areas. A further examination of the reaction mixture gave no evidence for the presence of any product which might arise from the reaction at C–H bond activated by the adjacent oxygen.

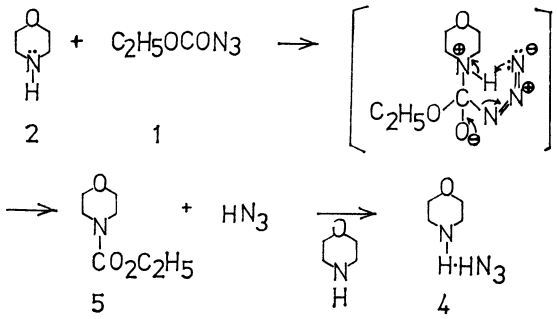

Scheme 1.

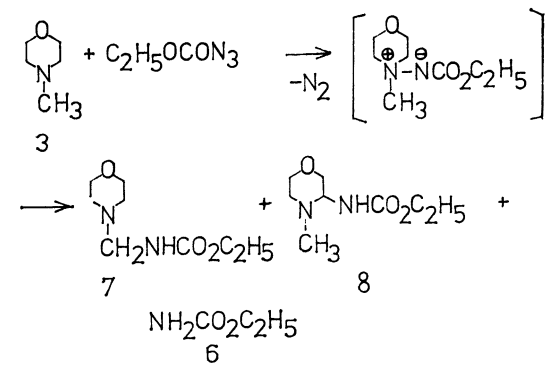

Scheme 2.

Of interest is the fact that the reaction occurs exclusively at C–H bonds adjacent to nitrogen. This can be rationalized in terms of the mechanism in which the N–N ylid is involved as an intermediate. Since nitrogen is a much stronger n-electron donor than oxygen and the N–N ylid is more stable than the O–N ylid, the electron-deficient nitrene attacks preferentially nitrogen over oxygen to give a more stable ylid followed by rearrangement leading to formal nitrene-insertion products, **7** and **8**, even though the detailed mechanism for the rearrangement has not been clear yet.

Experimental

IR spectra were recorded on a Hitachi Model EPI-G3 and ^1H NMR spectra on a JEOL JNM 4H 100 spectrometer.

Mass spectra were obtained by JEOL JMC OlSG-2 spectrometer.

Commercially available morpholine and 4-methylmorpholine were used after distillation. Ethyl azidoformate was prepared according to the method of Lwowski and Mattingly.[7]

Authentic 4-(ethoxycarbonyl)morpholine was prepared from morpholine and ethyl chloroformate by usual procedures.[7]

*Reaction of Ethyl Azidoformate (**1**) with Morpholine (**2**).* The azide **1** (2.0 g; 0.017 mol) was added at room temperature to **2** (7.5 g; 0.087 mol) with stirring. During the addition, a white solid rapidly separated without any evolution of gases. The mixture was then heated to 120 °C and kept at that temperature for 2 h. After cooling to room temperature the resulting solid was separated on a filter, washed with ether, dried *in vacuo* and recrystallized from hot methanol to give **4** as white needles, mp 129.2—130.2 °C (yield; 1.89 g; 86.1%). Soluble in water but insoluble in ether and benzene. IR (KBr) 2450 ($\overset{+}{N}H_2$), 2030 (N_3^-) and 1590 cm^{-1} ($\overset{+}{N}H_2$); ^1H NMR ($(CD_3)_2SO$) $\delta=3.15$ (4H, m, N-CH_2), 3.8 (4H, m, O-CH_2) and 7.35 (2H, br, NH_2, disappered by treatment with D_2O); MS *m/e*: 87 (M−HN_3) and 43 (HN_3); Found: C, 36.82; H, 7.58; N, 43.20%. Calcd for $C_4H_{10}ON_4$: C, 36.91; H, 7.74; N, 43.50%.

The filtrate was fractionally distilled *in vacuo* to give **5** (yield; 1.53 g; 57%): bp 111.2 °C/25 mmHg: IR (neat) 2950 (-CH_3), 1700 (C=O) and 1240 cm^{-1} (=C-O-C); ^1H NMR (CCl_4) $\delta=1.29$ (3H, t, CH_3-), 3.36—3.8 (8H, m, ring proton) and 4.1 (2H, q, -CH_2-); MS *m/e*: 159 (M); Found: C, 52.60; H, 8.49; N, 8.61%. Calcd for $C_7H_{13}O_3N$: C, 52,82; H, 8.23; N, 8.80%. IR spectrum of **5** was identical in all respects with that of an authentic sample.

*Thermolysis of **1** in 4-Methylmorpholine (**3**).* A stirred solution of **1** (2.3 g; 0.02 mol) in **3** (10.1 g; 0.1 mol) was heated to 115 °C and kept at this temperature for 3 h during which time nitrogen was smoothyl evolved. After the nitrogen evolution has ceased, removal of the excess **3** from the reaction mixture *in vacuo* left a residual oil (4.2 g). The residual oil was subjected to preparative VPC on a column (8 mm×2 m) packed with 5% Silicone OV-22 on 60/80 Uniport KS (oven temperature, initial: 110 °C, final: 230 °C, rate: 10 °C/min) to separate four components. Among them, three major components were identified as ethyl carbamate (**6**), 4-(ethoxycarbonylaminomethyl)morpholine (**7**) and 4-methyl-3-(ethoxycarbonylamino)morpholine (**8**), respectively. The product **6** was characterized by comparison of its VPC retention time and IR spectra with those of the authentic sample. The structural assignment of the components **7** and **8** was performed on the basis of their IR, ^1H NMR and mass spectral data. Analytical data for **7**: IR (neat) 3400 (NH), 1720 (C=O) and 1250 cm^{-1} (=C-O-C); ^1H NMR ($CDCl_3$) $\delta=1.28$ (3H, t, CH_3-), 2.05—3.08 (2H, m, N-CH_2), 3.5 (4H, m, H_2C-N-CH_2), 3.71 (4H, m, H_2C-O-CH_2) and 4.2 (2H, q, -CH_2-); MS *m/e* (rel intensity): 159 (M−C_2H_5 24.1), 115 (M−$CO_2C_2H_5$ 7.4), 100 (M−$NHCO_2C_2H_5$ 29.2) and 86 (M−$CH_2NHCO_2C_2H_5$ 30.7). Analytical data for **8**: IR (neat) 3325 (NH), 2800 (N-CH_3) and 1710 cm^{-1} (C=O); ^1H NMR ($CDCl_3$) $\delta=1.25$ (3H, t, CH_3-), 2.3 (3H, s, N-CH_3), 2.4—2.9 (3H, m, HC-N-CH_2), 3.3—3.85 (4H, m, H_2C-O-CH_2), 4.12 (2H, q, -CH_2) and 5.6 (1H, br, -NH-); MS *m/e* (rel intensity): 188 (M 45.5), 173 (M−CH_3 5.4), 159 (M−C_2H_5 69.7), 115 (M−$CO_2C_2H_5$ 17.2) and 100 (M−$NHCO_2C_2H_5$ 72.9).

The fourth component collected by preparative VPC was failed in its structural determination, although ^1H NMR spectra showed no peaks assignable to CH_3-, CH_2- or CH- adjacent to N.

References

1) T. Shingaki, M. Inagaki, N. Torimoto, and M. Takebayashi, *Chem. Lett.*, **1972**, 297.

2) H. Nozaki, S. Fujita, H. Takaya, and R. Noyori, *Tetrahedron*, **23**, 45 (1967).

3) H. Takeuchi, K. Kinoshita, S. M. A. Hai, M. Mitani, T. Tsuchida, and K. Koyama, *J. Chem. Soc., perkin Trans., 2* **1976**, 1201.

4) "Nitrenes," ed by W. Lwowski, Interscience Pubilshers, New York (1970), p. 206.

5) "Advances in Organic Chemistry Method and Results," ed by R. A. Raphael, E. C. Taylor, and H. Wynberg, Interscience Publishers, New York (1963), p. 171.

6) "Nitrenes," ed by W. Lwowski, Interscienec Publishers, New York (1970), p. 208.

7) W. Lwowski and T. W. Mattingly, *J. Am. Chem. Soc.*, **87** 1947 (1965).

Chemical Studies on Tuberactinomycin. XVII.[1] Synthesis of *threo*-γ-Hydroxy-L-β-lysine, Constituent Amino Acid of Tuberactinomycin A and N

Tadashi TESHIMA, Toshihiko ANDO, and Tetsuo SHIBA*

Department of Chemistry, Faculty of Science, Osaka University, Toyonaka, Osaka 560

(Received August 17, 1979)

Synopsis. *threo*-γ-Hydroxy-L-β-lysine which is a constituent amino acid of antibiotics tuberactinomycin A and N, was synthesized from *threo*-β-hydroxy-L-ornithine derivative by the Arndt-Eistert reaction. The synthetic amino acid was identical with the natural sample in all respects. Furthermore, a route was established to prepare a protected γ-hydroxy-β-lysine derivative useful for the peptide synthesis.

γ-Hydroxy-β-lysine is a constituent amino acid of peptide antibiotics, tuberactinomycin A and N.[2] Either *threo* or *erythro* isomer of this amino acid was obtained from both tuberactinomycin A and N depending on the hydrolysis conditions. Thus, *threo* isomer was obtained from a hydrolyzate with 6 M hydrochloric acid, whereas *erythro* isomer from that with concentrated sulfuric acid.[2] An intact configuration of the amino acid in the original antibiotics was supposed to be of *threo* form from an assumption of the reaction mechanisms in the acidolysis.[3-5]

Racemic *threo* and *erythro* forms of γ-hydroxy-β-lysine were synthesized from a key intermediate, β-methoxyornithine derivative, resulting in a confirmation of the structure of this amino acid.[6] In the present study, a genuine stereoisomer of the natural amino acid, *i.e.*, *threo*-γ-hydroxy-L-β-lysine, was synthesized via *threo*-β-hydroxy-L-ornithine according to a scheme shown in Fig. 1. An intermediate in the synthetic route, N^{β},N^{ϵ}-bis(benzyloxycarbonyl)-*O*-*t*-butyl-γ-hydroxy-L-β-lysine, was successfully used to the total synthesis of tuberactinomycin N, which will be reported elsewhere.[1]

In the Arndt-Eistert reaction for an elongation of the carbon chain, hydroxyl group must be blocked anyhow. Moreover, it was found in our previous study that γ-hydroxy-β-lysine was very liable to be lactonized.[2] Therefore, a protection of the hydroxyl group was necessary particularly for the purpose of the peptide synthesis. *t*-Butyl group was chosen as the protecting group because of a mildness in the introducing reaction. N^{δ}-Benzyloxycarbonyl-*threo*-β-hydroxy-L-ornithine (**1**) was obtained by a coupling of β-(benzyloxycarbonylamino)propionaldehyde with aqua[*N*-(1-carboxylatoethylidene)glycinato]copper(II) followed by a diastereomeric separation and then an optical resolution enzymatically according to the method reported previously.[7] The compound **1** was converted to bis(benzyloxycarbonyl) derivative **2**, and then to its methyl ester **3**. It was treated with isobutylene in the presence of an acid catalyst to give a fully protected derivative **4**. Saponification of **4** produced a free carboxylic acid **5**, which was treated with ethyl chloroformate and then diazomethane to afford a diazo ketone. Wolff rearrangement for the diazo ketone was carried out in the presence of silver benzoate in methanol. Hydrolysis of the product with 6 M hydrochloric acid gave *threo*-γ-hydroxy-L-β-lysine lactone dihydrochloride (**7**). The lactone dihydrochloride **7** thus synthesized was completely identical with the natural specimen obtained from the hydrochloric acid hydrolyzate of tuberactinomycin N[2] in all respects (Table 1). This is the first synthesis of the natural form of γ-hydroxy-β-lysine, and gave a confirmative conclusion for the supposed configurations of this natural amino acid.

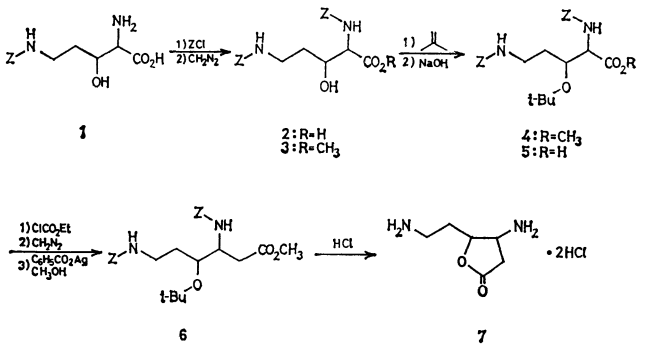

Fig. 1.

Table 1. Comparisons of the natural and synthetic γ-hydroxy-L-β-lysine lactone dihydrochlorides

	Synthetic	Natural
mp (°C, dec)	252—255	254—257
$[\alpha]_D^{25}$ (*c* 0.5, H_2O)	+63°	+65°
Thin-layer chromatography[a]	0.48	0.48
Paper electrophoresis[b]	13 cm	13 cm

a) R_f value on developing solvent: phenol-water-28% ammonia (30: 10: 1). b) Migration distance toward cathode. Buffer solution: pyridine-acetic acid-water (30: 4: 966).

Experimental

All melting points are uncorrected. NMR spectra were obtained with a Varian XL-100-15 spectrometer using sodium 2,2-dimethyl-2-silapentane-5-sulfonate as an internal standard. The optical rotations were measured with a Perkin-Elmer 141 polarimeter. IR spectra were obtained with a Hitachi EPI-G2 Grating Infrared Spectrophotometer. Thin-layer chromatographies were carried out by the ascending method on silica gel 60 F_{254} using developing solvent, phenol-water-28% ammonia (30:10:1). Paper electrophoreses were carried out at 750 V and 1 mA/cm 1 h on Toyo Roshi No. 51 paper using a buffer solution of pyridine–acetic acid–water (30:4:966).

N^{α}, N^{δ}-*Bis(benzyloxycarbonyl)*-threo-β-*hydroxy*-L-*ornithine* (**2**). To a suspension of N^{δ}-benzyloxycarbonyl-*threo*-β-hydroxy-L-ornithine (**1**)[7] (1.00 g, 3.55 mmol) and triethylamine (1.15 ml, 8.24 mmol) in 300 ml of water–tetrahydrofuran (2:1), was added benzyloxycarbonyl chloride (800 mg, 4.69 mmol) in 4 ml of tetrahydrofuran portionwise with stirring under ice cooling for 2.5 h. After the usual work up for

benzyloxycarbonylation, crystals of the product were obtained: yield 1.32 g (89.2%). It was recrystallized from ethyl acetate–hexane: yield 1.23 g (83.1%), mp 141.5—143 °C, $[\alpha]_D^{20}$+13.8° (c 1.04, CH_3OH).

Found: C, 60.80; H, 5.83: N, 6.62%. Calcd for $C_{21}H_{24}N_2O_7$: C, 60.57; H, 5.81; N, 6.73%.

N^{α},N^{δ} - *Bis(benzyloxycarbonyl)* - threo - *β* - *hydroxy* - L - *ornithine Methyl Ester* (**3**). To a solution of N^{α},N^{δ}-bis(benzyloxycarbonyl)-*threo*-*β*-hydroxy-L-ornithine (**2**) (1.20 g, 2.88 mmol) in 20 ml of methanol, a solution of diazomethane in ether was added until its yellow color remained. After excess diazomethane was decomposed with acetic acid, the reaction mixture was concentrated *in vacuo*. The oily residue was triturated with hexane to give crystals: yield 1.22 g (98.5%). It was recrystallized from ethyl acetate–hexane: yield 1.19 g (95.9%), mp 85—88 °C, $[\alpha]_D^{18}$+5.42° (*c* 1.02, CH_3OH).

Found: C, 61.40; H, 6.31; N, 6.28%. Calcd for $C_{22}H_{26}N_2O_7$: C, 61.38; H, 6.09; N, 6.51%.

N^{α},N^{δ}-*Bis(benzyloxycarbonyl)*-O - t - *butyl* - threo - *β*-*hydroxy*-L-*ornithine* (**5**). To a solution of N^{α},N^{δ}-bis(benzyloxycarbonyl)-*threo*-*β*-hydroxy-L-ornithine methyl ester (**3**) (1.00 g, 2.33 mmol) in 100 ml of dichloromethane and 300 ml of liquid isobutylene in a pressure bottle, 0.2 ml of concentrated sulfuric acid was added under cooling. The mixture was shaken at 37 °C for 11 d and then neutralized with triethylamine. The solution was concentrated *in vacuo*, and the oily residue was purified by silica gel column chromatography using a developing solvent of benzene–ethyl acetate (9:1); yield 910 mg (80.5%), a pale yellow oil. *O*-*t*-Butyl methyl ester (**4**) thus obtained was saponified with 2.81 ml of 1 M sodium hydroxide in 5 ml of *N*,*N*-dimethylformamide at 0 °C. After the usual work up, crystals of the carboxylic acid was obtained: yield 633 mg (71.6%). It was recrystallized from ethyl acetate–ether–hexane; yield 567 mg (64.1%), mp 92—95 °C, $[\alpha]_D^{21}$ −2.07° (*c* 5.07, CH_3OH).

Found: C, 63.65; H, 6.83; N, 5.92%. Calcd for $C_{25}H_{32}N_2O_7$: C, 63.55; H, 6.83; N, 5.93%.

threo-*γ*-*Hydroxy*-L-*β*-*lysine Lactone Dihydrochloride* (**7**). To a solution of N^{α},N^{δ}-bis(benzyloxycarbonyl)-*O*-*t*-butyl-*threo*-*β*-hydroxy-L-ornithine (**5**) (420 mg, 0.890 mmol) in 4 ml of ethyl acetate, *N*-methylmorpholine (0.100 ml, 0.890 mmol) and ethyl chloroformate (0.085 ml, 0.89 mmol) were added at −20 °C with stirring. The reaction mixture was stirred for 1 h, and insoluble material was filtered off. To the filtrate, excess diazomethane in ether was added at −20 °C with stirring. The reaction mixture was stirred at this temperature for 1 h and then at room temperature overnight. Insoluble material was filtered off and the filtrate was concentrated *in vacuo*. A diazo ketone was obtained as a yellow oil.

To a solution of this oily residue in 4 ml of methanol, silver benzoate (70 mg, 0.306 mmol) in 0.7 ml of triethylamine was added and the mixture was stirred at room temperature in the dark for 4 h and then concentrated *in vacuo*. After the residue was dissolved in ethyl acetate, insoluble inorganic material was filtered off. The filtrate was washed with 10% citric aicd, saturated sodium hydrogencarbonate, and water. Organic layer was dried over anhydrous magnesium sulfate and concentrated *in vacuo* to give a methyl ester **6**.

A suspension of **6** in 25 ml of hydrochloric acid was heated under reflux for 3 h, and concentrated *in vacuo*. The residue was triturated with ethanol and ether to give crystals: yield 58.1 mg (30.1%). It was recrystallized from ethanol–ether: yield 45 mg (23%), mp 252—255 °C (dec), $[\alpha]_D^{21}$ +63° (*c* 0.5, H_2O).

Found: C, 32.97; H, 6.59; N, 12.79; Cl, 32.33%. Cacld for $C_6H_{14}N_2O_2Cl_2$: C, 33.20; H, 6.50; N, 12.90; Cl, 32.66%.

References

1) Part XVI. T. Shiba, T. Ando, and T. Teshima, *J. Antibiot.*, **32**, 1078 (1979).

2) T. Wakamiya, T. Shiba, and T. Kaneko, *Bull. Chem. Soc. Jpn.*, **45**, 3668 (1972).

3) T. Wakamiya and T. Shiba, *J. Antibiot.*, **27**, 900 (1974).

4) T. Wakamiya, Y. Tarumi, and T. Shiba, *Chem. Lett.*, **1973**, 233.

5) T. Wakamiya, Y. Tarumi, and T. Shiba, *Bull. Chem. Soc. Jpn.*, **47**, 2686 (1974).

6) T. Wakamiya, T. Teshima, I. Kubota, T. Shiba, and T. Kaneko, *Bull. Chem. Soc. Jpn.*, **47**, 2292 (1974).

7) T. Shiba, T. Ukita, K. Mizuno, T. Teshima, and T. Wakamiya, *Tetrahedron Lett.*, **1977**, 2681.

Reaction of Dibenzyl Disulfide and Analogues with Na_2S_x–NaOH[1] Supplementary Data for Mechanism for Reaction of *p*-Nitrotoluene with Na_2S_x[2]

Yoshiro OGATA* and Yoshiaki NAKAGAWA

Department of Applied Chemistry, Faculty of Engineering, Nagoya University, Chikusa-ku, Nagoya 464

(Received August 31, 1979)

Synopsis. Reaction of dibenzyl disulfide with aquoethanolic NaOH gave benzaldehyde and α-toluenethiol. On the other hand, the reaction of dibenzyl disulfide with Na_2S_x in the presence of NaOH gave preferentially benzaldehyde alone. These facts are explained by the further reaction of α-toluenethiol with Na_2S_x giving benzaldehyde and support our mechanism proposed previously for the reaction of *p*-nitrotoluene with Na_2S_x.

In the previous article,[2] we reported the mechanism for the reaction of *p*-nitrotoluene with Na_2S_x. The mechanism involves a benzyl polysulfide derivative as one of the intermediates to give *p*-aminobenzaldehyde.

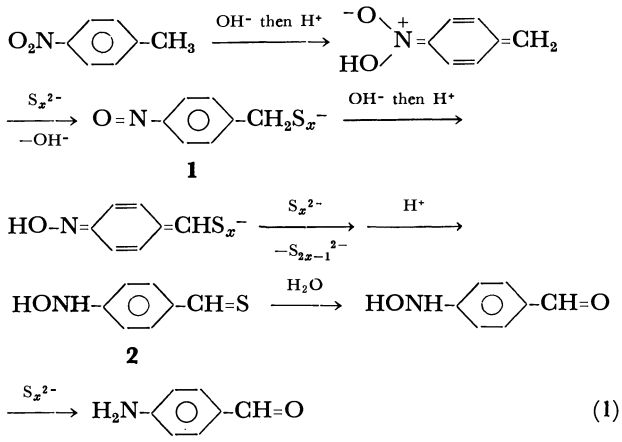

Among steps in this mechanism, there is no literature on the step for the formation of thioaldehyde (**2**) from benzyl polysulfide derivative (**1**) and, in the reaction path, there may be dibenzyl polysulfide derivatives produced from **1**. It has been reported that, for example, dithiodiacetic acid[3,4] or its ester[5] which has electron-withdrawing groups on the α-carbon to the dithio group decomposes by OH^- to give thioaldehyde and thiol, but the reaction of dibenzyl disulfide with OH^- is unknown. Hence dibenzyl disulfide and bis(*p*-nitrobenzyl) disulfide were selected as model compounds, and they were allowed to react with NaOH or Na_2S_x–NaOH. Further, the reaction of α-toluenethiol with Na_2S_x–NaOH was also examined.

TABLE 1. YIELDS OF PRODUCTS FROM A REACTION OF DIBENZYL DISULFIDE WITH NaOH OR Na_2S_x–NaOH IN H_2O–EtOH (2: 1) BY REFLUXING FOR 1 h

Products	Yield (%)	
	with NaOH[a]	with Na_2S_x–NaOH[b]
PhCHO	24.0	49.0
$PhCH_2SH$	24.4	trace
PhCOOH	3.1	4.5
$PhCH_2OH$	3.3	0.8

a) $[NaOH]_0 = 0.74$ M. b) $[NaOH]_0 = 0.70$ M, $[Na_2S \cdot 9H_2O]_0 = 0.17$ M, $[S]_0 = 0.65$ M; A mixture of Na_2S and S can form Na_2S_x ($x = 1$—5), its initial concentration being *ca.* 0.17 M as Na_2S_4.

Results and Discussion

Reaction with NaOH. The reaction of dibenzyl disulfide with aquoethanolic NaOH gave benzaldehyde, α-toluenethiol and a small amount of benzoic acid and benzyl alcohol. Yields of products are listed in Table 1.

$$PhCH_2SSCH_2Ph \xrightarrow{NaOH} PhCHO + PhCH_2SH + PhCOOH + PhCH_2OH \quad (2)$$

This type of reaction is expected from the alkaline decomposition of dithiodiacetic acid[3,4] or its ester[5] which gives $HSCH_2COOH$ and OHCCOOH.

Benzoic acid and benzyl alcohol appearing in Eq. 2 may be the products of Cannizzaro reaction of benzaldehyde.

Reaction with Na_2S_x–NaOH. The reaction of dibenzyl disulfide with aquoethanolic Na_2S_x, which was prepared from Na_2S and S *in situ* (see Experimental Section), in the presence of NaOH gave benzaldehyde and a small amount of benzoic acid and benzyl alcohol along with a trace amount of α-toluenethiol (Table 1). The yield of benzaldehyde (49%) in the reaction of dibenzyl disulfide with Na_2S_x–NaOH is nearly equal to the sum of yields of benzaldehyde (24%) and α-toluenethiol (24%) in the reaction with NaOH. Hence, the produced α-toluenethiolate ion may react further with Na_2S_x to give benzyl polysulfide ion, and then deprotonation occurs to facilitate the S–S bond fission as observed with other disulfide compounds such as dibenzyl disulfide (Eq. 3).

$$PhCH_2S^- \xrightarrow[-S^{2-}]{S_{x+1}^{2-}} PhCH_2S\text{-}S_x^- \xrightarrow{OH^-} \bar{P}hCH\text{-}S\text{-}S_x^- \quad (3a)$$

$$\bar{P}hCHS\text{-}S_x^- \xrightarrow{-S_x^{2-}} PhCH{=}S \xrightarrow{H_2O} PhCH{=}O \quad (3b)$$

Thiobenzaldehyde is easily hydrolyzed as reported previously by King[6] (Eq. 3b).

The reaction of *α-toluenethiol* with aquoethanolic Na_2S_x in the presence of NaOH gave mainly benzaldehyde, but no reaction occurred with NaOH. This fact supports the above mechanism, *i.e.*, polysulfide ion is necessary for the oxidation of thiol to the corresponding aldehyde.

In the reaction of *bis(p-nitrobenzyl) disulfide*, *p*-aminobenzaldehyde was identified by means of NMR as one of the products, which suggests that the analogous mechanism involving S–S cleavage followed by the

hydrolysis of thioaldehyde would operate.

These results suggest that the benzyl polysulfide derivatives or dibenzyl polysulfide derivatives, if produced during the reaction of *p*-nitrotoluene with Na_2S_x, should be easily converted into benzaldehyde derivatives by NaOH and Na_2S_x, so that the results support our mechanism previously postulated.

Experimental

Melting points were measured by a Yanagimoto micro melting point apparatus and were not corrected. NMR spectra were recorded on a Hitachi R-24B NMR spectrometer using Me_4Si as an internal standard. The GLC analysis was performed with a Yanagimoto G 180 gas chromatograph with a flame ionization detector.

Materials. Dibenzyl disulfide was prepared by the method of Minoura;[7] mp 69—70 °C (lit,[7] 71 °C); NMR ($CDCl_3$): δ 3.59 (s, 4H, CH_2), 7.24 (s, 10H, ArH). Bis(*p*-nitrobenzyl) disulfide was prepared according to Price;[8] mp 124.5—126 °C (lit,[8] 126.5 °C); NMR ($CDCl_3$): δ 3.69 (s, 4H, CH_2), 7.4 (d, 4H, ArH, J=9 Hz), 8.2 (d, 4H, ArH, J=9 Hz).

Reaction of Dibenzyl Disulfide with NaOH. A hot solution (14 ml) of NaOH (0.65 g, 16 mmol) was poured into a 100 ml round-bottomed flask containing a hot ethanolic solution (7 ml) of dibenzyl disulfide (1.00 g, 4.1 mmol). The mixture was heated under reflux for 1 h. Most of the products were extracted with diethyl ether from the alkaline solution and then the aqueous solution was acidified with dil. H_2SO_4. The acidic solution was also extracted with diethyl ether and the extract containing benzoic acid was esterified by diazomethane. Both extracts from alkaline and acidic solutions were analyzed by GLC, using two sorts of columns (2.5 mm × 1 m), PEG 20 M and Silicone OV 17, at 100—250 °C. Biphenyl was used as an internal standard.

Reaction of Dibenzyl Disulfide with Na_2S_x–NaOH. The analogous reaction of dibenzyl disulfide was done with a mixture of dibenzyl disulfide (1.00 g, 4.1 mmol), $Na_2S_x \cdot 9H_2O$ (0.83 g, 3.5 mmol), S (0.39 g, 1.2×10^{-2} g atom) and NaOH (0.65 g, 16 mmol). The products and their yields were listed in Table 1. All products were identified by comparison of GLC peaks with those authentic specimens.

References

1) Contribution No. 268.
2) Y. Ogata, A. Kawasaki, Y. Sawaki, and Y. Nakagawa, *Bull. Chem. Soc. Jpn.*, **52**, 2399 (1979).
3) N. A. Rosenthal and G. Oster, *J. Am. Chem. Soc.*, **83**, 4445 (1961).
4) J. P. Danehy and J. A. Kreuz, *J. Am. Chem. Soc.*, **83**, 1109 (1961).
5) E. G. Howard, *J. Org. Chem.*, **27**, 2212 (1961).
6) J. A. King and F. H. McMillan, *J. Am. Chem. Soc.*, **68**, 632, 1369 (1946).
7) Y. Minoura, *Nippon Kagaku Zasshi*, **73**, 131 (1952).
8) T. S. Price and D. F. Twiss, *J. Chem. Soc.*, **93**, 1403 (1908).

Synthesis of 3-Carbamoyl-4-[(β-D-ribofuranosyl)methyl]pyrazole, a Pyrazole Homo-*C*-nucleoside[1]

Tsuneo SATO and Ryoji NOYORI*

Department of Chemistry, Nagoya University, Chikusa, Nagoya 464

(Received September 17, 1979)

Synopsis. A facile, stereocontrolled synthesis of the title pyrazole homo-*C*-nucleoside is described.

Recently we have developed efficient routes to a variety of natural[2] and unnatural *C*-nucleosides.[3] Significant biological activities displayed by pyrazole nucleosides[4] have prompted us to make the related *C*-nucleoside analogues. Outlined herein is the stereospecific synthesis of a pyrazole homo-*C*-nucleoside.[5]

The readily accessible chiral lactone **1** was converted to **2**. The ester **2** was then reduced with diisobutylaluminum hydride[6] to give the corresponding aldehyde in a high yield, which in turn was condensed with methoxycarbonylmethylenetriphenylphosphorane[7] to produce **3**. 1,3-Dipolar cycloaddition across the electron-deficient double bond was effected by diazomethane and the resulting cycloadduct was aromatized by treating with bromine, giving rise to **4**. Ammonolysis of the ester function, giving **5**, and removal of the protective groups led to the desired homo-*C*-nucleoside **6**.

Experimental

General. All melting points are uncorrected. IR spectra were recorded on a JASCO IRA-1 spectrometer. ^1H and ^{13}C NMR spectra were obtained using a Varian HA-100D spectrometer and a Varian CFT-20 spectrometer, respectively. The chemical shifts are recorded in parts per million relative to tetramethylsilane as an internal standard. UV spectra were recorded on a Hitachi 323 recording spectrophotometer. Optical rotations were measured with a JASCO DIP-SL automatic polarimeter. Analytical thin-layer chromatography (TLC) was done using 0.25-mm layers of silica gel 60 PF_{254} (E. Merck) and preparative TLC was performed using 20×20 cm glass plates coated with a 1.0 mm layer of silica gel 60 PF_{254}. The position of spots is shown by R_f values. For column chromatography E. Merck Kiesergel 60 (70—230 mesh) was used.

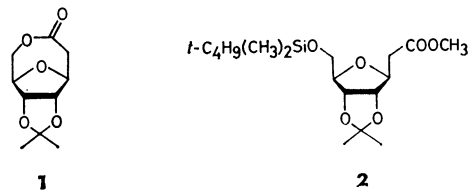

1

2

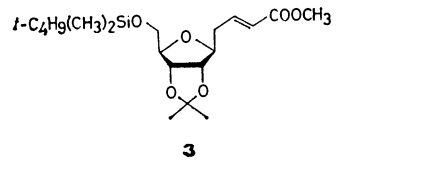

3

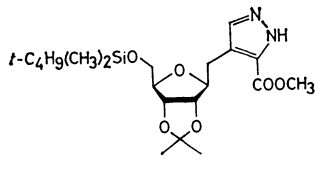

4

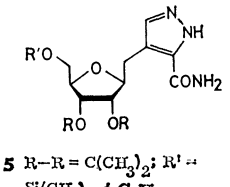

5 R–R = $C(CH_3)_2$; R' = $Si(CH_3)_2$-*t*-C_4H_9

6 R = R' = H

Methyl 2-(2,3-O-Isopropylidene-5-O-t-butyldimethylsilyl-β-D-ribofuranosyl)acetate (2). A mixture of methyl 2-(2,3-*O*-isopropylidene-β-D-ribofuranosyl)acetate[8,11a] (5.72 g, 23.3 mmol), *t*-butyldimethylsilyl chloride (5.41 g, 34.9 mmol), and imidazole (4.76 g, 69.8 mmol)[9] in 40 ml of dry DMF was stirred at 25 °C for 12 h, and then evaporated *in vacuo*. The residue was partitioned between ethyl acetate (100 ml) and brine (20 ml), and organic phase was filtered, dried (Na_2SO_4), and evaporated, leaving a syrup. Chromatography on a silica gel column using hexane–ethyl acetate (5:1) as an eluent gave 8.51 g (100%) of **2** as a colorless syrup. R_f=0.46 (hexane–ethyl acetate (2:1)); $[\alpha]_D^{21}$ −13.6° (*c* 1.62, $CHCl_3$); IR (neat) 1738 cm^{-1} (C=O); ^1H NMR ($CDCl_3$) δ 0.02 (s, CH_3), 0.85 (s, *t*-C_4H_9), 1.29 and 1.46 (s, isopropylidene CH_3), 2.58 (d-like, *J*=6.1 Hz, CH_2CO-OCH_3), 3.84 (s, OCH_3), 3.66 (d-like, *J*=3 Hz, $H_{5'}$), 4.02 (m, $H_{4'}$), 4.28 (m, $H_{1'}$), 4.38 (dd, *J*=4.1, 6.1 Hz, $H_{2'}$), 4.63 (dd, *J*=3.0, 6.1 Hz, $H_{3'}$); ^{13}C NMR ($CDCl_3$) δ 17.89, 25.52, 25.82, 27.36, 38.62, 51.34, 63.79, 81.18, 82.06, 84.66, 84.97, 113.74, 170.74.

Methyl 4-(2,3-O-Isopropylidene-5-O-t-butyldimethylsilyl-β-D-ribofuranosyl)crotonate (3). A freshly prepared solution of diisobutylaluminum hydride[6] in toluene (1.6 M, 17.0 ml, 27.1 mmol) was added dropwise over a period of 10 min to a slution of **2** (7.51 g, 20.9 mmol) in toluene (30 ml) at −78 °C under argon. The reaction mixture was then stirred at this temperature for additional 1 h. The mixture was diluted with ether (30 ml) and then saturated NH_4Cl solution (5 ml) was carefully added. The mixture was warmed to room temperature and filtered with a Celite 545 pad. The filtrate was evaporated under reduced pressure to give 2-(2,3-*O*-isopropylidene-5-*O*-*t*-butyldimethylsilyl-β-D-ribofuranosyl)acetaldehyde (6.32 g, 92%) as a colorless syrup. This material was subjected to the next reaction without purification. A mixture of this aldehyde (6.32 g, 19.2 mmol) and methoxycarbonylmethylenetriphenylphosphorane[7] (20.9 g, 65.6 mmol) in dry dichloromethane (60 ml) was stirred for 12 h at 25 °C. The reaction mixture was evaporated and the residue was chromatographed on a silica gel column using hexane–ethyl acetate (10:1) as an eluent. The resulting product was evaporated, leaving 3.98 g (54%) of **3** as a colorless syrup. In addition, the starting aldehyde was recovered (2.28 g, 36%). R_f=0.53 (hexane–ethyl acetate (2:1)); $[\alpha]_D^{21}$ −28° (*c* 0.62, $CHCl_3$); IR (neat) 1724 (C=O), 1660 cm^{-1} (C=C); ^1H NMR ($CDCl_3$) δ 0.03 and 0.83 (s, *t*-C_4H_9, $(CH_3)_2$), 1.26 and 1.45 (s, isopropylidene CH_3), 2.44 (m, CH_2CH=CH), 3.66 (d-like, *J*=3 Hz, $H_{5'}$), 3.66 (s, OCH_3), 3.94 (m, $H_{1'}$ and $H_{4'}$), 4.24 (dd, *J*=5.0, 6.3 Hz, $H_{2'}$), 4.58 (dd, *J*=4.0, 6.3 Hz, $H_{3'}$), 5.86 (dt, *J*=1.4, 16.0 Hz, CH=C<u>H</u>$COOCH_3$), 6.90 (dt, *J*=7.0, 16.0 Hz, C<u>H</u>=$CHCOOCH_3$); ^{13}C NMR ($CDCl_3$) δ 18.32, 25.57, 25.88, 27.47, 36.32, 51.16, 63.67, 81.99, 83.19, 84.53, 84.77, 114.08, 123.41, 144.30, 166.46. Found: *m/e* 371.1873. Calcd for $C_{18}H_{31}O_6Si$: (M−CH_3), 371.1890.

3-Methoxycarbonyl-4-[(2,3-O-isopropylidene-5-O-t-butyldimethylsilyl-β-D-ribofuranosyl)methyl]pyrazole (4). A solution of **3** (3.83 g, 9.92 mmol) in 10 ml of ether was cooled at 0 °C and to this was added a solution of diazomethane (49.6 mmol) in ether (50 ml). The resulting yellow solution was stirred at 25 °C for 12 h and then evaporated to dryness leaving 4.25 g (100%) of 3-methoxycarbonyl-4-[(2,3-*O*-isopropylidene-5-*O*-*t*-butyldimethylsilyl-β-D-ribofuranosyl)methyl]-2-pyrazoline as a yellow syrup. This material was not further purified. To the mixture of the pyrazoline (4.25 g, 9.92 mmol) and dry $NaHCO_3$ (4.17 g, 49.6 mmol) in dry chloroform (50 ml) was added drowpise a solution of bromine in chloroform (1.0 M solution, 16.9 mmol). The reaction mixture was stirred at 0 °C for 1 h. A solution of 10% sodium thiosulfate (30 ml) was added and the solution was stirred for additional 20 min. The organic phase was separated and the aqueous layer was extracted with ethyl acetate (3×20 ml). The combined extracts were dried (Na_2SO_4) and evaporated. The residue was chromatographed on a silica gel column using hexane–ethyl acetate (1:1) as an eluent. The pyrazole **4** was obtained as a colorless syrup (1.27 g, 30%). R_f=0.29 (hexane–ethyl acetate (1:1)); $[\alpha]_D^{21}$ −25° (*c* 1.5, $CHCl_3$); IR ($CHCl_3$) 3460 (NH), 1728 cm^{-1} (C=O); ^1H NMR ($CDCl_3$) δ 0.03 and 0.90 (s, *t*-C_4H_9, $(CH_3)_2$), 1.32 and 1.52 (s, isopropylidene CH_3), 3.10 (m, CH_2-pyrazole), 3.74 (d-like, *J*=4.0 Hz, $H_{5'}$), 3.94 (s, OCH_3), 4.0—4.3 (m, $H_{1'}$ and $H_{4'}$), 4.40 (dd, *J*=4.1, 6.1 Hz, $H_{2'}$), 4.66 (dd, *J*=3.8, 6.1 Hz, $H_{3'}$), 7.70 (br s, H_5); ^{13}C NMR ($CDCl_3$) δ 18.20, 25.53, 25.78, 27.37, 28.72, 51.30, 63.78, 82.05, 84.26, 84.67, 113.67, 120.02, 132.51, 138.26, 162.67; UV λ_{max} (CH_3OH) 221 nm (ε 7350). Found: *m/e* 426.2181. Calcd for $C_{20}H_{34}O_6N_2Si$: M, 426.2186. The NMR data of **4** are consistent with the assigned β structure. The signals due to the isopropylidene methyls occur at δ 1.32 and 1.52 in the ^1H spectrum (Δδ 0.20 ppm)[10] and δ 25.53 and 27.37 in the ^{13}C spectrum (Δδ 1.84 ppm),[11] and the observed chemical shift differences are apparently in the β range.

3-Carbamoyl-4-[(β-D-ribofuranosyl)methyl]pyrazole (6). A solution of the pyrazole **4** (1.00 g. 2.35 mmol) in methanol (50 ml) was saturated with ammonia at 0 °C and stirred at 25 °C for 4 d. Evaporation of the solvent gave yellow powder. Purification on silica gel plates eluting with hexane–ethyl acetate (1:2) gave 3-carbamoyl-4-[(2,3-*O*-isopropylidene-5-*O*-*t*-butyldimethylsilyl-β-D-ribofuranosyl)methyl]-pyrazole (**5**) (313 mg. 32%) as a white powder. This compound was recrystallized from ethyl acetate, mp 202—204 °C. In addition, unreacted **4** was recovered (630 mg, 63%). R_f=0.15 (hexane–ethyl acetate (1:1)); $[\alpha]_D^{20}$ −15° (*c* 0.15, CH_3OH); IR ($CHCl_3$) 3200—3540 (NH and NH_2). 1678 cm^{-1} (C=O); ^1H NMR (acetone-d_6) δ 0.05 and 0.91 (s, *t*-C_4H_9, $(CH_3)_2$), 1.15 and 1.33 (s, isopropylidene CH_3), 3.00 (m, CH_2–pyrazole), 3.64 (m, $H_{5'}$), 3.82 (m, $H_{1'}$), 4.08 (m, $H_{4'}$), 4.40 (dd, *J*=3.5, 6.5 Hz, $H_{2'}$), 4.55 (dd, *J*=3.2, 6.5 Hz, $H_{3'}$), 6.30 and 6.98 (br, NH_2), 7.60 (m, H_5), 11.10 (br, NH); ^{13}C NMR (dimethyl-d_6 sulfoxide) δ 17.96, 25.41, 25.79, 27.25, 28.31, 63.74, 81.71, 84.02, 84.15, 84.36, 112.78, 117.27, 130.52, 130.63, 164.55; UV λ_{max} (CH_3OH) 221 nm (ε 7800). Found: C, 55.69; H, 8.22; N, 10.14%. Calcd for $C_{19}H_{33}O_5N_3Si$: C, 55.45; H, 8.08; N, 10.21%.

The amide **5** (300 mg, 0.730 mmol) was stirred in 3 ml of 90% aqueous trifluoroacetic acid at 25 °C for 10 min and the mixture was evaporated to dryness *in vacuo*. The crude product was triturated with ether (3×3 ml). Compound **6** was obtained as a hygroscopic white powder (159 mg, 85%). ^1H NMR (dimethyl-d_6 sulfoxide) δ 2.92 (m, CH_2–pyrazole), 3.21 (m, $H_{5'}$), 3.64 (m, $H_{1'}$, $H_{2'}$, $H_{3'}$, and $H_{4'}$), 4.4—5.8 (br, OH), 7.10 (m, H_5), 7.10 and 7.64 (br, NH_2); ^{13}C NMR (dimethyl-d_6 sulfoxide) δ 29.18 (CH_2-pyrazole), 62.76 ($C_{5'}$), 72.34, 75.09, 84.02, 85.14 ($C_{1'}$–$C_{4'}$ of ribose), 119.38, 132.02, 132.15, 165.84; UV λ_{max} (CH_3OH) 222 nm.

This work was supported in part by the Ministry of Education, Japanese Government (Grant-in-Aid, No. 401538). We express our thanks to Fujisawa Pharmaceutical Co. for performing the elemental analysis and Ono Pharmaceutical Co. for obtaining the exact mass spectra.

References

1) *C*-Nucleoside Synthesis. IX. Part VIII: T. Sato and R. Noyori, *Heterocycles*, **13**, 141 (1979).

2) R. Noyori, T. Sato, and Y. Hayakawa, *J. Am. Chem. Soc.*, **100**, 2561 (1978); T. Sato, R. Ito, Y. Hayakawa, and R. Noyori, *Tetrahedron Lett.*, **1978**, 1829.

3) For example, T. Sato, M. Watanabe, and R. Noyori, *Tetrahedron Lett.*, **1979**, 2897.

4) For example, R. W. Sidwell, J. H. Huffman, G. P. Khare, L. B. Allen, J. T. Witkowski, and R. K. Robins, *Science*, **177**, 705 (1972).

5) Homo-*C*-nucleosides refer to a class of compounds that possess a methylene unit between the ribose moiety and an sp^2-carbon of the nitrogen heterocycles.

6) L. I. Zakharkin and I. M. Khorlina, *Tetrahedron Lett.*, **1962**, 619.

7) O. Isler, H. Gutmann, M. Montavon, R. Ruegg, G. Ryser, and P. Zeller, *Helv. Chim. Acta*, **40**, 1242 (1957).

8) T. Sato, K. Marunouchi, and R. Noyori, *Tetrahedron Lett.*, **1979**, 3669.

9) E. J. Corey and A. Venkateswarlu, *J. Am. Chem. Soc.*, **94**, 6190 (1972).

10) J. -L. Imbach, *Ann. N. Y. Acad. Sci.*, **255**, 177 (1975).

11) a) H. Ohrui, G. H. Jones, J. G. Moffatt, M. L. Maddox, A. T. Christensen, and S. K. Byram, *J. Am. Chem. Soc.*, **97**, 4602 (1975); b) J. A. Secrist III, *J. Org. Chem.*, **43**, 2925 (1978).

The Kinetics of the Darzens Reaction of *p*-Substituted Benzaldehydes and Phenacyl Chloride

Raj Kumar BANSAL* and Miss Kanta SETHI

9 *Department of Chemistry, Indian Institute of Technology, New Delhi, India*

(Received June 23, 1979)

Synopsis. The rate constants for the base-catalyzed Darzens reaction of *p*-substituted benzaldehydes and phenacyl chloride have been measured at two temperatures in aqueous dioxane. Enthalpies and entropies of activation have been evaluated. The reactivity of the *p*-substituted benzaldehydes was found to follow the order *p*-NO_2>*p*-Cl>*p*-Br>H>*p*-CH_3>*p*-OCH_3. The kinetic data can be correlated with ρ values according to the Hammett equation.

The Darzens reaction often involves the condensation between aldehyde or ketone and α-halogenomethylene compound to produce an oxirane containing derivative. The mechanism of the reaction between benzaldehyde and phenacyl chloride catalyzed by sodium hydroxide to form an epoxy ketone appears to be established from the work of Bartlett.[1] It is generally agreed that the following sequence of reactions is involved:

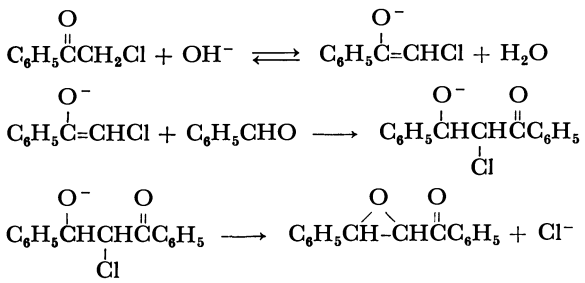

Furthermore, it is argued from non-kinetic methods that the second step is the rate-determining step of the reaction.[2]

A brief study of the methoxide ion catalyzed reaction between benzaldehyde and substituted phenacyl chlorides was made[3] to evaluate the effect of substituents on rate. There is no kinetic investigation, however, on the rate of the reaction when the substituents are located on benzaldehyde. In our continuing study[4] of the various aspects of the Darzens reaction we have measured the rates of the reaction between *p*-substituted benzaldehydes and phenacyl chloride using sodium hydroxide in dioxane–water solvent mixture. We have also examined the application of the Hammett equation in this reaction.

Experimental

Materials. All liquid aldehydes were purified by fractional distillation and stored under nitrogen: benzaldehyde, bp 62—62.5 °C/10 mmHg, *p*-methoxybenzaldehyde, (E. Merck), bp 88—89 °C/2 mmHg, *p*-methylbenzaldehyde (Fluka, A. G.), bp 72—73 °C/3 mmHg. *p*-Nitrobenzaldehyde (BDH) mp 105.5—106 °C (hexane), *p*-bromobenzaldehyde mp 67—67.5 °C (aq ethanol), phenacyl chloride (Fluka, A. G.), mp 56—57 °C (petroleum ether) were all purified by recrystallization. Analar grade dioxane was purified by refluxing with sodium metal followed by distillation.[5]

Experimental Procedure. From several initial preliminary runs it was established that the rate could be conveniently measured in 40% aq dioxane at 15 °C and 25 °C. Appropriate volumes of solutions of the components except phenacyl chloride were transferred to a nitrogen flushed, round bottomed flask fitted with a rubber septum and brought to the desired temperature. The reaction was initiated by injecting a required amount of concentrated solution of phenacyl chloride in dioxane with the help of a hypodermic syringe. The self-condensation of phenacyl chloride was precluded by using 9—15 fold excess of benzaldehyde. Five ml aliquots were withdrawn with the aid of a syringe and run into cold standard sulfuric acid. The remaining sulfuric acid was back-titrated against sodium hydroxide of known strength. The final reading was taken after the reaction flask was allowed to stand for 70 h. The rate constants were calculated from linear plots obtained by using the standard third order equation.[6]

Results and Discussion

All the runs were made at 15 °C and 25 °C in 40% aqueous dioxane (v/v). Sodium perchlorate of 0.01 M strength was employed to maintain a constant ionic strength. Duplicate runs were made in each case. The runs were carried out to about 60—70% completion, the reaction complies to a third order kinetics being first order in the concentration of each reactant. Rate constants were calculated from linear third order plots. Appropriate data are summarized in Table 1.

Table 1. Third order rate constants and activation parameters of base-catalysed condensation between *p*-substituted benzaldehydes and phenacyl chloride in aqueous dioxane

Compound	*p*-Substituent	$10^{-1}k/l^2$ mol^{-2} s^{-1} 15C°	25°C	ΔH / kcal mol^{-1}	$-\Delta S^*$ / e.u.
I	OCH_3	0.600±0.012	1.296±0.012	12.56±0.191	11.30±0.466
II	CH_3	0.676±0.017	1.397±0.029	11.76±0.249	13.97±0.838
III	H	0.764±0.012	1.484±0.010	10.98±0.134	16.33±0.418
IV	Br	0.965±0.019	1.854±0.026	10.47±0.046	17.58±0.150
V	Cl	0.989±0.016	1.878±0.028	10.28±0.070	18.20±0.222
VI	NO_2	1.768±0.015	2.890±0.033	7.74±0.042	25.88±0.141

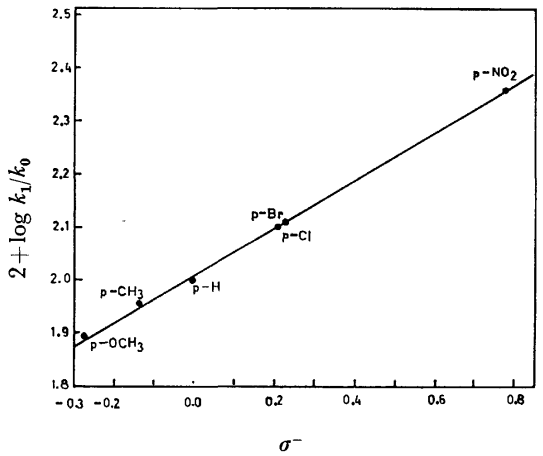

Fig. 1. Hammett plot of condensation of *p*-substituted benzaldehydes with phenacyl chloride.

There is a regular variation in the rates with the nature of the *p*-substituents. The order of reactivity being $NO_2 > Cl > Br > H > CH_3 > OCH_3$ *i.e.* electron-withdrawing groups increase while electron-donating groups decrease the rate. This fact is also borne out by the enthalpies of activation (ΔH^*) values calculated for these reactions which are 7.8 kcal/mol for the *p*-NO_2 and 12.56 kcal/mol for the *p*-OCH_3 groups.

The sign and magnitude of the reaction constant, ρ in the Hammett equation are often evaluated to assess the charge type of the transition state. The ρ value from the Hammett plot (Fig. 1) has been found to be $+0.446$ ($r=0.998$) by least squares method. The small value reflects a weak interaction between the substituent and the reaction site. It, however, does indicate the transition state has a negative character.

One of us (K.S.) is grateful to the Council of Scientific and Industrial Research (C.S.I.R.), New Delhi for financial assistance.

References

1) M. Ballester and P. D. Bartlett, *J. Am. Chem. Soc.*, **75**, 2042 (1953).

2) F. W. Bachelor and R. K. Bansal, *J. Org. Chem.*, **34**, 3600 (1969); M. Ballester and D. Perez-Blanco, *J. Org. Chem.*, **23**, 652 (1958).

3) Gy. Sipos, Gy. Schöbel, and F. Sirokman, *J. Chem. Soc., Perkin Trans. 2*, **1975**, 805.

4) R. K. Bansal, "Organic Reaction Mechanisms," Tata McGraw-Hill (1978); F. W. Bachelor and R. K. Bansal, *Ind. J. Chem.*, **15B**, 574 (1977); R. K. Bansal and K. Sethi, *Def. Sci. J.*, in press; R. K. Bansal and K. Sethi, *Monat Chem.*, Communicated.

5) A. I. Vogel, "A Text book of Practical Organic Chemistry," 3rd ed, Longman, London (1975).

6) A. A. Frost and R. G. Pearson, "Kinetics and Mechanism," John Wiley, New York (1961).

Adsorptive Mechanism on Activated Carbon in the Liquid Phase. III. The Relationship between the Physical Constants of Organic Compounds and Their Adsorbabilities on Activated Carbon from an Aqueous Solution[1)]

Ikuo Abe,* Katsumi Hayashi, Mutsuo Kitagawa,** and Toshihiro Urahata

Osaka Municipal Technical Research Institute, Ogimachi, Kita-ku, Osaka 530

***Society for Activated Carbon Research, Ogimachi, Kita-ku, Osaka 530*

(Received January 30, 1979)

In order to evaluate the adsorbability for a given activated carbon from a knowledge of the physical properties of the adsorbate, the partition coefficients (α) of 93 organic compounds between the solution and the adsorbed phases at an infinite dilution have been calculated and correlated with the various physical constants. For aliphatic monofunctional compounds, a good linear relationship is obtained between log α and the following physical constants: molecular weight, molar attraction constant, and modified organicity/inorganicity value. This indicates that these physical constants are useful for predicting the adsorbability of aliphatic monofunctional compounds and that a straight line represents the adsorption characteristics of a given activated carbon. The correlation coefficient between the log α value and the physical constants for multifunctional compounds is lower than that for monofunctional compounds. The adsorptive mechanism on activated carbon in an aqueous solution is discussed on the basis of the conclusion obtained in the previous paper.

The ability to predict the adsorbability for a given adsorbent from a knowledge of the physical properties of the adsorbate has long been an important objective in adsorbent-adsorbate interaction research. In gas-phase adsorption, the decisive component of the adsorption forces on an activated carbon surface is the dispersion component of the Van der Waals forces. Therefore, the adsorptive interaction is strongly dependent on the polarizability of the molecules. Since the polarizability of a molecule is approximately proportional to the volume of a molecule or molar volume, the adsorbability can also be evaluated in terms of the molar volume[2)] or the parachors.[3)] Reucroft *et al.*[4)] studied the relationship between the adsorbability and various physical constants and concluded that the molar refraction gives a good correlation. However, no similar investigation in liquid-phase adsorption has been thoroughly undertaken in contrast to that in the gas phase. A brief survey of adsorption from the liquid phase was, though, made by Hassler.[5)] He listed all the factors influencing adsorption at the carbon-liquid interface and noted that such physical properties as the molecular weight and the solubility significantly influenced the adsorbability. The significance of these factors has also been pointed out by numerous other investigators.[6–14)] Pouchly and Vavruch[15)] noted that the main factor was the general rule of the mutual affinity of substances with similar polarities. From this rule, it is expected that nonpolar substances will be more readily adsorbed on activated carbon, a nonpolar adsorbent, than polar substances. Wohleber and Manes[16)] presented a method for estimating the adsorbability of a partially miscible organic liquid from a water solution on an activated carbon by the knowledge of the adsorbability of the vapors of the solute and the solvent. The method, which is based on the Polanyi adsorption potential theory,[17)] suggests that the adsorbability in the liquid phase can be estimated from the molar volume, the parachor, or the molar refraction, which are used as the criteria of adsorbability in the gas phase. Abe *et al.*[18)] reported that the adsorption process of aliphatic monofunctional compounds is energetically similar to the precipitation process of the hydrocarbon portion of the solute. This suggests that the adsorbability can be estimated from the volume of the hydrocarbon portion of the solute. These discussions of the relationship between the adsorbability in the liquid-phase adsorption and the physical constants have been so far done almost always qualitatively, because they are based on limited data for a small number of compounds. Therefore, it is desirable to relate quantitatively the adsorbability to the physical constants for a large number of compounds. Giusti *et al.*[11)] have measured the amounts of adsorption of 90 organic compounds on an activated carbon, but have not discussed the subject thoroughly. Since a good correlation has been obtained between our adsorption data in the previous paper[18)] and Giusti's data, in this paper we have related the adsorbability to the physical constants quantitatively by using both sets of data. Furthermore, in order to find a physical constant with a good correlation with the adsorbability, we have also examined the physical constants which have been used for the prediction of the adsorbability on the other adsorption systems. For example, the inorganicity/organicity value has been used for predicting the affinity of dyes on fibers.[19,20)] The partition coefficient between water and 1-octanol has been used for estimating the affinity of organic compounds in the hydrophobic region in a protein molecule.[21,22)] The molar attraction constant, which gives a quantitative measure of the relative mutual attraction of organic molecules to one another as a result of dispersion forces, has been used as a physicochemical criterion for the sorption at the membrane-solution interface in reverse osmosis.[23)]

In this paper we have examined the correlation between the adsorbabilities of 93 organic compounds and these physical constants for predicting the adsorbability in terms of the physical constant. Furthermore, we have examined whether or not these results can be successfully explained by the adsorptive mechanism proposed in the previous paper.[18)]

TABLE 1. ADSORPTION OF ORGANIC COMPOUNDS FROM AN AQUEOUS SOLUTION ON CAL ACTIVATED CARBON, 25 °C

Compound No.	Compound	α[a]	$\frac{C_0-C}{C}$[b]	α[c]	Compound No.	Compound	α[a]	$\frac{C_0-C}{C}$[b]	α[c]
	[Alcohols]				48	Butyl acetate	15.7	5.49	4.98
1	Methanol		0.0373	0.0121	49	Pentyl acetate		7.28	6.99
2	Ethanol		0.110	0.0445	50	Isopropyl acetate		2.13	1.59
3	1-Propanol	0.184	0.233	0.110	51	Isobutyl acetate		4.56	3.98
4	1-Butanol	0.680	1.15	0.755	52	Vinyl acetate		1.80	1.30
5	1-Pentanol	2.25	2.55	1.98	53	2-Ethoxyethyl acetate		1.92	1.40
6	1-Hexanol	9.08	21.2	25.4	54	Ethyl acrylate		3.49	2.88
7	2-Propanol		0.144	0.0615	55	Butyl acrylate		22.3	27.0
8	2-Propene-1-ol		0.267	0.130		[Ethers]			
9	2-Methyl-1-propanol		0.721	0.430	56	Diethyl ether	0.548		
10	2-Methyl-2-propanol		0.418	0.223	57	Dipropyl ether	6.91		
11	2-Ethyl-1-butanol		5.90	5.43	58	Diisopropyl ether		4.04	3.44
12	2-Ethyl-1-hexanol		69.0	106		[Glycols & Glycol Ethers]			
	[Aldehydes]				59	Ethylene glycol		0.0730	0.0269
13	Formaldehyde		0.101	0.0401	60	Diethylene glycol		0.355	0.183
14	Acetaldehyde	0.0561	0.135	0.0569	61	Triethylene glycol		1.10	0.716
15	Propionaldehyde	0.151	0.383	0.200	62	Tetraethylene glycol		1.39	0.949
16	Butyraldehyde	0.641	1.12	0.732	63	1,2-Propanediol		0.131	0.0549
17	Valeraldehyde	2.41			64	Dipropylene glycol		0.198	0.0905
18	Acrylaldehyde		0.441	0.237	65	2-Methyl-2,4-pentanediol		1.59	1.12
19	Crotonaldehyde		0.838	0.516	66	2-Methoxyethanol		0.156	0.0678
20	Benzaldehyde		15.7	17.9	67	2-Ethoxyethanol		0.450	0.243
21	Paraldehyde		2.83	2.24	68	2-Butoxyethanol		1.27	0.852
	[Amines]				69	2-(Hexyloxy)ethanol		6.74	6.38
22	Dipropylamine		4.05	3.44	70	2-(2-Ethoxyethoxy)-ethanol		0.772	0.468
23	Butylamine		1.08	0.700	71	2-(2-Butoxyethoxy)-ethanol		4.78	4.21
24	Dibutylamine		6.69	6.31	72	3,6,9-Trioxaundecan-1-ol		2.30	1.74
25	Allylamine		0.458	0.249		[Halogenated Compounds]			
26	Ethylenediamine		0.120	0.0494	73	1,2-Dichloroethane		4.29	3.69
27	Diethylenetriamine		0.416	0.221	74	1,2-Dichloropropane		13.1	14.3
28	2-Aminoethanol		0.078	0.0292		[Ketones]			
29	2,2′-Iminodiethanol		0.380	0.199	75	Acetone	0.125	0.279	0.137
30	2,2′,2″-Nitrilotriethanol		0.493	0.272	76	2-Butanone	0.361	0.880	0.547
31	2-Amino-1-methylethanol		0.250	0.120	77	2-Pentanone	1.39	2.28	1.72
32	1,1′-Dimethyl-2,2′-iminodiethanol		0.842	0.519	78	2-Hexanone	5.13	4.17	3.57
	[Pyridines & Morpholines]				79	4-Methyl-2-pentanone		5.58	5.08
33	Pyridine		0.898	0.560	80	5-Methyl-2-hexanone		5.75	5.27
34	2-Methyl-5-ethylpyridine		8.35	8.26	81	Cyclohexanone		2.01	1.48
35	*N*-Methylmorpholine		0.739	0.443	82	Acetophenone		34.7	46.0
36	*N*-Ethylmorpholine		1.14	0.747	83	Isophorone		28.4	36.1
	[Aromatics]					[Acids]			
37	Benzene		18.8	21.7	84	Formic acid		0.307	0.153
38	Toluene		3.80	3.20	85	Acetic acid		0.316	0.159
39	Ethylbenzene		5.39	4.87	86	Propionic acid	0.230	0.484	0.266
40	Phenol		4.15	3.55	87	Butyric acid	0.813	1.47	1.01
41	Hydroquinone		4.99	4.44	88	Valeric acid	3.84	3.93	3.32
42	Aniline		2.98	2.38	89	Hexanoic acid	16.1	32.3	42.2
43	Styrene		9.00	9.03	90	Acrylic acid		1.82	1.31
44	Nitrobenzene		22.3	27.1	91	Benzoic acid		10.2	10.6
	[Esters]					[Oxides]			
45	Methyl acetate	0.274	0.355	0.183	92	Propylene oxide		0.353	0.182
46	Ethyl acetate	0.913	1.02	0.654	93	Styrene oxide		20.3	24.3
47	Propyl acetate	4.24	3.03	2.43					

a) Our data.[18] b) Giusti's data.[11] c) Calculated from Eq. 2.

Procedure

In a previous paper[18] the adsorption isotherms of 22 aliphatic monofunctional compounds from an aqueous solution on Pittsburgh Activated Carbon-grade CAL activated carbon have been determined, and the adsorbabilities of the solutes at an infinite dilution have been calculated. The adsorbability (α) has been defined as follows:

$$\alpha \equiv \lim_{C \to 0} \frac{X}{C}, \tag{1}$$

where X is the amount of adsorbed solute on carbon (mg/g) and C is the equilibrium concentration of the solute (mg/l). The constant, α, represents the partition coefficient between the solution and the adsorbed phases at an infinite dilution. The values of α for the 22 compounds are presented in Table 1. Giusti *et al.*[11] have reported the adsorption data for 90 compounds on Westvaco Nuchar Activated Carbon-grade WV-G activated carbon. They determined the adsorbability for each compound by measuring the amount of adsorption at an equilibrium concentration under the following conditions: a concentration of activated carbon of 5000 mg/l, and an initial concentration of the solute (C_0) of 1000 mg/l. We have calculated the value of $(C_0-C)/C$, which represents the partition coefficient at the equilibrium concentration, C, from their data.

Figure 1 shows the relationship between the value of $\log \alpha$ in our data and the values of $\log\{(C_0-C)/C\}$ calculated from Giusti's data for the common 19 compounds included in both sets of data. It can be seen from Fig. 1 that $\log \alpha$ is related to $\log\{(C_0-C)/C\}$ by the following equation:

$$\log \alpha = 1.21 \log \frac{C_0-C}{C} - 0.195. \tag{2}$$

The correlation coefficient (r) between $\log \alpha$ and $\log\{(C_0-C)/C\}$ obtained by the regression analysis was high, $r=0.957$, in spite of the difference in the carbon used. Assuming that Eq. 2 was applicable to the other 71 compounds, the α values for the 71 compounds were calculated from Eq. 2. These values are also tabulated in Table 1. In this manner, the values of α for all 93 organic compounds were determined.

The correlation between the adsorbabilities (α) and physical constants (x) were tested by means of the following linear relation:

$$\log \alpha = ax+b, \tag{3}$$

where a and b are constants. By regression analysis, the correlation coefficient (r) and the a and b constants were determined.

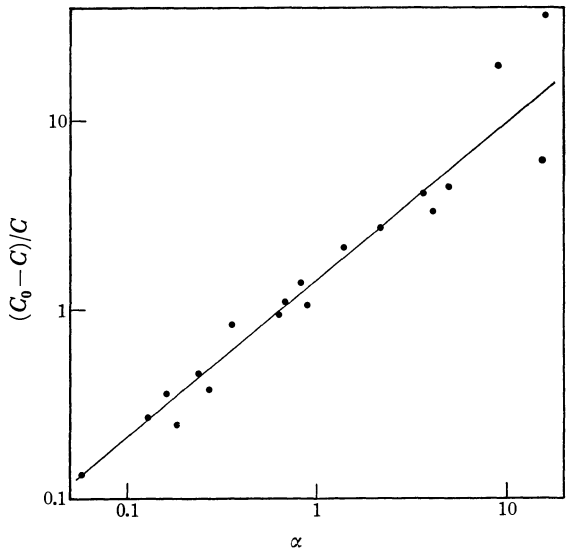

Fig. 1. Relationship between α in our data and $(C_0-C)/C$ calculated from Giusti's data.

Results

Molecular-size Parameters. The relationship between the molecular weight (M) and $\log \alpha$ is given in Fig. 2, while the results of the regression analysis are given in Table 2. The correlation coefficient was very high for the aliphatic monofunctional compounds and for all the aromatics except benzene, but for the aliphatic multifunctional compounds it was low. It can be seen from Table 2 or Fig. 2 that the α value for the aliphatic monofunctional compounds is approximately doubled for each rise of 10 in the molecular weight. As can be seen from Table 2, the correlation coefficient between the molar volume (V) and $\log \alpha$ was also high for aliphatic monofunctional compounds, and the correlation with the carbon number (N) of compound was good for all the compounds.

Aqueous Solubility (C_s). Figure 3 shows the relationship between $\log C_s$ and $\log \alpha$. The correlation

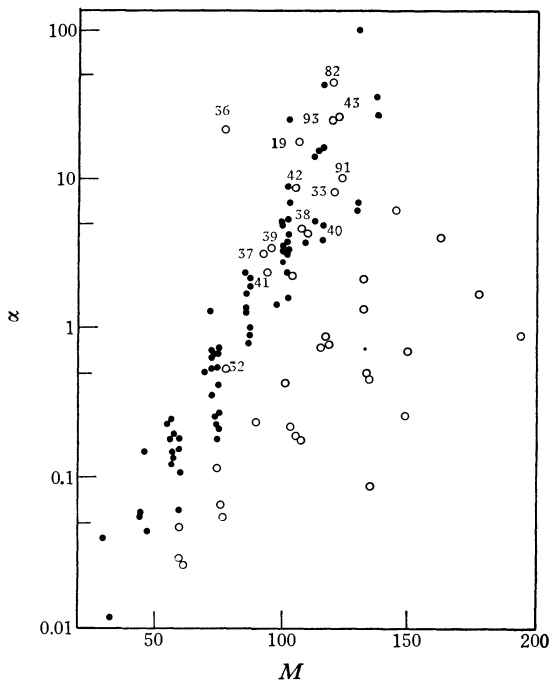

Fig. 2. Relationship between α and molecular weight. ●: Aliphatic monofunctional compounds, ○: aromatics and multifunctional compounds.

TABLE 2. RESULTS OF REGRESSION ANALYSIS FOR THE $\log \alpha = ax + b$ EQUATION

Physical constant	x	Compound	a	b	Number of data points n	Correlation coefficient r
Molecular weight	M	AMF[a]	0.0311	−2.60	73	0.943
		AMF+AR[b]	0.0315	−2.59	87	0.927
		AMF+AR*[c]	0.0317	−2.63	86	0.945
		T[d]	0.0175	−1.62	112	0.628
Molar volume[f]	V	AMF	0.0241	−2.38	59	0.868
		T	0.0206	−2.03	84	0.672
Carbon number	N	AMF	0.417	−1.79	73	0.864
		T	0.368	−1.72	112	0.818
Solubility[g]	$\log C_s$	L[e]	−1.03	0.816	15	−0.962
		AMF	−0.752	0.716	70	−0.842
		T	−0.647	0.656	108	−0.808
Molar-attraction constant	$\sum F$	AMF	0.00364	−3.17	68	0.932
		T	0.00267	−2.42	92	0.745
Organicity / Inorganicity	O/IO	AMF	0.302	−0.401	73	0.464
		T	0.204	−0.294	112	0.455
Modified O/IO value	A	AMF	2.30	−2.04	71	0.944
Partition coefficient (octanol-water system)	$\log P_{oct}$	AMF	0.932	−0.906	50	0.904
		T	0.523	−0.408	77	0.744
Dielectric constant[f]	D	AMF	−0.0495	0.564	55	−0.585
		T	−0.0441	0.577	76	−0.544
Molar refraction[f]	$[R]$	AMF	0.0968	−2.29	61	0.898
		T	0.0924	−2.30	80	0.825
Parachor[f]	$[P]$	AMF	0.0114	−2.51	45	0.889
		T	0.00925	−2.13	64	0.660

a) AMF: Aliphatic monofunctional compounds. b) AR: Aromatics. c) AR*: Aromatics except benzene. d) T: AMF+AR+Aliphatic multifunctional compounds. e) L: AMF in our work. f) These physical constants are cited from J. A. Riddick and W. B. Bunger, "Organic Solvents," Wiley-Interscience, New York (1970). g) Reference (f) and "International Critical Tables," McGraw-Hill, New York (1933).

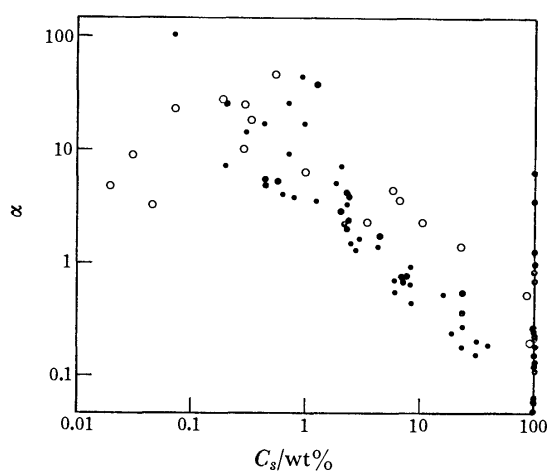

Fig. 3. Relationship between α and aqueous solubility.

coefficient was very high for the 15 linear aliphatic monofunctional compounds in our work. The value of a for these compounds was about −1, which suggests the following relationship;

$$\alpha \cdot C_s = \text{const.} \quad (4)$$

However, the correlation coefficient for all aliphatic monofunctional compounds was low because the compounds with 100 weight % aqueous solubility revealed a wide range of adsorbability.

Molar-attraction Constant (F). The concept of the cohesive energy of a liquid has been discussed extensively in the literature.[24,25] The molar cohesive energy, E, is given by this expression:

$$E \fallingdotseq \Delta H - RT \quad (5)$$

where ΔH is the heat of vaporization; R, the gas constant, and T, the absolute temperature. When the cohesion between molecules is due to dispersion forces, as is essentially the case with nonpolar molecules, E is related to the heat of mixing per cc (ΔH_{cc}) by Scatchard's[26] semi-empirical relation:

$$\Delta H_{cc} = \phi_1\phi_2\{(E_1/V_1)^{1/2} - (E_2/V_2)^{1/2}\}^2, \quad (6)$$

where ϕ is the volume ratio and the subscripts 1 and 2 represent a set of two dissimilar molecules. Equation 6 is equivalent to the statement that the cohesive energy, E, of a mixture of n_1 mol of Liquid 1 and n_2 mol of Liquid 2 can be given by this expression:

$$E^{1/2}(n_1V_1 + n_2V_2)^{1/2} = n_1(E_1V_1)^{1/2} + n_2(E_2V_2)^{1/2}, \quad (7)$$

which shows that $(EV)^{1/2}$ is an additive property. Assuming that this property might hold for the atoms

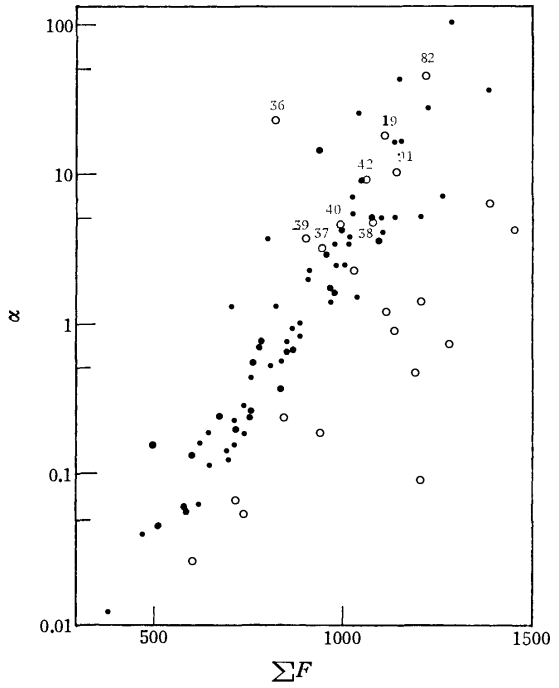

Fig. 4. Relationship between α and molar-attraction constant.

or groups constituting a molecule, Small[24] derived a set of additive constants for the common groups of organic molecules. These constants are called molar-attraction constants and are denoted by the symbol F. Then, ΣF summed over the present groups gives the value of $(EV)^{1/2}$ for 1 mol of the substance concerned.

Figure 4 shows the relationship between the ΣF values calculated from Small's F values for the compounds in Table 1 and log α. The correlation for the aliphatic monofunctional compounds and aromatics except benzene was very high, while that for aliphatic multifunctional compounds was low. This tendency is analogous to that of the molecular weight.

Organicity and Inorganicity. In order to estimate the solubility of organic compounds, Fujita[27] proposed the concept of organicity and inorganicity, where it is assumed that the organicity value per carbon atom is 20 and that inorganicity value for a hydroxyl group is 100. The inorganicity values for the other functional groups are determined in values relative to that for the hydroxyl group; they are given in Table 3. Since the organicity/inorganicity value (O/IO) is a criterion of the solubility, the value can also be used as a criterion of adsorbability. There existed a linear relationsihp between O/IO and log α for a homologous series of solutes, but the correlation coefficient for all the compounds in Table 1 was very low. This suggests that Fujita's IO value cannot be used as a criterion of adsorbability. In order to improve the correlation between the O/IO value and log α, the IO values for the functional groups were redetermined so as to fit the O/IO *vs.* log α plots of all the compounds to the straight line obtained for alcohols. These values are given in Table 3. Figure 5 shows the relationship between log α and the modified O/IO values calculated from the redetermined IO values and Fujita's O values. The correlation coefficient was very high for aliphatic monofunctional compounds.

Table 3. Inorganicity values for functional groups

Functional group		Inorganicity value	
		Fujita[10]	This work
Alcohols	-OH	100	100
Carboxylic aicds	-COOH	150	93
Ketones	>CO	65	109
Ethers	-O-	20	103
Esters	-COOR	60	93
Aldehydes	-CHO	65	98

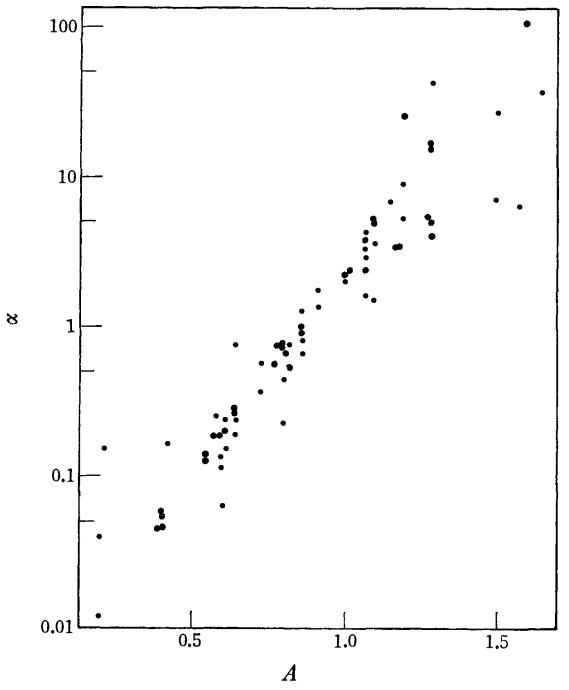

Fig. 5. Relationship between α and modified organicity/inorganicity.

Partition Coefficient between Water and 1-Octanol (P_{oct}). Assuming that the adsorption process is identical with the partition process between water and adsorbed phases, and that the polarity of the adsorbed phase is similar to that of 1-octanol, a high correlation between P_{oct} and α can be expected. Figure 6 shows the relationship between the log P_{oct} values calculated from Hansch's data[28] and log α. The correlation coefficient was high for aliphatic monofunctional compounds.

Polarity Parameters. The following empirical polarity parameters of organic compounds, among others, have been proposed by earlier investigators: $(D-1)/(2D+1)$ (D: dielectric constant, Kirkwood[29]), the E_T-values (Dimroth, Reichardt[30]), the Y-values (Winstein, Grunwald[31]), the Ω-values (Berson, Hamlet, Mueller[32]), the Z-values (Kosower[33]), and the S-values (Brownstein[34]). The relationship between the polarity parameters and log α were all similar in tendency, and the correlation coefficients were low.

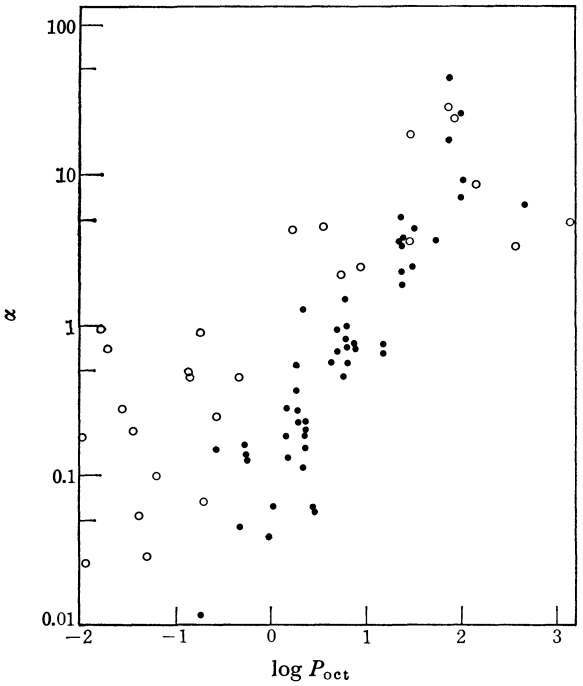

Fig. 6. Relationship between α and partition coefficient.

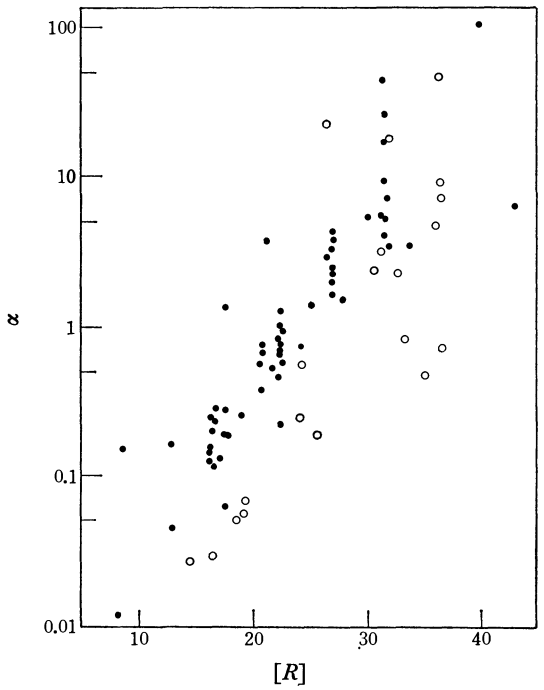

Fig. 7. Relationship between α and molar refraction.

Molar Refraction ([R]). The molar refraction is obtained from the Lorenz-Lorentz equation using the following form:

$$[R] = \frac{n^2-1}{n^2+2}\frac{M}{\rho} \tag{8}$$

where n is the refractive index and ρ is the density. Figure 7 shows the relationship between [R] and log α. The correlation coefficient for the 61 aliphatic monofunctional compounds was 0.898. In gas-phase adsorption, Reucroft *et al.*[4] obtained the high correlation coefficient of 0.94 for 15 organic vapors.

Parachor ([P]). Parachor is obtained approximately by the use of the following equation:

$$[P] = \frac{M}{\rho}\cdot\gamma^{1/4} \tag{9}$$

where γ is the surface tension. It can be seen from Table 2 that the correlation coefficient between [P] and log α is high, 0.889, for 45 aliphatic monofunctional compounds. In gas-phase adsorption, the value was 0.90 for 15 organic vapors.[4]

Discussion

In this work, the relationship between the adsorbability and various physical constants was examined for a large number of organic compounds, and it was found that, for aliphatic monofunctional compounds, there existed a good linear relationship between log α and the following physical constants: the molecular weight, the molar-attraction constant, and the modified *O/IO* value. This indicates that these physical constants are useful for predicting the adsorbability of aliphatic monofunctional compounds on activated carbon from an aqueous solution and that the *a* and *b* constants in Eq. 3 are useful for characterizing the adsorptive power of activated carbon. If the *a* and *b* constants are determined from the adsorption data of several compounds, the adsorbability for many other compounds can be predicted from only the physical constant. On the other hand, the adsorbability of multifunctional compounds could not be predicted from the physical constant and Eq. 3. The possibility of the prediction for aromatic compounds could not be ascertained because of the small number of compounds studied.

We will now consider the adsorptive mechanism on activated carbon in the water phase. In a previous paper[18] the free energy change of the adsorption process of 22 aliphatic monofunctional compounds on CAL activated carbon from aqueous solution was compared with the free energy of the precipitation process of the same compound from water to the pure liquid solute; the following results were obtained. 1) The adsorption process of the hydrocarbon portion of a solute molecule is analogous to the precipitation process of the portion. 2) The functional group situated in the terminal position of a solute molecule is appreciably hydrated, even in the adsorbed phase. 3) The functional group situated inside a solute molecule is not appreciably hydrated in the adsorbed phase. These results suggest that the adsorption of the solute takes place by means of the precipitation of the hydrocarbon portion of the solute from the aqueous solution and that the adsorbability depends mainly on the volume of the hydrocarbon. Since the free energy change for the precipitation process of the hydrocarbon is negative, the adsorbability increases with an increase in the volume of the hydrocarbon portion in a solute molecule. The fact that, for aliphatic monofunctional compounds, a high correlation coefficient was obtained between the adsorbability and the molecular weight, the molar volume, and the

modified O/IO value can be explained by the fact that the increase in these physical constants is approximately equal to the increase in the volume of the hydrocabon portion of a solute molecule. The high correlation with the molar-attraction constant, the molar refraction, and the parachor can also be accounted for by the fact that these physical constants are functions of the molar volume. Furthermore, the result that the correlation coefficient with the carbon atom number was high in spite of the variety of compounds suggests that the volume of the hydrocarbon was a dominant factor governing the adsorption. It can be seen from the modified IO values in Table 3 that the adsorbability does not appreciably depend on the kind of functional group.

The adsorbability of the multifunctional compounds was lower than that of the monofunctional compounds. This result can be explained by the facts that the functional group situated inside a solute molecule is somewhat dehydrated in the adsorbed phase and that the free energy change for the dehydration of the functional group is positive. In addition, the somewhat hydrated functional group may be considered to interfere with the dehydration of the adjacent hydrocarbon portion.

The low correlation with the polarity parameters suggests that the polarity is not the principal factor controlling the adsorbability on activated carbon and that the volume of the hydrocarbon portion of a solute molecule is not the principal factor controlling the polarity. Actually, the polarity is greatly influenced by the functional group.

Although, in this paper, we did not discuss the influence of the difference in activated carbon on the adsorbability of organic compounds, in a subsequent investigation[35] we obtained a similar result for a large number of activated carbons. It should be remembered, however, that surface oxides influence the adsorption of organic compounds.[5,7,11,36,37] In particular, the adsorption of strongly ionized low-molecular-weight compounds may be greatly influenced by surface oxides in a low or high pH solution.

The authors wish to express their thanks to Professor Nobuhiko Kuroki and Associate Professor Joichi Koga, the University of Osaka Prefecture, for their helpful discussions.

References

1) Part II: I. Abe, K. Hayashi, M. Kitagawa, and T. Urahata, *Nippon Kagaku Kaishi*, **1979**, 830.
2) M. M. Dubinin and D. P. Timofeyev, *Zh. Fiz. Khim.*, **22**, 133 (1948).
3) B. A. Vaskovsky; see M. M. Dubinin and E. D. Zaverina, *Dokl. Akad. Nauk SSSR*, **72**, 319 (1950).
4) P. J. Reucroft, W. H. Simpson, and L. A. Jonas, *J. Phys. Chem.*, **75**, 3526 (1971).
5) J. W. Hassler, "Activated Carbon," Chemical Publishing Company, New York (1963).
6) A. S. Weatherburn, G. R. F. Rose, and C. H. Bayley, *Can. J. Res.*, **27F**, 179 (1949).
7) J. S. Mattson and H. B. Mark, Jr., "Activated Carbon," Marcel Dekker, New York (1971).
8) M. Komori, K. Urano, and T. Nakai, *Nippon Kagaku Kaishi*, **1974**, 1795.
9) K. Urano, Y. Nishimura, and Y. Yanaga, *Nippon Kagaku Kaishi*, **1975**, 1444.
10) I. Abe, K. Hayashi, M. Kitagawa, and T. Urahata, *Nippon Kagaku, Kaishi*, **1978**, 1188.
11) D. M. Giusti, R. A. Conway, and C. T. Lawson, *J. Water Pollut. Control Fed.*, **46**, 947 (1974).
12) W. J. Weber, Jr., and J. C. Morris, *J. Sanit. Eng. Div.*, **89**, **SA2**, 31 (1963).
13) W. J. Weber, Jr., and J. C. Morris, *J. Sanit. Eng. Div.*, **90**, **SA3**, 79 (1964).
14) R. Lemieux and J. Morrison, *Can. J. Res.*, **25B**, 212 (1947).
15) J. Pouchly and I. Vavruch, "Physical Chemistry of Colloid Systems," SNTL, Prague (1960).
16) D. A. Wohleber and M. Manes, *J. Phys. Chem.*, **75**, 61 (1971).
17) M. Polanyi, *Verh. Deut. Phys. Ges.*, **16**, 1012 (1914); **18**, 55 (1916); *Z. Elektrochem.*, **26**, 370 (1920); *Z. Phys.*, **2**, 111 (1920).
18) I. Abe, K. Hayashi, M. Kitagawa, and T. Urahata, *Bull. Chem. Soc. Jpn.*, **52**, 1899 (1979).
19) N. Kuroki, "Senshoku Riron Kagaku," Maki-shoten, Tokyo (1969).
20) Z. Yoshida, S. Sagawa, and R. Oda, *Kogyo Kagaku Zasshi*, **63**, 305 (1960).
21) C. Hansch, K. Kiehs, and G. L. Lawrence, *J. Am. Chem. Soc.*, **87**, 5770 (1965).
22) K. Kiehs, C. Hansch, and L. Moore, *Biochemistry*, **5**, 2602 (1966).
23) "Reverse-Osmosis and Synthetic Membranes," ed by S. Sourirajan, National Research Council, Canada (1977), Chap. 2.
24) P. A. Small, *J. Appl. Chem.*, **3**, 71 (1953).
25) J. H. Hilderband, J. M. Prausnitz, and P. L. Scott, "Regular and Related Solutions," Van Nostrand Reinhold, New York (1970).
26) G. Scatchard, *Chem. Rev.*, **44**, 7 (1949).
27) A. Fujita, *Pharm. Bull. (Tokyo)*, **2**, 163 (1954).
28) A. Leo, C. Hansch, and D. Elkins, *Chem. Rev.*, **71**, 525 (1971).
29) J. G. Kirkwood, *J. Chem. Phys.*, **2**, 351 (1934).
30) K. Dimroth and C. Reichardt, "Palette," Publication of Sandoz AG., Basel, Switzerland (1962), No. 11, p. 28.
31) E. Grunwald and S. Winstein, *J. Am. Chem. Soc.*, **70**, 846 (1948).
32) A. Berson, Z. Hamlet, and W. A. Mueller, *J. Am. Chem. Soc.*, **84**, 297 (1962).
33) E. M. Kosower, *J. Am. Chem. Soc.*, **80**, 3253 (1958).
34) S. Brownstein, *Can. J. Chem.*, **38**, 1590 (1960).
35) I. Abe, K. Hayashi, M. Kitagawa, and T. Urahata, *Nippon Kagaku Kaishi*, **1980**, 545.
36) M. V. C. Sastri, *Indian Inst. Sci., Quart. J.*, **5**, 145, 162 (1942).
37) I. Abe, K. Hayashi, and M. Kitagawa, *Yukagaku*, **26**, 355 (1977).

Surface Composition of SnO_2–ZrO_2 Binary Oxide Catalyst and Its Selectivity for C_3H_6–NO Reaction

Toshinobu Imanaka, Takeshi Hashimoto, Katsumi Sakurai, Yasuaki Okamoto, and Shiichiro Teranishi*

Department of Chemical Engineering, Faculty of Engineering Science, Osaka University, Toyonaka, Osaka 560

(Received June 12, 1979)

The relation between the composition of outermost surface layer on SnO_2–ZrO_2 binary oxide catalyst and catalytic selectivity in the C_3H_6–NO reaction has been investigated by XPS technique. The composition of outermost surface layer was estimated from a comparison of the intensity ratios of X-ray induced Auger peak or XPS peak of Sn to XPS peak of Zr. A superficial enrichment of Zr was observed in these catalysts calcined at 600 °C in the air, while surface enrichment of Sn took place during the course of evacuation at 450 °C. The catalytic selectivity for formation of acrylonitrile showed a maximum with the catalyst containing Sn and Zr in the same concentration at the outermost surface layer of catalyst.

Enrichment of one component of a binary alloy occurs when the alloy is prepared in the air or reactive gases.[1,2] Knowledge of the surface composition of a binary catalyst is necessary for the clarification of heterogeneous catalytic reactions. Only a little evidence of the difference in surface and bulk compositions in cases of multicomponent oxide catalysts has been obtained.[3–6]

Studies with some binary oxide catalysts were carried out by means of X-ray photoelectron spectroscopy (XPS) in order to show the considerable difference occuring in the surface composition from the bulk composition of binary oxide catalysts such as SnO_2–MoO_3 and CoO–MoO_3 binary systems.[7–9] Only a few studies have been made to elucidate the influence of surface composition of solid catalysts on catalytic activity or selectivity.[7]

In the present work, the relation between the surface composition of some SnO_2–ZrO_2 binary oxide catalysts and the catalytic activity or selectivity for the C_3H_6–NO reaction has been studied. Special attention was attached to the role of the outermost surface layer of catalysts on catalytic activity and selectivity.

Experimental

The SnO_2–ZrO_2 binary oxide catalysts were prepared by impregnation and coprecipitation. The impregnated catalysts were prepared as follows: Powder of SnO_2 or ZrO_2 as a support was immersed in aqueous solutions of $ZrO(NO_3)_2$, $ZrOCl_2$, or $SnCl_2$ respectively, followed by evaporation to dryness at 100 °C and calcination in the air at 600 °C for 8 h. The SnO_2/ZrO_2 catalyst represents the SnO_2 supported on ZrO_2, the ZrO_2/SnO_2 catalysts representing the ZrO_2 supported on SnO_2.

Coprecipitated SnO_2–ZrO_2 catalysts were prepared by precipitation at pH~5 from a solution of $SnCl_2$ and $ZrO(NO_3)_2$ or $ZrOCl_2$ with dilute NH_4OH. The precipitates were washed, dried at 100 °C and then calcined in the air at 600 °C for 8 h. $SnCl_2 \cdot 2H_2O$, $ZrO(NO_3)_2 \cdot 2H_2O$, ZrO_2 (Nakarai Chemical Co.), $ZrOCl_2$, SnO_2, and a solution of NH_3 (Wako Pure Chem. Co.) were used.

Procedures

XPS spectra were measured on a Hitachi 507 photoelectron spectrometer equipped with a cylindrical mirror analyzer using Al $K\alpha_{1,2}$ radiation. The catalysts were mounted on a sample holder made of stainless steel. All binding energies were referred to the contaminant carbon [C 1s=285.0 eV]. The peak area intensities of Sn $3d_{5/2}$ and Zr 3d were used to obtain the Sn/Zr intensity ratio. The peak of Sn $3d_{5/2}$ (binding energy, *B.E.*, 486.6±0.2 eV) and Sn Auger (LMM, Kinetic energy; *K.E.*, 420 eV) were also used for obtaining information on depth profiles from the surface to the bulk of the catalysts. The surface compositions were determined by the intensity ratio Sn $3d_{5/2}$: Zr 3d or Sn Auger: Zr 3d using the calibration curve obtained by using mixtures of SnO_2 and ZrO_2 powder.

The reaction of C_3H_6–NO was studied over the SnO_2–ZrO_2 catalysts by using a reaction mixture, C_3H_6/NO=1/1, in a circulating system under 2.533×10^4 Pa (190 Torr) total pressure at 530 °C. Products were analyzed by GLC after 3 h.

Results and Discussion

Figure 1 shows the correlation between the content of Sn at the surface and that in bulk of SnO_2–ZrO_2 binary oxide catalysts prepared by coprecipitation.

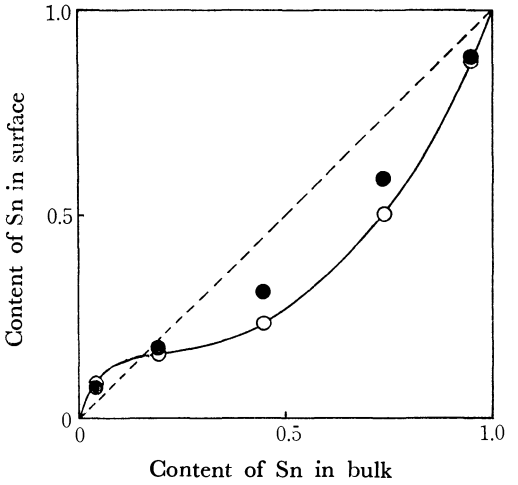

Fig. 1. Correlation between content of Sn in surface and that in bulk for coprecipitated SnO_2–ZrO_2 catalysts.
○: After calcination, ●: after evacuation at 450 °C for 2 h.

The value of surface composition was calculated from the intensity ratio of Sn Auger peak to Zr XPS peak, Zr 3d (*B.E.* 181.8±0.2 eV). The dotted straight line corresponds to the surface composition equal to bulk composition. A superficial enrichment of Zr was observed in these catalysts calcined in the air except for a small content of Sn (Sn/(Sn+Zr)<0.15 molar fraction). It is accepted that the surface is enriched by the constituent which has the lowest free energy under a surrounding gas. The surface enrichment of Zr during the course of preparation in the air would be due to the fact that the heat of formation of ZrO_2, 1079.5 kJ mol^{-1}, is larger than that of SnO_2, 574.9 kJ mol^{-1}. If the surface enrichment of Zr can be ascribed to the process in the formation of precipitate, the solubility product constant K_{sp} of $Sn(OH)_2$ should be smaller than that of $Zr(OH)_4$. However, the K_{sp} values of $Sn(OH)_2$[10] and $Zr(OH)_4$[11] are 1.8×10^{-15} and 8×10^{-52}, respectively, at 25 °C. The surface enrichment of Zr cannot be attributed to the difference of solubility in the formation of precipitates. A slight Sn enrichment was observed in the region less than 0.15 mole fraction of Sn in bulk. This might be due to the exclusion of Sn from the bulk of the catalyst by the crystallization of SnO_2. When evacuated at 450 °C for 2 h, the atomic intensity ratio Sn/(Sn+Zr) increased (Fig. 1), indicating that surface enrichment of Sn occurs during the course of evacuation.

The correlations between the content of Sn in surface and that in bulk of SnO_2–ZrO_2 binary catalysts prepared by the impregnation methods are shown in Fig. 2. As expected, the surface enrichment of Sn and Zr was observed in the SnO_2/ZrO_2 and ZrO_2/SnO_2 catalysts, respectively. After evacuation at 450 °C for 2 h, the surface enrichment of Sn was observed in both catalysts.

The surface is enriched by the constituent which has the lowest surface free energy, the surface composition being correlated with the surface tension of solids. Oresbury *et al.*[3] pointed out that the surface tension

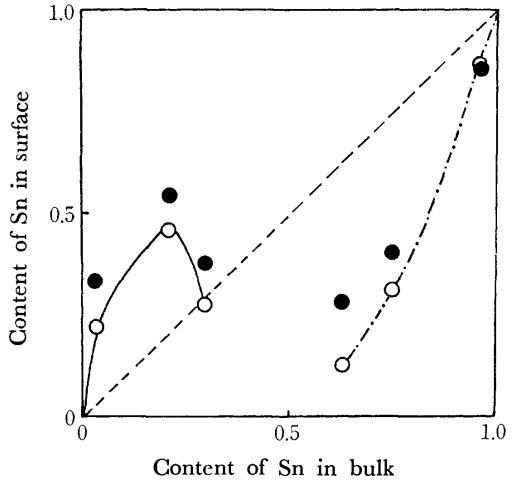

Fig. 2. Correlation between content of Sn in surface and that in bulk for impregnated SnO_2–ZrO_2 catalysts.
○: After calcination, ●: after evacuation at 450 °C for 2 h. ——: SnO_2/ZrO_2, —·—: ZrO_2/SnO_2.

of metals can be estimated from the heat of vaporization and sublimation, the surface tension of metals increasing with increase in the heat of vaporization and sublimation. The heat of vaporization of metals is correlated with the melting point of metals, the melting point increasing with increase in the heat of vaporization (*cf.* Zr: 581.6 kJ mol^{-1}, Sn: 290.4 kJ mol^{-1}). This relation might be applied to binary oxide catalysts. In the case of SnO_2–ZrO_2 binary catalysts, the surface enrichment of Sn seems to be due to the fact that the melting point of SnO_2, 1127 °C, is lower than that of ZrO_2, 2700 °C.[12] It might also be due to the fact that SnO_2 of the surface is reduced more easily than ZrO_2 since the heat of formation of SnO_2 is lower than that of ZrO_2.

It is necessary to estimate the composition of the outermost surface layer in relation to heterogeneous catalysis. The escape depth increases a great deal with increase in electron energy, characteristic of scattering length determined by electron-electron interactions.[13] The values for the escape depth is evaluated by using samples consisting of homogeneous films having uniform thickness.[14] The intensity, $I(d)$, of photoelectrons with a certain energy, expelled from a film of effective thickness d is given by $I(d)=I_\infty[1-\exp(-d/\lambda)]$, where λ is the electron escape depth in the film material and I_∞ the intensity of electrons expelled from a thick sample of the film material.

The energy dependence for the electron escape depth in the energy region of some kilovolts is expressed by the following relation obtained by Brundle,[13]

$$\lambda(E) \propto E^n$$

where n is 0.5±0.1[15] and E the kinetic energy, eV. Accordingly, the value of escape depth of the Sn Auger peak (kinetic energy: 420 eV) is *ca.* 8 Å, while the Sn XPS peak (kinetic energy: 1000 eV) is estimated to be *ca.* 12 Å. Thus, information on depth profiles is obtained from a comparison of both peak intensities.

A comparison of surface composition calculated from the intensity ratio of Sn Auger/Zr 3d to that of Sn 3d/Zr 3d is given in Fig. 3. The content of Sn obtained by using Sn Auger peak intensity is represented by r_1, and the content of Sn determined by Sn $3d_{5/2}$ by r_2. The surface layer in the impregnated and coprecipitated catalysts seems to be homogeneous. However, after evacuation at 450 °C, the surface enrichment of Sn is observed as shown in Figs. 1 and 2. The results indicate that the surface enrichment of Sn occurs in the surface layer of the SnO_2–ZrO_2 binary oxide catalysts during the course of evacuation at 450 °C.

In the presence of SnO_2–ZrO_2 catalysts, propylene reacts with NO to give CH_2=CHCN, CH_3CN, and CO_2. We have examined the relation between the composition of the outermost surface layer of the catalyst and the catalytic selectivity in this reaction (C_3H_6–NO).

Figure 4 shows the dependence of catalytic selectivity for the C_3H_6–NO reaction on the surface composition of the catalysts. In the catalysts prepared by both methods, the change in surface composition obtained from the intensity ratio Sn Auger/Zr 3d was not observed during contact with C_3H_6, NO, and

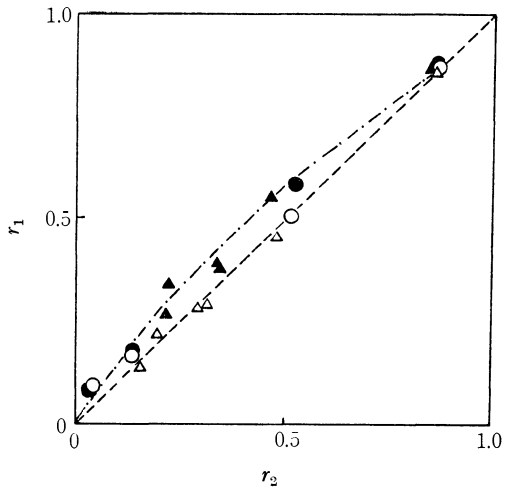

Fig. 3. Depth analysis of Sn in catalyst.
r_1: Content of Sn obtained by using Sn Auger intensity, r_2: content of Sn obtained by using Sn $3d_{5/2}$ intensity.
·····, ○: Coprecipitated catalysts, ·····, △: impregnated catalysts: SnO_2/ZrO_2 and ZrO_2/SnO_2. —·—, ●,▲: after evacuation at 450 °C for 2 h.

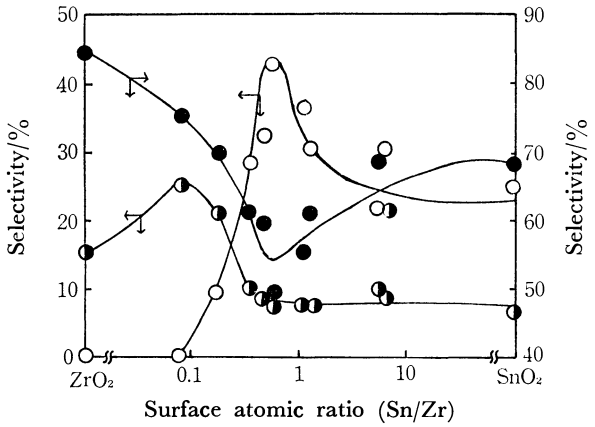

Fig. 4. Selectivity dependence of the reaction ($NO+C_3H_6$) on the surface composition of the catalyst.
○: CH_2=CHCN, ◑: CH_3CN, ●: CO_2.
Total pressure: 190 mmHg, Reaction mixtures: C_3H_6/NO=1/1 Reaction conditions: 530 °C for 3 h.

mixtures of C_3H_6 and NO. The selectivity for the formation of CH_2=CHCN becomes maximum at the atomic ratio, Sn/Zr=0.6, indicating that the catalytic selectivity is a function of surface composition of the catalyst irrespective of the method of preparation. The atomic ratios were estimated from the peak intensities of Sn Auger and Zr XPS, escape depths being 8 Å and 14 Å, respectively. The atomic ratio of Sn to that of Zr in the region near 3 Å from the outermost surface layer, $(Sn/Zr)_d$, was estimated by using the escape depths of Sn and Zr as follows.

$$(Sn/Zr)_d = f(I_{Sn}/I_{Zr})_d$$
$$= f(I_{Sn}/I_{Zr})_\infty[1-\exp(-d/\lambda_{Sn})]/[1-\exp(-d/\lambda_{Zr})]$$

where d=3 Å, λ_{Sn}=8 Å, λ_{Zr}=14 Å, and f is a constant.

The value of atomic ratio in the region near 3 Å from outermost surface layer can thus be estimated by

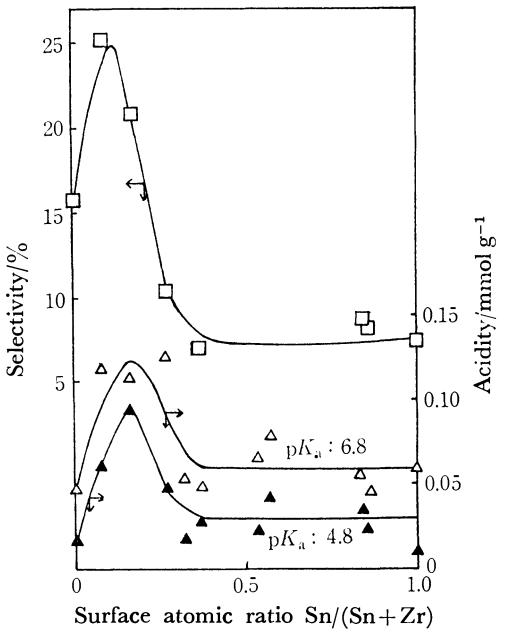

Fig. 5. Correlation between the selectivity for the formation CH_3CN as a function of the atomic ratio on the surface layer of the catalyst and its surface acidity.
□: Selectivity (%), △: pK_a: 6.8, ▲: pK_a: 4.8.

$(Sn/Zr)_{3Å}=0.96\simeq 1$.

This indicates that the catalytic selectivity for the formation of CH_2=CHCN becomes maximum with the same concentration of Sn and Zr of outermost surface layer on the catalyst.

On the other hand, the selectivity for the formation of CH_3CN becomes maximum near the atomic ratio 0.07 (Fig. 4). The results of acidity (amount of acid mmol/g) measured at pK_a=6.8 and 4.8 and the selectivity for formation of CH_3CN are shown in Fig. 5 as a function of the atomic ratio on the surface layer of the catalyst. The maximum selectivity agrees with that of acidity, indicating that the presence of acid sites on the surface of the catalysts results in the formation of CH_3CN produced by cracking reactions.

References

1) V. Ponec, *Catal. Rev.*, **11**, 1 (1975).
2) J. H. Sinfelt, *Acc. Chem. Res.*, **10**, 15 (1977).
3) S. H. Oresbury, P. A. Ertrand, and G. H. Somorjai, *Chem. Rev.*, **75**, 547 (1975).
4) I. Matsuura and M. W. J. Wolfs. *J. Catal.*, **37**, 174 (1975).
5) B. Grzybowska, J. Haber, W. Marczemski, and L. Unger, *J. Catal.*, **42**, 327 (1976).
6) T. S. R. Prasada Rao and P. G. Menon, *J. Catal.*, **51**, 64 (1978).
7) Y. Okamoto, T. Hashimoto, T. Imanaka, and S. Teranishi, *Chem. Lett.*, **1978**, 1035.
8) Y. Okamoto, T. Shimokawa, T. Imanaka, and S. Teranishi, *J. Chem. Soc., Chem. Commun.*, **1978**, 47.
9) Y. Okamoto, T. Shimokawa, T. Imanaka, and S. Teranishi, *J. Catal.*, **57**, 153 (1979).
10) "Solubilities of Inorganic and Organic Compounds, Binary Systems, Part I." Pergamon Press Ltd., (1963), Vol. 1, p. 43 (K_{sp} was calculated from the solubilities).

11) "Solubilities of Inorganic Compounds," American Chemical Society, Washington D. C. (1958), Vol. 2, p. 1695.
12) On the other hand, solid stannous oxide formed in a vacuum is unstable and decomposes into Sn and SnO_2, the treatment of the catalyst in a vacuum thus resulting in the segregation of Sn reduced on the surface layer. T. C. Platteauw and G. Meyer, *Trans. Faraday Soc.*, **52**, 1066 (1956).
13) C. R. Brundle, *Surf. Sci.*, **48**, 99 (1975).
14) M. Klasson A. Berndtsson, J. Hedman, R. Nilsson, R. Nyholm, and C, Nordling, *J. Electon Spectrosc. Relat. Phenom.* **3**, 427 (1974).
15) M. Klasson, J. Hedman, A. Berndtsson, R. Nilsson, C. Nordling, and P. Melnik, *Phys. Sci.*, **5**, 93 (1972).

Effect of Hydrogen Chloride on the Pyrolysis of Acetylene as Studied with a Single-pulse Shock Tube

Hiroo OGURA

Institute of Space and Aeronautical Science, The University of Tokyo, Komaba, Meguro-ku, Tokyo 153

(Received June 27, 1979)

The pyrolysis of acetylene in the presence of hydrogen chloride was investigated with a single-pulse shock tube in the temperature range 1100—1680 K. The hydrocarbons produced in the C_2H_2–HCl system were quite the same as those obtained in the C_2H_2–Ar system. The formation rate of the main pyrolysis product, 1-buten-3-yne, was reduced remarkably by the addition of hydrogen chloride, being of third-order and of inverse first-order with respect to the concentrations of acetylene and hydrogen chloride, respectively. The overall second-order rate constant obtained was

$$k(\mathrm{cm^3\ mol^{-1}\ s^{-1}}) = 2.9\times10^{12}\exp(-45800/RT).$$

As the chlorine atom containing product, only chloroacetylene was found in small amounts, its formation rate being of second-order with respect to acetylene. The inhibitory effect of hydrogen chloride on the 1-buten-3-yne formation rate was interpreted in terms of the change in the termination from the recombination reaction of 2-ethynylvinyl radical to the reaction of 2-ethynylvinyl radical with hydrogen chloride.

Hydrogen chloride has been used as an additive that may scavenge the chain carrier radicals in the system of decomposing hydrocarbons. Cullis *et al.*[1] studied the pyrolysis of acetylene in the presnece of hydrogen chloride at temperatures below 800 K, reporting that it may inhibit the pyrolysis of acetylene by a different mechanism from that of nitrogen monoxide. On the other hand, using a shock tube Bopp and Kern found that hydrogen chloride has no appreciable effect on the pyrolysis of acetylene at temperatures above 1650 K.[2]

A shock tube study on the pyrolysis of acetylene in the presence of nitrogen monoxide at intermediate temperatures showed that the nitrogen monoxide ceases to be an inhibitor with rise in temperature.[3] Analyses of both the yield-temperature plots of the pyrolysis products and the reaction products containing chlorine atom would be useful for a mechanistic study of the inhibitory effect of hydrogen chloride, as was found in the case of the C_2H_2–NO system.

Experimental

Apparatus and Procedure. The apparatus and procedure were the same as those described previously.[3] A 4-cm single-pulse shock tube was used, the driven section being 277 cm and the driver section 128.5 cm in length. Helium was used as a driver gas. The shocks were fired within 5 min after the test gases had been introduced into the driven section.

Materials. Four mixtures were prepared in a glass vessel of 10-l volume with the ratios of C_2H_2/HCl/Ar = 10/2/88; 10/0.5/89.5; 5/1/94; and 10/0/90. The test mixtures were stirred with a glass fan for 4 h. The mixing and storage time periods were kept constant for the three mixtures with hydrogen chloride, since too long storage resulted in the formation of vinyl chloride in a considerable amount. One mixture completely mixed was shock-heated within 2 d, the vinyl chloride formation being negligible.

Hydrogen chloride (Matheson Co.) was purified by bulb-to-bulb distillation. Argon and acetylene were purified according to the method reported.[3] The standard gas mixtures for the calibration of gas-chromatography were the same as those used previously.[3]

Chloroacetylene was synthesized from 1,2-dichloroethylene by the method of Bashford *et al.*[4] The chloroacetylene was purified by bulb-to-bulb distillation. The gas-chromatographic and mass spectrometric analyses showed that no detectable impurities were found. The purified chloroacetylene was diluted with a large amount of argon, and used as a gas-chromatographic standard gas.

Analytical. The reaction products were analyzed by gas-chromatography. The details of the hydrocarbon analysis were described elsewhere.[3] Chloroacetylene and vinyl chloride were analyzed in the same way as the hydrocarbons on a Porapak N column at 140 °C. The order of elution was CH_4, C_2H_6, C_2H_4, allene, propyne, chloroacetylene, vinyl chloride, 1,3-butadiene, 1-buten-3-yne, 1,3-butadiyne, and benzene. Hydrogen was analyzed at room temperature with a thermal conductivity cell on a 1.2 m column packed with molecular sieve 13X(80—100 mesh), argon being used as a carrier gas.

Results

The mixtures were subjected to shock-heating in the temperature range 1100—1680 K. The total densities behind the reflected shock waves were *ca.* 2.68×10^{-5} mol/cm^3, the reaction times being *ca.* 990 μs. The shock-heated samples were extracted into pre-evacuated bulbs of 60-ml volume, and analyzed by gas-chromatography.

Product analysis showed that the hydrocarbons produced with and without hydrogen chloride were the same; CH_4, C_2H_4, C_2H_6, allene, propyne, 1,3-butadiene, 1-buten-3-yne, 1,3-butadiyne, and benzene being formed. The major products were also 1-buten-3-yne, 1,3-butadiyne, and hydrogen in the presence of hydrogen chloride. The minor products were CH_4, C_2H_4, allene, propyne, and benzene, trace products being C_2H_6 and 1,3-butadiene as in the case of acetylene.

Chloroacetylene was produced in a small amount as a product containing chlorine atom. The chloroacetylene was identified by both gas-chromatographic and mass spectrometric comparison with the synthesized gas. Substances condensible at liquid nitrogen temperature in several runs at higher reaction temperatures were used for identification. No products which might contain chlorine atoms were detected in the substances condensible at liquid nitrogen temperature.

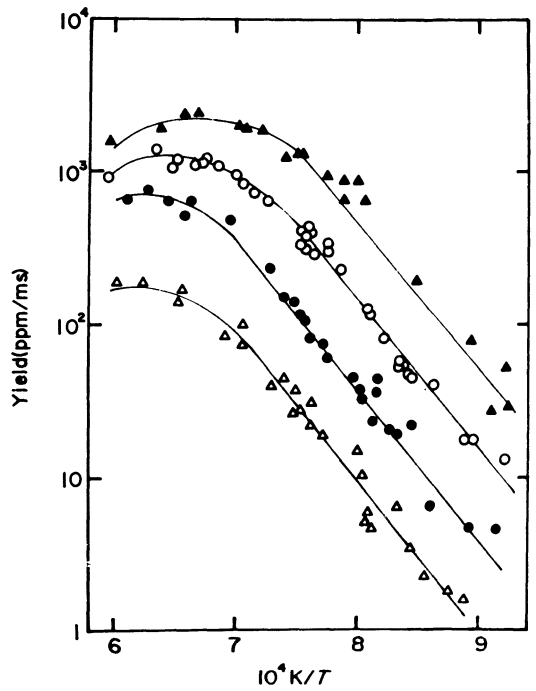

Fig. 1. Yield-temperature plots of 1-buten-3-yne formation.
●; C_2H_2/HCl/Ar=10/2/88, ○; C_2H_2/HCl/Ar=10/0.5/89.5, △; C_2H_2/HCl/Ar=5/1/94, ▲; C_2H_2/HCl/Ar=10/0/90.

Inhibited Rate of 1-Buten-3-yne Formation. The yields of 1-buten-3-yne(ppm/ms) for four mixtures with different composition of C_2H_2 and HCl are plotted as a function of temperature in Fig. 1. The yield-temperature plots show that the yields of 1-buten-3-yne are markedly decreased by the addition of hydrogen chloride at lower temperatures, and that they are significantly dependent on the amount of hydrogen chloride added. The rates of 1-buten-3-yne formation at temperatures below 1350 K are nearly of third order with respect to acetylene and of inverse first order with respect to hydrogen chloride. Apparent overall second-order rate constants for the inhibited 1-buten-3-yne formation at temperatures below 1350 K (58 experiments) are plotted in the Arrhenius form in Fig. 2. The best fit rate constant expression was obtained by the least-squares method as[5]

$$k_1(\mathrm{cm^3\ mol^{-1}\ s^{-1}}) = 2.9 \times 10^{12} \exp(-45800/RT)^*. \quad (1)$$

Formation Rate of Chloroacetylene. The formation of chloroacetylene was expected to have something to do with the reduction of 1-buten-3-yne yields. In order to determine the concentration dependence of the rate of chloroacetylene formation on acetylene and hydrogen chloride, the yields of chloroacetylene are plotted as a function of temperature in Fig. 3. We see that the rates of chloroacetylene formation are approximately of second-order with respect to acetylene and are little dependent on the hydrogen chloride concentration. Apparent second-order rate constants of 43 experiments are shown in the Arrhenius form in Fig. 4. The least-squares treatment of the data gives the best fit rate constant as[5]

$$k_2(\mathrm{cm^3\ mol^{-1}\ s^{-1}}) = 1.0 \times 10^{16} \exp(-67200/RT). \quad (2)$$

Only the data obtained at temperatures below 1350 K were adopted, since the yields of chloroacetylene decreased at higher temperatures and the temperatures where the yields began to decrease differed for the three mixtures with hydrogen chloride.

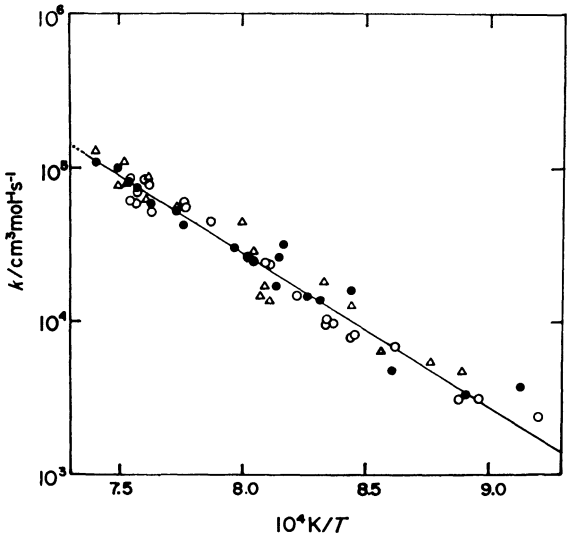

Fig. 2. Arrhenius plots of the second-order rate constants for 1-buten-3-yne formation.
Symbols are the same as in Fig. 1.

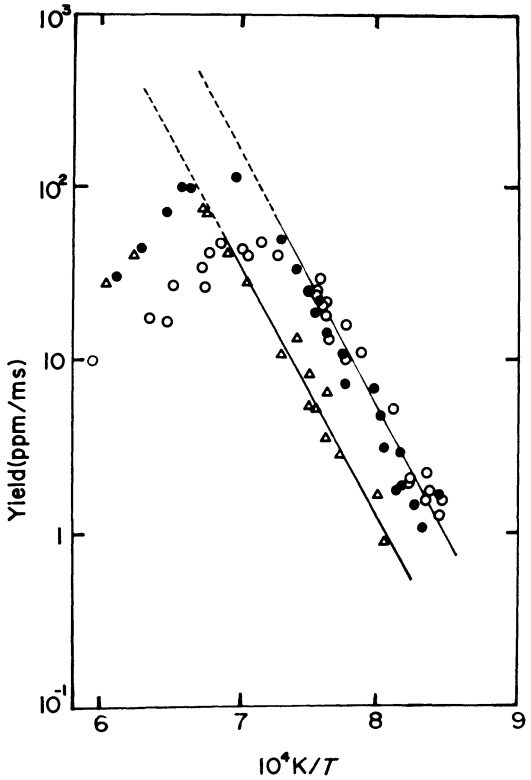

Fig. 3. Yield-temperature plots of chloroacetylene formation.
Symbols are the same as in Fig. 1.

* The activation energy is expressed in cal/mol (1 cal_{th} = 4.184 J).

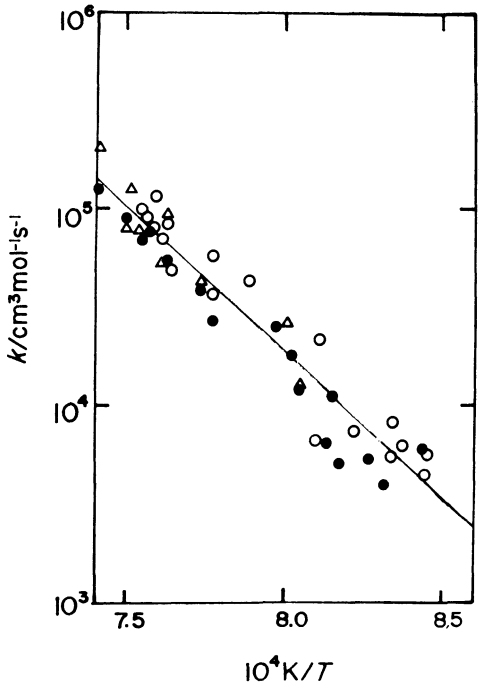

Fig. 4. Arrhenius plots of the second-order rate constants for chloroacetylene formation.
Symbols are the same as in Fig. 1.

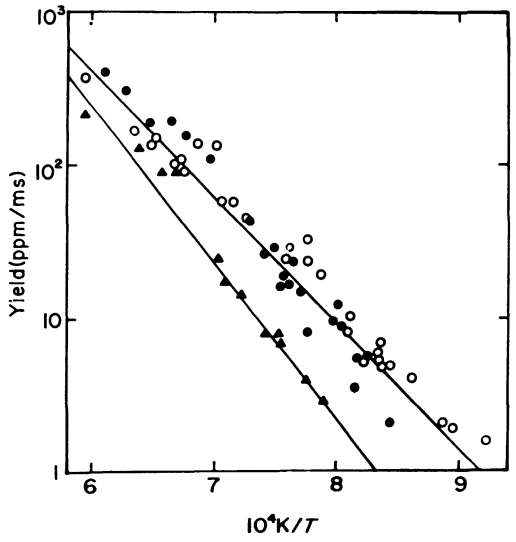

Fig. 5. Effect of hydrogen chloride on the yields of ethylene. Symbols are the same as in Fig. 1.

Effects on Other Products. Hydrogen chloride affects the yields of other products in two different ways: (a) in the case of 1,3-butadiyne, hydrogen, and ethylene, the yields increase considerably at lower temperatures, and at higher temperatures are little influenced by the concentration of hydrogen chloride added (Fig. 5); (b) in the case of allene, propyne, and benzene, the yields decrease significantly at lower temperatures, the decrease becoming smaller with rise in temperature.

Discussion

The hydrocarbons produced in the C_2H_2–HCl system are the same as those in the pyrolysis of acetylene. Although their yields are affected by the addition of hydrogen chloride, the forms of yield-temperature plots are similar to those in the absence of hydrogen chloride. This suggests that a mechanism similar to that of the pyrolysis alone is operative in the C_2H_2–HCl system. A pyrolysis mechanism for acetylene has been proposed from a thermochemical point of view,[6] and tested by the addition of nitrogen monoxide.[3] The mechanism is as follows:

$$2C_2H_2 \longrightarrow C_4H_3(1) + H \qquad \Delta H^\circ = 46.2 \quad (3)$$

$$C_4H_3(1) + C_2H_2 \longrightarrow C_6H_5 \qquad \Delta H^\circ = -20.5 \quad (4)$$

$$C_6H_5 \longrightarrow C_4H_4 + C_2H \qquad \Delta H^\circ = 53.1 \quad (5)$$

$$C_2H + C_2H_2 \longrightarrow C_4H_3(2) \qquad \Delta H^\circ = -44.8 \quad (6)$$

$$C_4H_3(2) + C_2H_2 \longrightarrow C_4H_4 + C_2H \qquad \Delta H^\circ = 11.7 \quad (7)$$

$$2C_4H_3(2) \longrightarrow \text{termination} \quad (8)$$

C_4H_3 (1) and C_4H_3 (2) stand for 1-ethynylvinyl and 2-ethynylvinyl radicals, respectively.

Inhibitory Effect of Hydrogen Chloride. A free-radical chain mechanism for the inhibited formation of 1-buten-3-yne could be constructed in line with that for the pyrolysis of acetylene. The inhibitory effect of hydrogen chloride can be interpreted by the reactions with the radicals present in the pyrolysis system of acetylene alone:[7]

$$C_4H_3(1) + HCl \longrightarrow C_4H_4 + Cl \qquad \Delta H^\circ = 23.8 \quad (9')$$

$$\longrightarrow C_4H_3(1)Cl + H \quad (9'')$$

$$C_2H + HCl \longrightarrow C_2H_2 + Cl \qquad \Delta H^\circ = -8.8 \quad (10')$$

$$\longrightarrow C_2HCl + H \qquad \Delta H^\circ = 11.3 \quad (10'')$$

$$C_4H_3(2) + HCl \longrightarrow C_4H_4 + Cl \qquad \Delta H^\circ = 2.0 \quad (11')$$

$$\longrightarrow C_4H_3(2)Cl + H \qquad \Delta H^\circ = 19.8 \quad (11'')$$

The reaction of C_6H_5 radical with HCl can be neglected, since the bimolecular reaction would be too slow to be competitive with the unimolecular decomposition of C_6H_5 radical (Reaction 5). The mechanism for the inhibited pyrolysis consists of three sets of competitive reactions of the radicals with C_2H_2 and HCl. The reaction of C_4H_3 (1) radical with HCl (Reactions 9′ and 9″) is referred to hereafter as Reaction 9.

The characteristic feature of the 1-buten-3-yne formation rates in the C_2H_2–HCl system is their concentration dependence on C_2H_2 and HCl. The formation rates are inversely proportional to the concentration of HCl. The inverse first-order dependence on an additive is observed when the termination reaction in its absence is replaced by a reaction of the predominant radical with the additive.[8] Thus Reaction 8, the major termination in the reaction C_2H_2–Ar system, would become a minor one in the C_2H_2–HCl system.

Assuming the steady-state concentrations of C_4H_3 (1), C_2H, C_6H_5, and C_4H_3 (2) radicals in Reactions 3—11, we get

$$R_3 = 2R_8^{HCl} + R_9 + R_{10} + R_{11}. \quad (12)$$

Since the contribution of Reaction 8 to the termination would be small, $2R_8^{HCl}$, R_8^{HCl} denoting the rate of Reaction 8 in the presence of HCl, can be neglected:

$$R_3 \simeq R_9 + R_{10} + R_{11}. \quad (12')$$

In the absence of hydrogen chloride, the steady-state concentrations of the radicals are expressed as follows:

$$[C_4H_3(1)]_{ss} = (k_3/k_4)[C_2H_2] \quad (13)$$

$$= 56 \exp(-40900/RT)[C_2H_2] \quad (13')$$

$$[C_2H]_{ss} = [C_4H_3(1)]_{ss} + (k_7/k_6)[C_4H_3(2)]_{ss} \quad (14)$$

$$\simeq 3.8 \times 10^2 \exp(-30900/RT)[C_2H_2] \quad (14')$$

$$[C_4H_3(2)]_{ss} = (k_3/2k_8)^{1/2}[C_2H_2] \quad (15)$$

$$= 3.0 \exp(-23700/RT)[C_2H_2] \quad (15')$$

The rate constants used in the above estimation are those adopted previously:[3]

$$k_3(\mathrm{cm^3\,mol^{-1}\,s^{-1}}) = 3.5\times10^{13} \exp(-47400/RT) \quad (16)$$

$$k_6(\mathrm{cm^3\,mol^{-1}\,s^{-1}}) = 6.5\times10^{11} \exp(-6500/RT) \simeq k_4 \quad (17)$$

$$k_7(\mathrm{cm^3\,mol^{-1}\,s^{-1}}) = 7.9\times10^{13} \exp(-22600/RT) \quad (18)$$

$$k_8(\mathrm{cm^3\,mol^{-1}\,s^{-1}}) = 2.0\times10^{12}. \quad (19)$$

From Eqs. 13′, 14′, and 15′, C_4H_3 (1) and C_4H_3 (2) are found to be the least and most abundant radicals in the C_2H_2–Ar system, respectively.

Although the change of concentration dependence of 1-buten-3-yne formation rate upon the addition of HCl might indicate that the hydrogen chloride added decreases the steady-state concentrations of the radicals in the C_2H_2–HCl system considerably, the C_4H_3 (2) radical would be the most predominant chain carrier radical even in the C_2H_2–HCl system. Neglecting the contribution of Reactions 9 and 10 to the termination, Eq. 12′ can be approximated by

$$R_3 = k_3[C_2H_2]^2 \simeq k_{11}[C_4H_3(2)]_{ss}^{HCl} = R_{11} \quad (12'')$$

from which we get the steady-state concentration of $C_4H_3(2)$ in the presence of HCl, $[C_4H_3(2)]_{ss}^{HCl}$:

$$[C_4H_3(2)]_{ss}^{HCl} \simeq (k_3/k_{11})[C_2H_2]^2/[HCl] \quad (20)$$

In the present mechanism 1-buten-3-yne is formed mainly by Reaction 7.

$$R_{C_4H_4}^{HCl} \simeq R_7^{HCl} \simeq k_7(k_4/k_{11})[C_2H_2]^3/[HCl], \quad (21)$$

where the formation rate of 1-buten-3-yne in the presence of HCl is denoted by $R_{C_4H_4}^{HCl}$. The formation rate derived from the present mechanism is in line with the observed one as regards concentration dependence.

Since no rate constants, estimated or observed, are available, k_{11} is calculated by a comparison with the observed (Eq. 1) and estimated (Eq. 21) rates for 1-buten-3-yne formation to be

$$k_{11}(\mathrm{cm^3\,mol^{-1}\,s^{-1}}) \simeq k_3k_7/k_1, \quad (22)$$

$$= 9.5\times10^{14} \exp(-24200/RT). \quad (22')$$

The rate constant estimated in Eq. 22′ is a representative one for both Reactions 11′ and 11″, its activation energy being greater than their heats of reaction. In view of the heat of reaction, the activation energy of Reaction 11″ is expected to be greater than that of Reaction 11′. When the activation energy of k_{11} is attributed to Reaction 11″, the activation energy for the inverse Reaction 11″ is estimated to be 4.4 kcal/mol from the heat of reaction. In the case of CH_3 radical reactions with HCl, the activation energies for the inverse reactions are obtained experimentally to be 4.6 kcal/mol for $H+CH_3Cl$ and 2.5 kcal/mol for $Cl+CH_4$.[9-11]

No detectable amount of chlorine atom containing products except for C_2HCl was found. $C_4H_3(2)Cl$ would undergo a unimolecular decomposition at temperatures above 1100 K as in the case of C_2H_3Cl.[12]

$$C_4H_3(2)Cl \longrightarrow C_4H_2 + HCl \qquad \Delta H^\circ = 20.4 \quad (23)$$

By this reaction the yields of C_4H_2 should increase upon addition of HCl, this being in line with the experimental results, In the present free-radical mechanism HCl catalizes the decomposition of the $C_4H_3(2)$ radical at temperatures above 1100 K.

The formation rate of 1-buten-3-yne in the absence of HCl has been reported:[6]

$$R_{C_4H_4} = 2.4\times10^{14} \exp(-46400/RT)[C_2H_2]^2. \quad (24)$$

In the present mechanism the steady-state concentrations of the $C_4H_3(2)$ radical with and without HCl are related to the observed 1-buten-3-yne formation rates as follows:

$$[C_4H_3(2)]_{ss}^{HCl}/[C_4H_3(2)]_{ss} = R_7^{HCl}/R_7 = R_{C_4H_4}^{HCl}/R_{C_4H_4} \quad (25)$$

$$= 1.2 \times 10^{-2} \exp(600/RT)[C_2H_2]/[HCl]. \quad (25')$$

In the presence of HCl the steady-state concentration of $C_4H_3(2)$ radical is reduced by a factor 0.1—0.3 of that in its absence (1100—1350 K and $[C_2H_2]/[HCl]=5$—20). The chain length of 1-buten-3-yne formation rate in the C_2H_2–Ar system is given by

$$R_{C_4H_4}/R_3 = R_{C_4H_4}/R_8 = 7.1 \exp(1000/RT), \quad (26)$$

$$\simeq 10(1100\text{—}1350\,\mathrm{K}). \quad (26')$$

The chain length in the C_2H_2–HCl system is shortened to *ca.* 1—3 under the present experimental conditions, since the 1-buten-3-yne formation rate is proportional to the steady-state concentration of C_4H_3 (2) radical. In the system with the composition of $[C_2H_2]/[HCl]=5$, the chain length is *ca.* 1.0 at temperatures 1100—1350 K, the chain being almost completely stopped.

The contribution of Reaction 8 to the termination in the C_2H_2–HCl system is estimated by means of Eqs. 12″ and 25.

$$R_8^{HCl} \simeq (1/10\text{—}1/100)R_8 \simeq (1/10\text{—}1/100)R_{11}.$$

As assumed in the derivation of Eq. 12″, Reaction 8 in the C_2H_2–HCl system is found to be an insignificant termination.

Formation Rate of Chloroacetylene. The steady-state approximation made in the derivation of Eq. 12 also gives the equation

$$R_8^{HCl} = R_7^{HCl} + R_{11} \quad (27)$$

from which the steady-state concentration of C_2H radical is obtained as

$$[C_2H]_{ss}^{HCl} = (1/k_6)(k_7+k_{11}[HCl]/[C_2H_2])[C_4H_3(2)]_{ss}^{HCl}. \quad (28)$$

In the present mechanism the chloroacetylene is formed by Reaction 10″. The formation rate is then expressed by

$$R_{C_2HCl} = (k_3k_{10''}/k_6k_{11})(k_7[C_2H_2]^2 + k_{11}[C_2H_2[HCl]), \quad (29)$$

$$= (k_3k_7/k_6)(k_{10''}/k_{11})[C_2H_2]^2(1+R_{11}/R_7^{HCl}). \quad (29')$$

Since the formation rate of chloroacetylene is little dependent on the hydrogen chloride concentration in the present experiments, to be compatible with the observed rate, Eq. 29′ can be approximated by

$$R_{C_2HCl} \simeq (k_3k_7/k_6)(k_{10}''/k_{11})[C_2H_2]^2. \quad (29'')$$

By a comparison of the estimated second-order rate constant with the observed one (Eq. 2), we obtain

$$k_{10}''/k_{11} = 2.3 \exp(-3700/RT), \quad (30)$$

$$\simeq 0.4—0.6\,(1100—1350\,K). \quad (30')$$

The rate constant k_{10}'' is then obtained from Eqs. 22' and 30:

$$k_{10}''(cm^3\,mol^{-1}\,s^{-1}) = 2.2\times10^{15}\exp(-27900/RT) \quad (31)$$

The frequency factors of k_{10}'' and k_{11} seem to be somewhat greater than that of the usual abstraction reaction, *i.e.*, 10^{13}—10^{14}. However, they might be reasonable as considered from the assumptions made in their derivation. The effective rate constants for Reactions 10 and 11 might be of comparable order of magnitude, since these reactions are of a similar type. This may be supported by Eq. 30'.

Using the estimated rate constants k_{10}'' and k_{11}' we can evaluate the relative importance of the competitive reactions of the radicals with C_2H_2 and HCl. The contribution of k_{10}' to k_{10} can be neglected in analogy with Reaction 11.

$$R_{10}/R_6^{HCl} \simeq (k_{10}''/k_6)[HCl]/[C_2H_2],$$
$$= 3.4\times10^3\exp(-21400/RT)[HCl]/[C_2H_2],$$
$$R_{11}/R_7^{HCl} = (k_{11}/k_7)[HCl]/[C_2H_2],$$
$$= 12\exp(-1600/RT)[HCl]/[C_2H_2],$$
$$(R_{10}/R_6^{HCl})/(R_{11}/R_7^{HCl}) \simeq (k_7/k_6)(k_{10}''/k_{11}),$$
$$= 3.0\times10^2\exp(-19800/RT),$$
$$\simeq 0.04—0.2(1100—1350\,K).$$

The equations show that the scavenging of C_2H radical by HCl molecule is less important than that of $C_4H_3(2)$ radical. This is in line with the assumption made in the derivation of 1-buten-3-yne formation rate.

Reactions of Other Radicals. In the absence of HCl, C_2H_4 is formed by the following reaction.[6]

$$H + C_2H_2 \longrightarrow C_2H_3, \quad \Delta H^\circ = -46.7 \quad (32)$$

$$C_2H_3 + C_2H_2 \longrightarrow C_2H_4 + C_2H, \quad \Delta H^\circ = 12.7. \quad (33)$$

In the presence of HCl, the C_2H_3 radical will react with HCl.

$$C_2H_3 + HCl \longrightarrow C_2H_4 + Cl, \quad \Delta H^\circ = 3.9 \quad (34')$$

$$\longrightarrow C_2H_3Cl + H, \quad \Delta H^\circ = 19.6 \quad (34'')$$

$$C_2H_3Cl \longrightarrow C_2H_2 + HCl. \quad \Delta H^\circ = 27.1 \quad (35)$$

As in the case of Reaction 11, the activation energy of Reaction 34' would be smaller than that of Reaction 34''. In view of the heat of reaction the activation energy of Reaction 34' would be smaller than that of Reaction 33, the yields of C_2H_4 thus increasing with the reaction of HCl at lower temperatures.

The C_2H_3 radical becomes a radical of greater molecular weight by successive reactions with C_2H_2 molecules. Its growth is suppressed considerably by Reaction 34 in the C_2H_2–HCl system, the yields of allene, propyne, and benzene decreasing.

$$C_2H_3 + C_2H_2 \longrightarrow C_4H_5 \xrightarrow{C_2H_2} C_6H_7,$$

$$C_6H_7 \longrightarrow C_3H_3 \xrightarrow{C_2H_2} C_3H_4,$$

$$\longrightarrow C_6H_6.$$

The reactions with HCl would produce excess atoms than in its absence. The yields of hydrogen will increase by

$$H + C_2H_2 \longrightarrow H_2 + C_2H.$$

Apparently a different effect of hydrogen chloride on the two groups would result from the same radical scavenging by hydrogen chloride. The main and characteristic features of acetylene pyrolysis inhibited by hydrogen chloride can be explained by the free-radical mechanism.

Comparison with Other Inhibitors. The small inhibitory effect of nitrogen monoxide was interpreted in terms of the scavenging and partial revival of the chain carrier radical.[3]

$$C_4H_4(2) + NO \longrightarrow C_2HCHO + HCN, \quad (36)$$

$$C_2HCHO \longrightarrow C_2H + CHO. \quad (37)$$

By a comparison with the estimated rate constants for Reactions 11 and 36, we get

$$k_{36}/k_{11} = 2.4\times10^{-2}\exp(9300/RT). \quad (38)$$

In the temperature range 1100—1350 K, the above values are 0.1—0.3, the scavenging effect of nitrogen monoxide being much smaller than that of hydrogen chloride. In the C_2H_2–NO system the steady-state concentration of $C_4H_3(2)$ radical is less reduced by Reaction 36, Reaction 8 being the predominant termination reaction.

The consumption rate of acetylene at temperatures below 800 K is inversely proportional to the hydrogen bromide concentration, while it is less dependent on the concentration of hydrogen chloride.[1] The activation energy of Reaction 11 is much greater than that of Reaction 8 (recombination reaction). Thus Reaction 8 can be faster than Reaction 11 at temperatures below 800 K, the scavenging effect of Reaction 11 being smaller. When hydrogen chloride is added in much smaller amounts than those in the present experiments. Reaction 8 predominates over Reaction 11 even at temperatures 1100—1350 K. In this case the inhibitory effect of hydrogen chloride would be similar to that reported.[1]

The author would like to express his gratitude to Prof. Kenji Kuratani, University of Tokyo, for his interest and valuable discussions.

References

1) C. F. Cullis, G. J. Minkoff, and M. A. Nettleton, *Trans. Faraday Soc.*, **58**, 1117 (1962).
2) A. F. Bopp and R. D. Kern, *J. Phys. Chem.*, **79**, 2579 (1975).
3) H. Ogura, *Bull. Chem. Soc., Jpn.*, **51**, 3418 (1978).
4) L. A. Bashford, H. J. Emeléus, and H. V. A. Briscoe, *J. Chem Soc.*, **1938**, 1358.
5) The least-squares method gives log $A_1 = 12.46\pm0.33$, $E_1 = 45800\pm1900$, log $A_2 = 16.00\pm0.51$, and $E_2 = 67200\pm3000$, where A, E, and errors denote frequency factor, activation energy, and standard deviation of the least-squares method, respectively.
6) H. Ogura, *Bull. Chem. Soc. Jpn.*, **50**, 1044 (1977).
7) The heats of formation, ΔH°(kcal/mol), are calculated at 298 K, the same heats of formation as those adopted[3]

being used. a) The heats of formation for HCl, Cl, and C_2HCl are −22.1, 28.9, and 51.1 kcal/mol. "JANAF Thermochemical Tables," 2nd ed, National Bureau of Standards NSRDS-NBS 37, U. S. Government Printing Office, Washington D. C. (1971); b) The heat of formation for C_2H_3Cl is 5.0 kcal/mol. Z. B. Alfassi, D. M. Golden, and S. W. Benson, *J. Chem. Thermodyn.*, **5**, 411 (1973); c) The heat of formation for $C_4H_3(2)Cl$ is estimated assuming the bond dissociation energy of C_4H_3-Cl is the same as that of C_2H_3-Cl (83.5 kcal/mol).

8) J. Esser and K. J. Laidler, *Int. J. Chem. Kinet.*, **2**, 37 (1970).

9) R. Manning and M. J. Kurylo, *J. Phys. Chem.*, **81**, 291 (1977).

10) W. Lange, H. Gg. Wagner, and C. Zetzsch, *Ber. Bunsenges. Phys. Chem.*, **79**, 861 (1975).

11) In analogy with the reaction of CH_3+HCl, the activation energy of Reaction 11′ would be estimated as 5.4 kcal/mol from the heat of reaction. If the contribution of Reaction 11′ to the rate of Reaction 11 is far greater than that of Reaction 11′, the activation energy of Reaction 11 would be close to that of Reaction 11′. In the product analysis no detectable amount of chlorine atom containing products except for C_2HCl was found. This might indicate the minor role of reactions with Cl atom in spite of their smaller heats of reaction.

12) F. Zabel, *Int. J. Chem. Kinet.*, **9**, 651 (1977).

Photoelectron Angular Distribution Measurements for Some Aliphatic Alcohols, Amines, and Halides

Chikatoshi UTSUNOMIYA,† Tsunetoshi KOBAYASHI,†† and Saburo NAGAKURA*,†,††

† *The Institute for Solid State Physics, The University of Tokyo, Roppongi, Minato, Tokyo 106*

†† *The Institute of Physical and Chemical Research, Wako, Saitama 351*

(Received July 9, 1979)

The angular distributions for the He I photoelectron spectra of some aliphatic alcohols, amines, and halides were measured in order to reexamine the assignments of the so-called p-type photoelectron spectral bands in the He I region of these molecules. The second band of methanol and the third band of ethanol were assigned to the in-plane n orbitals localized mainly on the oxygen atom. Furthermore, it was found that the angular distributions of photoelectrons were useful for the conformational analysis of molecules and that the sum of β values was conserved for these compounds.

The photoelectron differential cross-section ($d\sigma/d\Omega$) for an unpolarized light and an ensemble of randomly oriented molecules or atoms is given by

$$d\sigma/d\Omega \propto 1 + 0.5\beta(1.5\sin^2\theta - 1) \quad (1)$$

where β is an asymmetry parameter, and θ is the angle between the direction of an ejected photoelectron and that of an incoming photon.[1,2] The β value depends on the kinetic energy of the photoelectron and the character of the molecular orbital from which the photoelectron is ejected. Therefore, the β value is expected to be useful for the interpretation of photoelectron spectra. Actually, using the β values, we solved the problems of the photoelectron spectral band assignments of benzene[3] and pyridine[4] about which there had been disputes.

He I/II photoelectron spectra have been studied by a number of workers with methanol and ethanol[5-11] and also with methylamine and ethylamine.[5,9,11] However, studies of the assignments of all the bands in the He I region are few. Katsumata and coworkers[11] proposed the assignments of all the p-type bands in the He I region of these alcohols and amines on the basis of the sum rule.[12] As for methanol, Robin and Kuebler[10] assigned all the photoelectron spectral bands with the aid of an *ab initio* MO calculation.

Many photoelectron spectral studies have been made with alkyl halides.[8,12-19] Kimura and coworkers[12] studied systematically the photoelectron spectra of alkyl halides covering the higher alkyl chlorides, bromides, and iodides, and assigned all the p-type bands in the He I region with the aid of the sum rule.

In the present study, the photoelectron angular distributions have been measured for aliphatic amines, alcohols, and halides, and the band assignments have been reexamined from the standpoint of the photoelectron angular distributions. The correlation between the β value and the character of the orbital from which the photoelectron is ejected, and the existence of the sum rule for the β values are discussed.

Experimental

The details of a photoelectron spectrometer used for the angular distribution measurements in the present study were described in a previous paper.[3] The β values were obtained according to formula (1) using the intensities measured at two angles, $\theta=45°$ and 90°. The measurements were carried out at room temperature, and the vapor pressure of the samples was kept at 4×10^{-4} Torr.

Results and Discussion

Aliphatic Alcohols and Amines. The photoelectron spectra of methanol and ethanol are shown in Fig. 1, and those of methylamine and ethylamine in Fig. 2. The vertical ionization potentials (I_v) and the β values of methanol and ethanol are summarized in Table 1 together with the band assignments. It is known that ethanol and ethylamine take the *trans* and *gauche* forms in the gaseous state, the *trans* form being predominant for both compounds.[20,21]

The first band of methanol or ethanol is assigned to the out-of-plane n orbital (a″n′(O)) which is localized mainly on the oxygen atom.[6-8,10,11] As is seen in Table 1, the β values of these orbitals are nearly equal to each other. The second band of methanol was ascribed to the a′π(CH_3) orbital by Katsumata and coworkers[11] from the sum rule. However, from the comparative consideration of the second bands of methanol, water, and dimethyl ether, it is derived

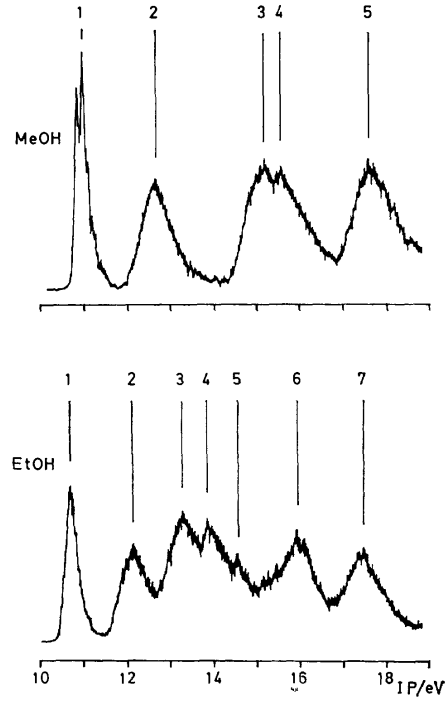

Fig. 1. Photoelectron spectra of methanol and ethanol.

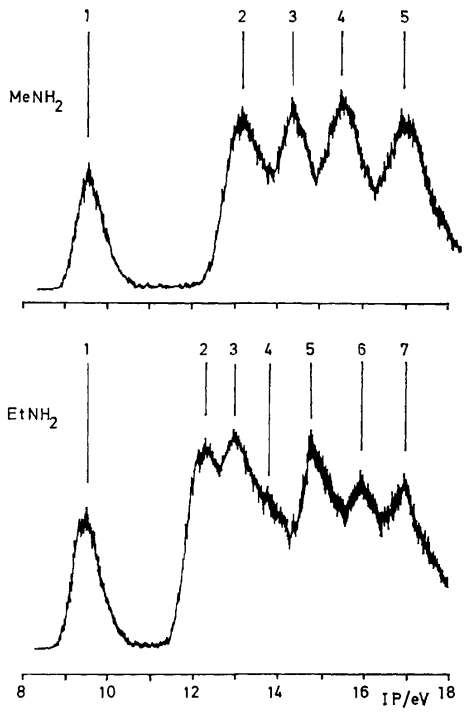

Fig. 2. Photoelectron spectra of methylamine and ethylamine.

that the band is assigned to the in-plane n orbital (a'n(O)) localized mainly on the oxygen atom. The second bands of water[13] and dimethyl ether[22] are assigned to the in-plane n(O) orbitals experimentally. The *ab initio* MO calculations of water[23] and dimethyl ether[24] also support the assignment. The β values and the ionization potentials of the second bands of water, methanol, and dimethyl ether are shown in Table 2. We can see from this table that the β value and ionization potential of the second band of methanol are intermediate between the corresponding values of water[25] and dimethyl ether. This shows that the second band of methanol is also assigned to the in-plane n(O) orbital. The MO calculation[26] is consistent with this assignment. The third, fourth, and fifth bands of methanol are assigned to the $a'\sigma(CO)$, $a''\pi'(CH_3)$, and $a'\pi(CH_3)$ orbitals, respectively, with the aid of the MO calculation.[26] As described later, these assignments are reasonable from the consideration of the β values and are consistent with Robin and Kuebler's result.[10]

As is seen in Table 1, the β values of the second and third bands of ethanol are 0.30 and 0.56, respectively. On the other hand, the β value of the $a'\sigma(CC)$ orbital of ethylamine is <0.37 (see the later discussion), and that of the in-plane n(O) orbital is 0.45 for methanol and 0.64 for dimethyl ether (Table 2). Therefore, the second band of ethanol should be assigned to the $a'\sigma(CC)$ orbital, and the third band to the in-plane n(O) orbital.

The fourth, fifth, and sixth bands of ethanol were assigned by Katsumata *et al.*[11] to the $a'\sigma(CO)$, $a''\pi^-(C_2H_5)$, and $a''\pi^+(C_2H_5)$ orbitals. These assignments are supported by the observed β values. Since the MO calculation of methanol[26] suggests that the energy of the $a'\pi(CH_3)$ orbital is higher than that of the $a'\sigma(OH)$ orbital, the seventh band of ethanol is preferably assigned to the $a'\pi(CH_3)$ orbital.

The band positions, β values, and assignments of the photoelectron spectra of methylamine and ethylamine are given in Table 3. The observed bands are assigned by considering the β values, the sum rule, and the MO's calculated with methylamine.[27]

According to the assignments given in Table 3, the β values of the pseudo π orbitals of the methyl group of methanol correspond to those of methylamine. This is also the case for the pseudo π orbitals of the ethyl groups of ethanol and ethylamine. The β value of the third band of ethylamine ($a'\sigma(CC)$) is 0.46 at the band maximum. This value, however, may conceivably be higher than the real value because this band is largely overlapped by the second band with the larger β value. The observed β value shows the energy dependence; 0.46 at 13.08 eV, 0.39 at

Table 1. Vertical ionization potentials (I_v in eV), β values, and band assignments of alkanols

	Band[a]	1	2	3	4	5	6	7
MeOH	I_v	10.95	12.65	15.17	15.53	17.57		
	β[b]	0.50±0.05	0.45±0.04	0.70±0.03	0.62±0.03	0.46±0.03		
	Assign. (sum rule)[c]	a''n'(O)	$a'\pi(CH_3)$	$a'\sigma(CO)$	$a''\pi'(CH_3)$	$a'\sigma(OH)$		
	Assign. (this work)	a''n'(O)	a'n(O)	$a'\sigma(CO)$	$a''\pi'(CH_3)$	$a'\pi(CH_3)$		
EtOH	I_v	10.64	12.16	13.28	13.85	14.55	15.96	17.45
	β[b]	0.44±0.03	0.30±0.03	0.56±0.03	0.64±0.04	0.57±0.03	0.69±0.05	0.68±0.05
	Assign. (sum rule)[c]							
	trans	a''n'(O)	$a'\sigma(CC)$	$a'\pi(CH_3)$	$a'\sigma(CO)$	$a''\pi^-(C_2H_5)$[e]	$a''\pi^+(C_2H_5)$[e]	$a'\sigma(OH)$
	gauche[d]	n'(O)	$\pi^-(C_2H_5)$	$\sigma(CC)$	$\pi(CH_3)$	$\pi^+(C_2H_5)$	$\sigma(CO)$	$\sigma(OH)$
	Assign. (this work)	a''n'(O)	$a'\sigma(CC)$	a'n(O)	$a'\sigma(CO)$	$a''\pi^-(C_2H_5)$	$a''\pi^+(C_2H_5)$	$a'\pi(CH_3)$

a) These numbers correspond to those shown in Fig. 1. b) The error of the β value denotes the mean square error. c) Ref. 11. d) The underlined orbitals of the *gauche* form are a'' like out-of-plane orbitals because ethanol has no symmetry in the *gauche* form. e) The π^+ and π^- denote the bonding and antibonding types of combinations of the methyl pseudo π and methylene pseudo π orbitals, respectively.

13.18 eV, and 0.37 at 13.28 eV. The band overlap decreases with increasing *IP*. This means that the real β value of the third band of ethylamine is smaller than 0.37 and corresponds well to the β value of the a'σ(CC) band of ethanol (0.3). Thus, the present band assignments of alcohols and amines given in Tables 1 and 3 are supported by the consistency of the β values determined for the corresponding bands.

From the above-mentioned consistency of β values, we can discuss the conformation of ethylamine as an example. On the assumption of the *gauche* form as the predominant conformation, the second band of ethylamine is assigned to the σ(CC) orbital (see Table 3) and its β value may be expected to be $\sim$0.3, being inconsistent with the observed value, 0.54. This seems to support the *trans* form as the predominant conformation.

From the comparison of the band assignments made by the present authors with those made by Katsumata *et al.* with the aid of the sum rule, we can see that

Table 2. Ionization potentials (I in eV) and β values of the second bands of water, methanol, and dimethyl ether

	H_2O[a]	MeOH	Me_2O
I	13.7	12.65	11.94
β[b]	0.3±0.1	0.45±0.04	0.64±0.03

a) Ref. 25. b) See footnote b) for Table 1.

Table 3. Vertical ionization potentials (I_v in eV), β values, and band assignments of alkylamines

	Band[a]	1	2	3	4	5	6	7
$MeNH_2$	I_v	9.58	13.18	14.32	15.46	16.83		
	β[b]	0.84±0.05	0.43±0.04	0.55±0.03	0.58±0.02	0.71±0.03		
	Assign. (sum rule)[c]	a'n(N)	a''π'(CH_3)	a'σ(CN)	a'π(CH_3)	a''π(NH_2)		
	Assign. (this work)	a'n(N)	a''π'(CH_3)	a'σ(CN)	a'π(CH_3)	a''π(NH_2)		
$EtNH_2$	I_v	9.50	12.27	12.98	13.8	14.80	15.81	16.75
	β[b]	0.93±0.04	0.54±0.03	0.46±0.03	0.55±0.02	0.53±0.03	0.62±0.03	0.62±0.03
	Assign. (sum rule)[c]							
	trans	a'n(N)	a''π^-(C_2H_5)	a'σ(CC)	a'π(CH_3)	a'σ(CN)	a''π^+(C_2H_5)	a''π(NH_2)
	gauche[d]	n(N)	σ(CC)	π(CH_3)	π^-(C_2H_5)	σ(CN)	π^+(C_2H_5)	π(NH_2)
	Assign. (this work)	a'n(N)	a''π^-(C_2H_5)	a'σ(CC)	a'π(CH_3)	a'σ(CN)	a''π^+(C_2H_5)	a''π(NH_2)

a) These numbers correspond to those shown in Fig. 2. b) See footnote b) for Table 1. c) Ref. 11. d) The underlined orbitals of the *gauche* form are a'' like out-of-plane orbitals because ethylamine has no symmetry in the *gauche* form.

Table 4. Vertical ionization potentials (I_v in eV), β values and band assignments of alkyl halides

	Band[a]	1	2	3	4	5	6	7
MeCl	I_v	11.29		14.46	15.48	16.10		
	β[b]	1.13±0.02		0.46±0.03	0.75±0.03	0.75±0.03		
	Assign.[c]	n(Cl)		σ(CCl)	π(CH_3)	π(CH_3)		
EtCl	I_v	11.01		12.99	13.45	14.46	15.64	16.32
	β[b]	1.04±0.05		0.61±0.04	0.54±0.04	0.44±0.07	0.66±0.03	0.76±0.03
	Assign.[d]	n(Cl)		σ(CCl)	σ(CC)	π^-(C_2H_5)	π(CH_3)	π^+(C_2H_5)
MeBr	I_v	10.53	10.85	13.47	15.13	15.79		
	β[b]	1.32±0.04	1.39±0.03	0.46±0.03	0.79±0.05	0.80±0.05		
	Assign.[c]	n(Br)	n(Br)	σ(CBr)	π(CH_3)	π(CH_3)		
EtBr	I_v	10.29	10.60	12.47	13.11	14.17	15.33	16.26
	β[b]	1.33±0.03	1.24±0.04	0.56±0.06	0.53±0.04	0.50±0.05	0.69±0.04	0.77±0.04
	Assign.[d]	n(Br)	n(Br)	σ(CBr)	σ(CC)	π^-(C_2H_5)	π(CH_3)	π^+(C_2H_5)
MeI	I_v	9.53	10.16	12.49	14.66	15.43		
	β[b]	1.60±0.03	1.56±0.03	0.66±0.02	0.82±0.04	0.87±0.03		
	Assign.[c]	n(I)	n(I)	σ(CI)	π(CH_3)	π(CH_3)		
EtI	I_v	9.33	9.92	11.60	12.98	13.89	15.00	15.97
	β[b]	1.50±0.03	1.49±0.04	0.69±0.02	0.58±0.04	0.51±0.04	0.76±0.02	0.87±0.02
	Assign.[d]	n(I)	n(I)	σ(CI)	σ(CC)	π^-(C_2H_5)	π(CH_3)	π^+(C_2H_5)

a) These numbers correspond to those shown in Figs. 3 and 4. b) See footnote b) for Table 1. c) Refs. 12—15, 19. d) Ref. 12.

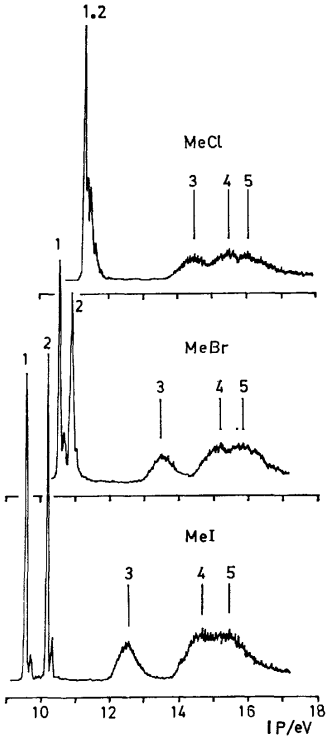

Fig. 3. Photoelectron spectra of methyl chloride, bromide, and iodide.

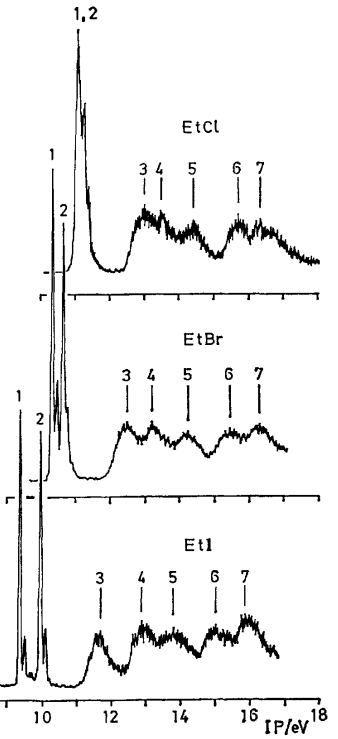

Fig. 4. Photoelectron spectra of ethyl chloride, bromide, and iodide.

the agreement is satisfactory for amines but some discrepancies due to the unreasonable assignments based on the sum rule are found for alcohols. This may be caused by the inadequate choice of parameters of the sum rule for the localized orbitals concerning the oxygen atom.

Alkyl Halides. The photoelectron spectra of methyl chloride, bromide, and iodide are shown in Fig. 3, and those of ethyl chloride, bromide, and iodide are in Fig. 4. The I_v's and the β values of these compounds are summarized in Table 4 together with the assignments made so far by other authors.[12-15,19] The β values of methyl halides were reported by Carlson and coworkers[25], and their values are consistent with ours. As is seen in Table 4, the consistency of β values among the related molecules is satisfied for the n(Cl), n(Br), n(I), σ(CCl), σ(CBr), and σ(CI) orbitals. This is also the case for the σ(CC) orbitals and the pseudo π orbitals of methyl and ethyl groups. These reasonable correspondences of the β values support the former assignments. The first and second bands of the bromides and iodides are caused by the spin-orbit splitting, and the fourth and fifth bands of the methyl halides are by the Jahn-Teller effect. The β values change scarcely by the splittings for the compounds.

Sum of β Values. The sums of the β values ($\sum\beta$) of all the p-type bands are shown in Table 5 for the alcohols, amines, and halides. The difference between the sum for methyl and ethyl derivatives ($\Delta\sum\beta$, see Table 5) is regarded to be the sum of the β values of the σ(CC) and $\pi(CH_2)$ orbitals. We can see from

Table 5. Sums of β values and their differences for aliphatic alcohols, amines, and halides

Compounds	$\sum\beta$[a]	$\Delta\sum\beta$[b]
MeOH	2.73±0.08	1.15±0.13
EtOH	3.88±0.10	
$MeNH_2$	3.11±0.08	1.14±0.11
$EtNH_2$	4.25±0.08	
MeCl	4.22±0.06	0.87±0.14
EtCl	5.09±0.12	
MeBr	4.76±0.09	0.86±0.15
EtBr	5.62±0.12	
MeI	5.51±0.07	0.89±0.11
EtI	6.40±0.08	

a), b) The errors for $\sum\beta$ and $\Delta\sum\beta$ denote mean square errors.

Table 5 that the values for the alcohols and the amines correspond well to each other. The values for the halides correspond well to one another and are equal to those for the alcohols and amines within the limits of experimental error as shown in Table 5. These results indicate that the sum of the β values is conserved for these molecules.

Finally, the β values of various orbitals of the molecules under consideration are summarized in Table 6. We can see from this table that a fluctuation of the β value from one molecule to another is small for the respective orbitals under consideration except for the $\pi(CH_3)$ orbital. Particularly the consistency of the β values is satisfied for the respective n orbitals.

From the above discussion, it is concluded that the photoelectron spectral bands can be assigned effectively with the aid of photoelectron angular distributions.

TABLE 6. β VALUES OF VARIOUS ORBITALS OF ALIPHATIC ALCOHOLS, AMINES, AND HALIDES

	n (Cl)	n (Br)	n (I)	n′ (O)	n (O)	n (N)	σ (CCl)	σ (CBr)	σ (CI)	σ (CC)	σ (CO)	σ (CN)	π (Me)	π^- (Et)	π^+ (Et)	π (NH_2)
MeOH				0.50	0.45						0.70		0.62 0.46			
EtOH				0.44	0.56					0.30	0.64		0.68	0.57	0.69	
$MeNH_2$						0.84						0.55	0.43 0.58			0.71
$EtNH_2$						0.93				0.46		0.53	0.55	0.54	0.62	0.62
MeCl	1.13						0.46						0.75 0.75			
EtCl	1.04						0.61			0.54			0.66	0.44	0.76	
MeBr		1.32 1.39						0.46					0.79 0.80			
EtBr		1.33 1.24						0.56		0.53			0.69	0.50	0.77	
MeI			1.60 1.56						0.66				0.82 0.87			
EtI			1.50 1.49						0.69	0.58			0.76	0.51	0.87	
Range of β[a]	1.04 | 1.13	1.24 | 1.39	1.49 | 1.60	0.44 | 0.50	0.45 | 0.56	0.84 | 0.93	0.46 | 0.61	0.46 | 0.56	0.66 | 0.69	0.30 | 0.58	0.64 | 0.70	0.53 | 0.55	0.43 | 0.87	0.44 | 0.57	0.62 | 0.87	0.62 | 0.71

a) The minimum and maximum values are shown.

References

1) J. C. Tully, R. S. Berry, and B. J. Dalton, *Phys. Rev.*, **176**, 95 (1968).
2) J. W. McGowan, D. A. Vroom, and A. R. Comeaux, *J. Chem. Phys.*, **51**, 5626 (1969).
3) T. Kobayashi and S. Nagakura, *J. Electron Spectrosc. Relat. Phenom.*, **7**, 187 (1975).
4) C. Utsunomiya, T. Kobayashi, and S. Nagakura, *Bull. Chem. Soc. Jpn.*, **51**, 3482 (1978).
5) M. I. Al-Joboury and D. W. Turner, *J. Chem. Soc.*, **1964**, 4434.
6) M. I. Al-Joboury and D. W. Turner, *J. Chem. Soc., B*, **1967**, 373.
7) M. J. S. Dewar and S. D. Worley, *J. Chem. Phys.*, **50**, 654 (1969).
8) A. D. Baker, D. Betteridge, N. R. Kemp, and R. E. Kirby, *Anal. Chem.*, **43**, 375 (1971).
9) A. W. Potts, T. A. Williams, and W. C. Price, *Faraday Discuss. Chem. Soc.*, No. 54, 104 (1972).
10) M. B. Robin and N. A. Kuebler, *J. Electron Spectrosc. Relat. Phenom.*, **1**, 13 (1972/73).
11) S. Katsumata, T. Iwai, and K. Kimura, *Bull. Chem. Soc. Jpn.*, **46**, 3391 (1973).
12) K. Kimura, S. Katsumata, Y. Achiba, H. Matsumoto, and S. Nagakura, *Bull. Chem. Soc. Jpn.*, **46**, 373 (1973).
13) D. W. Turner, C. Baker, A. D. Baker, and C. R. Brundle, "Molecular Photoelectron Spectroscopy," Wiley-Interscience, London (1970).
14) J. L. Ragle, I. A. Stenhouse, D. C. Frost, and C. A. McDowell, *J. Chem. Phys.*, **53**, 178 (1970).
15) A. W. Potts, H. J. Lempka, D. G. Streets, and W. C. Price, *Phil. Trans. R. Soc. London, Ser. A*, **268**, 58 (1970).
16) J. A. Hashmall and E. Heilbronner, *Angew. Chem. Int. Ed.*, **9**, 305 (1970).
17) A. D. Baker, D. Betteridge, N. R. Kemp, and R. E. Kirby, *Int. J. Mass Spectrom. Ion Phys.*, **4**, 90 (1970).
18) F. Brogli and E. Heilbronner, *Helv. Chim. Acta*, **54**, 1424 (1971).
19) L. Karlsson, R. Jadrny, L. Mattsson, F. T. Chau, and K. Siegbahn, *Phys. Scr.*, **16**, 225 (1977).
20) J. Michielsen-Effinger, *Ann. Soc. Sci. Bruxelles, Ser. 1*, **78**, 223 (1964).
21) M. Tsuboi, K. Tamagake, A. Y. Hirakawa, J. Yamaguchi, H. Nakagawa, A. S. Manocha, E. C. Tuazon, and W. G. Fately, *J. Chem. Phys.*, **63**, 5177 (1975).
22) S. Cradock and R. A. Whiteford, *J. Chem. Soc., Faraday Trans. 2*, **68**, 281 (1972).
23) R. M. Pitzer and D. P. Merrifield, *J. Chem. Phys.*, **52**, 4782 (1970).
24) W. J. Hehre, cited in W. L. Jorgensen and L. Salem, "The Organic Chemist's Book of Orbitals," Academic Press, New York (1973), p. 167.
25) T. A. Carlson, G. E. McGuire, A. E. Jonas, K. L. Cheng, C. P. Anderson, C. C. Lu, and B. P. Pullen, "Electron Spectroscopy," ed by D. A. Shirley, North-Holland, Amsterdam (1971), p. 207.
26) W. H. Fink and L. C. Allen, *J. Chem. Phys.*, **46**, 2261 (1967).
27) W. H. Fink and L. C. Allen, *J. Chem. Phys.*, **46**, 2276 (1967).

 © 1980 The Chemical Society of Japan Bull. Chem. Soc. Jpn., 53, 1221—1227 (1980)

The Syntheses, Electrical Resistivities, and Electronic Absorption Spectra of Cation-TCNQ-Crown Ether Complexes

Minoru Morinaga, Takashi Nogami,* Yasuhiro Kanda, Tsuruyoshi Matsumoto, Katsumi Matsuoka, and Hiroshi Mikawa

Department of Applied Chemistry, Faculty of Engineering, Osaka University, Yamadakami, Suita, Osaka 565

(Received July 23, 1979)

Crown ether complexes with alkali-metal–, ammonium–, and barium–TCNQ salts were isolated. Their electrical resistivities and electronic absorption spectra were measured. The simple salts, (crown ether)$_m$(M^+-$TCNQ^-$)$_n$, were almost all insulators with resistivities greater than 10^7 Ω cm. However, the complex salts, (Crown ether)$_m$(M^+TCNQ^-)$_n$(TCNQ), were much more conductive than simple salts with resistivities of 10^2—10^4 Ω cm. Three types of electronic-absorption spectra were observed for the simple salts. The simple salts with charge-transfer absorption bands were much more conductive than those without charge-transfer absorption bands.

Since tetracyanoquinodimethane (TCNQ) has been synthesized,[1] much attention has been paid to the high electrical conductivities and characteristic magnetic, optical, and structural properties of TCNQ complexes.[2] It has been clarified that a structure with segregated stacks of donor and acceptor molecules in the crystal greatly influences the physical properties. The modification of the crystal structure might, therefore, induce interesting properties. In order to confirm this, we chose to study metal-cation– and ammonium–TCNQ salts and have tried to surround the cation with crown ethers.[3] Surrounding the cation with crown ethers will weaken the interaction between the cation and TCNQ anion radicals,[4] leading to a change in the physical properties. We have isolated the complexes of alkali-metal–, ammonium–, and barium–TCNQ salts with crown ethers and cryptand, and have measured their electrical resistivities and electronic-absorption spectra.[5]

Results and Discussion

Isolation of Alkali-Metal–, Ammonium–, and Barium–TCNQ–Crown Ether Complexes. The following crown ethers, cryptand, and TCNQ salts were used for the preparation of the complexes: 12-crown-4 (**1**), 15-crown-5 (**2**), 18-crown-6 (**3**), dibenzo-18-crown-6 (**4**), dicyclohexyl-18-crown-6 (**5**), dibenzo-24-crown-8 (**6**), cryptand [2,2,2] (**7**), Li^+TCNQ^- (**8**), Na^+TCNQ^- (**9**), K^+TCNQ^- (**10**), Rb^+TCNQ^- (**11**), Cs^+TCNQ^- (**12**), $NH_4^+TCNQ^-$ (**13**), and $Ba^{2+}(TCNQ^-)_2$ (**14**). We have isolated two types of complexes *i.e.*, simple salts, expressed as (crown ether)$_m$(M^+TCNQ^-)$_n$, and complex salts, expressed as (crown ether)$_m$ (M^+-$TCNQ^-$)$_n$(TCNQ).[6] Table 1 lists the complexes isolated and their yields, melting points, stoichiometries, and analytical data, with some remarks. Most of the complexes were obtained as crystals. A variety of crystal colors were found for simple salts. As expected, the stoichiometry of a simple salt has a tendency for the crown ether with a cavity comparable to or larger than the cation size to have a one-to-one stoichiometry, while the crown ether with a cavity smaller than the cation size has a two-to-one stoichiometry arising from the cation sandwiched by crown ethers.[4] In spite of the above tendency, however, several exceptions to these rules exist for simple salts; 18-crown-6 and substituted 18-crown-6 make complexes of different stoichiometries with the same cation, as has been shown for Rb-cation complexes with **3**, **4**, and **5**, and Cs-cation complexes with **3**, **4**, and **5**. Most of the complex salts have the stoichiometry to be expected from those of simple salts. However, there are some exceptions, such as **2–11–15**, **3–12–15**, and **4–12–15**. In the case of the system with 15-crown-5 and Cs^+TCNQ^-, we could not isolate the simple salt, while the complex salt could be isolated easily. In this connection, we could isolate the complex salts of sodium and potassium cations, *i.e.*, **2–10–15**, **3–9–15**, **3–10–15**, and **4–10–15**, while the corresponding original complex salts, Na^+-$TCNQ^-$TCNQ and K^+TCNQ^-TCNQ, have not been obtained thus far. Besides the complexes in Table 1, we tried to obtain the following simple salts and complex salts: **2–13**, **6–13**, **4–14**, **2–9–15**, **4–9–15**, **7–9–15**, **3–10–15**, **7–10–15**, **4–11–15**, **7–11–15**, **7–12–15**, **2–13–15**, **6–13–15**, and **4–14–15**. However, the existence of these salts could not be verified.

The simple salts of purple, violet, and blue colors and all the complex salts were found to be stable in the air for several months. However, the greenish yellow, yellow, and green complexes were unstable, and the surfaces of the solids became brown in the air or in an oxygen atmosphere for several hours. They were stable in a vacuum or in an argon atmosphere. The change in the diffuse reflectance spectra of these complexes with time in the air showed the gradual disappearence of the absorption band in the near-infrared region and the appearence of the absorption band at 480 nm. The 480 nm band may be due to the α,α-dicyano-*p*-(cyanocarbonyl)-α-toluenide anion (DCT^-) produced by the following reaction:[7]

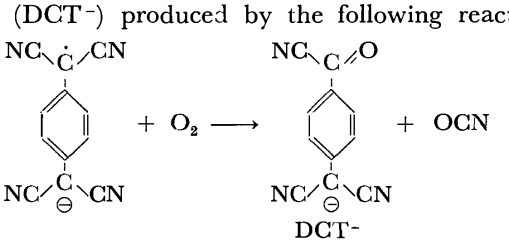

Electrical Resistivities. The electrical resistivities of the simple salts and complex salts measured with compressed samples are shown in Table 2. Table 3 shows the reported electrical resistivities, together with our measurements of the original TCNQ salts

Table 1. Cation-TCNQ-crown ether complexes

Complex	Yield/%[a]	Mp/°C[b]	Stoichiometry[c]	Found (Calcd) (%) C	H	N	Remark
Simple salts							
1-8			1 : 1	61.15 (62.02)	5.21 (5.20)	14.33 (14.46)	Black plates
1-9	48	183—185	2 : 1	57.94 (58.02)	6.21 (6.26)	9.51 (9.67)	Blue needles
2-9	19	150	1 : 1	58.86 (59.06)	5.36 (5.41)	12.35 (12.52)	Purple hexahedral
3-9		151—153	1 : 1	57.04 (58.65)	5.53 (5.74)	11.40 (11.40)	Blue needles
4-9	57	214—216	1 : 1	65.45 (65.41)	4.78 (4.80)	9.60 (9.54)	Yellow green plates
5-9	18	173—174	1 : 1	64.07 (64.09)	6.82 (6.72)	9.26 (9.34)	Purple plates
7-9	60	160—161	1 : 1	59.69 (59.69)	6.63 (6.68)	13.90 (13.92)	Yellow powder
2-10	46	210	2 : 1	56.17 (56.20)	6.65 (6.48)	8.29 (8.19)	Purple hexahedral
3-10	58	203—205	1 : 1	56.50 (56.79)	5.57 (5.56)	11.30 (11.04)	Purple needles
4-10	65	202—204	1 : 1	63.71 (63.67)	4.65 (4.68)	9.19 (9.28)	Yellow green plates
5-10		189—192	1 : 1	62.13 (62.42)	6.30 (6.55)	9.88 (9.10)	Violet plates
7-10	56	137	1 : 1	58.21 (58.14)	6.50 (6.51)	13.58 (13.56)	Blue hexahedral
2-11	58	202—203	2 : 1	52.62 (52.64)	6.14 (6.07)	7.68 (7.67)	Purple hexahedral
3-11	64	208—210	2 : 1	51.87 (52.04)	5.15 (5.09)	10.08 (10.11)	Violet needles
4-11	38	173—177	1 : 1	61.57 (61.81)	5.07 (5.19)	5.69 (5.54)	Green needles
5-11	39	190—192	1 : 1	58.01 (58.05)	6.18 (6.09)	8.30 (8.46)	Purple plates
6-11	43	106—108	1 : 1	58.07 (58.58)	4.84 (4.92)	7.81 (7.59)	Yellow green plates
7-11	43	146—148	1 : 1	53.97 (54.09)	6.05 (6.05)	12.60 (12.62)	Violet hexahedral
3-12	30	198—200	3 : 2	49.07 (49.12)	5.54 (5.50)	7.67 (7.64)	Yellow plates
4-12	42	156	2 : 1	59.33 (59.04)	5.04 (4.95)	5.57 (5.30)	Green needles
6-12	54	137—138	1 : 1	55.11 (55.04)	4.59 (4.62)	7.06 (7.13)	Yellow green plates
7-12	62	151—153	1 : 1	50.55 (50.50)	5.66 (5.65)	11.68 (11.78)	Violet hexahedral
2-13	36	140—142	2 : 1	57.82 (57.99)	7.46 (7.30)	10.57 (10.57)	Violet needles
3-13	15	170—172	1 : 1	59.01 (59.25)	6.41 (6.63)	14.16 (14.39)	Purple needles
4-13	60	168—170	2 : 1	65.91 (66.23)	5.77 (5.99)	7.64 (7.43)	Green needles
5-13	12	156—157	1 : 1	64.60 (64.63)	7.55 (7.46)	11.58 (11.78)	Blue hexahedral
2-14		253—255	2 : 1	53.43 (53.58)	5.09 (4.91)	11.42 (11.36)	Yellow green plates
3-14		249—251	1 : 1	52.73 (52.38)	4.04 (3.98)	13.70 (13.83)	Purple needles
Complex salts							
3-9-15	37		1 : 1 : 1	61.94 (62.15)	4.47 (4.64)	15.96 (16.11)	Black needles
2-10-15			2 : 1 : 1	59.49 (59.51)	5.42 (5.45)	12.41 (12.62)	Black needles

TABLE 1. (Continued)

Complex	Yield/%[a]	Mp/°C[b]	Stoichiometry[c]	Found (Calcd) (%) C	H	N	Remark
Complex salts							
4-10-15	36	224—225	1 : 1 : 1	65.18 (65.42)	3.92 (3.99)	13.91 (13.87)	Black hexahedral
2-11-15[d]		260	2 : 1 : 1	56.45 56.45 (56.56)	5.17 5.19 (5.18)	12.01 11.91 (11.99)	Black needles
3-11-15[d]	59	235	1 : 1 : 1	56.91 56.95 (57.03)	4.23 4.21 (4.25)	14.98 14.73 (14.78)	Black plates
2-12-15			2 : 1 : 1	53.99 (53.83)	4.83 (4.93)	11.68 (11.41)	Black hexahedral
3-12-15	58		1 : 1 : 1	53.56 (53.67)	3.93 (4.00)	14.00 (13.91)	Black needles
4-12-15		173—174	4 : 2 : 1	59.59 (60.05)	4.81 (4.69)	7.08 (7.24)	Black needles
3-13-15	20	160—162	1 : 1 : 1	62.39 (62.60)	5.23 (5.25)	18.20 (18.25)	Black hexahedral
4-13-15		162—164	2 : 1 : 1	67.98 (67.17)	4.63 (4.61)	15.93 (16.02)	Black needles
5-13-15	10	167	1 : 1 : 1	66.05 (66.15)	6.01 (6.06)	15.96 (15.78)	Black hexahedral
2-14-15		245—247	2 : 1 : 1	57.71 (57.99)	7.53 (7.30)	10.60 (10.57)	Black needles
3-14-15		287—289	1 : 1 : 1	56.47 (56.84)	3.62 (3.77)	16.53 (16.57)	Black powder

a) Unless specified, the yield is less than 10%. b) Unless specified, the melting point is higher than 300 °C. c) Crown ether: $M^{n+}(TCNQ^-)_n$ for simple salts. Crown ether: $M^{n+}(TCNQ^-)_n$: TCNQ for complex salts. d) The upper analytical data were obtained for the samples using the one-step method, and the lower ones, for the samples using two-step method. The other analytical data were obtained for the samples with the one-step method.

for the sake of comparison. Table 2 shows that the electrical resistivities of the simple salts are greater than 10^7 Ωcm. On the other hand, the complex salts are much more conductive than the corresponding simple salts, having electrical resistivities of 10^2—10^1 Ωcm. When we compare the values of Table 2 with those of Table 3, it is clear that simple salts are much less conductive than the corresponding original TCNQ salts. On the other hand, the electrical resistivities of the complex salts are of almost the same order as those of the original TCNQ salts. It is noteworthy that **3–9–15** and **3–13–15** are much more conductive than **9** and **13** respectively. Considering the fact that the complex salt can be easily produced for cation–TCNQ–crown ether complexes, these complexes may be expected to be good candidates for highly conductive organic materials.

We have found that a close correlation exists between the colors of the simple salts and their electrical resistivities. All the yellow or greenish-yellow complexes[8] have electrical resistivities greater than 10^{14} Ωcm.[9] On the other hand, blue, purple, violet, or green complexes[10] are much more conductive than the yellow or greenish-yellow complexes with the electrical resistivities of 10^7—10^{11} Ωcm. This is probably because of the difference in the strength of the interaction between adjacent TCNQ anion radicals in the crystal. The TCNQ anion radicals in the yellow or greenish-yellow crystals are almost completely isolated from each other. On the other hand, the overlap of the π-molecular orbitals of the neighboring TCNQ anion radicals occurs to some extent in the other simple salts.

We have also found evidence of complex-salt formation by only grinding a mixture of a simple salt and neutral TCNQ in an agate bowl. Figure 1 shows the plot of the electrical resistivities of the mixture against the initial neutral TCNQ molar fraction in **3–10** and **15** mixtures. The electrical resistivity drops about four orders of magnitude at the TCNQ molar fraction of *ca.* 0.7. The attained minimum electrical resistivities are one order of magnitude greater than in the pure complex salt, thus showing the complex-salt formation.

Electronic Absorption Measurements. The electronic absorption spectra were measured by the nujol-mull method. Figure 2 shows the electronic absorption spectra of **10** in an acetonitrile solution and in nujol mull. The absorption band at 7×10^3 cm^{-1} for the nujol-mull spectrum is ascribed to the charge-transfer (CT) transition between TCNQ anion radicals.[11] Table 2 summarizes the absorption-peak positions of the cation–TCNQ–crown ether complexes. Three types of absorption spectra were observed for the simple salts: Type A, purple, violet, or blue complexes with two absorption bands with comparable intensities below 20×10^3 cm^{-1}; Type B, yellow or greenish-yellow complexes with a sharp absorption peak around 12×10^3

Table 2. Electrical resistivities and electronic-absorption peak positions of cation-TCNQ-crown ether complexes

Complex	Resistivities	Absorption peak positions		
	Ω cm	10^3 cm^{-1}		
Simple salts				
Type A				
1-9	6.6×10^8	7.0	14.3	
2-9	1.3×10^{10}	9.3	14.3	
5-9		11.2	14.9	
2-10	8.5×10^{11}	9.6	15.2	
3-10	6.7×10^9	11.7	15.2	
5-10		10.8	14.8	
7-10	1.3×10^{10}	8.3	14.7	
2-11	1.3×10^9	10.5	14.6	
3-11	6.9×10^9	11.6	14.9	
5-11	2.8×10^{11}	10.4	14.8	
7-11	7.4×10^9	8.3	14.8	
7-12	2.4×10^{10}	8.1	14.7	
2-13	4.0×10^8	10.6	14.7	
3-13	2.3×10^9	11.8	14.9	
Type B				
4-9	$>10^{14}$	11.0	13.0	
7-9	$>10^{14}$	11.8	13.2	
4-10	$>10^{14}$	11.6	13.2	
6-11		11.3	12.9	14.5
3-12	$>10^{14}$	11.8	13.4	
6-12	$>10^{14}$	11.6	13.2	
Type C				
4-11	2.0×10^9	7.1	11.5	13.3
4-12	1.1×10^{11}	7.1	11.4	12.8
4-13	6.6×10^7	7.7	11.6	13.9
2-14		8.8	11.8	
Complex salts[a]				
3- 9-15	1.9×10^3	9.9	11.4	14.7
2-10-15		10.4		
4-10-15	4.4×10^3	9.9	11.4	
2-11-15	1.5×10^4	10.2	16.4	
3-11-15	1.2×10^4	10.6		
2-12-15		9.6	11.1	16.1
3-12-15	2.8×10^3	10.6		
3-13-15	4.6×10^2	10.8		
5-13-15		11.4	13.2	
2-14-15		11.2	15.2	

a) Besides these absorption peaks, all the complex salts have the absorption bands below 5×10^3 cm^{-1}.

Table 3. Electrical resistivities of cation-TCNQ salts[a]

Complex	Resistivities/Ω cm
8	2×10^5
9	3×10^4
10	5×10^3
11	2.8×10^3 [b]
12	3×10^4
13	3×10^4 [b]

a) D. S. Acker, Wayneshoro, Va., and D. C. Blomstrom, US Patent 3162641 (1964). b) Our measurements.

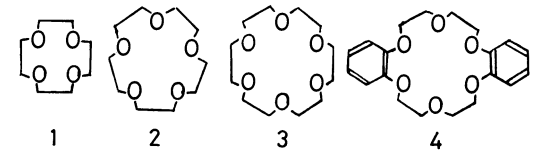

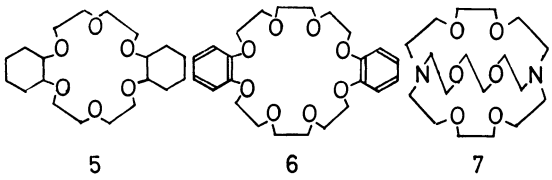

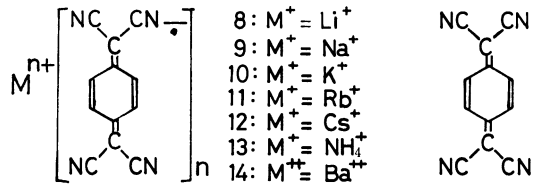

8,9,10,11,12,13,14 15

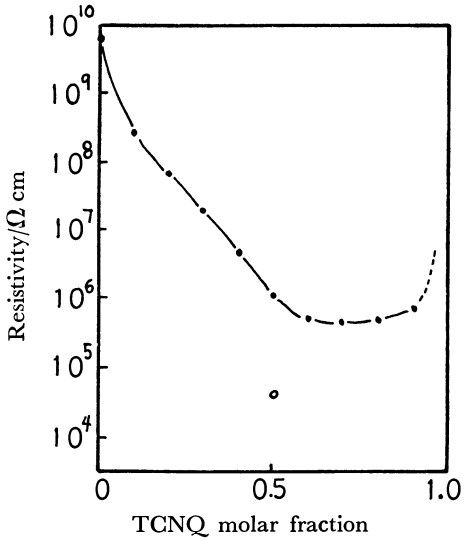

Fig. 1. The plot of the electrical resistivities of the mixture of **3–10** and **15** against initial neutral TCNQ molar fraction. Open circle denotes the electrical resistivity of the complex salt **3–10–15**.

cm^{-1} and no or weak absorption below 12×10^3 cm^{-1}, and Type C, green complexes with a sharp absorption peak around 12×10^3 cm^{-1} and a relatively strong absorption peak below 12×10^3 cm^{-1}. All the complex salts have a characteristic absorption below 5×10^3 cm^{-1}. Figures 3, 4, and 5 show the electronic absorption spectra of several simple salts of Types A, B, and C respectively as typical examples. Figure 6 shows the electronic absorption spectra of three complex salts.

Although crystallographic study and the polarized absorption spectra are needed for the assignment of the absorption bands, the most probable assignment for the Type A complex is that the lowest-energy

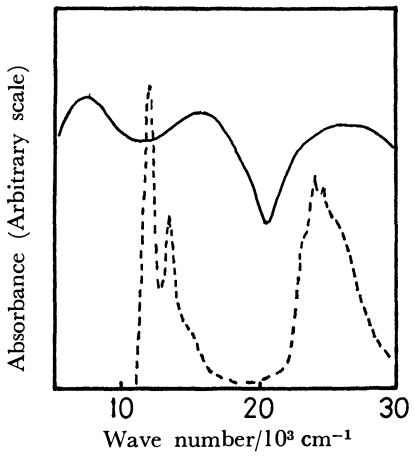

Fig. 2. The electronic absorption spectra of **10** in acetonitrile solution and in nujol mull.
---- in acetonitrile; —— in nujol mull.

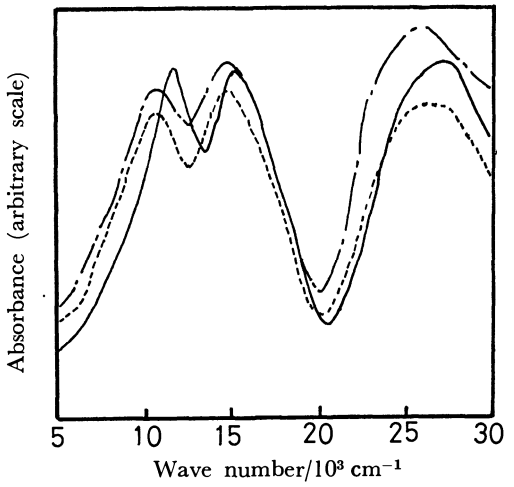

Fig. 3. The electronic absorption spectra of type A complexes in nujol mull.
—— **3–10**; ---- **2–11**; —— **2–13**.

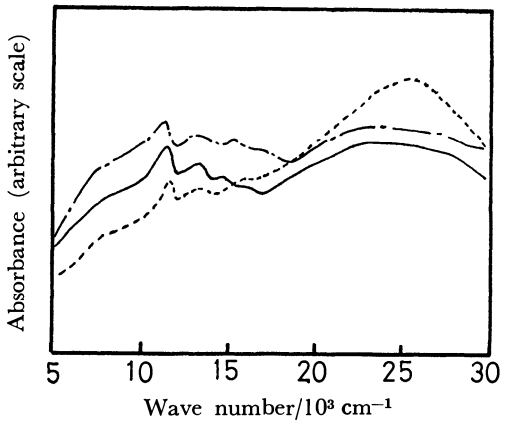

Fig. 4. The electronic absorption spectra of type B complexes in nujol mull.
—— **4–10**; —— **6–11**; ---- **7–9**.

band is due to the charge-transfer transition between TCNQ anion radicals, and the second band, to the local excitation within TCNQ anion radical. It is interesting to note that the absorption-peak positions

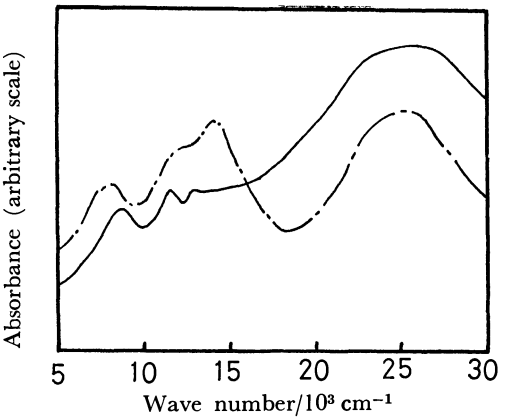

Fig. 5. The electronic absorption spectra of type C complexes in nujol mull.
—— **2–14**; —— **4–13**.

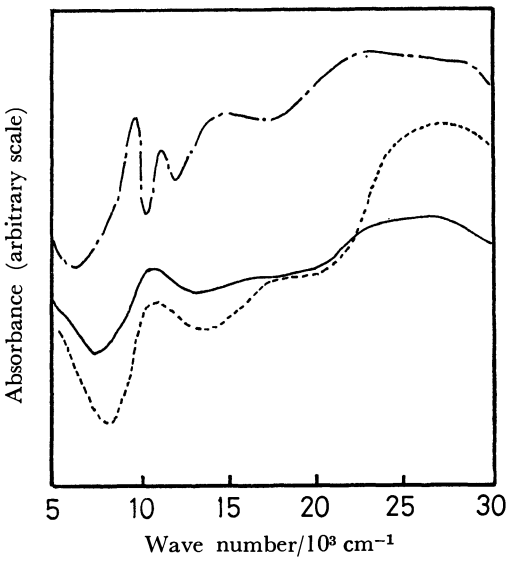

Fig. 6. The electronic absorption spectra of the complex salts in nujol mull.
—— **3–9–15**; —— **3–11–15**; ---- **3–13–15**.

of the lowest-energy band of the Type A complexes vary from complex to complex, ranging from 7.0×10^3 cm^{-1} to 11.8×10^3 cm^{-1}. If these bands are ascribed to the charge-transfer absorption, this fact will reflect the difference in the strength of the interaction between TCNQ anion radicals in Type A complexes. More exactly, the peak position of this band is affected by the crown ethers in the following order: 12-crown-4 complexes (7.0×10^3 cm^{-1})<cryptand [2,2,2]-complexes ($8.1—8.3\times10^3$ cm^{-1})<15-crown-5-complexes ($9.3—10.6\times10^3$ cm^{-1})<dicyclohexyl-18-crown-6-complexes ($10.4—11.2\times10^3$ cm^{-1})<18-crown-6-complexes ($11.6—11.8\times10^3$ cm^{-1}). In the 15-crown-5-complexes, an increase in the cation size results in a shift of the peak position to the higher-energy region, *i.e.*, 9.3×10^3 cm^{-1} for Na^+TCNQ^- ($R_{Na^+}=1.90$ Å)< 9.6×10^3 cm^{-1} for K^+TCNQ^- ($R_{K^+}=2.66$ Å)<10.5×10^3 cm^{-1} for Rb^+TCNQ^- ($R_{Rb^+}=2.96$ Å)<10.6×10^3 cm^{-1} for $NH_4^+TCNQ^-$ ($R_{HN_4^+}=2.84$ Å) Here, R_{M^+} indicates the ionic diameter of the M^+ cation. Contrary to this, a reverse order was found for the dicyclo-

hexyl-18-crown-6-complexes, *i.e.*, 11.2×10^3 cm^{-1} for Na$^+$TCNQ$^-$ > 10.8×10^3 cm^{-1} for K$^+$TCNQ$^-$ > 10.4×10^3 cm^{-1} for NH_4^+TCNQ$^-$. Although these clear correlations between the peak positions of the CT-bands and the molecular structures of the complexes are noteworthy, we can not discuss these characteristics any more without crystallographic data.

Type B complexes have almost the same absorption peaks, which resemble the absorption spectrum of TCNQ anion radical in shape and peak position (see Fig. 2). This fact suggests that TCNQ anion radicals are isolated in the Type B complexes. The unstable properties of these complexes in the air or in the oxygen atmosphere described before may also arise from the isolated structure of the TCNQ anion radical in the crystal.

The absorption spectra of the Type C complexes show an intermediate character between those of the Types A and B complexes, having a charge-transfer band and an isolated TCNQ$^-$ band.

All the complex salts have absorption bands below 5×10^3 cm^{-1}, as is evident from Fig. 6. These absorptions are to be ascribed to the charge-transfer transition from the TCNQ anion radical to neutral TCNQ.[11]

Correspondence between the Electrical Resistivities of the Complexes and Their Electronic Absorption Spectra. It has been clarified that the semi-conducting and, in some cases, metallic properties of several TCNQ complexes arise from the crystal structure with one-dimensional TCNQ columns, thereby having a large overlap of the π-electron clouds between adjacent TCNQ molecules.[2] The electronic absorption spectra of such complexes showed charge-transfer absorption bands between the adjacent TCNQ anion radicals[11] in the infrared region, reflecting the strong electronic interaction between TCNQ molecules.

We have found that simple salts may be divided into two groups from the viewpoint of the electrical resistivity, *i.e.*, the relatively conducting Types A and C complexes, and the insulating Type B complexes. Types A and C complexes have charge-transfer absorption bands showing an overlap of the π-electron clouds between TCNQ anion radicals. Thus, an electron can move through the overlap of the π-electron clouds in these complexes. On the other hand, the TCNQ anion radical is considered to be isolated in the Type B complexes, judging from their electronic absorption spectra. Thus, the π-electron on a TCNQ$^-$ can hardly move to the neighboring TCNQ, resulting in the insulating properties of Type B complexes.

The complex salts were much more conductive than simple salts. The observation of the charge-transfer absorption bands also shows a large overlap of the π-electron clouds between adjacent TCNQ molecules. Moreover, the Coulomb repulsion between the mobile electrons is much more reduced in the complex salt, resulting in much higher conductivities than in simple salts.

Experimental

Materials. All the crown ethers and cryptand were purchased from Nakarai Chemicals, Ltd. TCNQ and its cation salts were synthesized according to the literature.[12]

Isolation of Simple Salts. Most of the simple salts, (crown ether)$_m$(M$^+$TCNQ$^-$)$_n$, were isolated as follows. A cation-TCNQ salt and crown ether (1.2—2 molar ratio)[13] were dissolved in hot methanol and refluxed for 15 min with stirring, after which the hot solution was filtered. The filtrate was allowed to stand at room temperature, and then it was cooled at 0 °C for several hours. Crystals thus precipitated were collected, washed with a small amount of methanol, and dried in a vacuum. When crystals did not come out, the solution was cooled to −15 °C, or to 0 °C after being concentrated. In addition to the above general techniques, we used the following procedures if necessary: (i) In the case of cryptand [2,2,2], we used acetone as a solvent instead of methanol. (ii) After collecting the complexes of dibenzo-18-crown-6 and dibenzo-24-crown-8, they were washed first with benzene and then with methanol. (iii) Because the solubility of dibenzo-18-crown-6 and dibenzo-24-crown-8 is smaller than that of the other crown ethers, we used much more solvent. (iv) When the starting materials were recovered, we used more crown ether and less solvent the next time.

Isolation of Complex Salts. Complex salts, (crown ether)$_m$(M$^+$TCNQ$^-$)$_n$(TCNQ), were isolated by either a one-step method or a two-step method. In the one-step method, methanol containing cation-TCNQ salt and crown ether was mixed with an acetonitrile solution of neutral TCNQ (0.5—1.0 molar ratio),[14] after which the solution was refluxed with stirring for 15 min. The hot solution was filtered, allowed to stand at room temperature, and then cooled to 0 °C. The crystals thus precipitated were collected, washed with a small amount of methanol, and dried in a vacuum. In the two-step method, simple salt was first synthesized, and then the methanol solution of the simple salt was mixed with an acetonitrile solution of neutral TCNQ (0.5—1.0 molar ratio).[14] The solution was refluxed with stirring for 15 min, after which the hot solution was filtered. The filtrate was allowed to stand at room temperature and then cooled to 0 °C. The crystals thus precipitated were collected, washed with a small amount of methanol, and dried in a vacuum. In addition to the above techniques, we used the following procedures if necessary: (i) Crystallization should be done as slowly as possible. (ii) When neutral TCNQ came out initially, the crystallized TCNQ was filtered off, and then the solution was cooled again. (iii) When neutral TCNQ and complex salt came out together, we used either of two methods: (a) we separated the two materials by the use of spatula, or (b) if we could not separate them by the use of a spatula, we used more solvent and added either simple salt or crown ether and original TCNQ salt (M$^+$TCNQ$^-$). (iv) When complex salt and simple salt came out together, we added more solvent, or we added more solvent and a small amount of TCNQ.

Typical examples are shown below.

*Preparation of 18-Crown-6–K$^+$TCNQ$^-$, (**3**—**10**).* K$^+$-TCNQ$^-$ (150 mg) and 18-crown-6 (175 mg) were added to methanol (120 ml), after which solution was refluxed for 15 min. The hot solution was filtered, allowed to stand at room temperature, and then cooled to 0 °C overnight. The crystals were collected, washed with a small amount of methanol, and dried in a vacuum.

*Preparation of Dibenzo-18-crown-6–Na$^+$TCNQ$^-$, (**4**—**9**).* Na$^+$TCNQ$^-$ (100 mg) and dibenzo-18-crown-6 (165 mg) were added to methanol (200 ml), after which the solution was refluxed for 15 min. The hot solution was filtered, allowed to stand at room temperature, and then cooled to 0 °C overnight. The crystals were collected, washed

with a large amount of benzene and a small amount of methanol, and dried in a vacuum.

*Preparation of Cryptand [2,2,2]-Rb$^+$TCNQ$^-$, (**7—11**).* Rb$^+$TCNQ$^-$ (150 mg) and cryptand [2,2,2] (190 mg) were added to acetone (120 ml), after which the solution was refluxed for 15 min. The homogeneous solution was concentrated to about 30 ml by rotary evaporator and then filtered. The solution was allowed to stand at room temperature and then cooled to −15 °C overnight. The crystals were collected, washed with a small amount of acetone, and dried in a vacuum.

*Preparation of (18-Crown-6)$_2$(Cs$^+$TCNQ$^-$) (TCNQ), (**3—12—15**).* Cs$^+$TCNQ$^-$ (200 mg) and 18-crown-6 (300 mg) were added to methanol (160 ml), after which the solution was mixed with an acetonitrile solution (40 ml) of TCNQ (120 mg). The solution was refluxed for 15 min, and the hot solution was filtered. The solution was allowed to stand at room temperature and then cooled to 0 °C overnight. The crystals were collected, washed with a small amount of acetonitrile and methanol, and dried in a vacuum.

*Preparation of (18-Crown-6)$_2$(Rb$^+$TCNQ$^-$) (TCNQ), (**3—11—15**).* Rb$^+$TCNQ$^-$(18-crown-6)$_2$ (111 mg) in 80 ml of methanol was mixed with an acetonitrile solution (20 ml) of TCNQ (50 mg). The procedures were the same as in the preparation of **3—12—15**.

Measurement of Electrical Resistivity. A sample (150 mg) ground in an agate bowl was compressed at 2.2 t/cm^2 to obtain a pellet with a diameter of 13 mm and a thickness of about 0.8—0.9 mm. Silver paste was painted onto both surfaces of the pellet as electrodes, and the electrode area was measured by tracing the electrode shape on a section paper. The electrode area was usually about 50 mm^2. Copper wires were then attached to the electrodes by means of the silver paste. The electrical current was measured by means of Takeda-Riken TR-8651 Electrometer.

Electronic-absorption Measurements. The electronic-absorption spectra were measured by means of a Hitachi ESP-3T spectrometer. The nujol mull sample was sandwiched between the plates of two quartz cells.

We are grateful to Dr. Shinobu Ikeno, Research Division, Matsushita Electric Works Co., Ltd., for his helpful discussion. We are also grateful to Miss Junko Maenaka, Mr. Kazuaki Muneishi, and Miss Yuriko Sako, Faculty of Engineering, Osaka University, for the elementary analysis.

References

1) D. S. Acker and W. R. Hertler, *J. Am. Chem. Soc.*, **84**, 3370 (1962).

2) For example, "Synthesis and Properties of Low-Dimensional Materials," in *Annals of the New York Academy of Science*, ed by J. S. Miller and A. J. Epstein, The New York Academy of Sciences, New York (1978), Vol. 313; "Highly Conducting One-Dimensional Solids," ed by J. T. Devreese, R. P. Evrard, and V. E. van Doren, Plenum Press, New York and London (1979).

3) C. J. Pederson, *J. Am. Chem. Soc.*, **89**, 2495, 7017 (1967).

4) N. S. Poonia, *J. Am. Chem. Soc.*, **96**, 1012 (1974).

5) T. Nogami, M. Morinaga, Y. Kanda, and H. Mikawa, *Chem. Lett.*, **1979**, 111.

6) The possibility that the complex is only a mixture of M$^+$TCNQ$^-$ and crown ether is excluded by the fact that the stoichiometry of the isolated complex is invariable, regardless of the initial concentrations of crown ether and TCNQ salt.

7) W. R. Hertler, H. D. Martzler, D. S. Acker, and R. E. Benson, *J. Am. Chem. Soc.*, **84**, 3387 (1962); K. Mizoguchi, J. Tsuji, H. Tsuchida, and I. Shinohara, *Nippon Kagaku Kaishi*, **1977**, 395.

8) These complexes correspond to the Type B complex described in the electronic-absorption spectra of the complex.

9) The largest limit of the electrical resistivity in our measurement is $10^{14}\,\Omega$ cm.

10) These complexes correspond to Type A or Type C complexes, as has been described in the consideration of the electronic-absorption spectra of the complex.

11) J. Tanaka, M. Tanaka, T. Kawai, T. Takabe, and O. Maki, *Bull. Chem. Soc. Jpn.*, **49**, 2358 (1976).

12) L. R. Melby, R. J. Harder, W. R. Hertler, M. Mahler, R. E. Benson, and W. E. Mochel, *J. Am. Chem. Soc.*,,**84**, 3374 (1962).

13) When we used too much crown ether (more than a 2 molar ratio), we also got good crystals.

14) In the case of TCNQ molar ratios of greater than 1.0, complex salt was mixed with neutral TCNQ. In the case of TCNQ molar ratios of less than 0.5, however, the yield of the complex was reduced markedly.

Topological Index and Thermodynamic Properties. II.† Analysis of the Topological Factors on the Absolute Entropy of Acyclic Saturated Hydrocarbons

Hideyuki NARUMI and Haruo HOSOYA*,††

Department of Chemistry, Hokkaido University, Sapporo 060

†† *Department of Chemistry, Ochanomizu University, Bunkyo-ku, Tokyo 112*

(Received September 11, 1979)

The absolute entropy of acyclic saturated hydrocarbons is found to be well correlated linearly with the logarithm of the topological index (Z_G) of the graph of the carbon atom skeleton as, $S^\circ = a \log Z_G + b$, excpet for sterically overcrowded and highly symmetrical molecules. This relation is improved by taking the symmetry factor σ into account as, $S^\circ = a \log Z_G + b + c \log \sigma$. The physical meaning of these relations is clarified by analyzing the mathematical properties of Z_G and the rotational partition function proposed by Pitzer.

Recently importance of the topological or graph-theoretical aspects of molecules has been recognized and detailed analyses have been developed by many authors.[1-4] The problems discussed are, for example, enumeration of the number of the structural isomers,[1] analysis of the stability and the electronic distribution on π-electron networks,[5-7] coding and classification of the structures of molecules,[8,9] and interpretation of empirical rules on the thermodynamic properties of organic molecules.[10-12] Concerning the last problem one of the present authors has proposed the topological index[13] (Z_G) for the carbon atom skeleton of a saturated hydrocarbon and has shown that several empirical rules on the boiling point (bp) are interrelated to each other by assuming the relation

$$\text{bp} = a \log Z_G + b.^{12} \quad (1)$$

However, physical interpretation of Eq. 1 is not yet fully given.

It is practically very difficult to estimate the value of the boiling point of a compound from purely theoretical calculations based on an *a priori* model for the motions of molecular aggregates. Then a clue for solving this problem might be obtained by analyzing the topological aspects of other quantities, such as the entropy, critical pressure and volume, *etc.*, whose behaviors are similar to that of the boiling point but are more interpretable by the molecular theory.[14]

According to the theory developed by Pitzer,[15] the observed values of the absolute entropy S° of small acyclic saturated hydrocarbons can accurately be reproduced from the partition function obtained solely by the atomic and molecular constants and temperature.[15-19] However, from this theory and numerical calculations, it is difficult to draw generalized rules and their physical interpretation for the topological dependence of S°. Namely, so many different factors especially on the rotational conformations are entangled in the Pitzer's theory that practically the calculation of S° values is limited to small alkanes, say, with fewer than ten carbon atoms.

On the contrary, the topological index has been known to reflect the topological characteristics of the zig-zag chain especially on the degree of rotational freedom and to have a number of mathematically interesting properties. Namely, we have found that S° of saturated hydrocarbons is also related to the topological index as

$$S^\circ = a \log Z_G + b. \quad (2)$$

The purposes of the present paper are to obtain logical bases for the empirical relation 2 in terms of the Pitzer's partition function for clarifying the topological nature of the absolute entropy of van der Waals gases.

In Section I the mathematical properties of the topological index for tree graphs are reviewed with particular emphasis on the effect of branching including some additivity relationship. In Section II parallelism between the observed and calculated (by the topological index, Pitzer's partition function, and an empirical formula) entropies of small alkanes is presented and several important features of the branching effect on S° are exposed. It is also demonstrated that as the increase of the size of the molecule, to the extent where the Pitzer's theory cannot follow, the relation between $\log Z_G$ and observed S° gets better. In Section III by analyzing the relation between Z_G and the partition function the empirical relation 2 is justified.

I. Topological Index

Definition.[13] A graph G is composed of points and lines, or carbon atoms and C–C bonds of the carbon atom skeleton of a saturated hydrocarbon molecule. The non-adjacent number $p(G,k)$ for G is defined as the number of ways for choosing k ($0 \sim m$) disjoint lines, with $p(G,0)$ being defined as unity. The topological index Z_G is the sum of the $p(G,k)$'s,

$$Z_G = \sum_{k=0}^{m} p(G,k). \quad (3)$$

For a tree graph, or an acyclic hydrocarbon, $p(G,k)$ is nothing else but the coefficient of the characteristic polynomial of G

$$P_G(X) = (-1)^n \det(\boldsymbol{A} - X\boldsymbol{E}) = \sum_{k=0}^{n} a_k X^{n-k} = \sum_{k=0}^{[n/2]} (-1)^k p(G,k) X^{n-2k}, \quad (4)$$

where $\boldsymbol{A}$ is the adjacency matrix of G with elements

† Part I, *Bull. Chem. Soc. Jpn.*, **45**, 3415 (1972).

$$A_{rs} = \begin{cases} 1 & \text{if points r and s are neighbors} \\ 0 & \text{otherwise,} \end{cases} \quad (5)$$

$\boldsymbol{E}$ is the unit matrix of the same order n (the number of points in G) as $\boldsymbol{A}$, and det stands for a determinant. From Eqs. 3 and 4 one gets

$$Z_G = (-i)^n P_G(i) \quad (6)$$

for a tree graph.

Recursion Formulas.[13,20] The Z_G values for small tree graphs are given in Table 1, where the observed and calculated absolute entropy of the corresponding alkanes are compared for the later discussion.[21] For larger graphs, Z_G can easily be obtained from the values of smaller subgraphs by using the recursive relations described below.

Suppose that a graph G is obtained from graphs A and B by joining them with line l as in Fig. 1. The topological index Z_G of G can be given as

$$Z_G = Z_L \cdot Z_M + Z_A \cdot Z_B, \quad (7)$$

where L and M are the subgraphs obtained by deleting line l from G.

Suppose that a graph G is obtained from graphs A and B by joining them with point p as in Fig. 2. Graphs L and M which are obtained by adding point p to A and B, respectively, are the same as in Fig. 1. The topological index Z_G of G can be obtained by

$$Z_G = Z_L \cdot Z_B + Z_A \cdot Z_M - Z_A \cdot Z_B. \quad (8)$$

Branching Properties.[12] The topological indices of the various series of branched alkanes have a number of interesting mathematical properties which are in parallel with the experimentally known features of the absolute entropy. It is remarkable that these properties are maintained up to an infinitely large system. In the following discussion the carbon atom skeleton of an acyclic alkane is represented by a tree graph.

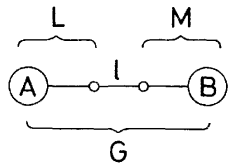

$$Z_G = Z_L \cdot Z_M + Z_A \cdot Z_B$$

Fig. 1. Recursion formula 1.

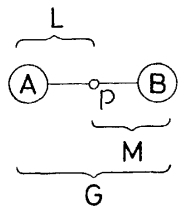

$$Z_G = Z_L \cdot Z_B + Z_A \cdot Z_M - Z_A \cdot Z_B$$

Fig. 2. Recursion formula 2.

Table 1. Topological index and observed and calculated absolute entropy of small alkanes

Alkane[b]	Z_G	Calculated $S°$ [a]			Observed $S°$ [f]
		$a \log Z_G + b$[c]	Pitzer[d]	P. & S.[e]	
4	5	74.41	74.10	74.1	74.07
2m3	4	70.12	70.48	69.9	70.60
5	8	83.44	83.18	83.1	83.52
2m4	7	80.87	82.27	81.2	82.13
22m3	5	74.41	73.04	71.8	73.11
6	13	92.76	92.32	92.4	92.91
3m5	12	91.23	91.48	90.3	91.52
2m5	11	89.55	90.80	90.3	91.03
23m4	10	87.72	87.32	85.4	87.43
22m4	9	85.70	85.66	84.6	85.62
7	21	101.98	101.45	101.5	102.29
3e5	20	101.04	97.87	97.2	98.36
3m6	19	100.05	101.38	100.8	101.80
2m6	18	99.02	100.04	99.4	100.48
23m5	17	97.92	98.79	97.3	99.08
33m5	16	96.75	95.83	94.5	95.16
24m5	15	95.51	94.64	94.5	94.86
22m5	14	94.19	93.34	93.7	93.83
223m4	13	92.76	92.27	90.2	91.62
s[g]	—	1.160	0.380	0.539	—
r[h]	—	0.9927	0.9993	0.9985	—

a) At 298.15 K in cal·K^{-1}·mol^{-1}. b) Abbreviated notation. For example, 24m5 stands for 2,4-dimethylpentane, and e for ethyl. See also Fig. 4. c) Equation 2 with $a=43.483$ and $b=44.240$. d) Equation 25 with $C_0=43.012$, $C_1=7.679$, $C_2=-1.068$, $C_3=-3.425$. See Table 3 for σ values ($a=500$ cal·mol^{-1}). e) Equation 30. See Table 3 for σ. f) Ref. 22. g) Standard deviation. h) Correlation coefficient.

TABLE 2. TOPOLOGICAL CHARACTERISTICS OF SEVERAL SERIES OF GRAPHS

Type	G_n	n_Y	n_X	Z_1	Z_2	a_G	b_G	$1000\delta_G = 1000 \log (a_N/a_G)$
N	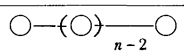	0	0	1	2	0.7236	0.2763	0
A	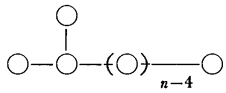	1	0	2	1	0.6180	−1.6180	68.5
B	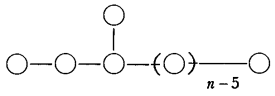			−1	3	0.6583	3.3417	41.0
C	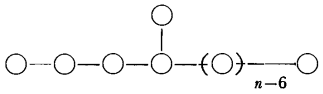			7	−2	0.6429	−9.6429	51.3
D	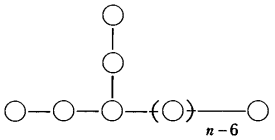			4	0	0.6833	−4.6833	24.9
								→ 46
E	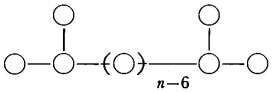	2	0	−5	5	0.5279	9.4721	137.0
F	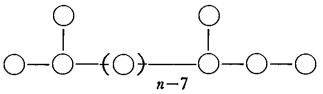			13	−6	0.5623	−19.5623	109.5
H	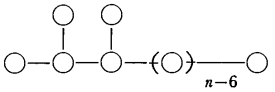			5	−1	0.5777	−6.5777	97.8
I	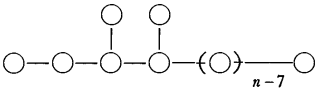			−11	9	0.6085	19.3915	75.2
J	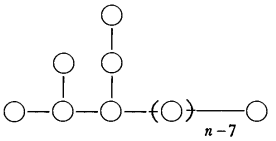			−3	4	0.5931	6.4069	86.4
								→101
K	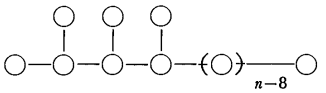	3	0	29	−16	0.5315	−45.5315	134.0 → 134
L	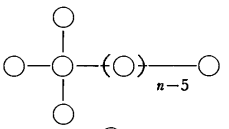	0	1	−2	3	0.4876	4.5124	171.5
M	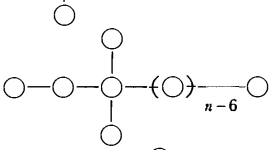			8	−3	0.5374	−11.5374	129.2
O	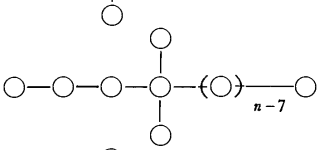			−18	13	0.5183	30.4817	144.9
P	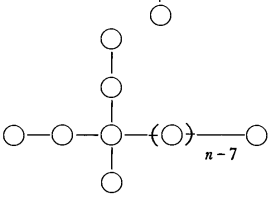			−16	12	0.5836	27.4164	93.4
								→135

TABLE 2. (Continued)

Type	G_n	n_Y	n_X	Z_1	Z_2	a_G	b_G	$1000\delta_G = 1000 \log (a_N/a_G)$	
Q	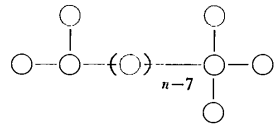	1	1	17	−9	0.4164	−26.4164	240.0	
R	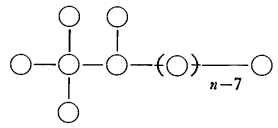			−7	6	0.4626	12.5374	194.3	→205
S	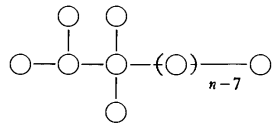			−15	11	0.4780	25.5220	180.1	
T	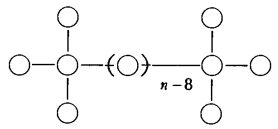	0	2	−45	29	0.3285	73.6715	343.0	→308
U	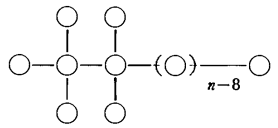			33	−19	0.3856	−52.3856	273.4	

Given a tree graph

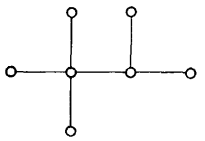

$Q_7 = R_7 = S_7$

and try to enlarge it to form a series of graphs with similar mode of branching by inserting points one by one in between certain prescribed lines. As in Fig. 3 there are three possible ways for doing so, since Q_7 has three topologically different types of lines.

In this way one gets three series of graphs, Q, R, and S. The original graph is turned out to be the smallest and the common member of the series Q, R, and S. As expected from this procedure, an infinite number of topologically different series of graphs are derived. In Table 2 are given twenty fundamental series of graphs with different modes of branching. They are subdivided into several classes with respect to the number of tertiary (n_Y) and quarternary (n_X) carbon atoms.

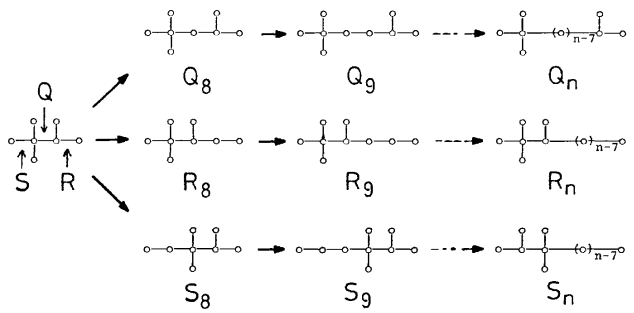

Fig. 3. Generation of different series of graphs from a parent graph.

Consider a series of graphs A-i-B composed of subgraphs A and B and i consecutive line of points. Successive application of Eqs. 7 and 8 gives the following recursive relation for the topological indices of these graphs.

A-i-B $(i \geq 0)$

$$Z_{A-(i+2)-B} = Z_{A-(i+1)-B} + Z_{A-i-B}. \quad (9)$$

Therefore, if the topological index of any series of graph G_n with n points as given in Table 2 is denoted by Z_n, a recursive relation similar to Eq. 9 can be written as

$$Z_{n+2} = Z_{n+1} + Z_n. \quad (10)$$

Although graph A-i-B has been defined for non-negative integers of i, the recursive relation 10 can formally be extended down to as small integers as one wishes irrespective of the existence of the corresponding graph. In Table 2 are given the Z_1 and Z_2 values for all the series of molecules studied. Although from these values the topological index Z_n for graph G_n can be obtained by the successive application of Eq. 10, one can obtain the closed and asymptotic forms of Z_n as in the following discussion.

It is known that if a series of numbers Z_n obey a recursive relation as 10, Z_n can be expressed explicitly by

$$Z_n = a\alpha^n + b\beta^n,^{23,24)} \quad (11)$$

where α and β are the roots of the equation

$$x^2 - x - 1 = 0,$$

namely,

$$\alpha = (1+\sqrt{5})/2 \text{ and } \beta = (1-\sqrt{5})/2. \quad (12)$$

The constants a and b are obtained if two of the members of the series $\{Z_n\}$ are given. Here by putting $n=1$ and 2 one gets

$$\begin{aligned} a &= (Z_1+\alpha Z_2)/(1+3\alpha) \\ b &= (Z_1+\beta Z_2)/(1+3\beta), \end{aligned} \quad (13)$$

which enables the calculation of any member of Z_n with Eq. 11. The values of a and b differ from series to series as in Table 2 and may be called as the structural factors.

For larger n the second term of Eq. 11 vanishes because of the relation $\alpha>1>|\beta|$. Then one gets

$$Z_n \rightarrow a\alpha^n \quad (14)$$

or

$$\log Z_n \rightarrow \log a + n \log \alpha. \quad (15)$$

The ratio Z_{n+1}/Z_n approaches to a constant value α for all the series of graphs,

$$Z_{n+1}/Z_n \rightarrow \alpha. \quad (16)$$

It is found from Table 2 that the value of a_G (a for a series G) is the largest for normal alkanes (series N) and is roughly determined by the number and mode of branching, whereas the value of b_G is scattered from series to series. This feature will be clarified if the value $\delta_G=\log(a_N/a_G)$ is compared with each other. Note that

$$\log Z_N - \log Z_G \rightarrow \log a_N - \log a_G = \delta_G. \quad (17)$$

As is evident from Table 2 the $\overline{\delta_G}$ averaged over a group of series with the same values of n_Y and n_X is roughly given by

$$100\,\bar{\delta}_G \fallingdotseq 5(n_Y+3n_X). \quad (18)$$

This means that the decrement of the logarithm of the topological index Z_G of a given graph from that of the linear graph with the same number of points is roughly determined by the number of the tertiary and quarternary carbon atoms in a simple manner as in Eq. 18. Recall that the effect of n_X on the lowering of the p(G, 2) number is three times as large as that of n_Y. See Eq. 12 of Ref. 13.

The effect of the quarternary carbon atom δ_X is three times larger than that of the tertiary carbon atom δ_Y. Namely,

$$\delta_L = 2.5\delta_A, \quad \delta_M = 3.2\delta_B, \quad \delta_O = 2.8\delta_C \quad (19)$$

or simply as

$$\delta_X \fallingdotseq 3\delta_Y. \quad (20)$$

Further inspection of the δ_X values reveals interesting additivity relationships. Namely, we have rigorous equalities as

$$\begin{aligned} \delta_E &= 2\delta_A \\ \delta_T &= 2\delta_L \\ \delta_Q &= \delta_A + \delta_L \ . \end{aligned} \quad (21)$$

That is, the value of δ for a graph with two branches is the sum of the δ values for the two graphs each with a single component branch, if the two roots of the branching are separated at least by one point, *i.e.*, one CH_2 unit. In Appendix I a general proof of this property of the δ value is given.

If two branches are adjacent the δ value is always smaller than the sum of the δ values for the component structures. For example, we can see

$$\begin{aligned} \delta_H &< \delta_A + \delta_B, \\ \delta_I &< \delta_B + \delta_C, \\ \delta_J &< \delta_A + \delta_D. \end{aligned} \quad (22)$$

Longer branching causes much smaller decrement in δ value than a shorter branching at the same root, for example,

$$\delta_D < \delta_B. \quad (23)$$

Finally the relations

$$\begin{aligned} &\delta_A > \delta_C > \delta_B, \\ \text{and} \quad &\delta_L > \delta_O > \delta_M \end{aligned} \quad (24)$$

show a zig-zag effect of the branching in going from the terminal to the center. All these properties can be deduced mathematically as in the case of the relation 20.

II. Relation between S° and Topological Quantities**

In Fig. 4 are shown the relations between the Z_G values and the observed absolute entropy S° of smaller ($n\leq 7$) acyclic saturated hydrocarbons. Similar plots are extended as in Fig. 5 for larger members of several series (normal (●), 3-methyl (△), 2,2-dimethyl (○), 2,3-dimethyl (+), and 2,4-dimethyl (□) alkanes) of saturated hydrocarbons. These two plots indicate several important aspects of the relation 2. Namely, Fig. 4 shows that the more the branching the smaller the value of S° as does Z_G. Introduction of a quarternary carbon atom causes much larger effect than that of two tertiary carbon atoms. It should also be noted here that as in the case of the boiling point 2-methyl substitution causes larger decrease in S° than does 3-methyl substitution in parallel with the behavior of Z_G. Inspection of the correlation

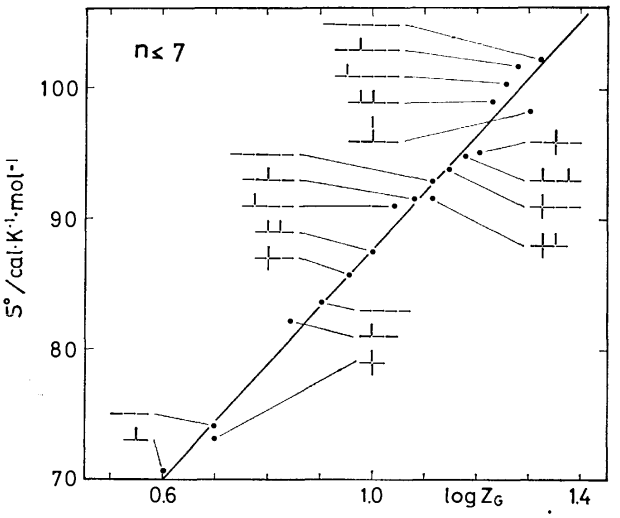

Fig. 4. $\log Z_G$—S° plot for smaller alkanes ($n\leq 7$).

** 1 cal=4.184 J.

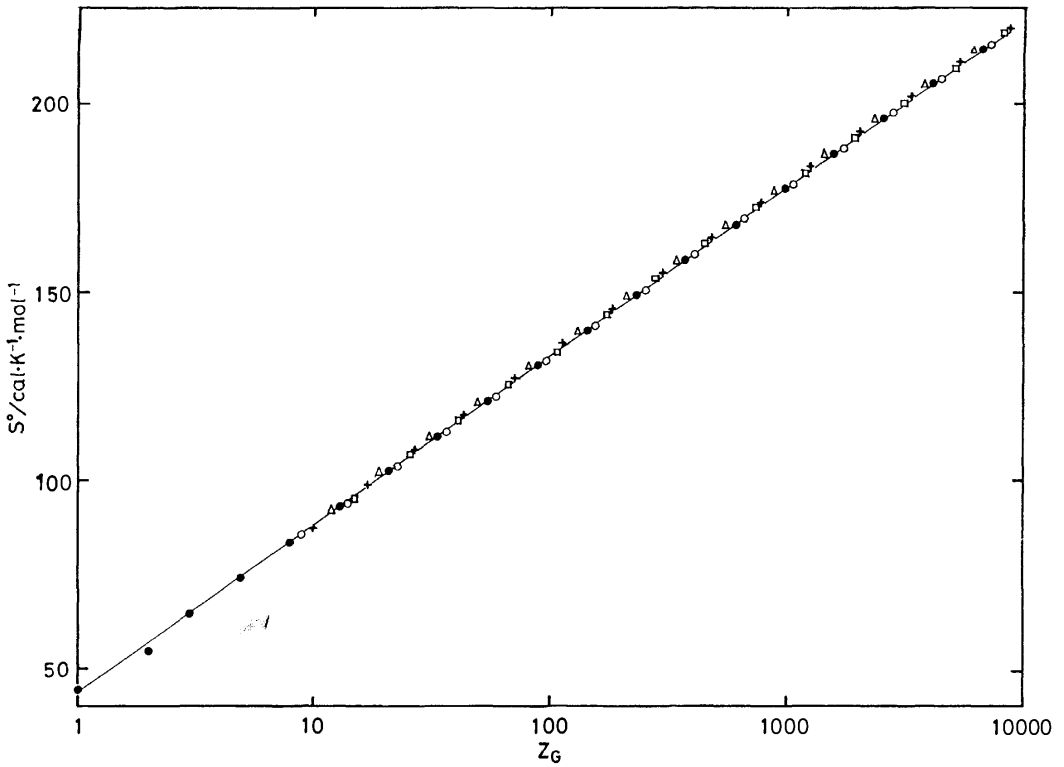

Fig. 5. log Z_G—$S°$ plot for larger members ($n \leq 20$) of several series of alkanes.
●: Normal, △: 3-methyl, ○: 2,2-dimethyl, +: 2,3-dimethyl, □: 2,4-dimethyl.

between the topological structure of alkane and entropy reveals that the effect of the tertiary and/or quarternary carbon atoms in lowering the $S°$ value is additive if there is at least a secondary (CH_2) carbon atom between these branching sites. Further, it is observed that the higher the symmetry, the smaller the $S°$ value. However, Z_G has nothing to do with the symmetry of a graph. The remarkably good linear relation between $S°$ and log Z_G, especially within each series, in Fig. 5 demonstrates that the growth of the chain length by one CC bond in eash series contributes the same amount (9.38 cal·K^{-1}·mol^{-1}) of increase in the entropy and that log Z_G has just the same property as has been shown above.

Although a number of empirical relations have been proposed for the topological dependence of the absolute entropy or the related quantities of branched compounds, especially of the saturated hydrocarbons, in this paper, we will discuss only three of them, namely, the relations proposed by the present author (topological index[12,13]), by Pitzer (partition function[15]), and by Pitzer and Scott (purely empirical one[18]), since the parameters involved in other theories do not seem to be easily interpretable.[4,10,11]

Pitzer has derived the expression of $S°$ of acyclic saturated hydrocarbons in terms of the molecular constants by enumerating the partition functions for the molecular motions. His original expression can be transformed into as

$$S° = C_0 + C_1 n + C_2 n_Y + C_3 n_X + \Delta, \tag{25}$$

$$\Delta = R(\ln Q + Q'/Q - \ln \sigma), \tag{26}$$

$$Q = \sum_{i}^{\text{conformations}} \exp(-\Delta\varepsilon_i/kT) = \sum_{j} g_j \exp(-\Delta\varepsilon_j/kT), \tag{27}$$

$$Q' = \sum_{i}^{\text{conformations}} \frac{\Delta\varepsilon_i}{kT} \exp(-\Delta\varepsilon_i/kT)$$

$$= \frac{a}{kT} \sum_{j} g_j \exp(-\Delta\varepsilon_j/kT), \tag{28}$$

$\Delta\varepsilon_i$=relative energy of i-th conformation
g_j=number of conformations with j excess *gauche* pairs relative to the conformation with the lowest energy, $\Delta\varepsilon_j$ being approximated as ja (a is the energy of a *gauche* form relative to the *trans* form)
σ=symmetry number=$\sigma_e \cdot \sigma_1 / I$
σ_e=symmetry number for external rotation
σ_1=symmetry number for internal rotation
I=number of racemic isomers (2 for racemic mixture, 1 for otherwise)
n=number of carbon atoms
n_Y=number of tertiary carbon atoms
n_X=number of quarternary carbon atoms.

The derivation of Eq. 25 will be given in Appendix II.

The numerical values of C_0, C_1, C_2, and C_3 for $S°$ at 298.15 K given in Table 1 are obtained from the paper by Person and Pimentel[16] and the book by Janz,[17] both of whom refined the Pitzer's original values.[25] Then Eq. 25 is expressed in the unit of cal·K^{-1}·mol^{-1} as

$$S°_{\text{thm}} = 43.012 + 7.679n - R\ln\sigma - 1.068\, n_Y - 3.425\, n_X + R(\ln Q + Q'/Q). \tag{29}$$

The data for calculating the values of σ, Q, and Q'

TABLE 3. STERIC AND SYMMETRY FACTORS OF SMALL ALKANES

Alkane[a]	Type[b]	g_j[c]						σ[c]			$R(\ln Q + Q'/Q)$[d]
		$j=0$	1	2	3	4	∞	σ_e	σ_i	I	
4	N	1	2				0	2	1	1	1.745
2m3	A	1					0	3	1	1	0
5	N	1	4	2			2	2	1	1	3.153
2m4	A	2	1				0	1	1	1	1.927
22m3	L	1					0	12	1	1	0
6	N	1	6	8	2		10	2	1	1	4.610
3m5	B			3	4		2	1	1	1	3.462
2m5	A		2	3			4	1	1	1	2.781
23m4	H			1	2		0	2	1	1	1.745
22m4	L			3			0	1	3	1	2.183
7	N	1	8	18	12	2	40	2	1	1	6.060
3e5	D				2	9	16	3	1	1	4.358
3m6	B			3	7	2	15	1	1	2	4.307
2m6	A		2	7	4		14	1	1	1	4.340
23m5	H				1	4	4	1	1	2	2.779
33m5	M				7		2	2	1	1	3.867
24m5	E			2			7	2	1	1	1.377
22m5	L			3			6	1	3	1	2.183
223m4	R					3	0	1	3	1	2.183

a) See Table 1. b) See Table 2. c) See Text for notations. d) $R=1.9872$ cal·K^{-1}·mol^{-1}, $T=298.15$ K, and $a=500$ cal·mol^{-1}.

are given in Table 3, where the g_j numbers have been obtained by the method of Balaban with 4-digit codes representing the direction of the C–C bond in the diamond lattice.[26,27]

Although Eq. 29 gives fairly good results (See Table 1) for the lower members of saturated hydrocarbons, it is a formidable task to get the g_j numbers for larger molecules. Then Pitzer and Scott have proposed the empirical formula

$$S^\circ_{emp} = 39.00 + 9.13n - R\ln\sigma - 3.5B \qquad (30)$$

where the value B is the number of branches.[18]

If one compares Eqs. 29 and 30 by noting that $B=n_Y+2n_X$, it is found that Eq. 30 does not properly take into account the effect of branching and also the rotational partition function. The effect of the site of the branching as discussed in Section I is completely neglected in Eq. 30.

The three different sets of calculated entropies, Eqs. 2, 29, and 30 are compared with the observed values in Table 1. As judged from the standard deviations (s) and the correlation coefficients (r) for the three different sets of calculations, the thermodynamic formula 29 gives the best and the topological formula 2 the worst agreement with experiments. Deviation of the plot of Z_G—S°_{top} from linearity in Fig. 4 is seen mostly for molecules with high symmetry.

In Figs. 6 and 7 the log Z_G—S°_{top} plots are also given for hydrocarbons with $n=8$ and 9, respectively,

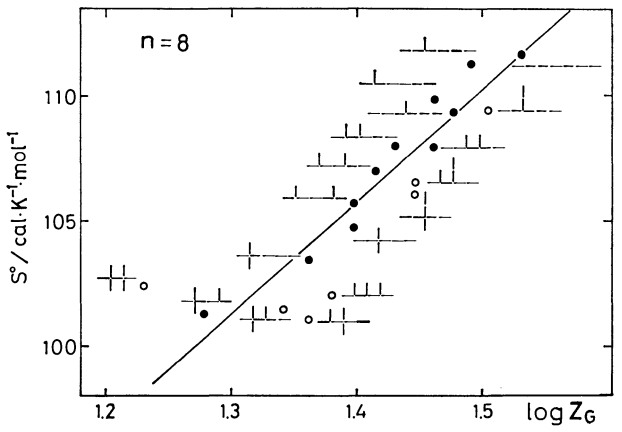

Fig. 6. log Z_G—S° plot for octane isomers.

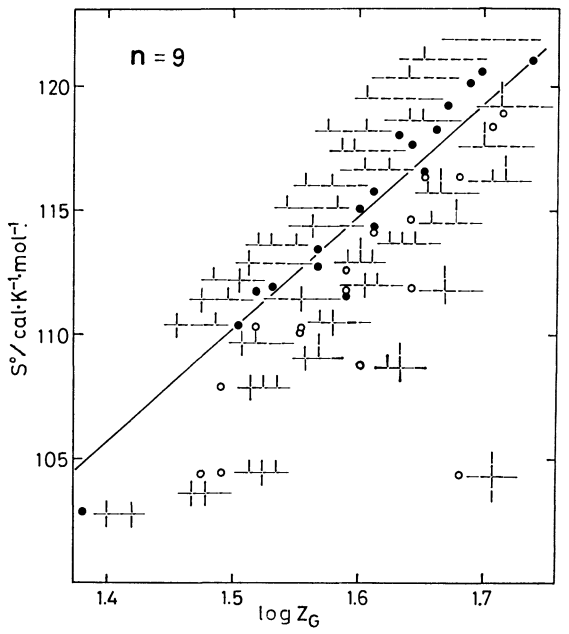

Fig. 7. log Z_G—S° plot for nonane isomers.

where those hydrocarbons containing skeletons

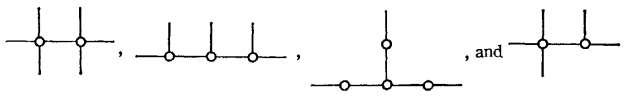

are marked with open circles, which tend to be scattered beneath the correlation line given in Fig. 5. Note that most of the rest of the molecules marked with filled circles are still on the straight line except for several melecules. Then as long as we are concerned with the fundamental analysis of the effect of branching and extension of the chain unit on the entropy, the topological index is found to be fairly effective, whereas the Pitzer's theory fails to be applied to larger molecules owing to the infeasibility of the enumeration of the steric factors.

III. Analysis of the Topological Dependence of the Entropy

As is found above, sterically overcrowded and/or highly symmetrical acyclic hydrocarbons are beyond the limit of the estimation of the absolute entropy by the use of only the topological index. If the symmetry factor σ is taken into consideration by adding the correction term to Eq. 2 for the set of data in Table 1, one gets

$$S^\circ_{top} = 46.453 + 42.100 \log Z_G - 2.9630 \log \sigma \qquad (31)$$

where the coefficients were obtained by the least squares calculation. The values of s=0.744 and r= 0.9970 show fair improvement from Eq. 2. In both of Eqs. 29 and 30, the contribution of the symmetry factor σ is given by $-R \ln \sigma = -4.576 \log \sigma$, which is 50 per cent larger than the corresponding term in Eq. 31. This means that the higher the symmetry of the molecule the smaller the topological index as the result of branching, but that this tendency of Z_G is not large enough for explaining the symmetry dependence of entropy completely.

With the above discussion in mind let us make term-to-term comparison of Eqs. 29 and 31 for larger alkanes. According to Relation 15, n can be substituted by

$$n = (\log Z_G - \log a)/\log \alpha. \qquad (32)$$

Equation 25 or 29 is then transformed as

$$S^\circ_{thm} = 43.012 + 36.744 \log Z_G - 4.5757 \log \sigma - (36.744 \log a + 1.068\, n_Y + 3.425\, n_X) + 1.9872\, (\ln Q + Q'/Q). \qquad (33)$$

There are observed small discrepancy between the corresponding coefficients of the first three terms of S°_{thm} and S°_{top}. Let us examine the relation between these discrepancies and the last two terms in S°_{thm}, which are missing from the expression of S°_{top}. As seen from Table 2 the fourth term is found to be constant as

$$-(36.744 \log a + 1.068\, n_Y + 3.425 n_X) = 6.9 \pm 1.4 \qquad (34)$$

throughout all the series studied. On the other hand, the last term seems to increase with n or $\log Z_G$ but with a few exceptions at least for small members of alkanes (See Table 3). Person and Pimentel[16] have noticed the linear increase of this term with respect to n for n-alkanes. One may then expect a rough estimate of this term as

$$R(\ln Q + Q'/Q) = 6.5 \log Z_G - 3.9 \pm 1.0 \qquad (35)$$

for larger alkanes. Now substitution of these two relations into Eq. 33 yields

$$S^\circ_{thm} = 46.0 + 43.2 \log Z_G - 4.6 \log \sigma \pm 2.4 \qquad (36)$$

which is turned out to be very close to the round-off experssion of Eq. 31 as

$$S^\circ_{top} = 46.5 + 42.1 \log Z_G - 3.0 \log \sigma. \qquad (37)$$

Large deviation from Eq. 34 is not expected, since the components in Eq. 34 are related with each other as in Eqs. 17 and 18. Although at the present stage we cannot draw any quantitative conclusion on Relation 35, this is qualitatively approved by the following discussion. The branching of the carbon atom skeleton diminishes the rotational degree of freedom mainly and additional decrement in the partition function is brought about by the increase of the overcrowded conformations. The above analysis shows that both the effects are reflected well in (the logarithm of) the topological index; the latter effect contributing by the amount of as large as fifteen per cent. The symmetry factor for a molecule with higher symmetry lowers further the entropy as much as a few per cent for each of additional symmetry operations.

One may well say that the above argument is based on superficial comparison of figures between experiments and models. However, the parallelism between the mathematical properties of S° and Z_G as discussed in Sections I and II ensures that these relations obtained in this paper can be used as the start for further analysis of the thermodynamic properties of van der Waals fluids.

Appendix I

Proof of Eq. 21

Consider four series of graphs, N, X, Y, and XY, as shown in Fig. A. Graph N_k is a path progression with k $(=l+m+n)$ points. Graph X_k, which is a member of the series X with k points, is composed of the root Ⓧ with l points and a path progression N_{m+n} $(m+n>0)$. Graph Y_k is composed of the root Ⓨ with m points and a path progression N_{l+m} $(l+m>0)$. The roots Ⓧ and Ⓨ characterize graphs X_k and Y_k, respectively, by their modes of branching. Graph XY_k is composed of the roots Ⓧ and Ⓨ and a path progression

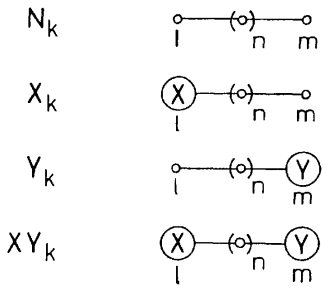

Fig. A. Four different series of graphs. The total number of points is $k=l+m+n$.

N_n ($n>0$).

If the topological indices of these graphs are denoted respectively as N_k, X_k, Y_k, and XY_k, these values can be expressed by using Eq. 8 as follows:

$$\begin{aligned} N_k &= N_{l+n}\cdot N_m + N_{l+n-1}\cdot N_{m+1} - N_{l+n-1}\cdot N_m \\ X_k &= X_{l+n}\cdot N_m + X_{l+n-1}\cdot N_{m+1} - X_{l+n-1}\cdot N_m \\ Y_k &= N_{l+n}\cdot Y_m + N_{l+n-1}\cdot Y_{m+1} - N_{l+n-1}\cdot Y_m \\ XY_k &= X_{l+n}\cdot Y_m + X_{l+n-1}\cdot Y_{m+1} - X_{l+n-1}\cdot Y_m. \end{aligned} \quad (A1)$$

Note that these relations are valid for the case with $n>0$, since graphs X_k and Y_k are defined, respectively, for the cases with $k\geq l$ and $k\geq m$. By combining these equations one gets

$$XY_k\cdot N_k - X_k\cdot Y_k = (X_{l+n}\cdot N_{l+n-1} - X_{l+n-1}\cdot N_{l+n}) \times (Y_m\cdot N_{m+1} - Y_{m+1}\cdot N_m). \quad (A2)$$

Division of the both sides of Eq. A2 by N_k^2 gives

$$\begin{aligned} \frac{XY_k}{N_k} - \frac{X_k}{N_k}\cdot\frac{Y_k}{N_k} &= \frac{X_{l+n}\cdot Y_m\cdot N_{l+n}\cdot N_m}{N_k^2} \\ &\times\left(\frac{N_{l+n-1}}{N_{l+n}} - \frac{X_{l+n-1}}{X_{l+n}}\right)\left(\frac{N_{m+1}}{N_m} - \frac{Y_{m+1}}{Y_m}\right) \\ &< \frac{X_{l+n}}{N_{l+n}}\cdot\frac{Y_m}{N_m}\left(\frac{N_{l+n-1}}{N_{l+n}} - \frac{X_{l+n-1}}{X_{l+n}}\right) \\ &\times\left(\frac{N_{m+1}}{N_m} - \frac{Y_{m+1}}{Y_m}\right). \end{aligned} \quad (A3)$$

The last inequality is obtained by using the relation

$$N_k > N_{l+n}\cdot N_m \quad \text{(from Eq. 7)}. \quad (A4)$$

Since the topological index of the path progression N_k is the largest among the isomeric graphs with the same number of points, we have

$$\frac{X_{l+n}}{N_{l+n}},\ \frac{Y_m}{N_m} < 1.$$

As k increases the remaining two terms in the parentheses individually approach to zero because of the asymptotic relation 14. Now Eq. A3 sharply converges to zero with increasing the size of the graph, or

$$\frac{XY_k}{N_k} \to \frac{X_k}{N_k}\cdot\frac{Y_k}{N_k}. \quad (A5)$$

With respect to the coefficient a defined in Eq. 11, a rigorous relation

$$\frac{a_{XY}}{a_N} = \frac{a_X}{a_N}\cdot\frac{a_Y}{a_N} \quad (A6)$$

holds, which completes the proof of Eq. 21.

Appendix II

Derivation of Eq. 25

According to Pitzer[15] the absolute entropy of an alkane is expressed as

$$S^\circ = f_0 + \sum_{i=1}^{7} f_i n_i + \Delta \quad (A7)$$

with

n_1=number of C–C stretching modes
n_2=number of C-C-C bending modes
n_3=number of internal rotations (C-C-C-C)
n_4=number of CH_3 groups
n_5=number of $-CH_2-$ groups
n_6=number of $-\overset{|}{C}H-$ groups$=n_Y$
n_7=number of $-\overset{|}{\underset{|}{C}}-$ atoms$=n_X$.

Δ is defined as Eq. 26. Person and Pimentel[16] give the coefficients f_i ($i=0\sim7$) for various temperatures. The values for $T=298.15$ K are:

$$f_0=57.473,\ f_1=0.792,\ f_2=2.173,$$
$$f_3=4.523,\ f_4=2.314,\ f_5=0.191,$$
$$f_6=-0.65,\ \text{and}\ f_7=-2.78$$

in units of cal·K^{-1}·mol^{-1}.

A simple combinatorial consideration on tree graphs gives the following relations among $n_1\sim n_7$ and n (the number of the carbon atoms),

$$\begin{aligned} n_1 &= n - 1 \\ n_2 &= n - 2 + n_6 + 2n_7 \\ n_3 &= n - 3 - n_6 - 2n_7 \\ n_4 &= 2 + n_6 + 2n_7 \\ n_5 &= n - 2 - 2n_6 - 3n_7. \end{aligned} \quad (A8)$$

By putting Relations A8 into Eq. A7 one gets Eq. 25 with

$$C_0=f_0-f_1-2f_2-3f_3+2f_4-2f_5=43.012$$
$$C_1=f_1+f_2+f_3+f_5=7.679$$
$$C_2=f_2-f_3+f_4-2f_5+f_6=-1.068$$
$$C_3=2f_2-2f_3+2f_4-3f_5+f_7=-3.425.$$

References

1) A. T. Balaban, Ed., "Chemical Application of Graph Theory," Academic Press, London (1976).
2) A. Graovac, I. Gutman, and N. Trinajstić, "Topological Approach to the Chemistry of Conjugated Molecules (Lecture Notes in Chemistry, No. 4)," Springer-Verlag, Berlin (1977).
3) H. Hosoya, *Kagaku No Ryoiki*, **26**, 989 (1972).
4) L. Kihr and L. H. Hall, "Molecular Connectivity in Chemistry and Drug Research," Academic Press, New York (1976).
5) H. Hosoya, K. Hosoi, and I. Gutman, *Theor. Chim. Acta*, **38**, 37 (1975); H, Hosoya and K. Hosoi, *J. Chem. Phys.*, **64**, 1065 (1976).
6) I. Gutman, M. Milan, and N. Trinajstić, *J. Am. Chem. Soc.*, **99**, 1692 (1977); I. Gutman and H. Hosoya, *Theor. Chim. Acta*, **48**, 279 (1978).
7) J. Aihara, *J. Am. Chem. Soc.*, **98**, 2750 (1978); **99**, 2048 (1977).
8) H. Hosoya, *J. Chem. Doc.*, **12**, 181 (1972).
9) M. Randić, *J. Chem. Phys.*, **60**, 3920 (1974); *J. Am. Chem. Soc.*, **97**, 6609 (1975).
10) H. Wiener, *J. Am. Chem. Soc.*, **69**, 17, 2636 (1947); *J. Chem. Phys.*, **15**, 766 (1947); *J. Phys. Chem.*, **52**, 425 (1948).
11) J. R. Platt, *J. Phys. Chem.*, **56**, 328 (1952).
12) H. Hosoya, K. Kawasaki, and K. Mizutani, *Bull. Chem. Soc. Jpn.*, **45**, 3415 (1972).
13) H. Hosoya, *Bull. Chem. Soc. Jpn.*, **44**, 2332 (1971).
14) H. Hosoya and Y. Maruyama, "Kōzō to Bussei," Asakura, Tokyo (1975).
15) K. S. Pitzer, *J. Chem. Phys.*, **8**, 711 (1940).
16) W. B. Person and G. C. Pimental, *J. Am. Chem. Soc.*, **75**, 532 (1953).
17) G. J. Janz, "Thermodynamic Properties of Organic Compounds—Estimation Methods, Principles and Practice," Academic Press, New York (1967).
18) K. S. Pitzer and D. W. Scott, *J. Am. Chem. Soc.*, **63**, 2419 (1941).
19) D. W. Scott, *J. Chem. Phys.*, **60**, 3144 (1974).
20) H. Hosoya, *Fibonacci Quart.*, **11**, 255 (1973).

21) Observed values of the absolute entropy of alkanes were taken from Ref. 22.
22) "Selected Values of Properties of Hydrocarbons and Related Compounds (API Report 44)," Thermodynamic Research Center, Texas A & M Univ. (1975).
23) N. N. Vorob'ev, "Fibonacci Numbers," Nauka Publ., Moskow (1964).
24) V. E. Hoggatt, Jr., "Fibonacci and Lucas Numbers," Houghton Mifflin Co., Boston (1969).
25) For several cases Pitzer gave wrong numbers for g_n. Although Person and Pimentel adjusted the parameters C_0, C_1, and C_2 for smaller normal alkanes, we did not use this sophisticated correction. Discrepancy of the $S°$ values from those of the previous papers might have arisen from the above alternatives.
26) A. T. Balaban, *Rev. Roum. Chim.*, **21**, 1049 (1976).
27) A number of conflicting theories have been proposed on the conformations of alkane skeletons. For example, Sheraga[28] claims that more than three potential minima exist around a C-C axis for larger alkanes, Scott[19] proposes a sophisticated method for estimating the steric repulsion energy in branched alkanes, Allinger[29] proposes another criterion for determining the conformations, *etc.*[30,31] However, according to some trial calculations of the steric factors for the various models, the topological dependence of the steric factor as a whole is not strongly dependent on the choice of these models.
28) R. A. Scott and H. A. Scheraga, *J. Chem. Phys.*, **44**, 3054 (1966).
29) N. L. Allinger, M. T. Tribble, M. A. Miller, and D. H. Wertz, *J. Am. Chem. Soc.*, **93**, 1637 (1971).
30) A. Abe, R. L. Jernigan, and P. J. Flory, *J. Am. Chem. Soc.*, **88**, 631 (1966).
31) A. L. Verma, W. F. Murphy, and H. J. Bernstein, *J. Chem. Phys.*, **60**, 1540 (1974).

Field Theoretical Treatment of the Proton hfs in Aromatic Ion Radicals

Shigeyuki Aono,* Kiyoshi Nishikawa, and Kisaburo Deguchi
Department of Chemistry, Faculty of Science, Kanazawa University, Marunouchi, Kanazawa 920
(Received September 13, 1979)

Field theoretical method to estimate the proton hfs in aromatic ion radicals is presented, and applied to explain why the proton hfs of the positive ion is larger than that of the negative ion of the same molecule. Since the Hartree-Fock orbitals of the neutral molecule are adequate for describing the negative ion state of this molecule, but not for the positive ion state, the correlation effect in the latter should be effectively taken into account, so that the particle propagators in the positive ion are renormalized. The hyperfine energy consists of two terms, the hyperfine self-energy term and the pole strength which is interpreted as the existence probability of the state under investigation. The electron correlation affects these differently between positive and negative ions.

It has been observed in aromatic compounds that absolute values of the proton hfs constants of the positive ions are larger than those of the corresponding negative ions.[1] Usually we adopt the simple relation that the hfs constant a_N is proportional to the spin density at the nucleus N;

$$a_N = Q\rho_N, \tag{1}$$

where Q is the proportionality constant, being estimated to be about -23 G. If we estimate ρ_N by means of the Hückel method or the PPP (Pariser-Parr-Pople) method, we can obtain

$$\rho_N^{(+)} = \rho_N^{(-)}. \tag{2}$$

That is, the spin density of the positive ion at the nucleus N, $\rho_N^{(+)}$ is equal to that of the negative ion, $\rho_N^{(-)}$. This relation is one of pairing properties widely found in the alternant hydrocarbons.[2]

Higuchi[3] tried a careful calculation taking into account the excess (shortage) of charge in the negative (positive) ion, and obtain the result reverse to the observation. Bolton[4] treated this problem from a intuitive aspect. His idea is that the orbital exponent of the wave function is larger (in absolute value) in the positive ion than in the negative ion, since there is an excessive nuclear attraction in the former.

It seems true that any theoretical effort to explain this problem would be in vain, so long as symmetrical character be kept in the alternant hydrocarbons. However, we should like to insist that it is preferable to treat both ions with common reference orbitals which are evaluated in the neutral molecule.

General

As is well known, the origin of the proton hfs in aromatic radicals is spin polarization due to the electron correlation at the nucleus in question. A little spin density produces magnetic energy due to the coupling between electron and nuclear spins.

A nice way to take the electron correlation effect into account in the spin polarization was introduced by Cederbaum.[5] This method will be briefly presented in the following.

We note that energy responsible for the proton hfs is a tiny part of the entire electron energy. In this sense, we wish to obtain the electron Green's function of which self-energy part contains the hyperfine energy. The total Hamiltonian of the system in question is written symbolically as

$$H = H_0 + H_V + H_{hf} \tag{3}$$

where H_0 is the HF (Hartree-Fock) Hamiltonian, H_V the electron correlation term and H_{hf} the hyperfine interaction between electron and nuclear spins.

Let us assume that we have already obtained in the HF approximation a set of one-particle orbitals, $\{\phi_n\}$ and that of orbital energies, $\{\varepsilon_n\}$. The Green's function in this approximation is

$$G^0_{ij}(\omega) = \frac{\delta_{ij}}{\omega - \varepsilon_i + i\eta \text{ sign } \varepsilon_i}, \tag{4}$$

where the orbital energy ε_i is counted from the chemical potential which is set at the mid-point between occupied and vacant orbital energies, and η the positive infinitesimal.

The Green's function for the total Hamiltonian (3) is written in matrix form as

$$G(\omega) = [G^0(\omega)^{-1} - \Sigma(\omega)]^{-1}, \tag{5}$$

and that for the first two terms of (3) is

$$G^V(\omega) = [G^0(\omega)^{-1} - \Sigma^V(\omega)]^{-1}, \tag{6}$$

where $\Sigma(\omega)$ and $\Sigma^V(\omega)$ are self-energy terms. It is obvious that

$$\Sigma(\omega) = \Sigma^V(\omega) + \Sigma^{hf}(\omega), \tag{7}$$

in which $\Sigma^{hf}(\omega)$ is the self-energy term concerning to the hyperfine interaction. $\Sigma^{hf}(\omega)$ arises in two ways: If the unpaired electron has finite density at the nucleus in question (the case of s electron), the electron spin directly couples with nuclear spin, while if not (the case of π electron, for example) the coupling takes place indirectly through intermediate states. In the latter case the electron correlation effect is especially important. However, even in the first case, we can show a correlation effect which is not given by current theories, but is given by the following field theoretical treatment.

Using relations (5) and (6) in (7), we obtain

$$G^V(\omega)^{-1} - G(\omega)^{-1} = \Sigma^{hf}(\omega). \tag{8}$$

Let $G^V(\omega)$ is diagonalized in the form

$$G^V_{ii}(\omega) = \frac{p(E^V_i)}{\omega - E^V_i}. \tag{9}$$

In the above, E^V_i is determined from

$$\det|G^V(\omega)| = 0, \tag{10}$$

and $p(E_i^{\mathrm{v}})$ is called the pole strength which is approximately evaluated as follows. Neglecting the off-diagonal terms in $G^{\mathrm{v}}(\omega)$, we obtain

$$G_{ii}^{\mathrm{v}}(\omega) = [\omega - \varepsilon_i - \Sigma_{ii}^{\mathrm{v}}(\omega)]^{-1}. \tag{11}$$

Then we set

$$\omega - \varepsilon_i - \Sigma_{ii}^{\mathrm{v}}(\omega) = (\omega - E_i^{\mathrm{v}})p(\omega)^{-1} \tag{12}$$

and differentiate both sides with respect to ω, and finally put $\omega = E_i^{\mathrm{v}}$. Thus it follows that

$$p(E_i^{\mathrm{v}}) = \left\{1 - \left.\frac{\partial \Sigma_{ii}^{\mathrm{v}}(\omega)}{\partial \omega}\right|_{\omega = E_i^{\mathrm{v}}}\right\}^{-1}. \tag{13}$$

Similarly we obtain

$$G_{ii}(\omega) = \frac{p(E_i)}{\omega - E_i}, \tag{14}$$

$$p(E_i) = \left\{1 - \left.\frac{\partial \Sigma_{ii}(\omega)}{\partial \omega}\right|_{\omega = E_i}\right\}^{-1}. \tag{15}$$

It should be stressed that the pole strength $p(E_i)$ is the probability that the state with an unpaired electron of which energy is E_i can exist.

The electron energy E_i consists of the energy containing up to the correlation effect, E_i^{v} and the hyperfine energy, Δ_i;

$$E_i = E_i^{\mathrm{v}} + \Delta_i. \tag{16}$$

Using (9) and (14) in (8), we get

$$\frac{\omega - E_i^{\mathrm{v}}}{p(E_i^{\mathrm{v}})} - \frac{\omega - E_i}{p(E_i)} = \Sigma_{ii}^{\mathrm{hf}}(\omega). \tag{17}$$

Here putting $\omega = E_i$, we have the result,

$$\Delta_i = p(E_i^{\mathrm{v}})\,\Sigma_{ii}^{\mathrm{hf}}(E_i). \tag{18}$$

Considering that $p(\omega)$ and $\Sigma_{ii}^{\mathrm{hf}}(\omega)$ are smooth and slowly varying function of energy parameter, we may be allowed to approximate as

$$\Delta_i \simeq p(\varepsilon_i)\,\Sigma_{ii}^{\mathrm{hf}}(\varepsilon_i). \tag{19}$$

This result shows us that the hyperfine energy is given by a product of two terms; the first is the pole strength which concerns electronic structure of the whole system, and the second is the hyperfine self-energy term which is determined from a rather local structure giving the hyperfine interaction. Therefore we can say that even if the hyperfine interaction is simple as in the case with an unpaired electron in the s orbital, the correlation effect is taken into account *via* the pole strength.

Case of Aromatic Ion Radicals

In order to discuss the difference of the proton hfs values between aromatic positive and negative ion radicals in terms of the pole strength and the hyperfine self-energy term as in (19), let us define:

$$\delta p = (p^{+} - p^{-})/p^{-},$$
$$\delta\Sigma^{\mathrm{hf}} = (\Sigma^{\mathrm{hf}+} - \Sigma^{\mathrm{hf}-})/\Sigma^{\mathrm{hf}-},$$

where + and − are added to clearly indicate positive and negative ions, respectively. Then it is found that

$$\delta\Delta \equiv (\Delta^{+} - \Delta^{-})/\Delta^{-} \simeq \delta p + \delta\Sigma^{\mathrm{hf}}, \tag{20}$$

neglecting the second order terms with respect to δp and $\delta\Sigma^{\mathrm{hf}}$.

Now we evaluate the hyperfine self-energy term. The current treatments in evaluating the hyperfine energy have been carried out under the condition that $p(\varepsilon_i) = 1$, so that the hyperfine self-energy term itself is the hyperfine energy. Since the π-orbital with an unpaired electron has a nodal plane on which the proton is, an exchange type interaction shown in Fig. 1a is invoked to cause the spin polarization at the proton. The magnetic interaction represented by a dotted line creates a particle-hole pair, then the hole propagator of it annihilates combined with the incomming particle propagator, i, while the particle propagator of the pair is scattered to i with the electronic interaction. This mechanism is called the σ-π exchange interaction. However, the direct type interaction in Fig. 1b has vanishing result to the spin polarization due to the possibility of arbitrary choice of spin directions of the polarization part.

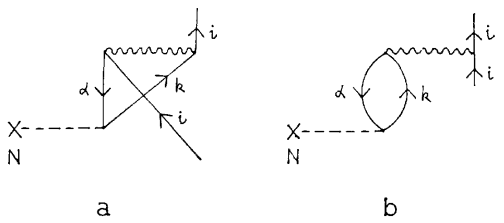

Fig. 1. Hyperfine self-energy terms.
a: Exchange type, b: direct type.

Observing the Fig. 1a, we can immediately obtain

$$\Sigma_{ii}^{\mathrm{hf}-}(\varepsilon_i) = -\sum_{k\alpha}(\mathrm{N};\ k\alpha)(ki;\ i\alpha)/\varepsilon_{\alpha k}, \tag{21}$$

$$\varepsilon_{\alpha k} = \varepsilon_\alpha - \varepsilon_k, \tag{21a}$$

where indices k and α denote the particle and hole states respectively, and

$$(\mathrm{N};\ k\alpha) = \int \mathrm{N}(\boldsymbol{r})\phi_k(\boldsymbol{r})\phi_\alpha(\boldsymbol{r})\mathrm{d}\boldsymbol{r}. \tag{22}$$

refering the magnetic interaction, and further

$$(ki;\ i\alpha) = \int \phi_k(\boldsymbol{r}_1)\phi_i(\boldsymbol{r}_1)\frac{1}{r_{12}}\phi_i(\boldsymbol{r}_2)\phi_\alpha(\boldsymbol{r}_2)\mathrm{d}\boldsymbol{r}_1\mathrm{d}\boldsymbol{r}_2. \tag{23}$$

In the above, the one-electron orbitals are assumed to be real without loss of generality.

We suppose the expression (21) refers to the negative ion, that is, an unpaired electron is in the lowest vacant orbital i. If we consider the positive ion in which an unpaired electron is in the highest occupied orbital η, we get a similar result,

$$\Sigma_{\eta\eta}^{\mathrm{hf}+}(\varepsilon_\eta) = -\sum_{k\alpha}(\mathrm{N};\ k\alpha)(k\eta;\ \eta\alpha)/\varepsilon_{\alpha k}. \tag{24}$$

In the corresponding diagram which leads to the above result, the direction of every line in Fig. 1a is reversed (see Fig. 2), and i is replaced by η.

Then using one of the pairing properties of the alternant hydrocarbons

$$(ki;\ i\alpha) = (k\eta;\ \eta\alpha) \tag{25}$$

we get

$$\Sigma_{ii}^{\mathrm{hf}-}(\varepsilon_i) = \Sigma_{\eta\eta}^{\mathrm{hf}+}(\varepsilon_\eta). \tag{26}$$

This is nothing but to reformulate the Mclachlan's result.[2]

To make steps further, a physical intuition is needed. Remember how to determine the HF orbitals. The HF functions of the particle state are determined for the state in which hole levels are already doubly occupied, then an extra electron is introduced. Therefore we can say that the HF functions are considerably suitable for describing the negative ion state. If we get a same order of approximation to the positive ion, we have to use the HF functions determined in the reference system which is the doubly ionized positive ion. Such consideration makes us use a different basis set for the positive ion from that for the negative ion. This is the Bolton's idea. However in the present treatment, we do not follow this, but want to use the identical basis set for both ions.

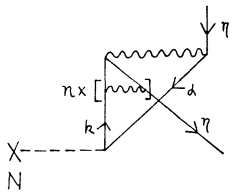

Fig. 2. Renormalization of the particle propagator in the hyperfine self-energy term of the positive ion.

When the basis set determined in the neutral molecule is employed, it is probable that the positive ion is more s nsitive to the electron correlation than the negative ion is. An extra positive charge in the positve ion works to decrease the virtual excitation energies, that is, the particle propagator should be renormalized with an extra hole propagator which arises only in the positive ion. To this end, in Fig. 2 the ladder type of particle-hole interactions are inserted n times (n tends to ∞). Combining this diagram and the corresponding exchange one, we can obtain

$$\begin{aligned}\Sigma_{\eta\eta}^{\mathrm{hf}+}(\varepsilon_\eta) &= -\sum_{k\alpha}(\mathrm{N};\, k\alpha)(k\eta;\, \eta\alpha)[\varepsilon_{\alpha k}+(\eta\eta;\, kk)-(\eta k;\, k\eta)]^{-1} \\ &= -\sum_{k\alpha}(\mathrm{N};\, k\alpha)(ki;\, i\alpha)[\varepsilon_{\alpha k}+(ii;\, kk)-(ik;\, ki)]^{-1},\end{aligned} \tag{27}$$

following the Kelly's technique to shift the energy denominator,[6] and using the pairing property to obtain the second equality. This is same as the expression of (21) for the negative ion except for the energy-shift terms of the denominator.

If we employ the CH fragment to estimate Σ^{hf}, the orbitals α and k are as usual restricted to the CH bonding and anti-bonding orbitals, respectively, so that we can remove the summation symbol. Consequently the second term of (20) becomes

$$\delta\Sigma^{\mathrm{hf}} = \{1+[(ii;\, kk)-(ik;\, ki)]/\varepsilon_{\alpha k}\}^{-1} - 1. \tag{28}$$

Since $\varepsilon_{\alpha k}$ is negative, it is obvious that the sign of (28) is positive, that is, at this stage the hfs value of the positive ion always larger than that of the negative ion.

We turn to evaluation of the pole strength, following

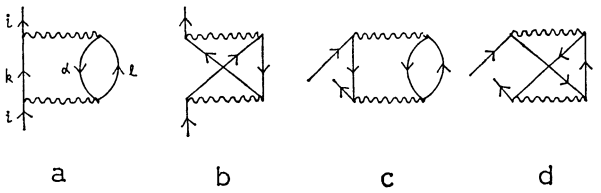

Fig. 3. Second order diagrams for the electron correlation (negative ion).

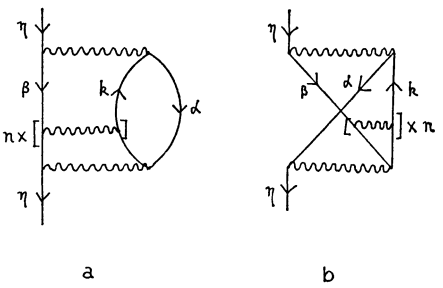

Fig. 4. Renormalization of the particle propagator in the electron correlation diagram (positive ion).

the spirit previously mentioned. To do so, the self-energy terms for the electron correlation will be calculated. Since we are using the HF orbitals, the first order diagrams are already included to infinite order. For the negative ion we are satisfied with an approximation displayed by Fig. 3, but the Fig. 3c and 3d can be neglected due to their small contributions (because of the large energy denominator). Therefore the second order correction in the negative ion becomes

$$\Sigma_{ii}^{\mathrm{V}}(\omega) = \sum_{\alpha kl} g(il;\, l\alpha)/(\omega+\varepsilon_\alpha-\varepsilon_k-\varepsilon_l), \tag{29}$$

$$g(ik;\, la) = 2(ik;\, l\alpha)(ki;\, \alpha l)-(ik;\, l\alpha)(k\alpha;\, li). \tag{29a}$$

In the case of the positive ion, the diagrams shown in Figs. 4a, 4b, and the corresponding exchange diagrams yield

$$\begin{aligned}\Sigma_{\eta\eta}^{\mathrm{V}}(\omega) = \sum_{\alpha\beta l} & g(\eta\beta;\, l\alpha)/[\omega+\varepsilon_l-\varepsilon_\alpha-\varepsilon_\beta-(\beta\beta;\, ll) \\ & +(\beta l;\, l\beta)].\end{aligned} \tag{30}$$

Then we get

$$\frac{\partial}{\partial\omega}\Sigma_{ii}^{\mathrm{V}}(\omega)\Big|_{\omega=\varepsilon_i} = -\sum_{\alpha kl} g(ik;\, l\alpha)/(\varepsilon_i+\varepsilon_\alpha-\varepsilon_k-\varepsilon_l)^2, \tag{31}$$

$$\begin{aligned}\frac{\partial}{\partial\omega}\Sigma_{\eta\eta}^{\mathrm{V}}(\omega)\Big|_{\omega=\varepsilon_\eta} &= -\sum_{\alpha\beta l} g(\eta\beta;\, l\alpha)/[\varepsilon_\eta-\varepsilon_\alpha-\varepsilon_\beta+\varepsilon_l \\ &\quad -(\beta\beta;\, ll)+(\beta l;\, l\beta)]^2 \\ &= -\sum_{\alpha kl} g(ik;\, l\alpha)/[\varepsilon_i+\varepsilon_\alpha-\varepsilon_k-\varepsilon_l \\ &\quad +(kk;\, ll)-(kl;\, lk)]^2,\end{aligned} \tag{32}$$

for the negative and positive ions, respectively. In obtaining the second equality of (32), use was made of the pairing properties,

$$\varepsilon_\eta = -\varepsilon_i, \qquad g(\eta\beta;\, l\alpha) = g(ik;\, l\alpha). \tag{33}$$

The expression of (32) is same as that of (31) except for additional terms in the denominator.

Using (31) and (32) in (15), we get δp of (20) as

Table 1. Proton hfs values of aromatic ion radicals. Experimental and theoretical results

		Experimental hf value/G			Theoretical		
		+ion	−ion	$\delta\Delta$	δp	$\delta\sum^{hf}$	$\delta\Delta$
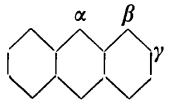	α	6.65	5.41	0.23	−0.051	0.340	0.189
	β	3.12	2.76	0.13	−0.051	0.107	0.056
	γ	1.40	1.53	−0.085	−0.051	0.051	0.
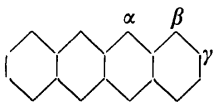	α	5.17	4.25	0.22	−0.060	0.173	0.113
	β	1.72	1.55	0.11	−0.060	0.060	0.
	γ	1.06	1.15	−0.078	−0.060	0.035	−0.025
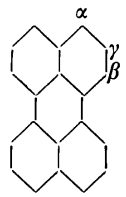	α	4.10	3.53	0.16	−0.066	0.121	0.055
	β	3.10	3.08	0.0065	−0.066	0.091	0.025
	γ	0.46	0.46	0.	−0.066	0.013	−0.053

$$\delta p \simeq \left.\frac{\partial\sum^{v}_{\eta\eta}(\omega)}{\partial\omega}\right|_{\omega=\varepsilon_\eta} - \left.\frac{\partial\sum^{v}_{ii}(\omega)}{\partial\omega}\right|_{\omega=\varepsilon_i}$$

$$= -\sum_{\alpha kl} g(ik;\, l\alpha)\{[\varepsilon_{i\alpha kl}+(kk;\, ll)-(kl;\, lk)]^{-2}-\varepsilon^{-2}_{i\alpha kl}\} \tag{34}$$

with

$$\varepsilon_{i\alpha kl} = \varepsilon_i+\varepsilon_\alpha-\varepsilon_k-\varepsilon_l. \tag{34a}$$

As $\varepsilon_{i\alpha kl}$ is negative, it is found that δp has the positive sign.

Comming back to (20), we discuss effects of two terms constructing the hyperfine energy difference between positive and negative ions: the first is δp which is negative and relates with the electron correlation of the whole system, and the second is $\delta\sum^{hf}$ which is positive, strongly depending upon the local situation where the magnetic nucleus under consideration is.

Numerical Results and Discussion

The present theory being semi-qualitative, the numerical procedure is simplified to save computer time. The π electron orbitals which are involved in our calculation are obtained by the Hückel method, and are regarded as the self-consistent HF orbitals in the PPP approximation. Then the electron-electron interactions are introduced with the Nishimoto-Mataga parametrization.[7] Therefore the orbital energies in (34a) are not Hückel ones, but are regarded as the HF orbital energies in the PPP approximation.

In evaluating the hyperfine self-energy term employing the CH fragment, the energy separation between the CH bonding and antibonding orbitals is needed. This is approximately estimated in the semi-empirical theory as $\varepsilon_{ak}\simeq -10$ eV. As to the electron repulsion terms, the exchange integral, $(ik;ki)$ is negligibly small, and the direct term, $(ii;kk)$ may be a little smaller than the one-center coulomb repulsion integral multiplied by the unpaired electron density at the carbon atom, ρ_{Ci}: $(ii;kk)\simeq 10\rho_{Ci}$ eV. These energy parametrizations make $\delta\sum^{hf}$ given by (28) simple as

$$\delta\sum^{hf} = (1-\rho_{Ci})^{-1} - 1 \tag{35}$$

We tabulate observations and theoretical results of a few species as explanational examples. In table we have given values of δp and $\delta\sum^{hf}$; for example in the case of anthracene radical, the negative value of δp is independent of sites, while values of $\delta\sum^{hf}$ which are positive rapidly decrease in order of α, β, and γ. The overall value at each site agrees qualitatively with observation. In other species, we can get the negative values at γ positions, which were never explained by the current theories.

Somebody will be suspicious of our theoretical result, claiming that parametrizations in the present treatment mask the reliability. However, we think that a theory would be successful, if it present any possibility to explain the observed values under reasonable (to some extent) assumptions.

References

1) J. P. Colpa and J. R. Bolton, *Mol. Phys.*, **6**, 273 (1963).
2) A. D. Mclachlan, *Mol. Phys.*, **4**, 49 (1961).
3) J. Higuchi, *J. Chem. Phys.*, **39**, 3455 (1963).
4) J. R. Bolton, *J. Chem. Phys.*, **43**, 309 (1965).
5) L. S. Cederbaum, F. E. P. Matschke, and W. von Niessen, *Phys. Rev.* *A***12**, 6 (1975).
6) M. P. Kelly, "Advances in Chemical Physics," Interscience Publishers (1968), XIV, p. 129.
7) K. Nishimoto and N. Mataga, *Z. Phys. Chem.*, **13**, 140 (1957).

The Preparation of Mesoporous Silica Gel and the Nature of the Modification of Its Surface with Organoalkoxysilane

Kazuo TANAKA,† Sumio SHINODA, Nobuharu TAKAI,
Hiroshi TAKAHASHI, and Yasukazu SAITO*

Institute of Industrial Science, The University of Tokyo, 22-1, Roppongi 7-Chome, Minato-ku, Tokyo 106

(Received September 26, 1979)

Mesoporous silica gel with a narrow pore-size distribution at the pore diameter of 200 Å has been prepared upon gelation in the presence of starch. Taking into account the effects on the geometrical properties of its surface, two typical surface-modifying procedures that utilize organoalkoxysilane were characterized. Procedure I retains the mesoporous structure, although the fixed amount of the organofunctional group is rather small. Procedure II introduces a large amount of the organofunctional group to the surface, but is accompanied by a pronounced reduction in both the B.E.T. surface area and the specific pore volume. The observed range of the apparent surface concentration of the organofunctional group and the scanning electron micrographs suggest that the surface is coated with highly crosslinked organosiloxane polymers in the latter case. Despite the contrasts between the two modified surfaces, the similarity of C-13 NMR line shapes, chemical shifts, and spin-lattice relaxation times between the respective surface organofunctional groups indicates that their microenvironment and mobility resemble each other.

The modification of the surface of porous adsorbents *via* the chemical bonding of the organofunctional group is now a common procedure to improve them for use as a stationary phase in liquid chromatography[1] or as a support of soluble complex catalysts.[2] A surface reaction with organoalkoxysilane is one of the most popular methods for this purpose, but scarcely physicochemical investigation has been undertaken to examine how the surface is actually "modified" by such a treatment.[1,3]

Since such geometrical properties as the specific pore volume and pore-size distribution govern the efficiency of chromatographic separations[4-6] and the activity and/or selectivity of catalytic reactions,[7] it is especially important to characterize appropriately the effect of the surface modification. From this viewpoint, we prepared mesoporous silica gel with a narrow pore-size distribution at the 200 Å pore diameter, and investigated the change in the geometrical properties associated with the coupling treatment with organoalkoxysilane. In an attempt to characterize the fixed organofunctional groups spectroscopically, C-13 NMR (CMR) spectroscopy was applied to them. Two typical procedures for fixation[8-11] were adopted, and the advantage of each procedure is discussed.

Experimental

Preparation of Mesoporous Silica Gel. Starch (15 g) was dissolved in warm water (500 cm^3), and the resulting solution was mixed with an aqueous solution of colloidal silica (Nissan Chem. Ind., Ltd.; Snowtex-30: SiO_2 content 30—31%; particle diameter 10—20 nm; pH 9.5—10.5; 500 cm^3). The mixed solution was poured into acetone (2.5 dm^3) with stirring and allowed to stand for 4 d with occasional stirring. During this procedure silica gel was precipitated, and the supernatant solution was replaced by acetone (2.5 dm^3) once a day. The silica gel thus formed was filtered, air-dried, milled in an α-alumina mortar, and calcined in air (120 °C, 24 h). After calcination, the color of the silica gel changed from white into light brown. It was decolorized by repeated washing with water, and then boiled three times. After cooling, the water was decanted and acid (concd HNO_3–concd H_2SO_4 150 cm^3; 9/1 Vol.) was added to the residual suspension of silica gel, which was then permitted to stand for 24 h. The treatment with acid was done twice. The sample was washed with water untill the solution became neutral and then dried in a drying oven. Silica gel was evacuated at 200 °C (4 h) immediately before the succeeding fixation treatment.

Procedure for the Fixation of Organofunctional Groups. The fixation of 3-aminopropyl or *N*-(2-aminoethyl)-3-aminopropyl groups to silica gel was effected in two ways. Procedure I: To a toluene solution (100 cm^3) of silane ($NH_2CH_2CH_2CH_2Si(OEt)_3$: Shin-Etsu Chem. Ind., Ltd.; 15.6 g), silica gel (10 g) was added with stirring, after which the suspended solution was refluxed for 24 h. The sample was then transferred to a Soxhlet apparatus, extracted with benzene for 24 h, and dried *in vacuo* (130 °C, 4 h). The fixation procedure for $NH_2CH_2CH_2NHCH_2CH_2CH_2Si(OMe)_3$ (Shin-Etsu Chem. Ind., Ltd.) was performed similarly using the following amounts of reagents: silane, 20.8 g; toluene, 100 cm^3, and silica gel, 15.0 g. Procedure II was the same as Procedure I except that water, in an amount equivalent to that necessary for hydrolyzing the alkoxyl group of the silane, was introduced into the toluene before the addition of silane. In Procedures I and II, about 20 and 70% of the added silane were consumed for fixation respectively.

Characterization of Silica Gels. The B.E.T. surface area (s_{BET}) was determined using the B.E.T. procedure (a_m (N_2) = 16.2 $Å^2$ $molecule^{-1}$). The specific pore volume (v_p) and the pore-size distribution were calculated from the nitrogen adsorption (or desorption) measurements at 77 K, based on the method of Cranston and Inkley,[12] or by means of mercury porosimetry (American Instrument Co., Ltd.; 60000 psi). The amounts of the fixed organofunctional groups were evaluated from the carbon and nitrogen contents of the modified silica gel, as determined from the elemental analysis. In the evaluation, alkoxyl carbons were omitted (*vide infra*), and the two values, coinciding within a 10% deviation, were averaged. Scanning electron micrographs were taken using a Hitachi HHS-2R SEM apparatus. CMR spectra were obtained with noise-modulated proton decoupling on a Fourier-transform pulsed NMR spectrometer (JEOL JNM-FX60), operating at 15.04 MHz.

† Present address: Mitsubishi Gas Chemical Company, Inc., 5—2, Marunouchi 2-Chome, Chiyoda-ku, Tokyo 100.

Results and Discussion

Geometrical Properties of the Surfaces. The prepared silica gel (original silica gel) has the values of 148 $m^2 g^{-1}$ for s_{BET} and 0.792 $cm^3 g^{-1}$ for v_p (calculated at the saturated vapor pressure). In particular, as revealed by mercury porosimetry, it has a maximum abundance of mesopores, amounting to 0.45 $cm^3 g^{-1}$, with an (entrance) pore diameter of about 200 Å (Fig. 1). This feature is probably derived from the effect of the incorporation of starch upon gelation.[13,14] The nitrogen adsorption and desorption isotherms on the silica gel showed hysteresis. The analysis of the isotherms gave the pore-size distributions depicted in Fig. 2. The cumulative pore volumes below 300 Å were 0.427 and 0.653 $cm^3 g^{-1}$ respectively. Since a distinctive peak with a maximum abundance at a pore diameter of about 200 Å appears only in the case of desorption, the mesopores with that pore diameter may be formed with various bottlenecks.

After the modification with Procedure I, the corresponding values became 0.332 $cm^3 g^{-1}$ (nitrogen adsorption), 0.483 $cm^3 g^{-1}$ (nitrogen desorption), and 0.46 $cm^3 g^{-1}$ (mercury porosimetry). As far as the 200 Å-mesopores are concerned, both the mercury porosimetry (Fig. 1) and the nitrogen desorption experiment (Fig. 2) showed distribution patterns similar to those of the original silica gel around this range, and their abundance, evaluated by the mercury porosimetry, was actually hardly affected at all. The application of the V_a-t plot,[15,16] however, showed that the micropores (<7 Å) present on the original silica gel with the surface area of 12 $m^2 g^{-1}$, where S_{total} was evaluated to be 151 $m^2 g^{-1}$, were lost after this modification. It can be said that Procedure I caused little change in the mesopore structure, although it disrupted most of the micropores.

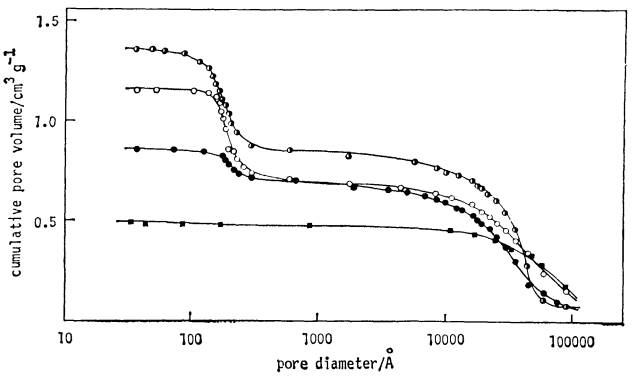

Fig. 1. Mercury intrusion pore size distribution of original and modified silica gels.
○: Original silica gel, ◑: after modification with Procedure I, ●: after modification with Procedure II, ■: Aerosil 380 after modification with Procedure II.

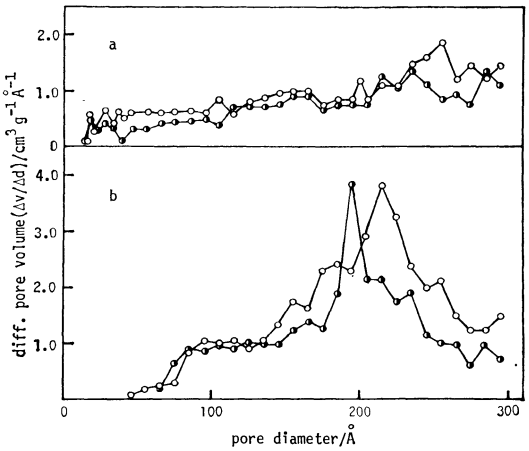

Fig. 2. Pore-size distributions determined from nitrogen adsorption (a) and desorption (b) isotherms.
○: Original silica gel, ◑: after modification with Procedure I.

It was found that Procedure II exerted a further influence on the surface geometrical properties because of the presence of water in the fixation treatment. Figure 1 shows that a large amount of mesopores of the original silica gel disappeared during the treatment. The cumulative pore volume below 300 Å was decreased as low as 0.082 $cm^3 g^{-1}$, and the V_a-t plot indicated that the micropores vanished also in this case. For reference, the result for the Aerosil 380 (Degussa) modified with Procedure II is shown in Fig. 1. Naturally, it exhibits no population in the mesopore range of about 200 Å. The distribution in the pore-size range around tens of thousands ång-

Table 1. Geometrical properities of modified silica gel surfaces and the amounts of fixed organofunctional groups

Fixation procedure	B.E.T. surface area / $m^2 g^{-1}$	Pore volume[a] / $cm^3 g^{-1}$	Fixed organofunctional group: Amount / mmol g^{-1}	Fixed organofunctional group: Apparent surface concentration[b] / Group/100 Å²
Procedure I	116	0.643	0.55	2.8
	95.7	0.566	0.85	5.3
	86.7	0.613	0.84	5.8
Procedure II	29.6	0.208	2.25	45.8
	13.1	0.128	2.70	124
	10.3[c]	0.055[c]	3.90[c]	228[c]

a) Evaluated at the saturated vapor pressure of nitrogen at 77 K. b) Calculated based on the B.E.T. surface area of modified surfaces. c) Modified with (3-aminopropyl)triethoxysilane.

stroms, which was observed in all the cases in Fig. 1, may correspond to the interstitial volume of agglomerated particles.

Table 1 presents the amount of the fixed organofunctional group, together with the values of s_{BET} and v_p, for the silica gels modified by the use of Procedure I or II in repeated runs. It is seen that Procedure II caused a pronounced reduction in both s_{BET} and v_p, but introduced an appreciable amount of organofunctional groups to the surface in comparison with Procedure I. The characteristic mesopores of the original silica gel are retained in Procedure I, whereas in Procedure II they are limited in return for the large amount of fixation. From this viewpoint, the trend shown in Table 1 is consistent with the data of the pore-size distribution.

The influence of these fixation procedures may be noticed plainly in the apparent surface concentration of the fixed organofunctional group (Table 1). In the case of Procedure I, the values have the same order of magnitude as the ordinary surface concentration of hydroxyl groups on silica gels (about 4.8 hydroxyl groups per 100 Å^2).[17] In contrast, Procedure II gave values far exceeding this value.

Scanning Electron Micrographs. Some representative scanning electron micrographs (SEM) of the original and modified silica gels are shown in Fig. 3. A remarkable feature is that the spherical shape of Aerosil 380 is completely lost by the modification with Procedure II. It appears that a number of Aerosil particles were combined and coated with a polymer-like substance, possibly an organosiloxane polymer. The marked decrease in s_{BET} (from 380 to 36 m^2 g^{-1}) seems to support this view. The SEM of the mesoporous silica gel modified with Procedure II also appears to indicate a similar surface coating. The observed range of the apparent surface concentration suggests that highly crosslinked organosiloxane polymers were formed as a result of the trifunctionality of the modifiers. The resemblance between the two silica gels, original and modified with Procedure I, is reasonable in view of the rather small change in the surface characteristics by this modification. It has been suggested that organoalkoxysilane molecules are fixed on silica surfaces in the monomeric form when the amount of physically adsorbed water is small.[1]

CMR Properties. The C-13 nuclear magnetic resonance of the fixed organofunctional group is detectable with high resolution if the solvent used to suspend the modified silica gel is properly chosen.[18] The CMR spectra of the fixed 3-aminopropyl groups are shown in Fig. 4. The absence of ethoxyl carbon resonances confirms that the ethoxyl groups were completely removed in the course of the fixation treatment. It is apparent that the two modified silica gels gave essentially identical spectra despite the salient contrasts between the geometrical properties of their surfaces. The situation was unaltered for the *N*-(2-aminoethyl)-3-aminopropyl group. The chemical shift data are tabulated in Table 2. The observed substantial low-field shift of the C_1 carbon atom seems reasonable in view of the fact that 2-butenes[19] and toluene[20] adsorbed on silica gel or Zeolite show low-field shifts for the carbon atoms pertinent to adsorption.

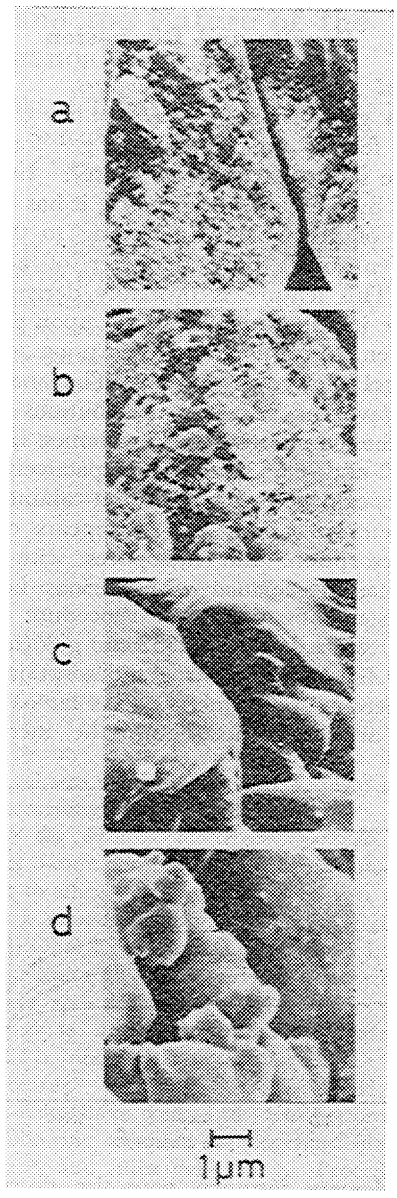

Fig. 3. Scanning electron micrographs of original and modified silica gels.
a: Original silica gel, b: after modification with Procedure I, c: after modification with Procedure II, d: Aerosil 380 after modification with Procedure II.

For the same samples, the spin-lattice relaxation times (T_1) of the carbon atoms were determined by the inversion-recovery method.[21] Table 3 shows that fixation caused a considerable reduction in T_1 values; here, too, there is no distiguishing difference between the two procedures.

The effect of possible paramagnetic impurities in the silica gel on the spin-lattice relaxation is small for the following reasons: (i) for both modified silica gels, the T_1 values of the C_1 carbon atom are significantly different between the two kinds of organofunctional groups, and (ii) the values of the ^{13}C–^1H nuclear Overhauser effect were determined to be 1.3 (C_1) and 1.6 (C_2) for the *N*-(2-aminoethyl)-3-amino-

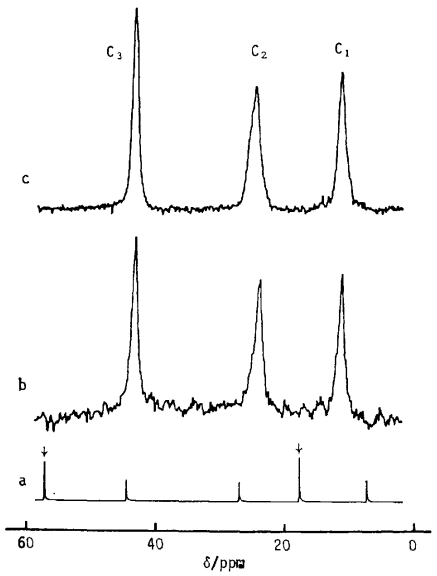

Fig. 4. C-13 NMR spectra of the 3-aminopropyl groups fixed on silica gel and of original alkoxysilane (15 MHz, 10 μs pulse width, 2.0 s pulse interval).
a: 3-Aminopropyltriethoxysilane (neat liquid, 1000 scans), b: fixed with Procedure I (0.96 mmol g^{-1}, D_2O suspension, 69000 scans), c: fixed with Procedure II (3.90 mmol g^{-1}, D_2O suspension, 22000 scans). Numbers are designated from the silicon atom. Arrows indicate the ethoxyl carbon resonances.

propyl group (fixed with Procedure II; $CDCl_3$ solvent), values which are close to the maximum value of this effect (1.988) and which indicate the predominance of ^{13}C–^{1}H dipole-dipole interactions in the relaxation of these carbon atoms.[21] We consider that the observed enhancement of relaxation rates is ascribable to the decrease in the freedom of motion of the organofunctional groups resulting from the anchoring of the silicon atom. The magnitude of T_1 is reasonable for the aliphatic carbon chain, whose translational motion is hindered, but whose internal rotation is almost free, when compared with those for the butyl group anchored in poly(butyl methacrylate) (T_1 in s: C_1 0.12, C_2 0.13, *etc.*).[22] The increase in T_1 from C_1 to C_2 to C_3 reflects the ease of motion, in that order.

It should be noted that the resemblance of line shapes between the spectra suggests that the fixed organofunctional groups obtained with Procedure II have a homogeneity similar to those obtained with Procedure I. This similarity seems noticeable in view of the high crosslinkage of organosiloxane polymers, which was suggested for the former case. Based on the CMR properties reported above, it may be concluded that the microenvironment and the mobility of the fixed organofunctional groups resemble each other in the D_2O solvent, irrespective of the difference in the method of surface modification.

Comparison of the Two Surface-modifying Procedures. The two procedures for surface modification have thus been characterized. In the case of Procedure

Table 2. C-13 chemical shifts of the organofunctional groups fixed on silica gel and of original alkoxysilane[a]

Sample		Medium	Chemical shift/ppm[b]				
Organofunctional group	State		C_1	C_2	C_3	C_4	C_5
$NH_2CH_2CH_2CH_2Si$-	Silane	neat	7.3	27.2	44.8		
	Silica (Procedure I)	D_2O	11.4	24.2	43.6		
	Silica (Procedure II)	D_2O	11.5	24.8	43.7		
$NH_2CH_2CH_2NHCH_2CH_2CH_2Si$-	Silane	neat	6.4	23.1	52.3	52.7	41.8
	Silica (Procedure I)	D_2O	11.6	22.6	50.6	51.8	40.0
	Silica (Procedure II)	D_2O	11.7	23.0	51.0	52.0	40.4

a) Numbers are designated from the silicon atom. b) Downfield from Me_4Si, where the original data, measured relative to 1,4-dioxane present in a concentrically placed capillary tube, are converted using $\delta_{dioxane}=67.4$ ppm. Accurate to ±0.3 ppm.

Table 3. Spin-lattice relaxation times of the organofunctional groups fixed on silica gel and of original alkoxysilane[a]

Sample		Medium	T_1/s[b]				
Organofunctional group	State		C_1	C_2	C_3	C_4	C_5
$NH_2CH_2CH_2CH_2Si$-	Silane	neat	2.27	3.03	3.16		
	Silica (Procedure I)	D_2O	0.25	0.36	0.36		
	Silica (Procedure II)	D_2O	0.21	0.35	0.36		
$NH_2CH_2CH_2NHCH_2CH_2CH_2Si$-	Silane	neat	0.98	0.98	0.97	1.28	1.49
	Silica (Procedure I)	D_2O	0.11	0.14	0.14	0.14	0.18
	Silica (Procedure II)	D_2O	0.10	0.14	0.20	0.14	0.37

a) Numbers are designated from the silicon atom. b) Accurate to ±0.02 s.

II, pores of silica gel as large as 200 Å in pore diameter are covered with organosiloxane polymers, but this procedure has the merit of producing a large quantity of fixation. This may be advantageous for its use as a silica support for preconcentration of trace metals,[23] affinity chromatography, or the immobilization of soluble complex catalysts with high density of active sites.

In contrast, modification with Procedure I retains the mesoporous structure of the silica gel surface. In this case, the ability to separate substances or to select substrates, through differentiating their molecular sizes, can be expected. If this characteristics is employed properly, the utility of the surface organofunctional groups may be enlarged.

The authors whish to thank Mr. Tatsuro Tsuru for the nitrogen adsorption and desorption measurements.

References

1) K. K. Unger, "Porous Silica," Elsevier, New York (1979), Chap. 3.
2) F. R. Hartley and P. N. Vezey, "Advances in Organometallic Chemistry," ed by F. G. A. Stone and R. West, Academic Press, New York (1977), Vol. 15, p. 189.
3) K. K. Unger, N. Becker, and P. Roumeliotis, *J. Chromatogr.* **125**, 115 (1976).
4) R. F. Nolte, S. Specht, and H.-J. Born, *J. Chromatogr.*, **110**, 239, 253 (1975).
5) Yu. A. Eltekov and A. S. Nazansky, *J. Chromatogr.*, **116**, 99 (1976).
6) J. R. Parrish, *Anal. Chem.*, **49**, 1189 (1977).
7) A. Martinec, K. Setinek, and L. Beranek, *J. Catal.*, **51**, 86 (1978).
8) K. G. Allum, R. D. Hancock, I. V. Howell, S. McKenzie, R. C. Pitkethly, and P. J. Robinson, *J. Organomet. Chem.*, **87**, 203 (1975).
9) K. Kochloefl and W. Liebelt, *J. Chem. Soc., Chem. Commun.*, **1977**, 510.
10) R. Jackson, J. Ruddlesden, D. J. Thompson, and R. Whelan, *J. Organomet. Chem.*, **125**, 57 (1977).
11) F. R. W. P. Wild, G. Gubitosa, and H. H. Brintzinger, *J. Organomet. Chem.*, **148**, 73 (1978).
12) R. W. Cranston and F. A. Inkley, "Advances in Catalysis," ed by D. D. Eley, H. Pines, and Paul B. Weisz, Academic Press, New York (1957), Vol. 9, p. 143.
13) J. C. Moore, *J, Polym. Sci. A.*, **2**, 835 (1964).
14) K. Unger and B. Scharf, *J. Colloid Interface Sci.*, **55**, 377 (1976).
15) B. C. Lippens and J. H. de Boer, *J. Catal.*, **4**, 319 (1965).
16) J. H. de Boer, B. G. Linsen, Th. van der Plas, and G. J. Zondervan, *J. Catal.*, **4**, 649 (1965).
17) A. V. Kiselev and V. I. Lygin, "Infrared Spectra of Surface Compounds," Wiley-Interscience, New York (1975).
18) K. Tanaka, S. Shinoda, and Y. Saito, *Chem. Lett.*, **1979**, 179.
19) I. D. Gay and J. F. Kriz, *J. Phys. Chem.*, **82**, 319 (1978).
20) D. Deininger, D. Geschke, and W.-D. Hoffmann, *Z. Phys. Chem.* (Leipzig), **225**, 273 (1974).
21) J. R. Lyerla, Jr., and G. C. Levy, "Topics in Carbon-13 NMR Spectroscopy," ed by G. C. Levy, Wiley-Interscience, New York (1974), Vol .1, p. 79.
22) G. C. Levy, *J. Am. Chem. Soc.*, **95**, 6117 (1973).
23) D. E. Leyden and G. H. Luttrell, *Anal. Chem.*, **47**, 1612 (1975).

 © 1980 The Chemical Society of Japan Bull. Chem. Soc. Jpn., 53, 1247—1251 (1980)

Synthesis and Electrical Properties of TCNQ Radical Anion Salts with *N,N'*-Ethylenedi(1,3-dithiolan-2-iminium) Dication and Related Dications

Yoshiji Yumoto, Ryoji Nishioka, and Toshio Tanaka*

Department of Applied Chemistry, Faculty of Engineering, Osaka University, Suita, Osaka 565

(Received September 27, 1979)

Simple and complex salts of the $TCNQ^{-}$ radical anion with *N,N'*-ethylenedi(1,3-dithiolan-2-iminium) dication and related dications, 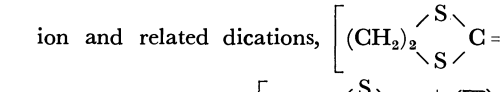 $(TCNQ)_m^{2-}$ (R=H, Me; n=2, 6; m=2, 3, or 4) and 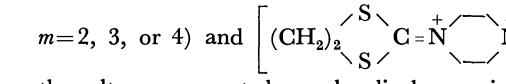 $(TCNQ)_m^{2-}$ (m=2, 3) were synthesized. All the salts as compacted samples display semiconducting behaviors in the 77—300 K range. Electrical resistivities of the simple salts are in the range of 1.8×10^{5}—9.8×10^{7} Ω cm at 25 °C. Electronic absorption spectra and magnetic susceptibilities suggest that the simple salts in the solid state involve $(TCNQ)_2^{2-}$ dimer. The 1 : 3 complex salt of *N,N'*-dimethyl-*N,N'*-ethylenedi(1,3-dithiolan-2-iminium) with TCNQ, 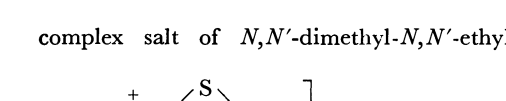 $(TCNQ)_3^{2-}$, exhibits a lower electrical resistivity (3.4 Ω cm) than other four complex salts (2.4×10—2.5×10^{3} Ω cm). Electronic absorption spectra and magnetic susceptibilities of the both 1 : 3 and 1 : 4 complex salts are interpreted in terms of the interaction between the TCNQ moieties.

According to the molecular requirements for obtaining highly conducting 7,7,8,8-tetracyanoquinodimethane (TCNQ) salts, for example, planar structure and high polarizability of the cation moiety, one of the authors recently prepared some simple and complex salts formed between *N,N*-dialkyl-1,3-dichalcogenacycloalkan-2-iminium cations and $TCNQ^{-}$ radical anion;

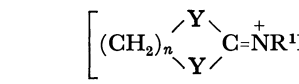

and

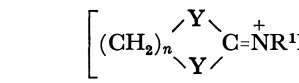

(n=2 or 3; Y=S or Se; R^1=R^2=Me, Et, *n*-Pr, *n*-Bu, *n*-C_6H_{13}, *n*-C_8H_{17}, *n*-$C_{10}H_{21}$, and Ph; R^1=Me and R^2=Ph).[1,2] All of these salts showed semiconducting behaviors. Electrical resistivities of the complex salts as compacted samples fell in the 2.4—90 Ω cm range at 25 °C with activation energies of 0.018—0.12 eV, whereas the simple salts exhibited the electrical resistivities of 4.4×10^{3}—1.3×10^{9} Ω cm with activation energies of 0.16—1.3 eV.

Thus, the iminium cations may be useful as cation sources in the synthesis of electrical conducting organic crystals. In this study, we have taken up di(1,3-dithiolan-2-iminium) dications, **A** and **B**, as the cation moieties of $TCNQ^{-}$ salts.

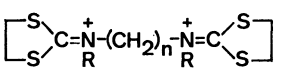

A

R= H, Me; n=2, 6

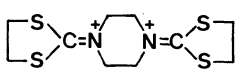

B

These dications are expected to have potential possibility of the formation of unusual stoichiometric $TCNQ^{-}$ salts with interesting electrical and magnetic properties. In fact, the stoichiometries of diquarternized 1,2-di(4-pyridyl)ethane and 1,2-di(4-pyridyl)-ethylene salts with TCNQ are 1:3,[3] 1:4,[4] 1:5,[5] and 2:5,[6] and the 1:4 complex salt of 1,2-bis(1-ethylpyridinim-4-yl)ethylene dication with the $TCNQ^{-}$ radical anion exhibit a metallic behavior below room temperature.[7]

This paper reports the preparation and electrical resistivity of some simple and complex salts of $TCNQ^{-}$ with the iminium dications. Electronic absorption spectra and magnetic susceptibilities of these salts are discussed in terms of the interaction between the TCNQ moieties.

Experimental

Disodium polymethylenebis(dithiocarbamate) (**1a—d**) were prepared as described in the literature.[8] Bis(triethylammonium) 1,4-piperazinebis(carbodithioate) (**2**) were obtained similarly by the reaction of piperazine in ethanol with triethylamine, followed by the addition of carbondisulfide.

N,N'-Ethylene-, *N,N'-Dimethyl-N,N'-ethylene-*, *N,N'-Hexamethylene-*, *N,N'-Dimethyl-N,N'-hexamethylenedi(1,3-dithiolan-2-iminium) and N,N'-Bis(1,3-dithiolan-2-ylidene)piperazine-1,4-dium Salts (**3a—d** and **4**).* To a suspension of **1a** (3.0 g, 12 mmol) in ethanol (20 ml) was added large excess 1,2-dibromoethane (5.1 g). The mixture was refluxed for 6 h, during which time white color of the suspension turned to yellow. A floating solid material in the suspension was collected by filtration and recrystallized from water to give white needles of *N,N'*-ethylenedi(1,3-dithiolan-2-iminium) dibromide (**3a**) in a 40% yield; mp 210—212 °C. Found: C, 22.26; H, 3.35; N, 6.60%. Calcd for $C_8H_{14}N_2S_4Br_2$: C, 22.54; H, 3.32; N, 6.57%. Similarly four other iminium dications were obtained as hexafluorophosphate or tetraphenylborate in 40—55% yields by the reaction of **1b—d** or **2** with excess 1,2-dibromoethane in ethanol, followed by the addition of ammonium hexafluorophosphate or sodium

tetraphenylborate. *N,N'*-Dimethyl-*N,N'*-ethylenedi(1,3-dithiolan-2-iminium) bis(hexafluorophosphate) (**3b**), mp 280—281 °C. Found: C, 20.26; H, 3.05; N, 4.68%. Calcd for $C_{10}H_{18}N_2S_4P_2F_{12}$: C, 20.55; H, 3.10; N, 4.79%. *N,N'*-Hexamethylenedi(1,3-dithiolan-2-iminium) bis(hexafluorophosphate) (**3c**), mp 198—200 °C. Found: C, 23.27; H, 3.58; N, 4.63%. Calcd for $C_{12}H_{22}N_2S_4P_2F_{12}$: C, 23.53; H, 3.62; N, 4.57%. *N,N'*-Dimethyl-*N,N'*-hexamethylenedi(1,3-dithiolan-2-iminium) bis(hexafluorophosphate) (**3d**), mp 225—227 °C. Found: C, 26.03; H, 4.02; N, 4.25%. Calcd for $C_{14}H_{26}N_2S_4P_2F_{12}$: C, 26.25; H, 4.09; N, 4.37%. *N,N'*-Bis(1,3-dithiolan-2-ylidene)piperazine-1,4-diium bis(tetraphenylborate) (**4**), mp 260—262 °C. Found: C, 74.10; H, 6.13; N, 3.23%. Calcd for $C_{53}H_{56}N_2S_4B_2$: C, 74.83; H, 6.06; N, 3.01%.

N,N'-Ethylene-, *N,N'-Dimethyl-N,N'-ethylene-*, *N,N'-Hexamethylene-*, *N,N'-Dimethyl-N,N'-hexamethylenedi(1,3-dithiolan-2-iminium) and N,N'-Bis(1,3-dithiolan-2-ylidene)piperazine-1,4-diium-TCNQ Simple Salts (5—9).* To a boiling ethanol (20 ml) solution of $Li^+TCNQ^{\cdot-}$ (0.50 g, 2.4 mmol) was added a hot aqueous (10 ml) solution of **3a** (0.50 g, 1.2 mmol). The mixture was allowed to stand in a refrigerator overnight. The resulting precipitate was recrystallized from acetonitrile to give **5** in a 71% yield. Other four simple salts **6—9** were prepared similarly by the equimolar reaction of $TCNQ^{\cdot-}$ in ethanol with the appropriate iminium dications in an acetonitrile/ethanol mixture (2:1 v/v), 67—85% yields.

N,N'-Ethylene-, *N,N'-Dimethyl-N,N'-ethylene-*, *N,N'-Haxamethylene-*, *N,N'-Dimethyl-N,N'-hexamethylenedi(1,3-dithiolan-2-iminium) and N,N'-Bis(1,3-dithiolan-2-ylidene)piperazine-1,4-diium-TCNQ Complex Salts (10—14).* To a boiling acetonitrile (50 ml) solution of the simple salt **5** (0.53 g, 0.78 mmol) was added two equivalent amounts of neutral TCNQ (0.32 g, 1.6 mmol) in boiling acetonitrile (25 ml). The mixture was allowed to stand at room temperature to afford **10** in a 75% yield. Similarly other complex salts **11—14** were prepared by the reactions of **6—9** with neutral TCNQ at the mole ratio of 1:2 in acetonitrile, respectively, 64—71% yields.

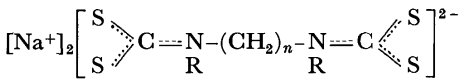

1a: R=H; n=2
1b: R=Me; n=2
1c: R=H; n=6
1d: R=Me; n=6

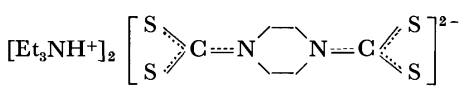

2

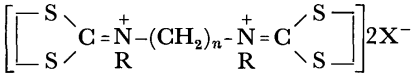

3a: R=H; n=2; X=Br
3b: R=Me; n=2; X=PF_6
3c: R=H; n=6; X=PF_6
3d: R=Me; n=6; X=PF_6

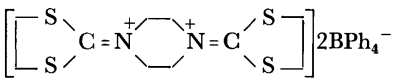

4

Table 1. Analytical data and properties of the $TCNQ^{\cdot-}$ salts

No.	Salt	Color	Mp(dec.) °C	%C Found (Calcd)	%H Found (Calcd)	%N Found (Calcd)	$TCNQ^{a)}/TCNQ^{\cdot-}$
5	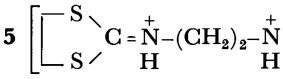	Violet microcrystals	195—197	57.21 (56.96)	3.45 (3.29)	20.43 (20.76)	
6	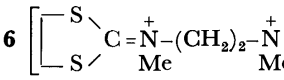	Dark-violet needles	228—230	56.99 (56.64)	3.56 (3.92)	19.46 (19.43)	
7	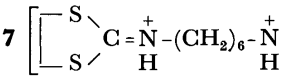	Dark-violet needles	155—157	58.93 (59.16)	4.08 (4.14)	19.30 (19.16)	
8	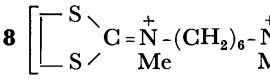	Dark-violet needles	177—181	59.16 (60.12)	4.33 (4.52)	18.06 (18.46)	
9	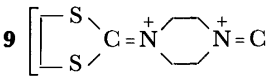	Violet needles	250—252	57.81 (58.28)	3.75 (3.67)	21.09 (20.79)	
10	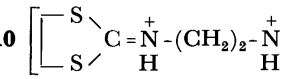	Black microcrystals	215—216	60.28 (60.05)	2.76 (3.18)	22.90 (22.84)	0.48
11	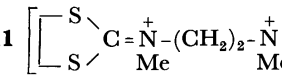	Black microcrystals	292—294	61.12 (60.92)	3.09 (3.33)	21.69 (21.62)	0.49
12	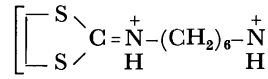	Black microcrystals	231—233	63.54 (63.25)	3.32 (3.36)	22.01 (22.13)	0.95
13	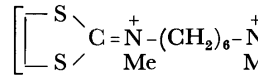	Black cubes	255—259	63.60 (63.78)	3.44 (3.63)	21.49 (21.60)	0.94
14	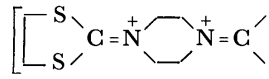	Black microcrystals	275—277	60.80 (61.05)	3.22 (3.12)	21.43 (21.67)	0.48

a) See text.

Physical Measurements. Electrical resistivities were measured as described previously,[1] in the 286—370 K range (for **5**—**9** and **12**) or using a OXFORD CF 104 cryostat equipped with digital temperature controller DTC-2 in the 77—300 K range (for **10**, **11**, **13**, and **14**). Electronic spectra were recorded on a HITACHI 340 spectrophotometer (3900—16700 cm^{-1}) and a UNION GIKEN SM 401 spectrophotometer (11100—50000 cm^{-1}). Infrared spectra were measured on a HITACHI 215 infrared spectrophotometer. Magnetic susceptibilities were measured for microcrystalline materials by a SHIMADZU MB-11 magnetic balance in the range of 77—300 K.

Results and Discussion

Synthesis and Characterization. Five *N,N'*-polymethylenedi(1,3-dithiolan-2-iminium) dications reacted with TCNQ$^{\cdot-}$ radical anion to give simple salts **5**—**9** with the composition of 1:2. Simple salts **5**, **6**, and **9** further reacted with neutral TCNQ in acetonitrile to afford the 1:3 complex salt, irrespective of the mole ratio of the reactants. On the other hand, the reactions of simple salts **7** and **8** with neutral TCNQ yield the 1:4 complex salts. This variation in compositions of the complex salts may reflect the distance between two cation sites in a given iminium dication.

The ratios of the TCNQ$^{\cdot-}$ radical anion to neutral TCNQ in these complex salts (Table 1) were determined by the absorbances at 395 and 842 nm in acetonitrile,[9] where the absorbance at 395 nm is a sum of those for the TCNQ$^{\cdot-}$ radical anion and neutral TCNQ and the absorbance at 842 nm is due to only the TCNQ$^{\cdot-}$ radical anion.

Electrical Properties. Temperature dependence of electrical resistivities for the simple and complex salts are illustrated in Fig. 1. The electrical resistivities (ρ) of simple and complex salts at 25 °C and the activation energies (E_a) calculated from the Arrhenius plots based on the equation, $\rho=\rho_0\exp(E_a/kT)$, are listed in Table 2, where ρ_0 is the constant value and k is the Boltzmann's constant. All the simple and complex salts showed typical semiconducting behaviors in the temperature range measured. The ρ values of simple salts **5**—**9** are in the same range as those of *N,N*-dialkyl-1,3-dithiolan-2-iminium-TCNQ$^{\cdot-}$ simple salts, 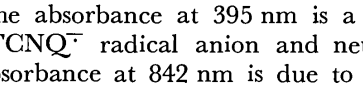 (R=Me, *n*-Pr, *n*-C_6H_{13}; $2.2\times10^5-1.3\times10^7$ Ω cm).[1,2] The ρ values shown in Table 2 indicate that the substitution of methyl group on the iminium nitrogen is more or less effective for obtaining organic salts with low electrical resistivities (compare **6**, **8**, **11**, and **13** with **5**, **7**, **10**, and **12**, respectively). On the other hand, the ρ values do not seem to be rationalized in terms of the methylene chain lengths (for instance, compare **12** and **13** with **10** and **11**, respectively), though more methylene groups between the two cation sites in a given iminium dications is possible to result in lowering planarity of the iminium dications. It should be noted that complex salt **11** exhibits a small ρ value, which is compared with those of *N,N*-dimethyl- and *N,N*-diethyl-1,3-dithiolan-2-iminium–TCNQ$^{\cdot-}$ complex salts, (3.8 and 3.3 Ω cm for R=Me and Et, respectively).[1] The resistivity, however, is larger by one order of magnitude than that of the highest conducting complex salt, quinolinium(TCNQ)$_2^{\cdot-}$ (0.5 Ωcm as compacted sample).[10]

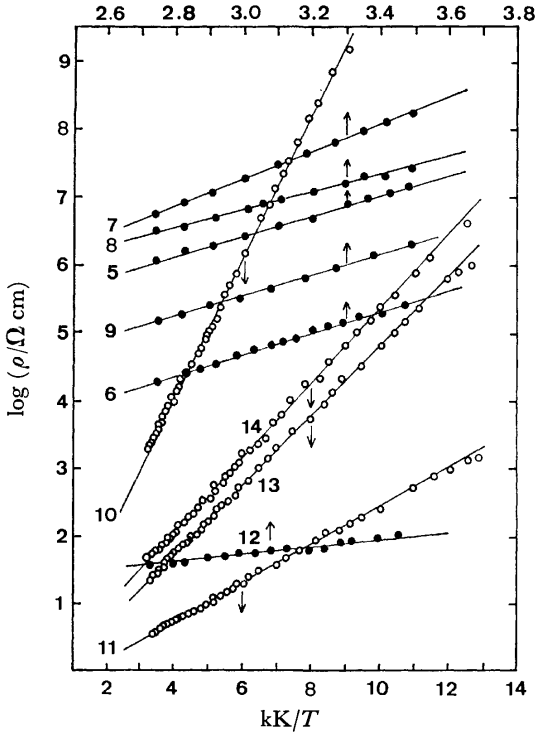

Fig. 1. Temperature dependence of the resistivity of the TCNQ$^{\cdot-}$ salts.

Table 2. Electrical resistivity (ρ) and activation energy (E_a) of the TCNQ$^{\cdot-}$ salts

Salt	$\rho_{25\,°C}$ / Ω cm	E_a / eV
Simple salt		
5	8.9×10^6	0.30
6	1.8×10^5	0.32
7	9.8×10^7	0.40
8	1.9×10^7	0.26
9	1.3×10^6	0.30
Complex salt		
10	2.5×10^3	0.21
11	3.4	0.058
12	9.2×10	0.12
13	2.4×10	0.10
14	5.3×10	0.11

Electronic Spectra and Magnetic Properties. Figure 2 illustrates the electronic absorption spectra of **6**, **11**, and **13** in the solid state. Simple salt **6** exhibits three absorption bands in the range of 4000—32000 cm^{-1}, of which the lowest energy band is assigned to the charge-transfer (CT) transition between the TCNQ$^{\cdot-}$ radical anions and the remaining two bands to the (TCNQ)$_2^{2-}$ dimer.[11] The presence of the (TCNQ)$_2^{2-}$ dimer in **6** is supported also from its diamagnetic property in the solid state at room temperature (χ_M=

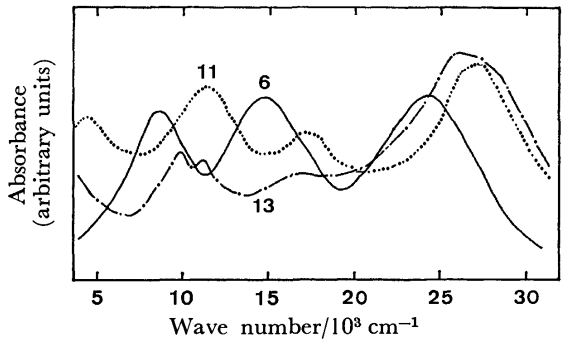

Fig. 2. Electronic absorption spectra of **6**, **11**, and **13** in Nujol mulls.

Table 3. Absorption maxima of the electronic spectra of the $TCNQ^{\cdot-}$ salts in nujol mulls

Salt	Wave number/10^3 cm^{-1} a)				
Simple salt					
5			8.3	15.1	24.7
6			8.5	14.5	24.4
7			9.0	15.0	25.2
8			8.3	15.3	25.5
9			8.9	14.9	24.5
Complex salt					
10	4.6		10.8	16.1	26.3
11	4.4		11.4	17.2	27.2
12		10.0	11.5	(17.0)	26.7
13		9.9	11.4	(16.7)	25.8
14	4.7		11.0	17.2	26.8

a) Shoulders in parentheses.

-3.0×10^{-4} emu mol^{-1}). Other four simple salts **5**, **7**, **8**, and **9** in the solid state showed electronic absorption spectra similar to that of **6**, as listed in Table 3. They also exhibited diamagentic properties at room temperature, which suggest that two $TCNQ^{\cdot-}$ radical anions are coupled completely with each other, resulting in the formation of the $(TCNQ)_2^{2-}$ dimer pair in solid **5**, **7**, **8**, and **9**.

The spectrum of **11** showed four absorption maxima in the 4000—32000 cm^{-1} range, of which the lowest energy band may be due to the CT transition between the $TCNQ^{\cdot-}$ radical anion and neutral TCNQ,[11] whereas the spectral appearance of the remaining three bands roughly resembles that of simple salt **6**, suggesting that the $TCNQ^{\cdot-}$ radical anions more or less interact with each other regardless of the additional TCNQ in neutral form. This is consistent with the diamagnetic property of **11** at room temperature ($\chi_M=-1.2\times10^{-4}$ emu mol^{-1}). In addition, the spectral features of **11** are very similar to those of $(Cs^+)_2(TCNQ)_3^{2\cdot-}$,[11] (morpholinium$^+$)$_2$(TCNQ)$_3^{2\cdot-}$,[11] and $\left[(CH_2)_2\begin{smallmatrix}S\\S\end{smallmatrix}C{=}\overset{+}{N}(n\text{-}C_{10}H_{21})_2\right]_2(TCNQ)_3^{2\cdot-}$.[2] Complex salt **11** is, therefore, suggested to have a stacking of TCNQ moieties similar to these 2:3 complex salts, where exists the unit consisting of two $TCNQ^{\cdot-}$ radical anions and one neutral TCNQ. The same conclusion can be drawn for **10** and **14** on the basis of their electronic spectra similar to that of **11** and diamagnetisms at room temperature.

The 1:4 complex salt **13** exhibits a spectrum similar to those of the 1:2 complex salts of *N*,*N*-dialkyl-1,3-dithiolan-2-iminium cations, $\left[(CH_2)_2\begin{smallmatrix}S\\S\end{smallmatrix}C{=}\overset{+}{N}R_2\right]$-$(TCNQ)_2^{\cdot-}$ (R= *n*-Pr, *n*-Bu, and Ph);[2] the intense absorption around 26000 cm^{-1} may be contributed from both the LE_2 state of the $TCNQ^{\cdot-}$ radical anion and the excited state of neutral TCNQ.[11] The band around 10000 cm^{-1} may be assigned to a transition to the LE_1 state[11] of the $TCNQ^{\cdot-}$ radical anion. The presence of monomeric $TCNQ^{\cdot-}$ is consistent with the fact that **13** showed a paramagnetism at room temperature ($\chi_M=6.6\times10^{-4}$ emu mol^{-1}). Another 1:4 complex salt **12** also exhibited essentially the same spectrum as **13** in the solid satte (Table 3). In addition, **12** and **13** showed a very broad band ranging from 4000 to 2500 cm^{-1}, which was never seen in the spectra of simple salts **5**—**9**. This band is assigned to the CT transition between $TCNQ^{\cdot-}$ and neutral TCNQ.[11]

Temperature dependence of the paramagnetic terms (χ_P) for complex salts **11** and **13** are illustrated in Fig. 3. The susceptibilities were obtained by subtracting the diamagnetic term calculated from Pascal's constants from the observed molar susceptibilities χ_M. Complex salt **11** obeys the Curie-Weiss' law. On the other hand, **13** shows a maximum near 160 K and its paramagnetic susceptibility increases as the temperature increases above 190 K. This behavior may indicate that the interaction between the unpaired electrons is changing irregularly with temperature. Whether the interaction is due to antiferromagnetic interaction, or the singlet-triplet equilibrium which

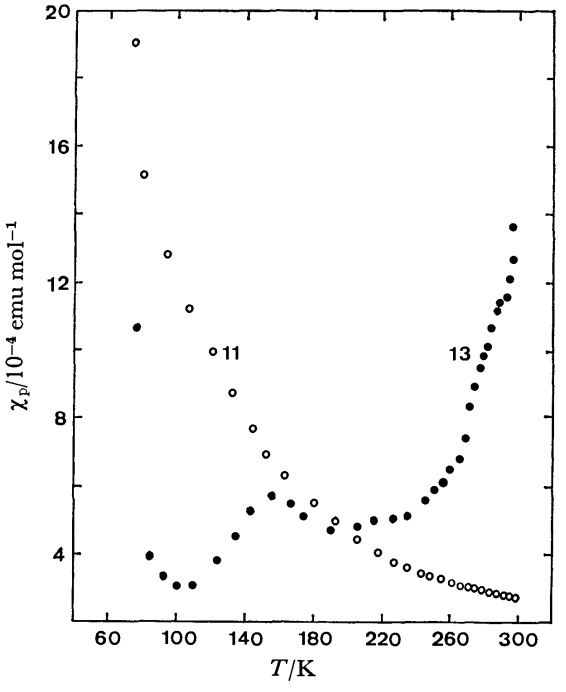

Fig. 3. Temperature dependence of paramagnetic susceptibilities of **11** and **13**.

has been reported in intermediate conductive 1:2 complex salts such as $Et_3\overset{+}{N}H(TCNQ)_2^{\cdot-}$,[12] is not clear in the present work. However, it is noted that the degree of the localization of the unpaired electrons (or spins) may be somewhat larger in **13** than **11**. This assumption may be correlated with the fact that **13** has a larger ρ value by one order of magnitude than **11**.

The authors wish to express their thanks to the Central Research Institute, Matsushita Electric Industrial Co., Ltd. for supplying a sample of TCNQ. They also would like to thank Professor Jiro Shiokawa of Osaka University for giving them the opportunity to use a magnetic balance. This work was carried out with a Grant-in-Aid for Scientific Research No. 347066 from the Ministry of Education, Science and Culture.

References

1) S. Araki, H. Ishida, and T. Tanaka, *Bull. Chem. Soc. Jpn.*, **51**, 407 (1978).
2) S. Araki and T. Tanaka, *Bull. Chem. Soc. Jpn.*, **51**, 1311 (1978).
3) A. Rembaum, A. M. Hermenn, F. E. Stewart, and F. Gutmann, *J. Phys. Chem.*, **73**, 513 (1969).
4) G. J. Ashwell, D. D. Eley, R. J. Fleming, S. C. Wallwork, and M. R. Willis, *Acta Crystallogr., Sect. B*, **32**, 2948 (1976); G. J. Ashwell, D. D. Eley, N. J. Drew, S. C. Wallwork, and M. R. Willis, *ibid.*, **33**, 2598 (1977).
5) G. J. Ashwell, D. D. Eley, A. Harper, A. C. Torrance, S. C. Wallwork, and M. R. Willis, *Acta Crystallogr., Sect. B*, **33**, 2258 (1977); G. J. Ashwell, D. D. Eley, N. J. Drew, S. C. Wallwork, and M. R. Willis, *ibid.*, **34**, 3608 (1978).
6) G. J. Ashwell, D. D. Eley, S. C. Wallwork, M. R. Willis, G. D. Welch, and J. Woodward. *Acta Crystallogr., Sect. B*, **33**, 2252 (1977).
7) G. J. Ashwell, D. D. Eley, and M. R. Willis, *Nature*, **259**, 201 (1976); G, J. Ashwell, D. D. Eley, M. R. Willis, and J. Woodward, *Phys. Status Solidi B*, **79**, 629 (1977).
8) H. L. Klöpping and G. J. M. Van der Kerk, *Recl. Trav. Chim. Pays-Bas*, **70**, 949 (1951).
9) M. Murakami and S. Yoshimura, *Bull. Chem. Soc. Jpn.*, **48**, 157 (1975).
10) L. R. Melby, R. J. Herder, W. R. Hertler, W. Mahler, R. E. Benson, and W. E. Mochel, *J. Am. Chem. Soc.*, **84**, 3374 (1962).
11) Y. Iida, *Bull. Chem. Soc. Jpn.*, **42**, 71, 637 (1969); J. Tanaka, M. Tanaka, T. Kawai, T. Takabe, and O. Maki, *ibid.*, **49**, 2358 (1976).
12) R. G. Kepler, *J. Chem. Phys.*, **39**, 3528 (1963); I. F. Shchegolev, *Phys. Status Solidi A*, **12**, 9 (1972).

Electronic Structures of Purine Bases Studied by Electrochemical-ESR Techniques. Spin Distribution in Purine Anion Radical

Hiroaki OHYA-NISHIGUCHI,* Yasunori SHIMIZU, Noboru HIROTA,† and Kohji WATANABE††

Department of Chemistry, Faculty of Science, Kyoto University, Kyoto 606

†† *Institute for Chemical Research, Kyoto University, Uji Kyoto 611*

(Received September 29, 1979)

We have investigated the ESR spectrum of anion radical of purine generated electrochemically using a helical electrode cell for low-temperature ESR measurements. The assignment of the hfcc was made with the aid of partial deuteration and MO calculations. The most notable observation is that about 45% of the spin density is localized at position 6. This correlates well with the preferential hydrogenation at this position. The McLachlan method reproduces the observed spin distribution well with $\beta_{N9C}/\beta_{CC}=1.0$, which indicates that the bonding between the nitrogen at 9 and carbons at 4 and 8 have large double bond characters. The INDO-MO calculations based on the two molecular geometries for 9*H*-purine also agree well with the experimental data. Finally the effect of tautomerism of purine on the spectrum is discussed.

Since Pullman-Pullman's first theoretical work[1] a wide variety of experimental and theoretical investigations[2] have been made on biologically important purine bases in order to elucidate their electronic strucutres. For example, the lowest excited singlet state has been identified as a $n\pi^*$ state from the electronic absorption spectrum of purine(I).[3] Nuclear magnetic resonance (NMR) spectroscopy of H, ^{13}C and ^{15}N in purines[4,5] has given useful information regarding their tautomeric behavior of the labile protons. Theoretical calculations using different methods have been made on excited state energies,[3,6] electron distribution,[2,7,8] dipole moments,[7,8] and zero field splittings in triplet states.[9,10]

In order to evaluate the results of various theoretical calculations it is important to have experimental data on the details of electronic wave functions, but such data have not been available on purines so far. Electron spin resonance (ESR) spectroscopy in solution is capable of providing the most direct information on the wave functions of π electrons through hyperfine studies, but their radical species in solution have not been detected before, presumably because of their instabilities. In 1974 Yao and Musha investigated the electrochemical reduction of I in nonaqueous solvents and reported an ESR spectrum which they ascribed to the purine anion radical($I^{\cdot-}$),[11] but this is questionable because of its unusually large hyperfine coupling constants.

One of the present authors (H. O.) recently developed a two-electrode electrolysis cell using a helix for low-temperature ESR measurements which has several advantages over the commonly used electrolysis cell for ESR in obtaining the spectra of unstable anion radicals.[12] Using this cell we have succeeded in obtaining an ESR spectrum which is assigned to $I^{\cdot-}$ with reasonable certainty. In this paper we first report the ESR spectra of the anion radicals of I, 8-deuteriopurine(I-*d*) and 6,8-dideuteriopurine(I-d_2) produced electrochemically at low temperatures and analyze them using the computer simulations. Secondly the hyperfine coupling constants (hfcc) obtained are compared with those calculated by McLachlan's method and INDO-MO method established by Pople and Beveridge.[13] Both calculations are carried out based on the two tautomeric forms, 7*H*- and 9*H*-purines. Thirdly we discuss the effect of tautomerism of I in relation to the NMR results.[4]

Experimental

Purine(Aldrich) was normally used without further purifications. Identical results were obtained by using purine purified by vacuum sublimation. I-*d* and I-d_2 were synthesized by heating purine in refluxing D_2O for 4 h and 72 h, respectively, according to the method by Schweizer *et al.*[14] From the proton NMR spectra it was shown that I-*d* was produced completely, but I-d_2 sample was found to contain I-*d* by 35%. Acetonitrile(AN) and butyronitrile(BN) were purified according to the method of Van Duyne and Reilly.[15] After being dried with molecular sieve 4A, *N*,*N*-dimethylformamide(DMF) was distilled over fresh molecular sieve 4A. Just before the preparation of the sample solution DMF was shaken with Na_2SO_4 to ensure complete dryness of the solvent and was transferred to the electrolysis cell with a pipet in an atmosphere of dry nitrogen gas. This process was effective of prolong the lifetime of the purine anion radical. As the supporting electrolyte tetrabutylammonium perchlorate(TBAP) or tetrabutylammonium tetrafluoroborate-(TBFB) (Nakarai Chemical Ltd., SP grade for polarography) was used without further purifications. Electrochemical reduction of I, I-*d* and I-d_2 were carried out inside the cavity using the cell consisting of a helix and a gold wire going through inside the helix. The details of the cell construction were given previously,[12] ESR spectra were taken with a JEOL PE-3 spectrometer equipped with a temperature controller.

Results and Discussion

ESR Spectra. After the temperature of the solution was decreased as low as −50 °C the voltage applied between the two electrodes was increased until the ESR signal could be observed on an oscilloscope or a recorder with the modulation amplitude of 1.0×10^{-4} T. As the voltage reached −6.0 V an ESR signal with hyperfine structures appeared. In view of the results of a electrochemical study of purine by Yao and Musha[11] the observed ESR spectrum is

† Also Department of Chemistry, State University of New York at Stony Brook, Stony Brook, N. Y. 11794, U.S.A.

most likely due to $I^{\cdot-}$. This appearance voltage(V_a) is appreciably lower than twice the half-wave reduction potential ($E^r_{1/2}$) of I measured by Yao and Musha (−2.30 V). However, the previous work[12] has shown that V_a is considerably lower than twice $E^r_{1/2}$, when the produced anion radical is unstable. Hence $I^{\cdot-}$ is likely to be highly reactive. For the observation of high resolution spectra a voltage of −7.0 V or lower was applied during the ESR measurements. ESR measurements were made with low modulation amplitude of the order of 0.1×10^{-4} T. The spectrum intensity reached its maximum in several minutes and disappeared at most in 20 minutes.

A typical example of the spectrum taken with the modulation amplitude of 10^{-5} T is shown in Fig. 1a. It can be satisfactorily interpreted in terms of the three doublet splittings of 10.46, 4.80 and 1.75×10^{-4} T due to protons, and the three triplet splittings of 4.47, 1.14 and 0.28×10^{-4} T due to nitrogen nuclei. This interpretation of the spectrum was confirmed by the computer simulation made by using these splittings and the linewidths of 0.45×10^{-4} T (Fig. 1b). It should be noticed that the observed spectrum consists of the hyperfine splittings due to only one species.

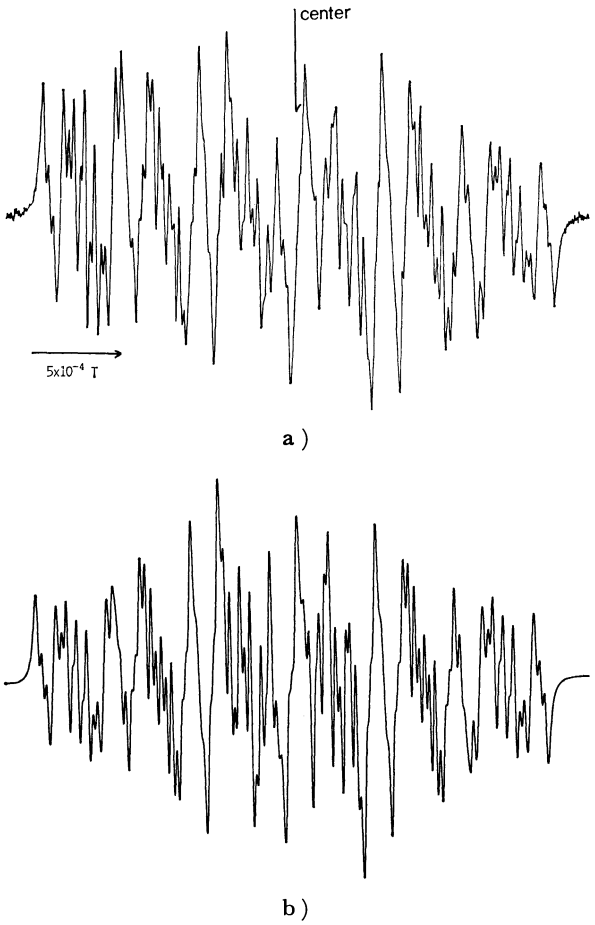

Fig. 1. a) ESR spectrum of $I^{\cdot-}$ generated electrochemically in DMF with 0.1 M TBAP at −50 °C, the applied voltage between two electrodes being −7.0 V. b) The simulation spectrum based on the data in Table 1. Total width: 28.79×10^{-4} T, line width: 0.450×10^{-4} T.

Recent evidence based on ^{13}C NMR indicates that I in dimethyl sulfoxide (DMSO) is in an equilibrium between 7*H*- and 9*H*-purine at room temperature, the ratio of the former to the latter being 4:6.[4] We have not detected so far any evidence for the existence of such tautomerism in our system. The experimental conditions, such as temperature, solvent used, supporting reagent, purification steps of I, have been altered, but the same spectrum was observed. The *g*-value of the spectrum was 2.0028, being close to that of free electron.

In order to ascertain the identification of the anion radical and to assign the proton hfcc, we have also taken the ESR spectra of I-$d^{\cdot-}$ and I-$d_2^{\cdot-}$ in DMF at −50 °C. Their spectra were resolved well enough to allow the analysis of hfcc (Fig. 2 and 3), though the spectrum of I-d_2 was superposed with the spectrum due to 35% of I-*d*. In table 1 the observed hfcc are summarized with those calculated by Hückel molecular orbital (HMO) modified with McLachlan's method.[16] From the comparison of the coupling constants of $I^{\cdot-}$ with those of I-$d^{\cdot-}$ and I-$d_2^{\cdot-}$ two coupling constants, 10.46 and 4.80G can be assigned unequivocally to positions 6 and 8, respectively. The others cannot be assigned experimentally but are tentatively assigned to the particular positions in the molecule

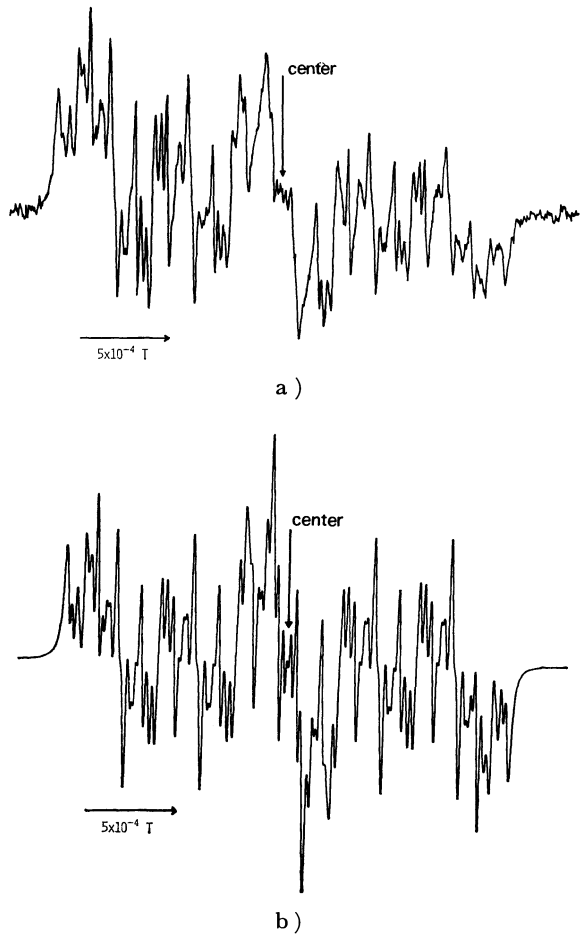

Fig. 2. a) ESR spectrum of I-$d^{\cdot-}$ generated with the same conditions as in Fig. 1a. b) The simulation spectrum based on the data in Table 1. Total width: 25.47×10^{-4} T, line width: 0.400×10^{-4} T.

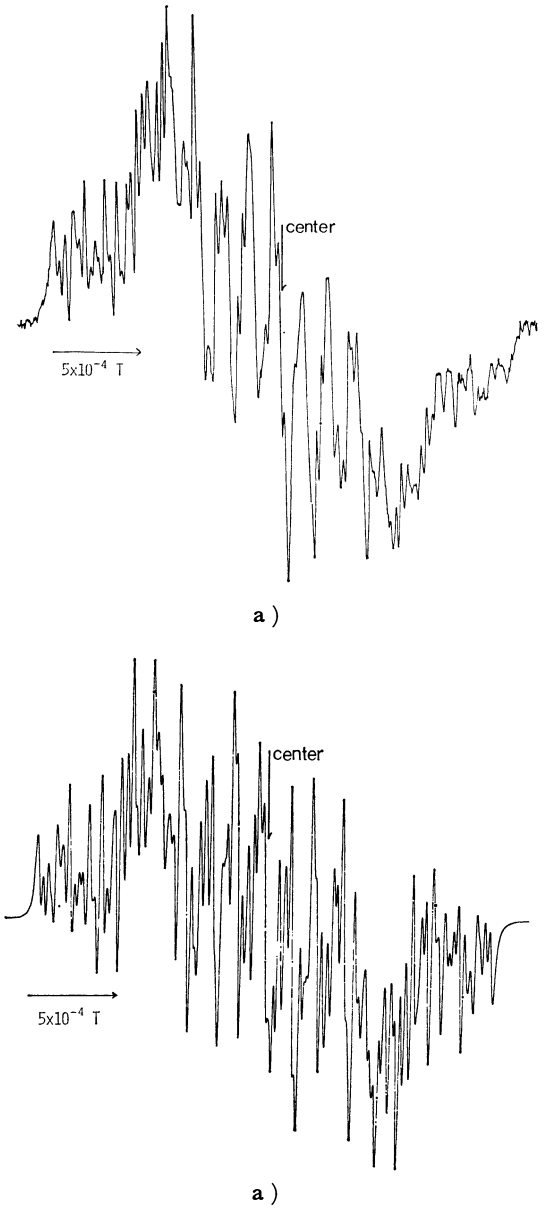

Fig. 3. a) ESR spectrum of I-d_2^- including 35% I-d^- generated with the same conditions as in Fig. 1a. b) The simulation spectrum based on the data in Table 1. Total width: 18.23×10^{-4} T for I-d_2^- and 25.47×10^{-4} T for I-d^-, The ratio of their intensities: 65:35, line width: 0.400×10^{-4} T.

from the comparison of the experimental data with those obtained by the MO calculations (Table 1).

Comparison with Molecular Orbital Calculations. The molecule of I is usually represented by the form in which the labile proton is attached to the N(9) nitrogen: 9*H*-purine. However, the chemical shift values in ^{13}C NMR spectra of I and its methyl derivatives in DMSO indicates that I in DMSO is a tautomeric mixture of 60% 9*H*-purine and 40% 7*H*-purine. It is necessary, therefore, to take these tautomers into account when we compare the experimental data with the calculated ones. We have calculated spin densities of these tautomers by McLachlan's methods, using the parameters derived empirically in pyridines and diazines by Talcot and Myers[17], except

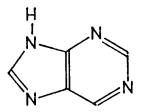

7*H*-purine

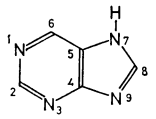

9*H*-purine

for the nitrogen to which the labile hydrogen atom is attached. The Coulomb integral of the nitrogen (α_N) in the NH fragment was estimated as $\alpha_N=\alpha_C+1.2\,\beta_{CC}$, based on the analysis of hfcc of radical cations of the dihydro derivatives of some diaza-aromatic compounds[18]. The resonance integrals between the nitrogen atom in this fragment and the adjacent carbon atoms (β_{NC}) were adjusted so as to fit to the experimental data. Spin densities of the 9*H*-purine anion radical were calculated by changing $\delta=\beta_{NC}/\beta_{CC}$ and the hfcc were calculated using $Q_N^N=27.3$, $Q_{NC}=-1.7$ and $Q_H=-42.5$G.[17] The obtained hfcc are given in Fig. 4 as functions of δ. Here $\delta=0.5$ corresponds to a model in which the NH fragment can be regarded as a secondary amine group. Then I is adequately described as 4,5-disubstituted pyrimidine with a strongly mesomeric substituent at position 5. This model is characterized by the largest spin density (48%) at position 8, followed by the next largest (26%) at position 6. As δ increases, spin densities at positions 6 and 3 increase appreciably accompanied by the decreases at positions 8 and 2. The best fit to the experimental results, shown by the dotted lines in Fig. 4, is obtained at $\delta=1.0$, which means that the

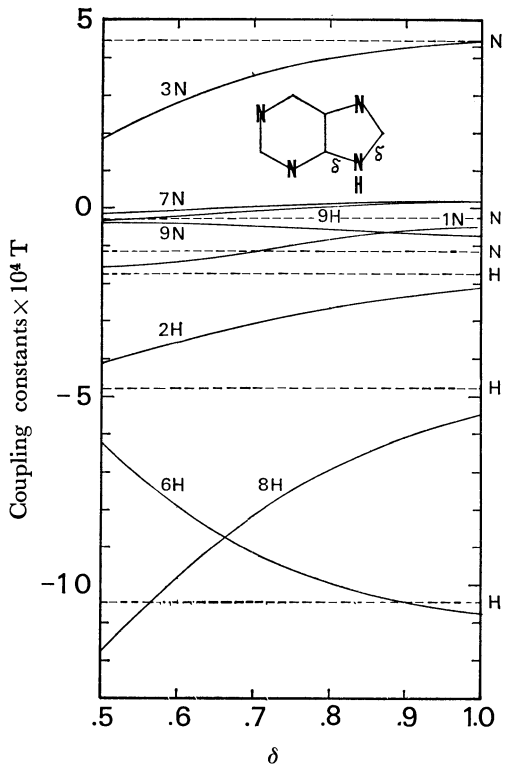

Fig. 4. Comparison of the hfcc of I$^-$ obtained experimentally (dotted lines) with those as functions of δ calculated by the McLachlan's method (see text).

Table 1. Measured hyperfine coupling constants[a] of purine, 8-deuterio- and 6,8-dideuteriopurine anion radicals at −50 °C, and calculated coupling constants[a] and spin densities of 7*H*- and 9*H*-purine anion radicals

Position	Purine		Purine-*d*	Purine-d_2	Calculated hfcc's[c] (McLachlan)	
	in AN+BN	in DMF	in DMF	in DMF	9*H*-Purine	7*H*-Purine
N1	0.28	0.28	0.28	0.28	−0.51 (0.014)	0.38 (0.043)
H2	1.79	1.75	1.75	1.75	−2.10 (0.086)	−1.07 (0.044)
N3	4.40	4.47	4.47	4.47	4.46 (0.172)	4.37 (0.170)
H6	10.75	10.46	10.46	D1.67	−10.76 (0.439)	−10.23 (0.418)
N7	<0.2[b]	<0.2[b]	<0.2[b]	<0.2[b]	0.16 (0.019)	0.26 (0.025)
H8	4.85	4.80	D0.74	D0.74	−4.55 (0.224)	−4.95 (0.243)
N9	1.18	1.14	1.14	1.14	−0.73 (−0.009)	−1.17 (−0.020)
Labile H	<0.2[b]	<0.2[b]	<0.2[b]	<0.2[b]	0.22	0.61

a) In unit of 10^{-4} T. b) Estimated from the line widths. c) Calculated by using the formula $a_H = Q_H\rho_C$, $a_N = Q_N^N\rho_N + Q_{NC}(\rho_C + \rho_{C'})$ and the parameters given in Ref. 17.

Table 2. Hyperfine coupling constants[a] of purine anion radical calculated by INDO method based on possible radical structure[b]

Position	7*H*-Purine		9*H*-Purine		Observed
	Watson	Inverted Spencer	Spencer	Inverted Watson	
N1	3.4999	3.0597	−0.0273	−0.3282	0.283
H2	0.2364	0.1089	−2.3398	−2.6486	1.750
N3	4.9997	4.9212	6.0115	6.2208	4.470
H6	−6.7342	−5.9061	−8.1522	−8.4456	10.46
N7	0.3073	0.4333	−0.1324	0.0677	<0.2
H8	−6.3173	−7.9999	−4.2455	−2.7192	4.80
N9	−2.4868	−2.4870	−1.6809	−1.5955	1.14
Labile H	−0.8193	−1.1284	0.7608	0.7699	<0.2
Total width	35.88	36.95	31.20	31.01	28.80

a) In unit of 10^{-4} T. b) See text.

electronic structure of $I^{\overline{\cdot}}$ should be regarded as one of a 10π-electron heterocyclic aromatics rather than that of a substituted pyrimidine with a strongly mesomeric substituent. In other words, the bonding between the nitrogen at 9 and carbons at 4 and 8 have double bond characters as much as an aromatic –C–C– bonding. This choice of δ is also supported by the result of the X-ray study by Watson *et al.*,[19] which showed that the bond lengths between N(9) and C(4), and N(9) and C(8) are 1.37 and 1.31 A, respectively, indicating double bond characters of these bonds. The hfcc of 7*H*-purine anion radical was also calculated using the same parameters as in the case of 9*H*-purine, which are also shown in Table 1. It should be noticed in Table 1 that the calculated coupling constants of two tautomers are quite similar to each other and are in good agreement with the experimental results except for that of the labile proton.

In order to further compare the experimentally determined hfcc with those calculated by MO methods we have also made INDO calculations. As is well known, the results of the calculations carried out by this method depends on the geometries adopted. Here we used the same geometries as those adopted by Pullman *et al.*;[7] Watson and inverted Spencer geometries for 7*H*-purine, and inverted Watson and Spencer geometries for 9*H*-purine. The Watson geometry was derived from the crystallographic data of purine which has 7*H*-form in crystal.[19] The Spencer geometry means the structure established by Spencer on the basis of a general study of purine derivatives which are in 9*H* forms.[20] The inverted Watson and the inverted Spencer geometries were obtained by inverting the lengths of the 7–8 and 8–9 bonds, those of the 5–7 and 4–9 bonds, and the corrsepond-ing angles, respectively. The hfcc of $I^{\overline{\cdot}}$ calculated with these geometries are listed in Table 2.

It is seen from the table that the calculated hfcc for 9*H*-purine are rather different from those for 7*H*-purine and are in better agreement with the experimental hfcc. The best agreement between the experimental and the calculated hfcc seems to be obtained in the case of Spencer geometry of 9*H*-purine. The inverted Watson model can predict a large hfcc for H6, but the agreement with the experimental results is somewhat poorer. The total width of the ESR spectrum calculated for 9*H*-purine also agrees reasonably well with the observed total width. On the other hand, the hfcc calculated for 7*H*-purine do not reproduce the observed features of hfcc. The total width of the spectra calculated are much larger than the observed one. Thus the results of the INDO

calculations seem to be in favor of the 9*H*-form for I^-.

The most remarkable feature of the spin distribution of the purine anion is that about 45% of the spin density is localized at position 6. Such a large localized spin density is very rare in a π electron system of the size of I and should have an important implication to its chemical reactivity. It is known that the reaction such as hydrogenation takes place preferentially at position 6.[11] This was rationalized from the result of MO calculation.[21] According to Fukui's frontier electron theory[22] such a reaction should take place at the position where the frontier electron density is the largest. Our result clearly shows a large electron density in the frontier orbital (LUMO) at position 6.

It is interesting to compare the unpaired electron spin distribution in LUMO of I with that of indole. Although its electron spin distribution is not known experimentally, the result of a semiempirical calculation[23] may be used for comparison. The spin densities at positions 2, 3, 6, and 8 of indole, the position numbers of which correspond to those of I, are 0.136, 0.220, 0.212 and 0.155, respectively. From the comparison with the data of I it may be deduced that aza-substitution to the particular ring carbons enhances the localization of the spin density to position 6.

Tautomerism of Purine. Sometimes in the ESR spectra the dynamic behaviors of radical species can be revealed from line-width alternation, or line-width variation which can be related to the lifetimes of the radical species under consideration. If we take into account the difference in the calculated coupling constants between two stable tautomers, two possibilities can be considered from the observed spectrum: one is the case that the anion radical formation stabilizes one of the two tautomers (7*H*- or 9*H*-purine) at the temperatures around -50 °C, and the other is that the exchange of the labile proton between the two tautomers is very rapid compared with the ESR time scale, 10^6 Hz s^{-1}. It is difficult at present, to say definitely which is appropriate for the interpretation of the observed spectrum, but the former case is more likely when we take into account the ^{15}N NMR result that only one very broad signal for N7 and N9 could be observed because of slow hydrogen exchange of the order of 10^2 Hz sec^{-1}.

References

1) A. Pullman and B. Pullman, *Bull. Soc. Chim. Fr.*, **1958**, 766.
2) For a review of experimental and theoretical aspects of purines, see, for example, B. Pullman and A. Pullman, *Adv. Heterocycl. Chem.*, **13**, 77 (1971).
3) M. J. Robey and I. G. Ross, *Photochem. Photobiol.*, **21**, 363 (1975).
4) M. Chenone, R. J. Pugmire, D. M. Grant, R. P. Panzica, and L. B. Townsend, *J. Am. Chem. Soc.*, **97**, 4627, 4636 (1975).
5) V. Markowski, G. R. Sullivan, and J. D. Roberts, *J. Am. Chem. Soc.*, **99**, 714 (1977).
6) W. Hug and I. Tinoco, Jr., *J. Am. Chem. Soc.*, **95**, 2803 (1973), **96**, 665 (1974).
7) B. Pullman, H. Berthod, F. Bergmann, Z. Neiman, Weiler-Feilchenfeld and E. D. Bergmann, *Tetrahedron*, **26**, 1483 (1970).
8) Z. Neiman, *J. Chem. Soc., Perkin Trans.* 2, **1972**, 585.
9) E. Kochanski and A. Pullman, *Int. J. Quantum Chem.*, **3**, 1055 (1969).
10) P. Daudey and A. Pullman, *Chem. Phys. Lett.*, **5**, 347 (1970).
11) T. Yao and S. Musha, *Bull. Chem. Soc. Jpn.*, **47**, 2650 (1974).
12) H. Ohya-Nishiguchi, *Bull. Chem. Soc. Jpn.*, **52**, 2064 (1979).
13) J. A. Pople and D. L. Beveridge, "Approximate Molecular Orbital Theory," McGraw-Hill, New York (1970).
14) M. P. Schweizer, S. I. Chan, G. K. Helmkamp, and P. O. Ts'o, *J. Am. Chem. Soc.*, **86**, 696 (1964).
15) R. P. Van Duyne and C. N. Reilly, *Anal. Chem.*, **44**, 142 (1972).
16) A. D. McLachlan, *Mol. Phys.*, **3**, 233 (1960).
17) C. L. Talcott and R. J. Myers, *Mol. Phys.*, **12**, 549 (1967).
18) B. L. Bolton and G. K. Fraenkel, *J. Chem. Phys.*, **41**, 1455 (1964).
19) D. G. Watson, R. M. Sweet, and R. E. Marsh, *Acta Crystallogr.*, **19**, 573 (1965).
20) M. Spencer, *Acta Crystallogr.*, **12**, 59 (1959).
21) T. Nakajima, and B. Pullman, *J. Am. Chem. Soc.*, **81**, 3876 (1959).
22) K. Fukui, T. Yonezawa, and H. Shingu, *J. Chem. Phys.*, **20**, 722 (1952).
23) R. G. Selsby and A. Grimson, *Int. J. Quantum Chem.*, **1977**, 527.

Effect of a Polar Solvent on the $^1J_{CH}$ Spin-coupling Constants in Chlorine-substituted Ethanes

Shosuke WATANABE* and Isao ANDO†

Minato High School of Technology, 18-13, Nishi-shinbashi 3-chome, Minato-ku, Tokyo 105

† *Department of Polymer Chemistry, Tokyo Institute of Technology, Ookayama, Meguro-ku, Tokyo 152*

(Received October 11, 1979)

The directly-bonded ^{13}C–H spin-coupling constants ($^1J_{CH}$) for two chlorine-substituted ethanes, $CHCl_2CHCl_2$ and $CHCl_2CH_2Cl$, have been measured in various solvents with a wide range of dielectric constants and/or as a function of the temperature. Also, these two effects were estimated by the finite perturbation theory based on the CNDO/2 approximation with the solvaton theory. Both experimentally and theoretically, the dielectric constant of a solvent affects the $^1J_{CH}$ more than the temperature. It is shown that the solvent effect on the $^1J_{CH}$ spin couplings in $CHCl_2CHCl_2$ and $CHCl_2CH_2Cl$ arises mainly from electronic changes in the solute molecules caused by intermolecular solute-solvent interaction, more than from the change in the population of the rotational isomers.

The effects of solvents on spin-coupling constants have been widely studied by many authors. Some excellent reviews[1] have been presented on these effects.

In a previous paper,[2] we have ourselves treated numerically the effect of a polar solvent on directly-bonded ^{13}C–H spin-coupling constants for molecules in which unsaturated bonds fix the relative spatial positions of the atoms with each other (*e.g.*, CH_2=CHCN), and for halomethanes, with the aid of the finite perturbation theory[3] (hereafter, an acronym FPT will be used) with the solvaton model.[4] This approach successfully provided a quantitative description of the solvent effects on $^1J_{CH}$, following the Johnston-Barfield approaches, the reaction field model,[5] the cluster model[6] and the rotating-point dipole model.[7]

There is another category of solvent effects of coupling constants, namely, the solvent effects of the coupling constants of molecules which can take into account two or more conformations. In this case, we must consider two effects on the coupling constants; one is due to solvent-induced electronic changes in the solute molecules, and the other, to the change in the relative populations between the isomers because of intermolecular solute-solvent interaction. Barfield and Johnston[1a] calculated the vicinal H-F coupling constants in 1,1,1-trifluoroethane using the reaction-field model and concluded that the contribution from the solvent-induced electronic changes on the observed solvent effect is by no means negligible. The purpose of the present work is to separate the above two effects both experimentally and theoretically, and to discuss the mechanism of the solvent effect on the $^1J_{CH}$'s of molecules with rotational isomerism. We will analyze this problem with the term of FPT considering the effect of the aprotic polar solvent on the $^1J_{CH}$ coupling constants in chlorine-substituted ethanes, $CHCl_2CHCl_2$ and $CHCl_2CH_2Cl$.

Experimental

The ^{13}C NMR spectra were measured by means of a JEOL PS-100 spectrometer with the PFT-100 Fourier transform system operating at 25.15 MHz. The Fourier-transformed spectra contain 4096 data points within spectra width of 1000 Hz. This indicates a limit of 0.25 Hz on the resolution. The temperatures are considered to be controlled within ±1 °C. The NMR tube used was 8 mm in diameter. The concentration of the sample in solution is 10% v/v.

The chlorine-substituted ethanes and solvents were obtained from the Tokyo Kasei Co. and were used without further purification.

Theoretical

Rotational Isomerism. Both $CHCl_2CHCl_2$ and $CHCl_2CH_2Cl$ take the three energetically-preferred isomeric states as follows;[8] $CHCl_2CHCl_2$:

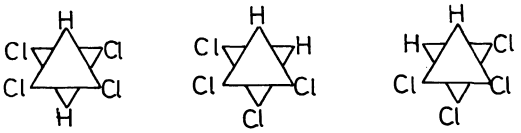

1-I 1-II 1-III

$CHCl_2CH_2Cl$:

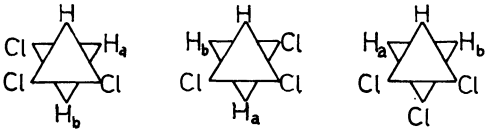

2-I 2-II 2-III

The observed coupling constant is given by[9]

$$\langle J_{CH}\rangle = X_I J^I_{CH} + X_{II} J^{II}_{CH} + X_{III} J^{III}_{CH}, \quad (1)$$

when the exchange rate is sufficiently larger than the difference between J_{CH}'s, where X_I, X_{II}, and X_{III} are the molar fractions of the three isomers, I—III, respectively. Each of the molar fractions can be expressed in terms of the relative energy, ΔE, of the isomer with respect to that of the reference conformer, III. Equation 1 can be reduced into the following forms if the coupling constants are assumed to be temperature-independent;[10]

$CHCl_2CHCl_2$:

$$\langle J_{CH}\rangle = [2J^{II}_{CH} + J^{I}_{CH}\exp(-\Delta E/RT)]/[2+\exp(-\Delta E/RT)] \quad (2)$$

$CHCl_2CH_2Cl$:

$$\langle J_{CH}\rangle = \frac{1}{2}[(J^{III}_{CH_a} + J^{III}_{CH_b}) + 2(J^{I}_{CH_a} + J^{I}_{CH_b})\exp(-\Delta E/RT)]/[1+2\exp(-\Delta E/RT)] \quad (3)$$

We can evaluate, in principle, the relative energies,

ΔE's of the isomers and the coupling constants, J_{CH}^{i}'s, from the temperature dependence of $\langle J_{CH}\rangle$'s. It is, however, hard to determine them because of the small change in $\langle J_{CH}\rangle$'s. Gutowsky *et al.*[9] have estimated the relative energies of the isomers through the temperature dependence of the vicinal proton-proton spin couplings in halogen-substituted ethanes by means of a least squares method with a computer. In our previous work, the values of the relative energies of the isomers were estimated by Gutowsky's treatment[9] from the temperature dependence of the vicinal proton-proton spin coupling[11] in calculating Eqs. 2 and 3.

$^1J_{CH}$ Spin-coupling Constant. In previous papers,[2,12] we have applied the solvaton model to interaction with a solvent with the aid of semi-empirical SCF calculations. The "solvaton" is convenient for the description of the distribution of the oriented solvent around each atom in a molecule. Only a few important basic assumptions are introduced there: i) A counter charge (the solvaton) is induced on the surface of the solute molecules upon the addition of the solute to an aprotic polar solvent: (ii) each solvaton is associated individually with each atom of the solute, and the charge is equal in magnitude, but opposite in sign, to that of the associated atom: (iii) there are no interactions between the solvatons themselves, and (iv) the solvent-solute interaction is approximated by the Born equation,[13] which describes the energy of the solvaton of an ion in a dielectric continuum.

We will calculate $^1J_{CH}$ coupling constants as a function of the dielectric constant(ε) with the aid of the CNDO/2 approximation[14] in consideration of the above-mentioned solvent-solute interaction using the FPT theory. In this calculation, we will consider only the Fermi contact interaction, which seems to be predominant in $^1J_{CH}$ coupling constants.

The spin-unrestricted SCF equations on the Fock matrices, $F_{\mu\nu}^{\alpha}$ and $F_{\mu\nu}^{\beta}$, for α and β electrons are given by

$$F_{\mu\nu}^{\alpha} = H_{\mu\nu}^{core} + \sum_{\lambda\sigma}[P_{\lambda\sigma}(\mu\nu|\lambda\sigma) - P_{\lambda\sigma}^{\alpha}(\mu\sigma|\lambda\nu)] + \frac{\varepsilon-1}{\varepsilon}\int\phi_{\mu}\left(\sum_{s}^{N}\frac{Q_s}{r_{s1}}\right)d\tau + \frac{8}{3}\pi\beta\mu\int\phi_{\mu}\delta(r_B)\phi_{\nu}d\tau \quad (4\text{-}1)$$

$$F_{\mu\nu}^{\beta} = H_{\mu\nu}^{core} + \sum_{\lambda\sigma}[P_{\lambda\sigma}(\mu\nu|\lambda\sigma) - P_{\lambda\sigma}^{\beta}(\mu\sigma|\lambda\nu)] + \frac{\varepsilon-1}{\varepsilon}\int\phi_{\mu}\left(\sum_{s}^{N}\frac{Q_s}{r_{s1}}\right)d\tau - \frac{8}{3}\pi\beta\mu\int\phi_{\mu}\delta(r_B)\phi_{\nu}d\tau \quad (4\text{-}2)$$

if the Fermi contact interaction[3] and the solvent-solute interaction are taken into account. The third terms including ε correspond to the solvent-solute interaction given by the solvaton theory, while the final terms in both equations correspond to the Fermi contact interaction. μ denotes the magnetic moment of the nucleus B, and $\delta(r_B)$, the Dirac delta function for the contact term between the electron and the nucleus B. The other symbols are used in the usual manner. The charge, Q_s, is defined by the (i) assumption. In a previous paper,[2] we assumed an inequality between Q^{α} and Q^{β} in the solvaton, but this assumption tends to overestimate the values of the $^1J_{CH}$ coupling constant. Thus, in this work, we modified this assumption by terms including ε in Eq. (4): that is, Q_s is handled without being separated into Q_s^{α} and Q_s^{β}. Further, r_{s1} is the solvaton-electron distance and is estimated as follows: (i) if the AO's and solvatons are associated with the same atomic center, the van der Waals' radius, r_v, of the corresponding atom can be used for the solvaton-electron distance, and (ii) if the AO's and solvatons are associated with different atomic centers with a separation of r_R, r_{s1} is approximated by:

$$\sqrt{r_v^2 + r_R^2}.$$

The expression for the coupling constant between A and B becomes:

$$J_{AB} = \frac{16}{9}h\gamma_A\gamma_B\beta^2 s_A^2(0)s_B^2(0)\left[\frac{\partial}{\partial h_B}\rho_{s_As_A}^{spin}(h_B)\right]_{h_B=0} \quad (5)$$

using the FPT theory, where:

$$h_B = \frac{8}{3}\pi\beta\mu_B s_B^2(0)$$

Here, γ is the gyromagnetic ratio, $s_B^2(0)$ is the density at the nucleus of the valence s orbital of the B atom, and $\rho_{s_As_A}^{spin}(h_B)$ is the spin-density matrix corresponding to the valence s orbital of the A atom.

In calculation, the bond lengths and bond angles used are the standard values proposed by Pople and Gordon[15] except for the C–Cl bond length, the value of the C–Cl is not given there. Instead, 1.71 Å, which appears elsewhere, is adopted.[16] The values used for the effective van der Waals' radii are 1.20, 1.59, and 1.8 Å in hydrogen, carbon, and chlorine atoms respectively.[17] All the calculations were carried out with the HITAC-M180 computer at the Tokyo Institute of Technology.

Results and Discussion

In Table 1 are shown the observed $^1J_{CH}$ values of $CHCl_2CHCl_2$ and $CHCl_2CH_2Cl$ in solvents with various dielectric constants. From these data, it is found that the $^1J_{CH}$ values increase with an increase in ε. The ε dependence of $^1J_{CH}$ in $CHCl_2CHCl_2$ is nearly equal to that in $CHCl_2CH_2Cl$. Also in $CHCl_2CH_2Cl$ the ε dependence of $^1J_{CH}$ for CH is larger than that for CH_2. In a previous paper[2] we have reported that the observed and calculated $^1J_{CH}$ values can be approximated by:

$$^1J_{CH} = a\left(\frac{\varepsilon-1}{\varepsilon}\right) + b\left(\frac{\varepsilon-1}{\varepsilon}\right)^2 + c \quad (7)$$

From the plot of $^1J_{CH}$ against $(\varepsilon-1)/\varepsilon$, the values of the a, b, and c parameters were obtained, they are tabulated in Table 2. The c parameter means the $^1J_{CH}$ value at $\varepsilon=1$, that is, for an isolated molecule. The a and b parameters provide measures of the magnitude of the solvent effect of $^1J_{CH}$ coupling. In the case of chlorine-substituted methanes,[2] the b parameter is nearly equal to zero. However, in $CHCl_2CHCl_2$

Table 1. The $^1J_{CH}$ spin coupling constants of $CHCl_2CHCl_2$ observed in various solvents with a wide range of dielectric constants (ε) at 25 °C

Solvents	ε	$CHCl_2CHCl_2$		$CHCl_2CH_2Cl$			
		CH		CH_2		CH	
		$^1J_{CH}$/Hz	ΔJ/Hz[d]	$^1J_{CH}$/Hz	ΔJ/Hz[d]	$^1J_{CH}$/Hz	ΔJ/Hz[d]
Hexane	2.02[a]	179.69	0	155.15	0	181.40	0
$CDCl_3$	4.806[a]	181.15	1.46	155.27	0.12	181.89	0.49
$CHCl_2CH_2Cl$	7.12[b]	—	—	155.64	0.49	181.98	0.58
$CHCl_2CHCl_2$	8.20[c]	181.15	1.46	—	—	—	—
Acetone	20.0[a]	184.08	4.39	155.88	0.73	183.59	2.19
Acetonitrile	35.8[a]	184.09	4.40	156.25	1.10	183.35	1.95
Dimethylsulfoxide	46.0[a]	185.54	5.85	156.66	1.51	184.04	2.64

a) National Bureau of Standards, Circular No. 514, 1951. b) Beil. E III, 1-154. c) J. A. Ridick and W. B. Bunger, "Organic Solvents", Wiley-Interscience, New York (1970). d) ΔJ is the difference between the coupling constants in the indicated solvent and in hexane.

Table 2. The values of the a, b, and c parameters in Eq. 7 for $CHCl_2CHCl_2$ and $CHCl_2CH_2Cl$

Parameter	$CHCl_2CHCl_2$	$CHCl_2CH_2Cl$	
	CH (Hz)	CH_2 (Hz)	CH (Hz)
a	3.5	0.5	2.0
b	4.0	1.3	3.0
c	178.3	154.9	180.3

Table 3. Temperature dependence of the $^1J_{CH}$ spin coupling constants of $CHCl_2CHCl_2$ and $CHCl_2CH_2Cl$ in neat liquid

Temp °C	$^1J_{CH}$/Hz		
	$CHCl_2CHCl_2$	$CHCl_2CH_2Cl$	
	CH	CH_2	CH
25	181.15	155.64	181.98
40	181.15	155.81	181.88
60	181.15	155.52	181.84
70	181.16	155.55	181.81
80	181.15	155.64	181.75
90	181.15	155.54	181.70
100	181.15	155.52	181.69

and $CHCl_2CH_2Cl$ the b parameter is finite, but larger than the value of the a parameter. The values of these parameters for CH are larger than those for CH_2. This fact coincides with the results for chlorine-substituted methanes,[2] in which an increase in the number of chlorine atoms induces an increase in the solvent effect.

Table 3 shows the temperature dependences of the $^1J_{CH}$ values of neat $CHCl_2CHCl_2$ and $CHCl_2CH_2Cl$. The $^1J_{CH}$ coupling is hardly dependent at all on the temperature. Thus, the temperature dependence for $^1J_{CH}$ is much smaller than the dependence on the polarity of the solvents. The difference in the $^1J_{CH}$ values in various solvents may not be the result of the difference in the populations of rotational isomers, but of the difference in electronic states in the molecules induced by the difference in solvent species. We will consider which difference is predominant through the calculation of the $^1J_{CH}$ couplings for a wide variety of dielectric constants and examples of rotational isomerism.

Before the numerical calculation, however, it is important to specify at the amounts of integral products, $s_C^2(0)s_H^2(0)$, chosen according to the FPT theory. The values will not only reflect the difference between the atomic or molecular environments of the nuclei, but will also be affected by the order of approximation in the molecular orbital theory. Thus, these values have often been proposed to coincide satisfactorily with the experimental results. Different values for the integral products seem to be different approximations inherent in the finite, self-consistent, and sum-over-states perturbation approximations. Two kinds of values will be used in this work: (i) Pople's value ($s_C^2(0)s_H^2(0)=1.5014$ a.u.),[3] and (ii) the ($s_C^2(0)s_H^2(0)=1.644$ a.u.) value, which gives the best agreement between the experimental results and our calculations. Table IV shows the calculated ε dependence of the $^1J_{CH}$ coupling constants of $CHCl_2CHCl_2$ and $CHCl_2CH_2Cl$ in *trans* and *gauche* conformations, using both values of the integral products. It is clear that the choice of the larger value (1.644 a.u.) for $s_C^2(0)s_H^2(0)$ decreases the difference between the calculated and experimental values. The dependence of the $^1J_{CH}$ coupling upon the dihedral angle, ϕ, is calculated at intervals of 10° as a function of ε, they are plotted in Fig. 1. The $^1J_{CH}$ value shows the dihedral-angle dependence as well as that of the coupling through three bonds. However, its dependence is very small compared with the latter case. Each of the dihedral-angle dependences for CH in $CHCl_2CHCl_2$ and $CHCl_2CH_2Cl$ have three minima and three maxima, while that for CH_2 in $CHCl_2CH_2Cl$ has two minima and two maxima. These positions are different in each case. The $^1J_{CH}$ values are not very much affected by $\phi(|^1J_{CH}(trans)-{}^1J_{CH}(gauche)|<0.5$ Hz). The $^1J_{CH}$ values in the *trans* and *gauche* positions are close to each other. From this, the temperature independence of the $^1J_{CH}$ couplings can be expected. On the other

hand, the ε dependence can be expected to be large.

The temperature dependences of $\langle {}^1J_{CH} \rangle$ were obtained using the calculated ${}^1J_{CH}$ couplings of *trans* and *gauche* conformations tabulated in Table 4, and Eqs. 2 and 3. In these equations the energy differences (ΔE) between the conformers in various solvents were determined with Gutowsky's treatment on vicinal proton-proton spin coupling:[11]

$CHCl_2CHCl_2$: 889 (in CCl_4), 919 (neat liquid), 1165 (in acetone) and 1352 cal/mol (in dimethylsulfoxide), while

$CHCl_2CH_2Cl$: 160 (in CCl_4), 200 (neat liquid), 217 (in acetone) and 504 cal/mol (in dimethylsulfoxide).

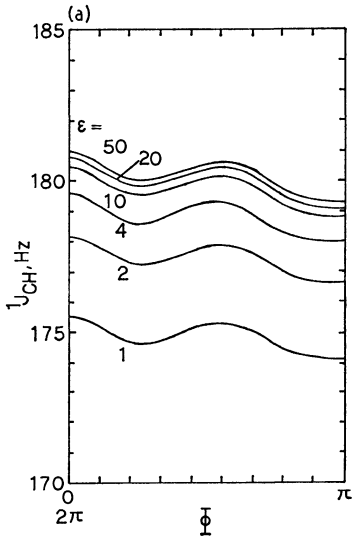

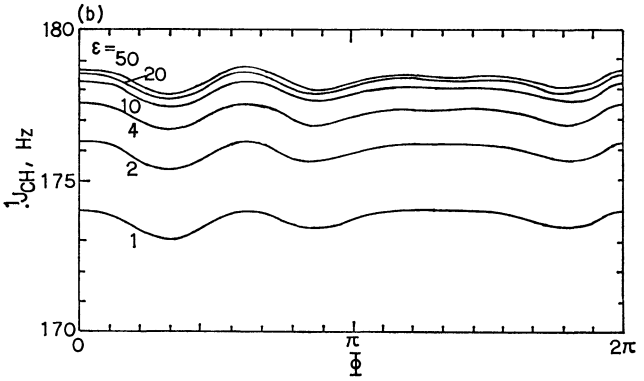

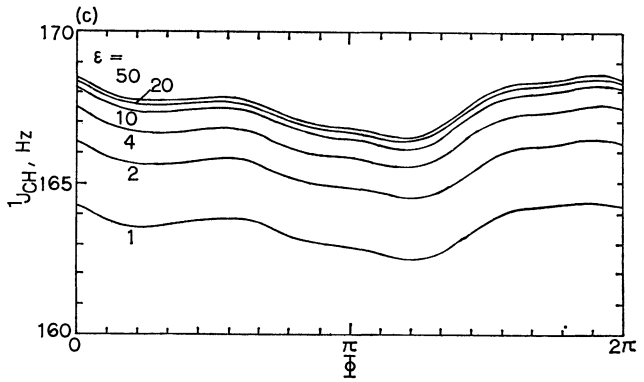

Fig. 1. The dihedral angle(Φ) dependences of the calculated ${}^1J_{CH}$ coupling constants of CH (a) in $CHCl_2$-$CHCl_2$ and CH (b) and CH_2 (c) in $CHCl_2CH_2Cl$ as a function of dielectric constant.

TABLE 4. THE CALCULATED ${}^1J_{CH}$ VALUES OF $CHCl_2CHCl_2$ AND $CHCl_2CH_2Cl$ IN *trans* AND *gauche* ISOMERS[a] AS A FUNCTION OF DIELECTRIC CONSTANT

	${}^1J_{CH}$/Hz											
	Pople' value $s_C^2(0)s_H^2(0)=1.5014$ a. u.						This work $s_C^2(0)s_H^2(0)=1.644$ a. u.					
	$\varepsilon=1$	2	4	10	20	50	$\varepsilon=1$	2	4	10	20	50
$CHCl_2CHCl_2$:												
trans ($\Phi=\Pi$)	105.95	107.49	108.30	108.81	108.99	109.09	174.18	176.71	178.05	178.88	179.18	179.34
gauche ($\Phi=\pm\Pi/3$)	106.28	107.87	108.72	109.25	109.43	109.54	174.72	177.34	178.74	179.61	179.90	180.04
$CHCl_2CH_2Cl$:												
CH												
trans ($\Phi=\Pi$)	105.65	107.02	107.74	108.20	108.35	108.44	173.69	175.94	177.12	177.88	178.13	178.28
gauche ($\Phi=\Pi/3$)	105.25	106.67	107.43	107.91	108.07	108.17	173.03	175.37	176.61	177.40	177.67	177.83
gauche ($\Phi=5/3\,\Pi$)	105.65	107.02	107.74	108.20	108.35	108.44	173.69	175.94	177.12	177.88	178.13	178.28
CH_2												
H_a												
trans ($\Phi=\Pi$)	99.13	100.29	100.90	101.28	101.41	101.49	162.97	164.88	165.88	166.50	166.72	166.85
gauche ($\Phi=\Pi/3$)	99.52	100.75	101.40	101.81	101.95	102.03	163.61	165.63	166.70	167.38	167.61	167.74
gauche ($\Phi=5/3\,\Pi$)	99.85	101.11	101.77	102.18	102.32	102.03	164.15	166.22	167.31	167.98	168.21	168.36

a) The definition of the dihedral angle, Φ, is as follows:

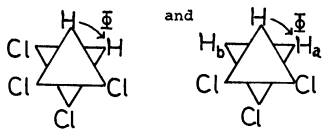

The results for $^1J_{CH}$ are shown in Table 5. The temperature dependence of the dielectric constants of the solvents is taken into account in Table 5 by the use of:

$$(\varepsilon+1)\cdot T \propto \text{constant} \quad (8)$$

after Wyman's study[18] of large classes of polar liquids. The calculated $\langle^1J_{CH}\rangle$ values are almost independent of the temperatures and can interpret the observed values qualitatively.

In order to obtain the calculated effect of the ε dependences of the $^1J_{CH}$, Eqs. 2 and 3 were used as well as the calculation of the temperature dependence. These results are shown in Table 6.

Table 5. Temperature dependences of the calculated $^1J_{CH}$ coupling constants of $CHCl_2CHCl_2$ and $CHCl_2CH_2Cl$ in neat liquid

Temp °C	$^1J_{CH}$/Hz		
	$CHCl_2CHCl_2$	$CHCl_2CH_2Cl$	
	CH	CH_2	CH
25	177.52	167.17	178.86
40	177.46	167.13	178.84
60	177.39	167.09	178.81
70	177.36	167.07	178.80
80	177.32	167.04	178.78
90	177.29	167.02	178.77
100	177.25	167.00	178.75

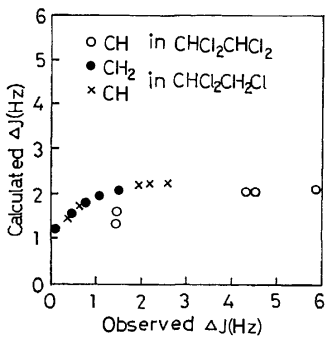

Fig. 2. The plots of calculated ΔJ against observed ΔJ.

For a further comparison of the calculated and experimental results, the differences, ΔJ, between the coupling constants in the indicated solvents and in hexane are shown in the table and also in Fig. 2. The calculated trends reproduce the observed ones in the solvent effect. However, the calculated values in the high-value range in ΔJ are underestimated. This seems to be a result of the exclusion of the one-center exchange integral in our calculation, because the inclusion of its integral leads to an increase in the magnitude of the directly-bonded coupling constant, as has been reported by Pople *et al.*[3]

As these results shows, the ε dependence is very large compared with the temperature dependence. This large dependence on ε is a proof of the larger contribution of the solvent-induced electronic changes of the solute molecules to the solvent effect on the $^1J_{CH}$, resulting from intermolecular solute-solvent interaction.

It can be concluded that there are good gross trends of agreement between the observed and calculated results. This would suggest a potential applicability of the solvaton theory in interpreting solvent effects in dipolar media.

The authors wish to thank Associate Professor R. Chûjô of our department for his many helpful suggestions and discussions.

References

1) a) M. Barfield and M. D. Johnston, Jr., *Chem. Rev.*, **73**, 53 (1973); b) S. L. Smith, *Fortsch. Chem. Forsch.*, **27**, 117 (1972); c) J. Kowalewski, *Prog. NMR Spectrosc.*, **11**, 1 (1977).

2) M. Kondo, S. Watanabe, and I. Ando, *Mol. Phys.*, **37**, 1521 (1979).

3) J. A. Pople, J. W. McIver, and N. S. Ostlund, *J. Chem. Phys.*, **49**, 2965 (1967).

4) a) G. Klopman, *Chem. Phys. Lett.*, **1**, 200 (1967); b) G. Klopman, *J. Am. Chem. Soc.*, **90**, 223 (1968); c) H. A. Germer, Jr., *Theor. Chim. Acta*, **34**, 145 (1974).

5) M. D. Johnston and M. Barfield, *J. Chem. Phys.*, **54**, 3083 (1971).

6) M. D. Johnston and M. Barfield, *J. Chem. Phys.*, **55**, 3483 (1971).

Table 6. The dielectric-constant dependences of the calculated $^1J_{CH}$ coupling constants of $CHCl_2CHCl_2$ and $CHCl_2CH_2Cl$

Solvents	ε	$CHCl_2CHCl_2$		$CHCl_2CH_2Cl$			
		CH		CH_2		CH	
		$^1J_{CH}$/Hz	ΔJ/Hz[a]	$^1J_{CH}$/Hz	ΔJ/Hz[a]	$^1J_{CH}$/Hz	ΔJ/Hz[a]
Hexane	2.02	175.92	0	165.52	0	177.03	0
$CDCl_3$	4.806	177.21	1.29	166.78	1.26	178.43	1.40
$CHCl_2CH_2Cl$	7.12	177.52	1.60	167.08	1.56	178.76	1.73
$CHCl_2CHCl_2$	8.20	177.60	1.68	167.16	1.64	178.85	1.82
Acetone	20.0	177.93	2.01	167.48	1.96	179.21	2.18
Acetonitrile	35.8	178.03	2.11	167.58	2.06	179.31	2.28
Dimethylsulfoxide	46.0	178.05	2.13	167.61	2.09	179.34	2.31

a) ΔJ is the difference between the coupling constants in the indicated solvent and in hexane.

7) M. D. Johnston and M. Barfield, *Mol. Phys.*, **22**, 831 (1971).
8) S. Mizushima, "Structure of Molecules and Internal Rotation," Academic Press, New York (1954).
9) H. S. Gutowsky, G. C. Beldford, and P. E. McMahon, *J. Chem. Phys.*, **36**, 3353 (1962).
10) J. C. Shug, P. E. McMahon, and H. S. Gutowsky, *J. Chem. Phys.*, **33**, 843 (1960).
11) I. Ando, unpublished data.
12) I. Ando, M. Kondo, and A. Nishioka, *J. Magn. Reson.*, **21**, 429 (1976).
13) M. Born, *Z. Phys.*, **1**, 45 (1920).
14) J. A. Pople and G. A. Segal, *J. Chem. Phys.*, **44**, 3289 (1967).
15) J. A. Pople and M. Gordon, *J. Am. Chem. Soc.*, **89**, 4253 (1967).
16) "Tables of Interatomic Distances and Configuration in Molecules and Ions. Supplement," ed by L. E. Sutton, The Chemical Society, London (1965).
17) L. Pauling, "The Nature of the Chemical Bond", 3rd ed, Cornell University Press, Ithaca (1960).
18) J. Wyman, *J. Am. Chem. Soc.*, **58**, 1482 (1936).

The Crystal and Molecular Structure of Epoxyisoacoragermacrone

Hideo UEDA,† Chuji KATAYAMA, and Jiro TANAKA*

Department of Chemistry, Faculty of Science, Nagoya University, Chikusa, Nagoya 464

(Received October 15, 1979)

The crystal and molecular structure of epoxyisoacoragermacrone, which is an important derivative of acoragermacrone isolated from *Acorus calamus* L. for the study of the structural organic chemistry and biogenetic reactions, has been determined by the X-ray method. The crystal is orthorhombic, $P2_12_12_1$, with lattice parameters $a=7.425(2)$, $b=26.604(8)$, and $c=7.150(2)$ Å. The ten-membered ring is in a boat-chair conformation similar to the highly strained *cis*, *trans*-germacradiene system. The methyl groups take the axial and *syn* arrangement, and are on the β-face of the medium ring.

Recently, many germacrane-type sesquiterpenes isolated from the plants have been investigated by X-ray analysis. The structures of these sesquiterpenes were discussed from a viewpoint of biogenetic reactions,[1-3] pharmacological activities,[4-8] and conformations of ten-membered ring skeleton.[9-14] As a series of studies on sesquiterpenes separated from sweet flag oil,[15b] Yamamura and his coworkers[15] isolated many sesquiterpenes from *Acorus calamus* L. (Japanese name "Shyobu") and determined the structures by chemical and spectroscopic methods. They reported that acoragermacrone (**1**), which had a ten-membered skeleton, is one of the most important precursor of sesquiterpenes in Shyobu, and in fact, germacrones and epoxides derived from **1** are sesquiterpenes having selenane-, cadinane-, guaiane-, and elemene-types by cyclization reactions.[15c,d]

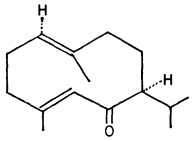

1

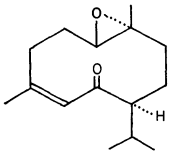

2

Epoxyisoacoragermacrone (**2**), 6,7-epoxy-10-isopropyl-3,7-dimethyl-2-cyclodecen-1-one derived from **1**, seems to be an important model compound for the biogenetic model reactions,[15d] and we undertook its X-ray crystal structure analysis.

Experimental

The crystals are of transparent prismatic forms. The space group was determined as $P2_12_12_1$ from the systematic absences observed on the oscillation and Weissenberg photographs. The unit-cell parameters were determined by the least-squares method, using twelve reflections measured on a Hilger & Watts four circle diffractometer with Ni-filtered Cu $K\alpha$ radiation ($\lambda=1.5418$ Å) The intensity data were collected on the diffractometer with the 2θ-ω scanning mode ($2\theta\leqq144°$) using the crystal of $0.3\times0.2\times0.3$ mm sealed in a glass capillary. The intensities of three standard reflections were monitored after every 100 reflections. The standard reflections were stable within 1% fluctuation from their mean values. Neither absorption nor extinction correction was made. The crystal data are given in Table 1.

TABLE 1. CRYSTAL DATA

Chemical formula:	$C_{15}H_{24}O_2$
M.W.:	236.36
Space group:	$P2_12_12_1$; $Z=4$
	$a=7.425(2)$, $b=26.604(8)$, $c=7.150(2)$ Å
D_c	$=1.111$ g cm^{-3}
μ	$=5.67$ cm^{-1} (for Cu $K\alpha$ radiation)

Determination and Refinement of the Structure

The structure was determined by the direct method with the program MULTAN[16] using 128 reflections with $|E|\geqq1.40$. An E map computed from the phase set with the highest figure of merit ($FOM=1.43$) revealed the locations of all non-hydrogen atoms. Hydrogen atoms were found on the difference Fourier map. The refinement was performed by the block-diagonal least-squares method with 960 independent reflections of $|F_o|\geqq3\sigma$. R-index converged to 0.060 with an equal weight for each reflection. The atomic scattering factors were taken from "International Tables for X-Ray Crystallography."[17] The least-squares program used for the refinement was written by Katayama, one of the authors. The program ORTEP[18] was used for drawing of Figs. 1—3. A part of the computation was performed at the Nagoya University Computation

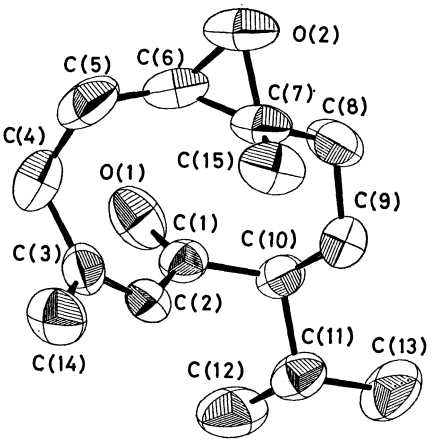

Fig. 1. The atomic numbering of **2**. Carbon and oxygen atoms are represented as thermal ellipsoids of a size such that the vibrating atoms have a 50% probability of being found them. The absolute configuration of the molecule was drawn to be in conformity with the established configuration by a chemical correlation method.

† Present address: Central Research Laboratory, Ube Industries Ltd., Nishihon-machi, Ube, Yamaguchi 755.

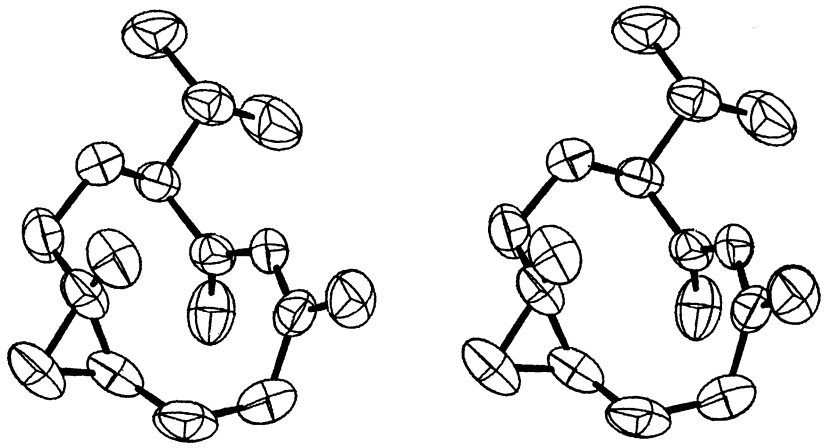

Fig. 2. A stereoscopic view of **2**. The absolute configuration and the criterion to the thermal ellipsoids of carbon and oxygen atoms are the same as in Fig. 1.

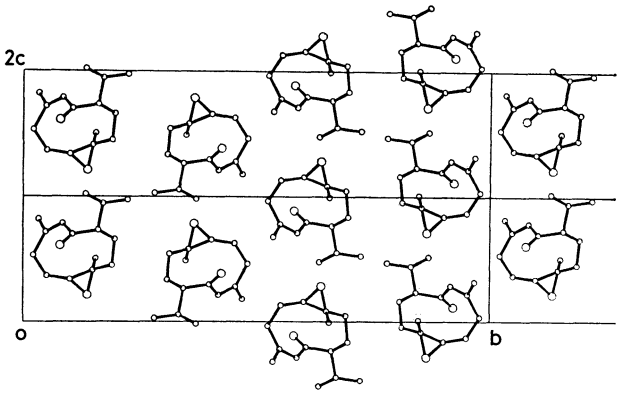

Fig. 3. The crystal structure projected along the a axis. Carbon atoms are depicted as small circles and oxygen atoms as large circles. The configuration is the same as in Fig. 1.

Center. The observed and calculated structure factors are given in Table 2.[19]

Results and Discussion

The molecular structure with atomic numberings is shown in Fig. 1, where each atom is represented by thermal ellipsoid as having 50% probability. The positional and thermal parameters of non-hydrogen atoms with their standard deviations are given in Tables 3 and 4, respectively. The coordinates and isotropic thermal parameters of hydrogen atoms are given in Table 5. The bond lengths and angles with their standard deviations are listed in Tables 6 and 7, respectively.

The molecule takes a "boat-chair" conformation. An α,β-unsaturated ketone chromophore takes a cisoid configuration, which is not planar, the torsion angle around C(1)–C(2) bond being 33°. The double bond C(2)=C(3) and epoxide group, equivalent to a double bond, are *cis* and *trans* configuration, respectively.

The methyl groups of germacradiene-type sesquiterpenes including *cis*, *trans*-double bonds are *anti* arrangement,[6] and of other ten-membered ring sesquiterpenes, shiromodiol[9] and pregeijerene[10] containing *trans,trans*-double bonds are *syn*, while those of melampodin[6] and haliangine,[14] *cis,trans*-double bonds, are *anti* arrangement. On the other hand, the conformations of the substituents of **2**, the epoxy and isopropyl groups, are semi equatorial and the two methyl groups are axial, *syn* arrangement, and β-orientation.

Ōsawa *et al.*[20] estimated the ground state conformation for all possible geometrical isomers of hedycaryol, one of the germacradiene-type sesquiterpenes, by the molecular mechanics calculations, and proposed that all the isomer might have more than two stable conformations. Takeda *et al.*[21] reported that several conformations of the ten-membered ring sesquiterpene should be considered in solution by temperature dependent NMR and NOE measurements. Yamamura *et al.*[15d] reported the C_{14} methyl group in **2** and in a reaction product of **2** by thiophenol protrudes into α-face of the macrocycle, which is contrary to our results. Therefore, it seems likely that the molecule

Table 3. Atomic coordinates and their standard deviations[a] of heavy-atoms

	x	*y*	*z*
O(1)	0.0487(6)	0.0782(2)	0.6129(6)
O(2)	0.4645(7)	0.1362(2)	0.2157(6)
C(1)	0.1535(8)	0.1044(2)	0.7017(8)
C(2)	0.3198(8)	0.0844(2)	0.7855(8)
C(3)	0.4251(8)	0.0481(2)	0.7192(8)
C(4)	0.3909(10)	0.0217(2)	0.5345(10)
C(5)	0.4788(11)	0.0500(2)	0.3698(9)
C(6)	0.3819(9)	0.0993(2)	0.3403(8)
C(7)	0.4475(9)	0.1479(2)	0.4159(8)
C(8)	0.3117(10)	0.1891(2)	0.4539(9)
C(9)	0.2592(9)	0.1944(2)	0.6223(9)
C(10)	0.1108(8)	0.1591(2)	0.7339(8)
C(11)	0.0671(9)	0.1696(2)	0.9442(8)
C(12)	−0.0635(11)	0.1322(3)	1.0197(10)
C(13)	−0.0074(11)	0.2215(2)	0.9734(11)
C(14)	0.5941(9)	0.0330(2)	0.8192(10)
C(15)	0.6282(9)	0.1538(2)	0.5078(9)

a) The standardard deviations are given in parentheses and refer to the last decimal position of respective values.

Table 4. Anisotropic thermal factors[a] ($\times 10^4$) and their standard deviations of heavy-atoms

	B_{11}	B_{22}	B_{33}	B_{12}	B_{23}	B_{31}
O(1)	226(9)	22(1)	359(13)	−25(5)	−58(6)	−14(22)
O(2)	329(12)	38(1)	161(10)	27(7)	1(6)	35(21)
C(1)	207(12)	16(1)	169(12)	−17(6)	−5(6)	85(25)
C(2)	217(13)	14(1)	175(12)	9(6)	18(6)	−18(24)
C(3)	251(14)	12(1)	246(15)	−2(6)	13(6)	76(29)
C(4)	335(18)	16(1)	346(19)	14(8)	−43(8)	25(39)
C(5)	354(20)	25(1)	258(17)	39(9)	72(8)	38(34)
C(6)	255(15)	29(1)	153(13)	2(8)	−28(7)	1(27)
C(7)	271(16)	25(1)	149(13)	10(8)	10(7)	63(28)
C(8)	313(18)	21(1)	206(15)	15(8)	39(7)	21(30)
C(9)	275(15)	14(1)	237(16)	3(7)	−12(7)	0(30)
C(10)	206(12)	16(1)	173(13)	24(6)	−17(6)	−49(24)
C(11)	199(13)	21(1)	213(14)	24(7)	−25(7)	−40(26)
C(12)	376(22)	34(2)	240(18)	−8(11)	−15(10)	182(37)
C(13)	398(23)	25(1)	350(20)	81(10)	−60(9)	29(42)
C(14)	263(16)	24(1)	301(18)	62(8)	21(9)	−20(35)
C(15)	198(14)	30(1)	262(17)	−35(8)	20(8)	−47(29)

a) The anisotropic thermal factors are of the form $\exp\{-(h^2B_{11}+k^2B_{22}+l^2B_{33}+hkB_{12}+hlB_{31}+klB_{23})\}$.

Table 5. Hydrogen atom parameters and their standard deviations

	x	y	z	B/Å^2
H(2)	0.357(7)	0.099(2)	0.880(7)	2.8(1.4)
H(4a)	0.448(8)	−0.014(2)	0.540(8)	3.7(1.4)
H(4b)	0.245(7)	0.019(2)	0.513(7)	2.4(1.3)
H(5a)	0.623(8)	0.055(2)	0.391(8)	4.9(1.6)
H(5b)	0.490(11)	0.026(2)	0.269(11)	9.8(2.3)
H(6)	0.251(7)	0.094(2)	0.325(8)	2.8(1.3)
H(8a)	0.361(9)	0.225(2)	0.422(9)	5.2(1.7)
H(8b)	0.205(8)	0.184(2)	0.387(8)	4.1(1.6)
H(9a)	0.212(8)	0.232(2)	0.678(8)	3.6(1.4)
H(9b)	0.376(8)	0.190(2)	0.725(8)	4.7(1.6)
H(10)	−0.012(8)	0.167(2)	0.662(7)	3.5(1.4)
H(11)	0.174(8)	0.169(2)	1.005(8)	4.1(1.5)
H(12a)	−0.089(9)	0.097(2)	0.995(9)	6.7(1.8)
H(12b)	−0.065(8)	0.134(2)	1.133(8)	5.1(1.7)
H(12c)	−0.202(8)	0.133(2)	0.970(9)	5.6(1.7)
H(13a)	−0.145(8)	0.227(2)	0.922(9)	5.0(1.7)
H(13b)	−0.023(9)	0.235(2)	1.071(9)	6.4(1.9)
H(13c)	0.050(9)	0.248(2)	0.903(8)	5.3(1.7)
H(14a)	0.588(9)	−0.008(2)	0.844(9)	6.4(1.9)
H(14b)	0.682(8)	0.030(2)	0.736(8)	4.4(1.6)
H(14c)	0.640(8)	0.056(2)	0.922(9)	5.2(1.7)
H(15a)	0.699(8)	0.121(2)	0.463(9)	5.4(1.7)
H(15b)	0.712(9)	0.189(2)	0.471(10)	7.3(2.0)
H(15c)	0.628(8)	0.147(2)	0.617(8)	3.6(1.5)

Table 6. Bond lengths and their standard deviations (Å)

O(1)-C(1)	1.223(7)	O(2)-C(6)	1.460(8)
O(2)-C(7)	1.471(8)	C(1)-C(2)	1.472(8)
C(1)-C(10)	1.506(8)	C(2)-C(3)	1.329(8)
C(3)-C(4)	1.517(10)	C(3)-C(14)	1.499(9)
C(4)-C(5)	1.544(11)	C(5)-C(6)	1.509(10)
C(6)-C(7)	1.484(9)	C(7)-C(8)	1.514(10)
C(7)-C(15)	1.502(9)	C(8)-C(9)	1.547(10)
C(9)-C(10)	1.535(9)	C(10)-C(11)	1.564(8)
C(11)-C(12)	1.490(10)	C(11)-C(13)	1.503(10)
C(i)-H(i)			
average	0.99		
range	0.80—1.15		

can take many conformations in solution.[21] The conformation of the medium ring of **2** is same as a less stable geometrical isomer of hedycaryol.[20]

Dunitz[22] distinguished between the conformers of ten-membered ring in terms of the endocyclic torsion angles. The torsion angles of some compounds having ten-membered ring are shown in Table 8. Each torsion angle of **2** is very similar to that of melampodin[6] and enhydrin,[8] which belongs to a highly strained *cis,trans*-germacradiene system. In dihydromikanolide[3] and pregeijerene,[10] however, several bonds are distorted in the opposite directions by about same magnitude compared with **2**.

The bond lengths are all normal except the C(6)–C(7) bond in the epoxide ring being significantly shorter than a normal single bond and the bond angle C(5)–C(6)–C(7), 123.3(6)°, indicates a remarkable deformation due to the epoxide ring formation. The similar distortion of the endocyclic bond angle was found in the other ten-membered ring epoxide, agerol diepoxide (127.2(6) and 125.0(5)),[1] dihydromikanolide (122.4(4)),[3] and elephantol *p*-bromobenzoate (124(1)°).[5]

Some of the non-bonded intramolecular distances are somewhat short, O(1)···C(6) being 3.199(8), C(1)···C(6), 3.094(9), C(1)···C(7), 3.206(9), C(2)···C(6), 3.240(9), and C(2)···C(7), 3.276(9)Å. A stereoview of the molecule is shown in Fig. 2, and the molecular packing in the crystal in Fig. 3. All intermolecular contacts are normal.

Table 7. Bond angles and their standard deviations (°)

C(6)-O(2)-C(7)	60.8(4)	O(1)-C(1)-C(2)	122.6(5)
O(1)-C(1)-C(10)	119.7(5)	C(2)-C(1)-C(10)	117.7(5)
C(1)-C(2)-C(3)	127.7(6)	C(2)-C(3)-C(4)	123.2(6)
C(2)-C(3)-C(14)	121.2(6)	C(4)-C(3)-C(14)	115.5(6)
C(3)-C(4)-C(5)	111.5(6)	C(4)-C(5)-C(6)	109.2(6)
O(2)-C(6)-C(7)	117.9(6)	O(2)-C(6)-C(7)	59.9(4)
C(5)-C(6)-C(7)	123.3(6)	O(2)-C(7)-C(6)	59.2(4)
O(2)-C(7)-C(8)	122.7(5)	O(2)-C(7)-C(15)	111.8(5)
C(6)-C(7)-C(8)	118.6(6)	C(6)-C(7)-C(15)	122.9(6)
C(8)-C(7)-C(15)	116.1(6)	C(7)-C(8)-C(9)	113.9(6)
C(8)-C(9)-C(10)	116.5(5)	C(1)-C(10)-C(9)	112.8(5)
C(1)-C(10)-C(11)	111.3(5)	C(9)-C(10)-C(11)	111.1(5)
C(10)-C(11)-C(12)	111.4(5)	C(10)-C(11)-C(13)	112.0(5)
C(12)-C(11)-C(13)	108.9(6)		

Table 8. Endocyclic torsion angles (°)[a] of some ten-membered ring

	(A)[b]	(B)[b]	(C)[b]	(D)[b]	(E)[b]
ω(1-2)	148	132	125	128	116
ω(2-3)	−2	13	4	−2	−2
ω(3-4)	−87	−97	−56	−86	−90
ω(4-5)	69	75	14	58	73
ω(5-6)	−98	−92	−54	66[c]	57[c]
ω(6-7)	154	147	155	−165[c]	−153[c]
ω(7-8)	−101	−119	−101	101[c]	66[c]
ω(8-9)	84	95	76	−59[c]	−3[c]
ω(9-10)	−56	−63	−71	−82	55[c]
ω(10-1)	−59	−56	−44	−150	−163

a) The sign is negative if an anticlockwise rotation is required of atom(1) to eclipse atom(4) whilst looking down the (2)-(3) bond. b) (A) present work; (B) enhydrin, renumbered from Ref. 8; (C) melampodin, renumbered and inverted from Ref. 6; (D) 1:1 adduct of pregeijerene with silver nitrate, renumbered from Ref. 10; (E) dihydromikanolide, renumbered from Ref. 3. c) The rotations of these bonds are in the opposite directions compared to (A).

The authors are grateful to Professor Shyosuke Yamamura, Meijo University, for his kind supply of the sample.

References

1) W. Messerotti, U. M. Pagoni, R. Trave, R. Zanasi, G. D. Andreetti, G. Bocelli, and P. Sgarabotto, *J. Chem. Soc., Perkin Trans. 2*, **1978**, 217.

2) S. F. Watkins, J. D. Korp, I. Bernal, D. L. Perry, N. S. Bhacca, and N. H. Fischer, *J. Chem. Soc., Perkin Trans. 2*, **1978**, 599.

3) P. J. Cox and G. A. Sim, *J. Chem. Soc., Perkin Trans. 2*, **1974**, 1355.

4) S. M. Kupchan, M. Maruyama, R. J. Hemingway, J. C. Hemingway, S. Shibuya, T. Fujita, P. D. Craswick, A. D. U. Hardy, and G. A. Sim, *J. Am. Chem. Soc.*, **93**, 4914 (1971).

5) A. T. McPhail and G. A. Sim, *J. Chem. Soc., Perkin Trans. 2*, **1972**, 1313.

6) S. F. Watkins, N. H. Fischer, and I. Bernal, *Proc. Natl. Acad. U. S. A.*, **70**, 2434 (1973).

7) W. Herz, R. Groote, and R. Murari, *J. Org. Chem.*, **43**, 3559 (1978).

8) G. Kartha and K. T. Go, *J. Chem. Soc., Chem. Commun.*, **1972**, 1327.

9) R. J. McClure and G. A. Sim, *Chem. Commun.*, **1970**, 128.

10) P. Coggon, A. T. McPhail, P. M. Gross, and G. A. Sim, *J. Chem. Soc., B*, **1970**, 1024.

11) P. J. Cox and G. A. Sim, *J. Chem. Soc., Perkin Trans. 2*, **1975**, 455.

12) P. J. Cox and G. A. Sim, *J. Chem. Soc., Perkin Trans. 2*, **1977**, 255.

13) M. E. Witt and S. F. Watkins, *J. Chem. Soc., Perkin Trans. 2*, **1978**, 204.

14) M. Nishikawa, K. Kamiya, A. Takabatake, H. Oshio, Y. Tomiie, and I. Nitta, *Tetrahedron*, **22**, 3601 (1966).

15) a) M. Niwa, A. Nishiyama, M. Iguchi, and S. Yamamura, *Bull. Chem. Soc. Jpn.*, **48**, 2930 (1975); b) S. Yamamura, M. Iguchi, A. Nishiyama, M. Niwa, H. Koyama, and Y. Hirata, *Tetrahedron*, **27**, 5419 (1971), and references cited therein; c) M. Niwa, M. Iguchi, and S. Yamamura, *Bull. Chem. Soc. Jpn.*, **49**, 3184 (1976); M. Niwa M. Iguchi, and S. Yamamura, *Tetrahedron Lett.*, **1975**, 3661; d) M. Niwa, M. Iguchi, and S. Yamamura, *Bull. Chem. Soc. Jpn.*, **49**, 3137 (1976).

16) G. Germain, P. Main, and M. M. Woolfson, *Acta Crystallogr., Sect. A*, **27**, 368 (1971).

17) "International Tables for X-Ray Crystallography," Birmingham, Kynoch Press (1974), Vol. IV, pp. 72—98.

18) C. K. Johnson, ORTEP, Report ORNL-3794, Ork Ridge National Laboratory, Tennessee (1965).

19) Table 2 is kept at the Office of the Editor of the Bulletin of the Chemical Society of Japan, Kanda, Surugadai, Chiyoda-ku, Tokyō (Document No. 8021).

20) E. Ōsawa, K. Shimada, M. Kodama, and S. Itô, *Tetrahedron Lett.*, **1979**, 2353.

21) K. Takeda, *Tetrahedron*, **30**, 1525 (1974); K. Tori, I. Horibe, Y. Tamura, H. Tada, and K. Takeda, *Tetrahedron Lett.*, **1976**, 387.

22) J. D. Dunitz, *Perspectives in Structural Chem.*, **2**, 7 (1968).

 © 1980 The Chemical Society of Japan Bull. Chem. Soc. Jpn., 53, 1267—1270 (1980)

Polymer-protected Colloidal Nickel Boride in Ethanol and Its Catalytic Activity for Hydrogenation

Yukimichi NAKAO* and Shoei FUJISHIGE

Research Institute for Polymers and Textiles, Yatabe-Higashi, Tsukuba-gun, Ibaraki 305

(Received October 26, 1979)

Colloidal nickel borides were prepared in ethanol from nickel(II) chloride and sodium borohydride using a polymer as a protective colloid. For atmospheric hydrogenation of olefins such as acrylamide at 30 °C, the colloid prepared by using poly(vinylpyrrolidone) exhibited catalytic activity 15—60 times that of the usual nickel boride prepared without using a polymer. The high activity of colloidal nickel borides was found to be due to the polymers, soluble nylon being the most effective. The colloids are stable under oxygen-free hydrogen, decomposing immediately on exposure to air.

Reduction of nickel(II) chloride ($NiCl_2 \cdot 6H_2O$) with sodium borohydride ($NaBH_4$) in aqueous solutions gives a black precipitate of nickel boride which is catalytically active for the hydrogenation of olefinic compounds[1] and the hydrolysis of $NaBH_4$.[2] Many variations for the preparation of nickel boride have been reported.[3] Although the form of precipitated nickel boride varies according to the mode of preparation, most of them consist of a common unit Ni_2B.[3] In general, the activity of a solid catalyst such as nickel boride is primarily controlled by its effective surface area which is dependent upon both particle size and dispersion state. A number of reports[4] have appeared on the colloidal noble metals prepared from the corresponding metal salts by treatment with a reductant such as molecular hydrogen in aqueous solution. The coagulation of colloidal metals can be prevented by the presence of a polymer.

Hydrosol of nickel boride was prepared by the reduction of nickel(II) nitrate with potassium borohydride in the presence of a fairly large amount (5%) of a polymer such as acid gelatin and poly(vinyl alcohol).[5] Sols of metals in alcohol have been prepared in a similar manner.[6] An extremely fine colloid of rhodium (9 Å in diameter) was prepared from a methanolic solution of rhodium(III) chloride by treatment with sodium hydroxide in the presence of poly(vinylpyrrolidone) as a protective colloid. The colloidal rhodium was a very effective catalyst especially for the atmospheric hydrogenation of internal olefins. A clear nickel boride sol was prepared by the reduction of $NiCl_2 \cdot 6H_2O$ with $NaBH_4$ in ethanol under hydrogen in the presence of a small amount (0.01%) of poly(vinylpyrrolidone).[7] It exhibited a much higher activity for the hydrogenation of olefins such as acrylamide than that of the nickel boride precipitate prepared without using polymers. In the present paper, the effects of materials and the mode of preparation on the colloidal nickel boride as regards its catalytic activity and stability against oxygen are described.

Experimental

Chemicals. Hydrogen was of 99.999% purity. Liquid chemicals (reagent grade) for reaction medium were degassed by refluxing under argon before use. Solid chemicals (reagent grade) were used without further purification.

Preparation of Colloidal Nickel Boride. A typical procedure for the preparation of colloidal nickel boride is as follows. Nickel(II) chloride ($NiCl_2 \cdot 6H_2O$, 0.020 mmol) and poly(vinylpyrrolidone) (PVP-K30, degree of polymerization 360, 2.0 mg) were dissolved in ethanol (18 ml) under hydrogen. To the solution was added an ethanolic solution (1 ml) of sodium borohydride ($NaBH_4$, 0.040 mmol) prepared under argon with stirring at 30.0 °C and atmospheric pressure of hydrogen. Dark brown sol (19 ml) of nickel boride was obtained. The formation was followed by hydrogen evolution which ceased within 15 min.

Hydrogenation of Acrylamide. An ethanolic solution (1 ml) of acrylamide (0.25 mmol) prepared under argon was added to the nickel boride sol (19 ml) with stirring at 30.0 °C and atmospheric pressure of hydrogen, hydrogen uptake starting. The progress of hydrogenation was followed by means of the uptake volume of hydrogen. The hydrogenation product was found to be propionamide by means of infrared spectra.

Results

Formation of Colloidal Nickel Boride. Addition of an ethanolic solutions of $NaBH_4$ (0.040 mmol) to ethanolic solutions of $NiCl_2 \cdot 6H_2O$ (0.020 mmol) and PVP-K30 at 30 °C under hydrogen resulted in the formation of colloidal nickel boride. On adding $NaBH_4$, a short induction period of 1—2 s ended with the formation of a colloid. Colloidal nickel borides were obtained at 0 °C and −20 °C with induction periods 5 s and 25 s, respectively. Hydrogen evolution began immediately after the colloid formation, ceasing in 15 min. The total evolution volume was 2.55 ml (0.104 mmol).

Catalytic Activity for Hydrogenation. Addition of acrylamide[8] to colloidal nickel boride resulted in hydrogen uptake. Figure 1 shows the time-course of the hydrogen uptake. Equimolar amount of hydrogen with acrylamide was taken up until the hydrogenation was completed in 4 min. The initial rate of hydrogen uptake (r_1(acam)) was determined from the curve to be 167 H_2 mmol/Ni_2B mol s,[9] giving a measure of the catalytic activity of colloid.

Available Materials. Various nickel(II) salts, borohydrides, and solvents were examined for the preparation of colloidal nickel boride using PVP-K30. The results are given in Table 1. Nickel(II) sulfate and nickel(II) acetate also give colloidal nickel borides with an almost equal activity to that from $NiCl_2 \cdot 6H_2O$. On the contrary, a black colloidal solution from nickel(II) nitrate exhibits a much lower activity.

The use of water as a solvent gives a gray turbid solution which is not so effective as the clear sol pre-

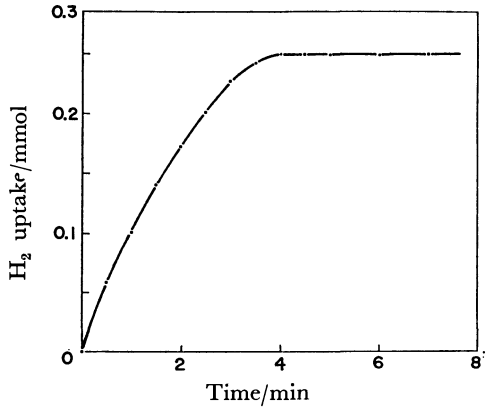

Fig. 1. Atmospheric hydrogenation of acrylamide in ethanol at 30 °C catalyzed by colloidal nickel boride.

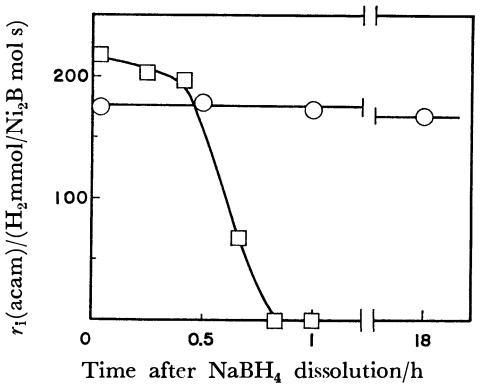

Fig. 2. Decrease in ability to produce colloidal nickel boride of ethanolic (○) and methanolic (□) $NaBH_4$ at 17 °C.

Table 1. Catalytic activity of colloidal nickel boride[a)]

Ni(II) salt	BH_4 salt	Solvent	r_i(acam)[b)] (H_2 mmol/Ni_2B mol s)
$NiCl_2 \cdot 6H_2O$	$NaBH_4$	EtOH	167
$NiSO_4 \cdot 7H_2O$	$NaBH_4$	EtOH	168
$Ni(OAc)_2 \cdot 4H_2O$	$NaBH_4$	95%EtOH	165
$Ni(NO_3)_2 \cdot 6H_2O$	$NaBH_4$	EtOH	2
$NiCl_2 \cdot 6H_2O$	$NaBH_4$	H_2O	11
$NiCl_2 \cdot 6H_2O$	KBH_4	MeOH	245
$NiCl_2 \cdot 6H_2O$	$NaBH_4$	MeOH	218

a) Prepared by using poly(vinylpyrrolidone)-K30. b) Initial rate of hydrogenation of acrylamide.

Table 2. Catalytic activity of colloidal nickel boride[a)]

Polymer	r_i(acam)[b)] (H_2 mmol/Ni_2B mol s)
Poly(vinylpyrrolidone)-K30[c)]	167
Poly(vinylpyrrolidone)-K15[d)]	180
Poly(vinylpyrrolidone)-K90[e)]	156
Soluble nylon[f)]	377
Poly(methyl vinyl ether)[g)]	74
Ethyl hydroxyethyl cellulose	193
Poly(vinyl alcohol)[h)]	170[i)]

a) Prepared by using $NiCl_2 \cdot 6H_2O$ and $NaBH_4$ in ethanol. b) Initial rate of hydrogenation of acrylamide. c) Degree of polymerization (DP)=360. d) DP=90. e) DP=3250. f) Ternary copolymer (6:66:610=3:4:3). g) DP=570. h) DP=500. i) Solvent=95% EtOH.

pared in ethanol. Potassium borohydride (KBH_4) is almost insoluble in ethanol, but soluble in methanol. A sol prepared in methanol with KBH_4 is more effective than that prepared with $NaBH_4$.

Borohydride salts are known to react with methanol.[10)] Ethanolic and methanolic solutions of $NaBH_4$ were examined for their ability to produce active colloidal nickel boride. The dependence of the ability of both $NaBH_4$ solutions upon time after $NaBH_4$ dissolution at 17 °C is shown in Fig. 2. Ethanolic $NaBH_4$ is still able to produce a colloid after being left to stand for 18 h, the ability of methanolic $NaBH_4$ being completely lost within 1 h. When methanolic $NaBH_4$ was added to $NiCl_2 \cdot 6H_2O$–PVP-K30 solutions 20 min after its dissolution, a highly active colloid was obtained. KBH_4 reacted with methanol more slowly than $NaBH_4$.

A series of ethanol-soluble polymers were examined as a protective colloid using $NiCl_2 \cdot 6H_2O$, $NaBH_4$, and ethanol. Poly(vinylpyrrolidone)s, soluble nylon, and poly(vinyl alcohol) gave dark brown colloids, while poly(methyl vinyl ether) and ethyl hydroxyethyl cellulose gave black colloids. The catalytic activity of these colloids is shown in Table 2. Poly(vinylpyrrolidone)s of degree of polymerization 90 (PVP-K15) and 3250 (PVP-K90) give dark brown colloids with a nearly equal activity to that prepared with PVP-K30. The catalytic activity of colloid varies with the kind of polymer. Colloidal nickel boride with soluble nylon is the most active among those listed in Table 2, exhibiting about five times the activity of that with poly(methyl vinyl ether). *N*-methylpyrrolidone, a monomeric compound having the same functional group as poly(vinylpyrrolidone), gave no colloid but a black precipitate. Absence of a polymer also resulted in the precipitation of nickel boride.

Effect of $NaBH_4$ to $NiCl_2 \cdot 6H_2O$ Ratio. Colloidal nickel borides were prepared in ethanol with varying amounts of $NaBH_4$, and used as a catalyst after being stirred under hydrogen for 15 min. Figure 3 (solid line) shows the dependence of catalytic activity of colloidal nickel boride upon the molar ratio of $NaBH_4$ to $NiCl_2 \cdot 6H_2O$ (B/Ni). When less than equimolar $NaBH_4$ with $NiCl_2 \cdot 6H_2O$ (B/Ni<1) was used, only unstable colloids were obtained. Thus, colloidal nickel boride, once formed on addition of $NaBH_4$, was gradually inactivated under hydrogen with fading of coloration during 15 min stirring. The catalytic activity of colloid increases remarkably with increase in the amount of $NaBH_4$ in the range of B/Ni ratio between 1 and 2, the dark brown coloration of the original solution remaining unchanged. By using not less than double molar $NaBH_4$ with $NiCl_2 \cdot 6H_2O$ (B/Ni≧2), a colloid with an almost constant activity was obtained.

Reduction of $NiCl_2 \cdot 6H_2O$ with $NaBH_4$ in ethanol in the absence of a polymer gave a suspension containing visible particles of precipitated nickel boride. Suspen-

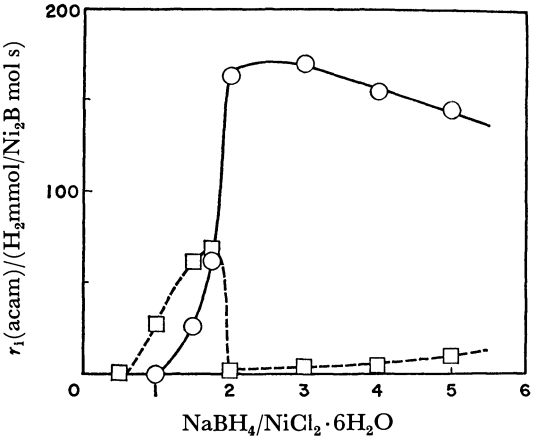

Fig. 3. Dependence upon $NaBH_4/NiCl_2 \cdot 6H_2O$ ratio of the catalytic activity of colloidal (○) and precipitated (□) nickel borides.

sions prepared with varying amounts of $NaBH_4$ were examined for their catalytic activity. The dependence of the catalytic activity of precipitated nickel boride upon B/Ni ratio (Fig. 3, broken line), is compared with that of colloidal nickel boride. Maximal activity is obtained with B/Ni ratio in the region 1.5—1.7, in which fine particles of nickel boride appear. On the other hand, the use of not less than double molar $NaBH_4$ with $NiCl_2 \cdot 6H_2O$ (B/Ni≧2) gives only a coagulated mass with a much lower activity. In this range of B/Ni ratio, colloidal nickel boride showed 15—60 times the catalytic activity of the precipitate.

Effect of the Amount of PVP-K30. The reduction of $NiCl_2 \cdot 6H_2O$ with $NaBH_4$ was carried out in ethanol in the presence of varying amounts of PVP-K30. As shown in Fig. 4, the presence of more than 0.5 mg (25 ppm) of PVP-K30 is important for obtaining colloidal nickel boride, otherwise a precipitate of nickel boride with a low activity is formed. The catalytic activity of colloidal nickel boride is nearly constant in the range of amount of PVP-K30 2—80 mg.

Decomposition by Oxygen. On exposure to the air, a dark brown solution of colloidal nickel boride was immediately converted into a light yellow inactive solution. In contrast, the colloid was stable under hydrogen and could be stored for 110 h with no change in coloration. The stored colloid exhibited 1.29 times the catalytic activity of the initial. Colloidal nickel boride was obtained under oxygen-free argon as well. Hydrogen was evolved by the hydrolysis of $NaBH_4$. So long as more than 4 vol% of evolved hydrogen was present in the atmosphere, the colloid was stable for a long period, exhibiting a considerable activity (r_i(acam)=150 H_2 mmol/Ni_2B mol s). Under argon containing less than 0.1 vol% of hydrogen, the colloidal nickel boride catalyst was completely inactivated within 1 h.

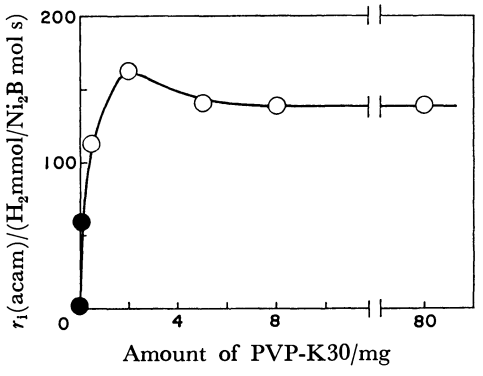

Fig. 4. Dependence upon the amount of PVP-K30 of the catalytic activity of nickel boride (○, colloidal; ●, precipitated).

Colloidal nickel borides prepared under hydrogen with 2 mg and 80 mg of PVP-K30 were exposed to the air at room temperature (20 °C). Decomposition of the colloids was followed by decrease in optical density at 750 nm of the colloidal solutions. The colloid with 80 mg of PVP-K30 always decomposed at a faster rate than that with 2 mg of PVP-K30.

Hydrogenation of acrylamide catalyzed by colloidal nickel borides with 2 mg and 80 mg of PVP-K30 was carried out in the presence of varying amounts of additional oxygen. The colloidal catalyst with 80 mg of PVP-K30 was inhibited more strongly than that with 2 mg of PVP-K30, the former being more sensitive to oxygen than the latter.

Discussion

The following stoichiometry was proposed for the progress of reduction of nickel(II) chloride with $NaBH_4$ in aqueous solution.[11]

$$NiCl_2 + 2NaBH_4 + 4.5H_2O \longrightarrow 0.5Ni_2B + 1.5H_3BO_3 + 6.25H_2 + 2NaCl \quad (1)$$

A similar process performed in ethanol under nitrogen gave a nickel boride precipitate having the formula $(Ni_2B)_2 \cdot H_3$.[12] It seems that colloidal nickel borides prepared in ethanol under hydrogen in the presence of a polymer contains a common structural unit Ni_2B. In the present case, the molar ratio of evolved hydrogen to $NiCl_2 \cdot 6H_2O$ charged was calculated to be 5.2, being smaller than that expected from Eq. 1. This gap between observed and theoretical amounts of evolved hydrogen is caused by the adsorption of hydrogen on the surface of colloidal nickel boride. Colloidal nickel borides were stable only in an oxygen-free atmosphere containing hydrogen. This indicates that the adsorption of hydrogen on the colloid surface might take part in the stability of the colloid. A black colloid prepared from nickel(II) nitrate was almost inactive (Table 1). On the other hand, colloidal nickel boride from $NiCl_2 \cdot 6H_2O$ was gradually inactivated when an alternative nitrate salt such as ammonium nitrate was added. In both cases, the inactivation process might be attributed to the loss of adsorbed hydrogen by oxidation with nitrate ion.

A reaction scheme involving $Ni(BH_4)_2$ intermediate was proposed for the process of nickel boride formation in aqueous solution.[11] During the induction period preceeding the formation of colloidal nickel boride, the conversion of $NiCl_2 \cdot 6H_2O$ into $Ni(BH_4)_2$ might occur.

In aqueous solution, nickel(II) hydroxide may be

formed in preference to nickel boride on account of the considerable basicity of the $NaBH_4$ solution. White turbidity appearing in the process using aqueous media (Table 1) might be due to polymeric nickel(II) hydroxide. However, nickel boride was predominantly produced in aqueous media when the reaction was carried out at low temperature (0 °C)[11] or in the presence of a large amount of polymers such as poly(vinyl alcohol)[5] owing to suppression of the formation of polymeric nickel(II) hydroxide.

The particle size of a colloidal catalyst is essential for the estimation of its turnover frequency. However, colloidal nickel boride was so unstable in a high vacuum as well as under hydrogen-free argon that the particle size of the colloid could not be determined by electron microscopy.

A precipitated nickel boride catalyst prepared without using polymers (B/Ni=1.5) was *ca.* 50% inhibited by the addition of 80 mg of PVP-K30. It seems that PVP-K30 acts as an inhibitor through locating on the catalytic surface of precipitated nickel boride. Polymers such as PVP-K30 existing in the solution of colloidal nickel boride are assumed to act as a protective colloid through covering the surface of colloidal particles.[13] Polymers existing in the solution of colloidal nickel boride are presumed to lower the catalytic activity to some extent. The widely varied activities of colloids prepared with a variety of polymers (Table 2) can be explained in terms of inhibition by polymers.

The degree of inhibition of a precipitated nickel boride catalyst increased with increase in the amount of PVP-K30. In contrary, the catalytic activity of colloidal nickel boride was independent of the amount of PVP-K30 (Fig. 4). A similar relationship was observed in the case of colloidal rhodium prepared by using poly(vinyl alcohol).[14] The discrepancy might be attributed to the variation of the size of colloidal particles with the amount of the polymer used.

The well-dispersed state of colloidal nickel boride due to the presence of PVP-K30 as a protective colloid is primarily responsible for its high activity. On the other hand, precipitated nickel boride formed with more than double molar $NaBH_4$ with $NiCl_2 \cdot 6H_2O$ gradually coagulated into a black mass with a very low activity. Well-dispersed suspension of precipitated nickel boride (B/Ni=1.5) coagulated on further addition of $NaBH_4$. Nickel borides were found to be very active catalysts for the hydrolysis of $NaBH_4$.[2]

$$NaBH_4 + 2H_2O \xrightarrow{Ni_2B} NaBO_2 + 4H_2 \quad (2)$$

It seems that excess or additional $NaBH_4$ is hydrolyzed to yield $NaBO_2$ which causes the coagulation of nickel boride precipitates.

Colloidal nickel borides prepared by using less than double molar $NaBH_4$ with $NiCl_2 \cdot 6H_2O$ exhibited a considerable activity when used immediately after preparation. Thus, acrylamide was hydrogenated at an initial rate of 46 H_2 mmol/Ni_2B mol s with the colloid which had been prepared 1 min before its use by using equimolar $NaBH_4$ with $NiCl_2 \cdot 6H_2O$. However, the colloid once formed was completely inactivated in 15 min with stirring under hydrogen (Fig. 3). The inactivation mechanism of the colloid under hydrogen has not been clarified.

References

1) R. Paul, P. Buisson, and N. Joseph, *Ind. Eng. Chem.*, **44**, 1006 (1952).

2) H. I. Schlesinger, H. C. Brown, A. E. Finholt, J. R. Gilbreath, H. R. Hoekstra, and E. K. Hyde, *J. Am. Chem. Soc.*, **75**, 215 (1953).

3) R. C. Wade, D. G. Holah, A. N. Hughes, and B. C. Hui, *Cat. Rev.*, **14**, 211 (1976), and the references cited therein.

4) For example, R. Zsigmondy, *Z. Anal. Chem.*, **40**, 697 (1901); C. Paal and C. Amberger, *Ber.*, **37**, 124 (1904); A. Skita, *Ber.*, **42**, 1627 (1909); W. P. Dunworth and F. F. Nord, *Adv. Cat.*, **6**, 125 (1954).

5) K. N. Machalov, A. T. Groisberg, and N. A. Palikhov, *Tr. Kazan. Khim.—Tekhnol. Inst.*, **1969**, 150; through *Chem. Abstr.*, **75**, 40844h (1971).

6) H. Hirai, Y. Nakao, and N. Toshima, *Chem. Lett.*, **1978**, 545.

7) Y. Nakao and S. Fujishige, *Chem. Lett.*, **1979**, 995.

8) Acrylamide was used as a substrate, since it is very soluble in both alcohols and water.

9) Since the stoichiometry of colloidal nickel boride is as yet unknown, a common unit of Ni_2B reported for precipitated nickel boride was applied for convenience to the molecular formula of colloidal nickel boride.

10) L. F. Fieser and M. Fieser, "Reagents for Organic Synthesis," John Wiley and Sons, Inc., New York (1967), p. 1050.

11) N. N. Mal'tseva, Z. K. Sterlyadkina, and V. I. Mikheeva, *Zh. Neorg. Khim.*, **11**, 720 (1966); through *Chem. Abstr.*, **65**, 1751f (1966).

12) P. C. Maybury, R. W. Mitchell, and M. F. Hauthorne, *J. Chem. Soc., Chem. Commun.*, **1974**, 534.

13) Y. Glazman and Z. Blashchuk, *J. Colloid Interface Sci.*, **62**, 158 (1977).

14) H. Hirai, Y. Nakao, and N. Toshima, *J. Macromol. Sci., Chem.*, **A12**, 1117 (1978).

The Oxidation Reaction of Tl(I) to Tl(III) by the Peroxodisulfate Ion. I. Kinetics and Mechanism in an Aqueous Solution

Masaru KIMURA,* Tsuneko AKAZOME, Kayo TAKENAKA, and Akiko KOBAYASHI

Department of Chemistry, Faculty of Science, Nara Women's University, Nara 630

(Received July 25, 1979)

The oxidation reaction of the thallium(I) ion to the thallium(III) ion by the peroxodisulfate ion has been studied in an aqueous acidic solution. The reaction constituted a chain reaction initiated by the thermal decomposition of the peroxodisulfate ion, the reaction involving no direct reactions between the thallium(I) and peroxodisulfate ions. At thallium(I) ion concentrations larger than 0.004 mol dm^{-3}, the reaction mechanism was assumed to be: $S_2O_8^{2-} \xrightarrow{k_1} 2SO_4^{\cdot-}$; $S_2O_8^{2-}+H^+ \xrightarrow{k_2} HSO_4^-+\frac{1}{2}O_2+SO_3$; $Tl(I)+SO_4^{\cdot-} \xrightarrow{k_3} Tl(II)+SO_4^{2-}$; $S_2O_8^{2-}+Tl(II) \xrightarrow{k_4} Tl(III)+SO_4^{\cdot-}+SO_4^{2-}$; $2Tl(II) \underset{k_{-5}}{\overset{k_5}{\rightleftharpoons}} Tl(I)+Tl(III)$. The rate of the reaction was described as $-d[S_2O_8^{2-}]/dt=(k_1+k_2[H^+])[S_2O_8^{2-}]+k_4(k_1/k_5)^{1/2}[S_2O_8^{2-}]^{3/2}$. The rate constants at an ionic strength of 0.16 mol dm^{-3} were determined to be $k_1=1.99\times10^{19}\exp[-157\text{ kJ mol}^{-1}/RT]\text{s}^{-1}$, $k_2=2.75\times10^{12}\exp[-103\text{ kJ mol}^{-1}/RT]\text{ dm}^3\text{ mol}^{-1}\text{ s}^{-1}$, and $k_4(k_1/k_5)^{1/2}=2.81\times10^{13}\exp[-108\text{ kJ mol}^{-1}/RT]\text{ dm}^{3/2}\text{ mol}^{-1/2}\text{ s}^{-1}$ in 0.01 mol dm^{-3} perchloric acid, the k_4 value being increased with a decrease in the hydrogen-ion concentration. The ionic strength (μ) dependence was described as $\log k_4(k_1/k_5)^{1/2}=-4.17-1.05\,\mu^{1/2}$ in 0.01 mol dm^{-3} perchloric acid at 40 °C. The reaction rate was completely retarded by the addition of 1% acrlyronitrile, 5×10^{-6} mol dm^{-3} cerium(III) sulfate, 1×10^{-3} mol dm^{-3} cerium(IV) sulfate, or 0.1 mol dm^{-3} sodium acetate, and it was also remarkably retarded by the addition of 1×10^{-3} mol dm^{-3} tetranitromethane. The copper(II) ion and molecular oxygen did not appreciably affect the reaction rate, but the iron(III) ion accelerated it greatly.

The peroxodisulfate ion is known as a powerful two-electron oxidizing agent, and the oxidation reactions of the organic and inorganic substrates by the peroxodisulfate ion have been extensively studied by a number of researchers and have been reviewed by House,[1] Wilmarth and Haim,[2] Wilson,[3] and Buist.[4] However, the investigation of the oxidation reaction of the thallium(I) ion by the peroxodisulfate ion has not been done previously. Bednar[5] studied the induced oxidation of the thallium(I) ion by the iron(II) ion-hydrogen peroxide reaction and concluded that the thallium(II) ion is formed as an intermediate by the reaction with the hydroxyl radical. The reaction of thallium(I) with the hydroxyl radical giving the thallium(II) ion also occurs during the photolysis[6] and radiolysis[7] of cerium(IV)-thallium(I) mixtures. It is now believed that the thallium(II) ion exists as an intermediate in the redox reaction of the thallium(I)-thallium(III) couple. In the oxidation reaction of the thallium(I) ion to the thallium(III) ion by the peroxodisulfate ion, three schemes for the reaction can be tentatively assumed: (1) a single step of the two-electron transfer by the direct reaction between the thallium(I) and peroxodisulfate ions; (2) two successive reactions of the one-electron transfer, involving the thallium(II) ion as the intermediate species, and (3) a reaction initiated only by the thermal decomposition of the peroxodisulfate ion, without any direct reactions between the reactants. The present paper intends to characterize each scheme and to ascertain the true mechanism of the reaction.

Experimental

Chemicals. Reagent-grade potassium peroxodisulfate of the Wako Pure Chemicals Co., Inc., was recrystallized twice from redistilled water and dried at 25 °C in a vacuum desiccator. Thallium(I) perchlorate was prepared by dissolving thallium(I) sulfate in a perchloric acid solution, recrystallizing it from an aqueous perchloric acid solution, washing it with ethanol, and drying it at 80 °C in a vacuum-drying oven. The thallium(I) perchlorate was confirmed to be free of sulfate ions. The sodium perchlorate used for adjusting the ionic strength was recrystallized twice from the redistilled water. The thallium(III) perchlorate was prepared by dissolving Tl_2O_3 in about 5 mol dm^{-3} perchloric acid at 60—70 °C for several hours. All the other chemicals used were guaranteed reagents. The redistilled water was prepared from the anion- and cation-exchange resin water by successive distillations from solutions with and without permanganate in a glass still.

Procedure. Most of the experiments were carried out in a solution of 0.1 mol dm^{-3} sodium perchlorate and 0.01 mol dm^{-3} perchloric acid at 40 °C; no buffer solutions were used in any experiments. The reaction vessel was covered with black adhesive-plastic tape to ensure darkness, and was placed in a thermostat bath. The aliquot samples were withdrawn at appropriate times and mixed with a cold solution of 1% acrylonitrile, so that the reaction was almost completely stopped and the temperature of the solution was reduced to about 25 °C. Then the concentrations of the peroxodisulfate and thallium(I) ions remaining were measured by means of polarography. The thallium(I)-ion concentration was determined by means of a.c. polarography at −0.45 V *vs.* SCE in a solution of 0.01 mol dm^{-3} perchloric acid, 0.1 mol dm^{-3} sodium perchlorate, and 0.01% gelatine at 25 °C. After the separation of the thallium(III) ion formed from the peroxodisulfate ion by filtering it through the cation-exchange resin, the peroxodisulfate-ion concentration was determined by means of d.c. polarography at 0.2 V *vs.* SCE in a solution with the same constituents as in the measurement of the thallium(I)-ion concentration. The method of the polarographic determination for the peroxodisulfate-ion concentration is essentially the same as that used in the previous studies.[8,9] The concentration of the thallium(III) ion formed was determined as follows. All the thallium(I) ion remaining in the reacting solution was once precipitated by the addition of a slight excess of CrO_4^{2-} in an acetate buffer solution with a 4.8 of pH. After the separation of the thallium(I) ion as Tl_2CrO_4, the thallium

(III) ion in the filtered solution was precipitated as $Tl(OH)_3$ in 0.1 mol dm^{-3} sodium hydroxide. The sediment of the hydroxo thallium(III) after filtration was dissolved in a perchloric acid solution. Then, the thallium(III)-ion concentrations were determined by means of d.c. polarography at 0.2 V *vs.* SCE under the conditions used for the measurements of the concentrations of the peroxodisulfate and thallium(I) ions. Blank experiments with mixtures of peroxodisulfate, thallium(I), and thallium(III) ions of the same constitutions as those in the reaction mixtures showed that this method of determination yields reliable results. It was also confirmed that no appreciable reaction of the peroxodisulfate ion with the thallium(I) ion occurred during the procedures for the determination of the concentrations.

Results

Stoichiometry. With concentrations of 8.0×10^{-3} mol dm^{-3} in potassium peroxodisulfate and 8.0×10^{-3} mol dm^{-3} in thallium(I) perchlorate, the concentrations of both peroxodisulfate and thallium(I) ions disappearing due to the reaction were determined and the results are shown in Table 1. The results in Table 1 indicate that, at the initial stages of reaction, the concentrations of the peroxodisulfate ion disappearing are almost equivalent to those of the thallium(I) disappearing, and that, at the later stages of reaction, those of the peroxodisulfate ion disappearing become larger than those of the thallium(I) ion disappearing. With 1.6×10^{-2} mol dm^{-3} in potassium peroxodisulfate and 4.0×10^{-3} mol dm^{-3} in thallium(I) perchlorate, the concentration of the peroxodisulfate ion disappearing and that of the thallium(III) ion being formed were determined and the results are shown in Table 2. At the initial stages of reaction, the concentrations of the peroxodisulfate ion disappearing are almost equivalent to those of the thallium(III) ion being formed, and, according to the progress of the reaction, those of the peroxodisulfate ion disappearing become larger than those of the thallium(III) ion being formed.

Reaction Order and Rate Law. The initial rate of the reaction (V_i) was determined at varied concentrations of the thallium(I) and peroxodisulfate ions under given conditions. The results are shown in Figs. 1 and 2. The plot of V_i *vs.* $[Tl(I)]_i$ in Fig. 1 indicates that the rate of the reaction increases linearly

TABLE 1. STOICHIOMETRY[a)]

Reaction time / h	$[S_2O_8^{2-}]_{disapp.}$ / 10^{-3} mol dm^{-3}	$[Tl(I)]_{disapp.}$ / 10^{-3} mol dm^{-3}	$[S_2O_8^{2-}]_{disapp.}$[b)] / 10^{-3} mol dm^{-3}
0.5	0.06	0.07	0.02
5	0.67	0.61	0.08
21	1.92	1.75	0.31
47	3.40	2.74	0.43
70	4.16	3.25	0.60
94	4.80	4.02	0.85
119	5.34	4.34	1.05
149	5.82	4.78	1.30

a) Initial concentrations of 8.0×10^{-3} mol dm^{-3} for both potassium peroxodisulfate and thallium(I) perchlorate, 0.01 mol dm^{-3} in perchloric acid, and 0.1 mol dm^{-3} in sodium perchlorate; 40 °C; dark. b) As in a), but in the absence of thallium(I).

TABLE 2.

Reaction time / h	$[S_2O_8^{2-}]_{disapp.}$ / 10^{-3} mol dm^{-3}	$[Tl(III)_{formed}$ / 10^{-3} mol dm^{-3}
1	0.35	0.38
2	0.70	0.70
3	1.05	1.1
4	1.42	1.3
5	1.67	1.6

a) Condition as in Table 1; except for 1.6×10^{-2} mol dm^{-3} in potassium peroxodisulfate, 4.0×10^{-3} mol dm^{-3} in thallium(I) perchlorate, and an ionic strength of 0.06 mol dm^{-3}.

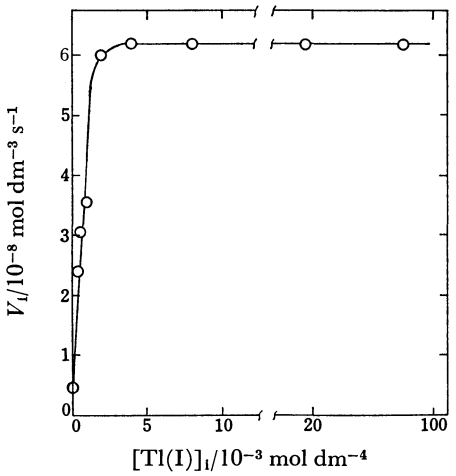

Fig. 1. Plot of V_i *vs.* $[Tl(I)]_i$.
Conditions as in Table 3; except varied concentrations of thallium(I) perchlorate.

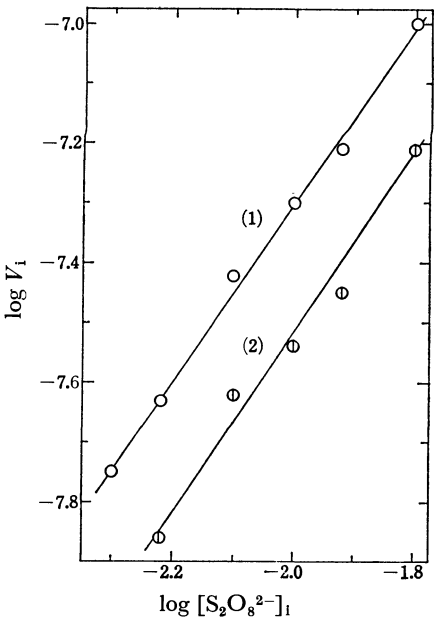

Fig. 2. Plot of log V_i *vs.* log $[S_2O_8^{2-}]_i$.
Conditions as in Table 3; except varied concentrations of potassium peroxodisulfate, and ionic strengths 0.06 and 0.16 mol dm^{-3} for lines 1 and 2, respectively.

with an increase in the thallium(I)-ion concentrations for the low concentrations, and that it then becomes independent of the thallium(I) ion over the range from 0.004 to 0.08 mol dm^{-3}. The plot of log V_i *vs.* log $[S_2O_8^{2-}]_i$ in Fig. 2 shows a straight line with a slope of 1.5±0.1. Those two results indicate that the rate of reaction between thallium(I) and peroxodisulfate ions at concentrations larger than 0.004 mol dm^{-3} thallium(I) is of zero and 1.5 order with respect to the concentrations of thallium(I) and peroxodisulfate ions respectively. Thus, the rate of reaction obeys Eqs. 7 and 9 (*vide infra*).

Effect of Radical Scavengers. The influence of the radical scavengers on the rate of reaction was examined, the results are shown in Table 3. The addition of 1% acrylonitrile completely inhibited the reaction rate, with the production of some amounts of a white sediment of polyacrylonitrile, indicating the existence of $SO_4^{\cdot-}$ and/or OH· radicals in the reacting solutions. Both the cerium(III) and cerium(IV) ions were very strong retarders of the reaction, even 5×10^{-6} mol dm^{-3} cerium(III) or 1×10^{-3} mol dm^{-3} cerium(IV) being able to reduce the reaction rate to the rate of the thermal decomposition of the peroxodisulfate ion. This clearly indicates the existence of both the oxidizing and reducing radicals in the reacting solution. Tetranitromethane was also a strong retarder of the reaction, indicating the existence of a thallium(II) species which can be act as a reducing agent for tetranitromethane. The acetate ion was also a retarder of the reaction, the reaction being completely inhibited by the addition of 0.1 mol dm^{-3} acetate. On the contrary, the iron(III) ion was an accelerator, and the copper(II) ion hardly affected the rate of reaction.

Acidity Dependence. The rate of the thermal decomposition of peroxodisulfate increased with an increase in the acidity of the reaction solution, while the rate of reaction between peroxodisulfate and thallium(I) ions decreased with an increase in the acidity. The results are tabulated in Table 4. The pH in the reacting solution become smaller according to the progress of reaction; this was because of the hydrolysis of the thallium(III) ion formed, *i.e.*, $H_2O+Tl^{3+}\rightarrow TlOH^{2+}+H^+$. However, the pH buffer solution was not used because most buffers may affect the reaction rate much as the acetate ion affects the rate of reaction (see Table 3).

Temperature Dependence. First, the rate of the thermal decomposition of the peroxodisulfate ion was

Table 3. Influence of radical Scavengers[a)]

Radical scavengers	$V_i/10^{-8}$ dm^{-3} mol s^{-1}
None	6.17
None	6.00 (in N_2 saturated)
None	0.45 (in the absence of Tl(I))
1% acrylonitrile	0.53[b)] (in the absence of Tl(I))
1% acrylonitrile	0.61[b)]
1×10^{-3} mol dm^{-3} tetranitromethane	2.50
1×10^{-6} mol dm^{-3} cerium(III)	3.56
5×10^{-6} mol dm^{-3} cerium(III)	0.44
1×10^{-5} mol dm^{-3} cerium(III)	0.40
1×10^{-4} mol dm^{-3} cerium(III)	0.47
1×10^{-4} mol dm^{-3} cerium(IV)	1.45
1×10^{-3} mol dm^{-3} cerium(IV)	0.72
1×10^{-4} mol dm^{-3} copper(II)	6.95
1×10^{-3} mol dm^{-3} copper(II)	7.12
1×10^{-4} mol dm^{-3} iron(III)	14.7
1×10^{-3} mol dm^{-3} iron(III)	19.7
0.01 mol dm^{-3} CH_3COONa	1.67 (pH 6.35)
0.01 mol dm^{-3} CH_3COONa	1.55 (pH 1.7 with 0.1 mol dm^{-3} $HClO_4$)
0.1 mol dm^{-3} CH_3COONa	0.4 (pH 2.4 with 0.1 mol dm^{-3} $HClO_4$)
0.2 mol dm^{-3} CH_3COONa	0.2 (pH 4.62 with 0.1 mol dm^{-3} $HClO_4$)

a) Initial concentrations of 0.016 mol dm^{-3} in potassium peroxodisulfate, 4.0×10^{-3} mol dm^{-3} in thallium(I) perchlorate, 0.01 mol dm^{-3} in perchloric acid, and 0.1 mol dm^{-3} sodium perchlorate; 40 °C; dark. b) A white sediment of polyacrylonitrile was formed in the reacting solution, irrespective of the presence or absence of the thallium(I) ion.

Table 4. Influence of the acidity[a)]

$[HClO_4]_{added}$ / mol dm^{-3}	pH[c)]	V_i / 10^{-8} dm^{-3} mol s^{-1}	V_i' / 10^{-8} dm^{-3} mol s^{-1}	k_b / 10^{-5} dm$^{3/2}$ mol$^{-1/2}$ s^{-1}	k_4[b)] / 10^3 dm^3 mol^{-1} s^{-1}
0.1		4.28	2.82	0.72	0.54
0.05	1.32—1.3	3.55	1.50	1.01	0.75
0.02	1.72—1.68	5.00	0.71	2.12	1.58
0.01	1.97—1.84	6.17	0.45	2.83	2.11
0.005	2.23—2.00	6.17	0.32	2.89	2.16
0.002	2.73—2.26	8.45	0.24	4.06	3.03
0	7 —2.34	10.3	0.10	5.04	3.76

a) Conditions as in Table 3, except for the varied concentrations of perchloric acid. V_i and V_i' indicate the initial rate of the decomposition of the peroxodisulfate ion in the presence and in the absence of the thallium(I) ion respectively. b) k_4 calculated by the relationship of $k_b=k_4(k_1/k_5)^{1/2}$ with $k_1=1.15\times10^{-7}$ s^{-1} and $k_5=6.4\times10^8$ dm^3 mol^{-1} s^{-1} at 40 °C. The k_5 was obtained from the data reported by Falcinella *et al.*[14] of 5.5×10^8 dm^3 mol^{-1} s^{-1} at 25 °C, with an activation free energy of 7.9 kJ mol^{-1}. c) The pH range indicates the pH changes at the time of reaction over the range from 0 to 5 h, for which the initial rate, V_i, has been determined.

TABLE 5. TEMPERATURE DEPENDENCE OF THE RATE OF THERMAL DECOMPOSITION OF THE PEROXODISULFATE ION[a)]

Temp	0.01 mol dm^{-3} NaOH	0.01 mol dm^{-3} $HClO_4$	
°C	$k_a/10^{-7}$ s^{-1}	$k_a/10^{-7}$ s^{-1}	$k_2/10^{-5}$ dm^3 mol^{-1} s^{-1}
40	1.15	2.8	1.65
45	3.45	7.95	4.5
50	8.70	14.8	6.1
55	18.5	27.7	9.2

a) 0.016 mol dm^{-3} in potassium peroxodisulfate, 0.1 mol dm^{-3} in sodium perchlorate, and 0.01 mol dm^{-3} in sodium hydroxide or 0.01 mol dm^{-3} in perchloric acid; varied temperatures; dark; $k_a=k_1+k_2[H^+]$.

TABLE 6. TEMPERATURE DEPENDENCE OF THE RATE OF THE REACTION OF THE PEROXODISULFATE ION WITH THE THALLIUM(I) ION[a)]

Temp	V_i	V_i'	k_b
°C	10^{-8} dm^{-3} mol s^{-1}	10^{-8} dm^{-3} mol s^{-1}	10^{-5} dm$^{3/2}$ mol$^{-1/2}$ s^{-1}
30	1.83	—	0.91
35	2.22	—	1.10
40	6.17	0.45	2.83
45	11.4	1.3	5.00
50	21.8	2.4	9.60
55	38.0	4.4	16.6

a) Conditions as in Table 4, except for 0.01 mol dm^{-3} perchloric acid and varid temperatures.

measured in 0.01 mol dm^{-3} sodium hydroxide and 0.01 mol dm^{-3} perchloric acid at an ionic strength of 0.16 mol dm^{-3} and at temperatures from 40 to 55 °C. Using the relationship of $-d[S_2O_8^{2-}]/dt=(k_1+k_2[H^+])[S_2O_8^{2-}]$ which has been reported by Kolthoff and Miller,[10] the values of k_1 and k_2 were evaluated to be as shown in Table 5. The activation energies for the k_1- and k_2-reactions were, respectively, 157 kJ mol^{-1} and 103 kJ mol^{-1}, the values being in good agreement with the 140 kJ mol^{-1} and 109 kJ mol^{-1} of the corresponding reactions reported by Kolthoff and Miller.[10] Next, the rate of the decomposition of the peroxodisulfate ion in the presence of the thallium(I) ion was measured in 0.01 mol dm^{-3} perchloric acid at an ionic strength of 0.16 mol dm^{-3} and at temperatures over the range from 30 to 55 °C (Table 6). The plot of ln k_b *vs.* T^{-1} gave a straight line, the k_b being described as $k_b=2.81\times10^{13}\exp[-108\text{ kJ mol}^{-1}/RT]$ dm$^{3/2}$ mol$^{-1/2}$ s^{-1}.

Ionic-strength Dependence. With concentrations of 1.6×10^{-2} mol dm^{-3} in potassium peroxodisulfate, 4.0×10^{-3} mol dm^{-3} in thallium(I) perchlorate, and 0.01 mol dm^{-3} perchloric acid, and with varied concentrations of sodium perchlorate at 40 °C, the initial rates of the disappearance of peroxodisulfate were 9.7×10^{-8}, 8.0×10^{-8}, 6.2×10^{-8}, 5.7×10^{-8}, and 5.2×10^{-8} dm^{-3} mol s^{-1} at ionic strengths of 0.06, 0.11, 0.16, 0.21, and 0.26 mol dm^{-3} respectively. The rate decreased with an increase in the ionic strength (μ), the plot of log k_b *vs.* $\mu^{1/2}$ being rectilinear with a slope of −1.05.

Discussion

The results of Fig. 1 and Table 3 absolutely deviated the schemes, 1 and 2, which were mentioned in the introduction section, but they could be well accounted for by Scheme 3, in which there are no direct reactions between peroxodisulfate and thallium(I) ions. Moreover, all the results obtained could be accounted for by the following reaction mechanism:

$$S_2O_8^{2-} \xrightarrow{k_1} 2SO_4^{\cdot-} \text{ [Initiation]} \quad (1)\,[10]$$

$$S_2O_8^{2-} + H^+ \xrightarrow{k_2} HSO_4^- + \frac{1}{2}O_2 + SO_3 \quad (2)\,[10]$$

$$Tl(I) + SO_4^{\cdot-} \xrightarrow{k_3} Tl(II) + SO_4^{2-} \quad (3)$$

$$S_2O_8^{2-} + Tl(II) \xrightarrow{k_4} Tl(III) + SO_4^{\cdot-} + SO_4^{2-} \quad (4)$$

$$2Tl(II) \underset{k_{-5}}{\overset{k_5}{\rightleftharpoons}} Tl(I) + Tl(III) \text{ [Termination]} \quad (5)\,[11\text{-}14]$$

Reactions 3 and 4 constitute a chain reaction in which Reaction 1 is the initiation reaction. The most probable termination reaction is a disproportionation of the thallium(II) ion. Schwarz *et al.*[11] reported the values for k_5 and k_{-5} to be 1.9×10^8 and 7.5×10^{-25} dm^3 mol^{-1} s^{-1} respectively in 1 mol dm^{-3} perchloric acid. Therefore, the backward reaction of Reaction 5 could actually be negligible. Thus, neglecting the backward reaction, and assuming steady-state concentrations for $SO_4^{\cdot-}$ and Tl(II), the following equations are derived:

$$[Tl(II)] = \sqrt{\frac{k_1[S_2O_8^{2-}]}{k_5}};$$

$$[SO_4^{\cdot-}] = \frac{2k_1[S_2O_8^{2-}]+k_b[S_2O_8^{2-}]^{3/2}}{k_3[Tl(I)]} \quad (6)$$

$$-d[S_2O_8^{2-}]/dt = k_a[S_2O_8^{2-}] + k_b[S_2O_8^{2-}]^{3/2} \quad (7)$$

$$-d[Tl(I)]/dt = k_1[S_2O_8^{2-}] + k_b[S_2O_8^{2-}]^{3/2} \quad (8)$$

where $k_a=k_1+k_2[H^+]$ and $k_b=k_4(k_1/k_5)^{1/2}$.
The first term on the right-hand side of Eq. 7 corresponds to the termal decomposition of the peroxodisulfate ion itself, and it is, except in a stlongly acidic

solution, much smaller than the second term (*e. g.*, see Fig. 1). When the first term on the right-hand side of Eq. 7 is negligible. Eqs. 9 and 10 are derived:

$$-\mathrm{d}[S_2O_8^{2-}]/\mathrm{d}t = k_b[S_2O_8^{2-}]^{3/2} \quad (9)$$

By integrating Eq. 9, we obtain:

$$\frac{1}{\sqrt{[S_2O_8^{2-}]}} = \frac{k_b}{2}t + \frac{1}{\sqrt{[S_2O_8^{2-}]_i}} \quad (10)$$

It may be seen from Fig. 3 that the relationship of Eq. 10 is experimentally satisfied, the slope in the plot of $[S_2O_8^{2-}]^{1/2}$ *vs.* t being unaffected by the initial concentrations of both the thallium(I) ion and the peroxodisulfate ion. The slight deviation from the straight line might be attributable to the first term of $k_a[S_2O_8^{2-}]$ in Eq. 7.

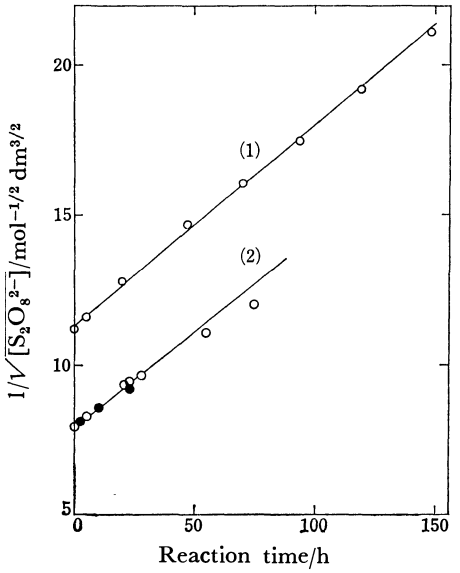

Fig. 3. Plot of $[S_2O_8^{2-}]^{-1/2}$ *vs.* t.
Conditions for line 1 are the same as in *a*) of Table 1 and those of line 2 are 1.6×10^{-2} mol dm^{-3} in potassium peroxodisulfate, 8.0×10^{-3} mol dm^{-3} in thallium(I) perchlorate for the plot ○, and 4.0×10^{-3} mol dm^{-3} in thallium(I) perchlorate for the plot ●. The other conditions are the same as in line 1.

The fact that the concentrations of the peroxodisulfate ion disappearing were larger than those of thallium(I) disappearing in Table 1 is due to the non-radical decomposition of the peroxodisulfate ion of Eq. 2. Thus, Eq. 7 is larger by the $k_2[H^+]\,[S_2O_8^{2-}]$ than Eq. 8. Reaction 3 is a reaction between the thallium(I) ion and the $SO_4^{\cdot-}$ radical. Therefore, when the thallium(I) ion concentration is extremely low, the rate of the whole reaction is controlled by Reaction 3, the rate being dependent on the thallium(I)-ion concentrations. This could, in practice, be observed at concentartions smaller than 2.0×10^{-3} mol dm^{-3} of thallium(I) (Fig. 1). Since the rate of Reaction 3 becomes slow at such low concentrations of the thallium(I) ion, Reactions 11 to 14 may occur together with Reactions 1 to 5, the reactions competing with each other:

$$H_2O + SO_4^{\cdot-} \rightleftharpoons HSO_4^- + OH\cdot \quad (11)^{10,16}$$

$$Tl(I) + OH\cdot \longrightarrow Tl(II) + OH^- \quad (12)^{15}$$

$$Tl(II) + OH\cdot \longrightarrow Tl(III) + OH^- \quad (13)$$

$$Tl(II) + SO_4^{\cdot-} \longrightarrow Tl(III) + SO_4^{2-} \quad (14)$$

The reaction mechanism at low concentrations of the thallium(I) ion is thought to be basically equivalent to that at the higher concentrations of the thallium(I) ion. When the thallium(I) ion concentrations were so high that Reaction 3 could be fast enough, Reactions 11 and 14, and accordingly all the reactions from 11 to 14, would be eliminated from the reaction scheme because the concentrations of $SO_4^{\cdot-}$ at the steady states are extremely low under such conditions. The strong inhibiting effect of acrylonitrile on the reaction rate, with a production of polyacrylonitrile, indicates that the chain-reaction mechanism is initiated by a radical. The inhibiting effect of the cerium(III) ion is due to the competitive reactions, 15 and 16, with Reactions 3, 4, and 5:

$$Ce(III) + SO_4^{\cdot-} \xrightarrow{k_{15}} Ce(IV) + SO_4^{2-} \quad (15)^{17}$$

$$Ce(III) + Tl(II) \underset{k_{-16}}{\overset{k_{16}}{\rightleftharpoons}} Ce(IV) + Tl(I) \quad (16)^{18}$$

Since the chain reaction in 4.0×10^{-3} mol dm^{-3} thallium(I) was completely inhibited by the addition of 5×10^{-6} mol dm^{-3} cerium(III), the rates of Reactions 15 and 16 are thought to be much faster than those of Reactions 3 and 4. The standard reduction potentials for the $Tl^{2+}+e^-\rightleftharpoons Tl^+$ and $Ce^{4+}+e^-\rightleftharpoons Ce^{3+}$ are 2.22 V[14] and 1.61 V[19] respectively at 25 °C. Therefore, Reaction 16 occurs very much towards the right, with an equilibrium constant of $\log K_{16}=10.9$. Thus, the rate constant k_{16} is estimated to be 9×10^5 dm^3 mol^{-1} s^{-1} by using the equilibrium constant with $k_{-16}=4.7\times10^{-5}$ dm^3 mol^{-1} s^{-1} at 50 °C.[18] The k_{16} value estimated is some hundreds times larger than the k_4 value. The cerium(IV) ion was also a strong retarder of the reaction between peroxodisulfate and thallium(I) ions. The inhibiting effect of the cerium(IV) ion is attributable to the occurrence of Reaction 17, which can be followed by Reactions 15 and 16:

$$Ce(IV) + Tl(II) \rightleftharpoons Ce(III) + Tl(III) \quad (17)$$

Since the standard reduction potential for the reaction of $Tl^{3+}+e^-\rightleftharpoons Tl^{2+}$ is 0.33 ± 0.05 V[14] at 25 °C, Reaction 17 occurs towards the extreme right-hand side, with an equilibrium constant of $\log K_{17}=21.7$. Tetranitromethane is an excellent electron-acceptor. Therefore, the inhibiting effect of tetranitromethane is attributable to the occurrence of Reaction 18, which competes with Reactions 4 and 5:

$$Tl(II) + C(NO_2)_4 \xrightarrow{k_{18}} Tl(III) + C(NO_2)_3^- + NO_2 \quad (18)$$

$k_{18} = 4\times10^8$ dm^3 mol^{-1} s^{-1} at pH 8—9[13]

The acceleration effect of the iron(III) ion could be due to the occurrence of Reactions 19, 20, and 21:

$$Tl(II) + Fe(III) \underset{k_{-19}}{\overset{k_{19}}{\rightleftharpoons}} Tl(III) + Fe(II) \quad (19)$$

$$Tl(II) + Fe(II) \xrightarrow{k_{20}} Tl(I) + Fe(III) \quad (20)$$

$$S_2O_8^{2-} + Fe(II) \xrightarrow{k_{21}} Fe(III) + SO_4^{\cdot-} + SO_4^{2-} \quad (21)$$

Schwarz *et al.*[11] reported the k_{19}, k_{-19}, and k_{20} to be 3.4×10^5, 0.0139, and 6.7×10^6 dm^3 mol^{-1} s^{-1} respectively in 1 mol dm^{-3} perchloric acid at 23 °C . The forward reactions of Eqs. 19 and 20 are competitive with Reactions 4 and 5. The rate constant k_{21} at 25 °C is 141 dm^3 mol^{-1} s^{-1} [20] and 25 dm^3 mol^{-1} s^{-1} [21] at an ionic strength of zero and 0.1 mol dm^{-3} respectively. Thus, the k_{21} value is somewhat smaller than the k_4 in Table 4. Nevertheless, the iron(III) ion greatly accelerated the reaction between peroxodisulfate and thallium(I) ions. By the addition of the iron(III) ion, the chain reaction may be carried out by Reactions 3, 4, 19, and 21, the chain termination being Reaction 20 in place of Reaction 5. The occurrence of Reactions 19 and 21, accompanied by the diminution in the termination Reaction 5, is thought to be a probable cause of the acceleration effect of the iron(III) ion. In the presence of the copper(II) ion, the equilibrium Reaction 22 will hold.

$$Tl(II) + Cu(II) \rightleftharpoons Tl(III) + Cu(I) \quad (22)$$

The equilibrium of Eq. 22 occurs towards the extremely left-hand side, with an equilibrium constant of log $K_{22}=-3$, the value being calculated by means of the redox potentials of 0.33 V[14] and 0.153 V[19] for the Tl^{3+}/Tl^{2+} and Cu^{2+}/Cu^{+} couples respectively. The rate constant for the reaction of $S_2O_8^{2-}+Cu(I)\rightarrow Cu(II)+SO_4^{\cdot-}+SO_4^{2-}$ has been reported to be 1.4×10^3 dm^3 mol^{-1} s^{-1} in 1 mol dm^{-3} KCl at 25 °C:[22] the value is almost the same magnitude as the k_4 values. The two conclusions above lead to the conclusion that the copper(II) ion could not be an effective accelerator for the reaction between peroxodisulfate and thallium(I) ions. The rate of the reaction between peroxodisulfate and thallium(I) ions decreased with an increase in the acidity in the reacting solution, whereas the rate of the thermal decomposition of the peroxodisulfate ion increased with an increase in the acidity (Table 4). Considering the relationship of Eq. 7, equation 23 may be assumed:

$$V_i = V_i' + k_b[S_2O_8^{2-}]_i^{3/2} \quad (23)$$

where V_i and V_i' indicate the initial rate of the disappearance of the peroxodisulfate ion in the presence and in the absence of the thallium(I) ion respectively. Equation 23 is satisfied, at least for the initial stages of reactions. The values of k_b and k_4 in Tables 4 and 6 where estimated by using Eq. 23 with the relatioship of $k_b=k_4(k_1/k_5)^{1/2}$. The pH dependence of k_4 may be attributable to the simultaneous reactions of $Tl^{2+}(aq)$ and $Tl(OH)^+$ with the peroxodisulfate ion.

$$S_2O_8^{2-} + Tl^{2+}(aq) \xrightarrow{k_{4a}} Tl(III) + SO_4^{\cdot-} + SO_4^{2-} \quad (4a)$$

$$S_2O_8^{2-} + TlOH^+ \xrightarrow{k_{4b}} Tl(III) + SO_4^{\cdot-} + SO_4^{2-} \quad (4b)$$

where Tl(III) indicates all the thallium(III) ions of the aquated and hydroxo species. The k_4 is described as:

$$k_4 = \frac{k_{4a}[H^+] + k_{4b}K_{TlOH}}{[H^+]+K_{TlOH}} \quad (24)$$

where $K_{TlOH}=[TlOH^+][H^+]/[Tl^{2+}(aq)]$.

Since K_{TlOH} is 3×10^{-5} mol dm^{-3} at 25 °C, Eq. 25 will be satisfied at concentrations larger than 3×10^{-3} mol dm^{-3} of $[H^+]$.

$$k_4 = k_{4a} + k_{4b}K_{TlOH}[H^+]^{-1} \quad (25)$$

The plot of k_4 *vs.* $[H^+]^{-1}$ showed a straight line, as in Fig. 4. The k_{4a} and k_{4b} were obtained as 250 and 9×10^5 dm^3 mol^{-1} s^{-1} from the intercept and the slope respectively. Thus, at a hydrogen-ion concentration of 0.01 mol dm^{-3}, 92% of k_4 corresponds to the second term of Eq. 25. The plot of k_4 *vs.* $[H^+]^{-1}$ greatly deviated from the linear line in the more alkaline region; thus, the $Tl(OH)_2$ species participated in the reaction.

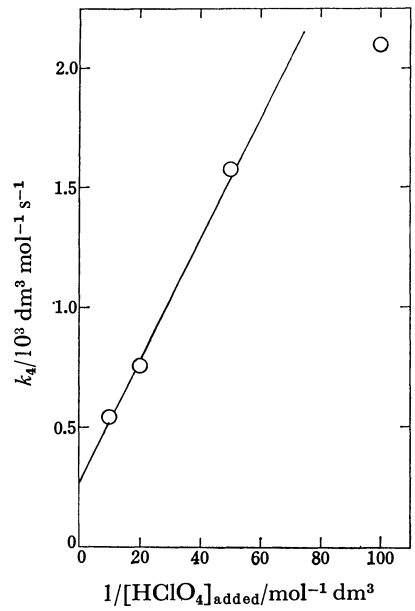

Fig. 4. Plot of k_4 *vs.* $1/[HClO_4]_{added}$ (Eq. 25). Conditions as in Table 4.

It should be noted here that the pH dependence of k_5 is so small as to be constant at hydrogen-ion concentrations over the range from 0.001 to 0.1 mol dm^{-3}. By the same treatments as used for the k_4 values, the following equations are obtained:

$$Tl^{2+}(aq) + Tl^{2+}(aq) \xrightarrow{k_{5a}} Tl(I) + Tl(III) \quad (5a)$$

$$Tl^{2+}(aq) + TlOH^+ \xrightarrow{k_{5b}} Tl(I) + Tl(III) \quad (5b)$$

$$k_5 = k_{5a} + k_{5b}K_{TlOH}[H^+]^{-1} \quad (26)$$

The k_5 at 25 °C is 3.0×10^9 dm^3 mol^{-1} s^{-1} at pH 5.6[13] and 5.2×10^8 dm^3 mol^{-1} s^{-1} at 0.1 mol dm^{-3} of $[H^+]$.[14] Thus, Eq. 26 is written as Eq. 27:

$$k_5 = 5.2\times10^8 + 6.2\times10^3[H^+]^{-1} \quad (27)$$

Equation 27 indicates that the k_5 is actually constant at hydrogen-ion concentrations larger than 6×10^{-4} mol dm^{-3}. Falcinella *et al.*[14] have reported that the k_5 value was independent of the acid concentrations over the range from 0.1 to 1.0 mol dm^{-3} and was slightly dependent on the temperature with an activation free energy, ΔG_5^*, of 7.9 ± 1.5 kJ mol^{-1}. From the temperature dependences for k_1 and k_b shown in Tables 5 and 6, the activation energies,

E_1 and E_b, derived from an Arrhenius plot were 157 and 108 kJ mol^{-1} respectively. Thus, the value of E_4 is obtained as 33 kJ mol^{-1} by the relationship of $E_b=E_4+(E_1-E_5)/2$.

Although Reaction 1 is not sensitive to the ionic strength, the k_4 and k_5 values are probably dependent on the ionic strength, because Reactions 4 and 5 are reactions between two ions of unlike and like signs. Thus, the k_b value which is composed of $k_4(k_1/k_5)^{1/2}$ may be thought to be largely dependent on the ionic strength. However, the ionic-strength dependence on k_b was not very large: the slope value for the plot of log k_b *vs.* $\mu^{1/2}$ was -1.05, an almost equivalent to the case of the reaction between two univalent-ions of unlike signs expected for the equation of log $k=\log k_0+1.02\ Z_-Z_+\ \mu^{1/2}$. As has been mentioned already, the k_{4b} term in Eq. 25 was calculated to be 92% of k_4 under the condition of a hydrogen-ion concentration of 0.01 mol dm^{-3}, this condition being the same as in the experiments for the ionic-strength dependence. Thus, the effective charges of the thallium(II) ion may be close to unity, smaller effective charges may cause the smaller dependence of the k_b on the ionic strength.

In a subscquent paper the reaction between thallium(I) and peroxodisulfate in alkaline solution will be discussed.

References

1) D. A. House, *Chem. Rev.*, **62**, 185 (1962).
2) W. K. Wilmarth and A. Haim, "Peroxide Reaction Mechanisms," ed by J. O. Edwards, Interscience, New York (1962), p. 175.
3) I. R. Wilson, "Comprehensive Chemical Kinetics," ed by C. H. Bamford and C. F. H. Tipper, Elsevier, N. Y. (1972), Vol. 6, p. 340.
4) G. J. Buist, "Comprehensive Chemical Kinetics," ed by C. H. Bamford and C. F. H. Tipper, Elsevier, N. Y. (1972), Vol. 6, p. 456.
5) J. Bednar, *Collect. Czech. Chem. Commun.*, **24**, 1240 (1959).
6) T. J. Sworski, *J. Am. Chem. Soc.*, **79**, 3655 (1957).
7) T. J. Sworski, *Radiat. Res.*, **4**., 483 (1956).
8) M. Kimura, *J. Phys. Chem.*, **77**, 1265 (1973).
9) M. Kimura, *Inorg. Chem.*, **13**, 841 (1974).
10) I. M. Kolthoff and I. K. Miller, *J. Am. Chem. Soc.*, **73**, 3055 (1951).
11) H. A. Schwarz, D. Comstock, J. K. Yandell, and R. W. Dodson, *J. Phys. Chem.*, **78**, 488 (1974).
12) P. O'Neill and D. Schulte-Frohlinde, *J. Chem. Soc., Chem. Commun.*, **1975** 387.
13) M. Bonifačić and K. -D. Asmus, *J. Chem. Soc., Dalton Trans.*, **1976**, 2074.
14) B. Falcinella, P. O. Felgata, and G. S. Laurence, *J. Chem. Soc., Dalton Trans.*, **1974**, 1367.
15) B. Cerek, M. Ebert, and A. J. Swallow, *J. Chem. Soc.*, **1966**, 612.
16) C. R. Giuliano, N. Schwarz, and W. K. Wilmarth, *J. Phys. Chem.*, **63**, 353 (1959).
17) S. Fronaeus and C. O. Östman, *Acta Chem. Scand.*, **9**, 902 (1955).
18) G. Wada and K. Tamaki, *Bull. Chem. Soc. Jpn.*, **47**, 1422 (1974).
19) W. M. Latimer, "Oxidation Potentials," 2nd ed, Prentice Hall, (1960), p. 344.
20) J. W. L. Fordham and H. L. Williams, *J. Am. Chem. Soc.*, **73**, 4855 (1951).
21) R. Woods, I. M. Kolthoff, and E. J. Meehan, *Inorg. Chem.*, **4**, 697 (1965).
22) I. M. Kolthoff and R. Woods, *J. Am. Chem. Soc.*, **88**, 1371 (1966).

Kinetic Studies of the Electron Transfer Reactions in Iron(II) and Iron(III) Systems. IX. Electron Transfer Reactions between Iron(II) and Iron(III) in Water Mixed with Ethanol, 1-Propanol, Ethylene Glycol, Glycerol, and Pentaerythritol

Goro WADA,* Youko OHTA, Sachiko HAYASHIDA, Harumi SUGINO, Toyomi MIZUI, and Yumiko AIHARA

Department of Chemistry, Faculty of Science, Nara Women's University, Nara 630

(Received August 9, 1979)

The rate constants of the electron transfer reactions between Fe(II) and Fe(III) were determined in mixed solvents of water and alcohols, such as ethanol, 1-propanol, ethylene glycol, glycerol, and pentaerythritol. From the acid concentration dependence of the rate, the predominant path of the reaction was estimated to be Fe^{2+}-$Fe(OH)^{2+}$ path with a rate constant k_H. The rate constant k_H increases with increase in the mole fraction x of ethanol and 1-propanol, and decreases with increase in x of methanol, ethylene glycol, glycerol, and pentaerythritol. A straight line is obtained when $\ln k_H$ is plotted against the reciprocal dielectric constant D^{-1} of the mixed solvents for the latter group of alcohols. From the slope of the straight line the distance between Fe^{2+} and $Fe(OH)^{2+}$ is estimated to be 7.8 Å at the intermediate stage of the reaction. Therefore, the reaction is mostly controlled by the electrostatic repulsive force, being influenced by D of the mixed solvents.

The electron transfer reactions between iron(II) and iron(III) in aqueous media proceed by a mechanism of hydrogen-atom transfer in the absence of catalyzing ligands which would make the reactions occur by either inner-sphere or outer-sphere mechanism.[1] In the hydrogen-atom transfer mechanism, an electron is transferred by a hydrogen atom, which can be regarded to behave as a proton carrying an electron, along a chain of hydrogen bondings between OH radicals of water or alcohol, with the oxidant and the reductant species at both ends.

If a foreign substance is added to the reaction system and the chain of hydrogen bondings is broken to some extent, the reactions by this mechanism would be retarded, causing a slowering of the reaction rate. This is what happens when substances such as nitromethane,[2] and some alcohols[3,4] are added. The effect of addition of methanol to the reaction system of the electron transfer between iron(II) and iron(III) was investigated in aqueous solutions.[5] In the present investigation, alcohols other than methanol, such as ethanol, 1-propanol, ethylene glycol, glycerol, and pentaerythritol were used for the purpose of clarifying the influence of the number of OH groups, the hydrophobicity of alkyl groups and the dielectric constants of the alcohols on the reaction rates, and confirming the reaction mechanism. The experimental results are discussed including data of the case of methanol.

Experimental

Materials. Alcohols of specially pure grade were purified as follows: ethanol and 1-propanol were redistilled under ordinary pressure, ethylene glycol and glycerol were redistilled under reduced pressures, and pentaerythritol was twice recrystallized from its aqueous solution. The method of preparation and purification of other materials used were the same as those already reported.[5,6]

Procedures. The hydrolysis constants of Fe^{3+} ion, $K_H=[Fe(OH)^{2+}][H^+]/[Fe^{3+}]$ and the rate constants of the electron transfer reaction, k, in mixed solvents of water and alcohols were determined in the same manner as reported.[5-7] The ionic association between Fe^{3+} ion and ClO_4^- ion was also checked in mixed solvents.[5] For the determination of optical densities, a Hitachi-Perkin-Elmer UV-VIS spectrophotometer Model 139 was used. The ionic strengths of the solutions were adjusted at 0.5 M by use of $NaClO_4$.

Results and Discussion

Hydrolysis Constants of Fe^{3+} Ion, K_H, in Mixed Solvents. In an aqueous solution containing iron(III) perchlorate and perchloric acid, Fe^{3+}_{aq} is partly hydrolyzed to $Fe(OH)^{2+}$ with a hydrolysis constant $K_H=[Fe(OH)^{2+}][H^+]/[Fe^{3+}]$, the following relation being established:[5]

$$\frac{[Fe(III)]}{A_H}=\frac{1}{\varepsilon_H}+\frac{[H^+]}{\varepsilon_H K_H} \quad (1)$$

where ε_H and A_H denote the molar absorption coefficient of $Fe(OH)^{2+}$ and the optical density due to $Fe(OH)^{2+}$ being equal to $\varepsilon_H[Fe(OH)^{2+}]$, respectively. [Fe(III)] and $[H^+]$ are the total concentration of iron(III) which is equal to the sum of $[Fe^{3+}]$ and $[Fe(OH)^{2+}]$ and the concentration of hydrogen ion which is also equal to the sum of the total concentration of perchloric acid added $[HClO_4]$ and the concentration of hydrolyzed species of iron(III), $[Fe(OH)^{2+}]$, respectively. The plot of $[Fe(III)]/A_H$ against $[H^+]$ would give a straight line with an intercept $1/\varepsilon_H$ and a slope $1/\varepsilon_H K_H$. First, the total optical density of the solution A was used instead of A_H, not known empirically, in order to obtain an approximate K_H, and the precise value of K_H could be obtained by means of successive approximations.

In order to determine A_H necessary for Eq. 1, the value of the molar absorption coefficient of Fe^{3+}, ε_0, should be known, since A_H has to be calculated by an equation $A_H=A-\varepsilon_0[Fe^{3+}]$. When acid concentration is varied from 0.01 M to 4 M, the apparent molar absorption coefficient $\varepsilon(=A/[Fe(III)])$ decreases abruptly, passes a broad minimum, and then increases approximately linearly. An example is shown in Fig. 1, for the case of 1-propanol, the curves being quite similar to the case of methanol.[5] The abrupt di-

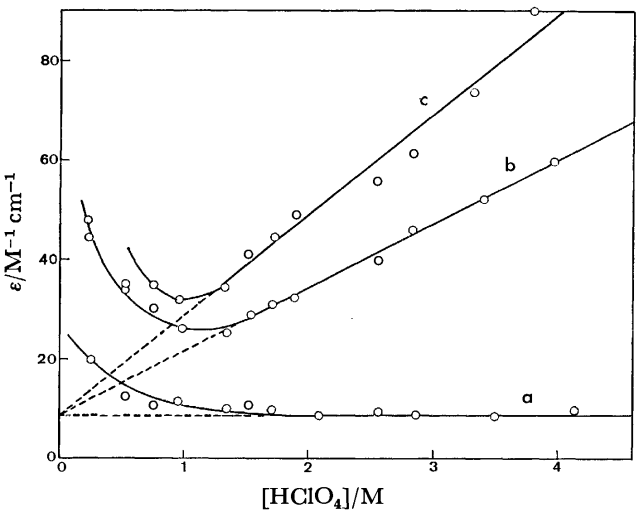

Fig. 1. Variation in apparent absorption coefficient ε of 1-propanol and water mixtures with perchloric acid concentration at $[Fe(III)]=1.5\times10^{-3}$ M, 330 nm, and 25 °C.
a: $x=0$, b: $x=0.10$, c: $x=0.18$.

minution of ε in the lower acid concentration range is due to the decrease in the concentration of hydrolyzed species of $Fe^{3+}{}_{aq}$, since ε_H is much larger than ε_0. On the other hand, the growth of ε in the higher acid concentration range is due to ionic association between Fe^{3+} and ClO_4^- ions, which does not occur in the absence of alcohol, this being observed more markedly at higher mole fraction of alcohol. Thus, ε is expressed by

$$\varepsilon=\frac{\varepsilon_0+\varepsilon_H K_H[H^+]^{-1}+\varepsilon_a K_a[H^+]}{1+K_H[H^+]^{-1}+K_a[H^+]}, \qquad (2)$$

where ε_a and K_a are the molar absorption coefficient and the formation constant of ion-pair, respectively.[5]

If the linear part of a curve is extended to $[HClO_4]=0$ the intercept of the extended straight line would give the value of ε_0 in the alcoholic solution. According to the extrapolation (broken lines in Fig. 1), ε_0 seems to have a constant value independent of the mole fraction of alcohol. In the cases of polyhydric alcohols, however, convergence to a common intercept does not generally take place; ε_0 seems to increase gradually with the increase in x. This might be due to the partial solvation of alcohol molecules into the hydration sphere of iron(III). At any rate, the ε_0 values estimated by this back extrapolation of the curves of ε against acid concentration were used for the calculation of A_H. In the present investigation, the acid concentration was so small that the occurrence of ion-pair formation was ignored.

The linearity of A_H^{-1} *vs.* $[H^+]$ is shown at constant $[Fe(III)]=1.0\times10^{-4}$ M at various mole fractions x of ethanol in Fig. 2. The values of K_H thus obtained are given in Table 1 for various mole fractions of alcohols. The value of K_H increases with the increase in x for all the alcohols studied.[5]

The Rate of Electron Transfer Reaction. The reaction proceeds with an apparent second-order rate constant k_{app} according to McKay's equation[8]

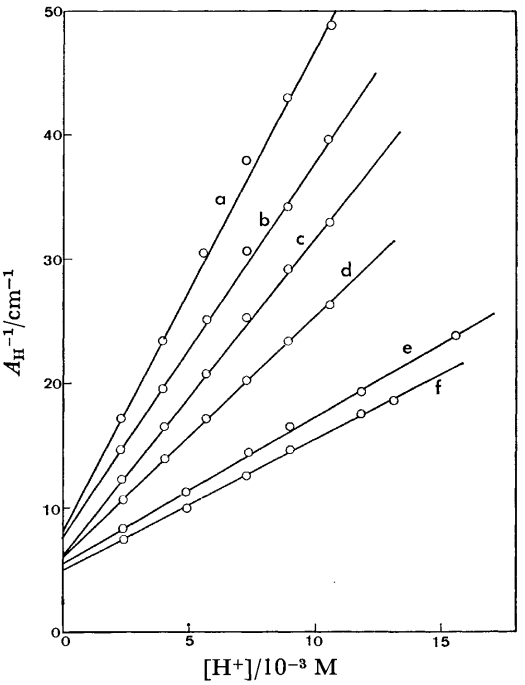

Fig. 2. Linear relationship of A_H^{-1} *vs.* $[H^+]$ at various mole fractions of ethanol x at $[Fe(III)]=1.0\times10^{-4}$ M and 25 °C.
a: $x=0$, b: $x=0.04$, c: $x=0.09$, d: $x=0.14$, e: $x=0.21$, f: $x=0.30$.

Table 1. Hydrolysis constants K_H and rate constants k_H at mole fractions of alcohols x and dielectric constants of mixed solvents D at $\mu=0.5$ M and 25 °C

Alcohol	x	D	K_H / 10^{-3} M	k_H / 10^3 M^{-1} s^{-1}
Ethanol	0	78.5	1.9	2.7
	0.04	72.8	2.0	3.1
	0.09	66.6	2.5	3.5
	0.14	61.0	3.2	3.7
	0.21	54.5	4.8	3.8
	0.30	47.8	4·7	3.7
1-Propanol	0.10	59.0	3.3	3.7
	0.18	48.5	4.7	3.9
Ethylene glycol	0.039	75.9	4.0	1.49
	0.085	72.7	4.9	1.40
	0.145	69.5	7.7	0.98
	0.206	66.0	10.8	0.76
	0.289	61.4	20.7	0.60
	0.394	56.0	32.2	0.33
Glycerol	0.027	75.0	2.8	—
	0.058	71.6	6.2	1.1
	0.096	68.6	8.9	—
	0.141	65.4	9.2	0.94
	0.198	61.6	13.4	—
	0.270	57.8	17.5	0.54
Pentaerythritol	0.00091	—	2.4	2.3
	0.00181	—	2.9	2.1
	0.00542	—	5.1	1.2

$$k_{app}=\frac{0.693}{([Fe(II)]+[Fe(III)])t_{1/2}} \qquad (3)$$

where $t_{1/2}$ represents the half period of the reaction,

which can be determined from the slope of a straight line obtained by plotting logarithms of the radioactivities caused by one of the reacting species against the reaction time. The variations of k_{app} in mixed solvents at various mole fractions of various alcohols are shown in Figs. 3—7. In the cases of ethanol (Fig. 3) and 1-propanol (Fig. 4), k_{app} increases with increase in x, contrary to the case of methanol,[5] in which k_{app} remains constant in the biginning, decreasing gradually with increase in x. In the cases of ethylene glycol (Fig. 5) and glycerol (Fig. 6), k_{app} first increases in a similar way to the cases of ethanol and 1-propanol, but then decreases. In the case of pentaerythritol (Fig. 7), k_{app} remains almost unchanged as far as its solubility in water permits the experiments. In all the measurements of k_{app} (Figs. 3—7), the values of k_{app} are always larger at lower acid concentrations.

Reaction Paths. Iron(III) might take part in the electron transfer reactions in two forms such as Fe^{3+}_{aq} and $Fe(OH)^{2+}$, the latter being produced in

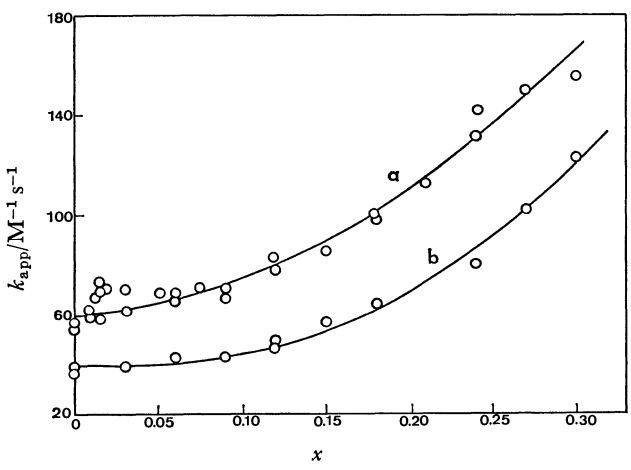

Fig. 3. Variation of k_{app} upon mole fraction of ethanol x at μ=0.5 M and 25 °C.
a: [H+]=0.10 M, b: [H+]=0.15 M.

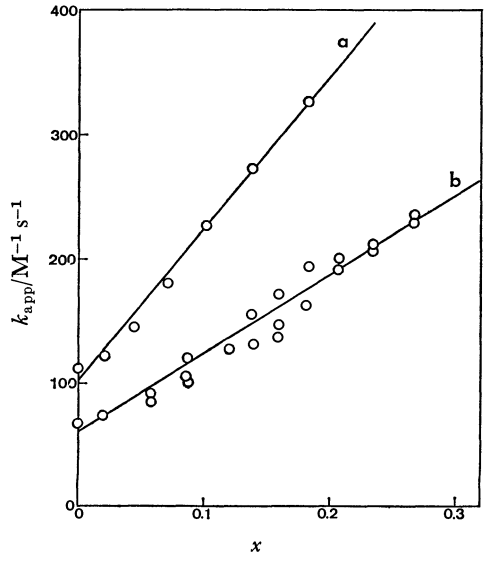

Fig. 4. Variation of k_{app} upon mole fraction of 1-propanol x at μ=0.5 M and 25 °C.
a: [H+]=0.05 M, b: [H+]=0.10 M.

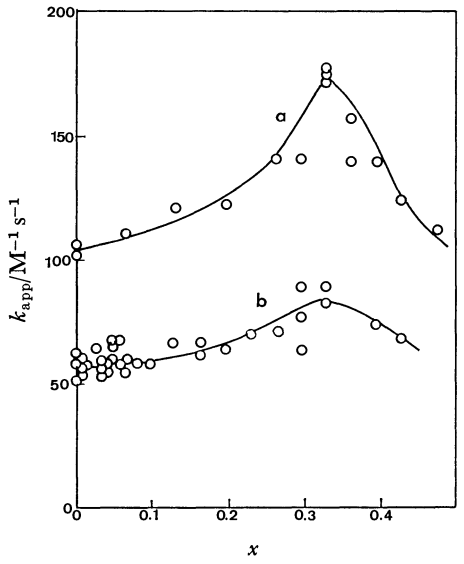

Fig. 5. Variation of k_{app} upon mole fraction of ethylene glycol x at μ=0.5 M and 25 °C.
a: [H+]=0.05 M, b: [H+]=0.10 M.

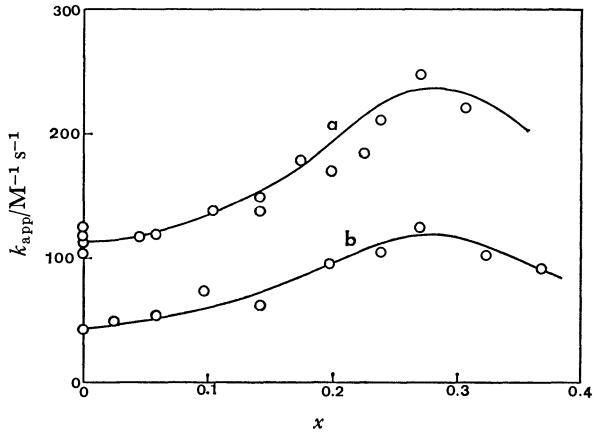

Fig. 6. Variation of k_{app} upon mole fraction of glycerol x at μ=0.5 M and 25 °C.
a: [H+]=0.05 M, b: [H+]=0.15 M.

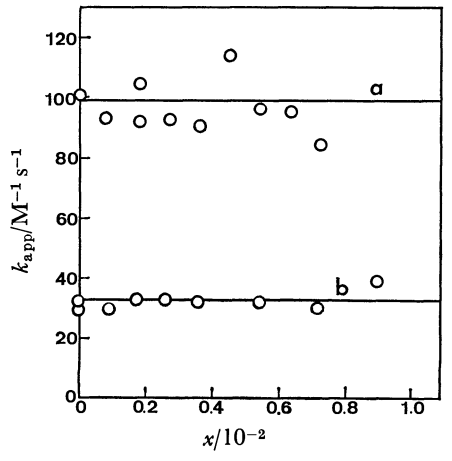

Fig. 7. Variation of k_{app} upon mole fraction of pentaerythritol x at μ=0.5 M and 25 °C.
a: [H+]=0.065 M, b: [H+]=0.20 M.

a greater amount in lower acid concentrations. The main reaction paths are considered to be as follows:

$$Fe^{2+} + {}^*Fe^{3+} \longrightarrow Fe^{3+} + {}^*Fe^{2+} \quad (k_0) \quad (4)$$

$$Fe^{2+} + {}^*Fe(OH)^{2+} \longrightarrow Fe(OH)^{2+} + {}^*Fe^{2+} \quad (k_H) \quad (5)$$

When the respective rate constants of Paths 4 and 5 are denoted by k_0 and k_H, the apparent second-order rate constant of the electron transfer reaction would be given by[5]

$$k_{app} = \frac{k_0 + k_H K_H [H^+]^{-1}}{1 + K_H [H^+]^{-1}}. \quad (6)$$

In order to confirm the mechanism, the values of $k_{app}(1+K_H[H^+]^{-1})$ were plotted against $[H^+]^{-1}$, linearity being obtained in each case. An example is shown in Fig. 8, where ethanol is adopted as a cosolvent in the $[H^+]$ range 0.03—0.3 M. The values of k_0 and $k_H K_H$ were obtained from the intercepts and the slopes. By using the values of K_H listed in Table 1, the values of k_H were obtained. The values of k_0 are usually very small and, consequently, inaccurate as compared with those of k_H. Therefore, the reaction rate via Path 5 is overwhelmingly greater than that via Path 4, except for the case in which very high acid concentration was used. The following discussion is thus restricted to Path 5.

The variation of k_H with x of various alcohols is shown in Fig. 9, along with that of methanol.[5] The k_H value decreases with increase in x of individual alcohol, the order of the depression effect being methanol<ethylene glycol<glycerol<pentaerythritol, in line with the order mono-<di-<tri-<tetra-hydric alcohols; k_H increases with increase in x in the cases of ethanol and 1-propanol.

Discussion. Both K_H and k_H vary with x (Table 1 and Fig. 9). However, when their logarithms are plotted against the reciprocals of dielectric constants of the mixed solvents,[9] the points lie on a straight line independent of the kind of alcohol with a positive and a negative slope corresponding to the plots of ln K_H and ln k_H respectively (Figs. 10 and 11). There are two exceptions: ethanol and 1-propanol. They give another straight line in Fig. 10 and deviate a great deal from linearity in Fig. 11.

Except for the cases of ethanol and 1-propanol,

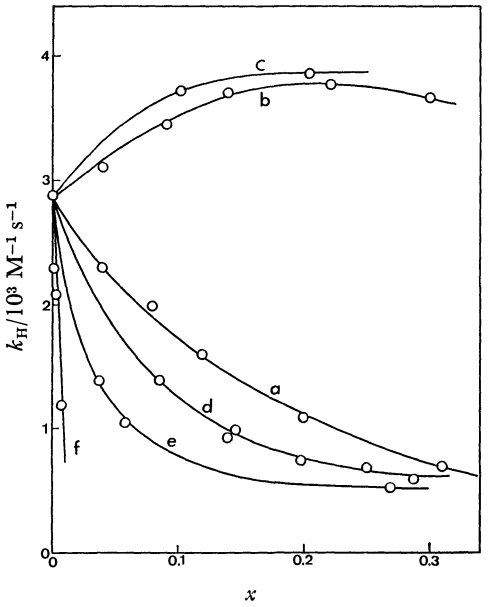

Fig. 9. Variation of k_H upon mole fraction of alcohols x at μ=0.5 M and 25 °C.
a: Methanol, b: ethanol, c: 1-propanol, d: ethylene glycol, e: glycerol, f: pentaerythritol.

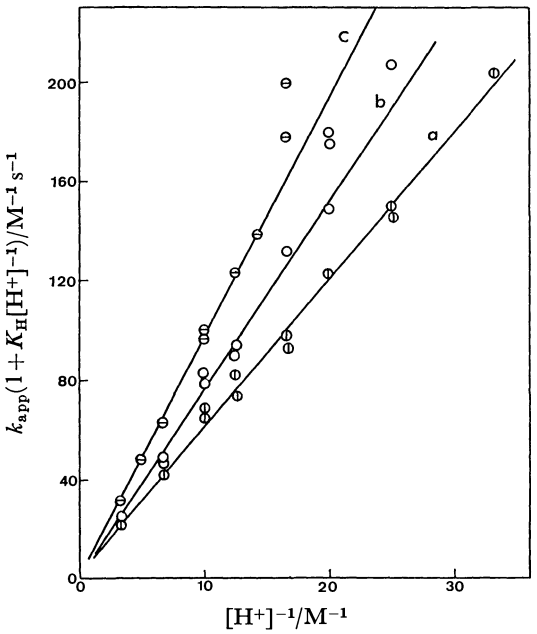

Fig. 8. Linear relation of $k_{app}(1+K_H[H^+]^{-1})$ with $[H^+]^{-1}$ at various ethanol mole fractions x at μ= 0.5 M and 25 °C.
a: x=0.04, b: x=0.09, c: x=0.14.

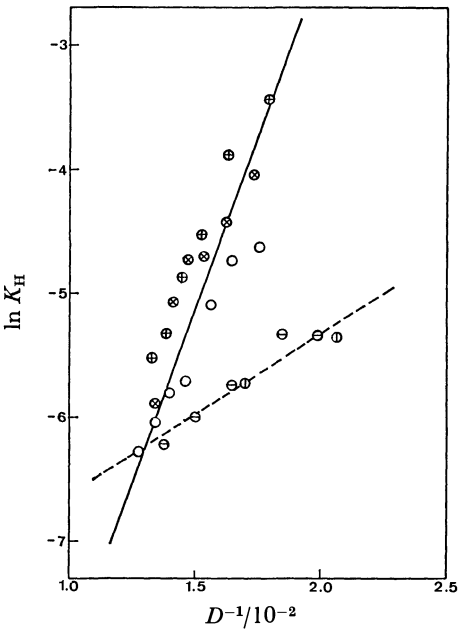

Fig. 10. Relationships between ln K_H and reciprocal dielectric constant D^{-1} in mixed solvents at μ=0.5 M and 25 °C.
○: Methanol, ⊖: ethanol, ◑: 1-propanol, ⊕: ethylene glycol, ⊗: glycerol.

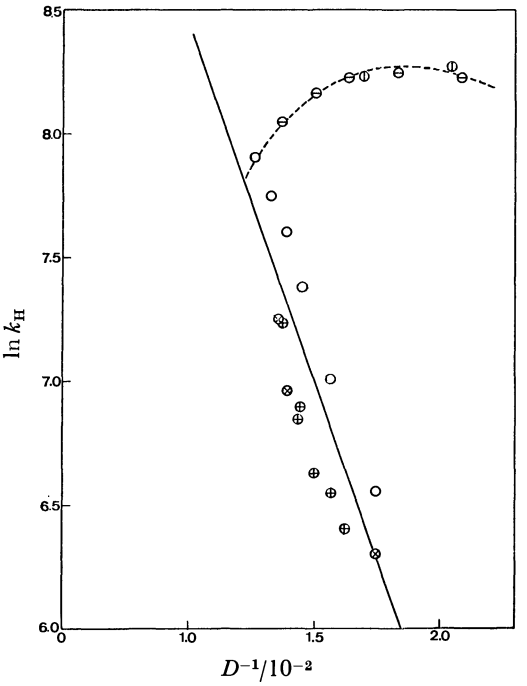

Fig. 11. Relationships between ln k_H and reciprocal dielectric constant D^{-1} in mixed solvents at $\mu=0.5$ M and 25 °C.
○: Methanol, ⊖: ethanol, ⓘ: 1-propanol, ⊕: ethylene glycol, ⊗: glycerol.

the fact that the plots of ln K_H and ln k_H *vs.* D^{-1} lie on a straight line indicates that both the hydrolysis reaction $Fe^{3+} \rightleftharpoons Fe(OH)^{2+} + H^+$ and Path 5 in the electron transfer reaction $Fe^{2+} + Fe(OH)^{2+} \rightarrow Fe(OH)^{2+} + Fe^{2+}$ are mostly influenced by electrostatic repulsion between the ions of the same sign, $Fe(OH)^{2+}$ and H^+, and Fe^{2+} and $Fe(OH)^{2+}$ respectively, in mixed solvents of different dielectric constants. According to Scatchard, these linear correlations are expressed by[10]

$$\ln K_H = \ln K_H^\circ + \frac{Z_A Z_B e^2}{kTd_H D}, \quad (7)$$

$$\ln k_H = \ln k_H^\circ - \frac{Z_C Z_D e^2}{kTd_{Fe} D}, \quad (8)$$

where Z_A, Z_B, Z_C, and Z_D are the numbers of electric charges on the reacting ions, e the elementary electric charge, k the Boltzmann constant, D the dielectric constant of the mixed solvents, and d_H and d_{Fe} the distances of the closest approach between the two reacting ions in the intermediate states during the course of hydrolysis and the electron transfer, respectively. K_H° and k_H° are hypothetical constants in solvents of infinite dielectric constant.

In the case of the hydrolysis, the reaction is the separation of an ion into two ions, $Fe(OH)^{2+}$ and H^+, bearing electric charges $Z_A=+2$ and $Z_B=+1$, while the electron transfer reaction of Path 5 is a collisional encounter of two ions, Fe^{2+} and $Fe(OH)^{2+}$, of $Z_C=Z_D=+2$. From the slopes of the straight lines in Figs. 10 and 11, we obtain the values $d_H=2.1$ Å and $d_{Fe}=7.8$ Å. By taking the approximate values of ionic radii $r(Fe^{2+})=0.8$ Å and $r(Fe^{3+})=0.7$ Å, and of molecular diameter $d(H_2O)=3.0$ Å into account, the values of d_H and d_{Fe} obtained are reasonable, since the intermediate approach in the former reaction might be the direct contact of two ions to each other with d_H nearly equal to the sum of $r(Fe^{3+})$ and $d(H_2O)$, while that in the latter reaction might be the outer-sphere contact of the two with d_{Fe} nearly equal to $r(Fe^{2+})+r(Fe^{3+})+2d(H_2O)$, which would support the plausibility of hydrogen-atom-transfer mechanism between aqua- and hydrolyzed-iron ions.†

The abnormal behavior of k_H observed in the cases of ethanol and 1-propanol has not been clarified. It might be related to the hydrophobicity of alkyl groups in alcohol molecules. The hydrophobic groups would promote the ice-like structure of water surrounding them,[11,12] and increase the hydrogen bondings between water molecules, which would increase the rate of the hydrogen-atom-transfer mechanism, k_H.

References

1) W. L. Reynolds and R. W. Lumry, *J. Chem. Phys.*, **23**, 2460 (1955).
2) A. G. Maddock, *Trans. Faraday Soc.*, **55**, 1268 (1959).
3) N. Sutin, *J. Phys. Chem.*, **64**, 1766 (1960).
4) R. A. Horne, "Exchange Reactions", International Atomic Energy Agency, Vienna (1965), p. 67.
5) G. Wada and A. Endo, *Bull. Chem. Soc. Jpn.*, **45**, 1073 (1972).
6) G. Wada, N. Yoshizawa, and Y. Sakamoto, *Bull. Chem. Soc. Jpn.*, **44**, 1018 (1971).
7) G. Wada, S. Nakago, and Y. Abe, *Bull. Chem. Soc. Jpn.*, **52**, 1381 (1979), Part VIII of this series.
8) H. A. C. McKay, *Nature*, **42**, 997 (1938).
9) G. Åkerlof, *J. Am. Chem. Soc.*, **54**, 4125 (1932).
10) G. Scatchard, *Chem. Rev.*, **10**, 229 (1932); E. S. Amis, "Solvent Effects on Reaction Rates and Mechanisms," Academic Press, New York (1966), Chap. 1.
11) G. Wada and S. Umeda, *Bull. Chem. Soc. Jpn.*, **35**, 646 (1962).
12) G. Wada, E. Nagao, N. Kawamura, and K. Kinumoto, *Bull. Chem. Soc. Jpn.*, **51**, 1937 (1978).

† An approximate straight line is drawn on the points for ethanol and 1-propanol (broken line, Fig. 10). From the slope $d_H=8.8$ Å is obtained by use of Eq. 7. This seems to correspond to a distance of $r(Fe^{3+})+nd(H_2O)$, n being approximately equal to 2.7. The physical meanings of this apparent distance are not clear. The exceptional characteristics of K_H for these two alcohols would partly reflect on k_H for the same alcohols as the exceptional behavior.

Crystal and Molecular Structure of (Ethyl methacrylate)-bis(triphenylphosphine)nickel(0)

Sanshiro KOMIYA,* Junichi ISHIZU, Akio YAMAMOTO, Takakazu YAMAMOTO,* Akio TAKENAKA,† and Yoshio SASADA†

Research Laboratory of Resources Utilization, Tokyo Institute of Technology, 4259 Nagatsuta, Midori-ku, Yokohama 227

† *Laboratory of Chemistry for Natural Products, Tokyo Institute of Technology, 4259 Nagatsuta, Midori-ku, Yokohama 227*

(Received August 30, 1979)

The crystal and molecular structure of (ethyl methacrylate)bis(triphenylphosphine)nickel, (CH_2=C(CH_3)-$COOC_2H_5$) $(PPh_3)_2Ni$, has been determined by single-crystal X-ray analysis. The crystals are monoclinic, space group $P2_1/c$, with unit-cell dimensions a=13.690(2), b=16.855(2), c=15.699(1)Å, β=105.09(1)°, and Z=4. The structure was solved by the heavy-atom method and refined by block-diagonal least-squares technique, using 4701 independent reflections, the final R value being 0.084 for $|F_o| \geq 3\sigma(F)$. The two phosphine ligands and the two olefinic carbon atoms comprise a distorted square-planar configuration about the Ni atom. The Ni–β-CH_2 bond (1.976(8)Å) is significantly shorter than the Ni–α-C bond (2.029(7)Å). The difference is explained by the contribution of polarized resonance structure in metal-olefin bonding.

Interaction of olefins with transition metals is of particular importance in organometallic and catalytic chemistry. Although extensive structural studies by X-ray analysis have been done on the group VIII transition metal complexes coordinated with olefins,[1-4] reports concerning nickel olefin complexes are rather limited, because of their thermal instability and high reactivity toward oxygen.[2-4] On the other hand, no report on the crystal structure of transition metal–α,β-unsaturated ester π complexes has been made to our knowledge[5] except for a Ru(0) complex with ethyl methacrylate, in which C–H oxidative addition of the ligand to Ru(0) has been found to give an unusual hydrido vinyl complex.[6]

We have studied the reactivities of zero valent nickel complexes with various vinyl compounds and found that the reaction of bis(1,5-cyclooctadiene)nickel with α,β-unsaturated ester (ethyl methacrylate, methyl methacrylate *etc.*) in the presence of tertiary phosphine ligands gives a convenient preparative method of various zerovalent nickel olefin complexes,[7] and the coordination through C=C bond has been postulated from the NMR and IR analyses and their chemical reactions.[8]

In order to get information concerning the bonding mode between nickel and α,β-unsaturated ester, an X-ray analysis of the (ethyl methacrylate)bis(triphenylphosphine)-nickel(0) crystal has been performed.

Experimental

(Ethyl methacrylate)bis(triphenylphosphine)nickel(0) was synthesized by the method previously reported.[7] A crystal suitable for X-ray diffraction, obtained by slow recrystallization from toluene at room temperature under nitrogen, was sealed in a capillary. Density of the crystal was determined by floatation in a mixture of CCl_4 and decalin. Data collection was carried out with a Rigaku computer-controlled four-circle diffractometer, using graphite-monochromated Cu $K\alpha$ radiation (λ=1.54178 Å) The unit-cell parameters were calculated with 37 high angle reflections. The crystallographic data are summarized in Table 1. Intensities were measured in ω-2θ scan mode with scan width of 1.5° (in ω) plus α_1-α_2 divergence at scan speed 4° (in 2θ) min^{-1}. Four reference reflections indicated no significant intensity variations throughout the experiment. Out of 4701 independent reflections in the range $5<2\theta<115°$, 362 weak reflections which gave the counts under background were considered as zero-reflections. The data were corrected for Lorentz and polarization factors but not for absorption effects. The standard deviation for each reflection was estimated by the equation, $\sigma^2(F)=\sigma_p^2+q|F_o|^2$, where σ_p is due to counting statistics and q is 4.39×10^{-6}, derived from the variation of the monitored reflections.

TABLE 1. CRYSTAL DATA

Compound	$Ni(CH_2=C(CH_3)COOC_2H_5)(PPh_3)_2$
Formula weight	697.53
Formula	$C_{42}H_{40}O_2P_2Ni$
Crystal system	Monoclinic
Space group	$P2_1/c$
a	13.690(2) Å
b	16.855(2) Å
c	15.699(1) Å
β	105.09(1)°
V	3497.7(6) Å^3
Z	4
Density	
exptl	1.31 g·cm^{-3}
calcd	1.32 g·cm^{-3}

Structure Determination

The structure was solved by the heavy-atom method and the atomic parameters were refined by block-diagonal least-squares technique. The quantity minimized was $\sum w(|F_o|-|F_c|)^2$, with $w=1/\sigma^2(F)$. All the hydrogen atoms assigned on a difference map were included. The zero reflections were included in the least-squares calculation by assuming $|F_o|=F_{1lm}$ where F_{1lm} is 2.67, an observational threshold value, but those for which $|F_c|<F_{1lm}$ were omitted. The final R was 0.098 (R=0.084 for $|F_o|>3\sigma(F)$). The final atomic parameters are listed in Table 2.[9] Atomic scattering factors used were taken from International Tables for X-ray Crystallography.[10]

Table 2. Fractional coordinates ($\times 10^5$; for H, $\times 10^3$) and thermal parameters ($\times 10^4$(/Å^2); for H, $\times 10^3$(/Å^2))

The anisotropic temperature factor has the form: $\exp\{-2\pi^2(h^2a^{*2}U_{11}+k^2b^{*2}U_{22}+l^2c^{*2}U_{33}+2hka^*b^*U_{12}+2hla^*c^*U_{13}+2klb^*c^*U_{23})\}$. The isotropic temperature factor has the form: $\exp\{-(8\pi^2U)\sin^2\theta/\lambda^2\}$.

ATOM	X	Y	Z	U11	U22	U33	U12	U13	U23
NI	79607(8)	50371(6)	31970(7)	506(6)	331(5)	759(7)	27(5)	131(5)	28(6)
P(1)	81023(13)	54132(9)	19105(12)	236(10)	171(8)	484(12)	2(8)	95(9)	13(8)
P(2)	72321(13)	59509(10)	38074(12)	275(10)	196(9)	441(12)	18(8)	87(9)	-3(8)
C(1)	86716(54)	40072(40)	33059(53)	406(47)	298(41)	852(62)	215(36)	164(43)	168(40)
C(2)	82667(51)	41033(36)	40401(45)	413(45)	221(37)	516(49)	94(33)	43(36)	119(33)
C(3)	89907(64)	42334(47)	49602(54)	683(63)	550(57)	677(63)	109(46)	-141(48)	185(45)
C(4)	73223(55)	37672(37)	40840(49)	530(51)	189(37)	712(58)	53(34)	180(43)	97(35)
C(5)	56719(71)	33907(59)	32337(73)	576(67)	869(77)	1461(101)	-345(58)	4(64)	98(68)
C(6)	50064(81)	35449(67)	23945(80)	790(84)	1082(90)	1664(119)	-287(72)	-156(77)	30(85)
C(7)	70888(50)	60364(37)	12223(44)	352(42)	286(38)	455(47)	25(32)	105(35)	62(33)
C(8)	69872(52)	68207(40)	14657(46)	347(44)	396(44)	517(52)	77(35)	14(38)	72(35)
C(9)	61556(59)	72673(42)	10147(56)	482(53)	374(46)	893(66)	87(39)	247(48)	160(43)
C(10)	54118(56)	69456(45)	3712(56)	325(47)	521(52)	890(68)	19(39)	25(44)	309(46)
C(11)	55019(57)	61776(50)	1292(53)	396(50)	752(62)	667(61)	-189(45)	-78(43)	165(47)
C(12)	63331(53)	57232(41)	5481(47)	399(47)	401(45)	549(53)	-54(36)	-7(39)	47(37)
C(13)	81564(46)	46349(35)	11080(41)	261(38)	288(36)	336(42)	46(30)	90(31)	36(31)
C(14)	86670(54)	46973(38)	5007(48)	445(48)	303(40)	609(54)	-65(34)	134(40)	-96(35)
C(15)	86604(59)	41066(47)	-1296(52)	548(56)	679(57)	642(59)	87(45)	290(46)	-74(45)
C(16)	80852(59)	34248(43)	-1063(50)	559(54)	454(48)	622(58)	6(40)	127(44)	-245(41)
C(17)	75740(58)	33435(42)	4860(51)	535(55)	370(45)	712(61)	-98(39)	76(45)	-128(40)
C(18)	75769(53)	39388(42)	11209(50)	381(47)	459(47)	710(59)	-30(38)	179(41)	-53(41)
C(19)	92442(47)	59844(35)	19544(44)	273(38)	220(34)	511(47)	22(30)	154(33)	-13(32)
C(20)	101236(52)	57783(38)	25921(48)	381(46)	347(43)	637(55)	44(35)	143(40)	105(37)
C(21)	109972(52)	62183(43)	27223(51)	270(43)	496(50)	766(61)	34(36)	82(40)	86(42)
C(22)	110158(54)	68768(41)	21934(52)	341(44)	378(44)	764(61)	-71(35)	179(41)	-77(40)
C(23)	101805(54)	70836(38)	15547(50)	429(48)	264(40)	710(58)	5(34)	229(42)	34(36)
C(24)	93019(48)	66311(38)	14310(44)	295(42)	324(40)	483(48)	5(32)	72(35)	-11(34)
C(25)	58706(49)	60913(35)	33176(45)	310(41)	214(37)	559(50)	-12(31)	118(35)	34(33)
C(26)	52363(55)	64733(43)	37282(52)	366(47)	415(47)	814(63)	-9(37)	143(43)	-164(42)
C(27)	42028(63)	65581(47)	32885(65)	534(59)	496(55)	1387(89)	106(44)	471(60)	-72(55)
C(28)	38220(59)	62575(48)	24839(57)	408(53)	613(58)	957(73)	-27(43)	52(48)	165(50)
C(29)	44325(59)	58726(50)	20695(52)	496(55)	815(64)	622(60)	-199(47)	131(45)	110(48)
C(30)	54560(53)	57717(42)	24833(48)	356(45)	501(48)	571(54)	-66(37)	130(39)	28(39)
C(31)	72879(52)	58524(35)	49649(45)	485(48)	194(36)	494(48)	17(32)	173(38)	-19(32)
C(32)	80519(57)	62012(41)	56296(49)	542(54)	409(46)	596(56)	24(39)	165(43)	46(39)
C(33)	81115(67)	60850(47)	65013(51)	866(70)	564(55)	505(57)	49(49)	8(48)	-40(43)
C(34)	74235(75)	56407(49)	67472(53)	1283(89)	574(57)	500(58)	132(56)	378(59)	158(44)
C(35)	66586(74)	52851(47)	61245(57)	1072(79)	514(55)	685(64)	-181(51)	351(57)	103(45)
C(36)	66115(62)	53881(43)	52650(49)	737(61)	404(45)	536(54)	-28(42)	230(46)	-14(39)
C(37)	78083(47)	69473(34)	38223(44)	265(39)	179(35)	539(50)	-45(29)	93(35)	-51(31)
C(38)	87492(52)	69989(39)	37307(48)	368(45)	351(43)	569(54)	-29(35)	75(39)	-129(36)
C(39)	92670(56)	77187(44)	37764(52)	391(50)	539(51)	698(61)	-127(40)	197(44)	-93(43)
C(40)	87385(63)	83865(43)	38995(53)	711(62)	391(47)	696(61)	-251(43)	111(49)	-30(41)
C(41)	78188(58)	83651(40)	39937(53)	520(53)	282(42)	855(65)	-12(37)	181(47)	11(40)
C(42)	72963(54)	76483(39)	39450(50)	386(48)	337(41)	730(58)	55(35)	258(42)	15(39)
O(1)	70595(44)	35937(30)	47301(37)	923(47)	498(35)	880(46)	-39(33)	433(37)	192(31)
O(2)	66807(40)	36725(31)	32507(36)	596(39)	597(37)	877(45)	-299(31)	2(33)	93(32)

ATOM	X	Y	Z	U	ATOM	X	Y	Z	U
H(31)	962(5)	438(4)	481(5)	53(25)	H(201)	1000(5)	548(4)	300(4)	33(21)
H(32)	924(5)	388(4)	528(5)	55(26)	H(211)	1158(5)	612(4)	321(4)	50(25)
H(33)	859(5)	461(4)	539(4)	41(23)	H(221)	1154(5)	718(4)	209(4)	43(23)
H(61)	412(7)	335(6)	231(6)	112(38)	H(231)	1019(5)	753(3)	113(4)	8(17)
H(62)	553(7)	335(6)	211(6)	111(38)	H(241)	870(4)	672(3)	103(3)	0(16)
H(63)	517(8)	400(6)	212(7)	141(44)	H(261)	550(4)	663(3)	427(3)	3(16)
H(51)	581(8)	289(6)	372(7)	131(43)	H(271)	392(5)	667(4)	364(4)	30(21)
H(52)	537(7)	377(6)	379(6)	111(37)	H(281)	306(6)	618(5)	220(6)	98(35)
H(11)	936(4)	404(3)	331(3)	2(16)	H(291)	422(5)	575(4)	152(4)	22(19)
H(12)	829(5)	361(4)	268(4)	51(25)	H(301)	586(4)	551(3)	212(3)	0(15)
H(81)	749(4)	702(3)	188(3)	0(16)	H(321)	842(4)	644(3)	545(3)	2(16)
H(91)	599(5)	773(4)	123(4)	41(23)	H(331)	835(4)	628(3)	674(3)	0(16)
H(101)	476(5)	726(4)	15(4)	29(21)	H(341)	742(5)	557(3)	724(4)	16(18)
H(111)	508(4)	597(3)	-23(4)	17(19)	H(351)	621(4)	505(4)	625(4)	20(18)
H(121)	650(5)	535(4)	28(4)	31(21)	H(361)	614(5)	518(4)	473(4)	43(24)
H(141)	903(4)	502(3)	42(3)	3(15)	H(381)	903(5)	665(4)	351(4)	39(23)
H(151)	905(4)	412(3)	-53(3)	0(16)	H(391)	993(4)	775(3)	364(4)	8(17)
H(161)	816(4)	316(3)	-51(4)	5(16)	H(401)	893(4)	868(3)	388(3)	1(16)
H(171)	719(5)	300(3)	52(4)	17(19)	H(411)	746(5)	863(4)	411(4)	28(20)
H(181)	722(4)	389(3)	145(3)	0(16)	H(421)	676(4)	764(3)	408(3)	0(16)

Results and Discussion

As shown in Fig. 1, the crystal structure consists of discrete molecules. All intermolecular contacts are normal, the shortest being 2.35 Å between H031 atoms related by the inversion center at (1,½, ½). Figure 2 shows a stereo view of the molecule. Tables 3 and 4 list the bond lengths and bond angles, respectively. All the C–C bond lengths and the C–C–C angles of the phenyl rings are normal, although some of these are contracted seemingly by the large thermal motion. The P–C bond distances and the Ni–P–C and C–P–C angles are comparable with those of the related compounds.[2-4]

As shown in Fig. 3, the nickel atom has a distorted square planar coordination of the two C and two P atoms, similar to the related Ni–ethylene complexes, $Ni(C_2H_4)L_2$.[2-4] Although the ethyl methacrylate molecule could coordinate in a variety of modes (*i.e.* through C=C, C=O, or both), only the carbon–carbon double bond has a linkage with the nickel atom, and the

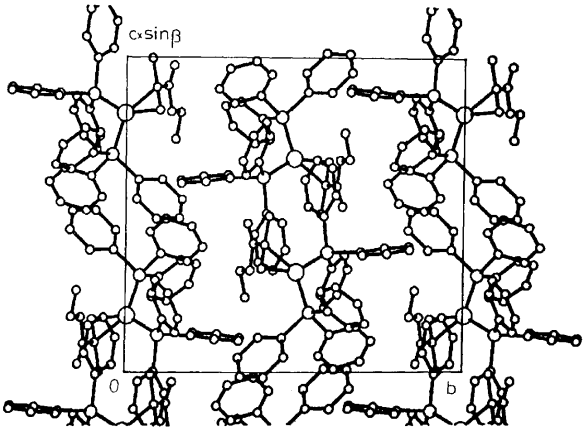

Fig. 1. Molecular packing projected along the a axis.

carbonyl group of the ester turns away from nickel. It seems to be reasonable that the C=C bond lies in the square coordination plane of zero valent metal olefin complex, M(olefin)L_2.[1b]

The coordination mode of ethyl methacrylate ligand mentioned above explains the NMR and IR results reasonably.[7] The large upfield shifts of olefinic protons and carbons in ^{1}H- and ^{13}C-NMR spectra are due to the strong interaction of nickel with the olefinic double bond. The absence of direct interaction between Ni and C=O group supports the slight shifts of ν(C=O) upon coordination.[7,8] The two methylene protons of the ethoxy group, H(51) and H(52), lie in the different circumstances, as indicated by ^{1}H-NMR spectra.[8]

The mean plane of the coordination is expressed by the equation, $0.8841X+0.4174Y+0.2101Z=13.322$ where X, Y, and Z are in Å taken along the directions a^*, b, and c, respectively. The deviations of atoms from the plane are −0.02 (Ni), −0.02 (P(1)), 0.03 (P(2)), 0.07 (C(1)), and −0.06 Å (C(2)). These slight but significant deviations are also described by the dihedral angle of 6.4(4)° between the planes through Ni, P(1), and P(2), and through Ni, C(1), and C(2). In the related Ni(0) and Pt(0) olefin complexes, the dihedral angles range from 1.3 to 18.5°.[2b] Such a twist may be mainly due to a steric effect between the bulky ligand molecules in addition to an electronic effect. The two Ni–P bond distances (2.173 Å and 2.187 Å), the P(1)–Ni–P(2) angle (111.29), the average of the Ni–C bond distances

Table 3. Bond distances (l/Å) and their standard deviation for the heavy atoms

Ni-P(1)	2.173(2)	Ni-P(2)	2.187(2)
Ni-C(1)	1.976(8)	Ni-C(2)	2.029(7)
C(1)-C(2)	1.412(10)	C(2)-C(3)	1.540(11)
C(2)-C(4)	1.430(10)	C(4)-O(1)	1.197(9)
C(4)-O(2)	1.382(9)	C(5)-O(12)	1.454(12)
C(5)-C(6)	1.417(16)		
Triphenylphosphine Ligands			
P(1)-C(7)	1.848(7)	C(7)-C(8)	1.393(10)
C(8)-C(9)	1.394(11)	C(9)-C(10)	1.347(11)
C(10)-C(11)	1.364(11)	C(11)-C(12)	1.387(11)
C(12)-C(7)	1.378(10)		
P(1)-C(13)	1.834(6)	C(13)-C(14)	1.325(10)
C(14)-C(15)	1.402(11)	C(15)-C(16)	1.399(11)
C(16)-C(17)	1.308(11)	C(17)-C(18)	1.408(11)
C(18)-C(13)	1.420(10)		
P(1)-C(19)	1.822(7)	C(19)-C(20)	1.395(9)
C(20)-C(21)	1.377(10)	C(21)-C(22)	1.390(11)
C(22)-C(23)	1.354(10)	C(23)-C(24)	1.392(10)
C(24)-C(19)	1.380(9)		
P(2)-C(25)	1.837(7)	C(25)-C(26)	1.369(10)
C(26)-C(27)	1.411(12)	C(27)-C(28)	1.335(12)
C(28)-C(29)	1.351(12)	C(29)-C(30)	1.393(10)
C(30)-C(25)	1.393(10)		
P(2)-C(31)	1.806(7)	C(31)-C(32)	1.400(10)
C(32)-C(33)	1.364(11)	C(33)-C(34)	1.336(12)
C(34)-C(35)	1.371(13)	C(35)-C(36)	1.345(12)
C(36)-C(31)	1.385(10)		
P(2)-C(37)	1.853(7)	C(37)-C(38)	1.336(10)
C(38)-C(39)	1.398(11)	C(39)-C(40)	1.379(11)
C(40)-C(41)	1.306(11)	C(41)-C(42)	1.396(11)
C(42)-C(37)	1.412(10)		

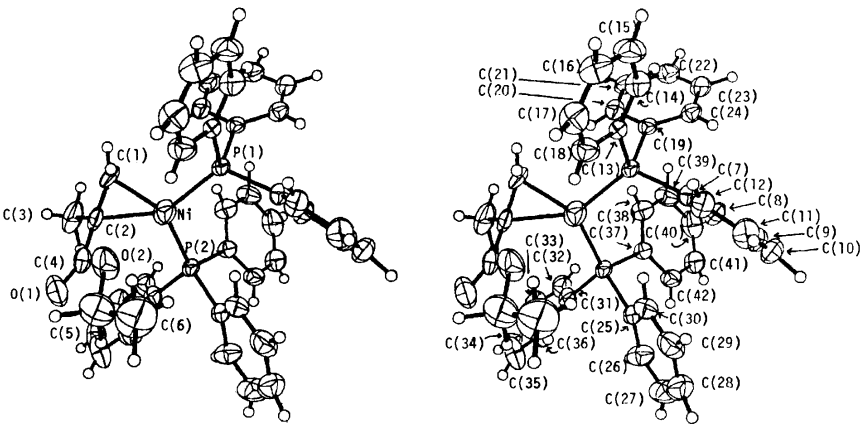

Fig. 2. Stereoscopic drawing of the molecule of (ethyl methacrylate)bis(triphenylphosphine)nickel. The non-hydrogen atoms are represented by their thermal ellipsoids with 50% probability, while the hydrogen atoms are represented by spheres of a fixed arbitrary radius.

Table 4. Bond angles (θ/°) and their standard derivations for the heavy atoms

P(1)-Ni-P(2)	111.3(1)	P(1)-Ni-C(1)	100.1(2)	P(1)-Ni-C(2)	141.1(2)
P(2)-Ni-C(1)	148.4(2)	P(2)-Ni-C(2)	107.5(2)	C(1)-Ni-C(2)	41.3(3)
Ni-P(1)-C(7)	118.3(2)	Ni-P(1)-C(13)	117.3(2)	Ni-P(1)-C(19)	113.7(2)
C(7)-P(1)-C(13)	99.4(3)	C(7)-P(1)-C(19)	103.2(3)	C(13)-P(1)-C(19)	102.5(3)
Ni-P(2)-C(25)	115.9(2)	Ni-P(2)-C(31)	118.1(2)	Ni-P(2)-C(37)	113.7(2)
C(25)-P(2)-C(31)	101.9(3)	C(25)-P(2)-C(37)	105.7(3)	C(31)-P(2)-C(37)	99.5(3)
Ni-C(1)-C(2)	71.4(4)	Ni-C(2)-C(1)	67.4(4)	Ni-C(2)-C(3)	118.3(5)
Ni-C(2)-C(4)	107.7(5)	C(1)-C(2)-C(3)	119.2(6)	C(1)-C(2)-C(4)	123.1(6)
C(3)-C(2)-C(4)	112.4(6)	C(2)-C(4)-O(1)	127.8(7)	C(2)-C(4)-O(2)	111.1(6)
O(1)-C(4)-O(2)	121.1(7)	C(6)-C(5)-O(2)	109.6(9)	C(4)-O(2)-C(5)	114.9(6)
Phenyl Rings					
P(1)-C(8)-C(8)	119.5(5)	P(1)-C(7)-C(12)	122.0(5)	C(8)-C(7)-C(12)	117.8(6)
C(7)-C(8)-C(9)	120.0(7)	C(8)-C(9)-C(10)	121.4(7)	C(9)-C(10)-C(11)	119.0(8)
C(10)-C(11)-C(12)	121.0(7)	C(7)-C(12)-C(11)	120.8(7)		
P(1)-C(13)-C(14)	124.1(5)	P(1)-C(13)-C(18)	117.3(5)	C(14)-C(13)-C(18)	118.5(6)
C(13)-C(14)-C(15)	122.9(7)	C(14)-C(15)-C(16)	117.7(7)	C(15)-C(16)-C(17)	120.6(7)
C(16)-C(17)-C(18)	122.1(7)	C(13)-C(18)-C(17)	118.2(7)		
P(1)-C(19)-C(20)	117.9(5)	P(1)-C(19)-C(24)	125.2(5)	C(20)-C(19)-C(24)	116.9(6)
C(19)-C(20)-C(21)	121.8(7)	C(20)-C(21)-C(22)	119.5(7)	C(21)-C(22)-C(23)	120.1(7)
C(22)-C(23)-C(24)	119.8(7)	C(19)-C(24)-C(23)	121.9(6)		
P(2)-C(25)-C(26)	124.2(5)	P(2)-C(25)-C(30)	117.7(5)	C(26)-C(25)-C(30)	118.1(6)
C(25)-C(26)-C(27)	119.7(7)	C(26)-C(27)-C(28)	121.3(8)	C(27)-C(28)-C(29)	120.0(8)
C(28)-C(29)-C(30)	120.5(8)	C(25)-C(30)-C(29)	120.4(7)		
P(2)-C(31)-C(32)	122.6(5)	P(2)-C(31)-C(36)	122.5(6)	C(32)-C(31)-C(36)	114.8(7)
C(31)-C(32)-C(33)	121.7(7)	C(32)-C(33)-C(34)	120.5(8)	C(33)-C(34)-C(35)	120.3(8)
C(34)-C(35)-C(36)	119.2(8)	C(31)-C(36)-C(35)	123.5(8)		
P(2)-C(37)-C(38)	118.5(5)	P(2)-C(37)-C(42)	122.4(5)	C(38)-C(37)-C(42)	119.1(6)
C(37)-C(38)-C(39)	122.8(7)	C(38)-C(39)-C(40)	116.0(7)	C(39)-C(40)-C(41)	123.4(8)
C(40)-C(41)-C(42)	120.9(7)	C(37)-C(42)-C(41)	117.8(7)		

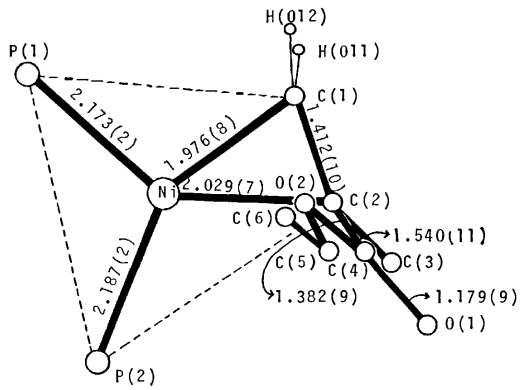

Fig. 3. Coordination geometry around the nickel for (ethyl methacrylate)bis(triphenylphosphine)nickel.

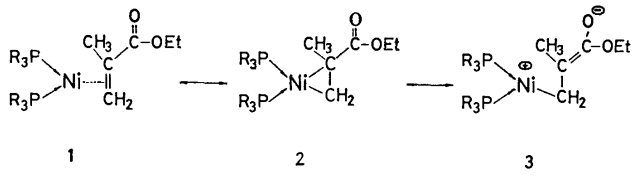

Fig. 4. Some possible resonance structures for (ethyl methacrylate)bis(triphenylphosphine)nickel.

(2.003 Å), and the C(1)–Ni–C(2) angle (41.3°) are comparable with those of the Ni–ethylene complex.[2a-b]

A closer examination, however, shows that the two Ni–C bonds are significantly different, the Ni–C(1) bond distance (1.976 Å) being shorter than Ni–C(2) bond distance (2.029 Å) (Figure 3). The C(1)=C(2) bond is lengthened, whereas the C(2)–C(4) bond is shortened from the normal distances (1.36 Å for C=C and 1.44 Å for C–C in C=C–C=O system)[12]. Although the C(4)–O(1) distance is contracted apparently due to the large thermal motion, a value corrected by the riding model[13] is 1.231 Å. These distances are interpreted by the contribution from three-membered metallacycle **2** and polarized structure **3**, in addition to **1** (see Figure 4)†. This scheme is consistent with the observation in ^{13}C-NMR spectra, that the chemical shift of C(1) varies to a higher field more significantly than that of C(2) with increasing the σ-donor property of tertiary phosphine ligands.[8] In addition the steric effect of the two substituents (methyl and ethoxycarbonyl) attached to C(2) and the two bulky triphenylphosphine ligands may facilitate the unequal coordination mentioned above. These two substituents are bent back away from nickel: the deviation of C(2) from the plane of C(1), C(3), and C(4) is 0.195 Å.

† Similar ionic contribution has been reported by Ibers *et al.* for a platinum(0) 1,1-dichloro-2,2-dicyanoethylene complex.[11] On the contrary, olefin shift to maximize the metal–olefin bond is postulated for Ni-acrylonitrile bond.[3] In the present complex a similar sliding of the olefin along the C=C bond is observed

This geometry suggests an increase of sp^3 character of C(1) and C(2).††

The Ni–P(2) distance is slightly longer than that of Ni–P(1) probably owing to the trans influence of closer C(1) to Ni than C(2).

Figure 1 was drawn by TSD:XTAL which is an interactive modeling program system for computer graphics.[14]

References

1) a) M. Herberhold, "Metal π-Complexes, Vol. II, Part 2," Elsevier Sci. Co., London, New York (1974); b) F. G. A. Stone and R. West, "Advances in Organometallic Chemistry," Academic Press, New York, London (1976), Vol. 14, p. 33.

2) a) P. T. Cheng, C. D. Cook, C. H. Koo, S. C. Nyburg, and M. T. Shiomi, *Acta Crystallogr., Sect B*, **27**, 1904 (1974); b) W. Dreissig and H. Dietrich, *Acta Crystallogr., Sect. B*, **24**, 108 (1968); c) C. Krüger and Y. H. Tsay, *J. Organomet. Chem.*, **34**, 587 (1972).

3) L. J. Guggenberger, *Inorg. Chem.*, **12**, 499 (1973).

4) S. D. Ittel and J. A. Ibers, *J. Organomet. Chem.*, **74**, 121 (1974).

5) Private Communication, recently Krüger solved the crystal structure of a nickel acrylic ester complex with 2,2′-bipyridine and showed the coordination through C=C double bond to nickel.

6) S. Komiya, T. Ito, M. Cowie, A. Yamamoto, and J. A. Ibers, *J. Am. Chem. Soc.*, **98**, 3874 (1976).

7) J. Ishizu, T. Yamamoto, and A. Yamamoto, *Bull. Chem. Soc. Jpn.*, **51**, 2646 (1978).

8) T. Yamamoto, J. Ishizu, S. Komiya, Y. Nakamura, and A. Yamamoto, *J. Organomet. Chem.*, **171**, 103 (1979).

9) A list of the observed and calculated structure factors are kept in the Office of the Chemical Society of Japan, (Document No. 8020).

10) "International Tables for X-Ray Crystallography," Vol. IV, The Kynoch Press, Birmingham (1974).

11) A. McAdam, J. N. Francis, and J. A. Ibers, *J. Organomet. Chem.*, **29**, 149 (1971).

12) "Tables of Interatomic Distances and Configuration in Molecules and Ions, Supplement," ed by L. E. Sutton, The Chemical Society, London (1965).

13) W. R. Busing and H. A. Levy, *Acta Crystallogr.*, **17**, 142 (1964).

14) A. Takenaka and Y. Sasada, *J. Cryst. Soc. Jpn.*, **21**, 214 (1980).

15) T. A. Albright, R. Hoffmann, J. C. Thibeault, and D. L. Thorn, *J. Am. Chem. Soc.*, **101**, 3801 (1979).

†† Recently molecular orbital consideration for the problem of asymmetry in metal–olefin bonding has been reported.[15]

Circular Dichroism Spectra and Their Relation to Asymmetric Distortion of Some Dimeric Molybdenum(V) Complexes Containing Optically Active Amino Carboxylate

Kimiko Z. Suzuki, Yoichi Sasaki,* Shun'ichiro Ooi,† and Kazuo Saito

Department of Chemistry, Faculty of Science, Tohoku University, Aoba, Aramaki, Sendai 980

† *Department of Chemistry, Faculty of Science, Osaka City University, Sugimoto-cho, Sumiyoshi-ku, Osaka 558*

(Received September 1, 1979)

Circular dichroism (CD) spectra of fifteen kinds of μ-X-μ-Y-bis(oxomolybdenum(V)) complexes, where X=Y=O, X=O and Y=S, and X=Y=S, containing optically active ligands such as (*S*)-cysteinate, its alkyl esters, (*R*)-penicillaminate (*R*-pen), (*S*)-histidinate, and (*R*)-propylenediaminetetraacetate, give two distinctive peaks with opposite signs at *ca.* 26000 and 33000 cm^{-1} in various media including KBr disks. Close examination of the known X-ray structural data of eight complexes indicated that the pseudo-octahedral coordination sphere of two molybdenum(V) ions are asymmetrically twisted around the Mo–Mo axis. The direction of such a twist for the complexes containing the ester ligands and *R*-pen, is opposite to that for the complexes with other ligands. The former and latter complexes give positive and negative, and negative and positive CD peaks at *ca.* 26000 and 33000 cm^{-1}, respectively. Thus the CD signs of the two peaks are related to the asymmetric distortion around the Mo–Mo axis.

Deviation of coordinated atoms from regular octahedron can cause a considerable effect on the circular dichroism(CD) spectra. Such an influence was demonstrated by the crystallographic data of some cobalt (III) complexes, *e.g.* tris(1,2-cyclopentanediamine)cobalt(III),[1] and also by theoretical considerations.[2,3] However, only a few examples are found,[1–4] which are limited to cobalt(III) complexes, and complexes of Schiff's bases with asymmetric diimine moiety.

Molybdenum(V) complexes give doubly bridged binuclear complexes with a μ-X-μ-Y-bis(oxomolybdenum (V)) core, $Mo_2O_2XY^{2+}$ (where X=Y=O, X=O and Y=S, and X=Y=S), and coordination number 5 or 6 depending on the ligands.[5] Their crystal structure exhibits considerable distortion from regular square pyramid or octahedron.[5–13] Such distortions can be asymmetrical when the ligand is optically active. The X-ray structure of $[Mo_2O_4(S\text{-cys})_2]^{2-}$,[8] $[Mo_2O_4(S\text{-hist})_2]$,[9] $[Mo_2O_4(S\text{-mecys})_2]$,[10] $[Mo_2O_2S_2(S\text{-cys})_2]^{2-}$,[11] $[Mo_2O_2S_2(S\text{-hist})_2]$[12], and $[Mo_2O_2S_2(S\text{-etcys})_2]$,[13] where *S*-cys^{2-}, *S*-hist$^-$, *S*-mecys$^-$, and *S*-etcys$^-$ are (*S*)-cysteinate, (*S*)-histidinate, *O*-methyl- and *O*-ethyl-(*S*)-cysteinate, respectively, are schematically shown in Fig. 1a to 1c. They have chelate rings containing asymmetric carbon atoms at the basal edges. The complexes of *O*-alkyl-(*S*)-cysteinate give coordination number 5, whereas those of the others 6. We have examined carefully the crystallographic data of these complexes and found asymmetric distortions around the $Mo_2O_2XY^{2+}$ core.

We have also prepared three (*R*)-propylenediaminetetraacetate (*R*-pdta) complexes with di-μ-oxo,[14] μ-oxo-μ-thio, and di-μ-thio bridges and determined the X-ray structure (Fig. 1d).[15] These complexes have structurally different feature from the hitherto known carboxylate complexes, with asymmetric chelate ring bridging the molybdenum(V) ions across the two apical sites of the dimer. These *R*-pdta complexes also show considerable asymmetric distortions.

The CD and optical rotatory dispersion spectra (ORD) of molybdenum(V) complexes have been reported with only a limited variety of species[14,16–18] and their relation with the structure has not been discussed. We have measured CD spectra of various amino carboxylate and their ester complexes including those mentioned above in various media. We report here a remarkable correlation between the asymmetric distortion around the $Mo_2O_2XY^{2+}$ core and the CD pattern in the ultraviolet region. The CD studies also provide useful informations on the assignment of the electronic absorption bands of the doubly bridged molybdenum(V) complexes.

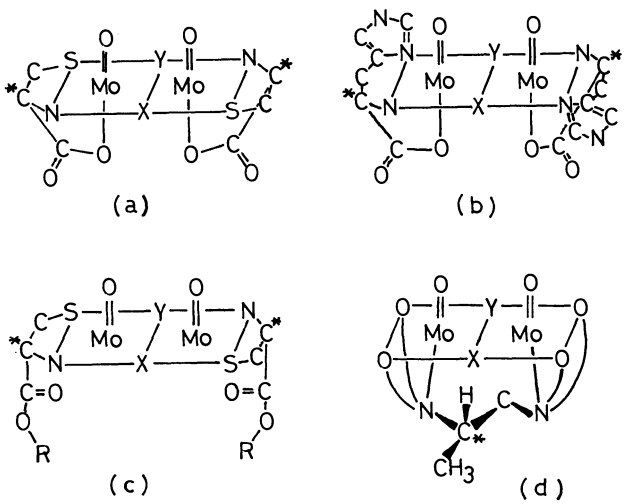

Fig. 1. Schematic drawings of the structure of $Mo_2O_2XY^{(2+)}$-type complexes (X=Y=O, X=O and Y=S, and X=Y=S). Asterisks indicate asymmetric carbons.
(a) $[Mo_2O_2XY(S\text{-cys})_2]^{2-}$, (b) $[Mo_2O_2XY(S\text{-hist})_2]$, (c) $[Mo_2O_2XY(S\text{-Rcys})_2]$ (R=CH_3 or C_2H_5), and (d) $[Mo_2O_2XY(R\text{-pdta})]^{2-}$.

Experimental

Preparation of the Complexes. The following seven complexes were prepared by the known methods; $Na_2[Mo_2O_4(S\text{-cys})_2]\cdot 5H_2O$,[19] $[Mo_2O_4(S\text{-hist})_2]\cdot 2H_2O$,[20] $[Mo_2O_4(S\text{-mecys})_2]$,[21] $[Mo_2O_4(S\text{-etcys})_2]$,[21] $Na_2[Mo_2O_4(R\text{-pdta})]\cdot 3H_2O$,[14,22] $Na_2[Mo_2O_3S(S\text{-cys})_2]\cdot 4H_2O$,[23] and $[Mo_2O_3S(S\text{-etcys})_2]$.[23]

The following three di-μ-thio-bis{oxomolybdenum(V)} complexes were prepared by modifying the methods in the literature.

Sodium di-μ-thio-bis[{(S)-cysteinato}oxomolybdate(V)] Tetrahydrate, $Na_2[Mo_2O_2S_2(S\text{-}cys)_2]\cdot 4H_2O$: A black solid was obtained by Mitchell's method,[19] which contained both soluble and insoluble components in *N,N*-dimethylformamide (DMF) (or dimethyl sulfoxide (DMSO)). The former seemed to be the expected complex. Insoluble component was not formed when the pH of the solution was adjusted carefully as follows. Hydrogen sulfide was slowly bubbled through 200 cm^3 of the solution of $Na_2[Mo_2O_4(S\text{-cys})_2]\cdot 5H_2O$ (2 g; 3 mmol) in water for 1 h, the pH of the solution being kept at *ca.* 7 by the addition of aqueous NaOH solution. The resulting reddish brown solution was evaporated to 25 cm^3 at 40 °C under a reduced pressure. Orange needles were collected after 3 days. Yield, 0.2 g. Found: C, 11.22; H, 2.71; N, 4.46%. Calcd for $C_6H_{18}N_2O_8S_4Na_2Mo_2$: C, 11.18; H, 2.82; N, 4.35%.

Di-μ-thio-bis[{(S)-histidinato}oxomolybdenum(V)] Dihydrate, $[Mo_2O_2S_2(S\text{-}hist)_2]\cdot 2H_2O$: The procedure reported by Spivack and Dori,[24] which involves the passage of H_2S through the aqueous solution of $[Mo_2O_4(S\text{-hist})_2]$, gave a black material, from which the pure complex was not obtained. The pure complex was prepared as follows. Sodium molybdate (2.4 g; 10 mmol) and (*S*)-histidine (1.6 g; 10 mmol) were dissolved in 100 cm^3 of water. Hydrogen sulfide was bubbled slowly through the solution for *ca.* 1 h, while 400 cm^3 of water was added in small portions. The reddish brown solution was purged with nitrogen gas to remove excessive H_2S, and evaporated in a rotary evaporator until yellow solid deposited, which was washed with water until the washing became colorless. The yield of yellow powder was 0.45 g. Found: C, 22.46; H, 2.93; N, 13.05%. Calcd for $C_{12}H_{20}N_6O_6S_2Mo_2$: C, 22.79; H, 3.19; N, 13.29%.

Di-μ-thio-bis[{O-methyl-(S)-cysteinato}oxomolybdenum(V)], $[Mo_2O_2S_2(S\text{-}mecys)_2]$: This was prepared by one of the three methods given by Mitchell,[19] from sodium molybdate (1.2 g, 5 mmol), (*S*)-cysteine methyl ester hydrochloride (3.4 g; 20 mmol) and H_2S. The crude product (0.6 g) was dissolved in acetonitrile, a small amount of insoluble materials was removed, and the solution was kept in air for two days. The brown precipitate was filtered off. Addition of methanol or water to the filtrate gave orange crystals. Found: C, 17.13; H, 2.82; N, 4.97%. Calcd for $C_8H_{16}N_2O_6S_4Mo_2$: C, 17.27; H, 2.90; N, 5.04%.

Five new complexes were prepared by the following methods. The data of elemental analysis and important infrared absorption bands of the new complexes are summarized in Table 1. Each complex shows characteristic infrared bands for its skeletal structure, $Mo_2O_2XY^{2+}$.[23,25]

Sodium di-μ-oxo-bis[{(R)-penicillaminato}oxomolybdate(V)] Dihydrate, $Na_2[Mo_2O_4(R\text{-}pen)_2]\cdot 2H_2O$: The complex ion, $[Mo_2O_4(R\text{-pen})_2]^{2-}$, was described previously,[26] but the preparation method has not yet been reported. Molybdenum pentachloride (3.1 g; 11 mmol) was dissolved in 25 cm^3 of 3 M (M=mol dm^{-3}) HCl. (*R*)-Penicillamine (5 g; 33 mmol) in 20 cm^3 of 3 M HCl was added to the solution. The pH was adjusted to 6—7 with 6 M NaOH, while the solution was cooled in an ice bath. Barium perchlorate (1.7 g; 5 mmol) in 20 cm^3 of water was added to the solution to give orange precipitate of $Ba[Mo_2O_4(R\text{-pen})_2]\cdot 3H_2O$. This barium salt (2.6 g) and a cation exchange regin Dowex 50W-X8 (Na^+-form, 120 cm^3) were stirred in 150 cm^3 of water for *ca.* 5 h. The regin was filtered off, and the filtrate was treated with ethanol (50 cm^3) to give orange precipitate (1.4 g). This was dissolved in a minimum amount of water and treated with acetonitrile to give first oily precipitate. The supernatant was removed by decantation and the oil was further treated with acetonitrile. Orange powder was collected and washed with acetonitrile and dried in air.

μ-Oxo-μ-thio-bis[{(S)-histidinato}oxomolybdenum(V)] Trihydrate, $[Mo_2O_3S(S\text{-}hist)_2]\cdot 3H_2O$: Hydrogen sulfide was bubbled slowly through the solution of molybdenum pentachloride (6.15 g; 23 mmol) in 100 cm^3 of 3 M HCl for *ca.* 2 h. The solution was purged with nitrogen gas to remove excessive H_2S, and a small quantity of brown solid was filtered off. (*S*)-Histidine (1.7 g; 11 mmol) was added to the filtrate. The pH was adjusted to *ca.* 6 with 8 M NaOH solution. Greenish brown precipitate was filtered off, and the filtrate was kept in an ice bath to give yellow crystals. They were dissolved in 50 cm^3 of 3 M HCl, and the pH was adjusted to *ca.* 6 with 8 M NaOH solution. The solution was filtered and kept in a refrigerator for 2 days to give yellow crystals.

μ-Oxo-μ-thio-bis[{O-methyl-(S)-cysteinato}oxomolybdenum(V)], $[Mo_2O_3S(S\text{-}mecys)_2]$: This was prepared by a similar method to that for the corresponding *S*-etcys complex.[23]

Sodium μ-oxo-μ-{(R)-propylenediaminetetraacetato}-μ-thio-bis{oxomolybdate(V)} Tetrahydrate, $Na_2[Mo_2O_3S(R\text{-}pdta)]\cdot 4H_2O$: The procedure for the preparation of $[Mo_2O_3S(S\text{-hist})_2]\cdot 3H_2O$ was followed until the addition of ligand. A solution of (*R*)-propylenediaminetetraacetic acid monohydrate[27] (2.8 g; 9 mmol) in 25 cm^3 of water was added to the molybdate solution, and the pH was adjusted to *ca.* 6 with 8 M NaOH solution. The solution was filtered to remove brown solid, and allowed to stand in a refrigerator for three days. A small quantity of black solid was removed, and the filtrate was evaporated to give first white solid, which was cooled in an ice-bath and filtered off, and then orange needles, which were recrystallized from water by adding ethanol.

Table 1. Elemental analysis and some infrared spectral data of the new compounds

Compound	Elemental analysis (%)			Infrared bands (cm^{-1})[a]		
	C Found(Calcd)	H Found(Calcd)	N Found(Calcd)	(Mo=O$_t$)	(Mo-O$_b$)	(Mo-S$_b$)[b]
$Ba[Mo_2O_4(R\text{-pen})\cdot 3H_2O$	16.26(16.19)	3.58(3.26)	3.85(3.78)			
$Na_2[Mo_2O_4(R\text{-pen})_2]\cdot 2H_2O$	11.53(11.42)	3.35(3.31)	4.64(4.44)	939 s	735m	
$[Mo_2O_3S(S\text{-hist})_2]\cdot 3H_2O$	22.68(22.72)	3.39(3.49)	13.49(13.25)	946 s	733m	467m
$[Mo_2O_3S(S\text{-mecys})_2]$	17.56(17.78)	2.91(2.99)	5.31(5.19)	939 s	738m	450w
$Na_2[Mo_2O_3S(R\text{-pdta})]\cdot 4H_2O$	19.17(19.08)	3.44(3.20)	3.96(4.05)	940 s	740m	460m
$Na_2[Mo_2O_2S_2(R\text{-pdta})]\cdot 3H_2O$	18.65(18.65)	2.93(3.13)	3.96(3.95)	941 s		480 s

a) Measured in KBr disks. b) Strongest band in the region 400—500 cm^{-1}, where several weak bands are also observed. The assignment should be tentative, according to the recent report on the resonance Raman spectra of some di-μ-thio complexes.[25]

Table 2. Torsion angles, θ_1, θ_2, θ_3, θ_4, and ξ,[a] and the chirality of the corresponding twist,[b] and the conformations of the gauche-like chelate rings of the ligands, for the $Mo_2O_2XY^{(2+)}$ type complexes

Complex	Torsion angles[c,d]					Chelate ring
	$\lvert\theta_1\rvert$	$\lvert\theta_2\rvert$	$\lvert\theta_3\rvert$	$\lvert\theta_4\rvert$	$\lvert\xi\rvert$	
$Na_2[Mo_2O_4(S\text{-cys})_2]\cdot 5H_2O$	4.0(8) Δ	1.5(7) Δ	1.7(7) Δ	11.7(5) Δ	0.1(4)*Δ	δ
$[Mo_2O_4(S\text{-etcys})_2]$	6.7(11)Δ	22.1(8) Δ	24.3(7) Δ		28.4(6) Δ	δ
$Na_2[Mo_2O_4(R\text{-pdta})]\cdot 3H_2O$	5.4(8) Δ	8.6(10)Δ	6.8(11)Δ	5.4(6) Δ	8.6(7) Δ	λ
$Na_2[Mo_2O_3S(R\text{-pdta})\cdot 4H_2O$	0.2(3)*Δ	10.0(3) Δ	11.6(4) Δ	9.1(2) Δ	11.5(2) Δ	λ
$Na_2[Mo_2O_2S_2(S\text{-cys})_2]\cdot 2H_2O$	4.7(14)Δ	1.4(11)Δ	0.6(11)*Δ	10.9(8) Δ	0.2(8)*Δ	δ
$[Mo_2O_2S_2(S\text{-mecys})_2]$	9.2(15)Δ	30.1(13)Δ	26.8(14)Δ		35.9(11)Δ	λ
$[Mo_2O_2S_2(S\text{-hist})_2]\cdot 1.5H_2O$	2.5(4) Δ	0.8(5) Δ	7.5(4) Δ	4.6(3) Δ	4.5(3) Δ	—
$Na_2[Mo_2O_2S_2(R\text{-pdta})]\cdot 4H_2O$	0.2(6)*Δ	9.3(6) Δ	9.2(7) Δ	10.8(4) Δ	10.4(5) Δ	λ

a) For the definition of θ_1, θ_2, θ_3, θ_4, and ξ, see Fig. 4a. b) See Fig. 4c. c) Estimated standard deviations in parentheses. d) Values with asterisks are too small to be valid for the discussion in the text.

Yield, 0.2 g.

Sodium μ-{(R)-Propylenediaminetetraacetato}-di-μ-thio-bis{oxomolybdate(V)} Trihydrate, $Na_2[Mo_2O_2S_2(R\text{-pdta})]\cdot 3H_2O$: An aqueous solution (400 cm³) of sodium molybdate (2.7 g; 10 mmol) and (*R*)-propylenediaminetetraacetic acid monohydrate[27] (1.6 g; 5 mmol) was treated with H_2S slowly until the color turned red, and then with nitrogen to remove excessive H_2S. The solution was evaporated under a reduced pressure to 50 cm³ and kept in a refrigerator for a week to give orange crystals. Yield, 0.1 g.

The Aqua Complex Ions, $[Mo_2O_2XY(H_2O)_6]^{2+}$:[28] These ions were obtained in solution by dissolving the corresponding *S*-cys complexes in 2 M $HClO_4$. Complete disappearance of CD indicated complete loss of (*S*)-cysteinate ligand. The absorption spectra of the di-μ-oxo and di-μ-thio complexes were in reasonable agreement with those reported previously.[29,30] The spectrum of $[Mo_2O_3S(H_2O)_6]^{2+}$ is reported for the first time.

Measurements. All the measurements were carried out at room temperature. Electronic absorption and CD spectra of the complexes were measured in water, DMF and DMSO, whenever soluble, and also in KBr disks. The neutral complexes were insoluble in water. The spectra of *O*-alkyl-(*S*)-cysteinato complexes were measured in acetonitrile, too. The spectra in water were measured under nitrogen atmosphere; otherwise the spectra changed slowly.

The electronic absorption spectra were recorded on a Hitachi 323 Recording Spectrophotometer and a Hitachi 124 Spectrophotometer with a Hitachi Recorder QPD-34. The CD spectra were recorded on a JASCO J-40 Automatic Recording Spectropolarimeter, and a JASCO ORD-UV-5 Spectrophotometer with a CD attachment, for compounds either in solutions or in KBr disks. Nitrogen gas was passed through the cell compartment during the measurement in the KBr disk. The infrared absorption spectra were recorded on a JASCO IR-A1 and a JASCO IR-A2 Spectrophotometer in KBr disks. The PMR spectra were measured with a Varian T-60 Spectrometer in D_2O with sodium 3-(trimethylsilyl)propanesulfonate as an internal standard.

The torsion angles listed in Table 2 were calculated using the atomic coordinates given in the literature.[8,10-13,15] The details of positional parameters have not been found for $[Mo_2O_4(S\text{-hist})_2]$.[9]

Results and Discussion

In the following, the X-ray structures are closely examined, first. Then the nature of absorption bands and the corresponding CD bands are discussed. Finally, the correlation between the structure and the CD spectra is discussed.

Geometrical Isomerism of the Complexes. Several geometrical isomers are possible for the *S*-cys complex. We have fractionally crystallized the sodium salt of $[Mo_2O_4(S\text{-cys})_2]^{2-}$ from aqueous solution by adding ethanol slowly. Aqueous solutions of all the precipitates gave almost identical CD spectra. Thus either all the fractions contained the same geometrical isomer, or a rapid isomerization took place in aqueous solution to give an isomeric mixture with the same composition. The CD spectra of the crystalline complex in KBr disk and in aqueous solution show similar pattern (Fig. 2) in visible region to eliminate the latter possibility. The isomer illustrated in Fig. 1a should have been formed stereoselectively. All the other com-

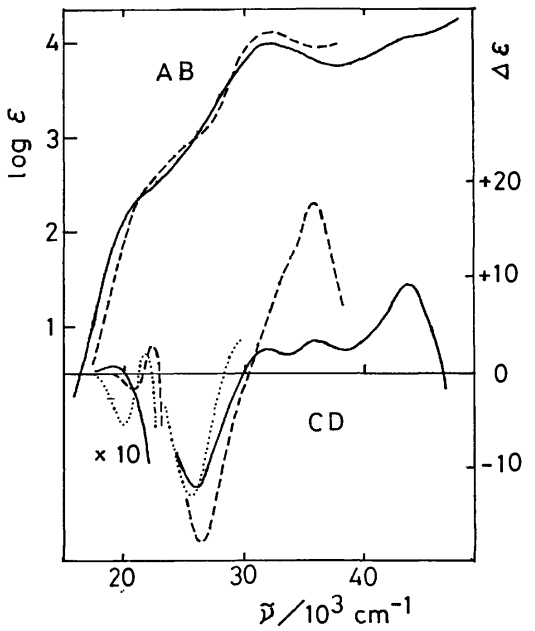

Fig. 2. Comparison in various media of absorption (AB) and CD spectra of $[Mo_2O_4(S\text{-cys})_2]^{2-}$; in water (——), in DMF (----), and in KBr disk (·····).

plexes of *S*-cys, its alkyl esters, *S*-hist and *R*-pen are believed to give the geometrical isomers in Fig. 1 exclusively.

The diamine part of the three *R*-pdta complexes is known to form a distorted λ gauche structure with the methyl group at equatorial direction.[15] The gauche structure of $[Mo_2O_4(pdta)]^{2-}$ was claimed to be fixed at 0—90 °C by the measurements of ^1H[31] and ^{13}C NMR spectra[32] in aqueous solution. Molecular model studies also indicated that the inversion of the gauche structure is difficult owing to the steric hindrance of methyl group with the oxide bridges.[31,32] We thus believe that the diamine part of all the three *R*-pdta complexes is fixed in aqueous solutions as found by X-ray crystallography.[15]

Two geometrical isomers are possible for $[Mo_2O_3S(R\text{-pdta})]^{2-}$ due to relative positions of the bridging oxo and sulfido ligands. The proton NMR spectrum of the complex in D_2O gave only one methyl signal (doublet), indicating only one isomer in the solution. Fractional crystallization failed to give any evidence for the existence of two isomers. The structure of stereoselectively formed isomer determined by X-ray diffraction method,[15] is shown in Fig. 1d.

Close Examination of the X-Ray Structures. Asymmetry caused by the arrangement of coordinated atoms around the $Mo_2O_2XY^{2+}$ core is considered first. A view of $[Mo_2O_4(R\text{-pdta})]^{2-}$ along the Mo–Mo axis (Fig. 3a, the axis perpendicular to the paper plane) clearly shows that the pseudo-octahedron of the molybdenum ion over the paper plane is rotated clockwise around the Mo–Mo axis from that underneath the paper plane. The extent of such a rotation may be expressed by the four torsion angles, θ_1, θ_2, θ_3, and θ_4, defined by the four pairs of metal ligand bonds, Mo–O_t, Mo–O_c, Mo–O_c', and Mo–N, respectively (Fig. 4a). The direction of rotation of each pair can be represented by the sign (P and M, suggested by IUPAC,[33] Fig. 4c) of the torsion angles.

Figure 3b shows the view of the same complex along the axis connecting two bridging oxygens. The coordinated four carboxylate oxygens show alternating

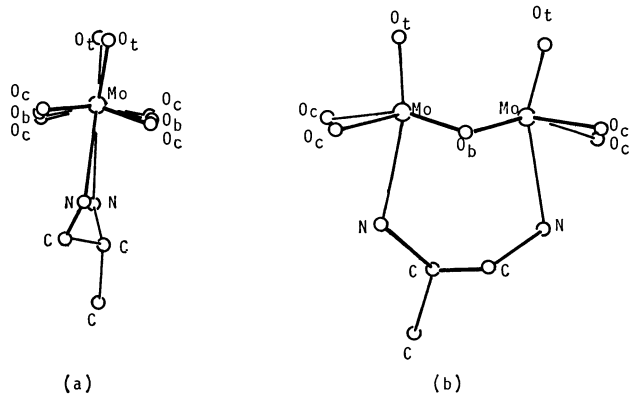

Fig. 3. (a) The projection from the Mo–Mo axis for $[Mo_2O_4(R\text{-pdta})]^{2-}$, and (b) the projection from the axis connecting two oxide bridges for the same ion. Acetate arms are omitted for clarity. (O_t=terminal oxide oxygen, O_b=bridging oxide oxygen, O_c=ligand carboxylate oxygen).

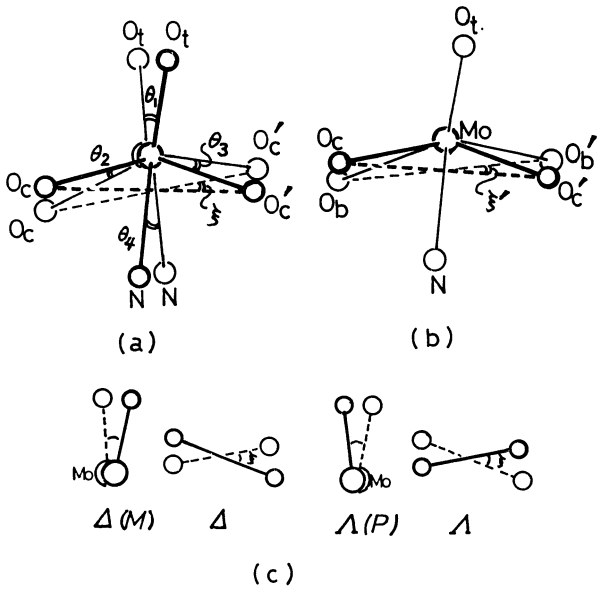

Fig. 4. (a) (b) The definition of torsion angles for $[Mo_2O_4(R\text{-pdta})]^{2-}$. ($O_t$, O_b, and O_c (O_c'), see legend of Fig. 3). (c) The definition of chirality used in this paper.

deviations from the mean plane of these four oxygen atoms. Such a distortion can be understood as a distortion of two basal edges, connecting two carboxylate oxygens, O_c and O_c', on a given molybdenum ion, and represented by the angle, ξ (Fig. 4a). These two basal edges give a skew arrangement, and the chirality of such a distortion can be expressed by the symbol, Δ or Λ.[34] The direction of the distortion of each Mo–ligand bond pair (Mo–O_t, Mo–O_c, Mo–O_c', and Mo–N) can be also expressed by use of Δ or Λ (Fig. 4c). Since the present asymmetry deals with 'conformation' of the two octahedrons of molybdenum(V) ions, δ and λ might be prefered to Δ and Λ. However, δ and λ are used for the conformation of ligand itself. Thus, the symbols, Δ and Λ, are tentatively used hereafter in this paper rather than P and M, since the latters are not always related to asymmetry. Table 2 lists the values of $|\theta_1|$, $|\theta_2|$, $|\theta_3|$, $|\theta_4|$, and $|\xi|$, and the 'chirality of the twist' for various doubly-bridged molybdenum(V) complexes containing optically active ligands. The angle ξ is closely related to θ_2 and θ_3, and is used hereafter as representing these angles.

The chirality of the twist of two Mo–O_t bonds (θ_1), and of the two basal edges (ξ), are the same for a given complex, except for $[Mo_2O_2S_2(S\text{-cys})_2]^{2-}$ and $[Mo_2O_2S_2(R\text{-pdta})]^{2-}$ whose ξ and θ_1, respectively, are negligibly small. It should be noted that the chirality of these twists of the bidentate *S*-cys ester complexes are different from those of the terdentate *S*-cys and *S*-hist complexes, despite of the same absolute configuration of these ligands themselves. The values of $|\xi|$ vary depending on the complex, and those for the *S*-cys ester complexes are considerably big as compared with those of the others. Variation in $|\theta_1|$ values is smaller. The chirality of the twist of two apical bonds (trans to terminal oxo bonds) is Δ for

the *R*-pdta complexes, and Λ for the *S*-cys and *S*-hist complexes, despite that the chirality of the twist of Mo–O_t bonds is Λ for all these complexes.

The asymmetries around each metal ion of the dimer are complicated by the highly distorted structure from the regular octahedron. The asymmetry of the basal plane involving two basal atoms and two bridging ligands may be most important, since the bond trans to Mo–O_t is longer than the others or fails to exist. Such asymmetry may be defined by the angle, ξ', in Fig. 4b. Under the definition the asymmetry around each metal ion of the dimer is considered similarly as that around the dimeric core defined by ξ. The five membered chelate rings at the basal edge form gauche like structure, whose absolute conformations are given in Table 2. The diamine part of *R*-pdta bridging the two apical sites of the $Mo_2O_2XY^{2+}$ core also form gauche like structure, whose absolute conformation is also given in Table 2.

There is no significant asymmetric spiral arrangement of more than two chelate rings in a given complex. No appreciable asymmetric distortion is seen within the $\begin{matrix}\diagup X \diagdown \\ Mo \quad Mo \\ \diagdown Y \diagup\end{matrix}$ core for all the complexes.

Medium Effects on the CD Spectra. The data of absorption and CD spectra of the di-μ-oxo complexes in various media are summarized in Table 3. The CD spectra in the region $<30000\ cm^{-1}$ for all the complexes are characterized by the strong peaks at *ca.* $26000\ cm^{-1}$. The CD pattern of a given complex in this region is very similar to one another regardless of the medium, although the peak in KBr disk shifts always to slightly lower wave number (Fig. 2). Such a similarity suggests that the basic skeletal structure of the complexes in crystals should be retained in the solutions; *i.e.* isomerization and ligand dissociation are not feasible upon dissolution, and the extent of donor atom distortion does not seem to change significantly. Similar conclusion was derived also for the μ-oxo-μ-thio and di-μ-thio complexes.

The CD spectrum of $[Mo_2O_4(S\text{-cys})_2]^{2-}$ in DMSO changed considerably as its concentration changed in less than 0.001 M solution. However, addition of free (*S*)-cysteine to the solution restored a pattern similar to that in solutions of higher complex concentration and that in DMF. Reversible ligand dissociation must take place in dilute DMSO solutions. A similar trend was observed also for $[Mo_2O_3S(S\text{-cys})_2]^{2-}$ in DMSO, but not for the other complexes in any of the solvents examined.

The CD spectrum of $[Mo_2O_4(S\text{-cys})_2]^{2-}$ in water is different from that in DMF in the region $>30000\ cm^{-1}$ (Fig. 2). Also the CD spectrum of $[Mo_2O_4(R\text{-pen})_2]^{2-}$ in water in the same region is significantly different from those in DMF and DMSO, the spectra in the latter two solvents being very similar to each other. Such a difference seems to be due to the difference in strength in the CD band at *ca.* $36000\ cm^{-1}$, the CD strength in DMF being *ca.* 5 times bigger than that in water. The origin of such a solvent effect is not certain. However, it is unlikely that the difference indicates the significant change in skeletal structure of the complex, since no significant change in the CD band in $26000\ cm^{-1}$ region, which is sensitive to the skeletal structure (*vide infra*), is observed. The CD spectra of two other *S*-cys complexes, $[Mo_2O_3S(S\text{-cys})_2]^{2-}$ and $[Mo_2O_2S_2(S\text{-cys})_2]^{2-}$, have similar patterns in water to those in the organic solvents. No significant change in CD spectra was observed for the *R*-pdta complexes in aqueous media and in DMF and DMSO.

The CD patterns of $[Mo_2O_4(S\text{-cys})_2]^{2-}$ and $[Mo_2O_4(R\text{-pen})_2]^{2-}$ are almost completely enantiomeric in a given solvent, suggesting that the replacement of two hydrogens with methyl groups at the adjacent carbon to $-S^-$ does not give significant influence on the CD spectrum.

The *S*-cys ester complexes have vacant apical sites (trans to terminal oxo), which might interact with solvent molecules. However, the solvent effects on the CD spectra of $[Mo_2O_4(S\text{-Rcys})_2]$ ($R=CH_3$, C_2H_5) is very small. No significant change was observed even in pyridine which has a strong donor ability. Probably the oxygen atoms of the ester ligands situate near the apical positions as in crystals,[10,13] to prevent the interaction of the solvent molecules.

The Nature of the Absorption Bands of the Di-μ-oxo Complexes. The $Mo_2O_4^{2+}$ complexes give different spectral patterns from those of the monomeric and single-bridged μ-oxo dimeric molybdenum(V) complexes.[5] The $Mo_2O_4^{2+}$ dimers are diamagnetic, indicating the interaction of the d-orbitals of the two metal ions.[5] The absorption spectrum of $[Mo_2O_4(R\text{-pdta})]^{2-}$ has two bands at 25800 and $33600\ cm^{-1}$, and a shoulder at *ca.* $20800\ cm^{-1}$ in water. Similar absorption patterns are observed for the complexes with the same core, $[Mo_2O_4(H_2O)_6]^{2+}$ (see Fig. 9),[29] $[Mo_2O_4(C_2O_4)_2(H_2O)_2]^{2-}$,[35] $[Mo_2O_4(edta)]^{2-}$,[36] and $[Mo_2O_4(hedta)(H_2O)]^-$,[37] where edta^{4-} and hedta^{3-} stand for ethylenediaminetetraacetate ion and *N*-(2-hydroxyethyl)ethylenediamine-*N*,*N*',*N*'-triacetate ion, respectively.

All the other complexes in this study also have absorption peaks at *ca.* $33000\ cm^{-1}$, but none in lower wave number region. However, they give CD bands in the region $<30000\ cm^{-1}$, suggesting the presence of electronic transitions of corresponding energies. The electronic transition energies of all the complexes can be estimated from either the absorption or the CD peaks, and are summarized in Table 3. Four common transitions are observed in the region from 12000 to $40000\ cm^{-1}$. The energies of these bands change only slightly from one complex to another. It is concluded that these transitions are mainly due to the $Mo_2O_4^{2+}$ core and to a much less extent to the variety of other ligands. Brown *et al.* calculated the electronic transition energies of $[Mo_2O_4(S\text{-cys})_2]^{2-}$ by the SCF-MO method and gave five transition energies, 13250, 20320, 27390, 30870, and $35700\ cm^{-1}$.[17] These transitions were claimed to involve the orbitals mainly located on the two molybdenum atoms, and hence common to other $Mo_2O_4^{2+}$ complexes.[17] The absorption and CD peaks at *ca.* $13250\ cm^{-1}$ should be very weak, if existed, since our results failed to indicate the transition at this wave number in <0.1 M aqueous solutions. The four transitions with the higher wave number

Table 3. The absorption (AB) and CD spectral data for of the di-μ-oxo-bis{oxomolybdenum(V)} complexes
(Wave number/10^3 cm^{-1}; absorption intensity ($\log \varepsilon$) and CD strength ($\Delta\varepsilon$) in parenthesis).[a,b]

Complex	Medium[c]	AB or CD	Band classification I	II	III	IV	V
$[Mo_2O_4(S\text{-cys})_2]^{2-}$	water	AB	21.0 s (2.31);		32.3 (4.03);		43.7 (4.05)
		CD	19.2 (+0.07);	26.1 (−12.2);	31.7 (+2.6);	36.0 (+3.1);	43.8 (+9.30)
	DMF	AB	21.0 s (2.25);	25.4 s (2.92);	32.0 (4.10);		— — — —
		CD	20.8 (−0.19); 22.6 (+0.3)	26.4 (−18.0);		36.0 (+17.9);	— — — —
	KBr	CD	20.0 (−) ; 21.8 (+)	25.5 (−)	— — — —	— — — —	— — — —
$[Mo_2O_4(R\text{-pen})_2]^{2-}$	water	AB	21.0 s (2.25);		32.2 (4.09);		44.4 (4.09)
		CD	18.6 (−0.07);	26.6 (+11.4);	31.9 (−4.4) ;	35.8 (−4.9);	43.6 (−11.7)
	DMF	AB			31.7 (4.06);		— — — —
	(DMSO)	CD	20.5 (+0.15); 22.4 (−0.29)	26.8 (+14.4);	30.0 s (−9.0) ;	36.0 (−22.0);	— — — —
$[Mo_2O_4(S\text{-hist})_2]$	DMSO	AB	21.1 s (1.87);	26.1 s (2.52);	33.0 (3.79);		— — — —
		CD	20.4 (+0.14);	26.9 (−3.0) ;	33.6 (+3.9);	38.0 (+7.3);	— — — —
	KBr	CD	20 (+) ;	26.7 (−)	— — — —	— — — —	— — — —
$[Mo_2O_4(S\text{-mecys})_2]$	AN	AB			34.0 s (3.95);	36.0 s (3.97);	45.5 (4.21)
		CD	22.3 (+0.85);	28.9 (+29.0);	34.4 (−22.0);	37.3 (+11.1);	40.5 (−4.20) 43.8 (+8.0) 46.9 (−9.2)
	DMF	AB	21.6 s (2.75);	29.2 s (3.48);	34.5 (3.94);		— — — —
		CD	22.4 (+1.42);	29.0 (+35.8);	34.0 (−22.0);	37.4 (+14.8);	— — — —
	KBr	CD	22.0 s (+) ;	27.5 (+) ;	32.6 (−) ;	— — — —	— — — —
$[Mo_2O_4(S\text{-etcys})_2]$	AN	AB		29.0 s (3.29);	34.2 s (3.95);	36.2 s (3.95);	45.0 s (4.20)
		CD	22.2 (+1.03);	28.8 (+30.5);	34.4 (−21.5);	37.4 (+10.2);	40.4 (−4.6) 44.0 (+10.0) 46.7 (−6.5)
	DMF	AB	22.1 s (2.18);	28.7 s (3.48);	34.4 (3.98);		— — — —
		CD	22.4 (+1.45);	29.0 (+36.2);	34.3 (−19.8);	37.6 (+12.5);	— — — —
	KBr	CD	22.5 s (+) ;	27.9 (+) ;	33.3 (−) ;	— — — —	— — — —
$[Mo_2O_4(R\text{-pdta})]^{2-}$	water	AB	20.8 s (2.00);	25.8 (2.60);	33.6 (4.00);		
		CD	20.8 s (−0.48);	26.0 (−5.5) ;	33.3 (+5.1) ;	37.1 (−1.6) ;	40.6 (+3.85) 45.2 (−5.10)
	DMF	AB		25.6 (2.60);	33.0 (3.99);		— — — —
		CD	20.6 (−0.38);	25.6 (−6.4) ;	32.8 (+5.7) ;		— — — —
	KBr	CD	19.8 (−) ;	25.2 (−) ;	31.8 (+) ;	35.9 (−) ;	— — — —

a) s indicates "shoulder". b) Dashed lines indicate the region where data cannot be obtained due to solvent absorption. c) DMF=*N*,*N*-dimethylformamide, DMSO=dimethyl sulfoxide, AN=acetonitrile, KBr=KBr disk.

must correspond to our four common transitions. These are denoted hereafter as band I, II, III, and IV from the low wave number (Table 3).

The band II of the two complexes containing the esters of *S*-cys are somewhat different from those of the other complexes: *i.e.* the position of the band is at a large wave number by nearly 3000 cm^{-1}, and the absorption strength is almost ten times of those of the other complexes. Such differences may be accounted for by the greater distortion of the *S*-cys ester complexes and the absence of apically ligating atoms. The nature of the band is not very different from those of the other complexes.[17]

Characteristics of the CD Spectra of the Di-μ-oxo Complexes. The CD data of the six $Mo_2O_4^{2+}$ complexes are listed in Table 3. The CD spectra in the band I region are weak in intensity and sensitive to the medium. There seems to be more than two components of electronic transitions, as judged from the CD spectra.

The CD sign of band II at *ca.* 26000 cm^{-1} are positive for $[Mo_2O_4(S\text{-mecys})_2]$, $[Mo_2O_4(S\text{-etcys})_2]$, and $[Mo_2O_4(R\text{-pen})_2]^{2-}$, and negative for the others. The CD pattern of this band is least affected by the medium. The $\Delta\varepsilon/\varepsilon$ value of this band is the biggest among those of the four transitions; *i.e.* the values are larger than those of the other bands by five to ten times except for the *S*-cys ester complexes. Therefore the band II should be the most important in considering the optical activity of the complexes. The CD signs at band III are always opposite to those at band II. Hence, the asymmetric source for these two transitions can be common.

No absorption peak is observed at band IV region, but one CD band is always observed. The CD sign of the band IV does not related to those of band II and III. In higher wave number region than 40000 cm^{-1}, a few absorption and CD peaks are observed, but the CD patterns are complicated. No further discussion is made in this study.

Relation between the CD Sign and the Structure of Di-μ-oxo Complexes. Comparison of the CD data in Table 3 with the structural data in Table 2 of three $Mo_2O_4^{2+}$ complexes, leads to the following findings.

The CD signs of the band II and III are related to the chirality of the twist of two Mo–O_t bonds (angle θ_1) and of the twist of the two basal edges (angle ξ). The negative and positive CD peaks at the band II and III regions, respectively, for the *S*-cys and *R*-pdta complexes reflect the Δ chirality of these twists, while the reverse CD signs for the *S*-etcys complex are related to the Λ chirality. It should be noted that the relationship is found for the three complexes which have different ligand environments. Such a relationship for the important band II transition suggests that the distortion around the Mo–Mo axis difined by the torsion angles, θ_1, θ_2, θ_3, and ξ, must be the most important asymmetric source of $Mo_2O_4^{2+}$ complexes.

The CD sign at band IV seems to be related to the absolute configuration of the ligand itself; *i.e.* positive CD peaks for the *S*-cys, *S*-hist, *S*-mecys, and *S*-etcys complexes, and negative CD peaks for the *R*-pdta and *R*-pen complexes. The CD sign at band IV seems to be also related to the conformation of the five membered chelate ring; *i.e.* positive and negative CD peaks corresponding to δ and λ conformations (Table 2), respectively. However, these relations concerning the band IV should be taken as tentative, since the location of relevant asymmetric centers in the molecules are different between the *R*-pdta complex and the others.

The twist of the two bonds trans to Mo–O_t (apical bond) would not be important in determining the CD patterns. These bonds are considerably longer, if existed, than the other bonds and would not give significant influence on the electronic transitions of the $Mo_2O_4^{2+}$ moiety. The asymmetry around each metal ion of the dimer represented by the torsion angle ξ', is parallel to the distortion of the dimer represented by ξ, and thus can also explain the CD signs of band II and III. However, such an explanation is less attractive since the nature of the absorption bands are now assigned to involve the transitions within the dimeric core rather than those within the orbitals of one metal ion.

Absorption and CD Spectra of the μ-Oxo-μ-thio and the Di-μ-thio Complexes. The absorption and CD spectra of $Mo_2O_4^{2+}$, $Mo_2O_3S^{2+}$, and $Mo_2O_2S_2^{2+}$ complexes containing *S*-cys, *S*-mecys, *S*-hist, and *R*-pdta are compared with one another in Figs. 5—8. Absorption spectra of $[Mo_2O_2XY(H_2O)_6]^{2+}$ are shown in Fig. 9. The numerical data of the μ-oxo-μ-thio and di-μ-thio complexes are summarized in Table 4 and 5, respectively.

General Features: The most characteristic feature of the absorption spectra is the remarkable increase in absorption intensity with increase in the number of bridging sulfide in the band II region (*ca.* 26000 cm^{-1}) except for the *S*-mecys complexes. The change in

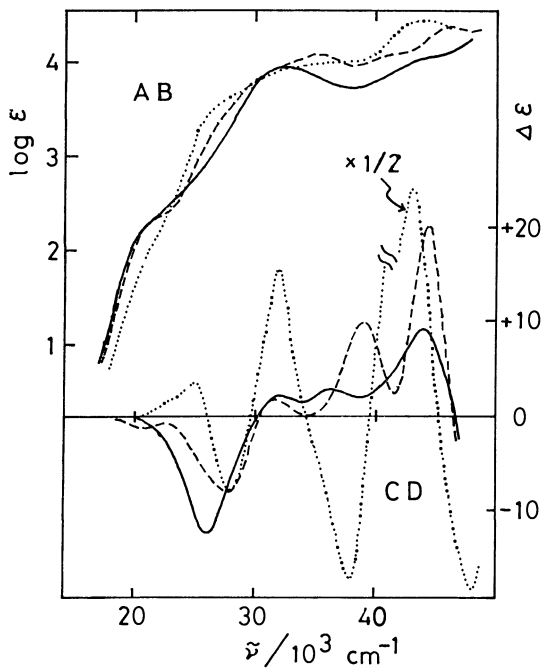

Fig. 5. Absorption (AB) and CD spectra of $[Mo_2O_2XY(S\text{-cys})_2]^{2-}$ in water; X=Y=O (——), X=O and Y=S (----), and X=Y=S (·····).

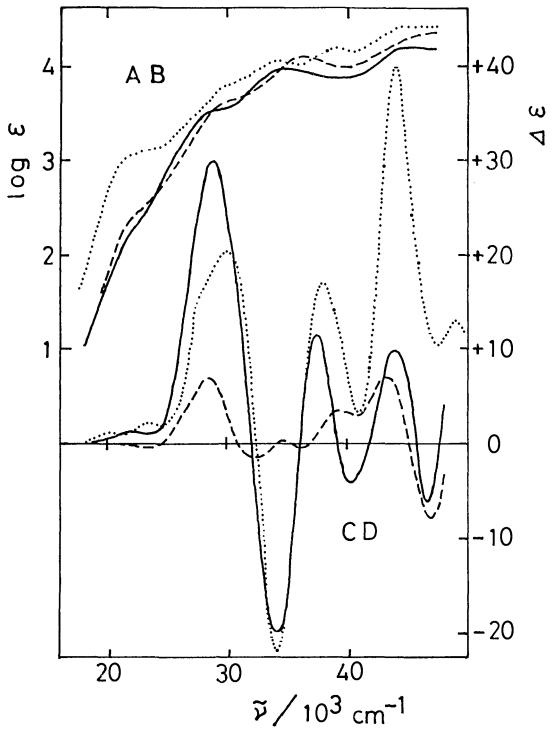

Fig. 6. Absorption (AB) and CD spectra of $[Mo_2O_2XY(S\text{-mecys})_2]$ in acetonitrile; X=Y=O (——), X=O and Y=S (----), and X=Y=S (·····).

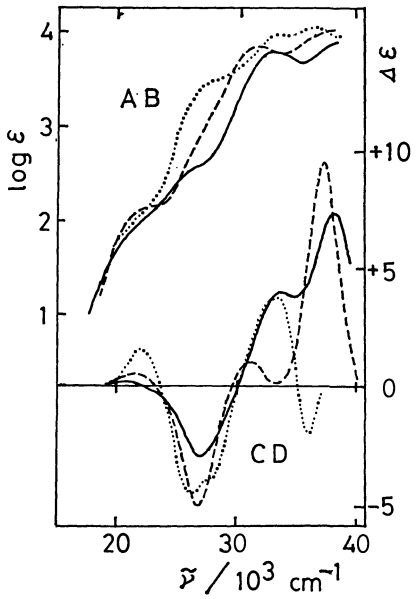

Fig. 7. Absorption (AB) and CD spectra of $[Mo_2O_2XY(S\text{-hist})_2]$ in DMSO; X=Y=O (——), X=O and Y=S (----), and X=Y=S (·····).

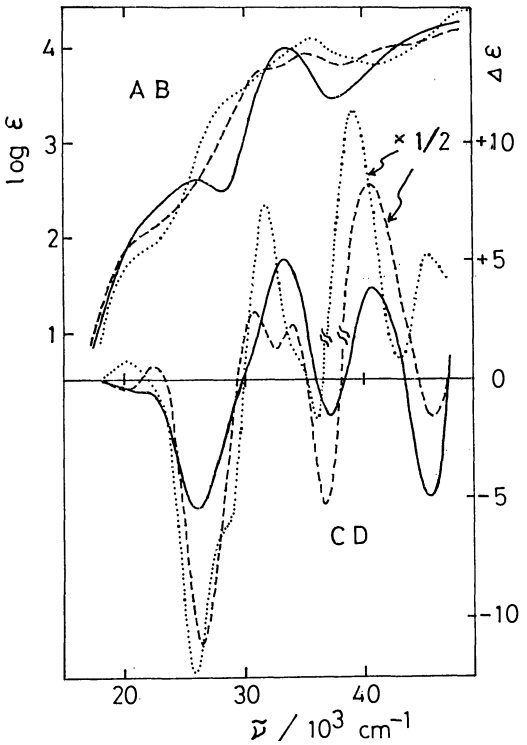

Fig. 8. Absorption (AB) and CD spectra of $[Mo_2O_2XY(R\text{-pdta})]^{2-}$ in water; X=Y=O (——), X=O and Y=S (----) and, X=Y=S (·····).

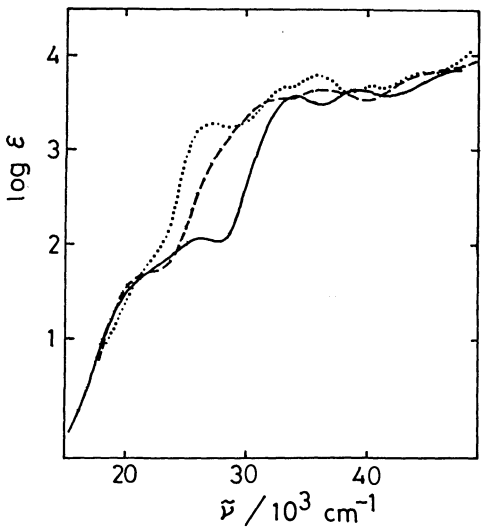

Fig. 9. Absorption spectra of $[Mo_2O_2XY(H_2O)_6]^{2+}$ in 2 M aqueous perchloric acid solution; X=Y=O (——), X=O and Y=S (----), and X=Y=S (·····).

CD spectra with change in the bridging group is rather modest in the band II and III region (25000—35000 cm^{-1}). The general pattern for the di-μ-oxo complexes (two distinctive CD bands with opposite signs) is also appreciated for the μ-oxo-μ-thio and di-μ-thio complexes. Such facts suggest that the nature of CD sensitive transitions at the band II and III region is common to all the complexes, regardless of the bridging groups. The difference in absorption spectra at the band II region is interpreted by the appearance of a strong new band which is less sensitive to CD, in the μ-thio complexes.

The following interpretations for the increase in absorption intensity at band II region, are not feasible, since the corresponding CD change is not accompanied; *i.e.* a) the intensity of 'band II' itself increased, and b) the 'band III' shifted its position to the band II region as the number of sulfide bridge increased.

Table 4. The numerical data of absorption (AB) and CD spectra of the μ-oxo-μ-thio-bis{oxomolybdenum(V)} complexes[a)]

Complex (solvent)	AB $\lambda/10^3$ cm^{-1} (log ε)	CD[b)] $\lambda/10^3$ cm^{-1} ($\Delta\varepsilon$)	
$[Mo_2O_3S(S\text{-cys})_2]^{2-}$ (water)	21.5 s (2.35)	21.0 (−1.10)	
	30.5 s (3.92)	27.7 (−8.00)*	
	35.0 (4.12)	31.7 (+2.19)*	
	41.0 s (4.10)	39.0 (+10.3)	
	46.3 (4.40)	44.3 (+20.1)	
$[Mo_2O_3S(S\text{-hist})_2]$ (DMF)	22.4 s (2.13)	21.7 (+0.18)	31.6 (+2.6)*
	31.4 (3.85)	26.9 (−3.8)*	
$[Mo_2O_3S(S\text{-mecys})_2]$ (acetonitrile)	23.0 s (2.50)	23.5 (−0.41)	36.2 (−0.3)
	30.0 s (3.63)	28.6 (+6.9)*	39.4 (+3.4)
	36.4 (4.10)	32.2 (−1.5)	43.3 (+7.0)
		34.8 (+0.2)	46.8 (−7.9)
$[Mo_2O_3S(S\text{-etcys})_2]$ (acetonitrile)	23.4 s (2.63)	23.4 (−0.42)	36.2 (−0.2)
	29.4 s (3.55)	28.6 (+6.7)*	39.4 (+3.4)
	36.2 (4.09)	32.0 (−1.9)	43.5 (+6.7)
	47.2 (4.34)	34.7 (+0.4)	47.0 (−7.7)
$[Mo_2O_3S(R\text{-pdta})]^{2-}$ (water)	21.6 s (2.05)	20.1 (−0.45)	34.0 (+2.2)
	32.0 s (3.77)	22.5 (+0.51)	36.5 (−5.4)
	35.3 (3.93)	26.1 (−11.1)*	40.7(+16.4)
	43.2 s (4.00)	30.8 (+2.8)*	45.5 (−3.5)

a) Data in only one solvent are given. Those in other solvents show similar values. b) Asterisk indicates the band which is assigned to have common nature to band II or III of the corresponding di-μ-oxo complex.

Table 5. The numerical data of absorption (AB) and CD spectra of the di-μ-thio-bis{oxomolybdenum(V)} complexes[a)]

Complex (solvent)	AB $\lambda/10^3$ cm^{-1} (log ε)	CD[b)] $\lambda/10^3$ cm^{-1} ($\Delta\varepsilon$)	
$[Mo_2O_2S_2(S\text{-cys})_2]^{2-}$ (water)	21.0 s (2.00)	19.3 (−0.04)	42.9 (+48.2)
	26.3 s (3.53)	25.0 (+3.95)	47.6 (−36.9)
	32.0 s (3.96)	27.8 (−7.88)*	
	35.8 (4.25)	31.5 (+15.7)*	
	43.7 (4.47)	37.8 (−16.8)	
$[Mo_2O_2S_2(S\text{-hist})_2]$ (DMSO)	22.2 s (2.13)	22.1 (+1.49)	36.0 (−2.02)
	27.4 s (3.40)	26.3 (−4.63)	
	33.6 (3.97)	28.2 s (−3.75)*	
	36.2 (4.03)	33.3 (+3.66)*	
$[Mo_2O_2S_2(S\text{-mecys})_2]$ (acetonitrile)	22.9 s (3.11)	17.0 (−0.05)	34.2 (−22.1)*
	30.5 s (3.84)	20.2 (+1.08)	38.0 (+17.0)
	34.3 (4.09)	23.6 (+2.18)	44.0 (+40.0)
	39.1 (4.20)	28.2 s (+17.2)*	49.1 (+13.2)
	45.1 s (4.44)	30.1 (+20.4)	
$[Mo_2O_2S_2(R\text{-pdta})]^{2-}$ (water)	21.0 s (1.82)	20.2 (+0.78)	36.0 (−1.8)
	28.6 s (3.62)	25.6 (−12.3)*	39.1 (+22.5)
	35.8 (4.08)	28.0 s (−6.4)	45.2 (+10.5)
	38.8 s (3.88)	31.7 (+7.4)*	
	48.4 (4.37)	34.4 s (+0.85)	

a) Data in only one solvent are given. Those in other solvents show similar values. b) Asterisk indicates the band which is assigned to have common nature to band II or III of the corresponding di-μ-oxo complex.

The absorption and CD spectra in the other regions (band I, IV, and V regions) do not show any systematic trend, the number and the energies of absorption or CD bands depending on the bridging structure and the ligand. The *S*-mecys complex gives only slight increase in absorption intensity with increase in the number of bridging sulfide in the band II region. However, the absorption intensity of the di-μ-thio *S*-mecys complex in the band I region is more than five times bigger than those of di-μ-oxo and μ-oxo-μ-thio *S*-mecys complexes.

Ott *et al.* claimed on the basis of absorption spectra that the absorption bands I—IV shift to higher wave number with increase in the number of sulfide bridge. However, the CD spectra do not conform with such a trend.

Band II Region: The CD bands for all the di-μ-thio complexes split into two components. They have opposite signs for the *S*-cys complex, and the same sign for the other complexes. The splitting is accounted for by the appearance of a new band. A comparison of the absorption spectra with the CD

spectra suggests that the CD component corresponding to the new band is the higher and lower wave number component for the *S*-cys and *S*-hist complexes, and for the *S*-mecys and *R*-pdta complexes, respectively. It is seen that the 'band II' not only remains at almost the same position as that for the di-μ-oxo complexes, but also keeps its sign unchanged, regardless of the change in bridging ligand. The new band has much smaller $\Delta\varepsilon/\varepsilon$ than the 'band II' does.

Band III Region: The CD peaks of μ-oxo-μ-thio and di-μ-thio complexes have same sign as those of the di-μ-oxo complexes, except for $[Mo_2O_3S(S\text{-etcys})_2]$ and $[Mo_2O_3S(S\text{-mecys})_2]$ which have no strong CD band in this region. Asymmetric distortion related to the CD strength at this region would be small for the μ-oxo-μ-thio *S*-cys ester complexes.

Relation between the CD Sign and the Structure of the μ-Thio Complexes. The CD bands with common nature to those of the di-μ-oxo complexes in band II and III region, are indicated with asterisks in Table 4 and 5. The same relation to that found for the di-μ-oxo complexes is also found for the μ-thio complexes. The negative and positive CD peaks for the 'band II' and 'band III', respectively, reflect the Δ chirality of the twist of two Mo–O_t bonds and of two basal edges, and the reverse CD patterns are related to Λ chirality of these twists. The relation is thus established for all the complexes regardless of the bridging structure, di-μ-oxo, μ-oxo-μ-thio and di-μ-thio.

Table 2 shows that $|\xi|$ values are much bigger than the $|\theta_1|$ values for most of the complexes. However, the ξ values for the di-μ-oxo and di-μ-thio cys complexes are nearly zero, and thus the twist of the two Mo–O_t bonds must be important in determining CD sign. On the other hand, the θ_1 values of μ-oxo-μ-thio and di-μ-thio complexes of *R*-pdta are practically zero. The donor atom distortion of the basal plane should be important for them. Intensity of the CD peaks of these complexes are not very different. These facts tell that neither the twist of Mo–O_t bonds nor the tetrahedral distortion of the basal plane alone can be the controlling factor of the CD sign at band II and III region. The CD sign must reflect the overall asymmetry caused by the twist of the two molybdenum coordination spheres around the Mo–Mo axis.

The present work was supported by a Grant-in-Aid for Science Research from the Ministry of Education, Science and Culture.

References

1) M. Ito, F. Marumo, and Y. Saito, *Acta Crystallogr., Ser. B.*, **27**, 2187 (1971).
2) F. S. Richardson, *Chem. Rev.*, **79**, 17 (1979), and references cited therein.
3) B. Bosnich and J. MacB. Harrowfield, *J. Am. Chem. Soc.*, **94**, 3425 (1972).
4) For example, a) R. M. Wing and R. Weiss, *J. Am. Chem. Soc.*, **92**, 1929 (1970); b) N. C. Payne, *Inorg. Chem.*, **12**, 1151 (1973); c) A. Pasini, M. Gullotti, and R. Ugo, *J. Chem. Soc., Dalton Trans.*, **1977**, 346.
5) E. I. Stiefel, *Progr. Inorg. Chem.*, **22**, 1 (1976), and references cited therein.
6) B. Spivack and Z. Dori, *Coord. Chem. Rev.*, **17**, 99 (1975), and references cited therein.
7) For recent examples, a) J. I. Gelder and J. H. Enemark, *Inorg. Chem.*, **15**, 1839 (1976); b) R. Mattes and G. Lux, *Z. Anorg. Allg. Chem.*, **424**, 173 (1976); c) B. M. Gatehouse, E. K. Nunn, J. E. Guerchais, and R. Kergoat, *Inorg. Nucl. Chem. Lett.*, **12**, 23 (1976); d) J. Dirand-Colin, M. Schappacher, L. Richard, and R. Weiss, *J. Less-Common Met.*, **54**, 91 (1977); e) B. Jezowska-Trzebiatowska, T. Glowiak, M. F. Rudolf, M. Sabat, and J. Sabat, *Russ. J. Inorg. Chem.*, **22**, 1590 (1977); f) I. G. Dance, A. G. Wedd, and I. W. Boyd, *Aust. J. Chem.*, **31**, 519 (1978); g) N. Kim, S. Kim, P. A. Vella, and J. Zubieta, *Inorg. Nucl. Chem. Lett.*, **14**, 457 (1978).
8) J. R. Knox and C. K. Prout, *Acta Crystallogr., Sect. B.*, **25**, 1857 (1969).
9) L. T. J. Delbaere and C. K. Prout, *J. Chem. Soc., Chem. Commun.*, **1971**, 162.
10) M. G. B. Drew and A. Kay, *J. Chem. Soc., A*, **1971**, 1846.
11) D. H. Brown and J. A. D. Jeffereys, *J. Chem. Soc., Dalton Trans.*, **1973**, 732.
12) B. Spivack, A. P. Gaughan, and Z. Dori, *J. Am. Chem. Soc.*, **93**, 5266 (1971).
13) M. G. B. Drew and A. Kay, *J. Chem. Soc., A*, **1971**, 1851.
14) R. M. Wing and K. P. Callahan, *Inorg. Chem.*, **8**, 2302 (1969).
15) A. Kojima, S. Ooi, Y. Sasaki, K. Z. Suzuki, and K. Saito, unpublished results.
16) D. H. Brown and J. McPherson, *J. Inorg. Nucl. Chem.*, **32**, 3309 (1970); **33**, 4203 (1971); **34**, 1705 (1972), and references cited therein.
17) D. H. Brown, P. G. Perkins, and J. J. Stewart, *J. Chem. Soc., Dalton Trans.*, **1972**, 1105.
18) D. H. Brown and P. G. Perkins, *Rev. Roum. Chim.*, **20**, 515 (1975).
19) A. Kay and P. C. H. Mitchell, *J. Chem. Soc., A*, **1970**, 2422.
20) L. R. Melby, *Inorg. Chem.*, **8**, 1539 (1969).
21) L. R. Melby, *Inorg. Chem.*, **8**, 349 (1969).
22) The complex was reported as an anhydrous salt, but we obtained a trihydrate which was confirmed by X-ray structural determination.[18]
23) V. R. Ott, D. S. Swieter, and F. A. Schultz, *Inorg. Chem.*, **16**, 2538 (1977).
24) B. Spivack and Z. Dori, *J. Chem. Soc., Chem. Commun.*, **1970**, 1716.
25) N. Ueyama, M. Nakata, T. Araki, A. Nakamura, S. Yamashita, and T. Yamashita, *Chem. Lett.*, **1979**, 421.
26) a) J. L. Corbin, N. Pariyadath, and E. I. Stiefel, *J. Am. Chem. Soc.*, **98**, 7862 (1976); b) V. Srinivasan, E. I. Stiefel, A. Ebsberry, and R. A. Walton, *J. Am. Chem. Soc.*, **101**, 2611 (1979).
27) F. P. Dwyer and F. L. Garvan, *J. Am. Chem. Soc.*, **81**, 2955 (1959).
28) The number of coordinated water, 6, is tentative, since the coordination of water at apical sites is not clarified.
29) M. Ardon and A. Pernick, *Inorg. Chem.*, **12**, 2484 (1973).
30) B. Spivack and Z. Dori, *J. Chem. Soc., Chem. Commun.*, **1973**, 909.
31) L. V. Haynes and D. T. Sawyer, *Inorg. Chem.*, **6**, 2146 (1967).
32) G. L. Blackmer, K. J. Johnson, and R. L. Roberts, *Inorg. Chem.*, **15**, 596 (1976).

33) IUPAC 1974 Recommendation for Section E, Fundamental Stereochemistry.
34) *Inorg. Chem.*, **9**, 1 (1970). The symbols, Δ and Λ, were suggested to be used for defining the asymmetry expressed by the two helically arranged lines. The original definition was extended to be applied to the present system. There seems to be no autherized rules for expressing the present asymmetries. However, new symbols $\tau(+)$ and $\tau(-)$ were suggested by private communication from Professor S. F. Mason. These symbols are related to the torsion angle (*e.g.* θ_1 in Fig. 4) and correspond to Λ and Δ, respectively, in the present system.
35) W. P. Griffith, *J. Chem. Soc., A*, **1969**, 211.
36) Y. Sasaki and A. G. Sykes, *J. Chem. Soc., Dalton Trans.*, **1974**, 1048.
37) Y. Sasaki and T. S. Morita, *Bull. Chem. Soc. Jpn.*, **50**, 1637 (1977).

Preparation of Copper(I)–Phosphine Complexes Having Cu–N Bonds and Their Reactions with Organic Halides

Takakazu YAMAMOTO,* Yoshio EHARA, Minoru KUBOTA, and Akio YAMAMOTO*

Research Laboratory of Resources Utilization, Tokyo Institute of Technology, 4259 Nagatsuta, Midori-ku, Yokohama 227

(Received September 7, 1979)

Reactions of a methylcopper complex $CH_3Cu(PPh_3)_2$(diethyl ether)$_{0.5}$ (PPh_3=triphenylphosphine) with active N–H compounds HNR^1R^2 give the corresponding copper derivatives formulated as $R^1R^2NCu(PPh_3)_n$ (n=2 for R^1R^2N=phthalimido, succinimido, *N*-phenylacetamido (**4**), acrylamido, phenylamido, and 2-oxo-1-pyrrolidinyl; n=1 for R^1R^2N=acetamido). The IR and NMR spectroscopic data of the complexes support the bonding of the R^1R^2N group to Cu through nitrogen. The reactions of the Cu(I)–N complexes with alkyl and aryl halides (RX) afford the corresponding *N*-substituted compounds RNR^1R^2 in high yields.

Copper and its compounds have been utilized as reagents or catalysts for various organic synthetic reactions such as the Ullmann reaction, Gattermann-Koch reaction, and Sandmeyer reaction.[1] Although some of the copper-promoted reactions are considered to proceed through the formation of intermediates having Cu–C, Cu–O, or Cu–N bonds, details of the mechanism of the reactions are still vague since chemistry of compounds having Cu–C, Cu–O, or Cu–N bonds has not developed sufficiently. In order to get detailed information concerning the copper-promoted synthetic reactions as well as to develop new copper-promoted synthetic reactions we have prepared Cu(I) complexes having Cu–C,[2] Cu–O,[3] or Cu–S[4] bonds and investigated chemical properties of these complexes. We wish to report on the preparation and properties of Cu(I) complexes having Cu–N bonds. In contrast to bivalent copper complexes for which imido complexes[5a–5b] are known since 1905 and the presence of Cu–N covalent bonds in the complexes has been established in some cases by X-ray crystallography,[5b] only a few reports[6] have appeared on the preparation of univalent Cu–N complexes, including *in situ* preparation[6b,6c] of complexes from CuX and R^1R^2NLi. Concerning other transition metal such as Ti, V, and Mo a number of NH_2– or dialkyl- (or diaryl)amido complexes have been prepared and the presence of metal–N covalent bonds has been demonstrated by X-ray crystallography.[7]

Results and Discussion

Preparation of Complexes. A methylcopper(I) complex $CuCH_3(PPh_3)_2$(diethyl ether)$_{0.5}$ **1**, convenient starting material reacting with active hydrogen compounds,[3,8] reacts smoothly at −20 to 0 °C with compounds having active N–H bond including phthalimide, succinimide, acetanilide, acrylamide, acetamide, aniline, and γ-butyrolactam to give complexes having Cu–N bonds with evolution of one equivalent of methane:

$$CH_3Cu(PPh_3)_2(Et_2O)_{0.5} + HNR^1R^2 \rightarrow \underset{\mathbf{1}}{}$$

$$Cu(NR^1R^2)(PPh_3)_n + CH_4 + 0.5\,Et_2O \qquad (1)$$

2—**8** n=1, 2

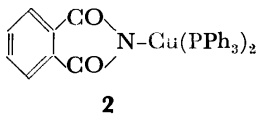

2

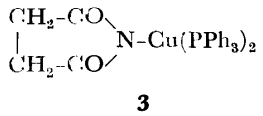

3

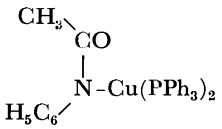

4

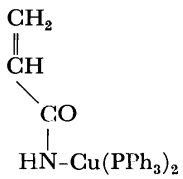

5

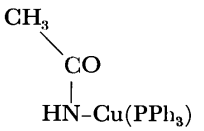

6

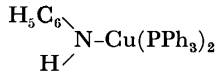

7

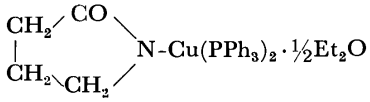

8

Generally the reaction with a compound having a more acidic N–H proceeds at a greater rate; the reaction with phthalimide takes only 10 min for completion, that with aniline taking *ca.* 10 h. Compounds with less acidic N–H such as $HN(C_2H_5)_2$ do not react with the methylcopper complex.

Physical properties and analytical data of the complexes are summarized in Table 1. Although most complexes are white, **7** is yellow, showing luminescence sometimes observed in Cu(I) compounds.[9] The complexes have high thermal stability but undergo gradual decomposition on exposure to the air, the decomposition proceeding much faster in solutions. The low electric conductivity of **2** in acetone excludes the possibility of an ionic structure such as $[Cu(PPh_3)_2]^+[N(CO)_2C_6H_4]^-$, suggesting that the imido group is covalently bonded to copper. The phthalimido–copper(I) complex **2** was found to be most stable. It could be prepared also by exchange reactions starting from $ROCu(PPh_3)_n$[3] or from other complexes **3**—**8** by treatment with 1 equiv of phthalimide to liberate ROH or R^1R^2NH. The number of the triphenylphosphine coordinated to copper can be controlled by the relative acidity of the amido or imido moiety as well as by steric factors. In the more acidic phthalimido (pK_a

TABLE 1. ANALYTICAL DATA OF Cu(I)-N COMPLEXES WITH PPh_3 LIGAND(S)

Complex	Color	Dp.[a] °C	Analysis Found (Calcd), %			
			C	H	N	Cu
2	light green	156—7	72.1 (72.0)	4.6 (4.7)	1.8 (1.9)	8.6 (8.7)
3	white	242—5	70.4 (70.0)	5.3 (5.0)	2.3 (2.0)	
4	white	151	72.7 (73.2)	5.5 (5.3)	2.3 (1.9)	
5	white	83—85	71.2 (71.2)	5.2 (5.2)	2.0 (2.1)	
6	white	172	62.1 (62.5)	5.1 (5.0)	3.8 (3.7)	15.7 (16.6)
7	yellow	69—70	73.8 (74.2)	4.9 (5.3)	2.0 (2.1)	
8	white	110	70.3 (71.1)	5.4 (5.8)	2.1 (2.0)	9.1 (9.0)

a) Decomposition point measured in glass capillaries.

TABLE 2. IR AND NMR SPECTROSCOPIC DATA OF THE Cu(I)-N COMPLEXES WITH PPh_3 LIGAND(S)

Complex	IR (ν/cm^{-1})[a]			^{1}H-NMR (δ/ppm)[b]
	ν(N-H)	ν(C=O)	$\Delta\nu$(C=O)[c]	
2		1650	100	7.4(PPh_3 and $-N(CO)_2C_6H_4$)
3		1610	110	2.44(s, 4H, CH_2), 7.4(m, 30H, PPh_3)
4		1685	−15	2.16(s, 3H), 7.0(m, 23H, *m*, *p*-H of PPh_3 and $C_6\underline{H}_5$-N), 7.6(m, 12H, *o*-H of PPh_3)
5	3270	1640[d] 1540[e]	50[f]	5.2(m, 1H, =CH), 6.1(m, 2H, $=CH_2$), 7.0(m, 19H, *p*-H of PPh_3 and NH), 7.7(m, 12H, *o*-H of PPh_3)
6	3450	1590[d] 1550[e]	80[f]	1.78(s, 3H, CH_3), 7.3(m, 16H, PPh_3 and NH)
7	3400			6.9(m, 5H, C_6H_5-N), 7.0(m, 19H, *m*, *p*-H of PPh_3 and NH), 7.6(m, 12H, *o*-H of PPh_3)
8		1590	100	1.60(q, 8 Hz, 2H, CH_2-$C\underline{H}_2$-CH_2), 2.00(t, 8 Hz, 2H, -CO-$C\underline{H}_2$-), 3.15(t, 7 Hz, 2H, -N-$C\underline{H}_2$-), 7.0(*o*, *p*-H of PPh_3), 7.5(*m*-H of PPh_3)

a) In KBr disk. b) Solvent: C_6D_6 for **3**, **4**, **5**, and **7**; $CDCl_3$ for **2**; CD_2Cl_2 for **6**; toluene-d_8 for **8**. c) $\Delta\nu$-(C=O)=ν(C=O)$_{free}$−ν(C=O)$_{complex}$. d) Amide I; e) Amide II.[13] f) Average of shifts in amide I and amide II bands.

of phthalimido=9.6) and succinimido (pK_a of succinimido=10.5) copper complexes two triphenylphosphine ligands are bonded, while the acetamido (pK_a of acetamido=16) complex contains one triphenylphosphine ligand. The complex containing 2-oxo-1-pyrrolidinyl moiety seems to be situated in the intermediate region; the complex initially formed (complex **8**) has a composition containing two triphenylphosphine ligands. Recrystallization of **8** from toluene gave a complex having one triphenylphosphine ligand based on elemental analysis and NMR data. The value for the carbon content of **8** somewhat lower than the calculated one might be due to the partial dissociation of PPh_3. The triphenylphosphine ligands contained in other bis(triphenylphosphine) complexes are held more firmly.

IR and NMR data of the complexes are summarized in Table 2. The ν(C=C) bands of amides and imides, except for acetanilide, are shifted to lower frequency by 50—110 cm^{-1} on complex formation. The lowering of ν(C=O) frequencies is accounted for by assuming the mixing of the following cannonical structure I and II in the ground state:

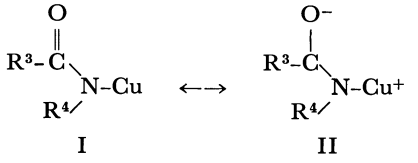

I II

In the cases of phthalimide and succinimide the magnitudes of the shifts are comparable to those observed with Pd and Pt imido complexes which have metal–N

σ-bonds.[10] In contrast to these amido and imido–copper complexes the IR spectrum of the *N*-phenylacetamido complex **4** was somewhat different, the ν(C=O) band being slightly shifted to higher frequency than that of the free acetanilide on complex formation. The reason for this is not clear. However, the IR spectrum may be accounted for by assuming the π-azaallylic type bonding between the *N*-phenyl entity and copper as in benzyl–transition metal complexes.[11]

The NMR spectrum of the succinimido complex **3** shows only one sharp singlet for the CH_2 groups, indicating that the two CH_2 groups are magnetically equivalent in line with the bonding of the succinimido ligand to Cu through nitrogen. The aliphatic C–H signals neighboring the amido group (CH_2 of succinimide, CH_3 of acetamide, and $-NC\underline{H}_2-$ and $-COC\underline{H}_2-$ of γ-butyrolactam) are shifted to higher field by 0.3—0.4 ppm on complex formation. This can be accounted for by the electron migration from Cu to the amido or imido ligands from the discussion on the IR spectra. The electron migration would decrease the an anisotropic paramagnetic effect of the C=O group and increase the diamagnetic shielding of atoms around the –NHCO– bond. A similar upfield shift by 0.4 ppm is observed for α-olefinic hydrogens of acrylamide. In contrast to these amido or imido ligands, no shift of the CH_3 signal in *N*-phenylacetamido is observed on complex formation beyond experimental error. This may be related to the unusual small shift of ν(C=O) to higher frequencies on complex formation.

Reactions with Organic Halides. Reactions of the Cu(I)–N complexes with alkyl or aryl halides lead to the substitution of Cu by the alkyl or aryl group, rendering further evidence for the bonding of the NR^1R^2 moiety to copper through nitrogen:

$$(PPh_3)_nCu\text{-}N\begin{matrix}R^1\\R^2\end{matrix} + RX \rightarrow R\text{-}N\begin{matrix}R^1\\R^2\end{matrix} \quad (2)$$

Results of the reactions are summarized in Table 3. The absence of *O*-substituted products excludes the possibility of a structure in which copper is bonded to an oxygen in an enolate form. In the reactions of **2** with aryl halides the yields depend drastically on temperature. For example, the reaction with C_6H_5Br(bp=155 °C) at 140 °C gives only a low yield, whereas that with C_6H_5I(bp=188 °C) or in diglyme (bp=186 °C) at 170 °C gives higher yields. Copper or its compounds are good catalysts for arylation of potassium phthalimide by aryl halides at 155—165 °C, the catalytic reaction being utilized to synthesize aromatic amines.[12] Occurrence of the arylation of **2** with aryl halides gives support to the proposed mechanism[12] involving the formation of a copper phthalimide intermediate during the course of the catalytic reaction.

Reactions of the Cu(I)–N complexes with alkyl halides proceed at much lower temperatures. Complex **2** affords *N*-alkylated phthalimides in almost quantitative yields under mild conditions. Acetyl chloride reacts with **7** to give acetanilide. The same product was obtained also by the reaction of **7** with $(CH_3CO)_2O$ in a 89% yield:

$$\mathbf{7} + CH_3COCl \text{ (or } (CH_3CO)_2O) \rightarrow \underset{89\text{—}92\%}{C_6H_5NHCOCH_3} \quad (3)$$

Experimental

General. Preparation and recrystallization of copper complexes were carried out under deoxygenated nitrogen or argon or in a vacuum. IR spectra were recorded on a Hitachi Model 295 using KBr discs under nitrogen, NMR spectra on a Japan Electron Optics Lab. JNM-PS-100 spectrometer (TMS as an internal standard). The gas evolved was analyzed with a Hitachi RMU 5B mass-spectrometer and a Shimadzu GC-5B gas chromatograph, its volume being measured with a Toepler pump. Microanalysis of carbon, hydrogen and nitrogen was performed by Mr. T. Saito in our laboratory with a Yanagimoto CHN Autocorder Type MT-2.

Material. $CH_3Cu(PPh_3)_2$(diethyl ether)$_{0.5}$ **1** was prepared as reported previously.[2] Solvents were dried by the usual procedure, distilled, and stored under argon or nitrogen. The N–H compounds were confirmed to be pure by gas chromatography.

Preparation of the Cu(I)–N Complexes. *N-Phthalimido-bis(triphenylphosphine)copper(I)* **2**: Diethyl ether (15 cm^3) was

Table 3. Reactions of thd Cu(I)-N complexes with organic halides[a]

Complex	Organic halide	Solv.	T/°C	t/h	Product (% yield/Cu)
2	*p*-$CH_3OC_6H_4Br$	diglyme	170	6	*p*-$CH_3OC_6H_4N(CO)_2C_6H_4$ 84
2	*p*-$CH_3C_6H_4Br$	diglyme	170	6	*p*-$CH_3C_6H_4N(CO)_2C_6H_4$ 48
2	C_6H_5Br	diglyme	170	6	$C_6H_5N(CO)_2C_6H_4$ 64
2	C_6H_5Br	none	140	0.7	$C_6H_5N(CO)_2C_6H_4$ 4
2	C_6H_5I	none	170	1.5	$C_6H_5N(CO)_2C_6H_4$ 46
2	*p*-FC_6H_4Br	diglyme	170	6	*p*-$FC_6H_5N(CO)_2C_6H_4$ 46
2	CH_3I	none	r. t.	3	$CH_3N(CO)_2C_6H_4$ 98
2	$C_6H_5CH_2Br$	none	170	4	$C_6H_5CH_2N(CO)_2C_6H_4$ 95
6	CH_3I	none	r. t.	1	$CH_3CONHCH_3$ 27
7	CH_3I	none	r. t.	5	$C_6H_5NHCH_3$ 24
7	CH_3COCl	none	r. t.	2	$C_6H_5NHCOCH_3$ 92
8	CH_3I	none	0	2	*N*-methyl-γ-butyrolactam 28

a) The reactions were carried out by using 0.15—1.0 mmol of the complex and 1—2 cm^3 of the organic halide in 2 cm^3 of the solvent.

added to a Schlenk tube containing 670 mg (1.0 mmol) of **1** and 154 mg (1.1 mmol) of phthalimide at −20 °C. Stirring of the mixture for 10 min at −20 °C gave a light green precipitate with evolution of CH_4. Filtration of the solution afforded 680 mg (89%) of the crude product. Recrystallization from acetone yielded light green prisms of **2** (460 mg, 35%). Equivalent conductivity of **2** in acetone at 0 °C was smaller than 1.0 S cm^2.

Succinimidobis(triphenylphosphine)copper(I) ***3***: The complex was prepared by the reaction of **1** (750 mg, 1.2 mmol) with succinimide (120 mg, 1.2 mmol) in a similar way to that for the preparation of **2**. The white precipitate obtained was washed with diethyl ether repeatedly and dried in a vacuum to give **3** (600 mg, 74%).

N-*Phenylacetamidobis(triphenylphosphine)copper(I)* ***4***: Acetanilide (0.200 g, 1.48 mmol) was added to a Schlenk type flask containing **1** (910 mg, 1.4 mmol) suspended in 5 cm^3 of diethyl ether. The yellow suspension was stirred at 0 °C for 0.5 h in the absence of air to give a white precipitate with evolution of methane (0.97 mol per Cu). The precipitate was crystallized from a mixture of diethyl ether and toluene and dried in a vacuum to give white crystals of **4** (800 mg, 76%).

Acrylamidobis(triphenylphosphine)copper(I) ***5***: The complex was prepared by the reaction of **1** (940 mg, 1.5 mmol) with acrylamide (110 mg, 1.5 mmol) in a similar way to that for the preparation of complex **4**. The white precipitate was crystallized from a mixture of diethyl ether and toluene to give white crystals of **5** (810 mg, 83%).

Acetamido(triphenylphosphine)copper(I) ***6***: Diethyl ether (15 cm^3) was added to a Schlenk tube containing 1050 mg (1.6 mmol) of **1** and 98 mg (1.7 mmol) of acetamide at −20 °C. Stirring of the mixture for 10 h at 0 °C gave a white precipitate, which was washed with diethyl ether repeatedly and dried in a vacuum to give **6** (610 mg, 97%).

Phenylamidobis(triphenylphosphine)copper(I) ***7***: Aniline (150 mg, 1.1 mmol) was added to **1** (670 mg, 1.1 mmol) suspended in 5 cm^3 of diethyl ether. Stirring of the yellow suspension at −10—0 °C for 1 day gave a pale-yellow precipitate, which was washed with diethyl ether repeatedly and dried in vacuum to give **7** (520 mg, 73%).

(2-Oxo-1-pyrrolidinyl)bis(triphenylphosphine)copper(I) ***8***: The complex was prepared by the reaction of **1** (1.6 g, 2.5 mmol) with γ-butyrolactam (0.19 cm^3, 2.5 mmol) in a similar way to that for the preparation of complex **7**. Yield=1.2 g (74%).

Reactions of the Cu(I)–N Complexes with Organic Halides: Bromobenzene (2 cm^3, 19 mmol) and diglyme (2 cm^3) were added to a reaction vessel containing 140 mg (0.19 mmol) of **2**. The mixture was stirred for 6 h under reflux. GLC analysis of the reaction mixture showed formation of 12 mmol (64%) of *N*-phenylphtalimide. The other reactions were carried out in a similar way under conditions given in Table 3.

References

1) a) T. Saegusa, T. Tsuda, and Y. Ito, *Kogyo Kagaku Zasshi*, **72**, 1627 (1969); b) J. F. Normant, *Synthesis*, **63** (1972); c) T. Kauffmann, *Angew. Chem.*, **86**, 321 (1974); d) R. Noyori, *Yuki Gosei Kagaku Kyokai Shi*, **34**, 675 (1976).

2) a) A. Yamamoto, A. Miyashita, T. Yamamoto, and S. Ikeda, *Bull. Chem. Soc. Jpn.*, **45**, 1583 (1972); b) A. Miyashita and A. Yamamoto, *ibid.*, **50**, 1102 (1977); c) T. Ikariya and A. Yamamoto, *J. Organometal. Chem.*, **72**, 145 (1974).

3) M. Kubota and A. Yamamoto, *Bull. Chem. Soc. Jpn.*, **51**, 2909 (1978).

4) A. Miyashita and A. Yamamoto, *J. Organometal. Chem.*, **113**, 187 (1976).

5) a) L. Tschugaeff, *Chem. Ber.*, **39**, 2897 (1905); b) N. P. Slabbert and D. A. Thornton, *J. Inorg. Nucl. Chem.*, **33**, 2933 (1971); c) N. Hojo, H. Shirai, and A. Suzuki, *Kogyo Kagaku Zasshi*, **73**, 2708 (1970); d) T. Tsukihara, Y. Kitsube, K. Fujimori, K. Kawashima, and Y. Kan-nan, *Bull. Chem. Soc. Jpn.*, **47**, 1582 (1974).

6) a) H. Bürger and U. Wannagat, *Monatsh. Chem.*, **95**, 1101 (1964); b) Th. Kauffmann, J. Albrecht, D. Berger, and J. Legler, *Angew. Chem.*, **79**, 620 (1967); c) T. Saegusa, T. Tsuda, K. Nishijima, and K. Isayama, *Tetrahedron Lett.*, **1968**, 3379.

7) a) G. W. A. Fowles, *Prog. Inorg. Chem.*, **6**, 1 (1964); b) D. C. Bradley, *Adv. Inorg. Chem. Radiochem.*, **15**, 259 (1972).

8) T. Yamamoto, M. Kubota, and A. Yamamoto, *Bull. Chem. Soc. Jpn.*, **51**, 1835 (1978).

9) A. R. Siedle, R. Velapoldi, and N. Erickson, *Inorg. Nucl. Chem. Lett.*, **15**, 33 (1979); *Appl. Surf. Sci.*, in press.

10) a) D. M. Roundhill, *J. Chem. Soc., Chem. Commun.*, **1969**, 567; b) D. M. Roundhill, *Inorg. Chem.*, **9**, 254 (1970).

11) a) D. G. H. Ballard and P. W. van Lienden, *Makromol. Chem.*, **154**, 177 (1972); b) R. B. King and A. Fronzaglia, *J. Am. Chem. Soc.*, **88**, 709 (1966); c) Y. Becker and J. K. Stille, *J. Am. Chem. Soc.*, **100**, 845 (1978).

12) a) R. G. R. Bacon and A. Karim, *J. Chem. Soc., Chem. Commun.*, **1969**, 578; b) R. G. R. Bacon and A. Karim, *J. Chem. Soc., Perkin Trans.*, **1973**, 272.

13) L. J. Bellamy, "The Infrared Spectra of Complex Molecules," Methuen, London (1964), p. 205.

 © 1980 The Chemical Society of Japan Bull. Chem. Soc. Jpn., 53, 1303—1307 (1980)

Performances of Lead and Copper(II) Ion-selective Electrodes in Metal Buffer Solutions and the Determination of the Stability Constants of Lead and Copper(II) Complexes

Genkichi NAKAGAWA,* Hiroko WADA, and Takeshi SAKO

Laboratory of Analytical Chemistry, Nagoya Institute of Technology, Gokiso-cho, Showa-ku, Nagoya 466

(Received September 8, 1979)

The behaviour of lead and copper(II) ion-selective electrodes (Denki Kagaku Keiki Co., Japan) at very low activity levels was examined in metal buffer solutions. In the absence of complexing agents, the Nernstian responses were obtained down to 10^{-6} mol dm^{-3} (μ=0.1) Pb^{2+} in the pH range from 4 to 7, and down to 10^{-7} mol dm^{-3} (μ=0.1) Cu^{2+} in the pH range from 4 to 6. The complexing agents which form stable complexes with Pb or Cu(II) were very effective in lowering the detection limits. The stability constants of the Pb and Cu(II) complexes with several ligands[CH_3COO^-, 1,10-phenanthroline(Phen), glycine(Hgly), iminodiacetic acid(H_2ida), nitrilotriacetic acid(H_3nta), *etc.*] were determined by measuring the activities of the free Pb or Cu(II) ion in metal buffer solutions. However, in spite of the high stability of the Pb- or Cu(II)-edta complex, the lower limit of the electrode response was abnormally high and the stability constant of Pb- or Cu(II)-edta complex could not be obtained. Some reasons for the abnormalities with EDTA were discussed.

The response of ion-selective electrodes at very low activity levels has been studied in metal buffer solutions.[1—4] Some authors have used ion-selective electrodes for the determination of the stability constants of metal complexes.[5,7] In these cases, measurements of the activitites of free metal ions at a very low level, *i.e.*, $<10^{-5}$ mol dm^{-3}, are usually required. On the other hand, in the potentiometric titrations of copper (II) or lead(II) with EDTA by the use of copper(II) or lead ion-selective electrodes, the electrode potentials after the equivalence point were found to be higher than the theoretical values.[6] This deviation implies that the determination of the stability constants of copper(II)- or lead-edta complex with copper(II) or lead ion-selective electrodes is impossible.

In our previous work,[7] the potential response of the Orion copper(II) ion-selective electrode Model 94-29 was examined in various copper(II) buffer solutions containing copper complexes and an excess of the ligand; the stability constants of copper(II) complexes were thus determined successfully. In the cases of the $edta^{4-}$ and nta^{3-} complexes, however, good results could not be obtained, while in the case of 1,10-phenanthroline the electrode responded to 10^{-16} mol dm^{-3} of the copper ion. Therefore, we suggested that, for the determination of the stability constants, the lower limits of the electrode response should be checked in a solution containing the same ligand in the same pH range. The use of the ion-selective electrode provides a simple and reliable method for determining the stability constants of metal complexes.

In the present work, the performance of the lead ion-selective electrode from the Denki Kagaku Keiki Co. (DKK), Japan, has been examined, and the stability constants of several lead complexes have been determined. The potential response of the copper(II) ion-selective electrode from the Denki Kagaku Keiki Co. has also been examined, and compared with that of the Orion copper(II) ion-selective electrode Model 94-29.

Experimental

Reagents. A lead(II) standard solution was prepared from analytical-grade lead nitrate and standardized against an EDTA solution by the use of Xylenol Orange as an indicator. A copper(II) standard solution was prepared from metallic copper (99.99% purity).

Ligands: Analytical-grade $Na_2H_2edta \cdot 2H_2O$ and H_3nta were recrystallized. The other ligands were of an analytical-grade and were used without further purification.

The potassium nitrate was recrystallized from distilled water.

Apparatus. Two Hitachi-Horiba F-5 Type pH Meters were used. One was equipped with a lead or copper(II) ion-selective electrode and a Horiba calomel electrode. Before the lead or copper(II) ion-selective electrode was used, the surface of the active membrane was polished with electrode polishing paper from the DKK Co.; then it was soaked in a *ca.* 0.2% CH_3COONa–CH_3COOH buffer (pH 6) containing 0.1% KNO_3 until the electrode potentials dropped down to -150——-170 mV for the lead ion-selective electrode and to 80—50 mV for the copper(II) ion-selective electrode. The electrodes were kept in distilled water. The calomel electrodes were connected to the test solution *via* a salt bridge of 0.1 mol dm^{-3} KNO_3 in agar-agar.

The following cell arrangement was used for measuring the lead or copper(II) ion activities:

Pb or Cu(II) ion-selective electrode	test solution	0.1 mol dm^{-3} KNO_3	calomel electrode (3.33 mol dm^{-3})

The ionic strength of the test solutions was maintained at 0.1 with KNO_3 except in the case of acetate, and measurements were made at 25 °C. During the potential measurements, magnetic stirring was done with a Teflon bar.

The equilibrium potential of this cell is expressed as Eq. 1 from the Nernst equation:

$$E = E' + \frac{RT}{2F}\ln[M^{2+}] \quad (1)$$

where E' is a constant consisting of the standard potential of the electrode, the junction potential and $(RT/2F)\ln\gamma_{M^{2+}}$, and where $[M^{2+}]$ is the concentration of the lead or copper(II) ion.

Response Time of Ion-selective Electrode. The constant potential reading were usually obtained within one minute for 10^{-2}—10^{-3} mol dm^{-3} metal ion solutions, within 5 minutes in 10^{-6} mol dm^{-3} solutions, and within 10 minutes in metal buffer solutions containing less than 10^{-10} mol dm^{-3} free metal ions.

Results

Potential Response of Pb and Cu(II) Ion-selective Electrodes. The potential response of a DKK lead ion-selective electrode was examined over the pH range between 3 and 9. The test solutions were prepared by stepwise dilution of a 10^{-2} mol dm^{-3} lead standard solution, and the pH was adjusted by adding a dilute HNO_3 or NaOH solution. As is shown in Fig. 1, the Nernstian response with a 29.0 mV slope was observed down to 10^{-6} mol dm^{-3} lead ion in the pH region of 4—7. The lowest line (D.L.) in Fig. 1 shows the detection limit of the electrode, which was obtained with the solution containing no lead ion. Below these potentials, the electrode no longer responded to the lead ion activity.

In the case of the copper(II) ion-selective electrode, the Nernstian response with a 29.2 mV solpe was obtained down to 10^{-7} mol dm^{-3} copper(II) ion in the pH range between 4 and 6 (Fig. 2). The detection limit of the DKK copper(II) ion-selective electrode used in this study was lower by one order than that of the Orion copper(II) ion-selective electrode employed in the previous work.

Effects of Complexing Agents on the Detection Limit. The electrode response was examined in a metal buffer solution containing an excess of complexing agents. The broken lines in Figs. 3 and 4 show the detection limits of the lead and copper(II) ion-selective electrodes in the solutions containing a complexing agent and no metal ion. Complexing agents which form stable complexes with the lead or copper(II) ion were very effective in lowering the detection limit, as was observed in the previous work with the Orion copper(II) ion-selective electrode.[7] With the DKK lead ion-selective electrode, the detection limit was

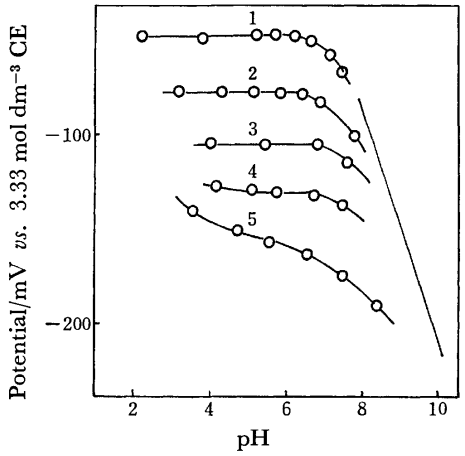

Fig. 1. Potential response of DKK Pb ion-selective electrode at μ=0.1, at 25 °C.
Pb^{2+}/mol dm^{-3}: 1: 10^{-3}, 2: 10^{-4}, 3: 10^{-5}, 4: 10^{-6} 5: detection limit.

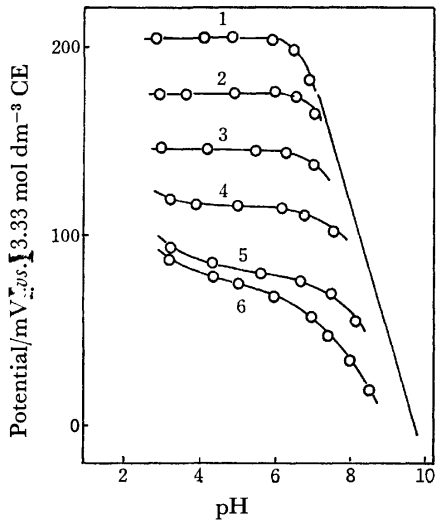

Fig. 2. Potential response of DKK Cu(II) ion-selective electrode at μ=0.1, at 25 °C.
Cu^{2+}/mol dm^{-3}: 1: 10^{-3}, 2: 10^{-4}, 3: 10^{-5}, 4: 10^{-6} 5: 10^{-7}, 6: detection limit.

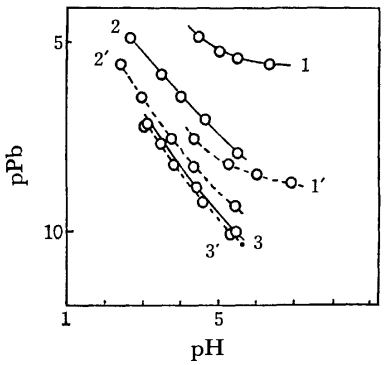

Fig. 3. Electrode response in lead buffer solutions. Broken lines show the detection limits in the solutions containing only complexing agents.
1: CH_3COO^-, C_{Pb}: 1.03×10^{-3} mol dm^{-3}, C_L: 5.93×10^{-2} mol dm^{-3}, 2: H_2nta C_{Pb}: 1.01×10^{-3} mol dm^{-3}, C_L: 5.04×10^{-3} mol dm^{-3}, 3: H_4edta C_{Pb}: 1.01×10^{-3} mol dm^{-3}, C_L: 5.19×10^{-3} mol dm^{-3}.

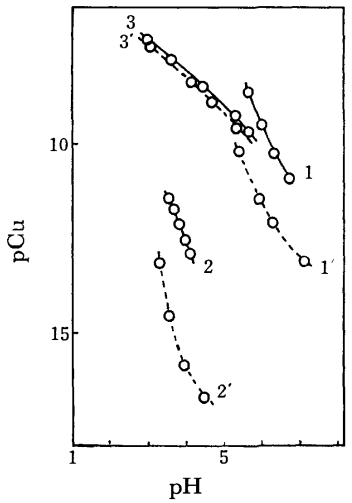

Fig. 4. Electrode response in copper(II) buffer solutions. Broken lines show the detection limits in the solutions containing only complexing agents.
1: NH_3, C_{Cu}: 1.08×10^{-3} mol dm^{-3}, C_L: 1.03×10^{-1} mol dm^{-3}. 2: phen, C_{Cu}: 1.08×10^{-4} mol dm^{-3}, C_L: 4.74×10^{-3} mol dm^{-3}. 3: H_4edta C_{Cu}: 1.08×10^{-3} mol dm^{-3}, C_L: 2.06×10^{-3} mol dm^{-3}.

around 10^{-6} mol dm^{-3} at pH 5 in the absence of complexing agents, while in the presence of 0.01 mol dm^{-3} H_2ida the detection limit was around 10^{-10} mol dm^{-3} at pH 7. Although H_4edta forms stable complexes with lead and copper(II) ions, the detection limits of both the DKK lead and copper(II) ion-selective electrode in H_4edta solutions were abnormally high, as with the Orion copper(II) ion-selective electrode.

The solid lines in Figs. 3 and 4 show the electrode potentials observed in lead and copper(II) buffer solutions respectively. The activities of the lead ion in the lead buffer solutions were much higher than the lower response limits of the lead ion-selective electrode except in the case of H_4edta. In H_4edta solutions the two curves almost coincided with each other; this means that the electrode potential does not give the correct activities of the lead ion in the solution. Again, the DKK copper(II) ion-selective electrode did not respond normally to the activities of the copper(II) ion in the H_4edta solution, as may be seen in Fig. 4.

Determination of Stability Constants of Lead Complexes. If the electrode potentials represent the true pPb values ($-\log[Pb^{2+}]$) in the lead-ion buffer solutions, the stability constants of the lead complexes in the buffer solutions can be determined from the electrode potential measured in the presence of the complexes and a large excess of the ligand, L, at different pH values (Fig. 3). The overall stability constants are defined as (charges are omitted for the sake of generality):

$$\beta_n = \frac{[PbL_n]}{[Pb][L]^n}. \quad (2)$$

Thus, the concentration of the free lead ion in a lead-ion buffer solution is given by:

$$pPb = \log \beta_n + n \log [L] - \log [PbL_n]. \quad (3)$$

$[PbL_n]$ and [L] are calculated by means of Eqs. 4 and 5 respectively;

$$[PbL_n] = C_{Pb} - [Pb], \quad (4)$$

$$[L] = [C_L - n(C_{Pb} - [Pb])]/\alpha_{L(H)}, \quad (5)$$

where C_L and C_{Pb} are the total concentrations of the ligand and the lead ion respectively, and where

$$\alpha_{L(H)} = 1 + \sum_{m=1}^{m} ([H]^m K_1 K_2 \cdots K_m), \quad (6)$$

the successive protonation constants of the ligand being represented as K_1, k_2,$\cdots K_m$. From the cell potential measured, pPb was obtained by means of Eq. 1; then β_n could be calculated. In Fig. 5 the pPb values are plotted against pL($-\log[L]$); straight lines with the slopes of 1 and 2 with CH_3COO^- and Hgly, of 1, 2, and 3 with phen, and of 1 with 8-hydroxy-5-quinolinesulfonic acid(H_2oxs), H_2ida, and H_3nta were obtained, while with H_4edta the slope was 0.4 instead of 1. Except for H_4edta, the values of the stability constants of the lead complexes obtained all agreed with the values reported in the literature.

Determination of the Stability Constants of Copper(II) Complexes. The relations between pCu and pL are plotted in Fig. 6. These plots yielded straight lines with slopes of 4 with NH_3, of 1 and 2 with H_2ida,

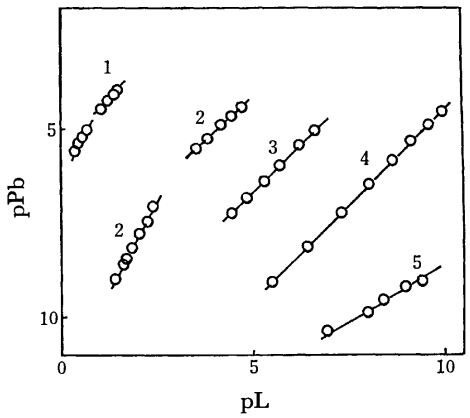

Fig. 5. Plots of pPb *vs.* pL.
1: CH_3COO^-, 2: Hgly, 3: H_2ida, 4: H_3nta, 5: H_4edta.

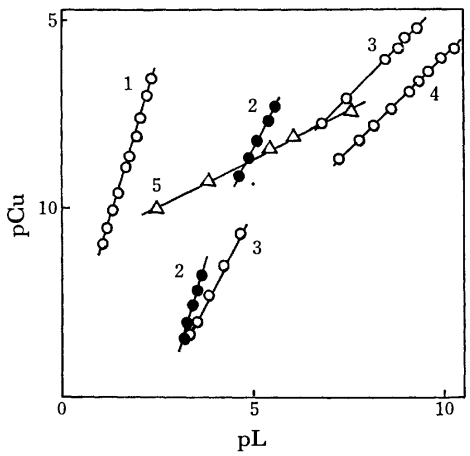

Fig. 6. Plots of pCu *vs.* pL.
1: NH_3, 2: phen, 3: H_2ida, 4: H_3nta, 5: H_4edta.

of 2 and 3 with phen, and of 1 with H_3nta, while it was 0.5 with H_4edta. Although the Orion copper(II) ion-selective electrode employed in the previous work did not give reliable results for the copper(II)–edta or nta complex, with the DKK copper(II) ion-selective electrode a good result was obtained for the H_3nta complex.

The stability constants of the lead and copper(II) complexes determined in this study are summarized in Table 1, along with the values in the literature.[8,9]

Application to EDTA Titrations. The potentiometric titration of lead with EDTA was carried out by means of the lead ion-selective electrode. The results are shown in Fig. 7. The electrode potentials after the equivalence point leveled out at the detection limit of the electrode and deviated from the theoretical titration curves in a way similar to that is the case with the Orion copper(II) ion-selective electrode.

Discussion

The active membranes of the DKK copper or lead ion-selective electrodes consist of mixed sulfides of copper(II) or lead and silver(I), as is the case of the Orion electrodes. Recently several papers have been published concerning the electrode potential of the mixed-sulfide membrane electrodes; however, the mechanism

TABLE 1. STABILITY CONSTANTS OF Pb OR Cu(II) COMPLEXES (25 °C, $\mu=0.1$)

Ligand	log β					
	Pb(II) Complexes (Determined)		(Literature)	Cu(II) Complexes (Determined)		(Literature)
CH_3COO^-	β_1	2.09	2.1	β_2	2.58 ($\mu=1.0$)	2.7
	β_2	3.29	3.3			
NH_3				β_4	12.49[a]	12.59
					12.53	
en				β_2	19.40	19.60
bpy				β_2	13.65	13.57
				β_3	16.75	17.0
phen	β_1	4.8	4.65	β_2	15.8	15.4
	β_2	7.8	7.5	β_3	19.8	20.4
	β_3	10.3	~9			
Hgly	β_1	5.00	5.1	β_2	15.28	15.1
	β_2	7.73	7.7			
H_2ida	β_1	7.67	7.45	β	10.54[a]	10.5
					10.48	
				β_2	16.35	16.5
H_3nta	β_1	11.56	11.39	β_1	12.97	12.96
H_2oxs	β_1	7.77	7.7			

a) Orion 94-29 Cu(II) electrode.

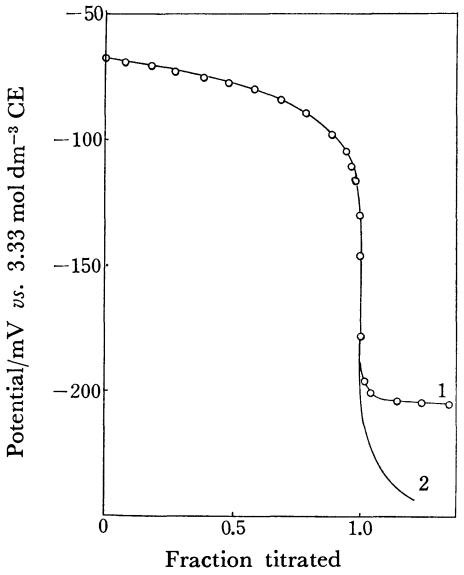

Fig. 7. Titration curve of Pb with EDTA.
1: Experimental, 2: theoretical, C_{Pb}: 1.01×10^{-3} mol dm^{-3}, C_{EDTA}: 1.04×10^{-2} mol dm^{-3}, pH 4.3 (CH_3-COOH-CH_3COONa buffer).

of potential response of these electrodes are not yet fully clarified. As an approximation, the potential response of these electrodes can be understood by considering these materials as the third class of electrodes for the silver(I) ion;

$$Ag_2S + M^{2+} \rightleftharpoons MS + 2Ag^+. \quad (7)$$

Thus, the electrode potentials are given by

$$E = {}^{\circ}E_{Ag^+/Ag} + \frac{RT}{2F}\ln\frac{K_{s(Ag_2S)}}{K_{s(MS)}} + \frac{RT}{2F}\ln a_{M^{2+}}. \quad (8)$$

The difference in the detection limits between the DKK copper(II) electrode and the Orion copper(II) electrode may be attributed to the differences in the methods of preparing the mixed sulfides and the membranes. Although the detection limits of ion-selective electrodes were determined by the solubility of the active materials of the electrode, the observed detection limits of the lead and copper(II) electrodes were much higher than the values calculated from solubility of PbS or CuS; for example, at pH 4 the solubilities of PbS and CuS are calculated to be around 10^{-9} mol dm^{-3} and 10^{-14} mol dm^{-3} respectively. This may be caused by the high activities of lead or copper (II) at the membrane surface resulting from the adsorption of these ions. The strong complexing agent reduces the activities of the copper(II) or lead ion at the membrane surface and shifts the detection limits to lower levels

In H_4edta solutions the detection limits of the lead and copper(II) ions were abnormally high compared with those in the solutions containing the other complexing agents. This fact is explained as follows. Since the stability of the silver complex with edta^{4-} is very small in comparison with the stability of the lead- or copper(II)-edta complex, the decrease in the activity of the silver ion at the membrane surface is not so marked as the decrease in the lead or copper(II) ion activity. Therefore, the equilibrium represented by Eq. 7 is shifted to the left, and finally the surface of the active membrane is converted to Ag_2S. Thus, the electrode would lose its selectivity toward the lead or copper(II) ion, and the detection limits may be determined by the activity of the silver ion at the membrane surface. On the other hand, complexing agents which form fairly stable complexes with both silver and lead or copper(II) ions, such as phen, may shift the detection limits of these electrodes to a very low level. If the electrode potential measured in the metal buffer solution is sufficiently higher than

the detection limits measured in the solution containing the same ligand, reliable stability constants of the metal complexes can be determined.

Recently, it was found that a mixed sulfide of copper(I) and silver(I) such as $Ag_{1.55}Cu_{0.45}S$ was formed in the active material of the copper(II) ion-selective electrode.[10,11] Since H_4edta forms weaker complex with the Cu(I) ion than with the Cu(II) ion, the high activities of the copper(I) ion at the membrane surface may also interfere with the measurement of the activities of copper(II) at very low levels.

Although some authors[1,12] have recommended the use of a metal buffer system which consists of copper (II)–edta or lead–edta for the calibration of the copper(II) or lead ion-selective electrode at low activitity levels, other metal buffer systems rather than H_4edta are to be preferred.

Part of this study was presented at the 26th International Congress of Pure and Applied Chemistry, Tokyo (1977).

References

1) E. H. Hansen, C. G. Lamm, and J. Růžička, *Anal. Chim. Acta*, **59**, 403 (1972).
2) E. H. Hansen and J. Růžička, *Anal. Chim. Acta*, **72**, 365 (1974).
3) P. Kivalo, P. Virtanen, K. Wickström, and M. Wilson, *Anal. Chim. Acta*, **87**, 401 (1976).
4) P. Kivalo, P. Virtanen, K. Wickström, and M. Wilson, *Anal. Chim. Acta*, **87**, 387 (1976).
5) E. H. Hansen and J. Růžička, *Talanta*, **20**, 1105 (1973).
6) G. J. M. Heijne and G. Den Boef, *Anal. Chim. Acta*, **89**, 287 (1977).
7) G. Nakagawa, H. Wada, and T. Hayakawa, *Bull. Chem. Soc. Jpn.*, **48**, 424 (1975).
8) L. G. Sillén and A. E. Martell, "Stability Constants of Metal-Ion Complexes" and "Supplement No. 1," The Chemical Society, London (1964; 1971).
9) A. Ringbom, "Complexation in Analytical Chemistry," Interscience Pub., New York (1963).
10) G. J. M. Heijne and W. E. van der Linden, *Anal. Chim. Acta*, **93**, 99 (1977).
11) K. Ito, N. Matsuda, S. Ikeda, and G. Nakagawa, Proceedings of 2nd Symp. of Solid-Ionics at Nagoya, Japan (1974); K. Ito, N. Matsuda, S. Ikeda, and G. Nakagawa, *Denki Kagaku*, **48**, 16 (1980).
12) R. Blum and H. M. Fog, *J. Electroanal. Chem.*, **34**, 485 (1972).

 © 1980 The Chemical Society of Japan Bull. Chem. Soc. Jpn., 53, 1308—1311 (1980) [Vol. 53, No. 5

Pyrolytic Sulfurization Gas Chromatography. VII. The Simultaneous Determination of the Atomic Ratio between C, H, O, and N in a Halo-organic Compound

Tadashi HARA,* Kaoru FUJINAGA, and Fujio OKUI

Department of Chemical Engineering, Fuculty of Engineering, Doshisha University, Karasuma Imadegawa, Kamigyo-ku, Kyoto 602

(Received October 24, 1979)

The halide produced from a halo-organic compound interferes with the simultaneous determination of the atomic ratio between C, H, O, and N in the compound by the pyrolytic sulfurization gas chromatography, but the interference can be eliminated by allowing the pyrolytic sulfurization of the compound to proceed in the presence of the sodium sulfide formed by the reaction between sodium azide and sulfur.

According to pyrolytic sulfurization gas chromatography (PSGC), which was originated by the present authors, the atomic ratio between C, H, O, and N in a usual organic compound,[1,2] a metallo-organic compound,[3] and a polymer[4] has been successfully and simultaneously determined.

The present study has been carried out to confirm whether or not PSGC can be applied to the analysis of a halo-organic compound. The chromatogram of a halo-organic compound obtained by PSGC was found to be different from that of the compound consisting of C, H, O, and N alone; that is, there were extra peaks which more or less overlapped with the peaks based on C, H, O, and N. This makes the application of PSGC to a halo-organic compound impossible. In order to eliminate the interference of halides, there seem to be two procedures; one is based on the fixation of halides in an ampule, and the other, on the fixation of halides after the crushing of the ampule. The former is better than the latter, since the flowing path in a gas chromatograph is made of stainless steel, which is apt to react with halides. Various substances were added to a sample for the fixation of halides in an ampule; the sodium sulfide (Na_2S) produced by the reaction between sodium azide (NaN_3) and sulfur(S) in a quartz tube which was closed at one end was found to be best for the present purpose. By this procedure, no peaks of halides were observed on the chromatogram, and a simultaneous determination of the atomic ratio between C, H, O, and N in a halo-organic compound could be successfully carried out.

Experimental

Apparatus and Reagents. The reagents and apparatus used were the same as those previously reported[3-6] except that NaN_3 of a guaranteed grade was newly used.

Samples. 5,7-Dibromo-8-quinolinol of a guaranteed grade was recrystallized from benzene for use. Bis(5,7-dibromo-8-quinolinolato)copper(II) and tris(5,7-dibromo-8-quinolinolato)iron(III) were prepared in accordance with the gravimetric procedure[7] by the use of purified 5,7-dibromo-8-quinolinol. The other samples were of a reagent grade for elemental analysis.

Procedure. After 6 mg of S and approximately 0.4 mg of NaN_3 had been placed in a quartz tube, one end of which was closed, the inside of the quartz tube was completely filled with helium by passing helium through it at the rate of 100 cm³/min; after 10 min the fused end of the tube was carefully heated in an electric furnace. This was followed by the formation of Na_2S by means of the reaction between NaN_3 and S in the tube. To the tube, 0.3—0.5 mg of a sample was then added, and the other end of the tube was fused after 10 minutes' passage of helium at the same flow rate as before, followed by the same operation as in the previous paper.

Results and Discussion

Interferences of Halides. Three typical halides were analyzed by the PSGC method; their chromatograms are shown in Fig. 1, in which (a), (b), and (c) correspond to the chromatograms of ammonium chloride (NH_4Cl), ammonium bromide, and ammonium

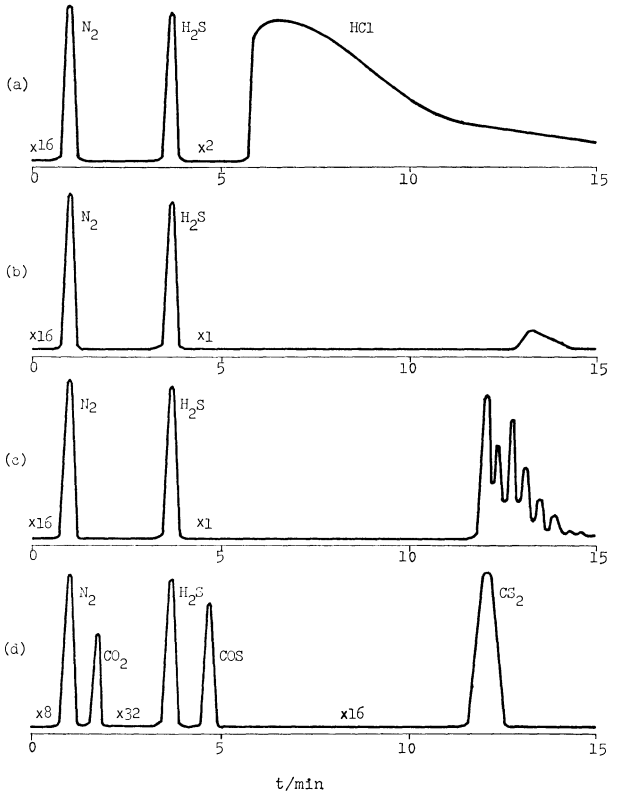

Fig. 1. Typical chromatograms of reaction products between S and ammonium halides by the conventional PSGC method.
(a) NH_4Cl, (b) NH_4Br, (c) NH_4I, (d) glycine as a halogen-free compound.

iodide respectively. As may be seen from Fig. 1, chloride and iodide interfere with the determination of carbon disulfide. Many peaks which appeared after a retention time of approximately 12 min were experimentally confirmed to be due to the compounds formed by the reaction between column packings of the gas chromatograph and iodine or iodide. These results made the application of PSGC to halo-organic compounds impossible. In order to eliminate the interference of halides, a procedure in which halides were fixed in an ampule was adopted, since the flowing path in a gas chromatograph is made of stainless steel, which is apt to react with the halides.

Fixation of Halides. Various substances were added to a sample for the fixation of halides in an ampule, and then the sample was analyzed (Table 1). Since halogen atoms had been completely captured on a silver wire or net in the conventional CH analysis, 1,2,3,4,5,6-hexachlorocyclohexane(γ-BHC) and NH_4Cl were analyzed by the PSGC method in the presence of powdered silver or silver sulfide (Ag_2S), but the peak of hydrogen chloride (HCl) was still observed. Furthermore, when silver chloride was analyzed by the PSGC method in the presence of glycine as a hydrogen source, the peak of HCl was observed. From these results, silver seemed to show a larger affinity for S than chlorine(Cl) and to produce Ag_2S under the present conditions. In these cases, a black solid which might be Ag_2S was observed in an ampule after the pyrolytic sulfurization, differing from the usual yellow contents. Sodium chloride (NaCl) was analyzed similarly as above in the presence of glycine, but no peak of HCl was observed. This suggested that soium (Na) showed a larger affinity for Cl than S under the present experimental conditions. Then γ-BHC and NH_4Cl were analyzed in the presence of the sodium acetate or NaN_3; no peak of HCl was observed, as the authors had expected. γ-BHC was further analyzed in the presence of the acetate of such alkaline earth metals as magnesium(Mg), calcium(Ca), strontium(Sr), and barium(Ba); most of HCl was fixed in all the reaction residues except magnesium acetate ($(CH_3COO)_2Mg$). According to the PSGC method, the acetates of Ca, Sr, and Ba were converted into their sulfides and volatile constituents, while $(CH_3COO)_2Mg$ was converted into its sulfide-oxide mixture and volatile constituents. There might be a correlation between the fixation of HCl and the reaction products obtained from the acetates of alkaline earth metals by the PSGC method. NH_4Cl was sealed into an ampule together with S and NaN_3 to give various atomic ratios of Na to Cl; the evolution of HCl was then investigated (Table 2). As may be seen from Table 2, the sulfide produced by the reaction between S and NaN_3 was found to react with chloride stoichiometrically to produce NaCl. To sum up these results, a basic sulfide was expected to be effective for the fixation of HCl, and so Na_2S was selected and used for the present study. Since Na_2S was very hygroscopic, however, and since its preparation in pure state was also difficult, an attempt was made to produce Na_2S by means of a reaction between S and NaN_3 in a quartz tube on the basis of the facts that NaN_3 decomposed into Na and nitrogen at about 300 °C[8] and Na_2S could be prepared from Na and S.[9,10] The reaction tube containing the Na_2S thus prepared was stable for at least 30 min in contact with air; therefore, the absorption of atmospheric moisture with Na_2S, which might take place during the insertion of the sample, was neglected for the simultaneous determination of the atomic ratio between C, H, O, and N. The present procedure thus established was applied to the three compounds shown in Fig. 1, but no peak based on halides was observed. The present procedure was the same as in the previous papers except for the coexistence of Na_2S, and it could be successfully applied to various halo-organic compounds.

Table 1. Effects of additives on the formation of HCl

Halides	Materials added	HCl
γ-BHC, NH_4Cl	Ag(powder)	+
γ-BHC, NH_4Cl	Ag_2S	+
AgCl	Glycine	+
NaCl	Glycine	−
γ-BHC, NH_4Cl	CH_3COONa	−
γ-BHC, NH_4Cl	NaN_3	−
γ-BHC	$(CH_3COO)_2Mg$	+
γ-BHC	$(CH_3COO)_2Ca$	trace
γ-BHC	$(CH_3COO)_2Sr$	trace
γ-BHC	$(CH_3COO)_2Ba$	trace

Table 2. Effects of the atomic ratio of Cl/Na on the formation of HCl in the NaN_3-NH_4Cl-S system

Atomic ratio		HCl
Na[a]	Cl[b]	
1.0	0.85	−
1.0	1.0	−
1.0	1.2	+

a) NaN_3. b) NH_4Cl.

Analysis of Various Compounds. Various halo-organic compounds, such as chloride, bromide, and iodide, were analyzed by the present procedure (Table 3); metallo-organic compounds containing a halo-organic compound as a ligand were also analyzed (Table 4). It was newly found (*cf.* Table 4) that the atomic ratio between C, H, O, and N in a metallo-organic compound containing both metal and halogen atom could be simultaneously determined.

Analysis of Fluoro-organic compounds. Fluoro-organic compounds were also analyzed by the present procedure (Table 5). As may be seen from Table 5, the result of oxygen was markedly positive. This might be attributed to the formation of water (H_2O) by Eq. 1 in which water hydrogen fluoride (HF) was made to react with the internal surface of a quartz tube, and to the subsequent conversion of H_2O into oxygen-containing compounds:

$$4HF + SiO_2 \longrightarrow SiF_4 + 2H_2O. \quad (1)$$

Table 3. Analytical results of halo-organic compounds

Sample[a]	C wt%			H wt%			O wt%			N wt%		
	Theor.	Found	Error	Theor.	Found	Error	Theor.	Found	Error	Theor.	Found	Error
1,2,3,4,5,6-Hexachlorocyclohexane $C_6H_6Cl_6$	92.26	92.52	+0.26	7.74	7.48	−0.26						
p-Chlorobenzoic acid C_7H_5Cl	69.42	69.30	−0.12	4.16	4.23	+0.07	26.42	26·46	+0.04			
S-Benzylthiouronium chloride $C_8H_{11}N_2ClS$	71.08	71.15	+0.07	8.20	8.06	−0.14	20.72	20.79	+0.07			
1-Chloro-2,4-dinitrobenzene $C_6H_3O_4N_2Cl$	43.13	43.19	+0.06	1.81	1.83	+0.02	38.30	38.32	+0.02	16.76	16.66	−0.10
1,2,3,4,5,6-Hexabromocyclohexane $C_6H_6Br_6$	92.26	92.33	+0.07	7.74	7.67	−0.07						
N-(α-Bromoisovaleryl)urea $C_6H_{11}O_2N_2Br$	50.34	50.66	+0.32	7.74	7.55	−0.19	22.34	22.43	+0.09	19.57	19.36	−0.21
p-Bromoacetanilide C_8H_8ONBr	71.63	71.61	−0.02	6.02	5.99	−0.03	11.92	11.77	−0.15	10.43	10.63	+0.20
o-Iodobenzoic acid $C_7H_5O_2I$	69.42	69.54	+0.12	4.16	4.11	−0.05	26.42	26.35	−0.07			

a) Halogen atoms were neglected in the calculation of the compositions of halo-organic compounds, since they could not be determined.

Table 4. Analytical results of metallo-organic compounds containing halogen atoms

Sample[a]	C wt%			H wt%			O wt%			N wt%		
	Theor.	Found	Error	Theor.	Found	Error	Theor.	Found	Error	Theor.	Found	Error
5,7-Dibromo-8-quinolinol $C_9H_5ONBr_2$	75.53	75.47	−0.06	3.51	3.59	+0.08	11.18	11.46	+0.28	9.78	9.48	−0.30
Bis(5,7-dibromo-8-quinolinolato)copper(II) $Cu(C_9H_4ONBr_2)_2$	76.04	76.13	+0.09	2.84	2.79	−0.05	11.26	11.41	+0.15	9.86	9.66	−0.20
Tris(5,7-dibromo-8-quinolinolato)iron(III) $Fe(C_9H_4ONBr_2)_2$	76.04	75.85	−0.19	2.84	2.74	−0.10	11.26	11.52	+0.26	9.86	9.89	+0.03

a) Metal atoms and halogen atoms were neglected in the calculation of the compositions of metallo-organic compounds, since they could not be determined.

Table 5. Analytical results of fluoro-organic compounds

Sample[a]	C wt%			H wt%			O wt%			N wt%		
	Theor.	Found	Error	Theor.	Found	Error	Theor.	Found	Error	Theor.	Found	Error
Fluoroacetamide C_2H_4ONF	41.37	39.04	−2.33	6.94	6.76	−0.18	27.56	30.91	+3.35	24.13	23.31	−0.82
Fluorobenzoic acid $C_7H_5O_2F$	69.42	67.21	−2.21	4.16	4.13	−0.03	26.42	28.65	+2.23			

a) The fluorine atom was neglected in the calculation of the compositions of fluoro-organic compounds, since it could not be determined.

Two experiments were further carried out; in one each ampule contained sodium fluoride (NaF) and S, while in the other each ampule contained NaF, S, and hydrogen. Gaseous oxygen did not evolve in the former, while it did in the latter. It is clear from these results that oxygen is not evolved until HF is produced in an ampule.

According to the present procedure, all the halogen atoms liberated from a halide sample were quantitatively captured in the reaction residues. This suggests a possibility of the simultaneous determination of the atomic ratio between C, H, O, N, and halogen atoms by the subsequent analysis of halogen atoms in the reaction residues.

References

1) K. Tsuji, K. Fujinaga, and T. Hara, *Bull. Chem. Soc. Jpn.*, **50**, 2292 (1977).
2) T. Hara, K. Fujinaga, and K. Tsuji, *Bull. Chem. Soc. Jpn.*, **51**, 1110 (1978).
3) T. Hara, K. Fujinaga, and K. Tsuji, *Bull. Chem. Soc. Jpn.*, **51**, 2951 (1978).
4) T. Hara, K. Fujinaga, and F. Okui, Abstr. ANAL 84, The ACS/CSJ Chemical Congress, Honolulu, Hawaii, April, 1979.
5) T. Hara, K. Fujinaga, K. Tsuji, and F. Okui, *Bull. Chem. Soc. Jpn.*, **51**, 3079 (1978).
6) T. Hara, K. Fujinaga, and F. Okui, *Bull. Chem. Soc. Jpn.*, **53**, 951 (1980).
7) R. Berg and H. Künstenmacher, *Z. Anorg. Allg. Chem.*, **204**, 215 (1932).
8) G. Brauer, "Handbuch der Präparativen Anorganishen Chemie," Ferdinand Enke Verlag, Stuttgart (1954), S. 362.
9) G. Brauer, "Handbuch der Präparativen Anorganishen Chemie," Ferdinand Enke Verlag, Stuttgart (1954), S. 279.
10) I. W. Klemm, H. Sodomann, and P. Langmesser, *Z. Anorg. Allg. Chem.*, **241**, 281 (1939).

Mössbauer Studies of the Gamma-ray-irradiation Effects of 1,10-Phenanthroline Compounds

Yonezo MAEDA, Hiroki OHSHIO,* and Yoshimasa TAKASHIMA

Department of Chemistry, Faculty of Science, Kyushu University, Hakozaki, Higashi-ku, Fukuoka 812

(Received July 23, 1979)

Mössbauer and infrared spectroscopies have been applied to the study of the gamma-ray-irradiation effects on eleven iron 1,10-phenanthroline compounds: $[Fe(phen)_2X_2]$ (X=Cl^-, $HCOO^-$, NCO^-, $\frac{1}{2}Ox^{2-}$, $\frac{1}{2}Mal^{2-}$, CN^-, and NO_2^-), $[Fe(phen)_3]X_2\cdot nH_2O$ (X=Cl^-, ClO_4^-, $HCOO^-$, and NO_2^-), $[Fe(phns)_2](ClO_4)_2\cdot 2H_2O$ and $[Fe(phnc)_2](ClO_4)_2\cdot H_2O$ (phen=1,10-phenanthroline, phns=1,10-phenantroline-2-carbothioamide, and phnc =1,10-phenantroline-2-carboxamide). For all the low-spin complexes except $[Fe(phen)_3](HCOO)_2\cdot 6H_2O$, no chemical changes were observed on the Mössbauer spectra after irradiation. All the iron(II) complexes in the high-spin state except $[Fe(phen)_2Cl_2]$ and $[Fe(phnc)_2](ClO_4)_2\cdot H_2O$ were, however, changed to iron(III) species under the influence of irradiation. Three iron(II) complexes in the intermediate-spin state were sensitive to gamma-rays.

A large number of investigations have been carried out by means of Mössbauer spectroscopy into the gamma-ray-irradiation effects on various compounds.

Friedt and Danon have reported that the principal effect of the radiolysis in iron(III) chelates could be interpreted in terms of the H radicals originating from the decomposition of the ligands, which had a high mobility and a high reducing property.[1] In iron(III) potassium oxalate, the reduction from iron (III) to iron(II) species by gamma-ray irradiation has been observed.[2] The primary process of this change is a charge transfer from the ligand to the iron, and the new oxidation state is stabilized by the destruction of the complex with an evolution of gases. In the emission Mössbauer spectroscopic study, the relation between the radiosensitivity and the degree of conjugation of the ligand has been elucidated.[3] The higher degree of conjugation a molecule possesses, the lower the probability of the radiolysis of its molecule.

In this work, in order to clarify the relationship of the radiation effect between the ligand field's strength (or the bond character) and the oxidation number (or the ground state of the iron complex), we synthesized several iron complexes with 1,10-phenanthroline and other related compounds as the ligands. The chemical changes which occurred in these complexes upon gamma-ray irradiation were investigated through Mössbauer spectroscopy. The following iron complexes were used; they were prepared according to the methods described in the literature: $[Fe(phen)_3]X_2\cdot nH_2O$ (X=ClO_4^-, $HCOO^-$, and NO_2^-)[4] $[Fe(phen)_2(CN)_2]$,[5] $[Fe(phen)_2(NO_2)_2]\cdot 1/2H_2O$,[6] $[Fe(phen)_2X_2]$ (X=Cl^-, $HCOO^-$, and NCO^-),[7] $[Fe(phen)_2X_2]\cdot nH_2O$ (X=1/2 oxalate, 1/2 malonate, and F^-),[8] $[Fe(phnc)_2](ClO_4)_2\cdot H_2O$,[9] and $[Fe(phns)_2](ClO_4)_2\cdot 2H_2O$.[10]

Experimental

The analytical data of the complexes prepared are listed in Table 1. The microanalyses were carried out at the Elemental Analysis Center of Kyushu University.

All the samples were sealed in glass tubes under a vacuum and were irradiated at a dose rate of 8.7×10^5 Rh^{-1} in a cylindrical tube of a 3500 Ci cobalt-60 unit of Kyushu University. All the irradiations were done at room temperature. The samples were kept at the temperature of

Table 1. Analytical data of the iron complexes

Complex	Calcd (%)			Found (%)			μ_{eff} (B.M.)
	C	H	N	C	H	N	
$[Fe(phen)_3](ClO_4)_2$	54.36	3.40	10.57	53.47	3.11	10.46	
$[Fe(phen)_3]Cl_2\cdot 5H_2O$	57.08	4.52	11.10	57.56	4.36	11.11	
$[Fe(phen)_3](NO_2)_2\cdot 5H_2O$	55.53	4.40	14.39	55.92	4.28	14.07	
$[Fe(phen)_3](HCOO)_2\cdot 6H_2O$	57.44	4.82	10.57	56.87	4.52	10.39	
$[Fe(phen)_2(NO_2)_2]\cdot 1/2H_2O$	55.73	3.11	16.24	55.24	3.18	15.84	
$[Fe(phen)_2(CN)_2]$	66.68	3.44	17.94	66.53	3.37	17.85	
$[Fe(phns)_2](ClO_4)_2\cdot 2H_2O$	40.58	2.88	10.92	40.32	3.00	10.30	
$[Fe(phen)_2Ox]\cdot 3H_2O$	55.39	3.97	10.03	55.70	3.66	9.62	3.8
$[Fe(phen)_2Mal]\cdot 3H_2O$	56.60	4.23	9.79	56.07	4.34	9.88	3.2
$[Fe(phen)_2F_2]\cdot 4H_2O$	54.76	4.59	10.64	55.25	4.84	10.72	2.8
$[Fe(phen)_2Cl_2]$	59.17	3·11	11.50	58.12	3.40	11.39	
$[Fe(phen)_2(HCOO)_2]$	61.58	3.58	11.07	61.54	3.60	11.19	
$[Fe(phen)_2(NCO)_2]$	62.41	3.22	16.80	62.38	3.23	16.86	
$[Fe(phnc)_2](ClO_4)_2\cdot H_2O$	43.41	2.80	11.68	43.20	2.77	11.50	
$[Fe(phen)_3](ClO_4)_3\cdot 2H_2O$	46.08	2.94	9.03	46.45	3.03	9.03	
$[Fe(phen)_2Cl_2](ClO_4)$	48.98	2.70	9.56	49.14	2.75	9.55	

liquid nitrogen from the end of the exposure to the start of the measurement of the Mössbauer and the infrared spectra in order to protect the radiation effect of the samples from thermal annealing. The total radiation dose was 1.0×10^9 R or 5.8×10^8 R.

A gas-chromatographic study was carried out under the conditions to be described below, by using a G-8 type apparatus of the Yanagimoto Co., Ltd. The sensing element consisted of thermal conductivity cells and the potentiometer was operated at 90 mV. The temperature of the conductivity cell block and the column 10 feet long were kept at the same temperature, either 40 or 170 °C. Gaseous products of the irradiated $[Fe(phen)_2(HCOO)_2]$ were injected directly by using a syringe connected to the carrier-gas-inlet line. Helium was used as the carrier gas at a flow rate of about 15 ml min^{-1}, while active carbon was used as the stationary phase.

The Mössbauer spectra of the unirradiated and irradiated samples were obtained at the temperature of liquid nitrogen using a constant-acceleration spectrometer made by Austin Science Associates. The data were stored in a 1024-channel analyser, type 5200 (Ino-tec, Inc). A 5-mCi cobalt-57 diffused into a Pd foil was used as the source. The isomer shift was calibrated relative to the center of the spectrum of an iron foil at 293 K. All the spectra were fitted to the Lorentzian line shape using the least-squares method.

The infrared spectra were obtained by using a Hitachi Grating Infrared Spectrophotometer, type 215, in the region from 650 to 4000 cm^{-1}. The KBr disk was used for the sample preparation.

Results and Discussion

Figures 1—7 show the Mössbauer absorption spectra of the unirradiated and irradiated samples: $[Fe(phen)_3](ClO_4)_3\cdot2H_2O$, $[Fe(phen)_3](HCOO)_2\cdot6H_2O$, $[Fe(phen)_2(HCOO)_2]$, $[Fe(phen)_2(NCO)_2]$, $[Fe(phen)_2Ox]\cdot3H_2O$, $[Fe(phen)_2Mal]\cdot3H_2O$, and $[Fe(phen)_2F_2]\cdot4H_2O$. The Mössbauer parameters before and after irradiation for all the samples are listed in Tables 2—5.

No chemical changes were observed in the Mössbauer spectra of $[Fe(phen)_3](ClO_4)_2$, $[Fe(phen)_3]Cl_2\cdot5H_2O$, $[Fe(phen)_2Cl_2]$, $[Fe(phnc)_2](ClO_4)_2\cdot H_2O$, $[Fe(phns)_2](ClO_4)_2\cdot2H_2O$, and $[Fe(phen)_2Cl_2](ClO_4)$. From these observations, it can be supposed that the radicals produced by the decomposition of 1,10-phenanthroline upon irradiation contribute to indetectable changes in the iron(II) ground state. On the other hand, the low-spin $[Fe(phen)_3](ClO_4)_3\cdot2H_2O$ was reduced to the low-spin iron(II) (55%) species. It is clearly observed that the high-spin complex $[Fe(phen)_2Cl_2](ClO_4)$ is not sensitive to radiation. This may indicate that the irradiation effect in this case depends upon the difference in the ground state of the iron atom, and the reduction from iron(III) to iron(II) species results from the electron transfer from the ligand to the central metal. $[Fe(phns)_2](ClO_4)_2\cdot2H_2O$ and $[Fe(phnc)_2](ClO_4)_2\cdot H_2O$, for which we could not detect any irradiation effect, are in high-spin and low-spin respectively. The difference between the ligands of

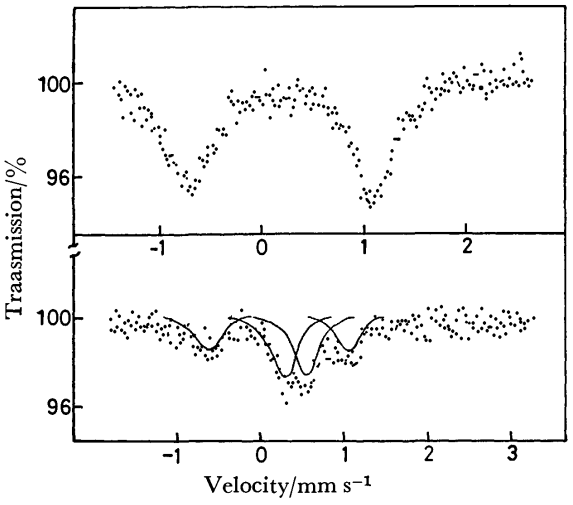

Fig. 1. Mössbauer spectra at 80 K of (a) non-irradiated and (b) irradiated $[Fe(phen)_3](ClO_4)_3\cdot2H_2O$.

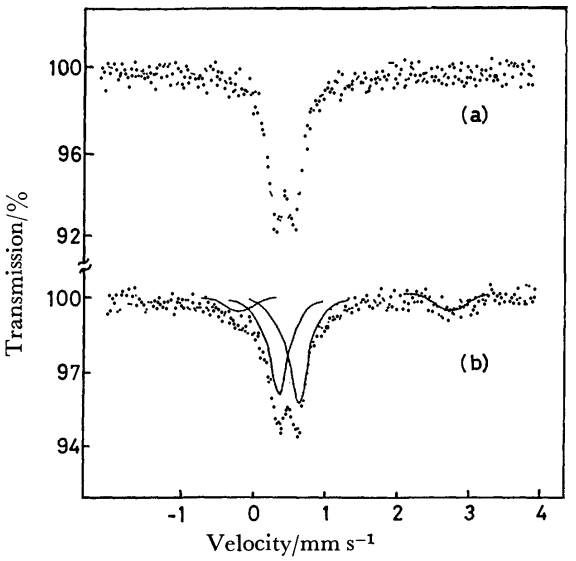

Fig. 2. Mössbauer spectra at 80 K of (a) non-irradiated and (b) irradiated $[Fe(phen)_3](HCOO)_2\cdot6H_2O$.

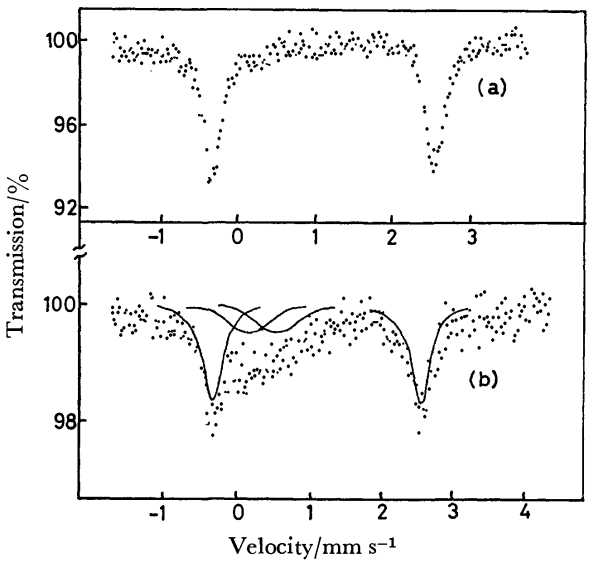

Fig. 3. Mössbauer spectra at 80 K of (a) non-irradiated and (b) irradiated $[Fe(phen)_2(HCOO)_2]$.

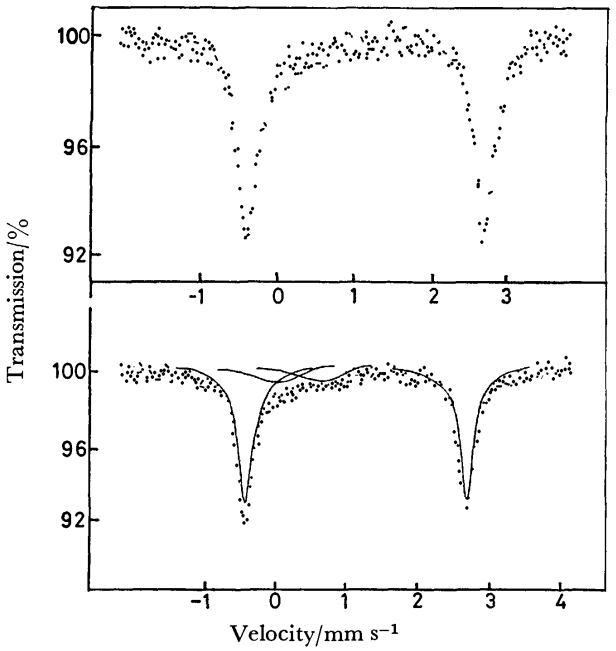

Fig. 4. Mössbauer spectra at 80 K of (a) non-irradiated and (b) irradiated $[Fe(phen)_2(NCO)_2]$.

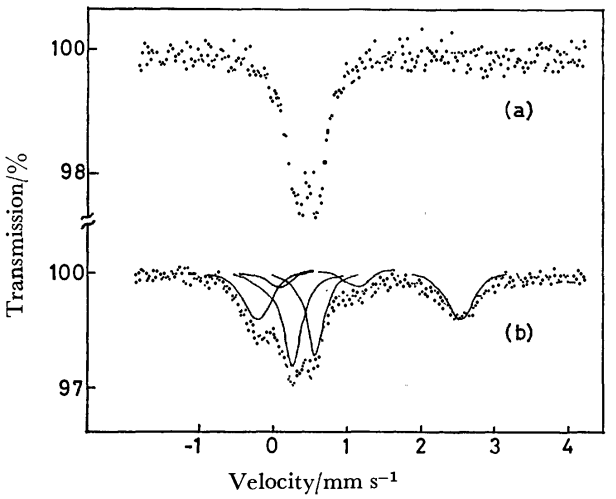

Fig. 5. Mössbauer spectra at 80 K of (a) non-irradiated and (b) irradiated $[Fe(phen)_2Ox]\cdot 3H_2O$.

the two samples is only that of carbonyl and thionyl groups, which were presumed to be sensitive to gamma-ray irradiation. It may be supposed that, even if the ligands are excited by gamma-rays, the decomposition of the ligands is suppressed because of the highly conjugated π-bond of the ligands.

Gütlich *et al.* have reported that high- and low-spin iron(II) species were observed in the emission spectra of $[^{57}Co(phen)_3](ClO_4)_2$.[11] The appearance of the high-spin iron(II) ion does not agree with the results of our external-irradiation experiment.

New peaks attributable to high-spin iron(II) species in the $[Fe(phen)_3](HCOO)_2\cdot 6H_2O$ and to high-spin iron(III) species in the $[Fe(phen)_2(HCOO)_2]$ and $[Fe(phen)_2(NCO)_2]$ appeared after the exposure to gamma-rays. There may be a possibility that the new peaks attributable to low-spin iron(II) species are hidden

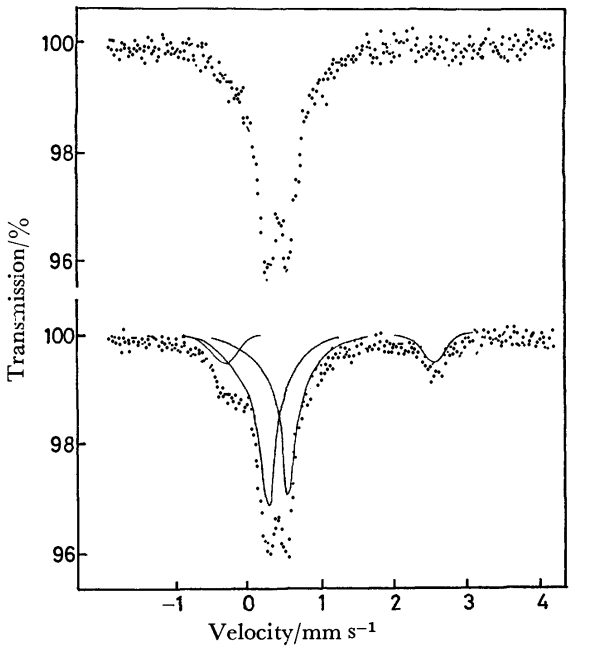

Fig. 6. Mössbauer spectra at 80 K of (a) non-irradiated and (b) irradiated $[Fe(phen)_2Mal]\cdot 3H_2O$.

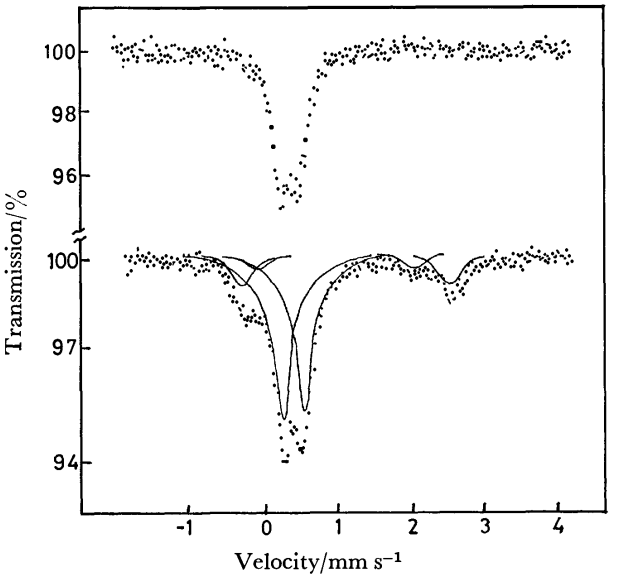

Fig. 7. Mössbauer spectra at 80 K of (a) non-irradiated and (b) irradiated $[Fe(phen)_2F_2]\cdot 4H_2O$.

in the absorption band of the high-spin iron(III) species, because their line widths are too broad to be resolved. However, we can not confirm the existence of the overlapping because of the technical difficulty in the curve fitting. The yield of high-spin iron(II) species produced in the irradiated $[Fe(phen)_3](HCOO)_2\cdot 6H_2O$ was 15%, while those of the high-spin iron(III) species in $[Fe(phen)_2(HCOO)_2]$ and $[Fe(phen)_2(NCO)_2]$ were 43% and 18% respectively. The small values of the isomer shift of iron(III) species in the above two samples suggest that there are four or five coordinated species with 1,10-phenanthroline as a result of the elimination of formate and isocyanate ions by gamma-ray irradiation. A gas-chromatograph-

Table 2. Mössbauer parameters of the samples before and after γ-ray irradiation measured at 80 K

Complex	Exp. $\times 10^8$R	δ [a] mm s^{-1}	Δ [b] mm s^{-1}	Γ [c] mm s^{-1}	
$[Fe(phen)_3](ClO_4)_2$	0	0.38	0.31		
	10.0	0.41	0.31		
$[Fe(phen)_3]Cl_2 \cdot 5H_2O$	0	0.35	0.26	0.29	0.28
	5.8	0.36	0.25	0.27	0.28
$[Fe(phen)_2Cl_2]$	0	1.08	3.26		
	10.0	1.12	3.30		
$[Fe(phnc)_2](ClO_4)_2 \cdot H_2O$	0	1.11	2.36	0.41	0.41
	10.0	1.12	2.54	0.48	0.48
$[Fe(phns)_2](ClO_4)_2 \cdot 2H_2O$	0	0.33	0.51	0.29	0.30
	10.0	0.33	0.49	0.29	0.34
$[Fe(phen)_3](ClO_4)_3 \cdot 2H_2O$	0	0.19	1.80		
	10.0	0.17	1.74		
		0.41	0.28		
$[Fe(phen)_2Cl_2](ClO_4)$	0	0.40	0		
	10.0	0.33	0		

a) Isomer shift. b) Quadrupole splitting. c) Full width at half-maximum.

Table 3. Mössbauer parameters of the samples before and after γ-ray irradiation measured at 80 K

Complex	Exp. $\times 10^9$R	δ mm s^{-1}	Δ mm s^{-1}	Γ mm s^{-1}	S S(total)	SSWR[a] Freedom
$[Fe(phen)_3](HCOO)_2 \cdot 6H_2O$	0	0.40	0.26	0.28 0.27		
	1	0.47	0.28	0.32 0.31	85	423/387
		1.26	2.94	0.47 0.35	15	
$[Fe(phen)_2(HCOO)_2]$	0	1.12	2.90	0.27 0.23		
	1	1.11	2.89	0.34 0.34	57	373/387
		0.29	0.35	0.74 0.74	43	
$[Fe(phen)_2(NCO)_2]$	0	1.14	3.10	0.33 0.29		
	1	1.13	3.10	0.27 0.27	82	388/391
		0.31	0.56	0.73 0.73	18	

a) SSWR: sum of the squares of the weighted residuals.

Table 4. Mössbauer parameters of the samples before and after γ-ray irradiation measured at 80 K

Complex	Exp. $\times 10^9$ R	δ mm s^{-1}	Δ mm s^{-1}	Γ mm s^{-1}	S S(total)	SSWR[a] Freedom
$[Fe(phen)_2Ox] \cdot 3H_2O$	0	0.41	0.27	0.32 0.23		
	1	0.40	0.28	0.32 0.27	46	
		1.15	2.74	0.47 0.47	44	388/391
		0.58	1.06	0.39 0.39	10	
$[Fe(phen)_2Mal] \cdot 3H_2O$	0	0.40	0.28	0.30 0.31		
	1	0.41	0.27	0.33 0.30	80	468/389
		1.14	2.84	0.34 0.34	20	
$[Fe(phen)_2F_2] \cdot 4H_2O$	0	0.41	0.25	0.27 0.28		
	1	0.41	0.27	0.27 0.29	73	
		1.15	2.86	0.35 0.35	22	405/385
		0.97	2.15	0.27 0.27	5	

Table 5. Mössbauer parameters of the samples before and after γ-ray irradiation measured at 80 K

Complex	Exp. $\times 10^8$ R	δ mm s^{-1}	Δ mm s^{-1}	Γ mm s^{-1}	
$[Fe(phen)_3](NO_2)_2 \cdot 5H_2O$	0	0.35	0.27	0.26	0.26
	5.8	0.38	0.26	0.32	0.32
$[Fe(phen)_2(NO_2)_2] \cdot 1/2H_2O$	0	0.33	0.43	0.27	0.28
	5.8	0.33	0.41	0.25	0.32
$[Fe(phen)_2(CN)_2]$	0	0.22	0.60	0.29	0.29
	5.8	0.21	0.60	0.35	0.34

ic study revealed that a large amount of carbon dioxide and a small amount of carbon monoxide existed in the irradiated $[Fe(phen)_2(HCOO)_2]$. It is considered that iron(III) species with a four- or five-coordinated structure are formed because of the decomposition of the formate ion. The radicals originating from the decomposition of 1,10-phenanthroline and hydrated waters of the second coordination sphere do not bring about the oxidation of the iron atom, because no irradiation effect was observed in $[Fe(phen)_3](ClO_4)_2$ and $[Fe(phen)_3]Cl_2 \cdot 5H_2O$. The new peaks attributable to the high-spin iron(II) species which appeared in $[Fe(phen)_3](HCOO)_2 \cdot 6H_2O$ after irradiation suggest that 1,10-phenanthroline has been decomposed by the reaction of 1,10-phenanthroline with some radicals or electrons arising from gamma-ray decomposition of the formate ion. This is true because the low-spin iron(II) state can be attained only in such a coordination situation as when the iron atom is coordinated with three 1,10-phenanthroline molecules. By comparing $[Fe(phen)_3](HCOO)_2 \cdot 6H_2O$ with $[Fe(phen)_2(HCOO)_2]$, it may be concluded that the oxidation reaction has occurred only in the latter complex. It is obscure, however, whether this difference is attributable to that in the ground states of the central metals, because we can not ignore the reaction of the iron ion with the decomposition products of the coordinated and uncoordinated $HCOO^-$, or the reaction of H_2O with the radicals produced. At present, the real reason why the high-spin iron(III) species appears in $[Fe(phen)_2(HCOO)_2]$ is ambiguous. The yields of high-spin iron(II) and iron(III) species appearing in $[Fe(phen)_3[(HCOO)_2 \cdot 6H_2O$ and $[Fe(phen)_2(HCOO)_2]$ after irradiation were 15% and 43% respectively. This indicates that the radiation effect on the central iron of $HCOO^-$ in the first coordination sphere is about three times as large as that in the second coordination sphere; this result is in good agreement with the result for other complexes done by Sano *et al.*[12]

As can be seen in Figs. 5, 6, and 7, the high-spin iron(II) and iron(III) species in $[Fe(phen)_2Ox] \cdot 3H_2O$, only the high-spin iron(II) species in $[Fe(phen)_2Mal] \cdot 3H_2O$, and two high-spin iron(II) species in $[Fe(phen)_2F_2] \cdot 4H_2O$ are observed after irradiation. The absence of high-spin iron(III) species in $[Fe(phen)_2Mal] \cdot 3H_2O$ after irradiation may be explained by the action of the carbon monoxide originating from the decomposition of the malonate ion, as has been reported in the cases of $M[Mn(mal)_2]$ ($M=NH_4^+$, Na^+, and K^+) and $K[Mn(mal)_2(H_2O)_2]$.[13] A comparison of the infrared spectrum of the unirradiated $[Fe(phen)_2Mal] \cdot 3H_2O$ with that of the irradiated one shows that the intensities of the C–O stretching appearing at 1610 and 1405 cm^{-1} were considerably decreased by the gamma-ray irradiation. This decrease suggests that carbonyl groups have been appreciably decomposed. The high-spin iron(II) species whose isomer shift is about 1.14 mm s^{-1} can be estimated to have a six-coordinated structure. The existence of the S=2 species in the irradiated $[Fe(phen)_2Ox] \cdot 3H_2O$ and $[Fe(phen)_2Mal] \cdot 3H_2O$ indicates that the ligand-field strength of the complex becomes weak. The configurational structure of a whole domain might retain the situation of total spin S=1, but in the spur formed in the path-way of ionizing radiation it might be changed to a state that is unable to maintain the situation of S=1 because of the local rearrangement of the configurational structure. The data obtained may support this assumption. Taking into account the value of the isomer shift (0.97 mm s^{-1}) of the newly produced species in $[Fe(phen)_2F_2] \cdot 4H_2O$ upon irradiation, it is reasonable to regard the species as a tetrahedral compound formed by the elimination of F^- from the coordination sphere. Such a tetrahedral species was not observed in the irradiated $[Fe(phen)_2Cl_2]$. This is because the atomic volume of Cl^- is too large in comparison with that of F^- to be removed from its coordination sphere.

No chemical changes were observed in all the samples listed in Table 5 except that the absorption intensities of $[Fe(phen)_3](NO_2)_2 \cdot 5H_2O$ and $[Fe(phen)_2(NO_2)_2] \cdot 1/2H_2O$ decreased after irradiation.

It may be concluded that in the series of the iron complexes containing 1,10-phenanthroline as a ligand, low- and high-spin iron(II) compounds and high-spin iron(III) compounds, which have ligands with highly conjugated structures, are stable to gamma-ray irradiation. On the other hand, low-spin iron(III) compounds are sensitive to radiation.

References

1) E. Baggio-Saitovitch, J. M. Friedt, and J. Danon, *J. Chem Phys.*, **56**, 1296 (1972).
2) A. Sugimori, *Bull. Chem. Soc. Jpn.*, **39**, 2583 (1966).
3) M. B. Misroch, C. J. Schramm, Jr., and A. Nath, *J. Chem. Phys.*, **65**, 1982 (1976).
4) J. F. Duncan and K. F. Mok, *J. Chem. Soc., A*, **1966**, 1493.
5) A. A. Schilt, *J. Am. Chem. Soc.*, **82**, 3000 (1960).
6) K. Madeja, *Chemicke Zvesti*, **19**, 186 (1965).
7) K. Madeja, W. Wilke, and S. Schmidt, *Z. Anorg. All. Chem.*, **346**, 306 (1966).
8) E. König and K. Madeja, *Inorg. Chem.*, **7**, 1848 (1968).
9) E. J. Halbert, C. M. Harris, E. Sinn, and G. J. Sutton, *Aust. J. Chem.*, **26**, 961 (1973).
10) H. A. Goodwin and F. E. Smith, *Aust. J. Chem.*, **25**, 37 (1972).
11) J. Ensling, B. W. Fitzsimmons, P. Gütlich, and K. M. Hasselbach, *Angew. Chem., Int. Ed. Engl.*, **9**, 637 (1970).
12) H. Sano and T. Ohnuma, *Chem. Phys. Lett.*, **26**, 348 (1974).
13) E. L. Simmons and W. W. Wendlandt, *Coord. Chem. Rev.*, **7**. 11 (1971).

 © 1980 The Chemical Society of Japan Bull. Chem. Soc. Jpn., 53, 1317—1320 (1980)

Mössbauer Spectroscopic Studies of the Chemical Effects Associated with ^{57}Co(Electron Capture)^{57}Fe Decay in Tris-β-diketonatocobalt(III) Compounds

Yoichi Sakai,† Kazutoyo Endo, and Hirotoshi Sano*

Department of Chemistry, Faculty of Science, Tokyo Metropolitan University, Fukasawa,, Setagaya-ku, Tokyo 158

(Received September 10, 1979)

Magnetic hyperfine structures (hfs) were found in the absorption Mössbauer spectra at 78 K of a paramagnetic iron(III) complex diluted in a diamagnetic cobalt(III) or aluminium(III) complex, such as ^{57}Fe(acac)$_3$ in Co(acac)$_3$, ^{57}Fe(oxin)$_3$ in Al(oxin)$_3$, and ^{57}Fe(dbm)$_3$ in Co(dbm)$_3$ (acac=acetylacetonato, oxin=8-quinolinolato, and dbm=dibenzoylmethanato), showing that the magnetic hfs is caused by the spin-spin relaxation through the surrounding diamagnetic species. In the emission Mössbauer experiments, magnetic hfs was observed at 78 K in ^{57}Co-labelled Co(dbm)$_3$, Co(oxin)$_3$, and polystyrene-diluted Co(acac)$_3$, while it was not observed in ^{57}Co-labelled Co(acac)$_3$ and Co(dpm)$_3$ (dpm=dipivaloylmethanato). The former possess π-conjugated systems to a greater extent than the latter, either in the ligands or in the vicinity of the ^{57}Co-labelled Co(III) species. These results were explained in terms of the radiolytic stabilities of the matrices as well as those of ^{57}Co-labelled compounds by showing that the paramagnetic radicals produced in a diamagnetic matrix quench the magnetic hfs because of the increased spin-spin interaction, as a consequence of the local radiolysis by EC-decay.

Emission Mössbauer spectroscopic studies have provided us with important information on the chemical fate of the decayed atom in a solid. We have ourselves reported on the chemical effects in the ^{57}Co(EC)^{57}Fe decay process in cobalt(III) coordination compounds by applying the technique. It was observed that the decayed ^{57}Fe species exist in one or more anomalous charge states within the lifetime of the nuclear excited level of ^{57}Fe.[1-3] It was also found that the yield of anomalous species, the high-spin ^{57}Fe(II) species, produced after the EC-decay and the subsequent Auger process is quite high in the ^{57}Co(III) coordination compounds containing the oxalato ligands or the oxalate anions, such as in $K_3[Co(C_2O_4)_3]\cdot 3H_2O$[1] and $[Co(NH_3)_6]_2(C_2O_4)_3$.[3] In order to explain the results, the local radiolytic process was proposed on the basis of absorption Mössbauer experiments in the γ-ray-irradiated $K_3[Fe(C_2O_4)_3]\cdot 3H_2O$.[4] In the local radiolytic process, the radical formation was assumed in the first stage (*e.g.*, CO_2^- from an oxalato ligand or an oxalate anion). Then, the radical may be stabilized by releasing an electron (*e.g.*, CO_2^- into CO_2+e^-), which results in the reduction of the ^{57}Fe(III) species, enhancing the yield of the ^{57}Fe(II) species. On the other hand, it has been reported that the magnetic hyperfine structure (hfs) caused by spin-spin relaxation was found in the absorption Mössbauer spectra of high-spin iron(III) (S=5/2) coordination compounds diluted in diamagnetic compounds—for example, in the spectra of tris(acetylacetonato)iron(III), Fe(acac)$_3$, diluted in Co(acac)$_3$[2] or Al(acac)$_3$[5]. However, in the emission Mössbauer spectra of ^{57}Co-labelled diamagnetic cobalt(III) coordination compounds, little or no magnetic hfs has been observed at the temperature of the absorption experiments, although the decayed ^{57}Fe(III) species remain in magnetically diluted environments of diamagnetic Co(III) compounds. The discrepancy between the results of the absorption and emission Mössbauer spectroscopic studies can be explained by assuming that the enhanced spin-spin interaction between ^{57}Fe atoms and the radicals produced in the local radiolysis through the EC and Auger processes should quench the magnetic hfs in the emission Mössbauer spectra of ^{57}Co-labelled cobalt(III) coordination compounds.

In the present paper, the emission Mössbauer spectroscopic studies of various tris(β-diketonato)cobalt(III) compounds are described in order to clarify the relation of the magnetic hfs, *i.e.*, the radical formation associated with the ^{57}Co(EC)^{57}Fe decay process, with the radiolytic property of the ligands or matrices in the vicinity of ^{57}Co-labelled compounds.

Experimental

Preparation of Materials Used. The mixed crystals of tris(8-quinolinolato)^{57}Fe(III), ^{57}Fe(oxin)$_3$, and Al(oxin)$_3$ were prepared by the co-precipitation method. The molar fraction of ^{57}Fe(oxin)$_3$ was 0.03; the homogeneity of Fe(oxin)$_3$ diluted in Al(oxin)$_3$ was confirmed by X-ray diffraction analysis to be as shown in Fig. 1, where the X-ray powder patterns of Fe(oxin)$_3$ and Al(oxin)$_3$ are different from each other and where the pattern of the mixed crystals shows that of Al(oxin)$_3$, but not Fe(oxin)$_3$, though the mixture of Fe(oxin)$_3$ and Al(oxin)$_3$ with the same molar fraction shows a small but clear contribution of Fe(oxin)$_3$ in the

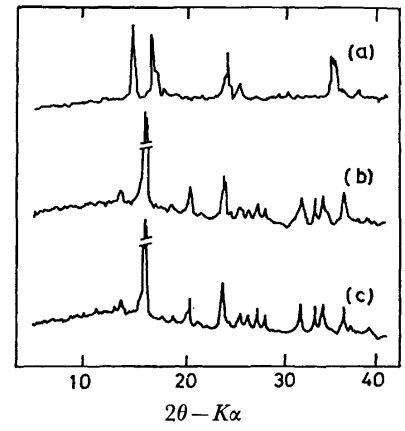

Fig. 1. X-Ray diffraction patterns of a) Fe(oxin)$_3$, b) Al(oxin)$_3$, and c) 3% mol (^{57}Fe-Al)(oxin)$_3$.

† Present address: Department of Chemistry, Faculty of Science, The University of Tokyo, Hongo, Tokyo 113.

diffraction pattern. The mixed crystals of tris(dibenzoylmethanato)^{57}Fe(III), ^{57}Fe(dbm)$_3$, and Co(dbm)$_3$ were prepared by the freeze-dry method, in which the molar fraction of ^{57}Fe(dbm)$_3$ was 0.03.

The ^{57}Co-labelled Co(acac)$_3$ was prepared according to the literature.[6] The mixture of $CoCO_3$ containing *ca.* 1.0 mCi of ^{57}Co and acetylacetone was refluxed at 90 to 100 °C by adding 10% H_2O_2. When the resultant green solution was cooled in an ice-bath, green crystals were deposited. The crystals were filtered and washed with water and methanol. The crude crystals were recrystallized from a benzene-hexane solution.

The ^{57}Co-labelled tris(dipivaloylmethanato)Co(III) complex, Co(dpm)$_3$, was prepared as follows: A mixture of $CoCO_3$ containing *ca.* 1.0 mCi of ^{57}Co and dipivaloylmethane was refluxed in ethanol by adding 10% H_2O_2. The crude green crystals thus separated were washed with ethanol. The resultant ^{57}Co(dpm)$_3$ was purified by the recrystallization of the benzene–hexane solution.

The ^{57}Co(dbm)$_3$ was prepared by an ordinary method. A mixture of $CoCO_3$ containing 1.0 mCi of ^{57}Co and dibenzoylmethane was strongly refluxed in ethanol by adding 10% H_2O_2. The crude product in the solution was filtered and washed with ethanol. The purification of ^{57}Co(dbm)$_3$ was carried out by alumina-column chromatography in a benzene solution.

The ^{57}Co-labelled Co(oxin)$_3$ was prepared according to Ablob's method;[7] that is, $CoCl_2 \cdot 6H_2O$ containing 1.0 mCi of ^{57}Co and 8-quinolinol were dissolved in ethanol, and the product was precipitated and collected. The purification was carried out by recrystallization.

The ^{57}Co(acac)$_3$ diluted in polystyrene was prepared as follows. The ^{57}Co(acac)$_3$ prepared with 5 mg of $CoCO_3$ containing 1.0 mCi of ^{57}Co was dissolved in benzene, to which a few hundred miligrams of polystyrene were added and dissolved homogeneously. The highly viscous solution was dried in air. The homogeneity of the Co(acac)$_3$ diluted in polystyrene was confirmed by X-ray diffraction analysis in cold experiments. The diffraction pattern of Co(acac)$_3$ diluted in polystyrene showed an amorphous state, while that of the mixture of Co(acac)$_3$ and polystyrene with the same contents as the diluted samples showed the peaks of both the crystalline Co(acac)$_3$ and the amorphous pattern of polystyrene.

The chemical structures of the metal(III) coordination compounds concerned in the present work are illustrated in Fig. 2.

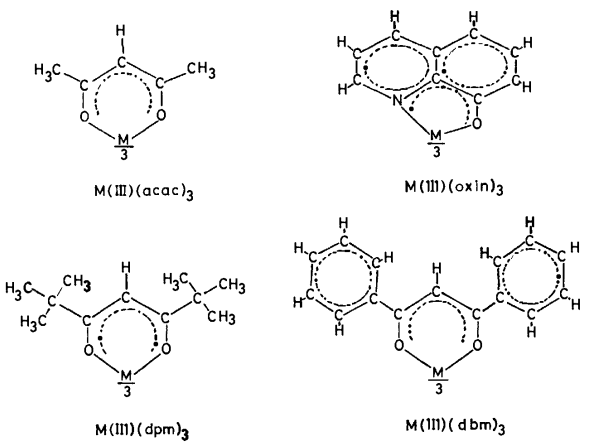

Fig. 2. Chemical structures of tris-β-diketonates of M(III) (M=Al, Fe, and Co).

Measurement of Mössbauer Spectra. The absorption Mössbauer spectra of the samples were measured at 78 K against a ^{57}Co(Pt) source moving in a mode of a constant-acceleration. Since all the emission Mössbauer spectra of the source materials kept at various temperatures (4.2 to 198 K) were measured against a moving ^{57}Fe-enriched stainless-steel as an absorber, both the emission and absorption spectra shown in Figs. 3—7 can be directly compared with each other. Velocity calibration was carried out by normalizing to iron metal in both the absorption and emission experiments.

Results

The absorption Mössbauer spectra at 78 K of ^{57}Fe(oxin)$_3$ diluted in diamagnetic Al(oxin)$_3$, ^{57}Fe(acac)$_3$ diluted in Co(acac)$_3$, and ^{57}Fe(dbm)$_3$ diluted in Co(dbm)$_3$ are shown in Figs. 3 (a), (b), and (c) respectively. The magnetic hfs is found in all the spectra of the mixed crystals at 78 K.

The emission Mössbauer spectra of crystalline ^{57}Co(dpm)$_3$, ^{57}Co(acac)$_3$, ^{57}Co(oxin)$_3$, and ^{57}Co(dbm)$_3$ at 78 K are shown in Figs. 4 (a), (b), (c), and (d) respectively. The magnetic hfs is observed in the spectra of ^{57}Co(oxin)$_3$ and ^{57}Co(dbm)$_3$, while almost no magnetic hfs is found in those of ^{57}Co(acac)$_3$ and ^{57}Co(dpm)$_3$ at 78 K. The emission Mössbauer spectra of ^{57}Co(dpm)$_3$, ^{57}Co(oxin)$_3$, and ^{57}Co(dbm)$_3$ at 4.2 K are shown in Figs. 5 (a), (b), and (c) respectively. The spectra of ^{57}Co(acac)$_3$ at 78 K and 4.2 K were reported by Nath *et al.*;[8] they are very similar to those of ^{57}Co(dpm)$_3$ shown in Figs. 4 and 5. The temperature-dependence of the emission Mössbauer spectrum is demonstrated for ^{57}Co(dbm)$_3$ in Fig. 6. The intensity of the magnetic hfs is found to increase with the decrease in the temperature. The emission

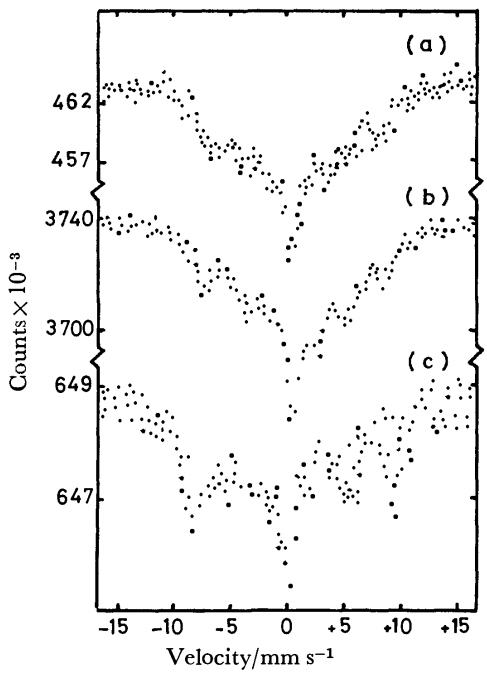

Fig. 3. Absorption Mössbauer spectra at 78 K of a) ^{57}Fe(oxin)$_3$ diluted in Al(oxin)$_3$, b) ^{57}Fe(acac)$_3$ diluted in Co(acac)$_3$, and c) ^{57}Fe(dbm)$_3$ diluted in Co(dbm)$_3$.

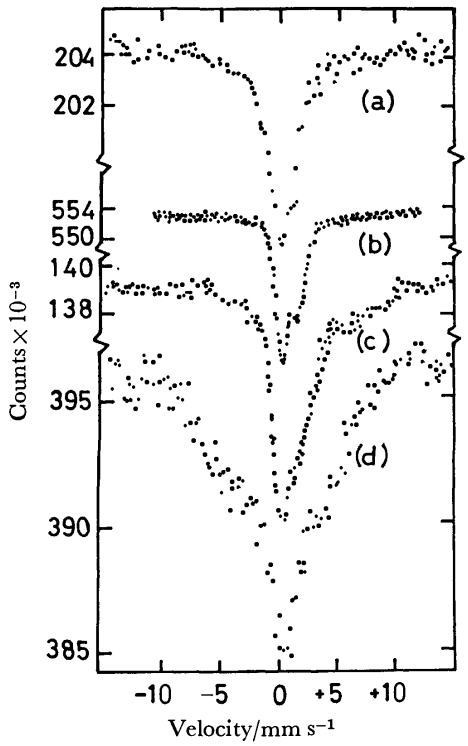

Fig. 4. Emission Mössbauer spectra at 78 K of a) $^{57}Co(dpm)_3$, b) $^{57}Co(acac)_3$, c) $^{57}Co(oxin)_3$, and d) $^{57}Co(dbm)_3$.

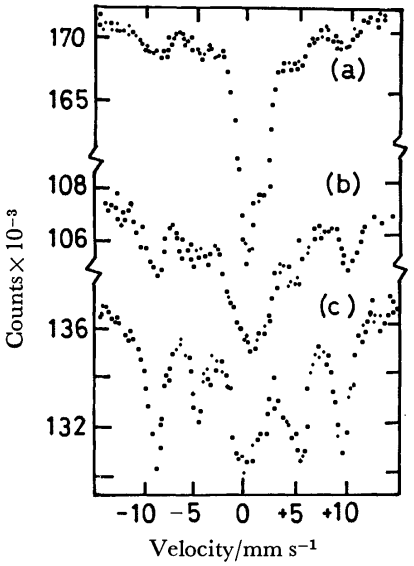

Fig. 5. Emission Mössbauer spectra at 4.2 K of a) $^{57}Co(dpm)_3$, b) $^{57}Co(oxin)_3$, and c) $^{57}Co(dbm)_3$.

spectrum at 78 K of $^{57}Co(acac)_3$ diluted in polystyrene is shown in Fig. 7, while the crystalline $^{57}Co(acac)_3$ is shown in Fig. 4 (b). The magnetic hfs is clearly found in the diluted sample.

Discussion

The magnetic hfs in the Mössbauer spectrum is known to arise from the interaction between the internal magnetic field caused by the electron-spin and the magnetic moment of the Mössbauer nucleus. In

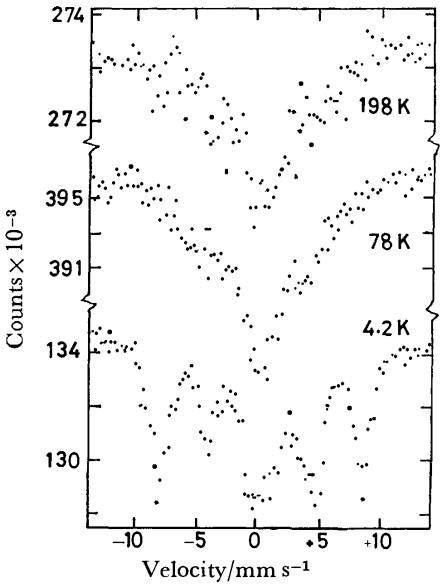

Fig. 6. Temperature-dependence of emission Mössbauer spectra for $^{57}Co(dbm)_3$.

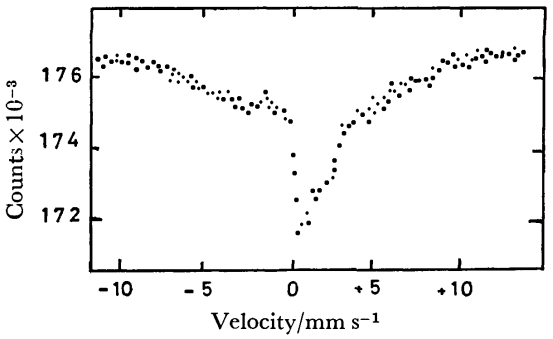

Fig. 7. Emission Mössbauer spectrum at 78 K of $^{57}Co(acac)_3$ diluted in polystyrene.

many paramagnetic iron compounds, however, the magnetic hfs is not observed in the absorption spectrum except at very low temperatures, because the internal magnetic field fluctuates in direction through the spin-spin and spin-lattice interactions with the surrounding atoms and/or molecules. Paramagnetic iron compounds diluted in diamagnetic compounds show the magnetic hfs at higher temperatures because of the decreased spin-spin interaction in the diluent diamagnetic compound. It is also known that a magnetic hfs of a small magnitude can be observed in the absorption spectra of the paramagnetic iron compounds with a large molecular size, as has been demonstrated by Wignall for $Fe(dbm)_3$ at 1.8 K.[9] We have previously reported that paramagnetic $Fe(acac)_3$ diluted in $Co(acac)_3$ shows the magnetic hfs in the absorption spectra at 78 to 230 K, but not $Fe(acac)_3$ diluted in paramagnetic $Mn(acac)_3$ or $Cr(acac)_3$ at the same temperature.[2]

In the present study, the absorption spectra at 78 K of paramagnetic $^{57}Fe(oxin)_3$ diluted in diamagnetic $Al(oxin)_3$ and $^{57}Fe(dbm)_3$ diluted in diamagnetic $Co(dbm)_3$ gave the magnetic hfs as well. As is known, the magnetic hfs is not clearly observed in the emission Mössbauer spectrum at 78 K in most ^{57}Co-labelled

cobalt(III) coordination compounds, such as hexammine cobalt(III), hexacyanocobaltate(III), tris(oxalato)-cobaltate(III), and tris(acetylacetonato)cobalt(III). When paramagnetic ^{57}Fe species produced through the EC-decay remain in environments diluted magnetically by diamagnetic cobalt(III) host compounds, the magnetic hfs might be expected to be observed to the same extent as in the paramagnetic Fe(III) species diluted in diamagnetic Co(III) compounds. In order to explain the experimental results (*i.e.*, that little or no magnetic hfs has been observed in most emission spectra at 78 K of the ^{57}Co-labelled cobalt(III) compounds), we have proposed that some species with an electron-spin should be formed in the vicinity of the decayed ^{57}Fe atoms and that the paramagnetic species with an electron spin should suppress the magnetic hfs through the spin-spin interaction with the paramagnetic ^{57}Fe species. The paramagnetic species were assumed to be radicals produced through the local radiolysis in the EC-decay and the subsequent Auger process.

As may be seen in Fig. 4, the magnetic hfs is observed in the emission spectra at 78 K in the source compounds, ^{57}Co(oxin)$_3$ and ^{57}Co(dbm)$_3$. The emission spectra at 4.2 K of these source compounds show the magnetic hfs to a much greater degree than at 78 K. The spectrum of ^{57}Co(dpm)$_3$ also shows the magnetic hfs at 4.2 K, but the intensity is apparently lower than those found in ^{57}Co(dbm)$_3$ and ^{57}Co(oxin)$_3$. The spectrum of ^{57}Co(acac)$_3$ at the temperature of liquid helium reported by Nath *et al.*[8] is very similar to that of ^{57}Co(dpm)$_3$. The intensities of the magnetic hfs at 4.2 K and 78 K decrease in the following order: ^{57}Co(dbm)$_3$ > ^{57}Co(oxin)$_3$ > ^{57}Co(dpm)$_3$ $\fallingdotseq$ ^{57}Co(acac)$_3$. The former two compounds have aromatic π-conjugated systems in the ligands, while the latter two compounds have no such aromatic system, as may be seen in Fig. 2. The appearance of the magnetic hfs might be related to the chemical structure of the source compound, especially to whether or not the source compound possesses π-conjugated systems in the ligands. Furthermore, the appearance of the magnetic hfs in the emission spectrum at 78 K of ^{57}Co(acac)$_3$ diluted in polystyrene shown in Fig. 7 can be explained in a similar way. The fact that fewer of the paramagnetic radicals are produced in the diluted sample of ^{57}Co(acac)$_3$ in polystyrene than in the neat crystalline ^{57}Co(acac)$_3$ may be ascribed to the effects of the many phenyl groups involved in polystyrene. It is well known in radiation chemistry that the radiolytic stability of compounds with π-conjugated systems is much larger than that of compounds with only σ-bond systems. The G-values of the free ion of various organic compounds in 2 MeV X-ray radiolysis were reported by Schmidt and Allen,[10] who showed that those values in aromatics and olefines are much smaller than in alkanes. From the radiation-chemical point of view, it may be concluded that the appearance of the magnetic hfs in the emission Mössbauer spectrum of a ^{57}Co-labelled cobalt(III) coordination compound proves the radical-formation hypothesis in the local radiolysis through the EC-Auger process.

References

1) H. Sano and T. Ohnuma, *Bull. Chem. Soc. Jpn.*, **44**, 726 (1975).
2) H. Sano, *J. Radioanal. Chem.*, **36**, 105 (1977).
3) H. Sano, M. Harada, and K. Endo, *Bull. Chem. Soc. Jpn.*, **51**, 2583 (1978).
4) N. Saito, H. Sano, and T. Tominaga, *Bull. Chem. Soc. Jpn.*, **38**, 681 (1965).
5) G. M. Bancroft, K. G. Dharmawardena, and A. J. Stone, *Chem. Commun.*, **1971**, 6.
6) J. Kleinberg, *Inorg. Synth.*, **5**, 188 (1957).
7) A. Ablob, *Memories Presentes Soc. Chem. T*, **53**, 234 (1933).
8) A. Nath, M. P. Klein, W. Kündig, and D. Lichtenstein, *Mössbauer Effect Methodology*, **5**, 163 (1966).
9) J. W. G. Wignall, *J. Chem. Phys.*, **44**, 2462 (1966).
10) W. F. Schmidt and A. O. Allen, *J. Chem. Phys.*, **52**, 2345 (1970).

 © 1980 The Chemical Society of Japan Bull. Chem. Soc. Jpn., 53, 1321—1326 (1980)

The Crystal Structure of Bis(2,2′-bipyridine)nitratocopper(II) Nitrate Monohydrate $[Cu(NO_3)(bpy)_2]NO_3 \cdot H_2O$

Hisayoshi NAKAI

Department of Chemistry, Hyogo College of Medicine, Mukogawa-cho, Nishinomiya, Hyogo 663

(Received September 19, 1979)

The crystal structure of the title compound has been redetermined from diffractometer data and refined by the least-squares method to $R=0.053$ for 2448 non-zero reflections. The crystal is triclinic, with $a=7.464(3)$, $b=10.002(5)$, $c=15.503(6)$ Å, $\alpha=111.50(5)$, $\beta=91.43(5)$, $\gamma=90.47(4)°$, space group $P\bar{1}$, and $Z=2$. The copper atom has a square-pyramidal coordination very distorted by the 4 N atoms of the bipyridine ligands and one of the O atoms of the nitrato ligand at the apical position. The disposition of the 4 N atoms at the basal plane is flattened tetrahedral. The Cu atom is displaced by 0.31 Å from the mean plane of the 4 N atoms towards the apical O atom. The Cu–O and the average Cu–N distances are 2.30 and 2.01 Å respectively. In both bipyridine molecules, the two pyridine planes are twisted slightly from each other; the interplanar angle is 2.6° in one bipyridine ligand and 6.0° in the other. The mean planes of the two bipyridine molecules make an angle of 44.6°.

The $Cu(bpy)_2^{2+}$ moiety in bis(bipyridine)copper(II) complexes has been shown to be unable to take a strictly coplanar disposition because of the interligand repulsion. Indeed, in these complexes, the planes of the two bipyridine ligands are usually twisted by 30—60° away from each other; consequently, the four nitrogen atoms are disposed tetrahedrally.[1-3] Such a situation, however, complicates the stereochemistry of penta-coordinate bis(bipyridine)copper(II) complexes; it is difficult to distinguish strictly between a trigonal-bipyramidal and a square-pyramidal structure. In the case of $[Cu(NO_3)(bpy)_2]NO_3 \cdot H_2O$, the coordination geometry of which has been reported briefly as a distorted trigonal bipyramid,[4] the reflectance spectrum is somewhat different from those of the other trigonal-bipyramidal complexes.[5]

In order to make a further investigation into the stereochemistry of bis(bipyridine)copper(II) complexes, a refinement of the crystal structure of the $[Cu(NO_3)(bpy)_2]NO_3 \cdot H_2O$ was performed using the diffractometer intensity data.

Experimental

The blue crystals of $[Cu(NO_3)(bpy)_2]NO_3 \cdot H_2O$ were prepared by Jeager's method[6] and were recrystallized from a water-methanol mixture. Found: C, 46.47; H, 3.67; N, 16.22%. Calcd for $Cu(bpy)_2(NO_3)_2 \cdot H_2O$: C, 46.38; H, 3.50; N, 16.23%.

Preliminary X-ray photographs taken with Cu $K\alpha$ radiation showed $\bar{1}$ Laue symmetry, indicating a triclinic space group. No systematic absences were observed. The space group is either $P\bar{1}$ or P1; the former was confirmed by a successful refinement of the structure.

A crystal with dimensions of $0.20 \times 0.20 \times 0.23$ mm was mounted on a glass fiber for data collection. The lattice constants were determined by a least-squares fit using 32 independent θ-values measured accurately on a diffractometer. Crystal data: $[Cu(NO_3)(bpy)_2]NO_3 \cdot H_2O$, $M.W.=517.9$, triclinic, $a=7.464(3)$, $b=10.002(5)$, $c=15.503(6)$ Å, $\alpha=111.50(5)$, $\beta=91.43(5)$, $\gamma=90.47(4)°$, $U=1076.4$ Å^3, $Z=2$, $D_c=1.60$, $D_m=1.60$ g·cm^{-3} (by flotation in a benzene–bromoform mixture), Mo $K\alpha$ radiation ($\lambda=0.71069$ Å), μ(Mo $K\alpha$)$=10.7$ cm^{-1}, space group $P\bar{1}$.

Intensity data with $2\theta \leqq 56°$ were collected at room temperature by means of the w-2θ scan technique on a Philips PW1100 four-circle diffractometer using graphite-monochromated Mo $K\alpha$ radiation. The scan speed and scan width were 0.03° s^{-1} and $(0.90+0.20\tan\theta)°$ respectively. The background was counted for 10 s at each end of the scan range. Three standard reflections (100, 040, and 002), monitored every 3 h throughout the data collection, showed no significant variation in intensity. A total of 2448 intensities with $I_{top}-2\sqrt{I_{top}}>I_{back}$ were classified as observed; I_{top} is the intensity (counts/s) measured at the top of the peak, while I_{back} is the mean background intensity (counts/s) obtained from the preliminary background measurement for 5 s on each side of the peak. The intensity data were processed with the computer program of Hornstra and Stubbe.[7] No absorption correction was made.

The reflectance spectrum of this compound was also measured, using a Hitachi 139 spectrophotometer fitted with a standard reflectance attachment.

Refinement of the Structure

The refinement of the structure was carried out by means of a block-diagonal least-squares method. The function minimized was $\Sigma w(|F_o|-|F_c|)^2$. A weighting scheme of the type suggested by Hughes[8] was applied, using $w=1.0$ for $F_o \leqq 20.0$ and $w=(20.0/F_o)^2$ for $F_o>20.0$. The atomic scattering factors were taken from Ref. 9.

The initial parameters were those reported earlier.[4] The refinement of the atomic positions and isotropic thermal parameters gave the R value of 0.127 after three least-squares cycles. Subsequent refinement in which each atom was allowed to vibrate anisotropically reduced the value of R to 0.064. The positions of all the hydrogen atoms were obtained from the difference Fourier map calculated at this point. These hydrogen atoms were included in the final refinement, with an isotropic thermal parameter of 4.0 Å^2. The final R value was 0.053 for 2448 observed reflections. All the parameter shifts were less than 0.2σ in the final cycle of the refinement. The atomic coordinates and thermal parameters are listed in Tables 1 and 2. The observed and calculated structure factors are preserved at the Chemical Society of Japan (Document Number 8013). The computer programs used in the calculations were as follows: HBLS-V[10] (least-squares calculation), RHOMAP[10] (Fourier synthesis), and DAPH[10] (interatomic distances and angles, least-squares plane, and coordinates of the H atoms). The calculations were made on the NEAC 2200-700 and

TABLE 1. ATOMIC PARAMETERS($\times 10^4$) FOR THE NON-HYDROGEN ATOMS AND THEIR STANDARD DEVIATIONS
The anisotropic thermal factors are of the form: $\exp\{-(h^2B_{11}+k^2B_{22}+l^2B_{33}+hkB_{12}+hlB_{13}+klB_{23})\}$.

Atom	x	y	z	B_{11}	B_{22}	B_{33}	B_{12}	B_{13}	B_{23}
Cu	1158(1)	3924(1)	2064(1)	256(2)	112(1)	43(1)	67(2)	48(1)	75(1)
N (1)	2825(7)	2776(5)	2562(3)	239(12)	104(6)	49(3)	−21(14)	3(9)	59(7)
C (1)	4431(9)	2245(7)	2230(5)	238(16)	134(9)	61(4)	21(19)	−18(12)	66(9)
C (2)	5438(11)	1422(7)	2604(5)	306(19)	116(9)	83(5)	82(20)	−62(15)	59(10)
C (3)	4750(12)	1145(8)	3358(6)	350(21)	143(10)	86(5)	3(23)	−104(17)	111(12)
C (4)	3137(11)	1723(7)	3716(5)	357(20)	143(9)	66(4)	−47(22)	−86(15)	117(11)
C (5)	2199(9)	2534(6)	3300(4)	248(15)	97(7)	45(3)	−73(16)	−31(11)	49(8)
N (2)	−187(7)	4018(5)	3172(3)	250(13)	125(7)	43(2)	−25(14)	16(9)	63(7)
C (6)	478(9)	3202(6)	3627(4)	270(16)	118(8)	43(3)	−82(18)	−10(11)	61(8)
C (7)	−457(11)	3034(8)	4351(4)	325(19)	185(11)	48(3)	−167(23)	−22(13)	97(10)
C (8)	−2043(11)	3720(9)	4607(5)	301(19)	222(13)	54(4)	−157(25)	51(14)	66(11)
C (9)	−2725(11)	4545(8)	4134(5)	288(18)	197(12)	49(4)	−74(23)	60(13)	39(10)
C (10)	−1785(9)	4658(7)	3415(4)	221(15)	145(9)	57(4)	−20(18)	46(12)	52(9)
N (3)	926(7)	5944(5)	2037(3)	203(11)	103(6)	48(3)	−10(13)	7(8)	47(6)
C (11)	337(10)	7137(7)	2704(4)	282(17)	107(8)	57(4)	13(18)	9(12)	46(9)
C (12)	351(10)	8464(7)	2622(5)	276(18)	114(8)	80(5)	46(19)	6(14)	57(10)
C (13)	1039(10)	8571(7)	1825(5)	295(18)	111(9)	83(5)	−47(20)	−47(15)	96(10)
C (14)	1698(9)	7371(7)	1146(5)	218(15)	123(8)	67(4)	−14(17)	−30(12)	89(9)
C (15)	1604(8)	6066(6)	1264(4)	172(13)	107(7)	48(3)	−42(15)	−26(10)	67(8)
N (4)	2235(7)	3575(5)	846(3)	222(11)	110(6)	46(2)	26(13)	21(9)	66(6)
C (16)	2238(8)	4713(6)	576(4)	180(13)	128(8)	43(3)	−20(16)	−1(10)	69(8)
C (17)	2822(9)	4577(7)	−296(4)	203(14)	157(9)	49(3)	−49(18)	12(11)	91(9)
C (18)	3358(9)	3265(8)	−889(4)	202(15)	199(11)	50(3)	−19(20)	33(11)	74(10)
C (19)	3321(9)	2088(8)	−618(4)	231(16)	172(10)	48(3)	19(20)	33(12)	26(9)
C (20)	2727(9)	2289(7)	258(4)	256(16)	125(8)	52(3)	39(18)	59(12)	49(9)
O (1)	−1491(7)	3165(4)	1231(3)	371(13)	108(5)	60(3)	−40(14)	−17(9)	70(6)
O (2)	−576(8)	1212(6)	1315(4)	344(15)	188(8)	114(4)	96(17)	−89(13)	152(10)
O (3)	−2903(7)	1206(5)	460(4)	282(13)	173(7)	93(4)	−109(15)	−77(11)	97(9)
N (5)	−1656(7)	1831(5)	995(3)	201(11)	131(7)	57(3)	26(14)	27(9)	86(7)
O (4)	4261(15)	5988(9)	3174(10)	787(38)	233(14)	399(16)	−213(36)	−788(44)	263(25)
O (5)	5920(15)	7652(12)	3204(8)	813(40)	427(21)	188(9)	34(46)	396(32)	232(23)
O (6)	4183(18)	8040(15)	4207(7)	956(49)	630(32)	144(8)	130(63)	214(32)	297(27)
N (6)	4772(11)	7126(9)	3471(6)	408(23)	269(14)	124(6)	66(29)	31(19)	184(16)
O(H_2O)	8102(16)	9781(14)	4750(8)	782(39)	619(30)	170(9)	−188(54)	5(29)	414(28)

TABLE 2. ATOMIC COORDINATES($\times 10^3$) OF THE HYDROGEN ATOMS AND THEIR STANDARD DEVIATIONS

Atom	x	y	z	Atom	x	y	z
H(C1)	485(6)	238(5)	158(3)	H(C12)	−9(7)	932(4)	316(3)
H(C2)	653(7)	90(5)	220(4)	H(C13)	103(7)	951(5)	179(4)
H(C3)	537(9)	61(6)	373(4)	H(C14)	199(7)	719(5)	42(3)
H(C4)	280(8)	159(5)	430(3)	H(C17)	285(6)	540(4)	−45(3)
H(C7)	3(7)	241(6)	461(3)	H(C18)	392(7)	311(6)	−154(3)
H(C8)	−282(8)	359(7)	509(3)	H(C19)	384(7)	107(5)	−105(3)
H(C9)	−384(7)	508(6)	430(3)	H(C20)	243(7)	150(5)	51(3)
H(C10)	−229(6)	526(5)	311(3)	H(H_2O)	693(18)	54(14)	517(7)
H(C11)	−11(7)	694(4)	330(3)	H(H_2O)′	785(20)	−6(17)	440(9)

ACOS-800 of Osaka University.

Results and Discussion

The crystal consists of discrete $[Cu(NO_3)(bpy)_2]^+$, NO_3^-, and H_2O. Figure 1 shows the a-axis projection of the crystal structure. The bond lengths and angles, with their estimated standard deviations, are given in Table 3.

Although the two chelate rings composed of Cu and the bpy have substantially the same structure, two Cu–N bonds in each ring are significantly different in length; the average value of the longer bond lengths is 2.034(5) Å, while that of the shorter ones is 1.983(5)

Å. The nitrato group is coordinated virtually as a unidentate ligand through the O(1) atom(Cu–O(1)= 2.299(5) Å), but one more oxygen atom, O(2), is located at a distance of 2.818(7) Å from the copper atom. The copper atom is thus five-coordinate, but the coordination polyhedron around the copper atom seems to be intermediate between a trigonal bipyramid and a square pyramid.

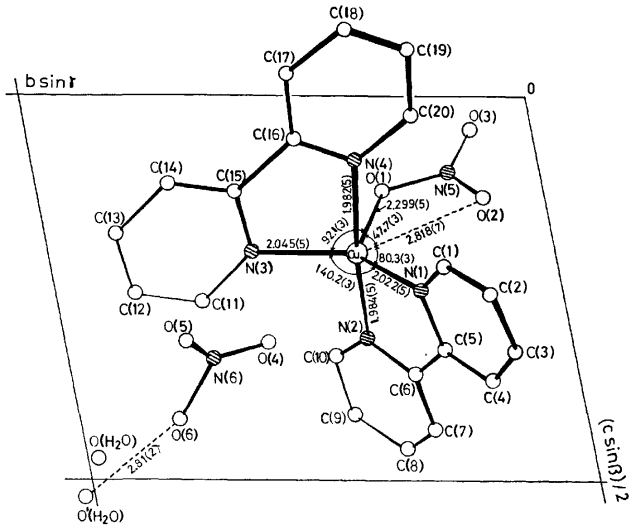

Fig. 1. The crystal structure viewed down the a axis.

If this complex is regarded as assuming a trigonal-bipyramidal structure, I, the N(2) and N(4) atoms can be said to occupy the axial positions, while the Cu, O(1), N(1), and N(3) atoms form an equatorial plane. However, in $[CuX(bpy)_2]^{n+}$-type complexes (X=I, NH_3, Cl, $CS(NH_2)_2$, and Cu^ICl_2) which have been classified as trigonal-bipyramidal structures on the bases of the spectral and X-ray studies,[5,11–15] it has been found that the axial Cu–N distances are significantly (0.06—0.12 Å) shorter than the equatorial ones except for the case of $[CuI(bpy)_2]^+$,[11] and also that the N–Cu–N angle in the equatorial plane is in the 109—123° range, which is close to the angle (120°) in the regular trigonal bipyramid. In the present complex, the difference between the axial and equatorial Cu–N bond distances is 0.038 Å, a little smaller than those in the trigonal-bipyramidal complexes mentioned above. Besides, the angle of N(1)–Cu–N(3) in the equatorial plane is 140.2(3)°; this value is considerably outside the range of 109—123°.

Table 3. Interatomic distances(l/Å) and angles(φ/°), with their estimated standard deviations in parentheses

Cu-N(1)=2.022(5)	C(16)-C(17)=1.390(9)	O(1)-Cu-N(4)=85.5(3)	C(6)-C(7)-C(8)=119.5(7)
Cu-N(2)=1.984(5)	C(17)-C(18)=1.367(11)	N(1)-Cu-N(2)=81.1(3)	C(7)-C(8)-C(9)=119.8(8)
Cu-N(3)=2.045(5)	C(18)-C(19)=1.389(11)	N(1)-Cu-N(3)=140.2(3)	C(8)-C(9)-C(10)=118.9(8)
Cu-N(4)=1.982(5)	C(19)-C(20)=1.382(10)	N(1)-Cu-N(4)=100.0(3)	N(2)-C(10)-C(9)=121.9(7)
Cu-O(1)=2.299(7)	N(5)-O(1)=1.251(7)	N(2)-Cu-N(3)=103.6(3)	C(11)-N(3)-C(15)=118.4(5)
Cu···O(2)=2.818(7)	N(5)-O(2)=1.222(8)	N(2)-Cu-N(4)=170.9(3)	N(3)-C(11)-C(12)=122.7(7)
N(1)-C(1)=1.350(9)	N(5)-O(3)=1.231(8)	N(3)-Cu-N(4)=81.4(3)	C(11)-C(12)-C(13)=118.2(7)
N(1)-C(5)=1.347(8)	N(6)-O(4)=1.119(18)	O(2)···Cu-O(1)=47.7(4)	C(12)-C(13)-C(14)=119.9(7)
C(1)-C(2)=1.385(11)	N(6)-O(5)=1.162(15)	O(2)···Cu-N(1)=80.3(4)	C(13)-C(14)-C(15)=118.8(7)
C(2)-C(3)=1.405(12)	N(6)-O(6)=1.264(18)	O(2)···Cu-N(2)=81.8(4)	N(3)-C(15)-C(14)=121.9(6)
C(3)-C(4)=1.379(12)	C(1)-H(C1)=1.12(5)	O(2)···Cu-N(3)=139.5(4)	N(3)-C(15)-C(16)=114.8(5)
C(4)-C(5)=1.391(10)	C(2)-H(C2)=1.06(6)	O(2)···Cu-N(4)=89.5(4)	C(14)-C(15)-C(16)=123.3(6)
C(5)-C(6)=1.467(9)	C(3)-H(C3)=1.02(6)	O(4)···Cu-N(1)=72.6(8)	Cu-N(3)-C(11)=128.4(5)
N(2)-C(6)=1.349(9)	C(4)-H(C4)=0.99(6)	O(4)···Cu-N(2)=95.3(8)	Cu-N(3)-C(15)=113.0(5)
N(2)-C(10)=1.354(9)	C(7)-H(C7)=0.93(6)	O(4)···Cu-N(3)=67.6(8)	Cu-N(4)-C(16)=115.0(4)
C(6)-C(7)=1.397(10)	C(8)-H(C8)=1.01(7)	O(4)···Cu-N(4)=93.6(8)	Cu-N(4)-C(20)=124.6(4)
C(7)-C(8)=1.366(12)	C(9)-H(C9)=0.98(5)	Cu-O(1)-N(5)=109.3(5)	C(16)-N(4)-C(20)=119.9(5)
C(8)-C(9)=1.382(12)	C(10)-H(C10)=0.96(5)	Cu···O(2)-N(5)=84.3(6)	C(15)-C(16)-N(4)=115.4(5)
C(9)-C(10)=1.370(11)	C(11)-H(C11)=1.07(5)	C(1)-N(1)-C(5)=119.0(6)	C(15)-C(16)-C(17)=123.9(6)
N(3)-C(11)=1.347(9)	C(12)-H(C12)=1.02(6)	N(1)-C(1)-C(2)=122.4(7)	N(4)-C(16)-C(17)=120.7(6)
N(3)-C(15)=1.357(8)	C(13)-H(C13)=0.96(6)	C(1)-C(2)-C(3)=118.0(7)	C(16)-C(17)-C(18)=119.3(7)
C(11)-C(12)=1.379(11)	C(14)-H(C14)=1.10(5)	C(2)-C(3)-C(4)=119.7(8)	C(17)-C(18)-C(19)=120.1(7)
C(12)-C(13)=1.389(12)	C(17)-H(C17)=0.94(6)	C(3)-C(4)-C(5)=118.9(7)	C(18)-C(19)-C(20)=118.1(7)
C(13)-C(14)=1.378(11)	C(18)-H(C18)=1.06(6)	N(1)-C(5)-C(4)=121.9(6)	N(4)-C(20)-C(19)=122.0(6)
C(14)-C(15)=1.384(9)	C(19)-H(C19)=1.07(5)	N(1)-C(5)-C(6)=114.7(6)	O(1)-N(5)-O(2)=118.2(6)
C(15)-C(16)=1.474(9)	C(20)-H(C20)=1.03(5)	C(4)-C(5)-C(6)=123.4(6)	O(1)-N(5)-O(3)=118.7(6)
N(4)-C(16)=1.349(8)	O(6)···O'(H_2O)[a]=2.81(2)	Cu-N(1)-C(1)=127.1(5)	O(2)-N(5)-O(3)=123.1(6)
N(4)-C(20)=1.337(9)		Cu-N(1)-C(5)=113.8(5)	O(4)-N(6)-O(5)=128.1(13)
		Cu-N(2)-C(6)=114.6(4)	O(4)-N(6)-O(6)=122.6(13)
O(1)-Cu-N(1)=127.8(3)	C(5)-C(6)-N(2)=115.2(6)	Cu-N(2)-C(10)=125.4(5)	O(5)-N(6)-O(6)=109.2(12)
O(1)-Cu-N(2)=86.7(3)	C(5)-C(6)-C(7)=124.4(6)	C(6)-N(2)-C(10)=119.4(6)	
O(1)-Cu-N(3)=92.1(3)	N(2)-C(6)-C(7)=120.5(6)		

a) $1-x$, $2-y$, $1-z$.

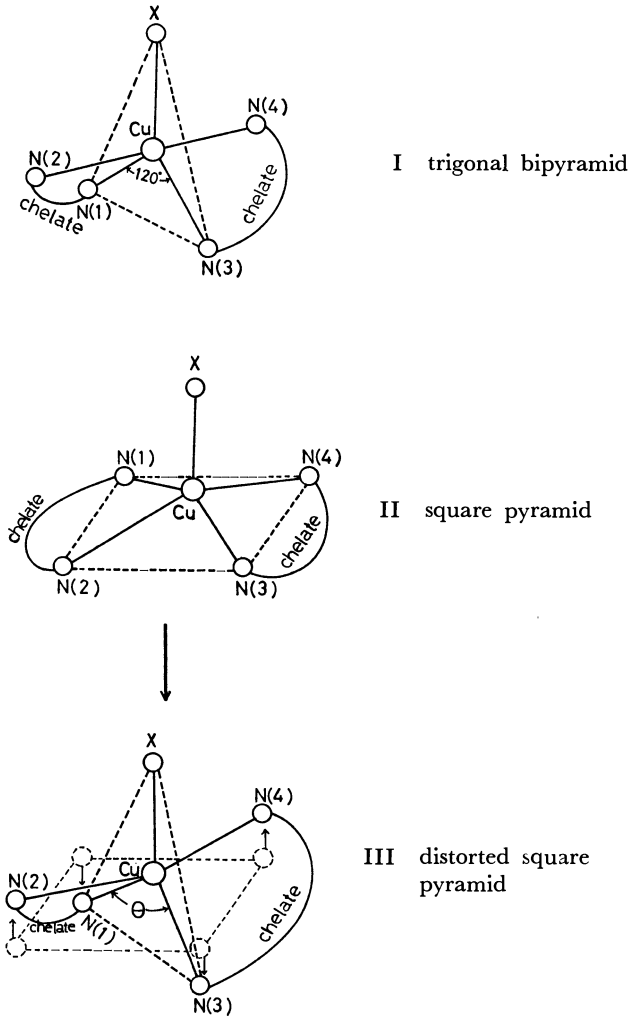

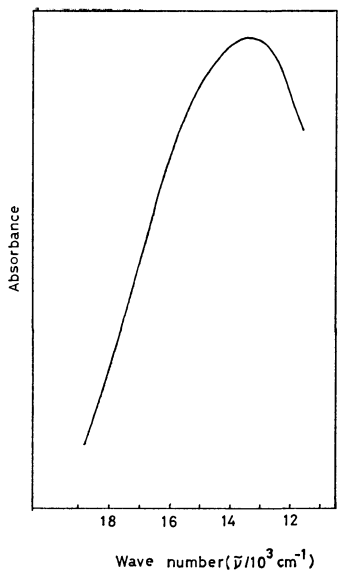

Fig. 2. Electronic reflectance spectrum of $[Cu(NO_3)(bpy)_2]NO_3 \cdot H_2O$.

The electronic reflectance spectrum of this complex in the range of $11.5—20.0 \times 10^3$ cm^{-1} shows a single peak at 13.2×10^3 cm^{-1}. The peak position is considerably different from those for the trigonal-bipyramidal Cu–bpy complexes,[5] in which the spectra have been known to show a single characteristic band with a maximum at $12.0—12.5 \times 10^3$ cm^{-1}. These structural and spectral features are not compatible with those of the trigonal-bipyramidal copper(II) chelates of the bpy.

On the other hand, if the coordination polyhedron of this complex is regarded as a square pyramid, II, the four nitrogen atoms should be taken as forming the basal plane, and the O(1) atom, as occupying the apical position. In this case, however, the nitrogen atoms can not take a planar disposition because of the interligand repulsion, and so presumably have a flattened tetrahedral arrangement, as is shown in III. The scaled model indicates that the N(1)–Cu–N(3)(=θ) and X–Cu–N(1)(=X–Cu–N(3)) angles in III (X= a donor atom in the fifth position) are 140—160° and 100—110° respectively. In the present complex, however, the O(1)–Cu–N(1) angle (127.8°), which corresponds to the X–Cu–N(1) angle in III, is larger than the expected value of about 110°, since the N(1)–Cu–N(3) angle corresponding to θ is 140.2°. On examining the significance of this observation in detail, it should be noted that the O(2) atom of the nitrato group almost lies on the plane, "A", defined by the Cu, O(1), N(1), and N(3) atoms (Fig. 1) and has short contacts with the atoms of the chelate rings: 3.178(8) Å to N(1), 3.205(8) Å to N(2), and 2.66(5) Å to H(C20). The steric interactions with the bipyridine ligands appear to prevent bidentate coordination of the nitrato group. Moreover, the O(2) atom results in the enlargement of the O(1)–Cu–N(1) angle by 35.7° as compared with the O(1)–Cu–N(3). On the basis of the structural features described above, the coordination geometry about the copper atom should

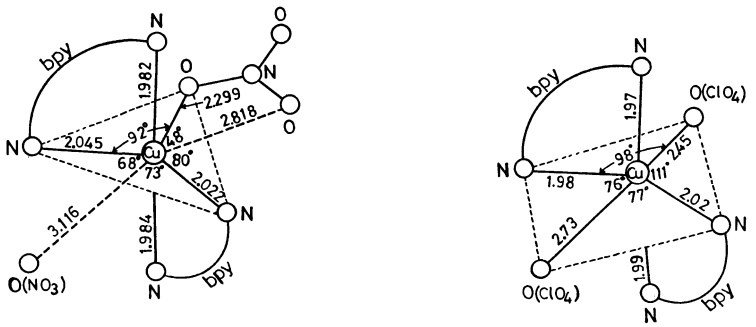

Fig. 3. The resemblance between the stereochemistries of $[Cu(NO_3)(bpy)_2]NO_3 \cdot H_2O$ and $[Cu(ClO_4)(bpy)_2]ClO_4$.

be regarded as a distorted square pyramid.

The copper atom is displaced by 0.31 Å towards the apical O(1) atom from the mean plane of the 4 N atoms. The Cu–N bond distances are 2.008 Å, on the average. The dihedral angle between the Cu$\begin{matrix}/N(1)\\ \backslash N(2)\end{matrix}$ and Cu$\begin{matrix}/N(3)\\ \backslash N(4)\end{matrix}$ planes is 42.8°. The structure of the present complex is thought to be related to that of the distorted *trans*-octahedral $[Cu(ClO_4)(bpy)_2]$-ClO_4.[1] This is illustrated in Fig. 3, which shows a schematic drawing of these two complexes. Although the O(4) atom of the uncoordinated NO_3^- ion is situated nearly at the sixth position in an octahedral coordination, it is 3.12 Å apart from the copper atom.

Table 4. Equation of the least-squares plane[a] and deviations of atoms from the planes (l/Å)

Pyridine ring I					
$-0.4432X-0.6450Y-0.6226Z+4.0435=0$					
N (1)	0.013	C (1)	−0.008	C (2)	−0.005
C (3)	0.013	C (4)	−0.009	C (5)	−0.004
Pyridine ring II					
$-0.4594X-0.6094Y-0.6462Z+4.1600=0$					
N (2)	−0.010	C (6)	−0.002	C (7)	0.010
C (8)	−0.007	C (9)	−0.005	C (10)	0.013
Bipyridine ligand I					
$-0.4550X-0.6260Y-0.6333Z+4.1181=0$					
N (1)	0.049	C (1)	0.013	C (2)	−0.019
C (3)	−0.020	C (4)	−0.025	C (5)	0.014
C (6)	0.006	C (7)	0.037	C (8)	0.011
C (9)	−0.016	C (10)	−0.018	N (2)	−0.031
Pyridine ring III					
$-0.8970X-0.0257Y-0.4414Z+1.9320=0$					
N (3)	0.008	C (11)	−0.011	C (12)	0.003
C (13)	0.008	C (14)	−0.012	C (15)	0.005
Pyridine ring IV					
$-0.9268X-0.0897Y-0.3646Z+2.1974=0$					
N (4)	−0.014	C (16)	0.009	C (17)	−0.001
C (18)	−0.003	C (19)	−0.001	C (20)	0.010
Bipyridine ligand II					
$-0.9121X-0.0641Y-0.4050Z+2.0784=0$					
N (3)	0.069	C (11)	0.060	C (12)	0.018
C (13)	−0.049	C (14)	−0.082	C (15)	−0.004
C (16)	−0.007	C (17)	0.050	C (18)	0.063
C (19)	0.015	C (20)	−0.040	N (4)	−0.079
Nitrato group					
$0.6082X+0.1645Y-0.7766Z+1.6931=0$					
O (1)	−0.001	O (2)	−0.001	O (3)	−0.001
N (5)	0.004				
Uncoordinated nitrate ion					
$-0.6632X+0.5074Y-0.5502Z+2.3854=0$					
O (4)	−0.004	O (5)	−0.004	O (6)	−0.004
N (6)	0.013				
Plane through N(1), N(2), N(3), and N(4)					
$-0.6884X-0.4547Y-0.5651Z+3.7622=0$					
N (1)	−0.293	N (2)	0.374	N (3)	−0.462
N (4)	0.560	Cu[b]	0.312		
Plane through Cu, N(1), N(3), and O(1)					
Cu	0.004	N (1)	−0.002	N (3)	−0.001
O (1)	−0.001	O (2) [b]	0.201	O (4) [b]	−0.131
Plane formed by Cu, N(1), and N(2)					
$-0.4800X-0.6873Y-0.5452Z+3.8742=0$					
Plane formed by Cu, N(3), and N(4)					
$-0.8885X-0.0910Y-0.4499Z+2.2572=0$					

a) Planes are defined as $AX+BY+CZ+D=0$, where X, Y, and Z are Cartesian coordinates which are related to the triclinic cell coordinates(x, y, z) by these transformations: $X=xa+yb\cos\gamma+zc\cos\beta$, $Y=yb\sin\gamma-zc\cos\alpha^*\sin\beta$, and $Z=zc\sin\alpha^*\sin\beta$. b) Atoms not used to define the least-squares plane.

The bipyridine ligands are not planar, but the individual pyridine moiety is planar within ±0.014 Å. The pyridine moieties of the bipyridine molecule are slightly twisted from each other about the 2,2′-carbon bond; the twist angle is 2.6° for the molecule comprising N(1) and N(2) and 6.0° for the other. Furthermore, the bond angle of α is larger than that of β by about 9°. A similar difference in these angles

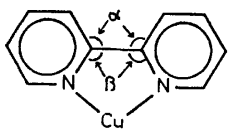

(5—10°) has also been observed in the crystal structure of the 2,2′-bipyridine molecule[16] and its copper(II) complexes.[1] The bond lengths in the bipyridine ligands range from 1.37(1) to 1.41(1) Å in the aromatic C–C bond, and from 1.34(1) to 1.36(1) Å in C–N, while the 2,2′-carbon bonds are about 1.47 Å long (Table 3). The bond angles of C–C–C, C–N–C, and C–C–N in pyridine rings are 119.1, 119.2, and 121.8° respectively, on the average. The H(C1)---H(C20) and H(C10)---H(C11) distances between the bipyridine chelates are 2.37(7) and 2.27(7) Å. These values are not very different from the sum of the van der Waals radii of the hydrogen atoms.

The nitrato group is planar and acts as a unidentate ligand through the O(1) atom; another O(2) atom is located at the distance of 2.818(7) Å from the copper atom. The angle of Cu–O(1)–N(5) is 109.3(5)°. This mode of coordination of the nitrato group has also been found in the complexes[17] containing unidentate nitrato groups (ex. $[Cu(NO_3)_2(phen)]$[18] and $[Cu(NO_3)(dach)_2]NO_3 \cdot [Cu(H_2O)(dach)_2](NO_3)_2$[19] (dach=1,4-diazacycloheptane)). The N(5)–O(1) bond distance is a little longer (0.02—0.03 Å) than the remaining N(5)–O(2) and N(5)–O(3) ones, and the O(2)–N(5)–O(3) angle is greater (4—5°) than those of O(1)–N(5)–O(2) and O(1)–N(5)–O(3). The dihedral angle between the nitrato plane and the "A" plane is about 10°.

The uncoordinated nitrate ion is linked to the water-oxygen atom, $O'(H_2O)[1-x, 2-y, 1-z]$, through O–H---O hydrogen bonding ($O'(H_2O)$---O(6)=2.81Å).

The author is very grateful to Professor Yukinao Noda for his kind advice and encouragement throughout the present work. The author is also grateful to Professor Emeritus Hisao Kuroya and Dr. Shun'ichiro Ooi of Osaka City University for their valuable discussions and advice, and to Dr. Keiji Matsumoto, Osaka City University, for the use of a Philips PW1100 dif-

fractometer.

References

1) H. Nakai, *Bull. Chem. Soc. Jpn.*, **44**, 2412 (1971).
2) M. B. Ferrari, G. G. Fava, and C. Pelizzi, *J. Chem. Soc., Chem. Commun.*, **1977**, 8.
3) W. D. Harrison and B. J. Hathaway, *Acta Crystallogr., Sect. B*, **34**, 2843 (1978).
4) H. Nakai, S. Ooi, and H. Kuroya, *Bull. Chem. Soc. Jpn.*, **43**, 577 (1970); H. Nakai, Ph. D. Thesis, Osaka City Univ., Osaka, Japan, 1971.
5) B. J. Hathaway, I. M. Procter, R. C. Slade, and A. A. A. Tomlinson, *J. Chem. Soc., A*, **1969**, 2219.
6) F. M. Jaeger and J. A. Dijik, *Z. Anorg. Chem.*, **227**, 273 (1936).
7) J. Hornstra and B. Stubbe, PW1100 Data Processing Program, Philips Research Laboratories, Eindhoven, Holland.
8) E. W. Hughes, *J. Am. Chem. Soc.*, **63**, 1737 (1941).
9) "International Tables for X-Ray Crystallography," Kynoch Press, Birmingham (1974), Vol. IV, pp. 71—98.
10) T. Ashida, The Universal Crystallographic Computing System-Osaka, The Computation Center, Osaka Univ. (1973), pp. 55, 63; N. Yasuoka and N. Tanaka, *ibid.*, p. 38.
11) G. A. Barclay, B. F. Hoskins, and C. H. L. Kennard, *J. Chem. Soc.*, **1963**, 5691.
12) F. S. Stephens, *J. Chem. Soc., Dalton Trans.*, **1972**, 1350.
13) F. S. Stephens and P. A. Tucker, *J. Chem. Soc., Dalton Trans.*, **1973**, 2293.
14) M. B. Ferrari, A. B. Corradi, G. G. Fava, C. G. Palmieri, M. Nardelli, and C. Pelizzi, *Acta Crystallogr., Sect. B*, **29**, 1808 (1973).
15) J. Kaiser, G. Brauer, and F. A. Schroder, *J. Chem. Soc., Dalton Trans.*, **1974**, 1490.
16) L. L. Merritt, Jr., and E. D. Schroeder, *Acta Crystallogr.*, **9**, 801 (1956).
17) C. C. Addison, N. Logan, S. C. Wallwork, and C. D. Garner, *Q. Rev. Chem. Soc.*, **25**, 289 (1971).
18) D. L. McFadden and A. T. McPhail, *J. Chem. Soc., Dalton Trans.*, **1975**, 1993.
19) M. S. Hussain and H. Hope, *Acta Crystallogr., Sect. B*, **25**, 1866 (1969).

An X-Ray Photoelectron Spectroscopic Study of Several Ligands in Coordination Compounds

Tooru YOSHIDA

Osaka Prefectural Industrial Research Institute, 2-1-53, Enokojima, Nishi-ku, Osaka 550

(Received October 13, 1979)

The N(1s) electron binding energies were measured by means of X-ray photoelectron spectroscopy for the complexes of 2-pyridinecarboxylic acid, 8-quinolinol, and anthranilic acid with a variety of bivalent metal ions. The correlations of their binding energies with the electronegativity and the ionic potential (Z/r) of the metal ion and the charge on the nitrogen atom, and the covalent character of the nitrogen-metal bond calculated on the basis of Pauling's concept were examined. The chemical shift in the N(1 s) binding energy was about 1 eV at most. However, it was suggested that it is possible to use the chemical shift to determine the nature and strength of the nitrogen-metal bond in a series of complexes of the same ligand.

X-Ray photoelectron spectroscopy (XPS) is now extensively used to study the electronic and geometric structures of coordination compounds. There have been many studies of the determinations of the oxidation state of elements, the donor-acceptor capacity of ligands, the mode of ligand coordination, the structure of valence levels, *etc.* However, there have been few studies in which the effect of a variety of metal ions of both transition and typical elements on the binding energy of inner-shell electrons of a ligand in a series of complexes of the ligand has been systematically examined.[1)]

The purpose of the present study is to determine the N(1s) electron binding energies of the complexes of the three bidentate ligands involving nitrogen and oxygen donor atoms—2-pyridinecarboxylic acid, 8-quinolinol, anthranilic acid, with various bivalent metal ions, and to examine the correlations of their binding energies with the electronegativity and the ionic potential of the metal ion and the charge on the nitrogen atom and the covalent character of the nitrogen–metal bond calculated based upon Pauling's concept.[2)]

Experimental

The X-ray photoelectron spectra were measured on an AEI ES200 spectrometer. Al k_α (1486.6 eV) and Mg k_α (1253.6 eV) X-ray radiations were used as the excitation sources. Samples were ground to powder and then dusted onto a double-backed adhesive tape. The measurements were run at room temperature under a vacuum of about 10^{-7} Torr. However, a freezing technique was used for a few volatile samples. All the free ligands (abbreviated as LH) were commercially available and of an analytical grade, and they were used after recrystallization from ethanol. The metal salts used were acetates except for the following salts: K_2PtCl_4, $PdCl_2$, $Fe(NH_4)_2(SO_4)_2$, $SnCl_2$, $BeSO_4$, and $Sr(NO_3)_2$. The complexes were prepared based upon the literature methods.[3)] In outline, the methods consisted of the addition of an ethanol or acetic acid solution of ligands to an aqueous solution of metal salts, in some cases followed by neutralization by an aqueous NaOH or ammonia. The ligand-metal ratios were 2:1 for all the complexes except for the beryllium complex of 2-pyridinecarboxylic acid. The composition of the beryllium complex of 2-pyridinecarboxylic acid was $Be_2OL_2\cdot 2H_2O$, as was the case with its 8-quinolinol complex.[4)] Instead of the beryllium complex of 8-quinolinol, that of 2-methyl-8-quinolinol was used; its composition was BeL_2.[5)] The sodium and perchlorate salts of each LH were obtained by treating LH with NaOH and $HClO_4$ in ethanol respectively. All the compounds were checked by elemental analysis. It is reasonable to assume that the C(1s) binding energy is nearly constant within the complexes of the same ligand. Furthermore, as only the relative energies were considered in the present study, the binding energy of the C(1s) electron peak was used as the energy standard throughout the present experiments; it was taken to be 285.0 eV. The reproducibilities of the values thus obtained were within ± 0.1 eV.

Binding-energy Correlations

It has been shown that, in the point-charge model, the core-electron binding energy (abbreviated as BE) can be expressed as follows in terms of the charge density, q_A, on the A atom of interest:[6)]

$$BE = k_A q_A + V + E_R + l_A, \quad (1)$$

where V denotes the electrostatic potential at the nucleus caused by the surrounding atoms, where E_R gives the relaxation energy attributable to photoionization, and where k_A and l_A are constants to be decided from experiments. Here, V is given by the equation: $V=\sum_{A\neq B} q_B/R_{A-B}$, where q_B is the charge on the surrounding atom, B, and where R_{A-B} is the interatomic distance from the B atom to the A atom. For the covalent compound, the summation may be restricted to atomic charges within one molecule. E_R can be expected to be almost constant as long as molecules in similar environments are being compared.[7)]

In this study, the structures of the compounds to be compared are so similar that the N(1s) binding energy may be approximately written as follows:

$$BE = k_N q_N + q_M/R_{M-N} + K \quad (2)$$

where q_N and q_M are the charges on the nitrogen and the metal respectively, where R_{M-N} is the interatomic distance of the metal and the nitrogen atoms, and where K is a constant. Here, all the other terms except for q_M/R_{M-N} in V were regarded as constants.

To a very rough approximation, the N(1s) binding energy is linearly related to the charge of the nitrogen atom.[6)] That is,

$$BE = k'_N q_N + l'_N \quad (3)$$

where k'_N and l'_N are constants.

Results and Discussion

All the compounds used and their N(1s) binding energies are given in Table 1. The electronegativities[8)]

Table 1. Measured N(1s) binding energies

Sample No.	Compound[a]	*BE*/eV 2-Pyridinecarboxylic acid	8-Quinolinol	Anthranilic acid
1	PtL_2	400.4	400.3	400.5
2	PdL_2	400.2	400.1	400.3
3	CuL_2	399.8	399.8	399.9
4	NiL_2	399.5	399.5	399.9
5	CoL_2	399.4	399.5	399.7
6	FeL_2	399.6	—	399.9
7	MnL_2	399.4	399.5	399.7
8	ZnL_2	399.4	399.6	399.8
9	CdL_2	399.5	399.5	399.8
10	HgL_2	400.0	—	400.1
11	SnL_2	399.5	—	399.8
12	PbL_2	399.3	399.5	399.6
13	BeL_2 or Be_2OL_2[b]	399.6	399.6	399.8
14	MgL_2	399.3	399.4	399.7
15	CaL_2	399.1	399.1	399.8
16	SrL_2	399.1	399.1	399.6
17	BaL_2	399.0	399.1	399.6
18	LNa	399.0	398.9	399.3
19	LH	399.2	399.1	399.6
20	LH_2ClO_4	401.4	401.5	402.0

a) Crystal waters in the structural formula were omitted because of the negligible effect of crystal water on the N(1s) binding energy. b) The formula corresponds to the complex of 2-pyridinecarboxylic acid.

and ionic[9] and atomic[10] radii adopted in this study are given in Table 2, along with the calculated charges and covalent characters.

All the N(1s) binding energies of the complexes of the three ligands were equal to, or higher than, those of the corresponding sodium salts, while they were lower than those of the corresponding perchlorates. The changes in the binding energy, the chemical shifts, were about 1 eV at most. These chemical shifts were considered to be attributable to the decreases in the electron density on the nitrogen atoms caused by the coordination of the lone-pair electrons of the nitrogen atoms to the metal.

In this study, the O(1s) binding energies were not discussed because of their small chemical shifts compared with those of the N(1s) binding energies.

Correlations between N(1s) Binding Energies and Electronegativities. Qualitatively, the electronegativity of an element is considered to be a measure of its ability to attract electrons. Therefore, it can be expected that, within the complexes of the same ligand, the binding energy of the donor atom of the ligand increases with the electronegativities of the metal ions involved.

The correlation between the N(1s) binding energy and the electronegativity in the complexes of 2-pyridinecarboxylic acid is shown in Fig. 1. An increase in the binding energy with the increase in the electronegativity could be observed, although the trend was weak. The correlations in the complexes of 8-

Table 2. Several physical constants and calculated charges

Element	Electronegativity[a] (χ)	Ionic radius r/Å	Atomic radius/Å	C(%)[b]	q_N[c]	q_M[c]	q_M/R_{M-N}
Pt	2.28	0.80	1.32	76.7	0.364	−0.963	−0.5
Pd	2.20	0.80	1.37	73.5	0.331	−0.831	−0.4
Cu	2.10	0.72	1.28	69.3	0.290	−0.663	−0.3
Ni	1.91	0.69	1.24	61.3	0.209	−0.339	−0.2
Co	1.88	0.72	1.25	60.0	0.196	−0.288	−0.1
Fe	1.83	0.74	1.35	57.8	0.175	−0.203	−0.1
Mn	1.55	0.80	1.36	46.1	0.057	0.259	0.1
Zn	1.65	0.74	1.37	50.2	0.099	0.098	0.0
Cd	1.69	0.97	1.52	51.9	0.115	0.032	0.0
Hg	2.00	1.10	1.55	65.1	0.248	−0.493	−0.2
Sn	1.80	0.93	1.58	56.5	0.162	−0.152	−0.1
Pb	1.87	1.21	1.74	59.5	0.192	−0.271	−0.1
Be	1.57	0.35	1.12	46.9	0.066	0.228 0.408[d]	0.1 0.2[d]
Mg	1.31	0.66	1.60	36.8	−0.036	0.621	0.3
Ca	1.00	0.99	1.96	26.3	−0.140	1.022	0.4
Sr	0.95	1.12	2.15	24.9	−0.155	1.079	0.4
Ba	0.89	1.34	2.24	23.1	−0.172	1.144	0.4
C	2.55						
N	3.04(3.31)[e]		0.74[f]				
O	3.44(3.80)[e]						
H	2.20						

a) Pauling's electronegativities. The values for the metal atom correspond to the +2 oxidation state. b) The covalent characters of the nitrogen-metal bonds estimated on the basis of Pauling's partial ionic character. c) The charges on the nitrogen and the metal atoms calculated based upon the Pauling's concept. d) The values correspond to the $Be_2OL_2 \cdot 2H_2O$ structure. e) The electronegativities of N^+ and O^+ estimated by Pauling's method. f) The covalent radius of the nitrogen atom.

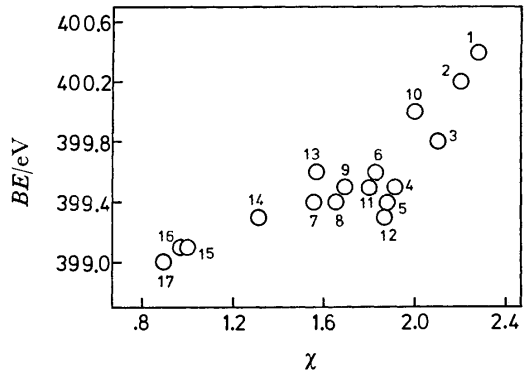

Fig. 1. Correlation between the N(ls) binding energies and the electronegativities of metals. Numbers refer to Table 1.

quinolinol and anthranilic acid were similar.

Correlations between N(1s) Binding Energies and Charges. The charges, q_N and q_M, in Eq. 2 were calculated by a method[11] utilizing Pauling's partial ionic character. That is, in general, the q_A on the A atom can be expressed as follows: $q_A=Q_A+\sum_{A\neq B} I_{AB}$, where Q_A is the formal charge on the A atom, and where I_{AB} is the partial ionic character of the A–B bond. Here, I_{AB} is given by the equation: $I_{AB}=1-\exp\{-0.25(\chi_A-\chi_B)^2\}$, where χ_A and χ_B are the electronegativities of the A and B atoms. In spite of a great deal of arbitrariness involved in obtaining the charge in this way, many good correlations have been reported between such a charge and the core-binding energy.[12] Because the bond length data for most of the compounds in Table 1 were not known, R_{M-N} in Eq. 2 was replaced for convenience by the sum of the atomic radius of the metal atom and the covalent radius of the nitrogen atom.

The values of q_N, q_M, and q_M/R_{M-N} thus obtained are given in Table 2. Here, the values of q_N in the table are for the complexes of 2-pyridinecarboxylic acid and 8-quinolinol; those for anthranilic acid are omitted.

For the complexes of 2-pyridinecarboxylic acid, the correlations of q_N with the binding energy and the corrected binding energy ($BE-q_M/R_{M-N}$) are shown in Figs. 2 and 3. In both figures, an increase in the binding energy with an increase in the charge was

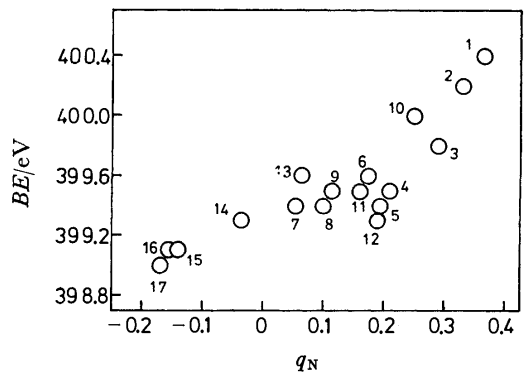

Fig. 2. Correlation between the N(ls) binding energies and the charges on nitrogen atoms. Numbers refer to Table 1.

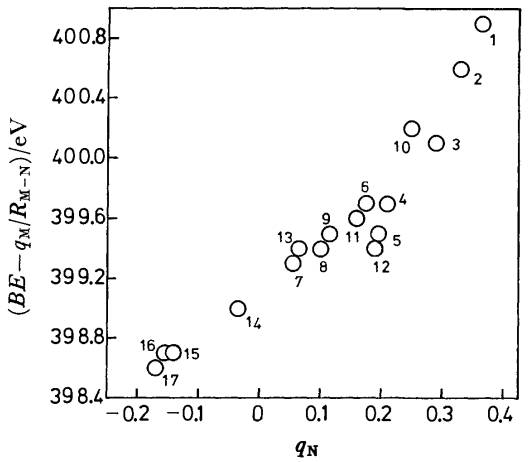

Fig. 3. Correlation between the corrected N(ls) binding energies and the charges on nitrogen atoms. Numbers refer to Table 1.

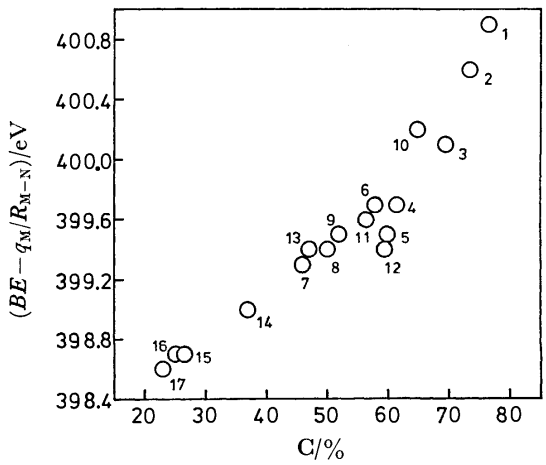

Fig. 4. Correlation between the corrected N(ls) binding energies and the covalent characters of the nitrogen–metal bonds. Numbers refer to Table 1.

observed, although its trend was not linear. As can be seen in Fig. 3, the inclusion of the correction term, q_M/R_{M-N}, slightly improves the correlation. For the complexes of 8-quinolinol and anthranilic acid also, similar correlations were observed.

Correlations between N(1s) Binding Energies and Covalent Characters. The covalent characters (abbreviated as C (%)) of the nitrogen–metal bonds, estimated on the basis of Pauling's partial ionic character,[2] are given in Table 2. That is, the covalent character corresponds to $100(1-I_{MN})$, where I_{MN} is the partial ionic character of the bond. For the complexes of 2-pyridinecarboxylic acid, the correlation between the corrected binding energy ($BE-q_M/R_{M-N}$) and the covalent character is shown in Fig. 4. An increase in the binding energy with the increase in the covalent character was observed. For the complexes of 8-quinolinol and anthranilic acid also, similar correlations were observed.

Considering the $\Delta H-T\Delta S=-RT\ln K$ relationship, it is seen that the stability constants of complexes, K, are functions of both the enthalpy change, ΔH, and the entropy change, ΔS. However, if the ligand is

the same, and there is also no significant difference in the size or structure of the complexes (*i.e.*, if ΔS is practically constant), the variation in their stabilities is primarily attributable to the difference in the strength of the metal-to-donor bond represented by ΔH. Therefore, in a bond in which pi bonding is not involved or in which sigma bonding is dominant, the stronger this bond is, that is, the more the covalent character of the bond, the more is the electron deficiency around the nitrogen atom, resulting in a corresponding increase in the N(ls) binding energy.

The higher binding energies of the complexes of the Pd and Pt of transition metal ions (Nos. 1—7 in the figure), of the Hg of zinc family ions (Nos. 8—10), and of the Be of alkaline earth ions (Nos. 13—17) compared with the other metal ions of each group seem to be consistent with the general trend that the above four metal ions form the more stable complexes in each group.

Correlations between N(1s) Binding Energies and Ionic Potentials. For the complexes of 2-pyridinecarboxylic acid, the correlation between the corrected binding energy and Z/r is shown in Fig. 5. The correlations for the complexes of 8-quinolinol and anthranilic acid were similar to Fig. 5. From the figure, the following facts were observed. In the group of alkaline earth ions, the binding energy increases linearly with Z/r. In the group of transition metal ions and zinc family ions, however, such no trend is observed at all. Furthermore, the binding energies of the latter group were considerably higher than those of the former metal ions with similar ionic potentials.

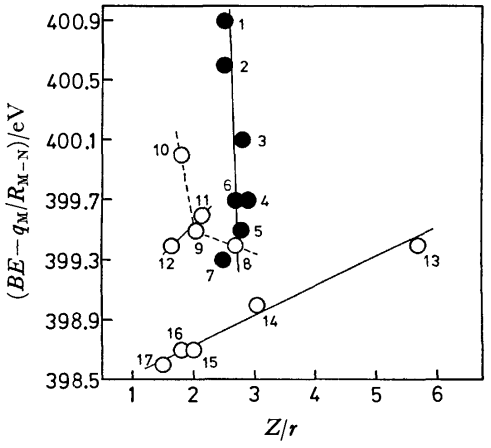

Fig. 5. Correlation between the corrected N(ls) binding energies and ionic potentials. Numbers refer to Table 1.
●: Complexes of transition elements, ○: complexes of typical elements.

These facts clearly suggest the difference in bonding type between the two groups. That is, the bonding type is ionic for the former metal ions and covalent for the latter.

The results of this study seem to support the conclusion that it is possible to use the chemical shift in the N(1s) binding energy by means of XPS, even if it is small, to determine the nature and strength of the nitrogen–metal bond in a group of carefully selected compounds.

The author wishes to thank Drs. Kiyoshi Yamasaki and Shigemasa Sawada for their helpful discussions and suggestions during this work, and Mr. Taichiro Hirohara for the elemental analysis.

References

1) V. I. Nefedov, *J. Mol. Structure*, **46**, 251 (1978).
2) L. Pauling, "The Nature of the Chemical Bond," 3rd ed, Cornell University Press, Ithaca, N. Y. (1960), p. 98.
3) a) A. Kleinstein and G. A. Webb, *J. Inorg. Nucl. Chem.*, **33**, 405 (1971); b) A. G. Hill and C. Curran, *J. Phys. Chem.*, **64**, 1519 (1960); c) Y. Kidani, R. Saito, and H. Koike, *Yakugaku Zasshi*, **92**, 1063 (1972); d) L. Sacconi and R. Cini, *Chem. Abstr.*, **47**, 11835 h (1953).
4) K. Motojima, *Nippon Kagaku Zasshi*, **77**, 95 (1956).
5) K. Motojima, *Bull. Chem. Soc. Jpn.*, **29**, 29 (1956).
6) K. Siegbahn *et al.*, "ESCA Applied to Free Molecules," North-Holland Pub. Co., Amsterdam (1969), p. 108.
7) D. W. Davis and D. A. Shirley, *J. Electron Spectrosc. Relat. Phenom.*, **3**, 137 (1974).
8) A. L. Allred, *J. Inorg. Nucl. Chem.*, **17**, 215 (1961).
9) L. H. Ahrens, *Geochim. Cosmochim. Acta*, **2**, 155 (1952).
10) H. Strunz, "Mineralogisch Tabellen," Akademisch Verlagesgesellschaft (1970).
11) R. Nordberg, R. G. Albridge, T. Bergmark, U. Ericson, J. Hëdman, C. Nordling, K. Siegbahn, and B. J. Lindberg, *Ark. Kemi*, **28**, 257 (1967).
12) K. Siegbahn *et al.*, "ESCA Atomic, Molecular and Solid State Structure Studied by Means of Electron Spectroscopy," Almqvist and Wiksells AB, Uppsala (1967).

The Collection of Uranium from Sea Water with Hydrous Metal Oxide. III. The Effects of Diverse Ions in Sea Water on Uranium Adsorption by Hydrous Titanium(IV) Oxide

Hisao YAMASHITA,* Yoshihiro OZAWA,** Fumito NAKAJIMA, and Toshifumi MURATA**

Hitachi Research Laboratory, Hitachi, Ltd., Kujimachi, Hitachi-shi 319-12

***Energy Research Laboratory, Hitachi, Ltd., Moriyama-cho, Hitachi-shi 316*

(Received April 2, 1979)

The effect of diverse ions present in sea water on the uranium adsorption is elucidated in the present paper. The uranium-adsorption experiments were conducted using sea water and a solution containing 0.72 mol dm^{-3} NaCl and 2.3×10^{-3} mol dm^{-3} $NaHCO_3$. The uranium uptake was about ten times larger from the NaCl–$NaHCO_3$ solution than from sea water. The ions which depressed the uranium uptake were the calcium, magnesium, and fluoride present in sea water. Among these ions, calcium had the largest effect on the uranium uptake. The analysis of calcium and carbonate in the adsorbent after the adsorption experiment has revealed that the molar ratio between calcium and carbonate was about one. It was considered that calcium carbonate was deposited on the adsorbent during the uranium adsorption. The specific surface area and the pore volume decreased after the deposition of calcium carbonate. It was supposed that the decrease in the uranium uptake was caused by the coverage of the surface of hydrous titanium(IV) oxide with calcium carbonate. Magnesium ions depressed the uranium uptake in the same manner as calcium ions. The effect of the magnesium ions, however, was relatively small compared with that of the calcium ions.

For the purpose of collecting uranium from sea water, several methods have been proposed; adsorption,[1-2] coprecipitation,[3] ion exchange,[4] ion floatation,[5] and solvent extraction.[4] The adsorption method has been thought to be most feasible. In the adsorption method, an adsorbent with a high adsorption capacity and selectivity is prerequisite, because the uranium concentration is very low (3 ppb), and a large amount of diverse ions are present in sea water. A large number of adsorbents have been examined. It has been reported that hydrous titanium(IV) oxide is the most suitable as a uranium adsorbent.[1-2]

More than sixty ions are present in sea water. Since hydrous titanium(IV) oxide serves as a cation exchanger in sea water, cations present in sea water may affect the uranium adsorption. Ogata *et al.*[6] reported that the uranium uptake decreased slightly in the presence of phosphate, fluoride, and copper. Kanno *et al.*[7] described that carbonate ions present in sea water had a negative effect on the uranium adsorption. However, these results can not satisfactorily account for the effect of diverse ions on uranium adsorption.

In the present work, the effect of diverse ions present in sea water on the uranium adsorption by hydrous titanium(IV) oxide is described.

Experimental

Preparation of Hydrous Titanium(IV) Oxide. Hydrous titanium(IV) oxide was prepared by adding 7% aqueous ammonia to a solution of 0.6 mol dm^{-3} titanium(IV) chloride at 90 °C. The precipitate was filtered off, washed with water, and dried at room temperature for about 10 d. The dried samples were crushed and sieved, a portion of 300—400 mesh being used in the experiments. The water content was determined by measuring the ignition loss at 800 °C; it was found to be 18%, which corresponded to $TiO_2\cdot H_2O$. X-Ray powder diffraction analysis showed the crystal form of anatase, with an apparent crystal size of 38 Å.

Adsorption Experiments. Sea water and a NaCl–$NaHCO_3$ solution were used in the adsorption experiments.

Table 1. Molar concentrations of uranium and major ions in sea water sampled at the Hitachi seashore

	Concentration/mol dm^{-3}
U	1.3×10^{-8}
Cl	5.4×10^{-1}
Na^+	4.6×10^{-1}
Mg^{2+}	5.2×10^{-2}
SO_4^{2-}	2.7×10^{-2}
Ca^{2+}	9.9×10^{-3}
K^+	9.7×10^{-3}
$HCO_3^-+CO_3^{2-}$	2.3×10^{-3}
pH	8.0—8.1

The molar concentrations of uranium and the major constituents of sea water used in the present work are shown in Table 1. In the case of a NaCl–$NaHCO_3$ solution, the concentration of NaCl was taken to be 0.72 mol dm^{-3} in order for it to be the same ionic strength as that of sea water while that of $NaHCO_3$ was ordinarily chosen to be 2.3×10^{-3} mol dm^{-3}, equal to that of sea water. The concentration of uranium in the solution was taken to be 3—60 ppb by adding a uranyl(VI) chloride solution. In the uranium-adsorption experiments, 40 mg of the adsorbent were introduced into 1000 ml of the solution. The solution was stirred by means of a vertical stirrer at 25 °C. Within 5 h, the adsorption equilibrium was achieved under the present experimental conditions. The adsorbent was separated from the solution, and the change of the uranium concentration in the solution was measured.

The carbonate, calcium, and magnesium uptake was measured by the following procedure; one-fifth gram of the adsorbent was introduced into 5000 ml of the solution, after which the solution was stirred for 5 h at 25 °C. The contents of calcium, magnesium, and carbonate in the adsorbent were then determined.

Analytical Method. The uranium in the solution was determined spectrophotometrically, with Arsenazo III as the indicator.[8] The determination of the carbonate in the

adsorbent was carried out by the following procedure. The adsorbent after the adsorption experiment was washed with distilled water and dried at room temperature. The dried samples were placed in a flask, where N_2 as carrier gas was passed through continuously, about 10 ml of 0.1 mol dm^{-3} HCl solution were then added to the flask at 50 °C. The carbon dioxide thus produced was introduced into the carbon analyzer, Kokusai Denki VK-1-type "Coulomatic C," and was determined by the coulometric titration. The limit of detection was 4.2×10^{-5} mmol as carbon, and the coefficient of variation was found to be 3.5% when 5 mg of calcium carbonate was analyzed by this procedure.

The determination of the calcium and magnesium adsorbed in the adsorbent was carried out by the following procedure; after the adsorption experiment, the dried samples were fused with sodium carbonate and boric acid and dissolved in an HCl solution. The concentration of calcium or magnesium in the HCl solution was then determined by atomic absorption spectrophotometry using a Hitachi 207 Atomic-absorption spectrophotometer.

The specific surface area and pore volume of the adsorbent were determined by means of the N_2 adsorption at −195 °C using a Carlo Erba Sorptomatic Series 1800.

Results and Discussion

Adsorption Isotherm of Uranium. The adsorption isotherm of uranium in sea water or a NaCl–$NaHCO_3$ solution is shown in Fig. 1. Kanno *et al.*[7] reported that the uranium adsorption from sea water gave a Freundlich-type isotherm. As is shown in Fig. 1, the same results were obtained in both sea water and the NaCl–$NaHCO_3$ solution.

The value of n in the Freundlich equation ($v=kC^{1/n}$) was found to be 1.4 and 1.3 for sea water and for the NaCl–$NaHCO_3$ solution respectively.

It is known that uranium in sea water exists in the form of tris(carbonato)dioxouranate(VI) ion $[UO_2(CO_3)_3]^{4-}$. The distributions of uranyl(VI) species in the NaCl–$NaHCO_3$ solution used in the present work were calculated from the stability constants;[9] they

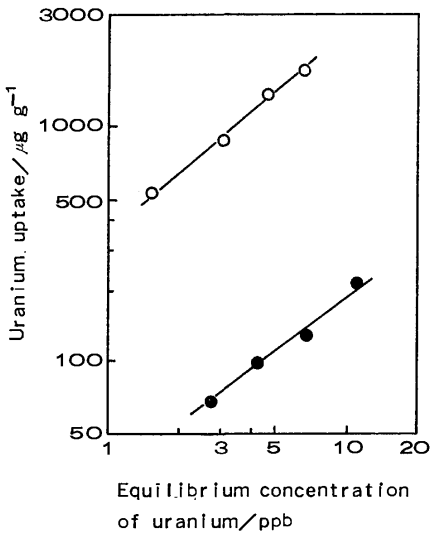

Fig. 1. Adsorption isotherm of uranium on hydrous titanium(IV) oxide.
Adsorption temperature: 25 °C, ○: NaCl–$NaHCO_3$ solution, ●: sea water.

Table 2. Distribution of uranyl complexes in the NaCl–$NaHCO_3$ solution at pH 8

Species	Ratio/%
UO_2^{2+}	0
$UO_2(OH)^+$	0.1
$UO_2(OH)_3^-$	14.1
UO_2Cl^+	0
$UO_2Cl_3^-$	0
$UO_2(CO_3)_2^{2-}$	0.9
$UO_2(CO_3)_3^{4-}$	84.9

are summarized in Table 2. The tris(carbonato)dioxouranate(VI) ion, which is the major uranyl(VI) species in sea water, is a predominant species in the NaCl–$NaHCO_3$ solution. Although the uranyl(VI) species and the type of adsorption are the same in sea water and in the NaCl–$NaHCO_3$ solution, the uranium uptake is found to be quite different. The difference in the uranium uptake is thought to be attributable to the diverse ions in sea water.

Effect of Diverse Ions in Sea Water. In order to investigate the effect of diverse ions in sea water on uranium adsorption, the uranium uptake was measured with NaCl–$NaHCO_3$ solutions containing 20 ppb uranium and a diverse ion at the concentration equal to that of sea water. The ion species examined are magnesium, calcium, strontium, potassium, borate, sulfate, fluoride, and bromide ions. The results are summarized in Table 3. The uranium uptake from an NaCl–$NaHCO_3$ containing K^+, Sr^{2+}, SO_4^{2-}, Br^-, or BO_3^{3-} was nearly equal to that from the NaCl–$NaHCO_3$ solution. The obtained results show that these ions have no effect on the uranium uptake. On the other hand, the uranium uptake was reduced by the presence of calcium, magnesium, and fluoride ions. Particularly, the presence of calcium ions hindered the uranium adsorption.

The uranium uptake from the solution containing all the ions together (No. 10 in Table 3) agreed well with that from sea water. The effects of calcium, magnesium, and fluoride ions on the uranium uptake

Table 3. Uranium uptake with a NaCl–$NaHCO_3$ solution containing 20 ppb of uranium and various ions at pH 8

Sample No.	Salt added	Concentration / mol dm^{-3}	Uranium uptake / μg g^{-1}
1	Not added	—	460
2	$MgCl_2$	5×10^{-2}	428
3	Na_2SO_4	3×10^{-2}	458
4	$CaCl_2$	1×10^{-2}	273
5	KCl	9×10^{-3}	462
6	KBr	8×10^{-4}	460
7	H_3BO_3	4×10^{-4}	460
8	$SrCl_2$	2×10^{-4}	457
9	NaF	7×10^{-5}	435
10	No. 2 to No. 9 added		223
11	Sea water		220

are discussed below.

It was reported in our previous paper[10] that the adsorption site of hydrous titanium(IV) oxide for $[UO_2(CO_3)_3]^{4-}$ may be supposed to be the surface hydroxo group [Ti–OH]. The fluoride ion reacts with Ti–OH to form Ti–F. The reaction is useful for the determination of the surface hydroxo group.[11] It may, therefore, be considered that fluoride ions reduce the uranium adsorption site by forming Ti–F. Since the concentration of fluoride ions in sea water is low, the effect of fluoride ions on the uranium uptake is small.

Figure 2 shows the variation in the uranium uptake with the concentration of calcium ions in NaCl–$NaHCO_3$ solutions containing 20 ppb of uranium. The uranium uptake decreases with an increase in the concentration of calcium ions. Since the deposition of the calcium compound was expected to take place on the adsorbent, the calcium uptake and carbonate uptake were measured in various solutions. The results are shown in Table 4. The calcium uptake was 0.56 mmol g^{-1} from the NaCl–$NaHCO_3$–$CaCl_2$ solution (No. 2 in Table 4) and 0.34 mmol g^{-1} from the NaCl–$CaCl_2$ solution (No. 3 in Table 4). Since hydrous titanium(IV) oxide behaves as a cation exchanger in an alkaline solution,[12] the calcium ion is thought to be adsorbed from the NaCl–$CaCl_2$ solution by means of an ion-exchange reaction. It is deduced that 0.34 mmol g^{-1} of the 0.56 mmol g^{-1} calcium uptake from the NaCl–$NaHCO_3$–$CaCl_2$ solution is attributable to the ion-exchange reaction, and 0.22 mmol g^{-1} (=0.56 mmol g^{-1}—0.34 mmol g^{-1}) to an other adsorption process. The carbonate uptake from the NaCl–$NaHCO_3$–$CaCl_2$ solution is found to be about 0.20 mmol g^{-1} (No. 2 in Table 4), while it is very small without calcium ions (No. 1 in Table 4).

The calcium uptake attributed to the adsorption process other than ion-exchange (0.22 mmol g^{-1}) is nearly equal to the carbonate uptake (0.20 mmol g^{-1}), indicating that calcium carbonate is deposited on the surface of the adsorbent. In the case of sea water, the calcium uptake and the carbonate uptake are in good agreement with those from the NaCl–$NaHCO_3$–$CaCl_2$ solution (No. 2 and No. 6 in Table 4).

The variation in the uranium, calcium, and carbonate uptake with the concentration of $NaHCO_3$ in the NaCl–$CaCl_2$ solution is shown in Fig. 3. The increase in the concentration of $NaHCO_3$ raises the calcium and carbonate uptakes while the uranium uptake markedly decreases. Regardless of the $NaHCO_3$ concentration, the difference between calcium and carbonate

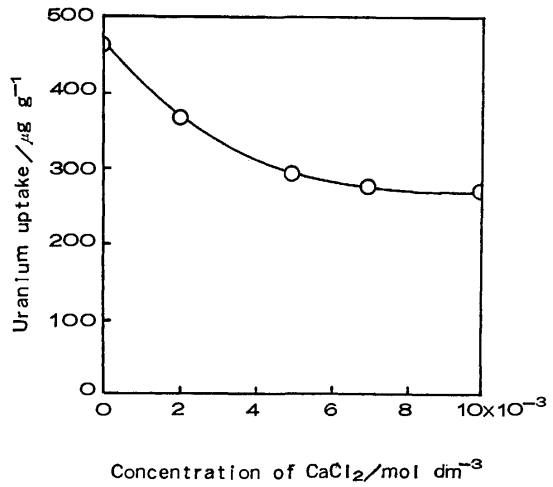

Fig. 2. Variation of uranium uptake with concentration of $CaCl_2$.
pH of the solution: 8.0, NaCl: 0.72 mol dm^{-3}, $NaHCO_3$: 2.3×10^{-3} mol dm^{-3}, uranium: 20 ppb.

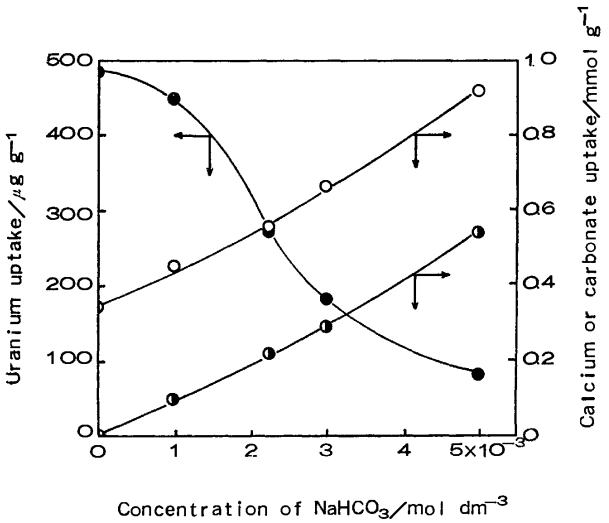

Fig. 3. Variation of uranium, calcium and carbonate uptake with concentration of $NaHCO_3$.
pH of the solution: 8.0, NaCl: 0.72 mol dm^{-3}, $CaCl_2$: 10^{-2} mol dm^{-3}, uranium: 20 ppb, ●: uranium uptake, ○: calcium uptake, ◑: carbonate uptake.

Table 4. Uptake of calcium, magnesium, and carbonate by hydrous titanium(IV) oxide with various solutions at pH 8

Sample No.	Solution[a]	Uptake/mmol g^{-1}		
		Calcium	Magnesium	Carbonate
1	NaCl-$NaHCO_3$	—	—	0.003
2	NaCl-$NaHCO_3$-$CaCl_2$	0.56	—	0.20
3	NaCl-$CaCl_2$	0.34	—	—
4	NaCl-$NaHCO_3$-$MgCl_2$	—	0.25	0.04
5	NaCl-$MgCl_2$	—	0.20	—
6	Sea water	0.51	0.18	0.22

a) NaCl: 0.72 mol dm^{-3}, $NaHCO_3$: 2.3×10^{-3} mol dm^{-3}, $CaCl_2$: 10^{-2} mol dm^{-3}, $MgCl_2$: 5×10^{-2} mol dm^{-3}.

TABLE 5. SPECIFIC SURFACE AREA(S) AND PORE VOLUME(V) OF HYDROUS TITANIUM(IV) OXIDE BEFORE AND AFTER URANIUM ADSORPTION

	Before adsorption	After adsorption		
		$NaCl$-$NaHCO_3$	$NaCl$-$NaHCO_3$-$CaCl_2$	Sea water
$S/m^2\ g^{-1}$	261	250	177	168
$V/cm^3\ g^{-1}$	0.34	0.33	0.26	0.24

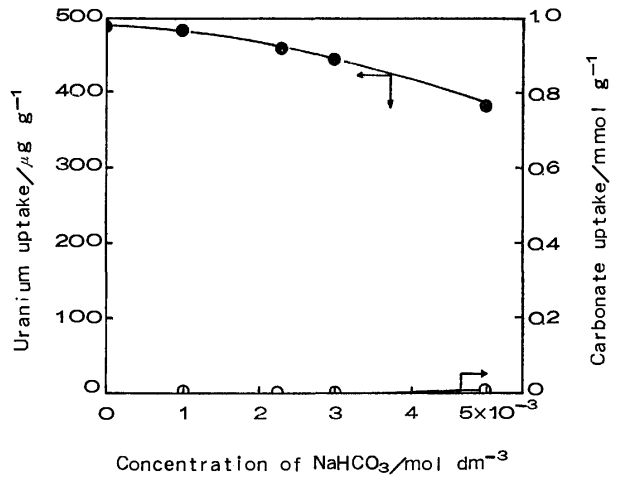

Fig. 4. Variation of uranium and carbonate uptake with concentration of $NaHCO_3$.
pH of the solution: 8.0, NaCl: 0.72 mol dm^{-3}, uranium: 20 ppb, ●: uranium uptake, ○: carbonate uptake.

uptakes remained constant (about 0.35 mmol g^{-1}); this value corresponds to the calcium uptake by the ion-exchange reaction. The variation in the uranium and carbonate uptakes with the $NaHCO_3$ concentration in the NaCl solution is shown in Fig. 4. In the absence of calcium ions, the carbonate uptake is very small, and the uranium uptake is slightly decreased with the concentration of $NaHCO_3$. It may be supposed that the decrease in the uranium uptake is due to the deposition of calcium carbonate on the adsorbent.

The magnesium uptake by the adsorbent is also shown in Table 4. The magnesium uptake in the presence and in the absence of $NaHCO_3$ were 0.25 mmol g^{-1} (No. 4 in Table 4) and 0.20 mmol g^{-1} (No. 5 in Table 4) respectively. Thus, the effect of carbonate ions on the magnesium uptake is rather small compared with that on the calcium uptake. It is considered that the deposition of magnesium carbonate is more difficult on the adsorbent than that of calcium carbonate. The specific surface area and pore volume of the adsorbent before and after the adsorption experiment are presented in Table 5. With the $NaCl$–$NaHCO_3$ solution, the changes in the surface area and the pore volume are very small.

On the other hand, with the $NaCl$–$NaHCO_3$–$CaCl_2$ solution and sea water, the decreases in the specific surface area and the pore volume are large. These results indicate that the decreases in the specific surface area and pore volume are due to the deposition of calcium carbonate on the adsorbent.

The present experimental results make it possible to conclude that the uranium uptake from sea water by hydrous titanium(IV) oxide is reduced mainly because of the calcium carbonate deposition.

The authors wish to thank Professor Shosuke Imoto of Osaka University for his many helpful discussions and suggestions.

References

1) N. J. Keen, *J. Brit. Nucl. Energy. Soc.*, **7**, 178 (1968).
2) N. Ogata and H. Kakihana, *J. At. Energy. Soc. Jpn.*, **11**, 82 (1969).
3) M. Ishibashi, T. Fujinaga, T. Kuwamoto, and Y. Ogino, *Nippon Kagaku Kaishi*, **88**, 73 (1967).
4) R. V. Davies, J. Kennedy, R. W. McIlroy, R. Spence, and K. M. Hill, *Nature*, **203**, 1110 (1964).
5) Y. S. Kim and H. Zeitlin, *Anal. Chem.*, **43**, 1390 (1971).
6) N. Ogata, N. Inoue, and H. Kakihana, *Nippon Kaisui Gakkai Shi*, **24**, 68 (1970).
7) M. Kanno, Y. Ozawa, and T. Mukaibo, *J. At. Energy. Soc. Jpn.*, **12**, 708 (1970).
8) Y. Miyake, Y. Sugimura, and T. Uchida, *Recod. Oceanog. Works. Jpn.*, **11**, 53 (1972).
9) L. G. Sillén and A. E. Martell, "Stability Constants of Metal-Ion Complexes," The Chem. Soc., London (1964), p. 138.
10) H. Yamashita, Y. Ozawa, F. Nakajima, and T. Murata, *Bull. Chem. Soc. Jpn.*, **53**, 1 (1980).
11) H. P. Boehm, *Adv. Catal.*, **16**, 179 (1966).
12) M. Abe, *Bunseki Kagaku*, **23**, 1254 (1974).

The Thermal Gas-phase Decomposition of Methyl Iodide

Ko Saito,* Hiroyuki Tahara, Osamu Kondo, Teiji Yokubo, Tetsuo Higashihara, and Ichiro Murakami

Department of Chemistry, Faculty of Science, Hiroshima University, Higashi Senda-machi, Naka-Ku, Hiroshima 730

(Received June 8, 1979)

The thermal gas-phase decomposition of methyl iodide diluted in Ar has been studied behind shock waves over the temperature range between 1050 and 1500 K and the total density range of 3.5×10^{-6}—3.9×10^{-5} mol cm^{-3}. The decomposition was monitored by means of the UV absorption of CH_3I at 259 or 275 nm. The initiation reaction was found to be the C-I bond fission, and the process proceeded in the low-pressure region under the present experimental conditions. The low-pressure limit rate constant was obtained as:

$$k_{2nd} = 10^{15.40\pm0.26}\exp\{-(42.56\pm1.50 \text{ kcal mol}^{-1})/RT\}\text{cm}^3 \text{ mol}^{-1} \text{ s}^{-1}.$$

Applying the RRKM strong collision theory, the collision efficiency factor was estimated to be 0.018 at 1300 K.

The thermal decomposition of methyl halides is of interest in connection with the decomposition mechanism and is an important test case for the theory of unimolecular reactions.[1] There have been reported many shock-tube studies of the pyrolysis of fluoro- and chloro-methanes.[2-5] In most cases, the decomposition of these molecules is initiated *via* the molecular elimination of HF and HCl.[6] Moreover, the unimolecular process was found in the fall-off region under the conditions available in shock waves.[7] On the other hand, there are few data on the decomposition of bromo- and iodo-methanes, although they are considered to offer proper kinetic data regarding simple bond-fission reactions of the C–Br and C–I bonds. It is important to determine the pressure dependence of the unimolecular process, because it depends on the energy-transfer efficiency in collisions between the reactant and diluent molecules. In the thermal unimolecular processes of relatively small molecules, at low pressures and at high temperatures the collisional activation is rate-determining. This allows us to derive information on the average energy transferred in collisions, which is difficult to describe theoretically. It is, therefore, necessary to accumulate many experimental data on the thermal unimolecular reactions of common molecules.

In the present work, we have studied the pyrolysis of CH_3I in Ar behind shock waves in order to obtain the unimolecular rate constant of the initiation reaction and to discuss the energy-transfer efficiency.

Experimental

The experiments were performed in shock tubes 5 cm and 9.4 cm in inner diameter. Detailed explanations of the equipment and the procedures have been given elsewhere.[8,9] The shocked gas properties were calculated by using the incident shock speed, assuming non-reaction conditions.

Liquid CH_3I (98% stated minimum purity) was purified by trap-to-trap distillation, while Ar (99.998%) was used as the diluent without further purification. Mixtures (0.2, 0.4, 1.25, 2.5, and 3.0 mol % CH_3I in Ar) were prepared in a 30-l glass flask. They were allowed to stand for more than 12 h before use.

Results

Measurements were performed behind incident and reflected shock waves which covered the following ranges: temperature=1050—1500 K; total density=3.5×10^{-6}—3.9×10^{-5} mol cm^{-3}; $[CH_3I]=4.5\times10^{-8}$—3.5×10^{-7} mol cm^{-3}. The disappearance of the shock-heated methyl iodide was followed by observing the absorption at 259 or 275 nm with FWHM=1.65 nm. The absorption due to the X→A transition of CH_3I has a maximum at 259.1 nm.[10] The absorption profiles obtained in a shock-heated mixture at 259 and 275 nm were essentially the same except for a slight difference which was observed at long reaction times. That is, it appeared that the absorption at 259 nm was largely influenced by some products in the later part of the reaction. Figure 1 shows a typical absorption profile at 275 nm and at the mean temperature of all the experimental runs. The absorption coefficient at this wavelength was about 4×10^5 cm^2 mol^{-1}, with a slight temperature dependence in the range of 1000—1500 K. Lambert-Beer's law was ascertained to hold in the concentration range studied. Values of the first-order rate constant were determined by two different procedures; *i.e.*, for the data obtained at 259 nm, the initial slope method was applied as: $k_{1st}=-\text{d}[CH_3I]/\text{d}t/[CH_3I]_0$, while for the data at 275 nm, the integration method was applied as: $k_{1st}=\ln([CH_3I]_0/[CH_3I])/\text{d}t$. As will be shown later, no

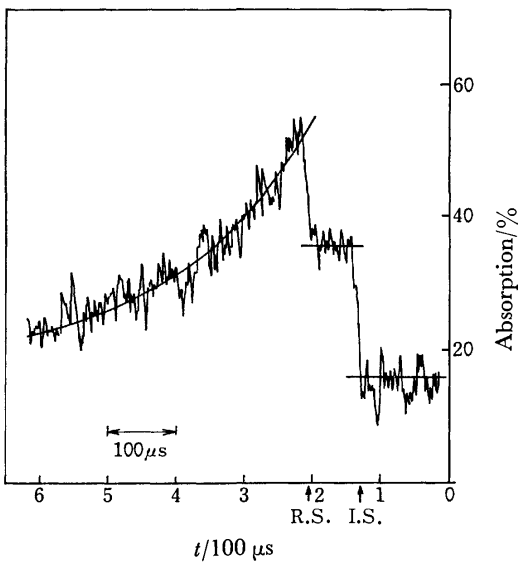

Fig. 1. Typical absorption profile obtained at 275 nm. 1.0 mol% in Ar, $P_1=100$ Torr, $P_5=3.01$ atm, $T_5=1300$ K, total density=2.82×10^{-5} mol cm^{-3}.

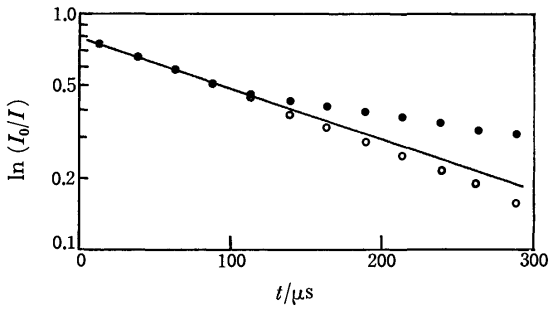

Fig. 2. Logarithmic plot of $\ln(I_0/I)$ *vs.* time for the data in Fig. 1.
● denotes the direct plot of the absorption profile and ○ denotes the corrected profile by substructing the absorption of C_2H_5I (see Ref. 15). The straight line gives $k_{1st}=4.78\times10^3$ s^{-1} and $k_{2nd}=1.71\times10^8$ cm^3 mol^{-1} s^{-1}.

difference is found between the k_{1st} values obtained by the two methods. Figure 2 shows the procedure of the integration method used for the data shown in Fig. 1. In the figure, the closed circles show the data directly obtained from the absorption profile, while the open circles correspond to the data corrected for the absorption of C_2H_5I, which will be discussed later. It appears that the plot (closed circles) shows a straight line at least 100 μs after the shock front passage; *i.e.*, the initial decomposition rate is first-order with respect to $[CH_3I]$ until 35% of the substance decomposes.[11] At higher temperatures, this value decreases slightly, but it is never less than 20%. It was ascertained that k_{1st} was independent of the concentration of CH_3I over the ten-fold range. An Arrhenius expression is given for the data at a total density of 1.6×10^{-5} mol cm^{-3} as:

$$k_{1st} = 10^{10.36\pm0.29}\exp\{-(41.57\pm1.67 \text{ kcal mol}^{-1})/RT\} \text{ s}^{-1},$$

where the error limits are the standard deviations. The value of the preexponential factor obtained is too low for us to consider that the initial process is in the high-pressure region. In fact, from the experiments in which the total density is changed over about ten-fold, k_{1st} was found to be fairly proportional to the total density over the whole range. Figure 3 shows an example of the Arrhenius plots of k_{1st} for three different total densities. They form three pallarel straight lines with the same slope as the above Arrhenius expression. The initial process is, thus, in the low-pressure region under the present experimental conditions. Therefore, the initial decomposition rate is expressed as:

$$-\text{d}[CH_3I]/\text{d}t = k_{2nd}[CH_3I][M],$$

where [M] denotes the total density. From the data of 40 runs, an Arrhenius expression for k_{2nd} is given as:

$$k_{2nd} = 10^{15.40\pm0.26}\exp\{-(42.56\pm1.50 \text{ kcal mol}^{-1})/RT\} \text{ cm}^3 \text{ mol}^{-1} \text{ s}^{-1}.$$

An Arrhenius plot of k_{2nd} is given in Fig. 4, where the data evaluated by the two procedures are in good agreement with each other.

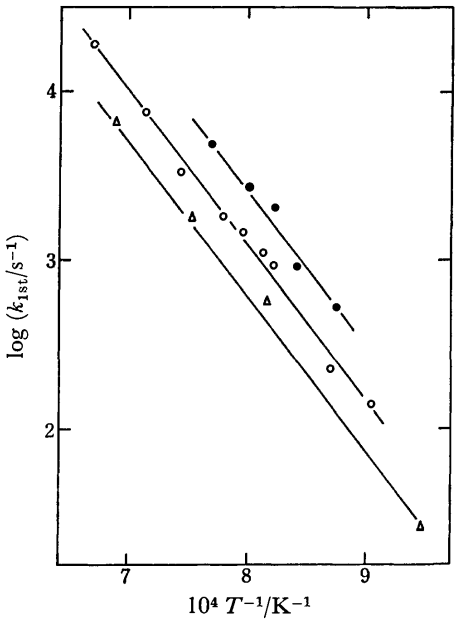

Fig. 3. Comparison of k_{1st} values for different total densities.
△: 0.58×10^{-5} mol cm^{-3}, ○: 1.32×10^{-5} mol cm^{-3}, ●: 2.73×10^{-5} mol cm^{-3}.

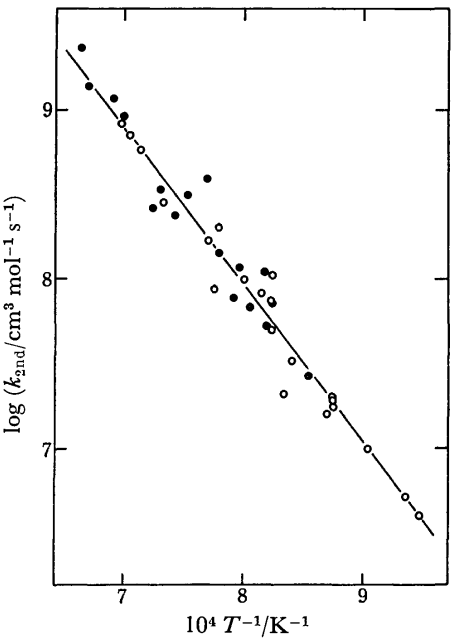

Fig. 4. Arrhenius plot of k_{2nd} evaluated by initial slope (●) and integration method (○).

Discussion

The initiation reaction is the C–I bond fission, not the molecular elimination of HI, because the heat of the reaction of the HI elimination is higher than the energy of the C–I bond fission by 38 kcal mol^{-1}.[12] Thus, the sequence of the reaction in the CH_3I decomposition is assumed to be as follows:

(1) $CH_3I + M \rightleftharpoons CH_3 + I + M$

(2) $CH_3I + I \rightleftharpoons CH_3 + I_2$

Table 1. Elementary reactions

Reaction	ΔH°_{298} / kcal mol^{-1}	ΔG°_T / kcal mol^{-1}	Rate constant / cm^3 mol^{-1} s^{-1}	Reference of rate constant
1	56.2	$-0.0357T+57.0095$	$k_1=10^{15.4}\exp(-42.6/RT)$	This work
2	20.1	$-0.00524T+20.2926$	$k_2=10^{14.0}\exp(-19.8/RT)$	a)
3	−0.2	$0.00166T-1.23$	$k_3=10^{11.8}\exp(-12.1/RT)$	Estimated
4	88.2	$-0.0393T+89.0048$	$k_4=10^{17.11}\exp(-89.6/RT)$	b)
5	36.1	$-0.02562T+37.2121$	$k_5=10^{13.99}\exp(-30.4/RT)$	a)
6	−94.1		$k_6=10^{13.5}$	Estimated
7	−54.5	$0.03067T-53.9849$	$k_{-7}=10^{16.0}\exp(-45.0/RT)$	Estimated
8	−18.4	$5.3541\times10^{-3}T-17.2616$	$k_8=10^{13.3}$	c)
9	−91.4		$k_9=10^{13.5}$	Estimated

a) T. Fueno, "Chemical Reaction Theory," Asakura Shoten (1975). b) J. Troe, "Fifteenth Symp. (Int.) on Combustion," The Combustion Institute, Pittsburgh (1975), p. 667. c) D. M. Golden and S. W. Benson, *Chem. Rev.*, **69**, 125 (1969).

(3) $CH_3I + CH_3 \rightleftharpoons CH_4 + CH_2I$

(4) $C_2H_6(+M) \rightleftharpoons 2CH_3(+M)$

(5) $I_2 + M \rightleftharpoons 2I + M$

(6) $2CH_2I(+M) \longrightarrow C_2H_4I_2(+M)$

(7) $CH_2I + I(+M) \rightleftharpoons CH_2I_2(+M)$

(8) $CH_2I + I_2 \rightleftharpoons CH_2I_2 + I$

(9) $CH_3 + CH_2I(+M) \longrightarrow C_2H_5I(+M)$.

This is based on the mechanism proposed for the photochemical reaction of CH_3I.[13] Table 1 lists the values of ΔH°_{298}, ΔG°_T, and the rate constants for the above reactions. Since there are no data for Reactions 3, 6, 7, and 9, the rate constants were estimated as follows. The value of k_3 was calculated by means of the BEBO method combined with the transition-state theory.[14] The values of k_6 and k_9 were assumed from the data of the recombination of CH_3 radicals. k_{-7} was estimated from the data of the present experiment. Computer simulations (Gear Program) were performed with the values in Table 1 by using the observed k_{2nd} value as the value of Reaction 1. As an example, Fig. 5 shows CH_3I profiles computed under the same conditions as those of the run shown in Fig. 1. It is found that there is no discrepancy between the profiles computed with Reaction 1 (solid line) and with the full reactions (dotted line) until 100 μs after the shock front (corresponding to about a 30% consumption of CH_3I). Therefore, the apparent second-order rate constant, k_{2nd}, which was measured at the early stage of the reaction, can be regarded as the low-pressure unimolecular rate constant of Reaction 1. The corresponding experimental profile is also shown in Fig. 5 by open circles. This is the one shown in Fig. 2 (open circles) connected by considering the effect of the products.[15]

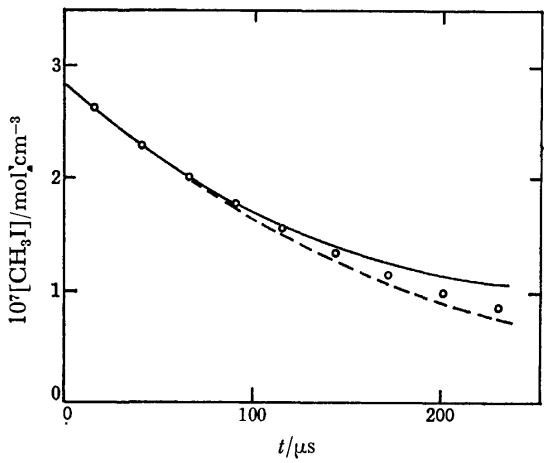

Fig. 5. Concentration profiles of CH_3I.
Conditions are the same as those in Fig. 1. ○: Experimental profile, ——: calculated by Reaction 1 alone, ----: calculated by using full reactions considered.

A rough estimation of the fall-off pressure, $P_{1/2}$, for Reaction 1 leads to $P_{1/2}\simeq 50$ atm at 1300 K (1 atm=101325 Pa).[16] Therefore, the pressure region in this work (0.4—3.2 atm) is considerably below the fall-off pressure. This is consistent with the experimental result that the rate constant of Reaction 1 was given as second-order. The activation energy of k_{2nd} (*i.e.*, k_1 at the low-pressure limit) is lower than the heat of reaction by about 13 kcal mol^{-1}. This may be explained by the low-pressure-limit unimolecular reaction theory. That is, a large part of the discrepancy could be compensated for by the participation of the internal energy in the decomposition. On the other hand, a small part of the discrepancy may be ascribed to the temperature dependence of the collision efficiency. The energy-transfer efficiency in collisions between the reactant and diluent molecules becomes small as the temperature rises. Moreover, at high temperatures available in shock waves, the collisional energy transfer becomes much less than the average thermal energy. From the experimental data of the low-pressure-limit rate constant, it is possible to estimate the collision efficiency and, in turn, the average energy $\langle\Delta E\rangle$ transferred per collision, on the basis of the strong collision rate constant. The value of $\langle\Delta E\rangle$ for a particular collision partner in one reaction is considered to be nearly constant, regardless of the temperature.[17] It is, therefore interesting to ascertain the $\langle\Delta E\rangle$ values for various collision pairs in one reaction.

It is possible to calculate an approximate value of the strong collision rate constant if it is not available from the experiments. An appropriate RRKM strong collision formulation is given as:[17]

$$k_o^{sc} = Z_{LJ}Q_{vib}^{-1}kT\rho_{vib}(E_o)F_E F_{rot}F_{anh}\exp(-E_o/RT),$$

where Z_{LJ} is the Lennard-Jones collision frequency; $\rho_{vib}(E_o)$, the vibrational energy level density at E_o; Q_{vib}, the vibrational partition function; E_o, the threshold energy; F_E, the energy dependence of the density of the states; F_{rot}, the centrifugal correction factor, and F_{anh}, the anharmonicity factor. Table 2 lists the calculated values of k_o^{sc} for several temperatures. The collision efficiency factor is defined as: $\beta_c \equiv k_o^{obs}/k_o^{sc}$, where k_o^{obs} is the low-pressure-limit rate constant obtained experimentally in a given heat bath. As is shown in Table 2, β_c is about 0.02 in the CH_3I–Ar system at the temperatures studied; this is comparable with the data for the simple bond fission of similar molecules (*e.g.*, β_c=0.016—0.020 for CH_4–Ar at 2000 K,[18,19] and β_c=0.020 for CH_3Cl–Ar at 2000 K[6]). The values of $-\langle\Delta E\rangle/kT$ are also listed in Table 2; they were evaluated by using this approximate relation:[17]

$$\beta_c/(1-\sqrt{\beta_c}) \simeq -\langle\Delta E\rangle/F_E kT.$$

The temperature dependence of β_c can be expressed as: $\beta_c \propto T^{-2.0}$. This agrees with the prediction of Tardy and Rabonovitch[20] rather than with the relation, $\beta_c \propto T^{-1}$, predicted by Luther and Troe.[21] The value of $-\langle\Delta E\rangle \simeq 70$ cal mol^{-1} obtained here for the CH_3I–Ar system is not unreasonable compared with the recent data for triatomic molecules diluted in Ar.[22]

It is found from the present results that, as a heat bath, Ar is inefficient in supplying the energy by means of both T-T and T-V energy-transfer processes.[23] Although uncertainties in the details of β_c and $\langle\Delta E\rangle$ remain, the data obtained in the present work make it quite clear that weak collision efficiencies are of importance for high-temperature reactions. Further investigations are needed for the CH_3I pyrolysis in various diluents including polyatomic molecules.

Table 2. Calculated results of k_o^{sc} a)

T/K	k_o^{sc}/cm^3 mol^{-1} s^{-1}	F_E	β_c	$-\langle\Delta E\rangle/kT$
1100	3.13×10^8	1.28	0.028	0.043
1200	2.11×10^9	1.31	0.021	0.033
1300	1.00×10^{10}	1.35	0.018	0.027
1400	3.79×10^{10}	1.38	0.015	0.024
1500	1.13×10^{11}	1.42	0.014	0.023

a) Input data for the calculation of k_o^{sc}: threshold energy, E_o=56.0 kcal mol^{-1}; Lennard-Jones collision diameters, $\sigma(CH_3I)$=4.23 Å[b], σ(Ar)=3.54 Å[c]; Lennard-Jones well depths, $\varepsilon(CH_3I)/k$=519 K[b], ε(Ar)/k=93.3 K[c]; vibrational frequencies of CH_3I, ν=2969.8, 3060.1 (2), 1251.5, 1435.5 (2), 532.8, 882.4 (2) cm^{-1}.[d] b) G. A. Millor and R. B. Bernstein, *J. Phys. Chem.*, **63**, 710 (1959). c) R. C. Reid, J. M. Prausnitz, and T. K. Sherwood, "The Properties of Gases and Liquids," 3rd ed, McGraw-Hill, N. Y. (1977). d) T. Shimanouchi, "Tables of Molecular Vibrational Frequencies," Vol. I, NSRDS-NBS 39 (1972).

References

1) For example, a) K. A. Holbrook, *Trans. Faraday Soc.*, **57**, 2151 (1961); b) W. Forst and P. St. Laurent, *Can. J. Chem.*, **43**, 3052 (1965); c) W. Forst and P. St. Laurent, *ibid.*, **45**, 3169 (1967).

2) a) E. Tschuikow-Roux and J. E. Marte, *J. Chem. Phys.*, **42**, 2049 (1965); b) E. Tschuikow-Roux, *ibid.*, **42**, 3639 (1965).

3) A. P. Modica and J. E. LaGraff, *J. Chem. Phys.*, **44**, 3375 (1966).

4) K. P. Schug and H. G. Wagner, *Z. Phys. Chem., N. F.*, **86**, 59 (1973).

5) K. P. Schug, H. G. Wagner, and F. Zabel, *Ber. Bunsenges. Phys. Chem.*, **83**, 167 (1979).

6) In the case of the CH_3Cl pyrolysis, the initiation reaction was found to be the C–Cl bond fission (O. Kondo, K. Saito, and I. Murakami, to be published).

7) Exceptionally, in the pyrolysis of CHF_3 (Ref. 2), second-order rate constants were measured at total pressures up to 18 atm.

8) T. Higashihara, K. Saito, and H. Yamamura, *Bull. Chem. Soc. Jpn.*, **49**, 965 (1976).

9) K. Saito, T. Yokubo, T. Fuse, H. Tahara, O. Kondo, T. Higashihara, and I. Murakami, *Bull. Chem. Soc. Jpn.*, **52**, 3507 (1979).

10) G. Herzberg, "Molecular Spectra and Molecular Structure," D. Van Nostrand Co., Princeton, N. J. (1967), Vol. 3.

11) The data reductions of all the experimental runs were performed without any corrections for the absorption of products.

12) In the decomposition of halomethanes, the following two channels are possible: (1) $CH_3X \rightarrow CH_3+X$ and (2) $CH_3X \rightarrow CH_2+HX$. The differences in the heats of reaction, $\Delta H_r^\circ(1)-\Delta H_r^\circ(2)$, are 27, −6, −22, and −38 kcal mol^{-1} for X=F, Cl, Br, and I respectively. In our preliminary experiments on the CH_3Cl and CH_3Br pyrolysis, it was found that these molecules decomposed *via* the C–X bond fission. From these facts, it can be expected that CH_3I also decomposes *via* the C–I bond fission.

13) S. W. Benson, "The Foundations of Chemical Kinetics," McGraw-Hill Co., N. Y. (1960), Chap. 8.

14) H. S. Johnston, "Gas Phase Reaction Rate Theory," The Ronald Press Co., N. Y. (1966).

15) Computer simulations showed that, during the pyrolysis of CH_3I, such products as CH_2I_2, C_2H_5I, and $C_2H_4I_2$ increase as the reaction proceeds. Among these products, which are considered to have an absorption at the UV region, the concentration of C_2H_5I increases up to the order of 10^{-10} mol cm^{-3}. On the other hand, the other two products are less than that of C_2H_5I by two orders; thus, they are negligible. In additional experiments, the absorption coefficient of C_2H_5I at 275 nm was measured to be about 4×10^6 cm^2 mol^{-1} in the temperature range of 1000—1300 K. Therefore, the absorption profile obtained for the CH_3I–Ar system was corrected by subtracting the absorption of C_2H_5I.

16) The value of the fall-off pressure was calculated by this relation:

$$P_{1/2} \simeq \nu(\lambda Z)^{-1}\{1+D_o/(n+1)RT\}^{-n}RT,$$

where ν is the mean frequency of the vibrations; D_o, the bond-dissociation energy; λ, the steric factor, and n, the effective number of the internal degrees of freedom for the

reaction. The values of λ and n were determined to be 0.016 and 5.75 respectively by using a classical collision theory.

17) J. Troe, *J. Chem. Phys.*, **66**, 4745, 4758 (1977).

18) P. Roth and T. Just, *Ber. Bunsenges. Phys. Chem.*, **79**, 682 (1975).

19) H. A. Olschewski, J. Troe, and H. G. Wagner, "Eleventh Symposium (International) on Combustion," The Combustion Institute, Pittsburgh (1967), p. 155.

20) D. C. Tardy and B. S. Rabinovitch, *Chem. Rev.*, **77**, 359 (1977).

21) K. Luther and J. Troe, "Seventeenth Symposium (International) on Combustion," The Combustion Institute, Pittsburgh (1979), p. 535.

22) H. Endo, K. Glänzer, and J. Troe, *J. Phys. Chem.*, **83**, 2083 (1979).

23) It is considered that the effective T-T process occurs when the masses of colliding molecules are nearly equal to each other, and that the effective T-V process occurs when the diluent molecule is so small as to have a high translational velocity.

Electron Transfer Reaction between $\Delta^{2,2'}$-Bi-1,3-dithiole (TTF) and 7,7,8,8-Tetracyanoquinodimethane (TCNQ). Electron Donating Property of TTF

Akihiko Yamagishi and Yôichi Iida*

Department of Chemistry, Faculty of Science, Hokkaido University, Sapporo 060

(Received July 2, 1979)

The reaction between $\Delta^{2,2'}$-bi-1,3-dithiole (TTF) and 7,7,8,8-tetracyanoquinodimethane (TCNQ) in acetonitrile solution, $TTF+TCNQ \rightleftharpoons TTF^{+\cdot}+TCNQ^{-\cdot}$, was analyzed spectrophotometrically. The thermodynamical data of chemical equilibrium were determined to be $K=(2.8\pm0.1)\times10^{-3}$ at 11 °C, $\Delta H=-6.7\pm1.3$ kJ mol^{-1} and $\Delta S=-72.8\pm17$ J K^{-1} mol^{-1}. The reaction-rate study of the equilibrium in several solvents was also made by temperature-jump technique. The difference in the electron-donating properties between TTF and *N,N,N',N'*-tetramethyl-*p*-phenylenediamine (TMPD) is discussed by comparing the results with those of the reaction between TMPD and TCNQ.

Formation of charge-transfer complexes from electron donor and acceptor molecules is well-known. A combination of strong donor and acceptor molecules often gives rise to separated ions (a cation radical of the donor and an anion radical of the acceptor) in solution.[1]

Attention has been paid to a charge-transfer complex of $\Delta^{2,2'}$-bi-1,3-dithiole (TTF)[2] with 7,7,8,8-tetracyanoquinodimethane (TCNQ) because of its unusually high electric conductivity in solid state.[3] TTF is a strong electron donor, and TCNQ a strong acceptor. In the solid complex, however, the charge transfer from TTF to TCNQ takes place incompletely, this being one cause for the TTF–TCNQ complex to show such high electric conduction. We have investigated the charge-transfer reaction from TTF to TCNQ in solution, only a few attempts having been made to study the behavior of the complex in solution. In order to clarify the charge-transfer interaction between TTF and TCNQ in solid state and in solution, we determined the thermodynamic equilibrium constants of reaction and also the kinetics of electron transfer in various solvents.

Experimental

Commercially available TTF (Aldrich Chem. Co.) and TCNQ (Kanto Chem. Co.) were purified by sublimation *in vacuo*. The temperature and concentration dependences of electronic absorption spectra of acetonitrile solutions containing TTF and TCNQ were measured with a Hitachi 808-Type spectrophotometer. The kinetic study of the electron transfer reaction in acetonitrile and dimethyl sulfoxide (DMSO) solution was made by the temperature-jump method, using a Union Giken temperature-jump apparatus. $NaClO_4$ was used as a supporting electrolyte. The detail of temperature-jump method is similar to that described previously.[4]

Results

Chemical Equilibrium of Electron Transfer Reaction. When TTF and TCNQ are mixed in acetonitrile, the observed electronic absorption spectrum almost comprises a superposition of the spectra of neutral TTF and TCNQ molecules. In addition, the spectra which are assigned to ionized TTF cation radical ($TTF^{+\cdot}$) and TCNQ anion radical ($TCNQ^{-\cdot}$) are observed faintly in the spectrum, no charge-transfer absorption due to TTF–TCNQ complex being detected. The observed absorptions around 700—900 nm are attributable to the absorptions of $TCNQ^{-\cdot}$, the absorptions around 600 nm to those of $TTF^{+\cdot}$.[5,6] Thus, the reaction between TTF and TCNQ in acetonitrile solution can be expressed by

$$TTF + TCNQ \rightleftharpoons TTF^{+\cdot} + TCNQ^{-\cdot}. \quad (1)$$

First we obtained the chemical equilibrium data of this electron transfer (*i.e.*, oxidation-reduction) reaction spectrophotometrically. Since the absorption at 842 nm is entirely assigned to that of $TCNQ^{-\cdot}$, the concentration of $TCNQ^{-\cdot}$ in its equilibrium state, $[TCNQ^{-\cdot}]$, was estimated by means of the optical density of the observed spectrum, together with the value of the molar extinction coefficient known for $TCNQ^{-\cdot}$ ($\varepsilon_{TCNQ^{-\cdot}}(842\text{ nm})=4.35\times10^4$). The equilibrium concentrations of the other molecular species in Eq. 1 were estimated by the relation, $[TTF^{+\cdot}]=[TCNQ^{-\cdot}]$, $[TTF]=[TTF]_0-[TCNQ^{-\cdot}]$ and $[TCNQ]=[TCNQ]_0-[TCNQ^{-\cdot}]$, where $[TTF]_0$ and $[TCNQ]_0$ indicate initial concentrations of TTF and TCNQ added, respectively. Assuming that the activity coefficients of these solutes are unity, the equilibrium constant of Eq. 1 is given by

$$K=\frac{[TTF^{+\cdot}]\,[TCNQ^{-\cdot}]}{[TTF]\,[TCNQ]}. \quad (2)$$

The K value thus estimated was found to be constant when $[TTF]_0$ was in the range $(3-0.3)\times10^{-5}$ M and $[TCNQ]_0$ in the range $(4-1)\times10^{-4}$ M, where 1 M= 1 mol dm^{-3}.

Next, we examined the temperature dependence of the observed K value and found almost linear relationship between $\ln K$ and $1/T$ values in the temperature range 11—25 °C. The following thermodynamic data were obtained for the chemical equilibrium of Eq. 1 in acetonitrile solution:

$$K=(2.8\pm0.1)\times10^{-3} \text{ at } 11\text{ °C},$$
$$\Delta H=-6.7\pm1.3\text{ kJ mol}^{-1},$$
$$\Delta S=-72.8\pm17\text{ J K}^{-1}\text{ mol}^{-1}.$$

The K value agrees with $K=2.5\times10^{-3}$ obtained by Tomkiewicz *et al.*[7] The large negative ΔS value indicates that the ordering of solvent molecules around $TTF^{+\cdot}$ and $TCNQ^{-\cdot}$ takes place upon ionization of TTF and TCNQ.

Kinetic Study of Electron Transfer Reaction. We measured the following forward, k_1, and backward, k_{-1}, rate constants by using temperature-jump technique,

$$\mathrm{TTF} + \mathrm{TCNQ} \underset{k_{-1}}{\overset{k_1}{\rightleftharpoons}} \mathrm{TTF}^{+\cdot} + \mathrm{TCNQ}^{-\cdot}. \quad (3)$$

In pure acetonitrile solution, however, the equilibrium constant K is very small. Thus the signal due to $TCNQ^{-\cdot}$ was so small that we could hardly detect any optical density change of $TCNQ^{-\cdot}$ upon temperature jumping.

In order to increase the concentrations of $TTF^{+\cdot}$ and $TCNQ^{-\cdot}$, we examined the chemical equilibrium of Eq. 1 in several mixed solvents of acetonitrile and DMSO, in view of the report that TTF and TCNQ are mostly ionized in *N,N*-dimethylformamide, DMSO and pyridine solutions.[7] In 27 vol% DMSO–acetonitrile mixed solvent, the equilibrium constant K increased to $(12\pm2)\times10^{-3}$ at 11 °C. In 37 vol % DMSO–acetonitrile mixed solvent, we obtained $K=(22\pm4)\times10^{-3}$ at 11 °C, $\Delta H=-10.0\pm1.7$ kJ mol^{-1} and $\Delta S=-67.4\pm20.9$ J K^{-1} mol^{-1}. The values of both K and $-\Delta H$ increased with increase in the ratio of DMSO in mixed solvent. The increase facilitated our observation of the rate constants of Eq. 3 by temperature-jump method. Figure 1 shows the result of the temperature-jump experiment in 37 vol % DMSO–acetonitrile solution; initial and final temperatures were 9 and 12 °C, respectively. The reciprocal of observed relaxation time, τ^{-1}, of the signal due to $TCNQ^{-\cdot}$ is plotted against the concentration of $[TCNQ^{-\cdot}]+[TTF^{+\cdot}]+K\{[TCNQ]+[TTF]\}$. In the reaction of Eq. 3, apparent relaxation time τ upon temperature jumping is given by

$$\begin{aligned}\tau^{-1} &= k_1([TTF]+[TCNQ])+k_{-1}([TTF^{+\cdot}]+[TCNQ^{-\cdot}]) \\ &= k_{-1}\{[TTF^{+\cdot}]+[TCNQ^{-\cdot}]+K([TTF]+[TCNQ])\},\end{aligned} \quad (4)$$

where we used the relation $K=k_1/k_{-1}$. Thus, we can obtain a linear relation between the τ^{-1} and $[TTF^{+\cdot}]+[TCNQ^{-\cdot}]+K([TTF]+[TCNQ])$ values, the slope giving k_{-1}. Our results almost agree with the linear relation. The backward rate constant, k_{-1}, was determined to be $k_{-1}=(5.3\pm1)\times10^8$ M^{-1} s^{-1} from the slope. The forward rate constant, k_1, was obtained as $k_1=k_{-1}K=(1.2\pm0.5)\times10^7$ M^{-1} s^{-1}.

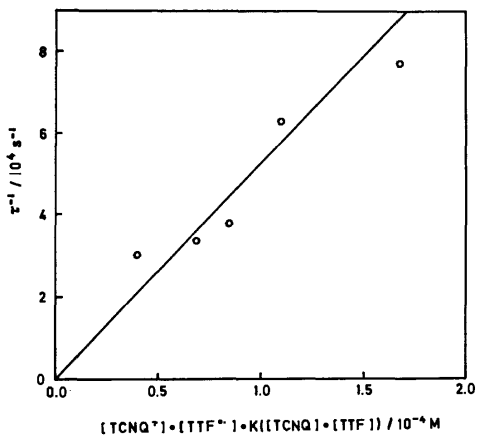

Fig. 1. Temperature-jump experimental result on the reaction of Eq. 3 in 37 vol % DMSO–acetonitrile solution around 11 °C.
Reciprocal of observed relaxation time of the signal due to $TCNQ^{-\cdot}$, τ^{-1}, was plotted against concentration of $[TCNQ^{-\cdot}]+[TTF^{+\cdot}]+K([TCNQ]+[TTF])$. See text.

Discussion

First, let us discuss the experimental result on the chemical equilibrium data. It is of interest to compare the electron transfer reaction of Eq. 1 in acetonitrile with the reaction between *N,N,N',N'*-tetramethyl-*p*-phenylenediamine (TMPD) and TCNQ in the same solvent. Since TMPD is a strong electron donor, comparison of the electron donating strength between TTF and TMPD is significant. Yamagishi *et al.* examined the following electron transfer reaction between TMPD and TCNQ in acetonitrile:[8]

$$\mathrm{TMPD} + \mathrm{TCNQ} \rightleftharpoons \mathrm{TMPD}^{+\cdot} + \mathrm{TCNQ}^{-\cdot}, \quad (5)$$

$$K' = \frac{[TMPD^{+\cdot}]\,[TCNQ^{-\cdot}]}{[TMPD]\,[TCNQ]}. \quad (6)$$

In this system, no absorption due to the charge-transfer complex of TMPD–TCNQ was detected. The thermodynamic data on the chemical equilibrium of Eq. 5 were obtained spectrophotometrically as follows:

$$K' = (7\pm2)\times10^{-2} \text{ at } 25\ ^\circ\mathrm{C},$$
$$\Delta H' = -17\pm4 \text{ kJ mol}^{-1},$$
$$\Delta S' = -71\pm21 \text{ J K}^{-1}\text{ mol}^{-1}.$$

Let us combine these data with those of the reaction between TTF and TCNQ of Eq. 1, and consider the following oxidation-reduction reaction between TTF and TMPD in acetonitrile solution:

$$\mathrm{TTF}^{+\cdot} + \mathrm{TMPD} \rightleftharpoons \mathrm{TTF} + \mathrm{TMPD}^{+\cdot}. \quad (7)$$

The equilibrium constant of this reaction, K'', can be derived from

$$K'' = \frac{[TTF]\,[TMPD^{+\cdot}]}{[TTF^{+\cdot}]\,[TMPD]} = \frac{K'}{K}, \quad (8)$$

where the relations of Eqs. 2 and 6 are used. We can also estimate the enthalpy change, $\Delta H''$, and the entropy change, $\Delta S''$, of Eq. 7. The results are:

$$K'' = (3.6\pm1.2)\times10 \text{ at } 11\ ^\circ\mathrm{C},$$
$$\Delta H'' = \Delta H' - \Delta H = -10.0\pm5.4 \text{ kJ mol}^{-1},$$
$$\Delta S'' = \Delta S' - \Delta S = +1.7\pm38 \text{ J K}^{-1}\text{ mol}^{-1}.$$

Let us consider the following equation in the chemical equilibrium of Eq. 7.

$$\begin{aligned}&E_0(\mathrm{TTF},\ \mathrm{TTF}^{+\cdot}) - \frac{RT}{F}\ln\frac{[TTF^{+\cdot}]}{[TTF]} \\ &\quad = E_0(\mathrm{TMPD},\ \mathrm{TMPD}^{+\cdot}) - \frac{RT}{F}\ln\frac{[TMPD^{+\cdot}]}{[TMPD]},\end{aligned} \quad (9)$$

where R and F are gas constant and Faraday constant, respectively, and $E_0(\mathrm{TTF},\ \mathrm{TTF}^{+\cdot})$ and $E_0(\mathrm{TMPD},\ \mathrm{TMPD}^{+\cdot})$ represent the oxidation potentials in the formation of the cation radicals of $TTF \rightleftharpoons TTF^{+\cdot}+$

e and TMPD⇌TMPD$^{+\cdot}$+e, respectively. The reactions are assumed to be reversible electrode reactions in acetonitrile solution. By use of Eq. 8 together with the K'' value, we obtain

$$E_0(\text{TTF, TTF}^{+\cdot}) = E_0(\text{TMPD, TMPD}^{+\cdot}) - 0.086\pm0.008\ \text{V}. \quad (10)$$

As regards the oxidation potentials, the following results were reported for acetonitrile solution.[9]

$$E_0(\text{TMB, TMB}^{+\cdot}) = E_0(\text{TMPD, TMPD}^{+\cdot}) - 0.28\ \text{V}, \quad (11)$$

$$E_0(\text{DMPD, DMPD}^{+\cdot}) = E_0(\text{TMPD, TMPD}^{+\cdot}) - 0.078\ \text{V}, \quad (12)$$

where TMB and DMPD denote *N,N,N',N'*-tetramethylbenzidine and *N,N*-dimethyl-*p*-phenylenediamine, respectively, and E_0(TMB, TMB$^{+\cdot}$) and E_0(DMPD, DMPD$^{+\cdot}$) refer to the reversible oxidation potentials in the formation of the cation radicals, TMB⇌TMB$^{+\cdot}$+e and DMPD⇌DMPD$^{+\cdot}$+e, in acetonitrile solution, respectively. Comparison of Eqs. 10—12 reveals that one-electron donating power of TTF is a little weaker than that of TMPD and is nearly equal to that of DMPD; the order of electron donating strengths is expressed by TMPD>DMPD≳TTF>TMB in acetonitrile solution.

Let us discuss the ionization potential of TTF. In the oxidation-reduction equilibrium of Eq. 7, the observed enthalpy change, $\Delta H''$, is given by

$$\Delta H'' = I_p(\text{TMPD}) - I_p(\text{TTF}) + \Delta\Delta H_{solv}(\text{TMPD}^{+\cdot}, \text{TMPD}) - \Delta\Delta H_{solv}(\text{TTF}^{+\cdot}, \text{TTF}), \quad (13)$$

where I_p(M) is the ionization energy of the neutral molecule, (M=TMPD or TTF), in gas phase, and $\Delta\Delta H_{solv}$(M$^{+\cdot}$, M) is the difference of solvation energy between M$^{+\cdot}$ and M in acetonitrile solution. Note that I_p(M) corresponds to an adiabatic ionization potential, since the reaction of Eq. 7 involves thermodynamic equilibrium. Thus, if we assume that the solvation energy, $\Delta\Delta H_{solv}$(TMPD$^{+\cdot}$, TMPD), is similar to $\Delta\Delta H_{solv}$(TTF$^{+\cdot}$, TTF), the difference of the ionization potentials between TMPD and TTF can be determined by means of Eq. 13. I_p(TMPD)=6.20 eV was chosen as a standard value for the adiabatic ionization potential of TMPD.[9] By use of the value, $\Delta H''=-10.0\pm5.4$ kJ mol^{-1}, the adiabatic ionization potential of TTF was estimated to be I_p(TTF)=6.30±0.06 eV, which is a little larger than that of TMPD, but almost the same as that of I_p(DMPD)=6.28 eV.[9] On the other hand, the vertical ionization potential of TTF has been determined to be 6.86 eV by photoionization method in gas phase.[10] The vertical energy of TTF exceeds the adiabatic energy by 0.56 eV. The vertical ionization potential of TMPD was found to be 6.75 eV by Nakato *et al.*[11] This is less than the 6.86 eV value of TTF by 0.11 eV, being in line with our finding that the adiabatic ionization potential of TMPD is also less than that of TTF by 0.1 eV.

The entropy change, $\Delta S''$, of the equilibrium of Eq. 7 is small. The reason for this is as follows. Although there is a significant entropy effect upon solvation of ion radicals in acetonitrile solution, the entropies due to the solvation of TMPD$^{+\cdot}$ and TTF$^{+\cdot}$ ions are almost the same and cancel each other, resulting in a small entropy change for the equilibrium of Eq. 7. There is some uncertainty in the value of $\Delta S''=+1.7\pm38$ J K^{-1} mol^{-1} obtained from $\Delta S'-\Delta S$ because of the accumulation of errors of $\Delta S'$ and ΔS. Thus, direct measurement of the equilibrium constant of Eq. 7 is desirable in order to obtain a more reliable value of $\Delta S''$ for the sake of confirmation.

The observed k_{-1} value of Eq. 3 in 37 vol% DMSO–acetonitrile solution is smaller than the $k_{-1}=(6\pm2)\times10^9$ M^{-1} s^{-1} value for the reaction of TMPD$^{+\cdot}$+TCNQ$^{-\cdot}$→TMPD+TCNQ in acetonitrile solution.[8] This might be explained in terms of the difference in the solvents used. Ionic species such as TTF$^{+\cdot}$ are solvated more strongly in DMSO than in acetonitrile. Since k_{-1} is for the electron transfer from ionic species to neutral molecules, the process involves release of solvation of the ionic species. Thus, the reaction in DMSO/acetonitrile requires more activation energy for k_{-1} than the reaction in pure acetonitrile, and the k_{-1} rate constant in the former solvent may be smaller than that in the latter. Except for this solvation effect, the reaction rates in the TTF/TCNQ system are almost of the same magnitude as those in the TMPD/TCNQ system. The difference in the molecular structures of TTF and TMPD may make a minor contribution to the kinetic difference.

Concluding Remarks

Let us consider the electronic states of solid TTF–TCNQ and TMPD–TCNQ complexes on the basis of the above discussions. In the TTF–TCNQ complex, there have been evidences for incomplete charge transfer, where 0.59 electron is transferred from TTF to TCNQ. Segregated columns composed of partially ionized TTF and TCNQ exist, giving rise to metallic properties in the TTF–TCNQ complex.[3] On the other hand, the TMPD–TCNQ complex shows almost ionic character of TMPD cation radical and TCNQ anion radical in the solid state. The X-ray analysis by Hanson,[12] ESR study by Kinoshita and Akamatu,[13] and measurement of the crystal spectra by Kuroda *et al.*[14] provide evidences for almost one electron transfer from TMPD to TCNQ. If the complete charge transfer occurs in the solid TMPD–TCNQ complex, the complex would show semiconductive properties of a Mott-Hubbard-type insulator. Actually, its electric conductivity has been reported to be as low as 10^{-6}—10^{-8} Ω^{-1} cm^{-1}.[5]

Since the acceptor TCNQ is common, the difference between incomplete charge transfer in the TTF–TCNQ complex and almost complete charge transfer in the TMPD–TCNQ complex might depend mostly on the difference in adiabatic ionization potentials between TTF and TMPD. In view of the magnitude of the estimated adiabatic ionization potentials of I_p(TMPD)=6.20 eV and I_p(TTF)=6.30±0.06 eV, the TMPD–TCNQ complex might undergo ionization more easily in the solid state than the TTF–TCNQ complex.

McConnell *et al.* showed that, under certain conditions, a slight change in the ionization potential of donor or the electron affinity of acceptor might sharply discriminate ionic state from non-ionic state in solid charge-transfer complex.[15] Recently, Soos reexamined their argument to improve crystal binding energy and found that the $TTF^{+\gamma}$ $TCNQ^{-\gamma}$ complex might be charged with $\gamma \approx 0.35$, the $TMPD^{+\gamma}TCNQ^{-\gamma}$ complex, with $\gamma \approx 0.6$—0.7.[16] Although the estimated $\gamma \approx 0.35$ value in the TTF–TCNQ complex is lower than the experimental $\gamma \approx 0.59$ value, the slight difference in the ionization potentials between TMPD and TTF causes considerable difference in the degree of charge transfer between TMPD–TCNQ and TTF–TCNQ complexes.

References

1) See, for example, G. Briegleb, "Elektronen-Donator-Acceptor Komplexe," Springer-Verlag, Berlin-Göttingen-Heidelberg (1961); L. J. Andrews and R. M. Keefer, "Molecular Complexes in Organic Chemistry," Holden-Day, Inc, San Francisco, London, Amsterdam (1964).

2) The name tetrathiafulvalene, abbreviated to TTF, is widely used in place of $\Delta^{2,2'}$-bi-1,3-dithiole.

3) See, for example, "Chemistry and Physics of One-Dimensional Metals," ed by H. J. Keller, Plenum Press, New York, London (1977).

4) A. Yamagishi, *Bull. Chem. Soc. Jpn.*, **48**, 2440 (1975).

5) L. R. Melby, R. J. Harder, W. R. Hertler, W. Mahler, R. E. Benson, and W. E. Mochel, *J. Am. Chem. Soc.*, **84**, 3374 (1962).

6) S. Hünig, G. Kiesslich, H. Quast, and D. Scheutzow, *Liebig's Ann. Chem.*, **1973**, 310.

7) Y. Tomkiewicz, J. B. Torrance, B. A. Scott, and D. C. Green, *J. Chem. Phys.*, **60**, 5111 (1974).

8) A. Yamagishi, F. Watanabe, and T. Masui, *J. Chem. Soc., Chem. Commun.*, **1977**, 273.

9) Y. Iida and A. Yamagishi, *Bull. Chem. Soc. Jpn.*, **52**, 2443 (1979). In this paper, we used an expression of reduction potential, $E_0(M^{+\cdot}, M)$, for $M^{+\cdot} + e \rightleftharpoons M$. Signs of the expression must be changed when we use the oxidation potential, $E_0(M, M^{+\cdot})$, for $M \rightleftharpoons M^{+\cdot} + e$.

10) B. A. Scott, F. B. Kaufman, and E. M. Engler, *J. Am. Chem. Soc.*, **98**, 4342 (1976).

11) Y. Nakato, M. Ozaki, A. Egawa, and H. Tsubomura, *Chem. Phys. Lett.*, **9**, 615 (1971).

12) A. W. Hanson, *Acta Crystallogr.*, **19**, 610 (1965); *Sect. B*, **24**, 768 (1968).

13) M. Kinoshita and H. Akamatu, *Nature*, **207**, 291 (1965).

14) H. Kuroda, S. Hiroma, and H. Akamatu, *Bull. Chem. Soc. Jpn.*, **41**, 2855 (1968).

15) H. M. McConnell, B. M. Hoffman, and R. M. Metzger, *Proc. Natl. Acad. Sci.*, **53**, 46 (1965).

16) Z. G. Soos, *Chem. Phys. Lett.*, **63**, 179 (1979).

Absolute Rate Constants for the Reactions of O(^{3}P) with Several Molecules

Ko-ichi SUGAWARA, Yo-ichi ISHIKAWA, and Shin SATO*

Department of Applied Physics, Tokyo Institute of Technology, Ookayama, Meguro-ku, Tokyo 152

(Received October 2, 1979)

Absolute rate constants were measured for several reactions of ground-state oxygen atoms at 296±2 K. The pulse-radiolysis of O_2, CO, or CO_2 in the He diluent was used to produce oxygen atoms, and the atomic concentration was monitored by the resonance absorption. The measurements were made in the pressure range from 50 to 950 Torr (1 Torr ≃133.3 Pa). The rate constants thus obtained were $(2.5\pm0.3)\times10^{-34}$ for O+O_2+He and $(1.0\pm0.2)\times10^{-35}$ for O+CO+He in units of cm^6 molecule^{-2} s^{-1} (1 cm^6 molecule^{-2} s^{-1}≃3.626×10^{35} m^6 mol^{-2} s^{-1}). For simple olefins, the following bimolecular rate constants (k/10^{-12} cm^3 molecule^{-1} s^{-1}) were obtained: Ethylene (1.0±0.2), propene (4.7±0.3), 1-butene (4.7±0.5), *trans*-2-butene (23±3), *cis*-2-butene (20±3), 2-methylpropene (17±2), 2-methyl-2-butene (55±5), 1,3-butadiene (20±2), (1 cm^3 molecule^{-1} s^{-1}≃6.022×10^{17} m^3 mol^{-1} s^{-1}). These rate constants were in fair agreement with the literature values.

The reactions of oxygen atoms with unsaturated hydrocarbons have been investigated by a variety of techniques. Cvetanović used a system of product analysis for the determination of the relative rate constants in his early studies.[1] For the production of oxygen atoms, the mercury-photosensitized decomposition of dinitrogen oxide and the photolysis of nitrogen dioxide were employed. The absolute rate constants were measured in discharge-flow systems combined with a mass spectrometer[2–5] or ESR.[6,7] This technique can, however, be used in only a limited low-pressure range, and it often needs stoichiometry corrections, because of the small difference in concentration between atoms and reactants in the reaction system.

Instead of the discharge-flow method, two other techniques have been employed so as to investigate the reactions under relatively high pressures, at which the concentration of the oxygen atoms is generally much lower than that of the reactants, and where no stoichiometry corrections are necessary. One is the flash-photolysis technique, which is often employed together with the method of resonance fluorescence[4,8–12] or the chemiluminescence of NO_2*[13–15] for the time-resolved measurement of the oxygen-atom concentration. The other is the modulation-phase shift technique, in which oxygen atoms are produced by the modulated mercury-photosensitization of dinitrogen oxide, and the rate constants are obtained as the phase shift between the incident radiation and the NO_2* chemiluminescence.[16–21]

Although a number of rate constants for the reactions of oxygen atoms with unsaturated hydrocarbons have been obtained by using these methods, there remain large discrepancies between the determined values. For example, the rate constant for the reaction of oxygen atoms with ethylene, which is one of the most investigated hydrocarbons, ranges from 5.0×10^{-13} to 1.2×10^{-12} cm^3 molecule^{-1} s^{-1}. Therefore, it is of interest to measure the rate constant using other techniques.

Recently we reported the absolute rate constants at room temperature for the reactions of H and D atoms with seven olefins, using a pulse radiolysis-resonance absorption technique.[22,23] The H and D atoms were generated in hydrogen and deuterium of some hundreds of Torr by the irradiation of an electron pulse, and were monitored by means of the light absorption at the Lyman-α line. This technique was initiated by Bishop and Dorfman[24] and developed by Mihelcic *et al.*[25] The results showed good agreement with those of previous works, and confirmed the validity of our apparatus and technique. This technique was extended to the rate constant measurements on the reactions of nitrogen atoms in the ground state with nitrogen monoxide, seven olefins, acetylene, and 1,3-butadiene.[26] The quenching rate coefficients of N(^{2}D) and N(^{2}P) by N_2 were also obtained.[27]

In the present work, this technique is extended to the measurement of the absolute rate constants for the reactions of oxygen atoms.

Experimental

The details of the apparatus and technique were given in the previous paper;[22] hence, only additional improvements and the major features will be described here.

Figure 1 shows the apparatus schematically. As the source of oxygen atoms, O_2(1.2—6.0 Torr), CO(≈11 Torr), or CO_2 (≈2.6 Torr) diluted with He (50—950 Torr) was used, and the gas mixture was irradiated with an electron pulse (pulse width, 3 ns; upper-limit energy, 600 keV) generated by Febetron 706 (Hewlett Packard Co.). The energy absorbed by 900 Torr He was estimated to be 4×10^{16} eV per pulse at a 25 kV DC charging voltage of

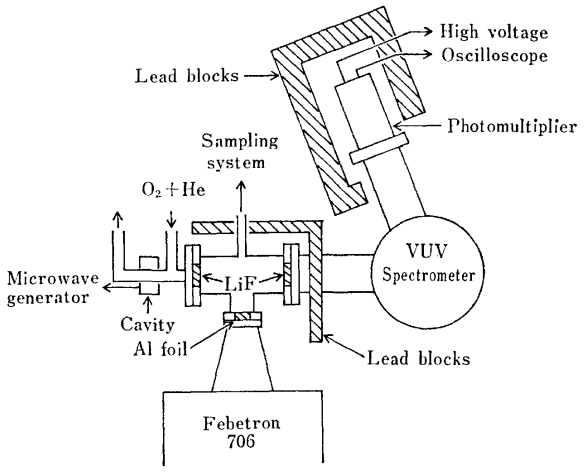

Fig. 1. Schematic diagram of the apparatus.

Febetron 706, on the basis of the measurement of the yields of nitrogen and oxygen in the pulse-irradiated dinitrogen oxide at 900 Torr. The values of 12.4 and 2.1 were taken as the G-values of nitrogen and oxygen,[28] and the energy absorption was assumed to be proportional to the electron density.

The concentration of oxygen atoms was followed by observing the light absorption of the resonance triplet lines of oxygen atoms around 130 nm. The resonance lamp used previously was a water-cooled capillary discharge lamp powered by a DC-current regulator. Since the output of the lamp fluctuated in the time range of μs ($S/N=5$ in the worst case), it was replaced by an electrodeless discharge lamp made of a Pyrex glass tube, 8 mm in inside diameter. A 2450 MHz microwave generator (Ito Chotanpa Co.) was operated at 70 W. A mixture of O_2 (10%) and He was made to flow at the total pressure of 5 Torr. Under these conditions, the highest intensity was obtained at the resonance line of the oxygen atoms. The resonance triplet lines ($^3S_1 \rightarrow {}^3P_{2,1,0}$: 130.217, 130.487, and 130.604 nm) emitted from the lamp passed through the reaction cell, on both sides of which LiF windows (Harshow Chem. Co.) were mounted, and were isolated with a vacuum ultraviolet spectrometer (Shimadzu, Model SGV-50). Since the slit width was open wide (1 mm), the triplet was not resolved. Consequently, the rate constants obtained in the present work are those of the overall reactions of oxygen atoms in the $^3P_2$, $^3P_1$, and $^3P_0$ states. The vacuum ultraviolet light was directly detected with a head-on-type photomultiplier (Hamamatsu TV Co., R976) amplified and monitored with an oscilloscope (Tektronix 465). Lead blocks were placed as is shown in Fig. 1 in order to protect the photomultiplier from the X-rays generated by the electron pulse.

The high-purity, dried He (Nihon Helium Co.) was passed through a trap filled with molecular sieve 4A at 77 K before use. The O_2 (Nihon Sanso Co.) and CO (Takachiho shoji Co.) were used without further purification. Research-grade olefins and CO_2 (Takachiho Shoji Co.) were used after thorough degassing.

Results

For the time-resolved measurements of the concentration of oxygen atoms, we used the resonance absorption method based on Lambert-Beer's law:

$$I_{tr} = I_0 \exp(-D), \quad \text{(I)}$$

$$D = \varepsilon[O]l. \quad \text{(II)}$$

The relative intensities of the incident and transmitted light, I_0 and I_{tr}, were evaluated from photographs such as Fig. 3a, and the optical density, D, was calculated by means of Eq. I. Since the molar absorption coefficient, ε, and the light-pass length, l, are constant, the oxygen-atom concentration, [O], should be proportional to D. However, Beer's law (II) does not always hold, because the line shape of the emission from a lamp is generally broader than that of the absorption in the reaction cell. Figure 2 shows the initial optical density as a function of the He pressure in the range from 50 to 950 Torr. The oxygen pressure was fixed at 3.0 Torr. In the present experiment, the absorption of energy by the gas mixture occurs through He, since O_2 is a minor component, and oxygen atoms are generated in proportion to the He pressure. Consequently, the plots shown in Fig. 2 correspond to the relationship between [O] and D. Evidently a linearity holds below the unity of D. In only this range of D, the photographs obtained were analyzed. As will be described below, the unity of D corresponds to the oxygen-atom concentration of 3×10^{13} cm^{-3}.

The System of O_2 in He. Figure 3a exhibits the transmittance, I_{tr}/I_0, as a function of the time obtained with the O_2 system in He. With this system, all the decay curves obtained fit a first-order decay plot, such as Fig. 3b. The slope of this linear rela-

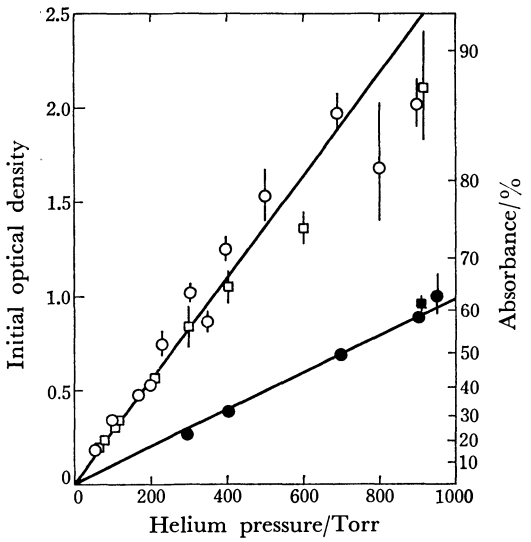

Fig. 2. Initial optical density and absorbance as a function of He pressure.
Charging voltage of Febetron is set at 25 kV (●, ■) and 28 kV (○, □). Circles were obtained with the mixture of 3 Torr oxygen and He. Squares were obtained with the same mixtures in the presence of 0.05 Torr ethylene.

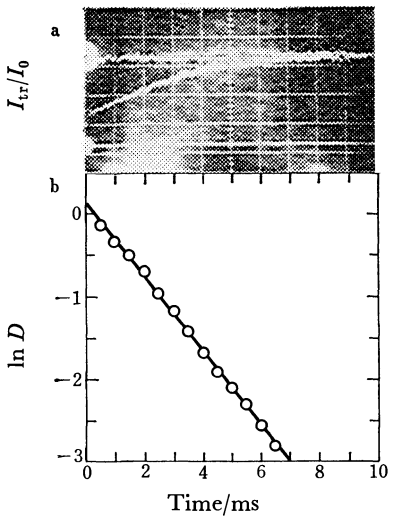

Fig. 3. Time dependence of the transmitted light at 130 nm (a) and the logarithm of the optical density (b).
This photograph was obtained within 10 ms with the mixture of 3.06 Torr oxygen and 604 Torr helium. Charging voltage of Febetron was 27 kV.

tionship gives the decay rate of the oxygen atoms. The reactions occuring in this system may be described by the next two termolecular reactions:

$$O + O_2 + He \longrightarrow O_3 + He, \quad (1)$$

$$O + O_2 + O_2 \longrightarrow O_3 + O_2. \quad (2)$$

The decay rate, k_{dr}, should, then, be given by this equation:

$$k_{dr} = k_1[O_2][He] + k_2[O_2]^2. \quad (III)$$

Here, k_1 and k_2 are the rate constants of Reactions 1 and 2 respectively. The He pressure dependence of the decay rate is shown in Fig. 4, where the oxygen pressures are fixed at 1.2 and 3.0 Torr. The slope and intercept of this linear relationship should correspond to $k_1[O_2]$ and $k_2[O_2]^2$ respectively. Figure 5 shows the O_2 pressure dependence of the decay rate, where the $k_{dr}[O_2]^{-2}$'s are plotted as a function of $[O_2]^{-1}$, with two fixed pressures of He. The slope and intercept should correspond to $k_1[He]$ and k_2 respectively. From these figures, k_1 and k_2 were obtained to be $(2.5\pm0.3)\times10^{-34}$ and $(1\pm3)\times10^{-33}$ cm^6 molecule^{-2} s^{-1} respectively. Since the pressure range of oxygen could not be changed widely, the error limit for k_2 was very large.

The System of CO in He. Figure 6a was obtained by the pulse radiolysis of the mixture of 10.5 Torr of CO and 905 Torr of He at 294 K. The first-order decay plot, Fig. 6b, exhibits that the decay of oxygen atoms seems to occur in two stages. In order to explain this decay curve, we considered the participation of carbon atoms in this reaction system:

$$C + CO + M \longrightarrow C_2O + M \ (M=He, CO) \quad (3)$$

$$O + CO + He \longrightarrow CO_2 + He \quad (4)$$

$$O + CO + CO \longrightarrow CO_2 + CO \quad (5)$$

$$O + C_2O \longrightarrow 2CO. \quad (6)$$

The decay rate of the concentration of oxygen atoms is, then, given by this equation:

$$k_{dr} = k_4[CO][He] + k_5[CO]^2 + k_6[C_2O]. \quad (IV)$$

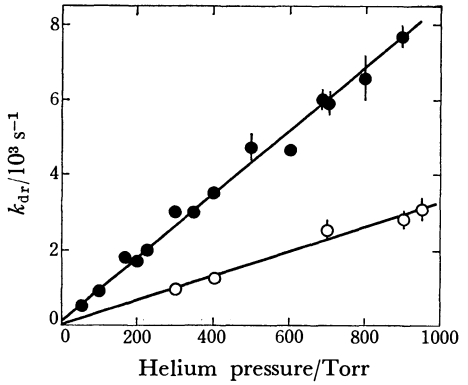

Fig. 4. Decay rate, k_{dr}, as a function of helium pressure.
The oxygen pressure is fixed at 1.2 Torr (○) and 3.0 Torr (●).

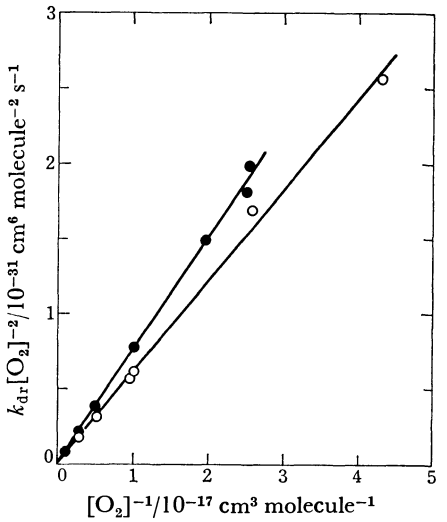

Fig. 5. $k_{dr}[O_2]^{-2}$'s as a function of $[O_2]^{-1}$.
The helium pressure is 700 Torr (○) and 900 Torr (●).

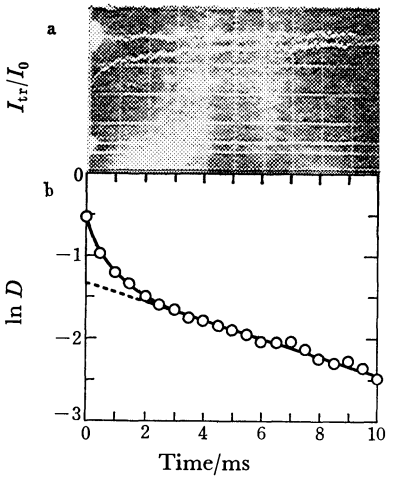

Fig. 6. Time dependence of the transmitted light at 130 nm (a) and the logarithm of the optical density (b).
Carbon monoxide pressure is 10.5 Torr and helium pressure 905 Torr.

TABLE 1. ABSOLUTE RATE CONSTANTS FOR THE $O+O_2+He\rightarrow O_3+He$ REACTION AT ROOM TEMPERATURE

Author[a]	KK	S	MW	DHK	This work
Method[b]	DF/CL	PR/AO_3	P, DF/CL	FP/RA	PR/RA
Pressure/Torr	0—5	$(2.0—5.7)\times10^4$	1—8	150—543	50—950
$k/10^{-34}$ cm^6 molecule^{-2} s^{-1}	4	1.9±0.3	6.3±0.3	4.6±2.6	2.5±0.3

a) KK: Kaufman and Kelso, Ref. 34; S: Sauer, Ref. 35; MW: Mulcahy and Williams, Ref. 36; DHK: Donovan, Husain, and Kirsch, Ref. 37. b) DF: Discharge flow; CL: chemiluminescence; PR: pulse radiolysis; AO_3: absorption of ozone; P: pyrolysis; FP: flash photolysis; RA: resonance absorption.

The initial fast decay of oxygen atoms shown in Fig. 6b may be due to the last term of Eq. IV.

Using the rate constant of Reaction 3 (6.3×10^{-32} cm^6 $molecule^{-2}$ s^{-1})[29] and the concentration of oxygen atoms, as will be stated below, we could estimate the rate constant of Reaction 6 to be larger than 5×10^{-11} cm^3 $molecule^{-1}$ s^{-1}.

If this reaction mechanism is correct, the rate constants of Reactions 4 and 5 can be estimated from the slow first-order decay shown in Fig. 6b, as has been done in the case of the O_2 in the He system. Figures 7 and 8 show the pressure dependence of k_{dr} on CO and He respectively. From these figures, the rate constants of Reactions 4 and 5 can be estimated as follows: $k_4=(1.0\pm0.2)\times10^{-35}$ and $k_5=(3\pm2)\times10^{-35}$ in units of cm^6 $molecule^{-2}$ s^{-1}.

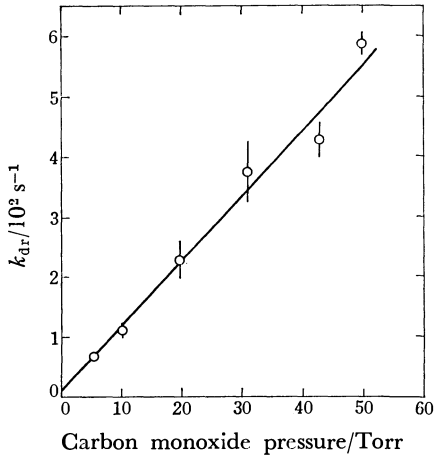

Fig. 7. The decay rate, k_{dr}, of oxygen atoms in the reaction O+CO+He as a function of carbon monoxide pressure. Helium pressure is 900 Torr.

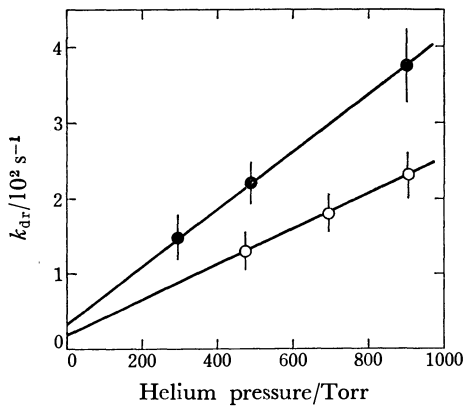

Fig. 8. The decay rate, k_{dr}, of oxygen atoms in the reaction O+CO+He as functions of helium pressure. The carbon monoxide pressures are fixed at 20 (○) and 30 (●) Torr.

The System of CO_2 in He. Similar measurements of the decay rate of oxygen atoms produced in the mixture of 2.6 Torr of carbon dioxide and He, the pressure ranging from 50 to 900 Torr, were carried out. Very slow first-order decays were found. If the oxygen atoms in this system react as follows:

$$O + CO_2 + He \longrightarrow CO_3 + He, \qquad (7)$$

then the upper limit of the rate constant of this reaction is estimated to be $(4\pm2)\times10^{-36}$ cm^6 $molecule^{-2}$ s^{-1}.

The Reactions with Olefins. When a small amount of an olefin is present in any of the three systems of O_2 in He, CO in He, and CO_2 in He, a fast decay of the oxygen atoms can be observed. Figures 9a and b show the decay curves obtained in the absence and presence of propene respectively, with the same sweep time of 0.2 ms per division. Figure 9c represents the first-order decay plots.

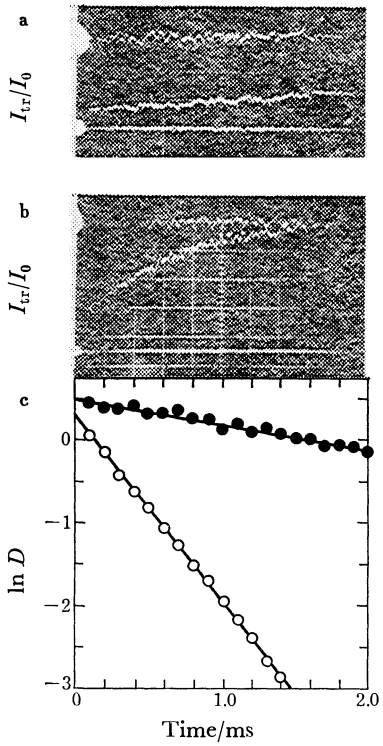

Fig. 9. Time dependence of the transmitted light at 130 nm. (a) was obtained with the mixture of 1.97 Torr O_2 and 904 Torr He, and (b) with the mixture of 0.010 Torr C_3H_6, 3.04 Torr O_2, and 903 Torr He. (c) is the first order plots of the decay curves of (a) (●) and (b) (○).

Table 2. Absolute rate constants for the O+CO+He→CO_2+He reaction at room temperature

Author[a]	DHK	SB	SN	This work
Method[b]	FP/RA	FP/RF	FP/CL	PR/RA
Pressure/Torr		30—200	20—450	300—950
$k/10^{-35}$ cm^6 $molecule^{-2}$ s^{-1}	<4.8	0.6±0.15	0.17±0.05	1.0±0.2

a) DHK: Donovan, Husain, and Kirsch, Ref. 37; SB: Slanger and Black, Ref. 38; SN: Stuhl aud Niki, Ref. 39. b) FP: flash photolysis; RA: resonance absorption; RF: resonance fluorescence; CL: chemiluminescence; PR: pulse radiolysis.

Figure 10 shows the decay rates of the oxygen atoms obtained by using four different sources of oxygen atoms as a function of the ethylene pressure. The slopes of these linear relationships correspond to the rate constant of the reaction of oxygen atoms with ethylene, and the intercepts, to the decay rates of oxygen atoms in each source of oxygen atoms in the absence of ethylene, *i.e.*, O_2 (3 and 6 Torr), CO (11 Torr), and CO_2 (2.6 Torr) in He (900 Torr). Evidently, the same rate constant for the reaction of the oxygen atoms with ethylene was obtained irrespective of the source of the oxygen atoms. Figure 11 shows that the rate constant is also independent of the helium pressure in the range from 50 to 1000 Torr. From these data, the rate constant of the addition reaction of the oxygen atoms to ethylene was estimated to be $(1.0\pm0.2)\times10^{-12}$ cm^3 molecule^{-1} s^{-1}. Table 3 compares previous studies of this reaction.

When the ratio of $[C_2H_4]/[He]$ was smaller than 10^{-4}, the apparent rate constant of the reaction of

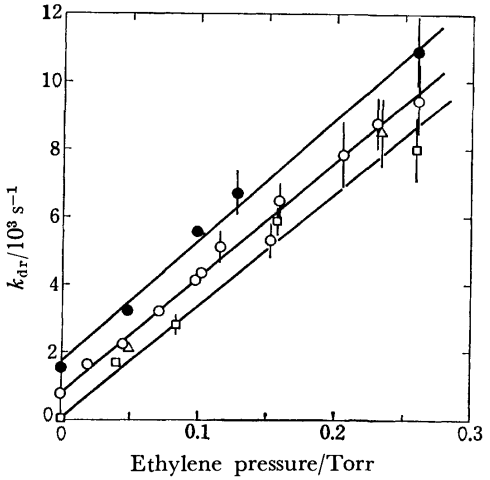

Fig. 10. The decay rates, k_{dr}, of oxygen atoms as a function of ethylene pressure.
The oxygen atom sources are 3.0 Torr O_2 (○), 6 Torr O_2 (●), 11 Torr CO (△), and 2.6 Torr CO_2 (□). Helium pressure is fixed at 900 Torr.

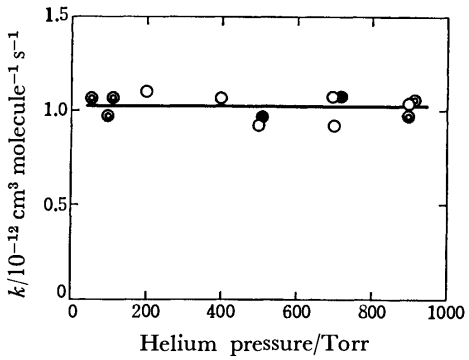

Fig. 11. The rate constant, k, for the reaction of O+ C_2H_4 as a function of helium pressure.
The ethylene pressures are 0.20 (○), 0.10 (●) and 0.05 (◎) Torr.

TABLE 3. RATE CONSTANT FOR THE REACTION OF OXYGEN ATOMS WITH ETHYLENE AT ROOM TEMPERATURE

Author[a)]	Method[b)]	Pressure/Torr	$[C_2H_4]/[O]_0$	$k/10^{-13}$ cm^3 molecule^{-1} s^{-1}
ES	DF/CL	0.25—7.5	0.30—2.3	12±4[c)]
E	DF/MS	1.4—2.4	0.38—1.6	9.5
BT	DF/ESR	1.4—2.8		5.3±0.7
NDW	DF/MS	1.0—2.3	0.010—0.047	5.2±0.4
WD	DF/ESR	0.90—1.33		7.5±0.5
DHHKB	DF/MS	1.30—2.27	0.33—0.54	8.67[d)]
SPG	DF/MS	0.78—2.14	0.010—0.018	7.7
SN	FP/CL	≈10	$>10^3$	$6.3\ ^{+0.3}_{-0.9}$
DHHKB	FP/RF	5—240	100—1500	8.36[d)]
DHHKB	FP/RA	≈50	>80	8.80[d)]
SN	FP/CL	5—20	40—1.6×10^5	6.25±0.63
KH	FP/RF		$>1.8\times10^4$	7.96±0.80
AP	FP/CL	≈26	500—2000	7.61±0.76
AC	HgS/PS	23—107		5.0±0.4
AP	HgS/PS	57—116		6.64±0.66
FACC	HgS/PS	30—50		7.18±0.75
SC	HgS/PS	30—90		6.67±0.85
This work	PR/RA	50—950	100—600	10±2

a) ES: Elias and Schiff, Ref. 40; E: Elias, Ref. 2; BT: Brown and Thrush, Ref. 6; NDW: Niki, Daby, and Weinstock, Ref. 3; WD: Westenberg and de Haas, Ref. 7; DHHKB: Davis, Huie, Herron, Kurylo, and Braun, Ref. 4; SPG: Slagle, Pruss, and Gutman, Ref. 5; SN: Stuhl and Niki, Refs. 13 and 14; KH: Kurylo and Huie, Ref. 8; AP: Atkinson and Pitts, Refs. 15, 20, and 21; AC: Atkinson and Cvetanović, Refs. 16 and 17; FACC: Furuyama, Atkinson, Colussi, and Cvetanović, Ref. 18; SC: Singleton and Cvetanović, Ref. 19. b) DF: discharge flow; FP: flash photolysis; HgS: Hg-photosensitization; CL: chemiluminescence; MS: mass spectrometry; ESR: electron-spin resonance; RF: resonace fluorescence; RA: resonance absorption; PS: phase shift. c) Calculated from the Arrhenius expression. d) Means of the data in the tables of Ref. 4.

the oxygen atoms was found to be a little larger than that obtained above. This is probably due to the fact that, since the amount of ethylene is small, the radicals produced in the reaction of the oxygen atoms with ethylene can compete with ethylene for the oxygen atoms. Therefore, we took the value obtained with the ratio, $[C_2H_4]/[He]$, larger than 10^{-4}. Such an anomaly could not be observed with any olefins other than ethylene.

Figure 12 summarizes the decay rates of oxygen atoms obtained with all olefins examined, as functions of olefin pressure. The rate constants thus obtained are summarized in Tables 4 and 5 together with those previously reported.

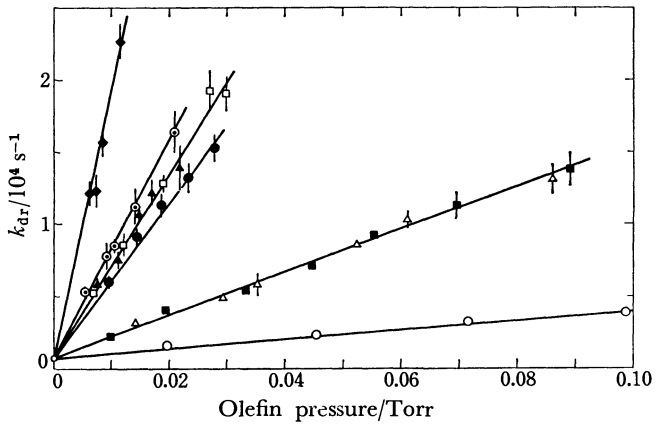

Fig. 12. The decay rates, k_{dr}, of oxygen atoms in the reactions of oxygen atoms with olefins.
Oxygen pressure is 3.0 Torr and helium pressure 900 Torr. ○: ethylene, ■: propene, △: 1-butene, ⊙: *trans*-2-butene, ▲: *cis*-2-butene, ●: 2-methylpropene, ◆: 2-methyl-2-butene, □: 1,3-butadiene.

Discussion

Initial Concentration of Oxygen Atoms. When helium containing a small amount of oxygen is irradiated with high-energy electrons, the ionization and excitation of helium occurs first, and then, the oxygen atoms in the ground (^{3}P) and metastable (^{1}D and ^{1}S) states are generated by the decomposition of oxygen through energy transfer from excited helium or through charge transfer from ionized helium, followed by neutralization with electrons.

Boyd *et al.* measured the *G*-value of ozone from a mixture of oxygen and helium, using Febetron 705 as the source of high-energy electrons; they found that $G(O_3)=16$ at total pressures higher than 300 Torr and with oxygen mole fractions ranging from 0.1 to 0.3.[30] In the present experiment, the mole fraction of oxygen is less than 0.06, so that the *G*-value of ozone may be smaller than 16.

In order to estimate the initial concentration of the oxygen atoms produced in a mixture of 3 Torr oxygen and 900 Torr helium, we used the following values: $G(O)=12.8$,[31] 4×10^{16} eV per pulse for absorbed dose, and 150 cm^3 for the effective volume of the reaction cell. The initial concentration of the oxygen atoms thus calculated was 3×10^{13} cm^{-3}, a value which corresponds to the unity of *D* in Fig. 2.

Influence of Other Active Species. When pulse radiolysis is used for the production of atoms, many different active species are generated together with the atoms required. As was discussed in a previous paper,[22] the participation of ionic species is completed within 10 μs after pulse irradiation; therefore, the only active species we have to consider here are two metastable oxygen atoms, ^{1}D and ^{1}S.

Resently Schofield summarized the rate constants

Table 4. Rate constants for the reactions of oxygen atoms with simple olefins at room temperature

Author[a]	Method[b]	Pressure /Torr	$k/10^{-12}$ cm^3 molecule^{-1} s^{-1}						
			Propene	1-Butene	*trans*-2-Butene	*cis*-2-Butene	2-Methyl-propene	2-Methyl-2-butene	1,3-Butadiene
E	DF/MS	0.75—3.0		5.2		21	16.5		
CS	FP/ACS	≈100		3.2±0.5			13±2		
AC	HgS/PS	23—107	1.96±0.10	2.57±0.20			10.3±2.5		
SN	FP/CL	≈10	$3.6\ ^{+0.2}_{-0.4}$						
K	FP/RF	25—258	3.69±0.21[c]						
FACC	HgS/PS	30—50	3.36±0.29	3.99±0.54		15.0±3.0	16.4±2.3	51.7±5.0	
AP	HgS/PS	57—116	3.34±0.37						
HHD	FP/RF	10—200		4.01±0.40[c]					
DHH	FP/RF	20—40				16.7±1.7[c]			
SC	HgS/PS	30—90	3.69±0.20	3.90±0.26		17.5±0.7	17.3±1.2		
ML	DF/RF	0.78—2.5	3.95±0.41						
AP	FP/CL	≈26	4.47±0.45	4.54±0.46	23.5±2.4	18.1±1.8	15.3±1.5		19.4±1.9
This work	PR/RA	200—1000	4.7±0.3	4.7±0.5	23±3	20±3	17±2	55±5	20±2

a) CS: Callear and Smith, Ref. 41; K: Kurylo, Ref. 11; ML: Michael and Lee, Ref. 42; HHD: Huie, Herron, and Davis, Refs, 9 and 10; DHH: Davis, Huie, and Herron, Ref. 12; for other abbreviations, see Table 3. b) ACS: absorption of CS radicals; for other abbreviations, see Table 3. c) Calculated from the Arrhenius expression.

TABLE 5. RELATIVE RATE CONSTANTS FOR THE REACTIONS OF OXYGEN ATOMS WITH SIMPLE OLEFINS AT ROOM TEMPERATURE

Author[a]	C	E	CS	AC	DHHKB HHD DHH	FACC	SC	AP	This work
Method[b]	HgS/PA	DF/MS	FP/ACS	HgS/PS	FP/RF	HgS/PS	HgS/PS	FP/CL	PR/RA
Ethylene	0.17	0.18		0.19	0.21	0.17	0.17	0.17	0.21
Propene	1.0			0.76		0.84	0.95	0.98	1.0
1-Butene	1	1	1	1	1	1	1	1	1
trans-2-Butene	4.9							5.2	4.9
cis-2-Butene	3.9	4.0			4.2	3.8	4.5	4.0	4.3
2-Methylpropene	4.3	3.2	4.0	4.0		4.1	4.4	3.4	3.6
2-Methyl-2-butene	14					13			12
1,3-Butadiene	4.2							4.3	4.3

a) C: Cvetanović, Ref. 1; for other abbreviations, see Tables 3 and 4. b) PA: product analysis; for other abbreviations, see Tables 3 and 4.

for the reactions of metastable oxygen atoms, ^1D and ^1S, with a number of molecules including oxygen, carbon monoxide, carbon dioxide, and olefins.[32] All rate constants reported are much larger than those obtained with the ground-state ^3P oxygen atoms. Simple calculations using these data can show that the reactions of the ^1D and ^1S oxygen atoms, even if they are produced in the present experimental systems, are all completed before the measurement of the decay of the ^3P oxygen atoms. For example, the O(^1D) atoms are quenched to O(^3P) atoms within 0.3 μs in the system containing 3 Torr of oxygen. Similarly, O(^1S) atoms, if produced in the system containing 0.1 Torr ethylene, are removed within one μs.

Influence of Secondary Reactions. Ozone, which is a product of the reaction of $O+O_2+M$, cannot affect the decay of oxygen atoms in the system of O_2 in helium, because the concentration of ozone produced is small ($<10^{13}$ cm^{-3}) and the rate constant for the reaction of $O+O_3$ is known to be not very large ($(2.5\pm0.5)\times 10^{-14}$ cm^3 molecule^{-1} s^{-1}).[33]

As has been stated in the Results section, when carbon monoxide was used as the source of oxygen atoms, the decay curve for the oxygen atoms was not a simple first-order one. We tentatively explained this as the result of the participation of C_2O in the reaction. This is obviously a subject for further investigation. This complication however, can be ignored in the measurement of the rate constants of the reactions of O+olefins, since the amount of olefins used was much larger than that of the C_2O produced and since the reactions of O+olefins are fast.

In the study of the reaction of oxygen atoms with ethylene, we found the anomaly presented in the Results section. Consequently, we made extensive measurements of this reaction. Some of the results are shown in Fig. 13, where it can be seen that the apparent rate constant for the reaction of oxygen atoms with ethylene increased with the decrease in the ratio of $[C_2H_4]/[O]_0$ below 100. Here, $[O]_0$ stands for the initial concentration of the oxygen atoms.

It is well known that the reaction of $O+C_2H_4$ does not give a stable addition product, but such radicals

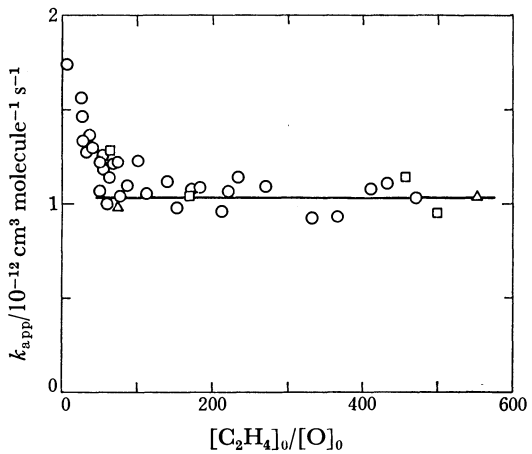

Fig. 13. The apparent rate constant, k_{app}, for the reaction of $O+C_2H_4$ as a function of the ratio, $[C_2H_4]/[O]_0$.
The O_2 (○), CO (△), and CO_2 (□) are used as the source of oxygen atoms.

as CH_3 and CHO, even at atmospheric pressure, while olefins larger than ethylene produce the corresponding addition products.[1] Consequently, the participation of radicals cannot be ignored in the case of ethylene. Let us consider the following simplified reaction mechanism:

$$O + C_2H_4 \longrightarrow R + \text{residue} \qquad k$$
$$R + O_2 + M \longrightarrow RO_2 + M$$
$$O + R \longrightarrow \text{products} \qquad k_R$$
$$O + RO_2 \longrightarrow \text{products} \qquad k_{RO_2}$$

Here, R stands for a radical, and k, k_R, and k_{RO_2}, for the rate constants for each reaction. The amounts of radicals are, of course, time-dependent, but they may be regarded as being in proportion to the initial concentration of the oxygen atoms. Then, the apparent decay rate, k_{app}, of the oxygen atoms may be written by the following equation:

$$k_{app} = k + k_R\frac{[R]}{[C_2H_4]} + k_{RO_2}\frac{[RO_2]}{[C_2H_4]}$$
$$\simeq k\left(1+\alpha(t)\frac{[O]_0}{[C_2H_4]}\right)$$

Therefore, we concluded that the k_{app} value obtained at higher ratios of $[C_2H_4]/[O]_0$ corresponds to the rate constant we are concerned with.

Comparison with Literature Values for the Reactions with Olefins. The rate constants previously obtained for the reaction of $O+C_2H_4$ are summarized in Table 3. They are classified by the method of measurement. The present result is slightly larger than those obtained by the flash-photolysis and modulation-phase-shift techniques, but within the limits of experimental error. Table 4 lists the rate constants for other olefins. The present results agree well with those obtained by Atkinson and Pitts.[15] In addition, the relative rate constants are tabulated in Table 5. All the data are in good agreement with each other, irrespective of the method of measurement.

References

1) R. J. Cvetanović, *Adv. Photochem.*, **1**, 115 (1963).
2) L. Elias, *J. Chem. Phys.*, **38**, 989 (1963).
3) H. Niki, E. E. Daby, and B. Weinstock, 12th Symp. Combust., Poitiers, France, 1968.
4) D. D. Davis, R. E. Huie, J. T. Herron, M. J. Kurylo, and W. Braun, *J. Chem. Phys.*, **56**, 4868 (1972).
5) I. R. Slagle, F. J. Pruss, Jr., and D. Gutman, *Int. J. Chem. Kinet.*, **6**, 111 (1974).
6) J. M. Brown and B. A. Thrush, *Trans. Faraday Soc.*, **63**, 630 (1967).
7) A. A. Westenberg and N. de Haas, 12th Sym. Combust., Poitiers, France, 1968.
8) M. J. Kurylo and R. E. Huie, *J. Chem. Phys.*, **58**, 1258 (1973).
9) R. E. Huie, J. T. Herron, and D. D. Davis, *J. Phys. Chem.*, **75**, 3902 (1971).
10) R. E. Huie, J. T. Herron, and D. D. Davis, *J. Phys. Chem.*, **76**, 3311 (1972).
11) M. J. Kurylo, *Chem. Phys. Lett.*, **14**, 117 (1972).
12) D. D. Davis, R. E. Huie, and J. T. Herron, *J. Chem. Phys.*, **59**, 628 (1973).
13) F. Stuhl and H. Niki, *J. Chem. Phys.*, **55**, 3954 (1971).
14) F. Stuhl and H. Niki, *J. Chem. Phys.*, **57**, 5403 (1972).
15) R. Atkinson and J. N. Pitts, Jr., *J. Chem. Phys.*, **67**, 38, 2492 (1977).
16) R. Atkinson and R. J. Cvetanović, *J. Chem. Phys.*, **55**, 659 (1971).
17) R. Atkinson and R. J. Cvetanović, *J. Chem. Phys.*, **56**, 432 (1972).
18) S. Furuyama, R. Atkinson, A. J. Colussi, and R. J. Cvetanović, *Int. J. Chem. Kinet.*, **6**, 741 (1974).
19) D. L. Singleton and R. J. Cvetanović, *J. Am. Chem. Soc.*, **98**, 6812 (1976).
20) R. Atkinson and J. N. Pitts, Jr., *Chem. Phys. Lett.*, **27**, 467 (1974).
21) R. Atkinson and J. N. Pitts, Jr., *J. Phys. Chem.*, **78**, 1780 (1974).
22) Y. Ishikawa, M. Yamabe, A. Noda, and S. Sato, *Bull. Chem. Soc. Jpn.*, **51**, 2488 (1978).
23) Y. Ishikawa and S. Sato, *Bull. Chem. Soc. Jpn.*, **52**, 984 (1979).
24) W. P. Bishop and L. M. Dorfman, *J. Chem. Phys.*, **52**, 3210 (1970).
25) D. Mihelcic, V. Schubert, F. Höfler, and P. Potzinger, *Ber. Bunsenges. Phys. Chem.*, **79**, 1230 (1975).
26) S. Sato, K. Sugawara, and Y. Ishikawa, *Chem. Phys. Lett.*, **68**, 557 (1979).
27) Y. Ishikawa, K. Sugawara, and S. Sato. The ACS/CSJ Chemical Congress, Hawaii, 1979.
28) C. Willis, A. W. Boyd, and P. E. Bindner, *Can. J. Chem.*, **50**, 1557 (1972).
29) D. Husain and L. J. Kirsch, *Trans. Faraday Soc.*, **67**, 2025 (1971).
30) A. W. Boyd, O. A. Miller, and E. B. Selkirk, *Can. J. Chem.*, **55**, 203 (1977).
31) C. Willis, A. W. Boyd, M. J. Young, and D. A. Armstrong, *Can. J. Chem.*, **48**, 1505 (1970).
32) K. Schofield, *J. Photochem.*, **9**, 55 (1978).
33) L. F. Phillips and H. I. Schiff, *J. Chem. Phys.*, **36**, 1509 (1962).
34) F. Kaufman and J. R. Kelso, *J. Chem. Phys.*, **46**, 4541 (1967).
35) M. C. Sauer, Jr., *J. Phys. Chem.*, **71**, 3311 (1967).
36) M. F. R. Mulcahy and D. J. Williams, *Trans. Faraday Soc.*, **64**, 59 (1968).
37) R. J. Donovan, D. Husain, and L. J. Kirsch, *Trans. Faraday Soc.*, **66**, 2551 (1970).
38) T. G. Slanger and G. Black, *J. Chem. Phys.*, **53**, 3722 (1970).
39) F. Stuhl and H. Niki, *J. Chem. Phys.*, **55**, 3943 (1971).
40) L. Elias and H. I. Schiff, *Can. J. Chem.*, **38**, 1657 (1960).
41) A. B. Callear and I. W. M. Smith, *Nature*, **213**, 382 (1967).
42) J. V. Michael and J. H. Lee, *Chem. Phys. Lett.*, **51**, 303 (1977).

Studies on 2-Aziridinecarboxylic Acid. IV. Total Synthesis of Actinomycin D (C_1) *via* Ring-opening Reaction of Aziridine

Takumi TANAKA, Kiichiro NAKAJIMA, and Kenji OKAWA*

Department of Chemistry, Faculty of Science, Kwansei Gakuin University, Nishinomiya 662

(Received June 18, 1979)

Actinomycin D (C_1) has been synthesized by a route involving the ester formation between two peptide fragments, (2*S*,3*S*)-1-(2-nitro-3-benzyloxy-4-methylbenzoyl)-3-methyl-2-aziridinecarbonyl-D-valylproline *t*-butyl ester and *N*-benzyloxycarbonylsarcosyl-*N*-methylvaline, *via* a ring-opening reaction of aziridine. Cyclization, followed by reduction and oxidation, gave actinomycin D (C_1). The synthetic actinomycin D (C_1) was indistinguishable from natural substance as regards physical properties and biological activity.

A number of cyclic peptide lactone antibiotics such as actinomycin group, etamycin, and echinomycin have been reported during the last few years. However, since they possess cyclic lactone structure and unusual amino acids, the synthetic approaches were limited.

It was found that the reaction of the peptide containing (2*S*, 3*S*)-3-methyl-2-aziridinecarboxylic acid with *N*-protected amino acids or dipeptides affords *O*-acylthreonine peptides.[1] This paper reports an application of the ester formation method to the synthesis of naturally occurring cyclic peptide lactone, actinomycin D (C_1) (Fig. 1).

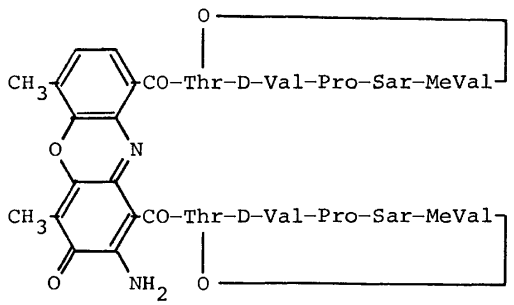

Fig. 1.

So far, the general synthetic method for peptide lactones involved formation of the ester bond (didepsipeptide) at the start, followed by peptide elongation and cyclization by the formation of the amide bond. A new route is designed in which linear pentapeptide ester **11** is directly formed by the ring-opening reaction of aziridinecarboxylic acid-containing peptide **8** with dipeptide **10** (Scheme 2). The method needs no activating reagent for the preparation of *O*-acylthreonine peptide, no racemization taking place during the course of direct introduction of *N*-protected dipeptide.

(2*S*,3*S*)-1-Trityl-3-methyl-2-aziridinecarboxylic acid (**4**) was prepared from threonine by the following route (Scheme 1). Tritylthreonine methyl ester (**1**) was treated with *p*-toluenesulfonyl chloride in a pyridine solution at −10 °C to give *O*-tosyl derivative **2**, which was refluxed in tetrahydrofuran with triethylamine to convert aziridinecarboxylic acid derivative **3**. Saponification of **3** with lithium hydroxide gave the desired amino acid **4**.

The aziridine segment **8**, (2*S*,3*S*)-1-(2-nitro-3-benzyloxy-4-methylbenzoyl)-3-methyl-2-aziridinecarbonyl-D-valylproline *t*-butyl ester, was synthesized as follows. Coupling of benzyloxycarbonyl-D-valine and proline

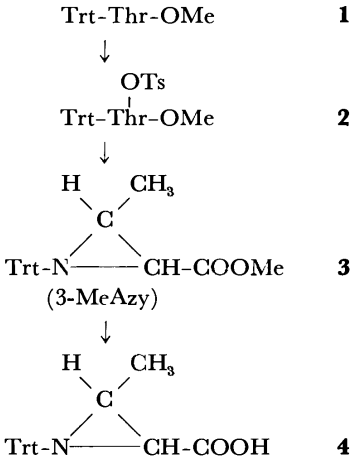

Scheme 1.

t-butyl ester using dicyclohexylcarbodiimide (DCC)[2] gave the dipeptide **5**. Hydrogenolysis of **5**, followed by coupling with **4** using DCC gave the tripeptide **6** in 91.5% yield. Selective removal of the trityl group of **6** with 85% formic acid containing a small amount of methanol gave **7** in 94.6% yield, which was then coupled, in the dark, with 2-nitro-3-benzyloxy-4-methylbenzoic acid *N*-hydroxysuccinimide ester. Compound **8** was obtained as colorless amorphous powder in 94.7% yield after purification by silica gel column chromatography using benzene–ethyl acetate (1 : 1 v/v). Benzyloxycarbonylsarcosine was coupled with *N*-methylvaline *t*-butyl ester using DCC to give the dipeptide **9**. *t*-Butyl group of **9** was removed by the action of trifluoroacetic acid to give the dipeptide acid **10** as an acid component.

The formation of the ester bond between *N*-methylvaline and threonine was carried out by heating **8** together with **10** at 110 °C for 5 h, in the dark. The coupling reaction afforded a mixture of **11** and the hydrolyzed product of **8** (threonine derivative), from which **11** was isolated in 45—55% yields by silica gel column chromatography. The *t*-butyl group of **11** was removed by the action of trifluoroacetic acid, the product **12** being treated with bis(*p*-nitrophenyl) sulfite in a pyridine solution to give the *p*-nitrophenyl ester **13**. Deprotection of benzyloxycarbonyl group of **13** with hydrogen bromide in dioxane, followed by neutralization, cyclization [0.98 mmol in 2 l pyridine, 60 °C, 8 h], and purification on Sephadex LH-20 column in methanol, gave cyclic pentapeptide lactone **14** in 21.4% yield. Catalytic hydrogenolysis of **14**,

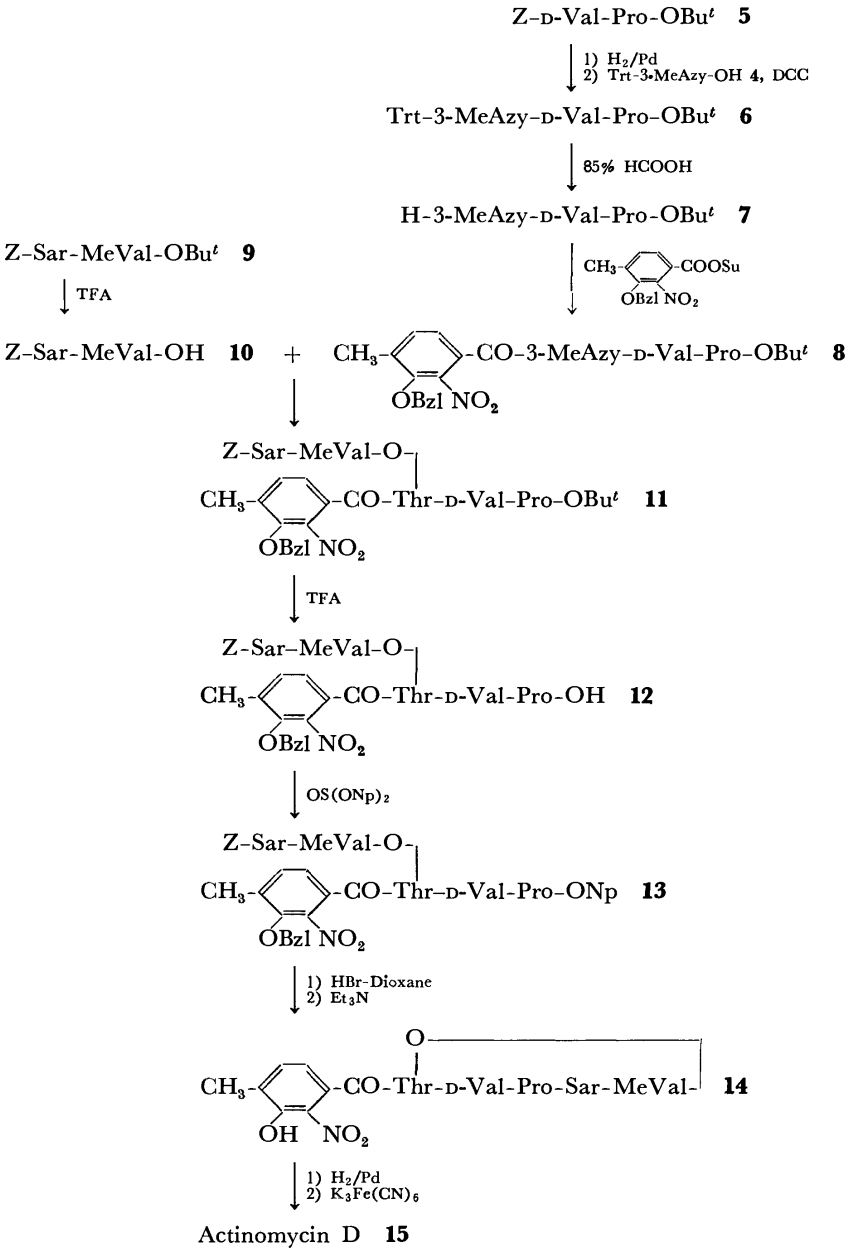

Scheme 2.

Table 1. Physical properties and biological activities of actinomycin D

Characteristics	Synthetic actinomycin D (**15**)	Natural actinomycin D (Lit.) a)	b)
Melting point/°C	242—243	241—243	246—247
Optical rotation ($[\alpha]_D^{23}$)[c]	−316	−323±10	−328±10
UV absorption	24900 (443)	24400 (443)	25000 (443)
[ε in methanol (λ/nm)]	35000 (240)	34100 (240)	34000 (231)
IR absorption (cm^{-1}, KBr)	1745 (lactone C=O)	1745	1760
	1620—1670 (amide)	1620—1670	1620—1670
	1580 (chromophore)	1580	1585
	1195 (lactone COC)	1195	1200[d]
Antibacterial activity (MIC, μg/ml)			
B. Subtilis ATCC-6633	0.78	0.78[e]	
E. Coli NIHJ	>100	—	

a) Ref. 3. b) Ref. 5. c) In methanol at *c* 0.21. d) Ref. 6. e) Ref. 7.

followed by oxidation with potassium hexacyanoferrate(III) in the 1:1 mixture of methanol and 0.067 M phosphate buffer, pH 7.1,[3] gave actinomycin D (C_1) (**15**), which was quantitatively crystallized from ethyl acetate–hexane.

The synthetic actinomycin D (C_1) was indistinguishable from the natural substance as regards physical properties and biological activity against *B. Subtilis*. The physical and biological data are summarized in Table 1.

The method using the ring-opening reaction of aziridine is an efficient means for synthesizing peptide lactone compounds.

Experimental

Melting points are uncorrected. Infrared spectra were obtained on a Hitachi EPI-G3 spectrometer, ultraviolet spectra on a Shimadzu UV-200 spectrophotometer. Optical rotations were determined at the D line on a Perkin-Elmer 141 polarimeter. Thin layer chromatography was carried out on silica gel G in the following solvent systems: R_f^1; chloroform–ethyl acetate (1:1), R_f^2; benzene–ethyl acetate (1:1), R_f^3; chloroform–methanol–acetic acid (8:1:1), R_f^4; chloroform–methanol–ethyl acetate (8:1:1), R_f^5; 1-butanol–acetic acid–water (4:1:1).

*Tritylthreonine Methyl Ester (**1**).* To a solution of threonine methyl ester hydrochloride (85.3 g, 0.5 mol) and triethylamine (140 ml, 1 mol) in $CHCl_3$ (280 ml) was added a solution of trityl chloride (139 g, 0.5 mol) in $CHCl_3$ (250 ml) at 0 °C. After being stirred for 24 h at 0 °C the solution was concentrated *in vacuo* and the residue was dissolved in ethyl acetate. The solution was washed with water, 10% citric acid and water. Drying over Na_2SO_4 and concentration gave an oil (186 g) of **1** in a theoretical yield, R_f^1 0.86, $[\alpha]_D^{23}$ +5.4 (*c* 0.94, $CHCl_3$).

*O-Tosyl-N-tritylthreonine Methyl Ester (**2**).* To a solution of **1** (5.72 g, 15.2 mmol) in dry pyridine (45 ml) was added at −10 °C a solution of *p*-toluenesulfonyl chloride (8.71 g, 45.7 mmol) in dry pyridine (50 ml). After being stirred for 3 d at −10 °C the reaction mixture was poured onto ice water (400 ml). The oily product was extracted with ethyl acetate. The extract was further washed with water, dried over Na_2SO_4, and concentrated *in vacuo*. The residue was crystallized from ethyl acetate–ether–hexane, 6.59 g (81.9%), mp 120—122 °C, $[\alpha]_D^{23}$ +87.7 (*c* 0.9, $CHCl_3$). Found: C, 70.21; H, 6.01; N, 2.50; S, 6.25%. Calcd for $C_{31}H_{31}O_5NS$: C, 70.30; H, 5.90; N, 2.64; S, 6.05%.

*(2S, 3S)-1-Trityl-3-methyl-2-aziridinecarboxylic Acid Methyl Ester (**3**).* A solution of **2** (16.5 g, 31.1 mmol) and triethylamine (36.4 ml, 93.3 mmol) in tetrahydrofuran (100 ml) was refluxed at 80 °C for 2 d. After removal of solvent the oily product was dissolved in ethyl acetate. The solution was washed with water, dried over Na_2SO_4, and concentrated *in vacuo*. The residue was crystallized from methanol, 10.1 g (90.4%), mp 109—110 °C, $[\alpha]_D^{23}$ −102.8 (*c* 1.0, $CHCl_3$). Found: C, 80.29; H, 6.39; N, 3.56%. Calcd for $C_{24}H_{23}O_2N$: C, 80.64; H, 6.48; N, 3.92%.

*(2S, 3S)-1-Trityl-3-methyl-2-aziridinecarboxylic Acid (**4**).* To a solution of **3** (6.0 g, 16.8 mmol) in acetonitrile (80 ml) and methanol (20 ml) was added drop by drop at 20 °C a solution of 2 M lithium hydroxide (24 ml, 84 mmol). After being stirred for 24 h at 20 °C the solvent was removed and the residue was dissolved in ethyl acetate. The solution was washed with 10% citric acid and water, dried over Na_2SO_4, and concentrated *in vacuo*. The residue was crystallized from hexane, 5.47 g (94.8%), mp 173—175 °C, $[\alpha]_D^{23}$ −77.3 (*c* 0.9, $CHCl_3$). Found: C, 79.54; H, 6.23; N, 3.80%. Cacld for $C_{22}H_{21}O_2N$: C, 79.73; H, 6.39; N, 4.23%.

*Benzyloxycarbonyl-D-valylproline t-Butyl Ester (**5**).* To a solution of benzyloxycarbonyl-D-valine (16.5 g, 70.5 mmol) and proline *t*-butyl ester (12.0 g, 70.5 mmol) in CH_2Cl_2 (150 ml) was added at −10 °C a solution of dicyclohexylcarbodiimide (DCC, 14.5 g, 70.5 mmol) in CH_2Cl_2 (50 ml). The reaction mixture was stirred at −10 °C for 3 h, and then overnight in a refrigerator. After removal of *N,N'*-dicyclohexylurea by filtration the filtrate was concentrated *in vacuo*. The residue was dissolved in ethyl acetate and the solution was washed with 10% citric acid, 1 M sodium hydrogencarbonate and water, dried over Na_2SO_4, and concentrated *in vacuo*. The residue was crystallized from ethyl acetate–ether–hexane. 24.5 g (89.9%), mp 90—91 °C, $[\alpha]_D^{23}$ −21.4 (*c* 1.0, MeOH). Found: C, 65.74; H, 8.58; N, 7.13%. Calcd for $C_{22}H_{32}O_5N_2$: C, 65.32; H, 7.97; N, 6.93%.

*(2S, 3S)-1-Trityl-3-methyl-2-aziridinecarbonyl-D-valylproline t-Butyl Ester (**6**).* Compound **5** (12.35 g, 30.5 mmol) was hydrogenated over palladium in methanol for 2 h to give N^{α}-free dipeptide. This was coupled with **4** (9.20 g, 28 mmol) in CH_2Cl_2 (150 ml) containing DCC (6.30 g, 30.5 mmol) using the same method as in the preparation of **5** to give **6**, which was crystallized from methanol, 15.3 g (91.5%), mp 93—94.5 °C, $[\alpha]_D^{23}$ −81.5 (*c* 0.82, MeOH). Found: C, 74.29; H, 7.85; N, 6.99%. Calcd for $C_{37}H_{45}O_4N_3$: C, 74.59; H, 7.61; N, 7.05%.

*(2S, 3S)-3-Methyl-2-aziridinecarbonyl-D-valylproline t-Butyl Ester (**7**).* **6** (12.0 g, 20 mmol) was added to an ice-cold solution of 85% formic acid (80 ml) containing metanol (20 ml), and the resulting solution was stirred for 3 h. After removal of solvent the residue was partitioned between ether and water. Sodium hydrogencarbonate was added to the aqueous layer producing alkaline solution, and the isolated oil was extracted with ethyl acetate. After being dried over Na_2SO_4 the solvent was concentrated *in vacuo* to give **7**, which was crystallized from methanol, 6.69 g (94.6%), mp 81—84 °C, $[\alpha]_D^{23}$ −39.0 (*c* 2.0, MeOH). Found: C, 61.42; H, 9.09; N, 11.79%. Calcd for $C_{18}H_{31}O_4N_3$: C, 61.17; H, 8.84; N, 11.89%.

*(2S, 3S)-1-(2-Nitro-3-benzyloxy-4-methylbenzoyl)-3-methyl-2-aziridinecarbonyl-D-valylproline t-Butyl Ester (**8**).* A mixture of **7** (4.8 g, 13.6 mmol) and 2-nitro-3-benzyloxy-4-methylbenzoic acid *N*-hydroxysuccinimide ester[4] (5.23 g, 13.6 mmol) was stirred in $CHCl_3$ (40 ml) in the dark at room temperature for 24 h. After removal of solvent the residue was dissolved in ethyl acetate, and the solution was washed with 10% citric acid and water, dried over Na_2SO_4, and concentrated *in vacuo*. The crude product was purified by silica gel column chromatography using benzene–ethyl acetate (1:1 v/v) to give **8** as an amorphous powder, 8.53 g (94.7%), R_f^2 0.65, $[\alpha]_D^{23}$ −81.1 (*c* 1.1, MeOH). Found: C, 63.85; H, 7.13; N, 8.71%. Calcd for $C_{33}H_{42}O_8N_4$: C, 63.65; H, 6.80; N, 9.00%.

*Benzyloxycarbonylsarcosyl-N-methylvaline t-Butyl Ester (**9**).* Benzyloxycarbonylsarcosine (17.6 g, 79 mmol), *N*-methylvaline *t*-butyl ester (14.8 g, 79 mmol), and DCC (19.6 g, 95 mmol) were allowed to react in CH_2Cl_2 (250 ml) using the same method as in the preparation of **5**. After purification of the residue by silica gel column chromatography using chloroform–ethyl acetate (1:1 v/v), **9** was obtained as an oil, 29.8 g (96.0%), R_f^1 0.80, $[\alpha]_D^{23}$ −75.8 (*c* 1.4, MeOH).

*Benzyloxycarbonylsarcosyl-N-methylvaline (**10**).* Trifluoroacetic acid (20 ml) was added to **9** (4.79 g, 12.2 mmol) at

−5 °C, and the reaction mixture was stirred for 3 h at the same temperature. After removal of trifluoroacetic acid *in vacuo* the residual oily product was partitioned between ethyl acetate and sodium hydrogencarbonate solution. Citric acid was added to the aqueous layer producing acidic solution, and the isolated oil was extracted with ethyl acetate. The ethyl acetate layer was washed with water successively, dried over Na_2SO_4, and concentrated *in vacuo* to give **10** as an oil, 3.7 g (90.0%), R_f[4] 0.58, $[\alpha]_D^{23}$ −77.7 (*c* 1.07, MeOH).

O-*(Benzyloxycarbonylsarcosyl*-N-*methylvalyl)*-N-*(2-nitro-3-benzyloxy-4-methylbenzoyl)threonyl*-D-*valylproline* t-*Butyl Ester (**11**)*. A mixture of **8** (1.87 g, 3 mmol) and **10** (4.0 g, 12 mmol), protected from light, was heated at 110 °C for 5 h in an oil bath. After cooling the reaction mixture was dissolved in ethyl acetate and the solution was washed with 1 M sodium hydrogencarbonate and water, dried over Na_2SO_4, and concentrated *in vacuo*. The residue was purified by silica gel column chromatography using chloroform–ethyl acetate (1:1 v/v) to give **11** as an amorphous powder, 1.54 g (53.6%), R_f[1] 0.59, $[\alpha]_D^{23}$ −6.47 (*c* 1.12, MeOH). Found: C, 62.65; H, 7.07; N, 8.23%. Calcd for $C_{50}H_{66}O_{13}N_6$: C, 62.61; H, 6.94; N, 8.76%. Another product possessing a lower R_f value (R_f[1] 0.23) was identified as *N*-(2-nitro-3-benzyloxy-4-methylbenzoyl)threonyl-D-valylproline *t*-butyl ester, 769 mg, amorphous powder, $[\alpha]_D^{23}$ −17.4 (*c* 0.9, MeOH). Found: C, 61.20; H, 6.88; N, 8.42%. Calcd for $C_{33}H_{44}O_9N_4$: C, 61.19; H, 6.92; N, 8.74%.

O-*(Benzyloxycarbonylsarcosyl*-N-*methylvalyl)*-N-*(2-nitro-3-benzyloxy-4-methylbenzoyl)threonyl*-D-*valylproline (**12**)*. Trifluoroacetic acid (15 ml) was added to **11** (1.30 g, 1.35 mmol) containing anisole (0.5 ml), and the reaction mixture was stirred for 1 h in the dark. After removal of trifluoroacetic acid, absolute ether was added. The solid precipitate was collected by filtration and washed throughly with absolute ether, 1.00 g (82.0%), R_f[3] 0.85, mp 118—121 °C, $[\alpha]_D^{23}$ −4.5 (*c* 1.0, MeOH). Found: C, 60.80; H, 6.44; N, 9.39%. Calcd for $C_{46}H_{58}O_{13}N_6$: C, 61.18; H, 6.47; N, 9.31%.

O-*(Benzyloxycarbonylsarcosyl*-N-*methylvalyl)*-N-*(2-nitro-3-benzyloxy-4-methylbenzoyl)threonyl*-D-*valylproline* p-*Nitrophenyl Ester (**13**)*. Bis(*p*-nitrophenyl)sulfite (4.4 g, 13.5 mmol) was added to a solution of **12** (1.20 g, 1.32 mmol) in pyridine (20 ml), and the reaction mixture was stirred at room temperature for 20 h in the dark. After removal of solvent the residue was dissolved in ethyl acetate, and the solution was washed with 1 M sodium hydrogencarbonate and water, dried over Na_2SO_4, and concentrated *in vacuo*. The crude product was purified by column chromatography on Sephadex LH-20 in ethyl acetate to give **13** as an amorphous powder, 1.09 g (80.8%), R_f[1] 0.42, $[\alpha]_D^{23}$ −1.7 (*c* 0.29, DMF). Found: C, 60.28; H, 6.00; N, 9.11%. Calcd for $C_{52}H_{61}O_{15}N_7$: C, 60.98; H, 6.00; N, 9.58%.

(2-Nitro-3-hydroxy-4-methylbenzoyl)threonyl-D-*valylprolylsarcosyl*-N-*methylvaline(threonine hydroxyl) Lactone (**14**)*. Hydrogen bromide gas was bubbled at 0 °C, in the dark, into a solution of **13** (1.0 g, 0.98 mmol) in dioxane (10 ml) for 15 min. The reaction mixture was allowed to stand at room temperature for 1 h. After removal of solvent the residue was dissolved in *N*,*N*-dimethylformamide (20 ml) and acetic acid (1 ml). The solution was added drop by drop over a period of 2.5 h to stirred pyridine (2000 ml) containing triethylamine (1 ml) at 60 °C. After being stirred for 5.5 h at the same temperature the pyridine was concentrated *in vacuo* and the residual oil was dissolved in ethyl acetate. The solution was washed with water, 10% citric acid, 1 M sodium hydrogencarbonate and water, dried over Na_2SO_4, and concentrated *in vacuo*. The crude product (568 mg) was purified by column chromatography on Sephadex LH-20 in methanol to give the desired product (159.8 mg, 24.8%), which was crystallized from ethyl acetate–hexane, 137.8 mg (21.4%), R_f[4] 0.38, mp 179—181 °C, $[\alpha]_D^{23}$ −21.0 (*c* 0.5, MeOH). IR (KBr) 1730 (ester C=O), 1655 (amide), 1190 cm^{-1} (ester COC). Found: C, 56.45; H, 6.71; N, 12.62%. Calcd for $C_{31}H_{44}O_{10}N_6$: C, 56.35; H, 6.71; N, 12.72%.

*Actinomycin D (C_1) (**15**)*. A solution of **14** (49 mg, 0.074 mmol) in methanol (10 ml) was hydrogenated over palladium black, in the dark. After 2 h, the mixture was filtered and the filtrate was added to an equal volume of stirred 0.067 M phosphate buffer pH 7.1 containing potassium hexacyanoferrate(III) (70.8 mg, 0.215 mmol). The mixture was stirred at room temperature for 20 min. It was then partitioned between ethyl acetate and water, the aqueous layer being separated and extracted three times with ethyl acetate. The combined ethyl acetate layer was washed successively with 1 M sodium hydrogencarbonate, 1 M HCl, and saturated NaCl, dried over Na_2SO_4, and concentrated *in vacuo* to afford a red crystalline residue, which was recrystallized from ethyl acetate–hexane to give actinomycin D, 44 mg (95.7%), R_f[5] 0.76. Physical and spectral data are given in Table 1. Found: C, 58.59; H, 6.96; N, 13.29%. Calcd for $C_{62}H_{86}O_{16}N_{12}\cdot H_2O$: C, 58.48; H, 6.97; N, 13.20%.

Microbiological Assay. The results of the assay and microorganism employed are given in Table 1. The minimum amount of the compound necessary for the complete inhibition of growth was determined by the Streak method using HI-agar.

The authors wish to express their thanks to the staff of Fujisawa Pharmaceutical Co., Ltd., for the elemental analysis and biological assay.

References

1) Part II. T. Tanaka, K. Nakajima, T. Maeda, A. Nakamura, N. Hayashi, and K. Okawa, *Bull. Chem. Soc. Jpn.*, **52**, 3579 (1979).

2) The abbreviations according to IUPAC-IUB commission, *J. Biol. Chem.*, **247**, 977 (1972), are used. *Z*: benzyloxycarbonyl, OBu^t: *t*-butyl ester, Trt: trityl. "Azyline" is used as the name of an 2-aziridinecarboxylic acid, "Azy" being its abbreviation. 3-MeAzy: (*2S*, *3S*)-3-methyl-2-aziridinecarboxylic acid.

3) J. Meienhofer, *J. Am. Chem. Soc.*, **92**, 3771 (1970).

4) J. Meienhofer, *J. Org. Chem.*, **32**, 1143 (1967).

5) H. Brockmann and H. Lackner, *Chem. Ber.*, **101**, 1312 (1968).

6) H. Brockmann and H. Lackner, *Angew. Chem.*, **66**, 1 (1954).

7) Natural actinomycin D was purchased from P-L Biochemicals, Inc., Lot No. 610111.

The Enantioface-differentiating Hydrogenation of the C=O Double Bond with Asymmetrically Modified Raney Nickel. XXXIII. The Preparation of (*R*)- and (*S*)-1,3-Butanediol from 4-Hydroxy-2-butanone

Shigeki MURAKAMI, Tadao HARADA, and Akira TAI*

Institute for Protein Research, Osaka University, Yamada-Kami, Suita, Osaka 565

(Received July 13, 1979)

The enantioface-differentiating hydrogenation of 4-hydroxy-2-butanone (I) to 1,3-butanediol(II) was conducted with asymmetrically modified metal catalysts. Among the modified catalysts examined, Raney nickel modified with a solution containing tartaric acid and NaBr (TA–NaBr–MRNi) gave the best results with respect to the optical and chemical yields. (*R*)-II, an optical purity of 69% was obtained in a quantitative chemical yield by the use of (*R,R*)-TA–NaBr–MRNi. (*S*)-II was also obtained by the use of (*S,S*)-TA–NaBr–MRNi. A simple method for the preparation of optically pure (*S*)-and (*R*)-II from the hydrogenation product was also developed.

1,3-Butanediol (II) is a biologically interesting compound as a synthetic source of dietary calories[1] and a hypoglycemic agent for diabetes.[2]

A recent study has indicated that (*R*)- and (*S*)-II show different physiological activities.[3] In order to make clear the relations between the absolute configuration and the biological activity of II, the development of a simple method of preparing optically active I was required.

This report will deal with our recent efforts to prepare (*S*)- and (*R*)-II by the enantioface-differentiating hydrogenation of 4-hydroxy-2-butanone (I) with an asymmetrically modified metal catalyst.

Results

The substrate of the present work was prepared from acetone and formaldehyde by a modification of Hays's method:[4]

$$CH_3\text{-}\underset{\underset{O}{\|}}{C}\text{-}CH_3 + CH_2O \xrightarrow{\text{Base}} CH_3\text{-}\underset{\underset{O}{\|}}{C}\text{-}CH_2CH_2OH \quad (1)$$

(I)

Since this reaction proceeds in a flow reactor with a short contact time, the large-scale production of the substrate is feasible.

The hydrogenation of I with various metal catalysts modified with (*R,R*)-tartaric acid easily proceeded at hydrogen pressures of 50—100 kg/cm² and at reaction temperatures of 80—140 °C to give II in good chemical yields.

$$CH_3\text{-}\underset{\underset{O}{\|}}{C}\text{-}CH_2CH_2OH \xrightarrow{H_2/cat} CH_3\text{-}\underset{\underset{OH}{|}}{CH}\text{-}CH_2CH_2OH \quad (2)$$

(I) (II)

However, the optical yields of the reaction were generally low except for the cases of nickel catalysts (Table 1). Thus, further studies were carried out with nickel catalysts.

Among the nickel catalysts examined, Raney nickel prepared by leaching the alloy with an alkaline solution at a high temperature (100 °C) was found to give the best-modified catalyst in terms of its enantiodifferentiating ability and the hydrogenating activity (Table 2). The selection of the favorable modifying reagent was carried out with the above-mentioned Raney nickel. As is shown in Table 3, tartaric acid

Table 1. Optical yield in the hydrogenation of I with a modified metal catalyst

Catalyst	Reaction temp °C	$[\alpha]_D^{20}$ of the product	Optical yield %	Chemical yield[c] %
RNi[a]	80	−8.27	27.3	80
RCo[a]	100	−0.23	0.8	82
RCu[a]	100	−0.38	1.3	80
RPd[a]	80	−0.10	0.3	85
Reduced NiO[b]	140	−4.7	15.9	45

a) A 1.5-g portion of Raney alloys (aluminium content: 50%) was leached with 20 ml of a 20% aqueous NaOH solution at 100 °C, and the resulting catalyst was modified with 100 ml of a 1% aq solution of (*R,R*)-tartaric acid at pH 4.0, at 85 °C. I (10 g) in 20 ml of THF and 0.2 ml of acetic acid was subjected to hydrogenation with each catalyst under a hydrogen pressure of 90 kg/cm². b) A 1-g portion of a nickel catalyst prepared from NiO[6] was modified in the same manner as above. c) Determined by GLC.

Table 2. Effect of leaching conditions of Raney alloy on the optical yield

	Amount of leaching solution[a] ml	Leaching temp of alloy °C	$[\alpha]_D^{20}$ of the product	Optical yield %
1	4	28	−2.88	9.8
2	4	50	−3.08	10.4
3	4	100	−4.58	15.5
4	20	100	−4.34	14.7
5	20	100	−8.69	27.3[b]

a) A 0.3-g portion of Raney alloy was leached with a 20% aqueous NaOH solution under the conditions listed in the table. Each catalyst was modified with 20 ml of 1% tartaric acid at pH 4 at 100 °C. I (2 g) in 3 ml of THF was subjected to hydrogenation at 100 °C under a hydrogen pressure of 90 kg/cm² for 14 h. b) The hydrogenation of I was carried out under the same conditions as above except for the addition of 0.04 ml of acetic acid to the reaction mixture.

Table 3. Optical yield of the hydrogenation of I with various sorts of modified Raney nickels[a]

	Modifying reagent	pH of modifying solution[b]	MRNi		NaBr-treated MRNi[d]	
			$[\alpha]_D^{20}$ of the product	Optical yield %	$[\alpha]_D^{20}$ of the product	Optical yield %
1	(*S*)-Valine	6.0	+1.88	6.3	+0.49	1.6
2	(*S*)-Proline	6.1	+0.34	1.1	—	—
3	(*S*)-Serine	5.7	+0.50	1.7	—	—
4	(*S*)-Threonine	6.5	+0.40	0.1	—	—
5	(*S*)-Aspartic acid	4	−0.18	0.6	−0.20	0.6
6	(*S*)-Glutamic acid	4	−0.65	2.2	—	—
7	(2*S*, 3*R*)-2-Amino-3-hydroxy-butanedioic acid	4	−0.45	1.6	−1.94	6.3
8	(2*S*, 3*S*)-2-Amino-3-hydroxy-butanedioic acid	4	+0.63	2.1	+2.65	8.6
9	(*R*,*R*)-Tartaric acid	4	−5.15	17.4	−15.6	50.0
10	(*R*,*R*)-2-Methyltartaric acid	4	−5.31	17.9	−17.2	55.9
11	(*S*)-Malic acid	4	+0.46	1.6	+0.29	0.9

a) A 0.3-g portion of Raney alloy was leached with 20 ml of a 20% aq NaOH solution at 100 °C. b) The pH was adjusted by the addition of NaOH to the solution of each modifying reagent. In the case of neutral amino acid, the aqueous solution was used without any pH adjustment. c) The catalyst was modified with 20 ml of an aqueous solution containing 0.2 g of each modifying reagent at 100 °C. I (2 g) in 3 ml of THF was subjected to hydrogenation with MRNi at 100 °C under H_2 pressure of 90 kg/cm² for 14 h. d) The catalyst was modified with 20 ml of a solution containing 1.6 g of NaBr and 0.2 g of each modifying reagent.

was one of the best modifying reagents in giving a highly enantio-differentiating catalyst.

The addition of sodium bromide to the modifying solution[5] resulted in a great increase in the enantio-differentiating ability of the catalyst when tartaric acid was used as the modifying reagent (Table 3).

Enhancements of the enantio-differentiating ability of the catalyst were observed by the addition of various sorts of inorganic salt to the modifying solution. Among the inorganic salts examined, sodium bromide was the most effective additive for the modifying solution in giving a catalyst with a high enantio-differentiating ability (Table 4).

Table 4. Optical yield of the hydrogenation of I with TA-inorganic salt-MRNi[a]

	Inorganic salt	Amount of salt in modifying solution[b]	Times of modification process	$[\alpha]_D^{20}$ of the product	Optical yield %
1	—	—	1	−9.00	27.3
2	NaF	1.6 g	1	−8.84	29.9
3	NaCl	1.6	1	−10.92	36.9
4	NaBr	1.6	1	−17.77	59.8
5	NaBr	1.6	2	−20.80	70.2
6	NaBr	1.6	3	−20.79	70.2
7	NaI	1.6	1	—	—[c]
8	NaI	4×10^{-4}	1	−5.3	17.7
9	$Na_2B_4O_7$	0.2	1	−5.91	20.0
10	CH_3COONa	0.2	1	−5.86	19.8
11	Na_2SO_4	1.6	1	−8.88	30.3

a) All the experimental conditions were the same as those described in Table 2. b) Into a 20-ml portion of a 1% solution of (*R*,*R*)-tartaric acid, the listed amount of each salt was dissolved. c) Hydrogenation did not proceed.

The relation between the enantio-differentiating ability of the catalyst and the concentration of sodium bromide in the modifying solution is shown in Fig. 1. The maximum enantio-differentiating ability was observed when the catalyst was modified with a solution containing 8% NaBr and 1% tartaric acid. A high concentration of sodium bromide resulted in a decrease in the enantio-differentiating ability. On the other hand, the repetition of the modification procedure under the best conditions of NaBr concentration resulted in an increase in the enantio-differentiating ability of the catalyst (Table 4, Entries 5 and 6).

Thus, the Raney nickel treated twice with a solution containing 8% NaBr and 1% tartaric acid was found to be the best enantio-differentiating hydrogenation catalyst (TA–NaBr–MRNi) for I.

The optical yield of the hydrogenation was also affected by the reaction conditions, such as the sort of solvent employed, the relative amounts of substrate,

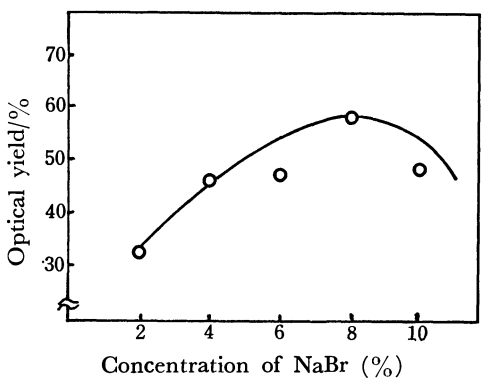

Fig. 1. The relation between optical yield and the concentration of NaBr in modifying solution.

catalyst, and solvent, and the reaction temperature.

As may be seen in Table 5, aprotic moderately polar solvents, such as THF, methyl propionate, and ethyl acetate, gave good optical yields. However, the use of methanol resulted in a poor optical yield.

As is shown in Fig. 2, the optical yields were constantly high over a wide range of the relative amounts of the catalyst, solvent, and substrate. However, the use of small amounts of a catalyst and/or a solvent resulted in poor optical yields.

The optimum optical yield was obtained at the reaction temperature of 85—100 °C (Fig. 3). This temperature was also favorable for giving a good chemical yield.

Under the conditions optimized from all the results mentioned before, (*R*)-II and (*S*)-II with an optical purity of 68—70% were obtained from I with (*R,R*)- and (*S,S*)-tartaric acid–MRNi's in almost quantitative chemical yields and with good reproducibility.

The reaction of the hydrogenation product with phenyl isocyanate gave 1,3-butanedioldicarbanilate (III) as crystals. When a saturated methanolic solution of III with an optical purity of 70% was kept in the presence of small pieces of crystals of optically pure III, optically pure III was crystallized out of the solution in a yield of 64%, based on the total weight of III. The reductive cleavage of the urethane group of optically pure III with $LiAlH_4$ gave optically pure II in a yield of 62% based on III. The overall yield of optically pure II was 40% based on I.

Table 5. Solvent effect on the optical yield of the reaction[a)]

Solvent	$[\alpha]_D^{20}$ of the product	Optical yield %
MeOH	−10.11	34.1
AcOEt	−16.74	56.6
$EtCO_2Me$	−17.76	60.0
THF	−20.50	69.4
THF/Benzene = 3/20	−17.65	59.6

a) The reaction conditions were the same as those described in Footnote a) of Table 1 except for the reaction time (14 h).

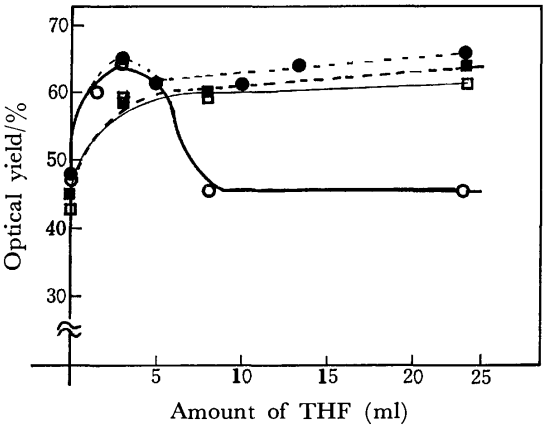

Fig. 2. The effect of the relative amounts of catalyst and solvent on the optical yield.
The substrate (2 g) was subjected to hydrogenation with the catalysts prepared from 0.3 g (–○–), 0.6 g (--●--), 0.9 g (–□–), and 1.5 g (--■--) of Raney alloy, respectively.

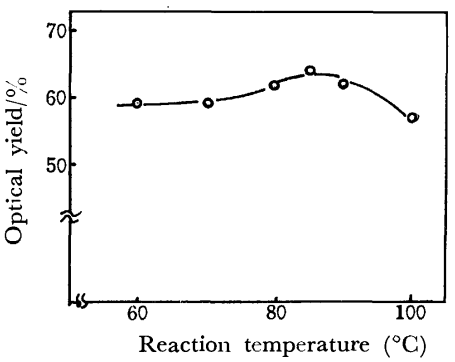

Fig. 3. The effect of reaction temperature on the optical yield.

Discussion

From the results of the present study, the optical yield of the reaction is considered to be determined by two major factors. The first factor is the differentiating ability of the modifying reagent, which depends mostly on the intermolecular interaction between the modifying reagent and the substrate adsorbed on the catalyst. The second factor is the ratio of the enantio-differentiating area to the non-enantio-differentiating area on the surface of the catalyst.

In the course of earlier studies of the enantio-differentiating hydrogenation of the β-ketoester, tartaric acid–MNi was found to be the best enantio-differentiating catalyst, as in the present work.[7)] The excellent result was attributed to the formation of two-site intermolecular interaction through hydrogen bondings between tartaric acid and the β-ketoester (Fig. 4a) in the enantioface-differentiating process.[8)] In a similar manner, tartaric acid can make hydrogen bondings with I, the hydroxyl group of I taking the place of the ester carbonyl group of the β-ketoester (Fig. 4b). The fact that both I and the β-ketoester gave the (*R*)-enantiomer in the hydrogenation over (*R,R*)-tartaric acid–MNi also strongly suggests that the mode of the enantioface-differentiating process of I is identical with that of the β-ketoester. From these considerations, it can be concluded that a high optical yield is obtained when a well-fitting intermolecular interaction is formed

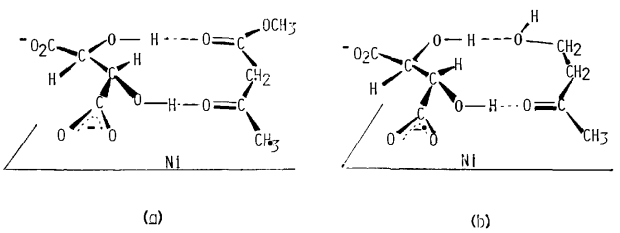

Fig. 4. Schematic representation of the complex of β-ketoester and (*R,R*)-tartaric acid (a) and that of I and tartaric acid (b).

between a modifying reagent and substrate adsorbed on the catalyst.

Such protic solvents as water and alcohol in the reaction system, which can take part in hydrogen bondings with I and/or tartaric acid, interfere with the formation of the rigid interaction between I and tartaric acid. Thus, the use of a protic solvent resulted in a significant decrease in the optical yield.

The dependence of the optical yield on the leaching temperature of the Raney alloy (Table 2) is closely related to the amount of aluminium remaining in the catalyst. It is well documented that Raney nickel prepared at a low temperature contains a large amount of aluminium and shows a high hydrogenation activity. The aluminium in the catalyst is considered to be in a polymeric form of aluminium hydroxide.[9] The hydroxyl groups of tartaric acid on the catalyst and the hydroxyl group of aluminium derivatives may compete in the formation of hydrogen bondings with the substrate. Under these conditions, the formation of a rigid tartaric acid-substrate interaction is disturbed to a large extent. For these reasons, the hydrogenation at the aluminium-enriched part of the catalyst gives the racemic product predominantly. Thus, the use of a Raney nickel leached at a low temperature resulted in a significant decrease in the optical yield.

A Raney nickel leached at a high temperature still contains some of an active nickel in the aluminium-enriched part of the catalyst. Partial poisoning with suitable substances is one way to remove such an active part of the catalyst.

In general, sodium bromide is considered to be a weakly poisoning reagent of a metal catalyst. This compound is apt to be adsorbed on the highly active nickel surface in the aluminium-enriched part of the catalyst. The remarkable increase in the optical yield on the treatment of the catalyst with sodium bromide is caused by the effective blocking of the non-enantiodifferentiating reaction site with sodium bromide.

Experimental

The GLC was carried out with a Shimadzu GC-4APF gas chromatograph using a 3-m, 5-mm-o.d. glass column packed with 5% Tween 80 on Shimalite W at the specified temperature.

The optical rotations were measured with a Perkin Elmer 241 polarimeter. The IR and ^{1}H-NMR spectra were taken with a Shimadzu IR-27G spectrometer and a Hitachi R-24 spectrometer respectively.

Substrate. 4-Hydroxy-2-butanone (I): This compound was obtained, by the aldol condensation of formaldehyde and acetone,[4] in a yield of 28%, based on formaldehyde; bp 56—58 °C/5 mmHg.** The GLC (130 °C) analysis of the distillate showed a 98% purity, with 2% of diacetone alcohol. The NMR and IR spectra of the product were compatible with those expected from the structure of I.

Modifying Reagent. (*R*,*R*)-Tartaric acid, (*S*,*S*)-tartaric acid, (*S*)-aspartic acid, (*S*)-glutamic acid, (*S*)-serine, (*S*)-threonine, (*S*)-valine, and (*S*)-malic acid were commercially purchased.

(2*S*,3*S*)-2-Amino-3-hydroxysuccinic acid ($[\alpha]_D^{20}$ 8.0° (*c* 1, 5 M HCl), lit,[7] 6.4° (*c* 1, H_2O). Anal. Found: C, 31.89; H, 4.73; N, 9.55%. Calcd for $C_4H_7O_5N$: C, 32.22; H, 4.73; N, 9.40%) and (2*S*,3*R*)-2-amino-3-hydroxysuccinic acid ($[\alpha]_D^{20}$ 46.5° (*c* 1, H_2O), lit,[10] 47.0° (*c* 1, H_2O). Anal. Found: C, 31.97; H, 4.71; N, 9.50%) were prepared by the previously reported method.[11]

Catalyst. Raney alloy was leached by adding it portion by portion, to a solution of NaOH under the conditions stated in the tables in the text.

The nickel catalyst was subjected to modification by soaking in the modifying solution for 1 h under the conditions stated in the table in the text.

After the removal of the modifying solution, the modified catalyst was rinsed successively with a 17-ml/(g-catalyst) portion of water, two 80-ml portions of methanol, and a 40-ml portion of the solvent used for the reaction.

Hydrogenation. Hydrogenation was carried out either in a 100-ml autoclave (the data in Tables 1 and 5 were thus obtained) or a 30-ml glass tube in the autoclave (the data in Tables 2,3 and 4 were thus obtained).

After the removal of the catalyst, the reaction prodcut was dried over anhydrous K_2CO_3 (overnight) and then distilled under reduced pressure to give II (bp 117 °C/40 mmHg). Subsequent GLC (130 °C) of the product showed a single peak at a retention time of 14 min. The IR and ^{1}H-NMR spectra of the product were identical with those of the racemic authentic sample (Wako Pure Chemical Co., Ltd.). A 1-g portion of the distillate was diluted in 10 ml of ethanol and, then the optical rotation was determined. The optical purity of the product was calculated based on the optical rotation of optically pure (*R*)-II, $[\alpha]_D^{20}$ −29.6° (*c* 10, EtOH).

Preparation of Optically Pure II. A mixture of II (8.8 g, $[\alpha]_D^{20}$ −20.7° (*c* 10, EtOH) and phenyl isocyanate (22.5 g) was heated at 100 °C for 1 h on an oil bath and then cooled to room temperature to give 30 g of crude III.

A 5-g portion of crude III was dissolved in 14 ml of boiling ethanol. The solution was cooled to room temperature and then mixed with 25 ml of hexane. The mixture was kept overnight at 5 °C. The separation of the crystals from the mixture gave 3.5 g of III ($[\alpha]_D^{20}$ −46.7° (*c* 5, EtOH). Three successive recrystallizations from ethanol–hexane under the same conditions as above gave 2.5 g of III ($[\alpha]_D^{20}$ −56.3° (*c* 5, EtOH)). Three further successive recystallizations resulted in no increase in the optical rotation.

The major portion of the crude III (25 g) was dissolved in 150 ml of methanol under reflux, after which the solution was kept at 5 °C overnight in the presence of small pieces of the crystals of III with $[\alpha]_D^{20}$ −56.3° (*c* 5, EtOH). The crystals were then collected and washed with a 10-ml portion of cold methanol. The crystals thus obtained amounted to 16 g. $[\alpha]_D^{20}$ −56.3° (*c* 5, EtOH), mp 130—131 °C. Found: C, 65.93; H, 6.15; N, 8.55%. Calcd for $C_{18}H_{20}N_2O_4$: C, 65.84; H, 6.14; N, 8.53%.

To the suspension of $LiAlH_4$ (30 g) in 300 ml of dry dioxane, which has been heated at 80 °C on an oil bath, a solution of 15 g of III ($[\alpha]_D^{20}$ −56.3°) in 300 ml of dioxane was added, drop by drop. The reaction mixture was heated for 3 h under reflux, cooled to 5 °C on an ice bath, and then hydrolyzed with 60 ml of water. The insoluble matter was separated by filtration and washed with 30 ml of methanol. The filtrate and washings were then combined and freed of the solvent under reduced pressure at 50 °C. The residue was mixed with 50 ml of water and then washed with three 15-ml portions of benzene. After the evaporation of water from the aqueous layer under reduced pressure, the residue was dried over zeolite 3 A (overnight) and then distilled

** 1 mmHg=133.322 Pa.

under reduced pressure to give 2.5 g II; bp 95—98 °C/10 mmHg, $[\alpha]_D^{20}$ −29.6° (*c* 10, EtOH), $[\alpha]_D^{20}$ −31.6° (*c* 1, EtOH) lit,[11] ($[\alpha]_D^{20}$ −29° (*c* 1, EtOH). The IR and NMR spectra, and the retention time in GLC were identical with those of the authentic sample.

The authors wish to express their thanks to Professor Yoshiharu Izumi and Dr. Hiroshi Ozaki, Institute for Protein Research, Osaka University, for their helpful suggestions. The present work was supported in part by a Grant in Aid for Scientific Research from the Ministry of Education (No. 303530).

References

1) H. A. Mehlman, *Fed. Proc., Fed. Am. Soc. Exp. Biol.*, **34**, 2166 (1975).
2) C. R. Mackerer, R. N. Saunders, J. R. Haettinger, and M. A. Mehlman, *Fed. Proc., Fed. Am. Soc. Exp. Biol.*, **34**, 2191 (1975).
3) H. Nakagawa, K. Nagai, T. Nishio, H. Tsubota, and A. Tai, *Seijinbyo Kenkyu*, **5**, 91 (1976).
4) J. A. Hays, G. F. Hager, H. M. Engelman, and H. M. Spurlin, *J. Am. Chem. Soc.*, **73**, 5369 (1951).
5) T. Harada and Y. Izumi, *Chem. Lett.*, **1978**, 1195.
6) T. Harada, S. Onaka, A. Tai, and Y. Izumi, *Chem. Lett.*, **1977**, 1131.
7) Y. Izumi, *Angew. Chem., Int. Ed. Engl.*, **10**, 871 (1971).
8) A. Tai, H. Watanabe, and T. Harada, *Bull. Chem. Soc. Jpn.*, **52**, 1468 (1979).
9) A. Kubomatsu and S. Komatsu, "Raney Shokubai," Kyoritsushuppan Co., Tokyo (1971).
10) H. Okai, N. Imamura, and N. Izumiya, *Bull. Chem. Soc. Jpn.*, **40**, 2154 (1967).
11) H. Gerlach, K. Oertle, and A. Thalmann, *Helv. Chim. Acta*, **59**, 755 (1976).

 © 1980 The Chemical Society of Japan Bull. Chem. Soc. Jpn., 53, 1361—1365 (1980)

Kinetic Studies on the *N,N*-Type Smiles Rearrangement

Junzo SUNAMOTO,* Hiroki KONDO, Fumihiro YANASE, and Hiroshi OKAMOTO

Department of Industrial Chemistry, Faculty of Engineering, Nagasaki University, Nagasaki 852

(Received July 28, 1979)

The Smiles rearrangement reaction of DL-2-aminododecanoic acid *N*-methyl-*p*-nitroanilide to DL-2-(*p*-nitrophenyl)aminododecanoic acid *N*-methylamide has been investigated in aqueous alkaline media containing 0—50% (v/v) acetonitrile or ethanol at 25 °C. It was found from the pH-rate profile that the reactive species is the free base form of the substrate. Acetonitrile content in the medium appreciably affected the rate with a maximum at *ca.* 20% in the acetonitrile content. The cationic CTAB micelles accelerated the rate 4.4-fold at pH 10, while the anionic SDS micelles suppressed the reaction almost completely. These effects of solvent and micelles were qualitatively correlated with the transition state of the reaction. A plausible mechanism for this reaction is the Smiles type rearrangement in which a spiro σ-complex is involved. The activation parameters obtained and suppression of the reaction rate by Cu(II) ion are in line with the proposed reaction mechanism.

Intramolecular nucleophilic aromatic substitution reaction (Eq. 1) is known as the Smiles rearrangement.[1]

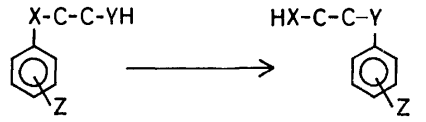

(1)

The original combination of SO_2 and OH for X and YH, respectively, was extended to a variety of combinations, *e.g.*, SO, S, and O for X and SH, NHR, and CONHR for YH.[1,2] Factors that influence the ease of the rearrangement are also well recognized.[2] Recent progress in this field has been achieved by the characterization of the common intermediate:[3,4]

However, detailed information on the reaction mechanism is restricted to a limited number of cases.

During the course of studies on the hydrolysis of carboxylate and carbonate esters or amides, we recently observed that in aqueous media DL-2-aminododecanoic acid *N*-methyl-*p*-nitroanilide (**1**) undergoes a rearrangement reaction, instead of normal hydrolysis, to give DL-2-(*p*-nitrophenyl)aminododecanoic acid *N*-methylamide (**2**). Gilman *et al.* suggested a similar

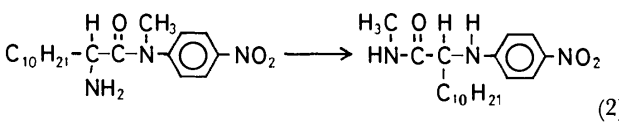

(2)

1 2

rearrangement in the reaction of 2-bromoacetanilides in methanolic ammonia.[5,6] Although they pointed out factors which affect the feasibility for the substrate to undergo the rearrangement, much remains to be clarified as regards the reaction mechanisms of the *N,N*-type rearrangement. The rearrangement reaction of **1** provides a good means for studying the micellar effects on organic reactions, since, a better understanding of the microscopic field effect that the aqueous micelles are expected to show will be obtained in unimolecular reactions such as the intramolecular rearrangement rather than bimolecular ones.[7,8] Since we obtained **1** as a stable hydrobromide, kinetic studies on the spontaneous and the micelle-catalyzed rearrangement of compound **1** have been performed. We have found that the reaction of **1** belongs to a normal Smiles-type rearrangement according to the S_Ni mechanism *via* an ionic transition state.

Experimental

Details of the synthesis of DL-2-aminododecanoic acid *N*-methyl-*p*-nitroanilide (**1**) were given in a previous paper.[9] DL-2-Aminododecanoic acid was prepared by α-bromination of dodecanoic acid followed by ammonolysis. After protection of the amino group with benzyloxycarbonyl group it was condensed with *N*-methyl-*p*-nitroaniline in the presence of phosphoryl chloride and pyridine. Removal of the protecting group with 12.6% HBr in acetic acid afforded the desired product (**1**) as the hydrobromide; mp 180—187 °C (dec); IR (KBr) 1640, 1580, 1465, 1330, 1100 cm^{-1}; NMR (DMSO-d_6) δ 0.88 (t, J=6 Hz, 3H, CH_3–), 1.24 (m, 16H, –$(CH_2)_8$–), 1.64 (m, 2H, –CH_2–CH–), 3.40 (s, 3H, *N*-CH_3), 4.06 (m, 1H, –CH–), 7.78 (d, J=8 Hz, 2H, phenyl), 8.30 (m, 3H, –NH_3^+), 8.32 (d, J=8 Hz, 2H, phenyl); UV (20% (v/v) aq acetonitrile) λ_{max} 285 nm (ε_{max} 9750). Found: C, 53.04; H, 7.53; N, 9.65%. Calcd for $C_{19}H_{32}N_3O_3Br$: C, 53.02; H, 7.49; N, 9.76%.

Product Analysis. A solution of **1** (402 mg) in 1.0 l of 3% (v/v) aqueous ethanol containing 0.01 M (1 M=1 mol dm^{-3}) sodium hydroxide and 1 M potassium chloride was kept at room temperature for 2 d. The precipitated crystalline mass was collected and recrystallized from carbon tetrachloride: yield, 299 mg (92%); mp 116—117 °C; IR (KBr) 3380, 3275, 1650 cm^{-1}; NMR (DMSO-d_6) δ 0.93 (t, J=6 Hz, 3H, CH_3–), 1.34 (m, 16H, –$(CH_2)_8$–), 1.81 (m, 2H, –CH_2–CH–), 2.75 (d, J=5 Hz, *N*-CH_3), 4.10 (m, 1H, –CH–), 6.98 (d, J=9 Hz, 2H, phenyl), 7.62 (m, 2H, NH), 8.32 (d, J=9 Hz, 2H, phenyl); UV (20% (v/v) aq acetonitrile) λ_{max} 387 nm (ε_{max} 21000); mass spectrum *m/e* 349 (M^+). Found: C, 65.12; H, 9.03; N, 11.70%. Calcd for $C_{19}H_{31}N_3O_3$ (349.48): C, 65.30; H, 8.94; N, 12.02%.

Kinetic Measurements. A three ml aqueous solution containing appropriate amounts of acetonitrile or ethanol, potassium chloride, and buffer salts (below pH 11) or sodium hydroxide (above pH 11) was placed in a cuvette and thermally equilibrated. Thirty μl of a substrate solution in acetonitrile was then injected and the whole mixture was stirred quickly and thoroughly with a slim Teflon rod. The

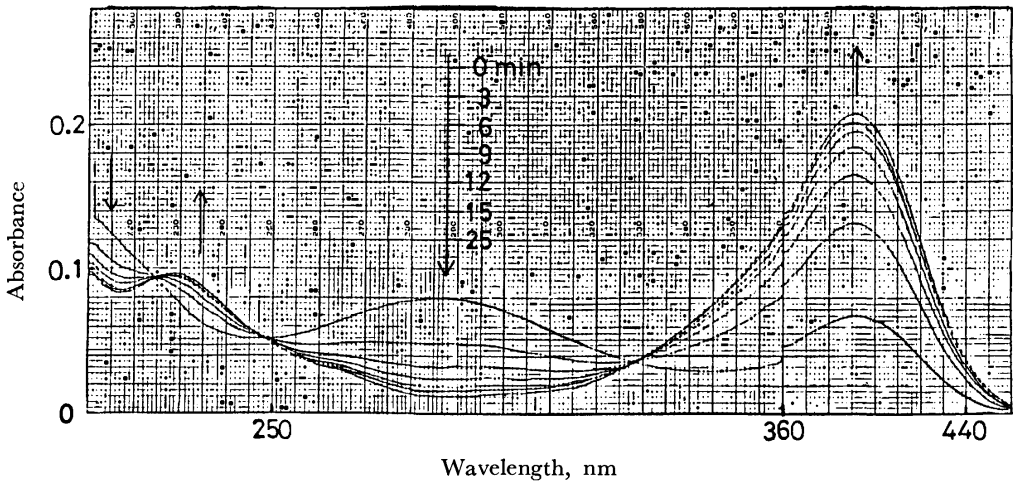

Fig. 1. Time-dependent spectral change in the rearrangement of **1** (9.90×10^{-6} M) in 29.7% (v/v) ethanol–1.0% (v/v) acetonitrile at 25 °C, μ=0.10 (KCl), and "pH" 10.

final concentration of each component in the reaction mixture is given under appropriate Figs. and/or Tables. The rate of rearrangement of **1** was followed spectrophotometrically by monitoring the appearance of the product **2** at 387 nm on a Hitachi 124 recording spectrophotometer. The reaction followed a good first-order kinetics and the apparent first-order rate constant was evaluated by the least-squares calculation. The correlation coefficients were better than 0.99. In some cases in which the concentration of organic solvent was low and precipitation of the product made it impossible to follow the appearance of product (387 nm), the disappearance of substrate was followed at 285 nm. The rapidly scanned spectra were measured on a Union Giken stopped-flow spectrophotometer Model RA-1300.

pH *Measurements.* The pH value of a reaction solution was determined with a TOA HM-5A pH meter connected to a TOA GS-135C combined electrode. For solutions containing a large amount of an organic solvent, the pH was calibrated by means of the conventional buffer salts dissolved in a medium of the same composition as that of the actual reaction solution. For this reason, the pH values given in this article are referred to as the apparent pH.

Results

Stoichiometry of Reaction. The product analysis indicates that **1** undergoes rearrangement in an aqueous alkaline medium to afford almost quantitatively the product **2** (see Experimental). The ^{1}H NMR spectrum of the product supports the structure of **2**: the original singlet of *N*-CH_3 proton signal changed to a doublet due to the coupling with the hydrogen attached to the amide nitrogen. In addition, signals of the hydrogens attached to 2- and 6-positions of the phenyl ring shifted upfield (0.8 ppm) upon the rearrangement. The absorption spectral change of the reaction as a function of time is shown in Fig. 1. The absorption at 285 nm decreased with the progress of reaction, a new band appearing at 387 nm. Isosbestic points were observed at 224.5, 248, and 328 nm throughout the reaction, indicating the absence or no accumulation of stable intermediate during the course of transformation of **1** into **2**. The potential hydrolysis product, *N*-methyl-*p*-nitroaniline was not detected by TLC analysis [silica gel, benzene–methanol (10:1 by volume)]. R_f-Values of **1**, **2**, and *N*-methyl-*p*-nitroaniline were 0.02, 0.16, and 0.55, respectively.

Effect of Solvent Content. The effect of acetonitrile content in the reaction medium on the rearrangement rate was studied at 25 °C and apparent pH 10. As seen in Fig. 2, the rate increases with acetonitrile content until the maximum rate is attained at a concentration of *ca.* 20% (v/v). Thereafter, the rate decreases almost linearly with the acetonitrile content.

pH-*Rate Profile.* The pH-rate profile of the rearrangement reaction was constructed as shown in Fig. 3. The profile is of typical sigmoid shape, indicating the presence of an acid dissociation process (pK_a= 10.34). The pK_a-value is quite reasonable for the acid dissociation constant of the primary amino group of **1**. The profile also demonstrates that the free base of **1** is by far the more reactive with the specific rate constant of 1.84×10^{-3} s^{-1} at 25.0 °C in 20% (v/v) aq acetonitrile. The reactivity of the ammonium species is too poor to estimate the specific rate constant

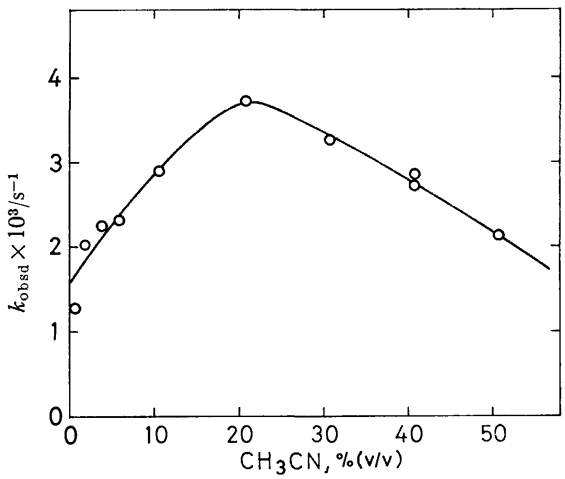

Fig. 2. Effect of acetonitrile content in the medium on the rearrangement rate of **1** (9.90×10^{-6} M) at 25 °C and "pH" 10.

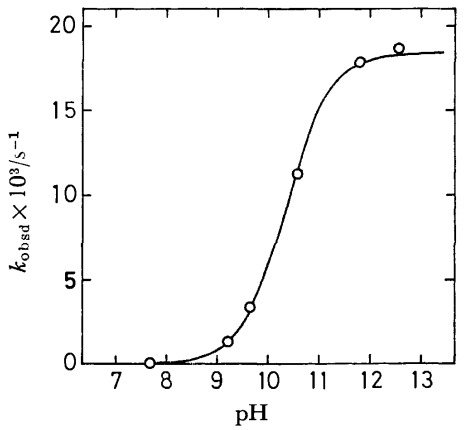

Fig. 3. pH-Rate profile for the rearrangement of **1** (9.90×10^{-6} M) in 20.8% (v/v) acetonitrile at 25 °C and μ=0.10 (KCl).

accurately under the present conditions.

Activation Parameters. In order to gain an insight into the energetics of the rearrangement, kinetic experiments were carried out in 29.7% ethanol–1.0% acetonitrile at pH 10 and at temperatures 20, 25, 30, and 35 °C (Table 1). The activation energy E_a obtained from the conventional Arrhenius plot was 17.7 kcal/mol, from which the following activation parameters were evaluated: 17.1 kcal/mol for the enthalpy of activation, 7.1 e.u. for the entropy of activation, and 14.9 kcal/mol for the free energy of activation at 303 K.

Effect of Additives. Since the substrate has several potential coordination sites, the effect of copper(II) ion on the reaction rate was investigated at 25 °C and pH 8 in 20.6% (v/v) acetonitrile. Addition of an equimolar amount of Cu(II) ion to the substrate showed little effect on the reaction rate, but 13-fold excess of Cu(II) ion brought about an appreciable suppression of the rate. That the reaction pathway was not changed even in the presence of Cu(II) ion was confirmed by product analysis.

Effects of three different micelles on the rate were also studied. The cationic CTAB micelles brought about 4.4-fold rate enhancement at pH 10.0, while the anionic SDS micelles almost completely suppressed the reaction. Nonionic Brij 35 micelles showed little effect. This difference among the three detergents should reflect the electrostatic nature of the intermediate or transition state of the reaction.

Table 1. Rate constants for the rearrangement of **1** at several different temperatures[a]

Temperature °C	$k_{obsd} \times 10^3$ s^{-1}
20	3.07, 3.33
25	5.38, 5.45
30	8.47, 9.12
35	13.2, 13.7

a) Experimental conditions: Medium, 29.7% (v/v) ethanol-1.0% (v/v) acetonitrile; μ=0.10 (KCl); pH 10.

Table 2. Effect of additives on the rate of rearrangement of **1** at 25 °C[a]

Additive	Concentration M	pH	$k_{obsd} \times 10^4$ s^{-1}
None[b]		8.01	1.42
Cu(II)[b]	1.09×10^{-5}	7.94	1.29
Cu(II)[b]	1.29×10^{-4}	8.09	0.763
None[c]		10.0	12.7±0.3
CTAB[c]	5.01×10^{-3}	10.0	55.3±0.8
SDS[c]	4.99×10^{-2}	10.0	≈0
Brij 35[c]	5.45×10^{-4}	10.0	13.5±0.6

a) Experimental conditions: Initial substrate concentration, 9.90×10^{-6} M; μ=0.10 (KCl) except for SDS. b) Medium, 20.6% (v/v) acetonitrile. c) Medium, 1.0% (v/v) acetonitrile.

Discussion

Gilman *et al.* reported the first example of *N,N*-type Smiles rearrangement.[5,6] However, they carried out the reaction in methanolic ammonia using 2-bromoacetanilides as a starting material for the most part, and postulated the intermediacy of 2-aminoacetanilides. In the present investigation, it was confirmed that amino acid *N*-methyl-*p*-nitroanilides undergo the rearrangement reaction and that the reactive species in the reaction is the free base of the substrate. It is well recognized that a strong base is required to generate a powerful nucleophile, Y^- species (Eq. 1), which brings about a rearrangement.[2] When YH is the amino group, it was suggested that a nitride ion might be necessary for the rearrangement to take place.[10] This, however, does not seem to be the case at least in our present system. The neutral amino group is a sufficiently strong nucleophile to displace the acylamido moiety.

As expected, the addition of Cu(II) ion to the system significantly prohibited the rearrangement, which is attributed to the masking of the reaction site by the coordination of the metal ion. The metal chelation seems to take place at the α-amino and amide carbonyl moieties (**3**), which might lead to facilitation of the amide bond cleavage.[11] Contrary to what might be

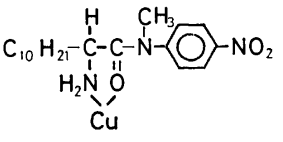

3

expected, no formation of hydrolyzates was observed during the course of reaction in the presence of Cu(II) ion. Hence, the chelation of copper(II) is not so effective as to alter the reaction pathway of the substrate **1**.

The Smiles rearrangement may be classified into two categories:[2] (a) the rearrangement proceeds in a concerted fashion through transition state **4**,[12] (b) the reaction proceeds through a stabilized intermediate **5** or **6** (Eq. 3). Depending on the stability of the intermediate σ-complex, either formation or decomposi-

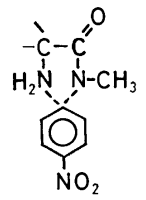

4

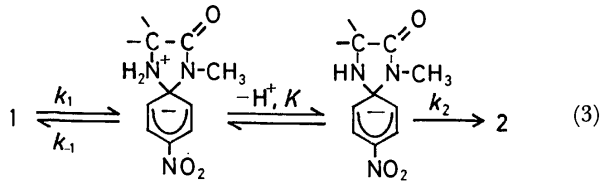

5 6

(3)

tion of the complex becomes the rate-determining step. When the complex is stable, it can be detected by conventional spectroscopy to verify that it takes part in the transformation of the substrate.[3,4] If the complex is not sufficiently stable, however, it is very difficult to confirm its existence.[6]

According to Okada and Sekiguchi,[4] the latter pathway appears to be plausible for the present rearrangement reaction. If we assume that the rate-determining step involves the formation of σ-complex ($k_1 \ll k_{-1}$, k_2), the pK_a obtained experimentally merely reflects the acid dissociation of the substrate, *i.e.*, ammonium$\rightleftarrows$free amine. Since no formation of intermediates was observed between **1** and **2** even by a rapid scanning spectroscopic technique, the subsequent steps should take place very rapidly.

When the decomposition of the complex is the rate-determining step ($k_2 \ll k_1$, k_{-1}), the observed rate constant (k_{obsd}) would be correlated with the specific rate constants of respective stages and equilibrium constant by

$$k_{obsd} = \frac{k_1 k_2 K}{(k_1+k_{-1})[H^+]+k_1 K} \tag{4}$$

which conforms to the observed pH-rate profile (see Results). Rearrangement of Eq. 4 leads to

$$\frac{1}{k_{obsd}} = \frac{k_1+k_{-1}}{k_1 k_2 K}[H^+] + \frac{1}{k_2}. \tag{5}$$

The intercept of the straight line based on the relationship between $1/k_{obsd}$ and $[H^+]$ gives the specific rate constant for the decomposition step (k_2), while a composite of rate and equilibrium constants (k_1, k_{-1}, and K) is obtained from the slope (120×10^{10} $s^{-1} M^{-1}$). Since we can not observe the individual steps independently, each constant can not be defined. However, on the basis of certain assumptions we can estimate roughly each constant as follows. The pK_a value of 10.34 obtained experimentally is too high to be assigned to intermediate **5**. If we arbitrarily assume as an upper limit that the pK of **5** is 7, the ratio k_1/k_{-1} becomes 4.5×10^{-4}. This indicates that the steady state concentration of the intermediates is very low to escape the conventional spectroscopic detection. If the pK value were close to the apparent pK_a and hence the ratio k_1/k_{-1} were somewhere around unity, we could have detected the intermediates **5** and/or **6**. Thus, these two mechanisms are kinetically indistinguishable.

Whichever mechanism is correct, the transition state has anionic or at least more polar character as compared with both the initial and final states. This is generally true for the Smiles rearrangement, polar solvents being favorable for the reaction.[2] The solvent effect observed over the acetonitrile concentration range higher than 20% (v/v) is in line with this consideration. Since substrate **1** carries a long alkyl chain it may entangle itself to form less reactive aggregates in the media of lower acetonitrile concentration,[13] resulting in the stabilization of the ground state. The increase in acetonitrile content defrosts the aggregation, leading to promotion of the rearrangement. Above *ca.* 20% of acetonitrile in the medium, the polarity effect of solvent to destabilize the polar transition state predominates and the reaction rate decreases with increasing acetonitrile concentration.

The observed positive effect of the cationic micelles is explicable in terms of the character of the transition state or intermediates. If the breakdown of the σ-complex intermediates is rate-determining, the CTAB micelles increase the steady state concentration of the anionic complex,[14,15] which is quite low in the absence of such micelles. This leads directly to enhancement of the observed rate constant.

According to the above discussion on the character of the transition state or intermediates, a negative value would be expected for the entropy of activation. The experimental value of +7.1 e.u. is apparently not compatible with this prediction. The discrepancy may have arisen from the fact that the experimental value contains several factors such as solvation to ground and transition states, not taken into consideration in the above argument. In any event, the value does not differ much from zero, indicating that the reaction is essentially unimolecular.

Thanks are due to Prof. Toyoki Kunitake, Department of Organic Synthesis, Kyushu University, for the use of his rapid scanning spectrophotometer.

References

1) L. A. Warren and S. Smiles, *J. Chem. Soc.*, **1930**, 956.
2) W. E. Truce, E. M. Kreider, and W. W. Brand, *Org. React.*, **18**, 99 (1970).
3) C. F. Bernasconi, R. H. de Rossi, and C. L. Gehriger, *J. Org. Chem.*, **38**, 2838 (1973).
4) K. Okada and S. Sekiguchi, *J. Org. Chem.*, **43**, 441 (1978) and their preceding papers cited therein.
5) N. W. Gilman, P. Levitan, and L. H. Sternbach, *Tetrahedron Lett.*, **1970**, 4121.
6) N. W. Gilman, P. Levitan, and L. H. Sternbach, *J. Org. Chem.*, **38**, 373 (1973).
7) J. H. Fendler and E. J. Fendler, "Catalysis in Micellar and Macromolecular Systems," Academic Press, New York (1975).
8) C. A. Bunton, M. J. Minch, J. Hidalgo, and L.

Sepulveda, *J. Am. Chem. Soc.*, **95**, 3262 (1973).
9) H. Kondo, R. Miyata, D. Horiguchi J. Kose, H. Okamoto, and J. Sunamoto, *Reports Fac. Eng. Nagasaki Univ.*, No. 9, 65 (1977).
10) G. E. Bonvicino, L. H. Yogodzinski, and R. A. Hardy, Jr., *J. Org. Chem.*, **27**, 4272 (1962).
11) J. P. Collman and D. A. Buckingham, *J. Am. Chem. Soc.*, **85**, 3039 (1963).
12) J. F. Bunnett and T. Okamoto, *J. Am. Chem. Soc.*, **78**, 5363 (1956).
13) F. M. Menger and L. E. Portony, *J. Am. Chem. Soc.*, **89**, 4698 (1967).
14) D. G. Herries, W. Bishop, and F. M. Richends, *J. Phys. Chem.*, **68**, 1842 (1964).
15) J. H. Fendler, E. J. Fendler, and M. V. Merritt, *J. Org. Chem.*, **36**, 2172 (1971).

Aldol Condensations with Metal(II) Complex Catalysts

Kazuo IRIE and Ken-ichi WATANABE*

Department of Chemistry, Faculty of Science, Tokyo Metropolitan University, Fukazawa, Setagaya-ku, Tokyo 158

(Received July 31, 1979)

Aldol condensations of aldehydes with ketones catalyzed by the first-row transition metal(II) complexes have been widely studied. Complexes of Co(II), Ni(II), Cu(II), and Zn(II) acetates with 2,2′-bipyridine were effective catalysts to afford cross-aldol condensation products, α,β-unsaturated ketones, in high yields without any self-condensation products. The reaction of 2-butanone, unsymmetrical aliphatic ketone, with benzaldehyde took place regioselectively to give base-catalyzed-type products.

Aldol condensation reactions catalyzed by transition metal(II) ions have been reported by several workers.[1] For example, Akabori reported that the aldol condensation of bis(glycinato)copper(II) with aldehydes gave copper(II) complexes of serine and so on under basic conditions.[1] In these reactions, however, no reaction products could be liberated without removing the Cu(II) ion from the complexes.

Recently, we have found that the copper(II)–2,2′-bipyridine(bpy) complex catalyzes the aldol condensation of aldehydes with ketones under neutral conditions to afford liberated α,β-unsaturated ketones without any by-product.[2] The product yield in this reaction increases remarkably in comparison with that catalyzed by the copper(II) ion itself. On the other hand, bpy itself has no catalytic activity at all.

It is of great importance that the reaction is largely affected by the kinds of ligands and counter ions of the complexes. We have examined the effects of the first-row transition metal(II) ions, various kinds of ligands, and some counter ions on the reactions. Furthermore, in order to ascertain the scope and limitation of the aldol condensations promoted by the metal(II) complexes, the reactions of various kinds of aldehydes and ketones were carried out. The results will be described in this paper.

Results and Discussion

Effects of Ligands on the Catalysis. In this study, the condensations of benzaldehyde and acetophenone in the presence of Cu(II) complexes were carried out. In order to examine the effects of ligands on the catalyst in the reaction, twelve kinds of ligands(L) were employed.

$$PhCH + CH_3CPh \xrightarrow[80\,^\circ C,\ 18\,h]{Cu(II)L,\ DMF} PhCH{=}CHCPh$$

A solution of benzaldehyde, acetophenone, copper(II) acetate, and a ligand in DMF was heated at 80 °C for 18 h. The complex formation in the solution was observed by means of the color change from the green of copper(II) acetate to other colors when the ligands were added. The amount of the complex catalyst was 16 mol% of the benzaldehyde used. The reaction product was chalcone, and the yield was determined by GLC analysis. The results are shown in Table 1.

The reaction catalyzed only by copper(II) acetate gave chalcone in a 53% yield. Then, upon the addition of Group I ligands, the yields decreased remarkably (Table 1). These carboxylic acids seem to be unfavorable ligands for the reaction. When Group II ligands (aliphatic amines) were employed, the yields of chalcone (53—54%) were similar to the case with copper(II) acetate itself. These results indicate that these aliphatic-amine ligands have no "ligand effect" on this reaction. When Group III ligands (tertiary aromatic amines) were employed, chalcone was formed in increased or decreased yields (22—82%). Such ligands as 2,2′-bipyridine(bpy), 1,10-phenanthroline (phen), and pyridine(py) were found to be fairly effective, since the yields increased predominantly (70—82%). On the other hand, such ligands as 6,6′-dimethyl-2,2′-bipyridine(dm-bpy) and 2,2′:6′,2″-terpyridine(terpy) seemed to inhibit the reactions (22—30%); this could be ascribed as steric hindrance by the bulky ligand molecules. These amines themselves did not catalyze the reaction.

Table 1. The yields of chalcone in the aldol condensation of benzaldehyde and acetophenone with Cu(II) complexes

Group No.	Ligand	Color of complex	Yield of chalcone/%[a]
	None	green	53
I	$(COOH)_2$	blue	0[b]
	$HSCH_2COOH$	black	0[b]
	NH_2CH_2COOH	red	17
II	$NH_2CH_2CH_2NH_2$	blue	53
	$(NH_2CH_2CH_2)_2NH$	blue	53
	$(CH_2NHCH_2CH_2NH_2)_2$	blue	54
	$(CH_3)_2NCH_2CH_2N(CH_3)_2$	dark green	53
III	(py)	blue	70
	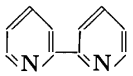 (bpy)	blue	82
	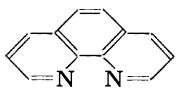 (phen)	blue	82
	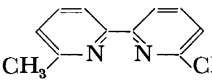 (dm-bpy)	yellow green	30
	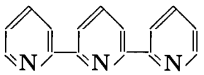 (terpy)	blue	22

a) Based on the amount of benzaldehyde. b) Heterogeneous solution.

Effects of Metal Ions on the Catalysis. Next, we

Table 2. The yields of chalcone in the reactions of benzaldehyde and acetophenone in the presence of various metal(OAc)$_2$-bpy complexes

$(bpy)_n$ / M(II)	Product yield/%[a]					
	Mn(II)	Fe(II)	Co(II)	Ni(II)	Cu(II)	Zn(II)
$n=0$	11	15	31	4	53	43
$n=1$	26	51	93	100	82	100
$n=2$	45	17	84	100	93	68
$n=3$	22	47	67	66	88	82

a) Based on the amount of benzaldehyde and determined by GLC. b) The reaction conditions were the same as those of Table 1.

Table 3. Effects of counter ions of metal(II)-bpy complexes on the yields of the aldol condensation of benzaldehyde with acetone

Counter ion	Yield of benzylideneacetone/%[a]					
	Mn(II)	Fe(II)	Co(II)	Ni(II)	Cu(II)	Zn(II)
AcO^-	52	60	78	65	47	67
NO_3^-	0	—	33	0	52	31
Cl^-	0	—	47	0	0	25

a) The yields of the reaction products were determined by NMR. In the cases with NO_3^- and Cl^-, 4-hydroxy-4-phenyl-2-butanone was formed predominantly, along with benzylideneacetone.

studied the catalytic effect of the first-row transition metal (II) acetates with the bpy ligand on the formation of chalcone, since it was found that bpy or phen was the most effective ligand for the reaction. The effects of the molar ratio of bpy on these metal(II) ions were also examined. The results are summarized in Table 2.

When a ligand was not added to the reaction mixture ($n=0$), the copper(II) acetate gave the highest yield. When the molar ratio of bpy to metal(II) acetate was 1:1 ($n=1$), the yields increased very much with all the metal(II) ions. Especially, the reactions with Co(II), Ni(II), and Zn(II) complexes gave quantitative yields. When the molar ratio of bpy to the metal was 2:1 ($n=2$), the yields decreased with Fe(II), Co(II), and Zn(II) and increased with Mn(II) and Cu(II). In the case of $n=3$, the yields decreased in comparison with that of $n=1$. In the case of $n=1$, the order of the product yields is in good agreement with the Irving-Williams series, which is known as the stabilization series of general complexes.[3] It is concluded that the more favorable combinations in the complex catalysts are bpy and Co(II), Ni(II), Cu(II), or the Zn(II) ion and that the molar ratio of M(II) to bpy of 1:1 ($n=1$) is the best.

Effects of Counter Ions on the Catalysis. In our previous report,[2] the yields of the condensation product were reported to be affected by the kinds of counter ions in the Cu(II)X_2-bpy catalysts. In order to clarify the effects of the counter ions of metal(II) complexes, nitrate, chloride, and acetate ions were chosen in M(II)-bpy complexes (1:1). In this study, the aldol condensation of benzaldehyde with acetone was examined in the presence of the complex catalysts at a reflux temperature for 18 h in DMF. The product yields were determined by NMR; the results are summarized in Table 3.

When the counter ion of the metal(II) complex was the acetate ion, benzylideneacetone was formed in a good yield. On the other hand, reactions catalyzed by the bpy-complex of metal(II) nitrate and chloride gave condensation products in a low yield. Therefore, the acetate ion was the best among these three counter ions, and the counter ion played a very important role in the aldol condensation with these metal(II) complex catalysts.

Solvent Effects. In this reaction system, the selection of solvent is important for dissolving the complex catalysts. The condensation of benzaldehyde with acetophenone in the presence of the Zn(II)-bpy complex was carried out in five kinds of polar solvents at 80 °C for 18 h, after which the reaction products were determined by GLC. The results showed that chalcone was formed in good yields in aprotic solvents, such as DMF (100%), DMSO (88%), and CH_3CN (78%). On the other hand, the yields of chalcone were low in protic solvents, such as MeOH (45%) and H_2O (18%). Thus, DMF was the best solvent for the complex-catalyzed reactions.

Condensations of Various Aldehydes with Acetophenone. Next, in order to develop this reaction system, we investigated further the aldol condensations of various kinds of aldehydes and ketones in the presence of the Co(II) acetate-bpy complex catalyst, one of the more favorable M(II) acetate-bpy complex catalysts (M(II): Ni, Co, Cu, Zn). First, the reactions of eighteen kinds of aldehydes with acetophenone were carried out.

To a solution of cobalt(II) acetate in DMF, an equimolar amount of bpy was added. The color of the solution was thus changed to reddish purple, indicating the complex formation. A mixture of aldehyde and acetophenone was then added to the complex solution, and the mixture was stirred at 80 °C for 18 h. The amount of the complex catalyst was 16 mol% of the aldehyde used. Each reaction product was isolated by preparative TLC and was identified as a α,β-unsaturated ketone by the NMR, IR, and the mp. The results are summarized in Table 4.

In the reactions of the *p*-substituted benzaldehydes, **1**—**8**, the substituted chalcones, **28**—**35**, were obtained in good yields, regardless of the kind of substituent group. Further, to examine the effects of substituted groups of aldehydes on the reactivity, the reactions of mono- and di-substituted benzaldehydes, such as *o*-anisaldehyde, **9**, salicylaldehyde, **10**, 2-hydroxy-3-methoxybenzaldehyde, **11**, and 4-hydroxy-3-methoxybenzaldehyde, **12**, were carried out. The reactions of **9** and **10** gave 2-methoxychalcone, **36**, and 2-hydroxychalcone, **37**, both in 72% yields. The reaction of **12** did not occur, the starting materials being recovered, while **11** gave 2-hydroxy-3-methoxychalcone, **38**, in a 47% yield. The difference in the reactivities of **11** and **12** seemed to account for the coordination

TABLE 4. REACTIONS OF VARIOUS ALDEHYDES WITH ACETOPHENONE IN THE PRESENCE OF THE Co(II)-bpy COMPLEX CATALYST

Aldehyde	Product	Yield/%	Mp/°C (lit,[4])
$(CH_3)_2N$-C$_6$H$_4$-CHO **1**	$(CH_3)_2N$-C$_6$H$_4$-CH=CHCO-C$_6$H$_5$ **28**	77	117.5—119 (114)
CH_3O-C$_6$H$_4$-CHO **2**	CH_3O-C$_6$H$_4$-CH=CHCO-C$_6$H$_5$ **29**	96	72—74 (72—74)
CH_3-C$_6$H$_4$-CHO **3**	CH_3-C$_6$H$_4$-CH=CHCO-C$_6$H$_5$ **30**	88	99—100 (96)
C$_6$H$_5$-CHO **4**	C$_6$H$_5$-CH=CHCO-C$_6$H$_5$ **31**	81	57—58 (57—58)
Cl-C$_6$H$_4$-CHO **5**	Cl-C$_6$H$_4$-CH=CHCO-C$_6$H$_5$ **32**	72	114—117 (114)
CN-C$_6$H$_4$-CHO **6**	CN-C$_6$H$_4$-CH=CHCO-C$_6$H$_5$ **33**	56	159—160[a]
NO_2-C$_6$H$_4$-CHO **7**	NO_2-C$_6$H$_4$-CH=CHCO-C$_6$H$_5$ **34**	86	158—160 (158—160)
NO_2 C$_6$H$_4$-CHO **8**	NO_2 C$_6$H$_4$-CH=CHCO-C$_6$H$_5$ **35**	67	143—145 (145—146)
OCH_3 C$_6$H$_4$-CHO **9**	OCH_3 C$_6$H$_4$-CH=CHCO-C$_6$H$_5$ **36**	72	61—61.5 (59—60)
OH C$_6$H$_4$-CHO **10**	OH C$_6$H$_4$-CH=CHCO-C$_6$H$_5$ **37**	72	152—153 (152—153)
CH_3O OH C$_6$H$_3$-CHO **11**	CH_3O OH C$_6$H$_3$-CH=CHCO-C$_6$H$_5$ **38**	43	112—113.5[a]
HO CH_3O C$_6$H$_3$-CHO **12**	—	none	
N C$_5$H$_4$-CHO **13**	N C$_5$H$_4$-CH=CHCO-C$_6$H$_5$ **39**	31	62—63 (60—61)
N C$_5$H$_4$-CHO **14**	N C$_5$H$_4$-CH=CHCO-C$_6$H$_5$ **40**	66	79—80 (70—71)
$(CH_3)_2CHCHO$ **15**	$(CH_3)_2CH$-CH=CHCO-C$_6$H$_5$ **41**	23	oil[b]
CCl_3CHO **16**	—	none	—
C$_6$H$_5$-CH_2CH_2CHO **17**	—	none	—
C$_6$H$_5$-CH=CHCHO **18**	C$_6$H$_5$-$(CH=CH)_2$CO-C$_6$H$_5$ **42**	80	104—105 (102—103)

The condensation reactions of aldehydes (1.875 mmol) with acetophenone (5 ml) were carried out in the presence of $Co(OAc)_2$+bpy(1:1)(0.300 mmol) at 80 °C for 18 h in DMF (5 ml).
a) Identified by elemental analysis. b) The reaction was carried out at the reflux temperature, and the product was identified by MS, NMR, and IR.

to Co(II). A chelation of the hydroxyl and formyl groups to Co(II) is possible in the reaction of **11**, since the hydroxyl group is in an ortho position to the formyl group. In **12**, the chelation of the *p*-hydroxyl and *m*-methoxyl groups to Co(II) seemed to be more predominant than that of the formyl group. The reaction of 2-pyridine-, **13**, or 4-pyridinecarbaldehyde, **14**, proceeded smoothly at room temperature for 3 d to give 1-phenyl-3-(2-pyridyl)-2-propen-1-one, **39** or 1-phenyl-3-(4-pyridyl)-2-propen-1-one, **40**, in a 31 or 66% yield respectively. The aldehyde, **14**, gave the reaction product to an extent similar to that in the reactions of *p*-substituted benzaldehyde, **1**—**8**, and no by-product was obtained. On the other hand, **13** gave three kinds of by-products besides the major product, **39**, by TLC. The reactions of the aliphatic-saturated aldehyde showed features different from those of aromatic aldehydes. The reactions of isobutanal, **15**, afforded 1-phenyl-4-methyl-2-penten-1-one, **41**, in a low yield (23%), and 3-phenylpropanal **17**, and chloral, **16**, did not react at all under similar reaction conditions. On the other hand, the reaction of α,β-unsaturated aldehyde, *trans*-cinnamaldehyde, **18**, gave 1,5-diphenyl-2,4-pentadien-1-one, **42**, in a good yield (80%). It may be concluded that the aldol condensations catalyzed by the Co(II)–bpy complex are smoothly promoted in the case of unsaturated aldehydes (aromatic, aliphatic).

Condensations of Various Ketones with Benzaldehyde. Since aromatic aldehydes are favorable substrates in a complex-catalyzed reaction system, the aldol condensations of ten kinds of ketones with benzaldehyde

Table 5. Reactions of various ketones with benzaldehyde in the presence of the Co(II)-bpy complex catalyst

Ketone and ester	Temp °C	DMF ml	Product	Yield/%	Mp/°C (lit,[4])
$PhCOCH_3$ **4**	80	5	$PhCH{=}CHCOPh$ **31**	81	57—58 (57—58)
CH_3COCH_3 **19**	reflux	6	$PhCH{=}CHCOCH_3$ **43**	63	41 (41.5)
$CH_3COCH_2CH_3$ **20**	reflux	5	$PhCH{=}CHCOCH_2CH_3$ **44** + $PhCH{=}C(CH_3)COCH_3$ **45**	95 [C_1:C_3 = 96:4]	39—40 (38.5—39.5) (C_1)
$CH_3COCH_2CH_2CH_3$ **21**	100	5	$PhCH{=}CHCOCH_2CH_2CH_3$ **46**	91	98—99 (99—100)[a]
$CH_3CH_2COCH_2CH_3$ **22**	100	5	—	none	—
23	80	2	PhCH= **47**	38	66—67 (67—68)
$CH_3COCH_2COCH_3$ **24**	80	10	$PhCH{=}C(COCH_3)_2$ **48**	19	oil[b]
$CNCH_2COOCH_2CH_3$ **25**	r.t.	5	$PhCH{=}C(CN)COOCH_2CH_3$ **49**	79	52—53 (66—67)
$BrCH_2COOCH_2CH_3$ **26**	r.t.	5	—	nono	—
$CH_3COOCH_2CH_3$ **27**	reflux	5	—	none	—

The condensation reactions of ketones (5 ml) with benzaldehyde (1.875 mmol) were carried out in the presence of $Co(OAc)_2$+bpy(1:1)(0.300 mmol) for 18 h in DMF.
a) Melting point of the phenylhydrazone derivative. b) Identified by NMR and IR.

were carried out. The reaction methods and conditions were almost the same as in Table 4. The results are shown in Table 5.

The reactions of benzaldehyde with methyl ketones, such as acetophenone, **4**, and acetone, **19**, gave chalcone, **31**, and benzylideneacetone, **43**, in 81 and 63% yields respectively. Thus, aliphatic and aromatic ketones showed similar reactivities toward benzaldehyde. The self-condensation reaction of acetone or acetophenone was also examined, but no condensation product was obtained and the starting material was recovered. The reaction of 2-butanone, **20**, an unsymmetrical aliphatic ketone, with benzaldehyde took place regioselectively.

$$PhCH{=}O + CH_3\overset{C_1}{C}(=O)\overset{C_3}{C}H_2CH_3 \xrightarrow[18\,h]{\text{cat., DMF}} PhCH{=}CHCOCH_2CH_3\ (C_1)\ \mathbf{44} + PhCH{=}C(CH_3)COCH_3\ (C_3)\ \mathbf{45}$$

cat: $Co(OAc)_2$+bpy(1:1)

A mixture of 1-phenyl-1-penten-3-one(C_1), **44**, and 3-methyl-4-phenyl-3-buten-2-one(C_3), **45**, was isolated in a 95% yield, and the ratio of C_1:C_3 was determined to be 96:4 by NMR. It was known that the base-catalyzed reaction of 2-butanone gave, preferentially, the condensation product at C_1 of ketone, while the acid-catalyzed reaction occurred preferentially at C_3.[4] The reaction of 2-pentanone, **21**, was also regiospecific, affording a C_1-condensation product, 1-phenyl-1-hexen-3-one, **46**, in a 91% yield. The reaction of the diethyl ketone, **22**, gave no condensation product, probably because it has no α-methyl group. This finding may explain why acyclic unsymmetrical methyl ketones gave regioselective products in these complex-catalyzed reactions. The reaction of cyclopentanone, **23**, as a cyclic α-unsubstituted methylene ketone gave the 2-benzylidenecyclopentanone, **47**, in a 38% yield. It seemed that the difference in the reactivities between cyclic and acyclic α-methylene ketones was ascribable to those pK_a values in the ketones. The reaction of acetylacetone, **24**, as a diketone gave 3-benzylidene-2,4-pentanedione, **48**, in a 19% yield. The reaction of ethyl cyanoacetate, **25**, was carried out at room temperature for 18 h. When a solution of **25** and benzaldehyde in DMF was added to a solution of the Co(II)-bpy complex in DMF, the reddish purple color of the complex was immediately changed to black. Similarly, the color of the reaction mixture of ethyl bromoacetate, **26**, changed to green. The reaction of **25** gave ethyl α-cyanocinnamate, **49**, in a 79% yield, while **26** gave no reaction product, and the starting materials were recovered. Similarly, the reaction of ethyl acetate, **27**, did not give any condensation product at all.

It is generally concluded that M(II)-bpy complexes catalyze cross-aldol condensations of aldehydes with ketones under neutral conditions in DMF to give α,β-unsaturated ketones in good yields. Further, the reactions give base-catalyzed-type products regioselectively. This catalyst system has also been applied to the polymer complex catalyst with good results.[5]

Conclusion. Several reactions catalyzed by the M(II)-bpy complex have been reported.[6] The methylation of ethylenediamine catalyzed by Pt(II)-amine complexes was examined; the *N*-methyl-substituted ethylenediamine was obtained only when the Pt(II)-bpy complex was used.[6a] In this reaction, the driving force of the catalytic activity by the bpy ligand was explained by attributing it to the back π-bonding in the Pt(II)-bpy complex. That is, a higher positive

charge is induced on the metal(II) ion by the coordination of the bpy ligand. Our results shown in Tables 1 and 2 also seem to be elucidated by this "ligand effect" of bpy. The oxygen atoms in the carbonyl groups of aldehyde and ketone may be more activated by coordination to the M(II)–bpy complex than by that to the M(II) ion itself.

It has been known that aldol condensations in a biological system are catalyzed by aldolase enzymes, Class I and Class II.[7] Class II aldolase is known as a metalloenzyme containing the Zn(II) ion at the catalytic site. However, in the reaction of Class II aldolase, the catalysis of Zn(II) ion has not been elucidated enough, since it has never been established that Zn(II) complexes catalyze the aldol condensations. Therefore, our reaction system with the Zn(II)–bpy gives a new clue for understanding the catalysis of Class II aldolase from the point of view of organic catalytic reactions. An investigation of the reaction mechanism is now in progress in connection with Class II aldolase.

Experimental

Materials. All the aldehyde, **1**—**18**, ketones, and esters were commercially available. The **13**—**18** aldehydes were purified by distillation before use. The ligand compounds, such as oxalic acid, mercaptoacetic acid, glycine, ethylenediamine, diethylenetriamine, triethylenetetramine, pyridine, 2,2′-bipyridine, 2,2′: 6′,2″-terpyridine, 1,10-phenanthroline, *N*,*N*,*N*′,*N*″-tetramethylethylenediamine, and 6,6′-dimethyl-2,2′-bipyridine, were provided by the Tokyo Kasei Co. Anhydrous metal(II) acetate(Kojundo Chemical Reseach) was used. In the reactions shown in Table 3, hydrous metal(II) salts (Wako Pure Chemicals) were used.

Instruments. The NMR and IR spectra were taken with a Hitachi Perkin-Elmer R-20A spectrophotometer (60 MHz) and a Hitachi 215 Grating Infrared spectrophotometer respectively. The mass spectra were determined on a Shimadzu-LKB 9000 gas chromatograph-mass spectrometer at 70 eV. The GLC was carried out with a Hitachi K-53 gas chromatograph with a flame ionization detector, using a 1.0 m stainless tube column packed with 10% Carbowax 20M on Diachrom A. The product yields were determined by the two methods of GLC and NMR analyses. Benzophenone and 1,1,2,2-tetrachroloethane were used as the internal standards in the GLC and NMR analyses respectively.

General Procedure of Metal-complex-catalyzed Aldol Condensation Reactions. Reaction of Benzaldehyde with Acetophenone: The Zn(II)–bpy complex was prepared by the addition of 2,2′-bipyridine (0.20 mmol) to a solution of anhydrous zinc(II) acetate (0.2 mmol) in DMF (1 ml), and then benzaldehyde (1.25 mmol) and acetophenone (5 ml) were added to a yellow solution of the complex. The reaction mixture was stirred for 18 h at 80 °C; then the solvent and the excess of acetophenone were removed under reduced pressure to give an oil which was subsequently purified by preparative TLC, using a 1:4 ether–hexane mixture as the eluent. The yellow crystals thus obtained were identified as chalcone by the mp of 55—56 °C (lit,[8a] 55—57 °C), the NMR, and the IR in comparison with an authentic sample. The isolated yield of chalcone was 86%, and the GLC-analyzed yield was 100%.

Reaction of Benzaldehyde with Acetone: The Zn(II)-bpy complex was prepared by the addition of 2,2′-bipyridine (4.0 mmol) to a solution of zinc(II) chloride ($ZnCl_2 \cdot H_2O$, 4.0 mmol) in DMF (10 ml), and then benzaldehyde (2.5 mmol) and acetone (10 ml) were added to a yellow solution of the complex. The reaction mixture was stirred for 18 h at the reflux temperature. Then, the solvent and the excess of acetone were removed under reduced pressure at room temperature to give an oil which was subsequently extracted with an ethyl acetate-and-water system. The organic layer was dried over anhydrous sodium sulfate and then evaporated under reduced pressure at room temperature to give an oil whose NMR showed a mixture of two kinds of products. The curde oil was recrystallized from petroleum ether to give colorless crystals which were identified as benzylideneacetone by the mp of 38—39 °C (lit,[8b] 40—42 °C), the NMR, and the IR in comparison with an authentic sample. The other product was identified as 4-hydroxy-4-phenyl-2-butanone on the basis of sepctroscopic evidence; Mass: *m/e* (%), 164 (M^+, 3), 146 (3), 131(26), 105(100); NMR (CCl_4); δ 2.10 (s, 3H, CH_3), 3.50 (s, OH, H-D-exchange), 5.00 (t, 1H, CH). The total yield of these two products (25%) was determined by its crude NMR, adding 1,1,2,2-tetrachloroethane as the internal standard; the product ratio of benzylideneacetone to 4-hydroxy-4-phenyl-2-butanone was 29:71.

Condensation Products. 4-(Dimethylamino)chalcone, **28**; Mp 117.5—119 °C (lit,[4] 114 °C); IR:1645 cm^{-1}; NMR ($CDCl_3$): δ 2.95 (6H, s, $N(CH_3)_2$).

4-Methoxychalcone, **29**; Mp 72—74 °C (lit,[4] 72—74 °C); IR 1660 cm^{-1} NMR (CCl_4): δ 3.75 (3H, s, CH_3).

4-Methylcahlcone, **30**; Mp 99—100 °C (lit,[4] 96 °C); IR 1650 cm^{-1}; NMR (CCl_4): δ 2.32 (3H, s, CH_3).

Chalcone, **31**; Mp 57—58 °C (lit,[4] 57—58 °C); IR 1650 cm^{-1}; NMR (CCl_4): δ 7.00—8.00 (aromatic proton).

4-Chlorochalcone, **32**; Mp 114—117 °C (lit,[4] 114 °C); IR 1660 cm^{-1}; NMR (CCl_4): δ 7.00—8.00 (aromatic proton).

4-Cyanochalcone, **33**; Mp 162.5—163 °C; IR 2200, 1660 cm^{-1}; NMR ($CDCl_3$): δ 7.50—8.13 (aromatic proton). Mass: *m/e*, 233 (M^+), 156 ($M^+ - C_6H_5$), 128 ($M^+ - C_6H_5CO$).

4-Nitrochalcone, **34**; Mp 158—160 °C (lit,[4] 158—160 °C); IR 1660 cm^{-1}; NMR ($CDCl_3$) δ 7.50—8.50 (aromatic proton).

3-Nitrochalcone, **35**; Mp 143—145 °C (lit,[4] 145—146 °C); IR 1660 cm^{-1}; NMR ($CDCl_3$), δ 7.20—8.20 (aromatic proton).

2-Methoxychalcone, **36**; Mp 61—61.5 °C (lit,[4] 59—60 °C); IR 1660 cm^{-1}; NMR (CCl_4) δ 3.78 (3H, s, OCH_3).

2-Hydroxychalcone, **37**; Mp 152—153 °C (lit,[4] 152—153 °C); IR 1640 cm^{-1}; NMR (DMSO-d_6) δ 7.00—8.00 (aromatic proton), 9.80 (br., OH, H-D exchange).

2-Hydroxy-3-methoxychalcone, **38**; Mp 112—113.5 °C; IR 1650 cm^{-1}; NMR (acetone-d_6) δ 3.87 (3H, s, OCH_3); Found: C, 75.21; H, 5.63%. Calcd for $C_{16}H_{14}O_3$: C, 75.57; H, 5.55%.

1-Phenyl-3-(2-pyridyl)-2-propen-1-one, **39**; Mp 62—63 °C (lit,[4] 60—61 °C); IR 1660 cm^{-1}; NMR (CCl_4) δ 7.00—8.50 (aromatic proton).

1-Phenyl-3-(4-pyridyl)-2-propen-1-one, **40**; Mp 79—80 °C (lit,[4] 70—71 °C); IR 1660 cm^{-1}; NMR (CCl_4) δ 7.30—9.00 (aromatic proton).

1-Phenyl-4-methyl-2-penten-1-one,, **41**; IR 1670, 1650 cm^{-1}; NMR ($CDCl_3$) δ 1.15 (6H, d, CH_3), 1.70 (1H, m, CH), 6.90—8.00 (aromatic proton); Mass: *m/e*, 174 (M^+), 159 ($M^+ - CH_3$), 144 ($M^+ - 2CH_3$), 131 ($M^+ - CH(CH_3)_2$).

Cinnamylideneacetophenone, **42**; Mp 104—105 °C (lit,[4] 102—103 °C); IR 1655 cm^{-1}; NMR (CCl_4) δ 7.00—8.10 (aromatic proton).

Benzylideneacetone, **43**; Mp 41 °C (lit,[4] 41.5 °C); NMR

($CDCl_3$) δ 2.30 (3H, s, CH_3), 6.62 (1H, d, =CH).

1-Benzylidene-2-butanone, **44**; Mp 39—40 °C (lit,[4] 38.5—39.5 °C); NMR ($CDCl_3$) δ 1.17 (3H, t, CH_3), 2.67 (2H, q, CH_2), 6.70 (1H, d, =CH).

1-Phenyl-1-hexen-3-one, **46**; Mp 98—99 °C (lit,[4] 99—100 °C, phenylhydrazone); IR 1690, 1660 cm^{-1}; NMR ($CDCl_3$) δ 0.92 (3H, t, CH_3), 1.60 (2H, m, CH_2), 2.66 (2H, t, CH_2).

2-Benzylidenecyclopentanone, **47**; Mp 66—67 °C (lit,[4] 67—68 °C); IR 1710 cm^{-1}; NMR ($CDCl_3$) δ 2.10 (4H, m, $-CH_2CH_2-$), 2.94 (2H, dt, $COCH_2$), 7.40—7.45 (aromatic proton).

3-Benzylidene-2,4-pentanedione, **48**; IR 1710 cm^{-1}; NMR (CCl_4) δ 2.22 (3H, s, CH_3), 2.38 (3H, s, CH_3).

Ethyl α-cyanocinnamate, **49**; Mp 52—53 °C (lit,[4] 66—67 °C); IR 2230, 1710 cm^{-1}; NMR ($CDCl_3$) δ 1.40 (3H, t, CH_3), 4.35 (2H, q, CH_2); Found: C, 71.55; N, 6.82; H, 5.49%. Calcd for $C_{12}H_{11}NO$: C, 71.63: N, 6.96; H, 5.51%.

The authors wish to express their thanks to Professor Masayoshi Nakahara of Rikkyo University and to Professor Akitsugu Nakahara and Shinnichiro Suzuki of Osaka University for their helpful advice.

References

1) M. Sato, K. Okawa, and S. Akabori, *Bull. Chem. Soc. Jpn.*, **30**, 937 (1957); S. Akabori, T. Otani, R. Marshall, M. Winitz, and J. P. Greenstein, *Arch. Biochem. Biophys.*, **83**, 1 (1959); T. Otani and M. Winitz, *ibid.*, **102**, 464 (1963); M. Iwata and S. Emoto, *Bull. Chem. Soc. Jpn.*, **49**, 1369 (1976).

2) K. Irie and K. Watanabe, *Chem. Lett.*, **1978**, 539.

3) H. Irving and R. J. P. Williams, *J. Chem. Soc.*, **1953**, 3192.

4) A. T. Nielsen and W. J. Houlihan, *Org. React.*, Vol. 16, (1968).

5) K. Irie, A. Imazawa, and K. Watanabe, *Chem. Lett.*, **1979**, 1401.

6) a) G. W. Watt and D. G. Upcharch, *J. Am. Chem. Soc.*, **90**, 914 (1968); b) H. Sigel and D. B. McCrmick, *Acc. Chem. Res.*, **3**, 201 (1970); c) J. W. Jauregg, B. E. Hackley, T. A. Lies, O. O. Owens, and R. Proper, *J. Am. Chem. Soc.*, **77**, 922 (1955).

7) B. L. Horecker, Orestes Tsalas, and C. Y. Lai, "The Enzymes," 3rd ed, ed by P. D. Boeyer, Academic Press, New York and London (1972), Vol. 7, p. 213.

8) a) N. L. Dranke and P. Allen Jr, *Org. Synth.*, Coll. Vol. 1, 78 (1941); b) E. P. Kohler and H. M. Chadwell, *ibid.*, Coll. Vol. 1, 77 (1941).

pyridine gave a crystalline 6-*O*-mesyl derivative (**15**) in 86% yield.

Treatment of **15** with sodium isopropoxide in isopropyl alcohol gave an epimino derivative, which was further converted into a crystalline *N*-acetylepimino derivative (**16**) in 84% yield. The presence of an aziridine ring was demonstrated by a characteristic IR absorption of an acylaziridine-carbonyl group at 1700 cm^{-1} [17] and by ^1H NMR spectroscopy. The configuration of **16** was proposed as 6,7-(*N*-acetylepimino)-6,7-dideoxy-L-*lyxo*-heptopyranoside, according to the stereochemistry of an aziridine ring formation which has been well studied by several investigators.[18-22]

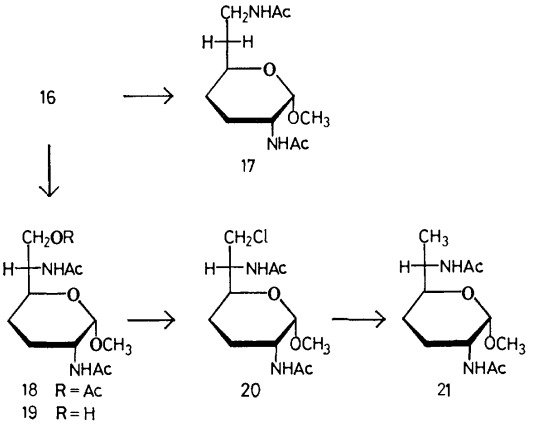

Scheme 4.

Catalytic hydrogenation of **16** in ethanol in the presence of Raney nickel gave a crystalline product (**17**) in a quantitative yield, which was found to be analytically pure. ^1H NMR spectrum of **17** revealed the presence of two acetamido and one methoxyl groups, but not a terminal methyl group. Thus **17** was identified as methyl 2,7-di-*N*-acetyl-2,3,4,6,7-pentadeoxy-α-D-*erythro*-heptopyranoside.

Methyl 2,6-di-*N*-acetyl-7-*O*-acetyl-2,3,4,6-tetradeoxy-β-L-*lyxo*-heptopyranoside (**18**) was obtained in 88% yield by heating **16** in glacial acetic acid. In the reaction, nucleophilic attack by an acetate ion on the aziridine ring occurs exclusively at C-7 position. This is in line with the fact that acetolysis of 6,7-(*N*-acetylepimino)-dideoxy-L-*glycero*-α-D-*galacto*-heptopyranoside derivative yielded 6-acetamido-7-*O*-acetyl-L-*glycero*-α-D-*galacto*-heptopyranoside derivative.[17]

De-*O*-acetylation of **18** in methanolic ammonia gave methyl 2,6-di-*N*-acetyl-2,3,4,6-tetradeoxy-β-L-*lyxo*-heptopyranoside (**19**) in 92% yield as crystals. Chlorination of **19** was performed by the triphenylphosphine–carbon tetrachloride procedure[23,24] to give a 7-chloro-7-deoxy derivative (**20**). Dehalogenation of **20** was carried out with tributylstannane[25-27] in the presence of α,α'-azobisisobutyronitrile under nitrogen atmosphere, methyl 2,6-di-*N*-acetyl-6-*epi*-α-D-purpurosamineide B (**21**) being obtained in 56% yield. Compound **21** was identical with an authentic sample prepared by methanolysis of tetra-*N*-acetylfortimicin B.[5]

Experimental

General Methods. Melting points were determined in capillary tubes and are corrected. Solutions were concentrated under reduced pressure below 40 °C. Optical rotations were measured with a Japan Spectroscopic DIS-SL polarimeter. ^1H NMR spectra were recorded with a Varian *EM360A* spectrometer at *60 MHz* or a Varian *XL-100* spectrometer at 100 MHz, peak positions being given in δ values. IR spectra were recorded with a Hitachi 225 spectrophotometer in KBr disks. TLC was performed on Wakogel B-10 (Wako Pure Chemical Co. Ltd.) plates, silica gel (Wakogel C-300) being used for column chromatography.

Methyl 2-Acetamido-2-deoxy-3,4-di-O-mesyl-6-O-trityl-α-D-glucopyranoside (6). Methanesulfonyl chloride (4.9 ml) was added to a stirred solution of methyl 2-acetamido-2-deoxy-6-*O*-trityl-α-D-glucopyranoside[15] (**5**, 10.0 g) in pyridine (50 ml). After being stirred for 2 h at 50 °C, the solution was concentrated, the residue being repeatedly extracted with chloroform and the combined chloroform solution washed with cold water. The chloroform layer was dried over Na_2SO_4 and concentrated. The residue was recrystallized from ethyl acetate to give 12.4 g (95%) of **6**, mp 184—185 °C (dec), $[\alpha]_D^{20}$ +53° (*c* 1.0, chloroform). ^1H NMR: δ 2.01 (s, 3, NAc), 2.52 (s, 3, SCH_3), 3.06 (s, 3, SCH_3), 3.41 (s, 3, OCH_3), 5.89 (d, 1, $J_{2,NH}$=9 Hz, NH).

Found: C, 57.08; H, 5.77; N, 1.95; S, 9.92%. Calcd for $C_{30}H_{35}NO_{10}S$: C, 56.85; H, 5.57; N, 2.21; S, 10.12%.

Methyl 2-Acetamido-2,3,4-trideoxy-6-O-trityl-α-D-erythro-hex-3-enopyranoside (7). Compound **6** (5.0 g) was heated with sodium iodide (50 g) and zinc powder (25 g) in DMF (280 ml) at 150 °C for 18 h with mechanical agitation under reflux. The reaction mixture was filtered and the filtrate was concentrated. The residue was dissolved in chloroform, the chloroform solution being washed repeatedly with 20% sodium thiosulfate solution and water. The solution was dried over Na_2SO_4 and concentrated. The residue was recrystallized from ether to give 2.3 g (64%) of **7**, mp 151—152 °C, $[\alpha]_D^{21}$ −34° (*c* 3.0, chloroform). ^1H NMR: δ 1.97 (s, 3, NAc), 4.80 (s, 1, H-1), 5.87 (d, 1, $J_{2,NH}$=10 Hz, NH).

Found: C, 75.89; H, 6.77; N, 3.12%. Calcd for $C_{28}H_{29}NO_4$: C, 75.82; H, 6.59; N, 3.16%.

By mild acid hydrolysis and subsequent acetylation, **7** was readily converted into methyl 2-acetamido-6-*O*-acetyl-2,3,4-trideoxy-α-D-*erythro*-hex-3-enopyranoside, mp 131—132 °C, $[\alpha]_D^{20}$ −37° (*c* 0.95, chloroform). ^1H NMR: δ 2.01 (s, 3, NAc), 2.10 (s, 3, OAc), 3.48 (s, 3, OCH_3).

Found: C, 54.37; H, 7.05; N, 5.86%. Calcd for $C_{11}H_{17}NO_5$: C, 54.31; H, 7.05; N, 5.76% .

Methyl 2-Acetamido-2,3,4-tridoxy-α-D-erythro-hexopyranoside (8). (*a*): Compound **7** (0.10 g) was hydrogenated in 80% aqueous methanol in the presence of palladium black at 50 °C overnight. After the catalyst had been filtered off, the filtrate was concentrated and the residue was fractionated on a silica gel column using 20:1 (v/v) benzene–ethanol as an eluant. Fractions moving fast on TLC in the same solvent system were combined and concentrated to give 10 mg (23%) of methyl 2-acetamido-2,3,4-trideoxy-6-*O*-trityl-α-D-*erythro*-hexopyranoside (**9**), mp 183—184 °C, $[\alpha]_D^{21}$ +38° (*c* 0.23, chloroform).

Found: C, 75.48; H, 7.03; N, 2.95%. Calcd for $C_{28}H_{31}NO_4$: C, 75.48; H, 7.01; N, 3.14%.

Fractions moving slowly on TLC were combined and concentrated to give 33 mg (72%) of **8** as a syrup, $[\alpha]_D^{21}$ +137° (*c* 1.76, methanol). ^1H NMR (CD_3OD): δ 1.91 (s, 3, NAc),

3.35 (s, 3, OCH_3), 4.54 (d, 1, $J_{1,2}$=3.2 Hz, H-1).

Found: C, 53.36; H, 8.37; N, 6.70%. Calcd for $C_9H_{17}NO_4$: C, 53.18; H, 8.43; N, 6.89%.

(*b*): Compound **7** (3.7 g) was catalytically hydrogenated as described in (a), and the residual mixture was hydrolyzed in 50% aqueous acetic acid (60 ml) at 60 °C for 1 h. The hydrolyzate was diluted with cold water (60 ml) and triphenylmethanol precipitated was removed by filtration. The filtrate was concentrated to give **8** in a quantitative yield as a crude syrup.

Compound **8** (83 mg) was acetylated and the product was recrystallized from ether–petroleum ether to give 70 mg (70%) of methyl 2-acetamido-6-*O*-acetyl-2,3,4-trideoxy-α-D-*erythro*-hexopyranoside, mp 106—107 °C, $[\alpha]_D^{20}$ +100° (*c* 1.0, chloroform). ^{1}H NMR: δ 1.97 (s, 3, NAc), 2.04 (s, 3, OAc), 3.38 (s, 3, OCH_3), 4.61 (d, 1, $J_{1,2}$=3.6 Hz, H-1), 5.67 (d, 1, $J_{2,NH}$=9.0 Hz, NH).

Found: C, 53.97; H, 7.70; N, 5.84%. Calcd for $C_{11}H_{19}NO_5$: C, 53.86; H, 7.81; N, 5.71%.

*Methyl 2-Acetamido-2,3,4-trideoxy-*α*-*erythro*-hexodialdo-1,5-pyranoside (**10**).* A solution of DCC (7.9 g) in DMSO (1 ml) was added under ice cooling to a stirred solution of **8** (2.6 g) in freshly distilled DMSO (4 ml) containing trifluoroacetic acid 0.5 ml) and pyridine (1 ml). Stirring was continued for 6 h at ambient temperature, and a solution of oxalic acid (2.3 g) in methanol (2 ml) was added to the reaction mixture. Dicyclohexylurea precipitated was filtered off and the filtrate containing **10** was used for the subsequent reaction.

A part of the filtrate was treated with 2,4-dinitrophenylhydrazine in phosphoric acid to give a hydrazone of **10**, mp 229—230 °C (dec).

Found: C, 47.27; H, 5.05; N, 18.32%. Calcd for $C_{15}H_{19}N_5O_7$: C, 47.24; H, 5.02; N, 18.37%.

*Methyl 2-Acetamido-2,3,4,7-tetradeoxy-7-nitro-*α*-*D*-ribo-heptopyranoside (**11**).* The filtrate containing **10** described above was diluted with methanol (10 ml). To the solution were added nitromethane (1.2 ml) and methanolic sodium methoxide (0.6 g Na in 5 ml of methanol) under ice cooling. After being settled overnight in a refrigerator, the pH of the solution was adjusted to 4 with Amberlite IR-120 (H^+) resin and concentrated. A solution of the residue in ethyl acetate was washed with cold water, dried over Na_2SO_4 and concentrated. The residue was recrystallized from ethyl acetate to give 1.52 g (45%) of **11**, mp 193—194 °C (dec), $[\alpha]_D^{21}$ +150° (*c* 1.0, methanol). The product showed a single spot at R_f 0.29 on TLC in 7:1 (v/v) benzene–ethanol. ^{1}H NMR (DMSO-d_6): δ 1.78 (s, 3, NAc), 3.24 (s, 3, OCH_3), 4.46 (d, 1, $J_{1,2}$=3.6 Hz, H-1).

Found: C, 45.94; H, 6.84; N, 10.71%. Calcd for $C_{10}H_{18}N_2O_6$: C, 45.79; H, 6.92; N, 10.68%.

From the mother liquor, a second crop of **11** (0.23 g, 7%) was obtained by column chromatography using 10:1 (v/v) benzene–ethanol as an eluant, followed by recrystallization from ethyl acetate.

*Methyl 2-Acetamido-7-amino-2,3,4,7-tetradeoxy-*α*-*D*-ribo-heptopyranoside (**12**).* Compound **11** (186 mg) was hydrogenated in methanol (6 ml) in the presence of Raney nickel overnight. After the catalyst had been filtered off, the filtrate was concentrated to give **12** as an amorphous solid in a quantitative yield, $[\alpha]_D^{21}$ +114° (*c* 2.28, methanol).

*Methyl 2,7-*N*-Acetyl-6-*O*-acetyl-2,3,4,7-tetradeoxy-*α*-*D*-ribo-heptopyranoside (**13**).* Compound **12** (89 mg) was acetylated and the product was recrystallized from ether–methanol to give 85 mg (70%) of **13**, mp 202—203 °C, $[\alpha]_D^{21}$ +101° (*c* 1.0, chloroform). ^{1}H NMR: δ 1.95 (s, 6, 2×NAc), 2.07 (s, 3, OAc), 3.33 (s, 3, OCH_3), 4.57 (d, 1, $J_{1,2}$=4 Hz, H-1), 4.83 (ddd, 1, $J_{6,7}$=6 Hz, $J_{6,7'}$=7 Hz, $J_{5,6}$=4 Hz, H-6), 5.86 (d, 1, $J_{2,NH}$=9.5 Hz, NH-2), 6.16 (t, 1, $J_{7,NH}$=5.5 Hz, NH-7).

Found: C, 52.89; H, 7.62; N, 8.82%. Calcd for $C_{14}H_{24}N_2O_6$: C, 53.15; H, 7.65; N, 8.86%.

^{1}H NMR spectrum of the corresponding 6-*O*-trideuterioacetyl derivative gave signals at δ 1.95 (s, 1, 6, 2×NAc) and 3.33 (s, 3, OCH_3).

*Methyl 2-Acetamido-7-*N*-benzyloxycarbonyl-2,3,4,7-tetradeoxy-*α*-*D*-ribo-heptopyranoside (**14**).* Benzyloxycarbonyl chloride (2.1 ml of 30% toluene solution) was added under ice cooling to a stirred solution of **12** (429 mg) in 94% aqueous ethanol (16 ml) containing sodium hydroxide (180 mg). After being settled in a refrigerator overnight, the reaction mixture was neutralized with 1 M hydrochloric acid and concentrated. The residue was purified on a silica gel column using 10:1 (v/v) benzene–ethanol as an eluant to give 498 mg (74%) of **14** as an amorphous solid, $[\alpha]_D^{21}$ +100° (*c* 1.0, methanol). ^{1}H NMR: δ 1.94 (s, 3, NAc), 3.32 (s, 3, OCH_3), 4.57 (d, 1, $J_{1,2}$=3.6 Hz, H-1), 5.09 (s, 2, benzyl CH_2), 5.48 (broad t, 1, NH-7), 5.81 (d, 1, $J_{2,NH}$=8.8 Hz, NH-2), 7.34 (s, 5, phenyl).

Found: C, 58.89; H, 7.08; N, 7.50%. Calcd for $C_{18}H_{29}N_2O_6$: C, 59.00: H, 7.15; N, 7.65%.

*Methyl 2-Acetamido-7-*N*-benzyloxycarbonyl-2,3,4,7-tetradeoxy-6-O-mesyl-*α*-*D*-ribo-heptopyranoside (**15**).* Methanesulfonyl chloride (0.08 ml) was added to a solution of **14** (336 mg) in pyridine (2 ml). After 3 h, the solution was concentrated and the residue was dissolved in chloroform. The chloroform solution was washed with water, dried over Na_2SO_4 and evaporated. The residue was recrystallized from ethyl acetate–petroleum ether to give 35 mg (86%) of **15**, mp 126—127 °C, $[\alpha]_D^{21}$ +75° (*c* 2.3, chloroform). ^{1}H NMR: δ 1.96 (s, 3, NAc), 2.99 (s, 3, SCH_3), 3.36 (s, 3, OCH_3), 4.61 (d, 1, $J_{1,2}$=3.6 Hz, H-1), 5.11 (s, 2, benzyl CH_2), 5.41 (broad t, 1, $J_{7,NH}$=6.0 Hz, NH-7), 5.71 (d, 1, $J_{2,NH}$=9.6 Hz, NH-2), 7.33 (s, 5, phenyl).

Found: C, 51.47; H, 6.24; N, 6.29; S, 6.99%. Calcd for $C_{19}H_{28}N_2O_8S$: C, 51.34; H, 6.35; N, 6.30; S, 7.21%.

*Methyl 2-Acetamido-6,7-(*N*-acetylepimino)-2,3,4,6,7-pentadeoxy-*β*-*L*-lyxo-heptopyranoside (**16**).* To a solution of **15** (323 mg) in dioxane (5 ml) was added a solution of sodium isopropoxide (40 mg of sodium) in isopropyl alcohol (2 ml). The solution was heated under reflux for 18 h, the progress of the reaction being monitored on TLC in 5:1 (v/v) benzene–ethanol. The starting material **15** (R_f 0.52) finally disappeared, three new spots appearing at R_f 0.10 (major), 0.16 (minor), and 0.64 (minor). The reaction mixture was filtered and the filtrate concentrated. The residue was acetylated with acetic anhydride in methanol, and after 10 min, pH of the solution was adjusted to 8. The solution was concentrated and the residue was extracted with ethyl acetate. The ethyl acetate solution was dried over Na_2SO_4 and concentrated. The residue was triturated in ether to give 156 mg (84%) of **16**, mp 174—175 °C, $[\alpha]_D^{21}$ +12° (*c* 1.0, chloroform). ^{1}H NMR: δ 1.95 (s, 3, NAc), 2.06 (d, 1, $J_{6,7}$=3.2 Hz, H-7), 2.16 (s, 3, AcN=), 2.24—2.59 (m, 2, H-6 and 7′), 3.36 (s, 3, OCH_3), 4.60 (d, 1, $J_{1,2}$=3.6 Hz, H-1), 5.77 (d, 1, $J_{2,NH}$=8.4 Hz, NH).

Found: C, 56.22; H, 7.66; N, 10.78%. Calcd for $C_{12}H_{20}N_2O_4$: C, 56.23; H, 7.87; N, 10.93%.

*Methyl 2,7-Di-*N*-acetyl-2,3,4,6,7-pentadeoxy-*α*-*D*-erythro-heptopyranoside (**17**).* Compound **16** (20 mg) was hydrogenated in ethanol (10 ml) in the presence of Raney nickel under hydrogen atmosphere (3.4 kg/cm^2) overnight. The catalyst was filtered off and the solution was concentrated. The residue was recrystallized from ether–methanol to give

19.5 mg (97%) of **17**, mp 207—208 °C, $[\alpha]_D^{20}$ +122.6° (*c* 0.47, methanol). ^{1}H NMR: δ 2.03 (s, 6, 2×NAc), 3.54 (s, 3, OCH_3), 4.79 (d, 1, $J_{1,2}$=3.2 Hz, H-1).

Found: C, 55.52; H, 8.43; N, 10.94%. Calcd for $C_{12}H_{22}N_2O_4$: C, 55.79; H, 8.59; N, 10.85%.

*Methyl 2,6-Di-*N*-acetyl-7-*O*-acetyl-2,3,4,6-tetradeoxy-β-*L*-lyxo-heptopyranoside (**18**).* A solution of **16** (109 mg) in glacial acetic acid (3 ml) was heated at 50 °C for 1 h and concentrated. The residue was neutralized with a $NaHCO_3$ solution and extracted with ethyl acetate. After being dried over Na_2SO_4, the ethyl acetate layer was concentrated. The residue was triturated in ether to give 119 mg (88%) of an amorphous product. A portion of the product was recrystallized from ether–methanol to give analytically pure **18** as needles, mp 195—196 °C, $[\alpha]_D^{21}$ +73.2° (*c* 1.0, chloroform). ^{1}H NMR: δ 1.97 (s, 3, NAc), 2.03 (s, 6, NAc and OAc), 3.32 (s, 3, OCH_3).

Found: C, 52.93; H, 7.46; N, 8.95%. Calcd for $C_{14}H_{24}N_2O_6$: C, 53.15; H, 7.65; N, 8.86%.

*Methyl 2,6-Di-*N*-acetyl-2,3,4,6-tetradeoxy-β-*L*-lyxo-heptopyranoside (**19**).* A solution of **18** (89 mg) in methanolic ammonia (5 ml) was settled overnight in a refrigerator and concentrated. The residue was purified on a silica-gel column using 4 : 1 (v/v) benzene–ethanol as an eluant. Fractions homogeneous on TLC (R_f 0.13) in the same solvent system were combined and concentrated. The residue was recrystallized from ether–methanol to give 71 mg (92%) of **19**, mp 181—182 °C, $[\alpha]_D^{20}$ +70° (*c* 1.0, chloroform). ^{1}H NMR: δ 1.97 (s, 3, NAc), 2.04 (s, 3, NAc), 3.37 (s, 3, OCH_3), 4.58 (d, 1, $J_{1,2}$=3.2 Hz, H-1), 5.83 (d, 1, $J_{2,NH}$=8.9 Hz, NH), 6.23 (d, 1, $J_{6,NH}$=8.5 Hz, NH).

Found: C, 52.58; H, 7.98; N, 10.15%. Calcd for $C_{12}H_{22}N_2O_5$: C, 52.54; H, 8.09; N, 10.21%.

*Methyl 2,6-Di-*N*-acetyl-7-chloro-2,3,4,6,7-pentadeoxy-β-*L*-lyxo-heptopyranoside (**20**).* To a solution of **19** (198 mg) in acetonitrile (4 ml) was added a solution of triphenylphosphine (247 mg) in carbon tetrachloride (8 ml). The reaction mixture was heated for 2 h and concentrated. The residue was purified on a silica gel column using 5:1 (v/v) benzene–ethanol as an eluant. Fractions homogeneous on TLC (R_f 0.38) in 4 : 1 (v/v) benzene–ethanol were combined and concentrated to give 129 mg (61%) of **20** as a syrup.

*Methyl 2,6-Di-*N*-acetyl-2,3,4,6,7-pentadeoxy-β-*L*-lyxo-heptopyranoside (Methyl 2,6-Di-*N*-acetyl-6-epi-α-*D*-purpurosaminide B) (**21**).* Tributylstannane (0.8 ml) and a small amount of α,α′-azobisisobutyronitrile were added to a solution of **20** (129 mg) in dry dioxane (20 ml). The mixture was heated at 80—90 °C for 2 h under nitrogen atmosphere and then concentrated. The residue was washed with hexane and purified on a silica-gel column using 5:1 (v/v) benzene–ethanol. Fractions homogeneous on TLC (R_f 0.32) in 4:1 (v/v) benzene–ethanol were combined and concentrated to give 64 mg (56%) of **21**, mp 212—213 °C, $[\alpha]_D^{20}$ +63.3° (*c* 1.0, methanol). (Found: C, 55.58; H, 8.46; N, 10.66%). The ^{1}H NMR and IR spectra were superimposable with those of an authentic sample prepared by methanolysis of tetra-*N*-acetylfortimicin B,[5] mp 212—213 °C, $[\alpha]_D^{20}$ +62.9° (*c* 0.98, methanol). The mixed melting point determination of **21** with the authentic sample showed no depression of melting point.

References

1) A preliminary communication presented at the American Chemical Society/Chemical Society of Japan Chemical Congress, Honolulu, Hawaii, April 5, 1979. Abstract CARB 9; T. Suami, Y. Honda, and T. Kato, *Chem. Lett.*, **1978**, 1125.

2) T. Nara, M. Yamamoto, I. Kawamoto, K. Takayama, R. Okachi, S. Takasawa, T. Sato, and S. Sato, *J. Antibiot.*, **30**, 533 (1977).

3) R. Okachi, S. Takasawa, T. Sato, S. Sato, M. Yamamoto, I. Kawamoto, and T. Nara, *J. Antibiot.*, **30**, 541 (1977).

4) P. J. L. Daniels, "Aminoglycoside antibiotics," ed by S. Mitsuhashi, Univ. of Tokyo Press. Tokyo (1975) pp 77—106.

5) R. S. Egan, R. S. Stanaszek, M. Cirovic, S. L. Mueller, J. Tadanier, J. R. Martin, P. Collum, A. W. Goldstein, R. L. De Vault, A. C. Sinclair, E. E. Fager, and L. A. Mitscher, *J. Antibiot.*, **30**, 552 (1977).

6) D. J. Cooper, M. D. Yudis, H. M. Marigliano, and T. Traubel, *J. Chem. Soc., C*, **1971**, 2876.

7) D. J. Cooper, P. J. L. Daniels, M. D. Yudis, H. M. Marigliano, R. D. Guthrie, and S. T. K. Bukhari, *J. Chem. Soc., C*, **1971**, 3126.

8) R. D. Guthrie and G. J. Williams, *J. Chem. Soc., Chem. Commun.*, **1971**, 923.

9) R. D. Guthrie and G. J. Williams, *J. Chem. Soc., Perkin Trans. 1*, **1972**, 2619.

10) S. Umezawa, T. Tsuchiya, and Y. Okazaki, *Bull. Chem. Soc. Jpn.*, **44**, 3494 (1971).

11) J. Cleophax, J. Leboul, A. Olesker, and S. D. Gero, *Tetrahedron Lett.*, **1973**, 4911.

12) J. S. Brimacombe, I. Da'aboul, and L. C. N. Tucker, *J. Chem. Soc., Perkin Trans. 1*, **1974**, 263.

13) J. S. Brimacombe, I. Da'aboul, and L. C. N. Tucker, *J. Chem. Soc., Perkin Trans. 1*, **1975**, 979.

14) M. Chmielewski, A. Konowal, and A. Zamojski, *Carbohydr. Res.*, **70**, 275 (1979).

15) R. W. Jeanloz, *J. Am. Chem. Soc.*, **74**, 4597 (1952).

16) G. H. Jones and J. G. Moffatt, "Methods in Carbohydrate Chemistry," Academic Press, New York (1972), Vol. 6, p. 315.

17) H. Saeki and E. Ohki, *Chem. Pharm. Bull.*, **18**, 789 (1970).

18) W. D. Rhoads and P. H. Gross, *Carbohydr. Res.*, **11**, 561 (1969).

19) J. S. Brimacombe, J. A. Miller, and U. Zakir, *Carbohydr. Res.*, **41**, C3 (1975).

20) D. H. Buss, L. Hough, and A. C. Richardson, *J. Chem. Soc.*, **1963**, 5295.

21) H. L. Spell, *Anal. Chem.*, **39**, 185 (1967).

22) C. F. Gibbs, L. Hough, and A. C. Richardson, *Carbohydr. Res.*, **1**, 290 (1965).

23) J. B. Lee and T. J. Nolan, *Can. J. Chem.*, **44**, 1331 (1966).

24) C. R. Haylock, L. D. Melton, K. N. Slessor, and A. S. Tracey, *Carbohydr. Res.*, **16**, 375 (1971).

25) G. J. M. Van der Kerk, J. G. Noltes, and J. G. A. Lujiten, *J. Appl. Chem.*, **7**, 366 (1957).

26) H. Arita and Y. Matsushima, *J. Biochem. (Tokyo)*, **70**, 795 (1971).

27) T. Suami, S. Nishiyama, Y. Ishikawa, and S. Katsura, *Carbohydr. Res.*, **53**, 239 (1977).

The Reaction of Olefins with Chloroalkoxyalkanes and Formic Acid in Ether

Kazuo NISHIURA,** Tsutomu TAGANO,** Yasuo WADA,**
Shigeo TANIMOTO, and Masaya OKANO*
Institute for Chemical Research, Kyoto University, Uji, Kyoto 611

(Received September 1, 1979)

The reaction of olefins with chloromethoxymethane (CMM) and excess formic acid in ether, in the presence of $ZnCl_2$ or $HgCl_2$, afforded mainly four products, 1-chloro- and 1-formyloxy-2-(formyloxymethyl)alkanes, and 3,5-dialkyl-4-chloro- and 3,5-dialkyl-4-(formyloxy)tetrahydropyrans, in various yields. In the case of styrene, the chief products were limited to the former two. Similar products were obtained from 1-chloro-1-ethoxyethane (CEE), but their yields were quite low.

In a previous paper,[1] we reported that the Lewis acid-catalyzed reaction of olefins with chloromethoxymethane(CMM) in acetonitrile gave *N*-[2-(methoxymethyl)alkyl]acetamides (**1**) after hydrolysis. When this reaction was carried out in a mixture of formic acid (a protic and good ionizing solvent) and ether, the expected product, **2** (Y=OCOH), was not formed; instead, two formyloxymethylated products, **3** (or **4**) (Y=Cl and OCOH), were obtained, together with substituted tetrahydropyrans, **5** (Y=Cl and OCOH). This paper will deal with these results.

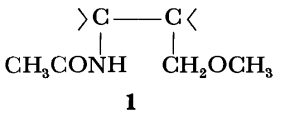

1

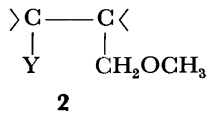

2

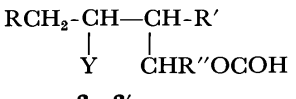

3, 3′

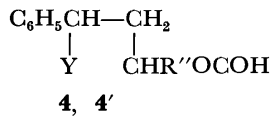

4, 4′

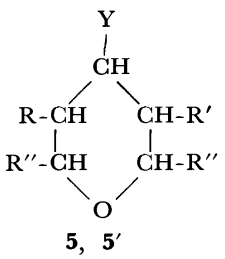

5, 5′

2, 3—5 (R″=H), **3′—5′** (R″=CH_3): Y=Cl or OCOH
3—5, 3′—5′ a: R, R′=$(CH_2)_3$, **b**: R=C_2H_5, R′=H, **c**: R=*n*-C_3H_7, R′=H

In this connection, it has been reported that the sulfuric acid-catalyzed reaction of olefins with formaldehyde in water or acetic acid (the Prins reaction) affords 1,3-dioxanes and 1,3-diols or their acetates (the homolog of **3** (Y=OCOH)) as the principal products,[2] whereas the reaction of terminal olefins with paraformaldehyde and hydrogen halides in anhydrous media yields mainly 3-alkyl-4-halotetrahydropyrans (correspond to **5** (Y=halogen)).[3]

Results and Discussion

When cyclohexene was allowed to react with CMM and excess formic acid in ether at room temperature for 24 h, in either the presence or absence of a metal chloride, the main distillate from the reaction mixture was found to consist of the following products: *trans*-1-chloro-2-(formyloxymethyl)cyclohexane (**3a**, Y=Cl), *trans*-1-formyloxy-2-(formyloxymethyl)cyclohexane (**3a**, Y=OCOH), and 9-chloro-3-oxabicyclo[3.3.1]nonane (**5a**, Y=Cl), accompanied by a slight amount of probably 9-formyloxy-3-oxabicyclo[3.3.1]nonane (**5a**, Y=OCOH). Besides, small amounts of cyclohexyl chloride and cyclohexyl formate (combined yield, *ca.* 15%) were found in the low-boiling fraction, and some tarry materials remained after distillation. For each of the products purely isolated, the structure was assigned by means of ^1H NMR and elemetal analyses. The presumed 3-oxabicyclo[3.3.1]nonane structure(A) for **5a**(Y=Cl) was confirmed by ^{13}C NMR study. The decoupled spectrum had five signals, as was to be expected from its symmetrical structure (the δ values are given in Table 3). If **5a** (Y=Cl) had the isomeric 3-oxabicyclo[4.3.0]nonane structure(B), it should give rise to eight separate signals.

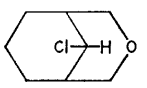

A

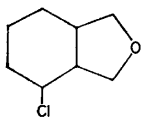

B

In the reaction without any additive, the total yield of **3a**(Y=Cl and OCOH) and **5a**(Y=Cl) was *ca.* 30%; a considerable amount of unreacted cyclohexene was also recovered. However, when $ZnCl_2$, $HgCl_2$, or $SnCl_4$ (1/4—1 eqiv.) was added to the reaction system, the total yield was improved up to around 50%, with the proportion of **3a**(Y=Cl) increasing considerably, and most of the cyclohexene was consumed. For equimolar addition, the above chlorides were nearly equal in their ability to carry Cl^-, but $ZnCl_2$ exhibited a slightly inferior tendency, and $AlCl_3$ and $BF_3 \cdot Et_2O$ were almost ineffective. When the ether solvent was replaced by dichloromethane, the yields of **3a** (Y=Cl and OCOH) decreased significantly. Further, when acetic acid (a less-ionizing solvent) was used in the place of formic acid, the reaction was quite slow and did not afford any of the products expected under the given conditions.

In cases where 1-hexene or styrene was used as an olefin component, the product distributions varied significantly. In the presence of $ZnCl_2$ or $HgCl_2$, the

** Koei Chemical Co., Ltd., Joto-ku, Osaka 536.

products **3c** and **5c** (Y=Cl and OCOH for both) were obtained from 1-hexene in a total yield of 55%. On the other hand, styrene, which does not contain an allylic H atom, gave mainly **4** (Y=Cl and OCOH) in a good total yield, without any accompanying tetrahydropyran derivatives, as had been expected. Here, the ring size for **5c** (Y=Cl and OCOH) was assigned mainly on the basis of the C–O–C stretching frequency (1090 cm^{-1} for both) in the IR spectrum, which corresponds fairly well to that exhibited by tetrahydropyran (1090 cm^{-1}), but not to that of tetrahydrofuran (1070 cm^{-1}).[4] Although both **5c**(Y=Cl and OCOH) were chromatographically (by GLC) homogeneous, the decoupled ^{13}C NMR spectrum of **5c** (Y=Cl) exhibited two similar sets of eight signals which can be assigned to a mixture of 4-chloro-3-propyltetrahydropyran and its isomer, probably 3-(1-chlorobutyl)tetrahydrofuran, in the ratio of *ca.* 4:1, while the ^{13}C analysis of **5c**(Y=OCOH) showed the existence of 4-formyloxy-3-propyltetrahydropyran alone (see Table 3). It should also be noted that the ratio of **3**(Y=Cl)+**3**(Y=OCOH)/**5**(Y=Cl)+**5** (Y=OCOH) varied from *ca.* 85/15 to *ca.* 35/65 as the olefin component was changed from cyclohexene to 1-hexene. The considerable difficulty in cyclization for the former olefin may be explained by the hindering effect in the ring-closure step (see Eq. 3).

Some typical data on the reaction of olefins with CMM and formic acid are shown in Table 1.

CMM is known to be accessible to the β-chloro-α-methoxymethylation of olefins in the presence of Lewis acids in aprotic solvents.[5] However, the present reaction showed quite a different pattern in which the introduction of a formyloxymethyl group, not a methoxymethyl group, occurred at an olefinic C; this might suggest that the formolysis of CMM leading to **6** is involved at an early stage of the reaction (Eq. 1).

$$CH_3OCH_2Cl \xrightarrow{\begin{array}{l}MCl_n\\ \longrightarrow [CH_3OCH_2^+ \cdot MCl_{n+1}^-]\\ HCOOH\ (\text{when } MCl_n \text{ is absent})\end{array}} \underset{\mathbf{6}}{CH_3OCH_2OCOH} + HCl \quad (1)$$

The formation of cyclohexyl chloride as a by-product and the following experimental result appear to support such a pathway *via* **6**: when an equimolar mixture of cyclohexene and **6** (prepared independently) was treated with HCl in formic acid in the presence of $ZnCl_2$, a mixture of **3a**(Y=Cl and OCOH) and **5a** (Y=Cl) was formed, analogous to the cyclohexene–CMM–formic acid reaction.

The succeeding protolysis of **6** may occur at the more basic ethereal O atom to afford the formyloxymethyl cation (**7**), and the addition of this cation and Cl^- (including MCl_{n+1}^-) or formic acid to olefins results in the formation of **3**(Y=Cl or OCOH respectively) (Eq. 2).

$$\left.\begin{array}{l} \mathbf{6} + H^+ \longrightarrow \underset{\mathbf{7}}{{}^+CH_2OCOH} + CH_3OH \\ RCH_2CH{=}CHR' + \mathbf{7} \longrightarrow \left[RCH_2\overset{+}{C}H\text{-}CH(CH_2OCOH)\text{-}R'\right] \\ \qquad\qquad \underset{\mathbf{8}}{} \\ \xrightarrow[\text{or HCOOH}]{Cl^-(\text{or } MCl_{n+1}^-)} \mathbf{3}\ (Y=Cl \text{ or } OCOH) \end{array}\right\} \quad (2)$$

Here, **3**(Y=Cl and OCOH) might be formed by another route, *via* the 1:1 olefin–CMM adduct (**2**, Y=Cl). However, such a possibility can be ruled out for the following reason: if **2**(Y=Cl) undergoes formolysis, the substitution would occur at the secondary C bearing Cl and would give rise to **2**(Y=OCOH),

Table 1. Reaction of olefins with CMM and formic acid in ether

Olefin 0.1 mol, CMM 0.1 mol, formic acid 1 mol, ether 45 ml.
Reaction conditions: 20—25 °C, 24 h.

Olefin	Additive (equiv.)	Product and yield (%)[a]			
		3 or **4** (Y=Cl)	**3** or **4** (Y=OCOH)	**5** (Y=Cl)	**5** (Y=OCOH)
Cyclohexene	None	8.9	22.3	2.4	
	$ZnCl_2$(1)	27.2	15.6	8.1	
	$ZnCl_2$(1/2)	26.2	18.7	7.2	
	$ZnCl_2$(1/4)	24.3	19.9	5.5	
	$ZnCl_2$(1/2)[b]	16.7	10.5	7.1	
	$HgCl_2$(1)[c]	27.9	15.4	6.3	
	$SnCl_4$(1/2)	27.8	17.3	8.1	
	$FeCl_3$(1)	21.9	14.7	7.5	
	$AlCl_3$(1/2)	11.7	18.4	2.7	
	$BF_3 \cdot Et_2O$(1)	7.4	20.3	3.3	
1-Hexene	$ZnCl_2$(1)	10.5	9.0	21.0[d]	14.7
	$HgCl_2$(1)[c]	11.0	10.0	18.9[d]	13.6
Styrene	$ZnCl_2$(1)	38.2	33.6	0	0

a) Based on olefin (determined by GLC). b) CH_2Cl_2(60 ml) was used as the solvent. c) Experiment on the scale of 1/2. d) A mixture of **5c** (Y=Cl) and its isomer (see Footnote d in Table 3).

not **3**(Y=Cl and OCOH). Moreover, it was proved by a blank experiment that the 1:1 cyclohexene–CMM adduct does not react with formic acid, at least under the given conditions.

A reasonable pathway to tetrahydropyrans **5**(Y=Cl and OCOH) is given below (Eq. 3), in which the route from **9** is essentially the same as that proposed by Stapp:[3]

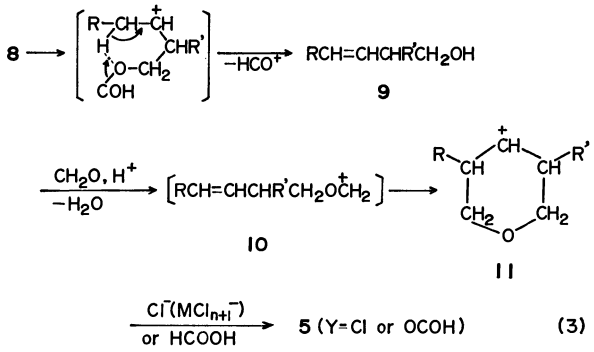

As to the transformation from **8** to **9**, another path involving the deprotonation of **8**, followed by hydrolysis, is possible. However, a separate experiment revealed that, in the cyclohexene–CMM reaction, the use of *dried* formic acid[6] did not cause any appreciable changes in the yields of all the products; this fact may suggest the participation of a process other than hydrolysis. For the same reason, the formaldehyde, which is required for the conversion of **9** to **10**, may be supposed to be formed by another reaction, such as the acid-catalyzed intramolecular methanolysis of **6** or the splitting of **7** itself, rather than by the acid hydrolysis of CMM or **6**. In view of the moisture-sensitive nature of **6**,[7] however, it seems to be difficult to rule out completely the possibility of its hydrolysis by external moisture.

The ring closure of the **10** cation may proceed in two ways to afford tetrahydropyran derivatives (*via* **11**) and/or tetrahydrofuran ones. In practice, the former type of product was formed either predominantly or exclusively, as has been described above. A quite similar trend has been observed in some related reactions. For example, the modification of the Prins reaction yields the above type of cyclic ethers as the main or side products, in which tetrahydropyran derivatives are either exclusive or predominant.[3,8] Further, in the intramolecular acylation of ω-arylalkanoic acids to give cyclic ketones, the fact that six-membered rings are formed in preference to five-membered ones has been demonstrated by several examples.[9]

Next, the reaction of olefins with 1-chloro-1-ethoxyethane(CEE) was examined under the same conditions as with CMM, but it was rather slow and the yields of products were generally very low (Table 2). Moreover, the ratios of the two formyloxyalkylated products differed from those in the case of CMM. Thus, in the reactions of 1-hexene with CMM and CEE (additive: $ZnCl_2$, 1 equiv.), the **3**(Y=Cl)/**3**(Y=OCOH) and **3'**(Y=Cl)/**3'**(Y=OCOH) ratios were 1.2 and 2.0 respectively, while in those of cyclohexene these ratios were 1.7 and 8.9 respectively. The large difference in the latter system may arise from a severe steric interference between the neighboring 1-(formyloxy)ethyl group of the cation corresponding to **8** and the attacking formic acid molecule (present as a cyclic dimer[11]).

Experimental

Except for the case of CEE, commercial organic materials were used after distillation. The CEE was prepared from paraaldehyde, ethanol, and HCl,[12] and was used after distillation. Commercial inorganic materials were used without further purification. The ^1H NMR spectra (in $CDCl_3$) were recorded with a Varian A-60 apparatus and a JEOL MH-100 apparatus. The ^{13}C NMR spectra were recorded on a JEOL FX-100 spectrometer in the pulse Fourier transform mode at 25.15 M Hz in $CDCl_3$. The IR spectra were determined with a Hitachi EPI-S2 spectrometer. The GLC analyses were carried out on a Shimadzu 5APTF apparatus, using EGSS-X (30%)-Chromosorb-W(lm) (with N_2 as the carrier gas).

Reactions of Olefins with CMM or CEE and Formic Acid. A typical example is given below. To a stirred mixture of cyclohexene (8.2 g, 0.1 mol), formic acid (46 g, 1 mol), and $ZnCl_2$ (13.6 g, 0.1 mol) in ether (45 ml), CMM (8.0 g, 0.1 mol) was added, drop by drop, at 0—5 °C. The mixture was stirred for 24 h at room temperature, and then it was slowly added to a suspension of $CaCO_3$ (50 g) in water. After this mixture had been stirred for 1 h, ether was added and inorganic precipitate was filtered off. The organic layer separated from the aqueous one was washed with aqueous NaCl and dried over $MgSO_4$,

Table 2. Reaction of olefins with CEE and formic acid in ether

Olefin 0.1 mol, CEE 0.1 mol, formic acid 1 mol, ether 45 ml.
Reaction conditions: 20—25 °C, 24 h.

Olefin	Additive (equiv.)	Product and yield (%)[a]			
		3' or **4'** (Y=Cl)	**3'** or **4'** (Y=OCOH)	**5'** (Y=Cl)	**5'** (Y=OCOH)
Cyclohexene	$ZnCl_2$(1)	8.9	1.0	2.5	
	$SnCl_4$(1/2)	7.0	0.8	1.4	
1-Pentene	$ZnCl_2$(1)	5.8	3.1	6.1	2.5
1-Hexene	$ZnCl_2$(1)	8.0	4.0	5.5	—[b]
Styrene	$ZnCl_2$(1)	11.5	5.4	0	0[c]

a) Based on olefin (determined by GLC). b) Not determined. c) Other product, $C_6H_5CH_2CH_2CH(CH_3)OCOH$ (29%).[10]

Table 3. Physical properties and analytical data of some representative products

Product	Bp (°C/Torr)	^{1}H- and ^{13}C-NMR, δ (ppm from TMS, in $CDCl_3$)		Found(Calcd) (%) C	H
3a (Y=Cl)[a]	118—120/20	^{1}H	8.05(s, 1H), 4.28(d, 2H), 3.77(d of t, 1H), 2.4—1.0(m, 9H)	54.86 (54.40)	7.67 (7.42)
3a (Y=OCOH)[a]	131—133/20	^{1}H	8.05(s, 2H), 4.80(d of t, 1H), 4.15(d, 2H), 2.3—0.9(m, 9H)	58.46 (58.05)	7.88 (7.58)
5a (Y=Cl)	132/70[b]	^{1}H	4.42(s, 1H), 4.04(d, 2H), 3.72(d, 2H), 2.3—1.4(m, 8H)	59.34 (59.81)	8.18 (8.15)
		^{13}C[c]	73.8(t, C-2,4), 63.8(d, C-9), 37.5(d, C-1,5), 24.2(t, C-6,8), 21.0(t, C-7)		
3c (Y=Cl)	98—100/13.5	^{1}H	8.00(s, 1H), 4.32(t, 2H), 3.98(m, 1H), 2.2—0.7(m, 11H)	54.44 (53.78)	8.98 (8.46)
3c (Y=OCOH)	84—86/2	^{1}H	8.05(s, 2H), 5.05(m, 1H), 4.20(t, 2H), 2.1—0.7(m, 11H)	57.77 (57.43)	8.88 (8.57)
5c (Y=Cl)[d]	199—201[e]	^{1}H	4.12—3.60(m, 3H), 3.6—3.0(m, 2H), 2.2—0.8(m, 10H)	60.10 (59.07)	9.89 (9.29)
		^{13}C[c]	71.0(t, C-2), 66.9(t, C-6), 61.9(d, C-4), 44.8(d, C-3), 36.6(t, C-5), 31.8(t, C-7), 19.8(t, C-8), 14.2(q, C-9)		
5c (Y=OCOH)[a]	108—109/18	^{1}H	8.06(s, 1H), 4.80(d of t, 1H), 4.1—3.8(m, 2H), 3.6—3.0(m, 2H), 2.2—0.8(m, 10H)	63.39 (62.76)	8.72 (9.37)
		^{13}C[c]	160.5(d, C-11), 73.6(d, C-4), 70.0(t, C-2), 65.7(t, C-6), 40.6(d, C-3), 31.3(t, C-5), 30.7(t, C-7), 19.9(t, C-8), 14.2(q, C-9)		
4 (Y=Cl)	122—124/9	^{1}H	8.05(s, 1H), 7.7—7.0(m, 5H), 5.05(t, 1H), 4.30(t, 2H), 2.40(q, 2H)	60.08 (60.46)	5.58 (5.58)
4 (Y=OCOH)	137/7	^{1}H	8.00(s, 2H), 7.4—7.1(m, 5H), 5.95(t, 1H), 4.15(t, 2H), 2.25(q, 2H)	63.66 (63.45)	6.02 (5.81)
3'a (Y=Cl)	—[f]	^{1}H	8.05(s, 1H), 5.50(q, 1H), 4.0—3.5(m, 1H), 2.4—1.4(m, 9H), 1.4—1.1(m, 3H)	58.08 (56.69)	8.25 (7.93)
3'a (Y=OCOH)	—[f]	^{1}H	8.05(s, 2H), 5.6—4.6(m, 2H), 2.4—0.7(m, 12H)	60.60 (59.99)	8.63 (8.04)
5'a (Y=Cl)	—[f]	^{1}H	4.38(s, 1H), 4.05—3.60(m, 2H), 2.3—1.4 (m, 8H), 1.22(d, 6H)	64.07 (63.65)	9.20 (9.08)
4' (Y=Cl)	—[f]	^{1}H	7.95(s, 1H), 7.4—7.1(m, 5H), 5.5—4.6 (m, 2H), 2.6—1.9(m, 2H), 1.32(d, 3H)	62.63 (62.11)	6.23 (6.16)
4' (Y=OCOH)	—[f]	^{1}H	8.02(s, 2H), 7.6—7.2(m, 5H), 5.92(t, 1H), 5.4—4.8(m, 1H), 2.6—1.8(m, 2H), 1.25(d, 3H)	65.72 (64.85)	6.61 (6.35)

a) *trans*-Isomer. b) Lit, 147 °C/110 Torr. [N. P. Volynskii, G. D. Galpern, and A. B. Urin, *Zh. Org. Khim.*, **2**, 1043 (1966); *Chem. Abstr.*, **65**, 15306 (1966)]. c) The numbering of C atoms is shown below. d) A mixture of **5c** (Y=Cl) and its isomer, probably 3-(1-chlorobutyl)tetrahydrofuran, in an approximate ratio of 4:1. The δ values (in ^{13}C NMR) of the isomer[c]: 67.1(t, C-2), 62.5(t, C-5), 60.8(d, C-6), 40.8(d, C-3), 30.8(t, C-4), 34.7(t, C-7), 19.3(t, C-8), 14.1(q, C-9). e) Lit,[3] 91—95 °C/15 Torr. f) Because of its small quantity, the bp could not be determined.

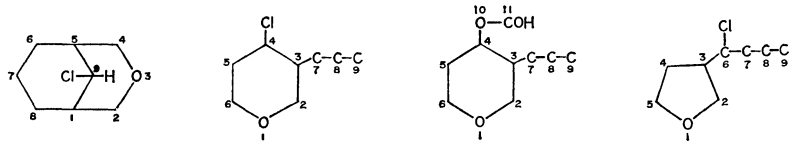

and most of the solvent was evaporated. Subsequent GLC analysis of the residue, using diphenylmethane as the internal standard, showed the presence of **5a** (Y=Cl) (1.3 g, 8.1 mmol) **3a** (Y=Cl) (4.8 g, 27.2 mmol), probably **5a** (Y=OCOH) (*ca.* 0.3 g), and **3a** (Y=OCOH) (2.9 g, 15.6 mmol). Each compound, except for **5a** (Y=OCOH), was isolated in an analytically pure state by duplicate distillation. The configuration and conformation of **3a** (Y=Cl and OCOH) were deduced from the splittings of the CHCl and CH-(OCOH) protons respectively in the ^{1}H NMR (100 MHz) spectrum, which indicate these protons are in an axial position, coupled strongly to two adjacent axial protons (δ=3.77, d of t, for CHCl; 4.80, d of t, for CHOCOH; and J=4 and 10 Hz for both).

In cases where the complete separation of the products by distillation was difficult, the analytically pure compounds were isolated from the corresponding raw distillates by column chromatography [Wakolgel, hexane–ether (5—10:1), petroleum ether–ether (10—20:1), or hexane–dichloromethane (20:1)].

The NMR spectra and analytical data of pure products satisfied all the given structures. Some representative data are given in Table 3.

*Reaction of Cyclohexene with Methoxymethyl Formate (**6**) and Formic Acid in the Presence of $ZnCl_2$ and HCl.* The formate, **6**, was prepared from CMM and $(HCOO)_2Pb$.[13] Into a

stirred mixture of cyclohexene (4.1 g, 50 mmol), formic acid (23 g, 0.5 mol), **6** (4.5 g, 50 mmol), and $ZnCl_2$ (6.8 g, 50 mmol) in ether (23 ml), dry HCl (*ca.* 2 g, 50 mmol) was introduced at −10——20 °C. The mixture was then kept for 24 h at room temperature under stirring. The work-up procedure was the same as above. Subsequent GLC analysis revealed the formation of **3a** (Y=Cl and OCOH) and **5a** (Y=Cl) (an approximate molar ratio, 11:4:5; total yield, *ca.* 35%).

Attempted Formolysis of 1-Chloro-2-(methoxymethyl)cyclohexane (1:1 Cyclohexene–CMM Adduct). The adduct was prepared by the reported method (in CS_2; cat., $ZnCl_2$).[14] To a stirred suspension of $ZnCl_2$ (6.8 g, 50 mmol) and formic acid (23 g, 0.5 mol) in ether (23 ml), the above adduct (8.1 g, 50 mmol) was added slowly, and then the mixture was stirred for 24 h at room temperature. GLC analysis after the usual work-up procedure showed that only the unreacted adduct was present.

We wish to thank Dr. Sakae Uemura, Institute for Chemical Research, Kyoto University, for his helpful discussions of the NMR data.

References

1) Y. Wada, T. Yamazaki, K. Nishiura, S. Tanimoto, and M. Okano, *Bull. Chem. Soc. Jpn.*, **51**, 1821 (1978).
2) For example, J. W. Baker, *J. Chem. Soc.*, **1944**, 296; A. T. Blomquist and J. Wolinsky, *J. Am. Chem. Soc.*, **79**, 6025 (1957).
3) P. R. Stapp, *J. Org. Chem.*, **34**, 479 (1969).
4) "Sadtler Standard Infrared Prism Spectra," Sadtler Research Lab. Inc., Philadelphia, Pa. (1968).
5) J. Mathien and J. Weill-Raynal, "Formation of C–C Bonds," Vol, 1, Georg Thieme Pub., Stuttgart (1973), p. 40.
6) Dried with sufficient anhydrous $CuSO_4$ twice [J. B. Garner, B. Saxton, and H. O. Parker, *Am. Chem. J.*, **46**, 236 (1911)].
7) M. H. Palomma and T. O. Herna, *Ber.*, **66**, 308 (1933).
8) L. J. Dolby, *J. Org. Chem.*, **27**, 2971 (1962).
9) See W. S. Johnson, *Org. React.* **2**, 114 (1944).
10) The formation of such an unusual product has also been reported in the $ZnCl_2$- or BF_3-catalyzed additions of acetoxychloromethane, (diethylamino)chloromethane, or (diethylamino)butoxymethane to styrene [R. Oda, K. Fujita, and I. Tabushi, *Nippon Kagaku Zasshi*, **87**, 756 (1966)].
11) For example, M. Koizumi, "Kagaku Ketsugo-ron" (tranlation of Pauling's "The Nature of Chemical Bonds"), Revised ed, Kyoritsu-Shuppan, Tokyo (1962), p. 431.
12) N. Rabjohn, *Org. Synth.*, Coll. Vol. IV, 748 (1963)
13) F. E. Clark, S. F. Cox, and E. Mack, *J. Am. Chem. Soc.*, **39**, 714 (1917).
14) C. D. Nenitzescu and V. Przemetzki, *Ber.*, **69**, 2707 (1936).

The Structure of Nitronitrosoaconitinic Acid, the Oxidation Product of Aconitine with Nitric Acid[1]

Takashi Amiya,* Yoshio Kanaiwa, Hideo Bando, Naomi Nakano, Takao Mori, and (the late) Harusada Suginome**

Hokkaido Institute of Pharmaceutical Sciences, 7-1 Katsuraoka-cho, Otaru 047-02

*** Department of Chemistry, Faculty of Science, Hokkaido University, Kita-10, Nishi-8, Kita-ku, Sapporo 060*

(Received October 4, 1979)

The structure of nitronitrosoaconitinic acid, which is an oxidation product of aconitine with nitric acid, was confirmed by spectroscopic methods. This compound is a new type of acid, a 2-nitro-2-cyclohexen-1-one, with a pK_a value comparable to that of carboxylic acids.

A study of the oxidation of aconitine (**1**) with nitric acid was first performed by Brady.[2,3a] The oxidation of aconitine (**1**), mesaconitine (**2**), and their derivatives has been found to yield a nitro *N*-nitroso derivative (**3**).[2,3b,4-7] Compound **3** has been called nitronitrosoaconitinic acid by Suginome.[4] Two alternative molecular formulae, $C_{31}H_{33}O_{13}N_3$[4] and $C_{31}H_{35}O_{13}N_3$,[5,7] have been proposed for **3** on the basis of the elemental analysis. Moreover, Suginome found that, although it retained both benzoyl and acetyl groups of **1**, one of the four methoxyl groups and alkyl group attached to the tertiary nitrogen of **1** are lost in the transformation.[4] Subsequently, extensive studies[5-7] have been carried out, but the structure still remains unknown. Compound **3** has now been subjected to modern structural analyses; in this paper, we wish to propose the **3** structure for this compound.

By field desorption mass spectrometry, **3** was confirmed to have a molecular formula of $C_{31}H_{35}O_{13}N_3$ [*m/e* 658 $(M+1)^+$]. The infrared spectrum exhibited bands attributable to hydroxyl groups at 3400—3700; to an α,β-unsaturated carbonyl and acyl carbonyl groups, at 1700 and 1720; to a nitro group, at 1373 and 1538, and to a benzene ring C–H bond, at 720 cm^{-1}. The UV spectrum in ethanol showed strong absorption bands at 230 (log ε; 4.2) and 343 nm (log ε; 3.4) attributable to an α,β-unsaturated carbonyl group. The ^1H NMR spectrum ($CDCl_3$, δ) showed the presence of an acetoxyl group (1.40, s, 3H), three methoxyl groups (3.18, 3.33, and 3.82, each 3H), and a benzoyloxy group and an olefinic proton (7.26—8.10, m, 6H). The removal of the two acyl groups by the alkaline hydrolysis of **3** afforded a compound (**4**), $C_{22}H_{29}O_{11}N_3$, designated as nitronitrosoaconinic acid,[4] [*m/e* 512 $(M+1)^+$]. The infrared spectrum exhibited bands attributable to hydroxyl groups at 3300—3700; to an α,β-unsaturated carbonyl group, at 1700, and to a nitro group at 1370 and 1535 cm^{-1}. The UV spectrum in ethanol showed strong bands at 230 (log ε; 4.1) and 343 nm (log ε; 3.1) attributable to an α,β-unsaturated carbonyl group. The ^1H NMR spectrum (D_2O, δ) revealed the presence of three methoxyl groups (3.30, 3.34, and 3.57, each 3H) and an olefinic proton (7.63, s, 1H) and indicated the generation of an olefinic proton in the transformation of **1** into **3**. On the acetylation of **4** with acetyl chloride, all of the four free hydroxyl and *N*-nitroso groups reacted and *N,O*-pentaacetyl derivative (**5**), dp 275—279 °C, was obtained as in the case of the acetylation of **3**.[4]

By chemical-ionization mass spectrometry, **5** was confirmed to have the molecular formula of $C_{32}H_{40}O_{15}N_2$ [*m/e* 710 $(M+NH_4)^+$]. The infrared spectrum exhibited bands attributable to an α,β-unsaturated carbonyl and acyl carbonyl groups at 1695 and 1740, and to a nitro group at 1362 and 1533 cm^{-1}. The UV spectrum in ethanol showed strong bands at 228 (logε; 4.3) (shoulder) and 343 nm (logε; 3.8) attributable to an α,β-unsaturated carbonyl group. The ^1H NMR spectrum ($CDCl_3$, δ) established the presence of four acetoxyl and an *N*-acetyl groups (2.00, 2.03, 2.09, 2.11, and 2.20, each 3H), three methoxyl groups (3.32, 3.36, and 3.40, each 3H), and an olefinic proton (7.18, s).

The strucutre of **3** was deduced by the correlation of the ^{13}C NMR signals of **1** with those of **3**. The reported[8] ^{13}C signal assignments of **1**, together with those of **3**, **4**, and **5**, are shown in Table 1. Assignments of the resonances to individual carbon atoms were achieved by using the ^1H single-frequency off-resonance decoupling technique, the chemical shift theory, and a comparison of their chemical shifts with those of aconitine type diterpenoid alkaloids.[8] A comparison of the ^{13}C signal assignments of **1** and **3** reveals the presence of the carbonyl group (singlet at 186.7 ppm) and the lack of C-3 carbon resonance at 70.4 ppm (doublet) in **3**. Thus, the carbonyl group was formed by the oxidation of the secondary hydroxyl group in Ring A. The low-field resonances at 142.8 and 148.8 ppm in **3** are assigned to the olefinic carbons, which correspond to a methine and a quarternaly carbon with a nitro group. The position of this double bond can be assigned to C-1 and C-2 on the basis of the observation of the UV spectrum of **3** and the lack of C-1 and C-2 carbon resonances at 83.4 and 36.0 ppm in **1**. The observation of the unexpected downfield shift (3.3 ppm) of the C-12 carbon in **3** relative to **1** suggests that it is preferable to interchange the chemical shifts of the C-2 and C-12 carbons in **1**.[8] By this interchange, this downfield shift is diminished to 1.3 ppm. On the other hand, on the basis of the observation of the spin-lattice relaxation-time (T_1) maesurements (C-17; 0.2 s and C-16; 0.6 s), the reported assignments of the chemical shifts of C-17 (61.0) and C-16′ (60.7)[8] have been interchanged.[1] The separation of the closely spaced peaks of C-17/C-16′ into positive and negative signals was observed. These data suggest that a large structural change took place only in the A-ring, more specifically, that

Table 1. ^{13}C chemical shifts of aconitine (**1**),[a] nitronitrosoaconitinic acid (**3**), nitronitrosoaconinic acid (**4**), and nitro-*N*-acetylaconinic acid tetraacetate (**5**)

Carbon	**1**[a,b]	**3**[b]	**4**[c]	**5**
1	83.4 (d)	142.8 (d)	145.8 (d)	144.1 (d)
2	34.0[g] (t)	148.8 (s)	150.7 (s)	149.1 (s)
3	70.4 (d)	186.7 (s)	189.0 (s)	188.4 (s)
4	43.2 (s)	48.5[d] (s)	50.4[d] (s)	49.0[d] (s)
5	46.6 (d)	51.1 (d)	55.4 (d)	50.3 (d)
6	82.3 (d)	81.1 (d)	82.5 (d)	82.0 (d)
7	44.8[d] (d)	48.0 (d)	49.2 (d)	47.9 (d)
8	92.0 (s)	89.5 (s)	78.7 (s)	87.9 (s)
9	44.2[d] (d)	42.1 (d)	48.1 (d)	41.9 (d)
10	40.8 (d)	36.7 (d)	38.6 (d)	37.2 (d)
11	49.8 (s)	50.5[d] (s)	51.7[d] (s)	51.7[d] (s)
12	36.0[g] (t)	37.3 (t)	39.7 (t)	37.9 (t)
13	74.0 (s)	74.1 (s)	77.6 (s)	79.9 (s)
14	78.9 (d)	78.3[e] (d)	80.0[e] (d)	76.1[e] (d)
15	78.9 (d)	78.5[e] (d)	81.5[e] (d)	77.6[e] (d)
16	90.1 (d)	89.9 (d)	92.9 (d)	88.2 (d)
17	60.7[f] (d)	62.6 (d)	64.8 (d)	52.5 (d)
18	75.6 (t)	70.5 (t)	72.2 (t)	70.1 (t)
19	48.8 (t)	42.7 (t)	44.0 (t)	46.6 (t)
N-CH_2	46.9 (t)	—	—	—
CH_3	13.3 (q)	—	—	—
1′	55.7 (q)	—	—	—
6′	57.9 (q)	58.3 (q)	58.4 (q)	59.1 (q)
16′	61.0[f] (q)	61.4 (q)	61.9 (q)	61.6 (q)
18′	58.9 (q)	59.2 (q)	59.5 (q)	59.1 (q)
C=O	172.2 (s)	172.0 (s)	—	C=O 168.2×2 (s)
CH_3	21.3 (q)	21.2 (q)	—	170.1×2 (s)
				170.3 (s)
C=O	165.9 (s)	165.7 (s)	—	CH_3 20.9 (q)
C_6H_5	129.8 (s)	129.2 (s)	—	21.9 (q)
	129.6 (d)	129.6 (d)	—	21.2×2 (q)
	128.6 (d)	128.8 (d)	—	21.6 (q)
	133.2 (d)	133.7 (d)	—	22.0 (q)

a) Results reported by Pelletier and Djarmati.[8] b) δ, ppm downfield from TMS in $CDCl_3$. c) δ, ppm downfield from TMS in CD_3OD. d) and e) These two values of each compound may be interchanged. f) and g) The reported assignments[8] of the chemical shifts of C-17 (61.0) and C-16′ (60.7) have been interchanged[1]; those of C-2 (36.0) and C-12 (34.0) are also interchanged.

the α,β-unsaturated carbonyl group was introduced into the A ring. The nitro group could be attached to either the α (C-2) or β (C-1) position of the α,β-unsaturated carbonyl group. Compound **3** can be obtained[6] from **2** *via* chromium trioxide oxidation to a ketone, followed by nitrosation at the carbon α to the carbonyl and oxidation with nitric acid. This sequence of reactions allows us to confirm that the nitro group is definitely attached to the C-2. Contrary to the significant differences observed in the chemical shifts of the C-1, C-2, and C-3 between **1** and **3**, only slight differences for C-4, C-5, C-7, C-10, C-18, and C-19 can be seen. These slight differences can be explained as results of the β and γ effects accompanying changes in the C-1, C-2, and C-3 carbons and the amino nitrogen in **1**. On the basis of all the results described above, the structure of nitronitrosoaconitinic acid is formulated as **3**; the series of reactions from **1** and **2** to afford **3**[6] are depicted in Scheme 1. According to this reaction process, the formation of **3** from oxonitine (**6**),[9,10] oxoaconitine (**7**),[5,7] and demethanolaconitinone (aconitoline) (**8**)[5-7] can be understood readily. These experimental data[6] suggest that Compound **9** is not demethanolanhydromesaconitinone $C_{32}H_{37}O_9N$,[6] but demethanolmesaconitinone $C_{32}H_{39}O_{10}N$, as is shown by the partial structure in Scheme 1. The chemical shifts of all of the carbons in **4** and **5** shown in Table 1 are in agreement with the assigned structures, **4** and **5**, considering the effects of using different solvents and the substitution of the hydroxyl for the acetoxyl groups.

The pK_a value of **3** was determined to be 4.9 by spectrophotometric measurements at a wavelength of 343 nm (λ max)[11] in buffer solutions. This value suggests that the acid strength of **3** is nearly equal to that of carboxylic acids. In the ^1H NMR spectrum, a signal due to an olefinic proton at δ 7.63 of **4** in D_2O disappeared slowly in the presence of a small

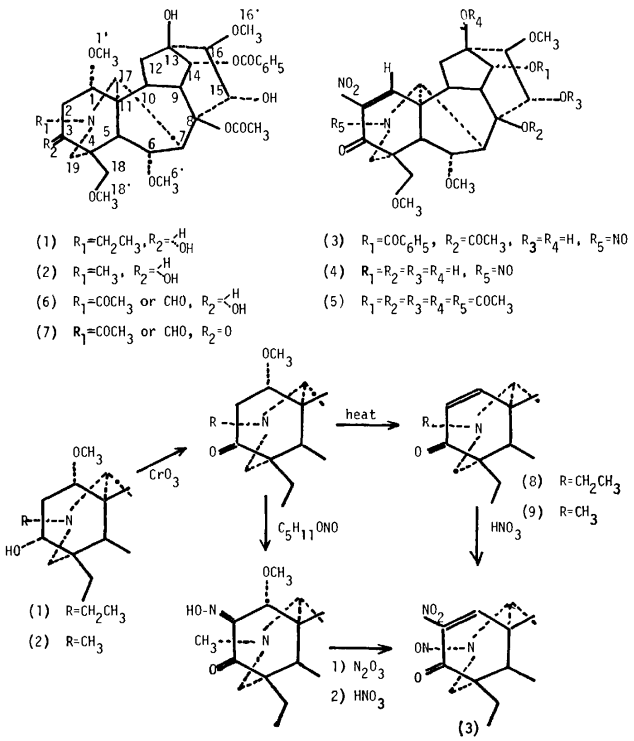

Scheme 1.

amount of alkali. Therefore, a system formed by the introduction of a nitro group into the α carbon of the double bond of the α,β-unsaturated carbonyl group is considered to be responsible for the acidity. No study concerning the acidity of such a structure has been reported, and further studies are presently in progress in our laboratories.

Experimental

The mps are uncorrected. The IR spectra were determined in KBr discs. The UV spectra were measured by means of a Shimadzu UV-300 spectrophotometer. The MS were measured by JEOL JMS-D300 and Shimadzu GCMS-9000 spectrometers. The Carbon-13 FT NMR spectra were taken at 25.00 MHz using a JEOL FX-100 spectrometer equipped with a JEC 980-24 K computer and 5 mm o. d. tubes. The FT-measurement conditions were: spectra width, 5 kHz; pulse width, 5 μs (45°); pulse repetition time, 1.0 s; number of data points, 8192; numbers of transients, 5000—40000. The values of pH were determined using a Corning model 7 pH meter.

Nitronitrosoaconitinic Acid (3). Mesaconitine (**2**) (2.3 g) was oxidized in 6 ml of HNO_3 (d 1.42) according to the method of a previous report[4] by heating in a water bath at 80 °C for 40 min. The precipitate (2.1 g) formed on the dilution of the reaction mixture was placed in a column of silica gel (100 g) and eluted with chloroform–methanol (100:1). This yielded **3** (575 mg) (needles of pale yellow) after recrystallization from acetone–water; dp 230 °C. UV: λ_{max}^{EtOH} 230 nm (log ε; 4.2) and 343 (log ε; 3.4); IR: ν_{max}^{KBr} 3700—3400, 1720, 1700, 1538, 1373, 720 cm^{-1}; NMR ($CDCl_3$, δ): 1.40 (3H, s, $OCOCH_3$), 3.18 (3H, s, OCH_3), 3.33 (3H, s, OCH_3), 3.82 (3H, s, OCH_3), 7.26—8.10 (6H, m, an olefinic and aromatic protons); MS: m/e 658 $(M+1)^+$. Found: C, 55.71; H, 5.09; N, 6.08%. Calcd for $C_{31}H_{35}O_{13}N_3 \cdot 1/2H_2O$: C, 55.85; H, 5.44; N, 6.30%.

Nitronitrosoaconinic Acid (4). Nitronitrosoaconitinic acid (**3**) was hydrolyzed according to previous report[4] by boiling it with 1 M barium hydroxide solution for 1 h. After cooling, the solution was passed through a column of an ion-exchange resin (Dowex-50W). The eluate was then evaporated. The residue was placed in a column of silica gel and eluted with ethanol. Recrystallization from water gave crystals: **4**; dp 287 °C. UV: λ_{max}^{EtOH} 230 nm (log ε; 4.1) and 343 (log ε; 3.1); IR: ν_{max}^{KBr} 3700—3300, 1700, 1535, 1370 cm^{-1}; ^1H NMR (D_2O, δ): 3.30 (3H, s, OCH_3), 3.34 (3H, s, OCH_3), 3.57 (3H, s, OCH_3) and 7.63 (1H, olefinic proton); MS: m/e 512 $(M+1)^+$. Found: C, 49.43; H, 5.60; N, 7.54%. Calcd for $C_{22}H_{29}O_{11}N_3 \cdot H_2O$: C, 49.90; H, 5.90; N, 7.93%.

Nitro-N-acetylaconinic Acid Tetraacetate (5). A mixture of nitronitrosoaconinic acid (**4**) (100 mg) and acetyl chloride (2 ml) was allowed to stand in a sealed tube for a week. After the subsequent removal of the acetyl chloride, methanol (1 ml) was added to the residue, and the resulting solution was added to ice-cold water. The precipitate (97 mg) thus formed was purified on a silica-gel column by eluting with chloroform–methanol; from the eluate, crystals (34 mg) were obtained; dp 275—279 °C. UV: λ_{max}^{EtOH} 228 nm (log ε; 4.3) (shoulder) and 343 (log ε; 3.8); IR: ν_{max}^{KBr} 1740, 1695, 1533 and 1362 cm^{-1}; ^1H NMR ($CDCl_3$, δ): 2.00, 2.03, 2.09, 2.11 and 2.20 (3H, singlet each, $OCOCH_3 \times 4$ and $NCOCH_3$), 3.32, 3.36 and 3.40 (3H, singlet each, $OCH_3 \times 3$) and 7.18 (1H, s, an olefinic proton); MS: m/e 710 $(M+NH_4)^+$. Found: C, 54.36; H, 5.60; N, 4.40%. Calcd for $C_{32}H_{40}O_{15}N_2 \cdot H_2O$: C, 54.08; H, 5.96; N, 3.94%.

Spectrophotometric Determination of the pK_a of Nitronitrosoacnitinic Acid (3). To a series of 5-ml portions of a saturated solution of **3** in water, 5-ml portions of 0.2 M buffers of different pH values were added, and then the resultant pH values of the mixtures were determined. A series of spectra were recorded at 22 °C. The pK_a value was determined at 343 nm according to the method described by Albert and Serjeant.[12] For the pH range of 4.1—5.6, acetate buffers were employed, and for that of 5.8—6.2, phosphate buffers. The spectra of the molecular and ionized species were determined in 0.005 M HCl and 0.005 M NaOH respectively.

Spectrometric Identification of the Olefinic Proton. To nitronitrosoaconinic acid (**4**) (30 mg) dissolved in 0.2 ml of D_2O, 0.05 ml of a solution of NaOD (60 mg) in D_2O (15.2 ml), divided into three protions, was added over a one-hour period at 22 °C. The NMR spectra were obtained during this period.

References

1) A preliminary account of this work has appeared in T. Amiya, Y. Kanaiwa, H. Bando, N. Nakano, and H. Suginome, *Chem. Lett.*, **1979**, 1163.

2) E. S. Stern, "The Alkaloids," ed by R. H. F. Manske and H. L. Holmes, Academic Press, New York, N. Y. (1954), Vol. IV, Chap. 37, p. 303; T. A. Henry, "The Plant Alkaloids," J. and A. Churchill, London (1949), pp. 674—681.

3) a) O. L. Brady, *J. Chem. Soc.*, **103**, 1821 (1913); b) A. Lawson, *ibid.*, **1936**, 80.

4) H. Suginome, *Ann.*, **533**, 172 (1938).

5) W. A. Jacobs and L. C. Craig, *J. Biol. Chem.*, **136**, 323 (1940).

6) R. Majima and K. Tamura, *Ann.*, **545**, 1 (1940).
7) W. A. Jacobs and S. W. Pelletier, *J. Am. Chem. Soc.*, **76**, 4048 (1954).
8) S. W. Pelletier and Z. Djarmati, *J. Am. Chem. Soc.*, **98**, 2626 (1976).
9) S. W. Pelletier and N. V. Mody, "The Alkaloids," ed by R. H. F. Manske and R. G. A. Rodrigo, Academic Press, New York, N. Y. (1979), Vol. XVII, Chap. 1, p. 5.
10) K. Wiesner and L. Fay, *Experientia*, **27**, 758 (1971).
11) The value in Ref. 1 is revised to this value.
12) A. Albert and E. P. Serjeant, "The Determination of Ionization Constants," 2nd ed, Chapman and Hall, London (1971), Chap. 4, p. 44.

The Palladium Catalyzed Nucleophilic Substitution of Aryl Halides by Thiolate Anions

Toshihiko MIGITA,* Tomiya SHIMIZU, Yoriyoshi ASAMI, Jun-ichi SHIOBARA, Yasuki KATO, and Masanori KOSUGI

Department of Applied Chemistry, Faculty of Technology, Gunma University, 1-5-1 Tenjincho Kiryu, Gunma 376

(Received December 8, 1979)

In the presence of a catalytic amount of tetrakis(triphenylphosphine)palladium, phenyl and methyl or methoxyphenyl iodides and bromides were found to react with thiolate anions in alcoholic solvents, to give the corresponding aryl sulfides in excellent yield. The reaction is useful to prepare symmetrical or unsymmetrical diaryl sulfides and aryl alkyl sulfides. The reaction mechanism does not involve aryl halide radical anions, but is thought to involve oxidative addition of aryl halide to Pd(0), nucleophilic substitution on the adduct followed by reductive elimination.

Aryl halides which are not activated by electron withdrawing substituents are inert to the usual nucleophilic reagents. Under special conditions, however, such unactivated aryl halides undergo substitution of halogens by nucleophiles. Besides the reactions *via* aryne intermediates under conditions involving high temperature or very strong bases, there have been noticed two kinds of substitution: aromatic $S_{RN}1$ which are stimulated by the presence of good electron donors,[1] and substitution catalyzed by the transition metal complexes.

As examples of the latter kind of reactions, there have been known that Pd(0) or Pd(II) catalyzes the substitution of aryl halides by cyanide,[2] acetylide anions,[3] π-nucleophiles,[4] and other organometallic reagents.[5] Ni(0) catalysts also promote the reaction with acetylide[3] or other carbanions[6] and halogen exchange with halide ions.[7]

As preliminarily reported, it has been found that in the presence of a catalytic amount of tetrakis(triphenylphosphine)palladium, $Pd(PPh_3)_4$, aryl bromides and iodides react easily with thiolate anions in dimethyl sulfoxide (DMSO) to give aryl sulfides in satisfactory yield.[8] Recently, similar reaction of alkenyl halide also has been developed.[9]

$$ArX + RS^- \xrightarrow{Pd(PPh_3)_4} ArSR + X^-$$

X: I, Br and R: Ph, Alkyl

On the other hand, quite similar reaction of aryl halides with arenethiolates giving sulfides has been known to proceed without metal complexes, in liquid ammonia under irradiation of Pyrex-filtered light, and the $S_{RN}1$ mechanism was proposed for the reaction.[10]

The present paper described the results of a further survey on the chemistry of the Pd(0) catalyzed reaction giving sulfides, comparing with that of the $S_{RN}1$ reaction.

Results

Table 1 shows the result of the reaction carried out by heating a solution of aryl halide (2 mmol), arene- or alkanethiol (2 mmol), sodium *t*-butoxide (4 mmol), and a catalytic amount of tetrakis(triphenylphosphine)-palladium in a solvent, the yield of the sulfide being obtained by GLC analysis.

Table 1 apparently shows the catalytic effect of $Pd(PPh_3)_4$. Without the catalyst, PhI, *p*-ClC_6H_4I, *p*-ClC_6H_4Br, and *m*-$MeOC_6H_4I$ reacted with PhS^- in DMSO to give low yield of the corresponding sulfides, and *p*-methyl and *p*-methoxy derivatives scarecely reacted and the aryl halides remained in the mixture under the same conditions. However, the presence of $Pd(PPh_3)_4$ in the reaction mixture converted all aryl halides into the corresponding sulfides in high yield. Palladium acetate also promotes the reaction, but seems inferior to $Pd(PPh_3)_4$ in the catalytic efficiency. Yield of diphenyl sulfide in the reaction of iodo benzene and PhS^- was still lower than that in the $Pd(PPh_3)_4$ catalyzed reaction, even when 10 mol% of $Pd(OAc)_2$ was present.

In preliminary experiments,[8] DMSO was chosen as a solvent, since in such an aprotic solvent nucleophile such as thiolate anion was considered to be more reactive than in a protic solvent. However, the results of the reaction of iodobenzene with benzenethiolate ion carried out in various easily available solvents indicate that alcohols are the most recommendable solvents.

Thus, the reaction in refluxing ethanol gave diphenyl sulfide in almost quantitative yield even in the presence of only 1 mol% of the catalyst, $Pd(PPh_3)_4$.

For preparative scale, it is most convenient to reflux a mixture made by adding aryl halide, thiol and then 1 mol% of $Pd(PPh_3)_4$ to a solution of sodium alcoholate prepared by dissolving sodium metal in the alcoholic solvent (see Experimental part). For the reaction of aryl iodide in ethanol, 4 h refluxing is sufficient to complete the reaction. Starting from iodobenzene (50 mmol), diphenyl sulfide and phenyl *t*-butyl sulfide were isolated in 88 and 65% yield, respectively.

Table 1 shows that the reaction proceeds with not only iodobenzene and its methyl or methoxy derivatives, but also with the corresponding unactivated aryl bromides. Aryl bromides react more slowly than aryl iodides. Thus, the reaction of bromobenzene in refluxing ethanol under which iodobenzene reacted smoothly, gave the sulfide only in low yield, but gave the excellent results under the conditions of refluxing alcohol of higher boiling point, *n*-BuOH.

Aryl chlorides are poor substrates toward the Pd(0) catalyzed substitution. Chlorobenzene was converted into the sulfide in only a trace amount under the same conditions. Chloronaphthalene and EtS^- gave a mod-

Table 1. $Pd(PPh_3)_4$ catalyzed sulfenylation of aryl halide

Run	ArX	Thiol	$Pd(PPh_3)_4$	Solvent	Temp/°C	Sulfide Yield/%	
1	C_6H_5I	PhSH	—	DMSO	100	22	(94)
2			0.08	DMSO	100	75	
3			0.08	DMSO	100	83	
4			0.08	DMF	100	59	
5			0.08	CH_3CN	reflux	11	
6			0.08	*n*-BuOH	reflux	100	
7			0.08	EtOH	reflux	100	
8			—	EtOH	reflux	0	
9			0.02	EtOH	reflux	97	
10	C_6H_5I	*t*-BuSH	0.08	EtOH	reflux	100	
11	C_6H_5I	*n*-BuSH	0.08	EtOH	reflux	42	
12			0.08	*n*-BuOH	reflux	90	
13	C_6H_5I	EtSH	0.08	*n*-BuOH	reflux	66	
14	*p*-$CH_3C_6H_4I$	PhSH	—	DMSO	100	0	
15			0.08	DMSO	100	78	
16			0.02	EtOH	reflux	85	
17	*m*-$CH_3C_6H_4I$	PhSH	0.02	EtOH	reflux	85	(81)
18	*o*-$CH_3C_6H_4I$	PhSH	0.02	EtOH	reflux	98	(72)
19	*p*-$CH_3OC_6H_4I$	PhSH	—	DMSO	100	6	
20			0.08	DMSO	100	78	(76)
21			0.02	EtOH	reflux	91	
22	*m*-$CH_3OC_6H_4I$	PhSH	—	DMSO	100	22	(88)
23			0.08	DMSO	100	83	
24			0.02	EtOH	reflux	100	
25	*o*-$CH_3OC_6H_4I$	PhSH	0.02	EtOH	reflux	65	
26	*p*-ClC_6H_4I	PhSH	—	DMSO	100	33	
27			0.08	DMSO	100	79	
28			0.02	EtOH	reflux	70	
29	2,6-$Me_2C_6H_3I$	PhSH	0.02	EtOH	reflux	16	(19)
30	PhBr	PhSH	—	DMSO	100	7	(23)
31			0.08	DMSO	100	82	
32			0.08	EtOH	reflux	19	
33			0.08	*n*-BuOH	reflux	100	
34	*p*-MeC_6H_4Br	PhSH	—	DMSO	100	4	
35			0.08	DMSO	100	51	
36			0.08	*n*-BuOH	reflux	100	
37	*p*-$MeOC_6H_4Br$	PhSH	—	DMSO	100	3	
38			0.08	DMSO	100	52	
39			0.08	*n*-BuOH	reflux	80	
40	*p*-ClC_6H_4Br	PhSH	—	DMSO	100	28	
41			0.08	DMSO	100	59	
42	PhCl	PhSH	0.08	DMSO	100	trace	
43	α-NaPhCl	EtSH	0.08	DMSO	100	46	
44			—	DMSO	100	38	

ArX: 2 mmol, thiol: 2 mmol, *t*-BuONa: 4 mmol, solvent: 20 ml.

erate yield of the sulfide, but the almost same results were obtained even without a catalyst.

As shown in Table 2 a), competitive experiments using large excess of substituted iodobenzenes showed somewhat retarding effects of the electron repelling substituents ($\rho \fallingdotseq +1.0$).

Alkanethiolates such as EtS^-, n-BuS^-, and t-BuS^- are also good substituting reagents. Semiquantitative competitive experiment on the reaction of iodobenzene with excess of a mixture of PhS^- and t-BuS^- showed t-BuS^- reacts about 9 times faster than PhS^- as shown in Table 2 b).

Discussion

The reactions of aryl iodides and bromides with thiolate anions in the presence of $Pd(PPh_3)_4$ were found to be useful for preparation of unsymmetrical diaryl or aryl alkyl sulfides. It should be noteworthy that the reaction can be applied to the aryl halides bearing electron repelling substituents.

The reaction needs no peculiar solvents, but the

Table 2. Competitive reaction

a) Reaction of PhS^- with PhI and XC_6H_4I

X	$[PhI]_i/[XC_6H_4I]_i$	$[XC_6H_4SPh]_f/[C_6H_5SPh]_f$	Relative rate k_X/k_H
p-Cl	1.00	1.80	1.8
p-CH_3	1.00	0.79	0.8
p-CH_3O	1.00	0.60	0.6

b) Reaction of PhI with PhS^- and *t*-BuS^-

$[PhSH]_i$	$[t\text{-BuSH}]_i$	$[PhSPh]_f$	$[t\text{-BuSPh}]_f$	Relative rate $k_{t\text{-BuS}^-}/k_{PhS^-}$
4.92	2.01	0.18	0.63	10.2
9.84	2.00	0.20	0.36	8.7

c) Reaction of $PhPdI(PPh_3)_2$ with PhS^- and *t*-BuS^-

$[PhSH]_i$	$[t\text{-BuSH}]_i$	$[PhSPh]_f$	$[t\text{-BuSPh}]_f$	Relative rate $k_{t\text{-BuS}^-}/k_{PhS^-}$
5.06	1.04	0.18	0.25	8.0

most common solvents, alcohols. Reaction temperature can be regulated by choosing the alcholic solvents depending on the reactivity of substrate. Thus, aryl iodides and bromides react smoothly in refluxing ethanol and 1-butanol, respectively. Work-up for separation of the products is reasonably easy as shown in the experimental part.

It is interesting to compare the features between the present reaction and the sulfenylation of unactivated aryl iodide proceeding through $S_{RN}1$ processes developed by Bunnett and Creary. At first glance on Table 1 in which yields of the sulfide produced through the $S_{RN}1$ is noted in parentheses, both the $S_{RN}1$ and the Pd(0) catalyzed sulfenylation of aryl halides seem to have resembling scope and limitation. Thus, unactivated aryl iodides react smoothly, aryl bromides react more slowly than iodides, and chlorides hardly react. In both reactions 2,6-dimethylphenyl iodide gave the corresponding sulfide, even though the yields are low presumably due to the steric hindrance, showing that both reactions do not proceed *via* elimination-addition involving intermediacy of arynes. However, there can be recognized some different features between these two types of reactions.

The Pd(0) catalyzed reaction is not inhibited by the presence of *p*-dinitrobenzene which has been known to be a good electron acceptor and to inhibit the $S_{RN}1$ processes.[1] The run (No. 3 in Table 1) carried out in the presence of *p*-dinitrobenzene (equimolar to the substrate) gave the excellent yield of diphenyl sulfide.

Secondly, the $S_{RN}1$ reactions of chlorophenyl iodides or bromides with PhS^- give almost exclusively disulfenylated products,[10] but in the Pd(0) catalyzed reaction, monosulfenylated products ClC_6H_4SPh are predominantly formed, even if excess of thiolate is used.

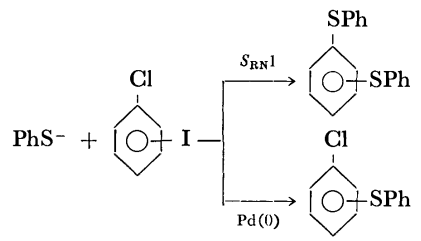

Inhibition by an electron acceptor, and disulfenylation of chlorophenyl halides are the striking features which strongly support the $S_{RN}1$ mechanism involving electron transfer to aryl halides giving anion radicals. Consequently, the present reaction lacking these features should be essentially different from the $S_{RN}1$ reaction, and not involving radical anions.

The most plausible mechanism of the Pd(0) catalyzed sulfenylation involves oxidative addition of aryl halide to Pd(0), followed by nucleophilic attack of thiolate anion on the adduct.

$$Ar\text{-}X + Pd(0) \longrightarrow Ar\text{-}Pd\text{-}X$$
$$RS^- + ArPdX \longrightarrow ArSR + Pd(0) + X^-$$

It has been established that aryl halide adds to $Pd(PPh_3)_4$ to give halo(aryl)bis(triphenylphosphine)-palladium(II), $ArPdX(PPh_3)_2$ in high yield.[11] The observed tendency of the substituent effects in the present reaction ($\rho \fallingdotseq 1.0$) concords with the qualitative observation of the substituent effects in the oxidative addition.[11] Then it is quite natural to consider the oxidative addition as the first step of the Pd(0) catalyzed reaction of aryl halide.

Actually, treatment of iodo(phenyl)bis(triphenylphosphine)palladium(II) prepared by the method of Fitton *et al.*[11] with a solution of PhS^- gave diphenyl sulfide almost quantitatively. Furthermore, competitive reaction of the adduct with excess amounts of PhS^- and *t*-BuS^- showed that *t*-BuS^- reacted about 8 times faster than PhS^-. This is in tolerable agreement with the result of the competitive reaction of iodobenzene with PhS^- and *t*-BuS^- described above. These facts strongly suggest intermediacy of the oxidative adducts between Pd(0) and aryl halide.

By the way, a mechanism involving an electron transfer to give anion radicals $ArX^{\cdot-}$ has been suggested as a initial step in the oxidative addition.[12] This possibility, however, seems unlikely at least in the addition of aryl halide to the Pd(0), because the Pd(0) catalyzed reaction of aryl halide with thiolate anion cannot be considered to involve generation of a radical anion, $ArX^{\cdot-}$. The anion radical once formed, would propagage $S_{RN}1$ reaction, which could show the features different from the present reaction, as discussed above.

The initial step of the reaction between the oxidative adduct and thiolate anion is thought to be a nucleophilic substitution on the palladium atom in the adduct. And reductive elimination on the substituted product may give aryl sulfide, regenerating Pd(0). Besides

$$ArPd\text{-}X + SR^- \longrightarrow Ar\text{-}Pd\text{-}SR + X^-$$

$$Ar\text{-}Pd\text{-}SR \longrightarrow ArSR + Pd(0)$$

thiolate and cyanide anions, triphenylphosphine also was found to react with the unactivated aryl halides in the presence of the Pd(0) catalyst, giving aryltriphenylphosphonium salts in high yield, as shown in Table 3.

Table 3. $Pd(PPh_3)_4$ catalyzed reaction of aryl halide with PPh_3

ArX	Product isolated yield/%	$ArP^+Ph_3X^-$ Mp/°C	Mp(lit)[a]/°C
PhI	93	325—328	328—326
p-MeC_6H_4I	80	208—209	207—209
p-$MeOC_6H_4I$	93	217—218	217—218
PhBr	7	286—288	288

ArX: 2 mm, PPh_3: 2 mmol, $Pd(PPh_3)_4$: 0.08 mmol, solvent: benzene: 3 ml.

a) L. Horner and H. Hoffman, *Chem. Ber.*, **91**, 45 (1958).

These three soft nucleophiles have been found to be particularly reactive toward the platinum atom of *trans*-$[Pt(py)_2Cl_2]$.[13] On the other hand, the Pd(0) catalyzed substitution of aryl halide by hard nucleophiles, for example, alkoxide and various types of carbanions such as $\bar{C}H_2CN$, $\bar{C}H(COOR)_2$, *etc.* was unsuccessful. These tendencies may be compatible with the mechanism involving nucleophilic attack on the palladium atom.

Experimental

All reagents were commercially available and, of reagent-grade quality, unless otherwise noted. Tetrakis(triphenylphosphine)palladium(0) was prepared according to the literature.[14] Reaction products, sulfides and phosphonium salts were identified by comparing their IR spectra with those of the authentic samples. GLC analysis was performed with a Ohkura model 710 gas chromatograph.

Reactions with Thiolate. *Small Scale Experiment*: A solution of aryl halide (2 mmol), thiol (2 mmol), sodium *t*-butoxide (4 mmol), and 1—4% molar amount of $Pd(PPh_3)_4$ in a solvent (20 ml) was heated at 100 °C or boiling points of solvents under a nitrogen stream with stirring. For the reactions of aryl iodides, reactions complete after 3 h, but prolonged heating does not affect yield of the sulfides. It takes more than 10 h to complete the reaction of aryl bromides. Yields of the products were determined by GLC analysis. The results (reaction time: 18 h) are shown in Table 1.

Preparative Scale Experiment: In a three necked flask (500 ml), a solution of sodium ethoxide was prepared by stirring a mixture of ethanol (200 ml) and sodium (3 g) for 30 min under nitrogen. To the solution was added a solution of iodobenzene (50 mmol) and thiophenol (50 mmol) in ethanol (50 ml), and then $Pd(PPh_3)_4$ (0.5 mmol). After refluxing the solution for 4 h with stirring, ethanol was driven off with a rotary evaporator. From the residue the product was extracted into pentane. After washing with water, usual work-up and distillation gave diphenyl sulfide (110—113 °C/5 mmHg) in 88% yield. Similarly the reaction with *t*-butyl mercaptane afforded *t*-butyl phenyl sulfide (85—90 °C/20 mmHg) in 65% yield.

Reaction with Triphenylphosphine. A solution of aryl iodide (2 mmol), triphenylphosphine (2 mmol), and $Pd(PPh_3)_4$ (0.08 mmol) in benzene (3 ml) was placed in a reaction tube. The tube was evacuated and sealed, and then immersed in a bath heated at 100 °C. After 18 h, aryl triphenylphosphonium salt crystallized from the mixture was filtered and washed with benzene. Yield and melting point observed are shown in Table 3.

Competitive Reactions. *Reactions of PhS^- with Large Excess of Aryl Iodides*: An equimolar mixture of iodobenzene (15 mmol) and substituted iodobenzene (15 mmol) was allowed to react with thiophenol (1 mmol) in the presence of alkoxide (2 mmol) and $Pd(PPh_3)_4$ (0.02 mmol) in ethanol (30 ml) at 100 °C for 18 h. From the molar ratio of the produced sulfides relative reactivity of the aryl iodide, k_{ArI}/k_{PhI} was estimated by the following equation.

$$k_{ArI}/k_{PhI} = [ArSPh]_f/[PhSPh]_f$$

Reaction of PhI with PhS^- and t-BuS^-: A solution of iodobenzene (0.5—1.0 mmol), thiophenol (5—10 mmol), 2-methyl-2-propanethiol (2 mmol), alkoxide (20 mmol), and $Pd(PPh_3)_4$ (0.02 mmol) in ethanol (20 ml) was refluxed for 1 h. Amounts of the produced sulfides were determined by GLC method. The relative reactivity $k_{t\text{-}BuS^-}/k_{PhS^-}$ was calculated by the following equation,

$$\frac{k_{t\text{-}BuS^-}}{k_{PhS^-}} = \log\frac{[t\text{-BuSH}]_i - [t\text{-BuSPh}]_f}{[t\text{-BuSH}]_i} \Big/ \log\frac{[PhSH]_i - [Ph_2S]_f}{[PhSH]_i}$$

where the suffixes i and f indicate the initial and final concentrations, respectively.

Reaction of $PhPdI(PPh_3)_2$ with PhS^- and t-BuS^-: Instead of iodobenzene and $Pd(PPh_3)_4$ in the above competitive experiment, $PhPdI(PPh_3)_2$ (0.5 mmol) was used.

The results of these competitive reactions were summarized in Table 2.

References

1) J. F. Bunnett, *J. Chem. Educ.*, **51**, 312 (1974) and the references cited therein.

2) K. Takagi, T. Okamoto, Y. Sakakibara, and S. Oka, *Chem. Lett.*, **1973**, 471; A. Sekiya and N. Ishikawa, *ibid.*, **1975**, 277.

3) L. Cassar, *J. Organomet. Chem.*, **93**, 253 (1975); H. A. Dieck and F. R. Heck, *ibid.*, **93**, 259 (1975); K. Sonogashira, Y. Tohda, and N. Hagiwara, *Tetrahedron Lett.*, **1975**, 4467.

4) C. B. Ziegler, Jr., and R. Heck, *J. Org. Chem.*, **43**, 2941, 2947, 2949, 2952 (1978).

5) Mg: K. Tamao, K. Sumitani, and M. Kumada, *J. Am. Chem. Soc.*, **94**, 4374 (1972); K. Tamao, K. Sumitani, Y. Koso, M. Zenbayashi, A. Fujioka, S. Kodama, I. Nakajima, A. Minato, and M. Kumada, *Bull. Chem. Soc. Jpn.*, **49**, 1958 (1976); R. J. P. Corrin and J. P. Masse, *J. Chem. Soc., Chem. Commun.*, **1972**, 144; Zn: A. O. King, and E. Negishi, *J. Org. Chem.*, **43**, 358 (1978), **42**, 1821 (1978); Al: S. Baba and E. Negishi, *J. Am. Chem. Soc.*, **98**, 6729 (1976); E. Negishi, and S. Baba, *J. Chem. Soc., Chem. Commun.*, **1976**, 596; Si: H. Matsumoto, S. Nagashima, K. Yoshihiro, and Y. Nagai, *J. Organomet. Chem.*, **85**, C1 (1975); Sn: M. Kosugi, K. Sasazawa, Y. Shimizu, and T. Migita, *Chem. Lett.*, **1977**, 301; B: N. Miyaura, K. Yamada, T. Yano, T. Yanagi, and A. Suzuki, 26th Symposium on Organometallic Chemistry Japan, **1979**, p. 199.

6) M. F. Semmelhack, R. O. Staraffer, and T. D. Rogerson, *Tetrahedron Lett.*, **1973**, 4519.

7) K. Takagi, N. Hayama, and T. Okamoto, *Chem. Lett.*, **1978**, 191.

8) M. Kosugi, T. Shimizu, and T. Migita, *Chem. Lett.*, **1978**, 13.
9) S. Murahashi, M. Yamamura, K. Yanagisawa, N. Mita, and K. Kondo, *J. Org. Chem.*, **44**, 2408 (1979).
10) J. F. Bunnett and X. Creary, *J. Org. Chem.*, **39**, 3173, 3611 (1974).
11) P. Fitton and E. A. Rick, *J. Organomet. Chem.*, **28**, 287 (1971).
12) J. K. Kochi, *Acc. Chem. Res.*, **7**, 351 (1974); I. H. Elson, D. G. Morell, and J. K. Kochi, *J. Organomet. Chem.*, **84**, C7 (1975).
13) R. G. Pearson, H. Sobel, and J. Songstad, *J. Am. Chem. Soc.*, **90**, 319 (1968).
14) *Inorg. Synth.*, Vol. XIII, 131.

The Chloroiodination of Deactivated Olefins with Antimony(V) Chloride–Iodine and Iodine Monochloride

Sakae UEMURA,* Shin-ichi FUKUZAWA, Masaya OKANO, and Seiji SAWADA**

Institute for Chemical Research, Kyoto University, Uji, Kyoto 611

** *Department of Chemistry, Kyoto University of Education, Kyoto 612*

(Received October 13, 1979)

By the reactions of olefins with an equimolar mixture of $SbCl_5$ and I_2 in carbon tetrachloride, various chloroiodoalkanes are obtained in fair to good yields. This method is applicable to various deactivated olefins, the reactions of which do not proceed by the reported method using a mixture of $CuCl_2$ and I_2. Iodine monochloride can aslo be used for this reaction, but in this case both the yield and the regiospecificity of the products are sometimes inferior.

During the course of the study of a facile method for preparing β-chloro-L-alanine or its analogue, a useful "suicide" substrate of current interest,[1] it became necessary for us to prepare α-iodo-β-chloro carboxylic acid or its ester as a precursor, which may be obtained by the chloroiodination of the corresponding α,β-unsaturated carboxylic acid or its ester. Baird *et al.*[2] have reported an efficient chloroiodination of olefins by using $CuCl_2$ and I_2 to produce chloroiodoalkanes, which have not generally been prepared by

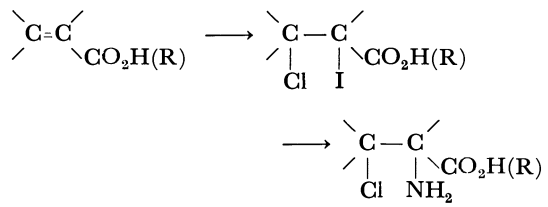

the addition of preformed iodine monochloride to olefins. The scope of this reaction is, however, restricted to olefins which have electron-donating substituents, such as alkyl and acetoxyl groups. It has previously been reported that a facile bromochlorination of olefins occurred with a mixture of antimony(V) chloride and bromine; this method is applicable to various deactivated olefins, such as fumaric and maleic esters and 1,2-dichloroethylene.[3] We have now found that a mixture of antimony(V) chloride and iodine can effect the chloroiodination of such deactivated olefins in carbon tetrachloride. It has also been shown that commercial iodine monochloride itself works as a chloroiodinating agent for such olefins, although the yield and the selectivity of the products were sometimes lower than with the $SbCl_5$–I_2 system. As one of a series of our studies of halogenation by the use of antimony(V) chloride,[3,4] we wish here to describe the details of the chloroiodination of olefins by using $SbCl_5$–I_2.

Results and Discussion

The reactions of activated olefins, such as 1-hexene, cyclohexene, and vinyl acetate, with an equimolar mixture of $SbCl_5$ and I_2 in carbon tetrachloride at the reflux temperature gave the corresponding chloroiodoalkanes in good to high yields, as in the cases with $CuCl_2$ and I_2. The stoichiometry of the reaction is given by Eq. 1. Here, the generation of two moles

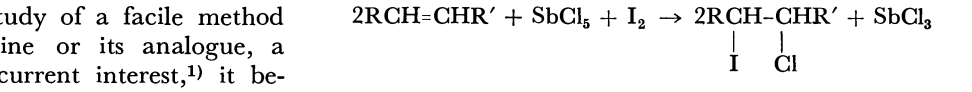

(1)

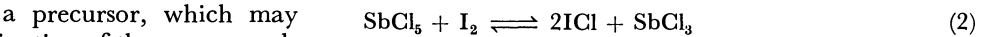

(2)

of ICl can be explained by assuming Eq. 2, as in the case of bromochlorination with $SbCl_5$ and Br_2.[3]

The application of this reaction to several deactivated olefins, such as α,β-unsaturated esters and nitriles, resulted in the formation of the expected chloroiodoalkanes in fair to good yields; this is in sharp contrast to the reaction with $CuCl_2$–I_2 system, which did not afford those products from several α,β-unsaturated esters under similar reaction conditions. Some typical results are shown in Table 1. As can be seen from the table, the yields of the products increased when the reaction temperature was raised in the case of α,β-unsaturated esters, while in the case of α,β-unsaturated nitriles the reaction at room temperature gave the most satisfactory results, though the yield was still low. In the latter case, the tarry compounds became almost the sole products at the reflux temperature, while only a trace amount of product was obtained at 0—5 °C.

Iodine monochloride is generally known as an iodinating agent for activated aromatic compounds, and there seem to have been no thorough studies of the chloroiodination of olefins by this reagent.[5] There is even a description in the literature[2] of how chloroiodoalkanes have not generally been prepared by the addition of iodine monochloride to olefins because of the dissociable nature of ICl, which frequently leads to high yields of unstable diiodides, along with small amounts of the desired product. However, when we treated the above olefins with commercial iodine monochloride, the desired chloroiodoalkanes were obtained; the yields of the products were even better for some olefins than those in the $SbCl_5$–I_2 system in the reaction at room temperature. The results are also listed in Table 1. When styrene was used as the substrate, chloroiodination proceeded with iodine monochloride, while (1-chloroethyl)benzene and polymeric tars were obtained by the use of $SbCl_5$–I_2 under the several sets of conditions we employed. It has previously been reported[2] that (1,2-dichloroethyl)benzene was the sole product in the reaction of styrene with $CuCl_2$–I_2. The isomer distributions of the products obtained

Table 1. Chloroiodination of various olefins in carbon tetrachloride

Olefin(25 mmol); halogenating agent, $SbCl_5$ or $CuCl_2$(12.5 mmol)+I_2(12.5 mmol), ICl(25 mmol); solvent(50 ml), CCl_4.

Olefin	Temp °C	Time h	Product	Yield/%[a] $SbCl_5+I_2$	ICl	$CuCl_2+I_2$
CH_2=$CHCO_2Et$	25	1	$CH_2ClCHICO_2Et$ (I) $CH_2ICHClCO_2Et$ (II)	31[b]	53[b]	0
CH_2=$CHCO_2Et$	76	1	$CH_2ClCHICO_2Et$ (I) $CH_2ICHClCO_2Et$ (II)	86[c,d]	69[e]	trace
trans-CH_3CH=$CHCO_2Me$	25	1	$CH_3CHClCHICO_2Me$ (I) $CH_3CHICHClCO_2Me$ (II)	51[g]	80[f]	0
trans-CH_3CH=$CHCO_2Me$	76	1	$CH_3CHClCHICO_2Me$ (I) $CH_3CHICHClCO_2Me$ (II)	63[g]		
CH_2=CHCN	25	1	$CH_2ClCHICN$	10	trace	
CH_2=$C(CH_3)CN$	25	1	$CH_2ClCI(CH_3)CN$ (I) $CH_2ICCl(CH_3)CN$ (II)	12[h]	8[h]	
cis-EtOOCCH=CHCOOEt	25	1	*threo*-EtOOCCHICHClCOOEt	13	18	
cis-EtOOCCH=CHCOOEt	76	3	*threo*-EtOOCCHICHClCOOEt	50	33	
trans-EtOOCCH=CHCOOEt	25	1	*erythro*-EtOOCCHICHClCOOEt	6	10	
trans-EtOOCCH=CHCOOEt	76	3	*erythro*-EtOOCCHICHClCOOEt	60	11	0
PhCH=CH_2	25	2	$PhCHClCH_2I$		79[e]	
PhCH=CH_2	25	16	$PhCHClCH_3$	34[e,i]		
n-C_4H_9CH=CH_2	30	0.2	*n*-$C_4H_9CHClCH_2I$ (I) *n*-$C_4H_9CHICH_2Cl$ (II)	30[e,j]	75[k]	91[h,l]
Cyclohexene	76	0.2	*trans*-1-Chloro-2-iodocyclohexane	94[e,m]		95[l]
CH_2=CHOAc	55	0.2	$CH_2ICH(Cl)OAc$	87[e]		88[l]

a) Determined by GLC unless otherwise stated. b) Ratio of I : II not known. c) Isolated yield. d) I : II=82 : 18. e) I : II=75 : 25. f) I : II=92 : 8. g) I : II=100 : 0. h) I : II=80 : 20. i) No $PhCHClCH_2I$; tarry products were formed. j) I : II=73 : 27. k) I : II=66 : 34. l) Ref. 2. m) Ref. 3.

from unsymmetrical olefins which were determined by ^{13}C NMR and/or GLC showed that I^+ attacked the electron-rich carbon solely or predominantly, as had been expected. For example, the chloroiodination of ethyl acrylate, methyl crotonate, acrylonitrile, and methacrylonitrile with $SbCl_5$–I_2 gave the corresponding chloroiodoalkanes with a selectivity of more than 80%. As to the isomer distributions of the products, there are not so many differences between the reaction with $SbCl_5$–I_2 and that with ICl, though the selectivity is slightly higher in the case of the $SbCl_5$–I_2 system. The reaction with $SbCl_5$–I_2 seems to involve the *in situ* formation of ICl by Eq. 2, followed by the attack of the ICl thus formed on olefins. Here, iodine monochloride may be activated by the $SbCl_5$ or $SbCl_3$ present in the reaction system to give more polarized species, as has been clarified in the chloroiodination of acetylenes with the same system.[4b]

Experimental

The GLC analyses were conducted on a Shimadzu 4CMPF apparatus, using Silicone DC QF-1 (1 and 3 m) and EGSS-X (1 m) columns (carrier gas, N_2). The ^1H NMR spectra were recorded with a JEOL MH-100 (100 MHz) and a Varian EM-360 (60 MHz) spectrometer in CCl_4, using TMS as the internal standard. The ^{13}C NMR spectra were recorded in the pulsed Fourier transform mode on a JEOL FX-100 spectrometer operating at 25.15 MHz in $CDCl_3$, using TMS as the internal standard.

Materials. All the starting materials—olefins, $SbCl_5$, $SbCl_3$, $CuCl_2$, I_2, iodine monochloride, and CCl_4—were commercially available and were used without further purification. Chloroiodoalkanes from cyclohexene, vinyl acetate, and 1-hexene were confirmed by a comparison of the ^1H NMR spectra and retention times on GLC with those of authentic samples prepared by the reported method.[2] All the other chloroiodoalkanes were isolated by distillation. Commercial 1-phenylethyl chloride was used as an authentic sample for GLC and ^1H NMR.

Syntheses of Chloroiodoalkanes. A typical experimental procedure and the spectral data and boiling points of the products are shown below.

Chloroiodination of Ethyl Acrylate with Antimony(V) Chloride–Iodine. To a dark brown, homogeneous solution of $SbCl_5$ (7.5 g, 25 mmol) and I_2 (6.3 g, 25 mmol) in CCl_4 (100 ml), ethyl acrylate (5.0 g, 50 mmol) was added, drop by drop, at the reflux temperature over a 10-min period, during which the color of the solution turned to purple. After stirring for 1 h, the reaction mixture was treated with water, and the white-to-pale yellow inorganic precipitate thus formed was removed by filtration. The CCl_4 layer was separated from the aqueous one, washed with aq $Na_2S_2O_3$, and dried over Na_2SO_4, and the solvent was evaporated. A liquid fraction boiling at 105 °C/20 mmHg (11.2 g) was collected; it consisted of ethyl 3-chloro-2-iodopropionate(I) and ethyl 2-chloro-3-iodopropionate(II) (I:II=82:18). The structural determination was carried out by means of ^1H and ^{13}C NMR and elemental analysis, while the isomer ratio was determined by ^{13}C NMR by comparing the peak intensities of the ethyl-group carbons of the two compounds. Found: C, 23.10; H, 2.89%. Calcd for $C_5H_8O_2ClI$: C, 22.88; H, 3.07%. ^1H NMR (CCl_4): δ 1.3 (t, 3H), 3.25—4.80 (m, 5H). ^{13}C NMR ($CDCl_3$): δ for I, 13.6 ($\underline{CH_3}$,

q), 16.9 (CHI, d), 44.7 (CH_2Cl, t), 62.1 (OCH_2, t), 168.7 (CO_2, s); δ for II, 2.5 (CH_2I, t), 13.9 (CH_3, q), 54.8 (CHCl, d), 62.4 (OCH_2, t), 168.7 (CO_2, s).

Methyl 3-Chloro-2-iodobutanoate(I) and Methyl 2-Chloro-3-iodobutanoate(II). Bp of I, 63—66 °C/3 mmHg. ^{1}H NMR of I (CCl_4): δ 1.7—1.9 (m, 3H), 3.73 (s, 3H), 4.17—4.45 (m, 2H). ^{13}C NMR ($CDCl_3$): δ for I, 24.6 (CH_3, q), 26.4 (CHI, d), 52.9 (OCH_3, q), 56.1 (CHCl, d), 169.4 (CO_2, s); δ for II, 22.1 (CHI, d), 24.6 (CH_3, q), 52.9 (OCH_3, q), 61.9 (CHCl, d), 169.4 (CO_2, s). Found: C, 23.17; H, 3.05%. Calcd for $C_5H_8O_2ClI$: C, 22.88; H, 3.07%.

3-Chloro-2-iodopropionitrile. Bp 95 °C/10 mmHg. ^{1}H NMR ($CDCl_3$): δ 3.87 (d, 1H, CH_2Cl), 3.90 (d, 1H, CH_2Cl), 4.52 (dd, 1H, CHI). ^{13}C NMR ($CDCl_3$): δ −5.4 (CHI, d), 45.2 (CH_2Cl, t), 116.9 (CN, s).

3-Chloro-2-iodo-2-methylpropionitrile(I) and 2-Chloro-3-iodo-2-methylpropionitrile(II). Bp of a mixture of I and II (I:II=80:20 by GLC), 40—44 °C/5 mmHg. ^{1}H NMR (CCl_4): δ 2.08 (s, CH_3 for II), 2.30 (s, CH_3 for I), 3.62 and 3.81 (d, J=10 Hz, CH_2 for II), 3.86 and 4.14 (d, J=12 Hz, CH_2 for I). ^{13}C NMR ($CDCl_3$): δ for I, 13.2 (s, quarternary C), 30.7 (q, CH_3), 52.9 (t, CH_2Cl), 119.8 (s, CN); δ for II, 11.7 (t, CH_2I), 30.0 (q, CH_3), 68.2 (s, quarternary C), 117.4 (s, CN).

Diethyl threo- *and* erythro-*2-chloro-3-iodosuccinate.* *threo*-Isomer: Bp 84 °C/3 mmHg. ^{1}H NMR (CCl_4): δ 1.3 (t, 6H), 4.18 (q, 4H), 4.4 (d, 1H), 4.8 (d, 1H). *erythro*-Isomer: Bp 100 °C/2 mmHg. ^{1}H NMR (CCl_4): δ 1.27 (t, 3H, CH_3), 1.30 (t, 3H, CH_3), 4.27 (q, 2H, CH_2), 4.30 (q, 2H, CH_2), 4.60—4.70 (m, 2H, CHCl and CHI).

(1-Chloro-2-iodoethyl)benzene. To a brown solution of iodine monochloride (4.05 g, 25 mmol) in CCl_4 (70 ml), we added styrene (2.61 g, 25 mmol) at 20 °C, after which the mixture was stirred for 2 h. After a usual work-up procedure, distillation afforded the product; 5.3 g (79% yield); bp 113 °C/6 mmHg, mp 41 °C (lit,[6] mp 46 °C). ^{1}H NMR ($CDCl_3$): δ 3.67 (d, 1H, CH_2I), 3.69 (d, 1H, CH_2I), 5.00 (dd, 1H, CHCl), 7.3 (m, 5H).

References

1) See, for example, "Enzyme-Activated Irreversible Inhibitors," ed by N. Seiler, M. J. Jung, and J. Koch-Weser, Elsevier/North-Holland Biomedical Press, Amsterdam (1978).

2) W. C. Baird, Jr., J. H. Surridge, and M. Buza, *J. Org. Chem.*, **36**, 2088, 3324 (1971).

3) S. Uemura, A. Onoe, and M. Okano, *Bull. Chem. Soc. Jpn.*, **47**, 143 (1974).

4) See, for example, a) S. Uemura, A. Onoe, and M. Okano, *Bull. Chem. Soc. Jpn.*, **47**, 147 (1974); S. Uemura, A. Onoe, H. Okazaki, and M. Okano, *ibid.*, **48**, 619 (1975); b) S. Uemura, H. Okazaki, A. Onoe, and M. Okano, *J. Chem. Soc., Perkin Trans. 1*, **1979**, 548, and the references therein.

5) See, for example, P. B. D. de la Mare, "Electrophilic Halogenation," Cambridge University Press, Cambridge (1976), pp. 161—166; L. F. Fieser and M. Fieser, "Reagents for Organic Synthesis," Wiley, New York (1967), p. 502.

6) H. Ingle, *J. Soc. Chem. Ind.*, **21**, 587 (1902).

Photolysis of Dibenzoyl Peroxide under Direct and Singlet Sensitized Irradiations. Mechanism for the Formation of the Geminate Product

Akihide KITAMURA, Hirochika SAKURAGI, Masayuki YOSHIDA,† and Katsumi TOKUMARU*

Department of Chemistry, The University of Tsukuba, Sakura-mura, Ibaraki 305

† *Department of Chemistry, Faculty of Science, The University of Tokyo, Hongo, Bunkyo-ku, Tokyo 113*

(Received October 16, 1979)

Attempts have been made to elucidate the mechanism for the efficient production of phenyl benzoate, the geminate product, from direct and singlet sensitized irradiations of dibenzoyl peroxide in solution. It is concluded that these irradiations produce a reactive state of the peroxide which can undergo two-bond cleavage of the O–O and C(α)–C(carbonyl) bonds to give a phenyl–benzoyloxy radical pair in a solvent cage, followed by the recombination of the component radicals to give the geminate product or by their diffusion out of the solvent cage to give diffusion products.

Although direct or aromatic hydrocarbon-sensitized photolysis[1-8] of dibenzoyl peroxide (BPO) has been shown to proceed through the singlet excited pathway,[9-15] some aspects of the reaction remain uncertain. Previously we reported[10] that direct photolysis and singlet sensitized decomposition of BPO give a noticeable amount of phenyl benzoate in contrast with triplet sensitization[4,8,16] and thermal decomposition[17,18] which give only a low yield of the ester. It has been shown that phenyl benzoate arises from the geminate recombination of benzoyloxy radicals and phenyl radicals on the basis of its noticeable formation from photolysis of BPO in toluene, *p*-xylene, and chlorobenzene[5] as well as CIDNP results.[11-15]

The efficient formation of the geminate product in the photolysis of BPO cannot be accounted for by the usual cleavage of the peroxide bond to give a pair of benzoyloxy radicals as results from thermolysis,[17,18] because benzoyloxy radicals decarboxylate too slowly[19] to afford a benzoyloxy–phenyl radical pair within the lifetime of the primary solvent-cage. The noticeable formation of the geminate product can be explained by a mechanism in which a significant fraction of excited peroxide molecules decomposes by either concerted or unusually rapid stepwise cleavage of the O–O and C(α)–C(carbonyl) bonds to give benzoyloxy–phenyl radical pairs followed by the cage recombination (Eq. 1).[3,8,20]

$$(PhCO_2)_2 \xrightarrow{h\nu} \overline{PhCO_2\cdot + \cdot OCOPh} \quad \overline{PhCO_2\cdot + Ph\cdot + CO_2} \rightarrow PhCO_2Ph \qquad (1)$$

Lemaire's group[8] investigated direct photolysis of BPO in solution, particularly in view of wavelength dependence of its quantum yield, and postulated that benzoyloxy radicals would be formed in the vibrationally excited state on 313-nm light irradiation, and that irradiation with shorter wavelength light would directly generate phenyl radicals which, in high concentrations of BPO, might attack the peroxide to give phenyl benzoate and benzoyloxy radicals.

On the other hand, McBride *et al.*,[21] by ESR spectroscopic investigation, reported that UV-irradiation of crystalline acetyl benzoyl peroxide at 64 K gave benzoyloxy–methyl radical pairs, and that subsequent irradiation with visible light led to the decarboxylation of the benzoyloxy radicals to give phenyl–methyl radical pairs, with the highest efficiency on irradiation with 750-nm light. The photo-induced decarboxylation of benzoyloxy radicals could explain the noticeable formation of phenyl benzoate in the photolysis of BPO.

In the present paper we report some features of the photolysis of BPO and attempts to elucidate the mechanisms for the formation of the geminate product. The present results will show that the simultaneous two-bond cleavage plays an important role in the noticeable formation of the geminate product, and that concurrent irradiation of visible light does not remarkably contribute to the formation of the geminate product.

Results

Thermal and Photochemical Decomposition of Substituted Dibenzoyl Peroxides. Dibenzoyl, bis(4-methoxybenzoyl), bis(4-methylbenzoyl), and bis(4-chlorobenzoyl) peroxides ($ArCO_2OCOAr$, 0.03 M) were thermally decomposed at 80, 90, and 100 °C and photolyzed at room temperature without any sensitizer in benzene and with chrysene (0.002 M) as a singlet sensitizer in benzene until the peroxides were completely decomposed. The resulting geminate products, $ArCO_2Ar$, were determined by GLPC analysis. The results are summarized in Table 1.[22]

CIDNP in Photolysis of BPO. In order to clearly observe a CIDNP spectrum due to the geminate product, deuterated BPO was employed to eliminate

Table 1. Yield of substituted phenyl benzoates in thermal and photochemical decompositions of bis(4-substituted benzoyl) peroxides

Mode of decomposition	Yield of substituted phenyl benzoate, $ArCO_2Ar$ (mol/mol-peroxide)			
	Ar = $MeOC_6H_4$	MeC_6H_4	C_6H_5	ClC_6H_4
Direct photolysis	0.047	0.072	0.13	0.074
Chrysene sensitized photolysis	0.037	0.056	0.12	0.044
Thermolysis at 80 °C	0.011	0.006	0.022	0.005
Thermolysis at 90 °C	0.011	0.006	0.023	0.004
Thermolysis at 100 °C	0.010	0.007	0.025	0.006

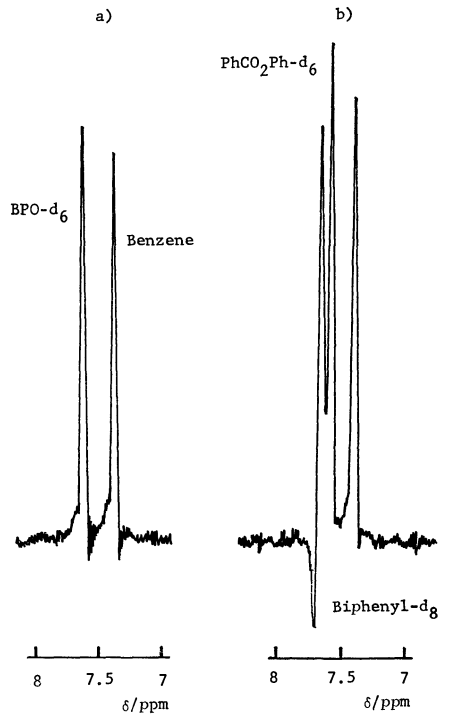

Fig. 1. CIDNP spectrum of BPO-d_6 in benzene-d_6 before irradiation (a) and during irradiation (b).

nuclear spin-spin couplings between aromatic ring protons and lengthen spin-lattice relaxation times of the products. When BPO-2,2′,4,4′,6,6′-d_6 was photolyzed in benzene-d_6 at room temperature with a 1 kW high pressure mercury lamp in the probe of an NMR spectrometer, a very clear polarized spectrum was observed as shown in Fig. 1. The enhanced absorption represents the meta protons on the phenoxyl segment of the geminate product, phenyl-2,4,6-d_3 benzoate-2,4,6-d_3, and the emission is assigned to biphenyl-2,2′,3,4,4′,5,6,6′-d_8. Irradiation of a solution of BPO-d_6 in the presence of naphthalene or chrysene in benzene-d_6 gave the same polarized NMR spectrum as the direct irradiation.

Sensitized Decomposition of BPO in the Presence of a Radical Scavenger. BPO (0.02 M) was irradiated with 366-nm light at room temperature in a mixed solvent consisting of varying fractions of styrene and benzene in the presence of chrysene (0.002 M) as a singlet sensitizer until the peroxide was completely decomposed (3.75 h). The yields of phenyl benzoate were determined by GLPC analysis to be 0.10, 0.10, 0.07, and 0.09 mol per 1 mol of the peroxide at the concentrations of styrene in 0, 1.74, 4.35, and 6.09 M, respectively.

Trapping of Carbon Dioxide in Thermal and Photochemical Decompositions of BPO in the Presence of a Radical Scavenger. In a mixture of varying fractions of benzene and styrene, BPO (0.02 M) was thermally decomposed at 80 °C and photolyzed at room temperature with a 400 W high pressure mercury lamp through a Pyrex wall. The resulting carbon dioxide was absorbed with an Ascarite tube and determined by gravimetry. The results are depicted in Fig. 2. The yields of carbon dioxide were suppressed to approach limiting values

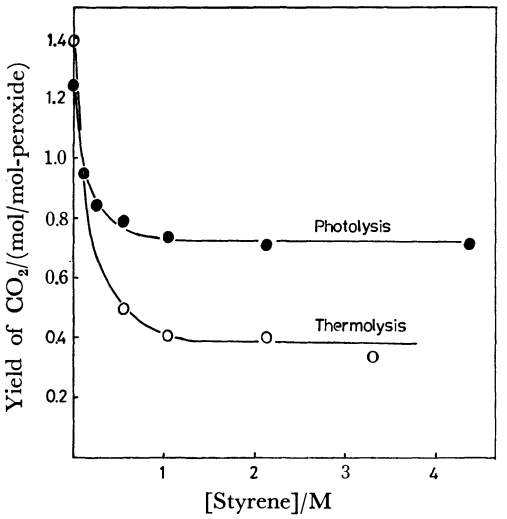

Fig. 2. Change of carbon dioxide yield in thermolysis and photolysis of BPO with concentration of styrene in benzene.

as the fraction of styrene increased in both photolysis and thermolysis. The limiting yields, however, are different between the photolysis (*ca.* 0.7 mol per 1 mol of the peroxide) and the thermolysis (*ca.* 0.3 mol).

Spin Trapping in Decomposition of BPO. When a solution of BPO (0.01 M) in benzene containing *N*-benzylidene-*t*-butylamine oxide (0.1 M) was irradiated in the cavity of an ESR spectrometer at room temperature with a 400 W high pressure mercury lamp for several minutes, signals due to both of the benzoyloxy spin adduct, *N*-*t*-butyl-α-benzoyloxybenzylaminyloxyl ($PhCO_2$–SA, a_N=14.0 G),[23] and the phenyl spin adduct, *N*-*t*-butyldiphenylmethanaminyloxyl (Ph-SA, a_N=15.5 G),[23] were observed in the ESR spectrum. The ratio of these spin adducts, $PhCO_2$–SA/Ph–SA, was determined to be *ca.* 5.6. This value was not varied with irradiation time (5—10 min). On the other hand, heating of a benzene solution of the same composition as above at 40 °C for 8 min gave only the signals due to the benzoyloxy spin adduct.

Effects of Singlet Excitation Energy of Sensitizers on the Geminate Product Yield. BPO (0.03 M) was irradiated in benzene at room temperature in the presence of aromatic hydrocarbons (1.3×10^{-4}—1.8×10^{-2} M) as sensitizers with a 1 kW high pressure mercury lamp through a Pyrex wall. The concentrations of the sensitizers were chosen so that the sensitizers absorbed more than 95% of incident light at 313 nm. Table 2 summarizes the yields of the products determined by GLPC analysis. The yield of phenyl benzoate tends to increase with increasing singlet excitation energy of the sensitizers.

Effects of Longer Wavelength Light on the Product Yields. In order to explore the contribution of the light-induced decarboxylation of benzoyloxy radicals to the formation of the geminate and diffusion products, in the course of the thermal decomposition, UV-irradiation, and nitrogen laser irradiation of BPO (0.03 M) in benzene, the solutions were concurrently irradiated with light of wavelengths longer than 400 nm. In this wavelength region neither BPO nor chrysene has

Table 2. Yields of products in hydrocarbon-sensitized photolysis of dibenzoyl peroxide (0.03 M) in benzene[a)]

Sensitizer	Singlet excitation energy of sensitizer[b)] /kcal mol^{-1}	Concentration of sensitizer /M	Yield (mol/mol-peroxide)		
			$PhCO_2Ph$	$PhCO_2H$	Ph-Ph
Naphthalene	91	1.8×10^{-2}	0.16	0.35	0.22
Triphenylene	83	6.7×10^{-3}	0.15	0.33	0.22
Fluoranthene	80	5.0×10^{-4}	0.10	0.31	0.22
Chrysene[c)]	79	2.0×10^{-3}	0.12		
Pyrene	77	1.3×10^{-4}	0.10	0.44	0.29
Anthracene	75	1.7×10^{-3}	0.091	0.46	0.27
9,10-Diphenylanthracene	70	1.2×10^{-3}	0.096	0.41	0.24
Perylene	65	3.2×10^{-3}	0.063	1.5	0.16

a) Irradiation was carried out through a Pyrex wall unless otherwise noted. b) S. L. Murov, "Handbook of Photochemistry," Marcel Dekker, Inc., New York, N. Y. (1973). c) Irradiated at 366 nm.

Table 3. Yields of products in thermal and photochemical decomposition of BPO (0.03 M) in benzene with concurrent irradiation of a tungsten-bromine lamp

Light source	Yield (mol/mol-peroxide)		
	$PhCO_2Ph$	$PhCO_2H$	Ph-Ph
HPML[a)]	0.13	0.45	0.23
HPML[a)]+BL[b)]	0.11	0.44	0.30
Thermal (80 °C)	0.02	0.31	0.26
Thermal (80 °C)+BL[b)]	0.02	0.22	0.33
N_2 Laser[c)]	0.16	0.45	0.30
N_2 Laser[c)]+BL[b)]	0.16	0.45	0.35

a) HPML stands for a high pressure mercury lamp. b) BL stands for a tungsten-bromine lamp. c) Sensitized with chrysene (6×10^{-3} M).

Table 4. Yields of products in photolysis of BPO with 313-nm light of varying intensity

Relative light intensity	Yield (mol/mol-peroxide)		
	$PhCO_2Ph$	$PhCO_2H$	Ph-Ph
0.23	0.21	0.51	0.33
0.37	0.17	0.48	0.42
0.58	0.17	0.48	0.44
0.61	0.08	0.47	0.29
0.68	0.17	0.45	0.37
1	0.14	0.45	0.30

any absorption band. Table 3 summarizes the yields of the products determined by GLPC analysis. The yield of biphenyl seems to be increased by irradiation of the longer wavelength light; however, no remarkable effects on the yield of phenyl benzoate are observed.

Effects of Light Intensity on the Product Yields. BPO (0.03 M) in benzene was irradiated with 313-nm light of varying intensity. The yields of the products determined by GLPC analysis are summarized in Table 4, which shows that the increase of light intensity in nearly five times does not remarkably affect the distribution of the products, although the yields of phenyl benzoate and benzoic acid tend to be slightly reduced with increasing light intensity.

In order to investigate the effect of strong laser pulses on the geminate product formation, an equimolar mixture of BPO (0.015 M) and deuterated BPO, $(C_6D_5CO_2)_2$, (0.015 M) was irradiated in toluene with chrysene with a nitrogen laser at room temperature. Mass spectrometric examination of the resulting ester showed that only the undeuterated ester, $C_6H_5CO_2C_6H_5$, and the ester deuterated on both of the aromatic rings, $C_6D_5CO_2C_6D_5$, were produced but even a trace amount of the ester with one deuterated aromatic ring, $C_6D_5CO_2C_6H_5$ or $C_6H_5CO_2C_6D_5$, was not produced.

Discussion

Production of phenyl benzoate from decomposition of dibenzoyl peroxide (BPO) in solutions under nitrogen remains in a low yield from thermolysis[17,18] but is noticeable from direct and singlet sensitized photolyses.[2,5,7,10] As Table 1 indicates, substituted dibenzoyl peroxides behave like unsubstituted BPO. Thus, the former peroxides also gave geminate products in higher yields in photolyses than in thermolyses. These findings suggest that the direct and singlet sensitized photolyses effectively produce benzoyloxy–phenyl radical pairs to give phenyl benzoate.

Formation of phenyl benzoate as the geminate product is further confirmed by the effect of styrene and CIDNP. As described above, increasing fractions of styrene added in the photolyzing system did not show any significant effect on the yield of phenyl benzoate. In addition, in CIDNP (Fig. 1), the sharp enhanced absorption due to the meta protons on the phenoxyl segment of the resulting phenyl-d_3 benzoate-d_3 indicates that the polarization must be due to phenyl-d_3 radicals which have escaped from the initial polarizing cage and retained some polarization through their recombination with benzoyloxy radicals.[13] This observation accords well with the prediction by Kaptein's[24] and Closs's[25] rules applied to the polarizing pair of benzoyloxy and phenyl radicals.

The effect of styrene and a spin trap revealed the effective decarboxylation taking place during the pho-

tolysis. Figure 2 indicates that as the fraction of styrene increases, the production of carbon dioxide is rapidly suppressed to approach limiting yields in both photolysis and thermolysis. The limiting yield is much higher in the photolysis (*ca.* 0.7 mol per 1 mol of the peroxide) than in the thermolysis (*ca.* 0.3 mol).

On decomposition of BPO in the presence of the spin trap, *N*-benzylidene-*t*-butylamine oxide, both phenyl spin adduct and benzoyloxy spin adduct were obtained in the photolysis in a ratio of 1:5.6, whereas only the benzoyloxy spin adduct was obtained in the thermolysis. The extent of the decarboxylation under spin trapping conditions is estimated to be $1/(1+5.6)=15\%$ and this figure is lower than that estimated from scavenging by styrene to measure carbon dioxide, $0.71/2=35\%$. This difference probably reflects the different ability between styrene and the nitrone to trap benzoyloxy radicals.

From the results mentioned above, it is obvious that the photolysis of BPO produces certain amounts of phenyl radicals and carbon dioxide without the intervention of benzoyloxy radicals of usual lifetimes which would be effectively scavenged by styrene or the spin trap. For the efficient formation of the benzoyloxy–phenyl radical pairs the following three possibilities can be envisaged.

The first possibility is a simultaneous two-bond cleavage of the peroxide in which the singlet excitation energy will be converted to vibrational energy enough to break both the oxygen-oxygen and carbon(α)-carbon(carbonyl) bonds giving simultaneously a benzoyloxy radical, a phenyl radical, and a carbon dioxide molecule (one-photon simultaneous process, Eq. 2). Direct excitation and excited singlet sensitizers seem to provide sufficient energies for the peroxide bond cleavage and the decarboxylation of benzoyloxy radicals in the thermal processes, *ca.* 31[26] and 13[19] kcal mol^{-1}, respectively.

The second possibility is a rapid successive two-bond cleavage in which the photolysis gives vibrationally[8] or electronically excited benzoyloxy radicals followed by their rapid decarboxylation within the lifetime of the solvent cage (one-photon successive process, Eq. 3).

A two-photon process is the third possibility where benzoyloxy radicals once formed are excited by continuing irradiation and decarboxylate within the lifetime of the solvent cage (two-photon successive process, Eq. 4).

$$\mathrm{PhCO_2OCOPh} \xrightarrow{h\nu} \overline{\mathrm{PhCO_2\cdot + CO_2 + Ph\cdot}} \quad (2)$$

$$\mathrm{PhCO_2OCOPh} \xrightarrow{h\nu} \overline{\mathrm{(PhCO_2\cdot)^* + PhCO_2\cdot}} \longrightarrow \overline{\mathrm{Ph\cdot + CO_2 + PhCO_2\cdot}} \quad (3)$$

$$\mathrm{PhCO_2OCOPh} \xrightarrow{h\nu} \overline{\mathrm{PhCO_2\cdot + PhCO_2\cdot}} \xrightarrow{h\nu} \overline{\mathrm{(PhCO_2\cdot)^* + PhCO_2\cdot}} \longrightarrow \overline{\mathrm{Ph\cdot + CO_2 + PhCO_2\cdot}} \quad (4)$$

In the singlet sensitization, the singlet excited hydrocarbon molecule will interact with the peroxide molecule to give a reactive exciplex.[9,10] In this exciplex the singlet excitation energy of the hydrocarbon moiety would be converted to the vibrational energy of the complex to cause the cleavage of the peroxide moiety into free radicals. Table 2 shows that the yield of phenyl benzoate tends to increase with increasing singlet excitation energy of the sensitizers. This result suggests that, on formation of the reactive exciplex, the higher the singlet excitation energy of the sensitizer, the more efficient the cleavage of both of the oxygen-oxygen and carbon-carbon bonds of BPO to give the geminate product.

Table 3 indicates that the concurrent irradiation with a tungsten-bromine lamp, which was used to increase light intensity in the visible region, gives no pronounced effect on the product distribution, although it seemingly enhances the formation of biphenyl in both photolysis and thermolysis. Consequently, under the present experimental conditions, the visible light illumination does not significantly accelerate the decomposition of benzoyloxy radicals in contrast with the reported results for crystalline acetyl benzoyl peroxide.[21]

Concurrent illumination of a tungsten-bromine lamp on the samples irradiated by a nitrogen laser was undertaken for the following intention. Thus, under laser irradiation, the excited peroxide molecules undergo decomposition almost during the nanosecond duration of the pulse, and the resulting benzoyloxy radicals would decarboxylate during the "dark period" of nearly 10 ms before the next pulse irradiation. Accordingly, the concurrent irradiation with a tungsten-bromine lamp could act during the "dark period" on the free radicals. However, as Table 3 indicates, the tungsten-bromine lamp was not effective to induce the decarboxylation of benzoyloxy radicals.

Furthermore, Table 4 shows that on irradiation at 313 nm the increase of light intensity in nearly five times does not remarkably affect the distribution of the products, although the yields of phenyl benzoate and benzoic acid tend to be slightly reduced with increasing light intensity. This finding suggests that 313-nm light also does not significantly induce the decarboxylation of benzoyloxy radicals.

On laser irradiation, it would be expected that the laser pulses, which supply 10^6—10^7 times as many photons as a 1 kW high pressure mercury lamp in a unit time, would transiently generate high concentrations of free radicals, and hence benzoyloxy and phenyl radicals diffused from the different initial solvent cages would combine to give phenyl benzoate as a diffusion product in addition to the geminate product. However, chrysene-sensitized laser irradiation of an equimolar mixture of BPO and BPO-d_{10} in toluene gave no diffusion products, $C_6H_5CO_2C_6D_5$ and C_6D_5-$CO_2C_6H_5$, but gave only a mixture of the geminate products, $C_6H_5CO_2C_6H_5$ and $C_6D_5CO_2C_6D_5$. This result shows that even on irradiation with light of strong intensity benzoyloxy–phenyl radical pairs effectively result in the geminate product, and that the radicals escaped from the solvent cage undergo decomposition or reactions with the solvent before they would randomly combine to give phenyl benzoate.

Therefore it is reasonable to conclude that in the decomposition of BPO from its excited singlet state,

the one-photon simultaneous (Eq. 2) or successive two-bond cleavage (Eq. 3) mainly contributes to the efficient formation of the benzoyloxy–phenyl radical pairs leading to the noticeable formation of the geminate product, and that the contribution of the two-photon process involving the light-induced decarboxylation of benzoyloxy radicals (Eq. 4) would be negligible.

Finally, it should be mentioned that both of the direct irradiation and singlet sensitized irradiation of BPO give nearly the same distribution of the products, suggesting that both photolytic reactions will proceed through the same reactive state of the peroxide. On direct photolysis, the initially produced (Franck-Condon-state), electronically excited peroxide molecule would relax into a reactive state which can dissociate at both of the O–O and C–C bonds. In the singlet sensitization, however, the singlet excited sensitizers do not have sufficient energies to be transferred to give electronically excited peroxide molecules as produced on direct photolysis. Consequently, the excited sensitizer molecules would complex with ground-state peroxide molecules to give reactive exciplexes, in which the electronic excitation energy would be relaxed through vibrational energy probably leading the peroxide moiety to the same reactive state as produced on direct photolysis.

Experimental

Materials. Dibenzoyl peroxide-2,2′,4,4′,6,6′-d_6, dibenzoyl peroxide-2,2′,3,3′,4,4′,5,5′,6,6′-d_{10}, bis(4-chlorobenzoyl), bis(4-methylbenzoyl), and bis(4-methoxybenzoyl) peroxides were prepared from the corresponding acyl chlorides and sodium peroxide, and recrystallized from dichloromethane-methanol. Dibenzoyl peroxide commercially obtained was purified similarly. Benzoyl-2,4,6-d_3 chloride was prepared in the following manner. A mixture of anilinium chloride and deuterated water was refluxed, and the anilinium salt was recovered. This process was repeated three times. Anilinium-2,4,6-d_3 chloride obtained was converted to benzonitrile-2,4,6-d_3 by the Sandmeyer reaction, and its hydrolysis and chlorination gave benzoyl-2,4,6-d_3 chloride. Other substituted benzoyl chlorides were prepared from the corresponding, commercially purchased acids in a usual manner. Aromatic hydrocarbons used as singlet sensitizers were purified by column chromatography and crystallization. Benzene and styrene were purified by distillation. Phenyl-2,4,6-d_3 benzoate-2,4,6-d_3 was prepared by irradiation of BPO-d_6 in carbon tetrachloride in the presence of naphthalene.

Photolysis. A solution of a peroxide (0.03 M) in benzene (3 ml) in a Pyrex tube was degassed by the usual freeze-thaw cycles or deaerated by bubbling of nitrogen, and irradiated by a 400 W or a 1 kW high pressure mercury lamp immersed in a Pyrex cooling well or furthermore surrounded by Toshiba UV-D36B glass filters when chrysene (0.002 M) was used as a sensitizer using a merry-go-round type Riko Rotary Photochemical Reactor, Model RH400-10W. Irradiation was continued for five times the half-life periods of the peroxide determined by iodometric analysis under the same conditions.

Thermolysis. A solution of a peroxide (0.03 M) in benzene (3 ml) in a Pyrex tube was degassed by the usual freeze-thaw cycles and heated in an air bath constantly maintained at 80, 90, and 100 °C for five times the half-life periods. The reaction times were chosen according to the reported decomposition rate constants of peroxides.[27]

Product Analyses. Phenyl benzoate, substituted phenyl benzoates, biphenyl, and benzoic acid were determined by GLPC analysis on a Shimadzu GC 4CM gas chromatograph equipped with a flame ionization detector. The following columns were used for quantitative analyses: Diethylene glycol succinate (5%) with H_3PO_4 (2%), Polyethylene Glycol 20 M (5%), and Silicone GE SE-30 (2%). Carbon dioxide was determined gravimetrically using an Ascarite tube.

Irradiation by a Tungsten-bromine Lamp during Thermolysis and Photolysis. A solution of BPO (0.03 M) in benzene (10 ml) was irradiated under nitrogen atmosphere at room temperature for 3 h by two lamps at the same time, a 1 kW high pressure mercury lamp immersed in a Pyrex cooling well and a 650 W tungsten-bromine lamp (Ushio, Type JCD) through a Toshiba Y-43 glass filter which transmits light longer wavelength than 400 nm.

Thermolysis under illumination of visible light was performed in a water bath kept at 80 °C for 23.75 h, during which the reacting solution was irradiated by the 650 W tungsten-bromine lamp through a water layer and a Toshiba Y-43 glass filter.

Irradiation of 313-nm Light of Varying Intensity. A solution of BPO (0.03 M) in benzene (10 ml) was irradiated under nitrogen atmosphere at room temperature for 11.5—51 h through a filter solution ($NiSO_4 \cdot 7H_2O$, 0.5 g/ml; transmittance, *ca.* 70% at 313 nm) and a Pyrex wall using a 1 kW high pressure mercury lamp. Light intensity was reduced by inserting piled silk cloth between a sample tube and the filter solution. Relative light intensity was calculated from half-life periods determined by iodometry.

CIDNP Measurements and ESR Spectra. CIDNP measurements were performed on a JEOL JNM-PX-100 NMR spectrometer and ESR spectra were recorded on a JEOL JES-ME-1X ESR spectrometer. A 1 kW and a 400 W high pressure mercury lamp were used as light sources in the CIDNP and ESR measurements, respectively.

Laser Photolysis. Nitrogen laser pulses were supplied from a 1 MW (3.5 mJ) Lambda Physik laser pulse generator. A solution of BPO (0.03 M) in benzene (2 ml) containing chrysene (0.006 M) was irradiated by the laser (100 pulses per second). Irradiation was continued for five times the half-life periods determined by iodometry in advance.

Mass Spectrometry. A solution of BPO and BPO-d_{10} (0.015 M, respectively) in toluene (2 ml) containing chrysene (0.006 M) was irradiated by the nitrogen laser. The photolyzed sample was examined by gas chromatography/mass spectrometry (Hitachi RMU-6M GC/MS). The relative intensities of the parent peaks of phenyl benzoate and phenyl-d_5 benzoate-d_5 were found to be different between the ascending part and descending part of the gas chromatographic peak (*e.g.*, 0.7 and 1.6, respectively), but in neither case a peak was detected at *m/e* 203 attributable to phenyl benzoate-d_5 or phenyl-d_5 benzoate.

The authors' thanks are due to Professor K. Maruyama and Dr. T. Otsuki in The University of Kyoto for their kind help in photo-CIDNP measurements. Thanks are also due to the Ministry of Education for their grant to support this research.

References

1) F. Fichter and A. Schnider, *Helv. Chim. Acta*, **13**, 1428 (1930).
2) Y. Ikeda, *Nippon Kagaku Zasshi*, **79**, 354 (1958).

3) J. C. Bevington and T. D. Lewis, *Trans. Faraday Soc.*, **54**, 1340 (1958).
4) C. Walling and M. J. Gibian, *J. Am. Chem. Soc.*, **87**, 3413 (1965).
5) T. Nakata, K. Tokumaru, and O. Simamura, *Tetrahedron Lett.*, **1967**, 3303.
6) H. C. Box, E. E. Sudzinski, and H. G. Freund, *J. Am. Chem. Soc.*, **92**, 5305 (1970).
7) J. D. Bradley and A. P. Roth, *Tetrahedron Lett.*, **1971**, 3907.
8) P. Lebourgeois, R. Arnaud, and J. Lemaire, *J. Chim. Phys.*, **1972**, 1633, 1643.
9) T. Nakata and K. Tokumaru, *Bull. Chem. Soc. Jpn.*, **43**, 3315 (1970).
10) K. Tokumaru, A. Ohshima, T. Nakata, H. Sakuragi, and T. Mishima, *Chem. Lett.*, **1974**, 571.
11) R. Kaptein, J. A. den Hollander, D. Antheunis, and L. J. Oostehoff, *J. Chem. Soc., Chem. Commun.*, **1970**, 1687.
12) S. R. Fahrenholtz and A. M. Trozzolo, *J. Am. Chem. Soc.*, **93**, 251 (1971).
13) S. R. Fahrenholtz and A. M. Trozzolo, *J. Am. Chem. Soc.*, **94**, 282 (1972).
14) H. D. Roth and M. L. Kaplan, *J. Am. Chem. Soc.*, **95**, 262 (1973).
15) C. F. Poranski, Jr., W. B. Moniz, and S. A. Sojka, *J. Am. Chem. Soc.*, **97**, 4275 (1975).
16) W. F. Smith, Jr., *Tetrahedron*, **25**, 2071 (1969).
17) D. H. Hey, M. J. Perkins, and G. H. Williams, *J. Chem. Soc.*, **1964**, 3412.
18) K. Tokumaru, *Nippon Kagaku Zasshi*, **92**, 887 (1971).
19) T. Suchiro and M. Ishida, *Bull. Chem. Soc. Jpn.*, **44**, 1692 (1971).
20) J. Saltiel and H. C. Curtis, *J. Am. Chem. Soc.*, **93**, 2056 (1971).
21) N. J. Karch, E. T. Koh, B. L. Whitsel, and J. M. McBride, *J. Am. Chem. Soc.*, **97**, 6729 (1975).
22) Bradley and Roth[7] reported that direct photolysis of bis(4-chlorobenzoyl) and bis(4-methylbenzoyl) peroxide gave the corresponding geminate products in the yields of 0.04 and 0.16 mol/mol-peroxide, respectively.
23) E. G. Janzen, C. A. Evans, and Y. Nishi, *J. Am. Chem. Soc.*, **94**, 8236 (1972).
24) R. Kaptein, "Chemically Induced Magnetic Polarization," ed by A. Leply and G. L. Closs, Wiley, New York, N. Y. (1973), Chap. 4.
25) G. L. Closs and M. S. Czerpski, *J. Am. Chem. Soc.*, **99**, 6127 (1977).
26) I. Jaffe, E. J. Prosen, and M. Szwarc, *J. Chem. Phys.*, **27** 416 (1957).
27) C. G. Swin, W. H, Stockmayer, and J. T. Clarke, *J. Am. Chem. Soc.*, **72**, 5426 (1950); A. T. Blomquist and A. J. Buselli, *ibid.*, **73**, 3883 (1951); W. Cooper, *J. Chem. Soc.*, **1951**, 3106.

Kinetic Studies on the Decomposition of the Most Typical Meisenheimer Complex of Sodium 1,1-Dimethoxy-2,4,6-trinitrocyclohexadienide in Methanol

Takehiro Abe

College of General Education, Tohoku University, Kawauchi, Sendai 980

(Received November 1, 1979)

The whole decomposition of the Meisenheimer complex formed from 2,4,6-trinitroanisole (TNA) and sodium methoxide proceeds in three steps and obeys the first-order kinetics in each step. The rate of the whole decrease of concentration of the complex is given by $-d([TNA\cdot CH_3ONa]+[TNA\cdot CH_3O^-])/dt=(k_1[H^+]+k_2[CH_3OH])\times[TNA\cdot CH_3ONa]+(k_3[H^+]+k_4[CH_3OH])\times[TNA\cdot CH_3O^-]-k_5[CH_3O^-]\times[TNA]$, where k denotes a rate constant. This leads to the modification of the conventional unimolecular mechanism shown by $TNA\cdot CH_3O^- \rightarrow TNA+CH_3O^-$.

The decomposition of the most typical Meisenheimer complex (**1**) formed from 2,4,6-trinitroanisole (**2**) and methoxide ion has been widely considered to be unimolecular as follows:[1]

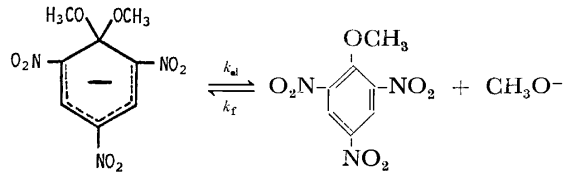

1 **2**

Here k denotes a rate constant. The values of k_d for the decomposition of 1,1-dimethoxy-2,4,6-trinitrocyclohexadienide (**1**) have been directly measured by dissolving appropriate quantities of the sodium or potassium salt of **1** in methanol.[2,3] The value (2.02×10^{-3} s^{-1}) measured by Abe *et al.*[2] for k_d at 25 °C is twice that (1.04×10^{-3} s^{-1}) of Fendler *et al.*[3] An attempt has, therefore, been made to reinvestigate the decomposition of the sodium salt of **1**. This will serve to elucidate the decomposition mechanisms of all the Meisenheimer complexes.

The k_d values have also been indirectly estimated by measuring the apparent pseudo-first-order rate constants (k_{obsd}) for the formation of **1** at various methoxide concentrations much higher than that of **2**, since $k_{obsd}=k_f[CH_3ONa]+k_d$.[3,4] This indirect estimation is, however, unfavorable in obtaining the precise values of k_d, because the estimation leads to noticeable error because of its very small value and **1** associates with cations such as Na^+, K^+, Ba^{2+} and Ca^{2+}.[5-7] At room temperature, the potassium salt of **1** was more easily crystallized from a methanolic solution than the sodium salt of **1**, while the former was less easily dissolved in methanol than the latter. The lithium salt of **1** could not be crystallized from a methanolic solution. The sodium salt of **1** is, therefore, the most appropriate for the present purpose. In comparison with the cases of the potassium salt, the decomposition of the sodium salt of **1** in methanol will be reinvestigated with the help of the results of the decompositions of the sodium salt in buffer solutions and in methanolic solutions containing sodium chloride, crown ether or dimethyl sulfoxide (DMSO).

Experimental

The sodium and potassium salts of **1** were crystallized from methanolic solutions resulting from adding methanolic solutions of sodium and potassium methoxide, respectively, into methanolic solutions of **2**. The IR and NMR spectra of the salts agreed with those of literatures.[1]

The methanolic solutions of the salts showed strong bands at 410—415 nm. The decompositions of the appropriate quantities of the salts in solutions were followed by measuring the absorbances (A) at 420 nm with a Hitachi 100-60 spectrophotometer equipped with a thermostated cell compartment and with a Hitachi 056 recorder (path length, 1.00 cm). In the present work, the rate of decrease of A *vs.* A has been obtained as a decomposition rate in order to discuss the decomposition mechanism easily by the rate of decrease of concentrations of the colored species. The decomposition rate is given by dA/dt which was obtained from a recorded A *vs.* t (time) curve according to $(A_{-\Delta t}-A_{\Delta t})/2\Delta t$. According to the required magnitude of the error in calculating $(A_{-\Delta t}-A_{\Delta t})$, the value of Δt was often taken from 30 s to 5 min in each run. All the linear relationships between the rates and other data were obtained by the least-squares method. All the errors indicated are probable errors with the 50% significance level.

The pH values of buffer solutions (KH_2PO_4–NaOH) of Tokyo Kasei were determined at 20.0 °C with a Hitachi-Horiba pH-meter D-5. Nisso 18-crown-6 (extra pure) was used without further purification.

Results

Decompositions of the Sodium and Potassium Salts of ***1*** *in Methanol.* The rates for four representative runs of decomposition of the sodium salt of **1** are shown in Fig. 1. In each run the rate and absorbance become low with time. The initial concentration of the salt varies with the runs of a, b, c and d. The error in the calculation of dA/dt for $A>1$ is twice that for $A<1$, because the absorbances higher than 1 were recorded on a half-reduced scale. Figure 1 shows that the decomposition of the salt in methanol apparently proceeds in three steps and obeys the first-order kinetics in each step. Of course, the plot of $\ln A$ *vs.* t for each run similarly gave the three first-order rate constants. The rate constants of k_A, k_B, and k_c for the first, second, and third steps, respectively, are listed in Table 1. These constants obtained from the results of six runs were independent of the initial

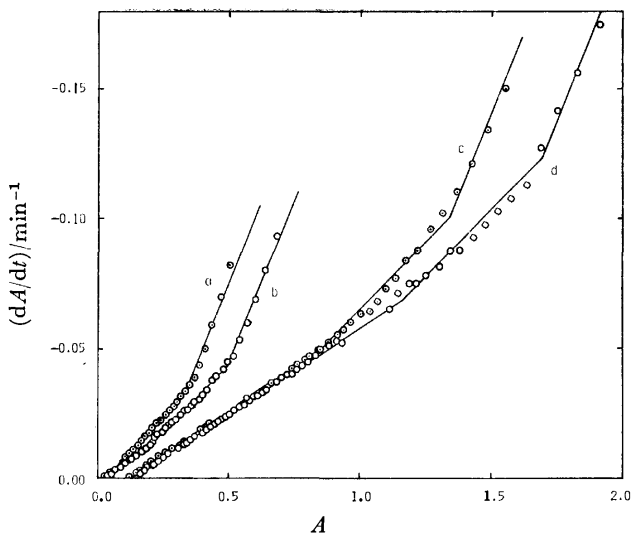

Fig. 1. Plots of dA/dt *vs.* A for the decomposition of the sodium salt of **1** in methanol (25.0 °C).
The initial concentrations of the salt: a; 2.4×10^{-5} M, b; 3.1×10^{-5} M, c; 7.0×10^{-5} M, d; 8.4×10^{-5} M.

TABLE 1. APPARENT RATE CONSTANTS OF k_A, k_B, AND k_C FOR THE DECOMPOSITIONS OF SODIUM SALT OF **1** IN METHANOL AND IN THE METHANOL CONTAINING DMSO (25.0 °C)

Mole fraction of DMSO	$k_A/10^{-3}$ s^{-1}	$k_B/10^{-3}$ s^{-1}	$k_C/10^{-3}$ s^{-1}
0	4.2±0.3	1.7±0.1	1.1±0.1
0.0594	2.9±0.2	1.3±0.1	0.83±0.03
0.1243	3.0±0.2	0.83±0.01	0.46±0.03
0.1949	1.3±0.1	0.57±0.03	0.30±0.02

concentrations of the salt whose absorbances were below 2. The values of k_B and k_c correspond to those of Abe *et al.*[2] and of Fendler *et al.*,[3] respectively.

The decomposition of the potassium salt of **1** in methanol gave the similar results to those of the sodium salt. The rate constants (25.0 °C) obtained from four runs for the potassium salt are $k_A=(3.2\pm0.1)\times10^{-3}$ s^{-1}, $k_B=(1.7\pm0.1)\times10^{-3}$ s^{-1} and $k_C=(1.3\pm0.1)\times10^{-3}$ s^{-1}. In this case the initial decreases in absorbance could not be recorded so early as those of the sodium salt, because the potassium salt was not easily dissolved as mentioned above. Therefore, the low value of k_A for the potassium salt compared with that for the sodium salt is not decisive.

Decomposition of the Sodium Salt of ***1*** *in Methanol Containing Sodium Chloride.* The decomposition of the sodium salt of **1** in the methanol containing sodium chloride (1.02×10^{-2} M (1 M=1 mol dm^{-3})) was the same as that of the salt in methanol without sodium chloride. Owing to the poor solubility of sodium chloride in methanol, the concentration of sodium chloride could not be higher than 10^{-2} M. Four runs at 25.0 °C gave $k_A=(4.0\pm0.1)\times10^{-3}$ s^{-1}, $k_B=(1.8\pm0.1)\times10^{-3}$ s^{-1} and $k_C=(1.2\pm0.1)\times10^{-3}$ s^{-1}.

From the ln A—t curves of the slow decompositions of the sodium salt of **1** in methanol at *ca.* 5 °C, the molar absorption coefficient of **1** in methanol was roughly estimated as 2.5×10^{4} cm^{-1} mol^{-1} at 420 nm by the extrapolation of the curve to the intercept. By using the coefficient value, the concentrations of the salts in the present study were estimated to be in the order of 10^{-5} M. Accordingly, the concentration of sodium chloride (1.02×10^{-2} M) was very higher than that of the sodium salt of **1**. In comparison with the results of the decomposition of the salt without sodium chloride, the presence of a small amount of sodium ion (1.02×10^{-2} M) does not apparently affect the decomposition of the salt. Fendler *et al.*[8] have, however, reported that the presence of excess sodium or potassium ion (2 M) slightly decreases the rates for the decomposition of **1** in water (pH=10.8).

Decompositions of the Sodium and Potassium Salts of ***1*** *in Buffer Solutions.* Figure 2 shows that all the decompositions of the sodium salt in the buffer solutions apparently proceed in the first and second steps for which the first-order rate constants of k_I and k_{II} can be given, respectively. In the case of the same buffer solution (pH=7.03), k_I and k_{II} were independent of the initial concentrations of the salt. The decomposition of the sodium salt of **1** in the buffer solution (pH=7.03) afforded a yellowish crude substance after evaporation and extraction with diethyl ether. The IR spectrum of the crude substance exhibited the absorption bands corresponding to **2**. The thin-layer chromatography of the diethyl ether solution of the substance showed the presence of **2** and of a trace of picric acid. The picric acid probably resulted from the further

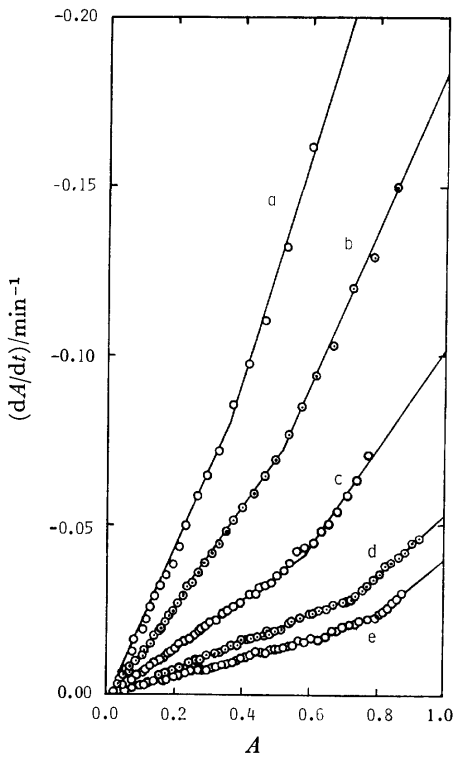

Fig. 2. Plots of dA/dt *vs.* A for the decomposition of the sodium salt of **1** in buffer solutions (20.0 °C).
The values of pH: a; 6.04, b; 6.23, c; 6.61, d; 7.03, e; 7.40.

reaction of **2** with hydroxide ion.[1)]

The decompositions of the potassium salt of **1** in the buffer solutions (pH=6.04, 6.23, and 6.61) gave the values of k_I and k_{II} roughly equal to the corresponding constants for the sodium salt.

Figure 3 shows that there is a linear relationship between k_I and k_{II} as follows:

$$k_I = (8.3\pm0.6) \times 10^{-4}\,s^{-1} + (1.2\pm0.1) \times k_{II}. \quad (1)$$

As shown in Fig. 4, both k_I and k_{II} are linearly proportional to the proton concentration of the buffer solution. The intersections of the straight lines at $[H^+]=0$, *i.e.*, $k_I=(1.2\pm0.1)\times10^{-3}\,s^{-1}$ and $k_{II}=(2.9\pm0.5)\times10^{-4}\,s^{-1}$ mean that the colored species react with not only H^+ but also water molecules (protic solvent molecules). However, even after 30 min the sodium salt of **1** showed the spectra quite identical to the initial ones in the aprotic solvents of DMSO, *N,N*-dimethylformamide, acetonitrile, and acetone. In order to make sure that no decompositions occured prior to records of the initial spectra, conformity to Beer's law was confirmed for the DMSO solution of the sodium salt.

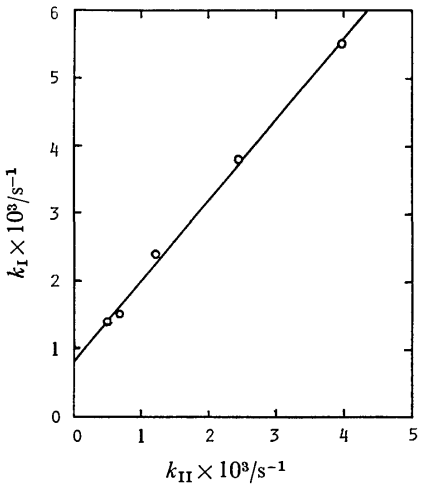

Fig. 3. Correlation of k_I with k_{II} for the sodium salt of **1** (20.0 °C).

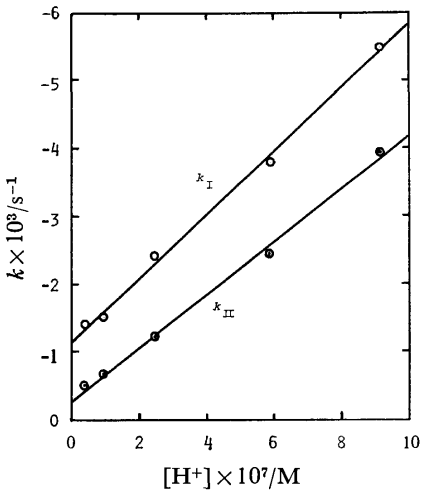

Fig. 4. Correlations of k_I and k_{II} with $[H^+]$ for the sodium salt of **1** (20.0 °C).

In the case of the potassium salt, both k_I and k_{II} were also proportional to $[H^+]$, although there were only three plots for each set of k_I and k_{II}. The plots of k_{II} were roughly similar to those for the sodium salt, while the plots of k_I were considerably scattered because of the hard solubility of the potassium salt.

*Decompositions of Sodium and Potassium Salts of **1** in Methanol Containing Crown Ether.* The sodium salt of **1** was decomposed at 25.0 °C in the methanolic solutions of 18-crown-6 at the concentrations of 4.8×10^{-4}, 2.13×10^{-3}, 6.43×10^{-3}, and 1.37×10^{-2} M. Representative examples for the decomposition rates are shown in Figs. 5 and 6. In the case of 2.13×10^{-3} M the whole decomposition of each run could be divided into three steps in a similar way to that in Fig. 5, while that in the case of 6.43×10^{-3} M was similar to that in Fig. 6. As shown in Fig. 5, the decomposition rates of the second and third steps are high with the decreasing initial concentration of the salt, though the concentration of the crown ether is constant. All the initial decompositions obeyed the first-order kinetics. As shown in Fig. 7, the initial first-order rate constant k_{init} is proportional to the initial concentration of 18-crown-6 ($[18\text{-Crown-6}]_0$).

The decompositions of the potassium salt of **1** in the methanolic solutions of 18-crown-6 at the concentrations of 4.8×10^{-4}, 2.13×10^{-3} and 6.43×10^{-3} M were roughly similar to the corresponding ones for the sodium salt.

*Decompositions of the Sodium Salt of **1** in Methanolic Solutions Containing DMSO.* The sodium salt of **1** was decomposed in the methanolic solutions containing 10, 20, and 30% (v/v) DMSO. Each decom-

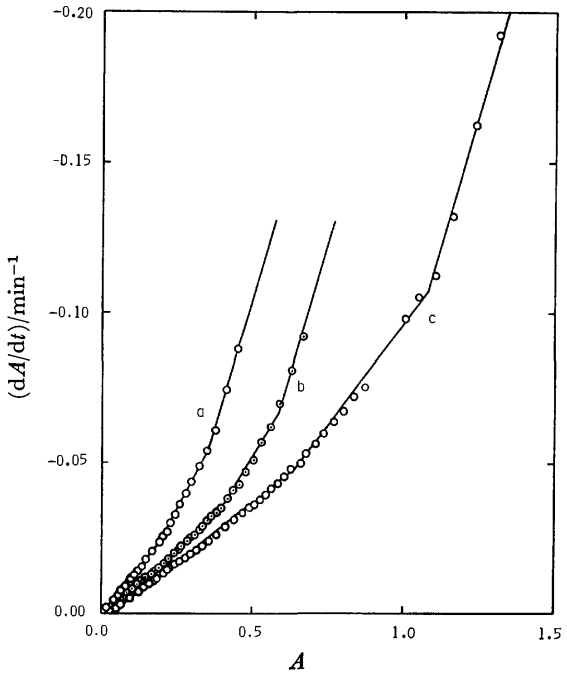

Fig. 5. Plots of dA/dt *vs.* A for the decomposition of the sodium salt of **1** in the methanol containing 18-crown-6 (4.8×10^{-4} M) (25.0 °C).
The initial concentrations of the salt: a; 2.2×10^{-5} M, b; 3.1×10^{-5} M, c; 6.1×10^{-5} M.

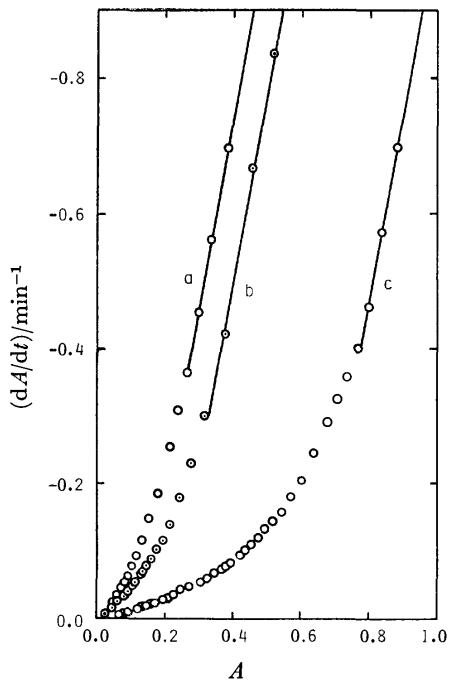

Fig. 6. Plots of dA/dt *vs.* A for the decomposition of the sodium salt of **1** in the methanol containing 18-crown-6 (1.37×10^{-2} M) (25.0 °C).
The initial concentrations of the salt: a; 3.1×10^{-5} M, b; 3.6×10^{-5} M, c; 5.1×10^{-5} M.

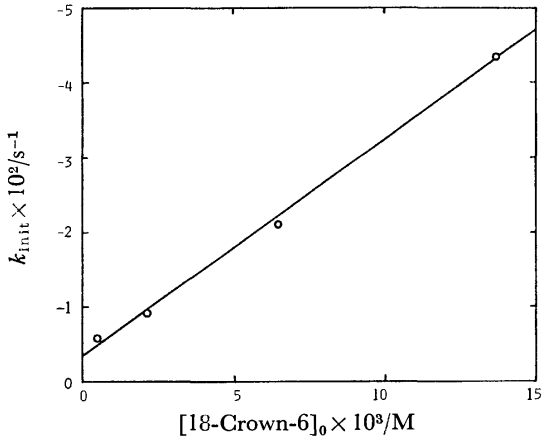

Fig. 7. Correlation of k_{init} with $[18\text{-Crown-6}]_0$ for the sodium salt of **1** (25.0 °C).

position proceeded in three steps like that of the salt in methanol. The apparent rate constants obtained from three or four runs for each DMSO solution are listed in Table 1. The plots of the rate constants against the mole fractions of DMSO (x_{DMSO}) are shown in Fig. 8. There is a linear relationship between the intersections (k_i°) and slopes of the three lines of Fig. 8 as follows:

$$k_i = k_i^\circ + [(1.02\pm0.03)\times10^{-3}\ s^{-1} - (3.02\pm0.01)\times k_i^\circ] \times x_{DMSO} \quad (2)$$

where i=A, B, or C. The term in the bracket on the right hand side of Eq. 2 is the slope of the ith line. Of course, k_i° corresponds to the ith rate constant for the decomposition of the salt in methanol. A

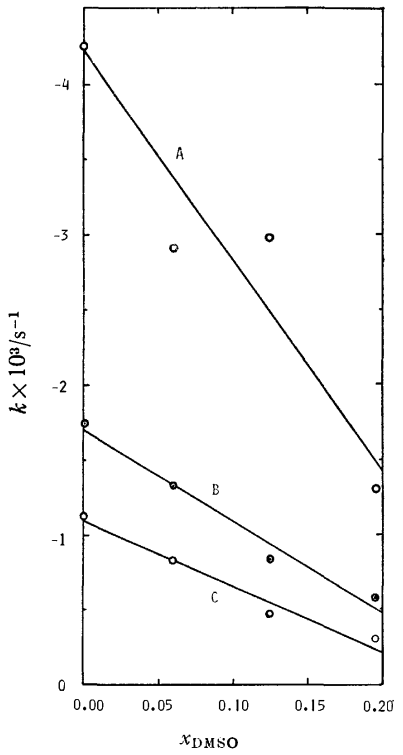

Fig. 8. Correlations of k_A, k_B, and k_C with x_{DMSO} for the sodium salt of **1** (25.0 °C).

good linear relationship has been found between the logarithmic values of apparent rate constants and x_{DMSO} for the decomposition of **1** in aqueous solutions containing DMSO.[9] In the present case, there was also a good relationship between $\log k_i$ and x_{DMSO}, but the relationship corresponding to Eq. 2 was very poor.

Discussion

According to the crystal structure determination of the potassium salt of **1**,[10] the potassium ion is located close to two oxygen atoms of the C_1–methoxyl groups and to an oxygen atom of the C_2– or C_6–nitro group. Crampton and Khan[5–7,11] have reported the ion-pair (**3**) formed from **1** and its counter ion even in the solution, where the cation is probably held by the four oxygen atoms of the methoxyl groups and *o*-nitro groups.

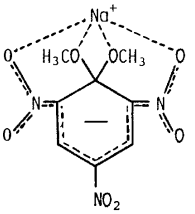

3

The appearance of the two steps in the decompositions of the salts in the buffer solutions (Fig. 2) needs to be interpreted to be due to the decompositions of both **1** and **3**, because the reformation of Meisenheimer complexes can be neglected in such buffer solutions. From the results of the decomposi-

tions of the salts in the buffer solutions (KH_2PO_4–NaOH), the decomposition mechanism can be written as Scheme 1. Here K denotes an equilibrium constant.

$$\mathbf{3} \overset{K_1^B}{\rightleftharpoons} \mathbf{1} + Na^+ \quad (3)$$

$$\mathbf{3} + H^+ \overset{k_1^B}{\longrightarrow} \mathbf{2} + CH_3OH + Na^+ \quad (4)$$

$$\mathbf{3} + H_2O \overset{k_2^B}{\longrightarrow} \mathbf{2} + CH_3OH + NaOH \quad (5)$$

$$\mathbf{1} + K^+ \overset{K_2^B}{\rightleftharpoons} \mathbf{1}\cdot K^+ \quad (6)$$

$$\mathbf{1}\cdot K^+ + H^+ \overset{k_3^B}{\longrightarrow} \mathbf{2} + CH_3OH + K^+ \quad (7)$$

$$\mathbf{1}\cdot K^+ + H_2O \overset{k_4^B}{\longrightarrow} \mathbf{2} + CH_3OH + KOH \quad (8)$$

$$\mathbf{1} + H^+ \overset{k_5^B}{\longrightarrow} \mathbf{2} + CH_3OH \quad (9)$$

$$\mathbf{1} + H_2O \overset{k_6^B}{\longrightarrow} \mathbf{2} + CH_3OH + OH^- \quad (10)$$

Scheme 1.

The absorbance observed at 420 nm was the sum of those of the colored species in the solution. Scheme 1 gives the rate of the total decrease of concentrations of **1**, **3**, and **1**·K^+ as follows:

$$-\frac{d}{dt}([\mathbf{1}] + [\mathbf{3}] + [\mathbf{1}\cdot K^+]) = (k_1^B[H^+] + k_2^B[H_2O]) \times [\mathbf{3}] + (k_3^B[H^+] + k_4^B[H_2O]) \times [\mathbf{1}\cdot K^+] + (k_5^B[H^+] + k_6^B[H_2O]) \times [\mathbf{1}]. \quad (11)$$

In the buffer solution, $[H^+]$ and $[H_2O]$ are constant. In the present study, the equal molar absorption coefficients are conveniently assumed for all **1**, **3**, and **1**·K^+, as made by Crampton and Khan.[5] Here one assumes the following relations:

$$k_1^B[H^+] + k_2^B[H_2O] = k_5^B[H^+] + k_6^B[H_2O] + \Delta_1$$

$$k_3^B[H^+] + k_4^B[H_2O] = k_5^B[H^+] + k_6^B[H_2O] + \Delta_2$$

where Δ_1 and Δ_2 are constant. Then, Eq. 11 can be written as

$$-\frac{dA}{dt} = \left[(k_5^B[H^+]+k_6^B[H_2O])+\Delta_1 \times \left(1+\frac{K_1^BK_2^B[K^+]}{[Na^+]}+\frac{K_1^B}{[Na^+]}\right)^{-1} + \Delta_2 \times \left(1+\frac{[Na^+]}{K_1^BK_2^B[K^+]}+\frac{1}{K_2^B[K^+]}\right)^{-1}\right] \times A. \quad (12)$$

Since $[Na^+]$ and $[K^+]$ can be assumed to be constant in the same buffer solution, Eq. 12 is reduced to

$$-\frac{dA}{dt} = (k_5^B[H^+]+k_6^B[H_2O]+\Delta_I) \times A, \quad (13)$$

where

$$\Delta_I = \Delta_1 \times \left(1+\frac{K_1^BK_2^B[K^+]}{[Na^+]}+\frac{K_1^B}{[Na^+]}\right)^{-1} + \Delta_2 \times \left(1+\frac{[Na^+]}{K_1^BK_2^B[K^+]}+\frac{1}{K_2^B[K^+]}\right)^{-1}.$$

The value of $[Na^+]$ varies with the pH value of the buffer solution. The contribution of Δ_I is, however, probably small compared with $k_5^B[H^+]$ and $k_6^B[H_2O]$ in Eq. 13, because **1**, **3**, and **1**·K^+ are the same complexes of **1** and both Δ_1 and Δ_2 are probably small. Then, Δ_I may be approximately assumed to be constant for all the buffer solutions. The value of $(k_5^B[H^+]+k_6^B[H_2O]+\Delta_I)$ corresponds to k_I. In the second step (Eqs. 6—10), **3** may vanish in the reaction system. Accordingly, the following final equation can be obtained in the same way as above:

$$-\frac{dA}{dt} = (k_5^B[H^+]+k_6^B[H_2O]+\Delta_{II}) \times A, \quad (14)$$

where Δ_{II} is approximately constant for all the buffer solutions. The value of $(k_5^B[H^+]+k_6^B[H_2O]+\Delta_{II})$ corresponds to k_{II}. Thus, the appearance of the two steps in the decompositions of the sodium salt of **1** in the buffer solutions can be accounted for. The empirical equation 1 may be explained by $k_I=(\Delta_I-\Delta_{II})+k_{II}$. The deviation of the coefficient 1.2 of k_{II} in Eq. 1 from 1 may be due mainly to an experimental error. Equations 13 and 14 show that both k_I and k_{II} should be proportional to the proton concentration in the buffer solution. In Fig. 4 the two straight lines are not completely parallel with each other, but the linear relationship between k_I and k_{II} is found in Fig. 3. The incompletely parallel lines in Fig. 4 seem to be due mainly to the pH dependences of Δ_I and Δ_{II}.

With the help of the results of the decompositions of the salts of **1** in the buffer solutions, the decomposition mechanism of the sodium salt of **1** in methanol can be written as shown in Scheme 2. The formation

$$CH_3OH \overset{K_M}{\rightleftharpoons} CH_3O^- + H^+ \quad (15)$$

$$\mathbf{3} \overset{K_1}{\rightleftharpoons} \mathbf{1} + Na^+ \quad (16)$$

$$\mathbf{3} + H^+ \overset{k_1}{\longrightarrow} \mathbf{2} + CH_3OH + Na^+ \quad (17)$$

$$\mathbf{3} + CH_3OH \overset{k_2}{\longrightarrow} \mathbf{2} + CH_3OH + CH_3ONa \quad (18)$$

$$\mathbf{1} + H^+ \overset{k_3}{\longrightarrow} \mathbf{2} + CH_3OH \quad (19)$$

$$\mathbf{1} + CH_3OH \overset{k_4}{\longrightarrow} \mathbf{2} + CH_3OH + CH_3O^- \quad (20)$$

$$\mathbf{2} + CH_3O^- \overset{k_5}{\longrightarrow} \mathbf{1} \quad (21)$$

Scheme 2.

of **3** from **1** and Na^+ may be essentially neglected, because the effect of the ion pairing has been considered to be small at the cation concentration below 10^{-3} M.[6] In the first and second steps $[CH_3O^-]$ may be neglected, because it is very low in these steps and may be consumed by the carbon dioxide dissolved in the reaction system not degassed. In the reaction system $[H^+]$ may be assumed to be stationary, because the rate of the reaction ($CH_3OH \rightarrow CH_3O^- + H^+$) can be expected to be lower than those of the ionic reactions such as $\mathbf{1}+H^+ \rightarrow \mathbf{2}+CH_3OH$ and $\mathbf{3}+H^+ \rightarrow \mathbf{2}+CH_3OH+Na^+$.

The rate of decrease of concentrations of **1** and **3** for the first step (Eqs. 15—20) is written as

$$-\frac{d}{dt}([\mathbf{1}]+[\mathbf{3}]) = (k_1[H^+]+k_2[CH_3OH])\times[\mathbf{3}] + (k_3[H^+]+k_4[CH_3OH])\times[\mathbf{1}]. \quad (22)$$

Here one writes the following equation:

$$k_3[H^+] + k_4[CH_3OH] = k_1[H^+] + k_2[CH_3OH] + \Delta, \quad (23)$$

where Δ is a constant. Using Eq. 23, one can reduce Eq. 22 to:

$$-\frac{dA}{dt} = (k_1[H^+] + k_2[CH_3OH] + \Delta') \times A, \quad (24)$$

where

$$\Delta' = \Delta \times (1+[Na^+]/K_1)^{-1}. \quad (25)$$

Here Δ' may be approximately constant, because the value of $[Na^+]$ is very small, though it increases with time. Then, k_A corresponds to:

$$k_A = k_1[H^+] + k_2[CH_3OH] + \Delta'. \quad (26)$$

Strictly speaking, Δ' is expected to be high with decreasing initial concentration of the salt, because $[Na^+]$ is low with the decreasing initial concentration. The value of k_A may, therefore, be high to some extent with the decreasing initial concentration. This behavior seems to appear in Fig. 1, since the initial plots for the runs of a and b slope more than the straight lines of k_A, while those of c and d are reverse.

In the second step (Eqs. 15, 19, and 20), **3** may disappear in the reaction system. Accordingly, the rate of decrease of concentration of **1** for this stage may be written as

$$-\frac{d[\mathbf{1}]}{dt} = (k_3[H^+]+k_4[CH_3OH]) \times [\mathbf{1}]. \quad (27)$$

This equation can be reduced to:

$$-\frac{dA}{dt} = (k_3[H^+]+k_4[CH_3OH]) \times A. \quad (28)$$

Then, the rate constant of k_B is written as

$$k_B = k_3[H^+] + k_4[CH_3OH]. \quad (29)$$

In the third step (Eqs. 15 and 19—21), the reverse reaction of formation of **1** may be finally observed, because the final equilibrium absorbances of c and d are more than 0.1 in Fig. 1. From Eq. 29, the value of $k_4[CH_3OH]$ is distinctly smaller than that of k_B (1.7×10^{-3} s^{-1} at 25 °C). On the other hand, the rate constant ($k_5=k_f$) for the formation of **1** is 17.3 s^{-1} M^{-1} at 25 °C.[3] The reaction of Eq. 20 is, therefore, probably much slower than that of Eq. 21 in Scheme 2, since $[CH_3OH]=24.6$ M at 25 °C. Then, $[CH_3O^-]$ may be assumed to be stationary. In the third step, therefore, the decrease of **1** due to the reaction of Eq. 20 may be approximately cancelled out by the reaction of Eq. 21. Accordingly, the rate of decrease of concentration of **1** may be written as

$$-\frac{d[\mathbf{1}]}{dt} = k_3[H^+][\mathbf{1}]. \quad (30)$$

This equation leads to

$$-\frac{dA}{dt} = k_3[H^+]A. \quad (31)$$

From Eq. 31, one obtains

$$k_C = k_3[H^+]. \quad (32)$$

Using the k_d value of Fendler *et al.*,[3] Crampton and Khan[6] have estimated the value of $1/K_1$ as 70 M^{-1} at 25 °C. As Crampton and Khan have described, the value should be regarded as giving the order of magnitude of the association constant rather a precise value. Actually the calculation with the use of 70 M^{-1} leads to the unfavorable result that almost no **3** exists at the initial stage when the sodium salt of **1** is dissolved in methanol at the concentration of 5×10^{-5} M. The precise value of $1/K_1$ will be smaller than 70 M^{-1}. Putting the value of $1/K_1$ smaller than 70 M^{-1} into Eq. 25, one can expect that only the value of k_A among k_A, k_B, and k_C becomes slightly low when the methanolic solution of the sodium salt of **1** contains the sodium chloride at the concentration of 1×10^{-2} M, because Eqs. 29 and 32 contain no $[Na^+]$. Therefore, the experimental results of the effect of sodium chloride on the decomposition of the sodium salt of **1** may be accounted for. Thus, the appearance of the pseudo-first-order rate constants of k_A, k_B, and k_C in the decomposition of the sodium salt of **1** in methanol can be explained by Scheme 2.

The formation of ion-pairs between alkali-polyether cations and anions has been known in an organic phase.[12] In the presence of a small excess of the crown ether, sodium ions have been considered to be taken off from the Meisenheimer complexes of 1,1-dimethoxy-2-methoxycarbonyl-4,6-dinitrocyclohexadienide in methanol.[11] Figure 7 shows that 18-crown-6 decomposes the colored species. Accordingly, the increase in the rate of decrease of concentrations of **1** and **3** in the methanol containing 18-crown-6 seems to be due to the following additional reactions together with those of Scheme 2:

$$Na^+ + \text{18-Crown-6} \rightleftharpoons Na^+\cdot\text{18-Crown-6},$$

$$CH_3O^- + Na^+\cdot\text{18-Crown-6} \rightleftharpoons CH_3O^-\cdot Na^+\cdot\text{18-Crown-6},$$

$$\mathbf{3} + \text{18-Crown-6} \rightleftharpoons \mathbf{1} + Na^+\cdot\text{18-Crown-6},$$

$$\mathbf{3} + \text{18-Crown-6} \longrightarrow \mathbf{2} + CH_3O^-\cdot Na^+\cdot\text{18-Crown-6},$$

$$\mathbf{1} + Na^+\cdot\text{18-Crown-6} \longrightarrow \mathbf{2} + CH_3O^-\cdot Na^+\cdot\text{18-Crown-6}.$$

At the present time, however, the detail of the mechanism for this case can not be discussed.

The pK_a value (27.9[13]) of methanol in DMSO at 25 °C is much larger than the logarithmic value (16.92[14]) of the minus autoprotolysis constant of methanol. Moreover, the activity coefficient of methanol in DMSO–methanol gradually decreases with the increasing mole fraction of DMSO.[15] The empirical equation 2 suggests that DMSO plays the same role in all the steps. Accordingly, the decreases in the apparent rate constants of k_A, k_B, and k_C with the increasing mole fraction of DMSO (Table 1) may be due mainly to the decrease in proton concentration and partly to the decrease in activity coefficient of methanol. The decrease of proton concentration in Eqs. 26, 29, and 32 can explain the decreasing apparent rate constants (Table 1) with the increasing mole fraction of DMSO. Thus, the effects of DMSO on the decomposition of the sodium salt of **1** in DMSO–

methanol can be explained by the mechanism shown in Scheme 2.

In view of the decomposition mechanism of the salt of **1** (Scheme 2), the rate of increase of concentrations of **1** and **3** may be written for the formation of the Meisenheimer complexes from **2** and CH_3ONa in methanol as follows:

$$\frac{d}{dt}([\mathbf{1}]+[\mathbf{3}]) = k_5[CH_3O^-][\mathbf{2}] - \left(k_3[H^+]+k_4[CH_3OH] + \frac{\Delta}{1+K_{-1}[Na^+]}\right) \times ([\mathbf{1}]+[\mathbf{3}]), \quad (33)$$

where K_{-1} is $1/K_1$. As usually made in obtaining the apparent first-order rate constants, one assumes that the initial concentration of sodium methoxide ($[CH_3ONa]_0$) is much higher than that of **2** ($[\mathbf{2}]_0$). Moreover, one assumes that $[CH_3ONa]_0$ is so low that the existence of $[CH_3ONa]$ can be ignored in the methanolic solution. Then, one can write Eq. 33 as

$$\frac{d}{dt}([\mathbf{1}]+[\mathbf{3}]) = \left(k_5[CH_3ONa]_0+k_3[H^+]+k_4[CH_3OH] + \frac{\Delta}{1+K_{-1}[Na^+]}\right) \times \{([\mathbf{1}]_e+[\mathbf{3}]_e)-([\mathbf{1}]+[\mathbf{3}])\}, \quad (34)$$

where the suffix e denotes an equilibrium concentration. Here Δ and $[Na^+]$ may be approximately constant in a methoxide solution, because $[H^+]$ is very low and $[CH_3ONa]_0 \gg [\mathbf{2}]_0$. Moreover, $k_3[H^+]$ may not contribute greatly in the case of the methoxide solution, because the autoprotolysis constant of methanol is very much small.[14] Therefore, the apparent psuedo-first-order rate constant k_{obsd} for the formation of the Meisenheimer complexes in methanol can be related to as follows:

$$k_{obsd} = k_5[CH_3ONa]_0 + k_3[H^+] + k_4[CH_3OH] + \frac{\Delta}{1+K_{-1}[Na^+]}. \quad (35)$$

Among the terms on the right hand side of Eq. 35, the contribution of $k_5[CH_3ONa]_0$ is, of course, the greatest in the case of the methoxide solution. According to Eq. 35, k_{obsd} should be proportional to $[CH_3ONa]_0$. The author obtains the following good linear relationship between k_{obsd} and $[CH_3ONa]_0$ for the data observed by Fendler *et al.*[3] at 410 nm in the range of $[CH_3ONa]_0$ from 1.05×10^{-3} M to 5.45×10^{-3} M:

$$k_{obsd} = (-0.4\pm3.8)\times10^{-3}\ s^{-1} + (18.5\pm1.0)\ s^{-1} \times [CH_3ONa]_0. \quad (36)$$

From Eq. 33, one obtains for the equilibrium state:

$$\frac{1}{[\mathbf{1}]_e+[\mathbf{3}]_e} = \frac{1}{[\mathbf{2}]_0} + \frac{1}{k_5[\mathbf{2}]_0} \times \left(k_3[H^+]_e+k_4[CH_3OH] + \frac{\Delta_e}{1+K_{-1}[Na^+]_e}\right) \times \frac{1}{[CH_3ONa]_0}. \quad (37)$$

Equation 37 shows that the equilibrium absorbance observed at a wavelength should be approximately proportional to $1/[CH_3ONa]_0$. This expectation is verified by using two sets of data[4,16] as shown in Fig. 9. From the intersections of the lines of a and b in Fig. 9, one obtains the values of 2.40×10^4 and $2.86\times10^4\ cm^{-1}\ M^{-1}$, respectively, for the molar extinction coefficient at 410 nm. These values roughly agree with the present coefficient of $2.5\times10^4\ cm^{-1}\ M^{-1}$ at 420 nm.

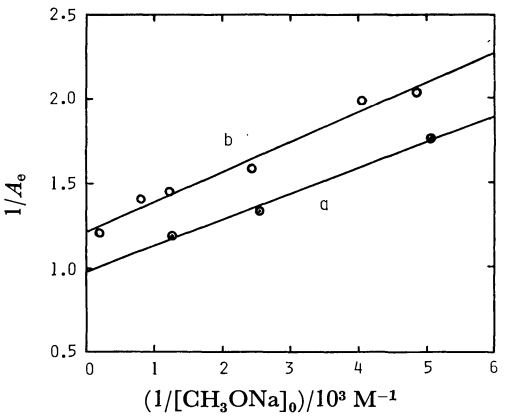

Fig. 9. Correlations of $1/A_e$ with $1/[CH_3ONa]_0$ (25 °C). The data used for the plots of a and b are taken from Refs. 4 and 16, respectively.

In conclusion, the decompositions of the Meisenheimer complexes of **1** and **3** in methanol are not unimolecular, but are due to the proton resulting from the dissociation of methanol and to the protic solvent molecule of methanol as shown in Scheme 2.

References

1) See the following reviews: (a) R. Foster and C. A. Fyfe, *Rev. Pure Appl. Chem.*, **16**, 61 (1966); (b) E. Buncel, A. R. Norris, and K. E. Russell, *Quart. Rev. Chem. Soc.*, **22**, 123 (1968); (c) M. R. Crampton, *Adv. Phys. Org. Chem.*, **7**, 211 (1969); (d) M. J. Strauss, *Chem. Rev.*, **70**, 667 (1970); (e) E. Buncel and H. Wilson, *Adv. Phys. Org. Chem.*, **14**, 133 (1977); (f) S. Sekiguchi, *Yuki Gosei Kagaku Kyokai Shi*, **36**, 633 (1978).

2) T. Abe, T. Kumai, and H. Arai, *Bull. Chem. Soc. Jpn.*, **38**, 1526 (1965).

3) J. H. Fendler, E. J. Fendler, and C. E. Griffin, *J. Org. Chem.*, **34**, 689 (1969).

4) P. Bemporad, G. Illuminati, and F. Stegel, *J. Am. Chem. Soc.*, **91**, 6742 (1969).

5) M. R. Crampton and H. A. Khan, *J. Chem. Soc. Perkin Trans. 2*, **1972**, 1173.

6) M. R. Crampton and H. A. Khan, *J. Chem. Soc. Perkin Trans. 2*, **1973**, 1103.

7) M. R. Crampton, B. Gibson, and F. W. Gilmore, *J. Chem. Soc. Perkin Trans. 2*, **1979**, 91.

8) J. H. Fendler, E. J. Fendler, and M. V. Merritt, *J. Org. Chem.*, **36**, 2172 (1971).

9) C. F. Bernasconi and M. C. Muller, *J. Am. Chem. Soc.*, **100**, 5530 (1978).

10) H. Ueda, N. Sakabe, J. Tanaka, and A. Furusaki, *Bull. Chem. Soc. Jpn.*, **41**, 2866 (1968).

11) M. R. Crampton, *J. Chem. Soc. Perkin Trans. 2*, **1975**, 825.

12) H. K. Frensdorff, *J. Am. Chem. Soc.*, **93**, 4684 (1971).

13) E. M. Arnett and L. E. Small, *J. Am. Chem. Soc.*, **99**, 808 (1977).

14) C. H. Rochester, "Acidity Functions," Academic Press, London (1970), p. 246.

15) J. R. Jones, *Prog. Phys. Org. Chem.*, **9**, 241 (1972).

16) V. Gold and C. H. Rochester, *J. Chem. Soc.*, **1964**, 1687.

Studies on Heterocyclic Analogs of Azulene. VI.[1] Cycloadditions of Styryl-substituted Aza Analogs of Azulene with Dimethyl Acetylenedicarboxylate[2]

Noritaka ABE* and Tarozaemon NISHIWAKI

Department of Chemistry, Faculty of Science, Yamaguchi University, Yamaguchi 753

(Received November 8, 1979)

8-[(*E*)-Styryl]-1-azaazulenes stereospecifically react with dimethyl acetylenedicarboxylate to form *trans*-7*H*-6a-azacyclobuta[*j*]cyclopent[*cd*]azulene (**3**), which undergoes thermal rearrangement into 3-[(*E*)-styryl]-3*H*-2a-azacyclopent[*cd*]azulene and 3a,4-dihydro-3*H*-2a-azadicyclopent[*cd, ij*]azulene (**7**), or isomerization into 3*H*-2a-azacyclopenta[*ef*]heptalene by silica gel. Compound **7** is oxidized during the course of reaction to yield 11-oxo-2a*H*-7,10b-methano-2a-azacyclopenta[*ab*]cycloundecene, compound **3** forming 5a,6-dihydro-3*H*-2a-azadicyclopenta[*ef, kl*]heptalene upon reaction with acetylene. The formation of **3** could be accounted for in terms of a symmetry-allowed thermal [$_{\pi}2_{s}+_{\pi}2_{a}+_{\pi}6_{a}$] cycloaddition.

Cycloaddition of nitrogen-heterocycles with alkynes, a versatile synthetic method of heterocycles which are otherwise difficult to obtain,[3] has been utilized recently in the azaazulene[4] and azapentalene ring systems.[5] We report on the cycloaddition of 8-styryl-substituted aza analogs of azulene with dimethyl acetylenedicarboxylate (DMAD).

8-Styryl-1-azaazulenes (**1a**—**d**) and 4-styryl-1,3-diazaazulene (**2**) were prepared by the reaction of the corresponding azaazulene with styrylmagnesium bromide. The (*E*)-configuration about the double bond of compounds **1a**—**c** and **2** follows from the presence of two pairs of 1H doublets at δ 7.5—8.7 (J=17 Hz) in their ^{1}H NMR spectra and an absorption at 970 cm^{-1} in their IR spectra. β-Bromo-β-ethylstyrene required for the preparation of **1d** was synthesized by the decarboxylation of the sodium salt of (*E*)-α,β-dibromo-α-ethylcinnamic acid. The stereochemistry of the styrene thus formed appears to depend on the water content of the solvent.[6] Our conditions (95% ethanol) favor the formation of a (*Z*)-isomer.

Four products were isolated when compound **1a** was heated under reflux with DMAD in benzene. They were characterized as 5-ethyl 8,9-dimethyl 6-chloro-7-phenyl-*trans*-7*H*-6a-azacyclobuta[*j*]cyclopent-[*cd*]azulene-5,8,9-tricarboxylate (**3a**) (24%), 1-ethyl 3,4-dimethyl 2-chloro-3-[(*E*)-styryl]-3*H*-2a-azacyclopent-[*cd*]azulene-1,3,4-tricarboxylate (**4a**) (9%), 1-ethyl 4,5-dimethyl 2-chloro-3-phenyl-3*H*-2a-azacyclopenta[*ef*]-heptalene-1,4,5-tricarboxylate (**5a**) (14%), and 1-ethyl 5,5a,6,7-tetramethyl 2-chloro-3-phenyl-5a,6-dihydro-3*H*-2a-azadicyclopenta[*ef, kl*]heptalene-1,5,5a,6,7-pentacarboxylate (**6a**) (7%), respectively, from consideration of their spectroscopic properties.

The ^{13}C NMR spectrum of **3a** exhibits signals assignable to sp^3 carbon atoms at δ 56.2 (s, C-9a), 61.5 (d, C-7a), and 65.1 ppm (d, C-7). Two 1H doublets (J=2 Hz) assignable to the H-7a and H-7 protons are observed at δ 3.87 and 5.49, respectively, in its ^{1}H NMR spectrum, whereas the protons at the seven-membered ring are observed at δ 5.60 (d, J=11 Hz, H-1), 6.0—6.3 (m, H-2 and H-3), and 7.22 (d, J=11 Hz, H-4). Large downfield shifts of 0.44 (H-7), 0.36 (H-7a), and 0.97 ppm (H-4) induced on addition of tris(dipivaloylmethanato)europium support these assignments. Further evidence supporting the structure **3a** is the fact that its mass spectrum displays intense

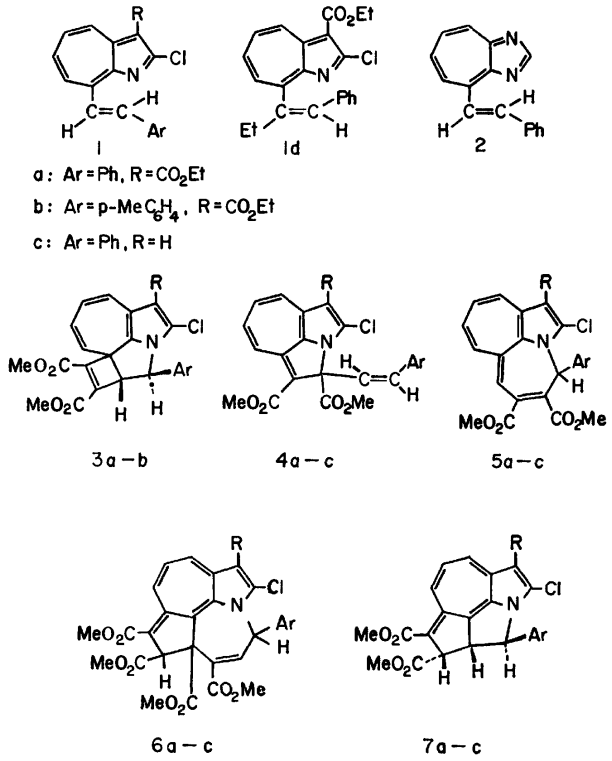

peaks at *m/e* 337 and 339 associated with the loss of dimethyl acetylenedicarboxylate or its equivalent from the molecular ion.[7] The $J_{7,7a}$ value indicates the H-7 and H-7a hydrogens to be situated *trans* to each other in the light of J_{cis} (10—13 Hz) and J_{trans} (2—10 Hz) values reported for the vicinal hydrogens of 2-pyrazolines.[8]

Two pairs of doublets at δ 6.0—7.1 (J=16 Hz) in the ^{1}H NMR spectrum of **4a** shows the presence of an (*E*)-styryl moiety, further confirmed by an IR absorption at 980 cm^{-1}, whereas the ^{1}H NMR spectrum of **5a** displays two 1H singlets at δ 5.31 and 6.11; the former is assigned to a benzylic H-3 proton and the latter to an olefinic H-6 proton. The presence of four aromatic protons in the seven-membered rings of **4a** and **5a**, respectively, is evident from their ^{1}H NMR spectra. The UV spectra of **4a** and **5a** are especially instructive for their structural determinations. The spectrum of **4a** is in line with that of 1-ethyl 3,4-dimethyl 2-chloro-3*H*-2a-azacyclopent[*cd*]azulene-1,3,4-

tricarboxylate[4] (**8**) and the spectrum of **5a** is in line with that of 1-ethyl 3,4,5,6-tetramethyl 2-chloro-3*H*-2a-azacyclopenta[*ef*]heptalene-1,3,4,5,6-pentacarboxylate[4] (**9**) except for the presence of additional low-intensity absorptions in the longer wavelength region for **5a**. The ^{13}C NMR spectral features of **4a** and **5a** are also in line with the proposed structures.

The ^1H NMR spectrum of **6a**, 1:2 adduct of **1a** and DMAD, shows the presence of three seven-membered ring protons at δ 6.22 (d, J=6 Hz, H-8), 6.37 (dd, J=10 and 6 Hz, H-9), and 7.39 (d, J=10 Hz, H-10). A singlet at δ 5.71 is assigned to a H-6 proton. There are two pairs of 1H doublets (J=3 Hz) at δ 4.66 and 5.29, the former being assigned to a benzylic H-3 proton and latter to a H-4 one. The ^{13}C NMR spectrum of **6a** exhibits signals assignable to sp^3 carbon atoms at δ 5.60 (s, C-5a), 65.4 (d, C-6), and 68.7 (d, C-3).

Whilst the reaction of **1b** with DMAD in benzene proceeded similarly to produce **3b**, **4b**, **5b**, and **6b**, the reaction of **1c** with DMAD under similar conditions afforded **4c**, **5c**, **6c**, and 4,5-dimethyl 2-chloro-3-phenyl-3a,4-dihydro-3*H*-2a-azadicyclopent[*cd*, *ij*]azulene-4,5-dicarboxylate (**7c**). The seven-membered ring protons of **7c** exhibit signals at δ 6.05 (dd, J=6.5 and 1 Hz, H-6), 6.17 (dd, J=10 and 6.5 Hz, H-7), and 6.84 (d, J=10 Hz, H-8) in its ^1H NMR spectrum. A singlet at δ 6.06 is assignable to a H-1 proton. The H-4 and H-3a protons give rise to the double doublets signals at δ 4.14 (J=8.5 and 1 Hz) and 4.39 (J=8.5 and 2 Hz), respectively. The former shows a long-range coupling with the H-6 proton, and the latter a vicinal coupling with the H-3 proton resonating at δ 5.27 (d, J=2 Hz). The $J_{3,3a}$ value indicates the H-3 and H-3a hydrogens to be situated *trans* to each other in the light of J_{cis} (10—13 Hz) and J_{trans} (2—10 Hz) value reported for the vicinal hydrogens of 2-pyrazolines.[8] The ^{13}C NMR spectrum of **7a** displays sp^3 carbon atoms at δ 42.7 (d, C-3a), 63.0 (d, C-4), and 66.3 (d, C-3).

The reaction of **1a** with DMAD in hot acetonitrile gave a similar result. However, when the reaction was carried out in hot xylene, the yields of the products changed remarkably. Thus, compounds **4a**, **6a**, and **7a** were obtained in 38, 10, and 24% yield, respectively, no compound **3a** being isolated. 1-Ethyl 5,6-dimethyl 2-chloro-3-phenyl-11-oxo-2a*H*-7,10b-methano-2a-azacyclopenta[*ab*]cycloundecene-1,5,6-tricarboxylate (**10a**) was isolated in 6% yield. Compound **10a** was also obtained by the oxidation of **7a** with 2,3-dichloro-5,6-dicyano-1,4-benzoquinone. Its ^1H NMR spectrum displays signals at δ 7.38 (dd, J=11 and 10 Hz, H-9), 8.79 (d, J=11 Hz, H-10), and 9.10 (d, J=10 Hz, H-8) for the seven-membered ring protons. A low-field resonating singlet at δ 7.42 is assignable to H-4 proton. The UV spectrum (λ_{max} 665 nm) suggests the presence of an extended chlomophore, and a ν(C=O) absorption at 1690 cm^{-1} in its IR spectrum the presence of a conjugated ketone. From the results, the structure was assigned.

Application of the forgoing reactions to the azaazulene (**1d**) possessing a (*Z*)-α-ethylstyryl group at C(8) gave a complicated mixture of products among

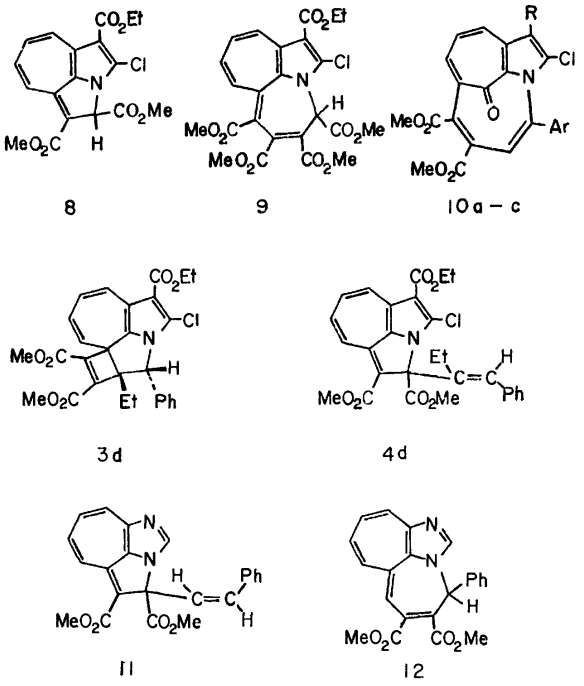

which the azacyclobuta[*j*]cyclopent[*cd*]azulene (**3d**) and the azacyclopent[*cd*]azulene (**4d**) were identified.

The study was further extended to 4-[(*E*)-styryl]-1,3-diazaazulene (**2**), which gave dimethyl 3-[(*E*)-styryl]-3*H*-1,2a-diazacyclopent[*cd*]azulene-3,4-dicarboxylate (**11**) and dimethyl 3-phenyl-3*H*-1,2a-diazacyclopenta-[*ef*]heptalene-3,4-dicarboxylate (**12**).

The ^1H NMR and ^{13}C NMR spectra of the majority of the compounds are summarized in Tables 1—7.

Mechanistic Discussion. There are two plausible mechanisms leading to the azacyclobuta[*j*]cyclopent-[*cd*]azulene ring system (**3**) from the 8-styryl-1-aza-azulene (**1**): symmetry-allowed thermal [$_\pi 2_s + _\pi 2_a + _\pi 6_a$] cycloaddition,[9] and the thermal [$_\pi 2_s + _\pi 2_a$] cycloaddition of DMAD with **13**, a valence tautomer of **1**, as shown in the scheme. However, the latter is not preferred, since the cyclobutene ring is disposed *trans* toward the five-membered ring and would have a high torsional energy. The experimental results support the first rationale: (i) the ^1H NMR spectrum of **1** lacks a benzylic proton which would be associated with the structure **13**, (ii) the UV spectrum of **1a**

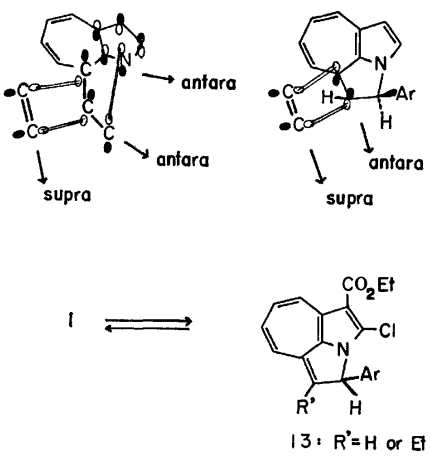

Table 1. ^{1}H NMR bands (δ values) of **1a—d** and **2**

Compound	H-2	H-3	H-4	H-5	H-6	H-7	Styryl H-α[a]	Styryl H-β[a]	Styryl Ar	CH_3CH_2[b]
1a			9.37 d; J=11 Hz	7.6—8.0 m		8.25 d; J=11 Hz	8.66 d	7.48 d	7.3—7.5 m (3H) 7.6—8.0 m (2H)	1.46 (3H), 4.44 (2H)
1b			9.42 d; J=10 Hz	7.55—8.1 m		8.28 d; J=10 Hz	8.68 d	7.51 d	2.37 s (3H) 7.18 d (2H)[c] 7.58 d (2H)[c]	1.48 (3H), 4.47 (2H)
1c		7.40 s	8.27 d; J=11 Hz	7.2—7.5 m		8.15 d; J=11 Hz	8.75 d	7.52 d	7.2—7.5 m (3H) 7.53—7.95 m (2H)	
1d			9.4—9.6 m		7.5—7.9 m			6.84—7.0 m	6.7—6.8 m (3H) 6.84—7.0 m (2H)	1.04 (3H), 2.87 (2H)[d] 1.48 (3H), 4.48 (2H)
2	9.07 s		8.87 d; J=11 Hz	7.55—8.1 m	8.2—8.6 m	7.55—8.1 m	8.71 d	7.77 d	7.3—7.5 m (3H) 7.55—8.1 m (2H)	

a) $J_{H\text{-}\alpha,\ H\text{-}\beta}$=17 Hz. b) Multiplicities and $J_{CH_3\text{-}CH_2}$ values are omitted. c) J=8 Hz. d) Double quartets; J=7 and 1 Hz.

Table 2. ^{1}H NMR bands (δ values) of **4a—d** and **11**

Compound	H-1	H-2	H-5	H-6	H-7	H-8	Styryl H-α[a]	Styryl H-β[a]	Styryl Ar	Ester[b] CH_3CH_2O	Ester[b] CH_3O
4a			7.46 d; J=12	6.70 dd; J=12, 8	6.34 dd; J=12, 8	7.62 d; J=12	7.14 d	6.00 d	7.15—7.4 m (5H)	1.40 (3H) 4.36 (2H)	3.76 (3H) 3.79 (3H)
4b			7.46 d; J=11	6.70 dd; J=11, 9	6.33 dd; J=11, 9	7.63 d; J=11	7.08 d	5.97 d	2.30 s (3H) 7.06 d (2H)[c] 7.24 d (2H)[c]	1.40 (3H) 4.36 (2H)	3.74 (3H) 3.78 (3H)
4c	6.34 s		7.41 d; J=12	6.67 dd; J=12, 9	6.21 dd; J=11, 9	6.85 d; J=11	7.16 d	5.98 d	7.2—7.4 m (5H)		3.75 (3H) 3.78 (3H)
4d			7.54 d; J=11	6.70 dd; J=11, 8	6.30 dd; J=11, 8	7.62 d; J=11		6.70[d]	7.27 s (5H)	1.39 (3H) 4.34 (2H)	3.75 (3H) 3.78 (3H)
11		7.41 s	7.25 d; J=10	6.73 t; J=10	6.18 t; J=10	7.10 d; J=10	7.52 d	6.71 d	7.17 s (5H)		3.98 (3H) 4.06 (3H)

a) J=16 Hz. b) Mutiplicities and $J_{CH_3\text{-}CH_2}$ values are omitted. c) J=8 Hz. d) J=2 Hz. The α-ethyl protons are observed at δ 0.72 t (3H) and 2.23 dq (J=8 and 2 Hz).

Table 3. ^{1}H NMR bands (δ values) of **5a—c** and **12**

Compound	H-1	H-2	H-3	H-6	H-7	H-8	H-9	H-10	Ar	Ester[a] CH_3CH_2O	Ester[a] CH_3O
5a			5.31 s	6.11 s	6.52 d; J=10	5.95—6.2 m	6.25—6.5 m	7.38 d; J=11	7.30 s (5H)	1.36 (3H) 4.23 (2H)	3.59 (3H) 3.84 (3H)
5b			5.31 s	6.06 s	6.52 d; J=10	6.0—6.2 m	6.25—6.5 m	7.41 d; J=11	2.32 s (3H) 7.09 d (2H) [b] 7.20 d (2H) [b]	1.32 (3H) 4.26 (2H)	3.58 (3H) 3.87 (3H)
5c	6.11 s		5.24 s	6.07 s	6.54 d; J=10	5.9—6.15 m	6.3—6.5 m	6.67 d; J=11	7.30 s (5H)		3.57 (3H) 3.88 (3H)
12		7.72 s	5.35 s	6.27 s		6.4—7.0 m			7.1—7.6 m (6H)		3.76 (3H) 3.82 (3H)

a) Multiplicities and $J_{CH_3\text{-}CH_2}$ values are omitted. b) J=8 Hz.

Table 4. ^{1}H NMR bands (δ values) of **6a—c**

Compound	H-1	H-3	H-4	H-6	H-8	H-9	H-10	Ar	Ester[a] CH_3CH_2O	Ester[a] CH_3O
6a		4.46 d; J=3	5.29 d; J=3	5.71 s	6.22 d; J=6	6.37 dd; J=10, 6	7.39 d; J=10	7.2—7.4 m (5H)	1.36 (3H) 4.31 (2H)	3.66 (3H), 3.68 (3H), 3.80 (3H), 3.87 (3H)
6b		4.63 d; J=3	5.27 d; J=3	5.69 s	6.21 d; J=7	6.35 dd; J=10.5, 7	7.39 d; J=10.5	2.35 s (3H) 7.13 s (4H)	1.36 (3H) 4.31 (2H)	3.65 (3H), 3.69 (3H), 3.80 (3H), 3.87 (3H)
6c	6.28 s	4.77 d; J=2	5.30 d; J=2	5.82 s		6.2—6.5 m	6.8—7.2 m	7.43 s (5H)		3.72 (3H), 3.76 (3H), 3.87 (3H), 3.93 (3H)

a) Multiplicities and $J_{CH_3\text{-}CH_2}$ values are omitted.

Table 5. ^{1}H NMR bands (δ values) of **7a—c**

Compound	H-1	H-3	H-3a	H-4	H-6	H-7	H-8	Ar	Ester[a] CH_3CH_2O	Ester[a] CH_3O
7a		5.34 d; J=2	4.40 dd; J=8, 2	4.10 dd; J=8, 1.5	6.09 dd; J=7, 1.5	6.31 dd; J=10, 7	7.1—7.4 m (6H)		1.36 (3H) 4.30 (2H)	3.83 (3H) 3.86 (3H)
7b		5.31 d; J=2	4.35 dd; J=8, 2	4.08 dd; J=8, 1.5	6.09 dd; J=7, 1.5	6.31 dd; J=10, 7	7.32 d; J=10	2.35 s (3H) 7.14 s (4H)	1.35 (3H) 4.28 (2H)	3.82 (3H) 3.85 (3H)
7c	6.06 s	5.27 d; J=2	4.39 dd; J=8.5, 2	4.14 dd; J=8.5, 1	6.05 dd; J=6.5, 1	6.17 dd; J=10, 6.5	6.84 d; J=10	7.2—7.4 m (5H)		3.81 (3H) 3.86 (3H)

a) Mutiplicities and $J_{CH_3\text{-}CH_2}$ values are omitted.

TABLE 6. ^{1}H NMR BANDS (δ VALUES) OF **10a—c**

Compound	H-1	H-4	H-8	H-9	H-10	Ar	Ester[a]	
							CH_3CH_2O	CH_3O
10a		7.42 s	9.10 d; J=10	7.38 dd; J=11, 10	8.79 d; J=11	6.85—7.0 m (2H) 7.15—7.3 m (3H)	1.44 (3H) 4.44 (2H)	3.83 (3H), 3.99 (3H)
10b		7.44 s	9.13 d; J=10	7.40 dd; J=11, 10	8.81 d; J=11	2.16 s (3H) 6.8—7.05 m (2H) 7.15—7.3 m (2H)	1.48 (3H) 4.48 (2H)	3.87 (3H), 3.99 (3H)
10c	6.74 s	7.33 s	9.12 d; J=10	7.29 t; J=10	7.98 d; J=10	6.9—7.05 m (2H) 7.1—7.25 m (3H)		3.86 (3H), 3.98 (3H)

a) Multiplicities and $J_{CH_3\text{-}CH_2}$ values are omitted.

TABLE 7. ^{13}C CHEMICAL SHIFTS OF THE COMPOUNDS (**3a**), (**3b**), (**4a**), (**4c**), (**5a**), (**6a**), AND (**7a**)

Carbon	**3a**	**3b**	**4a**	**4c**	**5a**	**6a**	**7a**
1	122.6 d	122.6 d	113.7 s	110.2 d	112.4 s	111.8 s	111.3 s
2	128.4 d	125.6 d	136.2 s	142.5 s	141.1 s	143.0 s	140.2 s
3	123.8 d	123.8 d	77.0 s	76.7 s	69.6 d	68.7 d	66.3 d
3a							42.7 d
4	130.8 d	130.7 d	115.5 s	114.3 s	119.0 s	123.8 d	63.0 d
4a	117.0 s	116.9 s	122.0 s	120.9 s			
5	112.1 s	112.0 s	125.8 d	126.1 d	120.2 s	123.6 s	113.1 s
5a						56.0 s	128.1 s
6	119.9 s	119.8 s	127.1 d	131.0 d	110.6 s	65.4 d	122.9 d
6a					124.2 s		
7	65.1 d	65.2 d	125.8 d	128.0 d	131.6 d	115.1 s	124.0 d
7a	61.5 d	61.3 d				126.5 s	
8	138.7 s	138.1 s	131.6 d	131.6 d	135.3 d	121.3 d	128.3 d
8a			124.4 s	121.8 s			136.0 s
8b			142.9 s	142.7 s			145.9 s
8c							118.2 s
9	139.6 s	138.8 s			136.0 d	127.9 d	
9a	56.2 s	56.1 s					
9b	149.5 s	149.5 s					
10					138.1 d	128.5 d	
10a					125.1 s	139.1 s	
10b					143.0 s	145.5 s	
10c						120.0 s	
C=O	163.4 s	163.3 s	167.1 s	167.8 s	168.5 s	166.3 s	164.8 s
	161.3 s	161.3 s	163.2 s	163.5 s	165.9 s	164.9 s	163.8 s
	160.6 s	160.6 s	162.7 s		162.7 s	164.2 s	163.6 s
						163.5 s	
						163.3 s	
MeO	52.4 q	52.3 q	53.2 q	53.3 q	52.7 q	52.7 q	52.6 q
	52.0 q	52.0 q	51.1 q	50.9 q	51.4 q	52.6 q	52.3 q
						52.4 q	
						52.1 q	
CH_2O	59.9 t	59.8 t	60.4 t		60.3 t	60.2 t	60.0 t
Me	14.4 q	21.1 q	14.4 q		14.2 q	14.4 q	14.4 q
		14.4 q					
-CH=CH-			136.7 d	136.3 d			
			124.4 d	124.2 d			
Phenyl	130.8 s[a]	136.7 s[c]	131.6 s[a]	136.1 s[a]	136.0 s[a]	134.6 s[a]	134.2 s[a]
	129.2 d[b]	129.8 d[b]	128.7 d[d]	128.5 d[e]	129.0 d[d]	129.1 d[b]	129.1 d[b]
	125.6 d[d]	129.1 s[a]	127.1 d[b]	126.8 d[b]	128.2 d[b]	126.4 d[d]	128.6 d[c]
		125.6 d[e]		125.1 d[c]			125.9 d[e]

a) C-1. b) C-3 and -5. c) C-4. d) C-2, -4, and -6. e) C-2 and -6.

differs a great deal from that of **8**,[4] (iii) the cycloaddition of 8-[(*E*)-styryl]-1-azaazulene (**1a**—**c**) proceeds stereospecifically producing the *trans*-isomer (**3**) only, (iv) no reaction took place even after heating of **4a** with DMAD for 6 d.

Compound **3a**, when heated under reflux in xylene, gave **4a**, **7a**, and **10a**, whereas compound **3d** underwent rearrangement into **4d** upon heating in a neat state. The results indicate that the azacyclopent[*cd*]azulene (**4**) is the thermal product of the azacyclobuta[*j*]-cyclopent[*cd*]azulene (**3**). Thus we can postulate that **4** was formed by the scission of the bond between nitrogen and benzylic carbon atoms of **3** followed by rapid stereospecific recyclization of the intermediate **14**;[10] the absence of a stereoisomer of **4** in the reaction products supports this assumption.

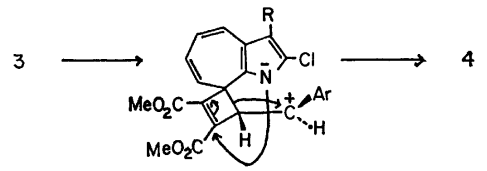

14

Compound **7** gives **10**, when oxidative cleavage occurs during the reaction, and compound **3** affords **6** upon further reaction with DMAD. However, we have been unable to rationalize the formation of **7** so far.

When a mixture of **3a** and silica gel in benzene was set aside for several days at room temperature, compound **3a** was found to undergo rearrangement into the azacyclopenta[*ef*]heptalene (**5a**) in 56% yield, revealing compound **5** to be a silica gel-induced rearrangement product of **3**.

Dimethyl 5-aryl-3*H*-2a-azacyclopenta[*ef*]heptalene-3,4-dicarboxylate (**16**) to be formed by the intramolecular cyclization of an extended dipolar species[4,11] (**15**) was not detected.

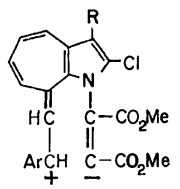

15

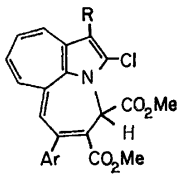

16

Experimental

Melting points were uncorrected. ^{1}H NMR spectra were taken with JEOL FX-100 (100 MHz), Hitachi R-40 (90 MHz), or Hitachi R-24B (60 MHz) spectrometers and ^{13}C NMR spectra with JEOL FX-100 or Hitachi R-26 spectrometers (solutions in $CDCl_3$ with Me_4Si as an internal standard). ^{1}H NMR spectral assignments were confirmed by decoupling techniques when necessary. UV spectra were measured for solutions in ethanol unless otherwise stated and IR spectra for Nujol mulls. Kiesel gel 60 was used for chromatography unless otherwise stated. (*E*)-*β*-Bromo-*p*-methylstyrene,[12] (*Z*)-α-ethylcinnamic acid[13] (mp 105—107 °C, lit,[14] mp 107 °C), and (*Z*)-*β*-bromo-*β*-ethylstyrene (bp 120—121 °C/17 Torr, lit,[14] bp 126—128 °C/23 Torr) were prepared by the reported methods.

*Syntheses of **1** and **2**.* A solution of ethyl 2-chloro-1-azaazulene-3-carboxylate (1.00 g) in tetrahydrofuran (30 ml) was slowly added to the Grignard solution prepared from magnesium (0.412 g), (*E*)-*β*-bromostyrene (3.11 g), and tetrahydrofuran (30 ml). The mixture was stirred for 5 min, hydrolyzed with methanol (8 ml) and 2 N-hydrochloric acid (40 ml), and extracted with benzene. The benzene solution was washed with dilute aqueous sodium hydroxide solution, stirred overnight with tetrachloro-*o*-benzoquinone (2.00 g), the solvent was evaporated, and alumina chromatography of the residue with benzene afforded **1a** (0.846 g, 59%). Crystallization from cyclohexane–dichloromethane gave yellow prisms, mp 161—162 °C, UV_{max} 225 nm (log ε 4.51), 295 (4.50), 322^{sh} (4.43), 392 (4.47), and 445^{sh} (3.59); IR 1700 (C=O) and 970 cm^{-1} (*trans* CH=CH). Found: C, 71.21: H, 4.74; Cl, 10.32; N, 3.92%. Calcd for $C_{20}H_{16}ClNO_2$: C, 71.11; H, 4.77; Cl, 10.50; N, 4.15%. By this procedure we made the following: (i) **1b** [81%, mp 147—148 °C (from cyclohexane–dichloromethane), UV_{max} 226 nm (log ε 4.41), 236 (4.41), 287^{sh} (4.40), 297 (4.41), 322^{sh} (4.31), 403 (4.43), and 455^{sh} (3.78); IR 1690 (C=O) and 970 cm^{-1} (*trans* CH=CH). Found: C, 71.81; H, 5.06; Cl, 10.18; N, 3.73%. Calcd for $C_{21}H_{18}ClNO_2$: C, 71.69; H, 5.16; Cl, 10.08; N, 3.98%.]; (ii) **1c** [62%, mp 90—91 °C (from petroleum ether), UV_{max} 247 nm (log ε 4.38), 282 (4.34), 325 (4.31), 385 (4.37), and 467 (3.36); IR 960 cm^{-1} (*trans* CH=CH). Found: C, 77.10; H, 4.54; Cl, 13.35; N, 5.23%. Calcd for $C_{17}H_{12}ClN$: C, 76.84; H, 4.55; Cl, 13.34; N, 5.27%.]; (iii) **1d** [81%, mp 128—129 °C (from cyclohexane–dichloromethane), UV_{max} 236 nm (log ε 4.55) 288 (4.66), 323 (4.10), 366^{sh} (3.46), and 442 (3.17); IR 1690 (C=O) and 835 cm^{-1} (trisubstituted ethylene). Found: C, 72.06; H, 5.75; Cl, 9.85; N, 3.70%. Calcd for $C_{22}H_{20}ClNO_2$: C, 72.23; H, 5.51; Cl, 9.69; N, 3.83%.]; (iv) **2** [87%, mp 148—149 °C (from cyclohexane–dichloromethane), UV_{max} 256 nm (log ε 4.41), 292^{sh} (4.23), 371 (4.31), and 433 (4.04); IR 965 cm^{-1} (*trans* CH=CH). Found: C, 82.77; H, 5.44; N, 11.85%. Calcd for $C_{16}H_{12}N_2$: C, 82.72; H, 5.21; N, 12.06%].

*Reaction of **1a** with DMAD.* (*a*): A solution of compound **1a** (0.25 g) and DMAD (1.052 g) in benzene (30 ml) was heated under reflux for 48 h and the solvent was evaporated. Chromatography of the residue with benzene gave **4a** [0.033 g (9%), red prisms (from cyclohexane), mp 172—173 °C, UV_{max} 252 nm (log ε 4.72), 375 (4.17), 393 (4.13), 440 (3.78), 468 (3.71), 502 (3.51), and 537 (3.06); IR 1750, 1700, and 1675 (C=O) and 980 cm^{-1} (*trans* CH=CH). Found: C, 64.91; H, 4.82; Cl, 7.50; N, 2.82%. Calcd for $C_{26}H_{22}ClNO_6$: C, 65.07; H, 4.62; Cl, 7.39; N, 2.92%]. Further elution afforded a mixture of products, which were fractionally crystallized from cyclohexane–dichloromethane to give **3a** [0.085 g (24%), yellow prisms (from petroleum ether–dichloromethane), mp 168—169 °C, UV_{max} 226^{sh} nm (log ε 4.51) and 290 (3.83); IR 1735, 1722, and 1690 cm^{-1} (C=O); ^{1}H NMR δ=1.35 (3H, t, *J*=7 Hz, Me), 3.70 (3H, s, Me), 3.87 (3H, s, Me), 3.87 (1H, d, *J*=2 Hz, H-7a), 4.28 (2H, q, *J*=7 Hz, CH_2), 5.49 (1H, d, *J*=2 Hz, H-7), 5.60 (1H, d, *J*=11 Hz, H-1), 6.0—6.3 (2H, m, H-2 and 3), 6.85—7.05 (2H, m, phenyl), 7.15—7.3 (3H, m, phenyl), 7.22 (1H, d, *J*=11 Hz, H-4); MS *m/e* 481 and 479 (M^+), 339 and 337 (M^+—DMAD). Found: C, 65.33; H, 4.77; Cl, 7.59; N, 2.88%. Calcd for $C_{26}H_{22}ClNO_6$: C, 65.07; H, 4.62; Cl, 7.39; N, 2.92%] and **5a** [0.05 g (14%), brown needles (from ethanol), mp 148—149 °C (dec), UV_{max}

228 nm (log ε 4.54), 260 (4.28), 434 (4.38), 492sh (3.95), 530 (3.74), and 570 (3.43); IR 1725, 1705, and 1700 cm^{-1} (C=O). Found: C, 65.33; H, 4.68; Cl, 7.25; N, 2.86%. Calcd for $C_{26}H_{22}ClNO_6$: C, 65.07; H, 4.62; Cl, 7.39; N, 2.92%]. Elution with chloroform gave a red oil, which solidified upon trituration with petroleum ether to give **6a** (0.034 g, 7%). Crystallization from ethanol afforded yellow prisms, mp 157—158 °C, UV_{max} 238 nm (log ε 4.28), 288 (3.84), 327 (3.91), and 380 (3.64); IR 1735, 1725, and 1705 cm^{-1}. Found: C, 61.79; H, 4.65; Cl, 5.51; N, 2.14%. Calcd for $C_{32}H_{28}ClNO_{10}$: C, 61.79; H, 4.54, Cl, 5.70; N, 2.25%.

(*b*): A solution of compound **1a** (0.50 g) and DMAD (2.10 g) in xylene (30 ml) was heated under reflux for 24 h and the solvent evaporated. Chromatography of the residue with benzene gave **4a** (0.27 g, 38%) followed by **7a** [0.17 g (24%), yellow needles (from ethanol), mp 177—178 °C, UV_{max} 263 nm (log ε 4.07), 323 (3.95), and 394 (3.58); IR 1735, 1710, and 1690 cm^{-1} (C=O). Found: C, 65.14; H, 4.49; Cl, 7.18; N, 2.87%. Calcd for $C_{26}H_{22}ClNO_6$: C, 65.07; H, 4.62; Cl, 7.39; N, 2.92%]. Further elution gave **10a** (0.046 g, 6%), which crystallized as blue prisms from ethanol, mp 187—188 °C, UV_{max} ($CHCl_3$) 267 nm (log ε 4.54), 301 (4.23), 313 (4.24), 349 (4.63), 391 (3.88), and 665 (3.30); IR 1715, 1690, and 1680 cm^{-1} (C=O). Found: C, 63.24; H, 4.02; Cl, 7.34, N, 2.73%. Calcd for $C_{26}H_{20}ClNO_7$: C, 63.23; H, 4.08; Cl, 7.18; N, 2.84%. Benzene–chloroform (1:1) eluted **6a** (0.088 g, 10%).

Reaction of ***1b*** *with DMAD.* (*a*): A solution of compound **1b** (0.50 g) and DMAD (2.02 g) in benzene (30 ml) was heated and worked-up as for **1a**. Elution with benzene gave **4b** [0.069 g (10%), red prisms (from cyclohexane), mp 198—199 °C, UV_{max} 253 nm (log ε 4.73), 375 (4.14), 394 (4.11), 441 (3.71), 470 (3.66), 503 (3.45), and 542 (3.00); IR 1750, 1695, and 1675 (C=O) and 980 cm^{-1} (*trans* CH=CH). Found: C, 65.83; H, 4.94; Cl, 7.25; N, 2.57%. Calcd for $C_{27}H_{24}ClNO_6$: C, 65.65; H, 4.90; Cl, 7.18; N, 2.84%]. Elution with benzene–chloroform (1:1) afforded a mixture of products, which was fractionally crystallized to yield **3b** [0.385 g (55%), yellow prisms (from cyclohexane), mp 151—152 °C, UV_{max} 240 nm (log ε 4.17) and 293 (3.82); IR 1735, 1720, and 1683 cm^{-1} (C=O); ^{1}H NMR δ=1.34 (3H, t, *J*=7 Hz, Me), 2.30 (3H, s, Me), 3.68 (3H, s, Me), 3.81 (1H, d, *J*=2 Hz, H-7a), 3.85 (3H, s, Me), 4.27 (2H, q, *J*=7 Hz, CH_2), 5.60 (1H, d, *J*=2 Hz, H-7), 5.60 (1H, d, *J*=10 Hz, H-1), 6.0—6.25 (2H, m, H-2 and 3), 6.84 (2H, d, *J*=8 Hz, phenyl), 7.08 (2H, d, *J*=8 Hz, phenyl), 7.18 (1H, d, *J*=10 Hz, H-4). Found: C, 65.72; H, 4.82; Cl, 7.44; N, 2.59%. Calcd for $C_{27}H_{24}ClNO_6$: C, 65.65; H, 4.90; Cl, 7.18; N, 2.84%] and **5b** [0.02 g (3%), brown needles (from ethanol), mp 116—118 °C, UV_{max} 260sh nm (log ε 4.20), 447 (3.92), 487sh (3.75), 530 (3.02), and 575 (2.97); IR 1735 and 1705 cm^{-1} (C=O). Found: C, 65.81; H, 4.95; Cl, 7.02; N, 2.54%. Calcd for $C_{27}H_{24}ClNO_6$: C, 65.65; H, 4.90; Cl, 7.18; N, 2.84%]. Elution with benzene–chloroform (1:2) gave **6b** (0.058 g, 6%). Crystallization from ethanol gave yellow needles, mp 175—176 °C, UV_{max} 262sh (log ε 4.12), 326 (3.92), and 385 (3.65); IR 1735, 1727, and 1705 cm^{-1} (C=O). Found: C, 62.02; H, 4.65; Cl, 5.78; N, 2.11%. Calcd for $C_{33}H_{30}ClNO_{10}$: C, 62.32; H, 4.75; Cl, 5.57; N, 2.20%.

(*b*): A solution of compound **1b** (0.25 g) and DMAD (1.01 g) in xylene (30 ml) was heated and worked-up as for **1a**. Elution with benzene gave **4b** (0.166 g, 47%), **7b** [0.038 g (11%), yellow needles (from ethanol), mp 188—189 °C, UV_{max} 238 nm (log ε 4.13), 264sh (4.05), 324 (3.90), and 395 (3.59); IR 1735, 1710, and 1690 cm^{-1} (C=O). Found: C, 65.59; H, 4.80; Cl, 7.19; N, 2.73%. Calcd for $C_{27}H_{24}ClNO_6$: C, 65.65; H, 4.90; Cl, 7.18; N, 2.84%] and **10b** [0.019 g (5%), blue needles (from ethanol), mp 191—192 °C, UV_{max} ($CHCl_3$) 269 nm (log ε 4.54), 301 (4.17), 313 (4.19), 351 (4.65), 390 (3.98), and 665 (3.18); IR 1725, 1690, and 1680 cm^{-1} (C=O). Found: C, 63.93; H, 4.32; Cl, 6.78; N, 2.88%. Calcd for $C_{27}H_{22}ClNO_7$: C, 63.85; H, 4.37; Cl, 6.98; N, 2.76%], successively. Elution with benzene–chloroform (1:1) gave **6b** (0.075 g, 17%).

Reaction of ***1c*** *with DMAD.* (*a*): A solution of compound **1c** (0.50 g) and DMAD (2.67 g) in benzene (30 ml) was heated and worked-up as for **1a**. Elution of benzene gave starting material **1c** (0.025 g) first. Further elution yielded four products: (i) **7c** [0.013 g (2%), yellow needles (from cyclohexane), mp 167—168 °C, UV_{max} 268 nm (log ε 4.10), 337 (3.85), and 415 (3.60); IR 1735 and 1710 cm^{-1} (C=O). Found: C, 67.89; H, 4.35; Cl, 8.97; N, 3.20%. Calcd for $C_{23}H_{18}ClNO_4$: C, 67.73; H, 4.45; Cl, 8.69; N, 3.43%]; (ii) **4c** [0.317 g (41%), red prisms (from cyclohexane), mp 133—134 °C, UV_{max} 242 nm (log ε 4.71), 282sh (4.24), 292sh (4.14), 375 (4.14), 395 (4.13), 438 (3.80), 466 (3.79), 498 (3.63), and 535 (3.20); IR 1757 and 1670 (C=O) and 965 cm^{-1} (*trans* CH=CH). Found: C, 68.03; H, 4.57; Cl, 8.68; N, 3.35%. Calcd for $C_{23}H_{18}ClNO_4$: C, 67.73; H, 4.45; Cl, 8.69; N, 3.43%]; (iii) **5c** [0.196 g (26%), brown prisms (from cyclohexane), mp 205 °C (dec), UV_{max} 215 nm (log ε 4.58), 250sh (4.34), 285sh (4.15), 440 (4.34), 456 (4.34), 488sh (4.13), 527 (3.97), 565 (3.69), and 618 (3.13); IR 1727 and 1695 cm^{-1} (C=O). Found: C, 67.71; H, 4.60; Cl, 8.63; N, 3.39%. Calcd for $C_{23}H_{18}ClNO_4$: C, 67.73; H, 4.45; Cl, 8.69; N, 3.43%]; (iv) **6c** [0.164 g (16%), yellow prisms (from cyclohexane), mp 182.5—184 °C, UV_{max} 337 nm (log ε 3.75) and 400 (3.52); IR 1735, 1728, and 1707 cm^{-1} (C=O). Found: C, 63.32; H, 4.24; Cl, 6.56; N, 2.51%. Calcd for $C_{29}H_{24}ClNO_8$: C, 63.34; H, 4.40; Cl, 6.45; N, 2.55%].

(*b*): A solution of compound **1c** (0.30 g) and DMAD (1.60 g) in xylene (30 ml) was heated and worked-up as for **1a**. Elution with benzene gave **7c** (0.036 g, 8%), **4c** (0.28 g, 61%), and **10c** [(0.014 g (3%), blue prisms (from ethanol), mp 207—208 °C, UV_{max} ($CHCl_3$) 273 (log ε 4.32), 301 (4.01), 314 (4.04), 353 (4.33), 398 (3.88), 410sh (3.84), and 665 (3.37); IR 1730, 1720, and 1690 cm^{-1} (C=O). Found: C, 65.62; H, 3.91; Cl, 8.36; N, 3.07%. Calcd for $C_{23}H_{16}ClNO_5$: C, 65.49; H, 3.82; Cl, 8.40; N, 3.32%], successively. Elution with benzene-chloroform (1:1) gave **6c** (0.025 g, 4%).

Reaction of ***1d*** *with DMAD.* (*a*): A solution of compound **1d** (0.40 g) and DMAD (1.55 g) in benzene (30 ml) was heated and worked-up as for **1a**. Elution with benzene gave **4d** [0.006 g (1%), red prisms (from petroleum ether), mp 113—114 °C, UV_{max} 246 nm (log ε 4.77), 252sh (4.77), 374 (4.14), 392 (4.10), 439 (3.72), 467 (3.69), 500 (3.51), and 537 (3.10); IR 1730 and 1695 (C=O) and 830 cm^{-1} (trisubstituted ethylene). Found: C, 66.04; H, 5.27; Cl, 7.01, N, 2.71%. Calcd for $C_{28}H_{26}ClNO_6$: C, 66.21; H, 5.16; Cl, 6.98; N, 2.76%]. Further elution afforded **3d** [0.247 g (45%), yellow needles (from petroleum ether), mp 141—142 °C, UV_{max} 238 nm (log ε 4.12) and 291 (3.79); IR 1730 and 1710 cm^{-1} (C=O); ^{1}H NMR δ=0.83 (3H, t, *J*=7 Hz, Me), 1.33 (3H, t, *J*=7 Hz, Me), 1.58 (2H, q, *J*=7 Hz, CH_2), 3.68 (3H, s, Me), 3.85 (3H, s, Me), 4.27 (2H, q, *J*=7 Hz, CH_2), 5.27 (1H, s, H-7), 5.54 (1H, d, *J*=9 Hz, H-1), 6.0—6.5 (2H, m, H-2 and 3), 7.1—7.4 (6H, m, H-4 and phenyl). Found: C, 65,91; H, 5.19; Cl, 7.27; N, 2.74%. Calcd for $C_{28}H_{26}ClNO_6$: C, 66,21; H, 5.16; Cl, 6.98; N, 2.76%]. Elution

with chloroform gave an unidentified red compound (0.127 g).

(*b*): A solution of compound **1d** (0.20 g) and DMAD (0.78 g) in xylene (30 ml) was heated and worked up as for **1a** to yield **4d** (0.009 g, 3%), **3d** (0.042 g, 15%), and a red compound (0.039 g).

Reaction of 2 with DMAD. A solution of compound **2** (0.50 g) and DMAD (3.059 g) in benzene (50 ml) was heated under reflux for 1 h, the solvent was evaporated, and the residue was chromatographed with benzene–chloroform (1:1) to give **11** (0.064 g, 8%), which crystallized from ethanol as yellow needles, mp 184—186 °C (dec), UV_{max} 233 (log ε 4.54), 291 (4.46), 354 (3.95), 370^{sh} (3.94), 415 (3.84), 441 (3.96), 466 (3.92), and 497 (3.67); IR 1725 and 1700 (C=O) and 970 cm^{-1} (*trans* CH=CH). Found: C, 70.49; H, 4.77; N, 7.20%. Calcd for $C_{22}H_{18}N_2O_4$: C, 70.58; H, 4.85; N, 7.48%. Elution with benzene–chloroform (1:2) gave **12** (0.138 g, 17%). which crystallized from cyclohexane as red prisms, mp 167—168 °C (dec), UV_{max} 293 nm (log ε 3.98) and 455 (3.64); IR 1720 cm^{-1} (C=O). Found: C, 70.73; H, 4.88; N, 7.29%. Calcd for $C_{22}H_{18}N_2O_4$: C, 70.58; H, 4.85; N, 7.48%.

Thermal Rearrangement of 3. (*a*): A solution of compound **3a** (0.10 g) in xylene (30 ml) was heated under reflux for 24 h. The work-up gave **4a** (0.04 g, 40%), **7a** (0.02 g, 20%), and **10a** (0.006 g, 6%).

(*b*): Compound **3d** (0.06 g) was heated at 200 °C in a neat state for 10 min and chromatographed. Elution with benzene gave **4d** (0.036 g, 60%).

Oxidation of 7a. A mixture of compound **7a** (0.04 g), 2,3-dichloro-5,6-dicyano-1,4-benzoquinone (0.019 g) in xylene (10 ml) was heated under reflux for 24 h, the solvent was evaporated, and the residue was chromatographed on alumina. Elution with benzene gave **10a** (0.007 g, 17%).

Rearrangement of 3 on Silica Gel. A mixture of compound **3a** (0.05 g) and silica gel (10 g) in benzene was left to stand at room temperature for five days and then chromatographed. Elution with benzene–chloroform (1:1) gave **5a** (0.028 g, 56%). In a similar mannar, a mixture of compound **3b** (0.10 g) and silica gel (20 g) gave **5b** (0.06 g, 60%).

We thank Prof. T. Asao and Dr. M. Yasunami, Tohoku University, and Dr. A. Mori, Kyushu University, for the NMR spectral determinations.

References

1) Part V, N. Abe and T. Nishiwaki, *Heterocycles*, **12**, 1031 (1979).
2) Preliminary communication, N. Abe and T. Nishiwaki, *J. Chem. Soc., Chem. Commun.*, **1979**, 476.
3) For a review see R. M. Acheson and N. F. Elmore, *Adv. Heterocyclic Chem.*, **23**, 263 (1978).
4) N. Abe, Y. Tanaka, and T. Nishiwaki, *J. Chem. Soc., Perkin Trans. 1*, **1978**, 429.
5) C. A. Ramsden, *Tetrahedron*, **33**, 3203 (1977); K. Matsumoto and T. Uchida, *Chem. Lett.*, **1978**, 1093; K. T. Potts, S. K. Datta, and J. L. Marshall, *J. Org. Chem.*, **44**, 622 (1979); H. Gotthardt and F. Reiter, *Chem. Ber.*, **112**, 266 (1979); H, Koga, M. Hirobe, and T. Okamoto, *Tetrahedron Lett.*, **1978**, 1291.
6) E. Grovenstein and D. E. Lee, *J. Am. Chem. Soc.*, **75**, 2639 (1953); S. J. Dristol and W. P. Norris, *ibid.*, **75**, 2645 (1953).
7) R. M. Acheson and G. Procter, *J. Chem. Soc., Perkin Trans. 1*, **1977**, 1924.
8) T. J. Batterham, "NMR Spectra of Simple Heterocycles," Wiley, New York (1973), p. 203.
9) Symmetry-allowed thermal multi-components cycloadditions are known: T. Machiguchi, Y. Yamamoto, M. Hoshino, and Y. Kitahara, *Tetrahedron Lett.*, **1973**, 2627; T. Kaneda, T. Ogawa, and S. Misumi, *ibid.*, **1973**, 3373; D. J. Pasto and J. K. Borchardt, *J. Am. Chem. Soc.*, **96**, 6944 (1974).
10) An alternative mechanism, symmetry-allowed [$_\pi 2_s + {}_\sigma 2_a + {}_\sigma 2_a$] rearrangement was suggested by a referee. However, we prefer the rapid bond scission-recyclization mechanism, since steric repulsion between an aryl group and an ester group would be greater in transition state for the referee's mechanism than ours.
11) J. J. Barr and R. C. Storr, *J. Chem. Soc., Perkin Trans. 1*, **1979**, 185; E. C. Taylor and Turch, *Chem. Rev.*, **79**, 181 (1979); see also references cited in Ref. 4.
12) K. Auwers and G. Keil, *Ber.*, **36**, 3908 (1903).
13) T. R. Johnson, *Org. React.*, **1**, 210 (1942).
14) M. T. Bogert and D. Davidson, *J. Am. Chem. Soc.*, **54**, 334 (1932).

Oxidation of Methyl (Methylthio)methyl Sulfoxide

Katsuyuki OGURA,*,† Michiyo SUZUKI, and Gen-ichi TSUCHIHASHI*

Sagami Chemical Research Center, Nishi-Ohnuma 4-4-1, Sagamihara Kanagawa 229

† *Department of Synthetic Chemistry, Faculty of Engineering, Chiba University, Yayoi-cho 1-33, Chiba 260*

(Received November 9, 1979)

Oxidation of methyl (methylthio)methyl sulfoxide (**2**) with hydrogen peroxide in acetic acid or methanol produced bis(methylsulfinyl)methane in high yield. Similar results were obtained in oxidation of **2** with ozone, sodium metaperiodate, and *m*-chloroperbenzoic acid. In contrast, methyl (methylthio)methyl sulfone (**4**) was exclusively formed when oxidation of **2** with hydrogen peroxide was carried out in methanol in the presence of sodium hydroxide. Furthermore, we established a convenient and efficient method of preparing **4** by oxidation of **2** with potassium permanganate.

Methyl (methylthio)methyl sulfoxide (**2**) can be easily obtained by oxidation of bis(methylthio)methane (**1**) with hydrogen peroxide in acetic acid[1] and this compound has been revealed to be a versatile reagent for synthesizing many kinds of organic compounds.[2]

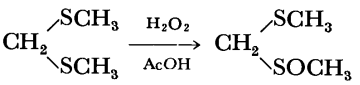

1 **2**

In order to search further uses for **2**, we examined oxidation of **2** with various oxidants and found an effective method leading to either bis(methylsulfinyl)-methane (**3**) or methyl (methylthio)methyl sulfone (**4**), both of which are expected to be useful synthetic reagents. Details of these oxidation reactions are described in the present paper.

Results and Discussion

Methyl (methylthio)methyl sulfoxide (**2**) was oxidized with one equiv-mol of hydrogen peroxide. In acetic acid, a smooth reaction took place and bis-(methylsulfinyl)methane (**3**) was given in 71% yield (86% yield based on the consumed **2**) as a mixture of its *meso* and *dl* diastereomers in the ratio of 61 : 39.[3] This ratio remained unchanged under moderate heating (150 °C) which is in sharp contrast with reported easy epimerization of bis(benzylsulfinyl)diphenylmethane.[4] In methanol, oxidation of **2** with hydrogen peroxide also afforded **3**, although the reaction proceeded rather slowly, and analogous results were obtained in oxidation of **2** with ozone, sodium metaperiodate, or *m*-chloroperbenzoic acid (MCPBA). The results are summarized in Table 1.

Table 1. Product distribution in oxidation of **2**

Oxidant	Solvent	Yield/%[a]	
		3	**4**
H_2O_2	AcOH	71 (61 : 39)	—
H_2O_2	MeOH	84 (61 : 39)	—
H_2O_2-NaOH	MeOH	—	78
O_3	CH_2Cl_2	90 (66 : 34)	—
$NaIO_4$	H_2O	85 (69 : 31)	—
MCPBA[b]	CH_2Cl_2	73 (64 : 36)	—
$KMnO_4$	CH_3COCH_3	—	97

a) The value in the parenthesis shows the ratio of the *meso* and *dl* forms. b) *m*-Chloroperbenzoic acid.

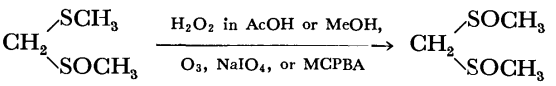

2 **3**

When oxidation of **2** with hydrogen peroxide was performed under alkaline conditions, methyl (methylthio)methyl sulfone (**4**) was exclusively produced in stead of **3**. Thus, large excess of hydrogen peroxide (utilized as a 35% aqueous solution) was dropwise added to a solution containing **2** and sodium hydroxide (one equiv to **2**) in methanol under keeping the reaction temperature below 50 °C and **4** was isolated in 78% yield. It is worth noting that **3** was not detected in the reaction mixture by NMR and TLC analyses. The structure of **4** was confirmed by the comparison of its IR and NMR spectra with an authentic specimen prepared by substitution of chloromethyl methyl sulfone with methanethiolate anion.[5]

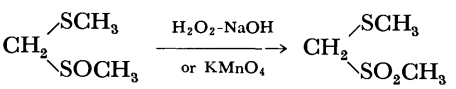

2 **4**

This exclusive formation of **4** from **2** can be explained in terms of nucleophilic oxidation with a peroxide anion formed by the reaction of hydrogen peroxide with sodium hydroxide, since perbenzoate anion in water–dioxane[6] and 1-phenylethylperoxide anion in a nonpolar solvent[7] were known to attack preferentially the positively-charged sulfur atom of a sulfoxide and convert it into the corresponding sulfone. Similar phenomena were also reported in the reactions with permanganate ion and osmium tetraoxide which could oxidize a sulfoxide without affecting a coexistent sulfide.[8,9] Hence, we tried to oxidize **2** with potassium permangante and established an efficient transformation of **2** into **4**. To a solution of **2** in acetone containing a small amount of water, was added an equiv-mol of potassium permanganate and the mixture was stirred at room temperature for 18 h. Usual work-up followed by column chromatography afforded **4** in 97% yield.

During the course of our investigation, Poje and Balenović reported that **4** was selectively obtained by oxidation of bis(methylthio)methane (**1**) with potassium permanganate.[10] However, the present method seems advantageous to the Poje-Balenović's method

from the synthetic viewpoint,[11] since the latter method requires controlling the reaction temperature at 0 °C for a longer period of time (8—10 d) and gives **4** in only moderate yield (70%).

Experimental

Oxidation of Methyl (Methylthio)methyl Sulfoxide (2) with Hydrogen Peroxide. a) In Acetic Acid: To a solution containing **2** (4.058 g: 32.7 mmol) in acetic acid (40 ml), was dropwise added a 30% aqueous solution (3.70 ml: 32.7 mmol) of hydrogen peroxide under cooling with ice-water and the resulting mixture was stirred for 7 h at room temperature. After addition of dichloromethane (500 ml), the acetic acid was neutralized with potassium carbonate (46.4 g) and the deposited solid was filtered off. The filtrate was dried (Na_2SO_4), evaporated *in vacuo*, and column-chromatographed on silica gel (using ethyl acetate–methanol as an eluent) to give the unconsumed **2** (729 ml: 5.88 mmol) and **3** (3.238 g: 23.1 mmol; 71%) as a colorless oil which crystallized on cooling. An NMR analysis showed that **3** consisted of two diastereomers in the ratio of 61:39:NMR ($CDCl_3$) of the major component: δ 2.94 (6H, s), 3.89 (1H, d, J=13.5 Hz), and 4.15 (1H, d, J=13.5 Hz);[3] NMR ($CDCl_3$) of the minor component: δ 2.85 (6H, s) and 4.09 (2H, s).

An analytical sample (*meso*:*dl*=57:43) was obtained by recrystallization from chloroform-diethyl ether: mp 44—84 °C[12] (lit,[3] mp of the *meso* form and the *dl* form 46—49 °C[13] and 92—94 °C, respectively); IR (neat) 1037 cm^{-1}. Found: C, 25.55; H, 5.80; S, 45.44%. Calcd for $C_3H_8O_2S_2$: C, 25.70; H, 5.75; S, 45.73%.

(b) In Methanol: To a solution of **2** (2.357 g:19.0 mmol) in methanol (10 ml), was added a 35% aqueous solution (2.0 ml: 20.6 mmol) of hydrogen peroxide and the resulting solution was stirred at room temperature for 81.5 h. After addition of dichloromethane (100 ml), the resulting mixture was dried (Na_2SO_4), and evaporated *in vacuo* to give a colorless oil (2.422 g), which was shown by an NMR analysis to consist of **2** (199 mg: 1.60 mmol) and two diastereomers (*meso*: *dl*=61:39) of **3** (2.223 g: 15.9 mmol; 84%).

c) In the Presence of NaOH: To a solution containing **2** (7.020 g: 56.6 mmol) and sodium hydroxide (2.25 g: 56.2 mmol) in methanol (20 ml), was dropwise added a 35% aqueous solution (8.0 ml: 82.3 mmol) of hydrogen peroxide over 40 min under keeping the reaction temperature below 50 °C. Further, a 35% aqueous solution (1.0 ml: 10.3 mmol) of hydrogen peroxide was added in one portion to cause gentle reflux for a time and then the reaction mixture was stirred at room temperature for 30 min. After addition of water (30 ml) and extraction with dichloromethane (70 ml×3), the organic layer was dried (Na_2SO_4), evaporated *in vacuo*, and subjected to column chromatography on silica gel, affording **4** (6.185 g: 44.2 mmol; 78%) as colorless crystals: mp 50—51.2 °C (from diethyl ether) (lit,[5] mp 50—51 °C); IR (KBr) 1293 and 1122 cm^{-1}; NMR ($CDCl_3$) δ 2.40 (3H, s), 3.01 (3H, s), and 3.82 (2H, s). Found: C, 25.78; H, 5.78; S, 45.83%. Calcd for $C_3H_8O_2S_2$: C, 25.70; H, 5.75; S, 45.73%.

These physical data were in complete agreement with those of an authentic sample prepared by substitution reaction of chloromethyl methyl sulfone with sodium methanethiolate as described below.

To a mixture containing dimethyl sulfoxide (19.7 g: 253 mmol) and potassium carbonate (10.0 g) in dichloromethane (150 ml), was portionwise added *N*-chlorosuccinimide (35.0 g: 262 mmol) over 30 min at room temperature under stirring. Then, the insoluble solid was filtered off and the filtrate was evaporated *in vacuo* to give an oil including crystals. After additon of carbon tetrachloride, the insoluble succinimide was removed by filtration and the filtrate was evaporated *in vacuo* to give a colorless oil which consisted mainly of chloromethyl methyl sulfoxide.[14] Without further purification, this oil was dissolved in acetic acid (45 ml) and, after additon of a 35% aqueous solution (45 ml) of hydrogen peroxide, the resulting solution was stirred at room temperature for 2 d. The reaction mixture was neutralized with an aqueous solution of potassium carbonate and extracted with dichloromethane. The extract was dried (Na_2SO_4), evaporated *in vacuo* and crystallized from ethanol to give chloromethyl methyl sulfone (27.43 g: 213 mmol; 79%) as colorless crystals: mp 55—56.5 °C (lit, mp 57.2—58.2 °C[15] and 55—56 °C[16]).

To a solution of chloromethyl methyl sulfone (2.57 g: 20.0 mmol) in *N*,*N*-dimethylformamide (45 ml), was added a 15% aqueous solution (15 ml: purchased from Tokyo Kasei Kogyo Co. Ltd.) of sodium methanethiolate and the resulting mixture was stirred at 50 °C for 3 h. After addition of water followed by extraction with dichloromethane, the organic layer was dried (Na_2SO_4) and evaporated *in vacuo*. The residue was recrystallized from ethanol to afford **4** (1.608 g:11.5 mmol; 57%) as colorless crystals: mp 48.5—50 °C.

Oxidation of 2 with m-Chloroperbenzoic Acid. *m*-Chloroperbenzoic acid (85% active; 1.08 g: 5.32 mmol) was added to a solution of **2** (620 mg; 5.0 mmol) in dichloromethane (10 ml), and then the resulting mixture was stirred for 1.5 h under cooling with ice-water. After addition of water (*ca.* 1 ml) and neutralization with potassium carbonate, the insoluble matter was filtered off and washed with ethyl acetate. The filtrate and the washings were combined and dried (Na_2SO_4). Evaporation *in vacuo* gave a colorless oil which was separated by column-chromatography on silica gel to give **3** (510 mg: 3.64 mmol; 73%). An NMR analysis showed that this product consisted of two diastereomers (*meso*: *dl*=64:36).

Oxidation of 2 with Ozone. Ozone, produced by silent discharge of oxygen, was passed through a solution of **2** (1.040 g: 8.39 mmol) in dichloromethane (10 ml) until the solution became blue. Evaporation *in vacuo* followed by column chromatography on silica gel gave **3** (1.051 g: 7.50 mmol; 90%) as a colorless oil which was shown by an NMR analysis to consist of two diastereomers (*meso*: *dl*=66:34).

Oxidation of 2 with Sodium Metaperiodate. A small amount (*ca.* 1 ml) of water and sodium metaperiodate (863 mg: 4.03 mmol) were added to **2** (498 mg: 4.02 mmol) and the resulting mixture was stirred for 4.5 h under cooling with ice-water. The insoluble solid was filtered off and washed with dichloromethane and ethyl acetate. The filtrate and the washings were combined, dried (Na_2SO_4), and evaporated *in vacuo*. The residue was subjected to column chromatography on silica gel to afford **3** (476 mg: 3.40 mmol; 85%) as a colorless oil which was shown by an NMR analysis to consist of two diastereomers (*meso*: *dl*=69:31).

Oxidation of 2 with Potassium Permanganate. To a solution containing **2** (1.327 g: 10.7 mmol) in acetone (50 ml) and water (2 ml), was added potassium permanganate (1.694 g:10.7 mmol) in several portions and the resulting mixture was stirred at room temperature for 19 h. The insoluble matter was filtered off and the filtrate was evaporated *in vacuo*. The residue was dissolved in dichloromethane and dried (Na_2SO_4). After evaporation *in vacuo*, the residue was subjected to column chromatography on silica gel (dichloromethane) to afford **4** (1.455 g: 1.03 mmol; 97%) as colorless crystals.

The authors would like to express their thanks to Professor Hirotada Iida of Chiba University for his encouragement and helpful discussion. We also wish to thank Mr. Shigeo Tomisawa and Mr. Hiroshi Kitazawa for their technical assistance.

References

1) K. Ogura and G. Tsuchihashi, *Bull. Chem. Soc. Jpn.*, **45**, 2203 (1972).

2) K. Ogura, Y. Ito, and G. Tsuchihashi, *Bull. Chem. Soc. Jpn.*, **52**, 2013 (1979) and the references cited therein.

3) **3** was obtained by periodate oxidation of **1** and the meso isomer of **3** showed nonequivalent diastereotopic methylene protons in the NMR spectrum: R. Louw and H. Nieuwenhuyse, *Chem. Commun.*, **1968**, 1561.

4) C. Y. Meyers and L. L. Ho, *Tetrahedron Lett.*, **1974**, 729.

5) P. Robson, P. R. H. Speakman, and D. G. Stewart, *J. Chem. Soc., C*, **1968**, 2180. We found that this substitution reaction proceeded more smoothly in *N,N*-dimethylformamide, compared with the reaction in ethanol previously reported (see Experimental Section).

6) R. Curci and G. Modena, *Tetrahedron Lett.*, **1963**, 1749 and **1965**, 863.

7) Y. Ogata and S. Suyama, *Chem. Ind. (London)*, **1971**, 707 and *J. Chem. Soc., Perkin Trans. 2*, **1973**, 755.

8) F. D. Chattaway and E. G. Kellett, *J. Chem. Soc.*, **1930**, 1352.

9) H. B. Henbest and S. A. Khan, *Chem. Commun.*, **1968**, 1036.

10) M. Poje and K. Balenović, *Tetrahedron Lett.*, **1978**, 1231.

11) **2** is commercially available and can be purchased from Nippon Soda Co. Ltd.

12) Since this mixture was very hygroscopic, the melting point was measured by using a sealed capillary tube in a H_2SO_4 bath and uncorrected. Other melting points reported herein were obtained with a Yanagimoto micro melting point apparatus and uncorrected.

13) This value was given for the melting point of the *meso* isomer containing a small amount of the *dl* isomer.[3]

14) G. Tsuchihashi and K. Ogura, *Bull. Chem. Soc. Jpn.*, **44**, 1726 (1971).

15) W. E. Truce, B. H. Birum, and E. T. McBee, *J. Am. Chem. Soc.*, **74**, 3594 (1952).

16) H. Richtzenhain and B. Alfredssohn, *Chem. Ber.*, **86**, 142 (1953).

Efficient Regioselective Aldol Condensation of Methyl Ketones Promoted by Organoaluminium Compounds, and Its Application to Muscone Synthesis

Jiro Tsuji,* Toshiro Yamada, Mitsumasa Kaito, and Tadakatsu Mandai
Department of Chemical Engineering, Tokyo Institute of Technology, Meguro, Tokyo 152

(Received November 16, 1979)

Dialkylaluminium aryloxide in combination with a tertiary amine was found to be a good reagent for regioselective aldol condensation of methyl ketones at the methyl side. Regioselective aldol condensation of 2-octanone was carried out using diisobutylaluminium phenoxide–pyridine. The intramolecular aldol condensation of 2,15-hexadecanedione promoted by the same reagent gave a mixture of dehydromuscones in 65% yield. Its hydrogenation produced muscone.

In our continuous effort to synthesize natural products from butadiene telomers, we attempted to synthesize muscone (3-methylcyclopentadecanone) (**3**). Muscone is a naturally occurring fragrant compound with musk odor. Many synthetic attempts for this unique 15-membered cyclic ketone have been made. One method carried out by Stoll is based on the intramolecular aldol condensation of 2,15-hexadecanedione (**1**) to form the 15-membered cyclic ketone (**2**).[1]

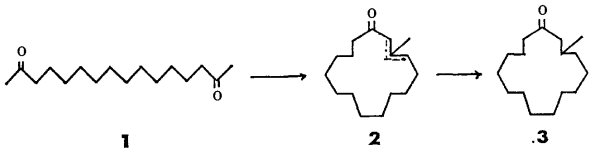

1 **2** **3**

Scheme 1.

Since the methyl group at 3-position of muscone need not be introduced separately, this synthetic scheme would be an elegant method if two inherent problems are solved. The first problem is a good synthetic method for the diketone **1** and the second one is a good method of aldol condensation. Concerning the first problem, the known methods are somewhat tedious.[2,3] We have reported new synthetic methods for this diketone using butadiene telomers.[4,5] Especially the synthesis starting from ethyl 3,8-nonadienoate is the convenient one.[6] The second problem of the intramolecular aldol condensation is an extremely difficult one. Aldol condensation is one of the most important means of carbon–carbon bond formation, but its utility in organic synthesis has been rather limited because of lack of selectivity.[7] The reaction is reversible and other competing reactions take place. Recently several ingenious methods have been reported on the controlled aldol condensation. In these methods, regioselective formation of enolate is essential. Regioselective formation of silyl enolates is a typical example. They are treated with titanium tetrachloride or ammonium fluoride to undergo regioselective cross aldol condensation.[8,9] However, these methods can not be applied to the present purpose of the intramolecular aldol condensation of diketone, because it is impossible to generate silyl enolate from the methyl side of one carbonyl group of the diketone, leaving the other carbonyl group intact. Also common bases such as alkyllithiums, and alkali alkoxides, are not suitable. In order to carry out the intramolecular aldol condensation of a diketone to form a macrocyclic ketone efficiently, the reaction must be rapid, irreversible, and regioselective. For this aldol condensation of the diketone, Stoll used magnesium amide derived from *N*-methylaniline and ethylmagnesium bromide.[1] This base presumably generates a magnesium enolate regioselectively which undergoes the aldol condensation. However, the desired aldol product having the 15-membered ring was obtained only in 17% yield, which is far from satisfaction. Thus it is imperative for us to devise a new method for the aldol condensation of this specific diketone. Our mechanistic consideration of the Stoll's method that the magnesium reagent generates magnesium enolate by coordinating to carbonyl group, while *N*-methylaniline assists the deprotonation leads us to a conclusion that magnesium is not a strong Lewis acid and some other metal compounds which have stronger Lewis acidity should be better. For this purpose, we selected organoaluminium compounds, because stronger Lewis acidity and high affinity to oxygen are expected with aluminium. We found our own organoaluminium compounds, which are very effective for regioselective aldol condensation, and successful aldol condensation of the diketone was achieved. Few studies have been reported on the aldol condensation using aluminium enolate.[10] Recently, successful cross aldol condensation *via* aluminium enolate generated by the treatment of carbonyl compounds with diethylaluminium 2,2,6,6-tetramethylpiperidide at low temperature has been reported.[11] By using our own organoaluminium compounds, successful aldol condensation of the diketone was achieved. A preliminary account of the work has already been given[12] and the details of the studies on the aluminium-promoted aldol condensation are presented in this paper.

Results and Discussion

Aldol Condensation of 2-Octanone. The first requisite in our studies is the regioselective aldol condensation at the methyl side of methyl ketones. For this purpose, we selected 2-octanone as a model compound and studied its aldol condensation using organoaluminium reagents. After considerable screening exper-

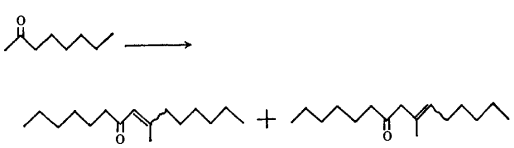

Scheme 2.

iments, we found that the aluminium compounds represented by a general formula R_2AlOAr afforded the desired enone as the aldol product selectively, but the yield was not high. The addition of tertiary amines as a proton capture produced the enone in high yields by suppressing undesired proton transfer. Then screening of the reaction conditions using R_2AlOAr–tertiary amine system was carried out by the addition of 2-octanone (1.0 mmol) in THF (3 ml) to a refluxing THF (6 ml) solution of R_2AlOAr–tertiary amine (3.0 mmol–3.0 mmol). The progress of the reaction was monitored by GLC. In this experiment, the aluminium reagent was used in an excess.

Concerning R in the reagent, ethyl and isobutyl were used, but no appreciable difference was observed (Fig. 1). Therefore, the most easily available isobutyl was used throughout this study. Then several phenols were tested as shown in Fig. 2. Phenol and *p*-cresol gave the highest yields, and *p*-*t*-butyl-, 2,6-dimethyl-, and *p*-methoxyphenol were less effective and *p*-nitrophenol was not satisfactory. From these results, phenol was our choice. As for the tertiary amines, no difference was observed among pyridine, 2,6-lutidine, and triethylamine as shown in Fig. 3. From the results of these screening experiments, we decided to adopt *i*-Bu_2AlOPh–pyridine system as the reagent throughout this study.

Then the effect of solvents was studied. The reaction proceeded at room temperature at moderate rate, but very rapidly by heating. The experiments were carried out at boiling temperatures of solvents. As shown in Figs. 4 and 5, nonpolar solvents such as benzene, toluene, and hexane seem to be the best solvents. In ethers, which coordinate to aluminium, the reaction was slower. In dioxane or 1,2-dimethoxyethane at their boiling temperatures, decomposition of the aldol product by secondary reactions took place at the same time. THF gave the better result at its boiling temperature. The reaction was slower in diethyl ether and dichloromethane. Consideration of the solubility of the aluminium reagent leads us to use a mixture of THF and hexane as a suitable solvent. In these experiments, an excess of the aluminium reagent was used, because in the desired intramolecular

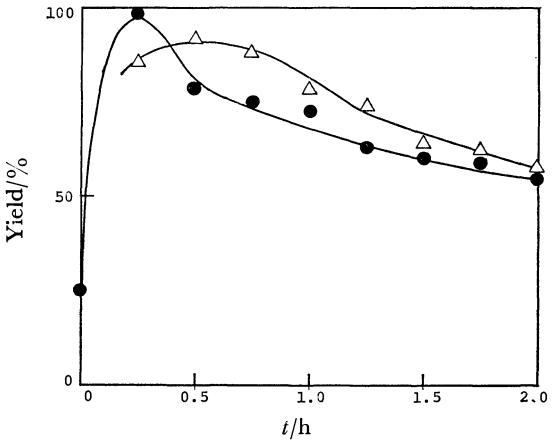

Fig. 1. Effect of alkyl groups in R_2AlOPh for aldol condensation of 2-octanone.
Conditions: R_2AlOPh/pyridine, THF reflux, △: R= ^{i}Bu, ●: R=Et.

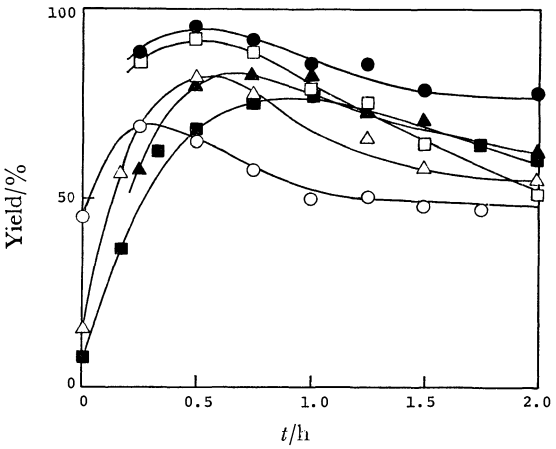

Fig. 2. Effect of aryloxy groups in $^iBu_2AlOAr$.
Conditions: $^iBu_2AlOAr$/pyridine, THF reflux, □: phenol, ▲: *p*-*t*-butylphenol, ■: 2,6-dimethylphenol, △: *p*-methoxyphenol, ○: *p*-nitrophenol, ●: *p*-cresol.

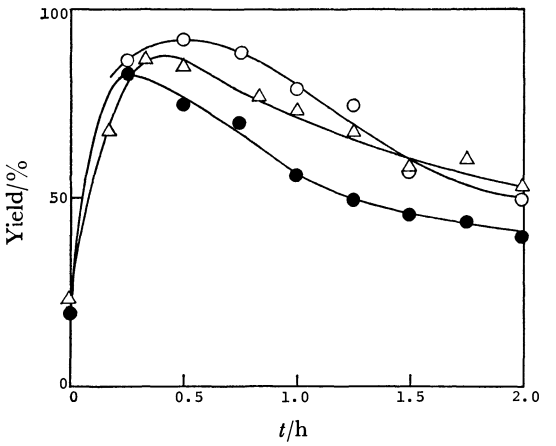

Fig. 3. Effect of amines.
Conditions: $^iBu_2AlOPh$/*t*-amine, THF reflux, △: triethylamine, ○: pyridine, ●: 2,6-lutidine.

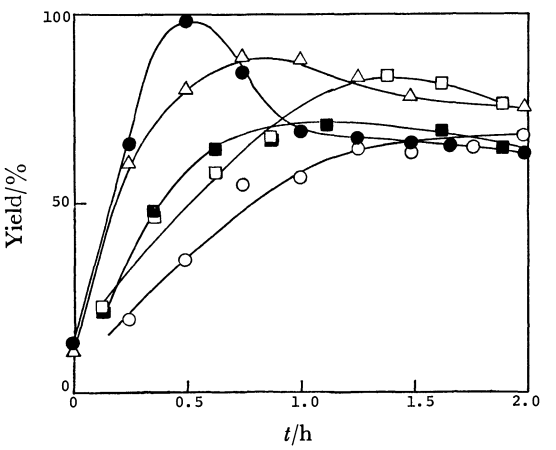

Fig. 4. Effect of solvents (1).
Conditions: $^iBu_2AlOPh$/pyridine, temp 52—57 °C, □: THF, △: benzene, ○: DME, ■: dioxane, ●: toluene.

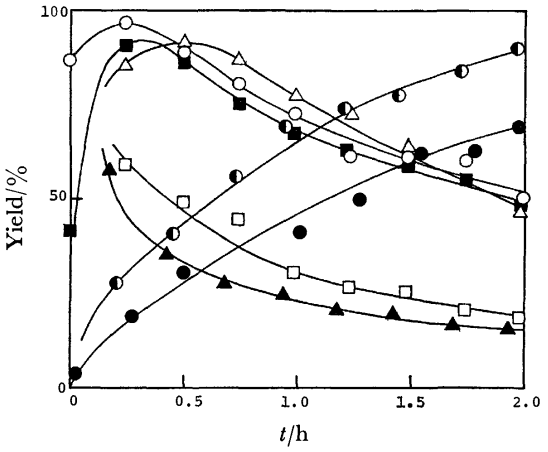

Fig. 5. Effect of solvents (2).
Conditions: $^{i}Bu_2AlOPh$/pyridine, reflux, ◐: Et_2O, ●: CH_2Cl_2, ○: hexane, ■: benzene, △: THF, □: DME, ▲: dioxane.

aldol condensation of the diketone, the aluminium reagent is present in an excess when the reaction is carried out under high dilution conditions by adding the diketone to the solution of the aluminium reagent, and the reaction conditions for the inter- and intramolecular reactions must be same. The yield of the desired aldol product reached at the maximum within one hour, and then other side reactions began to occur which decrease the yields of the aldol product. Therefore, the reaction must be stopped after short period of time.

Taking the above shown results into consideration, we have carried out the regioselective aldol condensation of 2-octanone in the following way. At first heptane solution of *i*-Bu_2AlH (7.6 mmol) was added at 0 °C to a solution of phenol (8.3 mmol) in THF. Then pyridine (9.0 mmol) was added at room temperature. The solution was brought to reflux and 2-octanone (10 mmol) was added in five minutes. After two hours, the reaction was quenched and the aldol product was isolated in 85% yield. The product was a mixture of 9-methyl-8-pentadecen-7-one and 9-methyl-9-pentadecen-7-one. Catalytic hydrogenation of the mixture afforded 9-methyl-7-pentadecanone as a single product. No product formed by the reaction at the methylene side was detected. 2-Butanone behaved similarly giving the expected aldol product.

Regioselective Aldol Condensation of 2,15-Hexadecanedione. We have confirmed that *i*-Bu_2AlOPh–pyridine is a good reagent for rapid, regioselective aldol condensation of 2-octanone and then we applied this reagent to the intramolecular aldol condensation of 2,15-hexadecanedione (**1**). Results of the experiments carried out under various conditions are summarized in table 1. In order to obtain a high yield of the aldol product, the use of 3—5 equivalents of the aluminium reagent was found to be essential, and the reaction was carried out under high dilution conditions by adding a diketone solution slowly. As the best yield, the desired aldol product was obtained in 65% after column chromatographic separation. In this case, some diketone was recovered, and the yield based on conversion was 78%, which seems to be satisfactory for this type of intramolecular aldol condensation to form the macrocyclic ketone. The reaction was carried out by adding the diketone solution (0.025 M, 40 ml) to *i*-Bu_2AlOPh/pyridine (0.04 M, 100 ml) by using a mechanically driven syringe over a period of 11 h under reflux. The product obtained was a mixture of double bond isomers **2**. Detailed analysis of the NMR spectrum showed that the mixture consists of *trans*-3-methyl-2-cyclopentadecenone (50%), *cis*-3-methyl-2-cyclopentadecenone (30%), and *trans*- and *cis*-3-methyl-3-cyclopentadecenone (20%). The mixture was hydrogenated using palladium on carbon to give muscone as a single product, which was identified by comparing its NMR and IR spectra with those of an authentic sample.

This efficient regioselective aldol condensation can be explained by the following mechanism. Coordination of aluminium to carbonyl oxygen and abstraction of proton from the less hindered methyl side with pyridine proceed concertedly to form the aluminium enolate **4**, which has a considerable life even at refluxing conditions. Then the attack of another carbonyl group forms the aldol product **5** which strongly coordinates to aluminium. Then liberation of diisobutylaluminium

Table 1. Intramolecular aldol condensation of 2,15-hexadecanedione

Entry	R_2AlOAr/R_3N (equiv./diketone[a])		Solvent/ml (b, c)		Yield/% d (e)
1	*i*-Bu_2AlOPh/Pyridine	(5)	THF	(50, 40)	42 (49)
2	*i*-Bu_2AlOPh/Pyridine	(5)	THF	(100, 40)	51 (75)
3	*i*-Bu_2AlOPh/Pyridine	(5)	Benzene	(100, 20)	32 (43)
4	*i*-Bu_2AlOPh/Pyridine	(5)	Benzene	(100, 40)	50 (61)
5	*i*-Bu_2AlOPh/Pyridine	(3)	THF Hexane	(20, 20) (80, 20)	47 (58)
6	*i*-Bu_2AlOPh/Pyridine	(4)	Hexane		65 (78)
7	*i*-Bu_2AlOPh/Pyridine	(5)	Hexane		59 (69)
8	Et_2AlOPh/2,6-Lutidine	(3)	Hexane		38 (41)
9	*i*-Bu_2AlOPh/2,6-Lutidine	(3)	Hexane		36 (43)
10	*i*-Bu_2AlOPh/2,6-Lutidine	(5)	Hexane		40 (50)

a) The diketone (1.0 mmol) was used. b) Solvent for the aluminium reagent. c) Solvent for the diketone. d) Isolated by column chromatography. e) Based on the consumed diketone.

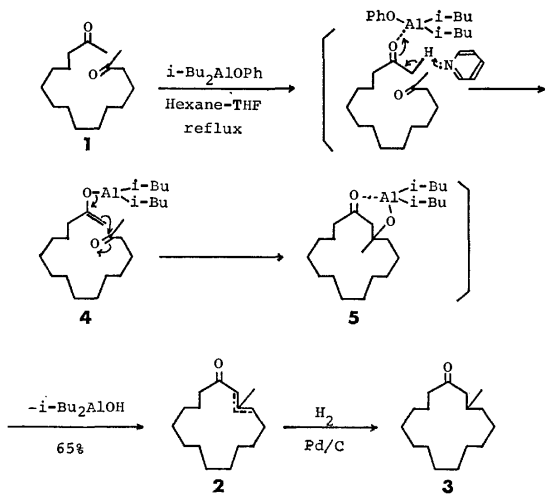

hydroxide forms the enone **2**.

Experimental

IR spectra were recorded as neat films on a JASCO-2 spectrometer. NMR spectra were recorded in CCl_4 on Hitachi R-24 (60 MHz) and Nippon Denshi PS-100 (100 MHz) with Me_4Si as an internal standard. Melting points were measured by Shibata (No. 297) melting point apparatus.

Materials: Diisobutylaluminium hydride was prepared by the thermal decomposition of triisobutylaluminium, followed by distillation, and used as a heptane solution (2.00 M). 2-Octanone, pyridine, and phenol were purified by distillation.

Aldol Condensation of 2-Octanone. A solution of phenol (880 mg, 8.3 mmol) in THF (10 ml) was placed in a 50 ml two-necked flask fitted with a reflux condenser and cooled to 0 °C. The heptane solution of *i*-Bu_2AlH (7.6 mmol, 3.8 ml) was added dropwise to the mixture at 0 °C with stirring. Then pyridine (9.0 mmol, 0.73 ml) was added at room temperature. The solution was gently refluxed and 2-octanone (1.28 g, 10 mmol) in THF (5 ml) was added dropwise in 5 min. After two hours, the mixture was cooled to 0 °C and 3 M-HCl was added. THF was removed *in vacuo*, and the residue was extracted with ether. The extract was washed with 5% NaOH, brine, and dried over $MgSO_4$. After removal of the solvent, the residue was purified by column chromatography (silica gel, hexane–ether 30/1) to give a mixture of 9-methyl-8-pentadecen-7-one and 9-methyl-9-pentadecen-7-one (1.01 g, 8.5 mmol, 85%). IR (neat) 2920, 1715, 1690, and 1620 cm^{-1}. NMR (CCl_4) δ 0.60—1.10 (m, 6H), 1.10—1.80 (m, 15.2H), 1.80—2.70 (m, 7H), 2.85—3.05 (m, 0.8H), and 5.90 (broad s, 1H).

Aldol Condensation of 2,15-Hexadecanedione. A solution of phenol (414 mg, 4.40 mmol) in THF (20.0 ml) was placed in a three-necked flask fitted with a reflux condenser and cooled to 0 °C. The heptane solution of *i*-Bu_2AlH (2.00 ml, 4.00 mmol) was added dropwise to the mixture at 0 °C with stirring. Then pyridine (0.40 ml, 379 mg, 4.80 mmol) and hexane (80.0 ml) were added at room temperature. A solution of 2,15-hexadecanedione (254 mg, 1.00 mmol) in THF–hexane (20 ml+20 ml) was added dropwise using a mechanically driven syringe over a period of 11 h at refluxing temperature with vigorous stirring. The reaction mixture was stirred for an additional hour. The mixture was cooled to 0 °C, and 3 M-HCl was added. The organic layer was separated, and the aqueous layer was extracted with ether (50 ml×3). The combined extracts were washed with 5% NaOH, brine, and dried over $MgSO_4$. Concentration of the extract gave a yellow oil, which was purified by column chromatography (silica gel, hexane–ether 20/1) to give a mixture of dehydromuscones **2** (156 mg, 65%). IR (neat) 2920, 1710, 1680, and 1605 cm^{-1}. NMR (CCl_4) δ 1.00—1.80 (m, 19.6H), 1.80 and 2.10 (s, 3H), 1.85—3.10 (m, 4.4H), 5.10—5.45 (m, 0.2H), and 6.00 and 6.05 (s, 0.8H); mass spectrum *m/e* 236 (M^+).

Preparation of Muscone. Catalytic hydrogenation of the dehydromuscones by Pd on carbon gave (±)-muscone in a quantitative yield. Its NMR and IR data, and GLC analysis were completely identical with those of an authentic sample. IR (neat) 2920 and 1710 cm^{-1}. NMR (CCl_4) δ 0.75—1.05 (m, 3H), 1.05—1.90 (broad s, 23H), and 1.90—2.45 (m, 4H). Semicarbazone mp 131.5—132.5 °C (Lit,[13] 131—132 °C).

References

1) M. Stoll and A. Rouve, *Helv. Chim. Acta*, **30**, 2019 (1947).
2) M. Stoll, *Helv. Chim. Acta*, **34**, 1817 (1951).
3) Y. Tsuzuki and S. Motoki, Japan Patent, 6626 (1957), *Chem. Abstr.*, **52**, 9821e (1958).
4) J. Tsuji, M. Mizutani, I. Shimizu, and K. Yamamoto, *Chem. Lett.*, **1976**, 773.
5) J. Tsuji, M. Kaito, and T. Takahashi, *Bull. Chem. Soc. Jpn.*, **51**, 547 (1978).
6) J. Tsuji, M. Kaito, T. Yamada, and T. Mandai, *Bull. Chem. Soc. Jpn.*, **51**, 1915 (1978).
7) A. T. Nealsen and W. J. Houlihan, *Org. React.*, **16**, 1 (1968).
8) T. Mukaiyama, K. Narasaka, and K. Banno, *Chem. Lett.*, **1973**, 1011; T. Mukaiyama, K. Banno, and K. Narasaka, *J. Am. Chem. Soc.*, **96**, 7503 (1974).
9) I. Kuwajima, E. Nakamura, and M. Shimizu, *J. Am. Chem. Soc.*, **99**, 1265 (1977).
10) E. A. Jeffery, A. Meisters, and T. Mole, *J. Organomet. Chem.*, **74**, 373 (1974) and literatures cited therin.
11) H. Nozaki, K. Oshima, K. Takai, and S. Ozawa, *Chem. Lett.*, **1979**, 379.
12) J. Tsuji, T. Yamada, M. Kaito, and T. Mandai, *Tetrahedron Lett.*, **1979**, 2257.
13) V. R. Mamdapur, P. P. Pai, K. K. Chakravarti, U. G. Nayak, and S. C. Bhattacharyya, *Tetrahedron*, **20**, 2601 (1964).

 © 1980 The Chemical Society of Japan Bull. Chem. Soc. Jpn., 53, 1421—1424 (1980)

Photochemical Type I and II Elimination Reactions of Dialkyl (Trichloromethyl)phosphonates

Nobutaka SUZUKI, Teruyuki KAWAI, Susumu INOUE,
Naoki SANO, and Yasuji IZAWA*

Chemistry Department, Faculty of Engineering, Mie University, Tsu 514

(Received December 7, 1979)

Irradiation of diisobutyl, dipropyl, and diethyl (trichloromethyl)phosphonates in MeCN gave corresponding monoesters and olefins *via* photochemical type II elimination. In addition, products *via* type I elimination were obtained from diisobutyl (trichloromethyl)phosphonate and its dimethyl ester.

In the previous paper, we briefly reported[1] that electron-withdrawing group attached on phosphorus atom of phosphonates compete with a double-bonded oxygen atom to attract electron, resulting in a stiffer P=O double bond and a higher frequence absorption and thus diisobutyl (trichloromethyl)phosphonate (**1a**) having a strongly electron-withdrawing group on phosphorus atom, photochemically decomposed by type II elimination to give the corresponding monoester and isobutylene.

In this paper, we wish to report further investigations on the photochemical elimination of dialkyl (trichloromethyl)phosphonates (**1a**, **1b**, and **1c**) in hope of exploring the exact nature of this reaction.

Results and Discussion

A solution of the phosphonates[2] (**1a**—**d**: 4.2 mmol: 24.7 mmol/l) in acetonitrile (170 ml) was flushed with nitrogen before and during irradiation to prevent photo-oxidation of the starting material and/or the product(s). During irradiation with a low-pressure mercury lamp (30 w; immersion type) the photo-reaction was monitored with GLC as the decrease of **1** (see Table 1).

The generated monoester (**2a**—**c**) and/or tetraalkyl hypophosphate (**4a** and **4d**) were isolated from the each resulting mixture by preparative TLC after evaporation. The R_f values of them were *ca.* 0.1 for **2a**—**c** and *ca.* 0.3—0.4 for **4a** and **4d**, respectively. The results and spectral data for the products, **2**, are shown in Tables 1 and 2, respectively.

Structure of **2a** had been reported in the previous paper[1] as a monoester of **1a** on the basis of its spectral properties. Both **2b** and **2c** showed very similar spectral properties to those of **2a**, respectively. Furthermore, the structures were confirmed by comparing IR spectra with the authentic samples prepared according

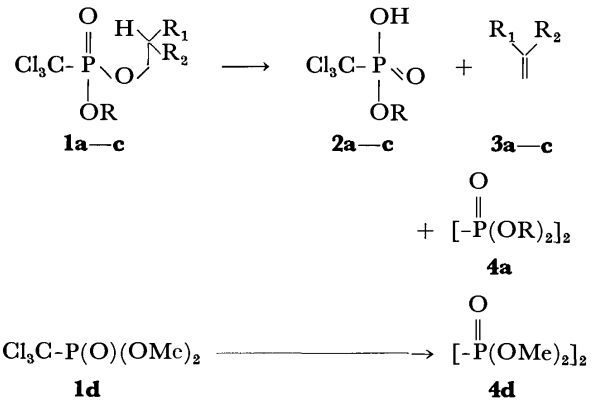

to the methods and analogous ones of Kamai and Kharasova[3] from thermal reactions of the parent phosphonic acid **5**[4] and the corresponding diesters (**1a**—**c**). (See Table 3). Thus, we conclude that **2b** and **2c** are the corresponding monoesters of **1b** and **1c**.

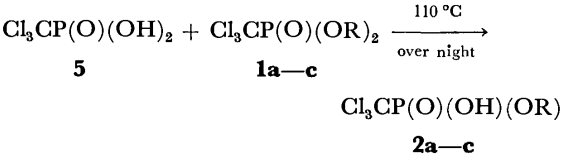

Obviously, the olefins and the monoesters are produced *via* the photochemical type II cleavage of **1**. Norrish type II reaction of carbonyl compounds having γ-hydrogen was now well documented,[5,6] however, that of phosphoryl compounds has been reported only in our preceding paper.[1] The present results reveal this type of reaction to be general in the (trichloromethyl)phosphonates.

In contrast, a product (**4d**) from photo-reaction of **1d** which can not give Norrish type II hydrogen abstraction by phosphoryl group, showed its molecular

Table 1. Photo-elimination of the phosphonates (**1a**—**e**)

1	R	R_1	R_2	Conv. %[a]	Time h	Yields/% 2[b]	3[c]	4[b]	Rel. ratio of Type II
a	*i*-Bu	Me	Me	28	2	7.2	15	60.7	0.83
b	*n*-Pr	Me	H	35	2	8.1	23.9	n.d.	0.66
c	Et	H	H	23	2	16.4	54.3	n.d.	1.00
d	Me	—	—	32	2	n.d.[e]	n.d.	92.5	
e	*n*-Bu	Et	H	18[d]	2	—	25.3[a]	n.d.	0.70

a) Determined by GLC. b) Isolated yield. c) Determined by GLC as dibromide. d) Irrad. externally in a quartz cell. e) Not detected.

Table 2. Spectral data for the generated and synthetic monoesters (**2a—c**)

	2a	**2b**	**2c**
MS	198.8877; $^{35}Cl_3CP(OH)_3^+$	198.8880	198.8880
(*m/z*)	198.889[a]		
	(calcd 198.889)	(calcd 198.889)	(calcd 198.889)
	137.0373; $P(O)(OH)(OC_4H_9)^+$	123.0223; $P(O)(OH)(OC_3H_7)^+$	109.0080; $P(O)(OH)(OC_2H_5)^+$
	137.037[a]		
	(calcd 137.036)	(calcd 123.021)	(calcd 109.006)
IR	1640, 1110 (P-OH)	1635, 1110	1630, 1085
(cm^{-1})	1245 (P=O)	1250	1245
	1040 (P-O-C)	1010	1040
	760 (P-C)	760	755
	550 (C-Cl)	550	545
NMR	identical with the appropriate starting material (**1a—c**) except the following signals.		
(δ ppm)	2.25 (1H, s)	2.19 (1H, s)	2.30 (1H, s)
	1.30 (1H, br.s)	1.30 (1H, br.s)	1.30 (1H, br.s)

a) Mass number of the photoproduct, see Ref. 1. b) On Silica gel PF_{254}-gipshaltig (Merck; thickness 2.2 mm; hexane-acetone, 5:1).

Table 3. Preparation of the monoesters (**2a—c**)

	R	**5**	**1a—c**	Yield/%[a]	Cryst.[b] color and form	Mp
a	*i*-Bu	100 mg	600.5 mg	92 mg (71.7%)	C-L	>250 °C
b	*n*-Pr	105	316	90 (70.8%)	C-CP	>300 °C
c	Et	115.7	318.6	80 (60.7%)	C-CP	228—229 °C

a) Based on **5**. b) C: colorless; L: leaflets; CP: crystalline powder.

peak at *m/z* 218 in MS. IR spectrum showed the presence of P=O bond and the absence of P–C and C–Cl bonds, and is identical with that of the authentic sample[7] prepared by the esterification of anhydrous hypophosphoric acid[8] (**6**) with diazomethane in ether. The NMR spectrum showed the presence of methyl protons which exhibited upfield shift by δ 0.32 ppm than that of **1d** and was very similar to that of $HP(O)(OMe)_2$ except P–H signal, and the Beilstein test was negative (Table 3). These data supported the structure, **4d**, which seems to be derived from the type I photo-elimination of **1d** as shown below. Photolysis of **1a** gave also an analogous compound, **4a**. Davies

$$\mathbf{1}^* \xrightarrow{\text{type I}} Cl_3C\cdot + \cdot P(O)(OR)_2$$

$$2\cdot P(O)(OR)_2 \longrightarrow \underset{\mathbf{4}}{[-P(O)(OR)_2]_2}$$

$$2Cl_3C\cdot \longrightarrow \underset{\mathbf{7}}{Cl_3C\text{-}CCl_3}$$

et al. observed the dialkoxyphosphinyl radicals, $\cdot P(O)(OR)_2$, by ESR spectra in photolysis of di-*t*-butyl peroxide in the presence of a dialkyl phosphonate, in the peroxide as solvent (R'=Me, Et, *i*-Pr, or *n*-Bu):[9] However,

$$t\text{-Bu-OO-}t\text{-Bu} \xrightarrow{h\nu} 2t\text{-BuO}\cdot$$

$$t\text{-BuO}\cdot + HP(O)(OR')_2 \longrightarrow t\text{-BuOH} + \cdot P(O)(OR')_2$$

product of hydrogen abstraction by the $\cdot P(O)(OR)_2$ radical, $H\text{-}P(O)(OR)_2$ was not detected in the present reactions. Thus, $\cdot P(O)(OR)_2$ radical would recombine with another one to afford **4**. On the other hand, hexachloroethane (**7**) was detected by GLC, which is supposed to be a coupling product of the partner radical, $\cdot CCl_3$.

The type **4** compounds, somehow, could not be detected in the photolyses of **1b** and **1c**.

The nitrogen streams bubbled through the each reaction mixture during irradiation were introduced into a bromine solution in carbon tetrachloride in order to trap the generated olefins, **3a—c**, and the resulting olefin dibromides (**8a—c**) were determined by GLC. For **1a** and **1e**, the olefin (**3a** and **3e**) in the reaction mixtures were also determined directly by GLC (Table 1).

The each yield of the corresponding **2** and **3** should be equal, if these compounds might be produced only *via* a type II reaction. However, the yields of **2** were lower than those of **3**. The lower yields may be explained by the difficulties on the determination of **2**. Thus, the monoesters (**2**) are very hygroscopic, hard to be eluated, and apt to be hydrolysed. In fact, when chromatographed on the silica-gel TLC, only 52% of the authentic sample of **2a** was recovered on elution. Thus, the yields of **3** were used to evaluate the type II elimination efficiency. For butyl derivative, **1e**, having secondary hydrogen as likely as **1b**, gave also **3** as much as from **1b**. This might suggest that the yield of **3b** reflected the true value of type II elimination.

As shown in Table 1, for **1b** and **1c** type II elimination exclusively occured, while competitive type I and II eliminations occured for **1a**. The competitive α-cleavage and γ-hydrogen abstraction of the phosphonates resemble to those of alkyl phenyl ketones[5c]

or alkanals.[5d] However, the relative rates of γ-hydrogen abstraction calculated from the yields of olefins slightly change as the γ-C–H bond strength, *i.e.*, 0.83, 0.66, and 1.00 for **1a**, **1b**, and **1c**. Comparing with those of phenyl alkyl ketones[6b] the reactivity of phosphoryl compounds is significantly different from that of ketones or alkanals.

Data of Turro and Weiss[5b] clearly demonstrate that the abstraction of the γ-hydrogen by alkyl ketones is most favorable when the hydrogen is directed toward the half-filled n orbital of the n-π^* excited carbonyl, that is, with on the hydrogen lying on the plane of the carbonyl group. The substituents at the γ-carbon atom may not affect sterically on the H-abstraction reaction rates. Therefore, reaction rates for the γ-hydrogen abstraction by an excited carbonyl group generally decrease in the order; tertiary>secondary>primary C–H bonds.

In contrast, for the type II elimination of dialkyl (trichloromethyl)phosphonates (**1**) a steric hindrance may play an important role in the reactivities. Thus, location of the γ-hydrogen near the phosphoryl oxygen atom seems to be sterically hindered by the bulky CCl_3 group. Examination of Dreiding models suggests that the co-planarity of the γ-hydrogen and O=P–C of the n-π^* excited states of phosphoryl group are sterically inhibited in the order; tert>sec≥prim C–H bonds, which probably reflect to the rates of type II elimination. In conclusion the efficiency of the present type II eliminations may be explained by both of the steric and the radical-stabilizing effects.

There were not great differences between the rates of the disappearnace of the starting materials (**1**). For the present reactions, it seems apparently that the type I elimination increases as the type II elimination decreases, which corresponds to that of carbonyl compound having been reported.[5b] Correlationship between the selectivity of the competitive α-cleavage and γ-hydrogen abstraction and their structure may be explained also by the steric hindrance mentioned above.

Experimental

All mp and bp were uncorrected. Following spectrometers were used for spectral measurements: IR: JASCO IR-G; UV: Shimadzu UV-200; NMR: JEOL JNM-MH-100 (100 MHz); MS: JEOL JMS-D-100; high MS were measured by JEOL Co. The spectral data are presented as follows: IR: in cm^{-1}; UV: in nm (ε given in parentheses); NMR: δ in ppm from int. TMS and J in Hz (accuracy ±0.3 Hz); and MS in m/z. GLC were carried out by Yanagimoto Yanaco G-80FP and G-1800F.

Materials. Dialkyl (trichloromethyl)phosphonates (**1a**—**e**) were prepared according to the literatures: **1a**: Colorless liquid, bp 72—74.5 °C/10^{-4} mmHg (lit, bp 109—110 °C/1 mmHg,[1] 144—145 °C/9 mmHg[2]) ν_{max}^{neat} 1280 (P=O), 1020 (P–O–C), 765 (P–C), 545 (C–Cl); λ_{max}^{MeCN} 256.5 (15.4), 300 (2.97); (ε_{254}^{MeCN} 14.9). **1b**: Colorless liquid, bp 59—61 °C/10^{-4} mmHg (lit,[2] bp 144—145 °C/12 mmHg), ν_{max}^{neat} 1275 (P=O), 1018 (P–O–C), 770 (P–C), 550 (C–Cl); (ε_{254}^{MeCN} 1.32). **1c**: Colorless liquid, bp 51—55 °C/5×10^{-3} mmHg (lit,[2] bp 122—123 °C/12 mmHg), ν_{max}^{neat} 1275 (P=C), 1018 (P–O–C), 765 (P–C), 550 (C–Cl); (ε_{254}^{MeCN} 0.39). **1d**: colorless liqiud, bp 52.5—54 °C/1.6×10^{-3} mmHg (lit,[2] bp 120—126 °C/12—13 mmHg; ν_{max}^{neat} 1282 (P=O), 1185, 1020 (P–O–C), 763 (P–C), 550 (C–Cl); (ε_{254}^{MeCN} 0.20). **1e**: Colorless liquid, bp 86—89 °C/4×10^{-3} mmHg (lit,[2] bp 145 °C/7 mmHg); ν_{max}^{neat} 1280 (P=O), 1028 (P–O–C), 768 (P–C), 552 (C–Cl); (ε_{254}^{MeCN} 0.48).

(Trichloromethyl)phosphonic acid (**5**) was prepared according to the literature; mp 158.5—161.5 °C (lit,[4] mp 163.2 °C).

Alkyl (trichloromethyl)phosphonates (**2a**—**c**) were prepared by analogous method of the literature[3] by thermal reactions (110 °C for 12 h in sealed tube) of the phosphonic acid (**5**) (1 equiv.) and the corresponding diester (**1a**—**c**, respectively; 2—3 equiv.). The results and spectral data of the products are summarized in Tables 2 and 3.

Tetramethyl hypophosphate (**4d**) was prepared by the method of the lit,[7] from the esterification of hypophosphoric acid (**7**)[8] with diazomethane in ether: Colorless liquid, bp 80 °C/2×10^{-4} mmHg (lit,[7] bp 85—87 °C/10^{-4} mmHg), m/z 218 (M^+) ν_{max}^{neat} 1460, 1260, 1180, 1020, 850, 825. Tetraisobutyl hypophosphate (**4a**) was prepared by the analogus method as above; colorless liquid, bp 92—94 °C/10^{-4} mmHg; m/z (M^+) 386; (Found: C, 49.42; H, 9.16%. Calcd for $C_{16}H_{36}O_6P_2$: C, 49.734; H, 9.391%).

Isobutylene (**3a**) was prepared with the general procedure dehydrating *t*-BuOH with anhydrous oxalic acid: Colorless liquid, δ (CCl_4) 1.70 (s, 6H), 4.62 (s, 2H). 1-Butene (**3e**) was prepared by the method of lit.,[10] reacting alkyl bromide with Grignard reagent (MeMgI): Colorless liquid, δ (CCl_4) 0.99 (t, 3H, J=7.0), 2.05 (m, 2H), 4.93 (m, 2H), 5.80 (m, 1H). 1,2-Dibromo-2-methylpropane (**8a**) was synthesized according to the lit,[11] Colorless liquid, bp 41—42.5 °C/17 mmHg (lit,[11] bp 165.6—166 °C). Propylene dibromide (**8b**) and ethylene dibromide (**8c**) were purchased from Tokyo Kasei Chem. Co.

Acetonitrile was dried over P_2O_5 and distilled from K_2CO_3 before use.

*Irradiation of Dialkyl (Trichloromethyl)phosphonates (**1a—d**):* Solution of the phosphonate (**1**) (4.2 mmol: 42.7 mM) in MeCN (170 ml) were irradiated directly with a low-pressure mercury lamp (Eikosha PIL-30; 30 w) in an immersion apparatus for 2—5 h at 20 °C. Nitrogen was bubbled through the solution before and during irradiation. Photoreaction was monitored by GLC as the decrease of the starting material (**1**) [10% SE-GE-31 on Diasolid L (60—80 mesh) in a stainless steel column 2.25 m, ϕ 2.5 mm; column temp, 180 °C; inj. temp, 250 °C; carrier gas (N_2); 50 ml/min; internal standard method].

The photoproducts were separated by preparative TLC [Silica gel PF_{254}-gipshaltig (Merck); 20×20 cm, thickness, 2.2 mm; 4-plates, hexane–acetone, 5:1], and the fractions were eluted with acetone. The results and spectral data of the products are summarized in Tables 1, 2, and 3.

The nitrogen streams bubbling through the solution during irradiation were introduced into bromine (0.5 g) solution of CCl_4 (20 ml) to trap the occuring olefins as olefin dibromides (**8**). These solutions were analyzed by GLC with the same column as above, [columm temp, 100 °C; inj. temp., 250 °C; carrier (N_2), 30 ml/min] and the olefin dibromides (**8a**—**c**) were assigned comparing the retention time in GLC with the corresponding authentic samples and the quantities were determined by the internal standard method.

The authors are grateful to JEOL Co. for the measurements of high mass spectra.

References

1) Previous paper in this series: Y. Ogata, Y. Izawa, and T. Ukigai, *Bull. Chem. Soc., Jpn.*, **46**, 1009 (1973), and references cited therein.

2) G. Kamai, and L. P. Egorova, *Zh. Obshch. Khim.*, **16**, 1521 (1946); *Chem. Abstr.*, **41**, 5439i (1947).

3) G. Kamai and F. M. Kharasova, *Zh. Obshch. Khim.*, **27**, 953 (1957); *Chem. Abstr.*, **52**, 3666a (1958).

4) A. Ya. Yakubovich and V. A. Ginsgurg, *Dokl. Akad. Nauk, SSSR*, **82**, 273 (1952); *Chem. Abstr.*, **47**, 2685 (1953); for IR: C. J. Pouchert, "The Aldrich Library of IR Spectra," Aldrich Chem. Co., Milwaukee, Wisconsin (1970), p. 410.

5) For examples: (a) J. A. Barltrop and J. D. Coyle, *Tetrahedron Lett.*, **1968**, 3235; (b) N. J. Turro and D. S. Weiss, *J. Am. Chem. Soc.*, **90**, 2185 (1968); (c) F. D. Lewis, R. W. Johnson, and D. E. Johnson, *ibid.*, **96**, 6090 (1974); (d) J. C. Dalton, M. W. Geiger, and J. J. Snyder, *ibid.*, **98**, 398 (1976).

6) (a) P. J. Wagner, *Tetrahedron Lett.*, **1968**, 5385; (b) *Acc. Chem. Res.*, **4**, 168 (1971): Photochemical abstraction of γ-hydrogen of phenyl alkyl ketones:

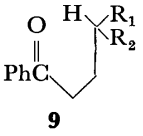

9

	R_1	R_2	Φ_{II}	$10^{-8} k_r(s^{-1})$
9a	Me	Me	0.25	4.8
b	Me	H	0.33	1.3
c	H	H	0.36	0.08

0.1 M ketone in benzene, 313 nm irradiation.

7) M. Baudler, *Z. Anorg. Allg. Chem.*, **288**, 171 (1956).

8) M. Baudler, *Z, Anorg. Allg. Chem.*, **279**, 115 (1955); E. Leininger and T. Chylski, *Inorg. Synth.*, **4**, 68 (1962).

9) A. G. Davies, D. Griller, and B. P. Roberts, *J. Am. Chem. Soc.*, **94**, 1782 (1972).

10) H. J. Lucas and R. T. Dillon, *J. Am. Chem. Soc.*, **50**, 1461 (1928).

11) M. S. Kharasch, W. Hered, and F. R. Mayo, *J. Org. Chem.*, **6**, 818 (1941).

 © 1980 The Chemical Society of Japan Bull. Chem. Soc. Jpn., 53, 1425—1434 (1980)

The Total Syntheses of Chamaecynone, Isochamaecynone, and Dihydroisochamaecynone[1)]

Masayoshi Ando,* Toyonobu Asao,[2)] Norio Hiratsuka,[3)]
Kahei Takase, and Tetsuo Nozoe[4)]

Department of Chemistry, Faculty of Science, Tohoku University, Aramaki-aza-Aoba, Sendai 980

(Received July 16, 1979)

A novel acetylenic nor-sesquiterpene, chamaecynone, and its related natural products, isochamaecynone and dihydroisochamaecynone, have been synthesized starting from α-santonin. In the base-induced equilibration of three pairs of compounds, chamaecynone and isochamaecynone, 4β*H*,5β-13-noreudesm-11-yn-3-one and 4α*H*, 5β-13-noreudesm-11-yn-3-one, and 4β*H*,5β-13-noreudesm-11-en-3-one and 4α*H*,5β-13-noreudesm-11-en-3-one, the ΔH values were determined to be +1.47 kcal/mol, +0.77 kcal/mol, and −2.28 kcal/mol respectively.

Chamaecynone (**1**), one of the nor-sesquiterpenes originally isolated from the essential oil of the Benihi tree (*Chamaecyparis formosensis* Matsum., Cupressaceae), has been shown to have a novel non-steroid *cis*-decalin conformation and to be one of the first examples of a natural acetylenic compound of terpenoid origin.[5)] Recently this compound has become of particular interest because of its efficient termiticidal activity without any significant toxicity on humans or domestic animals.[6,7)]

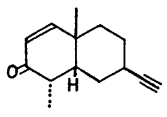

(1)

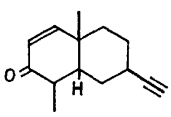

(2)

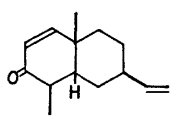

(3)

This paper will detail the total syntheses of chamaecynone and the related natural products, isochamaecynone (**2**) and dihydroisochamaecynone (**3**), in optically active forms.

Syntheses

We chose α-santonin (**4**) as the starting material of these syntheses mainly for the following four reasons: 1) Pure α-santonin is commercially available in large quantities, and its total synthesis has already been completed.[8)] 2) α-Santonin is conveniently functionalized as the starting material of the syntheses of chamaecynone and its related compounds, including the absolute configuration. 3) Since the *cis*-decalin intermediates in these syntheses are expected to be conformationally mobile, the optically active starting material is convenient for following the stereochemistry of intermediates by the analyses of CD or ORD curves. 4) Since chamaecynone is a bioactive compound, we want to get enough of chamaecynone and its related compounds in optically active forms for their bioassay.

In the syntheses of chamaecynone and its related compounds, there are three problems to overcome: 1) how to introduce the AB *cis*-ring junction, 2) how to introduce the terminal double bond (in dihydroisochamaecynone) or the terminal triple bond (in chamaecynone and isochamaecynone), and 3) how to introduce the α,β-unsaturated carbonyl moiety with an α-oriented methyl group (in chamaecynone) or a β-oriented methyl group (isochamaecynone and dihydroisochamaecynone) at the C_4-position. Keeping these problems in mind, we planned and carried out the syntheses according to the accompanying flow chart.

The first target was the preparation of the *cis*-decalone derivative (**7**). According to the method reported by Ishikawa,[9)] α-santonin was transformed into 6-episantonin (**5**), which was then easily reduced by zinc and acetic acid in methanol to give dienone carboxylic acid (**6**), although α-santonin had been recovered under the same conditions.[10)] Since the stereochemical course of the hydrogenation of α,β-unsaturated ketones is generally influenced by the presence of an acid or base, and by the solvent and catalyst employed,[11)] we examined the conditions of the catalytic hydrogenation of **6**; the best results will be presented below. The catalytic hydrogenation of **6** in ethanol containing potassium hydroxide (1.8 equiv) in the presence of 5% Pd/C gave a *ca.* 3:1 mixture of *cis*-**7** and *trans*-**20**. Fortunately, **7** was easily separated from the mixture by recrystallization. In agreement with the structure, the ORD curve of **7** exhibited a negative Cotton effect; on the contrary, the ORD curve of **20** showed positive Cotton effect.[15)]

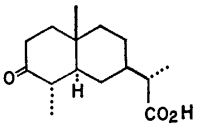

(20)

The next problem is the replacement of the carboxyl group of **7** with halogen. For this purpose, the Hunsdiecker reaction is well knwon. The silver salt of **7** was treated with bromine or iodine in carbon tetrachloride, but the results were disappointing. Probably the free halogen employed in this reaction attacked not only the silver salt of carboxyl group, but also the α-position of the carbonyl group to give a complex mixture. The application of Kochi's chlorodecarboxylation reaction[12)] to **7** gave an excellent result. Compound (**7**) was treated with lithium chloride (7 equiv) and lead tetraacetate (8 equiv) in refluxing benzene to give a desired chloro ketone (**8**) as a single stereoisomer, although the stereochemistry at C_{11} was not determined. When the ratio of lithium chloride to lead tetraacetate was increased, the chlorination of the α-position of the carbonyl group occurred, along with chlorodecarboxylation. When lithium bromide or lithium iodide was employed instead of lithium chloride, the reaction gave a complex mixture.

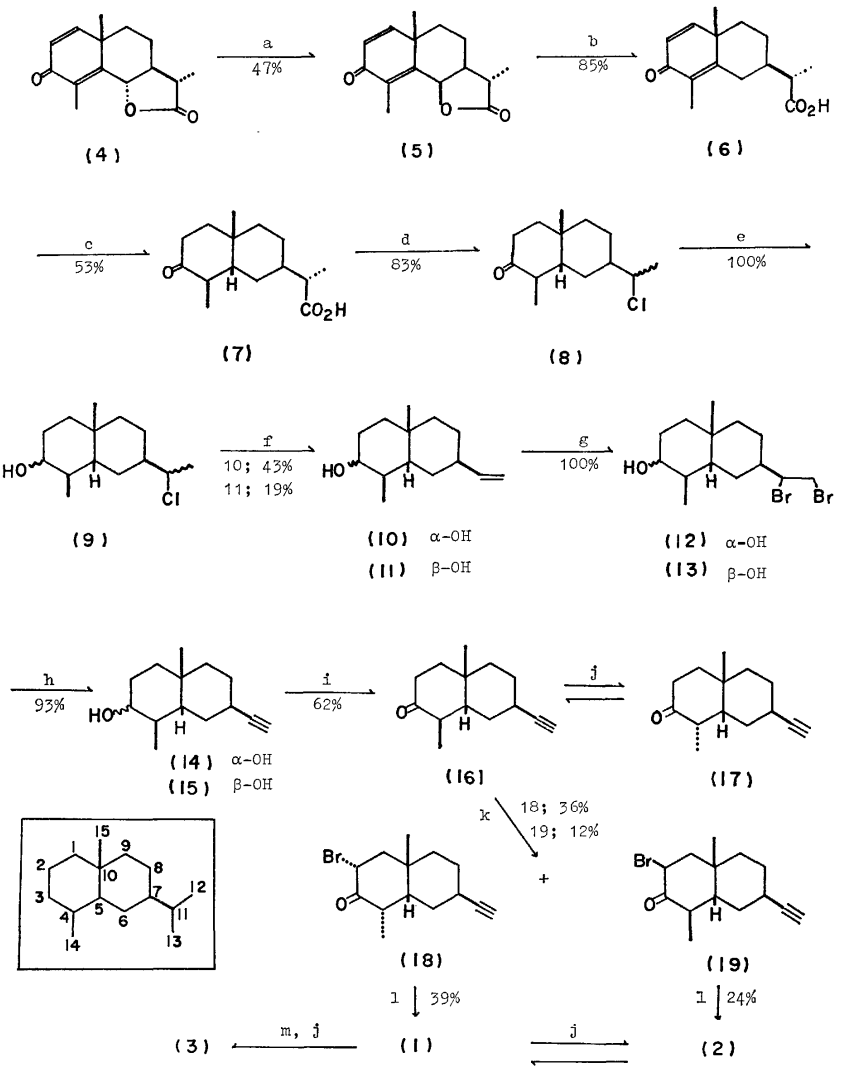

a: HCl gas, DMF; b: Zn, AcOH, MeOH; c: H_2, 5% Pd/C, KOH/EtOH; d: LiCl, $Pb(OAc)_4$, C_6H_6; e: $NaBH_4$, MeOH, ether; f: 1 M *t*-BuOK/*t*-BuOH; g: Br_2, CCl_4; h: 1 M *t*-BuOK/*t*-BuOH, C_6H_6; i: $CrO_3 \cdot 2Py$, Py; j: OH^- or H_3O^+; k: 48% HBr, Br_2, AcOH; l: LiBr, Li_2CO_3, DMF; m: H_2, Lindlar catalyst.

Scheme 1.

In the next step we envisioned the regioselective introduction of a double bond at the terminal position by the dehydrochlorination of **8** or an analogous method. Compound (**8**) was treated with lithium chloride and lithium carbonate in *N*,*N*-dimethylformamide to give a complex mixture of the double-bond isomers. Compound (**8**) was inert toward dehydrochlorination with such amines as *N*,*N*-dimethylaniline and collidines or toward substitution reactions with dimethylamine, bromide ions, and iodide ions. Since attempted dehydrochlorination of **8** with potassium *t*-butoxide gave unidentified acidic products by the air oxidation of the enolate anion of **8**,[13] we decided to try the same reaction after the protection of the carbonyl group.

The acetalization of **8** under standard conditions gave chloro acetal (**21**). The treatment of **21** with potassium *t*-butoxide gave the desired olefinic acetal (**22**). The deacetalization of **22** with dil. hydrochloric acid in ethanol gave a 2:1 mixture of **23** and **24**. The

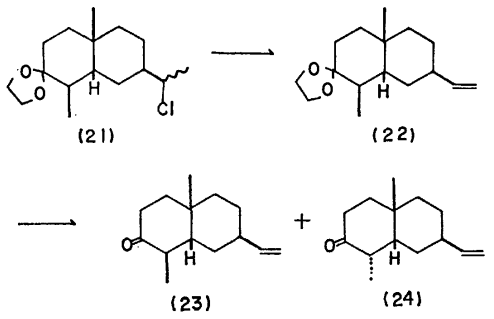

stereochemistry of **23** and **24** will be discussed below.

The dehydrochlorination of **8** was achieved by an alternate route. The reduction of **8** with sodium borohydride gave an oily mixture of epimeric alcohols (**9**). The dehydrochlorination of **9** with potassium *t*-butoxide gave a mixture of olefinic alcohols, which then afforded a 3α-alcohol (**10**) and 3β-alcohol (**11**) in 43% and 19% yields respectively after separation,

The oxidation of **10** and **11** gave the same ketone (**23**), while the catalytic hydrogenation of **23** afforded hexahydroisochamaecynone (**25**), which was identical with an authentic sample in its IR and NMR spectra.[5]

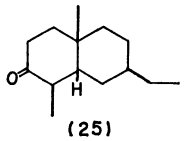

(25)

In the following steps we envisioned an approach to isochamaecynone which consisted of the bromination of **23** and the successive dehydrobromination of the resulting tribromide (**26**). The bromination of **23** with bromine (2 equiv) in carbon tetrachloride gave a tribromide (**26**). The dehydrobromination of **26** with potassium *t*-butoxide gave a complex mixture whose IR spectrum showed a strong absorption of the terminal triple bond at 3280 cm^{-1} but no absorption of an α,β-unsaturated carbonyl group. The treatment of **26** with lithium bromide and lithium carbonate in *N,N*-dimethylformamide or with such amines as *N,N*-dimethylaniline, collidines, and dimethylamine gave a mixture whose IR showed an absorption of an α,β-unsaturated carbonyl group, but no absorption of a triple bond. An attempted synthesis of dihydroisochamaecynone by the dehydrohalogenation of the bromo chloro ketone (**27**), which had been prepared

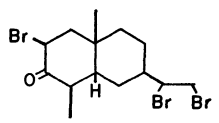

(26)

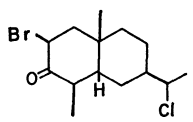

(27)

from **8**, gave analogous negative results. Since these results suggested that the reaction conditions of the formation of an α,β-unsaturated carbonyl moiety and a terminal triple bond were quite different, we decided to introduce these functional groups step by step.

The bromination of **10** gave a dibromide (**12**) as a diastereomeric mixture at C_{11}. The dehydrobromination of **12** with potassium *t*-butoxide gave an acetylenic alcohol (**14**), which was subsequently oxidized with the chromium trioxide–pyridine complex gave the desired acetylenic ketone (**16**). For practical purposes, **16** was prepared from **8** in a 32% overall yield without any separation or purification of the intermediates. The equatorial configuration of the C_4–Me group of **16** was suggested from the solvent effect in the NMR spectrum on passing from CCl_4 to benzene.[14] The ORD curve showed a negative Cotton effect, which was in accordance with the expected sign for **16**, with the steroid conformation bearing a $\beta(eq)$-methyl group at C_4.[15]

The bromination of **16** with bromine in acetic acid in the presence of hydrobromic acid afforded two kinds of unstable monobromides (**18** and **19**) after separation by column chromatography. The NMR spectrum of **18** in CCl_4 exhibited peaks at δ 0.98 (d, J=6.5 Hz, C_4–Me), 1.33 (s, C_{10}–Me), 1.85 (d, J=2.5 Hz, –C≡CH), and 4.57 (q, J=7.5 and 13.0 Hz, C_2–H). In particular, the bromine atom at C_2 was shown to be situated in an equatorial position by the magnitude of the coupling constans of C_2–H. This assignment was also supported by the IR absorption of the carbonyl group, which appeared a frequency higher by 20 cm^{-1} than that of **16**.[16] Judging from the reaction conditions, the C_4–Me group of **18** was deduced to be thermodynamically the more stable equatorial configuration. In addition, the $\alpha(eq)$-configuration of the C_4–Me group was confirmed by the transformation of **18** to chamaecynone, as will be shown later. The ORD curve of this compound showed a positive Cotton effect, which was in accordance with the expected sign for **18**, with the non-steroid conformation bearing an $\alpha(eq)$-bromine atom at C_2 and an $\alpha(eq)$-methyl group at C_4.

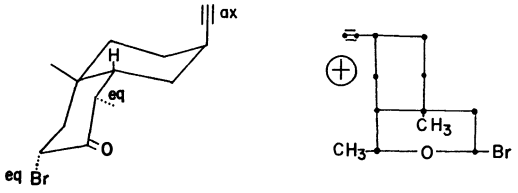

(18) Non-Steroid conformation

On the other hand, the NMR spectrum of **19** in carbon tetrachloride showed peaks at δ 1.09 (d, J=6.0 Hz, C_4–Me), 1.12 (s, C_{10}–Me), 1.90 (d, J=2.0 Hz, –C≡CH), and 4.75 (q, J=7.0 and 12.5 Hz, C_2–H). The coupling pattern and constant of the signal at δ 4.75 showed that the bromine atom at C_2 was equatorial. This assignment was also supported by the IR spectrum. The C_4–Me group of **19** was deduced to be thermodynamically the more stable equatorial configuration, considering the reaction conditions. In addition, the $\beta(eq)$-configuration of the C_4–Me group was confirmed by the transformation of **19** to isochamaecynone, as will be shown later. The ORD curve of this compound showed a negative Cotton effect, which was explained by the structure **19** in the steroid conformation bearing a $\beta(eq)$-bromine atom at C_2 and a $\beta(eq)$-Me group at C_4.

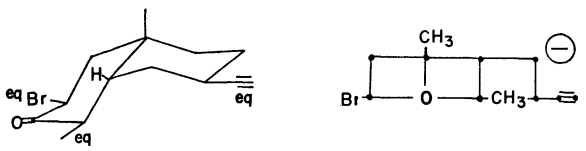

(19) Steroid conformation

The formation of the bromides **18** and **19** starting from **16** can reasonably be explained as follows. The ketone (**16**) was epimerized at C_4 in the presence of hydrobromic acid to give an equilibrium mixture of **16** and its C_4-epimer, **17**. The bromination of **16** and **17** in the reaction mixture at the C_2-position gave **19** and **18** respectively. The isolation of **17** and a detailed discussion of the stereochemistry will appear in a later section. The preferential formation of α-bromo ketones from **16** under those reaction conditions can also be reasonably explained by the reaction-rate difference between the bromination on an enol double bond and that on a termianl triple bond.[17] On the contrary, when **16** was brominated in acetic

acid in the presence of sodium acetate, **16** absorbed bromine slowly, giving a dibromide (**28**) as the sole product.

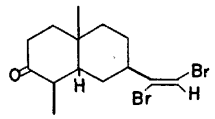

(28)

The dehydrobromination of **18** with lithium bromide and lithium carbonate in *N,N*-dimethylformamide produced chamaecynone, which was identical with natural material in its mixed melting point, thin-layer and gas-chromatographic behavior, and IR, NMR, and Mass spectra, and ORD curve.

The dehydrobromination of **19** with lithium bromide and lithium carbonate in *N,N*-dimethylformamide gave isochamaecynone (**2**). Although isochamaecynone was not isolated in a pure state from the natural surce,[5] these NMR absorptions were in accordance with those corresponding to isochamaecynone in the equilibrium mixture of chamaecynone and isochamaecynone, which was easily obtained by the base treatment of chamaecynone. In agreement with the structure **2** the product exhibited the absorption of a terminal triple bond at 3300 and 2123 cm^{-1} and the absorption of an α,β-unsaturated carbonyl group at 1672 cm^{-1} in its IR spectrum (KBr). The ORD curve (n-π^*) showed a negative Cotton effect which agreed with the sign expected from isochamaecynone, with the steroid conformation bearing a $\beta(eq)$-methyl group at C_4.[15,18]

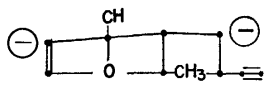

Octant Projection of **2**

Since the isolated yields of the bromides **18** and **19** were poor, probably because of their chromatographic unstability, we tried to prepare chamaecynone and isochamaecynone employing a crude mixture of bromides. In this case, *ca.* a 1:1 mixture of chamaecynone and isochamaecynone was obtained in a 65% yield, based on **16**, accompanied by a 10% yield of dehydrochamaecynone (**29**).

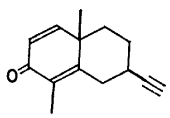

(29)

Since naturally occurring chamaecynone has already been converted to dihydroisochamaecynone, the total synthesis of **3** has also been completed formally.[5]

The Stereochemical Studies

In the course of the structural determination of chamaecynone, it was observed that hexahydrochamaecynone (**30**) was quantitatively isomerized to hexahydroisochamaecynone by base treatment. On the other hand, dihydrochamaecynone (**31**) gave an equilibrium mixture consisting of 10% of dihydrochamaecynone and 90% of dihydroisochamaecynone, whereas chamaecynone afforded an equilibrium mixture of 70% of chamaecynone and 30% of isochamaecynone.[5] These results strongly suggested that the relative stability of normal-series compounds (chamaecynone, dihydrochamaecynone, and hexahydrochamaecynone) to iso-series compounds (isochamaecynone, dihydroisochamaecynone, and hexahydroisochamaecynone) depended upon the bulkiness of the β-substituent at the C_7-position.

In this section we want to deal with the analyses of the energy difference between three pairs of normal- and iso-series compounds, chamaecynone and isochamaecynone, **17** and **16**, and **24** and **23**. The values for ΔH and ΔS of the equilibrium reaction were calculated using the values found for the equilibrium constant, K, and fitting a straight line to Eq. 1:

$$\ln K = -\left(\frac{1}{T}\right)\left(\frac{\Delta H}{R}\right) + \frac{\Delta S}{R} \quad (1)$$

Equilibration of Chamaecynone and Isochamaecynone. Chamaecynone was treated with a 2% potassium hydroxide solution of ethanol for 6 h and then quenched by the use of aqueous acetic acid solution. The ratio of chamaecynone and isochamaecynone was determined by gas-chromatographic analyses. A plot of $\ln K$ *vs.* $1/T$ was made and was found to be linear. From the slope and intercept of the line, the thermodynamic constants of the equilibrium reaction were determined.

ΔH and ΔS were determined to be +1.47 kcal/mol and +2.69 e.u. respectively. Although no equilibration data starting from isochamaecynone were obtained because of its limited aomunt, isochamaecynone gave the same composition mixture as chamaecynone at 25 °C in a 2% potassium hydroxide solution of ethanol.

*Equilibration of **17** and **16**.* The equilibration data for the **17**⇌**16** reaction, starting from **16** were determined to be as shown in Table 2 by the procedures mentioned above.

The C_4-epimer (**17**) was isolated from the equilibrium mixture by column chromatography. The small downfield shift [$\delta_{(CCl_4)}-\delta_{(C_6H_6)}$] of the C_4-methyl

Table 1. Equilibration data for the chamaecynone (**1**) ⇌ isochamaecynone (**2**) reaction, starting from **1**

Temp/°C	K (**2**/**1**)	ΔG/kcal mol^{-1}
25	0.321	0.67
52	0.397	0.60
80	0.472	0.53

Table 2. Equilibration data for the **17** ⇌ **16** reaction, starting from **16**

Temp/°C	K (**16**/**17**)	ΔG/kcal mol^{-1}
25	0.637	0.27
40	0.671	0.25
60	0.714	0.22
80	0.775	0.18

resonance in the NMR spectrum of **17** on passing from carbon tetrachloride to benzene suggested the equatorial configuration of the C_4-methyl group.[14] The ORD curve of **17** showed a positive Cotton effect ($[\phi]_{304}=+897$, $[\phi]_{265}=-1790$, $A=+26.9$), which could reasonably be explained by **17** with a non-steroid conformation bearing a $\beta(ax)$-ethynyl group at C_7 and an $\alpha(eq)$-methyl group at C_4.[14]

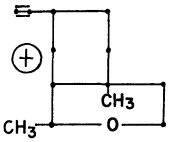

Octant Projection of **17**

The equilibration data for the **17**⇌**16** reaction, starting from **17** were also determined to be as shown in Table 3 by the same procedure. The results were in accordance with the results shown in Table 2. A plot of ln K *vs.* $1/T$ was made and found to be linear. From the slope and intercept of the line, ΔH and ΔS were determined to be +0.77 kcal/mol and +1.68 e. u. respectively.

Equilibration of ***24*** *and* ***23***. The equilibration data for the **24**⇌**23** reaction, were determined to be as shown in Table 4 by the procedure used in the cases of the equilibration of chamaecynone and iso-chamaecynone.

The plot of ln K *vs.* $1/T$ became linear, and from the slope and the intercept of the line ΔH and ΔS were calculated to be −2.28 kcal/mol and −3.87 e. u. respectively.

Consideration of the Results. The examination of Dreiding models showed there to be two Me–H and two R–H 1,3-diaxial interactions and two inner H–H interactions, as depicted by the arrows in the normal-series compounds. On the other hand, in the iso-series compounds there are two Me–H 1,3-diaxial interactions and three inner H–H interactions, as depicted by the arrows. Since two Me–H 1,3-diaxial interactions and two inner H–H interactions exist in both series of compounds, the observed ΔH values should reflect the difference between the two R–H 1,3-diaxial interactions in normal-series compounds and one inner H–H interaction in the iso-series compounds. Actually, the observed ΔH values reflect well the bulkiness of R at C_7. When R is the ethynyl group, **17** with non-steroid conformation bearing an axial ethynyl group is the favored isomer and ΔH is +0.77 kcal/mol. In this case, the R group is a linear ethynyl group and the magnitudes of the 1,3-diaxial interactions of this group and of two hydrogen atoms at C_5 and C_9 are the smallest of the three normal-series compounds. On the contrary, when R is a vinyl group, **24**, with a non-steroid conformation, is not the favored isomer and the observed ΔH is −2.28 kcal/mol. In this case, the vinyl group is planar and the magnitudes of the 1,3-diaxial interactions of this group and of the two hydrogen atoms at C_5 and C_9 are larger than that of the linear ethynyl group. When R is a three-dimensional ethyl group, the 1,3-diaxial interactions of R and the two hydrogen atoms at C_5 and C_9 may be expected to be far larger than that of the vinyl group. Actually, hexahydrochamaecynone (**30**) was completely isomerized to hexahydroisochamaecynone (**25**) by base treatment.

The equilibrium reaction of chamaecynone (**1**) and isochamaecynone (**2**) gave a tendency similar with that of the equilibrium reaction of **17** and **16**. The ΔH value is +1.47 kcal/mol, larger than the latter case, because in chamaecynone one Me–H interaction and two inner H–H interactions are eliminated compared with **17** by the introduction of a double bond at C_1, whereas in isochamaecynone one inner H–H interaction is eliminated compared with **16**.

Table 3. Equilibration data for the **17** ⇌ **16** reaction, starting from **17**

Temp/°C	K (**16**/**17**)	ΔG/kcal mol^{-1}
25	0.629	0.27
40	0.676	0.24
60	0.714	0.22
80	0.781	0.17

Table 4. Equilibration data for the **24** ⇌ **23** reaction, starting from **23**

Temp/°C	K (**23**/**24**)	ΔG/kcal mol^{-1}
25	6.30	−1.09
40	5.73	−1.08
62	4.59	−1.01
80	3.62	−0.90

Normal Series Compounds (Non-Steroid Conformation) Iso Series Compounds (Steroid Conformation)

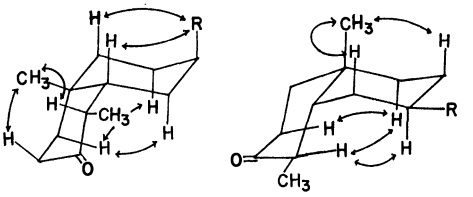

R= -C≡CH (17) ⟷ (16)

R= -CH=CH$_2$ (24) ⟵ (23)

R= -CH$_2$-CH$_3$ (30) ⟶ (25)

Normal Series Compounds (Non-Steroid Conformation) Iso Series Compounds (Steroid Conformation)

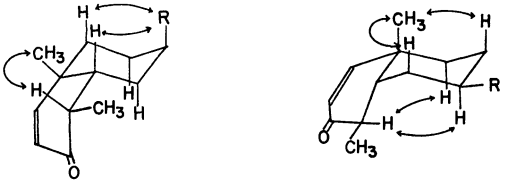

R= -C≡CH (1) ⟷ (2)

R= -CH=CH$_2$ (31) ⟵ (3)

Experimental

All the melting points are uncorrected. The IR spectra were determined on Shimadzu IR-27 and Hitachi EPI-S2 spectrophotometers. The NMR spectra were recorded on Varian A-60 and HA-100 spectrometers, employing tetramethylsilane as the internal reference. Gas-liquid partion chromatography (GLPC) analyses were performed on a Hitachi-Perkin Elmer F-6 apparatus. The ORD spectra were recorded on a Nihonbunko ORD/UV-5 spectrophotometer.

*3-Oxo-6αH,11βH-eudesma-1,4-dieno-13,6-lactone (**5**).* Compound **5** was prepared in a 47% yield as colorless plates by the method reported by Ishikawa;[9] mp 105 °C. IR (KBr): 1786, 1664, 1634, and 831 cm^{-1}. NMR ($CDCl_3$): δ 1.29 (3H, s, C_{10}–Me), 1.38 (3H, d, J=7.5 Hz, C_{11}–Me), 2.06 (3H, s, C_4–Me), 5.57 (1H, d, J=5.5 Hz, C_6–H), 6.25 (1H, d, J=10.0 Hz, C_2–H), and 6.78 (1H, d, J=10.0 Hz, C_1–H) ppm.

*(11S)-3-Oxo-eudesma-1,4-dien-13-oic Acid (**6**).* Compound **6** was prepared in an 85% yield as colorless columns by the method reported by Miki;[10] mp 102 °C. IR (KBr): 3200, 1739, 1650, 1616, 1595, and 836 cm^{-1}. NMR ($CDCl_3$): δ 1.21 (3H, s, C_{10}–Me), 1.23 (3H, d, J=6.5 Hz, C_{11}–Me), 1.83 (3H, s, C_4–Me), 6.17 (1H, d, J=10.0 Hz, C_2–H), and 6.71 (1H, d, J=10.0 Hz, C_1–H) ppm. Found: C, 72.70; H, 8.30; O, 19.31%. Calcd for $C_{15}H_{20}O_3$: C, 72.55; H, 8.12; O, 19.33%.

*(11S)-3-Oxo-4αH,5β-eudesman-13-oic Acid (**7**).* A mixture of **6** (7.41 g, 29 mmol), an ethanol solution (300 ml) of KOH (3 g, 54 mmol), and 5% Pd/C (3 g) was shaken under an atmosphere of hydrogen until the gas absorption had been completed. In 2 h, 1440 ml (1330 ml for one mole equiv) of hydrogen was consumed. After the filtration of the catalyst, the filtrate was poured into water, acidified with 6 M HCl (20 ml), and extracted with ether (200 ml×5). The combined extracts were washed with a satd. NaCl aq solution, dried ($MgSO_4$), and concentrated to give 7.0 g of a semisolid, which was then recrystallized from benzene–cyclohexane (1:2) to give 4.06 g (54%) of **7** as colorless prisms; mp 129 °C. IR (KBr): 1733 and 1675 (this band shifted to 1700 cm^{-1} in $CHCl_3$ or CS_2) cm^{-1}. NMR (CCl_4): δ 0.93 (3H, d, J=6.5 Hz, C_4–Me), 1.03 (3H, s, C_{10}–Me), 1.18 (3H, d, J=7.0 Hz, C_{11}–Me) ppm. ORD (MeOH): $[\phi]_{303}=-760$, $[\phi]_{260}=+2580$, $A=-33.4$.[19] Found: C, 71.12; H, 9.74%. Calcd for $C_{15}H_{24}O_3$: C, 71.39; H, 9.59%. The concentration of the mother liquor gave 3.35 g of a viscous oil, which was then dissolved in ether and methylated with a slight excess of CH_2N_2 in ether. The crude product was chromatographed over neutral alumina (170 g, activity grade 1) and eluted with benzene to give the oily methyl ester of (11*S*)-3-oxo-4*βH*,5α-eudesman-13-oic acid (**20**) (1.14 g, the faster running) and the oily methyl ester of **7** (0.75 g, the slower running). The methyl ester of **20** was hydrolyzed with 2 M KOH aq in EtOH to give 1.03 g of a crude crystalline compound, which was then recrystallized from benzene–cyclohexane (1:2, 5 ml) to give 0.45 g of **20** as colorless prisms; mp 109 °C. IR (KBr): 1727 and 1681 cm^{-1}. NMR (CCl_4): δ 0.91 (3H, d, J=6.5 Hz, C_4–Me), 1.06 (3H, s, C_{10}–Me), and 1.15 (3H, d, J=6.5 Hz, C_{11}–Me) ppm. ORD (MeOH): $[\phi]_{306}=+1010$. Found: C, 71.58; H, 9.78%. Calcd for $C_{15}H_{24}O_3$: C, 71.39; H, 9.59%.

*11-Chloro-4αH,5β-13-noreudesman-3-one (**8**).* A mixture of **7** (1 g, 4 mmol) dissolved in anhydrous benzene (50 ml), $Pb(OAc)_4$ (14.2 g, 32 mmol), and LiCl (1.2 g, 28 mmol) were placed in a round-bottomed flask equipped with a condenser and cooled in a dry ice–acetone bath to freeze the solvent. After the solvent had frozen, the system was evacuated and filled with N_2. The mixture was refluxed under vigorous stirring for 30 min, cooled to room temperature, and filtered. The filtrate was washed with 3 M HCl aq until it became colorless, and then 2 M Na_2CO_3 aq (10 ml×3), which had been acidified with a 6 M HCl aq solution; it was then extracted with ether, dried ($MgSO_4$), and concentrated to give 50 mg (5%) of the recovered **7**. The benzene layer was washed with a satd. NaCl aq solution, dried ($MgSO_4$), and concentrated to give 0.91 g of an oil, which was then chromatographed over silica gel (Merck, <230 mesh) and eluted with $CHCl_3$ to give 800 mg (83%) of **8** as a colorless oil. IR (neat): 1709 cm^{-1}. NMR (CCl_4): δ 0.93 (3H, d, J=7.0 Hz, C_4–Me), 1.04 (3H, s, C_{10}–Me), 1.49 (3H, d, J=6.5 Hz, C_{11}–Me), and 3.87 (1H, m, C_{11}–H) ppm. ORD (MeOH): $[\phi]_{303}=-870$, $[\phi]_{260}=+2470$, $A=-33.4$. Found: C, 68.86; H, 9.45%. Calcd for $C_{14}H_{23}OCl$: C, 69.19; H, 9.54%.

*11-Chloro-4αH,5β-13-noreudesman-3-ol (**9**).* To a solution of **8** (2.05 g, 8.4 mmol) in a mixture of ether (50 ml) and MeOH (34 ml), we added $NaBH_4$ (0.85 g, 22.5 mmol). The mixture was allowed to stand at room temperature for 2 h and then poured into a satd. NaCl aq solution (100 ml). The ether layer was separated after shaking, and the aqueous layer was further extracted with ether (50 ml×2). The combined extracts were washed with a satd. NaCl aq solution, dried ($MgSO_4$), and concentrated to give 2.03 g of **9** as an oil, which was then employed in the next step without any further purification.

A part of the product (152 mg) was chromatographed over silica gel (Merck, <230 mesh) and eluted with $CHCl_3$–CCl_4 (1:1) to give 127 mg of an oil. IR (neat): 3360 cm^{-1}. Found: C, 68.48; H, 9.90%. Calcd for $C_{14}H_{25}OCl$: C, 68.63; H, 10.29%.

*4αH,5β-13-Noreudesm-11-en-3α-ol (**10**) and 4αH,5β-13-Noreudesm-11-en-3β-ol (**11**).* A mixture of **9** (1.45 g, 5.92 mmol) and a 1 M *t*-BuOK/*t*-BuOH soln (60 ml) was refluxed for 44 h under N_2 and then concentrated *in vacuo*. The residue was poured into a satd. NaCl aq solution and extracted with ether (50 ml×3). The combined extracts were washed with a satd. NaCl aq solution, dried ($MgSO_4$), and concentrated to give 1.20 g of an oily crude product, which was then chromatographed over silica gel (Merck, <230 mesh) and eluted with CCl_4–$CHCl_3$ (2:1). The first running gave **11** (234 mg, 19%); mp 49—51 °C. IR (KBr): 3436, 3096, 1639, 993, and 900 cm^{-1}. NMR (CCl_4): 0.93 (3H, d, J=6.5 Hz, C_4–Me), 0.98 (3H, s, C_{10}–Me), 3.70 (1H, m, $W_{h/2}$=5.0 Hz, C_3–H), and 4.65—6.00 (3H, m, ABX pattern olefinic protons) ppm. Found: C, 80.85; H, 11.29%. Calcd for $C_{14}H_{24}O$: C, 80.71; H, 11.61%. The second running gave **10** (527 mg, 43%) as an oily material. IR (neat): 3378, 3115, 1642, 1000, and 909 cm^{-1}. NMR (CCl_4): δ 0.95 (3H, s, C_{10}–Me), 0.97 (3H, d, J=6.0 Hz, C_4–Me), 2.96 (1H, ddd, J=5.0, 9.0, and 9.0 Hz, C_3–H), and 4.65—6.00 (3H, m, ABX pattern olefinic protons) ppm. Found: C, 80.34; H, 11.15%. Calcd for $C_{14}H_{24}O$: C, 80.71; H, 11.61%.

*11,12-Dibromo-4αH,5β-13-noreudesman-3α-ol (**12**).* Into a stirred solution of **10** (0.798 g, 3.83 mmol) in CCl_4 (10 ml), we added a solution of Br_2 (0.70 g, 4.38 mmol) in CCl_4 (5 ml) at 0 °C. The mixture was stirred at 0 °C for 2 h, washed with a 10% Na_2CO_3 aq solution, dried ($MgSO_4$), and concentrated to give **12** (1.44 g, 100%) as a crystalline material, which was then employed in the next step without further purification. A part of this material was recrystallized from CCl_4 to give colorless needles; mp 127—128 °C. IR

(KBr): 3310 cm^{-1}. NMR (CCl_4); δ 0.97 (3H, s, C_{10}–Me), 0.98 (1H, d, J=5.5 Hz, C_4–Me of the minor isomer), 1.01 (2H, d, J=5.5 Hz, C_4–Me of the major isomer), 2.7—3.3 (1H, m, C_3–H), and 3.60—4.35 (3H, m, C_{11}–H, and C_{12}–H) ppm. Found: C, 45.81; H, 6.69%. Calcd for $C_{14}H_{24}OBr_2$: C, 45.65; H, 6.57%.

*4α*H,*5β-13-Noreudesm-11-yn-3α-ol (**14**).* A mixture of **12** (1.44 g, 3.91 mmol), dry benzene (30 ml), and a 1 M *t*-BuOK/*t*-BuOH solution (60 ml) was refluxed for 6.5 h under N_2. After the removal of a half of the volume of the solvent *in vacuo*, the mixture was poured into a satd. NaCl aq solution and extracted with ether (50 ml×3). The combined extracts were washed with a satd. NaCl aq solution, dried ($MgSO_4$) and concentrated to give **14** (754 mg, 93%) as an oily material, which was then employed in the next step without further purification. IR (neat): 3322 and 2123 cm^{-1}.

*4α*H,*5β-13-Noreudesm-11-yn-3-one (**16**).* A solution of **14** (282 mg, 1.37 mmol) in pyridine (2 ml) was added to a CrO_3–Py complex formed from CrO_3 (411 mg, 4.11 mmol) and anhydrous pyridine (6 ml), after which the mixture was allowed to stand at room temperature overnight. Petroleum ether (50 ml) was then added to the mixture, and the precipitate was filtered. The filtrate was washed successively with a satd. NaCl aq solution (50 ml×2), a 2 M HCl aq solution (50 ml×2), and a satd. NaCl aq solution (50 ml), dried ($MgSO_4$), and concentrated to give 251 mg of a crystalline material, which was then chromatographed over silica gel (Merck, <230 mesh, 12 g) and eluted with CCl_4–$CHCl_3$ (1:1) to give spectroscopically pure **16** (172 mg, 62%), mp 71—80 °C. This was recrystallized from pentane to give colorless prisms; mp 89—94 °C.[20] IR (KBr): 3279, 2119, and 1701 cm^{-1}. NMR (CCl_4): δ 0.98 (3H, d, J=6.2 Hz, C_4–Me), 1.08 (3H, s, C_{10}–Me), and 1.90 (1H, d, J=2.0 Hz, C_{12}–H) ppm. NMR (C_6H_6): δ 0.66 (3H, s, C_{10}–Me), 0.91 (3H, d, J=6.2 Hz, C_4–Me), and 1.90 (1H, d, J=2.0 Hz, C_{12}–H) ppm. ORD (MeOH): $[\phi]_{304}=-896$, $[\phi]_{265}=+1790$, $A=-26.9$.[19] MS (70 eV) *m/e*: 204 (M^+). Found: C, 82.20; H, 10.14%. Calcd for $C_{14}H_{20}O$: C, 82.30; H, 9.87%.

*Preparation of **16** from **8** without Purification in Each Step.* To a solution of **8** (637 mg, 2.60 mmol) in a mixture of ether and MeOH (10 ml and 16 ml each), we added $NaBH_4$ (300 mg, 7.93 mmol). The mixture was allowed to stand at room temperature for 2 h, poured into a satd. NaCl aq solution, and extracted with ether. The extract was washed with a satd. NaCl aq solution, dried, and concentrated to give **9** (580 mg, oil).

A mixture of **9** (580 mg) and 1 M *t*-BuOK/*t*-BuOH solution (30 ml) was refluxed for 45 h under N_2, concentrated *in vacuo*, and poured into a satd. NaCl aq solution. The mixture was extracted with ether, and the extract was washed with a satd. NaCl aq solution, dried ($MgSO_4$), and concentrated to give a mixture of **10** and its C_3-epimer (**11**) (370 mg, oil).

To a stirred solution of the resultant mixture of **10** and **11** (370 mg) in CCl_4 (5 ml), we added a solution of Br_2 (320 mg, 2.0 mmol) in CCl_4 (2.5 ml) at 0 °C. The mixture was stirred at room temperature for 2 h, washed with a 10% Na_2CO_3 aq solution, dried ($MgSO_4$), and concentrated to give a crystalline mixture of bromides (**12** and **13**) (658 mg).

A mixture of the resultant bromides (658 mg), anhydrous benzene (10 ml), and 1 M *t*-BuOK/*t*-BuOH solution (10 ml) was refluxed for 6.5 h under N_2. After the removal of a half of the volume of the solvent *in vacuo*, the mixture was diluted with a satd. NaCl aq solution and extracted with ether. The combined extracts were washed with satd. NaCl aq solution, dried ($MgSO_4$), and concentrated to give a mixture of oily alcohols (**14** and **15**) (270 mg).

A solution of the resultant alcohols (270 mg) in anhydrous pyridine (2 ml) was added to the CrO_3–Py complex formed from CrO_3 (411 mg, 4.11 mmol) and anhydrous pyridine (6 ml), after which the mixture was allowed to stand at room temperature overnight. Petroleum ether (50 ml) was then added to the mixture, and the precipitate was filtered. The filtrate was washed successively with a satd. NaCl aq solution, a 2 M HCl aq solution and a satd. NaCl aq solution, dried ($MgSO_4$), and concentrated to give a crude crystalline product (200 mg), which was then chromatographed over silica gel (10 g, Merck, <230 mesh) and eluted with $CHCl_3$–CCl_4 (1:1) to give **16** (171 mg, 32% overall yield from **8**).

*2α-Bromo-4β*H,*5β-13-noreudesm-11-yn-3-one (**18**) and 2β-Bromo-4α*H,*5β-13-noreudesm-11-yn-3-one (**19**).* To a solution of **16** (360 mg, 1.76 mmol) in AcOH (10 ml), we added 48% HBr (0.3 ml) and a solution of Br_2 (281 mg, 1.76 mmol) in AcOH (4 ml) successively. The mixture was stirred for 1 h at room temperature, poured into a satd. NaCl aq solution (100 ml), and extracted with ether (30 ml×3). The combined extracts were washed successively with a 10% Na_2CO_3 aq solution (20 ml×2) and a satd. NaCl aq solution (30 ml), dried ($MgSO_4$), and concentrated to give 467 mg of an oily product, which was then chromatographed over silica gel (30 g, Merck, <230 mesh) and eluted with CCl_4–$CHCl_3$ (4:1). The first running gave an unidentified oily mixture (58 mg). The second running gave 180 mg (36%) of **18** as a crystalline material. IR ($CHCl_3$): 3344, 2123, and 1724 cm^{-1}. NMR (CCl_4): δ 0.98 (3H, d, J=6.5 Hz, C_4–Me), 1.33 (3H, s, C_{10}–Me), 1.85 (1H, d, J=2.5 Hz, C_{12}–H), 4.57 (1H, q, J=7.5 and 13.0 Hz, C_2–H) ppm. ORD (MeOH): $[\phi]_{310}=+396$, $[\phi]_{270}=-1200$, $A=+16$. Found: C, 58.53, H, 6.89%. Calcd for $C_{14}H_{19}OBr$: C, 59.41; H, 6.77%. The third running gave 68 mg (14%) of **19** as a crystalline material.[21] IR ($CHCl_3$): 3344, 2132, and 1727 cm^{-1}. NMR (CCl_4): δ 1.09 (3H, d, J=6.0 Hz, C_4–Me), 1.12 (3H, s, C_{10}–Me), 1.90 (1H, d, J=2.0 Hz, C_{12}–H), and 4.75 (1H, q, J=7.0 and 12.5 Hz, C_2–H) ppm. ORD (MeOH): $[\phi]_{310}=-470$, $[\phi]_{260}=+604$, $A=-10.7$. Found: C, 59.62; H, 6.85%. Calcd for $C_{14}H_{19}OBr$: C, 59.41; H, 6.77%. The fourth running gave **a** complex mixture.

*Chamaecynone (**1**).* A mixture of **18** (105 mg, 0.37 mmol), Li_2CO_3 (90 mg, 1.22 mmol), and LiBr (90 mg, 1.04 mmol) in anhydrous DMF (18 ml) was stirred at 140—165 °C for 2 h under N_2, cooled, poured into a satd. NaCl aq solution (100 ml), and extracted with ether (30 ml×3). The combined extracts were washed successively with a 2 M HCl aq solution (30 ml) and a satd. NaCl aq solution, dried ($MgSO_4$), and concentrated to give 70 mg of an oily material, which was then chromatographed over silica gel (10 g, Merck, <230 mesh) and eluted with CCl_4–$CHCl_3$ (4:1) to give 29 mg (39%) of chamaecynone as a crystalline material, which was subsequently recrystallized from pentane to give colorless prisms; mp 88 °C. This material showed no depression in its melting point when admixed with an authentic specimen and was identical in all respects with the corresponding specimen in IR (KBr), NMR (CCl_4), ORD (MeOH), GLPC (SE 30), and MS (70 eV).

*Isochamaecynone (**2**).* A mixture of **19** (23 mg, 0.08 mmol), Li_2CO_3 (22 mg, 0.3 mmol), and LiBr (22 mg, 0.25 mmol) in anhydrous DMF (6 ml) was stirred at 140—165 °C for 6.5 h under N_2, cooled, poured into a satd. NaCl aq solution (20 ml), and extracted with ether (10 ml×3). The combined extracts were washed successively with **a** 2 M HCl aq solution (10 ml) and a satd. NaCl aq solution, dried ($MgSO_4$), and concentrated to give 18 mg of a crystalline

material, which was then chromatographed over silica gel (3 g, Merck, <230 mesh) and eluted with CCl_4–$CHCl_3$ (4:1) to give 4 mg (24%) of isochamaecynone; mp 79 °C. IR (KBr): 3300, 2123, 1672, and 834 cm^{-1}. NMR (CCl_4): δ 1.12 (3H, d, J=6.5 Hz, C_4–Me), 1.22 (3H, s, C_{10}–Me), 1.90 (1H, d, J=2.0 Hz, C_{12}–H), *ca.* 2.3 (1H, m, $W_{h/2}$= 24.0 Hz, C_7–H), 5.77 (1H, d, J=10.0 Hz, C_2–H), and 6.43 (1H, d, J=10.0 Hz, C_1–H) ppm. NMR (C_6H_6): δ 1.04 (1H, d, J=6.0 Hz, C_4–Me) and 0.71 (3H, s, C_{10}–Me) ppm. MS (70 eV) *m/e*: 202 (M^+). ORD (MeOH): $[\phi]_{340}=-870$.

Conversion of ***16*** *to Chamaecynone (****1****), Isochamaecynone (****2****), and Dehydrochamaecynone (13-Noreudesma-1,4-dien-11-yn-3-one,* ***29****) without the Isolation and Purification of the Corresponding Bromides.* A mixture of **16** (358 mg, 1.75 mmol), AcOH (30 ml), and a 48% HBr aq solution (0.5 ml) was stirred for 2 h at room temperature. To the mixture we then added a solution of Br_2 (290 mg, 1.80 mmol) in AcOH (2 ml). The mixture was stirred for 30 min at room temperature, poured into a satd. NaCl aq solution (100 ml), and extracted with ether (30 ml×3). The combined extracts were washed successively with a 10% Na_2CO_3 aq solution (20 ml×2) and a satd. NaCl aq solution (30 ml), dried ($MgSO_4$), and concentrated to give 494 mg of an oily product, which was then employed for the next reaction.

A mixture of the crude bromide (494 mg), Li_2CO_3 (420 mg, 5.68 mmol), and LiBr (420 mg, 4.83 mmol) in anhydrous DMF (80 ml) was stirred for 5 h at the refluxing temperature under N_2, cooled, poured into a satd. NaCl aq solution (300 ml), and extracted with ether (50 ml×4). The combined extracts were washed successively with a 2 M HCl aq solution (50 ml) and a satd. NaCl aq solution, dried ($MgSO_4$), and concentrated to give 320 mg of an oily material, which was then chromatographed over silica gel (50 g, Merck, <230 mesh) and eluted with CCl_4–$CHCl_3$ (4:1). The first running gave chamaecynone (99 mg). The second running gave a 1:1 mixture of chamaecynone and isochamaecynone (62 mg). The third running gave isochamaecynone (69 mg). The total yield of chamaecynone and isochamaecynone was 230 mg (65%), based on the **16**. The fourth running gave **29** (35 mg, 10%). NMR (CCl_4): δ 1.27 (3H, s, C_{10}–Me), 1.87 (3H, s, C_4–Me), 2.08 (1H, d, J=1.0 Hz, C_{12}–H), 6.09 (1H, d, J=9.8 Hz, C_2–H), and 6.66 (1H, d, J=9.8 Hz, C_1–H) ppm.

*11,12-Dibromo-4*α*H,5*β*-13-noreudesm-11-en-3-one (****28****).* To a mixture of **16** (113 mg, 0.55 mmol) and AcONa (100 mg, 1.22 mmol) in AcOH (100 ml), we added under mechanical stirring, a solution of Br_2 (90 mg, 0.56 mmol) in AcOH (5 ml). After stirring had continued for 4 h at room temperature, the mixture was poured into a satd. NaCl aq solution (100 ml) and extracted with ether (30 ml×3). The combined extracts were washed successively with 10% Na_2CO_3 (20 ml×2) and a satd. NaCl aq (30 ml) solution, dried ($MgSO_4$), and concentrated to give 195 mg of an oily material, which was then chromatographed over silica gel (15 g, Merck, <230 mesh) and eluted with a mixture of $CHCl_3$–CCl_4 (1:1) to give **28** (75 mg, 37%), which was subsequently recrystallized from hexane to give colorless prisms; mp 119 °C. IR (KBr): 3077, 1712, and 833 cm^{-1}. NMR (CCl_4): δ 1.01 (3H, d, J=6.5 Hz, C_4–Me), 1.10 (3H, s, C_{10}–Me), and 6.33 (1H, s, C_{12}–H) ppm. Found: C, 46.66; H, 5.57%. Calcd for $C_{14}H_{20}OBr$: C, 46.15; H, 5.53%.

*11-Chloro-3,3-ethylenedioxy-4*α*H,5*β*-13-noreudesmane (****21****).* A mixture of **8** (1.61 g, 6.63 mmol), ethylene glycol (24 ml), and *p*-toluenesulfonic acid (0.28 g) in dry C_6H_6 (60 ml) was refluxed in a flask equipped with a Dean-Stark column packed with anhydrous $MgSO_4$ for 2 h under N_2. The mixture was then cooled and diluted with a satd. NaCl aq solution (100 ml), and the benzene layer was drawn off. The aqueous layer was further extracted with C_6H_6 (30 ml×3). The combined extracts were washed with a NaCl aq solution, dried ($MgSO_4$), and concentrated to give 1.93 g (100%) of **21**, which was then recrystallized from pentane to give a crystalline material; mp 74 °C. NMR (CCl_4): δ 0.78 (3H, d, J=6.5 Hz, C_4–Me), 0.95 (3H, s, C_{10}–Me), 1.47 (3H, d, J=6.5 Hz, C_{11}–Me), and 3.83 (4H, s,) ppm. Found: C, 67.16; H, 9.39%. Calcd for $C_{16}H_{27}O_2Cl$: C, 66.95; H, 9.48%.

*3,3-Ethylenedioxy-4*α*H,5*β*-13-noreudesm-11-ene (****22****).* A mixture of **21** (1.93 g, 6.72 mmol) and a 1 M *t*-BuOK/*t*-BuOH solution (70 ml) was refluxed for 31 h under N_2, concentrated *in vacuo*, and diluted with a satd. NaCl aq solution. The mixture was then extracted with benzene (50 ml×3). The combined extracts were washed with a NaCl aq solution, dried ($MgSO_4$), and concentrated to give 1.58 g (94%) of **22**, which was then employed in the next step. IR (neat): 3110, 1642, 1000, and 918 cm^{-1}. NMR (CCl_4): δ 0.77 (3H, d, J=6.5 Hz, C_4–Me), 0.96 (3H, s, C_{10}–Me), 3.83 (4H, s,), 4.89 (1H, dd, J=3.5 and 18.0 Hz, C_{12}–H_a), 4.83 (1H, dd, J=3.5 and 10.0 Hz, C_{12}–H_b), and 5.70 (1H, ddd, J=6.0, 10,0, and 18.0 Hz, C_{11}–H) ppm.

Deacetalization of ***22****. The formation of a Mixture of 4*α*H, 5*β*-13-noreudesm-11-en-3-one (****23****) and 4*β*H,5*β*-13-noreudesm-11-en-3-one (****24****).* A mixture of **22** (1.58 g, 6.31 mmol) and a 2 M HCl aq solution (10 ml) in MeOH (50 ml) was refluxed for 4 h, concentrated to a half of the volume, poured into a satd. NaCl aq solution, and extracted with benzene (30 ml×3). The combined extracts were then washed with a satd. NaCl aq solution, dried ($MgSO_4$), and concentrated to give 1.23 g of an oily material, which was subsequently established by NMR and GLPC (SE 30) analyses to be a *ca* 1:2 mixture of **24** and **23**. The NMR (CCl_4) of **24** in the mixture of **24** and **23**: δ 0.88 (3H, d, J=6.5 Hz, C_4–Me), 1.08 (3H, s, C_{10}–Me), and 4.7–6.1 (3H, m, C_{11}– and C_{12}–H) ppm.

*4*α*H,5*β*-13-Noreudesm-11-en-3-one (****23****).* To the CrO_3–Py complex formed from CrO_3 (115 mg, 1.15 mmol) and anhydrous pyridine (2 ml), we added **10** (100 mg, 0.48 mmol) in anhydrous pyridine (4 ml). The mixture was then allowed to stand at room temperature overnight, diluted with petroleum ether (20 ml), and filtered. The filtrate was washed with a 2 M HCl aq solution (20 ml×2) and a satd. NaCl aq solution (30 ml), dried, and concentrated to give 90 mg (91%) of **23** as an oily material, which was then purified by pipe-to-pipe distillation. IR (neat): 3106, 1715, 1637, 995, and 908 cm^{-1}. NMR (CCl_4): δ 0.96 (3H, d, J=6.5 Hz, C_4–Me), 1.04 (3H, s, C_{10}–Me), and 4.7—6.1 (3H, m, C_{11}– and C_{12}–H) ppm. CD (MeOH): $[\theta]_{290}=-1875$. Found: C, 81.22; H, 10.92%. Calcd for $C_{14}H_{22}O$: C, 81.50; H, 10.75%. **11** also gave **23** in 87% in the same procedure.

*Hexahydroisochamaecynone (4*α*H,5*β*-13-Noreudesman-3-one,* ***25****).* A mixture of **23** (20 mg) and 5% Pd/C (20 mg) in MeOH (2 ml) was shaken under H_2 until the hydrogen uptake ceased. The oily crude product (22 mg) was chromatographed over silica gel (1 g, Merck, <230 mesh) and eluted with $CHCl_3$–CCl_4 (1:1) to give **25** (19 mg).

*2*β*,11,12-tribromo-4*α*H,5*β*-13-noreudesman-3-one (****26****).* To a CCl_4 solution (5 ml) of a mixture of **24** and **23** (1:2) (60 mg, 0.29 mmol) which had been formed by the deacetalization of **22**, we added Br_2 (96 mg, 0.60 mmol) in CCl_4 (2 ml). The mixture was stirred for 1 h at 0 °C, poured into a satd. NaCl aq solution (50 ml), and extracted with

benzene (10 ml×3). The combined extracts were washed successively with a 10% Na_2CO_3 aq solution (10 ml) and a satd. NaCl aq solution (20 ml), dried ($MgSO_4$), and concentrated to give 110 mg of an oily material, which was then chromatographed over silica gel (6 g, Merck, <230 mesh) and eluted with $CHCl_3$-CCl_4 (3:7) to give **26** (52 mg, 40%). NMR (CCl_4): δ 1.09 (3H, s, C_{10}–Me), 1.13 (3H, d, J=5.5 Hz, C_4–Me), 3.73 (1H, d, J=11.0 Hz, C_{12}–H_a), 3.80 (1H, d, J=4.5 Hz, C_{12}–H_b), 4.0—4.4 (1H, m, C_{11}–H), and 4.72 (1H, q, J=7.0 and 12.0 Hz, C_2–H) ppm.

2β-Bromo-11-chloro-4αH,5β-13-noreudesman-3-one (27). To a stirred solution of **8** (400 mg, 1.65 mmol) at 0 °C we added Br_2 (320 mg, 2.00 mmol) in CCl_4 (5 ml). The mixture was stirred for 1 h at 0 °C, poured into a satd. NaCl aq solution (100 ml), and extracted with ether (30 ml×3). The combined extracts were washed successively with a 10% Na_2CO_3 aq solution (30 ml) and a satd. NaCl aq solution (50 ml), dried ($MgSO_4$), and concentrated to give 640 mg of a crude, oily material, which was then chromatographed over silica gel (30 g, Merck, <230 mesh) and eluted with $CHCl_3$-CCl_4 (1:1) to give **27** (226 mg, 43%). NMR (CCl_4): δ 1.04 (3H, d, J=6.0, C_4–Me), 1.05 (3H, s, C_{10}–Me), 1.48 (3H, d, J=6.0 Hz, C_{11}–Me), 3.87 (1H, m, C_{11}–H), and 4.68 (1H, q, J=7.0 and 13.0 Hz, C_2-H) ppm.

4βH,5β-13-Noreudesm-11-yn-3-one (17). A solution of **16** (370 mg, 1.81 mmol) in 2% KOH–EtOH (25 ml) was allowed to stand at room temperature for 14 h and was then poured into a satd. NaCl aq solution (100 ml). The mixture was extracted with ether (30 ml×3). The combined extracts were washed with a satd. NaCl aq solution (50 ml), dried ($MgSO_4$), and concentrated to give a mixture of **16** and **17** (1:1.2), as ascertained by GLPC analysis (column: PEG 6000 on Diasolid M; oven temperature: 170 °C; N_2 flow rate: 30 ml/min; **16**: retention time, 16 min; **17**: retention time, 14 min). The mixture (mp 43—65 °C) was chromatographed over silica gel and eluted with CCl_4. The first running gave 111 mg of **17**, which was then recrystallized from pentane to give colorless prisms: mp 103—105 °C. IR (KBr): 3279, 2120, and 1701 cm^{-1}. NMR (CCl_4): δ 0.88 (3H, d, J=6.5 Hz, C_4–Me), 1.30 (3H, s, C_{10}–Me), and 1.91 (1H, d, J=2.5 Hz, C_{12}–H) ppm. NMR (C_6H_6): δ 0.92 (3H, d, J=6.0 Hz, C_4–Me), 0.98 (3H, s, C_{10}–Me) ppm. ORD (MeOH): $[\phi]_{304}$=+897, $[\phi]_{265}$=−1790, A=+26.9. MS (70 eV) *m/e*: 204 (M^+). Found: C, 81.77; H, 9.71%. Calcd for $C_{14}H_{20}O$: C, 82.30; H, 9.87%. The following running gave a mixture of **16** and **17**.

The Temperature Dependence of the Equilibrium in 16 and 17. Four portions of **16** and **17** (20 mg each) were dissolved separately in 2% KOH–EtOH (10 ml) in 100-ml Erlenmeyer flasks. The flasks were stoppered and kept in water baths thermostated at 25 °C, 40 °C, 60 °C, and 80 °C for 6 h. Each solution was then vigorously stirred into a mixture of AcOH (0.2 ml), ether (20 ml), and a satd.NaCl aq solution (60 ml). The ether layer was thus separated, and the aqueous layer was further extracted with ether (20 ml×3). The combined extracts were washed with a satd. NaCl aq solution (50 ml), dried (Na_2SO_4), and concentrated to give a mixture of **16** and **17** as a crystalline meterial. The ratio of **16** and **17** was determined by GLPC (3 mmϕ×1 m column containing 10% carbowax 20 M on diasolid M; oven temperature, 140 °C; N_2 flow rate, 40 ml/min). The retention times of **16** and **17** were 21 min and 18 min respectively.

The Temperature Dependence of the Equilibrium in Chamaecynone and Isochamaecynone. Three portions of chamaecynone (10 mg) were dissolved separately in 2% KOH–EtOH (10 ml) in 100-ml Erlenmeyer flasks. The flasks were stoppered and kept in water baths thermostated at 25 °C, 52 °C, and 80 °C for 6 h. Each solution was treated as has been described above to give a mixture of chamaecynone and isochamaecynone as a crystalline material. The ratio of chamaecynone and isochamaecynone was determined by GLPC (3 mmϕ×1 m containing 10% carbowax 20 M on diasolid M; oven temperature, 140 °C; N_2 flow rate, 40 ml/min). The retention times of chamaecynone and isochamaecynone were 19 min and 25.5 min respectively.

Isomerization of Isochamaecynone. A solution of isochamaecynone (7 mg) in 2% KOH–EtOH (1 ml) was allowed to stand at 25 °C and was then treated in the usual manner to give a mixture of chamaecynone and isochamaecynone (3:1), as determined by GLPC analysis (column: PEG 6000 on diasolid M; oven temperature, 170 °C; N_2 flow rate, 30 ml/min).

The Temperature Dependence of the Equiliblium in 23 and 24. Four portions of **23** (20 mg) were dissolved separately in 2% KOH–EtOH (10 ml) in 100-ml Erlenmeyer flasks. The flasks were then stoppered and kept in water baths thermostated at 25 °C, 40 °C, 60 °C, and 80 °C for 6 h. Each solution was then treated in the manner described above to give a mixture of **23** and **24** as an oily material. The ratio of **23** and **24** was determined by GLPC (3 mmϕ×1 m column containing 10% carbowax 20 M on diasolid M; oven temperature 140 °C; N_2 flow rate, 40 ml/min). The retention times of **23** and **24** were 54.5 min and 60 min respectively.

The authors wish to thank Dr. Takash Toda of the Department of Chemistry for his helpful discussion.

References

1) Preliminary report of this work: T. Nozoe, T. Asao, M. Ando, and K. Takase, *Tetrahedron Lett.*, **1967**, 2821.

2) Present address; Department of Chemistry, College of General Education, Tohoku University, Kawauchi, Sendai 980.

3) Present address: Analysis Group, Production Coordination Section, Kashima Division, Mitsubishi Petrochemical Co., Ltd., 17-1 Tōwada Kamisu-machi, Kashima-gun, Ibaragi 314-02.

4) Present address: Tokyo Research Laboratory of Kao Soap Co., Ltd., Bunka, Sumida-ku, Tokyo 131.

5) T. Nozoe, Y. S. Cheng, and T. Toda, *Tetrahedron Lett.*, **1966**, 3663.

6) I. Saeki, M. Sumimoto, and K. Kondo, *Holzforschung*, **27**, 93 (1973); T. Kondo, Japan Kokai 1973-92525 (*Chem, Abstr.* **81**, 59351r).

7) The total synthesis of *dl*-chamaecynone has been reported recently: T. Harayama, H. Cho, and Y. Inubushi, *Tetrahedron Lett.*, **1977**, 3273.

8) Y. Abe, T. Harukawa, H. Ishikawa, T. Miki, M. Sumi, and T. Toga, *J. Am. Chem. Soc.*, **78**, 1422 (1956).

9) H. Ishikawa, *Yakugaku Zasshi*, **76**, 504 (1956).

10) T. Miki, *Yakugaku Zasshi*, **75**, 410 (1955).

11) H. O. House, "Modern Synthetic Reactions," W. A. Benjamin, Melon Park, Calfornia (1972), p. 26, and the references there cited.

12) J. K. Kochi, *J. Am. Chem. Soc.*, **87**, 2500 (1965); *J. Org. Chem.*, **30**, 3265 (1965).

13) "Shin Jikken-kagaku Koza," ed by the Chemical Society of Japan, Maruzen, Tokyo (1978), Vol. 15 I–1, pp. 445—465, and the references there cited.

14) N. S. Bhacca and D. H. Williams, "Applications of NMR Spectroscopy in Organic Chemistry," Holden-Day, San Francisco (1964), Chap. 7.

15) Y. Hirata and T. Goto, "Senko-Bunsan," Hirokawa, Tokyo (1964).
16) K. Nakanishi, "Infrared Absorption Spectroscopy," Holden-Day, San Francisco (1962), p. 42.
17) J. Hine, "Physical Organic Chemistry," 2nd ed, McGraw-Hill Book Co., New York (1962), Chaps. 9 and 10.
18) "Kagaku No Ryoiki Zokan 80, Tennenbutsu-Kagaku '67," ed by Y. Kitahara, K. Nakanishi, and S. Ito, Nankodo, Tokyo (1967), pp. 159—178; K. Nakanishi, T. Goto, S. Ito, S. Natori, and S. Nozoe, "Natural Products Chemistry," Academic Press, New York (1974), Vol. 1, pp. 28—32, and the references there cited.
19) In the preliminary report, we reported incorrect maximum and minimum values of the ORD curves of **7** and **16** because of having made careless mistakes. The values reported there are not $[\phi]$ but $[\alpha]$ values.
20) The melting point of this compound was carelessly and erroneously reported to be 49 °C in the preliminary report.
21) Compound **19** was not identical with the crystalline compound with mp of 129 °C reported in the preliminary report.

© The Chemical Society of Japan

NOTES

Bull. Chem. Soc. Jpn., 53, 1435—1436 (1980)

Correlation between Electron Capture Detector Response and Chemical Structure for 1,2,3,4,5,6-Hexachlorocyclohexane

Yukikazu HATTORI,* Yoshio KUGE, and Shingo ASADA

Environmental Pollution Control Center of Osaka Prefecture, 1-3-62, Nakamichi, Higashinari-ku, Osaka-shi, Osaka 537

(Received May 2, 1979)

Synopsis. The relative sensitivities of an electron capture detector for four 1,2,3,4,5,6-hexachlorocyclohexane isomers were measured at different detector temperatures. The temperature dependence of the electron capture coefficients (K) for these compounds was determined. The K values of these compounds increased with a decrease in the detector temperature. These results show that the electron capture reactions of these compounds proceed non-dissociatively.

The electron capture detector (ECD), which exhibits a highly sensitive response to various organic compounds containing halogen, oxygen, and sulfur atoms, is widely used for environmental and other various analyses. Many reports about ECD sensitivities for various compounds have been published,[1-4] but the temperature dependence of the sensitivity was not considered in these studies.

Wentworth *et al.*[5-7] and Kojima *et al.*[8-11] studied the electron capture phenomena by using the pulse-sampling technique, thus elucidating the temperature dependence of the electron capture coefficients (K) for various compounds. They reported a correlation between the ECD response and the chemical structure for many compounds.

The present authors have previously studied[12-14] the ECD response and the temperature dependence for various aromatic halogeno and nitro compounds and for phthalate esters with the d.c. mode.

In this work, we have determined the ECD sensitivities and the temperature dependence for 1,2,3,4,5,6-hexachlorocyclohexane(BHC) isomers and studied the correlation between the ECD response and the chemical structure for these compounds. We intend to use these results for the identification and prediction of unknown compounds.

Experimental

Apparatus and Materials. A Varian aerograph 2100 type gas chromatography with an ECD (^{63}Ni, 8.5 mCi) was used in this experiment. Applied voltage was supplied with the d.c. mode. The glass column (2 mmϕ × 1.5 m) was packed with Gaschrom Q (100—120 mesh) coated with 2% Silicone OV-17. Extra pure nitrogen gas (Teikoku Sanso Co., Ltd.) was used as the carrier gas; it was purified by passage through two tubes packed with Molecular Sieve 5A and through an Oxy-trap tube (Alltech Associates Co., Ltd.), at the flow rate of 30 cm^3/min. The column temperature was set at 170 °C. The injector temperature was kept at 200 °C. The detector temperature was varied from 190 °C to 320 °C. BHC isomers (pesticides, analytical grade) and hexachlorobenzene (HCB)(special grade) were obtained from Wako Pure Chemical Co., Ltd. All the reagents were checked by gas chromatography.

Procedure. The relative sensitivity (RS) was obtained by calculating the relative peak area per mole of the compound, using HCB as a standard. The sample size was so chosen as to keep the peak area within a linear range on the calibration curve. The K values, the electron affinities (EA'), and the RS values were calculated by the method reported in a previous paper.[12]

Results and Discussion

Relative Sensitivities of ECD for BHC Isomers. The RSs of ECD for BHC isomers at three different detector temperatures are tabulated in Table 1. The RSs of the four isomers were in the order of $\alpha > \gamma > \delta \gg \beta$. Especially, the RS for β-BHC was less than those of the other isomers by a factor of about two or three. The RS's of BHC isomers are much larger than that of HCB, which has an equal number of chlorine atoms to BHC. These results may be attributed to the difference in the molecular skeleton and in the coformations of the C–Cl bonds in BHC and HCB.

Table 1. Relative sensitivities for ECD of BHC isomers and hexachlorobenzene

Compound	Relative sens. (230 °C)	Relative sens. (290 °C)	Relative sens. (320 °C)
α-BHC	7.68	4.74	6.21
β-BHC	2.46	1.99	2.74
γ-BHC	6.81	4.67	6.06
δ-BHC	6.27	3.99	4.99
Hexachlorobenzene	1.00	1.00	1.00

The Temperature Dependence of the ECD Response for BHC Isomers. Gas chromatograms of BHC isomers at three different detector temperatures are shown in Fig. 1. As the detector temperature is lowered, the peak heights showing ECD sensitivity become higher. Then the temperature dependences of ECD response were studied. Figure 2 shows the temperature dependence of the K values of four kinds of BHC isomer and HCB. It was found that the temperature dependence of the K values for these compounds showed positive slopes, but that of β-isomer showed an almost zero slope. If the plots of $\ln KT^{3/2}$ against $1/T$ show a positive slope, the electron capture reaction of the compound proceeds non-dissociatively.[6] Therefore, the electron capture reaction for BHC isomers appears to proceed non-dissociatively. These compounds were then supposed to capture an electron and to form stable negative ions. Aue *et al.*[15] studied the products of

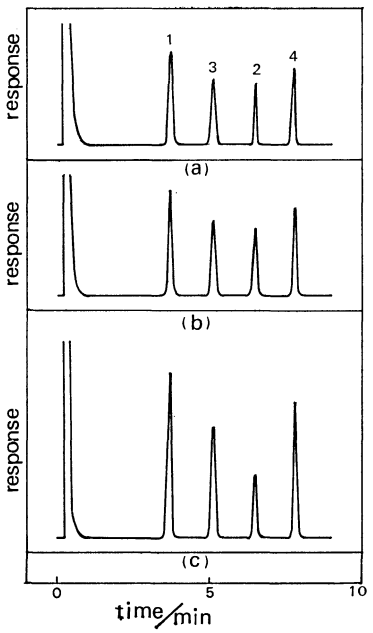

Fig. 1. Gas chromatograms of BHC isomers at different detector temperatures.
(a): 320 °C, (b): 290 °C, (c): 230 °C, 1: α-BHC, 2: β-BHC, 3: γ-BHC, 4: δ-BHC.

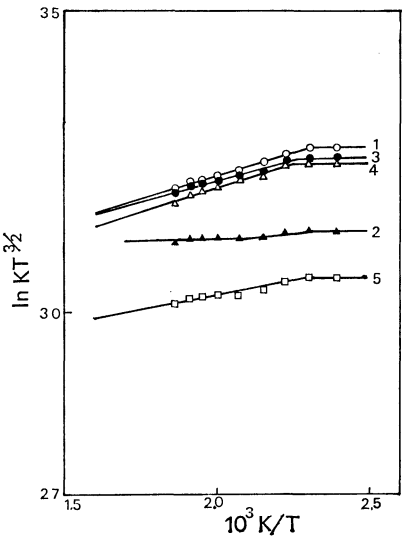

Fig. 2. Temperature dependence of K values.
1: α-BHC, 2: β-BHC, 3: γ-BHC, 4: δ-BHC, 5: hexachlorobenzene.

three BHC isomers and various polychlorobenzenes in an ECD. They suggested that BHC isomers were largely preserved in contrast to those of other polychlorobenzenes. This fact may support the idea that the electron capture reaction for BHC isomers proceeds non-dissociatively.

In Table 2, the values of the electron affinities (EA') calculated from the magnitude of the positive slopes plotted $\ln KT^{3/2}$ *vs.* $1/T$ and the conformations[16] of the C–Cl bonds in the molecule of BHC are listed. The EA' values of α,γ, and δ isomers were about 13 kJ/mol, while that of HCB was about 8 kJ/mol. The magnitude of the EA' values were in the order of

Table 2. Apparent electron affinities(EA') and conformations of BHC isomers and hexachlorobenzene

Compound	EA' / kJ mol^{-1}	Conformation of chlorine atoms[a] b) c)
α-BHC	12.68	aaeeee
β-BHC	5.06	eeeeee
γ-BHC	12.01	aaaeee
δ-BHC	13.85	aeeeee
Hexachlorobenzene	8.12	—

a) From Ref. 16. b) a: Axial bond. c) e: Equatorial bond.

δ>α>γ>HCB>β. Among the four kinds of BHC isomer, the temperature dependence of the K values, the ECD sensitivity, and the EA' value of β-isomer were very different from those of other isomers. Generally, cyclohexane derivatives adopt the most energetically favarable conformation, in which most substituents are equatorial.[17] All the chlorine substituents of β-isomer are equatorial and so β-isomer has the more stable structure compared with the other BHC isomers. Our experimental results concerning β-isomer may be related to the difference in the conformation. In this way, the electron capture reaction for BHC isomers is affected by the molecular conformations.

References

1) J. E. Lovelock, "Gas Chromatography," ed by N. Brenner, Academic Press, New York (1962), p 219.
2) W. L. Zielinski, Jr., and L. Fishbein, *J. Chromatogr.*, **28**, 293 (1967).
3) W. L. Zielinski, Jr., L. Fishbein, and R. O. Thomas, *J. Chromatogr.*, **30**, 77 (1967).
4) W. L. Zielinski, Jr., L. Fishbein, and L. Martin, Jr., *J. Gas Chromatogr.*, **5**, 552 (1967).
5) W. E. Wentworth, E. Chen, and J. E. Lovelock, *J. Phys. Chem.*, **70**, 445 (1966).
6) W. E. Wentworth and E. Chen, *J. Gas Chromatogr.*, **5**, 170 (1967).
7) W. E. Wentworth, L. W. Kao, and R. S. Becker, *J. Phys. Chem.*, **79**, 1161 (1975).
8) M. Satouchi and T. Kojima, *Anal. Lett.*, **5**, 931 (1972).
9) T. Kojima and M. Satouchi, *Bunseki Kagaku*, **22**, 1428 (1973).
10) M. Satouchi and T. Kojima, *Bunseki Kagaku*, **25**, 764 (1976).
11) T. Kojima, Y. Tanaka, and M. Satouchi, *Anal. Chem.*, **48**, 1760 (1976).
12) Y. Hattori, Y. Kuge, and S. Nakagawa, *Bull. Chem. Soc. Jpn.*, **51**, 2249 (1978).
13) Y. Hattori, Y. Kuge, and S. Asada, *Nippon Kagaku Kaishi*, **8**, 1102 (1978).
14) Y. Kuge, Y. Hattori, S. Asada, and S. Yamada, *Chem. Lett.*, **1979**, 208.
15) S. Kapita and W. A. Aue, *J. Chromatogr.*, **148**, 343 (1978).
16) R. D. Obrien, "Insecticides," Academic Press, New York (1967), p. 183.
17) S. Umezawa, "Yuki Kagaku," Maruzen (1962), pp. 6—14.

A Measurement of the Thermal Decomposition of CS_2 behind Reflected Shock Waves

Ko Saito,* Yoko Toriyama, Teiji Yokubo, Tetsuo Higashihara, and Ichiro Murakami
Department of Chemistry, Faculty of Science, Hiroshima University, Higashi Senda-machi, Hiroshima 730
(Received May 14, 1979)

Synopsis. The thermal decomposition of CS_2 in Ar was investigated in the temperature range of 2000—2900 K by monitoring both the UV absorption and the visible emission of CS_2. A typical induction zone was observed during the decomposition. It was found that the rate constant of the initiation reaction obtained from the induction zone was smaller than that reported by previous workers.

Shock-tube studies of the pyrolysis of CS_2 diluted in Ar have been reported by four research groups in the past.[1-5] In the low-pressure region, the rate of CS_2 disappearance is expressed generally as: $-d[CS_2]/dt=k[CS_2][Ar]+k'[CS_2]^2$, and for highly diluted mixtures, with only a small percentage of CS_2, the second term is neglected. k does not necessarily correspond to the rate constant of the $CS_2+Ar\rightarrow CS+S+Ar$ reaction. However, the values of k reported by the previous workers are consistent with each other within a factor of two, although different experimental conditions, techniques, and data analyses were employed. Among the previous experiments, Arnold *et al.*'s data[5] for k correspond clearly to the complex reaction after an induction period. In our present study by using the UV absorption technique, the induction zone was also found in the CS_2 concentration profile behind reflected shock waves below 3000 K. Moreover, it appeared that the second-order rate constant for the CS_2 decay rate in the induction zone was much smaller than the previous results. At temperatures higher than 3000 K, the induction period was so short that the CS_2 profile showed a simple decay curve, as if the decomposition proceeded *via* a simple mechanism. In this paper, therefore, only the case in which the induction zone apparently exists in the absorption profile is considered.

Experimental

Reaction mixtures containing 0.25 and 0.5 mol% CS_2 in Ar were heated by reflected shock waves in a shock tube 5 cm in inner diameter, previously described elsewhere,[6] and the CS_2 dissociation rate was deduced by monitoring the UV absorption at 220 ± 0.8 nm. In some experimental runs, the emission from the electronically excited CS_2 was monitored at 435 ± 5 nm simultaneously with the absorption record. The experimental conditions were as follows: temperature=1980—2930 K; total concentration=$(3.3—8.0)\times10^{-6}$ mol cm^{-3}; $[CS_2]=(1.5—4.0)\times10^{-8}$ mol cm^{-3}. At 220 nm, the observed absorption coefficient of CS_2 was around 1×10^7 cm^2 mol^{-1} and Lambert-Beer's law was ascertained to hold, at least up to 8×10^{-8} mol cm^{-3} of CS_2.

Results and Discussion

Figure 1 shows a typical trace of the UV absorption. The absorption of CS_2 rises to a maximum just behind the reflected shock front and then begins to decrease slightly; then, after a certain period (we call this the induction period of CS_2 decomposition), it rapidly falls to a steady value. From the two different slopes in the profile, as indicated by I and II in the figure, the corresponding rate constants, k_I and k_{II}, can be determined for each experiment. The visible emission, on the other hand, rose to a peak behind the reflected shock front with a relatively long rise time, while at the end of the induction zone it began to decrease towards a steady value. In the induction zone, the emission profile did not show any such gradient in its intensity as appeared in the simultaneous absorption record. Thus, from the emission profile, the rate of CS_2 disappearance was measured only from the slope behind the induction zone. Figure 2 shows an Arrhenius plot of the second-order rate constants, together with the previous data. The values of k_I and k_{II} were determined from the absorption profile as: $-d(ln[CS_2])/dt/[Ar]$, while the values of k_{III} were obtained by the emission profile as: $-d(lnI)/dt/[Ar]$, where I is the emission intensity. This figure shows that the second-order rate constants, k_{II} and k_{III}, fall in the range of the previous data, although our data show a somewhat larger scatter and, if k_{III} is considered alone, the data seem to have a different temperature dependence because of the lack of data over a wide temperature range. The plot of k_I, the apparent rate constant in the induction zone, lies below that of the previous data, but it shows the same temperature dependence.

An appropriate reaction mechanism was assumed for the CS_2 decomposition involving the 14 elementary reactions listed in Table 1. The simulation by using this mechanism clearly showed a radical chain behavior; thus, the existence of the induction zone, *i.e.*, a rapid decrease in CS_2, began after a time, and was followed by a rapid increase in the sulfur atom. A typical example of the calculation is shown in Fig. 3. Although the mechanism and the rate constants

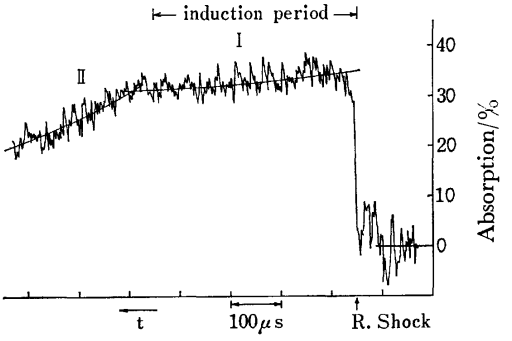

Fig. 1. Typical UV absorption trace.
Conditions: T=2460 K, $[Ar]=3.45\times10^{-6}$ mol cm^{-3}, $[CS_2]=1.73\times10^{-8}$ mol cm^{-3}. Rate constants: $k_I=1.06\times10^8$ cm^3 mol^{-1} s^{-1}, $k_{II}=7.45\times10^8$ cm^3 mol^{-1} s^{-1}.

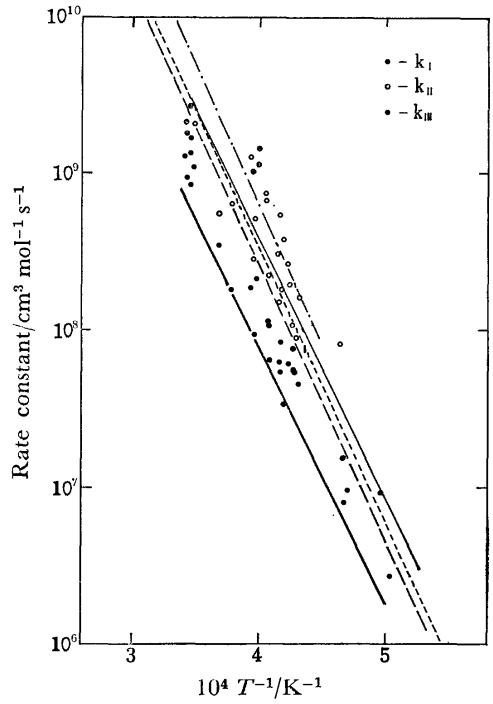

Fig. 2. Arrhenius plot of second order rate constants. k_I, k_{II}, and k_{III} are explained in the text. —·—: Ref. 1, ----: Ref. 2, — — —: Ref. 5, ——: Ref. 7, ——: k_1 determined in this work.

Table 1. Mechanism and kinetic data

	Reaction	Forwards rate constant[a] log A	E	Sources
1	$CS_2+Ar=CS+S+Ar$	14.4	74	a
2	$CS_2+S=CS+S_2$	14.0	4.07	b
3	$CS_2+CS_2=CS+S+CS_2$	14.22	43.7	c
4	$S_2+Ar=S+S+Ar$	13.6	80.2	d
5	$CS_2+S+Ar=CS_3+Ar$	$\log k=17.48$		e
6	$CS_2+S_2=CS+S_3$	$\log k=8.63$		f
7	$S_3+Ar=S_2+S+Ar$	14.39	22.7	g

a) Units: mol cm^{-3} for concentration, s for time, and kcal mol^{-1} for energy. The backwards rate constants were estimated using the equilibrium constants.
a. Obtained in this work. b. K. Howman, G. Krome, and H. Gg. Wagner, *Ber. Bunsenges. Phys. Chem.*, **74**, 650 (1970). c. Ref. 1. This reaction probably proceeds *via* a two-step process: $2CS_2\rightarrow CS_3+CS$ and $CS_3+Ar\rightarrow CS_2+S+Ar$. d. T. Higashihara, K. Saito, and I. Murakami, unpublished results. e. N. Basco and A. E. Peason, *Trans. Faraday Soc.*, **63**, 2684 (1967). f. Assumed from the data for $CO_2+O_2=CO+O_3$. g. Adjusted value to fit the experimental data.

used are not necessarily true, the simulation has significance in the sense that the induction period appears also in the calculation.

Since the rate of Reaction 1 is very small compared with that of Reaction 2, the concentration of sulfur atoms should rapidly reach a steady value. In fact, the computer simulation showed that a steady concentration was reached within 10 μs under the present experimental conditions (see Fig. 3). An Arrhenius expression for the initiation reaction rate constant

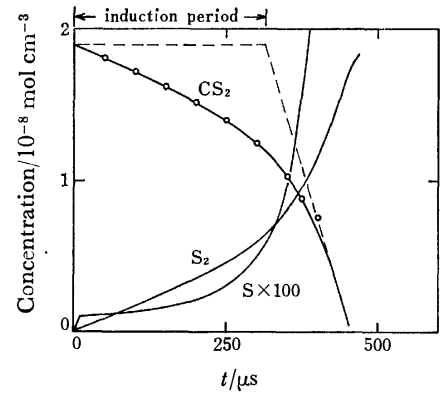

Fig. 3. Example of simulation.
Conditions: $T=2710$ K, $[Ar]=3.76\times10^{-6}$ mol cm^{-3}, $[CS_2]=1.88\times10^{-8}$ mol cm^{-3}. Open circles are the experimental profile of CS_2 under the same conditions.

was thus obtained from the $k_I=2k_1$ relation as:

$$k_1 = 10^{14.4\pm0.5}\exp\{-(74.3\pm6.5\text{ kcal mol}^{-1})/RT\}\ \text{cm}^3\text{ mol}^{-1}\text{ s}^{-1},$$

where the limits of error are the standard deviations. These results are shown in Fig. 2. The value of k_1 obtained in this study gives a collision efficiency factor, β_c,[8] of about 0.01 at 2500 K. This is considered satisfactory compared with the other spin-forbidden reactions of triatomic molecules.

The experimental conditions of Gaydon *et al.* and Arnold *et al.* are the same as those of the present work. Gaydon *et al.* obtained the rate of the CS_2 decomposition by observing the CS and S_2 absorption with relatively long time resolutions. Arnold *et al.* obtained the overall rate from the intensity gradient after the induction period in the emission profile at 450 nm. Therefore, the values of k_{II} and k_{III} measured in this work may be identified with the values of k measured by these workers. Olschewski *et al.* studied the decomposition rate by monitoring the CS_2 absorption at high total concentrations, 10^{-5}—10^{-4} mol cm^{-3}, while the CS_2 concentration was in the same range as in the present study. A calculation using the above assumed mechanism under their experimental conditions showed that the concentration of the sulfur atom reached a steady value within a very short time. Considering this fact, their k_1 values give an overestimate by at least a factor of two.

References

1) A. G. Gaydon, G. H. Kimbell, and H. B. Palmer, *Proc. R. Soc. London, Ser. A*, **279**, 313 (1964).
2) H. A. Olschewski, J. Troe, and H. Gg. Wagner, *Z. Phys. Chem. N. F.*, **45**, 329 (1965).
3) H. A. Olschewski, J. Troe, and H. Gg. Wagner, *Ber. Bunsenges. Phys. Chem.*, **70**, 1060 (1966).
4) P. R. Ryason, *Rev. Sci. Instr.*, **38**, 607 (1967).
5) S. T. Arnold, W. G. Brownlee, and G. H. Kimbell, *J. Phys. Chem.*, **74**, 8 (1970).
6) T. Higashihara, K. Saito, and H. Yamamura, *Bull. Chem. Soc. Jpn.*, **49**, 965 (1976).
7) D. L. Baulch, D. D. Drysdale, J. Duxbury, and S. Grant, "Evaluated Kinetic Data for High Temperature Reactions," Vol. 3, Butterworths, London (1976).
8) J. Troe, *J. Chem. Phys.*, **66**, 4745 (1977); **66**, 4758 (1977).

On the Thermal Decomposition of Shock-heated SO_2

Ko Saito,* Teiji Yokubo, Tetsuo Higashihara, and Ichiro Murakami
Department of Chemistry, Faculty of Science, Hiroshima University, Higashi Senda-machi, Hiroshima 730
(Received May 21, 1979)

Synopsis. The SO_2 pyrolysis was measured behind reflected shock waves under low SO_2 concentrations. A typical induction zone was observed in the decomposition process. It was found that the overall rate constants after the induction zone were in good agreement with the values for the primary reaction obtained by the following investigators: Just and Rimpel, Kiefer, and Grillo *et al.* This implies that, even in highly diluted mixtures at low pressures, the kinetics of the SO_2 decomposition is complicated.

The thermal decomposition of SO_2 behind shock waves has been investigated by many workers.[1-8] However, a problem regarding the second-order rate constant, k_1, for the primary reaction: $SO_2+M\rightarrow SO+O+M$, remains, since the decomposition has been found to proceed in a complex manner when high concentration mixtures are used. Olschewski *et al.*[2] measured the rate constant, k_1, for highly diluted mixtures (less than 0.1 mol % in Ar). Later, their results were revised slightly by Astholtz *et al.*[6] of the same laboratory by using mixtures of SO_2–Ar ranging from 100 to 2000 ppm SO_2 ($5\times10^{-10}<[SO_2]<\sim10^{-8}$ mol cm^{-3}). Just and Rimpel[5] measured k_1 by observing the O-atom production rate by means of atomic resonance absorption spectroscopy. Since they measured the rate for highly diluted mixtures (20—200 ppm SO_2 in Ar) and at low total pressures, corresponding to $\sim10^{-11}<[SO_2]<\sim10^{-10}$ mol cm^{-3}, they assumed that subsequent reactions play only a minor role in the process, and they obtained the k_1 values which were much higher than the values of Astholtz *et al.* (higher more than one order). The values of Just and Rimpel were, though, in rather good agreement with those obtained by Kiefer[4] (3—30% SO_2 in Kr) and by Grillo *et al.*[7] (0.13 and 0.26% SO_2 in Ar). It is considered that, under the experimental conditions in Kiefer's work ($[SO_2]>3\times10^{-8}$ mol cm^{-3}), the obtained data presumably relate to the complex reaction involving the bimolecular reaction of the reactant, not to the primary unimolecular process, although the rate constants were expressed simply as first order in $[SO_2]$, with a very high activation energy (close to the bond dissociation energy of OS–O). In the same sense, the experiments of Grillo *et al.* ($[SO_2]>1\times10^{-8}$ mol cm^{-3}) may also be considered to be connected with the complex reaction.

Thus, the experimental values of k_1 reported hitherto split into two groups, which differ from each other by a factor of about 20. There thus arises the question of whether or not the reaction is really simple in low-concentration mixtures, as in the Just and Rimpel work. There is another problem for the higher k_1 values as to the collision efficiency factor of 0.17 at about 3000 K,[5] which is considerably higher than in the other similar reactions.

Levitt and Sheen[3] observed the visible emission from shock-heated SO_2–Ar mixtures (5—10% SO_2) and obtained the overall rate of the SO_2 decomposition at around 3000 K on the basis of the proportionality between the emission intensity and the concentration of SO_2. This method is considered to give a good time and spatial resolution, without any large noises. In this study, therefore, we tried to measure the decomposition rate of SO_2 by monitoring the light emission from the shock-heated mixtures under the same conditions as those of Just and Rimpel.

Experimental

A shock tube 9.4 cm in inner diameter was used. The test section was evacuated to less than 1×10^{-6} Torr (1 Torr= 133.322 Pa) before each run. The gas conditions behind the reflected shock were calculated by using the incident shock speed in the manner reported in a previous paper.[9] The light emitted from the shock-heated gas was taken out of a quartz window through a slit 0.5 mm wide and was passed again through a second slit 0.5 mm wide placed at 15 cm apart from the window. Then the light was passed through a filter of 392.5±5 nm and was detected by means of a photomultiplier. The output signal was fed to a preamplifier and was recorded by a wave-memory with a sampling speed of 0.2 μs. Since, occasionally, the emission profile varies with a change in the optical arrangement and depends on the conditions of the inner wall of the tube,[10] we carefully checked to see that the field of view in the tube was less than 1 mm and that the reflection diffused by the opposite wall was removed completely.

Commercial SO_2 (99.0% minimum purity) was used after trap-to-trap distillation. Ar (99.998%) was used as the diluent, without any further purification. Mixtures of 0.01 and 0.05 mol% of SO_2 in Ar were prepared by diluting a premixed 5 mol % mixture.

Results and Discussion

The experiments were performed under these conditions: temperature=3000—4700 K; total density= 6.7×10^{-7}—3.3×10^{-6} mol cm^{-3}. Figure 1 shows typical emission records at different temperatures and $[SO_2]\simeq 9\times10^{-11}$ mol cm^{-3}. The peak height was ascertained to be the thermal emission from the electronically excited state of SO_2.[11] That is, a logarithmic plot of the peak intensity per unit of SO_2 concentration *vs.* 1/T agreed with the curve calculated theoretically, considering the temperature dependences of the partition functions of the ground and excited states.

The emission profiles obviously reveal the existence of an induction zone during the pyrolysis, as is shown in Fig. 1. The length of the induction zone decreases with an increase in the temperature, and at high temperatures it disappears from the profile (Fig. 1d).[12] The first-order rate constants, $k_{1st}=-d(\ln I)/dt$, were obtained from the decay curves after the induction

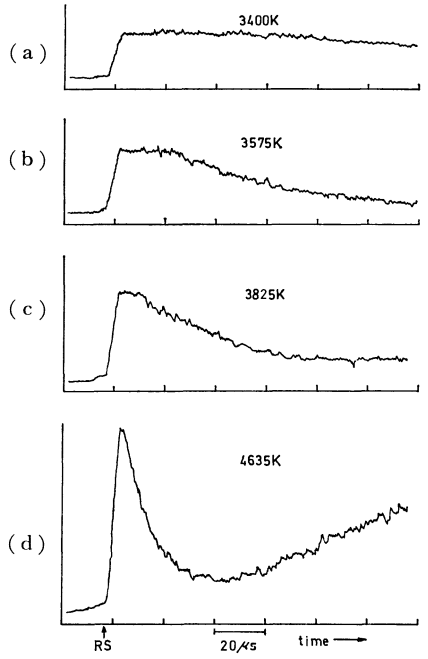

Fig. 1. Typical emission profiles at different temperatures.
Total densities are $(8.5\pm1)\times10^{-7}$ mol cm^{-3}. RS: reflected shock front.

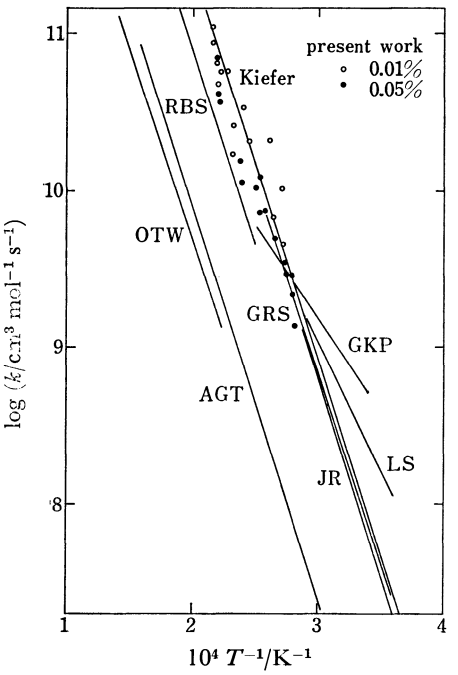

Fig. 2. Comparison of second-order rate constants.
GKP: Ref. 1, OTW: Ref. 2, LS: Ref. 3, Kiefer: Ref. 4, JR: Ref. 5, AGT: Ref. 6, GRS: Ref. 7, RBS: Ref. 8.

zone, where I is the emission intensity. Then, the values of the second-order rate constant were calculated as: $k_{2nd}=k_{1st}/[Ar]$. In this method, there arises no problem regarding the ambiguousness of the absolute SO_2 concentration in the mixture due to the adsorption of SO_2 on the walls of the reservoir and the shock tube. A plot of the second-order rate constant, k_{2nd}, is shown in Fig. 2, together with the previous data. It is obvious that our data points are near Kiefer's result and also the extended lines of the results of the Just and Rimpel and Grillo *et al.* The values of k_{2nd} correspond clearly to the complex decomposition rate of SO_2, since they were determined not from the initial decay, but from the decay behind the induction zone. The primary reaction rate is considered to reflect the initial decay rate at the earlier position in the induction zone; thus, it should give much smaller values than k_{2nd}. From the emission experiment, however, at least in our present work, no measurable decrease of the intensity was observed in the induction zone. From the present observations, it is likely that the primary reaction rate is as much as one order slower than the overall reaction rate behind the induction zone. In this respect, at the present time, Astholtz *et al.*'s data on the primary reaction rate constant are considered to be the most reliable. As has been described above, the data obtained by Kiefer and Grillo *et al.* obviously correspond to the complex reaction and, therefore, do not conflict with the present results. However, we cannot explain why the observation of the initial production rate of the O atom by Just and Rimpel gave such large values for k_1 under their experimental conditions.

Although, in this work we could not measure the value of k_1, it was confirmed that the decomposition of SO_2 proceeds in a complex manner, even in highly diluted mixtures and at low total pressures. Further investigations with more elaborate techniques will be needed to determine the true value of k_1.

References

1) A. G. Gaydon, G. H. Kimbell, and H. B. Palmer, *Proc. R. Soc. London, Ser. A*, **276**, 461 (1963).
2) H. A. Olschewski, J. Troe, and H. G. Wagner, *Z. Phys. Chem., N. F.*, **44**, 173 (1965).
3) B. P. Levitt and D. B. Sheen, *Trans. Faraday Soc.*, **63**, 2955 (1967).
4) J. H. Kiefer, *J. Chem. Phys.*, **62**, 1354 (1975).
5) T. Just and G. Rimpel, "Proceedings of the 11th International Symposium on Shock Tubes and Shock Waves," University of Washington, Seattle (1978), p. 226.
6) D. C. Astholz, K. Glänzer, and J. Troe, "Proceedings of the 11th International Symposium on Shock Tubes and Shock Waves," University of Washington, Seattle (1978), p. 232.
7) A. Grillo, R. Reed, and M. W. Slack, *J. Chem. Phys.*, **70**, 1634 (1979).
8) M. T. Raju, S. V. Babu, and V. S. Rao, preprint of the 12th International Symposium on Shock Tubes and Shock Waves, Israel (1979).
9) K. Saito, T. Yokubo, T. Fuse, H. Tahara, O. Kondo, T. Higashihara, and I. Murakami, *Bull. Chem. Soc. Jpn.*, **52**, 3507 (1979).
10) T. Just, private communication.
11) The emitting state at this wavelength was assumed to be the a $^3B_1$ state. According to the analysis by Levitt and Sheen (*Trans. Faraday Soc.*, **63**, 540 (1967)) the emission from the A^1B_2 state is slightly involved at this wavelength.
12) The increase in the intensity in the later part of the reaction period, appearing in Fig. 1d, is the emission due to the recombination of SO and O. The effect of this emission on the earlier part of the profile is considered to be negligible.

Reflectivity of Two-dimensional Cluster Compound, Nb_3I_8

Haruki KAWAMURA,* Ichimin SHIROTANI,† Masashi TANAKA,††
Kyoji TACHIKAWA, and Jiro TANAKA††

National Research Institute for Metals, 1-2-1, Sengen, Sakura Niihari-gun, Ibaragi 305
† *The Institute for Solid State Physics, The University of Tokyo, 7-22-1, Roppongi, Minato-ku, Tokyo 162*
†† *Department of Chemistry, Faculty of Science, Nagoya University, Chigusa-ku, Nagoya 464*

(Received September 25, 1979)

Synopsis. The reflectivity spectrum of two-dimensional cluster compounds, Nb_3I_8, is measured from 5×10^3 to 35×10^3 cm^{-1} and compared to that of Ag_2F. The spectrum has four peaks, at 7.5, 11.8, 20.0, and 28.6×10^3 cm^{-1}.

The physical properties of quasi-low-dimensional compounds have been a subject of considerable interest in recent years. Triniobium octaiodide, Nb_3I_8, is a two-dimensional semiconductor at atmospheric pressure. The resistivity on the ab plane of Nb_3I_8 is 50 Ω-cm, while that along the c axis is about 100 Ω-cm.[1] In a previous paper we have reported the reflectivity of two-dimensional metal Ag_2F and discussed the plasma frequency in the two-dimensional metal.[2] In this report we wish to present the reflectivity spectrum of the single crystal of Nb_3I_8 and compare it to that of Ag_2F.

The crystal structure of Nb_3I_8 is based on a hexagonal closed-packing of the iodine atoms, and three-eighths of the octahedral holes of the iodine octahedra are occupied by niobium atoms. Nb_3I_8 is crystallized in a layer structure similar to the CdI_2 structure. As is to be expected from the compositional ratio, one-fourth of the niobium atoms are left out from the niobium layers. Therefore, the metal atoms are arranged in triangular clusters. The distance between two iodine octahedron centers is 3.8 Å. The positions of the niobium atoms are shifted from the centers of the iodine octahedra. The Nb–Nb distance within a cluster are 3.0 Å, while the shortest Nb–Nb distance between clusters is 4.6 Å.[3] The magnetic property of Nb_3I_8 has also been reported in Ref. 3 to be a weak paramagnetism.

The single crystals of Nb_3I_8 were prepared by the known technique.[4] The crystals grew in the form of plates with a metallic dark gray appearance. The surface of a plate is found by X-ray diffraction analysis to be parallel to the layers of the triangular clusters. A detailed description of reflectivity measurement has already been presented in an earlier paper.[5]

Figure 1 shows the reflectivity spectrum of the Nb_3I_8 single crystal. The reflectivity reaches about 35% at its maximum point. This value is considerably lower than that of the two dimensional metal Ag_2F. The reflectivity spectrum of Ag_2F shows the typical metallic features which are to be expected from Drude's classical free electron theory. On the contrary, the reflectivity spectrum of Nb_3I_8 has four peaks at 7.5, 11.8, 20.0, and 28.6×10^3 cm^{-1}. The Drude-type spectrum is not observed in this two-dimensional semiconductor. Figure 2 shows the real, ε_1, and imaginary, ε_2, parts of the complex dielectric constant. These values are obtained by applying the Kramers-Kronig

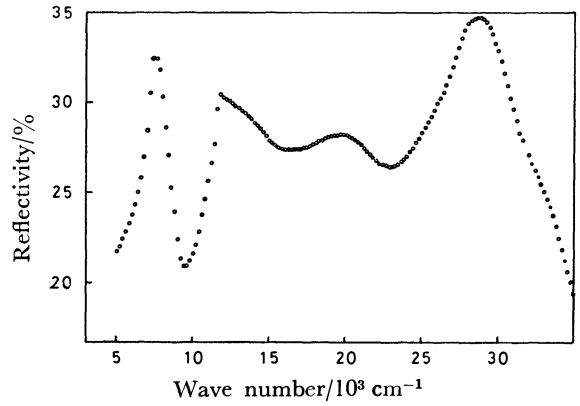

Fig. 1. Reflectivity spectrum of Nb_3I_8 against wave number.

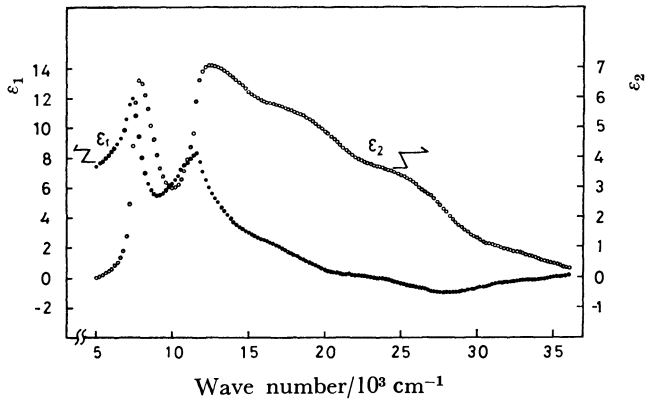

Fig. 2. Plot of the real part (ε_1, ●) and imaginary part (ε_2, ○) of the complex dielectric constant (ε).

analysis to the reflectivity data shown in Fig. 1. The absorption coefficient in Ag_2F increases with a decrease in the wave number in the near-infrared region. On the other hand, in Nb_3I_8, ε_2, which is proportional to the absorption coefficient, decreases with a decrease in the wave number. This suggests that Nb_3I_8 is a typical semiconductor. The resistivity on the ab plane of Nb_3I_8 is 50 Ω-cm, and the thermal-energy gap is about 0.52 eV. The metallic behaviour is not observed even at very high pressures.[1] The 4d electrons in niobium atoms hop among triangle clusters constructed from niobium atoms. The optical-energy gap estimated from the edge of the reflectivity spectrum is comparable to the thermal-energy gap obtained from the temperature dependence of the reflectivity. Therefore, we suggest that the near-infrared band at 7.5×10^3 cm^{-1} may arise from the charge transfer between niobium clusters.

Since NbI_4 is extremely sensitive to water and oxygen, the reflectivity spectrum of NbI_4 has been measured in dry nitrogen stream at room temperature.[7] A broad band was observed at around 21×10^3 cm^{-1}. Judging from the study of the absorption spectra of NbI_4 in pyridine,[8] the broad band in the NbI_4 single crystal may be assigned to the charge-transfer band between niobium and iodine atoms. Therefore, the band near 20×10^3 cm^{-1} in Nb_3I_8 must be attributable to the charge-transfer band between niobium and iodine atoms. Though it is very difficult to identify the two bands at 11.8 and 28.6×10^3 cm^{-1}, these bands may tentatively be assigned. The bond lengths between a central niobium atom and surrounding iodine atoms are listed in Table 1.[3] These bond lengths are divided into two groups. One group of lengths range in distance from 2.75 to 2.76 Å, with a mean distance of 2.75 Å, while the others range in distance from 2.92 to 3.02 Å, with a mean distance of 2.95 Å. On the other hand, the Nb–I lengths of NbI_4 are in the range of 2.65 to 2.90 Å,[6] and the mean length is 2.75 Å. The band 28.6×10^3 cm^{-1} may be assigned to the charge-transfer absorption of the longer-bond-length group. The niobium atoms in a Nb_3I_8 crystal are octahedrally surrounded by iodine atoms, and, according to the chemical analysis of Nb_3I_8, the I/Nb ratio was 2.82. Therefore, the valence state of a niobium atom is considered to be $Nb^{3+}(d^2)$. The bands at 11.8×10^3 cm^{-1} may be assigned to the d-d transition among energy levels split by the octahedral ligand field of iodine atoms.

Table 1. Interatomic distances/Å of Nb_3I_8

Nb–Nb	3.00, 4.60
Nb–I	2.75, 2.76
	2.92, 3.02

References

1) H. Kawamura, I. Shirotani, and K. Tachikawa, *J. Solid State Chem.*, **27**, 233 (1979).
2) H. Fujita, Y. Okada, H. Kawamura, I. Shirotani, and H. Inokuchi, *J. Phys. Soc. Jpn.*, **37**, 104 (1974).
3) A. Simon and H. G. von Schnering, *J. Less-Common Met.*, **11**, 31 (1966).
4) M. A. Kust, J. D. Corbett, and R. M. Friedman, *Inorg. Chem.*, **7**, 2081 (1968).
5) M. Tanaka, *Bull. Chem. Soc. Jpn.*, **51**, 1001 (1978).
6) L. F. Dahl and D. L. Wampler, *Acta Crystallogr.*, **15**, 903 (1962).
7) H. Kawamura, I. Shirotani, and M. Tanaka, to be published.
8) R. E. McCarley and B. A. Torp, *Inorg. Chem.*, **2**, 544 (1963).

Nitrogen 14 Nuclear Qnadrupole Resonance of Alloxan·H_2O

Takuya MARUIZUMI, Yukio HIYAMA, and Eiji NIKI*

Department of Industrial Chemistry, Faculty of Engineering, The University of Tokyo, Hongo, Tokyo 113

(Received September 26, 1979)

Synopsis. The ^{14}N nuclear quadrupole resonance spectra of alloxan·H_2O have been observed at room temperature. The predominant tautomer in a solid is concluded to be 5,5-dihydroxypyrimidine-2,4,6-trione. The NQR data were interpreted qualitatively by means of the Townes and Dailey theory.

Some nitrogen-containing heterocyclic compounds have been attracting pharmacological and biological interest because of thier pharmaceutical action, mainly attributable to the nitrogen atom's ability to make hydrogen bonds. For this reason, it seems important to obtain information about the electron density on the nitrogen nucleus, and, hence, about the chemical bonding of such heterocyclic compounds. Previously we have reported the ^{14}N NQR of sulfur-substituted uracils and analysed the valence-electron distribution around the nitrogen atom, using the Townes and Dailey theory.[1] In this paper we wish to report the first observation of the ^{14}N NQR of alloxan·H_2O. It is an analogue to barbituric acid and has been extensively studied in order to elucidate its ability to cause diabetes. For ^{14}N NQR, we can expect the three frequencies given in the following formulae,[2]

$$\nu_{\pm} = \frac{3}{4}e^2Qq/h\cdot\left(1\pm\frac{\eta}{3}\right)$$
$$\nu_0 = \nu_+ - \nu_- = \frac{1}{2}\eta\cdot e^2Qq/h \quad (1)$$

where e^2Qq/h is the quadrupole coupling constant and where η is the asymmetry parameter, which is the measure of the deviation from the axially symmetry of the electric field gradient (e.f.g.). The NQR data of alloxan·H_2O were interpreted qualitatively in terms of the Townes and Dailey theory.

Experimental

The nuclear magnetic double resonance in the laboratory frame[3] was employed to detect the NQR transitions. Before performing the double-resonance experiment, the high-field (about 0.6 T) and zero-field spin lattice relaxation times for alloxan·H_2O were measured in order to set the double-resonance time sequence, T-τ (cycle time and zero-field time respectively). NQR searching was carried out from 400 kHz to 4 MHz in 10 kHz steps, so the total experimental error may amount to about 10 kHz. The apparatus was a home-made one and has been described in detail in our previous paper.[4] The sample was a polycrystalline guaranteed-grade chemical obtained from the Tokyo Kasei Kogyo Co., Ltd. The sample volume was about 1 cm^3. All the experiments were performed at room temperature.

Results and Discussion

The proton high-field spin-lattice relaxation time, T_1, of alloxan·H_2O at room temperature was 25 s. In the zero field, the proton magnetization at first decreased quickly with the time constant, T_{1D} (6 s), and later more slowly with the time constant, T_{1N} (44 s). This slow decay of proton magnetization may be caused by the remagnetization of proton system by cross interaction with the ^{14}N system, which has a long spin-lattice relaxation time. From these data, the double-resonance cycle was set as $T=60$ s and $\tau=2$ s. The observed transition frequencies, the quadrupole coupling constants, e^2Qq/h, and the asymmetry parameters, η, of alloxan·H_2O are given in Table 1, together with the data of its analogue, barbituric acid.[5] Figure 1 shows the NQR spectrum of alloxan·H_2O. Before analysing the charge densities, the correct tautomeric structure for alloxan·H_2O must be settled. For alloxan·H_2O, Baeyer supposed the water molecule of alloxan·H_2O to be incorporated into the alloxan molecule as the hydroxyl group.[6] His assigned configurational formula of alloxan·H_2O is Illustration (A), shown below. For this formula, the keto or enol tautomeric forms through the migration of the hydrogen atoms may be possible; see Illustrations (B) and (C).

The nitrogens in (A) are both pyrrole-like, in (B) one is pyrrole-like and the other is pyridine-like, and in (C) both are pyridine-like. A simple criterion for distinguishing pyrrole-like and pyridine-like bond configurations is deduced when the nuclear quadrupole coupling constants of the pyridine-like and pyrrole-like nitrogens are compared, since the coupling constants of pyridine-like nitrogens are usually greater than 4

TABLE 1. NQR TRANSITION FREQUENCIES (kHz), QUADRUPOLE COUPLING CONSTANTS, e^2Qq/h (kHz), AND ASYMMETRY PARAMETERS, η, OF alloxan·H_2O AND ITS ANALOGUE, BARBITURIC ACID

Compound	[ν_+,	ν_-,	ν_0]	e^2Qq/h	η
Alloxan·H_2O	[2670,	2060,	610]	3150	0.39
	[2600,	1980,	620]	3050	0.41
Barbituric acid	[2575,	1895,	—]	2980	0.46
	[2480,	1755,	—]	2823	0.52

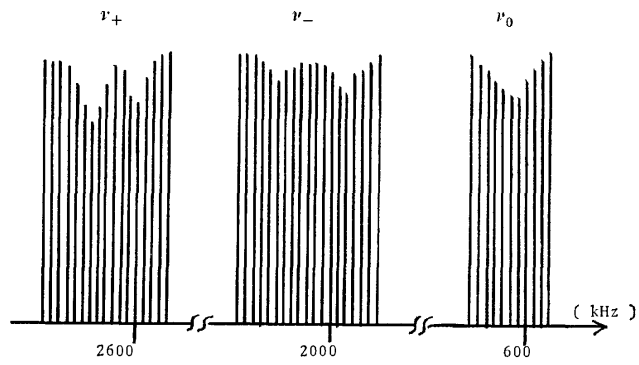

Fig. 1. ^{14}N NQR spectrum of alloxan·H_2O.

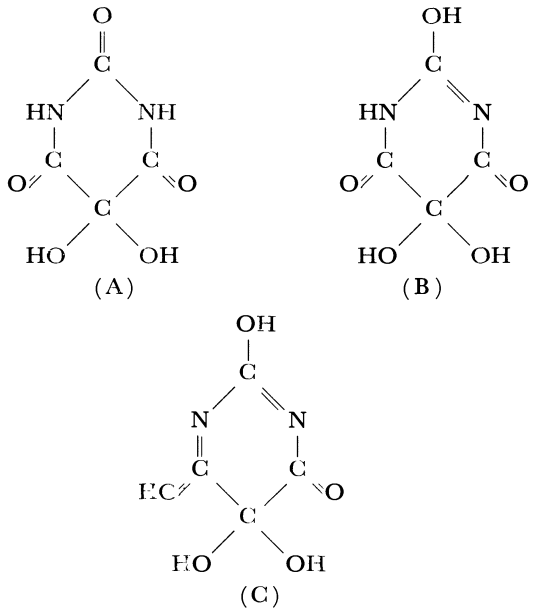

MHz. Additional insight can be obtained from the NQR spectrum shown in Fig. 1. In proton-nitrogen double-resonance experiments, nitrogen not directly bonded to hydrogen atoms gives weak absorption lines, and usually the ν_- lines are smeared out. From these considerations, we can decide that alloxan·H_2O exists predominantly in the triketo configuration (A) in its ground state; this decision agrees with the previous X-ray diffraction study.[7]

As the NC bond lengths and CNC angle for each nitrogen in alloxan·H_2O are quite similar, we can expect that the NQR coupling constants of two nitrogens of alloxan·H_2O are not very different. However the difference of coupling constants is 100 kHz, as may be seen in Table 1. This large difference can be explained by the difference in the intermolecular hydrogen bonds at each nitrogen atom. The two hydrogen bond lengths, N(1)–H(1)–O and N(3)–H(3)–O, differ by 0.164 Å.[7] This large difference would cause a large change in the coupling constants of the nitrogens. It would be possible tentatively to assign one set of observed lines to one particular site by considering the two different intermolecular hydrogen bonds at each nitrogen site and the NQR data experimentally obtained. However, any definitive assignment seems very difficult; therefore, we do not make any such assignment here.

With the Townes and Dailey theory, expressions relating the NQR data to the charge densities are derived as follows;

$$\pi - \sigma_{NC} = \frac{4}{3}\nu_+/(e^2Qq_0/h)$$
$$\sigma_{NH} - \sigma_{NC} = \frac{4}{3}\nu_0/(e^2Qq_0/h)\cdot[1/1-\cot^2\gamma] \quad (2)$$

Table 2. Values of π and σ_{NH} populations for alloxan·H_2O and barbituric acid. π and σ_{NH} are calculated assuming $e^2Qq_0/h=9.1$ MHz, and $\sigma_{NC}=1.200$

Compound	π	σ_{NH}	$[\eta]$[a]
Alloxan·H_2O	1.590	1.320	[0.39]
	1.581	1.322	[0.41]
Barbituric acid	1.577	1.334	[0.46]
	1.563	1.342	[0.52]

a) The asymmetry parameters are used to distinguish the two nitrogen sites in each molecule.

where π is the pi population, σ_{NH} is the NH sigma population, σ_{NC} is the averaged NC sigma population, 2γ is the CNC angle, and q_0 is the electric-field gradient caused by a 2p electron of the nitrogen atom. In order to estimate these charge densities, e^2Qq_0/h, σ_{NC}, and 2γ are set at 9.1 MHz,[8] 1.200, and 126°, the averaged values of the CNC angles for each nitrogen in alloxan·H_2O and barbituric acid.[7] The estimated values of the π and σ_{NH} populations are shown in Table 2. The great π populations and the small sigma populations of alloxan·H_2O compared with those of barbituric acid can easily be understood, since the hydroxyl group is known to be π-electron-donating and σ-electron-withdrawing.

Conclusion

In this paper, the following two conclusions were obtained;

1. Alloxan·H_2O exists predominantly in the 2,4,6-triketo-5,5-dihydroxy structure in a solid; this determination agreed with the results of the X-ray diffraction study.
2. The difference in coupling constants for nitrogens in alloxan·H_2O is attributable to the difference in intermolecular hydrogen bonds for each nitrogen.

References

1) T. Maruizumi, Y. Hiyama, N. Watanabe, and E. Niki, *Bull. Chem. Soc. Jpn.*, **51**, 978 (1978).
2) E. A. C. Lucken, "Nuclear Quadrupole Coupling Constants," Academic Press, London and New York (1969).
3) R. E. Slusher and E. L. Hahn, *Phys. Rev.*, **116**, 332 (1968).
4) Y. Hiyama, N. Watanabe, T. Maruizumi, and E. Niki, *Nippon Kagaku Kaishi*, **1979**, 961.
5) S. N. Subarao and P. J. Bray, *J. Chem. Phys.*, **67**, 1085 (1977).
6) A. Baeyer, *Liebigs Ann.*, **127**, 199 (1863).
7) C. Singh, *Acta Crystallogr.*, **19**, 759 (1965).
8) C. T. O'Konski and T. K. Ha, *J. Chem. Phys.*, **56**, 3169 (1972).

The Effects of Added Electrolytes on Mn^{2+}-ion Mobility in Micellar Solutions Studied by the ESR Method

Masako Ueki and Yuhei Uzu*

Department of Chemistry, Faculty of Science, Shinshu University, Asahi, Matsumoto 390

(Received November 1, 1979)

Synopsis. The effects of added electrolytes on manganese-ion mobility in manganese dodecyl sulfate solutions ($Mn(DS)_2$) were measured by means of the ESR method. The addition of aluminum chloride results in line-narrowing and an increase in the signal intensity in the ESR spectra at the concentrations above CMC of the $Mn(DS)_2$ solutions, while the addition of sodium chloride does not affect the ESR spectra.

To obtain information on counterion mobility in the interface between a micelle and the intermicellar solution, some investigations employing the manganese ion as an ESR probe of metal binding to sodium dodecyl sulfate (SDS) micellar solutions have been made by several groups of workers in recent years.[1,2] Above the CMC, it has been found that linewidth-broadening or signal-intensity loss in the ESR spectrum of the Mn^{2+} ion was caused by the Mn^{2+} ion in two environments surrounding the micelle: the manganese ion may be free in the intermicellar solution, or it may be attached to the micelles formed. In the hope of obtaining further corroborating evidence for this postulate, the present study, based on measurements of the linewidth and relative intensity of the Mn^{2+} ion, was performed for $Mn(DS)_2$ solutions, with and without added electrolytes.

The manganese dodecyl sulfate used was prepared by adding an excess of $MnSO_4$ to a SDS solution and by then cooling the solution in a dry ice–water bath. The SDS was synthesized according to the method of Dreger *et al.*[3]

The surface tensions on $Mn(DS)_2$ and SDS aqueous solutions were measured for the determination of the CMC by means of Kyowa Tensiometer. Surface-tension measurements in the redistilled water at 30 °C indicated no minima and CMC values of 8 mmol dm^{-3} for SDS and 1 mmol dm^{-3} for $Mn(DS)_2$, all in good agreement with those in the literature.[4] The inorganic electrolytes added, sodium and aluminum chlorides, were those of extra-pure reagents and had been purified by recrystallization.

For the preparation of the solution investigated, different amounts of the salts were dissolved in the $Mn(DS)_2$ solution at a given concentration above the CMC. For the concentrations below the CMC, the addition of the Al salt made precipitates, and so the measurements were made for solutions containing 5 mmol dm^{-3} and 10 mmol dm^{-3} $Mn(DS)_2$. The solutions thus obtained were directly inserted into a capillary tube 1.5 mm in o.d. and then sealed in the presence of air for the ESR measurements.

The ESR spectra were recorded with a Japan Electron Model JES-ME-3X spectrometer operating at the X band with 100-KHz field modulation.

In each measurement, six typical hyperfine lines were completely resolved. The linewidth (ΔH) was directly measured as the peak-to-peak distance of the fourth line from the low-field side.[5] For a Lorentzian resonance line, the intensity is proportional to the product of the height of the derivative curve and the square of the linewidth. The relative intensity was obtained by comparing the (height) × (linewidth)^2 product with that of the reference sample in the cavity. A sample of 0.01 wt % DPPH dispersed homogeneously in solid KCl was used as the reference standard.[2,6] All the intensity measurements were made with the same sample volume in order to obtain a good reproducibility. In addition, identical microwave power, crystal biasing current, field-scanning rate, and modulation amplitude were used. Figure 1 shows the dependence of the linewidth (ΔH) and the increment

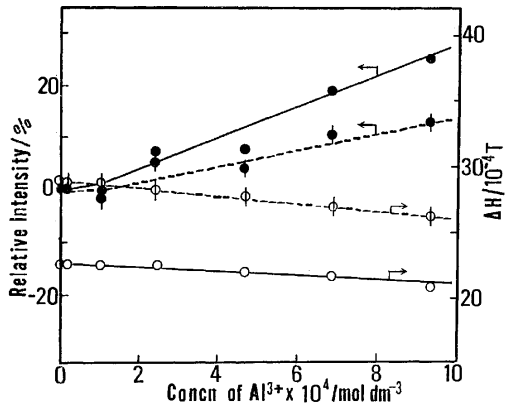

Fig. 1. Relative intensity (full points) and linewidth (open points) of Mn^{2+} as a function of added $AlCl_3$ concentration in $Mn(DS)_2$ solutions. —●—, —○—; 5 mmol dm^{-3} $Mn(DS)_2$, --●--, --○--; 10 mmol dm^{-3} $Mn(DS)_2$.

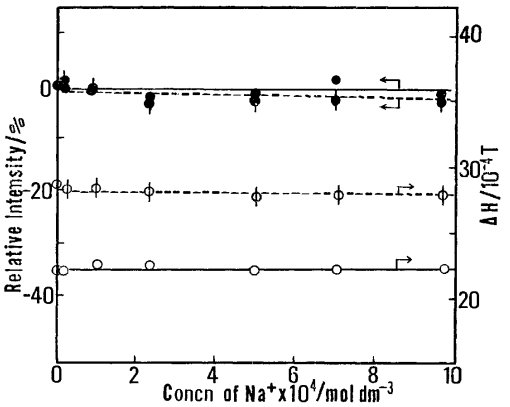

Fig. 2. Relative intensity (full points) and linewidth (open points) of Mn^{2+} as a function of added NaCl concentration in $Mn(DS)_2$ solutions. —●—, —○—; 5 mmol dm^{-3} $Mn(DS)_2$, --●--, --○--; 10 mmol dm^{-3} $Mn(DS)_2$.

in the relative intensity of the Mn^{2+} ion on the concentration of the added $AlCl_3$ at 30 °C, while in Fig. 2 the results for NaCl are presented. Although the figures show some scatter in the relative intensity, the much more pronounced effect of the Al^{3+} ion than that of the Na^+ ion at equimolar concentrations is immediatly obvious. On the further addition of the Al^{3+} ion, the linewidth tends to be appreciably narrower, whereas there is a corresponding increase in the relative intensity. On the contrary, no detectable changes in the ΔH and the intensity were observed upon the addition of NaCl in the range of the concentrations studied. This probably arises in part from the replacement of the Mn^{2+} ion with the more multivalent Al^{3+} ion in the electrical double layer at the micelle surface, followed by the increase in the average number of the free Mn^{2+} ion in the intermicellar solution. This fact was observed upon the addition of Mn^{2+} or VO^{2+} ion to a SDS solution.[1,7] Some support for this result may also be given by the observation of the ESR spectra for $Mn(DS)_2$ solutions with no added salts, as is shown in Fig. 3. In agreement with the earlier finding,[2] the line-broadening is observed at the CMC, and it increases as the concentration is raised. Simultaneously, the signal intensity seems to increase in proportion to the number of the free Mn^{2+} ion, irrespective of the loss in the intensity due to the micellar-bound Mn^{2+} ion above the CMC, as has been stated by Oaks.[2]

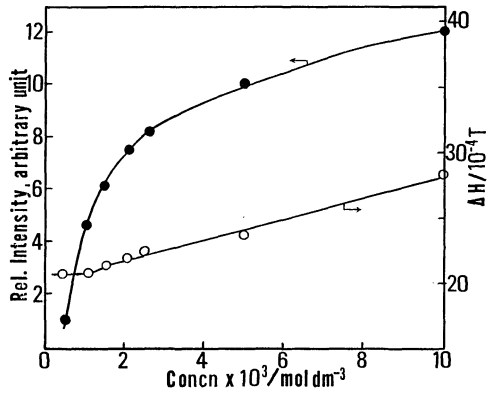

Fig. 3. Relative intensity and linewidth of Mn^{2+} as a function of $Mn(DS)_2$ concentration at 303 K.

On the basis of these deductions concerning the nature of the Mn^{2+} ion motion, the increase in the line-narrowing and intensity with the increase in the concentration of the added Al^{3+} ion can be explained in terms of a decrease in the amount of Mn^{2+} ions bound to the micelle relative to those "free" in the intermicellar solution.

References

1) A. Hasegawa, Y. Michihara, and M. Miura, *Bull. Chem. Soc. Jpn.*, **43**, 3116 (1970).
2) J. Oaks, *J. Chem. Soc. Faraday Trans.* 2, **69**, 1321 (1973).
3) E. E. Dreger *et al.*, *Ind. Eng. Chem.*, **36**, 610 (1944).
4) P. Mukerjee and K. J. Mysels, "Critical Micelle Concentrations of Aqueous Surfactant System," Nat. Stand. Ref. Data Series, Nat. Bur. Stand. (U. S.) NSRDS-NBS36, Feb., 1961.
5) B. B. Garret and L. O. Morgan, *J. Chem. Phys.*, **44**, 890 (1966).
6) S. I. Chan, B. M. Fung, and H. Lutje, *J. Chem. Phys.*, **47**, 2121 (1967).
7) P. Stilbs, J. Jermer, and B. Lindman, *J. Colloid Interface Sci.*, **60**, 232 (1977).

Ground-state Energy Stabilization in Solid Cation Radical Salts Derived from Some Aromatic Hydrocarbons

Yôichi IIDA

Department of Chemistry, Faculty of Science, Hokkaido University, Sapporo 060

(Received November 26, 1979)

Synopsis. The ground-state energy stabilization due to the charge-transfer interaction between cation radicals was examined with solid cation radical salts of 9,10-dimethylanthracene, 9,10-dichloroanthracene, and perylene with antimony pentachloride and perchlorate anions.

There have been made extensive investigations concerning the optical and magnetic properties of a number of crystalline ion radical salts.[1-7] In such ion radical salts, the planar ion radical moleucles are known to form, in themselves, a segregated stacking into one-dimensional columns so as to make a large overlap between their half-occupied moleuclar orbitals. The electronic and magnetic properties of those solid salts are interesting in comparison with those of ion radical monomer. The electronic spectrum of such solid salt is found to differ distinctly from the monomer spectrum of the corresponding ion radical molecule, but shows a charge-transfer transition between ion radicals in the low-energy region.[1-5] As for the magnetic properties, an antiferromagnetic spin exchange interaction between adjacent ion radicals is known to take place in such solid ion radical salt.[1-6] These optical and magnetic properties can be understood in terms of the charge-transfer interaction between ion radical molecules in segregated one-dimensional columns of solid ion radical salts. In the present paper, we shall examine the ground-state energy stabilization due to the charge-transfer interaction between cation radicals in solid aromatic hydrocarbon cation radical salts of 9,10-dimethylanthracene (DMA) with antimony pentachloride anion, 9,10-dichloroanthracene (DCA) with antimony pentachloride anion, and perylene with perchlorate anion.[2,8]

In a previous paper,[4] we applied Hubbard model to the segregated stack of the aromatic hydrocarbon cation radicals and explained the optical and magnetic behaviors of those solid cation radical salts. As for the DMA and DCA cation radical salts, non-alternant one-dimensional half-occupied Hubbard Hamiltonian was applied to the stack of the DMA or DCA cation radicals. The Hubbard Hamiltonian is given by

$$\mathscr{H} = \sum_{i,j,\sigma} T_{ij} C_{i\sigma}^{+} C_{j\sigma} + I \sum_{i} n_{i\downarrow} n_{i\uparrow}, \qquad (1)$$

where $n_{i\sigma} = C_{i\sigma}^{+} C_{i\sigma}$, and $C_{i\sigma}^{+}$ and $C_{i\sigma}$ are the creation and annihilation operators of an electron with σ-spin at the i-th site, respectively, and where T_{ij} is the electron transfer matrix element between the i-th and j-th sites, and the Coulomb repulsive potential, I, appears only when two electrons with up and down spins are at the same site. In this model, we take the half-occupied molecular orbital of the unpaired electron for one site of cation radical, and assume a model of regular one-dimensional column composed of infinite number of such sites. We further assume that the transfer matrix element of electron exists only between nearest neighbor sites and is denoted by $T(<0)$. In the case of regular one-dimensional half-occupied Hubbard model with $I \gg |T|$, the Hamiltonian of Eq. 1 becomes equivalent to the following effective Hamiltonian,[6]

$$\mathscr{H}_{\text{eff}} = \frac{4T^2}{I} \sum_{i} \left(\boldsymbol{S}_i \cdot \boldsymbol{S}_{i+1} - \frac{1}{4} \right) + 0\left(\frac{T^3}{I^2} \right), \qquad (2)$$

where $\boldsymbol{S}_i$, $(S=1/2)$, is the spin operator of an electron at the i-th site. In the limit of $I/|T| \to \infty$ and $N \to \infty$, where N is the number of sites in one-dimensional system, we can neglect such higher terms as $0(T^3/I^2)$, and the ground-state energy of Eq. 2 is given by

$$E = -\frac{4NT^2}{I} \ln 2. \qquad (3)$$

The ground-state energy of the one-dimensional system of the cation radicals is found to be stabilized by the charge-transfer interaction between cation radicals through the non-zero transfer matrix element, T. Rigorously speaking, the $I/|T|$ value of one-dimensional system of actual ion radical salt is large but not infinite, so that the approximation of E in Eq. 3 has some deviation from exact ground-state energy of Eq. 2. This deviation is caused by neglecting such terms as $0(T^3/I^2)$ in deriving Eq. 3. Therefore, relative error, $\Delta E/E$, in the approximation of Eq. 3 is, at most, of the order of T/I. An advantage of our application of Hubbard model is many-body treatment, so that we can obtain ground-state energy of one-dimensional stack composed of infinite number of ion radicals.

For the DMA cation radical salt, the experimental results of the charge-transfer absorption and the magnetic susceptibilities were well explained in terms of the parameter values of $I = 11600\ \text{cm}^{-1}$ and $T \approx -570\ \text{cm}^{-1}$.[4] In this case, since the magnitude of $I/|T| = 20.4$ is much larger than unity, we can apply, in place of Eq. 1, the effective Hamiltonian of Eq. 2 to the one-dimensional system of the DMA cation radicals. Then, by the use of the approximation of Eq. 3, the value of E was estimated to be $-0.93\ \text{kJ mol}^{-1}$, and the error of its value was within $\pm 0.046\ \text{kJ mol}^{-1}$. In a similar way, for the DCA cation radical salt, the values of $I = 11200\ \text{cm}^{-1}$ and $T \approx -560\ \text{cm}^{-1}$ were estimated with the one-dimensional system of the DCA cation radicals.[4] Then, the ratio of $I/|T| = 20.0$ is found to be much larger than unity, and the approximation with Eq. 3 is again applicable to our case. The ground-state energy was thus estimated as $E = -0.93 \pm 0.047\ \text{kJ mol}^{-1}$.

In the case of perylene cation radical salt, the perylene cation radicals are paired up to form dimers in the solid state.[2,4] Then, we applied a dimer model of Hubbard Hamiltonian, which can by written by

$$\mathscr{H} = \sum T(C_{1\sigma}^{+} C_{2\sigma} + C_{2\sigma}^{+} C_{1\sigma}) + I(n_{1\downarrow} n_{1\uparrow} + n_{2\downarrow} n_{2\uparrow}), \qquad (4)$$

where the notations are common to those in Eq. 1. The suffixes, 1 and 2, denote two sites of perylene cation radicals in a dimer, and $T(<0)$ is the electron transfer matrix element between the cation radicals in the dimer. If we only take the half-occupied molecular orbital of perylene cation radical for each site, there are six bases of the wave functions for the dimer. After solving the eigen value problem, the lowest s tate of the dimer is the singlet state whose energy is given by $E_s=I/2-\sqrt{(I/2)^2+(2T)^2}$.[3] The negative value of E_s means ground-state energy stabilization due to the charge-transfer interaction between cation radicals in the dimer through non-zero transfer matrix element, T. Earlier, we explained the optical and magnetic properties of the perylene cation radical salt with the above approach, and obtained the parameter values of $I=6330\ \mathrm{cm^{-1}}$ and $T=-1630\ \mathrm{cm^{-1}}$.[4] Therefore, the ground-state energy per one mole of perylene cation radicals can be estimated by summing the E_s value with half mole of the dimers, and is calculated to be $-8.19\ \mathrm{kJ\ mol^{-1}}$.

For the above three compounds, the ground-state stabilization energy due to the charge-transfer interaction between cation radicals becomes one of the factors for their cohesive energies. At the present time, there may be no other way to isolate and estimate its magnitude experimentally, but its magnitude is related to the absorption intensity of the charge-transfer transition between cation radicals in their solid-state spectra. In regular one-dimensional infinite stack of cation radicals, the absorption intensity is given, in the small $|T|$ limit, by $N\pi e^2aT^2/I$,[5] where a is the lattice separation. Therefore, the absorption intensity is approximately proportional to the magnitude of the ground-state stabilization energy. In the dimer model of cation radicals, the situation appears to be similar, and the magnitude of the ground-state stabilization energy is also nearly proportional to the charge-transfer absorption intensity of the dimer. In view of the estimated values of the stabilization energies of DMA, DCA, and perylene cation radical salts. the charge-transfer absorption intensity of the perylene cation radical salt will be about nine times stronger than those of the DMA and DCA cation radical salts, and the absorption intensities of the latter two compounds will be of the same magnitude. This prediction appears to be in agreement with the experimental result of the solid-state spectra reported by Sato *et al.*[2]

All of these compounds are ionic crystals and crystal Madelung energy will be the most important factor for their cohesive energies. Although there is no information on the values of Madelung energy for those compounds, the Madelung energies of several other cation radical salts such as Würster's Blue (*N,N,N',N'*-tetramethyl-*p*-phenylenediamine) perchlorate and iodide are of the order of $-4\times10^2\ \mathrm{kJ\ mol^{-1}}$.[6,7] In comparison with great contribution of the Madelung energy, the stabilization energy due to the charge-transfer interaction between cation radicals may make very small contribution to the total cohesive energy in our DMA, DCA, and perylene cation radical salts. However, it is important to note that the mechanism of the charge-transfer interaction does not act in usual ionic crystals such as alkali halides, but only takes place in solid ion radical salts.

References

1) See, for example, Z. G. Soos and D. J. Klein, "Molecular Association," ed by R. Foster, Academic Press, London, New York, San Francisco (1975) Vol. 1, Chap. 1; "Chemistry and Physics of One-Dimensional Metals," ed by H. J. Keller, Plenum Press, New York and London (1977).

2) Y. Sato, M. Kinoshita, M. Sano, and H. Akamatu, *Bull. Chem. Soc. Jpn.*, **42**, 3051 (1969).

3) Y. Iida, *Bull. Chem. Soc. Jpn.*, **51**, 2523 (1978).

4) Y. Iida, *Bull. Chem. Soc. Jpn.*, **52**, 1523 (1979).

5) Y. Iida, *Bull. Chem. Soc. Jpn.*, **52**, 2791 (1979).

6) Y. Iida, *Bull. Chem. Soc. Jpn.*, **52**, 3447 (1979).

7) R. M. Metzger, *J. Chem. Phys.*, **64**, 2069 (1976).

8) As for the DMA–$SbCl_5$ and DCA–$SbCl_5$ crystals, in view of their optical and magnetic properties shown in Ref. 2, ion radical species should be only cation radicals of DMA and DCA, and the counter anion of $SbCl_5$ will have some diamagnetic form. Concerning this anion form, Dr. Y. Sato, who is one of the authors of Ref. 2, suggested that the disproportionation to $SbCl_4^-$ and $SbCl_6^-$ might be most probable.

An X-Ray Photoelectron Spectroscopic Study of Several Metal Complexes of 2-Mercaptobenzimidazole and 2-Mercaptobenzoxazole

Tooru YOSHIDA

Osaka Prefectural Industrial Research Institute, 2-1-53, Enokojima, Nishi-ku, Osaka 550

(Received August 16, 1979)

Synopsis. The X-ray photoelectron spectra of several metal complexes of 2-mercaptobenzimidazole and 2-mercaptobenzoxazole were measured in order to examine the mode of coordination of the ligands. From their N(1s) and S($2p_{3/2}$) chemical shifts, it was suggested that the ligands are coordinated through both the sulfur and nitrogen atoms in most of the complexes.

Heterocyclic thiols, such as 2-mercaptobenzothiazole, **1**, 2-mercaptobenzimidazole, **2**, and 2-mercaptobenzoxazole, **3**, are widely used as organic reagents for inorganic ions. The complexing properties of these ligands, which exhibit thioketo-thiol tautomerism, have been studied by the use of a variety of techniques: IR, far IR, UV, magnetic measurements, and NMR.[1]

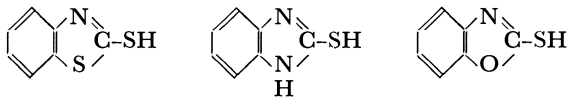

1 **2** **3**

X-Ray photoelectron spectroscopy (XPS) is sensitive to the charge distribution.[2] The XPS study of several metal complexes of **1** has been reported.[3] In that paper, it was proved that the copper was present in a (+1) oxidation state in the complexes obtained from Cu(II) salts and **1**.

The purpose of the present study is to examine the mode of the coordination of the ligands in several metal complexes of **2** and **3** and the oxidation state of copper in their copper complexes by means of XPS.

Experimental

The X-ray photoelectron spectra were measured on an AEI ES200 spectrometer. MgK_α (1253.6 eV) X-ray radiation was used as the excitation source. The samples were ground to powder and then dusted onto double-backed adhesive tape. The measurements were run at room temperature under a vacuum of about 10^{-7} Torr. The binding energy of the C(1s) electron peak was used as the energy standard throughout the present experiments; it was taken to be 285.0 eV. The reproducibilities of the values thus obtained were within ±0.1 eV. All the compounds used and their binding energies are given in Table 1.

Chemicals. Benzimidazole as a reference compound, 2-mercaptobenzimidazole, and 2-mercaptobenzoxazole (abbreviated as L", LH, and L'H respectively) were obtained commercially and were of an analytical grade. They were used after recrystallization from ethanol. The sodium salt (abbreviated as LNa) of LH was obtained by treating LH with NaOH, but the attempt to prepare L'Na was unsuccessful.

Preparations of Metal Complexes. *CuL*: A solution of LH (4 mmol) containing an equivalent amount of NaOH in ethanol (50 ml) was added to a solution of CuX_2 (X= Cl, NO_3, 1/2(SO_4), CH_3COO, ClO_4) (2 mmol) in water (50 ml). A grey-colored compound thus precipitated was digested on a water bath for an hour. The suspension was cooled, and then the precipitate was filtered and washed with ethanol. The yield of the complex was more than 95%, as in other copper complexes.

Cu(LH)Cl, $Cu(LH)_{1.5}(SO_4)_{0.5}$, and $Cu(LH)_{1.5}NO_3 \cdot H_2O$: A solution of LH (4—6 mmol) in ethanol (50 ml) was added to each solution of $CuCl_2$, $CuSO_4$, and $Cu(NO_3)_2$ (2 mmol) in water (50 ml). The ivory-white compounds thus precipitated were treated in a way similar to the procedure for CuL. *CuL'*: A solution of L'H (4 mmol) in ethanol (50 ml) was used instead of the solution of LH containing NaOH in the above procedure for preparing CuL. The color of the compound was ivory-white.

Pb(L–H): An ethanol solution of LH was added to an aqueous solution of $Pb(NO_3)_2$, and the mixed solution was neutralized with aqueous ammonia; a white complex was thus precipitated. *$PbL(CH_3COO)$*: An ethanol solution of LH was added to an aqueous solution of $Pb(CH_3COO)_2$, and then the solution was digested on a water bath; a pale yellow white compound was thus precipitated.

$NiL(OH) \cdot H_2O$ and $NiL'(OH) \cdot H_2O$: An aqueous solution of LH (L'H) containing an equivalent amount of NaOH was added to an aqueous solution of nickel salts, whereby a dark-brown (greenish-brown) compound was precipitated.

Other Metal Complexes: The other metal complexes were prepared based upon the literature.[1]

All the compounds used were dried in an air oven at 95 °C for at least 2 h and then analyzed elementally.

Results and Discussion

The N(1s) spectra of LH and L'H showed a single peak, and the peak could be assigned to the protonated nitrogen atom from its binding energy.[3] This indicates that both LH and L'H exist entirely in the thioketo form. This conclusion is consistent with the results obtained by IR.[4] The N(1s) spectra of LNa and L" showed two peaks with nearly equal intensities; these peaks could easily be assigned to protonated and deprotonated nitrogen atoms, based upon their binding energies.

The N(1s) binding energies of the protonated and deprotonated nitrogen atoms of LNa were 0.3—0.5 eV lower than those of L". The S($2p_{3/2}$) binding energy of LNa is fairly close to that of LH. These findings may suggest that, in LNa, the contribution of $-\overline{N}-\overset{|}{C}=S$ dominates that of $-N=\overset{|}{C}-\overline{S}$, and that an apparent unit negative charge on the nitrogen is delocalized by conjugation within the hetero five-membered ring.[5]

The N(1s) spectra of AgL, HgL_2, $CdL_2 \cdot 0.5H_2O$, $PbL(CH_3COO)$, CuL, $NiL(OH) \cdot H_2O$, $PdL_2 \cdot 2H_2O$, and $PtL_2 \cdot H_2O$ showed the presence of two kinds of nitrogen atoms, that is, protonated and deprotonated nitrogens, similarly to LNa. Those of the other metal complexes showed a single peak, indicating only one kind of nitrogen atom, that is, a deprotonated nitrogen atom for Pb(L–H), in addition to all the com-

TABLE 1. MEASURED BINDING ENERGIES

Compound	Binding energy/eV			
	N(1 s)	S($2p_{3/2}$)	O(1 s)	Cu($2p_{3/2}$)
LH	400.6	162.4		
LNa·H_2O	400.3, 398.5	162.2		
AgL	400.4, 398.9	162.7		
HgL_2	400.3, 398.9	162.9		
CdL_2·0.5H_2O	400.4, 399.0	162.5		
Pb(L-H)	398.9	162.7		
PbL(CH_3COO)	400.4, 398.8	162.4		
CuL	400.4, 399.0	162.8		933.4
Cu(LH)Cl	400.7	163.1		933.2
$Cu(LH)_{1.5}(SO_4)_{0.5}$	400.6	163.0		933.3
$Cu(LH)_{1.5}NO_3$·H_2O	400.6	163.0		933.4
NiL(OH)·H_2O	400.6, 399.1	162.7		
PdL_2·2H_2O	400.6, 399.5	162.9		
$Pd(LH)_2Cl_2$	400.6	163.0		
PtL_2·H_2O	400.6, 399.6	163.0		
$Pt(LH)_2Cl_2$	400.6	163.2		
L'H	400.9	162.5	534.6	
AgL'	399.4	162.8	534.5	
HgL'_2	399.3	163.1	534.6	
CdL'_2·H_2O	399.5	162.7	534.6	
PbL'_2	399.3	162.6	534.5	
CuL'	399.5	162.9	534.5	933.5
NiL'(OH)·H_2O	399.4	162.7	—	
PdL'_2	400.0	163.2	534.7	
PtL'_2	400.0	163.2	534.7	
L"	400.6, 399.0			

plexes of L'H, and a protonated nitrogen for the remaining complexes of LH.

In general, the coordination of a ligand to a metal ion causes a decrease in the electron density on the coordination atom, giving rise to an increase in the core-electron binding energy of the atom.

In the series of the complexes of LH, the chemical shifts of the N(1 s) binding energy of a deprotonated nitrogen atom or of the S($2p_{3/2}$), which are the differences between the N(1 s) or the S($2p_{3/2}$) binding energies of the complexes and LNa, were 0.2—1.1 eV. These chemical shifts were comparable with the values reported for the complexes with other ligands.[6] This seems to suggest that, in all the complexes, the ligand is coordinated through the sulfur atom, and that in the complex containing a deprotonated nitrogen atom the ligand is also coordinated through the nitrogen atom.

It was difficult to confirm the presence of the bond between a metal ion and a protonated nitrogen atom because of the absence of any appreciable difference between the N(1 s) binding energies of the protonated nitrogen atoms of a complex and LH.

In the series of the complexes of L'H, the N(1 s) and S($2p_{3/2}$) chemical shifts were 0.3—1.0 eV and 0.1—0.7 eV respectively. In this case, the N(1 s) binding energy (399.0 eV) of the deprotonated nitrogen atom of L" and the S($2p_{3/2}$) binding energy (162.5 eV) of L'H were used as the standard energies in determining the chemical shifts, because L'Na could not be obtained. The chemical shifts thus obtained seem to suggest that, in all the complexes, the ligand is coordinated through both the sulfur and nitrogen atoms. The O(1 s) electron spectra of all the complexes showed a single peak. There was no appreciable difference between the O(1 s) binding energies of a complex and L'H. This seems to suggest the absence of a metal–oxygen bond. These conclusions were consistent with the results obtained by IR and far IR.[1d]

The N(1 s) electron binding energies of L'H and its complexes were 0.3—0.5 eV higher than those of LH and the deprotonated nitrogen atom of its corresponding metal complexes. This finding suggests that the electron densities on the nitrogen atom of the former compounds are smaller than those of the latter. This seems to be consistent with the fact that the dissociation constant (pK_{N-H}=6.58) of L'H was smaller than that (pK_{N-H}=9.18) of LH.[7]

The Cu ($2p_{3/2}$) electron-region spectra of all the copper complexes in this study did not show at all a satellite characteristic of cupric compounds.[8] Furthermore, the Cu($2p_{3/2}$) binding energies were 2—4 eV lower than those of cupric compounds.[8] These findings indicate that the copper in the complexes is in a (+1) oxidation state, as in the copper complexes of 2-mercaptobenzothiazole.[3] This is apparent also from the stoichiometric analyses of the complexes in the present study.

The author wishes to thank Drs. Kiyoshi Yamasaki and Shigemasa Sawada for their helpful discussions and suggestions during this work, and Mr. Taichiro Hirohara for the elemental analysis.

References

1) a) J. Dehand and J. Jordanov, *Inorg. Chim. Acta*, **17**, 37 (1976); b) I. P. Khullar and U. Agarwala, *Can. J. Chem.*, **53**, 1165 (1975); c) F. Wilson and P. Merchant, *J. Inorg. Nucl. Chem.*, **29**, 1993 (1967); d) C. Preti and G. Tosi, *Can. J. Chem.*, **55**, 1409 (1977); e) C. Preti and G. Tosi, *ibid.*, **54**, 85 (1976); f) C. Preti and G. Tosi, *J. Inorg. Nucl. Chem.*, **38**, 1125 (1976).

2) a) K. Siegbahn *et al.*, "ESCA Atomic, Molecular and Solid State Structure Studied by Means of Electron Spectroscopy," Almqvist and Wiksells AB, Uppsala (1967); b) K. Siegbahn *et al.*, "ESCA Applied to Free Molecules," North-Holland Publ. Co., Amsterdam (1969).

3) T. Yoshida, K. Yamasaki, and S. Sawada, *Bull. Chem. Soc. Jpn.*, **52**, 2908 (1979).

4) a) D. Harrison and J. T. Ralph, *J. Chem. Soc., B*, **1967**, 14; b) M. St. C. Flett, *J. Chem. Soc.*, **1953**, 347.

5) G. R. Form, E. S. Raper, and T. C. Downie, *Acta Crystallogr., Sect. B*, **32**, 345 (1976).

6) a) V. Srinivasan and R. A. Walton, *Inorg. Chim. Acta*, **25**, L85 (1977); b) D. A. Edwards, R. Richards, R. E. Myers, and R. A. Walton, *Inorg. Chim. Acta*, **23**, 215 (1977); c) T. Yoshida and S. Sawada, *Bull. Chem. Soc. Jpn.*, **47**, 1024 (1974); d) T. Yoshida and S. Sawada, *ibid.*, **48**, 3379 (1975).

7) a) P. Lech and H. Hanna, *Chem. Abstr.*, **76**, 53995d (1972); b) L. N. Lomakina and I. P. Alimarin, *Chem. Abstr.*, **64**, 7426e (1966).

8) D. C. Frost, A. Ishitani, and C. A. Mcdowell, *Mol. Phys.*, **24**, 861 (1972).

Chemical Ionization Mass Spectrometry of Epoxides

Shin SUZUKI,* Yoshio HORI, Rebati C. DAS,† and Osamu KOGA

Department of Synthetic Chemistry, Faculty of Engineering, Chiba University, Yayoi-cho, Chiba 260

(Received June 20, 1979)

Synopsis. The chemical ionization mass spectrometry of epoxides using methane as a reagent gas produces quasi-molecular ions, $(M+1)^+$. This ion has maximum abundance for most epoxides except 1,2-epoxybutane. The method is useful for determination of the molecular weight of epoxides.

Although the behavior of olefines in the photochemical reactions of NO_x–hydrocarbon–O_2 system has attracted interest from the viewpoint of photochemical smog formation,[1–3] all the products from the above reactions were not identified. Epoxides are produced from the reaction of O radical and olefines.[1]

CI mass spectrometry, recently developed,[4] gives abundant quasi-molecular ions ($m/e=(M+1)^+$ or $(M-1)^+$) for many organic compounds, the method being useful for molecular weight determination.[4,5] The present paper gives the results of CI mass spectrometry of the epoxides, as a part of our overall program of identification and analysis of all the products formed in the NO_x–hydrocarbon–O_2 system.

Experimental

A Shimadzu GC-MS apparatus was used. C_2—C_4 epoxides were used as reference materials. Commercial ethylene oxide (Takachiho Chemical Industries), propylene oxide, 1,2-epoxybutane, 2-methyl-1,2-epoxypropane (Wako Pure Industries) and *cis*- and *trans*-2,3-epoxybutane (Tokyo Kasei) were used. All the compounds were separated in the GC column (PEG 400) at room temperature using helium as a carrier gas (flow rate 30 ml/min) before introduction to the ionization chamber.

Results and Discussion

Figures 1—6 give the EI and CI mass spectra of epoxides. The CI patterns were obtained with methane as a reagent gas. Methane gave relatively simple mass spectra for nitrites and nitrates as compared with i-C_4H_{10} as a reagent gas.[6] The spectra were obtained after subtraction of the background.

The operational conditions of the GC-MS apparatus are as follows. EI spectrum: Ion-source temperature 190 °C, Electron energy 70 eV, Pressure†† 7×10^{-7} Torr. CI spectrum: Ion-source temperature 190 °C, Electron energy 350—500 eV, Pressure†† 5×10^{-5} Torr.

The main reactant ions are CH_5^+ and $C_2H_5^+$ when methane is used as a reagent gas.[7] The proton and hydride transfer reactions of these ions are important for analytical purpose, since they generate the quasi-molecular $(M+1)^+$ and $(M-1)^+$ ions, respectively.

$$RH + CH_5^+/C_2H_5^+ \longrightarrow RH_2^+ + CH_4/C_2H_4 \quad (1)$$

$$RH + C_2H_5^+ \longrightarrow R^+ + C_2H_6 \quad (2)$$

All the compounds except 1,2-epoxybutane showed very simple CI mass spectra, giving $(M+1)^+$ ion most abundantly. 1,2-Epoxybutane also gives $(M+1)^+$ ion, but the peak at $m/e=55$ is the highest (Fig. 3). This might be related to the easier γ-cleavage of the 1,2-epoxybutane.[8] EI also gave rise to complex cleavage of epoxides, showing that CI is useful for determination of the molecular weight of epoxides.

A series of mass spectra of C_4H_8O isomers, 1,2-epoxybutane, *trans*- and *cis*-2,3-epoxybutane and 2-methyl-1,2-epoxypropane, are given in Figs. 3—6. Only 1,2-epoxybutane could be identified by the CI method, since it gives a different CI mass pattern. However, CI is useless to distinguish other three isomers. Ethylene oxide gives CI mass spectrum quite similar to that of its isomer, acetaldehyde, which is produced by the photochemical reaction of NO_x–hydrocarbon–air system.†††

Mass fragments other than stated above are as follows. $(2M+1)^+$ fragment ion appeared in ethylene oxide ($m/e=89$, Fig. 1) and *trans*- and *cis*-2,3-epoxybutane ($m/e=145$, Figs. 4 and 5). Such ions very often appear in the CI spectra.[9] Small amounts of $(M)^+$ and $(M-1)^+$ ions were found in C_3—C_4 epoxides. The peaks at $m/e=(M-17)$ are also common to all epoxides except ethylene oxides. This is the highest peak especially for 1,2-epoxybutane. For C_4 epoxides, the peak ($m/e=55$, Figs. 3—6) could be ascribed to $C_3H_3O^+$ or $C_4H_7^+$. C_3 epoxide (propylene oxide) gave the peak, $m/e=41$ (Fig. 2) which might be derived from C_2HO^+ or $C_2H_5^+$. This suggests alcoholic ion formation; certain alcoholic structures were found for ionized epoxides.[10] The peaks at $m/e=(M-13)$ exist in propylene oxide and 1,2-epoxybutane. They are tentatively assigned to $C_3H_7O^+$ for 1,2-epoxybutane and $C_2H_5O^+$ for propylene oxide. The peaks at $m/e=(M-29)$ are small, but appear in all the spectra except for ethylene oxide. They may be $C_2H_3O^+$ or $C_3H_7^+$ for C_4 ($m/e=43$, Figs. 3—6) and CHO^+ or $C_2H_5^+$ for C_3 ($m/e=29$, Fig. 2).

The present work is part of Special Research Project on Environmental Science supported by Grant in Aid for Scientific Research No. 303014 from the Ministry of Education, Science and Culture.

References

1) K. L. Demerjian, J. A. Kerr, and J. G. Calvert,

† Present address: Department of Chemistry, University College of Engineering, Burla, Orissa, India.

†† Pressure is monitored between the ionization chamber and the vacuum pump in the apparatus. The pressure is related only to the reagent gas pressure.

††† Acetaldehyde is passed into the solution containing 2,4-dinitrophenylhydrazine in order to precipitate its hydrazone. Ethylene oxide precipitate no hydrazone in the same solution. The precipitate can be analyzed by means of GC[11] or LC.[12] The application to air pollution analysis is under investigation in this laboratory.

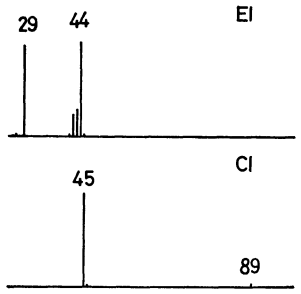

Fig. 1. Mass spectra of ethylene oxide (MW 44).

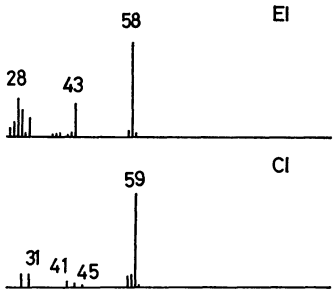

Fig. 2. Mass spectra of propylene oxide (MW 58).

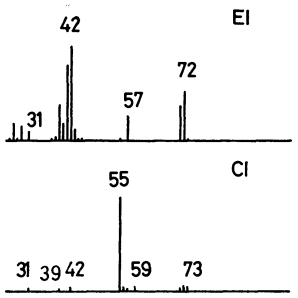

Fig. 3. Mass spectra of 1,2-epoxybutane (MW 72).

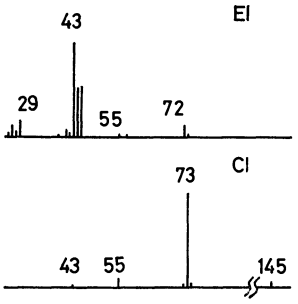

Fig. 4. Mass spectra of *trans*-2,3-epoxybutane (MW 72).

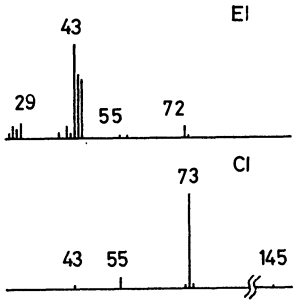

Fig. 5. Mass spectra of *cis*-2,3-epoxybutane (MW 72).

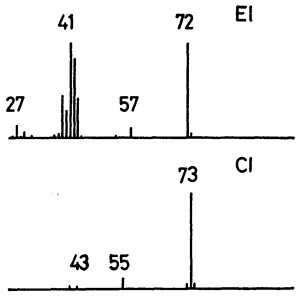

Fig. 6. Mass spectra of 2-methyl-1,2-epoxypropane (MW 72).

"Advances in Environmental Science and Technology," ed by J. N. Pitts, Jr., R. I. Metcalf, and A. Lloyd., John Wiley and Sons (1974) Vol. IV, p. 1.

2) A. P. Altshuller and J. J. Bufalini, *Environ. Sci. Technol.*, **5**, 39 (1971).

3) A. P. Altshuller and J. J. Bufalini, *Photochem. Photobiol.*, **4**, 97 (1965).

4) B. Munson, *Anal. Chem.*, **43**, 28A (1971).

5) F. W. McLafferty, "Interpretation of Mass Spectra" 2 ed W. A. Benjamin, Inc. (1973), p. 36.

6) R. C. Das, O. Koga, and S. Suzuki, *Bull. Chem. Soc. Jpn.*, **52**, 65 (1979).

7) M. S. B. Munson and F. H. Field, *J. Am. Chem. Soc.*, **88**, 2621 (1966).

8) P. Brown, J. Kossanyi, and C. Djerassi, *Tetrahedron. Suppl.* **8**, Part 1, 241 (1966).

9) F. Field, *J. Am. Chem. Soc.*, **91**, 2827 (1969).

10) C. C. Van de Sande and F. W. McLafferty, *J. Am. Chem. Soc.*, **97**, 4613 (1975).

11) L. J. Papa and L. P. Turner, *J. Chromatog. Sci.*, **10**, 744 (1972).

12) L. J. Papa and L. P. Turner, *J. Chromatog. Sci.*, **10**, 747 (1972).

The Liquid-Liquid Extraction of Zinc with Polyethylene Glycol and Poly(oxyethylene)-type Nonionic Surfactants

Toshio SUZUKI,* Naoyuki MURAKAMI, and Takeshi SOTOBAYASHI

Department of Chemistry, Faculty of Science, Niigata University, Ikarashi-Ninocho 8050, Niigata 950-21

(Received September 6, 1979)

Synopsis. The Zn(II) extraction was made from its acidic thiocyanate solution, using polyethylene glycol and its mono(alkylphenyl) ether as extractants. The effects of the number of oxyethylene groups (–O–CH_2–CH_2–) per molecule and of the kind of the counter cation of thiocyanate on the extractability are described, together with some other factors affecting the Zn(II) extraction.

Recently polyethylene glycol (PEG) and its derivatives have been found to useful as extractants in the liquid-liquid extraction of heavy metal and actinoid ions, and their extraction behavior has been briefly reported.[1–3] In the present paper, somewhat detailed results will be reported on the extraction behavior of a trace amount of Zn(II) from hydrochloric-acid solutions of several alkali and alkaline earth metal thiocyanates into some polar organic-solvent solutions of PEG and several poly(oxyethylene)-type nonionic surfactants.

Experimental

Reagents and Apparatus. The PEG, with a nominal molecular weight of 7500 ($HO(EO)_nH$, n: The number of oxyethylene groups (EO's), abbreviated as PEG 7500), and poly(oxyethylene)(–O–CH_2–CH_2–, POE) mono[(6-methylheptyl)phenyl] ether ($C_8H_{17}C_6H_4O(EO)_n$, $n=10$, abbreviated as Triton X-100) were supplied by the Wako Pure Chemicals Co., and the POE mono(nonylphenyl) ethers ($C_9H_{19}C_6H_4O$-$(EO)_nH$, $n=10$—120, abbreviated as NS (10—120), by the Nippon Oils & Fats Co. All these reagents were used for the extraction experiments without further purification. ^{65}Zn was used as a radioactive tracer to determine the distribution ratio of Zn(II) extraction, while the ^{65}Zn radioactivity was measured by means of a well-type NaI(Tl) detector (2.5× 3.0 in.) equipped with a multi-mode scaler (Aloka).

Extraction Procedure. Take 10 ml of an acidic aqueous thiocyanate solution containing a small amount of Zn(II) and 10 ml of a given organic solvent solution of a PEG or POE surfactant into a stoppered centrifuging tube, and then shake the tube for 2 h at 25±0.5 °C. It was proved by the preliminary experiment that the shaking time of 2 h was sufficient to attain the extraction equilibrium. After centrifuging, the radioactivity of a 5 ml aliquot of each phase was measured. The distribution ratio(D) of Zn(II) was determined by means of the radioactivity ratio of the two phases.

Results and Discussion

Effect of Organic Diluent. The extractability of Zn(II) was measured using various organic solvents as the diluent of PEG 7500 or Triton X-100, the results are shown in Table 1, together with the dielectric constants of the organic solvents used. As may be seen from this table, a polar diluent with a high dielectric constant (>10), like nitrobenzene and 1,2-dichloroethane(DCE), gave a high percentage extraction, but o-dichlorobenzene, with a dielectric constant of only 9.93, yielded a very low % E-value of 1.6. Thus, a 1,2-DCE solution of the extractant was used as the organic phase in this work.

Table 1. Effects of organic solvents

Solvent	Dielectric constant	Percentage extraction (%)	
		PEG 7500	Triton X-100
Nitrobenzene	34.8	>99	>99 (>99) [a]
1,2-Dichloroethane	15.1	>99	84.5 (>99)
o-Dichlorobenzene	9.93	1.6	94.8 (—)
Chlorobenzene	5.61	0.2	68.9 (>99)
Benzene	2.28	<0.1	16.8 (95.6)
Toluene	2.37	<0.1	13.6 (45.3)
Xylene	2.57	<0.1	— (15.6)
Carbon tetrachloride	2.23	<0.1	— (6.5)

Aqueous phase: 0.2 M KSCN, 0.01 M HCl, 0.001 M surfactant. a) Aqueous phase: 1.0 M KSCN, 0.01 M HCl, 0.05 M Triton X-100.

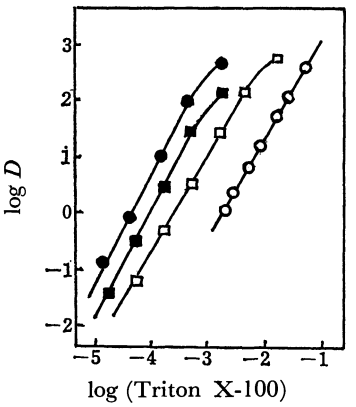

Fig. 1. Effect of surfactant concentration on the Zn(II) extraction.
Aqueous phase: 0.01 mol dm^{-3} HCl, 1.0 mol dm^{-3} thiocyanates. ●: KSCN, ■: NH_4SCN, □: NaSCN, ○: LiSCN. Organic phase: Triton X-100 in 1,2-DCE (w/v %).

Effect of the Extractant Concentration in the Organic Phase and the Kind of the Counter Cation of Thiocyanate in the Aqueous Phase. Figure 1 shows four log-log plots of the distribution ratio(D) of Zn(II) *vs.* the concentration (w/v %) in the organic phase of Triton X-100 for 4 different acidic aqueous phases, each containing an alkali metal and ammonium thiocyanates (1.0 mol dm^{-3}). When compared with each other at a given Triton X-100 concentration in the organic phase, the distribution ratios for these aqueous phases (4 thiocyanates) increased in the following order:

$$LiSCN < NaSCN < NH_4SCN < KSCN.$$

The log-log plots for Li^+, Na^+, NH_4^+, and K^+ give

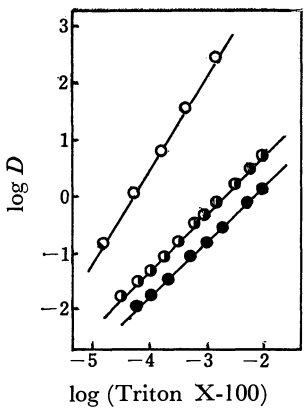

Fig. 2. Effect of surfactant concentration on the Zn(II) extraction.
Aqueous phase: 0.01 mol dm^{-3} HCl, 0.5 mol dm^{-3} thiocyanates. ○: $Ba(SCN)_2$, ◑: $Ca(SCN)_2$, ●: $Mg(SCN)_2$. Organic phase: Triton X-100 in 1,2-DCE.

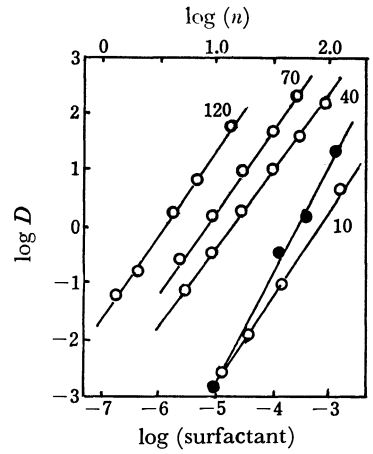

Fig. 3. Effect of the number(n) of EO's per molecule.
Aqueous phase: 0.5 mol dm^{-3} HCl, 1.0 mol dm^{-3} NH_4SCN. Organic phase: NS(10—120) in 1,2-DCE. ○: log *D* *vs.* log (surfactant), ●: log *D* *vs.* log (*n*). (The figures refer to the number of EO's.)

straight lines with slopes of 1.7, 1.7, 1.9, and 2.0 respectively. The plots for Na^+, however, show a tendency to deviate a little from their straight lines at high Triton concentrations of more than 10^{-2} mol dm^{-3}, the plots for NH_4^+ and K^+ show a similar tendency at concentrations of more than 10^{-3} mol dm^{-3}. Such a deviating tendency is not observed in the plot for Li^+, not even at high Triton concentrations of up to 8×10^{-2} mol dm^{-3}. In Fig. 2 the distribution ratio of Zn(II) is plotted against the concentration in the organic phase of Triton X-100, with the respective 0.01 mol dm^{-3} HCl solutions of 3 alkaline earth metal thiocyanates (1.0 mol dm^{-3}) being used as the aqueous phases. It can clearly be seen in Fig. 2 that the log-log plot for the aqueous phase of $Ba(SCN)_2$ has a slope of 1.7, about twice those for the aqueous $Mg(SCN)_2$ and $Ca(SCN)_2$ systems, and rather similar to those for the aqueous alkali metal thiocyanates (2.0—1.7). The *D*-value for the aqueous $Ba(SCN)_2$ system was larger than those for the $Mg(SCN)_2$ and $Ca(SCN)_2$ systems by a factor of at least 10—10^4 in the Triton X-100 concentration in the organic phase studied. The *D*-value for the aqueous phases of the these alkaline earth metal thiocyanates increased in this order:

$$Mg(SCN)_2 < Ca(SCN)_2 \ll Ba(SCN)_2.$$

Effect of the Number of EO's Per Molecule. Zn(II) was extracted from its 0.5 mol dm^{-3} HCl solution of NH_4SCN (1.0 mol dm^{-3}) with NS(10—120) in 1,2-DCE. Figure 3 shows the log-log plots of the distribution ratio(*D*) of Zn(II) *vs.* the formal molar concentration in the organic phase of NS (10—120), or the number of EO's per molecule. As can clearly be seen, at a given concentration in the organic phase of NS (10—120) the *D*-value increased with an increase in the EO number; the *D*-value for NS (120) was more than 10^4 times larger than that for NS(10), whereas the EO number for NS(10) is 12 times larger than that for NS(120). This finding is consistent with the U(VI) extraction dependence on the EO number for a series of PEG's of various molecular weights (200—20000)[3].

References

1) T. Sotobayashi, T. Suzuki, and S. Tonouchi, *Chem. Lett.*, **1976**, 585.
2) T. Sotobayashi, T. Suzuki, and K. Yamada, *Chem. Lett.*, **1976**, 77.
3) T. Sotobayashi, T. Suzuki, and H. Kudo, *J.Radioanal. Chem.*, **36**, 145 (1977).

Solid State Reactions between Rare Earth Orthophosphate and Oxide

Yasuo Hikichi,* Ken-iti Hukuo, and Jiro Shiokawa†

Materials Research Laboratory, Nagoya Institute of Technology, Gokiso-cho, Showa-ku, Nagoya 466

†*Department of Applied Chemistry, Faculty of Engineering, Osaka University, Yamadakami, Suita 565*

(Received September 17, 1979)

Synopsis. Solid state reactions between rare earth orthophosphate (RPO_4) and oxides (SiO_2, Al_2O_3, or CaO) in the air were studied by means of X-ray diffractometry. RPO_4 does not react with SiO_2, decomposing on heating above 1800 °C with Al_2O_3, or above 700 °C with CaO.

Anhydrous RPO_4 is stable in the air at temperatures near 2000 °C.[1,2] However, no study seems to have been carried out on the solid state reactions of RPO_4 with other oxides. The present study deals with such reactions between synthesized RPO_4 (R=La, Ce, Nd, Sm, Y, Dy, Er, or Yb) and oxides (SiO_2, Al_2O_3, or CaO) at temperatures in the range 600—1900 °C in the air.

Experimental

Starting Materials. Powder of monoclinic RPO_4 (R=La, Ce, Nd, or Sm) and that of tetragonal RPO_4 (R=Y, Dy, Er, or Yb), particle size less than 1 μm, and chemical composition very similar to that of theoretical RPO_4, were prepared by the methods reported[1,3-5]. Powder of SiO_2 (α-quartz, Wako Chemical Ind., Ltd.), Al_2O_3 (α-alumina, Nishio Ind., Ltd.) and CaO (Nakarai Chemicals, Ltd.), of high purity and less than 62 μm in length, were prepared from substances of reagent grade.

Solid State Reactions. Mixtures of RPO_4 and oxide in mole ratio 0.1—1 (RPO_4/oxide) were pressed at room temperature into pellets, *ca.* 10 mm diam. under the pressure 500 kgf/cm² (1 kgf/cm²=98.0665 kPa). The pellets were preheated at 600 °C, and then calcined in the temperature range 600—1900 °C for 60 min in an alumina crucible by using a SiC electric furnace (600—1500 °C) or an oxygen-propane gas furnace (1500—1900 °C).

Results and Discussion

Reaction with SiO_2. RPO_4 did not react with SiO_2 at temperature below 1700 °C. X-Ray diffraction patterns of the pellets calcined in the temperature range 600—1700 °C showed only the diffraction lines of the starting materials and none of new reaction products. The pellets softened with an increase in the amount of SiO_2 above 1713 °C (melting point of SiO_2) in the air.

Reaction with Al_2O_3. When the pellets were calcined below 1750 °C, X-ray diffraction patterns were those of the starting materials. However, some pellets (R=Nd, Sm, Y, Dy, Er, or Yb) calcined at 1800 °C and others (R=La, or Ce) calcined at 1850 °C for 60 min showed X-ray diffraction patterns of the reaction products (R_2O_3 or CeO_2).

The X-ray peak intensity of Al_2O_3 in the calcined pellets seems to be little affected by the calcining temperature and the decomposition of RPO_4, while that of R_2O_3 or CeO_2 was much affected, becoming strong with the decomposition of RPO_4. At 1900 °C, the X-ray diffraction lines of RPO_4 disappeared, only Al_2O_3 and R_2O_3 or CeO_2 becoming the main constituents of the calcined pellets. The amount of P of the calcined pellets determined by chemical analysis decreased gradually with the progress of the decomposition of RPO_4 above 1800 °C.

$AlPO_4$ is easily formed by heating mixtures of Al_2O_3 and P_2O_5 in the air. However, no $AlPO_4$ was detected in the pellets calcined at temperatures above 1800 °C for 60 min. Beck[6] reported that $AlPO_4$ is easily decomposed within a few minutes by heating at temperature above 1590 °C in the air, P component evaporating rapidly. Thus, even if $AlPO_4$ is formed in the pellets at temperatures above 1800 °C, it would be decomposed within a few minutes, its detection becoming difficult.

The reaction process might be expressed as follows:

$$2RPO_4 + Al_2O_3 \longrightarrow 2AlPO_4 + R_2O_3 \longrightarrow Al_2O_3 + R_2O_3 + (\text{P component}\uparrow)$$

$$\text{or}\quad 2CePO_4 + Al_2O_3 + 1/2O_2 \longrightarrow 2AlPO_4 + 2CeO_2 \longrightarrow Al_2O_3 + 2CeO_2 + (\text{P component}\uparrow) \quad (1)$$

$$2RPO_4 \xrightarrow{Al_2O_3} R_2O_3 + (\text{P component}\uparrow), \text{ or}$$

$$2CePO_4 \xrightarrow[1/2O_2]{Al_2O_3} 2CeO_2 + (\text{P component}\uparrow) \quad (2)$$

The process is based on the following assumptions: in (1) $AlPO_4$ can be formed in the calcined pellets in the early stages of reaction, and in (2) Al_2O_3 catalyzes the decomposition of RPO_4 in the calcined pellets, and no $AlPO_4$ can be formed because of high temperature.

It is apparent that RPO_4 can be decomposed by Al_2O_3 above 1800 °C in the air. However, which process takes place has not been clarified.

The melting points of Al_2O_3 and R_2O_3 or CeO_2 are higher than 1900 °C. However, the pellets softened at *ca.* 1900 °C, a part of the alumina crucible in contact with the pellets undergoing corrosion. The reason for the pellets softening at *ca.* 1900 °C can be explained by means of the phase diagrams of the systems Al_2O_3–R_2O_3 or CeO_2.[7] There are eutectic points such as 1720 °C (Al_2O_3 77 mol%+Nd_2O_3 23 mol%) or 1850 °C (Al_2O_3 20 mol%+Nd_2O_3 80 mol%) in the Al_2O_3–Nd_2O_3 system.

Reaction with CaO. RPO_4 reacted with CaO at temperatures above 700 °C, $Ca_3(PO_4)_2$ and R_2O_3 or CeO_2 being formed as new reaction products. The ratios of the decomposition of RPO_4 at temperature above 700 °C are expressed by means of the relative X-ray peak intensity ($I_1/(I_1+I_2)$) as shown in Fig. 1.

l_1 is the X-ray integrated peak intensity of RPO_4 ((200) diffraction line), and l_2 that of R_2O_3 or CeO_2 (diffraction line having the strongest intensity in the d range 2.95 (La_2O_3)—3.12 Å (CeO_2)(1 Å=0.1 nm).

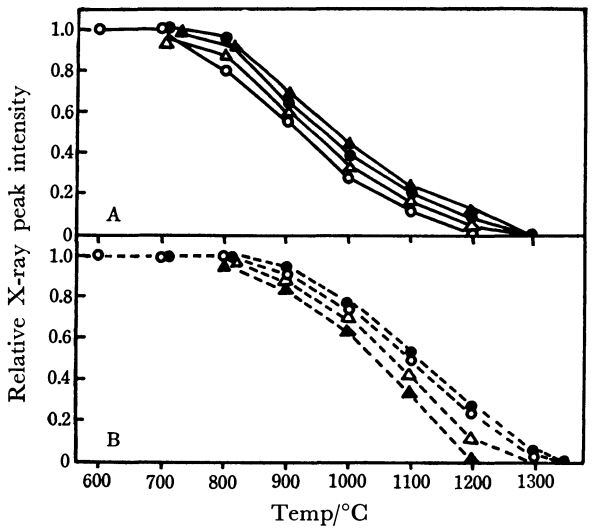

Fig. 1. Relation between the relative X-ray peak intensity and the firing temperature of the pellets[a] fired at various temperatures (600—1350 °C) for 60 min.
a) Mixing mole ratio (RPO_4/CaO) 0.6, A: Monoclinic form RPO_4, B: Tetragonal form RPO_4, ○—○: R=La, ●—●: R=Ce, △—△: R=Nd, ▲—▲: R=Sm, ○---○: R=Y, ●---●: R=Dy, △---△: R=Er, ▲---▲: R=Yb.

The relative X-ray peak intensity began to decrease at 700 °C, becoming O at 1350 °C (mixing mole ratio (RPO_4/CaO) below 0.6). The rate of decomposition of monoclinic RPO_4(A) seems to be slightly higher than that of tetragonal RPO_4(B) (Fig. 1).

The reaction products detected in the calcined pellets were only $Ca_3(PO_4)_2$ and R_2O_3 or CeO_2. The reaction process could be expressed by

$$2RPO_4 + 3CaO \longrightarrow Ca_3(PO_4)_2 + R_2O_3$$

or $$2CePO_4 + 3CaO + 1/2O_2 \longrightarrow Ca_3(PO_4)_2 + 2CeO_2 \quad (3)$$

The pellets softened at temperature below 1800 °C in the air since the melting point of $Ca_3(PO_4)_2$ is lower than that of RPO_4.

The work was partially carried out with Grant-in-Aid for Scientific Research No. 365280 from the Ministry of Education.

References

1) Y. Hikichi, K. Hukuo, and J. Shiokawa, *Nippon Kagaku Kaishi*, **1979**, 769.
2) Y. Hikichi and K. Hukuo, *Nippon Kagaku Kaishi*, **1976**, 88.
3) Y. Hikichi, K. Hukuo, and J. Shiokawa, *Bull. Chem. Soc. Jpn.*, **51**, 3645 (1978).
4) K. Hukuo and Y. Hikichi, *Nippon Kagaku Kaishi*, **1975**, 622.
5) Y. Hikichi, K. Hukuo, and J. Shiokawa, *Nippon Kagaku Kaishi*, **1977**, 1634.
6) W. R. Beck, *J. Am. Ceram. Soc.*, **32**, 147 (1949).
7) M. Mizuno, T. Yamada, and T. Noguchi, *Yogyo Kyokai Shi*, **85**, 24, 90, 374 (1977); **86**, 359 (1978).

Mechanical Strength and Thermal Expansion of Sintered Rare Earth Orthophosphate$(RPO)_4$

Yasuo HIKICHI,* Ken-iti HUKUO, and Jiro SHIOKAWA†

Materials Research Laboratory, Nagoya Institute of Technology, Gokiso-cho, Showa-ku, Nagoya 466

†*Department of Applied Chemistry, Faculty of Engineering, Osaka University, Yamadakami, Suita 565*

(Received September 18, 1979)

Synopsis. RPO_4 powders, obtained by heating a hexagonal form $RPO_4 \cdot 0.5H_2O$ (R=La, Ce, Pr, Nd, or Sm) or a monoclinic form $RPO_4 \cdot 2H_2O$ (R=Y, Er, or Yb) at 800 °C for 3 h, were pressed into plates or spheres at 500 kgf/cm² (1kgf/cm²=98.0665 kPa) and sintered at 1500 °C for 60 min in the air, the sintered bulk density being above 90% of the theoretical. The mechanical strength and thermal expansion of the sintered RPO_4 are : compressive strength 2300—3000 kgf/cm², bending strength 320—500 kgf/cm², and linear thermal expansion coefficients (30—900 °C) $(5.75—10)\times10^{-6}$.

In a previous paper,[1] a report was given on the freezing point of RPO_4 (R=La, Ce, Pr, Nd, Sm, Y, or Yb) measured by the specular reflection method with a heliostat type solar furnace. However, the mechanical strength and thermal expansion were not reported. The present study reports the compressive strength, bending strength and linear thermal expansion coefficients of RPO_4 sintered at 1500 °C in the air.

Experimental and Results

Starting Materials. Starting materials were powders of a monoclinic form RPO_4 (R=La, Ce, Pr, Nd, or Sm) and a tetragonal form RPO_4 (R=Y, Er, or Yb) prepared by heating a hexagonal form $RPO_4 \cdot 0.5H_2O$ (R=La, Ce, Pr, Nd, or Sm) or a monoclinic form $RPO_4 \cdot 2H_2O$ (R=Y, Er, or Yb) at 800 °C for 3 h in the air.[2-4] The particle sizes of the starting materials were less than 1 μm, the chemical composition being almost the same as the theoretical formula, RPO_4.

Sintering. No detailed study seems to have been reported on the sintering of RPO_4. Preliminary experiments were carried out in order to clarify the relation between the bulk density of the calcined RPO_4 pellets and the calcining temperature.

About 1 g of the starting material was pressed at room temperature into pellets of 10 mm diam. under the pressure of 500 kgf/cm². The bulk densities of the pellets were 2.49 ($LaPO_4$), 2.54 ($CePO_4$), 2.59 ($PrPO_4$), 2.61 ($NdPO_4$), 2.67 ($SmPO_4$), 1.82 (YPO_4), 2.69 ($ErPO_4$), and 2.74 g/cm³ ($YbPO_4$). The pellets were heated at 500 °C, and then calcined at various temperatures (900—1500 °C) for 60 min in an alumina crucible by using a SiC electric furnace. It was confirmed that the alumina crucible does not react with the pellets at temperature below 1500 °C in the air.

The bulk densities of the pellets calcined at 900 °C were the same as those of the starting pellets. However, the pellets began to shrink at temperature above 950 °C, their bulk densities increasing with rise in calcining temperature (Fig. 1). The theoretical densities are 5.04 ($LaPO_4$), 5.16 ($CePO_4$), 5.26 ($PrPO_4$),

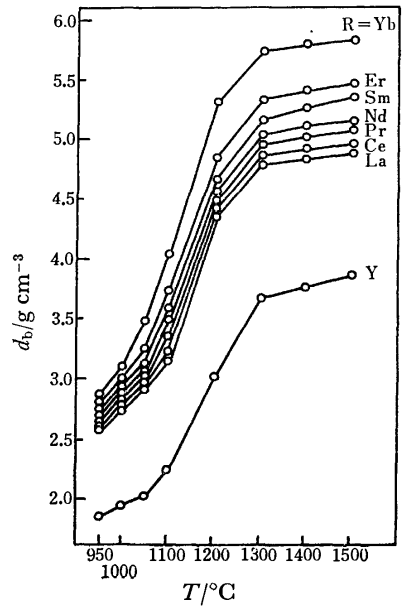

Fig. 1. Relation between the bulk density of the fired RPO_4 pellets and the firing temperature. Firing time: 60 min, d_b: Bulk density.

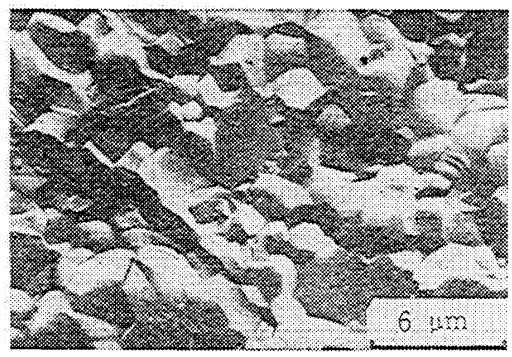

Fig. 2. The fractured surface of the sintered $CePO_4$ at 1400 °C for 60 min, studied by scanning electron microscopy.

5.40 ($NdPO_4$), 5.69 ($SmPO_4$), 4.26 (YPO_4), 6.12 ($ErPO_4$), and 6.36 g/cm³ ($YbPO_4$). The relative densities ((bulk density/theoretical density)×100%) increased rapidly above 1100 °C, becoming greater than 90% at 1500 °C: $LaPO_4$ 97%, $CePO_4$ 97%, $PrPO_4$ 97%, $NdPO_4$ 96%, $SmPO_4$ 94%, YPO_4 91%, $ErPO_4$ 90%, and $YbPO_4$ 92%. Apparent porosity of the pellets calcined at 1500 °C was below 5%. The results show that the sintering of RPO_4 is nearly completed by calcining at 1500 °C for 60 min in the air.

Scanning electron micrographs of the fractured surfaces of the sintered pellets show that the structure becomes dense (Fig. 2).

Mechanical Strength. The compressive strength

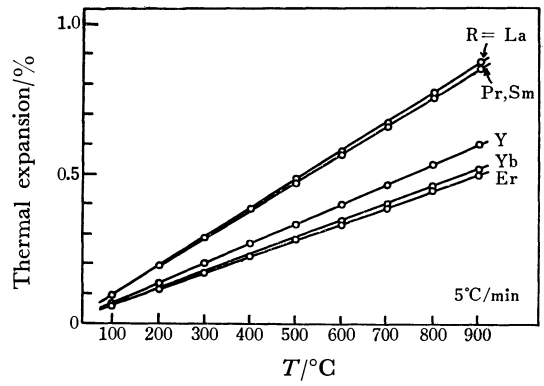

Fig. 3. Thermal expansion curves of the sintered RPO_4.

and 3-point bending strength (gauge length 30 mm) of the specimens sintered at 1500 °C for 60 min were measured. The specimens were cut into the 20 mm × 20 mm × 20 mm size for measurement of the compressive strength, and 50 mm × 20 mm × 10 mm for bending strength. Measurements were carried out for three samples of each sintered RPO_4.

The mean value of the compressive strength for each RPO_4 was in the range 2300—3000 kgf/cm^2, and that of the bending strength 320—500 kgf/cm^2. No definite relation has been found between the mechanical strength and the kind of rare earth element.

As compared with some commercial materials, the compressive strength and bending strength of the sintered RPO_4 seem to be larger than those of silica bricks (470—580 kgf/cm^2 and 27 kgf/cm^2)[5] or fire-clay bricks (340—445 kgf/cm^2 and 57—157 kgf/cm^2),[5] and almost the same as those of feldspathic porcelain (1700—3500 kgf/cm^2 and 100—450 kgf/cm^2)[5] or cordierite porcelain (1400—3100 kgf/cm^2 and 100—200 kgf/cm^2)[5] used for insulators.

Thermal Expansion Coefficient. A horizontal dilatometer with a dial gauge (0.001 mm) was used for measurement, the specimen holder and the extension rod being made of silica glass. The specimens sintered at 1500 °C for 60 min were cut into 4 mmϕ × 13 mm in size, and the measurements carried out in the temperature range 30—900 °C in the air with a heating rate about 5 °C/min.

Thermal expansion curves are shown in Fig. 3. The expansion ratio of the sintered $CePO_4$ and $NdPO_4$ at various temperature is close to that of $LaPO_4$, $PrPO_4$, or $SmPO_4$. The linear thermal expansion coefficients of the specimens calculated from these expansion curves are as follows: 10×10^{-6}($LaPO_4$), 9.90×10^{-6}($CePO_4$), 9.66×10^{-6} ($PrPO_4$), 9.77×10^{-6} ($NdPO_4$), 9.66×10^{-6} ($SmPO_4$), 6.90×10^{-6} (YPO_4), 5.75×10^{-6} ($ErPO_4$), and 5.98×10^{-6} ($YbPO_4$).

The thermal expansion coefficients of the sintered monoclinic form RPO_4 were larger than that of sintered Al_2O_3 (30—900 °C, 8.2×10^{-6}),[6] and smaller than that of fused MgO(30—900 °C, 13.9×10^{-6})[6] or fused CaO (30—900 °C, 12.8×10^{-6}),[6] those of the sintered tetragonal form RPO_4 being smaller than that of the sintered Al_2O_3.

The work was carried out with Grant-in-Aid for Scientific Research No. 365280 from the Ministry of Education.

References

1) Y. Hikichi, K. Hukuo, J. Shiokawa, M. Mizuno, and T. Noguchi, *Nippon Kagaku Kaishi*, **1979**, 769.
2) Y. Hikichi, K. Hukuo, and J. Shiokawa, *Bull. Chem. Soc. Jpn.*, **51**, 3645 (1978).
3) K. Hukuo and Y. Hikichi, *Nippon Kagaku Kaishi*, **1975**, 622.
4) Y. Hikichi, K. Hukuo, and J. Shiokawa, *Nippon Kagaku Kaishi*, **1977**, 1634.
5) N. Yamamoto, *Yogyo Kyokaishi*, **72**, 88, 108 (1964).
6) B. Yoshiki, "Taikabutsu Kogaku," Gihodo, Tokyo (1962), p. 170.

Preparation and ^{1}H-NMR Spectra of Dialkyl{tetrakis(1-pyrazolyl)borato}-thallium(III) Complexes

Masayoshi Onishi,* Katsuma Hiraki,* and Shigeki Nakagawa

Department of Industrial Chemistry, Faculty of Engineering, Nagasaki University, Bunkyo-machi, Nagasaki 852

(Received September 17, 1979)

Synopsis. Diethyl- and dibuthyl{tetrakis(1-pyrazolyl)-borato}thallium(III) complexes were prepared and characterized. The ^{1}H-NMR spectra of pyrazolyl protons of the BPz_4 ligand as well as the coupling constants between thallium and alkyl protons are discussed.

Trofimenko[1] reported several pyrazabole compounds, *i.e. boron* compounds of poly(1-pyrazolyl)borate. Storr *et al.* prepared sodium poly(1-pyrazolyl)aluminates and -indates,[2] and a few transition metal complexes of poly(1-pyrazolyl)gallates(III).[2,3] Some pyrazolyl-*N,N'*-bridged complexes of aluminum, gallium,[4] and thallium(III)[5] have also been reported. However, no study seems to have been reported on poly(1-pyrazolyl)borate complexes of IIIB group metals except boron[1] and thallium(I).[6]

This note deals with the preparation and ^{1}H-NMR study of two new dialkyl{tetrakis(1-pyrazolyl)borato} thallium(III) complexes, $[TlR_2(BPz_4)]$ {Pz=1-pyrazolyl, R=Et (**1**), and R=*n*-C_4H_9 (**2**)}.

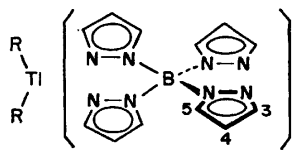

1, R = Et
2, R = *n*-C_4H_9

Experimental

General Procedure and Materials. Melting points were determined in capillary tubes on a Yanagimoto MP-S3 microstage apparatus and are uncorrected. IR spectra were recorded on a Hitachi model 285 spectrometer, and ^{1}H-NMR spectra on a JEOL model JNM-MH-100 spectrometer (100 MHz) using tetramethylsilane as an internal standard. Molecular weight was determined in dichloromethane using a Mechrolab model 301 vapor pressure osmometer. Molar conductivities were measured with a Toa Denpa CM-6A instrument. Solvents were dried and distilled by the standard methods, all the preparative operations being performed in an atmosphere of dry nitrogen.

Sodium tetrakis(1-pyrazolyl)borate, $\{Na(BPz_4)\}$[7] and dialkylthallium(III) bromides[8] were prepared according to reported procedures.

Reactions of Dialkylthallium(III) Bromides with Na(BPz_4). Sodium tetrakis(1-pyrazolyl)borate (1.66 mmol) was added to a THF solution of diethylthallium(III) bromide (1.46 mmol). After the mixture had been heated under reflux for 4 h, the solvent was evaporated under reduced pressure. The resulting residue was recrystallized from dichloromethane and hexane, affording a white powder of $[TlEt_2(BPz_4)]$ (**1**). A white powder of $[Tl(n\text{-}C_4H_9)_2(BPz_4)]$ (**2**) was prepared using dibuthylthallium(III) bromide in a similar way to that for **1**.

Results and Discussion

Diethyl- and dibutylthallium(III) bromides reacted with $Na(BPz_4)$ in THF under reflux to give **1** and **2**, respectively.[9] Complex **1** is considerably soluble in the usual organic solvents, the yield after recrystallization being fairly low. The molecular weight of **1** determined in dichloromethane was 526, in line with the monomeric structure formulated as $[TlEt_2(BPz_4)]$ (calcd 542). The non-ionic character of these two complexes was confirmed by low conductivity in common organic solvents (Table 1).

Mass spectra of **1** and **2** showed several peak-groups,

Table 1. Yields and properties of the new thallium(III) complexes

Complex	Yield[a] %	Mp °C	$\Lambda/(\Omega^{-1}\,cm^2/mol)$[b] CH_2Cl_2	THF	MeCOMe	EtOH	Found (Calcd), % C	H	N
1	8.8	194	0.25	—	0.55	2.7	35.66(35.48)	4.00(4.09)	21.01(20.69)
2	40	89—90	0.18	0.03	0.26	2.06	40.27(40.19)	5.03(5.06)	18.87(18.75)

a) Based on dialkylthallium(III) bromide. b) Molar conductivity in mol m^{-3} solution, at 25 °C.

Table 2. ^{1}H-NMR data of the thallium(III) complexes[a]

Complex	Alkyl group α-CH_2 δ/ppm	J_{HTl}/Hz	$J_{\alpha\beta}$/Hz	β-H δ/ppm	J_{HTl}/Hz	γ-CH_2 δ/ppm	δ-CH_3 δ/ppm	BPz_4 group[b] 3-H δ/ppm	4-H δ/ppm	5-H δ/ppm
1[c]	1.41(dq)	306	8.0	1.14(dt)	638	—	—	6.94(d)	6.28(t)	7.65(d)
2[d]	1.49(dt)	338	7.0	1.70(dm)[e]	538	1.25(m)[e,f,g]	0.86(t)[g]	6.94(d)	6.28(t)	7.65(d)

a) TMS as an internal standard. Abbreviations used; d=doublet, dm=double multiplet, dq=double quartet, dt=double triplet, m=multiplet, t=triplet. b) $^3J_{3,4}$ and $^3J_{4,5}$ are actually 2.0 Hz. c) In CD_2Cl_2. d) In $CDCl_3$. e) $^3J_{\alpha\beta}$ was not distinguished. f) The coupling to thallium was not distinguished. g) $^3J_{\gamma\delta}$=7.0 Hz.

Table 3. Solvent effect of the pyrazolyl proton resonances of **2**[a)]

Solvent	3-H	4-H	5-H
C_6D_6	7.21	6.12	7.48
CD_2Cl_2	6.88	6.25	7.59
$(CD_3)_2CO$	6.87	6.22	7.68

a) δ value (ppm) from TMS, at 25 °C. See Table 2, concerning the values in $CDCl_3$.

the pattern of each being characteristic of the isotopes of thallium (^{203}Tl and ^{205}Tl) and boron (^{11}B and ^{10}B). The highest peak of each peak-group, corresponding to a species containing both ^{205}Tl and ^{11}B was characterized as follows. Complex **1** showed four peaks at *m/e* 475, 513, 542, and 747 ascribable to the ethylthallium species, $[TlEt_2(BPz_3)]^+$, $[TlEt(BPz_4)]^+$, $[TlEt_2(BPz_4)]^+$ (the weak parent peak), and $[Tl_2Et_2(BPz_4)]^+$, respectively, and six peaks at *m/e* 350, 417, 484, 555, 622, and 689 to the dealkylated thallium species, $[Tl(BPz_2)]^+$, $[Tl(BPz_3)]^+$, $[Tl(BPz_4)]^+$, $[Tl_2(BPz_2)]^+$, $[Tl_2(BPz_3)]^+$(weak), and $[Tl_2(BPz_4)]^+$, respectively, the peak at *m/e* 614 not being ascribable to any species. Complex **2** showed four peaks at *m/e* 531, 541, 598, and 803 ascribable to the butylthallium species, $[Tl(C_4H_9)_2(BPz_3)]^+$, $[Tl(C_4H_9)(BPz_4)]^+$, $[Tl(C_4H_9)_2(BPz_4)]^+$ (weak parent peak), and $[Tl_2(C_4H_9)_2(BPz_4)]^+$, respectively, in addition to the six peaks ascribed to the dealkylated species and the unknown one at *m/e* 614 shown for complex **1**. It seems that the {poly(1-pyrazolyl)borato}dithallium fragments are formed in a considerable amount.

The pyrazolyl region in the ^1H-NMR spectrum of both **1** and **2** showed a virtual triplet for four 4-H's and two doublets for four 3-H's and 5-H's (Table 2). This indicates that the four pyrazolyl groups of the BPz_4 ligand are magneto-spectroscopically equivalent and fluxional in solution, similar to the case of $[Zn(BPz_4)_2]$[10] and $[Pd(1\text{-}3\text{-}\eta^3\text{-}C_3H_5)(BPz_4)]$.[10] On cooling to −31 °C,[11] the three signals broadened slightly, no slow-exchange limiting spectrum being obtained even at this temperature. ^1H-NMR data of the pyrazolyl protons of **2** in C_6D_6, CD_2Cl_2, and $(CD_3)_2CO$ are given in Table 3. Two doublets at δ 6.88 and 7.59 in CD_2Cl_2 were attributed to the 3-H's and the 5-H's, respectively, considering the fact that the environment of the outer 3-H's changes more significantly on switching the NMR solvent, than that of the inner 5-H's located near boron atom.

In the ^1H-NMR signals of alkyl groups, couplings to ^{203}Tl and ^{205}Tl were virtually identical (Table 2). Similar large and actually equal coupling constants of these two thallium isotopes were reported on some alkyl- or arylthallium(III) compounds by Maher and Evans, who found that a positive charge delocalized on the thallium atom increases the magnitude of the J(Tl-H) values, through the enhancement of s character upon the thallium atom.[12] The coupling constants of the α- and β-protons in **1** are actually comparable with the respective values [$^2J(H_\alpha Tl)=340$ Hz and $^3J(H_\beta Tl)=628$ Hz] of diethylthallium(III) sulfate,[12] this being the case with the dibutylthallium(III) homologues. This suggests that there is nearly one positive charge on the thallium atom in **1** or **2**, and the bonds between the thallium atom and the pyrazolyl-nitrogens are a kind of contact ion pair. This is in line with the fluxional behavior of the BPz_4 ligand in **1** and **2** at low temperature.

References

1) S. Trofimenko, *J. Am. Chem. Soc.*, **89**, 4948 (1967).
2) K. R. Breakell, D. J. Patmore, and A. Storr, *J. Chem. Soc., Dalton*, **1975**, 749.
3) D. J. Patmore, D. F. Rendle, A. Storr, and J. Trotter, *J. Chem. Soc., Dalton*, **1975**, 718.
4) A. Arduini and A. Storr, *J. Chem. Soc., Dalton*, **1974**, 503.
5) B. Walther, A Zschunke, B. Adler, A Kolbe, and S. Bauer, *Z. Anorg. Allg. Chem.*, **427**, 137 (1976).
6) M. I. Bruce, M. Z. Iqbal, and F. G. A. Stone, *J. Chem. Soc., (A)*, **1971**, 2820.
7) S. Trofimenko, *J. Am. Chem. Soc.*, **89**, 3170 (1967).
8) A. McKillop, L. F. Elson, and E. C. Taylor, *J. Organomet. Chem.*, **15**, 500 (1968).
9) The analytical data of **1** and **2** are satisfactory, as seen in Table 1. Their IR spectra were also consistent with the proposed formulae.
10) S. Trofimenko, *J. Am. Chem. Soc.*, **91**, 3183 (1969).
11) The temperature of the NMR samples was determined with methanol or 1,3-propanediol.
12) J. P. Maher and D. F. Evans, *J. Chem. Soc.*, **1965**, 637.

Reactions of 3-Acetyltropolone and Its Methyl Ethers with Methylhydrazine

Akio YAMANE,† Kimiaki IMAFUKU,* and Hisashi MATSUMURA

Department of Chemistry, Faculty of Science, Kumamoto University, Kurokami, Kumamoto 860

(Received August 27, 1979)

Synopsis. The reactions of 3-acetyltropolone and 3-acetyl-2-methoxytropone with methylhydrazine gave 1,3-dimethyl-1,8-dihydrocycloheptapyrazol-8-one (**3**) and 2,3-dimethyl-2,8-dihydrocycloheptapyrazol-8-one. 7-Acetyl-2-methoxytropone reacted with methylhydrazine to afford 1,3-dimethyl-1,8-dihydrocycloheptapyrazol-8-one methylhydrazone, besides a small amount of **3**.

In a previous paper,[1] we reported that 3-acetyltropolone (**1**) and 3-acetyl-2-methoxytropone (**2a**) reacted with hydrazine to afford 3-methyl-1,8-dihydrocycloheptapyrazol-8-one and that 7-acetyl-2-methoxytropone (**2b**) gave the hydrazone and azine of the above cycloheptapyrazolone. In this note, we wish to report the synthesis of 1,8- (**3**) and 2,8-dihydrocycloheptapyrazol-8-one (**4**), which have an additional methyl group at N_1 or N_2 atom, by the reactions of **1**, **2a**, and **2b** with methylhydrazine.

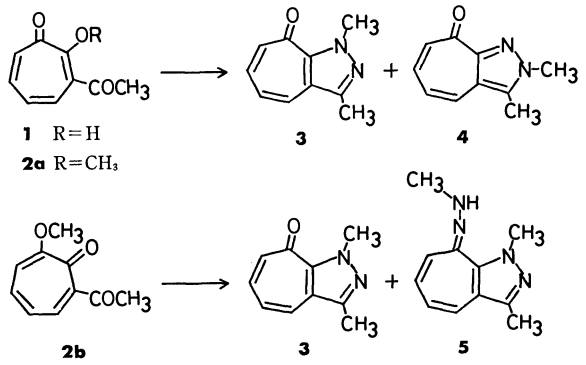

Scheme 1.

Results and Discussion

The refluxing of a mixture of 3-acetyltropolone (**1**) and methylhydrazine, which has two different nucleophilic nitrogen atoms, in methanol for 2 h gave two isomeric products, **3** (mp 96—98 °C) (60%) and **4** (mp 178—179 °C) (8%). The IR spectra of **3** and **4** show absorptions at 1643 and 1650 cm^{-1} respectively for the tropone carbonyl group. The UV spectra of the two isomers (**3** and **4**) are very similar to that of 3-methyl-1,8-dihydrocycloheptapyrazol-8-one,[1] as are shown in Fig. 1. The NMR spectra of **3** and **4** show peaks at δ 4.39 and 4.05 ppm respectively for the N-CH_3 group. The N-CH_3 peak of **3** is seen to shift to a lower field than that of **4** as a result of the anisotropic effect of the tropone carbonyl group. Thus, **3** and **4** were assigned to 1,3-dimethyl-1,8-dihydrocycloheptapyrazol-8-one and 2,3-dimethyl-2,8-dihydrocycloheptapyrazol-8-one respectively.

The refluxing of 3-acetyl-2-methoxytropone (**2a**) with methylhydrazine for 2 h gave the same products, **3** and **4** in 49 and 2% yields respectively.

† Present address: Wakunaga Pharmaceutical Co., Ltd., Koda-machi, Takata-gun, Hiroshima 729-64.

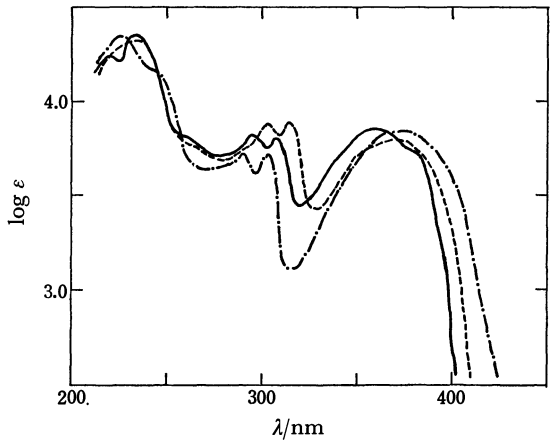

Fig. 1. UV Spectra.
——— 3-Methyl-1,8-dihydrocycloheptapyrazol-8-one,
------ **3**, —·—·— **4**.

A mixture of 7-acetyl-2-methoxytropone (**2b**) and methylhydrazine in methanol was refluxed for 2 h and then chromatographed on silica gel to afford **3** (trace) and **5** (29%). The IR spectrum of **5** shows no band near 1600 cm^{-1} for tropone, but it shows an NH band at 3260 cm^{-1}. Its UV spectrum is very similar to that of 3-methyl-1,8-dihydrocycloheptapyrazol-8-one hydrazone.[1] The NMR spectrum of **5** shows three singlet peaks at δ 2.16 for C-CH_3 and 3.72 for N-CH_3 in the pyrazole ring and 3.12 ppm for N-CH_3 of the methylhydrazono group. Consequently, **5** was assigned to 1,3-dimethyl-1,8-dihydrocycloheptapyrazol-8-one methylhydrazone.

No methylhydrazone (**5**) was obtained from the reaction of **1** and **2a** with methylhydrazine. Furthermore, **3** did not react with methylhydrazine either. It is thoguht that the methylhydrazone (**5**) was directly formed from **2b** by the mechanism shown in Scheme 2. In addition, the formation of the minor product (**3**) from **2b** might be considered to proceed as follows. The nucleophilic attack of methanol (*i.e.*, the solvent) on a C_2-atom of **2b** would give 3-acetyl-

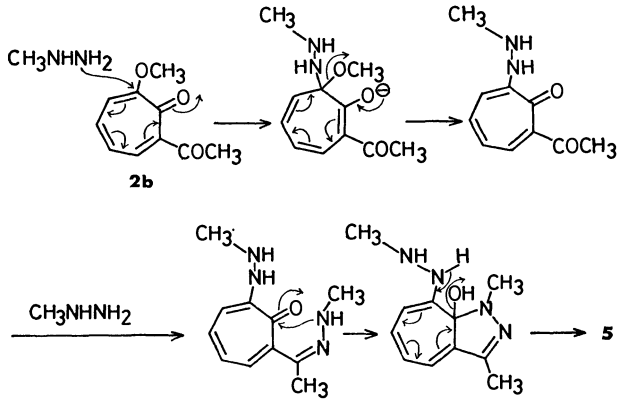

Scheme 2.

tropolone (**1**) which then reacts with methylhydrazine to afford **3**.

The NMR spectra of **3** and **4** in trifluoroacetic acid show a shift of the seven-membered ring protons by *ca.* 1.0—1.2 ppm, and one of the *N*- and *C*-CH_3 protons by *ca.* 0.4 ppm, towards a lower field. This indicates that the positive charge of the cations of **3** and **4** is delocalized over both the seven-membered ring and the pyrazole ring, as is shown in **3′** and **4′**:

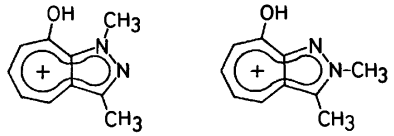

3′ **4′**

Experimental

Measurements. The melting points were determined with a Yanagimoto MP-S2 melting-point measuring apparatus and are uncorrected. The IR spectra were taken on a JASCO IRA-1 spectrophotometer, and the UV spectra on a Hitachi EPS-3T spectrophotometer. The NMR spectra were recorded with a Hitachi R-24 spectrometer (60 MHz), with TMS as the internal standard.

*Reaction of 3-Acetyltropolone (**1**) with Methylhydrazine.* A mixture of **1** (345 mg, 2.1 mmol) and methylhydrazine (185 mg, 4.1 mmol) in methanol (20 ml) was refluxed for 2 h. After the removal of the solvent, the residue was chromatographed on a Wakogel B-10 plate (30×30 cm^2) with ethyl acetate to give **3** (218 mg, 60%) and **4** (28 mg, 8%). 1,3-Dimethyl-1,8-dihydrocycloheptapyrazol-8-one (**3**): Pale yellow needles (from hexane); mp 96—98 °C; IR ($CHCl_3$): 1643, 1598 cm^{-1}; UV (MeOH): λ_{max} nm (log ε) 235 (4.33), 303 (3.89), 316 (3.89), 372 (3.80); NMR ($CDCl_3$): δ 2.50 (s, 3H, *C*-CH_3), 4.39 (s, 3H, *N*-CH_3), 6.4—7.5 ppm (m, 4H); NMR (CF_3COOH): δ 2.94 (s, 3H), 4.78 (s, 3H), 7.4—8.5 ppm (m, 4H). Found: C, 68.65; H, 5.76; N, 16.12%. Calcd for $C_{10}H_{10}N_2O$: C, 68.95; H, 5.79; N, 16.08%. 2,3-Dimethyl-2,8-dihydrocycloheptapyrazol-8-one (**4**): Pale yellow needles (from benzene-petroleum ether); mp 178—179 °C; IR ($CHCl_3$): 1650, 1603 cm^{-1}; UV (MeOH): λ_{max} nm (log ε) 226 (4.36), 244 (4.17), 252 (4.04), 290 (3.72), 303 (3.71), 377 (3.84); NMR ($CDCl_3$): δ 2.51 (s, 3H, *C*-CH_3), 4.05 (s, 3H, *N*-CH_3), 6.3—7.4 ppm (m, 4H); NMR (CF_3COOH): δ 2.95 (s, 3H), 4.49 (s, 3H), 7.5—8.5 ppm (m, 4H). Found: C, 68.91; H, 5.87; N, 16.16%. Calcd for $C_{10}H_{10}N_2O$: C, 68.95; H, 5.79; N, 16.08%.

*Reaction of 3-Acetyl-2-methoxytropone (**2a**) with Methylhydrazine.* A mixture of **2a** (423 mg, 2.4 mmol) and methylhydrazine (183 mg, 4.0 mmol) in methanol (20 ml) was refluxed for 2 h. The reaction mixture was then worked up as has been described above to afford **3** (205 mg, 49%) and **4** (8 mg, 2%).

*Reaction of 7-Acetyl-2-methoxytropone (**2b**) with Methylhydrazine.* A mixture of **2b** (357 mg, 2.0 mmol) and methylhydrazine (228 mg, 5.0 mmol) in methanol (20 ml) was refluxed for 2 h. After the removal of the solvent, the residue was chromatographed on two Wakogel B-10 plates (30×30 cm^2) with ether-chloroform (1:2) to give **3** (trace) and **5** (118 mg, 29%). 1,3-Dimethyl-1,8-dihydrocycloheptapyrazol-8-one methylhydrazone (**5**): Orange needles (from benzene-petroleum ether); mp 112—113 °C; IR ($CHCl_3$): 3260, 1530 cm^{-1}; UV (MeOH): λ_{max} nm (log ε) 260^{sh} (3.96), 270^{sh} (3.92), 350 (4.10); NMR ($CDCl_3$): δ 2.16 (s, 3H, *C*-CH_3), 3.12 (s, 3H, *NH*-CH_3), 3.72 (s, 3H, *N*-CH_3), 5.4—6.3 (m, 4H), 8.7—9.3 ppm (br, 1H, NH). Found: C, 65.31; H, 7.02; N, 27.79%. Calcd for $C_{11}H_{14}N_4$: C, 65.32; H, 6.98; N, 27.70%.

We wish to thank Dr. Tetsuo Nozoe, Professor Emeritus of Tohoku University, for his advice and encouragement.

Reference

1) A. Yamane, M. Nagayoshi, K. Imafuku, and H. Matsumura, *Bull. Chem. Soc. Jpn.*, **52**, 1972 (1979).

Two-phase Darzens Condensation Reaction with Octopus Compounds as a Catalyst

Sadatoshi AKABORI,* Michiko OHTOMI, and Seiichi YATABE

Department of Chemistry, Faculty of Science, Tōho University, Funabashi, Chiba 274

(Received September 27, 1979)

Synopsis. The octopus compound, readily derived from hexakis(mercaptomethyl)benzene and 1-chloro-3,6,9-trioxadecane, was effectively employed as a catalyst in the two-phase Darzens condensation of carbonyl compounds with chloroacetonitrile to afford the corresponding oxiranes in good yields.

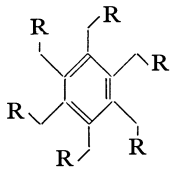

1a, R = -$SCH_2CH_2OCH_2CH_2OCH_2CH_2OCH_3$

1b, R = -$OCH_2CH_2OCH_2CH_2OCH_2CH_2OCH_3$

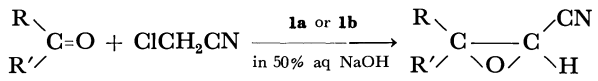

2 **3**

2 and 3	a	b	c	d	e
R	$(CH_2)_5$	CH_3CH_2-	Ph-	CH_3-	CH_3- Ph- and
R′		CH_3CH_2-	Ph-	CH_3-	Ph- CH_3-

In recent years, phase-transfer catalyses involving crown ether and quarternary ammonium halide have come into widespread use as a tool in organic synthesis.[1] The use of crown ether[2] and quarternary ammonium salts[3,4] to catalyze Darzens condensations with a wide variety of substrates has also been documented; however, to the best of the authors' knowledge, no mention has been made in the literature of condensation reactions catalyzed by an octopus compound. In the course of our studies of the phase-transfer reaction we have found[5] that octopus compounds are useful phase-transfer catalysts for the synthesis of nitriles from the reaction of alkyl halide and sodium cyanide. Therefore, we wish now to describe a convenient and efficient Darzens condensation of ketones with chloroacetonitrile catalyzed by octopus compounds.

The reaction was conducted by stirring a mixture of a carbonyl compound, an excess of chloroacetonitrile, and 50% aq. sodium hydroxide at 15 °C in the presence of an octopus-compound catalyst (**1a** or **1b**). The results are shown in Table 1. The maximum yields of the condensation products under our experimental conditions were obtained by using about 6—9% of the octopus compound by weight to the carbonyl compound. The reaction is exothermic, and the controlled addition of chloroacetonitrile is sometimes necessary. The octopus compounds functions as liquid-liquid phase transfer catalysts: however, the reaction proceeds at a slower rate in the absence of the catalyst. For example, cyclohexanone (**2a**) gives less than 9% of **3a** after 5 h at 15 °C when it is treated with chloroacetonitrile in the absence of **1**, whereas **3a** is formed in a 76% yield within 2 h when **1** is present. Thus, in the Darzens condensation of carbonyl compounds, it is most likely that octopus compounds transport the hydroxide anion into the organic phase, although the possibility of transforming the carbonyl compound into the aqueous phase can not be ruled out. When hexakis(2,5,8,11-tetraoxadodecyl)benzene (**1b**) was employed as the phase-transfer catalyst, the results were usually quite similar,

TABLE 1. DARZENS CONDENSATION IN THE PRESENCE OF OCTOPUS COMPOUNDS

Carbonyl compound ($\times 10^{-3}$ mol)	$ClCH_2CN$ (ml)	50% NaOH (ml)	Octopus compound ($\times 10^{-5}$ mol)	Reaction time h	Reaction temp °C	Product[a]	Yield %[b]
2a (1.2)	0.1	2.0	**1a** (7.0)	3	15	**3a**	76
2a (1.2)	0.1	2.0	**1a** (20.0)	3	15	**3a**	40
2a (1.2)	0.1	2.0	**1a** (3.5)	3	15	**3a**	32
2a (1.2)	0.1	2.0	**1b** (7.0)	3	15	**3a**	56
2b (1.0)	0.1	2.0	**1a** (7.0)	3	15	**3a**	45
2b (1.0)	0.1	2.0	**1a** (20.0)	3	15	**3b**	40
2b (1.0)	0.1	2.0	**1a** (3.5)	3	15	**3b**	28
2b (1.0)	0.1	2.0	**1b** (6.5)	3	15	**3b**	23
2c (1.2)	0.1	2.0	**1a** (8.1)	3	15	**3c**	56
2c (1.2)	0.1	2.0	**1b** (9.1)	3	15	**3c**	51
2d (1.2)	0.1	2.1	**1a** (8.2)	3	15	**3d**	59
2d (1.2)	0.1	2.0	**1b** (9.1)	3	15	**3d**	33
2e (1.2)	0.1	2.0	**1a** (7.3)	1	15	**3e**[c]	78[d]
2e (1.2)	0.1	2.0	**1b** (7.3)	1	15	**3e**[c]	75[d]

a) All the products show the same retention time with the authentic sample. b) The values are those obtained by GLC. c) The product (**3e**) was found to be a nearly 1:1 mixture of geometrical isomers (*E*- and *Z*-isomers). d) The total yield of *E*- and *Z*-isomers.

although rather less satisfactory. In the case of acetophenone, the condensation product was shown by the GLC analysis to be a 1:1 mixture of geometrical isomers (*E*- and *Z*-). The yield of **3c** shown in the table is the total yield of *E*- and *Z*-isomers. In further experiments, similar reactions of cyclohexanone (**2a**) or benzophenone (**2c**) with chloroacetonitrile in the presence of 18-crown-6 as a phase-transfer catalyst afforded 1-oxa-spiro-[2,5]-octane-2-carbonitrile (**3a**, 55% yield) or 3,3-diphenyloxirane-2-carbonitrile (**3c**, 47% yield).

Experimental

Analysis. The products were analyzed by gas chromatography. The chromatograms were obtained on a Hitachi 023 gas chromatograph, using 10% Polyester FF on a Chromosorb W AW/DMCS 1 m×3 mm column.

Materials. Hexakis(2-thia-5,8,11-trioxadodecyl)benzene (**1a**) and hexakis(2,5,8,11-tetraoxadodecyl)benzene (**1b**) were prepared according to the procedures described in a previous paper.[5] Authentic samples (1-oxa-spiro[2.5]-octane-2-carbonitrile (**3a**),[6] 3,3-diethyloxirane-2-carbonitrile (**3b**),[7] 3,3-diphenyloxirane-2-carbonitrile (**3c**),[7] 3,3-dimethyloxirane-2-carbonitrile (**3d**),[6] and 3-methyl-3-phenyloxirane-2-carbonitrile (**3e**, *E*-+*Z*-isomers))[6] were prepared according to the procedures described in the literature. Sodium hydroxide and ketones were used without further purification. The solvents used were purified by distillation.

General Procedure. A typical procedure for the reaction of cyclohexanone with chloroacetonitrile is as follows.

*Reaction of Cyclohexanone with Chloroacetonitrile in the Presence of **1a**.* A solution of 50% aq. sodium hydroxide (2 ml), cyclohexanone (1.2×10^{-3} mol), and hexakis(2-thia-5,8,11-trioxadodecyl)benzene (7.0×10^{-5} mol) was stirred for 10 min at 15 °C. Chloroacetonitrile (0.1 ml) was then added all at once, and the heterogeneous mixture (organic-water layers) was stirred for a further 2 h at 15 °C. The reaction mixture was diluted with water (10 ml) and extracted with ether (3×10 ml). The extract was washed with water and dried with anhydrous magnesium sulfate. The solvent was evaporated, and the residue in benzene was subjected to GLC analysis.

References

1) W. P. Weber and G. W. Gokel. "Phase-transfer Catalysis in Organic Synthesis," Springer-Verlag KG. (1977).
2) M. Makosza and M. Ludwikow, *Angew. Chem.*, **86** 744 (1974).
3) J. C. Hummelen and H. Wynberg, *Tetrahedron Lett.*, **1978**, 1089.
4) A. Jonczyk, A. Kwast, and M. Makosza, *J. Chem. Soc., Chem. Commun.*, **1977**, 902.
5) M. Ohtomi, S. Yoneyama, K. Arai, and S. Akabori, *Nippon Kagaku Kaishi*, **1976**, 1878.
6) A. Jonczyk, M. Fedorynski, and M. Makosza, *Tetrahedron Lett.*, **1972**, 2395.
7) V. F. Martynov and A. V. Shchelkunov, *Zh. Obshch. Khim.*, **28** 3248 (1958).

Comparison of Lewis Acids as Catalyst for the Alkylation of Benzene with *s*-Butyl Chloride

Masahito SEGI, Tadashi NAKAJIMA, and Sohei SUGA*

Department of Industrial Chemistry, Faculty of Technology, Kanazawa University, Kodatsuno, Kanazawa 920

(Received October 12, 1979)

Synopsis. The Friedel-Crafts alkylation of benzene with *s*-butyl chloride has been carried out in the presence of various Lewis acid catalysts. The relative order of catalyst activity is: $AlBr_3$, $AlCl_3$, $MoCl_5$, $SbCl_5 > TaCl_5 > NbCl_5 > FeCl_3 > ZrCl_4 > TiCl_4 \gg WCl_6$. The effect of addition of nitromethane on alkylation has been investigated.

Recently a report was given on the stereospecific Friedel-Crafts alkylation with optically active secondary alkyl chloride derivatives.[1] The reactions were so sensitive to moisture and the activity of aluminium chloride that it was difficult to control stereospecificity with sufficient reproducibility. The stereospecificity changed a great deal when iron (III) chloride was used as a catalyst instead of aluminium chlroide.[2] The results prompted us to compare Lewis acids as catalyst for the alkylation of benzene with *s*-butyl chloride.

The order of Lewis acid catalyst activity changes with reaction and/or reactant.[3] Comparison of Lewis acids in the Friedel-Crafts reaction has been reported with ethylene and hydrogen chloride,[4] benzyl chloride,[5] and acetyl chloride.[6] However, no report seems to have appeared on the reactions using secondary alkyl chloride as a reactant. The order of catalyst activity did not differ as compared with the case of primary alkyl chloride. Alkylation with $AlCl_3$–CH_3NO_2 catalyst proceeds through a homogeneous system, the catalytic activity of $AlCl_3$ decreasing moderately with the addition of nitromethane.[7] Nucleophiles which possess lone pair electrons, *e.g.* ethers and halides, are available as additives to $AlCl_3$ catalyst, but react with benzene as reactants. We have studied the effects of the addition of nitromethane to some active Lewis acids.

Results and Discussion

s-Butyl chloride and benzene were condensed at various temperatures by means of various Lewis acid catalysts for 10 min. The ratio *s*-butyl chloride : Lewis acid : benzene was kept 1 : 0.15 : 25 in each case. Below 5 °C, dichloromethane (4 ml) was added in order to prevent coagulation of benzene. 2-Phenylbutane produced was determined by GLC.

The Lewis acid catalysts were classified into four groups according to their activities in the alkylation with *s*-butyl chloride: (1) very active catalysts; (2) moderately active catalysts; (3) weak catalysts; (4) inactive catalysts (Table 1). In the case of (1), alkylation gave 2-phenylbutane with 100% conversion at −30 °C for 10 min. Figure 1 shows a comparison of the reaction rates of alkylation in the case of (2) and (3). The relative order of catalyst activity is: $NbCl_5 > FeCl_3 > FeCl_3$–CH_3NO_2 (10 times mol) $\simeq AlCl_3$–CH_3NO_2 (1.3 times mol) $> ZrCl_4 > AlCl_3$–CH_3NO_2 (10 times mol) $> AlCl_3$–$C_6H_5NO_2$ (10 times mol) $> TiCl_4 \gg WCl_6$. It seems that there is no relationship between the order and the configuration of electrons in the metal atom of catalysts. The difference in catalyst activity in the Friedel-Crafts alkylation has been elucidated mainly by means of the electrophilicity of catalyst-reactant complex formed.[8]

Table 1. Classification of Friedel-Crafts catalysts based on their activities in the alkylation with *s*-butyl chloride

(1)	Very active catalysts $AlBr_3$ (IIIa), $AlCl_3$ (IIIa), $MoCl_5$ (VIb), $SbCl_5$ (Va), $TaCl_5$ (Vb)
(2)	Moderately active catalysts $NbCl_5$ (Vb), $FeCl_3$ (VIII), $FeCl_3$-CH_3NO_2 (10 times mol), $AlCl_3$-CH_3NO_2 (1.3 times mol)
(3)	Weak catalysts $ZrCl_4$ (IVb), $AlCl_3$-CH_3NO_2 (10 times mol), $AlCl_3$-$C_6H_5NO_2$ (10 times mol), $TiCl_4$ (IVb), WCl_6 (VIb)
(4)	Inactive catalysts Cu_2Cl_2 (Ib), $ZnCl_2$ (IIb), $CdCl_2$ (IIb), $HgCl_2$ (IIb), $SnCl_4$ (IVa), $BiCl_3$ (Va), VCl_3 (Vb), $NiCl_2$ (VIII), $CoCl_2$ (VIII), $PdCl_2$ (VIII)

( ) is the group of periodic table.

In the presence of the aluminium chloride catalyst the reaction mixture is not homogeneous, due to the limited solubility of the catalyst. It becomes completely homogeneous by the addition of nitromethane, the catalytic activity becoming milder as compared with the case of aluminium chloride only. When $SbCl_5$, $FeCl_3$, $AlCl_3$, $AlBr_3$, $MoCl_5$, $TaCl_5$, or $NbCl_5$ in nitromethane solvent (10 times mol) was used as catalyst at 20 °C for 10 min, the conversion was 100, 100, 17.1, 7.9, 2.5, 2.3, 0%, respectively. It seems that the addition of nitromethane would form a Lewis acid–nitromethane (1:1) complex similar to the case of aluminium chloride,[9] tending to decrease the catalytic activity for alkylation.

Experimental

IR spectra were determined on a JASCO DS-301 spectrometer. GLC analysis was carried out on a 2 m column of 10% Carbowax 20 M on Diasolid L for 2-phenylbutane.

Aluminium chloride of commercial grade was purified by sublimation under nitrogen. Lewis acids of commercial grade were used without further purification. Benzene was washed with concentrated sulfuric acid and water, and distilled after being dried on sodium ribbon. Other solvents were dried[10] and distilled before use.

Reaction Procedures. To a stirred mixture of dry benzene (10 ml) and Lewis acid (0.81 mmol) was added a solution of *s*-butyl chloride (5.4 mmol) in benzene (2 ml) at the

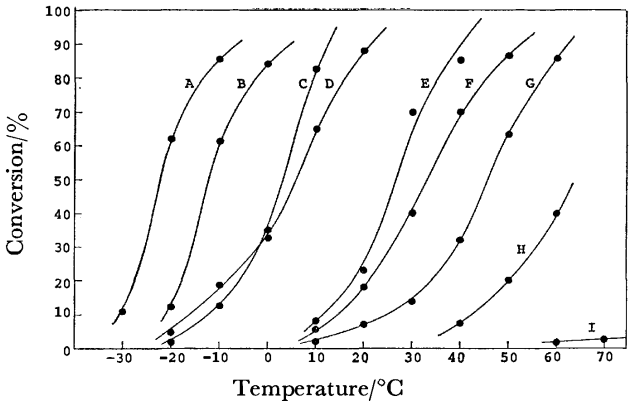

Fig. 1. Conversion percent in the alkylation of benzene with *s*-butyl chloride in the presence of catalysts in Groups 2 and 3 at −30 °C—70 °C for 10 min; A: $NbCl_5$, B: $FeCl_3$, C: $FeCl_3$–CH_3NO_2 (10 times mol), D: $AlCl_3$–CH_3NO_2 (1.3 times mol), E: $ZrCl_4$, F: $AlCl_3$–CH_3NO_2 (10 times mol), G: $AlCl_3$–$C_6H_5NO_2$ (10 times mol), H: $TiCl_4$, I: WCl_6.

rate required to maintain the desired temperature (Fig. 1). The reaction mixture was stirred at this temperature for 10 min, and then poured onto a mixture of crushed ice, concentrated hydrochloric acid (5 ml), and *p*-methylanisole (9.0 mmol) (internal standard). The benzene layer was separated and the aqueous layer extracted twice with 10 ml benzene. The combined organic layers were washed with water (15 ml) and dried over anhydrous sodium sulfate. The product was then determined by GLC by internal standardization technique.

References

1) T. Nakajima, S. Masuda, S. Nakashima, T. Kondo, Y. Nakamoto, and S. Suga, *Bull. Chem. Soc. Jpn.*, **52**, 2377 (1979).

2) S. Masuda, T. Nakajima, and S. Suga, *J. Chem. Soc., Chem. Commun.*, **1974**, 954.

3) G. A. Olah, "Friedel-Crafts and Related Reactions," Wiley-Interscience, New York (1963), Vol I, Chap. XI, p. 853.

4) A. V. Gross and V. N. Ipatiff, *J. Org. Chem.*, **1**, 599 (1936).

5) O. Tsuge and M. Tashiro, *Bull. Chem. Soc. Jpn.*, **40**, 119 (1967); G. A. Olah, S. Kobayashi, and M. Tashiro, *J. Am. Chem. Soc.*, **94**, 7448 (1972).

6) O. C. Dermer, D. M. Wilson, F. M. Johnson, and V. H. Dermer, *J. Am. Chem. Soc.*, **63**, 2881 (1941).

7) G. A. Olah, "Friedel-Crafts and Related Reactions," Wiley-Interscience, New York (1963), Vol I, Chap. IV, p. 246.

8) R. Nakane, *Yuki Gosei Kagaku Kyokai Shi*, **36**, 440 (1978).

9) L. Schmering, *Ind. Eng. Chem.*, **40**, 2072 (1948).

10) J. A. Riddick and E. E. Toops, Jr., "Organic Solvents," 2nd ed, Interscience Publishers, Inc., New York (1955).

Preparation and Properties of *N*-(Pentafluoropropionyl)amino Acid

Hajimu KAWA and Nobuo ISHIKAWA*

Department of Chemical Technology, Tokyo Institute of Technology, Ookayama, Meguro-ku, Tokyo 152

(Received November 12, 1979)

Synopsis. *N*-(Pentafluoropropionyl)amino acids, which were prepared by treating amino acids with hexafluoro-1,2-epoxypropane in diglyme, were found to be a versatile derivative of amino acids in gas chromatographic analysis.

N-Trifluoroacetylated α-amino acids are known to be useful derivatives for detection and separation of the parent amino acids.[1-7] Various esters of *N*-(trifluoroacetyl)-, *N*-(pentafluoropropionyl)- and *N*-(heptafluorobutyryl)-amino acids, which were prepared by perfluoroacylation with the corresponding perfluorocarboxylic anhydrides, were also reported to be useful in gas chromatographic resolution of the amino acids.[8] *N*-perfluoroacyl-L-α-amino acid chlorides are claimed to be resolving agents for asymmetric amines, as the gas chromatography of the complexes of these compounds provides a rapid, sensitive, and effective method for separating enantiomers.[9]

In the course of our studies on the reactivities of hexafluoro-1,2-epoxypropane, it was revealed that this perfluoro epoxide can be used as a versatile pentafluoropropionylating agent for alcohols, thiols and amines.[10] On extention of this reaction, the perfluoroacylation was applied for the preparation of pentafluoropropionylated amino acids, which are expected to be more volatile and more sensitive to gas chromatography than trifluoroacetyl derivatives.

Our previous method of pentafluoropropionylation of usual amines and alcohols using a hexafluoro-1,2-epoxypropane–triethylamine system in acetonitrile was not applicable to amino acids, as it gave only tarry material. Then we allowed amino acids to react with hexafluoro-1,2-epoxypropane without any amines using diglyme as a solvent. The reaction proceeded smoothly even at room temperature and after 2 or 3 h pentafluoropropionylamino acids were obtained in good yields (Table 1).

Thus by the aid of a fluorine ion hexafluoro-1,2-epoxypropane isomerized to pentafluoropropionyl fluoride, which reacted then with the amine to give pentafluoropropionyl derivative.[10]

$$CF_3CF(O)CF_2 \xrightarrow[\text{diglyme}]{F^-} CF_3CF_2C(=O)F$$

$$CF_3CF_2C(=O)F + H_2N\text{-}CHR\text{-}CO_2H \rightarrow CF_3CF_2C(=O)NH\text{-}CHR\text{-}CO_2H + HF$$

Though pentafluoropropionylamino acids have relatively higher melting points than the corresponding trifluoroacetyl derivatives, they are vaporized more rapidly on gas chromatography as expected (Table 2). It was also found that the pentafluoropropionyl group can be easily removed under mild alkaline conditions without racemization.

Experimental

Pentafluoropropionylation of Amino Acids. A mixture of L-phenylalanine (1.65 g, 10 mmol) and diglyme (10 ml) was placed in a glass pressure vessel and cooled to ≈ −70 °C. Liquefied hexafluoro-1,2-epoxypropane (bp −27 °C, 1.80 g, 10.9 mmol) was then introduced into the vessel and the whole was brought to room temperature with stirring. The mixture gradually became a clear solution, and the stirring was continued additional one hour. The reaction mixture was then poured into dilute aqueous hydrochloric acid, and the product was extracted with diethyl ether. The extract was dried over magnesium sulfate and the solvent was evaporated to give solid material. This crude product was subjected to column chromatography on silica gel using chloroform as an eluent. Pure *N*-(pentafluoropropionyl)-L-phenylalanine (2.18 g) was obtained in a yield of 70%.

Hydrolysis of Pentafluoropropionylamino Acid. A pentafluoropropionyl group was easliy removed under similar conditions to those reported in the case of a trifluoroacetyl group.[11] For example, *N*-(pentafluoropropionyl)-L-phenylalanine (0.62 g, 2 mmol) was added to an ethanol–water solution containing 5% sodium hydroxide, and the mixture was stirred for 1 h at room temperature. After neutraliza-

Table 1. Pentafluoropropionylamino acids and their derivatives (PFP = CF_3CF_2CO)

N-PFP-amino acid[a]	Yield[b] %	Mp °C	^{19}F NMR (ppm) CF_3	^{19}F NMR (ppm) CF_2	$[\alpha]_D^{20}$
N-PFP-glycine	75	122—123	+6.2	+45.3	
N-PFP-DL-phenylglycine	70	124—125	+6.0	+45.2	
N-PFP-L-alanine	60	86.5—87.5	+6.2	+45.3	−39° (c=0.4, Et_2O)
N-PFP-L-proline benzylamine salt	70	150—151	+6.3	+45.5	−315° (c=1, Me_2CO)
N-PFP-L-isoleucine benzylamine salt	65	98—98.5	+6.3	+45.3	+55° (c=1, EtOH)
N-PFP-DL-phenylalanine	63	128—129	+6.0	+45.1	
N-PFP-L-phenylalanine	72	122.5—123.5	+6.1	+45.3	+545 (c=1, Et_2O)

a) The microanalyses of these new compounds were in satisfactory agreement with calculated values (C±0.34%, H±0.14%, N±0.23%). b) Yield of isolated product. c) Upfield from external CF_3COOH in acetone.

Table 2. Gas chromatographic properties of perfluoroacylated amino acids[a)]

Amino acid	CF_3CO-derivative		CF_3CF_2CO-derivative		Retention time ratio C_2F_5CO/CF_3CO
	Mp °C	Retention time min	Mp °C	Retention time min	
Glycine	118	7.11[b)]	122—123	5.93[b)]	0.83
L-Alanine	65—67	5.37[b)]	85.5—87.5	4.98[b)]	0.92
L-Phenylalanine	120—121	4.50[c)]	122.5—123.5	4.13[c)]	0.91

a) G. L. C. analysis were carried out on a Shimadzu GC-3BT apparatus equipped with a TCD. The $4\phi \times 3$ steel column was packed with 10% Silicone GE-SE 30 on Chromosorb W. b) Helium gas was flowed at the rate of 19 ml/min, while the column was kept at 140 °C. c) The column was kept at 190 °C.

tion with aqueous hydrochloric acid, the solvent was removed. Residual solid was washed with water and recrystallized from water giving pure L-phenylalanine (0.16 g, 48%).

References

1) F. Weygand and E. Leising, *Chem. Ber.*, **87**, 248 (1954).
2) F. Weygand and W. Steglich, *Angew. Chem.*, **73**, 757 (1961).
3) F. Weygand, A. Prox, L. Schmidhammer, and W. König, *Angew. Chem.*, **75**, 282 (1963).
4) F. Weygand, B. Kolb, A. Prox, M. A. Tilak, and I. Tomida, *Z. Physiol. Chem.*, **332**, 38 (1960).
5) J. Wagner and G. Winkler, *Z. Anal. Chem.*, **183**, 1 (1961).
6) N. Ikekawa, *J. Biochem. (Tokyo)*, **54**, 279 (1963).
7) C. Zomzely, G. Marco, and E. Emery, *Anal. Chem.*, 1414 (1962).
8) D. R. Knapp, "Handbook of Analytical Derivatization Reactions," John Wiley, New York (1979), p. 249 and references cited therein.
9) R. W. Souter, U. S. Patent 3972925 (1976). *Chem. Abstr.*, **85**, 177984e.
10) N. Ishikawa and S. Sasaki, *Nippon Kagaku Kaishi*, **1976**, 1954.
11) E. E. Schallenberg and M. Calvin, *J. Am. Chem. Soc.*, **77**, 2779 (1955).

Catalytic Geometrical Isomerization of *cis*-Chrysanthemaldehyde and Related Ketones[1)]

Tadashi SASAKI,* Shoji EGUCHI, and Masatomi OHNO
Institute of Applied Organic Chemistry, Faculty of Engineering, Nagoya University, Furo-cho, Chikusa-ku, Nagoya 464
(Received November 14, 1979)

Synopsis. *cis*-Chrysanthemaldehyde isomerized cleanly to the *trans*-isomer catalyzed with methoxydimethylsulfonium iodide (**8**) at 25 °C. Zinc halides as well as silica gel were also demonstrated to be effective catalysts. Related aldehydes and ketones isomerized also with **8** at 80 °C but dihydrochrysanthemaldehyde did not isomerize at all.

Stereoisomerization of chrysanthemic acid **1** (2,2-dimethyl-3-(2-methylpropenyl)cyclopropanecarboxylic acid) and its derivatives has drawn much interest for many years because the insecticidal activity of the ester derivative is specific for *d*- and *trans*-isomers.[2)] These isomerizations were demonstrated in the nitrile derivative under anionic conditions,[3)] the ester derivative under thermolytic and photolytic conditions,[4a,b)] and the acid chloride derivative under Lewis acid catalytic conditions.[5)]

We wish to report in this paper facile and convenient geometrical isomerization of *cis*-chrysanthemaldehyde **2** under catalytic conditions, where no competing structural isomerizations[6)] were not observed.

cis-Aldehyde **2** was allowed to react at 25 °C in dimethyl sulfoxide containing a slight excess of methyl iodide to form *in situ* methoxydimethylsulfonium iodide **8**.[7)] After 24 h, ^{1}H NMR inspection indicated the quantitative isomerization to the *trans*-isomer. This clean geometrical isomerization of **2** was also catalyzed with zinc halides.[8)] The iodide, bromide, and chloride salts were all effective as far as used homogeneously in an appropriate solvent such as ether or dioxane. Interestingly, silica gel was found to be useful for this geometrical isomerization;[9)] contact of **2** with silica-gel column (Mallinckrodt 100 mesh) at room temperature for 18 h produced quantitatively the *trans*-isomer.

Several comparative experiments were carried out to test the general applicability of this simple method. Firstly the choice of catalyst for **2** was shown to be critical. The catalyst coordinating much or less with the aldehyde carbonyl did not give satisfactory results; boron trifluoride catalysis led to the formation of an intractable mixture and lithium iodide catalysis resulted in no reaction. *p*-Toluenesulfonic acid catalysis caused undesired ring opening.[11)] Secondly, reactivity of carbonyl compounds with the catalyst **8** was examined by using related aldehydes and ketones **3**—**7**: Chrysanthemyl methyl ketone **3** and phenyl ketone **4** were found to be less reactive than the aldehyde **2**, and thus underwent nearly quantitative isomerization on heating at 80 °C for 2 h and 7 h, respectively. Similarly, 2-phenylcyclopropanecarbaldehyde **5** and methyl ketone **6** isomerized to the corresponding *trans*-isomers in 83% and 46% yields, respectively, on heating as above for 7 h, although they were stable at 25 °C. However, dihydrochrysanthemaldehyde **7**, a saturated analogue of **2**, did not isomerize at all under the same catalytic conditions.

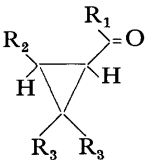

1 R_1=OH, R_2=CH=C$(CH_3)_2$, R_3=CH_3
2 R_1=H, R_2=CH=C$(CH_3)_2$, R_3=CH_3
3 R_1=CH_3, R_2=CH=C$(CH_3)_2$, R_3=CH_3
4 R_1=C_6H_5, R_2=CH=C$(CH_3)_2$, R_3=CH_3
5 R_1=H, R_2=C_6H_5, R_3=H
6 R_1=CH_3, R_2=C_6H_5, R_3=H
7 R_1=H, R_2=$CH_2CH(CH_3)_2$, R_3=CH_3

$(CH_3)_2\overset{+}{S}OCH_3$ I^-
8

These experimental facts suggest that the geometrical isomerization is significantly affected by a substituent on the cyclopropane ring through conjugation and by the nature of coordination of carbonyl group with catalyst. The reactivity trend of the observed isomerization, *i.e.*, aldehyde>methyl ketone>phenyl ketone and isobutenyl>phenyl>isobutyl substituent[10)] seems to reflect the ability to delocalize the positive charge to the cyclopropane ring. In addition, no deuterium incorporation was observed in the isomerization of **2** with **8** in 1:20 D_2O–DMSO (^{1}H NMR inspection) precluding an enolization pathway. Therefore, this stereoisomerization can be explained most reasonably as follows: The polarization of C=O double bond arising from the appropriate coordination of catalyst can generate a cyclopropylmethyl cation-like intermediate which caused the isomerization to thermally more stable *trans*-isomer. More activated intermediate carbonium ion may be responsible for the other reaction such as structural isomerization.[11)]

Above clean geometrical isomerization of *cis*-alkenylcyclopropanecarbonyl derivative is unprecedented to the best of our knowledge, and may be useful for obtaining pure *trans* isomer from, for instance, *cis* and *trans* mixture of carbonylcarbene adduct with conjugated olefins.

Experimental

Materials. Aldehydes **2**, **5**, and **7** were prepared by oxidation of the corresponding alcohols with pyridine–chromium trioxide.[12a,b,c)] Ketones **3**, **4**, and **6** were prepared from the corresponding carboxylic acids and methyl- or phenyllithium.[12a,d)]

^{1}H NMR Analyses. ^{1}H NMR spectra were obtained with a JEOL JNM-C-60HL spectrometer in carbon tetrachlo-

ride with tetramethylsilane as an internal standard. *Cis* and *trans* ratio was determined by the integral ratio of key signals at δ 5.36 (*cis*) and 4.89 (*trans*) (CH=C) for **2**, 5.28 (*cis*) and 4.82 (*trans*) (CH=C) for **3**, 5.36 (*cis*) and 4.16 (*trans*) (CH=C) for **4**, 8.53 (*cis*) and 9.25 (*trans*) (CHO) for **5**, and 1.87 (*cis*) and 2.19 (*trans*) ($COCH_3$) for **6**, respecuvely.

Geometrical Isomerization. (*A*): The aldehyde or ketone (1 mmol) was dissolved in a solution of methyl iodide (150 mg, 1.06 mmol) in dimethyl sulfoxide (3 ml) and the resulted solution was left in the dark at 25 °C or 80 °C. After the reaction time described in the text, the solution was poured onto water and the isomerized aldehyde or ketone was recovered nearly quantitatively by extraction with hexane, followed by usual work up. The *cis* and *trans* ratio was then determined by ^1H NMR spectra.

(*B*): The aldehyde **2** (152 mg, 1 mmol) was added to a solution of zinc iodide (160 mg, 0.5 mmol) in ether (5 ml), and the solution was left at 25 °C for 24 h. The catalyst was removed by extraction with water and usual work up gave almost quantitatively the *trans*-aldehyde. The reaction with zinc bromide or chloride under the same conditions except for using dioxane as a solvent gave similar results, but a small amount of contaminants was produced in the case of zinc chloride.

(*C*): The aldehyde **2** (152 mg, 1 mmol) was adsorbed on the silica gel (Mallinckrodt 100 mesh) column with chloroform. After 18 h at room temperature, the isomerized aldehyde was recovered quantitatively by eluting out with chloroform.

References

1) Studies on Chrysanthemic Acid. XII. Part XI: Ref. 12a.

2) M. Eliott, *J. Sci. Food Agric.*, **5**, 505 (1954).

3) S. H. Harper and K. C. Sleep, *J. Sci. Food Agric.*, **6**, 116 (1955).

4) a) T. Hanafusa, M. Ohnishi, M. Mishima, and Y. Yukawa, *Chem. Ind. (London)*, **1970**, 1050; b) K. Ueda and M. Matsui, *Tetrahedron*, **27**, 2771 (1971).

5) T. Nagase and G. Suzukamo, Ger. Offen, 2453639, 1975; *Chem. Abstr.*, **83**, 79414h (1975).

6) H. M. Walborsky and L. Plonsker, *J. Am. Chem. Soc.*, **83**, 2138 (1961).

7) a) S. G. Smith and S. Winstein, *Tetrahedron*, **3**, 317 (1958); b) W. W. Epstein and F. W. Sweat, *Chem. Rev.*, **67**, 247 (1967); For catalytic action of **8** on oxirane, see D. Bethell, G. W. Kenner, and P. J. Powers, *Chem. Commun.*, **1968**, 227.

8) For catalytic action of zinc halide, see for example, a) D. A. Evans, L. K. Truesdale, and G. L. Carroll, *Chem. Commun.* **1973**, 55; b) D. J. Creighton, J. Hajdu, and D. S. Sigman, *J. Am. Chem. Soc.*, **98**, 4619 (1976).

9) Recent review; M. Hojo and R. Masuda, *Yuki Gosei Kagaku Kyokai Shi*, **37**, 557 (1979).

10) T. Sasaki, S. Eguchi, M. Ohno, and T. Umemura, *Chem. Lett.*, **1972**, 503.

11) The reported structural isomerization of *trans*-isomers of **2** and **3** with *p*-toluenesulfonic acid may proceed *via* a fully opened cyclopropylmethyl cation intermediate; L. Cromble, P. A. Firth, R. P. Houghton, D. A. Whiting, and D. K. Woods, *J. Chem. Soc., Perkin Trans.* **1972**, 642. The aldehyde **2** is rearranged to 3,3-dimethyl-4,6-heptadienal at 80 °C with **8**, indicating that the temperature control is also important factor to avoid structural isomerization.

12) a) T. Sasaki, S. Eguchi, M. Ohno, and T. Umemura, *J. Org. Chem.*, **38**, 4095 (1973); b) G. Ohloff, *Tetrahedron Lett.*, **1965**, 3795; c) P. Scribe and J. Wisemann, *Bull. Soc. Chim. Fr.*, **1971**, 2268; d) I. G. Bolesov, Y. -H. Wu, N. P. Samoilva, and R. Ya. Levina, *Chem. Abstr.*, **70**, 11288w (1969).

The Reactions of Copper(I) 1-Alkenyltrimethylborates with Allylic Bromides or 2-Propynyl Bromide

Norio MIYAURA, Takashi YANO, and Akira SUZUKI*
Faculty of Engineering, Hokkaido University, Sapporo 060

(Received November 16, 1979)

Synopsis. The reactions between copper(I) 1-alkenyltrimethylborates (readily obtainable from 2-(1-alkenyl)-1,3,2-benzodioxaboroles and methyllithium) and allylic bromides or 2-propynyl bromide were found to give corresponding coupling products. These reactions provide new synthetic routes to 1,4-alkadienes or 1,2,7-alkatrien-5-ynes.

In a series of our investigations of the chemistry of copper(I) organoborate complexes,[1-7] we have now discovered a novel cross-coupling reaction of 1-alkenyltrimethylborates with allylic bromides or 2-propynyl bromide. The reactions provide new synthetic procedures for 1,4-alkadienes or 1,2,7-alkatrien-5-ynes from alkynes *via* hydroboration, respectively.

Addition of a solution of lithium (*E*)-1-hexenyltrimethylborate (**1**) prepared from 2-(1-hexenyl)-1,3,2-benzodioxaborole and three equivalents of methyllithium to a suspension of copper(I) iodide in tetrahydrofuran at −30 °C resulted in the disappearance of copper(I) iodide, and a clear solution was obtained as shown in Eqs. 1 and 2. Although we have not undertaken a detailed study of this complex, copper(I) 1-hexenyltrimethylborate (**2**) is considered to be formed *via* metal exchange reaction. No reaction occurred between allyl bromide and lithium 1-hexenyltrimethylborate (**1**) at room temperature, whereas when corresponding copper(I) borate (**2**) was used, the reaction proceeded smoothly (Eq. 3). VPC analysis revealed the formation of 1,4-nonadiene in a 97% yield.

The reaction was then applied to representative alkenylborates and allylic bromides. The results are summarized in Table 1. The 1,4-dienes thus obtained

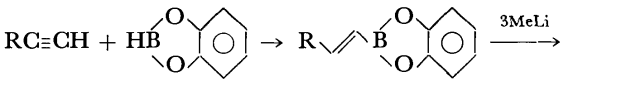

(1)

1

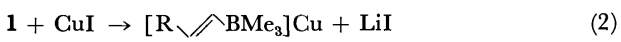

(2)

2

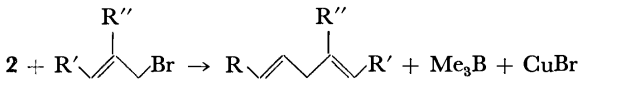

(3)

were indicated to be a single isomer in each case by VPC analysis, presumably *E*-isomer, because of IR (955 cm^{-1}) and direct comparison with authentic samples.

In the same way, copper(I) (*E*)-1-alkenyltrimethylborates react with 2-propynyl bromide (Eq. 5). At first, it was expected that the reaction of such copper(I) alkenylborates (**2**) with 2-propynyl bromide should give 4-alken-1-ynes (**3**) or 1,2,4-alkatrienes (**4**) as shown in Eq. 4. The reaction products actually obtained, however, were confirmed as 1,2,7-alkatrien-5-ynes (**5**).

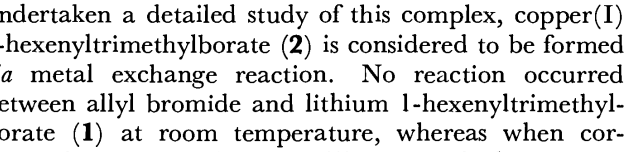

(4)

3 **4**

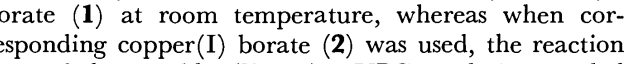

(5)

5

For example, 2-(1-hexenyl)-1,3,2-benzodioxaborole gave 1,2,7-dodecatrien-5-yne, the elemental analysis and mass spectrum (*m/e*=160, M^+) of which coincided with $C_{12}H_{16}$. The IR spectrum bands at 1955, 855 cm^{-1} due to –CH=C=CH_2, 955 cm^{-1} for *trans*-CH=CH–, and 2180 cm^{-1} for –C≡C– structure were observed. The NMR spectrum indicated the presence of two vinylic hydrogens (–CH_2CH^{α}=CH^{β}–), because H^{α} centered at 4.00 splits into doublet-triplet (J=16 and 6 Hz) and H^{β} at 4.62 splits into a doublet (J=16 Hz), and three allenic protones (–CH_2–CH^{γ}=C=$CH^{\delta}{}_2$),[5] H^{γ} centered at 4.93 splits into triplet-triplet (*J*=6 and 7 Hz) and two H^{δ} at 5.25 split into doublet-triplet (*J*=7 and 3 Hz). All of these data are in good agreement with the 1,2,7-alkatrien-5-yne structure.

Stereoselective formation of alkenylboranes *via* hydroboration of alkynes followed by transfer of stereodefined alkenyl groups to alkyl halides should provide one of the simplest method for the synthesis of stereodefined alkenes. Although it is evident that copper(I) alkenylborates[8] have a considerably high utility for such a purpose, the applicability of the present new reagents to coupling and addition reactions is now under further investigation.

TABLE 1. REACTION OF COPPER(I) ALKENYLTRIMETHYLBORATES WITH ALLYLIC BROMIDES AND 2-PROPYNYL BROMIDE

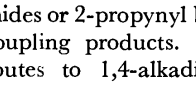 R^1=	R^2=	Allylic or 2-propynyl bromides[a]	Product	Yield[b] %
Butyl	H	CH_2=$CHCH_2$Br	1,4-Nonadiene	97
		CH_2=$C(CH_3)$-CH_2Br	2-Methyl-1,4-nonadiene	81
		CH_3CH=$CHCH_2$Br	2,5-Decadiene	46
			3-Methyl-1,4-nonadiene	52
Hexyl	H	CH_2=$CHCH_2$Br	1,4-Undecadiene	89
		2-Cyclohexenyl bromide	1-(2-Cyclohexenyl)-1-octene	42
Phenyl	H	CH_2=$CHCH_2$Br	1-Phenyl-1,4-pentadiene	92
Butyl	H	HC≡CCH_2Br	1,2,7-Dodecatrien-5-yne	54
Pentyl	H		1,2,7-Tridecatrien-5-yne	55
Hexyl	H		1,2,7-Tetradecatrien-5-yne	40
Ethyl	Ethyl		7-Ethyl-1,2,7-decatrien-5-yne	71

a) Allylic bromide/alkenylborane = 1.2. 2-Propynyl bromide/alkenylborane = 2.4.
b) Based on alkenylboranes employed.

Experimental

Materials. Commercial allylic bromides, alkynes, and 2-propynyl bromide were used. The tetrahydrofuran was

purified by distillation from $LiAlH_4$ before use. 1-Alkenylbenzodioxaboroles are prepared by Brown's method[9] from 1,3,2-benzodioxaborole and alkynes.

The IR and NMR spectra were taken on a Hitachi-Perkin Elmer Model 125 spectrophotometer and a Hitachi R-22 spectrometer at 90 MHz using tetramethylsilane as an internal standard, respectively.

General Procedure. The following procedures for the preparation of 1,4-nonadiene and 1,2,7-dodecatrien-5-yne are representative.

A dry 50 ml flask equipped with a septum inlet and a magnetic stirring bar was flushed with dry nitrogen. The flask was charged with 2-(1-hexenyl)-1,3,2-benzodioxaborole[9] (2.30 g, 10 mmol) and 10 ml of dry tetrahydrofuran. To this mixture was added methyllithium (22 ml of 1.26 M solution, 30 mmol) in ether at 0 °C and stirred for an additional 2 h to form lithium 1-hexenyltrimethylborate. Copper(I) iodide (3.8 g, 20 mmol) and 50 ml of dry THF were placed into a separate 200 ml-flask and cooled to −30 °C. The resultant lithium 1-hexenyltrimethylborate solution was gradually added under vigorous stirring. After 1 h, precipitated copper(I) iodide was completely disolved and a clear solution was obtained. To this solution was added allyl bromide (1.45 g, 12 mmol). The reaction mixture was allowed to warm up to room temperature and stirred for an additional 2 h. After the reaction was complete, the residual organoborane was oxidized with 3 ml of aqueous 3M-NaOH and 3 ml of 30%-H_2O_2 at room temperature for 2 h. The product was extracted by ether. The combined extract was washed with saturated NaCl solution and dried over magnesium sulfate. VPC analysis revealed the formation of 1,4-nonadiene (9.7 mmol, 97%).

The procedure for the preparation of 1,2,7-decatrien-5-yne is as follows: To the solution of copper(I) 1-hexenyltrimethylborate described above was added 2-propynyl bromide (2.86 g, 24 mmol) at −30 °C, and then the mixture was allowed to warm up to room temperature. After 2 h, residual organoborane was oxidized by alkaline hydrogen peroxide. VPC analysis of the ether extract indicated the presence of 5.4 mmol (54%) of 1,2,7-dodecatrien-5-yne.

Identification of the Products. In all cases analytically pure samples were obtained by preparative VPC with Varian autoprep Model-2800 and characterized by NMR, IR, and mass spectra,and refractive indices, and elemental analyses. *1,4-Nonadiene* and *1-phenyl-1,4-pentadiene* were characterized by direct comparison with authentic samples prepared by the methods reported by Negishi[10] and Speziale,[11] respectively.

2-Methyl-1,4-nonadiene: $n_D^{22}=1.4389$. Found: C, 86.74; H, 13.02%. Calcd for $C_{10}H_{18}$: C, 86.88; H, 13.12%. Mass: $m/e=138$ (M^+). IR (CCl_4): 3080, 1650, 975, 895, 965 cm^{-1}. NMR (CCl_4): τ, 9.1 (3H, t, $J=6$ Hz), 8.5—8.8 (4H, m), 8.31 (3H, s), 7.9—8.15 (2H, m), 7.36 (2H, d, $J=5$ Hz), 5.35 (2H, s), 6.59 (2H, m).

2,5-Decadiene: $n_D^{22}=1.4410$. Found: C, 86.65; H, 13.20%. Calcd for $C_{10}H_{18}$: C, 86.88; H, 13.12%. Mass: $m/e=138$ (M^+). IR (CCl_4): 3010, 965, 860 cm^{-1}. NMR (CCl_4): τ, 9.10 (3H, t, $J=6$ Hz), 8.5—8.8 (4H, m), 8.36 (3H, d, $J=4$ Hz), 7.9—8.15 (2H, m), 7.2—7.45 (2H, m), 4.5—4.7 (4H, m).

3-Methyl-1,4-nonadiene: $n_D^{22}=1.4390$. Found: C, 86.69: H, 13.21%. Calcd for $C_{10}H_{18}$: C, 86.88; H, 13.12%. Mass: $m/e=138$ (M^+). IR (CCl_4): 965, 910, 860 cm^{-1}. NMR (CCl_4): τ, 9.10 (3H, t, $J=6$ Hz), 8.93 (3H, d, $J=7$ Hz), 8.5—8.8 (4H, m), 7.85—8.1 (2H, m), 7.05—7.4 (1H, m), 5.09 (1H, d, $J=12$ Hz), 5.06 (1H, d, $J=16$ Hz), 4.55—4.70 (2H, m), 4.05—4.50 (1H, m).

1,4-Undecadiene: $n_D^{22}=1.4370$. Found: C, 86.70; H, 13.02%. Cacld for $C_{11}H_{20}$: C, 86.76; H, 13.24%. Mass: $m/e=152$ (M^+). IR (CCl_4): 3080, 1640, 965, 915, 860 cm^{-1}. NMR (CCl_4): τ, 9.10 (3H, t, $J=6$ Hz), 8.5—8.8 (8H, m), 7.85—8.1 (2H, m), 7.05—7.35 (2H, m), 5.01 (1H, d, $J=10$ Hz), 4.98 (1H, d, $J=16$ Hz), 4.51—4.64 (2H, m), 4.02—4.44 (1H, m).

1-(2-Cyclohexenyl)-1-octene: $n_D^{22}=1.4749$. Found: C, 87.38; H, 12.63%. Cacld for $C_{14}H_{24}$: C, 87.42; H, 12.58%. Mass: $m/e=192$ (M^+). IR (CCl_4): 3010, 970, 865 cm^{-1}. NMR (CCl_4): τ, 9.10 (3H, t, 6 Hz), 8.26—8.90 (12H, m), 7.89—8.17 (4H, m), 7.20—7.47 (1H, m), 4.58—4.73 (2H, m), 4.33—4.54 (2H, m).

1,2,7-Dodecatrien-5-yne: $n_D^{22}=1.5009$. Found: C, 89.93; H, 9.85%. Calcd for $C_{12}H_{16}$: C, 89.94; H, 10.06%. Mass: $m/e=160$ (M^+). IR (CCl_4): 2180, 1955, 955, 855 cm^{-1}. NMR (CCl_4): τ, 9.11 (3H, t, $J=6$ Hz), 8.45—8.9 (4H, m), 7.75—8.10 (2H, m), 6.9—7.17 (2H, m), 5.25 (2H, dt, $J=3$ and 7 Hz), 4.93 (1H, tt, $J=6$ and 7 Hz), 4.62 (1H, d, $J=16$ Hz), 4.00 (1H, dt, $J=6$ and 16 Hz).

1,2,7-Tridecatrien-5-yne: $n_D^{22}=1.4972$. Found: C, 89.39; H, 10.35%. Calcd for $C_{13}H_{18}$: C, 89.59; H, 10.41%. Mass: $m/e=174$ (M^+). IR (CCl_4): 2180, 1960, 950, 845 cm^{-1}. NMR (CCl_4): τ, 9.10 (3H, t, $J=6$ Hz), 8.5—8.85 (6H, m), 7.96 (2H, t, $J=6$ Hz), 6.91—7.13 (2H, m), 5.25 (2H, dt, $J=3$ and7 Hz), 4.93 (1H, tt, $J=6$ and7 Hz), 4.62 (1H, d, $J=16$ Hz), 3.99 (1H, dt, $J=6$ and 16 Hz).

1,2,7-Tetradecatrien-5-yne: $n_D^{22}=1.5012$. Found: H, 89.44; H, 10.78%. Calcd for $C_{14}H_{20}$: C, 89.29; H, 10.71%. Mass: $m/e=188$ (M^+). IR (CCl_4): 2180, 1960, 955, 860 cm^{-1}. NMR (CCl_4): τ, 9.09 (3H, t, $J=6$ Hz), 8.44—8.84 (8H, m), 7.73—8.05 (2H, m), 6.87—7.08 (2H, m), 5.22 (2H, dt, $J=3$ and 7 Hz), 4.90 (1H, tt, $J=6$ and 7 Hz), 4.60 (1H, d, $J=16$ Hz), 3.98 (1H, dt, $J=6$ and 16 Hz).

7-Ethyl-1,2,7-dodecatrien-5-yne: $n_D^{22}=1.5012$. Found: C, 88.76; H, 10.10%. Calcd for $C_{12}H_{16}$: C, 89.94; H, 10.06%. Mass: $m/e=160$ (M^+). IR (CCl_4): 2180, 1960, 860 cm^{-1}. NMR (CCl_4): τ, 9.02 (3H, t, $J=6$ Hz), 8.97 (3H, t, $J=6$ Hz), 7.76—8.07 (2H, m), 6.90—7.11 (2H, m), 5.25 (2H, dt, $J=3$ and 7 Hz), 4.93 (1H, tt, $J=6$ and 7 Hz), 4.37 (1H, t, $J=6$ Hz).

References

1) N. Miyaura, M. Itoh, and A. Suzuki, *Tetrahedron Lett.*, **1976**, 255.

2) K. Yamada, N. Miyaura, M. Itoh, and A. Suzuki, *Bull. Chem. Soc. Jpn.*, **50**, 3431 (1977).

3) N. Miyaura, M. Itoh, and A. Suzuki, *Synthesis*, **1976**, 655.

4) N. Miyaura, M. Sasaki, M. Itoh, and A. Suzuki, *Tetrahedron Lett.*, **1977**, 173.

5) N. Miyaura, M. Itoh, and A. Suzuki, *Bull. Chem. Soc. Jpn.*, **50**, 2199 (1977).

6) N. Miyaura, M. Sasaki, M. Itoh, and A. Suzuki, *Tetrahedron Lett.*, **1977**, 3369.

7) K. Yamada, T. Yano, N. Miyaura, and A. Suzuki, *Bull. Chem. Soc. Jpn.*, **52**, 275 (1979).

8) Y. Yamamoto, H. Yatagai, A. Sonoda, and S. Murahashi, *J. Chem. Soc., Chem. Commun.*, **1976**, 452.

9) H. C. Brown, "Organic Syntheses *via* Boranes," John-Wiley, New York (1975).

10) S. Baba, D. E. Van Horn, and E. Negishi, *Tetrahedron Lett.*, **1976**, 1927.

11) V. Speziale, and A. Lattes, *Bull. Soc. Chim. Fr.*, **1971**, 3057.

New Applications of Crown Ethers. II. Synthesis of 4'-Formylbenzocrown Ethers[1]

Fumio WADA,* Hiroshi HIRAYAMA, Hiroshi NAMIKI, Kiyoshi KIKUKAWA, and Tsutomu MATSUDA
Department of Organic Synthesis, Faculty of Engineering, Kyushu University, Hakozaki, Higashi-ku, Fukuoka 812
(Received December 10, 1979)

Synopsis. 4'-Formylbenzo-15-crown-5, -18-crown-6, and bis(4'-formylbenzo)-18-crown-6 were conveniently synthesized in excellent yields by Smith modification of Duff reaction: formylation with hexamethylenetetramine and trifluoroacetic acid or methanesulfonic acid.

4'-Formylbenzocrown ethers are considered to be useful intermediates for the preparation of various substituted benzocrown ethers with the use of the carbonyl function, and have been utilized for the preparation of 4'-(2-carboxyvinyl)-benzo-15-crown-5 (or 3-[3',4'-(1",4",7",10",13"-pentaoxacyclopentadeca-2"-ene)phenyl]acrylic acid),[2] phosphine derivatives,[3] bis(crown ether)s[3,4] and oximes.[5] 4'-Formylbenzo-15-crown-5 (**1**) and -18-crown-6 (**2**) were first prepared from 4-formylcatechol by Smid *et al.*,[6] using the conventional crown ring-forming cyclization. Direct formylation of benzo-15-crown-5 by Vilsmeyer reaction were reported recently by Hyde *et al.*[3] to give **1** in 54% yield. Electrophilic substitution in general seems to be promising for the synthesis of substituted benzocrown ethers. However, the reactions, especially those carried out under the catalysis of metal salts, frequently encounter with deactivation of the catalyst[7] and complexity in the isolation of the product[3] owing to the formation of crown ether complexes.

In our study to get a variety of substituted benzocrown ethers, we needed to disclose a simple method for the preparation of **1** and **2**. Among many reactions being attempted, formylation by Smith modification[8] of Duff reaction was found to be most promising because no inorganic reagent is required in the reaction, and preliminary experiments gave **1** and **2** in 58% and 32% yields, respectively. Other organic acids weaker than trifluoroacetic acid, except for methanesulfonic acid, gave only low yields. In the course of the study to optimize the reaction conditions it was found that the method of isolation of the products was also important factor and marked improvement of the yields could be attained by omission of neutralization of the reaction mixture. The results obtained under optimized conditions are summarized in Table 1. Formylation of dibenzo-18-crown-6 with excess reagents gave bis(4'-formylbenzo)-18-crown-6 (**3**) under similar reaction conditions. Methanesulfonic acid (98%) can be used in place of trifluoroacetic acid, but in certain cases it caused some problems in the isolation of the product due to the formation of emulsion, and led to a depressed yield.

One reason for lowering the yields in the conventional work-up containing neutralization of the excess acid is attributable to the increased solubility of sodium-crown ether complexes in aqueous phase. Another factor may be condensation of formylbenzocrown ethers during the repeated extractions from basic solution. The reasoning is based on the following observation that a mixture consisted of **1** and 4'-acetylbenzo-15-crown-5 in ethanolic sodium hydroxide gave 18% of 1,3-bis-[3',4'-(1",4",7",10",13"-pentaoxacyclopentadeca-2"-ene)phenyl]-propen-1-one after 3 h stirring at room temperature, but after 4 h oily condensation product was the principal product.

Experimental

Materials. Benzo-15-crown-5, -18-crown-6, and dibenzo-18-crown-6 were obtained according to the procedure of Pedersen.[7] Commercial trifluoroacetic acid (99%), methanesulfonic acid (98%) and hexamethylenetetramine were used as received.

*4'-Formylbenzo-15-crown-5 (**1**).* A mixture of benzo-15-crown-5 (2.0 g, 7.5 mmol), trifluoroacetic acid (5.6 ml) and hexamethylenetetramine (1.1 g, 7.5 mmol) was stirred at 85—90 °C under nitrogen for 12 h. The reaction mixture was added to the concentrate and stirred for 1 h. The mixture was extracted with benzene, and the extract was dried ($MgSO_4$). Concentration of the benzene extract under vacuum gave yellow oil, which on cooling solidified to faint yellow crystals, 1.8 g (82%), mp 78.2—81.0 °C. The product could be further purified by either extraction with hot heptane or chromatography on a short alumina column (chloroform–methanol) to give white crystals, mp 80.0—81.5 °C (lit,[6] mp 78—79 °C). When methanesulfonic acid

Table 1. Formylation of benzocrown ethers

Crown (mmol)		Acid (ml)		Hexamine (mmol)	Temp °C	Time h	Yield %
B15C5	7.5	CF_3CO_2H	5.6	7.5	85—90	12	82
	7.5	CH_3SO_3H	4.5	7.5	85—90	11	77
B18C6	7.5	CF_3CO_2H	5.6	7.5	85—90	24	86
	7.5	CH_3SO_3H	4.5	15.0	79—83	24	81
DB18C6	5.6	CF_3CO_2H	8.3	22	94—102	24	90[a]
	3.8	CH_3SO_3H	4.7	15	90—95	24	58[a]

a) 4',4"-Diformyl-DB18C6.

was used, the reaction mixture was poured into ice-water and extracted with benzene or benzene-chloroform.

The formylation of benzo-18-crown-6 under similar conditions gave **2**, mp 61.3—62.8 °C (after the purification) (lit,[6] mp 60—62 °C). The structure of **1** and **2** were identified by comparisons (mixed-melting point) with authentic samples prepared by the method of Smid *et al.*[6]

Formylation of dibenzo-18-crown-6 with **1** to 1.2 molar equivalent of hexamethylenetetramine gave a mixture of mono- and diformylated product along with the starting material. Use of excess amount of the amine afforded **3**, mp 231—233 °C. Found: C, 62.84; H, 5.77%. MS: *m/e*, 416, 169, 164, 163, 149. Calcd for $C_{22}H_{24}O_8$: C, 63.43; H, 5.76%.

References

1) Part I, F. Wada, R. Ishihara, Y. Kamohara, and T. Matsuda, *Bull. Chem. Soc. Jpn.*, **52**, 2959 (1979).

2) G. R. Brown and A. J. Foubister, *J. Med. Chem.*, **22**, 997 (1979).

3) E. M. Hyde, B. L. Shaw, and I. Shephered, *J. Chem. Soc., Dalton Trans.*, **1978**, 1696.

4) K. Kimura, H. Tamura, T. Tsuchida, and T. Shono, *Chem. Lett.*, **1979**, 611.

5) B. L. Shaw and I. Shephered, *J. Chem. Soc., Dalton Trans.*, **1978**, 1634.

6) R. Ungaro, B. El Haj, and J. Smid, *J. Am. Chem. Soc.*, **98**, 5198 (1976).

7) (a) W. W. Parish, P. E. Scott, and C. W. McCausland, *J. Org. Chem.*, **43**, 4577 (1978); (b) F. Wada and T. Matsuda, *Bull. Chem. Soc. Jpn.*, **53**, 421 (1980).

8) W. E. Smith, *J. Org. Chem.*, **37**, 3972 (1972).

The Removal of Arsenate in Waste Water with an Adsorbent Prepared by Binding Hydrous Iron(III) Oxide with Polyacrylamide

Yasumasa SHIGETOMI,* Yōichi HORI, and Takehiro KOJIMA
Department of Chemistry, Okayama College of Science, Ridai-chō, Okayama 700
(Received June 11, 1979)

Synopsis. Studies have been made to remove arsenate in waste water with an adsorbent prepared by binding hydrous iron(III) oxide with polyacrylamide. Arsenate anions were thus adsorbed over the pH range of 5—8; the adsorption capacity of arsenate was 43 mg per gram of the adsorbent.

The reaction of hydrous iron(III) oxide with several anions has been studied by several workers,[1-3] but the study of the reverse reaction, that is, the desorption or the decomposition, has been seen in only a few papers. It was observed that hydrous iron(III) oxide is a good anion exchanger and that such adsorbed anions as phosphate and fluoride are desorbed by treating them with a dilute solution of sodium hydroxide.[4]

On the other hand, our attempts to avoid the intricate filtration and precipitation of hydrous metal oxides, which detract from its utility for industrial application, have led us to make a proposal for utilizing a composite adsorbent, such a combination of polyacrylamide and hydrous metal oxides.[5] The present paper will report on fundamental work to remove arsenate in waste water by using a composite adsorbent prepared by binding hydrous iron(III) oxide with polyacrylamide.

Experimental

All the chemicals used were of an analytical grade. A stock solution of sodium arsenate was prepared by dissolving 4.1675 g of sodium arsenate in 100 cm^3 of water (1.33×10^{-1} mol dm^{-3} as As).

The most efficient adsorbent was prepared by the following procedure; to 100 cm^3 of water in which are dissolved 5.406 g of iron(III) chloride, we add a concentrated ammonia solution until the pH becomes 7. The precipitate is then separated from mother liquor by centrifuging, and, to the precipitate, 14 g of acrylamide, 4 g of *N,N'*-methylenediacrylamide, and 2 g of ammonium peroxodisulfate as a polymerization initiator, dissolved in 100 cm^3 of water, are added, after which the mixture is stirred vigorously at 70 °C on a water bath. The brown product thus obtained is ground to 50—80 mesh powder in water by using an electric mixer.

All the experiments for the adsorption were carried out by the following procedure, unless otherwise stated: place 50 cm^3 of a solution of sodium arsenate and 0.2 g of the adsorbent in a 100 cm^3 flask. Adjust the pH with an acetate buffer solution. When equilibrium is reached after shaking for 3 h, separate the adsorbent from the solution, determine spectrophotometrically the concentration of arsenate remaining in the solution by means of the molybdenum blue method, and then calculate the percentage of the adsorption from the difference between the initial and the remaining concentrations. In the experiment using a column ($\phi1.7\times2.5$ cm) loaded with 2.5 g of the adsorbent, the 1.33×10^{-3} mol dm^{-3} arsenate solution was passed through the column at a constant and known flow rate, 0.8 cm^3/min. Collect the effluent in a graduated cylinder, testing the outlet continually for the ions to be exchanged.

Results and Discussion

Figure 1 shows the percentage of the adsorption of arsenate as a function of the pH in the solution. Arsenate anions were collected with the adsorbent in amounts greater than 95% over the pH range of 5—6. It seems that the percentage tends to decrease at pH values lower than 4, because arsenic acid is too weak to dissociate.

Figure 2 shows a breakthrough curve when the 1.33×10^{-3} mol dm^{-3} arsenate solution was passed through the column. The breakthrough capacity, as calculated from the curve, is 43 mg per gram of the adsorbent.

The minimal volume of the 0.5 mol dm^{-3} sodium

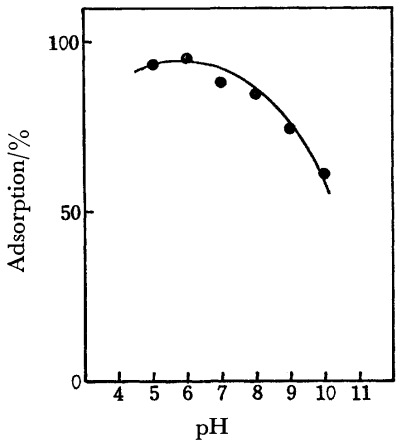

Fig. 1. Relation between pH and the adsorption of As(V).

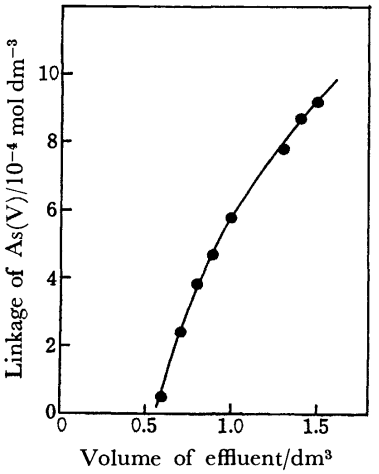

Fig. 2. Breakthrough curve of As(V).
Column: ϕ 1.7×26 cm; adsorbent: 2.5 g; flow rate: 0.83 cm^3/min; As(V): 1.33×10^{-3} mol dm^{-3}.

hydroxide solution required for the elution of arsenate anions can be determined as follows. Collect the effluent in fractions, determine the concentration of arsenate present in a fraction, and then plot the concentration against the volume of the effluent. The volume of the sodium hydroxide solution required for the generation can be determined from the elution curves; fifty cm^3 was sufficient to elute. Further, we examined how the capacity of the adsorption varied when the adsorbent was employed repeatedly. The results are shown in Fig. 3. The capacity was reduced to four-fifth its initial value by ten repetitions. That decrease is attributable to the contamination of the surface. However, if the 0.01 mol dm^{-3} hydrochloric acid is passed through and the adsorbent is washed, the capacity is restored to its original value. Also, we examined how the temperature in the solution affected the adsorption. Arsenate anions were adsorbed from the solution more easily and in greater quantities

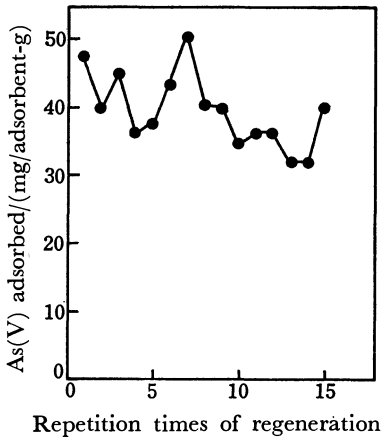

Fig. 3. Relation between repetition times of regeneration and the adsorption capacity of our efficient adsorbed for As(V).

Table 1. The adsorption capacity of our efficient adsorbent for various anions

Anions	Adspt. capacity of adsorbent for anions /mg g^{-1}	Initial concn. of anions/mol m^{-3}
AsO_4^{3-}	43 (as As)	2.67×10^{-3}
AsO_3^{3-}	46 (as As)	2.67×10^{-3}
$P_3O_{10}^{5-}$	26 (as P)	6.46×10^{-3}
F^-	24	2.10×10^{-2}
MoO_4^{2-}	12 (as Mo)	4.17×10^{-3}

The experiments were carried out at pH 4.

at a high temperature rather than at room temperature. Last, the adsorption capacities of the adsorbent for several anions were examined by a batch method using 2.67—5.34 mol dm^{-3} solutions of these anions. Table 1 show that the adsorbent can catch fluoride, phosphate, and molybdate, while it does not catch chloride and sulfate. Juging from these results, we can expect that the adsorbent can well be applied to the treatment of waste containing arsenate, such as geothermal waste water after the generation of electricity.

The present work was partially supported by the Scientific Grant from Nissan Science Foundation.

References

1) F. J. Hingston, A. M. Poner, and J. P. Quirk, *J. Soil. Sci.*, **23**, 177 (1972).
2) H. H. Stamm and H. W. Kohlschutter, *J. Nucl. Chem.*, **27**, 2103 (1965).
3) A. K. Moulik, S. N. Chkravarti, and S. K. Mukherjee, *J. Indian Chem.*, **47**, 149 (1970).
4) Y. Shigetomi, S. Watanabe, and Y. Hori, *Kankyo Gijyutsu*, **17**, 80 (1978).
5) Y. Shigetomi, T. Kojima, and M. Shinagawa, *J. Nucl. Sci. Technol.*, **14**, 811 (1977).

An Application of Microwave Treatment to the Dehydration of Manganese Dioxide for Lithium Nonaqueous Cells

Taketsugu HIRAI,* Isao TARI, and Tsutomu OHZUKU

Department of Synthetic Chemistry, Faculty of Engineering, Okayama University, Tsushima, Okayama 700

(Received October 11, 1979)

Synopsis. A new dehydration technique of manganese dioxide using 2.45 GHz microwave is presented. The so-called γ and γ,β-MnO_2, each containing less than 1 wt% water, which are not attainable by heat treatment, are obtained under specified conditions by this dehydration technique.

In recent years a number of metal oxide cathodes for lithium nonaqueous cells have been investigated.[1] Among them, the manganese dioxide (MnO_2) is one of the most promising cathode materials. The battery-grade electrolytic MnO_2 commercially available, however, originally contains 5 to 10 wt% water. As such water causes serious failures in the lithium-cell system, the development of a dehydration technique has been needed. In order to remove the water, Ikeda *et al.*[2] investigated the heat treatment of electrolytic MnO_2 for lithium-cell use. The continuous heating of electrolytic MnO_2, however, concomitantly caused a structural change in MnO_2.

As has been stated above, the heat treatment of electrolytic MnO_2 is not sufficient for the dehydration of MnO_2. For this reason, we used a microwave shower in the dehydration of electrolytic MnO_2 for a lithium nonaqueous cell. The objective of this study was to determine whether or not the application of 2.45 GHz microwaves to the dehydration of electrolytic MnO_2 is effective.

Experimental

Electrolytic γ-MnO_2, obtained from the Toyo Soda Manufacturing Corporation, had a particle size of 60—100 mesh and a relatively low equi-acidic point of 2.23 on a pH scale, as determined by Tari's pH-shift method.[3]

About 100 g of electrolytic MnO_2 in a 200-ml Pyrex beaker (*ca.* 60 mmϕ × 85 mm) were treated under 2.45 GHz microwave irradiation in a Kenmore microwave oven, model 99701, which had about a 600-W magnetron output and intermittent irradiation controls. In order to determine the effects of a microwave shower on electrolytic MnO_2, the weight loss, the X-ray diffractional pattern, and the water contents of the sample before and after the microwave treatment were measured. X-Ray data were obtained by using a Shimadzu X-ray diffractometer, type VD-11, with iron K_α radiation filtered with manganese. The water contents of the MnO_2 samples were determined by the following, indirect Karl Fischer titration: about 2 g of the MnO_2 sample, which had been crushed to a fine powder, were heated on a boat in a quartz tube at an elevated temperature under a stream of dry nitrogen carrier gas. The exhaust gas was then introduced into a vessel filled with an anhydrated solvent (Mitsubishi anhydrated solvent ME). Titration was automatically achieved by using a Karl Fischer automatic titration apparatus, model MK-AS (Kyoto Electronics Manufacturing Co., Ltd.). The differential thermal analysis and thermal gravimetry were also carried out by means of a Shimadzu Thermal Analyzer, type DT-30. For the sake of magnetron safety, a commercially available microwave absorber (60 mmϕ) was always located in the oven.

Results and Discussion

In the preliminary tests for the dehydration of the electrolytic MnO_2, we selected the intermittent microwave irradiation which consists of 15 s on and 10 s off. Although the continuous irradiation was also an effective method for the dehydration of electrolytic MnO_2, hardly no dehydrated γ or γ,β-MnO_2 was thus obtained. It sometimes caused the decomposition of MnO_2 to Mn_2O_3, which depended on the irradiation time, the microwave power, and the sample weight and/or the apparent volume.

After the preliminary examinations to avoid the decomposition of MnO_2 and to achieve the dehydration, the following conditions were decided on: intermittent microwave irradiation for 5 min, followed by radiation for 25 min; this two-stage treatment was repeated several times.

In order to confirm the effect of microwave irradiation on dehydration, the water content was measured. Figure 1 shows the water distribution of MnO_2 (No. 3 in Fig. 2 and Table 1) well dehydrated by microwave treatment compared with that of the original MnO_2. The water content of the MnO_2 sample shown in Fig. 1 was determined by calculating from the released water at an elevated temperature below 700 °C, assuming that the contained water was zero at 700 °C. The original electrolytic MnO_2 contained 8.3 wt% of water. The rapid decrease in water content below 200 °C was caused by adsorbed water. Because of the decomposition of MnO_2 to Mn_2O_3 up to 500 °C (typically 550 °C), which was confirmed by thermal

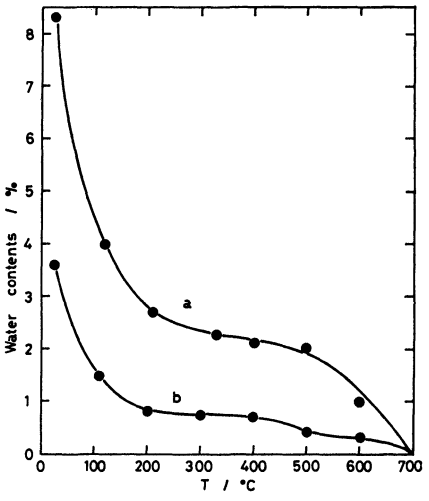

Fig. 1. Water distribution as a function of temperature. (a) Original electrolytic MnO_2, (b) microwave-treated MnO_2 (No. 3).

Table 1. Effect of microwave treatment on crystal structure and water contents

Sample No.	Microwave treatment	Classification from X-ray data	Water contents[a]/wt%
(Original)	—	γ-MnO_2	2.7±0.3
1	30 min	γ-MnO_2, trace of β-MnO_2?	1.2±0.1
2	60 min	γ-MnO_2, trace of β-MnO_2	0.9±0.1
3	90 min	γ,β-MnO_2	0.85±0.1
4	120 min	γ,β-MnO_2	0.6±0.1

a) Water removed below 200 °C was discarded.

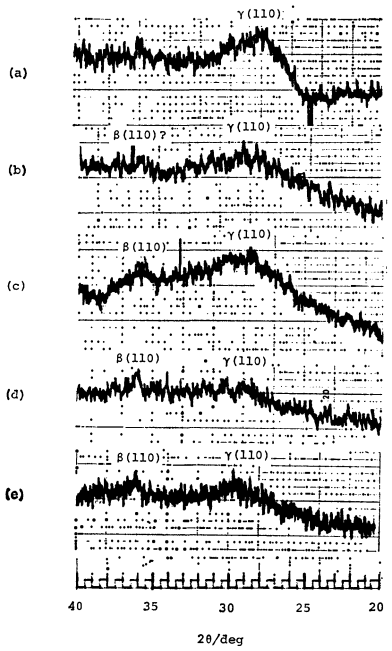

Fig. 2. Change of X-ray diffractional patterns by periodic microwave-treatment which consists of intermittent irradiation (15 s on, 10 s off) for 5 min, and the radiation for 25 min.
(a) Original MnO_2, (b) after 30 min (No. 1), (c) after 60 min (No. 2), (d) after 90 min (No. 3), (e) after 120 min (No. 4).

and X-ray analysis, a water content of less than 1.5 wt% was essentially not attainable by heat treatment.

The structural change caused by microwave treatment were also examined. The original MnO_2 showed the diffractional peaks (2θ) at about 28°, 47°, 54°, and 73°. The peaks at 47°, 54°, and 73° were not changed by microwave treatment. However, the diffused peak at about 28° was gradually decreased in its intensity, and a new peak at about 36° was observed. These delicate changes are shown in Fig. 2.

The above results are summarized in Table 1. The classification of MnO_2 was done according to the work of Fukuda.[4] The microwave treatment was concluded to be effective for the dehydration of MnO_2 from the fact that the so-called γ or γ,β-MnO_2, containing less than 1 wt% water, which could not be attained by heat treatment without the decomposition of MnO_2, was easily obtained by this treatment. Under these irradiation conditions, the water released below 200 °C was large in amount. Such adsorbed water, however, could be completely excluded by heat treatment at 200 °C, at which temperature the structural change in MnO_2 was proved not to occur.[2,3]

Further work related to lithium nonaqueous cells is now in progress in our laboratory.

The present work was supported by Grants-in-Aid for Scientific Research from the Ministry of Education (No. 475619) and the Asahi Garasu Kogyo Gijutsu Shorei-kai.

References

1) T. Ohzuku, Z. Takehara, and S. Yoshizawa, *Denki Kagaku*, **46**, 407, 411 (1978).
2) H. Ikeda, S. Ueno, T. Saito, S. Nakaido, and H. Tamura, *Denki Kagaku*, **45**, 314 391 (1977).
3) I. Tari, in "Surface Electrochemistry," ed by T. Takamura and A. Kozawa, Japan Scientific Societies Press (1978), p. 126.
4) M. Fukuda, *J. Electrochem. Soc. Jpn. (Overseas Ed.)*, **28**, E-38 (1960).

 © 1980 The Chemical Society of Japan Bull. Chem. Soc. Jpn., 53, 1479—1488 (1980)

The γ-Ray Induced Oxidation of Aromatic Hydrocarbons in Liquid Dinitrogen Oxide

Hidetoshi KARASAWA, Rei YUGETA, and Shin SATO*

Department of Applied Physics, Tokyo Institute of Technology, Ookayama, Meguro-ku, Tokyo 152

(Received April 4, 1979)

The γ-ray induced oxidation of aromatic hydrocarbons has been studied in liquid dinitrogen oxide, mainly at −18 °C. Various mixing ratios of dinitrogen oxide and four aromatic hydrocarbons have been examined. The main oxygen-containing products observed were the corresponding phenols and benzyl alcohols. The kinetic analysis showed that ionic species, probably N_2O^- ions, are the main precursors at low mole fractions of dinitrogen oxide and that oxygen atoms become important with an increase in the mole fraction. 1-Butene was used as a scavenger of oxygen atoms. The following rate constant ratios were obtained for the reactions of oxygen atoms and N_2O^- ions: $k(O+\text{toluene})/k(O+\text{1-butene})=0.02$, $k(O+\text{toluene})/k(O+\text{benzene})=2.0$, and $k(N_2O^-+\text{1-butene})/k(N_2O^-+\text{toluene})=2.5$. The relative rates for the formation of the corresponding phenols and benzyl alcohols through ionic reactions from aromatic hydrocarbons were obtained as follows: benzene, 1.0; toluene, 2.5; *p*-xylene, 2.2; 1,3,5-trimethylbenzene, 3.1. These values are quite different from the relative rate constants of the reactions of oxygen atoms with these aromatic hydrocarbons.

Recently much interest has been attracted to the γ-ray-induced oxidation of hydrocarbons in liquid carbon dioxide and dinitrogen oxide. The oxidizing species produced in the γ-radiolysis of a carbon dioxide solution are mainly oxygen atoms.[1-3] In a previous paper,[4] we reported on the reactions between oxygen atoms and several olefins in liquid carbon dioxide and discussed the relative rate constants of these reactions and the difference between gas- and liquid-phase reactions.

On the other hand, the oxidizing species produced in the γ-radiolysis of liquid dinitrogen oxide include not only oxygen atoms, but also N_2O^- ions and/or $N_2O_2^-$ ions.[5] When cyclohexene was used as a reactant, these oxidizing species formed different oxygen-containing products; oxygen atoms produced cyclohexene oxide and cyclohexanone, while ionic species led to the formation of cyclohexanol, 2-cyclohexenol, and probably water.

Aromatic hydrocarbons were also used as reactants in γ-ray-induced oxidation in liquid carbon dioxide.[6,7] The main products observed were the corresponding phenol. Sakurai *et al.* discussed the reaction mechanism and concluded that the oxidizing species are oxygen atoms when the mole fraction of carbon dioxide is higher than 0.9.[8-10]

About ten years ago, we studied the liquid-phase γ-radiolysis of benzene in the presence of dinitrogen oxide and measured the *G*-value of phenol.[11] The initial oxidizing species were concluded to be O^- or N_2O^- ions; *i.e.*, phenol seems to be formed from both oxidizing species, oxygen atoms and ionic species.

The present experiment attempted to confirm the formation of phenols in the reactions of ionic species with aromatic hydrocarbons and to obtain the relative rate constants of these reactions.

Experimental

The experimental procedure was the same as that described in a previous paper.[4] The dinitrogen oxide, purchased from the Takachiho Shoji Co., contained no detectable impurities; this was confirmed by means of a gas-chromatograph equipped with a 5-m dimethyl sulfolane column of 20% w/w on celite. The 1-butene, benzene (Merck Co.), toluene, *p*-xylene, and 1,3,5-trimethylbenzene (Tokyo Kasei Co.) were used after thorough degassing.

About 1 cm^3 of a liquid containing various mixing ratios of N_2O and hydrocarbons was irradiated with ^{60}Co γ-rays at −18 °C (sodium chloride–ice slush) except when otherwise stated. The dose was estimated by Fricke dosimetry on the assumption of a proportionality between the electron density and the dose.

The amount of the noncondensable product at 77 K was measured with a Toepler pump and a gas burrette. The other products were analyzed by gas-chromatography after the excess dinitrogen oxide had been removed at −78 °C. The columns used for the analysis were a 2-m Cresol-3M column (Nishio Kogyo Co.) for phenols and benzyl alcohols, and 2-m PEG-1500 and 2-m DNP columns (Gaschro Kogyo Co.) for 1-butene oxide, butanal, and 2-butanone.

Results and Discussion

Toluene–1-Butene–N_2O System. The main products observed in the γ-radiolysis of the mixture of toluene, 1-butene, and dinitrogen oxide are nitrogen, three isomeric cresols, benzyl alcohol, 1-butene oxide, butanal, and 2-butanone. The *G*-values of these products are shown in Figs. 1, 2, and 3 as functions of the electron fraction (ε) of dinitrogen oxide. It is noticeable that the electron-fraction dependence of cresols and benzyl alcohol is quite different from that of 1-butene oxide, butanal, and 2-butanone. This suggests that the two products, the product from toluene and that from 1-butene, are different in the mechanism of their formation.

The Precursor of 1-Butene Oxide. It is now well known that the reaction of oxygen atoms with olefins produces olefin oxides and their isomeric aldehydes and ketones.[12] In the case of 1-butene, 1-butene oxide (0.53), butanal (0.43), and 2-butanone (0.04) are produced. The numbers in parentheses are the fractions of the total addition products observed in the gas phase at room temperature. In a previous paper,[4] we investigated the γ-ray-induced oxidation of several olefins in liquid carbon dioxide at −18 °C and found, in the

case of 1-butene, that the fractions of the total addition products are 0.70 for 1-butene oxide, 0.25 for butanal, and 0.05 for 2-butanone. The difference between these fractions and those obtained in the gas-phase reaction may be attributed to the interaction between the intermediate biradical formed in the reaction of oxygen atoms with 1-butene and carbon dioxide.

When dinitrogen oxide was used in place of carbon dioxide, the formation of 1-butene oxide, butanal, and 2-butanone was again observed, as is shown in Fig. 2,

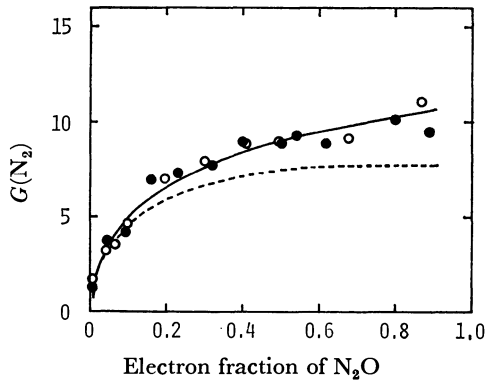

Fig. 1. The G-values of nitrogen from the two reaction systems; toluene (0.9)–1-butene(0.1)–N_2O (●) and benzene (0.6)–1,3,5-trimethylbenzene (0.4)–N_2O (○), as a function of the electron fraction ε of dinitrogen oxide.
The dotted line is the G-value of nitrogen produced by ionic process. Both solid and dotted lines are theoretical.

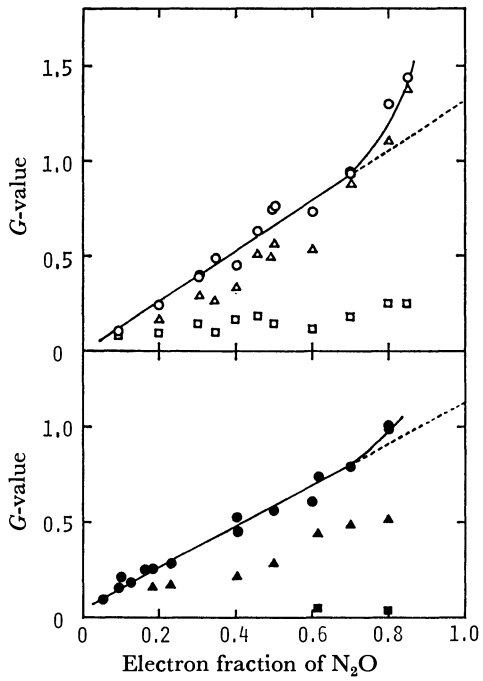

Fig. 2. The G-values of 1-butene oxide (○, ●), butanal (△, ▲), and 2-butanone (□, ■) as functions of the electron fraction ε of dinitrogen oxide.
Open symbols for the 1-butene–N_2O system and filled ones for the toluene (0.9)–1-butene (0.1)–N_2O system.

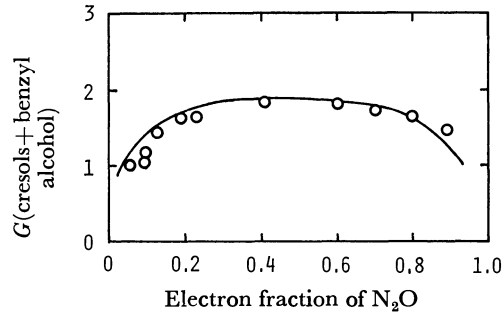

Fig. 3. The G-values of the sum of three kinds of cresols and benzyl alchol as a function of the electron fraction ε of dinitrogen oxide in the toluene (0.9)–1-butene (0.1)–N_2O system.
The solid line was calculated theoretically.

and the G-values were found to be proportional to the electron fraction of dinitrogen oxide up to 0.8, suggesting that these products are formed in the reaction of oxygen atoms generated by the radiolysis of dinitrogen oxide.

$$N_2O \rightsquigarrow N_2 + O \quad (1)$$

$$O + \text{1-Butene} \longrightarrow \text{1-Butene Oxide, Butanal, 2-Butanone} \quad (2)$$

The fractions of these products against the total addition products calculated from the slopes of the linear dependence of the G-values of these products on ε, however, are not the real fractions corresponding to Reaction 2, because a part of butanal and 2-butanone are believed to be formed by the reaction between 1-butene and the ionic species generated in this system. A similar observation has been made with regard to the formation of cyclohexanol in the γ-radiolysis of the mixture of cyclohexene and dinitrogen oxide.[1)]

Above 0.8 of the electron fraction of dinitrogen oxide, another process for the formation of oxygen atoms has to be considered, for which we propose the following reactions:

$$N_2O \rightsquigarrow N_2O^+ + e^- \quad (3)$$

$$e^- + N_2O \longrightarrow N_2O^- \quad (4)$$

$$N_2O^+ + N_2O^- \longrightarrow 2N_2 + 2O \longrightarrow N_2 + O + N_2O. \quad (5)$$

In the presence of a hydrocarbon, a charge transfer will occur, since the ionization potential of any hydrocarbon is smaller than that of dinitrogen oxide:

$$N_2O^+ + A \longrightarrow N_2O + A^+. \quad (6)$$

Here, A stands for a hydrocarbon. This process suppresses the formation of oxygen atoms.

As Fig. 2 shows, the formation of 1-butene oxide was reduced in the presence of toluene. Since toluene is also reactive to oxygen atoms, the decrease in G(1-butene oxide) allows us to estimate the relative rate constant of the oxygen atoms with 1-butene (k_B) and toluene (k_T) as follows:

$$(G_0 - G)/G = k_T[\text{toluene}]/k_B[\text{1-butene}].$$

Here, G and G_0 are the G-values of 1-butene oxide from the reaction system in the presence and in the absence of toluene. The substitution of the data shown in Fig. 2 gives the following ratio:

$$k_T/k_B = (1.30-1.12)/1.12\times 1/9 = 0.02.$$

The rate constants of the gas-phase reactions of oxygen atoms with hydrocarbons have been measured by Atkinson and Cvetanović[13] and by Atkinson and Pitts.[14,15] Using their data, we can estimate the rate constant ratio at −18 °C to be 0.008. Since the experimental error in activation energy is reported to be 30%, the ratio obtained in the present experiment may be regarded as being in agreement with the gas-phase data.

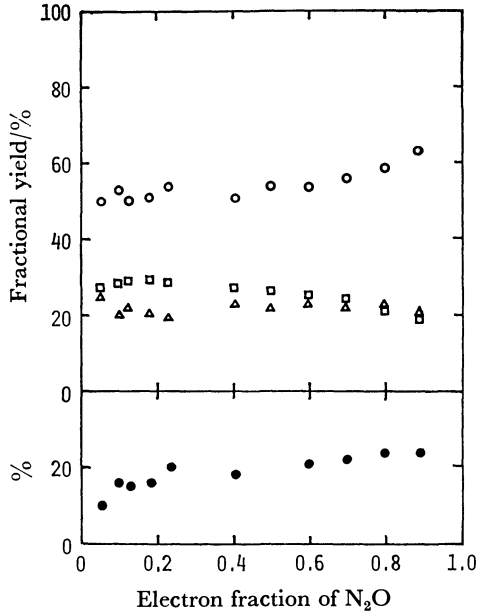

Fig. 4. The fractional yields of three kinds of cresols (○, ortho; □, meta; △, para) and benzyl alcohol (●) as functions of the electron fraction ε of dinitrogen oxide in the toluene (0.9)–1-butene (0.1)–N_2O system.

The Precursors of Cresols. Figure 4 shows the yield ratios of three kinds of cresols and benzyl alcohol from the toluene(0.9)–1-butene(0.1)–N_2O system as functions of the electron fraction of dinitrogen oxide. The numbers in parentheses are the mole fractions of the two hydrocarbons in the mixture. Since the ratio of ortho, meta, and para is dependent upon the electron fraction of dinitrogen oxide, we have to consider at least two precursors for the formation of these products. A comparison of Figs. 2 and 3 suggests that the precursors of cresols and benzyl alcohol are not oxygen atoms at low-electron fractions of dinitrogen oxide. Since dinitrogen oxide is a well-known electron scavenger, it may be natural to consider that the precursor is N_2O^- or O^- ions produced in the electron-scavenging reaction of dinitrogen oxide.

The reactions of N_2O^- ions in hydrocarbons, especially in cyclohexane, have been discussed by a number of researchers,[16–19] but they have not been established yet. In the present experiment, however, the similarity in the N_2O electron-fraction dependence of $G(N_2)$ and G(cresols+benzyl alcohol) at low values of ε strongly suggests that ionic species such as N_2O^- ions are the precursors of these products.

$$A \rightsquigarrow A^+ + e^- \quad (7)$$

$$e^- + N_2O \longrightarrow N_2O^- \quad (8)$$

$$N_2O^- + A \longrightarrow N_2 + AO^- \quad (9)$$

$$AO^- + A^+ \longrightarrow P + A \quad (10)$$

Here, A stands for an aromatic hydrocarbon, and P, for the addition product.

If this mechanism is operative, the ortho-meta-para ratio obtained in a low-electron fraction of dinitrogen oxide in the toluene–1-butene–N_2O system should correspond to the orientation of the addition of O^- to toluene. As Fig. 4 shows, the ratio at the lower limit of the electron fraction of dinitrogen oxide is 53: 27: 20.

In high-electron fractions, this ratio approaches 65: 15: 20 with the increase in ε. This ratio is close to that obtained in the gas-phase reaction of oxygen atoms with toluene (64: 17: 19).[20] In the previous section, we stated that oxygen-atom generation increases with the increase in ε above 0.8. Consequently, we may conclude that oxygen atoms become important precursors for cresols in high-electron fractions of dinitrogen oxide.

Below we will discuss a reaction mechanism which is applicable to all the range of ε; the kinetic treatment will be presented at that time.

Benzene–1,3,5-Trimethylbenzene–N_2O System.
Figure 5 shows the G-values of phenol, 2,4,6-trimethylphenol, and 3,5-dimethylbenzyl alcohol as functions of ε from the mixture of benzene (0.6), 1,3,5-trimethylbenzene (0.4), and N_2O. The numbers in parentheses are the mole fractions of the two hydrocarbons in the mixture. It may be worthwhile to mention here that the electron-fraction dependence of G(phenol) is similar to that of G(3,5-dimethylbenzyl alcohol), but different from that of G(2,4,6-trimethylphenol).

According to Grovenstein and Mosher,[20] the forma-

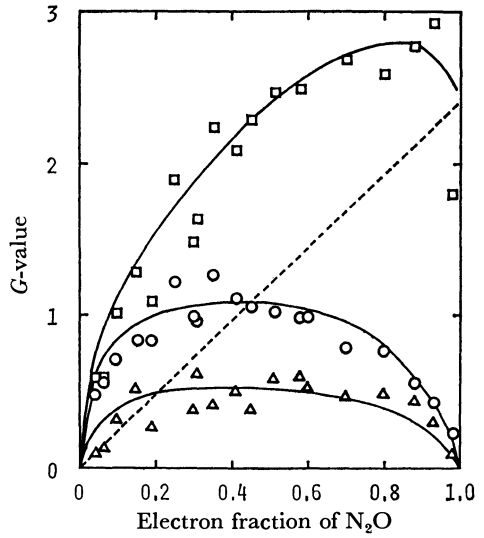

Fig. 5. The G-values of phenol (○), 2,4,6-trimethylphenol (□), and 3,5-dimethylbenzyl alcohol (△) as functions of the electron fraction ε of dinitrogen oxide in the benzene (0.6)–1,3,5-trimethylbenzene (0.4)–N_2O system.
Solid lines are theoretical. The dotted line is the G-value of 2,4,6-trimethylphenol formed in the reaction of oxygen atoms.

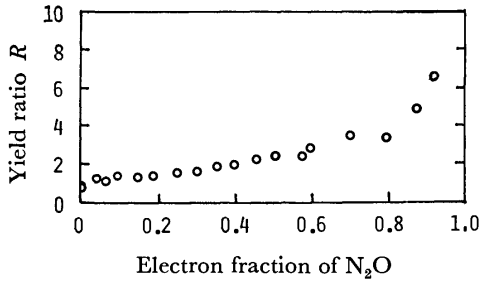

Fig. 6. The yield ratio R of [2,4,6-trimethylphenol]/[phenol] as a function of the electron fraction ε of dinitrogen oxide in the benzene (0.6)–1,3,5-trimethylbenzene (0.4)–N_2O system.

tion of phenols in the gas-phase reactions of oxygen atoms with aromatic hydrocarbons is faster for the more methyl-substituted ones. In the case of the competition between benzene and 1,3,5-trimethylbenzene, the reaction-rate ratio (R) for 2,4,6-trimethylphenol to phenol has been reported to be 77.5. The ratio obtained in the present experiment is plotted in Fig. 6 as a function of ε. As ε approaches unity, the ratio, R, seems to approach the value obtained by Grovenstein and Mosher, while at low values of ε, R is about unity.

In order to estimate the fractions of 2,4,6-trimethylphenol produced through two processes, one from the reaction of oxygen atoms and the other from the reaction of ionic species, we made a few experiments in which the mole fractions of benzene and 1,3,5-trimethylbenzene were changed in the presence of a constant electron fraction of dinitrogen oxide at 0.1. The results are shown in Fig. 7.

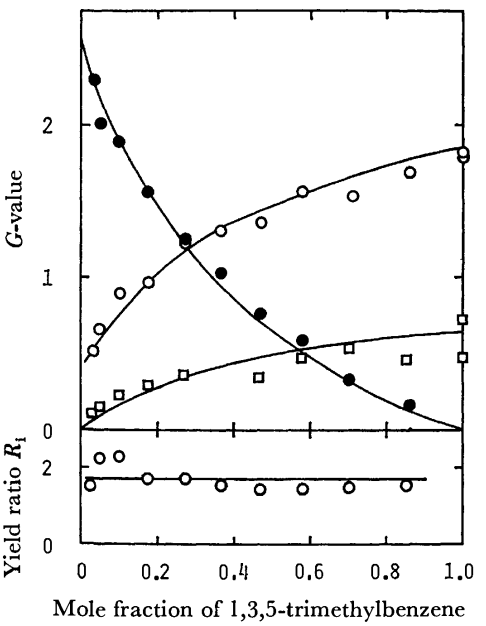

Fig. 7. The G-values of addition products from the benzene–1,3,5-trimethylbenzene system in the presence of dinitrogen oxide ($\varepsilon=0.1$) at 0°C and the yield ratio, R_1, as functions of the mole fraction of 1,3,5-trimethylbenzene.
●, Phenol; ○, 2,4,6-trimethylphenol; □, 3,5-dimethylbenzyl alcohol.

$$R_1=\frac{G_1(\text{2,4,6-trimethylphenol})}{G_1(\text{phenol})}\,\frac{[\text{benzene}]}{[\text{1,3,5-trimethylbenzene}]}$$

It is known in the gas-phase reaction that the phenol formation in the reaction of oxygen atoms with benzene is only 6% of the consumption of oxygen atoms.[21] This percentage may not be very different in the liquid-phase reaction. Moreover, benzene is much less reactive to oxygen atoms than is 1,3,5-trimethylbenzene. The phenol observed in the present experiment, therefore, may be assumed to be produced only from the reaction of ionic species with benzene:

$$\text{benzene} + N_2O^- \longrightarrow \text{phenol} \quad (11)$$

$$\text{1,3,5-trimethylbenzene} + N_2O^- \longrightarrow \text{2,4,6-trimethylphenol} \quad (12)$$

$$\text{1,3,5-trimethylbenzene} + O \longrightarrow \text{2,4,6-trimethylphenol.} \quad (13)$$

Since the formation-rate ratio of the 2,4,6-trimethylphenol produced by Reaction 12 to the phenol produced by Reaction 11 should be constant, this ratio can be calculated by using the data shown in Fig. 7 on the assumption that the extra amount of 2,4,6-trimethylphenol is produced by Reaction 13. The ratio thus estimated is 1.7. The plots for this estimation are also shown in Fig. 7.

Let us go back to the data shown in Fig. 5, where the mole-fraction ratio of benzene to 1,3,5-trimethylbenzene is 0.6: 0.4. Consequently, the G_i(2,4,6-trimethylphenol)/G_i(phenol) ratio in this experiment should be 1.1 ($=1.7\times0.4/0.6$). Here, G_i stands for the G-value of the product formed by the reaction of ionic species. Using this ratio, we can estimate the G-value of the 2,4,6-trimethylphenol produced by the reaction of oxygen atoms, on the assumption that the phenol observed is produced only from the reaction of ionic species. Figure 8 shows the G-values thus calculated as a function of the electron fraction of dinitrogen oxide. The G-values are obviously linearly dependent

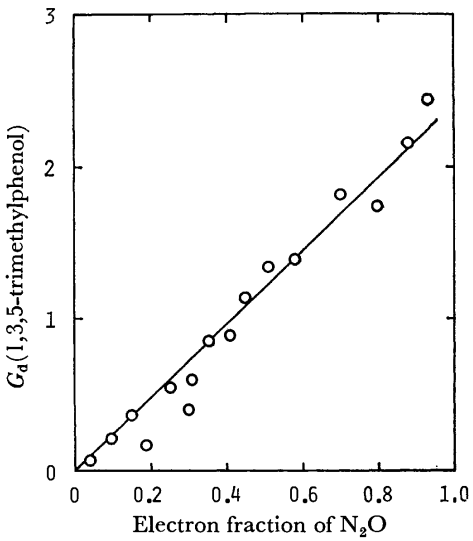

Fig. 8. The G-value of 2,4,6-trimethylphenol formed in the reaction of oxygen atoms produced by the direct radiolysis of dinitrogen oxide.

upon ε; this is consistent with the assumption made above that this part of the 2,4,6-trimethylphenol is produced by the reaction of oxygen atoms. The G-value of the 2,4,6-trimethylphenol produced by this process is calculated to be 2.4ε.

The Precursor of Benzyl-alcohol-type Products. So far two benzyl alcohol-type products have been found; one is benzyl alcohol from the toluene–N_2O system, and the other is 3,5-dimethylbenzyl alcohol from the benzene–1,3,5-trimethylbenzene–N_2O system. The dependence of G(benzyl alcohol) on the electron fraction of dinitrogen oxide was similar to that of G(cresols), although the absolute yield was very small when ε was close to unity. On the other hand, as Fig. 5 shows, the dependence of G(3,5-dimethylbenzyl alcohol) on ε was very similar to that of G(phenol).

According to Jones and Cvetanović,[22] no benzyl alcohol was formed in the gas-phase reaction of oxygen atoms with toluene. Consequently, we may conclude that both benzyl alcohol and 3,5-dimethylbenzyl alcohol are produced from the reaction with ionic species, although the mechanism cannot be specified in detail. In the following treatment, we tentatively assume that the mechanism of the formation of benzyl alcohols is similar to that of the isomeric phenols produced through the ionic process.

Kinetic Treatment. The neutralization reaction of geminate ion-pairs produced in the γ-irradiated system cannot be treated by a simple kinetic treatment in which the reaction rate is assumed to be always proportional to the reactant concentration in the solution. Consequently, several empirical equations have been proposed for the interpretation.[23–25] Among them, the so-called Schuler equation is the most famous.

In a previous paper,[26] we investigated the electron-scavenging process of bromobenzene in the γ-irradiated cyclohexane and 2,2,4-trimethylpentane, and concluded that the following Hummel empirical equation was better than Schuler's in explaining the wide range of concentrations of electron scavengers:

$$G(P) = G_{fi} + G_{gi}[1-\exp(-\sqrt{\alpha S})]. \quad \text{(I)}$$

Here, G(P) is the G-value of the electrons scavenged by a solute, with S as its concentration. G_{fi} and G_{gi} are the G-values of free and geminate electrons respectively, and α is an empirical constant proportional to the rate constant of the electron-scavenging reaction. The $\exp(-\sqrt{\alpha S})$ term on the right-hand side is the fraction which is not scavenged by the scavenger.

On the other hand, if the time distribution of the geminate electrons is denoted by $f_e(t)$, the fraction which is not scavenged by the scavenger may be written as follows:

$$\int_0^\infty f_e(t)\exp(-kSt)\mathrm{d}t = \exp(-\sqrt{\alpha S}). \quad \text{(II)}$$

Here, k is the rate constant of the electron scavenging and is related to α by $\alpha=k/\lambda$. λ is a constant depending on the solvent.[27] Using Eq. II, we can derive the concentration dependence of the electron-scavenging reaction without the knowledge of the time distribution of the geminate electrons.

In order to develop a theoretical treatment, we will now consider the phenol formation through the ionic process in the γ-radiolysis of a mixture of benzene and dinitrogen oxide. We propose the following reaction mechanism:[6]

$$C_6H_6 \rightsquigarrow C_6H_6^+ + e^- \quad (14)$$

$$N_2O \rightsquigarrow N_2O^+ + e^- \quad (15)$$

$$N_2O^+ + C_6H_6 \longrightarrow N_2O + C_6H_6^+ \quad (16)$$

$$e^- + N_2O \xrightarrow{k_e} N_2O^- \quad (17)$$

$$N_2O^- + N_2O \xrightarrow{k_s} N_2 + N_2O_2^- \quad (18)$$

$$N_2O^- + C_6H_6 \xrightarrow{k_a} N_2 + C_6H_6O^- \quad (19)$$

$$C_6H_6O^- + N_2O \xrightarrow{k_b} N_2 + C_6H_6O_2^- \quad (20)$$

$$C_6H_6^+ + e^- \longrightarrow Q \quad (21)$$

$$C_6H_6^+ + N_2O^- \xrightarrow{a} N_2 + P \quad (22)$$

$$C_6H_6^+ + N_2O_2^- \longrightarrow N_2 + Q \quad (23)$$

$$C_6H_6^+ + C_6H_6O^- \xrightarrow{b} P + C_6H_6 \quad (24)$$

$$C_6H_6^+ + C_6H_6O_2^- \xrightarrow{c} P + Q. \quad (25)$$

Here, Q stands for some products other than phenol, and P, for phenol. k_e, k_s, k_a, and k_b are the rate constants for the corresponding reactions. The a, b, and c shown in Reactions 22, 24, and 25 are the fractions of the phenol formation in these reactions. Reaction 20 was included to explain the large G-value of nitrogen. Reaction 22 is regarded as being similar to the reaction of oxygen atoms with benzene; therefore, the parameter, a, is taken to be equal to the conversion ratio of the phenol formation to the consumption of oxygen atoms. The phenol formation was not assumed in Reaction 23, since this reaction may be similar to the reaction of excited O_2 molecules with benzene. The reaction of $N_2O_2^-$ ions with benzene was not included, since the reactivity of $N_2O_2^-$ ions may be similar to that of superoxide ions. Superoxide ions are known not to be reactive to benzene.[28]

First, let us consider the lifetimes of negative species. The lifetime of a geminate electron produced in the system is denoted by t. If this electron is scavenged by N_2O at the time t', the lifetime of the negative charge will be prolonged, since the mobility of negative ions is much smaller than that of electrons. The lifetime of the N_2O^- ions thus produced may be expressed by $(t-t')r_D$, where $r_D=(\mu_e+\mu_+)/(\mu_-+\mu_+)$, and where μ_e, μ_+, and μ_- are the mobilities of electrons, $C_6H_6^+$ ions, and N_2O^- ions respectively. According to Reactions 18 and 19, N_2O^- ions react with N_2O or C_6H_6. If either of these reactions occurs at t'' after the formation of N_2O^- ions, the lifetime of the newly formed $N_2O_2^-$ or $C_6H_6O^-$ ions may be expressed by $[(t-t')r_D-t'']$. Here, we assumed that all of the negative ions have the same mobility, μ_-.

Since the probability that electrons are not scavenged by N_2O by the time t' is expressed by $\exp(-k_e[N_2O]t')$, and, similarly, the probability that N_2O^- does not react with N_2O or C_6H_6 by the time t'' after its generation is expressed by $\exp(-k_s[N_2O]t''-k_a[C_6H_6]t'')$, the fraction of the nitrogen formation by Reaction 18 may be expressed as follows:

$$F_{1s}(N_2) = \int_0^\infty f_e(t)dt \int_0^t k_e[N_2O] \exp(-k_e[N_2O]t')dt' \times \int_0^{(t-t')r_D} k_s[N_2O] \exp(-k_s[N_2O]t'' - k_a[C_6H_6]t'')dt''. \quad (III)$$

After the integrations are carried out, the use of Eq. II gives the following equation:

$$F_{1s}(N_2) = \frac{\beta S}{\beta S+\delta}\left[1-\exp(-\sqrt{\alpha S}) - \frac{\alpha S}{\alpha S-(\beta S+\delta)} \times \{\exp(-\sqrt{\beta S+\delta}) - \exp(-\sqrt{\alpha S})\}\right]. \quad (IV)$$

Here, $\alpha=k_e/\lambda$, $\beta=(k_s/\lambda)r_D$, and $\delta=(k_a[C_6H_6]/\lambda)r_D$. In similar manners, all of the fractions of the nitrogen formation through ionic processes can be derived. As for free electrons, we can use a usual kinetic treatment. Since the concentration of dinitrogen oxide used in the present experiment is not very small, all of the free electrons are assumed to be scavenged by N_2O. The fraction of the nitrogen formation initiated by free electrons may be written as follows:

$$F_{fi}(N_2) = \left(1+\frac{\beta S}{\beta S+\delta}+\frac{\delta}{\beta S+\delta}\frac{R_{20}}{R_{20}+R_{24}}\right). \quad (V)$$

Here, R_{20} and R_{24} are the reaction rates of the corresponding reactions. For simplicity, we assume the following expression for the ratio of R_{20}/R_{24}:[29]

$$R_{20}/R_{24} = [N_2O]/0.1 \quad (VI)$$

Ultimately we can obtain the following expression for the G-value of nitrogen produced through ionic processes:

$$G_i(N_2) = G_{fi}P_1 + G_{gi}[1-\exp(-\sqrt{\alpha S})]P_2 \quad (VII)$$

$$P_1 = F_{fi}(N_2) \quad (VIII)$$

$$P_2 = 2 - \frac{\alpha S}{\alpha S-(\beta S+\delta)}\left\{1-\frac{1-\exp(-\sqrt{\beta S+\delta})}{1-\exp(-\sqrt{\alpha S})}\right\} - \frac{\delta}{\beta S+\delta-\gamma S}\left[\frac{\alpha}{\alpha-\gamma}\left\{1-\frac{1-\exp(-\sqrt{\gamma S})}{1-\exp(-\sqrt{\alpha S})}\right\} - \frac{\alpha S}{\alpha S-(\beta S+\delta)}\left\{1-\frac{1-\exp(-\sqrt{\beta S+\delta})}{1-\exp(-\sqrt{\alpha S})}\right\}\right]. \quad (IX)$$

Here, $\gamma=(k_b/\lambda)r_D$. When this equation is applied to a very low concentration of a scavenger, the term for G_{fi} has to be accurately formulated.[30] In the present calculation, the contribution of G_{fi} is very small, since the G-values of the free electrons in aromatic hydrocarbons are known to be small:[31,32] for example, 0.06 for benzene, 0.05 for toluene, 0.07 for p-xylene, and 0.09 for 1,3,5-trimethylbenzene.

The expression for the phenol formation through an ionic process can similarly be derived as follows:

$$G_i(P) = G_{fi}Q_1 + G_{gi}[1-\exp(-\sqrt{\alpha S})][aQ_2+cQ_3+(b-c)Q_4] \quad (X)$$

$$Q_1 = \left[b+(c-b)\frac{S}{S+0.1}\right]\frac{\delta}{\beta S+\delta} \quad (XI)$$

$$Q_2 = \frac{\alpha S}{\alpha S-(\alpha S+\delta)}\left[1-\frac{1-\exp(-\sqrt{\beta S+\delta})}{1-\exp(-\sqrt{\alpha S})}\right] \quad (XII)$$

$$Q_3 = \frac{\delta}{\beta S+\delta}(1-Q_2) \quad (XIII)$$

$$Q_4 = \frac{\alpha}{\alpha-\gamma}\left[1-\frac{1-\exp(-\sqrt{\gamma S})}{1-\exp(-\sqrt{\alpha S})}\right] - Q_2. \quad (XIV)$$

Here, the phenol formation initiated by free electrons is assumed to result only from Reactions 24 and 25.

In order to determine the parameters appearing in the above expressions, we used two sets of experimental results; one consisted of the G-values of nitrogen and phenol obtained at low concentrations of dinitrogen oxide at room temperature, since benzene containing a small amount of dinitrogen oxide is crystallized at around 0 °C, while the other consisted of G(phenol)'s from a benzene–N_2O system at 0 °C.

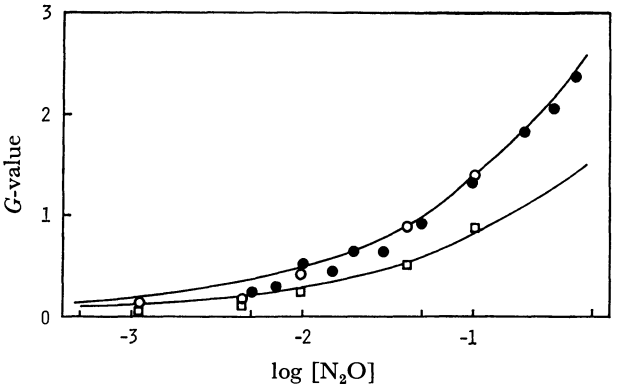

Fig. 9. The G-values of nitrogen (○, ●) and phenol (□) from the benzene–N_2O system at room temperature.
Solid lines are theoretical. Open symbols for the present work, and filled ones for the result of Hentz and Sherman.

Figure 9 shows $G(N_2)$ and G(phenol) at low concentrations of dinitrogen oxide, together with the results obtained by Hentz and Sherman.[33] The solid lines are the results of the calculation using Eqs. VII and X. The parameters used are $G_{fi}=0.06$, $G_{gi}=3.8$, $\alpha=0.5$ dm^3 mol^{-1}, $\beta=\gamma=1.0$ dm^3 mol^{-1}, $\delta=9.0[C_6H_6]$, $a=0.0$, and $b=c=1.0$. Here, we assumed $a=0.0$, since the fraction of the phenol formation against the consumption of oxygen atoms is known to be very small (6%) in the gas-phase reaction of oxygen atoms with benzene.

Figure 10 shows the G(phenol)'s as a function of ε from the benzene–N_2O system obtained at 0 °C. A solid line was calculated by using the same parameter as above. The deviation of the experimental plots at high-electron fractions above 0.9 might be due to the

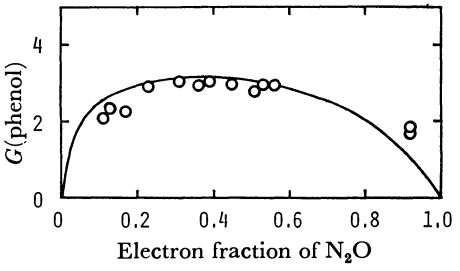

Fig. 10. The G-value of phenol from the benzene–N_2O system at 0°C. A solid line is theoretical.

phenol formation from the reaction of oxygen atoms with benzene. This point will be discussed later.

Now, let us go back to the data of $G(N_2)$ shown in Fig. 1. There are two origins of nitrogen in this reaction system, one is the direct radiolysis of dinitrogen oxide, $G_d(N_2)$, and the other, from the ionic process, $G_i(N_2)$:

$$G(N_2) = G_d(N_2) + G_i(N_2). \quad \text{(XV)}$$

$G_d(N_2)$ should be proportional to ε up to 0.8. The dotted line shown in Fig. 1 is $G_i(N_2)$ calculated by using Eq. VII. A solid line was drawn by adding 3.3ε to $G_i(N_2)$. Because of the scattering of the $G(N_2)$ data, only a wide range of the value, $G_d(N_2)/\varepsilon=3.0$—4.0, can be estimated from Fig. 1. The value of 3.3 was estimated as follows. In the 1-butene–N_2O system, we observed that G(1-butene oxide)$=1.4\varepsilon$. On the other hand, according to Cvetanović,[12] the yield of 1-butene oxide upon the consumption of oxygen atoms is about 0.42 in the gas-phase reaction. If we take this value for the present experiment, the G-value of the oxygen atoms produced by the direct radiolysis of dinitrogen oxide should be 3.3 ($=1.4/0.42$).

If we take this value, 3.3, as the G-value of the oxygen atoms from the direct radiolysis of dinitrogen oxide, the conversion yield, $a=G_d$(2,4,6-trimethylphenol)$/G_d$(oxygen atoms), in the benzene–1,3,5-trimethylbenzene–N_2O system is calculated to be 0.71 ($=2.4/3.3$).

It may be worthwhile here to make some comments on the parameters we have used above. When Hentz and Sherman analyzed $G(N_2)$,[33] they used Schuler's empirical equation, which is exactly the same as Hummel's equation at the lower limit of the scavenger concentration. The α parameter they obtained was about 0.7 dm^3 mol^{-1}. For the β parameter, they could not determine the exact value because of the scattering of data, but they suggested that it is larger than α. We have no knowledge to use for the estimation of the value of γ; however, Reactions 18 and 20 are similar in the mechanism of the oxygen-atom transfer, so that $\beta=\gamma$ may not be an absurd approximation. Reaction 19 is practically the addition reaction of O^- to benzene; therefore, $\delta/[C_6H_6]$ must be much larger than β and γ. We took 9.0 for this ratio.

The Competition of Aromatic Hydrocarbons for the Formation of the Corresponding Phenols by the Ionic Process. In order to investigate the competition of aromatic hydrocarbons for the formation of the corresponding phenols, the following three mixtures were γ-irradiated at various mixing ratios under a constant electron fraction of dinitrogen oxide ($\varepsilon=0.1$); benzene–toluene, benzene–*p*-xylene, and benzene–1,3,5-trimethylbenzene. The results for the last mixture have already been shown in Fig. 7.

When two aromatic hydrocarbons, A and B, are used in place of benzene in the reaction mechanism stated above, competition between A and B occurs in Reactions 19 and 20:

$$N_2O^- + A \xrightarrow{k_A} N_2 + AO^- \quad \text{(19A)}$$

$$N_2O^- + B \xrightarrow{k_B} N_2 + BO^- \quad \text{(19B)}$$

$$AO^- + N_2O \longrightarrow N_2 + AO_2^- \quad \text{(20A)}$$

$$BO^- + N_2O \longrightarrow N_2 + BO_2^-. \quad \text{(20B)}$$

The kinetic treatment including these reactions is somewhat complicated; however, when the electron fraction of dinitrogen oxide is not very large, the following approximate expression can be used:

$$G_i(P_A) = \frac{k_A[A]}{k_A[A]+k_B[B]}[b_A G_{fi} + c_A G_{gi}(1-e^{-\sqrt{aS}})] \quad \text{(XVI)}$$

$$G_i(P_B) = \frac{k_B[B]}{k_A[A]+k_B[B]}[b_B G_{fi} + c_B G_{gi}(1-e^{-\sqrt{aS}})]. \quad \text{(XVII)}$$

Here, the subscripts A and B correspond to the two hydrocarbons, A and B. Since G_{fi} is much smaller than G_{gi}, the contribution of the first term in brackets on the right-hand side is very small compared with the second one. The errors introduced in the estimation of k_A/k_B by using these approximate expressions were calculated numerically and estimated to be within 10%.

Since the gas-chromatographic analysis of products was not very reproducible, as will be shown below, we used the following procedure for the determination of the relative rate constants, k_A/k_B. This procedure has already been used in a previous paper,[4] where the relative rate constants of oxygen atoms with several olefins were determined.

In the case of benzene, the only addition product observed is phenol, but in the case of toluene we observed three kinds of cresols and benzyl alcohol, so that the process for the formation of addition products has to be divided:

$$N_2O^- + A \xrightarrow{m} P_{Am}$$
$$\xrightarrow{1-m} P_{A(1-m)}.$$

Here, m denotes the fraction of the P_{Am} product against the total addition products from the A hydrocarbon. Now, let us introduce a weighted mole fraction, x:

$$x = \frac{f[B]}{[A]+f[B]}, \quad \text{(XVIII)}$$

where f is the factor to be estimated. If the f factor is equal to the k_B/k_A ratio, the plots of $G(P_{Am})$ against x will give a straight line:

$$G(P_{Am}) = mG_A(1-x). \quad \text{(XIX)}$$

Here,

$$G_A = b_A G_{fi} + c_A G_{gi}(1-e^{-\sqrt{aS}}). \quad \text{(XX)}$$

A similar linearity can be obtained for the products of the reaction with the B hydrocarbon:

$$G(P_{Bn}) = nG_B x. \quad \text{(XXI)}$$

Here,

$$G_B = b_B G_{fi} + c_B G_{gi}(1-e^{-\sqrt{aS}}), \quad \text{(XXII)}$$

and n is the fraction of the P_{Bn} product. Such plots are made by varying the f factor until good linearities are obtained for all products.

Figures 11, 12, and 13 show the final plots thus obtained for the reaction systems of benzene–toluene, benzene–*p*-xylene, and benzene–1,3,5-trimethylbenzene respectively. Figure 13 clearly shows the intercept at [1,3,5-trimethylbenzene]$=0$ for the plots of 2,4,6-trimethylphenol. This is due to the reaction of the

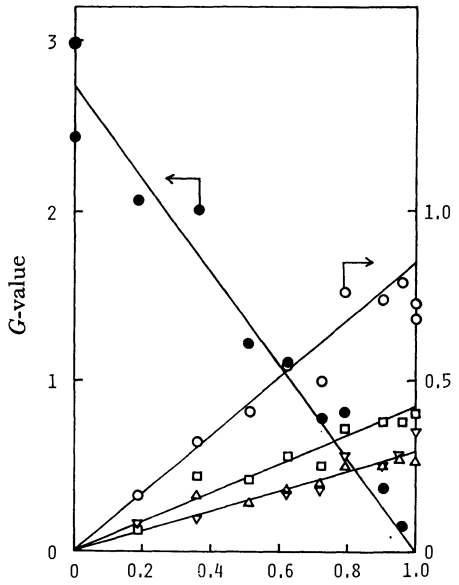

Fig. 11. The *G*-values of addition products from the mixture of benzene and toluene in the presence of dinitrogen oxide ($\varepsilon=0.1$) at 0°C as functions of the weighted mole fraction of toluene.
The value of f is taken as 2.5. ●, Phenol; ○, *o*-cresol; □, *m*-cresol; △, *p*-cresol; ▽, benzyl alcohol.

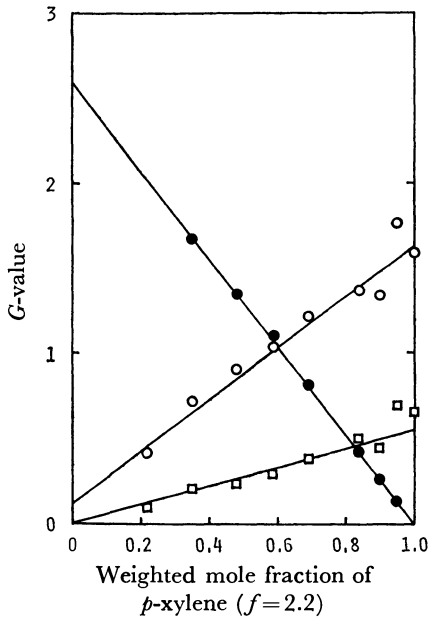

Fig. 12. The *G*-values of addition products from the mixture of benzene and *p*-xylene in the presence of dinitrogen oxide ($\varepsilon=0.1$) at room temperature as functions of the weighted mole fraction of *p*-xylene.
The value of f is taken as 2.2. ●, Phenol; ○, 2,5-dimethylphenol; □, *p*-methylbenzyl alcohol.

oxygen atoms produced in the direct radiolysis of N_2O. The relative rate constants of Reaction 19 thus obtained are summarized in Table 1.

Now, let us go back to Eq. X. Most of the parameters in this equation for the aromatic hydrocarbons are

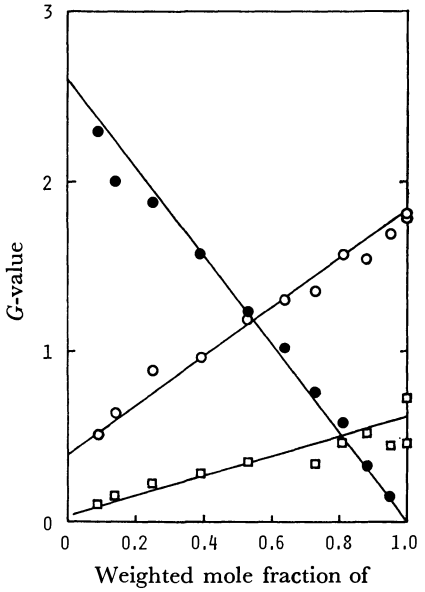

Fig. 13. The *G*-values of addition products from the mixture of benzene and 1,3,5-trimethylbenzene in the presence of dinitrogen oxide ($\varepsilon=0.1$) at 0°C as functions of the weighted mole fraction of 1,3,5-trimethylbenzene.
The value of f is taken as 3.1. ●, Phenol; ○, 2,4,6-trimethylphenol; □, 3,5-dimethylbenzyl alcohol.

TABLE 1. THE RELATIVE RATE CONSTANTS OF REACTIONS OF OXYGEN ATOMS AND N_2O^- IONS WITH SEVERAL HYDROCARBONS IN THE LIQUID PHASE

Reactions	Relative rate constants
O+benzene	1.0
O+toluene	2.0
O+1-butene	100
N_2O^-+benzene	1.0
N_2O^-+toluene	2.5
N_2O^-+*p*-xylene	2.2
N_2O^-+1,3,5-trimethylbenzene	3.1
N_2O^-+1-butene	6.25

known except for a, b, and c. Since ε is 0.1, we can neglect the phenol formation from the reaction of oxygen atoms with benzene, *i.e.*, $a=0.0$ in the case of the benzene system. Similarly, we assume here $a=0.0$ for the toluene system as well, since the ratio of the cresol formation to the consumption of oxygen atoms is known to be small (15%) in a gas-phase reaction.[22] As for 1,3,5-trimethylbenzene, we have already obtained $a=0.71$. For *p*-xylene, we tentatively assume $a=0.4$. As will be shown below, this value is consistent with the experimental results.

The total *G*-value of a specified product, P_α, may now be expressed as follows:

$$G(P_\alpha) = G_d(P_\alpha) + G_i(P_\alpha) \quad \text{(XXIII)}$$

$$G_d(P_\alpha) = laG_d(\text{oxygen atoms}) \quad \text{(XXIV)}$$

$$G_i(P_\alpha) = G_{fi}Q_1la + G_{gi}(1-e^{-\sqrt{aS}}) \times [laQ_2+mcQ_3+m(b-c)Q_4]. \quad \text{(XXV)}$$

TABLE 2. THE PARAMETERS ESTIMATED FOR THE THEORETICAL CALCULATION

$\alpha=0.5$ dm^3 mol^{-1}, $\beta=\gamma=1.0$ dm^3 mol^{-1}, $\delta/[C_6H_6]=9.0$

Reactant	a	$b=c$	Product	l	m
Benzene	0.17	1.0	Phenol	1.0	1.0
Toluene	0.36	0.74	*o*-Cresol	0.64	0.45
			m-Cresol	0.14	0.23
			p-Cresol	0.19	0.16
			Benzyl alcohol	0	0.16
			Phenol	0.03	0
p-Xylene	0.40	0.84	2,5-Dimethylphenol	1.0	0.75
			p-Methylbenzyl alcohol	0	0.25
1,3,5-Trimethylbenzene	0.71	0.81	2,4,6-Trimethylphenol	1.0	0.69
			3,5-Dimethylbenzyl alcohol	0	0.31

a: The fraction of the total addition products to the consumption of oxygen atoms; b: the fraction of the addition products to the consumption of N_2O^- ions; l: fractional yields of the addition products formed in the reaction of oxygen atoms; m: fractional yields of the addition products formed in the reaction of N_2O^- ions, followed by neutralization.

The expressions for Q_1, Q_2, Q_3, and Q_4 have already been shown in Eqs. XI, XII, XIII, and XIV respectively. l is the fraction of a specified product, P_α, against the total addition products formed in the reaction of oxygen atoms.

Table 2 summarizes all of the parameters used. These parameters can reproduce all the data shown in Figs. 11, 12, and 13 by the use of Eq. XXIII. As an example, the mole fraction dependence of the G-values of phenol, 2,5-dimethylphenol, and *p*-methylbenzyl alcohol is shown in Fig. 14. The dotted line shows the G-value of the 2,5-dimethylphenol produced through the ionic process (Eq. X).

The Phenol and Cresol Formations in the Reactions of Oxygen Atoms with Benzene and Toluene. In the above calculation, we assumed $a=0.0$ in the cases of benzene and toluene. In order to estimate the real values, we have investigated the phenol and cresol formations at a high electron fraction of dinitrogen oxide ($\varepsilon=0.92$), where the oxygen atoms produced from the direct radiolysis of dinitrogen oxide are important as the source of phenol formation. The results are shown in Fig. 15. The dotted lines are the G-values of the products formed through the ionic process, which have been calculated by using Eq. X.

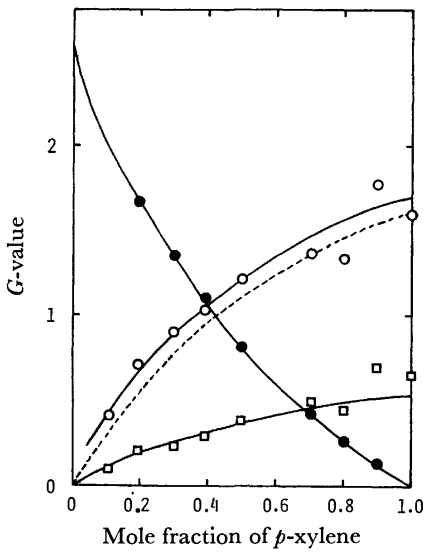

Fig. 14. The G-values of addition products from the benzene–*p*-xylene system in the presence of dinitrogen oxide ($\varepsilon=0.1$).
○, 2,5-Dimethylphenol; □, *p*-methylbenzyl alcohol; ●, phenol. Solid lines are theoretical. The dotted line is the G-value of 2,5-dimethylphenol produced through ionic process.

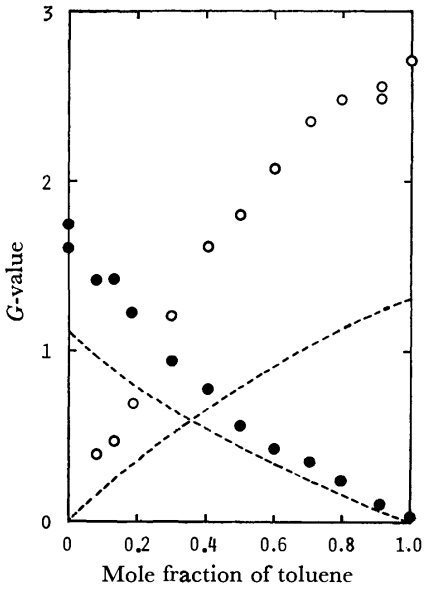

Fig. 15. The G-values of addition products from the benzene–toluene–N_2O system ($\varepsilon=0.92$).
○, The sum of cresols and benzyl alcohol; ●, phenol. Dotted lines are the G-values of each product formed through ionic process.

The difference in G-value between experiment and calculation is plotted in Fig. 16 by using the "weighted-mole-fraction" procedure. From this figure, we can estimate $a=0.17$ ($=0.52/(3.3\times0.92)$) for benzene and 0.36 ($=1.1/(3.3\times0.92)$) for toluene, and also

$$k(\mathrm{O}+\text{toluene})/k(\mathrm{O}+\text{benzene}) = 2.0.$$

Here, k is the rate constant of each reaction. Moreover, we can observe the intercept of G(phenol) at [benzene]=

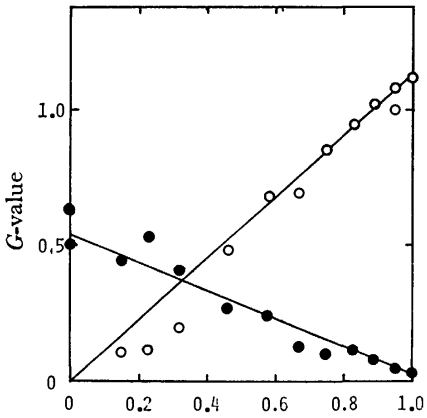

Fig. 16. The *G*-values of addition products formed in the reaction of oxygen atoms in the benzene–toluene–N_2O system (ε=0.92) as functions of the weighted mole fraction of toluene. ○, The sum of cresols; ●, phenol.

0, which suggests that a small amount of phenol is formed in the reaction of oxygen atoms with toluene. The *G*-value is calculated to be 0.03. This type of reaction has already been discussed by Sakurai *et al.*[8]

The Calculations of G(phenol)'s from the Toluene–1-Butene–N_2O System and of the G-values of the Addition Products from the Benzene–1,3,5-Trimethylbenzene–N_2O System. We now have all of the parameters necessary to calculate the *G*-values of the addition products shown in Figs. 3 and 5 by using Eq. XXIII, except for the rate-constant ratio, $k(N_2O^- + \text{1-butene})/k(N_2O^- + \text{toluene})$. For this ratio, we assumed 2.5 so as to explain the experimental data. The calculated results are shown in Figs. 3 and 5 as solid lines: the figures suggest that all the data are now explainable by the reaction mechanism proposed.

Although all the data shown in the present paper can be explained by the proposed reaction mechanism, this does not necessarily mean that such reactions as Reactions 19 and 20 are real reactions occurring in the system for the formation of the corresponding phenols. There might be another interpretation. In order to establish these reactions, we have to observe AO^- and AO_2^- ions directly, or, we have to investigate similar reactions with other aromatic compounds containing different substituents.

References

1) L. Wojnarovits, S. Hirokami, and S. Sato, *Bull. Chem. Soc. Jpn.*, **49**, 2956 (1976).
2) A. Hori, S. Takamuku, and H. Sakurai, *J. Chem. Soc., Chem. Commun.*, **1976**, 686.
3) A. Hori, S. Takamuku, and H. Sakurai, *J. Org. Chem.*, **42**, 2318 (1977).
4) H. Karasawa, T. Sasamoto, R. Yugeta, and S. Sato, *Bull. Chem. Soc. Jpn.*, **52**, 902 (1979).
5) S. Hirokami, L. Wojnarovits, and S. Sato, *Bull. Chem. Soc. Jpn.*, **52**, 299 (1979).
6) S. Sato, K. Hosoya, S. Shishido, and S. Hirokami, *Bull. Chem. Soc. Jpn.*, **45**, 2308 (1972).
7) K. Ishizaki and S. Sato, *Chem. Lett.*, **1975**, 123.
8) A. Hori, H. Matsumoto, S. Takamuku, and H. Sakurai, *J. Chem. Soc., Chem. Commun.*, **1978**, 16.
9) A. Hori, H. Matsumoto, S. Takamuku, and H. Sakurai, *Chem. Lett.*, **1978**, 467.
10) S. Goto, A. Hori, S. Takamuku, and H. Sakurai, *Bull. Chem. Soc. Jpn.*, **51**, 1569 (1978).
11) S. Hirokami, S. Shishido, and S. Sato, *Bull. Chem. Soc. Jpn.*, **44**, 1511 (1971).
12) R. J. Cvetanović, *Adv. Photochem.*, **1**, 115 (1962).
13) R. Atkinson and R. J. Cvetanović, *J. Chem. Phys.*, **55**, 659 (1971).
14) R. Atkinson and J. N. Pitts, Jr., *J. Phys. Chem.*, **79**, 295 (1975).
15) R. Atkinson and J. N. Pitts, Jr., *J. Chem. Phys.*, **67**, 38 (1977).
16) S. Sato, R. Yugeta, K. Shinsaka, and T. Terao, *Bull. Chem. Soc. Jpn.*, **39**, 156 (1966).
17) J. M. Warman, K. D. Asmus, and R. H. Schuler, *Adv. Chem. Ser.*, **82**, 25 (1968).
18) Y. Hatano, K. Takeuchi, and S. Takao, *J. Phys. Chem.*, **77**, 586 (1973).
19) G. R. Freeman and T. E. M. Sambrook, *J. Phys. Chem.*, **78**, 102 (1974).
20) E. Grovenstein, Jr., and A. J. Mosher, *J. Am. Chem. Soc.*, **92**, 3810 (1970).
21) G. Boocock and R. J. Cvetanović, *Can. J. Chem.*, **39**, 2436 (1961).
22) G. R. H. Jones and R. J. Cvetanović, *Can. J. Chem.*, **39**, 2444 (1961).
23) S. Sato and T. Oka, *Bull. Chem. Soc. Jpn.*, **44**, 856 (1971).
24) S. J. Rzad, P. P. Infelta, J. M. Warman, and R. H. Schuler, *J. Chem. Phys.*, **52**, 3971 (1970).
25) A. Hummel, *J. Chem. Phys.*, **49**, 4840 (1968).
26) H. Karasawa, E. R. Kim, and S. Sato, *Bull. Chem. Soc. Jpn.*, **50**, 1670 (1977).
27) M. Tachiya, *J. Chem. Phys.*, **70**, 4701 (1979).
28) Y. Moro-oka, P. J. Chung, H. Arakawa, and T. Ikawa, *Chem. Lett.*, **1976**, 1293.
29) S. Sato and S. Satoh, "Organic Scintillators and Liquid Scintillation Counting," ed by D. L. Horrocks and C. T. Peng, Academic Press (1971), p. 371.
30) The accurate expressions for G_{fl} (N_2) and G_{fl} (phenol) can be derived as follows:

$$G_{fl}(N_2) = \frac{1}{\sqrt{k_n D W}}\left\{2k_s[N_2O] + k_a[C_6H_6] + \frac{k_a k_b[N_2O][C_6H_6]}{k_b[N_2O] + \sqrt{k_n D/W}} + \sqrt{k_n D/W}\right\} \left\{1 + \frac{k_s[N_2O]}{\sqrt{k_n D/W}} + \frac{k_a[C_6H_6]}{k_b[N_2O] + \sqrt{k_n D/W}} \times \left(1 + \frac{k_b[N_2O]}{\sqrt{k_n D/W}}\right)\right\}^{-1}$$

$$G_{fl}(P) = \frac{1}{W}\left\{a + \frac{k_a[C_6H_6]}{k_b[N_2O] + \sqrt{k_n D/W}}\left(b + \frac{ck_b[N_2O]}{\sqrt{k_n D/W}}\right)\right\} \left\{1 + \frac{k_s[N_2O]}{\sqrt{k_n D/W}} + \frac{k_a[C_6H_6]}{k_b[N_2O] + \sqrt{k_n D/W}} \times \left(1 + \frac{k_b[N_2O]}{\sqrt{k_n D/W}}\right)\right\}^{-1}.$$

Here, k_n stands for the rate constant of the neutralization reaction between $C_6H_6^+$ ions and negative ions; *i.e.*, we assumed here $k_n = k_{22} = k_{23} = k_{24} = k_{25}$. D is the dose rate, and $W = 100/G_{fl}$; *cf.* K. Okazaki, R. Yugeta, and S. Sato, *Bull. Chem. Soc. Jpn.*, **46**, 2066 (1973).
31) C. Capellos and A. O. Allen, *J. Phys. Chem.*, **74**, 840 (1970).
32) A. Kira and J. K. Thomas, *J. Phys. Chem.*, **78**, 2094 (1974).
33) R. R. Hentz and W. V. Sherman, *J. Phys. Chem.*, **73**, 2676 (1969).

 © 1980 The Chemical Society of Japan Bull. Chem. Soc. Jpn., 53, 1489—1492 (1980)

An ESR Study of the Interaction of Copper(II) Octaethylporphyrin with π Acceptors

Hiroshi Yokoi* and Masamoto Iwaizumi

Chemical Research Institute of Non-aqueous Solutions, Tohoku University, Katahira, Sendai 980

(Received May 17, 1979)

The π-π interaction of octaethylporphyrincopper(II) (Cu(OEP)) with π acceptors has been investigated in solution and in magnetically-diluted crystals by ESR, and the perpendicular components of the ESR parameters for Cu(OEP) in various states have also been determined with considerable accuracy. It has been revealed that, upon the formation of charge-transfer complexes between Cu(OEP) and π acceptors, the g values decrease slightly, the copper hyperfine coupling constants remain almost unchanged, and the absolute values of the nitrogen superhyperfine coupling constants increase slightly. Accompanying changes in the electronic structure around the copper ion have been discussed. The ESR parameters of Cu(OEP) doped in Ni(OEP) have been noted to depend significantly upon the polymorphism of the diluent.

The dimerization and/or aggregation of planar metal complexes with π-ligands are phenomena in which the π-π interaction between the metal complexes plays an important role.[1-5] The π-π interaction of metal complexes with π acceptors or donors, which results in the formation of charge-transfer (CT) complexes in some cases, is also a subject of study aimed at elucidating the electron-transfer mechanisms, both in co-ordination chemistry and in biochemistry.[6,7] The CT complexes between metal porphyrins and various π acceptors are the best studied group.[8-10] Little work, however, has been done to investigate how the electronic structure of the metal complexes changes in the CT complexes. In the present work, such an attempt for a copper(II) porphyrin has been made by means of the ESR method.

In ESR studies of copper(II) porphyrins, we must know that it is not easy to determine precisely the perpendicular components of copper ESR parameters from the ESR spectra of frozen solutions and magnetically-diluted polycrystals. The usual computer-simulation method is not always useful for this purpose, since none of the simulated spectra thus far obtained for the systems have been fitted to the observed ones with any considerable accuracy.[11-14] This situation can further be understood from the fact that the $g_\perp$ and $|A_\perp|$ values previously reported for the copper(II) complexes of porphyrins and phthalocyanine are randomly distributed over the wide ranges of 2.031—2.072 and 0—54×10^{-4} cm^{-1} respectively.[11-18] In this work, those parameter values of octaethylporphyrincopper(II) in various states have been estimated on reasonable grounds.

Experimental

Materials. Octaethylporphyrin (abbreviated as $OEPH_2$) was obtained from the Stern Chemical Co., and its Cu(II) and Ni(II) complexes (Cu(OEP) and Ni(OEP) respectively) were prepared and purified according to the literature.[19] 1,3,5-Trinitrobenzene (TNB), 2,4,7-trinitrofluoren-9-one (TNF), piperidine (pip), and toluene were purchased from the Tokyo Kasei Co. and were purified by the standard literature methods. Doped samples were obtained by crystallization from 200: 1 mixtures of the diamagnetic matrix substance and the substituent one in dichloromethane and in *N*,*N*-dimethylformamide (DMF). The 1: 1 CT complexes of M(OEP)·TNF and $OEPH_2$·TNF were deposited as black needles immediately after the addition of an equimolar TNF to the dichloromethane solutions of M(OEP) and $OEPH_2$; the CT complexes were confirmed by elemental analyses. The sample of Cu(OEP) doped in Ni(OEP) will hereinafter be abbreviated as Cu/Ni(OEP); similar abbreviations will also be used for the other doped samples.

Physical Measurements. The ESR spectra at room temperature for both polycrystalline and solution samples and at 77 K for frozen solutions were recorded on a Varian E-4 X-band ESR spectrometer, the field strength being calibrated with an NMR probe and then with bis(2,4-pentanedionato)oxovanadium(IV) in benzene. The visible absorption spectra at room temperature were recorded on a Cary 14 spectrophotometer.

Results

The ESR spectrum of Cu(OEP) in toluene at 77 K is shown in Fig. 1(A). The undulation of the base-line, on which the monomer spectrum is superimposed, indicates the co-existence of triplet-state dimers; this was further evidenced by the half-field spectrum clearly observed around 1550 G.† The dimerization and/or polymerization of metal porphyrins in solution have been extensively studied by ESR[12,13,20-22] and by the other methods.[3-5] Their dimerization ability itself suggests that their molecules have the property

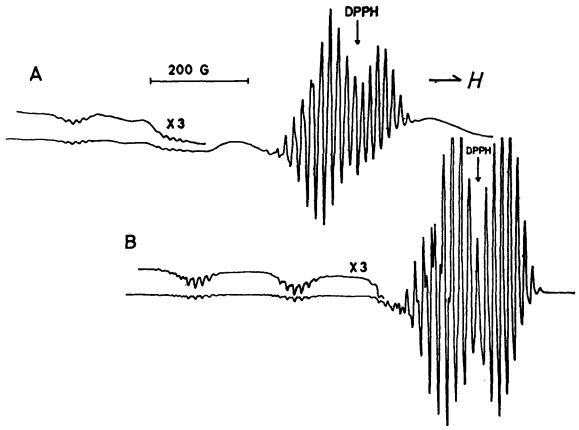

Fig. 1. X-Band ESR spectra of Cu(OEP) in toluene at 77 K.
(A) Without and (B) with an excess of TNB ([TNB]/[Cu(OEP)]=30).

† 1 G=10^{-4} T.

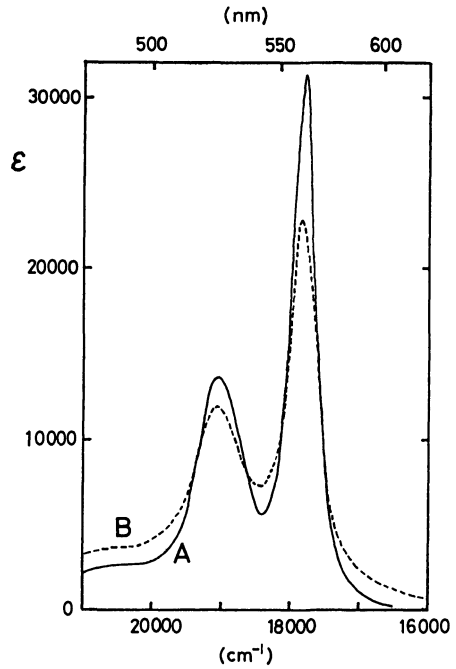

Fig. 2. Visible absorption spectra of Cu(OEP) in toluene at room temperature.
(A) and (B) correspond to those in Fig. 1 respectively.

of interacting readily with other π-systems. The frozen solution ESR spectrum of Cu(OEP) in toluene with excess TNB is shown in Fig. 1(B). This spectrum, in which dimer ESR signals disappear completely, is comparatively sharp in every absorption line. On the other hand, the visible absorption spectra of Cu(OEP) in toluene with and without excess TNB are as shown in Fig. 2. The spectral change on the addition of excess TNB is quite similar to that in the case of Co(OEP),[8] in which the 1:1 CT complex formation of Co(OEP)·TNB has been confirmed.

The ESR parameters determined directly and definitely from such ESR spectra as are shown in Fig. 1 number only three or four, $g_{//}$, $|A_{//}|$, $|A_{\perp}^{N}|$, and, possibly, $|A_{//}^{N}|$.[22] As has already been mentioned, the exact determination of the perpendicular components of g and A is not easy at present. Toluene is generally considered as an inert or non-co-ordinating solvent, and Cu(OEP) is a very stable square-planar complex with strong co-ordination bondings. In such a case, the relations of $g_0=(g_{//}+2g_{\perp})/3$ and $A_0=(A_{//}+2A_{\perp})/3$ hold well, where g_0 and A_0 are the parameters derived from fluid-solution ESR spectra and where the other parameters are those from their frozen-solution ESR spectra.[24] In Fig. 3, the observed ESR spectrum of Cu(OEP) in toluene at room temperature is shown, together with the simulated one, in which isotope effects due to the natural occurrence of ^{63}Cu and ^{65}Cu, a second-order correction of the resonance fields, and Lorentzian line shapes with M_I-dependent linewidths are taken into consideration.[25] The same simulation was done for the toluene solution of Cu(OEP) and excess TNB. The $g_{\perp}$ and $|A_{\perp}|$ values of both spectra shown in Fig. 1 were thus determined with a certain degree of reliability. The $g_{\perp}$ and $|A_{\perp}|$ values of the other frozen-solution type of spectra were obtained by a direct comparison between their spectra and the spectra shown in Fig. 1 in the perpendicular region. Some representative polycry-

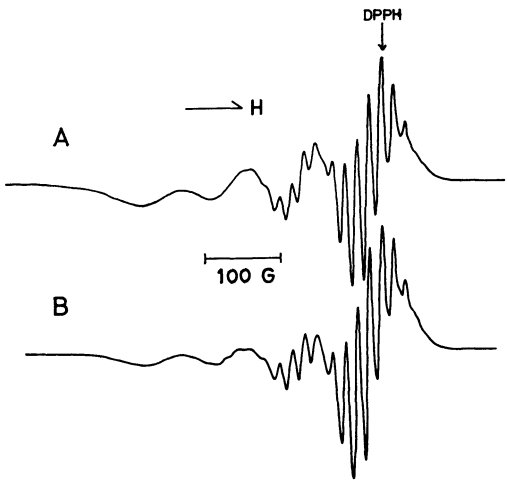

Fig. 3. X-Band ESR spectra of Cu(OPE) in toluene at room temperature.
(A), Observed; (B), simulated with $g_0=2.094$, $|A_0|=86.4$ G, $|A^N{}_0|=16.0$ G, and 3.5, 5.2, 6.9, and 8.7 G for the line widths of $M_I=3/2$, 1/2, $-1/2$, and $-3/2$ lines, respectively.

Table 1. ESR parameters[a] for Cu(OEP) in various states

Complex	Solvent or matrix	$g_{//}$	$g_{\perp}$	g_0	$10^3\|A_{//}\|$	$10^3\|A_{\perp}\|$	$10^3\|A_0\|$	$10^3\|A_{\perp}^{N}\|$ (cm^{-1})	$10^3\|A_{//}^{N}\|$	$10^3\|A_0^{N}\|$
Cu(OEP)	Toluene	2.187	2.047	2.094	20.4	2.4	8.4	1.45	1.83	1.57
Cu(OEP)·TNB	Toluene	2.181	2.045	2.092	20.4	2.5	8.5	1.46	1.85	1.58
Cu(OEP)·pip	Toluene	2.215	2.058		18.9			1.37	1.68	
Cu(OEP)	$OEPH_2$	2.190	2.048		19.8	2.3		1.43	1.70	
Cu(OEP)·TNF	$OEPH_2$·TNF	2.186	2.047		19.9	2.4		1.44	1.71	
Cu(OEP)[b]	Ni(OEP) (I)	2.190	2.049		19.9	2.3		1.46	1.75	
	Ni(OEP) (II)	2.175	2.044		20.2	2.5		1.49	1.75	
Cu(OEP)·TNF	Ni(OEP)·TNF	2.186	2.047		20.0	2.4		1.47	1.76	

a) All the values of copper hyperfine are given for ^{63}Cu. The estimated errors are ±0.001 for g, $\pm0.1\times10^{-3}$ cm^{-1} for A, and $\pm0.01\times10^{-3}$ cm^{-1} for A^N, but the respective relative errors among related complexes cited for comparison are less. All the A^N values were determined from partially enlarged spectra. b) (I), Crystallized from DMF; (II), crystallized from dichloromethane. All the other crystalline complexes were obtained by crystallization from dichloromethane.

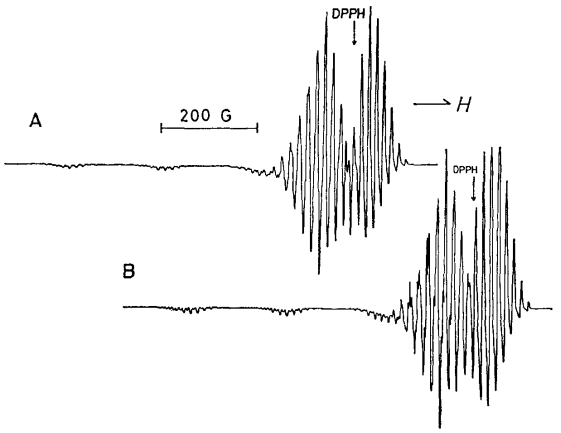

Fig. 4. X-Band polycrystalline powder ESR spectra of (A) Cu(OEP)/$OEPH_2$ and (B) Cu(OEP)·TNF/$OEPH_2$·TNF at room temperature.

stalline ESR spectra are shown in Fig. 4, just for information. All the ESR data thus determined are summarized in Table 1. The $g_\perp$ and $|A_\perp|$ values listed in the table agree well with those recently reported for copper(II) ^{15}N-etioporphyrin I in the free base.[18] This confirms the values in Table 1 to be reliable.

Discussion

Piperidine, which is a basic and saturated molecule with a nitrogen lone-pair, can co-ordinate apically to copper(II) porphyrins to form square-pyramidal five-co-ordinate complexes.[26] The ESR parameters change remarkably on the addition of piperidine to the toluene solution of Cu(OEP), as is shown in Table 1; the g and $|A|$ values remarkably increase and decrease respectively. These types of ESR changes for planar copper(II) complexes are generally caused by a change in the state of apical co-ordination.[27-29]

On the other hand, on the addition of an excess of TNB to the toluene solution of Cu(OEP), the ESR parameters changed, too, but in a different way; the g values decreased slightly, the $A_{//}$ value remained almost unchanged, and the $|A^N|$ values increased slightly. These facts show that piperidine and TNB have quite different types of interaction with Cu(OEP). A closer inspection of the table indicates that there are similar ESR changes in the crystalline states, too. In the case of Cu/Ni(OEP), however, (I) rather than (II) is adopted for comparison; this point will be discussed later. The same kind of ESR results for another complex in crystals can be found in the literature:[30] $g_{//}=2.212$, 2.206, and 2.206, and $10^3|A_{//}|=$ 19.98, 19.91, and 20.15 (cm^{-1}), for $Cu/PdOx_2$, $Cu/PdOx_2$·2TCNE, and $Cu/PdOx_2$·TCNQ respectively, where Ox, TCNE, and TCNQ are the abbreviations of 8-quinolinate, tetracyanoethylene, and 7,7,8,8-tetracyanoquinodimethane respectively. These data, however, have been discussed only from the point of view of a general understanding of host-lattice effects.

As to the host-lattice effects, it is interestingly found in Table 1 that the polycrystals of Cu/Ni(OEP) obtained by crystallization from DMF, (I), are remarkably different in ESR parameters from those crystallized from dichloromethane, (II). The difference is not the kind of difference which can be explained in terms of a change in the state of apical co-ordination. Ni(OEP) is well known to display polymorphism.[31,32] Two crystalline modifications with known X-ray analytical data have quite different molecular geometries and packings, although the complex is naturally very stable. Judging from the essence of polymorphism, however, the difference in energy between the crystalline modifications must not be large. The above-mentioned ESR result of Cu/Ni(OEP) shows that molecular-environmental effects due to polymorphism are sensitively reflected in the ESR parameters. It is noteworhy that the structure and properties of metal porphyrins depend to a marked extent on their molecular environment, and this seems to be of especial significance in view of the functional diversity of the complexes in biological systems. In Table 1, Cu(OEP)/$OEPH_2$ and (I) in Cu/Ni(OEP) have almost the same ESR parameters. This fact suggests that they are crystallographically similar, although the solvents of crystallization are different. In this study, accordingly, (I) in Cu/Ni(OEP), rather than (II), was adopted to compare with Cu/Ni(OEP)·TNF.

On the whole, it may be concluded that, when Cu(OEP) interacts with π acceptors, the g values decrease slightly and the $A_{//}$ value remains almost unchanged. In an axial molecular field, the σ antibonding wavefunction is:[33,34]

$$\psi_\sigma = \alpha d_{x^2-y^2} - (\alpha'/2)(\sigma_1-\sigma_2+\sigma_3-\sigma_4)$$
$$\alpha^2 + \alpha'^2 - 2\alpha\alpha' S = 1$$

where σ_i expresses the ith nitrogen lone-pair orbital and where the other symbols have their usual meanings. The bonding parameter, α, is a measure of the covalency of the in-plane σ bonding. To calculate α^2, an approximate formula based on the copper hyperfine term, $A_{//}$, can be used:[35]

$$\alpha^2 = -(A_{//}/P) + (g_{//}-2) + (3/7)(g_\perp-2) + C$$

where C is a small constant and where $P=2\gamma\beta_0\beta_n$ $\langle r^{-3}\rangle=0.0360$ cm^{-1}. According to this equation, the ESR changes mentioned above obviously lead to a slight decrease in value of α^2. The decrements ($\Delta\alpha^2$) are calculated to be -0.003——-0.008, meaning that the σ bonding becomes a little more covalent when Cu(OEP) interacts with π acceptors. This result is also supported by the experimental fact that both $|A^N_\perp|$ and $|A^N_{//}|$ values simultaneously increase slightly, as is shown in Table 1. The increments of $|A^N|$ are of a reasonable order of magnitude, in view of the relations of $\Delta\alpha'^2 \simeq -\Delta\alpha^2$ and the rough proportionality between $\Delta\alpha'^2$ and $\Delta|A^N|$.[34] This suggests that either of two changes in the electronic structure of Cu(OEP) may take place on the formation of its CT π-complexes. One of the changes is that the π-electron density at the four co-ordinating nitrogen atoms slightly increases in order for the σ co-ordination bonding to become a little more covalent.[24] The other change is that the electronic charge on the central copper atom increases slightly relatively in the CT complexes, so that the copper $d_{x^2-y^2}$ orbital level is lowered and, accordingly, the

orbital becomes easier to be mixed with the ligand σ orbitals.[36,37] These considerations do not seem unreasonable, since a small change in the distribution of π-electrons over the whole Cu(OEP) molecule must actually take place on the formation of its CT π-complexes. Further work will, however, be required to find a solution to this problem.

It is interesting to consider the differences between (I) and (II) in Cu/Ni(OEP) in Table 1, for instance, as to the value of α^2. If we assume $\alpha^2=0.803$ for (I),[25] the α^2 value of (II) can be calculated to be 0.794 from the above-described equation of α^2. This change in α^2, which is a host-lattice effect, is large compared with that in the CT complexes. This fact shows the importance of lattice effects or molecular environmental effects on the properties of metal prophyrins.

References

1) H. Yokoi and M. Chikira, *J. Chem. Soc., Dalton Trans.*, **1975**, 2101; M. Chikira and H. Yokoi, *ibid.*, **1977**, 2344; H. Yokoi and M. Chikira, *J. Am. Chem. Soc.*, **97**, 3975 (1975); M. Chikira, H. Yokoi, and T. Isobe, *Bull. Chem. Soc. Jpn.*, **47**, 2208 (1974); M. Chikira and T. Isobe, *ibid.*, **48**, 2052 (1975); H. Yokoi, Proceedings of III Intern. Symp. on Specific Interactions between Molecules or Ions, Poland (1976), p. 582.

2) T. D. Smith and J. R. Pilbrow, *Coord. Chem. Rev.*, **13**, 173 (1973), and the references cited therein.

3) R. J. Abraham, F. Eivazi, H. Pearson, and K. M. Smith, *J. Chem. Soc., Chem. Commun.*, **1976**, 698, 699.

4) K. A. Zachariasse and D. G. Whitten, *Chem. Phys. Lett.*, **22**, 527 (1973); R. J. Abraham, G. H. Barnett, G. E. Hawkes, and K. M. Smith, *Tetrahedron*, **32**, 2949 (1976).

5) R. F. Pasternack, L. Francesconi, D. Raff, and E. Spiro, *Inorg. Chem.*, **12**, 2606 (1973); R. R. Das, *J. Inorg. Nucl. Chem.*, **37**, 153 (1975).

6) R. J. P. Williams, "The Biochemistry of Copper," ed by J. Peisach, P. Aisen, and W. E. Blumberg, Academic Press, New York (1966), p. 131; M. Calvin, *J. Theoret. Biol.*, **1**, 258 (1961).

7) J. G. Heathcote, G. J. Hill, P. Rothwell, and M. A. Slifkin, *Biochim. Biophys. Acta*, **153**, 13 (1968).

8) H. A. Hill, A. J. Macfarlane, and R. J. P. Williams, *J. Chem. Soc., Chem. Commun.*, **1967**, 905.

9) H. A. O. Hill, P. J. Sadler, and R. J. P. Williams, *J. Chem. Soc., Dalton Trans.*, **1973**, 1663; C. D. Barry, H. A. O. Hill, P. J. Sadler, and R. J. P. Williams, *Proc. R. Soc. London, Ser. A*, **334**, 493 (1973); C. D. Barry, H. A. O. Hill, B. E. Mann, P. J. Sadler, and R. J. P. Williams, *J. Am. Chem. Soc.*, **95**, 4545 (1973).

10) G. P. Fulton and G. N. La Mar, *J. Am. Chem. Soc.*, **98**, 2119, 2124 (1976).

11) P. W. Lau and W. C. Lin, *J. Inorg. Nucl. Chem.*, **37**, 2389 (1975), and the references cited therein.

12) J. A. De Bolfo, T. D. Smith, J. F. Boas, and J. R. Pilbrow, *J. Chem. Soc., Dalton Trans.*, **1975**, 1523.

13) M. C. Findlay, L. C. Dickinson, and J. C. W. Chien, *J. Am. Chem. Soc.*, **99**, 5168 (1977).

14) In most simulation programs so far employed, the effects of the quadrupole interaction and second-order effects of the strong super-hyperfine interaction due to the four nitrogen nuclei have not been taken into consideration explicitly. Besides, there still seems to be much room for a re-consideration of the transition probability, the linewidth, and the convolution function. The simulated spectra in the perpendicular region may change remarkably according to how every problem mentioned above is settled.

15) A. Abkowitz, I. Chen, and J. H. Sharp, *J. Chem. Phys.*, **48**, 4561 (1968); I. Chen, M. Abkowitz, and J. H. Sharp, *ibid.*, **50**, 2237 (1969); A. MacCragh, C. B. Storm, and W. S. Koski, *J. Am. Chem. Soc.*, **87**, 1470 (1965).

16) J. Bohandy and B. F. Kim, *J. Magn. Reson.*, **26**, 341 (1977); J. Subramaian, J. H. Fuhrhop, A. Salek, and A. Gossauer, *ibid.*, **15**, 19 (1974).

17) T. G. Brown, J. L. Petersen, G. P. Lozos, J. R. Andersen, and B. M. Hoffman, *Inorg. Chem.*, **16**, 1563 (1977).

18) M. Momenteau, J. Mispelter, B. Loock, and J. M. Lhoste, *Can. J. Chem.*, **56**, 2598 (1978).

19) A. D. Adler, F. R. Longo, F. Kampas, and J. Kim, *J. Inorg. Nucl. Chem.*, **32**, 2443 (1969).

20) W. E. Blumberg and J. Peisach, *J. Biol. Chem.*, **240**, 870 (1965).

21) J. F. Boas, J. R. Pilbrow, and T. D. Smith, *J. Chem. Soc., A*, **1969**, 721; P. D. W. Boyd, T. D. Smith, J. H. Price, and J. R. Pilbrow, *J. Chem. Phys.*, **56**, 1253 (1972).

22) The spin Hamiltonian for the present systems is as follows:

$$\begin{aligned}\mathcal{H} = {} & \beta_0[{}''gH_zS_z + g_\perp(H_xS_x + H_yS_y)] + A_{//}S_zI_z \\ & + A_\perp(S_xI_x + S_yI_y) + S_x[A^N_{//}(I_{1x}+I_{3x}) + A^N_\perp(I_{2x}+I_{4x})] \\ & + S_y[A^N_\perp(I_{1x}+I_{3x}) + A^N_{//}(I_{2y}+I_{4y})] \\ & + S_z[A^N_\perp(I_{1z}+I_{2z}+I_{3z}+I_{4z})]\end{aligned}$$

where the four ligand nitrogen atoms on the xy plane are numbered 1 to 4.

23) M. Chikira, H. Kon, R. A. Hawley, and K. M. Smith, *J. Chem. Soc., Dalton Trans.*, **1979**, 245.

24) H. Yokoi, *Inorg. Chem.*, **17**, 538 (1978).

25) H. Yokoi and A. W. Addison, *Inorg. Chem.*, **16**, 1341 (1977).

26) E. W. Baker, M. S. Brookhart, and A. H. Corwin, *J. Am. Chem. Soc.*, **86**, 4587 (1964).

27) A. Astonik, N. M. D. Brown, A. A. McConnell, and A. L. Porte, *J. Chem. Soc., A*, **1969**, 545.

28) H. Yokoi, M. Sai, and T. Isobe, *Bull. Chem. Soc. Jpn.*, **43**, 1078 (1970).

29) J. I. Zink and R. S. Drago, *J. Am. Chem. Soc.*, **94**, 4550 (1972).

30) J. Ammeter, G. Rist, and H. H. Gunthard, *J. Chem. Phys.*, **57**, 3852 (1972).

31) E. F. Meyer, Jr., *Acta Crystallogr., Sect. B*, **28**, 2162 (1972).

32) D. L. Cullen and E. F. Meyer, Jr., *J. Am. Chem. Soc.*, **96**, 2095 (1974).

33) A. H. Maki and B. R. McGarvey, *J. Chem. Phys.*, **29**, 31, 35 (1958).

34) B. R. McGarvey, "Transition Metal Chemistry," ed by R. L. Carlin, Marcel Dekker, New York (1967), Vol. 3, p. 89.

35) D. Kivelson and R. Neiman, *J. Chem. Phys.*, **35**, 149 (1961).

36) C. J. Ballhausen and H. B. Gray, "Molecular Orbital Theory," Benjamin, New York (1964).

37) H. Yokoi and T. Isobe, *Bull. Chem. Soc. Jpn.*, **42**, 2187 (1969).

 © 1980 The Chemical Society of Japan Bull. Chem. Soc. Jpn., 53, 1493—1500 (1980)

Calorimetric Study of the Glassy State. XV.† Thermodynamic Study of Pinacol Hexahydrate and Pinacol-d_2 Hexadeuterate

Masaharu Oguni, Takasuke Matsuo, Hiroshi Suga,* and Syûzô Seki

Department of Chemistry, Faculty of Science, Osaka University, Toyonaka, Osaka 560

(Received July 16, 1979)

The heat capacities of pinacol hexahydrate and its deuterate analogue were measured in the temperature region between 13 and 260 K. A phase transition was found and the temperature of transition was determined to be 192.14 K for the hydrate and 191.17 K for the deuterate, respectively. The enthalpy and entropy of the transition were estimated to be 924 J mol^{-1} and 5.10 J K^{-1} mol^{-1} for the hydrate and 944 J mol^{-1} and 5.28 J K^{-1} mol^{-1} for the deuterate. The transition was interpreted as the order-disorder change of the orientations of the pinacol molecule. Besides the phase transitions, an additional anomaly was found around 150 K for the hydrate and two around 130 K and around 160 K for the deuterate, respectively. All of them are relaxational in their characteristics and interpreted as glass transitions due to freezing of reorientational motions of the water molecule and the pinacol molecule. The transition temperature and the activation enthalpy for the higher glass transition of the deuterate were estimated to be 167.2 K and (34±4) kJ mol^{-1}, respectively.

The existence of pinacol (2,3-dimethyl-2,3-butane diol) hexahydrate was first shown by Fittig[1] in 1859. The structural feature of the hydrate is that the crystal at room temperature involves two kinds of orientational disorder. X-Ray diffraction study by Kim and Jeffrey[2] revealed that the crystal has a three-dimensional hydrogen-bonded network composed of layers of water molecules and hydroxyl groups of the pinacol molecules. The diol molecules are entrapped in the voids in this framework with two-fold orientational disorder. Thus, the crystal is clathrate-like but not a genuine clathrate because the hydroxyl groups of the alcohol are incorporated in the host lattice.

The dielectric constants of the crystal were measured by Cook and Meakins[3] in the temperature range 240—290 K, and by Garrington and Williams,[4] who observed high values of ε'_0 exceeding 50. On the basis of the systematic measurements on partially dehydrated samples, they showed that the large value of ε'_0 is due to reorientational motions of the water molecules. It is noted in their work that the behaviour of dielectric dispersion and absorption is closely related to that in hexagonal ice crystal. Thus both the pinacol and the water molecules are in orientationally disordered states.

The present paper reports calorimetric studies on pinacol hexahydrate and its deuterate analogue and discusses the observed heat-capacity anomalies in terms of ordering and freezing of the different molecular disorders. This study was undertaken as an extension of the calorimetric investigation on the relaxational heat capacity anomalies observed in stable crystals,[5] including $SnCl_2 \cdot 2H_2O$, $SnCl_2 \cdot 2D_2O$,[6] H_2O,[7] D_2O,[8] H_3BO_3 and D_3BO_3.[9] A study on phase diagram of water-pinacol system is also reported.

Experimental

Pinacol (Aldrich Chem. Co.) was purified by vacuum-distillation at 50—60 °C. The water content of the purified crystal was analysed by use of Karl-Fischer's method to be 0.36 mg cm^{-3}. This crystal was used for the phase diagram study of the pinacol-water system. The hexahydrate crystal was prepared by recrystallization of the purified pinacol from the aqueous solution. The recrystallization was repeated three times for further purification. Excess water in the hexahydrate crystal was removed by equilibrating the crystal in a desiccator with the monohydrate.

Prior to the preparation of the hexadeuterate, the hydroxyl groups of the purified pinacol were deuterated by repeating alternately three times the dissolution of anhydrous pinacol into heavy water (99.75%) and the complete dehydration of the solution by the use of molecular sieve 3A. The anhydrous pinacol thus obtained was vacuum-distilled at 50—60 °C in order to remove the trace of molecular sieve. The hexadeuterate was recrystallized from the heavy water solution of the pinacol-d_2. The deuterated crystal was kept in a desiccator with the monodeuterate as in the case of the hexahydrate. The molecular formula of the deuterate crystal was $(CH_3)_2(OD)CC(OD)(CH_3)_2 \cdot 6D_2O$, and the deuteration level was estimated to be 99.5%.

The heat capacity measurements were carried out by using the calorimetric apparatus described before.[9,10] The crystal was loaded into the calorimeter cell in a polyethylene bag where the water vapor pressure was adjusted in advance so as to prevent dehydration of the crystal. The loaded cell was cooled to liquid nitrogen temperature in a glass vessel, evacuated for twenty minutes, and filled with one-atmospheric pressure of helium gas. The cell was taken out of the vessel and tightly sealed by screwing a cap with a gold gasket. The mass of the sample was 38.970 g for the hydrate and 43.075 g for the deuterate, respectively. The inaccuracy of the heat capacity measurement is estimated to be 1% at liquid hydrogen temperature and less than 0.3% above 40 K.

Results and Discussion

Phase Equilibrium in Water–Pinacol System. The equilibrium phase diagram between water and pinacol was investigated by Pushin and Glagoleva in 1922.[11] They found existence of the stable monohydrate in addition to the hexahydrate. Their interest was concentrated on melting (and eutectic) phenomena, while ours is directed to the transitions in the crystalline state. Figure 1 shows the present results of the phase relation examined by DTA. The melting point of the hexahydrate was found to be 318.5 K, in agreement with Pushin and Glagoleva. Those of the anhydrous pinacol and of the monohydrate were higher by 1.0 K and 0.4 K respectively, than the values determined by them.

As shown in the figure, phase transitions were found

† Part XIV. Bull. Chem. Soc. Jpn., **51**, 1691 (1978). Contribution No. 3 from Chemical Thermodynamics Laboratory.

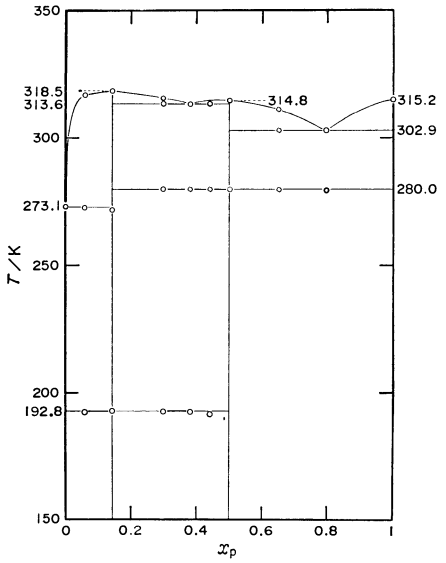

Fig. 1. Phase diagram of the system water–pinacol. x_p is the mole fraction of pinacol.

at 192.8 K and 280.0 K in the crystalline states of the hexahydrate and monohydrate, respectively. From the DTA curves the enthalpy of transition of the monohydrate was found to be larger by more than one order of magnitude than that of the hexahydrate. This is in good agreement with the observation that the room-temperature second moment[12] of the proton magnetic resonance of the monohydrate is considerably smaller than those of the hexahydrate and the anhydrous compound.

Heat Capacity. The heat capacities of the hexahydrate and the hexadeuterate were measured in the temperature region between 13 and 300 K. There appeared anomalies at 273 K and 277 K for the hydrate and the deuterate, respectively. These anomalies were interpreted as the melting of excess water contained in the crystal. Based on the assumption that this anomaly was attributed to melting of pure ice, the amount of excess water was estimated to be 127 mg for the hydrate and 69 mg for the deuterate corresponding to 0.33% and 0.16% of the sample masses,

Table 1. Molar heat capacity of pinacol hexahydrate

T_{av}/K	C_p/J K^{-1} mol^{-1}	T_{av}/K	C_p/J K^{-1} mol^{-1}	T_{av}/K	C_p/J K^{-1} mol^{-1}	T_{av}/K	C_p/J K^{-1} mol^{-1}	T_{av}/K	C_p/J K^{-1} mol^{-1}
13.07	8.458	65.76	107.6	(quenched)		(annealed)		192.37	979.7
14.09	10.01	67.49	110.8					192.57	859.6
15.11	11.59	69.22	114.0	125.98	207.9	126.35	208.6	192.86	425.9
16.14	13.21	70.97	117.2	127.93	211.0	128.83	212.5	193.29	309.8
17.20	14.95	69.73	114.9	129.89	214.2	131.31	216.2	194.21	306.0
18.28	16.77	71.50	118.2	131.78	216.9	133.75	220.1	196.06	309.1
19.39	18.81	73.32	121.4	133.61	219.7	136.16	223.9	197.90	311.2
20.58	20.82	75.15	124.7	135.45	222.7	138.57	227.8	199.72	312.5
21.83	23.13	76.95	127.9	137.31	225.3	141.00	232.4	201.54	316.1
23.01	25.39	78.76	131.1	139.18	228.2	143.43	237.2	203.37	318.3
24.23	27.75	80.55	134.4	141.03	231.1	145.87	242.7	205.22	321.0
25.51	30.19	82.34	137.5	142.87	233.6	148.27	247.3	207.16	323.3
26.75	32.68	84.14	140.7	144.68	236.7	150.62	251.3	209.27	326.3
28.07	35.20	85.95	143.8	146.47	239.4	152.95	254.8	211.45	329.1
29.58	38.18	87.76	146.9	147.73	241.5	155.25	258.5	213.62	332.2
31.19	41.36	89.60	150.1	148.54	242.7	157.52	262.1	215.76	335.2
32.74	44.48	91.45	153.1	150.08	247.7	160.43	266.4	217.90	337.9
34.29	47.58	93.26	156.2	152.23	252.1	163.31	270.7	220.01	340.7
35.85	50.64	95.07	159.2	154.34	256.0	165.22	273.4	222.77	344.5
37.46	53.85	96.96	162.3	156.42	259.5	167.30	276.8	224.85	347.4
39.08	56.91	98.89	165.5	158.48	263.3	169.38	280.2	226.92	350.1
40.65	59.98	100.84	168.5	160.52	266.4	171.46	283.6	228.97	353.2
42.27	63.10	102.79	171.8	162.54	269.2	173.56	287.3	231.01	356.0
43.93	66.29	104.73	174.9	164.49	272.6	175.68	291.0	233.04	358.7
45.58	69.44	106.67	178.0	166.52	275.4	177.77	294.9	235.07	361.4
47.23	72.69	108.61	181.2	168.51	279.1	179.85	298.8	237.05	364.0
48.87	75.81	110.54	184.3	170.52	282.2	181.90	303.1	238.80	366.5
50.47	78.91	112.48	187.1	172.57	285.3	183.93	307.2	241.02	369.8
52.11	82.03	114.42	190.3	174.59	288.7	185.93	312.2	243.39	372.8
53.78	85.28	116.34	193.1	176.50	292.9	187.88	318.0	245.75	376.3
55.45	88.41	118.25	196.2	178.49	296.3	189.42	322.9	248.09	379.3
57.12	91.55	120.18	199.0	180.40	300.2	190.34	326.9	250.42	382.7
58.80	94.70	122.10	202.3	182.29	303.9	190.90	330.2	252.72	385.6
60.51	97.98	124.04	204.3	184.16	307.9	191.35	333.7	255.02	389.1
62.27	101.23					191.80	336.8	257.29	392.3
64.04	104.49					192.15	754.1	259.55	395.6

Table 2. Molar heat capacity of pinacol hexadeuterate

T_{av}/K	C_p/J K^{-1} mol^{-1}	T_{av}/K	C_p/J K^{-1} mol^{-1}	T_{av}/K	C_p/J K^{-1} mol^{-1}	T_{av}/K	C_p/J K^{-1} mol^{-1}	T_{av}/K	C_p/J K^{-1} mol^{-1}
16.41	14.08	68.90	117.3	121.41	217.2	123.10	221.2	191.30	1263.5
17.27	15.60	70.57	120.5	123.70	221.1	125.19	225.4	191.47	997.8
18.16	17.13	70.79	120.9	125.98	225.9	127.25	229.1	191.72	517.3
19.13	18.97	72.44	124.1	128.27	229.9	129.61	233.6	192.08	354.1
20.18	20.89	74.01	127.1	130.53	234.9	131.83	237.8	192.51	341.0
21.31	23.03	75.55	129.9	132.74	239.0	134.02	242.0	192.96	340.6
22.44	25.29	77.20	133.2	134.96	243.8	136.18	246.1	193.50	341.5
23.51	27.61	78.96	136.5	137.23	247.3	138.31	249.8	194.74	342.8
24.65	29.70	80.67	139.7	139.46	251.8	140.41	253.6	196.39	345.6
25.93	32.29	82.34	143.0	141.63	255.9	142.48	257.3	198.43	348.4
27.35	35.22	83.98	146.3	143.81	259.6	144.50	261.2	200.72	352.2
28.77	38.01	85.64	149.4	146.00	264.0	146.78	265.3	203.24	355.8
30.15	40.88	87.32	152.6	148.16	267.5	148.93	269.5	205.73	359.8
31.56	43.81	88.97	155.8	150.30	271.6	151.05	273.9	208.23	363.2
33.03	46.78	90.64	158.9	152.42	275.5	153.22	279.3	210.74	367.4
34.52	49.86	92.44	162.3	154.50	279.7	155.44	284.7	213.23	371.2
36.00	52.91	94.25	165.8	156.16	281.8	157.71	289.5	215.69	374.6
37.45	55.81	95.97	169.0	157.28	284.3	159.87	294.1	218.14	378.8
38.84	58.53	97.75	172.3	158.80	289.1	162.01	297.8	220.57	382.2
40.21	61.29	99.58	175.9	160.79	294.9	164.12	301.4	222.99	385.7
41.58	64.01	101.38	179.2	162.79	299.2	166.20	304.8	225.39	389.1
43.08	66.96	103.21	182.7	164.80	301.8	168.27	308.8	227.77	392.6
44.69	70.15			166.80	306.3	170.31	312.8	230.13	396.0
46.25	73.16	(quenched)		168.78	309.5	172.67	318.2	232.47	400.0
47.87	76.40			170.73	313.4	174.58	320.8	235.15	404.0
49.51	79.60	96.54	169.7			176.48	325.2	237.47	407.0
51.12	82.70	98.19	173.3	(annealed)		178.36	329.4	239.78	411.0
52.69	85.72	99.94	176.6			180.22	333.5	242.07	413.9
54.23	88.84	101.83	180.1	105.29	186.6	182.06	338.3	244.34	417.6
55.77	91.80	103.78	183.8	106.79	189.5	183.87	342.5	246.76	421.1
57.27	94.73	105.76	187.4	108.51	192.9	185.76	347.3	249.34	424.9
58.82	97.72	107.80	191.4	110.63	196.6	187.45	353.6	251.89	429.0
60.42	100.83	109.93	195.0	112.70	200.6	188.77	358.6	254.42	432.5
62.09	104.01	112.13	199.7	114.73	204.6	189.55	362.8	256.98	436.1
63.83	107.53	114.42	204.5	116.77	208.6	190.16	367.7	259.58	440.6
65.55	110.85	116.75	208.3	118.85	212.6	190.67	372.1	262.16	444.0
67.24	114.08	119.09	212.6	120.97	217.1	191.07	604.8	264.72	447.6

respectively. The heat capacity contribution from the excess water was corrected for below 260 K by using the heat capacity data of the ice and heavy ice.[7,8] The heat capacity data are collected in Tables 1 and 2. Figure 2 gives the plots of the data together with those for the deuterate in an enlarged scale on the left side (110 K—145 K).

Both the hydrate and deuterate underwent a phase transition around 190 K as expected from the DTA result. Since the transitions are of the first order, all the measurements below the transition temperatures were made on the samples precooled slowly to 100 K in order to avoid incomplete conversion of the crystal into the low temperature phase. The temperature equilibration in the sample proceeded very slowly near the transition points, requiring a few days in the worst case. The temperature drift was followed for 12 h in most of the measurements in this region. The equilibrium temperature for the heat capacity calculation was determined by extrapolation of the temperature *vs.* time curve to the infinity of time assuming the exponential relation between them.

The heat capacity curves have additional small anomalies around 150 K for the hydrate and around 130 K and 160 K for the deuterate, respectively. The data in the anomalous regions are shown in Fig. 3 as the encraty (C_p/T) *vs.* the temperature. The equilibration time became extremely long in these regions, and either an exothermic or endothermic effect was observed depending on the thermal history of the sample. The following series of measurements was performed in order to study the hysteretic behavior in more detail. The hydrate sample was first equilibrated at 180 K and cooled with two different rates, $\simeq$8 mK min^{-1} and $\simeq$1.7 K min.$^{-1}$) The heat capacity measurement of the slowly cooled crystal was started at 125 K and continued up to 170 K by the step-by-step heating method in which the temperature increment was kept

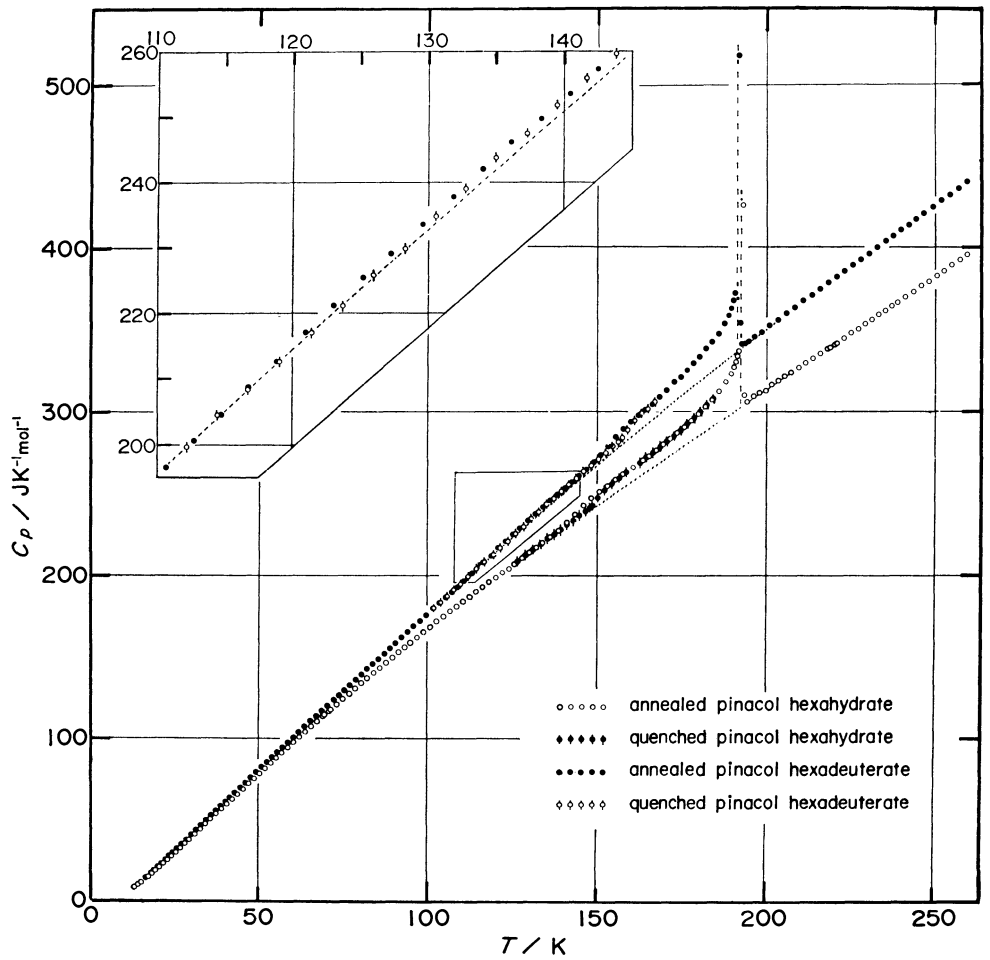

Fig. 2. Heat capacity of pinacol hexahydrate and pinacol hexadeuterate crystals.

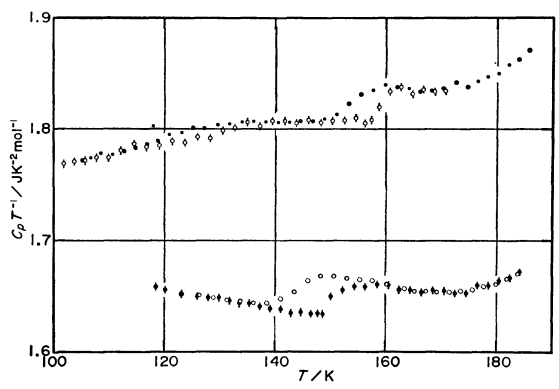

Fig. 3. Encraty (C_p/T) of pinacol hexahydrate (lower curve) and pinacol hexadeuterate (upper curve). The barred circles (⊖ and ●) represent the quenched crystal and the plain circles (○ and ●) the slowly cooled crystal.

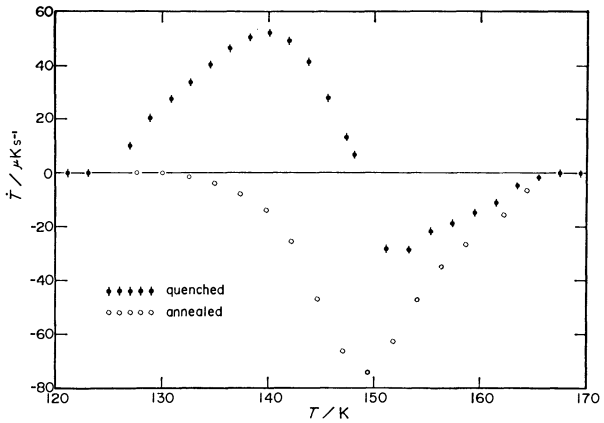

Fig. 4. Temperature drift *versus* temperature curves of pinacol hexahydrate.

approximately equal to 2 K and the drift followed for 35 min. Only endothermic drift was found in this series of measurement.

The measurement on the quenched sample was initiated at 120 K and followed the similar procedure up to 180 K. In this case the exothermic temperature drift occurred first and then an endothermic one as the temperature was raised. The former drift was followed for 40 min, and the latter for 60 min. The exothermic effect started around 125 K, reached the maximum rate at 140 K, decreased rapidly and disappeared around 149 K. The endothermic effect appeared above 149 K and remained appreciable up to 168 K, above which temperature the equilibration time

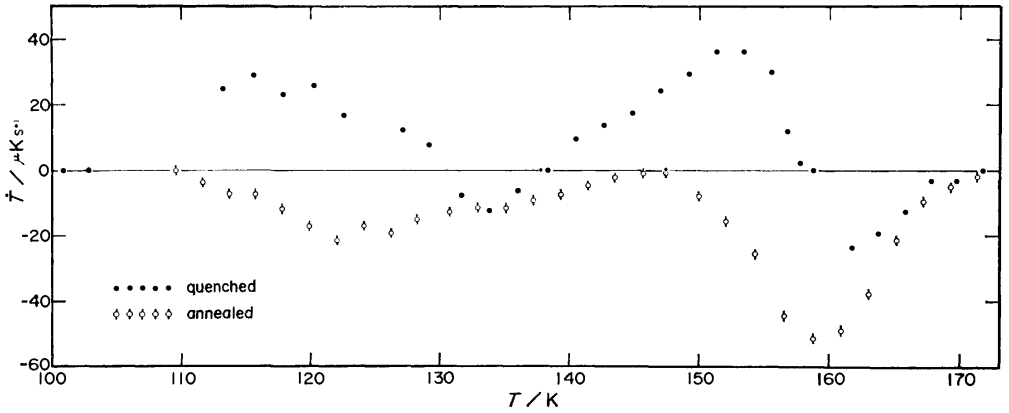

Fig. 5. Temperature drift *versus* temperature curves of pinacol hexadeuterate.

returned to its normal value. Figure 4 shows the rate of the temperature drift of the calorimeter cell determined at 30 min after turning off the heater.

For the deuterate, the temperature of the sample was equilibrated at 175 K where the equilibrium was reached rapidly, and decreased to the liquid nitrogen temperature at two different cooling rates. Measurement of the temperature drift was started at 110 K for the slowly cooled sample and at 100 K for the quenched one. The observed change of the drift rate with the temperature is shown in Fig. 5. In the case of the slowly cooled sample, only an endothermic effect was observed with two minima in the drift rate around 125 K and 160 K. In the quenched sample, positive and negative temperature drifts appeared alternately twice on heating. The drift approached the normal behavior above 170 K.

Appearance of different thermal drifts depending on the cooling rate is characteristic of a glass transition in the extended sense[5] as we have shown with tin chloride dihydrate,[6] hexagonal ice,[7,8] and orthoboric acid.[9] We interpret the relaxational anomalies in the present substances in the similar way. The main consequence of this interpretation is that a relaxational reorientation of the molecules is associated with the glass transition and that its relaxation time at the glass transition temperature is comparable with the time required for a single heat capacity measurement. The two relaxational anomalies in the deuterate crystal suggest that two different molecular processes are involved. The problem is then to assign molecular motions to the anomalies in the hydrate and deuterate and will be discussed later in this section. It should be added that there is an ambiguity in the determination of the heat capacity in the glass transition region due to irreversible changes occurring in the crystal. The values given in Tables 1 and 2 were calculated as elsewhere.[6,9]

Determination of Enthalpy and Entropy of the Transition. The anomalous part of the heat capacity was separated from the total by drawing a base-line which joins smoothly the heat capacity curves above 220 K and

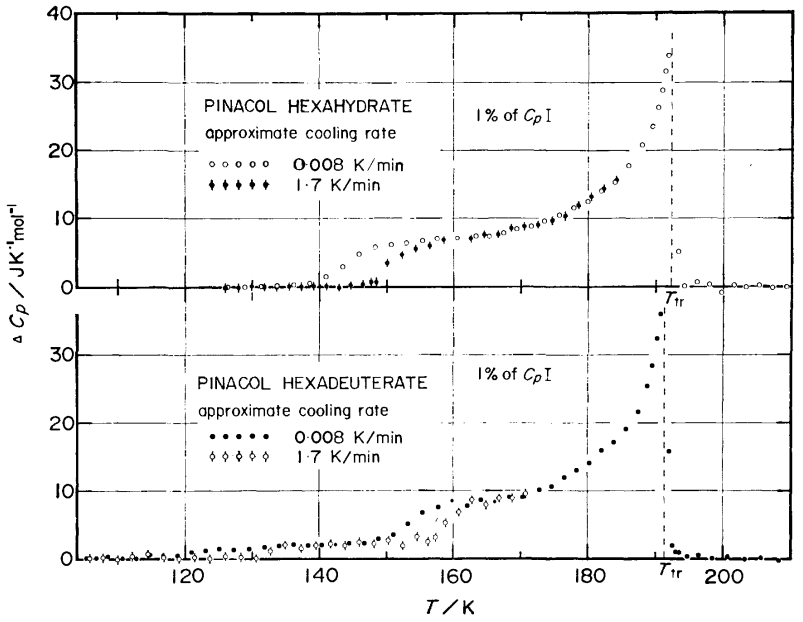

Fig. 6. Anomalous part of the heat capacity of pinacol hexahydrate and pinacol hexadeuterate.

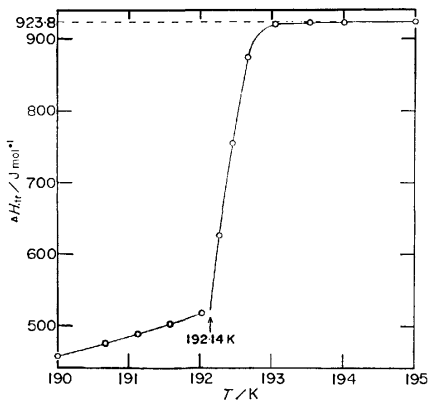

Fig. 7. Excess enthalpy *versus* temperature curve of pinacol hexahydrate.

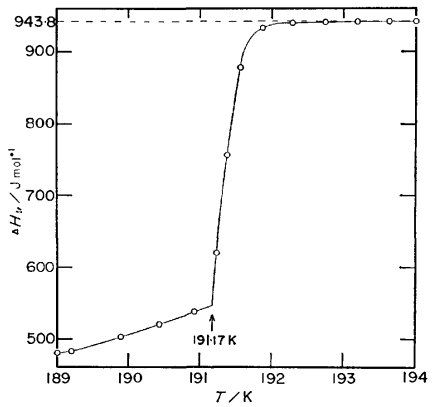

Fig. 8. Excess enthalpy *versus* temperature curve of pinacol hexadeuterate.

below the glass transition, as shown in Fig. 2. The anomalous part thus obtained is plotted in Fig. 6 where the upper half of the figure represents the hydrate and the lower the deuterate. The enthalpy and entropy of the transition were calculated by a numerical integration of the anomalous heat capacity for the slowly cooled sample and found to be 924 J mol^{-1} and 5.10 J K^{-1} mol^{-1} for the hydrate and 944 J mol^{-1} and 5.28 J K^{-1} mol^{-1} for the deuterate, respectively. The transition temperature was determined as the temperature at which the abrupt increase of the enthalpy occurred. Figures 7 and 8 show the excess enthalpy against the temperature around the transition point for the hydrate and the deuterate. The broken lines in the figures represent the total transition enthalpy. The transition temperature is 192.14 K for the hydrate and 191.17 K for the deuterate.

Mechanism of the Phase Transition and the Deuterium Isotope Effect on the Transition Temperature. In an NMR study published separately, we measured the proton spin-lattice relaxation times T_1 and $T_{1\rho}$ of the present substances.[13] The both substances showed almost the same magnitude of discontinuity in $T_{1\rho}$ at the transition temperature. This indicates that the phase transitions are closely related to the motion of the pinacol molecules rather than the water molecules. It has been shown by the X-ray study[2] at the room temperature that the pinacol molecules are in a disordered state. If the phase transitions are due to ordering of the orientational disorder of the molecules the transition entropy is expected to be $R\ln 2$ (=5.76 J K^{-1} mol^{-1}). The entropy change experimentally determined is approximately equal to this value. The phase transition can thus be interpreted in terms of the order-disorder change in the orientation of the pinacol molecules.

The transition temperature may be taken as a certain measure of the strength of the interaction among the pinacol molecules. The deuteration causes a slight decrease ($\simeq$1 K) in the transition temperature, indicating the corresponding decrease in the interaction. If we assume the inverse sixth power dependence of the interaction energy on the pinacol–pinacol distance, the isotope effect in the transition temperature is reproduced by 0.09% increase of the intermolecular separation on deuteration. The lattice constants of the deuterate have not been determined, but in the relatively short ($\simeq$0.26 nm) hydrogen bonds, the O–O distance in the deuterium bond is longer than in the corresponding hydrogen bond by up to 0.0022 nm or 0.8% of the bond length.[14] If a similar elongation of the hydrogen bonding occurs in the pinacol hexadeuterate, the negative isotope effect in the transition temperatures will be understood by the above argument based on the simple geometrical consideration.

The Relaxation Time and Activation Enthalpy. The exothermic and endothermic drift in the high temperature glass transition region of the deuterate were analysed by fitting an exponential function of time in which linear change of the temperature with the time was also taken into account to allow for the residual heat leak between the calorimeter cell and its surrounding. The relaxation times thus calculated are plotted in Fig. 9. The activation enthalpy determined from the plot was (33$\pm$4) kJ mol^{-1}. The relaxation time becomes 1 ks at 167.2 K.

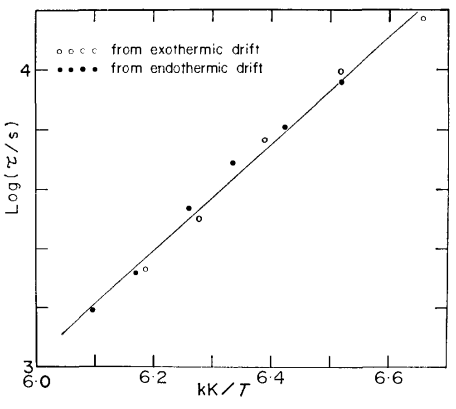

Fig. 9. Arrhenius plot of the enthalpy relaxation time derived from the calorimetric temperature drift at the upper glass transition of pinacol hexadeuterate. The open circles from the exothermic drift of the quenched crystal and the closed circles from the endothermic drift of the slowly cooled crystal.

Origin of the Glass Transitions. A glass transition takes place in principle whenever a molecular process involving passage by the molecule over a potential barrier occurs with the rate constant comparable with the inverse of the time scale of the experiment. There are two possibilities for such molecular motions in the pinacol hexahydrate. Kim and Jeffrey[2] suggested from the crystal symmetry that the hydrogen atoms in the hydrogen bonds are disordered. Cook and Meakins[3] pointed out a close similarity in the dielectric property between the pinacol hexahydrate and the ice I_h crystal. Namely, ε'_0 was found to be 77 along the water layer and 16 perpendicular to the layer, and the maximum absorption frequency at -5 °C is 6 kHz, comparable with 5 kHz in the ice. The large value of ε'_0 can be explained in terms of the reorientation of the water molecules. From the structural and dielectric evidences we can suppose that the hydrogen bonds are in dynamic disorder at the room temperature. At lower temperatures the dynamic disorder will change either to the order through a phase transition or to a static disorder by falling out of thermal equilibrium with other degrees of freedom of the substance. The dielectric study by Cook and Meakins shows that the latter is more likely. If we take 1 ks as the demarcation between the dynamic and static disorder and the Arrhenius parameters given by Cook and Meakins, the glass transition will occur at 170 K.

Another possibility for the molecular origin of the glass transition is the reorientational motion of the pinacol molecule. It was shown already that the orientation of the pinacol molecules orders at the phase transition. Thus, one may at first think that this degree of freedom need not be considered in the discussion of the origin of the glass transition because the orientation of the pinacol molecule is already ordered when the crystal is cooled to the glass transition temperature. However, the ordering can be incomplete at some temperature in the low temperature phase as is often the case in order-disorder transitions. The residual disorder would then cause a glass transition when it freezes into a static disorder. The glassy state so formed has a peculiar property that the frozen-in degree of freedom possesses a long range order. The magnitude of the heat capacity increment at the glass transition is determined by the temperature dependence of the transitional heat capacity and the relaxation time. The glass transitions in tin chloride dihydrate and orthoboric acid are of this kind. The phase transitions in the present substances are of the first order but there are excess heat capacities below the transition temperatures. Therefore the partial disorder in the low temperature phases can be responsible for the glass transitions.

As described in the experimental section, there are two glass transitions in the deuterate around 130 K and 160 K, whereas there is one in the hydrate around 150 K. Our previous experience on the hydrogen bonded systems show that if there is a glass transition in a hydrate crystal then there is a glass transition in the deuterate analogue and *vice versa*. Generalizing this observation to the present case, we assume that two different mechanisms are involved in the glass transition of the hydrate corresponding to the two glass transitions in the deuterate. This assumption is supported by the following evidence. First, the glass transition in the hydrate occurs at an intermediate temperature between the two glass transitions of the deuterate and none occurs above or below. Second, the glass transition region of the hydrate is broader than either of the glass transition regions of the deuterate (Figs. 3 and 4).

If one accepts that both the hydrate and deuterate undergo two glass transitions, the next step is to assign them to the two possible molecular motions discussed above. It was shown by the nuclear magnetic relaxation method that the reorientational motion of the water molecules occurs at higher temperature than the pinacol molecule.[13] The upper glass transition of the deuterate is attributed to the reorientation of the water molecule and the lower to the pinacol molecule. The activation enthalpy derived from the temperature drift data of the deuterate (33 ± 4) kJ mol^{-1} is equal to the activation enthalpy (33 kJ mol^{-1}) of the water reorientation in the hydrate obtained by NMR. In tin chloride dihydrate and ice I_h where reorientation of the water molecules is responsible to the glass transition, the glass transitions shift to higher temperature on deuteration.[6-8] The shifts (5—10 K) of the glass transitions in these compounds are comparable with the difference in temperature of the glass transition of the hydrate and the upper glass transition of the deuterate.

The lower glass transition in the deuterate is assigned to the second of the molecular motion discussed above, the reorientation of the pinacol molecule in the void of the clathrate-like structure. This motion is directly related to the phase transition. In the above, possibility of the lattice expansion on deuteration was discussed in relation to the negative isotope effect in the phase transition temperature. The same lattice expansion will enlarge the void in which the pinacol molecule reorients and thus decrease the height of the potential barrier hindering the molecular motion. This will result in faster reorientation of the pinacol molecule when compared at the same temperature and hence in the lower glass transition temperature in the deuterate than in the hydrate in agreement with above assignment of the molecular motion.

So far as has been known, the glass transition temperature increases invariably on deuteration. The present case is an exception in this respect. This will not be surprising if we consider that only the water and the hydroxyl part of the pinacol molecule were deuterated in the present crystal. The main part of the molecule responsible for the phase transition and the lower glass transition has not been deuterated. In contrast to this, motion of the deuterium itself is responsible for the glass transitions in those substances which undergo positive isotope effect on deuteration in the glass transition temperatures. Properties of the methyl-deuterated pinacol compounds will be interesting in this respect.

Conclusion

We have shown that pinacol hexahydrate and hexadeuterate undergo phase transitions and glass

transitions and discussed their molecular mechanisms from the calorimetric data. The molecular motions emerging from the discussion are generally consistent with the structural, dielectric, and NMR information available. However, a fundamental question of why the water molecules are disordered down to the lowest temperature has not been answered yet. This is closely related to the residual entropy of the ice I_h crystal and is in sharp contrast to the behavior of the layer hydrogen bonded crystals containing metal ions.[15] Low temperature study of other clathrate and clathrate-like hydrates formed by organic molecules will be interesting with regard to their transitional and relaxational properties.

References

1) R. Fittig, *Ann. Chem.*, **25**, 110 (1859).
2) H. S. Kim and G. A. Jeffrey, *J. Chem. Phys.*, **53**, 3610 (1970).
3) J. S. Cook and R. J. Meakins, *Trans. Faraday Soc.*, **51**, 1483 (1955).
4) D. C. Garrington and G. Williams, *J. Chem. Soc., Faraday Trans. 2*, **74**, 591 (1978).
5) H. Suga and S. Seki, *J. Non-Cryst. Solids*, **16**, 171 (1974).
6) T. Matsuo, M. Oguni, H. Suga, and S. Seki, *Bull. Chem. Soc. Jpn.*, **47**, 57 (1974).
7) O. Haida, T. Matsuo, H. Suga, and S. Seki, *J. Chem. Thermodyn.*, **6**, 815 (1974).
8) O. Haida, H. Suga, and S. Seki, *Proc. Jpn. Acad.*, **49**, 191 (1973); *J. Glaciology*, **22**, 155 (1979).
9) M. Oguni, T. Matsuo, H. Suga, and S. Seki, *Bull. Chem. Soc. Jpn.*, **50**, 825 (1977).
10) T. Matsuo, H. Suga, and S. Seki, *J. Phys. Soc. Jpn.*, **30**, 785 (1971).
11) N. A. Pushin and A. A. Glagoleva, *J. Chem. Soc.*, **121**, 2813 (1922).
12) A. S. C. Lawrence and M. P. McDonald, *Mol. Cryst.*, **1**, 205 (1966).
13) M. Oguni, T. Matsuo, H. Suga, and N. Nakamura, *J. Magn. Reson.*, **31**, 51 (1979).
14) "Hydrogen Bond," ed by P. Schuster, G. Zundel, and C. Sandorfy, North-Holland Publishing Company, Amsterdam, New York, Oxford (1976), Vol. II, p. 420.
15) T. Matsuo, Y. Kume, H. Suga, and S. Seki, *J. Phys. Chem. Solids.*, **37**, 499 (1977).

 © 1980 The Chemical Society of Japan Bull. Chem. Soc. Jpn., 53, 1501—1509 (1980)

Structural Studies of Asymmetric Hydrogenation. V. The Crystal Structures of [(*S*)-1-Cyanoethyl][(*S*)(−)-α-methylbenzylamine]-bis(dimethylglyoximato)cobalt(III) at 293 K and 173 K

Yuji Ohashi,* Yoshio Sasada, Seiji Takeuchi,** and Yoshiaki Ohgo**

Laboratory of Chemistry for Natural Products, Tokyo Institute of Technology, Nagatsuta, Midori-ku, Yokohama 227
***Niigata College of Pharmacy, 5829 Kamishinei-cho, Niigata 950-21*

(Received August 20, 1979)

The structure of [(*S*)-1-cyanoethyl][(*S*)(−)-α-methylbenzylamine]bis(dimethylglyoximato)cobalt(III) has been determined by X-ray analysis at 293 K and 173 K. The crystal is monoclinic, the space group being $P2_1$, $Z=2$, with $a=8.768(2)$, $b=13.356(2)$, $c=9.538(3)$ Å, and $\beta=96.73(3)°$ at 293 K, and $a=8.617(4)$, $b=13.222(4)$, $c=9.517(7)$ Å, and $\beta=96.26(7)°$ at 173 K. The structure was deduced by the heavy-atom method and was refined by the block-diagonal least-squares method to the final R values of 0.051 and 0.060 for 1878 and 1848 observed reflections at 293 K and 173 K respectively. The bis(dimethylglyoximato)cobalt moiety is twisted in the opposite way from that of [(*R*)-1-cyanoethyl][(*S*)(−)-α-methylbenzylamine]bis(dimethylglyoximato)cobalt(III). This supports the proposal that the asymmetry of the optically active amine is transferred into the substrate through the twist of the bis(dimethylglyoximato)cobalt moiety in the step of the σ-bond formation.

The serial crystal structures of the cobalt complexes have been determined by X-ray analysis[1-4] in order to clarify the mechanism of inducing asymmetry in the asymmetric hydrogenation of olefins.[5-10] In the crystal structures of [(*R*)-1-(methoxycarbonyl)ethyl][(*R*)(+)-α-methylbenzylamine]bis(dimethylglyoximato)cobalt-(III)[3] and [(*R*)-1-cyanoethyl][(*S*)(−)-α-methylbenzyl-amine]bis(dimethylglyoximato)cobalt(III)[4] (hereafter abbreviated as the R-R ester complex and the R-S cyano complex respectively), it has been shown that the bis(dimethylglyoximato)cobalt moiety (hereafter abbreviated as $Co(dmg)_2$ or cobaloxime) is twisted around its long axis because of the steric repulsion from the substituted alkyl group and α-methylbenzylamine. To examine the twisting of the $Co(dmg)_2$ moiety more closely, we attempted to determine the structure of the title complex, the S-S cyano complex, the only change from the R-S cyano complex in the previous paper being the inversion of the absolute configuration of the cyanoethyl group.

Preliminary experiments revealed that the crystalline-state racemization of the cyanoethyl group also occurs and that the thermal expansion of the crystal is abnormally anisotropic.[11] Therefore, the crystal structures at 293 K and 173 K were determined.

Experimental

Dark red, plate-like crystals of the S-S cyano complex, whose preparation will be reported in detail elsewhere, were obtained from the mother liquor after the fractional precipitation of the R-S cyano complex had been carried out from a solution containing the cyano complex with the racemic cyanoethyl group. A crystal $0.20\times0.25\times0.45$ mm³ in size was placed in a Rigaku four-circle diffractometer, Mo $K\alpha$ radiation monochromated by graphite ($\lambda=0.71069$ Å) being used. The unit-cell dimensions were obtained by the least-squares method with 15 high-angle reflections ($2\theta>20°$). Their values before and after the intensity data collection are shown in Table 1. The average values in the last column were used in this work. The crystal data are summarized in Table 2. The intensity data were collected in the same manner as that used for the R-S cyano complex.[4] A total of 1878 independent reflections, $|F_o|\geqq3\sigma(|F_o|)$, were obtained.

Table 1. The change in the unit-cell dimensions

	Start 1[a]	Start 2[b]	End[c]	Average[d]
a	8.768(2) Å	8.768(2)	8.774(2)	8.771
b	13.356(2) Å	13.380(2)	13.427(2)	13.404
c	9.538(3) Å	9.533(3)	9.520(3)	9.527
β	96.73(3)°	96.85(3)	97.05(4)	96.95
V	1109.2(5) Å³	1110.4(5)	1113.1(5)	1111.8

a) 2 h after the initiation of the X-ray irradiation. The data collection was unsuccessful because the change was so fast. b) After 4 h, at which time the data collection was started. c) After the data collection, about 30 h later. d) The average values between Columns 2 and 3. The structure factors and bond distances and angles are calculated using these values.

Table 2. Crystal data

Formula	$C_3H_4NC_8H_{11}N(C_4H_7N_2O_2)Co$	
F.W.	464.48	
a	8.768(2) Å (293 K)	8.617(4) Å (173 K)
b	13.356(2)	13.222(4)
c	9.538(3)	9.517(7)
β	96.73(3)°	96.26(7)°
V	1109.2(5) Å³	1077.9(10) Å³
Systematic absences	$0k0$; k odd	
Space group	$P2_1$	
Z	2	
D_m	1.396 g/cm³	
D_c	1.391 g/cm³	
μ(Mo $K\alpha$)	8.79 cm⁻¹	

The experimental details at 173 K, using a crystal $0.15\times0.15\times0.59$ mm³ in size, were the same as those for the R-S cyano complex. 1848 independent reflections, $|F_o|\geqq3\sigma(|F_o|)$, were obtained. Corrections for Lorentz and polarization factors were made, but no correction for absorption was applied.

Structure Determination

The structure at 293 K was deduced by the heavy-atom method and refined by the block-diagonal least-

Table 3. Fractional coordinates, with their standard deviations, multiplied by 10^4 for the non-hydrogen atoms and by 10^3 for the hydrogen atoms at 293 K

Atom	x	y	z
Co	125(1)	2500(0)	2655(1)
N(1)	14(6)	2819(4)	4571(5)
N(2)	1784(5)	3392(4)	2941(5)
N(3)	265(5)	2177(4)	746(5)
N(4)	−1560(6)	1609(4)	2369(5)
O(1)	−1103(5)	2475(5)	5294(4)
O(2)	2589(5)	3673(4)	1885(4)
O(3)	1299(5)	2592(5)	−7(4)
O(4)	−2465(5)	1425(4)	3361(4)
C(1)	1061(7)	3412(5)	5171(6)
C(2)	2107(7)	3771(5)	4206(6)
C(3)	−739(7)	1528(5)	145(7)
C(4)	−1806(7)	1192(5)	1122(7)
C(5)	1159(9)	3723(6)	6696(7)
C(6)	3353(8)	4528(6)	4576(8)
C(7)	−779(10)	1209(6)	−1343(7)
C(8)	−3078(9)	465(6)	703(8)
N(5)	−1170(5)	3742(4)	2070(5)
C(9)	−2862(7)	3752(6)	1669(7)
C(10)	−3524(8)	4773(7)	1893(8)
C(11)	−3357(7)	3414(5)	173(6)
C(12)	−2624(8)	3713(7)	−963(7)
C(13)	−3157(10)	3446(8)	−2310(8)
C(14)	−4439(10)	2845(7)	−2555(9)
C(15)	−5175(8)	2559(8)	−1471(8)
C(16)	−4641(8)	2810(5)	−100(8)
C(17)	1521(8)	1283(5)	3212(7)
C(19)	1117(8)	826(5)	4459(7)
N(6)	821(8)	430(5)	5469(7)
C(18)	3213(9)	1410(7)	3200(11)
H(01)	−181(9)	171(7)	480(8)
H(02)	196(7)	292(4)	63(6)
H(51)	198(8)	336(6)	725(7)
H(52)	47(8)	338(6)	704(7)
H(53)	132(8)	448(6)	681(7)
H(61)	427(8)	412(6)	483(8)
H(62)	355(9)	511(7)	381(8)
H(63)	304(10)	496(8)	523(9)
H(71)	28(7)	111(5)	−149(6)
H(72)	−144(8)	172(6)	−190(7)
H(73)	−130(9)	49(6)	−157(7)
H(81)	−364(7)	57(5)	−21(6)
H(82)	−375(8)	36(5)	138(7)
H(83)	−272(6)	−25(5)	72(6)
H(N51)	−103(7)	407(5)	280(6)
H(N52)	−87(6)	406(4)	132(6)
H(9)	−340(6)	324(4)	235(5)
H(101)	−330(7)	495(5)	284(6)
H(102)	−465(7)	490(6)	168(6)
H(103)	−319(11)	535(8)	124(9)
H(12)	−182(6)	414(4)	−90(6)
H(13)	−266(8)	372(6)	−304(8)
H(14)	−468(6)	273(5)	−345(6)
H(15)	−606(7)	211(5)	−168(6)
H(16)	−513(8)	259(7)	71(7)
H(17)	146(9)	79(6)	246(7)
H(181)	390(10)	67(7)	343(8)
H(182)	349(11)	200(7)	409(9)
H(183)	350(10)	151(8)	227(9)

Table 4. Fractional coordinates, with their standard deviations, multiplied by 10^4 for the non-hydrogen atoms and by 10^3 for the hydrogen atoms at 173 K

Atom	x	y	z
Co	168(1)	2500(0)	2656(1)
N(1)	50(8)	2814(5)	4571(6)
N(2)	1878(7)	3405(4)	2908(6)
N(3)	311(7)	2168(5)	744(6)
N(4)	−1538(7)	1608(5)	2392(7)
O(1)	−1097(5)	2467(6)	5317(5)
O(2)	2688(6)	3687(4)	1860(5)
O(3)	1367(6)	2585(6)	−22(5)
O(4)	−2466(6)	1428(4)	3395(6)
C(1)	1134(9)	3422(6)	5162(8)
C(2)	2169(9)	3774(7)	4176(8)
C(3)	−709(9)	1517(6)	142(8)
C(4)	−1815(10)	1185(6)	1141(8)
C(5)	1244(10)	3727(7)	6669(8)
C(6)	3450(11)	4539(7)	4519(10)
C(7)	−746(12)	1183(7)	−1333(9)
C(8)	−3085(10)	454(7)	741(9)
N(5)	−1143(7)	3771(5)	2088(7)
C(9)	−2888(9)	3752(6)	1669(8)
C(10)	−3560(10)	4793(7)	1887(9)
C(11)	−3295(9)	3418(7)	139(8)
C(12)	−2540(11)	3790(8)	−956(10)
C(13)	−3006(10)	3555(8)	−2352(10)
C(14)	−4268(11)	2916(8)	−2637(10)
C(15)	−5070(9)	2566(10)	−1568(9)
C(16)	−4597(9)	2807(6)	−160(9)
C(17)	1560(10)	1266(7)	3195(8)
C(19)	1131(10)	805(7)	4456(9)
N(6)	815(9)	421(6)	5479(7)
C(18)	3289(12)	1415(9)	3258(13)
H(01)	−189(13)	193(9)	457(12)
H(02)	232(13)	314(9)	84(11)
H(51)	216(8)	357(6)	707(7)
H(52)	69(9)	333(6)	721(8)
H(53)	137(9)	439(7)	682(9)
H(61)	442(11)	434(8)	477(11)
H(62)	378(10)	498(7)	374(9)
H(63)	330(9)	497(6)	505(8)
H(71)	30(8)	108(5)	−159(7)
H(72)	−116(10)	162(7)	−201(9)
H(73)	−145(14)	58(10)	−169(12)
H(81)	−372(9)	61(6)	−11(8)
H(82)	−373(8)	39(5)	138(7)
H(83)	−278(11)	−24(7)	73(10)
H(N51)	−101(9)	421(6)	275(8)
H(N52)	−77(9)	405(6)	124(8)
H(9)	−341(9)	330(6)	222(8)
H(101)	−324(10)	498(7)	287(9)
H(102)	−482(9)	493(6)	162(8)
H(103)	−314(8)	533(6)	128(8)
H(12)	−177(8)	425(5)	−72(7)
H(13)	−243(8)	377(6)	−325(7)
H(14)	−464(9)	270(7)	−354(8)
H(15)	−579(10)	223(7)	−181(9)
H(16)	−515(8)	268(6)	55(7)
H(17)	180(12)	75(8)	233(10)
H(181)	405(15)	69(10)	349(13)
H(182)	352(11)	177(8)	426(10)
H(183)	357(9)	176(7)	226(9)

squares method. All the hydrogen atoms were found on a difference map. The final refinement was made with the anisotropic and isotropic temperature factors for non-hydrogen and hydrogen atoms respectively. The weighting scheme employed was: $w=0.2$ if $|F_0|>96.91$ and $|F_0|<9.69$ and $w=(0.00211F_0^2-0.22423|F_0|+6.97531)^{-1}$ if $9.69\leqq|F_0|\leqq96.91$. The final R value became 0.051 for 1878 reflections. No peaks higher than 0.30 eÅ^{-3}, except for a peak of 0.45 eÅ^{-3} around the cobalt atom, were found on the final difference map.

The structure at 173 K was refined by the block-diagonal least-squares method using the parameters of the structure at 293 K as the starting parameters. The weighting scheme employed was: $w=0.2$ if $|F_0|>154.32$ and $|F_0|<15.43$ and $w=(0.00117F_0^2-0.19947|F_0|+9.46501)^{-1}$ if $15.43\leqq|F_0|\leqq154.32$. The final R value became 0.060 for 1848 reflections. No peaks higher than 0.45 eÅ^{-3}, except for peaks of 0.55 eÅ^{-3} around the cobalt atom, were found on the final difference map. The atomic scattering factors were taken from the International Tables for X-Ray Crystallography.[12] The final atomic coordinates and their standard deviations at 293 K and 173 K are given in Tables 3 and 4 respectively. Lists of the thermal parameters and the observed and calculated structure factors are kept in the Office of the Chemical Society of Japan (Document No. 8018). The computation was done on M-180 and M-160 computers at this Institute.

Description of the Structure

The equations of the mean planes for four nitrogen atoms and two dmg's are given in Table 5, together with the deviations of the atoms from the planes. The deviations are in good agreement between the two temperatures. The projection of the structure at 293 K on the plane (I) is shown in Fig. 1, in which the short contacts between the non-bonded atoms are also given. In Table 6, the short contacts at 173 K are compared with the corresponding ones at 293 K. The cyano and methyl groups are located over the gaps between the two dmg's. Such a conformation of the cyanoethyl group is also found in the R-S cyano complex,[4] although the locations of the methyl and cyano groups are exchanged because of the opposite configuration at C(17).

The four nitrogen atoms of $Co(dmg)_2$ are nearly coplanar, but the tetragon composed of them is slightly twisted in the opposite way from that of the R-S cyano complex. The twisting of the $Co(dmg)_2$ moiety will be discussed in detail in the following section. The diviation of the cobalt atom from the mean plane of $Co(dmg)_2$ is negligibly small. The oxygen atoms deviate downward to avoid the short contacts with the cyanoethyl group, whereas the carbon atoms deviate upward. These features are also observed in the R-S cyano complex.

The bond distances at 293 K are shown in Fig. 2, while they are compared with the corresponding ones at 173 K in Table 7. The bond angles at both temperatures are listed in Table 8. The Co–C(17) and Co–N(5) bonds at 293 K are longer by 0.011 Å, and shorter by 0.010 Å, respectively, than the corresponding ones at 173 K. This causes an increase in the bond angles of C(19)–C(17)–C(18) and Co–N(5)–C(9) at high temperatures. Considerable differences in the bond of N(5)–C(9) and the angle of N(2)–Co–C(17) are found

Table 5. Least-squares planes and deviations (l/Å) for equatorial ligands

X, Y, and Z in Å referred to **a**, **b**, and **c***) respectively.

(I) $Co(dmg)_2$ plane (293 K): $0.5806X-0.7619Y+0.2872Z+1.9444=0$.
(I′) $Co(dmg)_2$ plane (173 K): $0.5810X-0.7642Y+0.2802Z+1.8934=0$.
(II) dmg plane (293 K): $0.5741X-0.7783Y+0.2543Z+2.1319=0$.
(II′) dmg plane (173 K): $0.5765X-0.7789Y+0.2467Z+2.0748=0$.
(III) dmg plane (293 K): $0.5885X-0.7456Y+0.3126Z+1.8715=0$.
(III′) dmg plane (173 K): $0.5835X-0.7537Y+0.3023Z+1.8364=0$.

	(I)	(I′)	(II)	(II′)	(III)	(III′)
Co	−0.002	−0.005	0.049	0.044	0.042	0.028
N (1)	0.009[a]	0.011[a]	−0.005[a]	−0.006[a]		
N (2)	−0.009[a]	−0.011[a]	0.005[a]	0.006[a]		
N (3)	0.009[a]	0.011[a]			0.002[a]	−0.000[a]
N (4)	−0.009[a]	−0.011[a]			−0.002[a]	0.000[a]
O (1)	−0.062	−0.059	−0.083	−0.088		
O (2)	−0.103	−0.105	−0.069	−0.065		
O (3)	−0.042	−0.039			−0.050	−0.058
O (4)	−0.078	−0.089			−0.059	−0.062
C (1)	0.059	0.061	0.008[a]	0.010[a]		
C (2)	0.027	0.021	−0.008[a]	−0.010[a]		
C (3)	0.038	0.035			−0.004[a]	0.000[a]
C (4)	0.037	0.021			0.004[a]	−0.000[a]
C (5)	0.103	0.117	−0.001	0.012		
C (6)	−0.036	−0.040	−0.107	−0.102		
C (7)	0.039	0.052			−0.044	−0.018
C (8)	0.046	0.042			−0.022	−0.001

a) Atoms included in the least-squares calculation.

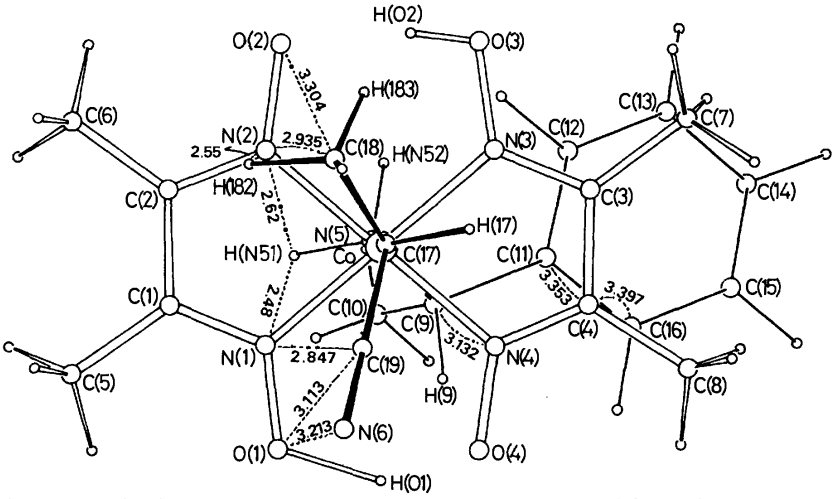

Fig. 1. Projection of the complex onto the mean plane of four nitrogen atoms of $Co(dmg)_2$ and the short contacts between non-bonded atoms (l/Å) at 293 K, their threshold values being 3.400 Å for the distances between the non-hydrogen atoms and 2.70 Å for those including hydrogen atoms.

Table 6. Short contacts between the non-bonded atoms (l/Å)

	293 K	173 K
N (1) ··· C (19)	2.847 (9)	2.822 (11)
N (1) ··· N (6)	3.368 (9)	3.327 (11)
N (1) ··· H (N51)	2.48 (6)	2.63 (8)
N (2) ··· C (18)	2.934 (12)	2.902 (14)
N (2) ··· H (N51)	2.62 (6)	2.70 (8)
N (2) ··· H (182)	2.55 (10)	2.81 (10)
N (4) ··· C (9)	3.132 (9)	3.113 (10)
N (4) ··· C (19)	3.074 (9)	3.048 (11)
O (1) ··· C (19)	3.112 (10)	3.086 (12)
O (1) ··· N (6)	3.213 (10)	3.162 (11)
O (2) ··· C (18)	3.303 (12)	3.304 (14)
O (4) ··· C (19)	3.288 (9)	3.259 (11)
C (4) ··· C (11)	3.353 (9)	3.315 (12)
C (4) ··· C (16)	3.397 (10)	3.352 (12)

between 293 K and 173 K. These differences may be due to the positional changes of the C(17) and N(5) atoms. The other corresponding distances and angles are in good agreement with each other.

The $Co(dmg)_2$ moiety in the methyl[(*R*)(+)-α-methylbenzylamine]cobaloxime, methyl complex, has the C_{2h} symmetry as a result of the steric repulsion from the amine ligand.[2] For the R-R ester complex, the symmetry of C_{2h} holds good with regard to the bond lengths of N–C and C–CH_3 and three angles around the *endo*-cyclic carbon atoms in the $Co(dmg)_2$ moiety. Such a symmetry is no longer conserved for the two cyano complexes, however. This may indicate that the steric and electrostatic interactions between $Co(dmg)_2$ and the substituted alkyl group in the cyano complexes are stronger than those in the methyl and R-R ester complexes.

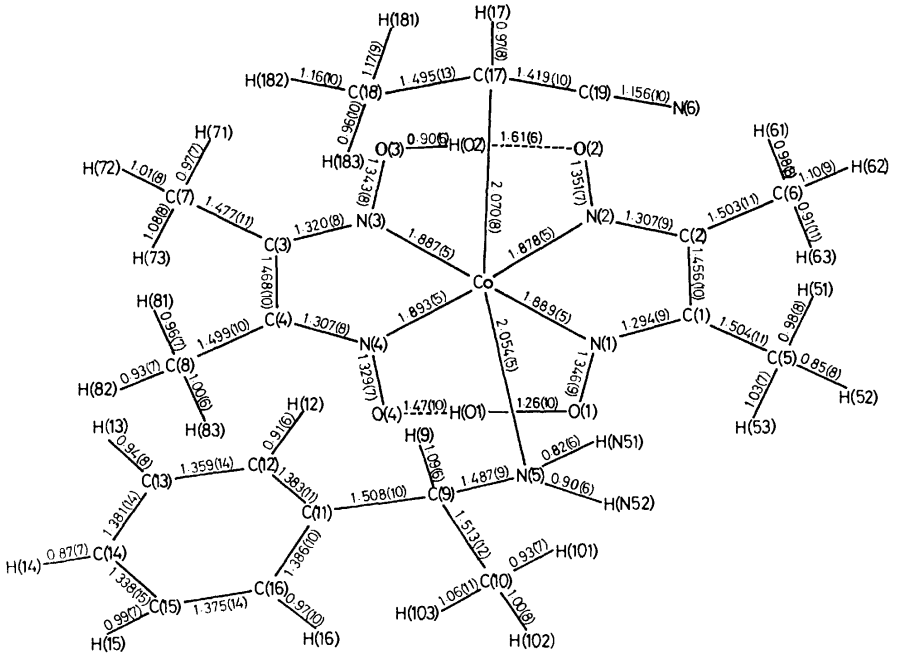

Fig. 2. Bond distances (l/Å) at 293 K. Their standard deviations are in parentheses.

Table 7. Bond distances (l/Å)
Esd's are in parentheses.

	293 K	173 K
Co–N(1)	1.889(5)	1.883(7)
Co–N(2)	1.878(5)	1.893(6)
Co–N(3)	1.887(5)	1.890(6)
Co–N(4)	1.893(5)	1.879(7)
Co–N(5)	2.054(5)	2.064(7)
Co–C(17)	2.070(8)	2.059(9)
N(1)–O(1)	1.346(9)	1.357(11)
N(1)–C(1)	1.294(9)	1.312(11)
N(2)–O(2)	1.351(7)	1.331(9)
N(2)–C(2)	1.307(9)	1.301(11)
N(3)–O(3)	1.343(8)	1.345(10)
N(3)–C(3)	1.320(8)	1.316(10)
N(4)–O(4)	1.329(7)	1.332(9)
N(4)–C(4)	1.307(8)	1.313(11)
C(1)–C(2)	1.456(10)	1.440(12)
C(1)–C(5)	1.504(11)	1.483(13)
C(2)–C(6)	1.503(11)	1.507(13)
C(3)–C(4)	1.468(10)	1.484(12)
C(3)–C(7)	1.477(11)	1.470(13)
C(4)–C(8)	1.499(10)	1.478(13)
N(5)–C(9)	1.487(9)	1.513(10)
C(9)–C(10)	1.513(12)	1.516(12)
C(9)–C(11)	1.508(10)	1.526(12)
C(11)–C(12)	1.383(11)	1.378(14)
C(11)–C(16)	1.386(10)	1.387(12)
C(12)–C(13)	1.359(14)	1.381(15)
C(13)–C(14)	1.381(14)	1.380(15)
C(14)–C(15)	1.338(15)	1.372(16)
C(15)–C(16)	1.375(14)	1.394(15)
C(17)–C(18)	1.495(13)	1.498(15)
C(17)–C(19)	1.419(10)	1.431(13)
C(19)–N(6)	1.156(10)	1.156(12)
O(1)–H(01)	1.26(10)	1.37(12)
O(2)–H(02)	1.61(6)	1.23(12)
O(3)–H(02)	0.90(6)	1.32(12)
O(4)–H(01)	1.47(10)	1.35(12)
C(5)–H(51)	0.98(8)	0.87(8)
C(5)–H(52)	0.85(8)	0.91(8)
C(5)–H(53)	1.03(7)	0.90(9)
C(6)–H(61)	0.98(8)	0.89(11)
C(6)–H(62)	1.10(9)	1.01(10)
C(6)–H(63)	0.91(11)	0.78(8)
C(7)–H(71)	0.97(7)	0.97(7)
C(7)–H(72)	1.01(8)	0.91(9)
C(7)–H(73)	1.08(8)	1.04(13)
C(8)–H(81)	0.96(7)	0.95(8)
C(8)–H(82)	0.93(7)	0.87(7)
C(8)–H(83)	1.00(6)	0.95(10)
N(5)–H(N51)	0.82(6)	0.86(8)
N(5)–H(N52)	0.90(6)	0.98(8)
C(9)–H(9)	1.09(6)	0.94(8)
C(10)–H(101)	0.93(7)	0.98(9)
C(10)–H(102)	1.00(8)	1.10(8)
C(10)–H(103)	1.06(11)	1.01(8)
C(12)–H(12)	0.91(6)	0.91(7)
C(13)–H(13)	0.94(8)	1.07(7)
C(14)–H(14)	0.87(7)	0.93(10)
C(15)–H(15)	0.99(7)	0.78(10)
C(16)–H(16)	0.97(10)	0.88(8)
C(17)–H(17)	0.97(8)	1.10(11)
C(18)–H(181)	1.17(9)	1.16(13)
C(18)–H(182)	1.16(10)	1.06(10)
C(18)–H(183)	0.96(10)	1.10(9)

The crystal structure viewed along the c axis is shown in Fig. 3, in which the short contacts are also given. There is a weak hydrogen bond between N(5) and N(6) in the unit of $(-x, 0.5+y, 1-z)$. The N···N distances are 3.246 and 3.171 Å for 293 and 173 K respectively. The distance of H(N51)···N(6) and the angle of N(5)–H(N51)···N(6) are 2.45 Å and 164° for 293 K, and 2.32 Å and 177° for 173 K. Such a hydrogen bond is also observed in the crystal of the R-S cyano complex. The other contacts are not unusually short.

Discussion

In Part III of this series, concerning the structure of the R-R ester complex, we proposed that the twisting of the $Co(dmg)_2$ moiety, caused by the steric repulsion from the methoxycarbonylethyl group and the amine, is one of the factors inducing asymmetry in the step of σ-bond formation.[3] This proposal must now be examined in connection with the R-S and S-S cyano complexes.

In Table 9, the deviations of the atoms in the $Co(dmg)_2$ moiety from the mean plane composed of four nitrogen atoms and the bond distances of Co–C(17) and Co–N(5) are listed for the complexes determined in this serial study. (The *exo*-cyclic atoms are omitted for the sake of clarity.) For the cyano complexes, the values at both room and low temperatures are given, because they change considerably with the temperature. As the absolute configurations of α-methylbenzylamine are different between the cyano complexes and the other two, the latter complexes are replaced by their enantiomers in the following discussion. Figure 4 shows the structures and the numberings of the atoms for the S-S (enantiomer of R-R) ester and the R-S cyano complexes. The amine is located below the $Co(dmg)_2$ plane, whereas the methyl and the substituted alkyl groups are placed above.

The tetragons, composed of four nitrogen atoms in the S-S ester and R-S cyano (293 K) complexes, are twisted in the same manner. Moreover, the magnitude of the twisting is equal. The tetragon in the S-S cyano (293 K) complex, on the other hand, is twisted in the opposite way, and the magnitude of the twisting is smaller than those of the S-S ester and R-S cyano (293 K) complexes. The methyl of the substituted alkyl group comes close to N(1) in the two structures of S-S ester and R-S cyano complexes. The unusually short contact between the methyl group and N(1) causes N(1) to deviate downward from the plane. The deviation of N(1) from the plane brings about the twist of the tetragon in such a manner that N(3) deviates downward, too, and N(2) and N(4), upward, the cobalt atom being fixed as a center. This twisting is called "clockwise twisting" for the S amine, viewed down along the axis perpendicular to the mean plane of $Co(dmg)_2$. In Fig. 5, the "clockwise twisting" is drawn schematically, the arrows being directed from the lower nitrogen atom to the upper one in each dmg. Although the twisting was defined in the previous paper as the distortion around the long axis of $Co(dmg)_2$, the above notation is more convenient, since the substrate should approach

Table 8. Bond angles (ϕ/°)

Esd's are in parentheses. Angles including methyl and phenyl hydrogen atoms are omitted.

	(293 K)	(173 K)		(293 K)	(173 K)
N(1)–Co–N(2)	81.1(2)	82.1(3)	N(4)–C(4)–C(3)	113.4(6)	112.8(7)
N(1)–Co–N(3)	179.2(2)	179.1(3)	N(4)–C(4)–C(8)	123.8(6)	124.6(8)
N(1)–Co–N(4)	98.7(2)	98.3(3)	C(3)–C(4)–C(8)	122.8(6)	122.5(8)
N(1)–Co–N(5)	89.3(2)	89.3(3)	Co–N(5)–C(9)	125.4(4)	123.7(5)
N(1)–Co–C(17)	91.6(3)	91.4(3)	N(5)–C(9)–C(10)	111.1(6)	109.4(7)
N(2)–Co–N(3)	98.4(2)	97.9(3)	N(5)–C(9)–C(11)	113.9(6)	112.0(6)
N(2)–Co–N(4)	179.5(2)	179.5(3)	C(9)–C(11)–C(12)	123.0(7)	122.7(8)
N(2)–Co–N(5)	85.3(2)	85.1(3)	C(9)–C(11)–C(16)	119.2(6)	117.5(7)
N(2)–Co–C(17)	87.8(3)	92.6(3)	C(12)–C(11)–C(16)	117.8(7)	119.4(8)
N(3)–Co–N(4)	81.8(2)	81.8(3)	C(11)–C(12)–C(13)	121.6(9)	122.4(10)
N(3)–Co–N(5)	91.3(2)	91.6(3)	C(12)–C(13)–C(14)	119.5(10)	117.9(10)
N(3)–Co–C(17)	87.8(3)	87.6(3)	C(13)–C(14)–C(15)	119.7(9)	120.7(10)
N(4)–Co–N(5)	94.3(2)	94.5(3)	C(14)–C(15)–C(16)	121.5(10)	121.2(11)
N(4)–Co–C(17)	88.1(3)	87.8(3)	C(11)–C(16)–C(15)	119.8(8)	118.4(9)
N(5)–Co–C(17)	177.2(3)	177.4(3)	Co–C(17)–C(18)	117.7(6)	117.2(7)
Co–N(1)–O(1)	122.9(5)	123.4(6)	Co–C(17)–C(19)	110.8(5)	110.5(6)
Co–N(1)–C(1)	116.7(5)	116.0(6)	C(18)–C(17)–C(19)	113.8(7)	111.7(8)
O(1)–N(1)–C(1)	120.5(6)	120.6(7)	C(17)–C(19)–N(6)	177.8(8)	178.5(10)
Co–N(2)–O(2)	122.3(4)	123.2(5)	N(1)–O(1)–H(O1)	116(4)	107(6)
Co–N(2)–C(2)	117.3(5)	115.0(6)	N(2)–O(2)–H(O2)	102(2)	108(5)
O(2)–N(2)–C(2)	120.3(6)	121.7(7)	N(3)–O(3)–H(O2)	105(4)	108(5)
Co–N(3)–O(3)	123.2(4)	123.1(5)	N(4)–O(4)–H(O1)	115(4)	108(5)
Co–N(3)–C(3)	116.8(4)	117.4(5)	O(1)–H(O1)–O(4)	133(7)	160(11)
O(3)–N(3)–C(3)	120.0(6)	119.5(7)	O(2)–H(O2)–O(3)	160(6)	156(10)
Co–N(4)–O(4)	122.5(4)	122.5(5)	Co–N(5)–H(N51)	101(4)	110(5)
Co–N(4)–C(4)	116.2(5)	116.8(6)	Co–N(5)–H(N52)	113(4)	108(5)
O(4)–N(4)–C(4)	121.3(5)	120.6(7)	C(9)–N(5)–H(N51)	105(4)	105(5)
N(1)–C(1)–C(2)	113.1(6)	112.5(7)	C(9)–N(5)–H(N52)	100(4)	101(5)
N(1)–C(1)–C(5)	123.4(7)	123.2(8)	H(N51)–N(5)–H(N52)	113(6)	109(7)
C(2)–C(1)–C(5)	123.5(7)	124.3(8)	N(5)–C(9)–H(9)	109(3)	113(5)
N(2)–C(2)–C(1)	111.8(6)	114.4(8)	C(10)–C(9)–H(9)	106(3)	107(5)
N(2)–C(2)–C(6)	123.3(7)	121.0(8)	C(11)–C(9)–H(9)	106(3)	106(5)
C(1)–C(2)–C(6)	124.8(7)	124.5(8)	Co–C(17)–H(17)	112(5)	117(6)
N(3)–C(3)–C(4)	111.8(6)	111.1(7)	C(18)–C(17)–H(17)	92(5)	81(6)
N(3)–C(3)–C(7)	123.0(6)	123.8(8)	C(19)–C(17)–H(17)	109(5)	117(6)
C(4)–C(3)–C(7)	125.2(6)	125.1(8)			

the Co atom along the axis perpendicular to the mean plane of $Co(dmg)_2$.

The asymmetric carbon atom, C(9), which comes most closely to $Co(dmg)_2$ among the atoms of the amine except for the coordinating amine group, comes near N(4). The steric repulsion between N(4) and C(9) should give rise to the twisting of the tetragon. The twisting is clockwise. In the two structures of the S-S ester and R-S cyano complexes, the steric repulsions of N(1)···C(18) and N(4)···C(9) result in the same twisting. On the other hand, the C(18) atom of the S-S cyano complex comes close to N(2). This causes a counterclockwise twisting of the tetragon. Because the repulsion of N(4)···C(9) would give a clockwise twisting, the $Co(dmg)_2$ moiety must have a more planar conformation than that of the R-S cyano complex. As the repulsion of N(2)···C(18) is stronger than that of N(4)···C(9), the tetragon shows the counterclockwise twisting.

The bond distance of Co–C(17) in the S-S cyano (293 K) complex is significantly longer than that of the R-S cyano (293 K) complex. Because the tetragon can not be twisted enough to avoid the short contact of N(2)···C(18), the Co–C(17) bond is lengthened. This may indicate that the strength of the Co–C bond is fairly weak.

At low temperatures, the Co–C(17) bonds in the R-S and S-S cyano complexes have the same distances, and the magnitude of the twisting in the R-S cyano complex becomes smaller than that at room temperature. As is shown in Table 10, the Co–C(sp^3) distance is lengthened with an increase in the number of the non-hydrogen substituents bonded to the coordinating carbon atom; that is, the Co–CH_3 and Co–CH_2R values are 2.00 and 2.04 Å respectively. As Table 10 shows, the Co–C(17) bond in the cyanoethyl complexes is estimated to have a distance between 2.04 and 2.067 Å, because the cyanoethyl group has two non-hydrogen substituents and the cyano and methyl groups are located over the gaps between two dmg's whereas the methoxycarbonyl

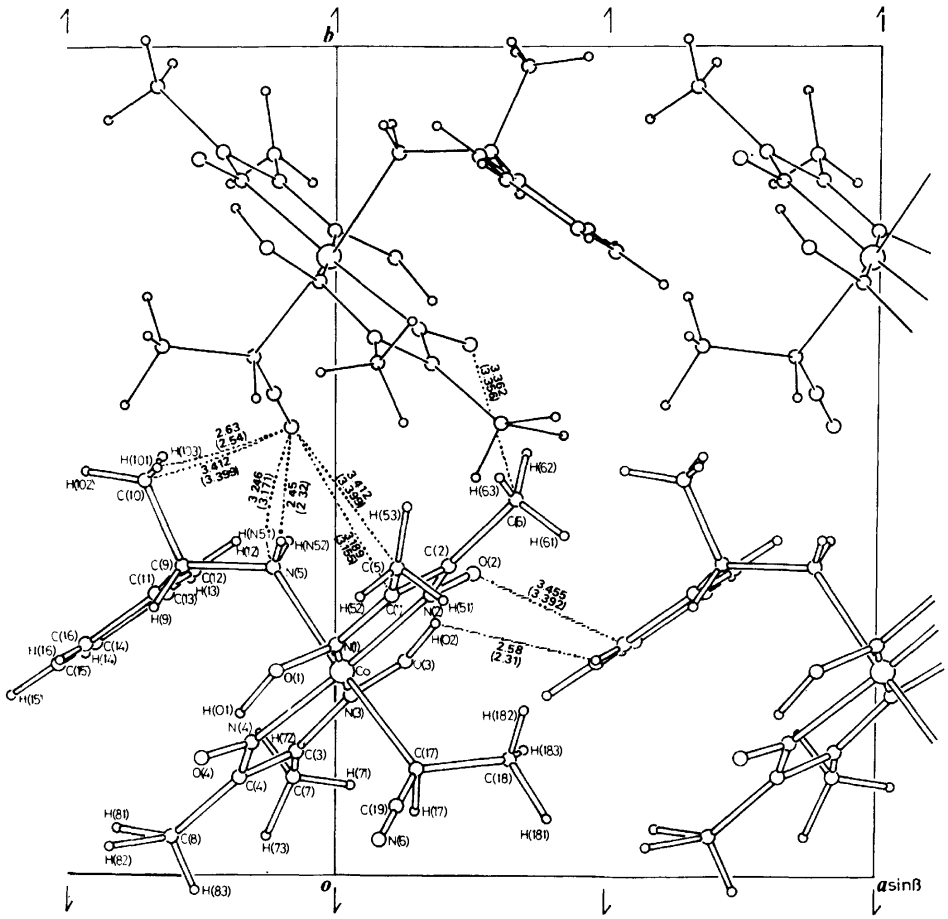

Fig. 3. Projection of the crystal structure along the c axis and the short contacts between complexes. The short contacts at 173 K are in parentheses.

TABLE 9. DEVIATIONS (l/Å) OF THE ATOMS FROM THE MEAN PLANE OF FOUR NITROGEN ATOMS, AND Co–C(17) AND Co–N(5) DISTANCES (l/Å), IN VARIOUS [SUBSTITUTED ALKYL][α-METHYLBENZYLAMINE]COBALOXIMES

	Methyl	S-S ester[a)]	R-S (293 K)	R-S (173 K)	S-S (293 K)	S-S (173 K)
Co	−0.04	0.041	0.008	0.003	−0.002	−0.005
N (1)	0.01	−0.020	−0.020	−0.014	0.009	0.011
N (2)	−0.01	0.020	0.020	0.014	−0.009	−0.011
N (3)	0.01	−0.020	−0.020	−0.014	0.009	0.011
N (4)	−0.01	0.020	0.020	0.014	−0.009	−0.011
C (1)	0.04	−0.178	0.029	0.033	0.059	0.061
C (2)	−0.03	−0.115	−0.007	0.019	0.027	0.021
C (3)	0.02	−0.113	0.003	0.012	0.038	0.035
C (4)	0.05	−0.089	0.107	0.053	0.037	0.021
Co–C (17)	1.988 (19)	2.067 (8)	2.036 (8)	2.056 (6)	2.070 (8)	2.057 (9)
Co–N (5)	2.089 (9)	2.066 (6)	2.088 (6)	2.070 (6)	2.054 (5)	2.064 (7)

a) The S-S ester is the enantiomer of the R-R ester complex.

and methyl groups in the S-S ester complex lie on the dmg rings. Therefore, the Co–C(17) distance of 2.057 Å at a low temperature seems to be a reasonable value. When the temperature is raised, the molecular packing in the crystal becomes loose and the strain in the molecule is released. For the R-S cyano complex, the tetragon composed of four nitrogen atoms is twisted to a greater extent and the Co–C bond becomes shorter, whereas the Co–C bond is lengthened for the S-S cyano complex. The abnormally anisotropic thermal expansion of the two cyano complexes may relate to the fact mentioned above. Because the reaction under investigation proceeds in solution, the conformation at room temperature may more closely resemble those in the intermediate state of the reaction.

It is noteworthy that the Co–N(5) bonds are altered

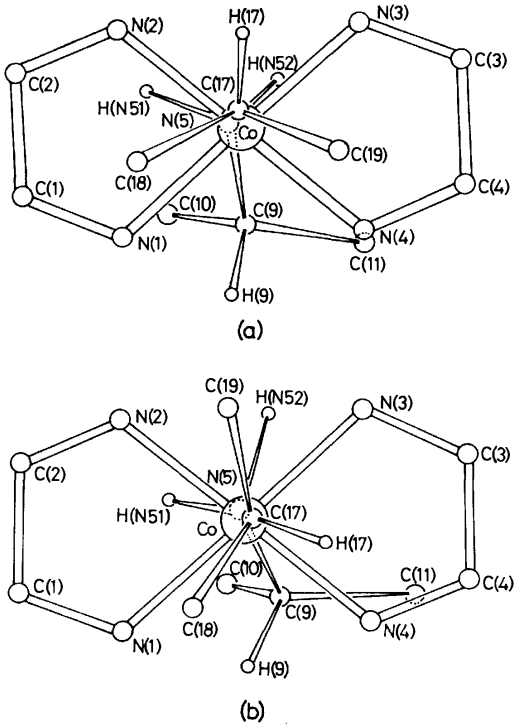

Fig. 4. Projections of the atoms around the Co atom onto the mean plane of four nitrogen atoms (a) for the S-S ester complex, the enantiomer of R-R,[3] and (b) for the R-S cyano complex.

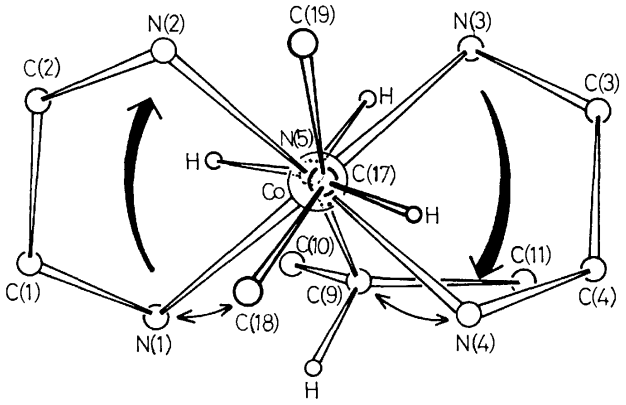

Fig. 5. Clockwise twisting of $Co(dmg)_2$ in the R-S cyano complex. The arrows are drawn from the lower nitrogen atoms to the upper ones in the Co-dmg rings. Such a twisting is brought about by the steric repulsions, N(1)···C(18) and N(4)···C(9).

in their lengths as the Co–C(17) distance in the cyano complexes is varied. All the sums of the Co–N(5) and Co–C(17) distances in both cyano complexes at low and room temperatures are nearly the same, the average value being 4.124 Å. This can be explained by the "trans influence" suggested by Brückner and Randaccio.[16]

In summary, the tetragon of $Co(dmg)_2$ is twisted significantly and the Co–C bond is shortened for the R-S cyano complex, while the tetragon has a slightly twisted conformation and the Co–N bond is shortened

Table 10. Co–C(sp^3) distances (l/Å) in various cobaloxime complexes

	Co–C distance	Ref.
$CH_3Co(dmg)_2(H_2O)$	1.990 (5)	13
$CH_3Co(dmg)_2(py)$	1.998 (5)	14
$CH_3Co(dmg)_2(nmeim)$	2.009 (7)	14
$CH_3Co(dmg)_2(mba)$	1.988 (19)	2
$(CH_2CO_2CH_3)Co(dmg)_2(py)$	2.04	15
$(CH_2CH_2CN)Co(dmg)_2(dphyea)$	2.04	1
$(CH(CH_3)CO_2CH_3)Co(dmg)_2(mba)$	2.067 (8)	3
$(CH(CH_3)CN)$- (293 K)	2.036 (8)	4
$Co(dmg)_2(mba)$ (173 K)	2.056 (6)	4
$(CH(CH_3)CN)$- (293 K)	2.070 (8)	present
$Co(dmg)_2(mba)$ (173 K)	2.057 (9)	present

py: pyridine, nmeim: 3-*N*-methylimidazole, dphyea: *erythro*-1,2-diphenyl-2-hydroxyethylamine, mba: α-methylbenzylamine.

Table 11. The short interatomic distances (l/Å) between $Co(dmg)_2$ and the axial ligands for the R-S and S-S cyano complexes

	R-S	S-S	Δ
C(9)···N(4)	3.176	3.132	0.044
C(18)···(N(1) or N(2))[a]	2.946	2.935	0.011
C(19)···(N(2) or N(1))[a]	2.863	2.847	0.016
C(19)···(O(2) or O(1))[a]	3.148	3.113	0.035
N(6)···(O(2) or O(1))[a]	3.284	3.212	0.071

a) The former atoms are for the R-S cyano complex, and the latter, for the S-S cyano complex.

for the S-S cyano complex. Table 11 shows the short interatomic distances between $Co(dmg)_2$ and the axial ligands for the two cyano complexes. Any distance of the R-S cyano complex is longer than the corresponding one of the S-S cyano complex. The repulsive energy of the former complex must be lower than that of the latter complex. The energy differences caused by the different lengths of the axial bonds, Co–C and Co–N, are considered to be compensated for the two cyano complexes, because the sums of the two bond distances are nearly the same.

In conclusion, the tetragon of the $Co(dmg)_2$ moiety is twisted because of the steric repulsion from the substituted alkyl group and the optically active amine. If the way of the twisting caused by the substituted alkyl group is in accord with that brought about by the amine, the tetragon is twisted and the steric repulsion between $Co(dmg)_2$ and the two axial ligands decreases. If both twistings are in the opposite way, on the other hand, the tetragon has a nearly planar conformation and the steric effect increases. The two σ-complexes have different repulsive energies, indicating that the two diastereomeric pathways in this reaction have different energies of activation in the "kinematically controlled asymmetric process."[17] This must be one of the factors inducing asymmetry in this asymmetric hydrogenation.

References

1) Part I: Y. Ohashi, Y. Sasada, Y. Tashiro, Y. Ohgo, S. Takeuchi, and J. Yoshimura, *Bull. Chem. Soc. Jpn.*, **46**, 2589 (1973).
2) Part II: Y. Ohashi and Y. Sasada, *Bull. Chem. Soc. Jpn.*, **50**, 1710 (1977).
3) Part III: Y. Ohashi and Y. Sasada, *Bull. Chem. Soc. Jpn.*, **50**, 2863 (1977).
4) Part IV: Y. Ohashi, Y. Sasada, S. Takeuchi, and Y. Ohgo, *Bull. Chem. Soc. Jpn.*, **53**, 627 (1980).
5) Y. Ohgo, S. Takeuchi, and J. Yoshimura, *Bull. Chem. Soc. Jpn.*, **44**, 283 (1971).
6) Y. Ohgo, S. Takeuchi, and J. Yoshimura, *Bull. Chem. Soc. Jpn.*, **44**, 583 (1971).
7) S. Takeuchi, Y. Ohgo, and J. Yoshimura, *Chem. Lett.*, **1973**, 265.
8) Y. Ohgo, S. Takeuchi, Y. Natori, and J. Yoshimura, *Chem. Lett.*, **1974**, 33.
9) Y. Ohgo, Y. Natori, S. Takeuchi, and J. Yoshimura, *Chem. Lett.*, **1974**, 709.
10) Y. Ohgo, Y. Natori, S. Takeuchi, and J. Yoshimura, *Chem. Lett.*, **1974**, 1327.
11) Y. Ohashi, Y. Sasada, and Y. Ohgo, *Chem. Lett.*, **1978**, 743.
12) "International Tables for X-Ray Crystallography," Vol. IV, The Kynoch Press, Birmingham (1974), p. 72.
13) D. L. McFadden and A. T. McPhail, *J. Chem. Soc., Dalton Trans.*, **1974**, 363.
14) A, Bigotto, E. Zangrando, and L. Randaccio, *J. Chem. Soc., Dalton Trans.*, **1976**, 96.
15) P. G. Lenhert, *Chem. Commun.*, **1976**, 980.
16) S. Brückner and L. Randaccio, *J. Chem. Soc., Dalton Trans.*, **1974**, 1017.
17) J. D. Morrison and H. S. Mosher, "Asymmetric Organic Reactions," Prentice-Hall, Englewood Cliffs, New Jersey (1971), p. 28.

Neutron Diffraction Study of Liquid Acetyl Chloride

Norio OHTOMO† and Kiyoshi ARAKAWA*

Research Institute of Applied Electricity, Hokkaido University, Sapporo 060

†*Faculty of Engineering, Hokkaido University, Sapporo 060*

(Received September 17, 1979)

The structure factor $S_m(Q)$ for liquid acetyl chloride at room temperature has been determined in the range Q, 0.9—27 Å^{-1}, by means of the time-of-flight (TOF) neutron diffraction method using the electron linear accelerator (LINAC). The structural parameters of CD_3COCl, bond distances, bond angles, and rms amplitudes, in liquid phase have been determined by a comparison of calculated curves with observed data, and it has been concluded that a molecule within the liquid takes an essentially identical conformation as a rotational isomer with that in gaseous phase, which was determined by microwave spectroscopy.

Studies on neutron diffraction have been extensively carried out during the last three decades. Neutron diffraction as well as X-ray and electron diffraction has turned out to be a powerful means for determining the structure of condensed matter directly.[1] The method has been applied to structural studies of molecular liquids recently. The positions of light atoms as hydrogen (deuterium) contained in the molecules of organic liquids can be determined. A typical molecular liquid as an object of studies by means of neutron diffraction is heavy water. Studies were carried out by Page and Powles,[2] Narten,[3] and the authors.[4,5]

Neutron diffraction studies on molecular liquids including water have provided useful information. Dore *et al.* studied diatomic liquids (N_2, O_2, and Br_2) and other non-hydrogenous and heteronuclear molecular liquids (C_2O_3, $VOCl_3$, and XCl_4: X=C, V, Si, Ti, Ge, and Sn). Structure factors $S_m(Q)$ for a wide range of momentum transfer Q were determined for these materials.[6] Bertagnolli *et al.* carried out measurements for hydrogenous molecular liquids (CD_3CN and $CDCl_3$) and determined $S_m(Q)$ in the range of low Q.[7] In order to determine the structure and conformation of molecules in liquids, it is necessary to obtain the $S_m(Q)$ data in a wide range of Q values. The neutron diffraction experiment by LINAC is extremely useful for obtaining data for higher Q values.

The result of a neutron diffraction study on liquid acetyl chloride is given in the present paper. Studies were carried out on the molecular structure of acetyl chloride in gaseous phase with use of electron diffraction and microwave spectroscopy,[8–10] Sinnott's[9] result by microwave spectroscopy being considered to be accurate. However, the structure and configuration of the molecule in liquid state have never been studied. Conformation of the molecule within the liquid is of interest in comparison with that in gaseous phase as considered from the viewpoint that strong molecular interactions within liquid may cause a change of conformation as a rotational isomer. The authors have been able to obtain the $S_m(Q)$ for a wide range of Q which is sufficient to make a precise determination of the structure of the molecule within the liquid.

Experimental

Procedure for Measurements. The experiment was performed by means of the TOF neutron diffraction method by LINAC.[4,5] Details of the apparatus and procedure were reported.[4,11]

Deuterated acetyl chloride CD_3COCl (purity of deuteration 99%, Stohler Isotope Chemicals (USA)) was used. The coherent scattering amplitude, scattering cross sections, and the absorption cross section for each atom are given in Table 1. The effect of strong absorption by chloride nuclei at lower Q can be corrected easily since the atoms absorb neutrons according to the $1/v$ law in the low energy region (v: neutron velocity).

Table 1. Coherent scattering amplitude (b_{coh}), scattering cross sections (σ_{coh} and σ_{inc}) and absorption cross section (σ_a)[a]

Element	b_{coh} (fermis)	σ_{coh} (barns)	σ_{inc} (barns)	σ_a (barns)
D	6.67	5.59	2.0	0.00046
C	6.65	5.56	0	0.0033
O	5.80	4.23	0	<0.002
Cl	9.6	11.58	3.5	33.6
V	−0.4	0.02	4.9	4.98

$\sigma_{coh}=4\pi b_{coh}^2$ and $\sigma_{inc}=4\pi b_{inc}^2$, where b_{inc} is the incoherent scattering amplitude. a) B. Dorner and R. Comès, "Dynamics of Solids and Liquids by Neutron Scattering," ed by S. W. Lovesey and T. Springer, Springer-Verlag, Berlin (1977), Chap. 3, pp. 136—141.

Measurements were carried out at room temperature (16 °C) at two different scattering angles (2θ=45° and 150°). Time-of-flight of neutrons was analyzed with a multi-channel time analyzer with channel widths of 20 μs and 10 μs at the scattering angles of 45° and 150°, respectively. Thin-walled cyrindrical quartz vessels were used to contain samples.

We obtained the $S_m(Q)$ data for low Q region (Q=0.95—14 Å^{-1}) and those for a higher Q region (Q=3.0—27 Å^{-1}) by measurement at each scattering angle. The count rate time-spectrum is given in Fig. 1 together with smoothed spectra for vanadium and background normalized in burst number of LINAC.

Corrections and Calibrations of Raw Scattering Data.[2,4] In order to determine structure factors, corrections for multiple scattering, absorption, background counting, and inelastic scattering are necessary. Absolute normalization of data was performed with use of scattering data from a standard vanadium rod of the same shape and dimensions as the sample.[4] $S_m(Q)$ data obtained after the correction except for inelastic scattering are given in Fig. 2.

A steady fall in $S_m(Q)$ values, caused by the inelastic scattering of neutrons by light nuclei, is observed at higher Q. For compensating of the effect, several conventional and useful

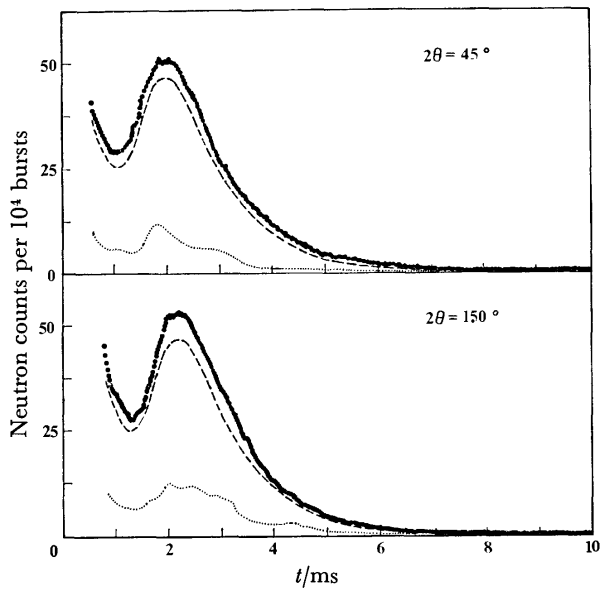

Fig. 1. Time-of-flight spectra.
●: CD_3COCl (16°C)+background, ------: vanadium +background, ·····: background.

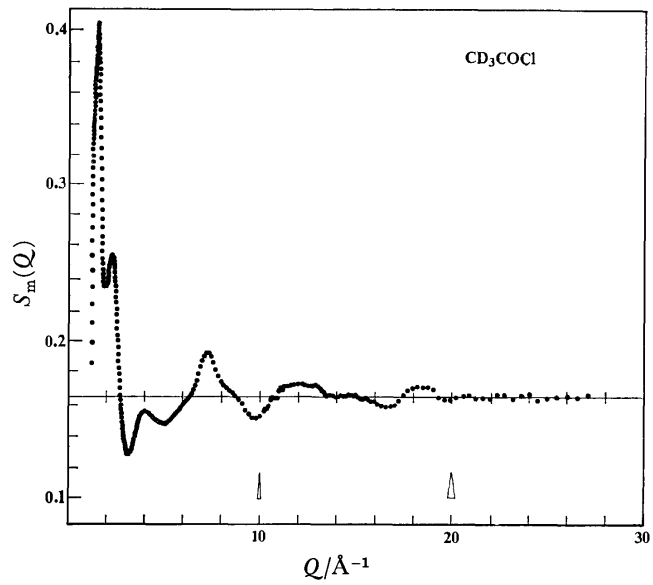

Fig. 3. The final structure factor $S_m(Q)$.
The magnitudes of the instrumental resolution are indicated by triangles at two points.

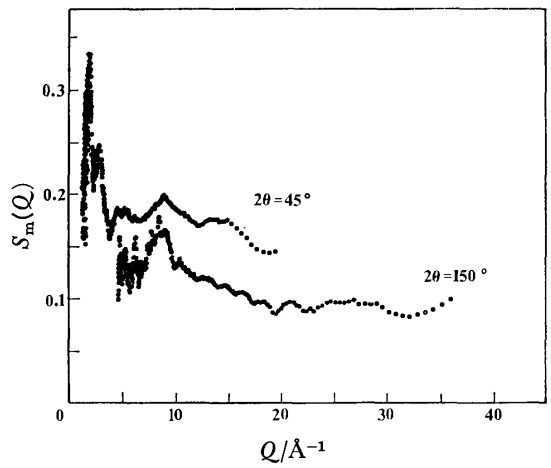

Fig. 2. The observed structure factor obtained after the application of corrections except that for inelastic scattering.

correction methods can be used. In the present study the Placzek method[12] was applied in a lower Q region and a dynamical correction method[13] in a higher Q region.

Calibration of absolute values for high Q data was performed considering the fact that $S_m(Q) \rightarrow \sum b_n^2/(\sum b_n)^2$ as $Q \rightarrow \infty$, where n ranges over all the nuclei in a molecule. Calibration for low Q data was made by overlapping the $S_m(Q)$ curves in the range 8—10 Å^{-1} for the two data sets. Thus, combining the two data sets,[6] we have obtained the final $S_m(Q)$ curve for the range of Q, 0.9—27 Å^{-1} (Fig. 3). The magnitudes of resolution ΔQ are given as triangles along the abscissa.[4] The statistical error was found to be smaller than 2.5% in the whole range of Q.

Results and Discussion

Analysis of Experimental Data. The structure factor $S_m(Q)$ for molecular liquids consists of an intramolecular structure factor $S_m^{(1)}(Q)$ and an intermolecular one $S_m^{(2)}(Q)$:

$$S_m(Q) = S_m^{(1)}(Q) + S_m^{(2)}(Q). \quad (1)$$

The higher the Q values, the smaller the $S_m^{(2)}(Q)$. Accordingly, structure factors for a higher Q region are characteristic of a single molecule, *viz.* the intramolecular structure factor

$$S_m(Q) \rightarrow S_m^{(1)}(Q) \text{ for high } Q. \quad (2)$$

For acetyl chloride the intramolecular structure factor becomes

$$S_m^{(1)}(Q) = (3b_D+2b_C+b_O+b_{Cl})^{-2}[3b_D^2+2b_C^2+b_O^2+b_{Cl}^2 + \sum_{i \neq j} b_i b_j j_0(Qr_{ij}) \exp(-\gamma_{ij}Q^2)], \quad (3)$$

where b_D, b_C, b_O, and b_{Cl} denote the coherent neutron scattering length of deuterium, carbon, oxygen, and chloride nucleous, respectively, $j_0(Qr)$ is a spherical Bessel function of zeroth order, and $(2\gamma_{ij})^{1/2}$ the rms amplitude to a bond length r_{ij}. The summation involved fifteen independent terms corresponding to different bond lengths.

The molecular model of acetyl chloride is shown in Fig. 4. The structure of the molecule except the methyl group is assumed to be a plane configuration,[9,10] and deuterium atoms in the methyl group are considered to

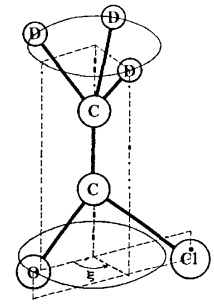

Fig. 4. The molecular model of acetyl chloride.

rotate about the C–C axis. At the rotational angle $\xi=0°$, a methyl deuterium atom eclipses oxygen atom (Fig. 4).

The structure of the molecule is characterized by the magnitudes of structural parameters: four bond lengths ($r_{C=O}$, r_{C-C}, r_{C-Cl}, and r_{C-D}), four rms amplitudes ($(2\gamma_{C=O})^{1/2}$, $(2\gamma_{C-C})^{1/2}$, $(2\gamma_{C-Cl})^{1/2}$, and $(2\gamma_{C-D})^{1/2}$), four bonding angles ($\angle$C–C=O, $\angle$C–C–Cl, $\angle$D–C–C, and $\angle$D–C–D), and a rotational angle ξ (Fig. 4). Values of these parameters determined so far for gas molecules of CH_3COCl by means of electron diffraction and microwave spectroscopy are summarized in Table 2,[8–10,14,15] the rms amplitudes being cited from the results of electron diffraction studies of formic acid (C=O)[14] and of *n*-propyl chloride (C–C, C–Cl, and C–H).[15]

TABLE 2. MOLECULAR PARAMETERS DETERMINED BY ELECTRON DIFFRACTION (ED) AND MICROWAVE (MW) METHODS

	ED[8]	MW[9]	$(2\gamma_{1j})^{1/2}$ [15]
Bond length (Å)			
C=O	1.22±0.04	1.192±0.010	<0.030[14]
C–C	1.50±0.04	1.499±0.010	0.036
C–Cl	1.77±0.02	1.789±0.005	0.051
C–H	1.09(assumed)	1.083±0.005	0.067
Bond angle			
$\angle$C–C=O		127°5′±10′	
$\angle$C–C–Cl	110°±3°	112°39′±30′	
$\angle$H–C–H		108°44′±30′ [a]	
$\angle$H–C–C	109.5°	110°21′±10′	

a) L. C. Krisher and E. B. Wilson, Jr., *J. Chem. Phys.*, **31**, 882 (1959).

Determination of the Intramolecular Structure within Liquid. In order to determine the molecular parameters and investigate the internal rotation of the methyl group by means of Eq. 2, $S_m^{(1)}(Q)$ was calculated for a number of structure models using Eq. 3, the magnitudes of the parameters being varied in reference to the values given in Table 2. The procedure of analysis is as follows.

Firstly, $S_m^{(1)}(Q)$ values were calculated with a variation of ξ successively at intervals of 10° from 0° to 80° and also for the averaged values corresponding to the free rotation of the methyl group about the C–C axis.[2,4] The parameters involving deuterium atom only (r_{C-D}, $\angle$D–C–D, and $\angle$D–C–C) were varied as follows: r_{C-D}, 1.085—1.105 Å at 0.005 Å step, $\angle$D–C–D, 108.5±1.0° and $\angle$D–C–C, 110.5±1.0°. The remainder of parameters were fixed to the values in Table 2. At the first stage we calculated the $S_m^{(1)}(Q)$ for 495 models. A typical example of the $S_m^{(1)}(Q)$ curves calculated with the variation of ξ is shown in Fig. 5. The best fit curve at the first stage of analysis with the experimental data is obtained at $\xi=0°$, $r_{C-D}=1.095$ Å, $\angle$D–C–D=108.5° and $\angle$D–C–C=110.0°.

Secondly, in order to determine more precisely the eight parameters (r_{C-C}, $r_{C=O}$, r_{C-Cl}, r_{C-D}, $\angle$C–C=O, $\angle$C–C–Cl, $\angle$D–C–D, and $\angle$D–C–C), keeping the value of ξ at 0° and fixing the values of rms amplitudes to the values in Table 2, we calculated $S_m^{(1)}(Q)$ for 435 models, the parameters being varied in the range given

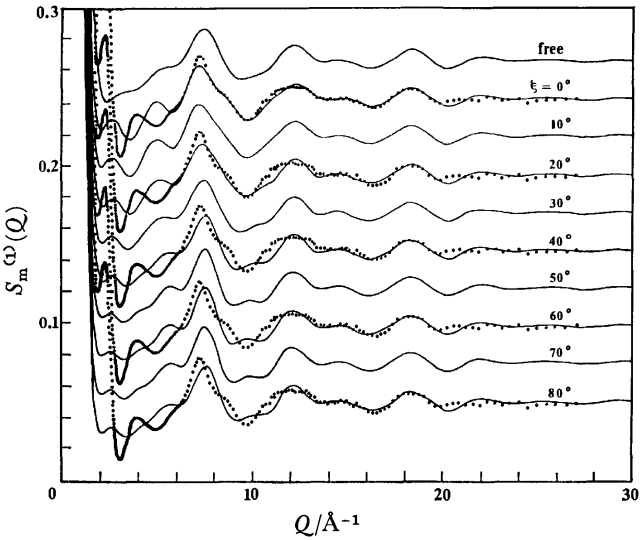

Fig. 5. The calculated $S_m^{(1)}(Q)$ with the variation of rotational angle ξ.
●: $S_m(Q)$ observed, ——: $S_m^{(1)}(Q)$ calculated.

TABLE 3. RANGE OF PARAMETERS

Parameter	Range	Interval of variation
	(Å)	(Å)
$r_{C=O}$	1.400—1.600	0.005
r_{C-C}	1.175—1.205	0.005
r_{C-Cl}	1.775—1.805	0.005
r_{C-D}	1.085—1.105	0.005
	(degree)	(degree)
$\angle$C–C=O	125.0—129.0	1.0
$\angle$C–C–Cl	110.5—113.5	1.0
$\angle$D–C–D	107.5—109.5	0.5
$\angle$D–C–C	109.5—111.5	0.5

TABLE 4. MOLECULAR PARAMETERS DETERMINED BY NEUTRON DIFFRACTION METHOD

	r_{1j} (Å)	$(2\gamma_{1j})^{1/2}$ (Å)		Bond angle (degree)
C=O	1.190±0.010	0.029	$\angle$C–C=O	127.0±1.0
C–C	1.500±0.005	0.036	$\angle$C–C–Cl	112.5±1.0
C–Cl	1.790±0.010	0.052	$\angle$D–C–D	108.5±0.5
C–D	1.095±0.005	0.066	$\angle$D–C–C	110.0±0.5

in Table 3. From a comparison of the calculated curves with experimental result, the parameters (except rms amplitudes) which gave the best fit model were determined (Table 4).

Finally, for the case of the parameter set thus determined calculations for 32 models with the variation of the rms amplitudes were carried out and the curves obtained compared with experimental results. The magnitudes of the rms amplitudes are also given in Table 4. The best fit curve with the experimental data is shown in Fig. 6. Agreement of both curves is excellent in the range of Q values, 5.5—20 Å^{-1}. The apparent deviations beyond $Q\gtrsim20$ Å^{-1} are insignificant and negligible. The deviation of the calculated $S_m^{(1)}(Q)$

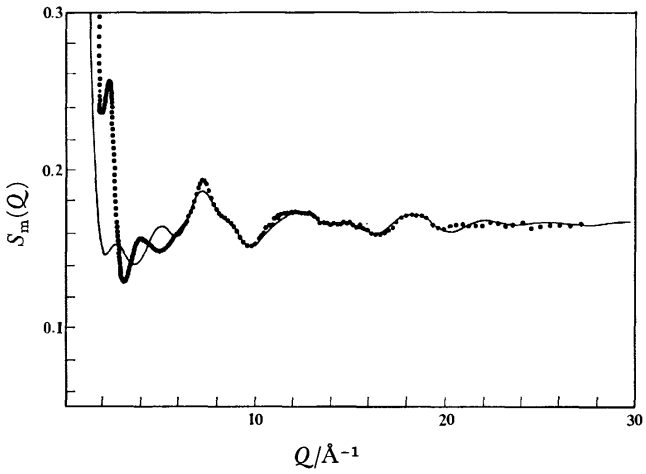

Fig. 6. Comparison of the calculated $S_m^{(1)}(Q)$ with the observed $S_m(Q)$.
●: $S_m(Q)$ observed, ——: $S_m^{(1)}(Q)$ calculated for the best model.

from the experimental curve in low Q region ($Q \lesssim 5.5$ Å^{-1}) is ascribed to the intermolecular contribution in liquid not included in the calculation (Eq. 3).

The results show that one methyl deuterium atom eclipses oxygen atom for the molecule in liquid as well as in gaseous phase. The molecular parameters assigned for liquid acetyl chloride (Table 4) are nearly identical with those determined for the molecule in gaseous phase by Sinnott.[9] The C–D bond length ($=1.095 \pm 0.005$ Å) is slightly larger than those in methyl groups.[9]

Conformation of a Molecule in Liquid Acetyl Chloride in Comparison with That in Gaseous Phase. A molecule within a system often changes its conformation through a phase transition. A typical example is the case of 1,2-dichloroethane ($C_2H_4Cl_2$) which has been studied fairly in detail.[16,17] A $C_2H_4Cl_2$ molecule in solid phase takes trans-conformation only; in liquid phase trans- and gauche-molecules are present at a ratio of *ca.* 1 : 1.92 in number; in gaseous phase the fraction of gauche-molecules decreases.

A molecule in gaseous phase seems to change its conformation as a rotational isomer in liquid and solid phase, as considered from the stronger effects of molecular interactions in condensed phases. According to the present result the situation for CD_3COCl differs from that for $C_2H_4Cl_2$. We have confirmed that all the CD_3COCl molecules in liquid phase take the conformation in which a deuterium atom in CD_3 group of the molecule eclipses the oxygen atom like that in gaseous phase.[18] A CD_3COCl molecule as a rotational isomer about the C–C axis does not change its conformation essentially through a phase change from gaseous to liquid state, the conformation being kept as shown in Fig. 4.

Microwave spectroscopy and electron diffraction have been used widely for determination of the structure of molecules, but application of the methods is mostly confined to gaseous systems. For determination of the molecular conformation within liquid, the neutron diffraction technique is considered important when used in combination with other techniques applicable to gases.

References

1) G. E. Bacon, "Neutron Diffraction," 3rd ed, Clarendon Press, Oxford (1975).
2) D. I. Page and J. G. Powles, *Mol. Phys.*, **21**, 901 (1971).
3) A. H. Narten, *J. Chem. Phys.*, **56**, 5681 (1972).
4) N. Ohtomo and K. Arakawa, *Bull. Chem. Soc. Jpn.*, **51**, 1649 (1978).
5) N. Ohtomo and K. Arakawa, *Bull. Chem. Soc. Jpn.*, **52**, 2755 (1979).
6) J. C. Dore, G. Walford, and D. I. Page, *Mol. Phys.*, **29**, 565 (1975); J. H. Clarke, J. C. Dore, and R. N. Sinclair, *ibid.*, **29**, 581 (1975); J. H. Clarke, J. C. Dore, G. Walford, and R. N. Sinclair, *ibid.*, **31**, 883 (1977); G. Stanton, J. H. Clarke, and J. C. Dore, *ibid.*, **34**, 823 (1977); G. Walford, J. H, Clarke, and J. C. Dore, *ibid.*, **36**, 1581 (1978); J. H. Clarke, J. R. Granada, and J. C. Dore, *ibid.*, **37**, 1263 (1979); I. P. Gibson and J. C. Dore, *ibid.*, **37**, 1281 (1979); J. R. Granada, G. W. Stanton, J. H. Clarke, and J. C. Dore, *ibid.*, **37**, 1297 (1979).
7) H. Bertagnolli, P. Chieux, and M. D. Zeidler, *Mol. Phys.*, **32**, 759: 1731 (1976); H. Bertagnolli, D. O. Leicht, and M. D. Zeidler, *ibid.*, **35**, 199: **36**, 1769 (1978).
8) Y. Morino, K. Kuchitsu, M. Iwasaki, K. Arakawa, and A. Takahashi, *Nippon Kagaku Zasshi*, **75**, 647 (1954).
9) K. M. Sinnott, *J. Chem. Phys.*, **34**, 851 (1961).
10) H. Takeo and C. Matsumura, *J. Chem. Phys.*, **64**, 4536 (1976).
11) T. Matsumoto, N. Ohtomo, and M. Senda, *J. Nucl. Sci. Technol.*, **15**, 863 (1978).
12) G. Placzek, *Phys. Rev.*, **86**, 377 (1952); J. G. Powles, *Mol. Phys.*, **36**, 1161: 1181 (1978).
13) G. C. Wick, *Phys. Rev.*, **94**, 1228 (1954); T. Matsumoto, *J. Nucl. Sci. Technol.*, **16**, 401 (1979).
14) I. L. Karle and J. Karle, *J. Chem. Phys.*, **22**, 43 (1954).
15) Y. Morino and K. Kuchitsu, *J. Chem. Phys.*, **28**, 175 (1957).
16) S. Mizushima, "Structure of Molecules and Internal Rotation," Academic Press Inc., New York (1954).
17) R. J. W. Le Fèrve and B. J. Orr, *Aust. J. Chem.*, **17**, 1098 (1964).
18) E. L. Eliel, N. L. Allinger, S. J. Angyal, and G. A. Morrison, "Conformational Analysis," Interscience Publishers (1965), pp. 19—20.

Structural Studies of Fortimicins. II.† Crystal and Molecular Structure of Fortamine

Noriaki HIRAYAMA,* Kunikatsu SHIRAHATA, Yuji OHASHI,†† and Yoshio SASADA††

Tokyo Research Laboratory, Kyowa Hakko Kogyo Co., Ltd., 3-6-6 Asahimachi, Machida, Tokyo 194

††*Laboratory of Chemistry for Natural Products, Tokyo Institute of Technology, Nagatsuta, Midori-ku, Yokohama 227*

(Received October 17, 1979)

Fortamine, L-3-amino-1-methoxy-6-methylamino-1,3,6-trideoxy-*chiro*-inositol, is a component of fortimicins which are potent aminocyclitol antibiotics. The space group is $P2_1$ with $a=9.454(1)$, $b=6.6957(8)$, $c=7.622(1)$ Å, $\beta=95.93(2)°$, and two $C_8H_{18}N_2O_4$'s per unit cell. The structure was solved by direct methods, least-squares refinement using 932 reflexions giving the final R value of 0.033. The ring conformation of fortamine is closer to the ideal chair form than that of the fortamine moiety in fortimicin B. The strain caused by the intramolecular hydrogen bond and glycosidic bond in fortimicin B is released in fortamine.

Fortimicins[1,2] are potent broad-spectrum aminocyclitol antibiotics produced by a strain of *Micromonospora olivoasterospona*.[3-5] The conformation of the 1,4-diaminocyclitol moiety of fortimicins is probably related to their activity.[1,3,4] We have determined the absolute configuration of fortimicin B (Fig. 1) by X-ray analysis.[6] An intramolecular hydrogen bond is formed between O(5)–H and N(2′), the fortamine ring being distorted from the ideal chair conformation. It is of interest to examine whether the ring distortion is due to the glycosidic bond or the intramolecular hydrogen bond. We have carried out an X-ray analysis of fortamine obtained by the hydrolysis of fortimicin B.

Experimental and Structure Determination

Fortamine was prepared by the hydrolysis of fortimicin B with hydrochloric acid. Crystals of fortamine were grown from a methanol solution. A $0.5\times0.3\times0.3$ mm³ crystal sealed in a glass capillary was used for data collection on a Rigaku four-circle automated diffractometer with graphite-monochromated Mo $K\alpha$ radiation ($\lambda=0.71069$ Å). Preliminary unit cell dimensions and space group were obtained from photographs. The space group was determined from systematic absence ($0k0$ for odd k). Accurate cell dimensions were determined by least-squares calculations with the 2θ values of 15 high-angle reflexions measured on the diffractometer. Crystal data are summarized in Table 1. All reflexions within the range $2\theta\leqq55°$ were collected by use of the ω-2θ scan mode with a scanning rate of $4°(2\theta)$ min^{-1}. Stationary background counts were accumulated for 10 s before and after each scan. Periodic checks of the intensity values of three standard reflexions showed no significant X-ray damage or crystal decay. Corrections for absorption or extinction were not applied. A total of 1191 independent reflexions were obtained, of which 932 ($|F_0|>3.0\sigma(|F_0|)$) were considered as observed.

The phases of 185 reflexions with $|E_0|\geqq1.2$ were assigned with MULTAN.[7] The best set of phases was used to calculate an E map, which gave 14 chemically significant peaks. The structural parameters were refined by block-diagonal least-squares methods with a modified HBLS program. At the stage $R=0.17$, all the hydrogen atoms were found by the difference Fourier synthesis. Refinement using anisotropic and isotropic temperature factors for the non-hydrogen and hydrogen atoms, respectively, gave the final R value 0.033 for 932 reflexions. The weighting system used in the final stage was $w=0.3$ for $|F_0|<1.51$ and $|F_0|>35.57$, and $w=(0.00792(F_0)^2-0.29822|F_0|+3.76458)^{-1}$ for $1.51\leqq|F_0|\leqq35.57$. Six strong reflexions, 1 −1 0, 1 −4 1, −1 −1 4, 1 0 0, −2 3 3, and −3 4 3, were excluded because they seemed to suffer from secondary extinctions. Atomic scattering factors were taken from "International Tables for X-Ray Crystallography".[8] The final positional and thermal parameters are given in Table 2. The tables of observed and calculated structure factors are kept as Document No. 8024 at the Chemical Society of Japan.

Table 1. Crystal data

$C_8H_{18}N_2O_4$	$b=6.6957(8)$
$M.W.=206.24$	$c=7.622(1)$ Å
$P2_1$	$\beta=95.93(2)°$
$Z=2$	$D_x=1.4276$ g·cm^{-3}
$a=9.454(1)$	μ(Mo $K\alpha$)$=1.221$ cm^{-1}

† Part I of the series: "Structure of Fortimicin B."[6]

Results and Discussion

Hydrogen Bond and Crystal Structure. The numbering system of atoms and the crystal structure viewed along the b axis are shown in Figs. 1 and 2, respectively. Hydrogen bond lengths and angles are given in Table 3. In the fortamine moiety of fortimicin B, only the O(2) hydroxyl group is involved in the intermolecular hydrogen bond. In fortamine, on the other hand, all functional groups except the methoxyl are involved in the intermolecular hydrogen bonds, there being no

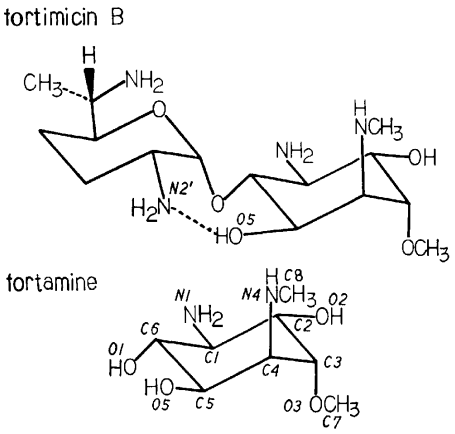

Fig. 1. Structures of fortimicin B and fortamine.

Table 2a. Final atomic coordinates with their estimated standard deviations, multiplied by 10^4 for non-hydrogen atoms and 10^3 for hydrogen atoms

Atom	x	y	z	Atom	x	y	z
C(1)	967(2)	3690(4)	2962(3)	HC(3)	368(2)	125(4)	135(3)
C(2)	1780(3)	1930(4)	2320(3)	HC(4)	420(2)	464(4)	35(3)
C(3)	3247(2)	2514(4)	1869(3)	HC(5)	301(3)	640(4)	236(3)
C(4)	3162(2)	4201(4)	502(3)	HC(6)	26(2)	500(4)	51(3)
C(5)	2372(3)	5985(4)	1179(3)	HAC(7)	528(3)	96(6)	407(4)
C(6)	897(3)	5422(4)	1642(3)	HBC(7)	602(3)	334(6)	475(4)
C(7)	5428(3)	2351(5)	3765(4)	HCC(7)	593(3)	249(6)	280(4)
C(8)	3352(3)	2146(5)	−2127(3)	HAC(8)	293(2)	207(4)	−336(3)
N(1)	−488(2)	3057(4)	3223(3)	HBC(8)	329(3)	75(5)	−149(4)
N(4)	2458(2)	3532(3)	−1229(2)	HCC(8)	434(2)	261(4)	−211(3)
O(1)	266(2)	7113(3)	2411(2)	HAN(1)	−100(3)	426(5)	367(3)
O(2)	1874(2)	399(3)	3640(2)	HBN(1)	−45(3)	209(5)	400(3)
O(3)	4074(2)	3243(3)	3421(2)	HN(4)	230(2)	467(4)	−192(3)
O(5)	2347(2)	7648(3)	1(2)	HO(1)	−50(2)	737(4)	189(3)
HC(1)	141(2)	418(4)	402(3)	HO(2)	144(3)	−59(4)	328(3)
HC(2)	127(2)	137(4)	122(3)	HO(5)	167(3)	751(5)	−92(3)

Table 2b. Final thermal parameters with their estimated standard deviations
Anisotropic thermal parameters (Å^2) are multiplied by 10^4 and isotropic ones (Å^2) multiplied by 10^3.

Atom	U or U_{11}	U_{22}	U_{33}	U_{12}	U_{13}	U_{23}
C(1)	284(1)	241(13)	226(11)	−30(11)	−7(9)	−13(11)
C(2)	371(13)	194(12)	197(11)	−4(12)	−40(10)	26(10)
C(3)	320(12)	280(15)	219(11)	50(12)	−36(9)	−74(11)
C(4)	215(11)	314(15)	276(12)	−43(11)	29(10)	−53(12)
C(5)	298(13)	235(13)	260(12)	−20(11)	−10(10)	−21(11)
C(6)	265(12)	213(12)	242(11)	34(11)	−3(9)	−35(11)
C(7)	302(14)	508(19)	488(16)	53(15)	−71(12)	12(16)
C(8)	433(15)	429(17)	275(13)	39(15)	67(11)	−59(14)
N(1)	343(11)	321(13)	330(11)	−7(11)	88(9)	39(11)
N(4)	275(10)	273(12)	224(9)	−1(10)	24(8)	5(10)
O(1)	286(8)	245(9)	386(9)	66(9)	−16(7)	−68(9)
O(2)	518(11)	215(9)	297(9)	−6(9)	−46(8)	55(9)
O(3)	290(9)	458(12)	336(9)	115(10)	−112(7)	−120(10)
O(5)	429(10)	257(10)	389(10)	−61(9)	13(8)	68(9)
HC(1)	23(6)					
HC(2)	25(6)					
HC(3)	24(7)					
HC(4)	22(6)					
HC(5)	44(8)					
HC(6)	21(6)					
HAC(7)	87(12)					
HBC(7)	78(11)					
HCC(7)	96(12)					
HAC(8)	38(7)					
HBC(8)	63(9)					
HCC(8)	43(8)					
HAN(1)	60(9)					
HBN(1)	53(8)					
HN(4)	27(7)					
HO(1)	51(8)					
HO(2)	43(8)					
HO(5)	58(9)					

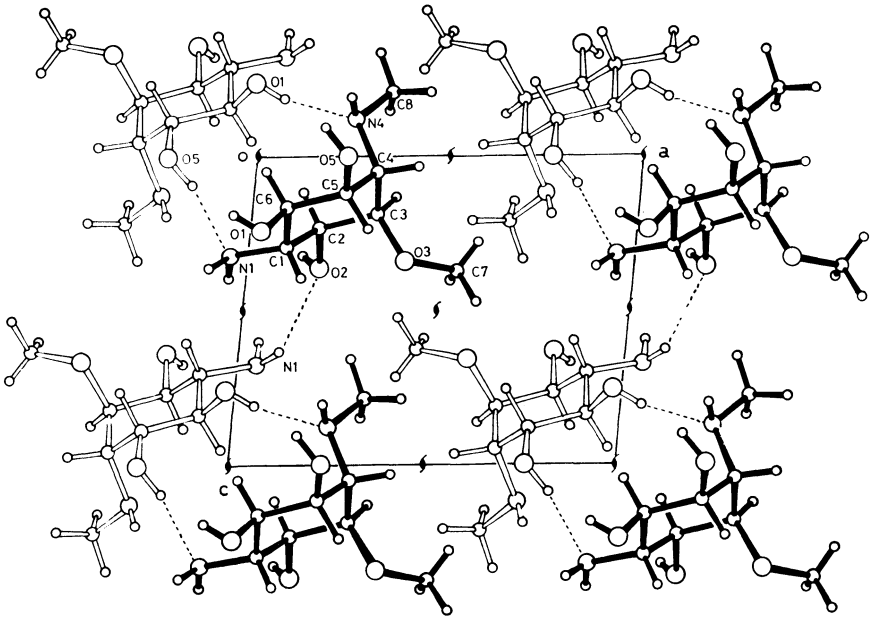

Fig. 2. The crystal structure projected along the b axis. The molecule composed of the numbering atoms corresponds to that given in Table 2.

TABLE 3. HYDROGEN BOND DISTANCES (l/Å) AND ANGLES (ϕ/°)

A–H···B	A···B	∠A–H···B
O(1)–H^{I}···N(4)^{II}	2.806(3)	163(3)
O(5)–H^{I}···N(1)^{II}	2.881(3)	160(3)
O(2)–H^{I}···O(1)^{III}	2.781(3)	177(3)
N(1)–H^{I}···O(2)^{IV}	3.246(3)	138(3)

I: (x y z)
II: ($-x$ 1/2+y $-z$)
III: (x $-1+y$ z)
IV: ($-x$ 1/2+y 1$-z$)

intramolecular hydrogen bond. The molecules related by the 2_1 screw axis through the origin are connected by the O(1)–H···N(4) and O(5)–H···N(1) hydrogen bonds. Along the b axis the molecules are linked by the O(2)–H···O(1) hydrogen bonds. The infinite columns thus formed are further interlinked by the weak N(1)–H···O(2) hydrogen bond to give double-layers. Boundary between the double-layers at (1/2, y, z) is held together mainly by the van der Waals forces of *N*-methyl and *O*-methyl groups.

Bond Lengths and Angles. Bond lengths and angles are given in Table 4, together with the corresponding values in fortimicin B. The average endocyclic

TABLE 4. BOND LENGTHS (l/Å) AND ANGLES (ϕ/°)

	Fortamine	Fortimicin B		Fortamine	Fortimicin B
C(1)–C(2)	1.505(4)	1.524(8)	C(1)–C(2)–C(3)	112.6(2)	110.4(5)
C(1)–C(6)	1.545(4)	1.510(8)	C(2)–C(3)–C(4)	111.1(2)	111.3(5)
C(2)–C(3)	1.513(4)	1.523(8)	C(3)–C(4)–C(5)	109.9(2)	109.3(5)
C(3)–C(4)	1.532(4)	1.526(9)	C(4)–C(5)–C(6)	112.0(2)	113.5(5)
C(4)–C(5)	1.528(4)	1.546(9)	C(5)–C(6)–C(1)	111.2(2)	113.9(5)
C(5)–C(6)	1.521(4)	1.501(8)	C(6)–C(1)–C(2)	111.4(2)	109.6(5)
C(1)–N(1)	1.470(4)	1.474(8)	N(1)–C(1)–C(2)	110.4(2)	110.2(5)
C(2)–O(2)	1.432(3)	1.410(7)	N(1)–C(1)–C(6)	108.7(2)	108.2(5)
C(3)–O(3)	1.434(4)	1.427(7)	O(2)–C(2)–C(1)	108.7(2)	111.1(5)
O(3)–C(7)	1.414(4)	1.389(10)	O(2)–C(2)–C(3)	110.7(2)	112.3(5)
C(4)–N(4)	1.485(4)	1.455(9)	O(3)–C(3)–C(2)	109.6(2)	113.6(5)
N(4)–C(8)	1.469(4)	1.486(9)	O(3)–C(3)–C(4)	107.2(2)	105.2(5)
C(5)–O(5)	1.429(3)	1.425(7)	C(7)–O(3)–C(3)	114.5(2)	116.6(5)
C(6)–O(1)	1.434(3)	1.439(7)	C(8)–N(4)–C(4)	112.2(2)	113.4(5)
			N(4)–C(4)–C(3)	111.8(2)	112.6(5)
			N(4)–C(4)–C(5)	110.3(2)	109.1(5)
			O(5)–C(5)–C(4)	112.0(2)	107.5(5)
			O(5)–C(5)–C(6)	112.5(2)	112.8(5)
			O(1)–C(6)–C(5)	109.1(2)	107.4(5)
			O(1)–C(6)–C(1)	109.1(2)	108.5(5)

C–C bond length, 1.522 Å, is equal to that of fortimicin B. The value is essentially the same as that of cyclohexane (1.532 Å)[9] and *myo*-inositol (1.521 Å).[10] The bond shortening of C(1)–C(6) and C(5)–C(6) in fortimicin B might be due to the glycosidic linkage. The long C(4)–C(5) distance of 1.546 Å in fortimicin B is probably caused by the strong intramolecular hydrogen bond. The results and geometries of cyclohexane rings in other compounds[9–13] suggest that the endocyclic C–C bond lengths can easily vary from 1.50 to 1.55 Å according to the intra- and intermolecular interactions.

The C(2)–O(2) and C(4)–N(4) bond lengths in fortamine are greater than those in fortimicin B by over 3σ. While O(2) in fortimicin B is weakly hydrogen bonded to solvent molecules with an O···O distance of 2.926(7) Å, that in fortamine is fairly strongly hydrogen bonded to the O(1) hydroxyl group with an O···O distance of 2.781(3) Å. Similarly, the N(4) atom in fortimicin B does not participate in a hydrogen bond, but that in fortamine is hydrogen bonded to the O(1) hydroxyl group. Such hydrogen bonds, therefore, seem to lengthen the bonds of C(2)–O(2) and C(4)–N(4) in fortamine.

The endocyclic bond angles C(1)–C(6)–C(5) and C(4)–C(5)–C(6) in fortimicin B are 113.9 and 113.5°, respectively, significantly larger than the average angle 111.5° in cyclohexane.[9] The corresponding values in fortamine having neither a glycosidic linkage nor an intramolecular hydrogen bond are 111.2 and 112.0°. The relatively large C(1)–C(2)–C(3) angle of 112.6° is probably due to the strong O(2)–H···O(1) hydrogen bond. The exocyclic bond angles of C(4)–C(5)–O(5) and O(5)–C(5)–C(6) are asymmetrical in fortimicin B because of the intramolecular hydrogen bond, while in fortamine they are symmetrical. Although O(3)–C(3)–C(4) and O(3)–C(3)–C(2) angles in fortimicin B are asymmetrical, they are symmetrical in fortamine.

Bond lengths and angles in fortamine are closer to the normal values than those in fortimicin B. Thus the glycosidic linkage and the intramolecular hydrogen bond might influence the local bond lengths and angles of fortamine ring.

Table 5. Torsional angles (τ/°)

	Fortamine	Fortimicin B
C(6)–C(1)–C(2)–C(3)	53.9	58.0
C(1)–C(2)–C(3)–C(4)	−56.1	−61.0
C(2)–C(3)–C(4)–C(5)	56.3	55.6
C(3)–C(4)–C(5)–C(6)	−56.4	−50.4
C(4)–C(5)–C(6)–C(1)	54.6	50.9
C(5)–C(6)–C(1)–C(2)	−52.6	−53.6
N(1)–C(1)–C(2)–O(2)	−62.2	−57.7
O(2)–C(2)–C(3)–O(3)	−59.8	−67.1
C(7)–O(3)–C(3)–C(4)	−110.1	−152.7
C(7)–O(3)–C(3)–C(2)	129.2	85.4
O(3)–C(3)–C(4)–N(4)	173.9	170.7
C(8)–N(4)–C(4)–C(5)	166.5	167.0
C(8)–N(4)–C(4)–C(3)	−70.9	−71.5
N(4)–C(4)–C(5)–O(5)	−60.1	−52.3
O(5)–C(5)–C(6)–O(1)	−57.9	−66.4
O(1)–C(6)–C(1)–N(1)	65.2	66.7

Conformation of the Molecule. A stereoscopic drawing of the molecule is shown in Fig. 3. The conformations of the ring and substituents of fortamine are essentially the same as those of fortimicin B. All torsional angles in the molecule are compared in Table 5. The overall flattening of fortamine rings is essentially the same in these two compounds with mean C–C–C–C torsional angles of 54.9° for fortimicin B and 55.0° for fortamine. These values are close to 54.9° in cyclohexane as determined by electron diffraction study.[9] In *epi*- and *myo*-inositol,[10] however, the ring is more puckered with the mean C–C–C–C torsional angles of 56.3 and 56.8°, respectively.

Closer examination shows that the present molecule takes a more symmetrical conformation than fortimicin B. The characteristics of the ring conformation are illustrated in Fig. 4, where the distance, d, is defined as the deviation of the two atoms from the least-squares plane of the other four atoms forming the seat of a chair. They are good indicies to show the puckering or the flattening of cyclohexane ring. The flattening, d= 0.601 Å, of the C(4)–C(5)–C(6) part in fortimicin B by the intramolecular hydrogen bond is accompanied

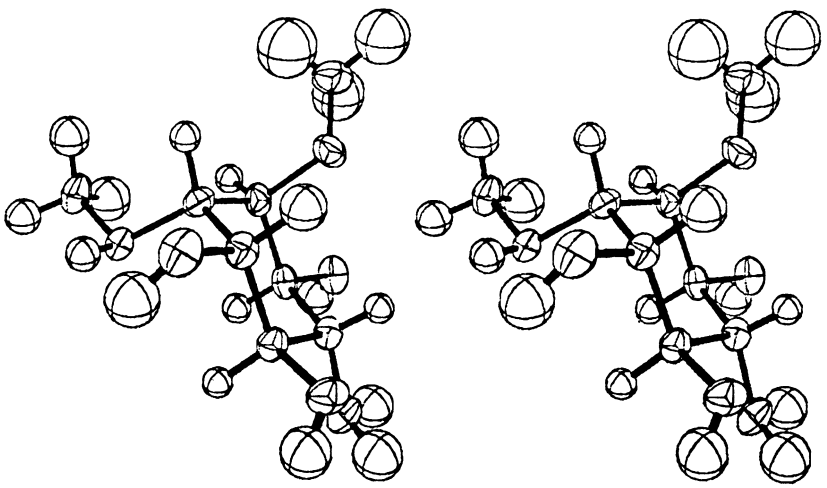

Fig. 3. Stereoscopic view with thermal ellipsoids at 50% probability.

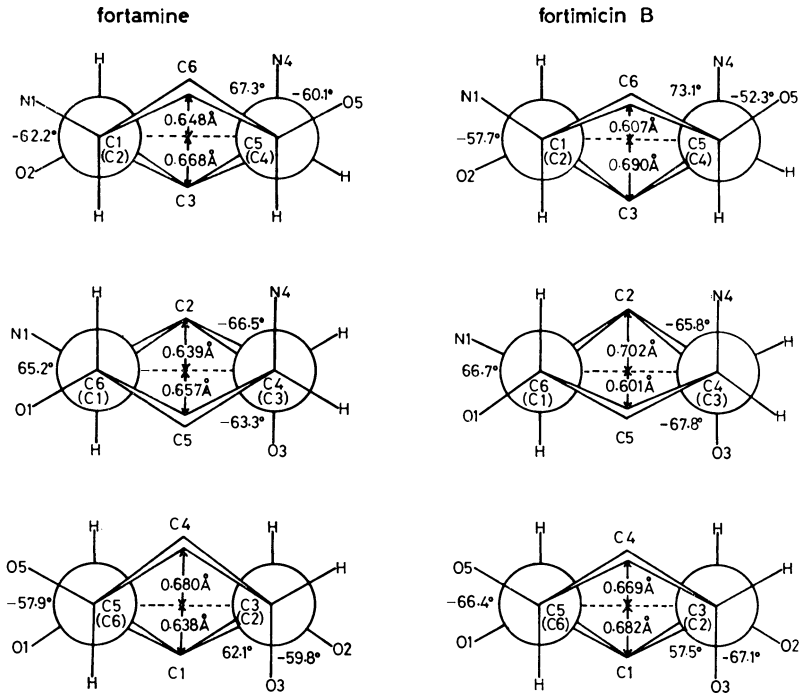

Fig. 4. Schematic drawing of chair forms of fortamine and fortimicin B.

by the puckering of the C(1)–C(2)–C(3) part, d=0.702 Å. The C(1)–C(6)–C(5) part in fortimicin B is flattened, (d=0.607 Å), probably due to the effect of the glycosidic bond, the flattening being followed by the puckering of the C(2)–C(3)–C(4) part, d=0.690 Å. In fortamine a slight puckering, d=0.680 Å, is seen at the *N*-methyl part but the ring as a whole takes essentially a symmetric structure.

These characteristics are related to the torsional angles. The C(3)–C(4)–C(5)–C(6), C(4)–C(5)–C(6)–C(1), C(1)–C(2)–C(3)–C(4) and C(6)–C(1)–C(2)–C(3) angles are significantly different between fortamine and fortimicin B. It seems that the remarkably small values of C(3)–C(4)–C(5)–C(6) and C(4)–C(5)–C(6)–C(1) angles in fortimicin B are mainly due to the intramolecular hydrogen bond. The effect of this local deformation of the chair geometry of the ring is discussed by calculating minimum energy conformation.[14] The calculation shows that the deformation of a torsional angle around an endocyclic bond induces an inverse deformation of the torsional angle around the opposite endocyclic bond in the ring. The extent is about 30% of the original deformation. The increase in C(1)–C(2)–C(3)–C(4) and C(6)–C(1)–C(2)–C(3) angles in fortimicin B are explained by this effect.

The results indicate that the glycosidic bond and the intramolecular hydrogen bond considerably flatten the fortamine ring locally.

References

1) R. S. Egan, R. S. Stanaszek, M. Cirovic, S. L. Mueller, J. Tadanier, J. R. Martin, P. Collum, A. W. Goldstein, R. L. De Vault, A. C. Sinclair, E. E. Fager, and L. A. Mitscher, *J. Antibiot.*, **30**, 552 (1977).

2) T. Iida, N. Sato, I. Matsubara, Y. Mori, and K. Shirahata, *J. Antibiot.*, in press.

3) T. Nara, M. Yamamoto, I. Kawamoto, K. Takayama, R. Okachi, S. Takasawa, T. Sato, and S. Sato, *J. Antibiot.*, **30**, 533 (1977).

4) R. Okachi, S. Takasawa, T. Sato, S. Sato, M. Yamamoto, I. Kawamoto, and T. Nara, *J. Antibiot.*, **30**, 541 (1977).

5) M. Sugimoto, S. Ishii, R. Okachi, and T. Nara, *J. Antibiot.*, **32**, 868 (1979).

6) N. Hirayama, K. Shirahata, Y. Ohashi, Y. Sasada, and J. R. Martin, *Acta Crystallogr., Sect. B*, **34**, 2648 (1978).

7) G. Germain, P. Main, and M. M. Woolfson, *Acta Crystallogr., Sect. A*, **27**, 368 (1971).

8) "International Tables for X-ray Crystallography," Kynoch Press, Birmingham (1974), Vol. IV, pp. 72—102.

9) O. Bastian, L. Fernholt, H. M. Seip, H. Kambara, and K. Kuchitsu, *J. Mol. Structure*, **18**, 163 (1973).

10) G. A. Jeffrey and H. S. Kim, *Carbohydr. Res.*, **15**, 310 (1970).

11) N. Goodhand and T. A. Hamor, *Acta Crystallogr., Sect. B*, **34**, 513 (1978).

12) G. Kartha, K. T. Go, A. K. Bose, and M. S. Tibbetts, *J. Chem. Soc., Perkin Trans. 2*, **1976**, 717.

13) M. D. Morse and J. P. Chesick, *Acta Crystallogr., Sect. B*, **32**, 954 (1976).

14) R. Bucourt, "Topics in Stereochemistry," An Interscience Publication John Wiley and Sons Ltd. (1974), pp. 160—183.

Direct Observation of the Type II Biradical and Triplet State of Valerophenone Excited by the Fourth Harmonic of a Nd:YAG Laser

Hisaharu HAYASHI and Saburo NAGAKURA*
Institute of Physical and Chemical Research, Wako, Saitama 351
(Received November 17, 1979)

The Norrish type II reaction of valerophenone was studied by the ns-laser photolysis technique, the fourth harmonic (266 nm) of a Q-switched Nd: YAG laser being used as an exciting light source. Transient absorptions due to the triplet state and 1,4-biradical of valerophenone were observed in both polar and nonpolar solvents. Quenching experiments with *cis*-1,3-pentadiene were also carried out. Transient absorptions due to the biradical were observed in the 350—300 nm region with the lifetimes of 103 ns (in methanol), 99 ns (in 2-propanol), 71 ns (in acetonitrile), and 31 ns (in 1,2-dichloroethane). Transient absorptions due to the triplet state were also observed in the 440—300 nm region.

Biradicals produced by the Norrish type II reaction of carbonyl molecules[1] have been regarded as important reaction intermediates in organic photochemistry. However, their existence had not been proved directly before the studies of Small and Scaiano with the aid of the ns-laser photolysis technique were carried out.[2-4] They used an N_2 laser (337.1 nm) as an exciting light source and observed the lifetimes of some type II biradicals through the rise curves of the absorptions of transient specimens produced by the electron transfer from the biradicals to some electron acceptors.

They also succeeded in observing directly transient absorptions due to the biradicals with a laser photolysis apparatus of very high sensitivity using a Q-switched frequency doubled ruby laser (347.1 nm) as an exciting light source.[5] They observed the transient absorptions of the biradicals in the 500—370 nm region, the spectra of which resembled that of the acetophenone ketyl radical.[6,7] Besides these weak bands, the ketyl radical has a much stronger band in the region below 370 nm.[6,7] From a similarity in the electronic structures of both specimens, the biradical might also be expected to have a strong band in the shorter wavelength region. However, it is very difficult to measure the transient absorption in the wavelength region shorter than that of the exciting light source. We recently constructed a ns-laser photolysis apparatus, the fourth (266 nm), third (355 nm), or second (532 nm) harmonics of a Q-switched Nd: YAG laser being used as an exciting light source. We have undertaken to measure the transient absorption due to the type II biradical of valerophenone extending the measurement region to 300 nm exciting the sample by the fourth harmonic of the laser.

The triplet-triplet (T_n-T_1) absorption of acetophenone overlaps the absorption of its ketyl radical.[7] A similar overlap is expected for the T_n-T_1 absorption of valerophenone and the absorption of the biradical, although Small and Scaiano did not consider the overlap.[5] In the present study, we have tried to measure the biradical absorption separately from the T_n-T_1 absorption by quenching experiments with *cis*-1,3-pentadiene.

Experimental

Valerophenone (Tokyo Kasei) was purified by distillation under reduced pressure. All solvents of spectrograde (Wako or Tokyo Kasei) were used without further purification. *cis*-1,3-Pentadiene (Tokyo Kasei Ultra Pure) purified by vacuum distillation was used for quenching studies. The samples contained in quartz cells with an optical length of 10 mm were degassed by four freeze-pump-thaw cycles. The concentration of valerophenone was 0.0065 mol dm^{-3}.

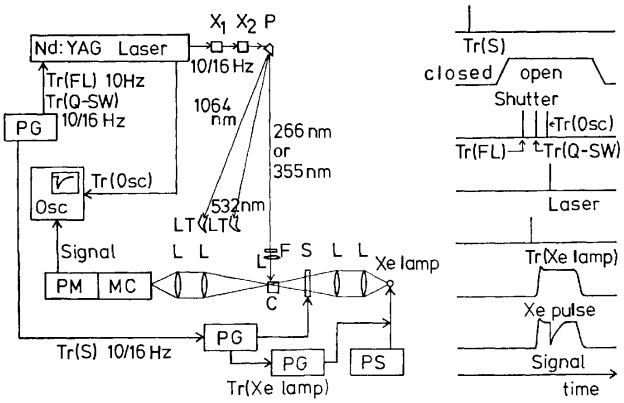

Fig. 1. Laser photolysis apparatus and time profiles of shutter, laser, and Xe pulse.
C: Sample cell, S: Electric shutter, L: Lenses, F: Filter (Toshiba UV-D33S), MC: Monochromator, PM: Photomultiplier, Osc: Oscilloscope, Tr(X): Trigger for X, PS: Power supply, PG: Pulse generator, FL: Flash lamps, Q-SW: Q-switching, X_1: Second harmonic generator, X_2: Third or fourth harmonic generator, P: Prism, LT: Light traps.

A block diagram of the laser photolysis apparatus is shown in Fig. 1. A Q-switched Quanta-Ray DCR-1 Nd: YAG laser was used as an exciting light source, a Quanta-Ray HG-1 harmonic generator providing the second, third, or fourth harmonics of the laser. The fourth harmonic was used as exciting light source, pulse width being 5 ns and maximum power 30 mJ. In order to avoid thermal lensing effects, the actual power was reduced as much as possible. Flash lamps for exciting the laser were discharged at 10 Hz, the maximum power being obtained. Its Q-switching was operated every 16 shots of the flash lamps (0.625 Hz) in order to prevent photochemical changes of the samples. The monitoring light with pulse width of 300 μs was obtained from a pulsed xenone arc (Ushio 150 W), irradiating the sample synchronously with the laser (0.625 Hz). Laser and monitoring light beams were crossed at right angles to each other. The monitoring light intensity was detected with

an HTV-R636 photomultiplier through a grating monochromator (Nikon G-250). An electronic shutter (Vincent 225L0A25X5[8] or Copal EMS #0[9]), opening synchronously with the laser pulse was used in order to protect the sample and the photomultiplier from continuous irradiation by the xenon arc. The time profiles of the shutter, monitoring light, and laser are also shown in Fig. 1. The transient signals were recorded by taking the photographs of the images on a Tektronix 7904 oscilloscope.

Results and Discussion

We have measured the transient absorption caused by the excitation of valerophenone in both polar and nonpolar solvents, in the region 440—300 nm. As examples, time-resolved absorption spectra were observed for the methanol and cyclohexane solutions (Fig. 2), the decay curve of the transient absorption being observed for these solutions (Fig. 3). We see that the decay curve for the methanol solution consists of two components:

$$I(t) = I_1 \exp(-t/\tau_1) + I_2 \exp(-t/\tau_2) \quad (1)$$

where τ_1 and τ_2 are the lifetimes of the fast and slow components, respectively, and I_1 and I_2 are the corresponding pre-exponential factors. The observed τ_1 and τ_2 values are given in Table 1.[10]

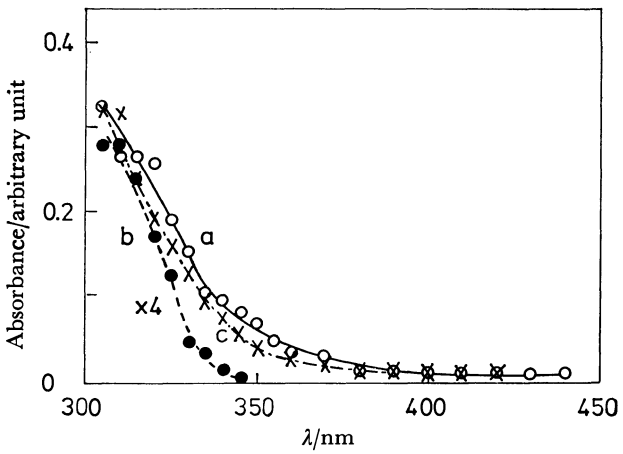

Fig. 2. Transient absorption spectra observed with valerophenone excited by the fourth harmonic of the Nd: YAG laser.
Curve a, observed with the methanol solution immediately after excitation: Curve b, observed with the methanol solution 100 ns after excitation: Curve c, observed with the cyclohexane solution immediately after excitation.

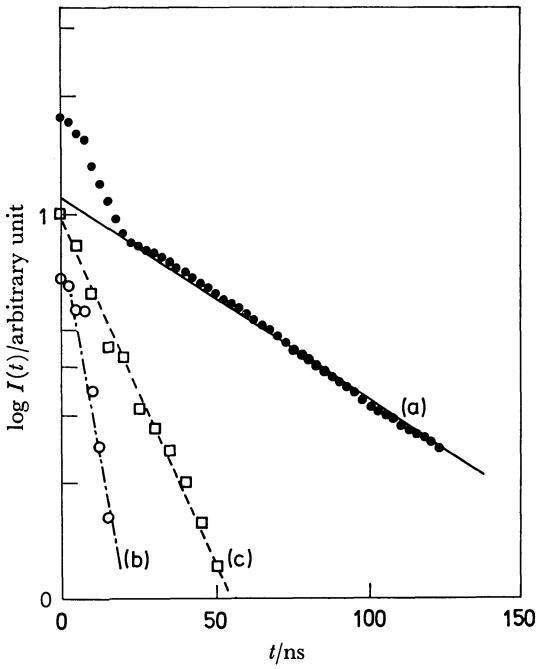

Fig. 3. Decay curves, $I(t)$, of the transient absorptions of valerophenone.
Curve a, the total decay curve observed at 318 nm in methanol: Curve b, the differnce between the observed curve in methanol and the fitted line for the slow decay component: Curve c, the decay curve observed at 320 nm in cyclohexane.

In order to assign the observed absorptions, we carried out quenching experiments with *cis*-1,3-penta-

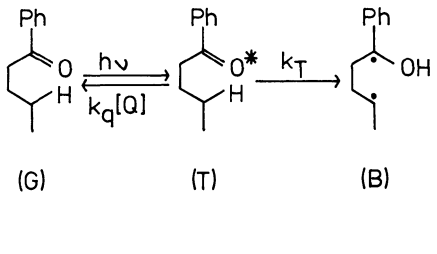

Scheme 1.

TABLE 1. LIFETIMES OF THE BIRADICAL AND TRIPLET STATE OF VALEROPHENONE

Solvent	Dielectric constant	η/cp	This work			Ref. 5	Ref. 3	
			τ_1/ns[a]	τ_2/ns[a]	τ/ns[a]	τ_B/ns[b]	τ_B/ns[b]	τ_T/ns[b]
Methanol	32.7[c]	0.5445[c]	12	103±7		93	102±15	16
2-Propanol	19.92[c]	1.765[d]	<9	99±10		—	—	—
Acetonitrile	37.5[e]	0.325[d]	<9	71±3		70	71±10	8.7
1,2-Dichloroethane	10.36[c]	0.730[d]	<9	31±6		—	—	—
Heptane	1.924[e]	0.3967[c]			30±6	—	—	—
Cyclohexane	2.023[e]	0.898[c]			23±3	38	—	—

a) See text. b) τ_B and τ_T are represented by the lifetimes of the biradical and triplet state of valerophenone, respectively. c) Values at 25 °C.[f] d) Values at 30 °C.[f] e) Values at 20 °C.[f] f) J. A. Riddick and W. B. Bunger, "Organic Solvents," John Wiley and Sons Inc., New York (1970).

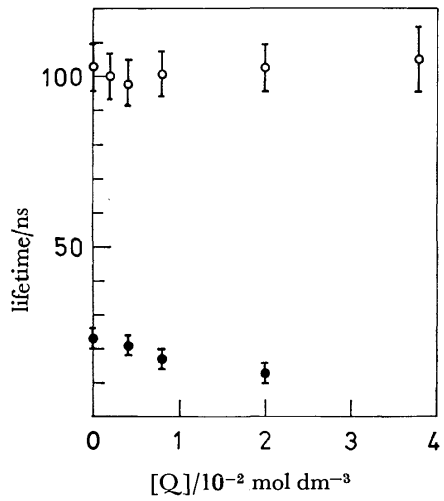

Fig. 4. Dependence of the lifetimes of the transient absorptions on [Q].
(○), For the slow lifetime, τ_2, observed with the methanol solution: (●), for the lifetime observed with the cylohexane solution.

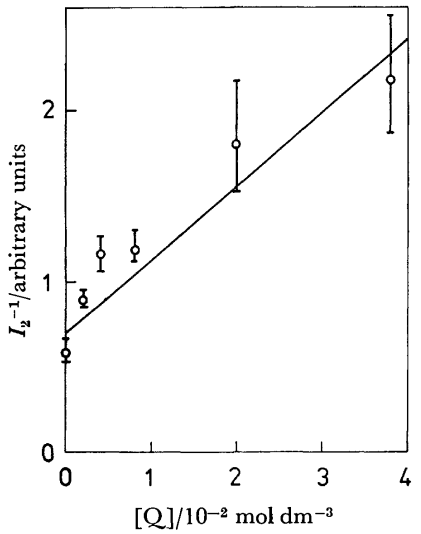

Fig. 5. Plot of $1/I_2$ observed for the methanol solution against [Q].

diene. The primary photochemical process of valerophenone in the ns-region is shown by Scheme 1, where G, T, and B denote the ground and triplet states of valerophenone and its biradical, respectively,[1] [Q] is the concentration of *cis*-1,3-pentadiene and k_T, k_B, and k_q are the respective rate constants. From measurement of the [Q] dependence of τ_1, τ_2, and I_2 (Figs. 4 and 5), we see that τ_2 is independent of [Q] and the inverse of the pre-exponential factor of the slow component, $1/I_2$, increases with increasing [Q]. This indicates that the slow component is safely assigned to the biradical and that curve b (Fig. 2) corresponds to its spectrum.[11] On the other hand, the fast component can be assigned to the triplet state, the only observable precursor of the biradical. Thus curve a (Fig. 2) can be considered to be a combination of curves due to the triplet state and the biradical. However, its 440—350 nm region may be mainly due to the triplet state, since the absorption intensity of the biradical is weak in this region.

When $k_T > k_B$, $1/I_2$ can be represented by (See Appendix)

$$1/I_2 = c[(k_T - k_B)/k_T + k_q[Q]/k_T] \quad (2)$$

where c is a constant. The following result is obtained from the $1/I_2$—[Q] line (Fig. 5):

$$k_q = (61 \pm 24) \times (k_T - k_B) \text{ mol}^{-1} \text{ dm}^3 \quad (3)$$

Since k_B and k_T were determined to be 0.97×10^7 s^{-1}, larger than 0.83×10^8 s^{-1}, respectively, k_q was calculated to be larger than $(4.5 \pm 1.8) \times 10^9$ s^{-1} mol^{-1} dm^3. This value is reasonable compared with the assumed one (5.5×10^9 s^{-1} mol^{-1} dm^3).[5]

We observed similar two component transient absorptions in acetonitrile, 2-propanol, and 1,2-dichloroethane. The observed fast and slow lifetimes are given in Table 1. The time-resolved spectra for these systems observed immediately and 100 ns after excitation are similar to those observed in methanol.

The cyclohexane solution also has a transient absorption in the region 420—300 nm (curve c, Fig. 2). Its decay curve, however, unlike that of the methanol solution, has only one component (Fig. 3). The lifetime, τ, for the cyclohexane solution was found to be 23±3 ns. The [Q] dependence of τ is also shown in Fig. 4. Since the observed τ values are not corrected, they are the upper limits of the real lifetimes, but we can conclude that τ decreases with increasing [Q]. Therefore, the observed transient absorption can be considered to be mainly due to the triplet state. Thus the spectrum obtained with the cyclohexane solution may be due to the triplet state, although possibility of contamination of the biradical absorption still remains.

We observed a similar one component decay curve of the transient absorption for the heptane solution (Table 1). The transient spectrum in heptane is similar to that in cyclohexane.

From the results, we conclude that the transient spectrum observed for valerophenone in the polar solvents in the 350—300 nm region can be assigned to the 1,4-biradical. It resembles that of the acetophenone ketyl radical.[7] Small and Scaiano observed the transient absorption spectra of the biradicals produced from γ-methylvalerophenone and valerophenone in the 500—370 nm region.[5] They are also similar to the spectrum of the acetophenone ketyl radical. The biradical absorption in this region is weak. We extended the wavelength region of the measurement to 300 nm, making it much easier to carry out such precise mechanistic works as quenching experiments.

As is shown in Table 1, the observed lifetimes for the biradical of valerophenone in polar solvents in this work agree with those obtained by Small and Scaiano with the indirect[3] and direct[5] methods. However, they could not observe the fast component in their transient absorption of valerophenone, and estimated the lifetime of the triplet state of valerophenone in methanol to be 16 ns through the indirect method.[3] This value is somewhat longer than the present result (less than 12 ns). The disagreement might be due to their underestimation of the k_q value.

In nonpolar solvents, Small and Scaiano also observed transient absorptions for γ-methylvalerophenone and valerophenone in the 500—370 nm region and assigned them to the biradical.[5] For example, the lifetimes of the biradicals of γ-methylvalerophenone and valerophenone in cyclohexane were reported to be 37 ns and 38 ns, respectively. The assignment for the former can be considered to be correct, since its triplet lifetime was confirmed to be much shorter than 37 ns,[5] but the assignment for the latter should be reexamined.

Appendix

The rate equations for [T] and [B] can be written as follows:

$$d[T]/dt = -k_T[T] - k_q[Q]\cdot[T], \quad \text{(A-1)}$$

$$d[B]/dt = k_T[T] - k_B[B]. \quad \text{(A-2)}$$

From Eq. (A-1), we get

$$[T] = [T]_0 \exp(-kt), \quad \text{(A-3)}$$

where $[T]_0$ is the initial concentration of [T] and k is given by

$$k = k_T + k_q[Q]. \quad \text{(A-4)}$$

When $t=0$, $[B]=0$. Thus [B] can be expressed by

$$[B] = A[\exp(-k_B t) - \exp(-kt)], \quad \text{(A-5)}$$

where A is a constant. When $k > k_B$, I_2 is proportional to A. Introducing Eqs. (A-3) and (A-5) into Eq. (A-2) we get

$$A = k_T[T]_0/(k-k_B). \quad \text{(A-6)}$$

Thus we can derive Eq. 1.

The authors' sincere thanks are due to Mr. Katsuo Nishi, the Institute of Physical and Chemical Research, for his kindness in designing the electric circuits of our laser photolysis apparatus. The present work was partially supported by Research Grant-in-Aids Nos. 412212 and 454135, the Ministry of Education, Science, and Culture.

References

1) P. J. Wagner, *Acc. Chem. Res.*, **4**, 168 (1971).
2) R. D. Small Jr., and J. C. Scaiano, *J. Phys. Chem.*, **81**, 829 (1977).
3) R. D. Small Jr., and J. C. Scaiano, *J. Phys. Chem.*, **81**, 2126 (1977).
4) R D. Small Jr., and J. C. Scaiano, *J. Phys. Chem.*, **82**, 2662 (1978).
5) R. D. Small Jr., and J. C. Scaiano, *Chem. Phys. Lett.*, **50**, 431 (1977).
6) A. Beckett, A. D. Osborne, and G. Porter, *Trans. Far. Soc.*, **60**, 873 (1964).
7) H. Lutz, E. Brehert, and L. Lindgvist, *J. Phys. Chem.*, **77**, 1758 (1973).
8) M. Kinoshita, *Kotaibutsuri*, **9**, 671 (1974).
9) K. Nishi and H. Hayashi, *Kagaku To Kogyo*, **32**, 942 (1979).
10) The obtained τ_1 may be the upper limit of the real lifetime, since no correction due to the laser pulse shape and the time delay of the measuring system were made.
11) Small and Scaiano observed the transient absorption spectra for the type II biradical in the 500—370 nm region. We also observed very weak transient absorption corresponding to the slow component in the 450—400 nm region.

 © 1980 The Chemical Society of Japan Bull. Chem. Soc. Jpn., 53, 1523—1529 (1980)

Studies on the Aqueous Solutions of Guanidinium Salts. XIV. Effect of Guanidinium Bromide on the Surface Tension of Aqueous Solutions of the Cationic Surfactants

Koichiro MIYAJIMA,* Hiromitsu YOSHIDA, Junko MAETANI, and Masayuki NAKAGAKI
Faculty of Pharmaceutical Sciences of Kyoto University, Yoshida Shimoadachi-cho, Sakyo-ku, Kyoto 606
(Received November 29, 1979)

The surface tensions of decyl-, tetradecyl-, and hexadecyl-trimethylammonium bromides were measured in the aqueous solutions of potassium bromide (KBr) and guanidinium bromide (GuBr). The critical micelle concentrations (CMC's) of the above surfactants decreased with increase of the concentration of KBr, while the CMC's showed minimum values in the aqueous GuBr solution, as the concentration of GuBr increased. The Langmuir coefficient, K_C, increased with decrease of the CMC. The influence of the salts on the surface tension and the micellization were well described in terms of the activity of the surfactant calculated by combining the Debye-Hückel law and Setschenow's equation.

A large number of studies have been reported on the effect of various electrolytes on the surface tension, the adsorption on the air-water interface and the micellization of surfactants.[1–9] The association and the adsorption to the air-water interface of ionic surfactant in aqueous solution are governed by two opposing forces. The hydrophobic force which is mainly due to the ordered water molecules around the hydrophobic tail of surfactant repelles the surfactant molecules or ions from the aqueous bulk solution to the interface or the micelle core. The polar head group favour the aqueous bulk phase rather than such ordered phase, because the electrostatic repulsive force between the head groups makes the surfactant molecule difficult to associate. In this connection, inorganic salts decrease the CMC and increase the adsorption to the air-water interface. The effect of the inorganic electrolytes were roughly described in terms of the change of the activity of surfactant in the presence of the salts.[10,11] In this treatment, however, the activity of surfactant was estimated by the Debye-Hückel theory and the effect of the salts on the hydrophobic hydration was ignored.

The organic salts, such as guanidinium and biguanide salts have been known to influence significantly the hydrophobic hydration.[12–14] The reduction of the hydrophobic hydration must decrease the activity of surfactant and increase the CMC.

From these point of view, we measured the surface tension of some alkyltrimethylammonium bromides (C_nBr) in aqueous solutions of guanidinium bromide (GuBr) and KBr, and obtained anomalous results for the C_nBr–GuBr–H_2O system. To interpret these results by the phase separation model, we introduced a new expression for the activity coefficient of ionic surfactant in salt solutions by taking into consideration the effects of salts on the hydrophobic group besides the ionic head group. Based on the activity thus obtained, the variations of CMC and surface tension depending on the concentration and the kind of salts were well interpreted in terms of the change of the activity of the surfactants in salts solutions.

Experimental

Materials. Dodecyl-, tetradecyl-, and hexadecyltrimethylammonium bromides were synthesized from corresponding alkyl bromides and trimethylamine by the method described elsewhere.[15] The crude product was recrystallized from ethanol two or three times. To remove the raw materials, Soxhlet's extracter was employed using ether as the solvent. After extraction, recrystallization from ethanol-ether mixture gave a white crystalline product. In elementary analysis, the experimental values were in good agreement with those of the calculated values as shown in Table 1. Guanidinium bromide used was the same compound reported previously.[12] Reagent grade 1-butanol, 1-hexanol, 1-octanol, and 1-decanol (Nakarai Chemical Co., Ltd.) were used without further purification. The purities of these alcohols were more than 98%. All solutes were dissolved in deionized and redistilled water. Aqueous solutions of GuBr and KBr were purified through activated charcoal powder before use.

Surface Tension Measurements. The surface tension was measured by Du Nouy tensiometer. The platinum ring with diameter 23 mm was heated by oxidizing flame before use. All glass apparatus were preserved in chromate-sulfric acid mixture and linsed well with distilled water before use. Temperature of the thermostat was maintained at 25 ± 0.2 °C. For the calculation of the surface tension of aqueous solutions, the value of 71.96 $mN \cdot m^{-1}$ was used as the surface tension of pure water at 25 °C. The experimental determination of the surface tension was precise to ±0.1 $mN \cdot m^{-1}$.

Table 1. Elementary analysis of cationic surfactants (%)

		H	C	N
Dodecyltrimethylammonium bromide ($C_{12}Br$)	Calcd	11.11	58.42	4.54
	Exp.	11.32	58.32	4.45
Tetradecyltrimethylammoniumbromide ($C_{14}Br$)	Calcd	11.38	60.69	4.16
	Exp.	11.64	60.74	4.02
Hexadecyltrimethylammonium bromide ($C_{16}Br$)	Calcd	11.61	61.61	3.84
	Exp.	11.70	62.86	3.77

Solubility Measurements. The saturated aqueous solutions of alcohols were obtained by mixing the excess amount of alcohol and water in a thermostat bath with magnetic stirrer at 25±0.1 °C. It took 2—3 d to reach equilibrium. After equilibrium, UV spectra of the saturated solutions were measured for the detection of the emulsification of alcohols. The differences of the intensities at 265 nm between water and the saturated aqueous alcohol solutions were not observed except for aqueous 1-butanol solution. The solubilized amount of alcohol was determined from the peak height of the gas chromatogram (GC). GC conditions are as follows; Column: 10% PEG20M on Chromosorb W, 100—200 mesh packed in 3 mm×1 m glass tubing; Column temperature: 120 °C; Carrier gas: He; Flow rate: 40 $cm^3 \cdot min^{-1}$; Injection temperature: 170—190 °C; Detector: FID.

Results

Surface Tensions of C_nBr Solutions. The surface tension, γ, at constant salts concentrations are shown as a function of logarithm of the concentration of $C_{14}Br$ in Figs. 1 and 2. The concentrations of surfactant and the added salts are expressed by C/mol·dm^{-3} and C_s/mol·dm^{-3}, respectively. At constant C_s, the surface tension decreased with increase of C. The break point for each curve is regarded as the critical micelle concentration (CMC) which is given in Table 2 together with those of $C_{12}Br$ and $C_{16}Br$. As shown in Fig. 1, the surface tension at a constant C decreases with increase of the concentration of KBr. Therefore, the curve of surface tension *vs.* log C shifts to the lower concentration region of surfactant with increase of C_s. However, as shown in Fig. 2, the behavior of the surface tension *vs.* log C curves for the $C_{14}Br$–GuBr–H_2O system is different from that of the $C_{14}Br$–KBr–H_2O system. At constant C, the surface tension decreases with increase of C_s up to about 1 mol·dm^{-3} and above this concentration,

TABLE 2. THE CMC VALUES OF ALKYLTRIMETHYLAMMONIUM BROMIDES IN AQUEOUS KBr AND GuBr SOLUTIONS

KBr; C_s/mM	CMC/mol·dm^{-3}	GuBr; C_s/mM	CMC/mol·dm^{-3}
	$C_{12}Br$		
0	1.10×10^{-2}	83.8	3.98×10^{-3}
0.96	1.07×10^{-2}	424	2.04×10^{-3}
9.58	2.88×10^{-3}	894	1.95×10^{-3}
95.8	8.71×10^{-4}	1392	2.69×10^{-3}
	$C_{14}Br$		
0	3.16×10^{-3}	0.79	2.95×10^{-3}
1.06	2.75×10^{-3}	7.87	1.48×10^{-3}
10.6	1.29×10^{-3}	78.7	3.89×10^{-4}
98.5	3.16×10^{-4}	394	2.14×10^{-4}
956	4.77×10^{-4}	1076	2.00×10^{-4}
		1685	3.24×10^{-4}
		2624	5.62×10^{-4}
	$C_{16}Br$		
0	9.42×10^{-4}	0.90	5.69×10^{-4}
0.96	6.08×10^{-4}	8.76	1.58×10^{-4}
10.0	1.32×10^{-4}	81.9	3.55×10^{-5}
95.4	2.60×10^{-5}	305	2.00×10^{-5}
820	5.96×10^{-6}	573	2.09×10^{-5}
		912	2.24×10^{-5}

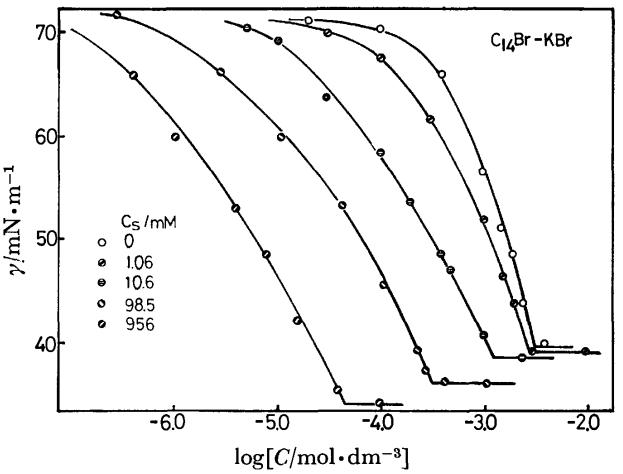

Fig. 1. The plot of the surface tension, γ, against the concentration of $C_{14}Br$, C, in aqueous KBr solution.

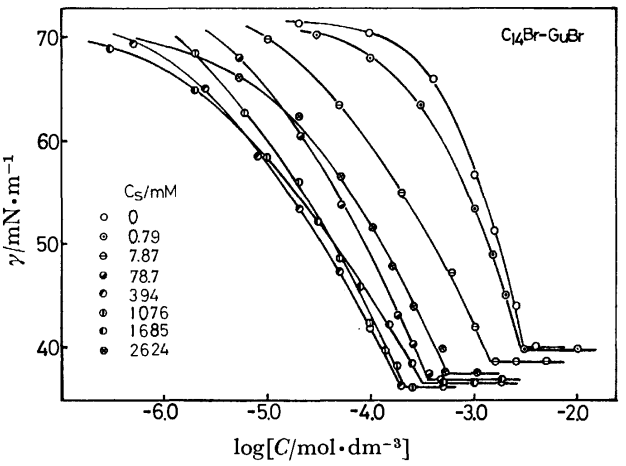

Fig. 2. The plot of the surface tension, γ, against the concentration of $C_{14}Br$, C, in aqueous GuBr solution.

the surface tension increases with the concentration of GuBr. This phenomenon was also observed in the $C_{12}Br$–GuBr–H_2O and $C_{16}Br$–GuBr–H_2O systems.

Effect of the Counter Ion Concentration on CMC. Using the CMC values obtained from Figs. 1 and 2, the values of log CMC were plotted against logarithm

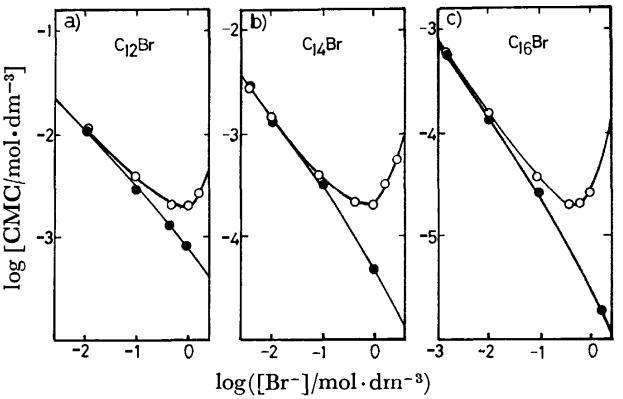

Fig. 3. The plot of log CMC against log [Br^-] in aqueous salt solution.
Salt; ○: GuBr, ●: KBr.

of counter ion concentration, log[Br^-].[1,3] They are shown in Figs. 3-a, 3-b, and 3-c. In the C_nBr–KBr–H_2O system, the values of log CMC decrease with increase of log[Br^-] values. The degree of CMC-lowering increases with the alkyl chain length. However, in the C_nBr–GuBr–H_2O system, the value of log CMC decreases with increase of log[Br^-], reaches a minimum and then increases with log[Br^-]. The concentrations of counter ion at the minimum points decrease with increase of alkyl chain length.

Adsorption at the Air-Water Interface. The adsorption amount of surfactant, Γ, is essentially defined by the Gibbs adsorption equation.[1,16]

$$\Gamma = -\frac{1}{RT}\left(\frac{\partial\gamma}{\partial \ln a}\right)_{T,P}, \quad (1)$$

where a is the activity of surfactant. If the activity coefficient can be regarded as unity, Eq. 1 is rewritten as Eq. 2,

$$\Gamma = -\frac{1}{iRT}\left(\frac{\partial\gamma}{\partial \ln C}\right)_{T,P}, \quad (2)$$

where

$$i = \nu_-\left(\frac{\nu_- C}{\nu_- C+\nu_{s-}C_s}\right) + \nu_+. \quad (3)$$

In Eqs. 1, 2, and 3, R, T, and P are the usual meanings,

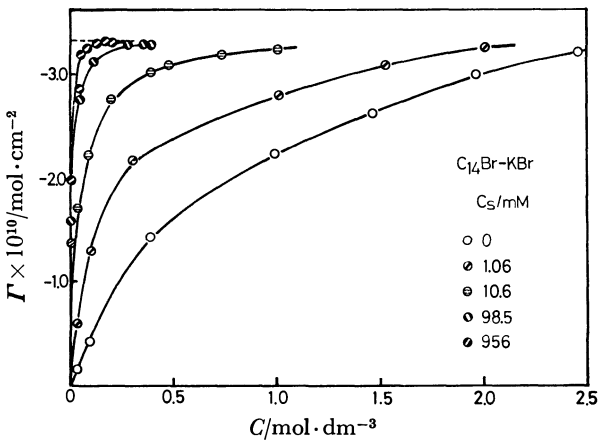

Fig. 4. Adsorption isotherms of $C_{14}Br$ in various concentrations of KBr solutions at 25°C.

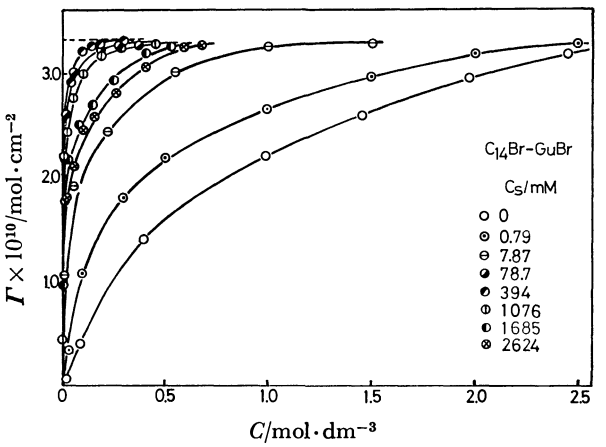

Fig. 5. Adsorption isotherms of $C_{14}Br$ in various concentrations of GuBr solutions at 25°C.

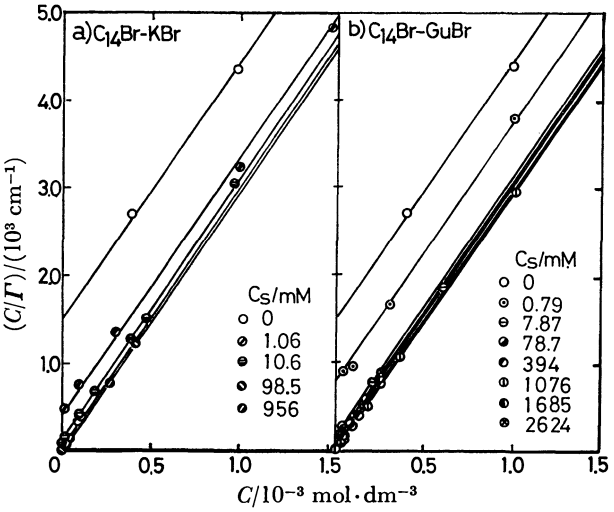

Fig. 6. Plots of C/Γ *vs.* C in various concentrations of salt solutions.

and ν_+ and ν_- are the number of moles of cation and anion formed from 1 mol of ionic surfactant, respectively, and ν_{s-} is the number of moles of anion fully dissociated from 1 mol of the added salt. As shown in Figs. 4 and 5, the Γ values of $C_{14}Br$ calculated from Eq. 2 are plotted against C at various C_s's. The Langmuir equation was applied to these systems.

$$\Gamma = \frac{\Gamma_s K_c C}{1+K_c C}, \quad (4)$$

where Γ_s is the saturated adsorption amount and K_c is the constant concerning the strength of adsorption. Equation 4 is rewritten as,

$$\frac{C}{\Gamma} = \frac{1}{\Gamma_s K_c} + \frac{1}{\Gamma_s}C. \quad (5)$$

The plot of C/Γ against C for the $C_{14}Br$–KBr–H_2O and $C_{14}Br$–GuBr–H_2O systems are shown in Figs. 6-a and 6-b, respectively. In accordance with Eq. 5, linear relationships exist between C/Γ and C. The values of Γ_s and K_c obtained from the slopes and the intercepts are shown in Table 3. In both the systems, Γ_s takes a constant value, 3.32×10^{-10} mol/cm^2, *i.e.* 50.1 Å^2/molecule. In the $C_{14}Br$–KBr–H_2O system, K_c values increase with the concentration of KBr, but in the $C_{14}Br$–GuBr–H_2O system, K_c values once increase and then decrease

Table 3. The values of K_c and Γ_s of $C_{14}Br$ in aqueous KBr and GuBr solutions

KBr		GuBr	
C_s/mM	K_c/dm^3·mol^{-1}	C_s/mM	K_c/dm^3·mol^{-1}
0	2.17×10^3	0.79	4.01×10^3
1.06	6.49×10^3	7.87	2.00×10^4
10.6	1.95×10^4	78.7	1.95×10^5
98.5	1.20×10^5	394	2.03×10^5
956	5.50×10^5	1076	9.80×10^4
		1685	3.64×10^4
		2624	2.96×10^4
Γ_s		Γ_s	
3.32×10^{-10} mol·cm^{-2}		3.32×10^{-10} mol·cm^{-2}	

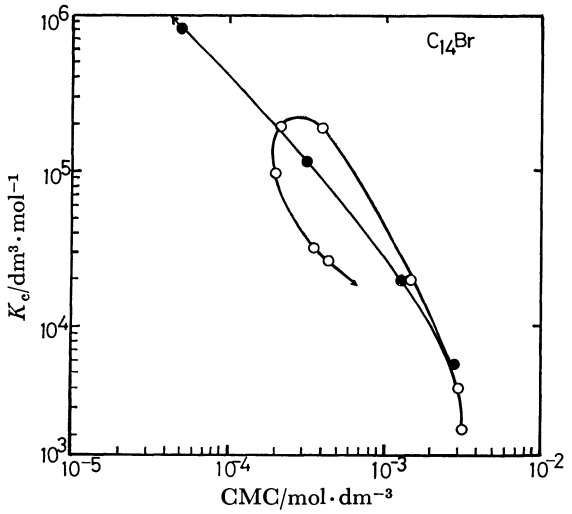

Fig. 7. The relationship between K_c and CMC.
Salt; ○: GuBr, ●: KBr.

with increase of the concentration of GuBr.

Relationship between CMC and K_c. In order to elucidate the relation between micelle equilibrium and adsorption equilibrium in aqueous salt solution, the values of log K_c were plotted against the values of log CMC. (Fig. 7) The arrow sign represents the direction of the increase of salt concentrations. Though the shapes of two curves are different from each other, the relation between K_c and CMC is similar, that is, the value of log K_c increases with decrease of the value of log CMC. This fact indicates that the adsorption at air-water interface is closely related to the micellization.

Discussion

Micellization. In most studies concerning the effect of electrolyte on the micelle formation, the plot of log CMC against the logarithm of counter ion concentration has been considered linear. The slope was regarded as a parameter related to the state of the dissociation of counter ion or the formation of ionic atmosphere by counter ions around the micelle. However, our investigation revealed that these plots are not linear in aqueous ternary system, especially in the C_nBr–GuBr–H_2O system. Therefore, it is not adequate to take into account the effect of electrolyte on micellization on the basis of only electrostatic effect of counter ion. Shinoda and Huchinson,[16] and Herraman[17] analyzed the experimental results thermodynamically, by regarding the micellization phenomenon as a kind of phase separation and met with success. Recently, it was pointed out that the activity, instead of the concentration, of surfactant should be used for the analysis of the experimental data.[10] Therefore, we used the activity of surfactant for the analysis of data. According to the phase separation model, it may be considered that the micelle formation occured when the activity of surfactant has reached a certain value.

The activity of cationic surfactant at CMC, a_m, in the aqueous solution of electrolyte with common anion may be written as,

$$a_m = f_\pm^{\nu}(CMC)^{\nu_+}(\nu_-(CMC)+\nu_{s^-}C_s)^{\nu_-}, \quad (6)$$

where $f_\pm$ is the mean ionic activity coefficient of surfactant and $\nu=\nu_+ + \nu_-$. In this work, $\nu_+=\nu_-=\nu_{s^-}=1$ and $\nu=2$. $f_\pm$ in Eq. 6 has been mostly determined from the Debye-Hückel equation for the activity coefficient.[18] However, only the electrostatic interaction is taken into consideration with the Debye-Hückel theory. In this respect, this law is originally suitable for inorganic electrolytes or their mixtures. Organic electrolytes such as surfactants have a large hydrophobic group besides an ionic head group. The hydrophobic group of surfactant is surrounded by the ice-like structure which decreases the entropy of the system and leads to the micelle formation. Inorganic electrolytes such as KBr and CsBr have a different effect from organic electrolytes such as guanidinium salts on the activity coefficient of hydrophobic compound. Alkali halides usually salt out the hydrophobic compound, while guanidinium halides salt in.[12] Therefore, when we discuss the activity coefficient of ionic surfactant in the presence of another salt, we must take into consideration the interaction between the hydrophobic moiety and ions, besides the interaction between the ionic head group and ions. In this connection, the salt effect on the activity of surfactant is considered to be the sum of these two contributions. The Debye-Hückel equation for $f_\pm$ represents the contribution from the interionic interaction. Güntelberg's approximation of the Debye-Hückel law[18] was used for the estimation of this interaction. In order to estimate the salt effect on the hydrophobic group, we introduced the Setschenow equation which represents the effect of salt on the solubility of nonelectrolyte.[19] This equation is written as,

$$\log(f_s/f_{s0}) = \log(S_0/S) = k_s'C_s, \quad (7)$$

where $f_s(f_{s0})$ and $S(S_0)$ are the activity coefficient and the solubility of nonelectrolyte in the presence (absence) of salt, respectively, and k_s' is the salting-out coefficient of nonelectrolyte. Assuming that the value of f_{s0} is

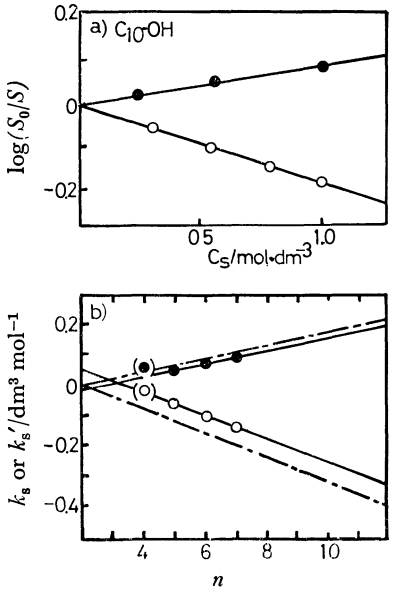

Fig. 8. a) The plot of $\log(S_0/S)$ of l-decanol against C_s.
b) k_s or k_s' value against carbon number of l-alcanols, n.
Salt; ○: GuBr, ●: KBr.

unity because of the low solubility of hydrophobic nonelectrolyte, Eq. 7 reduces to Eq. 8,

$$\log f_s = k_s' C_s. \quad (8)$$

Based on the above discussion, the activity coefficient of the ionic surfactant may be expressed by Eq. 9,

$$\log f_\pm = \frac{-A\sqrt{I}}{1+\sqrt{I}} + k_s C_s, \quad (9)$$

where I is the ionic strength and A is the constant, 0.5115 for 1:1 electrolyte at 25 °C, and k_s is the salting-out coefficient for the hydrophobic alkyl group. In order to obtain the k_s values for the hydrocarbon group of surfactant, the solubilities of n-alcohols with 6, 8, and 10 carbons were measured in the aqueous solutions of KBr and GuBr. As shown in Fig. 8, the value of $\log(S_0/S)$ for 1-decanol increases with the concentration of KBr and decreases with increase of the concentration of GuBr. From the slopes, the k_s' values were determined to be 0.092 and −0.147 for KBr and GuBr solutions, respectively. The values of k_s' of 1-hexanol and 1-octanol were obtained from the similar plots to 1-decanol. These values are shown in Table 4. To

Table 4. The values of salting-out coefficients of n-alkyl alcohols and n-alkyl groups in aqueous KBr and GuBr solutions

		k_s'/dm³·mol⁻¹ KBr	GuBr
Alcohol	1-Butanol	0.049	−0.023
	1-Hexanol	0.056	−0.066
	1-Octanol	0.069	−0.106
	1-Decanol	0.092	−0.147
Alkyl group	Dodecyl	0.12	−0.21
	Tetradecyl	0.14	−0.26
	Hexadecyl	0.16	−0.32

obtain the k_s values of dodecyl, tetradecyl, and hexadecyl groups, k_s' value was plotted against the carbon number of alcohols, n. As shown in Fig. 8-b, linear relationships exist between the k_s' values and n in each salt system. Therefore it is reasonable to determine the k_s' values of higher alcohols by extraporation. These k_s' values are not for the alkyl groups, but for alcohols, because they include the contribution of OH group. The salting-out coefficients of alkyl groups, k_s were obtained by subtracting the value of intercept from the k_s' values, on the assumption that the intercept represents the contribution of OH group. The k_s values of alkyl group thus obtained are also shown in Table 4. From the signs of k_s values, the effects of KBr and GuBr on the solubility of alcohols are consistent with those of these salts on the solubility of tetraalkylammonium salts.[20] Judging from the signs of k_s, the hydrophobic tails of surfactant molecules can associate more easily in the salt solution with a positive sign of k_s and less easily in the salt solution with a negative sign of k_s than in pure water. The difference of the sign of k_s indicates that the influence of KBr on the water structure in the vicinity of surfactant molecule is different from that of GuBr.[12,13]

From Eqs. 6 and 9, we obtain,

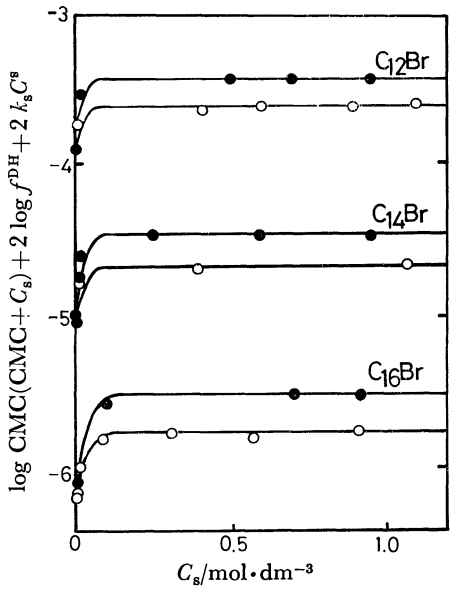

Fig. 9. The plot of log CMC (CMC+C_s)+2 log f^{DH}+2 k_sC_s against C_s in aqueous salts solutions.
Salt; ○: GuBr ●: KBr.

$$\log a_m = \log \mathrm{CMC}(\mathrm{CMC}+C_s) + 2\log f^{DH} + 2k_sC_s, \quad (10)$$

where $\log f^{DH}$ is the first term of the right hand side of Eq. 9. If the micellization occurs at constant activity in the aqueous solution, Eq. 10 must be constant. As shown in Fig. 9, the value of a_m is constant irrespective of C_s, except the low concentration of salt. Since the value of (CMC+C_s) is equal to [Br⁻], Eq. 10 is rewritten as,

$$\log \mathrm{CMC} + 2\log f^{DH} + 2k_sC_s = \log a_m - \log [Br^-]. \quad (11)$$

When Eq. 11 is applied to the $C_{14}Br$–KBr(or GuBr)–H_2O system, the slope of (log CMC+2 log f^{DH}+2 k_sC_s) *vs.* log [Br⁻] curve must be −1. As shown in Figs. 10-a and 10-b, the plots of log CMC or (log CMC+2 log f^{DH}) against log [Br⁻] are not linear, but the plot (log CMC+

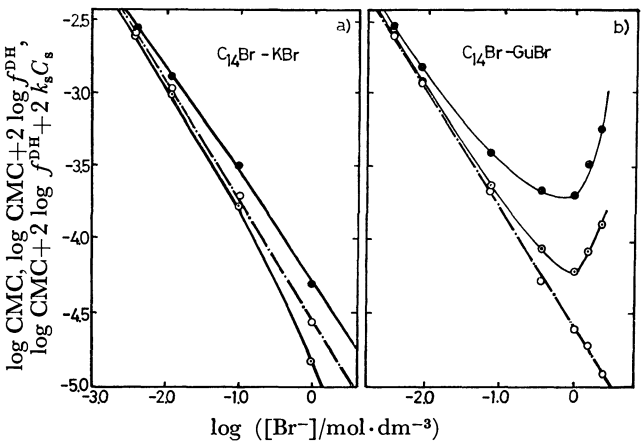

Fig. 10. The plot of log CMC, (log CMC+2 log f^{DH}), or (log CMC+2 log f^{DH}+2 k_sC_s) against log [Br⁻] for the $C_{14}Br$–salt–H_2O system.
Salt; a) KBr, b) GuBr.
●: log CMC *vs.* log [Br⁻],
⊙: log CMC+2 log f^{DH} *vs.* log [Br⁻],
○: log CMC+2 log f^{DH}+2 k_sC_s *vs.* log [Br⁻].

$2\log f^{DH}+2k_sC_s$) against log[Br^-] is linear in each ternary system and the slopes of both systems are -0.9, which is close to -1.

Surface Tension and Adsorption at Air-Water Interface. In the previous section, the micellization phenomena of cationic surfactants in salt solution were interpreted in terms of the constant activity of surfactant. Similarly, the behaviour of surfactant below CMC in salt solution was considered on the basis of the activity, a, defined by Eq. 12,

$$a = f_{\pm}^2 C(C+C_s) \quad (12)$$

where $f_{\pm}$ is the activity coefficient defined by Eq. 9.

The modified Szyszkowski equation obtained from the integration of Eq. 1 with the Langmuir equation by using a instead of C was applied to these ternary systems.[10]

$$\gamma_0 - \gamma = \Gamma_s RT \ln(1+K_a \cdot a), \quad (13)$$

where γ_0 and γ are the surface tension of pure water and surfactant solution, respectively, and K_a is the Langmuir coefficient. As shown in Figs. 11 and 12, the quantity of $\exp[(\gamma_0-\gamma)/\Gamma_s RT]-1$ is proportional to a. The values of K_a obtained from the slopes and Γ_s (3.32×10^{-10} mol/cm^2) are 4.16×10^6 dm^6·mol^{-2} and 3.82×10^6 dm^6·mol^{-2} for the $C_{14}Br$·KBr–H_2O and $C_{14}Br$–GuBr–H_2O systems, respectively. The value of K_a is a constant independent of C_s, while the K_c value varies with C_s.

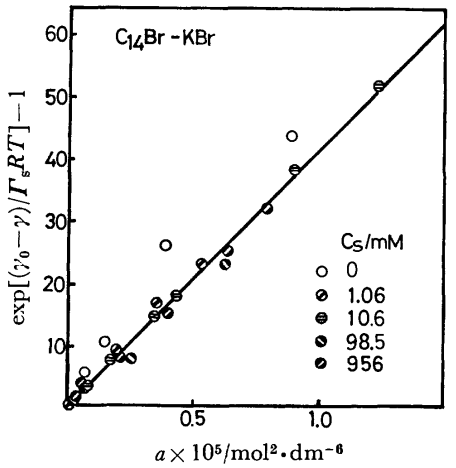

Fig. 11. The plot of $\exp[(\gamma_0-\gamma)/\Gamma_s RT]-1$ against a in aqueous KBr solution.

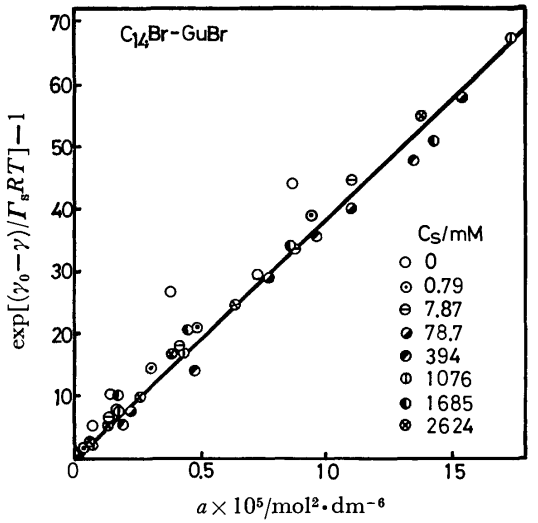

Fig. 12. The plot of $\exp[(\gamma_0-\gamma)/\Gamma_s RT]-1$ against a in aqueous GuBr solution.

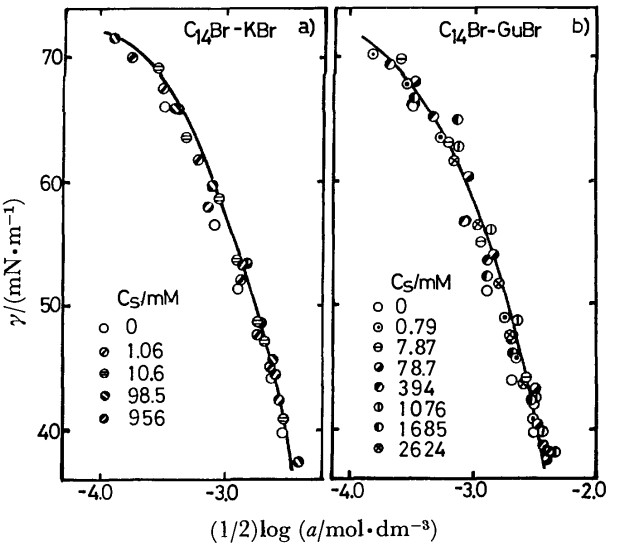

Fig. 13. The relationship between γ and 1/2 log a for the $C_{14}Br$– salt–H_2O system.

When the surface tension of $C_{14}Br$ is replotted against (1/2)log a as shown in Figs. 13-a and 13-b, every experimental value is located on the same curve obtained from Eq. 13 by using the values of K_a and Γ_s. The comparison of these figures with Figs. 1 and 2 indicates that the variation of curves in Figs. 1 and 2 is originally caused by the ignorance of the activity coefficient.

Conclusion

For the analysis of the salt effect on the CMC and the surface tension of cationic surfactant, we introduced a new expression for the activity coefficient in salt solution by taking into consideration the salt effect on the hydrophobic group of surfactant, besides the ionic head group. The electrostatic interaction between the ionic residue of surfactant and ions always decreases the activity of surfactant. However, the interaction between the hydrophobic group of surfactant and salt increases or decreases the activity of surfactant according to the sign of salting-out coefficient of salt. The salt with the negative sign of k_s decreases the activity coefficient of surfactant, resulting in the increase of CMC and the decrease of Γ, and *vice versa* for the salt with the positive sign. The opposite effect of GuBr to KBr on the CMC at relatively high concentration is mainly due to the difference of the sign of k_s.

Guanidinium salts denaturate proteins in aqueous solution. The main effect for the denaturation is believed to be the reduction of hydrophobic bonding in protein. Our experimental results are consistent with the above view of protein denaturation by guanidinium salts.

References

1) K. Shinoda, T. Nakagawa, B. Tamamushi, and T. Isemura, "Colloidal Surfactants," Academic Press, New York, (1973).
2) G. S. Hartley, *J. Chem. Soc.*, **1968**, 1938.
3) M. M. Corrin and W. D. Harkins, *J. Am. Chem. Soc.*, **69**, 683 (1947).
4) H. Lange, *Kolloid Z.*, **121**, 66 (1951).
5) E. W. Anacker, R. D. Geer, and E. H. Eylar, *J. Phys. Chem.*, **75**, 369 (1971).
6) J. F. Voeks and H. V. Tarter, *J. Phys. Chem.*, **59**, 1190 (1955).
7) J. M. Corkill and J. F. Goodman, *Trans. Faraday Soc.*, **58**, 206 (1962).
8) M. J. Shick, *J. Phys. Chem.*, **68**, 3585 (1964).
9) H. N. Singh, S. Swarup, and S. M. Saleen, *J. Colloid Interface Sci.*, **68**, 128 (1979).
10) M. Nakagaki, T. Handa, and S. Shimabayashi, *J. Colloid Interface Sci.*, **43**, 521 (1973).
11) S. Ozeki, M. Tunoda, and S. Ikeda, *J. Colloid Interface Sci.*, **64**, 28 (1978).
12) K. Miyajima, H. Yoshida, and M. Nakagaki, *Bull. Chem. Soc. Jpn.*, **51**, 2826 (1978).
13) K. Miyajima, H. Yoshida, and M. Nakagaki, *Bull. Chem. Soc. Jpn.*, **52**, 2880 (1979).
14) Unpublished data.
15) O. Westphal and D. Jercher, *Ber.*, **1940**, 1002.
16) K. Shinoda and E. Huchinson, *J. Am. Chem. Soc.*, **66**, 577 (1962).
17) K. W. Herraman, *J. Phys. Chem.*, **66**, 295 (1962).
18) R. A. Robinson and R. H. Stokes, "Electrolyte Solutions," 2nd ed, Butterworths, London (1959).
19) J. Setschenow, *Z. Phys. Chem.*, **4**, 117 (1889).
20) K. Miyajima, H. Yoshida, and M. Nakagaki, *Bull. Chem. Soc. Jpn.*, **50**, 2854 (1977).

Vibrational Distribution of HF Produced by Mercury Photosensitized Decomposition of Fluoroethylenes

Hajime WATANABE, Hiroyuki HORIGUCHI, and Soji TSUCHIYA*

Department of Pure and Applied Sciences, College of General Education, The University of Tokyo, Komaba, Meguro-ku, Tokyo 153

(Received December 15, 1979)

Distributions of vibrationally excited HF produced by Hg-photosensitized reactions of fluoroethylenes are determined by means of the IR emission measurement of HF fundamentals. The distributions are almost of Boltzmann type with temperatures of 11400, 13700, 7200, 5700, 5700, and 2200 K for respective parent molecules of CH_2=CHF, CH_3CF=CH_2, CH_2=CF_2, *cis*-, *trans*-CHF=CHF, and CHF=CF_2. The fractions of vibrational energy of HF† among the energies available for distribution in various degrees-of-freedom of product molecules are 19, 23, 11, 7.6, 7.6, and 1.7% for the above molecules, respectively. The statistical calculation results in much less energy disposal in HF vibration in the decompositions of CH_2=CHF, CH_3CF=CH_2, and CH_2=CF_2, while the distributions of HF† in CHF=CHF and CHF=CF_2 are closer to those predicted by the statistical calculation. The deactivation rate of HF† in CH_2=CHF is about three times larger than that in CH_2=CF_2, and the latter values resemble those in HF.

Experimental observations on energy partitioning among internal and external degrees-of-freedom of product molecules in chemical reactions have given deep insight into the mechanism and dynamics of the relevant molecular processes. In this paper, we discuss the energy partitioning in the Hg-photosensitized reaction of HF elimination from fluoroethylene (hereafter F-ethylene). The first experiment which demonstrated production of vibrationally excited HF (hereafter HF†) in photolysis of F-ethylenes was made by Berry and Pimentel,[1] who confirmed lasing actions of HF†. Almost at the same time, Clough, Polanyi, and Taguchi[2] determined the vibrational distribution of HF† produced by the reaction of Hg^*+CH_2=CF_2. The distribution shows relatively larger populations in higher levels than those predicted by the statistical calculation. The non-statistical vibrational energy disposal in the HCl produced by the UV photolyses of Cl-ethylenes was also reported by Berry,[3] who postulated a simple Golden Rule model to simulate the vibrational distribution of HCl. It was also reported that vibrationally excited HF was produced in reactions of H and O atoms with fluoroethylenes, and that the vibrational distribution of HF was predicted well by the model proposed by Berry.[4,5]

As for the mechanism of the present Hg-photosensitized reaction, Trobridge and Jennings[6] observed the quantum yield of CH≡CH from CH_2=CHF to be almost unity indicating the HF elimination as a dominant reaction channel. They also suggested two kinds of excited species as reaction intermediates. Discussion of the same line was given on the basis of the calculation of energy levels by Strausz *et al.*,[7] who postulated the mechanism: F-ethylene $\xrightarrow{Hg^*}$ $(\text{F-ethylene})^*_{\text{triplet}} \longrightarrow (\text{F-ethylidene})^*_{\text{triplet}} \longrightarrow (\text{F-ethylidene})^*_{\text{singlet}} \longrightarrow$ decomposition. Experimental studies to test this postulate were carried out by measuring yields of isomerization in *cis*- or *trans*-CHF=CHF[7] and of CH≡CH from CH_2=CHF.[8]

We report here observations of the vibrational distributions of HF formed by the Hg-photosensitized decompositions of CH_2=CHF, CH_2=CF_2, *cis*- and *trans*-CHF=CHF, CH_3CF=CH_2, and CHF=CF_2. The method is based on the IR emission measurement of HF† by the use of a modulation technique to separate the vibrational relaxation effect from the initial vibrational excitation. The results will be compared with the statistical partitioning of the excess energy among all degrees-of-freedom concerned.

Experimental

The apparatus is similar to that employed in the previous study.[9] A gas mixture of Ar and F-ethylene was made to flow through a quartz reaction cell (24 cm long and 3 cm dia.) *via* a liquid N_2 trap to a rotary vacuum pump (900 dm^3 min^{-1}). A pressure increase due to addition of F-ethylene to the main flow of Ar was monitored differentially by a capacitance manometer (M. K. S. Baratron, 210H). A trace of Hg vapor which was less than 1×10^{-3} Torr** was mixed to the flow. The reaction cell was surrounded by six low pressure Hg lamps (Toshiba, 10 W germicidal lamp) whose power was supplied through ballast resistor from an ac source (Elgar, 251) with variable frequencies in the range of 50 Hz—10 kHz in order to modulate the 253.7 nm intensity at twice the frequency of the ac source. One end of the reaction cell was sealed by a CaF_2 window from which the ac component of the IR emission spectrum of HF† was observed by a monochromator (Spex, 1700 III with a grating of 300 l mm^{-1}, blazed at 3 μm) equipped with a photovoltaic InAs detector (Santa Barbara Research Center). The output of the detector was treated by a preamplifier (P. A. R., 181) and a lock-in amplifier (Ithaco, 393) whose reference signal was taken from the modulated 253.7 nm radiation. Thus, both the intensity and the phase-delay angle of the emission were determined, and this made it possible to obtain information on both the production of HF† and its relaxation. Since an average residence time in the reaction cell was about 50 ms and the 253.7 nm radiation intensity was on the order of 10^{15} photon $cm^{-3}s^{-1}$, a fraction of decomposed F-ethylene did not exceed 10% when its partial pressure was less than 10^{-2} Torr. Vinyl fluoride, 1,1-difluoroethylene (Matheson, 99.9% and 99.0%, respectively), *cis*- and *trans*-1,2-difluoroethylene, 2-fluoropropene, and 1,1,2-trifluoroethylene (P.C.R.) were treated by repeated solidification at liquid N_2 temperature. Gas chromatographic analyses of the latter four compounds were made to confirm less than 1% of impurities included.

** 1 Torr ≈ 133.322 Pa.

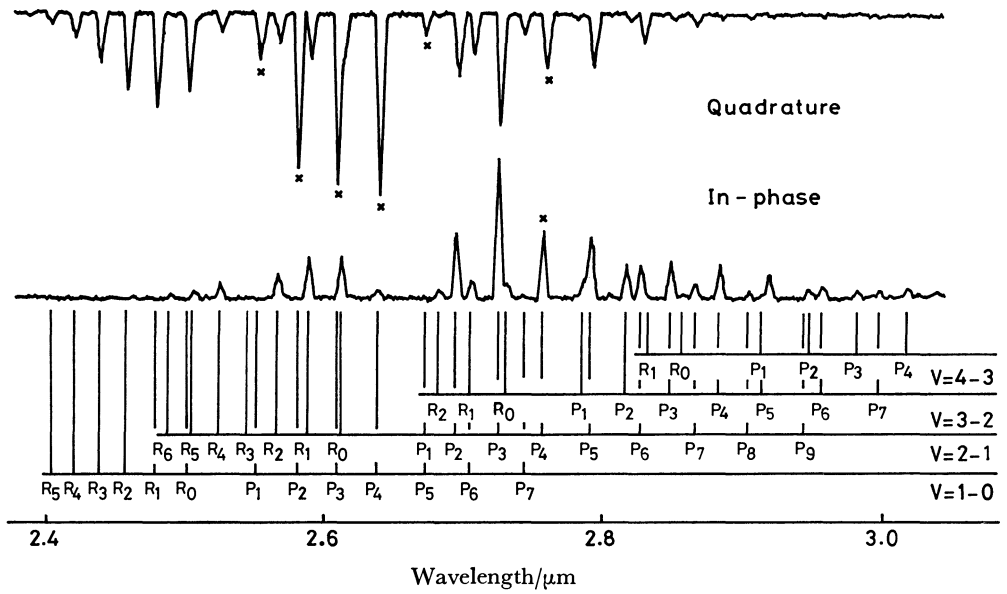

Fig. 1. AC components of emission spectrum of HF fundamentals observed in the mixture of 0.008 Torr CH_2=CHF+5 Torr Ar at 1.2 kHz modulation.
Lines marked by x are subjected to absorption of atmospheric water vapor.

Results

Analysis of Data. Figure 1 shows an example of the observed IR emission spectrum of HF†. Based on the molecular constants of HF given by Webb and Rao,[10] each emission line may be assigned to respective vibration-rotation transition as noted in Fig. 1. In order to determine a relative population in each vibration-rotation level from the spectrum, the spectroscopic data summarized by Meredith and Smith[11] and Herbelin and Emanuel[12] were employed. The emission intensity of the $v'J'$—$v''J''$ transition is formulated as

$$I_{v'J',v''J''} = [hc(\omega_{v'J',v''J''})^4/(2J'+1)(\omega_{v',v''})^3] \times S_{J',J''}F_{v'J',v''J''}A_{v',v''}N_{v'J'}, \quad (1)$$

where $\omega_{v'J',v''J''}$ and $\omega_{v',v''}$ are the wavenumbers of the relevant transition and the band center, respectively, and $S_{J',J''}$ represents the contribution of rotation to the dipole matrix element, and $A_{v',v''}$ is the spontaneous emission rate of the vibrational transition, and $N_{v',J'}$ is the population of the $v'J'$ state. In Fig. 2, plots of log $[I_{v'J',v''J''}/(\omega_{v'J',v''J''})^4 S_{J',J''}F_{v'J',v''J''}]$ are shown as a function of $J'(J'+1)$. The rotational equilibrium at room temperature is established in levels of $v'=1$—3 in the reaction system with the Ar pressure of more than 1 Torr. Thus, the rotational distribution in the level v' is described by

$$N_{v'J'} = N_{v'0} \exp[-B_{v'}J'(J'+1)/kT_{rot}]. \quad (2)$$

$N_{v'0}$ is determined by extrapolation of linear lines in Fig. 2, and is denoted hereafter as N_v. The population in the $v=4$ level is estimated from the line intensity of P(3 or 4) line of $v=4\rightarrow3$ transition assuming $T_{rot}=300$ K. As is seen from Fig. 2(b), a rotational non-equilibrium distribution is found in a low pressure reaction system. The observed distribution is almost in accord with that reported by Clough *et al.*,[2] and is partially relaxed due to collisional transitions in the gas phase as well as on the wall of the cell. Since it is difficult to estimate the selection rule for rotational transitions in collisions with the cell wall, the initial distribution may not be determined from the data obtained in the present flow apparatus.

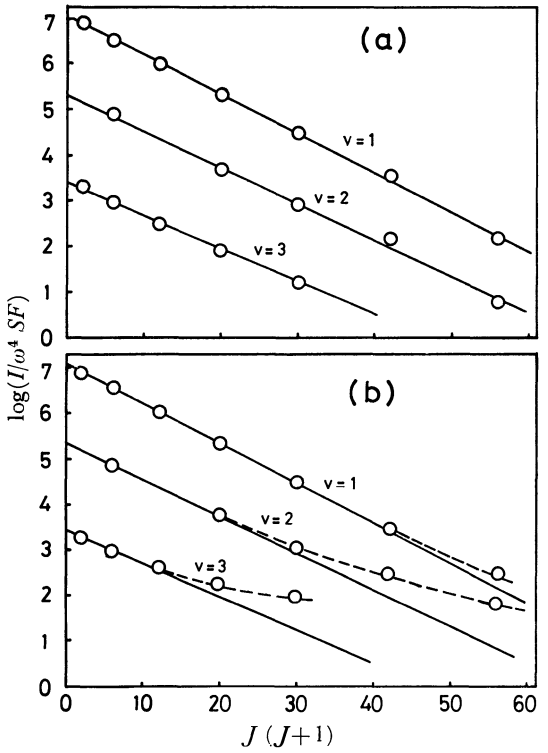

Fig. 2. Plots of $\log(I/\omega^4 SF)$ *vs.* $J(J+1)$.
The emission spectrum is observed at 1.2 kHz modulation in the mixtures of (a) 0.006 Torr CH_2=CF_2+3 Torr Ar and (b) 0.001 Torr CH_2=CF_2+0.2 Torr Ar. The slopes of the solid lines result in the rotational temperature of *ca.* 300 K.

Corresponding to the modulated 253.7 nm radiation intensity, the population in the level v is described as

$$N_v = \bar{N}_v + \tilde{N}_v \exp(i\omega t), \quad (3)$$

where the first term represents the DC component of N_v and the second the AC, and $\tilde{N}_v$ is a complex number to describe the quantity with a phase-delay angle. The kinetic equation for the population in the level v is formulated as follows.

$$dN_v/dt = K_v - R_{v,v-1}N_v + R_{v+1,v}N_{v+1}, \quad (4)$$

where K_v is the production rate of HF† in the level v, and $R_{v,v-1}$ the collisional plus radiative transition rate of $v \rightarrow v-1$. Here, it is assumed that a single quantum transition for the deactivation of HF†. An error caused by this assumption would not be very large, because the initial vibrational populations in higher levels are much smaller than those in lower levels as described later, and thus the contribution of multiple quantum transitions to the population in the relevant level v must be negligible. Equation 4 may be rewritten by the use of Eq. 3 as

$$i\omega\tilde{N}_v = \tilde{K}_v - R_{v,v-1}\tilde{N}_v + R_{v+1,v}\tilde{N}_{v+1}. \quad (5)$$

The imaginary part of this equation results in the equation

$$R_{v,v-1} = \omega(\cot\phi_v) + R_{v+1,v}(\tilde{N}^I_{v+1}/\tilde{N}^I_v), \quad (6)$$

where $\tilde{K}^I_v = 0$ and $\cot\phi_v = \tilde{N}^R_v/(-\tilde{N}^I_v)$ in which subscripts R and I denote the real and imaginary parts, respectively. The real part of Eq. 5 gives the formula

$$\tilde{K}^R_v = \omega(-\tilde{N}^I_v) + (R_{v,v-1}\tilde{N}^R_v - R_{v+1,v}\tilde{N}^R_{v+1}). \quad (7)$$

Thus, if the population in each level is obtained as a function of ω, the relaxation rate $R_{v,v-1}$ and the formation rate $\tilde{K}^R_v$ of HF† in respective vibrational level may be determined.

Vibrational Relaxation of HF†. In Fig. 3, tangent of the phase-delay angle of the R(1) line of the $v=1\rightarrow0$ transition is plotted against the modulation frequency. According to Eq. 6, tan ϕ_{vJ} is almost proportional to ω if the contribution of cascading supply to the population in the vJ level is not large. From Fig. 3, it is found that tan ϕ_{vJ} is not dependent on the Ar pressure if it exceeds 1 Torr, while tan ϕ_{vJ} is reduced at lower pressures of Ar. This means that Ar may not contribute to the deactivation of HF† and that the decrease of tan ϕ_{vJ} at a lower pressure may be attributed to deactivation of HF† by collisions on the wall of the cell. Thus, the later experiments were carried out in the mixture of Ar+F-ethylene at the total pressure of more than 1 Torr which is high enough to avoid the wall-collision effect.

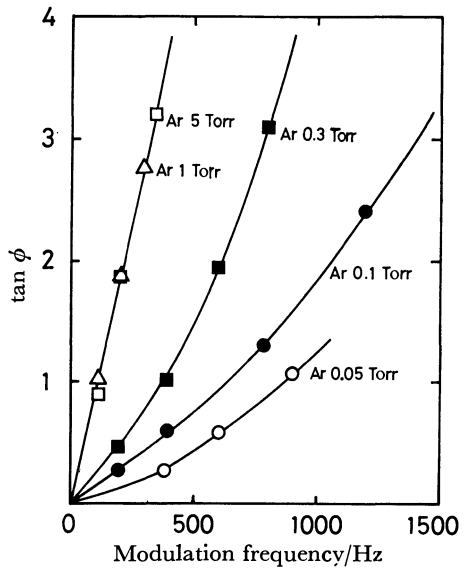

Fig. 3. Tangent of the phase -delay angle of R (1) line of $v=1\rightarrow0$ transition as a function of Ar pressure with the CH_2=CF_2 partial pressure of 0.006 Torr.

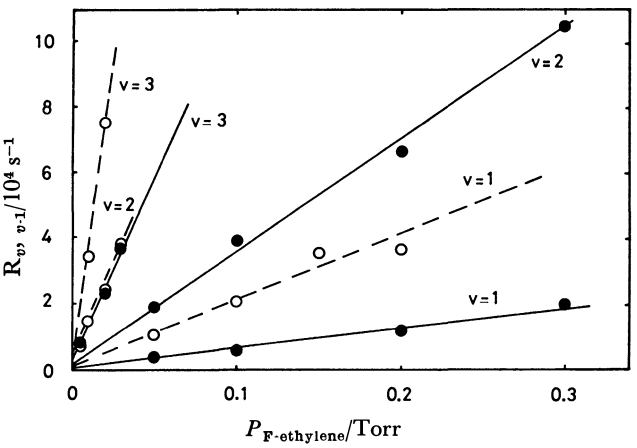

Fig. 4. The observed deactivation rate $R_{v,v-1}$ of HF† in the mixture of 5 Torr Ar +F-ethylene as a function of the partial pressure of F-ethylene.
Solid line: CH_2=CF_2, broken line: CH_2=CHF.

TABLE 1. DEACTIVATION RATE CONSTANT/$10^5\ s^{-1}\ Torr^{-1}$ OF HF† AT ROOM TEMPERATURE

v	Collision partner			
	CH_2=CHF	CH_2=CF_2	*cis*- and *trans*-CHF=CHF	HF
1	2.2±0.2	0.60±0.04	0.8±0.2	0.84[a]
2	11±2	3.5±0.3	4±1	4.2[b]
3	34±5	11±2	10±2	6.2[b]
4	40	30	—	10[b]

a) Ref. 13. b) Ref. 14.

In the analysis of the data by the use of Eq. 6, multiple quantum transitions are disregarded. However, the magnitude of the second term in the r.h.s. of Eq. 6 does not exceed 10% of the first term and thus, the error due to the above approximation must be much less than 10% and the obtained rate of $R_{v,v-1}$ may be interpreted as $\sum_{\delta\geq1} R_{v,v-\delta}$. The determined rates are plotted as a function of the partial pressure of F-ethylene in Fig. 4. The linear relation indicates that the dominant deactivation process occurs by collisions of HF† with F-ethylene. The slopes of these lines give the deactivation rate constants of HF† as summarized in Table 1. The deactivation of HF† in CH_2=CHF is about three times more efficient than in CH_2=CF_2, and the rate constants of HF($v=1,2$) are of the magnitude similar to those in HF.[13,14] While, larger rate constants of

HF(v=3,4) in F-ethylene than in HF indicate that the resonance effect is improved in higher levels of HF† for the V-V energy transfer from HF† to the CH stretching modes of F-ethylene.

Vibrational Distribution of HF. The observed sets of $|\tilde{N}_v|$ and ϕ_v of HF† produced from six kinds of F-ethylenes are given in Fig. 5. Values of ϕ_v's increase at higher modulation frequencies approaching to 90°, though they are relatively small for higher vibrational levels. The latter fact would be due to larger deactivation rates in higher levels. Contrary to this result, $|\tilde{N}_v|$ of v=1 or 2 is reduced very much as the modulation frequency increases. This means that the vibrational relaxation from upper vibrational levels contributes in large part to populations in lower levels. Thus, in order to determine the initial vibrational distribution, it is necessary to take into proper account the vibrational relaxation effect according to Eq. 7. First, $R_{v,v-1}$ is determined utilizing Eq. 6 and assuming no initial population in levels of $v \geqslant 5$. The data employed to estimate $R_{v,v-1}$ are obtained with a modulation frequency which results in ϕ_v's in the range of 30°—50°. This range is selected to obtain good accuracy of the determined $R_{v,v-1}$'s. Then, the relative magnitude of K_v may be determined by extrapolating the data of Fig. 5 to the case of infinitely fast modulation, where

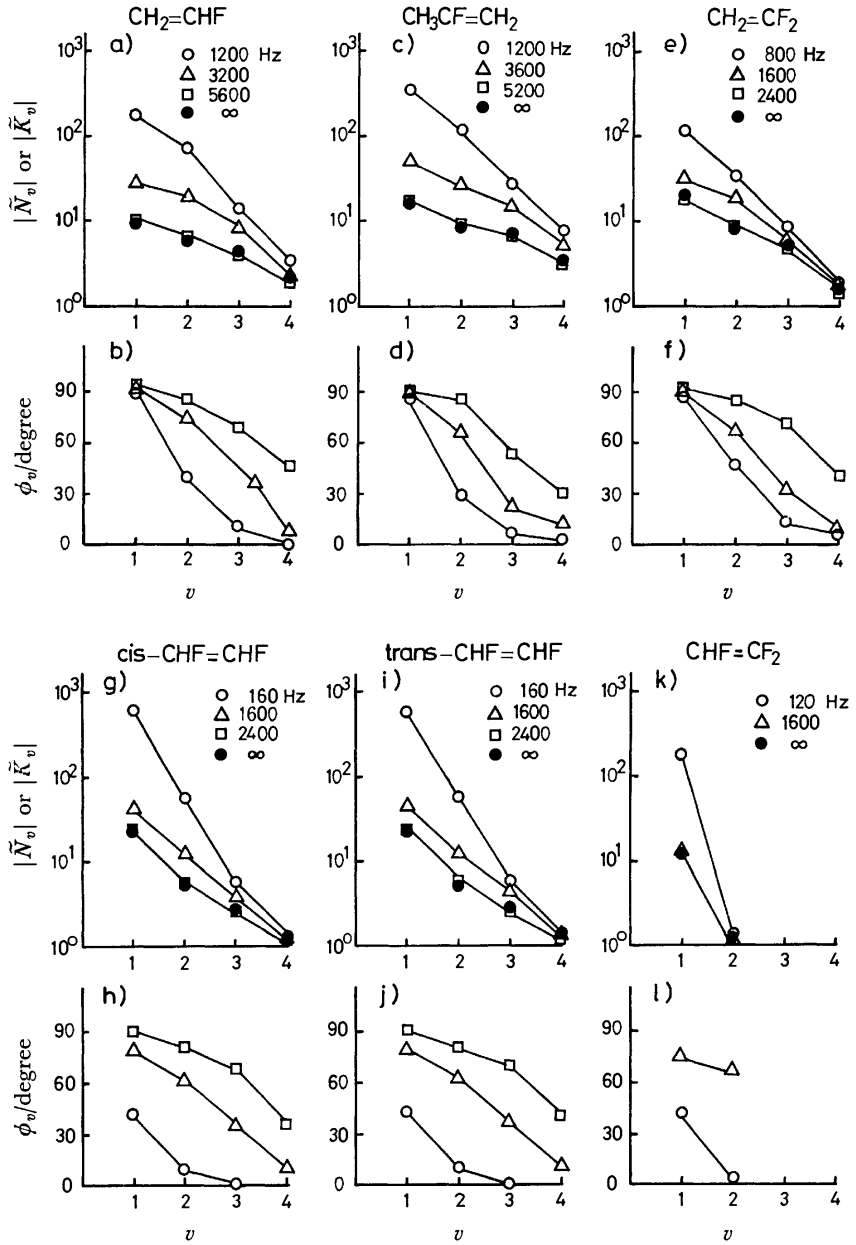

Fig. 5. Observed sets of $|\tilde{N}_v|$ and ϕ_v of HF† in the vibrational level v as a function of the modulation frequency. (a, b): CH_2=CHF 7 mTorr in Ar 5 Torr, (c, d): CH_3CF=CH_2 5 mTorr in Ar 5 Torr, (e, f): CH_2=CF_2 6 mTorr in Ar 3 Torr, (g, h): *trans*-CHF=CHF 7 mTorr in Ar 5 Torr, (i, j): *cis*-CHF=CHF 7 mTorr in Ar 5 Torr, (k, *l*): CHF=CF_2 5 mTorr in Ar 5 Torr.

TABLE 2. INITIAL VIBRATIONAL DISTRIBUTION OF HF† PRODUCED IN THE Hg-PHOTOSENSITIZED REACTION OF F-ETHYLENE

Parent molecule	CH_2=CHF	CH_3CF=CH_2	CH_2=CF_2	*cis*- and *trans*-CHF=CHF	CHF=CF_2
$v=1$	1.00	1.00	1.00	1.00	1.00
$v=2$	0.56±0.02	0.53±0.02	0.41±0.01	0.21±0.01	0.08±0.01
$v=3$	0.42±0.03	0.44±0.03	0.29±0.02	0.11±0.01	—
$v=4$	0.24±0.06	0.30±0.10	0.10±0.04	0.06±0.03	—
T_{vib}/K	11400	13700	7200	5700	2200
ΔH/kJ mol^{-1} a)	88	71	105	105	247
E_{avail}/kJ mol^{-1} b)	379	397	364	364	222
f_{vib}/% c)	19	23	11	7.6	1.7
f_{vib}^{calcd}/% d)	5.7	1.8	4.7	4.7	1.7

a) Heat of reaction at 298 K. b) Energy available for partitioning in product molecules. c) Observed fraction of energy converted to HF vibration from E_{avail}. d) Statistically calculated value of f_{vib}.

$\phi_v=90°$. The initial distributions of HF† are plotted also in Fig. 5 and their numerical values are given in Table 2. The values are close to the uncorrected ones of $|\tilde{N}_v|$ obtained at a modulation frequency of *ca.* 5 kHz. This fact rationalizes the procedure to uncover the initial vibrational distribution from the observed relaxed distribution. The initial distribution is almost of the Boltzmann type with 11400, 13700, 7200, 5700, 2200 K for respective parent molecules of CH_2=CHF, CH_3CF=CH_2, CH_2=CF_2, *trans*- and *cis*-CHF=CHF, and CHF=CF_2. The result for CH_2=CF_2 is in good agreement with that reported by Clough *et al.*[2]

Discussion

A schematic diagram explaining the energy levels of initial, intermediate, and final states in the reactions of CH_2=CHF and CH_2=CF_2 is given in Fig. 6. As pointed out already,[7] the triplet state of F-ethylene may be realized in the initial stage of the reaction. The lowest level of the triplet state is estimated by Coggiola *et al.*[15] to be around 420 kJ mol^{-1} from the ground state. Unfortunately, no information is obtained from the present experiment to judge whether the reaction proceeds *via* a second excited intermediate of F-ethylidene or it does through a vibrationally high state of the ground state F-ethylene.[17] Energetically, E_{avail} calculated from ΔH_f's listed in Table 3 must be shared among internal and external degrees-of-freedom of product molecules HF and CH≡CH or CH≡CF. E_{avail} for the reaction of CH_3CF=CH_2 is estimated assuming the products of HF + CH_3C≡CH though no experimental evidence is available. If HF and CH_2=C=CH_2 are produced, E_{avail} is reduced to 389 kJ mol^{-1}. Assuming the Boltzmann distribution of HF† with T_{vib} in Table 2, the amount of the HF† vibrational energy disposed may be calculated, although this procedure might overestimate populations in levels of $v\geqslant 5$. As noted in Table 2, 23—1.7% of E_{avail} is converted to the vibrational energy of HF†. It may be noticed that if a parent molecule involves more hydrogen atoms, a larger fraction of E_{avail} is disposed into the HF† vibration. Shock-tube experiments of thermal decomposition of F-ethylene were carried out to determine the activation energies listed in Table 3. It is only a speculation, however, that the activated state in the thermal decomposition is similar to the critical transition state in the Hg-photosensitized reaction. Two isomers of *cis*- and *trans*-CHF=CHF result in quite the same distribution of HF†. This leads to the conclusion that the critical state just before the decomposition is common to both isomers, and accords with the fact that the quantum yields for the *cis*↔*trans* isomerization are identical for both of the forward and backward directions.[7]

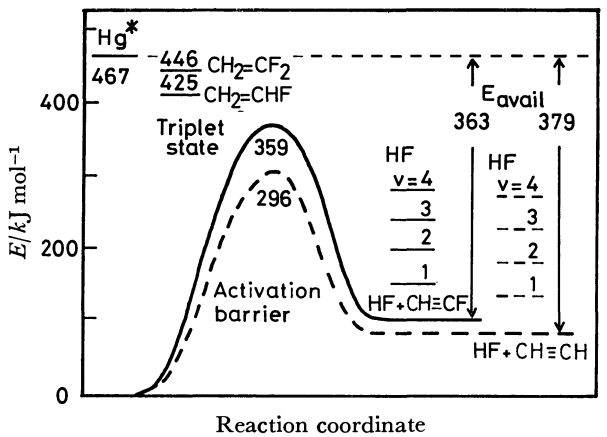

Fig. 6. Schematic potential energy diagram of HF elimination from CH_2=CHF and CH_2=CF_2.
The data source is given in Table 3.

A statistical calculation on the partitioning of E_{avail} in various degrees-of-freedom of product molecules is carried out for the Hg-photosensitized decompositions of F-ethylenes. In the calculation, the following assumptions are postulated. (1) A loose complex of HF and CH≡CH, CH≡CF, or CH_3C≡CH is assumed in the transition state for the decomposition. (2) The complex is formed on the top of the barrier which is realized in the effective potential composed of a long-range attractive potential due to a multipole interaction and the centrifugal force originating from the orbital angular momentum between HF and CH≡CH, CH≡CF, or CH_3C≡CH. (3) The angular momentum of the complex is in thermal equilibrium at the translational temperature of the reaction system. The vibrational state

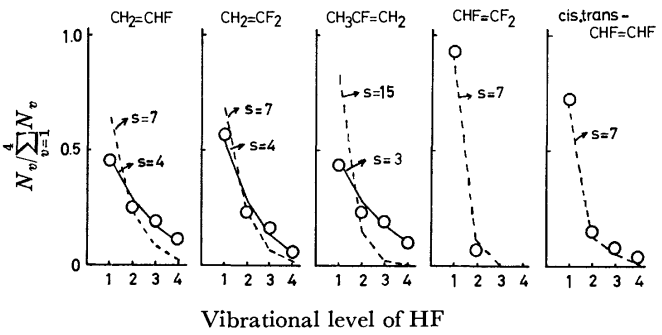

Fig. 7. The observed vibrational distribution (○) of HF† and the statistically calculated one.
Broken lines are the results calculated assuming total number of vibrational modes in a loose complex as active modes and solid lines are those assuming limited number of modes as active modes.

density is calculated by the Whitten-Rabinovitch equation[24] and the ones in another degrees-of-freedom are given in a book of Forst.[25] The calculation is based on the RRKM theory modified by Safron *et al.*[26] The vibrational frequencies of CH≡CH, CH≡CF, and $CH_3C{\equiv}CH$ are taken from Tables of Shimanouchi,[27] and CF≡CF from Ref. 20. The calculated results are shown in Fig. 7 together with the experimental data. The statistical calculation for CH_2=CHF, CH_3CF=CH_2, and CH_2=CF_2 gives much less populations in higher vibrational levels, while the calculation for *cis*- and *trans*-CHF=CHF and CHF=CF_2 results in the values close to the experimental ones.

The fact that the distributions of HF from *cis*-, *trans*-CHF=CHF and CHF=CF_2 are close to the statistical expectation may lead to the conclusion that the reaction scheme is different from that in other species. Strausz *et al.*[7] gave a speculation that CHF=CHF and CHF=CF_2 did not decompose *via* an intermediate of ethylidene type and resulted in primary products: C=CHF and HF in which HF was produced by the αα-elimination directly from excited F-ethylene. If this is the case, E_{avail} must be reduced very much causing less energy disposal to the HF vibration than that observed in the present experiment. According to Strausz *et al.*'s discussion, in the other molecules than CHF=CHF and CHF=CF_2, the decomposition occurs from the corresponding ethylidenes. However, more direct experimental information must be accumulated in order to discuss their speculation. As far as the present experiment is concerned, no positive evidence for their postulate was obtained.

The excess populations of HF† in comparison with the statistical expectation might be attributed to a non-random distribution of E_{avail} among the internal degrees-of-freedom of the CH≡CH·HF and CH≡CF·HF complexes. If the number of oscillating modes s is limited to three or four, the disagreement between the calculation and the experiment disappears as shown in Fig. 7. This may support the conclusion that E_{avail} is locally distributed among particular degrees-of-freedom in the complex. However, the disagreement may be caused by another mechanism. As described in Fig. 6, a potential barrier exists in the course of the decomposition. Hence, a strong force is possible to act upon the separating HF and CH≡CH or CH≡CF while sliding down the barrier. This possibility was suggested by Berry[3] as a cause for the vibrational excitation of HF in his bootstrap model. The similar type of discussion on energy partitioning has been made in F-substitution reactions of Cl- or Br-ethylenes. McDonald and coworkers[28] have made IR emission measurements of various modes of F-ethylenes produced, and found statistical distributions if a potential barrier does not exist on the passage to the reaction exit and non-statistical distributions if a barrier exists.

Table 3. Heats of formation ΔH_f, activation energies for thermal decomposition E_a, triplet energy level E_t of F-ethylenes and related species

Species	ΔH_f, 298 K/ kJ mol^{-1}	E_a/kJ mol^{-1}	E_t[h]/kJ mol^{-1}
CH_2=CHF	−135.2[a]	297[g]	426
CH_2=CF_2	−334.4[b]	359[e]	447
cis-CHF=CHF	−330[c]	288[e]	414
trans-CHF=CHF	−330[c]	276[e]	405
CHF=CF_2	−49[b]	—	426
CH_3CF=CH_2	−159[c]	—	—
CH≡CH	226.51[d]		
CH≡CF	42[e]		
CF≡CF	21[d]		
$CH_3C{\equiv}CH$	185.1[f]		
HF	−272.3[d]		

a) Ref. 17. b) Ref. 18. c) Estimated by a method described in Ref. 19. d) Ref. 20. e) Ref. 21. f) Ref. 22. g) Ref. 23. h) Ref. 15.

In Table 3, it is seen that the heat of the HF elimination reaction of CHF=CF_2 is much larger than those of CH_2=CHF and CH_3CF=CH_2, so that the barrier height for the backward reaction, $E_a-\Delta H$, is reduced to *ca.* 80 kJ mol^{-1} in the reaction of CHF=CF_2. Since no experimental data of ΔH_f is available for *trans*- and *cis*-CHF=CHF, an approximate method,[19] in which a mean contribution of each bond in F-ethylene molecules to ΔH_f is empirically estimated, is adopted to result in a common value of ΔH_f for three compounds of *trans*- and *cis*-CHF=CHF and CH_2=CF_2. However, $-\Delta H_f$ of CHF=CHF is probably between those of CH_2=CF_2 and CHF=CF_2, so that $E_a-\Delta H$ of CHF=CHF may not be of a smaller magnitude than that of CH_2=CF_2. Thus, it would be reasonable that the observed vibrational distributions of HF formed from *trans*- and *cis*-CHF=CHF and CHF=CF_2 are close to those calculated statistically, while the other F-ethylenes produce HF† with non-statistical vibrational distributions due to energy release through high exit barriers.

The above findings are supported by the crossed molecular beam reactions studied by Farrar and Lee.[29] Recently, they report a result slightly different from the IR chemiluminescence measurement of McDonald and coworkers. Non-statistical velocity distributions of products are found for both of CH_2=CHBr+F and +Cl reactions,[30] of which the product vibrational

distribution is statistical in the former reaction and nonstatistical in the latter on the basis of the IR emission measurement. If a molecule activated by a collision with a reactive or excited atom has a significant amount of energy exceeding a barrier height, the resulting short lifetime of the activated molecule may result in a non-statistical velocity distribution of product molecules. While, an intramolecular vibrational relaxation changes a non-statistical distribution to a statistical one before product molecules emit IR photons. This is an explanation for the discrepancy between the two experiments. However, since HF has discrete vibration-rotation levels in the present energy region and an intramolecular relaxation is impossible, the distribution observed in this experiment must be interpreted as the ones at the reaction exit. Thus, the observed vibrational distribution of HF is caused mainly by a dynamical force which acts on HF separating from CH≡CH or CH≡CF while sliding down from the barrier top.

This work was supported partly by a Grant-in-Aid for Scientific Research from the Ministry of Education (No. 211606).

References

1) M. J. Berry and G. C. Pimentel, *J. Chem. Phys.*, **51**, 2274 (1968); *IEEE J. Quantum Electron.*, **QE-6**, 176 (1970).
2) P. N. Clough, J. C. Polanyi, and R. T. Taguchi, *Can. J. Chem.*, **48**, 2919 (1970).
3) M. J. Berry, *J. Chem. Phys.*, **61**, 3114 (1974).
4) W. E. Jones, G. Matinopoulos, J. S. Wasson, and M. T. H. Liu, *J. Chem. Soc., Faraday Trans. 2*, **74**, 831 (1978).
5) W. E. Jones, G. Matinopoulos, and J. S. Wasson, *J. Chem. Soc., Faraday Trans. 2*, **74**, 2128 (1978).
6) A. R. Trobridge and K. R. Jennings, *Trans. Faraday Soc.*, **61**, 2168 (1965).
7) O. P. Strausz, R. J. Norstrom, D. Salahub, R. K. Gosavi, H. E. Gunning, and I. G. Csizmadia, *J. Am. Chem. Soc.*, **92**, 6395 (1970).
8) S. Tsunashima, H. E. Gunning, and O. P. Strausz, *J. Am. Chem. Soc.*, **98**, 1690 (1976).
9) H. Horiguchi and S. Tsuchiya, *J. Chem. Phys.*, **70**, 762 (1979).
10) D. U. Webb and K. N. Rao, *J. Mol. Spectrosc.*, **28**, 121 (1968).
11) R. E. Meredith and F. G. Smith, *J. Quant. Spectrosc. Rad. Transfer*, **13**, 89 (1973).
12) J. M. Herbelin and G. Emanuel, *J. Chem. Phys.*, **60**, 689 (1974).
13) R. A. Lucht and T. A. Cool, *J. Chem. Phys.*, **60**, 1026 (1974).
14) P. R. Pool and I. W. M. Smith, *J. Chem. Soc., Faraday Trans. 2*, **73**, 1434 (1977).
15) M. J. Coggiola, O. A. Mosher, W. M. Flicker, and A. Kuppermann, *Chem. Phys. Lett.*, **27**, 14 (1974).
16) According to the recent theoretical calculation of *ab initio* surface of CH_2=CHF by Kato and Morokuma, the triplet surface has a high barrier for reaction, so that non-adiabatic transition to the singlet surface must occur before decomposition. Kato and Morokuma, 14th Symposium on High Speed Reactions, Tokyo (1979).
17) V. P. Kolesov and T. S. Papina, *Zh. Fiz. Khim.*, **44**, 1101 (1970).
18) J. R. Lacher and H. A. Skinner, *J. Chem. Soc., A*, **1968**, 1034.
19) G. J. Janz, "Thermodynamic Properties of Organic Compounds," Academic Press, New York (1967).
20) "JANAF Thermochemical Tables," Nat. Stad. Ref. Data Ser., Nat. Bur. Stand., 37, U. S. Government Printing Office, Washington, D. C. (1972).
21) J. M. Simmie and E. Tschuikow-Roux, *J. Phys. Chem.*, **74**, 4075 (1970).
22) J. Collins and F. P. Lossing, *J. Am. Chem. Soc.*, **80**, 1568 (1958).
23) J. M. Simmie, W. J. Quiring, and E. T. Tschuikow-Roux, *J. Phys. Chem.*, **74**, 992 (1970).
24) G. Z. Whitten and B. S. Rabinovitch, *J. Chem. Phys.*, **38**, 2466 (1963).
25) W. Forst, "Theory of Unimolecular Reactions," Academic Press, New York (1973).
26) S. A. Sarfron, N. W. Weinstein, D. R. Herschbach, and J. C. Tully, *Chem. Phys. Lett.*, **12**, 564 (1972).
27) T. Shimanouchi, "Tables of Vibrational Frequencies," Consolidated Volume, Nat. Stand. Ref. Data Ser., Nat. Bur. Stand. 39, U. S. Government Printing Office, Washington, D. C. (1972).
28) J. G. Moehlmann and J. D. McDonald, *J. Chem. Phys.*, **62**, 3052 (1975); J. F. Durana and J. C. McDonald, *J. Chem. Phys.*, **64**, 2518 (1976).
29) J. M. Farrar and Y. T. Lee, *J. Chem. Phys.*, **65**, 1414 (1976).
30) R. J. Buss, M. J. Coggiola, and Y. T. Lee, *Faraday Discuss. Chem. Soc.*, **67**, 162 (1979).

Oxidation of Nitrotoluenes with Electro-generated Superoxide Ion

Hiromitsu SAGAE, Masamichi FUJIHIRA, Henning LUND,† and Tetsuo OSA*
Pharmaceutical Institute, Tohoku University, Aobayama, Sendai 980
(Received December 20, 1979)

The oxidation of *o*-, *m*-, and *p*-nitrotoluenes with electro-generated superoxide ion in dimethylformamide was studied using cyclic voltammetry and controlled potential macro-electrolysis. The electrochemical reduction of oxygen in the presence of *o*- and *p*-nitrotoluenes yielded the corresponding carboxylic acids because the methyl groups in these derivatives are activated by the nitro group. An intermediate in these oxidations should be the corresponding nitrobenzaldehyde. The reaction mechanism is discussed.

Recently superoxide ion, $O^{\cdot}$, has attracted a great deal of attention of organic and biological chemists, because it is novel activating reagent for organic synthesis and is one of the most important activated forms of molecular oxygen in biological systems.[1-3] Superoxide ion is produced by the electrochemical reduction of oxygen dissolved in non-aqueous solvents, such as pyridine, acetonitrile, and dimethylformamide (DMF) at −0.85 V *vs.* silver-silver chloride (Ag/AgCl)[2,3] as shown in Eq. 1:

$$O_2 + e \rightleftarrows O_2^{\cdot} \quad (1)$$

Alkali metal superoxides, such as potassium and sodium superoxides, are well known but their insolubility in the usual organic solvents makes them of little preparative use.[4] The electrochemical method is experimentally more convenient because the continuous generation of superoxide ion is possible on the electrode and the solubility of the superoxide ion in the presence of tetraethylammonium cations of the supporting electrolyte is sufficiently high.[5]

We have previously reported preliminary results on the reaction of nitrotoluenes and nitroethylbenzene with electro-generated superoxide ion.[6] In this paper, we describe in detail the reaction of nitrotoluenes with electro-generated superoxide ion in DMF solution, using macro-electrolysis and cyclic voltammetry.

There are many reports[7-10] on the oxidation of nitrotoluenes to nitrobenzoic acids using various oxidizing reagents and conditions, such as cobaltic salts,[7a] nitric acid,[8a] and basic condition.[7b] However, the oxidation with superoxide ion has not previously been reported. Advantageous characteristics of oxidation by electro-generated superoxide ion are two-fold; the oxidation proceeds under mild conditions and does not require any oxidizing chemicals. Elucidation of the reaction mechanism of the oxidation of nitrotoluenes with electro-generated superoxide ion should also prove to be useful in understanding the metabolism of such compounds in certain insects.[11]

Experimental

Materials. DMF was dried over anhydrous $CuSO_4$ for 24 h and then distilled under reduced pressure. Further purification was achieved by passage through a column of molecular sieves (4A 1/16) and activated alumina (both pre-treated by heating at 400 °C). Tetraethylammonium perchlorate (TEAP) was synthesized and purified in the usual manner.[12] Nitrotoluene, *p*-nitrobenzaldehyde, and nitrobenzoic acids of E. P. grade were purchased commercially (Wako Pure Chemical Industries) and were recrystallized before use.

Cyclic Voltammetry. Cyclic voltammetry was carried out in DMF solution containing 0.1 M (1 M=1 mol dm^{-3}) TEAP as a supporting electrolyte on a hanging mercury drop electrode (HMDE). The cathode potentials were referred to Ag/AgCl, aq 1 M KCl. Cyclic potential sweeps were generated by an NF Circuit Design Block FG-100AD function generator in conjunction with a potentiostat which was self-made according to the literature.[13]

Controlled Potential Macro-electrolysis. For controlled potential macro-electrolysis, a three compartment cell was employed in which cathodic and anodic chambers were separated by two porous glass disks and a reference electrode with a Luggin capillary was put near the cathode. A mercury pool with a surface area of 16 cm^2 was used as the cathode, and platinum gauze as the anode. The electrolyte solution (0.1 M TEAP) of 60 cm^3 containing 0.06 M substrate was placed in the cathodic chamber, 40 cm^3 of the electrolyte solution in the anodic chamber, and 10 cm^3 of the electrolyte solution in the middle chamber. Oxygen was bubbled through the cathode. The cathode potential was controlled with a Yanagimoto VE-8 controlled potential electrolyzer. The quantity of electricity passed was measured with a copper coulometer.

Separation of Nitrobenzoic Acid. The main products of the electrolyses, nitrobenzoic acids, were separated and identified by the following procedure. The catholyte was poured into 200 cm^3 of 10% aqueous $NaHCO_3$ solution. The starting material and products other than nitrobenzoic acids in this solution were removed by extraction with CH_2Cl_2. Since nitrobenzoic acids could not be precipitated by acidification of the aqueous layer due to the presence of DMF in the water, the aqueous layer was evaporated to dryness *in vacuo* to remove the DMF. The resulting solid was dissolved in water and acidified with 5% aqueous HCl to precipitate the nitrobenzoic acids. The products were purified by recrystallization from alcohol and identified as the expected carboxylic acids by comparing their melting points and infrared spectra (IR) with those of authentic samples. As described later, the peak potentials of the cyclic voltammograms of these products were also found to agree with those of the authentic carboxylic acids.

p-Nitrobenzoic Acid from p-*Nitrotoluene.* The macro-electrolysis of oxygen in the presence of 0.5 g of *p*-nitrotoluene was carried out at −0.9 V *vs.* Ag/AgCl. The electrolysis time was *ca.* 24 h and the total amount of charge passed was *ca.* 2000 C. About 0.22 g of *p*-nitrobenzoic acid was obtained using the method mentioned above, and about 0.11 g of *p*-nitrotoluene was recovered. The IR spectrum of the product

† On leave from Department of Organic Chemistry, University of Aarhus, DK-8000, Aarhus C, Denmark.

agreed with that of authentic *p*-nitrobenzoic acid. Mp 241—242 °C (lit, 242 °C)[14]

o-*Nitrobenzoic Acid from* o-*Nitrotoluene.* The macro-electrolysis of oxygen in the presence of 0.5 g of *o*-nitrotoluene was carried out at −0.9 V *vs.* Ag/AgCl. The electrolysis time was *ca.* 24 h and the total amount of charge passed was *ca.* 2050 C. About 0.21 g of *o*-nitrobenzoic acid was obtained using the method mentioned above, and about 0.12 g of *o*-nitrotoluene was recovered. The IR spectrum of the product agreed with that of authentic *o*-nitrobenzoic acid. Mp 146—147 °C (lit, 147—148 °C)[14]

p-*Nitrobenzoic Acid from* p-*Nitrobenzaldehyde.* The macro-electrolysis of oxygen in the presence of 0.5 g of *p*-nitrobenzaldehyde was carried out at −0.9 V *vs.* Ag/AgCl. The electrolysis time was *ca.* 24 h and the total amount of charge passed was *ca.* 1100 C. About 0.35 g of *p*-nitrobenzoic acid was obtained using the method mentioned above, and 0.08 g of *p*-nitrobenzaldehyde was recovered. The IR spectrum of the product agreed with that of authentic *p*-nitrobenzoic acid. Mp 241—242 °C (lit, 242 °C)[14]

m-*Nitrobenzoic Acid.* *m*-Nitrobenzoic acid was not obtained from the electrolysis of oxygen in the presence of *m*-nitrotoluene at −0.9 V *vs.* Ag/AgCl.

Results and Discussion

Controlled Potential Macro-electrolysis. The reduction peak potentials of nitrotoluenes, together with those for oxygen, nitrobenzoic acids, and *p*-nitrobenzaldehyde, in cyclic voltammetry are listed in Table 1.

Table 1. Reduction peak potentials of nitrotoluenes, *p*-nitrobenzaldehyde, and nitrobenzoic acids

Compound	E_p^1	E_p^2	E_p^3
o-Nitrotoluene	−1.23	−1.92	
m-Nitrotoluene	−1.14	−1.75	
p-Nitrotoluene	−1.10	−1.85	
p-Nitrobenzaldehyde	−0.82	−1.35	
o-Nitrobenzoic acid	−0.90	−1.20	−1.73
m-Nitrobenzoic acid	−0.92	−1.23	−1.75
p-Nitrobenzoic acid	−0.80	−1.16	−1.70
Cf. oxygen	−0.85	−1.75	

E/V *vs.* Ag/AgCl, solvent: DMF, supporting electrolyte: TEAP, electrode: HMDE.

The controlled potential macro-electrolyses of oxygen in the presence of nitrotoluenes were carried out at −0.9 V *vs.* Ag/AgCl in DMF solution. At −0.9 V *vs.* Ag/AgCl, only oxygen was reduced, to the superoxide ion, while nitrotoluenes were not reduced. The results of the electrolyses are collected in Table 2. *p*-Nitrotoluene reacted with electro-generated superoxide ion to yield *p*-nitrobenzoic acid (Eq. 2). Controlled potential macro-electrolysis of oxygen in the presence of *p*-nitrobenzaldehyde was carried out because *p*-nitrobenzaldehyde is predicted to be an intermediate in the oxidation of *p*-nitrotoluene to *p*-nitrobenzoic acid. As expected, the reaction of *p*-nitrobenzaldehyde with superoxide ion yielded *p*-nitrobenzoic acid fairly readily (Eq. 5), although *p*-nitrobenzaldehyde was not isolated when *p*-nitrotoluene was oxidized. These results indicated that the produced *p*-nitrobenzaldehyde reacts with electro-generated superoxide ion immediately, or is reduced at the electrode directly, owing to a more positive reduction potential (−0.82 V *vs.* Ag/AgCl) than that used for the controlled potential electrolysis. *o*-Nitrobenzaldehyde is also considered to be a most probable intermediate in the reaction of *o*-nitrotoluene with superoxide ion.

In order to investigate the positional effect of the nitro group attached to the benzene ring, macro-electrolyses of oxygen in the presence of *o*- and *m*-nitrotoluene were carried out. *o*-Nitrobenzoic acid was obtained from *o*-nitrotoluene, while *m*-nitrobenzoic acid was not obtained from *m*-nitrotoluene (Eqs. 3 and 4). This result indicates that the electro-generated superoxide ion reacts only with a methyl group which is activated by the nitro group attached to the benzene ring, to yield the corresponding carboxylic acid.

Cyclic Voltammetry of Nitrotoluenes. Cyclic voltammetry of nitrotoluenes, *p*-nitrobenzaldehyde, and *p*-nitrobenzoic acids in the presence and in the absence of oxygen was carried out in order to investigate the reaction mechanism. Cyclic voltammograms of *p*-nitrotoluene in the presence and in the absence of oxygen, together with that of oxygen, in DMF solution as shown in Fig. 1. In the cyclic voltammogram of oxygen, the first reversible reduction wave at −0.85 V *vs.* Ag/AgCl corresponded to the one-electron reduction of oxygen to the superoxide ion. The second irreversible reduction wave at −1.75 V *vs.* Ag/AgCl corresponded to the further one-electron reduction of superoxide ion to the peroxide ion, O_2^{2-}, followed by protonation. In the cyclic voltammogram of *p*-nitrotoluene under a nitrogen atmosphere, a reversible reduction wave at −1.1 V *vs.* Ag/AgCl and an irreversible reduction wave at −1.8 V *vs.* Ag/AgCl appeared. In the presence of oxygen, the first wave and the second wave are the corresponding first reduction waves of oxygen and *p*-nitrotoluene respectively. The second wave of oxygen

Table 2. Formation of carboxylic acids from nitrotoluenes

Starting material	Amount of nitrobenzoic acid produced/g	Yield/%	Selectivity/%	Current[a] efficiency/%
o-Nitrotoluene	0.21	45 (45—50)[b]	42 (42—96)[b]	52 (40—62)[b]
m-Nitrotoluene	undetected	—	—	—
p-Nitrotoluene	0.22	56 (50—60)	44 (44—95)	55 (45—65)
Cf. p-nitrobenzaldehyde	0.35	68 (55—70)	70 (70—90)	49 (49—65)

a) The current efficiency calculated as the electrons of 4 Faradays are necessary to obtain 1 mol of the corresponding acid from nitrotoluene, and 2 Faradays from nitrobenzaldehyde. b) The electrolysis was carried out several times and the range of the values are shown in parentheses.

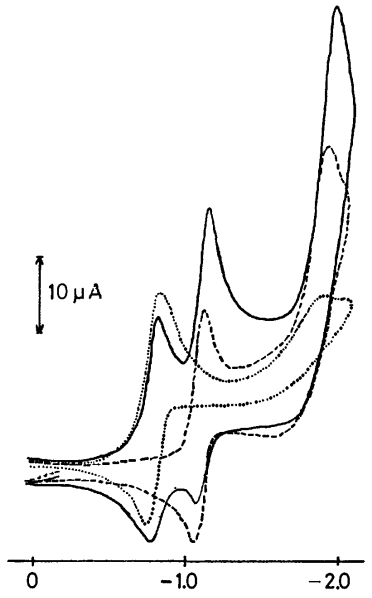

Fig. 1. Cyclic voltammograms of *p*-nitrotoluene. Concentration of *p*-nitrotoluene: *ca.* 10mM, electrolyte: 0.1 M TEAP/DMF, electrode: HMDE, sweep rate: 0.1 V s^{-1}, ------: in the absence of oxygen, ——: in the presence of oxygen. *Cf.* ·····: cyclic voltammogram of oxygen.

overlapped with the second wave of *p*-nitrotoluene at −1.8 V *vs.* Ag/AgCl. In this case no other reduction wave appeared except those for oxygen and *p*-nitrotoluene. Cyclic voltammetry of *o*- and *m*-nitrotoluenes in the presence and in the absence of oxygen gave similar results to those for *p*-nitrotoluene.

Cyclic Voltammetry of Nitrobenzoic Acids. The cyclic voltammogram of *p*-nitrobenzoic acid in DMF solution under a nitrogen atmosphere is shown in Fig. 2. The first and third reduction waves, whose reduction peak potentials are −0.8 V and −1.7 V *vs.* Ag/AgCl

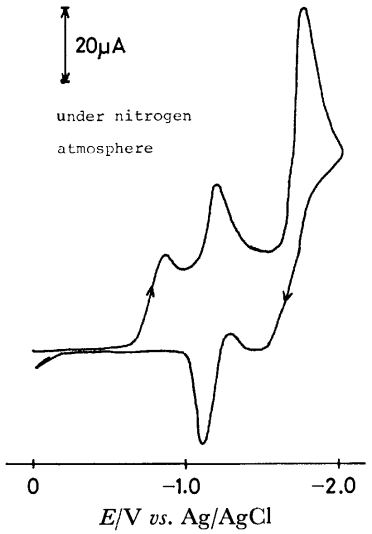

Fig. 2. Cyclic voltammogram of *p*-nitrobenzoic acid. Concentration of *p*-nitrobenzoic acid: *ca.* 10 mM, electrolyte: 0.1 M TEAP/DMF, electrode: HMDE, sweep rate: 0.1 V s^{-1}.

respectively, are irreversible. The second reduction wave is reversible with a reduction peak potential of −1.1 V *vs.* Ag/AgCl. Anomaly in shape of the corresponding reoxidation wave at *ca.* −1.1 V of the second reduction wave can be interpreted by the streaming phenonmenon, observed initially by Santhanam and Bard,[15] which occurs during oxidation of radical anion in cyclic voltammetric experiments. The cyclic voltammograms of *o*- and *m*-nitrobenzoic acids under a nitrogen atmosphere are similar to that of *p*-nitrobenzoic acid, and their reduction peak potentials are collected in Table 1.

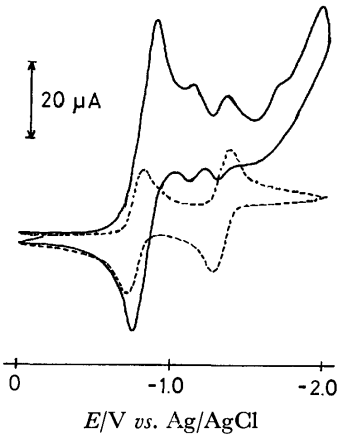

Fig. 3. Cyclic voltammograms of *p*-nitrobenzaldehyde. Concentration of *p*-nitrobenzaldehyde: *ca.* 10 mM, electrolyte: 0.1 M TEAP/DMF, electrode: HMDE, sweep rate: 0.1 V s^{-1}, ------: in the absence of oxygen, ——: in the presence of oxygen.

Cyclic Voltammetry of p-*Nitrobenzaldehyde.* Cyclic voltammetry of *p*-nitrobenzaldehyde, expected to be an intermediate in the oxidation of *p*-nitrotoluene, in the presence and in the absence of oxygen was carried out. The results are shown in Fig. 3. Two reversible reduction waves are observed under a nitrogen atmosphere with reduction peaks at −0.82 V and −1.35 V *vs.* Ag/AgCl. In the presence of oxygen a reversible reduction wave at −1.1 V and an irreversible reduction wave at −1.65 V *vs.* Ag/AgCl appeared as well as those for oxygen and *p*-nitrobenzaldehyde. These new reduction peak potentials corresponded to those of the second and third waves of *p*-nitrobenzoic acid. The first reduction wave of *p*-nitrobenzoic acid overlapped with the first wave of *p*-nitrobenzaldehyde and oxygen. This result indicates that *p*-nitrobenzoic acid was formed during cyclic voltammetry of *p*-nitrobenzaldehyde.

Cyclic Voltammetry of the Catholyte. In the course of macro-electrolysis of oxygen in the presence of *p*-nitrotoluene, cyclic voltammetry of the catholyte was carried out. The result is shown in Fig. 4. Since the *p*-nitrotoluene remained as a major substrate in the solution, two large reduction waves observed at −1.1 V and −1.9 V *vs.* Ag/AgCl should be due to *p*-nitrotoluene. The reduction waves at *ca.* −0.8 V and *ca.* −1.6 V *vs.* Ag/AgCl corresponded to the first and third

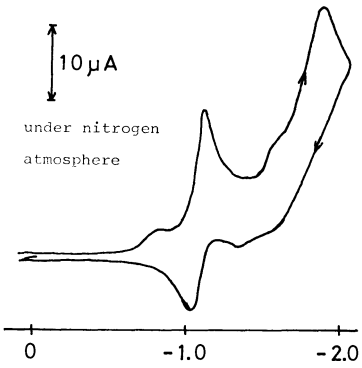

Fig. 4. Cyclic voltammogram of the catholyte in the course of the electrolysis in the presence of *p*-nitrotoluene. Electrolyte: 0.1 M TEAP/DMF, electrode: HMDE, sweep rate: 0.1 V s^{-1}.

reduction waves of *p*-nitrobenzoic acid. The second reduction wave of *p*-nitrobenzoic acid overlapped with the first reduction wave of *p*-nitrotoluene. In the cyclic voltammogram of *p*-nitrotoluene in the presence of oxygen (solid line in Fig. 1), no reduction wave appeared other than those for oxygen and *p*-nitrotoluene. These results indicate that *p*-nitrobenzoic acid was not formed during cyclic voltammetry, and consequently the reaction rate of the superoxide ion with *p*-nitrotoluene is deduced to be slow. Since the reduction wave corresponding to *p*-nitrobenzaldehyde did not appear in the course of macro-electrolysis in the presence of *p*-nitrotoluene as shown in Fig. 4, it is assumed that the produced *p*-nitrobenzaldehyde reacted instantaneously with electro-generated superoxide ion to yield *p*-nitrobenzoic acid. In the cyclic voltammogram of *p*-nitrobenzaldehyde in the presence of oxygen (solid line in Fig. 2), two reduction waves corresponding to those of *p*-nitrobenzoic acid appeared. The reaction rate of superoxide ion with *p*-nitrobenzaldehyde is therefore faster than that of superoxide ion with *p*-nitrotoluene.

$$O_2 + e \rightleftharpoons O_2^{\cdot-} \quad (1)$$

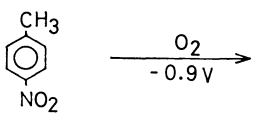

(2)

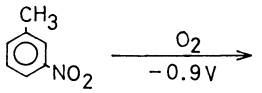

(3)

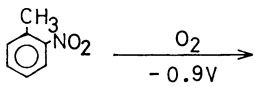

(4)

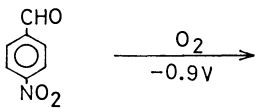

(5)

E/V *vs.* Ag/AgCl

$$RCH_3 + O_2^{\cdot-} \longrightarrow RCH_2\cdot + HO_2^- \quad (6)$$

$$RCH_2\cdot + O_2 \longrightarrow RCH_2OO\cdot \quad (7)$$

$$RCH_2OO\cdot + O_2^{\cdot-} \text{ (or e from electrode)} \longrightarrow RCH_2OO^- + O_2 \quad (8)$$

$$RCH_2OO^- \longrightarrow RCHO + OH^- \quad (9)$$

$$RCHO + O_2^{\cdot-} \text{ (or e from electrode)} \longrightarrow [RCHO]^{\cdot-} + O_2 \quad (10)$$

$$[RCHO]^{\cdot-} + O_2 \longrightarrow [RCOOOH]^{\cdot-} \quad (11)$$

$$RCHO + O_2^{\cdot-} \longrightarrow [RCOOOH]^{\cdot-} \quad (12)$$

$$RCHO + O_2^{\cdot-} \longrightarrow RCO\cdot + HO_2^{\cdot-} \quad (13)$$

$$RCO\cdot + HO_2^- \longrightarrow [RCOOOH]^{\cdot-} \quad (14)$$

$$[RCOOOH]^{\cdot-} \longrightarrow RCOO\cdot + OH^- \quad (15)$$

$$RCOO\cdot + O_2^{\cdot-} \text{ (or e from electrode)} \longrightarrow RCOO^- + O_2 \quad (16)$$

Scheme 1.

Reaction Scheme for the Oxidation. A reaction scheme for the oxidation of *p*- and *o*-nitrotoluenes with electro-generated superoxide ion can be suggested as shown in Scheme 1. One of the hydrogen atoms of the methyl group of the *o*- or *p*-nitrotoluene is abstracted by the electro-generated superoxide ion in DMF solution (Eq. 6). The resulting species reacts with oxygen (Eq. 7) and is further reduced to the peroxy anion by superoxide ion or by an electron from the electrode (Eq. 8). In a basic solvent such as DMF, release of hydroxy anion from this peroxy ion, which yields aldehyde (Eq. 9), occurs predominantly, rather than proton abstraction from the environment by the peroxy anion.[16] This hydrogen abstraction reaction by superoxide ion is similar to the reaction of the superoxide ion with 9,10-dihydroanthracene to yield anthraquinone.[17] The produced nitrobenzaldehyde can be reduced with superoxide ion as well as from the electron uptake at the electrode directly owing to its more positive reduction peak potential (−0.82 V *vs.* Ag/AgCl) (Eq. 10), and the formed anion radical reacts oxygen to produce hydrogen percarboxylic acid anion radical (Eq. 11). As the possible another route, superoxide ion reacts directly carbonyl group to yield addition product,[18] that is, hydrogen percarboxylic acid anion radical (Eq. 12). The nitrobenzaldehyde also reacts with superoxide ion instantly to yield an acyl radical (Eq. 13), which reacts with hydrogen peroxide anion (Eq. 14). The percarboxylic acid anion radical formed by Eqs. 11, 12, and 14 releases hydroxide anion, yielding the carboxyl radical (Eq. 15). This carboxyl radical is finally reduced to carboxyl anion by the superoxide ion or by an electron from the electrode (Eq. 16).

In conclusion, *o*- and *p*-nitrotoluene are considered to react with electro-generated superoxide ion in DMF solution to yield the corresponding nitrobenzoic acid *via* the nitrobenzaldehyde (Eq. 17) as described above.

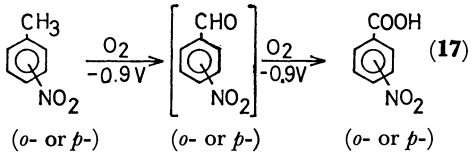

(17)

E/V *vs.* Ag/AgCl

We thank the Japan Society for the Promotion of Science for the provision of funds during the period

(Feb.—April 1976) when one of us (H.L.) was a Visiting Professor at Tohoku University. The present work was partially supported by a Grant-in-Aid for Scientific Reseach No. 47017 from the ministry of Education, Science and Culture.

References

1) G. A. Hamilton, "Chemical Models and Mechanisms for Oxygenases in Molecular Mechanisms of Oxygen Activation," ed by O. Hayaishi, Academic Press, New York (1975), p. 405.

2) R. Dietz, M. E. Peover, and P. Rothbaum, *Chem. Ing. Techn.*, **42**, 185 (1970).

3) T. Osa and M. Tezuka, *Denki Kagaku*, **44**, 2 (1976).

4) R. Dietz, A. E. J. Forno, B. E. Larcombe, and M. E. Peover, *J. Chem. Soc., B*, **1970**, 816.

5) J. W. Peters and C. S. Foote, *J. Am. Chem. Soc.*, **98**, 873, (1976).

6) H. Sagae, M. Fujihira, T. Osa, and H. Lund, *Chem. Lett.*, **1977**, 793.

7) a) R. Hasegawa and Y. Kamiya, *Bull. Chem. Soc. Jpn.*, **51**, 1490 (1978); b) G. A. Russell, A. J. Moye, E. G. Janzen, S. Mak, and E. R. Talaty, *J. Org. Chem.*, **32**, 137 (1976); c) T. A. Cooper and W. A. Waters, *J. Chem. Soc. B*, **1967**, 687; d) R. S. Barker and A. Saffer, U. S. Patent 3, 030, 414 (1962); *Chem. Abstr.*, **57**, 13689c (1962); e) K. A. Cherinskii, *Khim Tekhnol.*, **1968**, 60; *Chem. Abstr.*, **72**, 110572g (1970).

8) a) B. Srinivasan and S. B. Chanda, *Indian J. Technol.*, **1971**, 274; b) W. S. Trahanovsky and L. B. Young, *J. Org. Chem.*, **31**, 2033 (1966); c) L. A. Bigelow, *J. Am. Chem. Soc.*, **41**, 1559 (1919).

9) a) R. F. Dunbrook and A. Lowy, *Trans. Am. Electrochem.*, **45**, (pre-print) (1924); *Chem. Abstr.*, **18**, 1088 (1924); b) V. S. Kolevatova and S. A. Kolsova, *Sb. Nauchn. Tr. Permsk. Politekhn. Inst.*, **1963**, 54; *Chem. Abstr.*, **62**, 8670h (1965).

10) T. J. Wallace, J. E. Hofmann, and H. Pobiner, *Nature*, **204**, 376 (1964).

11) J. Chakraborty and J. N. Smith, *Biochem. J.*, **93**, 389 (1964).

12) a) T. Fujinaga, K. Izutsu, and K. Takaoka, *J. Electroanal. Chem.*, **12**, 203 (1966); b) S. Yamaguchi, Y. Yamakawa, and T. Tsukamoto, *Rev. Polarography*, **17**, 145 (1971).

13) T. Kuwana and J. W. Strojek, *Discuss. Faraday Soc.*, **45**, 134 (1968).

14) "Handbook of Chemistry and Physics," 54th ed, CRC Press, Cleveland, Ohio (1973), p. C–191.

15) K. S. V. Santhanam and A. J. Bard, *J. Am. Chem. Soc.*, **88**, 2669 (1966).

16) G. A. Russell, E. G. Janzen, A. G. Bemis, E. J. Geels, A. J. Moye, S. Mak, and E. T. Strom, *Adv. Chem. Ser.*, **51**, 112 (1965).

17) M. Tezuka, Y. Ohkatsu, and T. Osa, *Bull. Chem. Soc. Jpn.*, **48**, 1471 (1975).

18) M. J. Gibian, D. T. Sawyer, T. Ungermann, R. Tangpoonpholvivat, and M. M. Morrison, *J. Am. Chem. Soc.*, **101**, 640 (1979).

In Situ Measurement of Electrode Surface Change by Photoacoustic Spectroscopy

Hideki MASUDA, Akira FUJISHIMA,* and Kenichi HONDA

Department of Synthetic Chemistry, Faculty of Engineering, The University of Tokyo, Hongo, Bunkyo-ku, Tokyo 113

(Received December 25, 1979)

Photoacoustic spectroscopy (PAS) was used for the study of electrode-electrolyte interfaces *in situ*. The design of the PAS cell and the experimental procedure are given. The change in absorption at the interface during electrochemical reaction at Au electrodes, as measured by PAS technique, is described.

In resent years, there has been much interest in photoacoustic spectroscopy (PAS)[1-4] as a new tool for the investigation of the surface condition of various materials. One of the advantages of PAS is that absorption spectra can be obtained even for solid samples that are difficult to measure by conventional spectroscopic techniques on account of light scattering problems. We have noted this characteristics of PAS from the viewpoint of spectro-electrochemistry, and attemped to apply PAS to studies of the electrode surface *in situ*. Generally, spectro-electrochemical behavior is measured by using an electrode that is optically transparent,[5,6] internally reflective,[7,8] or specularly reflective,[9,10] by ellipsometric techniques,[11,12] and so on, for the purpose of characterizing the electrode-solution interfaces, or measuring the kinetic behavior of electrode reaction. It is expected that PAS will be more advantageous than conventional spectroscopic techniques in observing the electrode-solution interfaces, because preparation of a sample electrode is not difficult, that is, the surface does not need to be highly polished. Some work has been reported on the application of PAS to electrochemical studies,[13,14] but PAS was used in these cases to measure the absorption spectra of the electrode surface in the air after removal from the electrolysis cell. Here, we have applied PAS to study the surface behavior of metal electrode *in situ*.

In a conventional PAS cell, a sample is placed inside a closed chamber containing a suitable gas, and is illuminated through a window. For *in situ* investigation of an electrode surface that is in contact with the solution, such a cell can not be used in the usual way. Another technique for measuring electrode surfaces by PAS used a piezo electric pressure transducer,[15,16] but this method seems unsuitable for a solid-liquid system, especially an electrochemical one in which gas evolution may occur by electrolysis because the presence of bubbles in the solution would adversely affect the acoustic signal.

Therefore we constructed another type of cell, in which the sample was mounted outside the gas chamber. Heat on the surface of the sample resulting from radiationless transition due to irradiation with light is transported to the rear of the sample, causing the sealed gas to expand. Until now this technique has been scarcely used, because it has been thought that in the case of relatively thick samples the photoacoustic signal in this type of cell is liable to decrease during the conduction of heat from the active surface to the rear. As exceptional examples, Kanstad *et al.* measured the middle infrared region PAS spectra of specimens kept on a thin Al plate called open membrane spectrophone,[17] and Adams *et al.* applied this type of cell to determine the thermal diffusibility of thin polymer films.[18] Since even in these cells, the photoacoustic signals did not seem to decrease significantly, this technique can be put to practical use. The present work is concerned with the photoacoustic signal change in electrode-solution interfaces in the course of the electrode reaction, oxidation of an Au electrode or electrochemical deposition of other metals on the Au electrode.

Experimental

Figure 1 shows detail of the PAS cell employed in this study. The PAS cell was constructed from acrylic resin and used for spectroscopic measurement in electrolytic solutions. This PAS cell was 3.0 cm in width and 7.0 cm in height, and its internal volume was approximately 0.4 cm^3. An electret condenser microphone (Sony Model ECM-150) was employed in this cell as a pressure transducer. The working electrode was a flat gold plate 0.1 mm thick and 7.0 mm in diameter, which was polished to a bright surface with 3 μm alumina powder and then mounted on one side of the PAS cell by a silicone O-ring to ensure an air-tight seal. In this work, a PAS cell of the ordinary type was also used as a control for the results obtained using the cell shown in Fig. 1.

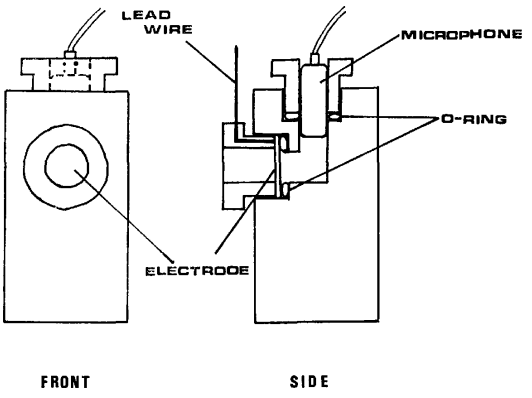

Fig. 1. PAS cell and sample arrangement.

Figure 2 shows the experimental set up. The light source was either a 500 W Xe lamp (Ushio Electric) or 3 W Ar ion laser (Spectra Physics Model 164). In measuring the photoacoustic spectrum using the Xe lamp, the radiation was focused on the electrode surface using a convex lens through a series of 10 nm bandwidth interference filters (Koshin Kogaku) and the light intensities of each wavelength were

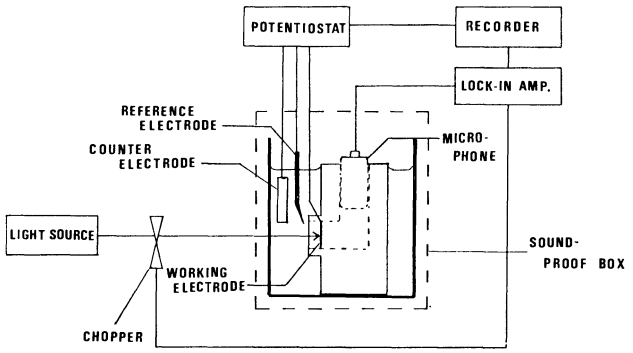

Fig. 2. Experimental set up for PAS–electrode system.

normalized by comparison with spectrum of carbon measured under identical conditions. The diameter of the laser beam was approximately 1.5 mm. The light beam was chopped mechanically by light chopper and the photoacoustic signal detected by the microphone was fed to a lock-in amplifier (Brookdeal Model 9501, or Nihon Bunko Model LA-120). The measurement was carried out using a chopping frequency of 125 Hz by considering both of the light power per pulse and the frequency characteristics of the microphone employed in this work. Electrolysis was carried out in a pyrex cell which had an optically flat window. This cell was held in a lead box to reduce external acoustic noises. A potentiostat (Nikko Keisoku Model NPGS-301) with a potential programmer (Nikko Keisoku Model NPS-2) was used to obtain current-potential curves. A saturated calomel electrode (SCE) was used as a reference electrode and the counter electrode was of platinum. A coulometer (Kowa Electronics Model DCM-150) was used to determine the total charge. The influence upon the photoacoustic signal of temperature changes resulting from electrode reactions, which is known as the electrochemical peltier effect,[19] was considered to be negligible because only the AC component of temperature change was detected by the lock-in amplifier. Current-potential, photoacoustic signal-potential and photoacoustic signal-charge curves were recorded on a X-Y-Y′ recorder (Riken Denshi Model D-72 or Yokokawa Model 3078).

Results and Discussion

Open Membrane Type Photoacoustic Cell. Before a measurement with the PAS cell shown in Fig. 1, we checked whether this cell could work well or not. Then, the photoacoustic signal at the open membrane type cell (Fig. 3A, the same type as that in Fig. 1) was compared with that of the conventional type cell

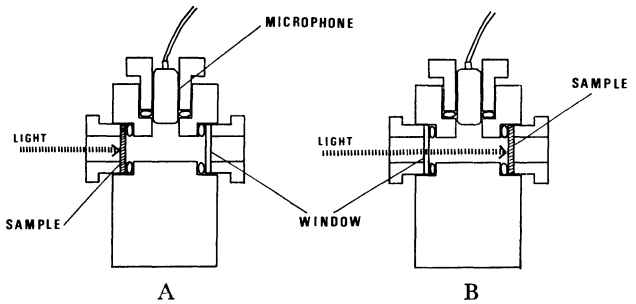

Fig. 3. Schematic diagram for measurement of signal magnitude. A) Open membrane type, B) conventional type.

Table 1. Comparison of the magnitudes of signals of PAS
(Irradiation by Ar ion laser, 0.5 W, 514.5 nm, 125 Hz)

	(A) Open membrane type	(B) Conventional type
Carbon (0.5 mm)	17 (μV)	44 (μV)
Au plate (0.1 mm)	19 (μV)	35 (μV)
Au plate (0.05 mm)	42 (μV)	35 (μV)

(Fig. 3B), where ways of irradiation to the sample were different. Table 1 shows the magnitude of the photoacoustic signal for a glassy carbon pellet and Au plates with the both cells. The signals were affected by the condition of the surfaces, especially in that of the Au plates. However, for the samples tested, the magnitude of the photoacoustic signals of the open membrane type cell was not significantly smaller than those of the conventional type cell. Further, for the thin Au plate (0.05 mm) the signal was observed to be larger than that of the conventional type cell, perhaps because in the latter illuminating intensity decreased on account of reflection at the glass window.

Even when the open membrane cell was immersed in the solution so that the sample surface was in contact with the solution, the photoacoustic signals did not decrease greatly. The signal ratio S(solution)/S(air) was approximately 0.9 in the case of the Au plate. These results show that the open membrane type PAS cell is well suited for practical use. Therefore, results shown below were obtained by use of the PAS cell shown in Fig. 1 (*i.e.* the open membrane type PAS cell).

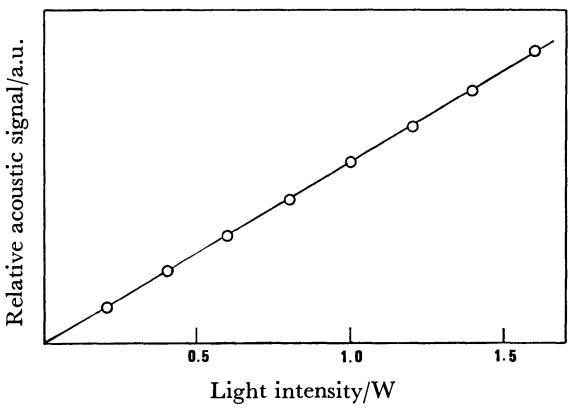

Fig. 4. Relationship between signal magnitude and incident light intensity for Au plate.

Figure 4 shows the relationship between the magnitude of the acoustic signal and the incident light intensity for the Au plate, where irradiation was carried out using the Ar ion laser (514.5 nm). The plot of the PAS signal against light intensity is relatively linear, and we consider that the photoacoustic signal does not appear to reach saturation even in high intensity region observed in this study.

Measurement of the Electrochemical Deposition of Cu on Au Electrode. Figure 5 shows the photoacoustic spectra

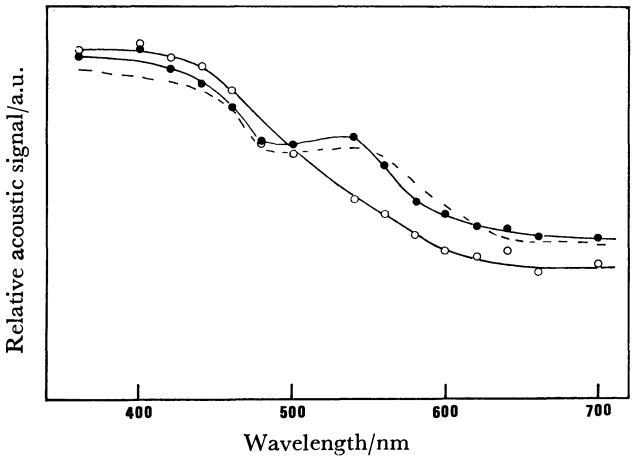

Fig. 5. Photoacoustic spectra of Au electrode; before (-○-), after (-●-) electrotysis in 5×10^{-3} M Cu^{2+} and of Cu plate (------).

of the Au electrode before and after electrolysis at −0.2 V *vs.* SCE in 1 M $HClO_4$ (1 M=1 mol/dm^3) containing 5×10^{-3} M Cu^{2+}, along with that of a 0.05 mm thick Cu plate, which was measured separately. Since the spectrum after electrolysis agreed with that of the Cu plate, it indicates that the Au electrode surface was covered with a Cu layer.

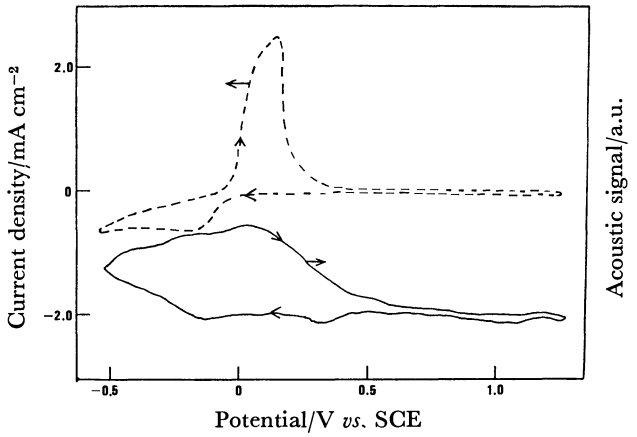

Fig. 6. Photoacoustic signal *vs.* potential (——) and current *vs.* potential (------) curves of Au electrode in the presence of Cu^{2+} ion.
5×10^{-3} M Cu^{2+}, 1 M $HClO_4$, potential sweep rate 40 s/V, λ=514.5 nm.

Figure 6 is a plot of the photoacoustic signal *versus* potential and current *versus* potential curves in the same electrolyte solution as in Fig. 5. The result in Fig. 5 shows that the light absorption of Cu is larger than that of Au when irradiated by a 514.5 nm Ar ion laser. The reduction current around −0.1 V in the cathodic sweep was due to the electrochemical deposition of Cu, and at almost the same potential it was observed that the photoacoustic signal began to increase. On the other hand, the anodic current peak at 0.20 V was attributed to the dissolution of the Cu layer. At that time the photoacoustic signal began to decrease

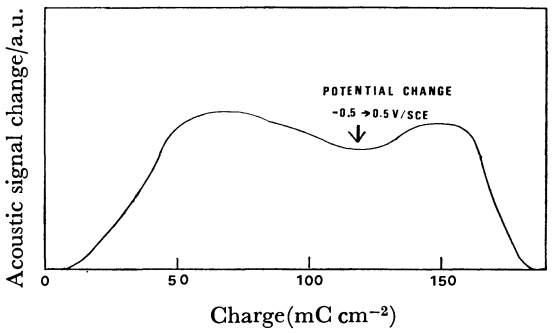

Fig. 7. Relative change in photoacoustic signal *vs.* charge for electrochemical deposition of Cu.
5×10^{-3} M Cu^{2+}, 1 M $HClO_4$, potential −0.5 V and +0.5 V *vs.* SCE. λ=514.5 nm.

and then returned to the value for the bare Au surface.

Figure 7 shows the change in the photoacoustic signal relative to the electric charge associated with the electrochemical deposition of Cu on the Au surface at −0.5 V. The photoacoustic signal increased in proportion to the charge and then became the constant value at about 50 mC/cm^2. At this charge, the thickness of the deposited copper layer was estimated to be 20 nm, assuming that the layer was uniform. The linear relationship between the photoacoustic signal and the charge can be interpreted on the basis of the McIntyre-Aspnes approximation,[20] in which the change in reflectivity is proportional to the thickness of thin film formed. In the flat region the photoacoustic signal would seem to be the result of absorption at the Cu layer alone. As shown in Fig. 7, the photoacoustic signal decreased a little in the region where the deposited layer became thicker. The reason for this is uncertain, but one can assume that one of the reasons is an increase in the surface heat radiation as the rough copper layer is formed. In anodic reaction, the photoacoustic signal decreased on a reverse path until it reached the value for the bare Au surface.

In *in situ* measurements such as those in Figures 6 and 7, the time constant of the phase sensitive detection is one of the significant factors. When the time constant is large compared with the reaction rate, a time lag is liable to be caused in the photoacoustic signal change.

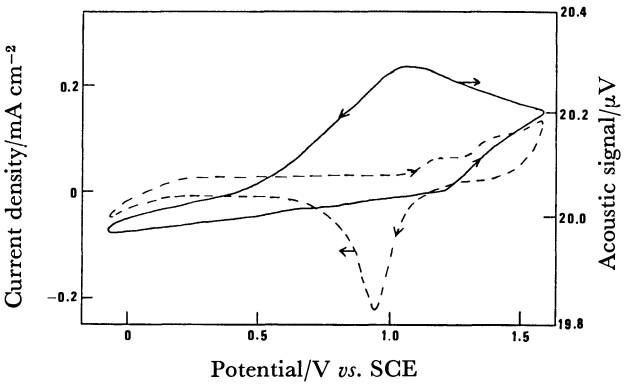

Fig. 8. Photoacoustic signal *vs.* potential (——) and current *vs.* potential (------) curves of Au electrode.
1 M $HClO_4$, potential sweep rate 40 s/V, λ=514.5 nm.

In this work, the photoacoustic signal was measured at a time constant of 1—3 s.

Measurement of Formation of an Oxide Layer at Au. Figure 8 shows the curve for the photoacoustic signal *versus* applied potential together with a current *versus* potential curve in 1 M $HClO_4$ solution on an Au electrode where photoacoustic signal was measured at a wavelength of 514.5 nm from the Ar ion laser with light intensity of 0.8 W. It has been widely reported that oxide layers are formed on the Au electrode with anodic polarization in an acid solution.[21-24] The anodic current at 1.2 V in the anodic sweep was attributed to the formation of the oxide layer on the Au electrode. As shown in Fig. 8 the increase in the photoacoustic signal began at almost the same potential as increase of the anodic current. The increase in the photoacoustic signal was mainly due to the increase in absorption resulting from formation of the oxide layer on the Au electrode, because the absorption coefficient of the oxide is greater than that of Au irradiated at 514.5 nm. On the other hand, in the cathodic sweep, a current peak was observed around 0.9 V due to the reduction of the oxide layer and at that time the photoacoustic signal decreased gradually depending on the amount of cathodic electricity. When the cathodic current decreased to the original value around 0.65 V, the photoacoustic signal also showed the same value as that on the bare Au surface.

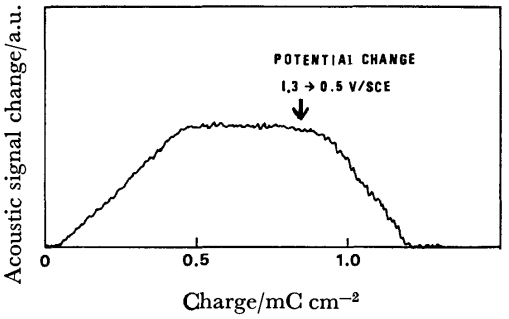

Fig. 9. Relative change in photoacoustic signal *vs.* charge for the formation of gold oxide.
1 M $HClO_4$, potential +1.3 V and 0.5 V *vs.* SCE. λ=514.5 nm.

Figure 9 shows the relationship between the change in the relative photoacoustic signal and the charge flowing. Figure 9 also showed the change in the photoacoustic signal, stepping the applied potential from 1.3 V to 0.5 V, at which potential the oxide is reduced. In Fig. 9 the photoacoustic signal increased linearly with the quantity of electricity for the oxidation process, and then reached a constant at about 0.5 C/cm^2, where the thickness of the oxide layer was estimated to be 0.5 nm, assuming the composition of the oxide layer to be Au_2O_3 with a bulk density of 6 g/cm^3.[24] In the rising region in Fig. 9, the acoustic signal seems to increase in proportion to the degree of surface coverage of the oxide layer. When the oxide layer was reduced by changing the applied potential from 1.3 V to 0.5 V, the photoacoustic signal decreased to the value at the bare Au surface.

Conclusion. The instrumentation used is simple and unsophisticated, but this technique was found to be useful for the study of electrode-solution interfaces *in situ*.[25] This PAS technique may be applicable for kinetic studies concerning electrode reactions, as well as for qualitative analysis by spectroscopic measurement. Sensitivity was fairly high, *e.g.*, in the order of monolayer change when using laser irradiation, and could be further improved by modification of the PAS cell, *e.g.*, smaller internal cell volume. Since PAS is influenced by external acoustic noises, exhaustive counterplan against the acoustic noise would be also required. In addition, by employing a double-beam PAS system, the signal to noise ratio could be expected to improve.

This technique is considered to be applicable to any type of samples (*e.g.* rough or porous surfaces) which are difficult to examine by conventional techniques. Since the metal electrodes employed in this work had flat, highly reflective surface, photoacoustic signals were relatively small. Semiconductors, however, have more definitive characteristics especially concerning their light effect, so this technique would be more useful for their electrode systems.

References

1) W. R. Harshbarger and M. B. Robin, *Acc. Chem. Res.*, **6**, 329 (1973).
2) A. Rosencwaig, *Anal. Chem.*, **47**, 592A (1975).
3) M. J. Adams, A. A. King, and G. F. Kirkbright, *Analyst*, **101**, 73 (1976).
4) R. C. Gray, V. A. Fishman, and A. J. Bard, *Anal. Chem.*, **49**, 697 (1977).
5) W. Benken and T. Kuwana, *Anal. Chem.*, **42**, 1114 (1970).
6) W. R. Heineman and T. Kuwana, *Anal. Chem.*, **43**, 1075 (1971).
7) W. N. Hansen and J. A. Horton, *Anal. Chem.*, **36**, 783 (1964).
8) W. N. Hansen, T. Kuwana, and R. A. Osteryoung, *Anal. Chem.*, **38**, 1810 (1966).
9) D. F. A. Koch, *Nature*, **202**, 387 (1964).
10) J. D. E. McIntyre, "Advance in Electrochemistry and Electrochemical Engineering," J. Wiley and Sons, New York (1973), Vol. 9, pp. 61—166.
11) J. Kruger, *J. Electrochem. Soc.*, **110**, 654 (1963).
12) W. Paik, M. A. Genshaw, and J. O'M. Bockris, *J. Phys. Chem.*, **74**, 4266 (1970).
13) P. Nordal and S. O. Kanstad, *Opt. Commun.*, **24**, 95 (1978).
14) M. Fujihira, T. Osa, D. Hursh, and T. Kuwana, *J. Electroanal. Chem.*, **88**, 285 (1978).
15) W. Lahmann, H. J. Ludewig, and H. Welling, *Anal. Chem.*, **49**, 549 (1977).
16) S. Oda, T. Sawada, and H. Kamada, *Anal. Chem.*, **50**, 865 (1978).
17) S. O. Kanstad and P. Nordal, *Opt. Commun.*, **26**, 367 (1978).
18) M. J. Adams and G. F. Kirkbright, *Analyst*, **102**, 281 (1977).
19) R. Tamamushi, *J. Electroanal. Chem.*, **45**, 500 (1973); **65**, 263 (1975).
20) J. D. E. McIntyre and D. E. Aspnes, *Surf. Sci.*, **24**, 417 (1971).

21) W. E. Reid and J. Kruger, *Nature*, **203**, 402 (1964).
22) R. S. Sirohi and M. A. Genshaw, *J. Electrochem. Soc.*, **116**, 910 (1969).
23) T. Takamura, K. Takamura, W. Nippe, and E. Yeager, *J. Electrochem. Soc.*, **117**, 626 (1970).
24) D. M. Kolb and J. D. E. McIntyre, *Surf. Sci.*, **28**, 321 (1971).
25) A. Fujishima, H. Masuda, and K. Honda, *Chem. Lett.*, **1979**, 1063.

 © 1980 The Chemical Society of Japan Bull. Chem. Soc. Jpn., 53, 1547—1549 (1980)

A Spectrophotometric Study of Tributyl Phosphate Adducts of Three Bis(β-diketonato)copper(II) Complexes in Carbon Tetrachloride

Tatsuya SEKINE* and Teruyuki TOSAKA

Department of Chemistry, Science University of Tokyo, Kagurazaka, Shinjuku-ku, Tokyo 162

(Received August 23, 1979)

Adduct formation equilibria between bis(2-thenoyltrifluoroacetonato)-, bis(trifluoroacetylacetonato)-, and bis(hexafluoroacetylacetonato)copper(II) chelates and tributyl phosphate (TBP) in water-saturated carbon tetrachloride were studied spectrophotometrically at 25 °C. The chelates added one TBP molecule and decreased the absorption, but not very much. The formation constants obtained from the changes in the absorption, given as a function of the TBP concentration, agreed very well with those obtained previously by a solvent-extraction method.

The adduct formation of uncharged metal chelates with neutral ligands in the organic phase in solvent-extraction systems enhances the metal-chelate extraction; this enhancement is often called "synergism." The equilibria of the adduct formation can be measured from an analysis of the enhancement of the extraction, which is determined as a function of the ligand concentration in the organic phase; also, the formation constants of the adduct metal chelates have been determined in several systems under various conditions.[1–4]

The formation of adducts may affect the spectral properties of the complex. This has been observed in several metal chelate systems,[5] especially when the adduct-forming ligands were organic bases, such as homologues or derivatives of pyridine and quinoline. The appearance of strong absorptions upon the addition of organic bases to metal chelates in the organic phase in solvent-extraction systems has been used in the colorimetry of the metal ion; the sensitivity has thus been found to be much higher than in the absence of the adduct-forming ligand.[6,7]

The change in the absorption by adduct formation as a function of the ligand concentration may also be used in the determination of the formation constants. In studies of the synergism of metal extraction as chelates on the addition of heterocyclic organic bases, the adduct-formation constants have been spectrophotometrically determined and discussed in relation to the synergism.[8,9] Such quantitative spectrophotometric studies of adduct chelate formation equilibria with heterocyclic organic bases have been reported several times.[10–22]

Another group of ligands which have been studied frequently in connection with their ability to form adduct chelates are neutral phosphorus compounds such as tributyl phosphate (TBP); the changes in the absorptions have also been discussed in relation to the enhancement of the extraction.[23,24] However, not much quantitative analysis of the changes in the absorption has been done, and few spectrophotometric determinations of the adduct formation constants with such neutral organophosphorus compounds have been made.

In the course of a series of studies of metal-chelate extraction with several β-diketones and their synergism with neutral ligands in our laboratory, it was found that the optical absorption also changed upon adduct-formation in the copper(II) extraction systems with β-diketones in conjunction with TBP and that the equilibrium constants obtained from these spectrophotometric data agreed very well with those obtained from the solvent-extraction data.

Experimental

The experimental conditions were the same as in the previous solvent-extraction study,[25,26] except that the changes in the absorption spectra were measured instead of those in the distribution ratio.

The bis(β-diketonato)copper(II) ($Cu(acac)_2$) and the β-diketones were supplied by the Dojindo Co., Kumamoto. The tributyl phosphate was supplied by the Tokyo Kasei Co., Tokyo, and was purified by the same method as before.[25,26] The carbon tetrachloride was an analytical-grade solvent. Two UV-VIS spectrophotometers (Hitachi type-556 and -139) were used.

A weighed amount of $Cu(acac)_2$ was dissolved in water-saturated carbon tetrachloride containing 0.1 mol dm^{-3} of 2-thenoyltrifluoroacetone (Htta), trifluoroacetylacetone (Htaa), or hexafluoroacetylacetone (Hhfa) and converted into $Cu(tta)_2$, $Cu(taa)_2$, or $Cu(hfa)_2$. These solutions were used as the stock solutions. A portion of a stock solution and a portion of a water-saturated carbon tetrachloride solution of TBP were mixed; when necessary, another portion of carbon tetrachloride was added in order to bring the initial concentrations of the bis(β-diketonato)copper(II), the β-diketone and TBP up to the wanted values. The solution was stored for 1 h, and the absorption spectrum was measured using a glass cell with a 1 cm light path. The temperature was kept at 25±0.3 °C.

Statistical

In this paper, the chemical species with the subscript "aq" are those in aqueous solutions, while the lack of any subscript indicates those in carbon tetrachloride solutions.

The ligand-exchange equilibria of acetylacetonate ions in $Cu(acac)_2$ with a β-diketone, Ha, may be written as:

$$Cu(acac)_2 + Ha \rightleftarrows Cu(acac)(a) + Hacac \quad (1)$$

$$Cu(acac)_2 + 2Ha \rightleftarrows Cu(a)_2 + 2Hacac \quad (2)$$

$$K_{x1} = [Cu(acac)(a)][Hacac][Cu(acac)_2]^{-1}[Ha]^{-1} \quad (3)$$

$$K_{x2} = [Cu(a)_2][Hacac]^2[Cu(acac)_2]^{-1}[Ha]^{-2}. \quad (4)$$

The values of K_{x1} and K_{x2} can be obtained from the solvent-extraction constants as follows:

$$Cu^{2+}(aq) + 2Hacac \rightleftarrows Cu(acac)_2 + 2H^+(aq) \quad (5)$$

$$Cu^{2+}(aq) + Hacac + Ha \rightleftarrows Cu(acac)(a) + 2H^+(aq) \quad (6)$$

$$Cu^{2+}(aq) + 2Ha \rightleftarrows Cu(a)_2 + 2H^+(aq) \quad (7)$$

$$K_{ex(acac)} = [Cu(acac)_2][H^+]_{aq}^2[Cu^{2+}]_{aq}^{-1}[Hacac]^{-2} \quad (8)$$

$$K_{ex(mix)} = [Cu(acac)(a)][H^+]_{aq}^2[Cu^{2+}]_{aq}^{-1} \times [Hacac]^{-1}[Ha]^{-1} \quad (9)$$

$$K_{ex(a)} = [Cu(a)_2][H^+]_{aq}^2[Cu^{2+}]_{aq}^{-1}[Ha]^{-2}. \quad (10)$$

Here, the statistical values of $K_{ex(mix)}$ are obtained as:[27]

$$K_{ex(mix)} = 2\sqrt{K_{ex(acac)}K_{ex(a)}}. \quad (11)$$

Although the statistical value of $K_{ex(mix)}$ could, to some extent, be different from the experimental value, it may be used in this study, taking its concentration as an approximate value.

$$K_{x1} = K_{ex(mix)}K_{ex(acac)}^{-1} \quad (12)$$

$$K_{x2} = K_{ex(a)}K_{ex(acac)}^{-1}. \quad (13)$$

The formation equilibrium of the adduct can be written as:

$$Cu(a)_2 + tbp \rightleftarrows Cu(a)_2(tbp) \quad (14)$$

$$\beta_{1(org)} = [Cu(a)_2(tbp)][Cu(a)_2]^{-1}[tbp]^{-1}. \quad (15)$$

When the molar extinction coefficients of the $Cu(a)_2$ and $Cu(a)_2(tbp)$ species at a certain wavelength are ε_0 and ε_1 respectively, then the optical density can be written as:

$$E = \varepsilon_0[Cu(a)_2] + \varepsilon_1[Cu(a)_2(tbp)]. \quad (16)$$

The following equations may be valid in these systems:

$$[Cu(II)]_{total} = [Cu(a)_2] + [Cu(a)_2(tbp)] \quad (17)$$

$$[tbp]_{total} = [tbp] + [Cu(a)_2(tbp)]. \quad (18)$$

By using a least-squares program, the values of $\beta_{1(org)}$ and ε_1 can be computed by successive approximation procedures.

Results and Discussion

The equilibrium constants for the ligand exchange in Eqs. 3, 4, 12, and 13 were calculated from the extraction constants in the literature, as listed in Table 1. Since the maximum amount of Hacac produced by the ligand exchange should be twice that of the $Cu(acac)_2$ chelate added, it should be lower than 1×10^{-3} mol dm^{-3}. Thus, it may be seen from Eqs. 12 and 13 and the values of the constants in Table 1 that more than 99% of the initial bis(acetylacetonato)copper(II) should be converted into the complexes when the β-diketone concentration is 0.1 mol dm^{-3}. It was also confirmed by spectrophotometric measurements that the optical-absorption spectrum of the solution thus obtained by the ligand exchange was identical to that of the solution of each β-diketone complex within the limits of experimental error. This exchange formed free acetylacetone and decreased the concentration of that β-diketone. The change in the absorption caused by the changes in these concentrations was corrected on the basis of the molar extinction coefficients of the β-diketones and the concentration of copper(II).

Table 1. Equilibrium constants for the ligand exchange of copper(II) chelates in CCl_4

Ligand	log K_{ex}[a]	log $K_{ex(mix)}$[b]	log K_{x1}	log K_{x2}
Hacac	−3.47	—	—	—
Htta	−1.08	−1.98	1.49	2.39
Htaa	−1.12	−2.00	1.47	2.35
Hhfa	−0.26	−1.57	1.90	3.21

a) When the aqueous phase was 0.1 mol dm^{-3}, (Na, H)ClO_4. Taken from refs. 25 and 26. b) Calculated statistical values.

The total copper(II) concentration was maintained at 5×10^{-4} mol dm^{-3}. Optical measurements were carried out in the region where the molar extinction coefficient is higher than 2×10^2 and where the absorption due to the reagent is not high. This region was from 400 to 420 nm at twenty-one different points for the $Cu(tta)_2$ chelate, from 350 to 400 nm at fifty-one different points for the $Cu(taa)_2$ chelate, and from 370 to 390 nm at twenty-one different points for the $Cu(hfa)_2$ chelate. The absorption of the $Cu(hfa)_2$ chelate and its TBP adduct could not be measured below 370 nm because, in this region, the absorption of the reagent was very high. Absorptions were also measured up to 800 nm, but no high absorption due to the adduct formation ($\varepsilon_1 > 200$) was found in this region. Thus, the range of the wavelengths of the data used for the calculation was narrow in all the cases, as can be seen from Fig. 1. Several sets of data of the optical absorption, E, in Eq. 16 at this copper(II) concentration and various total TBP concentrations were obtained at each wavelength.

The least-squares calculation of the values of $\beta_{1(org)}$

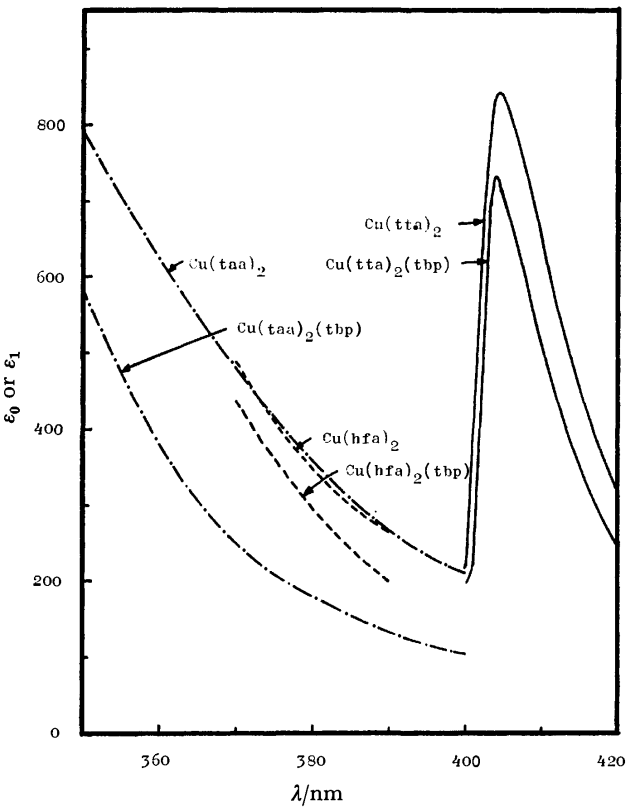

Fig. 1. Absorption spectra of bis(β-diketonato)copper (II) chelates and their tbp adducts given by molar absorptivity as a function of wavelength.

Table 2. Summary of formation constants of TBP adduct chelate complexes

Chelate	$\log \beta_{1(org)}$ [a] (by spectrophotometry)	$\log \beta_{1(org)}$ [b] (by solvent extraction)
$Cu(tta)_2$	2.21±0.1	2.27
$Cu(taa)_2$	2.15±0.1	2.16
$Cu(hfa)_2$	4.63±0.1	4.60

a) Present work; the limit of error is 3σ. b) Refs. 25 and 26.

and ε_1 at each wavelength were carried out from the set of data, together with the ε_0 of that bis(β-diketonato)-copper(II) which was determined at that wavelength in the absence of TBP. The variation in the values of $\beta_{1(org)}$, the formation constants of the TBP adducts, obtained from the data at different wavelength was rather small; the values are listed in Table 2, together with the corresponding values obtained by the solvent-extraction method in the previous study. The constants obtained by these two different methods agreed very well, as may be seen in Table 2. The values of ε_1, the molar extinction coefficient of the TBP adducts, were also obtained from the experimental data by these calculations. The values of ε_1 are shown in Fig. 1, together with the values of ε_0 of the bis(β-diketonato)-copper(II) complexes.

Since the carbon tetrachloride solutions were saturated by water, the effect of water in the carbon tetrachloride on the adduct-formation equilibrium should be identical with that in solvent extraction systems. However, if spectrophotometric experiments were to be made at various water concentrations, the effect of water in the solvent which can not be made by the solvent extraction method could be determined.

As may be seen from Fig. 1, the absorption spectra of each bis(β-diketonato)copper(II) complex and its TBP adduct are rather similar, although the absorption curve of the bis(hexafluoroacetylacetonato)complex and of its TBP adduct become a little closer in the lower-wavelength region. In all the cases, the molar extinction coefficient of the adduct is smaller than that of the chelate ($\varepsilon_1/\varepsilon_0$ is 0.75 to 0.85 with $Cu(tta)_2$, 0.50 to 0.65 with $Cu(taa)_2$, and 0.75 to 0.90 with $Cu(hfa)_2$). However, the $\varepsilon_1/\varepsilon_0$ values are not far from 1, so the adduct formation by TBP seems to have only a slight effect on the electronic state of the complex. This is quite different from the observation that, by the formation of bis(β-diketonato)complexes with organic bases, a strong absorption appears in the higher wavelength region.[6,7]

The difference in the two absorption spectra is not large, but the adduct-formation constants, $\beta_{1(org)}$, could be determined accurately in the present study. This indicates that the spectrophotometric determination may be used for the adduct-formation equilibria in several other systems. However, since the metal concentration can not be lowered very much for accurate optical measurements, the error in the constants must be larger than those obtained by the solvent extraction method, which can be studied even at tracer metal concentrations, if the value of $\beta_{1(org)}$ is very large, for example, as in the case of the $Cu(hfa)_2$ chelate.

The authors are grateful to Dr. Yuko Hasegawa and Dr. Naohiko Ihara for their contributions to this work in the preliminary stage and for their valuable discussions.

References

1) T. V. Healy, "Solvent Extraction Research, Proceedings of the 5th International Conference on Solvent Extraction Chemistry, Jerusalem, 1968," ed by A. S. Kertes and Y. Marcus, Wiley, New York (1969), p. 257.
2) H. Irving, "Solvent Extraction Chemistry, Proceedings of the International Conference on Solvent Extraction Chemistry, Goteborg, 1966," ed by D. Dyrssen, J.-O. Liljenzin, and J. Rydberg, North Holland, Amsterdam (1969), p. 91.
3) A. S. Kertes and Y. Marcus, "Solvent Extraction Research," Wiley, New York (1969).
4) T. Sekine and Y. Hasegawa, "Solvent Extraction Chemistry," Marcel Dekker, New York (1977).
5) G. Duyckaerts and J. F. Desreux, "Int. Solvent Extraction Conf.," Toronto (1977), p. 52.
6) H. Akaiwa and H. Kawamoto, *Anal. Chim. Acta*, **40**, 407 (1968).
7) H. Kawamoto and H. Akaiwa, *Nippon Kagaku Zasshi*, **89**, 585 (1968).
8) H. Irving and N. S. Al-Niaimi, *J. Inorg. Nucl. Chem.*, **27**, 2231 (1965).
9) H. Irving and N. S. Al-Niaimi, *J. Inorg. Nucl. Chem.*, **27**, 1671 (1965).
10) J. Csaszer and J. Szeghalmi, *Acta Univ. Szeged., Acta Phys. Chem.*, **12**, 117 (1966).
11) R. J. Casey and W. R. Walker, *J. Inorg. Nucl. Chem.*, **29**, 1301 (1967).
12) V. A. Alekseevskii and A. G. Muftakhov, *Tr. Samarkand. Gos. Univ.*, **167**, 139 (1969).
13) A. F. Garito and B. B. Wayland, *J. Am. Chem. Soc.*, **91**, 866 (1969).
14) A. Choplin-Gast and R. Hugel, *Bull. Soc. Chim. Fr.*, **8**, 2840 (1970).
15) A. G. Muftakhov, V. A. Alekseevskii, and L. M. Naumova, *Zh. Neorg. Khim.*, **16**, 2705 (1971).
16) A. Choplin and R. Hugel, *J. Inorg. Nucl. Chem.*, **34**, 3739 (1972).
17) M. Sato and T. Kwan, *Bull. Chem. Soc. Jpn.*, **46**, 3745 (1973).
18) N. S. Al-Niaimi, A. R. Al-Karaghouli, S. M. Aliwi, and M. G. Jalhoom, *J. Inorg. Nucl. Chem.*, **36**, 283 (1974).
19) M. Chikuma, A. Yokoyama, and H. Tanaka, *J. Inorg. Nucl. Chem.*, **36**, 1243 (1974).
20) N. S. Al-Niaimi and H. A. A. Rasoul, *J. Inorg. Nucl. Chem.*, **36**, 2051 (1974).
21) E. Kwiatkowski and J. Trojanowski, *J. Inorg. Nucl. Chem.*, **38**, 131 (1976).
22) V. A. Alekseevskii, O. A. Ramazanova, and L. A. Deryabina, *Zh. Neorg. Khim.*, **23**, 545 (1978).
23) S. M. Wang, W. R. Walker, and N. C. Li, *J. Inorg. Nucl. Chem.*, **28**, 875 (1966).
24) N. N. Kazanova, I. I. Antipova-Karataeva, O. M. Petrukhin, and Yu. A. Zolotov, *Izv. Akad. Nauk SSSR, Ser. Khim.*, **8**, 1716 (1973).
25) T. Sekine and D. Dyrssen, *J. Inorg. Nucl. Chem.*, **26**, 1727 (1964).
26) T. Sekine and N. Ihara, *Bull. Chem. Soc. Jpn.*, **44**, 2942 (1971).
27) T. Sekine and D. Dyrssen, *J. Inorg. Nucl. Chem.*, **26**, 2013 (1964).

Synthesis of Crown Ether Dyes[1)]

Toshiro YAMASHITA, Hiroshi NAKAMURA, Makoto TAKAGI,* and Keihei UENO

Department of Organic Synthesis, Faculty of Engineering, Kyushu University, Hakozaki, Higashi-ku, Fukuoka 812

(Received September 13, 1979)

Crown ether dyes were synthesized in order to develop photometric reagents which are highly selective to alkali and alkaline earth metals. They contain dissociable protons attached to the chromophores of crown ether molecule. Their extraction behavior for alkali and alkaline earth metal ions as neutral complex was examined. The dyes extract potassium and alkaline earth metals, respectively. Dyes with picrylamino chromophore are effective for extractive photometric determination of potassium. A molecular design of colorimetric reagents is discussed on the basis of crown ethers.

In view of the recent success in extraction photometric determination of alkali metals by crown ether-based chromogenic reagents,[2,3)] a series of crown ethers dyes with dissociable protons attached to the chromophores were synthesized, and their extraction behavior for alkali and alkaline earth metal ions was examined. Since only a very few chromogenic crown ethers are known,[4)] development of this type of compound is highly desirable for its use as a crown ether reagent in analysis.

Results and Discussion

Synthesis. The dyes synthesized are summarized in structural formulae **1**—**6**, and the synthetic routes are illustrated in (1)—(6). Since the reactions involved are the chemical transformations, no details are given except for the method of purification. Most of the dyes were isolated and purified by column chromatography followed by recrystallization. Readily crystallizable compounds, *e.g.*, **1a**, **1b**, **1d**, **5a**, or **5b**, were isolated by recrystallization, the yields being often very low, due to loss by repeated recrystallization (**1b** and **1d**). It is preferable to carry out a rough separation of the reaction product first by column procedure either on silica gel or alumina. The recrystallization of the main product then becomes easier. Preparation of crown ether dyes was difficult due to the difficulty in isolation. For example, the synthesis of benzein dye from 4′-formylbenzo-15-crown-5 and phenol by reactions similar to (4) could not be achieved, since the isolation of triarylmethane precursor of the dye was unsuccessful. The compound is difficult to handle, being both hydrophilic and lipophilic as regards solubility.

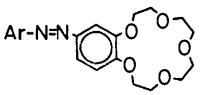

1, Ar= 2-hydroxy-1-naphthyl (a)
4-hydroxyphenyl (b)
3-*t*-butyl-4-hyroxyphenyl (d)
3-chloro-4-hydroxyphenyl (e)

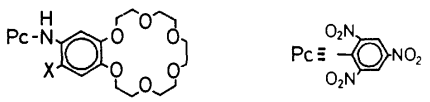

2, X = H (a)
NO_2 (b)

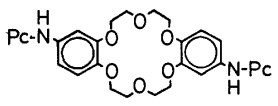

3

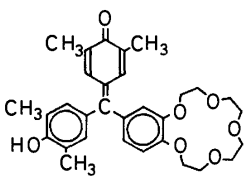

4

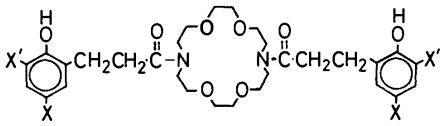

5, X= H H, X′= H (a)
NO_2 H (b)
-N=N- H (c)
-N=N-NO_2 H (d)
-N=N-NO_2 -N=N-NO_2 (e)

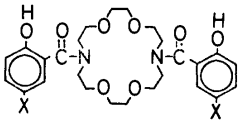

6, X = H (a)
NO_2 (b)

Acid Dissociation and Metal Extraction. The acid dissociation constants (K_{HA}) of crown ether dyes were determined photometrically in water containing 20% dioxane by volume. The results, together with the λ_{max}

Table 1. Physical properties of crown ether dyes

Dyes	pK_{HA}[a)]	λ_{max}, nm[b)]	$\varepsilon(\lambda_{max})\times 10^{-3}$ [b)]
1a	11.6	473	13.2
1b	8.6	363	22.9
1c	9.7	368	22.4
1d	7.3	370	17.2
2a	10.6[c)]	400	11.5
2b	8.8[c)]	425	14.6
4	7.9	465[d)]	4.6[d)]

a) 20% Dioxane, μ=0.10 (LiCl), 25 °C. b) Chloroform. c) 10% Dioxane, μ=0.10 (LiCl), 25 °C. d) Dioxane.

and ε values for the undissociated dyes in chloroform solution, are summarized in Table 1. The dissociation constants reflect the structural characteristics of the dyes.

The dyes sythesized are sparingly soluble in water but appreciably soluble in most organic solvents. Some of the dyes (**3**, **5b**, **5c**, **6a**, and **6b**) are not very soluble in the usual solvents and it is difficult to increase the concentration sufficient for spectrophotometry. The extraction behavior of the dyes **1**—**4** toward potassium, an element which seems to be the most easily extracted[2,3] was studied under various conditions. No spectral change was observed for azo dyes **1** dissolved in organic solvents such as chloroform, isobutyl methyl ketone, nitrobenzene or 1-pentanol, when the solution was brought in contact with 1 M K^+ aqueous solution buffered at pH 9.5—12.5 with carbonate (K_2CO_3) or borate ($Li_2B_4O_7$–LiOH). The spectra of the organic solution remained as those of HA (undissociated form), indicating that no extraction of K^+A^- type species took place. The azo crown ether dye **7** (pK_a, 9.2; 10% dioxane)[5] was found to behave similarly (no extraction).

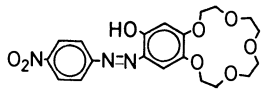

7

In the presence of potassium in aqueous solution the dye partially leaked out from organic into aqueous phase for **1b**. This suggests that with azo dyes **1a** and **1d**, complexation of potassium with the benzo-15-crown-5 function occurs, but the resulting complex of zwitter ion structure M^+A^- is hardly distributed in either organic or aqueous phase. At most, the complex partially goes into aqueous phase with relatively less lipophilic dye such as **1b**.

In contrast to azo dyes **1**, the picrylamino-substituted benzo-18-crown-6 (**2**) extracts potassium successfully. This is in line with the behavior of benzo-15-crown-5 homologues.[2,3] In fact, **2** is an extraction reagent for potassium, more effective than benzo-15-crown-5 homologues, and can be used for the determination of ppm level of potassium.[6] The dibasic ether dye **3** behaves similarly, but a detailed study could not be made because of the low solubility of the compound (in chloroform) and the precipitation of metal complex at high concentration of potassium. No alkaline earth metal ions were extracted by **3**.

The benzein dye **4** was studied in a similar way for the extraction of potassium. The absorbance of the organic phase at 600 nm was 0.02 (optical path, 1 cm) when 3.8×10^{-5} M solution of **4** in isobutyl methyl ketone was shaken with an equal volume of 0.1 M Li_3EDTA–OH (trilithium salt of *N'*-(2-hydroxyethyl)-ethylenediamine-*N,N,N'*-triacetic acid, pH 10.1). On addition of potassium chloride, the absorbance increased to 0.09 (0.01 M KCl) and 0.19 (0.1 M KCl), indicating the extraction of K^+A^-. However, the dye was unstable in alkaline solution, probably because of the irreversible oxidation of ionized species.

The difference in extraction behavior between hydroxyarylazo- and picrylamino-substituted benzo crown ethers should be mentioned. Both types of dyes would extract metals by forming complexes of the zwitter-ion structure, *e.g.*, **8** and **9**, as in the following.

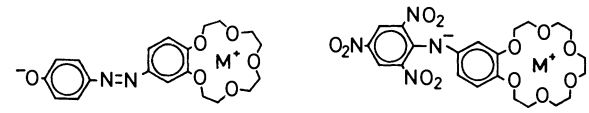

8 **9**

8 and **9** each represent perhaps the most important of the many canonical formulae for the resonance stabilized zwitter-ion complexes from the corresponding azo and picrylamino crown ether dyes, respectively. In **9**, there is a steric congestion around anionic nitrogen, and the hydration would be considerably hindered. On the other hand, the phenolate oxygen in **8** may be easily hydrated and this canonical structure should be greatly stabilized in aqueous solution. In other words, negative charge of the dye would be more delocalized in **9** than in **8**. A negative-positive charge separation in the complex might be smaller with the picrylamino crown ether complexes than with azo crown ether complexes. This might increase the distribution of the picrylamino metal complexes in organic solution. That the benzein dye extracts potassium to some extent suggests the better charge delocalization than in azo dyes.

Compounds **5** and **6** were synthesized with the hope that chelate-type coordination by phenolate anion to the crown ether-encapsulated metal might help increase both stability and extractability of the alkali as well as alkaline earth metals.

The extraction of alkali and alkaline earth metal ions by dyes **5c**, **5d**, **5e**, **6a**, and **6b** was studied, only **5e** being found to extract the metals. Figure 1 shows the spectra of 9.4×10^{-6} M **5e** in chloroform in contact

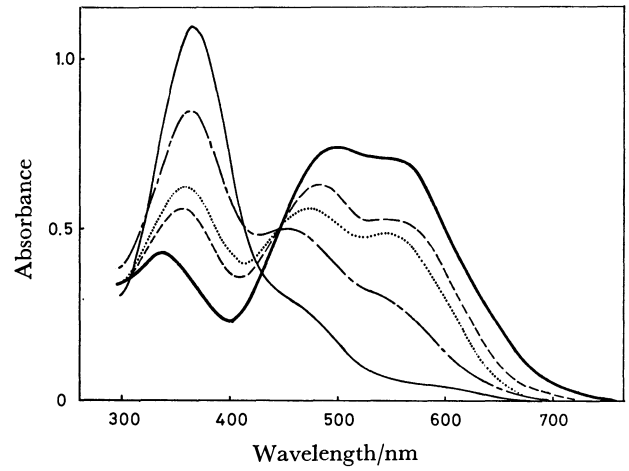

Fig. 1. Absorption spectra of 9.4×10^{-6} M **5e** in chloroform contacted with an equal volume of 1 M metal chloride solution buffered with 1 M triethanolamine at pH 10.9.
——, Without metal chloride (blank); –·–·–, LiCl; ·····, $CaCl_2$; – – –, $BaCl_2$; ——, 9.4×10^{-6} M **5e** in 0.1 M LiOH (20% dioxane), 25 °C.

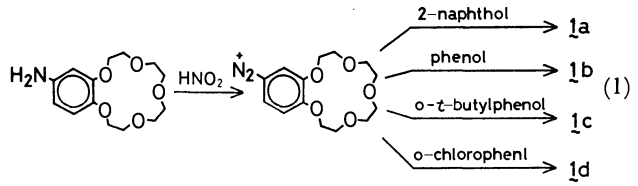

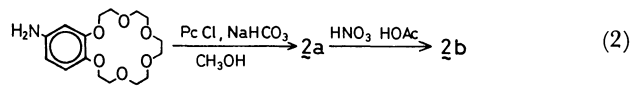

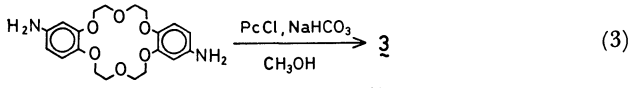

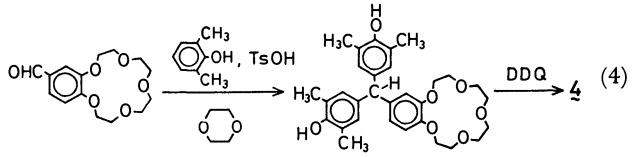

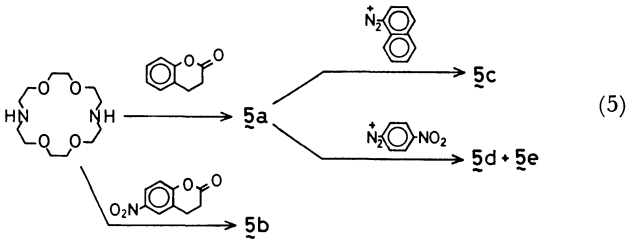

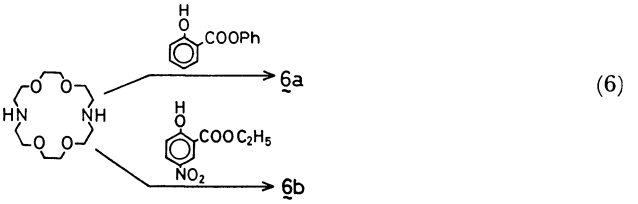

with an equal volume of 1 M LiCl, $CaCl_2$ or $BaCl_2$ solution buffered with 1 M triethanolamine at pH 10.9. Change in spectrum from the blank (1 M metal being absent) to that in the presence of 1 M metal chlorides is irregular (no apparent isosbestic point) due to the distribution of the dye to aqueous phase. However, a regular increase in absorbance at 500—550 nm region is observed from lithium to calcium and barium. From a comparison of the result with a limiting spectra taken in 0.1 M LiOH (20% dioxane), the metals seem to be extracted as $M^{II}A$ or M^{I}_2A (**5e**=H_2A) type complexes. With potassium salt a considerable fraction of the dye is distributed into aqueous phase. Dyes **5c**, **5d**, **6a**, and **6b** are distributed completely into aqueous solution under similar extraction conditions.

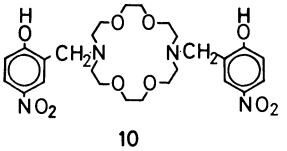

10

While **6b** does not extract alkaline earth metals, the analogous crown ether dye **10** does.[7] The difference might be due to the lower donor property of the amide nitrogen combined with an unfavorable orientation of phenolic group in **6b** for coordination. The phenolic hydroxyl would be coplanar with the amide group because of conjugation and hydrogen bonding, prohibiting access of the phenolate group to the center of the diaza-18-crown-6 ring where the metal ions are to be captured. The introduction of the two methylene groups between the amide carbonyl and aromatic nucleus in **5e** releases the steric constraint enforced by the amide bonding, making it possible for phenolate anions to occupy the axial positions of the encapsulated metal. The increased acidity of phenolic hydroxyl groups assisted by two *p*-nitrophenylazo groups for each aromatic neucleus also helps increase the degree of formation of metal complex at a lower pH. That the phenolate anion in **10** can reach the encapsulated metal is readily envisaged by stereomodel inspection. The unusually high stability of alkaline earth metal complexes from *N,N'*-dipropionic acid derivative of the diaza-18-crown-6[8] supports this view.

In conclusion, the two factors seem to be most important in the molecular design of crown ether based extraction photometric reagents for alkali and alkaline earth metals: an extensive delocalization of anionic charge and a minimum distance of positive-negative charge separation in the resulting metal complex. Both factors are essential if the metal complexes are of zwitter-ion structure as with **2**. The charge delocalization factor would not be essential if the metal complexes can assume a chelate-type coordination structure (**5e** and **10**). In this case, however, a structural requirement which allows the coordination of the dye anion to the metal should be considered.

Experimental

Apparatus and Instruments. IR spectra were recorded on a JASCO DS-403G infra-red spectrophotometer, UV and visible absorption spectra on a Hitachi 200 double beam spectrophotometer and a Hitachi 556 dual wave-lengths double beam spectrophotometer. ^{1}H-NMR spectra were measured with either a Varian A-60 or a Bruker WH-90. The pH measurements were made on an Orion 801A ion-analyzer equipped with TOA GST-155C hybrid glass electrode.

Acid Dissociation Constant. Several miligrams of the dye sample was weighed and dissolved in 20 ml dioxane in a 100 ml measuring flask. Lithium chloride (0.42 g) was then added along with a small amount of aqueous acetic acid to make ionic strength and pH of the final solution 0.10 and $\leq$5, respectively, the mixture being diluted with water to 100 ml. One tenth molar lithium hydroxide was added, and the pH and the absorption spectra were measured. The effect of lithium salt and organic solvent (dioxane) on pH measurements was not corrected. The acid dissociation constant was obtained from the slope of the plot, $\Delta A[H^+]/[HA]_t$ *vs.* $\Delta A/[HL]_t$, by means of the equation

$$\frac{\Delta A[H^+]}{[HA]_t} = K_a\left(\Delta\varepsilon - \frac{\Delta A}{[HA]_t}\right).$$

Where $\Delta A(=A-A_0)$ is the increment of absorbance at any pH from the initial absorbance (A_0) where all the dye molecule (HA) exist in undissociated form. $[HA]_t$ is the total concentration of the dye and $\Delta\varepsilon$ is the difference between ε_A-

and ε_{HA}.

Synthesis of Dyes. The synthetic procedures are not optimized for the maximum yield of the product.

1a. 4′-Nitrobenzo-15-crown-5 was hydrogenated in ethanol over Pd/C catalyst.[9] After removal of the catalyst, 3—5 times molar excess of fluoroboric acid was gradually added and the mixture stored in a refrigerator overnight. The fluoroborate salt of 4′-aminobenzo-15-crown-5 was obtained as white needles. Yield, 90%. The salt (0.30 g, 0.82 mmol) and 1.6 ml of 1 M HCl were dissolved in 10 ml water and diazotized in the usual manner. 2-Naphthol (117 mg, 0.82 mmol) dissolved in 2.7 ml of 1M NaOH was chilled below 5° C. To this solution was added the diazotized solution under stirring. After being stirred for an hour, the mixture was acidified by addition of acetic acid, and the red precipitates formed were collected. The crude product was then digested in a small amount of hot methanol, turning into fine red crystals. Yield, 0.28 g, 66%; mp 162—163 °C; IR(KBr) 3440(OH), 1600(aromatic nuclei), and 1130 cm^{-1} (C–O–C); NMR($CDCl_3$) δ=3.76 (8H, s, OCH_2CH_2O), 3.85—4.10 (4H, m, OCH_2CH_2O), 4.10—4.30 (4H, m, OCH_2-CH_2O), 6.80—7.90 (9H, m, aromatic H). Found: C, 63.75; H, 5.93; N, 6.22%. Calcd for $C_{24}H_{26}N_2O_2$: C, 63.62; H, 5.94; N, 6.39%.

1b. Phenol and benzo-15-crown-5-4′-diazonium salt were allowed to react by a procedure similar to that for **1a**. Crystals with blackish-green sheen: yield 11%; mp 72—74 °C; IR(KBr) 3480(OH), 1590, 1502 (aromatic nuclei), 1261, and 1120 cm^{-1} (C–O–C); NMR ($CDCl_3$) δ=3.76 (8H, s, OCH_2CH_2O), 3.86—4.10 (4H, m, OCH_2CH_2O), 4.10—4.30 (4H, m, OCH_2-CH_2O), 6.82—7.87 (9H, m, aromatic H). Found: C, 54.62; H, 6.87; N, 6.38%. Calcd for $C_{20}H_{24}N_2O_6\cdot 3H_2O$: C, 54.29; H, 6.76; N, 6.31%.

1c. *o-t*-Butylphenol and benzo-15-crown-5-4′-diazonium salt were reacted by a procedure similar to that for **1a**. The crude product was passed through an alumina column with chloroform/ether (1/1, v/v), the main band being collected. The product was recrystallized from ethanol. Orange powder; yield 34%; mp 107—108 °C; IR(KBr) 3440(OH), 1590, 1502 (aromatic nuclei), 1265, and 1125 cm^{-1} (C–O–C); NMR ($CDCl_3$) δ=1.36 (9H, s, $C(CH_3)_3$), 3.80 (8H, s, OCH_2-CH_2O), 3.88—4.11 (4H, m, OCH_2CH_2O), 4.11—4.36 (4H, m, OCH_2CH_2O), 6.71—7.98 (6H, m, aromatic). Found: C, 62.15; H, 7.48; N, 5.90%. Calcd for $C_{24}H_{32}N_2O_6\cdot H_2O$: C, 62.33; H, 7.66; N, 6.01%.

1d. The compound was synthesized by reacting benzo-15-crown-5-4′-diazonium salt with *o*-chlorophenol. The product was purified by recrystallization from aqueous acetone. Needles with blackish-green sheen; yield 11%; mp 62—64 °C; IR(KBr) 3480 (OH), 1592, 1502 (aromatic nuclei), 1260, and 1120 cm^{-1} (C–O–C); NMR (acetone-d_6) δ=3.76 (8H, s, OCH_2CH_2O), 3.82—4.07 (4H, m, OCH_2CH_2O), 4.07—4.36 (4H, m, OCH_2CH_2O), 6.98—8.17 (6H, m, aromatic H). Found: C, 54.14; H, 5.31; N, 6.34%. Calcd for $C_{20}H_{23}N_2O_6Cl\cdot H_2O$: C, 54.45; H, 5.23; N, 6.36%.

2a. 4′-Nitrobenzo-18-crown-6[9] (0.50 g, 1.5 mmol) was hydrogenated on Pd/C in ethanol. The reaction mixture after removal of the catalyst was concentrated under reduced pressure, the residue being redissolved in a small amount of methanol. Picryl chloride (0.4 g, 1.7 mmol) and sodium hydrogencarbonate (0.15 g) were added in succession. After being stirred for 30 min, the mixture was acidified by hydrochloric acid and then concentrated to dryness under reduced pressure. The residue was taken into chloroform, washed with water, dried, concentrated, and applied to a silica-gel column. Elution with chloroform/ether (1/1, v/v) gave the main band, from which a dark reddish mass was obtained by concentration. A careful recrystallization (several days) from aqueous acetone or aqueous methanol gave dark-red needles. Yield, 0.52 g, 45%; mp 55—56 °C; IR(KBr) 3300 (NH), 1620 (aromatic nuclei), 1510, 1330 (NO_2), and 1128 cm^{-1} (C–O–C); NMR ($CDCl_3$) δ=3.70 (4H, s, OCH_2-CH_2O), 3.76 (8H, s, OCH_2CH_2O), 3.85—4.35 (8H, m, OCH_2CH_2O), 6.35—6.9 (3H, m, aromatic H) and 9.05 (2H, s, aromatic H). Found: C, 48.81; H, 4.91; N, 10.58%. Calcd for $C_{22}H_{26}N_4O_{12}$: C, 49.07; H, 4.87; N, 10.41%.

2b. To a chloroform solution (25 ml) of **2a** (0.85 g) was added dropwise a mixture of 1.5 ml each of glacial acetic acid, chloroform, and fuming nitric acid (*d*, 1.42) at room temperature. The reaction mixture was then washed four times with 20 ml water, and the chloroform solution was evaporated to dryness. The residue was recrystallized from aqueous acetone. Orange crystals; yield, 0.30 g, 32%; mp 160—161 °C; IR (KBr) 1620 (aromatic nuclei), 1520, 1330 (NO_2) and 1130 cm^{-1} (C–O–C); NMR ($CDCl_3$) δ=3.69 (4H, s, OCH_2CH_2O), 3.73 (8H, s, OCH_2CH_2O), 3.85—4.35 (8H, m, OCH_2CH_2O), 6.38 (1H, s, aromatic H), 7.76 (1H, s, aromatic H), 9.19 (2H, s, aromatic H), 11.76 (1H, s, NH). Found: C, 45.24; H, 4.29; N, 11.80%. Calcd for $C_{22}H_{25}N_5O_{14}$: C, 45.29; H, 4.30; N, 12.00%.

3. *trans*-Dinitrodibenzo-18-crown-6[10,11] (1.0 g, 2.2 mmol) was suspended in acetic acid (10 ml) and hydrogenated over Pd/C catalyst. The catalyst was removed by filtration, and the acetic acid solution was concentrated under reduced pressure to a thick oil, which was redissolved in a small amount of methanol and neutralized with excess sodium hydrogen carbonate (0.85 g). Picryl chloride (1.5 g 6 mmol) was added and stirred at room temperature for a half hour. The reaction mixture was worked up in a similar manner to that for **2**. The compound becomes less soluble in chloroform with increase in purity. Recrystallization from aqueous *N,N*-dimethylformamide gave reddish brown crystalline powder. Yield, 1.2 g, 67%; mp 222—226 °C; IR(KBr) 1620 (aromatic nuclei), and 1130 cm^{-1} (C–O–C); NMR (DMSO-d_6) δ=3.76, 4.25 (16H, broad, OCH_2CH_2O), 6.67, 6.89 (6H, s, aromatic H), 8.79 (4H, s, aromatic H), 10.21 (2H, s, NH). Found: C, 47.03; H, 3.54; N, 13.33%. Calcd for $C_{32}H_{28}$-$N_8O_{18}\cdot 1/4H_2O$: C, 47.03; H, 3.49; N, 13.72%.

4. 4′-Formylbenzo-15-crown-5[9] (0.50 g, 1.7 mmol), 2,6-dimethylphenol (0.60 g, 4.9 mmol), and *p*-toluenesulfonic acid (0.32 g, 1.7 mmol) were refluxed in 25 ml dioxane for 30 h. After removal of dioxane under reduced pressure, the residue was taken into chloroform and subjected to silica gel column chromatography with an eluting solvent starting from chloroform, chloroform/ether (1/1, v/v), ether to ether/ethanol (1/1, v/v). The main band appeared in ether fraction, giving light yellowish needles by recrystallization from aqueous acetone. The compound was found to be 4′-[bis(3,5-dimethyl-4-hydroxyphenyl)methyl]-benzo-15-crown-5, the precursor compound of **4**, from the analytical data. Yield, 0.37 g, 42%; mp 171—172.5 °C; IR(KBr) 3450 (OH), 1580 (aromatic nuclei), and 1150 cm^{-1} (C–O–C); NMR ($CDCl_3$) δ=2.05 (12H, s, CH_3), 3.5—4.1 (16H, m, OCH_2CH_2O), 4.48 (2H, s, OH), 5.05 (1H, –CH–), 6.51 (7H, s, aromatic H). Found: C, 70.61; H, 7.33%. Calcd for $C_{31}H_{38}O_7\cdot 1/4H_2O$: C, 70.65; H, 7.31%. The compound (λ_{max}, 410 nm; ε, 480; $CHCl_3$) is slightly contaminated with **4** due to the air-oxidation during the work-up. One tenth gram (0.19 mmol) of the dye precursor obtained above was dissolved in 10 ml anhydrous methanol, and 43 mg (0.19 mmol) of DDQ (dichlorodicyano-*p*-benzoquinone) was added under stirring. The color of the solution turned red, and red crystalline power precipitated after stirring for 10 min. Yield, 90 mg, 90%; mp 244—245 °C; IR(KBr) 3400 (OH), 1620, 1590 (aromatic nuclei), 1265, and

1140 cm^{-1} (C–O–C); NMR ($CDCl_3$) δ=2.15 (12H, s, CH_3), 3.75 (8H, s, OCH_2CH_2O), 3.85—4.05 (4H, m, OCH_2CH_2O), 4.05—4.30 (4H, m, OCH_2CH_2O), 6.65—7.35 (5H, m, aromatic H). Found: C, 70.83; H, 6.97%. Calcd for $C_{31}H_{36}O_7 \cdot 1/4H_2O$: C, 70.92; H, 6.96%.

5a. 3,4-Dihydrocoumarin (0.90 g, 6.1 mmol) and Kryptofix 22 (E. Merck, 7,16-diaza-1,4,10,13-tetraoxacyclooctadecane) (0.30 g, 1.1 mmol) were mixed and heated at 200 °C for 18 h under nitrogen. The excess dihydrocoumarin was then removed under reduced pressure, and the residue recrystallized from ethyl acetate to give white plates. Yield, 0.52 g, 80%; mp 131—131.5 °C; IR (KBr) 3400 (OH), 1620 (amide), 1590 (aromatic nuclei), 1285, and 1120 cm^{-1} (C–O–C); NMR ($CDCl_3$) δ=2.65—2.85 (8H, m, CH_2CH_2-CO), 3.15—3.65 (24H, m, OCH_2CH_2O), 6.80—7.25 (8H, m, aromatic H). Found: C, 64.22; H, 7.59; N, 4.91%. Calcd for $C_{30}H_{42}N_2O_8$: C, 64.52; H, 7.64; N, 5.02%.

5b. 6-Nitro-3,4-dihydrocoumarin (0.60 g, 3.0 mmol)[12] and Kryptofix 22 (0.20 g, 0.7 mmol) were mixed and heated at 140 °C for 15 h under nitrogen. After removal of excess 6-nitro-3,4-dihydrocoumarin by vacuum sublimation, the residue was recrystallized from a mixed solvent consisting of *N,N*-dimethylformamide, methanol and water. Yellow powder; Yield, 0.24 g, 48%; mp 124—125 °C; IR(KBr) 3400 (OH), 1620 (amide), 1510, 1345 (NO_2), 1285, and 1120 cm^{-1} (C–O–C); NMR (DMSO-d_6) δ=2.65, 2.85 (8H, m, CH_2CH_2CO), 3.15—3.65 (24H, m, OCH_2CH_2O), 6.85, 7.05 (2H, m, aromatic H), 7.90, 8.10 (4H, m, aromatic H).

5c. **5a** was reacted with 1-naphthalene diazonium salt in the usual manner at pH ≈9 for 1 h. The crude product was treated with a silica gel column with an eluting solvent starting from chloroform and ether to ethyl acetate. The main product appeared in ether fractions, from which brown powder was obtained by recrystallization. Yield, 0.20 g, 43%; mp 88—92 °C; IR(KBr) 3400 (OH), 1620 (amide), 1595 (aromatic nuclei), 1250, and 1130 cm^{-1} (C–O–C); NMR ($CDCl_3$) δ=2.65—2.85 (8H, m, CH_2CH_2CO), 3.15—3.65 (24H, m, OCH_2CH_2O), 6.90—8.0 (20H, m, aromatic H). Found: C, 68.99; H, 6.57; N, 9.10%. Calcd for $C_{30}H_{56}N_6O_8 \cdot 1/4H_2O$: C, 68.77; H, 6.48; N, 9.63%.

5d and *5e*. *p*-Nitroaniline (0.20 g, 1.5 mmol) was diazotized in the usual manner and added to an ice-cooled solution of **5a** (0.20 g, 0.36 mmol) in 1M LiOH (10 ml). The mixture was stirred at pH 8—9 for a half hour and acidified by acetic acid to give brownish powder. The precipitates were collected, washed with water and dried. The crude product (0.30 g) was dissolved in chloroform and chromatographed on a column of silica gel with an eluting solvent chloroform/ethyl acetate (1/1, v/v). The first fraction contained **5d** and the second fraction **5e**. **5d**. Yellowish brown crystalline powder; yield, 0.15 g, 49%; mp 196—203 °C (dec); IR (KBr) 1640 (amide), 1590 (aromatic nuclei), 1520, 1340 (NO_2), 1280, and 1095 cm^{-1} (C–O–C); NMR ($CDCl_3$) δ=2.65—2.85 (8H, m, CH_2CH_2CO), 3.15—3.65 (24H, m, OCH_2CH_2O), 6.75—7.15 (6H, aromatic H), 7.65—8.65 (8H, m, aromatic H). Found: C, 57.67; H, 5.50; N, 13.19%. Calcd for $C_{42}H_{48}N_8O_{12} \cdot H_2O$: C, 57.66; H, 5.72; N, 12.81%. *5e*. Blackish brown powder; yield, 70 mg, 14%; mp 144 °C (dec); IR (KBr) 3400 (OH), 1640 (amide), 1520, 1340 (NO_2), 1280 and 1105 cm^{-1} (C–O–C); NMR ($CDCl_3$) δ=2.60—2.90 (4H, m, CH_2Ar), 2.92—3.14 (4H, m, CH_2CO), 3.40—3.76 (24H, m, OCH_2CH_2O), 7.80—8.10 (10H, m, aromatic H), 8.20—8.50 (10H, m, aromatic H). Found: C, 54.56; H, 4.80; N, 15.77%. Calcd for $C_{54}H_{54}N_{14}O_{16} \cdot 2H_2O$: C, 54.45; H, 4.87; N, 16.47%. A contamination from tris(*p*-nitrophenylazo) derivative could not be excluded.

6a. Phenyl salicylate (0.90 g, 6.9 mmol) and Kryptofix 22 (0.30 g, 1.1 mmol) were mixed and heated (melted) under nitrogen at 160 °C for 16 h. The excess phenyl salicylate was hydrolyzed by the addition of water followed by heating (3 h). Salicylic acid and phenol were removed by vacuum sublimation, and the residue was recrystallized from ethyl acetate/ether. White crystalline powder; yield, 0.21 g, 36%; mp 141—142 °C; IR(KBr) 3400 (OH), 1625 (amide), 1595 (aromatic nuclei), 1255, and 1140 cm^{-1} (C–O–C); NMR ($CDCl_3$) δ=3.05—3.75 (24H, m, OCH_2CH_2O), 6.65—7.30 (8H, m, aromatic H), 9.55 (2H, s, OH). Found: C, 61.61; H, 6.98; N, 5.32%. Calcd for $C_{26}H_{34}N_2O_8 \cdot 1/4H_2O$: C, 61.60; H, 6.72; N, 5.53%.

6b. Ethyl 5-nitrosalicylate (0.65 g, 3.0 mmol) was allowed to react with Kryptofix 22 (0.20 g, 0.8 mmol) at 140 °C for 15 h under nitrogen. The excess ethyl 5-nitrosalicylate was removed by vacuum sublimation, and the residue was recrystallized from ethanol to given yellowish powder. It was found by analysis that the preparation is contaminated by the mono *N*-salicyloyl-substituted product. Reactions under prolonged reaction time introduced decomposition products. Yield, 0.17 g, 38%; mp 114.5—117 °C; IR (KBr) 3400 (OH), 1620 (amide), 1590 (aromatic nuclei), 1315 (NO_2), and 1120 cm^{-1} (C–O–C); NMR ($CDCl_3$) δ=3.20—4.10 (24H, m, OCH_2CH_2O), 6.95 (1H, d, aromatic H), 8.25 (1H, q, aromatic H), 8.81 (1H, d, aromatic H). Found: C, 51.69; H, 6.42; N, 8.15%. Calcd for $C_{26}H_{32}N_4O_{12} \cdot 1/2H_2O$: C, 51.19; H, 5.36; N, 9.31%.

The present work was partially supported by Grant-in-Aid for Scientific Research B-347055 from the Ministry of Education.

References

1) Photometric Reagents for Alkali Metal Ions Based on Crown Ether Complex Formation 4; Previous paper, Ref. 3.
2) M. Takagi, H. Nakamura, and K. Ueno, *Anal. Lett.*, **10**, 1115 (1977).
3) H. Nakamura, M. Takagi, and K. Ueno, *Talanta*, **26**, 921 (1979).
4) J. P. Dix and F. Vögtle, *Angew. Chem. Int. Ed. Engl.*, **17**, 857 (1978).
5) The authors thank Dr. Fumio Wada of the Department of Organic Synthesis, Kyushu University, for the supply of sample.
6) M. Takagi, H. Nakamura, and K. Ueno, Abstract Anal-193, ACS/CSJ Chemical Congress, Honolulu, Hawaii, April, 1—6, 1979.
7) M. Tazaki, M. Takagi, and K. Ueno, unpublished work.
8) M. Takagi, M. Tazaki, and K. Ueno, *Chem. Lett.*, **1978**, 1179.
9) R. Ungaro, B. El Haj, and J. Smid, *J. Am. Chem. Soc.*, **98**, 5198 (1976).
10) W. M. Feigenbaum and R. H. Michel, *J. Polym. Sci. A-1*, **9**, 817 (1971).
11) E. Shchori, J. Jagur-Grodzinski, and M. Shporer, *J. Am. Chem. Soc.*, **95**, 3842 (1973).
12) T. R. Ingle and B. V. Bhide, *J. Univ. Bombay*, **23**, *Pt.* 3, *Sci.*, No., Sect. A, No. 36, 33 (1954); *Chem. Abstr.*, **50**, 322 (1956).

 © 1980 The Chemical Society of Japan Bull. Chem. Soc. Jpn., 53, 1555—1559 (1980)

Metal Complexes in Acetic Acid. I. Kinetics and Mechanism of Reactions of Tetra-μ-acetato-dicopper(II) with Lithium Chloride and Hydrogen Chloride

Shigenobu FUNAHASHI, Tetsuo NISHIMOTO, Pradyot BANERJEE,[1a]
Kiyoshi SAWADA,[1b] and Motoharu TANAKA*
Laboratory of Analytical Chemistry, Faculty of Science, Nagoya University, Chikusa-ku, Nagoya 464
(Received September 28, 1979)

Kinetics of reactions of tetra-μ-acetato-dicopper(II) (copper(II) acetate dimer: $Cu_2(OAc)_4$) with lithium chloride and hydrogen chloride (XCl where X denotes Li or H) in acetic acid have been studied spectrophotometrically by using a stopped-flow technique with a computer-assisted averaging device. The rate of decomposition of copper(II) acetate dimer to the monomeric chloro complex is expressed as $-d[Cu_2(OAc)_4]/dt=k^{XCl}[Cu_2(OAc)_4][XCl]$. At 25 °C $k^{LiCl}=(3.5\pm0.6)\times10^5$ mol^{-1} kg s^{-1} ($\Delta H^*=50\pm10$ kJ mol^{-1} and $\Delta S^*=30\pm20$ J mol^{-1} K^{-1}) and $k^{HCl}=(4.8\pm1.0)\times10^5$ mol^{-1} kg s^{-1} ($\Delta H^*=23\pm10$ kJ mol^{-1} and $\Delta S^*=-60\pm20$ J mol^{-1} K^{-1}). Mechanisms are proposed for the decomposition of copper(II) acetate dimer and some discussions are made on the difference in reactivities of LiCl and HCl.

Acetic acid has been used as a convenient solvent for the titration of weak bases.[2] It is a non-dissociating solvent having low dielectric constant ($D=6.18$ at 20 °C[3]), while it is similar in nature to water for its amphiprotic character. Grunwald and co-workers have studied kinetic behavior of proton exchange and ion-pair exchange (metathesis) in acetic acid.[4] Although plenty of information has been so far gathered on equilibria of metal complexes in anhydrous acetic acid media,[5-7] kinetic and mechanistic studies of metal complexes are scarce.[8,9] It appeared of particular interest for us to make a kinetic and mechanistic study of the reactions of the tetra-μ-acetato-dicopper(II) (henceforth we call it copper(II) acetate dimer) with lithium chloride and hydrogen chloride in acetic acid. The present study should provide some information on the reactivity of the dimeric copper entity.

Experimental

All starting chemicals were of reagent grade. Solutions of reagents were prepared in a glove box filled with dried air.

Reagents. *Acetic Acid:* Potassium permanganate (30 g) was added to acetic acid (3 dm^3) and after refluxing for *ca.* 10 h, the solution was distilled. The distillate was then refluxed again with about 200 g of boron triacetate for 12 h and distilled. Calculated amount of acetic anhydride was added to remove residual water in the acetic acid, and it was allowed to stand for *ca.* 4 d at 110 °C.[10] The resultant acetic acid contained at most 1.5×10^{-3} mol dm^{-3} of water and presumably the same amount of acetic anhydride as that of remaining water.

Copper(II) Acetate: Copper(II) acetate was recrystallized from water. Then it was recrystallized first from reagent grade acetic acid and then from anhydrous acetic acid, and dried in a desiccator over sodium hydroxide for a few days under a reduced pressure. The copper(II) acetate solution was prepared by weighing crystals, and standardized by EDTA after evaporating excess acetic acid and then adding NH_3 to make the pH buffered at *ca.* 4.3. The determination of copper in copper(II) acetate crystals by electrolysis confirmed the composition of $Cu_2(CH_3CO_2)_4$.

Lithium Chloride: Lithium chloride was recrystallized twice from distilled water and dried at 120 °C. The solution was prepared by weighing. Its concentration was checked by the Mohr method with K_2CrO_4 as indicator.

Hydrogen Chloride Solution: Hydrogen chloride generated from NaCl with concentrated H_2SO_4 was dried with concentrated H_2SO_4 and was led to anhydrous acetic acid. A hydrogen chloride solution was handled as gently and carefully as possible in order to avoid volatilization of hydrogen chloride. The concentration of each hydrogen chloride solution for kinetic measurements was determined by means of mercury(II) thiocyanate method[11] after dilution of the acetic acid solution with water.

Perchloric Acid Solution: Aqueous solution of perchloric acid (*ca.* 60%, super special grade, Wako Pure Chemical Industries, Ltd.) was diluted with acetic acid, and acetic anhydride equivalent to water was added dropwise to the perchloric acid solution keeping temperature of the solution below 25 °C. The concentration of perchloric acid was standardized against potassium hydrogen phthalate, Crystal Violet being used as indicator.

Lithium Acetate: Lithium acetate was recrystallized twice from acetic acid. Crystals were dried over sodium hydroxide *in vacuo*. The lithium acetate crystals were dissolved in acetic acid and the concentration was determined with a standard perchloric acid in acetic acid using Crystal Violet as indicator.

Measurements. Spectral measurements were performed on a highly sensitive spectrophotometer (SM 401, Union Giken Co. Ltd., Osaka) which enables us to measure spectra at a full scale of 0.01 optical density. The concentration of water was determined by the Karl-Fisher aquametry.

Dynamic reactions were followed by means of a stopped-flow technique using a highly sensitive stopped-flow spectrophotometer with a computer-assisted averaging device,[12] which enable us to follow reactions slower than around 1 ms of half-life. Although the sensitivity of the instrument is very high by itself (0.01 absorbance/full scale per cm path length of light), it gives a poor SN ratio when used as a detector of a stopped-flow apparatus. Then by repeating the flow up to 500 times and averaging signals in a microcomputer, it was possible to improve considerably the SN ratio and to obtain a smooth reaction trace even at highest sensitivity of the instrument. The requirement for signal averagers is that the signal be repetitive. In this apparatus, since reactant solutions was driven by nitrogen gas pressure controlled by solenoid valves, the flow was easily controlled for repeated mixing of reactant solutions. Hence a high

reproducibility of each signal was attained. In the present study, the averaged trace obtained from 10—50 flows was recorded on an X-Y recorder.

Equilibria. There have been some studies on the monomer-dimer equilibrium of copper(II) acetate in acetic acid

$$Cu_2(OAc)_4 \overset{K_{dim}}{\rightleftharpoons} 2Cu(OAc)_2 \quad (1)$$

Cheng and Howald,[13] and Grasdalen and Svare[14] determined the monomer-dimer equilibrium constant as a function of the water concentration in acetic acid. According to them, the dissociation constant K_{dim} is less than 5×10^{-6} mol dm^{-3} at 25 °C in dry acetic acid. We have measured the absorbance of copper acetate solution at 680 nm, where the dimer has an absorption maximum and the dissociation products absorb little. Over the copper(II) acetate concentration range from 10^{-5} to 10^{-2} mol kg^{-1}, the molar absorption coefficient of copper(II) acetate remained almost constant (Fig. 1). The spectra of the solution remained unchanged and showed the characteristic absorption maxima at 370 nm and 680 nm, indicating the dimeric structure of copper(II) acetate. We estimated $K_{dim}\leq10^{-7}$ mol dm^{-3}. Thus the copper(II) acetate exists solely as a dimer under our experimental conditions.

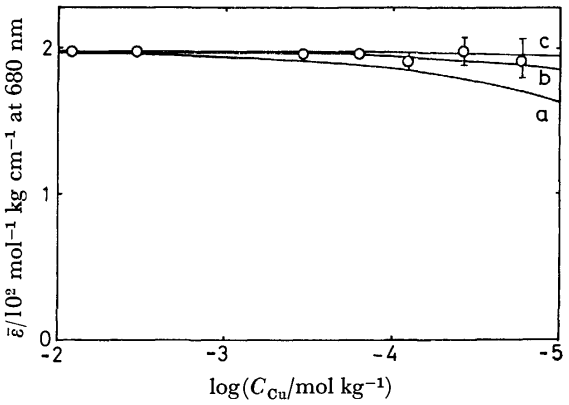

Fig. 1. Dependence of apparent molar absorption coefficient ($\bar{\varepsilon}$) on copper (II) acetate concentration (C_{Cu}). C_{Cu} refers to the concentration per copper atom in mol kg^{-1}. Curves a, b, and c are calculated with $K_{dim}=10^{-6}$, 10^{-7}, and 10^{-8} mol kg^{-1}, respectively.

The presence of a small amount of water (*ca.* 10^{-3} mol kg^{-1}) is inevitable in the present reaction systems. Water in acetic acid can behave as a base, but it is very weak. Perchloric acid and hydrogen chloride, reacting with water, produce their corresponding hydrates $H_3O^+ClO_4^-$ and $H_3O^+Cl^-$. However, these reactions do not occur to an appreciable extent under our experimental conditions. Judging from the equilibrium constant (0.6 ± 0.3 mol^{-1} dm^3) for the replacement of one of the two acetic acid molecules on the axial sites of the copper(II) acetate dimer by water in acetic acid:[6]

$$Cu_2(OAc)_4(HOAc)_2 + H_2O \rightleftharpoons Cu_2(OAc)_4(H_2O)(HOAc) + HOAc \quad (2)$$

the monohydrate may be excluded under our experimental conditions. The equilibria of copper(II) acetate dimer with hydrogen chloride, perchloric acid and lithium acetate in acetic acid have been investigated in detail:[7]

$$Cu_2(OAc)_4 + 2HCl \rightleftharpoons 2CuCl(OAc) + 2HOAc \quad (10^{4.7}\ \text{mol}^{-1}\ \text{kg}) \quad (3)$$

$$Cu_2(OAc)_4 + 4HCl \rightleftharpoons 2CuCl_2 + 4HOAc \quad (10^{15.2}\ \text{mol}^{-3}\ \text{kg}^3) \quad (4)$$

$$Cu_2(OAc)_4 + 2HClO_4 \rightleftharpoons 2Cu(OAc)(ClO_4) + 2HOAc \quad (10^{3.5}\ \text{mol}^{-1}\ \text{kg}) \quad (5)$$

$$Cu_2(OAc)_4 + 4HClO_4 \rightleftharpoons 2Cu(ClO_4)_2 + 4HOAc \quad (10^{10.4}\ \text{mol}^{-3}\ \text{kg}^3) \quad (6)$$

$$Cu_2(OAc)_4 + 2LiOAc \rightleftharpoons Li_2Cu_2(OAc)_6 \quad (10^{0.89}\ \text{mol}^{-2}\ \text{kg}^2) \quad (7)$$

$$Cu_2(OAc)_4 + 4LiOAc \rightleftharpoons 2Li_2Cu(OAc)_4 \quad (10^{-0.4}\ \text{mol}^{-3}\ \text{kg}^3) \quad (8)$$

where the values of equilibrium constants for the relevant over-all reactions are given in parentheses. Coordinating solvent molecules are omitted for simplicity. The constant for the formation of chloro copper(II) complex from $Cu_2(OAc)_4$ and LiCl not being available, it was confirmed spectrally that the equilibrium was much favored to the formation of monomeric chloro complex under our experimental conditions. Comparison of the spectrum of $Cu_2(OAc)_4$ with that of the reaction mixture revealed that it was reasonable to follow the rate of the reaction at 300—320 nm, where the change in absorbance was large. Most of the runs were thus performed at 315 nm for LiCl and at 305 nm for HCl. From knowledge of the equilibria mentioned above we were able to set the appropriate conditions for kinetic measurements.

Results

The kinetics have been followed under conditions where the reverse reaction can be neglected in the kinetic study. The increase in absorbance with reaction time in the presence of a large excess of XCl was satisfactorily fitted to a pseudo-first-order rate law. Conditional first-order rate constants, k_0^{XCl}, were obtained from linear plots according to $\ln (A_\infty-A_0)/(A_\infty-A_t) = k_0^{XCl} t$, where A_0, A_t, and A_∞ denote respectively the absorbances at zero, at time t and at infinite time. Thus rate equation for the appearance of monomeric chloro copper complex (Cu–Cl) or decomposition of copper(II) acetate dimer is given by

$$\frac{1}{2}\frac{d[Cu\text{–}Cl]}{dt} = -\frac{d[Cu_2(OAc)_4]}{dt} = k_0^{XCl}[Cu_2(OAc)_4], \quad (9)$$

where $[Cu_2(OAc)_4]$ refers to a concentration of copper(II) acetate dimer ($Cu_2(OAc)_4\cdot2HOAc$), and two solvent molecules coordinated to the axial sites are omitted for simplicity. Conditional rates were found to be unaffected by the initial Cu(II) concentration (4.31×10^{-6}—7.48×10^{-5} mol kg^{-1}), while the increase in the XCl concentration resulted in the increase in k_0^{XCl}. The plot of k_0^{XCl} against total concentration of XCl, C_{XCl}, is linear with no intercept (Fig. 2). Then the rate law is

$$-\frac{d[Cu_2(OAc)_4]}{dt} = k^{XCl}[Cu_2(OAc)_4][XCl], \quad (10)$$

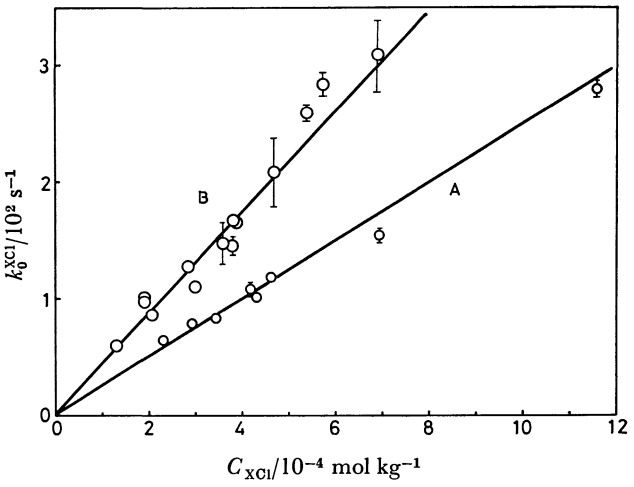

Fig. 2. Plots of conditional first-order rate constant (k_0^{XCl}) against the concentration of XCl (C_{XCl}). A: LiCl, B: HCl, at 20 °C.

Table 1. Effect of added water on the conditional rate constants

LiCl system[a]		HCl system[b]	
$10^2C_{H_2O}$/mol kg^{-1}	k_0^{LiCl}/s^{-1} ($\pm$10)[c]	$10^2C_{H_2O}$/mol kg^{-1}	k_0^{HCl}/s^{-1} ($\pm$15)[c]
<0.2[d]	151$\pm$25[e]	<0.2[d]	120$\pm$25[e]
0.43	151	0.28	108
1.3	170	0.61	105
2.3	177	0.89	105
3.4	191	1.4	106
6.1	233	1.9	119
9.8	244	3.1	140
		3.9	156

a) Conditions: $C_{Cu}=9.64\times10^{-6}$ mol kg^{-1}, $C_{LiCl}=4.31\times10^{-4}$ mol kg^{-1}, 25 °C. b) Conditions: $C_{Cu}=8.52\times10^{-6}$ mol kg^{-1}, $C_{HCl}=2.50\times10^{-4}$ mol kg^{-1}, 25 °C. c) Deviation from an average value of several experimental points. d) No added water. The concentration of water was less than 2×10^{-3} mol kg^{-1}. e) This value was estimated from data at 25 °C in Table 2.

where k^{XCl} is a second-order rate constant. Some kinetic experiments were carried out to have an idea of the effect of added water in the present reaction (Table 1). There was no effect of water at least up to 10^{-2} mol kg^{-1}. As the amount of water in our reaction systems is at most 3×10^{-3} mol kg^{-1}, the contribution of water to reaction rates can be neglected. From the temperature dependence of k^{XCl} (Eyring's plot), the activation parameters are calculated, and tabulated in Table 2.

The reaction of copper(II) acetate dimer ($C_{Cu}=9.39\times10^{-6}$ mol kg^{-1}) with LiCl ($C_{LiCl}=4.95\times10^{-4}$ mol kg^{-1}) was followed in the presence of lithium acetate over the concentration range from 3.59×10^{-5} to 1.20×10^{-4} mol kg^{-1}, which does not appreciably favor equilibria 7 and 8 to the right. We found no kinetic effect of lithium acetate, which is one of the strongest bases in acetic acid. The kinetic run of $Cu_2(OAc)_4$ (8.45×10^{-6} mol kg^{-1}) with HCl (2.72×10^{-4} mol kg^{-1}) was carried out in the presence of up to 1.2×10^{-5} mol kg^{-1} of $HClO_4$. Perchloric acid at such a concentration level does not appreciably favor equilibria of $Cu_2(OAc)_4$ shown in Eqs. 5 and 6. The rate constant remained unchanged in the presence of such amounts of $HClO_4$, which is the strongest acid in acetic acid.

Table 2. Second-order rate constants and activation parameters

Temp/°C	$10^{-5}k^{LiCl}$/mol^{-1} kg s^{-1}	$10^{-5}k^{HCl}$/mol^{-1} kg s^{-1}
17	1.9$\pm$0.3 (8)[a]	4.0$\pm$0.7 (6)
20[b]	2.5$\pm$0.5 (8)	4.2$\pm$0.9 (14)
25	3.5$\pm$0.6 (22)	4.8$\pm$1.0 (19)
30	4.8$\pm$0.8 (2)	6.0$\pm$1.5 (4)
35	6.0$\pm$1.0 (2)	7.3$\pm$1.5 (4)
$\Delta H^{\ddagger}$/kJ mol^{-1}	50$\pm$10	23$\pm$10
$\Delta S^{\ddagger}$/J mol^{-1} K^{-1}	30$\pm$20	$-$60$\pm$20

a) Figure in parenthesis indicates number of runs carried out at different XCl concentrations. b) Data for this are given in Fig. 2.

The reaction of copper(II) acetate dimer with perchloric acid ($Cu_2(OAc)_4+4HClO_4\rightarrow2Cu(ClO_4)_2$) was followed at 680 nm where the difference in absorbance of $Cu_2(OAc)_4$ and $Cu(ClO_4)_2$ is maximum. The reaction was too fast to be followed in the present conditions ($C_{HClO_4}=10^{-3}$ mol kg^{-1}, $C_{Cu}=10^{-4}$ mol kg^{-1}, 25 °C). Judging from the dead time of our apparatus, we presume the half life time is less than 0.5 ms. Then, provided the order is first with respect to $HClO_4$, the second-order rate constant (k^{HClO_4}) seems to be larger than 3×10^6 mol^{-1} kg s^{-1}.

Discussion

The values of activation enthalpy and entropy for k^{LiCl} and k^{HCl} are very different. We shall consider the present results in the light of the exchange of acetic acid at the axial positions of copper(II) acetate dimer. Grasdalen[15] has studied the exchange rate of acetic acid at the axial positions of the dimeric copper(II) acetate by measuring ^{1}H NMR line width and line shift in acetic acid/ethanol solutions ($k_{ex}=3.0\times10^4$ s^{-1} (25 °C), $\Delta H^{\ddagger}_{ex}=44.8$ kJ mol^{-1} and $\Delta S^{\ddagger}_{ex}=9.2$ J mol^{-1} K^{-1}). We have also made measurements of the temperature dependence of the solvent acetic acid proton line broadening and shift for solutions of copper(II) acetate dimer in acetic acid, acetic acid/chloroform and acetic acid/dichloromethane solutions. Activation parameters for acetic acid exchange were determined to be $k_{ex}=(1.2\pm0.2)\times10^4$ s^{-1}, $\Delta H^{\ddagger}_{ex}=50\pm4$ kJ mol^{-1} and $\Delta S^{\ddagger}_{ex}=2\pm5$ J mol^{-1} K^{-1} for both HOAc/$CDCl_3$ solution ([HOAc]=5.24 mol kg^{-1}) and HOAc/CD_2Cl_2 solution ([HOAc]=1.79 mol kg^{-1}).[16] The values of activation enthalpy $\Delta H^{\ddagger}_{ex}$ for the exchange of acetic acid are the same even in different diluent solvent (ethanol, chloroform and dichloromethane) and even for different concentration of acetic acid in the bulk. The fact clearly indicates that the rate-determining step for k_{ex} should be the same in these mixed solvents and also,

most probably in pure acetic acid solution.

In ethanol solution the axial ethanol molecule on the copper acetate dimer is readily replaced by acetic acid.[14] This is contrary to the prediction based on the difference in the basicity between acetic acid and ethanol: the latter is much more basic than the former. The geometry should thus favor the coordination of acetic acid by an extra hydrogen bonding with the bridging acetate.[14] This hydrogen bonding appears to account for the unexpectedly slow exchange rate of acetic acid at the copper acetate dimer without recourse to the exchange between axial and bridging ligands.[15,17]

In view of the fact that the activation enthalpy for the reaction of copper acetate dimer with lithium chloride is the same as that for the acetic acid exchange, it seems reasonable to suppose that the reaction of copper acetate dimer with lithium chloride is a dissociative interchange mechanism: in the transition state the chloride ion in LiCl[18] enters the apical coordination site vacated in the solvent dissociation. Positive activation entropy for k^{LiCl} is in harmony with this dissociative mode of activation. The coordination of chloride to copper initiates the decomposition of the dimeric structure, followed by fast reactions leading to monomeric chloro complexes.

The activation enthalpy for k^{HCl} is smaller than for k_{ex}, while the activation enthalpy for k^{LiCl} is identical with that for k_{ex} within experimental errors. The rate for the reaction of $Cu_2(OAc)_4$ with $HClO_4$ is much faster than that with HCl. At this stage it is of interest to consider the role of ionization and dissociation of reactants in the present reaction systems. Dissociation of AB is written as

$$AB \rightleftharpoons A^+B^- \rightleftharpoons A^+ + B^-$$

with the overall dissociation constant K_D:

$$K_D = \frac{[A^+]+[B^-]}{[AB]+[A^+B^-]} = \frac{K_iK_d}{1+K_i}$$

where K_i is an ionization constant and K_d is a dissociation constant.[19] Available values of K_d are $10^{-7.10}$ for LiCl,[20,21] $10^{-6.78}$ for LiOAc,[20,22] $10^{-8.55}$ for HCl,[20] $10^{-10.1}$ for H_2O,[20] and $10^{-5.87}$ for $HClO_4$.[20] K_d can be calculated by an equation of the type derived by Fuoss for ion-pair formation.[23] Therefore unknown K_d values may be predicted, at least to a correct order of magnitude. On this basis, K_d is estimated to be about 10^{-6} mol dm^{-3} for all of these 1 : 1 electrolytes. Then values of K_i for LiCl, LiOAc, HCl, and H_2O can be estimated to be $10^{-1.1}$, $10^{-0.8}$, $10^{-2.6}$, and $10^{-4.1}$, respectively. Hydrogen chloride and water are largely unionized, while lithium chloride and lithium acetate are to a considerable extent in the form of undissociated ion-pair. It should be noted that the extent of ionization is largest for perchloric acid.

It seems likely that the rate-determining step for HCl and $HClO_4$ is the proton-assisted cleavage of a copper-oxygen bond. Since perchloric acid is ionized to a much larger extent than hydrogen chloride, it may act more effectively on copper–oxygen bond than un-ionized HCl molecule. The addition of a proton from HCl to a bridged oxygen results in a polarized transition state leading to the cleavage of a copper–oxygen bond. Subsequent formation of monomeric chloro copper(II) complexes should be fast. The negative activation entropy for k^{HCl} is consistent with preequilibrium involving HCl addition: polarized transition state should favor the solvation of the activated complex.

We are grateful to the Ministry of Education, Science and Culture for financial support through Grant No. 347029. P. B. thanks Japan Society for the Promotion of Science for the award of a Fellowship, which enabled his visit and study in Japan.

References

1) a) On leave from Department of Inorganic Chemistry, Indian Association for the Cultivation of Science, Jadavpur, Calcutta-32, India; b) Laboratory of Analytical Chemistry, Faculty of Science, Niigata University, Niigata 950-21.

2) G. Charlot and B. Trémillon, "Chemical Reactions in Solvents and Melts," Pergamon Press (1969), p. 205.

3) W. Dannhauser and R. H. Cole, *J. Am. Chem. Soc.*, **74**, 6105 (1952).

4) a) E. Grunwald and E. Price, *J. Am. Chem. Soc.*, **86**, 2965, 2970 (1964); b) E. Grunwald and M. S. Puar, *ibid.*, **89**, 6842 (1967); c) M. R. Crampton and E. Grunwald, *ibid.*, **93**, 2987 (1971); d) "Dynamic Nuclear Magnetic Resonance Spectroscopy," ed by L. M. Jackman and F. A. Cotton, Academic Press, Inc., New York (1975), E. Grunwald and E. K. Ralph, "Proton transfer processes," pp. 643—647.

5) a) Ref. 2, p. 194; b) M. Hronec, R. Přikryl, and V. Veselý, *Chem. Zvesti*, **29**, 440 (1975); c) O. W. Kolling and J. L. Lambert, *Inorg. Chem.*, **3**, 202 (1964); d) K. Sawada, M. Okazaki, H. Hirota, and M. Tanaka, *ibid.*, **15**, 1976 (1976).

6) K. Sawada and M. Tanaka, *J. Inorg. Nucl. Chem.*, **35**, 2455 (1973).

7) K. Sawada, H. Ohtaki, and M. Tanaka, *J. Inorg. Nucl. Chem.*, **34**, 625, 3455 (1972).

8) D. J. Kingham and D. A. Brisbin, *Inorg. Chem.*, **9**, 2034 (1970).

9) A. W. Chester, *Inorg. Chem.*, **9**, 1743, 1746 (1970).

10) According to our preliminary experiments, the half-life times for the reactions of acetic anhydride and water in acetic acid with excess acetic anhydride (0.2 mol kg^{-1}) at 25 °C were 35 h and 5 m in the absence and in the presence of $HClO_4$ (2×10^{-2} mol kg^{-1}), respectively.

11) S. Utsumi, *Nippon Kagaku Zasshi*, **73**, 835 (1952).

12) M. Tanaka, S. Funahashi, and T. Nagamura, Paper No. 63, Abstracts of 1977 Pittsburgh Conference on Analytical Chemistry and Applied Spectroscopy.

13) A. T. A. Cheng and R. A. Howald, *Inorg. Chem.*, **7**, 2100 (1968).

14) H. Grasdalen and I. Svare, *Acta Chem. Scand.*, **25**, 1089 (1971).

15) H. Grasdalen, *Acta Chem. Scand.*, **25**, 1103 (1971).

16) S. Funahashi, T. Nishimoto, A. Hioki, and M. Tanaka, to be published elsewhere.

17) The exchange between axial and bridging ligands has been proposed as the rate-determining step in the trifluoroacetate exchange with tetrakis(μ-trifluoroacetato)dimolybdenum in acetonitrile (K. Teramoto, Y. Sasaki, K. Migita, M. Iwaizumi and K. Saito, *Bull. Chem. Soc. Jpn.*, **52**, 446 (1979)). It is unfortunate that no separate NMR signal of acetic acid attached to copper acetate dimer can be observed in any solvents studied because of the low solubility

of the dimer.

18) Grunwald *et al.* showed molecular structure of ion-pairs in acetic acid from electric dipole moments. The solvated ion-pair of LiCl is best described as monodentate attachment of *cis*-HOAc to cation: Cl^-–$Li^+\cdots O(=C(CH_3)-O-H)$ (E. Grunwald, M. R. Crampton, A. Effio, and T.-P. I, *J. Am. Chem. Soc.*, **98**, 1716 (1976).

19) I. M. Kolthoff and S. Bruckenstein, *J. Am. Chem. Soc.*, **78**, 1 (1956).
20) S. Bruckenstein and I. M. Kolthoff, *J. Am. Chem. Soc.*, **78**, 2974 (1956).
21) T. L. Smith and J. H. Elliott, *J. Am. Chem. Soc.*, **75**, 3566 (1953).
22) O. W. Kolling and H. E. Gracey, *Inorg. Chem.*, **11**, 2556 (1972).
23) R. M. Fuoss, *J. Am. Chem. Soc.*, **80**, 5059 (1958).

Dissociation of μ-Oxo-bis[oxobis(8-quinolinolato)vanadium(V)] and μ-Oxo-bis[oxobis(4-isopropyltropolonato)-vanadium(V)] in Chlorobenzene

Akio YUCHI, Hiroshi MURANAKA, Shinkichi YAMADA, and Motoharu TANAKA*

Laboratory of Analytical Chemistry, Faculty of Science, Nagoya University, Chikusa-ku, Nagoya 464

(Received November 15, 1979)

Dissociation of dimeric vanadium(V) complexes with 8-quinolinol(Hox) and 4-isopropyltropolone(Hipt), $V_2O_3(ox)_4$ and $V_2O_3(ipt)_4$, in organic solvents was studied spectrophotometrically. The equilibrium is found to be

$$V_2O_3L_4 + H_2O \rightleftarrows 2VO_2L + 2HL$$

with the following logarithmic equilibrium constants: log $K = -12.9$ for $L = ox^-$ and -12.8 for $L = ipt^-$ in chlorobenzene. VO_2L was synthesized and characterized by IR, UV, and visible spectroscopy for these ligands and also for 2-methyl-8-quinolinol.

Vanadium(V) reacts with 8-quinolinol(Hox) in weakly acidic media to form a black precipitate. This complex was thought to be $VO(OH)(ox)_2$ and has been the subject of a number of studies.[1–8]

In the preceding papers we have studied the complexation of vanadium(V) with 8-quinolinolate ion in aqueous solutions, and established the formation of the following species: $VO_3(ox)^{2-}$, $VO_3H(ox)^-$, $VO_2(ox)$, and $VO_2(ox)_2^-$.[9] Then taking these findings into consideration we have analyzed the extraction behavior of vanadium(V) with 8-quinolinol, and the extracted species from less acidic media is identified to be $V_2O_3(ox)_4$.[10] Furthermore by IR spectroscopy in solid state this complex is shown to have an oxo-bridged dimeric structure, $VO(ox)_2$–O–$VO(ox)_2$.[10]

In this paper dissociation of $V_2O_3(ox)_4$ dissolved in organic solvents are investigated spectrophotometrically. The 1:1 complex synthesized from $V_2O_3(ox)_4$ is characterized with UV, visible, and IR spectroscopy. Furthermore, 4-isopropyltropolone (Hipt) and 2-methyl-8-quinolinol(Hmeox) complexes are also studied and compared with the 8-quinolinolate complex.

Experimental

Reagent. 4-Isopropyltropolone was recrystallized twice from ligroin and dried under reduced pressure.

Chlorobenzene and nitrobenzene were shaken three times with sulfuric acid, sodium hydroxide solution, and finally with distilled water. Then the solvents were dehydrated over calcium chloride, refluxed over phosphorus pentaoxide, and distilled. The middle 80% was collected for use. The concentration of water in these solvents was about 4×10^{-3} mol dm^{-3}. Water saturated solvents were obtained by shaking these solvents with distilled water again, which contained about 2×10^{-2} mol dm^{-3} water. Solvents of different concentrations of water were obtained by mixing these two solvents.

Ammonium metavanadate, 8-quinolinol, and 2-methyl-8-quinolinol were purified as described previously.[10]

Measurement. All the experiments were carried out in a room thermostated at 25±0.5 °C. All the measurements were performed in a thermoelectric circulating bath at 25±0.1 °C.

UV, visible, and IR spectra were recorded on a UNION High Sens spectrophotometer SM-401 with a thermostated cell compartment and a JASCO infrared spectrophotometer IR-S, respectively. The absorbance was measured with a Karl Zeiss spectrophotometer model 1 PMQ II.

Thermogravimetric analysis was performed using a Shimadzu thermogravimeter TGA-30 and a Shimadzu thermal analyzer DT-30B.

The concentration of water was determined by the Karl-Fischer method with the coulometric generation of iodine. Vanadium(V) was determined spectrophotometrically with PAR.[11]

Preparation. *μ-Oxo-bis[oxobis(8-quinolinolato)vanadium(V)]*: $VO(ox)_2$–O–$VO(ox)_2$ was prepared as described previously.[3,4]

Dioxo-8-quinolinolatovanadium(V): $VO_2(ox)$ was prepared by heating the above complex in Abderhalden's dryer with sodium hydroxide as a trap for vaporized 8-quinolinol. Crude complex was recrystallized from chlorobenzene.

μ-Oxo-bis[oxobis(4-isopropyltropolonato)vanadium(V)]: $VO(ipt)_2$–O–$VO(ipt)_2$ was prepared by mixing dioxovanadium(V) perchlorate solution and 4-isopropyltropolone and adjusting pH at 3.5 by the addition of ammonia. After standing overnight the precipitate was filtered off and dried at 80 °C. Prolonged heating over 100 °C resulted in the gradual weight loss.

Dioxo-4-isopropyltropolonatovanadium(V): $VO_2(ipt)$ was prepared as in the corresponding 8-quinolinolate complex.

Hydroxooxobis(2-methyl-8-quinolinolato)vanadium(V) Dihydrate: $VO(OH)(meox)_2\cdot2H_2O$ was prepared as described previously.[5]

Dioxo-2-methyl-8-quinolinolatovanadium(V): $VO_2(meox)$ was prepared as in the case of $VO_2(ox)$.

Results

Vanadium(V)-8-quinolinolate complex, dissolved in chlorobenzene (about 10^{-4} mol dm^{-3}), shows a broad absorption maximum at around 550 nm. The spectrum of this solution changes under different conditions: the concentration of water, the concentration of excess 8-quinolinol, and the total concentration of the vanadium(V) complex.

Reaction with Water. The reaction of the complex with water results in the decrease of the absorbance in all the visible region. After the completion of this reaction (one or two hours) the absorbance was measured. Because of the limited change of water concentration (0.006—0.018 mol dm^{-3}), we were not able to obtain sufficient data for precise analysis. However, the reaction proceeds to a larger extent and more rapidly with increasing water concentration. It

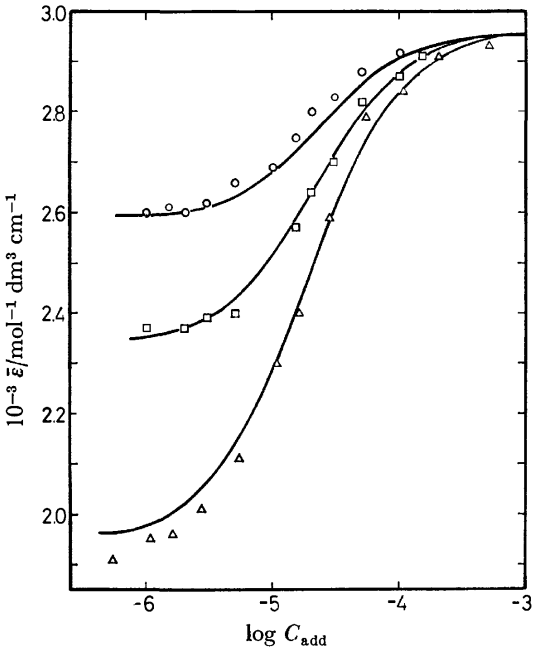

Fig. 1. Molar absorbance change at 480 nm as a function of log C_{add}.
$C_{H_2O}=1.13\times10^{-2}$ mol dm^{-3}; C_V/mol dm^{-3}: ○: 1.19×10^{-4}, □: 5.95×10^{-5}, △: 2.98×10^{-5}. The solid lines are curves calculated with the constants obtained.

should be noted that in the presence of excess amounts of 8-quinolinol we observe no reaction. The chlorobenzene solution of vanadium(V)-8-quinolinolate showed the absorption spectrum very similar to the reflection spectrum of the complex. Thus it may be concluded that we are dealing with the same compound in solution as in solid state.

Reaction with Excess 8-Quinolinol. The reaction of the complex with 8-quinolinol results in the increase of the absorbance in all the visible region. The reaction completes within a minute. The absorbance at 480 nm was then measured. Apparent molar absorbance, $\bar{\varepsilon}$, was plotted against the logarithmic concentration of added 8-quinolinol, log C_{add} (Fig. 1).

In the absence of the added 8-quinolinol, $\bar{\varepsilon}$ is smaller for lower total concentration of the complex and/or for higher water concentration. $\bar{\varepsilon}$ increases with increasing concentration of 8-quinolinol, and it becomes constant beyond 10^{-3} mol dm^{-3} regardless the conditions. These facts point to the presence of only one species, $V_2O_3(ox)_4$, under these conditions.

Dependence of the Absorbance on the Total Concentration of the Complex. Dependence of $\bar{\varepsilon}$ on the total concentration of the vanadium(V) complex, C_V, in the absence of excess 8-quinolinol and at constant amounts of water was studied using quartz cells with light path lengths of 10 and 50 mm (Fig. 2) Upon dilution of the complex solution Beer's law is not obeyed, and the apparent molar absorbance decreases. The limiting values of $\bar{\varepsilon}$ at lower ligand concentration in Fig. 1 are well accommodated in the plot given in Fig. 2.

On the other hand in the presence of sufficient amount of 8-quinolinol, as seen from Fig. 2, $\bar{\varepsilon}$ values are constant for different complex concentrations.

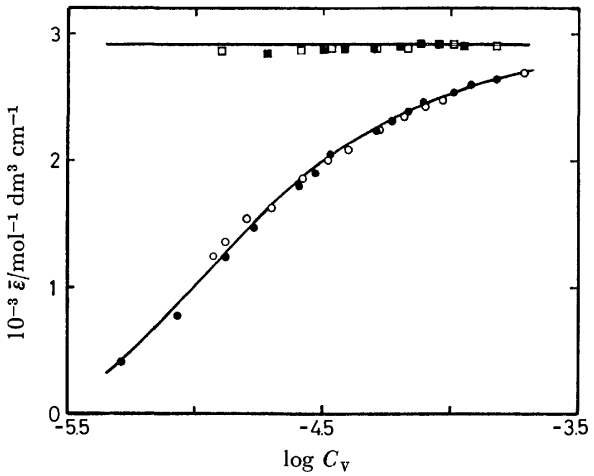

Fig. 2. Molar absorbance change at 480 nm as a function of log C_V.
C_{H_2O}/mol dm^{-3}: ○, □: 1.00×10^{-2}, ●, ■: 1.13×10^{-2}, C_{add}/mol dm^{-3}: ○, ●: 0, □, ■: 2.60×10^{-3}. The solid lines are curves calculated with the constants obtained.

Treatment of Equilibria. The reaction of $V_2O_3(ox)_4$ with water to its lower complex is expressed by Eq. 1 (see below about the composition of the lower complex).

$$V_2O_3(ox)_4 + H_2O \overset{K}{\rightleftharpoons} 2VO_2(ox) + 2Hox \qquad (1)$$

The concentration of water being in large excess compared with the other species and kept constant, the conditional dissociation constant, K', is given by Eq. 2:

$$K' = K[H_2O] = \frac{[VO_2(ox)]^2[Hox]^2}{[V_2O_3(ox)_4]}. \qquad (2)$$

The apparent molar absorbance at 480 nm is expressed by Eq. 3:

$$\bar{\varepsilon} = \frac{\varepsilon_{24}[V_2O_3(ox)_4] + \varepsilon_{11}[VO_2(ox)]}{2[V_2O_3(ox)_4]+[VO_2(ox)]}, \qquad (3)$$

where ε_{11} and ε_{24} are the molar absorbances of $VO_2(ox)$ and $V_2O_3(ox)_4$, respectively. The value of ε_{11} and K' were refined to give minimum error square sum of data, $U=\Sigma(\bar{\varepsilon}_{obsd}-\bar{\varepsilon}_{cald})^2$, with an electronic computer. The value of ε_{11} approached to zero, which is consistent with the spectrum of $VO_2(ox)$.

Then the obtained logarithmic conditional dissociation constants under various conditions were plotted against

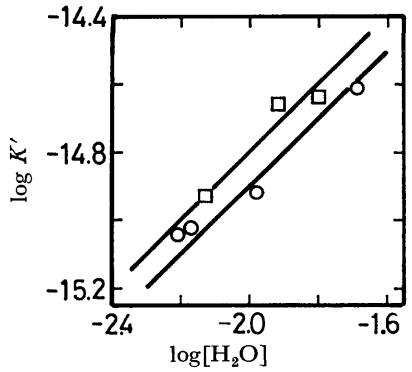

Fig. 3. The plot of log K' against log[H_2O].
○: 8-Quinolinolate complex, □: 4-isopropyltropolonate complex.

the logarithmic concentration of water (Fig. 3). The plot falls along a straight line with a slope of unity. This confirms the validity of Eq. 1. From the intercept the dissociation constant is obtained:

$$V_2O_3(ox)_4 + H_2O \rightleftarrows 2VO_2(ox) + 2Hox$$
$$: \log K = -12.9.$$

The possibility for the formation of the lower complex, $V_2O_4(ox)_2$, given by Eq. 4 was also examined. The assumption of this species lead to a systematic deviation from the experimental data.

$$V_2O_3(ox)_4 + H_2O \rightleftarrows V_2O_4(ox)_2 + 2Hox \quad (4)$$

Dissociation of 4-Isopropyltropolonate Complex ($V_2O_3(ipt)_4$). Similar measurements were performed on 4-isopropyltropolonate complex under various conditions. All the data were analyzed by the same treatment as in the case of 8-quinolinolate complex to give K' and ε_{11}. The value of ε_{11} is close to zero, which is also consistent with the spectrum of VO_2(ipt) (see below). The plot of log K' against log[H_2O] falls along a straight line with a slope of unity (Fig. 3). From the intercept the following dissociation constant is obtained:

$$V_2O_3(ipt)_4 + H_2O \rightleftarrows 2VO_2(ipt) + 2Hipt$$
$$: \log K = -12.8.$$

Properties of Crystals. Thermogravimetry and Visible Spectroscopy: For the 8-quinolinolate complex, a weight loss was observed about 240 °C as reported by Borrel and Pâris.[1] (Fig. 4a) But the form of the thermogram depends upon the rate of heating, and no distinct plateau was observed at 240 °C at 0.5 °C min^{-1}. Thus no definite species can be found at this temperature. On the other hand, over 500 °C it approached to a constant weight corresponding to VO_2(ox). At 240 °C we have a mixture of the species VO_2(ox) with free 8-quinolinol, which gives a characteristic yellow solution just after dissolution in chlorobenzene. This solution, having an absorption maximum at 398 nm and no absorption at longer wavelength than 450 nm, returned to black in a day. The reaction was accelerated by the addition of 8-quinolinol. Thus the complex heated at 240 °C is the molten mixture of VO_2(ox) and Hox, and vaporization of 8-quinolinol occurs at higher temperature.

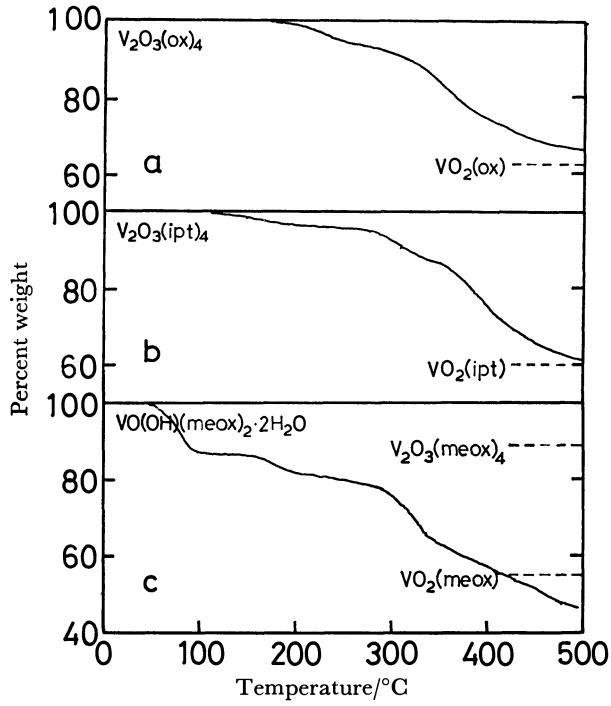

Fig. 4. Thermograms of vanadium (V) complexes.
a: 8-Quinolinolate complex, b: 4-isopropyltropolonate complex, c: 2-methyl-8-quinolinolinolate complex.

For the 4-isopropyltropolonate complex, the thermogram approached to a constant weight corresponding to VO_2(ipt) beyond 500 °C (Fig. 4b). The complex dried at 240 °C, when dissolved in chlorobenzene, showed an absorption maximum at 366 nm and no absorption at longer wavelength than 450 nm, and also returned to black in a day.

For the 2-methyl-8-quinolinolate complex, a weight loss corresponding to 2.5 water molecules from VO(OH)(meox)$_2 \cdot 2H_2O$ to $V_2O_3(meox)_4$ was observed below 100 °C.[10,12] Further heating also dissociates the complex into VO_2(meox) and Hmeox (Fig. 4c), which is overlapped with oxidative decomposition of the ligand.

Table 1. Summary of the properties of vanadium(V) complexes

Complex	λ_{max}[a] / nm	ν(V=O)[b] / cm^{-1}	ν(V–O–V)[c] / cm^{-1}
8-Quinolinolate			
$V_2O_3(ox)_4$	550	950	715
VO_2(ox)	398	990[e]	—
4-Isopropyltropolonate			
$V_2O_3(ipt)_4$	530	950	715
VO_2(ipt)	366	990[e]	—
2-Methyl-8-quinolinolate			
VO(OH)(meox)$_2 \cdot 2H_2O$	340	925	—
$V_2O_3(meox)_4$	—[d]	960	715
VO_2(meox)	388	980[e]	—

a) λ_{max} is the wavelength of the absorption maximum in the UV and visible spectrum. b, c) ν(V=O) and ν(V–O–V) are the wavenumbers of the IR spectrum of V=O and V–O–V, respectively. d) The spectrum was unmeasurable in solution because of rapid change to the monomeric complex. e) The absorption was very broad and unsymmetric.

Infrared Spectra: IR bands of ν(V=O) and ν_{asym} (V–O–V) of the complexes are summarized in Table 1. All the dimeric compounds have ν(V=O) near 950 cm^{-1} in addition to ν_{asym}(V–O–V) at 715 cm^{-1} as in oxo-bridged dimeric Mo(V) complexes.[13]

The lower complexes are expected to have tetrahedral configuration. As the bonds between vanadium and oxo groups are much stronger than those of vanadium and organic ligands, the O–V–O skelton may be approximated as bent triatomic system and expected to have two vibrational mode in metal-oxo double bond region. But the symmetric and antisymmetric modes in bent triatomic system having similar wavenumber in many cases, the broad bands near 990 cm^{-1} seems to consist of these two bands and should not be

compared with those of dimeric compounds. The absence of a band near 715 cm^{-1} excludes the possibility of a dioxo-bridged dimeric structure, $VO(ox)\langle{}^{O}_{O}\rangle VO(ox)$ for the lower complex.

Discussion

The visible spectrum of vanadium(V)–8-quinolinolate complex has been reported by many authors. The molar absorbance at 480 nm calculated from the literature are listed in Table 2. In the presence of excess amounts of 8-quinolinol the value of $\bar{\varepsilon}$ of extracted species or dissolved complex is well consistent with ours. In the absence of excess ligand the molar absorbance varies with experimental conditions, as evident from our findings.

Table 2. The molar absorbance of vanadium(V)-8-quinolinolate complex in the literature

$\bar{\varepsilon}$ / mol^{-1} dm^3 cm^{-1}	C_v / mol dm^{-3}	C_{add} / mol dm^{-3}	Remarks	Ref.
2450—2500	1.96×10^{-4}	0	dissolved	3
2250—2500	—	0	dissolved	5
2950	2.0×10^{-4}	6.76×10^{-3}	dissolved	14
2640	1.1×10^{-4}	0	extracted	15
2910	1.1×10^{-4}	5.01×10^{-3}	extracted	15
3000	0.8×10^{-4}	7.94×10^{-3}	extracted	16

The dissociation constants of the two complexes, $V_2O_3(ox)_4$ and $V_2O_3(ipt)_4$, differ little: the difference is not large enough to discuss the effect of donor atoms: N and O for 8-quinolinolate, and O and O for 4-isopropyltropolonate. With this constant it is well understood that no lower complex was found in the extraction of vanadium(V) with 8-quinolinol.[10]

This type of ligand dissociation is anticipated to be promoted by heating. Actually the nitrobenzene solution of $V_2O_3(ox)_4$ changes to yellow when heated and it returns to black reversibly in cold.[17] The products of this reaction should not be identified as V_2O_5 and Hox but as $VO_2(ox)$ and Hox. Heating of solid complex also promote dissociation and, when the dissociated ligand is removed by NaOH, $VO_2(ox)$ is obtained.

We have shown the presence of $VO_2(ox)$ in aqueous solution, and proposed the structure of $VO(OH)_2(ox)(H_2O)$ from the comparison of pK_a between vanadic acid and complexes.[9] Accordingly the equilibria given by Eq. 5 is shifted completely to the right in aqueous solutions, while it is much favored to the left in organic solvents.

$$VO_2(ox) + 2H_2O \rightleftarrows VO(OH)_2(ox)(H_2O) \quad (5)$$

The 1 : 1 vanadium(V) complexes with β-diketonates have been reported.[18,19] They were identified as $VOL\langle{}^{O}_{O}\rangle VOL$ or VO_2L (L: β-diketonate) depending upon the presence or absence of infrared absorption near 715 cm^{-1} ascribed to the oxo bridging.

The visible spectrum of vanadium(V)-4-isopropyltropolonate complex has been reported from an analytical point of view by a few authors as $VO(OH)(ipt)_2$.[20–22] The spectrum of extracted species in the presence of excess amounts of 4-isopropyltropolone has an absorption maximum at 520 nm,[22] which is consistent with ours, whereas that of extracted species from strongly acidic media (6.6 mol dm^{-3} HCl) has an absorption maximum at 590 nm.[21] This blue shift is ascribed to the protonation of the complex, which has been found in the extraction of the 8-quinolinolate complexes.[10]

In the extraction of vanadium(V) with 4-isopropyltropolone, the extracted species was identified to be $VO(OH)(ipt)_2$.[23] The characteristics of UV, visible, and IR spectra,[10] however, point to the dimeric structure, $V_2O_3(ipt)_4$, as in the case of the 8-quinolinolate complex.

We gratefully acknowledge the Grand-in-Aid from Ministry of Education, Science and Culture (No. 347029).

References

1) M. Borrel and R. Pâris, *Anal. Chim. Acta*, **4**, 267 (1950).
2) H. J. Bielig and E. Bayer, *Ann. Chem.*, **584**, 96 (1953).
3) A. J. Blair and D. A. Pantony, *Anal. Chim. Acta*, **13**, 1 (1955).
4) A. J. Blair, D. A. Pantony, and G. J. Minkoff, *J. Inorg. Nucl. Chem.*, **5**, 316 (1958).
5) H. Nakamura, Y. Shimura, and R. Tsuchida, *Bull. Chem. Soc. Jpn.*, **34**, 1143 (1961).
6) R. P. Henry, P. C. H. Mitchell, and J. E. Prue, *Inorg. Chim. Acta*, **7**, 150 (1973).
7) L. W. Amos and D. T. Sawyer, *Inorg. Chem.*, **13**, 78 (1974).
8) T. L. Riechel and D. T. Sawyer, *Inorg. Chem.*, **14**, 1869 (1975).
9) A. Yuchi, S. Yamada, and M. Tanaka, *Bull. Chem. Soc. Jpn.*, **52**, 1643 (1979).
10) A. Yuchi, S. Yamada, and M. Tanaka, *Anal. Chim. Acta*, **115**, 301 (1980).
11) Y. Shijo and T. Takeuchi, *Bunseki Kagaku*, **14**, 115 (1965).
12) M. Borrel and R. Pâris, *Anal. Chim. Acta*, **5**, 573 (1951).
13) E. I. Stiefel, "Progress in Inorganic Chemistry," John Wiley and Sons, Inc. (1977), Vol. 22.
14) M. Tanaka, *Talanta*, **5**, 162 (1960).
15) M. Tanaka and I. Kojima, *Anal. Chim. Acta*, **36**, 522 (1966).
16) V. P. R. Rao and Y. Anjaneyulu, *J. Inorg. Nucl. Chem.*, **33**, 3567 (1971).
17) M. Tanaka and T. Katsurai, *Naturwissenschaften*, **48**, 48 (1961).
18) A. Doadrio and A. G. Carro, *Anales Real Soc. Espan. Fis. Quim. Ser. B*, **60**, 495 (1964).
19) A. Doadrio and C. Molina, *Anales Real Soc. Espan. Fis. Quim. Ser. B*, **64**, 253 (1970).
20) M. Tanaka and I. Kojima, *Anal. Chim. Acta*, **41**, 75 (1968).
21) G. H. Rizvi and R. P. Singh, *Talanta*, **19**, 1198 (1972).
22) I. Kojima and Y. Miwa, *Anal. Chim. Acta*, **83**, 329 (1976).
23) O. Menis, B. E. McClellan, and D. S. Bright, *Anal. Chem.*, **43**, 431 (1971).

Selective Ester-exchange Reactions of Dibenzyl-aspartate and -glutamate in the Coordination Sphere of Copper(II) Ion

Yasuo NAKAO,*,† Masaaki DEMICHI, and Akitsugu NAKAHARA

Institute of Chemistry, College of General Education, Osaka University, Toyonaka, Osaka 560

†*Chemical Laboratory, Faculty of Education, Okayama University, Okayama 700*

(Received September 29, 1979)

Copper(II) complexes of the Schiff bases derived from salicylaldehyde and dibenzyl aspartate or glutamate have been prepared for the first time. Upon refluxing the solution of these complexes in methanol for 30 min, bis(α-methyl β-benzyl *N*-salicylideneaspartato)copper(II) and bis(α-methyl γ-benzyl *N*-salicylideneglutamato)-copper(II) were obtained. The mechanism of these selective ester-exchange reactions in the metal-coordination sphere has been discussed. Several Schiff bases were obtained and characterized.

Many reactions of amino acids, such as transamination, racemization, substitution of α-hydrogen and decarboxylation, proceed *via* formation of metal Schiff base chelates as intermediates, most of them being useful as models for pyridoxal-dependent enzymatic reactions.[1,2]

A number of studies have been carried out on the ligand reactivities of the metal complexes of Schiff bases derived from amino acid esters and carbonyl compounds. The ester-exchange reaction was reported by Pfeiffer *et al.*,[3] extended by other investigators.[4—7] However, most of the studies have been confined to the reactions of those containing simple amino acid esters. Nakao and Nakahara studied the selective ester-exchange reaction in copper(II) chelate of the Schiff base composed of salicylaldehyde and dibenzyl DL-aspartate.[8] In this paper we report on the mechanism of selective ester-exchange reactions occurring in the coordination sphere of copper(II) ion, on the basis of our recent study on the other copper(II) chelates.

Experimental

Benzyl Glycinate Benzenesulfonate was prepared by the method of Cipera and Nicholls.[9]

p-*Toluenesulfonates of Benzyl β-Alaninate and γ-Aminobutyrate* were prepared according to the reported method.[10]

Dibenzyl L- *and* DL-*Aspartate Benzenesulfonate* were obtained by a similar procedure to that for benzyl glycinate benzenesulfonate.[9] Melting points and analytical data of these compounds recrystallized from ethanol are as follows: L-Asp(OBzl)$_2$·$C_6H_5SO_3H$: mp 113—114 °C. Found: C, 60.99; H, 5.41; N, 3.01%. DL-Asp(OBzl)$_2$·$C_6H_5SO_3H$: mp 134—134.5 °C. Found: C, 60.81; H, 5.47; N, 3.05%. Calcd for $C_{24}H_{25}O_7NS$: C, 61.12; H, 5.35; N, 2.97%

Dibenzyl L- *and* DL-*Glutamate Benzenesulfonate* were prepared according to the reported method.[10]

Dibenzyl DL-*Glutamate Hydrochloride* was obtained from the corresponding benzenesulfonate described above.[11]

α-Methyl-β-benzyl L- *and* DL-*Aspartate Hydrochloride.* β-Benzyl L- and DL-Aspartate were prepared by the procedure reported by Izumiya *et al.*[12] The L-compound was identified by a comparison of melting point. Melting point and analytical data of β-benzyl DL-aspartate recrystallized from hot water containing a small volume of triethylamine are as follows: mp 211—214 °C (dec.). Found: C, 59.25; H, 5.89; N, 6.30%. Calcd for $C_{11}H_{13}O_4N$: C, 59.18; H, 5.87; N, 6.28%.

β-Benzyl N-*Benzyloxycarbonyl*-L- *and* -DL-*aspartate*: The L-compound was obtained by the method reported by Ariyoshi *et al.*[13] from β-benzyl L-aspartate. The DL-compound was prepared by the same method, being recrystallized from ethyl acetate-petroleum ether. Mp 99—101 °C. Found: C, 63.60; H, 5.39; N, 3.95%. Calcd for $C_{19}H_{19}O_6N$: C, 63.86; H, 5.36; N, 3.92%.

β-Benzyl-N-*carboxy*-L- *and* -DL-*aspartate Anhydride*: The compounds were prepared from β-benzyl *N*-benzyloxycarbonyl-L- and -DL-aspartate by the method of Berger and Katchalski.[14] The L-compound was identified by comparing the melting point with that reported.[14] Melting point and analytical data of DL-compound washed with petroleum ether are as follows: mp 150—153 °C. Found: C, 57.70; H, 4.54; N, 5.66%. Calcd for $C_{12}H_{11}O_5N$: C, 57.82; H, 4.46; N, 5.62%.

α-Methyl β-benzyl L- and DL-Aspartate Hydrochloride were prepared according to the method of Ariyoshi *et al.*[13] DL-Asp(α-OMe)(β-OBzl)·HCl: mp 120—121 °C. Found: C, 52.72; H, 5.97; N, 5.13%. Calcd for $C_{12}H_{16}O_4NCl$: C, 52.66; H, 5.90; N, 5.12%.

α-Methyl-γ-benzyl L-*Glutamate Hydrochloride.* γ-Benzyl L-Glutamate,[15] γ-Benzyl *N*-Benzyloxycarbonyl-L-glutamate[16] and γ-Benzyl *N*-carboxy-L-glutamate Anhydride[16] were prepared according to the reported method.

α-Methyl γ-benzyl L-Glutamate Hydrochloride was prepared by the same method as that for the corresponding α-methyl β-benzyl L-aspartate hydrochloride,[13] using γ-benzyl-*N*-carboxy-L-glutamate anhydride instead of β-benzyl-*N*-carboxy-L-aspartate anhydride. Mp 129—131 °C. Found: C, 53.81; H, 6.25; N, 5.03%. Calcd for $C_{13}H_{18}O_4NCl$: C, 54.26; H, 6.32; N, 4.87%.

Copper(II) Complex of the Schiff Base Derived from Salicylaldehyde and Benzyl Glycinate, [*Cu(Sal=GlyOBzl)*$_2$], ***1a***. A mixture of 6.4 g (0.02 mol) of benzyl glycinate benzenesulfonate and 3.1 g (0.01 mol) of bis (salicylaldehydato)copper (II) was dissolved in 40 cm^3 of water. The reaction mixture was then stirred at 40 °C for 2 h. After it had been cooled, a brownish green crystal was filtered, and washed several times by water, yield 60%. IR(KBr) 1735 cm^{-1} (ester C=O). Found: C, 63.44; H, 5.06; N, 4.69%. Calcd for [Cu($C_{32}H_{28}O_6N_2$)]: C, 64.04; H, 4.71; N, 4.67%.

Copper (II) Complexes of the Schiff Bases Derived from Salicylaldehyde and Benzyl β-Alaninate and γ-Aminobutyrate, [*Cu(Sal=β-AlaOBzl)*$_2$], ***1b*** *and* [*Cu(Sal=γ-N-BuOBzl)*$_2$], ***1c***. These complexes were prepared in a similar manner using benzyl β-alaninate *p*-toluenesulfonate and benzyl γ-aminobutyrate *p*-toluenesulfonate, respectively. [Cu(Sal=β-AlaOBzl)$_2$]: yield 60%. IR (KBr) 1730 cm^{-1} (ester C=O). Found: C, 64.80; H, 5.47; N, 4.29%. Calcd for [Cu($C_{34}H_{32}O_6N_2$)]: C, 65.00; H, 5.14; N, 4.46%. [Cu(Sal=γ-*N*-BuOBzl)$_2$]: yield 43%. IR (KBr) 1725 cm^{-1} (ester C=O). Found: C, 64.58; H, 5.31; N, 4.00%. Calcd for [Cu($C_{36}H_{36}O_6N_2$)]·1/2H_2O: C, 64.99;

H, 5.62; N, 4.21%.

The Reactions of Copper(II) Complexes ***1a, 1b, and 1c*** *with Methanol.* The reaction mixture of 1 g of the complex **1a**, **1b**, or **1c** and methanol (200 cm³)–chloroform (100 cm³) was heated under reflux for 30 min. After it had been filtered, the filtrate was cooled to give brownish green crystals. They were collected by filtration, the same additional product being obtained by removing the solvent. The products were identified as the copper(II) chelates of the Schiff bases derived from salicylaldehyde and methyl glycinate, β-alaninate, and γ-aminobutyrate, respectively, from the results of elemental analyses. [Cu(Sal=GlyOMe)$_2$]: 92% yield. IR(KBr.) 1750 cm^{-1} (ester C=O). Found: C, 53.20; H, 4.76;N, 6.14%. Calcd for [Cu($C_{20}H_{20}O_6N_2$)]: C, 53.62; H, 4.51; N, 6.25%. [Cu(Sal=β-AlaOMe)$_2$]: 66% yield. IR(KBr) 1720 cm^{-1} (ester C=O). Found: C, 55.16; H, 5.33; N, 5.95%. Calcd for [Cu($C_{22}H_{24}O_6N_2$)]: C, 55.50; H, 5.09; N, 5.88%. [Cu(Sal=γ-*N*-BuOMe)$_2$]: 60% yield. IR(KBr) 1730 cm^{-1} (ester C=O). Found: C, 55.45; H, 5.78; N, 5.57%. Calcd for [Cu($C_{24}H_{28}O_6N_2$)]·H_2O: C, 55.21; H, 5.80; N, 5.37%.

Copper(II) Complexes of Schiff Bases Derived from Salicylaldehyde and Dibenzyl L- *and* DL-*Aspartates,* [*Cu(Sal=*L- *or* DL-*Asp(OBzl)$_2$)$_2$*], ***3a.*** To a mixture of 5.6 g (0.012 mol) of dibenzyl L- or DL-aspartate benzenesulfonate and 60 cm³ of water was added 1.9 g (0.006 mol) of bis(salicylaldehydato)-copper (II). The reaction mixture was stirred at 40 °C for 3 h, and allowed to stand for a few hours at room temperature. The precipitate was collected by filtration, and washed with water and ethanol. [Cu(Sal=L-Asp(OBzl)$_2$)$_2$]: 40% yield. Mp 130.5—132 °C. IR(KBr) 1735 cm^{-1} (ester C=O). Found: C, 67.04; H, 5.11; N, 3.30%. Calcd for [Cu($C_{50}H_{44}$-$O_{10}N_2$)]: C, 66.98; H, 4.96; N, 3.13%. [Cu(Sal=DL-Asp-(OBzl)$_2$)$_2$]: 96% yield. Mp 138—140 °C. IR(KBr) 1735 cm^{-1} (ester C=O). Found: C, 67.30; H, 5.12; N, 3.17%. Calcd for [Cu($C_{50}H_{44}O_{10}N_2$)]: C, 66.98; H, 4.96; N, 3.13%.

Copper(II) Complexes of Schiff Bases Derived from Salicylaldehyde and Dibenzyl L- *and* DL-*Glutamate,* [*Cu(Sal=*L- *or* DL-*Glu(OBzl)$_2$)$_2$*], ***3b.*** The complexes were prepared by a similar procedure to that for **3a** using dibenzyl L-glutamate benzenesulfonate and dibenzyl DL-glutamate hydrochloride. [Cu(Sal=L-Glu(OBzl)$_2$)$_2$]: 82% yield. Mp 105—107 °C. IR (KBr) 1740, 1710 cm^{-1} (ester C=O). Found: C, 66.70; H, 5.29; N, 3.03%. Calcd for [Cu($C_{52}H_{48}O_{10}N_2$)]·1/2H_2O: C, 66.90; H, 5.30; N, 3.00%. [Cu(Sal=DL-Glu(OBzl)$_2$)$_2$]: 86% yield. Mp 98—100 °C. IR(KBr) 1745, 1710 cm^{-1} (ester C=O). Found: C, 67.70; H, 5.34; N, 2.75%. Calcd for [Cu($C_{52}H_{48}O_{10}N_2$)]: C, 67.55; H, 5.24; N, 3.03%.

Reactions of Copper(II) Complexes ***3a*** *and* ***3b*** *with Methanol.* Complex **3a** (1 g) was refluxed in a mixture of methanol (200 cm³)–chloroform (30—50 cm³) for 30 min, and then filtered. The filtrate was cooled to give brownish green needles. After removing the solvent from the mother liquor, the same prcduct was also isolated. A similar treatment was carried out for **3b**. The reaction prouduct from [Cu(Sal=L-Asp-(OBzl)$_2$)$_2$] and CH_3OH: 30% yield. Mp 134—135.5 °C. IR (KBr) 1740 cm^{-1} (ester C=O). Found: C, 60.83; H, 4.88; N, 3.91%. Calcd for [Cu($C_{38}H_{36}O_{10}N_2$)]: C, 61.32; H, 4.89; N, 3.76%. The reaction product from [Cu(Sal=DL-Asp(OBzl)$_2$)$_2$] and CH_3OH: 63% yield. Mp 130—131 °C. IR (KBr) 1740 cm^{-1} (ester C=O). Found: C, 61.00; H, 5.03; N, 3.98%. Calcd for [Cu($C_{38}H_{36}O_{10}N_2$)]: C, 61.32; H, 4.89; N, 3.76%. The reaction product from [Cu(Sal=L-Glu(OBzl)$_2$)$_2$] and CH_3OH: 40% yield. IR(KBr) 1730, 1710 cm^{-1} (ester C=O). Mp 114—115 °C. Found: C, 61.88; H, 5.41; N, 3.91%. Calcd for [Cu($C_{40}H_{40}O_{10}N_2$)]: C, 62.20; H, 5.23; N, 3.63%. The reaction product from [Cu(Sal=DL-Glu(OBzl)$_2$)$_2$] and CH_3OH: 52% yield. IR (KBr) 1740, 1715 cm^{-1} (ester C=O). Mp 102—104 °C. Found: C, 61.72; H, 5.56; N, 3.70%. Calcd for [Cu($C_{40}H_{40}$-$O_{10}N_2$)]: C, 62.20; H, 5.23; N, 3.63%.

Copper(II) Complexes of the Schiff Bases Derived from Salicylaldehyde and α-Methyl β-benzyl L- *and* DL-*Aspartate,* [*Cu(Sal=*L- *or* DL-*Asp(α-OMe)(β-OBzl))$_2$*], ***4a.*** A mixture of 0.81 g (0.0030 mol) of α-methyl β-benzyl L- or DL-aspartate hydrochloride and 0.45 g (0.0015 mol) of bis(salicyladehydato)copper (II) was dissolved in 10 cm³ of water. The mixture was stirred at 30—40 °C for 3 h, and then cooled. A brownish green crystalline product was filtered and washed several times with water containing a small amount of ethanol. [Cu(Sal=L-Asp(α-OMe) (β-OBzl))$_2$]: 43% yield. Mp 132—132.5 °C. IR(KBr) 1740 cm^{-1} (ester C=O). Found: C, 61.16; H, 4.89; N, 3.82%. Calcd for [Cu($C_{38}H_{36}O_{10}N_2$)]: C, 61.32; H, 4.89; N, 3.76%. [Cu(Sal=DL-Asp(α-OMe) (β-OBzl))$_2$]: 56% yield. Mp 131—133 °C. IR(KBr) 1740 cm^{-1} (ester C=O). Found: C, 61.41; H, 4.94; N, 3.95%. Calcd for [Cu($C_{38}H_{36}O_{10}N_2$)]: C, 61.32; H, 4.89; N, 3.76%.

Copper(II) Complex of the Schiff Base Derived from Salicylaldehyde and α-Methyl γ-benzyl L-*Glutamate,* [*Cu(Sal=*L-*Glu(α-OMe) (γ-OBzl))$_2$*], ***4b*** was prepared in the same way as that for chelate **4a**. 32% yield. IR(KBr) 1740, 1710 cm^{-1} (ester C=O). Found: C, 60.61; H, 5.27; N, 3.76%. Calcd for [Cu($C_{40}H_{40}O_{10}N_2$)]·H_2O: C, 60.78; H, 5.37; N, 3.55%.

Isolation of Schiff Bases ***5a—d*** *from Various Copper (II) Chelates.* To a solution of 0.5 g of each copper(II) chelate in 20 cm³ of chloroform was added 10% aqueous solution of disodium ethylenediaminetetracetate (20 cm³). The mixture was stirred at room temperature for several hours (Scheme 3). After the chloroform fraction had been dried over anhydrous magnesium sulfate, the filtrate was evaporated to dryness. Characterization of the yellow crystals or oily products obtained is given in Table 1. The results of elemental analysis are as follows. SalH=DL-Asp(OBzl)$_2$: Found: C, 72.19; H, 5.26; N, 3.50%. Calcd for $C_{25}H_{23}O_5N_2$: C, 71.92; H, 5.56; N, 3.36%. SalH=L-Asp(OBzl)$_2$: Found: C, 72.06; H, 5.26; N, 3.50%. Calcd for $C_{25}H_{23}O_5N$: C, 71.92; H, 5.56; N, 3.36%. SalH=DL-Asp(α-OMe) (β-OBzl): Found: C, 66.21; H, 5.69; N, 4.09%. Calcd for $C_{19}H_{19}O_5N$: C, 66.65; H, 5.89; N, 4.09%. SalH=L-Glu(OBzl)$_2$: Found: C, 72.37; H, 5.82; N, 3.23%. Calcd for $C_{26}H_{25}O_5N$: C, 72.37; H, 5.84; N, 3.25%.

*Direct Synthesis of SalH=*DL-*Asp(OBzl)$_2$.* The Schiff base was also synthesized from salicylaldehyde and dibenzyl DL-aspartate benzenesulfonate. The dibenzyl DL-aspartate[11] prepared from 4.7 g (0.01 mol) of dibenzyl DL-aspartate benzenesulfonate was dissolved in 50 cm³ of chloroform. To the mixture was added 1.2 g (0.01 mol) of salicylaldehyde and refluxed for 2 h. After it had been filtered, the filtrate was evaporated to dryness. The dry residue obtained as a syrup was rubbed with petroleum ether, and the resulting crystalline suspension filtered. The other Schiff bases were obtained by the same method.

*Reduction of SalH=*L-*Asp(OBzl)$_2$.* Sodium cyanohydroborate was added to a cold solution of SalH=L-Asp(OBzl)$_2$ (1 g) in methanol (200 cm³) until the yellow color of the solution disappeared. The reaction mixture was evaporated to dryness *in vacuo*, and the residue was washed several times with water and then extracted with chloroform. After the chloroform fraction had been dried over anhydrous magnesium sulfate, the solvent was removed from the filtrate under reduced pressure to give the ligand **11**, as a pale yellow oily product. IR(Nujor) 3300 cm^{-1} (N–H) and 1740 cm^{-1} (ester C=O). NMR($CDCl_3$) δ 2.74 (2H, d, –CH-C$\underline{H}_2$), 3.69 (1H, t, -C$\underline{H}$–CH_2), 4.61 (2H, s, -C$\underline{H}_2$–NH–), 5.03 and 5.10 (2H, s, Ar–C$\underline{H}_2$), and 7.26—6.59 ppm (14H, m, Ar-$\underline{H}$).

This substance was used for subsequent reaction without further purification.

Copper(II) Chelate **12**. To a solution of 0.8 g (0.002 mol) of **11** in 20 cm³ of chloroform was added 0.13 g (0.001 mol) of anhydrous copper (II) chloride. The mixture was stirred at room temperature for 3 h. After it had been filtered, the filtrate was evaporated to give a greenish oily product, which was washed with petroleum ether. IR (Nujor) 3300 cm^{-1} (N–H) and 1735 cm^{-1} (ester C=O).

Reaction of Copper(II) Complex **12** *with Methanol*. A mixture of complex **12** (0.5 g) and methanol (150 cm³) was heated under reflux for 30 min. After it had been filtered, a green-brown oily product, **13**, was obtained upon removal of methanol from the filtrate. IR(Nujor) 3300 cm^{-1} (N–H) and 1735 cm^{-1} (ester C=O).

Isolation of **14** *from Copper(II) Complex* **13**. Isolation was carried out in the same way as that for **3a**—**b** or **4a**—**b** (Scheme 3). Compound **14** was obtained as an oily product. IR (Nujor) 3300 cm^{-1} (N–H) and 1740 cm^{-1} (ester C=O). NMR ($CDCl_3$) δ 2.82 (2H, d, –CH–C$\underline{H}_2$), 3.68—3.79 (4H, m, –C$\underline{H}$–C$\underline{H}_2$ and –COOC$\underline{H}_3$), 4.71 (2H, s, –C$\underline{H}_2$–NH–), 5.18 (2H, s, –COOC$\underline{H}_2$–Ar), and 7.42—6.82 ppm (9H, m, Ar–$\underline{H}$).

*Reaction of SalH=*L*-Asp(OBzl)₂,* **5a**, *with Methanol in the Presence of* $CuCl_2$. A typical reaction is as follows: To a solution of **5a** (0.8 g, 0.002 mol) in 200 cm³ of methanol was added 0.0027 g (0.00002 mol) of anhydrous copper (II) chloride. The reaction mixture was heated under reflux for 30 min. After it had been filtered, the filtrate was evaporated to dryness. A greenish oily product obtained was treated by the same procedure as for the isolation of **14** from **13**. Evaluation of the extent of the ester-exchange reaction occurred in the system was carried out on the basis of each peak area for –COOC$\underline{H}_3$, –COOC$\underline{H}_2$–Ar and –CH=N in PMR spectrum.

Measurements. Melting points were determined on a micro melting point apparatus and are uncorrected. IR spectra were recorded with a Hitachi 215 grating infrared spectrophotometer with KBr disk and Nujor mull, UV absorption spectra with a Union Giken SM-401 high sensitivity recording spectrophotometer, and PMR spectra with a JEOL JNM-MH-100 spectrometer with TMS reference. Thin layer chromatography (TLC) was carried out on silica gel (Merck Silica Gel 60 F_{254}). Chloroform was used as a solvent in all cases.

Results and Discussion

Ester-exchange Reactions in the Copper(II) Chelates of the Schiff Bases derived from Salicylaldehyde and Benzyl Glycinate, β-Alaninate or γ-Aminobutyrate. The copper(II) chelates of benzyl *N*-salicylidene-glycinate, -β-alaninate, and -γ-aminobutyrate, **1a**—**c**, were prepared by the condensation of bis(salicylaldehydato)copper(II) with benzyl ester of each amino acid. When chelates **1a**—**c** were refluxed in methanol for 30 min, the copper(II) chelates **2a**—**c** of methyl *N*-salicylidene-glycinate, -β-alaninate, and -γ-aminobutyrate were obtained in good yields. This indicates that the benzyl ester groups at α-, β-, or γ-position in the copper(II) chelates **1a**—**c** can be replaced by a methyl ester group (Scheme 1).

Selective Ester-exchange reactions in the Copper(II) Chelates of the Schiff Bases derived from Salicylaldehyde and Dibenzyl Aspartate or Glutamate. The copper(II) chelates of dibenzyl *N*-salicylidene-aspartate and -glutamate, **3-a** and **-b**, were prepared by warming a mixture of bis(salicylaldehydato)copper(II) and dibenzyl aspartate or glutamate. A methanol–chloroform solution of complex **3a** was refluxed for 30 min to yield a copper(II) chelate, of which half of the original benzyl groups were replaced by methyl groups. Elemental analysis of the reaction product shows that ester-exchange reaction takes place, though it is not clear in what position. We therefore, synthesized separately the copper(II) chelates of the Schiff bases derived from salicylaldehyde and α-methyl β-benzyl-DL- or -L-aspartates **4a**. The IR spectra of the authentic complexes thus obtained and the products of ester-exchange reaction agree with each other. The melting points for both the compounds showed no essential difference. From the results it can be concluded that the ester-exchange reaction in the complexes **3a** occurs selectively at the α-position in dibenzyl L- and DL-aspartate moiety (Scheme 2). No ester-exchange reaction in compound **5a**, the ligand of complex **3a**, was observed in the absence of copper(II). The α-ester group in dibenzyl L- and DL-glutamate moiety of the complexes **3b** is also preferably replaced in the same way by methyl groups.

For the sake of confirmation, the Schiff bases were isolated from the copper(II) complexes **3**- and **4-a** and **-b** (Scheme 3). The physical properties of Schiff bases **5a**—**d** are given in Table 1 and the PMR spectra of the L-isomers in Figs. 1 and 2. By comparing Figs. 1-a and -b we see that ligand **5a** of the original complex **3a** exhibits two peaks around 5 ppm (5.05 and 5.14 ppm), and ligand **5b** of the reaction product **3b** only one peak (5.08 ppm) in the same region. Since these peaks are caused by benzyl groups, the decrease in the number of peaks from 2 to 1 shows that the ester-exchange reaction takes place at only one of the two benzyl

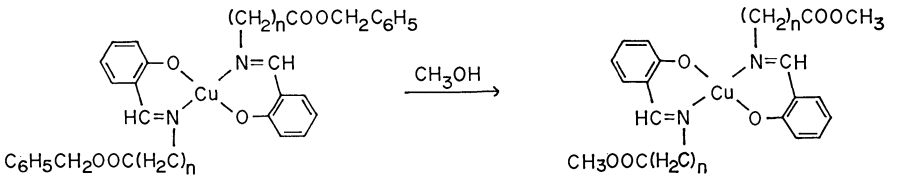

1a, n=1
1b, n=2
1c, n=3

2a, n=1
2b, n=2
2c, n=3

Scheme 1.

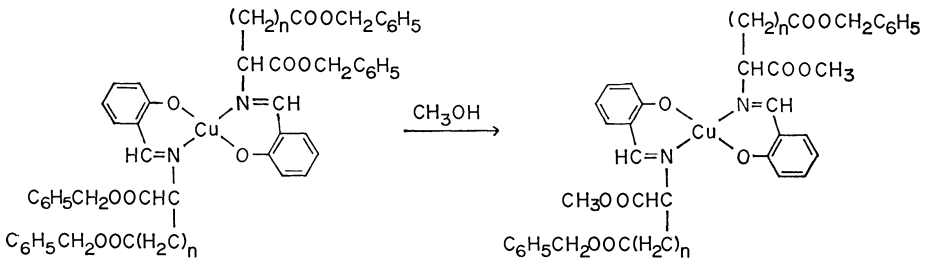

3a, n=1
3b, n=2

4a, n=1
4b, n=2

Scheme 2.

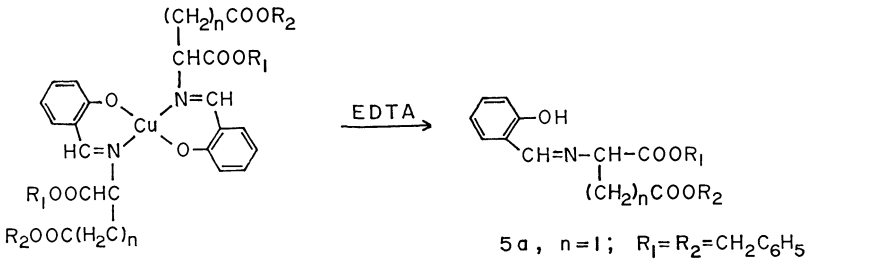

3- and 4-a and -b

5a, n=1; $R_1=R_2=CH_2C_6H_5$
5b, n=1; $R_1=CH_3$, $R_2=CH_2C_6H_5$
5c, n=2; $R_1=R_2=CH_2C_6H_5$
5d, n=2; $R_1=CH_3$, $R_2=CH_2C_6H_5$

Scheme 3.

Table 1. Physical properties of schiff bases, **5a—d**

Compound	Mp/°C	UV($CHCl_3$) λ_{max}/nm	UV($CHCl_3$) log ε	IR, ν/cm^{-1} C=O(ester)	IR, ν/cm^{-1} C=N
5a(DL–)	69—70.5	260	4.1	1730	1625
		324	3.6		
5a(L–)	69.5—70.5	260	4.1	1730	1620
		324	3.6		
5b(DL–)	46—47	260	4.2	1740	1630
		323	3.7		
5b(L–)	a)	260	4.1	1735	1630
		325	3.6		
5c(DL–)	a)	260	4.1	1740	1630
		324	3.7		
5c(L–)	46—51	260	4.1	1735	1625
		323	3.7		
5d(DL–)	a)	260	4.1	1735	1630
		323	3.7		
5d(L–)	a)	259	4.3	1730	1625
		323	3.8		

a) Oily product.

Table 2. TLC for schiff bases[a] of L-aspartate

R_1	R_2	R_f
$C_6H_2C_6H_5$	$CH_2C_6H_5$	0.41[b]
CH_3	$CH_2C_6H_5$	0.32[c]
CH_3	$CH_2C_6H_5$	0.32[d]
CH_3	CH_3	0.23[e]

a) 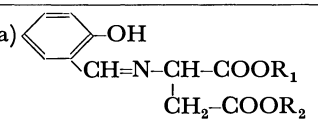

b) $[Cu(Sal=L\text{-}Asp(OBzl)_2)_2] \xrightarrow{EDTA}$ reaction product. c) Salicylaldehyde + L-Asp(α-OMe)(β-OBzl) → reaction product. d) $[Cu(Sal=L\text{-}Asp(OBzl)_2)_2] \xrightarrow[\text{reflux, 30 min}]{CH_3OH}$ reaction product $\xrightarrow{EDTA}$ reaction product. e) Salicylaldehyde + L-$Asp(OMe)_2$ → reaction product.

ester groups. This is also supported by the following facts. The peak (3.69 ppm, s, 3H) due to methoxyl group is seen in the spectrum for ligand **5b** of the reaction product, the number of protons of aromatic rings decreasing from 14 to 9 with the exchange reaction. The results of TLC for the Schiff bases consisting of salicylaldehyde and some diesters of L-aspartic acid are summarized in Table 2. It was confirmed from the R_f values that the ester-exchange reaction takes place selectively at the α-position in the chelates **3a**. The same variation in PMR spectra was also observed in glutamate-Schiff base chelates (Fig. 2). The two peaks at 5.02 and 5.12 ppm arising from the methylene protons of benzyl groups in **5c** decrease to one peak (5.08 ppm) in the ligand **5d** of the reaction product. Appearance of a new peak (3.72 ppm) due to the methoxyl group and decrease of the peak for protons of aromatic rings with the ester-exchange reaction were also observed.

Reaction Mechanism. Two essentially different mechanisms have been proposed[5,7] to elucidate the ester-exchange reactions occurring in the presence of metal ion. Although both mechanisms were proposed

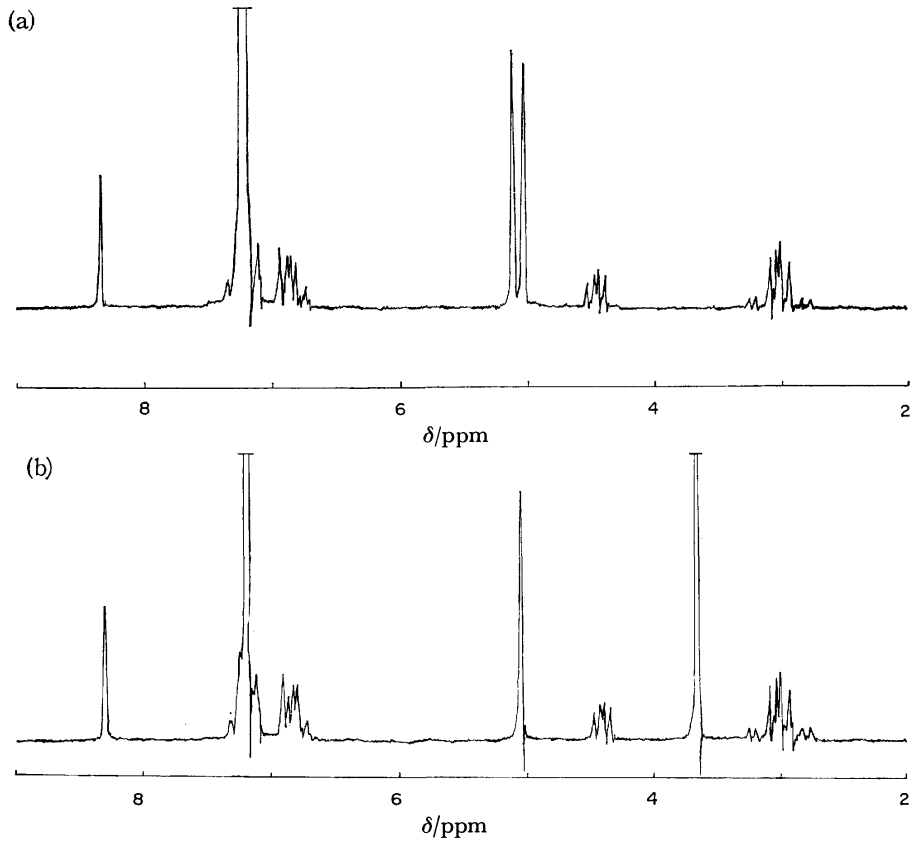

Fig. 1. PMR spectra of; a) SalH=L-Asp(OBzl)$_2$ **5a** and b) SalH=L-Asp(α-OMe) (β-OBzl) **5b.**

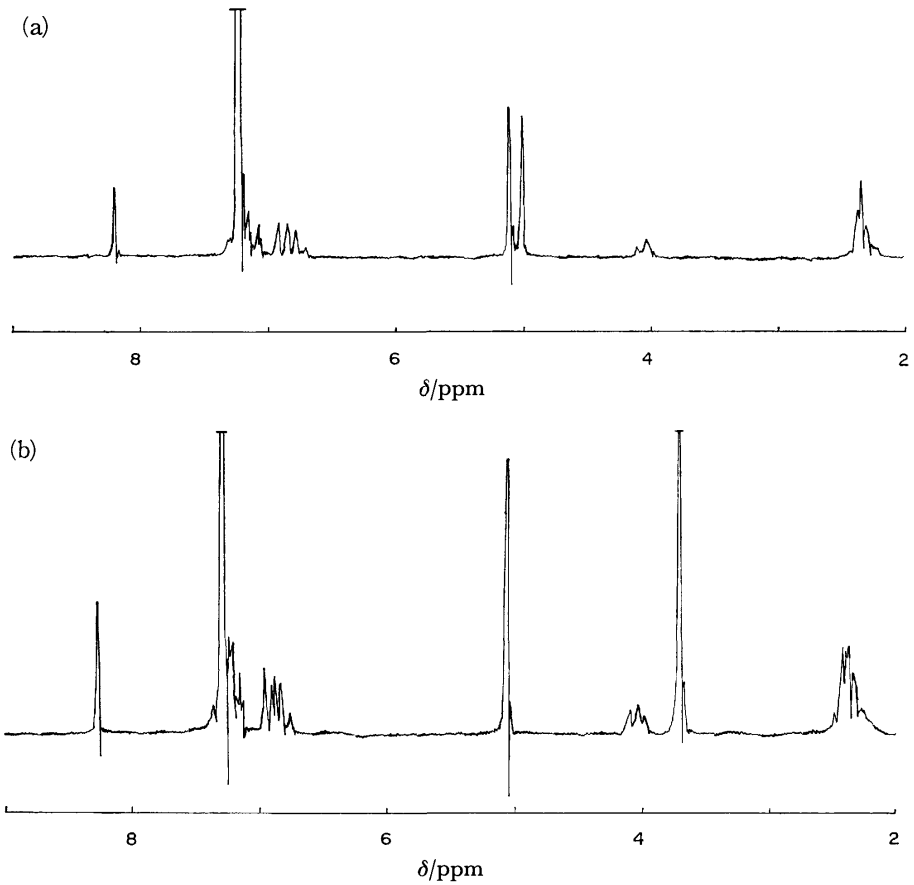

Fig. 2. PMR spectra of; a) SalH=L-Glu(OBzl)$_2$ **5c** and b) SalH=L-Glu(α-OMe) (γ-OBzl) **5d.**

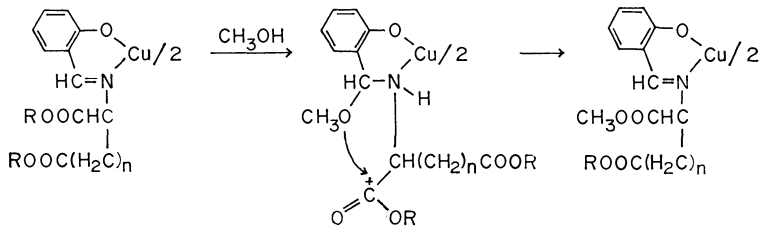

3-a and -b 6 4-a and -b

$R = CH_2C_6H_5$, n = 1 or 2

Scheme 4.

for the esters of the neutral amino acids such as glycine, α- and β-alanine, they were applied to explain the present kind of diesters of acidic amino acids. In the mechanism of Gillard and Wootton[7] (Scheme 4), the addition of methanol molecule would first take place at the azomethine double bond. In the structure of the intermediate **6**, the oxygen atom of the methoxyl group would readily attack nucleophilically the carbon atom of the α-ester group, since the methoxyl group is located very closely to the α-ester group. On the other hand, the attacking of the same methoxyl group seems to be difficult against the β- or γ-ester group because of its distant location. Furthermore, there might be a steric interruption of the α-ester group. The reason why the selective ester-exchange reaction occurs is thus reasonably explained on the basis of the mechanism of Gillard and Wootton.[7] The selective and highly catalytic activity of enzyme reactions are said to be understandable on the basis of the proximity and the orientation effects of the functional groups in enzymes and substrates. In this respect, the present mechanism bears a resemblance to the enzyme reactions. In the mechanism according to Houghton and Pointer[5] (Scheme 5), the reaction begins with a dissociation of one of the two Schiff base ligands in complex **3a**, followed by the formation of tridentate chelation of the remainder ligand. In structure **7** (or **8**) the carbon atom of α-ester group would be readily attacked by oxygen atom of methanol because of the electrophilic character of the former and the nucleophilic character of the latter. Although coordination of the ester group at the β- or γ-position is also possible, it would be much more difficult than that of the α-ester group, in view of the structure-stability relationship in the fused chelate ring system.[10,17] In the Houghton and Pointer mechanism, preferential formation of the terdentate chelate **7** (or **8**) would play an important role for the selective ester-exchange reaction. If the selective ester-exchange reactions of the present kind proceed *via* the Gillard and Wootton mechanism, the reactions would not occur in chelates **12** which lacks azomethine double bonds. As a matter of fact, the selective ester-exchange reaction in **12** was observed under the same conditions. Accordingly, the possibility of the Gillard and Wootton mechanism is slight. Further, the reactions of **5a** with methanol in the presence of catalytic concentrations of copper(II) chloride indicate that a slight amount of copper(II) ion is insufficient to cause the ester-exchange reaction, while increasing amount of copper(II) chloride promotes it (Table 3). The mechanism of Houghton and Pointer has the advantage of interpreting the result described above. Though the efficiency of the ester-exchange reaction is low in the presence of minute quantities of copper(II), it is understandable in view of the observa-

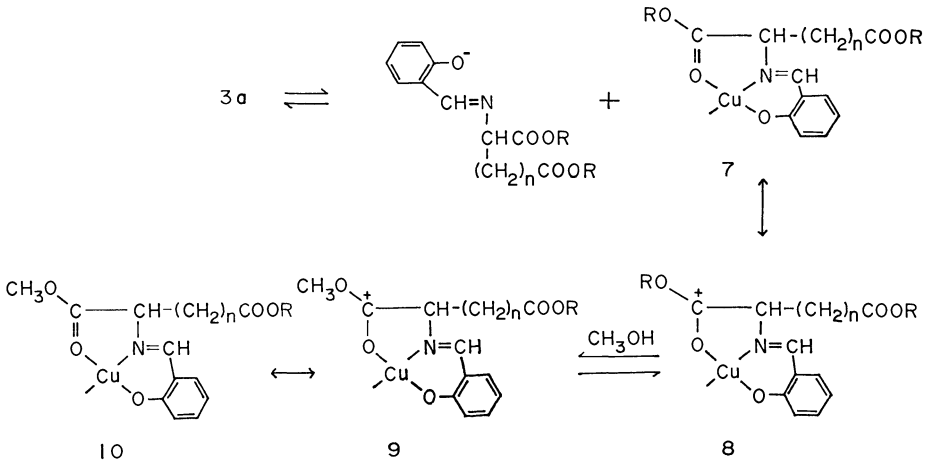

10 9 8

$R = CH_2C_6H_5$, n = 1 or 2

Scheme 5.

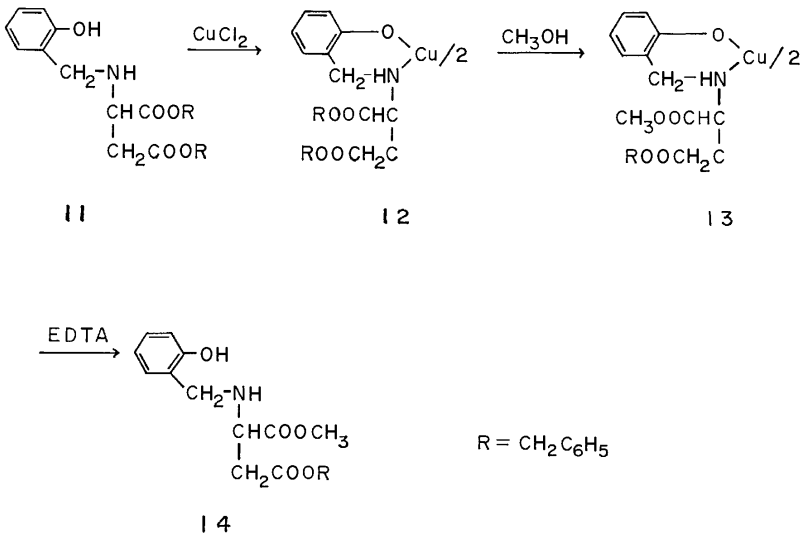

11 12 13 14

Scheme 6.

TABLE 3. RELATION BETWEEN THE AMOUNTS OF $CuCl_2$ USED AND THE EXTENT OF ESTER-EXCHANGE REACTION OCCURRING[a)]

	Amount of $CuCl_2$ used (mol/mol % against Schiff base)		
	1/100	1/10	1/5
Extent of ester-exchange reaction occurring (%)	0	5	10

a) 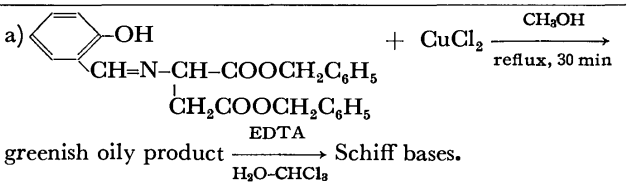

greenish oily product $\xrightarrow[H_2O\text{-}CHCl_3]{EDTA}$ Schiff bases.

tion that the major complex in solution is probably **3a** rather than **7** which are the active species for ester-exchange reaction. In conclusion, we are more in line with the Houghton and Pointer mechanism, which involves the dissociation and recoordination of Schiff base ligand.

We are grateful to Mr. Yoshio Terawaki of the Faculty of Engineering Science of this university for PMR measurements. Expense for this work were defrayed in part by grants from the Takeda Science Foundation and the Ministry of Education.

References

1) "Pyridoxal Catalysis: Enzymes and Model Systems," ed by E. E. Snell, A. E. Braunstein, E. S. Severin, Y. M. Torchinsky, John Wiley and Sons, New York (1968).
2) R. H. Holm, "Inorganic Biochemistry," ed by G. L. Eichhorn, Elsevier Sci. Publ., Amsterdam (1973), Vol. 2, p. 1137.
3) P. Pfeiffer, W. Offerman, and H. Werner, *J. Pract. Chem.*, **159**, 313 (1942).
4) H. S. Verter and A. E. Frost, *J. Am. Chem. Soc.*, **82**, 85 (1960).
5) R. P. Houghton and D. J. Pointer, *J. Chem Soc.*, **1964**, 3302.
6) G. A. Auld and A. Davison, *Inorg. Chem.*, **7**, 306 (1968).
7) R. D. Gillard and R. Wootton, *J. Chem. Soc.*, (B), **1970**, 364.
8) Y. Nakao and A. Nakahara, *Chem. Lett.*, **1977**, 145.
9) J. D. Cipera and R. V. V. Nicholls, *Chem. Ind.*, **1955**, 16.
10) Y. Nakao and A. Nakahara, *Bull. Chem. Soc. Jpn.*, **51**, 3522 (1978).
11) H. K. Miller and H. Waelsch, *J. Am. Chem. Soc.*, **74**, 1092 (1952).
12) N. Izumiya, H. Uchio, and T. Yamashita, *Nippon Kagaku Zassi*, **79**, 420 (1958).
13) Y. Ariyoshi, T. Shiba, and T. Kaneko, *Bull. Chem. Soc. Jpn.*, **40**, 1709 (1967).
14) A. Berger and E. Katchalski, *J. Am. Chem. Soc.*, **73**, 4084 (1951).
15) J. P. Greenstein and M. Winitz, "Chemistry of the Amino Acid," Wiley, New York (1961), Vol. 2, p. 943.
16) W. E. Hanby, S. G. Waley, and J. Watson, *J. Chem. Soc.*, **1950**, 3239.
17) Y. Nakao and A. Nakahara, *Bull. Chem. Soc. Jpn.*, **46**, 187 (1973).

Diastereomers and Circular Dichroism Spectra of the Tris(*trans*-1,2-cyclopentanediamine)cobalt(III) Complex

Mihoko KUNIMATSU, Hideaki KANNO,† Masaaki KOJIMA, Kazuo KASHIWABARA, and Junnosuke FUJITA*

Department of Chemistry, Faculty of Science, Nagoya University, Chikusa, Nagoya 464

(Received October 13, 1979)

The (lel_3), (lel_2ob), and ($lelob_2$) isomers of $[Co(rac\text{-cptn})_3]^{3+}$ were obtained by the reaction of *trans*-$[CoCl_2(pyridine)_4]^+$ with *rac*-cptn, where cptn denotes *trans*-1,2-cyclopentanediamine. No indication for the formation of the (ob_3) isomer was found. The isomers were resolved into optical isomers by SP-Sephadex column chromatography. The circular dichroism spectra of these optical isomers were measured and the results compared with those of the related complexes. The anomalous circular dichroism pattern of the (lel_3) isomer in the region of the first absorption band was found to result from the contribution of the strong vicinal effect of the chiral cptn chelate ligand as compared with that of the configurational effect.

The tris(*rac-trans*-1,2-cyclopentanediamine)cobalt(III) ion, $[Co(rac\text{-cptn})_3]^{3+}$ has four possible diastereomers, each of which exists in a pair of enantiomers (Δ and Λ). Since the ligand forms a gauche-type (δ and λ) chelate ring upon coordination, these diastereomers can be designated as lel_3($\Delta(\lambda\lambda\lambda)$ and $\Lambda(\delta\delta\delta)$), lel_2ob ($\Delta(\lambda\lambda\delta)$ and $\Lambda(\delta\delta\lambda)$), $lelob_2$($\Delta(\lambda\delta\delta)$ and $\Lambda(\delta\lambda\lambda)$), and ob_3($\Delta(\delta\delta\delta)$ and $\Lambda(\lambda\lambda\lambda)$).[1]

Jaeger and Blumendal[2] found in their studies on metal complexes with *rac*-cptn that $[M(rac\text{-cptn})_3]^{3+}$ (M=Co(III), Rh(III)) exists in only one pair of enantiomers, $(+)_{589}$-$[M((-)\text{-cptn})_3]^{3+}$ and $(-)_{589}$-$[M((+)\text{-cptn})_3]^{3+}$. Ito *et al.*[3] prepared $(-)_{589}$-$[Co((+)\text{-cptn})_3]^{3+}$ and determined its absolute configuration by the X-ray method to be $\Lambda(\delta\delta\delta)(lel_3)$-$[Co(S,S\text{-cptn})_3]^{3+}$. They found that this isomer shows a main circular dichroism (CD) band with the negative sign in the region of the first absorption band in contrast with Λ-$[Co(en)_3]^{3+}$ (en=ethylenediamine) and other Λ-tris(1,2-diamine)cobalt(III) complexes whose main CD bands are always positive in this region. Toftlund and Pedersen[4] found that the reaction of *trans*-$[CoCl_2py_4]^+$ (py=pyridine) with (*R,R*)-cptn gives $\Delta(\lambda\lambda\lambda)(lel_3)$- and $\Lambda(\lambda\lambda\lambda)(ob_3)$-$[Co(R,R\text{-cptn})_3]^{3+}$ in the formation ratio 10: 1. The Λ-ob_3 isomer, although it was not isolated as crystals but only separated as a fraction in the column chromatography, also showed an anomalous CD pattern in the region of the first absorption band, its main CD being negative.

In order to elucidate such anomalous CD spectra of $[Co(cptn)_3]^{3+}$, it is desirable to isolate all diastereomers of this complex. This paper deals with the preparation and resolution of diastereomers of $[Co(rac\text{-cptn})_3]^{3+}$ and their CD spectra.

Experimental

Ligands. *Trans*-1,2-cyclopentanediamine (cptn) was prepared and resolved by the method of Toftlund and Pedersen.[4] The (+)-cptn isomer has (*S,S*)-configuration, forming a δ-gauche chelate ring upon coordination.[3]

$[Co(cptn)_3]^{3+}$. *a)*: *Trans*-$[CoCl_2py_4]Cl\cdot 6H_2O$ was mixed with (−)-cptn in 2-methoxyethanol.[4] The product was carefully chromatographed by use of a column of SP-Sephadex C-25 (ϕ 2.7×130 cm). By elution with 0.15 mol/dm³ disodium hydrogenphosphate, 0.2 mol/dm³ sodium sulfate, or 0.15 mol/dm³ sodium $(+)_{589}$-tartratoantimonate (III), the column always gave only one band of the $\Delta(\lambda\lambda\lambda)(lel_3)$ isomer. No indication for the presence of the $\Lambda(\lambda\lambda\lambda)(ob_3)$ isomer was observed.

b): An *N,N*-dimethylformamide solution (50 cm³) containing *trans*-$[CoCl_2(R,R\text{-cptn})_2]ClO_4$[5] (0.55 g, 1.3 mmol) and *R,R*-cptn (0.13 g, 1.3 mmol) was stirred at room temperature for a day. The resulting red solution was diluted with water to 1 dm³, adjusted to pH 4 with hydrochloric acid, and poured on a column of SP-Sephadex C-25 (ϕ 2.7×130 cm). The adsorbed band was eluted by the same method as the above to give only one $\Delta(\lambda\lambda\lambda)(lel_3)$ isomer, no $\Lambda(\lambda\lambda\lambda)(ob_3)$ isomer being detected on the column.

c): To a 2-methoxyethanol solution (3 cm³) of *rac*-cptn (3 g, 30 mmol) was added dropwise a 2-methoxyethanol solution (10 cm³) of *trans*-$[CoCl_2py_4]Cl\cdot 6H_2O$ (5 g, 8.5 mmol). The red $[Co(cptn)_3]Cl_3$ complex was precipitated immediately and filtered at 0 °C after 1 h. It was washed three times with 3 cm³ portion of ethanol and air dried. (yield: 85%). A small portion (*ca.* 0.2 g) of this crude complex was dissolved in water and the solution was poured on a column of SP-Sephadex C-25 (ϕ 2.7×130 cm). By elution with a 0.2 mol/dm³ Na_2SO_4 solution, three red bands, T_1, T_2, and T_3 were obtained in succession. Each eluate was diluted with 10^{-2} mol/dm³ HCl and poured again on a small column of SP-Sephadex C-25. The adsorbed band was eluted with 2 mol/dm³ HCl after the column had been washed thoroughly with 10^{-2} mol/dm³ HCl in order to remove Na^+ ions. The eluate was evaporated to dryness in a vacuum desiccator over NaOH and P_2O_5. The residue was washed with a small amount of ethanol and recrystallized from water to give red crystals. T_1, T_2, and T_3 formed in the ratio 10: 4: 1, are racemates of the lel_3, lel_2ob, and $lelob_2$ diastereomers, respectively.

The diastereomers were resolved by SP-Sephadex column chromatography.[6] The T_1 isomer adsorbed on a column of SP-Sephadex C-25 (ϕ 2.7×130 cm) was eluted with a 0.3 mol/dm³ sodium $(+)_{589}$-hydrogentartrate solution. Two bands were separately eluted. From the fast and the slowly eluted fractions, $(-)_{589}$-$\Lambda(\delta\delta\delta)(lel_3)$-$[Co(S,S\text{-cptn})_3]Cl_3\cdot 4H_2O$ and $(+)_{589}$-$\Delta(\lambda\lambda\lambda)(lel_3)$-$[Co(R,R\text{-cptn})_3]Cl_3\cdot 4H_2O$, respectively, were isolated by a method similar to that for the racemates described above. Elution with sodium $(+)_{589}$-tartratoantimonate (III) resulted in poor separation between the bands of the enantiomers.

The T_2 and T_3 isomers were resolved similarly with an eluent, a 0.15 mol/dm³ sodium $(+)_{589}$-tartratoantimonate (III)

† Present address: Department of Chemistry, Faculty of Science, Shizuoka University, Shizuoka 420.

TABLE 1. ANALYTICAL DATA OF THE cptn COMPLEXES

Complex	C/%		H/%		N/%	
	Found	Calcd	Found	Calcd	Found	Calcd
T_1: $(+)_{589}$-$[Co(cptn)_3]Cl_3\cdot 4H_2O$	33.44	33.49	8.15	8.26	15.46	15.63
T_2: $(+)_{589}$-$[Co(cptn)_3]Cl_3\cdot 5H_2O$	32.61	32.40	8.03	8.36	15.42	15.12
T_3: $(-)_{589}$-$[Co(cptn)_3]Cl_3\cdot 3H_2O$	34.32	34.65	8.04	8.16	15.90	16.17
$(+)_{589}$-Δ-$[Co(en)_2((-)\text{-cptn})]Cl_3\cdot H_2O$	26.78	26.77	7.69	7.51	21.00	20.82
$(+)_{589}$-Λ-$[Co(en)_2((-)\text{-cptn})]Cl_3\cdot 1.5H_2O$	26.57	26.19	7.26	7.59	20.02	20.37
$[Co(NH_3)_4((-)\text{-cptn})]Cl_3\cdot 1.5H_2O$	17.05	16.65	7.98	7.56	23.61	23.31

cptn=$C_5H_{12}N_2$.

solution, and the optical isomers were isolated by the same method as that for the T_1 isomer. The fast eluting enatiomers of T_2 and T_3 are $(-)_{589}$-$\Lambda(\delta\delta\lambda)(lel_2ob)$-$[Co(S,S\text{-cptn})_2(R,R\text{-cptn})]Cl_3\cdot 5H_2O$ and $(+)_{589}$-$\Lambda(\delta\lambda\lambda)(lelob_2)$-$[Co(S,S\text{-cptn})(R,R\text{-cptn})_2]Cl_3\cdot 3H_2O$, respectively. Their antipodes obtained from the slowly eluted bands are thus $(+)_{589}$-$\Delta(\lambda\lambda\delta)(lel_2ob)$-$[Co(R,R\text{-cptn})_2(S,S\text{-cptn})]Cl_3\cdot 5H_2O$ and $(-)_{589}$-$\Delta(\lambda\delta\delta)(lelob_2)$-$[Co(R,R\text{-cptn})(S,S\text{-cptn})_2]Cl_3\cdot 3H_2O$.

[Co(en)$_2$(R,R-cptn)]$^{3+}$. This complex was prepared from *trans*-$[CoCl_2(en)_2]Cl$ and (*R,R*)-cptn in dimethyl sulfoxide by a method similar to that reported.[7] The isomers were separated by an SP-Sephadex column chromatographic method. By elution with a 0.2 mol/dm^3 Na_2SO_4 solution, two orange bands of $\Delta(\lambda)$- and $\Lambda(\lambda)$-$[Co(en)_2(R,R\text{-cptn})]^{3+}$ were eluted in succession. From the eluates, orange crystals of the complex chlorides were obtained by the same method as that for the tris(cptn) complex. Both isomers showed positive rotation at 589 nm.

[Co(NH$_3$)$_4$(R,R-cptn)]$^{3+}$. This complex was prepared from $[Co(NH_3)_5(H_2O)](ClO_4)_3$ and (*R,R*)-cptn by a method similar to that for the corresponding en complex.[8] Since an orange fraction obtained by chromatography with an eluent, 0.2 mol/dm^3 Na_2SO_4, was contaminated with the starting aqua complex, the fraction was rechromatographed with a 0.2 mol/dm^3 disodium tartrate solution. The complex chloride was isolated by the same method as that for the tris(cptn) complex and recrystallized from a mixture of water and methanol. Analytical data of all the complexes are given in Table 1.

Measurements. Absorption and CD spectra were recorded in aqueous solutions on a Hitachi 323 spectrophotometer, and a JASCO J-40 spectropolarimeter, respectively. Optical rotations were measured with a JASCO DIP-4 polarimeter. ^{13}C-NMR spectra were obtained with a Jeol JNM FX-60 spectrometer using TMS as an external reference in aqueous solutions by locking to D_2O. For the measurements, the tris (cptn) complex chlorides were converted into acetates with QAE-Sephadex A-25 anion exchanger in the acetate form in order to increase the solubility.

Results and Discussion

The Isomers of [Co(cptn)$_3$]$^{3+}$. Toftlund and Pedersen[4] obtained $\Delta(\lambda\lambda\lambda)(lel_3)$- and $\Lambda(\lambda\lambda\lambda)(ob_3)$-$[Co(R,R\text{-cptn})_3]^{3+}$ in the ratio 10: 1 by the reaction of *trans*-$[CoCl_2py_4]Cl\cdot 6H_2O$ with *R,R*-cptn in 2-methoxyethanol. However, all attempts to prepare the (ob_3) isomer were unsuccessful (Experimental). On the other hand, three (T_1, T_2, and T_3) of the four possible diastereomers (lel_3, lel_2ob, $lelob_2$, and ob_3) were obtained in the ratio 10: 4: 1, by a method similar to that of Toftlund and Pedersen using *rac*-cptn instead of *R,R*-cptn. No indication for the presence of more than three isomers was observed in the column chromatography. The isomers were completely resolved by SP-Sephadex column chromatography.

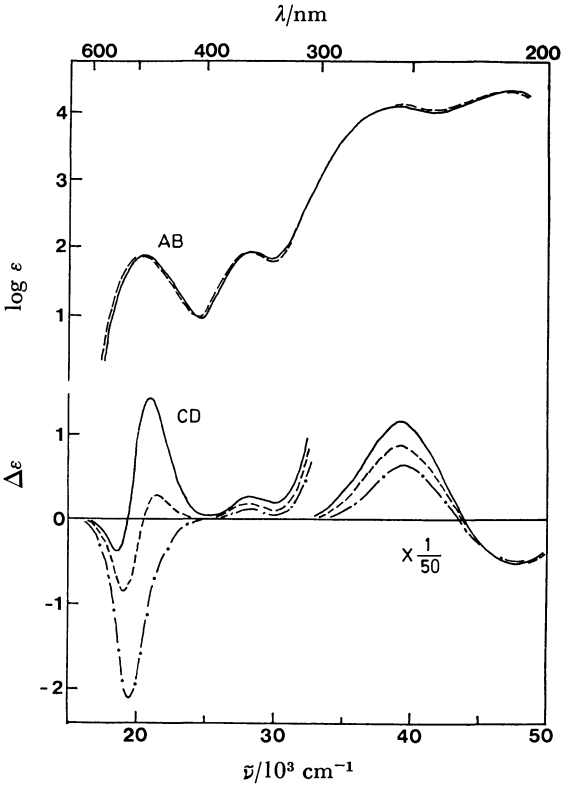

Fig. 1. Absorption and CD spectra of $[Co(cptn)_3]^{3+}$.
——: $(+)_{589}$-$\Delta(\lambda\lambda\lambda)$ (lel_3)-$[Co(R,R\text{-cptn})_3]^{3+}$ (T_1), ------: $(+)_{589}$-$\Delta(\lambda\lambda\delta)$ (lel_2ob)-$[Co(R,R\text{-cptn})_2(S,S\text{-cptn})]^{3+}$ (T_2), -·-·-: $(-)_{589}$-Δ $(\lambda\delta\delta)$ $(lelob_2)$-$[Co$ $(R,R\text{-cptn})$ $(S,S\text{-cptn})_2]^{3+}$ (T_3).

The CD spectra of the enantiomers obtained from the more slowly eluted bands on the columns are given in Fig. 1 and the spectral data in Table 2. The CD spectrum of T_1 is the mirror image of that of $\Delta(\delta\delta\delta)(lel_3)$-$[Co(S,S\text{-cptn})_3]^{3+}$ whose absolute configuration has been determined by the X-ray method.[3] Thus T_1 is assigned to $\Delta(\lambda\lambda\lambda)(lel_3)$-$[Co(R,R\text{-cptn})_3]^{3+}$. The other T_2 and T_3 isomers (Fig. 1) can be assigned to $\Delta(\lambda\lambda\delta)(lel_2ob)$-$[Co(R,R\text{-cptn})_2(S,S\text{-cptn})]^{3+}$ and $\Delta(\lambda\delta\delta)(lelob_2)$-$[Co(R,R\text{-cptn})(S,S\text{-cptn})_2]^{3+}$, respectively, for the following reasons: 1) The CD spectra in the region of the first absorption band change remarkably but regularly in the order T_1, T_2, and T_3, but those in the ultraviolet

Table 2. Absorption and CD spectral data

	Absorption $\bar{\nu}/10^3$ cm^{-1} (log ε)	CD $\bar{\nu}/10^3$ cm^{-1} ($\Delta\varepsilon$)
$(+)_{589}$-$\Lambda(\lambda\lambda\lambda)(lel_3)$-$[Co(R,R\text{-cptn})_3]^{3+}(T_1)$	20.3(1.88)	18.6(−0.39)
		21.0(+1.46)
	28.3(1.92)	28.3(+0.27)
	39.0(4.08)	39.2(+58.2)
	47.4(4.28)	47.6(−25.4)
$(+)_{589}$-$\Lambda(\lambda\lambda\delta)(lel_2ob)$-$[Co(R,R\text{-cptn})_2(S,S\text{-cptn})]^{3+}(T_2)$	20.2(1.90)	19.0(−0.88)
		21.5(+0.29)
	28.3(1.93)	28.1(+0.19)
	39.1(4.08)	39.3(+43.7)
	46.7(4.28)	47.6(−25.1)
$(-)_{589}$-$\Lambda(\lambda\delta\delta)(lelob_2)$-$[Co(R,R\text{-cptn})(S,S\text{-cptn})_2]^{3+}(T_3)$	20.1(1.88)	19.5(−2.13)
	28.3(1.93)	27.8(+0.10)
	39.1(4.08)	39.5(+30.2)
	47.2(4.28)	47.6(−25.2)
$(+)_{589}$-$\Lambda(\lambda)$-$[Co(en)_2(R,R\text{-cptn})]^{3+}$	21.1(1.93)	19.9(−1.41)
		22.4(+0.46)
	29.1(1.90)	28.4(−0.17)
	47.2(4.31)	44.5(+30.5)
$(+)_{589}$-$\Lambda(\lambda)$-$[Co(en)_2(R,R\text{-cptn})]^{3+}$	21.1(1.93)	20.4(+1.95)
	29.1(1.90)	27.8(+0.08)
	47.6(4.33)	38.8(+3.68)
		45.9(−21.0)
$[Co(NH_3)_4(R,R\text{-cptn})]^{3+}$	20.8(1.81)	21.1(+0.71)
	29.1(1.77)	28.2(−0.02)
	41.9(3.68)	41.7(+6.76)
	47.2(3.97)	

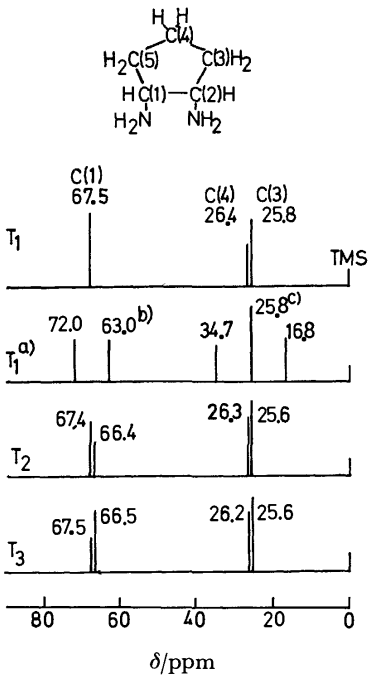

Fig. 2. ^{13}C-NMR spectra of the three isomers of [Co(cptn)$_3$] $(CH_3COO)_3$ in D_2O (15.04 MHz, The signals due to CH_3COO^- are omitted).
a) The off-resonance spectrum, b) J_{C-H}=135.5 Hz. c) J_{C-H}=134.3 Hz.

region are very similar to one another, indicating the same absolute configuration.[9] 2) The reactions with optically active *R,R*-cptn give only one isomer of (*lel*$_3$), no (*ob*$_3$) isomer being obtained. 3) The yields of T_1, T_2, and T_3 decrease in this order. Since the stability of (*lel*$_{3-n}$*ob*$_n$) isomers of [Co(1,2-diamine)$_3$]$^{3+}$ decreases with an increase in the number of the *ob* ligands,[1,10] the order suggests the *lel*$_3$, *lel*$_2$*ob*, *lelob*$_2$ isomers for T_1, T_2, and T_3, respectively. The assignments are supported by ^{13}C-NMR spectroscopy (Fig. 2). The peak assignment can be made on the basis of the off-resonance and a comparison of relative intensities of the peaks. The T_1(*lel*$_3$) isomer which has D_3 symmetry[3] shows three kinds of carbons of the ligands. In the off-resonance spectrum, the lowest field peak at 67.52 ppm splits into two, while the two high field peaks at 26.37 and 25.80 ppm give a triplet due probably to accidental degeneracy of two triplets. The latter two peaks show a remarkable difference in intensity. Thus, the peaks at 67.52, 26.37, and 25.80 ppm can be assigned to the C(1), C(4), and C(3) atoms, respectively (Fig. 2). The T_2(*lel*$_2$*ob*) and T_3(*lelob*$_2$) isomers, both of which should have C_2 symmetry, each exhibits two C(1) peaks of different intensity. The T_2(*lel*$_2$*ob*) isomer shows a strong peak at a similar frequency value to that of the T_1(*lel*$_3$) isomer, and a weak peak in a little higher magnetic field. The T_3(*lelob*$_2$) isomer shows two similar peaks, but whose relative intensities are reversed (Fig. 2). Thus, the ^{13}C-NMR spectra strongly support the previous assignment that T_1, T_2, and T_3 are the *lel*$_3$, *lel*$_2$*ob*, and *lelob*$_2$ isomers, respectively.

The $\Lambda(\lambda\lambda\lambda)(ob_3)$ isomer reported[4] seems to be the $\Lambda(\lambda\lambda\delta)(lel_2ob)$ isomer, the formation of which might have resulted from incomplete resolution of the ligand. The CD spectrum reported for this isomer is very similar to that of our $\Lambda(\lambda\lambda\delta)(lel_2ob)$ isomer. The reason for the *ob*$_3$ isomer not being formed under the experimental conditions given is not known. However, the formation ratio of T_1, T_2, and T_3 (10:4:1) suggests that the stability of isomer decreases a great deal with an increase in the number of the *ob* ligands. The analogous [Co(chxn)$_3$]$^{3+}$ (chxn=*trans*-1,2-cyclohexanediamine) complex gives the *lel*$_3$, *lel*$_2$*ob*, *lelob*$_2$, and *ob*$_3$ isomers in the formation ratio of *ca.* 14:11:4:1 in equilibrium at 100 °C.[11] The differences among these values are small as compared with those of [Co(cptn)$_3$]$^{3+}$. The difference in the stability caused by replacing the *lel* ligand with the *ob* one in [Co(cptn)$_3$]$^{3+}$ would be much larger than that in [Co(chxn)$_3$]$^{3+}$. Attempts to equilibrate the isomers of [Co(cptn)$_3$]$^{3+}$ were unsuccessful because of the decomposition of the complex.

Absorption and CD Spectra. The three isomers of [Co(cptn)$_3$]$^{3+}$ give very similar absorption spectra, but the first absorption bands shift toward the smaller wavenumber side by *ca.* 100 cm^{-1} as the number of the *ob* ligands increases by one (Fig. 1 and Table 2). The magnitude of the shift is fairly large as compared with that of other tris(1,2-diamine) complexes. For [Co(chxn)$_3$]$^{3+}$ [11] and [Co(pn)$_3$]$^{3+}$ (pn=propylenediamine),[12] the differences in the absorption maxima between the *lel*$_3$ and *ob*$_3$ isomers are only 50 and 20 cm^{-1}, respectively. The large shift of the first absorption

band due to replacement of the *lel* ligand with the *ob* one in $[Co(cptn)_3]^{3+}$ also suggests that the complex becomes unstable rapidly with an increase in the number of the *ob* ligands.

The red $[Co(cptn)_3]^{3+}$ complex gives all the absorption bands at wavenumbers smaller than those of the corresponding bands of the orange $[Co(chxn)_3]^{3+}$ [11] and $[Co(pn)_3]^{3+}$.[12] The red shift of the charge-transfer band, in particular, amounts to 5000—8000 cm^{-1}. Such red shifts might be brought about by a strained structure of the cptn chelate ring as pointed out by Ito *et al.*;[3] the N–N distance of 3.14 Å in a strain-free, free ligand decreases in length to 2.76 Å on forming a chelate ring, which give considerable strain in bond angles of the chelate ring. In cobalt(III) complexes with strain caused by various factors such as congestion due to bulky ligands or steric requirement, as in the case of cptn, the d-d absorption bands shift to the small wavenumber side.[13] The shift of the charge-transfer band might also be correlated with such a strained structure of the cptn chelate ring. No appreciable strain is observed for bond angles of the chelate rings in $[Co(chxn)_3]^{3+}$ [14] and $[Co(pn)_3]^{3+}$.[15]

The CD spectra of three isomers of the $[Co(cptn)_3]^{3+}$ complex are compared in Fig. 1. If we assume that all the isomers have the same Δ-configuration, the CD contributions due to the configurational and the vicinal effects can be estimated by the equations

$$\Delta\varepsilon(\Delta) = 1/2[\Delta\varepsilon(T_2: \Delta\lambda\lambda\delta) + \Delta\varepsilon(T_3: \Delta\lambda\delta\delta)]$$

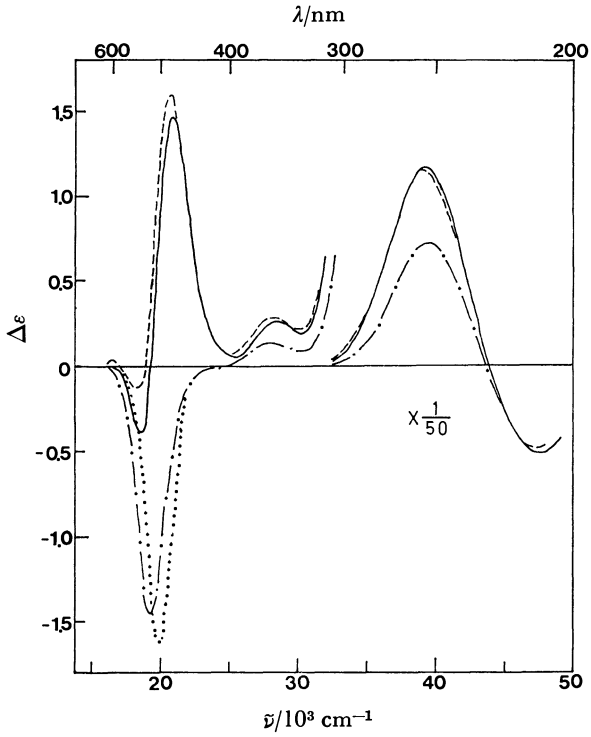

Fig. 3. Configurational effect CD ($\Delta\varepsilon(\Delta)$) of $[Co(cptn)_3]^{3+}$.
——: Observed CD of $\Delta(\lambda\lambda\lambda)$-$[Co(R,R\text{-cptn})_3]^{3+}$ (T_1), –·–·–: Calculated $\Delta\varepsilon(\Delta) = 1/2[\Delta\varepsilon(T_2: \Delta\lambda\lambda\delta) + \Delta\varepsilon(T_3: \Delta\lambda\delta\delta)]$, – – –: Calculated $\Delta\varepsilon[\Delta(\lambda\lambda\lambda)] (= \Delta\varepsilon(\Delta) + 3\Delta\varepsilon(\lambda))$, ……: Calculated $\Delta\varepsilon(\Delta)$ from $\Delta(\lambda)$- and $\Lambda(\lambda)$-$[Co(en)_2(R,R\text{-cptn})]^{3+}$ ($1/2\{\Delta\varepsilon[\Delta(\lambda)] - \Delta\varepsilon[\Lambda(\lambda)]\}$).

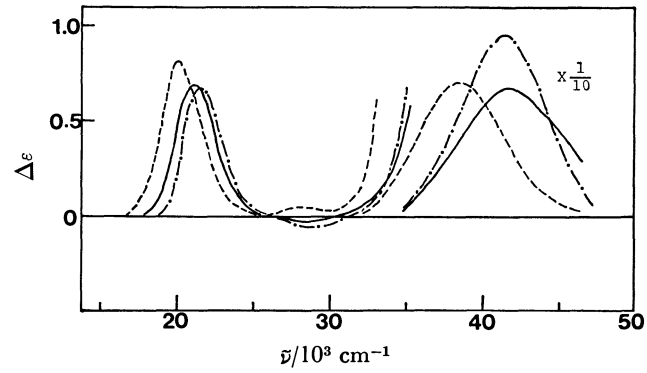

Fig. 4. Vicinal effect CD ($\Delta\varepsilon(\lambda)$) of the $\lambda(R,R$-cptn) ligand.
——: Observed CD of $[Co(NH_3)_4(R,R\text{-cptn})]^{3+}$, – – – –: Calculated $\Delta\varepsilon(\lambda) = 1/2[\Delta\varepsilon(T_2: \Delta\lambda\lambda\delta) - \Delta\varepsilon(T_3: \Delta\lambda\delta\delta)]$, –·–·–: Calculated $\Delta\varepsilon(\lambda)$ from $\Delta(\lambda)$- and $\Lambda(\lambda)$-$[Co(en)_2(R,R\text{-cptn})]^{3+}$ ($1/2\{\Delta\varepsilon[\Delta(\lambda)] + \Delta\varepsilon[\Lambda(\lambda)]\}$).

$$\Delta\varepsilon(\lambda) = 1/2[\Delta\varepsilon(T_2: \Delta\lambda\lambda\delta) - \Delta\varepsilon(T_3: \Delta\lambda\delta\delta)]$$

where $\Delta\varepsilon(T_2: \Delta\lambda\lambda\delta)$ and $\Delta\varepsilon(T_3: \Delta\lambda\delta\delta)$ are the observed CD for $(+)_{589}$-T_2 and $(-)_{589}$-T_3 isomers, respectively, and $\Delta\varepsilon(\Delta)$ and $\Delta\varepsilon(\lambda)$ the CD of the Δ-configurational and the $\lambda(R,R$-cptn)-vicinal effects, respectively. The calculated CD curves of these two effects are shown in Figs. 3 and 4 in which CD curves of the related complexes are given for comparison. The CD curve calculated for $\Delta\varepsilon[\Delta(\lambda\lambda\lambda)] (= \Delta\varepsilon(\Delta) + 3\Delta\varepsilon(\lambda))$ agrees with the observed CD spectrum of $(+)_{589}$-$T_1\Delta(\lambda\lambda\lambda)(lel_3)$-$[Co(R,R\text{-cptn})_3]^{3+}$ over the whole region (Fig. 3). This indicates that the additivity[9,16] in CD between the configurational and the vicinal effects holds in the CD of $[Co(cptn)_3]^{3+}$. The $\Delta\varepsilon(\Delta)$ curve also resembles the Δ-configurational CD curve obtained similarly from the CD spectra of a diastereomeric pair, $\Delta(\lambda)$- and $\Lambda(\lambda)$-$[Co(en)_2(R,R\text{-cptn})]^{3+}$ ($1/2\{\Delta\varepsilon[\Delta(\lambda)] - \Delta\varepsilon[\Lambda(\lambda)]\}$). On the other hand, the $\lambda(R,R$-cptn)-vicinal CD curve, $\Delta\varepsilon(\lambda)$, is very similar in pattern and strength to the observed CD spectrum of $[Co(NH_3)_4(R,R\text{-cptn})]^{3+}$, and also to the vicinal CD curve obtained from $\Delta(\lambda)$- and $\Lambda(\lambda)$-$[Co(en)_2(R,R\text{-cptn})]^{3+}$ ($1/2\{\Delta\varepsilon[\Delta(\lambda)] + \Delta\varepsilon[\Lambda(\lambda)]\}$). All the results support the validity of the additivity. Hence the configurational and the vicinal CD of the $[Co(cptn)_3]^{3+}$ complex can be compared with those of other diamine complexes.

The configurational ($\Delta\varepsilon(\Delta)$) and the vicinal ($3\Delta\varepsilon(\lambda)$) CD curves of $[Co(R,R\text{-cptn})_3]^{3+}$ in the region of the first absorption band are compared with those of $[Co(R,R\text{-chxn})_3]^{3+}$ [11,17] and $[Co(R\text{-pn})_3]^{3+}$ [9,17] (Fig. 5). The signs of the configurational and the vicinal CD of the R,R-cptn complex are the same as those of the corresponding CD of the other complexes. However, there is a big difference in the relative CD strength of these two effects. In the $[Co(R,R\text{-cptn})_3]^{3+}$ complex, the vicinal CD is much stronger than the configurational CD, the relation being reversed in the other complexes. However, if the CD strength is neglected, there is no anomaly in the CD of the R,R-cptn complex; the Δ-configurational and the λ-gauche vicinal effects give CD with negative and positive signs, respectively, in the region of the first absorption band, in line with the

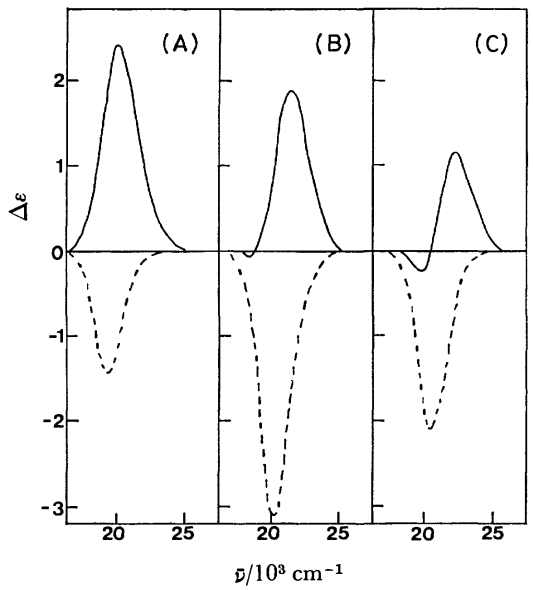

Fig. 5. Comparison of configurational ($\Delta\varepsilon(\Delta)$) (——) and vicinal ($3\Delta\varepsilon(\lambda)$) (——) effect CD of the $\Delta(lel_3)$-[Co(diamine)$_3$]$^{3+}$ complexes.
Diamine: (A) *R,R*-cptn, (B) *R,R*-chxn, (C) *R*-pn.

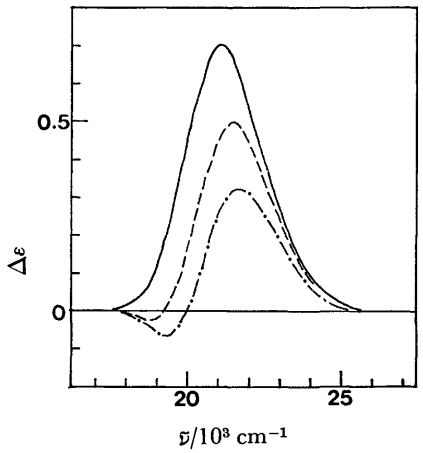

Fig. 6. CD spectra of the [Co(NH$_3$)$_4$(diamine)]$^{3+}$ complexes.
Diamine: *R,R*-cpth (——), *R,R*-chxn (——), *R*-pn (-•-•-).

general rule concerning the CD sign in this region and the absolute configuration of a cobalt(III) complex. It is therefore concluded that the anomalous CD pattern, the positive sign of the main CD band of $\Delta(\lambda\lambda\lambda)$-[Co(*R,R*-cptn)$_3$]$^{3+}$ results from the contribution of the stronger positive vicinal effect than the negative configurational effect. The Δ-[Co(*R,R*-chxn)$_3$]$^{3+}$ and Δ-[Co(*R*-pn)$_3$]$^{3+}$ complexes which give the negative main CD band in line with the general rule have a strong negative configurational CD as compared with the positive vicinal CD.

The reason why the cptn complex shows such anomalous CD differing from those of the chxn and pn complexes is not clear. Ito *et al.*[3] suggested from a comparison of the data of X-ray crystal analyses on several tris(diamine) complexes that the important factor governing the rotatory strength of d-d transitions in metal complexes is the cumulative effect of various distortions of the ligand atoms. The cptn chelate ring involves strain. The bond angles, NC(1)C(5)(119°) and C(2)C(1)C(5)(110°) deviate from the normal tetrahedral angle.[3] The [Co(tn)$_3$]$^{3+}$ complex (tn=trimethylenediamine) exhibiting an extremely weak CD in the region of the first absorption band[18] is also strained in the bond angle (CoNC=117.4°),[19] although the complex consists of six-membered chelate rings in the chair form. These strained complexes show CD spectra in the region of the first absorption band differing from those of other strain-free complexes. On the other hand, the vicinal effect CD of a 1,2-diamine chelate ligand depends on the chiral gauche conformation rather than on the asymmetric carbon atom.[20,21] The conformation of the chelate ring should be achiral, when it is in a *cis*, planar conformation. Thus the CD strength due to the vicinal effect of a chiral 1,2-diamine chelate ligand would depend on the dihedral angle of the N–C–C–N moiety of the puckered chelate ring. The strength of the vicinal CD increases in the order of the *R*-pn, *R,R*-chxn, and *R,R*-cptn complexes (Figs. 5 and 6). The order agrees with an increasing order of the observed dihedral angles of the chelate rings in (lel_3)-[Co(diamine)$_3$]$^{3+}$; *R*-pn(51°),[15] *R,R*-chxn(59°),[14] and *R,R*-cptn(61.5°).[3] Thus, the anomalous CD pattern in the region of the first absorption band of $\Delta(\lambda\lambda\lambda)(lel_3)$-[Co(*R,R*-cptn)$_3$]$^{3+}$ is understandable in terms of the strong vicinal effect of the cptn chelate ligand.

The authors wish to thank Dr. Shunji Utsuno, Shizuoka University, for the ^{13}C-NMR spectra. The work was partially supported by a Grant-in-Aid for Scientific Research from the Ministry of Education (No. 243013).

References

1) E. J. Corey and J. C. Bailar, Jr., *J. Am. Chem. Soc.*, **81**, 2620 (1959).
2) F. M. Jaeger and H. B. Blumendal, *Z. Anorg. Chem.*, **175**, 161 (1928); *Proc. Akad. Amsterdam*, **37**, 412 (1928); F. M. Jaeger, *Proc. Kon. Ned. Akad. Wetensch.*, **40**, 2, 108 (1937).
3) M. Ito, F. Marumo, and Y. Saito, *Inorg. Nucl. Chem. Lett.*, **6**, 519 (1970); *Acta Crystallogr., Sect. B*, **27**, 2187 (1971).
4) H. Toftlund and E. Pedersen, *Acta Chem. Scand.*, **26**, 4019 (1972).
5) M. Goto, M. Takeshita, and T. Sakai, *Bull. Chem. Soc. Jpn.*, **52**, 2589 (1979).
6) Y. Yoshikawa and K. Yamasaki, *Inorg. Nucl. Chem. Lett.*, **6**, 523 (1970).
7) H. Ogino and J. Fujita, *Bull. Chem. Soc. Jpn.*, **48**, 1836 (1975).
8) H. Ogino, *Bull. Chem. Soc. Jpn.*, **50**, 2459 (1977).
9) K. Ogino, K. Murano, and J. Fujita, *Inorg. Nucl. Chem. Lett.*, **4**, 351 (1968).
10) F. P. Dwyer, F. L. Garvan, and A. Shulman, *J. Am. Chem. Soc.*, **81**, 290 (1959).
11) S. E. Harnung. B. S. Sφrensen, I. Creaser, H. Maeqaard, U. Pfenninger, and C. E. Schaffer, *Inorg. Chem.*, **15**, 2123 (1976).
12) S. E. Harnung, S. Kallesφe, A. M. Sargeson, and C. E. Schaffer, *Acta Chem. Scand.*, **A28**, 385 (1974).

13) F. Mizukami, H. Ito, J. Fujita, and K. Saito, *Bull. Chem. Soc. Jpn.*, **45**, 2129 (1972).
14) F. Marumo, Y. Utsumi, and Y. Saito, *Acta Crystallogr., Sect. B*, **26** 1492 (1970).
15) H. Iwasaki and Y. Saito, *Bull. Chem. Soc. Jpn.*, **39**, 92 (1966).
16) C. T. Liu and B. E. Douglas, *Inorg. Chem.*, **3**, 1356 (1964).
17) M. Kojima and J. Fujita, unpublished data.
18) J. R. Gollogly and C. J. Hawkins, *J. Chem. Soc., Chem. Commun.*, **1968**, 689.
19) T. Nomura, F. Marumo, and Y. Saito, *Bull. Chem. Soc. Jpn.*, **42**, 1016 (1969).
20) C. J. Hawkins, E. Larsen, and I. Olsen, *Acta Chem. Scand.*, **19**, 1915 (1965).
21) B. Bosnich and J. MacB. Harrowfield, *J. Am. Chem. Soc.*, **94**, 3425 (1972).

 © 1980 The Chemical Society of Japan Bull. Chem. Soc. Jpn., 53, 1577—1583 (1980)

Kinetics and Mechanism of the Reactions of Bis(acetylacetonato)-palladium(II) with Alkylamines

Shinichi MATSUMOTO and Shinichi KAWAGUCHI*

Department of Chemistry, Faculty of Science, Osaka City University, Sumiyoshi-ku, Osaka 558

(Received October 15, 1979)

The reactions of bis(acetylacetonato)palladium(II), $Pd(acac)_2$, with alkylamines (L) such as butyl-, cyclohexyl-, diethyl-, and dipropylamines in methanol to afford $[Pd(acac)L_2](acac)$ obey the usual two-term rate law, rate$=(k_0+k_1[L])[Pd(acac)_2]$. On the other hand, the rate of reaction of $Pd(acac)_2$ with diethylamine in THF and benzene is expressed by rate$=(k_1+k_2[L])[L][Pd(acac)_2]$. A mechanism is proposed which presumes the hydrogen-bonding interaction of $Pd(acac)_2$ with methanol and amine. Intermediacy of Pd(acac)(acac-C^3)L in these reactions was denied on the basis of the kinetic studies, and the carbon-bonded complex was concluded to be produced *via* $[Pd(acac)L_2](acac)$. The equilibrium constants for the reactions, $Pd(acac)_2+2Et_2NH\rightleftarrows[Pd(acac)(Et_2NH)_2](acac)$ and $Pd(acac)(acac\text{-}C^3)(Et_2NH)+Et_2NH\rightleftarrows[Pd(acac)(Et_2NH)_2](acac)$ were determined in dichloromethane and methanol.

The central-carbon-bonded complexes of acetylacetone and other β-dicarbonyl compounds have long been known for platinum, mercury, and other rather soft metal ions.[1] Strange to say, the palladium(II) complex of this sort had not been reported before 1971, when Baba *et al.* found that bis(acetylacetonato)palladium(II), $Pd(acac)_2$,** reacts with bases such as triphenylphosphine, pyridine, and diethylamine to convert one of the chelating ligands into the central-carbon-bonded state.[2] The molecular structure of Pd(acac)(acac-C^3)PPh_3 was confirmed by X-ray analysis.[3] Similar reactions have been successfully carried out with $Pt(acac)_2$,[4] $AuMe_2(acac)$,[5] and $Pd(etac)_2$ (etac=O,O'-chelated monoanion of ethyl acetoacetate)[6] to obtain the central-carbon-bonded complexes of β-dicarbonyl compounds.

When bis(β-diketonato)palladium(II) was reacted with excess nitrogen bases (L), *e.g.* in neat liquid, the β-diketonate anion, (β-dik), such as acetylacetonate, trifluoroacetylacetonate, and hexafluoroacetylacetonate was expelled from the coordination sphere to produce $[Pd(\beta\text{-dik})L_2](\beta\text{-dik})$ or $[PdL_4](\beta\text{-dik})_2$ depending on the nature of L.[7] In order to clarify whether or not the chelated β-diketonate ligand dissociates *via* the central-carbon-bonded state, kinetic and equilibrium studies on the reactions of $Pd(acac)_2$ with several alkylamines have been performed by the spectrophotometric method.

Experimental

Materials. Bis(acetylacetonato)palladium(II) was prepared according to the literature[8] and recrystallized twice from benzene. Found: C, 39.52; H, 4.64%. Calcd for $C_{10}H_{14}O_4Pd$: C, 39.46; H, 4.59%. All of the amines used in the following preparation of complexes were dried with sodium sulfate and distilled before use. Methanol and benzene were dried with Linde Molecular Sieves 3A and 4A, respectively, and distilled. Tetrahydrofuran (THF) was kept standing with lithium aluminium hydride for several days prior to distillation. The distillate was dried with Linde Molecular Sieve 3A and redistilled. Dichloromethane was treated with potassium carbonate, dried with Linde Molecular Sieve 4A and distilled. Water contents of organic solvents were checked with an MCI digital water microanalyzer CA-OI to be $1—2\times10^{-3}$ mol dm^{-3} in benzene and $3—4\times10^{-3}$ mol dm^{-3} in other solvents employed.

Acetylacetonatobis(diethylamine)palladium(II) acetylacetonate, $[Pd(acac)(Et_2NH)_2](acac)$, was prepared by the method reported by Okeya *et al.*[7]; $Pd(acac)_2$ (0.400 g) was dissolved in hot diethylamine (5 ml) and the solution was cooled to -20 °C to deposit the product in a 22% yield. Found: C, 47.86; H, 8.08; N, 6.02%. Calcd for $C_{18}H_{36}O_4N_2Pd$: C, 47.97; H, 8.05; N, 6.21%.

Acetylacetonato(acetylacetonato-C^3)(diethylamine)palladium(II), Pd(acac)(acac-C^3)(Et_2NH), was prepared according to Baba *et al.*[2] and recrystallized from dichloromethane–petroleum ether (bp *ca.* 50 °C). Found: C, 47.11, H, 5.07; N, 3.71%. Calcd for $C_{14}H_{25}O_4NPd$: C, 47.11; H, 5.00; N, 3.65%.

Acetylacetonatobis(cyclohexylamine) palladium(II) acetylacetonate, $[Pd(acac)(cyhxNH_2)_2](acac)$, was obtained as pale yellow fuzzy needles in a 68% yield on addition of diethyl ether to a reaction mixture of $Pd(acac)_2$ (0.200 g) with cyclohexylamine (2 ml) in dichloromethane (10 ml) after 30 min stirring at room temperature, and recrystallized from dichloromethane–diethyl ether. Found: C, 52.74; H, 8.15; N, 5.80%. Calcd for $C_{22}H_{40}O_4N_2Pd$: C, 52.57; H, 8.02; N, 5.57%.

Preparation and recrystallization of these mixed-ligand complexes must be carried out quickly to obtain pure substances. Prolonged handling in solution induces side reactions. Acetylacetonatobis(butylamine)palladium(II) and acetylacetonatobis(dipropylamine) palladium(II) acetylacetonates were also prepared but did not give satisfactory analyses, probably owing to contamination with by-products containing the carbon-bonded acetylacetonate ligand.

Kinetic and Equilibrium Measurements. Absorption spectra were measured with a Hitachi EPS-3T recording spectrophotometer. The reactions of $Pd(acac)_2$ with alkylamines were followed spectrophotometrically at 330 nm, the absorption maximum of the startimg complex. A large excess (50—10000 times) of amine was employd against $Pd(acac)_2$ ($6—50\times10^{-5}$ mol dm^{-3}) to attain the pseudo first order condition. The reaction of Pd(acac)(acac-C^3)(Et_2NH) with diethylamine was also followed spectrophotometrically at 295 nm and the pseudo first order condition was fulfilled by using 5000—15000 times amine against the complex ($8—11\times10^{-5}$ mol dm^{-3}).

** In this paper, acac represents an acetylacetonate anion chelated to a metal ion through two oxygen atoms, and acac-C^3 and acac-O stand for acetylacetonate anions bonded as a unidentate to a metal ion through the central carbon and an oxygen, respectively.

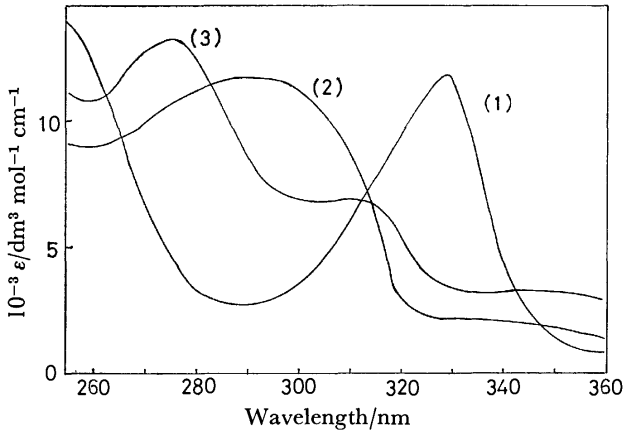

Fig. 1. Absorption spectra of $Pd(acac)_2$ (1), [Pd(acac)-$(Et_2NH)_2$] (acac) (2), and Pd (acac) (acac-C^3) (Et_2NH) (3) in dichloromethane.

In the experiments to determine the equilibria in dichloromethane, solutions containing [Pd(acac)$(Et_2NH)_2$] (acac) (1—4×10^{-2} mol dm^{-3}) and diethylamine (0—4×10^{-2} mol dm^{-3}) were kept at 25 °C for 24 h. Absorption spectra were measured immediately after dilution of the equilibrated solution to *ca.* 10^{-4} mol dm^{-3}, and absorbances at 290, 300, 320, and 330 nm were used to determine concentrations of three complexes, $Pd(acac)_2$, Pd(acac)(acac-C^3)(Et_2NH), and [Pd-(acac)$(Et_2NH)_2$](acac) on the basis of their spectra displayed in Fig. 1. Equilibria in methanol were attained by mixing solutions of $Pd(acac)_2$ (2—8×10^{-5} mol dm^{-3}) and diethylamine (2—15×10^{-4} mol dm^{-3}) and keeping the mixture at 25 °C for 24 h. Absorbances at 330 nm were utilized to obtain the equilibrium concentrations of Pd $(acac)_2$ and [Pd(acac)$(Et_2NH)_2$] (acac).

Results

Kinetics of the Reactions of Pd(acac)$_2$ with Alkylamines. Figure 2 shows, as an example, the change of absorption

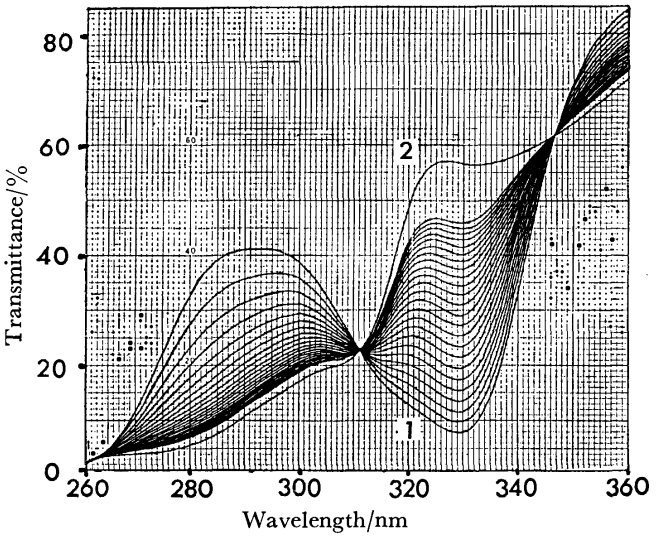

Fig. 2. The change of absorption spectrum with time during the reaction of $Pd(acac)_2$ (6.860×10^{-5} mol dm^{-3}) with diethylamine (2.039×10^{-1} mol dm^{-3}) in THF at 25.0 °C, curves 1 and 2 being spectra 2 min and *ca.* 4 h after commencement of the reaction, respectively.

TABLE 1. PSEUDO FIRST ORDER RATE CONSTANTS FOR THE REACTIONS OF $Pd(acac)_2$ WITH AMINES AT 25 °C

Solvent	10^5[Pd(acac)$_2$] / mol dm^{-3}	10^2[amine] / mol dm^{-3}	10^3k_{obsd} / s^{-1}
		butylamine	
CH_3OH	8.925	0.3475	1.60
		0.4545	2.05
		0.6621	2.77
		0.7848	3.33
		1.059	4.36
		1.324	5.37
		2.119	8.28
		cyclohexylamine	
	9.104	0.1753	0.742
		0.2566	0.924
		0.5006	1.54
		0.6632	1.92
		0.9340	2.66
		1.151	3.20
		1.476	3.93
		1.802	4.63
		dipropylamine	
	9.012	1.741	1.47
		2.176	1.76
		2.611	1.99
		2.901	2.22
		3.482	2.59
C_6H_6	8.431	27.53	0.4669
		59.00	1.710
		68.33	2.365
	11.10	42.93	0.9471
		91.86	4.467
		diethylamine	
CH_3OH	6.198	1.600	1.62
		2.188	2.19
		3.733	3.20
	7.273	0.8615	1.10
		1.354	1.58
		1.586	1.69
	7.622	1.805	1.75
		2.557	2.29
		2.858	2.48
		4.362	3.64
	50.12	1.285	1.34
		1.531	1.60
		3.365	3.10
C_6H_6	7.458	17.74	0.4332
		32.39	1.121
		46.08	2.110
	11.28	44.54	1.977
		55.67	3.302
		74.23	5.086
		89.08	7.471
		133.6	15.69
THF	6.860	20.39	0.636
		28.88	1.22
		34.66	1.61
		51.99	3.25
		69.32	5.44

spectrum with time during the reaction of $Pd(acac)_2$ with excess diethylamine in THF at 25 °C. Two distinct isosbestic points are observed at 311 and 347 nm, and curve 2 recorded *ca.* 4 h after the commencement of reaction coincides with the spectrum of authentic $[Pd(acac)(Et_2NH)_2](acac)$. These facts indicate that the overall reaction followed spectrophotometrically is expressed by Eq. 1 and there is no absorbing species involved in an appreciable amount except the starting and final complexes.

$$Pd(acac)_2 + 2Et_2NH \longrightarrow [Pd(acac)(Et_2NH)_2](acac) \quad (1)$$

Plots of $\log(A_t - A_\infty)$ *vs.* time gave straight lines over four half lives. Here A_t and A_∞ denote absorbances of the reaction mixture at time t and after completion of reaction, respectively. The same reaction in methanol and benzene also obeyed the pseudo first order kinetics.

Reactions of $Pd(acac)_2$ with other bases were carried out mainly in methanol. Reactions with cyclohexylamine and dipropylamine gave the final spectra, of which the former coincided with the spectrum of authentic $[Pd(acac)(cyhxNH_2)_2](acac)$. For the reaction with butylamine, a satisfactory spectrum at the infinite time could not be obtained owing to the succeeding reactions to yield $[Pd(BuNH_2)_4](acac)_2$, and the Guggenheim method[9] was employed to analyze the kinetic data.

Table 1 shows that the pseudo first order rate constants increase with the concentration of amine. However the exact dependence varies with the nature of solvent. As is seen in Fig. 3, the rate constants obtained from the reactions of several alkylamines in methanol increase with the amine concentration in accordance with the two term rate equation(2) which is characteristic of the ligand substitution reactions of square planar complexes which proceed according to the associative (**A**) mechanism.[10]

$$k_{obsd} = k_0 + k_1[amine] \quad (2)$$

These straight lines gave a practically common non-zero intercept, indicating the contribution of the solvent path. As is listed in Table 2, the second order rate constants exhibit a remarkable difference between the primary and secondary amines, the former reacting several times faster than the latter. The basicities of these amines are not so different; the pK_a values of the

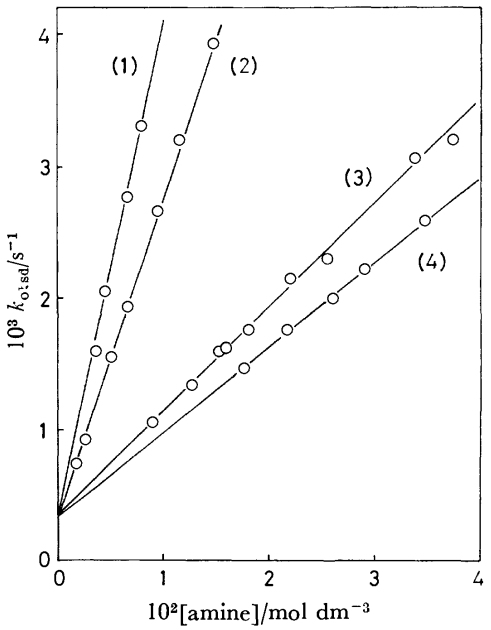

Fig. 3. Variation with the amine concentration of the pseudo first order rate constants for the reactions of $Pd(acac)_2$ with butylamine (1), cyclohexylamine (2), diethylamine (3), and dipropylamine (4) in methanol at 25 °C.

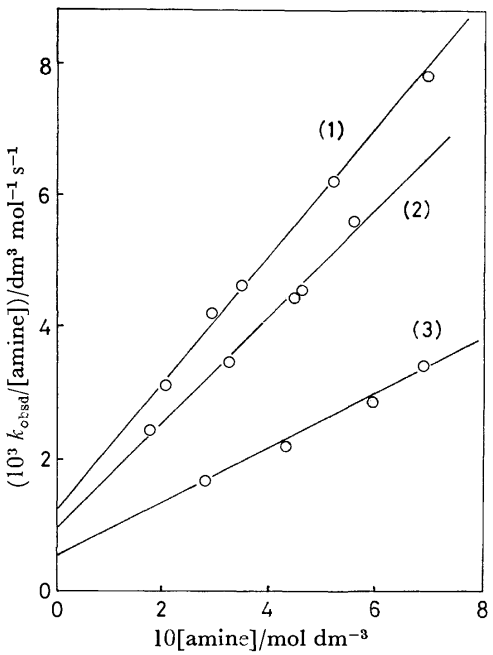

Fig. 4. Dependence on the amine concentration of the pseudo first order rate constants for the reactions of $Pd(acac)_2$ with diethylamine in THF (1) and benzene (2), and with dipropylamine in benzene (3) at 25 °C.

Table 2. Rate data for the reactions of $Pd(acac)_2$ with various amines at 25 °C

Solvent	Amine	10^4k_0 / s^{-1}	10^2k_1 / $dm^3\ mol^{-1}\ s^{-1}$	10^3k_2 / $dm^6\ mol^{-2}\ s^{-1}$
CH_3OH	butylamine	3.30±0.08	37.7 ±0.2	
	cyclohexylamine	3.32±0.07	24.3 ±0.2	
	diethylamine	3.40±0.09	8.27 ±0.09	
	dipropylamine	3.48±0.09	6.40 ±0.08	
THF	diethylamine		0.114±0.009	9.75±0.11
C_6H_6	diethylamine		0.094±0.007	8.10±0.08
	dipropylamine		0.035±0.007	4.80±0.07

conjugate acids are recorded as 10.64, 10.64, 10.93, and 11.00 at 25 °C for butylamine, cyclohexylamine, diethylamine, and dipropylamine, respectively.[11] The weaker nucleophilicity of the secondary amines than the primary amines seems to stem from their bulkiness. Steric influences of the entering as well as the leaving ligands have been established for amine substitution reactions of some platinum(II) complexes.[12]

On the other hand, the kinetic data obtained for the secondary amines in benzene and THF did not give linear plots similar to those in Fig. 3, but instead gave straight lines when k_{obsd}/[amine] was plotted against the amine concentration (Fig. 4), thus conforming to Eq. 3.

$$k_{obsd} = (k_1 + k_2[\text{amine}])[\text{amine}] \quad (3)$$

In these non-coordinating solvents the solvent path is not observed. The first term in Eq. 3 may correspond to the second term in Eq. 2, representing the reagent path. It should be noted, however, that the values of k_1 for the reactions of diethylamine in benzene and THF are about 1/80 of k_1 in methanol and k_1 for the dipropylamine reaction in benzene is less than 1/180 of that in methanol (Table 2). The k_2 path showing the second order dependence of the rate on the amine concentration has not been observed for usual substitution reactions of the square planar complexes. Some kind of specific interaction between $Pd(acac)_2$ and amine might assist the displacement of the acetylacetonate ligand. Table 3 lists the rate constants for the reaction of diethylamine at various temperatures and the kinetic parameters obtained from the Eyring plots.

Table 3. Rate constants at various temperatures and kinetic parameters for the reaction of $Pd(acac)_2$ with diethylamine

	10^2k_1 in CH_3OH / $dm^3\ mol^{-1}\ s^{-1}$	10^3k_1 in C_6H_6 / $dm^3\ mol^{-1}\ s^{-1}$	10^3k_2 in C_6H_6 / $dm^6\ mol^{-2}\ s^{-1}$
25 °C	8.27±0.09	0.94±0.07	8.10±0.08
30 °C	9.59±0.10	1.07±0.10	10.1±0.1
35 °C	10.3 ±0.1	1.24±0.11	11.9±0.2
40 °C	11.8 ±0.2	1.51±0.12	13.5±0.2
ΔH^*/KJ mol^{-1}	15±1	21±2	23±1
ΔS^*/J K^{-1} mol^{-1}	−20±4	−33±5	−9±5

With the aim of gaining an insight into the solvent effect, the reaction of $Pd(acac)_2$ with diethylamine was followed in mixtures of methanol and THF at various compositions. Figure 5 indicates that the rate equation (1) holds for the reactions in mixed solvents containing more than 4 mol dm^{-3} methanol, giving the k_0 and k_1 values as listed in Table 4. When the methanol content is as low as 0.485 mol dm^{-3}, on the other hand, the rate data deviate remarkably from linearity, but conform to the rate law (3) with $k_1 = 4.39 \times 10^{-3}$ $dm^3\ mol^{-1}\ s^{-1}$ and $k_2 = 1.05 \times 10^{-2}$ $dm^6\ mol^{-2}\ s^{-1}$. The rate data in solutions containing 2.25 and 1.18 mol dm^{-3} methanol well lie on straight lines, but gave negative k_0 values. The quadratic term with respect to the amine

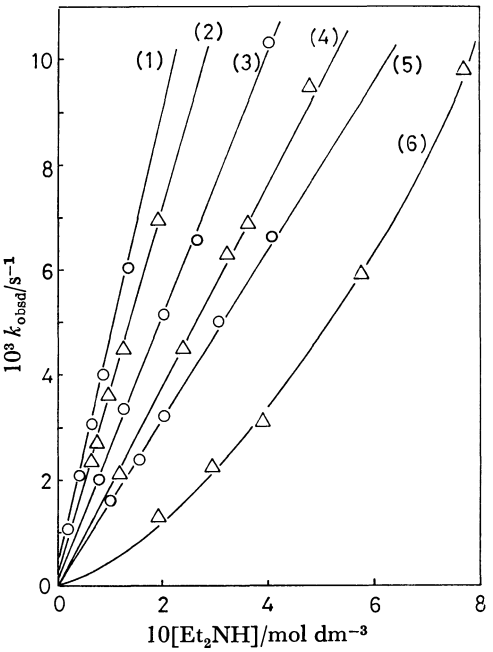

Fig. 5. Variation with the amine concentration of the pseudo first order rate constants for the reactions of $Pd(acac)_2$ with diethylamine in methanol-THF mixed solvents containing 12.4 mol dm^{-3} (1), 8.24 mol dm^{-3} (2), 4.12 mol dm^{-3} (3), 2.25 mol dm^{-3} (4), 1.18 mol dm^{-3} (5), and 0.485 mol dm^{-3} (6) methanol at 25 °C.

Table 4. Rate data for the reactions of $Pd(acac)_2$ with diethylamine in mixtures of methanol and THF at 25 °C

Mole fraction of CH_3OH	$[CH_3OH]$ / mol dm^{-3}	10^4k_0 / s^{-1}	10^2k_1 / $dm^3\ mol^{-1}\ s^{-1}$	10^2k_2 / $dm^6\ mol^{-2}\ s^{-1}$
1	24.7	3.40±0.09	8.27±0.09	
0.668	12.4	1.92±0.10	4.66±0.05	
0.501	8.24	1.04±0.10	3.58±0.04	
0.263	4.12	0.45±0.11	2.56±0.04	
0.151	2.25		2.07±0.02	
0.082	1.18		1.60±0.02	
0.034	0.485		0.439±0.011	1.05±0.01
0	0		0.114±0.009	0.975±0.011

concentration might contribute to the observed rates progressively with increase in the amine concentration, thus making slopes of the straight lines steeper than expected from Eq. 2. In the region where the methanol concentration is smaller than 1 mol dm^{-3}, k_1 decreases suddenly and the k_2 term contributes appreciably to the overall rate.

Kinetics of the Reaction of Acetylacetonato(acetylacetonato-C³)(diethylamine)palladium(II) with Diethylamine. Although the spectral change exemplified by Fig. 2 appears to correspond to a simple reaction, the reaction of $Pd(acac)_2$ with two molecules of amine such as Eq. 1 can not occur as an elementary reaction, but must consist of at least two steps, involving an intermediate which contains a unidentate acetylacetonate ligand.

$$Pd(acac)_2 + Et_2NH \longrightarrow Pd(acac)_2(Et_2NH) \quad (4)$$

$$Pd(acac)_2(Et_2NH) + Et_2NH \longrightarrow [Pd(acac)(Et_2NH)_2](acac) \quad (5)$$

As stated already, the reaction of $Pd(acac)_2$ with diethylamine in the preparative scale gave Pd(acac)-(acac-C^3)(Et_2NH) in a high yield.[2] In order to clarify whether the carbon-bonded acetylacetonato complex is involved as an intermediate in reaction (1), the rate of reaction (6) was measured in methanol at 25 °C.

$$Pd(acac)(acac\text{-}C^3)(Et_2NH) + Et_2NH \longrightarrow [Pd(acac)(Et_2NH)_2](acac) \quad (6)$$

The pseudo first order rate constants listed in Table 5 conform to the two term rate law (2) with $k_0=(9\pm3)\times10^{-6}$ s^{-1} and $k_1=(9.70\pm0.08)\times10^{-4}$ dm^3 mol^{-1} s^{-1}. Contribution of the solvent path (k_0) is negligibly small and the value of k_1 is two orders of magnitude smaller than that for the overall reaction (1). Thus the mixed-ligand complex containing a carbon-bonded acetylacetonate anion can not be an intermediate in reaction (1).

Table 5. Pseudo first order rate constants for the reaction of Pd(acac)(acac-C^3)Et_2NH with diethylamine in methanol at 25 °C

10^5[complex] / mol dm^{-3}	[amine] / mol dm^{-3}	$10^4 k_{obsd}$ / s^{-1}
11.08	0.656	6.19
	0.765	7.50
	1.129	10.7
8.524	0.921	8.64
	1.301	12.20

Equilibrium Studies. When a solution of [Pd(acac)(Et_2NH)$_2$](acac) in dichloromethane was kept standing for 24 h at 25 °C, an equilibrium was attained. Concentrations of three complexes involved were determined spectrophotometrically and used to calculate the equilibrium constants. The least-squares treatment of six sets of data gave the values $K_1=32.9\pm1.1$ dm^6 mol^{-2} for

$$Pd(acac)_2 + 2Et_2NH \overset{K_1}{\rightleftharpoons} [Pd(acac)(Et_2NH)_2](acac) \quad (7)$$

and $K_2=0.224\pm0.007$ dm^3 mol^{-1} for

$$Pd(acac)(acac\text{-}C^3)(Et_2NH) + Et_2NH \overset{K_2}{\rightleftharpoons} [Pd(acac)(Et_2NH)_2](acac). \quad (8)$$

Similar experiments were also performed in methanol, but the carbon-bonded complex was not involved in the equilibrium mixtures, the spectra being analyzed almost satisfactorily as mixtures of $Pd(acac)_2$ and [Pd(acac)(Et_2NH)$_2$](acac). A more precise value of K_1 in methanol at 25 °C was obtained as $(3.93\pm0.04)\times10^6$ dm^6 mol^{-2} from seven determinations started with a mixture of $Pd(acac)_2$ and diethylamine. The value is five orders of magnitude larger than that in dichloromethane, indicating an overwhelming stability of the salt-like complex in polar solvents such as methanol. In dichloromethane, on the other hand, the salt-like complex is unfavorable and converted into the carbon-bonded complex.

In order to see whether the carbon-bonded acetylacetonate can be transformed to the usual *O,O'*-chelate, *ca.* 10^{-5} mol dm^{-3} solutions of Pd(acac)(acac-C^3)-(Et_2NH) in dichloromethane and methanol were left standing. Spectroscopic assays at intervals over a period of several hours revealed no sign of production of $Pd(acac)_2$ but a slow decomposition was noticed. Thus the direct mutual conversion between the *O,O'*-chelated and the central-carbon-bonded states of acetylacetonate in palladium(II) complexes does not occur at all, but is reallized only *via* the outer-sphere complex.

Discussion

Kinetic studies on the bonding mode transformation of the β-diketonate ligand in metal complexes have scarcely been performed. Fish prepared a two-coordinate mercury(II) complex of 1,1,1,2,2,3,3-heptafluoro-7,7-dimethyl-4,6-octanedione and determined the rates at several temperatures of transformation of one of the two central-carbon-bonded ligands to the unidentate oxygen-bonding by means of the ^{1}H NMR spectroscopy.[13] He suggested a *C,C,O*-trihapto transition state for the intramolecular keto-enol tautomerization. Ito, *et al.* determined rates and kinetic parameters of three steps in the following reactions by ^{1}H NMR.[14]

$$Pt(acac)_2 \overset{+py}{\longrightarrow} Pt(acac)(acac\text{-}C^3)py \overset{+py}{\underset{-py}{\rightleftharpoons}} Pt(acac\text{-}C^3)_2(py)_2 \quad (9)$$

They also presumed a η^3-oxoallylic intermediate for the conversion of the *O,O'*-chelate to central-carbon-bonding.

In the present palladium(II) case, however, the kinetic studies unequivocally denies the intramolecular mechanism and supports the intermolecular one, one of the chelated acetylacetonate ligands leaving the coordination sphere first (Eq. 7), and then making a counterattack upon the metal atom as a carbanion (the reverse reaction of Eq. 8). Nucleophilic attack by the acetylacetonate carbanion upon the coordinated organic ligand has been occasionally demonstrated.[15,16] Although similar reactions of acetylacetonate with metal centers have not been documented explicitly thus far, the nucleophilic attack of the carbanion must be involved in preparation of the carbon-bonded acetylacetonato complexes with various metal ions.[1]

Reaction (8) is reversible and the carbon-bonded acetylacetonate can be displaced by an amine molecule. Thus formation and dissociation of the carbon-bonded acetylacetonate complex proceed *via* the outer-sphere complex, and the former can not be an intermediate in the formation reaction of the latter from $Pd(acac)_2$. The exact nature of the unidentate bonding of acetylacetonate in the intermediate complex (Eq. 4) is not clear, since the intermediate is not involved in an appreciable amount to allow the spectroscopic detection. However, the acetylacetonate in question may

be bonded to palladium *via* an oxygen atom. Such an ether-like bonding was first reported for the trialkyl(acetylacetonato-*O*)silicon complexes,[17] and was more recently found in Pt(acac-*O*)$_2$(PEt$_3$)$_2$[18] and Pt(acac-*O*)$_2$-(piperidine)$_2$.[19]

Pearson and Johnson[20] studied hydrolysis and other substitution reactions of Pd(acac)$_2$ in 91% water—9% methanol. A rapid equilibrium is assumed between the starting bis-chelate and an intermediate containing an oxygen-unidentate acetylacetonate ligand, which is displaced by a water molecule in the succeeding rate determining step. If this is the case for the present system, that is, if reaction (4) proceeds much faster and (5) is rate-determining, then reaction (4) should attain an equilibrium. When the equilibrium concentration of the intermediate is not negligibly small, it should be detected spectrophotometrically. On the other hand, when the equilibrium is not favorable to the intermediate, its concentration will increase with amine and the overall rate should be second order with respect to amine. In reality, the intermediate is not observed (Fig. 2) and the second order rate concerning amine is not observed for reactions in methanol. Thus reaction (4) is considered to be rate-determining, (5) proceeding faster.

The rate equation obtained in methanol (Eq. 2) and that in THF and benzene (Eq. 3) differ from each other. Although Eq. 2 involves the solvent term, Eq. 3 does not in spite of the fact that the donor number of THF (20.0) is similar to that of methanol (19.0).[21] Furthermore, k_1 which expresses the rate of the so-called reagent path increases quite remarkably when methanol is added to THF (Table 4). These results suggest some kind of interaction between Pd(acac)$_2$ and methanol to assist the attack of an amine molecule upon the palladium atom and/or the splitting of the Pd–O(acac) bond. Davis and Fackler showed from IR measurements that methanol forms hydrogen bonds with β-diketone chelates of various metal ions.[22] Recently Murthy and Shah found a slight blue shift and absorbance increase in the spectrum of tetrakis(acetylacetonato)thorium(IV) in dichloromethane on addition of methanol and other alcohols, and determined equilibrium constants for the adduct formation reactions, K for methanol being 2.0 dm^3 mol^{-1} at 30.0 °C.[23] Unfortunately the present Pd(acac)$_2$—methanol system showed no appreciable IR or electronic spectral change, but the hydrogen bond formation between them is conceivable and the scheme depicted in the upper part of Fig. 6 is proposed to the reaction in methanol. Analogously the second order term in Eq. 3 is presumed to originate from the hydrogen-bond interaction between Pd(acac)$_2$ and amine, and the lower part of Fig. 6 is proposed to the reaction in aprotic solvents.

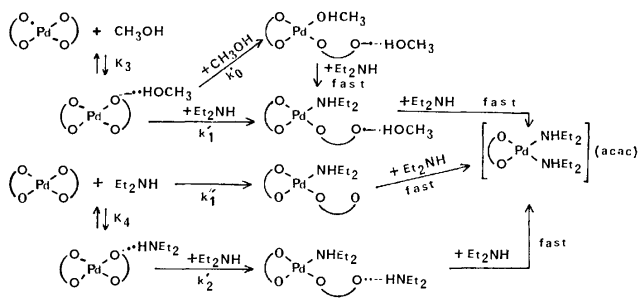

Fig. 6. Proposed mechanism for the reactions of Pd(acac)$_2$ with diethylamine in methanol and other aprotic solvents such as THF and benzene.

According to the proposed scheme the pseudo first order rate constant is calculated to be

$$k_{obsd} = \frac{k_0'K_3[CH_3OH]^2+(k_1'K_3[CH_3OH]+k_1''+k_2'K_4[amine])[amine]}{1+K_3[CH_3OH]+K_4[amine]}. \quad (10)$$

For the reaction in THF or benzene, this reduces to

$$k_{obsd} = \frac{(k_1''+k_2'K_4[amine])[amine]}{1+K_4[amine]}, \quad (11)$$

which coincides with Eq. 3 when $1 \gg K_4[amine]$, resulting in

$$k_1 = k_1'' \text{ and } k_2 = k_2'K_4. \quad (12)$$

In methanol $K_3[CH_3OH] \gg 1+K_4[amine]$, that is all of the Pd(acac)$_2$ molecules are presumed to interact with methanol, and Eq. 10 reduces to Eq. 2, k_0 and k_1 being $k_0'[CH_3OH]$ and k_1', respectively.

For reactions in mixed solvents which obey the rate equation (2) rather than (3), the pseudo first order rate constant will be expressed by

$$k_{obsd} = \frac{k_0'K_3[CH_3OH]^2+(k_1'K_3[CH_3OH]+k_1'')[amine]}{1+K_3[CH_3OH]}, \quad (13)$$

giving, on comparison with Eq. 2,

$$k_0 = \frac{k_0'K_3[CH_3OH]^2}{1+K_3[CH_3OH]} \quad (14)$$

$$\frac{[CH_3OH]}{k_0} = \frac{1}{k_0'} + \frac{1}{k_0'K_3[CH_3OH]},$$

and

$$k_1 = \frac{k_1'K_3[CH_3OH]+k_1''}{1+K_3[CH_3OH]} \quad (15)$$

$$\frac{1}{k_1-k_1''} = \frac{1}{k_1'-k_1''} + \frac{1}{(k_1'-k_1'')K_3[CH_3OH]}.$$

Although the plot of $[CH_3OH]/k_0$ *vs.* $1/[CH_3OH]$ shows a straight line except one point (Fig. 7), the k_0 data are insufficient and include larger uncertainties with

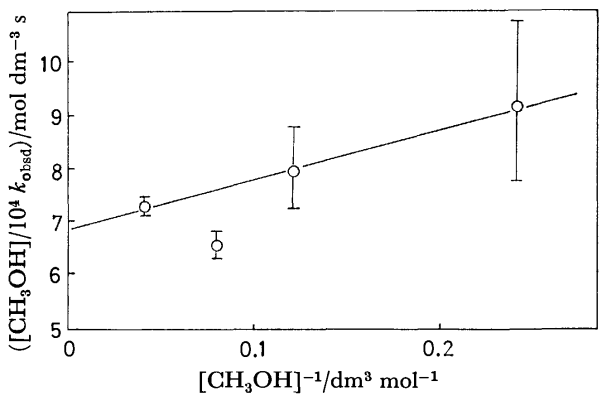

Fig. 7. Plot of k_0 with respect to the methanol concentration in methanol–THF solutions.

decreasing methanol concentration, precluding assignment of reliable values to k_0' and K_3. The trial to find an appropriate value for k_1'' to obtain a good linear plot according with Eq. 15 has also failed. Contrary to expectation based on Eq. 15, k_1 increases almost linearly with the concentration of methanol (Table 4). The rate constants k_1' and k_1'' might change intrinsically with the nature of medium. It is regrettable that various kinds of solvents can not be used for the present reaction owing to the solubility trouble.

We wish to thank the Ministry of Education for the Grant-in-Aid for Scientific Research (No. 243014).

References

1) D. Gibson, *Coord. Chem. Rev.*, **4**, 225 (1969).
2) S. Baba, T. Ogura, and S. Kawaguchi, *Inorg. Nucl. Chem. Lett.*, **7**, 1195 (1971); *Bull. Chem. Soc. Jpn.*, **47**, 665 (1974).
3) M. Horike, Y. Kai, N. Yasuoka, and N. Kasai. *J. Organomet. Chem.*, **72**, 441 (1974).
4) T. Ito, T. Kiriyama, and A. Yamamoto, *Bull. Chem. Soc. Jpn.*, **49**, 3250 (1976).
5) S. Komiya and J. K. Kochi, *J. Am. Chem. Soc.*, **99**, 3695 (1977).
6) S. Okeya and S. Kawaguchi, *Inorg. Chem.*, **16**, 1730 (1977).
7) S. Okeya, Y. Onuki, Y. Nakamura, and S. Kawaguchi, *Chem. Lett.*, **1977**, 1305.
8) A. A. Grinberg and L. K. Simonova, *Zhur. Priklad. Khim.*, **26**, 880 (1953); *Chem. Abst.*, **47**, 11060 g (1953).
9) A. A. Frost and R. G. Pearson, "Kinetics and Mechanism," 2 nd ed, Wiley, New York (1961), p. 49.
10) *E. g.* F. Basolo and R. G. Pearson, "Mechanism of Inorganic Reactions," 2 nd ed, Wiley, New York (1967), Chapt. 5.
11) J. A. Riddick and W. B. Bungel, "Organic Solvents," 3rd ed, Wiley-Interscience, New York (1970).
12) A. L. Odell and H. A. Raethel, *Chem. Commun.*, **1968**, 1323; **1969**, 87.
13) R. H. Fish, *J. Am. Chem. Soc.*, **96**, 6664 (1974).
14) T. Ito, T. Kiriyama, Y. Nakamura, and A. Yamamoto, *Bull. Chem. Soc. Jpn.*, **49**, 3257 (1976).
15) B. F. G. Johnson, J. Lewis, and M. S. Subramanian, *J. Chem. Soc., A*, **1968**, 1993; B. F. G. Johnson, T. Keating, J. Lewis, M. S. Subramanian, and D. A. White, *ibid.*, **1969**, 1793.
16) L. A. P. Kane-Maguire, *J. Chem. Soc., A*, **1971**, 1602; C. A. Mansfield and L.A.P. Kane-Maguire, *J. Chem. Soc., Dalton Trans.*, **1976**, 2187.
17) J. J. Howe and T. J. Pinnavaia, *J. Am. Chem. Soc.*, **91**, 5378 (1969); T. J. Pinnavaia, W. T. Collins, and J. J. Howe, *ibid.*, **92**, 4544 (1970).
18) T. Ito, T. Kiriyama, and A. Yamamoto, *Chem. Lett.*, **1976**, 835.
19) S. Okeya, F. Egawa, Y. Nakamura, and S. Kawaguchi, *Inorg. Chim. Acta*, **30**, L319 (1978).
20 R. G. Pearson and D. A. Johnson, *J. Am. Chem. Soc.*, **86**, 3983 (1964).
21) V. Gutman and R. Schmid., *Coord. Chem. Rev.*, **12**, 263 (1974).
22) T. S. Davis and J. P. Fackler, Jr., *Inorg. Chem.*, **5**, 242 (1966).
23) A. S. N. Murthy and S. B. Shah, *J. Inorg. Nucl. Chem.*, **40**, 1948 (1978).

Equilibrium, X-Ray, and ^{1}H-NMR Studies of the $ZrCr_2$–H System

Hideo Imoto,† Motoshige Sasaki,†† Taro Saito, and Yukiyoshi Sasaki*

Department of Chemistry, Faculty of Science, The University of Tokyo, Hongo, Bunkyo-ku, Tokyo 113

(Received October 16, 1979)

The pressure isotherms of the $ZrCr_2$–H system (20—200 °C, 10—700 Torr) and powder X-ray diffraction have shown the occurrence of two phases, cubic $ZrCr_2H_x$ ($x<1.0$) and hexagonal $ZrCr_2H_x$ ($2.5<x<3.5$). From the gradual change in the diffraction pattern with x, it has been concluded that samples with a low hydrogen concentration ($x<0.8$) contain another hexagonal phase. All these phases have Laves-type structures (C14 and C15). At 106 K, $ZrCr_2H_{2.66}$ has a much smaller second moment (7.2 G) of ^{1}H-NMR than the value calculated from the random-distribution model (77.9 G), which shows that the nearest sites can not be filled by hydrogen atoms at the same time. The system of $TiCr_2$–H has also been studied for comparison.

In 1961, Beck reported that the intermetallic compound $ZrCr_2$ absorbs hydrogen up to $ZrCr_2H_{3.42}$.[1] More recently, Pebler and Gulbransen have studied the equilibria of the system and have established the formation of a solid solution of hydrogen in the hexagonal-metal phase.[2] They observed at lower temperature, a tendency for phase separation which may occur below 0 °C, but no new phase was detected by X-ray diffraction studies. The present paper will show evidence for the formation of three different phases on the hydrogenation of $ZrCr_2$ by the use of X-ray and dissociation-pressure measurements. The results of the study of the $TiCr_2$–H system will be mentioned only briefly, because more extended data have been published after the completion of this work.[3] It is, though, worthy of note that our samples of $TiCr_2$ were of the C14 type and not the C15 type used by Reilly in Ref. 3.

$ZrCr_2$ and $TiCr_2$ are the only intermetallic phases in Zr– and Ti–Cr systems, and both form Laves phases. The low-temperature form of $TiCr_2$ has the cubic $MgCu_2$ (C15) structure, and it is transformed into the hexagonal $MgZn_2$ (C14) structure at 1220 °C. About the polymorphic nature of the $ZrCr_2$ compound, the literature presents conflicting reports. For instance, Rostoker reported that the transformation from the low-temperature form with the $MgCu_2$ structure to the form with the $MgZn_2$ structure occurs at 990—994 °C.[4] However, according to Alisova *et al.*, the $MgZn_2$-type structure is the low-temperature form and the transition temperature is 1480±10 °C.[5] As will be discussed later, the $ZrCr_2$ used in this work contained both the cubic and hexagonal forms.

Experimental

Materials. The starting materials were electrolytic chromium (99.2%), sponge titanium (99.8%), and sponge zirconium (99.8%). Intermetallic compounds were prepared by non-consumable arc-melting in an atomsphere of argon, the buttons being inverted and remelted several times to ensure homogeneity. X-Ray diffraction analyses showed both samples to contain only the intermetallic phases. It was found by X-ray fluorescence analysis that the non-iron impurity did not exceed 0.05% in the $ZrCr_2$ sample; the results of the chemical analyses were: Zr, 46.83% (calcd. 46.73%); Fe, 0.091%. The hydrogen for the experiments was obtained by the thermal decomposition of titanium hydride, which had been prepared from sponge titanium and high-purithy hydrogen (99.9999%). The titanium hydride was stored in a vacuum and had never been taken out into the atmosphere before experiments.

Equilibrium Studies and Preparation of Hydrided Samples. The apparatus for the measurements of the dissociation pressure and for the preparation of hydrided samples was a vacuum line made of glass equipped with four gas reservoirs, a silica tube in which samples were laid, and another silica tube for the generation of hydrogen from titanium hydride. The vacuum of the system before the experiments was under 10^{-6} Torr. The pressure of hydrogen was measured with a mercury manometer. The hydrogen composition (x) was calculated from the changes in the quantity of hydrogen gas, as determined by the pressure measurements. Corrections for the volume change of the manometer and for the temperature of the heated part of the sample tube had been previously determined. The temperature of the sample was controlled within ±1 °C by the use of a thermostat and an oil bath. For the measurements of the dissociation pressures, several grams of the intermetallic compounds crushed into grains (10—20 mesh) with an Ellis mortar were used. The samples for X-ray and ^{1}H-NMR studies were prepared as follows: after preliminary hydrogenation, the intermetallic compound was powdered, dehydrided and hydrided again to give samples containing certain quantities of hydrogen. The samples were not crushed or powdered after the final preparation.

X-Ray and ^{1}H-NMR Studies. The X-ray studies were performed with a powder diffractometer using Ni-filtered Cu K_α radiation at an ambient temperature. Silicon was used as the internal standard. For the intensity measurements, samples were sprinkled on sample holders coated with adhesive agent. The least squares of the lattice parameters and the calculation of the reflection intensities were performed on a HITAC 8700/8800 computer at the Computer Centre of the University of Tokyo. The ^{1}H-NMR was measured with a Varian VF-16 wide-line spectrometer with a Varian variable-temperature accessory.

Results

The observed isotherms of the $ZrCr_2$–H and $TiCr_2$–H systems are shown in Fig. 1 and Fig. 2. The enthalpy and entropy changes of the reaction:

$$1/1.5\ ZrCr_2H_{1.0} + 1/2\ H_2 \longrightarrow 1/1.5\ ZrCr_2H_{2.5}$$

were calculated as $\Delta H = -11$ kcal/mol and $\Delta S = -26$ cal/K/mol (1 cal=4.184 J) from the temperature

† Present address: Max-Planck-Institut für Festkörperforschung, 7000 Stuttgart 80, BRD.

†† Present adderss: Ministry of Labor, Tokyo 100.

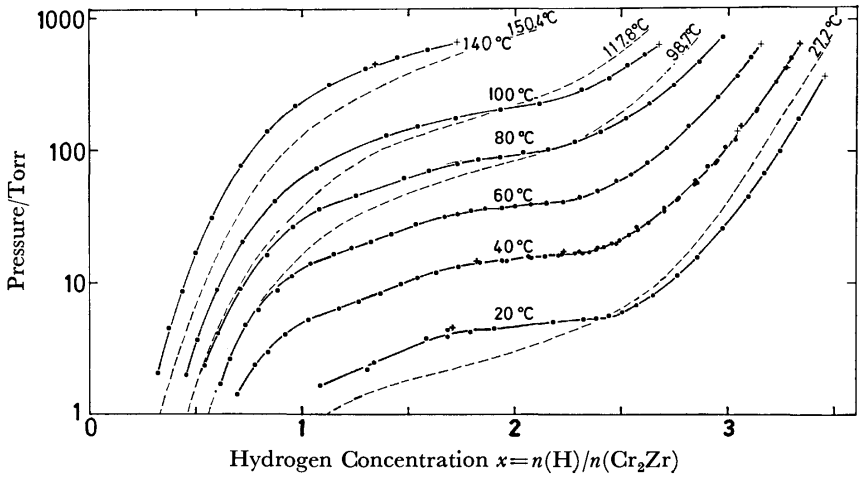

Fig. 1. Pressure-composition isotherms for the system of $ZrCr_2$–H.
+Dehydriding; ● hydring.

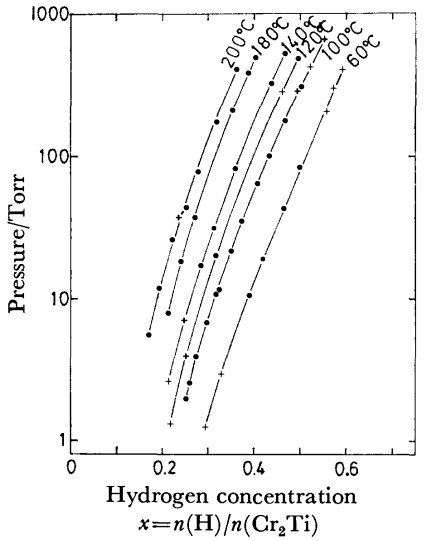

Fig. 2. Pressure-composition isotherms for the system of $TiCr_2$–H.
+ Dehydriding; ● hydriding.

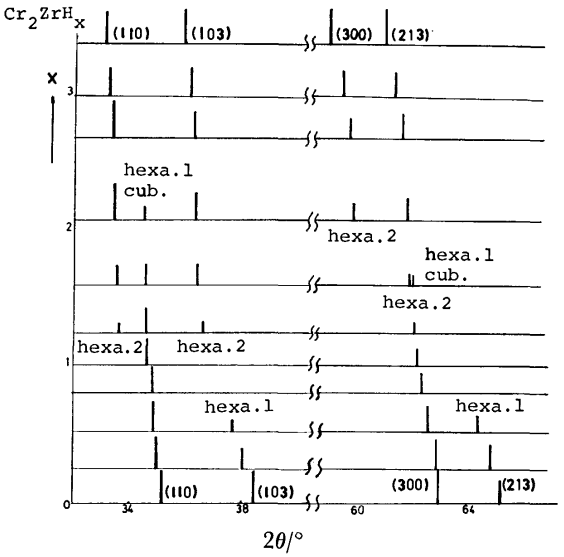

Fig. 3. Observed reflection-angles and -intensities of the powder X-ray diffration of $ZrCr_2H_x$.

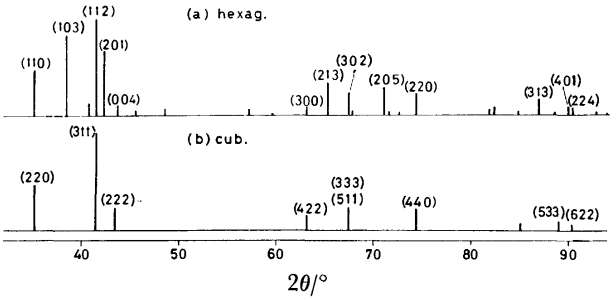

Fig. 4. Calculated reflection-angles and -intensities of the powder X-ray diffraction of $ZrCr_2$.
(a) The structure is assumed to be hexagonal Laves phase; (b) The structure is assumed to be cubic Laves phase.

dependence of the plateau pressure. The isotherms for the $ZrCr_2$–H system with plateaus showed that two phases coexist in the samples in the $1<x<2.5$ region, and the X-ray data confirmed it. A hydrogen-rich phase (α' phase) with a hexagonal $MgZn_2$-type structure (C14) and a hydrogen-poor phase with a cubic $MgCu_2$-type structure were observed with the X-ray techniques in the samples in the two-phase region. While the powder pattern of the hydrogen-rich phase did not change with the x value except for the lattice expansion, a gradual variation in the powder pattern was observed in the samples with low hydrogen concentrations, as is shown in Fig. 3. The powder pattern of the sample with $x=1.0$ is identical with the calculated pattern of the cubic structure (C15), while the pattern of the sample with a very low hydrogen concentration is similar to the hexagonal structure (C14) (Fig. 4). The sample with x value between these two extremes have powder patterns generated by the superposition of these two patterns. Though the calculated patterns of the hexagonal and cubic structures are very similar, some reflections, such as (103) and (213), of the hexagonal structure do not correspond to any reflection of the cubic phase. From the measurements of the intensities

of these reflections, the following was concluded: the starting material, $ZrCr_2$, which has been prepared by the dehydrogenation of $ZrCr_2H_x$, as has been described in the Experimental section, consists *ca.* 40% of the cubic (α_c) and *ca.* 60% of the hexagonal (α_h) phase. The samples with $x<0.8$ also consist of cubic (α_c) and hexagonal (α_h) phases, but the percentage of the cubic phase increase with the x value until it reaches 100% at $x=0.8$.

Table 1. Lattice constants of $ZrCr_2H_x$ and $TiCr_2H_x$
Standard deviations in parentheses.

	a/Å	c/Å
$ZrCr_2$ (α_h)	5.107(3)	8.290(8)
$ZrCr_2H_{0.250}$ (α_h)	5.119(2)	8.356(6)
$ZrCr_2H_{0.516}$ (α_h)	5.141(3)	8.383(8)
$ZrCr_2H_{1.582}$ (α')	5.342(2)	8.747(6)
$ZrCr_2H_{2.047}$ (α')	5.354(1)	8.746(10)
$ZrCr_2H_{2.824}$ (α')	5.376(1)	8.774(3)
$ZrCr_2H_{2.953}$ (α')	5.386(1)	8.801(3)
$ZrCr_2H_{3.340}$ (α')	5.420(1)	8.856(6)
$TiCr_2$	4.923(2)	7.990(4)
$TiCr_2H_{0.171}$	4.938(3)	8.026(10)
$TiCr_2H_{0.318}$	4.946(3)	8.074(12)
$TiCr_2H_{0.526}$	4.967(5)	8.131(14)
$ZrCr_2$ (α_c)	7.211(3)	
$ZrCr_2H_{0.250}$ (α_c)	7.237(2)	
$ZrCr_2H_{0.516}$ (α_c)	7.264(1)	
$ZrCr_2H_{0.795}$ (α_c)	7.298(4)	
$ZrCr_2H_{1.012}$ (α_c)	7.306(2)	
$ZrCr_2H_{1.232}$ (α_c)	7.322(3)	
$ZrCr_2H_{1.582}$ (α_c)	7.328(3)	

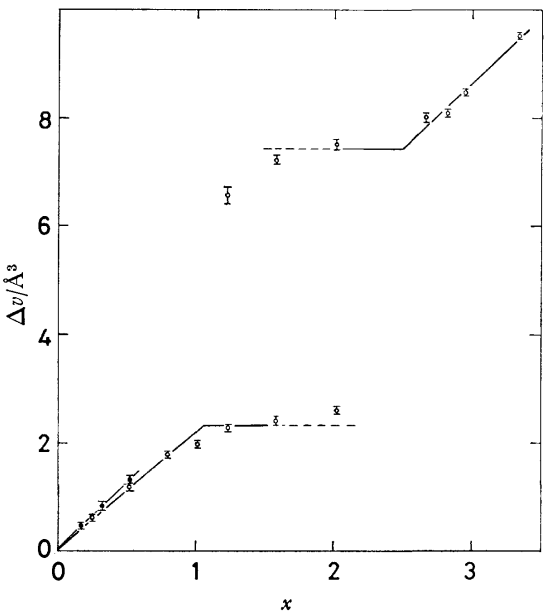

Fig. 5. Hydrogen-concentration dependence of the volume of MCr_2H_x with standard derviations.
M is Ti (filled circles) or Zr (unfilled circles). Δv means $\Delta V/Z$, where ΔV is the increase of the unit-cell volume of MCr_2H_x and Z is the number of MCr_2H_x units in a unit cell. $ZrCr_2H_x$) $0<x<1$) has two stuructures, but their Δv's are practically equal.

In contrast with $ZrCr_2H_x$, $TiCr_2H_x$ ($x<0.6$) had only a hexagonal $MgZn_2$-type structure (C14). The lattice constants of $ZrCr_2H_x$ and $TiCr_2H_x$ are shown in Table 1, while the increase of the volumes with the x value is shown in Fig. 5. The volume increase per hydrogen atom was 2.5 Å^3 for $TiCr_2H_x$ and 2.2 Å^3 for $ZrCr_2H_x$. These values are a little smaller than the values for palladium alloy–hydrogen systems reported by Baranowski *et al.* (11.5/4 Å^3=2.9 Å^3).[6]

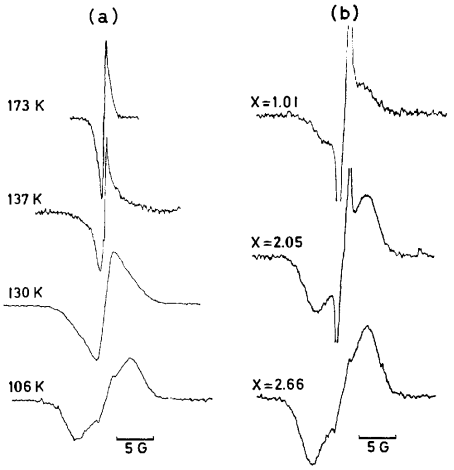

Fig. 6. ^{1}H-NMR spectrum of $ZrCr_2H_x$ at 3700 G.
(a) Temperature-dependence of the ^{1}H-NMR spectrum of $ZrCr_2H_{2.66}$; (b) Hydrogen-concentration dependence of the ^{1}H-NMR spectrum of $ZrCr_2H_x$ at 106 K.

The temperature dependence of the ^{1}H-NMR spectrum of $ZrCr_2H_x$ is shown in Fig. 6. A widening of the signal of hydrogen in the α' phase was observed at 173—106 K, but the signal of hydrogen in the α_c and α_h phases showed motional-narrowing even at 106 K. The second moment of the $ZrCr_2H_{2.66}$ sample at 106 K was 7.2 G^2 (1 G=10^{-4} T).

Discussion

The dissociation pressures of the $ZrCr_2$–H system obtained by the present authors are higher than those reported by Pebler and Gulbransen, as is shown in Fig. 1. To explain this discrepancy, the present authors assume some width of the nonstoichiometry of the $ZrCr_2$ phase, as in the case of $TiCr_2$, though it has not yet been reported how wide the phase is. Therefore, the difference in the dissociation pressure of $ZrCr_2H_x$ probably depends on the composition of the $ZrCr_2$ phase. A very small difference may be enough to explain the discrepancy in these two sets of data. The small variation in the dissociation pressure in the two-phase region ($1.0<x<2.5$) may also be caused by the nonstoichiometry of $ZrCr_2$, since a small inhomogeneity may inevitably be brought about in the sample prepared by arc-melting, which causes a fluctuation in the dissociation pressure of the sample.

In a Laves-phase compound, AB_2, if it has the ideal structure of the Laves phase, there are 24 tetrahedral holes around one larger atom, A, whether its structure is the $MgZn_2$ type or the $MgCu_2$ type. All these holes

have the same size, and hydrogen atoms are assumed to enter into these holes, because they are the largest ones. If all these holes were filled with hydrogen atoms, the composition of the compound would be AB_2H_{12}. Because the c/a ratios of the lattice constants of hexagonal $ZrCr_2$ and $TiCr_2$ are very close to the value of the ideal structure, $2\sqrt{6}/3$, and since they change very slightly with the x value, we can assume in the following discussions that they have the ideal structure of the Laves phase.

The tetrahedral holes in $ZrCr_2$ and $TiCr_2$ are all of almost the same size. Strictly speaking, the radii of the largest spheres that these holes can hold are calculated to be 0.349 Å for $ZrCr_2$ and 0.360 Å for $TiCr_2$ if we assume the atomic radii to be 1.2866 Å for chromium, 1.4615 Å for titanium, and 1.6027 Å for zirconium,[7] and if we assume the unit-cell volumes to be equal to the observed values of $ZrCr_2$ and $TiCr_2$. Therefore, the difference in the hydrogen-absorption ability between $ZrCr_2$ and $TiCr_2$ can not be attributable to the difference in the size of the holes of each intermetallic compound.

Since, around 106 K, the ^{1}H-NMR spectrum of $ZrCr_2H_{2.66}$ did not broaden as the temperature decreased, the hydrogen atoms are thought to form a rigid lattice. Therefore, the second moment of the spectrum can be compared with the theoretical value calculated using the following equation:[8]

$$M = \frac{9}{10}\gamma^2 N^{-1} \sum_{j \neq k} r_{jk}^{-6}$$

where M, γ, N, and r_{jk} are the second moment, the magnetic moment of a proton, the number of protons, and the distance between the protons j and k respectively. If we assume a random distribution of hydrogen atoms in all of the tetrahedral holes mentioned above, we get 77.9 G^2 as M, which is much larger than the observed value (7.2 G). This discrepancy suggests that a hydrogen atom occupying a hole prevents other hydrogen atoms from entering the neighboring holes. This seems probable, because the distance between the nearest holes are only about 1.2 Å. For the purpose of getting an approximate value of the second moment for the restricted random distribution in which a hydrogen atom has no neighbor within 1.5 Å, the above equation, excluding the terms in which r_{jk} is less than 1.5 Å has been calculated. The result of this calculation was 14.2 G^2; this value agrees better with the observation.

The transformation from the hexagonal α_h phase to the cubic α_c phase shown by the intensity variation in the X-ray diffraction in $ZrCr_2H_x$ is not analogous to any other found in metal–hydrogen systems, but the facts described below may support the occurrence of this transformation. The only difference between the two structures is their stacking order, the cubic phase having the ABCABC....order and the hexagonal phase having the ABAB....order.[9] Therefore, the transformation between the two structures may take place easily by means of a shear mechanism; indeed, in the $TiFe_2$ system a martensitic transformation between these structures has been proposed on the basis of the temperature dependence of the electric conductivity at low temperatures.[10] The reason why the coexistence of these two phases has not been shown by the isotherms may be that the plateau pressure is lower than the measured pressure range.

The authors gratefully acknowledge Dr. Keiichi Nakamura for his help in preparing samples and in NMR measurements at the Research Institute for Metals.

References

1) R. L. Beck, quoted by E. A. Aitken, "Intermetallic Compounds," ed by J. H. Westbrook, Wiley, New York (1967).
2) A. Pebler and E. A. Gulbransen, *Trans. Metall. Soc. AIME*, **239**, 1953 (1967).
3) J. R. Johnson and J. J. Reilly, *Inorg. Chem.*, **17**, 3103 (1978).
4) W. Rostoker, *Trans. AIME*, **197**, 304 (1953).
5) S. P. Alisova, P. B. Budberg, and K. I. Shakohova, *Sov. Phys. Crystallogr.*, **9**, 343 (1964).
6) B. Baranowski, S. Majchrzak, and T. B. Flanagan, *J. Phys., F*, **1971**, 258.
7) J. Donohue, "The Structures of Elements." Wiley-Interscience, New York (1974).
8) A. Abragam, "The Principle of Nuclear Magnetism," Clarendon Press, Oxford (1961).
9) W. B. Pearson, "The Crystal Chemistry and Physics of Metals and Alloys," Wiley-Interscience, New York (1972).
10) K. Ikeda, T. Nakamichi, and M. Yamamoto, *J. Phys. Soc. Jpn.*, **30**, 1504 (1971).

Circular Dichroism and Stereochemistry of Tetranuclear Cobalt(III) Complexes of Hexol Type. III.[1] The *meso*-2,3-Butanediamine, (*R*)-1,2-Propanediamine, and (*R,R*)-1,2-Cyclohexanediamine Complexes

Tomikatsu KUDO* and Yoichi SHIMURA

Department of Chemistry, Faculty of Science, Osaka University, Toyonaka, Osaka 560

(Received October 24, 1979)

Eight, six, and four optical isomers of diamine hexols $[Co\{(OH)_2Co(diamine)_2\}_3]^{6+}$ containing *meso*-2,3-butanediamine, (*R*)-1,2-propanediamine, and (*R,R*)-1,2-cyclohexanediamine, respectively, were separated by column chromatography. The absorption and CD (circular dichroism) spectra were measured in the visible and ultraviolet regions in 0.01 mol dm^{-3} HCl, the absolute configurations being determined mainly on the basis of the CD spectra. Assuming that the configurational chiralities are identical to those of the corresponding ethylenediamine hexol isomers, it has been established that the *lel* and *ob* orientations of the (*R*)-diamine ligand show different vicinal CD curves due to the asymmetric carbon atom in the ligand.

Eight optical isomers $\Lambda(\Lambda\Lambda\Lambda)$, $\Lambda(\Delta\Lambda\Lambda)$, $\Lambda(\Delta\Delta\Lambda)$, $\Lambda(\Lambda\Lambda\Delta)$, $\Lambda(\Delta\Delta\Delta)$, $\Lambda(\Delta\Lambda\Delta)$, $\Lambda(\Delta\Delta\Lambda)$, and $\Lambda(\Lambda\Delta\Lambda)$ are theoretically possible for a hexakis(diamine)-hexa-μ-hydroxo-tetracobalt(III) ion $[Co\{(OH)_2Co(diamine)_2\}_3]^{6+}$. All the eight isomers of $[Co\{OH)_2Co(en)_2\}_3]^{6+}$ (en hexol) were separated by column chromatography,[1] CD (circular dichroism) spectra being studied in comparison with that of the corresponding ammine hexol $[Co\{(OH)_2Co(NH_3)_4\}_3]^{6+}$.[2] Only a few investigations have been reported for hexol complexes containing optically active diamines; for example, Masuda and Douglas[3] reported only two and one of the possible eight optical isomers of $[Co\{(OH)_2Co((S)$- and (*R*)-1,2-propanediamine$)_2\}_3]^{6+}$, respectively. The present paper deals with the preparation and separation of $[Co\{(OH)_2Co(diamine)_2\}_3]^{6+}$ isomers, assignment of their absolute configurations, and discussion on the so-called vicinal CD curves due to the optically active diamines. (*R*)-(−)-1,2-propanediamine (*R*-pn), (*R,R*)-(−)-1,2-cyclohexanediamine (*R,R*-chxn), and *meso*-2,3-butanediamine (*meso*-2,3-bn) were used as diamine ligands.

Experimental

Preparation and Separation of Isomers. *1)* $[Co\{(OH)_2Co(meso\text{-}2,3\text{-}bn)_2\}_3]^{6+}$: The complex nitrate was prepared by a modification of the method for the corresponding ethylenediamine complex.[4] To 17.4 g of $Co(NO_3)_2\cdot 6H_2O$ in 20 cm^3 of water was slowly added 40 cm^3 of a 10% ice-cold aqueous solution of *meso*-2,3-butanediamine with stirring in an ice-bath. The mixture was vigorously stirred and oxidized by blowing compressed air on the surface for *ca.* 2h after cooling, the remaining solid being filtered off and washed with a small amount of water. The filtrate and washings were poured into a column (5 × 135 cm) of strong-acid ion-exchanger (SP Sephadex C-25, Na^+ form). After a broad pink-red band had been swept out with 0.1 M (1 M = 1 mol dm^{-3}) sodium d-tartrate solution, the adsorbed band was eluted with a sodium d-tartrate solution (0.17 M in the early stage of elution, and then 0.25 and 0.34 M successively in the later stages). During the course of elution the column was cooled by flushing cold (5 °C) water. The eluted eight brown bands were numbered B-1, B-2, ···, and B-8 in the order of elution. Each eluate was diluted about ten times with cold water which had been acidified to pH 4 with $HClO_4$, and the solution was passed through a small amount of strong-acid ion-exchanger (SP Sephadex C-25, Na^+ form). The complex on the exchanger was washed with a cold 0.01 M $NaClO_4$ solution and eluted with a cold 5 M $NaClO_4$ solution which had been acidified to pH 4 with $HClO_4$. Powdered sodium perchlorate was added to this eluate, and the solution was kept in a refrigerator. The desired complex was collected by filtration and washed with a cold ethanol–water (1: 1) solution, ethanol, and then ether. The brown crystals were dried in a vacuum desiccator over calcium chloride. Found for isomer B-1: C, 19.20; H, 5.48; N, 11.14%. Calcd for $[Co\{(OH)_2Co(meso\text{-}2,3\text{-}bn)_2\}_3](ClO_4)_6\cdot 2H_2O = C_{24}H_{78}N_{12}O_{30}Cl_6Co_4\cdot 2H_2O$: C, 19.22; H, 5.51; N, 11.21%. Found for isomer B-2: C, 19.22; H, 5.56; N, 11.08%. Calcd for $C_{24}H_{78}N_{12}O_{30}Cl_6Co_4\cdot 2.5H_2O$: C, 19.11; H, 5.55; N, 11.14%. The other isomers underwent mutarotation in the coures of crystallization, the products obtained showing the same CD pattern as that of the isomer B-1 or B-2 in the region 740—200 nm.

2) $[Co\{(OH)_2Co(R\text{-}pn)_2\}_3]^{6+}$: The isomers were prepared and separated by a similar procedure to that described in *1)* using (*R*)-1,2-propanediamine instead of *meso*-2,3-butanediamine. Eleven brown bands were confirmed on the chromatograph. Measurements of absorption and CD spectra confirmed that the first four and the next three bands give identical CD curves, respectively. Because of their low yields, the first four and the next three bands were combined respectively. They are denoted by P-1 and P-2, the remaining four bands being denoted by P-3, P-4, P-5, and P-6 in the order of elution. Crystallization was carried out as described in *1)*. Found for isomer P-1: C, 14.55; H, 4.89; N, 11.23%. Calcd for $[Co\{(OH)_2Co(R\text{-}pn)_2\}_3](ClO_4)_6\cdot 3H_2O\cdot 0.5NaClO_4 = C_{18}H_{66}N_{12}O_{30}Cl_6Co_4\cdot 3H_2O\cdot 0.5NaClO_4$: C, 14.47; H, 4.89; N, 11.23%. Found for isomer P-2: C, 15.01; H, 4.97; N 11.52%. Calcd for $C_{18}H_{66}N_{12}O_{30}Cl_6Co_4\cdot 2.5H_2O\cdot 0.25NaClO_4$: C, 14.86; H, 4.92; N, 11.55%. Found for isomer P-3: C, 13.66; H, 5.25; N, 10.61%. Calcd for $C_{18}H_{66}N_{12}O_{30}Cl_6Co_4\cdot 8H_2O\cdot 0.5NaClO_4$: C, 13.64; H, 5.22; N, 10.61%. Found for isomer P-4: C, 14.22; H, 5,34; N, 11.30%. Calcd for $C_{18}H_{66}N_{12}O_{30}Cl_6Co_4\cdot 7H_2O$: C, 14.36; H, 5.36; N, 11.17%. Found for isomer P-5: C, 13.93; H, 4.62; N, 10.90%. Calcd for $C_{18}H_{66}N_{12}O_{30}Cl_6Co_4\cdot 2.5H_2O\cdot NaClO_4$: C, 13.98; H, 4.63; N, 10.87%. Found for isomer P-6: C, 14.67; H, 5.14; N, 11.17%. Calcd for $C_{18}H_{66}N_{12}O_{30}Cl_6Co_4\cdot 5H_2O\cdot 0.25NaClO_4$: C, 14.41; H, 5.11; N, 11.21%.

3) $[Co\{(OH)_2Co(R,R\text{-}chxn)_2\}_3]^{6+}$: The isomers were prepared and separated by a similar procedure to that described in *1)* using (*R,R*)-1,2-cyclohexanediamine instead of *meso*-2,3-

butanediamine. The four brown bands on the chromatographic column are denoted by C-1, C-2, C-3, and C-4 in the order of elution. Each eluate was diluted *ca.* ten times with cold water which had been acidified to pH 4 with HCl, and was then adsorbed again on a small amount of strong-acid ion-exchanger (SP Sephadex C-25, Na^+ form). This was washed with a cold 0.01 M NaCl solution and eluted with a cold 3 M NaCl solution which had been acidified to pH 4 with HCl. Powdered sodium chloride was added to the eluate, and the solution was kept in a refrigerator. The desired complex was collected by filtration and washed with a cold ethanol–water (1: 2) solution ,ethanol, and then ether. The brown needle crystals were dried in a vacuum desiccator over calcium chloride. Isomer C-3 was obtained in a low yield because of its high solubility. Found for isomer C-1: C, 31.25; H, 7.60; N, 12.06; Cl, 16.79%. Calcd for $[Co\{(OH)_2Co(R,R\text{-chxn})_2\}_3]Cl_6 \cdot 7.5H_2O \cdot 0.5NaCl = C_{36}H_{90}N_{12}O_6Cl_6Co_4 \cdot 7.5H_2O \cdot 0.5NaCl$: C, 30.89; H, 7.56; N, 12.01; Cl, 16.46%. Found for isomer C-2: C, 32.05; H, 7.80; N, 12.13; Cl, 15.96%. Calcd for $C_{36}H_{90}N_{12}O_6Cl_6Co_4 \cdot 7.5H_2O$: C, 31.54; H, 7.72; N, 12.26; Cl, 15.52%. Found for isomer C-3: C, 31.01; H, 7.61, N, 12.07; Cl, 16.64%. Calcd for $C_{36}H_{90}N_{12}O_6Cl_6Co_4 \cdot 7.5H_2O \cdot 0.5NaCl$: C, 30.89; H, 7.56; N, 12.01; Cl, 16.46%. Found for isomer C-4: C, 31.90; H, 7.53; N, 12.30; Cl, 17.17%. Calcd for $C_{36}H_{90}O_6N_{12}Cl_6Co_4$ $6H_2O \cdot 0.5NaCl$: C, 31.49; H, 7.49; N, 12.24; Cl, 16.78%.

Measurements. The visible and ultraviolet absorption spectra were measured with a Shimadzu UV-200 spectrophotometer, and CD spectra with a JASCO MOE-1 spectropolarimeter. Measurements were carried out at room temperature in 0.01 M HCl and 0.15 M Na_2SeO_3.

Results and Discussion

Characterization of Isomers. The absorption and CD data of $[Co\{(OH)_2Co(meso\text{-}2,3\text{-}bn)_2\}_3]^{6+}$ isomers are summarized in Table 1. Since isomers B-3 to B-8 were not obtained as solid salt, their CD values were estimated on the basis of concentration which was calculated from the absorbance at 618 nm assuming the molar absorption coefficient $\varepsilon_{618} = 115$ mol^{-1} dm^3 cm^{-1}, which is the value for B-1 and B-2. The absorption intensities of eight en hexol isomers were almost equal at this wave-length.[1] It is evident from the CD data that B-1 is enantiomeric to B-2, as is B-3 to B-4, B-5 to B-6, and B-7 to B-8. The CD curves of isomers B-1, B-3, B-5, and B-7, all of which have a positive CD band at about 16200 cm^{-1}, are shown in Fig. 1. The data for the isomers of *R*-pn and *R,R*-chxn hexols are summarized in Tables 2 and 3, and the absorption and CD curves are shown in Figs. 2 and 3.

The absorption and CD spectra of the present hexols remained unchanged in the eluting solution at room temperature for *ca.* 24 h, being the same as those in 0.01 M HCl and in H_2O. All isomers, except for P-5, are fairly stable against mutarotation in 0.01 M HCl, in 0.15 M Na_2SeO_3, and in H_2O. P-5 undergoes mutarotation rather rapidly in 0.15 M Na_2SeO_3 and slowly in H_2O, but is fairly stable in 0.01 M HCl. In the column chromatography, P-1 and P-2 consist of four and three subbands, respectively. The subbands of each isomer show the same CD spectra in 0.01 M HCl. This indicates the occurrence of geometrical isomers due to the difference in arrangements of the asymmetric carbons. MacDermott[5] and Kojima

Table 1. Absorption and CD data of $[Co\{(OH)_2Co(meso\text{-}2,3\text{-}bn)_2\}_3]^{6+}$ in 0.01 M HCl

Wave numbers are given in 10^3 cm^{-1} unit, log ε or $\Delta\varepsilon$ values (in parentheses) in mol^{-1} dm^3 cm^{-1}.

Isomer	Absorption σ_{max} (log ε)	CD σ_{ext} ($\Delta\varepsilon$)
B-1		14.62 (−2.45)
	16.17 (2.06)	16.34 (+17.9)
	20.14 (2.64)	20.24 (−32.0)
		26.09 (+2.03)
	32.00 (3.78)	31.19 (−4.63)
		37.49 (+11.6)
	48.80 (4.81)	44.31 (+143)
B-2		14.59 (+2.47)
	16.15 (2.06)	16.36 (−18.1)
	20.13 (2.65)	20.24 (+31.8)
		26.16 (−2.01)
	31.98 (3.77)	31.19 (+4.68)
		37.59 (−11.5)
	48.92 (4.81)	44.42 (−148)
B-3		14.41 (−2.27)
	16.19	16.20 (+18.7)
	20.21	20.03 (−29.5)
		25.68 (+1.50)
	32.01	31.37 (−7.51)
		36.19 (+3.33)
		39.78 (−14.3)
	48.32	44.43 (+132)
B-4		14.38 (+2.32)
	16.20	16.23 (−18.5)
	20.21	20.05 (+29.8)
		25.62 (−1.59)
	32.00	31.40 (+7.56)
		36.25 (−3.26)
		39.69 (+14.6)
	48.41	44.53 (−137)
B-5		14.47 (−2.57)
	16.18	16.25 (+17.6)
	20.25	20.04 (−22.8)
		25.59 (+1.10)
	31.99	31.86 (−11.6)
		40.04 (−35.0)
	48.74	44.52 (+78.0)
B-6		14.44 (+2.53)
	16.19	16.28 (−17.6)
	20.23	20.04 (+22.6)
		25.63 (−1.07)
	32.00	31.80 (+11.3)
		40.13 (+35.3)
	48.68	44.62 (−78.4)
B-7		14.51 (−2.64)
	16.21	16.40 (+17.7)
	20.16	20.20 (−20.0)
		25.72 (+1.30)
	32.01	31.68 (−14.7)
		40.67 (−62.1)
	48.62	45.33 (+70.7)
B-8		14.53 (+2.63)
	16.19	16.39 (−17.9)
	20.18	20.21 (+19.7)
		25.72 (−1.34)
	32.00	31.71 (+14.8)
		40.60 (+62.6)
	48.73	45.41 (−71.6)

TABLE 2. ABSORPTION AND CD DATA OF $[Co\{(OH)_2Co(R\text{-pn})_2\}_3]^{6+}$ IN 0.01 M HCl

Wave numbers are given in 10^3 cm^{-1} unit, log ε or $\Delta\varepsilon$ values (in parentheses) in mol^{-1} dm^3 cm^{-1}.

Isomer	Absorption σ_{max} (log ε)	CD σ_{ext} ($\Delta\varepsilon$)
P-1		14.56 (−2.25)
	16.18 (2.03)	16.39 (+18.5)
	20.22 (2.60)	20.13 (−31.8)
		26.01 (+2.15)
	32.14 (3.78)	31.08 (−6.72)
		37.74 (+10.8)
	49.20 (4.76)	44.58 (+168)
P-2		14.61 (+2.26)
	16.11 (2.07)	16.36 (−22.0)
	20.25 (2.57)	20.16 (+33.9)
		25.86 (−1.15)
	32.06 (3.79)	30.92 (+6.22)
		37.52 (−8.38)
	49.20 (4.79)	44.51 (−137)
P-3		14.58 (−2.53)
	16.18 (2.03)	16.04 (+16.9)
	20.31 (2.55)	20.15 (−24.8)
		25.81 (+2.13)
	32.20 (3.77)	31.39 (−10.3)
		36.52 (+1.96)
		40.32 (−17.8)
	48.97 (4.76)	44.96 (+129)
P-4		14.54 (+2.36)
	16.11 (2.07)	16.34 (−19.5)
	20.30 (2.54)	20.24 (+29.4)
		25.76 (−0.91)
	32.13 (3.77)	31.34 (+7.10)
		36.44 (−2.58)
		40.13 (+13.9)
	48.97 (4.79)	44.90 (−132)
P-5		14.61 (+2.96)
	16.07 (2.11)	16.40 (−18.9)
	20.28 (2.50)	20.23 (+20.5)
		25.64 (−1.19)
	32.20 (3.77)	31.67 (+17.7)
		40.95 (+78.9)
	48.43 (4.76)	45.48 (−57.4)
P-6		14.57 (+2.60)
	16.08 (2.09)	16.36 (−18.1)
	20.29 (2.52)	20.23 (+22.9)
		25.62 (−0.89)
	32.14 (3.78)	31.76 (+11.7)
		40.54 (+41.9)
	48.61 (4.78)	45.02 (−90.3)

TABLE 3. ABSORPTION AND CD DATA OF $[Co\{(OH)_2Co(R,R\text{-chxn})_2\}_3]^{6+}$ IN 0.01 M HCl

Wave numbers[a] are given in 10^3 cm^{-1} unit, and log ε or $\Delta\varepsilon$ values (in parentheses) in mol^{-1} dm^3 cm^{-1}.

Isomer	Absorption σ_{max} (log ε)	CD σ_{ext} ($\Delta\varepsilon$)
C-1		14.41 (−2.15)
	16.3[sh] (2.00)	16.23 (+17.2)
	20.12 (2.65)	19.96 (−35.8)
		25.73 (+2.70)
	31.90 (3.82)	30.36 (−3.33)
		37.0[sh] (+22.0)
	46.20 (4.82)	43.29 (+160)
C-2		14.57 (+2.30)
	16.19 (2.08)	16.33 (−20.9)
	20.08 (2.56)	20.02 (+35.4)
		25.63 (−1.11)
	31.80 (3.82)	31.06 (+5.94)
		36.63 (−6.54)
	46.19 (4.84)	43.20 (−93.4)
C-3		14.51 (+2.57)
	16.10 (2.10)	16.30 (−19.9)
	20.10 (2.53)	20.04 (+26.8)
		25.50 (−1.09)
	31.80 (3.81)	31.41 (+12.6)
		39.68 (+33.9)
	45.60 (4.82)	43.60 (−52.2)
C-4		14.52 (−2.22)
	16.19 (2.06)	16.35 (+16.8)
	20.08 (2.56)	19.99 (−24.5)
		25.68 (+2.45)
	31.85 (3.81)	31.06 (−9.58)
		36.40 (+4.77)
		39.06 (−4.33)
	46.30 (4.81)	43.67 (+123)

a) sh=shoulder.

et al.[6-8] separated such geometrical isomers of mononuclear complexes *Δ*- and *Λ*-$[Co(R\text{-pn})_3]^{3+}$, *Λ*-$[Co(i\text{-bn})_3]^{3+}$, and *Λ*-$[Co(meso\text{-2,3-bn})_3]^{3+}$ by column chromatography (*i*-bn=2-methyl-1,2-propanediamine), but found their separation to be difficult, the absorption and CD spectra of the separated isomers being nearly identical. A similar kind of geometrical isomerism was expected for the *meso*-2,3-bn hexol, but no band separation was observed in the chromatography.

Absorption and CD Spectra. The absorption and CD spectra of the present hexols are similar to those of $[Co\{(OH)_2Co(en)_2\}_3]^{6+}$.[1] The absorption bands at *ca.* 16200 and 20200 cm^{-1} are assigned to the first d-d transition bands of CoO_6 and CoN_4O_2 chromophores, respectively. The second d-d transition bands of both chromophores seem to be masked by an intense band at *ca.* 32000 cm^{-1}, which is due to the charge transfer transition from the oxygen atom of the OH bridge groups to the central metal, $p_\pi(O)\rightarrow e_g(Co)$. The CD spectra show two extrema (the A_2 and E_a components of approximate D_3 symmetry) in the first d-d transition region of CoO_6 chromophore and one extremum (combined $B_1+A_2+B_2$ components) in the region of CoN_4O_2 chromophore. The CD intensity of CoN_4O_2 chromophore band at *ca.* 20000 cm^{-1} varies widely from isomer to isomer. The CD patterns in the d-d transition region are very similar, while those in the charge transfer transition region somewhat differ (Figs. 1—3).

When the CD spectrum of each isomer of *meso*-2,3-bn hexol is compared with that of the isomer of en hexol with the same fraction-number, *e.g.*, B-1 with E-1, the CD intensity and band shape in the d-d transition region are almost identical but the CD extremum

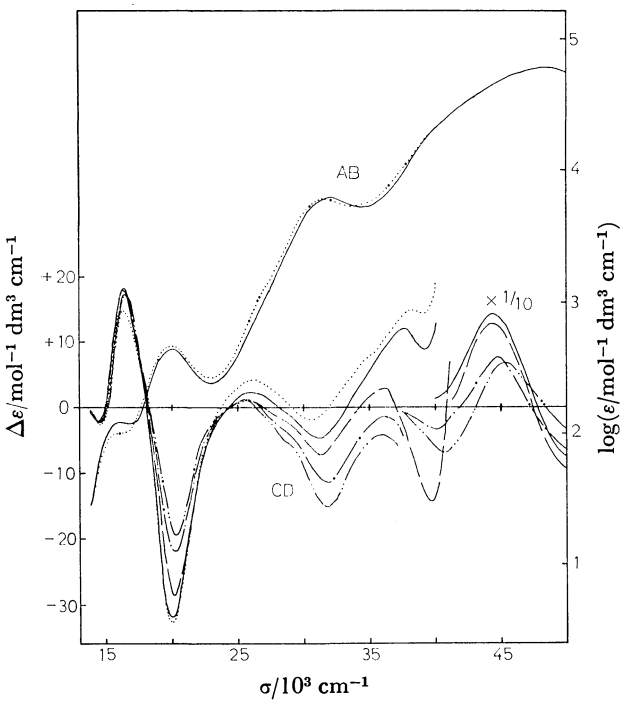

Fig. 1. Absorption (AB) and CD curves of $[Co\{(OH)_2Co(meso\text{-}2,3\text{-}bn)_2\}_3]^{6+}$.
Isomer B-1 (——), B-3 (——), B-5 (–·–·–), and B-7 (–··–··) in 0.01 M HCl and B-1 (------) in 0.15 M Na_2SeO_3.

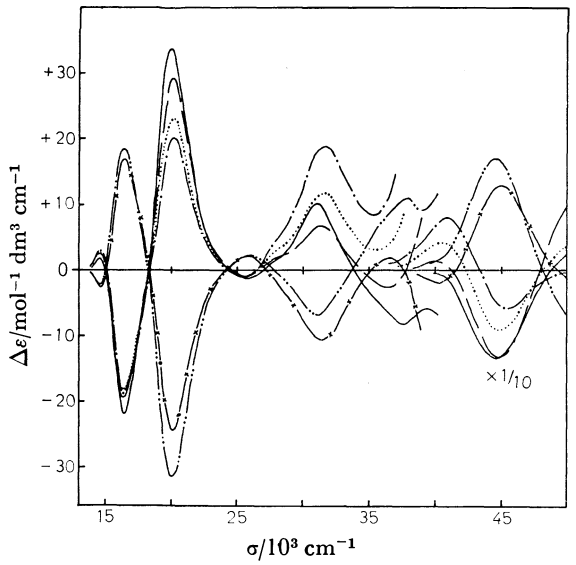

Fig. 2. CD curves of $[Co\{(OH)_2Co(R\text{-}pn)_2\}_3]^{6+}$.
Isomer P-1 (–··–··), P-2 (——), P-3 (–x–x–), P-4 (——), P-5 (–·–·–), and P-6 (------) in 0.01 M HCl.

positions shift to lower energy side in the isomer of *meso*-2,3-bn hexol. The shift approximately corresponds to the difference between the absorption peaks of *meso*-2,3-bn hexol and en hexol in the CoN_4O_2 chromophore region. The CD bands of not only CoN_4O_2 chromophore but also of CoO_6 chromophore shift to lower energy side. The d-d absorption peak of CoN_4O_2 chromophore varies in the following order of energy: NH_3[2]$<$*R,R*-chxn$\lesssim$*meso*-2,3-bn$<$*R*-pn$\lesssim$en.[1] The order coincides

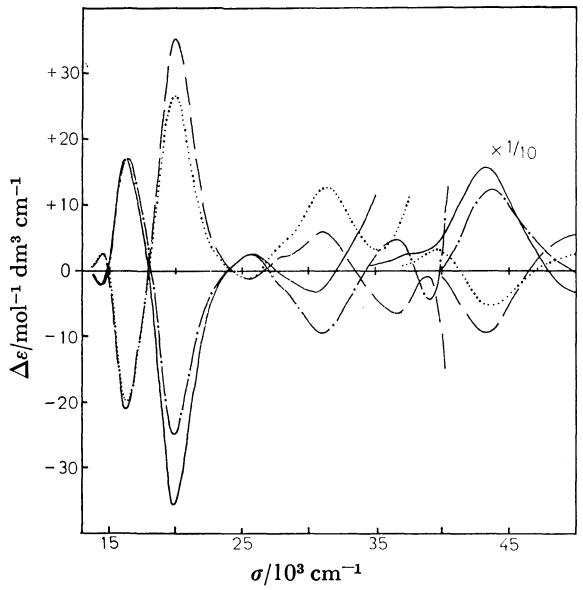

Fig. 3. CD curves of $[Co\{(OH)_2Co(R,R\text{-}chxn)_2\}_3]^{6+}$.
Isomer C-1 (——), C-2 (——), C-3 (------), and C-4 (–·–·–) in 0.01 M HCl.

approximately with that for mononuclear complexes of CoN_6 type.

Absolute Configuration. From the close resemblance between the CD spectra of $[Co\{(OH)_2Co(meso\text{-}2,3\text{-}bn)_2\}_3]^{6+}$ and $[Co\{(OH)_2Co(en)_2\}_3]^{6+}$ isomers, isomers B-1, B-3, B-5, and B-7 are assigned to $\Lambda(\Lambda\Lambda\Lambda)$, $\Lambda(\Delta\Lambda\Lambda)$, $\Lambda(\Delta\Delta\Lambda)$, and $\Lambda(\Delta\Delta\Delta)$, respectively, and B-2, B-4, B-6, and B-8 to $\Delta(\Delta\Delta\Delta)$, $\Delta(\Delta\Delta\Lambda)$, $\Delta(\Delta\Lambda\Lambda)$, and $\Delta(\Lambda\Lambda\Lambda)$, respectively. In a similar way, the absolute configurations of isomers P-1 and P-3 of $[Co\{(OH)_2Co(R\text{-}pn)_2\}_3]^{6+}$ are assigned to $\Lambda(\Lambda\Lambda\Lambda)$ and $\Lambda(\Delta\Delta\Lambda)$, respectively, and P-2, P-4, P-5, and P-6 to $\Delta(\Delta\Delta\Lambda)$, $\Delta(\Lambda\Lambda\Lambda)$, $\Delta(\Delta\Lambda\Lambda)$, and $\Delta(\Lambda\Delta\Lambda)$, respectively. Isomer P-5 underwent mutarotation in aqueous solution in a manner similar to that of the corresponding $\Delta(\Delta\Lambda\Lambda)$ isomer of en hexol. Isomers C-1, C-2, C-3, and C-4 of $[Co\{(OH)_2Co(R,R\text{-}chxn)_2\}_3]^{6+}$ are assigned to the absolute configurations $\Lambda(\Lambda\Lambda\Lambda)$, $\Delta(\Delta\Delta\Lambda)$, $\Lambda(\Delta\Delta\Lambda)$, and $\Delta(\Lambda\Lambda\Lambda)$, respectively. C-4 might be assigned alternatively to $\Delta(\Delta\Lambda\Lambda)$ from the CD pattern, particularly in the region of charge transfer transitions. The $\Delta(\Delta\Lambda\Lambda)$ isomers of en, *meso*-2,3-bn, and *R*-pn hexols underwent mutarotation, but not the isomer C-4. In view of vicinal effect, it is not adequate to assign this isomer to the $\Delta(\Delta\Lambda\Lambda)$ configuration. The absolute

Table 4. Absolute configurations of $[Co\{(OH)_2Co(diamine)_2\}_3]^{6+}$ isomers

Absolute configuration	en	*meso*-2,3-bn	*R*-pn	*R,R*-chxn
$\Lambda(\Lambda\Lambda\Lambda)$	E-1	B-1	P-1	C-1
$\Delta(\Delta\Delta\Delta)$	E-2	B-2	P-2	C-2
$\Lambda(\Delta\Delta\Delta)$	E-3	B-3	P-3	C-3
$\Delta(\Lambda\Lambda\Lambda)$	E-4	B-4	P-4	
$\Lambda(\Delta\Lambda\Lambda)$	E-5	B-5		
$\Delta(\Delta\Lambda\Lambda)$	E-6	B-6	P-6	C-4
$\Lambda(\Delta\Lambda\Lambda)$	E-7	B-7		
$\Delta(\Delta\Delta\Lambda)$	E-8	B-8	P-5	

configurations of all the hexol isomers containing diamines are given in Table 4.

The numbers of isomers of individual hexols obtained decrease in the order of diamines en>*R*-pn>*R,R*-chxn, the reverse order of bulkiness of the *C*-substituent groups. The repulsion between the non-bonded atoms seems to exist in the remaining less stable isomers, this being partly confirmed by the construction of molecular models of the missing isomers.

Additivity of CD Contributions. Assuming that the chromophore and configurational chirality of an *R*-pn (or *R,R*-chxn) hexol isomer are identical to those of the corresponding en hexol isomer, we get the following equation for the CD of these complexes:

$$\left.\begin{aligned} \Lambda(\Delta\Delta\Delta)^{R} &= \Lambda(\Delta\Delta\Delta)^{\mathrm{en}} + 6(R) \\ \Lambda(\Delta\Delta\Lambda)^{R} &= \Lambda(\Delta\Delta\Lambda)^{\mathrm{en}} + 6(R) \\ &\cdots\cdots\cdots\cdots \\ \Lambda(\Lambda\Lambda\Lambda)^{R} &= \Lambda(\Lambda\Lambda\Lambda)^{\mathrm{en}} + 6(R) \end{aligned}\right\} \quad (1)$$

where $\Lambda(\Delta\Delta\Delta)^{R}$ and $\Lambda(\Delta\Delta\Delta)^{\mathrm{en}}$ denote the CD of isomers $\Lambda(\Delta\Delta\Delta)$ of *R*-pn (or *R,R*-chxn) and en hexol, respectively, and (R) is the vicinal contribution of an *R*-pn (or *R,R*-chxn) ligand. By applying the observed CD curves of *R*-pn (*R,R*-chxn) and en hexol isomers to Eq. 1, the vicinal contribution curves (R) can be calculated (Figs. 4 and 5). The calculation was performed by using the observed CD curves of en hexol isomers, which were shifted by α (in cm^{-1}) to lower energy side (Table 5). The shift α was estimated from the difference between the CoN_4O_2 absorption peaks of the diamine and en hexol isomers. In the case of

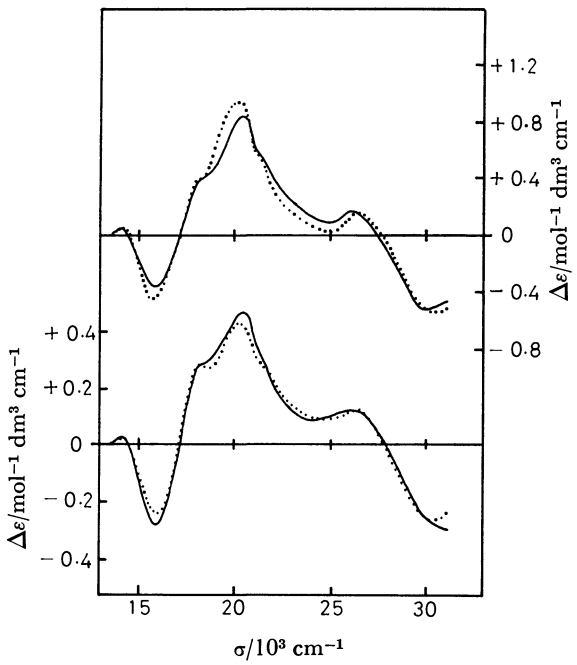

Fig. 4. Calculated vicinal CD curves $(R)_{tet}$.
$(R)^{R,R\text{-chxn}}_{\Delta\Delta\Delta} = \Delta\varepsilon\{(\text{C-2}) - \Delta\varepsilon(\text{E-2})\}/6$ (——), and $(R)^{R,R\text{-chxn}}_{\Delta\Delta\Delta} = \{\Delta\varepsilon(\text{C-3}) - \Delta\varepsilon(\text{E-3})\}/6$ (------) (upper curves); and $(R)^{R\text{-pn}}_{\Delta\Delta\Delta} = \{\Delta\varepsilon(\text{P-2}) - \Delta\varepsilon(\text{E-2})\}/6$ (——), and $(R)^{R\text{-pn}}_{\Delta\Delta\Delta} = \{\Delta\varepsilon(\text{P-3}) - \Delta\varepsilon(\text{E-3})\}/6$ (------) (lower curves).

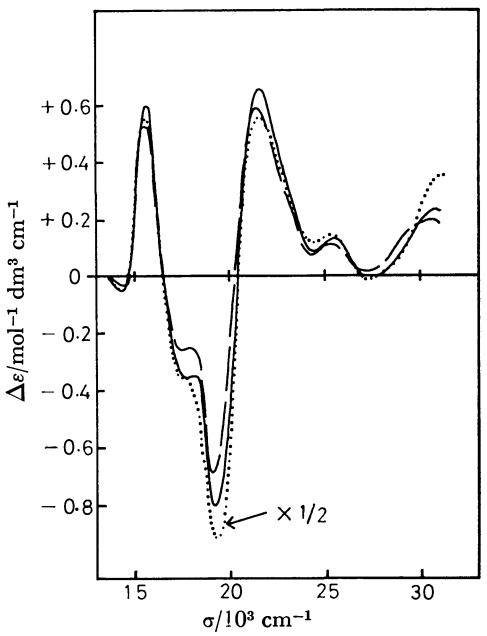

Fig. 5. Calculated vicinal CD curves $(R)_{ob}$.
$(R)^{R\text{-pn}}_{\Lambda\Lambda\Lambda} = \{\Delta\varepsilon(\text{P-1}) - \Delta\varepsilon(\text{E-1})\}/6$ (——), $(R)^{R\text{-pn}}_{\Lambda\Lambda\Lambda} = \{\Delta\varepsilon(\text{P-4}) - \Delta\varepsilon(\text{E-4})\}/6$ (——), and $(R)^{R,R\text{-chxn}}_{\Lambda\Lambda\Lambda} = \{\Delta\varepsilon(\text{C-1}) - \Delta\varepsilon(\text{E-1})\}/6$ (------).

TABLE 5. α VALUES REPRESENTING THE SHIFT OF CD PEAK OF DIAMINE HEXOL ISOMER TO LOWER ENERGY SIDE RELATIVE TO THAT OF THE CORRESPONDING ISOMER OF en HEXOL

Isomer	α/cm^{-1}	Isomer	α/cm^{-1}	Isomer	α/cm^{-1}
B-1	170	P-1	90	C-1	190
B-2	160	P-2	40	C-2	210
B-3	120	P-3	20	C-3	230
B-4	120	P-4	30	C-4	250
B-5	120	P-5	50		
B-6	110	P-6	40		
B-7	120				
B-8	130				

meso-2,3-bn hexol, the ligand has two asymmetric carbons of opposite chiralities, (R) and (S), no contribution of vicinal chiralities being expected in total. The calculated vicinal contribution is zero in the region 13800—30000 cm^{-1}.

As is seen in Figs. 4 and 5, the calculated vicinal contributions are equal when the isomers have the same absolute configuration in the three CoN_4O_2 chromophores, regardless of the absolute configuration of CoO_6 chromophore. However, the calculated vicinal CD curves are not equal when the absolute configuration of the three CoN_4O_2 chromophores is reversed, *viz.*, $(R)_{\Delta\Delta\Delta} \neq (R)_{\Lambda\Lambda\Lambda}$. The calculated vicinal CD curves of the *R*-pn and *R,R*-chxn hexol isomers with the same absolute configuration of CoN_4O_2 chromophores have very similar patterns, the CD intensity of vicinal contribution of *R,R*-chxn being about twice that of *R*-pn; thus the intensity is proportional to the number of asymmetric carbons.

The *R*-pn and *R,R*-chxn chelate rings have a λ

conformation. In the light of the *lel* and *ob* orientations[9] of C–C bonds of diamine chelate rings relative to the pseudo C_3 axis of individual CoN_4O_2 tris(chelate) chromophores, it is evident that the isomer $\{\Delta(\lambda\lambda)\Delta(\lambda\lambda)\Delta(\lambda\lambda)\}$ has the $lel_2lel_2lel_2$ form, $\{\Delta(\lambda\lambda)\Delta(\lambda\lambda)\Delta(\lambda\lambda)\}$ $lel_2lel_2ob_2$, $\{\Delta(\lambda\lambda)\Lambda(\lambda\lambda)\Delta(\lambda\lambda)\}$ $lel_2ob_2ob_2$, and $\{\Delta(\lambda\lambda)\Lambda(\lambda\lambda)\Lambda(\lambda\lambda)\}$ $ob_2ob_2ob_2$. Thus, Eq. 1 should be rewritten as follows:

$$\left.\begin{aligned}
\Delta(\Delta\Delta\Delta)^R &= \Delta(\Delta\Delta\Delta)^{en} + 6(R)_{lel} \\
\Delta(\Delta\Delta\Lambda)^R &= \Delta(\Delta\Delta\Lambda)^{en} + 4(R)_{lel} + 2(R)_{ob} \\
\Delta(\Delta\Lambda\Lambda)^R &= \Delta(\Delta\Lambda\Lambda)^{en} + 2(R)_{lel} + 4(R)_{ob} \\
\Delta(\Lambda\Lambda\Lambda)^R &= \Delta(\Lambda\Lambda\Lambda)^{en} + 6(R)_{ob} \\
&\cdots\cdots\cdots\cdots \\
\Lambda(\Lambda\Lambda\Lambda)^R &= \Lambda(\Lambda\Lambda\Lambda)^{en} + 6(R)_{ob},
\end{aligned}\right\} \quad (2)$$

where $(R)_{lel}$ and $(R)_{ob}$ denote the vicinal contribution due to the *lel* and *ob* forms of *R*-pn (or *R*,*R*-chxn) ligand, respectively. Thus, the vicinal CD curves calculated from isomers P-1, P-4, and C-1 are $(R)_{ob}$, and the curves calculated from isomers P-2, P-3, C-2, and C-3 are $(R)_{lel}$. The $(R)_{lel}$ curve differs definitely from the $(R)_{ob}$ one.

The vicinal contributions, $(R)_{lel}$ and $(R)_{ob}$, can be also calculated from the observed CD curves of isomers $\Delta(\Delta\Delta\Delta)$ and $\Delta(\Delta\Delta\Lambda)$ by applying Eq. 2:

$$(R)_{lel} = [2\{\Delta(\Delta\Delta\Lambda)^R - \Delta(\Delta\Delta\Lambda)^{en}\} - \{\Delta(\Delta\Lambda\Lambda)^R - \Delta(\Delta\Lambda\Lambda)^{en}\}]/6, \text{ and}$$

$$(R)_{ob} = [2\{\Delta(\Delta\Lambda\Lambda)^R - \Delta(\Delta\Lambda\Lambda)^{en}\} - \{\Delta(\Delta\Delta\Lambda)^R - \Delta(\Delta\Delta\Lambda)^{en}\}]/6.$$

As is seen in Fig. 6, the vicinal CD curves calculated from isomers $\Delta(\Delta\Delta\Lambda)$ and $\Delta(\Delta\Lambda\Lambda)$ agree with those calculated from $\Delta(\Delta\Delta\Delta)$, $\Delta(\Delta\Lambda\Lambda)$, $\Lambda(\Delta\Delta\Delta)$ or $\Lambda(\Lambda\Lambda\Lambda)$. This shows that the two vicinal contributions, $(R)_{lel}$ and $(R)_{ob}$, are additive.

Both vicinal contribution curves, $(R)_{lel}$ and $(R)_{ob}$, show rather strong CD even in the absorption region of CoO_6 chromophore which is separated far from the asymmetric carbons.

It was difficult to assign exactly the absolute configuration of the isomer C-4 of $[Co\{(OH)_2Co(R,R\text{-chxn})_2\}_3]^{6+}$ only from the CD pattern; it might be assigned to either $\Delta(\Delta\Delta\Lambda)$ or $\Delta(\Delta\Lambda\Lambda)$. If we apply the additivity between $(R)_{lel}^{R,R\text{-chxn}}$ and $(R)_{ob}^{R,R\text{-chxn}}$ obtained from C-1, C-2, or C-3 isomers, it is possible to see which of the following two relations is adequate:

a) $\{\Delta\varepsilon(\text{C-4}) - \Delta(\Delta\Delta\Lambda)^{en}\}/6 = \{2(R)_{lel}^{R,R\text{-chxn}} + (R)_{ob}^{R,R\text{-chxn}}\}/3$

b) $\{\Delta\varepsilon(\text{C-4}) - \Delta(\Delta\Lambda\Lambda)^{en}\}/6 = \{(R)_{lel}^{R,R\text{-chxn}} + 2(R)_{ob}^{R,R\text{-chxn}}\}/3.$

We see from Fig. 7 that the calculated curve $\{\Delta\varepsilon(\text{C-4}) - \Delta(\Delta\Lambda\Lambda)_{en}\}/6$ is very similar to the curve $\{(R)_{lel}^{R,R\text{-chxn}} + 2(R)_{ob}^{R,R\text{-chxn}}\}/3$. The calculated curve in this case is very similar to the curve calculated (intensity was doubled) from P-6 ($\Delta(\Delta\Lambda\Lambda)$). The absolute configuration of the isomer C-4 is therefore exactly assigned to $\Delta(\Delta\Lambda\Lambda)$.

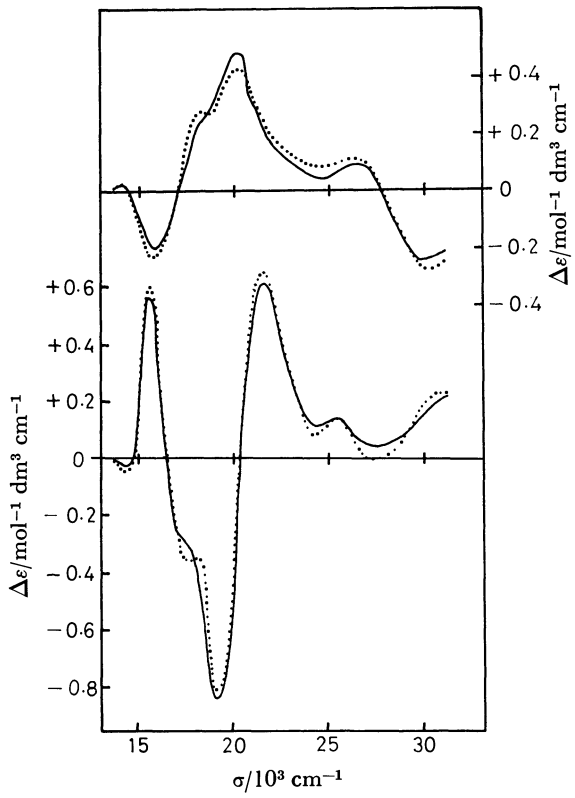

Fig. 6. Calculated vicinal CD curves.
$(R)_{lel}^{R\text{-pn}} = [2\{\Delta\varepsilon(\text{P-6}) - \Delta\varepsilon(\text{E-6})\} - \{\Delta\varepsilon(\text{P-5}) - \Delta\varepsilon(\text{E-8})\}]/6$ (——), and $\{\Delta\varepsilon(\text{P-3}) - \Delta\varepsilon(\text{E-3})\}/6$ (------) (upper curves); and $(R)_{ob}^{R\text{-pn}} = [2\{\Delta\varepsilon(\text{P-5}) - \Delta\varepsilon(\text{E-8})\} - \{\Delta\varepsilon(\text{P-6}) - \Delta\varepsilon(\text{E-6})\}]/6$(——), and $\{\Delta\varepsilon(\text{P-1}) - \Delta\varepsilon(\text{E-1})\}/6$ (------) (lower curves).

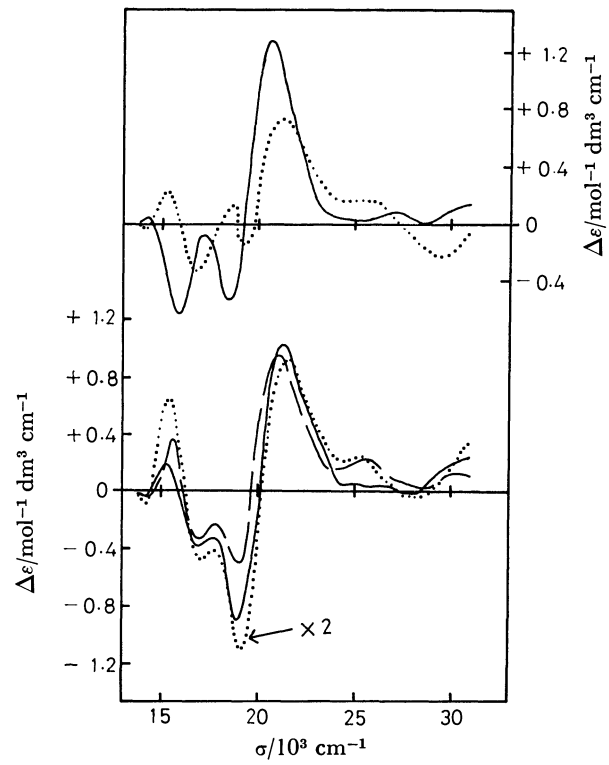

Fig. 7. Calculated CD curves.
$\{\Delta\varepsilon(\text{C-4}) - \Delta\varepsilon(\text{E-8})\}/6$ (——) and $\{2(R)_{lel}^{R,R\text{-chxn}} + (R)_{ob}^{R,R\text{-chxn}}\}/3$ (------) (upper curves), and $\{\Delta\varepsilon(\text{C-4}) - \Delta\varepsilon(\text{E-6})\}/6$ (——), $\{(R)_{lel}^{R,R\text{-chxn}} + 2(R)_{ob}^{R,R\text{-chxn}}\}/3$ (——), and $\{\Delta\varepsilon(\text{P-6}) - \Delta\varepsilon(\text{E-6})\}/6$ (------) (lower curves).

TABLE 6. EXTREMUM DATA (MEAN VALUES) OF OBTAINED VICINAL CD CONTRIBUTIONS
Wave numbers[a] are given in 10^3 cm^{-1} unit and $\Delta\varepsilon$ values (in parentheses) in mol^{-1} dm^3 cm^{-1}.

Assignment	$\frac{(R)_{lel}^{R\text{-pn}}}{\sigma_{ext}\ (\Delta\varepsilon)}$	$\frac{(R)_{lel}^{R,R\text{-chxn}}}{\sigma_{ext}\ (\Delta\varepsilon)}$	$\frac{(R)_{ob}^{R\text{-pn}}}{\sigma_{ext}\ (\Delta\varepsilon)}$	$\frac{(R)_{ob}^{R,R\text{-chxn}}}{\sigma_{ext}\ (\Delta\varepsilon)}$
A_2 (CoO_6)	14.18 (+0.02)	14.20 (+0.05)	14.41 (−0.05)	14.40 (−0.10)
E_a (CoO_6)	15.92 (−0.26)	15.84 (−0.41)	15.57 (+0.57)	15.61 (+1.11)
B_1 (CoN_4O_2)	18.20 (+0.27)	18.1^{sh} (+0.36)	17.48 (−0.31)	17.5^{sh} (−0.71)
A_2+B_2 (CoN_4O_2)	20.42 (+0.44)	20.34 (+0.90)	19.11 (−0.75)	19.23 (−1.87)
	21.8^{sh} (+0.12)	21.6^{sh} (+0.48)	21.56 (+0.63)	21.60 (+1.11)
2nd d-d transition	26.30 (+0.12)	26.41 (+0.17)	25.43 (+0.12)	25.51 (+0.29)

a) sh=shoulder.

The vicinal contribution of an (*R*)-diamine ligand consists of the conformational one (λ) and the vicinal one in a limited sence (*R*) due to the asymmetric carbons. Thus the vicinal contribution of an *R*-pn or *R,R*-chxn is presented by $(\lambda)+(R)$, the (*R*) being proportional to the number of asymmetric carbon atoms, *viz.*, $(R)^{R,R\text{-chxn}}=2(R)^{R\text{-pn}}$. On the other hand, the intensity of vicinal curves calculated by Eq. 2 for *R,R*-chxn hexol is about twice that of the *R*-pn hexol. The vicinal contribution due to the asymmetric carbons should be a dominant factor in this case, the conformational contribution hardly contributing at all to the overall vicinal CD. This indicates that the diamine conformation in en hexol is identical to that in *R*-pn or *R,R*-chxn hexol. An alternative but more plausible explanation is that the conformational contributions of diamine chelate rings are negligibly small in all the hexol type complexes. In many mononuclear complexes, the conformational effect contributes mainly to the overall vicinal CD.[10,11] In a limited number of mononuclear complexes, however, the vicinal contribution due to asymmetric carbons becomes a dominant factor.[12] The diamine hexols present an interesting example of the latter case.

Numerical data (mean values) of the individual vicinal CD contributions are given in Table 6.

References

1) Part II of this series: T. Kudo and Y. Shimura, *Bull. Chem. Soc. Jpn.*, **52**, 3553 (1979).
2) T. Kudo and Y. Shimura, *Bull. Chem. Soc. Jpn.*, **52**, 1648 (1979).
3) I. Masuda and B. E. Douglas, *J. Coord. Chem.*, **1**, 189 (1971).
4) A. Werner, *Chem. Ber.*, **40**, 2103 (1907).
5) T. E. MacDermott, *Inorg. Chim. Acta*, **2**, 81 (1968).
6) M. Kojima, Y. Yoshikawa, and K. Yamasaki, *Bull. Chem. Soc. Jpn.*, **46**, 1687 (1973).
7) M. Kojima, Y. Yoshikawa, and K. Yamasaki, *Inorg. Nucl. Chem. Lett.*, **9**, 689 (1973).
8) M. Kojima, Y. Yoshikawa, and K. Yamasaki, *Bull. Chem. Soc. Jpn.*, **48**, 2801 (1975).
9) J. Corey and J. C. Bailar, Jr., *J. Am. Chem. Soc.*, **81**, 2620 (1959).
10) C. J. Hawkins, E. Larsen, and I. Olsen, *Acta Chem. Scand.*, **19**, 1915 (1965).
11) C. J. Hawkins, "Absolute Configuration of Metal Complexes," Wily-Interscience, New York (1970).
12) H. Ito, J. Fujita, and K. Saito, *Bull. Chem. Soc. Jpn.*, **40**, 2584 (1967).

Stereoselective Association between Acetylacetonatobis(ethylenediamine)cobalt(III) and Malonate Ions as Studied by Nuclear Magnetic Resonance[1]

Hiroshi NAKAZAWA, Ushio SAKAGUCHI, and Hayami YONEDA*
Department of Chemistry, Faculty of Science, Hiroshima University, Hiroshima 730
(Received October 27, 1979)

The effect of added malonate upon the chemical shift and the exchange rate of amine hydrogens of acetylacetonatobis(ethylenediamine)cobalt(III) ion, $[Co(acac)(en)_2]^{2+}$, have been investigated by ^1H and ^{13}C NMR spectroscopy. In the absence of malonate, the amine groups give rise to two signals in the ^1H spectra and two rate constants of amine exchange due to *trans* and *cis* (to coordinated oxygen) amine groups. Upon addition of malonate, the *trans* NH_2 undergoes a down-field shift, the *cis* NH_2 resonance splitting into two peaks. In the presence of malonate, all of the four kinds of amine hydrogens of $[Co(acac)(en)_2]^{2+}$ exhibit different exchange rates. The following conclusion was obtained from the results coupled with ^{13}C NMR data. (i) The malonate ion works in two ways in amine exchange, as a general base catalyst and to form an exchange-inert ion-pair. (ii) The two *trans* hydrogens that are directed approximately parallel to the two-fold axis of the complex ion hydrogen-bond simultaneously to the two carboxyl groups of malonate, leading to a retardation of amine exchange rates. (iii) The rates of the other *trans* hydrogens and *cis* hydrogens are determined by a compromise between acceleration due to general base catalysis and deceleration due to forming ion-associated species. (iv) The conformation of coordinated ethylenediamine is fixed as either ($\delta\delta$) or ($\lambda\lambda$) in the hydrogen-bonded species.

The amine groups of *cis*-$[CoX_2(en)_2]^+$ ions give rise to two broad singlets in their proton NMR spectra. However, the assignment of these singlets to *cis* and *trans* amines, which are *cis* and *trans* to coordinated X ligands, respectively, is not straightforward owing to their equal intensities. A method of assigning these signals on the assumption that the chemical shifts of amine hydrogens are determined primarily by the magnetic anisotropy of the central cobalt(III) ion was proposed.[2] Although the theory based on the magnetic anisotropy could explain the chemical shift variations for a series of pentaamminecobalt(III) ions, the agreement was not good for *cis*-$[CoX_2(en)_2]^+$ type of complexes.

While ion-associated species in solution are believed to have well-defined structures, little evidence seems to have been obtained, particularly in the case of diamagnetic metal complexes.[3] A limited number of structures of ion-pairs in solution are proposed[4] mainly from studies of circular dichroism spectra. The circular dichroism technique is limited to optically active compounds. The kinetic behavior of amine hydrogen exchange of *cis*-$[CoX_2(en)_2]^+$ ions might be affected by added anions. Thus stereochemical information obtained from the effects of added anions on the hydrogen exchange kinetics, could be applied to many complexes irrespective of optically active and inactive complexes.

The aim of this work is twofold: (a) to obtain evidence in support of the postulated NMR assignments and (b) to obtain stereochemical information on the ion-paired species. We chose the system $[Co(acac)(en)_2]^{2+}$ and malonate, mal^{2-} for the following reason. Since the cation carries a higher positive charge than most *cis*-$[CoX_2(en)_2]^+$ compounds which are usually univalent, it will interact more strongly with added anions and the effects of ion association would be significant.

Experimental

$[Co(acac)(en)_2]I_2 \cdot H_2O$ was prepapared and recrystallized analytically pure.[5] Extra pure sodium malonate (Katayama Kagaku Kogyo Co. Ltd.) was used without further recrystallization. Sample solutions were made by dissolving the materials in D_2O (Merck, 99.75 atom % D minimum). The concentration of $[Co(acac)(en)_2]I_2$ of all solutions was 0.1 mol dm^{-3} and that of Na_2mal was varied from 0 to 1.0 mol dm^{-3} at suitable intervals.

^1H NMR spectra were measured on a Varian T-60 spectrometer operating at 60 MHz. The rate of amine hydrogen exchange was determined by measuring the NMR signal intensities of *cis* NH_2 and *trans* NH_2 at suitable time intervals. Proton chemical shifts are referred to internal sodium 2,2-dimethyl-2-silapentane-5-sulfonate, DSS. All measurements were made at 36.4 °C. Proton noise decoupled and undecoupled ^{13}C NMR spectra were recorded for H_2O solutions at 22.6 MHz on a Hitachi R-42 spectrometer by the FT technique. The pH of the sample solution was measured with a Hitachi-Horiba Model F-7 pH meter using a microelectrode immediately after kinetic measurements.

Results

Chemical Shifts. The ^1H NMR spectra of $[Co(acac)(en)_2]I_2$ in D_2O contain two broad signals at 5.02 ppm and 4.42 ppm from internal DSS, due to *cis* NH_2 and *trans* NH_2, respectively, which denote amine hydrogens *cis* and *trans* to oxygen atoms of coordinated acetylacetone.

Figure 1 shows the amine hydrogen portion of the ^1H NMR spectra of $[Co(acac)(en)_2]I_2$ with 0, 0.4, 0.8, and 1.0 mol dm^{-3} of Na_2mal taken immediately after dissolution in D_2O. Chemical shift values of each peak are given in Table 1. With an increase in the concentration of Na_2mal, the signal of *trans* NH_2 shifted to low fields. While *cis* NH_2 appeared as a single peak in the absence of Na_2mal, the *cis* peak became broader, its height being almost half of that of *trans* NH_2 when 0.4

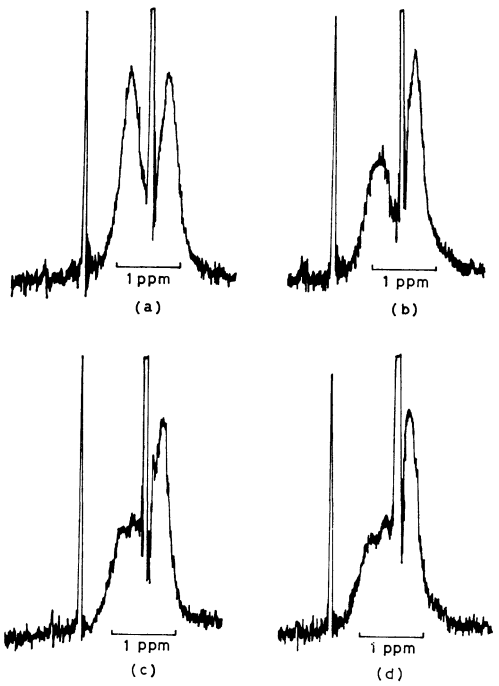

Fig. 1. The amine hydrogen portion of the ^1H NMR spectra of $[Co(acac)(en)_2]I_2$ with 0 (a), 0.4 (b), 0.8 (c), and 1.0 mol dm^{-3} (d) of Na_2mal, taken immediately after dissolution in D_2O. The strong central singlet is due to solvent HDO and to the left of the spectrum is the methine hydrogen of acac.

Table 1. ^1H chemical shifts in δ(ppm) from internal DSS for *cis* and *trans* NH_2

Two peaks appear for *cis* NH_2 when Na_2mal exceeds 0.4 mol dm^{-3}.

Na_2mal (mol dm^{-3})	0	0.4	0.8	1.0
cis NH_2	5.02	5.07	5.11	5.13
		4.97	4.90	4.89
trans NH_2	4.42	4.47	4.52	4.53

mol dm^{-3} of Na_2mal was added. With 0.8 and 1.0 mol dm^{-3} of Na_2mal, the *cis* resonance eventually split into two peaks. The chemical shift difference of these two peaks increased with increasing concentration of Na_2mal. However, the average of their chemical shift values remained unaffected, being equal to the position of *cis* NH_2 without Na_2mal. The ^{13}C chemical shifts of $[Co(acac)(en)_2]I_2$ in the absence and presence of Na_2mal, referred to the methyl carbon resonance of internal methanol, are given in Table 2. The assignment was based on the splitting pattern of each resonance in the undecoupled spectrum.

Rates of Amine Hydrogen Exchange. In the absence of Na_2mal, the plots of ln(intensity) *vs.* time were linear for both *cis* and *trans* NH_2. The result for the solution with 0.1 mol dm^{-3} Na_2mal is shown in Fig. 2, where plots for *trans* NH_2 turn out to be a curve in contrast with a straight line for *cis* NH_2. Analysis of the rate data for *trans* NH_2 gave two pseudo-first-order rate

Table 2. ^{13}C chemical shifts in ppm of $[Co(acac)(en)_2]I_2$ in H_2O referred to the methyl carbon of internal methanol

The concentration of $[Co(acac)(en)_2]I_2$ and Na_2mal is 0.1 and 1.0 mol dm^{-3}, respectively. s, d, t, and q stand for singlet, doublet, triplet, and quartet signals in proton coupled spectra.

	CO(acac)	$COO^-(mal^{2-})$	CH(acac)	CH_3OH	$CH_2(mal^{2-})$	CH_2(en)	CH_2(en)	CH_3(acac)
Without Na_2mal	142.67(s)	——	49.45(q)	0	——	−3.77(t)	−5.66(t)	−22.83(q)
With Na_2mal	142.50(s)	128.02(s)	no signal	0	−2.06(t)	−3.86(t)	−5.75(t)	−22.83(q)

Table 3. First-order rate constants (s^{-1})

$k_{t(f)}$ and $k_{t(s)}$ denote faster and slower rate constants of *trans* NH_2, respectively. Without Na_2mal only one rate is obtained. $k_{c(L)}$ and $k_{c(H)}$ denote *cis* NH_2 when appeared separately at lower and higher fields, respectively. The signal of *cis* NH_2 does not split into two peaks when Na_2mal is 0 and 0.1 mol dm^{-3}.

Na_2mal (mol dm^{-3})	0	0.1	0.1	0.4	0.4
Apparent pH	6.72	6.18	6.44	5.91	5.80
$k_{t(f)}$	1.31×10^{-3}	2.89×10^{-3}	2.55×10^{-3}	9.78×10^{-4}	5.69×10^{-4}
$k_{t(s)}$		4.88×10^{-4}	5.29×10^{-4}	8.00×10^{-5}	7.80×10^{-5}
$k_{c(L)}$	4.57×10^{-4}	3.48×10^{-4}	3.23×10^{-4}	1.70×10^{-4}	7.54×10^{-5}
$k_{c(H)}$					2.15×10^{-5}

Na_2mal (mol dm^{-3})	0.6	0.6	0.8	0.8	1.0
Apparent pH	5.99	5.93	5.84	5.84	5.88
$k_{t(f)}$	7.70×10^{-4}	9.06×10^{-4}	5.29×10^{-4}		
$k_{t(s)}$	7.28×10^{-5}	8.53×10^{-5}	8.10×10^{-5}		
$k_{c(L)}$	8.67×10^{-5}	1.33×10^{-4}	7.73×10^{-5}	8.60×10^{-5}	7.35×10^{-5}
$k_{c(H)}$	6.47×10^{-5}	1.08×10^{-4}	2.44×10^{-5}	4.77×10^{-5}	4.02×10^{-5}

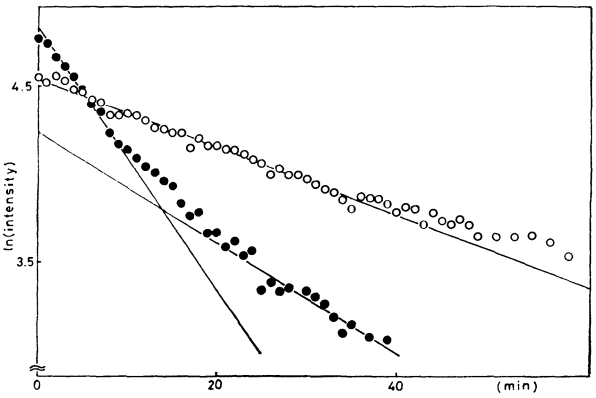

Fig. 2. The plots of ln (intensity) *vs.* time for *cis* (○) and *trans* (●) NH_2 of $[Co(acac)(en)_2]^{2+}$ with 0.1 mol dm^{-3} of Na_2mal.

constants $k_{t(f)}$ and $k_{t(s)}$, which denote faster and slower exchange rates of *trans* NH_2, respectively. The rate constants with varying concentration of Na_2mal are given in Table 3, along with apparent pH. The *trans* NH_2 peak underwent a down-field shift with Na_2mal and at 0.8 mol dm^{-3} of Na_2mal was too close to the strong HDO peak, making the measurement difficult. Since the *cis* resonance splits into two peaks when the Na_2mal concentration exceeds *ca.* 0.5 mol dm^{-3}, two rate constants, $k_{c(H)}$ and $k_{c(L)}$, refer to the peaks at higher and lower magnetic fields, respectively.

Discussion

The Assignment of Amine Signals. In a previous paper a method was proposed for assigning two NH_2 signals of *cis*-$[CoX_2(en)_2]^+$ ions.[2] It was based on the assumption that the chemical shifts of amine hydrogens are primarily determined by the magnetic anisotropy of the central cobalt(III) ion. It has been proposed that for *cis*-$[CoX_2(en)_2]^+$ ions the *cis* NH_2 resonates at a field lower than the *trans* NH_2 if the ligand X is ranked lower, like acac, than en in the spectrochemical series. Thus the *trans* NH_2 of $[Co(acac)(en)_2]^{2+}$ is expected to appear at higher magnetic field than the *cis* NH_2. On the other hand, in a kinetic study of amine hydrogen exchange for several *cis*-$[CoX_2(en)_2]^+$ type of complexes,[6] it was found that the *trans* amine hydrogens are exchanged much faster than the *cis* hydrogens if X is a weaker ligand than en (acac is an example). In the absence of malonate the high field NH_2 signal decreased in intensity more rapidly than the low field one, indicating assignment of the high field signal to the *trans* NH_2.

The results suggest that the high field resonance at δ 4.42 is due to the *trans* NH_2 of $[Co(acac)(en)_2]^{2+}$. The effect of added malonate on amine exchange kinetics can be consistent only when we adopt this assignment.

HD Exchange Kinetics. The *trans* NH_2 exhibits two exchange rates in the presence of Na_2mal, in contrast with only one rate in the absence of malonate. This indicates that two kinds of hydrogens of *trans* NH_2 are discriminated by mal^{2-} in solution. A molecular

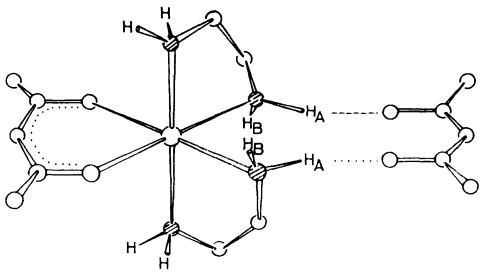

Fig. 3. The proposed structure of ion-associated species, $[Co(acac)(en)_2]^{2+}\cdots\cdots mal^{2-}$.
H_A is approximately parallel to the C_2-axis. Malonate ion approaches from the side opposite to acac along the C_2-axis and hydrogen bonds only to H_A.

model shows that *trans* NH_2 has two kinds of hydrogens, H_A (pointing approximately parallel to the molecular two-fold axis of $[Co(acac)(en)_2]^{2+}$) and H_B, and that two carboxyl groups of mal^{2-} can hydrogen-bond simultaneously to two H_A's (Fig. 3). It is reasonable that mal^{2-} approaches the complex electrostatically from the side opposite acac along the two-fold axis because minus charge is localized on acac. The shift of *trans* NH_2 to low fields caused by addition of Na_2mal supports this view since hydrogen bonding causes downfield shifts.[7] We thus assign the slower exchange rate, $k_{t(s)}$, to H_A and the faster one, $k_{t(f)}$, to H_B. Since double hydrogen bonding would greatly stabilize the chelate structure, we might expect that *trans* H_A is not exchanged while retaining the hydrogen bond.[8]

HD exchange rate constants of coordinated amine groups are proportional to the concentration of OD^- ion.[9]

$$k \propto [OD^-]$$

The equation still holds for such situations where a stable ion-associated species is formed between the metal complex and added anions. In such cases the second-order rate constant $k'=k/[OD^-]$ decreases gradually with an increasing anion concentration. This has been ascribed to an increase in the number of ion-associated species for which amine hydrogen exchange is considered extremely slow. Yamatera and Fujita[10] utilized this behavior to obtain the association constant between *Λ*- and *Λ*-$[Co(en)_3]^{3+}$ and *d*-tartrate ions. Their result can be rationalized by invoking the face-to-face multifunctional hydrogen bonding in solution, as found in the crystal structure of *Λ*-$[Co(en)_3]Br$(*d*-tartrate)$\cdot 5H_2O$.[11] We will discuss our results in terms of the second-order rate constants $k_i'=k_i/[OD^-]$ (i=c, t(s), t(f)), which were derived by using $K_w(D_2O)$,[12,13] corrected according to the ionic strength of the solution extending from 0.3 to 2.5. k' values were plotted against $[Na_2mal]/[complex]$ in order to see the dependence of k' on the concentration of malonate (Fig. 4).

The $k'_{t(f)}$ values for *trans* H_B increase sharply upon addition of Na_2mal, followed by a gradual decrease in the concentration of Na_2mal. Since the rate enhancement can not be due to pH-effect, mal^{2-} and $Hmal^-$ work as general base catalysts, enhancing the rate of *trans* H_B. This may be performed through an ion-pair such as

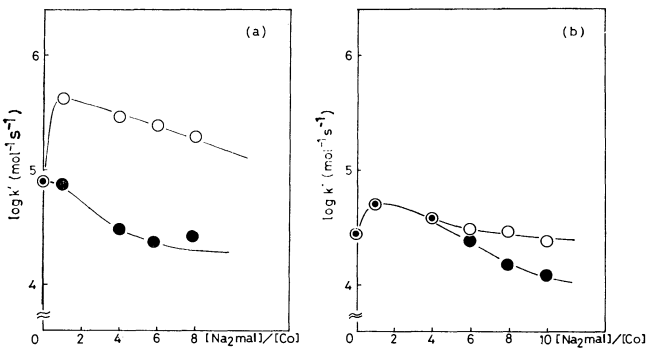

Fig. 4. The plots of logarithms of second-order rate constants (mol^{-1} s^{-1}) *vs.* the molar concentration ratio of Na_2mal to [Co(acac) $(en)_2$]I_2.
(a) For *trans* NH_2; Two rates, $k'_{t(f)}$ (○) and $k'_{t(s)}$ (●), are detected in the presence of Na_2mal. (b) For *cis* NH_2; Addition of Na_2mal brought about a splitting of the *cis* peak into two peaks, hence $k'_{c(L)}$ (○) and $k'_{c(H)}$ (●).

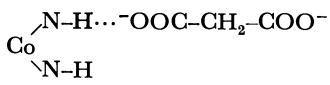

where one of the carboxyl groups hydrogen-bonds to an amino group, the other dangling and not interacting with amino hydrogens. A similar rate enhancement due to general base catalysis by acetate and malonate has been confirmed for *cis*-$[CoX_2(en)_2]^+$ ions with X_2= mal^{2-}, $(CN)_2$, $(NO_2)_2$.[14] The gradual reduction of $k_{t(f)}$ may be interpreted as follows. The number of predominant ion-associated species increases with an increase in the concentration of malonate (Fig. 3). Since associated species have zero electric charge, it is improbable that mal^{2-} or $Hmal^-$ ion approaches this associated species, acting as general base catalysis on the associated complexes.

The $k_{t(s)}$ value, which refers to *trans* H_A, decreases with an increase in the concentration of Na_2mal, indicating that the number of the species in which mal^{2-} associates with two *trans* H_A through hydrogen bond, increases with increasing concentration of Na_2mal. However, the steady decrease of $k_{t(s)}$ seems to indicate not the inaccessibility of general base to H_A but retardation due to ion-pairing offsetting the effect of general base catalysis.

For *cis* NH_2, an average of $k'_{c(H)}$ and $k'_{c(L)}$ increases up to 0.1 mol dm^{-3} of Na_2mal, though the increase is about one-fourth of that of $k'_{t(f)}$ at the same Na_2 mal concentration; the increments are 1.6 and 6.6 times for k'_c and $k'_{t(f)}$, respectively, as compared with the corresponding values in the absence of malonate. Although the increase of k'_c indicates that the malonate ion works as general base catalysis on *cis* NH_2, the effect on k'_c is smaller than that on $k'_{t(f)}$. This suggests that the malonate ion approaches *cis* NH_2 less frequently, which is quite likely from electrostatic consideration. The subsequent gradual decrease of k'_c may be explained in a manner similar to that for $k'_{t(f)}$.

The results can be summarized as follows. Malonate ion can work as general base catalyst for exchanging amine hydrogens. The values of $k'_{t(f)}$ for *trans* H_B and k'_c for *cis* NH_2 would be taken as a compromise of two opposing factors: rate acceleration due to general base catalysis by malonate ion and rate retardation due to ion-pairing (Fig. 3). The initial increase of $k'_{t(f)}$ and k'_c is due to general base catalysis and the subsequent gradual retardation to additional hydrogen bond effect. The steady decrease of $k'_{f(s)}$ for *trans* H_A caused by malonate ions is explained by the selective hydrogen bond between mal^{2-} and *trans* H_A.

Conformation of Ethylenediamine Chelates. With an increase in the concentration of Na_2mal, the ^1H signal of *cis* NH_2 split into two peaks, the separation increasing. In ^{13}C NMR spectra, both peaks assigned to en carbons underwent high field shifts by about 0.1 ppm upon addition of Na_2mal. This suggests that the conformational equilibrium of the two en chelates is driven toward either ($\delta\delta$) or ($\lambda\lambda$) by the presence of mal^{2-}.

The conformation of ethylenediamine coordinated to metal ions is rapidly interconverting between the δ and λ forms in aqueous solution.[15] If the conformations of two ethylenediamine rings are fixed as ($\delta\lambda$) or ($\lambda\delta$), the number of expected resonance peaks may be up to four for *cis* NH_2 on ^1H NMR spectra and also four for CH_2 resonance of en on ^{13}C NMR. However, the energy difference between ($\delta\lambda$) and ($\delta\delta$) or between ($\delta\lambda$) and ($\lambda\lambda$) is generally accepted as very small and the relative populations of these two conformations would be virtually 1 : 1. Thus the observed ^{13}C chemical shift, being an average with 1 : 1 weights, should be the midpoint between the shifts expected for the δ and λ conformers. On the other hand, if the conformation of two ethylenediamine is fixed as ($\delta\delta$) or ($\lambda\lambda$), the corresponding ^1H and ^{13}C spectra should consist of only two peaks. Since our system would be in rapid dynamical equilibrium between free and the associated species, and the conformation of en ring would be considered to be constrained by hydrogen bonding with mal^{2-} in the associated species, the observed spectra should be an average weighted by the abundance of respective species.

The signals split upon addition of malonate are not those with which malonate is proposed to be interacting, *i.e.*, *trans* NH_2. However, if we accept the view that conformational equilibrium is shifted to either ($\delta\delta$) or ($\lambda\lambda$) upon addition of malonate, the two kinds of hydrogens of *cis* NH_2 will have stereochemically different disposition, especially with respect to the cobalt-acac chelate; one of the *cis* NH_2 is poised over the chelate ring and the other is not. This will bring about a large chemical shift difference for the two *cis* hydrogens but not for the two *trans* ones. The effect of the magnetically anisotropic ring current of the chelate ring has not been clarified. However, the former hydrogen might be to a greater extent shielded than the latter.[16] On electrostatic grounds the *cis* NH poised over the chelate ring might undergo exchange more slowly. Experimentally, of the two *cis* signals the high field one is exchanged more slowly than the other, which is in line with our assumption.

The authors would like to thank Dr. Y. Uchio and Prof. S. Hayashi for ^{13}C NMR measurements. One

of the authors (U. S.) acknowledges financial support from the Ministry of Education under Grant No. 446-7054-364214 and the Matsunaga Research Grant.

References

1) This work is Proton Magnetic Resonance Spectra of Metal Ammine Complexes. 11. Part of this work was communicated in preliminary form; U. Sakaguchi, H. Nakazawa, and H. Yoneda, *J. Chem. Soc., Chem. Commun.*, **1979**, 356.

2) U. Sakaguchi, S. Yamazaki, and H. Yoneda, *Bull. Chem. Soc. Jpn.*, **49**, 402 (1976).

3) For NMR techniques for paramagnetic metal complexes, see, *e.g.*, G. N. La Mar in "NMR of Paramagnetic Molecules," ed by G. N. La Mar, W. Dew. Horrocks, Jr., and R. H. Holm, Academic Press, New York, N. Y. (1973), Chap. 10.

4) S. F. Mason, "Optical Rotatory Dispersion and Circular Dichroism," ed by F. Ciardelli and P. Salvadori, Heyden and Son Ltd., London (1973), Chap. 2.1, and references cited therein.

5) I. K. Reid and A. M. Sargeson, *Inorg. Synth.*, **9**, 167 (1967).

6) U. Sakaguchi, K. Maeda, and H. Yoneda, *Bull. Chem. Soc. Jpn.*, **49**, 397 (1976), and references cited therein.

7) J. A. Pople, W. G. Schneider, and H. J. Bernstein, "High-resolution Nuclear Magnetic Resonance," McGraw-Hill, N. Y. (1959), Chap. 15.

8) M. Eigen and W. Kruse, *Z. Naturforsh.*, **18b**, 857 (1963).

9) (a) J. S. Anderson, H. V. A. Briscoe, and N. L. Spoor, *J. Chem. Soc.*, **1943**, 361; (b) H. Block and V. Gold, *J. Chem. Soc.*, **1959**, 966; (c) J. W. Palmer and F. Basolo, *J. Inorg. Nucl. Chem.*, **15**, 279 (1960).

10) (a) H. Yamatera and M. Fujita, *Bull. Chem. Soc. Jpn.*, **42**, 3043 (1967); (b) M. Fujita and H. Yamatera, *ibid.*, **50**, 2672 (1977).

11) Y. Kushi, M. Kuramoto, and H. Yoneda, *Chem. Lett.*, **1976**, 135.

12) H. S. Harned and W. J. Hamer, *J. Am. Chem. Soc.*, **55**, 2149 (1933).

13) W. F. K. Wynne-Jones, *Trans. Faraday Soc.*, **32**, 1397 (1936).

14) U. Sakaguchi, H. Nakazawa, K. Sakai, Y. Morimoto, and H. Yoneda, unpublished results.

15) J. K. Beattie, *Acc. Chem. Res.*, **4**, 253 (1971).

16) F. A. Bovey, "Nuclear Magnetic Resonance Spectroscopy," Accademic Press, New York, N. Y. (1969), Chap. 3.

Effects of Sodium Tetraborate as an Additive on the Reaction of α-Alumina with Sodium Carbonate

Byong-Tae CHANG,* Jae-Gun OH, and Suk-Ja OM
Department of Chemistry, Korea University, Kodaira, Tokyo 187
(Received November 2, 1979)

Effects of sodium tetraborate as an additive in the reaction of α-alumina with molten sodium carbonate have been studied mainly in a N_2 atmosphere. Addition of sodium tetraborate accelerates the reaction, the α-alumina reacted increasing from 31.7% to 99.3% by addition of sodium tetraborate corresponding to the initial B_2O_3/Na_2O molar ratio of only 1/15 under the other same conditions. By means of the Jander equation the activation energy was found to be 53 kcal/mol for the α-Al_2O_3–Na_2CO_3–$Na_2B_4O_7$ system, which was lower by 10 kcal/mol than that for the α-Al_2O_3–Na_2CO_3 system. X-Ray diffraction and thermal data were analyzed in relation to the phase equilibrium of the melt.

Production of alumina from resources other than bauxite is becoming important. A number of reports have appeared on the production of alumina from various low-grade sources such as clay, aluminous shale, anorthosite, nephelite, *etc.*[1–8]

A lime-soda sinter process is one of the most important methods for extracting alumina from low-grade sources to which the Bayer process can not be applied because of high silica content. Raw materials reacted with molten sodium carbonate form sodium aluminate which is soluble in both acidic and basic aqueous solutions. The reaction of various types of alumina with sodium carbonate is fundamental in the complex lime-soda sinter process.

In a previous paper the lime-soda sinter process was discussed with use of Korean diaspore, cyanite and kaolinite as starting materials.[9] Christie *et al.* studied the reaction rate of α-alumina with sodium carbonate in relation to gasification of coal in melts containing sodium carbonate, showing that the reaction process is considerably hindered by diffusion.[10]

Sodium tetraborate is often used as a flux for the decomposition of minerals by molten Na_2CO_3. The purpose of the present work is to clarify the promoting action of sodium tetraborate on the reactivity of α-alumina with sodium carbonate.

Experimental

Reagent grade α-alumina was ground and sized into −150 —+200 mesh (No. 1) and −200 mesh (No. 2). The specific surface area of No. 2 was found to be 0.90 m^2/g by the BET method. Reagent grade anhydrous sodium carbonate and sodium tetraborate decahydrate (borax) were dried at 500 °C for 1 h. Nitrogen and oxygen were purified by the usual methods. Other materials were of reagent grade and used without further purification.

The percentage of α-alumina reacted with sodium carbonate, η, was determined as follows: Samples in a platinum boat were laid in an electric furnace at 900—1250 °C. The sinter was cooled down to room temperature as fast as possible in N_2 gas, and leached with hot 1 mol/dm^3 HCl solution for 30 min. The leachate was filtered. $Al(OH)_3$ was precipitated by adding aqueous ammonia to the filtrate and weighed in the form of Al_2O_3 after heating. The value of η was calculated from the weight of alumina leached.

Results and Discussion

Effect of Gas Atmosphere. α-Alumina reacts with sodium carbonate to form sodium aluminate:

$$Al_2O_3(s) + Na_2CO_3(l) = 2NaAlO_2(s) + CO_2(g). \quad (1)$$

From the large negative value of Gibbs free energy for this reaction[11] α-alumina is expected to react completely with molten Na_2CO_3 at temperatures above 900 °C. However, the experimental results (Fig. 1)

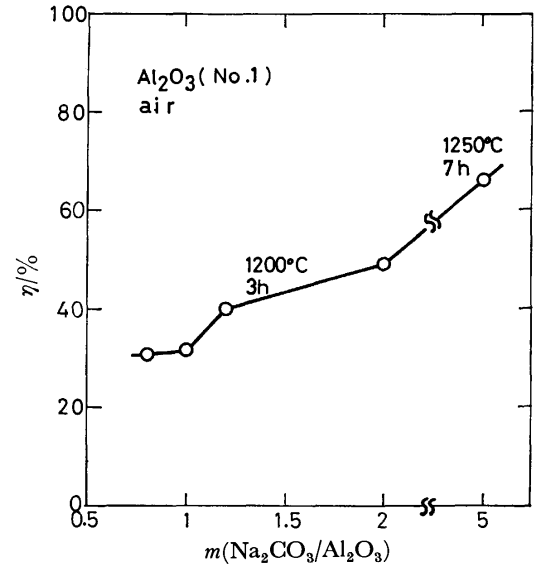

Fig. 1. Variation of the percents of α-alumina reacted with initial Na_2CO_3/Al_2O_3 molar ratio.

indicate that the reaction is not complete in the air. For example, the value of η was found to be low at 66% even for the initial molar ratio(m) 5 of Na_2CO_3/Al_2O_3 and reaction time 5 h at 1250 °C. The sinters obtained in the air were colored brown, the Pt boat containing the sinter being considerably corroded. In spite of the disappearance of α-alumina in X-ray diffraction patterns of the sample sintered for a long time, the value of η was much lower than 100% (Fig. 3a).

Maegawa found that the atmosphere influences the sintering process, and that H_2O gas atmosphere enhances the rate of reaction of α-alumina with sodium carbonate in comparison with O_2, H_2+CO, or CO_2 gas atmos-

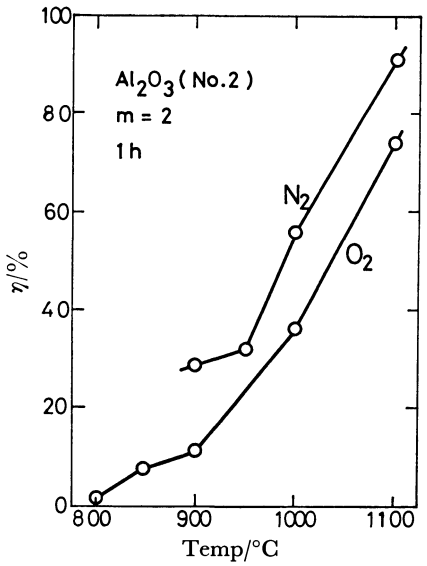

Fig. 2. Difference between the effect of N_2 and O_2 gas atmospheres on the reaction of Al_2O_3 with Na_2CO_3.

phere.[12] Figure. 2 shows changes in the η values with reaction temperature in purified N_2 and O_2 with constant flow rates of 80 ml/min. The values of η obtained in O_2 were found to be lower than those obtained in N_2, the corrosion of the Pt boat being much enhanced in O_2. The sinter obtained in N_2 remained white with no corrosion of the Pt boat; those obtained in O_2 were colored red-brown as in the air. The same results were obtained when a Ni boat was used. By comparing Fig. 3a with 3b, we see that there are compounds other than α-Al_2O_3(a), Na_2CO_3(n), and $NaAlO_2$(na). Carbon dioxide,[10] as well as O_2 seems to hinder the sinter process.

Effect of Additives. Sodium tetraborate and aluminium fluoride were used as additives to facilitate Reaction 1. Addition of sodium tetraborate was found to be very effective (Fig. 4). The greater the initial

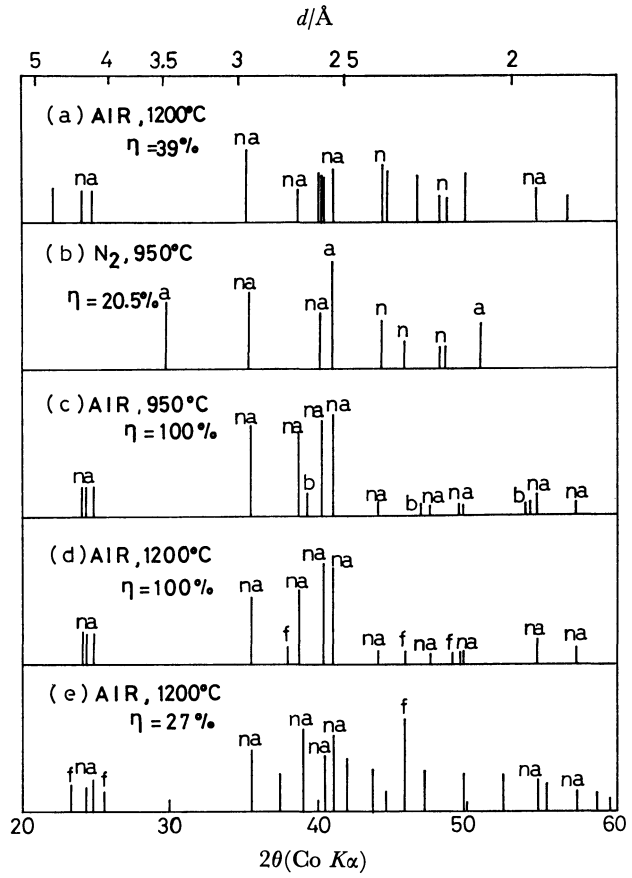

Fig. 3. X-Ray diffraction data for the sinters obtained under conditions as follows: (a) α-Al_2O_3 (No.1)+Na_2CO_3, m=5 (b) α-Al_2O_3 (No. 1)+Na_2CO_3, m=2 (c) α-Al_2O_3 (No.1)+Na_2CO_3+$Na_2B_4O_7$, m=1.7 and n=1/15 ($X_{B_2O_3}$=0.053) (d) α-Al_2O_3 (No. 1)+Na_2CO_3 +AlF_3 (20 wt%), m=2 (e) α-Al_2O_3 (No. 1)+Na_2CO_3 +AlF_3 (20 wt%), m=1, 1 Å=0.1 nm.

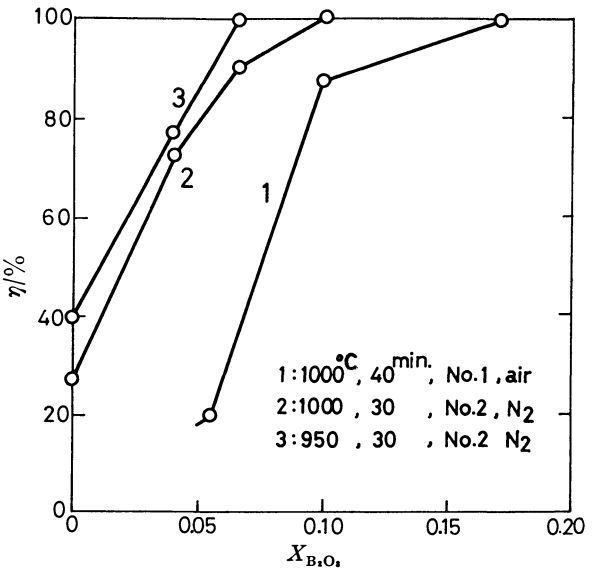

Fig. 4. Effect of the addition of borax on the reaction of α-Al_2O_3 with Na_2CO_3.

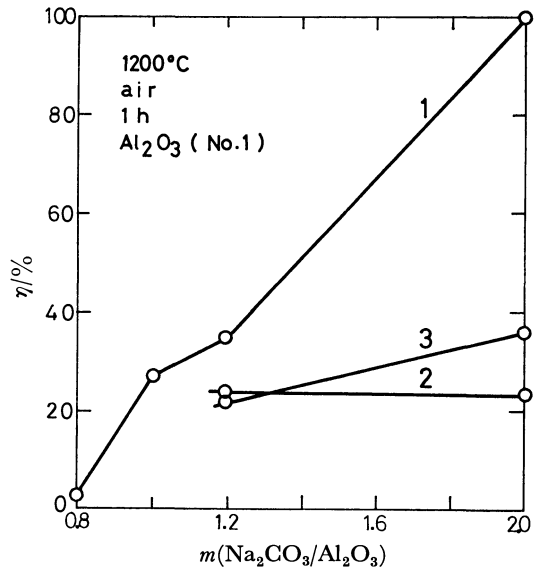

Fig. 5. Effect of the addition of AlF_3 and NaF on the reaction of Al_2O_3 with Na_2CO_3.
Curve 1; α-Al_2O_3+Na_2CO_3+AlF_3 (20 wt%), 2; α-Al_2O_3+Na_2CO_3+NaF(20 wt%), 3; α-Al_2O_3+Na_2CO_3.

B_2O_3/Na_2O molar ratio(n), the greater the effect. The sinters to which sodium tetraborate had been added remained white, causing no corrosion of the Pt boat. The sinter having $\eta=100\%$ obtained for the Al_2O_3–Na_2CO_3–$Na_2B_4O_7$ system gave only the diffraction patterns of $NaAlO_2$ and probably sodium borate(b) (Fig. 3c).

The effects of AlF_3 and NaF as additives were also studied. The effect of AlF_3 on Reaction 1 depends a great deal on the value of m (Fig. 5). When 20 wt% AlF_3 was added to a mixture with m of 2.0, the value of η increased from 36% to 100%. Aluminium fluoride reacts with molten Na_2CO_3 partly to form $NaAlO_2$:

$$AlF_3 + 2Na_2CO_3 = 3NaF + NaAlO_2 + 2CO_2, \quad (2)$$

$$AlF_3 + 3NaF = Na_3AlF_6. \quad (3)$$

If all the AlF_3 added were converted into NaF, the effect of NaF would be observed similar to that of AlF_3. However, this was not the case (Fig. 5). X-Ray diffraction analysis of the sinter obtained in the case of $m=2$ and $\eta=100\%$ showed the presence of $NaAlO_2$ and a fluoride compound(f), probably Na_3AlF_6. In the case of $m=1$ and $\eta=27\%$, η was found to be low, in spite of the absence of the diffraction pattern for α-Al_2O_3. This suggests that α-Al_2O_3 might merely dissolve in Na_3AlF_6 formed by the reaction of AlF_3 with Na_2CO_3.

Reaction Rate as a Function of Temperature. Figures 6 and 7 show changes in η with reaction time, t, at three temperatures for α-Al_2O_3–Na_2CO_3($m=2$) and α-Al_2O_3–Na_2CO_3–$Na_2B_4O_7$($m=2$ and $n=1/15$).

Since a protective layer of sodium aluminate having very low solubility in molten Na_2CO_3,[10] is formed on alumina, the diffusion of CO_3^{2-} ion through the sodium aluminate layer would be the rate-determining step.[10,12] The results were analyzed by means of the Jander equation

$$[1-(1-\eta)^{1/3}]^2 = kt, \quad (4)$$

$$k = \frac{2DC_0}{\rho r_0^2}, \quad (5)$$

where k is a rate constant, D diffusion coefficient, C_0 the concentration of CO_3^{2-} ion in the bulk, ρ is the density of

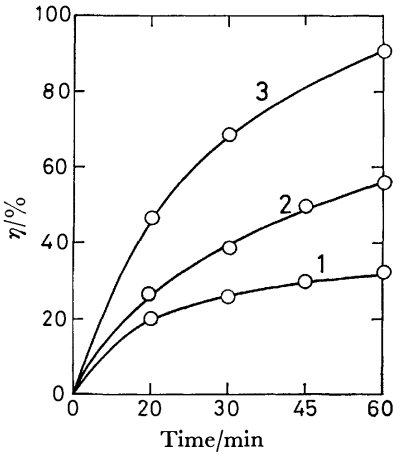

Fig. 6. Changes in the percents of α-alumina reacted *vs.* time in the N_2 atmosphere for α-Al_2O_3–Na_2CO_3 system ($m=2$).
Curve 1: 950 °C, 2: 1000 °C, 3: 1100 °C.

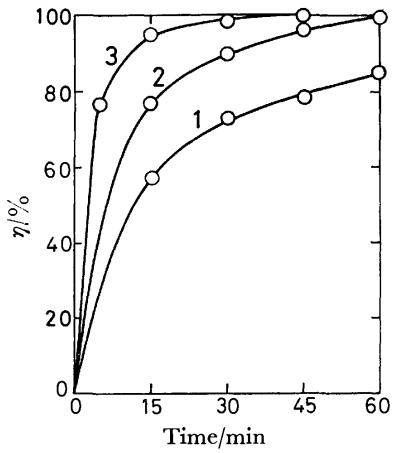

Fig. 7. Changes in the percents of α-alumina reacted *vs.* time in the N_2 atmosphere for α-Al_2O_3–Na_2CO_3–$Na_2B_4O_7$ system ($m=2$, $n=1/15$).
Curve 1: 900 °C, 2: 950 °C, 3: 1000 °C.

$NaAlO_2$ layer (2.72 g/cm³), and r_0 the average size of α-Al_2O_3 (0.28 μm) calculated from the special area of 0.09 m²/g. Figures 8 and 9 show linear relationships,

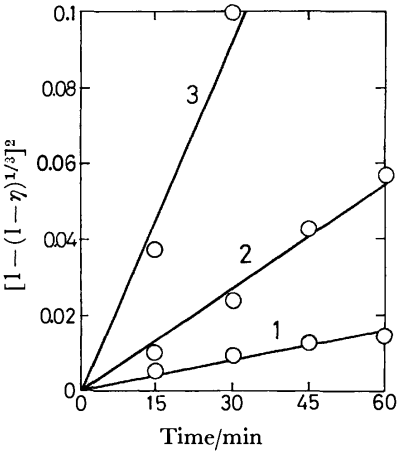

Fig. 8. $[1-(1-\eta)^{1/3}]^2$ *vs.* reaction time for α-Al_2O_3–Na_2CO_3 system.
1: 950 °C, 2: 1000C°, 3: 1100 °C.

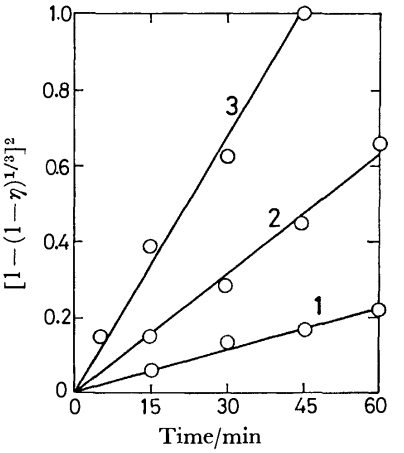

Fig. 9. $[1-(1-\eta)^{1/3}]^2$ *vs.* reaction time for α-Al_2O_3–Na_2CO_3–$Na_2B_4O_7$ system.
1: 900 °C, 2: 950 °C, 3: 1000 °C.

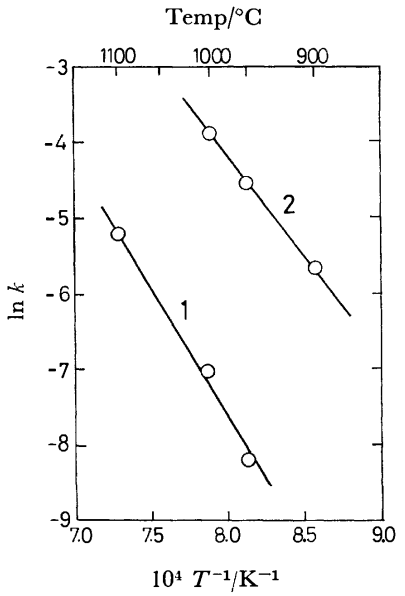

Fig. 10. Variation of rate constant, k, with temperature. 1: α-Al_2O_3–Na_2CO_3 system, 2: α-Al_2O_3–Na_2CO_3–$Na_2B_4O_7$ system.

the slopes giving the k values. At 1000 °C the k value for α-Al_2O_3–Na_2CO_3–$Na_2B_4O_7$ system is larger by *ca.* 11 times than that for α-Al_2O_3–Na_2CO_3 system. Figure 10 shows Arrhenius-type plots of k *vs.* $10^4/T$. The activation energy calculated from the slopes is 53 kcal/mol for the former, lower by 10 kcal/mol than that for the latter (kcal means $kcal_{th}$; 1 $kcal_{th}$=4184 J). For the Arrhenius activation energy for the reaction of α-Al_2O_3 with Na_2CO_3, Christie *et al.*[10] and Maegawa *et al.*[12] reported the values of 62±3 and 58.8 kcal/mol, respectively, which agree with our results.

Discussion on the Effect of Sodium Tetraborate as an Additive. Molten Na_2CO_3 is completely ionized and consists of species such as Na^+, CO_3^{2-}, and ion pair $(Na^+CO_3^{=})^-$, the dissociation of CO_3^{2-} into CO_2 and O^{2-} ion being finite at temperatures above melting point.[13] Thus the reaction of α-alumina with Na_2CO_3 can be expressed by a series of elementary steps as follows:

$$Na_2CO_3(l) = Na^+(l) + (Na^+CO_3^{=})^-(l), \quad (6)$$

$$(Na^+CO_3^{=})^-(l) = Na^+(l) + CO_3^{2-}(l), \quad (7)$$

$$CO_3^{2-}(l) = O^{2-}(l) + CO_2(g), \quad (8)$$

$$Al_2O_3(s) + O^{2-}(l) = 2AlO_2^-(l), \quad (9)$$

$$Na^+(l) + AlO_2^-(l) = NaAlO_2(s). \quad (10)$$

According to the Lux-Flood concept of basicity of oxides,[14,15] a base is defined as an oxide donor and an acid as an oxide acceptor:

$$(acid) + O^{2-} = (base) \quad (11)$$

The reaction of α-alumina with sodium carbonate might be the neutralization between acidic Al_2O_3 and basic Na_2O. Thus pO^{2-}[*i.e.* $-\log a(O^{2-})$] was chosen as a scale of basicity. According to the calculation of the relative basicity of oxides by Yagisawa *et al.*, B_2O_3 is more acidic than Na_2O and Al_2O_3.[16] Duffy and Ingram,[17] who presented a concept of optical basicity for the melt, reported that an increase in B_2O_3 content lowers the basicity of Na_2O–B_2O_3 melt; B_2O_3 has a

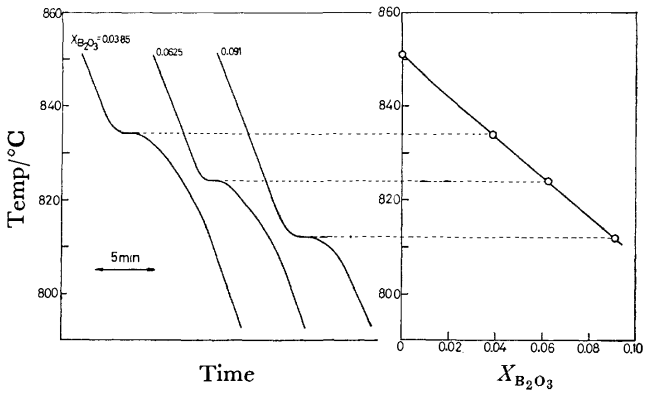

Fig. 11. Cooling curves for mixed melts of Na_2CO_3 and $Na_2B_4O_7$, and the melting points *vs.* $X_{B_2O_3}$.

tendency to consume O^{2-} ion:

$$B_2O_3 + 5O^{2-} = 2BO_4^{5-} \quad (12)$$

It is thus concluded that the effect of the addition of sodium tetraborate is not caused by the increase in the basicity of the melt.

The phase diagram of Na_2O–B_2O_3 system has been reported only for the region $B_2O_3 \geq 50\%$.[18] Basic sodium borates such as $5Na_2O \cdot B_2O_3$, $2Na_2O \cdot B_2O_3$, and $3Na_2O \cdot B_2O_3$ are known in the region $B_2O_3 \leq 50\%$. Figure 11 shows cooling curves for Na_2CO_3–$Na_2B_4O_7$ melts. Addition of sodium tetraborate to sodium carbonate give rise to the lowering of solidification point of the melt in proportion to the molar fraction of B_2O_3. With the progress of Reaction 1, the concentration of B_2O_3 in the melt increases as a result of consumption of Na_2CO_3, lowering the melting point; the nearer the reaction approaches 100% completion, the greater the lowering in melting point. The activation energy for diffusion is approximately proportional to melting point.[19] The activation energy for the α-Al_2O_3–Na_2CO_3–$Na_2B_4O_7$ system, having lower melting points, was found to be lower by 10 kcal/mol than for the α-Al_2O_3–Na_2CO_3 system. The lowering of the melting point results in the lowering of the viscosity of the melt, promoting the contact of α-alumina with the melt and the diffusion of CO_3^{2-} and/or $(Na^+CO_3^{=})^-$ ion(s) through a porous layer of $NaAlO_2$ formed on the surface of α-alumina.

References

1) F. T. Peters, R. C. Kirby, and K. B. Hibie, *J. Metals*, **19**, 26 (1967).
2) R. V. Lundquist, *Bumines Rept. of Inv.*, **6288** (1963).
3) F. A. Peters, P. W. Johnson, J. J. Henn, and R. C. Kirby, *Bumines Rept. of Inv.*, **6927** (1966).
4) S. G. Ampian, *Bumines Rept. of Inv.*, **6933** (1967).
5) G. P. Tkachenko, N. S. Shmorgunenko, L. E. Finkelishtein, V. V. Krasavin, V. Ya. Abramov, and B. I. Arlyuk, USSR. Patent, 476227 (1973).
6) A. I. Lainer, M. A. Kolenkova, L. V. Mirkin, O. S. Ignatiev, L. B. Samaryanova, and V. G. Morozov, USSR. Patent, 285911 (1967).
7) H.-U. Kang, D.-H. Bak, S.-S. Hong, and O.-S. Sin, *Hwahakgwa Hwahakgongop* (Chemistry and Chemical Industry,

D. P. R. of Korea), **14**, 18 (1971).
8) C.-B. Yang, R.-R. Choe, R.-M. Chang, and N.-S. Choe, *Bull. Academy of Science of D. P. R. of Korea*, **21**, 28 (1973).
9) B.-T. Chang, J.-G. Oh, Y.-G. Do, and J.-D. Kwon, *Reports of Korea University*, No. 6, 76 (1976).
10) J. R. Cristie, A. J. Darnell, and D. F, Dustin, *J. Phys. Chem.*, **82**, 33 (1976).
11) D. R. Stull and H. Prophet, *Natl. Stand. Ref. Data Ser., Natl. Bur. Stand.*, No. 37 (1971).
12) Y. Maegawa and T. Matsumura, *Kogyo Kagaku Zasshi*, **46**, 1075, 1078 (1943).
13) G. J. Janz and M. R. Lorenz, *J. Electrochem. Soc.*, **108**, 1052 (1961).
14) H. Lux, *Z. Elektrochem.*, **45**, 303 (1939).
15) H. Flood and T. Forland, *Acta Chem. Scand.*, **1**, 592 (1947).
16) S. Yagisawa, Y. Watanabe, and M. Seki, *J. Met. Soc. of Japan*, **15**, 339 (1951).
17) J. A. Duffy and M. D. Ingram, *J. Am. Chem. Soc.*, **93**, 6448 (1971).
18) G. W. Morey and H. E. Merwin, *J. Am. Chem. Soc.*, **58**, 2252 (1936).
19) J. O' M. Bockris and A. K. N. Reddy, "Modern Electrochemistry," Plenum, New York (1970), vol. 1, Chap. 6-4.

 © 1980 The Chemical Society of Japan Bull. Chem. Soc. Jpn., 53, 1605—1609 (1980)

The Chromatographic Concentration of Mercury in Sea Water with 2-Mercaptobenzothiazole Supported on Silica Gel

Kikuo TERADA,* Kumiko MORIMOTO, and Toshiyasu KIBA

Department of Chemistry, Faculty of Science, Kanazawa University, Kanazawa 920

(Received August 29, 1979)

A solid chelating material, 2-mercaptobenzothiazole supported on silica gel (MBT-SG), was prepared and used for the preconcentration of inorganic and organic mercury compounds from a sea-water sample. The chelating capacity of the material was 12 μeq. Hg/g. The mercury(II) ion, the methylmercury ion, and the ethylmercury ion were quantitatively retained on the MBT-SG at pH values of 1.0, 5.0, and 4.0 respectively from an aqueous solution, and at pH values of 4.0, 4.5, and 5.0 respectively from a sea-water. A column packed with the material provided a quantitative recovery of these ions from a sea-water sample at a high flow rate (1—3 l h^{-1}). Mercury was eluted by the use of a acetone–hydrochloric acid mixture (25: 1) or a 1% thiourea solution in 0.1 mol dm^{-3} hydrochloric acid. The latter effluent was submitted atomic-absorption spectrometry after reductive vaporization for the determination of mercury.

The analytical data on mercury in sea water which have been obtained up to the present time vary widely, from 2 to 2800 ng l^{-1}.[1-6] Such a wide variation in the values may be attributed to the following factors; i) contamination from an acid added to the sample for preservation;[7,8] ii) a change in chemical species, accompanied by an acidification of the sample,[9-11] iii) contamination from the container material,[12] iv) loss by vaporization and adsorption from the water sample[13,14] and contamination from air-borne particulate in the laboratory.[15-19] Therefore, it is preferable that mercury be concentrated as early as possible after sample collection in order to minimize the loss and contamination during storage.[20,21]

Previously, a simple method for the preconcentration and determination of several metals in natural waters was reported by Terada *et al.*[22] By their method, copper, zinc, lead, and cadmium in sea water could be rapidly concentrated on a column of a newly prepared chelating material, 2-mercaptobenzothiazole supported on silica gel (MBT-SG). This material was also found to be useful for the rapid concentration of inorganic and organic mercury compounds from sea water. A simple method for the rapid concentration, followed by the atomic-absorption spectrometric determination, of mercury in sea water using the MBT-SG column will be described in the present paper.

Experimental

Reagents. 2-Mercaptobenzothiazole-silica gel (MBT-SG) was prepared in the same way as was described in a previous paper.[22] Before use, the silica gel was washed with hydrochloric acid (1+1), nitric acid (1+2), and deionized water, succesively.

Standard Solution of Mercury (II) Nitrate. A 0.5 g of distilled mercury was dissolved in 30 ml of nitric acid and then diluted to 250 ml with deionized water.

Chloromethylmercury and Chloroethylmercury Labelled with ^{203}Hg.[23] About 0.3 g of dimethylmercury or diethylmercury was dissolved in about 2 ml of cold ethanol (Solution A). About 0.3 g of mercury (II) chloride was dissolved in about 2 ml of cold ethanol and spiked with ^{203}Hg (Solution B). To Solution A, Solution B was added, then, after a few seconds, the product separated as a white crystalline precipitate was filtered through a filter paper, Toyo No. 5C, washed with cold ethanol, and then dried by means of an air current at the pump. Finally, the labelled chloromethylmercury or chloroethylmercury was crystallized from a hot ethanol solution. The specific activities of these compounds were 1.3×10^8 cpm g^{-1} and 2.7×10^8 cpm g^{-1} respectively. The radioactive tracer ^{203}Hg was purchased from the Radiochemical Centre, Amersham (England). The radioactive purity of this tracer was checked by means of a Ge (Li) detector coupled with a 1024 multichannel analyzer.

Standard Solution of Chloromethylmercury. 40.2 mg of labelled chloromethylmercury was dissolved in water, and then 8 ml of hydrochloric acid was added. The solution was diluted to 100 ml with deionized water. This solution was diluted to the desired concentration with deionized water before every use.

Standard Solution of Chloroethylmercury. 50.3 mg of labelled chloroethylmercury was dissolved in a small volume of ethanol (1 ml), and the then mixture was diluted with deionized water. Eight milliliters of hydrochloric acid were then added to this solution, and the solution was diluted to 100 ml with deionized water. This solution was diluted to the desired concentration before every use.

1% Thiourea Solution in 0.1 mol dm^{-3} Hydrochloric Acid.

10% Tin (II) Chloride Solution in 1 mol dm^{-3} Hydrochloric Acid. The solution was bubbled by the air pump for 10 min at a flow rate of 0.5 l min^{-1}.

10 mol dm^{-3} Sodium Hydroxide Solution.

Apparatus. The apparatus used included two Hitachi-Horiba pH meters, M-5 and M-7; a Kobe Kogyo Co., Model STL-200 (44.5×50.8 mm NaI (Tl) crystal), well-type scintillation counter; a Hitachi 170-50 atomic-absorption spectrometer with a 18-cm-long quartz-absorption cell (this apparatus was connected to a Hitachi recorder).

The chromatographic column was a glass tube 12 mm in diameter and 140 mm in length, with a coarse sintered-glass disc and a stop-cock at the bottom.

A Toyo E-E SF200A fraction collector was also used.

Procedure for Batch Experiments. Two milliliters of the mercury test solution, (50 ppm, containing ^{203}Hg for mercury (II), 37.4 ppm and 46.5 ppm as mercury for chloromethylmercury and chloroethylmercury respectively), 10 ml of a buffer solution, and 0.5 g of MBT-SG were put into a 50-ml centrifuge tube and mixed. The mixture was then agitated mechanically at 340 strokes min^{-1} for 5 min at room temperature. The supernatant was filtered through a dry sheet of Toyo No. 5C filter paper. Each 3 ml of the filtrate was submitted to gamma-ray counting, afetr which the retention recovery was calculated.

Procedure for Column Method. The chromatographic tube (12 mm in diameter) was filled with 5 g of dried MBT-SG, and then a piece of filter paper was placed on the top of the column. In this case, the bed length became about 7 cm. A given volume of sea water containing individual mercury species was adjusted to a suitable pH, and then percolated through the column at a flow rate of 1—3 l h^{-1}. After washing the column with about 10 ml of deionized water, the mercury was eluted by the use of a 1% thiourea solution in 0.1 mol dm^{-3} hydrochloric acid or a solvent mixture of acetone and hydrochloric acid (25: 1) at the flow rate of about 1 ml min^{-1}. Then the effluent was made up to 25 ml, and a 3-ml aliquot of the solution was pipetted into a test tube for the measurement of its radioactivity by means of a gamma-ray scintillation counter.

Recommended Analytical Procedure. The following procedure is recommended: after the sample is collected, a 1- to 2-l portion is immediately adjusted to *ca.* pH 5.5 with hydrochloric acid and then pessed through the MBT-SG column (2 g of the material), which had been washed with 25 ml of the thiourea eluting solution and 25 ml of mercury-free sea water successively, at the flow rate of 1 to 2 l h^{-1} under gentle suction. Mercury-free sea water is prepared by passing sea water through the MBT-SG column. Subsequently, about 25 ml of the 1% thiourea eluting solution is passed through the column at the flow rate of about 1 ml min^{-1}. Then, the column is washed with about 10 ml of deionized water. The effluent and the washing are collected in a 100-ml Erlenmyer flask, and an additional 10 ml of deionized water is added to the flask. In a 50-ml beaker, about 6 ml of 10 mol dm^{-3} sodium hydroxide solution is placed, and then 5 ml of a 10% tin (II) chloride solution in hydrochloric acid is added under vigorous stirring, after which the solution is poured into the above Erlenmyer flask containing the column effluent. The flask is immediatly closed with a silicon rubber stopper provided with inlet- and outlet-tubes, the former being connected to a small air pump, and the latter, to a glass tube containing magnesium perchlorate. Then, the content is submitted to the determination of mercury by means of atomic-absorption spectrometry. The front of the magnesium perchlorate tube has been connected to a quartz atomic absorption cell 18 cm in length. After the flask has been shaken for 1.5 min, the air is bubbled through the solution at the flow rate of 0.5 l min^{-1} using an air pump. The absorbance is measured at 254 nm.

The reagent blank test has to be carried out throughout the whole procedure except for passing the sample water down the column.

Results and Discussion

Characteristics of the Chelating Material. The chelating capacity of MBT-SG for mercury, as measured by the column method, was found to be about 12 μmol per g of MBT-SG. This is comparable with that obtained for copper(II) (10 μmol per g of MBT-SG) and appears to be enough to collect mercury from a large amount of sea water, because 1 l of sea water is estimated to contain as little as about 0.3 μmol of heavy metal ions in all. This is compatible with 0.03 g of MBT-SG.

This solid chelating material also showed no loss of the mercury once retained on it even after a storage period of about one year. Therefore, this material can be submitted to atomic-absorption spectrometry or radioactivation analysis for mercury after carrying back it to laboratory without any loss and contamination of the element. An ordinary disposable syringe tube (5 ml) may be conveniently used as a column tube on board ship.

Recovery of Mercury(II), Methylmercury, and Ethylmercury ions at Various pH *Values.* The recovery of each individual mercury species was examined for a simple aqueous solution and for sea water of various pH values by the batch-experiment technique, as has been described previously. The pH of the solution was adjusted by sodium acetate plus hydrochloric acid for pH 1—5, and potassium dihydrogen phosphate plus sodium hydroxide for pH 6—8.

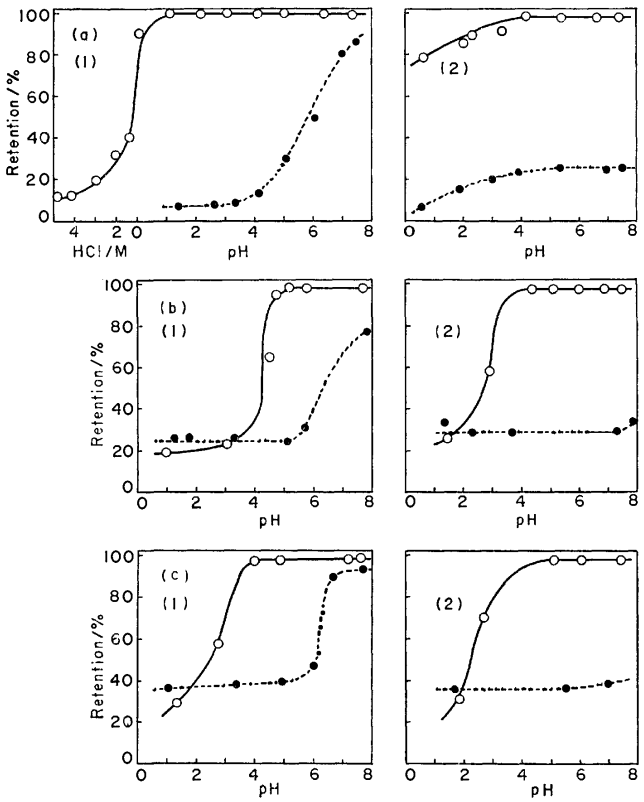

Fig. 1. Effect of pH on retention of (a) mercury(II), (b) methylmercury(I), and (c) ethylmercury(I).
(1): Aqueous solution, (2): sea water;
—○— MBT-SG; ---●--- untreated silica gel.

The results are shown in Fig. 1, along with those obtained by using untreated silica gel. The pH value mentioned is that measured after the equilibration. The mercury(II) ion was found to be retained completely on the chelating material at pH 1 for the aqueous solution and at pH 4 for sea water, but when untreated silica gel was put into an aqueous solution, the mercury-(II) ion began to be adsorbed at pH 4. In the case of sea water, however, a recovery of 30% was only obtained at pH values of 6 or above.

The complete retention of the methylmercury ion from an aqueous solution and sea water were achieved at pH 4.5 and 4 respectively with MBT-SG, and a remarkable difference in adsorbability between the

two adsorbents was observed. In the aqueous solution, the ethylmercury ion behaved quite similarly to the methylmercury ion, but in sea water a quantitative retention of ethylmercury on MBT-SG was obtained at pH 5.

Consequently, the pH value of 5 to 5.5 was chosen as the operating pH for the column experiments.

Retention of Individual Ions on the Column. One-liter portion of sea water containing a metal ion in various concentration were passed through the column at different flow rates. Each mercury species retained on the column was eluted with 20 ml of a mixture of acetone and hydrochloric acid (25: 1). The effluent was made up to 25 ml, and then a 3 ml portion of the aliquot was pipetted into a test tube for gamma-ray counting. Table 1 shows that the quantitative recovery of the mercury(II) ion in the concentration range of 0.032—20 ppb was attained from 1 l of sea water.

Table 1. Recovery of mercury(II), methylmercury(I), and ethylmercury(I) by the column method[a)]

Ion	Concentration / ppb	Flow rate / $l\ h^{-1}$	Recovery / %
Hg(II)	20	1—2	100
	1	2—3	100
	0.032	1—3	100
$CH_3Hg(I)$	200	1—2	100
$C_2H_5Hg(I)$	200	1—2	100

a) MBT-SG: 5 g; column: $\phi 12 \times 70$ mm.

In the cases of methylmercury and ethylmercury ions, their quantitative retention was also observed from 1 l of sea water of a very low concentration (below 0.2 ppm), and they were easily released from the column with the same mixed solution of acetone and hydrochloric acid. Thus, the preconcentration of the inorganic and organic mercury from 1 l of a sample solution is easily attainable within only 20 to 30 min.

Effect of Various Ions and Organic Substances on the Adsorption of Mercury. Since various metal ions are well-known to react with MBT, copper(II), lead(II), zinc(II), cadmium(II), nickel(II), cobalt(II), and iron(III) were examined for their effects on this preconcentration procedure of mercury. One liter of sea water, containing the mercury(II) ion in a concentration of 1 ppb, both methylmercury and ethylmercury ions in a concentration of 0.2 ppm, and one of the above-mentioned ions in a concentration of 1 ppm, was passed through a column containing 5 g of MBT-SG (70 mm long) at the flow rate of 2 l h^{-1}. As shown in Table 2, none of these metal ions at the 1 ppm level had any effect on the adsorption of any mercury species. Sea water generally contains only 50 ppb of heavy metal ions in all; therefore, the effects of these metal ions on the adsorption of mercury from sea water may, for practical purposes, be disregarded.

Table 2. Effect of diverse ions on the recovery of mercury compounds by the column method

Ion	Concn. / ppm	Recovery/% Hg(II)	$CH_3Hg(I)$	$C_2H_5Hg(I)$
Cu(II)	1	100	100	100
Pb(II)	1	100	100	100
Zn(II)	1	100	100	100
Cd(II)	1	100	100	100
Ni(II)	1	100	100	100
Co(II)	1	100	100	100
Fe(III)	0.1	100	100	100

Table 3. Effect of various substances on the recovery of mercury(II) by the column method[a)]

Substance	Concentration / mol dm^{-3}	Recovery / %
Cysteine	10^{-4}	83
Cystine	10^{-4}	80
EDTA	10^{-4}	100
Citric acid	10^{-4}	98
Tartaric acid	10^{-4}	99
SCN^-	10^{-4}	96

a) MBT-SG: 3 g; column: $\phi 12 \times 50$ mm.

Some organic compounds were also examined for their effects. In this case, a solution containing mercury in a concentration of 20 ppb and the organic compounds in a concentration of about 100 times that of mercury was passed through the column. The results are shown in Table 3. Several organic ligands such as EDTA, citric acid, and tartaric acid, did not interfere, and thiocyanate slightly reduced the adsorbability of mercury on MBT-SG. On the other hand, cysteine and cystine appreciably reduced the recovery of mercury. Apparently, this is due to the higher affinity of these ligands to mercury. For methylmercury and ethylmercury ions, similar experiments were not done because each specific activity of their labelled compounds became too low to perform the test of a reasonably low concentration of mercury. However, comparable recoveries of them with the mercury(II) ion can be expected from the results shown in Fig. 1 and Table 2.

Since, in sea water, these organic substances are never found beyond the concentration shown in the Table, the interference of these substances may also be negligible. In fact, in the present recovery experiment, the quantitative retention of each of the three kinds of mercury ions was achieved from a sea-water sample which had been collected at Tsukumo Bay, Noto Peninsula, and assumed to be more polluted by domestic activity than open sea water.

Elution of Mercury. Mercury was retained intimately on the column, therefore, elution with a single mineral acid, such as hydrochloric acid or nitric acid, gave a poor recovery of mercury. Various kinds of solvents and their mixtures were tested for adoption as the eluent by the batch method; the results are shown in Table 4. Among the various kinds of solutions tested, a solvent mixture of acetone and hydrochloric acid (in a mixing ratio of 9: 1 or 25: 1)[22] and a 1% thiourea solution in 0.1 mol dm^{-3} hydrochloric acid[21] were found to be most adequate for the elution of

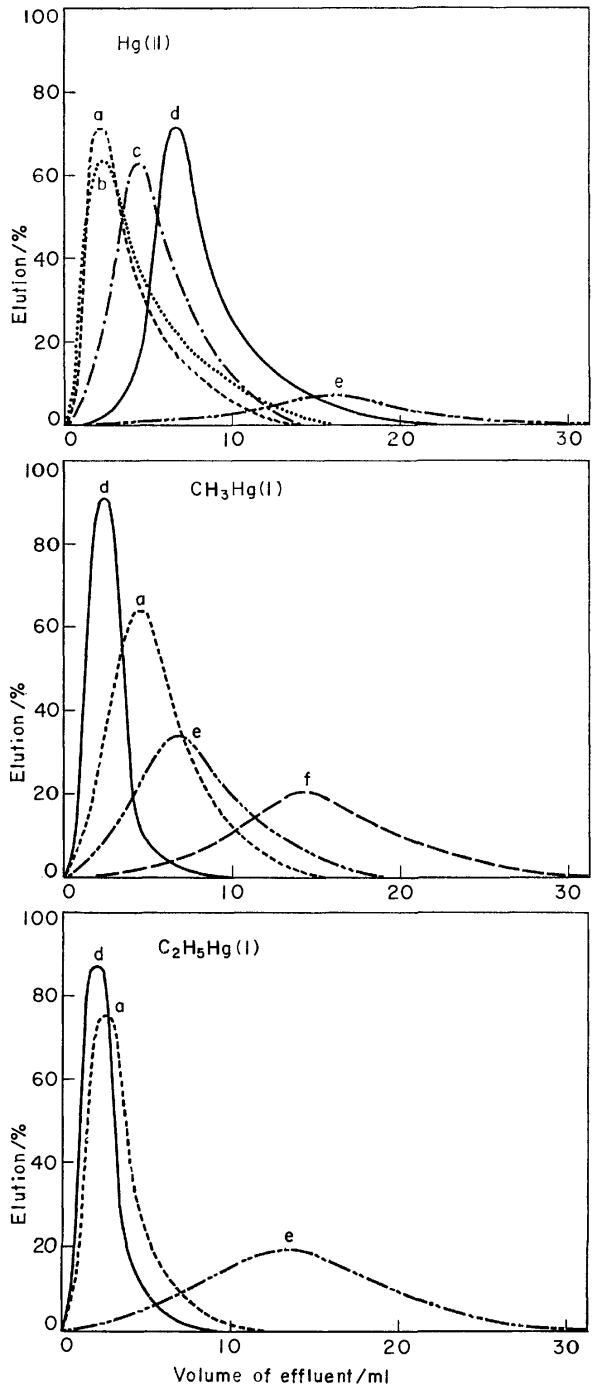

Fig. 2. Elution of mercury(II), methylmercury(I), and ethylmercury(I) retained on MBT-SG.
(a) Ethanol, (b) 1% thiourea in HCl (0.1 mol dm^{-3}), (c) acetone–HCl (9: 1), (d) acetone–HCl (25: 1), (e) HCl (1 mol dm^{-3}), (f) HCl (0.1 mol dm^{-3}).

mercury from the column.

The elution curves with various eluting solutions are shown in Fig. 2, from which about 20 ml of the solvent mixture of acetone and hydrochloric acid, and 20 ml of the 1% thiourea solution in hydrochloric acid seem to be suitable for obtaining quantitative recovery of mercury from the column. The former solvent mixture, however, released not only mercury, but also the chelating reagent from the column to some extent, and became difficult to submit the eluate to the subsequent atomic-absorption spectrometry of mercury because of the interference of the coexisting reagent, which was likely to give a higher value of mercury. On the other hand, the latter solvent could not dissolve the chelating reagent, and no interference occured in the atomic-absorption spectrometry of mercury in the effluent.

Table 4. Release of mercury(II) retained on MBT-SG (Batch Experiment)

Substance	Released/%
HCl (1 mol dm^{-3})	5.4
HCl (6 mol dm^{-3})	12.4
HCl (10 mol dm^{-3})	7.9
HCl (1 mol dm^{-3})+NaCl	23.2
HNO_3 (1 mol dm^{-3})	8.8
HNO_3 (6 mol dm^{-3})	49.6
H_2SO_4 (3 mol dm^{-3})	15.0
Ascorbic acid	6.8
Ethanol	50.7
Acetone–HCl (9: 1)	76.4
Acetone–HCl (25: 1)	75.0
1% thiourea in HCl (0.1 mol dm^{-3})	76.0

Shaking time: 5 min.

Blanks were usually obtained when MBT and thiourea were employed. However, if the column was washed with the thiourea eluting solution by passing it through the column prior to the passage of the sample, a rather higher blank attributable to the MBT reagent was completely eliminated, and the overall blank value reached that caused by thiourea (about 2 ng of mercury).

Reductive Vaporization of Mercury. According to Umezaki *et al.*,[24] both inorganic and organic mercury compounds can be reduced to metal by the use of the tin(II) ion in a 1 mol dm^{-3} sodium hydroxide solution containing a trace amount of the copper(II) ion; also, the mercury can be driven off by the aeration of this solution. In the present study, this treatment was directly applied to the effluent containing a radioactive tracer of mercury, and the mercury thus evolved was introduced into 10 ml of the 1% potassium permanganate solution. After diluting this solution to 25 ml, a 3 ml portion was taken out and its gamma activity was counted. About 93% of the mercury in the effluent vaporized and was absorbed in the permanganate solution. Therefore, the result obtained by this procedure has to be corrected by this factor. On the other hand, when the initial effluent was made up to 1 mol dm^{-3} in a hydrochloric acid solution containing tin(II) chloride, mercury was not vaporized at all.

Table 5. Analysis of sea water

Method	Preconcentration factor	Mercury content ng/l
Direct analysis after MnO_4^- oxidation[a]	—	280±40
The present method[b]	8	280±20

a) Sample: 50 ml. b) Sample: 200 ml.

Analysis of Sea Water for Mercury. The present method was applied to a sea-water sample collected from a very shallow beach near Kanazawa Harbour. The sea water was filtered through cleaned absorbent cotton and analyzed after preconcentration by a factor of eight. The results are given in Table 5, along with those obtained by direct analysis without preconcentration after the permanganate oxidation of the sample. The mercury content is rather high for coastal water, but the two sets of results show a good agreement.

Conclusion

2-Mercaptobenzothiazole-silica gel(MBT-SG) provides an easy means for the preconcentration of mercury(II), methylmercury(I), and ethylmercury(I) prior to the ordinary cold-vapor atomic-absorption spectrometry. The great advantages of this chelating material, in spite of its relatively low chelating capacity, are the ease of preparation and the fast adsorptions of mercury compounds from the water sample. Moreover, mercury retained on MBT-SG can be preserved without any loss or any contamination for one year. The loss of the reagent from the column during the passage of a large volume of sample solution is inappreciably small, so 2—5 l of sea water can be treated with a relatively small column. The mercury ion preconcentrated in this way can be eluted from the column with a small volume of an eluent with a high concentration factor. Furthermore, as mercury compounds in sample water rapidly react with MBT on the column, the time necessary for the preconcentration is considerably shorter than in the other method. By the present method, mercury in concentration range of 2—50 ng can be determined.

The authors wish to thank the Ministry of Education for a Grant-in-Aid (Special Project Research, "Fundamental Research for the Preservation of the Marine Environment," Project No. 111313).

References

1) H. Hamaguchi, R. Kuroda, and K. Hosohara, *Nippon Kagaku Zasshi*, **82**, 347 (1961).
2) T. M. Letherland, J. D. Burton, M. J. McCartoney, and F. Culkin, *Nature*, **232**, 112 (1972).
3) J. D. Burton and T. M. Letherland, *Nature*, **231**, 440 (1971).
4) R. E. Cranston and J. D. Burton, *Environ. Sci. Tech.*, **6**, 274 (1972).
5) H. V. Weiss, S. Yamamoto, T. E. Crocier, and J. H. Methewson, *Environ. Sci. Tech.*, **6**, 644 (1972).
6) D. Gardner and J. P. Riley, *Nature*, **241**, 526 (1973).
7) M. Zief and J. W. Mitchell, "Contamination Controll in Trace Element Analysis," John Wiley and Sons, New York (1976).
8) A. R. Byrne, M. Dermelj, and L. Kosta, *J. Radioanal. Chem.*, **6**, 325 (1970).
9) M. Nishimura and S. Konishi, *Kaiyokagaku*, **8**, 820 (1976).
10) I. Sanemasa, T. Deguchi, K. Urata, J. Komodo, and H. Nagai, *Anal. Chim. Acta*, **87**, 479 (1976).
11) R. A. Carr and P. E. Wilkniss, *Environ. Sci. Tech.*, **7**, 62 (1973).
12) W. F. Fitzgerald, W. B. Lyons, and C. D. Hunt, *Anal. Chem.*, **46**, 1882 (1974).
13) R. E. Rosian and C. M. Wai, *Anal. Chim. Acta*, **65**, 279 (1973).
14) S. Shimomura, Y. Nishihara, and Y. Tanase, *Bunseki Kagaku*, **17**, 1148 (1968).
15) R. S. Foote, *Science*, **177**, 513 (1972).
16) S. J. Long, D. R. Scott, and R. J. Thompson, *Anal. Chem.*, **45**, 2227 (1973).
17) P. Schramel, K. Samsahl, and J. Pavlu, *J. Radioanal. Chem.*, **19**, 329 (1974).
18) M. H. Borthner and D. E. Robertson, *Anal. Chem.*, **47**, 592 (1975).
19) I. Sanemasa, *Bull. Chem. Soc. Jpn.*, **48**, 1795 (1975).
20) R. Coyne and J. Collin, *Anal. Chem.*, **44**, 1093 (1972).
21) K. I. Mahan and S. E. Mahan, *Anal. Chem.*, **49**, 662 (1977).
22) K. Terada, A. Inoue, J. Inamura, and T. Kiba, *Bull. Chem. Soc. Jpn.*, **50**, 1060 (1977).
23) W. K. Wilde, *J. Chem. Soc.*, **1949**, 72.
24) Y. Umezaki and K. Iwamoto, *Bunseki Kagaku*, **20**, 173 (1971).

Binuclear Metal Complexes. XXXI.[1] Synthesis and Magnetic Property of Binuclear Manganese(III) Complexes with 3-Salicylideneamino-1-propanol and Its Homologues[2]

Naoyuki TORIHARA, Masahiro MIKURIYA, Hisashi OKAWA,* and Sigeo KIDA
Department of Chemistry, Faculty of Science, Kyushu University, Hakozaki, Higashiku, Fukuoka 812
(Received November 19, 1979)

Binuclear manganese(III) complexes with 3-salicylideneamino-1-propanol and its homologues, MnL(ac) and $MnLXH_2O$ (L=Schiff base dianion; ac=acetate ion; $X^-=Cl^-$, Br^-, N_3^-), were synthesized. It was shown that manganese(III) ions were bridged by the deprotonated alcoholic oxygen of the Schiff base in the equatorial plane and coordinated by bidentate acetate ion or X^- and H_2O groups in apical positions to form six-coordination. Cryomagnetic measurements indicated that an antiferromagnetic spin-exchange interaction operates between a pair of manganese(III) ions; exchange integral being evaluated at -13.5——-20.4 cm^{-1}.

Binuclear manganese(III) complexes are of interest in studying spin-exchange interaction of d^4–d^4 system. Recently di-μ-oxo bridged binuclear manganese(III) complexes were found to be a model of photosystem-II in green plant photosynthesis, where manganese functions as a redox catalyst for the oxidation of water to molecular oxygen.[3] In spite of the growing interests in magnetism and in bioinorganic aspect, characterized binuclear manganese(III) complexes with di-μ-oxo bridging system are very few.[4-6]

Zelentsov *et al.*[5] prepared manganese(III) complexes with 2-(salicylideneamino)ethanol and its homologues. The magnetic moments of these complexes are higher at room temperature but lower near liquid nitrogen temperature than the spin-only value. They assumed that the complexes have a di-μ-oxo bridged binuclear structure, in which a ferromagnetic spin-exchange interaction is operating between the metal ions. In general binuclear metal complexes with 2-(salicylideneamino)ethanol markedly differ in magnetic property from those of 3-salicylideneamino-1-propanol. For example, copper(II) complex with 3-salicylideneamino-1-propanol forms a discrete binuclear structure which displays a very strong antiferromagnetic spin-exchange interaction.[7,8] On the other hand, the complex with 2-(salicylideneamino)ethanol shows a normal magnetic moment at room temperature and obeys the Curie-Weiss law with a positive Weiss constant.[7] The latter complex was considered to have a "cubane-type" tetranuclear structure, which has been confirmed for the copper(II) complex with the Schiff base derived from acetylacetone and 2-aminoethanol.[9] Thus, it was aimed in this study to prepare binuclear manganese(III) complexes with 3-salicylideneamino-1-propanol and its homologues and to investigate their magnetic property in comparison with the complexes obtained by Zelentsov *et al.*

The ligands used in this study are Schiff bases obtained by condensing salicylaldehyde, *o*-vaniline, 5-bromosalicylaldehyde, or 2-hydroxy-1-naphthaldehyde with 3-amino-1-propanol. They are abbreviated as H_2spa, H_2vpa, H_2brspa, and H_2npa respectively. Two types of binuclear complexes, MnL(ac) and $MnLXH_2O$ (H_2L=Schiff base; $X^-=Cl^-$, Br^-, N_3^-), were synthesized in this study. Mononuclear complexes, $Mn(Hspa)_2ClO_4$ and $Mn(Hspa)_2NCS$, were also prepared.

Experimental

Syntheses. *$Mn(Hspa)_2ClO_4$*: A solution of salicylaldehyde (2.4 g), 3-amino-1-propanol (1.5 g) and manganese(II) perchlorate hexahydrate (14.4 g) in methanol (300 ml) were refluxed for 2 h. A deep black-green solution thus obtained was slowly concentrated at a temperature below 20 °C to give black prisms. They were collected by suction and dried under reduced pressure.

Found: C, 46.87; H, 4.67; N, 5.49%. Calcd for $C_{20}H_{24}N_2O_8ClMn$: C, 47.02; H, 4.74; N, 5.48%.

$Mn(Hspa)_2NCS$: $Mn(Hspa)_2ClO_4$ (1.0 g) was dissolved in methanol (50 ml) and to this solution was added NaNCS (0.8 g). The mixture was refluxed for 30 min, filtered while hot and allowed to stand over night. Black prisms which separated were collected and dried under reduced pressure.

Found: C, 53.53; H, 5.11; N, 9.01%. Calcd for $C_{21}H_{24}N_3O_4SMn$: C, 53.73; H, 5.15; N, 8.95%.

Mn(spa)(ac). To a solution of salicylaldehyde (2.4 g) and 3-amino-1-propanol (1.5 g) in methanol (300 ml) was added manganese(II) acetate tetrahydrate (9.8 g) to give a deep green solution. After refluxing for 5 h, the volume of the solution was concentrated to *ca.* 30 ml at a temperature lower than 20 °C to give black-green prisms. They were collected and recrystallized from methanol.

Found: C, 49.06; H, 4.79; N, 4.72%. Calcd for $C_{12}H_{14}NO_4Mn$: C, 49.50; H, 4.85; N, 4.81%.

Mn(vpa)(ac). This complex was obtained as black-green prisms in the same way as that of Mn(spa)(ac) except for using *o*-vaniline instead of salicylaldehyde.

Found: C, 48.67; H, 5.03; N, 4.20%. Calcd for $C_{13}H_{16}NO_5Mn$: C, 48.61; H, 5.02; N, 4.36%.

Mn(brspa)(ac)·MeOH. This complex was obtained as green prisms in the same way as that of Mn (spa) (ac) except for using 5-bromosalicylaldehyde instead of salicylaldehyde.

Found: C, 38.79; H, 4.25; N, 3.50%. Calcd for $C_{13}H_{17}NO_5BrMn$: C, 38.83; H, 4.26; N, 3.48%.

Mn(npa)(ac)·MeOH. This complex was obtained as black prisms by reacting 2-hydroxy-1-naphthaldehyde, 3-amino-1-propanol and manganese(II) acetate tetrahydrate in methanol.

Found: C, 54.72; H, 5.15; N, 3.77%. Calcd for $C_{17}H_{20}NO_5Mn$: C, 54.70; H, 5.13; N, 3.75%.

$Mn(spa)ClH_2O$. A solution of salicylaldehyde (2.4 g), 3-amino-1-propanol (1.5 g) and manganese(II) perchlorate hexahydrate (14.4 g) in methanol (300 ml) was refluxed for 2 h. To a black-green solution thus obtained was added sodium hydroxide (1.6 g) and the mixture was stirred for 5 d

to give reddish black solution. When the solvent was evaporated, there remained an oily substance. It was dissolved in methanol (50 ml) to which lithium chloride (4.2 g) was added. The mixture was stirred under reflux for 30 min and filtered. The filtrate was allowed to stand over night to give deep green crystals, which were collected by suction and dried under reduced pressure.

Found: C, 41.96; H, 4.60; N, 4.90%. Calcd for $C_{10}H_{13}NO_3ClMn$: C, 42.05; H, 4.59; N, 4.90%.

Mn(spa)BrH$_2$O. This complex was obtained as deep green prisms in the same way as that of Mn(spa)ClH$_2$O except for using sodium bromide instead of lithium chloride.

Found: C, 36.10; H, 3.94; N, 4.31%. Calcd for $C_{10}H_{13}N_4O_3Mn$: C, 36.39; H, 3.97; N, 4.24%.

Mn(spa)N$_3$H$_2$O. This complex was obtained as deep green crystals in the same way as that of Mn(spa)ClH$_2$O except for using sodium azide instead of lithium chloride.

Found: C, 41.30; H, 4.49; N, 19.03%. Calcd for $C_{10}H_{13}N_4O_3Mn$: C, 41.11; H, 4.48; N, 19.18%.

Measurements. Infrared spectra of the complexes were measured with a Hitachi infrared spectrophotometer Model 215 on a KBr disk and a nujol mull. Electronic spectra were measured with a Shimadzu multipurpose spectrophotometer Model MSP-5000 by a reflection on a powder sample. Magnetic susceptibilities were measured by Faraday method in a temperature range from liquid nitrogen temperature to room temperature. Magnetic moments were calcualted by the expression, $\mu_{eff}=2.828\sqrt{\chi_A \times T}$, where χ_A is the magnetic susceptibility per one manganese ion corrected for diamagnetism using Pascal's constants.

Results and Discussion

In general manganese(II) complexes with Schiff bases are air-sensitive and easily oxidized to manganese(III) complexes by molecular oxygen. All complexes obtained in this study must be manganese(III) complexes judging from their elemental analyses and deep color.

Infrared spectrum of mononuclear Mn(Hspa)$_2$ClO$_4$ shows a strong band around 3400 cm^{-1}, which is attributed to the non-coordinated alcoholic OH group. This fact implies that Hspa$^-$ acts as a bidentate ligand. The Cl–O stretching frequency of perchlorate ion splits into three (1130, 1080, and 1040 cm^{-1}). This suggests that the perchlorate ion coordinates to manganese(III) ion as a bidentate ligand, because the splitting is quite similar to that (1130, 1093, and 1058 cm^{-1}) of blue form of Ni(en)$_2$(ClO$_4$)$_2$ in which perchlorate ion functions as a bidentate ligand.[10] On the other hand, two OH-stretching bands were found for Mn(Hspa)$_2$NCS at 3500 and 3250 cm^{-1}. It is likely that one Hspa$^-$ acts as a bidentate ligand and the other as a tridentate ligand. The C–N and C–S stretching bands of NCS$^-$ ion were observed at 2070 and 810 cm^{-1}, respectively, indicating the donation of NCS$^-$ ion to the metal at the nitrogen atom.[11] Thus, the infrared spectra and the compositions of the mononuclear complexes indicate that they possess structures of six-coordination.

Electronic spectrum of Mn(Hspa)$_2$ClO$_4$ shows bands at 15600 and 20600 cm^{-1}. The spectrum of Mn(Hspa)$_2$NCS shows bands at 12500, 15600, 20800, and 22200 cm^{-1}. The bands in the region 12000—16000 cm^{-1} are assigned to the d-d transitions. Although the correct intensities of the bands in the region 20000—23000 cm^{-1} are not known from reflectance spectrum, they are much weaker than the intra-ligand band near 28000 cm^{-1}. In addition to this, many manganese(III) complexes show d-d bands whose frequencies are higher than 20000 cm^{-1}. Thus, we tentatively assigned the bands in the region 20000—23000 cm^{-1} to d-d transitions. Since manganese(III) ion under O_h symmetry should show only one spin-allowed d-d band, it is likely that the geometry around the metal is much distorted from regular octahedron. Magnetic moments of Mn(Hspa)$_2$ClO$_4$ and Mn(Hspa)$_2$NCS at room temperature are 4.88 and 4.82 BM respectively, which are quite common for high-spin manganese(III) complexes.

Infrared spectra of the binuclear complexes do not show OH-stretching band of the alcoholic group. For the binuclear complexes with 3-salicylideneamino-1-propanol, alcoholic oxygen-bridged and phenolic oxygen-bridged binuclear structures are known.[12] The phenolic oxygen-bridged structure can be characterized by a skeletal band near 1550 cm^{-1},[12] which is higher in frequency than that of its related mononuclear complex. Although the skeletal band of MnL(ac) is concealed from a strong C–O band of carboxyl group, the band of MnLXH$_2$O is well resolved and observed at 1550 cm^{-1}. This frequency is almost the same as that of mononuclear Mn(Hspa)$_2$ClO$_4$ and Mn(Hspa)$_2$NCS. Thus, we may conclude that the complexes possess the 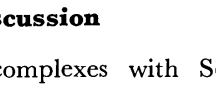 skeleton bridged by the alcoholic oxygen. This is compatible with the result of Miners and Sinn that the alcoholic oxygen-bridged binuclear structure is prefered to the phenolic oxygen-bridged structure when the complex is formed in alkaline media.[12]

The antisymmetric and the symmetric C–O stretching bands of acetate group in MnL(ac) were found at 1550 and 1400 cm^{-1} respectively. In general the antisymmetric and the symmetric C–O stretching bands of carboxylate ion coordinated to a metal as a unidentate ligand shifts to higher and to lower frequencies respectively, as the metal–O bond becomes strong.[13] On the other hand, both of the carbonyl bands shift in the same direction with a change of the metal–O bonding, when the carboxylate ion bridges metal ions.[13] The carboxyl bands of the present complexes seem to belong to the class of the latter type of bonding. Therefore, it is assumed that the acetate group in MnL(ac) functions as a bridge. Coordination of water molecule and azide ion to the metal for Mn(spa)N$_3$H$_2$O was confirmed by IR bands at 3250 and 2050 cm^{-1}. Coordination of chloride and bromide ions is supposed for Mn(spa)ClH$_2$O and Mn(spa)BrH$_2$O by the analogy of the above case. Based on these facts we assumed that two types of the binuclear complexes possess the structures given in Fig. 1.

Reflectance spectra of binuclear complexes of MnL(ac) and MnLXH$_2$O are similar to each other in that they have four absorption bands in the visible region. These bands are tentatively assigned to d-d

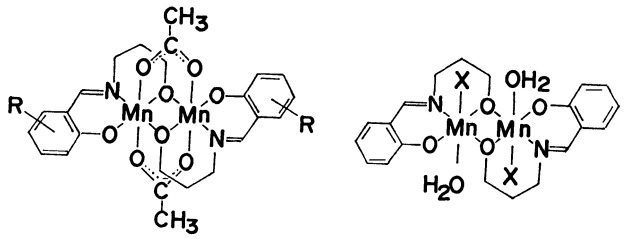

Fig. 1. Possible structures of binuclear complexes.

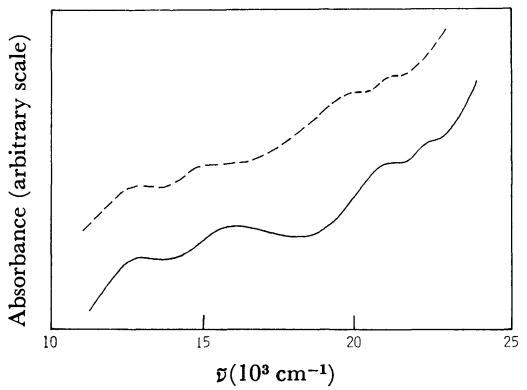

Fig. 2. Reflectance spectra of (——) Mn(spa)(ac) and (-----) Mn(spa)ClH_2O.

Table 1. Magnetic parameters of complexes

	J/cm^{-1}	g
Mn(spa)(ac)	−19.1	1.99
Mn(vpa)(ac)	−20.4	2.00
Mn(brspa)(ac)·MeOH	−13.5	1.99
Mn(npa)(ac)·MeOH	−18.9	1.99
Mn(spa)ClH_2O	−16.0	2.00
Mn(spa)BrH_2O	−16.8	2.00
Mn(spa)N_3H_2O	−14.4	2.00

transitions. Typical examples of electronic spectra are shown in Fig. 2. It is likely that the coordination geometry of the complexes is distorted from regular octahedron so that the ^5E_g and the $^5T_{2g}$ states of an octahedral manganese(III) ion split into five orbitally singlet states.

Effective magnetic moments of MnL(ac) and $MnLXH_2O$ at room temperature fall in the range 3.84—4.22 BM, which are lower than the moments (4.8—5.0 BM) found for most high-spin manganese(III) complexes. The operation of antiferromagnetic spin-exchange interaction between a pair of manganese(III) ions appears to be the main reason for the subnormal magnetic moments. Cryomagnetic measurements have shown that the magnetic susceptibility of the complexes has a maximum around 100 K. These magnetic behaviors can be well interpreted in terms of the magnetic susceptibility expression for the high-spin d^4–d^4 system based on the isotropic spin-exchange model ($\mathcal{H}=-2J\sum\hat{s}_i\hat{s}_j-g\beta s_z'H$, total spin s_z' being calculated by Kambe's approach),

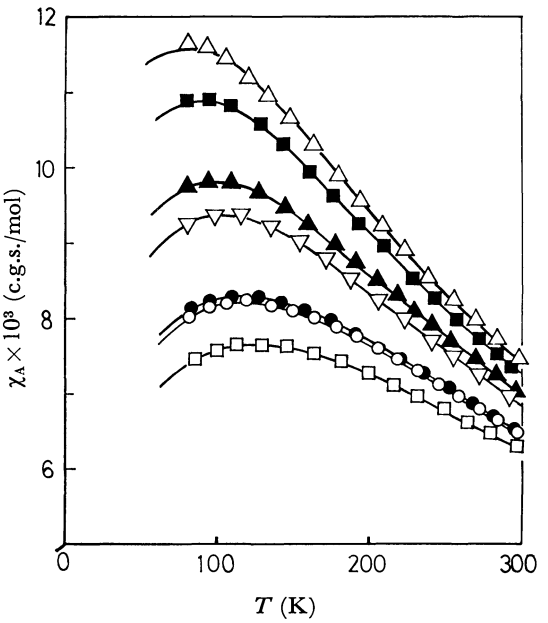

Fig. 3. Temperature variations of magnetic susceptibilities. (○) Mn(spa)(ac), (□) Mn(vpa)(ac), (△) Mn(brspa)(ac)·MeOH, (●) Mn(npa)(ac)·MeOH, (▲) Mn(spa)ClH_2O, (▽) Mn(spa)BrH_2O, and (■) Mn(spa)N_3H_2O.

where J is the exchange integral and other symbols have their usual meanings. Good agreements between the experimental and the theoretical susceptibilities are shown in Fig. 3. Magnetic parameters, g and J, determined from the best-fit technique, assuming $N\alpha$ at zero, are given in Table 1. Thus, it may be concluded that the manganese(III) complexes with 3-salicylideneamino-1-propanol and its homologues possess a discrete binuclear structure in which an appreciably strong antiferromagnetic spin-exchange interaction is operating between the metal ions.

In contrast to the above, the magnetisms of manganese(III) complexes with 2-(salicylideneamino)-ethanol and its homologues are quite strange. According to Zelentsov *et al.*,[5] the complexes consist of binuclear units and their magnetisms can be interpreted in terms of intramolecular ferromagnetic spin-exchange interaction (J=20—30 cm^{-1}) and a large zero-field splitting (*ca.* 8 cm^{-1}). However, the presence of such a large zero-field splitting is unlikely, since magnetisms of most mononuclear manganese(III) complexes obey the Curie-Weiss law with a small Weiss constant (θ= 0——25K).[14] When we plotted the inverse magnetic susceptibilities measured by Zelentsov *et al.* against the temperature, nearly straight lines were drawn in the temperature range 80—300K and the Weiss constants were estimated at −40——−120K. Very large negative Weiss constants can most naturally be explained in terms of a predominantly operating antiferromagnetic spin-exchange interaction in the molecule.

$$\chi_A=\frac{Ng^2\beta^2}{kT}\times\frac{30+14\exp(-8J/kT)+5\exp(-14J/kT)+\exp(-18J/kT)}{9+7\exp(-8J/kT)+5\exp(-14J/kT)+3\exp(-18J/kT)+\exp(-20J/kT)}+N\alpha,$$

Authors are grateful to the Ministry of Education for a Scientific Research Grant-in-Aid.

References

1) Part XXX: H. Okawa, T. Yoshida, N. Torihara, and S. Kida, *Mem. Fac. Sci., Kyushu Univ., Ser. C*, **12**, 71 (1979).
2) Presented at the 29 th Meeting of Coord. Chem. in Japan, Hamamatsu, Oct. 1, 1979.
3) D. T. Sawyer, M. E. Bodini, L. A. Willis, T. L. Riechel, and K. D. Magers, "Bioinorganic Chemistry -II,"ed by K. N. Raymond, Am. Chem. Soc., Washington (1977), p. 330.
4) A. Mangia, M. Nardelli, C. Pelizzi, and G. Pelizzi, *J. Chem. Soc., Dalton Trans.*, **1973**, 1141.
5) V. V. Zelentsov, I. K. Somova, R. S. Kurtanidze, and N. V. Semanina, *Soviet J. Corod. Chem.*, **3**, 1448 (1977).
6) D. K. Rastogi, S. K. Sahni, V. B. Rana, and S. K. Dua, *J. Coord. Chem.*, **8**, 97 (1978).
7) T. Tokii, Y. Muto, M. Kato, K. Imai, and H. B. Jonassen, *J. Inorg. Nucl. Chem.*, **34**, 3377 (1972).
8) M. Kato, Y. Muto, H. B. Jonassen, K. Imai, and A. Harano, *Bull. Chem. Soc. Jpn.*, **41**, 1864 (1968).
9) J. A. Bertrand and J. A. Kelley, *Inorg. Chim. Acta*, **4**, 203 (1970).
10) M. E. Farago, J. M. James, and V. C. G. Trew, *J. Chem. Soc., A*, 820 (1967).
11) K. Nakamoto, "Infrared Spectra of Inorganic and Coordination Compound," John Wiley and Sons, New York (1970), p. 187.
12) J. O. Miners and E. Sinn, *Bull. Chem. Soc. Jpn.*, **46**, 1457 (1973).
13) K. Nakamoto, Y. Morimoto, and A. E. Martell, *J. Am. Chem. Soc.*, **83**, 4528 (1961).
14) A. T. Casey and S. Mitra, "Theory and Application of Molecular Paramagnetism," ed by E. A. Boudreaux and L. N. Mulay, John Wiley and Sons, New York (1976), p. 178.

Thermal Square Planar-to-Octahedral Transformation of Nickel(II) Complexes Containing 2-Aminobenzimidazole in the Solid Phase[1)]

Yoshinori IHARA* and Ryokichi TSUCHIYA†

Laboratory of Chemistry, Faculty of Education, Kanazawa University, Kanazawa 920
†*Department of Chemistry, Faculty of Science, Kanazawa University, Kanazawa 920*

(Received November 30, 1979)

Thermal reactions of the complexes, $[Ni(abi)_4]X_2 \cdot nH_2O$ (abi, 2-aminobenzimidazole; X, Cl, Br, I, NO_3, ClO_4, or $1/2SO_4$; *n*, 3 for chloride and bromide, 1 for nitrate, and 0 for others) were investigated. Distinct color changes from orange to green were observed in the three complexes of chloride, bromide, and nitrate upon heating. It was found from the changes in absorption and far-IR spectra and magnetic susceptibilities under the thermal reactions that the complexes undergo transformation from square planar to tetragonally distorted octahedral structures, involving an increase in the coordination number from four to six. No such transformation could be found in the corresponding iodide, perchlorate, and sulfate. The effect of the introduced amino group on the structural conversion reactions of the abi complexes is discussed as compared with the corresponding benzimidazole complexes, $[Ni(bimd)_4]X_2$, which underwent transformation from square planar to octahedral structure upon heating when X is I or NO_3.[2)]

Nickel(II) ion forms complexes of various structures, *e.g.*, octahedral, tetrahedral, and square planar structures, depending on the ligand, mutual transformation often occurring among them.[3)] Few studies in the solid phase, however, are known.

Tsuchiya *et al.* reported the structural transformation of $[Ni(H_2O)_2(NN\text{-deen})_2]X_2$, where *NN*-deen is *N,N*-diethylethylenediamine and X halide ion.[4)] The chloride, upon heating, evolved two moles of coordinated water accompanied by anation of chloride ions with retention of the original octahedral structure, whereas the bromide underwent transformation from octahedral to square planar structure without anation of bromide ions after the liberation of water molecules. In addition to nickel(II) complexes containing *N*-substituted diamine, the thermal behavior of the complexes with the *C*-substituted diamines, 2-methyl-1,2-propanediamine and 1,2-diphenylethylenediamine, has been studied in the solid phase by Farago *et al.*[5)] and Lifschitz *et al.*,[6)] respectively. Transformation from octahedral to square planar structure was also observed in these complexes. The studies deal with the structural transformation of nickel(II) complexes containing diamine derivatives, accompanied by the change of the coordination number from six to four, upon heating in the solid phase.

Interesting thermal, mutual transformations have been reported as regards spectral measurements. The structure of bis(*N,N*-diethylethylenediamine)copper(II) tetrafluoroborate, perchlorate, and nitrate turns to square planar with fall in temperature, and to octahedral with rise in temperature.[7)] Tsuchiya *et al.* found a new transformation from square planar to octahedral structure in the benzimidazole complexes, $[Ni(bimd)_4](NO_3)_2 \cdot 2.5C_2H_5OH$ and $[Ni(bimd)_4]I_2$, in the solid phase.[2)] The study is characterized by the reactions involving the increase in the coordination number from four to six upon heating, and by the use of imine derivatives as the ligand which acts as a unidentate one.

The present study was undertaken to prepare the square planar nickel(II) complexes containing 2-aminobenzimidazole, and to investigate their thermal transformation into octahedral structure in the solid phase, and the effect of the amino group introduced to benzimidazole on the thermal reactions.

Experimental

Preparation. The ligand, 2-aminobenzimidazole, and the nickel (II) complexes were prepared by the methods reported,[8,9)] their chemical formulas being identified by elemental analyses and spectral measurements.

Thermal Analysis. TG and DSC measurements were carried out with a Rigaku Denki standard TG-DSC apparatus. All the measurements were carried out under constant flow of nitrogen at a heating rate 1.25 °C min^{-1}.

Isothermal Measurements. The green products were obtained by isothermal heating using the electrical furnace in static air.

Spectral Measurements. The electronic spectra in the solid state were measured by a diffuse reflectance method with a Hitachi EPU-2A spectrophotometer equipped with a standard Hitachi reflection attachment (Type R-3). The far-IR spectra were measured by the Nujol method with a JASCO IR-F far-infrared spectrophotometer.

Measurements of Magnetic Susceptibilities. The effective magnetic moments were evaluated from the magnetic susceptibilities measured by the Gouy method at room temperature. $Hg[Co(NCS)_4]$ was employed as a reference material. The susceptibilities of the complexes were corrected by using Pascal's constants for each element or atomic group contained.

Results and Discussion

Thermal Analyses. Since a distinct color change from orange to green was found for the three complexes, chloride, bromide, and nitrate, by the qualitative thermal technique, thermal analyses were carried out by TG-DSC measurements. The results are shown in Figs. 1—3. On the other hand, the iodide, perchlorate, and sulfate complexes decomposed without obvious color change upon heating.

Chloride turns from orange to green at the endothermic peak near 215 °C, at which melting seems to occur (Fig. 1). The exothermic peak near 150 °C seems to be attributable to a slight change in the packing of the crystal, since the changes in color and thermo-

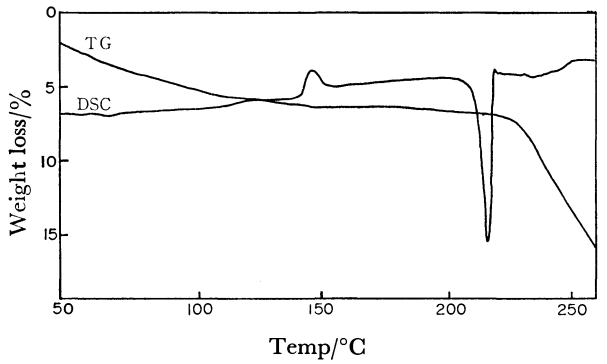

Fig. 1. Thermal analysis of $[Ni(abi)_4]Cl_2 \cdot 3H_2O$.

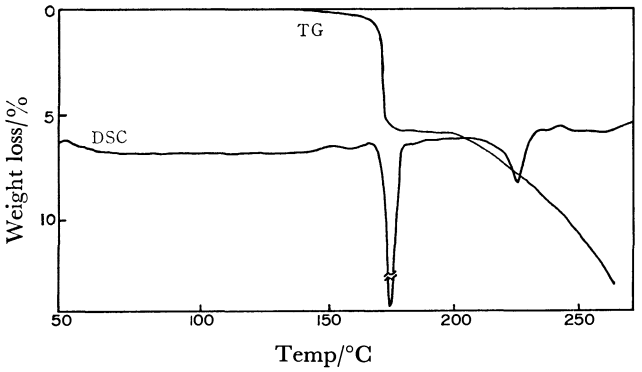

Fig. 2. Thermal analysis of $[Ni(abi)_4]Br_2 \cdot 3H_2O$.

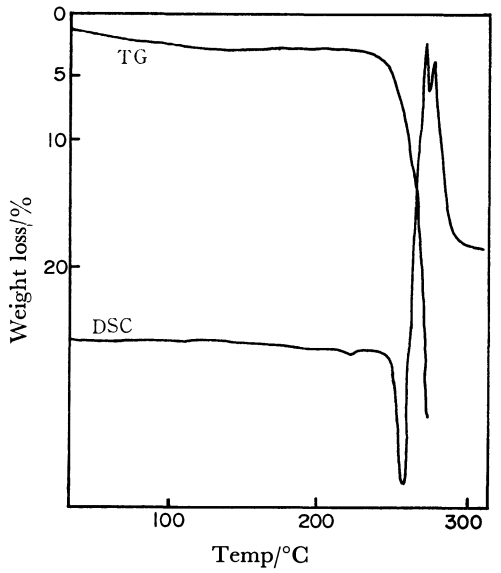

Fig. 3. Thermal analysis of $[Ni(abi)_4](NO_3)_2 \cdot H_2O$.

gravimetric curve are scarcely found in the complex at temperatures lower and higher than that of the peak. Bromide was converted into green completely at 175 °C, accompanied by the liberation of three moles of lattice water, decomposing gradually (TG curve, Fig. 2). For nitrate, no plateau predicting the formation of the stable product was observed (TG curve, Fig. 3), moss-green product being obtained by means of isothermal technique. The endothermic peak involving melting just before the exothermic peak appears with abrupt weight loss near 250 °C seems to indicate simultaneous occurrence of the structural transformation.

The most suitable conditions of isothermal heating for obtaining the products for identification of their structures are as follows: at 200 °C for 2—3 min, at 170 °C for 4—5 min, and at 230 °C for 2—3 min for chloride, bromide, and nitrate, respectively.

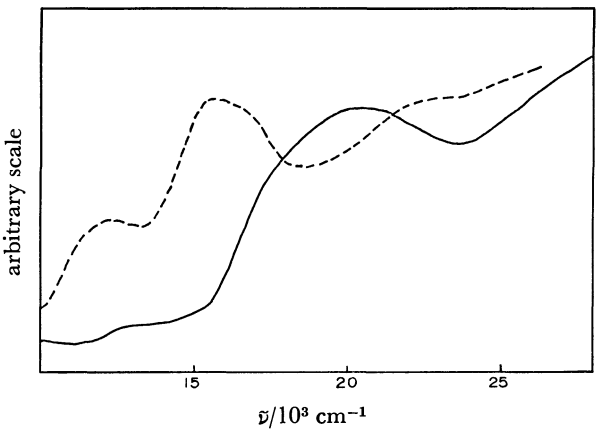

Fig. 4. Electronic spectra of $[Ni(abi)_4]Cl_2 \cdot 3H_2O$ before heating (——) and after heating (– – –).

Electronic Spectra. The electronic spectral change of chloride in the solid phase upon heating is shown in Fig. 4, the spectral data of all the green products being summarized in Table 1, together with the magnetic moments and the analytical data.

The chloride, before heating, has a broad absorption band near 20×10^3 cm^{-1} due to the square planar structure of nickel(II) complexes, and a charge transfer band characteristic to the complexes containing imidazole derivatives (Fig. 4). After heating, the chloride shows three absorption bands in visible region, but they slightly deviate from the general feature of the spectral pattern of octahedral nickel(II) complexes. This is similar to the case of $[Ni(NCS)_2(abi)_4]$ considered to have a tetragonally distorted octahedral structure[9]

Table 1. Electronic spectra data, magnetic moments, and analytical data of the heated products

Products	C(%)		H(%)		N(%)		Absorption Maxima ($\tilde{\nu}/10^3$ cm^{-1})			μ_{eff}(B.M.)
	Found	Calcd	Found	Calcd	Found	Calcd				
$[NiCl_2(abi)_4] \cdot H_2O$	49.48	49.44	4.33	4.45	24.64	24.71	12.5w	16.3	23.1sh	1.98
$[NiBr_2(abi)_4]$	46.55	44.77	3.56	3.76	23.44	22.38	12.5w	16.4	22.5sh	1.56
$[Ni(NO_3)_2(abi)_4] \cdot H_2O$	46.21	45.85	3.79	4.13	26.90	26.74	12.4w	16.5	23.4sh	2.12
$[Ni(NCS)_2(abi)_4]$							13.3w	16.3	22.2sh 26.5	

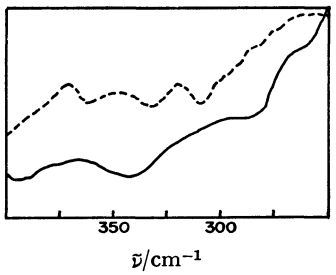

Fig. 5. Far-IR spectra of $[Ni(abi)_4](NO_3)_2 \cdot H_2O$ before heating (——) and after heating (-----).

(Table 1). Some of the octahedral benzimidazole complexes, $[NiX_2(bimd)_4]$, prefer tetragonal distortion.[10] All the products are expected to have the same structure.

Far-IR Spectra. Figure 5 shows the far-IR spectra of nitrate before and after heating. A distinct difference in their spectra lies in the appearance of the peak at 310 cm^{-1} after heating. Ferraro and Walker[11] pointed out that anhydrous metal nitrates, $Cu(NO_3)_2$ and $Co(NO_3)_2$, exhibit a peak in the range 250—350 cm^{-1} assigned to metal-oxygen vibration owing to the coordination of nitrate ion to central metal. The new peak, appearing in the nitrate heated can be ascribed to Ni–O(NO_3) stretching vibration. If so, the nitrate ions situated in the outer sphere before heating approach the central metal making the coordinated bond in the product.

Magnetic Moments. The magnetic moments of the products are given in Table 1. The complexes, showing diamagnetism before heating, are converted into paramagnetic ones upon heating. The values 1.56—2.12 BM are considerably lower than those of the nomal paramagnetic octahedral nickel(II) complexes. However, the values for the tetragonally distorted octahedral structures fall below 2.0 BM.[12] The data of magnetic moments together with the results of the electronic spectra suggest the formation of the tetragonally distorted octahedral complexes by thermal treatment.

Thermochromism of the three complexes, chloride, bromide, and nitrate, from orange to green is considered to result from the structural transformation from square planar to octahedral structures, involving considerably tetragonal distortion. The transformation can be represented by the following scheme.

$$[Ni(abi)_4]X_2 \cdot nH_2O \xrightarrow[\Delta]{-nH_2O} [NiX_2(abi)_4]$$

(X=Cl, Br, NO_3)

The analytical data of the products (Table 1) give no confirmation on the decomposition of 2-aminobenzimidazole in coordination sphere upon heating.

One mol of the lattice water appearing in the products of chloride and nitrate is that adsorbed when the products are placed at room temperature. They give the weight loss corresponding to 1 mol of water when heated again at 50 °C.

Enthalpy Changes. The enthalpy changes and the reaction temperatures of the structural transfer reactions determined by the DSC analyses are given in Table 2. Though all the reactions proceed endothermically, no reversibility of the transfer reactions was observed.

Table 2. Enthalpy changes and reaction temperatures

Starting complexes	ΔH(kJ/mol)	Reaction temp/°C
$[Ni(abi)_4]Cl_2 \cdot 3H_2O$	8.8	215
$[Ni(abi)_4]Br_2 \cdot 3H_2O$	8.8	175
$[Ni(abi)_4](NO_3)_2 \cdot H_2O$	7.1	250

The enthalpy changes seem too small for bromide to be caused by the dehydration of three moles of the lattice water alone. It can be explained in terms of the simultaneous occurrence of the structural transformation presumed to proceed exothermically besides the dehydration reaction. In the case of chloride and nitrate the enthalpy changes can be interpreted to be due to the structural transfer reactions being accompanied by endothermic melting.

Table 3. Possibility of square planar-to-octahedral transformation

X	bimd	abi
Cl	(not prepared)	possible
Br	(not prepared)	possible
I	possible	decomposed
NO_3	possible	possible
ClO_4	decomposed	decomposed
SO_4	(not prepared)	decomposed

Comparison with bimd Complexes. The possibilities of the transformation from square planar structure to octahedral one of bimd and abi complexes by the thermal treatment are summarized in Table 3. One striking difference between bimd and abi complexes is the possibility of formation of the square planar structure in the latter complexes containing chloride or bromide ion. The green octahedral dihalogenotetrakis (benzimidazole) complexes were prepared without appearance of the square planar structure for the chloride or bromide, whereas the complexes containing the iodide or nitrate ion were converted from square planar structure into the octahedral diacido complexes by thermal treatment. The results suggest that the ionic radii of anions in bimd complexes are important in stereochemical requirement for the preparation of the starting complexes and structural transformation, *viz.*, the smaller ion fits to a greater extent the packing of the *trans* sites of the coordination plane surrounded by the four bimd molecules.

The square planar species are formed in abi complexes. This seems to depend on steric hinderance by the amino group introduced and on the higher basicity in the abi ligand surrounding a nickel(II) ion. Another feature of the abi complexes is that thermal structural transformation prefers tetragonal distortion in the products heated than in the bimd complexes.

We wish to thank Mr. Hiroyasu Imai, Department of Pharmaceutical Science, Hokuriku University, for the TG-DSC measurements.

References

1) Presented at the 29 th Symposium of Coordination Compounds of the Chemical Society of Japan, Hamamatsu, October, 1979.

2) R. Tsuchiya, E. Kyuno, A. Uehara, S. Joba, and S. Ohba, *Chem. Lett.*, **1976**, 911.

3) C. W. Everett, Jr., and R. H. Holm, *J. Am. Chem. Soc.*, **87**, 2118 (1965).

4) R. Tsuchiya, S. Joba, A. Uehara, and E. Kyuno, *Bull. Chem. Soc. Jpn.*, **46**, 1454 (1973).

5) K. E. Farago, J. M. James, and V. C. G. Trew, *J. Chem. Soc., A*, **1968**, 48.

6) I. Lifschitz, J. C. Bos, and K. M. Dijkema, *Z. Anorg. Allg. Chem.*, **242**, 97 (1936).

7) A. B. P. Lever, E. Mantovani, and J. C. Donini, *Inorg. Chem.*, **10**, 2424 (1971).

8) P. Biddle, E. S. Lane, and J. L. Willans, *J. Chem. Soc.*, **1960**, 2369.

9) M. J. M. Cambell, D. W. Card, and R. Grzeskowiak, *J. Chem. Soc., Dalton Trans.*, **1972**, 1687.

10) D. M. L. Goodgame, M. Goodgame, and M. J. Weeks, *J. Chem. Soc., A*, **1967**, 1125.

11) J. R. Ferraro and A. Walker, *J. Chem. Phys.*, **42**, 1273 (1965).

12) a) S. L. Holt, Jr., R. J. Bouchard, and R. L. Carlin, *J. Am. Chem. Soc.*, **86**, 519 (1964); b) S. L. Holt, Jr. and R. L. Carlin, *ibid.*, **86**, 3017 (1964); c) G. A. Melson and D. H. Busch, *ibid.*, **86**, 4830 (1964).

The Extraction of Several Anions by Methyltrioctylammonium into Various Solvents

Yasushi INOUE* and Osamu TOCHIYAMA

Department of Nuclear Engineering, Faculty of Engineering, Tohoku University, Aramaki-aza-aoba, Sendai 980

(Received September 7, 1979)

The back extraction of methyltrioctylammonium chloride (MTOACl) from ten kinds of organic solvents was investigated as a function of the MTOACl concentration. The chemical species of the ammonium salt in the organic phase were found to be in the form of dissociated ions, of ion pairs, or of dimeric ion pairs, according to the dielectric constant of the solvent. MTOACl was better extracted into more polar and acidic solvents, such as nitrobenzene, 3-methyl-1-butanol, and chloroform. The selectivity coefficients ($K_{X/Cl}$) of MTOA for the exchange of Br^-, I^-, ClO_4^-, *vs.* Cl^- were obtained from the study of the distribution of several organic color reagents; they were found to increase with the anion size, irrespective of the organic solvent used. For all but acidic solvents, the values of $K_{X/Cl}$ were similar to each other. Such acidic solvents as 3-methyl-1-butanol and chloroform, however, reduced the selectivity of the extraction for anions.

Quaternary ammonium salts have been extensively used for metal extractions[1] and more recently have received attention as phase transfer catalysts[2] and exchangers for ion-selective electrodes.[3] However, our knowledge of the properties of substituted ammonium salts in solution is too limited to give a general guide for such applications. Knowledge of their property of extracting simple anions is, above all, most important in understanding many related reactions.

In this paper, the extraction of simple anions, such as chloride, bromide, iodide, and perchlorate, by methyltrioctylammonium (MTOA) into various organic solvents was investigated. MTOA was chosen as a representative long-chain alkylammonium because MTOA and closely related tertiary amine, trioctylamine (TOA) have been commonly used in extraction studies. The organic solvents were selected so as to furnish a wide variation in character. The extraction of chloride was first investigated by the analysis of the distribution of MTOACl between two phases to obtain the general idea of the extraction reaction. The extraction of other anions by MTOA was then indirectly studied through the ion-exchange reaction between the ion to be studied and the anions of several organic reagents, such as thenoyltrifluoroacetone (TTA), tetrabromophenol sulfonephthalein (Bromophenol Blue, BPB), and *p*-nitrophenol (*p*-NP), which coexisted in the system (hereafter, these reagents are referred to as "indicators"). These results were integrated in terms of the selectivity coefficients against chloride and discussed on the basis of various properties of the solvents and anions, as will be described below.

Experimental

Reagents. Methyltrioctylammonium chloride (Capriquat, Dotite reagent) was used as received. The effective concentration of the quaternary ammonium base was determined by acid-base titration in acetic acid.[4] All the other reagents were of a reagent grade and were used without further purification.

Apparatus. A shaker (Takabayashi Rika RL-6) and a centrifuge (Kubota KH-180) were used for the extraction experiment. A pH meter (Tōa Dempa HM-6A) was used for the pH measurements. The absorption spectra were measured with a Hitachi EPS-3 recording spectrophotometer using a quartz cell (1 cm light path).

Procedures. *General Procedure*: Equal volumes (4 cm^3) of an aqueous and an organic solution with the desired compositions were brought into contact in a glass tube and shaken mechanically for 15 min (140 times/min) at room temperature (23±2 °C). If necessary, the phase separation was accelerated by centrifugation. After phase separation, the concentration of the solute of interest was measured by a suitable analytical method. The aqueous phase was used for the pH measurements.

Distribution Ratio of MTOACl: An organic solution containing a definite concentration of MTOACl and an aqueous solution were equilibrated, and the concentration of MTOA in the aqueous phase was determined. The MTOA in the aqueous solution was extracted with BPB into xylene at pH about 11 ($[Na_2CO_3]=0.05$ mol dm^{-3}),[5] then the absorbance of the xylene solution was measured at 607 nm. The concentration of MTOA was calculated from the calibration curve, which obeyed Beer's law over the range from 2.5×10^{-6} to 2.5×10^{-5} mol dm^{-3}. The concentration of MTOA in the organic phase was calculated from the difference between the initial added concentration and the concentration in the aqueous phase after equilibration.

Extraction Exchange Constants: An organic solution containing MTOACl was equilibrated with an aqueous solution containing the desired concentrations of a certain anion (as a sodium salt) and buffer reagents (0.05 mol dm^{-3} of acetic acid, plus a variable concentration of ammonium hydroxide or 0.05 mol dm^{-3} sodium carbonate, depending on the pH of the solution to be studied) in the presence of an indicator which had been added to the organic (TTA) or the aqueous phase (BPB, *p*-NP). When TTA was used as an indicator, the absorption spectrum of TTA in the organic phase was measured to give the ratio of the salt to the acid form of TTA.[6] When BPB or *p*-NP was used as an indicator, the distribution ration was obtained from the measurement of the absorbance of the organic phase (at 600—608 nm for BPB) or the aqueous phase (at 402 nm for *p*-NP).

Results and Discussion

Extraction of MTOACl. Since the extracted ammonium salt may be in the form of dissociated ions, of ion pairs, or of still higher ion associations, the concentration of MTOA in the organic phase can be expressed as:

$$C_{Q,o} = [Q^+]_o + [QCl]_o + 2[Q_2Cl_2]_o + \cdots, \quad (1)$$

assuming that Cl^- is the only anion present. Here, Q^+ denotes the cation of MTOA; square brackets show the concentration of the enclosed species; the subscript o stands for the organic phase; the absence of any subscript indicates the aqueous phase. C is the total (analytical) concentration; in this case, the subscript a stands for the aqueous phase, and the absence of any subscript represents the total of C_0 plus C_a. As the electrical neutrality relation in the organic phase,

$$[Q^+]_o = [Cl^-]_o, \quad (2)$$

holds, Eq. 1 can be transformed into:

$$C_{Q,o} = K_{1/2}([Q^+][Cl^-])^{1/2} + K_1[Q^+][Cl^-] + 2K_2([Q^+][Cl^-])^2 + \cdots, \quad (3)$$

where $K_{1/2}$, K_1, and K_2 are these concentration quotients:

$$K_{1/2} = ([Q^+]_o[Cl^-]_o/[Q^+][Cl^-])^{1/2}, \quad (4)$$

$$K_1 = [QCl]_o/[Q^+][Cl^-], \quad (5)$$

$$K_2 = [Q_2Cl_2]_o/([Q^+][Cl^-])^2. \quad (6)$$

When no excess anions exist in the system, the relation in the aqueous phase:

$$[Q^+] = [Cl^-], \quad (7)$$

also holds and Eq. 3 can be expressed as:

$$C_{Q,o} = K_{1/2}[Q^+] + K_1[Q^+]^2 + 2K_2[Q^+]^4 + \cdots. \quad (8)$$

As it is obvious that

$$C_{Q,a} = [Q^+], \quad (9)$$

the plot of log $C_{Q,o}$ *vs.* log $C_{Q,a}$ will show the slopes according to the predominant species in the organic phase: 1 (dissociated ions), 2 (ion pairs), or 4 (dimers). When a large excess of chloride over Q^+ is present in the system, $[Cl^-]$ in Eq. 3 is considered to be constant and the slopes are 1/2 (dissociated ions), 1 (ion pairs), and 2 (dimers). Figures 1—3 show the results obtained in the back extraction of MTOACl from various organic solvents into water or 0.1 mol dm^{-3} of NaCl. The distribution behavior of MTOACl can be grouped into three classes according to the organic solvents used.

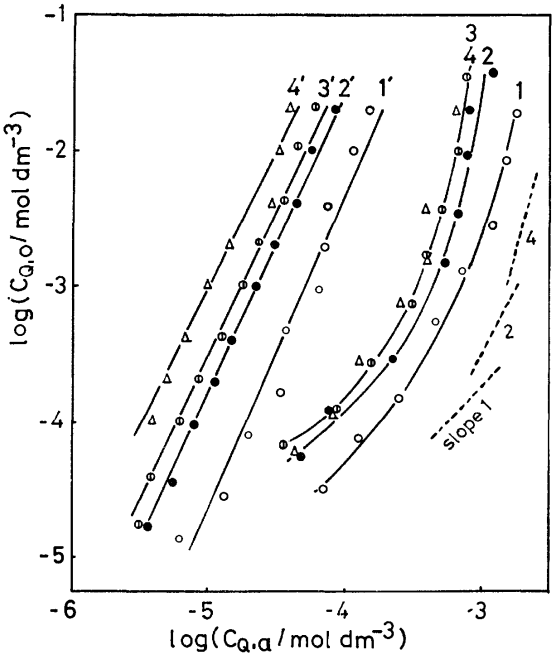

Fig. 1. Extraction of MTOACl (1).
1,1′: Hexane, 2,2′: xylene, 3,3′: carbon tetrachloride, 4,4′: benzene, 1—4: *vs.* water, 1′—4′: *vs.* 0.1 mol dm^{-3} NaCl.

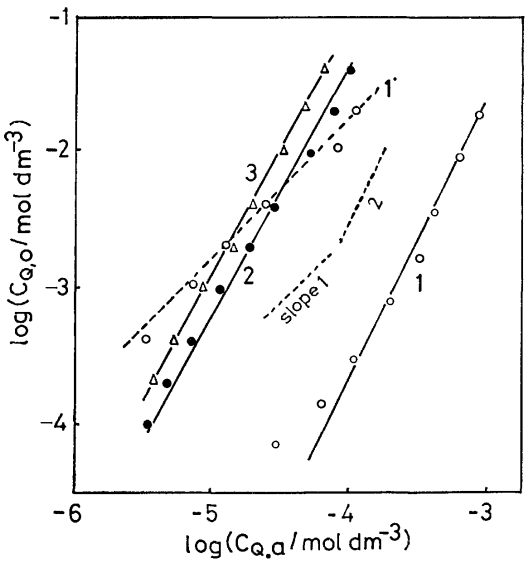

Fig. 2. Extraction of MTOACl (2).
1,1′: Butyl acetate, 2: dichloromethane, 3: chloroform, 1—3: *vs.* water, 1′: *vs.* 0.1 mol dm^{-3} NaCl.

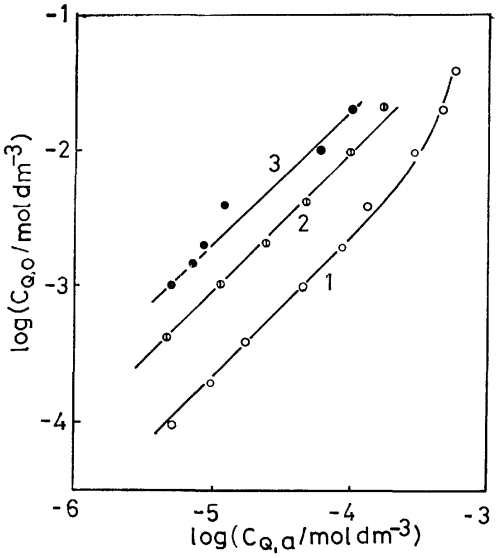

Fig. 3. Extraction of MTOACl (3).
1: 4-Methyl-2-pentanone, 2: nitrobenzene, 3: 3-methyl-1-butanol, 1—3: *vs.* water.

Figure 1 shows the distribution behavior of MTOACl between water or 0.1 mol dm^{-3} NaCl and four so-called "inert solvents." The slope of 2 obtained for 0.1 mol dm^{-3} NaCl and the maximum slope of 4 for water suggest that MTOACl is in the form of dimers in the organic phase. For water, however, the slope of the curves varies from 1 to 4, depending on the C_Q. As the pH of the aqueous phase was found to decrease slightly after the equilibration, species containing hydroxide

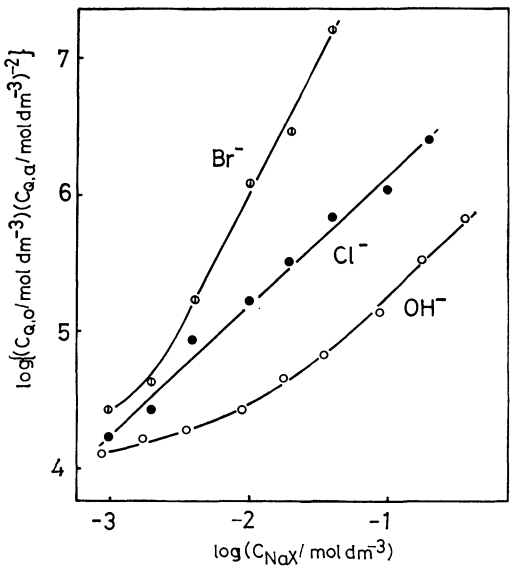

Fig. 4. Effect of anions on the extraction of MTOA into xylene.
$C_Q = 8 \times 10^{-3}$ mol dm^{-3}.

ions may also participate in the extraction of MTOA. If we consider that only dimers are present in the organic phase, it can easily be deduced that the slope of the log $(C_{Q,o}/C_{Q,a}^2)$ *vs.* log [X^-] (X^- denotes anions participating in the extraction) plot will give the mean number of anions in the extracted species. Figure 4 clearly indicates that a mixed dimer such as Q_2ClOH was also extracted along with Q_2Cl_2, while Q_2Br_2 was extracted when a considerable amount of bromide was present. Therefore, the smaller slopes in the lower concentration range of MTOA, shown by Curves 1—4 in Fig. 1, do not mean the extraction of a monomer nor dissociated ions, but the extraction of the mixed dimer. The approximate values of the extraction constants, K_2, were estimated from the data over the concentration range where the slope of Curves 1—4 equals 4, as is shown in Table 1.

Figure 2 shows the results for three solvents which are considered to have intermediate polarity. The slopes of 2 and 1 for the curves obtained for water and for 0.1 mol dm^{-3} NaCl (for butyl acetate) respectively indicate the existence of ion pairs over the concentration range studied. For butyl acetate, however, the contribution of hydroxide ions may not be neglected in the lower concentration range of MTOA.

Figure 3 shows the results for highly polar solvents, such as 4-methyl-2-pentanone, nitrobenzene, and 3-methyl-1-butanol. The slope of 1 observed for these solvents suggests the dissociation of ion pairs, except for 4-methyl-2-pentanone in the higher concentration range of MTOA, where some degree of ion-pair formation is considered to occur since the plots deviate upward from the straight line.

Table 1 summarizes the results of the extraction of MTOACl. To compare the extractability of organic solvents for MTOACl, the logarithms of the distribution ratios of MTOA, log D_Q=log $(C_{Q,o}/C_{Q,a})$, at $C_Q = 2 \times 10^{-3}$ mol dm^{-3} are also given. The general features of the extraction of MTOACl are quite similar to those of hydrohalic acids by tridodecylamine (TDA), as investigated by Müller and Diamond.[8] The dielectric constant of the organic solvents directly affects the degree of association or dissociation of ion pairs. In the extraction of TDAHX (X^-=Cl^-, Br^-, I^-, SCN^-), the presence of ion pairs (in chloroform), ion pairs and higher ion aggregates (in benzene, carbon tetrachloride, and cyclohexane), and ion pairs and free ions (in nitrobenzene) have been reported. In the extraction of MTOACl, however, the existence of only one chemical form for one solvent was verified under the experimental conditions adopted; dimers alone in benzene, carbon tetrachloride and hexane, ion pairs in chloroform, and free ions alone in nitrobenzene. The difference in the results for nitrobenzene between TDAHX and MTOACl may be attributable to the presence of the hydrogen bond in the ion pairs. The dielectric constant of the solvents plays an important role also in determining the extractability; polar solvents are favorable for the

Table 1. Extraction constants of MTOA chloride

Species in organic phase and solvent	ε[a]	AN[b]	Extraction constant	log D_Q[d]
Q_2Cl_2 (or Q_2ClOH)			log (K_2 mol^3 dm^{-9})	
Hexane	1.89	0	8.9	0.2
Xylene	2.37	—	10.1	0.5
Carbon tetrachloride	2.24	8.6	10.5	0.6
Benzene	2.28	8.2	10.6	0.6
QCl			log (K_1 mol dm^{-3})	
Butyl acetate	5.01	—	4.35	0.79
Dichloromethane	9.08	20.4	6.76	2.03
Chloroform	4.81	23.1	7.07	2.18
$Q^+ + Cl^-$			log $K_{1/2}$	
4-Methyl-2-pentanone	13.11	—	1.32	1.32
Nitrobenzene	34.82*	14.8	1.97	1.97
3-Methyl-1-butanol	14.7*	(33.5)[c]	2.30	2.30

a) Relative dielectric constant at 20 °C or 25 °C (marked by *) from Ref. 7. b) Acceptor number from Ref. 9; for water, AN=54.8. c) Value for 2-propanol. d) At $C_Q = 2 \times 10^{-3}$ mol dm^{-3}.

extraction of MTOACl and TDAHX. Furthermore, it is certain that the acidic properties of the solvents influence the extraction, as evidenced by the correlation between the extraction constants and the acceptor numbers which have been introduced by Gutmann[9] as a measure of the acidity of electrophilic solvents. As a whole, MTOACl is better extracted by the more polar and acidic (as a Lewis acid) solvents.

Ion-exchange Selectivity of MTOA. As has been discussed above, the extraction of MTOACl shows complex features depending upon the solvents and upon the concentrations of MTOA and anions. In order to compare the extraction of various anions by MTOA, therefore, it is preferable to apply a method which can simplify both the experimental and theoretical treatments. For this purpose, we have studied the exchange property of MTOA for several anions. If we assume that the concentration of exchangeable counter anions in the organic phase governs the equilibrium,[10] the exchange reaction may be described as follows:

$$(\cdots Y^{m-})_o + mX^- = m(\cdots X^-)_o + Y^{m-}, \quad (10)$$

where Y denotes the anion with the charge m and where $(\cdots Y^{m-})_o$ and $(\cdots X^-)_o$ indicate the exchangeable anions in the organic phase; *i.e.*,

$$[\cdots X^-]_o = C_{X,o}, \quad (11)$$

$$[\cdots Y^{m-}]_o = C_{Y,o}, \quad (12)$$

when the charge of these anions balances with that of MTOA cations in the organic phase. The constant for the exchange reaction (10) is defined as:

$$(K_{X/Y})^m = (C_{X,o})^m[Y^{m-}]/C_{Y,o}[X^-]^m. \quad (13)$$

When $m=1$, Eq. 13 can be written as follows according to the predominant species of MTOA salt in the organic phase:

(*i*) For free ions,

$$K_{X/Y} = [X^-]_o[Y^-]/[Y^-]_o[X^-], \quad (14)$$

(*ii*) for monomers,

$$K_{X/Y} = [QX]_o[Y^-]/[QY]_o[X^-], \quad (15)$$

(*iii*) and for dimers,

$$K_{X/Y} = \frac{(2[Q_2X_2]_o+[Q_2XY]_o)[Y^-]}{(2[Q_2Y_2]_o+[Q_2XY]_o)[X^-]}, \quad (16)$$

In the case of (*i*) or (*ii*), it can be easily seen that $K_{X/Y}$ gives a constant value. On the other hand, in the case of dimers, it is doubtful if the right-hand side of Eq. 16 gives a constant value. It is clear that the combination of the extraction constant for pure dimers,

$$K_{2,X} = [Q_2X_2]_o/([Q^+][X^-])^2, \quad (6')$$

$$K_{2,Y} = [Q_2Y_2]_o/([Q^+][Y^-])^2, \quad (6'')$$

leads to the following relationship:

$$K_{2,X}/K_{2,Y} = [Q_2X_2]_o[Y^-]^2/[Q_2Y_2]_o[X^-]^2. \quad (17)$$

The assumption made for Eq. 10 means that the two exchange sites in dimers do not interact with each other; in other words, the dimerization from QX and QY to Q_2X_2, Q_2Y_2, or Q_2XY occurs statistically. Therefore, the concentration of each species in the organic phase can be described as:

$$[Q_2X_2]_o = (C_{X,o})^2/2(C_{X,o}+C_{Y,o}) = (C_{X,o})^2/2C_{Q,o}, \quad (18)$$

$$[Q_2XY]_o = C_{X,o}C_{Y,o}/(C_{X,o}+C_{Y,o}) = C_{X,o}C_{Y,o}/C_{Q,o}, \quad (19)$$

$$[Q_2Y_2]_o = (C_{Y,o})^2/2(C_{X,o}+C_{Y,o}) = (C_{Y,o})^2/2C_{Q,o}. \quad (20)$$

The substitution of these equations into Eq. 17 gives the relationship as:

$$K_{2,X}/K_{2,Y} = (C_{X,o})^2[Y^-]^2/(C_{Y,o})^2[X^-]^2 = (K_{X/Y})^2. \quad (21)$$

Therefore, we can now understand that Eq. 16 gives a constant value, which may in turn be written as:

$$K_{X/Y} = [Q_2XY]_o[Y^-]/[Q_2Y_2]_o[X^-] = [Q_2X_2]_o[Y^-]/[Q_2XY]_o[X^-]. \quad (22)$$

Hence, we can conclude that Eq. 13 holds regardless of the form of the predominant species in the organic phase if the dimer formation occurs statistically. Furthermore, Eq. 13 can be applied when monomers coexist with dimers. When free ions and monomers coexist, however, Eq. 13 no longer holds as long as QX and QY differ in the dissociation constant in the organic phase. The assumption made here was warranted by the fact that Eq. 13 could be successfully applied to the experimental results, as will be described later. Therefore, we can simply compare the extraction of various anions by MTOA under the notion of the exchange reaction, Eq. 10, except when free ions coexist with monomers.

From Eq. 13, the distribution ratio of Y can be represented as follows:

$$D_Y = C_{Y,o}/[Y^{m-}] = (1/K_{X/Y})^m(C_{X,o}/[X^-])^m. \quad (23)$$

When D_Y is obtained for an indicator Y, $C_{X,o}$, and $[X^-]$ can be calculated from the respective initial concentrations as follows:

$$C_Y = C_{Y,o} + [Y^{m-}], \quad (24)$$

$$C_Q = mC_{Y,o} + C_{X,o} = mC_Y(1+1/D_Y)^{-1} + C_{X,o}, \quad (25)$$

$$C_X = C_{X,o} + [X^-]. \quad (26)$$

Then the exchange constant of X against Y can be obtained from the plot of log D_Y *vs.* log $C_{X,o}/[X^-]$. When TTA is used as an indicator, the constant, $K'_{X/T}$ was obtained from the next relationships:

$$K'_{X/T} = ([HT]_o/[\cdots T^-]_o)(C_{X,o}/[H^+][X^-]), \quad (13')$$

$$D'_T = [\cdots T^-]_o/[HT]_o = (1/K'_{X/T})(C_{X,o}/[H^+][X^-]), \quad (23')$$

$$C_T = [\cdots T^-]_o + [HT]_o + [T^-], \quad (24')$$

$$C_Q = [\cdots T^-]_o + C_{X,o}, \quad (25')$$

$$C_X = C_{X,o} + [X^-]. \quad (26)$$

The distribution ratios of BPB or *p*-NP, or the ratios of the salt to the acid form of TTA in the organic phase, were measured at various concentrations of NaX or at various pH values. From the experimental plots thus obtained, some of which are shown in Figs. 5—7, the exchange constants were estimated to be as is shown in Tables 2—4. HT, H_2B, and HR denote the acid forms of TTA, BPB, and *p*-NP respectively. The straight lines obtained by the method of least squares have the slopes to be expected from the number of acidic hydrogen in the indicators, that is, close to 1 for the TTA and *p*-NP systems and 2 for the BPB system. In some exceptional cases, however, the slopes deviate somewhat from

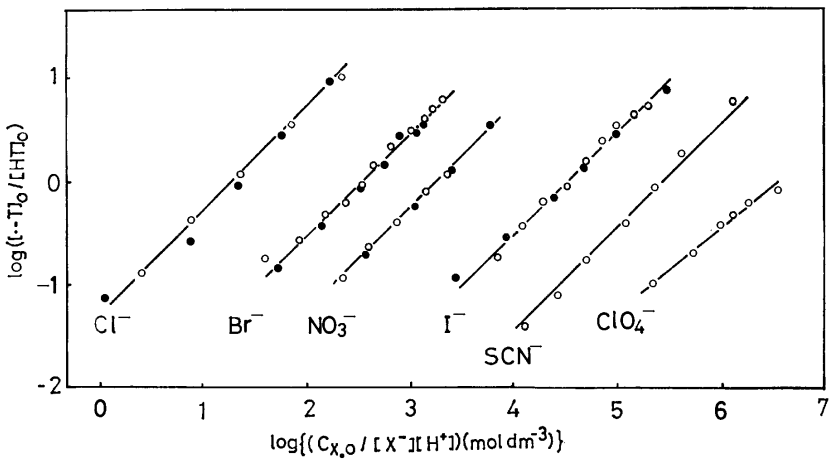

Fig. 5. Plot of Eq. 23′ for TTA–xylene system.
○: Obtained by varying C_{NaX} (at pH 4—6), ●: obtained by varving pH (at C_X=0.01—0.1 mol dm^{-3}), C_Q=(5—10)×10^{-5} mol dm^{-3}, C_T=6×10^{-5} mol dm^{-3}.

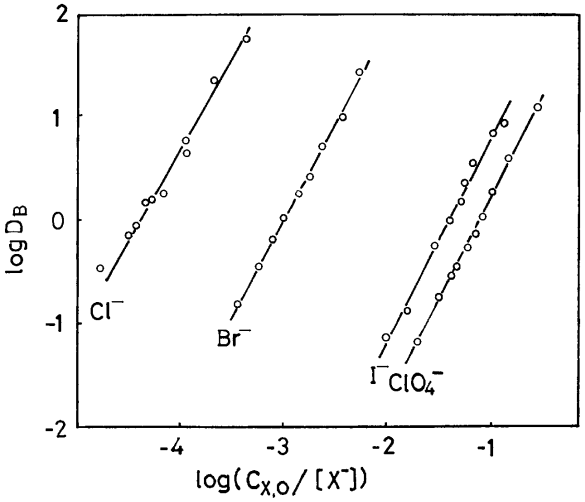

Fig. 6. Plot of Eq. 23 for BPB–chloroform system.
C_Q=4×10^{-5} mol dm^{-3}, C_B=10^{-5} mol dm^{-3}.

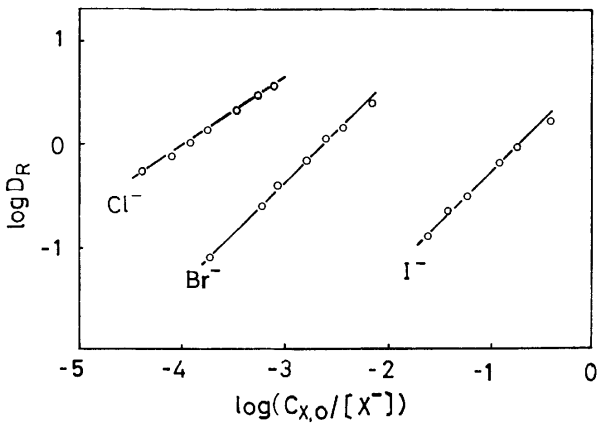

Fig. 7. Plot of Eq. 23 for *p*-NP–MIBK system.
C_Q=10^{-4} mol dm^{-3}, C_R=5×10^{-5} mol dm^{-3}.

these values; the reason for this is not clear, but the difference in the degree of dissociation of ion pairs, or the extraction of some other species, such as QHB, QNaB, and QHR_2, may be considered to be responsible. As long as the slopes are similar for a certain pair of anions, however, it is possible for us to obtain the selectivity coefficient for the pair because the method adopted is based on the comparison of the concentrations of anions which give D_Y (or D'_T)=1 for the distribution of the indicator. The standard deviations for the values of the exchange constants in Tables 2—4 were around 0.06. They amounted to about 0.1 for exceptional cases where the experimental conditions were such that it was difficult to obtain the data with a satisfactory accuracy. From Tables 2—4, the logarithm of the selectivity coefficient for X_1 *vs.* X_2 can be estimated by means of the following equation:

TABLE 2. EXCHANGE CONSTANTS OF MTOA SALT (TTA)[a]

Solvent	log $K'_{X/T}$ (Eq. 13′)					
	Cl	Br	I	ClO_4	NO_3	SCN
Hexane	1.18 (0.9)[b]	2.09 (1.0)	3.90 (1.0)	5.41 (1.1)		
Xylene	1.26 (1.0)	2.49 (1.0)	4.51 (1.0)	6.57 (0.8)	3.25 (1.0)	5.44 (1.0)
	1.30*(1.0)	2.61*(1.0)	4.49*(0.9)		3.25*(0.9)	
Benzene	1.45 (0.8)	2.84 (1.0)	5.03 (1.0)	7.06 (0.9)		
Chloroform	4.22 (1.0)	5.60 (1.0)			5.48 (1.0)	6.84 (1.2)

a) Obtained from data at various C_X values at a constant pH (4—6), except for values marked with *, which were obtained from data at various pH values at a constant C_X (0.01—0.1 mol dm^{-3}), both at C_Q=(5—10)×10^{-5} mol dm^{-3} and C_T=5×10^{-5} mol dm^{-3}. b) Numbers in parentheses indicate the slope, *m*, obtained by the method of least squares.

Table 3. Exchange constants of MTOA salt (BPB)[a]

Solvent	log $K_{X/B}$ (Eq. 13)			
	Cl	Br	I	ClO_4
Xylene			−3.00(2.0)[b]	−1.32(1.7)
Benzene			−2.84(2.0)	−1.20(2.0)
Carbon tetrachloride			−2.61(2.1)	−1.90(2.0)
Butyl acetate		−4.04(1.8)	−2.27(2.1)	−0.43(2.0)
Dichloromethane	−4.90(1.4)	−3.30(2.0)	−1.41(2.1)	−0.12(1.9)
Chloroform	−4.37(1.8)	−3.00(1.9)	−1.42(2.0)	−1.13(2.0)
4-Methyl-2-pentanone	−4.72(1.2)	−3.24(1.8)	−1.36(2.0)	1.26(1.4)
Nitrobenzene		−3.67(2.4)	−1.47(2.2)	0.71(1.7)
3-Methyl-1-butanol[c]	−2.56(1.2)	−2.10(1.3)	−1.36(1.4)	−1.11(1.3)

a) Obtained from data at various C_X values at $C_Q=4\times10^{-5}$ mol dm^{-3} and $C_B=10^{-5}$ mol dm^{-3}. b) See Note b) in Table 2. c) Obtained at $C_Q=2\times10^{-4}$ mol dm^{-3} and $C_B=1.5\times10^{-5}$ mol dm^{-3}.

Table 4. Exchange constants of MTOA salt (*p*-NP)[a]

Solvent	log $K_{X/R}$ (Eq. 13)		
	Cl	Br	I
Carbon tetrachloride	−2.40(0.8)[b]	−0.76(0.9)	1.53(0.8)
Butyl acetate	−3.72(0.6)	−2.50(0.8)	−0.79(0.8)
4-Methyl-2-pentanone	−3.98(0.7)	−2.64(1.0)	−0.73(1.0)
Nitrobenzene	−3.75(0.9)	−2.10(1.0)	0.16(1.0)

a) Obtained from data at various C_X values at $C_Q=10^{-4}$ mol dm^{-3} and $C_R=5\times10^{-5}$ mol dm^{-3}. b) See Note b) in Table 2.

Table 5. Comparison of selectivity coefficients obtained by different reagents

Solvent	X_1	X_2	log K_{X_1/X_2} (Eq. 27)		
			HT	BPB	*p*-NP
Xylene	ClO_4	I	2.07	1.68	
Benzene	ClO_4	I	2.03	1.64	
Butyl acetate	I	Br		1.77	1.71
Chloroform	Br	Cl	1.38	1.37	
4-Methyl-2-pentanone	Br	Cl		1.48	1.34
	I	Br		1.88	1.91
Nitrobenzene	I	Br		2.20	2.26

$$\log K_{X_1/X_2} = \log K_{X_1/Y} - \log K_{X_2/Y}. \quad (27)$$

As is shown in Table 5, the values obtained through the use of different indicators agreed with each other within the limits of experimental error, except for the cases of log $K_{ClO_4/I}$ in xylene and benzene. These last two disagreements are beyond the limits of experimental errors, and further experiments must be carried out to understand the reason for these disagreements.

The selectivity coefficients of MTOA for the exchange of anions *vs.* Cl^- are summarized in Table 6, as are those of Dowex-1X8—10[11] for purposes of comparison. The table indicates that the values of log $K_{X/Cl}$ increase in the order $Br^-<I^-<ClO_4^-$ and are similar to each other for most of the solvents used in spite of the marked difference in their extraction power and in the chemical species of MTOACl in these solvents.

However, it is interesting to note that the solvent with a higher acceptor number has a lower selectivity for anions; such acidic solvents as 3-methyl-1-butanol and chloroform are inferior in selectivity to other solvents. Because of the specific interaction of alcohols in alkylammonium systems,[12] 3-methyl-1-butanol is a good solvent for the extraction of MTOA salts, but its selectivity for anions is inferior to that of other solvents (about the same degree as solid-ion exchangers). Carbon tetrachloride and chloroform have abnormally small log $K_{ClO_4/I}$ values. One possible explanation is the specific reaction of alkylammonium salt with halo-

Table 6. Summary of selectivity coefficients of MTOA salt[a] and TDAH salt[b]

Solvent	log $K_{X/Cl}$				
	MTOA			TDAH	
	Br	I	ClO_4	Br	I
Hexane	0.91	2.72	4.23		
Cyclohexane				0.96	2.40
Xylene	1.27	3.22	5.1		
Carbon tetrachloride	1.64	3.93	4.64	1.19	3.44
Benzene	1.39	3.58	5.4	1.00	2.48
Butyl acetate	1.22	2.96	4.80		
Dichloromethane	1.60	3.49	4.78		
Chloroform	1.37	2.95	3.24	0.80	1.75
4-Methyl-2-pentanone	1.41	3.31	5.93		
Nitrobenzene	1.65	3.88	6.06	0.92	2.22
3-Methyl-1-butanol	0.46	1.20	1.45		
Dowex-1[c]	0.48	1.00	1.48		

a) When values obtained by different reagents disagreed, mathematical means were adopted. b) Calculated from K_{app} in Ref. 8. $K_{app}=C_{TDAH,o}/C_{TDA,o}a_{HX}$ at a total TDAHX concentration of 0.1 mol dm^{-3}. c) Ref. 11.

genated hydrocarbons,[13] for example, the deprotonation of chloroform producing CCl_3^- anions and finally dichlorocarbene in a strongly alkaline solution, which is the important reaction in phase-transfer catalysis.[2]

MTOA salts and trialkylammonium salts, $(alkyl)_3NH^+X^-$, resemble each other in the general features of these selectivity. In Table 6, the selectivity coefficients of tridodecylammonium for the exchange of anions *vs.* Cl^- are also shown; they were estimated from the apparent extraction constant of TDAHX obtained by Müller and Diamond.[8] On the whole, the selectivity of MTOA for anions is higher than that of TDAH; the difference increases with both the polarity of the solvents and the size of the anions. These findings are compatible with the common understanding[1] that the higher substituted alkylammonium have higher selectivities.

In conclusion, a better extraction of MTOA salts can be obtained by the use of polar and acidic solvents; in the case of acidic solvents, however, there should be a low selectivity for anions. Therefore, in the extraction of anionic complexes of metal ions in the presence of a large excess of such acids as HCl and HNO_3, aromatic solvents will meet the requirement of selectivity at the cost of extractability. On the other hand, acidic solvents such as chloroform and alcohols may be used for the extraction of chelate complexes of metal ions from aqueous solutions at the sacrifice of selectivity. Polar, aprotic solvents, such as nitrobenzene and 4-methyl-2-pentanone, are considered to be the best, although they have other disadvantages in practical use.

References

1) W. Müller, *Actinides Rev.*, **1**, 71 (1967).
2) W. P. Weber and G. W. Gokel, "Phase Transfer Catalysis in Organic Synthesis," Springer-Verlag KG (1977); translated into Japanese by I. Tabushi and T. Nishiya, Kagaku Dojin (1978).
3) R. P. Buck, *Anal. Chem.*, **48**, 23R (1976).
4) C. W. Pifer and E. G. Wollish, *Anal. Chem.*, **24**, 300 (1952).
5) M. E. Auerbach, *Ind. Eng. Chem. Anal. Ed.*, **15**, 492 (1943).
6) Y. Inoue, O. Tochiyama, and I. Oda, *J. Inorg. Nucl. Chem.*, **41**, 1375 (1979).
7) J. A. Riddick and W. B. Bunger, "Organic Solvents," 3rd ed, in "Technique of Chemistry," ed by A. Weissberger, Wiley-Interscience, New York (1970), Vol. II.
8) W. Müller and R. M. Diamond, *J. Phys. Chem.*, **70**, 3469 (1966).
9) V. Gutmann, *Coord. Chem. Rev.*, **18**, 225 (1976).
10) Y. Marcus, *J. Inorg. Nucl. Chem.*, **28**, 209 (1966).
11) I. Eliezer and Y. Marcus, *J. Inorg. Nucl. Chem.*, **25**, 1465 (1963).
12) G. Schill, "Isolation of Drugs and Related Organic Compounds by Ion-pair Extraction," in "Ion Exchange and Solvent Extraction," ed by J. A. Marinsky and Y. Marcus, Marcel Dekker, New York (1974), Vol. 6, Chap. 1, pp. 1—57.
13) Y. Marcus and A. S. Kertes, "Ion Exchange and Solvent Extraction of Metal Complexes," Wiley-Interscience, New York (1969), p. 742.

New Synthesis and Hydroboration of Vinylphosphonates

Mitsuji YAMASHITA,* Mitsumasa KOJIMA, Hiroshi YOSHIDA,
Tsuyoshi OGATA, and Saburo INOKAWA*,**

Department of Synthetic Chemistry, Faculty of Engineering, Shizuoka University, Hamamatsu 432
***Department of Chemistry, Faculty of Science, Okayama University, Okayama 700*

(Received July 30, 1979)

The Arbuzov reaction of trimethyl and triethyl phosphites with acyl chlorides gave 1-oxoalkylphosphonates in 57—80% yields. The Wittig reaction of the phosphonates with methylenetriphenylphosphorane gave vinylphosphonates in 25—59% yields. Hydroboration of vinylphosphonates in oxolane gave 2-hydroxyethylphosphonates in 50—65% yields. The procedure seems to be a good synthetic method to afford 1-alkyl-substituted 2-hydroxyethylphosphonates which have one more carbon atom than the starting 1-oxoalkylphosphonates.

5,6-Dideoxy-5-*C*-(phenylphosphinyl)-D-glucose derivatives have been synthesized by the development of information on the chemical modification of sugars.[1,2] Methods for preparing a phosphorus–carbon bond on a secondary carbon of the sugar skeleton played a key role. Methods for preparing primary carbon–phosphorus bonds are comparatively simple, the yields being usually high, *e.g.*, Arbuzov and Becker reactions.[3] The present paper deals with the synthesis of 1-oxoalkylphosphonates, Wittig reaction of the 1-oxoalkylphosphonates to make a secondary carbon–phosphorus bonds, and hydroboration of vinylphosphonates to synthesize 2-hydroxyethylphosphonates, which have a partial structure of phosphorus-sugars.

Results and Discussion

1-Oxoalkylphosphonates were synthesized by the reaction of trialkyl phosphites with 1.2 mol equivalent of acyl halides at room temperature for 12 h or at 40—60 °C for 2—3 h.[4]

$$RC(=O)Cl + P(OR')_3 \longrightarrow RC(=O)P(=O)(OR')_2 + R'Cl$$

1a: R=Me, R'=Me
1b: R=Et, R'=Me
1c: R=*c*-C_6H_{11}, R'=Me
1d: R=$PhCH_2CH_2$, R'=Me
1e: R=Ph, R'=Me
1f: R=Me, R'=Et
1g: R=Et, R'=Et

The Wittig reaction of 1-oxoalkylphosphonates with methylenetriphenylphosphorane to prepare secondary alkylphosphonate derivatives was studied. Treatment of methylenetriphenylphosphonium bromide suspended in anhydrous benzene with sodium amide at room temperature for 15 h followed by filtration gave a solution of methylenetriphenylphosphorane. To this was added compound **1** under ice cooling. After the coloration of ylide had vanished, the temperature was raised to room temperature, stirring being continued for additional 4—5 h. Removal of benzene *in vacuo* gave compound **2**. The yields and boiling points are summarized in Table 1.

$$\underset{\mathbf{1}}{RC(=O)P(=O)(OR')_2} \xrightarrow{Ph_3P=CH_2} \underset{\mathbf{2}}{RC(=CH_2)P(=O)(OR')_2} + Ph_3PO$$

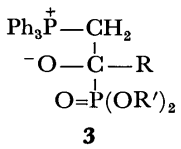

3

The betaine intermediate of the formula **3** should be stabilized when R is an electron-withdrawing substituent (*e.g.*, Ph), and protonated by a 1-oxo-3-phenylpropyl group bearing active methylenes. The successive cleavage process to give olefin and phosphine oxide could be so depressed that the yields of compounds **2d** and **2e** are lowered.[5]

Wittig reactions of ethylidenetriphenylphosphorane with 1-oxoethylphosphonates **1a** and **1f** were carried out under various conditions. The reactions seem to be less effective to produce 1-methyl-1-propenylphosphonates. The Horner type reaction of compound **1a** with diethyl ethylphosphonate in the presence of butyllithium in oxolane gave no expected olefinic product, probably because of abstraction of proton from 1-oxoethylphosphonate by the phosphonate carbanion. Reactions of compounds **1a** and **1f** with ethylidene- and methoxymethylenetriphenylphosphoranes were also

Table 1. Preparation of 1-alkylvinylphosphonates (**2**) *via* Wittig reaction

Compound	R	R'	Yield/%	Bp(°C/mmHg)
2a	Me	Me	50	38—41/1 (66.5—57/8)[a]
2b	Et	Me	55[b]	——
2c	*c*-C_6H_{11}	Me	42	46—49/0.9—1.0
2d	$PhCH_2CH_2$	Me	25	80—81/1
2e	Ph	Me	22[b]	—— (103—107/0.07)[c]
2f	Me	Et	45	44—47/1 (46—47/1)[d]
2g	Et	Et	59	50—52/0.1

a) Ref. 17. b) Obtained by NMR spectra. c) Ref. 16. d) Ref. 19.

unsuccessful. The Wittig reaction of methylenetriphenylphosphorane with 1-oxoalkylphosphonates seems to be a convenient method for preparing 1-alkylvinylphosphonates under mild conditions.

Hydroboration of compound **2f** was carried out according to the method of Brown and his co-workers.[6] To the oxolane solution containing compound **2f** and 20% mole excess of sodium tetrahydroborate was added 20% mole excess of trifluoroborane etherate at 0—5 °C. Coolant was removed after the addition of the etherate. Allowing the reaction mixture to stand for 2 h followed by oxidation with hydrogen peroxide, work-up, and distillation gave 22% yield of diethyl 2-hydroxy-1-methylethylphosphonate (**4f**) and 50% of unreacted **2f**.

When 2.4 fold excess amount of sodium tetrahydroborate and trifluoroborane etherate were used, consumption of almost all the starting phosphonate was revealed by TLC and NMR analyses after 15 h reaction period. The reaction rate of sterically hindered olefin with borane decreases a great deal at the third addition stage of borane, *i.e.*, formation of trialkylborane.[7] This seems to be the reason for the excess amount of hydroboration reagents being required for complete consumption of the starting phosphonates. The results of hydroboration are summarized in Table 2.

Table 2. Hydroboration of vinylphosphonates (**2**)

Compound	R	R′	Yield of compound **4**[a] %		Bp(°C/mmHg)
2c	*c*-C_6H_{11}	Me	65	(20)[b]	——
2f	Me	Et	50	(30)[b]	87—90/0.2
2g	Et	Et	58	(33)[b]	87—89/0.15
2h	Ph	Et	Not isolated		——

a) Determined by means of NMR with chloroform as an internal standard. b) Isolated yields.

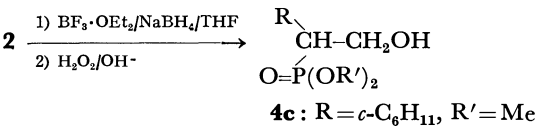

4c: R=*c*-C_6H_{11}, R′=Me
4f: R=Me, R′=Et
4g: R=Et, R′=Et

Hydroboration of compound **2h** (R=Ph, R′=Et) gave a complicated result. TLC analysis of the reaction mixture showed at least three components, which should consist of diethyl 2-hydroxy-[8] and 1-hydroxy-1-phenylethylphosphonates. In the hydroboration of styrene, α- and β-hydroxy compounds were produced, where electron-withdrawing substituents such as *p*-Cl depressed the β-hydroxy product, increasing the portion of the α-hydroxy compound.[9] The effect should be an important factor for making the hydroboration reaction of compound **2h** complicated.

Diethyl 2-hydroxy-1-methylethylphosphonate (**4f**) was treated with acetic anhydride–pyridine at room temperature for 3 d. The NMR spectrum of the product purified by TLC on silica gel (43% isolated yield) showed the presence of one acetoxyl group (δ, 2.20 ppm). IR (ν_{max}, 1740 cm^{-1}, C=O) and mass spectra [*m/e*, 238 (M^+)] also supported the view that the compound is diethyl 2-acetoxy-1-methylethylphosphonate as given by

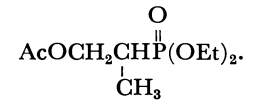

5f

The reaction sequence seems to be satisfactory for preparing β-hydroxyalkylphosphonates having one carbon atom more than that of the starting phosphonates.

Experimental

Measurements. Melting and boiling points were uncorrected. ^{1}H-NMR spectra were measured on Hitachi-Perkin-Elmer R-20 (60 MHz) and Hitachi R-24 (60 MHz) spectrometers with tetramethylsilane as an internal standard, and IR spectra on a Japan Spectroscopic Co. Ltd. A-3 infrared spectrophotometer. Optical rotations were measured with a DIP-4 polarimeter.

Materials. The following materials were synthesized according to reported methods: dimethyl 1-oxoethylphosphonate (**1a**, 60% yield, bp 58—61 °C/1 mmHg),[10] dimethyl-1-oxo-1-phenylmethylphosphonate (**1e**, 68% yield, bp 144—146 °C/3.5 mmHg),[10] diethyl 1-oxoethylphosphonate (**1f**, 61% yield, bp 54—55 °C/0.5 mmHg),[11] diethyl 1-oxopropyl phosphonate (**1g**, 57% yield, bp 69—73 °C/0.3 mmHg),[12] ethyltriphenylphosphonium iodide (mp 166—168.5 °C)[13] and bromide (mp 202—204 °C),[14] diethyl ethylphosphonate (bp 45 °C/1.5 mmHg),[15] and diethyl 1-phenylvinylphosphonate (**2h**, bp 93—95 °C/0.05 mmHg).[16]

*Synthesis of Dimethyl 1-Oxopropylphosphonate (**1b**).* Propionyl chloride (5.4 g) was added to trimethyl phosphite (6.0 g) at 0 °C. The mixture was allowed to stand overnight at room temperature. Distillation under reduced pressure gave compound **1b** (4.7 g) in 59% yield, bp 58—61.5 °C/0.5 mmHg. ^{1}H-NMR ($CDCl_3$) δ 1.10 (t, J=7.1 Hz, 3H, $CH_2\underline{Me}$), 2.94 (q, J=7.1 Hz, 2H, CH_2), 3.96 (d, J=10.8 Hz, 6H, OMe); IR ν_{max}^{neat} 1704 cm^{-1} (C=O).

Found: C, 36.08; H, 6.93%. Calcd for $C_5H_{11}O_4P$: C, 36.14; H, 6.63%.

*Synthesis of Dimethyl Cyclohexylcarbonylphosphonate (**1c**).* Reaction of trimethyl phosphite (3.4 g) with cyclohexanecarbonyl chloride (3.7 g) under the same conditions as mentioned above gave compound **1c** (5.5 g) in 64% yield, bp 90—93 °C/0.5 mmHg.[4] ^{1}H-NMR ($CDCl_3$) δ 1.0—2.2 [m, 10H, $(CH_2)_5$], 2.4—3.3 (m, 1H, CH), 3.85 (d, J_{POCH}=11.7 Hz, 6H, POMe), IR ν_{max}^{neat} 1693 cm^{-1} (C=O).

*Synthesis of Dimethyl 1-Oxo-3-phenylpropylphosphonate (**1d**).* Treatment of trimethyl phosphite (3.9 g) with 3-phenylpropionyl chloride (4.4 g) at 0 °C to room temperature as mentioned for the synthesis of compound **1b** gave compound **1d** (3.0 g) in 48% yield, bp 127—129 °C/0.5 mmHg. ^{1}H-NMR ($CDCl_3$) δ 2.96 (t, J=5.3 Hz, 2H, CH_2), 2.99 (t, J=5.3 Hz, 2H, CH_2), 3.77 (d, J_{POCH}=11.4 Hz, 6H, POMe), 7.0—7.4 (m, 5H, Ph); IR ν_{max}^{neat} 1698 cm^{-1} (C=O).

Found: C, 54.38; H, 6.41%. Calcd for $C_{11}H_{15}O_4P$: C, 54.55; H, 6.20%.

*Synthesis of Dimethyl Isopropenylphosphonate (**2a**) by Wittig Reaction.* Methyltriphenylphosphonium bromide (6.0 g) in benzene (60 ml) was treated with sodium amide (1.8 g) at room temperature for 15 h. The sodium bromide formed and sodium amide unreacted were filtered off under nitrogen flow, the ammonia formed being removed *in vacuo*. To the solution of methylenetriphenylphosphorane was added compound **1a** (2.0 g) dropwise under ice cooling and the mixture

was allowed to react at room temperature for 5 h. Removal of benzene followed by distillation *in vacuo* afforded 1.0 g of compound **2a** (50% yield), bp 38—41 °C/1 mmHg (lit,[17] bp 66.5—67 °C/8 mmHg).

*Synthesis of Dimethyl 1-Ethylvinylphosphonate (**2b**) via Wittig Reaction.* To a benzene solution of methylenetriphenylphosphorane prepared from methyltriphenylphosphonium bromide (6.0 g) and sodium amide (1.8 g) was added compound **1b** (2.2 g) dropwise. Processing of the reaction mixture as described above followed by vacuum distillation gave 1.2 g of compound **2b** (55% yield), bp 46—49 °C/0.9—1.0 mmHg. ^{1}H-NMR ($CDCl_3$) δ 1.11 (t, J=7.5 Hz, 3H, Me), 1.90—2.6 (m, 2H, CH_2), 3.73 (d, J_{POCH}=10.4 Hz, 6H, POMe), 5.80 [ddt, $J_{PC=CH(trans)}$=48.0 Hz, $J_{HC=CCH}$=1.8 Hz, $J_{HH(gem)}$=1.5 Hz, 1H, PC=CH(*trans*)], 6.04 [ddt, $J_{PC=CH(cis)}$=22.5 Hz, $J_{HC=CCH}$=1.1 Hz, $J_{HH(gem)}$=1.5 Hz, 1H, PC=CH(*cis*)].[18]

Found: C, 43.82; H, 8.10%. Calcd for $C_6H_{13}O_3P$: C, 43.90; H, 7.93%.

*Synthesis of Dimethyl 1-Cyclohexylvinylphosphonate (**2c**).* Wittig reaction of compound **1c** (2.4 g) with methylenetriphenylphosphorane at room temperature for 5 h followed by a similar procedure to that above and distillation *in vacuo* afforded compound **2c** (1.0 g, 42% yield), bp 80—81° C/1 mmHg. ^{1}H-NMR ($CDCl_3$) δ 0.5—2.5 (m, 11H, C_6H_{11}), 3.74 (d, J_{POCH}=11.1 Hz, 6H, POMe), 5.88 [d, $J_{PC=CH(trans)}$=50.3 Hz, 1H, PC=CH(*trans*)], 6.09 [d, $J_{PC=CH(cis)}$=24.0 Hz, 1H, PC=CH(*cis*)].[18]

Found: C, 54.88; H, 9.10%. Calcd for $C_{10}H_{19}O_3P$: C, 55.05; H, 8.72%.

*Synthesis of Diethyl 1-Methylenepropylphosphonate (**2g**).* To methylenetriphenylphosphorane, prepared from methyltriphenylphosphonium bromide (6.5 g) and sodium amide (2.1 g) in benzene (70 ml) was added compound **1g** (2.9 g) under ice cooling. The reaction at room temperature for 4 h followed by the work-up mentioned above and distillation gave 1.7 g of compound **2g** (59% yield), bp 50—52 °C/0.1 mmHg. ^{1}H-NMR ($CDCl_3$) δ 1.12 (t, J=7.5 Hz, 3H, $CCH_2C\underline{H}_3$), 1.32 (t, J=7.1 Hz, 6H, $OCH_2C\underline{H}_3$), 2.27 (dqdd, J_{PCCH}=12.0 Hz, J_{HCCH}=7.5 Hz, $J_{HC=CCH}$=1.0 and 1.8 Hz, 2H, CH_2), 4.06 (dq, J_{POCH}=7.1 Hz, J_{HH}=7.1 Hz, 4H, $POCH_2$), 5.72 [ddt, $J_{PC=CH(trans)}$=46.6 Hz, $J_{HC=CCH}$=1.8 Hz, $J_{HH(gem)}$=1.3 Hz, 1H, PC=CH(*trans*)], 6.98 (ddt, $J_{PC=CH(cis)}$=21.3 Hz, $J_{HC=CCH}$=1.0 Hz, $J_{HH(gem)}$=1.3 Hz, 1H, PC=CH(*cis*)].[18]

Found: C, 49.84; H, 8.62%. Calcd for $C_8H_{17}O_3P$: C, 49.98; H, 8.93%.

Compound **1f** was converted into compound **2f** (45% yield) by the same procedure, bp 44—47 °C/1 mmHg (lit,[19] bp 46.5—47.0 °C/1 mmHg).

*Reaction of Compounds **1a** and **1f** with Phosphoranes.* Reaction of compounds **1a** and **1f** with ethyltriphenylphosphonium iodide in the presence of base (sodium amide or sodium hydride in benzene, oxolane, or dimethyl sulfoxide) gave only a trace amount of 1-methyl-1-propenylphosphonate, the reaction with methoxymethylenetriphenylphosphorane giving no corresponding vinylphosphonates.

Hydroboration of Diethyl Isopropenylphosphonate. To an oxolane solution (15 ml) of sodium tetrahydroborate (0.60 g) and compound **2f** (4.5 g) was added trifluoroborane etherate (2.9 g) in oxolane (3.0 ml) dropwise at 0—5 °C over a period of 1 h. The reaction mixture was kept at room temperature until the complete consumption of compound **2f** was confirmed by TLC and NMR analyses (15 h), 3 mol dm^{-3} sodium hydroxide (45 ml) and 30% hydrogen peroxide (45 ml) then being added at 0—5 °C for oxidation. Evaporation of oxolane followed by extraction with chloroform and distillation *in vacuo* afforded 1.5 g of diethyl 2-hydroxy-1-methylethylphosphonate (**4f**, 30% yield), bp 87—90 °C/0.2 mmHg. ^{1}H-NMR ($CDCl_3$) δ 1.30 (t, J_{HH}=7.5 Hz, 6H, $OCH_2C\underline{H}_3$), 1.40 (dd, J_{PCCH}=13.5 Hz, J_{HH}=7.5 Hz, 3H, $CHC\underline{H}_3$), 1.70—2.15 (m, 1H, $C\underline{H}CH_3$), 3.55—3.95 (m, 2H, $C\underline{H}_2OH$), 4.15 (s, 1H, OH), 4.20 (dq, J_{HH}=7.5 Hz, J_{POCH}=7.5 Hz, 4H, $POCH_2$); IR ν_{max}^{neat} 3320 cm^{-1} (OH); mass spectrum, *m/e*, 196 (M$^+$).

Found: C, 43.58; H, 8.85%. Calcd for $C_7H_{17}O_4P$: C, 42.86; H, 8.73%.

Hydroboration of Diethyl 1-Ethylvinylphosphonate. Treatment of compound **2g** (3.0 g) with sodium tetrahydroborate (0.4 g) and trifluoroborane etherate (1.8 g) in oxolane (8 ml) followed by oxidation with 30% hydrogen peroxide (1.7 ml) and 3 mol dm^{-3} sodium hydroxide (1.7 ml), similar work-up and distillation to that described above afforded diethyl 2-hydroxy-1-ethylethylphosphonate (1.1 g, 33% yield), bp 87—89 °C/0.15 mmHg. ^{1}H-NMR ($CDCl_3$) δ 0.98 (t, J=7.5 Hz, 3H, $CHCH_2C\underline{H}_3$), 1.33 (t, J=6.8 Hz, 6H, $POCH_2C\underline{H}_3$), 1.50—2.0 (m, 3H, $C\underline{H}C\underline{H}_2CH_3$), 3.5—4.2 (m, 2H, $C\underline{H}_2OH$), 4.05 (s, 1H, OH), 4.16 (bq, J_{POCH}=6.9 Hz, J_{HH}=6.9 Hz, 4H, $POC\underline{H}_2CH_3$); IR ν_{max}^{neat} 3300 cm^{-1} (OH).

Found: C, 45.51; H, 9.31%. Calcd for $C_8H_{18}O_4P$: C, 45.70; H, 9.13%.

Hydroboration of Dimethyl 1-Cyclohexylvinylphosphonate. Hydroboration of compound **2c** (1.9 g) with sodium tetrahydroborate (0.3 g) and trifluoroborane etherate (1.3 g) in 7 ml of oxolane followed by oxidation with 30% hydrogen peroxide (1.2 ml) and 3 mol dm^{-3} sodium hydroxide (1.2 ml) at 0—5 °C as mentioned for the preparation of compound **4f** and separation of the products by preparative TLC (silica gel; eluent, acetone: petroleum ether=3: 1) gave dimethyl 1-cyclohexyl-2-hydroxyethylphosphonate (0.41 g, 20% yield). ^{1}H-NMR ($CDCl_3$) δ 0.60—2.15 (m, 12H, $C_6\underline{H}_{11}$–$C\underline{H}$), 3.72 and 3.75 (pair of d, J_{POCH}=10.5 Hz, 6H, POMe), 3.85 (s, 1H, OH), 3.60—3.90 (m, 2H, $C\underline{H}_2OH$); IR ν_{max}^{neat} 3260 cm^{-1} (OH); mass spectrum, *m/e*, 236 (M$^+$).

*Hydroboration of Diethyl 1-Phenylvinylphosphonate (**2h**).* Hydroboration of compound **2h** gave three products, R_f values on TLC being 0.50, 0.30, and 0.15 (silica gel; eluent, ethyl acetate: chloroform=3: 2). Separation of the products by TLC followed by NMR measurement showed an OH group at 2.83 ppm. The integrated signal for phenyl ring protons seemed to be *ca.* 10% less than that for the expected product. The result indicates the presence of impurities in the sample.

*Acetylation of Compound **4f**.* Treatment of compound **4f** (0.60 g) in anhydrous pyridine (0.90 g) with 1.3 g of acetic anhydride at room temperature for 3 d followed by removal of volatile materials *in vacuo* and washing the chloroform solution with water afforded a crude product, which was subjected to chromatography on silica gel giving dimethyl 2-acetoxy-1-methylethylphosphonate (0.30 g) in 43% yield. ^{1}H-NMR ($CDCl_3$) δ 1.22 (dd, J_{PCCH}=17.2 Hz, J_{HH}=7.2 Hz, 3H, $CHC\underline{H}_3$), 1.34 (t, J=6.6 Hz, 6H, $POCH_2C\underline{H}_3$), 2.08 (s, 3H, COMe), 2.1—2.8 (m, 1H, PCH), 4.14 (dq, J_{POCH}=7.2 Hz, J_{HH}=7.2 Hz, 4H, $POCH_2$), 4.40—4.65 (m, 2H, $C\underline{H}_2OAc$); IR ν_{max}^{neat} 1742 cm^{-1} (C=O), 1217 (P=O); mass spectrum, *m/e*, 238 (M$^+$).

Found: C, 45.05; H, 8.23%. Calcd for $C_9H_{19}O_5P$: C, 45.38, H, 8.04%.

References

1) H. Takayanagi, K. Seo, M. Yamashita, H. Yoshida, T. Ogata, and S. Inokawa, *Carbohydr. Res.*, **63**, 105 (1978).

2) M. Yamashita, Y. Nakatsukasa, H. Yoshida, T. Ogata,

and S. Inokawa, *Carbohydr. Res.*, **70**, 247 (1979).
3) K. H. Worms and M. S. Schmidt-Dunker, "Organic Phosphorus Compounds," Wiley-Interscience, New York (1976), p. 22.
4) M. Kojima, M. Yamashita, H. Yoshida, T. Ogata, and S. Inokawa, *Synthesis*, **1979**, 147.
5) F. Ramirez and S. Derschowitz, *J. Org. Chem.*, **22**, 41 (1957).
6) H. C. Brown, K. J. Murray, L. J. Murray, and J. A. Snover, *J. Am. Chem. Soc.*, **82**, 4233 (1960).
7) H. C. Brown and B. C. S. Rao, *J. Am. Chem. Soc.*, **81**, 6428 (1959).
8) L. Fagerlind and L. E. Tammelin, *Acta Chem. Scand.*, **14**, 1353 (1960).
9) H. C. Brown and G. Zweifel, *J. Am. Chem. Soc.*, **82**, 4708 (1960).
10) a) M. I. Kabachnik and P. A. Rossiiskaja, *Bull. Acad. Sci. U. R. S. S., Classe Sei Chim.*, **1945**, 364; *Chem. Abstr.*, **40**, 4688 (1946); b) 1 MmHg=133.322 Pa.
11) A. Takamizawa, Y. Sato, and S. Tanaka, *Yakugaku Zasshi*, **85**, 298 (1965).
12) K. D. Berlin, D. M. Hellwege, and M. Nagabhushanam, *J. Org. Chem.*, **30**, 1265 (1965).
13) L. Horner and H. Moser, *Chem. Ber.*, **99**, 2789 (1966).
14) L. Horner and A. Mentrup, *Justus Liebigs Ann. Chem.*, **646**, 65 (1961).
15) M. S. Kharasch, R. A. Mosher, and I. S. Bengelsdorf, *J. Org. Chem.*, **25**, 1000 (1960).
16) W. E. Krueger, M. B. McLean, A. Rizwaniuk, J. R. Maloney, G. L. Behelfer, and B. E. Boland, *J. Org. Chem.*, **43**, 2877 (1978).
17) A. N. Pudovik, I. P. Gozman, and V. I. Nikitina, *Zh. Obshch. Khim.*, **33**, 3201 (1963); *Chem. Abstr.*, **60**, 4178c (1964).
18) Vinyl protons were assigned in reference to data of chemical shifts and coupling constants for vinylphosphonic acids.[20]
19) T. Gomyo, H. Yoshida, T. Ogata, H. Inokawa, and S. Inokawa, *Nippon Kagaku Kaishi*, **1974**, 1093.
20) G. L. Kenyon and F. M. Westheimer, *J. Am. Chem. Soc.*, **88**, 3557 (1966).

 © 1980 The Chemical Society of Japan Bull. Chem. Soc. Jpn., 53, 1629—1631 (1980)

The Synthesis of Tedanin and Its Isomer, 3-Hydroxy-2,3-didehydro-β,φ-caroten-4-one[1]

Mitsuki YASUHARA,[2] Kazuko INANAGA, Takashi KUMAE, Hemat Rysona BRAHMANA, Nobuhisa OKUKADO, and Masaru YAMAGUCHI*

Department of Chemistry, Faculty of Science, Kyushu University, Hakozaki, Higashi-ku, Fukuoka 812

(Received August 13, 1979)

The structure, 3-hydroxy-2,3-didehydro-β,χ-caroten-4-one, assigned to tedanin, the main carotenoid pigment of the marine sponge "*Tedania digitata* (O. Schmidt)," has been confirmed by total synthesis starting with β,χ-carotene. An isomer, 3-hydroxy-2,3-didehydro-β,φ-caroten-4-one, was also synthesized from β,φ-carotene.

Tedanin was first isolated as the main carotenoid from the sea sponge "*Tedania digitata* (O. Schmidt)," and its chemical structure has been established to be 3-hydroxy-2,3-didehydro-β,χ-caroten-4-one (**1**)[3] by Okukado on the basis of chemical and spectroscopic evidence.[4] This pigment was also found in a sea sponge, "*Clathria frondifera* (Bowerbank)," by Tanaka and Katayama.[5]

In this paper, we wish to report a total synthesis of tedanin which has unambiguously confirmed the proposed structure. We also wish to report the synthesis and characterization of the isomer, 3-hydroxy-2,3-didehydro-β,φ-caroten-4-one (**2**), in which a χ-ring end group of tedanin was replaced by a φ-end group. Although its natural existence has not yet been established, the isomer can be expected to exist in nature with a high probability since a φ-end group has often been encountered in natural carotenoids.[6]

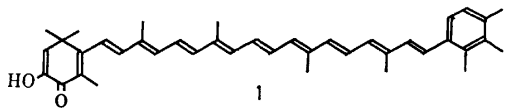

1

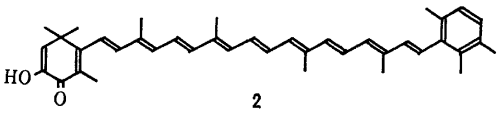

2

Results and Discussion

The synthesis of tedanin started with β,χ-carotene (β-isorenieratene) (**5**). The latter compound had previously been synthesized by Weedon *et al.*[7] and later reported to occur in some species of photosynthetic brown bacteria (*Phaebium*).[8] The synthesis by Weedon *et al.* was carried out according to the $C_{10}+C_{20}\rightarrow C_{30}$, $C_{30}+C_{10}\rightarrow C_{40}$ building scheme; however, a different construction principle, $C_{15}+C_{25}\rightarrow C_{40}$, was used in the present study. Thus, the Wittig reaction of 5-(2,6,6-trimethyl-1-cyclohexenyl)-3-methyl-2,4-pentadienylidenetriphenylphosphorane (**3**)[9] with 12'-apo-χ-caroten-12'-al (**4**), which we had previously used for the synthesis of 7,8-didehydrorenieratene,[10] gave β,χ-carotene (**5**) in a 51% yield after purification by column chromatography on alumina. The physical and spectroscopic properties were identical with those reported by Weedon *et al.* The treatment of **5** with *N*-bromosuccinimide and glacial acetic acid in chloroform, followed by saponification with methanolic potassium hydroxide,[11] afforded an alcohol (**6**) in a 74% yield. The alcohol has the molecular formula of $C_{40}H_{52}O$, which was determined by elemental analysis and mass spectrum; it shows ^1H NMR signals at δ 1.02(3H), 1.04(3H), 1.85(3H), and 4.02(1H), which can be assigned to protons of the 4-hydroxy-2,6,6-trimethyl-1-cyclohexenyl moiety.[12] The treatment of **6** with active manganese dioxide prepared by Attenburrow's method[13] gave a ketone (**7**) as purplish black crystals in a 61% yield. When γ-manganese dioxide[14] was used for this oxidation, no desired ketone (**7**) was obtained; the reaction products consisted of several components with shorter wavelength absorptions than those of the alcohol (**6**). The oxidation from **6** to **7** resulted in a bathochromic shift (8 nm), accompanied by a complete loss of fine structures in the UV spectrum.[15] Finally, the oxidation of **7** by oxygen in the presence of potassium *t*-butoxide[16] yielded tedanin (**1**) in a 71% yield after purification by chromatography on silica gel. The identity of the synthetic material with the natural specimen was established by a mixed melting-point determination and mixed chromatography as well as by a comparison of the IR, UV, NMR, and mass spectra.

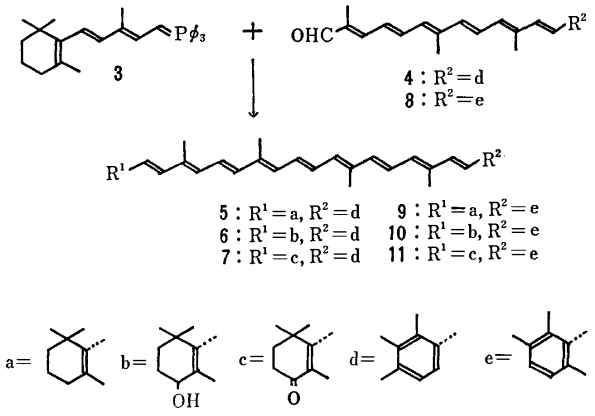

The synthesis of 3-hydroxy-2,3-didehydro-β,φ-caroten-4-one (**2**) was carried out starting from β,φ-carotene (**9**) by the route adopted for the synthesis of tedanin. The chromatographic behavior of **2** was very similar to that of tedanin. The physical and spectroscopic properties will be described in the Experimental section. As expected, the isomer (**2**) showed its absorption maximum in benzene at 483 nm, shorter by 7 nm than that of tedanin (**1**), which has a χ-end group. This can be explained on the basis of the fact that the chromophore system of **2** was more distorted than that of **1** because of the steric interference between the polyene chain

and two methyl substituents at the 1- and 5-positions in the ϕ-end group compared with one substituent at the 1-position in the χ-end group.[7]

Experimental

All the melting points are uncorrected. All the reactions and operations were carried out under an atmosphere of nitrogen as far as possible. The instruments and solvents used for the measurements of the spectra were as follows: UV spectra: Hitachi, Model EPS-3T (benzene). IR spectra: Hitachi, Model R-215 (KBr). NMR spectra: Hitachi, Model R-20B ($CDCl_3$, with TMS as the internal standard). Mass spectra: Hitachi, Model RMU-6MG.

β,χ-Carotene (5). An ethereal solution of phenyllithium (1.1 mol dm^{-3}, 9 ml) was added, at room temperature, to a stirred suspension of 5-(2,6,6-trimethylcyclohexenyl)-3-methyl-2,4-pentadienyltriphenylphosphonium bromide[9] (3.015 g) in dry ether (40 ml). After 5 min, dry dichloromethane (5 ml) was added to destroy the excess phenyllithium. To this deep red solution of the ylid we then added a solution of 12′-apo-χ-caroten-12′-al[10] (**4**) (900 mg) in dichloromethane (30 ml). The mixture was stirred for 2 h at room temperature, poured into water, and extracted with benzene. The extract was dried with sodium sulfate and evaporated. The reddish residue was chromatographed on neutral alumina [Merck, deactivated by the addition of water (2%)], with a benzene–petroleum benzine mixture (3 : 7) as the developer. The main red zone was eluted with a benzene–methanol mixture (9: 1), and the eluate was concentrated under reduced pressure to give a crude product, which was then recrystallized from a dichloromethane–ethanol mixture. Red crystals (51%); mp 165 °C (lit,[7] mp 164 °C). Found: C, 89.92; H, 9.81%. Calcd for $C_{40}H_{52}$: C, 90.15; H, 9.85%. λ_{max} 506, 474 nm ($\varepsilon = 1.31 \times 10^5$); IR 3040, 2980, 2950, 1655, 970, 835 cm^{-1}; NMR δ 1.04 (6H, s, 1, 1-dimethyl), 1.75 (3H, s, 5-methyl), 2.00, and 2.09 (9H, s, and 3H, s, respectively; chain methyls), 2.23, and 2.32 (3H, s, and 6H, s, respectively; aryl methyls); MS 532 (M), 453, 440, 426, 399, 395, 374, 133, 106, 105, 92, 91.

β,χ-Caroten-4-ol (6). A cooled solution of NBS (109 mg) in a mixture of glacial acetic acid (0.49 ml) and chloroform (13 ml) was stirred into a solution of **5** (300 mg) in dry chloroform (33 ml) which had been cooled at −60 °C with Dry Ice–chloroform bath. After stirring at −60 °C for 2 h, *N*-ethylmorpholine (1.45 ml) was added; the mixture was stirred for 2 h at 0 °C and then heated under reflux for 2 h. The mixture was washed three times with aqueous hydrochloric acid (0.1 mol dm^{-3}), aqueous sodium hydrogencarbonate, and then water. After the removal of the solvent, the residue was dissolved in benzene (30 ml) and treated overnight with a 15% methanolic potassium hydroxide solution (33 ml) at room temperature. The mixture was then diluted with water, and the organic layer was washed with water, dried, and evaporated. The residue was chromatographed on alumina [deactivated by the addition of water (5%)] with benzene. The main red zone was eluted with a benzene–methanol mixture (9 : 1); the subsequent removal of the solvent gave a crude product, which was purified by recrystallization with a benzene–ethanol mixture. Purplish red needles (74%); mp 153—154 °C. Found: C, 87.22; H, 9.54%. Calcd for $C_{40}H_{52}O$: C, 87.53; H, 9.55%. λ_{max} 506, 474 ($\varepsilon = 1.28 \times 10^5$), 449 nm; IR 3460, 3040, 2950—2850, 1560, 1445, 960, 816, 804 cm^{-1}; NMR δ 1.02 and 1.04 (each 3H, s, 1,1-dimethyl), 1.85 (3H, s, 5-methyl), 1.99 and 2.07 (9H, s and 3H, s, respectively; chain methyls), 2.21 and 2.31 (3H, s and 6H, s, respectively; aryl methyls), 4.02 (1H, m, 4-methin), 6.18—7.10 (16H, m, olefinic and aromatic protons); MS 548 (M), 530, 515, 438, 424, 372, 133, 106, 105, 92, 91.

β,χ-Caroten-4-one (7). A solution of **6** (143 mg) in acetone (12 ml) and dichloromethane (24 ml) was stirred into a suspension of active manganese dioxide[13] (1.43 g) in acetone (12 ml), after which the mixture was stirred for 2.5 h at room temperature. After the filtration of the manganese dioxide and the removal of the solvent, the resulting red solid was recrystallized from a dichloromethane–ethanol mixture. Purplish black prisms (77%); mp 197—198 °C. Found: C, 87.66; H, 9.38%. Calcd for $C_{40}H_{50}O$: C, 87.86; H, 9.22%. λ_{max} 482 nm ($\varepsilon = 1.05 \times 10^5$); IR 3040, 2980—2850, 1655, 970, 835 cm^{-1}; NMR δ 1.20 (6H, s, 1,1-dimethyl), 1.89 (3H, s, 5-methyl), 2.01 and 2.08 (9H, s and 3H, s, respectively; chain methyls), 2.22 and 2.32 (3H, s and 6H, s, respectively; aryl methyls), 2.54 (2H, m, 3-methylene), 6.20—7.42 (16H, m, olefinic and aryl protons); MS 546 (M), 531, 459, 440, 388, 343, 158, 133, 106, 105, 92, 91,

Tedanin (1). A solution of potassium *t*-butoxide in *t*-butyl alcohol (*ca.* 1 mol dm^{-3}, 2.5 ml) was added to a solution of **7** (20.5 mg) in a mixture of dry benzene (12 ml) and *t*-butyl alcohol (18 ml); after stirring at room temperature for 20 min, dry oxygen gas was bubbled into the mixture for 6 h at 45 °C. The reaction mixture was then diluted with benzene, and the solution was washed successively with water, aqueous hydrochloric acid (0.1 mol dm^{-3}), aqueous sodium hydrogencarbonate, and water. After the removal of the solvent, the resulting residue was chromatographed on silica gel with a chloroform–benzene mixture (3 : 7). The elution of the main red zone and the removal of the solvent gave a crude product, which was subsequently recrystallized from a dichlomethane–ethanol mixture. Purplish black prisms (71%); mp 189—190 °C (lit,[4] mp 188—189 °C), undepressed by admixture with a natural specimen. Mixed chromatography of the synthetic and the natural pigment showed no separation on silica gel and sucrose columns. Found: C, 85.39; H, 8.67%. Calcd for $C_{40}H_{48}O_2$: C, 85.66; H, 8.63%. The spectral properties, such as the UV, IR, and NMR, were also identical with those of natural tedanin previously reported.

β,φ-Carotene (9). This was prepared by a method similar to that described above for the synthesis of β,χ-carotene (**5**), starting with **3** and 12′-apo-φ-caroten-12′-al[10] (**8**) (244.2 mg). Red plates (46%); mp 137—138 °C (lit,[7] 128 °C). Found: C, 90.02; H, 9.78%. Calcd for $C_{40}H_{52}$: C, 90.16; H, 9.84%. λ_{max} 494, 465 ($\varepsilon = 1.14 \times 10^5$), 437 nm; IR 3030, 3000—2850, 970, 955, 830, 810 cm^{-1}; NMR δ 1.04 (6H, s, 1,1-dimethyl), 1.72 (3H, s, 5-methyl), 2.00 and 2.10 (9H, s, and 3H, s, respectively; chain methyls), 2.25 and 2.28 (3H, s and 6H, s, respectively; aryl methyls), 6.15—6.90 (14H, m, olefinic protons), 6.97 (2H, s, aryl protons); MS 532 (M) 440, 426, 374, 317, 133, 105, 91.

β,φ-Caroten-4-ol (10). This was obtained from **9** (212.3 g) by a method similar to that used for β,χ-caroten-4-ol (**6**). Purplish red needles (57%); mp 136—136.5 °C. Found: C, 87.24; H, 9.29%. Calcd for $C_{40}H_{52}O$: C, 87.53; H, 9.55%. λ_{max} 492, 463 ($\varepsilon = 1.28 \times 10^5$), 436 nm; IR 3450, 3033, 2922—2858, 1560, 1445, 964, 808 cm^{-1}; NMR δ 1.03 and 1.06 (each 3H, s, 1,1-dimethyl), 1.87 (3H, s, 5-methyl), 2.00 and 2.11 (9H, s and 3H, s, respectively; chain methyls), 2.25 and 2.28 (3H, s and 6H, s, respectively; aryl methyls), 4.03 (1H, m, 4-methin), 6.05—6.85 (14H, m, olefinic protons), 6.98 (2H, s, aromatic protons); MS 548 (M), 530, 424, 372, 133, 105, 92, 91.

β,φ-Caroten-4-one (11). This was prepared from **10** (108 mg) by the same method as **7**. Purplish black needles

(62%); mp 178—179 °C. Found: C, 87.99; H, 9.22%. Calcd for $C_{40}H_{50}O$: C, 87.86; H, 9.22%. λ_{max} 469 nm ($\varepsilon=1.70\times10^5$); IR 3030, 2970—2790, 1645, 975, 830, 810 cm^{-1}; NMR δ 1.20 (6H, s, 1,1-dimethyl), 1.89 (3H, s, 5-methyl), 2.00 and 2.10 (9H, s and 3H, s, respectively; chain methyls), 2.25 and 2.28 (3H, s and 6H, s, respectively; aryl methyls), 2.49 (2H, m, 3-methylene), 6.10—6.85 (14H, m, olefinic protons), 6.98 (2H, s, aromatic protons); MS 546 (M), 454, 133, 119, 91, 84.

3-Hydroxy-2,3-didehydro-β,φ-caroten-4-one (**2**). This was obtained from **11** (38 mg) by a method similar to that used for tedanin (**1**). Purplish black needles (49%); mp 170—171 °C. Found: C, 85.63; H, 8.61%. Calcd for $C_{40}H_{48}O_2$: C, 85.67; H, 8.63%. λ_{max} 483 nm ($\varepsilon=1.87\times10^5$); IR 3425, 3030, 2990—2830, 1695, 1620, 972, 830, 808 cm^{-1}; NMR δ 1.30 (6H, s, 1,1-dimethyl), 2.02 and 2.04 (each 6H, s; chain methyls), 2.24 and 2.28 (3H, s and 6H, s, respectively; aryl methyls), 6.06—6.85 (15H, m, olefinic protons), 6.98 (2H, s, aromatic protons); MS 560(M), 544, 468, 454, 408, 204, 157, 119, 105, 91.

This work was partially supported by a Grant-in-Aid for Scientific Research from the Ministry of Education, Science, and Culture.

References

1) Presented at the 5 th International Symposium on Carotenoids, Madison, Wisconsin, USA, July, 1978.

2) Present adderss: Mitsui Petrochemical Industries, Ltd., Chigusakaigan, Ichihara, Chiba 299-01.

3) For the nomenclature used in this article; see the IUPAC Commission on the Nomenclature of Organic Chemistry and the IUPAC-IUB Commission on Biochemical Nomenclature, *Biochemistry*, **10**, 4827 (1971).

4) N. Okukado, *Bull. Chem. Soc. Jpn.*, **48**, 1061 (1975).

5) Y. Tanaka and T. Katayama, *Nippon Suisan Gakkai Shi*, **42**, 801 (1976).

6) M. Yamaguchi, *Bull. Chem. Soc. Jpn.*, **31**, 51, 739 (1958); S. Liaaen-Jensen, E. Hegge, and L. M. Jackman, *Acta Chem. Scand.*, **18**, 1703 (1964); F. Arcamone, B. Camerino, G. Franceschi, and S. Penco, *Gazz. Chim. Ital.*, **100**, 581 (1970); T. Hamasaki, N. Okukado, and M. Yamaguchi, *Bull. Chem. Soc. Jpn.*, **46**, 1884 (1973).

7) R. G. D. Cooper, J. B. Davis, and B. C. L. Weedon, *J. Chem. Soc.*, **1963**, 5637.

8) S. Liaaen-Jensen, *Acta Chem. Scand.*, **19**, 1025 (1965).

9) W. Sarnecki and H. Pommer, U. S. Patent 2950321 (1960); *Chem. Abstr.*, **55**, 4577 (1961).

10) T. Ike, J. Inanaga, A. Nakano, N. Okukado, and M. Yamaguchi, *Bull. Chem. Soc. Jpn.*, **47**, 350 (1974).

11) R. Entschel and P. Karrer, *Helv. Chim. Acta*, **41**, 402 (1958); J. D. Surmatis, A. Walser, J. Gibas, U. Schwieter, and R. Thommen, *ibid.*, **53**, 974 (1970).

12) W. Vetter, G. Englert, N. Rigassi, and U. Schwieter, "Carotenoids," ed by O. Isler, H. Gutmann, and U. Solms, Birkhauser, Basel (1971), p. 207.

13) J. Attenburrow, A. F. B. Cameron, J. H. Chapman, R. M. Evans, B. A. Hems, A. B. A. Jansen, and T. Walker, *J. Chem. Soc.*, **1952**, 1094.

14) L. I. Vereshchagin, S. R. Gainulina, S. A. Podskrebysheva, L. A. Gaivoronskii, L. L. Okhapkina, V. G. Vorob'eva, and V. P. Latyshev, *J. Org, Chem. USSR*, **8**, 1143 (1972).

15) Ref. 12, p. 194.

16) J. B. Davis and B. C. L. Weedon, *Proc. Chem. Soc.*, **1960**, 182; R. G. D. Cooper, J. B. Davis, A. P. Leftwick, C. Price, and B. C. L. Weedon, *J. Chem. Soc., Perkin Trans. 1*, **1975**, 2195.

Studies of Polymeric Flocculants. XI.[1] The Preparation and Properties of Polyampholytes

Takamasa NONAKA* and Hiroaki EGAWA

Department of Industrial Chemistry, Faculty of Engineering, Kumamoto University, Kurokami, Kumamoto 860

(Received August 23, 1979)

The polyampholytes were prepared by treating potassium polymethacrylate with (3-chloro-2-hydroxypropyl)-trimethylammonium chloride. The solution viscosity behavior and the potentiometric titration of the polyampholytes were studied. The flocculating ability of the polyampholytes was also investigated by the use of kaolin suspensions. The amine/acid ratio could be varied as desired to some extent by means of changing the reaction temperature. However, the polyampholytes containing more amino groups than about 46% could not be obtained. The resulting polyampholytes showed characteristic viscosity behavior. The results of the flocculation of kaolin suspensions with the polyampholytes showed that the polyampholytes can be expected to become a new type of polymeric flocculants, in which the chain expansion and the charge sign can be varied by changing the pH values of the solutions.

Some polyampholytes have been prepared and studied by a number of investigators,[2-8] but the flocculation of suspensions with polyampholytes had not been investigated. In the present paper, the preparation and properties of potassium methacrylate–[2-hydroxy-3-(methacryloyloxy)propyl]trimethylammonium chloride copolymer as a new polyampholyte were investigated. Furthermore, the flocculating ability of the polyampholytes was studied by the use of kaolin suspensions.

Experimental

Preparatoin of Potassium Polymethacrylate. The pH values of a methacrylic acid aqueous solution were adjusted to 7.0—7.2 by adding a 2-mol dm^{-3} KOH aqueous solution. Potassium methacrylate in an aqueous solution was polymerized at 40 °C for 48 h, and then the aqueous solution was poured into an excess of ethanol in order to precipitate potassium polymethacrylate. The intrinsic viscosity was measured in a 2-mol dm^{-3} $NaNO_3$ aqueous solution at 25 °C. The number-average molecular weight of the potassium polymethacrylate was calculated by means of the following equation: $[\eta]=KM^a$.[9]

Preparation of (3-Chloro-2-hydroxypropyl)trimethylammonium Chloride. (3-Chloro-2-hydroxypropyl)trimethylammonium chloride (**1**) was prepared by a method described previously.[10] At first, 9.6 g of trimethylammonium hydrochloride was dissolved in 10 cm^3 of water. Into this solution 9.3—14.0 g of epichlorohydrin were then stirred, drop by drop, at 40—50 °C, after which the reaction mixture was heated at the same temperature for an additional hour. The product was purified by crystallization from methanol. The total chlorine content of **1** was determined by means of a flask-combustion method.[11] The chloride-ion content was determined by means of the Mohr method.[12]

Preparation of Polyampholytes. The potassium methacrylate–[2-hydroxy-3-(methacryloyloxy) propyl] trimethylammonium chloride copolymers were prepared by treating potassium polymethacrylate with **1** at 40—120 °C for 2—10 h. The reaction mixture was poured into an excess of ethanol in order to precipitate the polyampholytes. The polyampholytes were then purified by Soxhlet extraction with ethanol for 30 h. The amine content of the polyampholytes was calculated on the basis of the nitrogen content of the polyampholytes thus obtained. The polyampholytes for an elemental analysis were obtained as follows: about 0.5 g of the polyampholytes was dissolved in 50 cm^3 of a 1-mol dm^{-3} HCl solution, after which the solution was poured into an excess of ethanol in order to precipitate the polyampholyte. The polyampholyte was purified by Soxhlet extraction with ethanol for 30 h and dried *in vacuo* at 50 °C for 5 h.

Measurement of Solution Viscosity of Polyampholytes. The viscosities were measured in an aqueous solution of various concentrations of the polyampholytes at different pH values. In order to determine the isoelectric point of the polyampholytes, the viscosities were also measured by varying the pH values of the aqueous solution of the polyampholytes. All the viscosities were measured by means of an Ostwald viscosimeter at 30 °C.

Potentiometric Titration. The polyampholytes, dissolved in 50 cm^3 of a 0.1 mol dm^{-3} KCl solution, were titrated with a 0.1 mol dm^{-3} KOH (or 0.1 mol dm^{-3} HCl)–0.1 mol dm^{-3} KCl solution. The pH values of the solution were then measured by means of a Hitachi-Horiba pH meter.

Flocculation Tests. The flocculating ability was studied by observing the sedimentation rate and the sedimented volume by a test tube. The kaolin was supplied by the Wako Junyaku Kogyo Co. Ltd.,; its composition and particle size distribution are shown in Table 1 and Fig. 1 respectively. The pH value of a 5% suspension of this kaolin in water was 4.15. The sedimentation data were obtained at room temperature using a 25-cm^3 graduated test tube (1.7 cm

Table 1. Components of kaolin

Component	Weight percentage
SiO_2	78.1
Al_2O_3	13.9
Fe_2O_3	0.1
Ignition loss	3.0

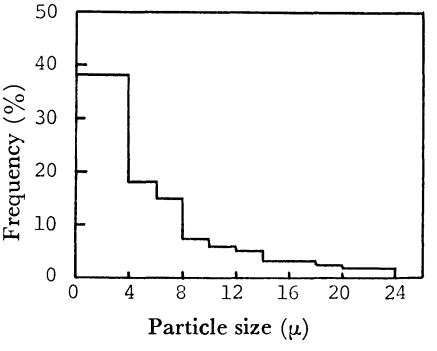

Fig. 1. Particle size distribution of kaolin.

inner diameter and 18.0 cm long). 20 cm^3 of a 6.25% (w/v) kaolin suspension was poured into the test tube. An aqueous solution of a polymer was added, and then water was added to the test tube until the total volume amounted to 25 cm^3. The contents were mixed by inverting the test tube 25 times at a speed of one time per 4 seconds. Then it was allowed to settle. The sedimentation rate was determined by plotting the height of the solid-liquid boundary as a function of the time. The sedimented volume was determined by measuring the volume of the kaolin after 24 h.

Results and Discussion

Potassium Polymethacrylate and **1**. Potassium polymethacrylate with a different degree of polymerization was obtained by an aqueous-solution polymerization of potassium methacrylate using a different amount of the initiator (ammonium persulfate). **1** was prepared by the method described previously.[10] When **1** was prepared by treating 1.2 mol of epichlorohydrin with 1 mol of trimethylamine hydrochloride, the values of the elemental analysis of the products were in good agreement with the values calculated for $C_6H_{15}NOCl_2$. Found: C, 38.43; H, 7.97; N, 7.42; Cl, 37.70%. Calcd for $C_6H_{15}NOCl_2$: C, 38.29; H, 7.98; N, 7.45; Cl, 37.70%. The chloride-ion content was 50.19 per cent of the total chlorine of the product.

Preparation of Polyampholytes. In order to prepare polyampholytes containing both amino groups and carboxyl groups in the desired ratio, the reaction of potassium polymethacrylate with **1** was carried out under a variety of conditions. The reaction equation was as follows:

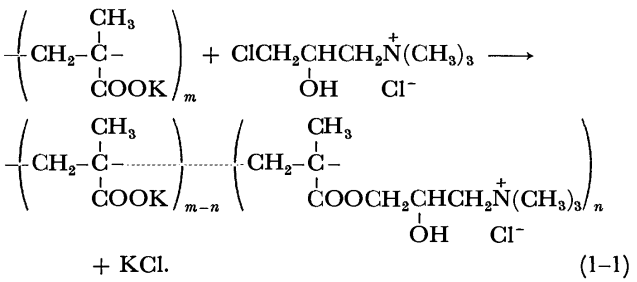

+ KCl. (1-1)

The results are shown in Table 2. It was found that the conversion (amine content) was greatly affected by the reaction temperature. The conversion decreased to 37.9% when the reaction was carried out at 120 °C. The reason why the conversion decreased can not be explained at present. The conversion was, on the other hand, little affected by the other conditions. Consequently, the polyampholytes containing more amino groups than about 46% could not be obtained. This is probably due to the steric hindrance of the bulky amine compound to be introduced into potassium polymethacrylate.

The reaction of potassium polyacylate with **1** was carried out under the same conditions as those used for potassium polymethacrylate. Some results are shown in Table 2. In this case, it was found that the conversion was also affected by the reaction temperature. The polyampholytes obtained at temperatures above 80 °C were insoluble in water. Therefore, a more detailed investigation was not carried out with this polyampholyte.

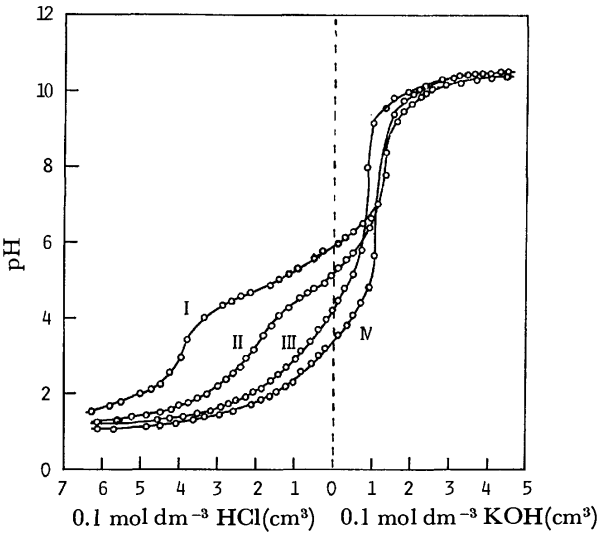

Fig. 2. The pH titration curves of the polyampholytes. Polymer concentration: *ca.* 0.16 g/100 cm^3.

	I	II	III	IV
Polyampholyte	**A**	**B**	**C**	**D**
Amine/Acid mole ratio	8.1/91.8	29.2/70.8	37.6/62.4	45.5/54.5

pH *Titration Curves of the Polyampholytes*. The pH titration curves of the polyampholytes obtained are shown in Fig. 2. The pH titration curves show that each potassium methacrylate–[2-hydroxy-3-(methacryloyloxy)propyl]trimethylammonium chloride copolymer contained about 0.56 meq/g of the acid form of carboxyl groups. An obvious inflection point in the titration curves can be observed with the polyampholyte **A** (amine/acid mole ratio=8.1/91.9) obtained at 40 °C and the polyampholyte **B** (amine/acid mole ratio= 29.2/70.8) obtained at 60 °C in the low pH region. These points probably correspond to the completed change from potassium salt to the acid form of carboxyl groups in the polyampholytes. However, such an obvious inflection point in the titration curves can not

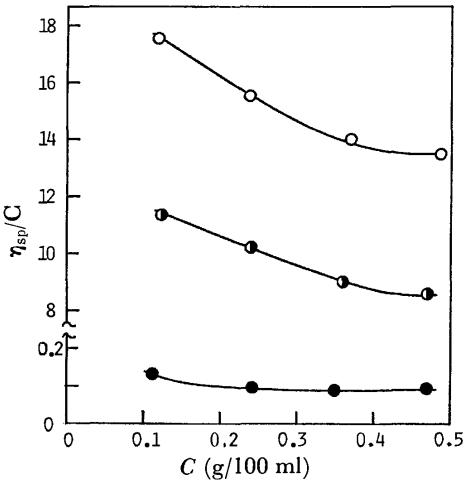

Fig. 3. Relation between the reduced viscosity and the polymer concentration at different pH values. Polymer: Polyampholyte **A**; pH, ●: 4, ◑: 7, ○: 10.

TABLE 2. PREPARATION OF POLYAMPHOLYTES

Expt. No.	PMAK[a] g	I[b] g	H_2O cm^3	Temp °C	Time h	Yield g	Amine[c] / Acid mole ratio
1	1.24	1.88	40	40	6	0.80	8.1/91.9
2	1.24	1.88	40	60	6	1.13	29.2/70.8
3	1.24	1.88	40	80	6	1.17	37.6/62.4
4	1.24	1.88	40	100	6	1.63	45.5/54.5
5	1.24	1.88	40	80	2	1.08	32.9/67.1
6	1.24	1.88	40	80	4	1.09	37.6/62.4
7	1.24	1.88	40	80	6	1.17	37.6/62.4
8	1.24	1.88	40	80	10	1.34	37.7/62.3
9	1.24	1.88	40	80	6		37.6/62.4
10	1.24	3.76	40	80	6		38.5/61.5
11	1.24	1.88	20	80	6		41.8/58.2
12	1.24	1.88	40	80	6		37.6/62.4
13	1.24	1.88	80	80	6		33.5/66.5
	PAK[d]						
14	1.10	1.88	30	40	6	1.15	4.4/95.6
15	1.10	1.88	30	60	6	1.15	21.6/78.4
16	1.10	1.88	30	80	6	1.15	34.4/65.6
17	1.10	1.88	30	100	6	1.45	41.4/58.6

a) Potassium polymethacrylate with the degree of polymerization of 600. b) (3-Chloro-2-hydroxypropyl)trimethylammonium chloride. c) The amine content was calculated on the basis of the nitrogen content of the polyampholytes. d) Potassium polyacrylate.

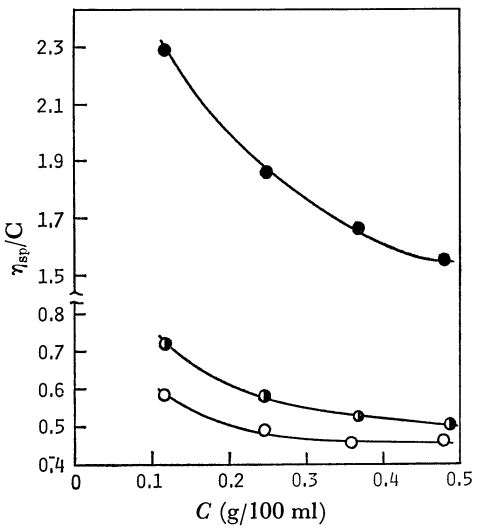

Fig. 4. Relation between the reduced viscosity and the polymer concentration at different pH values.
Polymer: Polyampholyte **D**; pH; ●: 4, ◑: 7, ○: 10.

be observed with the polyampholyte **C** (amine/acid mole ratio=37.6/62.4) obtained at 80 °C and the polyampholyte **D** (amine/acid mole ratio=45.5/54.5) obtained at 100 °C.

The Solution Viscosity and the Isoelectric Point of the Polyampholytes. The relation between the reduced viscosities and the concentrations of the polyampholytes **A** and **D** are shown at different pH values in Figs. 3 and 4 respectively. It was found that the polyampholytes showed viscosity vehavior typical of common polyelectrolytes. A difference in the order of the reduced viscosities at different pH values was observed with the polyampholytes with different amine/acid mole ratios. In the cases of the polyampholytes **A** and **B**, the reduced viscosities at different pH values increased in the order of pH 10>pH 7>pH 4. In the cases of the polyampholytes **C** and **D**, the reduced viscosities increased in the order of pH 4>pH 7>pH 10. These phenomena are characteristic of polyampholytes. The relation between the reduced viscosities of these polyampholytes and the pH values are shown in Fig. 5. Figure 5 shows that the reduced viscosities of the polyampholytes **A** and **B** increased with an increase in the pH values in the pH region from 5.3 to 8.2. This viscosity increase is ascribed to the chain expansion caused by the repulsion of the negatively charged carboxyl groups. On the other hand, the reduced viscosities increased a little with a decrease in the pH values in the pH region from

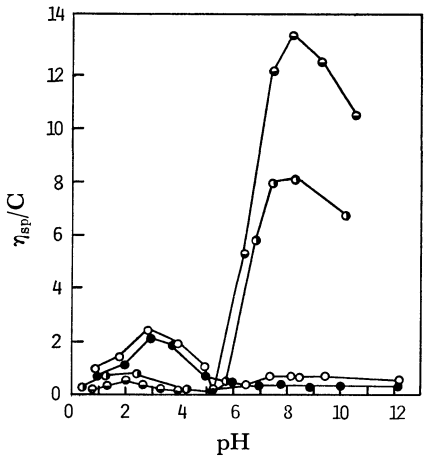

Fig. 5. Relation between the reduced viscosities of the polyampholytes with the different amine/acid ratio and pH values.
Polyampholyte; ◒: **A**, ◑: **B**, ○: **C**, ●: **D**.

5.3 to 2.0. This viscosity increase is ascribed to the chain expansion caused by the repulsion of a small amount of the positively charged amino groups in the polyampholytes. The reduced viscosities decreased at pH values above 8.2 and below 2.0. This viscosity decrease is ascribed to the chain contraction of the polyampholytes caused by the increase in the ionic strength by the addition of KOH or HCl to adjust the pH values of the solution. The reduced viscosities of the polyampholytes **C** and **D** scarcely increased at pH values above 5.3. As the amino groups in the polyampholytes obtained are quaternary amino groups, they dissociate even in an aqueous solution with the pH values above 7. Therefore, the viscosity decrease is ascribed to the chain contraction of the polyampholytes caused by the formation of the polyioncomplexes by means of interaction between the amino groups and carboxyl groups in the polyampholytes in the high pH region.

The isoelectric point, characterized by a minimum in the solution viscosity, of the polyampholytes **A** and **B** was obvious, but the isoelectric point of the polyampholytes **C** and **D** could not be obviously observed.

The Flocculation of Kaolin Suspension with the Polyampholytes. We have previously reported the preparation of cationic polymers and their flocculating ability.[13-15] The flocculation of suspensions with polyampholytes has not, however, been reported. The polyampholytes are expected to become a new type of flocculants, as the chain expansion and the charge sign of the polyampholytes can be varied by changing the pH values of the solution. Therefore, the flocculating ability of the polyampholytes was investigated by the use of kaolin suspensions at different pH values (3, 5.5, and 8). These pH values correspond, respectively, to the pH values at which the maximum, minimum, and maximum in the reduced viscosities of the polyampholytes were observed (Fig. 5). The polymers used are the polyampholytes **A**, **B**, **C**, and **D**. The results are shown in Figs. 6, 7, and 8. Figure 6 shows that the sedimentation rate of kaolin at pH 3 with the polyampholytes increased in the order of the polyampholytes **A**>**B**>**C**>**D** when more than 0.02% of the polyampholytes were added to kaolin. This order of the sedimentation rate was not in agreement with the order of the reduced viscoisities of the polyampholytes in pH 3. The sedimentation rate and the sedimented volume of kaolin with potassium polymethacrylate with the same degree of polymerization (600) as the polyampholytes are also shown in Fig. 6. The sedimentation rate of kaolin with potassium polymethacrylate increased slightly with an increase in the amount of the polymers added, but the sedimented volume of kaolin was almost the same as that in the case of no addition of a polymer. It is said that the flocculation of kaolin with sodium polyacrylate in a low pH region was brought about by a hydrogen bonding between the polymers and kaolin particles.[16] In the flocculation of kaolin with the polyampholytes at pH 3, it is considered that the flocculation was brought about with both amino groups and carboxyl groups in the polyampholytes.

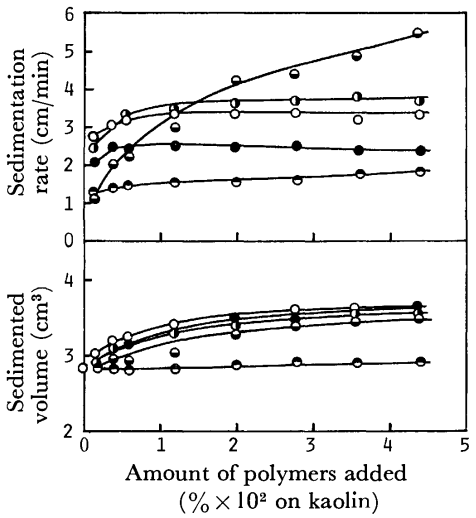

Fig. 6. Relation between sedimentation rate (or sedimented volume) and the amount of the polymer added at pH 3.
Polyampholyte; ◒: **A**, ◑: **B**, ○: **C**, ●: **D**, ◓: PMAK (potassium polymethacrylate).

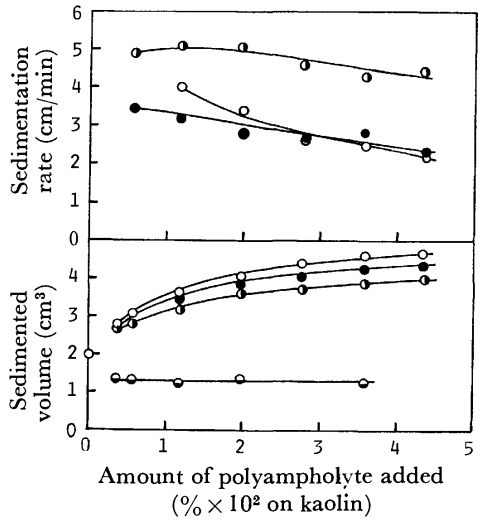

Fig. 7. Relation between sedimentation rate (or sedimented volume) and the amount of the polymer added at pH 5.5.
Polyampholyte; ◒; **A**, ◑: **B**, ○: **C**, ●: **D**.

Figure 7 shows that the highest sedimentation rate, at pH 5.5, was observed with the polyampholyte **B**. At pH 5.5, the kaolin suspension was not flocculated with the polyampholyte **A** and potassium polymethacrylate. The sedimented volume of kaolin with the polyampholyte **A** was smaller than that in the case of the addition of no polymer. These data show that the polyampholyte **A** acted as a dispersing agent of the negatively charged kaolin particles.

Figure 8 shows that, at pH 8, the kaolin suspension was not flocculated with the polyampholytes **A** and **B**, but was flocculated with the polyampholytes **C** and **D**, when a large amount of the polyampholytes was added. It is considered that, at pH 8, the polyampholytes (**A** and **B**) containing many carboxyl groups acted as dispersing agents of the negatively charged kaolin particles. This consideration was also confirmed by the

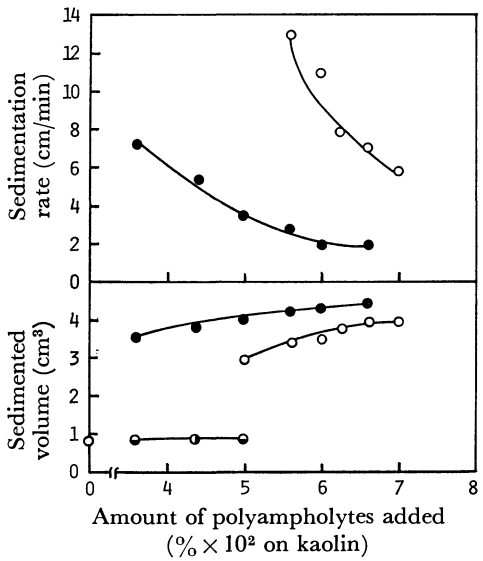

Fig. 8. Relation between sedimentation rate (or sedimented volume) and the amount of the polymer added at pH 8.
Polyampholyte; ◒: **A**, ◑: **B**, ○: **C**, ●: **D**.

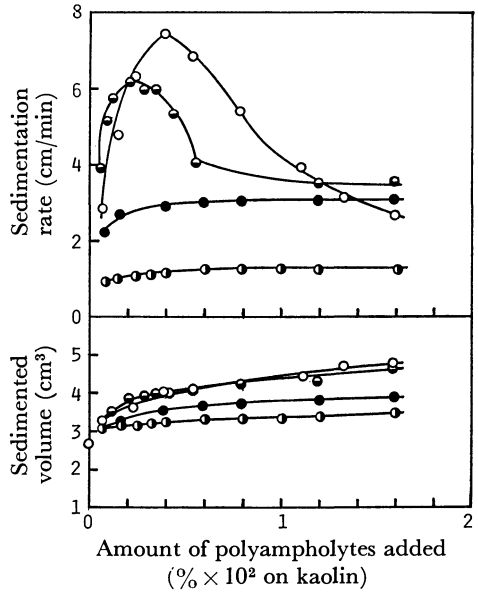

Fig. 9. Effect of the degree of polymerization of the polyampholytes on the flocculation of kaolin.

	◒	●	◑	○
$\bar{P}n$	1960	600	310	Primafloc C-7
Amine/Acid mole ratio	44.3/55.7	41.1/58.9	35.6/64.4	(Rohm and Haas Co.)

small sedimented volume of kaolin with the polyampholytes **A** and **B**. Consequently, the polyampholytes **A** and **B** may be said to be excellent polymeric flocculants for positively charged particles in a high pH region, although the flocculation of positively charged particles with the polyampholytes was not investigated in this paper.

The sedimentation rate of kaolin with the polyampholyte **C** was higher than that with the polyampholyte **D**. On the other hand, the sedimented volume of kaolin with the polyampholyte **C** was smaller than that with the polyampholyte **D**. In the flocculation of kaolin with the polyampholytes, no definite relation between the sedimentation rate and the sedimented volume was observed.

Effect of the Degree of Polymerization of the Polyampholytes on the Flocculation. Many investigators have reported that the flocculating ability increased with an increase in the degree of polymerization of polymeric flocculants.[13,14,17,18] The flocculation of the kaolin suspension was investigated with polyampholytes with different degrees of polymerization at pH 3. The results are shown in Fig. 9. Figure 9 shows that the flocculating ability of the polyampholytes increased with an increase in the degree of polymerization of the polymers, in the same manner as with cationic[13,14] or nonionic[17,18] polymeric flocculants. For comparison, the sedimentation rate and the sedimented volume of kaolin with Primafloc C-7,[19,20] which is a commercial cationic polymeric flocculant, *i.e.*, a polyvinylimidazoline with the molecular weight of more than a million, prepared by Rohm and Haas Co., America, are also shown in Fig. 9.

As has been mentioned above, the polyampholytes could be prepared by treating potassium polymethacrylate with **1** and the amine/acid ratio could be varied as desired to some extent by means of changing the reaction temperature. The polyampholytes can be expected to become a new type of polymeric flocculant, in which the chain expansion and the charge sign can be varied by changing the pH values of the solution.

References

1) Part X: T. Nonaka and H. Egawa, *Nippon Kagaku Kaishi*, **1980**, 121.
2) T. Matsumoto, *Kobunshi Kagaku*, **8**, 412 (1951).
3) T. Alfrey, Jr., and H. Morawetz, *J. Am. Chem. Soc.*, **74**, 436 (1952).
4) T. Alfrey, Jr., R. M. Fouss, H. Morawetz, and H. Pinner, *J. Am. Chem. Soc.*, **74**, 438 (1952).
5) M. Vranken and G. Smets, *J. Polym. Sci.*, **14**, 521 (1954).
6) C. H. H. Neufeld and C. S. Marvel, *J. Polym. Sci.*, A-**1**, **5**, 537 (1967).
7) M. Kamachi, M. Kurihara, and J. K. Stille, *Macromolecules*, **5**, 161, (1972).
8) L. van der Does, J. Hofman, and T, E. C. van Utteren, *Polym. Lett. Ed.* **11**, 169 (1973).
9) R. Arnold and S. R. Caplan, *Trans. Faraday Soc.*, **51**, 857 (1955).
10) A. Ohnishi, J. Kubo, T. Kurosaki, and J. Noguchi, *Kobunshi Kagaku*, **25**, 618 (1968).
11) Yuki Biryo Bunseki Kenkyu Kondankai Henshu, "Yuki Biryo Teiryo Bunseki," Nankodo, Tokyo (1969), p. 383.
12) S. Hirano, "Kogyo Bunseki Kagaku Jitsuken," Kyoritsu Shutsupan, Tokyo (1962), p. 243.
13) H. Egawa, T. Nonaka, and N. Ikeguchi, *Nippon Kagaku Kaishi*, **1972**, 184.
14) H. Egawa and T. Nonaka, *Nippon. Kagaku Kaishi*, **1973**, 1201.
15) T. Nonaka and H. Egawa, *Nippon Kagaku Kaishi*, **1974**, 1771; **1975**, 1955; **1976**, 1304; **1977**, 882.

16) "Mizushori No Kobunshikagaku To Gijyutsu (Ge), Kobunshi Mizushorizai," ed by The Society of Polymer Science, Japan, Chishojinkan, Tokyo (1975), p. 150.
17) Y. Toyoshima, *Nippon Kagaku Zasshi*, **82**, 1297 (1961).
18) F. Linke and R. B. Booth, *Trans. Am. Soc. Mech. Engrs.*, **217**, 364 (1960).
19) E. Ohmori, "Kobunshi Gyoshuzai," Kobunshi Kankokai, Kyoto (1973), p. 49.
20) Rohm and Haas Co., "Technical Bulletin," (1966), p. 1.

N-Acylimidazoles-Trifluoroacetic Acid System as the Acylating Agent for Aromatic Hydrocarbons

Takashi KEUMI,* Hiroshi SAGA, and Hidehiko KITAJIMA

Department of Fiber and Dyestuff Chemistry, Faculty of Engineering, Fukui University, Bunkyo, Fukui 910

(Received September 20, 1979)

N-Benzoylimidazole in trifluoroacetic acid could benzoylate electron-rich aromatic compounds, such as durene, *p*-dimethoxybenzene, mesitylene, anisole, thiophene, and fluorene, to give the corresponding benzophenone derivatives in good yields. It was further elucidated, in the reaction of fluorene, that *N*-acylimidazoles composed of a variety of acyl groups also could be used for the ketone synthesis. Therein, the imidazolides of aliphatic carboxylic acids or substituted benzoic acids with an electron-donating group gave ketones in high yields. The above-mentioned aromatic compounds were also acylated with *N*-trifluoroacetylimidazole and free carboxylic acids in trifluoroacetic acid. The mechanism for these reactions was assumed to proceed *via* a mixed anhydride between trifluoroacetic acid and carboxylic acid.

Acylation is one of the most important reactions in organic chemistry. Many kinds of procedures for the acylation of hetero atoms of amines or alcohols, and for that of aliphatic carbons are available[1] but only a few routes for aromatic carbons are known. Of them, the Friedel-Crafts reaction using aluminum chloride as the catalyst is the most famous and the most useful.[2] However, the Friedel-Crafts acylation generally requires molar amounts of a catalyst which is a hygroscopic solid and which forms complexes with the product. A work-up, consequently, is needed to decompose these complexes, and the catalyst is usually non-recoverable. In addition, a large amount of hydrochloric acid evolves during the reaction and at the hydrolysis of the complexes. Therefore, the use of aluminum chloride as the catalyst for ketone synthesis is sometimes inconvenient, particularly when carrying out a large-scale reaction.

Recently, some methods capable of acylating aromatic hydrocarbons with a small amount of a catalyst or none at all have been developed.[3–5] Above all, it is very interesting, in the reports by Bourne[4] and Effenberger,[5] that a mixed anhydride of carboxylic acid with trifluoroacetic acid or trifluoromethanesulfonic acid can be used for the acylation of aromatic hydrocarbons without the use of aluminum chloride. We ourselves have previously reported that trifluoromethylsulfonyloxypyridine can be used for the condensation of carboxylic acid and aromatic hydrocarbon to give the ketone.[6] In the present paper, we will report that *N*-acylimidazoles are useful as acylating agents for some aromatic compounds in trifluoroacetic acid.

Results and Discussion

The chemistry of imidazolides has been well established and reviewed precisely by Staab.[8] *N*-Acylimidazoles generally are very powerful acylating agents for hetero atoms of alcohols or amines, but they can not be used with aromatic carbons. Ried and Shubert[9] attempted the application of *N*-acylimidazoles as the acylating agents in the Friedel-Crafts ketone synthesis, and they observed that the imidazolides were not more suitable than acyl chlorides or acid anhydrides for the reactions. We also attempted the benzoylation of fluorene with *N*-benzoylimidazole, using aluminum chloride as the catalyst in dichloromethane at room temperature, but little benzoylfluorene was obtained.

The enhanced reactivities of *N*-acylimidazoles to the hetero atoms can be explained as being due to the delocalization of the lone-pair electron of the amide-nitrogen to make up the aromatic sextet and the electron-withdrawing effects of the other one, behaving like pyridine-nitrogen.[8] If the imidazolide is used together with a strong Brönsted acid, the pyridine-like nitrogen is protonated to form an imidazolium ion, so the electrophilicity of the acyl group might be increased. Thus, we found that *N*-acylimidazoles could acylate aromatic hydrocarbons in conjunction with trifluoroacetic acid to give ketones in good yields. For example, 2-benzoylfluorene was isolated in a yield of 80% by heating under reflux for 5 h a mixture of fluorene, *N*-benzoylimidazole, and trifluoroacetic acid in a molar ratio of 1: 1.2: 10 respectively. Under the same conditions, other aromatic compounds, such as durene, *p*-dimethoxybenzene, anisole, mesitylene, and thiophene, were benzoylated to give the corresponding ketones in good yields. However, benzophenone could not be obtained by this procedure. The results are summarized in Table 1 (Method A).

The validity of *N*-acylimidazoles as the acylating agent for aromatic substrates was further investigated by an examination of the reaction of fluorene with a wide variety of *N*-acylimidazoles. The results are summarized in Table 2 (Method A). The reactions were carried out under the same conditions, that is, by heating, under reflux for 10 h, a mixture of fluorene, *N*-acylimidazole, and trifluoroacetic acid in a molar ratio of 1: 1.2: 10 respectively.

All the imidazolides, except for *N*-(*p*-nitrobenzoyl)-imidazole, gave the corresponding 2-acylfluorenes in satisfactory yields. The imidazolides of aliphatic carboxylic acids or aromatic carboxylic acids containing an electron-donating group gave 2-acylfluorenes in especially high yields. Although we can not discuss the results in detail, for this work is not a quantitative one, the Hammett plots for the logarithm of ketone yields indicated a correlation with the reaction constant of -1.62 ($r=0.872$, $n=8$). If the *N*-acylimidazole generates an acyl cation which attacks the aromatic nucleus, as in usual Friedel-Crafts reactions, or if the acyl group of the imidazolide attacks directly through a cooperative activation by trifluoroacetic acid (Eq. 1

Table 1. Benzoylation of aromatic hydrocarbons with *N*-benzoylimidazole or *N*-trifluoroacetylimidazole and benzoic acid in trifluoroacetic acid

Aromatic substrate	Ketone yield/%		Isolated product			IR $\nu_{C=O}$ (cm^{-1}) (KBr or Neat)
	Method A[a]	Method B[b]	Mp or Bp/°C/Torr		Compound	
			Found	Reported		
Durene(D)	77	99	119—120	119[14]	3-Benzoyl-D	1670
p-Dimethoxybenzene(DMB)	73	95	50—52	51[15]	2-Benzoyl-DMB	1665
Mesitylene(M)	78	98	156—157/6	189/17[16]	2-Benzoyl-M	1670
Thiophene(TH)	80	100	55—56	56—57[17]	2-Benzoyl-TH	1625
Anisole(A)	86	98	61—63	61—63[18]	4-Benzoyl-A	1650
Fluorene(F)	80	91	122—123	122[19]	2-Benzoyl-F	1645
Anthracene(AT)	—	82	145—146	148[20]	9-Benzoyl-AT	1660
m-Xylene(MX)	—	66	140/5	321/744[21]	4-Benzoyl-MX	1660
p-Xylene(PX)	—	8[c]	36	36[22]	2-Benzoyl-PX	1668
Toluene(T)	—	5[c]	oil	55[23]	4-Benzoyl-T	1645
Benzene	0	—				

a) Purified ketone yield. b) Crude ketone yield. c) Determined by GLC.

Table 2. Acylation of fluorene with *N*-acylimidazoles or *N*-trifluoroacetylimidazole and carboxylic acids in trifluoroacetic acid

Acyl group in the product	Isolated 2-acylfluorene							
	Yield/%[a]		Mp/°C (Reported)	IR $\nu_{C=O}$(cm^{-1}) (KBr)	Elemental analysis			
					Found (%)		Calcd (%)	
	Method A	Method B			C	H	C	H
CH_3CO	89	82	130—131 (128—129)[24]	1678	86.66	5.93	86.51	5.81
CH_3CH_2CO	86	82	118—119 (120—121)[25]	1675	86.53	6.30	86.45	6.35
$CH_3CH_2CH_2CO$	96	92	118—119	1670	86.48	6.64	86.40	6.82
m-$CH_3OC_6H_4CO$	80	88	99—100	1645	83.94	5.30	83.98	5.37
p-$CH_3OC_6H_4CO$	93	95	155—156	1640	83.87	5.35	83.98	5.37
o-$CH_3C_6H_4CO$	84	92	138—139 (138)[26]	1660	88.77	5.76	88.70	5.67
m-$CH_3C_6H_4CO$	90	88	115—116	1655	88.64	5.54	88.70	5.67
p-$CH_3C_6H_4CO$	95	93	118—119	1645	88.82	5.55	88.70	5.67
C_6H_5CO	80	91	122—123 (122)[27]	1645	88.85	5.19	88.86	5.22
m-ClC_6H_4CO	65	72	149—151	1650	78.85	4.33	78.82	4.30
p-ClC_6H_4CO	76	79	177—179	1648	78.86	4.40	78.82	4.30
p-$NO_2C_6H_4CO$	16	15	184—186	1644	76.15	4.09	76.18	4.16

a) The remainder was the unreacted fluorene.

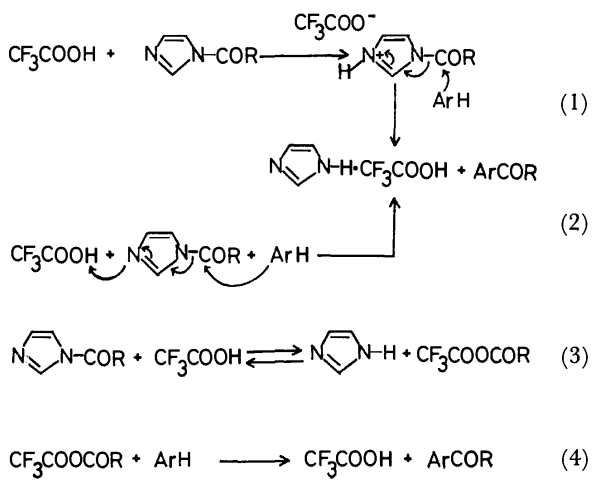

or 2), the reaction constant should be a positive value, because the reaction constants for the aluminum chloride-catalyzed Friedel-Crafts benzoylation[10] and the hydrolysis of the *N*-benzoylimidazoles[11] have been reported to be +1.858 and +1.85 respectively. Hence, this reaction mechanism does not to be a direct electrophilic attack on the aromatic nucleus by either the acyl cation or the *N*-acylimidazole.

It is well known that imidazolides generally react with carboxylic acids to give acid anhydrides.[12] Furthermore, according to Bourne,[4] a mixed anhydride between trifluoroacetic acid and carboxylic acid can work as the acylating agent for some aromatic hydrocarbons in the presence of trifluoroacetic acid. Therefore, it can be considered that this kind of mixed anhydride, *i.e.*, carboxylic trifluoroacetic anhydride, could be yielded

at the first of the reaction and that it then attacks the aromatic carbon to give ketone (Eqs. 3 and 4). A cleavage of the carbon–oxygen bond between the trifluoroacetate and the acyl group would be involved in the transition state, so that the yield of the ketone would be lower in the reaction with mixed anhydrides containing a strong electron-withdrawing group, because the bond in such anhydrides is difficult to break down. If this assumption is correct, results similar to those observed above should be obtained in the reaction of an aromatic substrate with carboxylic acid and *N*-trifluoroacetylimidazole which affords the carboxylic trifluoroacetic anhydride according to Eq. 5:

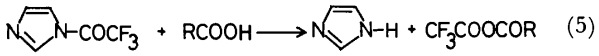

(5)

Thus, the acylation reactions of aromatic compounds with *N*-trifluoroacetylimidazole and carboxylic acids were examined. The reactions were carried out by heating, under reflux for 10 h, a mixture of an aromatic substrate, carboxylic acid, and *N*-trifluoroacetylimidazole, in a molar ratio of 1: 1.2: 1.2 respectively, in trifluoroacetic acid. The results are summarized in Tables 1 and 2 (Method B).

As expected, the aromatic compounds shown in Table 1, except for toluene and *p*-xylene, were benzoylated in good yields with free benzoic acid and *N*-trifluoroacetylimidazole in trifluoroacetic acid. This method was also established to be useful in reactions with a variety of carboxylic acids. The substituent effects of substituted benzoic acids on the ketone yield were similar to those which were obtained in the reaction with the *N*-acylimidazole–trifluoroacetic acid system. Consequently, the acylation with the *N*-acylimidazole–trifluoroacetic acid system is considered to proceed *via* the carboxylic trifluoroacetic anhydride. It has already been shown by Bourne[4] that the mixed anhydride can be used as the acylating agent for some aromatic compounds. However, the use of the mixed anhydride as the starting material is, in general, troublesome because these compounds are sensitive to moisture and tend to be disproportionate.[13] In addition, excess trifluoroacetic anhydride must be used to prepare them. We have now established that we can acylate aromatic hydrocarbons with *N*-acylimidazoles in trifluoroacetic acid without the use of this kind of mixed anhydride nor trifluoroacetic anhydride. Trifluoroacetic acid, which is now very popular, has a moderate boiling point, making it easy to recover from the reaction mixture by distillation. *N*-Acylimidazoles can also be easily prepared and are relatively stable.

In conclusion, the *N*-acylimidazole–trifluoroacetic acid system seems to offer one method capable of acylating aromatic hydrocarbons without the use of the classical Friedel-Crafts catalyst. Above all, the *N*-trifluoroacetylimidazole–trifluoroacetic acid system is superior as a reagent for a condensation between aromatic compounds and free carboxylic acids to give aromatic ketones.

Experimental

Materials and Measurements. All the *N*-acylimidazoles used for the acylation were synthesized according to the procedure described in the literature.[7] All the other materials were commercially available and were purified, when necessary, by distillation or recrystallization. All the acylated products were identified by comparing their physical data with those of authentic samples synthesized by Classical Friedel-Crafts reactions. All the melting points are uncorrected. The infrared spectra were obtained on a Hitachi EPI-S2 model infrared spectrophotometer.

Method A; *Benzoylation of Anisole by* N-*Benzoylimidazole in Trifluoroacetic Acid.* To a mixture of 8.9 mmol of *N*-benzoylimidazole and 7.5 mmol of anisole, 5 ml of trifluoroacetic acid were added, after which the new mixture was heated under reflux for 5 h. After cooling, water was added. The resulting precipitates were collected by filtration, washed with water and aqueous sodium carbonate, and dried to obtain 1.54 g of crude benzoylanisole (mp 52—57 °C; 96% yield). Crystallization from ethanol gave pure *p*-methoxybenzophenone (1.38 g; mp 61—63 °C; 86% yield).

Butyrylation of Fluorene by N-*Butyrylimidazole in Trifluoroacetic Acid.* To a mixture of 6 mmol of fluorene and 7.2 mmol of *N*-butyrylimidazole, 5 ml of trifluoroacetic acid were added, after which the new mixture was heated under reflux for 5 h. After cooling, water was added to the mixture, the unreacted fluorene was distilled off with steam, and the residue was separated by filtration to obtain butyrylfluorene (1.37 g; mp 112—115 °C; 96% yield). Crystallization from ethanol gave 2-butyrylfluorene (mp 118—119 °C). Unreacted fluorene was recovered (3%) from the distillate.

Method B; *Benzoylation of Durene by* N-*Trifluoroacetylimidazole and Benzoic Acid in Trifluoroacetic Acid.* To a mixture of 7.5 mmol of durene, 9 mmol of benzoic acid, and 5.5 ml of trifluoroacetic acid, 9 mmol of *N*-trifluoroacetylimidazole were added, after which the new mixture was heated under reflux for 10 h. Then water was added, and the resulting precipitates were collected by filtration, washed with water, and dried to obtain benzoyldurene (1.76 g; mp 118—120 °C; 99% yield). Crystallization from ethanol gave 3-benzoyldurene (mp 119—120 °C).

Butyrylation of Fluorene by N-*Trifluoroacetylimidazole and Butyric Acid in Trifluoroacetic Acid.* To a mixture of 6 mmol of fluorene, 7.2 mmol of butyric acid, and 5 ml of trifluoroacetic acid, *N*-trifluoroacetylimidazole (7.2 mmol) was added, after which the new mixture was heated under reflux for 5 h. After cooling, water was added to the mixture, then, after the unreacted fluorene had beed distilled off with steam, the residue was collected by filtration, washed with water, and dried to obtain butyrylfluorene (1.30 g; mp 112—114 °C; 92% yield). Crystallization from ethanol gave 2-butyrylfluorene (mp 118—119 °C). Unreacted fluorene was recovered in a 7% yield from the distillate.

References

1) S. R. Sandler and W. Karo,"Organic Functional Group Preparations," Academic Press, New York (1968), pp. 245, 270; A. Buehler and D. E. Pearson, "Survey of Organic Syntheses," John Wiley and Sons, New York (1970), pp. 801, 894; H. O. House, "Modern Synthetic Reactions," Benjamin, Menlo Park (1972), p. 734.

2) P. H. Gore, *Chem. Rev.*, **55**, 233 (1955); "Friedel-Crafts and Related Reactions," ed by G. A. Olah, John Wiley and Sons, New York (1964), Vol. III, p. 1.

3) D. E. Pearson and C. A. Buehler, *Synthesis*, **1972**, 533.

4) E. J. Bourne, M, Stacey, J. C. Tatlow, and R. Worrall, *J. Chem. Soc.*, **1954**, 2006; *ibid.*, **1951**, 718.

5) F. Effenberger and G. Epple, *Angew. Chem.*, **1972**, 294.

6) T. Keumi, H. Saga, R. Taniguchi, and H. Kitajima, *Chem. Lett.*, **1977**, 1099.
7) H. A. Staab, *Chem. Ber.*, **89**, 1927 (1956).
8) H. A. Staab and W. Rohr, "Newer Methods of Preparative Organic Chemistry," ed by W. Foerst, Academic Press, New York (1962), Vol. 5, p. 61.
9) W. Ried and H. J. Schubert, *Liebigs Ann. Chem.*, **653**, 181 (1962).
10) P. J. Slootmaekers, A. Rasschaert, and W. Janssens, *Bull. Soc. Chim. Belges.*, **75**, 199 (1966).
11) H. A. Staab, W. Otting, and A. Ueberle, *Z. Elektrochem.*, **61**, 1000 (1957).
12) H. A. Staab, G. Walther, and W. Rohr, *Chem. Ber.*, **95**, 2073 (1962).
13) C. D. Hurd and M. F. Dull, *J. Am. Chem. Soc.*, **54**, 3427 (1932).
14) C. Friedel, J. M. Crafts, and E. Ador, *Ann. Chim. Phys.*, **1**, 511 (1884).
15) M. T. Bogert and H. P. Howell, *J. Am. Chem. Soc.*, **52**, 837 (1930).
16) M. S. Kharasch, R. Morrison, and W. H. Urry, *J. Am. Chem. Soc.*, **66**, 368 (1944).
17) H. D. Hartough and A. I. Kosak, *J. Am. Chem. Soc.*, **68**, 2639 (1946).
18) S. Chodroff and H. C. Klein, *J. Am. Chem. Soc.*, **70**, 1647 (1948).
19) K. Dziewonski and A. Obtulowiez, *Bull. Int. Acad. Polon.*, **1930A**, 339.
20) J. W. Cook, *J. Chem. Soc.*, **1926**, 1284.
21) K. Elbs, *J. Prakt. Chem.*, **35**, 469 (1887).
22) K. Elbs, *J. Prakt. Chem.*, **35**, 473 (1887).
23) H. Staudinger, *Ber.*, **49**, 1926 (1916).
24) G. Rieveschl and F. E. Ray, *Org. Synth.*, Coll. Vol. III, 420 (1955).
25) K. Dziewonski and J. Schweiger, *Bull. Int. Acad. Polon.*, **1932A**, 293.
26) I. G. Farbenind, D. R. Patent 481819.
27) K. Dziewonski and A. Obtulowiez, *Bull. Int., Acad. polon.*, **1930A**, 339.

Stereochemistry of Nucleophilic Addition Reactions. VIII.[1] Preparation of 1,5-Anhydro-4,6-*O*-benzylidene-2,3-dideoxy-3-nitro-D-*erythro*-hex-2-enitol and Its Reactions with Some Nucleophiles

Tohru SAKAKIBARA,* Yutaka NOMURA, and Rokuro SUDOH

Department of Chemistry, Faculty of Science, Tokyo Institute of Technology, Ookayama, Meguro-ku, Tokyo 152

(Received October 15, 1979)

The title compound was synthesized from 1,5-anhydro-D-glucitol *via* nitromethane cyclization. The reduction of the compound with sodium borodeuteride afforded a mixture of saturated nitro compounds having an axial and equatorial deuterium atom at C-2 in an approximate ratio of 2: 1. On the other hand, the reaction with hydrogen cyanide gave predominantly the adduct with the *manno* configuration, together with small amounts of a cyano olefin. The reaction with hydrazoic acid yielded addition products with the *gluco* and *manno* configurations; the ratio was strongly affected by the solvent used.

Our own studies of nucleophilic addition reactions to methyl 4,6-*O*-benzylidene-2,3-dideoxy-3-nitro-β-D-*erythro*-hex-2-enopyranoside (**1**)[2] and its α-anomer **2**,[3] 1-*O*-acetyl-4,6-*O*-benzylidene-2,3-dideoxy-3-nitro-β-D-*erythro*-hex-2-enopyranose (**3**), and its α-anomer **4**,[4] and methyl 6-*O*-benzoyl-2,3-dideoxy-α-D-*glycero*-hex-2-enopyranosid-4-ulose,[5] as well as other reports,[6] strongly suggest that these reactions are controlled by steric hindrance, stereoelectronic control, and electrostatic interaction. In the reactions of **1** with nucleophiles, we have proposed an important role of electrostatic interaction between the incoming nucleophile and both C_1–O_1 and C_1–O_5 bonds.[2a] If a nucleophile is an anion or has nonbonded electron pairs, electrostatic repulsion becomes the decisive factor, but if a nucleophile is electronically neutral, it becomes less important and the reaction is probably controlled by other factors. Furthermore, if a nucleophile has a cationic part, attractive forces such as hydrogen bonding may be operative. On the basis of this surmise, we can explain the results of many reactions.

In order to confirm this surmise and to elucidate whether or not both C_1–O_1 and C_1–O_5 bonds are required to control the approach of a nucleophile at C-2, we have synthesized the title compound **8** and performed some nucleophilic addition reactions.

Results and Discussion

Oxidation of 1,5-anhydro-D-glucitol (**5**)[7] with sodium metaperiodate, followed by nitromethane cyclization in the presence of catalytic amounts of sodium methoxide, afforded a syrup, the subsequent benzylidenation of which gave 1,5-anhydro-4,6-*O*-benzylidene-3-deoxy-3-nitro-D-glucitol (**6**) in 40% yield from **5**. Acetylation of **6** with pyridine–acetic anhydride or sodium acetate–acetic anhydride afforded the acetate **7** in good yield. In contrast to the corresponding methyl α-[8] and β-pyranoside,[9] treatment of **7** with sodium hydrogencarbonate in refluxing benzene caused a partial double-bond migration from C-2 to C-1, giving the glucal **9** besides the desired nitro olefin **8**, before the completion of the elimination of acetic acid. The double-bond migration was observed even when **8** was warmed in a methanol–DMSO solution at 50 °C. The reaction, therefore, was stopped at the stage where the intensities of the absorption bands of the unsaturated and saturated nitro groups were nearly equal in the IR spectrum. After the separation of most **7** by crystallization from carbon tetrachloride, these compounds were separated by column chromatography. The nitro olefin structure for **8** was deduced from elemental analysis, IR (1525 cm^{-1} conjugated nitro olefin), and the NMR spectrum (olefinic proton at δ 7.00 in chloroform-*d*). The glucal structure for **9** was determined from the IR (1640 and 1560 cm^{-1} nonconjugated carbon–carbon double bond and saturated nitro group respectively) and the NMR spectrum (olefinic proton at δ 6.48 and 4.37 in chloroform-*d*), together with elemental analysis.

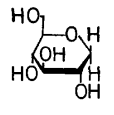

5

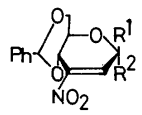

1: R^1 = OMe, R^2 = H
2: R^1 = H, R^2 = OMe
3: R^1 = OAc, R^2 = H
4: R^1 = H, R^2 = OAc
8: R^1 = R^2 = H

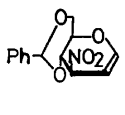

9

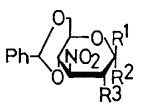

6: R^1 = R^2 = H, R^3 = OH
7: R^1 = R^2 = H, R^3 = OAc
10: R^1 = OMe, R^2 = H, R^3 = D
12: R^1 = H, R^2 = OMe, R^3 = D
14: R^1 = R^2 = H, R^3 = D
19: R^1 = R^2 = H, R^3 = N_3

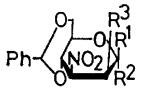

11: R^1 = H, R^2 = OMe, R^3 = D
13: R^1 = R^2 = H, R^3 = D
15: R^1 = R^2 = R^3 = H
16: R^1 = R^2 = H, R^3 = CN
18: R^1 = R^2 = H, R^3 = N_3

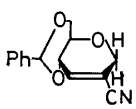

17

Selective reduction of the double-bond moiety of **1** and **2** was achieved by Baer and Rank; however, its stereochemistry was not investigated.[10] Reduction of **1** and **2** with sodium borodeuteride in methanol-d_4 exclusively afforded the saturated nitro compounds, **10** and **11**, respectively. The signals for the H-1 of **10** and **11** appeared as doublets with splitting of 9.8 and <1.0 Hz respectively. A similar reduction of the 2-deuterated derivative of **2** with sodium borohydride afforded the compound **12** ($J_{1,2}$=3.5 Hz).[11] These results showed that the deuteride ion exclusively entered from the opposite side of the glycosidic group. An

TABLE 1. CHEMICAL SHIFT (δ)[a] AND FIRST-ORDER COUPLING CONSTANTS (Hz) AT 100 MHz ($CDCl_3$)

Compd	H-1a	H-1e	H-2	H-3	H-4	H-5	H-6a	H-6e	PhCH
7	3.28(q)	4.22(q)	5.40(se)	4.77(t)	4.09(t)	3.40(m)	3.73(t)	4.33(q)	5.50(s)
	$J_{1a,1e}=11.3$, $J_{1a,2}=10$, $J_{1e,2}=6.0$, $J_{2,3}=J_{3,4}=J_{4,5}=J_{5,6a}=J_{6a,6e}=10$, $J_{5,6e}=5.0$								
8	←4.40—4.46→		7.00(m)	—	4.65(m)	3.57(m)	3.85(t)	4.34(q)	5.68(s)
	$J_{1a,1e}$, $J_{1a,2}$, $J_{1e,2}$, $J_{1a,4}$, $J_{1e,4}$, $J_{2,4}<3.0$, $J_{4,5}=7.5$, $J_{5,6a}=J_{6a,6e}=10$, $J_{5,6e}=4.4$								
9	6.48(q)		4.87(q)	5.23(se)	4.43(t)	←3.8—4.5→			5.58(s)
	$J_{1,2}=6.3$, $J_{1,3}=1.9$, $J_{2,3}=2.2$, $J_{3,4}=8.2$, $J_{4,5}=8.9$								
15[b]	2.62(se)	3.38(o)	c		4.26(o)	3.84(t)	2.89(se)	3.35(t)	4.02(q) 5.17(s)
	$J_{1a,2a}=11.9$, $J_{2a,3}=11.9$, $J_{2e,3}=5.2$, $J_{3,4}=J_{4,5}=9.7$, $J_{5,6a}=8.9$, $J_{5,6e}=5.2$, $J_{6a,6e}=10.8$								
16[d]	3.61(q)	4.22(q)	3.55(m)	4.75(q)	4.44(q)	3.44(se)	3.87(t)	4.35(q)	5.67(s)
	$J_{1a,1e}=12.7$, $J_{1a,2}=2.2$, $J_{1e,2}=1.9$, $J_{2,3}=5.2$, $J_{3,4}=10$, $J_{4,5}=J_{5,6a}=J_{6a,6e}=10.5$, $J_{5,6e}=4.9$								
17	←4.3—4.4→		—	3.76(q)	4.24(m)	3.50(o)	3.76(t)	4.35(q)	5.58(s)
	$J_{1a,3}$, $J_{1e,3}$, $J_{1a,4}$, $J_{1e,4}$, $J_{3,4}<2.0$, $J_{4,5}=8.2$, $J_{5,6a}=J_{6a,6e}=9.7$, $J_{5,6e}=4.1$								
18[d]	3.69(q)	4.21(q)	4.29(q)	4.67(q)	4.47(t)	3.41(se)	3.84(t)	4.39(q)	5.69(s)
	$J_{1a,1e}=12.7$, $J_{1a,2}=1.5$, $J_{1e,2}=2.0$, $J_{2,3}=3.7$, $J_{3,4}=J_{4,5}=J_{5,6a}=J_{6a,6e}=9.7$, $J_{5,6}=4.5$								
19	3.35(t)	4.19(q)	4.24(m)	4.57(t)	4.03(t)	3.37(m)	3.72(t)	4.34(q)	5.50(s)
	$J_{1a,1e}=12.5$, $J_{1a,2}=12.5$, $J_{1e,2}=5.0$, $J_{2,3}=J_{3,4}=J_{4,5}=J_{5,6a}=J_{6a,6e}=10$, $J_{5,6e}=5.0$								

a) Me_4Si as the internal standard; (se) and (o) indicate sextet and octet respectively. b) This compound was recorded in benzene-d_6. c) $\delta=1.78$ (o, 1, H-2a) and 1.34 (m, 1, H-2e); $J_{1a,2e}=2.5$, $J_{1e,2a}=5.2$, $J_{1e,2e}=1.5$, and $J_{2a,2e}=12.7$ Hz. d) The assignments of H-1a and H-1e were tentative.

important role of the anomeric methoxyl group in such a highly stereoselective reduction was proved by a similar reduction of **8**, in which a mixture of saturated nitro compounds with axial and equatorial deuterio groups was formed in an approximate ratio of 2: 1, as judged from the NMR spectrum. It is noteworthy that the C-3 position of the crude product, produced by sodium borodeuteride reduction of **1** in methanol-d_4, was also deuterated; however, this deuterium atom was exchanged for a hydrogen atom after purification by column chromatography on silica gel.

On the other hand, a selective axial approach, as in the cases of **2**[3a] and **4**,[4] was observed in the reaction of **8** with hydrogen cyanide. When the nitro olefin **8** was treated with hydrogen cyanide in acetonitrile in the presence of small amounts of aqueous potassium cyanide, three products were formed which were detectable by TLC and NMR spectroscopy. Separation by column chromatography afforded the *manno* isomer **16** as the major product, together with trace amounts of an unidentified product and a cyano olefin **17**. The *manno* configuration for **16** was deduced from the NMR data, analyzed by the help of the decoupling technique; $J_{1a,2}=2.2$, $J_{1e,2}=1.9$, $J_{2,3}=5.2$, and $J_{3,4}=10$ Hz. The structure of the cyano olefin **17**, which was obtained in good yield by treatment of **16** with triethylamine, was determined from the IR (2210 cm^{-1}; CN) and NMR data (olefinic proton at δ 3.76). This reaction was proved to be insensitive to the solvents used (THF, dioxane, acetonitrile, and DMF), giving the *manno* isomer **16** as the major product. When trace amounts of triethylamine were used as a catalyst, double-bond migration predominantly occurred to give the glucal **9**, together with small amounts of the addition products, as judged from the NMR spectrum.

More complicated results were obtained in the reaction of **8** with hydrazoic acid. Treatment of **8** with hydrazoic acid in THF afforded a mixture of the *manno* **18** and the *gluco* isomer **19** in an approximate ratio of 1.2: 1, as judged by NMR spectroscopy. Under the

TABLE 2. SOLVENT EFFECTS ON THE REACTION OF **8** WITH HYDRAZOIC ACID[a]

Entry	Solvent (ml)		Product ratios 0.5 h	1.5 h	5 h	20.5 h[b]
1	Benzene	(0.15)	r	r	r	r
2	$CDCl_3$	(0.15)	r	r	r	r
3	$CDCl_3$	(0)[c]	r	r	r (t of **19**)	8 : 1 (t of **8**)
4	THF	(0.15)	r	1 : 1.2 (70% r)	1 : 1.2 (55% r)	1 : 1.2
5	Acetone-d_6	(0.15)	1 : 1.2 (70% r)	1 : 1.2 (35% r)	1 : 1.2	1 : 1.2
6	DMSO-d_6	(0.15)	1 : 5	1 : 5	1 : 5	1 : 5

a) The nitro olefin **8** (13 mg, 0.05 mmol) was treated with hydrazoic acid (*ca.* 0.08 mmol) in $CDCl_3$ (0.05 ml) in a NMR sample-tube at room temperature, and the ratio was determined by NMR spectroscopy. b) Reaction time. c) Without dilution, 0.2 ml of a $CDCl_3$ solution containing hydrazoic acid was used. d) r and t indicate recovery and trace amounts respectively.

same conditions, the reaction of **1**[12] and **3**[4] with hydrazoic acid exclusively affordcd the *gluco* isomer (90 and 84% yields respectively), whereas the same reaction of **2**[3a] and **4**[4] predominantly afforded the *manno* isomer (76 and 82% respectively). The present finding, therefore, indicated the important role of the substituent at the anomeric carbon for the approach of the azide ion to C-2.

Compounds **18** and **19** were separated by column chromatography on silica gel. The IR spectra of both compounds showed the presence of an azide (2110 cm^{-1}) and a nitro group (1560 cm^{-1}). The *manno* and *gluco* structures for **18** and **19** were assigned from the coupling constants; $J_{1a,2}=1.5$, $J_{1e,2}=2.0$, $J_{2,3}=3.7$, and $J_{3,4}=9.7$ Hz for **18** and $J_{1a,2}=12.5$, $J_{1e,2}=5.0$, $J_{2,3}=10$, and $J_{3,4}=10$ Hz for **19**.

As shown in Table 2, the product ratios and the rates were strongly affected by the solvents. In such a relatively nonpolar solvent as chloroform, the reaction did not occur even after 20.5 h (Entries 1 and 3); however, in the presence of excess hydrazoic acid (*ca.* 6 equiv.), it slowly proceeded to give the *gluco* isomer **19**, as the major product (Entry 3). On the other hand, in DMSO the reaction occurred readily to afford the *manno* isomer **18**, as the major product (Entry 6). Furthermore, in THF and acetone it was somewhat retarded, affording nearly equal amounts of **18** and **19** (Entries 4 and 5). Similar solvent effects had previously been observed in the case of **2**[3a] and **4**;[4] the exceptional, predominant formation of the *gluco* isomer in a chloroform solution was attributed to hydrogen bonding between hydrazoic acid and the oxygen atom (O-1) at the anomeric carbon atom. However, this explanation is not applicable to the present reaction, because compound **8** has no such oxygen atom. Presently we can not give any reasonable explanation of these solvent effects.

Because the reactions of the 1,5-anhydro sugar **8** as well as the α-anomers (**2** and **4**) with hydrazoic acid were affected by the solvents, the similar reaction of the β-anomer **1** was performed in several solvents (DMSO, THF, and chloroform). It was found to be insensitive to these solvents, affording exclusively the *gluco* isomer.

As had previously been described, nucleophiles predominantly entered from the axial side of **8**, except in one case, to give the *manno* isomer. Therefore, the stereoselective approach of nucleophile from the equatorial side of the β-anomers (**1** and **3**) requires, at least, an equatorially orientated anomeric methoxyl or acetoxyl group.

Experimental

The melting points were determined in capillaries and are uncorrected. The IR spectra were recorded on KBr discs with a Hitachi 215 IR spectrometer. The NMR spectra were determined for solutions in chloroform-*d* (tetramethylsilane as internal standard), unless otherwise noted, with a JNM-PS-100 (JEOL) spectrometer. The solutions were evaporated under reduced pressure. Column chromatography was carried out on silica gel (C-300, Wakogel, Japan). Silica gel CF-254 was used for the TLC.

*1,5-Anhydro-4,6-O-benzylidene-3-deoxy-3-nitro-*D*-glucitol (6).* A solution of sodium metaperiodate (47 g, 0.22 mol) in 300 ml of water was cooled in an ice–water bath, and then a mixture of 1,5-anhydro-D-glucitol (**5**) (16.4 g, 0.1 mol)[7] and sodium hydrogencarbonate (8.4 g, 0.1 mol) was added in portions over 20 min with stirring. The mixture was allowed to warm to 21 °C and was stirred for additional 3 h, and then the precipitated sodium iodate was removed by filtration. The filtrate was concentrated to a partly crystalline mass, to which 100 ml of ethanol was added. After the removal of the insoluble material, the solution was evaporated to a syrup, which was subsequently dissolved in ethanol; the solution was then filtered from the remnant salt and evaporated. This procedure was repeated if the dissolution of the resulting syrup in ethanol caused an appreciable quantity of salt to separate. The syrupy dialdehyde was dissolved in 200 ml of methanol, and 6 ml (0.11 mol) of nitromethane was added. This solution was cooled in an ice–water bath, and 1 mol dm^{-3} sodium methoxide was added until the solution showed pH 9. The solution was brought to 21 °C, kept at that temperature for overnight, and then deionized by Amberlite IR-120 (H^+) cation-exchange resin. After the removal of the resin, the solution was evaporated completely to a syrup, the IR spectrum of which showed the presence of a nitro group (1560 cm^{-1}). Without further purification, the syrup was benzylidenated. Powdered anhydrous zinc chloride (26 g) was added to a flask containing the syrup and benzaldehyde (60 ml). The mixture was stirred at 21 °C for 20 h and then poured into a solution of water (100 ml) and hexane (250 ml) with stirring, whereby the crude acetal was precipitated. The precipitate was washed well with water and hexane. Recrystallization from ethanol afforded 11.8 g of **6** (40.4% from **5**); mp 154—155.5 °C; $[\alpha]_D^{21}$ −36.2 (*c* 1, $CHCl_3$); IR 3545, 3450, 3210 (OH), and 1555 cm^{-1} (NO_2).

Found: C, 55.57; H, 5.43; N, 5.13%. Calcd for $C_{13}H_{15}NO_6$: C, 55.51; H, 5.38; N, 4.98%.

*2-i-O-Acetyl-1,5-anhydro-4,6-O-benzylidene-3-deoxy-nitro-*D*-glucitol (7).* *a*): A solution of **6** (9 g, 0.032 mol) in 90 ml of anhydrous pyridine was cooled in an ice–water bath, and to this solution was added slowly 26 ml of acetic anhydride. The mixture was brought to 21 °C, kept at that temperature for 3 h, and then poured into 300 ml of ice–water. The precipitate was filtered and washed with water. Recrystallization from ethanol gave 7.6 g (73.8%) of **7**; mp 199—199.5 °C; $[\alpha]_D^{21}$ −31.7° (*c* 1, $CHCl_3$); IR 1760 (CO) and 1560 cm^{-1} (NO_2).

Found: C, 56.04; H, 5.36; N, 4.37%. Calcd for $C_{15}H_{17}NO_7$: C, 55.72; H, 5.30; N, 4.33%.

b): The nitro alcohol **6** (100 mg, 0.36 mmol) and sodium acetate (200 mg) in acetic anhydride (2 ml) were heated at *ca.* 100 °C for 5 min, until the solution turned orange. The mixture was then poured into ice–water, and the precipitate that separated was collected and washed with water. Recrystallization from ethanol gave 64 mg (55.6%) of **7**.

Elimination of Acetic Acid from the Acetate **7**. The acetate **7** (646 mg, 2 mmol, desiccator-dried) and sodium hydrogencarbonate (1.5 g, desiccator-dried) were added to distilled benzene (10 ml). The mixture was heated under reflux with stirring. From time to time, a small test sample was withdrawn from the supernant solution and allowed to evaporate on a sodium chloride plate for inspection by means of IR spectroscopy. A gradual decrease in the relative intensity of the carbonyl band at 1760 cm^{-1} and a gradual increase in the nitro olefin band at 1530 cm^{-1} and in the carbon–carbon double bond at 1635 cm^{-1} indicated that the isomerization of **8** to **9** occurred before the completion of the elimination of acetic acid. When the intensities of the bands of the unsaturated and saturated nitro group were almost the same

(*ca.* 7 d), the reaction was stopped. After cooling, the inorganic material was filtered off and washed with acetone. The filtrate was evaporated to give a solid residue (610 mg). Most of the starting material, **7** (270 mg), was removed by the addition of carbon tetrachloride (10 ml), followed by filtration. The filtrate was evaporated and chromatographed on silica gel, eluting with benzene. Each fraction was inspected by IR spectroscopy. The first fraction consisted of 90 mg of crystalline **9**, which was recrystallized from diisopropyl ether; 79 mg (15%); mp 90.0—91.0 °C; $[\alpha]_D^{21}$ −158° (*c* 1, $CHCl_3$); IR 1635 (C=C) and 1550 cm^{-1} (NO_2); R_f 0.61 (benzene)

Found: C, 59.09; H, 4.98; N, 5.21%. Calcd for $C_{13}H_{13}NO_5$: C, 59.31; H, 4.98; N, 5.32%.

The second fraction was a mixture of **8** and **9** (52 mg) (1.5: 1 from NMR spectroscopy).

The third fraction consisted of 145 mg of **8**, which was recrystallized from diisopropyl ether; 128 mg (24.3%); mp 87.5—88.0 °C; $[\alpha]_D^{21}$ −238° (*c* 1, $CHCl_3$); IR 1530 cm^{-1} (NO_2); R_f 0.36 (benzene).

Found: C, 59.57; H, 5.03; N, 5.26%. Calcd for $C_{13}H_{13}NO_5$: C, 59.31; H, 4.98; N, 5.32%.

The fourth fraction consisted of 35 mg of **7** (total 305 mg, 47.2%); R_f 0.28 (benzene).

*Reduction of the Nitro Olefiins **1**, **2**, and **8** with Sodium Borodeuteride.* To a solution of **1** (20 mg, 0.07 mmol) in methanol-d_4 (0.4 ml) was added sodium borodeuteride (5 mg, 0.12 mmol) at 21 °C. The mixture was allowed to stand for 20 min and then concentrated. The NMR spectrum of the crude product showed that it was deuterated both at C-2 (equatorial position) and C-3; NMR δ=4.55 (d, 1, $J_{1,2}$=9.8 Hz, H-1), 2.18 (d, 1, H-2a) and 4.17 (d, 1, $J_{4,5}$=9.7 Hz, H-4). The crude product was chromatographed on silica gel, eluting with benzene-ethyl acetate (10: 1, v/v), to give 17 mg (84%) of **10**; NMR δ=4.55 (d, 1, $J_{1,2}$=9.8 Hz, H-1), 2.18 (q, 1, $J_{2,3}$= 11.9 Hz, H-2a), 4.78 (q, 1, $J_{3,4}$=9.7 Hz, H-3), 4.17 (t, 1, $J_{4,5}$=9.7 Hz, H-4), 3.46 (m, 1, H-5), 3.86 (t, 1, $J_{5,6a}=J_{6a,6e}$= 10.4 Hz, H-6a), and 4.38 (q, 1, $J_{5,6e}$=4.5 Hz, H-6e).

A similar reduction of **2** (20 mg) afforded **11** in 91% yield (after purification with column chromatography); NMR δ= 4.87 (broad s, 1, $J_{1,2}$ <1.0 Hz, H-1), 2.46 (broad d, 1, $J_{2,3}$= 5.2 Hz, H-2e), and 5.06 (q, 1, $J_{3,4}$=10 Hz, H-3).

A similar reduction of methyl 4,6-*O*-benzylidene-2,3-dideoxy-2-deuterio-3-nitro-α-D-*erythro*-hex-2-enopyranoside (20 mg)[13] with sodium borohydride (5 mg) yielded **12** (89%, after column chromatography); NMR (60 MHz) δ=4.85 (d, 1, $J_{1,2}$=3.5 Hz, H-1), 2.34 (q, 1, $J_{2,3}$=11.2 Hz, H-2a), and 5.04 (q, 1, $J_{3,4}$=9.7 Hz, H-3).

A similar reduction of **8** (56.3 mg. 0.21 mmol) with sodium borohydride (15.6 mg, 0.41 mmol) in methanol (1.2 ml) afforded 45 mg (79%) of a syrup (after column chromato, graphy). Crystallization from diisopropyl ether–hexane afforded 30 mg (52.6%) of **15**; mp 71—71.5 °C; $[\alpha]_D^{24}$ −26° (*c* 0.5, $CHCl_3$); IR 1545 cm^{-1} (NO_2); R_f 0.41 (benzene).

Found: C, 58.84; H, 5.70; N, 5.14%. Calcd for $C_{13}H_{15}NO_5$: C, 58.86; H, 5.70; N, 5.28%.

A similar reaction of **8** (18 mg, 0.07 mmol) with sodium borodeuteride (5 mg) afforded a mixture (14 mg) of **13** and **14** as a syrup. Although the H-2a and H-2e signals overlap in chloroform-*d*, they separate in benzene-d_6; the ratio of **13**: **14**=2: 1 was determined. The assignment of the signals of these compounds was performed by comparison with the deuterated and the corresponding undeuterated products.

*1,5-Anhydro-4,6-O-benzylidene-2-cyano-2,3-dideoxy-3-nitro-D-mannitol (**16**).* To an acetonitrile solution (3.3 ml) containing hydrogen cyanide (*ca.* 6 equiv.) was added **8** (78.9 mg, 0.3 mmol) and an aqueous solution of potassium cyanide (0.06 ml, 1.9 mg) at 28 °C. The mixture was stirred at the ambient temperature for 2.5 h and then evaporated to give a residue. The residue was dissolved in chloroform and washed with water. The organic layer was evaporated to give a residue, which was subsequently crystallized from ethanol to give 74 mg of **16**. Recrystallization from isopropyl alcohol afforded 65 mg (74.7%) of **16**; mp 124—125 °C; $[\alpha]_D^{20}$ −154° (*c* 1, $CHCl_3$); IR 2230 (CN) and 1565 cm^{-1} (NO_2); R_f 0.41 (benzene–ethyl acetate, 10: 1, v/v).

Found: C, 57.75; H, 4.93; N, 9.63%. Calcd for $C_{14}H_{14}N_2O_5$: C, 57.93; H, 4.86; N, 9.65%.

The mother liquor was concentrated and chromatographed on silica gel, eluting with benzene–ethyl acetate (30: 1, v/v); the first fraction consisted of 6 mg of **17**, which was found to be identical with an authentic sample by a comparison with the IR and NMR spectral data. The second fraction consisted of 5 mg of an undetermined product, although it seems to be the *gluco* isomer, as judged from IR and NMR spectroscopy. The third fraction was composed of 5 mg of **16** (total yield of **16**: 80.4%).

*1,5-Anhydro-4,6-O-benzylidene-2-cyano-2,3-dideoxy-D-erythro-hex-2-enitol (**17**).* To a solution of **16** (22 mg, 0.067 mmol) in acetone (1.5 ml) was added triethylamine (0.2 ml). The mixture was stirred at 30 °C for 6 h and then evaporated to give a solid residue (18.4 mg). Recrystallization from isopropyl alcohol gave 13 mg (70.6%) of **17**; mp 170.5—171.5 °C; $[\alpha]_D^{20}$ +36.9° (*c* 1, $CHCl_3$); IR 2210 cm^{-1} (CN); R_f 0.69 (benzene–ethyl acetate, 10: 1, v/v).

Found: C, 69.15; H, 5.37; N, 5.96%. Calcd for $C_{14}H_{13}NO_3$: C, 69.12; H, 5.39; N, 5.76%.

*Attempt at the Direct Preparation of **17** from **8**.* To an ice–water-cooled chloroform solution (2.1 ml) of **8** (13 mg, 0.05 mmol) containing hydrogen cyanide (5 equiv.) was added 0.02 ml of triethylamine. The mixture was kept for 23 h in a refrigerator and then washed with *ca.* 1 mol dm^{-3} HCl solution and water. The NMR spectrum of the crude product showed that it consisted of **9** (>60%) and small amounts of **16** and **17**.

*1,5-Anhydro-2-azido-4,6-O-benzylidene-2,3-dideoxy-3-nitro-D-mannitol (**18**) and glucitol (**19**).* *a) From the Nitro Olefin **8**:* To a solution of **8** (26.3 mg, 0.1 mmol) in acetone (0.5 ml) was added a chloroform solution containing hydrazoic acid (0.3 mmol) at 21 °C. The mixture was allowed to stand at that temperature for 21 h and then evaporated to give a syrup (30 mg), the NMR spectrum of which showed the presence of only **18** and **19** in a ratio of 1.2 : 1. The syrup (30 mg+28 mg) was chromatographed on silica gel, eluting with benzene; the first fraction consisted of 20 mg of NMR spectroscopically pure **19**. Recrystallization from ethanol gave 16 mg (26%) of **19**; mp 126.5—127.5 °C; $[\alpha]_D^{20}$ —66.9° (*c* 0.5, $CHCl_3$); IR 2110 (N_3) and 1560 cm^{-1} (NO_2); R_f 0.59 (benzene).

Found: C, 51.14; H, 4.48; N, 18.18%. Calcd for $C_{13}H_{14}N_4O_5$: C, 50.98; H, 4.61; N, 18.29%.

The second fraction was a mixture of **18** and **19** (8 mg).

The third fraction was composed of 28 mg of pure **18**, which crystallized from diisopropyl ether to afford 20 mg (32.7%) of **18**; mp 127.5—128.5 °C; $[\alpha]_D^{20}$ −170° (*c* 0.5, $CHCl_3$); IR 2100 (N_3) and 1560 cm^{-1} (NO_2); R_f 0.47 (benzene).

Found: C, 51.15; H, 4.50; N, 18.03%. Calcd for $C_{13}H_{14}N_4O_5$: C, 50.98; H, 4.61; N, 18.29%.

*b) From the Acetate **7**:* To a solution of **7** (83 mg, 0.26 mmol) in acetonitrile (4 ml)–water (0.5 ml) was added sodium azide (19 mg, 0.29 mmol). The mixture was stirred at 28 °C for 24 h and then evaporated to give a residue. The residue was dissolved in dichloromethane and washed with water.

The organic layer was dried over $MgSO_4$ and evaporated to give a solid residue, which was similarly chromatographed on silica gel to give a mixture (52 mg) of **18** and **19** (3.1: 1, as judged from NMR spectroscopy), besides the starting material (14 mg).

References

1) Part VII. For this series, see Ref, 13.

2) a) T. Sakakibara and R. Sudoh, *J. Org. Chem.*, **42**, 1746 (1977); b) T. Sakakibara, R. Sudoh, and T. Nakagawa, *ibid.*, **38**, 2179 (1973); c) T. Sakakibara, M. Yamada, and R. Sudoh, *ibid.*, **41**, 736 (1976); d) T. Sakakibara, R. Sudoh, and T. Nakagawa, *Bull. Chem. Soc. Jpn*, **51**, 1189 (1978).

3) a) T. Sakakibara and R. Sudoh, *J. Chem. Soc., Chem. Commun.*, **1974**, 69; *Carbohydr. Res.*, **50**, 191 (1976); b) T. Sakakibara and R. Sudoh, *J. Org. Chem.*, **40**, 2823 (1975); c) T. Sakakibara and R. Sudoh, *J. Chem. Soc., Chem. Commun.*, **1977**, 7; *Bull. Chem. Soc. Jpn*, **51**, 1193 (1978); d) T. Sakakibara, A. Seta, Y. Tachimori, T. Takamoto, and R. Sudoh, *Chem. Lett.*, **1977**, 1365.

4) T. Sakakibara and R. Sudoh, *Carbohydr. Res.*, **58**, 31 (1977).

5) T. Sakakibara, T. Kawahara, and R. Sudoh, *Carbohydr. Res.*, **58**, 39 (1977).

6) *E.g.*, H. H. Baer and W. Rank, *Can. J. Chem.*, **49**, 3192 (1971); **52**, 2257 (1974); H. Paulsen and W. Koebernick, *Carbohydr. Res.*, **56**, 53 (1977); H. Paulsen and W. Greve, *Chem. Ber.*, **107**, 3013 (1974): S. D. Gero, E. Jegou-Aumont, J. Leboul, E. Jegou, and D. Mercier, *J. Chem. Soc., Chem. Commun.*, **1975**, 11; B. Fraser-Reid, *Acc. Chem. Res.*, **8**, 192 (1975); P. M. Collins, D. Gardiner, S. Kumar, and W. G. Overend, *J. Chem. Soc., Perkin Trans. 1*, **1972**, 2596.

7) R. K. Ness, H. G. Fletcher, Jr., and C. S. Hudson, *J. Am. Chem. Soc.*, **72**, 4547 (1950).

8) H. H. Baer and F. Kienzle, *Can. J. Chem.*, **45**, 983 (1967).

9) H. H. Baer and T. Neilson, *Can. J. Chem.*, **43**, 840 (1965).

10) H. H. Baer and W. Rank, *Can. J. Chem.*, **50**, 1292 (1972).

11) B. Coxon, *Tetrahedron*, **21**, 3481 (1965).

12) T. Sakakibara and R. Sudoh, unpublished data.

13) Y. Tachimori, T.Sakakibara, and R. Sudoh, *Carbohydr. Res.*, in press.

The Reaction of 2-Chloroazulene Derivatives with Lithium Acetylide in Liquid Ammonia

Tadayoshi MORITA, Taira FUJITA, and Kahei TAKASE*

Department of Chemistry, Faculty of Science, Tohoku University, Aramaki-aza-Aoba, Sendai 980

(Received October 18, 1979)

The reaction of diethyl 2-chloroazulene-1,3-dicarboxylate (**1a**) with lithium acetylide in liq ammonia gave diethyl 4- and 6-ethynylazulene-1,3-dicarboxylates by an abnormal substitution reaction. In a similar manner, some 2-chloroazulenes, possessing alkoxycarbonyl and/or cyano substituents at the 1- and 3-positions of azulene nucleus, gave the corresponding 4 (or 8)- and 6-ethynylazulenes. The same type reaction proceeded when lithium phenylacetylide, sodium indenide, and sodium fluorenide were used as the reagents, **1a** giving diethyl 4- and 6-(phenylethynyl)-, 6-(3-indenyl)-, and 6-(9-fluorenyl)azulene-1,3-dicarboxylates, respectively.

The halogeno substituents of haloazulenes are directly replaced by some nucleophilic reagents, such as alkoxides, amines, thiolates, or carbanions derived from active methylene compounds, to give the corresponding "normal substitution products."[1-3] On the other hand, no replacement of the chloro substituent occurred in the reaction of 2-chloroazulene derivatives with Grignard reagents.[4] Addition of the reagents took place at the 4- or 6-position with formation of the dihydrozulene-type addition products, whose dehydrogenation with tetrachloro-*o*-benzoquinone afforded 4- and 6-substituted azulene derivatives in which the chloro substituent at the 2-position remained.

We have recently found a third type of reaction of haloazulene derivatives with nucleophilic reagents; the reaction of 2-chloroazulene derivatives with alkali metal acetylide in liq ammonia yielded 4- and 6-ethynylazulene derivatives by an abnormal substitution reaction.[5] This paper describes the details of the reaction of 2-chloroazulene derivatives with lithium acetylide and its related carbanions in liq ammonia.

Results and Discussion

Diethyl 2-chloroazulene-1,3-dicarboxylate (**1a**),[2] when allowed to react with lithium acetylide in liq ammonia at −40 °C for 1 h, gave a mixture of diethyl 4- (**2a**) and 6-ethynylazulene-1,3-dicarboxylates (**3a**) in good yields. A similar result was obtained with use of sodium acetylide instead of lithium acetylide. 2-Chloroazulenes (**1b**, **1c**, **1d**, and **1e**) also readily reacted with lithium acetylide to give mixtures of isomeric 4-, 6-, and 8-ethynylazulenes (**2b**, **3b**, and **4b**), (**2c** and **3c**), (**2d** and **4d**), and (**2e** and **4e**), respectively. Each product was isolated from a mixture by silica-gel chromatography (Table 1).

The structures of the ethynylazulene derivatives were determined on the basis of spectral data (Tables 2, 3, and 4), as well as the results of elemental analyses. The electronic spectra indicate that the compounds are azulene derivatives.[6] The presence of the ethynyl group is shown by the sharp absorption bands in IR spectra corresponding to the $\nu_{C\equiv C}$ and $\nu_{\equiv CH}$ (ethynylic). The NMR spectra also reveal the singlets assignable to ethynylic protons. The positions of the substituents in the compound are deduced from the NMR signal patterns corresponding to the ring protons: an AA'BB'-type signal is found in the NMR spectra of symmetrical 6-ethynyl derivatives (**3a**, **c**) and two AB-type signals with long-range coupling in the unsymmetrical 6-ethynyl derivative (**3b**), together with a singlet due to H-2.

Table 1. Reaction of 2-chloroazulene derivatives with lithium acetylides

2-Chloro-azulene derivatives	Products (yield/%)		
	4-Ethynyl-	6-Ethynyl-	8-Ethynyl-
1a	**2a** (25.2)	**3a** (35.7)	
1b	**2b** (30.7)	**3b** (25.6)	**4b** (1)
1c	**2c** (44.5)	**3c** (4.9)	
1d	**2d** (73.3)		**4d** (4.5)
1e	**2e** (43.2)		**4e** (14.9)
1f		**3f** (58.3)	
1g		**3g** (39.9)	
1a	**5** (44.8)[a]	**6** (38.3)	

a) (Phenylethynyl)azulene.

On the other hand, a complex multiplet due to the adjacent four-proton system is found in the spectra of 4- (**2a**, **b**, **c**, **d**, **e**) and 8-ethynyl derivatives (**4b**, **d**, **e**), together with a singlet due to H-2 (**2a**, **b**, **c**) or an AB-type signal due to H-2 and H-3 (**2d**, **e** and **4d**, **e**). The structural correlations between pairs of the isomeric 4-ethynyl (**2b**, **d**, **e**) and 8-ethynyl derivatives (**4b**, **d**, **e**) were confirmed by the fact that the NMR peaks corre-

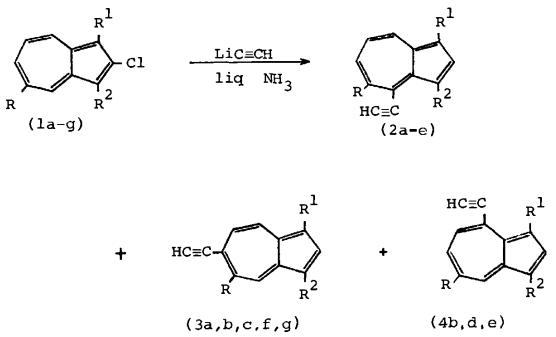

a: R=H, $R^1=R^2=CO_2Et$
b: R=H, $R^1=CO_2Me$, $R^2=CN$
c: R=H, $R^1=R^2=CN$
d: $R=R^2=H$, $R^1=CO_2Et$
e: $R=R^2=H$, $R^1=CN$
f: R=Me, $R^1=R^2=CO_2Et$
g: R=*iso*-Pr, $R^1=R^2=CO_2Et$

Table 2. Electronic spectral data of ethynylazulene derivatives

Compound	Solvent	λ_{max} nm (log ε)				
2a	Cyclohexane	254(4.48)	272(4.32)^{sh}	309(4.50)	320(4.52)	370(3.88)
		388(3.90)	565(2.86)			
3a	Cyclohexane	230(4.57)	270(4.36)	305(4.78)^{sh}	320(5.00)	353(4.17)
		378(3.92)	514(2.68)	540(2.76)	582(2.68)	644(2.27)
2b	Cyclohexane	250(4.39)	263(4.06)	278(4.13)	315(4.31)	360(3.62)
		390(3.65)	540(2.62)^{sh}	558(2.67)	605(2.61)	655(2.26)
3b	Chloroform	260(4.09)	309(4.67)^{sh}	317(4.78)^{sh}	321(4.87)^{sh}	345(4.05)
		353(4.10)	358(4.08)	376(3.61)	545(2.77)	580(2.70)^{sh}
4b	Cyclohexane	265(4.40)	310(4.60)^{sh}	318(4.64)	365(3.95)	383(3.78)
		578(2.81)				
2c	Chloroform	245(4.46)	275(4.33)	310(4.50)	325(4.44)^{sh}	355(3.95)
		365(3.91)	373(3.87)	382(3.99)	440(3.38)	530(2.88)^{sh}
		550(2.90)	560(2.88)	600(2.71)	640(2.39)	650(2.32)^{sh}
3c	Chloroform	260(2.79)	310(4.23)	324(4.36)	353(3.70)	370(3.71)
		380(3.66)	450(2.36)	525(2.48)	570(2.39)	600(2.67)
		620(2.07)	640(1.98)			
2d	Cyclohexane	265(4.38)	304(4.70)	318(4.75)	365(3.77)	375(3.61)
		387(3.65)	576(2.67)	628(2.56)		
4d	Cyclohexane	270(4.49)	305(4.50)	350(3.57)	363(3.65)	380(3.10)
		440(2.30)	550(2.51)	605(2.62)	660(2.50)	
2e	Chloroform	268(4.62)	303(4.72)	317(4.74)	353(3.72)	367(3.78)
		370(3.65)	382(3.58)	460(2.17)	505(2.47)	575(2.70)
		620(2.60)				
4e	Chloroform	272(4.65)	303(4.59)	315(4.58)	350(3.75)	360(3.82)
		378(3.73)	580(2.77)	630(2.68)		
3f	Cyclohexane	237(4.42)	276(4.27)	313(4.70)^{sh}	325(4.84)	355(4.40)
		382(3.82)	552(2.86)	590(2.80)^{sh}	645(2.46)^{sh}	
3g	Cyclohexane	240(4.66)	275(4.40)	318(4.83)^{sh}	323(4.91)	354(4.16)
		383(3.97)	549(2.89)	585(2.83)	645(2.44)	
5	Cyclohexane	255(4.53)	300(4.51)	365(4.36)	570(3.02)	590(3.00)
6	Methanol	235(4.54)	270(4.14)	310(4.43)^{sh}	348(4.70)	530(2.99)

Table 3. IR spectral data of ethynylazulene derivatives (KBr tablet, in cm^{-1})

Compound	$\nu_{C\equiv CH}$	$\nu_{C\equiv C}$	$\nu_{C\equiv N}$	COOR			
2a	3230	2090		1690	1200	1049	1031
3a	3230	2090		1690	1190	1044	
2b	3250	2100	2220	1696	1210	1040	
3b	3260	2090	2200	1697	1210	1041	
4b[a)]	3250	2100	2220	1725			
2c	3230	2090	2220				
3c	3260	2100	2220				
2d	3300	2090		1685	1220	1042	
4d	3330	2100		1710	1210	1025	
2e	3270	2090	2200				
4e	3240	2090	2220				
3f	3250	2090		1680	1210	1040	1028
3g	3250	2090		1680	1200	1041	1028
5		2200		1712	1210	1040	
				1690	1190	1017	
6		2208		1684	1203	1037	

a) In chloroform.

sponding to H-8 of 4-ethynyl derivatives are found at lower field, because of the diamagnetic anisotropy due to the CO_2R or CN group in the peri-position, than those corresponding to H-4 of 8-ethynyl derivatives. In a similar manner to that of **1a**, 5-alkyl-2-chloroazulenes (**1f**[7] and **1g**[8]) also reacted with lithium acetylide to give the 6-ethynylazulenes (**3f**) and (**3g**), respectively. In these cases only 6-ethynyl derivatives, whose structures were confirmed by spectral data (Tables 2, 3, and 4), were obtained in spite of the presence of the alkyl group at the 5-position of the azulene nucleus.

From the results, it was found that the reaction of 2-chloroazulenes (**1a—g**) with lithium acetylide in liq ammonia gave no 2-ethynylazulene derivatives, normal substitution product, but 4(or 8)- and 6-ethynylazulenes, abnormal substitution products, which were formed in such a way that the reagent entering into a position not that at which the leaving chloro substituent was attached. A mechanism for this abnormal substitution reaction seems to involve the additional-elimination process (Scheme 1). The acetylide attacks 2-chloroazulenes (**1**) at the 4(or 8) or 6-position of the azulene nucleus to give an anionic intermediate (**A** or **A'**) of a cyclopentadienide structure. Such attack of the reagent would be facilitated by the aid of electron-withdrawing alkoxycarbonyl or cyano groups at the 1- and/or 3-positions, because of stabilization of the anion (**A** or **A'**). This is supported by the fact that 2-chloroazulene did not react with acetylide under the same conditions.

TABLE 4. NMR SPECTRAL DATA OF ETHYNYLAZULENE DERIVATIVES
(at 60 MHz, in $CDCl_3$, Chemical shifts in δ/ppm from TMS, J/Hz)

Compound	C≡CH	Ring protons							$J_{2,3}$	$J_{4,5}$	$J_{7,8}$	OCH_2-CH_3 J=7.0 (Others)
		H_2	H_3	H_4	H_5	H_6	H_7	H_8				
2a	3.77s	8.58s			7.50	—	7.90m	9.80m				4.49q 1.40t 1.42t
3a	3.47s	8.78s		9.63d	7.83d		7.83d	9.63d		11.0	11.0	4.43q 1.46t
2b	4.07s	8.58s			7.80	—	7.95m	9.82m				(3.98s OCH_3)
3b[a]	3.56s	8.52s		8.62d	7.86dd		7.92dd	9.63d		10.2	10.5	(3.96s OCH_3)
4b	3.88s	8.30s		8.77m	7.63	—	8.00m					(3.95s OCH_3)
2c[b]	4.15s	8.36s			7.66	—	8.00m	8.76d			9.3	
3c	4.18s	8.28s		8.34d	7.59d		7.59d	8.34d		10.0	10.0	
2d	3.58s	8.27s	7.51d		7.20	—	7.57m	9.63m	4.0			4.38q 1.43t
4d	3.78s	8.23d	7.40d	8.53d	7.33	—	7.60m		4.0	11.0		4.40q 1.43t
2e	3.76s	8.10d	7.55d		7.35	—	7.80m	8.67d	4.0		10.0	
4e	3.96s	8.12d	7.33d	8.46d	7.23	—	7.78m		4.0	10.0		
3f	3.76s	8.76s		9.80s			7.88d	9.46d			10.5	4.43q 1.45t (2.90s CH_3 on C-5)
3g	3.71s	8.80s		10.27s			7.92d	9.45d			11.0	4.42q 1.43t 4.43q 1.45t (4.02sept 1.46d $CH(CH_3)_2$)
5		8.56s			7.28	—	7.87m	9.76m				4.40q 1.42t on C-1 4.29q 1.29t on C-3 (7.2—7.8 C_6H_5)
6		8.60s		9.85d	8.00d		8.00d	9.45d		11.0	11.0	4.50q 1.40t (7.4—7.7 C_6H_5)

Multiplicity, s: singlet; d: doublet; t: triplet; q: quartet; sept: septet; m: multiplet.
a) 100 MHz. b) Pulse Fourier transform mode.

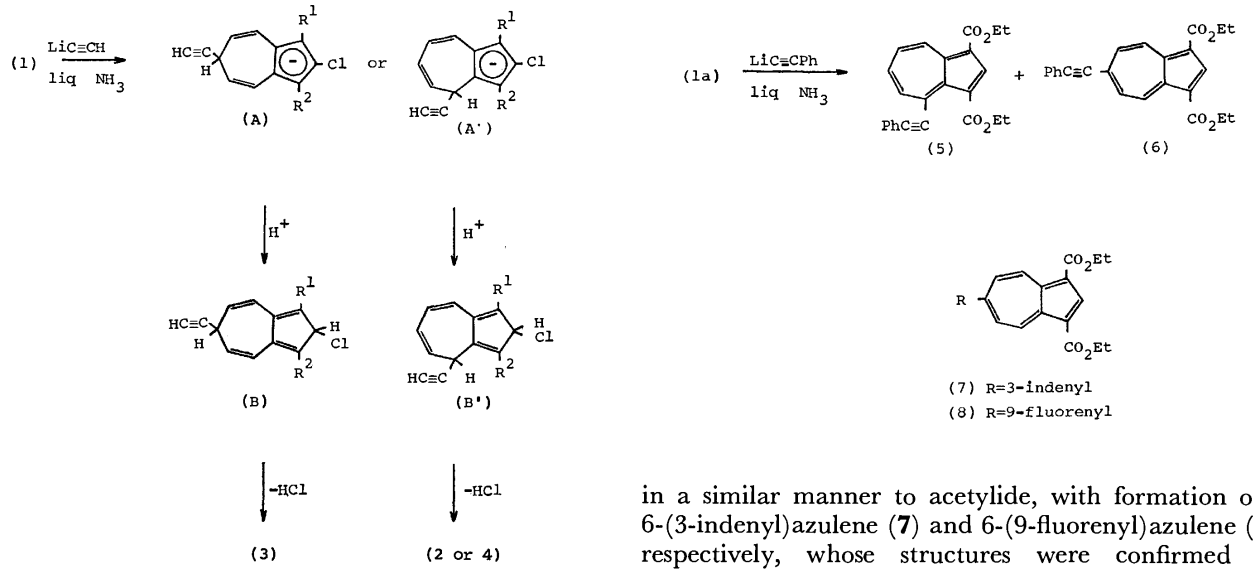

Scheme 1. A mechanism for the reaction of 2-Chloroazulene derivatives with lithium acetylide.

Dehydrochlorination from the protonated intermediate (**B** or **B'**), produced from the anion (**A** or **A'**) afforded 4(or 8)-ethyl- (**2** or **4**) or 6-ethynylazulenes (**3**). The same type of reaction proceeded when lithium phenylacetylide was used as a reagent instead of lithium acetylide; **1a** easily reacted with this reagent to give 4-(phenylethynyl)- (**5**) and 6-(phenylethynyl)azulene (**6**) in 44.8 and 38.3% yields, respectively. The structures of these products were determined on the basis of spectral data (Tables 2, 3, and 4).

Sodium indenide and fluorenide also reacted with **1a** in a similar manner to acetylide, with formation of a 6-(3-indenyl)azulene (**7**) and 6-(9-fluorenyl)azulene (**8**), respectively, whose structures were confirmed by spectral data (Experimental).

It is evident that such bulky groups could attack only the less hindered 6-position rather than the more hindered 4(or 8)-position with two ethoxycarbonyl groups in the peri-position.

Experimental

Melting points are uncorrected. The electronic spectra were measured on a Hitachi EPS-3 Spectrometer and IR spectra on a Shimadzu IR-27 infracord. The NMR spectra were measured with a Varian A-60D Spectrometer; in some cases on a JNM-100 instrument in the Fourier transform mode. TMS was used as an internal standard. The mass spectra were recorded on Hitachi RMU-6 mass spectrometer

at 25 eV. The THF employed was distilled from calcium hydride before use.

*Methyl 2-Chloro-3-cyanoazulene-1-carboxylate (**1b**).* Dry HCl gas was bubbled into a benzene solution (600 ml) of methyl 2-amino-3-cyanoazulene-1-carboxylate[9] (4.5 g, 19.9 mmol) at 5 °C for 15 min. To the solution was added isopentyl nitrite (4.5 g) with stirring. After stirring for 2 d at room temp, water (600 ml) was added to the mixture. The reaction mixture was extracted with benzene. The organic layer was washed with water, satd. $NaHCO_3$ aq, dried (Na_2SO_4), and evaporated to give a reddish brown residue. Chromatography (alumina, with benzene) of the residue gave **1b** (4.3 g, 87.95 mmol), red prisms (from ethanol), mp 207—209 °C; λ_{max} (chloroform), nm (log ε): 297 (4.89), 307 (4.98), 353 (4.15), 370 (3.99), 496 (3.09), 510 (3.08); IR (KBr) 2210 (C≡N), 1690 cm^{-1} (C=O); NMR ($CDCl_3$): δ 4.03 (s, CO_2Me), 7.67—8.27 (m, H-5,6, and 7), 8.72 (dm, J=10 Hz, H-4), 9.75 (dm, J=10 Hz, H-8). Found: C, 63.48; H, 3.14; N, 5.56%. Calcd for $C_{13}H_8ClNO_2$: C, 63.55; H, 3.28; N, 5.70%.

*2-Chloro-1,3-dicyanoazulene (**1c**).* A mixture of 1,3-dicyano-2-hydroxyazulene[10] (100 mg, 0.54 mmol), $POCl_3$ (5 ml), and a trace of pyridine was heated in a sealed tube at 150 °C for 8 h. After distillation of excess $POCl_3$, the residue was treated with ice and water, and extracted with a large amount of chloroform. The organic extract was washed with water, dried (Na_2SO_4), and concentrated. The residue was chromatographed on alumina with chloroform to give **1c** (84 mg, 73.4%), red prisms (from ethanol), mp over 300 °C. $\lambda_{max}^{chloroform}$ nm (log ε): 297 (4.70), 310 (4.83), 347 (3.89), 353 (3.89), 372 (3.71), 498 (2.86), 520 (2.85). IR (KBr): 2200 cm^{-1} (C≡N). Found: C, 67.67; H, 3.32; N, 13.36%. Calcd for $C_{12}H_5ClN_2$: C, 67.78; H, 3.37; N, 13.18%.

*2-Chloro-1-cyanoazulene (**1e**).* A mixture of **1b** (2.0 g) and 75% H_2SO_4 (40 ml) was heated at 70 °C until the evolution of CO_2 ceased, and the mixture was poured into ice and water, and then extracted with chloroform. The organic layer was washed with satd. NaCl aq, dried (Na_2SO_4), and concentrated to give a red residue. Chromatography of the residue on alumina with chloroform gave **1e** (1.3 g, 85%), red needles (from ethanol), mp 160—162 °C. $\lambda_{max}^{chloroform}$ nm (log ε): 290 (4.78), 303 (4.88), 340 (3.74), 353 (3.86), 365 (3.47), 520 (2.72), 550 (2.69). IR (KBr): 2200 cm^{-1} (C≡N). NMR ($CDCl_3$): δ 7.30 (s, H-3), 7.67—8.07 (m, H-5—7), 8.50 (dm, J=10 Hz, H-4), 8.70 (dm, J=10 Hz, H-8). Found: C, 70.74; H, 3.81; N, 7.49%. Calcd for $C_{11}H_6NCl$: C, 70.63; H, 3.21; N, 7.45%.

Reaction of 2-Chloroazulene Derivatives with Lithium Acetylides: General Procedure. The reaction of 2-chloroazulene derivatives with alkali metal acetylides was carried out as follows: A stream of acetylene gas was introduced into a blue colored fresh lithium metal in liq ammonia at −40 °C until the blue color of the solution disappeared. After stirring for 5 min, a solution of the 2-chloroazulene derivatives in dry THF was added to the solution of lithium acetylide. The mixture was kept at −40 °C for 1 h with stirring. Methanol was then added and excess ammonia was removed by evaporation at room temperature. The residue was mixed with ice–water, acidified slightly with 6 mol dm^{-3} HCl and extracted with benzene. The organic extract was washed with satd. $NaHCO_3$ aq, water, and dried (Na_2SO_4). The benzene solution, after concentration to a small volume, was chromatographed (silica gel, with benzene as an eluent). The yields of the ethynylazulene derivatives are given in Table 1, their electronic spectral data in Table 2, IR spectral data in Table 3, and NMR spectral data in Table 4.

*Reaction of **1a**[2] with Lithium Acetylide.* A solution of **1a** (550 mg, 1.8 mmol) in dry THF (30 ml) was treated with a lithium acetylide solution, prepared from lithium metal (69 mg, 10 mmol), liq NH_3 (20 ml) and gaseous acetylene. The reaction mixture was worked up. The first elution from chromatography afforded **3a** as reddish violet crystals (190 mg, 35.7%), which were recrystallized from ethanol to give reddish violet needles, mp 164—165 °C (Found: C, 73.14; H, 5.62%. Calcd for $C_{18}H_{16}O_4$: C, 72.96; H, 5.44%). The second elution gave **2a**, blue crystals (134 mg, 25.2%), which were recrystallized from ethanol to give blue prisms, mp 81—82 °C (Found: C, 72.65; H, 5.54%. Calcd for $C_{18}H_{16}O_4$: C,72.96; H, 5.44%). Treatment of **1a** (1.50 g, 4.89 mmol) with a sodium acetylide solution (prepared from 500 mg of sodium metal, 30 ml of liq NH_3, and acetylene) gave **3a** (580 mg, 40.0%) and **2a** (610 mg, 42.1%).

Reaction of **1b** (1.000 g, 4 mmol) in dry THF (50 ml) with lithium acetylide (prepared from 110 mg of Li, 30 ml of liq NH_3, and acetylene) yielded 245 mg (25.6%) of methyl 3-cyano-6-ethynylazulene (**3b**), violet needles, mp over 300 °C, from ethanol (Found: C, 76.97; H, 3.79; N, 6.03%. Calcd for $C_{15}H_9NO_2$: C, 76.58; H, 3.86; N, 5.96%), 295 mg (30.7%) of methyl 3-cyano-4-ethynylazulene-1-carboxylate (**2b**), violet needles, mp over 300 °C, from ethanol (Found: C, 76.45; H, 3.54; N, 6.02%. Calcd for $C_{15}H_9NO_2$: C, 76.58; H, 3.86; N, 5.96%), and 10 mg (1%) of methyl 3-cyano-8-ethynylazulene-1-carboxylate (**4b**), violet needles, mp over 300 °C, from ethanol[mass: *m/e* 235 (M^+, 100%)].

Reaction of 2-chloro-1,3-dicyanoazulene (**1c**) (426 mg, 2 mmol) with lithium acetylide (prepared from 42 mg of Li, 30 ml of liq NH_3, and acetylene) yielded 20 mg (4.9%) of 1,3-dicyano-6-ethynylazulene (**3c**), red prisms, mp over 300 °C, from ethanol (Found: C, 83.54; H, 3.02; N, 13.72%. Calcd for $C_{14}H_6N_2$: C, 83.15; H, 2.99; N, 13.85%) and 180 mg (44.5%) of 1,3-dicyano-4-ethynylazulene (**2c**), reddish violet prisms, mp over 300 °C, from ethanol (Found: C, 82.83; H, 3.06; N, 14.03%. Calcd for $C_{14}H_6N_2$: C, 83.15; H, 2.99; N, 13.85%).

Reaction of **1d** (702 mg, 3 mmol) in dry THF (30 ml) with lithium acetylide (prepared from 63 mg of Li, 20 ml of liq NH_3, and acetylene) gave 492 mg (73.2%) of ethyl 4-ethynylazulene-1-carboxylate (**2d**), violet needles, mp 60—61 °C, from light petroleum ether [mass: *m/e* 244 (M^+, 82.6%), 179 (M^+ −45, 100%), 152 (42.1%)] and 30 mg (4.5%) of ethyl 8-ethynylazulene-1-carboxylate (**4d**), blue oil [mass: *m/e* 244 (M^+, 100%)].

Reaction of **1e** (760 mg, 4 mmol) in dry THF (30 ml) with lithium acetylide (prepared from 100 mg of Li, 30 ml of liq NH_3, and acetylene) afforded 307 mg (43.2%) of 1-cyano-4-ethynylazulene (**2e**), blue needles, mp 150—153 °C, from ethanol [mass: *m/e* 177 (M^+, 100%)] and 107 mg (14.9%) of 1-cyano-8-ethynylazulene (**4e**), blue needles, mp 85—86 °C, from ethanol [mass: *m/e* 177 (M^+, 100%)].

Reaction of diethyl 2-chloro-5-methylazulene-1,3-dicarboxylate (**1f**)[7] (115 mg, 0.36 mmol) in 20 ml of THF with lithium acetylide (prepared from 10 mg of Li) yielded 965 mg (58.3%) of diethyl 6-ethyl-5-methylazulene-1,3-dicarboxylate (**3f**), reddish violet needles, mp 169—170 °C, from ethanol (Found: C, 73.31; H, 5.84%. Calcd for $C_{19}H_{18}O_4$: C, 73.53; H, 5.85%).

Reaction of diethyl 2-chloro-5-isopropylazulene-1,3-dicarboxylate (**1g**)[8] (1.050 g, 3 mmol) in 30 ml of THF with lithium acetylide (prepared from 63 mg of Li) yielded 407 mg (39.9%) of diethyl 6-ethynyl-5-isopropylazulene-1,3-dicarboxylate (**3g**), reddish violet needles, mp 122—123 °C, from ethanol (Found: C, 74.29; H, 6.43%. Calcd for $C_{21}H_{22}O_4$: C, 74.53; H, 6.55%).

Reaction of **1a** (3.00 g, 9.79 mmol) in 50 ml of THF with

phenylacetylide (prepared from 207 mg (29.5 mmol) of Li, 4.0 g of phenylacetylene, 30 ml of liq NH_3) gave 1.394 g (38.3%) of diethyl 6-(phenylethynyl)azulene-1,3-dicarboxylate (**6**), reddish violet needles, mp 160—161 °C, from ethanol (Found: C, 77.24; H, 5.73%. Calcd for $C_{24}H_{20}O_4$: C, 77.40; H, 5.41%) and 1.631 g (44.8%) of diethyl 4-(phenylethynyl)-azulene-1,3-dicarboxylate (**5**), bluish violet needles, mp 104—105 °C, from ethanol (Found: C, 77.24; H, 5.37%. Calcd for $C_{24}H_{20}O_4$: C, 77.40; H, 5.41%).

Diethyl 6-(3-Indenyl)azulene-1,3-dicarboxylate (7). A solution of **1a** (352 mg, 1.1 mmol) in 30 ml of THF was added with stirring to a solution of sodium indenide prepared from 138 mg of Na, 20 ml of liq NH_3, and 700 mg of indene in 50 ml of THF at −40 °C. After being stirred for 90 min, the reaction mixture was quenched with 30 ml of MeOH and worked up. The first elution from chromatography gave unreacted indene. The second elution gave 222 mg (52.3%) of **7**, red prisms, mp 130—131 °C, from ethanol, $\lambda_{max}^{chloroform}$ nm (log ε): 247 (4.48), 268 (4.44), 309 (4.63), 348 (4.39), 372 (4.29), 516 (2.91), 552 (2.80 sh), 605 (2.42 sh); IR (KBr): 1680 (C=O), 1195 (C–C(=O)–O), 1039 (O–C–C) cm^{-1}; NMR ($CDCl_3$): δ 1.45 (t, J=7.0 Hz, 2 $OCH_2C\underline{H}_3$), 4.45 (q, J=7.0 Hz, 2 $OC\underline{H}_2CH_3$), 3.58 (2H, d, J=2.0 Hz, H-1′), 6.80 (d, J=2.0 Hz, H-2′), 7.67—7.25 (4H, m, phenyl protons), 7.97 (br d, J=11.0 Hz, H-5,7), 8.83 (s, H-2), 9.80 (br d, J=11.0 Hz, H-4,8). Found: C, 77.34; H, 5.76%. Calcd for $C_{25}H_{22}O_4$: C, 77.70; H, 5.74%.

Diethyl 6-(9-Fluorenyl)azulene-1,3-dicarboxylate (8). A solution of **1a** (306 mg, 1 mmol) in 20 ml of THF was added with stirring to a solution of sodium fluorenide prepared from 75 mg of Na, 20 ml of liq NH_3, and 500 mg of fluorene in 20 ml of THF at −40 °C. After being stirred for 1h, the reaction mixture was worked up. The first elution from the chromatography gave 108 mg (18.5%) of **8**, red prisms, mp 192—193 °C, from cyclohexane. λ_{max}^{MeCN} nm (log ε): 233 (4.71), 270 (4.66), 310 (4.79), 375 (3.42), 500 (2.88). IR (KBr): 1684 (C=O), 1208 (C–C(=O)–O), 1028 (O–C–C) cm^{-1}. NMR ($CDCl_3$): δ 1.40 (t, J=7.0 Hz, 2 $OCH_2C\underline{H}_3$), 4.36 (q, J=7.0 Hz, 2 $OC\underline{H}_2CH_3$), 5.18 (s, H-9′), 7.00—7.37 (6H, m, H-2′—7′), 7.83 (m, H-1′, 8′), 7.35 (br d, J=11.0 Hz, H-5,7), 8.76 (s, H-2), 9.51 (br d, J=11.0 Hz, H-4,8). Found: C, 79.60; H, 5.49%. Calcd for $C_{26}H_{24}O_4$: C, 79.79; H, 5.54%.

References

1) K. Hafrner, H. Patzelt, and H. Kaiser, *Justus, Liebigs, Ann. Chem.*, **656**, 24 (1962).

2) T. Nozoe, S. Seto, and S. Matsumura, *Bull. Chem. Soc. Jpn.*, **35**, 1990 (1962).

3) T. Nozoe, K. Takase, and M. Tada, *Bull. Chem. Soc. Jpn.*, **38**, 247 (1965); M. Tada, *ibid.*, **39**, 1954 (1966); T. Arai, Ph. D. Thesis, Tohoku University (1970).

4) N. Abe, T. Morita, and K. Takase, *Tetrahedron Lett.*, **1973**, 3883; N. Abe and K. Takase, ibid., **1973**, 4739.

5) T. Fujita, T. Morita, and K. Takase, *Tetrahedron Lett.*, **1974**, 2585.

6) E. Heilbronner, "Non-benzenoid Aromatic Compounds," ed by D. Ginsburg, Interscience Publishers, New York (1959), pp. 217—276; T. Nozoe, K. Takase, H. Matsumura, T. Asao, K. Kikuchi, and S. Ito, "Dai-yuki-Kagaku (Comprehesive Organic Chemistry)," ed by M. Kotake, Asakura Shoten, Tokyo (1960), Vol. 13, pp. 439—528.

7) H. Akino, *Sci. Rept. Hirosaki University*, **11**, 18 (1964); *Chem. Abstr.*, **63**, 1754 (1965); Ph. D. Thesis, Tohoku University (1961).

8) T. Asano, Ph. D. Thesis, Tohoku University (1958).

9) This compound was prepared from 3-methoxycarbonyl-2*H*-cyclohepta[*b*]furan-2-one in a 93% yield by a modification of the method of Nozoe *et al. cf.* T. Nozoe, K. Takase, T. Nakazawa, and S. Fukuda, *Tetrahedron*, **27**, 3357 (1971).

10) T. Nozoe, S. Seto, S. Matsumura, and T. Asano, *Proc. Jpn. Acad.*, **32**, 339 (1959); T. Nozoe, S. Seto, S. Matsumura, and Y. Murase, *Bull. Chem. Soc. Jpn.*, **35**, 1179 (1962).

The Reactions of (1-Halo-1-alkenyl)dialkylboranes with Lead(IV) Acetate or (Diacetoxyiodo)benzene. A Stereoselective Synthesis of 1-Halo-1,2-dialkylethylenes

Yuzuru Masuda, Akira Arase,* and Akira Suzuki**

Department of Applied Chemistry, Kitami Institute of Technology, Kitami 090

***Department of Applied Chemistry, Faculty of Engineering, Hokkaido University, Sapporo 060*

(Received October 30, 1979)

The reaction of (1-halo-1-alkenyl)dialkylboranes with lead(IV) acetate or (diacetoxyiodo)benzene was studied. (1-Bromo-1-alkenyl)dialkylboranes gave 1-bromo-1,2-dialkylethylenes. When alkyl groups on the boron atom of vinylboranes were bulky or the reaction temperatures were low, *Z*-isomers were afforded, whereas when alkyl groups on the boron atom were small or the reaction temperatures were relatively high, *E*-isomers were afforded as the main products. (1-Chloro-1-alkenyl)dialkylboranes gave (*Z*)-1-chloro-1,2-dialkylethylenes regardless of the reaction conditions. (1-Iodo-1-alkenyl)dialkylboranes failed to give satisfactory yields of 1-iodo-1,2-dialkylethylenes.

The authors previously reported a stereospecifically defined synthesis of 1-bromo-1,2-dialkylethylenes by the reaction of (1-bromo-1-alkenyl)dialkylboranes with lead(IV) acetate (LTA) or (diacetoxyiodo)benzene (DIB).[1]

$$R_2BCBr{=}CHR' \xrightarrow{Pb(OAc)_4 \text{ or } PhI(OAc)_2} RCBr{=}CHR' \ (Z \text{ or } E)$$

Alkenyl halides are potentially important compounds in organic synthesis because of their wide use as reaction intermediates for introduction of some substituents to alkenyl group *via* alkenylmagnesiums,[2] lithiums,[3] and coppers.[4] Several synthetic methods for alkenyl halide have hitherto been reported. Brown and his co-workers described a route to terminal and internal alkenyl halides from alkynes by the reaction of alkenyldialkylborane[4] and alkenylboronic ester[5] with molecular halogen. In these reactions, "anti-Markownikoff" addition of hydrogen halide to alkyne was realized. On the other hand the reaction reported by us,

$$RC{\equiv}CR' \xrightarrow{HBR_2''} RCH{=}CR'BR_2'' \xrightarrow{X_2} RCH{=}CR'X$$

involves a migration of an alkyl group from the boron atom to the alkenyl carbon atom. Thus the latter reaction has a great advantage in that the several types of internal alkenyl bromide can be synthesized almost arbitrarily by selecting the combination of starting alkyne and alkene. Thus in this report, more detailed studies including some related reactions are presented.

Results and Discussion

The reactions of organoborane with oxidizing agents at times give peculiar reaction products. Among those, the reaction with LTA or DIB is one of interesting classes, because in the reaction with such reagent, trialkylborane affords corresponding alkyl acetate,[6] whereas in the reaction of 1-alkenyldialkylborane (I) an intramolecular migration of one alkyl group from boron atom to the alkenyl carbon atom adjacent to the boron atom occurs to give a corresponding *E*-alkene (II) (Table 1).

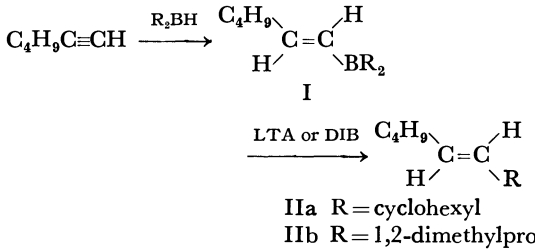

IIa R = cyclohexyl
IIb R = 1,2-dimethylpropyl

Although stereoselective syntheses of internal alkene from alkenyldialkylboranes have been achieved by Zweifel *et al.*,[7] Negishi *et al.*,[8] and Yatagai *et al.*,[9] these reactions are carried out under strong basic conditions. Consequently, they can not be used when organoboranes have alkyl groups sensitive to base. In contrast, there are no problems even for such organoboranes in the present reaction, because the reaction proceeds under almost neutral conditions. Further, our findings suggest the possibility that a combination of alkyl group with haloalkenyl group occurs by the reaction of (1-halo-1-alkenyl)dialkylboranes with above reagents.

Thus, 1-bromo-1-hexyne, readily prepared from 1-hexyne in a high yield,[10] was hydroborated by dicyclohexylborane or bis(1,2-dimethylpropyl)borane to (1-bromo-1-hexenyl)dialkylborane (III),[7a,8] and LTA or DIB was added to the reaction mixture. As was expected, (*Z*)-1-bromo-1-cyclohexyl-1-hexene (IVa) or 4-bromo-2,3-dimethyl-4-nonene (IVb) was obtained in a moderate yield with a high stereoselectivity (Table 2).

Table 1. Reaction[a] of 1-hexenyldialkylboranes with LTA or DIB

R	Reagent	Solvent	Product (*E* : *Z*)	Yield/%[b]
Cyclohexyl	DIB	$CHCl_3$	IIa (92 : 8)	60 (54)[c]
	LTA	C_6H_6	IIa (85 : 15)	45
1,2-Dimethylpropyl	LTA	CH_2Cl_2	IIb (93 : 7)	53 (50)[c]

a) Carried out at 0—25 °C for 4 h. Mole ratio; organoborane/reagent=1. b) Determined by GLPC based on BH_3 employed. c) Isolated by elution with hexane on silica-gel column.

Table 2. Reaction[a] of (1-bromo-1-hexenyl)dialkylboranes, derived from sterically hindered olefin, with LTA or DIB

R	Reagent	Solvent	Temp/°C	Time/h	Product (Z : E)	Yield/%[b]
Cyclohexyl	DIB	CH_2Cl_2	0	4	IVa (95 : 5)	55 (51)[c]
	DIB	CH_2Cl_2	−25	4	IVa (98 : 2)	58 (54)[c]
	LTA	CH_2Cl_2	−50	8	IVa (98 : 2)	43
1,2-Dimethylpropyl	DIB	CH_2Cl_2	−25	4	IVb (96 : 4)	42
	LTA	CH_2Cl_2	−50	8	IVb (98 : 2)	56 (50)[c]
	LTA	C_6H_6 / n-C_6H_{14}	0	4	IVb (97 : 3)	40

a) Mole ratio; organoborane/reagent=1. b) Determined by GLPC based on BH_3 employed.
c) Isolated by elution with hexane on silica-gel column.

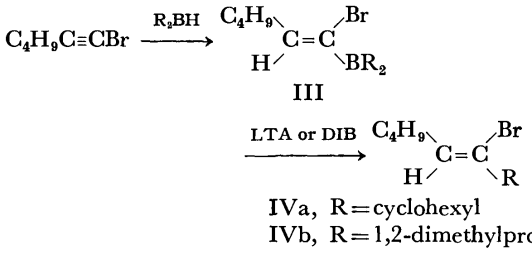

IVa, R=cyclohexyl
IVb, R=1,2-dimethylpropyl

It is apparent that the utility of this reaction depends on the availability of the starting dialkylborane. However, dialkylboranes prepared by the simple hydroboration of alkenes with borane in THF is limitted to only sterically hindered olefins such as cyclohexene, 2-methyl-2-butene, and α-pinene.[11] Several methods for the general synthesis of dialkylboranes have been proposed.[12] However, they did not give satisfactory results in the present reaction, probably because of the complexity of the procedure or contaminations of some compounds which were liable to inhibit the reactions.

Accordingly, we employed another easier procedure for the synthesis of dialkylborane. Brown *et al.*[13] have reported that the reaction of 2 mol of 1-pentene and 1 mol of borane in THF at room temperature results in the formation of a mixture containing 63.3% of dipentylborane. Consequently, the introduction of a solution of such a hydroboration stage to our reaction

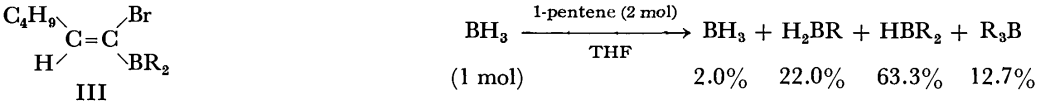

seemed togive corresponding alkenyl bromides. Actually, acceptably pure 1-bromo-1,2-dialkylethylenes (IVc, IVd, and IVe) were obtained in about 50—60% yields uncontaminated with by-products which obstructed the isolation of the alkenyl bromides in column chromatography. The results are summarized in Table 3.

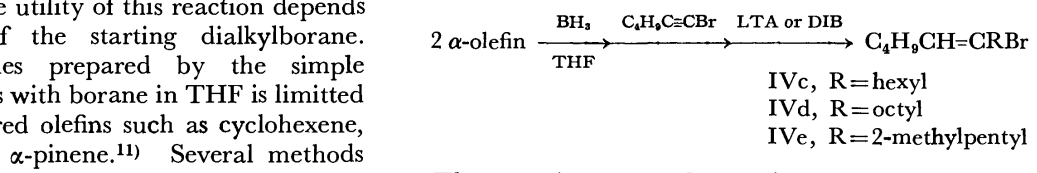

IVc, R=hexyl
IVd, R=octyl
IVe, R=2-methylpentyl

The most important feature in the results is the fact that stereospecifically defined bromoalkenes were obtained by merely controlling the reaction conditions, such as temperature and solvent, when LTA was employed. That is, (*Z*)-(1-bromo-1-hexenyl)dialkylborane, obtained *via* the hydroboration of 1-bromo-1-hexyne with dialkylborane, gave (*Z*)-6-bromododecene at −50 °C in dichloromethane, while the same organoborane gave *E*-isomer at 0 °C in a mixture of benzene and hexane (1: 1). Similar results were obtained when 1-octene and 2-methyl-1-pentene were employed as the starting alkene, suggesting the wide applicability of the

Table 3. Reaction of (1-bromo-1-hexenyl)dialkylboranes, derived from 1-alkyne, with LTA or DIB

R	Reagent[a]	Solvent	Temp/°C	Time/h	Product (Z : E)	Yield/%[b]
Hexyl[d]	DIB	CH_2Cl_2	0	4	IVc (48 : 52)	40
	DIB	CH_2Cl_2	−50	4	IVc (49 : 51)	10
	LTA	CH_2Cl_2	0	4	IVc (21 : 79)	36
	LTA	CH_2Cl_2	−50	4	IVc (96 : 4)	65 (56)[c]
	LTA	C_6H_6 / n-C_6H_{14}	0	4	IVc (5 : 95)	55 (52)[c]
Octyl[d]	LTA	CH_2Cl_2	−50	4	IVd (97 : 3)	(54)[c]
	LTA	C_6H_6 / n-C_6H_{14}	0	4	IVd (4 : 96)	(45)[c]
2-Methylpentyl[e]	LTA	CH_2Cl_2	−50	4	IVe (97 : 3)	54 (51)[c]
	LTA	C_6H_6 / n-C_6H_{14}	0	4	IVe (10 : 90)	42 (35)[c]

a) Mole ratio; organoborane/reagent=1. b) Determined by GLPC based on BH_3 employed. c) Isolated by elution with hexane on silica-gel column. d) Carried out by using a following solution; 2 × 1-alkene + BH_3: THF $\xrightarrow{25\,°C,\ 24\,h}$ R_2BH (63%). e) Carried out by using a following solution; 2 × 2-methyl-1-pentene + BH_3: THF $\xrightarrow{0\,°C,\ 2\,h}$ $(2\text{-methylpentyl})_2BH$ (60—70%).

Table 4. Reaction of (1-chloro-1-hexenyl)dialkylboranes with LTA or DIB

R	Reagent[a)]	Solvent	Temp/°C	Time/h	Product (Z : E)	Yield/%[b)]
Cyclohexyl	DIB	CH_2Cl_2	−50—0	8	VIa (97 : 3)	55 (52)[c)]
	LTA	CH_2Cl_2	−50	4	VIa (97 : 3)	48
1,2-Dimethyl propyl	LTA	CH_2Cl_2	−50—0	8	VIb (97 : 3)	42 (40)[c)]
Hexyl	LTA	CH_2Cl_2	−50—0	8	VIc (97 : 3)	53 (51)[c)]
	LTA	[C_6H_6 / n-C_6H_{14}]	0	4	VIc (97 : 3)	31

a) Mol ratio; organoborane/reagent=1. b) Determined by GLPC based on BH_3 employed. c) Isolated by elution with hexane on silica-gel column. d) Carried out by using a following solution: 2×1-hexene+ BH_3: THF $\xrightarrow{25\,°C,\ 24\,h}$ (hexyl)$_2$BH (63%).

present reaction for the syntheses of several types of 1-bromo-1,2-dialkylethylene.

On the other hand, in the Zweifel reaction,[7] the migration of alkyl group from the boron atom of 1-alkenyldialkylborane to the alkenyl carbon atom adjacent to the boron atom with iodine under alkaline solutions, was applied on the same (1-bromo-1-hexenyl)-dialkylborane, but only a small amount of the corresponding Z-isomer was found to be obtained.

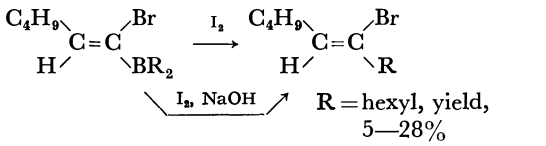

Then we undertook the reaction of (1-chloro-1-alkenyl)dialkylborane(V), obtained from 1-chloro-1-hexyne[14] and dialkylboranes, with LTA or DIB. The results are shown in Table 4. In all cases examined, corresponding (Z)-1-chloro-1,2-dialkylethylenes were afforded in moderate yields with high stereoselectivities. Unfortunately, E-isomers could not be obtained as predominant products, even by controlling the reaction conditions, such as temperature and solvent.

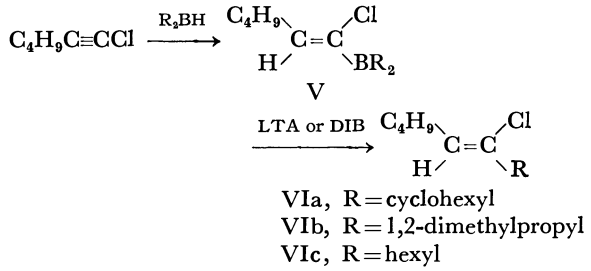

(1-Iodo-1-hexenyl)dialkylborane failed to give satisfactory yields of 1-iodo-1,2-dialkylethylenes in the similar treatment with LTA. In these cases appreciable amounts of by-products, such as alkyl acetate and trisubstituted alkene, presumably formed by a migration of two alkyl groups, were contaminated.

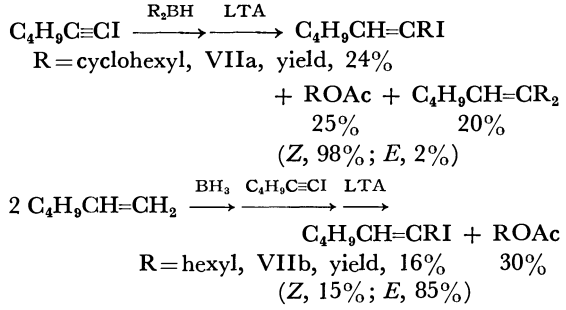

The present reaction provides a new method for the stereoselective synthesis of (Z)- or (E)-1-bromo-1,2-dialkylethylene, and also of (Z)-1-chloro-1,2-dialkylethylene. It is interesting that sterically defined (Z)- or (E)-1-bromo-1,2-dialkylethylene is obtained by controlling the reaction conditions when LTA is used. The manner of the elimination of the dialkylboryl group from the carbon atom seems to influence the stereochemistry of the product. A further work involving such a mechanistic study is now under investigation.

Experimental

Instruments. IR spectra (film) were recorded by using a Hitachi-285 spectrometer. PMR (CCl_4, TMS) were run on a Hitachi R-20A spectrometer. Mass spectra were recorded by using a Hitachi M-52 mass spectrometer.

Reagents. Cyclohexene, 1-hexene, and 1-octene were distilled under argon stream after drying over lithium aluminium hydride. Commercial 2-methyl-2-butene, 2-methyl-1-pentene, and 1-hexyne were used without any purification. Solvents were purified by appropriate methods respectively and they were distilled before use. 1-Chloro-1-hexyne,[14] 1-bromo-1-hexyne,[10] and 1-iodo-1-hexyne[15] were prepared by the methods described in the literatures. Borane in THF, [11c] lead (IV) acetate,[16] above 98% purity,[17] and (diacetoxyiodo)benzene[18] were prepared by the methods described in the literatures.

Identification of the Products. E- and Z- isomers were isolated respectively from the reaction mixture by repeated applications on the column chromatography, and subjected to the analysis. They were identified by reference to literatures.[2,19]

1-Bromo-1-cyclohexyl-1-hexene (IVa). A 100-ml round bottomed flask, equipped with a gas inlet for argon, a sample inlet with a serum cap, a dropping funnel and a magnetic stirring bar, was flushed with argon, and then in the flask dicyclohexylborane was prepared by the addition of cyclohexene (1.64 g, 20 mmol) to BH_3 (10 mmol) in THF. To the solution, 1-bromo-1-hexyne (1.61 g, 10 mmol) was slowly added at −10 °C and then the solution was stirred for 3 h at 0 °C. Then DIB (3.2 g, 10 mmol) in dichloromethane (30 ml) was dropped at −25 °C and the reaction mixture was stirred at the same temperature. After completion of the reaction, hexane (20 ml) was added, and the solution was washed with NaCl-saturated water once and then dried over anhydrous sodium sulfate. After the removal of the solvent under reduced pressure, the reaction mixture was put on a column packed with silica gel (Wako gel Q-50) giving 1.32 g (5.4 mmol, 54%) of IVa (Z, 98%; E, 2%) by elution with benzene. Z-Isomer was isolated by repeated applica-

tions on column chromatography of the above mixture: n_D^{20} 1.4940; PMR δ 5.52 (t, 1H); [2,19] IR $\nu_{c=c}$ 1655 cm^{-1};[2] mass spectrum *m/e* 244, 246 (M^+). Found: C, 59.11; H, 8.69%. Calcd for $C_{12}H_{21}Br$: C, 58.78; H, 8.63%.

4-Bromo-2,3-dimethyl-4-nonene (IVb). To the solution of (1-bromo-1-hexenyl)bis(1,2-dimethylpropyl)borane, obtained in the similar manner as described above, LTA (4.5 g, 10 mmol) in dichloromethane (50 ml) was dropped at −50 °C and the stirring was continued for 8 h at the same temperature. Then, water (5 ml) and hexane (20 ml) were added to the solution at 0 °C. By the same procedure as described in the synthesis of IVa, 1.17 g (5.0 mmol, 50%) of IVb (*Z*, 98%; *E*, 2%) was obtained. *Z*-isomer was isolated by column chromatography of the above mixture: n_D^{20} 1.4638; PMR δ 5.53 (t, 1H);[2,19] IR $\nu_{c=c}$ 1655 cm^{-1};[2] mass spectrum *m/e* 232, 234 (M^+). Found: C, 56.50; H, 9.02%. Calcd for $C_{11}H_{21}Br$: C, 56.66; H, 9.08%.

(Z)-6-Bromo-5-dodecene (IVc-Z). In the same reaction apparatus as described above, flushed with argon, 1-bromo-1-hexyne (1.61 g, 10 mmol) was placed, and then the solution, prepared by the hydroboration (25 °C, 24 h) of 1-hexene (1.68 g, 20 mmol) with BH_3 (10 mmol, in THF), was dropped into the flask by using a syringe at −25 °C followed by the stirring for 2 h at −10 °C. Then LTA (4.5 g, 10 mmol) in dichloromethane (50 ml) was slowly added at −65 °C and the solution was stirred at −50 °C for 4 h. After the reaction, a mixture of water (3 ml) and THF (5 ml) was added to the solution at −50 °C, and then the solution was allowed to return to room temperature. By the same procedure as described in the synthesis of IVa, 1.38 g (5.6 mmol, 56%) of IVc (*Z*, 96%; *E*, 4%) was obtained. *Z*-isomer was isolated by column chromatography: n_D^{20} 1.4682; PMR δ 5.51 (t, 1H);[2,19] IR $\nu_{c=c}$ 1655 cm^{-1};[2] mass spectrum *m/e* 246, 248 (M^+). Found: C, 58.46; H, 9.29%. Calcd for $C_{12}H_{23}Br$: C, 58.30; H, 9.38%.

(Z)-6-Bromo-5-tetradecene (IVd-Z). This compound was obtained in the similar manner as described in the synthesis of IVc-*Z*; PMR δ 5.51 (t, 1H);[2,19] IR $\nu_{c=c}$ 1660 cm^{-1};[2] mass spectrum *m/e* 274, 276 (M^+). Found: C, 61.18; H, 9.80%. Calcd for $C_{14}H_{27}Br$: C, 61.09; H, 9.89%.

(Z)-6-Bromo-8-methyl-5-undecene (IVe-Z). This compound was obtained in the similar manner as described in the synthesis of IVc-*Z*; PMR δ 5.52 (t, 1H);[2,19] IR $\nu_{c=c}$ 1660 cm^{-1};[2] mass spectrum *m/e* 246, 248 (M^+). Found: C, 58.39; H, 9.36%. Calcd for $C_{12}H_{23}Br$: C, 58.30; H, 9.38%.

(E)-6-Bromo-5-dodecene (IVc-E). To the solution of (1-bromo-1-hexenyl)dialkylborane, prepared by the procedure as described in the synthesis of IVa, a mixture of benzene (20 ml) and hexane (20 ml) was added, and then powdered LTA (4.5 g, 10 mmol) was introduced slowly to the solution at −10 °C, followed by stirring for 4 h at 0 °C. Then, water (5 ml) was added. By the similar procedure as described in the synthesis of IVa, 1.28 g (5.2 mmol, 52%) of a mixture (*Z*, 5%; *E*, 95%) was obtained. *E*-Isomer was isolated by column chromatography: n_D^{20} 1.4718; PMR δ 5.71 (t, 1H);[2,19] IR $\nu_{c=c}$ 1645 cm^{-1};[2] mass spectrum *m/e* 246, 248 (M^+). Found: C, 58.48; H, 9.31%. Calcd for $C_{12}H_{23}Br$: C, 58.30; H, 9.38%.

(E)-6-Bromo-5-tetradecene (IVd-E). This compound was obtained in the similar manner as described in the synthesis of IVc-*E*; PMR δ 5.72 (t, 1H);[2,19] IR $\nu_{c=c}$ 1645 cm^{-1};[2] mass spectrum *m/e* 246, 248 (M^+). Found: C, 58.35; H, 9.38%. Calcd for $C_{12}H_{23}Br$: C, 58.30; H, 9.38%.

(Z)-1-Chloro-1-cyclohexyl-1-hexene (VIa), (Z)-4-Chloro-2,3-dimethyl-4-nonene (VIb), (Z)-6-Chloro-5-dodecene (VIc), (Z)-1-Iodo-1-cyclohexyl-1-hexene (VIIa) and (E)-6-Iodo-5-dodecene (VIIb). These compounds were synthesized in the similar manners as described in the syntheses of the corresponding bromo compounds. Analytical data are as follows.

VIa: PMR δ 5.31 (t, 1H);[2,19] IR $\nu_{c=c}$ 1660 cm^{-1};[2] mass spectrum *m/e* 200, 202 (M^+). Found: C, 71.87; H, 10.53%. Calcd for $C_{12}H_{21}Cl$: C, 71.80; H, 10.54%.

VIb: PMR δ 5.31 (t, 1H);[2,19] IR $\nu_{c=c}$ 1660 cm^{-1};[2] mass spectrum *m/e* 188, 190 (M^+). Found: C, 70.03; H, 11.16%. Calcd for $C_{11}H_{21}Cl$: C, 70.00; H, 11.21%.

VIc: PMR δ 5.03 (t, 1H);[2,19] IR $\nu_{c=c}$ 1655 cm^{-1};[2] mass spectrum *m/e* 202, 204 (M^+). Found: C, 71,12; H, 11.41%. Calcd for $C_{12}H_{23}Cl$: C, 71.08; H, 11.43%.

VIIa: PMR δ 5.30 (t, 1H);[2,19] IR $\nu_{c=c}$ 1640 cm^{-1};[2] mass spectrum *m/e* 292 (M^+). Found: C, 49.38; H, 7.20%. Calcd for $C_{12}H_{21}I$: C, 49.33; H, 7.24%.

VIIb: PMR δ 6.03 (t, 1H);[2,19] IR $\nu_{c=c}$ 1630 cm^{-1};[2] mass spectrum *m/e* 294(M^+). Found: C, 49.03; H, 7.84%. Calcd for $C_{12}H_{23}I$: C, 48.99; H, 7.88%.

References

1) Y. Masuda, A. Arase, and A. Suzuki, *Chem. Lett.*, **1978**, 665.

2) T. H. Chan, P. W. Law, and W. Mychajlowsky, *Tetrahedron Lett.*, **1977**, 3317

3) a) J. F. Normant, *Synthesis*, **1972**, 63; b) G. Cahiez, D. Bernard, and J. F. Normant, *ibid.*, **1976**, 245.

4) H. C. Brown, D. H. Bowman, S. Misumi, and M. K. Unni, *J. Am. Chem. Soc.*, **89**, 4531 (1967).

5) H. C. Brown, T. Hamaoka, and N. Ravindran, *J. Am. Chem. Soc.*, **95**, 5786, 6456 (1973).

6) Y. Masuda and A. Arase, *Bull. Chem. Soc. Jpn.*, **51**, 901 (1978).

7) a) G. Zweifel, H. Arzomanian, and C. C. Whitney, *J. Am. Chem. Soc.*, **89**, 3652 (1976); b) G. Zweifel, R. P. Fischer, J. T. Snow, and C. C. Whitney, *ibid.*, **93**, 6309 (1971).

8) E. Negishi, J. J. Katz, and H. C. Brown, *Synthesis*, **1972**, 555.

9) H. Yatagai, Y. Yamamoto, K. Maruyama, A. Sonoda, and S. Murahashi, *J. Chem. Soc., Chem. Commun.*, **1977**, 852.

10) K. E. Schulte and M. Goes, *Arch. Pharm.*, **290**, 118 (1959).

11) a) H. C. Brown, "Hydroboration," W. A. Benjamin, Inc., New York (1962); b) G. M. L. Cragg, "Organoboranes in Organic Synthesis," Marcel Dekker, New York (1973); c) H. C. Brown, "Organic Syntheses *via* Boranes," J. Wiley and Sons, New York (1975).

12) a) H. C. Brown, E. Negishi, and S. K. Gupta, *J. Am. Chem. Soc.*, **92**, 6648 (1970); b) H. C. Brown and S. K, Gupta, *ibid.*, **93**, 1818 (1971); c) A. Pelter, K. Rowe, and K. Smith, *J. Chem. Soc., Chem. Commun.*, **1975**, 531.

13) H. C. Brown, A. Tsukamoto, and D. B. Bigley, *J. Am. Chem. Soc.*, **82**, 4703 (1960).

14) a) H. Normant and T. Cuvigny, *Bull. Soc. Chim. F.*, **1957**, 1447; b) D. J. Pflaum and H. H. Wenzke, *J. Am. Chem. Soc.*, **56**, 1106 (1934).

15) P. L. Southwick and J. R. Kirchiner, *J. Org. Chem.*, **27**, 3305 (1962).

16) J. C. Bailar, Jr., *Inorg. Synth.*, Vol. 1, 47 (1939).

17) L. F. Fieser and M. Fieser, "Reagent for Organic Synthesis," J. Wiley and Sons, New York (1967) Vol. 1, p. 537.

18) K. H. Pausker, *J. Chem. Soc.*, **1953**, 107.

19) L. M. Jackman and S. Sternhell, "Application of Nuclear Magnetic Resonance Spectroscopy in Organic Chemistry," 2 nd ed, Pergamon, Oxford (1969), p. 184.

Enolate Anions. II. Substituent Effects of Sodium Ethyl Phenylacetates in DMSO[1]

Syun-ichi KIYOOKA,* Yoshinobu UEDA, and Kojiro SUZUKI
Department of Chemistry, Faculty of Science, Kochi University, Akebono-cho, Kochi 780
(Received October 31, 1979)

The UV-visible, IR, and ^{1}H-NMR spectra of the sodium enolates of ethyl phenylacetates (substituents; *p*-CH_3O, *p*-CH_3, *m*-CH_3, H, *p*-Cl, *p*-CH_3CO, *m*-CH_3CO, *p*-$COOC_2H_5$, *p*-CN, and *p*-NO_2) in DMSO were measured at room temperature. The derivatives with electron-attracting groups at the *para* position exhibit their absorption maxima with $\varepsilon > 10^4$ in visible regions above 400 nm. The visible spectra suggest the presence of a resonance between their electron-attracting groups at the para position and the enolate anion parts through the benzene ring. The carbonyl-stretching vibrations of the enolates in the IR spectra and the chemical shifts of the residual methine proton of the enolates in the ^{1}H-NMR spectra can be well explained by using the substituent constants, σ and σ^-. The ρ values of the *meta* and *para* lines are extremely different. In the case of the *p*-NO_2 derivative, the ^{1}H-NMR spectra of the benzene-ring protons indicate that the free rotation of the partially double bond between the benzene ring and the enolate-anion part is fixed at room temperature.

The methylene protons adjacent to the electron-attracting groups, such as the nitro, cyano, and ester groups, are acidic enough to give anions when treated with sodium hydride.[2] Such an anion is not a localized carbanion, but a delocalized enolate anion, as well as one derived from ketone.[3] Studies of the structure of the metal enolate anions are rapidly increasing in number, though they are almost entirely restricted to mono- and diketones.[4] Zaugg *et al.* have pointed out that the reactivity of enolate anions depends on the states of the ions and ion-pairs. However, spectroscopic studies of enolate anions have not given more definitive results about the states of ions and ion-pairs than about those of carbanions.[5,6]

The states of the ions and ion-pairs of enolate anions were mainly presumed on the basis of kinetic evidence. In the alkylation of enolate anions, the reaction rate was greatly accelerated by the addition of dipolar aprotic solvents, such as DMSO and DMF. The enhanced rate was explained on the basis of the presence of more dissociated species (free ions and solvent-separated ion-pairs) in the reaction.[5]

In DMSO, the ^{13}C-NMR spectra of the enolate anions of some diethyl alkylmalonates apparently gave a simple pattern which could be assigned to only one species at room temperature.[1] So long as sodium metal is used as a counter cation, the metal cation can be sufficiently solvated with the dipolar aprotic solvent. Therefore, the apparent species in the ^{13}C-NMR spectra seem to depend on the equilibrium among some predominant configurations of the enolate anion on an NMR time scale. The structure of the sodium enolate anions, derived from ethyl phenylacetates, may be determined by means of the steric and electronic stabilities of the configuration and/or the conformation of the enolate-anion part in DMSO.

In spite of the importance of the electronic perturbation in estimating the reactivity of enolate anions, the substituent effects have scarcely been investigated at all. This paper will deal with the substituent effects in the UV-visible, IR, and ^{1}H-NMR spectra of enolate anions and the correlation between the effects and their configurations.

Results and Discussion

Molecular spectroscopy (UV-visible and IR) can generally reflect the configurations and conformations of substrates in solution, while magnetic resonance spectroscopy gives some informations about structure, including the proportions of the configurations and dynamic information about the transformation process among the configurations. A systematic examination of substituent effects in the UV-visible, IR, and ^{1}H-NMR spectra of enolate anions can clarify the alteration in their structure by substituents.

UV-Visible Spectra. In writing the resonance structures for the benzylic anion, the coplanarity of the ring with the α-methylene group is implied, because there can be an effective overlap between the p-orbital of the α-carbon with the unshared pair of electrons and the p_π-orbitals of the benzene ring.[7] The UV-visible spectrum of benzyllithium was observed at 330 nm (λ_{max}) with an absorption intensity of log $\varepsilon = 3.98$ (yellow color).[8] The enolate anion of ethyl phenylacetate gave the absorption maximum at 345 nm. It can, therefore, be presumed that this enolate anion has a resonance structure, analogous to the benzyl anion.

Table 1 shows the data of the UV-visible spectra of the enolate anions. The absorption maxima of the

Table 1. UV-visible spectra of enolate anions of ethyl (*p*-substituted phenyl)acetates[a]

Substituent	λ_{max}	ε_{max}	Color
MeO	340	—[b]	yellow
Me	345	—[b]	yellow
H	345	—[b]	yellow
Cl	350	—[b]	yellow
COOEt	428	0.84×10^4	yellow
CN	405	2.17×10^4	yellow-green
MeCO	453	1.73×10^4	yellow-red
NO_2	548	3.30×10^4	violet
	580	3.00×10^4	

a) These original esters have no absorption bands in the UV-visible region (300—700 nm). b) Accurate ε_{max} values could not be obtained at low concentrations (10^{-5} mol/dm^3).

enolate anion with electron-releasing substituents and hydrogen at the *para* position are present at the range of 340—350 nm. The overlaps between the p-orbital of α-carbon and the p_π-orbitals of the benzene ring are of nearly the same degree as in these enolate anions because of similar λ_{max}. The absorption maxima of these enolate anions are mostly extinguished by dilution with DMSO to a concentration of 10^{-5} mol/dm^3, so that the accurate ε_{max} can not be obtained. This may be attributed to the presence of an equilibrium between the enolate anions and DMSO.

On the other hand, the enolate anions which have electron-attracting substituents at the *para* position are stable at low concentrations (10^{-5} mol/dm^3) because of the high acidity enhanced by these substituents. The more bathochromic shifts of λ_{max} were observed in the region above 400 nm for the more electron-attracting groups, which are conjugated with the enolate-anion part through the benzene ring. The marked tendency of the enolate anions to show a bathochromic effect is similar to that of phenolate anions.[9] Hence, the pattern of the additional resonance of the enolate anions seems not to be far from that of the phenolate anions. Two adsorption maxima with nearly equal intensities were observed in the case of the enolate anions of ethyl *p*-nitrophenylacetate; these are characteristic of *para* nitro substituents.[10]

Table 2. IR spectra of ethyl phenylacetates and these enolate anions in DMSO
Carbonylstretching vibration (cm^{-1}).

Substituent	Original ester	Enolate anion
p-MeO	1727	1588
p-Me	1726	1588
m-Me	1726	1587
H	1724	1589
p-Cl	1725	1591
p-COOEt[a]	1728	1617
p-CN[a]	1728	1622
p-MeCO[a]	1727	1618
m-MeCO	1726	1593
p-NO_2[a]	1730	1640

a) The other characteristic absorption bands were observed in the enolate anions with electron-attracting substituents at the *para*-position.

p-COOE	1555, 1515 cm^{-1}
p-CN	1555, 1510 cm^{-1}
p-MeCO	1550, 1515 cm^{-1}
p-NO_2	1575, 1520 cm^{-1}

IR Spectra. Table 2 shows the wave numbers of the carbonyl (CO) stretching vibrations in the ethyl phenylacetates and their enolate anions. These wave numbers are very important in examining the electron density at the CO double bond. The original esters have definite wave numbers (1724—1730 cm^{-1}) in spite of the variation in the substituents. The CO stretching vibration bands of enolate anions are illustrated by some typical representative spectra (*p*-Cl and *p*-CN) in Fig. 1.

The enolate anions with substituents other than *para* electron-attracting substituents give only one absorption band with a strong intensity in the region of 1587—1593 cm^{-1}, like the *p*-Cl derivative in Fig. 1. In the enolate anion of ethyl phenylacetate, the CO absorption band was observed at a lower frequency, 135 cm^{-1}, than in the original ester. This low-frequency shift indicates an increase in the electron density of the polarized CO bond in the enolate anion.

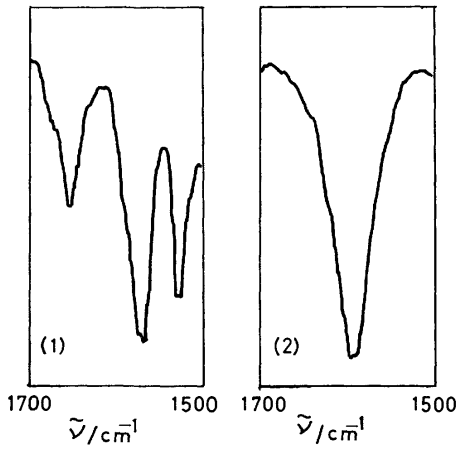

Fig. 1. The carbonyl streching vibration bands (1500—1700 cm^{-1}) of enolate anions; (1) *p*-CN derivative, (2) *p*-Cl derivative.

In contrast, the enolate anions with *para* electron-attracting substituents gave one CO absorption band with a medium intensity, together with two other absorption bands (1575—1550 and 1520—1510 cm^{-1}) which seem to be attributable to the resonance. The stronger electron-attracting ability of the substituent shifts the CO stretching absorption band of the enolate anion to a higher frequency region; in the *para* nitro derivative, the absorption band was obtained 51 cm^{-1} higher than in the *para* hydrogen derivative. This high-frequency shift suggests that the delocalized electrons flow into the benzene ring rather than being present in the polarized CO bond.

^{1}H-NMR Spectra. The ^{1}H-NMR measurements of enolate anions are useful for the investigation of the structures in solution.[11] On the basis of a consideration of molecular models of the enolate anion derived from ethyl phenylacetate, one of the stable configurations is illustrated below:

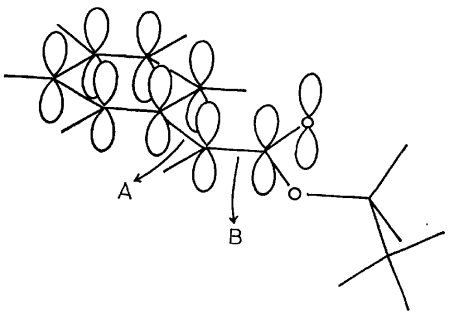

In the above figure, the A bond forms the maximum overlap between the p-orbital of the enolate-anion part and the p_π-orbitals of the benzene ring, while the benzene ring is located at a position *trans* to the ethoxyl group with respect to B bond. For detailed descriptions

TABLE 3. ^{1}H-NMR CHEMICAL SHIFTS OF ETHYL PHENYLACETATES IN DMSO-d_6
The chemical-shift values are indicated by means of a δ scale.

Substituent		$X-C_6H_4-\overset{\alpha}{C}H_2-COO-\overset{\beta}{C}H_2-\overset{\gamma}{C}H_3$		
		α	β	γ
p-MeO	a)	3.61	4.14	1.19
	b)	3.34	3.60	1.11
	c)	+0.27	+0.54	+0.08
p-Me	a)	3.69	4.14	1.18
	b)	3.38	3.98	1.13
	c)	+0.31	+0.16	+0.05
m-Me	a)	3.65	4.15	1.20
	b)	3.38	3.64	1.20
	c)	+0.27	+0.51	0.00
H	a)	3.71	4.41	1.18
	b)	3.45	3.59	1.14
	c)	0.26	+0.55	+0.04
p-Cl	a)	3.75	4.18	1.21
	b)	3.42	3.75	1.13
	c)	+0.33	+0.43	+0.08
p-COOEt	a)	3.83	4.18	1.21
	b)	4.01	3.54	1.11
	c)	−0.18	+0.64	+0.10
p-CN	a)	3.94	4.20	1.24
	b)	4.14	3.90	1.13
	c)	−0.20	+0.30	+0.11
p-MeCO	a)	3.85	4.18	1.23
	b)	4.28	3.90	1.13
	c)	−0.43	+0.28	+0.10
m-MeCO	a)	3.85	4.19	1.23
	b)	3.50	3.54	1.10
	c)	+0.35	+0.65	+0.13
p-NO_2	a)	3.94	4.22	1.24
	b)	4.75	4.01	1.18
	c)	−0.81	+0.21	+0.06

a) Chemical shifts of original esters. b) Chemical shifts of enolate anions. c) Differences (a—b). A plus sign represents a high-field shift.

of the configurations, these two partially double bonds (A and B) are very important.

As the rotational barrier of the B bond in the enolates derived from ethyl phenylacetates is assumed to be of a similar degree to that of the partially double bond in lithio isobutyrophenone (>27 kcal mol^{-1}),[12] the rotation about the B bond may be restricted and fixed to a preferential *trans* configuration at room temperature. On the other hand, the A bond would be allowed to rotate at room temperature, because the analogous partially double bond in stryl anions has rotational barriers (11—14 kcal mol^{-1})[13] which are clearly connected with the delocalization of the negative charge into the benzene rings. Table 3 shows the ^{1}H-NMR chemical shifts of the alkyl parts in enolate anions derived from ethyl phenylacetates. From the simple pattern of the observed spectra of the alkyl parts, the species in the solution can be attributed to only one structure, which presumably corresponds to the *trans* configuration.[14] The chemical shifts of $-CH_2-$ and $-CH_3$ in the enolate anions are observed at higher fields (+0.2—+0.6 and <+0.1 ppm, respectively) than those of the original esters. The chemical shifts of the residual active methine proton are obtained at fields +0.2—+0.6 ppm higher than those of original esters; these shifts evidently show substituent effects.

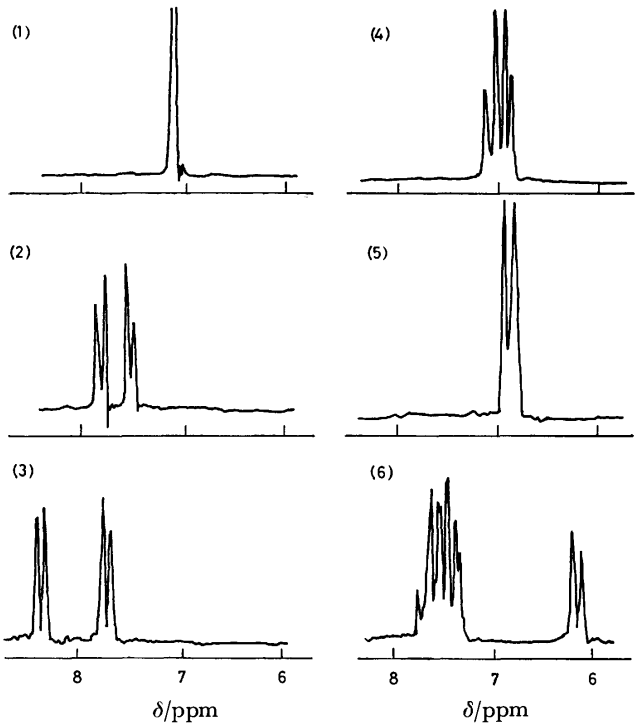

Fig. 2. The ^{1}H-NMR spectra of original esters [(1), (2), (3)] and enolate anions [(4), (5), (6)] at δ 6—8 ppm; (1), (4): *p*-Me derivative, (2), (5): *p*-CN derivative, (3), (6): *p*-NO_2 derivative.

The ^{1}H-NMR spectra of benzene-ring protons are shown in Fig. 2 (*p*-CH_3, *p*-CN, and *p*-NO_2 compounds). In the *p*-CH_3 derivative, the apparent singlet pattern of benzene-ring protons in the original ester is changed to the AB pattern in the enolate anion. In the *p*-CN derivative, the apparent AB pattern of benzene-ring protons in the original ester is changed to a doublet pattern with a large high-field shift in the enolate anion. The ^{1}H-NMR patterns of the benzene-ring protons in these enolate anions are symmetrical, as has been mentioned above. Such observations suggest that the partially double bond A has a free rotation because of the equivalence in the magnetic environments of two *ortho* protons and two *meta* protons. In the *p*-NO_2 derivative, however, the symmetric AB pattern of the benzene-ring protons in the starting ester changed to a dissymmetric pattern with an extreme high-field shift (at 6.32 ppm) of one proton, distinguished from three benzene-ring protons, in the enolate anion. The partially double bond A in the *p*-NO_2 enolate anion is assumed to be almost fixed on the basis of this observation.[14] Such a greatly enhanced double-bond character of the A bond is also supported by the chemical shift (4.75 ppm) of the residual methine proton in the *p*-NO_2 enolate anion, measured in the olefinic regions.

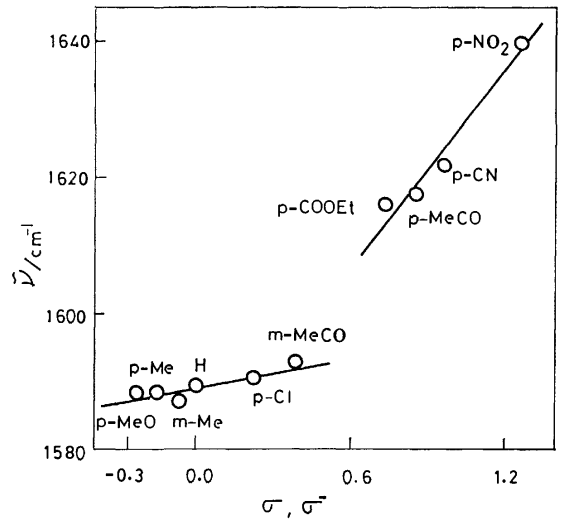

Fig. 3. Hammett plot of the frequencies of carbonyl stretchings in enolate anions of ethyl substituted phenylacetates.

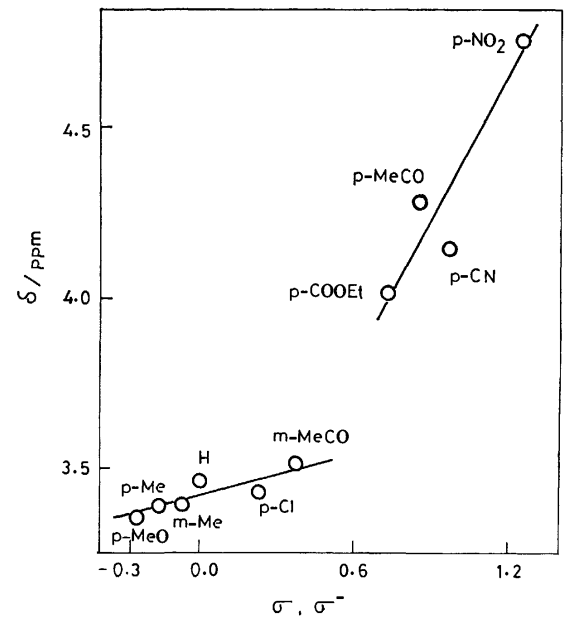

Fig. 4. Hammett plot of the chemical shifts of residual methine proton in enolate anions of ethyl substituted phenylacetates.

Substituent Effects. It has been reported[15] that there is a good linear correlation between the CN stretching-vibration bands of the anions derived from substituted benzyl cyanides and the substituent constants, σ^-. The substituent effects related to anion system are generally correlated by σ^- constants.[16] The CO stretching-vibration bands of the enolate anions derived from ethyl phenylacetates are plotted against σ and σ^- in Fig. 3, which shows two characteristic lines. The plot of the chemical shifts of the residual methine protons *vs.* σ and σ^- is similar to that of the CO wave numbers, as is shown in Fig. 4.

These two lines, which constitute a meta-line of both meta substituents and para electron-releasing substituents for σ and a *para*-line of *para* electron-attracting substituents for σ^-, have extremely different ρ values, suggesting that two different mechanism are required to account for the substituent effects in a sodium-phenylacetate system. The behavior promoted by *para* electron-attracting substituents is consistent with all the observations of the UV-visible, IR, and ^{1}H-NMR spectra of the enolate anions presented above.

Experimental

Materials. Substituted phenylacetic acids and the ethyl esters were prepared according to the following routes:

1. The phenylacetic acids (*p*-CH_3O, *p*-CH_3, and *m*-CH_3) were synthesized by the Willgerodt reaction of the acetophenones[17,18] derived from the corresponding substituted benzoic acids.

2. The ethyl phenylacetates (*p*-CH_3CO and *m*-CH_3CO) were synthesized by the acetylation[19] of ethyl phenylacetate.

3. The phenylacetic acids (*p*-Cl, *p*-NO_2, *p*-CN, and *p*-$COOC_2H_5$) were synthesized by the nitration[20] of phenylacetonitrile, hydrolysis,[21] reduction,[22] and a Sandmyer reaction.[23] Thease synthesized compounds were identified by means of the IR and ^{1}H-NMR spectra and by CHN elementary analysis. The bp's or mp's of the esters are shown in Table 4, together with the literature values.

Preparation of Enolate Anions. Sodium hydride (NaH), the mineral oil having been washed out with dry DMSO, was added to DMSO (2—3 cm^3) in a 50 cm^3 three-necked flask equipped with a gas-inlet tube, a condenser, and a magnetic stirrer. Under an argon atmosphere, ethyl phenylacetates, equivalent to the NaH, in dry DMSO (1 cm^3) were added to the solution, and the resulting mixture was stirred for 30 min at room temperature. According to the above

Table 4. Physical constants of ethyl phenylacetates

Compound	Bp or mp
p-MeO	bp 120 °C/4 mmHg[g] (bp 143—144 °C/11 mmHg)[a,b]
p-Me	bp 88—90 °C/4.5 mmHg (bp 134—135 °C/25 mmHg)[b]
m-Me	bp 90—94 °C/5 mmHg (bp 122—123 °C/18 mmHg)[b]
p-Cl	bp 100—102 °C/2 mmHg (mp 33—33.5 °C)[b,c]
p-COOEt	bp 144—146 °C/3 mmHg (bp 312—313 °C)[d]
p-CN	mp 93 °C (mp 87—88 °C)[c]
p-MeCO	bp 110—117 °C/2 mmHg (mp 67—68 °C)[e]
m-MeCO	bp 156 °C/5 mmHg (bp 118 °C/0.5 mmHg)[e]
p-NO_2	mp 64 °C (mp 63 °C)[f]

a) Ref. 18. b) R.O.C. Norman, G.K. Radda, D.A. Brimacombe, P.D. Ralph, and E.M. Smith, *J. Chem. Soc.*, **1961**, 3247. c) Ref. 22. d) M. Fileti and G. Basso, *Gazz. Chim. Ital.*, **21**, 52 (1891). e) Ref. 19. f) Ref. 21. g) 1 mmHg=133.322 Pa.

procedures, the solution of the enolate anions was about 0.5 mol/dm^3. Spectral-grade DMSO (Dojinyaku Kagaku) was used for the measurements of the visible and IR spectra, and DMSO-d_6 (Merck), for the measurements of the ^{1}H-NMR spectra.

Measurement of Visible Spectra. The prepared enolate solution was diluted to 10^{-4} mol/dm^3, transferred into a crystal cell (d=1 cm), covered with argon, and measured over the range of 300—700 nm, using a Hitachi 557 Double-wavelength Double-beem Spectrophotometer.

Measurement of IR Spectra. The prepared enolate solution was diluted to 0.2 mol/dm^3, transferred into a liquid cell (d=0.2 mm), and measured using a JASCO A-302 Diffraction Grating Infrared Spectrophotometer.

Measurement of ^{1}H-NMR Spectra. The prepared enolate solution (0.5 mol/dm^3) was transferred into a NMR tube (ϕ=5 mm) filled with argon, sealed, and measured using a JEOL MH-100 NMR Spectrometer (100 MHz). The proton signals present in the solvent, 99% DMSO-d_6, were employed as an internal standard for the chemical shifts.

References

1) Previous paper in this series: Part 1, S. Kiyooka and K. Suzuki, *Chem. Lett.*, **1975**, 793.

2) H. O. House, "Modern Synthetic Reactions," 2nd ed, W. A. Benjamin, Menlo Park, Calif. (1972).

3) a) D. J. Cram, "Fundamentals of Carbanion Chemistry," Academic Press, New York (1965); b) E. Buncel, "Carbanions, Mechanistic and Isotopic Aspects," Elsevier Scientific Publishing Comp., Amsterdam (1975).

4) a) L. M. Jackman and B. C. Lange, *Tetrahedron*, **33**, 2737 (1977); b) V. M. Depalma and E. M, Arnett, *J. Am. Chem. Soc.*, **100**, 3514 (1978).

5) H. E. Zaugg, B. W. Horrom, and S. Borgwardt, *J. Am. Chem. Soc.*, **82**, 2895 (1960).

6) "Ion and Ion Pairs in Organic Reactions," ed by M. Szwarc, Wiley, New York (1972), Vol. 1.

7) G. Fraenkel, J. G. Russell, and Y. H. Chen, *J. Am. Chem. Soc.*, **95**, 3208 (1973).

8) R. Waack and M. A. Doran, *J. Am. Chem. Soc.*, **85**, 1651 (1963).

9) H. E. Zaugg and A. D. Schaefer, *J. Am. Chem. Soc.*, **87**. 1857 (1965).

10) E. F. Caldin, M. Kasparian, and G. Tomalin, *Trans. Faraday Soc.*, **64**, 2802 (1968).

11) a) A. A. Petrov, S. M. Esakov, and B. A. Ershov, *J. Org. Chem., USSR* (Eng.), **12**, 774 (1976); b) M. Raban, E. A. Noe, and G. Yamamoto, *J. Am. Chem. Soc.*, **99**, 6527 (1977).

12) L. M. Jackman and R. C. Haddon, *J. Am. Chem. Soc.*, **95**, 3687 (1973).

13) S. Brownstein and D. J. Worsfold, *Can. J. Chem.*, **50**, 1246 (1972).

14) ^{1}H-NMR measurements at various temperatures are still being done. They will clarify the detailed structures of the enolate anions, derived from ethyl phenylacetates.

15) I. N. Juchnovski, I. G. Binev, and T. M. Kolev, *Tetrahedron Lett.*, **1976**, 1519.

16) Y. Yukawa and Y. Tsuno, *Nippon Kagaku Zasshi*, **86**, 873 (1965).

17) a) J. Munch-Peterson, *Org. Synth.*, Coll. Vol. IV, 715 (1963); b) G. A. Reynolds and C. R. Hauser, *ibid.*, Coll. Vol. IV, 708 (1963).

18) J. A. King and F. H. McMillan, *J. Am. Chem. Soc.*, **68**, 2335 (1946).

19) D. Papa, E. Schwenk, and A. Klinsberg, *J. Am. Chem. Soc.*, **68**, 2133 (1946).

20) G. R. Robertson, *Org. Synth.*, Coll. Vol. I, 396 (1932).

21) G. R. Robertson, *Org. Synth.*, Coll. Vol. I, 406 (1932).

22) G. R. Robertson, *Org. Synth.*, Coll. Vol. I, 52 (1932).

23) a) C. S. Marbel and S. M. McElvain, *Org. Synth.*, Coll. Vol. I, 170 (1932); b) H. T. Clarke and R. R. Read, *ibid.*, Coll. Vol. I, 514 (1932).

Heterofulvalenes. II. Synthesis and Reaction of 2,3 : 7,8-Dibenzo-1,4-dithia-6-azafulvalene

Juzo NAKAYAMA,* Mimiko IMURA, and Masamatsu HOSHINO
Department of Chemistry, Faculty of Science, Saitama University, Urawa, Saitama 338
(Received November 7, 1979)

Reaction of 2-isopentyloxy-1,3-benzodithiole with indole in acetic acid gave a 93% yield of 3-(1,3-benzodithiol-2-yl)indole (**4a**) which was converted to 2-(3-indolyl)-1,3-benzodithiolylium tetrafluoroborate (**5a**) in a 77% yield by treatment with trityl tetrafluoroborate. **5a** was also prepared by reaction of indole with 2 molar amounts of 1,3-benzodithiolylium tetrafluoroborate. Treatment of **5a** with triethylamine afforded the title compound **6a** in 93% yield. **6a** was protonated, methylated, and benzoylated at its 6-position by tetrafluoroboric acid, methyl iodide, and benzoyl chloride, respectively. Reaction of **6a** with dimethyl acetylenedicarboxylate gave a 1,6-dipolar intermediate which was trapped as an adduct with ethanol. **6a** was smoothly reduced by sodium borohydride to give its 5,6-dihydro derivative.

In recent years synthetic studies of tetrathia- and tetraselenafulvalenes and their derivatives have been extensively done in order to find excellent organic semiconductors.[1] In this connection, 1,4-dithia-azafulvalenes seem to be compounds of current interest, although only slight attention has been paid to their chemistry.[2] In Part I of this series, we reported the synthesis of 1,4-dithia-5-aza- and 6-azafulvalenes (**1** and **2**), and their spectroscopic properties are suggestive of the considerable contribution of the polarlized structures (**1′** and **2′**) to the ground state of these compounds.[3] We now report the synthetic studies of dibenzo analogs of **1** and **2** and the reaction of the title compound.

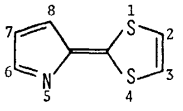

1

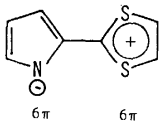

1′

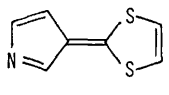

2

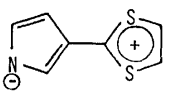

2′

Results and Discussion

Synthesis. 2-Isopentyloxy-1,3-benzodithiole (**3**) which has recently become readily obtainable[4] can react with a wide variety of nucleophiles.[5] Thus, **3** reacted with indole at room temperature to give 3-(1,3-benzodithiol-2-yl)indole (**4a**) in a 93% yield. Similarly, **3** reacted with 2-methyl- and 1-methylindoles giving **4b** (98%) and **4c** (95%), respectively. 3-Methylindole, carrying a methyl at its most reactive position towards electrophiles, reacted at its 2-position to give **4d** in a 96% yield.[6]

In the light of the reaction of 1,3-benzodithiole with trityl tetrafluoroborate (**7**) producing 1,3-benzodithiolylium tetrafluoroborate (**8**) in a good yield,[8] treatment of **4a** with **7** seems to be a promising route to 2-(3-indolyl)-1,3-benzodithiolylium tetrafluoroborate (**5a**). Thus, **4a** smoothly reacted with an equivalent of **7** to give the desired product **5a** in a 77% yield. Similarly,

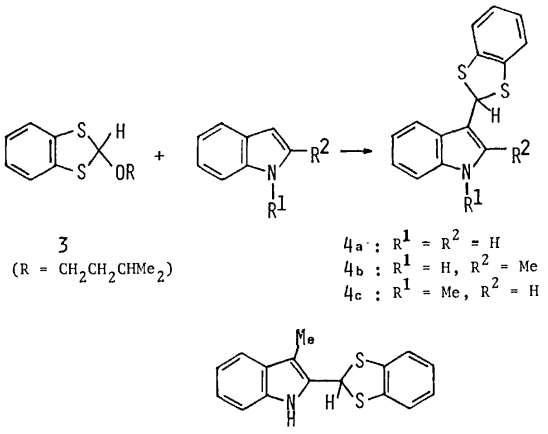

3 (R = $CH_2CH_2CHMe_2$)

4a : $R^1 = R^2 = H$
4b : $R^1 = H$, $R^2 = Me$
4c : $R^1 = Me$, $R^2 = H$

4d

treatment of **4b** and **4c** with **7** gave **5b** (75%) and **5c** (71%), respectively. However, the reaction of **4d** with **7** failed to furnish **5d** (a 68% yield of **4d** was recovered

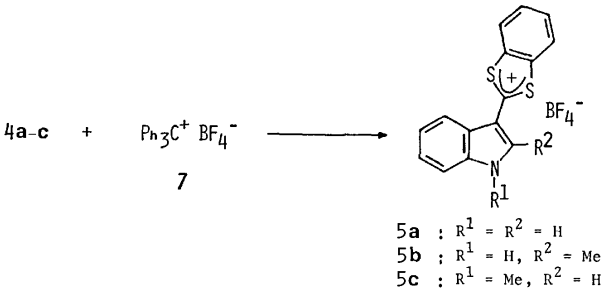

5a : $R^1 = R^2 = H$
5b : $R^1 = H$, $R^2 = Me$
5c : $R^1 = Me$, $R^2 = H$

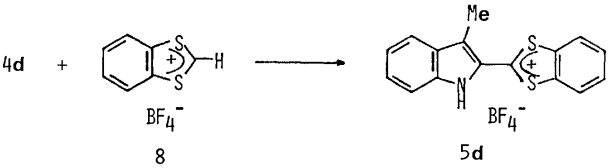

8

5d

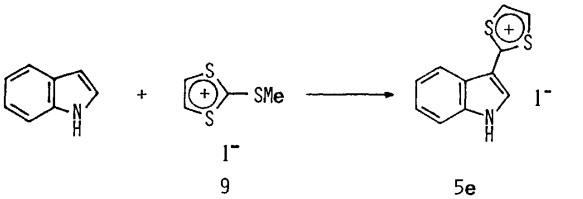

9

5e

and the yield of triphenylmethane resulting from hydride abstraction by trityl cation was only 15%).

Recent studies have shown that **8** can abstract a hydride from 2-substituted 1,3-benzodithioles yielding 2-substituted 1,3-benzodithiolylium tetrafluoroborates.[3,9] In fact, treating **4d** with an equivalent of **8** afforded **5d** in a 63% yield. This result, together with the fact that the formation of **4** from **3** and indoles involves 1,3-benzodithiolylium ion as intermediate,[7] is indicative that treatment of indoles with 2 molar amounts of **8** would produce **5** in a single step; one mole of **8** reacts with indoles to give **4** and another mole of **8** abstracts a hydride from **4** to yield **5**. Expectedly, the reaction of 3-methylindole with 2 molar amounts of **8** furnished **5d** in a 54% yield. In a similar way, **5a** (60%) and **5b** (51%) were also obtained.

We also prepared 2-(3-indolyl)-1,3-dithiolylium iodide (**5e**); heating indole with the salt **9** at 50 °C in acetonitrile gave **5e** in a 58% yield. However, **9** failed to react with 3-methylindole.

The final step is the deprotonation of **5**. In the case of **5a** and **5b**, this was easily achieved by treating them with triethylamine in acetonitrile at 0 °C; the title compound **6a** and its methyl derivative **6b** were obtained in 93 and 92% yields, respectively. However, treatment of an acetonitrile solution of **5d** with triethylamine resulted in the black reaction mixture, from which an unstable compound, which was converted to the starting material **5d** on treatment with tetrafluoroboric acid, was isolated in a good yield. We could not detect the presence of the desired product **6d**. Attempted trapping of **6d** by dimethyl acetylenedicarboxylate was also unsuccessful. Treatment of **5e** with 1,8-diazabicyclo-[5.4.0]undec-7-ene (DBU) as base yielded **6e** quantitatively.

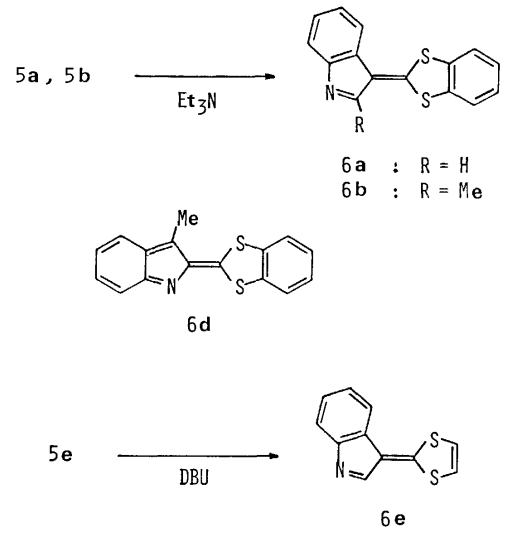

Reaction. Broadly speaking, the spectroscopic features of compounds **5** and **6** are similar to those observed with **1**, **2**, and their protonated species[3] (see Experimental section).

Treatment of **6a** with tetrafluoroboric acid gave **5a** quantitatively. Heating **6a** with methyl iodide and then treating the resulting product with tetrafluoroboric acid gave **5c** in a 91% overall yield. When **6a** was allowed to react with benzoyl chloride in acetonitrile and then the mixture was treated with tetrafluoroboric acid, a 70% yield of 2-(1-benzoyl-3-indolyl)-1,3-benzodithiolylium tetrafluoroborate (**5f**) was obtained.

Heating **6a** with dimethyl acetylenedicarboxylate in boiling chloroform containing ethanol produced compound **10** in a 60% yield. The IR spectrum of **10** has absorptions at 1735 and 1705 cm^{-1} due to the ester carbonyl groups. The NMR spectrum determined in $CDCl_3$ showed two singlets of methyls at 3.80 and 3.96 ppm, a triplet of methyl at 1.26 ppm, and a quartet of methylene at 3.67 ppm. The *trans* geometry of the methoxycarbonyl groups was elucidated from the chemical shift value of the olefinic proton which appeared at 6.27 ppm. It is documented that the olefinic proton of the *trans* form of this type of compounds appears at 5.99—6.27 ppm, whereas that of the *cis* form resonates at 6.63—6.94 ppm.[10] The formation of **10** can best be rationalized by capture of the 1,6-dipolar intermediate **11** by ethanol.

In all the examples described above, **6a** easily reacted at its 6-position with electrophiles. This can be understood as a result of the contribution of polarlized structure corresponding to **2'** to the ground state of **6a**.

Reaction of **6a** with nucleophiles was next examined. **6a** resisted reaction with phenylmagnesium bromide, but it smoothly reacted with sodium borohydride at

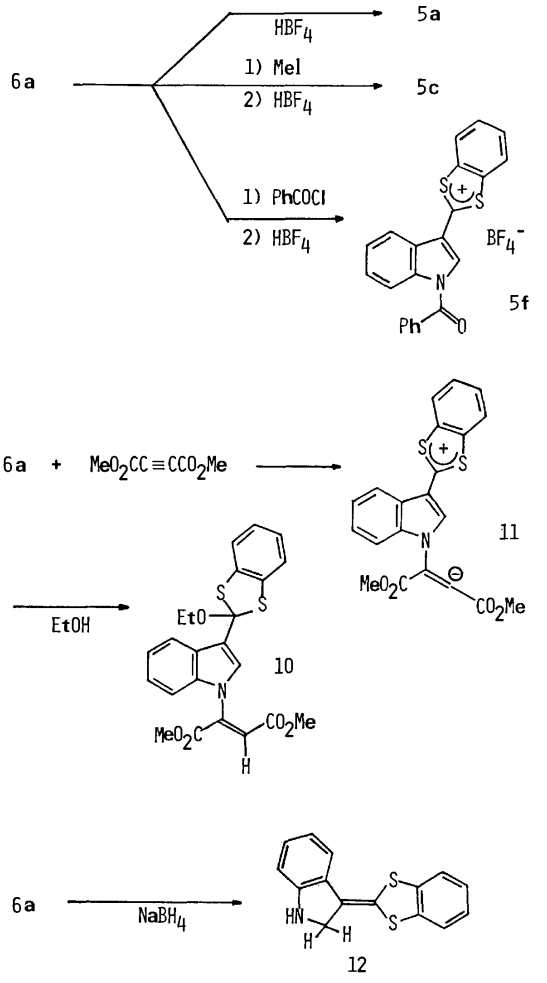

room temperature in a mixture of tetrahydrofuran and water. Workup of the mixture gave **12**, the dihydro derivative of **6a**, in an 89% yield as unstable compound in solution. Structure of **12** was determined by spectroscopic and elemental analyses. The result indicates that hydride ion as nucleophile attacks on the 5-position of **6a** rather than the dithiole ring carbon. This is not in harmony with the expected reactivity of **6a** from the contribution of the canonical structure like **2'** and further investigation, emphasis placed on this point, will be needed.

Experimental

2-Isopentoxy-1,3-benzodithiole (**3**),[4] trityl[11] and 1,3-benzodithiolylium[8] tetrafluoroborates (**7** and **8**), and 2-methylthio-1,3-dithiolylium iodide (**9**)[12] were prepared by reported methods. Acetonitrile was refluxed over and distilled from calcium hydride.

Preparation of 4. 3-(1,3-Benzodithiol-2-yl)indole (**4a**). A solution of 1.17 g (10 mmol) of indole and 2.64 g (11 mmol) of **3** in 30 ml of acetic acid was allowed to stand at room temperature for 4 h. The solution was diluted with 100 ml of water, and the resulting precipitate was triturated, collected, washed with water, and dried to give 2.50 g (93%) of **4a**, which melted at 96—98 °C after recrystallization from cyclohexane. NMR ($CDCl_3$) δ 6.60 (1H, s, methine), 6.9—7.4 (8H, m), and 7.7—7.9 (2H, m). Found: C, 66.95; H, 4.19; N, 5.18; S, 23.78%. Calcd for $C_{15}H_{11}NS_2$: C, 66.91; H, 4.12; N, 5.20; S, 23.77%.

In a similar way as described with **4a**, compounds **4b—d** were prepared in 98, 95, and 96% yields, respectively.

3-(1,3-Benzodithiol-2-yl)-2-methylindole (**4b**), mp 120—121 °C (from ethanol). NMR ($CDCl_3$) δ 2.30 (3H, s, Me), 6.90 (1H, s, methine), 6.95—7.30 (7H, m), 7.65 (1H, broad s, NH), and 7.95 (1H, m). Found: C, 67.30; H, 4.65; N, 4.95; S, 22.70%. Calcd for $C_{16}H_{13}NS_2$: C, 67.84; H, 4.63; N, 4.95; S, 22.59%.

3-(1,3-Benzodithiol-2-yl)-1-methylindole (**4c**), mp 139—140 °C. NMR ($CDCl_3$) δ 3.60 (3H, s, Me), 6.58 (1H, s, methine), 6.8—7.3 (8H, m), and 7.7 (1H, m). Found: C, 67.70; H, 4.66; N, 5.01; S, 22.57%. Calcd for $C_{16}H_{13}NS_2$: C, 67.84; H, 4.63; N, 4.95; S, 22.59%.

2-(1,3-Benzodithiol-2-yl)-3-methylindole (**4d**), mp 127—128 °C (from cyclohexane). NMR ($CDCl_3$) δ 2.26 (3H, s, Me), 6.64 (1H, s, methine), 7.0—7.3 (7H, m), 7.45—7.55 (1H, m), and 8.3 (1H, broad s, NH). Found: C, 67.96; H, 4.68; N, 4.89; S, 22.45%. Calcd for $C_{16}H_{13}NS_2$: C, 67.84; H, 4.63; N, 4.95; S, 22.59%.

2-(3-Indolyl)-1,3-benzodithiolylium Tetrafluoroborate (5a).
a) From 4a and 7: A solution of 2.59 g (7.85 mmol) of **7** in 15 ml of anhydrous acetonitrile was added dropwise over a period of 15 min to a stirred and ice-cooled solution of 2.11 g (7.85 mmol) of **4a** in 15 ml of anhydrous acetonitrile. The mixture was warmed to room temperature and stirred for 1 h. The resulting crystalline precipitate was collected and washed with a small amount of acetonitrile to give 2.17 g (77%) of **5a**, which melted at 246—247 °C (dec) (orange needles) after recrystallization from acetonitrile. IR (Nujol) 3300 (NH) and 1000—1120 cm^{-1} (BF_4^-); NMR (CF_3CO_2D, 65 °C), δ 7.5—7.7 (3H, m), 7.7—8.2 (4H, AA'XX'm), 8.02 (1H, m), and 8.70 (1H, s, -NH-CH=); UV (CH_3CN) (log ε) 453 nm (4.69). Found: C, 50.57; H, 2.85; N, 3.85%. Calcd for $C_{15}H_{10}NS_2BF_4$: C, 50.72; H, 2.84; N, 3.94%.

b) From Indole and 2 Molar Amounts of 8: A soliuton of 2.40 g (10 mmol) of **8** in 15 ml of anhydrous acetonitrile was added dropwise during 10 min to a stirred and ice-cooled solution of 0.59 g (5 mmol) of indole in 5 ml of anhydrous acetonitrile. After stirring for 4 h at room temperature, the resulting crystalline precipitate was collected and washed with a small amount of acetonitrile to give 0.85 g of **5a** as orange crystals. The filtrate was diluted with 10 ml of ether and the resulting precipitate was collected to give another crop of **5a** (0.23 g); total yield (60%). **5a**, thus obtained, agreed in all respects with a specimen obtained from **4a** and **7**.

2-(2-Methyl-3-indolyl)-1,3-benzodithiolylium Tetrafluoroborate (5b). Under the same conditions as described with **5a**, 1.42 g (5 mmol) of **4b** and 1.65 g (5 mmol) of **7** gave 1.38 g (75%) of **5b**, mp 284—286 °C (dec), yellow needles (from acetonitrile). IR (Nujol) 3270 (NH) and 1000—1120 cm^{-1} (BF_4^-); NMR (CF_3CO_2D) δ 2.93 (3H, s, Me), 7.4—7.6 (3H, m), 7.7—8.2 (4H, AA'XX'm), and *ca.* 8.0 (1H, m); UV (CH_3CN) (log ε) 441 nm (4.57). Found: C, 52.04; H, 3.33; N, 3.63%. Calcd for $C_{16}H_{12}NS_2BF_4$: C, 52.05; H, 3.28; N, 3.79%.

5b was also obtained from 2-methylindole and 2 molar amounts of **8** in a 51% yield.

2-(1-Methyl-3-indolyl)-1,3-benzodithiolylium Tetrafluoroborate (5c). Under the same conditions as described with **5a**, 1.42 g (5 mmol) of **4c** and 1.65 g (5 mmol) of **7** gave 1.32 g (71%) of **5c**, mp 276—278 °C, orange needles (from acetonitrile). NMR (CF_3CO_2D) δ 4.02 (3H, s, Me), 7.5—8.2 (8H, m), and 8.62 (1H, s, -NMe-CH=). Found: C, 52.17; H, 3.25; N, 3.63%. Calcd for $C_{16}H_{12}NS_2BF_4$: C, 52.05; H, 3.28; N, 3.79%.

2-(3-Methyl-2-indolyl)-1,3-benzodithiolylium Tetrafluoroborate (5d). *a) From 4d and an Equivalent of 8*: A solution of 576 mg (2.4 mmol) of **8** in 4 ml of anhydrous acetonitrile was added dropwise over a period of 10 min to a stirred and ice-cooled solution of 680 mg (2.4 mmol) of **4d** in 10 ml of acetonitrile. The mixture was stirred for 3 h while warmed to room temperature. The resulting precipitate was collected to give 557 mg (63%) of **5d**, mp 236—237 °C (dec), violet needles (from acetonitrile). NMR (CF_3CO_2D) δ 2.74 (3H, s, Me), 7.13 (1H, m), 7.45 (2H, m), 7.69 (1H, d), and 7.76—8.30 (4H, m, AA'XX'm); UV (CH_3CN) (log ε) 467 nm (4.70). Found: C, 52.21; H, 3.40; N, 3.52; S, 17.33%. Calcd for $C_{16}H_{12}NS_2BF_4$: C, 52.05; H, 3.28; N, 3.79; S, 17.37%.

b) From 3-Methylindole and 2 Molar Amounts of 8: Under the same conditions as described with **5a**, 1.31 g (10 mmol) of 3-methylindole and 5.28 g (22 mmol) of **8** gave 1.98 g (54%) of **5d**, mp 231—233 °C (dec).

c) Attempted Synthesis from 4d and 7: A solution of 0.83 g (2.5 mmol) of **7** in 10 ml of anhydrous acetonitrile was added dropwise over a period of 10 min to a stirred and ice-cooled solution of 0.71 g (2.5 mmol) of **4d** in 20 ml of anhydrous acetonitrile. After stirring for 2 h, the mixture turned dark red without precipitation of product. Dilution of the mixture with 30 ml of anhydrous ether also caused no precipitation. Therefore, the mixture was poured into 100 ml of ice water and extracted with three 100 ml portions of ether. The extract was washed with water, dried, and evaporated. The residure was chromatographed on a column of silica gel, which afforded 0.10 g (15%) of triphenylmethane, mp 93—94 °C, 0.47 g (68%) of **4d**, and 0.36 g (53%) of triphenylmethanol, mp 161—162 °C.

2-(3-Indolyl)-1,3-dithiolylium Iodide (5e). A mixture of 117 mg (1 mmol) of indole and 276 mg (1 mmol) of **9** in 15 ml of anhydrous acetonitrile was heated at 50 °C for 8 h. The resulting crystalline precipitate was collected to give 200 mg

(58%) of **5e**, mp 280 °C, reddish brown needles (from DMF–nitromethane). UV (CH_3CN) (log ε) 438 nm (3.53); NMR (DMSO-d_6) δ 7.3—8.2 (4H, m), 8.50 (2H, s, dithiole ring), and 9.07 (1H, s, –NH–CH=). Found: C, 38.30; H, 2.29; N, 4.01; S, 18.75%. Calcd for $C_{11}H_8INS_2$: C, 38.27; H, 2.34; N, 4.06; S, 18.57%.

2,3 : 7,8-Dibenzo-1,4-dithia-6-azafulvalene (6a). To a stirred and ice-cooled solution of 0.71 g (2 mmol) of **5a** in 20 ml of anhydrous acetonitrile was added dropwise 0.5 ml of triethylamine. The reaction occurred immediately with precipitation of yellow crystals. After stirring for 1 h at room temperature, the precipitate was collected and washed with acetonitrile to give 0.50 g (93%) of **6a**, which melted at 212—213 °C (yellow needles) after recrystallization from benzene. IR (Nujol) 1600, 1578, 1566, 1538, 1460, 1438, 1290, 1220, 1195, 875, 765, and 740 cm^{-1}; UV (C_6H_6) (log ε) 417 nm (4.55); MS *m/e* 267 (M^+); NMR ($CDCl_3$) δ 7.2—7.4 (4H, m), 7.4—7.7 (4H, m), and 8.20 (1H, s, –N–CH=). Found: C, 67.76; H, 3.61; N, 5.24; S, 23.83%. Calcd for $C_{15}H_9NS_2$: C, 67.41; H, 3.39; N, 5.24; S, 23.95%.

5-Methyl-2,3: 7,8-dibenzo-1,4-dithia-6-azafulvalene (6b). Treatment of 0.74 g (2 mmol) of **5b** with 0.5 ml of triethylamine at 0 °C gave 0.52 g (92%) of **6b**, mp 183—184 °C (dec), yellow needles (from benzene). UV (C_6H_6) (log ε) 400 nm (4.40); MS *m/e* 281 (M^+); MNR ($CDCl_3$) δ 2.58 (3H, s, Me), 7.15—7.36 (4H, m), and 7.40—7.70 (4H, m). Found: C, 68.72; H, 4.02; N, 4.83; S, 22.67%. Calcd for $C_{16}H_{11}NS_2$: C, 68.32; H, 3.94; N, 4.98; S, 22.75%.

7,8-Benzo-1,4-dithia-6-azafulvalene (6e). To a stirred solution of 200 mg (0.58 mmol) of **5e** in 20 ml of anhydrous acetonitrile was added 0.1 ml of DBU. The mixture was stirred for 0.5 h and diluted with 100 ml of ice water. The resulting precipitate was collected, washed with water, and dried to give 108 mg (100%) of **6e** as golden yellow crystals, mp 134—135 °C. MS *m/e* (%) 217 (M^+, 100), 159 (8), 149 (32), 78 (22), and 76 (33); NMR ($CDCl_3$) 6.85 (2H, s, dithiole ring), 7.15—7.80 (4H, m, benzene ring), and 8.17 (1H, d, –N–C=H–). Found: C, 60.95; H, 3.31; N, 6.22%. Calcd for $C_{11}H_7NS_2$: C, 60.79; H, 3.25; N, 6.45%.

Attempted Synthesis of 6d. To a stirred and ice-cooled suspension of 369 mg (1 mmol) of **5d** in 13 ml of anhydrous acetonitrile was added 0.3 ml of triethylamine. The yellow suspension turned dark red immediately. The mixture was stirred for 1.5 h at room temperature and a small amount of tarry insoluble material was filtered off. The dark filtrate was diluted with water and the resulting precipitate was collected and washed with methanol to give 200 mg of a pink solid, mp 154—156 °C; IR (Nujol) 3380 (NH) and 1115 cm^{-1} (aliphatic ether). Attempted purification of this compound by recrystallization or reprecipitation suffered extensive decomposition. The addition of 1 ml of 42% tetrafluoroboric acid to a solution of 209 mg of this compound in 10 ml of acetic anhydride resulted in the formation of 154 mg of **5d**.

To a stirred and ice-cooled solution of 156 mg (1.1 mmol) of dimethyl acetylenedicarboxylate and 0.2 ml of triethylamine in 20 ml of anhydrous acetonitrile was added 369 mg (1 mmol) of **5d** in small portions. The mixture was warmed to room temperature and heated at 50 °C for 5 h. Workup of the mixture gave only intractable tars.

Treatment of 6a with Tetrafluoroboric Acid. A mixture of 67 mg (0.25 mmol) of **6a** in 2 ml of 42% tetrafluoroboric acid was stirred for 0.5 h and the resulting precipitate was collected and washed with anhydrous ether to give 87 mg (98%) of **5a**.

Treatment of 6a with Methyl Iodide. To a stirred suspension of 195 mg (0.73 mmol) of **6a** in 10 ml of acetonitrile was added 0.5 ml of methyl iodide and the mixture was heated under reflux for 1 h. The resulting precipitate was collected to give 278 mg (93%) of 2-(1-methyl-3-indolyl)-1,3-benzodithiolylium iodide as red crystals, whose IR spectrum is essentially the same as that of **6a**. This compound (123 mg) was stirred in a mixture of 1 ml of 42% tetrafluoroboric acid and 5 ml of acetic anhydride for 20 min to give 109 mg of **5c**, mp 275—277 °C, whose IR spectrum agreed in all respects with that of a specimen obtained from **4c** and **7**.

Tretment of 6a with Benzoyl Chloride. A mixture of 134 mg (0.5 mmol) of **6a** and 141 mg (1 mmol) of benzoyl chloride in 10 ml of acetonitrile was stirred at room temperature for 0.5 h. The mixture was cooled to 0 °C and a mixture of 1 ml of 42% tetrafluoroboric acid and 10 ml of acetic anhydride was added. After stirring for 1 h at room temperature, the resulting precipitate was collected and washed with ether to give 161 mg (70%) of 2-(1-benzoyl-3-indolyl)-1,3-benzodithiolylium tetrafluoroborate (**5f**), mp 240 °C, yellowish orange needles (from acetonitrile). IR (Nujol) 1700 (C=O) and 1000—1120 cm^{-1} (BF_4^-). Found: C, 57.32; H, 3.00; N, 2.83; S, 14.07%. Calcd for $C_{22}H_{14}NOS_2BF_4$: C, 57.53; H, 3.07; N, 3.05; S, 13.96%.

Reaction of 6a with Dimethyl Acetylenedicarboxylate. To a stirred solution of 267 mg (1 mmol) of **6a** in 15 ml of chloroform containing 0.5—0.9% of ethanol as a stabilizer was added a solution of 312 mg (2.2 mmol) of dimethyl acetylenedicarboxylate in 5 ml of chloroform. The mixture was stirred for 0.5 h at room temperature and then refluxed for 2 h. Analysis by TLC showed the formation of a single product. Evaporation of the solvent left a yellow solid, which was washed with ether to give 216 mg (60%) of **10**, mp 171.5—172 °C (from CCl_4), colorless needles. IR (Nujol) 1735 and 1705 cm^{-1} (C=O); NMR ($CDCl_3$) δ 1.26 (3H, t, J=7 Hz, Me), 3.67 (2H, q, J=7 Hz, CH_2), 3.80 (3H, s, Me), 3.96 (3H, s, Me), 6.27 (1H, s, olefinic), 7.1—7.6 (8H, m), and 7.9 (1H, m). Found: C, 60.42; H, 4.51; N, 3.13; S, 13.86%. Calcd for $C_{23}H_{21}NO_5S_2$: C, 60.66; H, 4.65; N, 3.08; S, 14.05%.

Reduction of 6a with Sodium Borohydride. To a stirred mixture of 80 mg (2.1 mmol) of sodium borohydride in 20: 1 tetrahydrofuran/water (21 ml) was added 267 mg (1 mmol) of **6a** in small portions. The mixture was stirred for 0.5 h and a trace amount of insoluble material was filtered off. The filtrate was diluted with 20 ml of water and the resulting precipitate was collected and dried to give 240 mg (89%) of **12** as faint yellow crystals, mp 128—129 °C. This compound is unstable in solution; when it was dissolved in chloroform, yellow polymeric material, scarcely soluble in organic solvents, deposited a few minutes later. This made it impossible to obtain a good NMR spectrum; δ ($CDCl_3$) 4.10 (2H, s, CH_2) and 6.5—7.4 (8 or 9H, m). IR (KBr) 3380 (NH), 3050, 2870, and 2840 (CH_2), 1605, 1585, 1475, 1445, 1320, 1280, 1250, and 740 cm^{-1}. Found: C, 66.64; H, 4.17; N, 5.44; S, 23.71%. Calcd for $C_{15}H_{11}NS_2$: C, 66.91; H, 4.12; N, 5.20; S, 23.77%.

References

1) M. Narita and C. U. Pittman, Jr., *Synthesis*, **1976**, 489.
2) R. Gompper and R. Weiss, *Angew. Chem., Int. Ed. Engl.*, **7**, 296 (1968); R. Weiss and R. Gompper, *Tetrahedron Lett.*, **1970**, 481.
3) J. Nakayama, Y. Watabe, and M. Hoshino, *Bull. Chem. Soc. Jpn.*, **51**, 1427 (1978).
4) J. Nakayama, *Synthesis*, **1975**, 38.
5) J. Nakayama and M. Hoshino, *Yuki Gosei Kagaku Kyokai Shi*, **37**, 655 (1979) and references cited therein.
6) The synthesis of these compounds was preliminary reported.[7]

7) J. Nakayama, M. Imura, and M. Hoshino, *Chem. Lett.*, **1975**, 1319.
8) J. Nakayama, K. Fujiwara, and M. Hoshino, *Bull. Chem. Soc. Jpn.*, **49**, 3567 (1976).
9) J. Nakayama, K. Yamashita, M. Hoshino, and T. Takemasa, *Chem. Lett.*, **1977**, 789.
10) N. F. Chamberlain, "The Practice of NMR Spectroscopy," Plenum Press, New York and London (1974), p. 155.
11) H. J. Dauben, Jr., L. R. Honnen, and K. M. Harmon, *J. Org. Chem.*, **25**, 1442 (1960).
12) E. Klingsberg, *J. Am. Chem. Soc.*, **86**, 5290 (1964).

Studies on 1-(Thiosulfinylaminothio)piperidines

Syoji MORIMURA, Hideo HORIUCHI, Chihiro TAMURA, and Takao YOSHIOKA
Central Research Laboratories Sankyo Co., Ltd., Hiromachi Shinagawa-ku, Tokyo 140

(Received November 7, 1979)

Hindered piperidine derivatives with a new functional group(–S–N=S=S), 2,2,6,6-tetramethyl-1-(thiosulfinylaminothio)piperidines (**4**) were obtained from the corresponding piperidines **1**, sulfur monochloride and ammonia. These compounds were also prepared from bis(2,2,6,6-tetramethylpiperidino) disulfides or bis(2,2,6,6-tetramethylpiperidino) trisulfides under similar reaction conditions. In much lower yields, unhindered 1-(thiosulfinylaminothio)piperidines (**8**) were also obtained. The photochemical and thermal stabilities of **4** and **8** were nearly the same. Reaction pathways were disucssed.

Recently the reaction of hindered amines such as 2,2,6,6-tetramethylpiperidine (**1b**) with sulfur chlorides has been studied by Bennett *et al.*[1] who found that sulfur dichloride (SCl_2) curiously gave bis(2,2,6,6-tetramethylpiperidino) disulfide (**2b**) in the presence of triethylamine and *N*,*N*-dimethylformamide (DMF) (Eq. 1), and that sulfur monochloride (S_2Cl_2) gave bis(2,2,6,6-tetramethylpiperidino) trisulfide (**3b**) in

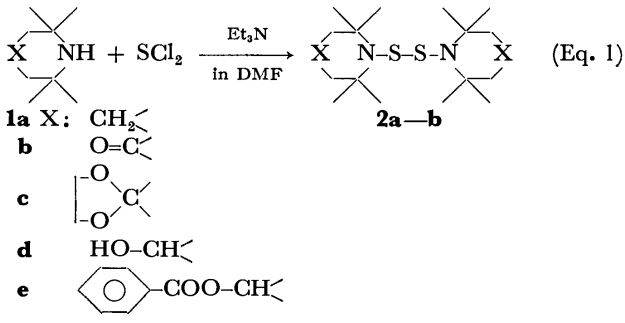

1a X: CH_2
b O=C
c cyclic O–C–O
d HO–CH
e C6H5–COO–CH

(Eq. 1)

2a—b

1 + S_2Cl_2 → **3a—b** (Eq. 2)

hexane or ether (Eq. 2). The disulfides **2** have been shown by us to be effective stabilizing reagents for polyurethane.[2] While trying to find an improved means of synthesizing **2**, it was found that in the presence of

1 + S_2Cl_2 ⟶ **2** (Eq. 3)

DMF and an excess amount of **1**, S_2Cl_2 normally gives the disulfides **2** in excellent yields (Eq. 3).[2] During this research, we further found that piperidine derivatives with a new functional group (–S–N=S=S), 2,2,6,6-tetramethyl-1-(thiosulfinylaminothio)piperidines (**4**) are obtained when equimolar amounts of **1** and S_2Cl_2 are allowed to react and the resulting mixture is quenched with aqueous ammonia. In this paper, we wish to report the preparation and properties of **4** as well as possible reaction pathways for formation of **4**.

Results and Discussion

Compounds **4** was prepared not only from **1** but also from the disulfide **2** or the trisulfide **3**, under similar reaction conditions.

*Preparation of 2,2,6,6-Tetramethyl-1-(thiosulfinylaminothio)piperidines (**4a—d**) from 2,2,6,6-Tetramethylpiperidines (**1a—d**).* The reaction mixture of **1** with S_2Cl_2 was pale yellow. When the mixture was treated with 10% aqueous ammonia, the color turned to deep red immediately. The red mixture contained the trisulfide **3** (major product) accompanied by a small amount of the disulfide **2** (Eq. 4). However pure **2** and **3** are colorless.

1 $\xrightarrow[\text{ii) aq } NH_3]{\text{i) } S_2Cl_2}$ red subst. **4** + **3**(maj.) + **2**(min.) (Eq. 4)

A comparative experiment showed that similar treatment of the reaction mixture (from **1b**) with a 10% aqueous solution of potassium hydrogencarbonate instead of aqueous ammonia gave a colorless mixture containing **3b** (major product) and **2b** (minor product) (Eq. 5). Thus it became apparent that ammonia is

Table 1. Properties of compounds **4a—d**

No.	X, Y (N–S–N=S=S)	Mp/°C	Vis. spectrum λ_{max}/nm(log ε)	R_f-SiO_2 (Solvent)
4a	H, H	(red oil)	413 in E	0.75 (B/H:1)
4b	O=C	116.5—118 (red prisms)	409(4.11) in H 411(4.11) in E	0.13(B)
4c	cyclic O–C–O	98—99 (red prisms)	412(4.14) in H 414(4.14) in E	0.50(B)
4d	H, C_6H_5COO	99—100 (red prisms)	411(4.15) in H 413(4.15) in E	0.62(B)

H: hexane, E: EtOH, B: benzene.

$$\mathbf{1b} \xrightarrow[\text{ii) ap } KHCO_3]{\text{i) } S_2Cl_2} \mathbf{3b}(\text{maj.}) + \mathbf{2b}(\text{min.}) \qquad \text{(Eq. 5)}$$

the cause of the coloration. In order to clarify the cause of the coloration, the red substances were isolated and their structures were determined. Chromatographic separation of the mixture gave small amounts (Y=6—14 %) of red oils or prisms (**4a**—**d**) whose physical properties are given in Table 1. Typical structure determination was carried out as follows. **4c** has the formula, $C_{11}H_{20}N_2O_2S_3$, based on the satisfactory elemental analysis and molecular weight determination (308), as shown both by VPO method and mass spectrum. Since the NMR spectrum showed three singlets at δ 1.45 (12H), 1.92 (4H), and 3.97 (4H), the "$C_{11}H_{20}NO_2$" part of **4c** ("$C_{11}H_{20}NO_2$"+"NS_3") was characterized as both the piperidine part with four methyl groups and the ethylene acetal part ($CDCl_3$). However, the "NS_3" part of **4c** ($C_{11}H_{20}NO_2$+"NS_3") could not be characterized by spectroscopic analysis. Thus the whole structure determination was carried out by X-ray crystallographic analysis.[3a] Phases were assignable by the symbolic addition procedure, and structure factors were refined by the block-diagonal least-squares technique to a final R-factor of 6.7%. Consequently, **4c** was determined as 7,7,9,9-tetramethyl-1-(thiosulfinylaminothio)-1,4-dioxa-8-azaspiro[4.5]-decane (**4c**), containing the new thiosulfinylaminothio group, –S–N=S=S (Fig. 1). Structures **4a**, **4b**, and **4d** were analogously assigned on the basis of visible, mass, NMR spectra and/or elemental analyses. The new compounds **4a**—**d** indicated fungicidal activity,[3b] besides offering UV protecting in polyolefins, like polypropylene.

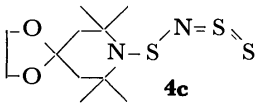

4c

Fig. 1.

Preparation of 4 from Bis(2,2,6,6-tetramethylpiperidino) disulfide (2) or Bis(2,2,6,6-tetramethylpiperidino) trisulfide (3). First, we wanted to see whether 1-(thiosulfinylaminothio)piperidine (**4**) was the secondary product given by an interaction of ammonia with the disulfide **2** and/or trisulfide **3**. This is because, as shown in Eqs. 4 and 5, treatment of the reaction mixture with 10% aqueous ammonia gave **4**, **3**, and **2**; whereas treatment of the same mixture with 10% aqueous $KHCO_3$ gave **3** and **2** without **4**.

The desired examination was carried out as follows. Treatment of pure, freshly prepared **2a** or **3a** with 10% aqueous ammonia caused no reaction under reaction conditions similar to those used in Eq. 4. However, in the presence of equimolar amounts of S_2Cl_2 relative to **2a** or **3a**, similar treatment with ammonia gave the expected **4a** (Eq. 6) in a yield of 35.2 or 32.7%, respectively, higher than that of 8.6% from **1a**. The yields were based on the assumption that 1 mol of the starting **1**, **2**, or **3** gives 1 mol of **4**. Thus **2** and/or **3** may be the precursor of **4**. The relatively low yield of **4** from **1** is reasonably explained by assuming that **1** consumes sulfur monochloride to give **2** and/or **3**.

$$\mathbf{2a} \xrightarrow[\text{ii) aq } NH_3]{\text{i) } S_2Cl_2} \mathbf{4a} \qquad \mathbf{3a} \xrightarrow[\text{ii) aq } NH_3]{\text{i) } S_2Cl_2} \mathbf{4a} \qquad \text{(Eq. 6)}$$

Although the reaction of secondary amines with sulfur monochloride has been shown in many papers to give bis(disubstituted amino) polysulfides,[4] no compounds having the –S–N=S=S group have yet been reported. For primary amines, on the contrary, the analogous function, the thiosulfinylamino group (–N=S=S) was recently reported by Barton *et al.*[5] and Inagaki *et al.*[6] Aromatic primany amines having an electron-donating group at the *p*-position, or bulky groups at the 2 and 6-positions, *e.g.* *p*-dimethylaminoaniline or 2,4-di-*t*-butyl-6-methylaniline, react with sulfur monochloride to give the corresponding *N*-thiosulfinylaniline **5** or **6**, as shown in Fig. 2, which was relatively stable. Interestingly, substituted aniline with less bulky groups at the 2 and 6 positions, such as 2,4,6-trimethylaniline, gives the corresponding *N*-thiosulfinylaniline in a low yield. They explained the stability of *N*-thiosulfinylaniline in term of the steric effect.[6]

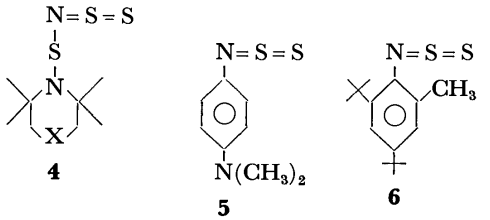

4 **5** **6**

Fig. 2.

Formation of Non-Hindered 1-(Thiosulfinylaminothio)-piperidines (8). In order to investigate whether the contribution of the steric effect by the tetramethyl group is necessary for the formation of 1-(thiosulfinylaminothio)piperidines (**8**), piperidines unsubstituted at the 2 and 6-positions (**7a** and **7b**) were examined. **7a** and **7b** similarly gave the corresponding 1-thiosulfinylaminothio derivatives **8a** and **8b** (Eq. 7), respectively, in much

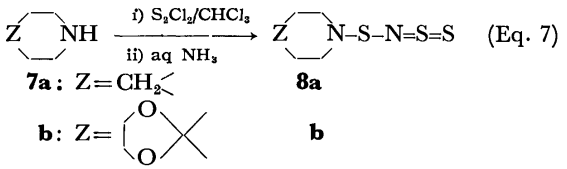

7a: Z=CH_2 **8a**

b: Z= **b**

(Eq. 7)

lower yield (*ca.* 0.4%),[7] under the same reaction conditions as described in Eq. 4. The isolated **8a** was characterized by its high resolution mass spectrum exhibiting an M^+ peak at *m/e* 193.9986, which consisted with the calculated value for $C_5H_{10}N_2S_3$ (194.0006), and by its visible spectrum (410 nm in ethanol). Additionally, the compound **8a** was also prepared in 2.8% yield[7] from the corresponding disulfide **9** (Eq. 8)

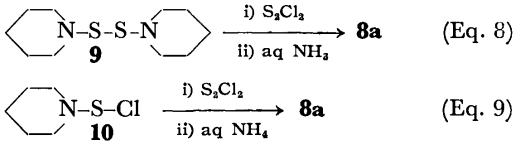

9 **10**

(Eq. 8) (Eq. 9)

in a manner similar to that shown in Eq. 6.

As will be discussed later, 1-sulfenylpiperidine chloride (**10**)[8] may be one of the precursors of **8a** (Eq. 9). In order to examine this assumption, freshly prepared **10** was treated by a method similar to that described in Eq. 6. Expectedly **10** also gave **8a** (Eq. 9) in 1.2% yield.[7]

Thus it was found that **8a** was obtained from **7a**, **9**, or **10**. However the yield of **8a** is much lower than that of **4a**. The difference may depend upon that of the stability of **4a** and **8a**. In order to check this explanation, we tried following experiments.

The Photo- and Thermal Behavior of Hindered (4) and Nonhindered (8) 1-(Thiosulfinylaminothio)piperidines. The photochemical behavior of sterically hindered 1-(thiosulfinylaminothio)piperidines (**4**) and unhindered 1-(thiosulfinylaminothio)piperidines (**8**) under natural diffused light at room temperature was studied. Relative fading rates of both **4** and **8** were compared at a concentration of $5—10\times10^{-5}$ M in hexane or ethanol for a period of 1 h, measuring the decrease in visible absorption at 410 nm (Table 2). Blank experiments on **4** and **8** in the dark at room temperature showed no detectable change in hexane and ethanol. Table 2 shows that the photochemical behavior of **4** and **8** are nearly the same, and therefore, their photochemical behavior does not depend on the bulk of the substituents at the 2 and 6 positions.

Table 2. Photochemical behavior of 1-(thiosulfinylaminothio)-piperidines, **4** and **8**

Compound	% Loss during 1 h[a,b]	Solvent[c]
4a	5	H and E
4b	5	H and E
4c	7	H and E
4d	7	H and E
8a	5	H and E

a) On allowing to stand under natural diffused light. b) By measuring the decrease at 410 nm. c) H: hexane; E: ethanol.

Thermal behavior of **4** and **8** was similarly studied. Refluxing a $5—10\times10^{-5}$ M solution of **4** or **8** in chloroform for 3 h showed no detectable change in visible absorption.

Accordingly the much lower yield of **8** than **4** could not be explained in terms of the product stability. Thus the difference in the yield of **4** or **8** seems to depend on other causes, *e.g.*, properties of an uncertain intermediate to be discussed later.

Possible Reaction Pathways. Equation 2, along with as described in Eqs. 4, 5, and footnote 9 shows that piperidines, **1** or **7**, react with sulfur monochloride to give the corresponding disulfides, **2** or **9**, and the trisulfide **3**. The resulting **2**, **3**, or **9** may further react with sulfur monochloride at the first stage (Fig. 3) to give the corresponding 1-sulfenyl chloride **10** or **12**, since sulfur monochloride has been known to polarize to $Cl^{\delta-}.....^{\delta+}S_2Cl$.[4] Additionally, a presumed compound, **11** simultaneously prepared from **2**, **3**, or **9** may also give **10** or **12**. Equations 6 and 8 show that the di- and trisulfides **2**, **9**, and **3** actually give the corresponding 1-(thiosulfinylaminothio)piperidines **4** and **8**. Further Eq. 9 also shows that the sulfenyl chloride **10** actually gives **8**.

Thus it can be explained that the new 1-(thiosulfinylaminothio)piperidines **4** or **8** are prepared *via* the corresponding disulfides **2** or **9** and/or the trisulfides **3** and, subsequently, such sulfenyl chloride as **10**. Tentatively it is assumable that **4** and **8** may be prepared *via* the postulated intermediates **13** and **14** derived from the sulfenyl chloride **12** or **10** (Fig. 3) although the intermediary presence of **13** and **14** are unconfirmed. From this assumption, the much lower yield of **8** (R=H), described above, may be explained by the decrease of stability of the intermediate **13** or **14** (R=H).

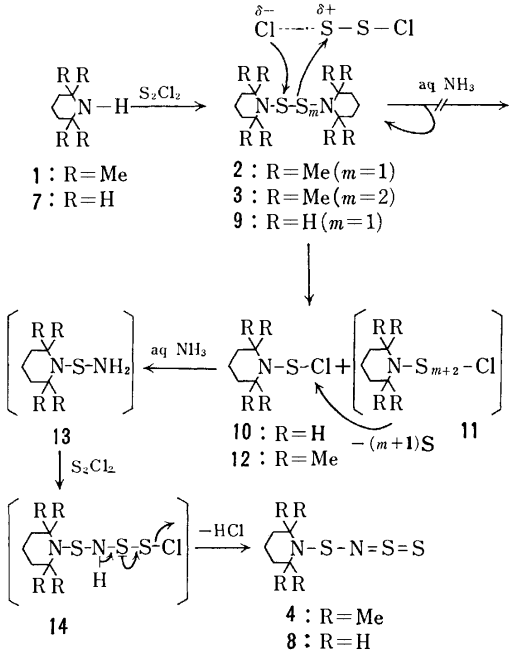

Fig. 3.

Experimental

Mps were not corrected.

NMR spectra were obtained using a Varian A-60 NMR spectrometer, using TMS as an internal standard.

Mass spectra were obtained using a JEOL-JMS-OISG mass spectrometer with an ionizing energy of 75 eV.

Thin-layer chromatography (TLC) was performed on TLC-plates Silica Gel F_{254} (0.25 mm) (Merk).

Bis(2,2,6,6-tetramethylpiperidino) Disulfide (2a) (X: $CH_2<$). Into a solution of 48 g (0.34 mol) of 2,2,6,6-tetramethylpiperidine (**1a**) (X: $CH_2<$) in 120 ml of DMF and 350 ml of hexane was added dropwise a solution of 4.58 g (0.034 mol) of sulfur monochloride in 40 ml of hexane with stirring at −20——25 °C for 30 min. After the addition was completed, the internal temperature was gradually raised to room temperature over a period of 30 min. The reaction mixture was then poured into ice and extracted with benzene. The benzene layer was washed with a 3% aqueous solution of hydrochloric acid and three times with water and dried over sodium sulfate. Evaporation of the benzene under diminished pressure gave 11.2 g of the crude product **2a** which was recrystallized from methanol to give 9.4 g of an

analytically pure colorless compound (needles), mp 83—84 °C, [lit,[1] mp 84—85 °C]. The combined yield of crystalline product (80.2%) and of the residue in solution (as determined by NMR using anisol as an internal standard) was 88.8% based on the starting sulfur monochloride. Found: C, 62.49; H, 10.71; N, 7.97; S, 18.60%. Calcd for $C_{18}H_{36}N_2S_2$: C, 62.73; H, 10.52; N, 8.12; S, 18.60%.

Bis(4-oxo-2,2,6,6-tetramethylpiperidino) Disulfide (2b) (X: O=C<) was prepared by our improved method described in Refs. 2a and 2c.

Bis trisulfides 3a and 3b were prepared by the method of Bennett *et al.*[1]

Isolation of 1-(Thiosulfinylaminothio)piperidines (4) and Detection of Bis(2,2,6,6-tetramethylpiperidino) Disulfides (2) and Bis(2,2,6,6-tetramethylpiperidino) Trisulfides (3). (Eq. 4)

4-Oxo-2,2,6,6-tetramethyl-1-(thiosulfinylaminothio) piperidine (4b): Into a solution of 31 g (0.2 mol) of **1b** in 500 ml of toluene was added dropwise a solution of 27 g (0.2 mol) of sulfur monochloride in 80 ml of hexane with stirring at 10—15 °C over a period of about 2 h. After the addition was completed, the reaction mixture was poured into 300 g of ice and 200 g of 35% aqueous ammonia. The organic phase was then separated, washed with water and dried over magnesium sulfate. Evaporation of the solvent under diminished pressure gave a red solid, which was chromatographed on 1.5 kg of Silica Gel 60 (Merck, 70—230 mesh) with benzene to give red crude crystals in 14% yield. Recrystallization of the crude crystals from hexane gave analytically pure red prisms, mp 116.5—118 °C. NMR (CCl_4) δ 1.47 (S, 12H), 2.60 (S, 4H). MS *m/e* 264 (M^+). Found: C, 40.52; H, 6.00; N, 10.61; S, 36.04%. Calcd for $C_9H_{16}N_2OS_3$: C, 40.87; H, 6.09; N, 10.59; S, 36.73%.

The trisulfide 3b and a trace amount of the disulfide 2b were detected in the reaction mixture by TLC and NMR-analysis.

4-Benzoyloxy-2,2,6,6-tetramethyl-1-(thiosulfinylaminothio)-piperidine, (4d). Into a solution of 4.8 g (0.0184 mol) of 4-benzoyl-2,2,6,6-tetramethylpiperidine **1d** in 20 ml of chloroform was added dropwise a solution of 2.5 g (0.0185 mol) of sulfur monochloride in 10 ml of chloroform with stirring at 10—15 °C over a period of 20 min. After the addition was completed, the reaction mixture was poured into 30 g of ice and 20 g of 35% aqueous ammonia. Then the chloroform was separated, washed with water, and dried over magnesium sulfate. Evaporation of the chloroform under diminished pressure gave a red solid, which was chromatographed on 150 g of Silica Gel 60 (Merck, 70—230 mesh) with a mixture of benzene and hexane (1: 1) to give red crude crystals in 6% yield. Recrystallization of the crude crystals from hexane gave analytically pure red prisms, mp 99—100 °C. NMR ($CDCl_3$) δ 1.46 (S, 6H), 1.54 (S, 6H), 1.75 (br. d, 2H), 2.27 (dd, 2H, J=12 and 4.5 Hz), 5.58 (tt, J=12 and 4.5 Hz), 7.3—8.3 (m, 5H). MS *m/e* 370 (M^+). Found: C, 51.53; H, 5.91; N, 7.68; S, 26.21%. Calcd for $C_{16}H_{22}N_2O_2S_3$: C, 51.86; H, 5.98; N, 7.55; S, 25.95%.

1-(Thiosulfinylaminothio) piperidines, 4a, 4c, 8a, and 8b, were prepared from the corresponding amines by a method similar to that described for **4b** and **4d**. **4a** (Y=8.6%) was identified visible, NMR, and mass spectra. NMR ($CDCl_3$) δ 1.40 (S, 12H), 1.5—1.8 (m, 6H). MS *m/e* 250 (M^+). Data of **4c** (Y=7%) were given in the text. Found: C, 42.83; H, 6.31; N, 9.00; S, 31.46%. Calcd for $C_{11}H_{20}N_2O_2S_3$: C, 42.82; H, 6.53; N, 9.08; S, 31.18%. Unhindered **8a** and **8b**, separated by column chromatography, were identified by visible, mass, and/or high resolution mass spectra. Data of **8a** was given in the text. R_f-value (SiO_2-TLC/hexane) was 0.25. **8b:** The mass spectrum (*m/e* 252, M^+) was consistent with the theoretical value. λ_{max} (in EtOH): 410 nm.

Experiment A (Eq. 5). The reaction mixture, which was obtained during the preparation of **4b**, was poured into ice and 10% aqueous potassium hydrogencarbonate instead of ammonia. In the resulting organic phase, **3b** and a trace amount of **2b** were observed by TLC and NMR analysis.

Experiment B (Eqs. 6, 8, and 9). Under the same reaction conditions as used in Eq. 4, an equimolar mixture of **2a**, **2b**, **3a**, **9**, or **10** and sulfur monochloride were treated with aqueous ammonia. The results were shown in the text.

7b was prepared from the corresponding 1-methylpiperidine by the modified method of Fischer *et al.*[12]

9 was prepared by the method of Dogadkin *et al.*[10]

10 was prepared by the method of Weiss *et al.*[8]

The authors thank Director of Central Research Laboratories, Dr. Keisuke Murayama, and Director of Fine Chemical Research in these Laboratories, Dr. Nobuo Soma for their encouragement and valuable comments throughout this study. The authors are also indebted to the members of the analytical section of these laboratories for the elemental analyses and spectral data.

References

1) J. E. Bennett, H. Sieper, and P. Tavs, *Tetrahedron*, **23**, 1697 (1967).

2) a) K. Murayama, S. Morimura, T. Yoshioka, K. Matsui, T. Kurumada, I. Watanabe, and N. Ohta, German Patent 1929928 (08 Jan 1970); *Chem. Abstr.*, **72**, 67726 w (1970); b) I. Suzuki, K. Ichikawa, K. Murayama, and S. Morimura, German Patent 1928915 (11 Dec 1969); *Chem. Abstr.*, **72**, 44815 k (1970); c) S. Morimura, *Nippon Kagaku Kaishi*, **1980**, 289.

3) a) C. Tamura, K. Aiba, S. Sato, T. Hata, S. Morimura, and T. Yoshioka, *Acta, Cryst.*, **B33**, 3918 (1977); b) N. Soma, S. Morimura, T. Yoshioka, and T. Nishimura, Jpn Patent S52—38908.

4) L. A. Wiles and Z. S. Ariyan, *Chem. Ind. (London)*, **1962**, 2102.

5) D. H. R. Barton and M. J. Robson, *J. Chem. Soc., Perkin Trans. 1*, **1974**, 1245.

6) a) Y. Inagaki, R. Okazaki, and N. Inamoto, *Tetrahedron Lett.*, **1975**, 4575; **1977**, 293; b) Y. Inagaki, R. Okazaki, and N. Inamoto, *Bull. Chem. Soc. Jpn.*, **52**, 2002, 2008 (1979).

7) Yields were measured by visible absorption (410 nm), and were based on the assumptions that equimolar **4a** and **8a** should show the same ε-value and that 1 mol of the starting **7**, **9**, and **10** should give 1 mol of **8a**.

8) G. Weiss and G. Schulze, German Patent, 1131222 (14, June 1962); *Chem. Abstr.*, **57**, 13771 e (1962).

9) Piperidine **7a** has been known to react with sulfur monochloride giving the corresponding disulfide **9**.[10]

10) B. A. Dogadkin, M. S. Feldstein, I. I. Eitington, and D. M. Pevzner, *Rudd. Chem. Technol.*, **32**, 976 (1959).

11) J. G. Fischer, and G. Mikite, *Acta Chim. Acad. Sci. Hung.*, **68**, 261 (1971).

The Reaction of Alkenylboranes with Palladium Acetate. Stereoselective Synthesis of Olefinic Derivatives†,[1]

Hidetaka YATAGAI

Department of Chemistry, Faculty of Science, Kyoto University, Kyoto 606

(Received November 14, 1979)

The reactions of alkenylboranes with palladium acetate were investigated. Alkenyldialkylboranes, derived from terminal alkynes, underwent intramolecular migration reaction in the presence of an equimolar amount of palladium acetate and triethylamine to give (*E*)-olefins. On the other hand, under the same conditions as above or even in the presence of catalytic amounts of palladium acetate, alkenyldialkylboranes derived from internal alkynes underwent protonolysis reaction to produce (*Z*)-olefins. An alkenylpalladium intermediate which was presumably involved in the latter reaction was trapped by allylic chloride to give 1,4-dienes.

Organic syntheses *via* boranes have been broadening the synthetic applicability of olefinic or acetylenic derivatives, since organoboranes are easily obtainable *via* hydroboration. Especially, application of alkenylboranes toward organic syntheses may enchant synthetic chemists in view of introduction of alkenyl groups with *trans* configuration into organic molecules. Indeed, various synthetic methods using alkenylboranes have been developed.[2] As for the C–C bond formation which is accomplished by the intramolecular migration reaction as shown in Eq. 1,[3] there lies a limitation

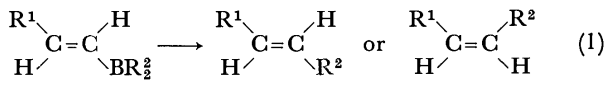

(1)

concerning to the R^2 group; R^2 is limited to the secondary. The methodology of transmetallation from less reactive B–C bond to a reactive other metal-carbon bond seems to exclude this limination and provide a possibility of versatile intermolecular C–C bond formations.[4] It was reported in previous papers that such a transmetallation was realized in the case of copper by the reaction between methylcopper and alkenylboranes.[4a] This result prompted to investigate other transition metal such as palladium,[5,7] which was of potentially wide applicability to organic synthesis.[6] In this paper the reactions of alkenylboranes with various palladium complexes are examined and three types of reactions, 1) intramolecular migration reaction,[1a] 2) protonolysis reaction,[1b] and 3) cross-coupling reaction are reported.

Results and Discussion

Intramolecular Migration Reaction Promoted by Palladium Acetate. First, alkenyldialkylboranes (**1**) derived from terminal alkynes were tried to react with an equimolar amount of various palladium complexes such as $PdCl_2$, $Pd(AcAc)_2$, $Pd_2(DBA)_3$, $Pd(PPh_3)_4$[7] and $Pd(OAc)_2$. Quite interestingly, only palladium acetate reacted smoothly at room temperature with **1** to produce (*E*)-olefins (**2**) as the coupling product between alkenyl and alkyl groups. (Eq. 2).

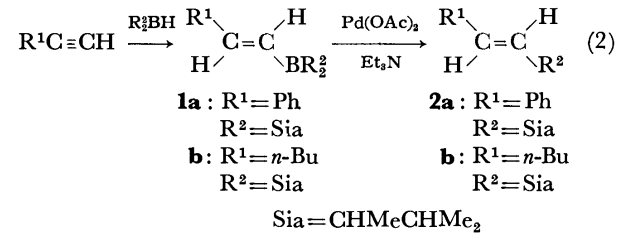

(2)

1a: R^1=Ph, R^2=Sia; **1b**: R^1=*n*-Bu, R^2=Sia

2a: R^1=Ph, R^2=Sia; **2b**: R^1=*n*-Bu, R^2=Sia

Sia=$CHMeCHMe_2$

This reaction essentially needed triethylamine and the yield of **2** depended upon the amount of triethylamine. When catalytic amounts of triethylamine (7 mol %) were used in the reaction of (*E*)-styryldisiamylborane (**1a**), **2a** was obtained in the highest yield. In contrast to this, when R^1 was alkyl such as (*E*)-1-hexenyldisiamylborane (**1b**), an equimolar amount of triethylamine gave the best result. (see, Table 1).

Table 1. Reaction of **1** with $Pd(OAc)_2$ in the presence of various amounts of amine[a]

1 (**1a** or **1b**)	Product (**2a** or **2b**)	Et_3N mmol	Yield of **2**[b] %
1a	**2a**	2	64
		1	68
		0.35	79
		0.07	98
		0	60
1b	**2b**	2	55
		1	74
		0.05	33
		0	10

a) **1** (1 mmol), $Pd(OAc)_2$ (1 mmol).
b) By GLPC yield.

Taking account of these results, various types of (*E*)-olefins (**2**) were synthesized from alkynes (Table 2). The stereochemistry of the products in each case was over 96% *trans* as determined by the strong absorption at 965 cm^{-1} region in IR spectra and GLPC examination in comparison with the corresponding *Z*-isomer.

Previously, Zweifel and his co-workers reported the stereoselective synthesis of (*E*)-olefins from alkenylboranes using BrCN.[3a] Attempts to apply this procedure to styrylboranes (Table 2 entries 1, 3, and 4) resulted in failure; reaction of **1a** with BrCN gave

† Thesis submitted by the author (H. Y.) to Kyoto University in partial fulfillment of the requirements for the degree of Rigaku-Hakushi (Ph. D.).

Table 2. Reaction of **1** with $Pd(OAc)_2$–Et_3N[a]

Entry	Acetylene	Borane[c]	Product[d]	Yield[e] (Isoln)[b]
1[f]	PhC≡CH	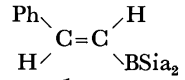 **1a**	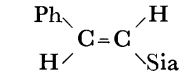 **2a**	94 (86)
2[g]	*n*-BuC≡CH	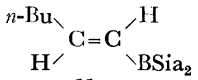 **1b**	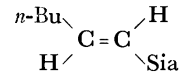 **2b**	74 (58)
3[f]	PhC≡CH	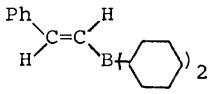 **1c**	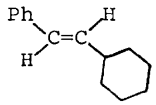 **2c**	58 (35)
4[f]	PhC≡CH	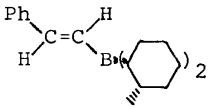 **1d**	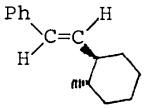 **2d**	(86)
5[g]	$Cl(CH_2)_3C{\equiv}CH$	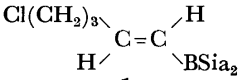 **1e**	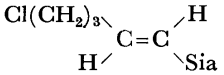 **2e**	(62)

a) All reactions were performed on a 1 mmol scale. b) Isolation was carried out on a 5 mmol scale. c) Sia=CHMeCHMe$_2$. d) Identified by IR and NMR spectroscopies, elemental analyses, and/or comparison with authentic materials. e) By GLPC based on the acetylenes. f) Catalytic amounts of Et_3N (7 mol %) were used. g) Stoichiometric amounts of Et_3N were used.

styrene instead of **2a**. Consequently, the present reaction offers a noteworthy improvement in the existing methodology of intramolecular migration reaction.

By the hydroboration method for the preparation of alkenyldialkylboranes, the alkyl groups are limited to secondary groups. Thus, the introduction of the primary alkyl group was achieved by the two methods as shown in Eqs. 3 and 4. Although the desired (*E*)-5-decene (**4**) was obtained by both methods, yields were low and the reaction in Eq. 4 gave 1,3-diene (**6**) as a by-product.

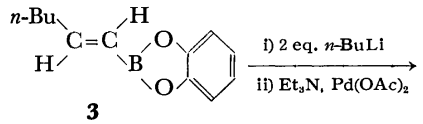

3 → *n*-BuCH=CH(*n*-Bu) **4** (3)

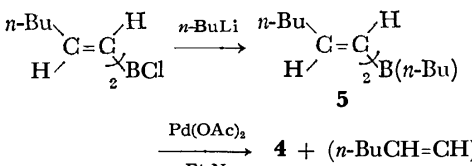

5 → **4** + (*n*-BuCH=CH)$_2$ **6** (4)

31% 57%

Two mechanisms appear reasonable to consider for this transformation; a) intermolecular coupling process *via* the alkenylpalladium acetate on the analogy of transmetallation to Hg[4c] and Pd[5] (Eq. 5), and b) intramolecular process *via* acetoxypalladation-migration-elimination (Eq. 6). Although a mixture of **1a** and dicyclohexylacyloxyborane was treated with $Pd(OAc)_2$–Et_3N, cross-coupling product (β-cyclohexylstyrene) could

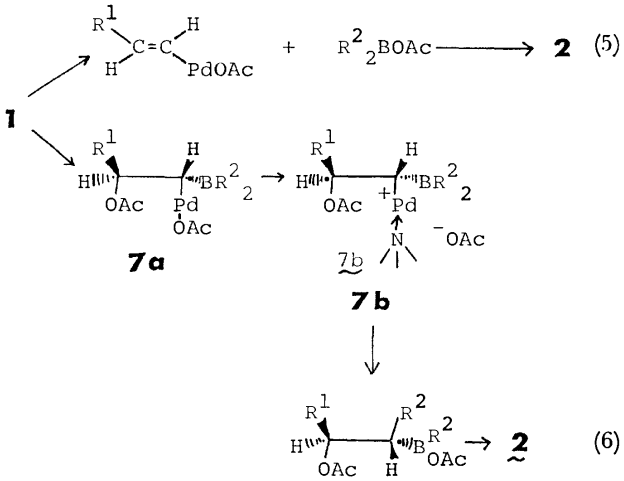

(5)

(6)

not be obtained thus excluding the intermolecular mechanism. Therefore, intramolecular migration is reasonable. There remain the following two possibilities; 1) *cis* acetoxypalladation-migration[3] from boron to the α-carbon with inversion at the migration terminus syn elimination[3a,8,9] or 2) *trans* acetoxypalladation-inversion anti elimination.[3b,8a] The hitherto known migrations proceed with inversion of configuration and the anti β-elimination is restricted to the reaction in the presence of strong base. Consequently, intramolecular process 1) demanding the *cis*-acetoxypalladation is favorable.[10]

The orientation of the acetoxypalladation may be explained as follows. The vacant p orbital of boron atom interacts with π-electrons of the double bond[11] to make the β-carbon of alkenylborane electropositive.

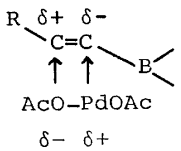

Fig. 1.

Therefore the nucleophilic acetoxyl group can attack this β-carbon to give **7** (Fig. 1).[12]

The investigation of effect of various amines showed that the yield of **2b** had a relation with coordination ability of amines with trimethylborane (Table 3). That is, the present reaction can proceed smoothly under the conditions in which amine coordinates with palladium rather than boron. Et_3N could satisfy these conditions and coordinate with palladium to give cationic palladium complex (**7b**) which may induce alkyl migration more easily.[13]

Table 3. Reaction of **1b** with $Pd(OAc)_2$ in the presence of amine[a]

Amine	Yield of **2b** (%)	Amine: BMe_3 dissociation const.[b]
	32	0.301
Me_3CNH_2	49	9.46
Et_3N	74	—[c]

a) **1b** (1 mmol), $Pd(OAc)_2$ (1 mmol), amine (1 mmol). b) H. C. Brown, "Boranes in Organic Chemistry," Cornel Univ. Press **1972**, p. 59. c) Too highly dissociated to be measured.

Application of this type of reaction to alkenyldialkylboranes (**8**), derived from internal alkynes, resulted in failure giving (*Z*)-olefins (**9**) instead which were formed *via* retentive protonalysis of the alkenylgroup of **8** (Eq. 7).

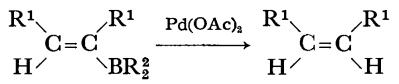

(7)

8a: R^1=*n*-Bu, R^2=Sia **9a**: R^1=*n*-Bu

Protonolysis of Alkenyldialkylboranes (8) Catalyzed by Palladium Acetate. As mentioned above, treatment of (*E*)-5-decenyldisiamylborane (**8a**) with an equimolar amount of palladium acetate and triethylamine produced **9a** in a yield of 71%. Quite interestingly, this protonolysis reaction proceeded successfully even in the presence of catalytic amounts of palladium acetate (5—10 mol%). The results are summarized in Table 4. Judging from Table 4, applicability of this method appears to be general for internal alkynes. However, similar treatment of alkenylborane derived from terminal alkyne gave unsatisfactory result.

Previous methods for the protonation of alkenylboranes under acidic[14] or basic[15] conditions have several disadvantages; *e.g* incompatibility with various acid or base sensitive functional groups. The present procedure under a neutral and mild conditions can give a solution to this problem.

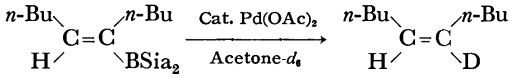

(8)

8a *d*-Content 88%

The experiment using acetone-d_6 as a solvent gave deuterium incorporated olefin[16] (Eq. 8). Accordingly, the proton source was confirmed to be the solvent. A mechanistic rationale which readily accounts for the observed catalytic process and deuterium labelling in

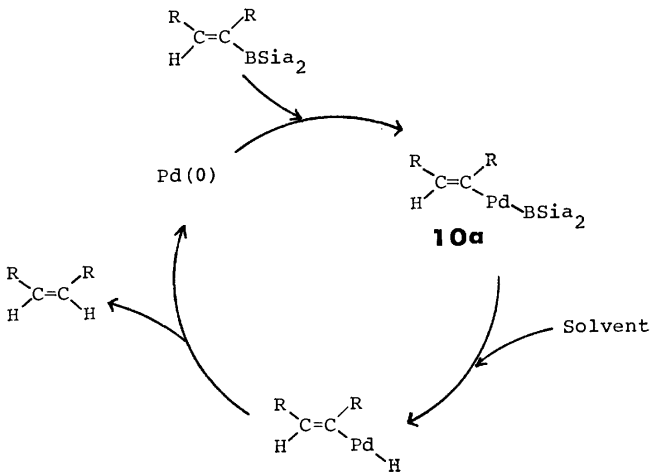

Scheme 1.

Table 4. Protonolysis of **8** with catalytic amounts of $Pd(OAc)_2$[a]

Acetylene	Hydroborating reagent[b]	Product	Yield/% (Isoln)[d]
n-BuC≡Cn-Bu	Sia_2BH	(*Z*)-5-Decene	95
n-BuC≡Cn-Bu	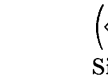	(*Z*)-5-Decene	94
n-HexC≡CEt	Sia_2BH	(*Z*)-3-Decene	(70)
PhC≡CPh	Sia_2BH	(*Z*)-Stilbene	69[e]
n-OctC≡C$(CH_2)_7$COOMe	Sia_2BH	Methyl oleate	91
n-BuC≡CH	Sia_2BH	1-Hexene	30[f]

a) All reactions were carried out at room temperature overnight. b) Sia=$CHMeCHMe_2$. c) All products were identified by NMR, IR, and comparison with the authentic materials. d) By GLPC yield. Yields were based on alkynes. e) Starting material was recovered in 24% yield, owing to incomplete hydroboration. f) The starting borane was recovered in 70% yield.

TABLE 5. CROSS-COUPLING OF **8** WITH ALLYLIC CHLORIDE[a)]

Entry	Alkenylborane	Halide	Product[c)]	Yield[d)] (Isoln)[b)] **11**	**9**
1	**8a**	CH_2=$CHCH_2Cl$	**11a**	23	65
2	**8b**	CH_2=$CHCH_2Cl$	**11a**	70	13
3	**8b**	CH_2=$CHCHMeCl$	*n*-Bu, *n*-Bu, H, CH_2CH=$CHMe$ **11b** [e)]	60	20
4	**8b**	$MeCH$=$CHCH_2Cl$	—	—	47
5	**8c** R^1=$Cl(CH_2)_3$, BR^2_2=9-BBN	CH_2=$CHCH_2Cl$	**11c** R^1=$Cl(CH_2)_3$	(30)	
6	n-Hex, H, H, B	CH_2=$CHCH_2Cl$	*n*-Hex, H, H, CH_2CH=CH_2	trace	30

a) All reactions were performed on a 1 mmol scale. b) Isolation was carried out on a 5 mmol scale. c) Identified by IR, NMR, and/or comparison with the authentic materials. d) By GLPC, based on alkenylboranes. e) Mixture of 2*E* and 2*Z*-isomers.

acetone-d_6 is shown in Scheme 1; a) oxidative insertion of Pd(0) into the C–B bond followed by b) H-abstraction from the solvent and c) reductive elimination. Supposedly, in contrast to the alkenylboranes derived from terminal alkynes, migration of the alkyl group of **8** to the α-carbon must proceed quite sluggishly due to bulky alkenyl group of **8** compared to that of **1**.

Cross-coupling of Alkenylboranes Catalyzed by Palladium Acetate. The mechanistic consideration of the protonolysis reaction as suggested above indicates that this reaction might proceed *via* an alkenylpalladium intermediate such as **10**. It appears possible that such an intermediate may be trapped by an appropriate olefin. Actually, allyl chloride reacted with the intermediate to give (*E*)-1,4-dienes (**11**) stereoselectively. The protonolysis reaction, however, competed with the cross-coupling reaction (Eq. 9). This problem was solved by using alkenyl-9-borabicyclo[3.3.1]nonane (alkenyl-9-BBN) as a starting material. (see, Table 5).

$$\underset{\textbf{8a}:\ R^1=n\text{-Bu},\ R^2=\text{Sia}\quad \textbf{8b}:\ R^1=n\text{-Bu},\ BR^2_2=\text{9-BBN}}{R^1CH{=}CHBR^2_2} \xrightarrow[\text{Cat. Pd(OAc)}_2]{\text{Allyl chloride}} \underset{\textbf{11a}:\ R^1=n\text{-Bu}}{R^1CH{=}CHCH_2CH{=}CH_2} + \underset{\textbf{9a}}{R^1CH{=}CHH} \quad (9)$$

From	**8a**:	23%	65%
	8b:	70%	13%

Allyl chloride and 3-chloro-1-butene underwent the effective cross-coupling (entries 2, 3, and 5), while crotyl chloride gave a poor result (entry 4). The cross-coupling reaction proceeded completely as S_N2' process and with retention of configuration of the double bond of alkenylboranes. Unfortunately the reaction of 1-alkenyl-9-BBN derived from terminal alkynes with allyl chloride gave only trace amounts of desired diene.

This reaction nearly completed within 30 min at room temperature, and at this time di-π-allyl-μ,μ'-dichlorodipalladium (**12**) was formed. Since it was confirmed that **12** did not react with **8a** or **8b**, **12** was not a real catalyst. Two catalytic cycles are possible for the reaction (Scheme 2); a) direct transmetallation of the B–C bond followed by insertion and elimination which is a process similar to Heck's[17] and Larock's[18] reaction, might be involved; b) oxidative addition of alkenyl boranes to Pd(0) produces **10**, which is considered to be an intermediate in the protonolysis reaction, and the subsequent insertion of allylic chloride and elimination give the product. The reaction of stoichiometric

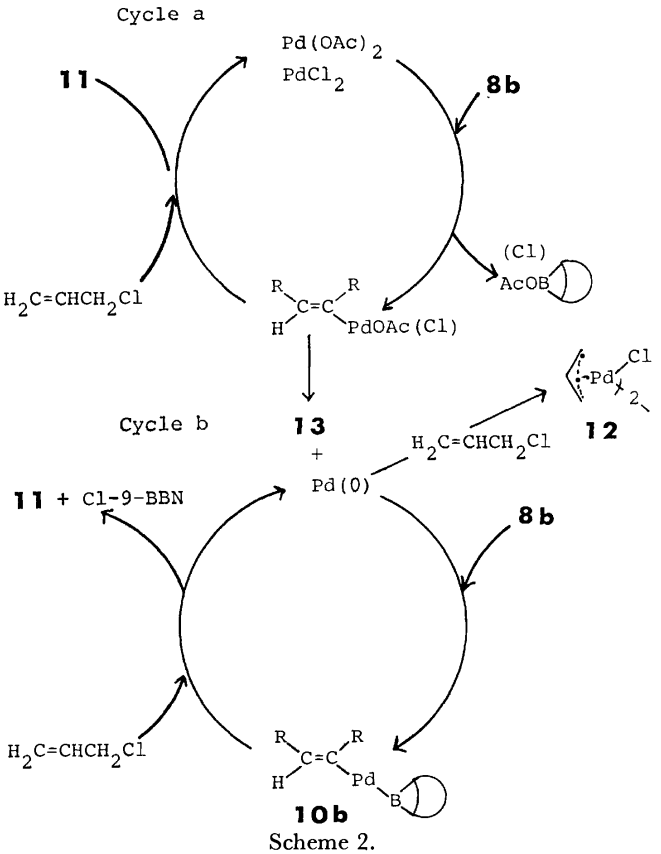

Scheme 2.

amounts of palladium acetate with **8b** gave the dimeric product (**13**), presumably *via* alkenylpalladium acetate. In the presence of methyl acrylate[5] the cross-coupling product (**14**) was also obtained (Eq. 10). Therefore, there might be a possibility for the cycle a. However, cycle b can not be discarded on the basis of the following results; the addition of allyl chloride, after stirring the mixture of **8b** and catalytic amounts of palladium acetate for 1 h, also produced **11a** in a yield of 45%. In this system catalytic species is considered to be Pd(0) since palladium acetate must be reduced by the initial reaction[20] *via* the transmetallation and dimerization as shown in Eq. 10[21] Accordingly it is favorable to

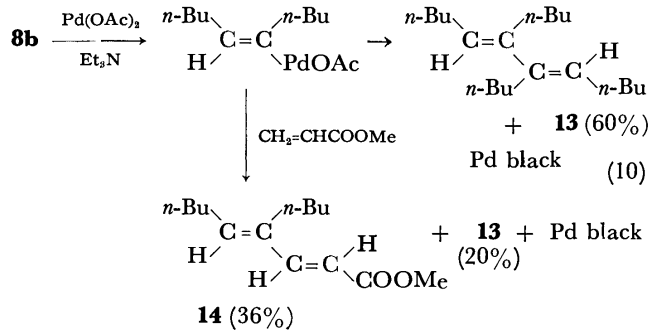

consider that b is a main cycle for this reaction and formation of **12** extinguishes Pd(0) species. In the reaction with crotyl chloride, the formation of **12** might prevail over the insertion of crotyl chloride into **10b** owing to its steric effect.[22]

Experimental

NMR spectra were recorded on a JEOL-PS-100 spectrometer; chemical shifts in CCl_4 are expressed in parts per Million relative to Me_4Si. IR spectra were recorded on a JASCO-IR A-1 and GLPC analyses were performed on a JEOL-JGC-20K instrument, using a 2m column packed with SE-30 or Silicone DC-550 on Celite 545 AW. GC-MS were measured on a HITACHI-MR-1 using a 1 m column (SE-30). Elemental analyses were performed by the Microanalytical Laboratory of Kyoto University, Kyoto, Japan. Air sensitive materials were handled *via* the standard techniques described in Chapter 9 of Ref. 14. The reaction flasks were fitted with a side arm capped with a rubber septum. All reactions were carried out under a static pressure of nitrogen.

Reagent-grade solvents were purified by standard techniques and kept over a drying reagent. BH_3: THF and 9-borabicyclo[3.3.1]nonane (9-BBN) were prepared according to Ref. 14. Alkenylboranes[14] were prepared *in situ* without distillation. (*E*)-5-Decenyl-9-BBN,[23] di[(*E*)-1-hexenyl]chloroborane,[24] and 2-[(*E*)-1-hexenyl][1,3,2]benzodioxaborole[13] were distilled and their physical data are listed in Ref. 25. Commercially available *n*-BuLi was titrated by Eastham's method.[26] $Pd(OAc)_2$,[27] $Pd_2(DBA)_3$,[28] $Pd(PPh_3)_4$,[29] and $Pd(AcAc)_2$[30] were prepared according to the known procedures. Spectral data of products are listed in Table 6.

General Procedure for Synthesis of **2**. Syntheses of **2a**, **2c**, and **2d** were as follows. To a solution of $Pd(OAc)_2$ (5 mmol) and triethylamine (0.35 mmol) in THF (20 ml), **1** (5 mmol) was added. Palladium black soon precipitated from the resulting mixture. After stirring overnight at room

Table 6. Spectral data of products

Product	NMR	(IR cm^{-1})	Anal. (%) or MS
(*E*)-3,4-Dimethyl-1-phenylpentene (**2a**)	7.38—7.05 (5H, m), 6.35 (1H, d, J=15 Hz), 6.09 (1H, d-d, J=15, 7.5 Hz), 2.31—1.95 (1H, m), 1.80—1.35 (1H, m), 1.05 (3H, d, J=7 Hz), 0.93 (6H, d, 7 Hz)	965	Found: C, 89.88; H, 10.47 Calcd: C, 89.59; H, 10.41
(*E*)-2,3-Dimethyl-4-nonene (**2b**)	5.45—5.20 (2H, m), 2.20—1.70 (3H, m), 1.70—1.13 (5H, m), 1.13—0.95 (9H, m)	965	a)
(*E*)-1-Cyclohexyl-2-phenylethylene (**2c**)	7.41—7.08 (5H, m), 6.33 (1H, d, J=15 Hz), 6.03 (1H, d-d, J=15, 7 Hz), 2.37—2.01 (1H, m), 2.01—1.53 (6H, m), 1.53—1.02 (4H, m)	965	Found: H, 90.33; H, 9.71 Calcd: C, 90.26; H, 9.74
(*E*)-1-(*trans*-2-Methylcyclohexyl)-2-phenylethylene (**2d**)	7.41—7.05 (5H, m), 6.33 (1H, d, J=15.5 Hz), 5.94 (1H, d-d, J=15.5, 7.5 Hz), 1.98—1.53 (5H, m), 1.53—0.99 (5H, m), 0.92 (3H, d, J=6 Hz)	965	Found: C, 89.95; H, 10.19 Calcd: C, 89.94; H, 10.06
(*E*)-8-Chloro-2,3-dimethyl-4-octene (**2**)	5.40—5.16 (2H, m), 3.48 (2H, t, J=6 Hz), 2.34—1.98 (2H, m), 2.04—1.20 (4H, m), 1.05—0.75 (9H, m)	965	a)
(5*E*)-5-Butyl-2,5-decadiene (**11b**)	5.40—5.20 (2H, m), 5.02 (1H, bt, J=6 Hz), 2.70—2.50 (2H, m), 2.10—1.80 (4H. m), 1.62 (*E*-Me, d, J=4 Hz), 1.56 (*Z*-Me, d, J=4 Hz), 1.40—1.20 (8H, m), 0.90 (6H, bt, J=6 Hz)	965	M^+ (196)
(*E*)-8-Chloro-4-(chloropropyl)-1,4-octadiene (**11c**)	5.90—5.50 (1H, m), 5.20—4.80 (3H, m), 3.60—3.30 (4H, m), 2.70 (2H, d, J=6 Hz), 2.30—2.10 (4H, m), 1.80—1.70 (4H, m)	1635 990 910	M^+ (220) M^+—Cl (185)

a) Comparison with an authentic material prepared by Zweifel method.[3a]

temperature the mixture was concentrated under reduced pressure. Essentially pure products were obtained simply by passing this residue through an alumina column. **2b** and **2e** were isolated by the same method using 5 mmol of triethylamine. The investigation of the effect of amine was performed on 1 mmol scale and the reaction mixture was analyzed by GLPC. IR and NMR spectra of **2b** and **2e** were identified with those of authentic materials, prepared by the Zweifel method.[3a] Other products exhibited the expected spectroscopic characteristics.

Isomeric Purity of 2. In every case, the corresponding *Z*-isomers were synthesized by the Zweifel method; iodine-promoted intramolecular migration reaction.[3b] The GLPC examination (DC-550) revealed that each of **2a**, **2c**, and **2d** had longer retention time than that of corresponding *Z*-isomer. On the other hand, each of **2b** and **2e** had almost the same retention time as that of the corresponding *Z*-isomer, making the analysis difficult. It was found, however, that the corresponding epoxides of these compounds were easily separated by GLPC (DC-550).[31] Each Epoxide of *E*-isomers had shorter retention time than that of *Z*-isomers.

Synthesis of 4. *a*): *n*-BuLi in hexane (2 mmol) was added to **3** (1 mmol) in THF (2 ml) at 0 °C. The resulting mixture was stirred for 30 min at 0 °C and then triethylamine (1 mmol) and $Pd(OAc)_2$ (1 mmol) were added. The mixture was stirred overnight. The formation of **4** was confirmed by GC-MS in comparison with an authentic material and GLPC examination by internal standard method revealed this solution contained **4** in 27% yield.

b): **6** (1 mmol) was prepared in situ by the slow addition of *n*-BuLi (1 mmol) to di[(*E*)-1-hexenyl]chloroborane (1 mmol) in THF at −78 °C. To this solution, $Pd(OAc)_2$ (1 mmol) and triethylamine (1 mmol) were added at room temperature. GLPC examination by the same method as above revealed that this solution contained **4** in 31% yield accompanied by **6** in 57% yield.

General Procedure for the Synthesis of 9. Alkynes (5 mmol) were hydroborated by disiamylborane (5 mmol) to form alkenyldisiamylboranes (**8**). To this solution, $Pd(OAc)_2$ (0.5—0.1 mmol) was added under a static pressure of nitrogen at room temperature and the resulting mixture was stirred overnight. THF was removed under reduced pressure. The products were isolated through an alumina column. All products were identified by comparison with authentic materials which were obtained commercially or by the reduction of the corresponding alkynes.[32] IR spectra of all products showed no absorption at 965 cm^{-1}.

Deuterium Labelling Study. 5-Decyne was hydroborated by disiamylborane (1 mmol). THF was removed under reduced pressure. To remove THF completely, BCl_3 (2 mmol) in hexane was added to this residue and precipitated THF: BCl_3 was filtrated. The solvent and excess BCl_3 were removed under reduced pressure and the residue was utilized for the protonolysis reaction in acetone-d_6 (2 ml) catalyzed by $Pd(OAc)_2$ (0.1 mmol). The deuterium content was determined by GC-MS and NMR to be 88%.

General Procedure for (E)-1,4-Dienes (11). To a solution of alkenyl-9-BBN (5 mmol) and allyl chloride (5 mmol), $Pd(OAc)_2$ (0.5—0.1 mmol) was added and the resulting mixture was stirred overnight at room temperature. The products were isolated through an alumina column. Stereochemistry of **11a** was determined as follows. An authentic sample of **11a** was prepared according to Eisch method;[33a] NMR (δ, CCl_4) 5.65 (d-d, J=18, 10 Hz, 1H), 5.00 (t, J=6 Hz, 1H), 4.98—4.76 (m, 2H), 2.66 (d, J=6 Hz, 2H), 2.10—1.80 (m, 4H), 1.52—1.08 (m, 8H), 0.90 (t, J=6 Hz, 6H). IR (cm^{-1}), 990, 910. (*Z*)-4-Butyl-1,4-nonadiene, stereoisomer of **11a**, was prepared by the Zweifel method;[33b] 5-decyne (5 mmol) was hydroaluminated by $(i\text{-Bu})_2$-AlHMeLi, prepared from $(i\text{-Bu})_2AlH$ and MeLi. Then allyl bromide (10 mmol) in THF was added and resulting mixture was refluxed for 2 h. After addition of aq H_2SO_4 (0.5 M), the resulting mixture was extracted several times with hexane. The hexane solution was washed with aq $NaHCO_3$ and sat. solution of NaCl. Hexane was evaporated and the residue was chromatographed over alumina by using petroleum ether. Kuhgel rohr distillation gave (*Z*)-4-butyl-1,4-nonadiene; bp 140—160 °C/20 mmHg (40% yield), NMR (δ, CCl_4), 5.65 (d-d, J=10 Hz, 1H), 5.10 (t, J=6 Hz, 1H), 5.06—4.80 (m, 2H), 2.73 (d, J=6 Hz, 2H), 2.16—1.80 (m, 4H), 1.52—1.14 (m, 8H), 0.88 (bt, J=6 Hz, 6H), IR (cm^{-1}) 1630, 990, 905. Consequently, these isomers could be clearly discriminated by the chemical shift at the region between 2.66 and 2.73 ppm and NMR spectrum of the reaction product completely accorded with that of 4*E*-isomer. Furthermore, these isomers could be separated by GLPC (3m, 30% of Apiezon on Celite 545 AW). The retention time of 4*Z*-isomer was shorter than that of 4*E*-isomer, and the GLPC analysis of the reaction product showed a single sharp peak, whose retention time accorded with that of 4*E*-isomer. Accordingly, the reaction product can be assigned to pure 4*E*-isomer. This result indicates that the cross-coupling products retain the stereochemistry of the starting alkenyl-9-BBN. The stereochemical result could apply to other cross-coupling reaction. **11b** was assigned to a mixture of 2*E* and 2*Z*-isomers, since the IR spectrum showed a weak absorption at 965 cm^{-1} region.

Synthesis of 13. To a THF solution (4 ml) of Et_3N (1 mmol) and $Pd(OAc)_2$ (1 mmol), **8b** (1 mmol) was added. After stirring for 1 h at room temperature, palladium black was precipitated. GLPC examination revealed that **13** was formed in 60% yield, the structure of which was confirmed by GC-MS in comparison with an authentic material.[34]

Synthesis of 14. To a THF solution (4 ml) in which $Pd(OAc)_2$ (1 mmol), Et_3N (1 mmol), and methyl acrylate (2 mmol) were dissolved, **8b** (1 mmol) was added at room temperature. After stirring for 1 h, GLPC examination revealed that **14** and **13** were formed in 36 and 20% respectively. **14** was isolated through an alumina column by using hexane; NMR (δ, CCl_4), 7.10 (d, J=16 Hz, 1H), 5.80 (t, J=6 Hz, 1H), 5.68 (d, J=16 Hz, 1H), 3.64 (s, 3H), 2.30—2.00 (m, 4H), 1.60—1.20 (m, 8H), 1.00—0.80 (m, 6H). MS; 223 (M^+).

Mechanistic Study. THF solution (2 ml) of $Pd(OAc)_2$ (10 mg) showed an absorption at 400 nm (ε=30). By the addition of **8a** or **8b** (1 mmol) this absorption disappeared, and then the solution was stirred for 1 h. After addition of allyl chloride (1 mmol), a new absorption at 350 nm appeared in UV spectrum. This absorption corresponded with that of di-π-allyl-μ,μ'-dichlorodipalladium (**12**) in THF. In the stoichiometric reaction (1 mmol scale), **12** was isolated in 10% yield by column chromatography (alumina-hexane). GLPC examination revealed that the cross-coupling took place within 30 min and yield was 45%.

References

1) For a preliminary report on some aspects of the present study, see, a) H. Yatagai, Y. Yamamoto, K. Maruyama, A. Sonoda, and S-I. Murahashi, *J. Chem. Soc., Chem. Commun.*, **1977**, 852; H. Yatagai, Y. Yamamoto, and K. Maruyama, *ibid.*, **1978**, 702.

2) For a review, see P. F. Hudrilik and A. M. Hudrilik "The Chemistry of the Carbon-carbon Triple Bond," ed by

S. Patai, John Wiley and Sons, N. Y., (1978), Part 1, Chap. 7.

3) For synthesis of (*E*)-olefins, a) G. Zweifel, R. P. Fisher, J. T. Snow, and C. C. Whitney, *J. Am. Chem. Soc.*, **94**, 6560 (1972). (*Z*)-Olefins, b) G. Zweifel, R. P. Fisher, J. T. Snow, and C. C. Whitney, *J. Am. Chem. Soc.*, **93**, 6310 (1971).

4) Transmetallation to copper, a) Y. Yamamoto, H. Yatagai, and I. Moritani, *J. Am. Chem. Soc.*, **97**, 5606 (1975); Y. Yamamoto, H. Yatagai, A. Sonoda, and S-I. Murahashi, *J. Chem. Soc., Chem. Commun.*, **1976**, 452: Y. Yamamoto, H. Yatagai, K. Maruyama, A. Sonoda, and S-I. Murahashi, *Bull. Chem. Soc. Jpn.*, **50**, 3427 (1977); Y. Yamamoto, H. Yatagai, K. Maruyama, A. Sonoda, and S-I. Murahashi, *J. Am. Chem. Soc.*, **97**, 5606 (1977). Magnesium, b) K. Kondo and S-I. Murahashi, *Tetrahedron Lett.*, **1979**, 1237. Mercury, c) R. C. Larock and H. C. Brown, *J. Am. Chem. Soc.*, **92**, 2467 (1970); R. C. Larock, S. K. Gupta, and H. C. Brown, *ibid.*, **94**, 4371 (1972).

5) Heck and Dieck reported the transmetallation of *Z*-alkenylboric acid to alkenylpalladium acetate in the stoichiometric reaction but not fully investigated, H.A. Dieck and R. F. Heck, *J. Org. Chem.*, **40**, 1083 (1975).

6) B. M. Trost, *Tetrahedron*, **1977**, 2615.

7) Recently Miyaura and Suzuki reported that $Pd(PPh_3)_4$ catalyzed the cross-coupling reaction of alkenylboranes with alkenyl halides in the presence of bases, such as NaOMe; N. Miyaura, K. Yamada, and A. Suzuki, *Tetrahedron Lett.*, **1979**, 3437; N. Miyaura and A. Suzuki, *J. Chem. Soc., Chem. Commun.*, **1979**, 866.

8) a) E. Negishi, G. Lew, and T. Yoshida, *J. Org. Chem.*, **39**, 2321 (1974); b) G. L. Larson and A. Hernandez, *J. Organomet. Chem.*, **102**, 123 (1975).

9) Regarding the migration step, it is known that the nucleophilic substitution of π-allylpalladium complexes proceeds with inversion; B. M. Trost and L. Weber, *J. Am. Chem. Soc.*, **97**, 1611 (1975). Many other examples that the displacement of Pd(II) occurs in S_N2 fashion can also be found in Ref 10.

10) Normally, the acetoxypalladation which proceeds in a trans fashion is carried out in the presence of a large excess of acetic acid; P. M. Henry, *Adv. Organomet. Chem.*, **13**, 363 (1975).

11) Y. Yamamoto and I. Moritani, *J. Org. Chem.*, **40**, 3434 (1975).

12) Olefins substituted with electron-withdrawing groups add palladium at the α carbon; G. Henrici-Olive and S. Olive "Coordination and Catalyst," Verlag Chemie, (1977), Chap 7.

13) In Ref. 6, Trost suggested that cationic palladium complexes may be attacked by nucleophiles more easily.

14) H. C. Brown, "Organic Syntheses *via* Boranes," John Wiley and Sons, New York, (1975).

15) E. Negishi and K-W. Chin, *J. Org. Chem.*, **41**, 3484 (1976).

16) Initially, THF was removed by an aspirator for 5 h and replaced by actone-d_6. However, deuterium content of the olefin was 50%. It was considered that THF could not be removed by this method. Thus, the residue was treated with strong Lewis acid (BCl_3) to remove the THF as the BCl_3: THF complex. According to this method, deuterium content reached to 88%. See also experimental section.

17) R. F. Heck, *J. Am. Chem. Soc.*, **90**, 5531 (1968).

18) R. C. Larock, J. C. Bernhardt, and R. J. Driggs, *J. Organomet. Chem.*, **156**, 45 (1978).

19) Although π-allylpalladium was isolated in the stoichiometric reaction, it was analyzed by means of UV spectroscopy.

20) The Reaction in Eq. 10 proceeded within 1 h. Accordingly the initial reaction should reduce $Pd(OAc)_2$ to Pd(0) in less than 1 h, since the ratio of borane to palladium is much grater than that in Eq. 10.

21) Indeed, only trace amounts of dimer **13** were obtained in every cross-coupling reaction in Table 6.

22) Ref. 12, Chap 8.

23) H. C. Brown, C. G. Scouten, and R. Liotta, *J. Am. Chem. Soc.*, **98**, 1785 (1976).

24) H. C. Brown and N. Ravindran, *J. Am. Chem. Soc.*, **98**, 1785 (1976).

25) H. Yatagai, Y. Yamamoto, and K. Maruyama, *J. Org. Chem.*, **44**, 2567 (1979).

26) S. C. Watson and J. F. Eastham, *J. Organomet. Chem.*, **9**, 165 (1967).

27) T. A. Stephenson, S. M. Morehouse, A. R. Powell, J. P. Heffer, and G. Wilkinson, *J. Chem. Soc.*, **1965**, 3632.

28) Y. Ukai, H. Kawazura, and Y. Ishii, *J. Organomet. Chem.*,**165**, 253 (1974).

29) D. R. Caoulson, *Inorg. Synth.*, **13**, 121 (1972).

30) A. A. Grinberg and L. K. Shimonova, *Zh. Prikl. Khim.*, **26**, 880 (1953).

31) T. Tokuyama and T. Yamashita, "Shin-Jikken Kagaku Koza," ed by K. Maruyama, Maruzen, Tokyo (1976), Vol. 15, Chap 12.

32) The reduction of alkynes was performed by hydrogenation using Lindler catalyst.

33) a) J. J. Eisch and G. A. Damasevitz. *J. Org. Chem.*, **41**, 2214 (1976); b) G. Zweifel and R. B. Steele, *J. Am. Chem. Soc.*, **89**, 5085 (1967).

34) This authentic material was previously prepared (see Ref. 4a).

 © 1980 The Chemical Society of Japan Bull. Chem. Soc. Jpn., 53, 1677—1682 (1980)

Layered Compounds. LXIII.[1] Bromination of Double- and Triple-layered Paracyclophanes

Tetsuo Otsubo,† Hisanori Horita, Yosuke Koizumi, and Soichi Misumi*
The Institute of Scientific and Industrial Research, Osaka University, Suita, Osaka 565
(Received November 19, 1979)

[*m.m*][*n.n*]Triple-layered paracyclophanes underwent bromination to give exclusively monobromo derivatives substituted to the inner benzene. The reactions were markedly accelerated by the transannular electronic interaction as compared to [*n*]- and double-layered paracyclophanes, and their enhanced reactivities were demonstrated by some competitive reactions. The relative rates of [2.2] and [3.3]systems are in reverse order for the triple-layered and double-layered series. Their reaction mechanisms were discussed.

It is well-known that layered compounds exhibit unique properties originated from the transannular π-electronic interaction of the faced benzene rings.[2] The enhancement in chemical reactivities based on the interaction was observed in some studies on the electrophilic aromatic substitution of double-layered compounds such as [*n.n*]paracyclophanes[3] and janucene.[4] Since multilayered cyclophanes show a stronger π-electronic interaction than double-layered series,[2] it is very interesting to study their chemical properties. Multilayered [2.2]paracyclophanes are expected to be highly reactive for electrophilic aromatic substitutions. However, their severe strain prevents normal Friedel-Crafts reaction and leads to unusual reactions such as skeletal rearrangement.[5]

[3.3]Paracyclophane and its derivatives are expected to show a reactivity reflecting the transannular π-electronic interaction alone because they have far less strain than those of the corresponding [2.2]phane systems. In addition, they may give some of the information on the reactions, in which the formation of π-complex is an important step of aromatic substitution, since [3.3]paracyclophane show a strong π-basicity.[6] In these regards we have investigated the bromination of double and triple-layered paracyclophanes with [2.2] and [3.3]types of bridging chains and related cyclophanes.

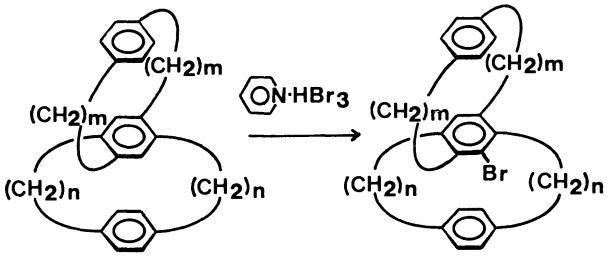

1, m = n = 2
2, m = 2, n = 3
3, m = n = 3
4, m = n = 2
5, m = 2, n = 3
6, m = n = 3

Scheme 1.

Results and Discussion

Bromination. Triple-layered paracyclophanes **1**—**3**[1,7,8] gave easily the corresponding monobromo derivatives **4**—**6** as a sole product by non-catalytic bromination. In the reactions, pyridinium hydrobromide perbromide afforded the bromides in better yields than with bromine alone. These brominations were complete in a shorter time than for [*n*]paracyclophane or double-layered paracyclophane, indicating an acceleration of the reaction based on strong transannular electronic stabilization in the transition state. No dibromo derivative was formed even if an excess of the reagent was used or the reaction time was prolonged. The first-introduced bromine substituent may prevent the following substitution because the steric requirement and the inductive effect of the very bromo group probably makes difficult the formation of the second σ-complex at the inner benzene.

On the other hand, bromination of 4,7-dimethyl-[2.2][2.2]paracyclophane **7**[7] afforded an equimolar mixture of inner-bromo derivative **8** and outer-bromo derivative **9**. Both reaction sites, the inner and the dimethylated outer benzenes, are in a similar electronic state with regard to alkyl substituent effect, but the outer benzene is of greater advantage than the inner with regards to steric surroundings. This sterical disadvantage for bromo-substitution at the inner benzene must be compensated by a stabilization of the intermediate due to a larger transannular electronic interaction to yield an equal amount of **8** and **9**.

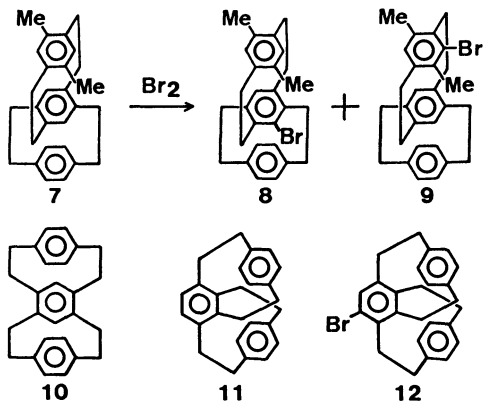

Scheme 2.

Treatment of **1** with bromine in the presence of iron powder gave skeletal rearrangement products **10**—**12**[5] together with **4**. Our previous papers reported that **1**

† Present address: Department of Applied Chemistry, Faculty of Engineering, Hiroshima University, Sendamachi, Hiroshima 730.

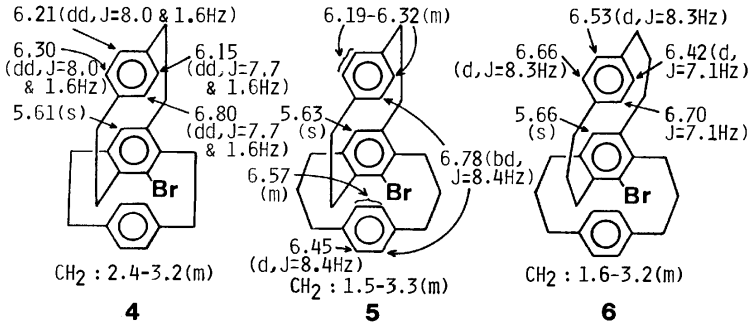

Fig. 1. NMR data of monobromo triple-layered paracyclophanes **4**—**6** in deuteriochloroform (δ, 100 MHz).

underwent the same skeletal rearrangement by catalysis of a variety of Brønsted acids such as tin(IV) chloride–hydrogen chloride.[5] So, it can be presumed that a similar acid, *e.g.*, iron(III) bromide–hydrogen bromide, was formed in the bromination reaction and acted as a catalyst for the rearrangement.

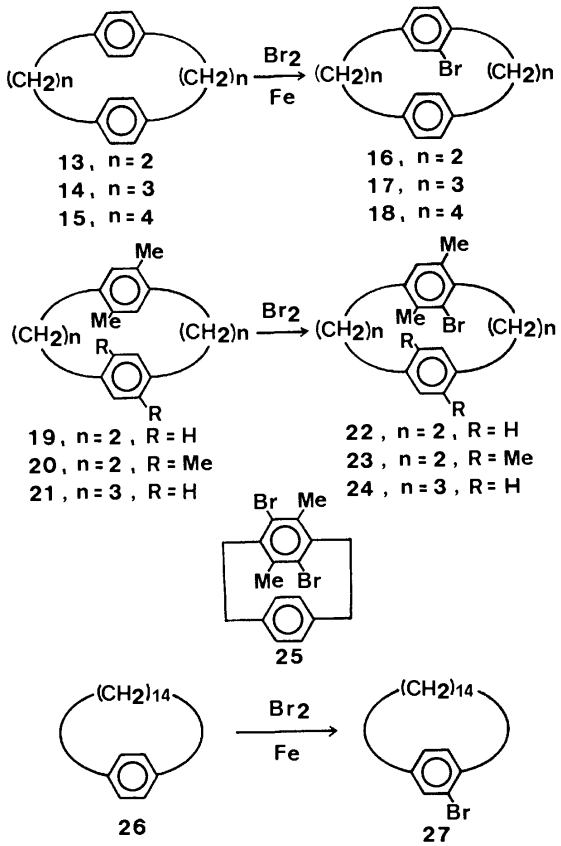

Scheme 3.

Monobromination of [*n.n*]paracyclophanes, **13**,[9] **14**,[10] and **15**, and [14]paracyclophane **26** was accomplished by bromine and iron catalyst. Methyl substituted [*n.n*]paracyclophanes **19**—**21**, on the other hand, were readily brominated by bromine alone. In this case, use of excess reagent provided dibromo derivative as represented by **25**, and pyridinium hydrobromide perbromide was less reactive.

Physical Properties of Bromo Derivatives. The structures of all the bromo derivatives were confirmed by NMR and mass spectra and elemental analyses. The NMR spectra of bromo triple-layered paracyclophanes show a characteristic pattern (Fig. 1). The aromatic signals of the parent triple-layered compounds appear at higher field due to the anisotropic effect of the faced aromatic rings,[11] but the introduction of bromine atom gives rise to a considerable downfield shift of the proton pseudo-gem to the bromine (0.65 ppm for the [2.2][2.2]system and 0.30 ppm for the [3.3][3.3]-system).[10,12] This may be explained in terms of steric compression effect of the bromine atom.

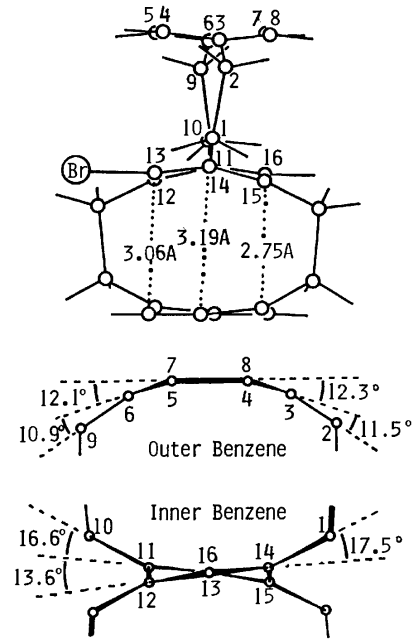

Fig. 2. Molecular structure of monobromo triple-layered [2.2]paracyclophane **4**.

An exact molecular structure of **4** was determined by X-ray crystallographic analysis (Fig. 2).[13] Its structural features are described below. The bending of the outer benzenes are almost the same as those of [2.2]paracyclophane **13**[14] and tetramethyl quadruple-layered [2.2]-paracyclophane,[15] and the inner benzene is twisted by a nearly equal twisting angle, *ca.* 13°, as that of the quadruple-layered paracyclophane. The non-bonding distance between the bromine and the pseudo-gem proton is an unexpectedly large value, 3.218 Å which is equal to or rather longer than ordinary van der Waals

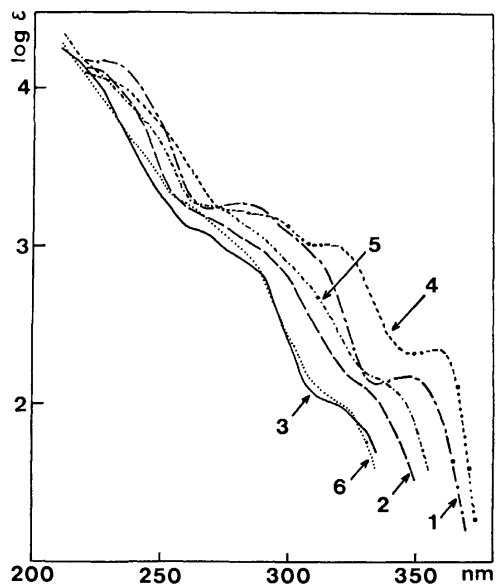

Fig. 3. The electronic spectra of triple-layered [*m.m*]-[*n.n*]paracyclophanes **1**—**3** and their monobromo derivatives **4**—**6** in tetrahydrofuran.

contact. Accordingly, it is concluded that the introduction of a bromine atom exerts less influence on the original structure of the parent hydrocarbon than expected from NMR analysis.

As shown in Fig. 3, the strong transannular electronic interactions of triple-layered paracyclophanes are indicated by marked bathochromic shifts of bands in their electronic spectra.[7,16] Although the spectrum of benzene itself is little affected by bromo substituent,[17] the substitution to triple-layered paracyclophanes gives rise to further bathochromic shifts of the longer wavelength bands except the [3.3][3.3]system. Thus, the substituent effect is dependent on the interplanar distance in the parent compounds, *viz.*, [2.2][2.2]PC **1**>[2.2][3.3]PC **2**>[3.3][3.3]PC **3** (PC=paracyclophane). Figure 4 shows the electronic spectra of monobromo dimethyl derivatives **8** and **9**. The inner bromo derivative **8** exhibits a significant red shift, whereas the outer bromo derivative **9** a hypsochromic shift of the longest wavelength band, supporting a much larger transannular electronic interaction due to the bromo substitution at the inner benzene as described above.

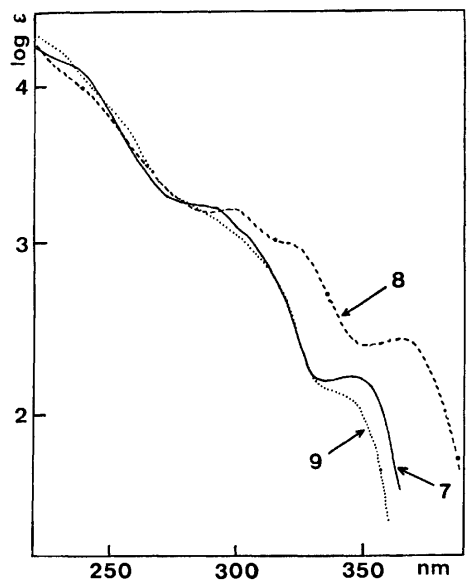

Fig. 4. The electronic spectra of dimethyl triple-layered [2.2]paracyclophane **7** and its monobromo derivatives **8** and **9** in tetrahydrofuran.

Table 1. Competitive reactions of paracyclophanes

Run	Compounds	Reagent[a]	Product ratio
1	**1** and **2**	A or B	**4** : **5**=20 : 1
2	**2** and **3**	A	**5** : **6**= 3 : 1
3	**7**	B	**8** : **9**= 1 : 1
4	**1** and **7**	B	**4** : **8**+**9**= 1.5 : 1
5	**13** and **14**	C	**16** : **17**= 1 : 2
6	**13** and **15**	C	**16** : **18**= 9 : 1
7	**15** and **26**	C	**18** : **27**= 1.4 : 1
8	**19** and **20**	B	**22** : **23**= 1 : 3
9	**19** and **21**	B	**22** : **24**= 1 : 1.2
10	**1** and **19**	B	**4** : **22**= 1 : 0
11	**1** and **20**	B	**4** : **23**= 1 : 0
12	**2** and **19**	B	**5** : **22**= 1 : 0
13	**3** and **21**	B	**6** : **24**= 1 : 0
14	**7** and **20**	B	**8**+**9** : **23**= 1 : 0

a) A: Pyridinium hydrobromide perbromide. B: Bromine. C: Bromine and iron powder.

Competitive Reactions. The bromination of layered paracyclophanes is surely accelerated by the transannular electronic interaction in the transition state. The magnitude of the acceleration was estimated by competitive reactions summarized in Table 1. The reactions are obviously speeded up with an increase of the layer number regardless of kinds of reagent. Especially the reactions of triple-layered series are overwhelmingly faster than those of double-layered series (Runs 10—14). The relative rate of triple-layered series is [2.2][2.2]PC **1**: [2.2][3.3]PC **2**: [3.3][3.3]PC **3**=60: 3: 1 (Runs 1 and 2). This order is in accord with the relative strength of transannular electronic interaction above-stated in the electronic spectra.

On the other hand, the relative rate of double-layered series using [14]paracyclophane **26** as a standard is as follows; [3.3]PC **14**: [2.2]PC **13**: [4.4]PC **15**: [14]PC **26**=29: 13: 1.4: 1 (Runs 5—7). The rather higher reactivity of [3.3]system **14** than [2.2]system **13** is particularly surprising and in conflict with the results of triple-layered series. The difference between iron-catalytic and non-catalytic conditions can be ruled out for interpretation of the above problem because a non-catalyzed competitive reaction of the dimethyl series, **19** and **21**, gave also the same order, although the advantage of [3.3]system becomes relatively smaller in the presence of methyl groups having a large substituent effect.

The difference in relative rates of the two series may be explained by a mechanism described below. In the substitution reaction of triple-layered cyclophanes **1**—**3**, the formation of π-complex on the inner benzenes is

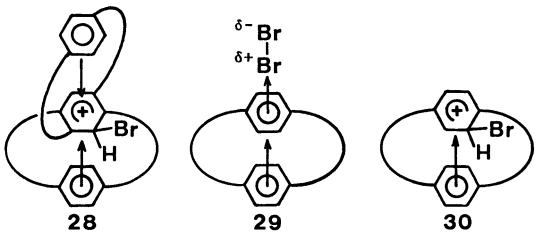

Scheme 4.

sterically impossible although their π-basicities are increased by four alkyl substituents. Therefore, the electrophile must directly attack the inner benzenes to form σ-complex **28** which is stabilized by transannular charge delocalization to both outer benzenes. Since the transition state resembles the σ-complex, the relative rate of triple-layered series reflects the transannular electronic interaction of σ-complex. On the other hand, the reactions of double-layered paracyclophanes are expected to proceed *via* the formation of π-complex **29** followed by σ-complex **30** like an ordinary electrophilic aromatic substitution. The transannular electronic interaction must be more effective in the σ-complex having ionic structure than in the π-complex having charge-transfer character. When the σ-complex is highly stabilized by such an interaction, its potential energy may be at lower level than that of the π-complex. This consideration is consistent with Olah's proposal that in highly exothermic electrophilic aromatic substituion the reaction state with the highest energy leads to the formation of a π-complex.[18] On taking account of a noticeable property that [3.3]paracyclophane **14** interacts as a much stronger π-base than [2.2]paracyclophane **13**,[6] the reaction pathways are understood by the diagram shown in Fig. 5. The figure reveals that the formation of π-complex is rate-determining and the [3.3]system takes a lower energy path than the [2.2]system. Thus, the rate-determining step resembles σ-complex for triple-layered series and π-complex for double-layered series, respectively.

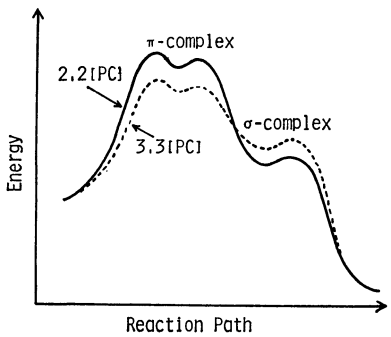

Fig. 5. A reaction diagram for bromination of [2.2]- and [3.3]paracyclophanes.

The above explanation is also supported from a viewpoint of steric effect. The introduction of methyl groups at the outer benzene of triple-layered [2.2][2.2]-paracyclophane **1** results in a 66% reduction of the rate for the inner substitution (Run 4). The methyl group must block the formation of σ-complex or the elimination of proton from σ-complex. On the other hand, such a steric blocking of pseudo-methyl group is not recognized in the reactions of double-layered cyclophanes. In a competitive reaction of **19** and **20**, (Run 8), **20** having pseudo-gem methyl group is rather more reactive than **19**. This also confirms that the formation of π-complex is rate-determining because the pseudo-gem methyl group does not sterically prevent the formation of π-complex but accelerates it due to larger stabilization resulted from an increased transannular electron release of the attached, non-complexed benzene.

Experimental

Melting points are uncorrected. All the solvents are of reagent grade unless otherwise stated. NMR spectra were taken with Hitachi Perkin-Elmer R-20 (60 MHz) and JEOL FX-100 (100 MHz) spectrometers using TMS as an internal standard, MS with Hitachi RMU-7 spectrometer at 70 eV using a direct insertion technique, and UV with Hitachi EPS-3T spectrophotometer.

The syntheses of all the starting material except **21** were reported in the previous papers.[7,8,19,20] 5,8-Dimethyl[3.3]-paracyclophane **21** was prepared in the same way as that used for [3.3]paracyclophane **14**;[19] colorless scales from hexane, mp 119—120.5 °C, MS *m/e* 264 (M^+). NMR ($CDCl_3$, 100 MHz): δ 1.8—2.3 (m, 4H, CH_2), 2.17 (s, 6H, CH_3), 2.4—2.9 (m, 8H, benzylic CH_2), 6.38 (s, 2H, ArH), 6.65 (dd, J=7.8 and 1.8 Hz, 2H, ArH), 6.89 (dd, J=7.8 and 1.8 Hz, ArH).

12-Bromo[2.2][2.2]paracyclophane **4**. *a) With Pyridinium Hydrobromide Perbromide*: A mixture of [2.2][2.2]paracyclophane **1**[7] (1 g, 2.95 mmol) and pyridinium hydrobromide perbromide (2.36 g, 7.39 mmol) in 80 ml of dry dichloromethane was stirred for 2.5 h at 0 °C. The reaction mixture was filtered through a column of neutral alumina and recrystallized from benzene to give colorless prisms, 0.909 g (74%), mp 236 °C (dec. in sealed tube), MS *m/e* 416, 418 (M^+). Found: C, 74.82; H, 5.86; Br, 18.73%. Calcd for $C_{26}H_{25}Br$: C, 74.82; H, 6.04; Br, 19.14%.

b) With Bromine–Iron: Into a solution of **1** (100 mg, 0.30 mmol) in 15 ml of dry dichloromethane was dropwise added bromine (101 mg, 0.63 mmol) in 2.8 ml of carbon tetrachloride. The mixture was stirred for 20 min at room temperature and filtered through a short column of neutral alumina. Recrystallization of the eluted product from benzene gave colorless prisms, 44 mg (36%).

c) With Bromine–Iron: Iron powder (11 mg) was stirred with 4 ml of dichloromethane and 0.5 ml of a solution of bromine (133 mg, 0.83 mmol) in 4 ml of carbon tetrachloride for 2.5 h at 25 °C. Dichloromethane (18 ml) was added and the resulting mixture was brought to reflux. [2.2][2.2]-Paracyclophane **1** (245 mg, 0.72 mmol) was added in one portion and the remaining bromine solution was added dropwise within 10 min to the refluxing, stirred solution. The mixture was stirred under reflux for 30 min and quenched with 10% $NaHSO_3$ solution. The organic layer was separated and washed with water, sat. $NaHCO_3$ solution, and water, successively. After dryness over anhyd magnesium sulfate, the solvent was condensed and the remainder was chromatographed on alumina with 1:9 dichloromethane–hexane. The main fraction consisted of a mixture of four products **4**, **10**, **11**, and **12**. Careful rechromatography on silica gel with 1: 50 benzene-hexane gave first **4** (14.4 mg,

4.8%), secondly **11**[5] (23.0 mg, 9.4%), and finally a mixture of **10** and **12**. Separation of the mixture was accomplished by gel permeation liquid chromatography, **10**[5] (8.4 mg, 3.4%) and **12**[5] (9.2 mg, 3.1%).

12-Bromo[2.2][3.3]paracyclophane ***5***. A mixture of [2.2]-[3.3]paracyclophane **2**[19] (25.2 mg, 0.07 mmol) and pyridinium hydrobromide perbromide (43.5 mg, 0.14 mmol) in 2.5 ml of dry dichloromethane was stirred for one hour at room temperature. The solution was washed with dil sodium sulfite solution and then sat sodium chloride solution. After drying over anhyd magnesium sulfate, the solvent was evaporated. The residue was chromatographed on silica gel with benzene and the eluted product was recrystallized from hexane–benzene to give colorless plates, 22.6 mg (74%), mp 186—188 °C, MS *m/e* 444, 446 (M^+). Found: C, 75.31; H, 6.41; Br, 17.92%. Calcd for $C_{28}H_{29}Br$: C, 75.50; H, 6.56; Br, 17.94%.

14-Bromo[3.3][3.3]paracyclophane ***6***. [3.3][3.3]Paracyclophane **3**[8] (9.6 mg, 0.024 mmol) was treated with pyridinium hydrobromide perbromide (15 mg, 0.047 mmol) in 2 ml of dry dichloromethane for 7 h at room temperature. The mixture was worked up as described for **5**. Recrystallization from hexane gave colorless prisms, 5.0 mg (44%), mp 207—208 °C, MS *m/e* 472, 474 (M^+). Found: C, 75.93; H, 7.08; Br, 16.64%. Calcd for $C_{30}H_{33}Br$: C, 76.10; H, 7.02; Br, 16.88%.

12-Bromo- and 5-Bromo-4,7-dimethyl[2.2][2.2]paracyclophanes ***8*** *and* ***9***. Into a stirred solution of bromine (116 mg, 0.73 mmol) in 3 ml of carbon tetrachloride and 20 ml of dichloromethane was added 4,7-dimethyl[2.2][2.2]paracyclophane **7**[7] (100 mg, 0.27 mmol) in one portion. The mixture was stirred for 30 min at 19 °C. After evaporation of the solvents, the residue was chromatographed on silica gel with hexane, 1: 50 benzene–hexane, and 1: 20 benzene–hexane, successively. From the first eluate was obtained one isomer **9**, 9.9 mg (8%), colorless prisms from benzene–hexane, mp 193—194 °C, MS *m/e* 444, 446 (M^+). NMR ($CDCl_3$, 60 MHz): δ 1.92 (s, 3H, CH_3), 1.97 (s, 3H, CH_3), 2.1—3.5 (m, 16H, CH_2), 5.68 (s, 1H, inner ArH), 5.72 (s, 1H, inner ArH), 5.91 (s, 1H, outer ArH), 6.24 (s, 4H, outer ArH). Found: C, 75.24; H, 6.43; Br, 18.14%. Calcd for $C_{28}H_{29}Br$: C, 75.50; H, 6.56; Br, 17.94%.

From the second eluate was obtained another isomer **8**, 9.9 mg (8%), colorless prisms from hexane, mp 172—173 °C, MS *m/e* 444, 446 (M^+). NMR ($CDCl_3$, 60 MHz): δ 1.97 (s, 3H, CH_3), 2.15 (s, 3H, CH_3), 2.3—3.4 (m, 16H, CH_2), 5.79 (s, 1H, inner ArH), 5.92 (s, 1H, outer ArH), 5.94 (s, 1H, outer ArH), 6.14 (dd, J=8 and 2 Hz, 1H, outer ArH), 6.25 (dd, J=9 and 2 Hz, 1H, outer ArH), 6.36 (dd, J=9 and 2 Hz, 1H, outer ArH), 6.87 (dd, J=8 and 2 Hz, 1H, outer ArH). Found: C, 75.57; H, 6.46; Br, 17.90%. Calcd for $C_{28}H_{29}Br$: C, 75.50; H, 6.56; Br, 17.94%.

Bromination of [n.n]paracyclophanes. The preparation of 4-bromo[2.2]paracyclophane **16**[9] is described below as a typical experiment.

Iron powder (8 mg) was added in a solution of bromine (156 mg, 1 mmol) in 3.8 ml of carbon tetrachloride and stirred for one hour at room temperature. [2.2]Paracyclophane **13** (166 mg, 0.8 mmol) in 20 ml of dry dichloromethane was added, and the stirring was continued for 4 h. The reaction was quenched with dil sodium hydrogensulfite soln, washed with sat. aq sodium chloride soln, and dried over magnesium sulfate. After evaporation of the solvents, the residue was chromatographed on silica gel with benzene and recrystallized from hexane to give almost pure 4-bromo[2.2]-paracyclophane **16**, 167 mg (73%). An analytical sample was purified by gel permeation liquid chromatography and again recrystallization from hexane, colorless plates, mp 133—134 °C, MS *m/e* 286, 288 (M^+). NMR ($CDCl_3$, 100 MHz): δ 2.6—3.7 (m, 8H, CH_2), 6.48 (dd, J=7.9 and 2.0 Hz, 1H, pseudo-ortho ArH), 6.50 (m, 4H, ArH), 7.14 (dt, J=7.9, 2.0, and 2.0 Hz, 1H, pseudo-gem ArH). Found: C, 66.69; H, 5.04; Br, 27.81%. Calcd for $C_{16}H_{15}Br$: C, 66.91; H, 5.26; Br, 27.82%.

5-Bromo[3.3]paracyclophane ***17***: Yield 73%, colorless crystals from hexane, mp 149—150 °C (lit,[10] mp 153—154 °C), MS *m/e* 314, 316 (M^+). NMR ($CDCl_3$, 100 MHz): δ 1.7—3.2 (m, 12H, CH_2), 6.61 (s, 2H, meta and para ArH), 6.66 (d, J=8.4 Hz, 1H, pseudo-ortho ArH), 6.75 (s, 2H, pseudo-meta and -para ArH), 6.90 (s, 1H, ortho ArH), 7.03 (d, J=8.4 Hz, 1H, pseudo-gem ArH).

6-Bromo[4.4]paracyclophane ***18***: Yield 81%, colorless plates from pentane, mp 89—89.5 °C, MS *m/e* 342, 344 (M^+). NMR ($CDCl_3$, 100 MHz): δ 1.1—3.0 (m, 16H, CH_2), 6.58 (dd, J=7.6 and 1.5 Hz, 1H, para ArH), 6.6—6.9 (m, 5H, ArH), 6.96 (d, J=1.5 Hz, ortho ArH). Found: C, 69.85; H, 6.67; Br, 23.00%. Calcd for $C_{20}H_{23}Br$: C, 69.97; H, 6.75; Br, 23.27%.

5-Bromo-4,7-dimethyl[2.2]paracyclophane ***22*** *and 5,8-Dibromo-4,7-dimethyl[2.2]paracyclophane* ***25***. Into a solution of 4,7-dimethyl[2.2]paracyclophane **19**[7] (300 mg, 1.27 mmol) was added bromine (234 mg, 1.46 mmol) in 6 ml of carbon tetrachloride. The mixture was stirred for 2.5 h at 35 °C, and worked up as described in the bromination of [*n.n*]paracyclophanes. Chromatography of the crude product on silica gel with hexane gave dibromo product **25** from the first eluate and monobromo derivative **22** from the following few fractions.

22: yield 310 mg (78%), colorless plates from hexane, mp 97.5—98.5 °C, MS *m/e* 314, 316 (M^+). NMR ($CDCl_3$, 60 MHz): δ 2.11 (s, 3H, CH_3), 2.15 (s, 3H, CH_3), 2.4—3.5 (m, 8H, CH_2), 6.14 (s, 1H, ArH), 6.44 (dd, J=8 and 2 Hz, 1H, ArH), 6.68 (dd, J=8 and 2 Hz, 1H, ArH), 6.80 (dd, J=8 and 2 Hz, 1H, ArH), 6.95 (dd, J=8 and 2 Hz, 1H, ArH). Found: C, 68.50; H, 5.97; Br, 25.05%. Calcd for $C_{18}H_{19}Br$: C, 68.56; H, 6.08; Br, 25.36%.

25: yield 30 mg (6%), colorless scales from benzene–hexane, mp 168.5—169.5 °C, MS *m/e* 392, 394 (M^+). NMR ($CDCl_3$, 60 MHz): δ 2.21 (s, 3H, CH_3), 2.8—3.6 (m, 8H, CH_2), 6.64 (dd, J=8 and 2 Hz, 2H, ArH), 6.91 (dd, J=8 and 2 Hz, 2H, ArH). Found: C, 54.67; H, 4.43; Br, 40.06%. Calcd for $C_{18}H_{18}Br_2$: C, 54.83; H, 4.61; Br, 40.56%.

5-Bromo-4,7,12,15-tetramethyl[2.2]paracyclophane ***23***. 4,7,12,15-Tetramethyl[2.2]paracyclophane **20**[7] (246 mg, 0.93 mmol) in 20 ml of dry dichloromethane was treated with bromine (151 mg) in 5 ml of carbon tetrachloride at 28 °C. After 60 min from the start, the mixture was worked up as usual. The main product **23** was purified by column chromatography on silica gel with hexane and recrystallization from hexane, 237 mg (74%), colorless plates, mp 159.5—160 °C, MS *m/e* 342, 344 (M^+). NMR ($CDCl_3$, 60 MHz): δ 2.03 (s, 3H, CH_3), 2.12 (s, 3H, CH_3), 2.18 (s, 3H, CH_3), 2.28 (s, 3H, CH_3), 2.4—3.8 (m, 8H, CH_2), 6.40 (bs, 3H, ArH). Found: C, 69.93; H, 6.78; Br, 22.97%. Calcd for $C_{20}H_{23}Br$: C, 69.97; H, 6.75; Br, 23.28%.

6-Bromo-5,8-dimethyl[3.3]paracyclophane ***24***. 5,8-Dimethyl[3.3]paracyclophane **21** (26.4 mg, 0.10 mmol) in 3 ml of dry dichloromethane was treated with bromine (20 mg, 0.13 mmol) in 0.5 ml of carbon tetrachloride at room temperature. After 4 h, the mixture was worked up as usual. The main product **24** was purified by gel permeation liquid chromatography and then column chromatography on silica gel with hexane, 16 mg (46%), colorless scales from ethanol, mp 108—109 °C, MS *m/e* 342, 344 (M^+). NMR ($CDCl_3$, 100 MHz): δ 1.7—3.2 (m, 12H, CH_2), 2.18 (s, 3H, CH_3),

2.29 (s, 3H, CH_3), 6.27 (s, 1H, ArH), 6.71 (ABd, J=9 Hz, 1H, ArH), 6.75 (ABd, J=9 Hz, 1H, ArH), 6.91 (ABbd, J=9 Hz, 2H, ArH). Found: C, 69.73; H, 6.61; Br, 23.09%. Calcd for $C_{20}H_{23}Br$: C, 69.97; H, 6.75; Br, 23.27%.

16-Bromo[14]paracyclophane **27**. Bromine (20 mg, 0.13 mmol) in 0.5 ml of carbon tetrachloride was stirred with iron powder (5 mg) for 30 min at room temperature. [14]Paracyclophane **26**[20] (29 mg, 0.105 mmol) in 5 ml of dry dichloromethane was added at once. The mixture was stirred for 1.5 days and worked up in the usual way. The main product **27** was purified by column chromatography on silica gel with hexane and gel permeation liquid chromatography, 15 mg (40%), colorless oil, MS *m/e* 350, 352 (M^+). NMR ($CDCl_3$, 100 MHz): δ 0.6—1.8 (m, 24H, CH_2), 2.4—3.0 (m, 4H, benzylic CH_2), 7.01 (dd, J=7.7 and 0.5 Hz, 1H, ArH), 7.08 (d, J=7.7 Hz,1H,ArH),7.33 (d, J=0.5 Hz,1H,ArH). Found: C, 68.14; H, 9.11; Br, 23.04%. Calcd for $C_{20}H_{31}Br$: C, 68.37; H, 8.89; Br, 22.74%.

Competitive Reactions. An equimolar mixture of two cyclophanes (2 mol) was treated with a reagent (1 mol) indicated in Table 1. The reaction conditions were essentially the same as in the experimental part above-stated for the bromination of each cyclophane. The reaction time was controlled in such a way that about one-half amount of the more reactive component was consumed. Analysis of the reaction mixture was carried out by proton NMR measurement. The product ratio was determined on the basis of the integration of the isolated, appropriate peaks. On the other hand, carbon NMR analysis was performed for Run 6 alone, because nothing was clearly isolated peaks in the PMR spectrum of the products.[21]

CMR datum of **16** ($CDCl_3$, TMS standard, JEOL FX-100):[22] δ 33.477 (C-1), 34.793 (C-2), 35.475 and 35.816 (C-9,10), 126.941 (C-4), 128.648 (C-13), 131.424 (C-7), 132.203, 132.835, and 133.225 (C-12,15,16), 134.980 (C-8), 137.170 (C-5), 139.026 (double) and 139.268 (C-6,11,14), 141.513 (C-3).

CMR datum of **18**:[22] δ 26.460 (C-3), 28.458, 28.653, and 28.848 (C-2,12,13), 34.842 (C-1), 35.134 (double) and 35.280 (C-4,11,14), 123.386 (C-6), 127.186 (C-17), 128.063 (C-9), 128.352 (double) and 128.843 (C-16,19,20), 130.839 (C-10), 132.936 (C-7), 137.809 (C-8), 139.026 and 139.268 (C-15,18), 141.607 (C-5).

References

1) Part LXII: T. Otsubo, T. Kohda, and S. Misumi, *Bull. Chem. Soc. Jpn.*, **53**, 512 (1980).

2) S. Misumi and T. Otsubo, *Acc. Chem. Res.*, **11**, 251 (1978) and references cited therein.

3) D. J. Cram, W. J. Wechter, and R. W. Kierstead, *J. Am. Chem. Soc.*, **80**, 3126 (1958).

4) S. J. Cristol and W. Y. Lim, *J. Org. Chem.*, **34**, 1 (1969).

5) H. Horita, N. Kannen, T. Otsubo, and S. Misumi, *Tetrahedron Lett.*, **1974**, 501; H. Horita, Y. Koizumi, T. Otsubo, Y. Sakata, and S. Misumi, *Bull. Chem. Soc. Jpn.*, **51**, 2668 (1978).

6) D. J. Cram and R. H. Bauer, *J. Am. Chem. Soc.*, **81**, 5971 (1959); M. Sheehan and D. J. Cram, *ibid.*, **91**, 3553 (1969).

7) T. Otsubo, S. Mizogami, I. Otsubo, Z. Tozuka, A. Sakagami, Y. Sakata, and S. Misumi, *Bull. Chem. Soc. Jpn.*, **46**, 3519 (1973). U

8) T. Otsubo, T. Kohda, and S. Misumi, *Tetrahedron Lett.*, **1978**, 2507.

9) D. J. Cram and A. C. Day, *J. Org. Chem.*, **31**, 1227 (1966).

10) M. Sheehan and D. J. Cram, *J. Am. Chem. Soc.*, **91**, 3544 (1969).

11) T. Otsubo, S. Mizogami, Y. Sakata, and S. Misumi, *Bull. Chem. Soc. Jpn.*, **46**, 3831 (1973).

12) H. J. Reich and D. J. Cram, *J. Am. Chem. Soc.*, **91**, 3534 (1969).

13) Y. Koizumi, T. Toyoda, H. Horita, and S. Misumi, presented at 32nd National Meeting of the Chemical Society of Japan, Tokyo, April 1975, Summary I, p. 184.

14) C. J. Brown, *J. Chem. Soc.*, **1953**, 3265; D. K. Lonsdale, H. J. Milledge, and K. V. Rao, *Proc. Roy. Soc. London, Ser. A*, **255**, 82 (1960); H. Hope, J. Bernstein, and K. N. Trueblood, *Acta Crystallogr., Sect. B*, **28**, 1733 (1972).

15) H. Mizuno, K. Nishiguchi, T. Otsubo, S. Misumi, and N. Morimoto, *Tetrahedron Lett.*, **1972**, 4981: H. Mizuno, K. Nishiguchi, T. Toyoda, T. Otsubo, S. Misumi, and N. Morimoto, *Acta Crystallogr., Sect. B*, **33**, 329 (1977).

16) I. H. Miller, L. Glass, and S. A. Rice, *J. Am. Chem. Soc.*, **88**, 5063 (1966); S. Iwata, K. Fuke, M. Sasaki, S. Nagakura, T. Otsubo, and S. Misumi, *J. Mol. Spectrosc.*, **46**, 1 (1973).

17) H. H. Jaffé and M. Orchin, "Theory and Applications of Ultraviolet Spectroscopy," John Wiley and Sons, Inc., New York, N. Y. (1962), p. 247.

18) G. A. Olah, *Acc. Chem. Res.*, **4**, 240 (1971).

19) T. Otsubo, M. Kitasawa, and S. Misumi, *Chem. Lett.*, **1977**, 977.

20) T. Otsubo and S. Misumi, *Synth. Commun.*, **8**, 285 (1978).

21) For CMR data of [*n*]-, [*n.n*]-, and multilayered paracyclophanes, see, T. Kaneda, T. Otsubo, H. Horita, and S. Misumi, *Bull. Chem. Soc. Jpn.*, **53**, 1015 (1980).

22) For the numbering of cyclophanes, see B. H. Smith, "Bridged Aromatic Compounds," Academic Press Inc., New York, N. Y. (1964).

 © 1980 The Chemical Society of Japan Bull. Chem. Soc. Jpn., 53, 1683—1688 (1980)

Photochemical Reactions of Dicyanobenzenes with Aliphatic Amines

Mamoru OHASHI,* Kentaro MIYAKE, and Kazuo TSUJIMOTO
Department of Materials Science, The University of Electro-Communications, Chofu, Tokyo 182
(Received November 22, 1979)

Upon irradiation, *p*-dicyanobenzene reacted with primary, secondary, and tertiary aliphatic amines to give substitution products in which one of the cyano groups was replaced by the amine at α-CH position or by an alkyl group of the amine. *o*-Dicyanobenzene reacted similarly, but the *meta*-isomer did not react under similar conditions. The rates of the fluorescence quenching of *p*-dicyanobenzene with the amines are close to the diffusion-controlled rate, but are somewhat dependent on the ionization potentials of the amines. When the substitution product was irradiated, the corresponding alkylation product was obtained. The mechanisms of these reactions have been investigated by the use of such proton donors as MeOH(MeOD); on the basis of those investigations, new photochemical reactions involving charge-transfer, followed by proton-transfer and then addition-elimination, are proposed, as well as a new type of photo-induced Birch reduction.

Since Bryce-Smith and his co-workers first reported the photoaddition of aliphatic amines to benzene in 1967,[1] a number of photochemical reactions of arenes with amines have been extensively studied. For instance, naphthalene,[2] stilbene[3] and anthracene[4] undergo photoaddition of various amines. It has been well-documented that these photochemical reactions proceed through exciplexes or solvated radical anion-radical cation pairs.

For several years we also have examined the photochemical reactions of charge-transfer complexes and have established several new reactions which proceed through radical anion-radical cation pairs. For instance, on charge-transfer excitation, such typical electron acceptors as tetracyanobenzene (TCNB),[5] tetracyanoquinodimethane (TCNQ),[6] and tetracyanoethylene (TCNE),[7] react with π-donor toluene derivatives, or n-donor ethers, to give substitution or addition products. Here, irradiation within the charge-transfer absorption bands of the system produces a donor radical cation as well as an acceptor radical anion. Subsequent proton-transfer from the donor to the acceptor yields a radical pair, which then couples to lead to an addition product. The energy required for the electron transfer is related to the ionization potential of the donor and the electron affinity of the acceptor according to the Weller equation.[8] It has been shown that the smaller the donor's ionization potentials, and the larger the acceptor's electron affinity, the easier the charge-transfer reaction. In accordance with this, strong donor-acceptor pairs, such as TCNQ or TCNE–amine systems, undergo addition reactions upon only heating,[9] while the reaction of TCNE, TCNQ, or TCNB with aromatic hydrocarbons or ethers takes place only in the excited state, not in the ground state.

Now we have examined photochemical reactions of dicyanobenzenes, relatively weak electron acceptors, with amines, strong electron donors.[10] Since the ultraviolet spectra of dicyanobenzene–amine systems do not exhibit any charge-transfer absorption band, charge-transfer complex formation in the ground state is either absent or very weak. In this case, the electron-transfer reactions do take place upon irradiation.

Results and Discussion

Photochemical Reactions of Dicyanobenzenes with Triethylamine. The irradiation of a mixture of *o*-dicyanobenzene (0.05 M, **1**) and triethylamine (0.5 M) in acetonitrile with a low-pressure mercury arc gave a substitution product (**4**) in 79% yield, together with small amounts of *o*-ethylbenzonitrile (**5**, 9%) and benzonitrile (trace). The quantum yield of the disappearance of the starting material was measured at 0.15 by means of trioxalatoferrate (III) actinometry. Similarly, *p*-dicyanobenzene (**3**) reacted with triethylamine under similar conditions to give the corresponding substitution product (**8**) and *p*-ethylbenzonitrile (**9**) in 18 and 56% yields respectively. A trace amount of benzonitrile was also detected. Again, the quantum yield of disappearance of *p*-dicyanobenzene was 0.15. On the contray, *m*-dicyanobenzene (**2**) was inert under similar conditions: after long irradiation (20 h), only a trace amount of *m*-ethylbenzonitrile (**7**) was detected by gas chromatography-mass spectrometry and a large amount of the starting materials was recovered.

Although the photochemical reactivities of **1** and **3** were similar, their product distributions were different; *i.e.*, in the photochemical reaction of **1**, the substitution product, **4**, was the major one, while the alkylated product, **9**, was the major one in the case of **3**. It is also remarkable that the *meta*-isomer (**2**) has a very low reactivity in comparison with that of the *ortho*- or

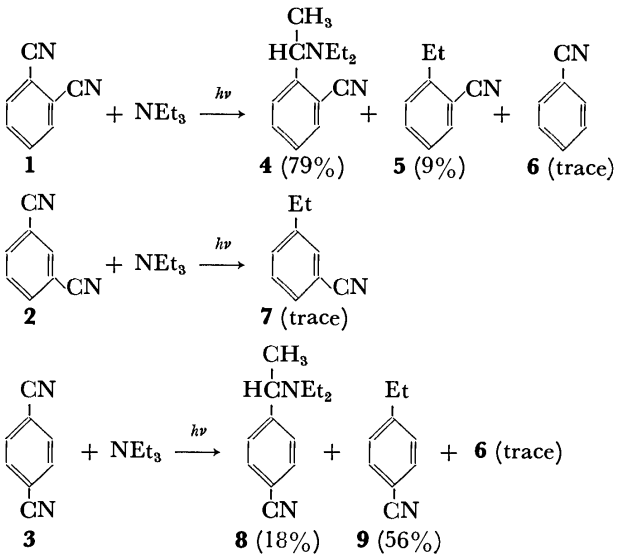

Scheme 1.

para-isomer. The difference in the reactivities of the isomers may suggest that a complication is involved in the reactions.

Reactions analogous to those in Scheme 1, but using tetramethylurea in place of triethylamine, have been reported.[11]

Photochemical Reactions of p-*Dicyanobenzene with Primary and Secondary Amines.* It has been reported that the photoaddition of primary and secondary amines to benzene or the photosubstitution in a difluorobenzene–diethylamine system occurs at the NH group in the amine.[1,12] Similar results have been reported in anthracene-amine systems.[4] We ourselves have found that, in contrast with the benzene or anthracene-primary or secondary amine systems, cyclohexylamine, a primary amine, and diisopropylamine, a secondary amine, reacted with **3** upon irradiation not at the NH group, but at the α-CH instead.[10b] Recently, it has also been reported that the photoamination of pyridine or chlorobenzene resulted in the formation of substitution derivatives at the α-CH position of the amine.[13]

The irradiation of a solution of **3** (0.046 M) and cyclohexylamine (2.6 M) in acetonitrile with a medium-pressure mercury arc for 13 h gave *p*-cyclohexylbenzonitrile (**10**), along with a substitution product (**11**), in 11 and 10% yields respectively. Similarly, the irradiation of **3** in acetonitrile in the presence of diisopropylamine (0.87 M) under similar conditions gave *p*-isopropylbenzonitrile (**12**) and a substitution product (**13**) in 30 and 25% yields respectively. A small amount of benzonitrile was also detected in both reaction mixtures by gas chromatography-mass spectrometry. The reactivities of the amines, however, were very low in comparison with that of triethylamine. The reaction scarcely occured under the same irradiation conditions as those of the aforementioned **3**-triethylamine system. The structures of the alkylated products, **10** and **12** were confirmed by direct comparison with the authentic specimens. Structures of **11** and **13** were assigned to the substitution products on the basis of elementary analyses and spectral investigations; the IR spectrum of **11** shows peaks at 3380 and 3310 cm^{-1}, characteristic of a NH_2 groups, while **13** shows a peak at 3330 cm^{-1} (NH) in the IR spectrum and a singlet 6H peak ($>CMe_2$) at δ 1.40 in the NMR spectrum, indicating that the compounds have structures substituted at the α-CH groups of the amines. Structures **14** and **15** were ruled out by the spectroscopic evidence (see Experimental section). No products corresponding to the adducts of **3** at the NH groups of the amines have been detected.

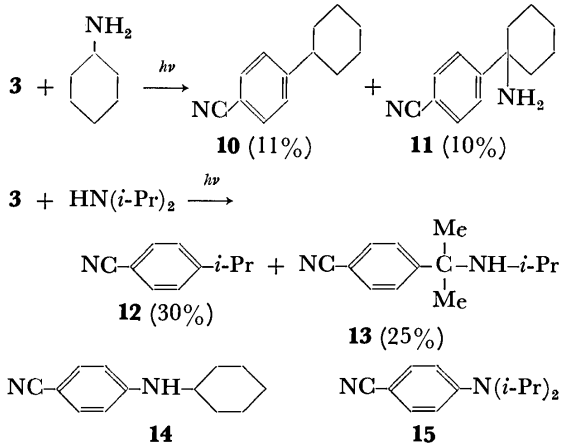

Scheme 2.

Mechanism for the Substitution Reactions. When the reaction of **1** with triethylamine was carried out in CH_2Cl_2, the reaction did not proceed; this suggested that the reaction takes place *via* a dipolar intermediates. Methanol also quenched the reaction. This behavior is similar to the case of the photo-induced substitution of TCNB–toluene systems, implying the participation of a proton-transfer process.[5a,b] When the reaction of **3** with triethylamine was carried out with oxygen bubbling through the mixture, **8** and **9** were not detected as products in the reaction mixture, but a trace amount (<1%) of *p*-cyanobenzamide was obtained instead, along with a large amount of the recovered starting materials. The quenching action of oxygen suggests that the reaction proceeds through a triplet state or an ion-radical intermediate. 1,3-Pentadiene (0.01 M), however, failed to quench the reaction. In order to clarify the multiplicity of the reactive state, fluorescence quenching experiments were performed.

The results of the Stern-Volmer treatments of the fluorescence quenching of **3** with the amines are summarized in Table 1. The kq values obtained are close to the diffusion-rate constant. The trend for amines with lower ionization potentials to be more efficient quenchers resembles that to be found in anthracene–amine systems and other general electron donor–acceptor systems.[4] Neither charge-transfer absorption nor exciplex emission was observed in these systems. The fluorescence of *o*-dicyanobenzene (**1**) was similarly quenched by triethylamine with a $k_q\tau$ value of 133 M^{-1}. It may be concluded from these experiments that the reactive species is a singlet state of the dicyanobenzene and that the primary photochemical step must be electron-transfer from the amine to the aromatics, as is usual in arene–amine systems.

The mechanisms of the fluorescence quenching of arenes by amines are probably the same in these systems, but those of the subsequent substitution differ. For instance, while the quenching of anthracene fluorescence by secondary amines and by tertiary amines proceeds *via* the same mechanism, the photochemical reactions of anthracene with secondary amines proceed *via* a different mechanism from that with a tertiary amine.[4] Concerning the molecularities of these reactions, it has been suggested that the excited charge-transfer species of a benzene–secondary amine system decay through proton-transfer in which two molecule of the amine participate,[1] while the photo-induced reaction of anthracene with *N*,*N*-dimethylaniline takes place *via* a triple exciplex.[4] It has also been demonstrated that

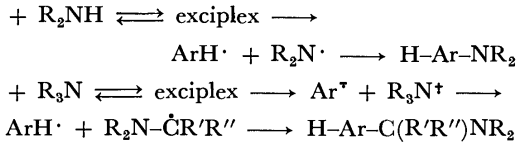

Scheme 3.

Table 1. Fluorescence quenching of **3** with amines

Amine	Solvent	k_q (M^{-1})[a]	k_q ($\times 10^9$ M^{-1} s^{-1})[a]	Concn of **3** ($\times 10^{-4}$ M)	*Ip* (eV)
a) Triethylamine	MeCN	158	8.8	2.18	7.50
b) Triethylamine	CH_2Cl_2	116	6.4	9.97	75.0
c) Diisopropylamine	MeCN	145	8.1	1.09	7.73
d) Cyclohexylamine	MeCN	126	7.0	2.18	8.86

a) The k_q values were calculated, based on τ being 18 ns.[15] See Fig. 1 for the amine-concentration range. Exciting light at 283 nm. Fluorescence at 394 nm.

the reactions of arene with secondary amines seem to proceed through exciplexes in which hydrogen transfer, followed by radical coupling, takes place; consequently, the 1,2- or 1,4-addition of the NH group in the amine results (Scheme 3).[3,4] Unlike the case of secondary amines, electron-transfer from the amine to the arene occurs in an arene–tertiary amine systems to form a pair of solvated radical ions, which then collapse to radicals *via* proton-transfer and subsequently couple to give the addition product at the α-CH bond of the amine to the arene. These mechanisms are shown in Scheme 3. A full electron-transfer is necessary to render the α-CH bond sufficiently acidic for proton-transfer to occur.[3]

In view of those investigations, two possible mechanisms are conceivable. One is that, since the electron affinity of **3** is larger than that of benzene, electron-transfer from the amine to the aromatics must be easier than in the hydrocarbon–amine systems and the pair of radical ions can be produced even by using the secondary or primary amine as an electron donor. Subsequent proton-transfer occurs predominantly from the α-CH position rather than from the NH group, though the acidities of the α-CH and the NH group of diisopropylamine or cyclohexylamine radical cation have not yet been determined. A similar hydrogen-transfer from the α-CH position has been observed in the photochemical reactions of ketones with primary amines.[14] The other is that, as is the case with a secondary amine–arene system, hydrogen-transfer from the NH group occurs in the exciplex or the radical ion pair, with the resulting radicals coupling to give an unstable *N*-addition product (**16**) as an intermediate. If the elimination of HCN occurs, an *N*-substitution product, **14** or **15**, will be produced. On the other hand, if the elimination of the amine takes place, the starting materials will be recovered, with the photochemical reactions working as radiationless decay processes of the excited species. This is probably the actual case. This mechanism accounts for the low reactivities of the primary and the secondary amines in comparison with those of triethylamine. The quenching of the reaction of **3** with triethylamine by methanol is also accounted for by a similar mechanism; methanol protonates the anion radical in the exciplex or the ion pair to give the neutral radical, from which the back transfer of an electron to the cation radical, followed by deprotonation, then gives the starting materials again.

Although the reduction potential of *m*-dicyanobenzene (−2.17 V) is similar to those of the *o*- or *p*-isomers (−2.12 and −1.97 V respectively),[15] the fact that the meta-isomer has much less reactivity than the *ortho*- and *para*-isomers is remarkable. In order to account for this fact, we assume that a proton from the radical cation transfers to the *ipso*-position of the dicyano compounds, and that the resulting radical is stabilized by conjugation with the cyano group in the *ortho*- and *para*-isomers, but not in the *meta*-isomer. Since the proton-transfer step is supposed to determine the rate for these reactions,[6] the stabilization of the radical intermediate may control the reactivity of the acceptor employed. A similar trend has been reported in the light-induced hydrogen isotope exchange in benzonitrile, where the exchange occurred mainly at the para(89.8%) and ortho(10%) positions, but scarcely at all at the meta(0.2%) position, in the benzonitrile–triethylamine–tritiated water system.[16] It was concluded from those results that the stability of the inter mediate radical is in the order of $I_p > I_o > I_m$, which is in accord with our assumption (Scheme 4).

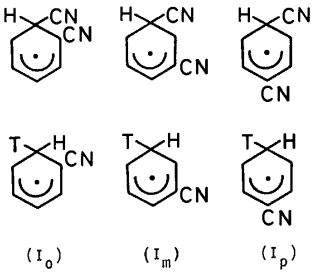

Scheme 4.

On the basis of these results, we propose the following mechanism, in which the two processes involved in the hydrogen-transfer step compete with each other. Hydrogen- or proton-transfer from the NH group probably results in the recovery of the starting materials, while proton-transfer from the α-CH position gives the substitution products, as is shown in Scheme 5.

Mechanism of the Formation of Alkylated Products. To identify the route to the alkylated products, the substitution product, **4**, was irradiated in acetonitrile under nitrogen with a low-pressure mercury arc; the alkylated product, **5**, was thus obtained in a good yield. Triethylamine added to the system slightly increased (1.4 times) the yield of the product, while methanol slightly decreased it (0.7 times). From these results, it is clear that the alkylated products have been derived from the corresponding substitution products through a new photo-induced reductive cleavage of the benzylic C–N bond.

Although many studies have been reported on the photolytic solvolysis of benzyl acetate,[17] alcohols,[18] ammonium salts,[19] halides[20] and sulfonium salts,[21] the photo-induced reductive cleavage of benzylic C–O or C–N bonds by electron donor has scarcely been examined at all.[22] Recently it was reported that

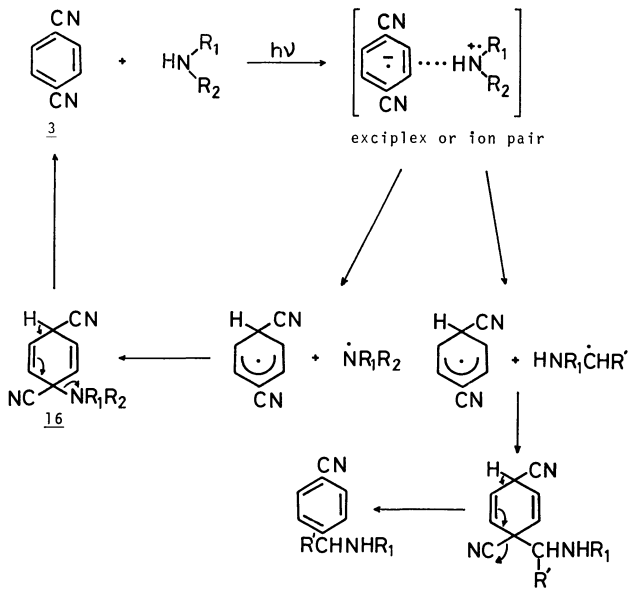

Scheme 5.

photo-induced intramolecular charge-transfer gives rise to the cleavage of benzylic C–O bonds through a carbonium-ion mechanism.[17]

In our case, the intramolecular charge-transfer excitation from the amino group to the aromatic moiety is negligible, because the absorption spectrum of **4** is identical to that of *o*-tolunitrile. The emission spectrum of **4**, however, exhibits a broad weak band at 350—400 nm, along with a strong band at 316 nm. The former may be assigned to the fluorescence from the excited singlet state of the intramolecular charge-transfer configuration. The Stern-Volmer treatments of the quenching of both emission bands by triethylamine gave linear plots with a $k_q\tau$ value of 163 M^{-1}. Here again, a charge-transfer interaction between the singlet state of **4** and triethylamine is conceivable.

When the reaction was carried out in MeOD in place of acetonitrile, 0.51 atoms of deuterium were incorporated in the product, **5**, indicating that a proton-transfer step participated in the reaction process. A similar deuterium incorporation (0.55 atoms) was obtained in the case of the acetonitrile–MeOD–triethylamine system. The NMR spectrum of the deuterated **5** indicated that the incorporated deuterium was located mainly in the benzylic methylene group. The irradiation of **5** under similar conditions showed that no significant incorporation of deuterium by H–D exchange occurred.

Barltrop has shown that the photo-induced Birch reduction of naphthalene by triethylamine in the presence of D_2O resulted in the formation of a dihydro product in which 1.6 atoms were deuterated. He concluded that the naphthalene radical anion produced by photoinduced electron-transfer picks up the deuterium and that the resulting deuterated radical is reduced in two parallel paths, *i.e.*, one proceeding by means of electron-transfer, followed by deuterium-transfer giving a dideuterated product, and the other involving hydrogen-atom transfer.[2b]

Referring to those observations, we propose a reduction-elimination mechanism for the present unique reduction. The reaction probably proceeds through an excimer of **4** or an exciplex between **4** and triethylamine when the amine is present in the system. Electron-transfer, followed by proton-transfer in the excited donor-acceptor system, gives a radical intermediate with the ejection of diethylamine, from which two parallel paths, as in the case of the naphthalene–triethylamine system, proceed; hydrogen-transfer, and electron-transfer followed by proton-transfer. Scheme 6 represents the possible mechanism for the photochemical reaction of **4** with triethylamine in the presence of MeOD. The intramolecular charge-transfer excitation may only result in an increase of the radiation-less decay; it may be that no chemical reactions proceed from this configuration.[23]

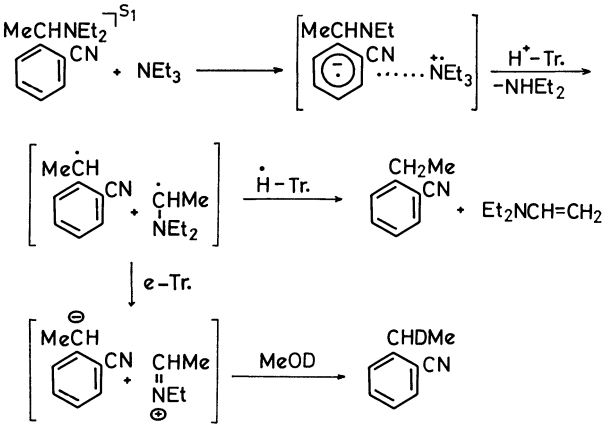

Scheme 6.

Experimental

Melting points were determined with a Kofler hot-stage apparatus and are uncorrected. IR spectra were taken with a JASCO model IRA-1 instrument, while UV spectra were obtained with a Hitachi 124 spectrophotometer. ^1H NMR spectra were recorded with Hitachi R-24 and R-20B instruments, with tetramethylsilane as the internal standard. Mass spectra were recorded with a Hitachi RMU-6MG single-focusing instrument equipped with a direct/in-beam ion source; ionizing energy, 70 or 20 eV, source temperature, *ca.* 200 °C. Fluorescence spectra were measured with a Hitachi 204 fluorescence spectrophotometer. Irradiations for photochemical reactions were carried out with a low-pressure mercury lamp(Ushio ULO-6DQ, 6 W) or with a medium-pressure mercury lamp(Ushio UM-102, 100W). A merry-goround spparatus (Taika-Kogyo MGR) was used for the actinometry.

The dicyanobenzenes, purchased from the Tokyo Kasei Co., were recrystallized from benzene. The amines, purchased from the Wako-Junyaku Co., were reagent-grade and were distilled befor use.

Photochemical Reactions of o-Dicyanobenzene with Triethylamine. A solution of *o*-dicyanobenzene (955 mg, 7.5 mmol) in acetonitrile (70 ml) in the presence of triethylamine (7 g, 70 mmol) was irradiated with a low-pressure mercury lamp (6 W) for 16 h under nitrogen. The solvent was then evaporated *in vacuo*, and the residue was chromatographed on silica gel (Wako C-200) to give **4** (657 mg, 79%), **5** (50 mg, 9%), **6** (trace, detected by gas chromatography-mass spectrometry, identified by a mass spectral comparison with an authentic

sample), and the starting material (534 mg).

o-[*1-(Diethylamino)ethyl*]*benzonitrile* (**4**). Bp 70 °C (17 mg Hg); IR (liq) 2230 cm^{-1}; NMR (CCl_4) δ 0.96 (t, 6, J= 7.0 Hz), 1.32 (d, 3, J=7.0 Hz), 2.58 (q, 4, J=7.0 Hz), 4.14 (q, 1, J=7.0 Hz), 7.06—7.77 (m, 4); mass spectrum, 70 eV, m/z (rel. intensity) 204 (14), 187 (100), 159 (3), 130 (36), 103 (3), 72 (4), 58 (48), mass spectrum calcd for $C_{13}H_{18}N_2$: m/z 202.1470, found: 202.1455.

o-*Ethylbenzonitrile* (**5**).[24] Identified by direct comparison with the authentic specimen synthesized according to the Bissell[25] and Newman[26] methods.

Photochemical Reaction of m-*Dicyanobenzene with Triethylamine.* A solution of *m*-dicyanobenzene (1.02 g, 5.63 mmol) and triethylamine (11 g, 1.09 mmol) in acetonitrile (170 ml) was irradiated for 20 h under similar conditions. A usual work-up gave a trace amount of *m*-ethylbenzonitrile[24] [3 mg, mass spectrum, 20 eV, m/z (rel. intensity) 132 (12), 131 (47), 130 (9), 117 (17), 116 (100), 104 (15), 103 (20), 89 (12)]. The retention time of this compound in the gas chromatography-mass spectrometry was different from those of **5** and **9**.

Photochemical Reaction of p-*Dicyanobenzene with Triethylamine.* A solution of *p*-dicyanobenzene (744 mg, 5.81 mmol) and triethylamine (9.0 g, 89.1 mmol) in acetonitrile (170 ml) was irradiated with a low-pressure mercury arc (6 W) for 6 h under nitrogen. The solvent was removed *in vacuo*, and the residue was chromatographed on silica gel to give **8** (138 mg, 18%), **9** (282 mg, 56%), **6** (trace), and the starting material (257 mg).

p-[*1-(Diethylamino)ethyl*]*benzonitrile* (**8**). IR (liq) 2220 cm^{-1}; NMR (CCl_4) δ 0.95 (t, 6, J=7.0 Hz), 1.27 (d, 3, J= 7 Hz), 2.49 (q, 4, J=7.0 Hz), 3.83 (q, 1, J=7.0 Hz), 7.04—7.91 (m, 4); mass spectrum, 70 eV, m/z (rel. intensity) 202 (20), 187 (100), 173 (9), 130 (21), 116 (5), 103 (21); mass spectrum calcd for $C_{13}H_{18}N_2$: m/z 202.1470, Found: 202.1476.

p-*Ethylbenzonitrile* (**9**).[24] Identified by direct comparison with the authentic specimen synthesized according to the Bissell[25] and Newman[26] methods.

Photochemical Reaction of p-*Dicyanobenzene with Cyclohexylamine.* A mixture of *p*-dicyanobenzene (501 mg, 3.91 mmol) and cyclohexylamine (21.7 g, 219 mmol) in acetonitrile (60 ml) was irradiated with a medium-pressure mercure arc (100 W) for 13.5 h under nitrogen. A usual work-up gave pale yellow crystals **11** (31 mg, 10%), an oil **10** (32 mg, 11%), **6** (trace), and the starting material (305 mg).

p-(*1-Aminocyclohexyl*)*benzonitrile* (**11**). Mp 61—63 °C (from benzene–cyclohexane); IR (KBr) 3380, 3310, 2230, 1605 cm^{-1}; NMR (CCl_4) δ 0.90—2.20 (m, 10), 7.59 (d, 2, J=9.5 Hz), 7.69 (d, 2, J=9.5 Hz); mass spectrum, 20 eV, m/z (rel. intensity) 200 (20), 184 (2), 171 (8), 157 (100), 144 (6), 129 (6), 116 (3), 103 (1). Found: C, 77.48; H, 8.28; N, 13.87%. Calcd for $C_{13}H_{16}N_2$: C, 77.96; H, 8.05; N, 13.99%.

p-*Cyclohexylbenzonitrile* (**10**). IR (liq) 2215 cm^{-1}; NMR (CCl_4) δ 0.80—3.20 (m, 11), 7.20 (d, 2, J=9.0 Hz), 7.46 (d, 2, J=9.0 Hz); mass spectrum, 20 eV, m/z (rel. intensity) 185 (59), 159 (9), 143 (13), 129 (100), 117 (15), 116 (12), 103 (3), 102 (3). The structure was identified by a direct comparison of the spectra with those of the authentic specimen synthesized as follows: cyclohexylbenzene (25 g, 156 mmol) was treated with bromine (26 g, 163 mmol) in the presence of iodine (1.7 g, 6.5 mmol) according to Bissell's method[25] to give *p*-bromocyclohexylbenzene[10 g, 27%, bp 85 °C (1 mmHg)], which was then treated with copper (I) cyanide (4.0 g, 44.6 mmol) in pyridine (10 ml) according to Newman's method[25] to give **10** (1.9 g).

Photochemical Reaction of p-*Dicyanobenzene with Diisopropylamine.* A solution of *p*-dicyanobenzene (1.00 g, 7.81 mmol) and diisopropylamine (15 g, 149 mmol) in acetonitrile (150 ml) was irradiated with a medium-pressure mercury arc (100 W) for 9 h under nitrogen. A work-up in the usual manner gave an oil **12** (258 mg, 30%), an other oil **13** (294 mg, 25%), **6** (trace), and the recovered starting material (241 mg).

p-(*1-Isopropylamino-1-methylethyl*)*benzonitrile* (**13**). IR (liq) 3330, 2230 cm^{-1}; NMR (CCl_4) δ 0.86 (d, 6, J=6.5 Hz), 1.40 (s, 6), 2.69 (sep, 1, J=6.5 Hz), 7.05—7.85 (m, 4); mass spectrum, 20 eV, m/z (rel. intensity) 202 (4), 187 (100), 173 (2), 159 (3), 145 (48), 144 (22), 130 (4), 116 (9), 104 (3), 100 (8), 44 (31). Picrate, mp 196—199 °C (dec from ethanol). Found: C, 52.54; H, 4.86; N, 15.90%. Calcd for $C_{19}H_{25}N_5O_7$: C, 52.90; H, 4.91; N, 16.23%.

p-*Isopropylbenzonitrile* (**12**).[24] The structure was confirmed by a direct comparison of the spectra with those of the authentic material, synthesized by alternative method; the bromination of cumene (20 g, 167 mmol) with bromine (27 g, 169 mmol) and iodine (3.4 g, 13.4 mmol) according to the method in the literature[25] gave the bromide (18 g, 54%), which was then treated with copper(I) cyanide (10 g, 112 mmol) in pyridine (15 ml) for 22 h under nitrogen according to Newman's method[26] to give **12** (2.0 g, 16%).

Photochemical Reaction of p-*Dicyanobenzene with Triethylamine under Oxygen.* A solution of *p*-dicyanobenzene (720 mg, 5.63 mmol) and triethylamine (12 g, 119 mmol) in acetonitrile (120 ml) was irradiated with a low-pressure mercury arc (6 W) for 17 h. Oxygen was bubbled through the solution during the course of irradiation. A work-up in the usual manner gave *p*-cyanobenzamide (3 mg, 1%); colorless crystals; mp 224—226 °C (lit,[27] 224 °C).

Solvent Dependency of the Photochemical Reaction of **1** *with Triethylamine.* Each solution of **1** (90 mg, 0.703 mmol) and triethylamine (1 ml), dissolved in 10 ml of acetonitrile, methanol, or dichloromethane, was irradiated by means of a merry-go-round apparatus with a low-pressure mercury arc (10 W) for 22 h. The relative yields of the product, **4**, were estimated by means of gas chromatography (Degs 1.5% on Diasolid ZF 80-100), using 2-methoxynaphthalene as the internal standard. The complete quenchig of the reaction in methanol and in dichloromethane was determined.

Quantum Yields of the Disappearance of **3** *in the Photochemical Reaction of* **3** *with Triethylamine.* A solution of **3** (80 mg, 0.625 mmol) and triethylamine (1.0 g, 9.91 mmol) in acetonitrile (10 ml) was irradiated by means of a merry-go-round apparatus with a low-pressure mercury arc (10 W) for 6 h. The amount of unreacted **3** was then determined by means of gas chromatography, the conversion of **3** was found to be less than 10%. Trioxalatoferrate(III) actinometry was used (1.15×10^{16} quanta/s) to determine the quantum yields of the consumption of **1** and **3**, they were both 0.15.

Photochemical Reaction of **4**. Various solutions (Table 2) of **4**, isolated and purified by vacuum distillation, were irradiated by means of a merry-go-round apparatus with a low-pressure mercury arc (10 W) for 3.5 h. The yields of **5** was then determined by means of gas chromatography.

Table 2. Relative yields of **5** in the photolysis of **4** under different conditions

	4 (mg)	CH_3CN (ml)	NEt_3 (ml)	MeOH (ml)	Yield
a	24.5	5.0	—	—	1.0
b	24.5	4.7	0.3	—	1.4
c	24.7	4.0	0.3	0.7	0.65

The results are summarized in Table 2.

Photochemical Reaction of 4 in the Presence of MeOD. **4** (80 mg) was irradiated under various conditions (Table 3) by means of a merry-go-round apparatus with a low-pressure mercury arc (10 W) for 20 h. The solvent was then removed, and the residue was chromatographed on silica gel to give **5**. The isotopic purity of each specimen was determined by mass spectrometry. The results are summarized in Table **3**. The methanol-d_1 was purchased from the Wakenyaku Co., its isotopic purity was better than 99%.

Table 3. Deuterium incorporation of **5**

	CH_3CN (ml)	MeOD (ml)	NEt_3 (ml)	D-incorporation(%)
a	—	12	—	51
b	—	11	1	53
c	11	1	—	40
d[a)]	10	1	1	55

a) In the case of d), the NMR spectrum exhibited the following peaks of the relative intensities: δ 7.30 (m, 4.0H), 2.84(q, 1.4H), and 1.25(t, and d, 3.2H).

This work was supported by a Grant-in-Aid for Scientific Research of the Ministry of Education (No. 247018).

References

1) a) M. Bellas, D. Bryce-Smith, and A. Gilbert, *Chem. Commun.*, **1967**, 263, 862; b) D. Bryce-Smith, *Pure Appl. Chem.*, **34**, 193 (1973); c) M. Bellas, D. Bryce-Smith, M. T. Clarke, A. Gilbert, G. Klunkin, S. Krestonosich, C. Manning, and S. Wilson, *J. Chem. Soc., Pekin Trans. 1*, **1977**, 2571; d) D. Bryce-Smith and A. Gilbert, "Terahedron Reports No. 40, Organic Photochemistrv of Benzene-II," Pergamon Press, Oxford (1978).

2) a) J. A. Barltrop and R. J. Owers, *Chem. Commun.*, **1970**, 1492; b) J. A. Barltrop, *Pure Appl. Chem.*, **33**, 179 (1983).

3) a) M. Kawanishi and K. Matunaga, *J. Chem. Soc., Chem. Commun.*, **1972**, 313; b) T. Kubota and H. Sakurai, *Chem. Lett.*, **1972**, 923, 1249; c) A. Couture, A. Lablache-Combier, and H. Oftenberg, *Tetrahedron*, **21**, 2023 (1975); d) F. D. Lewis and T. I. Ho, *J. Am. Chem. Soc.*, **99**, 7991 (1977); e) F. D. Lewis, *Acc. Chem. Res.*, **12**, 152 (1979).

4) a) R. S. Davidson, *Chem. Commun.*, **1969**, 1450; b) N. C. Yang and J. Libman, *J. Am. Chem. Soc.*, **95**, 5783 (1973); c) N. C. Yang, D. M. Shold, and B. Kim, *ibid.*, **98**, 6587 (1976).

5) a) A. Yoshino, M. Ohashi, and T. Yonezawa, *Chem. Commun.*, **1971**, 97; b) A. Yoshino, K. Yamasaki, T. Yonezawa, and M. Ohashi, *J. Chem. Soc., Perkin Trans. 1*, **1975**, 735; c) M. Ohashi and K. Tsujimoto, *Chem. Lett.*, **1975**, 829; d) M. Ohashi and N. Nakayama, *ibid.*, **1976**, 1143; e) S. Yamada, Y. Kimura, and M. Ohashi, *J. Chem. Soc., Chem. Commun.*, **1977**, 667; f) M. Ohashi, K. Tsujimoto, and Y. Furukawa, *J. Chem. Soc., Perkin Trans. 1*, **1979**, 1147.

6) a) K. Yamasaki, A. Yoshino, T. Yonezawa, and M. Ohashi, *J. Chem. Soc., Chem. Commun.*, **1973**, 9; b) K. Yamasaki, T. Yonezawa, and M. Ohashi, *J. Chem. Soc., Perkin Trans. 1*, **1975**, 93; c) M. Ohashi, N. Nakayama, and K. Yamasaki, *Chem. Lett.*, **1976**, 1131.

7) a) M. Ohashi, S. Suwa, and K. Tsujimoto, *J. Chem. Soc., Chem. Commun.*, **1976**, 404; b) M. Ohashi, S. Suwa, and K. Tsujimoto, *ibid.*, **1977**, 348; c) M. Ohashi, S. Suwa, Y. Osawa, and K. Tsujimoto, *J. Chem. Soc., Perkin Trans. 1*, **1979**, 2219.

8) D. Rehm and A. Weller, *Israel J. Chem.*, **8**, 259 (1970).

9) a) B. C. McKusick, R. E. Heckert, T. L. Cairns, D. D. Coffman, and H. F. Mower, *J. Am. Chem. Soc.*, **80**, 2806 (1958); b) W. R. Hertler, H. D. Hartler, D. S. Acker, and R. E. Benson, *J. Am. Chem. Soc.*, **84**, 3387 (1962).

10) Preliminary communications: a) K. Tsujimoto, K. Miyake, and M. Ohashi, *J. Chem. Soc., Chem. Commun.*, **1976**, 387; b) M. Ohashi and K. Miyake, *Chem. Lett.*, **1977**, 615.

11) Y. Tsujimoto, M. Hayashi, Y. Nishimura, T. Miyamoto and Y. Odaira, *Chem. Lett.*, **1977**, 677.

12) D. Bryce-Smith, A. Gilbert, and S. Krestonosich, *J. Chem. Soc., Chem. Commun.*, **1976**, 405.

13) D. Bryce-Smith, A. Gilbert, and S. Krestonosich, *Tetrahedron Lett.*, **1977**, 385.

14) S. G. Cohen and R. J. Baumgarten, *J. Am. Chem. Soc.*, **89**, 3471 (1967).

15) P. H. Rieger, I. Bernal, W. H. Reinmuth, and G. K. Frankel, *J. Am. Chem. Soc.*, **85**, 685 (1963).

16) M. Yoshida, H. Kaneko, A. Kitamura, T. Ito, K. Oohashi, N. Morikawa, H. Sakuragi, and K. Tokumaru, *Bull. Chem. Soc. Jpn.*, **49**, 1697 (1976).

17) a) H. E. Zimmerman and V. R. Sandel, *J. Am. Chem. Soc.*, **85**, 915 (1963); b) S. Fujita, Y. Ozaki, and H. Nozaki, *Bull. Chem. Soc. Jpn.*, **45**, 257 (1972); c) D. A. Jaeger, *J. Am. Chem. Soc.*, **97**, 902 (1975); d) R. B. Ivanov, V. L. Ivanov, and M. G. Kuzmin, *Mol. Photochem.*, **6**, 125 (1974); e) D. A. Appleton, B. Brocklehurst, J. McKenna, J. M. McKenna, M. J. Smith, P. S. Tayor, S. Thackeray, and A. R.Walley, *J. Chem. Soc., Chem. Commun.*, **1977**, 108.

18) C. I. Lin, P. Singh, and E. F. Ullman, *J. Am. Chem. Soc.*, **98**, 6711 (1976).

19) V. Lillis, J. McKenna, J. M. McKenna, and I. H. Williams, *J. Chem. Soc., Chem. Commun.*, **1974**, 473, 494.

20) S. J. Cristol and G. C. Schloemer, *J. Am. Chem. Soc.*, **94**, 5916 (1972).

21) A. L. Maycock and G. A. Berchtold, *J. Org. Chem.*, **35**, 2532 (1970).

22) M. Ohashi, K. Tsujimoto, and Y. Furukawa, *Chem. Lett.*, **1977**, 543.

23) a) D. Bryce-Smith, A. Gilbert, and G. Klunklin, *J. Chem. Soc., Chem. Commun.*, **1973**, 330; b) R. S. Davidson and K. R. Trethewey, *ibid.*, **1976**, 827.

24) L. Eberson, S. Nilsson, and B. Rietz, *Acta Chem. Scand.*, **26**, 3870 (1972).

25) E. R. Bissell and R. E. Spenger, *J. Org. Chem.*, **21**,1146 (1959).

26) M. S. Newman, *Org. Synth.*, Coll. Vol. III, 631 (1955).

27) F. E. Digangi and O. Gisvold, *J. Am. Pharm. Assoc.*, **38**, 154 (1949).

 © 1980 The Chemical Society of Japan Bull. Chem. Soc. Jpn., 53, 1689—1693 (1980)

The Synthesis of Unsubstituted Crown Ethers by the Reaction of Oligoethylene Glycols with Arenesulfonyl or Alkanesulfonyl Chlorides

Ping-Lin Kuo, Norio Kawamura, Masaki Miki, aud Mitsuo Okahara*

Department of Applied Chemistry, Faculty of Engineering, Osaka University, Yamadakami, Suita, Osaka 565

(Received November 29, 1979)

A new facile method of synthesizing crown ethers from oligoethylene glycols by treating them with arenesulfonyl or alkanesulfonyl chlorides in the presence of alkali metal hydroxide or alkoxide was described. 15-Crown-5 and 21-crown-7 were synthesized from pentaethylene glycol and heptaethylene glycol respectively in good yields, while 18-crown-6 was obtained from both hexaethylene glycol and triethylene glycol. Although the main product was 24-crown-8 in the reaction of tetraethylene glycol/TsCl/Na(K)OH in dioxane, 12-crown-4 was obtained in a moderate yield from the reaction of tetraethylene glycol/benzenesulfonyl chloride/*t*-BuOLi in *t*-BuOH. Furthermore, the analogous treatment of PEG 200 afforded a mixture of 15-, 18-, 21-, and 24-crown ethers. The reaction conditions were investigated, and the scope of the reaction was discussed.

One feature of the remarkable recent developments in the field of macrocyclic compounds has been the publication of numerous reports during the past ten years.[1,2]

The various methods proposed for the synthesis of crown compounds may be classified into two categories: 1) A modified Williamson ether synthesis by means of a reaction between oligoethylene glycols or aromatic dihydroxy compounds, and oligoethylene glycol dichlorides or ditosylates, in the presence of alkali, which has the appropriate template atom,[3-7] and 2) a Lewis acid-catalyzed cyclo-oligomerization of ethylene oxide using special metal salts.[8,9]

Although the former method has been widely adopted for the synthesis of crown compounds, the intramolecular cyclization of a polyoxyethylene compound with a hydroxyl group at one end and a leaving group at the other end, which corresponds to the intermediate in the former method, may be a more convenient way to get crown compounds.[10]

In view of this, an attempt was undertaken in our laboratory to get such compounds,[11] and we have recently reported a new method of obtaining a variety of crown compounds through the *in situ* formation of such precursors.[12,13]

The detailed results of the synthesis of unsubstituted crown ethers from oligoethylene glycols by treatment with arenesulfonyl or alkanesulfonyl chlorides in the presence of alkali metal hydroxide will be described in this paper.

Experimental

The IR and ^{1}H NMR spectra were recorded on a JASCO IR-E spectrophotometer and a JEOL JMN-PS-100 spectrometer respectively. The GLC analyses were performed on a Shimadzu gas chromatograph GC-3BF, equipped with a flame-ionization detector.

Oligoethylene Glycols. The penta-, hexa-, and heptaethylene glycols were each purely separated from a polyethylene glycol mixture with an average molecular weight of 250 by distillation at a reduced pressure. The di-, tri-, and tetraethylene glycols were commercial products and were used without purification.

Synthesis of 15-Crown-5 (IIc) from Pentaethylene Glycol. Pentaethylene glycol (4.8 g, 0.02 mol) and *p*-toluenesulfonyl chloride (4.0 g, 0.02 mol) were dissolved in 30 ml of monoglyme, after which the solution was slowly added, drop by drop, into a suspension of powdered sodium hydroxide (6.0 g, 0.15 mol) in 30 ml of monoglyme over a period of 2 h at room temperature. After the addition was complete, the reaction was continued for one more hour, and the reaction product was filtered. The precipitate was washed with dichloromethane, and then the solvent was removed from the combined solution of filtrate and washings to leave the 15-crown-5 complex as an almost colorless liquid. It was found by GLC to consist 61% of 15-crown-5 (10% Carbowax 20 M or Silicone DC 550 on Celite 545, 220 °C, carrier gas N_2). When a part of the complexes (3.6 g) was thermolyzed using Kugelrohr distillation apparatus, free 15-crown-5 (IIc, 1.7 g, 50%) was obtained as a viscous liquid. NMR (CCl_4, δ): 3.53 s, MS (*m/e*): 220 (M^+).

Small-scale experiments for the investigation of the reaction conditions were carried out using 1.0 g (4.2 mmol) glycol in 60 ml of a solvent in manner similar to that described above.

Synthesis of 18-Crown-6 (IId) from Hexaethylene Glycol. Hexaethylene glycol (3.0 g, 0.011 mol) and *p*-toluenesulfonyl chloride (2.0 g, 0.011 mol) were dissolved in 40 ml of dioxane, after which the solution was added, drop by drop, into a suspension of powdered potassium hydroxide (2.4 g, in 40 ml dioxane) at 40 °C. The white solid (4.8 g) thus obtained was found to contain 2.68 g (92%) of 18-crown-6 (IId) and no unreacted glycol by GLC. When a part of the crude product (3.5 g) was thermolyzed by means of a Kugelrohr apparatus at reduced pressure, IId (1.6 g, 75%) was isolated in a pure state. MS (*m/e*): 264 (M^+), NMR (CCl_4, δ): 3.50 s.

Synthesis of 21-Crown-7 (IIe) from Heptaethylene Glycol. Heptaethylene glycol (3.0 g, 9.2 mmol) was treated with *p*-toluenesulfonyl chloride (1.75 g, 9.2 mmol) in 80 ml of dioxane in a manner simmlar to that described above at 50 °C. The crude complex (3.3 g) was extracted by the use of hexane in a continuous extractor to give 1.67 g (59%) of pure 21-crown-7 (IIe) as a colorless liquid. IR (neat): 2880 s, 1465 m, 1360 m, 1300 m, 1255 m, 1115 s, 945 m, and 850 w cm^{-1}. MS (*m/e*, rel. intensity): 308 (M^+, amplified), 133 (20), 89 (49), 87 (29), 73 (21), 72 (13), 59 (18), 58 (17), 45 (100), 44 (23), and 43 (29). NMR (CCl_4, δ): 3.54 s. Analysis for $C_{14}H_{28}O_7$: C, 53.98 (Calcd. 54.53); H, 8.99 (9.15).

Reaction of Tetraethylene Glycol with Sulfonyl Chloride. a): A solution of tetraethylene glycol (3.9 g, 0.02 mol) and *p*-toluenesulfonyl chloride (4.0 g, 0.02 mol) in monoglyme (30 ml) was added into a suspension of sodium hydroxide

(6.0 g) in 30 ml of monoglyme at 20 °C. The crude product (3.3 g), which was found by GLC to contain 3% of 12-crown-4, was treated on a silica-gel column to give a low-melting solid (0.42 g) from an acetone–hexane eluent. IR (neat): 2880 s, 1460 w, 1350 m, 1300 w, 1250 w, 1150—1110 s, 950 w, and 850 w cm^{-1}. MS (*m/e*, rel. intensity): 352 (M^+, 5), 177 (5), 133 (24), 117 (24), 101 (14), 89 (60), 87 (37), 73 (30), 59 (25), 58 (25), 45 (100), 44 (32), and 43 (40). NMR (CCl_4, δ): 3.52 s. From the above spectral data, it was identified as 24-crown-8 (IIf). Yield: 12%, b): Tetraethylene glycol (7.77 g, 0.04 mol) and benzenesulfonyl chloride (7.36 g, 0.04 mol) were dissolved in 90 ml of *t*-butyl alcohol, after which the solution was added, drop by drop, into a suspension of lithium *t*-butoxide (12.8 g, 0.16 mol) in 90 ml of *t*-butyl alcohol over a period of 2 h. After the reaction was complete, the *t*-butyl alcohol was removed *in vacuo* and dichloromethane (100 ml) was added to the residue and filtrate. After the solvent had then been removed, the crude complex was thermolyzed to give a colorless liquid (3.5 g). It was further purified by distillation at reduced pressure. IIb, 1.93 g (27%). IR (neat): 2925 s, 1465 w, 1375 m, 1300 m, 1255 m, 1140 s, 1100 s, 1095 m, 1020 m, 920 m, and 850 m cm^{-1}. MS (*m/e*, rel. intensity): 176 (M^+, amplified), 133 (8), 89 (30), 87 (18), 73 (15), 59 (15), 58 (19), 57 (11), 45 (100), 44 (33), 43 (40), and 28 (29). NMR (CCl_4, δ): 3.56 s.

Also, the crude complex of IIb (3.95 g; IIb content, 38%), obtained in another reaction, was dissolved in methanol (10 ml), after which the solution was extracted continuously by hexane for 9 h. The colorless liquid thus obtained (1.96 g) was distilled under reduced pressure to afford IIb (0.65 g, 31%) in a pure state.

Reaction of Mixture of Glycols with Sulfonyl Chloride. a): Tetraethylene glycol (3.9 g, 0.02 mol), triethylene glycol (3.0 g, 0.02 mol), *p*-toluenesulfonyl chloride (8.0 g, 0.04 mol), and potassium hydroxide (10 g) was allowed to react at 60 °C in dioxane to afford a crude product (9.8 g). It was found by GLC determination to contain three kinds of crown ethers: 18-crown-6 (1.02 g, 19%), 21-crown-7 (2.06 g, 33%), and 24-crown-8 (0.98 g, 14%), *b)*: Tetraethylene glycol (1.94 g, 0.01 mol), diethylene glycol (1.06 g, 0.01 mol), *p*-toluenesulfonyl chloride (4.0 g, 0.02 mol), and potassium hydroxide (2.7 g) were allowed to react in dioxane at 60 °C. The crude complex (2.2 g) was analyzed by GLC and found to contain 18-crown-6 (0.60 g, 23%) as the major product, together with small amounts of 24-crown-8 (3%) and 12-crown-4 (<1%).

Conversion of Polyethylene Glycol 200 to Crown Ethers. 3.0 g of commercial polyethylene glycol 200, which was a mixture of di- (1 wt%), tri- (26%), tetra- (36%), penta- (29%), and hexaethylene glycol (8%), was treated with *p*-toluenesulfonyl chloride (2.9 g) in the presence of sodium hydroxide (1.3 g)

Table 1. Synthesis of 15-crown-5 from pentaethylene glycol

Exp. No.	Solvent	Concn mol/l	Sulfonyl chloride	Alkali	React. temp/°C	Yield/%[a]
1	Monoglyme	0.07	*p*-$CH_3C_6H_4SO_2Cl$	NaOH	0	36
2	Dioxane	0.07	*p*-$CH_3C_6H_4SO_2Cl$	NaOH	20	70 (50)[b]
3	THF	0.07	*p*-$CH_3C_6H_4SO_2Cl$	NaOH	20	69
4	Dioxane	0.35[c]	*p*-$CH_3C_6H_4SO_2Cl$	NaOH	20	62 (48)
5	Dioxane	0.70[d]	*p*-$CH_3C_6H_4SO_2Cl$	NaOH	20	55 (45)
6	Dioxane	0.07	*p*-$CH_3C_6H_4SO_2Cl$	NaOH	40	81
7	Monoglyme	0.07	*p*-$CH_3C_6H_4SO_2Cl$	NaOH	40	82
8	Diglyme	0.07	*p*-$CH_3C_6H_4SO_2Cl$	NaOH	40	81
9	THF	0.07	*p*-$CH_3C_6H_4SO_2Cl$	NaOH	40	81
10	Ether	0.07	*p*-$CH_3C_6H_4SO_2Cl$	NaOH	f)	63
11	Benzene	0.07	*p*-$CH_3C_6H_4SO_2Cl$	NaOH	40	44
12	Hexane	0.07	*p*-$CH_3C_6H_4SO_2Cl$	NaOH	40	15
13	Dioxane	0.07	*o*-$CH_3C_6H_4SO_2Cl$	NaOH	40	79
14	Dioxane	0.07	*p*-Cl-$C_6H_4SO_2Cl$	NaOH	40	68
15	Dioxane	0.07	$C_6H_5SO_2Cl$	NaOH	40	85
16	Dioxane	0.07	CH_3SO_2Cl	NaOH	40	64
17	Dioxane	0.07	$C_2H_5SO_2Cl$	NaOH	40	55
18	Dioxane	0.07	*p*-$CH_3C_6H_4SO_2Cl$	NaOH	60	82
19	Dioxane	0.07	*p*-$CH_3C_6H_4SO_2Cl$	NaOH	80	80
20	Dioxane	0.28[e]	*p*-$CH_3C_6H_4SO_2Cl$	NaOH	80	82 (75)
21	Diglyme	0.07	*p*-$CH_3C_6H_4SO_2Cl$	NaOH	100	82
22	Diglyme	0.07	*p*-$CH_3C_6H_4SO_2Cl$	NaOH	120	59
23	Monoglyme	0.07	*p*-$CH_3C_6H_4SO_2Cl$	KOH	0	26
24	Dioxane	0.07	*p*-$CH_3C_6H_4SO_2Cl$	KOH	20	37
25	Dioxane	0.07	*p*-$CH_3C_6H_4SO_2Cl$	KOH	40	53
26	Dioxane	0.07	*p*-$CH_3C_6H_4SO_2Cl$	KOH	60	57
27	Dioxane	0.07	*p*-$CH_3C_6H_4SO_2Cl$	KOH	80	54
28	Dioxane	0.07	*p*-$CH_3C_6H_4SO_2Cl$	KOH	100	53
29	Diglyme	0.07	*p*-$CH_3C_6H_4SO_2Cl$	KOH	120	48

a) Determined by GLC. b) Values in parentheses are the purified, isolated yields obtained by thermolysis (Nos. 2, 4, and 20) or by hexane extraction (No. 5). c) Glycol 5.0 g/TsCl 4.1 g/NaOH 3.6 g/dioxane 60 ml. d) Glycol 5.0 g/TsCl 4.1 g/NaOH 3.6 g/dioxane 30 ml. e) Glycol 47 g/TsCl 38 g/NaOH 32 g/dioxane 700 ml. f) Reflux temperature.

Table 2. Synthesis of crown ethers from oligoethylene glycols

Exp. No.	PEG	Solvent	Concn mol/l	Sulfonyl chloride	Alkali	React. temp/°C	Yield of crown ether/%[a]	
1	Hexa E.G.	dioxane	0.060	TsCl	NaOH	20	18-crown-6	44
2	Hexa E.G.	dioxane	0.060	TsCl	NaOH	40	18-crown-6	57
3	Hexa E.G.	dioxane	0.060	TsCl	NaOH	60	18-crown-6	71
4	Hexa E.G.	dioxane	0.060	TsCl	NaOH	80	18-crown-6	70
5	Hexa E.G.	diglyme	0.060	TsCl	NaOH	100	18-crown-6	67
6	Hexa E.G.	diglyme	0.060	TsCl	NaOH	120	18-crown-6	50
7	Hexa E.G.	dioxane	0.060	TsCl	KOH	20	18-crown-6	77 (52)[b]
8	Hexa E.G.	dioxane	0.060	TsCl	KOH	40	18-crown-6	95
9	Hexa E.G.	dioxane	0.138	TsCl	KOH	40	18-crown-6	92 (75)
10	Hexa E.G.	dioxane	0.060	TsCl	KOH	60	18-crown-6	98 (75)
11	Hexa E.G.	dioxane	0.060	TsCl	KOH	80	18-crown-6	94
12	Hexa E.G.	diglyme	0.060	TsCl	KOH	100	18-crown-6	89
13	Hexa E.G.	diglyme	0.060	TsCl	KOH	120	18-crown-6	84
14	Hepta E.G.	dioxane	0.052	TsCl	NaOH	40	21-crown-7	28
15	Hepta E.G.	dioxane	0.052	TsCl	NaOH	60	21-crown-7	38
16	Hepta E.G.	dioxane	0.052	TsCl	NaOH	80	21-crown-7	36
17	Hepta E.G.	dioxane	0.052	TsCl	KOH	20	21-crown-7	48
18	Hepta E.G.	dioxane	0.052	TsCl	KOH	40	21-crown-7	73
19	Hepta E.G.	dioxane	0.115	TsCl	KOH	50	21-crown-7	75 (59)
20	Hepta E.G.	dioxane	0.052	TsCl	KOH	60	21-crown-7	79
21	Hepta E.G.	dioxane	0.052	TsCl	KOH	80	21-crown-7	80
22	Hepta E.G.	diglyme	0.052	TsCl	KOH	100	21-crown-7	73
23	Hepta E.G.	diglyme	0.052	TsCl	KOH	120	21-crown-7	62
24	Tetra E.G.	dioxane	0.085	TsCl	NaOH	20	12-crown-4 24-crown-8	3 18 (12)
25	Tetra E.G.	dioxane	0.085	TsCl	*t*-BuOLi	60	12-crown-4	22
26	Tetra E.G.	dioxane	0.085	TsCl	*t*-BuOLi	80	12-crown-4	25
27	Tetra E.G.	*t*-BuOH	0.220	TsCl	*t*-BuOLi	80[c]	12-crown-4	39 (27)
28	Tetra E.G.	*t*-BuOH	0.085	$BzSO_2Cl$	*t*-BuOLi	40	12-crown-4	34
29	Tetra E.G.	*t*-BuOH	0.085	$BzSO_2Cl$	*t*-BuOLi	60	12-crown-4	41
30	Tetra E.G.	*t*-BuOH	0.085	$BzSO_2Cl$	*t*-BuOLi	80[c]	12-crown-4	49

a) Determined by GLC. b) Values in parentheses are the yields of crown ethers isolated by thermolysis (Nos. 7, 9, 10, and 27), hexane extraction (No. 19), or column chromatography (No. 24). c) Reflux temperature.

and potassium hydroxide (3.0 g) in 60 ml of dioxane at 60 °C. The crude complex (3.5 g) thus obtained was found by GLC analysis to contain 15-crown-5 (0.67 g), 18-crown-6 (0.38 g), 21-crown-7 (0.49 g), and 24-crown-8 (0.40 g).

Results and Discussion

The overall reaction scheme for the synthesis of crown ethers is shown in Scheme 1.

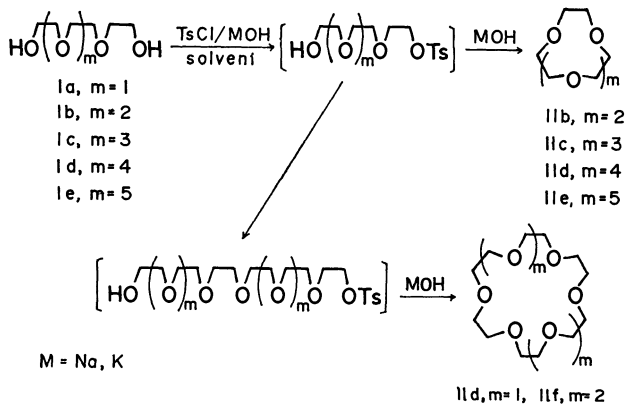

Scheme 1. Synthesis of crown ethers from oligoethylene glycols.

Pentaethylene glycol, hexaethylene glycol, and heptaethylene glycol were converted easily to the corresponding crown ethers, *i.e.*, 15-crown-5, 18-crown-6, and 21-crown-7 respectively. The results are shown in Tables 1 and 2.

On the other hand, tetraethylene glycol gave only a very small amount of 12-crown-4 (3%) under reaction conditions similar to those of the higher homologues, in spite of complete consumption of the starting glycol. Instead, 24-crown-8 was isolated in a 12% yield from the reaction product, suggesting that the template effect was not effective for the cyclization of tetraethylene glycol to 12-crown-4.[14]

However, the yield of 12-crown-4 could be increased up to 49% by altering the alkali/solvent system from Na(K)OH/dioxane to *t*-BuOLi/*t*-BuOH.

The solvent may play an important role in this reaction.[15] In the reactions in dioxane, THF, monoglyme, and diglyme, the yields of crown ethers were almost all the same and well satisfactory, while the reactions in ether, acetonitrile, and benzene gave somewhat poorer yields, and in hexane, the yield was very low, probably because of the limited solubility of

glycol. On the other hand, although a slight amount of 15-crown-5 was obtained in the reaction in DMF, no crown ether was obtained in the DMSO solvent and the glycols were recovered unchanged. Sulfonyl chlorides seemed to react with these solvents in preference to glycols when alkali metal hydroxide was present.

The kind of sulfonyl chloride also has some effect on the reaction. Among the sulfonyl chlorides investigated, benzenesulfonyl chloride was most effective with the *o*- and *p*-toluenesulfonyl chlorides following. The alkanesulfonyl chlorides seemed less effective than arenesulfonyl chlorides.

With respect to the effect of the alkali metal cation as the template ion, results almost the same as in the previous investigations were obtained.[5,6] The order of the effectiveness of sodium cation for the oligoethylene glycol was: *penta*>*hexa*>*hepta*>*octa*≫*tetra*, while that of the potassium cation was: *hexa*>*hepta*>*penta*>*octa*≫*tetra*. Other cations, such as Li^+, Ba^{++}, and Ca^{++} were found to be ineffective.

The temperature effect has already been reported briefly.[16] A temperature of around 60 °C was found to be optimum for the synthesis of most of the crown ethers investigated.

The concentration of the glycols and the addition rate may also affect the reaction, because the intramolecular cyclization to a crown ether may be preferable to the intramolecular oligomerization in a dilute solution. However, the addition time was settled as 2 h for the convenience of comparison, while the concentration was changed over the range from 0.07 to 0.7 mol/l in the synthesis of 15-crown-5.

Although the yield was observed to decrease slightly in concentrations (0.7 mol/l) higher than that in the dilute solution (0.07 mol/l), the difference in the yields between the concentrations was not so remarkable that, by controlling the addition rate, a satisfactory result can be expected even in production on a large scale.

Furthermore, as to such glycols as tri- and tetraethylene glycol, which are difficult to cyclize to the corresponding crown ethers, cyclization was observed to occur after the dimerization or trimerization of glycol, as 24-crown-8 instead of 12-crown-4 was obtained in the reaction of tetraethylene glycol. Thus, when triethylene glycol was treated with an equimolar amount of *p*-toluenesulfonyl chloride, 18-crown-6 was obtained in the maximum yield of 72%, as is shown in Fig. 1 (Curve II).

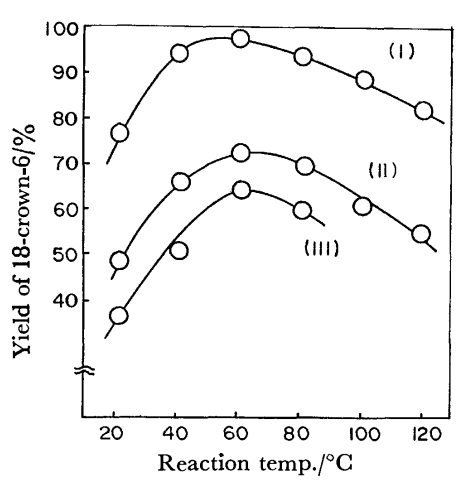

Fig. 1. Yield of 18-crown-6 in various reactions.
Curve I : Cyclization of hexaethylene glycol by TsCl.
Curve II : Condensation of two moles of triethylene glycol by TsCl.
Curve III: Condensation of triethylene glycol and triethylene glycol ditosylate.

The yield was somewhat lower than that of the cyclization of hexaethylene glycol (Curve I), but better than that of the condensation between triethylene glycol and triethylene glycol ditosylate (Curve III).[4,16]

Similarly, the three expected crown ethers, *i.e.*, 18-crown-6, 21-crown-7, and 24-crown-8, were obtained in the molar ratio of 4: 7: 3 from the reaction of an equimolar mixture of triethylene glycol and tetraethylene glycol (Scheme 2 and Table 3).

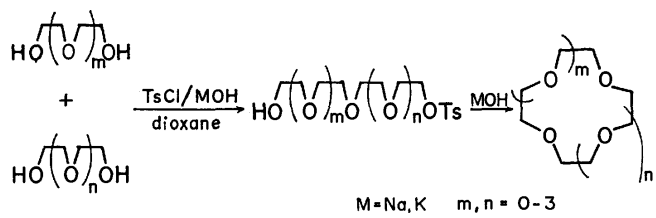

Scheme 2. Synthesis of crown ethers from mixtures of oligoethylene glycols.

Table 3. Synthesis of crown ethers by the coupling reaction of glycols

Exp. No.	*m*	*n*	MOH	Product	Yield/%[a]
1	3	0	NaOH	15-crown-5	trace[b]
2	3	1	KOH	18-crown-6	23[b]
3	3	2	NaOH	18-crown-6	19
			KOH	21-crown-7	33
				24-crown-8	14
4	3	3	KOH	12-crown-4	2
				24-crown-8	24

a) Determined by GLC. b) The presence of a small amount of 24-crown-8 was detected.

However, our attempts to prepare crown ethers using ethylene glycol or diethylene glycol were not successful because of their prompt conversion to ethylene oxide or dioxane.

Furthermore, the treatment of the commercial polyethylene glycol 200, which is composed mainly of tri-, tetra-, penta-, and hexaethylene glycols, with *p*-toluenesulfonyl chloride at 60 °C in the presence of

Table 4. Synthesis of crown ethers from polyethylene glycol 200

Product	PEG Source	Yield/wt%[a]
15-Crown-5	penta	26
18-Crown-6	hexa, tri×2	15
21-Crown-7	tri+tetra	20
24-Crown-8	tetra×2, tri+penta	16

a) Determined by GLC.

NaOH/KOH afforded a mixture of 15-, 18-, 21-, and 24-crown ethers, with the complete consumption of the glycols (Table 4).

Free crown ethers were isolated from their complexes with sodium (potassium) chloride or *p*-toluenesulfonate by thermal decomposition under reduced pressure using a Kugelrohr distillation apparatus, column chromatography or continuous extraction by hydrocarbon solvents. The last means was preferable to the others, especially for the separation of 15- and 21-crown ethers from their complexes.

References

1) R. M. Izatt and J. J. Christensen, "Synthetic Multidentate Macrocyclic Compounds," Academic Press (1978).

2) M. Hiraoka, "Crown Compounds," Kodansha Scientific (1978).

3) C. J. Pedersen, *J. Am. Chem. Soc.*, **89**, 7017 (1967).

4) J. O. Dale and P. O. Christiansen, *Chem. Commun.*, **1971**, 670; *Acta. Chem. Scand.*, **26**, 1471 (1972).

5) R. N. Green, *Tetrahedron Lett.*, **1972**, 1793.

6) F. L. Cook, T. C. Caruson, M. P. Byrne, C. W. Bowers, D. H. Speck, and C. L. Liotta, *Tetrahedron Lett.*, **1974**, 4029.

7) G. Jones, C. R. Ransom, and C. B. Reese, *Synthesis*, **1976**, 515.

8) J. Dale, G. Bogen, and K. Dassvath, *Acta. Chem. Scand.*, **B 28**, 378 (1974).

9) J. Dale and K. Daasvath, *Chem. Commun.*, **1976**, 515.

10) The initial attempt by Pedersen[3] to obtain 18-crown-6 by the intramolecular cyclization of hexaethylene glycol monochloride was unsuccessful because of the low yield (1.8%) of the objective product. Recently Mondolini and Masci[17,18] have also reported some results along these lines.

11) M. Okahara, M. Miki, S. Yanagida, I. Ikeda, and K. Matsushima, *Synthesis*, **1977**, 854.

12) P.-L. Kuo, M. Miki, and M. Okahara, *Chem. Commun.*, **1978**, 504.

13) P.-L. Kuo, M. Miki, I. Ikeda, and M. Okahara, *Tetrahedron Lett.*, **1978**, 4273.

14) The formation of 24-crown-8 instead of 12-crown-4 in the reaction of diethylene glycol and diethylene glycol ditosylate was also reported by Dale.[4]

15) Remarkable differences in the yield of 18-crown-6 by solvents were also noticed by Green.[5]

16) N. Kawamura, M. Miki, I. Ikeda, and M. Okahara, *Tetrahedron Lett.*, **1979**, 535.

17) L. Mandolini and B. Masci, *J. Am. Chem. Soc.*, **99**, 7709 (1977).

18) L. Mandolini and B. Masci, *Synth. Commun.*, **9**, 851 (1979).

Nucleophilic Reactions of Hexafluoro-1,2-epoxypropane with 1,2-Bifunctional Ethanes

Hajimu KAWA, Hamdy A. HAMOUDA, and Nobuo ISHIKAWA*

Department of Chemical Technology, Tokyo Institute of Technology, Ookayama, Meguro-ku, Tokyo 152

(Received December 12, 1979)

Reactions between hexafluoro-1,2-epoxypropane and 1,2-bifunctional ethanes were studied. Ethylenediamine, 2-aminoethanol and 2-aminoethanethiol gave corresponding *N*- and *O*-pentafluoropropionylated products, while ethylene glycol, 2-mercaptoethanol, and 1,2-ethanedithiol afforded ring closed products, such as 1,4-dioxanone, 1,4-oxathianone, and 1,4-dithianone compounds.

Hexafluoro-1,2-epoxypropane (**1**) is easily attacked by nucleophiles usually at the 2-position, and the resulting carboxylic acid fluorides (**2**) further react with another molecule of the nucleophile to give 2-substituted tetrafluoropropanoic acid derivatives (**3**).[1-3] Utilizing

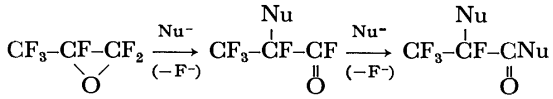

these reactivities of **1** for nucleophiles, we have prepared several fluorinated 2,3-benzo-fused 1,4-diheteracyclic compounds (**4**) by the reaction between **1** and 1,2-bifunctional benzenes.[4] Another example of the

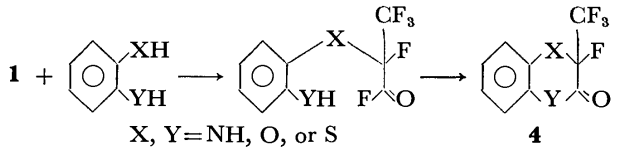

preparation of fluorinated heterocycles from **1** is the condensation with mercaptobenzimidazoles giving thiazolobenzimidazolones which are interesting from the pharmaceutical point of view.[5] Since the formation of

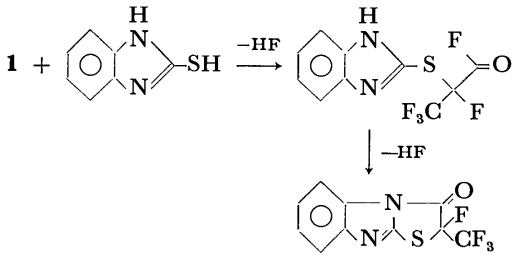

other kind of 1,4-diheteracyclic compounds had been expected, these works have now been extended and reactions between **1** and 1,2-bifunctional ethanes were examined. The reactions were, however, not so simple like those with 1,2-bifunctional benzenes and some interesting behaviors of 1,2-bifunctional ethanes were observed.

Results and Discussion

Reactions of Hexafluoro-1,2-epoxypropane with Ethylenediamine, 2-Aminoethanol and 2-Aminoethanethiol. Hexafluoro-1,2-epoxypropane is known to isomerize easily into pentafluoropropanoic acid fluoride (**6**) by the aid of a fluoride ion or a strong base.[6,7]

The reaction with an alkylamine is reported to give some amount of *N*-alkylpentafluoropropionamide (**7**)

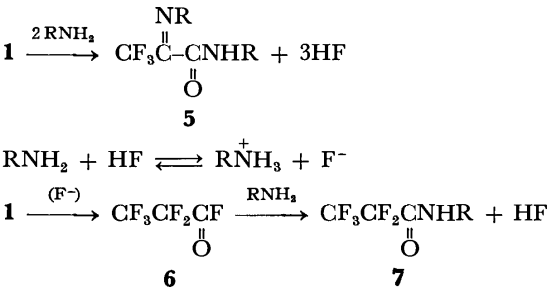

together with the main 2-substituted amide (**5**). When we allowed **1** to react with an equimolar amount of ethylenediamine, 2-aminoethanol or 2-aminoethanethiol in diglyme at room temperature, only *N*- and *O*-pentafluoropropionylated products were obtained and no 2-substituted tetrafluoropropanoic acid derivatives.

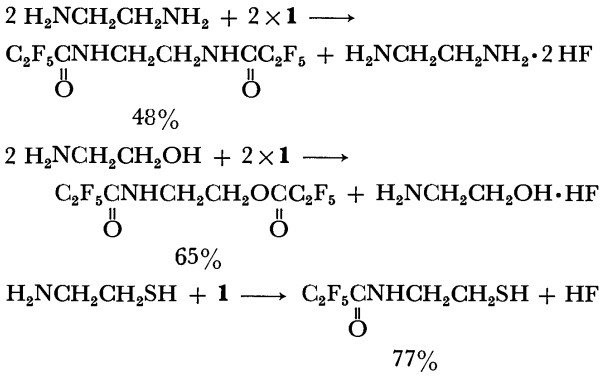

Thus, by the nucleophilic reactions of **1** with 2-functional ethylamines, none of heterocyclic compounds were obtained. This is in contrast to those with *ortho*-functional anilines which gave 2,3-benzo-fused 1,4-diheteracyclic compounds in good yields.[4] The difference should be ascribed to the stronger basicities of aliphatic amines than those of the aromatic amines. The strong basicity of ethylenediamine or 2-aminoethanol must have promoted the isomerization of **1** to **6** rather than the nucleophilic reaction at the 2-position of **1**.

Reactions of Hexafluoro-1,2-epoxypropane with Ethylene Glycol, 2-Mercaptoethanol, and 1,2-Ethanedithiol. As described above, the amino group of 2-functional ethylamines was found to accelerate the formation of acid fluoride **6**. Then we examined the reaction of **1** with non-basic 1,2-bifunctional ethanes, *i.e.*, ethylene glycol, 2-mercaptoethanol and 1,2-ethanedithiol.

Ethylene glycol reacted smoothly with **1** in diglyme and 3-fluoro-3-trifluoromethyl-1,4-dioxan-2-one (**8**) was

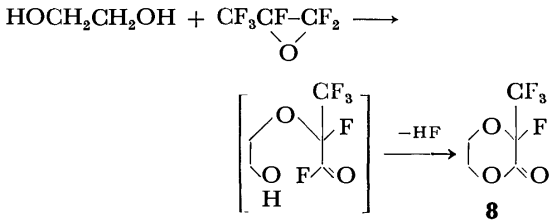

expectedly obtained. In the case of mercaptoethanol, two isomers of 1,4-oxathianone (**9**, **10**) were obtained in almost similar yields.

It is evident that **9** was formed by the nucleophilic attack by the OH group of mercaptoethanol first, while **10** was formed by that of the SH group first. In addition to these two heterocyclic compounds, a considerable amount (11%) of *O*-pentafluoropropionyl compound (**11**) was isolated from the reaction mixture.

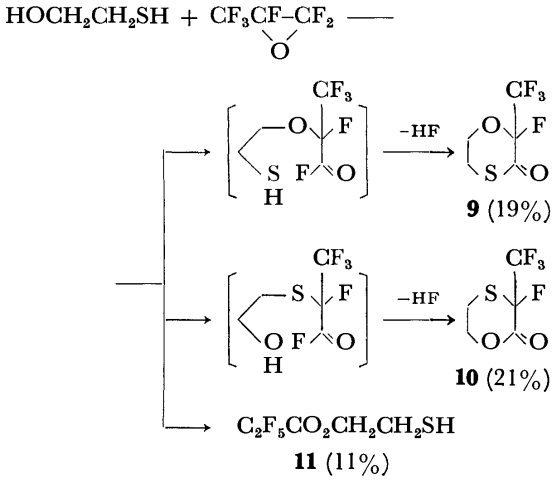

With 1,2-ethanedithiol, 2-fluoro-2-trifluoromethyl-1,4-dithian-3-one (**12**) was expectedly formed, though the yield was rather poor (26%), and a larger amount of *S*-pentafluoropropionyl compound (**13**) was obtained.

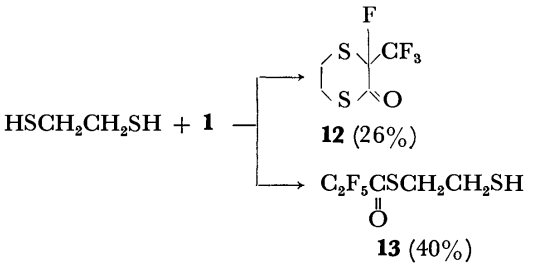

The formation of pentafluoropropionylated products in the case of reactions with the thiol and the dithiol should have resulted from the partial isomerization of **1** to **6** by the aid of the mercapto group, which behaved as a weak base.

Equilibrium among N-, O- *and* S-*Pentafluoropropionyl Groups.* From the results obtained heretofore, we noticed that there are differences among *N*-, *O*-, and *S*-pentafluoropropionyl groups in their thermodynamic stabilities.

For example, when *N*,*O*-bis(pentafluoropropionyl)-2-aminoethanol was treated with an equimolar amount of 2-aminoethanol, proportionation reaction occurred, and the *N*-(pentafluoropropionyl) compound was obtained quantitatively.

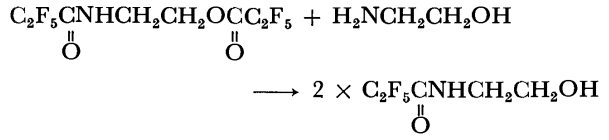

Further, we examined pentafluoropropionylation of 1,2-bifunctional ethanes by having them react with **1** in acetonitrile in the presence of triethylamine, the reaction which was used for the pentafluoropropionylation of

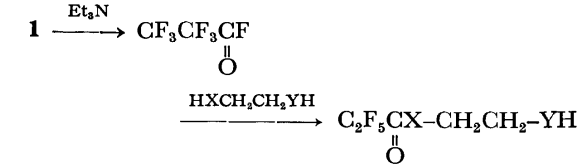

alcohols and amines.[8] The results are shown in Table 1. It is notable that when two different kinds of groups present in a molecule, only one group of them was exclusively pentafluoropropionylated. An amino group was always predominantly pentafluoropropionylated rather than a hydroxyl or a mercapto group, and between the latter two groups, a hydroxyl group was more readily perfluoroacylated. From these results, it was evident that the order of thermodynamic stabilities of pentafluoropropionyl groups is C_2F_5CONH> $C_2F_5CO_2$>C_2F_5COS. This order is in accordance with the general stabilities of acyl compounds,[9] but the trend seems to be more remarkable in a series of perfluoroacyl compounds.[10]

Table 1. Pentafluoropropionylation of 1,2-bifunctional ethanes

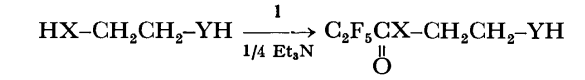

Product		Yield[a]/%
C_2F_5COX	YH	
C_2F_5CONH	C_2F_5CONH	42
C_2F_5CONH	OH	92
C_2F_5CONH	SH	95
$C_2F_5CO_2$	OH	90
$C_2F_5CO_2$	SH	53[b]
C_2F_5COS	SH	72

a) Based on ^{19}F-NMR signal intensities. b) Low yield is due to the formation of thiirane:

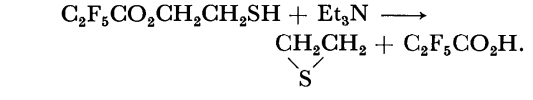

The ^{19}*F-NMR Spectra.* Most of the qualitative and quantitative analyses of reaction products in this work were easily done by means of the ^{19}F-NMR spectra.

In a series of $-X-CF-CF_3$ moieties, the NMR signals for C<u>F</u> and C<u>F</u>$_3$ of X=O compounds were characteristically distinguishable from those of X=S compounds. Thus, in comparison with those of X=O compounds, the signals due to <u>F</u> and C<u>F</u>$_3$ of X=S compounds shift considerably up and down field

TABLE 2. THE ^{19}F-NMR FOR Et–X–CF(CF$_3$)–CO$_2$Et

X	Chem. Shift (ppm)[a]		J_{CF-CF_3} (Hz)
	CF	CF_3	
O	+53.3	+5.0	2.8
S	+72.0	−3.5	10.8

a) Upfields from ext. CF_3CO_2H in Et_2O.

respectively, and the coupling constants J_{F-CF_3} were much larger. The results are shown in Table 2.

The fluorine atom of the S–CF group is supposed to be more shielded than that of the O–CF group due to the more positive character of the sulfur atom than the oxygen atom. In the case of the –N=C–CF_3 group, the signal due to CF_3 appeared, of course, as a singlet at about −20 ppm.

As to the ^{19}F chemical shifts for $CF_3CF_2C(=O)XR$, characteristic patterns were observed depending on the X atom, as shown in Table 3. In general, the signals due to CF_2 in X=NH, O, and S compounds appeared at 45—46, 43—44, and 42—43 ppm upfield from CF_3CO_2H standard respectively. These values could be used for the identification of the pentafluoropropionyl groups.

TABLE 3. THE ^{19}F-NMR CHEMICAL SHIFTS FOR $CF_3CF_2C(=O)–XR$

δ ppm upfield from ext. CF_3CO_2H in acetonitrile.

X	R	CF_2	CF_3
NH	*n*-Pr	+45.4	+6.2
NH	$PhCH_2$	+45.2	+5.7
NH	Ph	+45.1	+5.8
O	*n*-Pr	+44.3	+6.4
O	$PhCH_2$	+44.3	+6.2
O	Ph	+44.4	+6.2
S	*n*-Pr	+42.3	+5.3
S	$PhCH_2$	+42.5	+5.2
S	Ph	+42.4	+5.0

Experimental

All the ^{19}F-NMR chemical shifts throughout this article are given in δ ppm upfield from external CF_3CO_2H.

N,N'-Bis(pentafluoropropionyl)ethylenediamine. A mixture of ethylenediamine (1.20 g, 20 mmol) and diglyme (20 ml) was placed in a glass pressure vessel and cooled to≈ −70 °C. Liquefied hexafluoro-1,2-epoxypropane (bp −27 °C, 3.50 g, 21 mmol) was then introduced into the vessel and the whole was brought to room temperature. After stirring of 1 h, the reaction mixture was poured into water and an oily material was extracted with diethyl ether. The extract was dried over magnesium sulfate and the solvent was removed, yielding a solid material. The crude product was recrystallized from aqueous methanol to give pure *N,N'*-(bispentafluoropropionyl)-ethylenediamine (1.69 g, 48%), mp 169 °C. IR: 3315 (NH), 1690 (C=O) cm^{-1}. ^{19}F-NMR (in acetone): δ 5.5 (CF_3), 44.5 (CF_2) ppm. Found: C, 27.43; H, 1.81; N, 7.76%. Calcd for $C_8H_6N_2O_2F_{10}$: C, 27.29; H, 1.72; N, 7.96%.

N,O-Bis(pentafluoropropionyl)-2-aminoethanol. 2-Aminoethanol (1.22 g, 20 mmol) instead of ethylenediamine was used in the above procedure. Reaction was continued for 2 h at room temperature and worked up similarly. Distillation gave 1.70 g (66%) of *N,O*-bis(pentafluoropropionyl)-2-aminoethanol, bp 81—82 °C/3 mmHg. IR (film): 3310 (NH), 1710 (C=O), 1700 (C=O) cm^{-1}. ^{19}F NMR (neat): δ 7.0 (2× CF_3), 45.0, 47.0 (CF_2) ppm. Found: C, 27.64; H, 1.65; N, 4.33%. Calcd for $C_8H_5NO_3F_{10}$: C, 27.21; H, 1.43; N, 3.97%.

N-Pentafluoropropionyl-2-aminoethanol. 2-Aminoethanol (0.30 g, 5 mmol) was added to a mixture of *N,O*-bis(pentafluoropropionyl)-2-aminoethanol (1.29 g, 5 mmol) and diglyme (10 ml) at room temperature. After 30 min of stirring the solvent was removed, and almost pure *N*-pentafluoropropionyl-2-aminoethanol (1.56 g, 98%), bp 99—100 °C/5 mmHg was obtained. IR: 3500—3300 (NH, OH), 1700 (C=O) cm^{-1}. ^{19}F-NMR (neat): δ 6.0 (CF_3), 45.5 (CF_2) ppm. Found: C, 29.11; H, 2.87; N, 6.76%. Calcd for $C_5H_6NO_2F_5$: C, 28.99; H, 2.92; N, 6.76%.

N-Pentafluoropropionyl-2-aminoethanethiol. Pentafluoro-1,2-epoxypropane (3.50 g, 21 mmol) and 2-aminoethanethiol (1.54 g, 20 mmol) were allowed to react at room temperature for 2 h in diglyme (20 ml). *N*-Pentafluoropropionyl-2-aminoethanethiol (3.60 g, 77%), bp 108—109 °C/11 mmHg was obtained after usual treatment. IR: 3310 (NH), 2550 (SH), 1700 (C=O) cm^{-1}. ^{19}F-NMR (neat): δ 6.0 (CF_3), 45.5 (CF_2), ppm. Found: C, 26.13; H, 2.57; N, 5.82%. Calcd for $C_6H_5NOSF_5$: C, 26.91; H, 2.71; N, 6.28%.

When a mixture of this compound (1.11 g, 5 mmol), 2,4-dinitrochlorobenzene (1.01 g, 5 mmol), potassium hydroxide (0.3 g, 5 mmol) and ethanol (30 ml) was refluxed for 3 h, *S*-(2,4-dinitrophenyl)derivative (1.4 g, 72%) was obtained. Recrystallization from chloroform gave a pure material, mp 138 °C. IR: 3310 (NH), 1700 (C=O) cm^{-1}. ^{19}F-NMR (acetone): δ 6.0 (CF_3), 45.5 (CF_2) ppm. Found: C, 33.68; H, 2.08; N, 10.73%. Calcd for $C_{11}H_8N_3O_5SF_5$: C, 33.94; H, 2.07; N, 10.79%.

3-Fluoro-3-trifluoromethyl-1,4-dioxan-2-one (8). A mixture of pentafluoro-1,2-epoxypropane (5.81 g, 35 mmol), ethylene glycol (1.86 g, 30 mmol) and diglyme (20 ml) in a sealed glass tube was allowed to react for 50 h at room temperature. The reaction mixture was poured into water and the resulting organic layer was separated and dried over magnesium sulfate. Vacuum distillation gave pure dioxanone (2.25 g, 40%), bp 100—101 °C/25 mmHg. IR: 1780 (C=O) cm^{-1}. ^{19}F-NMR (neat): δ 3.6 (CF_3), 35.4 (CF) ppm. Found: C, 31.74; H, 2.10%. Calcd for $C_5H_4O_3F_4$: C, 31.91; H, 2.13%.

2-Fluoro-2-trifluoromethyl-1,4-oxathian-3-one (9) and 3-Fluoro-3-trifluoromethyl-1,4-oxathian-2-one (10). 2-Mercaptoethanol (2.34 g, 30 mmol) was allowed to react with pentafluoro-1,2-epoxypropane (5.81 g, 35 mmol) in diglyme (20 ml) for 20 h at room temperature. The reaction mixture was poured into water and the separated oil was dried ($MgSO_4$) and distilled carefully to give the following products:

O-Pentafluoropropionyl-2-mercaptoethanol (0.74 g, 11%), pb 68 °C/77 mmHg. IR: 1785 (C=O) cm^{-1}. ^{19}F-NMR (neat): δ 4.8 (CF_3), 43.1 (CF_2) ppm. Found: C, 26.48; H, 2.42%. Calcd for $C_5H_5O_2SF_5$: C, 26.79; H, 2.42%.

The mixture of two isomers 1,4-oxathianone (2.45 g, 40%), bp 60—85 °C/2 mmHg. The ratio of these two isomers, **9**: **10**= 1: 1, was determined by ^{19}F-NMR and they were practically separated by column chromatography (Silica Gel) using hexane as an eluent.

9: bp 93.5—94.5 °C/16 mmHg. IR: 1680 (C=O) cm^{-1}.

^{19}F-NMR (neat): δ 2.9 ($C\underline{F}_3$), 36.0 ($C\underline{F}$) ppm.

Found: C, 29.16; H, 1.90%. Calcd for $C_5H_4O_2SF_4$: C, 29.41; H, 1.96%. **10**: bp 84—85 °C/2 mmHg. IR: 1770 (C=O) cm^{-1}. ^{19}F-NMR (neat): δ −1.2 ($C\underline{F}_3$), 55.0 (CF) ppm. Found: C, 29.21; H, 1.88%.

*2-Fluoro-2-trifluoromethyl-1,4-dithian-3-one (**12**).* The reaction of 1,2-ethanedithiol (2.82 g, 30 mmol) and pentafluoro-1,2-epoxypropane (5.81 g, 35 mmol) in diglyme (20 ml) was carried out for 12 h at room temperature. The reaction mixture was then poured into water and worked up as usual. Fractional distillation gave the following two porducts:

S-Pentafluoropropionyl-1,2-ethanedithiol (2.88 g, 40%): bp 69—70 °C/30 mmHg. IR: 1680 (C=O) cm^{-1}. ^{19}F-NMR (neat): δ 4.7 ($C\underline{F}_3$), 42.0 ($C\underline{F}_2$) ppm. Found: C, 24.66, H, 2.00%. Calcd for $C_5H_5OS_2F_5$: C, 25.00; H, 2.08%. **12** (1.72 g, 26%): bp 83—84 °C/6 mmHg. IR: 1680 (C=O) cm^{-1}. ^{19}F-NMR (neat): δ −3.0 ($C\underline{F}_3$), 52.5 ($C\underline{F}$) ppm. Found: C, 27.03; H, 1.80%. Calcd for $C_5H_4OS_2F_4$: C, 27.27; H, 1.82%.

Reaction of 1,2-Biflunctional Ethanes with Hexafluoro-1,2-epoxypropane in the Presence of Triethylamine. General Procedure. A solution of 1,2-bifunctional ethane (10 mmol) and triethylamine (0.25 g, 2.5 mmol) in acetonitrile (10 ml) was cooled to −70 °C, then liquefied pentafluoro-1,2-epoxypropane (1.66 g, 10 mmol) was introduced into the vessel and the whole was brought to room temperature. After 30 min of stirring, benzylidyne trifluoride (1.46 g, 10 mmol) was added as an internal standard and the yield was determined by ^{19}F-NMR spectral analysis (Table 1).

For the isolation of the product, the reaction mixture was poured into water and the separated oily material was subjected to vacuum distillation. *O*-Pentafluoropropionylethylene glycol, for example, was obtained in 63% yield. bp 44 °C/5 mmHg. IR: 3350 (OH), 1710 (C=O) cm^{-1}. ^{19}F-NMR (neat): δ 5.5 ($C\underline{F}_3$), 44.5 (CF_2) ppm. Found: C, 27.08; H, 2.42%. Calcd for $C_5H_5O_3F_5$: C, 26.80; H, 2.25%.

References

1) D. Sianesi, A. Pasetti, and F. Tarli, *J. Org. Chem.*, **31**, 2321 (1966).
2) A. Pasetti, F. Tarli, and D. Sianesi, *Gazz. Chim. Ital.*,**98**, 277, 290 (1968).
3) I. L. Knunyants, V. V. Shokina, and I. V. Galakhov, *Khim. Geterotsikl. Soedin*, **1966**, 873.
4) N. Ishikawa and S. Sasaki, *Bull. Chem. Soc. Jpn.*, **50**, 2164 (1977).
5) H. A. Hammouda and N. Ishikawa, *Bull. Chem. Soc. Jpn.*, **51**, 3091 (1978).
6) R. A. Bekker, G. V. Asratyan and D. L. Dyatkin, *Zhur. Org. Khim.*, **9**, 1644 (1973).
7) Du Pont, Brit. Patent 1019788 (1966).
8) N. Ishikawa and S. Sasaki, *Nippon Kagaku Kaishi*, **1976**, 1954.
9) S. Patai, "The chemistry of carboxylic acids and esters," John Wiley and Sons (1969), p. 726.
10) R. Hershfield and G. L. Schmir, *J. Am. Chem. Soc.*, **95**, 3994 (1973).

Wittig-type Reaction of Dimetallated Carbodianion Species as Produced by Zinc Reduction of *gem*-Polyhalogen Compounds in the Presence of Lewis Acids

Kazuhiko TAKAI, Yuji HOTTA, Koichiro OSHIMA,* and Hitosi NOZAKI

Department of Industrial Chemistry, Faculty of Engineering, Kyoto University, Yoshida, Kyoto 606

(Received December 27, 1979)

Treatment of R^1COR^2 with a suspension prepared from diiodomethane, trimethylaluminum and excess zinc in tetrahydrofuran at room temperature affords olefins $R^1R^2C{=}CH_2$ in fair (R^1,R^2=alkyl) to good (R^1=alkyl, R^2=H) yields. The ketone methylenation is better carried with another system consisting of CH_2Br_2–Zn–$TiCl_4$. Ketones and aldehydes are transformed into α-chloro α,β-unsaturated esters or α,β-unsaturated esters in good yields on treatment with methyl trichloroacetate or *t*-butyl dichloroacetate (ethyl dibromoacetate) in the presence of diethylaluminum chloride and zinc.

Metallic zinc is widely used in organic synthesis[1] and often activated by plating the surface with such metals as copper, mercury or silver.[2] The organoaluminum compounds have been found to facilitate the reduction of α-halo carbonyl compounds with zinc greatly and the dramatic effect of co-existing diethylaluminum chloride on the Reformatsky type aldol reaction has been observed.[3] We report here further exploitation for (1) terminal olefin synthesis[4] and (2) α,β-unsaturated ester synthesis by means of species as produced upon zinc reduction of *gem*-polyhalogen compounds in the presence of certain Lewis acid reagents.

Terminal Olefin Synthesis. The Wittig type carbonyl methylenation by means of CH_2I_2–Zn has been described already especially in the presence of a large excess of zinc,[5,6] although the recorded yields are far from satisfactory from the preparative point of view. We wish to report that a mixture of CH_2I_2, Zn, and trimethylaluminum (1 : 3 : 0.2 mol ratio) reacts with carbonyl compounds to produce olefins much more effectively as summarized in Table 1.

Table 1. Reaction of R^1COR^2 with CH_2I_2–Zn–Me_3Al affording $R^1R^2C{=}CH_2$[a]

Entry	R^1COR^2		Temp	Time	$R^1R^2C{=}CH_2$
	R^1	R^2	°C	h	Y/%[b]
1	Ph	H	25	1	86[c]
2	Ph	Me	25	2	67[c]
3	PhCH=CH–	H	0	1	75
4	$CH_3(CH_2)_{10}$–	H	0	4	81
5	$CH_3(CH_2)_7$–	$CH_3(CH_2)_2$–	25	2	62
6	–$(CH_2)_{11}$–		25	6	65
7	(citral)		25	4	80

a) Three mol of CH_2I_2, nine mol of Zn and 0.6 mol of Me_3Al were employed per mol of carbonyl compounds. b) Isolated yield unless otherwise specified. c) GLPC yield by internal standard method.

Rather surprisingly, careful examination of the products failed to prove any traces of cyclopropane derivatives, which should be ascribed to the Simmons-Smith reaction of the olefinic linkage of the carbonyl components (entry 3, 7) or of the resulting $R^1R^2C{=}CH_2$. Although the reaction of the Simmons-Smith reagent with Me_3SnCl gives ICH_2SnMe_3,[7] the present reagent has been found to afford $CH_2(SnMe_3)_2$[8] exclusively under the same conditions and no ICH_2SnMe_3.

We therefore are tempted to attribute the formation of Wittig type olefins to the carbodianion species, although the identity of counter ions attached are still not clear. This *gem*-dimetallic nature of the present reactive intermediate has been further confirmed by the fact that preformed iodohydrin $PhCH(OH)CH_2I$[9] was recovered practically unchanged after treatment with excess of the reagent prepared as above. Olefination of aldehyde and ketone carbonyls by *gem*-dimetallic reagent of the type Mtl–CH_2–Mtl′ has been described to afford variable yields.[10] Exclusive carbonyl methylenation of enals (entry 3, 7) is unprecedented.

The yields of the methylenated products from ketones could not be improved over 70% in spite of various attempts made by means of the CH_2I_2, Zn, and R_3Al system. Other Lewis acids have been examined in the

Table 2. Effects of various lewis acid on the transformation of 4-dodecanone to 2-propyl-1-decene[a]

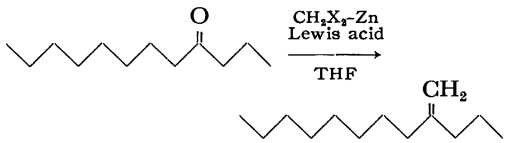

Lewis acid	Yield/% of 2-Propyl-1-decene	
	CH_2I_2	CH_2Br_2
Me_3Al	62	14
Et_3Al	55	27
Et_2AlCl	56	23
$AlCl_3$	42	<5
$TiCl_4$	83	89
VCl_4	73	20
$ZrCl_4$	34	<5
WCl_6	<5	<5

a) Three mol of CH_2I_2 or CH_2Br_2, 9 mol of Zn and 1 mol of Lewis acid were employed per mol of 4-dodecanone. Reaction mixture was stirred for 12 h at 25 °C and 2-propyl-1-decene was isolated by column chromatography.

transformation of 4-dodecanone to 2-propyl-1-decene with CH_2X_2 and zinc (Table 2). Among them, $TiCl_4$ has proved to be the best enabling to use CH_2Br_2 instead of CH_2I_2.

The results of methylenation with CH_2Br_2, Zn, $TiCl_4$ system are shown in Table 3. Neither cyclopropane compounds nor isomerized olefins were isolated. Entry 3[11] and 4[12] showed the superiority of the method over the Wittig reaction. The reductive coupling of the carbonyl component[13] was observed only with an aldehyde (entry 6), although the desired olefin was still predominant.

Both systems of CH_2I_2–Zn–Me_3Al and CH_2Br_2–Zn–$TiCl_4$ are complementary. The mild conditions and high yields characterize the two systems as a useful alternative for the Wittig carbonyl methylenation.[14]

Table 3. Reaction of R^1COR^2 with CH_2Br_2–Zn–$TiCl_4$ affording $R^1R^2C{=}CH_2$[a]

Entry	R^1COR^2		Temp	Time	$R^1R^2C{=}CH_2$
	R^1	R^2	°C	h	Y/%[b]
1	$CH_3(CH_2)_7$–	$CH_3(CH_2)_2$–	25	12	89
2	–$(CH_2)_{11}$–		25	12	80
3	–$(CH_2)_6$–		25	6	83[c]
4	(camphor)		25	40	92[c]
5	(geranylacetone)		25	12	83
6	$CH_3(CH_2)_{10}$–	H	0	4	55[d]

a) One and a half mol of CH_2Br_2, 4.5 mol of Zn and 1.1 mol of $TiCl_4$ were employed per mol of carbonyl compounds. b) Isolated yield. c) GLPC yield by internal standard method. d) $CH_3(CH_2)_{10}CH(OH)$-$CH(OH)(CH_2)_{10}CH_3$ was also obtained (24%).

α-Chloro α,β-Unsaturated Ester and α,β-Unsaturated Ester Syntheses. The reaction between ethyl trichloroacetate and carbonyl compounds in the presence of zinc[15] or Mg–$HgCl_2$[16] has been reported to result in the formation of α,α-dichloro β-hydroxy esters or the further reduced β-hydroxy esters. Meantime, we have disclosed that co-existence of diethylaluminum chloride in these classical Reformatsky reaction changes the reaction path dramatically to afford α-chloro α,β-unsaturated esters[17] instead. The results are summarized in Table 4.

$$CCl_3COOR^1 + R^2COR^3$$

Mg–$HgCl_2$ | Zn | Zn–Et_2AlCl

$$\begin{array}{ccc} \overset{OH}{\underset{R^3}{\overset{R^2}{\diagdown}}}\!\!\diagup\!\!\underset{H}{\overset{H}{\diagdown}}\!\!-\!\!COOR^1 & \overset{OH}{\underset{R^3}{\overset{R^2}{\diagdown}}}\!\!\diagup\!\!\underset{Cl}{\overset{Cl}{\diagdown}}\!\!-\!\!COOR^1 & \overset{R^2}{\underset{R^3}{\diagdown}}\!\!C{=}C\!\!\overset{Cl}{\diagup}\!\!\diagdown\!\!COOR^1 \end{array}$$

Remarkably, a Reformatsky product $Me_2C{=}CHCH_2$-$CH_2C(CH_3)(OH)CCl_2COOMe$ prepared by the conventional way has been recovered unchanged on treatment with the Zn–Et_2AlCl system. Furthermore, α,β-unsaturated esters were produced in the similar reaction of dichloro- or dibromoacetate with carbonyl in fair yields, which are shown in Table 5. The present method provides an alternative for the Emmons-Wadsworth-Horner reaction[18] and would very probably involve a Mtl–C(X)=C(OMtl')OR (X=Cl or H) type species. It should be noted that the presence of diethylaluminum chloride is crucial to the formation of α,β-unsaturated esters, since its absence results in ordinary Reformatsky products, halohydrins.[24]

Table 4. Synthesis of α-chloro α,β-unsaturated esters

$$CCl_3COOMe + R^1COR^2 \xrightarrow[THF]{Zn,\ Et_2AlCl} \overset{R^1}{\underset{R^2}{\diagdown}}\!\!C{=}C\!\!\overset{Cl}{\diagup}\!\!\diagdown\!\!COOMe$$

Entry	R^1COR^2		Conditions		Product	
	R^1	R^2	°C	h	Y/%[a]	E/Z
1	Ph	H	0	4	51	<5/>95
2	–$(CH_2)_5$–		0	6	81	—
3	$Me_2C{=}CH(CH_2)_2$–	CH_3	0	6	90	28/72
4	Ph	CH_3	0	4	86	9/91

a) Isolated yields.

Table 5. Synthesis of α,β-unsaturated esters

$$X_2CHCOOR^1 + R^2COR^3 \xrightarrow[THF]{Zn,\ Et_2AlCl} \overset{R^2}{\underset{R^3}{\diagdown}}\!\!C{=}C\!\!\overset{H}{\diagup}\!\!\diagdown\!\!COOR^1$$

Ester		R^2COR^3		Conditions		Product	
X	R^1	R^2	R^3	°C	h	Y/%[a]	E/Z
Cl	^{t}Bu	Ph	CH_3	25	6	67	62/38
Cl	^{t}Bu	–$(CH_2)_{11}$–		25	8	61	—
Cl	^{t}Bu	$Me_2C{=}CH(CH_2)_2$–	CH_3	25	6	52	59/41
Br	Et	Ph	H	25	3	42	>95/<5
Br	Et	$CH_3(CH_2)_{10}$–	H	25	3	43	>95/<5

a) Isolated yields.

Experimental

The IR spectra were determined on a Shimadzu IR-27-G spectrometer; the mass spectra, on a Hitachi RMU-6L machine; and the NMR spectra, on a JEOL C-60-H or a Varian EM-390H spectrometer. The chemical shifts are given in δ, with TMS as the internal standard. The analyses were carried out by the staff at the Elemental Analyses Center of Kyoto University. Commercial zinc dust was washed several times with 5% hydrochloric acid, washed in turn with water, methanol, and ether, and dried.[19] Tetrahydrofuran (THF) was dried on benzophenone ketyl and distilled. All the experiments were carried out under an argon atmosphere. Purification of products were performed by preparative thin layer chromatography (TLC) or column chromatography on silica gel (Merck Kieselgel 60). Analytical GLPC was performed with a Yanagimoto GCG-550-F. Product percentages were calculated from peak area ratios without correction for detector response. Preparative GLPC was performed with a JEOL-JGC-20K apparatus.

Preparation of Terminal Olefins by Means of CH_2I_2–Zn–Me_3Al System. To a suspension of zinc dust (1.18 g, 18 mmol) and diiodomethane (1.61 g, 6.0 mmol) in dry THF (10 ml) was added a hexane solution of trimethylaluminum (1.0 M, 1.2 ml, 1.2 mmol) at 25 °C. The resulting mixture was stirred until the exothermic reaction had subsided (10 min). A solution of carbonyl compound (2.0 mmol) in THF was added dropwise at 25 °C (0 °C). After stirring at this temperature for an appropriate time described in Table 1, the reaction mixture was diluted with ether (10 ml), poured into 1 M hydrochloric acid (20 ml), and extracted with ether. The separated organic layer was washed with brine (2×20 ml), dried over anhydrous sodium sulfate, and concentrated under reduced pressure. The crude product was purified by column chromatography on silica gel (20 g) using hexane as an eluent.

Preparation of Terminal Olefins by Means of CH_2Br_2–Zn–$TiCl_4$ System. To a suspension of zinc dust (0.59 g, 9.0 mmol) and dibromomethane (0.52 g, 3.0 mmol) in THF (10 ml) was added a dichloromethane solution of titanium tetrachloride (1.0 M, 2.2 ml, 2.2 mmol) at 25 °C. Instantaneous reaction occurred under evolution of heat and rapid color change to dark brown. After 15 min, a THF solution of carbonyl compound (2.0 mmol) was added dropwise and the resulting mixture was stirred at 25 °C (0 °C) for an appropriate time described in Table 3. The reaction mixture was diluted with ether (10 ml), poured into 1 M hydrochloric acid (20 ml), and extracted with ether. The separated organic layer was washed with brine (2×20 ml), dried over anhydrous sodium sulfate, and concentrated under reduced pressure. The crude product was purified by column chromatography on silica gel (20 g) using hexane as an eluent.

2-Propyl-1-decene: Bp 82 °C (bath temp, 2 Torr); IR (neat): 3080, 1643, 1470, 890 cm^{-1}; NMR (CCl_4): δ 0.90 (t, J=6 Hz, 6H), 1.15—1.55 (bm, 14H), 1.94 (t, J=6 Hz, 4H), 4.60 (s, 2H); MS *m/e* (%): 182 (M^+, 4), 139 (5), 97 (12), 56 (100); Found: C, 85.73; H, 14.62%. Calcd for $C_{13}H_{26}$: C, 85.63; H, 14.37%.

Methylenecyclododecane: Bp 85 °C (bath temp, 2 Torr); IR (neat): 3080, 1645, 1485, 1445, 890 cm^{-1}; NMR (CCl_4): δ 1.15—1.60 (bm, 18H), 1.93—2.20 (bt, 4H), 4.80 (s, 2H); MS *m/e* (%): 180 (M^+, 18), 109 (32), 97 (66), 82 (82), 55 (100). The compound was identical with the authentic sample.[20]

4,8-Dimethyl-1,3,7-nonatriene: Bp 53 °C (bath temp, 2 Torr); IR (neat): 3080, 1648, 1600, 1450, 990, 892 cm^{-1}; NMR (CCl_4): δ 1.60 (s, 3H), 1.67 (s, 3H), 1.74 (s, 3H), 1.95—2.17 (bm, 4H), 4.80—5.15 (bm, 3H), 5.76 (d, J=10 Hz, 1H), 6.46 (ddd, J=10, 10, 17 Hz, 1H); MS *m/e* (%): 150 (M^+, 7), 135 (6), 107 (11), 81 (18), 69 (100); Found: C, 87.87; H, 12.21%. Calcd for $C_{11}H_{18}$: C, 87.93; H, 12.07%.

Methylenecycloheptane: Bp 135 °C (1 atm); IR (neat): 3100, 1640, 1450, 880 cm^{-1}; NMR (CCl_4): δ 1.53 (bm, 8H), 2.23 (bt, 4H), 4.60 (s, 2H); MS *m/e* (%): 110 (M^+, 19), 95 (55), 82 (74), 67 (100). The compound was identical with the authentic sample.[21]

2-Methylenebornane: Mp 67—70 °C (sublimes appreciably at room temperature); IR (neat): 3070, 1655, 1450, 870 cm^{-1}; NMR (CCl_4): δ 0.77 (s, 3H), 0.88 (s, 6H), 1.08—2.60 (m, 7H), 4.40—4.65 (bdd, 2H); MS *m/e* (%): 150 (M^+, 25), 135 (45), 121 (24), 107 (100), 79 (79). The compound was identical with the authentic sample.[12]

2,6,10-Trimethyl-1,5,9-undecatriene: Bp 78 °C (bath temp, 2 Torr); IR (neat): 3080, 1650, 1450, 885, 825 cm^{-1}; NMR (CCl_4): δ 1.57, 1.65, 1.67, 1.70 (s, 12H), 1.85—2.20 (bm, 8H), 4.62 (s, 2H), 4.90—5,14 (bm, 2H); MS *m/e* (%): 192 (M^+, 3), 177 (3), 136 (9), 121 (9), 81 (52), 69 (100); Found: C, 87.20; H, 12.82%. Calcd for $C_{14}H_{24}$: C, 87.42; H, 12.58%.

1-Phenyl-1,3-butadiene and 1-Tridecene: These compounds were identical with the authentic samples.[22,23]

Reaction of Dodecanal with the Reagent Prepared from CH_2Br_2–Zn–$TiCl_4$ System. Dodecanal (0.37 g, 2.0 mmol) was treated with the reagent prepared from dibromomethane (0.52 g, 3.0 mmol), zinc (0.59 g, 9.0 mmol), and titanium tetrachloride (2.2 ml of a 1.0 M dichloromethane solution, 2.2 ml) in THF (10 ml) at 25 °C. The crude product was submitted to preparative TLC (hexane–ether, 1: 1) on silica gel. The faster-moving band (R_f=0.79) provided the desired olefin, 1-tridecene (0.20 g, 55%). The slower-moving band (R_f=0.25) consisted of 12,13-tetracosanediol (89 mg) as a solid; mp 88 °C; IR (KBr): 3300, 2900, 1470, 1068, 708 cm^{-1}; NMR ($CDCl_3$): δ 0.89 (t, J=6 Hz, 6H), 1.10—1.52 (m, 40H), 3.30—3.60 (m, 2H); Found: C, 77.77; H, 13.82%. Calcd for $C_{24}H_{50}O_2$: C, 77.77; H, 13.60%. The compound was identical with the authentic sample.[13]

Reaction of Trimethyltin Chloride with the Reagent Derived from CH_2I_2–Zn–Me_3Al in THF. The reagent was prepared from diiodomethane (0.54 g, 2.0 mmol), zinc (0.39 g, 6.0 mmol), and trimethylaluminum (0.5 ml of a 1.0 M hexane solution, 0.5 mmol) in THF (10ml) as mentioned before. After stirring at 25 °C for 30 min, the mixture was allowed to stand for 20 min and the supernatant was transformed to an another flask. To this was added a THF solution of trimethyltin chloride (0.80 g, 4.0 mmol) at *ca.* 40 °C and the resulting mixture was stirred at the same temperature for 4 h. After a usual workup, the crude product was purified by column chromatography on silica gel (10 g) using hexane as an eluent (R_f=0.55 (hexane)). Successive distillation gave methylenebis (trimethylstannane) (0.18 g, 27%) as a colorless oily liquid; bp 63 °C (bath temp, 5 Torr); IR (neat): 1465, 1262, 1190, 1100, 1025, 955, 760, 600 cm^{-1}; NMR (CCl_4) δ 0.05 (Sn–CH_3, 18H, J_{Sn-H}=51 Hz), −0.29 (Sn–CH_2–Sn, 2H, J_{Sn-H}=55 Hz); MS *m/e* (%): 329 (56), 327 (67), 325 (M^+–CH_3, 64), 165 (100). Values of *m/e* are given for the isotope ^{118}Sn. The relative intensities of the peaks of the isotopic varieties of the ions correspond to the calculated values; Found: C, 24.63; H, 6.17%. Calcd for $C_7H_{20}Sn_2$: C, 24.61; H, 5.90; Sn, 69.49%. The compound was identical with the authentic sample.[8]

Preparation of α-Chloro α,β-Unsaturated Esters by Means of CCl_3COOMe–Zn–Et_2AlCl System. To a stirred suspension of zinc dust (0.39 g, 6.0 mmol) and diethylaluminum chloride (0.67 ml of a 1.5 M hexane solution, 1.0 mmol) in THF (10

ml) was added a THF solution of methyl trichloroacetate (0.43 g, 2.4 mmol) and carbonyl compound (2.0 mmol) at 0 °C over a period of 3 h. After stirring for an additional 1 h, the resulting mixture was diluted with ether (20 ml), poured into 1 M hydrochloric acid (20 ml), and extracted with ether. The separated organic layer was washed with brine (2×20 ml), dried over anhydrous sodium sulfate, and concentrated under reduced pressure. The crude product was purified by column chromatography (hexane–ether, 20: 1) on silica gel (20 g).

Methyl (Z)-2-Chloro-3-phenylpropenoate: Bp 87 °C (bath temp, 2 Torr); IR (neat): 2955, 1730, 1620, 1495, 1450, 1438, 1265, 1040, 765, 690 cm^{-1}; NMR (CCl_4): δ 3.83 (s, 3H), 7.20—7.90 (m, 6H); MS *m/e* (%): 198 (M^++2, 21), 196 (M^+, 62), 165 (22), 161 (73), 160 (24), 137 (35), 129 (52), 102 (100); Found C, 61.38; H, 4.69%. Calcd for $C_{10}H_9O_2Cl$: C, 61.08; H, 4.61%. (*E*)-Isomer was not detected by GLPC.

Methyl Chlorocyclohexylideneacetate: Bp 80 °C (bath temp, 3 Torr); IR (neat): 2950, 1725 ,1610, 1438, 1270, 1245, 1210, 1030, 760 cm^{-1}; NMR (CCl_4): δ 1.50—1.80 (m, 6H), 2.38—2.55 (bt, J=6 Hz, 2H), 2.55—2.75 (bt, J=6 Hz, 2H), 3.75 (s, 3H); MS *m/e* (%): 190 (M^++2, 32), 188 (M^+, 91), 157 (54), 156 (50), 134 (65), 121 (96), 93 (100), 91 (64); Found: C, 57.29; H, 7.32%. Calcd for $C_9H_{13}O_2Cl$: C, 57.30; H, 6.95%.

Methyl (E)- and (Z)-2-Chloro-3,7-dimethyl-2,6-octadienoate: GLPC (20% PEG 6000, 2 m, 150 °C) indicated two peaks, T_r=14.1 min ((*E*)-isomer, 28%), T_r=12.4 min ((*Z*)-isomer 72%). The analytically pure samples of both isomers were prepared by preparative GLPC (20% PEG 6000). (*E*)-Isomer: bp 70 °C (bath temp, 2 Torr); IR (neat): 2940, 1772, 1645, 1438, 1260, 1020, 760 cm^{-1}; NMR (CCl_4): δ 1.62 (s, 3H), 1.68 (s, 3H), 1.95—2.67 (m, 4H), 2.15 (s, 3H), 3.76 (s, 3H), 5.07 (bt, 1H); MS *m/e* (%): 218 (M^++2, 1), 216 (M^+, 3), 181 (9), 148 (14), 139 (9), 116 (10), 69 (100), 53 (10); Found: C, 61.24; H, 8.15%. Calcd for $C_{11}H_{17}O_2Cl$: C, 60.97; H, 7.91%. (*Z*)-Isomer: bp 72 °C (bath temp, 2 Torr); IR (neat): 2940, 1722, 1615, 1438, 1250, 1025, 775 cm^{-1}; NMR (CCl_4): δ 1.63 (s, 3H), 1.69 (s, 3H), 2.02 (s, 3H), 2.05—2.70 (m, 4H), 3.27 (s, 3H), 5.08 (bt, 1H); MS *m/e* (%): 216 (M^+, 1), 181 (12), 148 (13), 139 (7), 116 (10), 69 (100), 41 (51); Found: C, 60.93; H, 8.09%. Calcd for $C_{11}H_{17}O_2Cl$: C, 60.97; H, 7.91%.

Methyl (E)- and (Z)-2-Chloro-3-phenyl-2-butenoate: GLPC (10% PEG 20 M, 2 m, 140 °C) indicated two peaks, T_r=27.0 min ((*E*)-isomer, 9%), T_r=19.6 min ((*Z*)-isomer, 91%). The analytically pure samples of both isomers were prepared by preparative GLPC (30% PEG 20 M). (*E*)-Isomer: bp 85 °C (bath temp, 2 Torr); IR (neat): 2960, 1730, 1492, 1440, 1250, 1048, 760, 695 cm^{-1}; NMR (CCl_4): δ 2.39 (s, 3H), 3.80 (s, 3H), 7.00—7.40 (m, 5H); MS *m/e* (%): 212 (M^++2, 15), 210 (M^+, 44), 180 (24), 179 (30), 178 (56), 116 (19), 115 (100); Found: C, 63.01; H, 5.41%. Calcd for $C_{11}H_{11}O_2Cl$: C, 62.72; H, 5.26%. (*Z*)-Isomer: bp 87 °C (bath temp, 2 Torr); IR (neat): 2960, 1735, 1620, 1495, 1440, 1240, 1090, 695 cm^{-1}; NMR (CCl_4): δ 2.26 (s, 3H), 3.46 (s, 3H), 7.00—7.38 (m, 5H); MS *m/e* (%): 212 (M^++2, 13), 210 (M^+, 40), 180 (23), 179 (24), 178 (66), 116 (21), 115 (100); Found: C, 62.87; H, 5.36%. Calcd for $C_{11}H_{11}O_2Cl$: C, 62.72; H, 5.26%.

Preparation of α,β-Unsaturated Esters from Ketones by Means of Cl_2CHCOO^tBu–Zn–Et_2AlCl System. To a stirred suspension of zinc dust (0.59 g, 9.0 mmol) and diethylaluminum chloride (2.0 ml of a 1.5 M hexane solution, 3.0 mmol) in THF (10 ml) was added a THF solution of *t*-butyl dichloroacetate (0.56 g, 3.0 mmol) and ketone (2.0 mmol) at 25 °C over a period of 3 h. After stirring for additional 3 h, the resulting mixture was diluted with ether (10 ml), poured into 1 M hydrochloric acid (20 ml), and extracted with ether. The separated organic layer was washed with brine (2×20 ml), dried over anhydrous sodium sulfate and evaporated to remove solvent. The crude product was purified by column chromatography (hexane–ether, 20: 1) on silica gel (20 g) and distilled *in vacuo*.

t-Butyl (E)- and (Z)-3-Phenyl-2-butenoate: TLC (hexane–ether, 10: 1) showed two UV active bands, R_f=0.28 ((*E*)-isomer, 62%), R_f=0.42 ((*Z*)-isomer, 38%). (*E*)-Isomer: bp 61 °C (bath temp, 2 Torr); IR (neat): 2980, 1725, 1720, 1640, 1368, 1300, 1145, 960, 860 cm^{-1}; NMR (CCl_4): δ 1.20 (s, 9H), 2.12 (s, 3H), 5.72 (s, 1H), 7.05—7.40 (bm, 5H); MS *m/e* (%): 218 (M^+, 3), 162 (100), 161 (72), 145 (50), 144 (72), 117 (22), 116 (26), 115 (34), 57 (30): Found: C, 77.06; H, 8.44%. Calcd for $C_{14}H_{18}O_2$: C, 77.03; H, 8.31%. (*Z*)-Isomer: bp 60 °C (bath temp, 2 Torr); IR (neat): 2970, 1710, 1632, 1368, 1274, 1145, 870, 768 cm^{-1}; NMR (CCl_4): δ 1.48 (s, 9H), 2.50 (s, 3H), 5.96 (s, 1H), 7.20—7.50 (bm, 5H); MS *m/e* (%): 218 (M^+, 4), 162 (100), 161 (70), 145 (63), 144 (71), 117 (25), 116 (29), 115 (41), 57 (42); Found: C, 77.07; H, 8.54%. Calcd for $C_{14}H_{18}O_2$: C, 77.07, H, 8.31%.

t-Butyl Cyclododecylideneacetate: Bp 120 °C (bath temp, 1.5 Torr); IR (neat): 2980, 1712, 1640, 1470, 1364, 1240, 1130, 874, 708 cm^{-1}; NMR (CCl_4): δ 1.20—1.40 (bm, 18H), 1.43 (s, 9H), 2.13 (t, J=6 Hz, 2H), 2.62 (t, J=6 Hz, 2H), 5.53 (s, 1H); MS *m/e* (%): 224 ($M^+-(H_2C{=}CMe_2)$, 64), 207 (38), 164 (56), 100 (48), 57 (88), 55 (60), 41 (100); Found: C, 77.36; H, 11.77%. Calcd for $C_{18}H_{32}O_2$: C, 77.09; H, 11.50%.

t-Butyl (E)- and (Z)-3,7-Dimethyl-2,6-octadienoate: GLPC (10% PEG 20 M, 2 m, 120 °C) indicated two peaks, T_r=7.4 min ((*E*)-isomer, 59%), T_r=9.7 min ((*Z*)-isomer, 41%). The analytically pure samples of both isomers were prepared by preparative GLPC (30% PEG 20 M). (*E*)-Isomer: bp 65 °C (bath temp, 2 Torr); IR (neat): 2980, 1710, 1648, 1450, 1364, 1240, 1144, 852 cm^{-1}; NMR (CCl_4): δ 1.44 (s, 9H), 1.60 (s, 3H), 1.65 (s, 3H), 2.00—2.10 (bm, 7H), 5.10 (bt, 1H), 5.48 (s, 1H); MS *m/e* (%): 224 (M^+, trace), 168 ($M^+-(H_2C{=}CMe_2)$, 17), 151 (16), 123 (22), 100 (33), 69 (100), 57 (30); Found: C, 74.84; H, 10.97%. Calcd for $C_{14}H_{24}O_2$: C, 74.95; H, 10.78%. (*Z*)-Isomer: bp 67 °C (bath temp, 2 Torr); IR (neat): 2990, 1715, 1670, 1368, 1230, 1135, 865 cm^{-1}; NMR (CCl_4): δ 1.44 (s, 9H), 1.57 (s, 3H), 1.66 (s, 3H), 2.00—2.20 (bm, 7H), 5.02 (bt, 1H), 5.48 (s, 1H); MS *m/e* (%): 168 ($M^+-(H_2C{=}CMe_2)$, 20), 151 (16), 125 (9), 123 (24), 100 (44), 69 (100), 57 (40); Found: C, 74.96; H, 10.95%. Calcd for $C_{14}H_{24}O_2$: C, 74.95; H, 10.78%.

Preparation of α,β-Unsaturated Esters from Aldehydes by Means of $Br_2CHCOOEt$–Zn–Et_2AlCl System. To a stirred suspension of zinc dust (0.91 g, 14.0 mmol) and diethylaluminum chloride (2.0 ml of a 1.5 M hexane solution, 3.0 mmol) in THF (10 ml) was added a THF solution of ethyl dibromoacetate (0.98 g, 4.0 mmol) and aldehyde (2.0 mmol) at 25 °C over a period of 2 h. After stirring for an additional 1 h, the resulting mixture was diluted with ether (20 ml), poured into 1 M hydrochloric acid (20 ml), and extracted with ether. The separated organic layer was washed with brine (2×20 ml), dried over anhydrous sodium sulfate, and evaporated to remove solvent. The crude product was purified by column chromatography (hexane–ether, 20: 1) on silica gel (20 g).

Ethyl (E)-2-Tetradecenoate: Bp 115 °C (bath temp, 2 Torr); IR (neat): 2925, 1725, 1660, 1604, 1470, 1264, 1234, 1040, 975 cm^{-1}; NMR (CCl_4): δ 0.87 (t, J=6 Hz, 3H), 1.27 (bm, 23H), 2.03—2.33 (bt, 2H), 4.08 (q, J=6 Hz, 2H), 5.66 (d, J=16 Hz, 1H), 6.82 (dt, J=6, 16 Hz, 1H); MS *m/e* (%): 254 (M^+, 7), 209 (33), 166 (25), 127 (29), 101 (63), 55 (93), 43 (100);

Found: C, 75.67; H, 11.92%. Calcd for $C_{16}H_{30}O_2$: C, 75.54; H, 11.89%. The product was contaminated by <5% of the (*Z*)-isomer (by NMR).

References

1) N. Kawabata, *Kagaku*, **33**, 205 (1978); I. Nishiguchi, *Yuki Gosei Kagaku Kyokai Shi*, **37**, 966 (1979).

2) J. M. Denis, C. Girard, and J. M. Conia, *Synthesis*, **1972**, 549 and references cited therein.

3) K. Maruoka, S. Hashimoto, Y. Kitagawa, H. Yamamoto, and H. Nozaki, *J. Am. Chem. Soc.*, **99**, 7705 (1977).

4) K. Takai, Y. Hotta, K. Oshima, and H. Nozaki, *Tetrahedron Lett.*, **1978**, 2417.

5) H. Hashimoto, M. Hida, and S. Miyano, *J. Organomet. Chem.*, **10**, 518 (1967); **12**, 263 (1968); S. Miyano, T. Ohtake, H. Tokumasu, and H. Hashimoto, *Nippon Kagaku Kaishi*, **1973**, 381. Although aldehydes provide reasonable yields, ketones are almost unreactive.

6) P. Turnbull, K. Syhora, and J. H. Fried, *J. Am. Chem. Soc.*, **88**, 4764 (1966); I. T. Harrison, R. J. Rawson, P. Turnbull, and J. H. Fried, *J. Org. Chem.*, **36**, 3515 (1971). The recorded high yields of hydroxy ketone reaction are ascribed to the assistance by hydroxyl being sterically allowed.

7) D. Seyferth and S. B. Andrews, *J. Organomet. Chem.*, **30**, 151 (1971).

8) The ^1H NMR spectrum in CCl_4 with $CHCl_3$ as an internal standard showed the signals for the methyl protons (δ 0.05) and the methylene protons (−0.29) with relative intensities of 9: 1. The elemental analysis gave a satisfactory result. A. A. Buyakov, T. K. Gar, and V. F. Mironov (*Zh. Obshch. Khim.*, **43**, 801 (1973)) recorded the compound to exhibit δ 0.29 CH_2 signal. Prof. V. F. Mironov kindly informed us that minus sign is missing in their paper.

9) C. Golumbic and D. L. Cottle, *J. Am. Chem. Soc.*, **61**, 996 (1939).

10) F. Bertini, P. Grasselli, and G. Zubiani, *Tetrahedron*, **26**, 1281 (1970) and references cited therein.

11) A. Schriesheim, R. J. Muller, and C. A. Rowe, Jr., *J. Am. Chem. Soc.*, **84**, 3164 (1962).

12) R. Greenwald, M. Chaykovsky, and E. J. Corey, *J. Org. Chem.*, **28**, 1128 (1963).

13) T. Mukaiyama, T. Sato, and J. Hanna, *Chem. Lett.*, **1973**, 1041.

14) A. Maercker, *Org. React.*, **14**, 270 (1965); A. W. Johnson, "Ylid Chemistry," Academic Press, New York, N. Y. (1966).

15) B. Castro, J. Villieras, and N. Ferracutti, *Bull. Soc. Chim. Fr.*, **1969**, 3521.

16) R. E. Miller and F. F. Nord, *J. Org. Chem.*, **16**, 728 (1951).

17) J. Villieras, P. Perriot, and J. F. Normant, *Synthesis* **1978**, 31; T. H. Chan and M. Moreland, *Tetrahedron Lett.*, **1978**, 515; F. Karrenbrock and H. J. Schaefer, *ibid.*, **1979**, 2913.

18) W. S. Wadsworth, Jr., and W. D. Emmons, *Org. Synth.*, Coll. Vol. V, 547 (1973); K. Shimoji, H. Taguchi, K. Oshima, H. Yamamoto, and H. Nozaki, *J. Am. Chem. Soc.*, **96**, 1620 (1974).

19) The zinc dust was purified: L. F. Fieser and M. Fieser, "Reagents for Organic Synthesis," John Wiley and Sons, Inc., New York, N. Y. (1967),Vol. 1, p. 1276.

20) J. Casanova and B. Waegell, *Bull. Soc. Chim. Fr.*, **1971**, 1295.

21) Y. Hata and M. Watanabe, *J. Am. Chem. Soc.*, **95**, 8450 (1973).

22) O. Grummitt and E. I. Becker, *Org. Synth.*, Coll. Vol. IV, 771 (1963).

23) A. P. Kozacik and E. E. Reid, *J. Am. Chem. Soc.*, **60**, 2436 (1938).

24) Financial support by the Ministry of Education, Science, and Culture, Japanese Government, (Grant-in-Aid #247077, 303023, 403022) is acknowledged.

The Electronic Spectra of Intramolecular Charge-transfer Compounds and Their Marked Solvatochromism in a Strong Hydrogen-bonding Solvent: 2-(Arylmethylene)-1,3-indandiones and 2-(1-Naphthyl)-*p*-benzoquinone

Kazuhiko CHIBA, Jun-ichi AIHARA,* Kotaro ARAYA, and Yoshio MATSUNAGA

Department of Chemistry, Faculty of Science, Hokkaido University, Sapporo 060

(Received September 6, 1979)

The first electronic absorption bands of the title compounds can all be assigned to the intramolecular charge-transfer transitions. The solvent effects on these bands are quite analogous to those on the absorption bands characteristic of binary charge-transfer complexes. Especially, when the title compounds are dissolved in trifluoroacetic acid, marked bathochromic shifts of the first bands are observed, in harmony with their charge-transfer character. Such solvatochromism is obviously due to the hydrogen-bond formation between the solute and the solvent molecules. When strong hydrogen bonding occurs, the electron affinity of the 2-methylene-1,3-indandione moiety increases by about 0.41 eV.

Very many papers have so far been published concerning binary charge-transfer (CT) complexes in the solution phase.[1] The physical and chemical properties of these complexes have thus been clarified widely. However, our understanding of intramolecular CT compounds in solution is still far from satisfactory.[2–4] Here, an intramolecular CT compound is an organic compound in which an electron-attracting group with a large electron affinity is attached to an electron-donor molecule, forming a single conjugated system as one whole.[3] This kind of compound has the following two characteristics. First, as in the case of binary CT complexes, the first electronic absorption bands are mostly related to the charge-transfer, each within a single conjugated system. Second, such compounds are structurally much less flexible in solution than binary CT complexes. This might make the analysis of the electronic spectra much less ambiguous than that of binary CT complexes. It is noteworthy that some aspects of the solution spectra of binary CT complexes remain elusive.[5] This is primarily due to the fact that the general response of a CT transition to a solvent is inconsistent with the dielectric theory of solute-solvent interactions.[6] In this context, we can fully expect that some intramolecular CT compounds might be useful in exploring further the intrinsic features of CT-type transitions.

In this paper, we would like to present the first systematic survey of the electronic transitions typical of the intramolecular CT compounds. The first absorption bands of 2-(arylmethylene)-1,3-indandiones (**A**) and 2-(1-naphthyl)-*p*-benzoquinone (**B**) will be examined below in conjunction with the solvent effects on binary CT complexes.

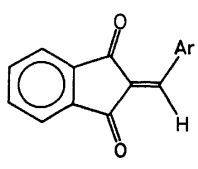

A

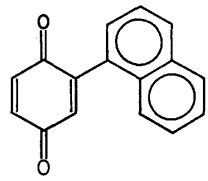

B

Experimental

The 2-(arylmethylene)-1,3-indandiones listed in Table 1 and 2-(1-naphthyl)-*p*-benzoquinone were prepared and purified according to the procedures found in the literature.[7,8] In each of them, a ring system with two carbonyl groups bonds a benzenoid compound. The absorption spectra of these compounds were measured using a Beckman DK-2A spectrophotometer. All the solvents were of a guaranteed grade and were used without further purification.

Intramolecular CT Character of the First Absorption Bands

An intramolecular CT transition is defined as an electronic transition from an occupied molecular orbital localized in a part of a conjugated system to an unoccupied molecular orbital localized in the other part of the same conjugated system.[2–4] All the 2-(arylmethylene)-1,3-indandiones (**A1—7**) and 2-(1-naphthyl)-*p*-benzoquinone (**B**) exhibit intramolecular CT bands isolated on the low-energy side of the electronic absorption spectra. The intramolecular CT character of the first absorption bands was verified as follows.

First, the molecular orbital (MO) calculations provide theoretical evidence for it. The Pariser-Parr-Pople MO calculations carried out by Meyer[9] and by us[10] indicate that, for all compounds investigated, the highest occupied molecular orbital (HOMO) is localized mainly at the benzenoid ring, whereas the lowest unoccupied molecular orbital (LUMO) is localized mainly at the 2-methylene-1,3-indandione (or *p*-benzoquinone) ring. Accordingly, the benzenoid ring can be considered as a good electron donor, as usual, and the methyleneindandione (or *p*-benzoquinone) ring as a good electron acceptor. Meyer has already assigned the first absorption band of 2-benzylidene-1,3-indandione to the lowest intramolecular CT transition.[9] The situation is exactly the same for the other compounds.

The MO calculations show that a geometrical HOMO-LUMO separation depends straightforwardly upon the dihedral angle between a benzenoid donor ring and an acceptor ring.[10] For most of the compounds

Table 1. Intramolecular CT absorption bands of 2-(arylmethylene)-1,3-indandiones in chloroform

Aryl group (Ar)	$h\nu_{ICT}$ / 10^3 cm^{-1}	ε[a]	I_p[b]/eV
Phenyl (**A1**)	29.09	33400	9.24[c]
Styryl (**A2**)	25.95	45100	8.60[d]
1-Naphthyl (**A3**)	24.81	17600	8.12[c]
2-Naphthyl (**A4**)	27.35	29100	8.12[c]
p-Dimethylaminophenyl (**A5**)	20.78	86400	7.51[e]
1-Pyrenyl (**A6**)	20.51	43700	7.41[f]
9-Anthryl (**A7**)	20.25	10700	7.40[c]

a) Extinction coefficient. b) Vertical ionization potential. c) Ref. 12. d) R. A. W. Johnstone and F. A. Mellon, *J. Chem. Soc., Faraday Trans. 2*, **69**, 1155 (1973). e) Ref. 13. f) Ref. 14.

in Table 1, it is not possible to take a planar configuration because of serious steric hindrance. This structural feature is quite favorable to the HOMO-LUMO separation, thus improving the intramolecular CT character of the first absorption band. Especially, a large dihedral angle between the two parts of 2-(9-anthrylmethylene)-1,3-indandione (**A7**) can be inferred from the small extinction coefficient of the first absorption band.

In a simplified MO treatment,[11] the overlap integral between two bonded $2p_z$ orbitals which belong to different chromophores is found to be proportional to $\cos\Theta$, where Θ is the dihedral angle between them, and the absorption intensity may be expected to be proportional to $\cos^2\Theta$. The extinction coefficient of the first band of **A7** is about one-eighth that of 2-(*p*-dimethylaminobenzylidene)-1,3-indandione (**A5**) and about one-fourth that of 2-(1-pyrenylmethylene)-1,3-indandione (**A6**). We may assume that the donor ability is almost the same for these three compounds, since the ionization potentials of the isolated donors (*i.e.*, anthracene, *N,N*-dimethylaniline, and pyrene) are nearly equal to each other.[12-14] Therefore, if we assume **A5** and/or **A6** to be planar in shape, the dihedral angle in **A7** must be at least 60°. This angle can be justified by inspecting a molecular model of this compound.

Next, the good acceptor ability of a methyleneindandione ring is supported by the crystal structure of **A5**.[15] The methyleneindandione ring of each molecule is therein in close contact with the *p*-dimethylaminophenyl ring of its adjacent molecule, the two forming a CT-type self-complex. Since the donor part has a good electron-donating character, such a self-complex formation in the solid phase witnesses the good acceptor ability of the methyleneindandione ring.[2,4,16] The electron affinity of *p*-benzoquinone is 1.89 eV;[17] it is also a good electron acceptor, even if it becomes a part of a larger conjugated system, as in the case of 2-(1-naphthyl)-*p*-benzoquinone. The intramolecular CT character of the first absorption bands of several 2-aryl-*p*-benzoquinones has previously been confirmed experimentally.[4,16]

Finally, the most conclusive proof of the intramolecular CT character is obtained by plotting the electronic absorption maximum against the ionization potential of the donor part for **A1—7**. In general, a CT transition energy is linearly related to an ionization potential of the donor molecule if the acceptor molecule is common to all the CT complexes concerned.[18,19] In the case of intramolecular CT compounds with common acceptor parts, an intramolecular CT transition energy, $h\nu_{ICT}$, may analogously be expressed as:

$$h\nu_{ICT} = a_1 I_p - b_1, \quad (1)$$

where a_1 and b_1 are constants characteristic of the acceptor part and where I_P is, of course, an ionization potential of the donor part, *e.g.*, an ionization potential of anthracene in the case of **A7**.

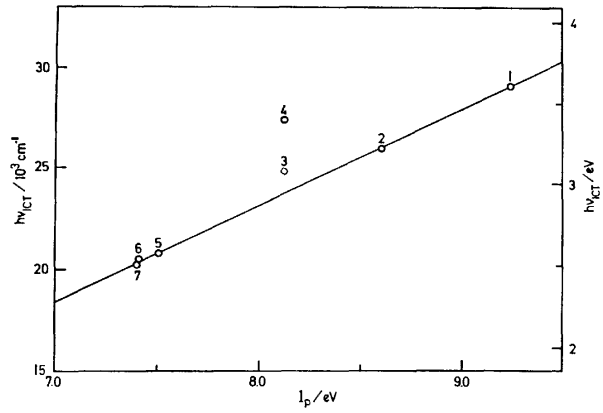

Fig. 1. Correlation of the intramolecular CT absorption maxima with the donor ionization potentials: 1, **A1**; 2, **A2**; 3, **A3**; 4, **A4**; 5, **A5**; 6, **A6**; **7**, **A7**.

As is shown in Fig. 1, this relationship was found to hold well for most 2-(arylmethylene)-1,3-indandiones dissolved in chloroform. The two exceptions are the 1- and 2-naphthylmethylene derivatives (**A3** and **A4**). For the other compounds, a_1=0.592 and b_1=1.840 when $h\nu_{ICT}$ and I_P are given in units of eV. Although the absorption maxima of the two exceptional compounds deviate upward from Eq. 1, there are clear absorption shoulders near the energy predicted by this relationship. They are located at 23500 cm^{-1} for **A3** and at 25000 cm^{-1} for **A4**. There may be some structural factor in these intramolecular CT compounds which causes a marked change in the Franck-Condon envelope. The appearance of such a vibrational structure is not unusual when an intramolecular CT compound is dissolved in a relatively inert solvent.[4] Accordingly, we can safely say that Eq. 1 is valid for all 2-(arylmethylene)-1,3-indandiones. It is, then, quite natural to attribute the first absorption band of every compound in Table 1 to an intramolecular CT transition between HOMO and LUMO. For binary CT complexes in solution, the a_1 value lie in the 0.83—0.97 range,[1] a little larger than that for the intramolecular CT bands considered above. According to Flurry's MO description of CT transitions,[19] the a_1=0.592 value indicates that 1.592 of the two frontier electrons reside in the donor ring in the ground state. Consequently, these intramolecular CT compounds can really be regarded as undissociable CT complexes.

Solvatochromism Caused by a Strong Hydrogen-Bonding Solvent

If a given electronic absorption band is of the CT type, its solvent dependence might be similar to that of binary CT complexes.[5] In order to examine this possibility, the first absorption maxima of **A7** in various solvents were plotted against the dielectric constants of the solvents[20] (*cf.* Fig. 2). In general, *n*-donor solvents,

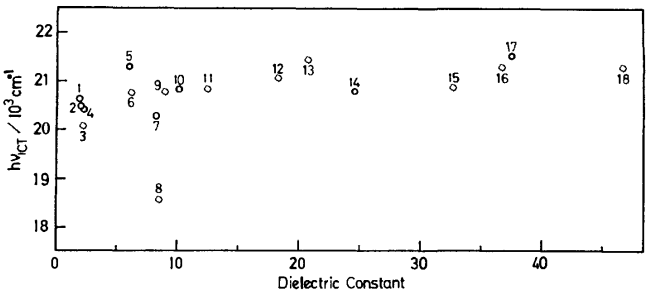

Fig. 2. The first absorption maximum of **A7** as a function of solvent dieletric constant: 1, hexane; 2, cyclohexane; 3, carbon tetrachloride; 4, benzene; 5, ethyl acetate; 6, acetic acid; 7, 1,2,2,2-tetrachloroethane; 8, trifluoroacetic acid; 9, dichloromethane; 10, 1,2-dichloroethane; 11, pyridine; 12, cyclohexanone;13, acetone; 14, ethanol; 15, methanol; 16, *N*,*N*-dimethylformamide; 17, acetonitrile; 18 dimethyl sulfoxide.

such as ketones, alcohols, and nitriles, shifted the intramolecular CT band to the higher-energy side. This spectral aspect is quite consistent with that of binary CT complexes,[1] but is evidently contrary to the prediction of the dielectric theory of solute-solvent interactions.[6] Such a response to solvents further supports the CT character of the electronic transition concerned.

When the intramolecular CT compounds were dissolved in trifluoroacetic acid (TFAA), an unusually large bathochromic shift of the first absorption band occurred. In 1975, Sep *et al.* observed very large bathochromic shifts of the CT bands when anthracene complexes with typical acceptors were dissolved in TFAA.[21] The same effect can be seen in Fig. 2, where TFAA (8) marks a singular point, as in the case of binary CT complexes.[21] In order to analyze such bathochromism induced by TFAA, we used dichloromethane (DCM) as the reference solvent. The dielectric properties of these two solvents are quite similar to each other.[20] The dielectric constants are 8.55 for TFAA and 8.93 for DCM. The refractive indexes are 1.285 for TFAA and 1.421 for DCM. This pair of solvents, therefore, lend themselves to the study of specific solvation effects.

It is noteworthy that, for the compounds investigated, the energy difference between the first absorption bands of the DCM and the TFAA solution amounts to 1270—2400 cm^{-1}. By the way, the second absorption band of **A7** is a local-excitation band, in the sense that the molecule is excited locally at the anthracene ring.[10] The 0–0 vibrational component of this band is located at 26400 cm^{-1}, while that of the first band of anthracene is located at 26400 cm^{-1}, too, both in DCM. The vibrational spacing of the former band is about 1380 cm^{-1}, which is comparable to that of the latter band (1415 cm^{-1}). In contrast to the first band of **A7**, the TFAA-to-DCM shift of the second band (*i.e.*, the local-excitation band) is about 200 cm^{-1}, about one-tenth that of the first intramolecular CT band. The TFAA-to-DCM solvent shift of the intramolecular CT band is thus an order of magnitude larger than that of an allowed excitation band localized in a nonpolar conjugated hydrocarbon ring.

Such an anomalous bathochromic shift of the intramolecular CT band begins to occur when only a drop of TFAA is added to a few ml of the DCM solution. When the amount of TFAA reaches a certain mol %, the TFAA effect on the absorption spectrum becomes substantially saturated. After that, the absorption peak remains almost unmoved. In other words, the curve of a peak position versus the solvent composition is linear, with essentially no slope, as long as the concen-

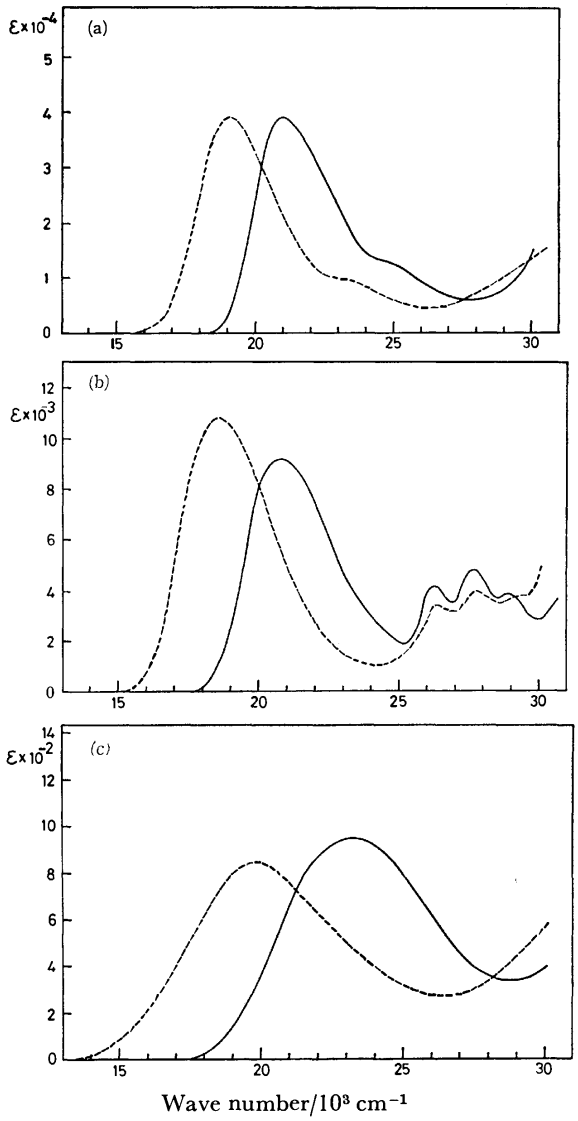

Fig. 3. Absorption spectra of the dichloromethane solutions (——) and the trifluoroacetic acid solutions (——): (a), **A6**; (b), **A7**; (c), **B**.

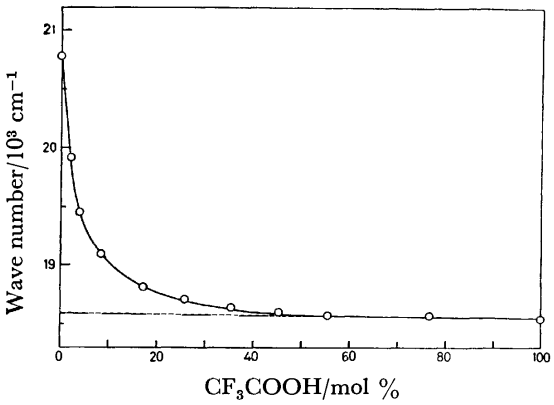

Fig. 4. The intramolecular CT absorption maximum as a function of solvent composition of the CH_2Cl_2–CF_3COOH–**A7** system.

tration of TFAA is sufficiently high. Figures 3 and 4 illustrate this situation. Let the linear portion in the curve be extrapolated to the 100% pure DCM solution, and we can, in principle, estimate the peak position of the TFAA solution which would be exhibited if TFAA had exactly the same dielectric properties as DCM. The slope of this linear portion, if any, might be interpreted as due to a slight difference in dielectric properties between TFAA and DCM.

Accordingly, an extrapolated point in the energy scale, $h\nu_0$, can be taken as the reference energy in evaluating the degree of specific solvatochromism caused by TFAA. A net bathochromic shift not due to the dielectric properties of TFAA can, then, be expressed as:

$$\Delta h\nu_{ICT} = h\nu_{ICT} - h\nu_0. \quad (2)$$

Here, $h\nu_{ICT}$ indicates the energy of the first absorption maximum of the TFAA solution. The numerical values concerning Eq. 2 are all listed in Table 2. As for this expression, one exceptional compound may be 2-(1-naphthyl)-*p*-benzoquinone, for which there is little linear portion in the band-peak *versus* solvent-composition curve. In this case, the tangent at the 100% pure TFAA solution was extrapolated to the other end of the solvent composition. Fortunately, the tangent had no inclination.

Table 2. Bathochromic shifts of intramolecular CT bands of 2-(arylmethylene)-1,3-indandiones and 2-(1-naphthyl)-*p*-benzoquinone in trifluoroacetic acid

Compd[a]	$h\nu_{ICT}/10^3$ cm^{-1}		$\Delta h\nu_{ICT}$	ΔE_a
	CH_2Cl_2	CF_3COOH[b]	10^3 cm^{-1}	eV
A1	29.15	27.88(27.88)	1.27	0.27
A2	26.02	24.13(24.13)	1.89	0.40
A3	25.00	22.60(22.60)	2.40	0.50
A4	27.83	25.88(25.88)	1.95	0.41
A6	20.92	19.01(19.01)	1.91	0.40
A7	20.78	18.54(18.59)	2.19	0.46
B	23.22	19.80(19.80)	3.42	—

a) See Table 1 for abbreviations. b) Values for $h\nu_0$ are given in parentheses.

As may be seen from Table 2, $\Delta h\nu_{ICT}$ is almost the same as the energy difference between the first absorption bands of the DCM and the TFAA solution. The value of $\Delta h\nu_{ICT}$ stays in the 1270—2400 cm^{-1} range for 2-(arylmethylene)-1,3-indandiones and is somewhat larger for 2-(1-naphthyl)-*p*-benzoquinone.

It has been established that a protic solvent often shifts the CT absorption band to the blue side.[5] However, the direction of the TFAA solvent shift, defined by Eq. 2, is obviously the opposite of that expected on going from DCM to a protic solvent. The primary effect of TFAA on the intramolecular CT bands is totally different from that of familiar protic solvents. On the other hand, the strong hydrogen-bonding ability of TFAA has been proved by C-13 NMR investigations of various ketones.[22] The chemical shifts show that TFAA molecules attach selectively to carbonyl oxygens in a hydrogen-bonding manner. Sep *et al.* also observed such an effect on acid anhydrides by means of C-13 NMR spectrometry.[21] In this sense, TFAA is in marked contrast to ethanol, which may act as a proton acceptor rather than as a proton donor.[23] The same situation must be true in the present case. The $\Delta h\nu_{ICT}$ quantity can, hence, be interpreted as due to hydrogen bonding between the solute and the solvent molecules.

Here, we should note that, when hydrogen bonding effectively occurs between solvent molecules and a molecule of the type shown in Table 1, the acceptor ability related to the LUMO of the solute is improved because of the increased core charge on each carbonyl oxygen.[21] The donor ability related to the HOMO can, nevertheless, be expected to remain almost unchanged because of the geometrical HOMO-LUMO separation. Therefore, the energy shift of the intramolecular CT band in TFAA can be ascribed mostly to a change in the electron affinity of the acceptor part.

By analogy with Eq. 1, the following expression may hold for intramolecular CT compounds with common donor parts:

$$h\nu_{ICT} = -a_2E_a + b_2, \quad (3)$$

where E_a is the electron affinity of the acceptor part and where a_2 and b_2 are constants characteristic of the common donor part. In the CT-excited state, the charge on the donor part decreases to the same extent as the charge on the acceptor part increases. As both a_1 in Eq. 1 and a_2 in Eq. 3 are determined principally by the degree of charge transfer,[18,19] we can assume that a_2 is close to a_1 for the same group of intramolecular CT compounds. Thus, the change in the acceptor electron affinity on going from DMC to TFAA can be evaluated as:

$$\Delta E_a = -\Delta h\nu_{ICT}/a_1. \quad (4)$$

By the use of experimental values for $\Delta h\nu_{ICT}$, an increase in the electron affinity of the methyleneindandione part, on the average, is calculated to be 0.41 eV in TFAA. A larger amount of change in electron affinity is conceivable for 2-(1-naphthyl)-*p*-benzoquinone in TFAA.

It has been inferred from analogous bathochromic shifts of the intermolecular CT bands that the electron

affinities of typical acceptor molecules in association with anthracene might also be enhanced in the same solvent.[21] However, in the case of binary CT complexes, the position and the orientation of an acceptor, relative to those of a donor, are not firmly fixed in the solution phase because the binding energy between the two components is very small.[1] Both components must be fluctuating rather independently as a result of thermal agitation. Strong hydrogen bonding may further deform the shape of the complex when it is dissolved in TFAA. For binary CT complexes, a linear portion in the band-peak versus solvent-composition curve has an appreciable slope, although the same pair of solvents (*i.e.*, TFAA and DCM) are employed[21]. This may reflect the nonrigidity of binary CT complexes in solution. On the other hand, the present results on intramolecular CT compounds are mostly free from ambiguities arising from these factors. The distance between the donor and the acceptor is kept unchanged because of the existence of a direct bond between them. Therefore, we might safely say that the shift of an intramolecular CT absorption band is indeed due to the increased electron affinity of the acceptor part, but a similar conclusion with regard to binary CT complexes[21] appears a bit less decisive.

Remarks

In addition to 2-(arylmethylene)-1,3-indandiones and 2-(1-naphtyl)-*p*-benzoquinone, we have examined the solvatochromism of many other compounds of the intramolecular CT type. However, when one or more hetero atoms were present in the π-electron framework of the donor part, it was not easy to analyze the resulting solvation effect in detail. For example, solvent effects on **A5** are not simple because specific interactions occur between solvent molecules and hetero atoms in both the donor and acceptor parts. When more than a small amount of the solvent effect on the acceptor side is cancelled by that on the donor side, it is quite difficult to separate the overall solvent shift between the two sides of the molecule. The absorption spectrum of **A5** in TFAA is totally different from that in DCM. For this reason, the present study had to be limited strictly to intramolecular CT compounds in which there are no hetero atoms in the donor part. The donor parts of these compounds are supposedly inert to the hydrogen-bonding effect of TFAA. Such compounds, each with a single kind of substituent on the acceptor side, were, hence, most suitable for analyzing a specific solvation effect induced by TFAA.

According to the simple CT theory,[1] a vibrational structure of a CT absorption band might be characteristic of the acceptor component because a CT transition may naively be viewed as an electron jump to the LUMO localized in the acceptor.[24] In the present case, the band shape scarcely changes even when a strong hydrogen bonding occurs between solute and solvent molecules. This may imply that the vibrational modes which determine the contour of the intramolecular CT absorption band are little affected by the hydrogen-bond formation. In line with this, there is no drastic change in the absorption intensity, either.

In this context, Kuboyama *et al.* assigned the first absorption band of 4-pyrone to the intramolecular CT transition from the ethereal oxygen to the carbonyl group.[25] The solvent shift induced on going from heptane to 1,1,1,3,3,3-hexafluoro-2-propanol (HFP) is quite large (*ca.* 1200 cm^{-1}). HFP is also a strong hydrogen-bonding solvent.[21] However, the shape of the intramolecular CT band is somewhat deformed in this solvent. This is probably due to a considerable reorganization of the π-electron framework of 4-pyrone, since its whole conjugated system is very compact. The existence of a second, but very weak, absorption band was predicted near the intramolecular CT band;[25] it may also be responsible for the deformation of the CT band.

One of us (J.A.) is grateful to the Ministry of Education, Science, and Culture, Japan, for a Scientific Research Grant-in-Aid (No. 164116).

References

1) See, *e. g.*, G. Briegred, "Elektronen-Donator-Acceptor-Komplexe," Springer-Verlag, Berlin (1961); R. Foster, "Organic Charge-Transfer Complexes," Academic Press, London (1969); "Molecular Complexes," Vol. I, Elek Science, London (1973); Vol. II (1974); K. M. C. Davis, "Molecular Association," ed by R. Foster, Academic Press, London (1975), Vol. I, Chap. 3.

2) See, *e. g.*, J. Freimanis, "Progress and Some Prospects in Charge-Transfer Complex Chemistry," Wrocław Technical University, Wrocław (1978).

3) See, *e. g.*, S. Nagakura and J. Tanaka, *J. Chem. Phys.*, **22**, 236 (1954); S. Nagakura, *Pure Appl. Chem.*, **7**, 79 (1963).

4) J. Aihara, G. Kushibiki, and Y. Matsunaga, *Bull. Chem. Soc. Jpn.*, **46**, 3584 (1973); J. Aihara, *ibid.*, **47**, 2063 (1974); A. Sasaki, J. Aihara, and Y. Matsunaga, *ibid.*, **47**, 2926 (1974); K. Araya and J. Aihara, *ibid.*, **52**, 935 (1979).

5) H. W. Offen and M. S. F. A. Abidi, *J. Chem. Phys.*, **44**, 4642 (1966); J. Aihara, M. Tsuda, and H. Inokuchi, *Bull. Chem. Soc. Jpn.*, **42**, 1824 (1969); O. B. Nagy, J. B. Nagy, and A. Bruylants, *J. Chem. Soc., Perkin Trans. 2*, **1972**, 968; S. Dupire, J. M. Mulindabyuma, J. B. Nagy, and O. B. Nagy, *Tetrahedron*, **31**, 135 (1975).

6) Y. Ooshika, *J. Phys. Soc. Jpn.* **9**, 594 (1954); E. G. McRae, *J. Phys. Chem.*, **61**, 562 (1957).

7) N. A. Dimond and T. K. Mukherjee, *Disc. Faraday Soc.*, **51**, 102 (1971).

8) P. Brassard and P. L'Ecuyer, *Can. J. Chem.*, **36**, 700 (1958).

9) A. Y. Meyer, *J. Chem. Soc., B*, **1970**, 986.

10) We calculated the Pariser-Parr-Pople-type MO patterns of 2-arylmethylene-1,3-diones and 2-(1-naphthyl)-*p*-benzoquinone using a computer program published in: O. Kikuchi, "Bunshikidoho," Kodansha, Tokyo (1971), Chap. 2. However, the detailed results are not cited here because quite tentative molecular geometries were adopted.

11) H. H. Jaffé and M. Orchin, "Theory and Applications of Ultraviolet Spectroscopy," Wiley, New York (1962), Chap. 15.

12) P. A. Clark, F. Brogli, and E. Heilbronner, *Helv. Chim. Acta*, **55**, 1415 (1972).

13) A. D. Baker, D. P. May, and D. W. Turner, *J. Chem.*

Soc., B, **1968**, 22.
14) R. Boschi and W. Schmidt, *Tetrahedron Lett.*, **1972**, 2577.
15) N. S. Magomedova and Z. V. Zvonkova, *Kristallografiya*, **23**, 281 (1978).
16) G. R. Desiraju, I. C. Paul, and D, Y. Curtin, *J. Am. Chem. Soc.*, **99**, 1594 (1977).
17) C. D. Cooper, W. T. Naff, and R. N. Compton, *J. Chem. Phys.*, **63**, 2752 (1975).
18) H. McConnell, J. S. Ham, and J. R. Platt, *J. Chem Phys.*, **21**, 66 (1953).
19) R. L. Flurry, Jr., *J. Phys. Chem.*, **69**, 1927 (1965); **73**, 2111 (1969).
20) R. L. Schneider, *Eastman Org. Chem. Bull.*, **47**, (1) 1 (1975).
21) W. J. Sep, J. W. Verhoeven, and Th. J. de Boer, *Tetrahedron*, **31**, 1065 (1975).
22) See, *e. g.*, G. L. Nelson, G. C. Levy, and J. D. Cargioli, *J. Am. Chem. Soc.*, **94**, 3089 (1972); P. B. Koster, J. Runsink, and M. J. Janssen, *J. Chem. Soc., Perkin Trans. 2*, **1979**, 393.
23) J. Figueras, *J. Am. Chem. Soc.*, **93**, 3255 (1971).
24) A. H. Kadhim and H. W. Offen, *Mol. Cryst.*, **3**, 311 (1968).
25) A. Kuboyama, Y. Sato, and H. Arano, *Bull. Chem. Soc. Jpn.*, **49**, 3685 (1976).

 © 1980 The Chemical Society of Japan Bull. Chem. Soc. Jpn., 53, 1709—1713 (1980)

Polymer Effects under Pressure. IV. The Hydrolysis of Phenyl Esters Catalyzed by α-Chymotrypsin up to 2000 bar[1)]

Yoshihiro TANIGUCHI* and Keizo SUZUKI

Department of Chemistry, Faculty of Science and Engineering, Ritsumeikan University, Kita-ku, Kyoto 603

(Received October 16, 1979)

The rates of the hydrolysis of 2-valeryloxy(C_5)- and 2-heptanoyloxy(C_7)-benzoic acids catalyzed by α-chymotrypsin (α-CHT) were measured at pressures up to 2000 bar at 30 °C and pH 7.8 in a 0.05 M Tris buffer solution. The apparent Michaelis constant, K_m^{app}, was estimated to vary from 5.9 to 9.9 mM, and k_{cat} from 11×10^{-3} to 52×10^{-3} s^{-1}, for the C_5 ester, and K_m^{app}, from 4.7 to 10 mM, and k_{cat} from 37×10^{-3} to 200×10^{-3} s^{-1}, for the C_7 ester, between 1 and 2000 bar. From the pressure dependences of K_m^{app} and k_{cat}, the volume changes accompanying the dissociation of the enzyme–substrate complex and the activation volume for the process of the product formation were calculated to be -6.3 ± 2 and -20 ± 2 cm^3/mol for the C_5 ester and -9.5 ± 2 and -21 ± 2 cm^3/mol for the C_7 ester. The effects of the pressure on the hydrolysis of *p*-nitrophenyl acetate (PNPA) catalyzed by α-CHT have also been measured up to 3000 bar at pH 7.8 in a 0.05 M Tris buffer solution and at 25 °C and 35 °C. The activation volumes were -3 cm^3/mol at 25 °C and -4 cm^3/mol at 30 °C and 25 °C. These results were discussed on the basis of the X-ray study of the enzyme–substrate complex.

Werbin and McLaren[2)] have studied the effect of the pressure on the rate of the α-chymotrypsin-catalyzed hydrolysis of casein and of the L-tyrosine ethyl ester over a limited range of substrate concentrations. The activation volume of the former was -13.8 cm^3/mol for the apparent first-order rate constant, while that of the latter was -13.5 cm^3/mol for the zeroth-order rate constant. Recently Lockyer *et al.*[3)] have studied the pseudo-first-order rate of the hydrolysis of *p*-nitrophenyl esters. The activation volumes for the deacylation of the corresponding acyl-enzymes, were -6, -3, and -2 cm^3/mol for the *p*-nitrophenyl esters of acetic, isobutyric, and pivalic acid respectively. The relationship between these negative volume changes and the mechanism of the enzyme reaction was not clarified in detail. While there was no loss of activity of α-CHT in the pH 7.8 Tris buffer solution after pressure treatment for 1 h at 2000 bar and at 22 °C (this result was also supported by Miyagawa and Suzuki[4)]), it is not clear whether or not α-CHT undergoes reversible inactivation.

In the present study, the enzyme activity was first measured in the hydrolysis of PNPA catalyzed by α-CHT up to 3000 bar at three temperatures. The hydrolysis rate of 2-valeryloxy(C_5)- and 2-heptanoyloxy-(C_7)-benzoic acids catalyzed by α-CHT was measured up to 2000 bar at 30 °C. The results were compared with those of PNPA in order to discuss the reaction mechanism of the α-CHT-catalyzed hydrolysis.

Experimental

Materials. The 2-valeryloxy(C_5)- and 2-heptanolyoxy-(C_7)-benzoic acids were obtained by the method of Hofstee.[5)] The products, recrystallized five times from ethanol, were freed from unchanged 2-hydroxybenzoic acid, as checked by the absorption at 300 nm of 2-hydroxybenzoic acid. C_5 ester: mp 84—85 °C (lit,[5)] mp 86 °C); MS (75 eV); Found: *m/e* 222.0888. Calcd for $C_{12}H_{14}O_4$: M, 222.1082. C_7 ester: mp 72.5—73.0 °C (lit,[5)] 70 °C); MS (75 eV); Found: *m/e* 250.1200. Calcd for $C_{14}H_{18}O_4$: M, 250.1398. The PNPA (Aldrich Chemical Co., Inc.) was recrystallized twice from hexane; mp 79—80 °C (lit,[6)] mp 79.5—80 °C). The α-CHT was obtained from the Nutritional Biochemicals Co. (3× crystallized, Lot #6373). The methanol and acetonitrile were distilled before use.

Apparatus and Procedure. The high-pressure apparatus and procedure have been reported in detail in a previous paper.[1a)] The hydrolysis was performed at pH 7.8 in a 0.05 M Tris-HCl buffer up to 3000 bar for PNPA and up to 2000 bar at 30 ± 0.1 °C for 2-acyloxybenzoic acids. The hydrolysis was monitored by observing the change in the optical density at 400 nm due to the *p*-nitrophenolate ion and at 300 nm due to 2-hydroxybenzoic acid by means of a Hitachi-Perkin Elmer EP 139-type spectrophotometer directly under pressure. The sample cell for the measurement of the UV region was made up of a quartz window, and the pressure-transmitting fluid was silicone oil (Shinetsu Chemicals Co.), which was found to be free from absorbance near 300 nm. The enzyme stock solutions were assayed using PNPA before each experiment. The data used from all the enzyme hydrolyses were taken during the first 30 min of each run.

Results

Hydrolysis of C_5 and C_7 Esters. These esters are hydrolyzed spontaneously in the absence of the enzyme. The rate of the spontaneous hydrolysis was proportional to the ester concentration. Therefore, the rate of hydrolysis in the presence of the enzyme, V_{app}, is separated into two terms, the uncatalyzed rate, V_w, and the enzyme-catalyzed rate, V_{cat}:

$$V_{app} = V_{cat} + V_w. \quad (1)$$

At each pressure, the hydrolysis rates, V_{cat}, for the enzyme reaction obtained by means of Eq. 1 increase with the substrate concentration, then level off at higher concentrations, thus following the Michaelis-Menten kinetics as is shown in Eq 2:

$$E + S \underset{K_m^{app}}{\rightleftharpoons} ES \xrightarrow{k_{cat}} E + P, \quad (2)$$

where E is the enzyme; S, the substrate; ES, the Michaelis complex, and P, the product. When $[E]\ll[S]$, the rate of the product formation is expressed as:

$$V_{cat} = \frac{k_{cat}\cdot[E]\cdot[S]}{K_m^{app}+[S]}, \quad (3)$$

where [E] and [S] denote the enzyme and substrate

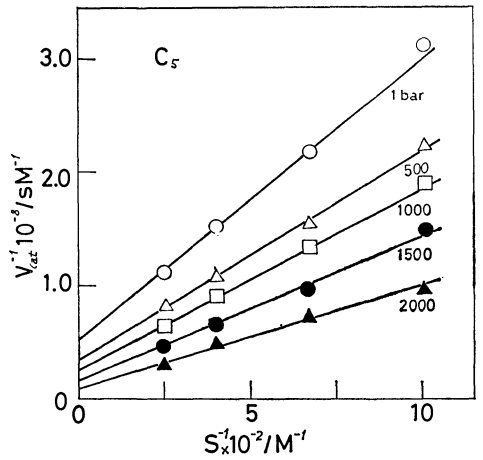

Fig. 1. Lineweaver-Burk plots of the enzyme hydrolysis of C_5 ester at pH 7.8 (0.05 M Tris–HCl) in 9% methanol–water at 30 °C. The enzyme concentration is 2×10^{-6} M.

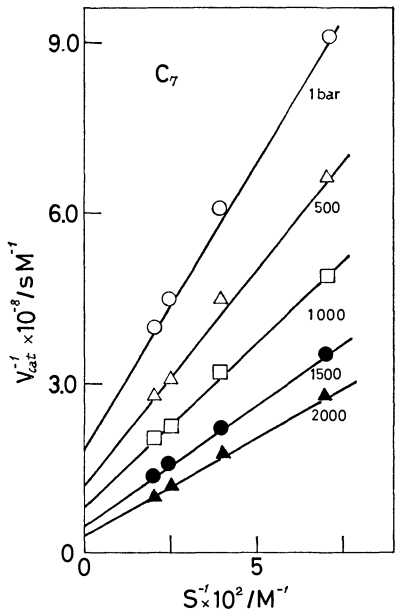

Fig. 2. Lineweaver-Burk plots of the enzyme hydrolysis of C_7 ester at pH 7.8 (0.05 M Tris–HCl) in 9% methanol–water at 30 °C. The enzyme concentration is 2×10^{-6} M.

concentrations. K_m^{app} and k_{cat} were determined by the least-squares method from the Lineweaver-Burk plots between $1/V_{cat}$ and $1/[S]$ in Eq. 4, as is shown in Figs. 1 (C_5) and 2 (C_7):

$$\frac{1}{V_{cat}} = \frac{K_m^{app}}{k_{cat}[E]}\cdot\frac{1}{[S]} + \frac{1}{k_{cat}[E]} \quad . \qquad (4)$$

These values are shown in Table 1. From the linear relationship of the logarithms of K_m^{app} and of k_{cat} *vs.* the pressure established in Figs. 3 and 4, the volume change ΔV accompanying the dissociation of the Michaelis complex and the activation volume, ΔV^*, accompanying the process of the product formation were determined to be -6.3 ± 2 and -20 ± 2 cm³/mol for

Table 1. Kinetic parameters of the hydrolysis of C_5 and C_7 esters catalyzed by α-CHT at various pressures and 30 °C[a)]

Pressure	K_m^{app}/mM		$k_{cat}\times10^3/s^{-1}$	
bar	C_5	C_7	C_5	C_7
1	5.9, 6.1[b)]	4.7, 3.0[b)]	11	37
500	6.7	5.6	16	57
1000	7.4	6.9	23	78
1500	8.4	8.3	35	122
2000	9.9	10	52	200

a) Reaction conditions: pH 7.8 in a 0.05 M Tris buffer solution, 9% methanol; the enzyme concentration, 2×10^{-6} M. b) Ref. 8.

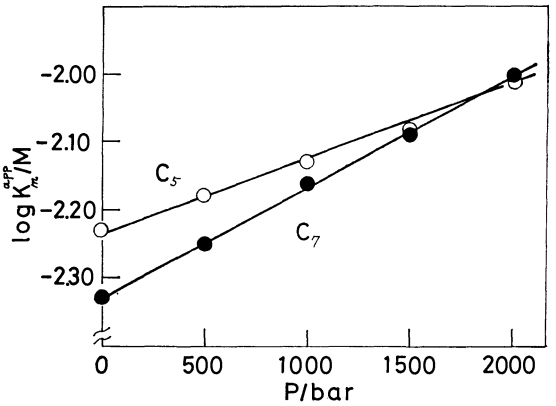

Fig. 3. Pressure *vs.* log K_m^{app} at 30 °C.

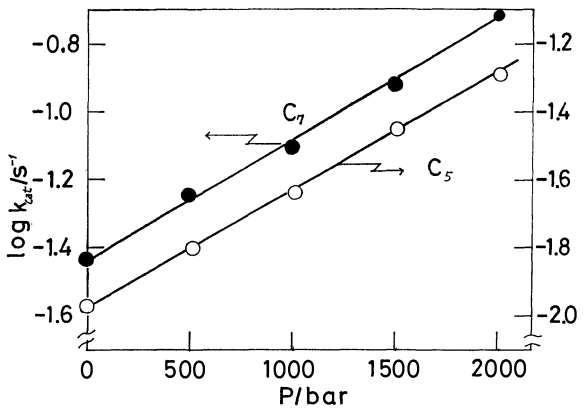

Fig. 4. Pressure *vs.* log k_{cat} at 30 °C.

the C_5 ester -9.5 ± 2 and -21 ± 2 cm³/mol for the C_7 ester respectively.

Hydrolysis of PNPA. PNPA is also hydrolyzed spontaneously in the absence of the enzyme. The rate of the spontaneous hydrolysis is proportional to the PNPA concentration. Therefore, the enzyme rate, V_{cat}, was obtained by means of Eq. 1. When $[E]\ll[S]$ at PNPA concentrations higher than $[S]=1.6\times10^{-5}$ M,[6] the reaction rate can be considered to be substrate-independent and to be proportional to the enzyme concentration. At each pressure, the rate constants, k_{cat}, were obtained by means of Eq. 5:

$$k_{cat} = V_{cat}/[E]. \qquad (5)$$

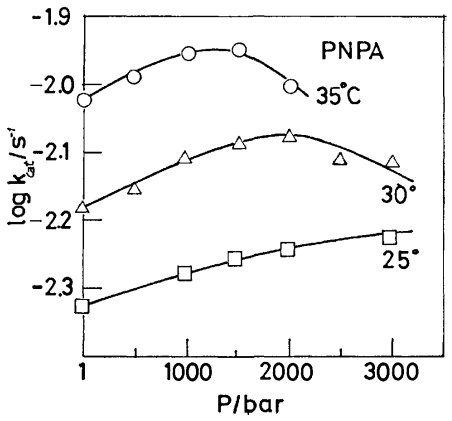

Fig. 5. Pressure effects of log k_{cat} for enzyme hydrolysis of PNPA at pH 7.8 (0.05 M Tris-HCl) in 1.6% acetonitrile–water at 25 °C, 30 °C, and 35 °C, respectively. The enzyme concentration is 2×10^{-6} M, and PNPA concetration is 9.56×10^{-5} M.

The relationship between the logarithm of k_{cat} and the pressure at 30 °C and 35 °C in Fig. 5 shows the maxima at a certain pressure, while at 25 °C it simply increases up to 3000 bar. Lockyer *et al.*[3] reported that the value of log k_{cat} for PNPA increases linearly up to 2000 bar at 20 °C and that the activation volume is −6 cm³/mol. Therefore, phenomena in which the k_{cat} values decrease above a certain pressure (2000 bar at 30 °C and 1500 bar at 35 °C) indicate the loss of the activity of α-CHT under pressure. This interpretation is also directly supported by a recent study of the pressure denaturation based on the measurement of the fluorescence of α-CHT up to 5000 bar.[7] The activation volumes at 1 bar are −3 cm³/mol at 25 °C and −4 cm³/mol at 30 °C and 35 °C respectively.

Discussion

In the hydrolysis catalyzed by α-CHT, the pathway containing acylation and deacylation is shown by Eq. 6:

$$\begin{array}{l} E + S \underset{k_{-1}}{\overset{k_1}{\rightleftharpoons}} ES \xrightarrow{k_{acyl}} Acyl\text{-}E + P_1 \\ \qquad\qquad\qquad\qquad\qquad\quad \Big\downarrow k_{deacyl} \\ \qquad\qquad\qquad\qquad\qquad\quad E + P_2. \end{array} \tag{6}$$

The kinetic parameters can, then, be expressed by:

$$K_m^{app} = K_m \cdot k_{deacyl}/(k_{acyl}+k_{deacyl}), \tag{7}$$

$$k_{cat} = k_{acyl} \cdot k_{deacyl}/(k_{acyl}+k_{deacyl}), \tag{8}$$

where:

$$K_m = (k_{-1}+k_{acyl})/k_1. \tag{9}$$

Then,

$$K_m^{app} = K_m \cdot k_{cat}/k_{acyl}. \tag{10}$$

From the pressure dependences of K_m^{app} and k_{cat}, ΔV and ΔV^* are given by the following equations:

$$\Delta V = \Delta V_m + \Delta V^* - \Delta V^*_{acyl}, \tag{11}$$

$$\Delta V^* = \Delta V^*_{acyl} + \Delta V^*_{deacyl} + RT\partial \ln (k_{acyl}+k_{deacyl})/\partial P. \tag{12}$$

From the study of the pH effect on the hydrolysis of 2-acyloxybenzoic acids catalyzed by α-CHT, Hofstee[8] suggested that the rate-determining step for the overall reaction of the rate constant, k_{cat}, is the acylation. The k_{acyl} value is nearly equal to the k_{deacyl} for 2-acyloxybenzoic acids catalyzed by α-CHT because the k_{cat} values for C_5 and C_7 esters, as shown in Table 1, are approximately half of the k_{deacyl} values: 16.8×10^{-3} s^{-1} for the C_5 ester and 69×10^{-3} s^{-1} for the C_7 ester,[9] respectively. The ΔV^* values of −20 cm³/mol for the C_5 ester and −21 cm³/mol for the C_7 ester at 30 °C agree with those of −20 cm³/mol, accompanied by the hydrolysis of 3-nitro-4-butyryloxybenzoic acid (NBBA) and 3-nitro-4-valeryloxybenzoic acid (NPeBA) catalyzed by the copolymer of 1-vinyl-2-methylimidazole with 1-vinylpyrrolidone (MI-VP),[1a] in which the deacylation process is not the rate-determining step, at least. In the hydrolysis of the PNPA ester, in which the deacylation process is the rate-determinig step,[6] the ΔV^* values are −3 cm³/mol at 25 °C and −4 cm³/mol at 30 °C and 35 °C. The difference in the sizes of the activation volume between the two process, acylation and deacylation, is of interest.

The detailed mechanism of the charge-relay system accompanying the acylation and the deacylation of α-CHT was proposed by Blow *et al.*[10] Following the model of the acylation step in Fig. 6, the formation of one hydrogen bond between the NH group of the imidazole ring of His-57 and the carbonyl oxygen atom of the substrate, and one covalent bond between the alkoide anion of Ser-195 and the carbonyl carbon atom of the substrate is expected to be established on the transition state, accompanied by the formation of the tetrahedral intermediate between the substrate and α-CHT. The volume changes accompanying the formation of such bonds are established to be about from −10 to −15 cm³/mol for one covalent bond[11,12] and from −5 to −7 cm³/mol for one hydrogen bond.[13,14] Therefore, the value of −20 cm³/mol accompanying the acylation process, which is independent of the length of the alkyl chain of the substrate, is reasonable.

In the deacylation step shown in Fig. 7, at first there occur the formation of one covalent bond between the oxygen atom of the H_2O molecule and the carbon atom of the carbonyl group, and the rupture of one covalent bond, accompanied by the release of the acyl group from acyl-α-CHT. Secondly, there occur a breaking of the weak interaction (ionic bonds, hydrogen bonds, and hydrophobic interactions) between the acyl group and the side-chain groups of amino acids around the active center of α-CHT. As the volume change, accompanied by the appearance and the disappearance of covalent bonds, can be expected to cancel each other out, the observed activation volumes for each substrate, −13 cm³/mol for L-tyrosyl-,[2] −7 cm³/mol for 3-(3-indolyl)-acryloyl-,[15] −6 to −4 cm³/mol for acetyl[3] −3 cm³/mol for isobutyryl,[3] and −2 cm³/mol for pivaloyl-α-CHT,[3] would come from the latter term. The differences in these volume changes can be discussed from the point of view of the detailed structure of the active center of acyl-α-CHT, as determined in the X-ray studies.

From the structure of 3-(3-indolyl)acryloyl-α-CHT

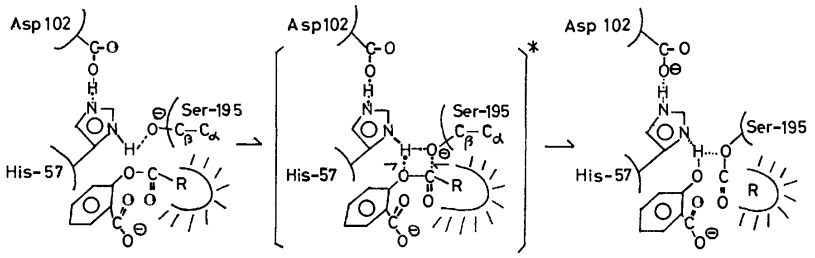

Fig. 6. Modified mechanism for the acylation step of α-CHT proposed by Blow *et al.*, (1969). R is the alkyl chain.

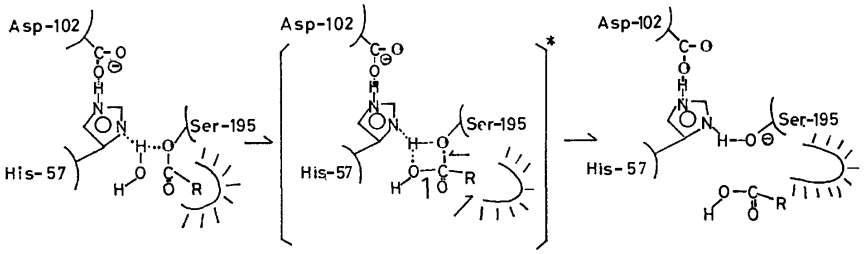

Fig. 7. Modified mechanism for the deacylation step of acyl-α-CHT proposed by Blow *et al.*, (1969). R is the alkyl chain.

determined by Henderson,[16] it is clear that one H_2O molecule acts as a hydrogen bond bridge between the acyl oxygen atom and the NH group of the imidazole ring of His-57 and that the indole ring exists in the hydrophobic cavity. Simultaneously with rupture of the hydrophobic interactions in the deacylation process, the NH group of the indole ring is freed from hydrophobic interaction and can form a hydrogen bond with a H_2O molecule. If a hydrogen bond connected to the carbonyl oxygen atom does not change, the value of -7 cm^3/mol for the 3-(3-indolyl)acryloyl group corresponds to the formation of a hydrogen bond between the NH group of indole and a H_2O molecule, because the rupture of such hydrophobic interaction does not contribute to the volume change; *i.e.*, the volume change accompanied by the formation of hydrophobic interaction containing the benzene ring is nearly zero.[17]

In the deacylation of L-tyrosinyl-α-CHT, the OH group of tyrosine ($pK_a=10$) ionizes when the tyrosine residue is transferred from the hydrophobic cavity of α-CHT to the pH 7.8 buffer solution. The volume change accompanied by the ionization of the tyrosine residue was estimated to be -11.3 cm^3/mol from the study of the pressure effect on the ionization of *p*-nitrophenol.[18] Therefore, the value of -13 cm^3/mol can be explained as being due to the ionization of the tyrosine residue.

The volume changes accompanying the deacylation of acyl (acetyl, isobutyryl, pivaloyl, valeryl, heptanoyl)-α-CHT come mainly from the rupture of the hydrophobic interaction between the alkyl chain of acyl-α-CHT and the hydrophobic cavity of α-CHT. This view is supported by the two facts of a negative volume change accompanied by the rupture of the hydrophobic interaction[19] and of the observed negative values of the experimental activation volume for the deacylation of acyl-α-CHT. Moreover, the observed binding constants of the esters and α-CHT increase with an increase in the length of the alkyl chain of the acyl group up to the size of C_7, which is the optimum hydrocarbon chain.[8] Therefore, it is to be expected that the longer the hydrocarbon chain, the more negative the value of the volume change will be on the rupture of hydrophobic interaction. The expected volume change is -6.3 cm^3/mol for the C_5 ester and -9.5 cm^3/mol for the C_7 ester, judging from a study of the pressure effect on K_m^{app} to be described later. As the value of -20—-21 cm^3/mol accompanying the process of the product formation is too small to explain the rupture of the hydrophobic interaction between the acyl groups of the esters and the hydrophobic pocket of α-CHT, the rate-determining step in this experimental system seems not to be the deacylation step. On the other hand, the amount of the volume change expected from the rupture of hydrophobic interaction between the acetyl, isobutyryl, or pivaloyl group and the hydrophobic pocket of α-CHT is opposite to the experimental results (-6 to -4 cm^3/mol for acetyl, -3 cm^3/mol for isobutyryl, and -2 cm^3/mol for pivaloyl)[3]; *i.e.*, the larger the hydrophobicity of acyl groups, the less negative the value of the activation volume. This fact can be explained in terms of the relationship between the molecule size of acyl groups and the size of the hydrophobic pocket of α-CHT. The X-ray study of Steitz *et al.*[20] determined the size of the pocket to be approximately 1.0—1.2 nm × 0.55—0.65 nm × 0.33—0.45 nm. The van der Waal's radius of the acetyl group is 0.40 nm, while those of isobutyryl and pivaloyl are over 0.5 nm. Therefore, the acetyl group can fit into the pocket, but the bulky groups of isobutyryl and pivaloyl are too large to do so. The ΔV^* values, which are -4 to -6 cm^3/mol for acetyl, -3 cm^3/mol for isobutyryl, and -2

cm^3/mol for pivaloyl groups, are explained by the ratio of the hydrophobic contact of the acyl groups of the esters to the hydrophobic pocket of α-CHT.

When the acylation step is the rate-determining one, the value of K_m^{app} is found by Eq. 7 to be equal to the value of K_m. If k_{-1} were larger than k_{acyl} is Eq. 9, the value of K_m would be the true dissociation constant of the Michaelis complex. The values of -6.3 cm^3/mol for the C_5 ester and -9.5 cm^3/mol for the C_7 ester correspond to the volume change accompanying the dissociation of the Michaelis complex. The amino acids surrounding the hydrophobic pocket in contact with the acyl group through the hydrophobic interaction are Met-195, Val-213, and Try-215. As the contribution of such aromatic compounds as Try-215 to the volume change accompanied by the formation of the hydrophobic interaction is negrigibly small (nearly zero),[17] the average number of the alkyl chain of the side chains of Met-195 and Val-213 is three. Therefore, the estimated volume change for the interaction between the hydrocarbon part of C_3 and the valeryl or heptanoyl groups are in the range of -5 to -10 cm^3/mol, as established by the study of the model compounds.[19] Thus, the driving force of the association of the substrate to the enzyme, α-CHT is shown to be primarily the hydrophobic interaction, as has already been described.

It is concluded that the negative volume change accompanying the dissociation of the Michaelis complex is due primarily to the hydrophobic interaction between the substrates and α-CHT. The value of ΔV^*_{acyl} is explained by the formation of the tetrahedral intermediate in the transition state of the acylation process. These values of ΔV^*_{deacyl} are derived by breaking weak interactions between the acyl groups and side-chain groups of amino acids around the active center of α-CHT, as deduced from the X-ray study of the enzyme-substrate complex.

One of the present authors (Y. T.) is grateful for financial support from the Matsunaga Memorial Science Foundation. We are both also grateful to Dr. R. K. Williams, University of Guelph, Canada, for his advice and continuous encouragement; to Dr. S. Kunugi, Kyoto University, for his advice, and to Miss K. Saeki, Kobe Women's College of Pharmacy, Japan, for the measurement of the molecular weight of the C_5 and C_7 esters using the mass spectrometer.

References

1) a) Part 2: Y. Taniguchi, K. Shimokawa, H. Hisatomi, S. Tanamachi, and K. Suzuki, *Macromolecules*, **11**, 829 (1978); b) Part 3: Y. Taniguchi, O. Inoue, and K. Suzuki, *Bull. Chem. Soc. Jpn.*, **52**, 1327 (1979).
2) H. Werbin and A. D. McLaren, *Arch. Biochem. Biophys.*, **31**, 285 (1951).
3) G. D. Lockyer, Jr., D. Owen, D. Crew, and R. C. Neuman, Jr., *J. Am. Chem. Soc.*, **96**, 7303 (1974).
4) K. Miyagawa and K. Suzuki, *Rev. Phys. Chem. Jpn.*, **32**, 51 (1963).
5) B. H. J. Hofstee, *J. Biol. Chem.*, **199**, 357, 365 (1952).
6) F. J. Kezdy and M. L. Bender, *Biochemistry*, **1**, 1097 (1962).
7) T. Ishibashi, M. Dissertation, Ritsumeikan University, Kyoto, 603.
8) B. H. J. Hofstee, *Biochim. Biophys. Acta*, **32**, 182 (1959).
9) K. Martinek, V. N. Darovska, S. D. Varfolomeyer, and I. V. Berezin, *Biochim. Biophys. Acta*, **271**, 80 (1972).
10) D. M. Blow, J. J. Birktaft, and B. S. Hartley, *Nature*, **221**, 337 (1969).
11) K. R. Brower, *J. Am. Chem. Soc.*, **83**, 4370 (1961).
12) C. Walling and M. Naiman, *J. Am. Chem. Soc.*, **84**, 2628 (1962).
13) Y. Taniguchi and K. Suzuki, *J. Phys. Chem.*, **78**, 759 (1974).
14) E. Fishman and G. H. Drickamer, *J. Chem. Phys.*, **24**, 548 (1956).
15) R. C. Neuman, Jr., D. Owen, and G. D. Lockyer, Jr., *J. Am. Chem. Soc.*, **98**, 2982 (1976).
16) R. Henderson, *J. Mol. Biol.*, **54**, 341 (1970).
17) M. E. Friedman and H. A. Scheraga, *J. Phys. Chem.*, **69**, 3795 (1965).
18) R. C. Neuman, Jr., W. Kauzmann, and A. Zipp, *J. Phys. Chem.*, **77**, 2687 (1973).
19) K. Suzuki, Y. Taniguchi, and T. Watanabe, *J. Phys. Chem.*, **77**, 1918 (1973).
20) T. A. Steitz, R. Henderson, and M. Blow, *J. Mol. Biol.*, **46**, 337 (1969).

Chiral Mesophases of 12-Hydroxyoctadecanoic Acid in Jelly and in the Solid State. I. A New Type of Lyotropic Mesophase in Jelly with Organic Solvents

Taro TACHIBANA,* Tomoko MORI, and Kayako HORI*
Department of Chemistry, Ochanomizu University, Otsuka, Bunkyo-ku, Tokyo 112
(Received October 26, 1979)

Thermally reversible jellies of optically active 12-hydroxyoctadecanoic acid (12HOA) with CCl_4 or aromatic solvents form a lyotropic mesophase, which shows enantiomeric circular dichroism (CD) and induced CD due to achiral molecules added to the jellies, indicating that the jellies have a supramolecular helicoidal structure. The X-ray examination revealed that the jellies are composed of a number of small, ordered domains with such a lamellar structure as is observed in the crystalline solid. The supramolecular helicoidal structure was associated with the lamellar structure; as a result, it was suggested that the lyotropic mesophase has a chiral smectic structure and, furthermore, that the mesophase is present in thin, fibrous aggregates of 12HOA molecules within which the jellies are enmeshed.

Optically active 12-hydroxyoctadecanoic acids (12HOA) form thermally reversible jellies with aromatic solvents or carbon tetrachloride, while the racemic 12HOA separates out as crystals from the saturated solution in these solvents. We have recently found that the jellies present images very similar to that of the liquid crystalline phase under a polarizing microscope, and that they exhibit an enantiomeric circular dichroism (CD) in a region of wavelengths where the molecules have no absorption.[1] These hitherto undescribed observations led us to infer that the jellies form a lyotropic mesophase with a supramolecular chiral structure. The best-known example of such mesophases is a cholesteric (chiral nematic) mesophase formed by such synthetic polypeptides as poly(γ-benzyl glutamate) (PBG) in organic solvents.[2] Lyotropic mesophases with a cholesteric structure composed of a low-molecular-weight compound were recently reported for swelling gels of *N*-acylamino acids in aromatic solvents.[3] We found that the jellies of 12HOA were composed of a chiral smectic mesophase structure which exists locally as small domains with randomly-oriented helical axes. This paper will describe a new chiral mesophase, which is different from the cholesteric mesophase of PBG or *N*-acylamino acids.

Experimental

Materials. The crystalline samples of (*R*)-12HOA were purified from commercial products, as has been described previously.[4] The (*S*)-12HOA was prepared by a method described previously from the methyl ester of (*R*)-12HOA.[4] The purities, as estimated from the results of gas chromatography, the melting point, and the specific rotatory power ($[\alpha]_D^{25}$/deg dm^{-1} cm^3 g^{-1} (in pyridine)), of these samples were as follows: (*R*), 99.1%, 353.4 K (lit,[4] 353.6 K), −0.46 (lit,[5] −0.41); (*S*), 97.2%, 352.3 K, +0.44 (lit,[5] +0.3±0.1). The solvents for jelly formation were of a reagent grade and were further purified by the standard method.

Methods. The mesomorphic textures were observed by using an Olympus POM polarizing microscope. The CD spectra were recorded on a JASCO J-20A spectropolarimeter using 1—10 mm thick cells, depending on the concentration (25—120 mmol l^{-1}). The CD were expressed by the molar ellipticity $[\theta]$/deg dm^2 dmol^{-1}. The absorption spectra were measured on a Shimadzu UV-200S spectrophotometer. The X-ray diffraction patterns of jellies were obtained using a Rigaku Rotaflex 2078 diffractometer with Cu $K\alpha$ radiation, with 50 kV and 200 mA. Jellies about 1 mm thick were formed in the opening of an aluminum sample holder and were sandwiched by two poly(ethylene terephthalate) films 7 μm thick. X-Ray diffraction patterns for jellies with benzene were successfully obtained by a transmission method, which was carried out for samples fixed vertically to an incident beam. By this method, the obtained patterns were almost uninfluenced by poly(ethylene terephthalate) films in the range of $2\theta = 1°$—$30°$. However, the transmission method was unsuccessful for jellies with CCl_4 because of the large scattering power of the Cl atoms. In this case, a conventional reflection method was available, but the peaks at low diffraction angles were very much smaller than those for jellies with benzene measured by means of a transmission method, because of the absorption of X-rays due to their long path in a poly(ethylene terephthalate) film cover at a low-angle incidence.

Results and Discussion

Jelly Formation. Chiral 12HOA dissolves readily in aromatic solvents and chlorinated solvents, such as carbon tetrachloride, chloroform, or dichloromethane, at high temperatures. These solutions set to jellies, on cooling, in a reversible way. Jellies with benzene or carbon tetrachloride are almost transparent; therefore, these are used as samples for optical studies. Solutions above 25 mmol l^{-1} in carbon tetrachloride and above 33 mmol l^{-1} in benzene set to jellies at 25 °C. The transition between solution and jelly occurred over a narrow temperature range and showed hysteresis because of the slow rate of the transition. The jellies were thixotropic, indicating that the jelly structure is held by weak bondings.

According to our previous infrared spectroscopic study,[6] the jellies are held by molecular association involving intermolecular hydrogen bonding in which almost all the hydroxyl groups take part; isotropic solutions of chiral 12HOA in carbon tetrachloride exhibited the absorption bands due to the free hydroxyl groups in addition to the absorption bands due to the hydrogen-bonded hydroxyl groups, while the jellies gave only the absorption bands due to the hydrogen-bonded

hydroxyl groups. Furthermore, the infrared spectral results led us to conclude that the hydroxyl groups link the chiral molecules by multiple hydrogen bonding, forming long sequences of hydrogen bonds. Such hydrogen bonding was also found for both the crystalline solids and the built-up multilayers, and it was assumed to exist also in the monolayers at the air-water interface.

When hot solutions of 12HOA were rapidly cooled in an ice-bath, the jellies thus formed were found to scatter a bluish light, which disappeared at room temperature after a short period. This indicates a heterogeneous structure of the jellies; the scattering centers grow to such various sizes that the centers scatter light over a wide range of wavelengths. A bluish scattering light was also observed for the crystalline powder of 12HOA immersed in benzene or carbon tetrachloride. This indicates that the dissolution of crystals of 12HOA into the solvents occurs through the jelly formation.

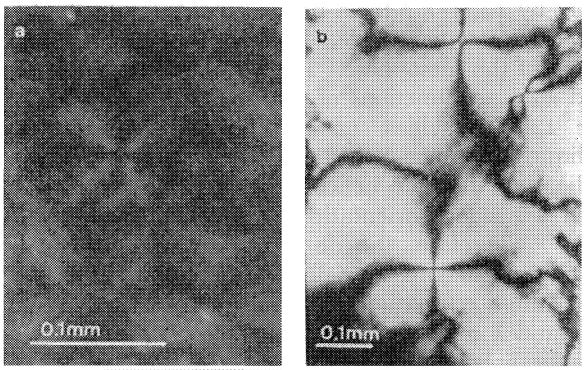

Fig. 1. Microscopic textures of jellies of (*R*)-12HOA–CCl_4 between crossed polarizers.
(a): Spherulitic texture (43 mmol l^{-1}); (b): Schlieren texture (318 mmol l^{-1}).

Microscopic Examination. Hot solutions of (*R*)-12HOA in carbon tetrachloride were placed between two glass plates and cooled to room temperature. The resultant thin films of the jellies were examined by means of a polarizing microscope. The jellies were birefringent; however, the sign of birefringence was not determined because of the difficulty of preparing the oriented single domain samples. The jellies displayed a spherulitic or Schlieren texture between crossed polarizers. The microscopic textures are shown in Fig. 1. The surface treatment of supporting plates had no effect on these textures. There was a general tendency for the spherulitic texture to occur in the jellies prepared by the slow cooling of the solutions of a lower concentration and for the Schlieren texture to occur in the jellies prepared by the rapid cooling of the solutions of a higher concentration. These textures are similar to the patterns observed previously in thermotropic[7] or lyotropic liquid crystals.[8] Thus, the microscopic observation indicates that the jellies have local orders with a mesomorphic structure. Generally, it is difficult to determine from the microscopic texture whether the type of lyotropic mesophase is nematic, smectic, or cholesteric.

The spherulitic domains showed an extinction cross, which was unchanged on the rotation of the stage of the polarizing microscope. The optical sign of the spherulitic domains, as determined by using a sensitive color plate, was negative. A similar spherulite-like phase with optically negative sign has also been observed for the *N*-octadecanoyl-L-glutamic acid–dimethyl phthalate system, which was regarded as a liquid crystalline phase of the cholesteric type.[3]

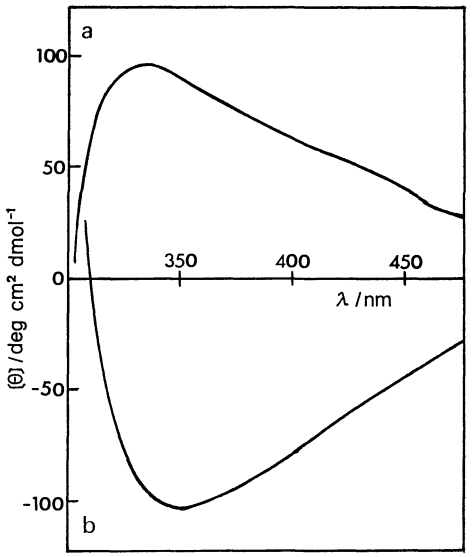

Fig. 2. Enantiomeric CD bands of jellies of 12HOA–CCl_4 at room temp.
(a): (*S*)-12HOA, 25.7 mmol l^{-1}; (b): (*R*)-12HOA, 35.7 mmol l^{-1}.
The location of the CD maximum was insensitive to change of temperature (see Fig. 6).

Circular Dichroic Studies. The jellies exhibited a weak, but definite CD band with a peak around 370 nm, a range of wavelengths in which they absorbed no light. The sign was negative for the *R*-enantiomer and positive for the *S*-enantiomer, irrespective of the solvents used. Figure 2 shows a typical example of the enantiomeric CD bands for jellies of (*R*)- and (*S*)-12HOA with carbon tetrachloride. This enantiomeric relationship was observed quite reproducibly, though the intensities, $[\theta]$, and the locations of the CD maximum, λ_{max}, were rather scattered. This indicates that the CD bands originate from the chirality of the 12HOA molecule. A similar CD spectrum was also observed for jellies with other solvents, such as benzene (λ_{max}: around 480 nm) and toluene (λ_{max}: around 470 nm). Linear dichroism, which is attributable to any strain introduced on jelly formation, was little observed when examination was done by means of the procedure of Tunis-Schneider and Maestre.[9] The observed CD spectrum is thus ascribed to the selective reflection of circularly polarized light in one sence by the chiral jellies. The same optical phenomenon has been observed for cholesteric liquid crystals and explained by assuming a supramolecular helicoidal structure with a twist determined by the chirality of the constituent molecules.[7]

An enantiomeric induced circular dichroism (ICD) could also be observed for some achiral molecules when

they were dissolved in jellies of chiral 12HOA. Figure 3 shows the ICD bands (superimposed on the CD curve of the jelly) and the electronic spectra between 330 and 395 nm for anthracene dissolved in a jelly of (*R*)-12HOA. The ICD bands show a single sign (negative for (*R*)-12HOA and positive for (*S*)-12HOA) and follow the electronic spectral bands closely. Such ICD characteristics have also been observed for lyotropic cholesteric mesophases of PBG[10] and other polypeptides, and more recently for those of *N*-acylamino acids.[3] Figure 4 shows similar ICD results obtained for a cyanine dye, pynacyanole chloride, which was not soluble in carbon tetrachloride, but was solubilizable in solutions or jellies of 12HOA with the same solvent. These ICD results support the assumption that 12HOA jellies are composed of a type of lyotropic chiral mesophase with a supramolecular helicoidal structure.

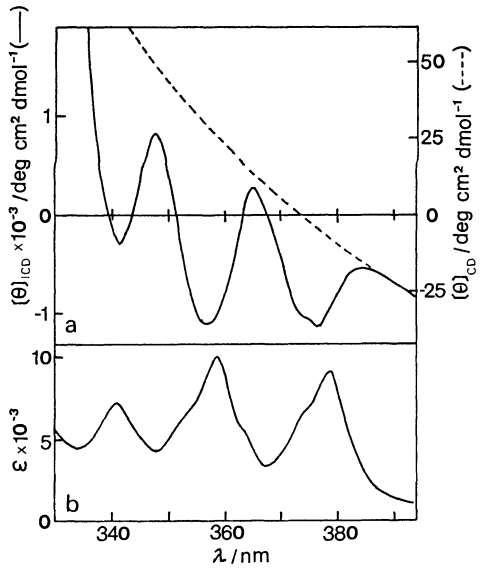

Fig. 3. (a) ICD spectral bands (——) for anthracene (8.8 mmol l^{-1}) superimposed on the CD curve (-----) of the jelly of (*R*)-12HOA- CCl_4.
Enantiomeric ICD bands of jellies of (*S*)-12HOA–CCl_4 are omitted from the figure.
(b) Electronic spectra of anthracene.

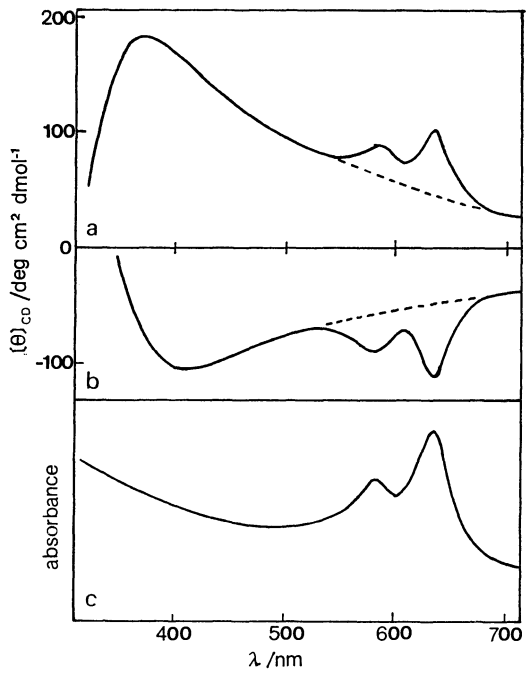

Fig. 4. (a) ICD spectral band for pynacyanole chloride superimposed on the CD band of a jelly of (*S*)-12HOA–CCl_4 (52.7 mmol l^{-1}). (b) Those of a jelly of (*R*)-12HOA–CCl_4 (42.3 mmol l^{-1}). (c) Electronic spectral bands for pynacyanole chloride in the jelly.

The dimensions of the structure may be estimated assuming the model of the helicoidal structure proposed by de Vries.[11] The model postulates only a helical stacking of birefringent layers, regardless of whether or not the helicoidal structure is a cholesteric type. The CD band is due to the selectively reflected light with circular polarization in one sense. In this case, λ_{max} is simply related to the pitch, p, of the supramolecular helix by $\lambda_{max}=\bar{n}.p$ for a normal incidence to the layers in a homeotropic sample, where $\bar{n}$ is an average refractive index of the mesophase. For an oblique incidence, $[\theta]$ and λ_{max} are functions of the angle of incidence. For the 12HOA jellies, no angular dependence for an oblique incidence could be found in $[\theta]$ and λ_{max}, indicating that the helicoidal structures are dispersed, with a random orientation of the helical axes in the jelly. Therefore, the de Vries equation can not be strictly applied to the jellies of 12HOA. However, a very rough estimation of p from the observed values of λ_{max} and $\bar{n}$ may be possible. For example, p was 250 nm for a jelly with carbon tetrachloride with $\lambda_{max}=$ 370 nm and $\bar{n}=1.46$, while p was 320 nm for a jelly with benzene with $\lambda_{max}=480$ nm and $\bar{n}=1.50$. Though λ_{max} appeared in a visible wavelength region, the band ranged within a wide region of wavelengths, so that such an iridescent color as was observed for cholesteric liquid crystals was not exhibited. The CD maximum for a jelly sample containing any additive was found to be shifted to a longer wavelength than that for the original jelly. Since little differences in $\bar{n}$ were found between additive-free and additive-containing jellies with carbon tetrachloride (for example, n_D^{22} is 1.4600 for the former and 1.4603 for a jelly containing 8.8 mmol l^{-1} of anthracene), the shift of λ_{max} is ascribed to an increase in the pitch of the helicoid with the incorporation of additive molecules into the helicoidal structures.

The chirality of the chiral mesophase can be found by determining the handedness of the reflected or transmitted light with circular polarization from the CD band (the pitch band). In the case of jellies of (*R*)-12HOA, the sign of the CD is negative, as is shown in Fig. 2, indicating that right-hand circularly polarized light is selectively reflected by the jelly. Therefore, the screw sense of the molecular helical arrangement is right-handed.[12] That is, the sense of the supramolecular helix is right-handed (P-helicity) for (*R*)-12HOA and left-handed (M-helicity) for (*S*)-12HOA.

The above-mentioned results indicate that there is a striking similarity between jellies of 12HOA and typical cholesteric mesophases. However, there are several differences in CD characteristics between two systems.

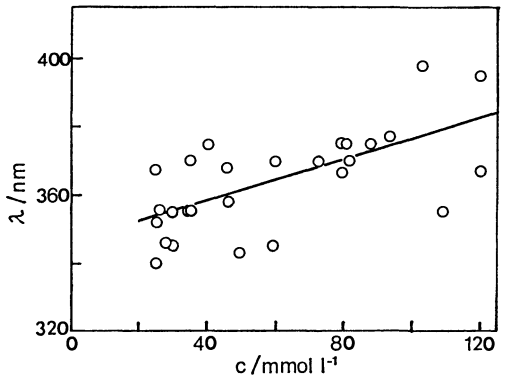

Fig. 5. Concentration dependence of λ_{max} of jellies of (*R*)-12HOA–CCl_4.

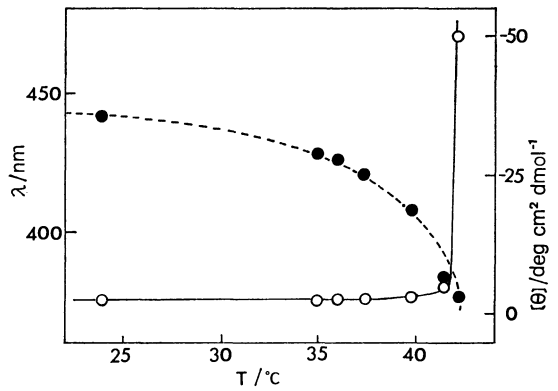

Fig. 6. Temperature dependence of λ_{max} (○) and $[\theta]$ (●) of a jelly of (*R*)-12HOA–CCl_4 jelly (81.7 mmol l^{-1}).
The jelly melted into isotropic soln. at 42 °C.

First, the magnitude of ICD for anthracene is about 2000 deg cm^2 $dmol^{-1}$, which is small compared to the values for thermotropic cholesteric liquid crystals ($\approx 10^6$)[13] and to those for lyotropic cholesteric liquid crystals such as PBG ($\approx 10^4$).[10] Second, the value of λ_{max}, which is related to p, increased slightly with an increase in the concentration of 12HOA, as is shown in Fig. 5. This is quite different from the result observed for the lyotropic cholesteric mesophase of PBG, since Robinson reported[14] that p was proportional to $1/C^2$, where C is the volume fraction of the polymer in the lyotropic cholesteric mesophase. Thirdly, the location of λ_{max} was independent of the temperature in the range from 22 to 41 °C, just below the melting point of the jelly, as is shown in Fig. 6. The temperature independence of λ_{max} is remarkably in contrast with the observations for thermotropic or lyotropic cholesteric mesophases. These facts suggest that the chiral mesophase of 12HOA is different from the chiral nematic phase. Figure 6 shows also that $[\theta]$ decreases rapidly to zero, only when the temperature approaches the melting point of the jelly.

X-Ray Diffraction Studies. Figure 7 shows the X-ray diffraction patterns for jellies with benzene and for a specimen of the crystalline powder of (*R*)-12HOA. The jelly patterns exhibited comparably sharp reflections corresponding to a long spacing of 4.67 nm, together with a wide, diffuse reflection corresponding to a short spacing of 0.46 nm. Similar patterns have often been obtained for lyotropic liquid crystals composed of amphiphilic compounds,[15] in which the values of the long spacing becomes larger with a decrease in the concentration of the solute. However, it was found that, in contrast with such lyotropic liquid crystals, the long spacing obtained for the jellies was almost in accord with that obtained for the crystalline powder, independent of the concentration of 12HOA. Therefore, the jelly pattern obtained is essentially the same as the powder pattern, although the former is, as a whole, broader. This indicates that the jellies are composed of a number of small domains with a lamellar structure similar to that in the crystalline solids, though the diffuse reflection with spacing corresponding to 0.46 nm indicates that the organization of the hydrocarbon chains in the lamellar structure of the small domains in the jellies is less ordered than that in the crystalline solids. The gel patterns are generally known to be similar to the powder patterns, as has been shown, for example, in the case of the aluminum dilaurate–cyclohexane gels.[16]

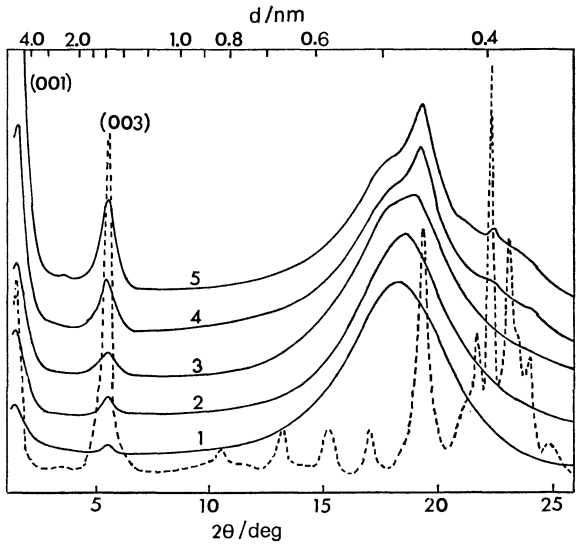

Fig. 7. X-Ray diffraction patterns for jellies of (*R*)-12HOA–benzene (——) and for a specimen of crystalline powder of (*R*)-12HOA (------).
(1) 24.3 mmol l^{-1}, (2) 57.6 mmol l^{-1}, (3) 64.1 mmol l^{-1}, (4) 160 mmol l^{-1}, (5) 257 mmol l^{-1}.

The long spacing, 4.67 nm, is interpreted as the distance between double plane layers of oriented amphiphilic molecules. The extended length of the bimolecule of 12HOA can be inferred from that of octadecanoic acid, which is an analogue of 12HOA. The latter is estimated from the length of the crystallographic c axis, it having been reported to be 4.938 nm for the B-form[17] and 5.07 nm for the C-form.[18] A comparison of these values with 4.67 nm leads us to conclude that, both in small domains in jellies and in crystalline solids, the bimolecules of 12HOA are packed in layers, with the long axis of the molecule tilting at about 21° from normal to the layer plane.

The crystal structure of 12HOA has not been analyzed, because it was not obtained as single crystals of a suitable size. However, a tentative interpretation has been given[6] on the basis of the powder patterns, in combination with the infrared spectral results and the concept of the subcell introduced by Vand.[19] The molecular chains of 12HOA can be closely packed, with a simultaneous formation of hydrogen-bond sequences extending along the b_s axis, in the triclinic subcell, whose dimensions, a_s, b_s, and γ_s, are 0.45 nm, 0.54 nm, and 120°. Assuming the remaining subcell dimensions, c_s, α_s, and β_s, to be 0.26 nm, 70°, and 108°, which are typical values previously reported for triclinic subcells,[20] the short spacings between a_sc_s planes and between b_sc_s planes are calculated to be 0.46 nm and 0.39 nm respectively. These values are consistent with those corresponding to strong reflections observed for the crystalline powder sample, as is shown in Fig. 7.

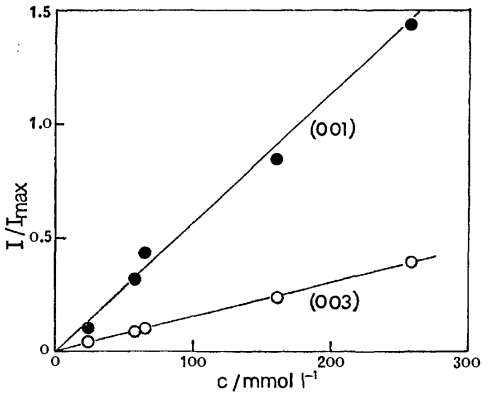

Fig. 8. Concentration dependence of the ratio of the peak height (I) of the (001) or (003) reflection relative to the maximal height (I_{max}) of the reflection corresponding to the short spacings.

The reflection peaks corresponding to the long spacing were found to become greater with an increase in the concentration. For convenience, the ratio of the peak height of the (001) or (003) reflection relative to the maximal height of the wide, diffuse reflection corresponding to a series of short spacings was plotted against the concentration. Figure 8 shows that the ratio is linearly proportional to the concentration, indicating that the lamellar structure becomes more ordered as the concentration is increased. It can also be seen from Fig. 7 that the peak corresponding to a spacing of 0.46 or 0.39 nm, which represents the spacing between a_sc_s planes or between b_sc_s planes respectively, comes to appear on the broad reflection curve with an increase in the concentration. This suggests that a crystalline order develops as the concentration is increased. Similar X-ray results were also obtained for the jellies with carbon tetrachloride by using a reflection method described in the Experimental section.

X-Ray studies were done also for the jellies containing anthracene or pynacyanole chloride, which gave the ICD. On adding the additives, it was found that the reflection peaks corresponding to the long spacing decreased remarkably in intensity without any alternation in the position of the peak, and that the peak of the broad reflection tended to shift slightly to a lower diffraction angle. This fact indicates that the lamellar structure in the jellies becomes less ordered when the additives are included. On the other hand, the CD maximum for the jellies containing any additive shifted to a longer wavelength than that for the additive-free jellies. This shift implies an increase in the helical pitch in supramolecular helicoidal structures, that is, a decrease in the helicoidal order in the jellies. The X-ray studies and the CD results strongly suggest that the supramolecular helicoidal structure exists in the lamellar structure constituting the small domains locally dispersed in the jellies. As has been described previously, the bimolecules of 12HOA in the domains are packed in layers with the long axis of the molecule tilting from normal to the layer. Therefore, one can consider the possibility that tilted chiral amphiphilic molecules of 12HOA in adjacent parallel layers are slightly skewed rather than parallel, so that a helicoidal structure is formed with a helical axis normal to the molecular layers. Such a structure has recently been found[21] in some thermotropic smectic liquid crystals; it is called the twisted smectic C mesophase or the chiral smectic C mesophase. It is thus possible to consider that 12HOA in jellies forms a lyotropic mesophase with a chiral smectic structure, a new kind of mesophase. Further studies are required to establish the details of such a mesophase and to locate the additive molecules which give rise to the ICD by becoming involved into the helicoidal lamellar structure.

Chiral Structure in Jellies. Jellies are composed of a continuous network of molecular aggregates or polymer chains in which the solvent is trapped.[22] The presence of helically twisted fibers in the jellies of 12HOA has been demonstrated by the use of an electron microscope after the removal of the solvent by evaporation.[4] It was then found that fibers were of a uniform thickness of about 10—100 nm and that the pitch of the helical twisting was about 80—1000 nm. There is no doubt that such fibers provide the crystalline domains responsible for the X-ray diffraction, although the fibers enmeshing the jellies may be thinner than the fibers seen by an electron microscope.

A very interesting and relevant question is the relation between the supramolecular helicoidal structure in the chiral mesophase and the macro-helical structure of twisted fibers observed under an electron microscope. With regard to the one enantiomer, the two helices are reversed; in the case of the *R*-enantiomer, the screw sense is right-handed for the chiral mesophase and left-handed for the macro-helix of the fibers. Therefore, the twisting of the fibers itself is not the origin of the CD in the jellies.

When the jellies on the supporting plates are dried, solid films were formed. As will be described in detail in Part 2, the solid films exhibited a CD band and X-ray diffraction patterns similar to those observed in the jellies. Therefore, the molecular arrangement in the solid films is considered to be essentially the same as

that in fibers within the jellies. It may thus be concluded that a chiral smectic structure giving rise to the CD exists in the structure of molecular layers constituting the solid films or the fibers. Such a chiral structure of 12HOA is formed only through the jelly state. It was impossible to obtain the chiral mesophase by heating the crystals or by cooling the isotropic melt.

The optical properties of the chiral smectic mesophase are known to be identical with those of cholesteric mesophases for the normal incidence of light.[23] The same optical properties would be expected to be displayed by the chiral mesophase of 12HOA. However, the fibers of 12HOA are randomly dispersed in the jellies, so that the chiral mesophase in the jellies is present locally as small domains which are dispersed with randomly-oriented helical axes within the jellies. This would explain the broadening and the weak intensity of the observed CD band compared with the effect in planar cholesteric mesophases.

Electron microscopy in our laboratory has shown that large ribbon-like fibers tend to be split into many thinner and helically twisted fibers.[24] This indicates that the double molecular layers of 12HOA are stacked approximately parallel to the direction of the width of the fibers. The helical axis of the chiral smectic structure in the molecular layers is directed to the width of the fibers.

It is also interesting to note that the chiral amphiphilic molecules such as 12HOA form helically organised systems in such different stages as a helical mesophase and helically twisted fibers. A similar relationship has also been seen in the case of synthetic polypeptides; the polymer molecules of the α-helix form a lyotropic cholesteric liquid crystal[2] and helically twisted fibers.[25]

The jellies of chiral 12HOA are a two-phase system, composed of the solvent and the fibers comprising the chiral smectic mesophase. In this point, the jellies of 12HOA are a unique chiral system of matter. This interesting chiral mesophase may provide an asymmetric medium in which any asymmetric reactions can occur.

The present work was partially supported by a Grant-in-Aid for Scientific Research from the Ministry of Education (No. 254129).

References

1) T. Tachibana, T. Mori, and K. Hori, *Nature*, **278**, 578 (1979).
2) E. T. Samulski and A. V. Tobolsky, "Liquid Crystals and Plastic Crystals," ed by G. W. Gray and P. A. Winsor, Ellis Horwood, Chichester (1974), pp. 175—198.
3) K. Sakamoto, R. Yoshida, M. Hatano, and T. Tachibana, *J. Am. Chem. Soc.*, **100**, 6898 (1978).
4) T. Tachibana and H. Kambara, *J. Colloid Interface Sci.*, **28**, 173 (1968); *Bull. Chem. Soc. Jpn.*, **42**, 3422 (1968).
5) K. Serck-Hanssen, *Chem. Ind. (London)*, **1958**, 1554.
6) T. Tachibana, T. Yoshizumi, and K. Hori, *Bull. Chem. Soc. Jpn.*, **52**, 34 (1979).
7) A. Saupe, "Liquid Crystals and Plastic Crystals," ed by G. W. Gray and P. A. Winsor, Ellis Horwood, Chichester (1974), pp. 18—47.
8) F. B. J. Rosevear, *J. Am. Oil Chem. Soc.*, **31**, 628 (1954).
9) M. J. B. Tunis-Schneider and M. F. Maestre, *J. Mol. Biol.*, **52**, 521 (1970).
10) F. D. Saeva and G. R. Olin, *J. Am. Chem. Soc.*, **95**, 7882 (1973).
11) H. de Vries, *Acta Crystallogr.*, **4**, 219 (1951).
12) M. Aihara and H. Inaba, *Opt. Commun.*, **3**, 77 (1971).
13) F. D. Saeva, P. E. Sharpe, and G. R. Olin, *J. Am. Chem. Soc.*, **95**, 7656 (1973).
14) C. Robinson, Tetrahedron, **13**, 219 (1961).
15) F. Husson, H. Mustacchi, and V. Luzzati, *Acta Crystallogr.*, **13**, 668 (1960).
16) S. S. Marsden, Jr., K. J. Mysels, and G. H. Smith, *J. Colloid Sci.*, **2**, 265 (1947).
17) E. von Sydow, *Acta Crystallogr.*, **8**, 557 (1955).
18) V. Malta, G. Celotti, R. Zannetti, and A. F. Martelli, *J. Chem. Soc., B*, **1971**, 548.
19) V. Vand, *Acta Crystallogr.*, **4**, 104 (1951).
20) E. von Sydow, *Ark. Kemi*, **9**, 231 (1956).
21) S. L. Arora, J. L. Fergason, and A. Saupe, *Mol. Cryst. Liq. Cryst.*, **11**, 243 (1970).
22) B. Jirgensons and M. E. Straumanis, "A Short Textbook of Colloid Chemistry," 2nd ed, Pergamon Press, Oxford (1962), Chap. 15.
23) D. W. Berreman, *Mol. Cryst. Liq. Cryst.*, **22**, 175 (1973); O. Parodi, *J. Phys. (Paris), Colloq.*, **36**, Cl-325 (1975); M. Brunet, *ibid.*, Cl-321. The second and third papers show that de Vries' analysis for cholesterics can be applied to chiral smectics C, both theoretically and experimentally respectively.
24) T. Tachibana, S. Kitazawa, and H. Takeno, *Bull. Chem. Soc. Jpn.*, **43**, 2418 (1970).
25) T. Tachibana and H. Kambara, *Kolloid-Z.*, **219**, 40 (1967).

 © 1980 The Chemical Society of Japan Bull. Chem. Soc. Jpn., 53, 1720—1722 (1980) [Vol. 53, No. 6

A Conductance Study of the Complexation Reaction of Dibenzo-24-crown-8 with Alkali Metal Ions in Propylene Carbonate and Methanol

Yasuyuki TAKEDA* and Hisao YANO

Department of Chemistry, Faculty of Science, Chiba University, Yayoi-chō, Chiba 260

(Received November 16, 1979)

The formation constants (K_{ML^+}) for 1:1 complexes of dibenzo-24-crown-8 (DB24C8) with alkali metal ions (Na^+, K^+, Rb^+, and Cs^+) in propylene carbonate (PC) and methanol have been determined conductometrically at different temperatures in order to obtain the values of the enthalpy (ΔH) and entropy changes (ΔS). The complexation reactions between DB24C8 and the alkali metal ions in PC and methanol are all exothermic, and the ΔS values of these systems are all negative. In the case of the PC system, there is no considerable difference in ΔS among the alkali metal ions (Na^+, K^+, Rb^+, and Cs^+); thus, the K_{ML^+} sequences depend entirely on the $-\Delta H$ sequences. Since, in methanol, the $-\Delta H$ and $-\Delta S$ values for K^+ are nearly equal to those for Cs^+, and since the largest $-\Delta H$ value for Rb^+ is balanced by the largest $-\Delta S$ value, DB24C8 shows no selectivity for the alkali metal ions (K^+, Rb^+, and Cs^+) in methanol.

The complexation reaction between dibenzo-24-crown-8 (DB24C8) and metal ions has been investigated by different methods, *e.g.*, calorimetry,[1] conductometry,[2] and solvent extraction.[3] Moreover, solvent extraction with DB24C8 has been used in the separation of barium(II) from strontium(II).[4]

DB24C8 forms stoichiometrically stable complexes with metal ions. They are mostly 1:1 complexes in solution. Since DB24C8, whose configuration is termed cylindrically symmetrical,[5] is a flexible crown ether and has a large cavity size (4.5—5.0 Å[6]), great conformational changes are required to fold around the metal ion on complexation. In the DB24C8 complex, the metal ion held in the cavity is partially wrapped around by DB24C8.[7] The stability of the complexes depends largely on the solvent medium[2] and the flexibility of the DB24C8 ring.[1]

The present study was undertaken in order to understand in detail the thermodynamics of the complexations of DB24C8 with alkali metal ions in nonaqueous solvents. In this paper, the formation constants for 1:1 complexes of DB24C8 with alkali metal ions in propylene carbonate (PC) and methanol have been determined conductometrically at different temperatures in order to obtain the values of the enthalpy and entropy changes.

Experimental

Materials. The method of the purification of DB24C8 (Nisso Co., Ltd.) was as has previously been described.[4] Lithium, sodium, and potassium perchlorates were obtained commercially. Rubidium and caesium perchlorates were prepared by adding an equimolar perchloric acid solution to an aqueous solution of rubidium bromide and caesium chloride respectively. All these perchlorates were recrystallized from water five times and, before use, dried at 150 °C in a vacuum oven. PC was distilled twice under nitrogen at about 12 mmHg. Methanol was allowed to stand in contact with molecular sieves for several days and then distilled twice. In each case of PC and methanol the middle 70% of the distillate was used. The water contents of the finally purified PC and methanol determined by the Karl Fischer titration were less than 0.01 and 0.03% respectively. The conductivities of the final products of PC and methanol were less than 5×10^{-8} and 1×10^{-7} ohm^{-1} cm^{-1} respectively.

Apparatus and Procedure. The conductance measurements were made on a Yanagimoto conductivity outfit, model MY-7, in a thermostated water bath at 10, 15, 20, 25, 30, and 35 ± 0.02 °C. Two cells were used with cell constants of 0.09317 and 0.2046 cm^{-1}.

The experimental procedure to obtain formation constants of DB24C8 complexes with alkali metal ions is as follows; a solution of the alkali metal perchlorate (5×10^{-4} M; 1 M= 1 mol dm^{-3}) 200 cm^3 was placed in the cell (volume 300 cm^3) and the resistance of the solution was measured. Then a step-by-step increase in the DB24C8 concentration was effected by a quick transfer with a pipet from the solution of DB24C8 (PC: 1×10^{-2} M, methanol: 5×10^{-3} M) to the cell, until the total concentration of DB24C8 was about two-and-a-half (methanol) or four times (PC) as large as that of the alkali metal perchlorate. The resistance of the solution in the cell was remeasured after each transfer.

Results

The molar conductivity, Λ, *vs.* $[L]_t/[M]_t$ plots for caesium perchlorate at 10, 15, 20, 25, 30, and 35 °C in PC and in methanol are given in Figs. 1 and 2 respectively, where $[L]_t$ and $[M]_t$ are the total concen-

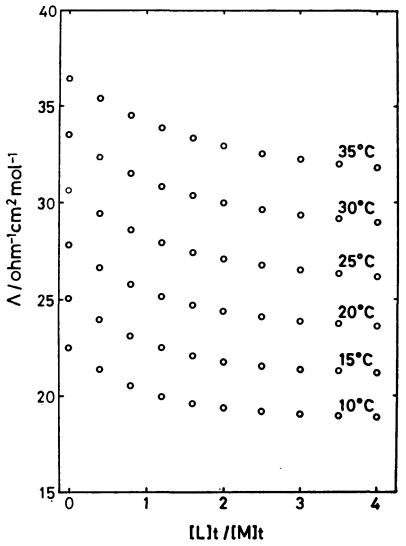

Fig. 1. Λ *vs.* $[L]_t/[M]_t$ plots for caesium perchlorate in PC at different temperatures.
$[M]_t=5\times10^{-4}$ M.

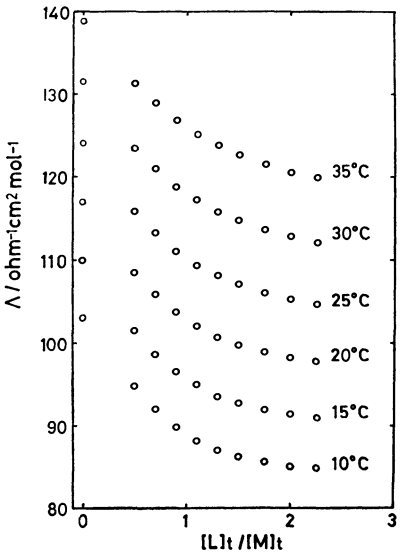

Fig. 2. Λ *vs.* $[L]_t/[M]_t$ plots for caesium perchlorate in methanol at different temperatures.
$[M]_t = 5 \times 10^{-4}$ M.

trations of DB24C8 and the alkali metal ion respectively. The Λ *vs.* $[L]_t/[M]_t$ plots show a decrease in Λ with an increase in the DB24C8 concentration. The experimental plots of the other alkali metal perchlorates in PC and methanol are similar, and so have been omitted. In the cases of the Li^+–PC and methanol and the Na^+–methanol systems, since hardly any change in Λ is found in spite of an increase in the DB24C8 concentration, the conductometric determination of the complex formation constant is impossible. It is assumed that the association between the cation and the perchlorate ion in PC and methanol is negligible under these highly dilute experimental conditions and that, in this work, DB24C8 forms the 1 : 1 complexes with the alkali metal ions in PC and methanol.

The equilibrium equation is given by:

$$\begin{array}{ccccc} M^+ & + & L & \rightleftarrows & ML^+ \\ \alpha[M]_t & & [L]_t-(1-\alpha)[M]_t & & (1-\alpha)[M]_t, \end{array} \quad (1)$$

where M^+, L, and α are the alkali metal ion, DB24C8, and the fraction of free alkali metal ions. Accordingly, the complex formation constant, K_{ML^+}, is defined by:

$$K_{ML^+} = [ML^+]/[M^+][L] = (1-\alpha)/\alpha[L]. \quad (2)$$

The observed conductivity, κ, is written as:

$$\kappa = \kappa_{MClO_4} + \kappa_{MLClO_4}, \quad (3)$$

where κ_{MClO_4} and κ_{MLClO_4} are the conductivities of alkali metal perchlorate and alkali metal DB24C8 perchlorate respectively. The molar conductivities are given by:

$$\Lambda_{MClO_4} = \kappa_{MClO_4}/[M^+] = \kappa_{MClO_4}/\alpha[M]_t, \quad (4)$$

$$\Lambda_{MLClO_4} = \kappa_{MLClO_4}/[ML^+] = \kappa_{MLClO_4}/(1-\alpha)[M]_t, \quad (5)$$

where Λ_{MClO_4} and Λ_{MLClO_4} are the molar conductivities of alkali metal perchlorate and alkali metal DB24C8 perchlorate respectively. As a consequence of Eqs. 4 and 5, Eq. 3 can be transformed into:

$$\Lambda = \kappa/[M]_t = \alpha\Lambda_{MClO_4} + (1-\alpha)\Lambda_{MLClO_4}. \quad (6)$$

Since the DB24C8 concentration was kept low ($<2.5 \times 10^{-3}$ M) during these experiments, corrections for viscosity changes were neglected. As a consequence of Eq. 6, Eq. 2 can be transformed into:

$$K_{ML^+} = (\Lambda_{MClO_4}-\Lambda)/(\Lambda-\Lambda_{MLClO_4})[L], \quad (7)$$

where $[L] = [L]_t - [M]_t(\Lambda_{MClO_4}-\Lambda)/(\Lambda_{MClO_4}-\Lambda_{MLClO_4})$.

The procedure for obtaining the K_{ML^+} value is as follows. The Λ_{MLClO_4} value is estimated from the Λ values at the points of large $[L]_t$ to $[M]_t$ ratios. Using this Λ_{MLClO_4} value, the K_{ML^+} value in Eq. 7 is calculated. The actual K_{ML^+} and Λ_{MLClO_4} values are calculated by a nonlinear least-squares analysis.[8] In each system the K_{ML^+} values increase monotonously with a decrease in temperature. The $\log K_{ML^+}$ *vs.* T^{-1} plot shows a linear relationship for each system. By way of example, the $\log K_{ML^+}$ *vs.* T^{-1} plots for the caesium–PC and methanol systems are given in Fig. 3. The values of the enthalpy change, ΔH, and the entropy

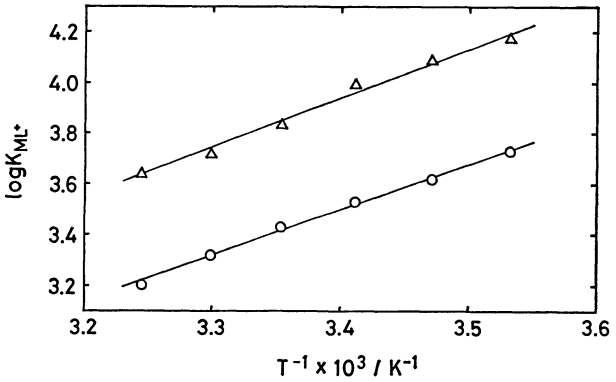

Fig. 3. $\log K_{ML^+}$ *vs.* T^{-1} plots for caesium–PC and methanol systems.
○: PC, △: methanol.

Table 1. $\log(K_{ML^+}/\text{mol}^{-1}\,\text{dm}^3)$, ΔH, and ΔS values for the complexation of alkali metal ions with DB24C8 in various solvents

Crown ether	Cation	Solvent	$\log K_{ML^+}$ (at 25 °C)	$-\Delta H$ / kJ mol^{-1}	$-\Delta S$ / JK^{-1} mol^{-1}
DB24C8	Na^+	PC	4.1_6	$37._7$	$46._0$
		70 wt% CH_3OH in H_2O[1]	1.54	32.4	79.1
	K^+	PC	3.7_3	$34._5$	$44._4$
		CH_3OH	3.5_7	$35._3$	$49._4$
		70 wt% CH_3OH in H_2O[1]	2.42	35.7	73.6
	Rb^+	PC	3.5_5	$32._9$	$42._3$
		CH_3OH	3.8_6	$39._4$	$57._7$
		70 wt% CH_3OH in H_2O[1]	2.55	36.5	73.6
	Cs^+	PC	3.4_6	$32._3$	$42._3$
		CH_3OH	3.8_4	$36._8$	$49._0$
		70 wt% CH_3OH in H_2O[1]	2.48	37.4	77.8
DB30C10[9]	Cs^+	CH_3OH		53.22	95.48

change, ΔS, calculated from these data are summarized in Table 1, together with the $\log K_{ML}^+$ values at 25 °C and the literature values.

Discussion

The complexation reactions between DB24C8 and the alkali metal ions in PC and methanol are all exothermic, and the ΔS values of these systems are all negative (Table 1). DB24C8 is a large crown ether and has a great ligand-ring flexibility. The uncomplexed DB24C8 may be more flexible than the complexed DB24C8. It thus appears that the negative ΔS values are largely attributable to the great conformational changes when a complexation reaction occurs. It may be seen from Table 1 that, in methanol, the ΔS value of Cs^+ for DB24C8, which is smaller than dibenzo-30-crown-10 (DB30C10), is much larger than that for DB30C10. The $-\Delta H$ sequences of the alkali metal ions with DB24C8 in PC are $Na^+ > K^+ > Rb^+ \geq Cs^+$, while those in 70 wt% CH_3OH are completely the reverse. In the case of the DB24C8–PC system, there is no considerable difference in ΔS among the alkali metal ions; thus, the $\log K_{ML}^+$ sequences entirely depend on the $-\Delta H$ sequences (Table 1). Since, in methanol, the $-\Delta H$ and $-\Delta S$ values of DB24C8 for K^+ are nearly equal to those for Cs^+, and since the largest $-\Delta H$ value for Rb^+ is balanced by the largest $-\Delta S$ value, DB24C8 shows no selectivity for the alkali metal ions in methanol. In methanol, the ΔH value of Cs^+ for DB24C8, which has smaller donor oxygen atoms than DB30C10, is much larger than that for DB30C10.

Among the solvents, the $-\Delta S$-value series for the Na^+–, the K^+– and Cs^+–, and the Rb^+–DB24C8 systems are given in the order PC$\ll$70 wt% CH_3OH, PC$<$methanol$\ll$70 wt% CH_3OH, and PC$<$methanol$<$70 wt% CH_3OH, respectively (Table 1). It may be attributed chiefly to the solvent structural influences of methanol and water that, in the case of each alkali metal ion-DB24C8 system, the $-\Delta S$ value increases on moving from PC to 70 wt% CH_3OH. Moreover, in the cases of the K^+, Rb^+, and Cs^+–DB24C8 systems, the large increase in $-\Delta S$ on going from methanol to 70 wt% CH_3OH may be largely due to the stronger water structural influences compared to methanol. For the Na^+–DB24C8 system, the larger $-\Delta H$ and the much smaller $-\Delta S$ values of PC result in the much greater $\log K_{ML}^+$ value compared to 70 wt% CH_3OH. Although, in the cases of the K^+, Rb^+, and Cs^+–DB24C8 systems, there is no considerable difference in ΔH, the K_{ML}^+ values in PC and methanol are as large as one order of magnitude larger than that in 70 wt% CH_3OH. This is largely attributed to the much smaller $-\Delta S$ values in PC and methanol compared to 70 wt% CH_3OH (Table 1). Since, in each case of the K^+ and Cs^+–DB24C8 systems, there are no significant differences in ΔH and ΔS between PC and methanol, the $\log K_{ML}^+$ values in PC and methanol are nearly equal. For the Rb^+–DB24C8 system, the larger $-\Delta H$ value in methanol is canceled by the larger $-\Delta S$ value compared to PC; thus, there is no considerable difference in $\log K_{ML}^+$ in PC and methanol.

TABLE 2. ($\Lambda_{MLClO_4}/\Omega^{-1}$ cm^2 mol^{-1}) VALUES IN METHANOL AT DIFFERENT TEMPERATURES

Temp/°C	Λ_{MLClO_4}		
	K^+	Rb^+	Cs^+
	$[M]_t =$ 5.054×10^{-4} M	$[M]_t =$ 5.044×10^{-4} M	$[M]_t =$ 5.041×10^{-4} M
10	82.41	81.53	82.11
15	88.76	87.39	87.52
20	93.90	93.27	93.68
25	100.2	99.15	98.97
30	106.5	104.8	105.4
35	112.9	111.8	112.3

The Λ_{MLClO_4} values of K^+, Rb^+, and Cs^+ in methanol at different temperatures are given in Table 2. As can be seen from Table 2, the $[M]_t$ values of K^+, Rb^+, and Cs^+ are nearly equal to one another, and there is scarcely any difference in Λ_{MLClO_4} among K^+, Rb^+, and Cs^+ at the same temperature, suggesting that the charge of the alkali metal ion held in the DB24C8 cavity is effectively shielded by the DB24C8 and that the DB24C8 complexes with the alkali metal ions in methanol are approximately equal to each other in size.

References

1) R. M. Izatt, R. E. Terry, D. P. Nelson, Y. Chan, D. J. Eatough, J. S. Bradshaw, L. D. Hansen, and J. J. Christensen, *J. Am. Chem. Soc.*, **98**, 7626 (1976).
2) Y. Takeda, H. Yano, M. Ishibashi, and H. Isozumi, *Bull. Chem. Soc. Jpn.*, **53**, in press (1980).
3) Y. Takeda, *Bull. Chem. Soc. Jpn.*, **52**, 2501 (1979).
4) Y. Takeda, K. Oshio, and Y. Segawa, *Chem. Lett.*, **1979**, 601.
5) C. J. Pedersen, *J. Am. Chem. Soc.*, **89**, 7017 (1967).
6) C. J. Pedersen, *J. Am. Chem. Soc.*, **92**, 386 (1970).
7) N. S. Poonia, *J. Am. Chem. Soc.*, **96**, 1012 (1974).
8) D. F. Evans, S. L. Wellington, J. A. Nadis, and E. L. Cussler, *J. Solution Chem.*, **1**, 499 (1972).
9) M. Shamsipur and A. I. Popov, *J. Am. Chem. Soc.*, **101**, 4051 (1979).

 © 1980 The Chemical Society of Japan Bull. Chem. Soc. Jpn., 53, 1723—1727 (1980)

The Thermal Stability of Metal Cation-TCNQ Anion Radical Salts

Yoshio KISHIMOTO* and Wataru SHIMOTSUMA

Materials Research Laboratory, Matsushita Electric Industrial Co., Ltd., Moriguchi, Osaka 570

(Received September 17, 1979)

To study the thermal stability of several metal cation–TCNQ salts (mainly alkali metal salts), the variation in the electrical resistivity and the characteristics of the chemical degradations by heating were measured. Most metal–TNCQ salts do not melt and are not sublimated, but have decomposition points at about 320 °C. Na(TCNQ) has a stable resistivity, even after heating for 500 hours at 200 °C, and is the most stable among the metal–TCNQ salts tested. Metal–TCNQ salts are gradually damaged from the surfaces of the crystalline powders by heating, and the TCNQ molecule is oxidized, thus losing CN groups. The crystallization process of the TCNQ salts has a great influence upon their thermal stabilities. In the complex salt $Cs_2(TCNQ)_3$, the application of d.c. voltage gives rise to the polarization current at a temperature near 200 °C, and the TCNQ molecules tend to migrate in the electric field.

Charge-transfer complexes based on 7,7,8,8-tetracyanoquinodimethane (TCNQ) have been extensively studied as organic metals or one-dimensional conductors in recent years; they have also received considerable interest in connection with their possible use as electronic materials.[1,2] Considering the life as electronic material or the compounding process with polymeric materials in practical use, the thermal stability of a TCNQ complex is highly important. Many TCNQ complexes with organic electron-donors are susceptible to thermal decomposition; metal–TCNQ salts are thermally more stable because of the low ionization potentials of metals. However, the thermal stability of the metal–TCNQ salts has been studied only by DTA and TGA.[3,4]

In this paper, in order to ascertain the upper limit of the thermal stability of TCNQ complexes, the thermal stabilities of several metal cation–TCNQ anion radical salts (mainly alkali metal salts) have been studied from both sides of their electrical resistivities and chemical degradations. The thermal stabilities have mainly been studied at the comparatively high temperatures of 200—250 °C in air; after the heating at 200—250 °C, the resistivity and chemical degradation of the TCNQ salts were measured at room temperature (RT). To study the variation in the resistivity, the dependence of the RT resistivity on the heating time, the temperature dependence of the resistivity, the d.c. polarization currents at temperatures ranging from RT to 200 °C, and the differences in the variation in the resistivity with several crystallization methods were measured. Moreover, the chemical degradations were analyzed by means of DTA, TGA, IR spectra, elemental analysis, or X-ray powder diffraction patterns.

Experimental

Synthesis of Metal–TCNQ Salts. Polycrystalline samples of Li(TCNQ), Na(TCNQ), K(TCNQ), $Cs_2(TCNQ)_3$, Ba(TCNQ)$_2$, and Cu(TCNQ) were prepared by refluxing for 4 h mixed acetonitrile solutions of TCNQ and metal iodides.[3] CsI and $BaI_2 \cdot 2H_2O$, which are insoluble in acetonitrile, were dissolved in a small amount of methanol, after which the solutions were added to TCNQ solutions. The hot mixed solutions were cooled to 0 °C, and the polycrystalline powders of the TCNQ salts thus deposited were filtered off and washed with acetonitrile.

Electrical Measurements. About constant weights of the polycrystalline powder samples were introduced into glass capillaries 1.5 mm in inner diameter and were packed to a saturated thickness of about 1 mm by pressing them repeatedly (about thirty times) under a weight of 230 g. Under a pressure of 13 kg/cm^2 and using electrodes composed of stainless steel sticks, the resistances for d. c. voltage were measured. In order to check the correctness of electrical measurements, the following measurements were carried out. The resistance was influenced by the pressure and electrode materials, but was over the wide range of 0.3—300 V/cm and showed a linear dependence on the thicknesses of the samples in the capillaries. When graphite powders were used as elctrodes instead of stainless steel, the samples showed lower resistivities, but the temperature dependence of their resistivities had the same temperature coefficients. Further, both these samples showed constant currents for 1 h under a voltage of 10 V at 30, 45, 60, 80, and 100 °C.

Analysis of Degradated Products. The IR spectra were measured by means of a JASCO Model DS-403G infrared spectrophotometer using the KBr-wafer technique. The DTA and TGA were performed by using an electric microbalance(Rigaku Electric Co., Ltd.), and each sample was measured under the following two conditions: by increasing the temperature at the rate of 10 °C/min from RT to 1000 °C, or by holding the temperature at 250 °C for 1 h after increasing temperature at the rate of 2.5 °C/min from 200 °C to 250 °C. The X-ray diffraction patterns were measured by means of a Philips PW-1009 X-ray diffractometer, using Cu $K\alpha$ radiation as the X-ray source(35 kV, 10 mA).

Results and Discussion

Thermal Stability of Resistivity. The temperature dependences of the resistivity of metal–TCNQ salts are shown in Fig. 1. All these curves except that of K-(TCNQ) are in accord with Arrhenius' equation at temperatures below 120 °C, but crystals of K(TCNQ) show unstable non-linear characteristics. The time dependence of the resistivity at 200 °C under a d.c. voltage of 10 V (about 100 V/cm) is shown in Fig. 2; $Cs_2(TCNQ)_3$ shows a remarkable variation in the current based on the polarization of the carriers. The variation in the resistivities with the time at 200 °C is faster, probably because of the existence of the electric field, than that (Fig. 3(1)) of the salts loaded only with heat at 200 °C. The resistivities of metal–TCNQ salts cooled from 200 °C to RT become higher than those shown in Fig. 1 as well as in Ref. 5, but the

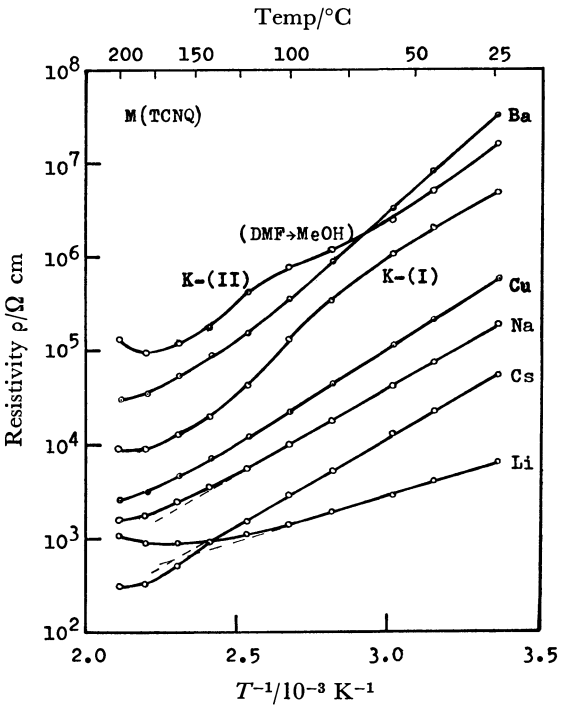

Fig. 1. Temperature dependence of resistivity of metal–TCNQ salts.

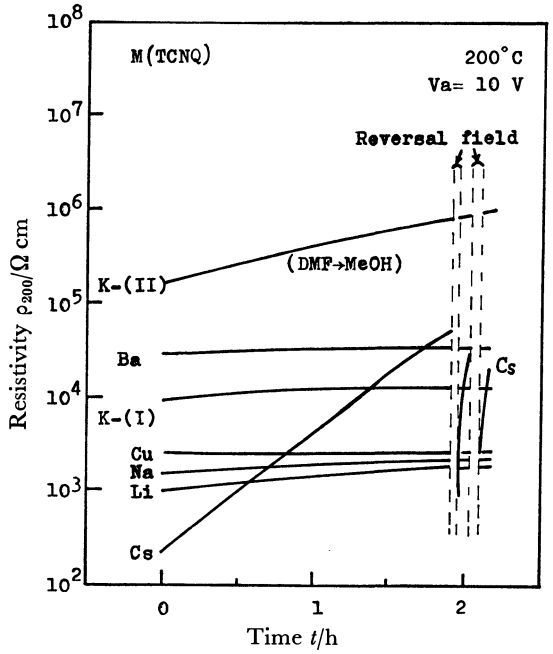

Fig. 2. Dependence of resistivity on time at 200 °C under d.c. voltage of 10 V (about 100 V/cm).

variations in the resistivities of Na(TCNQ), Cu(TCNQ), and $Ba(TCNQ)_2$ were only small.

After the six kinds of metal–TCNQ salts were heated at 200, 220, and 250 °C, their resistivities were measured at the RT of 24 °C. The results are shown in Fig. 3 and Table 1. Here, Li(TCNQ)-A and Na(TCNQ)-A are new samples synthesized at the same time as the other metal salts, while Li(TCNQ)-B and Na(TCNQ)-B are old samples synthesized about 9 years ago and kept

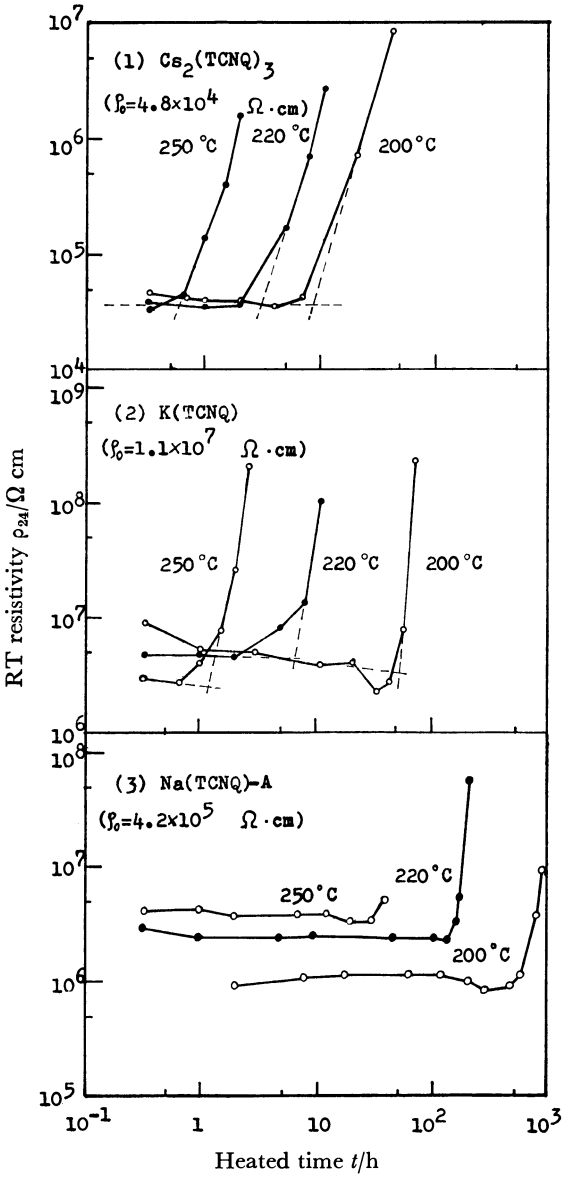

Fig. 3. Stability of RT resistivity of metal–TCNQ salts heated at each temperature.
ρ_0: Initial resistivity and RT: 24 °C.

TABLE 1. ELECTRICAL LIFE OF METAL–TCNQ SALTS UPON HEATING

Metal–TCNQ salt	Electrical life, t_{th}/h		
	250 °C	220 °C	200 °C
Li(TCNQ)-A[a)]	—	—	64
Li(TCNQ)-B[b)]	(1.2)	(6.3)	(15)
Na(TCNQ)-A	35	170	600
Na(TCNQ)-B	(11)	(72)	(175)
K(TCNQ)	1.25	6.8	55
$Cs_2(TCNQ)_3$	0.6	3	9
$Ba(TCNQ)_2$	2.3	8	24
Cu(TCNQ)	2	9	24

a) A: New sample. b) B: Sample synthesized 9 years ago.

in air for that long period. These results are characterized by the retention of comparatively constant resistivities, followed by rapid increases in the resistivities, with a resemblance to the induction period of thermal degradation in the stabilizer-filled polymer.[6] Here, the threshold times at the variation points in these figures are evaluated from the intersecting points of the dashed lines and are here termed the "electrical life," t_{th}. The values of t_{th} are tabulated in Table 1. Na(TCNQ) has the longest life among the metal–TCNQ salts tested. These values of t_{th} belong to a very stable class of organic materials, and so the tested metal–TCNQ salts have been shown to have a satisfactory stability in practical use as electronic materials.

The t_{th}-1/T plots of K(TCNQ) shows straight lines, but the life at RT estimated from the linear characteristics of K(TCNQ) is too long. The t_{th}-1/T values of other metal–TCNQ salts, plotted from the data shown in Table 1, do not show straight lines, but the slopes of the plots are almost all the same. In order to estimate the life at RT, the t_{th}-1/T characteristics need to be measured over a range of temperatures wider than 200—250 °C. In Fig. 3, except for the case of $Cs_2(TCNQ)_3$, the value of ρ_{24} of each sample, which was heated at the temperatures of 200, 220, and 250 °C, varies even though the material is the same, but the results seem to be based on the change in the crystal state by heating at a different temperature or on the stresses of the crystal at the time of the drop in the temperature.

Thermal Degradation of Complex Salt – $Cs_2(TCNQ)_3$. $Cs_2(TCNQ)_3$ shows a remarkable variation in the current at temperatures near 200 °C, as is shown in Fig. 2, although the results of the elemental analysis of a sample heated for only 7.2 h at 200 °C show the same composition as virgin $Cs_2(TCNQ)_3$. Also after the reversal of the electric field, a remarkable variation in the current, the so-called absorption current, also occurs. Such characteristics are examples of ionic behavior based on the polarization of the carrier by an electric field, different from the constant current under a d.c. electric field in the case of electronic conduction, and show that TCNQ molecules in crystal of $Cs_2(TCNQ)_3$ easily migrate at temperatures close to 200 °C in response to the electric field. These factors coincide with the behavior shown in Ref. 7. Besides, needle crystals of $Cs_2(TCNQ)_3$ are gradually pulverized to microcrystals with the sublimation of a liberated molecule such as $TCNQ^0$ during the heating of 200—250 °C. The X-ray diffraction peaks of the heated $Cs_2(TCNQ)_3$ are also gradually lowered, while keeping the same peak pattern. Therefore, the thermal degradation of the salt is surmised to occur gradually from the surface of the crystal powders. After a longer heating, the composition of the degradated product seems to come close to the value of Cs(TCNQ) judging from the composition of elements shown in Table 2.

Thermal Degradation of Simple Salts. As is shown in Table 3, the DTA data indicate that the decomposition points are above 285 °C and that heating for 1 h at 250 °C does not cause any peak in the DTA curve. The weight losses also occur to only a small extent in that condition. However, upon heating for several hours at that temperature (250 °C), a rapid increment of resistivity occurs except in the case of Na(TCNQ), as is shown in Fig. 3 and Table 1. Na(TCNQ), whose electrical life, t_{th}, is 600 h at 200 °C has a very excellent stability. The high stability of Na(TCNQ) is considered to be related to the finding that the beginning temperature, T_{h2}, of the second peak in the DTA data is higher than that of the other salts by about 100 degrees. This high stability is probably due to the pertinence of the ionic radius of sodium, which has a low ionization potential in the crystal.

Many of these alkali or alkali earth metal–TCNQ salts whose metals have low ionization potentials are

Table 2. Elemental analysis, weight loss, and solubility of metal–TCNQ salts heated at 200 °C

Sample[a]		Color	Elemental analysis[b]			Oxygen[c] content	Weight loss	Solubility (Color of solution)[d]	
			C/%	H/%	N/%	%	%	CH_3CN	H_2O
K(TCNQ)-I	0 h	deep red	59.56 (59.23)	1.48 (1.65)	23.45 (23.04)	0	0	△ (green)	×
	35 h	deep red	59.01	1.72	23.32	0	2.0	—	—
	71.5 h	black	56.65	1.76	20.76	3.59	6.7	—	—
	235 h	amber	48.22	2.08	11.92	18.3	17.3	—	—
K(TCNQ)-II	0 h	deep red	59.18 (59.23)	1.76 (1.65)	23.01 (23.04)	0	0	△ (green)	×
	4 h	deep red	56.77	1.74	20.88	4.87	2.8	—	—
	11.5 h	black	50.77	2.11	14.68	15.0	7.8	△ (light green)	△ (yellow)
	22 h	dark green	48.36	2.16	11.90	19.2	12.4	—	—
	40 h	amber	46.87	2.36	9.56	21.9	17.6	×	○ (amber)
	112.5 h	amber	45.26	2.35	8.96	23.1	20.8	×	○ (amber)
$Cs_2(TCNQ)_3$	0 h	purple	49.32 (49.21)	1.20 (1.37)	18.92 (19.14)	0	0	△ (light green)	×
	7.2 h	purple	49.52	1.30	19.38	0	0.6	—	—
	42 h	dark purple	44.14	1.48	14.95	6.03	9.4	×	○ (amber)
Na(TCNQ)-B	345 h	black	54.06	2.08	11.2	—	—	△ (light green)	△ (light green)

a) Time(h) is the heating time of the sample at 200 °C. b) Calculated value in parentheses. c) Value calculated from elemental analysis and weight loss. d) ○: Easily soluble, △: slightly soluble, and × : insoluble.

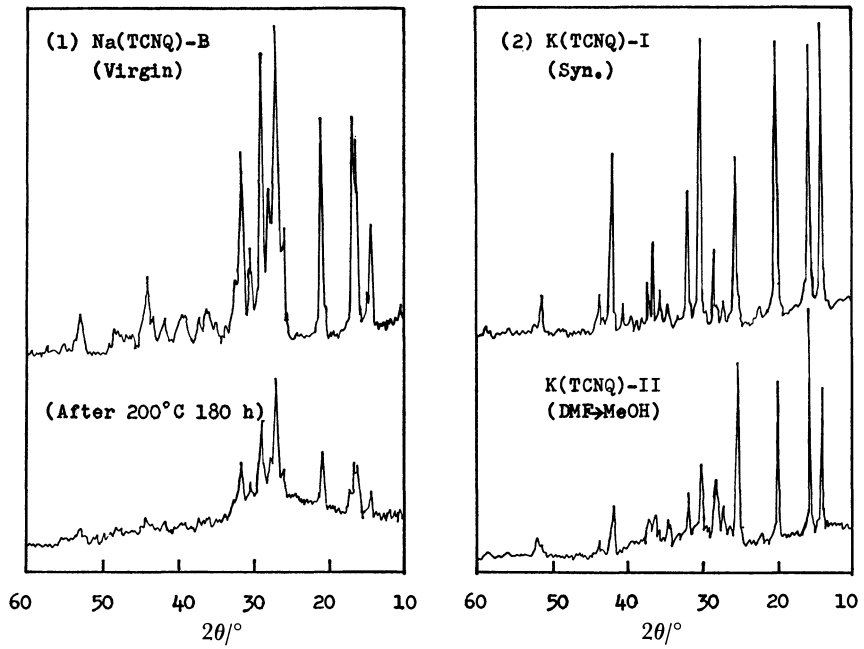

Fig. 4. Variation of X-ray diffraction patterns of Na(TCNQ) and K(TCNQ).

degradated to become black without any evaporation or sublimation, but K(TCNQ) changes its color variously with the degree of degradation, as will be shown below. Cu(TCNQ) sublimes near 355 °C, and its thermally decomposed product upon long heating at 200 °C seems to include metallic copper. This is probably due to the weak ionization tendency of copper. The results of elemental analysis are shown in Table 2. The metal–TCNQ salts are degradated to lose CN groups. In numerous cases of color changes of salts occurring with degradation, the degradation is characterized by a variation in the resistivity immediately after the color change. It is clear that the color change reflects the variation in the composition of TCNQ salt.

The X-ray diffraction peaks of Na(TCNQ) are lowered with its degradation, showing the same patterns as are shown in Fig. 4(1). Therefore, the thermal degradation is considered to occur gradually from the surface of the crystalline powders. Besides, the data of IR spectrophotometry on the degradated products of Na(TCNQ) and K(TCNQ) show peaks at the wave numbers of 750, 1380, 1670, 1740, and 3400 cm^{-1}. These peaks are deduced to show a hydrogen bond, carbonyl group, or carboxyl group formed by the oxidation of the TCNQ molecule, but the correct molecular structures of the degradated products of TCNQ salts are still not clear. The solubilities of the tested metal–TCNQ salts and their degradated products in water and in acetonitrile are tabulated in Table 2, along with the colors of the solutions. K(TCNQ) and $Cs_2(TCNQ)_3$ change to very water-soluble substances upon heating.

Thermal Stabilities of Various K(TCNQ) Crystals. K(TCNQ)-I was synthesized in acetonitrile by using the above-described method. By means of the recrystallization or reprecipitation of the K(TCNQ)-I, the following four kinds of K(TCNQ) were prepared:

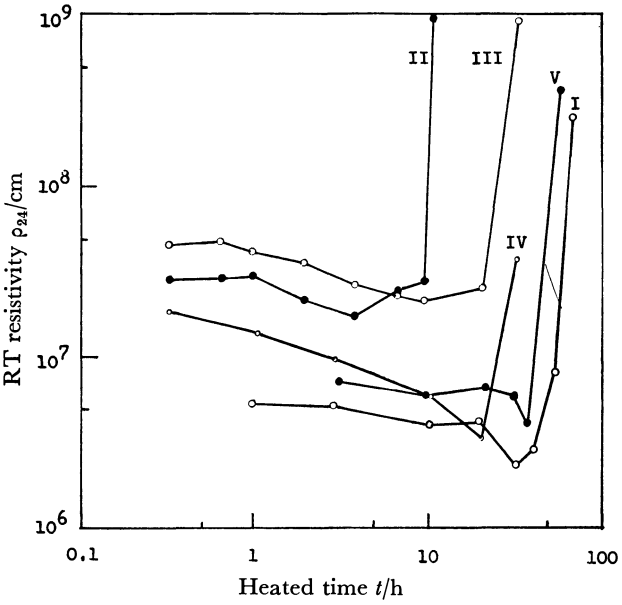

Fig. 5. Stability of RT resistivity of various K(TCNQ) crystals heated at 200 °C.
ρ_0: Initial resistivity and RT: 24 °C.
ρ_0/Ωcm: I 1.1×10^7, II 2.9×10^7, III 4.3×10^7, IV 2.8×10^7, V 6.2×10^7.

K(TCNQ)-II....reprecipitated from a DMF solution of K(TCNQ)-I of 100 °C by dilution with much methanol at 0 °C.

K(TCNQ)-III....recrystallized from a DMF solution of K(TCNQ)-I.

K(TCNQ)-IV....once recrystallized from an acetonitrile solution of K(TCNQ)-I.

K(TCNQ)-V....twice recrystallized from an acetonitrile solution of K(TCNQ)-I.

These crystals of K(TCNQ) have the virgin resistivities, ρ_0, shown in Fig. 5, but it is strange that their

Table 3. Thermal analysis of metal–TCNQ salts by DTA and TGA

	T_h/°C			Weight loss/%[a]			Residue at 1000 °C/%	Weight loss/%[b]	
	T_{h1}	T_{h2}	T_{h3}	T_w	$T_w \rightarrow T_{h2}$	$T_{h2} \rightarrow 1000$ °C		Before 250 °C	After 250 °C 1 h
K(TCNQ)-I	315	450	630	310	9.5	71	19.5	0	1.0
K(TCNQ)-II	285	450	590	275	14	66.5	19.5	0	14.2
K(TCNQ)-IV	310	450	660	300	10	74.5	15.5	0	8.0
K(TCNQ)-V	320	450	680	315	9.5	78	22.5	0	4.0
Na(TCNQ)-B	340	545	660	330	18.5	60.5	21	0	2.6
Li(TCNQ)-B	325	430	475	315	19	62.5	18.5	2	3.5
$Cs_2(TCNQ)_3$	320	455	—	310	11.5	61.5	27	0	3.5
Cu(TCNQ)	355			355	80	—	20	0	0.3
$Ba(TCNQ)_2$	370	430	—	355	23.5	46.5	30	0	0.5

T_h and T_w are the beginning temperatures of the exothermic peak and the weight loss respectively. a) 10 °C/min from RT to 1000 °C. b) 2.5 °C/min from 200 °C to 250 °C and hold at 250 °C for 1 h.

resistivites are about one order of magnitude higher than the values measured immediately after compacting the crystalline powders into a capillary. The variation in the RT resistivities of these K(TCNQ) crystals upon heating at 200 °C is also shown in Fig. 5. K(TCNQ)-II shows the most unstable result among the samples (I—V) in the figure; the results have a tendency similar to that of the DTA data shown in Table 3. Since the K(TCNQ)-II does not show any weight loss at temperatures below 250 °C, but does show low peaks in the X-ray powder pattern, as is shown in Fig. 4(2), this instability may be deduced to be based on the difference is crystal states rather than a residual DMF solvent.

Figure 5 shows that the crystallization processes exert great influences upon their thermal stabilities; it is interesting that K(TCNQ)-I, prepared in synthesis, shows a fairly stable result. In the heating process, K(TCNQ) crystals show various color changes different from those of many metal–TCNQ salts, as is shown in Table 2; the color changes of K(TCNQ)-(I—V) correspond to the variation in resistivities shown in Fig. 5.

In conclusion, the thermal stabilities of metal–TCNQ salts may be summarized as follows:

(1) Na(TCNQ) has a stable resistivity, even after heating for 500 h at 200 °C, and is the most stable among the metal–TCNQ salts tested.

(2) Most of the metal–TCNQ salts do not melt and are not sublimated, but have a decomposition point at about 320 °C.

(3) Metal–TCNQ salts are considered to be gradually damaged from the surface of crystalline powders by heating, and the TCNQ molecule is oxidized, losing CN groups.

(4) The crystallization process and the crystal state of the salts have a great influence upon the thermal stabilities.

(5) In the $Cs_2(TCNQ)_3$ complex salt, the application of the voltage gives rise to a polarization current at a temperature near 200 °C, and the TCNQ molecules tend to migrate in the electric field and to be slightly sublimated at that temperature.

(6) When the voltage is applied to metal–TCNQ salts at temperatures above 150 °C, the salts often suffer irreversible variations in their resistivities.

References

1) S. Yoshimura and M. Murakami, *Ann. N. Y. Acad. Sci.*, **313**, 269 (1978).

2) Y. Kishimoto, T. Hayashi, M. Hashimoto, and T. Ohshima, *J. Appl. Polym. Sci.*, **21**, 2721 (1977).

3) L. R. Melby, R. J. Hertler, W. Mahler, R. E. Benson, and W. E. Mochel, *J. Am. Chem. Soc.*, **84**, 3374 (1962).

4) A. I. Sherle, S. M. Mezhikovskii, V. V. Kuzina, and A. A. Berlin, *Izv. Akad. Nauk SSSR, Ser. Khim.*, 554 (1974).

5) N. Sakai, I. Shirotani, and S. Minomura, *Bull. Chem. Soc. Jpn.*, **45**, 3321 (1972).

6) W. L. Hawkins, "Polymer Stabilization," Wiley, New York (1972), p. 422.

7) J. S. Blakemore, U. Bernstein, J. E. Lane, and D. A. Woodburg, Int. Conf. Phys. Semecon. (NLD), 13 th, 345 (1976).

Temperature Dependence of Structural Propensity of 1-Butanol in Water

Neriyanuri Manohara Murthy and Saraswatula Venkata Subrahmanyam*

Department of Physics, SVU Autonomous Post-Graduate Centre, Anantapur 515003, India

(Received July 9, 1979)

The temperature dependence of structural propensity of 1-butanol has been studied by investigating its effect on the temperature of sound velocity maximum (TVM) in aqueous mixtures of glycerol and pyridine. The structural contribution to the shift in TVM of binary solution, $[\Delta T_{str}]_{exp}$ was found to be positive at low concentrations of 1-butanol for aqueous pyridine solutions whose TVM are 37.6 °C and 23.7 °C. For aqueous glycerol solutions whose TVM is 43.3 °C, $[\Delta T_{str}]_{exp}$ values, in the entire concentration range of 1-butanol studied, are found to be negative. The results indicate that below 40 °C 1-butanol behaves as a structure promoter while above 40 °C it behaves as a structure breaker.

The effect of solutes (electrolytes or nonelectrolytes) in promoting the hydrogen bonded structure of water is a function of temperature. Structure makers at low temperatures are known to behave as structure breakers at high temperatures.[1-4] Our earlier studies[5,6] on the effect of 1-butanol on the temperature of adiabatic compressibility minimum and sound velocity maximum of water indicate structure breaking property at high temperatures (around 60 and 75 °C) where as the density maximum studies by Wada and Umeda[7] (around 4 °C) indicate structure making propensity for this solute.

To understand the temperature dependence of structural propensity of 1-butanol, we have taken up a study of the effect of 1-butanol on the temperature corresponding to the sound velocity maximum of aqueous mixtures of glycerol (TVM=43.3 °C) and pyridine (TVM 37.6 and 23.7 °C) and the results are presented in this paper. Glycerol and pyridine which are known to be effective structure breakers[8] were chosen simply to lower TVM of water to any desired value at which the effect of 1-butanol could be studied to delineate its temperature dependence of structural propensity.

Experimental

Triple distilled degassed water was used to prepare stock solutions of aqueous glycerol and pyridine. These solutions were used to prepare ternary solutions of 1-butanol of desired concentration. The concentration of 1-butanol in the ternary solution was calculated by considering the aqueous binary stock solution as a solvent of effective molecular weight M_{12} given by $X_wM_w+X_sM_s$ where M_w, M_s and X_w, X_s represent the molecular weights and mole fractions respectively of water and glycerol and or pyridine. Ultrasonic velocity in binary solutions of aqueous glycerol and pyridine and in the ternary solutions with 1-butanol as the third component was determined using a single crystal variable path interferometer working at 3 MHz with an accuracy of ±0.003%. The details of the experimental technique and the method of measurement of velocity and temperature of the experimental liquid were discussed elsewhere.[5] The velocity measurements were confined to a temperature range of ≃5 °C on either side of TVM at intervals of ≃2 °C. AR grade glycerol, pyridine, and 1-butanol were used in the present study after necessary purification following the procedure given by Weissberger.[9]

Results

Diffraction corrected ultrasonic velocity as a function of temperature at different concentrations of 1-butanol in aqueous glycerol (M_{12}=24.7455, X_s=0.0909) and in aqueous pyridine solutions (M_{12}=20.5599, X_s=0.0416 and M_{12}=21.7209, X_s=0.0606) are presented graphically in Figs. 1 to 3. In all the solutions since the shape of the velocity temperature curves are similar to that of pure water, the template of the velocity-temperature curve for pure water was used to fix TVM and the accuracy in fixing TVM is ±0.2 °C.

Discussion

The shift in the temperature corresponding to the sound velocity maximum in the binary solutions of aqueous glycerol or pyridine due to the addition of 1-butanol may be given by

$$\Delta T = (T_{exp})_{ternary\ sol} - (T_{exp})_{binary\ sol.} \quad (1)$$

ΔT may be thought of as arising due to two effects namely dilution effect and structural effect. The dilution effect is always to lower TVM but the structural effect may be positive or negative depending on whether the nonelectrolyte promotes or disrupts the binary solution structure. These two effects may be separated by considering the expressions representing the temperature dependence of velocity in aqueous glycerol

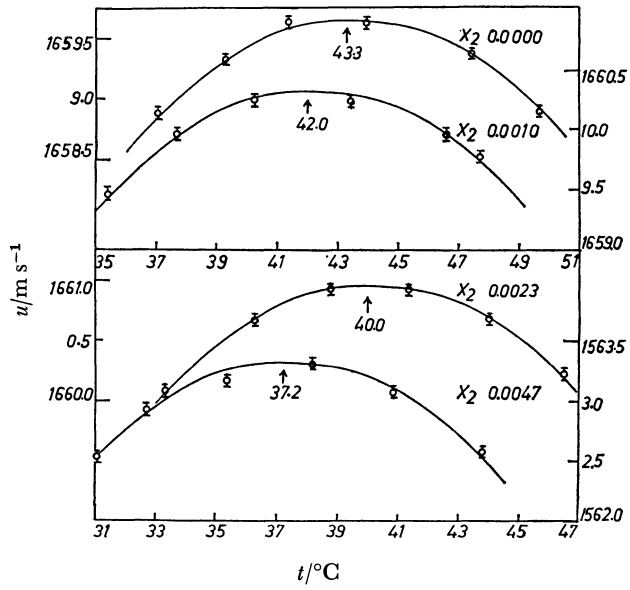

Fig. 1. Ultrasonic velocity *versus* temperature in aqueous solutions of glycerol at different molefractions of 1-butanol.

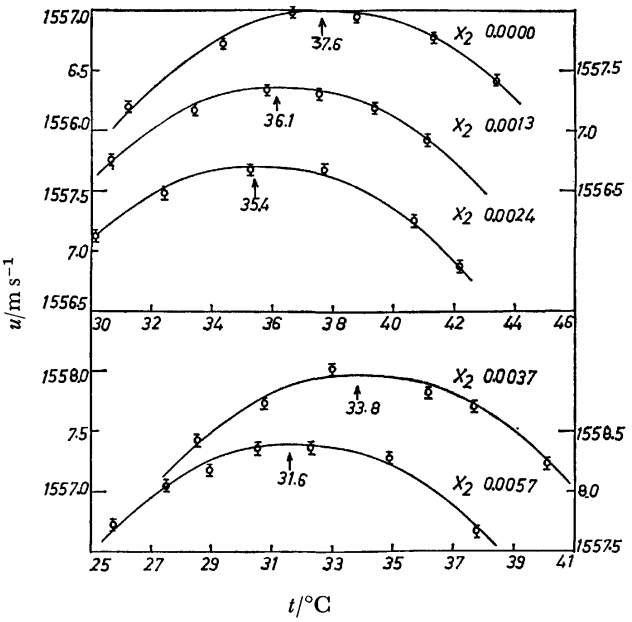

Fig. 2. Ultrasonic velocity *versus* temperature in aqueous solutions of pyridine at different molefractions of 1-butanol.

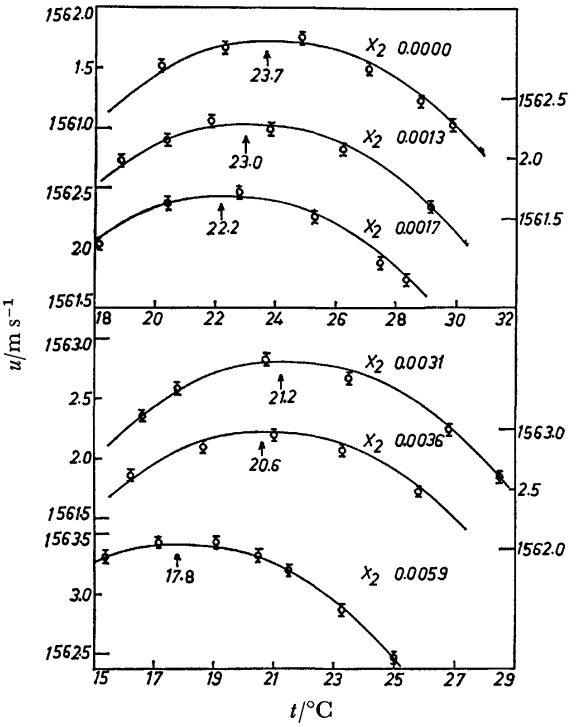

Fig. 3. Ultrasonic velocity *versus* temperature in aqueous solutions of pyridine at different molefractions of 1-butanol.

or pyridine and the nonelectrolyte.

The structural contribution to the shift in the temperature of sound velocity maximum in the ternary solution can be calculated using the following expressions that may be obtained on the same lines as that for pure water.[6]

$$[\Delta T_{str}]_{exp} = T_{exp} - T_{id}, \quad (2)$$

where

$$T_{id} = T_{\text{binary sol}} - \left(\frac{\phi_2}{\phi_{12}}\right)^2\left(\frac{W_{12}}{W_2}\right)\frac{\alpha}{(2\beta)}\left(\frac{u_{12}}{u_2}\right)^3, \quad (3)$$

where ϕ_{12}, ϕ_2 and W_{12}, W_2 represent the volume fractions and weight fractions of binary aqueous solution and 1-butanol respectively in the ternary solution. α represents the temperature coefficient of sound velocity in 1-butanol and u_{12} and u_2 the velocities in the aqueous binary solution and solute respectively. For 1-butanol u_2 is given by

$$u_2 = u_2^\circ - \alpha t, \quad (4)$$

where u_2° and α are 1323.58 m s^{-1} and 3.3644 m s^{-1} °C^{-1} respectively and t represents the temperature in °C. u_{12} may be written as

$$u_{12} = u_{12}^\circ - \beta(T-t)^2. \quad (5)$$

The values of u_{12}°, β, and T for stock solutions of aqueous glycerol and pyridine are given in Table 1.

Table 1. Values of u_{12}°, β, and T for aqueous binary solutions

Solvent	X_s	u_{12}° / m s^{-1}	β / m s^{-1} °C^{-2}	T / °C
Aqueous glycerol	0.0909	1559.67	0.0204	43.3
Aqueous pyridine	0.0416	1556.99	0.0204	37.6
	0.0606	1561.72	0.0184	23.7

In all cases T_{id} was calculated using the method of successive approximations. Table 2 gives the values of T_{exp}, T_{id}, ΔT, and $[\Delta T_{str}]_{exp}$ at different concentrations of 1-butanol. The variation of $[\Delta T_{str}]_{exp}$ *versus* molefraction X_2 of 1-butanol in different aqueous binary solutions are shown graphically in Fig. 4 along with the $[\Delta T_{str}]_{exp}$ *versus* X_2 of 1-butanol in pure water taken from literature.[6] From the figure it is clear that below 40 °C 1-butanol behaves as a structure maker since $[\Delta T_{str}]_{exp}$ values are positive for solutions in which the TVM are 37.6 and 23.7 °C. $[\Delta T_{str}]_{exp}$

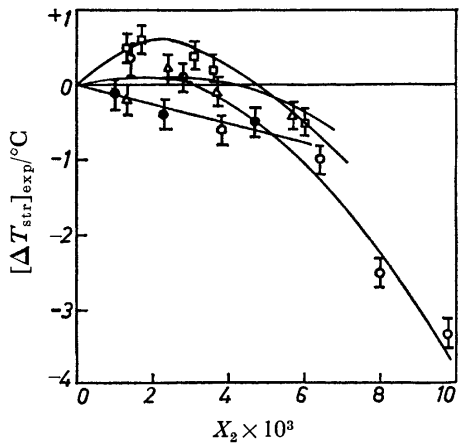

Fig. 4. $[\Delta T_{str}]_{exp}$ *versus* molefraction X_2 of 1-butanol in different solvents.
○: Pure water TVM 74 °C,
●: aqueous glycerol TVM 43.3 °C,
△: aqueous pyridine TVM 37.6 °C,
□: aqueous pyridine TVM 23.7 °C.

Table 2. T_{exp}, T_{id}, ΔT, and $[\Delta T_{str}]_{exp}$ at different molefractions X_2 of 1-butanol in binary aqueous mixtures

Solvent	X_2	T_{exp} °C	T_{id} °C	ΔT °C	$[\Delta T_{str}]_{exp}$ °C
Aqueous glycerol of TVM 43.3 °C	0.0010	42.0	42.1	−1.3	−0.01
	0.0023	40.0	40.4	−3.3	−0.4
	0.0047	37.2	37.7	−6.1	−0.5
Aqueous pyridine of TVM 37.6 °C	0.0013	36.1	36.3	−1.5	−0.2
	0.0024	35.4	35.2	−2.2	+0.2
	0.0037	33.8	33.9	−3.8	−0.1
	0.0057	31.6	32.0	−6.0	−0.4
Aqueous pyridine of TVM 23.7 °C	0.0013	23.0	22.5	−0.7	+0.5
	0.0017	22.2	21.6	−1.5	+0.6
	0.0031	21.2	20.8	−2.5	+0.4
	0.0036	20.6	20.4	−3.1	+0.2
	0.0059	17.8	18.3	−5.9	−0.5

Table 3. Comparison of the shifts produced in the TVM of water due to the addition of organic solutes with the observed shift in the ternary solution, treating aqueous binary solutions as aqueous

X_B	X_G/X_P	$(\Delta T)_{X_B}$ °C	$(\Delta T)_{X_G/X_P}$ °C	$\Delta T_{calcd} = (\Delta T)_{X_B} + (\Delta T)_{X_G/X_P}$ °C	$\Delta T_{obsd} = T_w - T_{t\,sol}$ °C
		Water+Glycerol+1-Butanol			
0.0010	0.0908	1.3±0.4	30.7±0.4	32.0±0.8	32.0±0.4
0.0023	0.0907	3.1+0.4	30.6±0.4	33.7±0.8	34.0±0.4
0.0047	0.0905	6.6±0.4	30.5±0.4	37.1±0.8	36.8±0.4
		Water+Pyridine+1-Butanol			
0.0013	0.0416	1.7±0.4	36.4±0.4	38.1±0.8	37.3±0.4
0.0024	0.0415	3.2±0.4	36.3±0.4	39.5±0.8	38.6±0.4
0.0037	0.0415	5.1±0.4	36.3±0.4	41.4±0.8	40.2±0.4
0.0057	0.0414	8.1±0.4	36.2±0.4	44.3±0.8	42.4±0.4
0.0013	0.0605	1.7±0.4	50.1±0.4	51.8±0.8	51.0±0.4
0.0017	0.0605	2.2±0.4	50.1±0.4	52.3±0.8	51.8±0.4
0.0031	0.0604	4.3±0.4	50.0±0.4	54.3±0.8	52.8±0.4
0.0036	0.0604	5.0±0.4	50.0±0.4	55.0±0.8	53.4±0.4
0.0059	0.0602	8.4±0.4	49.9±0.4	58.3±0.8	56.2±0.4

X_B: Molefraction of 1-butanol when aqueous glycerol or aqueous pyridine is treated as cosolvents of effective molecular weights $M_{G,W}$ or $M_{P,W}$. X_G/X_P: Molefraction of glycerol/pyridine when aqueous 1-butanol is treated as cosolvent of effective molecular weight $M_{B,W}$.

values are negative for solutions in which the values of TVM are 43.3 and 74 °C indicating that above 40 °C 1-butanol behaves as a structure breaker. The behaviour of 1-butanol above 40 °C as a structure breaker was also confirmed from the studies on volumetric behaviour of aqueous isomeric butyl alcohols.[10] Hence the results of the present study indicate that as temperature increases the structure making efficiency of 1-butanol decreases and at temperatures above 40 °C it behaves as a structure breaker.

It is necessary to note that the assignment of structure making or breaking nature to 1-butanol as a function of temperature is valid only when 1-butanol has little interaction with glycerol or pyridine in the ternary system and interacts only with the water. Our results are based on the assumption that the aqeuous glycerol or pyridine as seen by 1-butanol is aqueous and the interactions between 1-butanol and glycerol or pyridine in the presence of water are negligible when compared with the interaction of 1-butanol with the aqueous nature of the solution structure. To know whether this is the actual situation prevailing in the ternary system, we have calculated the shift in TVM of water due to the addition of the two organic solutes (independently) namely glycerol or pyridine and 1-butanol to water, ΔT_{calcd}, and a comparison is made with the observed shift, ΔT_{obsd}, (74 °C− T_{exp} in the ternary solution) to see whether the shift ΔT is additive with respect to them. Our earlier data[6,8] on TVM of aqueous glycerol, pyridine, and 1-butanol are taken for the evaluation of the shifts corresponding to the concentrations of these solutes in the ternary systems. The shifts in the TVM of water corresponding to the concentrations of the present study are obtained

by least square fitting of the data.[6,8] As per the data presented in Table 3, the agreement between the calculated and observed shifts is quite good in the case of the ternary system water+glycerol+1-butanol. In the case of the ternary system water+pyridine+1-butanol, except when the concentrations of 1-butanol and pyridine are 0.0057 and 0.0414 and 0.0059 and 0.0602, the agreement between the calculated and experimental shifts is quite good. These observations indicate that ΔT is additive with respect to each solute and the effect of 1-butanol, glycerol, and pyridine on TVM of pure water is respectively independent of each other coexisting solute. However, the difference between the calculated and observed shifts for the ternary systems in which $X_B=0.0057$, $X_P=0.0414$ and $X_B=0.0059$, $X_P=0.0602$; which is about 2%, in our view, is due to the effect of temperature on the structure making or breaking power of the solutes being different in aqueous solution and in the ternary system and may not be considered as due to the influence of pyridine on 1-butanol or *vise versa* in their efficiency to shift the TVM of the solution. We would like to mention at this juncture that this point needs extensive study of ternary systems containing the two organic solutes which are both either structure breakers or structure makers. Further experimentation in this direction is in progress.

References

1) F. Franks and D. J. G. Ives, *Quart. Rev.*, **20**, 1 (1966).
2) F. Franks, "Hydrogen Bonded Solvent Systems," Taylor and Francis, London (1968).
3) R. K. Mohanty, T. S. Sarma, S. Subramaniyan, and J. C. Ahluwalia, *Trans. Faraday Soc.*, **67**, 305 (1971).
4) B. Kingston and M. C. R. Symons, *J. Chem. Soc., Faraday Trans. 2*, **69**, 978 (1973).
5) S. V. Subrahmanyam and N. Manohara Murthy, *J. Solution Chem.*, **4**, 347 (1975).
6) N. Manohara Murthy and S. V. Subrahmanyam, *Bull. Chem. Soc. Jpn.*, **50**, 2589 (1977).
7) G. Wada and S. Umeda, *Bull. Chem. Soc. Jpn.*, **35**, 646, 1797 (1962).
8) S. V. Subrahmanyam and N. Manohara Murthy, *Z. Phys. Chem. (N. F.)*, **88**, 116 (1974).
9) A. Weissberger, "Physical Methods of Organic Chemistry," 2nd ed, Interscience, New York (1955), Vol. III.
10) F. Franks and H. T. Smith. *Trans. Faraday Soc.*, **64**, 2962 (1968).

Macroscopic Viscosity and Dielectric Relaxation Process of Ethyl and Butyl Acetates

Sudhir Kumar Saxena, Jagdish Prasad Shukla, and Mahesh Chandra Saxena*
Department of Physics, Lucknow University, Lucknow, India
(Received October 13, 1979)

Dielectric constants and losses have been measured at 9.8 GHz microwave frequency for ethyl and butyl acetates in benzene and benzene-paraffin oil mixtures at 18 °C. The data obtained has been analysed in terms of the two relaxation times $\tau_{(1)}$ and $\tau_{(2)}$ using Higasi, Koga, and Nakamura method and their dependence on the viscosity has been examined. Since the observed values of $\tau_{(1)}$ and $\tau_{(2)}$ are significantly different, the systems studied represent two Debye type dispersions. It has been found that the relaxation behaviour giving rise to $\tau_{(1)}$ in both the ester molecules is not effected to any appreciable extent by the increased macroscopic viscosity. The dielectric relaxation time $\tau_{(2)}$ associated with the molecular process lengthens with the increasing macroscopic viscosity of the medium.

Dielectric relaxation process in aliphatic esters (acetates) have been studied by a number of workers[1-5] both in pure liquids and in solutions. The absorption process in these systems have been attributed to the molecular as well as the group rotations. Dependence of the dielectric relaxation time on the viscosity of the medium has been extensively examined by several workers[6-10] and various empirical relations have been proposed. Grubb and Smyth[11] studied some substituted naphthalene, anisole, primary and secondary amines and diamines in paraffin oil and have estimated the relaxation times τ_1 and τ_2 associated with the molecular and group processes. The enthalpies were evaluated for methyl iodide, chlorobenzene, cyanocyclopropane *etc.* by Balogun and Cumper[12] using benzene+liquid paraffin oil as solvents. In study, Crossley and Srivastava[13] reported the value of 'x' ($=\Delta H_\gamma/\Delta H_\varepsilon$) for acetophenone, anisoles, bromobenzene, and *p*-dimethoxybenzene in the mixture of solvents, paraffin oil and heptane, and paraffin oil and hexadecane. Recently in another study[14] using solvent of high viscosity they have resolved the dielectric data of 1-butanol and 1-decanol into two relaxation process (τ_1) and (τ_2). It has been observed that molecular relaxation time changes rapidly with the changing viscosity of the solvent–solute mixture. However, the relaxation time (τ_2) practically remains constant. The effect of the macroscopic viscosity of the solvent on the process which probably arises from the group rotation have been examined only for a few cases with varying high viscosity.

Aliphatic esters have been examined for their dielectric behaviour using various methods.[1-5] The investigations were however confined only to the studies relating to the relaxation mechanism and their structure. It was, therefore, considered worthwhile to examine ethyl acetate and butyl acetate in the solvent mixtures of paraffin oil and benzene which provide a high viscous medium for the dipolar rotations. The dielectric data was resolved into two absorption processes, $\tau_{(1)}$ being an implicit function of τ_1 and τ_2 and weight factor C_1 and $\tau_{(2)}$ associated with the molecular process and the effect of macroscopic viscosity on $\tau_{(1)}$ has been examined. This has been found to be in agreement with the earlier studies of Crossley *et al.*[14] on 1-butanol and 1-decanol.

Experimental

The dielectric constant ε' and dielectric loss ε'' have been measured at x-band at frequency 9.8 GHz by the technique of Robert and von-Hippel[15] as modified by Dakin and Works.[16] The refractive indices of different dilute solutions at infinite frequency was measured by Abbe's refractometer. The dielectric constant at infinite frequency was obtained by squaring the refractive indices of different dilute solutions respectively. The possibility of Poley absorption is ruled out as the microwave frequency used for the measurement is comparatively much low. The static dielectric constant have been measured by the calibrated dipolemeter based on the principle of heterodyne beat method. The measurement of ε' and ε'' are accurate upto $\pm 2\%$ and $\pm 5\%$ respectively.

Average viscosity of the solvent solute mixture was obtained by taking the mean of six values for a group of solutions of various solvents obtained by measuring the fall time of liquid in the capillary of the Ostwald's viscometer.

Chemicals. The chemicals used were of purest quality available, both the ethyl acetate and butyl acetate were obtained from the British Drug House (Ltd.) England. The physical properties of both the esters were checked against the literature values. The solvent benzene were distilled twice before use. The benzene (A. R. grade) was obtained from B. D. H. (England) and medicinal liquid paraffin oil was obtained from Liberty Pharmaceutical (Ltd.) Bombay (India). The mixture of benzene and paraffin oil in the following percentage were used as solvent for the measurements.

1: 100% paraffin oil
2: 10% benzene+90% paraffin oil
3: 20% benzene+80% paraffin oil
4: 30% benzene+70% paraffin oil.

Theory: The slopes a_0, a', a'', and a_∞ have been obtained by plotting the weight fraction *versus* ε_0, ε', ε'', and ε_∞ for both the compounds. The values have been reported in Table 1. The slopes are defined by the set of Eq. 1.

$$\begin{aligned} \varepsilon_0 &= \varepsilon_{10} + a_0 W_2 \\ \varepsilon' &= \varepsilon_1' + a' W_2 \\ \varepsilon'' &= a'' W_2 \\ \varepsilon_\infty &= \varepsilon_{1\infty} + a_\infty W_2. \end{aligned} \quad (1)$$

The subscripts 1 and 2 refer to pure solvent and solute respectively. Similarly ε_∞ refers to the dielectric constant at infinite frequency. ε_0 is the dielectric constant at static field and W_2 is weight fraction of the solute.

The most probable relaxation time τ_{OH} and the distribution

Table 1. The slopes a_0, a', a'', and a_∞ for ethyl and butyl acetate in benzene and paraffin oil (p.o.) mixture at 18 °C

Compound	Concentration	a_0	a'	a''	a_∞
(A) Ethyl acetate	100% p.o.	3.33	2.66	1.05	−0.28
	90% p.o.+10% benzene	2.86	2.35	0.95	−0.26
	80% p.o.+20% benzene	2.50	2.12	0.80	−0.256
	70% p.o.+30% benzene	2.20	1.90	0.70	−0.25
(B) Butyl acetate	100% p.o.	2.96	2.10	1.00	−0.265
	90% p.o.+10% benzene	2.58	1.80	0.83	−0.25
	80% p.o.+20% benzene	2.12	1.50	0.70	−0.21
	70% p.o.+30% benzene	1.74	1.30	0.55	−0.19

Table 2. Distribution parameter 'α', most probable relaxation time τ_{OH} by Higasi method, $\tau_{(1)}$, $\tau_{(2)}$, and $\tau_{(0)}$ obtained by Higasi, Koga, and Nakamura method and dipole moment at 18 °C

Compound	Concentration	α	η poise	τ_{OH} ps	$\tau_{(1)}$ ps	$\tau_{(2)}$ ps	$\tau_{(0)}$ ps	$\mu_{(D)}$ expt Debye	$\mu_{(D)}$ Lit.
(A) Ethyl acetate	100% p.o.	0.14	0.233	5.7	5.8	10.5	7.8	1.81	1.86
	90% p.o.+10% benzene	0.12	0.070	5.4	5.7	9.3	7.2	1.76	
	80% p.o.+20% benzene	0.07	0.038	5.3	5.5	7.8	6.6	1.66	
	70% p.o.+30% benzene	0.06	0·024	5.1	5.3	7.0	6.1	1.56	
(B) Butyl acetate	100% p.o.	0.25	0.240	7.1	6.9	16.3	10.6	1.98	1.84
	90% p.o.+10% benzene	0.24	0.090	6.8	6.6	15.5	10.1	1.80	
	80% p.o.+20% benzene	0.22	0.059	6.6	6.5	14.6	9.7	1.65	
	70% p.o.+30% benzene	0.20	0.025	6.1	6.1	13.1	8.9	1.45	

parameter 'α' have been calculated from the Eq. 2, given by Higasi *et al.*[17]

$$\tau_{OH} = \frac{1}{W}\left[\frac{A^2+B^2}{C^2}\right]^{1/2(1-\alpha)}$$
$$1-\alpha = \frac{2}{\pi}\tan^{-1}\frac{A}{B}, \quad (2)$$

where

$$A = a''(a_0-a_\infty)$$
$$B = (a_0-a')(a'-a_\infty) - a''^2 \quad (3)$$
$$C = (a'-a_\infty)^2 + a''^2.$$

Having obtained the appreciable value of distribution parameter 'α', the dielectric relaxation mechanism has been further resolved by Higasi, Koga, and Nakamura method[18] in terms of the two relaxation times $\tau_{(1)}$ and $\tau_{(2)}$ defined by the Eqs. 4 and 5:

$$\tau_{(1)} = \frac{1}{W}\frac{a''}{(a'-a_\infty)}, \quad (4)$$

$$\tau_{(2)} = \frac{1}{W}\frac{(a_0-a')}{a''}. \quad (5)$$

The slopes a_0, a', a'', and a_∞ are defined by the set of Eq. 1. The average probable relaxation time $\tau_{(0)}$ is obtained by the geometrical mean of $\tau_{(1)}$ and $\tau_{(2)}[\tau_{(0)}=\sqrt{\tau_{(1)}\tau_{(2)}}]$.

The apparent dipole moment was calculated by Higasi's method[19] employing Eq. 6.

$$\mu^2 = \frac{27kT}{4\pi N}\frac{M_2}{d_1}\frac{a_0-a_\infty}{(\varepsilon_1'+2)^2}$$
$$= B^2(a_0-a_\infty), \quad (6)$$

where

$$B = \left\{\frac{27kTM_2}{4\pi Nd_1}\right\}^{1/2}\frac{1}{(\varepsilon_1'+2)}$$

M_2 is the molecular weight of the substance and d_1 is the density of the solvent, and other symbols have their usual meaning.

Discussion

(A) Ethyl Acetate. An examination of Table 2 shows that the distribution parameter 'α' for ethyl acetate has a variation (0.14—0.06) when the concentration of paraffin oil varies from 100% to 70% in benzene. The highest value of distribution parameter 'α' is 0.14 in 100% p.o. and the lowest value, 0.06 has been observed in 70% p.o. in benzene. These observations are in agreement with the earlier investigations of Smyth *et al.*[1] The appreciable value of the distribution parameter 'α', indicates the existence of more than one relaxation process occurring in the system. The most probable relaxation time τ_{OH} evaluated using Higasi method[17] has been found to vary from 5.1—5.7 ps in the range of concentration changing from 70% p.o. in benzene to 100% p.o. The dielectric

dispersion has been further resolved by Higasi, Koga, and Nakamura method,[18] into two separate processes which gave rise to two relaxation time $\tau_{(1)}$ and $\tau_{(2)}$. $\tau_{(1)}$, which is related to the group process has been found to vary from 5.3—5.8 ps when the concentration varies from 70% p.o. in benzene to 100% p.o. $\tau_{(2)}$, which represent the molecular process has been found to vary from 7.0—10.5 ps in the same concentration range. The average relaxation time $\tau_{(0)}=\sqrt{\tau_{(1)}\tau_{(2)}}$ for the overall process was found to vary from (6.1—7.8 ps). An examination of Table 2 reveals that the relaxation time $\tau_{(1)}$ associated with the group process for all the concentrations remains almost constant, whereas, the other relaxation time $\tau_{(2)}$ related to the molecular process varies appreciably with the concentration of the solvent. These results are in agreement with the previous studies of Srivastava and Crossley[14] on alcohols and of Grubb and Smyth[11] on substituted anisoles, naphthalene, and substituted amines. It has also been observed that $\tau_{(0)}$ the average relaxation time is slightly greater than the most probable relaxation time τ_{OH}. They are consistent with the previous observation of Higasi *et al.*[5] on alkyl acetates.

The dipolemoment of the compound has been calculated in various solvents. It has been observed that the dipolemoment varies from 1.56—1.81 D for the concentration of p.o. varying from 70% p.o. to 100% p.o. These values are not much different from the literature value[20] of dipolemoment (=1.86 D) for ethyl acetate in solution. The value is highest in 100% p.o. and is decreasing with the dilution of paraffin oil with benzene. This is in agreement with the reports on similar data by Srivastava and Crossley[14] for 1-butanol and 1-decanol in paraffin oil and heptane mixture.

(B) Butyl Acetate. The distribution parameter 'α' for butyl actate shows variation (0.20—0.25) in the concentration range of 70% p.o. in benzene to 100% p.o. The 'α' values are found to decrease with the dilution of paraffin oil with benzene, which is in agreement with the previous study by Smyth *et al.*[1] The most probable relaxation time τ_{OH} has been found to vary from 6.1—7.1 ps, while the concentration of paraffin oil and benzene mixture changes from 70% p.o.+30% benzene to 100% p.o. The most probable relaxation time τ_{OH} for butyl acetate is found to be longer than ethyl acetate. This is as expected due to the bigger size of this molecule. On further resolving the absorption by Higasi, Koga, and Nakamura method[18] the two relaxation times obtained were $\tau_{(1)}$ (=6.1—6.9 ps) and $\tau_{(2)}$ (=13.1—16.3 ps) in the concentration range used. The two distinct values for $\tau_{(1)}$ and $\tau_{(2)}$ indicate the existence of two distinct relaxation processes in the system. It has been observed that $\tau_{(1)}$ for butyl acetate is longer than $\tau_{(1)}$ for ethyl acetate for the same concentration range. This is as expected since $\tau_{(1)}$ arises perhaps from the rotation of the heavier group-C_4H_9 around the carbon–carbon bond. Similar results were reported by Grubb and Smyth[11] on α- and β-methoxy- and ethoxy-naphthalenes in the solution of decalin and Nujol. Further it is observed that the relaxation time $\tau_{(1)}$ is practically constant with the varying macroscopic viscosity of the solvent, which is in agreement with the earlier investigations of Srivastava and Crossley[14] on alcohols and Grubb and Smyth[11] on amines, naphthalene, and anisole.

$\tau_{(2)}$ and $\tau_{(0)}$ both are found to be larger for butyl acetate than the values obtained for ethyl acetate in the same concentration range. This follows the usual dependence on the shape and size of molecules in process.

The dipolemoment in the various solvents have been calculated by Higasi method.[19] It is found to vary from (1.45—1.98 D) when the concentration varies from 70% p.o. in benzene to 100% p.o. The value resembles well within the experimental error from the literature value[20] 1.84 D for the butyl acetate in the solution. The highest value for dipolemoment was observed in 100% p.o. which is decreasing with the dilution of paraffin oil with benzene.

A graph has drawn between log $\tau_{(1)}$ and log η_s and log $\tau_{(2)}$ and log η_s (Figs. 1 and 2). It has been observed that the relaxation time $\tau_{(1)}$ is practically constant with the macroscopic viscosity of solvent and solute. A line of greater slope has been observed for $\tau_{(2)}$ showing that molecular relaxation time is varying appreciably with the viscosity for both the ester molecules. It is in agreement with the earlier observations by several workers.[11,14,21]

Conclusion

The microwave absorption studies on ethyl and butyl acetates in high viscous solvents exhibit a flexible behaviour. The two relaxation time $\tau_{(1)}$ and $\tau_{(2)}$ for both the systems have been found to be appreciably distinct. The effect of average macroscopic

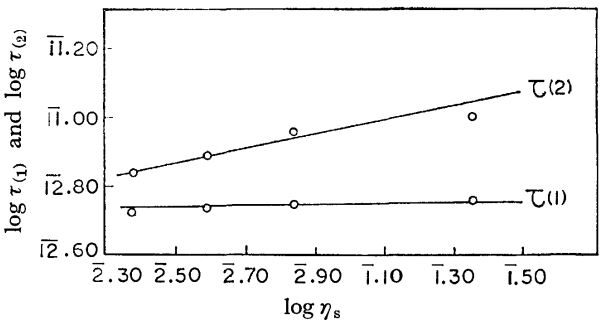

Fig. 1. Plot of log $\tau_{(1)}$ and log $\tau_{(2)}$ *vs.* log η_s (ethyl acetate).

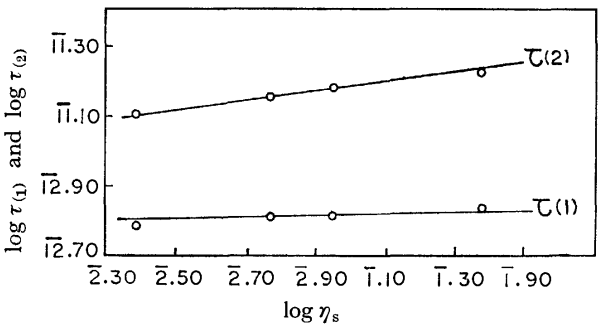

Fig. 2. Plot of log $\tau_{(1)}$ and log $\tau_{(2)}$ *vs.* log $\eta_{(s)}$ (butyl acetate).

viscosity of the medium has been observed for both the molecules. $\tau_{(1)}$ for ethyl acetate varies from (5.3—5.8 ps) while the viscosity changes from (0.024—0.233 poise). $\tau_{(2)}$ for the same system changes from (7.0—10.5 ps). Similarly for butyl acetate, $\tau_{(1)}$ has been found to be slightly longer, in the range 6.1 to 6.9 ps for the viscosity variations from 0.025 to 0.243 poise whereas $\tau_{(2)}$ varies from 13.1 ps to 16.3 ps. This clearly indicates that $\tau_{(1)}$ for both the systems practically remains constant with the macroscopic viscosity of the medium whereas $\tau_{(2)}$ varies in different media according to the size and shape of the molecules. The two straight lines, drawn for the variation of $\tau_{(1)}$ and $\tau_{(2)}$ with viscosity show the similar effect. It can, therefore, be concluded that the viscosity of the medium has hardly any effect so far as the process giving rise to the relaxation time $\tau_{(1)}$ is concerned. This perhaps can be associated with the internal rotation of the group attached to the two species. This is in agreement with the earlier studies on a few other molecular species.[11,14,21]

One of us (S. K. Saxena) is grateful to University Grant Commission, New Delhi (India) for the award of financial assistance and the Teacher fellowship under "faculty improvement programme" to complete this work.

References

1) P. L. Mc. Geer, A. J. Curtis, G. B. Rathmann, and C. P. Smyth, *J. Am. Chem. Soc.*, **74**, 3541 (1952).
2) B. S. Rajyam, C. R. K. Murty, *Indian J. Pure Appl. Phys.*, **11**, 28 (1973).
3) R. L. Patil and K. S. Rao, *Cur. Sci. (India)*, **44** (16), 579 (1975).
4) V. Rao Murlidhara, "Development of the 8 m.m. technique and the measurement of dielectric dispersion of certain liquids," D. Sc., thesis, Andhara University, Waltair, 1962.
5) Y. Koga, H. Takahashi, and K. Higasi, *Bull. Chem. Soc. Jpn.*, **47**, 84 (1974).
6) W. H. Whiffen and H. W. Thomson, *Trans. Faraday Soc.*, **42** A, 122 (1946).
7) J. Y. H. Chau., R. J. W. Le Fever, and J. Tardif, *J. Chem. Soc.*, **1957**, 2293.
8) J. Bhattacharya, B. Sinha, S. B. Roy, and G. S. Kastha, *Indian J. Phys.*, **38**, 413 (1964).
9) B. Sinha, S. B. Roy, and G. S. Kastha, *Indian J. Phys.*, **40**, 101 (1966).
10) N. E. Hill, *Proc. Phys. Soc., B*, **67**, 149 (1954).
11) E. L. Grubb and C. P. Smyth., *J. Am. Chem. Soc.*, **83**, 4873, 4879 (1961).
12) G. A. Balogun and C. W. N. Cumper; *J. Chem. Soc., Faraday. Trans. 2*, **1973**, 1172.
13) S. C. Srivastava and J. Crossley, *Can. J. Chem.*, **54**, 1418 (1976).
14) J. Crossley and S. C. Srivastava, *Adv. Mol. Relax. Process*, **8**, 111 (1976).
15) S. Roberts and A. von-Hippel, *J. Appl. Phys.*, **17**, 610 (1946).
16) T. W. Dakin and C. N. Works, *J. Appl. Phys.*, **18**, 789 (1947).
17) K. Higasi; *Bull. Chem. Soc. Jpn.*, **39**, 2157 (1966).
18) K. Higasi, Y. Koga, and M. Nakamura, *Bull. Chem. Soc. Jpn.*, **44**, 988 (1971).
19) Y. Koga, H. Takahashi, and K. Higasi, *Bull. Chem. Soc. Jpn.*, **46**, 3359 (1973).
20) C. P. Smyth, "Dielectric Behaviour and Structure," McGraw-Hill, New York (1955), p. 304.
21) K. Higasi and C. P. Smyth, *J. Am. Chem. Soc.*, **82**, 4759 (1960).

Hydroxyamidine as a Highly Selective Extractant for Spectrophotometric Determination of Molybdenum with Thiocyanate

Raghunandan Singh KHARSAN and Rajendra K. MISHRA*
Department of Chemistry, Ravishankar University, Raipur-492010, India

(Received April 16, 1979)

A highly selective method for the extractive-spectrophotometric determination of molybdenum is described. Molybdenum is reduced with ascorbic acid in strongly acidic media (2.0—4.5 mol dm^{-3} HCl), and complexed with N^1-hydroxy-N^1-*p*-tolyl-N^2-(3,4-dimethylphenyl)benzamidine in the presence of thiocyanate. The stoichiometry of mixed complex is found to be 1:2:2 (metal:reagent:thiocyanate). The red-orange molybdenum complex shows a sharp maximum at 470 nm having molar absorptivity 3800 dm^3 mol^{-1} cm^{-1}. All the metal ions associated with a matrix of molybdenum such as Ni(II), Co(II), Cu(II), Mn(II), Ti(IV), Zr(IV), V(V), Nb(V), Ta(V), and W(VI) do not interfere. The applicability of the method has been tested with an ore and various alloys.

A number of reagents such as thiocyanate–tin(II) chloride,[1] thiocyanate–copper(I) chloride,[1] toluene-3,4-dithiol,[1] phenylhydrazine,[1] chloranilic acid,[1] mercaptoacetic acid,[1,2] dithiooxamide,[3] 4-methyl-2-pentanol,[4] 2-mercapto-4*H*-1-benzothiopyran-4-one,[5] potassium ethylxanthate,[6] monooctyl α-anilinobenzylphosphonate thiocyanate,[7] and salicylhydroxamic acid[8] have been reported for extraction photometric determination of molybdenum. N^1-hydroxy-N^1,N^2-diarylbenzamidines, monobasic and bidentate chelating agents have been used for gravimetric determination[9-11] of nickel, copper, and molybdenum and colorimetric determination[12-14] of manganese, iron, and vanadium. N^1-Hydroxy-N^1-*p*-tolyl-N^2-(3,4-dimethylphenyl)benzamidine (abbreviated as Hhtdb), a newly synthesized monobasic and bidentate chelating agent is found to be a selective chromogenic reagent for extractive-photometric determination of molybdenum(V)–thiocyanate complex into benzene (using ascorbic acid as a reducing agent).

The present method is compared with the other methods mentioned above. All the methods except for those using thiocyanate–tin(II) chloride and thiocyanate–copper(I) chloride suffer either from interference of one or more elements such as iron, copper, nickel, cobalt, tin, titanium, zirconium, niobium, chromium, and tungsten, or absorbance due to reagent at wavelength of maximum absorption. The thiocyanate–tin(II) chloride is commonly used for extractive-photometric determination of molybdenum. However, a serious drawback of this method is that the colour intensity produced by a constant quantity of molybdenum depends upon a number of factors such as volume of the aqueous phase, coefficient of expansion of isopentyl alcohol, concentration of iron, and tin(II). The thiocyanate–copper(I) chloride method also has a number of drawbacks from a practical standpoint. The original volume of the sample solution should not exceed a few millilitres and iron should not be present in more than minute amounts. The disadvantages are overcome successfully in the present *N*-hydroxyamidine thiocyanate method. The *N*-hydroxyamidine thiocyanate method is simple, rapid and highly selective. Moreover, it is free from volume ratio of aqeuous phase, concentration of reagents, order of addition of reagents, temperature, standing time and correlation of colour intensity with iron concentration.

The present paper reports the solvent extraction and photometric determination of molybdenum(V)–thiocyanate complex with htdb, various optimization constants and nature of complex separation from various diverse ions and its application to the analysis of ore and alloys.

Experimental

Apparatus. Absorbance measurements were made with an ECIL UV-VIS spectrophotometer model-865 matched with 1-cm silica and quartz cuvettes. All pH measurements were made with a Systronic pH meter type-322.

Standard Molybdenum Solution. A 1000-ppm molybdenum solution was prepared by dissolving 1.8401 g of A. R. ammonium molybdate tetrahydrate in glass distilled water and diluting to 1 dm^3. The metal content of the solution was determined with use of 8-quinolinol.[15] The stock solution was diluted to desired concentration.

Preparation of Reagent. The reagent was prepared by condensation of equimolar ratio of *N*-(3,4-dimethylphenyl)-benzimidoyl chloride and *N*-*p*-tolylhydroxylamine in ether medium.[13,16] The resulting hydrochloride was treated with dilute ammonia to liberate the corresponding free base. The free base was crystallized from benzene:petroleum ether (2:1). Mp 154 °C; yield 68%. Found: C, 79.64; H, 6.42; N, 8.22%. Calcd for $C_{22}H_{22}N_2O$: C, 80.00; H, 6.66; N, 8.48%.

A 0.1% w/v solution of reagent in benzene was used. A 10 and 5% w/v aqueous solution of ascorbic acid and potassium thiocyanate respectively, were used throughout the experiment.

Procedure. Place an aliquot of solution containing 200 μg of molybdenum on a 100-cm^3 separatory funnel. To this add 5 cm^3 of ascorbic acid followed by 5 cm^3 of potassium thiocyanate in final dilution of 25 cm^3 aqueous volume with subsequent adjustment of the acidity to 3.5 mol dm^{-3} HCl. Add 25 cm^3 benzene solution of reagent and equilibrate for 3 min. Allow the phases to separate and transfer the benzene layer to a 50-cm^3 beaker containing 2 g of anhydrous sodium sulfate. Measure the absorbance at 470 nm against a reagent blank.

Results and Discussion

Absorption Spectra. The absorption spectra of reagent and mixed complex are shown in Fig. 1. The reagent shows a negligible absorption in the region 450—700 nm. In the presence of thiocyanate a stable orange-red Mo(V)–htdb–SCN mixed complex is formed into benzene, showing a molar absorptivity of 3800 dm^3 mol^{-1} cm^{-1} at 470 nm.

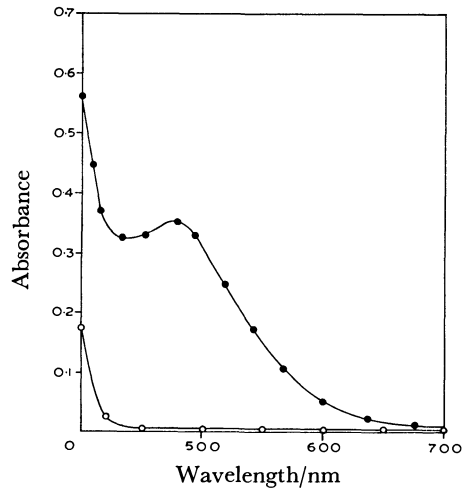

Fig. 1. Absorption spectra.
●: Mo(V)–htdb–SCN (8.33 10^{-5} M C_{Mo}), ○: 0.1% (w/v) Hhtdb in benzene.

Effect of Experimental Variables. Various water immiscible organic solvents such as benzene, toluene, carbon tetrachloride, and chloroform were examined for extracting the molybdenum mixed complex. Benzene was found to be the best solvent because of high extractability of mixed complex of molybdenum into it.

The acidity of aqueous phase was maintained with hydrochloric acid. Other mineral acids are unsuitable for extraction. If the concentration of hydrochloric acid in aqueous phase lies between 0.5—8.0 mol dm^{-3} the position of the absorption band of benzene extract remains intact but the absorbance value is affected. The optimum acidity range was found to be 2.0—4.5 mol dm^{-3} HCl.

A 30 and 300 fold molar excess of Hhtdb and thiocyanate were necessary for quantitative extraction of molybdenum. Addition of more reagents (100 and 2000 fold molar excess of Hhtdb and thiocyanate, respectively) has no adverse effect on the absorption and maximum wavelength of the coloured complex.

The period of equilibration was varied from 3 to 30 min. Extraction being quantitative after 3 min, it is recommended that the mixture be shaken for at least 3 min.

Variation in volume of aqueous phase in the range 10—60 cm^3 and temperature range 20—35 °C caused no measurable change in the absorbance of the molybdenum mixed complex. The benzene extract was stable for at least 20 h at 27±2 °C.

Beer's Law, Optimum Concentration Range and Precision. The molybdenum concentration range which follows Beer's law was found to be 3—20 ppm of metal. The optimum concentration range evaluated on the basis of the Ringbom plot[17] was 5—18 ppm of molybdenum. The precision of the system was checked by measuring the absorbance values of 10 samples, each containing 200 μg molybdenum/25 cm^{-3}. The relative standard deviation of the method was found to be 0.98%.

Composition. In molybdenum–thiocyanate–htdb mixed complex the ratio of molybdenum to reagent and thiocyanate was determined by the curve fitting method[18] (log absorbance *vs.* log [M] of reagent/thiocyanate). The results showed the formation of a 1:2:2 (metal:reagent:thiocyanate) mixed complex in benzene (Figs. 2 and 3).

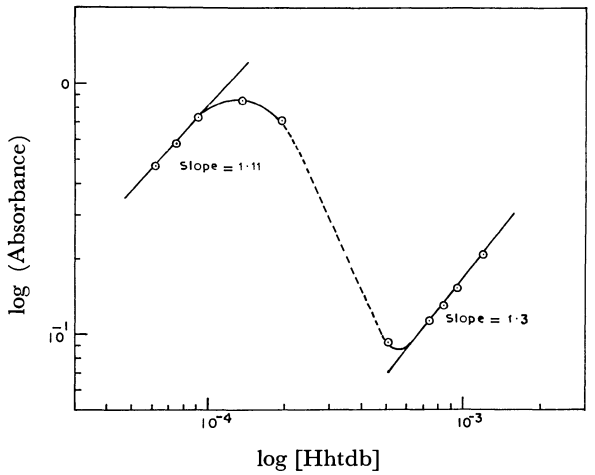

Fig. 2. Curve fitting method to determine the ratio of Mo(V) to $HOC_{22}H_{21}N_2$ in Mo(V)–$OC_{22}H_{21}N_2$–SCN complex.
0.1 mol dm^{-3} SCN, 3.0 mol dm^{-3} HCl.

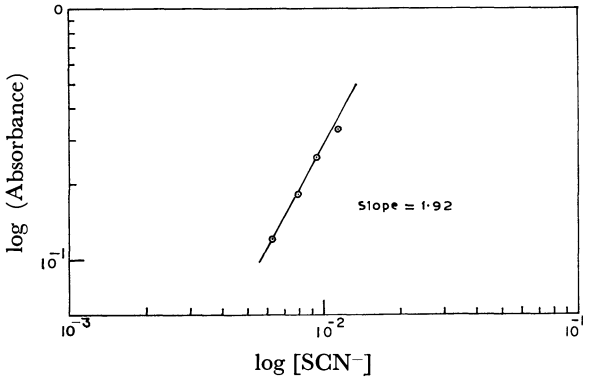

Fig. 3. Curve fitting to determine the ratio of Mo(V) to SCN^- in Mo(V)–$OC_{22}H_{21}N_2$–SCN complex.
0.003 mol dm^{-3} $HOC_{22}H_{21}N_2$, 3.0 mol dm^{-3} HCl.

The absorbance of Mo(V)–htdb–SCN mixed complex varies with the amount of reagent. Absorbance increases up to 2 fold molar excess of reagent, then a sudden decrease in absorbance is observed in 3—6 fold molar excess and beyond 6 fold molar excess the absorbance gradually increases. The results indicate that 1:1:2 and 1:2:2 (metal:htdb:SCN) stable complexes are formed (Fig. 2). However, if the reagent is added in excess only a 1:2:2 mixed complex is formed.

The overall extraction equilibrium may be expressed as follows:[19]

$$MoO^{3+} + 2SCN^- + 2Hhtdb_o \rightleftharpoons MoO(SCN)_2OC_{22}H_{21}N_2(HOC_{22}H_{21}N_2)_o + H^+,$$

where $HOC_{22}H_{21}N_2$ denotes hydroxyamidine and subscript o, the organic phase.

Effect of Foreign Ions. In order to study the effect of diverse ions on the determination, an aliquot of molybdenum solution containing 200 μg of the metal was transferred to a 100-cm^3 separatory funnel and to this was added a solution containing a known

amount of diverse ions. The acidity was adjusted to 3.5 mol dm^{-3} with hydrochloric acid and the total volume to about 25 cm^3, molybdenum being extracted with the reagent as described above. Chloride, bromide, nitrate, sulfate, urea, thiourea, tin(II), triethanolamine, borate, phthalate, selenate, alkali, and alkaline earth elements and lanthanoid elements have no interfering effect up to 3000 ppm. The tolerance limits for other ions are given in Table 1.

Application of the Method. In order to test the validity of method, two alloy steels obtained from Bureau of Analysed Sample Ltd., Newham Hall, Middlesbrough, Yorks, and an ore from Indian Bureau of mines, Nagpur, India, have been employed. The results are given in Table 2.

Table 1. Tolerance limit for diverse ions

Ions added	Tolerated amount[a] / ppm	Ions added	Tolerated amount[a] / ppm
Fe(III)	1500	Ce(IV)	500
Ti(IV)	120	V(V)	120
Zr(IV)	700	Nb(V)	200
W(VI)	70	Ta(V)	250
Pd(II)	900	U(VI)	1600
Zn(II)	2200	Al(III)	2200
Ni(II)	2000	Co(II)	2000
Mn(II)	1600	Th(IV)	1500
Cr(III)	1600	Cu(II)	1200
Oxalate	800	Citrate	800
Tartrate	800	Phosphate	1500
Fluoride	900	Iodide	1000
Thiosulfate	700	EDTA	1000

a) Less than 2% error.

Table 2. Determination of molybdenum in ore and alloy steels

Sample	Certified value / %	Found,[a] %	Standard deviation
Ore[b]	2.9	2.89	±0.0328
Steel, BCS[c] No. 64a	4.11	4.08	±0.0469
Steel, BCS[c] No. 241/1	0.52	0.495	±0.0636

a) An average of 6 determinations. b) Obtained from Indian Bureau of Mines, Nagpur. c) British Chemical Standard.

Dissolve an appropriate weight of the sample (1 g for 0.5% of molybdenum, 0.1—0.3 g for 5% of molybdenum) in 50 cm^3 sulfuric acid, and oxidize with concentrated nitric acid. The solution is evaporated almost to dryness 3—4 times and diluted with water. Undissolved silica and inorganic matter are filtered off and the solution is diluted to a definite volume in a calibrated flask. Take an aliquot of this solution, add 5 cm^3 of ascorbic acid solution and determine the molybdenum content by the procedure given above.

References

1) E. B. Sandell, "Colorimetric Determination of Traces of Metals," 3rd ed, Interscience Publisher Inc., New York (1959), pp. 644, 650, 652, 653.
2) R. Pribil and J. Adam, *Talanta*, **18**, 349 (1971).
3) D. A. Willian, I. J. Holcomb, and D. F. Boltz, *Anal. Chem.*, **47**, 2025 (1975).
4) S. P. Patil and V. M. Shinde, *Anal. Chim. Acta*, **67**, 473 (1973).
5) C. P. Savariar, M. K. Arunachalam, and T. R. Hariharan, *Anal. Chim. Acta*, **69**, 305 (1974).
6) M. K. Arunachalam and M. K. Kumaran, *Talanta*, **21**, 355 (1974).
7) B. Tamhina, M. J. Herak and V. Tagodic, *Anal. Chim. Acta*, **76**, 417 (1975).
8) C. K. Pal and A. K. Chakraburthy, *J. Indian Chem. Soc.*, **52**, 138 (1975).
9) K. K. Deb and R. K. Mishra, *Curr. Sci.*, **47**, 341 (1978).
10) K. S. Patel and R. K. Mishra, *J. Indian Chem. Soc.*, **55**, 462 (1978).
11) K. K. Deb and R. K. Mishra, *J. Indian Chem. Soc.*, **55**, 733 (1978).
12) K. S. Patel and R. K. Mishra, *J. Indian Chem. Soc.*, **55**, 773 (1978).
13) K. Satyanarayana and R. K. Mishra, *Anal. Chem.*, **46**, 1609 (1974).
14) K. Satyanarayana and R. K. Mishra, *J. Indian Chem. Soc.*, **53**, 63 (1976).
15) A. I. Vogel, "A Textbook of Quantitative Inorganic Analysis," Longmans Green and Co. Ltd., London (1964), p. 508.
16) K. K. Deb and R. K. Mishra, *J. Indian Chem. Soc.*, **53**, 178 (1976).
17) A. Ringbom, *Z. Anal. Chem.*, **115**, 332 (1938).
18) L. G. Sillen, *Acta Chem. Scand.*, **10**, 185 (1956).
19) D. D. Parrin, *J. Am. Chem. Soc.*, **80**, 3540 (1958).

Stereochemistry of Base-catalysed Addition of Methyl Mercaptoacetate to Acetylenic Ketones and Esters. Effects of Activating Groups and Solvents

Mohamed Nabih BASYOUNI,* Mohamed Tawfik OMAR, and Edwar Amin GHALI
Chemistry Department, Faculty of Science, Ain Shams University, Abbassia, Cairo, Egypt
(Received May 1, 1979)

Piperidine-catalysed addition of methyl mercaptoacetate to benzoyl- and *p*-chlorobenzoyl-phenylacetylenes in ethanol gave the corresponding (*Z*)-1-aryl-3-(methoxycarbonylmethylthio)-3-phenyl-2-propen-1-one. However, *p*-anisoylphenylacetylene gave a mixture of (*Z*)- and (*E*)-3-(methoxycarbonylmethylthio)-1-(*p*-methoxyphenyl)-3-phenyl-2-propen-1-ones in the ratio of 4: 1. This ratio was completely inverted when the latter addition was carried out in dry benzene. Rationalisation of these results is presented which depends on the effect of activating groups and solvents on the stereochemistry of addition. Piperidine-catalysed addition of methyl mercaptoacetate to methyl phenylpropiolate in ethanol gave methyl (*Z*)-3-(methoxycarbonylmethylthio)cinnamate. Hydrazine hydrate converted some of the above mono-adducts into some pyrazole derivatives.

As the continuation of our work[1,2] on the stereochemistry of the base-catalysed addition of thiols to non-terminal acetylenes, we now report the results obtained from such addition of methyl mercaptoacetate to aroylphenylacetylenes, which has not been investigated previously. Furthermore, the addition to methyl phenylpropiolate was also investigated. The work was undertaken primarily to obtain more precise information on the effect of activating groups and solvents on the stereochemistry of the addition.

Thus, when methyl mercaptoacetate was added to benzoyl- and *p*-chlorobenzoyl-phenylacetylenes Ia and Ib in the presence of a catalytic amount of piperidine in ethanol at room temperature, the solid products obtained were proved to be (*Z*)-3-(methoxycarbonylmethylthio)-1,3-diphenyl-2-propen-1-one IIa and (*Z*)-3-(methoxycarbonylmethylthio)-1-(*p*-chlorophenyl)-3-phenyl-2-propen-1-one IIb, respectively. However, *p*-anisoylphenylacetylene Ic reacted with methyl mercaptoacetate under the same experimental conditions, giving two mono-adducts, that is, (*Z*)-3-(methoxycarbonylmethylthio)-1-(*p*-methoxyphenyl)-3-phenyl-2-propen-1-one IIc and its (*E*)-isomer III in the ratio of about 4: 1.

C_6H_5–C≡C–COR + $HSCH_2CO_2CH_3$ ⟶

Ia—d

a: R = C_6H_5
b: R = C_6H_4Cl-*p*
c: R = $C_6H_4OCH_3$-*p*
d: R = OCH_3

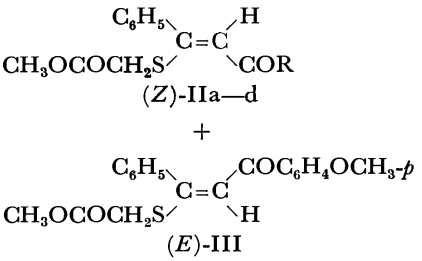

(*Z*)-IIa—d

+

(*E*)-III

The structures of the mono-adducts IIa—c and III were determined from the following evidence: i) analytical data, ii) the infrared spectra, which show,

TABLE 1. SPECTRAL DATA FOR COMPOUNDS II AND III

Compound	Infrared spectra $\nu_{C=O}$ / cm^{-1}	Electronic spectra λ_{max} / nm	ε_{max}	NMR spectra (in $CDCl_3$) δ	Assignment
IIa	1780 (sh)	327	18475		
	1760	256	9105		
	1640				
IIb	1760 (sh)	330	18150	7.07—8.0	(10H, m, Ar–H and –C=CH)
	1740	272	9790	3.27	(2H, s, SCH_2)
	1640			3.6	(3H, s, CO_2CH_3)
IIc	1760	332	24500	6.8—8.14	(10H, m, Ar–H and –C=CH)
	1740	≈280—285	12100	3.23	(2H, s, SCH_2)
	1640			3.6	(3H, s, CO_2CH_3)
				3.9	(3H, s, OCH_3)
IId[a]	1760 (sh)	276	10625		
	1730	210	10915		
III	1740 (sh)	323	19825	6.8—8.0	(10H, m, Ar–H and –C=CH)
	1725			3.63	(2H, s, SCH_2)
	1660			3.83	(3H, s, CO_2CH_3)
				3.9	(3H, s, OCH_3)

a) Lit,[5] $\nu_{C=O}$ at 1730 cm^{-1} and λ_{max} (ε) 275(10500), 211(10580).

inter alia, the bands at 1640—1660 cm^{-1} and 1725—1780 cm^{-1}. The low frequency band may be correlated with $\nu_{C=O}$ of α,β-unsaturated ketones[3] and the higher frequency one with $\nu_{C=O}$ of saturated esters,[3] iii) the electronic spectral data exhibit absorption maxima at 323—332 nm characteristic of chalcones[4] and iv) the NMR spectra of the mono-adducts IIb, IIc, and III agree quite well with the structures assigned to them (*cf.* Table 1).

Tentative assignment of configuration to the mono-adducts IIc and III, obtained from methyl mercaptoacetate and *p*-anisoylphenylacetylene, as (*Z*) and (*E*), respectively, was based on the following: it has been reported by Bohlmann and Bresinsky[5] that in (*Z*)- and (*E*)-sulfones IV and V, respectively, the signal for SCH_2 protons in the former appears at higher field than that for the corresponding protons of the latter. Also, Halphen and Owen[6] have found that the signals for SCH_2 and $C\underline{H}_2CO_2CH_3$ in ethyl *cis*-3-[2-(methoxycarbonyl)ethylthio]acrylate VI appear at higher field when compared with those of the corresponding *trans* isomer. Since in the present investigation the signal for the SCH_2 protons in the major isomer appears at relatively higher field than that for the minor isomer, the former may be similarly assigned the (*Z*)-configuration and the latter the (*E*)-configuration. It is worth noting that the signal for the ester methyl protons of the (*Z*)-isomer appears at higher field than that of the corresponding protons of the (*E*)-isomer whereas the signals for the methoxyl groups of both isomers appear at the same position (with same strength) (*cf.* Table 1).

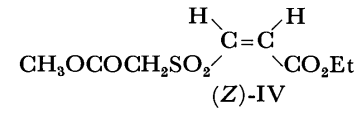

(*Z*)-IV

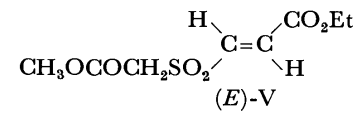

(*E*)-V

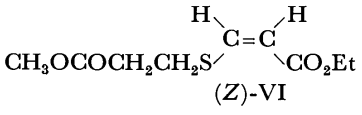

(*Z*)-VI

However, this tentative assignment was further confirmed from the following evidence: a) the electronic spectral data of the two isomers IIc and III. Thus, it is evident from Table 1 that the absorption maxima of IIc are shifted slightly to longer wave lengths with increasing strength, compared with those of III. This indicates that III has the (*E*)-configuration whereas IIc must have the (*Z*)-configuration which is consistent with the cis-trans relationship[7] on the one hand and with the configurations of *cis*- and *trans*- chalcones[4] on the other, and b) the infrared spectra of the two isomers which show $\nu_{C=O}$ of α,β-unsaturated ketone system at 1640 and 1660 cm^{-1} (Table 1). The higher value must be of the (*E*)-isomer III and the lower of the (*Z*)-isomer IIc. This is consistent with those of transoid and cisoid enones,[8] respectively.

Similarly, the mono-adducts IIa and IIb were assigned the (*Z*)-configuration on the basis of the results that their electronic spectra are similar to that of (*Z*)-IIc and also from the value of $\nu_{C=O}$ of the α,β-unsaturated ketone system (*cf.* Table 1). Moreover, the signals for SCH_2 and CO_2CH_3 protons in IIb are the same as those of (*Z*)-IIc in position and strength.

Formation of only the (*Z*)-isomers IIa and IIb in the case of addition of methyl mercaptoacetate to acetylenic ketones Ia and Ib, respectively, and (*Z*)-IIc as a major product in the case of Ic is in accord with the rule of *trans* nucleophilic addition.[9] However, formation of some (*E*)-isomer III from the addition of methyl mercaptoacetate to *p*-anisoylphenylacetylene Ic merits explanation, since it has been reported[2] that the piperidine-catalysed addition of arenethiols to Ic under the same experimental conditions, gives only the (*Z*)-mono-adducts, namely (*Z*)-3-arylthio-1-(*p*-methoxyphenyl)-3-phenyl-2-propen-1-ones, *via* a concerted mechanism. It seems, therefore, that the mercaptoalkanoate moiety had played a role that facilitates formation of the (*E*)-isomer III and that a different mechanism, most probably a stepwise one might be operating in such addition. According to this mechanism, the mercaptoalkanoate anion adds first to Ic to give the anion (A) in which an interaction between the positively polarized carbon atom of the ester carbonyl group and the negatively charged α-acetylenic carbon atom is possible (*cf.* transition state A′). As a result of this interaction, proton abstraction from the protic solvent is no longer localized on the α-acetylenic carbon atom but can occur at the ketonic carbonyl oxygen atom as well, since the basicity of the latter is enhanced owing to the activating effect of the *p*-methoxyl group. Thus, addition of the proton can occur either to the α-acetylenic carbon atom or to the oxygen atom of the ketonic group. It is evident that in the former case addition of the proton will lead to formation of only the (*Z*)-isomer IIc, whereas in the latter case an enolate A″ is formed. Tautomerisation of A″ to the carbonyl compound can then lead to a mixture of the (*Z*)-IIc and its (*E*)-isomer III.

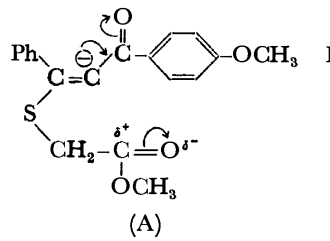

(A)

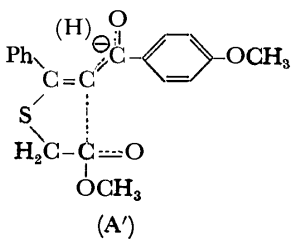

(A′)

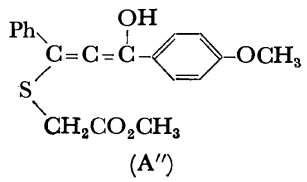

(A″)

Formation of only the (*Z*)-isomers IIa and IIb on treating Ia and Ib, respectively, with methyl mercaptoacetate under the same experimental conditions can be explained on the basis that in the transition state, the proton will add preferentially to the α-acetylenic carbon atom, since in these cases the basicity of the oxygen atom of the ketonic group is not enhanced as a result of the absence of activating *p*-substituent groups.

It is worth noting that the degree of *trans* stereoselectivity for nucleophilic additions of arenethiols to terminal acetylenes of the type H–C≡C–Y in methanol has been reported,[10] depending on the nature of the activating group Y and decreasing in the case that Y is a carbonyl-containing group, *i.e.* CO_2CH_3 or $COCH_3$. An enolate intermediate has also been proposed in these cases.[10]

Since (*Z*)-IIc is configurationally stable under the same experimental conditions (see Experimental), formation of its (*E*)-isomer III could not arise from it by post-isomerisation.

If concerted addition of a proton from a protic solvent is indeed a major factor in *trans* addition, a change of solvent might produce a change in product stereochemistry. An aprotic solvent would be incapable of making such an involvement and, if in such a solvent a thiol and a basic catalyst were to behave as thiolate-protobase ion pair, protonation might, perforce, take place on the same side as thiolate coordination, so that a *trans* product might be formed by *cis* addition. This postulate has been tested previously by Halphen and Owen[6] who studied the addition of mercaptoalkanoic acid to ethyl propiolate in different solvents and concluded that the base-catalysed addition of thiols to terminal acetylenes, *i.e.* propiolates, in dilute solution of aprotic solvents will, in general, favour the formation of *trans* enesulfides (by *cis* addition). The results obtained from the present investigation may be taken as an added proof for the validity of this mechanism in the case of addition of thiolates to non-terminal acetylenes in an aprotic solvent. Thus, when methyl

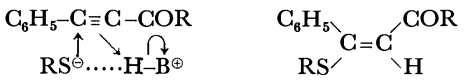

mercaptoacetate was allowed to add at room temperature to *p*-anisoylphenylacetylene Ic in dry benzene and in the presence of piperidine as a catalyst, two mono-adducts were separated (see Experimental), the major product (45%) being identical (mp, mixed mp, and IR spectroscopy) with (*E*)-3-(methoxycarbonylmethylthio)-1-(*p*-methoxyphenyl)-3-phenyl-2-propen-1-one III and the minor product (10%) being identical with (*Z*)-3-(methoxycarbonylmethylthio)-1-(*p*-methoxyphenyl)-3-phenyl-2-propen-1-one IIc. It is worth noting that the ratio of the (*Z*)-isomer IIc to its (*E*)-isomer III when the addition was carried out in ethanol at room temperature was found to be 4: 1.

It may, therefore, be concluded that the presence of the activating groups, namely COAr, in conjugation with the triple bond of non-terminal acetylenes can affect the stereochemistry of the base-catalysed addition of methyl mercaptoacetate in such a manner as to permit some *cis* addition, and that the change of solvent from a protic to an aprotic solvent can produce a dramatic change in product stereochemistry, *i.e.* gives predominantly *trans* or (*E*)-mono-adducts resulting from *cis* addition. Furthermore, a total stereoselectivity was observed during the addition of the same nucleophile to the non-terminal acetylenic ester, namely methyl phenylpropiolate.

Thus, piperidine-catalysed addition of methyl mercaptoacetate to methyl phenylpropiolate Id in ethanol gave methyl 3-(methoxycarbonylmethylthio)cinnamate IId which was analytically pure and showed the infrared-spectral bands for $\nu_{C=O}$ at 1760 (sh), 1730, and 1720 cm^{-1}, which may be correlated with $\nu_{C=O}$ of saturated esters[3] and α,β-unsaturated esters.[3] It is worth noting that Bohlmann and Bresinsky[5] have studied the addition of methyl mercaptoacetate to ethyl phenylpropiolate in dimethyl sulfoxide containing potassium *t*-butoxide as a catalyst and obtained a mono-adduct whose spectral data (see Table 1) are in good agreement with those of the product obtained from the present investigation, namely IId. They[5] did not assign any configuration to the mono-adduct. However, the compound in our hands may be tentatively assigned the (*Z*)-configuration on the basis of the results that similar addition of thiolates to ethyl phenylpropiolate proceeded exclusively by *trans* addition.[11]

The mono-adducts IIa and IIc reacted with hydrazine hydrate to give 3,5-diphenylpyrazole VIIa and 1*H*- or 2*H*-3-(*p*-methoxyphenyl)-5-phenylpyrazole VIIb, respectively. The reaction may be represented as involving an *in situ* formation of the hydrazone (B) whose NH_2 group then attacked the β-carbon atom to give the cyclised product with elimination of methyl mercaptoacetate or alternatively the hydrazine may attack the β-carbon atom first with expulsion of methyl mercaptoacetate to give (C), not isolated, which is tautomeric with (C'). Condensation of the NH_2 group with the carbonyl group can then lead to the pyrazole derivative.

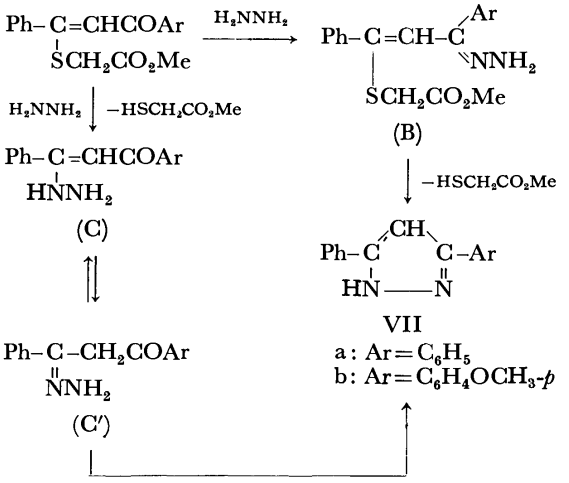

Experimental

All melting points are not corrected. Infrared and electronic spectra were measured on a Unicam SP 1200 spectrophotometer (KBr discs) and Beckmann DK 2 spectrophotometer (in ethanol), respectively. NMR spectra (in $CDCl_3$) were determined on a Varian T 60 instrument using TMS as an internal reference.

(Z)-IIa—c and (E)-III 1-Aryl-3-(methoxycarbonylmethylthio)-3-phenyl-2-propen-1-ones. To a solution of the ketone Ia, b, or c (0.005 mol) in ethanol (10 ml) was added a solution of methyl mercaptoacetate (0.005 mol) in ethanol (10 ml) followed by one drop of piperidine. The reaction mixture was then allowed to stand at room temperature for *ca.* 20 h. The precipitated solids were filtered off and recrystallized from an

Table 2. (*Z*)-1-Aryl-3-(methoxycarbonylmethylthio)-3-phenyl-2-propen-1-ones IIa—c and (*E*)-3-(methoxycarbonylmethylthio)-1-(*p*-methoxyphenyl)-3-phenyl-2-propen-1-one III

Compound	Melting point °C	Yield %	Formula	Found (%) C	H	S	Calcd (%) C	H	S
IIa	108—109[a]	65	$C_{18}H_{16}SO_3$	69.6	5.3	10.3	69.2	5.1	10.25
IIb	94—95[b]	60	$C_{18}H_{15}ClSO_3$	62.7	4.6	9.1	62.3	4.3	9.2
IIc	88—89[c]	47	$C_{19}H_{18}SO_4$	66.5	5.4	9.4	66.7	5.3	9.35
III	112—113[d]	12	$C_{19}H_{18}SO_4$	66.6	5.3	9.8	66.7	5.3	9.35

a) From light petroleum (bp 80—100 °C). b) From light petroleum (bp 60—80 °C). c) From light petroleum (bp 60—80 °C), mixed mp with III 60—65 °C. d) From benzene–light petroleum (bp 60—80 °C).

appropriate solvent to give the *(Z)-title compounds*. Evaporation of the mother-liquor at room temperature after separation of the (*Z*)-IIc gave a solid residue which was fractionally recrystallized from light petroleum (bp 60—80 °C) to which had been added few drops of benzene to give (*E*)-III. The combined mother-liquors after isolation of (*E*)-III were evaporated at room temperature to give a small amount of (*Z*)-IIc. The results are given in Table 2.

When dry benzene was used as a solvent in the case of addition of methyl mercaptoacetate to *p*-anisoylphenylacetylene Ic, the precipitated solid was fractionally crystallized from benzene–light petroleum (bp 60—80 °C) to give the (*E*)-3-(methoxycarbonylmethylthio)-1-(*p*-methoxyphenyl)-3-phenyl-2-propen-1-one III in 45% yield, mp and mixed mp with the sample obtained from the addition in ethanol 112—113 °C. The mother-liquors gave a precipitated solid which was recrystallized from light petroleum (bp 60—80 °C) to give the (*Z*)-3-(methoxycarbonylmethylthio)-1-(*p*-methoxyphenyl)-3-phenyl-2-propen-1-one IIc in 10% yield, mp 88—89 °C, not depressed upon admixture with the (*Z*)-IIc obtained from the reaction using ethanol as a solvent.

Attempted Isomerisation of (Z)-3-(Methoxycarbonylmethylthio)-1-(p-methoxyphenyl)-3-phenyl-2-propen-1-one, IIc. Piperidine (0.1 ml) was added to a solution of the *title compound* (0.001 mol) in ethanol or benzene (5 ml) and the solution kept at room temperature for 20 h. The solid obtained after allowing the solvent to evaporate at room temperature was crystallized from light petroleum (bp 60—80 °C) to give unchanged starting material (mp, mixed mp, and IR spectroscopy) in *ca.* 95% recovery.

Methyl (Z)-3-(Methoxycarbonylmethylthio)cinnamate, IId. To a solution of methyl phenylpropiolate Id (0.01 mol) in ethanol (20 ml) was added methyl mercaptoacetate (0.01 mol) followed by one drop of piperidine and the solution was allowed to stand at room temperature until crystallization occurred. Recrystallization of the filtered solid product from benzene–light petroleum (bp 60—80 °C) gave the title compound as colourless crystals in 55% yield, mp 97—98 °C. Found: C, 58.5; H, 5.3; S, 12.4%. Calcd for $C_{13}H_{14}SO_4$: C, 58.6; H, 5.3; S, 12.0%. Evaporation of the mother-liquors left an oil which contained unchanged starting materials since infrared spectroscopy shows, *inter alia*, $\nu_{C\equiv C}$ at 2200 cm^{-1}.

3,5-Diphenylpyrazole, VIIa, and 1H- or 2H-3-(p-Methoxyphenyl)-5-phenylpyrazole, VIIb. To a solution of the monoadducts IIa or IIc (0.003 mol) in ethanol (20 ml) was added excess hydrazine hydrate and the reaction mixture was refluxed for 2.5 h. After 24 h the solid product was collected by filtration and recrystallized from ethanol. 3,5-Diphenylpyrazole VIIa was obtained as colorless crystals in 86% yield, mp 199—200 °C, undepressed upon admixture with an authentic specimen.[12] 1*H*- or 2*H*-3-(*p*-methoxyphenyl)-5-phenylpyrazole VIIb was obtained in 82% yield, mp 155—156 °C, undepressed upon admixture with an authentic specimen.[12]

References

1) M. T. Omar and M. N. Basyouni, *Bull. Chem. Soc. Jpn.*, **47**, 2325 (1974).
2) M. N. Basyouni and M. T. Omar, *Egypt. J. Chem.*, **18**, 469 (1975).
3) L. J. Bellamy, "The Infrared Spectra of Complex Molecules," Methuen, London (1966).
4) W. BruceBlack and R. E. Lutz, *J. Am. Chem. Soc.*, **77**, 5134 (1955).
5) F. Bohlmann and E. Bresinsky, *Chem. Ber.*, **97**, 2109 (1964).
6) P. D. Halphen and T. C. Owen, *J. Org. Chem.*, **38**, 3507 (1973).
7) F. A. Miller in H. Gilman, "Organic Chemistry," John Wiley and Sons, Inc., New York, N. Y. (1953), Vol. III, Chap. 2, p. 168.
8) G. Eglinton in "Physical Methods in Organic Chemistry," J. C. P. Schwarz, Oliver and Boyd, Edinburgh and London (1964), Chap. 3, p. 65.
9) W. E. Truce, J. A. Simms, and M. M. Boudakian, *J. Am. Chem. Soc.*, **78**, 695 (1956); W. E. Truce, M. M. Boudakian, R. F. Heine, and R. J. McManimia, *ibid.*, **78**, 2743 (1956); W. E. Truce and J. A. Simms, *ibid.*, **78**, 2756 (1956); S. I. Miller, *ibid.*, **78**, 6091 (1956).
10) W. E. Truce and G. J. Tichenor, *J. Org. Chem.*, **37**, 2391 (1972).
11) W. E. Truce and D. L. Goldhamer, *J. Am. Chem. Soc.*, **81**, 5795 (1959).
12) F. G. Baddar, M. N. Basyouni, F. A. Fouli, and W. I. Awad, *J. Indian Chem. Soc.*, **50**, 589 (1973).

NMR Studies of Zerovalent Metal π-Complexes of Dibenzylideneacetone. III. Conformation and Bonding of the Mononuclear Palladium and Platinum Complexes

Hisao TANAKA and Hiroshi KAWAZURA*

Faculty of Pharmaceutical Sciences, Josai University, Sakado, Saitama 350-02

(Received July 20, 1979)

Synopsis. ^{1}H-NMR spectorscopy of the M[$(C_6H_5$-CH=CH)$_2$CO]$_3$ (M=Pd,Pt) complexes revealed that the coordinated olefinic moieties are fixed in the *s-trans* form, while the uncoordinated ones are fluxional around the *s-cis* form. The fluxional behavior of the uncoordinated olefins was explained in terms of the π-back donation in the complexes.

The dibenzylideneacetone (dba) ligand provides a unique series[1,2] of zerovalent Pd and Pt complexes in which only the olefinic double bond participates in the bonding to the metal. As has been reported in the preceding papers,[3,4] the binuclear complexes, M(dba)$_3$ (M=Pd, Pt), retain a rigid structure, even in solution, where the two olefinic double bonds of dba are separately joined to the two metal atoms. However, the mononuclear complexes, M(dba)$_3$ (M=Pd, Pt), are expected to be in a more flexible form because of the existence[5] of olefinic portions free from coordination. We wish to report here on the fluxional behavior of the free olefinic portions, seen by ^{1}H-NMR spectroscopy, and on its correlation with the π-back bonding nature in the complexes.

Results and Discussion

Figure 1 shows the ^{1}H-NMR spectra of the compounds, M[$(C_6D_5$CH=CH)$_2$CO]$_3$ (M=Pd, Pt). Two kinds of AB quartet patterns are found in both spectra, where the high-field one and the low-field one originate from the protons of the coordinated olefin and from those of the free olefin in a given dba ligand respectively. The NMR parameters are gathered in Table 1, where δ_A and δ_B are the chemical shift of the proton on the carbonyl side (H_A) and that on the phenyl side (H_B) respectively.

As has previously been discussed,[3,4,6] the conformation of the olefinic moiety of the dba ligand can be discriminated from the magnitude of the internal shift $\delta_{AB}(=\delta_B-\delta_A)$; $\delta_{AB}\leqslant 0.4$ for the *s-cis* form and $\delta_{AB}\geqslant 1.0$ ppm for the *s-trans* form. Therefore, the coordinated olefins with δ_{AB} of 1.22 for the Pd complex and that of 1.08 ppm for the Pt complex are found to be in the *s-trans* form. On the other hand, the uncoordinated olefins have δ_{AB}'s of 0.50 and 0.82 ppm for the respective complex, comparable to that of 0.63 ppm for free dba.

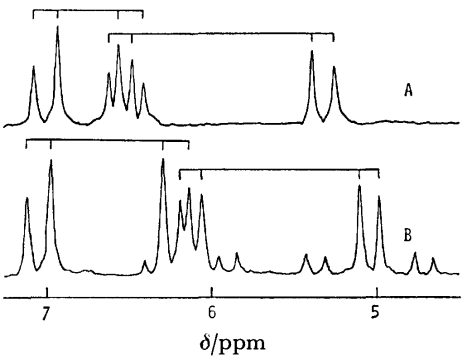

Fig. 1. ^{1}H-NMR spectra of Pd[$(C_6D_5$CH=CH)$_2$CO]$_3$ (A) and Pt[$(C_6D_5$CH=CH)$_2$CO]$_3$ (B), measured in $CDCl_3$ at −60 °C.

Table 1. ^{1}H-NMR parameters of Pd(dba)$_3$, Pt(dba)$_3$, and free dba in $CDCl_3$ at −60 °C

	Olefins	J_{AB} Hz	δ_A ppm	δ_B ppm	δ_{AB} ppm	$\bar{\delta}_H$ ppm
Pd(dba)$_3$	C[a]	13.3	5.343	6.562	1.219	5.953
	U[b]	15.4	6.517	7.017	0.500	6.767
Pt(dba)$_3$	C[c]	11.7	5.075	6.153	1.078	5.614
	U	15.3	6.257	7.076	0.819	6.666
Free dba		16.0	7.188	7.821	0.633	7.504

a) C; coordinated. b) U; uncoordinated. c) J_{Pt-A}; 65.9 and J_{Pt-B}; 44.3 Hz. δ_A and δ_B; in ppm with tetramethylsilane. $\delta_{AB}=\delta_B-\delta_A$ and $\bar{\delta}_H=(\delta_A+\delta_B)/2$.

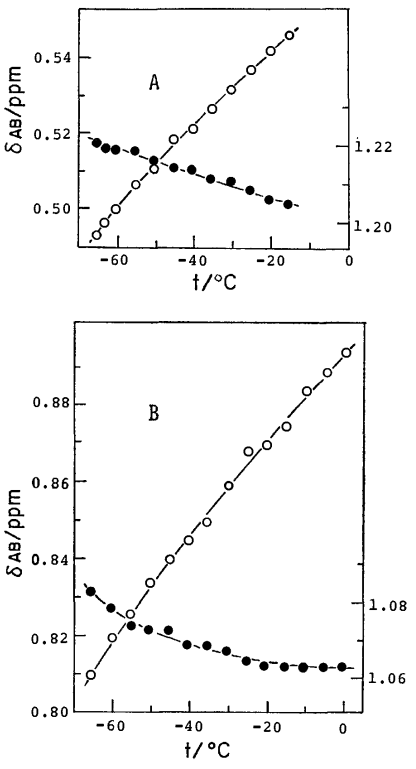

Fig. 2. Temperature dependence of the δ_{AB} for the coordinated (●; right ordinate) and uncoordinated olefins (○; left ordinate): A; Pd(dba)$_3$ and B; Pt(dba)$_3$ in $CDCl_3$.

In order to ascertain the detail of the ligand conformation, we have examined the temperature dependence of δ_{AB} (Fig. 2). With an increase in the temperature, the δ_{AB}'s for the coordinated olefins decrease slightly, indicating a characteristic aspect of the behavior[4] of the fixed *s-trans* form,[7] while the δ_{AB}'s for the uncoordinated olefins increase markedly, as in free dba, in which the olefins are in an equilibrium[6] between the major *s-cis* and minor *s-trans* forms. Thus, the temperature dependence of δ_{AB} for the uncoordinated olefins was analyzed assuming the following equilibrium and thermodynamic relation:

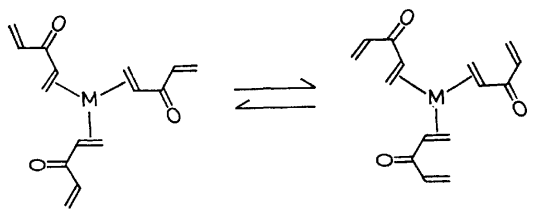

$$\ln \frac{\delta_{AB}^{obsd}-\delta_{AB}^{t}}{\delta_{AB}^{c}-\delta_{AB}^{obsd}} = -\frac{\Delta H}{RT} + \frac{\Delta S}{R},$$

$$\delta_{AB}^{obsd} = c^{c}\delta_{AB}^{c} + c^{t}\delta_{AB}^{t} \quad (c^{c}+c^{t}=1).$$

Here, δ_{AB}^{c} and δ_{AB}^{t} are the intrinsic values of δ_{AB} for the *s-cis* and *s-trans* forms. When the optimal values[8] of ΔH and ΔS are adopted, δ_{AB}^{c} and δ_{AB}^{t} are 0.44 and 1.48 ppm for the Pd complex and 0.50 and 1.47 ppm for the Pt complex; the values are close to the corresponding values[6] of 0.44 and 1.59 ppm for free dba. The conformer populations of the *s-cis* form (c^{c}) are 0.90(−15°) and 0.94(−60°) in the Pd complex and 0.62(−15°) and 0.67(−60°C) in the Pt complex.

Thus, the dba ligands of the Pd complex might exist almost entirely in the *s-cis*, *s-trans* form, as in the crystalline state,[5] while those of the Pt complex could contain an appreciable amount of the *s-trans*, *s-trans* form. The conformational difference between the two complexes can be understood in terms of the metal-olefin π-back donation. As has already been clarified by an INDO calculation of the dba molecule,[6] the *s-trans*, *s-trans* form has a highly repulsive interaction arising mainly from the proximity of the two H_B protons, and so becomes destabilized in the free state. The coordination to the metal, however, causes a little change in the geometry of the dba molecule, such as an out-of-plane bending[9] of the olefinic hydrogens, which diminishes the core repulsion within the ligand and makes feasible the existence of the *s-trans*, *s-trans* form. Such a stabilization effect of *s-trans*, *s-trans* form would be more effective in the Pt complex than in the Pd complex, since the π-back donation is stronger in the Pt complex, as is confirmed[4] by the values of the *trans*-olefinic coupling, J_{AB}, and the mean shift, $\bar{\delta}_{H}[=(\delta_{A}+\delta_{B})/2]$. We conclude that the π-back donation not only plays a major role in determining the bonding strength of the coordinated olefin in the zerovalent metal complex, but also determines the conformational attitude of the uncoordinated counterpart.

Experimental

The complexes, $M[(C_6D_5CH{=}CH)_2CO]_3$ (M=Pd,Pt), were prepared by the method of Moseley and Maitles,[10] using the dba-d_{10}.[6] To assign δ_A and δ_B, the $M[(C_6D_5CD{=}CH)_2CO]_3$ and $M[(C_6D_5CH{=}CD)_2CO]_3$ compounds were synthesized by a similar method. The samples were prepared at *ca.* −60 °C and were measured on a JEOL PFT/EC 100 spectrometer. Least-squares calculations for the analysis of δ_{AB} were performed on an IBM 1130 machine at Josai University.

References

1) T. Ukai, H. Kawazura, Y. Ishii, J. Bonnet, and J. A. Ibers, *J. Organomet. Chem.*, **65**, 253 (1974).

2) C. G. Pierpont and M. C. Mazza, *Inorg. Chem.*, **13**, 1891 (1974).

3) H. Kawazura, H. Tanaka, K. Yamada, Y. Takahashi, and Y. Ishii, *Bull. Chem. Soc. Jpn.*, **51**, 3466 (1978).

4) H. Tanaka and H. Kawazura, *Bull. Chem. Soc. Jpn.*, **52**, 2815 (1979).

5) M. C. Mazza and C. G. Pierpont, *Inorg. Chem.*, **12**, 2955 (1973).

6) H. Tanaka, K. Yamada, and H. Kawazura, *J. Chem. Soc., Perkin Trans. 2*, **1978**, 231.

7) The framework molecular model shows the rotation about C–C(O) bond in the coordinated olefinic portion to be restricted because of a sterical hindrance among the neighbouring ligands.

8) ΔH=6.1 in $Pd(dba)_3$, 2.5 kJ mol^{-1} in $Pt(dba)_3$, and $\Delta S = R\ 1n2 = 5.76$ J K^{-1} mol^{-1} in both complexes. For the procedure used to evaluate the thermodynamic relation, see Ref. 6.

9) J. H. Nelson, K. S. Wheelock, L. C. Cusachs, and H. B. Jonassen, *Inorg. Chem.*, **11**, 422 (1972).

10) K. Moseley and P. M. Maitlis, *J. Chem. Soc., Dalton Trans.*, **1974**, 169.

A Re-investigation of the Conformational Interconversion in the 1,2,3,6,7,8-Hexahydropyrene Anion Radical by ENDOR

Masamoto Iwaizumi,* Shouichi Kita, Masahiro Kohno,† and Taro Isobe
Chemical Research Institute of Non-Aqueous Solutions, Tohoku University, Katahira, Sendai 980
†*Analytical Instrument Division, JEOL, Ltd., Akishima, Tokyo 196*

(Received August 14, 1979)

Synopsis. The ENDOR spectra of the 1,2,3,6,7,8-hexahydropyrene anion radical were measured at −94—−60 °C. Based on the computer simulation of the temperature-dependent ENDOR spectra, the thermodynamic constants of the conformational interconversion of the anion radical were determined and compared with those previously obtained by ESR spectroscopy.

Magnetic resonance spectroscopy has been used as one of the most effective techniques for the investigation of chemical-dynamic processes. Many papers have been reported on the ESR investigation of the conformational intercoversion of radical molecules. Iwaizumi *et al.*[1] and de Boer *et al.*[2] have reported on the line-width-alternation effect on the ESR spectra of the anion radical of 1,2,3,6,7,8-hexahydropyrene (HP) (Fig. 1);

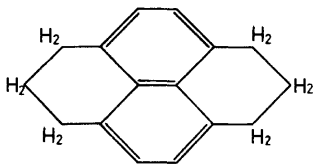

Fig. 1. 1,2,3,6,7,8-Hexahydropyrene, HP.

they attributed the effect to the conformational interconversion of the $HP^{\cdot}$ molecule between a chair form and a boat form. Claridge *et al.*[3] and Pijpers *et al.*[4] made more detailed kinetic studies and obtained the thermodynamic constants of the conformational interconversion through a computer simulation of the ESR spectra, depending on the temperature. However, appreciably different thermodynamic parameters were reported by the two groups (see Table 1). Both groups measured the ESR spectra of $HP^{\cdot}$ in the same solvent, but they used different counter ions in their experiments; *i.e.*, Claridge *et al.* treated $HP^{\cdot}$ in 1,2-dimethoxyethane (DME) with the sodium ion, while Pijpers *et al.* treated $HP^{\cdot}$ in DME with the potassium ion. In our experiment, however, no differences in the ESR spectra could be found between those two solvent and counter-ion systems to give such different thermodynamic constants. In the present work, we attempted a reexamination of the conformational interconversion of $HP^{\cdot}$ by means of ENDOR spectroscopy. Shain has also examined $HP^{\cdot}$ by the use of ENDOR, but he could not observe the ENDOR spectra at various temperatures.[5]

The magnitude of ENDOR enhancement depends on all the possible transition rates in the spin system; it changes with the temperature and with the viscosity of the solvents, and in some cases the observation of the ENDOR spectra is limited to a narrow temperature region. In Shain's experiment, where DME was used as the solvent, the observation of the ENDOR spectra was possible only in the vicinity of the freezing point of the solution (up to about 10 °C above the freezing point). In the present work, we used bis(2-methoxyethyl) ether (diglyme), with a higher viscosity than DME, and DME as the solvents. The latter was used for the measurements at temperatures below the freezing point of the former.

Results and Discussion

The ENDOR spectra were recorded with a JEOL ES-EDX-1 ENDOR spectrometer. By the use of diglyme, the ENDOR spectra could be observed up to about −60 °C. Over the temperature range used (−60 — −94 °C), the line widths, positions, and shapes of the ENDOR signals due to the β and γ protons change with the temperature; the signals due to the β protons broaden, and the separation between the two lines attributable to the axial and equatorial ones becomes smaller with an increase in the temperature, representing that the dynamic process of the β protons is in the slow-rate region, $\Delta\omega_{\beta}\tau \ll 1$, while the two ENDOR lines attributable to the axial and equatorial γ protons observed at the low temperatures collapse into a single line with an increase in the temperature, representing that the dynamic process of the γ protons ranges from the slow- to the fast-rate region, $\Delta\omega_{\gamma}\tau \gg 1$—$\Delta\omega_{\gamma}\tau \ll 1$. Here, τ is the mean lifetime of each conformation, and $\Delta\omega_{\beta}$ and $\Delta\omega_{\gamma}$ are $2\pi|(a_{\beta ax}-a_{\beta eq})/2|$ and $2\pi|(a_{\gamma ax}-a_{\gamma eq})/2|$ respectively, the hyperfine coupling constants for the axial and equatorial β and γ protons, $a_{\beta ax}$, $a_{\beta eq}$, $a_{\gamma ax}$, and $a_{\gamma eq}$, being measured in Hz. We obtained τ values as a function of the temperature, based on the computer simulation of the line shape, for the β- and γ-proton ENDOR lines. It is known that the line-shape for ordinary ENDOR lines of radicals should be a saturated Lorentzian.[6] In the present case, however, we ignored such an effect and simply assumed that the line-shape for the ENDOR signals under the dynamic process are expressed by the

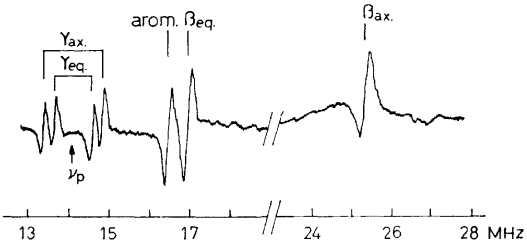

Fig. 2. ENDOR spectrum of $HP^{\cdot}$ in DME with K^+ at −94 °C. ν_p is free proton frequency and β_{ax}, β_{eq}, γ_{ax}, γ_{eq}, and arom. indicate the signals due to the axial and equatorial β and γ protons and aromatic protons, respectively.

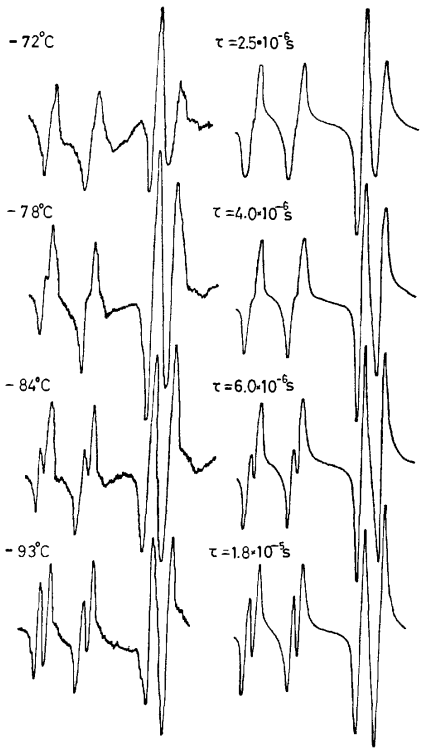

Fig. 3. Temperature dependence of the ENDOR spectra and the computer simulations. The spectrum at −93 °C was observed from $HP^{\bullet}$ in DME with K^+ and the others from $HP^{\bullet}$ in diglyme with K^+.

modified Bloch equation.[7] The line shapes were calculated by using the four-jump model[8] and using the $a_{\beta ax}$, $a_{\beta eq}$, $a_{\gamma ax}$, and $a_{\gamma eq}$ values obtained from the spectrum at the lowest temperature in the experiment. For the evaluation of τ, we also applied the following equations for the β-proton ENDOR signals:

$$1/T_2'(\text{ENDOR}) = k'$$

$$\Delta\omega = (\Delta\omega_{\beta}^2 - 8k'^2)^{1/2}$$

where $1/T_2'$ (ENDOR) is an additional line-broadening in the ENDOR signals, $\Delta\omega$ is the observed separation between the ENDOR lines due to the axial and equatorial β protons, and $k'=1/2\tau$.[9] Figure 3 shows the temperature dependence of the ENDOR signals in the

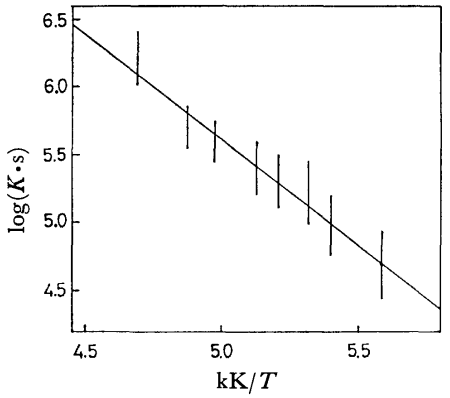

Fig. 4. The Arrehnius plot of the rate constant for the interconversion process of $HP^{\bullet}$.

Table 1. Thermodynamic parameters for conformational interconversion of $HP^{\bullet}$

	This work (by ENDOR)	Claridge *et al.* (by ESR)	Pijpers *et al.* (by ESR)
E_{act}/kJ mol^{-1}	29.9±2.6	26.8±2.5	41.8±1.7
k_0/s	$2.51\times 10^{13\pm0.8}$	$3.16\times 10^{13\pm0.8}$	$2.5\times 10^{14}\pm5\%$
$\Delta H^{\pm}$/kJ mol^{-1}	28.3±2.6[a]		39.7±1.7[b]
ΔS/J mol^{-1} K^{-1}	7.6±3.7[a]		21.8±0.4[b]
ΔG/kJ mol^{-1}	26.9±3.2[a]		33.9±2.1[b]

a) At 190 K. b) At 273 K.

14—17 MHz region, and the computer simulations of the spectra, the ENDOR signals due to the aromatic protons being expressed as having the same intensity over the present temperature range. The Arrehnius plot is shown in Fig. 4. The thermodynamic constants thus obtained are listed in Table 1. It may be seen that the obtained thermodynamic constants are in rather good agreement with Claridge *et al.*'s values, and that the activation energy, E_{act}, obtained in the present work for $HP^{\bullet}$ is smaller than the value reported by Pijpers *et al.* Pijpers *et al.* have indicated that the E_{act} for $HP^{\bullet}$ is larger than that for HP^{+}; *i.e.*, the E_{act} for $HP^{\bullet}$ is 41.8 kJ mol^{-1}, while the E_{act} for HP^{+} is 14.6 kJ mol^{-1}.[4] However, such a large difference in the E_{act} between the anion and the cation radicals seemed quite surprising, though in our ESR studies of the conformational interconversion of 4,5,9,10-tetrahydropyrene ion radicals, too, a larger activation energy has been observed for the anion radical.[10] The E_{act} value obtained in the present work indicates that the difference between the E_{act} for the anion and the corresponding cation radical may be rather smaller than that reported by Pijpers *et al.* It may also be noted that the E_{act} for $HP^{\bullet}$ is smaller than that for the intercoversion between a chair and a boat form of the neutral cyclohexane molecule, 42.3 kJ mol^{-1}.[11]

References

1) M. Iwaizumi and T. Isobe, *Bull. Chem. Soc. Jpn.*, **38**, 1547 (1965).
2) E. de Boer and A. P. Praat, *Mol. Phys.*, **8**, 291 (1964).
3) R. F. C. Claridge and B. M. Peake, *J. Magn. Reson.*, **6**, 29 (1972).
4) F. W. Pijpers, M. R. Arick, B. M. P. Hendriks, and E. de Boer, *Mol. Phys.*, **22**. 781 (1971).
5) A. L. Shain, *Mol. Phys.*, **22**, 733 (1971).
6) N. M. Atherton, "Electron Spin Resonance, Theory and Application," John Wiley and Sons, New York (1973), Chap. 10, pp. 379—389.
7) H. S. Gutowsky, D. W. McCall, and C. P. Slichter, *J. Chem. Phys.*, **21**, 279 (1953); H. S. Gutowsky and C. H. Holm, *ibid.*, **25**, 1288 (1956).
8) A. Carrington, *Mol. Phys.*, **5**, 425 (1962).
9) C. von Borczyskowski, K. Mobius, and M. Plato, *J. Magn. Reson.*, **17**, 202 (1975).
10) M. Iwaizumi and T. Isobe, *Mol. Phys.*, **29**, 546 (1975).
11) F. R. Jensen, D. S. Noyce, C. H. Sederholm, and A. J. Berlin, *J. Am. Chem. Soc.*, **84**, 386 (1962).

The ENDOR Spectrum of 1,7,7-Trimethylbicyclo[2.2.1]heptane-2,3-dione Semiquinone in Solution

Reiko Tosa,*† Yashige Kotake, Masaharu Okazaki, Hideo Shikata,†† and Keiji Kuwata

Department of Chemistry, Faculty of Science, Osaka University, Toyonaka, Osaka 560

(Received September 3, 1979)

Synopsis. The ENDOR spectra of 1,7,7-trimethylbicyclo[2.2.1]heptane-2,3-dione semiquinone (camphorsemiquinone anion) showed a sharp temperature variation in the intensity of each ENDOR line. The relationship between the optimum temperature for the ENDOR enhancement and the relaxation mechanisms was discussed on the basis of the experimental results.

Sharp variations with the temperature in the relative intensities of ENDOR signals have been a problem of much interest in connection with the discussion of the relaxation mechanism[1–4] and finding the optimum conditions for ENDOR experiments[3] in solution. Generally, the nuclear relaxation due to the electron-nuclear dipolar (END) interaction[2] and the flip-flop transition due to the modulation of isotropic hyperfine interaction[4] are known to be effective for ENDOR enhancement in solution. The camphorquinone anion has a rigid structure, as is shown in Fig. 1; therefore, the hyperfine interaction can hardly be expected to be modulated by the internal motions of the molecule.[4] Moreover, an unpaired electron delocalizes in the O–C–C–O moiety, and the END interaction is estimated to be small because β, γ, and δ-protons are distant from the unpaired electron. Thus, it seemed it would be interesting to observe the ENDOR of this anion and discuss the mechanisms of ENDOR.

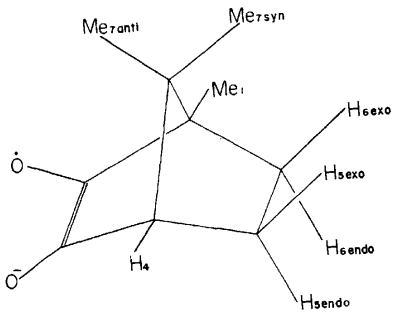

Fig. 1. The molecular structure of camphorquinone.

1,7,7-Trimethylbicyclo[2.2.1]heptane-2,3-dione (camphorquinone) was reduced with sodium (or potassium)-isopropoxide in isopropyl alcohol, which had been dehydrated by refluxing with calcium hydride, and then transferred to a sample tube by vacuum distillation. Samples were diluted until the effect of the Heisenberg spin exchange or intermolecular dipolar interaction on the ESR spectrum became negligible. For ENDOR observation, the magnetic field was fixed at an intense

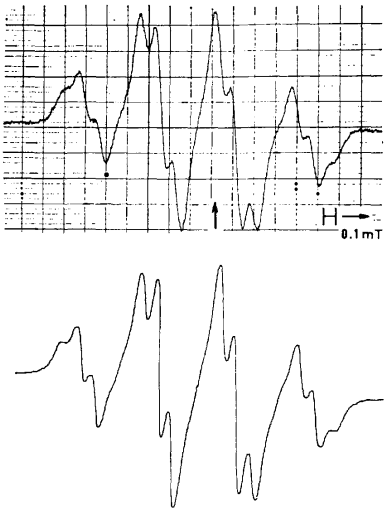

Fig. 2. ESR spectrum of camphorquinone anion in isopropyl alcohol. Upper, experimental spectrum; lower, spectrum simulation using A_{iso}'s given in Table 1.

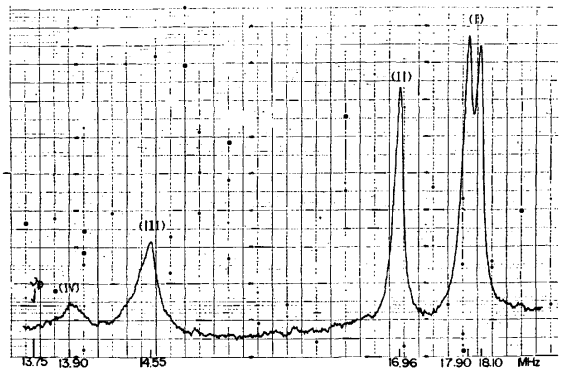

Fig. 3. ENDOR spectrum of camphorquinone anion in isopropyl alcohol at −40 °C.

peak of the high-field side, as is indicated in Fig. 2.

The ENDOR spectrum at frequencies higher than that of the free proton frequency (ν_p=13.75 MHz) is shown in Fig. 3, where the ENDOR lines are numbered from I through IV from the high-frequency side. The doublet at 18 MHz showed a tendency to enlarge the incision as the microwave power decreased. This doublet may result from two hyperfine interactions of a similar, but slightly different magnitude; it is not caused by the coherence effect because of the absence of any change in the splitting on a decrease in the rf power.

For a series of compounds with a molecular frame similar to camphorquinone, by the varying substituents, the ESR spectra were analysed in detail by Russell.[5] In the ENDOR spectrum of camphorquinone, a slight

† Present address: Doshisha High School, Iwakura, Sakyo-ku, Kyoto 606.

†† Present address: College of Liberal Arts and Science, Ehime University, Matsuyama 790.

Table 1. The values of A_{iso} and A_{aniso}

Proton	A_{iso}/mT	A_{aniso}[a]/mT
H_{exo}	0.309 0.297	0.03
H_{endo}	0.015	0.14
H_4	0.23	0.22
$Me_{7\,syn}$	0.058	—
$Me_{7\,anti}$	0.015	—

a) The largest value among the anisotropic hyperfine coupling constants.

difference in the hyperfine splittings for two *exo*-protons, which had been assumed by Russell to be equivalent, came to light (see Table 1). This difference may be due to the slight asymmetry of the structure of this ion. The broadening of the ENDOR lines, (III) and (IV), seems to show an overlap of ENDOR lines for the protons with slightly different hyperfine splitting constants from each other, but no further resolution could be obtained.

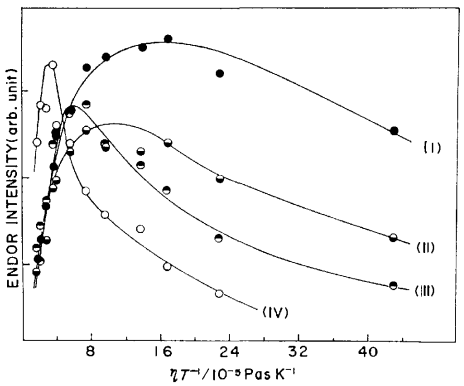

Fig. 4. Dependence of ENDOR intensity on η/T in isopropyl alcohol.
(I) *exo*-protons, (II) proton at 4 position, (III) *syn*-protonin the methyl group at 7 position, (IV) *endo*-protons (also *anti*-proton in the methyl group at 7 position).

For each peak of the ENDOR spectrum, the dependency of the intensity on η/T, where η is the viscosity coefficient of the solvent, was examined, and the optimum temperature where ENDOR enhancement reaches its maximum was obtained (Fig. 4). According to the assignment with the values of A_{iso}, which give adequate ESR simulation, it was presumed that the (I)—(IV) ENDOR lines correspond to H_{exo}, H_4, $Me_{7\,syn}$, and H_{endo} (also $Me_{7\,anti}$) protons respectively.

The END term and isotropic term for each proton are given in Table 1. The isotropic term was determined from the ESR spectrum simulation and then confirmed more minutely by ENDOR. The END term was estimated by the theory of McConnell and Strathdee,[6] using the unpaired electron density calculated by the HMO method.

When the END mechanism dominates for α protons on the aromatic ring, it has been found that the proton with the larger END term shows a maximum ENDOR intensity at a lower value of η/T than the proton with the smaller END term.[3] In the present system, the same relationship was found on H_{exo}'s and H_4 protons, but not on H_{endo} and H_4 protons. As the reason for this discrepancy, it was postulated that the $Me_{7\,anti}$ proton has an A_{iso} value very close to those for $H_{5\,endo}$ and $H_{6\,endo}$; thus, the multiplicity of the electron-spin state increases and the optimum temperatures of the H_{endo}'s shift to higher values.[7]

The anisotropic interaction of the $Me_{7\,anti}$ protons with an unpaired electron may be supposed to be fairly large when these methyl protons move to the vicinity of the π-conjugate system in the semiquinone anion in the course of the internal rotation of the methyl group. Then, the relaxation of the nuclear spins of the methyl protons may be greatly accelerated by the modulation of the anisotropic interaction due to the molecular motion or internal motions of the methyl group. This possibility, however, is not supported at the present stage of experiments, for no clear difference in the relaxation behavior has been found between the $Me_{7\,anti}$ protons and the $Me_{7\,syn}$ protons, which have a much smaller anisotropic interaction. This is probably due to the shorter correlation times of the motions induced by the Brownian motion of the solvent molecules.

In the $H_{5\,exo}$, $H_{6\,exo}$, and H_4 protons, a smaller difference was found between the optimum temperatures for the H_{exo}'s and H_4 than would be expected from the difference between their END terms; this may be due to the shift of the optimum temperature for H_{exo}'s to a higher value because of the higher multiplicity for H_{exo} protons.

References

1) J. H. Freed, "ESR Saturation and Double Resonance in Liquid," in "Electron Spin Relaxation in Liquids," ed by L. T. Muus and P. W. Atkins, Plenum Press New York (1972), pp. 503—530.
2) R. D. Allendoerfer and A. H. Maki, *J. Magn. Reson.*, **3**, 396 (1970).
3) Y. Kotake and K. Kuwata, *Bull. Chem. Soc. Jpn.*, **47**, 45 (1974).
4) N. M. Atherton and B. Day, *Mol. Phys.*, **29**, 325 (1975).
5) G. A. Russell and K. Y. Chang, *J. Am. Chem. Soc.*, **87**, 4381 (1965).
6) H. M. McConnell and J. Strathdee, *Mol. Phys.*, **2**, 192 (1959).
7) J. H. Freed, *J. Chem. Phys.*, **58**, 3089 (1973).

The Configuration of the Adsorbed Polymer at the Solid-Liquid Interface as Depicted by ESR and IR Studies

Harutoshi SAKAI* and Yoshio IMAMURA

Department of Chemistry, Faculty of Science, Science University of Tokyo, Kagurazaka, Shinjuku-ku, Tokyo 162

(Received October 16, 1979)

Synopsis. Bound segment fractions of adsorbed poly(methyl methacrylate) on silica in CCl_4 were determined by both the spin-labeling technique and infrared spectroscopy. The ESR method yielded considerably larger values than the IR, indicating a highly flattened structure of the adsorbed polymer. However, the greater reliability of the ESR method was pointed out.

Problems of the configurational properties of chain polymer molecules adsorbed at the solid-liquid interface have been receiving much attention in both theoretical and practical fields. In many of the theoretical treatments, it has been predicted that the fraction of the bound segments, p, becomes close to unity in the case of a strong attractive force between the segment and the surface.[1] The experimental estimation of p was first reported by Fontana and Thomas using IR spectroscopy.[2] They obtained values of p from 0.3 to 0.4 for the adsorbed poly(alkyl methacrylate) on silica in organic solvents. Later experiments showed a similar tendency.[3,4] Recently, an ESR technique, the spin-label method, has been employed by Robb *et al.*[5] for studies of the adsorption of poly(vinylpyrrolidone) onto silica, mainly from aqueous solutions. The ESR values of p from 0.6 to 0.9 were appreciably higher than the results from the IR method. A comparison of the ESR and IR techniques was attempted by Robb and Smith, mainly from the standpoint of utility.[6] However, it could not be decided whether the large difference in the estimated values of p comes from the differences in the adsorption systems (polymer, solvent, and solid) or from those in the evaluating methods, since they had merely compared their ESR observations with the published data obtained by the IR method. In the present work, we will deal with an experimental comparison of ESR and IR methods using the case of adsorbed poly(methyl methacrylate) on silica from a CCl_4 dilute solution.

Experimental

Spin-labeled PMMA was prepared by the anionic copolymerization of methyl methacrylate and 4-methacryloyloxy-2,2,6,6-tetramethyl-1-piperidyloxyl (molar ratio 450: 1) with a phenylmagnesium bromide catalyst in toluene at 0 °C.[7] One fraction of the narrow molecular-weight distribution, obtained by repeated fractional precipitation, was used throughout the adsorption experiments. The number-average mol wt of the fraction used was determined to be 1.22×10^5 by membrane osmometry. The spin-label concentration in the polymer was about one label per 400 monomer residues. Cabosil M-5 supplied by Cabot, Far East, Inc., was used as the adsorbent; it had a specified surface area of 220 m^2/g for nitrogen adsorption. The polymer was adsorbed onto the silica from a CCl_4 dilute solution at 25 °C. Measurements of the ESR spectra were performed on a JEOL JES FE-3X spectrometer, while the corresponding IR spectra were recorded on a JASCO, DS 403G spectrometer.

Results and Discussion

In Fig. 1, (a) shows a typical IR absorption of the adsorbed PMMA, while (b) shows the normal spectrum of the free polymer in the CCl_4 solution. The spectrum (c), which was attributed to the H-bonded carbonyl, was obtained by graphical subtraction of (b) from (a), after conversion into a suitable intensity scale. In this case, the H-bonding seems to bring about a frequency shift from 1736 to 1712 cm^{-1} and a line broadening. The fraction of the H-bonded carbonyl groups in the adsorbed polymer was determined by a modification of the method of Kalnin'sh *et al.*[3] The integrated absorption intensity was used for the calculation instead of the extinction coefficient.

A typical ESR spectrum of the adsorbed PMMA is shown in Fig. 2(e). The line shape indicates that the spectrum is composed of several portions which are easily distinguishable in their molecular motion. These arise from differences in the configurational states of the segments in the adsorbed polymer chain. From the analysis of the line shape, we concluded that the spectrum of the adsorbed polymer could be separated into three component spectra. On the other hand, we obtained three different spectra of PMMA which have different degrees of motional freedom. These are shown in Fig. 2(a), (b), and (c);

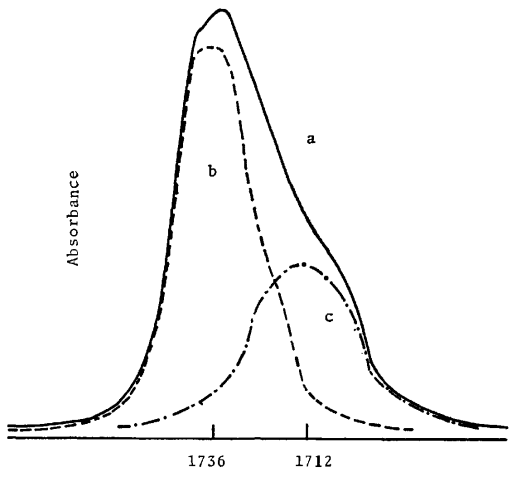

Fig. 1. IR absorption spectra of PMMA at the C=O stretching frequency.
a: Adsorbed on silica in CCl_4, b: in free CCl_4 solution, c: produced by graphycal subtraction of (b) from (a).

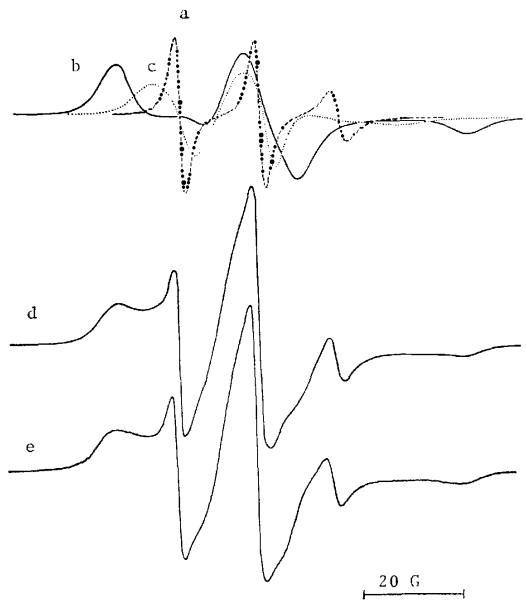

Fig. 2. ESR spectra of spin-labeled PMMA.
Top: a; in CCl_4 solution at 10 °C, b; in the frozen solution at −120 °C, c; of the molten state at 146 °C. Center: d; reproduced by superposition of above three model spectra. Bottom: e; adsorbed on silica in CCl_4 at 25 °C.

(a): a free polymer solution of a low viscosity at 10 °C (2 mg/ml), (b): a solution cooled to the frozen state at −120 °C, (c): a highly viscous polymer in the molten state at 146 °C. Apparently, the chain mobility decreased in the order of (a), (c), and (b). From the observation of the apparent line shape, the three spectra were found to correspond roughly to the three components of the adsorbed polymer. These three reference spectra were superimposed upon one another with suitable intensity ratios to reproduce the observed spectrum (e). The reproduced spectrum (d) closely fits in the observed line shape. In the polymer chain lying on the solid surface, the sequences of the segments directly bound to the surface should have restricted motion, while the detached segments should be much more mobile. Therefore, the component in a very strongly immobilized state was assigned to the train segments directly bound to the surface. The other two components, in relatively mobile states, were assigned to the free segments which are forming a short loop or a long loop. Our experimental evidence that the spin labels do not have a stronger affinity for the silica surface than the original MMA monomer demonstrates that specific adsorption through the nitroxide labels does not proceed during the polymer-adsorption process.

The values of p obtained by the ESR analysis are plotted against θ in Fig. 3. Here, θ is the amount of adsorption relative to the saturated adsorption, By our preliminary experiments, the saturated amount of adsorption was almost independent of the molecular weight of the polymer, while p decreased moderately with an increase in the mol wt. The fractions of the H-bonded carbonyl groups obtained by the IR analysis are also plotted in Fig. 3. The results from ESR exhibit a much higher level than the IR results. Both ESR and

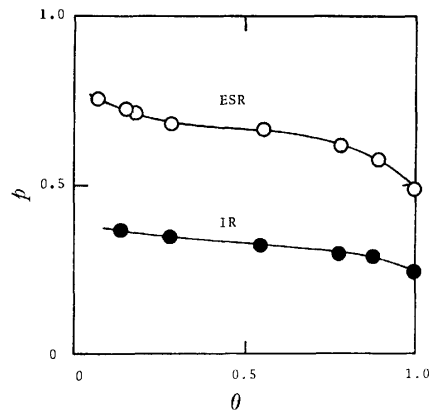

Fig. 3. Fraction of bound segments (p) *vs.* relative amount of adsorption (θ).

IR values of p were moderately decreased with an increase in θ. At the initial stage of a small amount of adsorption, θ=0.27, the ESR value of p was 0.67, which showed an appreciably flattened structure of the adsorbed polymer.

Cabosil silica has, as is well known, a partially hydrolized surface and a relatively small density of silanol groups on its surface. Most of those silanol groups are "isolated hydroxide" groups which are distant from one another beyond 4 Å. The density of the surface silanol available for the H-bonding with the polymer carbonyl was estimated to be about 3 OH per 100 Å^2 or less from the results obtained for the saturation adsorption (1.77 mg/m^2), where 24% of the carbonyls of the adsorbed PMMA were H-bonded. If a sequence of the segments is anchored only by the H-bonding with such dilute silanols, the absorbed sequence should be highly elongated along the surface.

One possible explanation for the large differences in our results from ESR and IR methods is as follows; some of the segments in a train interact with the silanol groups, while the remaining train segments interact with "non-hydroxylic sites"[8] on the silica surface. The IR method evaluates only the segments adsorbed through the H-bonding between the carbonyl and the silanol, whereas the ESR method evaluates the segments adsorbed in any mechanism. Therefore, the conventional IR method tends to estimate p values smaller than the actual values. On the other hand, we consider that the ESR method is more advantageous, as it visualizes the actual structure of the adsorbed polymer.

References

1) A. Silberberg, *J. Chem. Phys.*, **46**, 1105 (1967).
2) B. J. Fontana and J. R. Thomas, *J. Phys. Chem.*, **65**, 480 (1961).
3) K. Kalnin'sh, A. N. Krasovskii, B. G. Belen'kii, and G. A. Andreyeva, *Vysokomol. Soedin., Ser. A*, **18**, 2304 (1976).
4) P. Peyser, D. J. Tutas, and R. R. Stromberg, *J. Polym. Sci., A-1*, **5**, 651 (1967).
5) K. K. Fox, I. D. Robb, and R. Smith, *J. Chem. Soc., Faraday Trans. 1*, **70**, 1186 (1974).
6) I. D. Robb and R. Smith, *Polymer*, **18**, 500 (1977).
7) O. H. Griffith, J. F. W. Keana, S. Rottschaefer, and T. A. Warlich, *J. Am. Chem. Soc.*, **89**, 5072 (1967).
8) A. N. Sidorov, *Opt. Spektrosk.*, **8**, 806 (1960).

Simple Topological Theory of Aromaticity for Annulenes and Radialenes

Jun-ichi AIHARA

Department of Chemistry, Faculty of Science, Hokkaido University, Sapporo 060

(Received January 5, 1980)

Synopsis. Simple theory of aromaticity for annulenes and radialenes is developed by means of generalized total π-electron energy indexes, and is used to rationalize thermochemical stability and diamagnetic susceptibility exaltation of these compounds.

Total π-electron energy, E_π, is one of the fundamental quantities in chemistry of conjugated compounds. It is essential to the estimation of their thermochemical stability and reactivity. Molecular orbital (MO) theory has so far provided much information concerning total π-electron energies of conjugated hydrocarbons.[1] In parallel with this, a considerable amount of effort has been devoted to correlating the total π-electron energy E_π with particular structural features of a conjugated system.[2] Coefficients of the Hückel MO characteristic polynomial P(X) also reflect E_π in a like manner.[2-5] They can easily be evaluated by inspection of a molecular geometry.[5-7] Hosoya *et al.* previously proposed a modified topological index for E_π as a function of most coefficients of $P(X)$.[3] We later generalized it so as to include contributions from all the coefficients.[4] Our generalized total π-electron energy index Z^* is formally defined as

$$Z^* = |P(\mathrm{i})|, \tag{1}$$

where $\mathrm{i}=\sqrt{-1}$. In the case of alternant hydrocarbons, Z^* exactly agrees with Hosoya's modified topological index.[3,4] The total π-electron energy can nicely be approximated as[4]

$$E_\pi \approx E_\pi^* = 6.0846 \log Z^*, \tag{2}$$

in units of β. In this note I would like to show that Eqs. 1 and 2 are very useful for elucidating aromatic character of annulenes and radialenes.

TABLE 1. π-ELECTRON ENERGIES PER UNIT STRUCTURE OF ANNULENES ($2E_\pi/N$) IN UNITS OF β

N	Z^*	$2E_\pi/N$	
		$2E_\pi^*/N$	Hückel MO
4	5.00	2.1265	2.0000
6	20.00	2.6387	2.6667
8	45.00	2.5148	2.4143
10	125.00	2.5518	2.5889
12	320.00	2.5405	2.4880
14	845.00	2.5441	2.5680
16	2205.00	2.5429	2.5137
18	5780.00	2.5433	2.5595
20	15125.00	2.5432	2.5255
22	39605.00	2.5432	2.5552
24	103680.00	2.5432	2.5319
26	271445.00	2.5432	2.5527
28	710645.00	2.5432	2.5358
30	1860500.00	2.5432	2.5511
∞	∞	2.5432	2.5465

First, the Z^* value of [N]annulene is given in a general form as

$$Z^* = \frac{1}{\sqrt{5}}\left(\frac{1+\sqrt{5}}{2}\right)^{N+1} - \frac{1}{\sqrt{5}}\left(\frac{1-\sqrt{5}}{2}\right)^{N+1} - 2(-1)^{N/2}. \tag{3}$$

Derivation of this expression is based on the recursion formula for obtaining topological indexes of annulenes.[8] Individual Z^* values are presented in Table 1. Since E_π^* represents estimated total π-electron energy of [N]-annulene, the π-electron energy per annulene unit structure is given as $2E_\pi^*/N$. This quantity corresponds to a sum of π-electron energies of the C=C bond and its adjacent C–C bond in the canonical structure.[9,10] As easily seen from Table 1, the $2E_\pi^*/N$ value oscillates about the limiting value of 2.5432β. This limiting value is an estimated π-electron energy per unit structure for an infinitely large annulene, which is evidently free from aromaticity.

Accordingly, annulenes with $2E_\pi^*/N < 2.5432\beta$ are predicted to be aromatic, and those with $2E_\pi^*/N > 2.5432\beta$ to be antiaromatic. Although these predictions seem very rough, they are in good accord with Hückel's $(4n+2)$ rule of aromaticity.[11] All annulenes predicted to be aromatic possess $(4n+2)$ π-electrons, and those predicted to be antiaromatic possess $4n$ π-electrons. Such a way of aromaticity consideration is exactly the same as those presented by Aihara,[10] Cocordano,[12] and Haddon.[13] The Hückel MO π-electron energies per unit structure are favorably compared with the $2E_\pi^*/N$ values in Table 1. Another important point is that the π-electron energy per unit structure becomes nearly constant for annulenes with $N \geq 20$. This aspect of our total π-electron energy index Z^* is quite consistent with the finding of Dewar *et al.*[14] and Hess and Schaad[9] that bond energies are additive for nonaromatic species.

Next, the Z^* value of [N]radialene is expressed as

$$Z^* = \begin{cases} (1+\sqrt{2})^{N+1} + (1-\sqrt{2})^{N+1} - 2(-1)^{N/2} & \text{for } N = 2n \\ \{[(1+\sqrt{2})^{N+1} + (1-\sqrt{2})^{N+1}]^2 + 4\}^{1/2} & \text{for } N = 2n+1, \end{cases} \tag{4}$$

where n is an integer. Derivation of this expression is also based on the recursion formula for obtaining topological indexes of radialenes.[8] Individual Z^* values are listed in Table 2. A radialene unit structure is a combination of the CH_2=C bond and its adjacent C–C bond in the canonical structure.[9,10] Unlike annulenes, radialenes appear substantially olefinic in nature except for slightly antiaromatic [4]radialene. All the π-electron energies per unit structure (E_π^*/N) are very close to the limiting value of 2.3290β. Comparison with MO π-electron energies per unit structure[9,10,14] supports nonaromatic character of radialenes thus predicted. These results are of course

Table 2. π-Electron energies per unit structure of radialenes (E_π/N) in units of β

N	Z^*	E_π/N	
		E_π^*/N	Hückel MO
3	14.14	2.3333	2.4335
4	32.00	2.2896	2.4142
5	82.02	2.3291	2.4320
6	200.00	2.3335	2.4335
7	478.00	2.3290	2.4320
8	1152.00	2.3285	2.4319
9	2786.00	2.3290	2.4320
10	6728.00	2.3291	2.4320
11	16238.00	2.3290	2.4320
12	39200.00	2.3290	2.4320
13	94642.00	2.3290	2.4320
14	228488.00	2.3290	2.4320
15	551614.00	2.3290	2.4320
∞	∞	2.3290	2.4320

consistent with our graph theory of aromaticity.[15]

An NMR criterion of aromaticity has also been used according to which diamagnetic ring currents indicate aromaticity while paramagnetic ring currents indicate antiaromaticity.[16] We can show that such a magnetic criterion of aromaticity is identical with the above energetic criterion. When an external magnetic field, H, is applied perpendicularly to the molecular plane, our total π-electron energy index of [N]annulene becomes[17]

$$Z^* = \frac{1}{\sqrt{5}}\left(\frac{1+\sqrt{5}}{2}\right)^{N+1} - \frac{1}{\sqrt{5}}\left(\frac{1-\sqrt{5}}{2}\right)^{N+1} - 2(-1)^{N/2}\cos\Theta_N H, \quad (5)$$

where $\Theta_N = 2\pi e S_N/hc$. Here, S_N is the area enclosed by the [N]annulene ring, and e, h, and c are the standard constants with these symbols. When $N=4n+2$, the applied magnetic field decreases Z^*, so it decreases E_π^*. Conversely, when $N=4n$, the applied magnetic field increases both Z^* and E_π^*. Thus the effect of the magnetic field H on [$4n+2$]annulenes is exactly opposite to that on [$4n$]annulenes. This gives the reason why [$4n+2$]annulenes are diamagnetic while [$4n$]annulenes are paramagnetic.[16] Note that the second derivative of the total π-electron energy with respect to H gives the magnetic susceptibility of a conjugated system.[17] It should be noted that the sign of the susceptibility obtained from Eq. 5 agrees with experiment, so does the sign of the ring current.[16]

On the other hand, for [N]radialene in the magnetic field,

$$Z^* = \begin{cases} (1+\sqrt{2})^{N+1} + (1-\sqrt{2})^{N+1} - 2(-1)^{N/2}\cos\Theta_N H & \text{for } N = 2n \\ \{[(1+\sqrt{2})^{N+1} + (1-\sqrt{2})^{N+1}]^2 + 4\cos^2\Theta_N H\}^{1/2} & \text{for } N = 2n+1. \end{cases} \quad (6)$$

When N is even, the field effect on [N]radialene is in principle analogous to that on [N]annulene, but the former is much smaller than the latter. When N is odd, the field effect is essentially negligible. These suggest that marked diamagnetic susceptibility exaltation cannot be anticipated for radialenes. This is in harmony with their olefinic character.[9,10,14,15] We have thus been able to elucidate two major features of aromaticity, *i.e.*, specific stability and enhanced diamagnetism, in terms of our generalized total π-electron energy index Z^*.

Since 1971, Hosoya and coworkers have been interpreting various molecular properties in terms of topological indexes.[3,6,8,18] The present theory of aromaticity can hence be regarded as a practical extension of their topological chemistry. Simplicity and elegance are characteristics common to all these works.

References

1) A. Streitwieser, Jr., "Molecular Orbital Theory for Organic Chemists," Wiley, New York, N. Y. (1961); L. Salem, "The Molecular Orbital Theory of Conjugated Systems," W. A. Benjamin, New York, N. Y. (1966); M. J. S. Dewar, "The Molecular Orbital Theory of Organic Chemistry," McGraw-Hill, New York, N. Y. (1969).

2) References in this field have been exhaustively collected in: I. Gutman, *Match*, **4**, 195 (1978).

3) H. Hosoya, K. Hosoi, and I. Gutman, *Theor. Chim. Acta*, **38**, 37 (1975).

4) J. Aihara, *J. Org. Chem.*, **41**, 2488 (1976).

5) J. Aihara, *J. Am. Chem. Soc.*, **98**, 6840 (1976).

6) H. Hosoya, *Theor. Chim. Acta.* **25**, 215 (1972).

7) A. Graovac, I. Gutman, N. Trinajstić, and T. Živković, *Theor. Chim. Acta*, **26**, 67 (1972),

8) H. Hosoya, *Fibonacci Quart.*, **11**, 255 (1973).

9) B. A. Hess, Jr., and L. J. Schaad, *J. Am. Chem. Soc.*, **93**, 305, 2413 (1971).

10) J. Aihara, *Bull. Chem. Soc. Jpn.*, **48**, 517 (1975).

11) E. Hückel, *Z. Phys.*, **70**, 204 (1931); **78**, 628 (1932).

12) M. Cocordano, *C. R. Acad. Sci., Ser. C*, **284**, 441 (1977).

13) R. C. Haddon, *J. Am. Chem. Soc.*, **101**, 1722 (1979).

14) M. J. S. Dewar and G. J. Gleicher, *J. Am. Chem. Soc.*, **87**, 685, 692 (1965); M. J. S. Dewar and C. de Llano, *ibid.*, **91**, 789 (1969).

15) J. Aihara, *J. Am. Chem. Soc.*, **98**, 2750 (1976); I. Gutman, M. Milun, and N. Trinajstić, *ibid.*, **99**, 1692 (1977).

16) R. C. Haddon, V. R. Haddon, and L. M. Jackman, *Top. Curr. Chem.*, **16**, 103 (1971); F. Sondheimer, *Acc. Chem. Res.*, **5**, 81 (1972).

17) J. Aihara, *J. Am. Chem. Soc.*, **101**, 558, 5913 (1979).

18) H. Hosoya, *Bull. Chem. Soc. Jpn.*, **44**, 2332 (1971); H. Hosoya, K. Kawasaki, and K. Mizutani, *ibid.*, **45**, 3415 (1972); H. Hosoya and M. Murakami, *ibid.*, **48**, 3512 (1975); H. Hosoya and K. Hosoi, *J. Chem. Phys.*, **64**, 1065 (1976); I. Gutman, T. Yamaguchi, and H. Hosoya, *Bull. Chem. Soc. Jpn.*, **49**, 1811 (1976).

The Back-extraction Behavior of Chelate Compounds. III.† The Extraction and the Back-extraction of the Metal (II) Diethyldithiocarbamates

Takaharu HONJO* and Hisanori IMURA

Department of Chemistry, Faculty of Science, Kanazawa University, Kanazawa 920

(Received October 2, 1979)

Synopsis. The behavior of trace amounts of cadmium(II), cobalt(II), copper(II), iron(II), mercury(II), manganese(II), nickel(II), lead(II), and zinc(II) in backextraction has been examined in order to establish the basic conditions for the separation of metals as their diethyldithiocarbamates by back-extraction.

A number of papers and reviews concerning the solvent extraction of metal diethyldithiocarbamates have been presented, but scarcely no back-extraction techniques have been examined and applied to the separation of metals.[1] In the present work, the behavior of trace amounts of cadmium(II), cobalt(II), copper(II), iron(II), mercury(II), manganese(II), nickel(II), lead(II), and zinc(II) in back-extraction has been examined in order to establish the basic conditions for the separation of metals as their diethyldithiocarbamates by back-extraction.

Experimental

Extraction. Extraction was carried out with a buffered solution containing a radioactive tracer; the pH was adjusted to the desired value by mixing an appropriate amount of 10^{-2} M (1M=1 mol dm^{-3}) of hydrochloric acid, acetic acid, sodium acetate, and sodium hydroxide. A solution of 5×10^{-3} M of DDDC (diethylammonium diethyldithiocarbamate) in carbon tetrachloride (10 cm^3) was shaken by means of a mechanical shaker (340 strokes/min) with an equal volume of an aqueous solution containing 10^{-4} M of each metal for 5 min at room temperature (20—25 °C). After centrifugation, a 3-cm^3 portion of each phase was pipetted out into a test tube, after which the radioactivity was counted with a NaI(Tl) scintillation counter. The distributions of Cu(II) and Ni(II) were spectrophotometrically determined by measuring the absorbance of $Cu(DDC)_2$ at 436 nm and that of $Ni(DDC)_2$ at 440 nm respectively. The concentration of uncomplexed DDDC in the organic phase was spectrophotometrically determined as a copper chelate in carbon tetrachloride. The pH of the aqueous phase was measured again after extraction by means of the pH meter.

Back-extraction. Since an organic phase which had been prepared by the standard extraction procedure contained an uncomplexed DDDC in a different quantity because of its decomposition, the organic phase was shaken with a buffered solution of pH 8—9 in order to remove the uncomplexed DDDC just before the back-extraction procedure. Then a 5-cm^3 aliquot of the organic phase was shaken with a 5-cm^3 portion of an aqueous solution adjusted to the desired pH or acidity for 5 min at room temperature. The distribution was determined as in the case of the extraction.

Percent Extraction. The percentage of extraction, %E, and the percentage of back-extraction, $\%E_{back}$ can be calculated by means of these equations: $\%E=D(1+D)\times100$ and $\%E_{back}=D^*(1+D^*)\times100$, where D and D^* are the net distribution ratios of a metal in the extraction and the back-extraction respectively.

Results and Discussion

The shaking time of 5 min was preferred in the extraction process, because the decomposition of DDDC and its metal chelates seems quite small within this time, as is shown in Fig. 1. The Mn–DDC chelate extracted was the most unstable among all the metal–DDC chelates in carbon tetrachloride, and decomposed gradually just after the extraction. The extraction of 10^{-4} M of 9 divalent metals was carried out with 5×10^{-3} M of DDDC in carbon tetrachloride for each, while the back-extraction of the metal diethyldithiocarbamates extracted was done with various acidic and basic aqueous solutions. The results are shown in Fig. 2 as a function of the pH or HCl(M) of the aqueous phase. The symbols in the two figures, A→O and O→A,

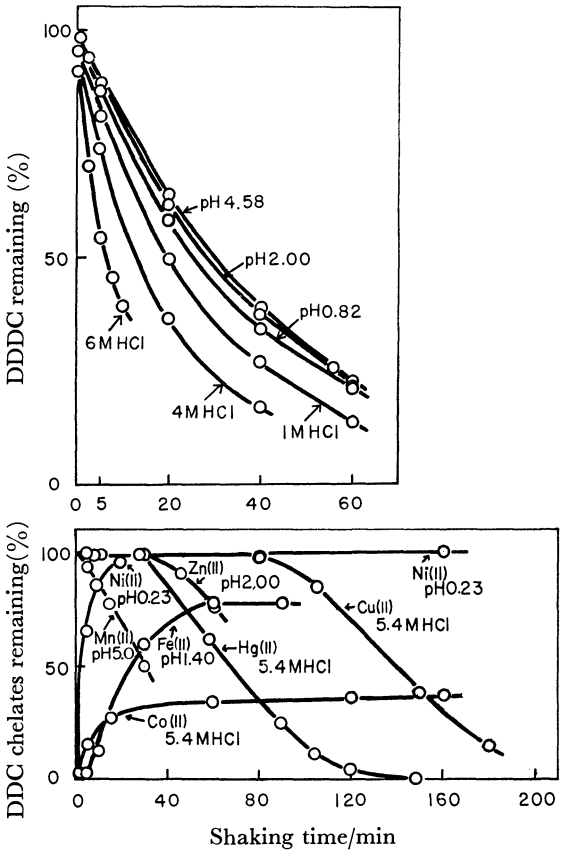

Fig. 1. Percentage of remaining of 10^{-3} —10^{-2} M of DDDC and its metal chelates in carbon tetrachloride on continuous shaking with an aqueous solution of various pH or various concentration of hydrochloric acid.

† Part II: T. Honjo*, T. Unemoto, and T. Kiba, *Bull. Chem. Soc. Jpn.*, **48**, 1651 (1975).

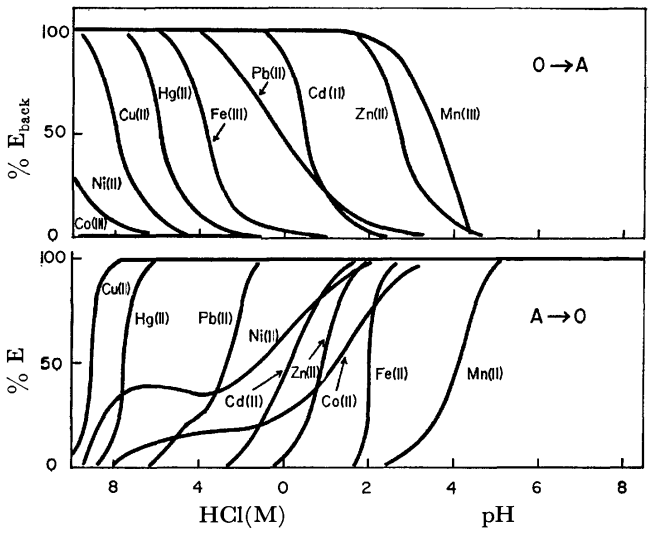

Fig. 2. Extraction and back-extraction curves of metal–5×10^{-3} M of DDDC–carbon tetrachloride systems.

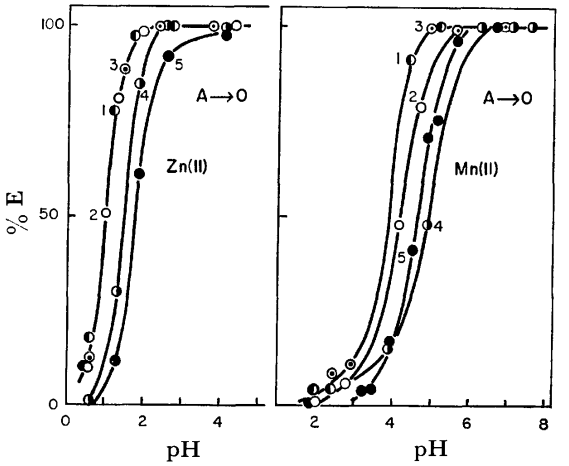

Fig. 3. Effect of diluent on the extraction of Zn(II) and Mn(II) with DDDC in various organic solvents.
1 —◐— Nitrobenzene, 2 —○— carbon tetrachloride, 3 —⊙— benzene, 4 —◑— chloroform, 5 —●— methyl isobutyl ketone.

denote the extraction and the back-extraction of the chemical species respectively. The data on the $pH_{1/2}$ values (the pH of the half-extraction) and the $HCl_{1/2}$ (the concentration of hydrochloric acid of the half-extraction of metal diethyldithiocarbamates) obtained in the present extraction system are summarized in Table 1. The disagreement of the $pH_{1/2}$ and the $HCl_{1/2}$ values appearing in the liquid-liquid extraction of Cu(II), Hg(II), Pb(II), Cd(II), and Zn(II) with DDDC may be due to the fact that the concentration of DDDC is equivalent to those of metals in carbon tetrachloride in the back-extraction. The curves of Mn(II), Fe(II), Co(II), and Ni(II) in the extraction and the back-extraction give asymmetrical forms, suggesting an irreversible extraction process, *i.e.*, the oxidation of the metals or a slow rate of chelate formation during extraction. However, the curves of Zn(II) and Hg(II) in the extraction and the back-extraction became exactly symmetrical when the back-extraction was carried out with 5.0×10^{-3} M of DDDC in carbon tetrachloride. The solvent effect on the extractions of Zn(II) and Mn(II) with DDDC has also been investigated. As is shown in Fig. 3, Zn(II) and Mn(II) are readily extracted with non-polar solvents, such as benzene and carbon tetrachloride. The extractability of Zn(II) and Mn(II) with DDDC in nitrobenzene was found to be enhanced. The unstable $Mn(DDC)_3$ in carbon tetrachloride after extraction was not decomposed for at least 15 min with 12% nitrobenzene and not for 1 h with 80% nitrobenzene. This fact may result from the solvation effect of nitrobenzene, which has polarity; this polarity decreases the decomposition of DDDC and its metal chelates.

Table 1. $pH_{1/2}$ and $HCl_{1/2}$ values determined by the extraction and the back-extraction of metals with 5×10^{-3} M of DDDC in carbon tetrachloride

Metal	$pH_{1/2}$ or $HCl_{1/2}$	
	Extraction	Back-extraction[a]
Cd(II)	0.1	0.4
Co(II)	1.2	>10 M[b]
Cu(II)	9.0 M	7.8 M
Fe(II)	2.1	3.8 M[b]
Hg(II)	7.5 M	5.8 M
Mn(II)	4.3	3.6[b]
Ni(II)	1.3 M	>10 M
Pb(II)	2.6 M	0 M
Zn(II)	1.0	2.7

a) Without uncomplexed DDDC. b) The (III) valent metals of the extract ascertained by means of mass spectrometry. Conditions: electron energy, 75 eV; current, 200 μA; temperature, 140—160 °C; parent peaks (*m/e*): 503 for $Co(DDC)_3^+$, 450 for $Fe(DDC)_3^+$, and 499 for $Mn(DDC)_3^+$.

The authors wish to thank Professor Emeritus Toshiyasu Kiba of Kanazawa University for his helpful advice.

References

1) T. Sekine and Y. Hasegawa, "Solvent Extraction Chemistry: Fundamentals and Applications," Marcel Dekker, New York (1977).

The Crystal Structures of Monoclinic and Triclinic Forms of Bis[(*R*)-1,2-propanediame]platinum(II) Chloride Dihydrate

Choji MAEDA, Keiji MATSUMOTO, and Shun'ichiro OOI*

Department of Chemistry, Faculty of Science, Osaka City University, Sumiyoshi-ku, Osaka 558

(Received October 8, 1979)

Synopsis. The crystal structures of monoclinic and triclinic forms of $[Pt(R\text{-pn})_2]Cl_2\cdot 2H_2O$ have been determined from diffractometer data. Despite the difference in crystal systems, the complex cations in the two kinds of crystals have essentially the same structure. The disposition of the CH_3 groups is *trans*. One of the chelate rings is of the λ conformation, with an equatorial CH_3 group, while the other has the δ conformation, with an axial CH_3 group.

The bis[(*R*)-1,2-propanediamine]platinum(II) ion ($[Pt(R\text{-pn})_2]^{2+}$) may exist in *trans* and *cis* isomers. The 100 MHz PMR spectrum of $[Pt(R\text{-pn})_2]Cl_2$ shows one methyl doublet at 1.35 ppm, indicating either that the compound comprises only one isomer or that methyl signals due to the *trans* and *cis* isomers are virtually superimposed in the 100 MHz spectrum.[1] The X-ray structure analysis of the title compound has disclosed that the compound contains only the *trans* isomer.

Experimental

$[Pt(R\text{-pn})_2Cl_2\cdot 2H_2O$ was prepared in two different ways. i) $[Pt(Cl)_2(R\text{-pn})]$ was treated with an excess of *R*-pn; subsequent recrystallization from water yielded predominantly monoclinic crystals, with a small amount of triclinic crystals. ii) The reaction of $PtCl_2$ with an excess of *R*-pn in water gave a compound with the same formula as that obtained in i), but in this case the quantity of triclinic crystals was larger than that of monoclinic ones. Both the monoclinic and triclinic crystals gave satisfactory analyses.

Crystal Data: 1) Monoclinic form (**1**), $a=5.181(2)$, $b=21.142(11)$, $c=6.776(2)$ Å, $\beta=96.50(3)°$, $D_m=2.02$, $D_c=2.03$ g cm^{-3}, $Z=2$, space group $P2_1$, μ(Mo $K\alpha$)$=103.6$ cm^{-1}: 2) Triclinic form (**2**), $a=10.688(9)$, $b=6.786(4)$, $c=5.174(3)$Å, $\alpha=96.27(6)°$, $\beta=96.54(6)°$, $\gamma=86.19(4)°$, $D_m=2.02$, $D_c=2.02$ g cm^{-3}, $Z=1$, space group P1, μ(Mo $K\alpha$)$=103.1$ cm^{-1}.

The intensities were measured on an automated diffractometer by means of the ω-2θ scan method, with graphite-monochromated Mo $K\alpha$ radiation. Crystal size: $0.20\times 0.20\times 0.25$ mm for **1**, $r=0.07$ mm for **2** (ground spherically); scan speed: 0.017° s^{-1} for **1** and **2**; scan range: $(0.8+0.2\tan\theta)°$ for **1**, $(1.0+0.2\tan\theta)°$ for **2**; background measurement at each end of the scan range: 20 s for **1** and **2**; maximum 2θ value: 55° for **1**, 50° for **2**; number of reflections with $F_0^2>3\sigma(F^2_0)$: 1576 for **1**, 1691 for **2**.

The refinement of the structures were performed by means of the block-diagonal least-squares method. The function minimized was $\sum w(F_0-|F_c|)^2$. The convergence was attained with $R=0.033$ ($R_w=0.042$) for **1** and $R=0.039$ ($R_w=0.048$) for **2**. w for **1**: $w=0.7$ for $F_0<13.0$, $w=1.0$ for $13.0\leq F_0\leq 32.0$, $w=(32.0/F_0)^2$ for $F_0>32.0$. w for **2**: $w=0.7$ for $F_0<17.0$, $w=1.0$ for $17.0\leq F_0\leq 40.0$, $w=(40.0/F_0)^2$ for $F_0>40.0$. No attempt was made to locate the H atoms. The atomic scatterings factors, with corrections for anomalous scattering of Pt^0 and Cl^-, were taken from Ref. 2. The F_0-F_c tables are deposited as Document No. 8015 at the Chemical Society of Japan. The atomic coordinates are listed in Table 1. All the computations were performed by using programs in UNICS[3] on a FACOM 230-60 computer at this University.

Results and Discussion

The crystal structures of **1** and **2** are shown in Fig. 1. Both the monoclinic and triclinic crystals comprise only the *trans* isomer with substantially identical

TABLE 1. POSITIONAL AND THERMAL PARAMETERS

Atom	Monoclinic form (1)				Triclinic form (2)			
	10^4x	10^4y	10^4z	B/Å^2	10^4x	10^4y	10^4z	B/Å^2
Pt	1423.6(6)	0	4261.6(5)	a)	0	0	0	a)
Cl(1)	8010(6)	−796(2)	8870(5)	a)	−1639(5)	−4416(7)	−6953(9)	a)
Cl(2)	4776(6)	819(2)	−299(5)	a)	1562(5)	4474(7)	-2991(9)	a)
N(1)	2944(20)	−489(5)	2039(15)	2.7(2)	−1027(14)	2241(22)	−1691(29)	3.0(3)
N(2)	2477(21)	−796(5)	5875(15)	2.7(2)	−1600(14)	−1469(22)	−1402(29)	3.1(3)
N(3)	−190(20)	479(5)	6449(15)	2.5(2)	937(13)	−2289(20)	1853(26)	2.6(2)
N(4)	237(20)	776(5)	2611(15)	2.5(2)	1529(13)	1523(21)	1562(27)	2.8(2)
C(1)	4249(31)	−1075(7)	2858(24)	3.6(2)	−2145(20)	1649(32)	−3285(42)	4.0(4)
C(2)	2755(28)	−1331(7)	4470(21)	3.3(2)	−2670(20)	−26(30)	−1982(40)	3.8(4)
C(3)	3934(35)	−1914(10)	5518(27)	4.6(3)	−3765(24)	−912(37)	−3531(49)	5.1(5)
C(4)	−1939(26)	983(6)	5482(20)	2.9(2)	1971(17)	−1407(26)	3799(34)	3.9(3)
C(5)	−622(27)	1293(7)	3831(20)	3.0(2)	2578(17)	141(27)	2571(36)	3.1(3)
C(6)	1687(31)	1708(8)	4657(25)	4.0(3)	3397(21)	−687(33)	482(43)	4.3(4)
O(1)	4144(36)	−2718(9)	676(24)	7.1(4)	4561(20)	4158(33)	−3413(43)	7.0(5)
O(2)	−828(40)	−2218(10)	452(29)	7.9(4)	5613(23)	4081(37)	1789(48)	8.2(6)

a) Anisotropic thermal parameters ($\times 10^4$) in the form of; $\exp[-(B_{11}h^2+B_{22}k^2+B_{33}l^2+B_{12}hk+B_{13}hl+B_{23}kl)]$ with these parameters:

	Atom	B_{11}	B_{22}	B_{33}	B_{12}	B_{13}	B_{23}
1	Pt	163(1)	14.8(1)	89.2(6)	−4(1)	22(1)	−2(1)
	Cl(1)	245(10)	24.9(8)	168(6)	−20(5)	63(13)	19(4)
	Cl(2)	229(10)	22.4(8)	149(6)	−22(5)	51(12)	13(4)
2	Pt	75.5(4)	86.3(8)	215(2)	−27(1)	63(1)	−10(2)
	Cl(1)	102(5)	166(9)	308(17)	−62(11)	93(14)	10(20)
	Cl(2)	96(5)	168(9)	310(17)	−56(11)	72(14)	32(20)

TABLE 2. SELECTED BOND DISTANCES (l), BOND ANGLES (ϕ), AND TORSION ANGLES (τ)

Bond lengths (l/Å)	1	2	Bond angles (ϕ/°)	1	2
Pt–N(1)	2.06(1)	2.03(2)	N(1)–Pt–N(2)	82.9(4)	80.9(7)
Pt–N(2)	2.05(1)	2.06(2)	N(3)–Pt–N(4)	82.9(4)	83.6(6)
Pt–N(3)	2.05(1)	2.06(2)			
Pt–N(4)	2.04(1)	2.03(2)			

N–H···Cl hydrogen bonds

N–H[a)]···Cl	1[b)]	2[b)]	N···Cl (l/Å) 1	N···Cl (l/Å) 2	H···Cl (l/Å) 1	H···Cl (l/Å) 2	N–H···Cl (ϕ/°) 1	N–H···Cl (ϕ/°) 2
N(1)–H···Cl(2)	I	I	3.38(1)	3.41(2)	2.52	2.54	144	145
N(1)–H···Cl(1)	III	IV	3.21(1)	3.24(2)	2.22	2.25	173	174
N(2)–H···Cl(1)	I	I	3.32(1)	3.31(2)	2.34	2.34	167	166
N(2)–H···Cl(1)	II	V	3.25(1)	3.22(2)	2.28	2.25	162	162
N(3)–H···Cl(1)	II	V	3.34(1)	3.34(2)	2.41	2.41	155	155
N(3)–H···Cl(2)	IV	III	3.27(1)	3.25(1)	2.30	2.28	163	163
N(4)–H···Cl(2)	I	I	3.24(1)	3.26(2)	2.31	2.33	153	155

Torsion angles (τ/°)

	1	2		1	2
N(1)–C(1)–C(2)–N(2)	52	49	N(3)–C(4)–C(5)–N(4)	50	52
N(1)–C(1)–C(2)–C(3)	3	5	N(3)–C(4)–C(5)–C(6)	71	72
Pt–N(2)–C(2)–C(3)	9	13	Pt–N(4)–C(5)–C(6)	93	87

a) The coordinates of H atoms were calculated on the assumption of N–H=1.00 Å. b) Roman numerals denote the following equivalent positions for Cl^- ions: **1** I x, y, z; II $-1+x, y, z$; III $-1+x, y, -1+z$; IV $x, y, -1+z$ **2** I x, y, z; II $x, y, 1+z$; III $x, -1+y, z$; IV $x, 1+y, 1+z$; V $x, y, 1+z$.

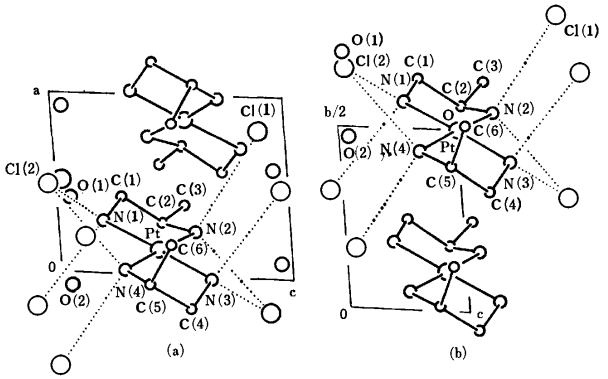

Fig. 1. The crystal structures of the monoclinic form (a) and the triclinic form (b).
The dotted lines indicate N–H···Cl hydrogen bonds.

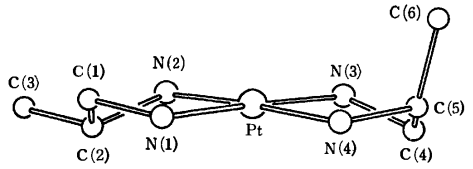

Fig. 2. The structure of $[Pt(R\text{-pn})_2]^{2+}$ ion.

structures. Moreover, the environments of the complex ions in the two structures have a close resemblance to one another. Furthermore, the two-dimensional crystal structure parallel to (010) in **1** is similar to that parallel to (100) in **2**, though the three-dimensional structures are different from each other in the stacking modes along the axes perpendicular to the respective planes. Such hircumstances are reflected in the interrelation between cte unit-cell dimensions of the two kinds of crystals; the a, b, c, and β in **1** are very close in magnitude to c, $2a$, b, and α in **2**. All the amino H atoms are involved in N–H···Cl hydrogen bonds, which are rather weak in view of the N···Cl distances.

One chelate ring has a λ conformation, with an equatorial CH_3 group, while in the other the conformation is δ, with an axial CH_3 group (Fig. 2). There have been two conflicting views regarding the behavior of the 5-membered chelate ring composed of Pd(II) or Pt(II) with the pn ligand. The observed coupling constants among the CH_2 and CH protons have been shown to be consistent with theoretical ones obtained from the conformationally fixed ring model with an equatorial CH_3 group.[1] On the other hand, the ^1H–^1H[4] and ^{195}Pt–^{13}C coupling constants,[5] as well as the circular dichroism intensity,[6] have been utilized to estimate the abandance ratio of the λ conformer to the δ conformer in the Pt(or Pd)-pn ring on the assumption that a rapid $\lambda \leftrightarrow \delta$ inversion takes place in the chelate ring. The λ: δ ratios were estimated to be 50: 50 and 70: 30 from the analyses of the ^1H–^1H and ^{195}Pt–^{13}C coupling constants respectively, and 3: 1, from that of the CD data, indicating the presence of a considerable amount of the axial CH_3 conformer in solution. Although the structure in a solid is not always held in solution, the axial CH_3 ring found in this work is indicative of the flexibility of the Pt-pn ring. From the point of view of the inverting ring model, the $\lambda\delta$ conformer is favorable in entropy term by $RT\ln 2$ over the $\lambda\lambda$ or $\delta\delta$ conformer. Provided that there exists no significant difference between the strain energies of the λ and δ rings, and that the two rings in the bis chelate are inverted independently from each other, the $\lambda\delta$ conformer is the most abundant species in solution. The finding that both kinds of crystals contain only the $\lambda\delta$ conformer implies that the assumption is not far from the real situation, although the conformation is largely dependent on the crystal packing.

This research was supported by a Grant-in-Aid for Scientific Research from the Ministry of Education.

References

1) S. Yano, H. Ito, Y. Koike, J. Fujita, and K. Saito, *Bull. Chem. Soc. Jpn.*, **42**, 3184 (1969).
2) "International Tables for X-Ray Crystallography," Kynoch Press, Birmingham (1974), Vol. IV, pp. 71, 148.
3) "The Universal Crystallographic Computation Program System," The Crystallographic Society of Japan (1969).
4) C. J. Hawkins and R. M. Peachey, *Aust. J. Chem.*, **29**, 33 (1976).
5) L. E. Erickson, J. E. Sarneski, and C. N. Reilly, *Inorg. Chem.*, **14**, 3007 (1975).
6) C. J. Hawkins, "Absolute Configuration of Metal Complexes," Wiley-Interscience (1971), Chap. 5.

Reaction of Bis[1-(2-pyridylazo)-2-naphtholato]cobalt(III) Chloride, $[Co^{III}(pan)_2]Cl$, with Hyperoxide in Dimethyl Sulfoxide†

Katsura MOCHIZUKI, Taira IMAMURA, and Masatoshi FUJIMOTO*

Department of Chemistry, Faculty of Science, Hokkaido University, Sapporo 060

(Received October 18, 1979)

Synopsis. The complex $[Co^{III}(pan)_2]^+$ was found to react in DMSO with hyperoxide, O_2^-, to give a bivalent cobalt complex $[Co^{II}(pan)_2]^0$. The oxidation of $[Co^{II}(pan)_2]^0$ to $[Co^{III}(pan)_2]^+$ by oxygen did not proceed in DMSO in the absence of water and/or H^+. The standardization of O_2^- in DMSO were also described.

In aqueous solution the cobalt(II) complex $[Co^{II}(pan)_2]^0$ formed by the reaction of Co^{2+} and 1-(2-pyridylazo)-2-naphthol, PAN, was found to be successively oxidized to the cobalt(III) complex by dissolved oxygen.[1,2] In the present report the reaction of $[Co^{III}(pan)_2]^+$ and O_2^- in DMSO was investigated, where hyperoxide acts as a reducing agent.

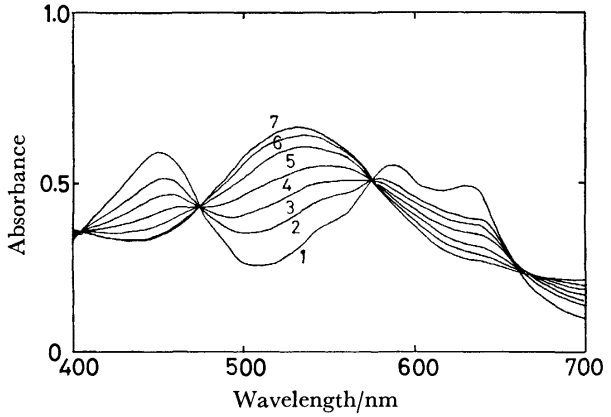

Fig. 1. The spectral change in the reaction of $[Co^{III}(pan)_2]Cl$ with O_2^- in DMSO. Initial concentrations of the complex and O_2^- are 2.18×10^{-5} and 2.99×10^{-4} mol dm^{-3}, respectively. The solution contains 1.42×10^{-3} mol dm^{-3} dicyclohexyl-18-crown-6 as a solubilizing agent. The spectrum was recorded at 0 (1), 0.5 (2), 4 (3), 11 (4), 30 (5), 60 (6), and 125 min (7).

Reaction of $[Co^{III}(pan)_2]Cl$ with O_2^-. Figure 1 shows a typical example of the spectral change for the reaction of $[Co^{III}(pan)_2]^+$ and O_2^- in DMSO. Each spectrum was recorded at appropriate time intervals. The spectra changed with isosbestic points at 475, 575, and *ca.* 650 nm.[3] The absorptions around 450 and 600 nm due to $[Co^{III}(pan)_2]^+$ decreased with the increase of a new absorption around 530 nm. The spectrum due to the free ligand PAN was not observed in the course of the reaction. The final spectrum of the reaction was essentially the same as the spectrum of (1) $[Co^{II}(pan)_2]^0$ observed as an intermediate in the course of the reaction between Co^{2+} and PAN,[2] (2) $[Co^{II}(pan)_2]^0$ observed in the deoxygenated system,[2] and (3) the final product obtained by the electrolytic reduction of $[Co^{III}(pan)_2]Cl$.[4] These results suggest the formation of $[Co^{II}(pan)_2]^0$ ($\lambda_{max}=530$ nm, $\varepsilon=28000$ mol^{-1} dm^{-3} cm^{-1} in DMSO) by the reaction of $[Co^{III}(pan)]^+$ with O_2^-.

The changes in the absorbance *vs.* time for the reaction of $[Co^{III}(pan)_2]^+$ with O_2^- in deoxygenated media and in undegassed solution were compared with each other. For the deoxygenated system the solutions of the two reactants were separately degassed beforehand by freezing several times. No difference in the rates of the reduction was observed between these two systems. This result suggests that the oxygen dissolved in the solution does not affect the rate of the reduction of $[Co^{III}(pan)_2]^+$ by O_2^-.

Kinetic measurements were carried out using a stopped-flow method under the conditions of O_2^- in large excess over the ligand. The pseudo-first-order rate constant, k_{obsd}, showed a first-order dependence on the total concentrations of $[O_2^-]_0$ (1.3×10^{-4}—6.3×10^{-4} mol dm^{-3}). From the slope and the intercept of the linear plots of k_{obsd} against $[O_2^-]$ the forward and the backward rate constants, k_f and k_d, were evaluated to be 5.2×10^2 mol^{-1} dm^3 s^{-1} and $<10^{-2}$ s^{-1}, respectively.

Stability of $[Co^{II}(pan)_2]^0$ in DMSO. When dry oxygen was passed for 1—2 h through a dry DMSO solution of $[Co^{II}(pan)_2]^0$ obtained by electrolytic reduction, no oxidation was observed, the spectrum remaining unchanged at least for 1 h. However the addition of a small amount of water (0.5 cm^3 H_2O to 3.5 cm^3 DMSO) changed the spectrum gradually to that of $[Co^{III}(pan)_2]^+$. Marked acceleration of the oxidation to $[Co^{III}(pan)_2]^+$ was observed by the addition of a slight excess of perchloric acid over $[Co^{II}(pan)_2]^0$; a large excess of perchloric acid dissociated the ligand PAN from cobalt(II) complex. These results suggest that the oxidation of $[Co^{II}(pan)_2]^0$ by oxygen does proceed in the presence of H_2O and/or H^+. The considerable stability of $[Co^{II}(pan)_2]^0$ in dry non-protonic solvent as DMSO and also the small value of k_d in dry DMSO support the following mechanism:

$$Co^{2+} + 2PAN \overset{H^+}{\rightleftharpoons} [Co^{II}(pan)_2]^0$$
$$\underset{O_2^- \text{ in DMSO}}{\overset{O_2,\ H_2O \text{ and/or } H^+}{\rightleftharpoons}} [Co^{III}(pan)_2]^+,\ k_d,\ k_f.$$

This mechanism is the same as that postulated for the reaction of copper phenanthroline complex with oxygen and hyperoxide.[5]

Experimental

Materials. The complex $[Co^{III}(pan)_2]Cl$ was pre-

† Presented in part at the 1979 Winter Meeting in Hokkaido of the Chemical Society of Japan and the Japan Society for Analytical Chemistry, Sapporo, February 2, 1979, Abstract, p. 25.

pared from cobalt(II) chloride and PAN (Dojindo, Kumamoto). Stoichiometric amount of cobalt(II) chloride in water and PAN in dioxane were slowly mixed with stirring. The solution was diluted with a large amount of water. Precipitates formed were filtered, washed successively with dioxane–water (1:20) and water, and dried *in vacuo*. Found: C, 58.66; H, 3.70; N, 13.57; Cl, 5.92%. Calcd for $C_{30}H_{20}N_6O_2CoCl \cdot H_2O$: C, 59.17; H, 3.64; N, 13.80; Cl, 5.82%.

Dicyclohexyl-18-crown-6 (perhydrodibenzo-18-crown-6) (Nippon Soda) and KO_2 (ICN Pharmaceuticals) were used without further purification. Dimethyl sulfoxide was dried with calcium hydride, distilled under reduced pressure, and stored under argon atmosphere. The solution of O_2^- was prepared by dissolving KO_2 in DMSO by adding dicyclohexyl-18-crown-6 in DMSO.[5]

Standardization of O_2^- in DMSO with Iodine. The concentration of O_2^- in DMSO solution was determined titrimetrically. To three cubic centimeters of a *ca.* 1×10^{-3} mol dm^{-3} solution of O_2^- in a capped optical cell a freshly-prepared standard DMSO solution of iodine (2.0×10^{-2} mol dm^{-3}) was added using a microsyringe, and the absorbance at 400 nm was measured after 15 min. The final absorbance was plotted against the amounts of I_2 solution added, showing the gradual decrease until it began to increase at the end point **A** in proportion to the concentration of an excess of iodine (see the inset of Fig. 2). The concentration of O_2^- was determined from the amount of iodine consumed at **A** based on the following reaction.

$$2O_2^- + I_2 \longrightarrow 2O_2 + 2I^-$$

Stability of O_2^- in DMSO. Figure 2 shows the change in the concentration of O_2^- in DMSO with the lapse of time stored at room temperature in a tightly-sealed flask in the dark as described in the literature.[5] Seventy percent of O_2^- based on the weighed amount of KO_2 was found to remain unchanged even a day after preparation. After 2 weeks the concentration of O_2^- decreased to 60%.

Measurements. Absorption spectra were measured at 25±0.2 °C with a Hitachi recording spectrophotometer Model EPS-3T. Platinum electrodes were used for the electrolytic reduction of the complex. Kinetic measurements were carried out with a Union Giken stopped-flow spectrophotometer Model 1300.

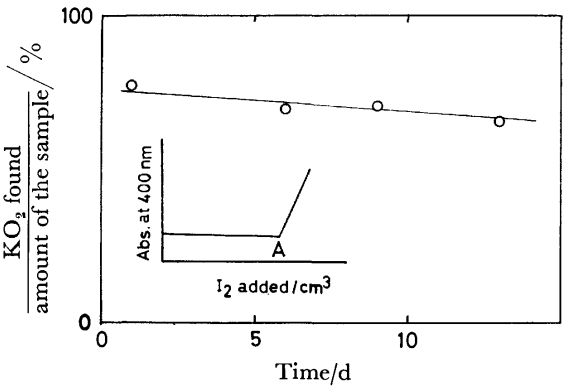

Fig. 2. The change in the concentration of O_2^- in DMSO solution with the lapse of time. The initial concentration of O_2^- was *ca.* 1×10^{-3} mol dm^{-3}. The inset shows a typical pattern for the change in absorbance at 400 nm against the volume of standard I_2 added (see the text).

References

1) K. L. Cheng and R. H. Bray, *Anal. Chem.*, **27**, 782 (1955).

2) K. Mochizuki, T. Imamura, T. Ito, and M. Fujimoto, *Bull. Chem. Soc. Jpn.*, **51**, 1743 (1978).

3) New absorption bands appeared around 600—700 nm after standing for long time may be ascribed to the decomposition of the ligand by excess of O_2^-.

4) The electrolytic reduction was carried out at 1.5 V for 12 h in DMSO under anaerobic conditions in the presence of 0.1 mol dm^{-3} Et_4NClO_4 as a supporting electrolyte.

5) J. S. Valentine and A. B. Curtis, *J. Am. Chem. Soc.*, **97**, 224 (1975).

Studies on the Solvent Extraction of Metal Perchlorates. I. Partition of Sodium(I) between Aqueous Perchlorate, Thiocyanate, and Iodide Solution and Hexane Containing Trioctylphosphine Oxide

Satoshi KUSAKABE and Tatsuya SEKINE*

Department of Chemistry, Science University of Tokyo, Kagurazaka, Shinjuku-ku, Tokyo 162

(Received November 26, 1979)

Synopsis. Extraction equilibria of sodium (I) in aqueous 1 mol dm^{-3} sodium salt–hexane containing trioctylphosphine oxide systems were measured at 25 °C. The extracted species was always trisolvate, the extraction being improved in the order $NaClO_4$>NaSCN>NaI>$NaNO_3$. This is explained in terms of the hydrofobic and hydrophilic tendencies of the anions.

The solvent extraction behavior of metal perchlorates with solvating type extractants differs somewhat from that of other salts in which the interactions between the metal ion and the anions are to some extent coordinative. We have measured the distribution ratio of sodium(I) between aqueous perchlorate solutions and hexane containing trioctylphosphine oxide (TOPO). In the present paper, the results are compared with those in other systems containing other kinds of anion.

Experimental

All the reagents were of reagent grade. A weighed amount of TOPO, supplied by Dojindo Laboratories, Kumamoto, was dissolved in hexane and washed with 0.1 mol dm^{-3} sodium hydroxide, the supernatant portion of organic phase being washed with water. Sodium perchlorate was recrystallized three times from water. The sodium salts were dissolved in water and the concentration was measured by gravimetry.

The distribution measurements were carried out in a room thermostated at 25±0.3 °C. A 5—7 cm^3 portion of a 1 mol dm^{-3} sodium salt solution and the same volume of a TOPO–hexane solution were placed in stoppered glass tube, agitated mechanically and centrifuged. A portion of the organic phase was transferred into another tube and the sodium (I) was back-extracted into 0.01 or 1 mol dm^{-3} nitric acid. The sodium content was measured by flame photometry.

Results and Discussion

The extraction of sodium(I) as ion-pairs with an anion, X^-, with TOPO can be expressed by

$$Na^+ + X^- + n\text{TOPO(org)} \rightleftarrows Na(TOPO)_n{}^+X^-\text{(org)}, \quad (1)$$

where "org" denotes chemical species in the organic phase. When the organic phase is an essentially nonpolar solvent, the dissociation of the extracted ion-pairs can be neglected. Since the solvation number was always three, we obtain the equation

$$D = [Na(I)]_{org}/[Na(I)] = [Na(TOPO)_3{}^+X^-]_{org}/[Na^+] = K_{ex3}[X^-][TOPO]^3_{org}, \quad (2)$$

where K_{ex3} is the extraction constant defined by

$$K_{ex3} = [Na(TOPO)_3{}^+X^-]_{org}/[Na^+][X^-][TOPO]^3_{org}. \quad (3)$$

Since perchloric acid[1] as well as thiocyanic and hydroiodic acid[2] are well extracted with TOPO, we get

$$[TOPO]_{total} = [TOPO]_{org} + m[HX(TOPO)_m]_{org} + 3[Na(TOPO)_3{}^+X^-]_{org} \quad (4)$$

$$= [TOPO]_{org} + mK_h[H^+][X^-][TOPO]^m_{org} + 3K_{ex3}[Na^+][X^-][TOPO]^3_{org} \quad (5)$$

where K_h is given by

$$K_h = [HX(TOPO)_m]_{org}/[H^+][X^-][TOPO]^m_{org}. \quad (6)$$

When the extraction of the acid is negligible, we have

$$[TOPO]_{org} = [TOPO]_{total} - 3K_{ex3}[Na^+][X^-][TOPO]^3_{org}. \quad (7)$$

Equation 5 indicates that the "free" TOPO concentration decreases with an increase in acidity and consequently a decrease in metal extraction. This was experimentally confirmed. For example, when the total TOPO concentration was 0.1 mol dm^{-3} and the aqueous phase was a perchlorate medium, the log D was −2.3 if the aqueous phase was neutral. However, it turned out to be −2.6 and −3.4 when the acid concentration in the initial aqueous phase was 0.01 and 0.03 mol dm^{-3}, respectively.

The free TOPO concentration and extraction constants were calculated by a successive approximation procedure by means of Eqs. 2 and 7 using a least squares computer program. A good fit of the calculated values and experimental data was obtained only when an extraction of trisolvates, $Na(TOPO)_3{}^+X^-$, was assumed. The constants obtained are:

$NaClO_4$: $\log K_{ex3} = 1.01 \pm 0.14$

NaSCN: $\log K_{ex3} = 0.38 \pm 0.11$

NaI: $\log K_{ex3} = -0.46 \pm 0.14$

where the limit of the error is 3σ. Figure 1 shows the dependence of the distribution ratio on the calculated free TOPO concentration. The solid lines were calculated by introducing these values into Eq. 2.

Attempts were made to analyze the acid dependence of the perchlorate extraction by means of Eqs. 2 and 5 using the K_h value of perchloric acid,[1] $10^{3.15}$. However, the results were lower than the calculated ones when the TOPO and/or acid concentration was high. This may be due to changes in the activity coefficients of the chemical species in the organic phase. When both the acid and TOPO concentrations were high (*e.g.* initial TOPO and acid concentrations 0.1 mol dm^{-3}), a second organic phase appeared.

Experiments were carried out with sodium nitrate, bromide, and chloride. The extractions were very poor. After careful purification of TOPO by the procedure

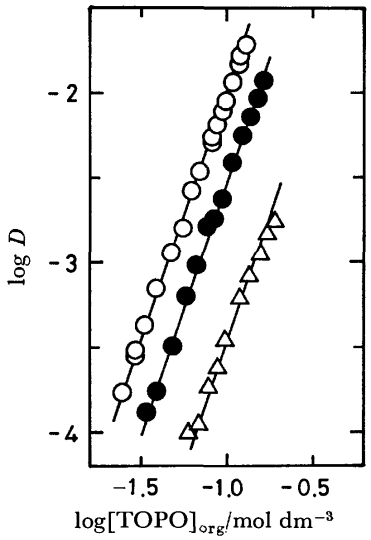

Fig. 1. The distribution of sodium perchlorate (○), thiocyanate (●), and iodide (△) as a function of the calculated free TOPO concentration in hexane. The aqueous phase was 1.0 mol dm^{-3} solution of each salt.

described, the distribution ratio was, in all cases, lower than 10^{-4} with 0.1 mol dm^{-3} TOPO.

The interactions between sodium ion and the anion in the ion-pairs might mainly be electrostatic and thus the effect of the anion on the solvation of the metal ion should be slight. This may be the reason why only the solvation number of 3 was found among the three sodium salts in the present study, differing from the findings previously reported: the solvation number of perchlorates of cobalt(II),[3] nickel(II),[4] and zinc(II)[5] with TOPO is larger than that of their thiocyanates. It is also different from the TOPO extraction of mineral acids into hexane. The solvation number of TOPO of thiocyanic and nitric acid was unity while that of perchloric and hydrohalogenic acid was two. This can be explained on the assumption that the interactions between the proton and the anion of the acid is not purely electrostatic in this nonpolar solvent.

The distribution ratio of sodium(I) under identical conditions is higher in the order, perchlorate>thiocyanate>iodide>nitrate. In all cases, the nature of the cations in the ion-pairs, $Na(TOPO)_3^+X^-$, should be similar and the extraction is mainly affected by the extractability of the anion. The large size and small tendency of hydration of perchlorate ion are favorable for its extraction. Thiocyanate ion is also large, and not as hydrophilic as to interfere with its extraction. The two anions differ from nitrate ion: although nitrate ion is large, its hydrophilic nature should make its extraction much poorer. The order observed among the halides may also be explained from this standpoint.

It should be noted that the extraction of sodium perchlorate from 1 mol dm^{-3} sodium perchlorate solution is not very poor when the TOPO concentration is high. Even at high pH where the extraction of perchloric acid is negligible, the sodium perchlorate extraction somewhat decreases the TOPO concentration. For example, when the initial TOPO concentration in hexane is 0.1 and 0.2 mol dm^{-3}, the extraction of sodium perchlorate from its 1 mol dm^{-3} solution decreases the free TOPO concentration to 0.083 and 0.13 mol dm^{-3}, *viz.*, the free TOPO concentration decreases to 83 and 65% under these conditions. However, when the TOPO concentration is lower than 0.018 mol dm^{-3}, the decrease is calculated to be less than 1%. The same is true in the thiocyanate and iodide extraction systems though the effect is smaller than in the perchlorate system.

Several reports have appeared on the solvent extraction of sodium(I).[6] However, only a few deal with that of sodium salts;[7-9] no quantitative analysis seems to have been made on their extraction equilibria. However, since sodium perchlorate solutions are often employed as the ionic media of solvent extraction of metal ions with solvating type extractants in nonpolar solvents, this type measurement is indispensable for a precise analysis of metal extraction equilibria in such systems.

The authors are grateful to Messrs. Yuichi Ishida and Kenji Ohira for their assistance in the experiments.

References

1) M. Niitsu and T. Sekine, *J. Inorg. Nucl. Chem.*, **37**, 1054 (1975).

2) M. Niitsu and T. Sekine, *Bull. Chem. Soc. Jpn.*, **50**, 1015 (1977).

3) T. Sekine, R. Murai, and M. Iguchi, *Nippon Kagaku Zasshi*, **92**, 412 (1971).

4) R. Murai, S. Iwahori, and T. Sekine, *Bull. Chem. Soc. Jpn.*, **50**, 1315 (1977).

5) H. Moriya and T. Sekine, *Bull. Chem. Soc. Jpn.*, **45**, 1626 (1972).

6) T. Sekine and Y. Hasegawa, "*Solvent Extraction Chemistry*," Marcel Dekker, New York (1977), p. 501.

7) G. M. Arcand and W. R. Carroll, *J. Phys. Chem.*, **66**, 1014 (1962).

8) Y. Hasegawa, T. Ishii, and T. Sekine, *Bull. Chem. Soc. Jpn.*, **44**, 275 (1971).

9) I. L. Krupatkin, L. D. Vorobeva, V. P. Maskhliya, and M. E. Veselova, *Zh. Obshck. Khim.*, **45**, 985 (1975); *Chem. Abstr.*, **83**, 66250 (1975).

The Glucosylation of Several Alcohols with Tetra-*O*-benzyl-α-D-glucopyranose and a Mixture of *p*-Nitrobenzenesulfonyl Chloride, Silver Trifluoromethanesulfonate, and Triethylamine

Shinkiti KOTO,* Tadaaki SATO, Naohiko MORISHIMA, and Shonosuke ZEN
School of Pharmaceutical Sciences, Kitasato University, Shirokane, Minato-ku, Tokyo 108
(Received September 20, 1978)

Synopsis. A novel glucosylation of several alcohols using 2,3,4,6-tetra-*O*-benzyl-α-D-glucopyranose and a ternary mixture of *p*-nitrobenzenesulfonyl chloride, silver trifluoromethanesulfonate, and triethylamine is presented.

The development of methods for the glycosylation is important in carbohydrate chemistry.[1] Recently, several syntheses of glucosides using 2,3,4,6-tetra-*O*-benzyl-α-D-glucopyranose (**1**) have been reported.[2] We ourselves have briefly communicated a two-stage glucosylation using a novel procedure for generating the reactive sulfonate[3] from **1** and a ternary mixture of *p*-nitrobenzenesulfonyl chloride (NsCl), silver trifluoromethanesulfonate (AgOTf), and triethylamine (Et_3N).[4] This report will present a further finding that the one-stage treatment of an equimolar mixture of **1** and an alcohol with the ternary mixture in dichloromethane afforded the corresponding glucosides containing the β-anomer predominantly, as is shown in Table 1. This

Table 1. Glucosylation of alcohols with tetra-*O*-benzyl-α-D-glucopyranose (**1**) and a mixture of *p*-nitrobenzenesulfonyl chloride, silver trifluoromethanesulfonate, and triethylamine

Run	R[b]	Method[c]	Yield/% Glucosides (α/β)	(Net Yield)[d]	**7a**+**7b**	Recov./% **1**
1	Me	/2/	76 (16/60)	(83)	16	8
2	Me	/1/	68 (11/57)	(96)	0	29
3	Cm	/2/	67 (18/49)	(72)	23	7
4	Cm	/1/	75 (15/60)	(96)	0	22
5	Ch	/2/	64 (17/47)	(78)	21	18
6	Ch	/1/	69 (19/50)	(84)	12	18
7	Ct	/1/	56 (16/40)	(72)	17	22[e]
8	Dh	/1/	76 (13/60)	(93)	0	18[f]

a) Yields are based on the weight of products separated chromatographically, referring to that of **1** charged. b) Ch=cyclohexyl, Cm=cyclohexylmethyl, Ct=5α-cholestan-3β-yl, Dh=6-(2,4-dinitroanilino)hexyl, Me=methyl. c) /1/=one-stage treatment, /2/=two-stage treatment. d) Yields based on the **1** used. e) The recovery of the alcohol was 37%. f) The recovery of the alcohol was 23%.

constitutes a convenient method for the preparation of β-glucoside from **1**. The self-condensation of **1**, yielding octa-*O*-benzyl-α,α- and α,β-trehalose (**7a** and **7b**),[5] was prevented in the one-stage glucosylation of alcohols with a primary hydroxyl group. Silver chloride and *p*-nitrobenzenesulfonic acid were deposited in the course of the reaction. Thus, the overall reaction is written by Eq. 1, where G denotes the tetra-*O*-benzyl-D-glucopyranosyl moiety:

	R^1	R^2
1	H	OH
2a	H	OMe
2b	OMe	H
3a	H	OCm
3b	OCm	H
4a	H	OCh
4b	OCh	H
5a	H	OCt
5b	OCt	H
6a	H	ODh
6b	ODh	H
7a	H	OαG
7b	OαG	H

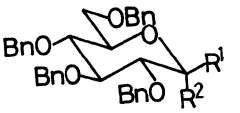

Bn=benzyl
Ch=cyclohexyl
Cm=cyclohexylmethyl
Ct=5α-cholestan-3β-yl
Dh=6-(2,4-dinitroanilino)hexyl
Me=methyl
αG=2,3,4,6-tetra-*O*-benzyl-α-D-glucopyranosyl

$$\alpha\text{GOH} + \text{ROH} + \text{NsCl} + \text{AgOTf} + \text{Et}_3\text{N} \longrightarrow \alpha,\beta\text{GOR} + \text{AgCl} + \text{NsOH} + \text{Et}_3\text{N}\cdot\text{TfOH}. \quad (1)$$

It should be noted that the self-condensations of **1** were unavoidable in the one-stage glucosylation of alcohols with a secondary hydroxyl group. The ternary mixture cannot be stored even at 0 °C, since an appreciable amount of bis(*p*-nitrophenyl) sulfoxide is formed.[6]

Experimental

General. The instruments used are identical with those mentioned in the foregoing papers,[5,7] except for the JEOL JDX-7F X-ray powder diffractometer (Cu *K*α ray, λ=153.2 pm, Ni filter). The dichloromethane (Wako), cyclohexylmethanol (Tokyo Kasei), cyclohexanol (Koso), and triethylamine (Wako) were distilled and stored over molecular sieves (Linde 3A) before use. Compound **1**,[7] *p*-nitrobenzenesulfonyl chloride (Tokyo Kasei), 5α-cholestan-3α-ol (Tokyo Kasei), and 6-(2,4-dinitroanilino)-1-hexanol (mp 76—77 °C, Found: C, 50.55, H, 6.05, N, 15.03%. Calcd for $C_{12}H_{17}N_3O_5$: C, 50.88, H, 6.05; N, 14.83%), prepared by the treatment of 6-amino-hexanol (Aldrich) with 2,4-dinitrofluorobenzene (Wako) and $NaHCO_3$ in aq ethanol, as well as silver trifluoromethanesulfonate, made by the neutralization of Ag_2CO_3 (Wako) with aq trifluoromethanesulfonic acid (Kanto Denka Kogyo), were stored *in vacuo* over P_2O_5.

General Procedure for One-stage Glucosylation. To a mixture of **1** (180 mg, 0.33 mmol), alcohol (0.33 mmol), *p*-nitrobenzenesulfonyl chloride (74 mg, 0.33 mmol), and silver trifluoromethanesulfonate (86 mg, 0.33 mmol) in dichloromethane (1.8 ml), we added triethylamine (47 μl, 0.33 mmol) at −40 °C (bath temperature) and the resulting mixture was stirred well. The bath temperature gradually rose at the rate of 1.0 °C/min to 0 °C, at which temperature the mixture was then stirred for 3 h. After the addition of powdered $NaHCO_3$ (*ca.* 0.1 g) and stirring at room temperature, the mixture was filtered, evaporated, and chromatographed on silica gel (Kanto Kagaku), using three kinds of solvent systems: benzene and butanone (Solvent A), hexane and ethyl acetate (Solvent B), and chloroform and ethyl acetate (Solvent C),

TABLE 2. PHYSICAL DATA OF GLUCOSIDES

	Solvents for Chromatog.[a]		Mp/°C (Recryst. from)[b]	$[\alpha]_D^{20}$ (c, $CHCl_3$)	Found (%) C H N	Calcd for: (%)	C H N
2a[c]	Solv. A	s	—	+28° (1.0)	75.73; 6.92		
2b[d]		f	74—75 (HX)	+11° (5.6)	75.85; 6.92	$C_{35}H_{38}O_6$	75.79; 6.90
3a	Solv. B	s	—	+33° (1.0)	76.73; 7.48		
3b		f	103—104 (HX)	+4° (1.6)	77.52; 7.56	$C_{41}H_{48}O_6$	77.36; 7.55
4a	Solv. B	s	—	+45° (1.3)	77.26; 7.44		
4b		f	105—106 (IP)	+8° (1.6)	77.40; 7.50	$C_{40}H_{46}O_6$	77.14; 7.45
5a	Solv. B	s	123—125 (IP)	+67° (0.5)	80.44; 9.07		
5b		f	120—123 (IP)	+20° (1.0)	79.89; 8.90	$C_{61}H_{82}O_6$	80.40; 9.01
6a	Solv. C	f	—	+25° (1.0)	68.32; 6.08; 4.95		
6b		s	—	+9° (1.0)	68.43; 6.26; 5.06	$C_{46}H_{51}N_3O_{10}$	68.55; 6.38; 5.21

a) For the solvent systems, see **Experimental**. f=faster-moving, s=slower-moving. b) HX=hexane, IP=isopropyl ether. c) O. T. Schmidt, T. Auer, and H. Schmadel, *Chem. Ber.*, **93**, 556 (1960), $[\alpha]_D^{20}$ +32.2° (*c* 5, $CHCl_3$). d) P. W. Austin, F. E. Hardy, J. G. Buchanan, and J. Baddiley, *J. Chem. Soc.*, **1964**, 2128, mp 68—69 °C, $[\alpha]_D^{20}$ +11° (*c* 5.3, dioxane).

respectively; these solvents were also used for TLC on silica gel (Merck, 7731).

General Procedure for Two-stage Glucosylation.[4,8] To an equimolar mixture of **1** (180 mg, 0.33 mmol), *p*-nitrobenzenesulfonyl chloride (74 mg), and silver trifluoromethanesulfonate (86 mg) in dichloromethane (1.8 ml), we added triethylamine (47 μl, 0.33 mmol) at −40 °C. After the bath temperature was risen to −10 °C, the mixture was stirred for 30 min. An alcohol (0.33 mmol) was then added, and agitation was continued at 0 °C for 3 h. Work-up was done as has been described above.

*Self-condensation of **1** with the Ternary Mixture.* To a mixture of **1** (90 mg, 0.17 mmol), *p*-nitrobenzenesulfonyl chloride (37 mg), and silver trifluoromethanesulfonate (43 mg) in dichloromethane (0.9 ml), we added triethylamine (24 μl) at −40 °C. The bath temperature rose to room temperature at the rate of 1.0 °C/min. The processed reaction mixture was chromatographed using Solvent A (gradient, 100: 1—20: 1) to give **7a** (17.5 mg, 20%) and then **7b** (36.6 mg, 42%). Compounds **7a** and **7b** were identified with those prepared before.[7]

*Alternative Synthesis of **5a**.* Ethyl 2.3,4,6-tetra-*O*-benzyl-1-thio-α-D-glucopyranoside[9] (40 mg, 0.83 mmol) in dichloromethane (0.5 ml) was treated with Br_2 in dichloromethane (0.62 g/ml, 22 μl) at room temperature for 10 min. After evaporation to dryness, the syrup thus obtained was reacted with 5α-cholestan-3β-ol (32 mg, 0.083 mmol), tetrabutylammonium bromide[10] (27 mg, 0.083 mmol), and 2,6-lutidine (10 μl, 0.083 mmol) in dichloromethane (0.5 ml) overnight. Chromatography using Solvent A (40: 1), followed by recrystallization from hexane, afforded **5a** (59 mg, 78%) (Found: C, 79.39; H, 8.83%).

*Alternative Synthesis of **5b**.* A mixture of 3β-(2,3,4,6-tetra-*O*-acetyl-β-D-glucopyranosyloxy)-5α-cholestan[11] (0.14 g, 0.2 mmol), KOH (0.35 g), and benzyl chloride (1.4 ml) was heated at 100 °C for 16 h. After processing, chromatography sing Solvent A (40: 1) and recrystallization from hexane gave **5b** (0.08 g, 73%) (Found: C, 79.44; H, 8.70%).

Isolation of p-*Nitrobenzenesulfonic Acid and Silver Chloride.* The reaction mixture of glucosylation carried out on a 0.33-mmol scale using cyclohexylmethanol was filtered to give a solid. Subsequent washings of solid with methanol on evaporation afforded hydroscopic crystals of *p*-nitrobenzenesulfonic acid (42 mg, 62%), identified with the authentic sample by determining their IR (KBr) spectra. A washed solid (≈40 mg, >80%) on the filter was identified with AgCl by determining its X-ray powder diffraction.

Examination of the Stability of the Ternary Mixture. To a mixture of *p*-nitrobenzenesulfonyl chloride (73.8 mg, 0.33 mmol) and silver trifluoromethanesulfonate (85.7 mg, 0.33 mmol) in dichloromethane (1.8 ml), we added triethylamine (47 μl, 0.33 mmol) at −40 °C; the bath temperature was programmed as it was in the one-stage treatment. The mixture was then directly poured onto a column of silica gel, which was subsequently chromatographed with benzene. Bis(*p*-nitrophenyl)sulfoxide (8.2 mg, 17%) (mp 181.5 °C, UV_{max} (95% C_2H_5OH) 268 nm (ε 1.8×10^4) [lit,[12] mp 178—180 °C, UV_{max} (95% (C_2H_5OH) 268 nm (ε 1.82×10^4)], Found: C, 49.33, H, 2.66; N, 9.71. M^+ − 16. 276,[13] Calcd for $C_{12}H_8N_2O_5S$: C, 49.32; H, 2.76; N, 9.58%, MW 292. 27) and the slower-moving *p*-nitrobenzenesulfonyl chloride (55.7 mg, 75%), identified with an authentic sample by determining the mp, IR (KBr), and MS (M^+ 221, M^++2. 223), were thus obtained.

We wish to thank the Kanto Denka Kogyo Co. for their gift of trifluoromethanesulfonic acid and Mr. Yoshio Hamada for his technical assistance.

References

1) K. Igarashi, *Adv. Carbohydr. Chem. Biochem.*, **34**, 243 (1977).
2) J. Leroux and A. S. Perlin, *Carbohydr. Res.*, **47**, C8 (1976), **67**, 163 (1978); W. A. Szarek, H. C. Jarrell, and J. K. N. Jones, *ibid.*, **57**, C13 (1977); H. Tsutsumi, Y. Kawai, and Y. Ishido, *Chem. Lett.*, **1978**, 629.
3) F. J. Kronzer and C. Schuerch, *Carbohydr. Res.*, **27**, 379 (1973); R. Eby and C. Schuerch, *ibid.*, **34**, 79 (1974).
4) S. Koto, Y. Hamada, and S. Zen, *Chem. Lett.*, **1975**, 587.
5) S. Koto, N. Morishima, and S. Zen, *Bull. Chem. Soc. Jpn.*, **52**, 784 (1979).
6) Studies of the formation of sulfoxide are in progress.
7) S. Koto, N. Morishima, Y. Miyata, and S. Zen, *Bull. Chem. Soc. Jpn.*, **49**, 2639 (1976).
8) In the early phase of the study (Ref. 4), 1,2-dichloroethane was used. Later, less freezing dichloromethane was used.
9) F. Weygand and H. Ziemann, *Ann.*, **657**, 179 (1962).
10) R. U. Lemieux, K. B. Hendriks, R. V. Stick, and K. James, *J. Am. Chem. Soc.*, **97**, 4056 (1975).
11) R. P. Linstead, *J. Am. Chem. Soc.*, **62**, 1766 (1940).
12) H. H. Szmant and J. O. McIntosh, *J. Am. Chem. Soc.*, **73**, 4246 (1951).
13) This peak was not detected in the MS of the NsCl used.

The Formation of Two Kinds of Thiophene Derivatives by the Reaction of the 4*H*-Pyran-4-thione Derivative with Dimethyloxosulfonium Methylide in a One-pot Process

Hiroshi YAMAOKA,* Ikuhiro MISHIMA, and Terukiyo HANAFUSA

Department of Chemistry, Faculty of Science, Hiroshima University, Higashi-senda-machi, Naka-ku, Hiroshima 730

(Received July 21, 1979)

Synopsis. The reaction of 2,6-dimethyl-3,5-diphenyl-4*H*-pyran-4-thione with dimethyloxosulfonium methylide occurred facilely to give two kinds of 2-thienylacetones, accompanied by a five-membered α,β-unsaturated thione, a naphtho-[2,1-*b*]thiophene derivative, and a hemithioacetal.

In our previous report, the reaction of the 4*H*-1-benzopyran-4-thione (chromothione) derivatives with dimethyloxosulfonium methylide (DOSM) was reported to give 3,4-benzo-5-methylene-2-oxabicyclo[4.1.0]hept-3-enes (vinylcyclopropanes), with the increment of two methylene groups, accompanied by the removal of the sulfur in a one-pot procedure, although there have been few reports on the addition of DOSM to thioketones.[1] There is, thus, interest in the study of the behavior of DOSM toward the parent 4*H*-pyran-4-thione derivative, **1**, in comparison with the benzo-condensed chromothione system.

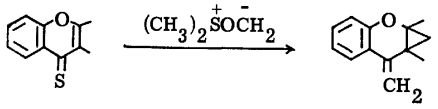

Experimental

The mps are uncorrected. The IR and the UV spectra were measured with Hitachi 215 and 124 model apparatuses respectively. The ^{1}H-NMR spectra were measured on a Varian T-60 spectrometer in $CDCl_3$, using tetramethylsilane as the internal standard. We are indebted to Drs. Shizuko Eguchi and Yasuhito Uchio, Hiroshima Univ., for obtaining the mass and the ^{13}C-NMR spectra respectively.

Preparation of Thione **1**. The treatment of 2,6-dimethyl-3,5-diphenyl-4*H*-pyran-4-one[2] with P_2S_5 in 1,2-dichloroethane under reflux for 2 h afforded pinkish prisms. Mp 224—226 °C (80% yield, from 2-propanol) (see Table 1).

Reaction of 4H-Pyran-4-thione **1** *with DOSM*. To DOSM in dimethyl sulfoxide (15 ml), prepared from NaH (66% in oil, 130 mg, 3.57 mmol) and trimethyloxosulfonium iodide (850 mg, 3.86 mmol), dry ether (5 ml) and **1** (500 mg, 1.71 mmol) were added, after which the mixture was stirred at room temperature for several minutes under a nitrogen atmosphere. After the usual work-up process, the crude product was purified by the use of a silica-gel column, followed by preparative TLC using ether-light petroleum as the eluent, to give five products (see Table 1): **2**, violet oil (15 mg, 3%, λ_{max} 355 nm (log ε 3.42), unstable; a facile isomerization occurred to give **3** quantitatively); **3**, colorless oil (80 mg, 15%; monooxime, mp 180—182 °C from methanol–water); **4**, mp 40—42 °C (38 mg, 7%, from light petroleum); **5**, mp 117—119 °C (trace, from light petroleum, λ_{max} 243 (4.58), 285 (3.92), 315 (3.28), 329 nm (3.41)); **6**, mp 110—112 °C (110 mg, 19%, from light petroleum, λ_{max} 297 nm (3.47); monoacetate, *m/e* 380 (M^+), 338, 205 (base), calcd for $C_{23}H_{24}O_3S$ (Mw 380); δ 7.58—7.13 (10H, m), 3.80 (2H, s, methylene), 2.10 (3H, s), 2.02 (3H, s), 1.98 (3H, s), 1.92 (3H, s)).

Results and Discussion

The treatment of **1** with DOSM in dimethyl sulfoxide (DMSO) afforded five products, **2**, **3**, **4**, **5**, and **6**, whose structures were assigned to a five-membered α,β-unsaturated thione, two kinds of thienylacetones, a naphthothiophene, and a hemithioacetal, respectively, on the basis of their microanalyses and spectral data, as shown in the table (see also Experimental section). The production of two kinds of 2-thienylacetone derivatives, **a**, was expected by comparing the spectral characteristics of **3** and **4** with those of the related 2-furylacetones.[3] The UV spectrum of **5** agreed well with the parent naphtho[2,1-*b*]thiophene reported in the literature.[4] Therefore, it is noteworthy that all these compounds in our present work contain sulfur, while vinylcyclopropanes have been obtained by the reaction of chromothione with DOSM.[1]

Now let us discuss the structural problem of two kinds of thiophene derivatives, **3** and **4**. As it has been reported that the acid-catalyzed deuterium exchange of α-hydrogen on the thiophene ring took place 10^3 times as fast as that of β-hydrogen,[5] **3** and **4** were subjected to deuterium exchange in acetic acid-d_4 at 140 °C for 1.5 h; it was found that a vinyl signal (δ=6.87 in **3**) completely disappeared, while, on the contrary, another signal (δ=6.65 in **4**) appeared sufficiently in the ^{1}H-NMR spectra. Accordingly, **3** possesses α-hydrogen on the thiophene ring, while there is no such hydrogen in **4**.

Compound **2** rearranged facilely into **3** quantitatively under neat conditions. Ketone, **7**,[3] was treated with P_2S_5 in carbon tetrachloride at room temperature for 6 h to give **4**, but **3** could not be detected. It may, therefore, be expected that there are two kinds of formation routes, where **3** and **4** are derived from a five-membered thione, **2** (Path A), and a six-membered one, **b** (Path B), *via* the Michael adduct, **c**, at the first stage; nonetheless, there is a high reactivity of the thiocarbonyl group at the C-4 position of **1**. One of the plausible pathways for understanding the production of these materials is presented in the Scheme 1.

It is interesting that **2** was isolated as the sole product (30%) from **1** and DOSM, concomitant with the recovery of **1**, when DMSO was diluted with tetrahydrofuran (THF) (1:2 v/v) at 0 °C for 30 min; this is probably because of the stabilization of the intermediate desirable for five-membered α,β-unsaturated thione formation.

Table 1. The IR, NMR, mass, and elemental analyses data

Compound	IR ν_{max} (cm^{-1})	^{1}H-NMR δ (ppm) in $CDCl_3$	Mass (*m/e*)	Found (Calcd) % C	H	S	Formula
1	1630, 1240, 870, 750	7.50—7.05 (10H, m), 2.30 (6H, s)	292 (M^+)	77.79 (78.05)	5.53 (5.52)	11.09 (10.97)	$C_{19}H_{16}OS$
2	1585, 1495, 1250, 975	7.77—7.20 (10H, m), 5.20 (2H, broad s)[a] 2.37 (3H, s), 1.83 (3H, s)	306 (M^+) 288, 205[c]		b)		$C_{20}H_{18}OS$
3*	1715, 1600	7.47—6.93 (10H, m), 6.87 (1H, s), 5.07 (1H, s, methine), 2.0 (6H, s)	306 (M^+) 277, 263[c]	74.37[d] (74.73)	5.97[d] (5.96)	4.34[d,e] (4.36)[e]	$C_{20}H_{18}OS$ ($C_{20}H_{19}NOS$)[d]
4*	1715	7.25 (10H, s), 6.65 (1H, s), 5.28 (1H, s, methine), 2.43 (3H, s), 2.08 (3H, s)	306 (M^+) 279, 263	78.39 (78.01)	5.92 (6.20)	10.46 (9.99)	$C_{20}H_{18}OS$
5	1440, 900, 730, 690	8.10—7.87 (1H, m), 7.70—7.5 (1H, m), 7.47—7.07 (7H, m), 7.02 (1H, s, vinyl), 2.85 (3H, broad s), 2.22 (3H, s)	288 (M^+)[c] 272, 246	83.00 (83.29)	5.81 (5.59)	9.98 (11.12)	$C_{20}H_{16}S$
6*	3500, 1670, 1490, 940, 750	7.92—7.63 (2H, m), 7.53—7.10 (8H, m), 5.02 (OH), 3.50 (1H, d)[f] [7.0],[g] 2.67 (1H, d)[f] [3.2], 2.37 (3H, s) [2.3], 1.92 (3H, s) [1.2], 0.80 (3H, s) [4.0]	338 (M^+) 295, 205[c]	74.52 (74.55)	6.55 (6.67)	9.48 (9.45)	$C_{21}H_{22}O_2S$

* ^{13}C-NMR ($CDCl_3$) δ: **3**, 205.1 (s), 141.3, 138.2, 137.1, 136.7, 130.6, 129.8, 129.4, 128.8, 128.5, 128.1, 127.9, 127.5, 120.3 (d), 58.9 (d), 29.2 (q), 15.4 (q). **4**, 205.1 (s), 140.6, 138.8, 138.5, 136.8, 133.1, 128.7, 128.5, 127.9, 127.4, 127.2, 58.3 (d), 29.0 (q), 15.0 (q). **6**, 211.8 (s), 149.0 (s), 137.2 (s), 136.7 (s), 130.4, 128.6, 128.5, 128.3, 127.3, 81.9 (s), 78.7 (s), 51.7 (t), 30.0 (q), 26.4 (q), 18.4 (q). a) It was separated to δ 5.42 and 5.17 in C_6D_6. b) Too unstable to obtain an analytically pure sample. c) Base peak. d) Monooxime. e) Nitrogen. f) J=16 Hz. g) Downfield shifts (δ, ppm) caused by the addition of Eu(fod)$_3$ (1 equiv.) are shown in brackets.

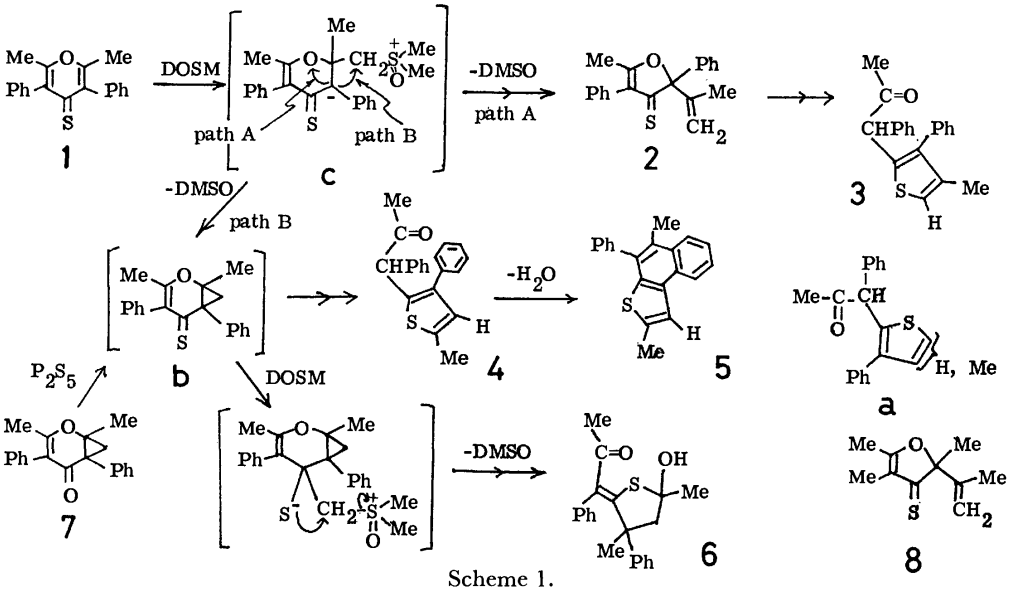

Scheme 1.

The reaction of DOSM to 2,3,5,6-tetramethyl-4*H*-pyran-4-thione in DMSO did not afford any vinylcyclopropanes, but only complicated mixtures difficult to identify, when THF–DMSO was used as the solvent, a five-membered unsaturated thione, **8**, could be isolated in a 5% yield: λ_{max} 345 nm; $\delta(CCl_4)$ 4.98 (1H, s), 4.83 (1H, s), 2.20 (3H, s), 1.82 (3H, s), 1.55 (6H, s); *m/e* 182 (M^+), 167, 139.[6]

In summary, the reactivity of 4*H*-pyran-4-thiones to DOSM is found to be quite different from that of the corresponding benzo-condensed reactants.

We are indebted to the Ministry of Education for two Scientific Research Grants in Aid (374168 and 447022).

References

1) H. Yamaoka, Y. Yamada, S. Ono, and T. Hanafusa, *Chem. Lett.*, **1979**, 523, and the references cited therein.
2) T. L. Emmick and R. L. Letsinger, *Org. Syn. Coll. Vol.*, **V**, 450 (1973).
3) H. Yamaoka, I. Mishima, M. Miyamoto, and T. Hanafusa, *Bull. Chem. Soc. Jpn.*, **53**, 469 (1980).
4) C. E. Loader and C. J. T. Timmons, *J. Chem. Soc., C*, **1967**, 1677; F. Momicchioli and A. Rastelli, *ibid., B*, **1970**, 1353.
5) B. Östman and S. Olsson, *Arkiv. Kemi.*, **15**, 275 (1960); R. Halvarson and L. Melander, *ibid.*, **8**, 29 (1955); see also Y. Kitahara, T. Kametani, and H. Horita, eds., *Kagaku no Ryoiki Zokan*, **94**(3), 7 (1971).
6) Unpublished.

The Copper(I) Iodide-assisted Reaction of Nonactivated Aryl Iodides with Some Alkali Metal Pseudohalides[1]

Hitomi SUZUKI,* Keiko MIYOSHI, and Misao SHINODA**

Department of Chemistry, Faculty of Science, Ehime University, Bunkyo-cho, Matsuyama 790

***Department of Industrial Chemistry, Faculty of Engineering, Toyama University, Nakagawa-sonomachi, Takaoka 933*

(Received October 30, 1979)

Synopsis. Copper(I) iodide dissolves into warm hexamethylphosphoric triamide to give a black solution, in which polymethylated iodobenzenes undergo nucleophilic attack by azide and selenocyanate ions, giving the corresponding aryl azides and selenocyanates in low to good yields. In the absence of copper(I) salt, however, the reaction does not take place. Cyanide, cyanate, thiocyanate, and fluoride ions bring about a decoloration of the reaction mixture and no displacement reactions ensue, while the tellurocyanate ion affords the corresponding aryl cyanides while liberating elemental tellurium.

The traditional methods for converting organic halides to the corresponding pseudohalides involve displacement reactions with alkali metal pseudohalides; these methods are unsatisfactory or even fail with most aryl halides. The most commonly employed procedures of preparing aryl pseudohalides are thus based on the reaction of diazotized aromatic amine with pseudohalide ions, preferably in the presence of an appropriate catalyst.[2] However, these methods are often limited by the availability of the starting amines, especially in the case of polysubstituted systems.

During the course of preparing some polyalkylbenzene derivatives, we have found that copper(I) iodide dissolved in hexamethylphosphoric triamide (HMPA) can induce the reaction of nonactivated aryl iodides with some pseudohalide ions, such as azide and selenocyanate ions. This reaction has not previously been reported in the literature, but it seems to have some potential as an alternative route to aryl azides and selenocyanates.[3,4]

Copper(I) iodide dissolves into warm HMPA to give a black solution, in which polymethylated iodobenzenes are activated to such an extent as to undergo nucleophilic attack by azide and selenocyanate ions, giving the corresponding aryl azides or aryl selenocyanates in low to good yields. Curiously, the reaction does not proceed to completion even in the presence of a large excess of a nucleophilic reagent. Without copper(I) salt, no displacement reaction takes place. Moreover, when other dipolar aprotic solvent systems, including *N*,*N*-dimethylformamide, *N*,*N*-dimethylacetamide, and *N*-methylpyrrolidone, are used, the reaction fails to occur.

The replacement of copper(I) iodide by copper(I) chloride or bromide, as expected,[5] leads to a facile halogen exchange, and the corresponding aryl chloride or bromide are obtained in nearly quantitative yields. Several attempts to accomplish similar reactions between aryl chloride and pseudohalide ions in the presence of copper(I) chloride have, however, been unsuccessful. With this combination, the characteristic coloration of the reaction mixture is not observed.

Of considerable interest is the finding that the addition of other pseudohalide ions, *i.e.*, cyanide, cyanate, or thiocyanate ions, to a black solution of aryl iodide and copper(I) iodide in HMPA results in a decoloration of the reaction mixture, and no displacement reactions ensue. These results are in contrast to those obtained from the reactions of aryl iodides with copper(I) cyanide and thiocyanate in warm HMPA, in which aryl cyanides[6] and diaryl disulfides[7] respectively are obtained in high yields. Alkali fluorides also produce decoloration.

In one procedure, potassium tellurocyanate[8] is allowed to react with aryl iodides in a mixture of HMPA and dimethyl sulfoxide (DMSO). In the presence of copper(I) iodide, tellurocyanate undergoes immediate decomposition, with the deposition of a dark grey tellurium powder, and aryl cyanide is the sole identifiable product obtained. Since potassium cyanide does not react with aryl iodide, not even in the presence of copper(I) iodide, the copper(I) cyanide resulting from the decomposition of the initially formed copper(I) tellurocyanate seems to be responsible for the formation of aryl cyanide.[6] The mechanism of the activation of polyalkylated aryl iodides by copper(I) iodide is not clear at present, although one may expect a possible role of the *in situ*-formed copper(I) azide or selenocyanate.

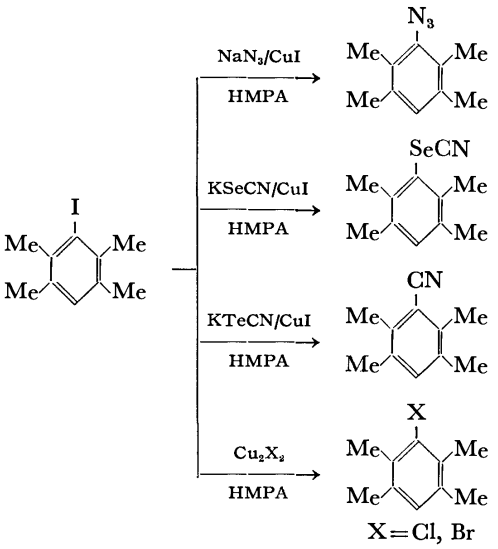

Scheme 1.

Experimental

The melting points were determined on a hot-stage apparatus and are uncorrected. The infrared spectra were run as Nujol mulls on a Hitachi 215 spectrophotometer; only

prominent peaks were recorded. The ^{1}H-NMR spectra were measured in deuteriochloroform with a Varian T-60 spectrometer, using TMS as the internal standard, unless otherwise stated. The mass spectra were obtained on a Hitachi RMS-4 mass spectrometer with an ionizing potential of 70 eV, and selenium-containing peaks are reported for ^{80}Se.

The iodoarenes were prepared by the direct iodination of the corresponding arenes with iodine/periodic acid.[9] Hexamethylphosphoric triamide was dried over phosphorus pentaoxide and distilled prior to use. The alkali azide, cyanide, cyanate, thiocyanate, and selenocyanate were used as received. The potassium tellurocyanate was obtained by gently heating tellurium powder and potassium cyanide in dry DMSO and was used in solution.[8]

The mode of reaction is illustrated below by the representative preparations of pentamethylphenyl selenocyanate and 2,3,5,6-tetramethylphenyl azide. No effort was made to optimize the reaction.

Pentamethylphenyl Selenocyanate. A mixture of iodopentamethylbenzene (1.37 g; 5 mmol), copper(I) iodide (0.48 g; 2.5 mmol), and HMPA (7 ml) was heated with stirring at 100—110 °C until a black solution resulted, to which potassium selenocyanate (1.44 g; 10 mmol) was then added in one portion. The mixture was stirred for 7—12 h at this temperature and then poured into water. The milky solution gradually separated a precipitate, which was filtered off and extracted with hexane using a Soxhlet extractor. From the concentrated extract, the selenocyanate separated as pale yellow plates. Yield, 0.59—0.91 g (47—72%). Mp 123—124 °C. ^{1}H-NMR: δ 2.27 (s, 3Me) and 2.62 ppm (s, 2Me); IR: ν_{max} 2145, 1055, 1005, and 910 cm^{-1}. Found: C, 57.02; H, 6.00; N, 5.42%; M$^+$, 253. Calcd for $C_{12}H_{15}NSe$: C, 57.15; H, 5.99; N, 5.55%; M$^+$, 252.2.

In a similar fashion, 2,3,5,6-tetramethylphenyl selenocyanate was obtained from iododurene in 45—61% yields. Pale yellow plates; mp 88—89 °C. ^{1}H-NMR: δ 2.25 (s, 2Me), 2.52 (s, 2Me), and 7.02 ppm (s, 1H$_{arom}$); IR: ν_{max} 2150, 995, 875, and 790 cm^{-1}. Found: C, 55.39; H, 5.64; N, 5.66%; M$^+$, 239. Calcd for $C_{11}H_{13}NSe$: C, 55.47; H, 5.50; N, 5.88%; M$^+$, 238.2.

2,3,5,6-Tetramethylphenyl Azide. To a black homogenious solution of iododurene (0.68 g; 2.6 mmol) and copper(I) iodide (0.48 g; 2.5 mmol) in HMPA (5 ml), sodium azide (1.3 g; 20 mmol) was added in one portion. The deep red mixture was heated at 70—90 °C for 24 h and then quenched by the addition of water. Heating at higher temperatures led to the extensive decomposition of the azide formed. The product was extracted with ether, washed with water, and dried over sodium sulfate. The subsequent removal of the solvent gave a white crystalline mass, which showed a sharp IR band due to the azide group at 2100 cm^{-1}. Since the pure azide could not be obtained by fractional crystallization and chromatography over alumina, the product mixture was treated with an excess of lithium aluminum hydride in tetrahydrofuran; the resulting 2,3,5,6-tetramethylaniline was isolated and identified as an *N*-acetyl derivative. Mp 205—207 °C (lit,[10] 207 °C). The displacement reaction by the azide ion proceeded slowly, and the conversion, as calculated from the integration area of the ^{1}H-NMR peaks of the methyl groups, never exceeded 15% under the above conditions.

By a similar treatment, iodopentamethylbenzene was converted into the corresponding azide (10—15% conversion calculated from the ^{1}H-NMR peak area), which was reduced to pentamethylaniline and identified as an *N*-acetyl derivative. Mp 212—214 °C (lit,[11] 213 °C).

Reaction with Potassium Tellurocyanate. To a solution of iododurene (1.30 g; 5 mmol) and copper(I) iodide (0.48 g; 2.5 mmol) in HMPA (10 ml), a fresh solution of potassium tellurocyanate (1.92 g; 10 mmol) in DMSO (10 ml)[8] was added all at once. The mixture, which had turned dark brown with the liberated tellurium powder, was heated with stirring at 100—110 °C for 12 h and then poured into water. A dark grey precipitate was filtered off and extracted with hexane using a Soxhlet extractor. The extract was evaporated under reduced pressure, and the residue was recrystallized from ethanol to give white needles (0.08 g; 10%); it was identified as 2,3,5,6-tetramethylbenzonitrile by direct comparison with an authentic specimen. Mp 74—75 °C (lit,[12] 76—77 °C). ^{1}H-NMR: δ 2.22 (s, 2Me), 2.41 (s, 2Me), and 7.08 ppm (s, 1H$_{arom}$); IR (KBr): ν_{max} 2200, 1470, 1375, and 1000 cm^{-1}.

Reaction with Copper(I) Chloride. A mixture of iododurene (0.78 g; 3 mmol), copper(I) chloride (0.40 g; 4 mmol), and HMPA (6 ml) was kept at 90—100 °C for 4 h and then diluted with water. A grey precipitate was filtered off and extracted with hexane using a Soxhlet extractor. The extract was evaporated to give chlorodurene as a white mass (0.50 g; 99%) which, on recrystallization from aqueous ethanol, melted at 45—47 °C (lit,[13] 47.5—48 °C).

References

1) The reaction of polysubstituted aromatics. Part LVI. Part LV: H. Suzuki, M. Usuki, and T. Hanafusa, *Nippon Kagaku Kaishi*, **1980**, 38.

2) For a review of the displacement of the diazonium group by pseudohalide ions, see "The Chemistry of Diazonium Compounds," ed by S. Patai, Interscience, London (1978).

3) For a general survey of organic azides, see "The Chemistry of the Azide Group," ed by S. Patai, Interscience, London (1971).

4) For a review of organoselenium compounds, see H. Rheinboldt, "Houben-Weyl Methoden der Organischen Chemie," 4th ed, E. Müller, Georg Thieme Verlag, Stuttgart (1955), Vol IX, p. 942.

5) W. B. Hardy and K. B. Fortenbaugh, *J. Am. Chem. Soc.*, **80**, 1716 (1958).

6) H. Suzuki and T. Hanafusa, *Synthesis*, **1974**, 53.

7) H. Suzuki and M. Shinoda, *Bull. Chem. Soc. Jpn.*, **50**, 321 (1977).

8) H. K. Spencer, M. V. Lakshmikantham, and M. P. Cava, *J. Am. Chem. Soc.*, **99**, 1470 (1977).

9) H. Suzuki, *Org. Synth.*, **51**, 94 (1971).

10) R. Willstätter and H. Kubli, *Chem. Ber.*, **42**, 4151 (1909).

11) A. W. Hofmann, *Chem. Ber.*, **18**, 1821 (1885).

12) H. Suzuki, M. Koge, A. Inoue, and T. Hanafusa, *Bull. Chem. Soc. Jpn.*, **51**, 1168 (1978).

13) L. I. Smith and C. L. Moyle, *J. Am. Chem. Soc.*, **58**, 1 (1936).

The Reductive Coupling of Organic Halide Using Hydrazine and a Palladium Amalgam Catalyst. I. The Preparation of Biaryls

Riichiro NAKAJIMA,* Yuji SHINTANI, and Tadashi HARA

Department of Chemical Engineering, Faculty of Engineering, Doshisha University, Karasuma Imadegawa Kamikyo-ku, Kyoto 602

(Received November 6, 1979)

Synopsis: Iodoarenes could be converted to the corresponding biaryls in high yields by the use of a catalytic amount of a palladium amalgam in place of a palladium–calcium carbonate catalyst in Busch's reaction. The 2,3′-isomer content in the bitolyls obtained by the homo-coupling of *o*-iodotoluene was 15% when palladium was used, while it was 1% when a palladium amalgam was used, and the latter was re-usable. The present method is further applicable to some iodoalkanes.

The preparation of symmetrical biaryls with haloarenes is ordinarily accomplished by either one-step or two-step procedures in which the former uses a metal, as in the Ullmann reaction,[1] or a zerovalent metal complex, as in the reaction discovered by Semmelhack *et al.*;[2] while the latter uses the Grignared reagent. The Ullmann reaction is applicable to ortho-halo-substituted arenes, but it is greatly inhibited or prevented by the presence of such substituents as amino, hydroxyl, and free carboxyl groups.[1] Moreover, the reaction does not usually proceed under mild conditions. In Semmelhack's reaction, the zerovalent complex is very sensitive to air and heat, and the presence of ortho substituents in the haloarenes slows down the reaction velocity.[2] The method reported by Taylor *et al.*,[3] involving the reaction *via* the Grignard reagent, is a good one for the preparation of biaryls in respect to the yield, but it can not be used for ortho-halo-substituted arenes.

In the methods described above, a stoichiometric amount or an excess amount of metal are required, and a reaction which proceeds with a catalytic amount of the metal is desirable for the preparation of biaryls. Busch's reaction[4] has not been used for the preparation of biaryls since the reaction proceeds in accordance with a radical reaction mechanism and the yield of biaryls is low except for biquinolyls,[5–7] which have not been prepared by other methods. On the other hand, Jullia[8] and Norman[9] have recently reported the coupling of haloarenes in the presence of palladium supported on activated charcoal[8] and of palladium metal prepared *in situ* from palladium acetate.[9] However, these reaction conditions are not suitable for the preparation of the biaryls, because the hydrogenation and the dimerization of the haloarenes take place at the same time. This investigation has, therefore, been carried out in order to find suitable conditions for preparing the biaryl.

The reductive homo-coupling of iodoarenes with hydrazine was found to proceed in a high yield under mild conditions by the use of a palladium amalgam catalyst and to be further applicable to ortho-substituted iodoarenes. The present method is simple and easy to operate in comparison with the ordinary method; also, it is a useful method for preparing biaryls.

Results and Discussion

Carriers other than the calcium carbonate in Busch's reaction have been examined for the preparation of biaryls, but no better results were obtained. Although Busch's reaction had not been examined without using a carrier,[4–7] the coupling of iodo-*p*-xylene (**1**) with hydrazine gave 2,2′,5,5′-tetramethylbiphenyl (**2**) in an 18.9% yield and *p*-xylene by the use of the palladium prepared *in situ* from palladium chloride (**3**). The coupling of **1** with a palladium–calcium carbonate catalyst in place of the palladium metal gave **2** in an 11.8% yield. Therefore, the reductive coupling with hydrazine did not always require a carrier. Nickel, copper, and mercury, which had been prepared *in situ* from the corresponding metal chloride, were not observed to catalyze the coupling of iodobenzene under the same conditions. The use of the palladium amalgam prepared *in situ* from mercury(II) chloride (**4**) (0.43 mmol) and **3** (0.50 mmol) as the catalyst enhanced the yield of **2** to 70.6%, about four times as large as that in the absence of mercury. In this case, the hydrogena-

Table 1. Coupling of haloarenes with hydrazine by the use of a palladium amalgam or palladium metal

Haloarene	Yield of biaryl/%[a]	
	Pd–Hg (Method B)	Pd (Method C)
Chlorobenzene		Trace
Bromobenzene	4	30
Iodobenzene	90	49
o-Iodotoluene (T)[b]	67[c]	17[d]
o-Iodotoluene (W)[b]	77[c]	54[e]
m-Iodotoluene	83[f]	28[e]
p-Iodotoluene	102	48
Iodo-*p*-xylene	74	19
3-Iodo-*o*-xylene	64[g]	
4-Iodo-*o*-xylene	78[g]	56[g]
Iodomesitylene	0	0[h]
p-Iodoethylbenzene	82	
p-Iodoaniline	26	
4-Iodo-1,2-dimethoxybenzene	51	

a) Isolated weight. b) Obtained from the Tokyo Chemical Industry Co., Ltd. and Wako Chemical Industries, Ltd., respectively. c—g) The biaryl contained the following isomers: c) 1.3% of the 2,3′-isomer, d) 15.3% of the 2,3′-isomer, e) 16.3% of the 2,3′-isomer, f) 0.7% of the 2,3′-isomer, and g) 0.5% of the 2,3,3′,4′-isomer. h) 2,3′,4,5′,6-Pentamethyldiphenylmethane was detected in a 1% yield.

tion was depressed. Some representative results of haloarenes are shown in Table 1. The use of the palladium amalgam in place of palladium increased the yield of biaryl in the coupling of all the iodoarenes listed in Table 1, but decreased that of bromobenzene. It was further found in the coupling of *o*-iodotoluene that the use of the amalgam catalyst hindered the migration of the bonding position which occurred on the intermediate complex [Ph–Pd–X] in the absence of mercury and decreased the contents of 2,3′-dimethylbiphenyl from 15% to 1.3%. The present method was applicable to the synthesis of 2,2′-disubstituted biaryls much like the Ullmann reaction, but iodomesitylene, which had substituents at both ortho positions, did not give the biaryl, in contrast with the Ullmann reaction.

Since **3** as well as **4** was reduced with hydrazine in the initial reaction stage to give the metal, and since the produced amalgam was present throughout the reaction, the reuse of the recovered amalgam as the catalyst was examined for the preparation of **2**. As is shown in Table 1, **1** gave **2** in a 74% yield with **3** and **4**. **2** was obtained in yields of 45% and 53% with the first recovered palladium amalgam (97.5% of the theoretical amount) and with the second recovered one (79.6% of the theoretical amount) respectively. The recoveries of **1** in these reactions were 0.4%, 12.2%, and 1.8% respectively. The use of palladium and mercury in place of these chlorides gave **2** in a 47% yield. Therefore, the following conclusions may be drawn: (1) Both the salts and the metals (amalgam) can be used as catalysts. (2) The activity of the catalyst does not decrease very much even after the reaction, and so the catalyst is re-usable. Since the present method is operationally simple, highly selective, and widely applicable, it offers advantages over the previous methods for the preparation of symmetrical biaryls.

As is shown in Table 2, the present method is also applicable to the reductive coupling of iodoalkanes, but the yield is still unsatisfactory. Further experiments are now in progress.

Experimental

Materials. The reagents and solvent employed were of a commercially available grade except those noted below. Iodo-*p*-xylene,[10] 3-iodo-*o*-xylene,[11] 4-iodo-*o*-xylene,[11] iodomesitylene,[10] *p*-iodoethylbenzene,[10] 4-iodo-1,2-dimethoxybenzene,[12] and 1-iododecane[13] were prepared by the methods given in the literature. The purity of all the halo compounds was determined by GLPC to be over 98%.

Table 2. Coupling of iodoalkanes with hydrazine by the use of a palladium amalgam catalyst (Method B)

Iodoalkane	Coupling product	Yield/%
1-Iodohexane	dodecane	0.2
Iodocyclohexane	bicyclohexyl	6.7
1-Iododecane	eicosane	2.5

Reductive Coupling of **2** *with Palladium (Method A).* A mixture of **1** (21.7 mmol), **3** (0.51 mmol), 85% hydrazine hydrate (**5**) (9.8 mmol), and sodium hydroxide (**6**) (101 mmol) in methanol (12 ml) was refluxed for 6.5 h with stirring. The resulting mixture was filtered, and the residual metal was washed with benzene and water. **2** was obtained by the steam distillation of the filtrate. The amount of **2** was determined by GLPC, using biphenyl as the internal standard. The palladium–calcium carbonate catalyst, prepared by a usual method from calcium carbonate (1.0 g) and **3** (0.51 mmol), was also used in place of **3**.

Reductive Coupling of Organic Halide with a Palladium Amalgam Catalyst (Method B). A mixture of organic halide (25 mmol), **3** (0.50 mmol), **4** (0.50 mmol), and **6** (125 mmol) in 16 ml of methanol containing **5** (15 mmol) was stirred for 6 h under refluxing. The resulting mixture was filtered, and the inorganic residues were washed with benzene and water. After the organic layer had separated from the aqueous layer of the filtrate, the dimer was obtained by either the evaporation of the solvent or distillation *in vacuo*, followed by weighing. After 6 hs' reaction, almost no organic halide was recovered from the reaction mixture. The purity of the reaction products was determined by GLPC to be over 98% except in the case of 4,4′-diaminobiphenyl (97%). The reaction products were identified by their retention time, GC-MS (EI and CI), and NMR spectra in comparison with those of authentic samples.

Reductive Coupling of Haloarenes with a Palladium Catalyst (Method C). The experiment was carried out in the same manner as in Method B except that only **3** (2.5 mmol) was used in place of **3** and **4**.

References

1) P. E. Fanta, *Synthesis*, **1974**, 9.
2) M. F. Semmelhack, P. M. Helquit, and L. D. Jones, *J. Am. Chem. Soc.*, **93**, 5908 (1971).
3) A. McKillop, L. F. Elsom, and E. C. Taylor, *Org. Synth.*, **55**, 48 (1976); *Tetrahedron*, **26**, 4041 (1970).
4) M. Busch and W. Schmidt, *Ber.*, **62**, 2612 (1929); M. Busch and W. Weber, *J. Prakt. Chem.*, **146**, 1 (1936).
5) K. Ueda, *Yakugaku Zasshi*, **51**, 495 (1931); **57**, 180, 184 (1937).
6) F. H. Case and J. J. Lafferty, *J. Org. Chem.*, **23**, 1375 (1958).
7) S. Nakano, *Yakugaku Zasshi*, **79**, 310, 314 (1959); **80**, 1510, 1515 (1960).
8) M. Jullia, M. Dutell, C. Grard, and E. Kuntz, *Bull. Soc. Chim. Fr.*, **1973**, 2791.
9) F. R. S. Clark, R. O. C. Norman, and C. B. Thomas, *J. Chem. Soc., Perkin Trans. 1*, **1975**, 121.
10) H. Suzuki, K. Nakamura, and R. Goto, *Bull. Chem. Soc. Jpn.*, **39**, 128 (1966).
11) L. I. Smith and J. W. Opie. *J. Org. Chem.*, **6**, 427 (1941).
12) D. E. Janssen and C. V. Wilson, *Org. Synth.*, Coll. Vol. IV, 547 (1963).
13) H. Stone and H. Shechter, *Org. Synth.*, Coll. Vol. IV, 323 (1963).

The Reactions of 2-Phenyl-2*H*-1-benzopyrans and 2-Phenyl-4*H*-1-benzopyrans with Lead(IV) Acetate

Kazu KUROSAWA,* Katsutoshi YAMAGUCHI, Yasuyuki NAGATA, and Hisatake OHKI

Department of Chemistry, Faculty of Science, Kumamoto University, Kurokami 2-39-1, Kumamoto 860

(Received November 8, 1979)

Synopsis. The reactions of 7-methoxy-2-phenyl-2*H*-1-benzopyran and 7-methoxy-2-phenyl-4*H*-1-benzopyran with lead(IV) acetate gave 2-benzoyl-6-methoxybenzofuran and 6-acetoxy-3-methoxy-6-(3-oxo-3-phenyl-1-propenyl)-2,4-cyclohexadien-1-one. The reactions of 7-methoxy-2-(*p*-methoxyphenyl)-2*H*-1-benzopyran and 7-methoxy-2-(*p*-methoxyphenyl)-4*H*-1-benzopyran with lead(IV) acetate also gave the corresponding benzofuran and cyclohexadienone. The reaction pathway is discussed.

As a continuation of the previous reports[1,2] on the oxidations of 2-phenyl-2*H*-1-benzopyrans and 2-phenyl-4*H*-1-benzopyrans with potassium permanganate, which gave flavones in excellent yields, we have now investigated the reactions of these benzopyrans and related compounds with lead(IV) acetate in various organic solvents and with different molar ratios of the oxidant to the substrate.

When 7-methoxy-2-(*p*-methoxyphenyl)-2*H*-1-benzopyran (**1b**) was oxidized with lead(IV) acetate in boiling benzene, two compounds (**5b** and **6b**) were isolated. The NMR spectrum of **5b**, $C_{17}H_{14}O_4$ (mp 149 °C), indicated that the structure is 6-methoxy-2-(*p*-methoxybenzoyl)benzofuran (Fig. 1), which was confirmed by independent synthesis: the reaction of 2-hydroxy-4-methoxybenzaldehyde with 2-bromo-*p*-methoxyacetophenone gave **5b**. The structure of **6b** was confirmed by means of a study of its NMR spectrum to be 6-acetoxy-3-methoxy-6-[3-(*p*-methoxyphenyl)-3-oxo-1-propenyl]-2,4-cyclohexadien-1-one (Fig. 1), in which the configuration of the C=C double bond in the side chain is *trans* (J=16.0 Hz). TLC showed that there were many other products, which, however, could not be purified. Similarly, the reaction of 7-methoxy-2-phenyl-2*H*-1-benzopyran (**1a**) gave the corresponding 2-benzoyl-6-methoxybenzofuran (**5a**) (mp 105—106 °C) and 6-acetoxy-3-methoxy-6-(3-oxo-3-phenyl-1-propenyl)-2,4-cyclohexadien-1-one (**6a**). The reaction of such other 2-phenyl-2*H*-1-benzopyrans as 2-(*p*-methoxyphenyl)-2*H*-1-benzopyran, which has no methoxyl group at the 7-position, resulted in a complex mixture of products and failed to give the corresponding benzofuran and cyclohexadienone. Therefore, it seems that the presence of a methoxyl group at the 7-position of 2-phenyl-2*H*-1-benzopyran is necessary to give the above products. We were particularly interested in the fact that the ring contraction took place to form a benzofuran ring, and so we subsequently studied its reaction pathway.

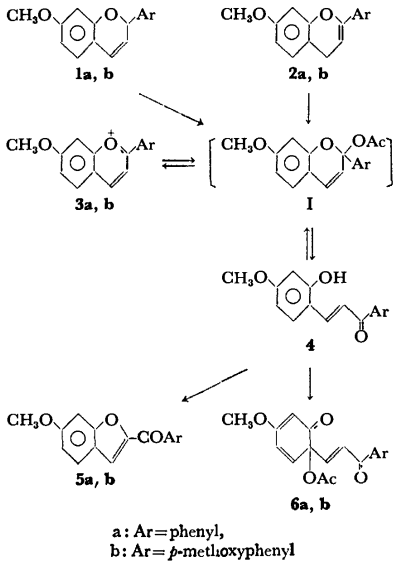

Fig. 1.

It was found that the reactions of 2-phenyl-4*H*-1-benzopyrans (**2a** and **2b**) with lead(IV) acetate in benzene also gave the benzofurans (**5a** and **5b**) and the cyclohexadienones (**6a** and **6b**) in yields similar to those in the reactions of **1a** and **1b** (Entries 3, 4, 9, and 10). When the reaction of **2b** was conducted in chloroform, the yields were practically the same as those in benzene (Entry 11). In acetic acid, however, the yield of **5b** decreased, whereas the yield of **6b** increased, and a characteristic fluorescence of flavylium ion was observed. This may suggest that either the flavylium ion (**3**) or 2-acetoxy-2-phenyl-2*H*-1-benzopyran (I) could be a reaction intermediate. Thus, the oxidation of **3b** was carried out under various reaction conditions. As has been mentioned above, the yield of **5b** in the reaction of **2b** in acetic acid was lower than in any other solvent, but the reactions of **3a** and **3b** in acetic acid containing two equivalents of potassium acetate gave **5a** and **5b** in improved yields (Entries 6 and 14—16). This indicates that I is a more adequate reaction intermediate. It is well known that the hydrolysis of the flavylium ion (**3**) gives an equilibrium mixture of 2-hydroxy-2-phenyl-2*H*-1-benzopyran and (*Z*)- and (*E*)-2-hydroxychalcone;[3] in fact, the treatment of **3b** with acetic acid containing potassium acetate did give (*E*)-2-hydroxy-4,4′-dimethoxychalcone (**4**). The reaction of **4** with lead(IV) acetate gave **5b** and **6b**. It has been reported that the reaction of *o*-substituted phenols with lead(IV) acetate gave 6-acetoxy-2,4-cyclohexadienones[4] and that the reaction of phenols with a double bond in the side chain with this reagent gave a cyclized compound, as has been shown in the cases of 2′-hydroxychalcones,[5] 2-hydroxystilbene,[6] 3-(*o*-hydroxyphenyl)-coumarin,[7] and 2′-hydroxyisoflavone.[8] Thus, it may be concluded that the reaction pathway of this interesting ring-contraction is as is shown in Fig. 1. **1** and **2** are oxidized by lead(IV) acetate to give I. Isomerization between **1** and **2** is not likely to occur under the present reaction conditions, as both **1b** and **2b** were recovered unchanged on heating in benzene.

Table 1. Reactions of 2-phenyl-2*H*-1-benzopyrans (**1**), 2-phenyl-4*H*-1-benzopyrans (**2**), flavylium perchlorates (**3**), and 2-hydroxy-4,4′-dimethoxychalcone (**4**) with lead (IV) acetate

Entry	Substrate	Reaction conditions: Molar ratio of substrate and oxidant	Reaction conditions: Solvent[a]	Reaction conditions: Temp[b] °C	Product (yield[c])/% 5	Product (yield[c])/% 6
1	**1a**	1 : 2	B	reflux	10	7
2	**1a**	1 : 3	B	reflux	12	18
3	**2a**	1 : 2	B	reflux	11	11
4	**2a**	1 : 3	B	reflux	12	15
5	**3a**	1 : 2	A	100	3	28
6	**3a**	1 : 2	A, K	100	3	43
7	**1b**	1 : 2	B	reflux	11	13
8	**1b**	1 : 3	B	reflux	9	8
9	**2b**	1 : 2	B	reflux	9	8
10	**2b**	1 : 3	B	reflux	8	10
11	**2b**	1 : 3	C	reflux	9	10
12	**2b**	1 : 3	A	100	3	14
13	**3b**	1 : 2	A	100	4	35
14	**3b**	1 : 1.5	A, K	100	5	34
15	**3b**	1 : 2	A, K	100	7	44
16	**3b**	1 : 2.5	A, K	100	7	42
17	**4**	1 : 2	A	100	7	14
18	**4**	1 : 2	C	reflux	9	9

a) A: acetic acid, B: benzene, C: chloroform, and K: potassium acetate (2 mmol). b) Heating was continued for 30 min. c) Isolated yield, based on the amount of the substrate used.

I can also be formed by the addition of the acetate ion to **3**. I then becomes a mixture of (*Z*)- and (*E*)-chalcones, the latter being oxidized to give **5** and **6**.

Experimental

All the ^{1}H-NMR spectra were recorded for the deuteriochloroform solution with a Hitachi R-24 NMR spectrometer, with TMS as the internal standard. The IR spectra were recorded for the chloroform solution with a JASCO IRA-1 spectrometer, while the UV spectra were recorded for the methanol solution on a Hitachi EPS-3T UV spectrophotometer. The melting points were determined on a Yanagimoto hot-stage and are uncorrected.

Materials. 7-Methoxy-2-phenyl-2*H*-1-benzopyran (**1a**),[1] 7-methoxy-2-(*p*-methoxyphenyl)-2*H*-1-benzopyran (**1b**),[9] 7-methoxy-2-phenyl-4*H*-1-benzopyran (**2a**),[2] 7-methoxy-2-(*p*-methoxyphenyl)-4*H*-1-benzopyran (**2b**),[10] 7-methoxyflavylium perchlorate (**3a**),[11] 4′,7-dimethoxyflavylium perchlorate (**3b**),[12] and (*E*)-2-hydroxy-4,4′-dimethoxychalcone (**4**)[13] were prepared by the literature methods.

*Oxidations of 2-Phenyl-2*H*-1-benzopyrans (**1a** and **1b**), 2-Phenyl-4*H*-1-benzopyrans (**2a** and **2b**), Flavylium Perchlorates (**3a** and **3b**), and (E)-2-Hydroxy-4,4′-dimethoxychalcone (**4**).* To a mixture of a substrate (1 mmol) and a solvent (20 ml), lead(IV) acetate[14] (1.5—3 mmol) was added, after which the mixture was heated for 30 min. The reaction mixture was filtered (in the case of a reaction using acetic acid as the solvent, the acetic acid was removed *in vacuo* and the residue was extracted with chloroform), and the filtarte was concentrated and chromatographed on TLC, with chloroform as the developing solvent. **5a** and **5b** were further purified by recrystallization.

*2-Benzoyl-6-methoxybenzofuran (**5a**)*: Mp 105—106 °C (MeOH); IR 1640 cm^{-1} (C=O); UV λ_{max} (log ε) 236^{sh} (3.99), 259 (4.00), and 345 nm (4.34); NMR δ=3.87 (3H, s, OCH_3), 6.8—7.1 (2H, m, $H_{(5)}$ and $H_{(7)}$), 7.4—7.7 (5H, m), and 7.9—8.1 (2H, m, $H_{(2')}$ and $H_{(6')}$). Found: C, 75.96; H, 4.81%. Calcd for $C_{16}H_{12}O_3$; C, 76.18; H, 4.80%.

*6-Methoxy-2-(p-methoxybenzoyl)benzofuran (**5b**)*: Mp 149 °C (MeOH); IR 1645 cm^{-1} (C=O); UV λ_{max} (log ε) 228^{sh} (4.23), 259^{sh} (3.81), 307^{sh} (4.07), and 347 nm (4.33); NMR δ=3.89 (6H, s, 2×OCH_3), 6.8—7.2 (4H, m, $H_{(3')}$, $H_{(5)}$, $H_{(5')}$, and $H_{(7)}$), 7.45 (1H, s, $H_{(3)}$), 7.57 (1H, d, J=8.5 Hz, $H_{(4)}$), and 8.08 (2H, m, $H_{(2')}$ and $H_{(6')}$). Found: C, 72.33; H, 5.01%. Calcd for $C_{17}H_{14}O_4$; C, 72.33; H, 5.00%.

*6-Acetoxy-3-methoxy-6-(3-oxo-3-phenyl-1-propenyl)-2,4-cyclohexadien-1-one (**6a**)*: Mp 116—117 °C; IR 1680 and 1758 cm^{-1} (OAc); UV λ_{max} (log ε) 260 (3.93) and 308^{sh} nm (3.72); NMR δ=2.21 (3H, s, OAc), 3.82 (3H, s, OCH_3), 5.59 (1H, t, J=1.5 Hz, $H_{(2)}$), 6.26 (2H, d, J=1.5 Hz, $H_{(4)}$ and $H_{(5)}$), 6.67 (1H, d, J=17.6 Hz, $H_{(1')}$), 7.37 (1H, d, J=17.6 Hz, $H_{(2')}$), 7.3—7.7 (3H, m) and 7.8—8.0 (2H, m); MS *m/e* 312.0941 (calcd for $C_{18}H_{16}O_5$; 312.0998), 284, 270, 202, 165, 160, 152, 111, and 105.

*6-Acetoxy-3-methoxy-6-[3-(p-methoxyphenyl)-3-oxo-1-propenyl]-2,4-cyclohexadien-1-one (**6b**)*: Liquid; IR 1680 (C=O) and 1760 cm^{-1} (OAc); UV λ_{max} (log ε) 225 (4.26) and 295 nm (4.19); NMR δ=2.21 (3H, s, OAc), 3.81 (3H, s, OCH_3), 3.87 (3H, s, OCH_3), 5.61 (1H, t, J=1.5 Hz, $H_{(2)}$), 6.27 (2H, d, J=1.5 Hz, $H_{(4)}$ and $H_{(5)}$), 6.65 (1H, d, J=16.0 Hz, $H_{(2')}$), 7.01 (2H, m, $H_{(3'')}$ and $H_{(5'')}$), 7.37 (1H, d, J=16.0 Hz, $H_{(1')}$), and 8.04 (2H, m, $H_{(2'')}$ and $H_{(6'')}$); MS *m/e* 342.1088 (calcd for $C_{19}H_{18}O_6$; 342.1103), 314, 300, 282, 190, 165, 161, 111, 135, and 92.

*Preparation of 6-Methoxy-2-(p-methoxybenzoyl)benzofuran (**5b**).* To a hot, ethanolic solution (20 ml) of 2-hydroxy-4-methoxybenzaldehyde (456 mg) and potassium hydroxide (168 mg), we added 2-bromo-*p*-methoxyacetophenone (689 mg), after which the reaction mixture was heated under reflux for 2 h. The reaction mixture was then acidified with dilute hydrochloric acid, and the precipitates were collected. The subsequent recrystallization of the crude product from ethanol gave colorless needles (375 mg, 44%); mp 149 °C.

*Treatment of 4′,7-Dimethoxyflavylium Perchlorate (**3b**) with Potassium Acetate in Acetic Acid.* **3b** (367 mg) was heated in acetic acid (10 ml) containing potassium acetate (200 mg) for 5 min. The reaction mixture was then diluted with water (60 ml), and the precipitates were collected by filtration to give **4** (240 mg, 85%), found to be identical with an authentic sample in all respects.

The authors wish to thank Dr. Shinzaburo Hishida at Hitachi, Ltd., Katsuda, for his measurements of the mass spectra.

References

1) Y. Ashihara, Y. Nagata, and K. Kurosawa, *Bull. Chem. Soc. Jpn.*, **50**, 3298 (1977).
2) K. Kurosawa and Y. Ashihara, *Bull. Chem. Soc. Jpn.* **51**, 1175 (1978).
3) L. Jurd, "The Chemistry of Plant Pigments," ed by C. O. Chichester, Academic Press (1972), p. 123.
4) R. Criegee, *Angew. Chem.*, **70**, 173 (1958).
5) K. Kurosawa and J. Higuchi, *Bull. Chem. Soc. Jpn.*, **45**, 1132 (1972).
6) K. Nogami and K. Kurosawa, *Bull. Chem. Soc. Jpn.*, **47**, 505 (1974).
7) K. Kurosawa and K. Nogami, *Bull. Chem. Soc. Jpn.*, **49**, 1955 (1976).
8) K. Kurosawa and F. Araki, *Bull. Chem. Soc. Jpn.*, **52**, 529 (1979).
9) J. W. Clark-Lewis and E. J. McGarry, *Austr. J. Chem.*, **26**, 2447 (1973).
10) L. Jurd, *Chem. Ind. (London)*, **1966**, 1683.
11) A. W. Johnson and R. M. Melhuish, *J. Chem. Soc.*, **1947**, 246.
12) W. Sperling, F. C. Werner, and H. Kuhn, *Ber. Bunsenges Phys. Chem.*, **70**, 530 (1966); *Chem. Abstr.*, **65**, 7129b (1966).
13) L. Jurd, *Tetrahedron*, **25**, 2367 (1969).
14) L. F. Audrieth, *Inorg. Synth.*, **3**, 47 (1950).

Reactions of Thionitrites or Thionitrates with Carbanions

Koichi SHINHAMA, Yong Hae KIM, and Shigeru OAE*

Department of Chemistry, The University of Tsukuba, Niiharigun, Ibaraki 305

(Received November 10, 1980)

Synopsis. Reaction of several thionitrites (RSNO) or thionitrates ($RSNO_2$) with carbanions such as Grignard reagents, alkyllithium, or the carbanion of diethyl malonate gave *C*-alkylthio derivatives such as sulfides or diethyl (alkylthio)malonates.

In the course of our studies on the synthetic applications of thionitrites (RSNO)[1] and thionitrates ($RSNO_2$),[2] the two initial key intermediates in the oxidation of thiols with dinitrogen tetraoxide (N_2O_4), we found that both thionitrites and thionitrates reacted rapidly with carbanionic species such as Grignard reagents, alkyllithium, and the carbanion of diethyl malonate below room temperature. This paper deals with these reactions.

When thionitrites (**1**) or *t*-butyl thionitrate (**2a**) were treated with phenylmagnesium bromide (**3a**) or methylmagnesium iodide (**3b**) in diethyl ether, the corresponding sulfides (**4**) were obtained as the main products, besides small amounts of disulfides (**5**) and thiols (**6**).

RSNO or $RSNO_2$ + R′MgX ⟶

1 **2** **3**

1a: R=*p*-Tol **2a**: R=*t*-Bu **3a**: R′=Ph, X=Br
1b: R=*t*-Bu **3b**: R′=CH_3, X=I

RSR′ + $(RS-)_2$ + RSH

4 **5** **6**

4a: R=*p*-Tol, R′=Ph **5a**: R=*p*-Tol **6a**: R=*p*-Tol
4b: R=*p*-Tol, R′=CH_3 **5b**: R=*t*-Bu **6b**: R=*t*-Bu
4c: R=*t*-Bu, R′=Ph

When thionitrite **1a** was treated with methyllithium (**7a**) or benzyllithium (**7b**)[3] in diethyl ether, nearly the same results were obtained as in the reaction with the Grignard reagents. Sulfide **4b** and benzyl *p*-tolyl sulfide (**4d**) were the major products, as summarized in Table 1.

These reactions were considered to proceed *via* the nucleophilic attack of the carbanionic species on the sulfur atoms of **1** or **2a**. The carbanions do not seem

p-TolSNO + RLi ⟶

1a **7**

7a: R=CH_3
7b: R=$PhCH_2$

p-TolSR + $(p\text{-TolS-})_2$ + *p*-TolSH

4 **5a** **6a**

4b: R=CH_3
4d: R=$PhCH_2$

to attack the nitrogen atom, in view of the lack of formation of the *C*-nitroso or *C*-nitro compound. **1** and **2a** were found to decompose during the reaction to give small amounts of the corresponding disulfides **5**. The thiols **6** are considered to be formed by the reaction of disulfides **5** with carbanions.

When **2a** was treated with diethyl malonate (**8**) in the presence of potassium hydroxide, diethyl (*t*-butylthio)malonate (**9**) was obtained in a good yield. This reaction did not proceed without potassium hydroxide. The reaction of **1b** with diethyl malonate (**8**) in the presence of potassium hydroxide did not give **9** but uncharacterized products.

$$t\text{-BuSNO}_2 + CH_2(CO_2Et)_2 \xrightarrow[\text{in EtOH}]{\text{KOH}} t\text{-BuSCH}(CO_2Et)_2$$

2a **8** **9**

Meanwhile, treatment of 1.4 equiv. of *p*-chlorophenyl thionitrate (**2b**) with diethyl malonate (**8**) in the presence of potassium hydroxide gave diethyl bis(*p*-chlorophenylthio)malonate (**10**) as the major product. However, when this reaction was carried out in the presence of a large amount of potassium hydroxide, ethyl (*p*-chlorophenylthio)acetate (**12**), which might be formed by partial hydrolysis of diethyl (*p*-chloro-

$$p\text{-Cl-C}_6H_4\text{-SNO}_2 + CH_2(CO_2Et)_2 \xrightarrow[\text{in EtOH}]{\text{KOH}}$$

2b **8**

$(p\text{-Cl-C}_6H_4S-)_2C(CO_2Et)_2$ + *p*-Cl-$C_6H_4SCH(CO_2Et)_2$

10 **11**

+ *p*-Cl-$C_6H_4SCH_2CO_2Et$

12

TABLE 1. REACTIONS OF THIONITRITES **1a—b**, OR THIONITRATE **2a** WITH CARBANIONS **3a—b** OR **7a—b**

Substrate	Carbanion	[Carbanion]/[Substrate]	Temp/°C	Time/min	Product[a]	Isolated yield/%
1a	**3a**	3	−70	3	**4a**[b,d]	57
1a	**3b**	3	−70	3	**4b**[b,e]	43
1a	**7a**	1	−70	3	**4b**[b,e]	57
1b	**3a**	1	0—5	5	**4c**[c,f]	72
2a	**3a**	1.1	0—5	5	**4c**[c,f]	79
1a	**7b**	1	−70	3	**4d**[b,g]	32

a) IR and NMR spectra of all these sulfides were identical with those of authentic samples. b) Small amounts of disulfide **5a** and thiol **6a** were also obtained. c) A small amount of disulfide **5a** was confirmed by GC-MS spectrum. d) Bp (bath temp) 135—140 °C/3 mmHg (lit,[4] 163—163.5 °C). e) Bp (bath temp) 90 °C/3 mmHg (lit,[5] 104—104.5 °C/20 mmHg). f) Bp (bath temp) 85—90 °C/3 mmHg (lit,[6] 73 °C/5 mmHg). g) Bp (bath temp) 100—110 °C/2 mmHg, mp 44 °C (lit,[7] 46 °C).

Table 2. Reactions of thionitrates **2a—b** with diethyl malonate **8** in the presence of potassium hydroxide

Thionitrate	Thionitrate: KOH: **8**	Temp °C	Time min	Product	Isolated yield/%
2a	5 : 8 : 6	25	3	**9**	79[a]
2a	10 : 16 : 5	0—5	3	**9**	74[b]
2b	7 : 8 : 5	0—5	3	**10**[d]	29[b,c]
2b	5 : 16 : 5	0—5	3	**12**[e]	72[b]

a) Based on thionitrate **2a**. b) Based on diethyl malonate **8**. c) After recrystallization from EtOH solution. d) Small amounts of compounds **11** and **12** were also formed. e) Small amounts of compounds **10** and **11** were also formed.

phenylthio)malonate (**11**) followed by decarboxylation, was obtained as the major product. These results are listed in Table 2.

Experimental

All the melting points and boiling points were uncorrected. Elemental analyses were carried out by the Chemical Analysis Center at our University. Analytical determinations by GLC were performed on a Hitachi 163 gas chromatograph fitted with the following column (3 mm o.d. × 3 m): 10% SE-30 on Chromosorb W. ^{1}H-NMR spectra were taken at 60 MHz on a Hitachi R-24 A or R-24 apparatus. IR spectra were recorded with a Hitachi 215 spectrometer. Mass spectra were recorded with a Hitachi RMU-6M spectrometer.

*Thionitrites (**1a—b**).* These compounds were prepared from the corresponding thiols with dinitrogen tetraoxide following the procedure reported by us.[1,2b] Pure thionitrite **1a** was quite unstable at room temperature, and hence this compound was used as a solution in diethyl ether immediately after preparation. Pure thionitrite **1b** was rather stable at room temperature.

*Thionitrates (**2a—b**).* Thionitrates **2a—b** were prepared from the corresponding thiols with excess dinitrogen tetraoxide.[2] Thionitrate **2a** was stable and remaining almost in pure form at room temperature for several weeks. Thionitrate **2b** was unstable at room temperature and hence was used immediately (within 30 min) after recrystallization from diethyl ether.

*Reactions of Thionitrites (**1a—b**) or Thionitrates (**2a—b**) with Grignard Reagents (**3a—b**) or Alkyllithium (**7a—b**).* The following is a typical procedure. The Grignard reagent **3a** (7 mmol) in diethyl ether (5.4 ml) was added to a stirred solution of thionitrite **1b** in dry diethyl ether (5 ml) for a few minutes at 0—5 °C. The solution was stirred further for *ca.* 3 min. The red solution of thionitrite **1b** turned to a white suspension. A cold HCl aq solution was added to the solution and then the mixture was extracted with diethyl ether. The ethereal extract was dried ($MgSO_4$), concentrated, purified by TLC (silica gel, hexane), and distilled giving 835 mg (72%) of the sulfide **4c**: bp (bath temp) 85—90 °C/3 mmHg (1 mmHg = 133.322 Pa) (lit,[6] 73 °C/5 mmHg).

*Diethyl (t-Butylthio)malonate (**9**).* A mixture of thionitrite **2a** (675 mg, 5 mmol) and diethyl malonate **8** (961 mg, 6 mmol) was added for a few minutes to a stirred solution of potassium hydroxide (450 mg, 8 mmol) in ethanol (3 ml) at room temperature. The solution was stirred further for *ca.* 3 min, and then cold HCl aq solution was added and the mixture was extracted with diethyl ether. The ethereal extract was dried ($MgSO_4$), concentrated, purified by TLC (silica gel, hexane: ether = 10: 1), and distilled, giving 980 mg (79%) of the compound **9**: bp (bath temp) 100—110 °C/3 mmHg. IR (neat): 1725, 1365, 1242, 1150, 1075, and 1030 cm^{-1}. NMR (CCl_4): δ 1.28 (t, 6H, CH_3-), 1.35 (s, 9H, *t*-Bu), 4.00 (s, 1H, -C<u>H</u>), and 4.13 (q, 4H, -C<u>H</u>$_2$-). MS (70 eV), *m/e* (rel. intensity), 245 (5, M$^+$), 191 (41, $^+$SCH-$(CO_2Et)_2$), 159 (16, $^+CH(CO_2Et)_2$), 118 (23, $^+SCHCO_2Et$), and 57 (100, *t*-Bu$^+$). Found: C, 52.82; H, 8.18%. Calcd for $C_{11}H_{20}O_4S$: C, 53.20; H, 8.11%.

*Diethyl Bis(p-chlorophenylthio)malonate (**10**).* A mixture of thionitrate **2b** (1.41 g, 7 mmol) and diethyl malonate **8** (0.80 g, 5 mmol) was added for a few minutes to a stirred solution of potassium hydroxide 0.45 g, 8 mmol) in ethanol (3 ml) at 0—5 °C. The solution was stirred further for *ca.* 3 min, and then cold HCl aq solution was added and the mixture was extracted with diethyl ether. The crude product was purified by TLC (silica gel, hexane: ether = 10: 1) and recrystallization (from ethanol) to give 643 mg (29% from diethyl malonate **8**) of compound **10**: mp 89—90 °C. IR (KBr): 1725, 1260, 1090, 1038, 1009, and 815 cm^{-1}. NMR (CCl_4): δ 1.14 (t, 6H, CH_3-), 4.01 (q, 4H, -C<u>H</u>$_2$-), 7.25 (d, J=8 Hz, 4H, ring protons), and 7.55 (d, J=8 Hz, 4H, ring protons). MS (70 eV), *m/e* (rel. intensity), 443 (16, M$^+$), 370 (4, $(p\text{-Cl-}C_6H_4S\text{-})_2C(CO_2Et)^+$), and 300 (100, *p*-Cl-$C_6H_4SC(CO_2Et)_2^+$). Found: C, 51.58; H, 4.04%. Calcd for $C_{19}H_{18}Cl_2O_4S_2$: C, 51.24; H, 4.07%.

*Ethyl (p-Chlorophenylthio)acetate (**12**).* A mixture of thionitrate **2b** (5 mmol), and diethyl malonate **8** (5 mmol) was added for a few minutes to a stirred solution of potassium hydroxide (16 mmol) in ethanol (8 ml) at 0—5 °C. The solution was stirred further for *ca.* 3 min, then cold HCl aq solution was added and the mixture was extracted with diethyl ether. Then the product was distilled giving 825 mg (72%) of compound **13**: bp 140—143 °C/2 mmHg (lit,[8] 126—130 °C/1 mmHg). IR (neat): 1720, 1260, 1140, 1085, 1020, and 820 cm^{-1}. NMR (CCl_4): δ 1.25 (t, 6H, CH_3-), 4.18 (q, 4H, -C<u>H</u>$_2$-), 4.35 (s, 1H, -C<u>H</u>), and 7.13—7.70 (m, 4H, ring protons). MS (70 eV), *m/e* (rel. intensity), 230 (55, M$^+$) and 157 (100, $p\text{-Cl-}C_6H_4SCH_2^+$). Found: C, 51.86; H, 4.99%. Calcd for $C_{10}H_{11}ClO_2S$: C, 52.06; H, 4.80%. Small amounts of compound **10** and **11** were also confirmed by GC-MS spectra. Compound **11**: MS (70 eV), *m/e* (rel. intensity), 302 (53, M$^+$), 229 (35, $p\text{-Cl-}C_6H_4SCHCO_2Et^+$), and 156 (100, $p\text{-Cl-}C_6H_4SCH^+$).

References

1) a) S. Oae, D. Fukushima, and Y. H. Kim, *J. Chem. Soc., Chem. Commun.*, **1977**, 407; b) S. Oae, Y. H. Kim, D. Fukushima, and K. Shinhama, *J. Chem. Soc., Perkin Trans. 1*, **1978**, 913.

2) a) S. Oae, K. Shinhama, and Y. H. Kim, *Chem. Lett.*, **1979**, 1077; b) S. Oae, K. Shinhama, K. Fujimori, and Y. H. Kim, *Bull. Chem. Soc. Jpn.*, **53**, 775(1980).

3) D. Seyferth, R. Suzuki, C. J. Murphy, and C. R. Sabet, *J. Organometal. Chem.*, **2**, 431 (1964).

4) H. Lecher, F. Holschneider, K. Köberle, W. Speer, and P. Stoeklin, *Ber.*, **58**, 409 (1925).

5) H. Gilman and N. J. Beaber, *J. Am. Chem. Soc.*, **47**, 1449 (1925).

6) V. N. Ipatieff, H. Pines, and B. S. Friedman, *J. Am. Chem. Soc.*, **60**, 2731 (1938).

7) H. Gilman and W. B. King, *J. Am. Chem. Soc.*, **47**, 1136 (1925).

8) B. Roth and G. H. Hitching, *J. Org. Chem.*, **26**, 2770 (1961).

Studies on Heterocyclic Analogs of Azulene. VII.[1] Regioselective Cycloadditions of Cycloheptimidazole to Electron-deficient Olefins

Noritaka ABE* and Tarozaemon NISHIWAKI

Department of Chemistry, Faculty of Sciences, Yamaguchi University, Yamaguchi 753

(Received November 19, 1979)

Synopsis. Cycloheptimidazole reacted with electron-deficient olefins (*e.g.*, ethyl acrylate or acrylonitrile) to give the regioselective [6+2] cycloadducts, which were readily dehydrogenated to give 2a,3-dihydro-1,2a-diazacyclopent[*cd*]-azulenes.

We have recently reported[2] that the reaction of aza analogs of azulene with dimethyl acetylenedicarboxylate affords cycloadducts, the formation of which is accounted for in terms of an intramolecular cyclization of an extended dipolar species.[3] This paper is concerned with the regioselective cycloadditions of cycloheptimidazole with electron-deficient olefins.

When a mixture of cycloheptimidazole (**1**) and ethyl acrylate was heated under reflux for 20 h, two products, ethyl 2a,3-dihydro-1,2a-diazacyclopent[*cd*]azulene-4-carboxylate (**2a**) (24%) and ethyl 2a,3,4,4a-tetrahydro-1,2a-diazacyclopent[*cd*]azulene-4-carboxylate (**3a**) (48%), were isolated as red needles and an unstable pale yellow oil, respectively. The ^{1}H-NMR spectrum of the former (**2a**) shows two 1H doublets at δ 6.89 (H-8) and 7.23 (H-5) (J=11 Hz) and two 1H double doublets at δ 6.12 (H-7) and 6.51 (H-6) (J=11 and 9 Hz) assignable to seven-membered ring protons, and a 2H doublet at δ 5.07 (J=1.5 Hz, H-3) which shows a long-range coupling with the H-2 proton resonating at δ 7.62 (t, J=1.5 Hz), in addition to signals for an ethyl group. An absorption at 1675 cm^{-1} in its IR spectrum indicates the presence of a conjugated ester carbonyl. These observations allow the ester group to be assigned at C-4. The latter compound was found to be rather unstable and changed into **2a** on storage in air or by dehydrogenation with 2,3-dichloro-5,6-dicyano-1,4-benzoquinone supporting the structure of **3a**. IR spectrum of picrate of **3a** shows an absorption of unconjugated ester carbonyl at 1720 cm^{-1}, and ^{1}H-NMR spectrum of the picrate accords with the structure in spite of its quite complex feature.

Since the presence of a dehydrogenation catalyst such as palladium–charcoal may stimulate[4] the formation of **2a**, the reaction was repeated in the presence of palladium–charcoal. As expected, **2a** was obtained in higher yield and **3a** was not isolated at all.

Acrylonitrile similarly reacts with **1** in the absence of palladium–charcoal to yield **2b** as red prisms (15%), according to the manner of the regioselective [6+2] cycloaddition reaction. This reaction was sluggish than that of ethyl acrylate, *i.e.*, 73% of the starting material **1** was recovered even after reflux for 48 h.

In these reaction, the electrophilic olefin attacks the ring nitrogen to give a dipolar species (**4**) followed by the intramolecular cyclization reaction. These results further lend support the mechanism we advanced previously for the reaction of **1** with dimethyl acetylenedicarboxylate.[2]

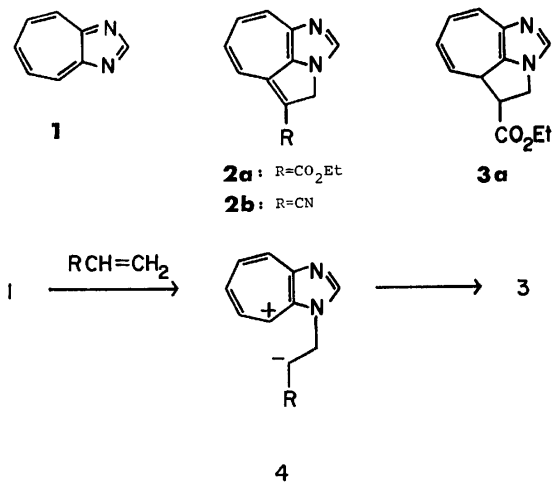

4

Experimental

Melting points were uncorrected. IR spectra were recorded for Nujol mulls. ^{1}H-NMR spectra were recorded with JEOL FX-100 (100 MHz) or Hitachi R-24B (60 MHz) spectrometers. UV spectra were measured for ethanol solutions. Kiesel gel 60 was used for chromatography unless otherwise stated. Yields are based on consumed starting material.

*Reaction of **1** with Ethyl Acrylate.* (*a*): A mixture of **1** (1.00 g) and ethyl acrylate (4.00 g) was heated under reflux for 20 h. Reaction mixture was evaporated under reduced pressure, and the residue was chromatographed. Elution with chloroform gave **2a** (0.176 g, 24%), red needles (from petroleum ether), mp 80—82 °C, UV_{max} 223 nm (log ε 4.36), 253^{sh} (4.18), 359 (4.13), 375 (4.08), 424 (3.57), 448 (3.61), 477 (3.55), 513 (3.35), 555^{sh} (2.95). IR 1675 cm^{-1} (ester C=O). ^{1}H-NMR ($CDCl_3$) δ=1.32 (3H, t, J=7 Hz, CH_3), 4.22 (2H, q, J=7 Hz, OCH_2), 5.07 (2H, d, J=1.5 Hz, H-3), 6.12 (1H, dd, J=11 and 9 Hz, H-6), 6.51 (1H, dd, J=11 and 9 Hz, H-7), 6.89 (1H, d, J=11 Hz, H-8), 7.23 (1H, d, J=11 Hz, H-5), 7.62 (1H, t, J=1.5 Hz, H-2). Found: C, 68.39; H, 5.58; N, 12.08%. Calcd for $C_{13}H_{12}N_2O_2$: C, 68.41; H, 5.30; N, 12.27%. Picrate of **2a**, red needles (from ethanol), mp 195—197 °C (dec.). IR 1680 cm^{-1} (ester C=O). Found: C, 49.85; H, 3.40; N, 15.04%. Calcd for $C_{19}H_{15}N_5O_9$: C, 49.89; H, 3.31; N, 15.31%. Elution with ethyl acetate gave **3a** as a pale yellow oil (0.349 g, 48%). Picrate of **3a**, orange needles (from ethanol), mp 166—167 °C. IR 1720 cm^{-1} (ester C=O). ^{1}H-NMR (DMSO-d_6) δ=1.27 (3H, t, J=7 Hz, CH_3), 4.18 (2H, q, J=7 Hz, OCH_2), 4.2—4.7 (4H, m, H-3, 4, and 4a), 5.5—6.8 (5H, m, H-2, 5, 6, 7, and 8), and 9.00 (1H, s, OH), and phenyl proton of picric acid appeared at δ 8.55 (2H, s). Found: C, 49.75; H, 3.97; N, 15.00%. Calcd for $C_{19}H_{17}N_5O_9$: C, 49.67; H, 3.73; N, 15.25%. Further elution gave the starting material **1** (0.579 g). (*b*): A mixture of **1** (0.30 g), ethyl acrylate (4.00 g), and 5% palladium–charcoal (0.10 g) was heated under reflux for 20 h. The mixture was cooled and filtered. The filtrate was evaporated under reduced pressure and the residue was similarly chro-

matographed as above to afford **2a** (0.129 g, 41%) and the starting material **1** (0.120 g).

*Reaction of **1** with Acrylonitrile.* A mixture of **1** (0.60 g) and acrylonitrile (4.00 g) was heated under reflux for 48 h. The mixture was evaporated under reduced pressure, and the residue was chromatographed. Elution with chloroform gave **2b** (0.034 g, 15%), red prisms (from cyclohexane), mp 149—150 °C, UV_{max} 223 nm (log ε 4.16), 256^{sh} (4.04), 354 (3.93), 370^{sh} (3.85), 424 (3.34), 452 (3.33), 483 (3.25), 520 (3.06), 560^{sh} (2.74). IR 2200 cm^{-1} (C≡N). ^{1}H-NMR ($CDCl_3$) δ=5.07 (2H, d, J=1 Hz, H-3), 6.12 (1H, dd, J=11 and 8 Hz, H-6), 6.44 (1H, dd, J=11 and 8 Hz, H-7), 6.66 (1H, d, J=11 Hz, H-5), 6.90 (1H, d, J=11 Hz, H-8), 7.64 (1H, t, J=1 Hz, H-2). Found: C, 73.05; H, 3.85; N, 23.02%. Calcd for $C_{11}H_7N_3$: C, 72.91; H, 3.89; N, 23.19%. Elution of ethyl acetate gave the starting material **1** (0.438 g).

*Oxidation of **3a**.* A mixture of **3a** (0.050 g) and 2,3-dichloro-5,6-dicyano-1,4-benzoquinone (0.055 g) in benzene (20 ml) was heated under reflux for 24 h, then chromatographed on alumina. **2a** (0.035 g, 71%) was eluted with chloroform.

We thank Dr. Masafumi Yasunami, Tohoku University, for NMR spectral determination.

References

1) Part VI, N. Abe and T. Nishiwaki, *Bull. Chem. Soc. Jpn*, **53**, 1406 (1980).

2) N. Abe, Y. Tanaka, and T. Nishikawaki, *J. Chem. Soc., Perkin Trans. 1*, **1978**, 429.

3) J. J. Barr and R. C. Storr, *J. Chem. Soc., Perkin Trans. 1*, **1979**, 185; E. C. Taylor and I. J. Turchi, *Chem. Rev.*, **79**, 181 (1979); see also references cited in Ref. 2.

4) A. Galbraith, T. Small, R. A. Barnes, and V. Boekelheide, *J. Am. Chem. Soc.*, **83**, 453 (1961); A. Galbraith, T. Small, and V. Boekelheide, *J. Org. Chem.*, **24**, 582 (1959); V. Boekelheide and A. Miller, *ibid.*, **26**, 431 (1961).

Synthesis Using Allylidenedihydropyridines. VIII.[1] Facile Preparation of 2-Alkylthio-3-vinylpyrazolo[1,5-*a*]pyridines

Akikazu KAKEHI,* Suketaka ITO, and Kozo WATANABE

Department of Industrial Chemistry, Faculty of Engineering, Shinshu University, Wakasato, Nagano 380

(Received December 12, 1979)

Synopsis. Reactions of 1-[bis(alkylthio)methyleneamino]-2-methylpyridinium iodides with activated ethoxymethylene compounds in the presence of alkali gave the corresponding 1-[bis(alkylthio)methyleneamino]-2-allylidene-1,2-dihydropyridines in considerable yields, and their thermolyses in benzene afforded 2-alkylthio-3-vinylpyrazolo[1,5-*a*]-pyridine derivatives.

In a previous paper a report was given on a simple preparation method of 2-alkylthio-1-vinylindolizine derivatives from the corresponding pyridinium 1-[(alkylthio)thiocarbonyl]methylides.[2] The extension of this route for synthesizing its azaanalogue, 2-alkylthio-3-vinylpyrazolo[1,5-*a*]pyridine, should be possible if an appropriate starting material such as pyridinium 1-[(alkylthio)thiocarbonyl]aminide is available.[3] In contrast with pyridinium 1-[(alkylthio)thiocarbonyl]-methylide,[4] however, such type of pyridinium 1-aminide has not been reported. In this paper we wish to report the syntheses of pyridinium 1-[(alkylthio)thiocarbonyl]-aminides and of the title compounds using them.

Since the smooth formation of *S*-involving pyridinium betaines from the reactions of various pyridinium 1-methylides with carbon disulfide are well known,[4] the preparation of pyridinium 1-[(alkylthio)thiocarbonyl]aminide by a similar procedure was attempted and accomplished well when the reaction of pyridinium 1-aminide with carbon disulfide was carried out in the presence of a certain alkylating agent: When a mixture of 1-amino-2-methylpyridinium iodide (**1**), carbon disulfide, and dimethyl or diethyl sulfate was treated with potassium hydroxide in ethanol, the expected 2-methylpyridinium 1-[(methylthio)- (**2**) or 1-[(ethylthio)-thiocarbonyl]aminide (**3**) was obtained in 59 or 65% yield. The respective reactions of **2** and **3** with methyl and ethyl iodide gave the *S*-alkylated products, 1-[bis(methylthio)- (**4**) and 1-[bis(ethylthio)-methyleneamino]-2-methylpyridinium iodide (**5**), in quantitative yields. The reactions of the pyridinium salts (**4** and **5**) with ethyl (ethoxymethylene)cyanoacetate (**6**) and 3-(ethoxymethylene)pentane-2,4-dione (**7**) in the presence of potassium carbonate afforded the corresponding 1-[bis(alkylthio)methyleneamino]-2-allylidene-1,2-dihydropyridine derivatives (**8**—**11**) in 47—56% yields. These compounds (**8**—**11**) were then thermolysed smoothly in refluxing benzene to give 2-alkylthio-3-vinylpyrazolo[1,5-*a*]pyridines (**12**—**15**) with the elimination of methanethiol or ethanethiol. Interestingly, pyrazolopyridines (**12**—**15**) were very stable and unchanged even in dilute hydrochloric acid or aqueous sodium hydroxide. However, **13** and **15** were decomposed by the treatments of conc. hydrochloric acid to yield products (**16** and **17**), and **12** and **14** under similar conditions gave only intractable tarry substances. These results are summarized in the following Scheme.

The structures of these compounds (**2** and **3**, **4** and **5**, **8**—**11**, and **12**—**15**) were determined by their physical and spectral analyses and by comparisons with spectral data of known pyridinium 1-aminides, pyridinium salts, 2-allylidene-1,2-dihydropyridines, and 3-vinylpyrazolo-[1,5-*a*]pyridines, respectively.[3] On the other hand, those of **16** and **17** were concluded to be the monodeacetylated compounds of starting pyrazolopyridines (**13** and **15**), because their NMR spectra exhibited a characteristic AB quartet signal coupled with 16.0 Hz at δ 7.89, 7.62, 6.78, and 6.50 (**16**) or at δ 7.90, 7.82, 6.79, and 6.51 (**17**) and only one acetyl singlet at δ 2.35

Table 1. IR Spectral data and elementary analyses

Compd No.	Formula	Calcd (%)			Found (%)			ν^{KBr} (cm^{-1})	
		C	H	N	C	H	N		
2	$C_8H_{10}N_2S_2$	48.45	5.08	14.13	48.21	5.04	14.40	1399	971
3	$C_9H_{12}N_2S_2$	50.91	5.70	13.20	51.02	5.68	13.07	1392	978
4	$C_9H_{13}IN_2S_2$	31.77	3.85	8.23	31.65	3.87	8.35	1476	1235
5	$C_{11}H_{17}IN_2S_2$	35.87	4.65	7.45	36.02	4.61	7.45	1470	1230
8	$C_{15}H_{17}N_3O_2S_2$	53.70	5.11	12.53	53.81	5.15	12.47	2210	1668
9	$C_{15}H_{18}N_2O_2S_2$	55.86	5.63	8.69	55.87	5.92	8.40	1583	1506
10	$C_{17}H_{21}N_3O_2S_2$	56.19	5.83	11.57	56.10	5.93	11.59	2215	1667
11	$C_{17}H_{22}N_2O_2S_2$	58.25	6.33	7.99	58.29	6.39	7.89	1590	1505
12	$C_{14}H_{13}N_3O_2S$	58.52	4.56	14.63	58.28	4.59	14.52	2215	1721
13	$C_{14}H_{14}N_2O_2S$	61.29	5.14	10.21	61.00	5.11	10.21	1674	1492
14	$C_{15}H_{15}N_3O_2S$	59.78	5.02	13.94	59.85	5.05	13.92	2210	1718
15	$C_{15}H_{16}N_2O_2S$	Oil						1679	1500[a]
16	$C_{12}H_{12}N_2OS$	62.04	5.21	12.06	62.02	5.18	12.11	1603	1259
17	$C_{13}H_{14}N_2OS$	63.91	5.78	11.47	63.80	5.78	11.49	1602	1252

a) Neat.

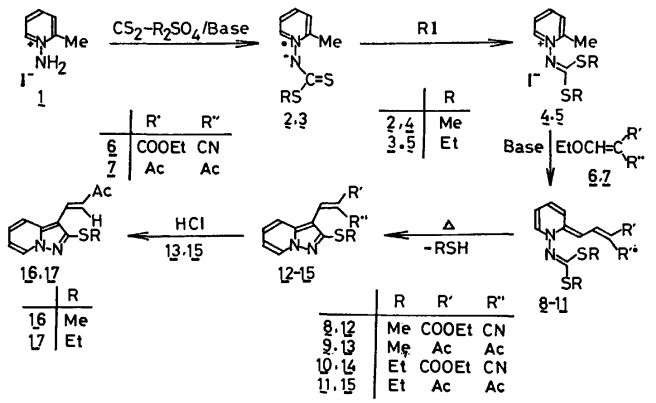

(**16**) or 2.37 (**17**) due to the protons of the 3-vinyl moiety.[5] Furthermore, the configuration of the 3-vinyl group was determined to be *trans* by the large coupling constant (16.0 Hz) between the olefinic protons.

Experimental

Melting points were measured with a Yanagimoto micro-melting point apparatus and are uncorrected. Microanalyses and IR spectra were measured with a Perkin-Elmer 240 Elemental Analyzer and a Hitachi 260-10 Infrared Spectrophotometer, respectively, and are listed in the Table. The NMR spectra were determined with a Varian EM360A Spectrometer in deuteriochloroform with tetramethylsilane as an internal standard. The chemical shifts are expressed in δ values.[6]

Preparations of 2-Methylpyridinium 1-[(Alkylthio)thiocarbonyl]-aminides (2 and 3). To an ethanolic solution (50 ml) of 1-amino-2-methylpyridinium iodide (**1**, 4 mmol), carbon disulfide (6 mmol), and dimethyl or diethyl sulfate (6 mmol) aqueous potassium hydroxide (9 mmol in 5 ml of water) was added dropwise under stirring at room temperature. After the addition the mixture was stirred for additional 1 h, and then poured into ice–water (200 ml). The resulting solution was extracted two times with chloroform (100 ml) and the combined extract was washed with water, dried over anhydrous sodium sulfate, and concentrated at reduced pressure. Column separation (alumina) of the residue and recrystallization from chloroform–hexane gave **2**, 59%, mp 128—129 °C, δ 2.57 (3H, s, SMe), and 2.64 (3H, s, C_2–Me), and **3**, 65%, mp 113—115 °C, δ 1.37 (3H, t, J=7.0 Hz, $SCH_2\underline{CH_3}$), 2.62 (3H, s, C_2–Me), and 3.13 (2H, q, J=7.0 Hz, $S\underline{CH_2}CH_3$), as colorless crystals.

Preparations of 2-Alkylthio-3-vinylpyrazolo[1,5-a]pyridine Derivatives (12—15). To a chloroform solution (30 ml) of **2** or **3** (2 mmol) methyl or ethyl iodide (2 ml) was added at room temperature and the solution was allowed to stand for 20 min. The reaction mixture was then concentrated and the residue was recrystallized from chloroform–ether to give **4**, mp 134—136 °C, and **5**, mp 131—132 °C, as slightly brown crystals in almostly quantitative yields. The mixture of salt (**4** or **5**, 2 mmol) and ethoxymethylene compound (**6** or **7**, 2 mmol) was treated with potassium carbonate (5 g) in chloroform (50 ml) at room temperature for 3 d and, then, the reaction solution was filtered to remove insoluble substances. The filtrate was concentrated at reduced pressure and the residue was separated by column chromatography (alumina) using ether and then chloroform as eluents. Recrystallizations from chloroform–hexane of the crude products gave **8**, 50%, mp 116—117 °C, δ 1.30 (3H, t, J=7.0 Hz, $OCH_2\underline{CH_3}$), 2.57 and 2.73 (each 3H, s, SMe), 4.22 (2H, q, J=7.0 Hz, $O\underline{CH_2}CH_3$), 5.57 (1H, d, J=14.0 Hz, vinyl-H), and 8.19 (1H, d, J=14.0 Hz, vinyl-H), **9**, 47%, mp 93—95 °C, δ 2.40 (6H, s, 2×COMe), 2.56 and 2.80 (each 3H, s, SMe), 6.85 (1H, d, J=14.0 Hz, vinyl-H), and 7.98 (1H, d, J=14.0 Hz, vinyl-H), **10**, 51%, mp 108—109 °C, δ 1.28, 1.32, and 1.49 (each 3H, t, J=7.0 Hz, $OCH_2\underline{CH_3}$ and 2×$SCH_2\underline{CH_3}$), 3.10 and 3.33 (each 2H, q, J=7.0 Hz, $S\underline{CH_2}CH_3$), 4.51 (2H, q, J=7.0 Hz, $OCH_2\underline{CH_3}$), 5.53 (1H, d, J=14.0 Hz, vinyl-H), and 8.18 (1H, d, J=14.0 Hz, vinyl-H), and **11**, 56%, mp 101—102 °C, δ 1.30 and 1.49 (each 3H, t, J=7.0 Hz, $SCH_2\underline{CH_3}$), 2.33 (6H, s, 2×COMe), 3.10 and 3.39 (each 2H, q, J=7.0 Hz, $S\underline{CH_2}CH_3$), 6.73 (1H, d, J=14.0 Hz, vinyl-H), and 8.01 (1H, d, J=14.0 Hz, vinyl-H). A benzene solution (30 ml) of 2-allylidene-1,2-dihydropyridine (1 mmol) was heated under reflux until the TLC spot of the material disappeared (about 3—6 h). The reaction mixture was then concentrated and separated by column chromatography (alumina) using ether. Recrystallizations from ether-hexane afforded 2-alkylthio-3-vinylpyrazolopyridines (**12**—**15**) as yellow needles: **12**, 57%, mp 169—170 °C, δ 1.39 (3H, t, J=7.0 Hz, $OCH_2\underline{CH_3}$), 2.70 (3H, s, SMe), 4.37 (2H, q, J=7.0 Hz, $O\underline{CH_2}CH_3$), and 8.34 (1H, s, vinyl-H), **13**, 43%, mp 104—105 °C, δ 2.29 and 2.42 (each 3H, s, COMe), 2.68 (3H, s, SMe), and 7.73 (1H, s, vinyl-H), **14**, 55%, mp 143—144 °C, δ 1.40 and 1.43 (each 3H, t, J=7.0 Hz, $OCH_2\underline{CH_3}$ and $SCH_2\underline{CH_3}$), 3.27 (2H, q, J=7.0 Hz, $SCH_2\underline{CH_3}$), 4.38 (2H, q, J=7.0 Hz, $O\underline{CH_2}CH_3$), and 8.39 (1H, s, vinyl-H), **15**, 53%, oil, δ 1.44 (3H, t, J=7.0 Hz, $SCH_2\underline{CH_3}$), 2.31 and 2.47 (each 3H, s, COMe), 3.29 (2H, q, J=7.0 Hz, $S\underline{CH_2}CH_3$), and 7.88 (1H, s, vinyl-H).

Acid Hydrolyses of 13 and 15. Pyrazolopyridines (**13** or **15**, 100 mg) was dissolved in 10 ml of concd hydrochloric acid and kept for 3 h at room temperature. The solution was concentrated to dryness at reduced pressure and the residual oil was separated by column chromatography (alumina) using ether and then chloroform as eluents. Recrystallizations of the crude products from chloroform–hexane gave 2-methylthio-(**16**), 65%, mp 142—144 °C, and 2-ethylthio-3-(3-oxo-1-butenyl)pyrazolo[1,5-*a*]pyridine (**17**), 79%, mp 107—109 °C, as pale yellow needles. On the other hand, similar treatments of **12** and **14** gave only tarry substances and the separation of any significant products from them was unsuccessful.

References

1) For part 7 of this series, see A. Kakehi, S. Ito, K. Watanabe, T. Ono, and T. Miyazima, *J. Chem. Res.*, (*S*), 18 (1980), (*M*), 401—425 (1980).

2) A. Kakehi, S. Ito, T. Maeda, R. Takeda, M. Nishimura, M. Tamashima, and T. Yamaguchi, *J. Org. Chem.*, **43**, 4837 (1978).

3) A. Kakehi, S. Ito, K. Uchiyama, and K. Kondo, *J. Org. Chem.*, **43**, 2896 (1978).

4) a) F. Kröhnke and K. Gerlach, *Chem. Ber.*, **95**, 1108 (1962); b) F. Kröhnke, K. Gerlach, and K.-K. Schnalke, *Chem. Ber.*, **95**, 1118 (1962); c) Y. Tominaga, Y. Miyake, H. Fujito, Y. Matsuda, and G. Kobayashi, *Yakugaku Zasshi*, **97**, 927 (1977).

5) The facile elimination of an acetyl substituent on the carbon-carbon double bond is very interesting.

6) The proton signals on the pyridine ring appeared at δ 7.5—8.5 (**2** and **3**), 8.1—9.3 (**4** and **5**), 6.4—7.7 (**8**—**11**), 6.8—8.6 (**12**—**15**), and 6.8—8.4 (**16** and **17**), respectively.

Photochemical Reductive Acylation and Oxidative Acyl Activation on Phenazine and Related Nitrogen Heterocycles[1)]

Makoto TAKAGI,* Setsuo GOTO, and Tsutomu MATSUDA*

Department of Organic Synthesis, Faculty of Engineering, Kyushu University, Hakozaki, Higashi-ku, Fukuoka 812

(Received December 17, 1979)

Synopsis. Irradiation of phenazine in acetaldehyde or propionaldehyde solution gave an *N*-acylated 5,10-dihydrophenazine. Acridine similarly gave 9-acyl-9,10-dihydroacridine, and 10-methylacridinium salt gave 9-acyl-10-methyl-9,10-dihydroacridine. In methanol *N*-acylated dihydrophenazines reacted with *N*-bromosuccinimide to give phenazine and methyl carboxylates in quantitative yield.

p-Benzoquinones are known to undergo reductive acylation with aldehydes under photo-irradiation.[2)] When the resultant hydroquinone monocarboxylates are oxidized in the presence of appropriate nucleophiles, oxidative acyl activation takes place, and the acyl group is transferred to the nucleophile with a concurrent reproduction of *p*-benzoquinones.[3)] The entire process, the reductive acylation followed by the oxidative acyl transfer, constitutes a cycle which converts aldehydes into activated acyl compounds by means of a quinone-hydroquinone redox pair as an acyl carrier. A similar process has been disclosed recently by us for a 1,2-dithiolane-1,3-dithiol redox pair, and a formal resemblance of the process to the reaction of coenzyme lipoic acid in pyruvate dehydrogenase has been pointed out (Eq. 1).[4–7)] In living organisms there are several redox coenzymes which contain nitrogen heterocycles, *e.g.*, flavin and nicotinamide, and it would be interesting to study nigrogen heterocycles for the reaction similar to quinones and 1,2-dithiolanes.

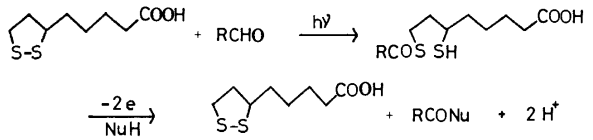

(1)

Results and Discussion

The results of photo-reactions are summarized in Table 1. Besides the heterocycles in Table 1, 1,10-phenanthroline, quinoxaline, quinoline, and benzothiazole were subjected to photo-irradiation in propionaldehyde solution, but the starting heterocycles were recovered unreacted. *N*-alkylated quinolinium and 1-benzyl-3-carbamoylpyridinium chlorides gave intractable complex mixtures. The reactions in Table 1 generally gave complicated mixtures, and the isolation of the products was attained by recrystallization and column chromatography.

The mechanism of the present photochemical reductive acylation is yet to be studied. In contrast to the reaction of 1,2-dithiolanes which was effected under both photochemical and thermal (in the presence of AIBN as radical initiator) conditions,[7)] the reaction of phenazine proceeded only under photo-irradiation. The photo-reduction of acridine[8)] and phenazine[9)] has been reported. The reductive photo-alkylation of acridine by aliphatic carboxylic acid has also been described.[10)] The present reaction may be related to these reactions in mechanism. The acylation reaction will find a synthetic use for the preparation of acylphenazines, since the synthesis of acetyl- and propionylphenazine has not been described in the literature reflecting the difficulty of the direct acylation of the phenazine nucleus.

Table 1. Photo-reaction of nitrogen heterocycles with aldehydes

Heterocycle	Aldehyde	Irradiation time/h	Product (yield/%)
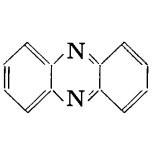	CH_3CHO	6	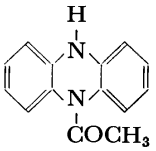 **1** (35)
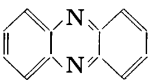	C_2H_5CHO	5	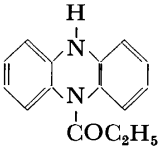 **2** (20)
			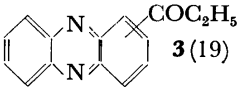 **3** (19)
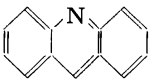	CH_3CHO	2	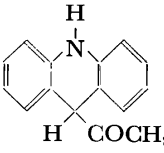 **4** (36)
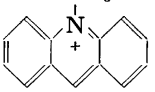	C_2H_5CHO	3	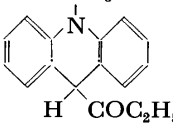 **5** (52)

The 5-acyl-5,10-dihydrophenazines **1** and **2** in methanol were allowed to react with *N*-bromosuccinimide (NBS) at room temperature. The oxidation proceeded in a few minutes to give a quantitative yield of methyl carboxylates and phenazine. The plausible mechanism is formulated in Eq. 2. Thus, it is concluded that phenazine undergoes the same type of reductive acylation and oxidative acyl transfer reactions as those

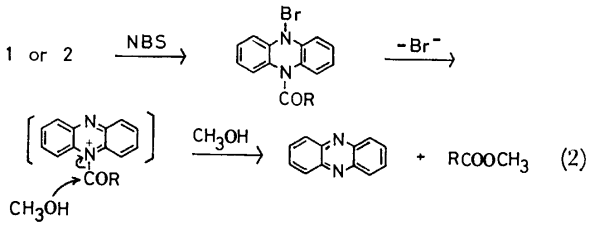

(2)

of quinones and 1,2-dithiolanes.

The oxidation of **4** or **5** did not bring about such an acyl activation. The compound **5** was found to be gradually oxidized in the air, even in the isolated crystalline state, to give 10-methyl-9(10*H*)-acridinone. The reaction most probably involved the formation of a 9-hydroperoxy derivative **6** by air oxidation and its subsequent decomposition to propionic acid and 10-methyl-9(10*H*)-acridinone.

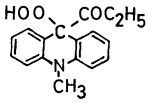

6

Experimental

Photo-reaction of Phenazine with Acetaldehyde. Phenazine (0.40 g) was dissolved in acetaldehyde (200 ml), and the mixture was irradiated under nitrogen at $\leq$10 °C by a 100W immersion type high pressure mercry lamp.[4,6] The light shorter than 330 nm in wavelength was eliminated by a liquid filter (NaBr–Pb $(NO_3)_2$–H_2O).[6] After 6 h irradiation, the red reaction mixture was evaporated, the residue was digested in 5 ml of benzene, and the insoluble red solid was collected. Recrystallization from ethanol gave reddish crystals, 0.22 g (**1**, 35%). For further purification, the product dissolved in chloroform was passed through a short column of silica gel. Another recrystallization from ethanol gave white grannular crystals. mp 258—260 °C (254—255 °C[11]); IR (Nujol) 3280 (NH) and 1650 cm^{-1} (CO); NMR (CF_3CO_2H) δ=2.58 (3H, s, CH_3), 7.0—7.6 (8H, m, aromatic H). Found: C, 74.90; H, 5.46; N, 12.48%. Calcd for $C_{14}H_{12}N_2O$: C, 74.98; H, 5.39; N, 12.49%.

Photo-reaction of Phenazine with Propionaldehyde. The reaction was carried out in a similar manner to the above procedure using 0.55 g of phenazine in 150 ml of propionaldehyde. After 5 h photo-irradiation, the mixture was concentrated. The solid product was filtered and recrystallized from ethanol. Yellow needles (**3**). Yield, 0.14 g, 19%; mp 123—123.5 °C; IR (Nujol) 1685 cm^{-1} (CO); NMR (CCl_4) δ=1.29 (3H, t, J=7.0 Hz, CH_3), 3.43 (2H, q, CH_2), 7.6—8.4 (7H, m, aromatic H); MS (*m/e*) 236 (M^+), 179 ($M^+-C_2H_5CO$). Found: C, 75.88; H, 5.14; N, 11.82%. Calcd for $C_{15}H_{12}N_2O$: C, 76.25; H, 5.12; N, 11.85%. The filtrate from the concentrated reaction mixture was further evaporated to dryness, and the residue was dissolved in a small amount of ethanol. The addition of hexane produced precipitates, which were recrystallized from ethanol to give reddish crystals. **2**. Yield, 0.15 g, 20%. Another recrystallization from ethanol after passing through a short column of silica gel in chloroform gave white grannular crystals. mp 193—194 °C; IR (Nujol) 3250 (NH) and 1650 cm^{-1} (CO); NMR ($CDCl_3$) δ=1.10 (3H, t, J=7.0 Hz, CH_3), 2.52 (2H, q, CH_2), 6.12 (1H, s, NH, D-exchange), 6.6—7.5 (8H, m, aromatic H); MS (*m/e*) 238 (M^+), 181 ($M^+-C_2H_5CO$). Found: C, 75.49; H, 5.97; N, 11.72%. Calcd for $C_{15}H_{14}N_2O$: C, 75.61; H, 5.92; N, 11.75%.

Photo-reaction of Acridine with Acetaldehyde. Acridine (2.01 g) dissolved in acetaldehyde (200 ml) was irradiated for 2 h. The white precipitates formed (9,9′,10,10′-tetrahydro-9,9′-biacridine,[12] 0.12 g, 12%) were filtered off, and the filtrate was concentrated to dryness. The residue was subjected to column chromatography (silica gel, benzene) to yield **4** as colorless crystals. Yield, 0.45 g, 36%; mp 92—93 °C (benzene); IR (KBr) 3350 (NH) and 1687 cm^{-1} (CO); NMR ($CDCl_3$) δ=1.98 (3H, s, CH_3), 4.90 (1H, s, HC←), 6.27 (1H, s, NH) 7.5—8.4 (8H, m, aromatic H). Found: C, 80.93; H, 5.86; N, 6.45%. Calcd for $C_{15}H_{13}NO$: C, 80.69; H, 5.87; N, 6.27%.

Photo-reaction of 10-Methylacridinium Chloride with Propionaldehyde. 10-Methylacridinium chloride (1.02 g) in propionaldehyde (100 ml) was irradiated for 3 h. A part of the salt remained undissolved. The reaction mixture was filtered and concentrated to dryness. The residue was taken in chloroform and sujected to column chromatography (silica gel, chloroform) to give pale yellow crystals of **5**. Yield, 0.36 g, 52%; mp 60—63 °C; IR (Nujol) 1710 cm^{-1} (CO); NMR ($CDCl_3$) δ=0.83 (3H, t, J=7.0 Hz, $CH_2\underline{CH_3}$), 2.35 (2H, q, CH_2), 3.37 (3H, s, NCH_3), 4.85 (1H, s, HC←), 6.7—7.4 (8H, m, aromatic H). Found: C, 81.10; H, 6.87; N, 5.58%. Calcd for $C_{17}H_{17}NO$: C, 81.24; H, 6.82; N, 5.57%. The sample stored in the dark in a desiccator turned to high-melting yellow crystals in a year. A recrystallization from ethanol gave yellow needles, mp 202—204 °C, which proved to be 10-methyl-9(10*H*)-acridinone (mp 199 °C[13]) by comparing with an authentic sample.[13]

Oxidation of 1 by NBS. **1** was dissolved in 5—10 mmol/dm^3 concentration in 10 ml methanol. The methanol contained hexane as internal standard for the subsequent GLC analysis. NBS was added in twice molar excess of **1**, and the mixture was stirred at room temperature (—20 °C). UV spectra showed the formation of phenazine to be complete in 5 min according to Eq. 2. The GLC analysis on 10% tetraethyleneglycol on Celite at room temperature indicated 80—100% formation of methyl acetate. Both hexane and methyl acetate peaks appeared before the solvent (methanol) peak under these GLC conditions. The oxidation of **2** similarly confirmed the reaction in Eq. 2.

References

1) Presented at the 34 th national meeting of the Chemical Societhy of Japan, Hiratsuka, April 1—4, 1976.

2) J. M. Bruce, E. Cutts, *J. Chem. Soc., C*, **1966**, 449.

3) M. Takagi, M. Tazaki, and T. Matsuda, *Bull. Chem. Soc. Jpn.*, **50**, 2704 (1977) and references cited therein.

4) M. Takagi, S. Goto, and T. Matsuda, *J. Chem. Soc., Chem. Commun.*, **1976**, 92.

5) M. Takagi, S. Goto, R. Ishihara, and T. Matsuda, *J. Chem. Soc., Chem. Commun.*, **1976**, 993.

6) M. Takagi, *Methods Enzymology*, Vol. 62, part D, 145 (1979).

7) M. Takagi, S. Goto, M. Tazaki, and T. Matsuda, *Bull. Chem. Soc. Jpn.*, in submission.

8) S. Kato, S. Minagawa, and M. Koizumi, *Bull. Chem. Soc. Jpn.*, **34**, 1026 (1961).

9) C. Dufraisse, A. Etienne, and E. Toromanoff, *Compt. Rend.* **235**, 759 (1952).

10) R. Noyori, M. Kato, M. Kawanishi, and H. Nozaki, *Tetrahedron*, **25**, 1125 (1969).

11) Z. V. Pushikareva and L. B. Radina, *Dokl. Akad. Nauk S. S. S. R.* **123**, 301 (1958); *Chem. Abstr.*, **53**, 7184i (1959).

12) H. Göth, P. Cerutti, and H. Schmid, *Helv. Chim. Acta*, **48**, 1395 (1965).

13) K. Lehmstedt and H. Hundertmark, *Chem. Ber.*, **64**, 2386 (1931).

Synthesis of 1,6-Dioxadispiro[2.0.4.4]dodecan-7-one

Kiyomi KAKIUCHI,* Yasuhiro HIRAMATSU, Yoshito TOBE, and Yoshinobu ODAIRA
Department of Petroleum Chemistry, Faculty of Engineering, Osaka University, Suita, Osaka 565

(Received December 20, 1979)

Synopsis. 1,6-Dioxadispiro[2.0.4.4]dodecan-7-one, a useful intermediate of dispiro-α-methylene-γ-butyrolactones, was synthesized in a good overall yield by the cycloaddition of dichloroketene to 1,2-dimethylenecyclohexane, and the zinc dust reduction of the chlorine atoms, followed by the Baeyer-Villiger oxidation with *m*-chloroperbenzoic acid.

Recently, much attention has been paid on the chemistry of α-methylene-γ-butyrolactones, especially, concerning the structure-biochemical activity relationship, because a number of naturally occurring sesquiterpene lactones display antitumor and/or cytotoxic activity attributed to this moiety.[1] From the above point of view, we previously reported on the synthesis of the dispiro-γ-butyrolactone (**2**), being a useful intermediate of the dispiro-α-methylene-γ-butyrolactone (**3**) having a spiro cyclopropane ring,[2] by the acid catalyzed or thermally induced cyclobutyl-cyclopropylcarbinyl type rearrangement of the propellalactone (**1**).[5] As part of the study on the synthesis of various types of dispiro-γ-butyrolactones, we wish to report here a convenient synthesis of 1,6-dioxadispiro[2.0.4.4]-dodecan-7-one (**4**) having a spiro epoxide linkage which is expected to enhance the reactivity of the conjugated lactone toward biological nucleophiles.[1a]

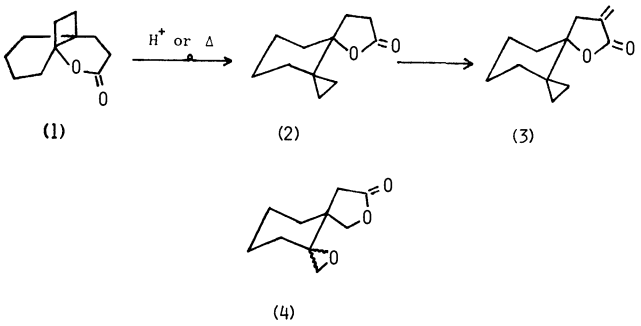

The epoxy-γ-lactone **4** was prepared as outlined in Scheme 1; i) the cycloaddition of dichloroketene to 1,2-dimethylenecyclohexane employing the high-dilution method,[6] ii) the reductive removal of the chlorine atoms with zinc dust–acetic acid,[7] iii) the epoxidation with *m*-chloroperbenzoic acid (MCPBA), and iv) the Baeyer-Villiger oxidation.

A solution of equal amounts of trichloroacetyl chloride and phosphoryl chloride in ether was added dropwise over a period of 5 h to an ethereal solution of 1,2-dimethylenecyclohexane (**5**), which was readily available from *cis*-1,2-cyclohexanedicarboxylic anhydride, and excess of activated zinc, and the mixture was refluxed for 30 h. The 1: 1 cycloadduct, that is the spiro dichlorocyclobutanone (**6**), was obtained in a 61% yield.[8] The reductive removal of the chlorine atoms from **6** with excess of zinc dust and acetic acid in ether at room temperature gave the spiro cyclobutanone (**7**) in a 71% yield. The epoxidation of **7** with 1.2 equivalent of MCPBA in chloroform at room temperature for 3 h afforded the epoxy cyclobutanone (**8**) in a 71% yield.[9] Finally, the Baeyer-Villiger oxidation of **8** with 1.2 equivalent of MCPBA in chloroform at room temperature for 6 d gave a 1: 1 mixture of two epoxy-γ-lactones **4**[10] in a 70% yield. The γ-lactone **4** was also obtained directly from the cyclobutanone **7** by the oxidation with 3-fold excess of MCPBA for 6 d (77%).

In this way, 1,6-dioxadispiro[2.0.4.4]dodecan-7-one **4**, a key compound for the synthesis of dispiro-α-methylene-γ-butyrolactones having an epoxide linkage, was synthesized in a good yield by means of the efficient dichloroketene addition.

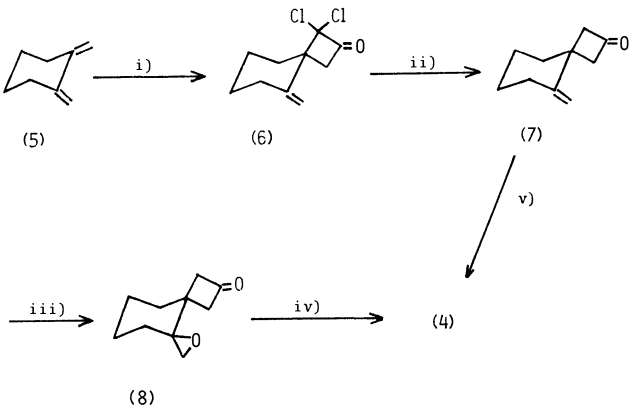

Scheme 1.

i) Cl_3CCOCl, Zn(Cu), $POCl_3$, Et_2O, 30 h; ii) Zn, AcOH, Et_2O, 30 h; iii) MCPBA (1.2 eq.), $CHCl_3$, 3 h; iv) MCPBA (1.2 eq.), $CHCl_3$, 6 d; v) MCPBA (3 eq.), $CHCl_3$, 6 d.

Experimental

IR spectra were recorded using a JASCO IR-G spectrometer. ^1H NMR spectra were obtained on a JEOL JNM-PS-100 spectrometer, using Me_4Si as an internal standard and CCl_4 as a solvent. MS spectra were measured with a Hitachi RMU-6E spectrometer.

1,2-Dimethylenecyclohexane (**5**)[11] was prepared in a similar method to that of Davalian *et al.*,[12] and purified by distillation using a spinning-band distillation column.

1,1-Dichloro-5-methylenespiro[3.5]nonan-2-one (6). A solution of 8.1 ml (0.078 mol) of freshly distilled trichloroacetyl chloride and 6.8 ml (0.078 mol) of phosphoryl chloride (distilled from K_2CO_3) in 440 ml of dry ether was added dropwise over 5 h to a mixture of 8.4 g (0.078 mol) of **5** and 7.6 g (0.114 mol) of activated zinc in 600 ml of dry ether under a nitrogen atmosphere. The reaction mixture was stirred at reflux for additional 30 h. The excess zinc was filtered and washed with ether. The filtrate was concentrated *in vacuo* to *ca.* 25% of its original volume, an equal volume of pentane added, and

the solution stirred for 1 h to precipitate zinc salts. The solution was decanted from the residue, washed successively with water, a cold saturated $NaHCO_3$ solution and brine, and dried (Na_2SO_4). The solvent was removed *in vacuo* and the residue was distilled under reduced pressure. After recovery of 2.6 g of **5** (bp 60 °C/90 Torr), 7.1 g of **6** was obtained as pale yellow oil (61%): bp 86—88 °C/0.8 Torr; IR 1800, 1635 cm^{-1}; NMR δ 1.16—2.50 (m, 8H), 2.66 (d, J= 17 Hz, 1H), 3.62 (d, J=17 Hz, 1H), 4.80 (s, 1H), 5.08 (s. 1H); MS *m/e* 222 (M^++4), 220 (M^++2), 218 (M^+). Found: C, 54.91; H, 5.56%. Calcd for $C_{10}H_{12}OCl_2$: C, 54.82; H, 5.52%.

5-Methylenespiro[3.5]nonan-2-one (7). A mixture of 7.0 g (0.032 mol) of **6**, 10 g of zinc, and 10 ml of acetic acid in 150 ml of dry ether was stirred at room temperature for 30 h.[13] The reaction mixture was filtered and the filtrate was washed with saturated $NaHCO_3$ solution, brine, and dried (Na_2SO_4). The solvent was removed *in vacuo* and the residue was distilled under reduced pressure to give 3.4 g of the cyclobutanone **7** (71%): bp 68—69 °C/3 Torr; IR 1775, 1635 cm^{-1}; NMR δ 1.45—1.82 (m, 6H), 2.02—2.28 (m, 2H), 2.45—2.80 (m, 2H), 2.88—3.24 (m, 2H), 4.68 (s, 1H), 4.78 (s, 1H); MS *m/e* 150 (M^+). Found: C, 79.84; H, 9.54%. Calcd for $C_{10}H_{14}O$: C, 79.95; H, 9.39%.

1-Oxadispiro[2.0.3.4]undecan-6-one (8). A solution of 250 mg (1.7 mmol) of **7** and 440 mg (2.0 mmol) of 80% MCPBA in 10 ml of chloroform was stirred at room temperature for 3 h. The solution was washed with saturated Na_2SO_3 solution, saturated $NaHCO_3$ solution, water, and dried (Na_2SO_4). The solvent was evaporated *in vacuo* to give 197 mg of **8** as colorless oil (71%). Analytical sample was obtained by preparative GLC: IR 1775 cm^{-1}; NMR δ 1.20—2.08 (m, 8H), 2.24—3.12 (m, 6H); MS *m/e* 166 (M^+). Found: C, 72.05; H, 8.70%. Calcd for $C_{10}H_{14}O_2$: C, 72.26; H, 8.49%.

1,6-Dioxadispiro[2.0.4.4]dodecan-7-one (5). A solution of 100 mg (0.65 mmol) of **8** and 170 mg (0.78 mmol) of 80% MCPBA in 10 ml of chloroform was stirred at room temperature and the progress of the reaction was monitored by GLC. After 6 d, the solution was treated as described above. Chromatography on silica gel (20% ether–petroleum ether) gave 87 mg of **4** as colorless oil (74%).[10] 471 mg of **4** was also obtained in 77% yield from the reaction of 500 mg (3.3 mmol) of **7** and 2.2 g (9.9 mmol) of 80% MCPBA in 27 ml of chloroform for 6 d: IR 1765 cm^{-1}; NMR δ 1.20—2.00 (m, 8H), 2.04—2.72 (m, 4H), 3.60—4.20 (m, 2H); MS *m/e* 182 (M^+). Found: C, 65.72; H, 7.75%. Calcd for $C_{10}H_{14}O_3$: C, 65.91; H, 7.74%.

References

1) a) E. Rodriguez, G. H. N. Towers, and J. C. Mitchell, *Phytochemistry*, **15**, 1573 (1976); b) K. H. Lee, E. S. Huang, C. Piantadosi, J. S. Pagano, and T. A. Geissman, *Cancer Res.*, **31**, 1649 (1971).

2) α-Methylenation of **2** was readily conducted by the usual procedure[3] to afford **3** in a good yield.[4]

3) P. A. Grieco, J. A. Noguez, Y. Masaki, K. Hiroi, M. Nishizawa, A. Rosowsky, S. Oppenheim, and H. Lazarus, *J. Med. Chem.*, **20**, 71 (1977).

4) Unpublished results.

5) a) Y. Tobe, K. Kakiuchi, Y. Kawakami, Y. Sakai, K. Kimura, and Y. Odaira, *Chem. Lett.*, **1978**, 1027; b) K. Kakiuchi, Y. Tobe, and Y. Odaira, *J. Org. Chem.*, **45**, 729 (1980).

6) L. R. Krepski and A. Hassner, *J. Org. Chem.*, **43**, 2879 (1978).

7) D. A. Bak and W. T. Brady, *J. Org. Chem.*, **44**, 107 (1979).

8) The 1: 2 cycloadduct was not obtained.

9) Trace of **4** was also obtained besides the epoxide **8**.

10) Though **4** consisted of two isomers (**A**) and (**B**) they could not be separated completely by GLC or column chromatography; therefore they were characterized as a mixture. Attempt on their separation and structure assignment is in progress.

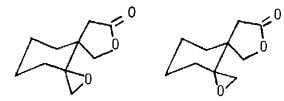

(A) (B)

11) P. D. Bartlett, A. S. Wingrove, and R. Owyang, *J. Am. Chem. Soc.*, **90**, 6067 (1968).

12) D. Davalian and P. J. Garratt, *J. Am. Chem. Soc.*, **97**, 6883 (1975). **5** was prepared by esterification of *cis*-1,2-cyclohexanedicarboxylic anhydride, reduction with $LiAlH_4$, and treatment with methanesulfonyl chloride followed by reaction with $KOBu^t$.

13) After 2 h, the monochlorocyclobutanone was obtained as a main product which was purified by preparative GLC: bp 107—108 °C/5 Torr; IR 1785, 1635 cm^{-1}; NMR δ 1.16—2.20 (m, 8H), 2.85 (s, 2H), 4.82 (s, 1H), 4.86 (s, 1H), 4.95 (s, 1H); MS *m/e* 186 (M^++2), 184 (M^+). Found: C, 64.90; H, 7.13%. Calcd for $C_{10}H_{13}OCl$: C, 65.04; H, 7.10%.

Diazoalkane Complexes of Molybdenum†

Yasushi MIZOBE, Yasuzo UCHIDA, and Masanobu HIDAI*
Department of Industrial Chemistry, The University of Tokyo, Hongo, Tokyo 113
(Received January 14, 1980)

Synopsis. The hydrazido(2-) complexes $[MoX_2(NNH_2)(PMe_2Ph)_3]$ (X=Cl or Br) derived from bis(dinitrogen) complex and HX react with aldehydes or ketones to give a series of diazoalkane complexes $[MoX_2(\rightleftharpoons N{-}N{=}CRR')(PMe_2Ph)_3]$.

Extensive studies on the reactions of coordinated dinitrogen in well defined complexes to form C–N bonds have been undertaken in order to open a new chemistry of dinitrogen. Aroyl, acyl, and alkyl halides have been shown to react with the dinitrogen complexes of molybdenum and tungsten, *trans*-$[M(N_2)_2(dpe)_2]$ (M=Mo or W; dpe=$Ph_2PCH_2CH_2PPh_2$), to afford the complexes containing organo-nitrogen ligands.[1] The same reactions with the dinitrogen complexes of mono(tertiary) phosphines $[M(N_2)_2(L)_4]$ (M=Mo or W; L=PMe_2Ph or $PMePh_2$), however, released the coordinated dinitrogen as dinitrogen gas.[2] We have recently found a more versatile route to the formation of C–N bonds from coordinated dinitrogen, which involved the condensation of the hydrazido (2-) complexes $[MF(NNH_2)(dpe)_2][BF_4]$ derived from *trans*-$[M(N_2)_2(dpe)_2]$ (M=Mo or W) and HBF_4 with a variety of aldehydes or ketones (RR′ C=O) to yield the diazoalkane complexes $[MF(\rightleftharpoons N{-}N{=}CRR')(dpe)_2][BF_4]$.[3] We report here preparation of diazoalkane complexes of molybdenum containing PMe_2Ph by the similar condensation reactions.

Results and Discussion

The hydrazido(2-) complexes $[MoX_2(NNH_2)(PMe_2Ph)_3]$ (X=Cl or Br) which are readily obtained from *cis*-$[Mo(N_2)_2(PMe_2Ph)_4]$ and aqueous HX in methanol[4] condense with aldehydes or ketones to give

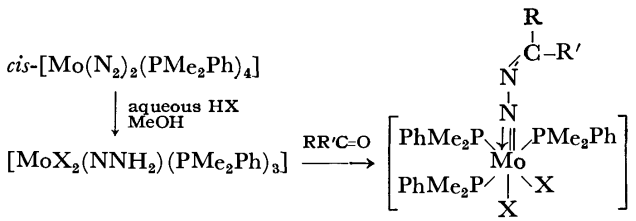

diazoalkane complexes. The condensation reactions are markedly accelerated by catalytic amount of acids, though the reaction of aldehydes occurs smoothly even in the absence of acids. Spectroscopic data of the diazoalkane complexes are given in Table 1. These complexes give rise to strong ν(C=N) bands in the 1520—1570 cm^{-1} region of the infrared spectra. The ^1H-NMR spectra show two triplets and one doublet with intensity 6H each which are characteristic of virtually coupled *meridional* phosphine methyls in a complex lacking a plane of symmetry containing the phosphines. As observed in the diazoalkane complexes reported previously,[3,5] the substituents R and R′ are in inequivalent positions. Thus, the complex $[MoCl_2(N_2CMe_2)(PMe_2Ph)_3]$ exhibits two singlets at 1.5 (intensity 3H) and 1.7 ppm (intensity 3H) assignable to the methyls on the nitrogen-bearing carbon.

Acetophenone readily condenses with the complexes $[MoX_2(NNH_2)(PMe_2Ph)_3]$, though it does not react with the hydrazido(2-) complexes $[MF(NNH_2)(dpe)][BF_4]$ (M=Mo or W) probably because of a steric effect.[3] In the case of acetylacetone, one of the two carbonyl groups condenses with the $MoNNH_2$ group and other remains free (ν(C=N), 1570; ν(C=O), 1720 cm^{-1}). The complex dissolved in CD_2Cl_2 shows a complicated NMR spectrum, which is interpreted in

Table 1. New diazoalkane complexes of molybdenum $[MoX_2(N_2CRR')(PMe_2Ph)_3]$

X	R	R′	Yield (%)	Analytical data[a] C	H	N	ν(C=N) (cm^{-1})	NMR (alkyl region) (ppm)
Cl	Ph	H	41	53.04 (53.23)	5.79 (5.63)	3.83 (4.01)	1530	
Cl	Me	Me	42	50.06 (49.78)	6.50 (6.05)	4.26 (4.30)	1570	1.5s(3H), 1.7s(3H)
Cl	$(CH_2)_5$		90	52.36 (52.10)	6.67 (6.28)	4.29 (4.05)	1560	1.4—2.4m(10H)
Br	$(CH_2)_5$		71	46.74 (46.17)	5.95 (5.56)	3.96 (3.59)	1555	1.3—2.3m(10H)
Cl	Me	Ph	71	53.41 (53.86)	6.15 (5.80)	3.39 (3.93)	1525	2.1s(3H)
Br	Me	Ph	86	47.86 (47.90)	5.38 (5.16)	3.49 (3.49)	1520	1.9s(3H)
Cl	Me	CH_2COMe	45	50.12 (51.41)	6.14 (6.11)	4.18 (4.14)	1570	

a) Calculated values are in parenthesis. b) Methyl protons of PMe_2Ph are omitted. s=singlet, m=multiplet.

† Preparation and Properties of Molybdenum and Tungsten Dinitrogen Complexes. 12.

terms of an equilibrium between keto and enol forms ($C\underline{H}_3CO$–, $C\underline{H}_3C(OH)$=, $C\underline{H}_3CN$–, 1.9—2.2; –$C\underline{H}$=C(OH)–, 4.8; –$C\underline{H}_2COCH_3$, 3.3 ppm). Chatt and Hidai *et al.*[5] have recently shown that diazoalkane complexes of tungsten containing PMe_2Ph are prepared by the similar condensation reactions and treatment of the complex $[WBr_2(N_2CMe_2)(PMe_2Ph)_3]$ with HBr gas in CH_2Cl_2 yields hydrazine and acetone azine in moderate yields. On the other hand, when the diazoalkane complex of molybdenum $[MoCl_2(N_2CMe_2)(PMe_2Ph)_3]$ are treated with an excess of HCl gas in CH_2Cl_2, 0.22 mol of ammonia and 0.32 mol of hydrazine per metal atom are formed, together with a trace of acetone azine.[6]

Experimental

All reactions were carried out under dry dinitrogen using standard Schlenk-tube techniques. The complexes *cis*-$[Mo(N_2)_2(PMe_2Ph)_4]$ and $[MoX_2(NNH_2)(PMe_2Ph)_3]$ (X= Cl or Br) were prepared by published methods.[4] Analytical data of the diazoalkane complexes of molybdenum are shown in Table 1.

Preparation of $[MoCl_2(N_2CHPh)(PMe_2Ph)_3]$. To a suspension of $[MoCl_2(NNH_2)(PMe_2Ph)_3]$ (183 mg, 0.300 mmol) in CH_2Cl_2 (3 ml) was added benzaldehyde (121 μl, 1.20 mmol) at room temperature. After stirring for several minutes, a greenish-brown homogeneous solution was produced. After a further 6 h, hexane (3 ml) was added to the solution to give greenish-brown crystals, which were filtered off, washed with ether, and then dried *in vacuo* (86 mg, yield 41%).

Preparation of $[MoCl_2\{N_2C(CH_2)_5\}(PMe_2Ph)_3]$. To a suspension of $[MoCl_2(NNH_2)(PMe_2Ph)_3]$ (212 mg, 0.347 mmol) in CH_2Cl_2 (3 ml) was added cyclohexanone (0.29 ml, 2.8 mmol) and one drop of concentrated (*ca.* 35%) hydrochloric acid. A red homogeneous solution was immediately obtained. After stirring for 15 min, the volume was reduced *in vacuo* to *ca.* 1 ml and hexane (4 ml) was added. Red needles precipitated from the solution, which were filtered off, washed with ether, and dried *in vacuo* (215 mg, yield 90%).

In similar fashion were prepared $[MoBr_2\{N_2C(CH_2)_5\}(PMe_2Ph)_3]$, $[MoCl_2(N_2CMePh)(PMe_2Ph)_3]$, $[MoBr_2(N_2CMePh)(PMe_2Ph)_3]$, $[MoCl_2(N_2CMe_2)(PMe_2Ph)_3]$, and $[MoCl_2\{N_2CMe(CH_2COMe)\}(PMe_2Ph)_3]$.

References

1) J. Chatt, A. A. Diamantis, G. A. Heath, N. E. Hooper, and G. J. Leigh, *J. Chem. Soc. Dalton Trans.*, **1977** 688 and references therein; T. Tatsumi, M. Hidai, and Y. Uchida, *Inorg. Chem.*, **14**, 2530 (1975); M. Sato, T. Tatsumi, M. Hidai, and Y. Uchida, *J. Organomet. Chem.*, **152**, 239 (1978).

2) P. C. Bevan, J. Chatt, G. J. Leigh, and E. G. Leelamani, *J. Organomet. Chem.*, **139**, C59 (1977).

3) M. Hidai, Y. Mizobe, and Y. Uchida, *J. Am. Chem. Soc.*, **98**, 7824 (1976); M. Hidai, Y. Mizobe, M. Sato, T. Kodama, and Y. Uchida, *ibid.*, **100**, 5740 (1978).

4) J. Chatt, A. J. Pearman, and P. L. Richards, *J. Chem. Soc. Dalton*, **1978**, 1766 and references therein.

5) P. C. Bevan, J. Chatt, M. Hidai, and G. J. Leigh, *J. Organomet. Chem.*, **160**, 165 (1978).

6) M. Hidai, Y. Mizobe, T. Takahashi, and Y. Uchida, *Chem. Lett.*, **1978**, 1187.

Synthesis of Dihydrosphingosine

Yutaka SAITOH, Yoshihiko MORIYAMA,** Hiroshi HIROTA, and Takeyoshi TAKAHASHI*

Department of Chemistry, Faculty of Science, The University of Tokyo, Hongo, Bunkyo-ku, Tokyo 113

***Institute of Chemistry, Kyoto Prefectural University of Medicine, Taishogun, Kita-ku, Kyoto 603*

(Received January 18, 1980)

Synopsis. A conversion of (*S*)-3-acetoxy-2-phthalimidopropanal into dihydrosphingosine is described.

A number of syntheses of sphingosine (**1**), dihydrosphingosine (**2**), and related compounds have been reported.[1-3] This paper deals with a convenient synthesis of dihydrosphingosine [**2**; (2*S*,3*R*)-*erythro*-2-aminooctadecane-1,3-diol] from (*S*)-3-acetoxy-2-phthalimidopropanal (**3**).

The chiral aldehyde (**3**) was prepared from L-serine (**4**) *via* (*S*)-3-acetoxy-2-phthalimidopropanoic acid (**5**) by the known procedure.[2] The Grignard reaction of **3** with pentadecylmagnesium bromide in ether at a temperature between −88 and −45 °C gave a mixture of diol monoacetates (**6a** and **6b**). This mixture was subjected to acid hydrolysis and the product mixture was separated by column and thin-layer chromatography to afford (2*S*,3*R*)-*erythro*-2-phthalimidooctadecane-1,3-diol (**7a**) and (2*S*,3*S*)-*threo*-2-phthalimidooctadecane-1,3-diol (**7b**) in 13% and 1% yields from **3**, respectively.

The *erythro* and *threo* configurations were shown for **7a** and **7b**, respectively, on the basis of the following evidence. Treatment of **7a** with 2,2-dimethoxypropane in the presence of *p*-toluenesulfonic acid gave an acetonide (**8a**) in an almost quantitative yield. Acetalization of **7b** gave the corresponding acetonide (**8b**) in 55% yield. The coupling constant between a C-4 proton and a C-5 proton was determined to be 10 Hz and 5 Hz for **8a** and **8b**, respectively; the two protons should be in a *trans* relationship for **8a** and in *cis* one for **8b**. Acid hydrolysis of these acetonides (**8a** and **8b**) gave the diols (**7a** and **7b**), respectively.

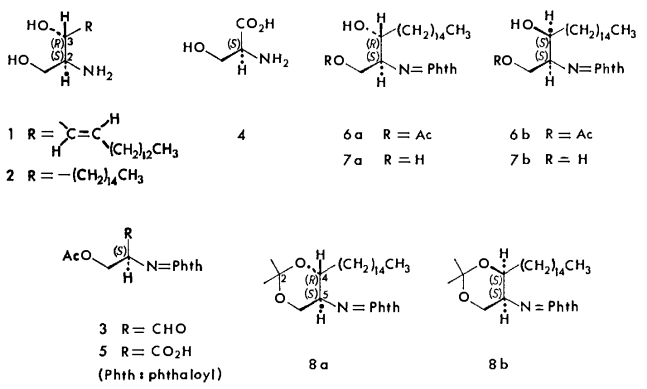

These results suggest that a stereoselective attack[2] of the Grignard reagent to the aldehyde (**3**) was effected preferentially from the less hindered side of **3** to give predominantly the desired *erythro* derivative (**6a**).

Finally, hydrazinolysis of **7a** afforded dihydrosphingosine (**2**) in 81% yield.

Experimental

IR spectra were measured with a Hitachi EPI-G2 spectrometer, ^{1}H-NMR spectra with a JEOL PS-100 (100 MHz), a Varian EM-390 (90 MHz), or a Hitachi R-20B (60 MHz) spectrometer in deuteriochloroform solution containing tetramethylsilane as an internal standard, high resolution and chemical ionization (CI-MS) mass spectra with a JEOL JMS-D300 mass spectrometer. Measurements of optical rotation were carried out with a JASCO polarimeter DIP-SL, and high performance liquid chromatography (HPLC) analyses with a Waters liquid chromatograph model ALC-GPS 202-401. For column chromatography Wakogel C-200 (Wako Pure Chemical Industries) was used. Thin-layer chromatography (TLC) was carried out on Kieselgel GF_{254} (E. Merck, Darmstadt) in 0.25 mm thickness.

Grignard Reaction of (S)-3-Acetoxy-2-phthalimidopropanal (3) with Pentadecylmagnesium Bromide. A solution of pentadecylmagnesium bromide (3.6 mmol) in ether (60 ml) was added dropwise to a solution of the aldehyde (**3**; 0.94 g, 3.6 mmol) in ether (3.6 ml) with stirring under an argon atmosphere at a temperature between −88 and −80 °C. After the mixture had been stirred at −78 °C for 2 h and then at −45 °C for 30 min, a saturated aqueous solution (10 ml) of ammonium chloride was added at −45 °C. The reaction mixture was treated in the usual way to give a residue (1.90 g) which was chromatographed on a column of silica gel (60 g). Elution with hexane–ethyl acetate (17: 3) gave a mixture (410 mg) of crude diol monoacetates (**6a** and **6b**). This mixture was purified by preparative TLC to give a sample for spectral measurements; this sample showing one spot on TLC gave two peaks at R_t=28.4 min (major product; **6a**) and R_t=27.7 min (minor product; **6b**) on HPLC examination [column: μ-PORASIL, 1/4(inch) × 1(foot); solvent system: 30% ether–hexane; flow rate: 1 ml/min]. However, separation of each of two diastereomers (**6a** and **6b**) was unsuccessful due to proximity of their retention times. Mixture of **6a** and **6b**: mp 60 °C (crystallized from acetone): IR (KBr) 3400, 2920, 2850, 1780, 1750, 1710, 1560, 1380, 1370, 1250, 1240, and 720 cm^{-1}; ^{1}H-NMR ($CDCl_3$) δ 0.90 (3H, t-like; $-CH_2C\underline{H}_3$), 1.97 (3H, s; CH_3-CO–), 3.77 (1H, br. s; disappeared on addition of D_2O; –OH), 4.10 (1H, br. s; –C<u>H</u>–OH), 4.35 (1H, m; –C<u>H</u>–N–), 4.60 (2H, m; $-C\underline{H}_2OAc$), and 7.85 (4H, m; aromatic H's).

In the column chromatography described above, successive elution with hexane–ethyl acetate (4: 1) gave a residue (*ca.* 450 mg) showing ^{1}H-NMR signals at δ 6.58 (2H, s; $-\underline{C}=CH_2$), 7.75 (4H, m; aromatic H's), and 9.63 (1H, s; –CHO). This suggested that the unchanged starting material (**3**) suffered elimination of acetic acid to give 2-phthalimido-2-propenal. Further purification of the residue was not carried out.

Treatment of **3** with the Grignard reagent at room temperature resulted in a formation of a complex mixture probably due to an attack of the reagent to the phthaloyl grouping. Further examination of the mixture was not effected. In the reaction at a temperature between −88 and −45 °C, this kind of product mixture was not formed,

*Acid Hydrolysis of the Mixture of Diol Monoacetates (**6a** and **6b**).* The mixture of crude diol monoacetates (**6a** and **6b**; 410 mg) was added to a solution (30 ml) prepared from 1 M hydrochloric acid and methanol (1:9 v/v), and the whole mixture was refluxed for 3 h. The reaction mixture was neutralized with aqueous sodium hydrogencarbonate solution and extracted thrice with chloroform. The combined chloroform solution (total 30 ml) was treated in the usual way to give a solid (380 mg), which was chromatographed on a column of silica gel (12 g). Elution with hexane–ethyl acetate (7:3) gave a mixture of **7a** and **7b**, and then pure **7a** (125 mg). This mixture was subjected to separation by TLC to afford **7a** (71 mg) and **7b** (16.4 mg; 1% yield from **3**). The *erythro*-diol (**7a**; total 196 mg) was obtained in 13% yield from **3**. (2*S*,3*R*)-*erythro*-2-Phthalimidooctadecane-1,3-diol (**7a**), mp 69—70 °C (crystallized from hexane–ethyl acetate), $[\alpha]_D^{24}$ −6° (*c* 0.18; EtOH); IR (Nujol) 3400, 1780, and 1705 cm^{-1}; ^{1}H-NMR ($CDCl_3$) δ 0.89 (3H, t-like; $-CH_2C\underline{H}_3$), 3.1—3.6 (2H, broad signal; 2×OH), 4.18 [4H, m; HO–C<u>H</u>–C<u>H</u>($C\underline{H}_2$OH)–N–], and 7.81 (4H, m; aromatic H's); CI-MS (using methane as reactant gas) *m/e* 432 $(M+1)^+$. Found: *m/e* 431.3033. Calcd for $C_{26}H_{41}NO_4$: M, 431.3034. (2*S*,3*S*)-*threo*-2-Phthalimidooctadecane-1,3-diol (**7b**), mp 46—48 °C (crystallized from hexane–ethyl acetate), $[\alpha]_D^{23}$ +3° (*c* 0.24; $CHCl_3$); IR (KBr) 3450, 2920, 2850, 1780, 1710, 1470, 1400, 1380, and 720 cm^{-1}; ^{1}H-NMR ($CDCl_3$) δ 0.89 (3H, t-like; $-CH_2C\underline{H}_3$), 3.3—3.6 (2H, broad signal; 2×OH), 4.05 (3H, m; $-C\underline{H}_2$OH and –C<u>H</u>OH), 4.35 (1H, m; –C<u>H</u>–N–), and 7.81 (4H, m; aromatic H's); CI-MS *m/e* 432 $(M+1)^+$. Found: *m/e* 431.3034. Calcd for $C_{26}H_{41}NO_4$: M, 431.3034.

Acetalization of the erythro-*Diol (**7a**).* A solution of the *erythro*-diol (**7a**; 50 mg) in 2,2-dimethoxypropane (1.5 ml) containing a trace of *p*-toluenesulfonic acid was stirred at room temperature for 10 h. The reaction mixture was treated in the usual way to give a residue, which was subjected to purification by preparative TLC giving an acetonide (**8a**; 53.9 mg) in an almost quantitative yield. (4*R*,5*S*)-2,2-Dimethyl-4-pentadecyl-5-phthalimido-1,3-dioxane (**8a**), mp 65—65.5 °C (crystallized from ethanol), $[\alpha]_D^{30}$ +18° (*c* 0.21; EtOH); IR (Nujol) 1780, 1720, 1260, 1200, 1160, 1120, 1105, 1090, 1075, and 800 cm^{-1}; ^{1}H-NMR ($CDCl_3$) δ 0.89 (3H, t-like; $-CH_2C\underline{H}_3$), 1.48 and 1.67 (each 3H, s; *t*-CH_3), 3.73 [1H, dd, J=10 and J=5 Hz, $C_{(6a)}$–H], 4.28 [1H, td, J=10 and J=5 Hz; $C_{(5a)}$–H], 4.53 [1H, t, J=10 Hz; $C_{(6\beta)}$–H], 4.65 [1H, m; $C_{(4\beta)}$–H], and 7.86 (4H, m; aromatic H's); CI-MS *m/e* 472 $(M+1)^+$; MS *m/e* 456.3114 $(M-15)^+$. Found: C, 74.12; H, 9.64; N, 3.17%. Calcd for $C_{29}H_{45}NO_4$: C, 73.84; H, 9.62; N, 2.97%.

Acetalization of the threo-*Diol (**7b**).* The *threo*-diol (**7b**; 28 mg) was dissolved in 2,2-dimethoxypyropane (1.5 ml) containing a trace of *p*-toluenesulfonic acid, and the solution was stirred at room temperature for 12 d. The reaction mixture was treated in the usual way to give a residue. This was subjected to separation by preparative TLC to afford the corresponding acetonide (**8b**; 16.7 mg) in 55% yield, besides unchanged **7b** (11.1 mg). When the reaction was carried out for 12 h, almost all the starting material (**7b**) was found to be unchanged. (4*S*,5*S*)-2,2-Dimethyl-4-pentadecyl-5-phthalimido-1,3-dioxane (**8b**), mp 59—60 °C (crystallized from ethanol), $[\alpha]_D^{25}$ −20° (*c* 0.15; $CHCl_3$); IR (Nujol) 1780, 1710, 1230, 1170, 1140, 1120, and 880 cm^{-1}; ^{1}H-NMR ($CDCl_3$) δ 0.90 (3H, t-like; $-CH_2C\underline{H}_3$), 1.45 and 1.61 (each 3H, s; *t*-CH_3), 3.96 [1H, dd, J=11 and J=7 Hz; $C_{(6)}$–H], 4.16 [1H, m; $C_{(4a)}$–H], 4.41 [1H, dd, J=11 and J=7 Hz; $C_{(6)}$–H], 4.70 [1H, td, J=7 and J=5 Hz; $C_{(5a)}$–H], and 7.90 (4H, m; aromatic H's); CI-MS *m/e* 472 $(M+1)^+$; MS *m/e* 456.3106 $(M-15)^+$.

*Acid Hydrolysis of the Acetonides (**8a** and **8b**).* The (4*R*,5*S*)-acetonide (**8a**; 38 mg) was added to a solution (5 ml) prepared from 1 M hydrochloric acid and methanol (1:9 v/v), and the mixture was refluxed for 2 h. The reaction mixture was neutralized with aqueous sodium hydrogencarbonate solution and extracted with chloroform. The chloroform solution was treated in the usual way to give the *erythro*-diol (**7a**; 20.9 mg). The *threo*-diol (**7b**) was obtained from the (4*S*,5*S*)-acetonide (**8b**) by the same acid hydrolysis.

Hydrazinolysis of the erythro-*Diol Phthalimide (**7a**).* Hydrazine hydrate (80%; 0.2 ml) was added to a solution of the *erythro*-diol phthalimide (**7a**; 70.5 mg) in ethanol (1.3 ml), and the mixture was refluxed for 1.5 h. The reaction mixture was extracted with dichloromethane (5 ml) after addition of water (1 ml) and potassium hydroxide (0.2 g). The organic layer was treated in the usual way to give a residue, which crystallized from chloroform to afford an *erythro*-amine (**2**; 39.8 mg) in 81% yield. (2*S*,3*R*)-*erythro*-2-Aminooctadecane-1,3-diol (**2**; dihydrosphingosine), mp 76.5—77.5 °C (lit,[4] 78.5—79 °C), $[\alpha]_D^{21}$ +5° [*c* 0.40; $CHCl_3$–EtOH (9:1)] (lit[4] +6°); IR (Nujol) 3350, 3300, 1620, 1580, 1070, and 1040 cm^{-1}; ^{1}H-NMR ($CDCl_3$) δ 0.88 (3H, t-like; $-CH_2C\underline{H}_3$), 2.87 [5H, broad signal; H<u>O</u>–CH_2–C<u>H</u>($N\underline{H}_2$)–C<u>H</u>(O<u>H</u>)–], and 3.70 (3H, broad signal; $-C\underline{H}_2$OH and –C<u>H</u>OH). Found: *m/e* 301.2964. Calcd for $C_{18}H_{39}NO_2$: M, 301.2979.

References

1) D. Shapiro, H. Segal, and H. M. Flowers, *J. Am. Chem. Soc.*, **80**, 1194 and 2170 (1958), and references cited therein; K. Sisido, N. Hirowatari, and T. Ishida, *J. Org. Chem.*, **29**, 2783 (1964); E. J. Reist and P. H. Christie, *ibid.*, **35**, 3521 and 4127 (1970).

2) H. Newman, *J. Am. Chem. Soc.*, **95**, 4098 (1973).

3) H. Newman, *J. Org. Chem.*, **39**, 100 (1974).

4) G. Sticht, D. Lekim, and W. Stoffel, *Chem. Phys. Lipids*, **8**, 10 (1972); *Chem. Abstr.*, **76**, 71968b (1972).

Determination of Stoichiometry and Formation Constant of Molecular Complexes by Differential Refractometry

Ram SAHAI* and Vinod SINGH
Department of Chemistry, V. S. S. D. College, Kanpur 208002, India
(Received September 8, 1979)

Synopsis. A more adequate method has been proposed to determine the stoichiometry and equilibrium constant of molecular complexes by Job method using differential refractometry in modification of Yoshida and Ōsawa method. This method has been verified on phenol–naphthalene system in cyclohexane at 35 °C. The equilibrium constant (K_1=4.9±0.20 dm^3 mol^{-1}), obtained by this method is in good agreement with the literature value.

In our previous investigations to determine the formation constants of molecular complexes, nuclear magnetic resonance,[1] spectrophotometric,[2] refractometric,[3,4] and differential refractometric[5] methods have been used. Yoshida and Ōsawa[6] have also used the refractometric method to determine the equilibrium constant of 1:1 molecular complexes by Job method. In their approach they have plotted n^2 *versus* molar ratio of the solutes [donor(D) and acceptor(A)] and observed the maximum deviation from the additive line (k). As they have pointed out that due to limited accuracy of the instrument, they could not get the reliable value of the equilibrium constant (K_1) because of increased solute concentration (10^{-1} mol dm^{-3}). In this communication an alternate method has been suggested to get the reliable value of K_1 under the conditions of Yoshida and Ōsawa, using the differential refractometry in Job method.

Reagent grade (BDH) phenol, naphthalene were used after further purification. A. R. grade cyclohexane was purified by standard procedures.[7] Stock solutions of phenol (0.10 mol dm^{-3}) and naphthalene (0.10 mol dm^{-3}) were prepared by weighing on an analytical balance and then diluted to the required volume in volumetric flask by cyclohexane.

The refractive indices have been measured by Bausch and Lomb refractometer with an accuracy of ±0.0002. All the measurements were carried out at 35±0.1 °C. The experiment has been carried out for two sets. Firstly, the refractive indices of phenol and naphthalene (0.0 mol dm^{-3}—0.6 mol dm^{-3}) were observed separately and then the refractive indices of mixed solution (phenol+naphthalene), keeping the total concentration constant (0.6 mol dm^{-3}). Secondly, the refractive indices of phenol and naphthalene (0.0 mol dm^{-3}—1.0 mol dm^{-3}) were measured separately and then the refractive indices of mixed solution (phenol+naphthalene), keeping the total concentration constant (1.0 mol dm^{-3}). The refraction per cm^3 due to charge-transfer ($\Delta\Omega C_{DA}$) has been calculated for each set by using Eq. 1 as suggested by Sahai and Singh.[5]

$$10^3(\phi-\phi_D) - \Omega_A C_A^\circ = 6000(n-n_D)n_D/(n_D^2+2)^2 - \Omega_A C_A^\circ = \Delta\Omega C_{DA}. \quad (1)$$

In Eq. 1 $\Omega_A C_A^\circ$ may be calculated by Eq. 2.

$$\Omega_A C_A^\circ = 10^3(\phi_A-\phi_0) = 6000(n_A-n_0)n_0/(n_0^2+2)^2 \quad (2)$$

The quantity Ω_j for the jth solute is defined as

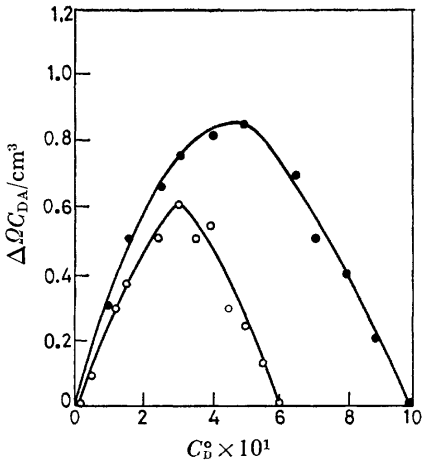

Fig. 1. A Plot of the refraction per cm^3 due to charge-transfer, $\Delta\Omega C_{DA}$/cm^3 *versus* molar ratio of solutes indicating 1:1 stoichiometry of phenol–naphthalene complex.

$\Omega_j=R_j-V_j\phi_0$; where R_j is the apparent molar refraction and V_j the apparent molar volume of the jth solute.[5] The refraction per cm^3 of solvent (ϕ_0), acceptor (ϕ_A), donor (ϕ_D), and solution (ϕ) may be calculated by the relations: $\phi_0=(n_0^2-1)/(n_0^2+2)$; $\phi_A=(n_A^2-1)/(n_A^2+2)$; $\phi_D=(n_D^2-1)/(n_D^2+2)$; $\phi=(n^2-1)/(n^2+2)$, where n_0, n_A, n_D, and n are the refractive indices of solvent, acceptor, donor and solution (donor+acceptor) respectively.[3] A plot of $\Delta\Omega C_{DA}$ *versus* molar ratio of solutes for phenol naphthalene complex has been shown in Fig. 1 which suggests 1:1 stoichiometry of this complex. After getting a more reliable value of k from this plot, the equilibrium constant (K_1) has been calculated by Yoshida & Ōsawa's[6] equation (Eq. 3).

$$K_1 = 2\sqrt{k}\{\sqrt{k}(C+C')-(C+kC')\}/(C-kC')^2, \quad (3)$$

where k is the maximum deviation from the base line for two different concentrations of solutes (C and C').

The refractive index of phenol as well as that of naphthalene increases in cyclohexane with concentration. When phenol solution is mixed with naphthalene, a neutral complex is formed. The plot of Δn, the difference in refractive indices of calculated and observed values, against (complex) is linear indicating that there is no interaction between the complex and individual species.

A change in electron cloud density in the neutral atom or molecule will lead to a change in the polarizability. Since the complex is generally more polar than the components, the electronic polarizability or refractive index increases and the deviation depends upon the extent of interaction between the donor and acceptor. Therefore stronger the complex, the larger the deviation in the refractive index value.

The small deviation in refractive index of the mixed system of phenol and naphthalene in cyclohexane shows that the interaction between phenol and naphthalene is weak. In the present case the deviation is positive and the maximum is observed at 1:1 molar ratio. The K value obtained thus is 5.8 ± 0.20 dm^3 mol^{-1} at 35 °C which is slightly higher compared to the value calculated from the available data.[8] But the K value obtained from the plot of $\Delta\Omega C_{DA}$ *versus* molar ratio of solutes is 4.9 ± 0.20 dm^3 mol^{-1} at 35 °C which is almost comparable with that of the calculated value. As the refractive index for visible light varies with the wavelength, the electron polarization is somewhat uncertain. So the K value obtained by the plot of n^2 *versus* molar ratio of solutes must be accepted with care.

Due to the limited accuracy of the instrument, the solute concentration was raised (0.10 mol dm^{-3}) in order to get k value sufficient to fit in Eq. 3. At this higher concentration, the solute aggregation occurs which prevents to get the reliable value of K_1. But this problem has been resolved in the present scheme in which instead of the plot of n^2 *versus* molar ratio, the refraction per cm^3 due to charge-transfer, ($\Delta\Omega C_{DA}$), has been calculated and plotted against molar ratio. The equilibrium constant obtained by the plot of $\Delta\Omega C_{DA}$ *versus* molar ratio of solutes ($K_1=4.9\pm0.20$ dm^3 mol^{-1}) is more reliable than that of K_1 obtained by the plot of n^2 *versus* molar ratio of the solutes ($K_1=5.8\pm0.20$ dm^3 mol^{-1}) which is in agreement with that of literature value.[9] In the present scheme, the refraction per cm^3 due to solvent, acceptor and donor has been considered whereas in the earlier methods[6,10,11] the square of refractive indices (n^2) of solution was taken into account only. Thus the data obtained by the present scheme are more reliable than that of earlier one. It, therefore, appears that the present method may prove better to calculate the equilibrium constant (K_1) of the weak complexes within the limited accuracy of the instrument for which the concentration of the solutes is ought to be high. Though the present scheme involves a lot of complexity in the experimental procedure but the data obtained are more reliable compared to the earlier method.[6]

One of us (V.S.) is thankful to Kanpur University, Kanpur for the award of U.G.C. Fellowship. The authors are grateful to Professor P.C. Nigam (I. I. T., Kanpur) for providing some experimental facilities to carry out this work.

References

1) R. Sahai, G. L. Loper, S. H. Lin, and H. Eyring, *Proc. Natl. Acad. Sci. U.S.A.*, **71**, 1499 (1974).
2) R. Sahai and V. N. Badoni, *Indian J. Chem.*, **15A**, 731 (1977).
3) R. Sahai, P. C. Pande, and V. Singh, *Indian J. Chem.*, **18A**, 217 (1979).
4) R. Sahai and V. Singh, *Indian J. Pure Appl. Phys.*, in press.
5) R. Sahai and V. Singh, *Indian J. Chem.*, in press.
6) Z. Yoshida and E. Ōsawa, *Bull. Chem. Soc., Jpn.*, **38**, 140 (1965).
7) J. A. Riddick and W. B. Bunger, "Techniques of Chemistry," Vol. II. "Organic Solvents," ed by A. Weissberger, Wiley-Interscience, New York (1970).
8) A. S. N. Murty and C. N. R. Rao, *Appl. Spectr. Revs.*, **2**, 69 (1969).
9) Z. Yoshida and E. Ōsawa, *J. Am. Chem. Soc.*, **88**, 4019 (1966).
10) R. A. Singh and S. N. Bhat, *Indian J. Chem.*, **15A**, 1106 (1977).
11) R. A. Singh and S. N. Bhat, *J. Phys. Chem.*, **82**, 2323 (1978).

Studies on Complexes of Metal(II) Carboxylates with Donor Molecules. IV.[1] Complexes of Nickel(II) Chloroacetates with Pyridine *N*-Oxides and Triphenylphosphine Oxide

Narsingh KUMAR,* Piyara Lal KACHROO, and Rama KANT
Department of Chemistry, University of Jammu, Jammu 180001, India
(Received June 16, 1979)

Synopsis. Twelve green crystalline complexes with the general formula $[Ni(O_2CR)_2 \cdot L]_2$ were prepared by the reaction of stoichiometric amounts of pyridine *N*-oxide, 2-methylpyridine *N*-oxide, 3-methylpyridine *N*-oxide, and triphenylphosphine oxide with nickel(II) mono-, di-, and trichloroacetates in methanol. The complexes were characterized by elemental analyses, conductance, magnetic moments, IR and electronic spectra as neutral, binuclear, carboxylato bridged species identical to those of copper(II) acetate monohydrate. The complexes involve varying degrees of magnetic interaction which diminishes with increasing chlorine substitution in the chloroacetate moiety.

Studies on binuclear metal(II) carboxylate complexes of the type $[M(O_2CR)_2 \cdot L]_2$ (especially, when M=Cu) reveal that the extent of magnetic interaction in these systems is largely determined by the nature of the carboxylate anion and the addend ligand.[2-4] However, in complexes of nickel(II) propionate and butyrate with aromatic amine oxides, we found that the magnetic moments of these complexes are independent of the nature of the alkanoate anion.[5] Since chloroacetic acids widely differ in acid strength, their nickel(II) complexes have been examined in order to assess the effect of varying basicity of the carboxylate anions on magnetic and other properties of the resulting complexes. The results of these studies are presented in this paper.

Experimental

Materials. Trinickel(II) carbonate tetrahydroxide tetrahydrate was repeatedly washed with hot water and then dried in the air. The chloroacetic acids and the amine oxide ligands were purified by vacuum distillation. Triphenylphosphine oxide hemihydrate was heated at 105 °C in a vacuum for 3 h and subsequently recrystallized from dry acetone to give the anhydrous compound (mp 154—155 °C). Nickel(II) chloroacetates were prepared as hydrates by the method of Lever and Ogden[6] and its modifications. The anhydrous samples obtained after drying in a vacuum over phosphorus pentaoxide gave satisfactory results in elemental analyses.

Complexes. The complexes were prepared by the direct interaction of the appropriate nickel(II) chloroacetate and the ligand in methanol, using the same general technique as given in the following example.

Bis(chloroacetato)(pyridine N-oxide)nickel(II). To a solution containing 1.48 g (6 mmol) nickel(II) chloroacetate in methanol (125 cm^3) was added, with stirring, a solution of 0.93 g (6.5 mmol) of freshly purified pyridine *N*-oxide in methanol (10 cm^3). The resulting green solution was concentrated to *ca.* 30 cm^3 and filtered while hot. Anhydrous diethyl ether (30 cm^3) was added to the cold filtrate and the green solid which separated out on allowing the filtrate to stand overnight was recrystallized from a 2:1 ethyl acetate–benzene mixture (60 cm^3) containing a small amount of pyridine *N*-oxide (0.15 g). The crystalline product was collected, washed with a 2:1 ethyl acetate–benzene mixture and then dried in a vacuum over phosphorus pentaoxide to yield 1.38 g (68% based on nickel(II) chloroacetate) of the required product.

The remaining nickel(II) chloroacetate complexes were prepared similarly in 50—80% yields. Reactions were also carried out using ligands in higher molar ratio of 1:2, 1:3, and a large excess but the products obtained were invariably of 1:1 stoichiometry, identical to those obtained with reactants in equimolar ratio.

Analyses. Nickel was determined gravimetrically as bis(dimethylglyoximato)nickel(II). Carbon and hydrogen analyses were carried out in the departmental microanalytical laboratory. For chlorine analysis, a sample containing 20—25 mg of chlorine was fused with a mixture of anhydrous sodium carbonate (0.5 g), sodium hydroxide (0.25 g) and sodium (0.1 g) at 700—900 °C for *ca.* 30 min in a platinum crucible. The resulting mass was extracted with distilled water, and the chloride contents of the alkaline extract were determined gravimetrically as silver chloride.

Measurements. Magnetic measurements were carried out at room temperature by the Gouy method using Hg-$[Co(NCS)_4]$ as a calibrant. The electronic spectra were recorded in acetone over 8000—28500 cm^{-1} on a Beckman DK-2A spectrophotometer, while the infrared spectra were scanned on Perkin-Elmer 337 and 621 instruments as Nujol mulls in sodium chloride and polyethylene plates.

Results and Discussion

The results of elemental analyses indicate that the complexes are of 1:1 stoichiometry and can be formulated as $[Ni(O_2CR)_2 \cdot L]$. The complexes are light green to green in color. They are moderately soluble in polar solvents, but are generally insoluble in nonpolar solvents. Molar conductance values of the millimolar solutions of the complexes in methanol are of the order 20–40 S cm^2 mol^{-1} suggesting that the complexes are nonelectrolytic in nature. Molecular weights could not be determined by the cryoscopic method because of insufficient solubility of the complexes in benzene and nitrobenzene.

Electronic Spectra. The electronic spectra of the complexes show the usual three bands (I, III, and IV) around 9000, 15000, and 25000 cm^{-1} as observed in octahedral complexes of nickel(II); these bands are assigned to $^3T_{2g} \leftarrow {}^3A_{2g}$, $^3T_{1g}(F) \leftarrow {}^3A_{2g}$, and $^3T_{1g}(P) \leftarrow {}^3A_{2g}$ transitions.[7] An important feature of the electronic spectra of these complexes is that an additional band (II) is observed at ≈ 14000 cm^{-1}. The band is usually of lower intensity assigned to the spin forbidden, singlet transition $^1E_g(D) \leftarrow {}^3A_{2g}$, gaining intensity through configurational interaction or spin-orbit coupling.[7] The molar extinction coefficient values of the bands fall in the range 2.3—17 dm^3 cm^{-1} mol^{-1} similar to those reported for trans octahedral nickel(II) complexes.[6,7]

TABLE 1. ANALYSES, MAGNETIC MOMENTS, ELECTRONIC SPECTRA, AND IR-BANDS OF THE COMPLEXES

Complex	Found (Calcd) (%)				μ_{eff}[a]	$\nu/10^3$ cm^{-1}				Important IR-band/cm^{-1}			
	C	H	Cl	Ni	B. M.	I	II	III	IV	$\nu_{NO\|P=O}$	$\nu_{COO}(as)$	$\nu_{COO}(sy)$	$\Delta\nu_{COO}$
$[Ni(O_2CCH_2Cl)_2(C_5H_5NO)]_2$	32.05 (31.70)	3.05 (2.64)	20.36 (20.84)	17.15 (17.23)	2.64	9.0	13.9	15.2	24.6	1217	1630	1374	256
$[Ni(O_2CCH_2Cl)_2(2\text{-}CH_3C_5H_4NO)]_2$	— (33.83)	— (3.10)	19.11 (20.02)	16.38 (16.55)	—	8.9	14.0	15.1	24.8	1209	1622	1372	250
$[Ni(O_2CCH_2Cl)_2(3\text{-}CH_3C_5H_4NO)]_2$	33.60 (33.83)	3.55 (3.10)	19.87 (20.02)	16.56 (16.55)	2.63	9.0	13.7	15.2	25.1	1258	1634	1376	258
$[Ni(O_2CCH_2Cl)_2(C_6H_5)_3PO]_2$	49.90 (50.41)	4.05 (3.63)	13.11 (13.56)	11.02 (11.21)	2.79	8.9	13.7	15.0	24.9	1168	1638	1376	262
$[Ni(O_2CCHCl_2)_2(C_5H_5NO)]_2$	26.05 (26.36)	2.50 (1.71)	34.21 (34.66)	14.28 (14.33)	2.82	9.0	14.0	15.4	25.4	1222[b] 1210	1645	1355	290
$[Ni(O_2CCHCl_2)_2(2\text{-}CH_3C_5H_4NO)]_2$	27.90 (28.32)	2.55 (2.12)	32.72 (33.51)	14.05 (13.86)	2.80	9.0	14.1	15.3	25.1	1208	1647	1355	292
$[Ni(O_2CCHCl_2)_2(3\text{-}CH_3C_5H_4NO)]_2$	28.20 (28.32)	2.55 (2.12)	32.96 (33.51)	13.72 (13.86)	2.80	9.0	13.7	15.3	25.1	1220	1651	1360	291
$[Ni(O_2CCHCl_2)_2(C_6H_5)_3PO]_2$	— (44.54)	— (2.81)	23.01 (23.96)	9.76 (9.91)	—	8.8	13.6	15.1	25.0	1168	1645	1350	295
$[Ni(O_2CCCl_3)_2(C_5H_5NO)]_2$	22.55 (22.56)	1.15 (2.04)	43.87 (44.49)	12.46 (12.26)	3.07	8.8	13.6	15.2	25.6	1218	1695	1346	349
$[Ni(O_2CCCl_3)_2(2\text{-}CH_3C_5H_4NO)]_2$	24.50 (24.35)	1.50 (1.42)	42.44 (43.23)	11.80 (11.92)	3.11	9.0	13.5	15.0	25.1	1220	1690	1345	345
$[Ni(O_2CCCl_3)_2(3\text{-}CH_3C_5H_4NO)]_2$	24.60 (24.35)	1.55 (1.42)	42.67 (43.23)	11.40 (11.92)	3.12	8.9	13.7	15.3	25.2	1257	1690	1344	346
$[Ni(O_2CCCl_3)_2(C_6H_5)_3PO]_2$	39.85 (39.90)	2.50 (2.27)	32.19 (31.67)	8.67 (8.87)	3.21	8.9	13.8	15.1	25.5	1170	1690	1340	350

a) At room temperature, 290 K. b) Shoulder.

Magnetic Properties. The magnetic moments of the complexes (Table 1) fall in the range 2.60—3.21 BM which are, in general, less than the magnetic moments of 3.15—3.30 BM observed for magnetically normal, octahedral nickel(II) carboxylate complexes.[8] This suggests that the complexes involve some metal–metal interaction and may have a binuclear (or polynuclear), carboxylato bridged structure similar to some nickel(II) trihaloacetate complexes.[9]

The magnetic moment values of the present complexes are significantly higher than the values of 2.35—2.63 BM observed for nickel(II) alkanoate complexes,[7] showing a regular increase from mono-, to di- and trichloroacetate complexes. This indicates that the magnetic interaction in these complexes decreases sharply as the basicity of the chloroacetate anion decreases with increasing chlorine substitution in the acetate moiety.

Infrared Spectra. The N–O stretching frequency which occurs at 1250, 1244, and 1278 cm^{-1} in pyridine *N*-oxide, 2-methylpyridine *N*-oxide, and 3-methylpyridine *N*-oxide is shifted to lower frequencies by 20—60 cm^{-1} in the nickel(II) chloroacetate complexes. This indicates monodentate coordination of pyridine *N*-oxide ligands.[10] δ_{N-O} and γ_{C-H} also show some positive or negative shifts confirming the coordination of *N*-oxide ligands through their oxygen atoms. The P=O stretching vibration shows a negative shift of 19—21 cm^{-1}, while $\delta_{P=O}$ and γ_{C-H} also undergo small shifts indicating that triphenylphosphine oxide is coordinated through its P=O oxygen atom in its complexes.[11]

The asymmetric carboxyl stretching frequency in nickel(II) mono-, di-, and trichloroacetate complexes occurs as a very strong peak at 1638—1622, 1651—1645, and 1695—1690 cm^{-1}, while the symmetric carboxyl stretching frequency is observed at 1376—1372, 1360—1350, and 1346—1340 cm^{-1}, respectively. The upwards shift of $\nu_{COO}(as)$ and downward shift of $\nu_{COO}(sy)$ noted in these complexes is ascribed to the increasing chlorine substitution in the chloroacetate anion.[12] The position and nature of the carboxyl stretching frequencies, as well as their separation, are comparable to the frequencies reported by Lever and Ogden for nickel(II) complexes containing bidentate bridging chloroacetato groups.[6] All this corroborates the view that the complexes under investigation are binuclear, carboxylato bridged species identical to copper(II) acetate monohydrate.[13]

The authors wish to thank Professor O. P. Vig, Head of the Chemistry Department, Panjab University, Chandigarh, for laboratory facilities. One of the authors (R. K.) was granted a Junior Research Fellowship from the University Grants Commission, India.

References

1) Part III: N. Kumar, P. L. Kachroo, and R. Kant, *Transition Metal Chem.*, in press.
2) M. Kato, H. B. Jonassen, and J. C. Fanning, *Chem. Rev.*, **64**, 99 (1964).
3) J. Drew, M. B. Hursthouse, P. Thornton, and A. J. Welch, *J. Chem. Soc., Chem. Commun.*, **1973**, 52.
4) D. H. Hibdon and J. H. Nelson, *Inorg. Chim. Acta*, **7**, 629 (1973).
5) N. Kumar, P. L. Kachroo, and R. Kant, *Indian J. Chem.*, **18A**, 265 (1979).
6) A. B. P. Lever and D. Ogden, *J. Chem. Soc., A*, **1967**, 2041.
7) A. B. P. Lever, "Inorganic Electronic Spectroscopy," Elsevier, New York, N. Y. (1968).
8) B. N. Figgis and J. Lewis, *Prog. Inorg. Chem.*, **6**, 37 (1964).
9) S. Amasa, D. H. Brown, and D. W. A. Sharp, *J. Chem. Soc., A*, **1969**, 2892.
10) N. M. Karayannis, L. L. Pytlewski, and C. M. Mikulski, *Coord. Chem. Rev.*, **11**, 93 (1973).
11) D. R. Cousins and F. A. Hart, *J. Inorg. Nucl. Chem.*, **29**, 1745 (1967).
12) E. Spinner, *J. Chem. Soc.*, **1964**, 4217.
13) J. N. Van Niekerk and F. R. L. Schoening, *Acta Crystallogr.*, **6**, 227 (1953); *Nature*, **171**, 6 (1953).

Neutron Diffraction Study of Aqueous Ionic Solutions. II. Aqueous Solutions of Sodium Chloride and Potassium Chloride

Norio Ohtomo† and Kiyoshi Arakawa*

Research Institute of Applied Electricity, Hokkaido University, Sapporo 060

† *Faculty of Engineering, Hokkaido University, Sapporo 060*

(Received September 20, 1979)

The structure factors $S_m(Q)$ for aqueous solutions of NaCl and KCl at room temperature have been determined by means of the LINAC-TOF-neutron diffraction method. A revised subtraction method was applied to diffraction data of the solutions. Results obtained for the structure of the nearest hydration shell around ions are as follows. (a) The coordination numbers are 8 for Na^+ and 6 for Cl^- in the NaCl solution and 8 for K^+ and 6 for Cl^- in the KCl solution; (b) the average ion-oxygen distances are 2.50 ± 0.10 Å for Na^+, 2.70 ± 0.10 Å for K^+, and 3.10 ± 0.05 Å for Cl^-; (c) around chloride ions water molecules take the configuration to orient the vector which bisects the D–O–D angle on a straight line joining an oxygen atom and the anion. Analysis was performed on the data of LiCl and CsCl solutions.

Neutron diffraction studies have recently been carried out on aqueous ionic solutions.[1–3] It was found that the method is useful for the determination of the structures of ionic solutions, in particular the structure parameters of the hydration shell around ions such as coordination numbers, ion-oxygen distances, and orientational arrangements of water molecules within the first hydration shell.

The recent development of the TOF-neutron diffraction method, associated with the proposition of improved correction procedures for inelastic scattering, has made it possible to provide more accurate data.[1,4–6] On neutron diffraction data of aqueous ionic solutions, there is no general method of analysis. Three procedures have been proposed so far: the near-neighbor model method by Narten *et al.*,[2] the first-order-difference spectroscopy by Soper *et al.*,[3] and the subtraction method by the authors.[1] However, the method of Narten *et al.* has been questioned especially concerning the nature of the near-neighbor model itself,[4,7,8] while the method of Soper *et al.* using isotopes of nuclear species in the sample is clearly restricted in applicability.

In our study of aqueous solutions of LiCl and CsCl by the subtraction method (Paper I)[1] we obtained information on the structure of the first hydration shell around ions. In order to elucidate the structure of the shell about univalent ions, we have carried out a neutron diffraction study on aqueous solutions of NaCl and KCl, a revised subtraction method being used to confirm the accuracy of the results.

Experimental

The experiment was performed by means of the TOF-neutron diffraction method by LINAC. Details of the apparatus and procedures were reported.[1,4,9]

Two 1.0 M alkali halide solutions (1 M = 1 mol dm^{-3}) were prepared by the addition of extra pure anhydrous sodium chloride and potassium chloride to heavy water. Samples composed of naturally occurring elements were used, the values of coherent scattering amplitudes of the elements being 0.36×10^{-12} cm for Na, 0.37×10^{-12} cm for K, and 0.96×10^{-12} cm for Cl.[10]

Measurements were carried out at room temperature (20.5 °C) at the scattering angle, $2\theta=45°$. We obtained the $S_m(Q)$ data for a range of low Q, 0.9—10.0 $Å^{-1}$ ($Q=4\pi/\lambda\sin\theta$). $S_m(Q)$ curves of NaCl and KCl solutions including that of D_2O are given in Fig. 1. The change in the bump at *ca.* 4 $Å^{-1}$ as well as that in the main peak accompanied by a shoulder at 2.8 $Å^{-1}$ indicate the main effects of ions on the structure of the first hydration shell.

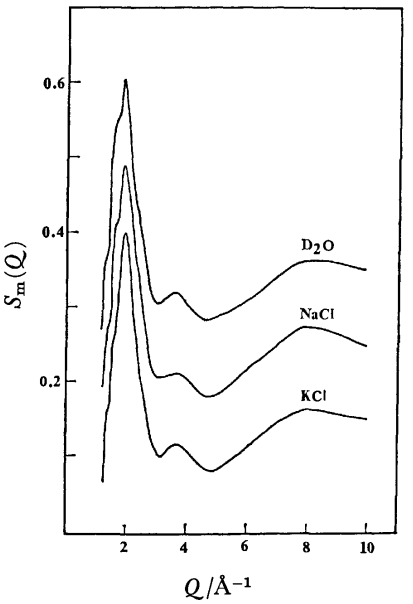

Fig. 1. Observed structure factors for NaCl and KCl solutions at 1 M, compared with the factor for D_2O.

The statistical errors are the same as those reported:[1] 0.5—0.6% in the Q range 2—5 $Å^{-1}$ and 0.9% at *ca.* 8 $Å^{-1}$.

Analysis of Aqueous Solutions of Alkali Chlorides

Subtraction Method of Analysis. In order to analyze the data of comparatively dilute aqueous solutions for determination of the structure of the first hydration shell, we have used a subtraction method in which the structure factor $S_m(Q)_{D_2O}$ of D_2O multiplied by an appropriate fraction is subtracted from the total structure factor $S_m(Q)_{total}$ of solutions.[1] The remaining factor $\Delta S_m(Q)$ thus obtained has been compared with the $\Delta S_m(Q)_{calcd}$ calculated for a structure model of the hydration shell, the structure model which gives the best fit curve being determined. In applying the subtraction method we modify Eq. 2, Paper I,

in an attempt to make the method more available. By introducing a term multiplied by a coefficient a which indicates a contribution of the interactions between water molecules within the first hydration shell and environmental molecules outside of the shell in addition to Eq. 2, Paper I, the remaining factor $\Delta S_m(Q)$ for the first hydration shell becomes

$$\Delta S_m(Q) = S_m(Q)_{total} - \left(\frac{N_w'}{N_w} - x\right) S_m(Q)_{D_2O} - axS_m(Q)_{D_2O}, \quad (1)$$

$$x = \frac{c(n_+ + n_-)}{55.3}, \quad (2)$$

where N_w and N_w' are the mole numbers of water in 1 dm^3 of pure water and those of water in 1 dm^3 of the solutions, respectively, x is the mole fraction of D_2O molecules coordinated in the first hydration shell around ions, n_+ and n_- are the coordination numbers around the cation and the anion, respectively, and c is concentration in M. The second term in Eq. 1 shows the contribution from bulk water outside of the hydration shells, and the third one that from the pairs between molecules within hydration shells and bulk water molecules. In aqueous solutions as dilute as 1 M, we can assume $N_w'/N_w \simeq 1$,[11] and we get

$$\Delta S_m(Q) = S_m(Q)_{total} - (1-x)S_m(Q)_{D_2O} - axS_m(Q)_{D_2O}. \quad (3)$$

In order to study the contribution of the interactions between water molecules in the first hydration shell ($c(n_+ + n_-)$mol) and those outside, the magnitude of a is estimated as follows. The contribution of the interactions to $S_m(Q)$ is supposed to be equal to that of $c(n_+ + n_-)/2$ mol of bulk water molecules on the average, since $c(n_+ + n_-)$ mol of the water molecules in the nearest hydration shell are in contact with ions on the one side, the contribution to the total water-water interactions then becoming approximately half as much as that of the same mol of bulk water. Thus, the magnitude of a is 1/2 in this case. In the analysis used in Paper I, the contribution was neglected, and Eq. 2 in the paper is identical with the case of $a=0$ in Eq. 3 above. We will now compare the two cases, $a=1/2$ and $a=0$.

Calculation of $\Delta S_m(Q)$. In order to determine the structure of the nearest hydration shell in the NaCl and KCl solutions, the observed values of $\Delta S_m(Q)$ are compared with those calculated for various structure models assumed.

The structure of the hydration shell is characterized by several parameters, coordination numbers, ion-oxygen distances, and orientational arrangements of water molecules around ions. The coordination numbers and ion-oxygen distances reported so far are located given in Tables 1 and 2 together with the tables in Paper I. As regards the configuration of water molecules around ions, two forms, linear and bifurcated, are assumed for cations where lone-pair electrons are located in the vicinity of the ions (Paper I, Figs. 5 (a) and (b)) and also for anions where deuterium atoms are located in the vicinity of the ions (Paper I, Figs. 5(c) and (d)).

The calculated remaining factor, $\Delta S_m(Q)_{calcd}$, we have

$$\Delta S_m(Q)_{calcd} = \sum_{\alpha=\pm} [x'_\alpha (\sum_{n=1}^{m_\alpha} b_n)^{-2} \sum_{i=1}^{m_\alpha} \sum_{j=1}^{m_\alpha} b_i b_j \times \exp(-\gamma_{\alpha ij} Q^2) j_0(Q r_{\alpha ij})], \quad (4)$$

where

$$j_0(Qr) = \frac{\sin(Qr)}{Qr}, \quad (5)$$

with summation for α over two contributions from the hydrated structure of cation (+) and anion (−). m_α is the number of atoms within the hydrated structure labelled by α, x'_α the mole fraction of D_2O molecules coordinated in the shell around cation and anion, and b_i the coherent scattering length of nucleus i. $r_{\alpha ij}$ is the distance between nuclei i and j within the hydrated structure labelled by α and their mean-square variations $2\gamma_{\alpha ij}$.

Table 1. Coordination numbers of Na^+ and K^+ determined from X-ray (X) diffraction study as well as from molecular dynamics (MD) and monte calro (MC) calculations

Ion	Coordination number	Solute	Concentration / M	Method	Ref.
Na^+	5—6			MC	iii
	4±1.5	NaI	7	X	v
	5			MD	vi
	6.6±0.1	NaCl	2.2	MD	vii
	7.3		0.55	MD	viii
	4.3			MC	ix
K^+	4	KOH	12	X	i
	5.3	KCl	2—4	X	ii
	5—7			MC	iii
	3.2—1.7	KJ	0.5—5	X	iv
	5.1			MC	ix

i) E. W. Brady, *J. Chem. Phys.*, **28**, 464 (1958). ii) D. S. Terekhova, A. I. Ryss, and I. V. Radchenko, *Zh. Strukt. Khim.*, **10**, 923 (1969). iii) H. Kistenmacher, H. Popkie, and E. Clementi, *J. Chem. Phys.*, **61**, 799 (1974). iv) M. Ya Fishkis and T. E. Soboleva, *Zh. Strukt. Khim.*, **15**, 186 (1974). v) M. Maeda and H. Ohtaki, *Bull. Chem. Soc. Jpn.*, **48**, 3755 (1975). vi) Ref. 9. vii) Ref. 8. viii) Ref. 10. ix) E. Clementi and R. Barsotti, *Chem Phys. Lett.*, **59**, 21 (1978).

Table 2. Average ion-oxygen distances of the first hydration shell determined from X-ray (X) diffraction study as well as from molecular dynamics (MD) and monte calro (MC) calculations

Ion	Distance / Å	Solute	Concentration / M	Method	Ref.[a]
Na^+	2.3±2.4			MC	iii
	2.40±0.03	NaI	7	X	v
	2.31	NaCl	2.2	MD	vii
	2.59			MC	ix
K^+	2.8±2.9			MC	iii
	3.27			MC	ix

a) References are the same as those in Table 1.

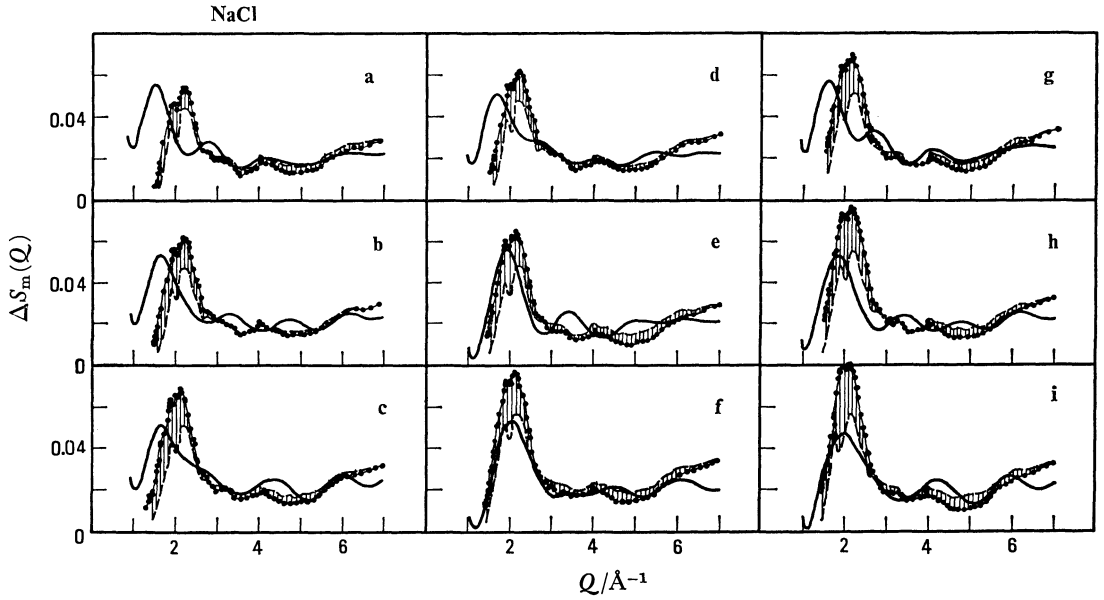

Fig. 2. Changes in the calculated $\Delta S_m(Q)$ with variation of the coordination number for NaCl solution,
•: observed $\Delta S_m(Q)$ ($a=0$), ----: observed $\Delta S_m(Q)$ ($a=1/2$),
(a) $n_+=4$, $n_-=4$, (b) $n_+=6$, $n_-=4$, (c) $n_+=8$, $n_-=4$, (d) $n_+=4$, $n_-=6$, (e) $n_+=6$, $n_-=6$,
(f) $n_+=8$, $n_-=6$, (g) $n_+=4$, $n_-=8$, (h) $n_+=6$, $n_-=8$, (i) $n_+=8$, $n_-=8$.

Table 3. Range of parameters for structure models

Ion	Coordination number	Ion-oxygen distance/Å	Type of configurations around ions	(ϕ/degree)
Na^+	4, 6, 8	2.20—2.70	linear	(44.75—64.75)
			bifurcated	(0.0 —20.0)
K^+	4, 6, 8	2.70—3.40	linear	(44.75—64.75)
			bifurcated	(0.0 —20.0)
Cl^-	4, 6, 8	3.00—3.20	linear	(0.0 —20.0)
			bifurcated	(0.0 —20.0)

The contribution from the hydrated structure for each kind of ion is calculated by a similar procedure to that for the water structure previously described,[4] constructed for the corresponding structure models. The model consists of several parameters varying in a range of magnitude (Table 3). For example, in the case of $n_\pm=4$, 6, and 8, tetrahedral, octahedral, and cubic coordination is assumed, respectively, with the variation of ion-oxygen, ion-deuterium, oxygen-oxygen, and oxygen-deuterium distances and the orientational angles.

We calculated $\Delta S_m(Q)$ for a number of structure models with various magnitudes of parameters (Table 3). For both solutions, 36 different structure models with respect to the coordination number and type of orientational configuration were assumed; for each structure model, ion-oxygen distances and the angle ϕ were varied successively at intervals of 0.05 Å and 10°, respectively. In all, we calculated the $\Delta S_m(Q)$ curves for 1,680 different structure models of the first hydration shell in the NaCl solution and for 1,824 different models in the KCl solution, the best structure model being then determined by a comparison of the $\Delta S_m(Q)_{calcd}$ curves with those observed for both solutions.

Table 4. Coordination numbers, ion-oxygen distances and configurations around ions determined in the present study

Ion	Coordination number	Ion-oxygen distance/Å	Configuration around ions (ϕ/degree)
Na^+	8	2.50±0.10	undetermined
K^+	8	2.70±0.10	undetermined
Cl^-	6	3·10±0.05	bifurcated (0.0)

Results of Analysis. The $\Delta S_m(Q)_{calcd}$ curves for different sets of coordination numbers for NaCl and KCl solutions are shown in Figs. 2 and 3, respectively, two sets of observed values of $\Delta S_m(Q)$ being plotted for $a=1/2$ and $a=0$ and the interval between those being hatched. The best fit curves with observed $\Delta S_m(Q)$ are obtained in the case of $n_{Na^+}=8$ and $n_{Cl^-}=6$ for the NaCl solution (Fig. 2 (f)) and in the case of $n_{K^+}=8$ and $n_{Cl^-}=6$ for the KCl solution (Fig. 3 (f)). The curves other than the best fit ones deviate appreciably from both observed $\Delta S_m(Q)$ ($a=1/2$ and $a=0$) (Figs. 2 and 3).

The $\Delta S_m(Q)$ curves with various magnitudes of parameters are shown in Figs. 4 (a)—(d) for $n_{Na^+}=8$ and $n_{Cl^-}=6$ for the NaCl solution, and in Figs. 4 (a')—(d') for $n_{K^+}=8$ and $n_{Cl^-}=6$ for the KCl solution.

The calculated $\Delta S_m(Q)$ curves of the best models thus determined for both solutions are given in Figs. 2 (f) and 3 (f) for NaCl and KCl solutions, respectively. The magnitudes of parameters and orientational configurations for the best models of the first hydration shell are given in Table 4. Concerning the configurations of water molecules within the first hydration shell around Cl^-, we have confirmed that the bifurcated type is predominant for both solutions (Figs. 4 (d) and (d')).[12] However, with respect to the configurations around cations, we could not determined which

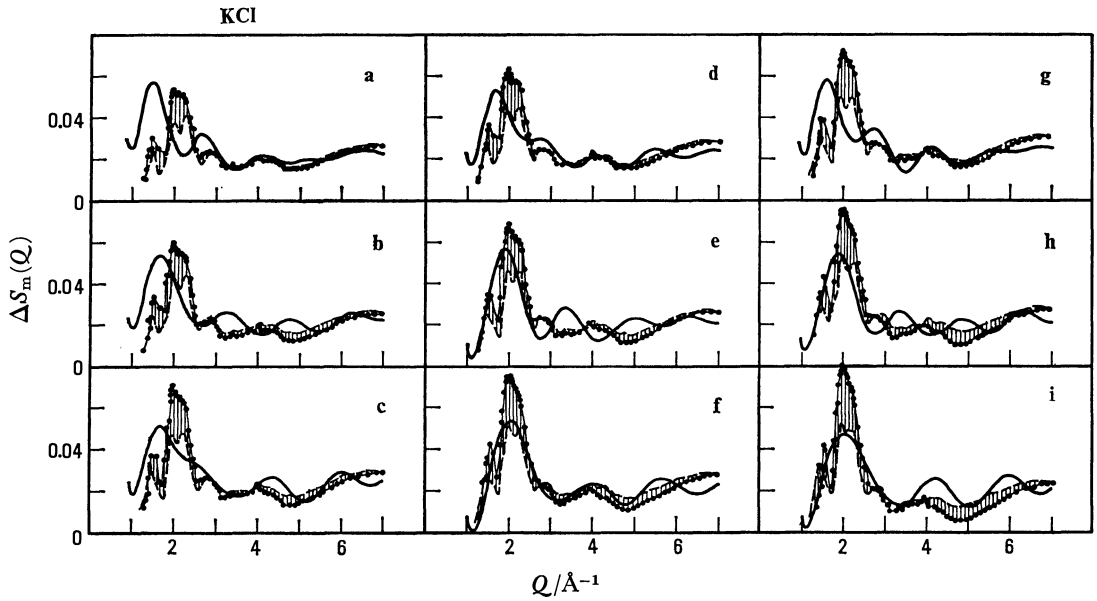

Fig. 3. Changes in the calculated $\Delta S_m(Q)$ with variation of the coordination number for KCl solution, •: observed $\Delta S_m(Q)$ ($a=0$), ----: observed $\Delta S_m(Q)$ ($a=1/2$),
(a) $n_+=4$, $n_-=4$, (b) $n_+=6$, $n_-=4$, (c) $n_+=8$, $n_-=4$, (d) $n_+=4$, $n_-=6$, (e) $n_+=6$, $n_-=6$, (f) $n_+=8$, $n_-=6$, (g) $n_+=4$, $n_-=8$, (h) $n_+=6$, $n_-=8$, (i) $n_+=8$, $n_-=8$.

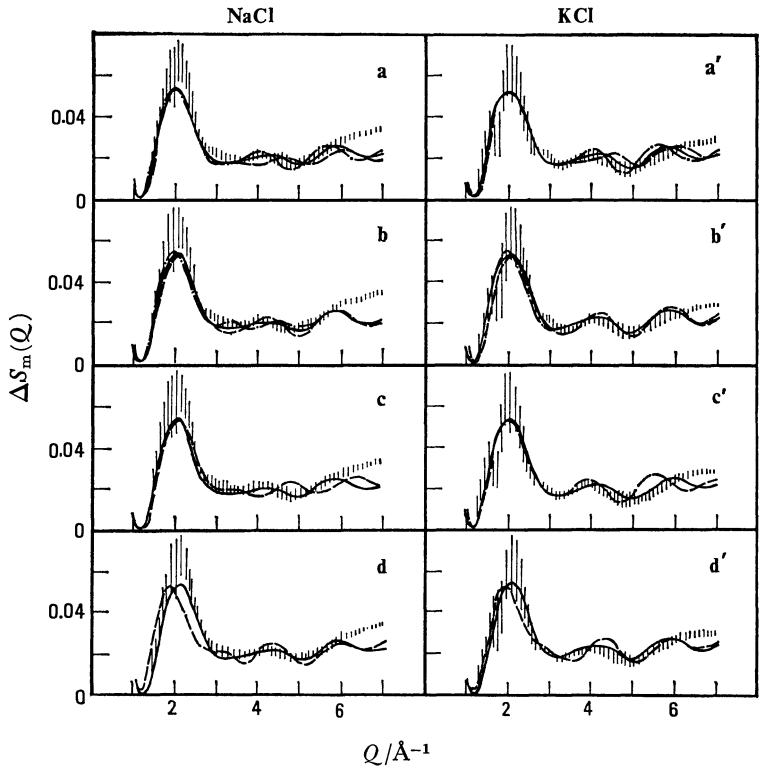

Fig. 4. Changes in the calculated $\Delta S_m(Q)$ with variation of physical parameters for NaCl (a—d) and KCl (a′—d′) solutions. The vertical lines indicate the intervals between two sets of observed values of $\Delta S_m(Q)$ ($a=0$ and $a=1/2$).
(a) $r_{Na^+\text{-}O}$ (all other parameters are identical with those given in Table 4), ----: 2.40 Å, ——: 2.50 Å, —·—: 2.60 Å, (b) $r_{Cl^-\text{-}O}$ (all other parameters are identical with those given in Table 4), ----: 3.00 Å, ——: 3.10 Å, —·—: 3.20 Å, (c) configurations around Na^+ (all other parameters are identical with those given in Table 4), ——: bifurcated, ----: linear, (d) configurations around Cl^- (all other parameters are identical with those given in Table 4), ——: bifurcated, ----: linear, (a′) $r_{K^+\text{-}O}$ (all other parameters are identical with those given in Table 4), ----: 2.60 Å, ——: 2.70 Å, —·—: 2.80 Å, (b′) $r_{Cl^-\text{-}O}$ (all other parameters are identical with those given in Table 4), ----: 3.00 Å, ——: 3.10 Å, —·—: 3.20 Å, (c′) configurations around K^+ (all other parameters are identical with those given in Table 4), ——: linear, ----: bifurcated, (d′) configurations around Cl^- (all other parameters are identical with those given in Table 4), ——: bifurcated, ----: linear.

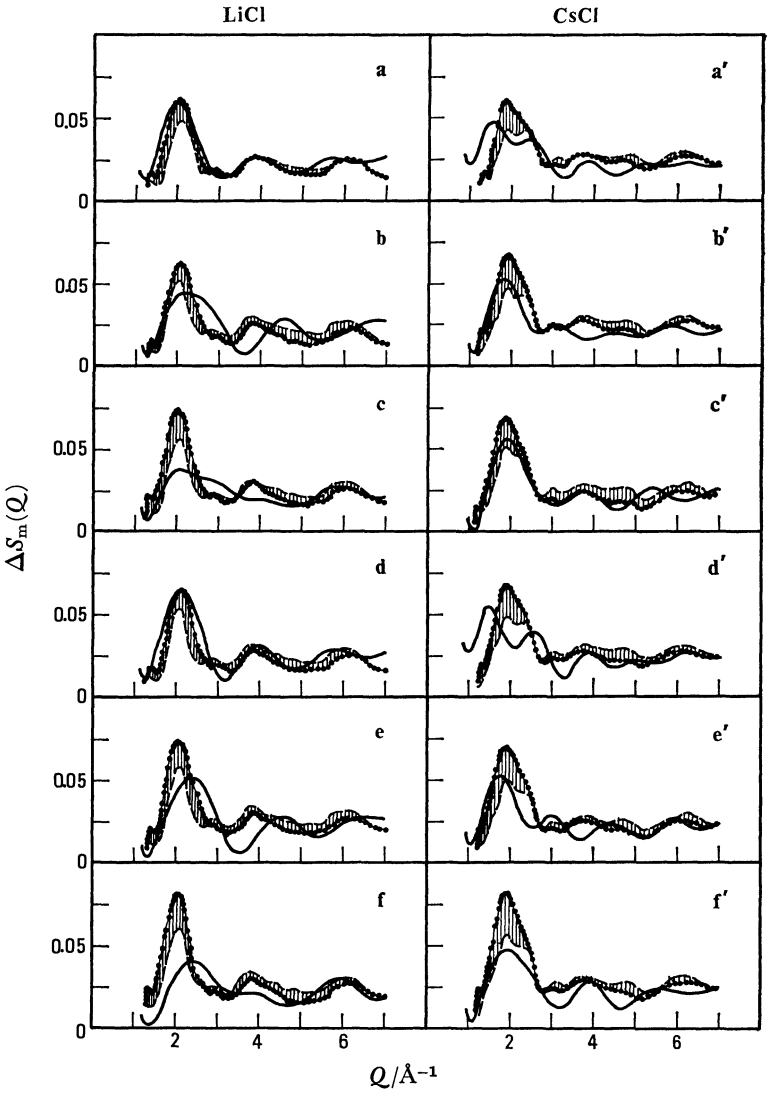

Fig. 5. Changes in the calculated $\Delta S_m(Q)$ with variation of the coordination number for LiCl (a—f) and CsCl (a'—f') solutions.
•: Observed $\Delta S_m(Q)$ ($a=0$), ----: observed $\Delta S_m(Q)$ ($a=1/2$),
(a), (a') $n_+=4$, $n_-=6$, (b), (b') $n_+=6$, $n_-=6$, (c), (c') $n_+=8$, $n_-=6$, (d), (d') $n_+=4$, $n_-=8$, (e), (e') $n_+=6$, $n_-=8$, (f), (f') $n_+=8$, $n_-=8$.

type, linear or bifurcated, is predominant (Figs. 4 (c) and (c')).

From the structure analysis where the parameters have been varied systematically (Table 3), we conclude that structure models shown in Table 4 give the best fit curves with those observed for the NaCl and KCl solutions at 1 M.

The same analysis was performed for the LiCl and CsCl solutions according to the present procedure in order to re-examine the results given in Paper I. The $\Delta S_m(Q)$ curves calculated for different sets of coordination numbers are shown in Fig. 5 and the best fit curves with observed $\Delta S_m(Q)$ are obtained in the case of $n_{Li^+}=4$ and $n_{Cl^-}=6$ for the LiCl solution (Fig. 5 (a)) and in the case of $n_{Cs^+}=8$ and $n_{Cl^-}=6$ for the CsCl solution (Fig. 5 (c')). For the LiCl solution, in the case of a set of coordination numbers which gives the best fit curve ($n_{Li^+}=4$ and $n_{Cl^-}=6$), the $\Delta S_m(Q)$ curves with various magnitudes of parameters are shown in Fig. 6. The adequacy shown in Figs. 5 (a) and (c') is the same as that given in Table 4, Paper I.

We have calculated the difference $\Delta S_m(Q)_{obsd}-\Delta S_m(Q)_{calcd}$ for two cases: $a=1/2$ and $a=0$, where $\Delta S_m(Q)_{obsd}$ is the observed value of the remaining factor (Eq. 3), $\Delta S_m(Q)_{calcd}$ being the calculated value for various models. It was found that the difference is practically independent of over Q all the range. The magnitude of $\Delta S_m(Q)_{obsd}-\Delta S_m(Q)_{calcd}$ is primarily determined by the factor (n_++n_-). $\Delta S_m(Q)_{obsd}-\Delta S_m(Q)_{calcd}$ becomes nearly identical for both cases: ($n_+=4$, $n_-=8$) and ($n_+=6$, $n_-=6$), for example. In Fig. 7, the differences are plotted against (n_++n_-) which is an important factor characterizing various models. For the assignment of $a=1/2$, the differences are essentially zero (Fig. 7). This supports adequacy of the assignment superior to the case of $a=0$.

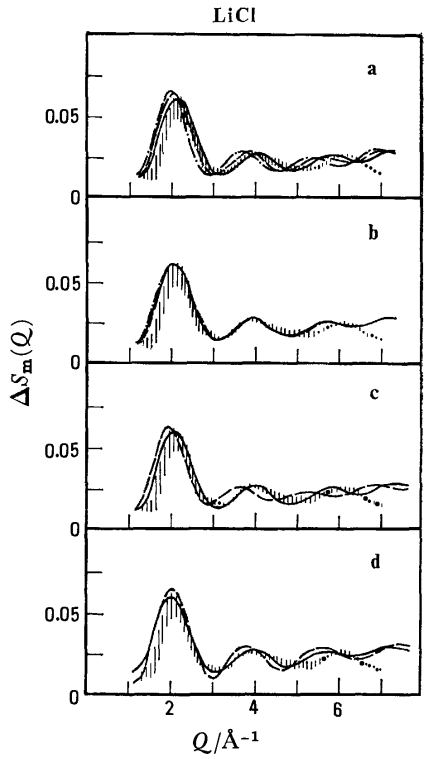

Fig. 6. Changes in the calcualted $\Delta S_m(Q)$ with variation of physical parameters for the LiCl solution. The vertical lines indicate the intervals between two sets of observed values of $\Delta S_m(Q)$ ($a=0$ and $a=1/2$). (a) r_{Li^+-O} (all other parameters are identical with those given in Table 4), ——: 1.90 Å, ----: 2.00 Å, —·—: 2.10 Å, (b) r_{Cl^--O} (all other parameters are identical with those given in Table 4), ----: 3.05 Å, ——: 3.10 Å, —·—: 3.15 Å, (c) configurations around Li^+ (all other parameters are identical with those in Table 4), ——: linear, ----: bifurcated. (d) configurations around Cl^- (all other parameters are identical with those in Table 4), ——: linear, ----: bifurcated.

Discussions and Concluding Remarks

Concerning the structure within the first hydration shell in aqueous solutions of alkali halides, we have determined coordination numbers and average ion-oxygen distances as well as orientational arrangements of water molecules around ions by analyzing the neutron diffraction data. A summary is given herewith on the results of this study and those given in Paper I.

Coordination Number and Ion-oxygen Distances. For Cl^- the coordination numbers are six in all solutions at 1 M, while the number is four for Li^+ and eight for other cations (Na^+, K^+, and Cs^+). The value for Li^+ determined is in line with those reported so far.[1] The values for Na^+, K^+, and Cs^+ reported so far are found to be very diversified. However, according to recent results obtained by molecular dynamics studies for these cations,[13–15] the coordination numbers around the univalent cations are 7—8 except that around Li^+, which is essentially in agreement with ours. From the results of our two studies, the unique behavior of Li^+ in water as compared with that of other alkaline cations has been clarified.

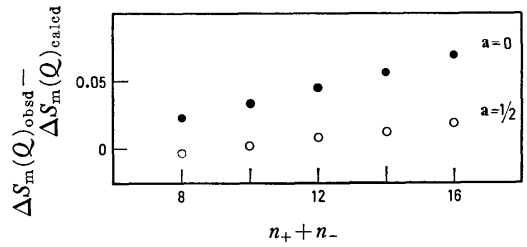

Fig. 7. $\Delta S_m(Q)_{obsd} - \Delta S_m(Q)_{calcd}$ plotted against $(n_+ + n_-)$.

The average ion-oxygen distances for Li^+, Na^+, K^+, Cs^+, and Cl^- within the first hydration shell have been found to be 1.90±0.05 Å, 2.50±0.10 Å, 2.70±0.10 Å, 2.95±0.10 Å, and 3.10±0.05 Å, respectively.

Orientational Configurations around Ions. As regards the orientational configuration of water molecules around ions, it is widely believed that the molecules take either of the two forms, linear or bifurcated, on the average within the hydration shell. we have little experimental knowledge concerning the question.

Our results show that water molecules within the nearest hydration shell take a linear configuration for Li^+ and Cs^+ in LiCl and CsCl solutions and a bifurcated one for Cl^- in NaCl and KCl solutions. Complete determination of the orientational configuration around all ions in solutions has not been achieved.

References

1) N. Ohtomo and K. Arakawa, *Bull. Chem. Soc. Jpn.*, **52**, 2755 (1979).
2) A. H. Narten, F. Vaslow, and H. A. Levy, *J. Chem. Phys.*, **58**, 5017 (1973).
3) A. K. Soper, G. W. Neilson, J. E. Enderby, and R. A. Howe, *J. Phys. C, Solid State Phys.*, **10**, 1793 (1977).
4) N. Ohtomo and K. Arakawa, *Bull. Chem. Soc. Jpn.*, **51**, 1649 (1978).
5) N. Ohtomo and K. Arakawa, *Bull. Chem. Soc. Jpn.*, **53**, 1510 (1980).
6) J. H. Clarke, J. R. Granada, and J. C. Dore, *Mol. Phys.*, **37**, 1263 (1979); G. Walford, J. H. Clarke, and J. C. Dore, *ibid.*, **36**, 1581 (1978).
7) G. Licheri, G. Piccaluga, and G. Pinna, *J. Chem. Phys.*, **64**, 2437 (1976).
8) J. G. Powles, *Adv. Phys.*, **22**, 1 (1973).
9) T. Matsumoto, N. Ohtomo, and M. Senda, *J. Nucl. Sci. Technol.*, **15**, 863 (1978).
10) B. Dorner and R. Comès, "Dynamics of Solids and Liquids by Neutron Scattering," ed by S. W. Lovesey and T. Springer, Springer-Verlag, Berlin (1977), Chap. 3, pp. 113—141.
11) At 1 M solutions, for instance, the magnitude of error due to an approximation of $N_{w'}/N_w \simeq 1$ is smaller than that of the experimental error.
12) The bifurcated configuration of water molecules around Cl^- is significant, since the linear type has been reported so far only for more concentrated solutions.[2,3]
13) K. Heinzinger and P. C. Vogel, *Z. Naturforsch.*, **31a**, 463 (1976).
14) C. L. Briant and J. J. Burton, *J. Chem. Phys.*, **64**, 2888 (1976).
15) P. Bopp, K. Heinzinger, and G. Jancso, *Z. Naturforsch.*, **32a**, 620 (1977).

 © 1980 The Chemical Society of Japan Bull. Chem. Soc. Jpn., 53, 1795—1800 (1980)

Correlation Functions Calculated by Using Reference Interaction Site Model Equations for Diatomic Molecular Fluids

Kazumitsu KOJIMA and Kiyoshi ARAKAWA*

Research Institute of Applied Electricity, Hokkaido University, Sapporo 060

(Received September 25, 1979)

The reference interaction site model (RISM) theory was applied to diatomic molecular fluids, by using three different forms of approximation for site-site direct correlation function. Applicability of the three forms of RISM equation, RISM-1, RISM-2, and RISM-3, was examined, site-site pair correlation functions being calculated from them and a comparison of the results with those of computer simulations being made. Structure factor for liquid nitrogen, oxygen, and bromine were obtained from the solution of the RISM-2 equation and compared with experimental results.

In the preceding paper[1] the authors solved the RISM equation coupled with the Percus-Yevick (PY) and the hypernetted chain (HNC) approximations [referred to as the RISM-1 equation] and applied the result to fluids composed of homonuclear diatomic molecules. Johnson and Hazoumé[2] have also applied the RISM-1 equation coupled with the PY approximation to liquid nitrogen and benzene, and obtained identical results. The original RISM-1 equation was given first intuitively by Chandler and Andersen[3] for molecular fluids composed of fused hard spheres. Chandler[4] derived another form of the equation by means of a systematic functional Taylor expansion [referred to as RISM-2 equation].

The original RISM-1 equation was first solved numerically by Lowden and Chandler[5] for homonuclear diatomic fluids with hard sphere potentials, and used in several numerical works since then. The results were found to be of use for interpreting the behavior of polyatomic fluids.[1,6-9] The result given in the preceding paper[1] shows that the RISM-1 equation can be applied to molecular fluids with an arbitrary site-site pair potential. A graph theoretical interpretation of the RISM-1 equation was given by Chandler.[10]

So far no application of the RISM-2 equation to fluid systems seems to have been carried out. We have undertaken to solve it in combination with a PY and a HNC approximation for fluids composed of homonuclear diatomic molecules in order to compare the results with those obtained from the RISM-1 equation.

The model and three forms of the RISM equation are presented, where a new version of the RISM equation (RISM-3) is proposed in Sec. I, and computational procedures in Sec. II. The results are discussed and compared with those of computer simulations,[11,12] as well as with those of other calculations[13] and experimental studies[14,15] in Sec. III. The HNC approximation for RISM-2 equation are given in Appendix by means of the functional Taylor expansion.

Theory

Model and Definition of Statistical Mechanical Functions.[1] Let us consider the same system as that treated previously.[1] The molecular shape is shown in Fig. 1. An intermolecular potential, $w(i,j)$, is expressed as the sum of site-site pair interaction potentials $u_{\alpha\gamma}(|\boldsymbol{r}_i^\alpha-\boldsymbol{r}_j^\gamma|)$.

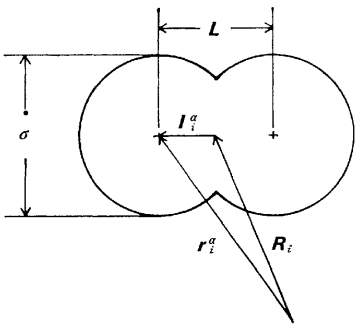

Fig. 1. Shape of RISM molecule.

Two types of site-site pair potentials were chosen: the Lennard-Jones potential[1] and the hard sphere potential,

$$\left.\begin{aligned} u_{\alpha\gamma}(r) &= \infty, \quad r<\sigma, \\ &= 0, \quad r>\sigma, \end{aligned}\right\} \tag{1}$$

where σ is the diameter of the hard sphere.

The site-site total correlation function, $h_{\alpha\gamma}(r)=g_{\alpha\gamma}(r)-1$, is considered, the site-site pair correlation function, $g_{\alpha\gamma}(r)$, being defined as reported.[1] The site-site direct correlation function, $c_{\alpha\gamma}(r)$, is defined by an Ornstein-Zernike type equation[4,10] as

$$\boldsymbol{h}(\boldsymbol{r}) = \boldsymbol{\omega}*\boldsymbol{c}*\boldsymbol{\omega}(\boldsymbol{r}) + \rho\boldsymbol{\omega}*\boldsymbol{c}*\boldsymbol{h}(\boldsymbol{r}) \tag{2}$$

where the * denotes a convolution, ρ the number density and the matrices $\boldsymbol{h}(\boldsymbol{r})$, $\boldsymbol{\omega}(\boldsymbol{r})$, and $\boldsymbol{c}(\boldsymbol{r})$ have element $h_{\alpha\gamma}(r)$, $\omega_{\alpha\gamma}(r)$, and $c_{\alpha\gamma}(r)$, respectively. The first term of $h_{\alpha\gamma}(r)$ in Eq. 2 is expressed as

$$\sum_{\eta,\nu}\int d\boldsymbol{r}'\int d\boldsymbol{r}''\omega_{\alpha\eta}(\boldsymbol{r}'')c_{\eta\nu}(|\boldsymbol{r}''-\boldsymbol{r}'|)\omega_{\nu\gamma}(|\boldsymbol{r}'-\boldsymbol{r}|). \tag{3}$$

The function, $\omega_{\alpha\gamma}(r)$, for the rigid diatomic molecule is expressed as

$$\omega_{\alpha\gamma}(r) = \delta_{\alpha\gamma}\delta(r) + (1-\delta_{\alpha\gamma})(4\pi L_{\alpha\gamma}^2)^{-1}\delta(r-L_{\alpha\gamma}),^{18)} \tag{4}$$

where, $\delta(r)$ and $\delta_{\alpha\gamma}$ are the Dirac delta function and the Kronecker delta, respectively. The Fourier transform representation of Eq. 2 is

$$\hat{\boldsymbol{h}}(\boldsymbol{k}) = \hat{\boldsymbol{\omega}}(\boldsymbol{k})\hat{\boldsymbol{c}}(\boldsymbol{k})\hat{\boldsymbol{\omega}}(\boldsymbol{k})[\boldsymbol{I}-\rho\hat{\boldsymbol{c}}(\boldsymbol{k})\hat{\boldsymbol{\omega}}(\boldsymbol{k})]^{-1}, \tag{5}$$

where $\boldsymbol{A}^{-1}$ denotes the matrix inverse of a matrix $\boldsymbol{A}$ and $\boldsymbol{I}$ the identity matrix.

PY and HNC Approximations. The PY and HNC approximations for the RISM-1 equations[1] are expressed as

$$c_{\alpha\gamma}(r) = y'_{\alpha\gamma}(r)f_{\alpha\gamma}(r) \tag{6}$$

and

$$c_{\alpha\gamma}(r) = y'_{\alpha\gamma}(r)[f_{\alpha\gamma}(r)+1] - \ln y'_{\alpha\gamma}(r) - 1, \quad (7)$$

respectively. Here the $f_{\alpha\gamma}(r)$ and the $y'_{\alpha\gamma}(r)$ are defined by

$$f_{\alpha\gamma}(r) = \exp[-\beta u_{\alpha\gamma}(r)] - 1, \quad (8)$$

and

$$y'_{\alpha\gamma}(r) = g_{\alpha\gamma}(r)[f_{\alpha\gamma}(r)+1]^{-1}, \quad (9)$$

respectively, where the β^{-1} is equal to the Boltzmann constant multiplied by temperature.

Chandler[4] derived the PY approximation for the RISM-2 equation by means of a systematic functional Taylor expansion. The functional form of the PY approximation for the RISM-2 equation is

$$[\boldsymbol{\omega}*\boldsymbol{c}*\boldsymbol{\omega}(\boldsymbol{r})]_{\alpha\gamma} = y_{\alpha\gamma}(r)\bar{f}_{\alpha\gamma}(r), \quad (10)$$

where the $y_{\alpha\gamma}(r)$ and the $\bar{f}_{\alpha\gamma}(r)$ are defined by

$$y_{\alpha\gamma}(r) = g_{\alpha\gamma}(r)[\bar{f}_{\alpha\gamma}(r)+1]^{-1}, \quad (11)$$

and

$$\bar{f}_{\alpha\gamma}(r) = \int d\boldsymbol{1}d\boldsymbol{2}\delta(\boldsymbol{r}^{\alpha})\delta(\boldsymbol{r}^{\gamma}-\boldsymbol{r})\{\prod_{\eta,\nu}[f_{\eta\nu}(r)+1]-1\}, \quad (12)$$

respectively. The $\bar{f}_{\alpha\gamma}(r)$ is the averaged Mayer function when site α on molecule 1 and site γ on molecule 2 are held fixed at a distance r from each other. Let us propose the HNC approximation for the RISM-2 equation expressed as

$$[\boldsymbol{\omega}*\boldsymbol{c}*\boldsymbol{\omega}(\boldsymbol{r})]_{\alpha\gamma} = y_{\alpha\gamma}(r)[\bar{f}_{\alpha\gamma}(r)+1] - \ln y_{\alpha\gamma}(r) - 1. \quad (13)$$

The equation is derived by means of the functional Taylor expansion (see Appendix).

Further, let us propose new approximations (RISM-3) in analogy with Eqs. 6, 10 (PY), and Eqs. 7, 13 (HNC) as follows:

$$[\boldsymbol{\omega}*\boldsymbol{c}*\boldsymbol{\omega}(\boldsymbol{r})]_{\alpha\gamma} = y'_{\alpha\gamma}(r)f_{\alpha\gamma}(r), \quad (14)$$

and

$$[\boldsymbol{\omega}*\boldsymbol{c}*\boldsymbol{\omega}(\boldsymbol{r})]_{\alpha\gamma} = y'_{\alpha\gamma}(r)[f_{\alpha\gamma}(r)+1] - \ln y'_{\alpha\gamma}(r) - 1, \quad (15)$$

respectively. Equations 14 and 15 are similar to the PY and HNC approximations in their functional form, respectively.

Three Forms of the RISM Equation. Various forms of integral equations are given by combining Eq. 5 (Ornstein-Zernike type equation) with one of several types of the PY and HNC approximations. We call Eq. 5 coupled with Eq. 14 or Eq. 15 the RISM-3 equation. The RISM-1 equation[1] is expressed as Eq.5 coupled with Eq. 6 or Eq. 7. The RISM-2 equation[4] is expressed as Eq. 5 coupled with Eq. 10 or Eq. 13. The RISM-1 equation was solved[1] in the case of fluids composed of homonuclear diatomic molecules (Fig. 1), interacting through the Lennard-Jones site-site pair potential. Solutions of the RISM-2 and 3 equation have been obtained for the first time in the case of homonuclear diatomic fluids.

Computational Procedure

Computational Methods. The procedure to solve the RISM-1 equation was reported.[1] The RISM-2 equation was solved by means of an iteration procedure. The functions $h_{\alpha\gamma}(r)$ and $[\boldsymbol{\omega}*\boldsymbol{c}*\boldsymbol{\omega}(\boldsymbol{r})]_{\alpha\gamma}$ have a discontinuity at $r=\sigma_{\alpha\gamma}$. Thus, we define a new function $\gamma_{\alpha\gamma}(r)$,

$$\gamma_{\alpha\gamma}(r) \equiv h_{\alpha\gamma}(r) - C_{\alpha\gamma}(r), \quad (16)$$

where

$$C_{\alpha\gamma}(r) \equiv [\boldsymbol{\omega}*\boldsymbol{c}*\boldsymbol{\omega}(\boldsymbol{r})]_{\alpha\gamma}. \quad (17)$$

$\gamma_{\alpha\gamma}(r)$ is a continuous function of r. By use of it, the RISM-2 equation can be written as

$$\hat{\boldsymbol{\gamma}}(\boldsymbol{k}) = \hat{\boldsymbol{C}}(\boldsymbol{k})\hat{\boldsymbol{\omega}}^{-1}(\boldsymbol{k})\hat{\boldsymbol{C}}(\boldsymbol{k})[\boldsymbol{I}-\rho\hat{\boldsymbol{\omega}}^{-1}(\boldsymbol{k})\hat{\boldsymbol{C}}(\boldsymbol{k})]^{-1}, \quad (18)$$

and

$$\gamma_{\alpha\gamma}(r) = y_{\alpha\gamma}(r) - 1 \quad \text{(PY)},$$
$$= \ln y_{\alpha\gamma}(r) \quad \text{(HNC)}. \quad (19)$$

The initial choise for $y_{\alpha\gamma}(r)$ is $y_{\alpha\gamma}(r)=1$, because the $h_{\alpha\gamma}(r)$ is equal to $\bar{f}_{\alpha\gamma}(r)$ at the low density limit. The iteration has been continued until the self-consistency of

$$\left|\frac{y^{\text{out}}_{\alpha\gamma}(r)-y^{\text{in}}_{\alpha\gamma}(r)}{y^{\text{in}}_{\alpha\gamma}(r)}\right| < 10^{-7} \quad (20)$$

is satisfied.

Calculation of the Function $\bar{f}_{\alpha\gamma}(r)$. For the diatomic molecule, the $\bar{f}_{\alpha\gamma}(\boldsymbol{r}_1^{\alpha}, \boldsymbol{r}_2^{\gamma})$ is represented by Ladanyi and Chandler[16] as follows.

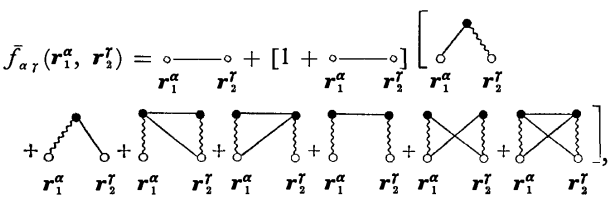

(21)

where ○——○ and ○~~~○ represent $f_{\alpha\gamma}(\boldsymbol{r}_1^{\alpha}, \boldsymbol{r}_2^{\gamma})$ and $s_{\alpha\gamma}(\boldsymbol{r}_1^{\alpha}, \boldsymbol{r}_2^{\gamma})$, respectively. White circles are labeled since they represent particular interaction site at specific locations. Black circles are circles which have been integrated over space and summed over interaction site, *i.e.*

$$\bullet = \sum_{\alpha=1}^{m}\int d\boldsymbol{r}_1^{\alpha}[\mathrm{O}_1].$$

For example, the diagram represents the integral $\sum_{\eta=1}^{m}\int d\boldsymbol{r}^{\eta} f_{\alpha\eta}(\boldsymbol{r}_1^{\alpha}, \boldsymbol{r}^{\eta})s_{\eta\gamma}(\boldsymbol{r}^{\eta}, \boldsymbol{r}_2^{\gamma})$. The last two diagrams of Eq. 21 are omitted because the contribution of these two terms is negligible in the case of hard sphere site-site pair potential.[16]

Calculation of Structure Factors. Neutron scattering experiments can determine the structure factor, $S(k)$, which is expressed in terms of site-site pair correlation functions:

$$S(k) = (\sum_{\alpha=1}^{m} b_{\alpha})^{-2}\sum_{\alpha,\gamma}^{m} b_{\alpha}b_{\gamma}[\hat{\omega}_{\alpha\gamma}(k) + \rho\hat{h}_{\alpha\gamma}(k)], \quad (22)$$

where the b_{α} denotes the coherent neutron scattering amplitude for a nucleus of type α. We carried out the calculations of the structure factors for liquid nitrogen, oxygen and bromine. In order to compare the results with those obtained from experimental studies,[14,15] it is neccesary to determine two molecular

Table 1.

	σ/nm	L/nm	L/σ
N_2	0.33	0.11	0.3
O_2	0.295	0.12	0.407
Br_2	0.33	0.228	0.691

parameters, σ and L, of these diatomic molecules. Hsu *et al.*[9] used the best parameters of the molecules by a comparison of the structure factors calculated with those obtained by experiments.[14,15] The molecular parameters in the present calculations are given in Table 1.

Results and Discussion

Correlation Functions. Figure 2 shows the function, $g_{11}(r)$, calculated by means of the RISM-1, 2, and 3 equations by the use of the PY approximation for diatomic fluids with the hard sphere site-site pair potentials. The $g_{11}(r)$ calculated from the RISM-3 equation is similar in shape to a $g(r)$ of simple hard-sphere fluids. The $g_{11}(r)$ calculated from the RISM-2 equation is in good agreement with that calculated by means of the RISM-1 equation except in the vicinity of first peak. It seems that the difference in the vicinity of the two first peaks results from the use of the two different forms of PY approximations, Eqs. 6 and 10. Figure 3 shows the function $g_{11}(r)$ calculated by the RISM-1, 2, and 3 equations for fluids with the Lennard-Jones site-site pair potentials by the use of the PY approximations as well as the curve obtained by molecular dynamics study.[11] The function $g_{11}(r)$ calculated from the RISM-1 equation is in best agreement with the result of molecular dynamics. It is evident from Fig. 2 that two $g_{11}(r)$ curves calculated by the use of the RISM-1 and 2 equations for hard-sphere fluids are nearly identical with each other over the region $r \geqq \sigma + L$, in sharp contrast to the cases of the Lennard-Jones fluids (Fig. 3).

Figure 4 shows $g_{11}(r)$ calculated by the RISM-2 equation with use of the PY approximation for the fluid with the hard sphere site-site pair potential at two densities. $g_{11}(r)$ at $\rho\sigma^3=0.4$ has a sharp cusp at $r=\sigma+L$, while at a higher density, $\rho\sigma^3=0.65$, a weak square shoulder appears at the same position. At a higher density, the shape of the first peak of the RISM-2 equation differs to some extent from that of the RISM-1 equation as seen by a comparison of Figs. 2 and 4. Figure 5 shows $g_{11}(r)$ calculated by the RISM-2 equation with use of the PY approximation for fluids with the Lennard-Jones site-site pair potentials at two densities, $\rho\sigma^3=0.4$ and 0.65, and at the same temperature, $kT/\varepsilon=4.03$.

Johnson[13] derived a new equation analogous to the RISM-1 equation from the Ornstein-Zernike equation using Fourier-Wigner series, and calculated $g_{11}(r)$ for fluids with hard-sphere site-site potentials. Figure 6 shows a comparison of $g_{11}(r)$ we obtained with Johnson's. Our $g_{11}(r)$ has a shoulder at $r=\sigma+L$ in contrast to the results obtained by Johnson.

Figure 7 shows $g_{11}(r)$ calculated by the RISM-2

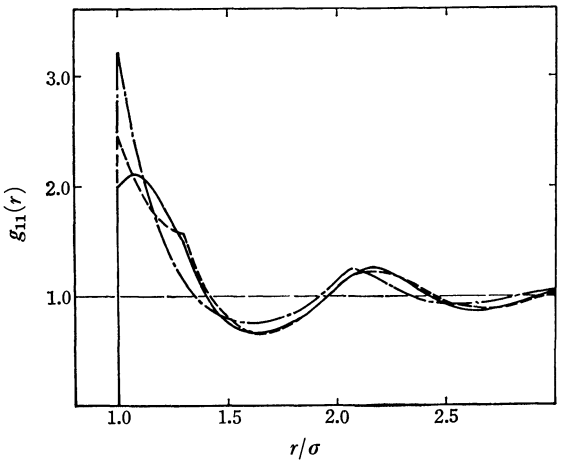

Fig. 2. Site-site pair correlation functions calculated by using the PY like approximation for diaomic molecular fluids with the hard sphere potential: $L/\sigma=0.3$ and $\rho\sigma^3=0.6964$.
----: RISM-1, ——: RISM-2, ——: RISM-3.

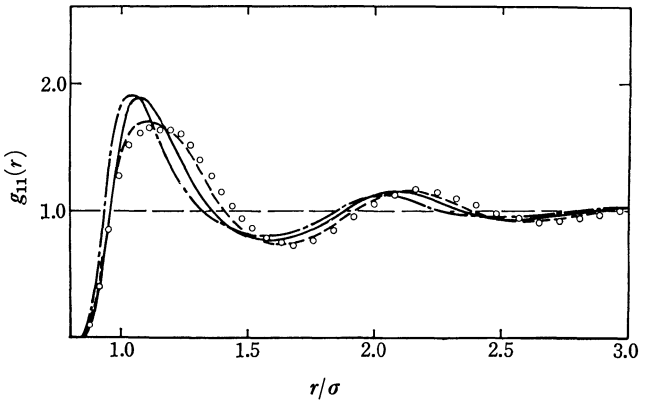

Fig. 3. Site-site pair correlation functions calculated by using the PY like approximation for diatomic molecular fluids with the Lennard-Jones potential: $L/\sigma=0.3$, $\rho\sigma^3=0.6964$ and $kT/\varepsilon=4.03$.
----: RISM-1, ——: RISM-2, ——: RISM-3, ○○○○: molecular dynamics result of Ref. 11.

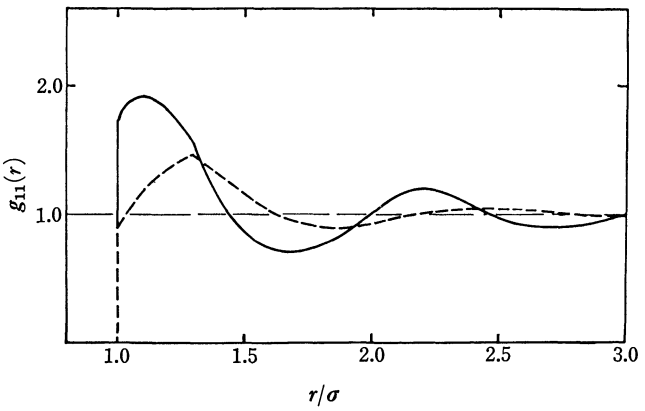

Fig. 4. Site-site pair correlation functions calculated from the RISM-2 equation by using the PY like approximation for diatomic molecular fluids with the hard-sphere potential: $L/\sigma=0.3$.
----: $\rho\sigma^3=0.4$, ——: $\rho\sigma^3=0.65$.

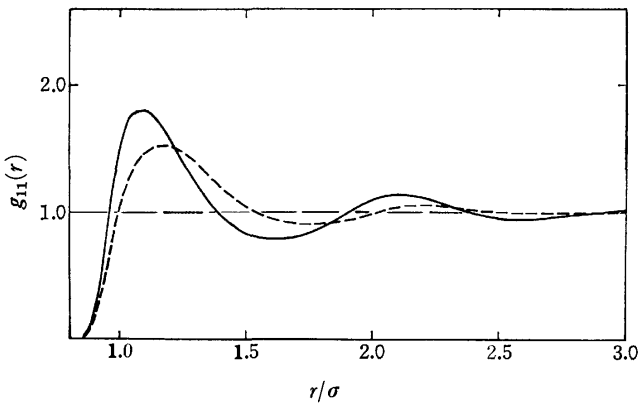

Fig. 5. Site-site pair correlation functions calculated from the RISM-2 equation by using the PY like approximation for diatomic molecular fluids with the Lennard-Jones potential: $L/\sigma=0.3$ and $kT/\varepsilon=4.03$. ——: $\rho\sigma^3=0.4$, ——: $\rho\sigma^3=0.65$.

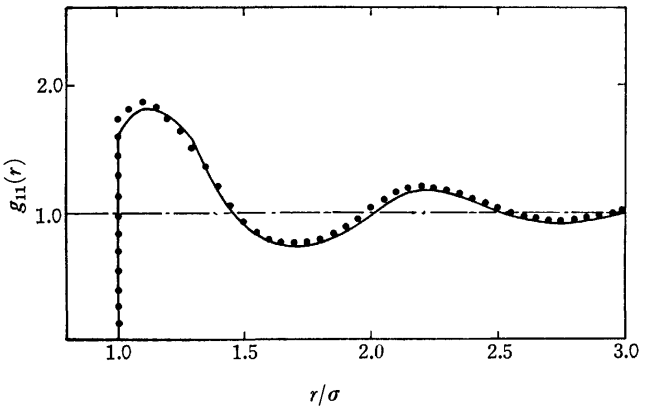

Fig. 6. Site-site pair correlation functions for diatomic molecular fluids with the hard sphere potential: $L/\sigma=0.3$ and $\rho\sigma^3=0.6214$.
——: This work (RISM-2, PY like approximation), ••••: calculated result of Ref. 13.

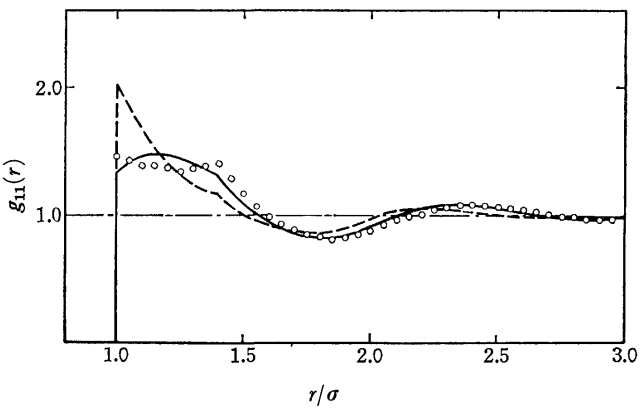

Fig. 7. Site-site pair correlation functions calculated from the RISM-2 equation for diatomic molecular fluids with the hard-sphere potential: $L/\sigma=0.4$ and $\rho\sigma_3=0.4875$.
——: PY like approximation, ----: HNC like approximation, ○○○○: Monte Carlo result of Ref. 12.

equation with use of the PY approximation as well as that obtained by the Monte Carlo (MC) method.[12] $g_{11}(r)$ calculated with use of the PY approximation is in better agreement with the result of MC calculation as compared with that calculated with use of the HNC approximation. Figure 8 shows a comparison of the site-site direct correlation function, $c_{11}(r)$, with results calculated with use of the PY and HNC approximations, including those of MC calculation. $c_{11}(r)$ calculated with use of the PY approximation is in agreement with that obtained by the MC calculation within the range from the origin to $r=\sigma-L$.

Structure Factors. Structure factors calculated with use of the RISM-2 equation are compared with those determined by neutron scattering experiments (Figs. 9—11). Calculations were carried out with use of the RISM-2 equation with the PY approximation

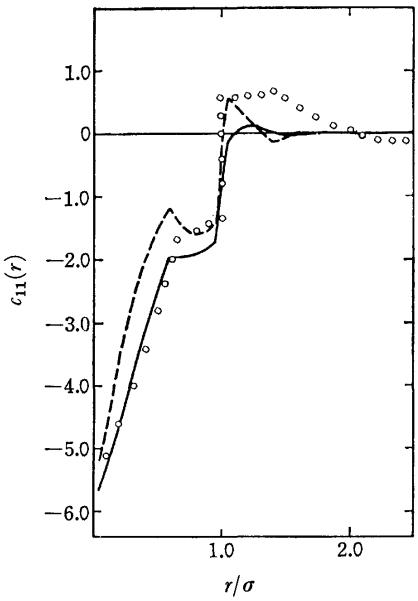

Fig. 8. Site-site direct correlation functions, $c_{11}(r)$, calculated from the RISM-2 equation for diatomic molecular fluids with the hard-sphere potential: $L/\sigma=0.3$ and $\rho\sigma^3=0.4875$.
——: PY like approximation, ----: HNC like approximation, ○○○○: Monte Carlo result of Ref. 12.

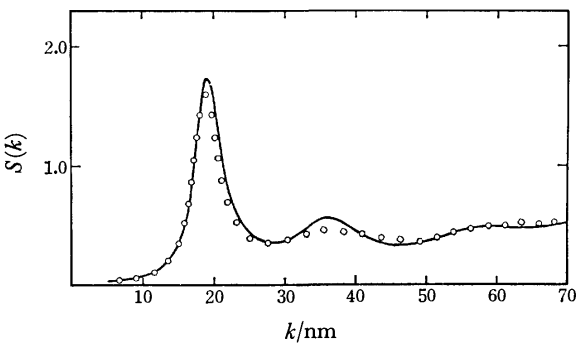

Fig. 9. Comparison of structure factors between calculated and experimental results for liquid nitrogen.
——: This work, ○○○○: experimental result of Ref. 14.

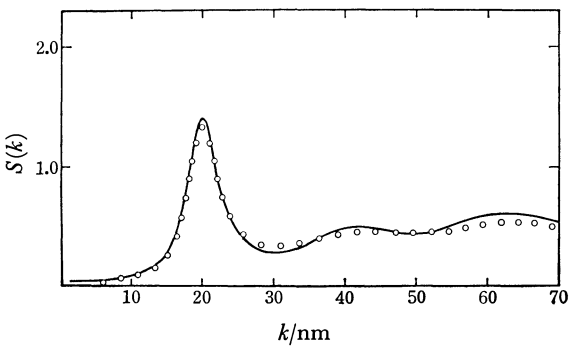

Fig. 10. Comparison of structure factors between calculated and experimental results for liquid oxygen. ——: This work, ○○○○: experimental result of Ref. 14.

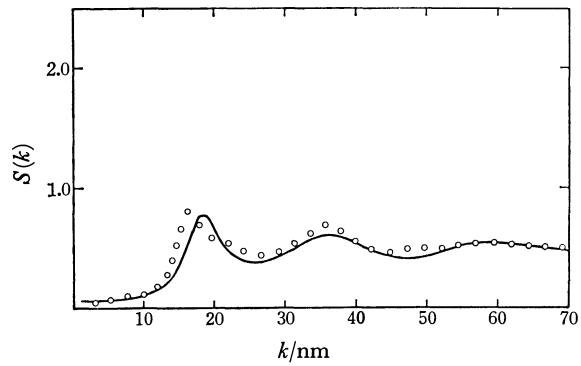

Fig. 11. Comparison of structure factors between calculated and experimental results for liquid bromine. ——: This work, ○○○○: experimental result of Ref. 15.

for diatomic molecular fluids with hard sphere site-site pair potentials. The experimental results are those for liquid nitrogen,[14] oxygen,[14] and bromine[15] under the conditions given in Table 2. The molecular parameters for these liquids[12] are given in Table 1.

The agreement between calculated and experimental results is satisfactory in the cases of liquid nitrogen and liquid oxygen. In liquid bromine, the calculated values deviate from the experimental ones in the vicinity of the first and second peaks. Experimental studies[15] show that the behavior of $S(k)$ of liquid bromine is in sharp contrast to that of liquid nitrogen and liquid oxygen.

The $S(k)$ curves calculated by the RISM-1 and the RISM-2 equations are in good agreement with those obtained from experiment,[1,6,9] for liquid nitrogen and liquid oxygen. The discrepancy between calculated and experimental results for liquid bromine seems to be ascribed to some characteristic of the liquid.[17]

Comparison of the Three Forms of the RISM Equation. Summarizing the results in the present and preceding paper,[1] we can say that the RISM-1 equation gives the best results, *viz.*, the presence of a cusp or a shoulder at $r=\sigma+L$ in $g_{\alpha\gamma}(r)$ curves and agreement of the curves with those given by MD calculations. The numerical results of $g_{\alpha\gamma}(r)$ show that the RISM-1 equation is the best of the three equations, the RISM-2 coming next. Concerning the structure factor curves, the RISM-2 equation seems to give as good results as the RISM-1 equation (Fig. 9 and 10, and Ref. 1).

Table 2.

	ρ/nm^{-3}	T/K
N_2	17.29	77.4
O_2	21.98	84
Br_2	11.76	293

Of the three equations the RISM-1 equation behaves the best on the whole, but it contains some "unallowed diagrams" as stated by Chandler from the viewpoint of topological reduction scheme.[10] In a strict sence the RISM-1 equation contains inconsistensy in its theoretical scheme Thus the RISM-2 equation derived by systematic functional Taylor expansion[4] might be superior to the RISM-1 equation, though the latter is fairly easy to treat in calculation as compared with the other two equations.

Appendix

The HNC approximation for the RISM-2 equation is derived as follows by means of the method of a generalized functional Taylor expansion proposed by Chandler.[4]

Consider the quantity

$$Q_{\alpha\gamma}(\boldsymbol{r},\phi)=\langle\rho_\gamma(\boldsymbol{r})\rangle_\phi\Big[\int d\boldsymbol{I}d\boldsymbol{2}\delta(\boldsymbol{r}_1^\alpha)\delta(\boldsymbol{r}_2^\gamma-\boldsymbol{r})\times\exp\{-\beta\sum_{\eta,\nu}\phi_{\eta\nu}(\boldsymbol{r}_2^\nu-\boldsymbol{r}_1^\eta)\}\Big]^{-1},\tag{A-1}$$

where the function $\phi_{\eta\nu}(\boldsymbol{r}_2-\boldsymbol{r}_1)$ denotes an arbitrary site-site potential function.

At the end points

$$\int d\boldsymbol{I}\delta(\boldsymbol{r}_1^\alpha)Q_{\alpha\gamma}(\boldsymbol{r},\phi=0)=\rho\tag{A-2}$$

and

$$\int d\boldsymbol{I}\delta(\boldsymbol{r}_1^\alpha)Q_{\alpha\gamma}(\boldsymbol{r},\phi=u)=\rho g_{\alpha\gamma}(r)[\bar{f}_{\alpha\gamma}(r)+1]^{-1}.\tag{A-3}$$

We define a new quantity, $Q'_{\alpha\gamma}(\boldsymbol{r},\phi)$, by

$$Q'_{\alpha\gamma}(\boldsymbol{r},\phi)\equiv\ln\Big[\int d\boldsymbol{I}\delta(\boldsymbol{r}_1^\alpha)Q_{\alpha\gamma}(\boldsymbol{r},\phi)\Big].\tag{A-4}$$

If we expand $Q'_{\alpha\gamma}(\boldsymbol{r},\phi)$ in powers of the response $\langle\rho_\eta(\boldsymbol{r}')\rangle_u-\rho$:

$$Q'_{\alpha\gamma}(\boldsymbol{r},u)=Q'_{\alpha\gamma}(\boldsymbol{r},0)+\sum_\eta\int d\boldsymbol{r}'\frac{\delta Q'_{\alpha\gamma}(\boldsymbol{r},\phi)}{\delta\langle\rho_\eta(\boldsymbol{r}')\rangle_\phi}\Big|_{\phi=0}[\langle\rho_\eta(\boldsymbol{r}')\rangle_u-\rho]+\cdots\tag{A-5}$$

Truncating the right hand side of Eq. (A-5) at linear term, we can calculate the term by the use of the relations Eqs. (3.4) and (3.5) in Ref. 4, and obtain

$$\sum_\eta\int d\boldsymbol{r}'\frac{\delta Q'_{\alpha\gamma}(\boldsymbol{r},\phi)}{\delta\langle\rho_\eta(\boldsymbol{r}')\rangle_\phi}\Big|_{\phi=0}[\langle\rho_\eta(\boldsymbol{r}')\rangle_u-\rho]=h_{\alpha\gamma}(r)-[\boldsymbol{\omega}*\boldsymbol{c}*\boldsymbol{\omega}(\boldsymbol{r})]_{\alpha\gamma}.$$

Substituing Eqs. A-2, A-3, and A-6 into Eq. A-5, we get

$$[\boldsymbol{\omega}*\boldsymbol{c}*\boldsymbol{\omega}(\boldsymbol{r})]_{\alpha\gamma}=h_{\alpha\gamma}(r)-\ln g_{\alpha\gamma}(r)[\bar{f}_{\alpha\gamma}(r)+1]^{-1}.$$

The relation is the HNC approximation for RISM-2 equation.

References

1) K. Kojima and K. Arakawa, *Bull. Chem. Soc. Jpn.*, **51**, 1977 (1978).
2) E. Johnson and R. P. Hazoumé, *J. Chem. Phys.*, **70**, 1599 (1979).
3) D. Chandler and H. C. Andersen, *J. Chem. Phys.*, **57**, 1930 (1972).
4) D. Chandler, *J. Chem. Phys.*, **59**, 2742 (1973).
5) L. J. Lowden and D. Chandler, *J. Chem. Phys.*, **59**, 6587 (1973).
6) L. J. Lowden and D. Chandler, *J. Chem. Phys.*, **61**, 5228 (1974).
7) B. C. Freasier, D. Jolly, and R. J. Bearman, *Mol. Phys.*, **32**, 1463 (1976).
8) C. S. Hsu and D. Chandler, *Mol. Phys.*, **36**, 215 (1978).
9) C. S. Hsu, D. Chandler, and L. J. Lowden, *Chem. Phys.*, **14**, 213 (1976).
10) D. Chandler, *Mol. Phys.*, **31**, 1213 (1976).
11) J. Barojas, D. Levesque, and B. Quentrec, *Phys. Rev. A*, **7**, 1902 (1972); B. Quentrec and C. Brot, *ibid.*, **12**, 272 (1975).
12) W. B. Streett and D. J. Tildesley, *J. Chem. Phys.*, **68**, 1275 (1978).
13) E. Johnson, *J. Chem. Phys.*, **67**, 3194 (1977).
14) J. C. Dore, G. Walford, and D. I. Page, *Mol. Phys.*, **29**, 565 (1975).
15) J. H. Clarke, J. C. Dore, G. Walford, and R. N. Sinclair, *Mol. Phys.*, **31**, 883 (1976); G. W. Stanton, J. H. Clarke, and J. C. Dore, *ibid.*, **34**, 823 (1977).
16) B. M. Ladanyi and D. Chandler, *J. Chem. Phys.*, **62**, 4309 (1975).
17) Clarke *et al.* state that "the difference may be attributed to the increased anisotropy and vibrational properties of bromine molecules."[15]
18) We correct the careless mistake of dropping the power index 2 of $L_{\alpha\gamma}$ in Eq. 6 of the preceding paper.[1]

ESR Study of the Phosphorescent State of Benzo[*f*]quinoline

Hiroshi Sekiya, Yasuhiko Gondo,* and Yoshiya Kanda

Department of Chemistry, Faculty of Science, Kyushu University, Hakozaki, Higashi-ku, Fukuoka 812

(Received October 1, 1979)

Electron spin resonance absorption has been observed in a single-crystal solid solution of benzo[*f*]quinoline in biphenyl under irradiation at 120 K with light from a high-pressure mercury lamp. The fine structure of the resonance spectrum observed at 9.25 GHz can be described by the spin Hamiltonian

$$\mathbf{H} = \beta \boldsymbol{H} \cdot \boldsymbol{g} \cdot \boldsymbol{S} + D\left[S_z^2 - \frac{1}{3}S(S+1)\right] + E(S_x^2 - S_y^2)$$

in which $S=1$, $D=\pm 0.09926(18)$ cm^{-1}, $E=\mp 0.04781(6)$ cm^{-1}, $g_{xx}=2.0024(6)$, $g_{yy}=2.0018(4)$, and $g_{zz}=2.0018(4)$; the z axis is normal to the molecular plane, the x and y axes being the in-plane fine-structure principal axes. The principal x axis deviates by $\pm 4°$ from the biphenyl long axis and the principal z axis by 7° from the biphenyl out-of-plane axis. The phosphorescence spectra and lifetimes have been measured both at 77 K and at 4.2 K. Marked doublet splittings were observed in the phosphorescence bands at 4.2 K, suggesting a large guest-host interaction.

This work deals with the determination of the principal axes of the zero-field splitting (ZFS) tensor for benzo[*f*]quinoline (BFQ) in its lowest excited triplet state. In order to investigate the nature of the triplet-state wave function, it is important to determine the directions of the principal axes, not to speak of the principal values. However, the number of compounds for which the ZFS principal axes were determined are limited.[1-4] Vincent and Maki[1] showed that the ZFS parameters of quinoxaline, quinoline, and isoquinoline in durene closely resemble those of naphthalene in durene, whereas the principal axes of quinoline and isoquinoline are no longer coincident with the durene axes. Such deviation of the ZFS principal axes has also been found in 1,5-naphthyridine in durene,[2] and 1,6-diazanaphthalene in durene.[3] As for tetramethylpyrazine in durene, de Groot *et al.*[4] showed that the principal axes deviate largely from the durene axes, suggesting that the molecular symmetry does not necessarily specify the principal axes.

The electronic states of BFQ and benzo[*h*]quinoline have been studied extensively in our laboratory, in particular the delayed fluorescence of BFQ in biphenyl host,[5] the concentration depolarization of phosphorescence in ethanol glass,[6] the dipole moments and pK_a values in the ground and first excited singlet states,[7] and the temperature and solvent dependence of the phosphorescence lifetime.[8] The most relevant finding is the fact that no sign of the spin alignment could be detected in these benzoquinolines in their lowest excited triplet states in hexane at 1.3 K, and in biphenyl even at 1.18 K[5,8] According to Antheunis,[9] phenanthrene in its lowest excited triplet state in both biphneyl and fluorene provides intriguing examples; even at 1.2 K the spin-lattice relaxation times are about 1 ms, approximately one thousand times faster than the decay of the lowest excited triplet state to the ground state. The results may justify the claim that the phenanthrene-type compounds are important in the study of the spin-alignment mechanism in the triplet state.

Thus, it seems significant to obtain fundamental information on the lowest excited triplet state of BFQ, in particular, on the ZFS parameters, ZFS principal axes, and ***g***-tensor, from the electron spin resonance (ESR) spectra observed for the single-crystal solid solutions of BFQ in biphenyl. For identification of the triplet state, we have also studied the phosphorescence spectra of BFQ in biphenyl and biphenyl-d_{10} at 77 K and 4.2 K.

Experimental

Materials. BFQ (Tokyo Kasei Kogyo Co., Ltd.) was treated with sulfuric acid and sodium hydroxide as described previously,[10] and then zone-refined extensively. Biphenyl (Wako Pure Chem. Ind., Ltd.) was recrystallized from ethanol or sublimed and then zone-refined. Biphenyl-d_{10} (Merck, Sharp and Dohme Canada, Ltd.) was zone-refined. The sample crystals were grown in Pyrex tubes from the melts in a Bridgman furnace. The initial concentration of BFQ in biphenyl was *ca.* 1.2 mol%, the final concentration in the grown crystals not being known. Samples, sealed in a vacuum into Pyrex tubes, were lowered in the furnace at a rate of 30 mm a day.

Measurements. The ESR spectrometer (Echo Electronics Co., Ltd.) essentially consists of a microwave unit (EWG-10), a 100-kHz phase sensitive detector (E-100D), and a klystron power supply (EKS-1PS). Measurements were carried out using a microwave frequency of 9.25 GHz and a magnetic field modulation of 100 kHz. The microwave frequency was determined with a calibrated cavity wavemeter, the external magnetic fields being determined with a proton NMR gaussmeter. Irradiation of the sample crystals was made with a 250-W high-pressure mercury lamp (USH-250D, Ushio Electric Inc.).

Values of direction cosines of the biphenyl molecular axes in the crystal required for mounting the sample crystals properly in the cavity, were obtained from the molecular planes least-squares fitted to the X-ray diffraction data given by Trotter[11a] (Table 1). The unit cell of the biphenyl crystal is shown in Fig. 1. Main features of the biphenyl

Table 1. Biphenyl direction cosines[a]

	L′	M′	N′
a	−0.30311	−0.51754	0.80017
b	0.00662	0.83747	0.54645
c′	−0.95293	0.17550	−0.24723

a) Ref. 11a. Axis c′ is normal to the ab plane. See Fig. 1.

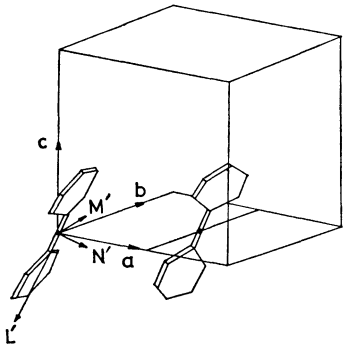

Fig. 1. Biphenyl crystal structure and axis systems.

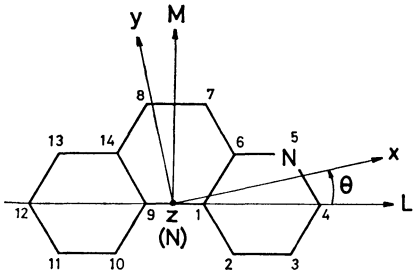

Fig. 2. Molecular axes, L, M, N, ZFS principal axes, x, y, z, and numbering scheme for the benzo[*f*]quinoline molecule.

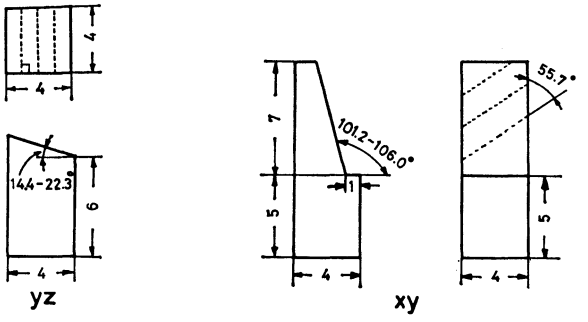

Fig. 3. Quartz wedges used to mount the sample crystals.
The ab plane was attached to the surfaces with the dotted lines which specify the b-axis direction. Lengths are given in mm. With the wedges (a) and (b), the external magnetic field lies in the yz and xy planes, respectively.

crystal are as follows: (1) It is a monoclinic crystal of the space group $P2_1/a$ with two molecules in a unit cell. (2) The crystal cleaves in the ab plane. (3) The long axes of the two molecules in a unit cell are parallel to each other within 3°.[11b,12] Figure 2 shows the molecular axes adopted and designation of the ZFS principal axes, x, y, and z.

Several quartz wedges were devised in order to rotate the static external magnetic field in the fine-structure xy and yz planes of one of the two molecules in a unit cell. Typical wedges, whose geometries are based on the direction cosines given in Table 1, are shown in Fig. 3. A biphenyl crystal doped with BFQ was mounted with its cleavage plane, *viz.*, ab plane, against the surface of a wedge by use of a varnish (GE-7031, General Electric Co.), the wedge being attached to a quartz rod directly connected to a conventional crystal-rotating device. The sample crystals were cooled by a flow of cold nitrogen gas. The sample temperature was estimated to be 120±10 K by putting a thermocouple in place of the sample crystals in the cavity. The ESR signal decays were observed at 77 K with crystals directly immersed in the liquid nitrogen in a Dewar vessel with a finger.

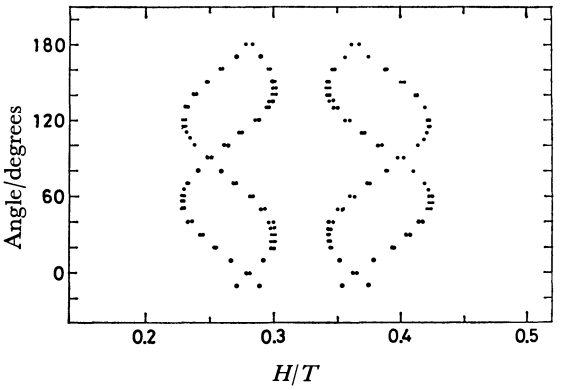

Fig. 4. Angular dependence of the resonance field strength. The magnetic field ***H*** is rotated in the ab plane.

For optical measurements, a 500-W xenon lamp was used for irradiation of the sample crystals directly immersed in the coolant. A saturated aqueous solution of nickel sulfate of 30-mm path length was used to cut the infrared radiation. Emissions from the samples were dispersed with a 750-mm Czerny-Turner-type spectrometer (RM-L21, Nalumi Co., Ltd.). The input signal to a picoammeter (TR-8651, Takeda Riken Industry Co., Ltd.) was obtained with a photomultiplier (R375, Hamamatsu TV Co., Ltd.). The spectra were recorded on a strip chart recorder (model 056, Hitachi, Ltd.), the phosphorescence decay curves being displayed on an oscilloscope (DS-5016, Iwatsu Electric Co., Ltd.) and photographed.

Results and Discussion

ESR Spectra in the ab Plane. Measurements with the external magnetic field ***H*** in the ab plane were carried out in order to confirm the mounting of the sample crystals, without using any particular wedge; the sample crystals were mounted with their cleavage surfaces directly attached to the bottom of the quartz rod. The results are shown in Fig. 4, where the zero degree on the ordinate axis approximately corresponds to the b axis. They closely resemble the corresponding results reported on phenanthrene in biphenyl,[12] except for the fact that eight resonances were found for BFQ, in general, instead of four for phenanthrene. As reported on quinoline, isoquinoline, 1,6-diazanaphthalene, *etc.*,[1-4] the doubling of the number of the resonances can be taken as an evidence for the deviation of fine-structure principal axes from the host molecular axes. It indicates that two magnetically inequivalent orientations are possible for the BFQ molecule at each of the two biphenyl lattice sites. For the sake of convenience, the two sites in a unit cell are designated as site A and site B, respectively, the quartz wedges in Fig. 3 being assumed to fit site A. Arabian numerals, 1 and 2, stand for the two inequivalent

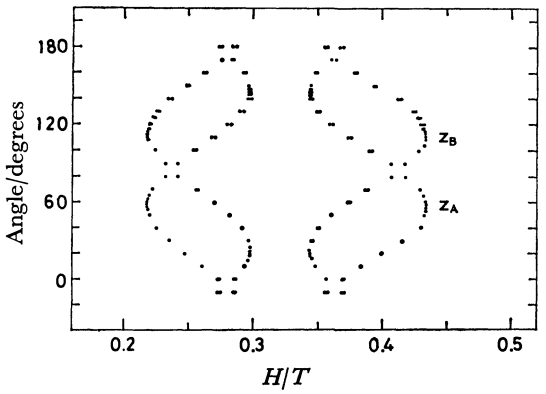

Fig. 5. Angular dependence of the resonance field strength. The magnetic field $\boldsymbol{H}$ is rotated nearly in the yz plane. The inclination of the wedge is 17.6°.

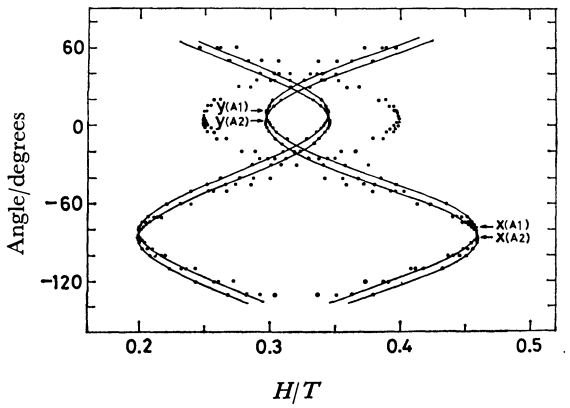

Fig. 6. Angular dependence of the resonance field strength. The mangetic field $\boldsymbol{H}$ is rotated nearly in the xy plane. The dihedral angle of the wedge is 104.8°. Points are experimentally obtained, while solid curves are drawn using the experimental D, E, and g values.

orientations at each site, respectively. Thus, magnetically the orientations of the BFQ molecules are distinguished from each other by the notations, A1, A2, B1, and B2. One of the two patterns (Fig. 4) corresponds to the lattice site for A1 and A2, and the other to that for B1 and B2. The two patterns are essentially the same except for the phase difference, as expected from the crystal structure of biphenyl. This shows that the ab plane has been identified properly in the mounting of sample crystals.

ESR Spectra in the yz Plane. On the basis of results from X-ray diffraction of the biphenyl crystal,[11a] the inclination of the surface of an appropriate wedge should be 17.7° (Fig. 3(a)), for rotation of the external magnetic field $\boldsymbol{H}$ in the M'N' plane of any one of the two biphenyl molecules in a unit cell. Four wedges of inclination in the range 14.4°—22.3° were used. The resonance fields obtained by rotating $\boldsymbol{H}$ nearly in the yz plane are shown in Fig. 5. The apparent principal value of the fine-structure tensor reaches a maximum for the inclination of 17.6° of the wedge surface, *viz.*, the largest separations correspond to the resonances with $\boldsymbol{H}$ on the z axes, the smallest those nearly on the y axes. The low-field transitions with $\boldsymbol{H}$ nearly parallel to the z axes shift to the higher fields for wedge inclinations differing from 17.6°. The spectra corresponding to orientations 1 and 2 are seen to draw closer togerher, coalescing into one spectrum as the directions of $\boldsymbol{H}$ rotates to coincide with the z axis, showing that the molecular planes of the two inequivalent guests at each of the two lattice sites, A and B, are parallel to each other within experimantal errors. Consequently, the angle between the two fine-structure z axes may lead to the dihedral angle between the planes of the A-site and B-site BFQ molecules. From the phase difference in the two distinct patterns (Fig. 5), the dihedral angle can immediately be estimated to be 55.0°, in contrast to 69.3° found for the corresponding dihedral angle between the two biphenyl molecules in a unit cell.[11] Thus, the molecular plane of BFQ is not parallel to that of biphenyl. In particular, the difference of 14.3° in the two angles indicates a decrease of 7° in the relative tilt of the guest plane as compared with the host. Similar observations have been reported by Vincent and Maki[1] for isoquinoline in durene, and by Brandon *et al.*[12] for phenanthrene in biphenyl. Hutchison and McCann studied in detail the system of phenanthrene-d_{10} in biphenyl with the aid of ENDOR at 2 K, reporting that a site of biphenyl is replaced by four differently oriented phenanthrene molecules, and that a maximum difference of 5° is found in the angles defined for the guest and host molecular planes.[13]

ESR Spectra in the xy Plane. Five wedges were used for measurements with $\boldsymbol{H}$ in the xy plane, *viz.*, LM plane, their dihedral angles being in the range 101.2°—106.0° (Fig. 3(b)); a maximum resonance field was realized with a wedge of the dihedral angle 104.8°, and with the b-axis orientation of 55.7° on the wedge surface. In these initial measurements in the xy plane, no account was taken of the fact that the molecular plane of BFQ deviates from that of biphenyl, the external magnetic field not being rotated exactly in the xy plane. In order to bring the external magnetic field exactly in the xy plane, we assumed that the host and guest molecular planes at each site make an angle in the range 6°—7°, on the basis of the finding on the yz-plane experiments. The angle determines the b-axis orientation on the wedge surface; for the angle 6°, the b-axis orientation should be 61.2° instead of 55.7° shown in Fig. 3(b), and for the angle 7°, it should be 62.2°. Measurements were carried out with the wedge of dihedral angle 104.8° and with the two b-axis orientations of 62.0° and 62.8°. Figure 6 shows the results obtained with the orientation of 62.0°. The separations for the resonance fields with $\boldsymbol{H}$ on the y axes are larger than the minimum separations in the yz-plane experiments (Fig. 5), reflecting the fact that the experiments did not sweep the y axes exactly. The L axes of the two sites A and B are parallel to each other, since the four resonances draw closer together and coalesce into one as $\boldsymbol{H}$ moves to the x axes. The coalescence makes it impossible to determine the angle between the principal x axes of A1 and A2 exactly. As for $\boldsymbol{H}$ parallel to the y

Table 2. Observed zero-field splitting parameters[a)]

	Benzo[*f*]quinoline[b)] in biphenyl	Phenanthrene[c)] in biphenyl	Benzo[*f*]quinoline[d)] in ethanol
D/cm^{-1}	$\pm 0.09926(18)$	$\pm 0.100430(10)$	$+0.1023$
E/cm^{-1}	$\mp 0.04781(6)$	$\mp 0.046576(9)$	-0.0477
$\lvert E/D \rvert$	0.4817	0.46377	0.466
g_{xx}	2.0024(6)	2.0041	
g_{yy}	2.0018(4)	2.00279(5)	
g_{zz}	2.0018(4)	2.00209(5)	
θ/degrees	± 4	0	

a) Numbers in parentheses are estimated standard deviations in units of the last signfiicant digit. b) This work. c) Ref. 12. d) Ref. 15.

axes, the relative deviation of the principal y axis of A1 from that of A2 was found to be 8° in the xy plane, so that the corresponding deviation of the x axes should also be 8°. In view of the observations on other aromatic nitrogen heterocyclic compounds,[1-4)] we assume that the deviation of the x axis from the L axis in A1 is as large in magnitude as and opposite in sign to that in A2. We thus obtain an in-plane rotation of 4° in the ZFS tensor, due to the introduction of a nitrogen atom in the phenanthrene skeleton.

ZFS Parameters. The ZFS parameters were determined by means of the procedure developed by Hutchison and Mangum.[14)] The canonical resonance fields H_{1x}, H_{2x}, H_{1y}, and H_{2y}, were determined from the measurements in the xy plane, whereas H_{1z} and H_{2z} were determined from those in the yz plane, where subscripts 1 and 2 refer to the low- and high-field resonances, respectively. The principal axes of the $\boldsymbol{g}$-tensor have been assumed to coincide with those of the fine-structure tensor, *viz.*, the ZFS tensor. The parameters fitting the spin Hamiltonian

$$\mathbf{H} = \beta \boldsymbol{H} \cdot \boldsymbol{g} \cdot \boldsymbol{S} + D\left[S_z^2 - \frac{1}{3}S(S+1)\right] + E(S_x^2 - S_y^2)$$

are given in Table 2.

The ZFS parameters of BFQ resemble those of phenanthrene in biphenyl,[12)] which confirms that the lowest excited triplet state of BFQ is of the $\pi\pi^*$ type. A remarkeble feature of the ZFS parameters in the phenanthrene-type compounds is the large E value. The E value of BFQ is slightly larger than that of phenanthrene, and the ratio $|E/D|$ of BFQ increases as compared with that of phenanthrerne by *ca.* 4%, suggesting that the spin distribution in BFQ would be more assymmetric than that in phenanthrene. In the ESR study of BFQ in ethanol glass performed by Gondo and Maki,[15)] the signs of D and E were determined to be plus and minus, respectively, by means of magnetophotoselection. The E value in the crystal is almost identical to that in the ethanol glass, whereas the D value is smaller than that in the ethanol glass by *ca.* 2%. Such variations were reported on quinoxaline[1a)] and on phenoxazine by Löhste *et al.*[16)] who suggested that the variations of the ZFS energies in phenoxazine might be due to the solvent polarities and the hydrogen bonding which may induce some change in the molecular geometry. It is not clear, however, what interaction is operative in the case of BFQ.

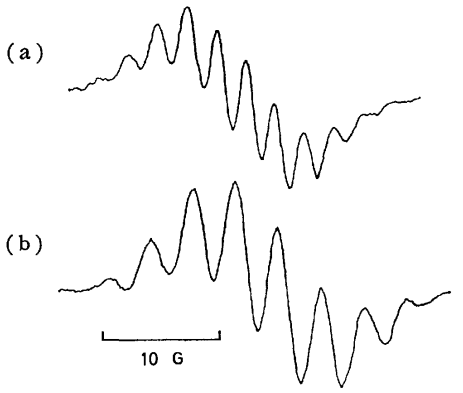

Fig. 7. Observed hyperfine structure of the triplet benzo[*f*]quinoline.
(a): High-field transition with $\boldsymbol{H}$//y, (b): low-field transition with $\boldsymbol{H}$//y.

Gondo and Kanda calculated the principal values and axes of the ZFS tensors for the $\pi\pi^*$ excited triplet states of some aromatic compounds, by employing the Pariser-Parr-type two-center Coulomb repulsion integrals and the core integrals of $\beta_{CC} = -2.39$ eV and $\beta_{CN} = -2.576$ eV.[17)] The results obtained for BFQ are $+0.1105$ cm^{-1}, -0.0582 cm^{-1}, and $+0.6°$, for D, E, and θ, respectively, where θ is the angle defined in Fig. 2(a). The calculated principal values confirm that the observed triplet state is of the $\pi\pi^*$ type. On the other hand, the calculated θ value would not determine the sign of the observed θ of $\pm 4°$, since the value is absolutely small.

Hyperfine Structure. The hyperfine structure of the triplet BFQ was observed for the magnetic field nearly parallel to the fine-structure x axis as well as y axis. The observed spectra are shown in Fig. 7. Although the hyperfine structure is apparently well resolved for the x axis, it is in fact complicated owing to overlapping of the signals due to the different sites. In order to aid the computer simulation of the hyperfine structure, the triplet spin densities given in Table 3 were calculated by an LCAO-SCF-MO-CI approach in which all the singly excited configurations were taken into account, and the Pariser-Parr and Nishimoto-Mataga approximations were adopted for the two-center Coulomb repulsion integrals. It should be noted that these two approximations give essentially the same spin densities for the nitrogen atom, although the Nishimoto-Mataga approximation gives much more

Table 3. Theoretical normalized spin densities ρ based on the Pariser-Parr (PP) and Nishimoto-Mataga (NM) approximations for Coulomb repulsion integrals

Atomic position[a)]	ρ(PP)	ρ(NM)
1	0.0411	0.0429
2	0.0433	0.0524
3	0.0621	0.0615
4	0.0148	0.0260
5	0.0614	0.0690
6	0.0248	0.0261
7	0.2104	0.1869
8	0.2064	0.1826
9	0.0418	0.0436
10	0.0668	0.0718
11	0.0716	0.0705
12	0.0225	0.0354
13	0.1024	0.1016
14	0.0277	0.0296

a) See Fig. 2(a).

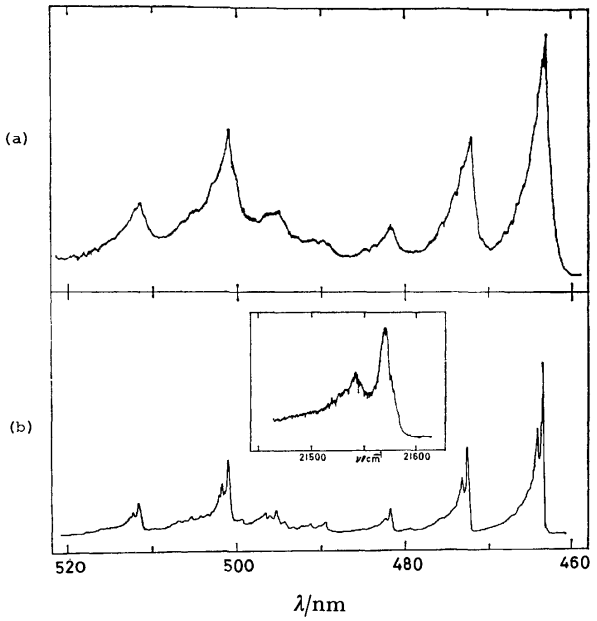

Fig. 8. Phosphorescence spectra of benzo[*f*]quinoline in biphenyl host; (a) at 77 K and (b) at 4.2 K. The insert in (b) shows the details around the 0,0-bands.

uniformly distributed spin densities for the carbon atoms than the Pariser-Parr.[18)]

Simulation of the hyperfine structure was performed by combining the calculated spin densities with the experimentally determined principal values of the hyperfine coupling tensor.[1,19)] The simulated spectra disagree definitely with those observed. The hyperfine structure of BFQ is expected to be complicated owing to its low molecular symmetry; even a small change in the spin distribution tends to provide quite a different hyperfine spectrum. Thus, for further clarification of the hyperfine structure and spin distribution, study on deuterated BFQ's is important.

Table 4. Phosphorescence lifetimes τ of benzo[*f*]-quinoline in biphenyl single crystals

Host	At 4.2 K		At 77 K	
	$\nu_{0,0}$/cm^{-1}	τ/s	$\nu_{0,0}$/cm^{-1}	τ/s
Biphenyl	21573	2.90	21575	2.08 (2.2) [a)]
	21544	2.61		
Biphenyl-d_{10}	21570	2.83	21576	2.29 (2.2) [a)]
	21540	2.57		

a) The values in parentheses were obtained from ESR signal decays.

Phosphorescence Spectra and Lifetimes. Figure 8 shows the phosphorescence spectra of BFQ in biphenyl observed at 77 K and 4.2 K. The obvious difference between the spectra is the multiplet splitting in the spectrum at 4.2 K, each vibronic band apparently consisting of a doublet. Hochstrasser and Noe reported similar multiplet splittings in the fluorescence and phosphorescence spectra of phenanthrene–biphenyl mixed crystals at 1.8 K.[20)] Enlarged features (Fig. 8(b)) are shown around the 0,0-band observed at 4.2 K, the splitting amounting to 29 cm^{-1} in biphenyl and to 30 cm^{-1} in biphenyl-d_{10}. These are considerably larger than the corresponding value of 11 cm^{-1} found for phenanthrene in biphenyl.[20)] The paramagnetic species observed as the triplet BFQ can be identified in part by the phosphorescence lifetimes (Table 4). The phosphorescence lifetime has been found to depend markedly on the solvents as well as temperature.[8)]

Orientation of the Guest Molecule in the Crystal. The angle of rotation of the z axis, *viz.*, N axis, of BFQ in biphenyl is slightly larger than that of phenanthrene in biphenyl.[12)] Such deviation of the principal axes of the guest molecules in the host crystal was studied by Hochstrasser and Small[21)] in connection with the site splittings in the electronic spectra. Their calculations suggest that we should not in general expect exact alignment of the principal axes of a guest and a host molecule. Since the volume occupied by a BFQ molecule is larger than that occupied by a biphenyl molecule, there would naturally be intermolecular interactions which would tilt the z axis of the guest molecule. Incidentally, the z axis of isoquinoline is tilted by 13° in durene,[1)] while that of 1,5-naphthyridine is tilted by 2° also in durene. These results indicate that the z-axis tilting in the aromatic nitrogen heterocyclic compounds would depend on the location of the nitrogen atoms in a complicated manner.

The present work was partially supported by the Ito Science Foundation and by Grants-in-Aid for Scientific Research Nos. 334026 and 347014 from the Ministry of Education, Science and Culture.

References

1) J. S. Vincent and A. H. Maki, *J. Chem. Phys.*, **39**, 3088 (1963); **42**, 865 (1965).
2) J. S. Vincent, *Chem. Phys. Lett.*, **8**, 37 (1971).
3) R. Bramley and B. J. McCool, *Mol. Phys.*, **29**, 649

(1975).
4) M. S. de Groot, I. A. M. Hesselmann, F. J. Reinders, and J. H. van der Waals, *Mol. Phys.*, **29**, 37 (1975).
5) Y. Kusumoto, Y. Gondo, and Y. Kanda, *Chem. Lett.*, **1974**, 81; *Bull. Chem. Soc. Jpn.*, **49**, 2706 (1976).
6) Y. Gondo, M. Hirai, T. Iwao, T. Kakibaya, T. Kuroi, H. Nagatomo, and Y. Kanda, *Chem. Lett.*, **1975**, 463; *J. Lumin.* **12/13**, 825 (1976).
7) H. Sekiya, Y. Gondo, and Y. Kanda, Preprint of the Symposium on Photochemistry, Fukuoka, October 1976, p. 59 (2A14); M. Nakamizo, *Spectrochim. Acta*, **22**, 2039 (1966).
8) T. Masuda, H. Sekiya, Y. Gondo, and Y. Kanda, *Mem. Fac. Sci., Kyushu Univ., Ser. C*, **12**, 7 (1979).
9) D. Antheunis, Thesis, Leiden University, 1974, p. 108.
10) Y. Kanda and R. Shimada, *Spectrochim. Acta*, **15**, 211 (1959).
11) a) J. Trotter, *Acta Crystallogr.*, **14**, 1135 (1961); b) A. Hargreaves and S. H. Rizvi, *ibid.*, **15**, 365 (1962).
12) W. Brandon, R. E. Gerkin, and C. A. Hutchison Jr., *J. Chem. Phys.*, **41**, 3717 (1964).
13) C. A. Hutchison Jr., and V. H. McCann, *J. Chem. Phys.*, **61**, 820 (1974).
14) C. A. Hutchison Jr., and B. W. Mangum, *J. Chem. Phys.*, **34** 908 (1960).
15) Y. Gondo and A. H. Maki, *J. Phys. Chem.*, **72**, 3215 (1968).
16) J. M. Löhste, C. Helen, and M. Ptak, "The Triplet State," ed by A. B. Zahlan, Cambridge Univ. Press, London (1967), p. 479.
17) Y. Gondo and Y. Kanda, Preprint of the 10th ESR Symposium, Osaka, October 1971, p. 84; *Bull. Chem. Soc. Jpn.*, **43**, 3943 (1970).
18) Y. Gondo and Y. Kanda, *Bull. Chem. Soc. Jpn.*, **45**, 1612 (1972).
19) N. Hirota, C. A. Hutchison Jr., and P. Palmer, *J. Chem. Phys.*, **40**, 3717 (1964).
20) R. M. Hochstrasser and L. J. Noe, *Chem. Phys. Lett.*, **6**, 27 (1975).
21) R. M. Hochstrasser and G. J. Small, *J. Chem. Phys.*, **48**, 3612 (1968).

Reactions of Pentane and 2-Methylbutane over Solid Super Acids Prepared by Different Conditions

Osamu Takahashi, Takashi Yamauchi,† Toshihiko Sakuhara, Hideshi Hattori,* and Kozo Tanabe

Department of Chemistry, Faculty of Science, Hokkaido University, Sapporo 060

† *Nishiki Research Center, Kureha Chem. Ind. Co., Iwaki 974*

(Received October 8, 1979)

The reaction of pentane to 2-methylbutane was carried out at 0 °C over solid super acid catalysts which were prepared by treatment of various metal oxides with SbF_5 under different conditions, and the preparation conditions that affect the catalytic behavior of the catalyst were examined. Among the different base metal oxides, TiO_2–ZrO_2 became the most active catalyst when treated with SbF_5. The maximum conversion to 2-methylbutane which appeared in the reaction of pentane was high when a base metal oxide was treated with SbF_5 at a low temperature, and also when the reaction temperature was low. At the maximum conversion, the selectivity of the catalysts for the skeletal isomerization was almost 100%. As the reaction of pentane proceeded, the catalytic activity for the skeletal isomerization to 2-methylbutane was decreased but that for the formation of 2-methylpropane from 2-methylbutane was increased. The reaction mechanism is briefly discussed.

Recently, many attempts have been made to prepare solid super acids which show catalytic activity for skeletal isomerization of alkanes at low temperature, and most of them are patented. Other than the patents, Magnotta *et al.* reported that a complex of $AlCl_3$ with polystyrene sulfonic acid is active for the cracking and isomerization of hexane at 85 °C.[1,2] Olah *et al.* presented Nafion-H as a solid super acid.[3–5] Ono *et al.* reported that mixtures of aluminum halides with metal sulfates or with metal chloride showed high activities for the isomerization of pentane at room temperature.[6–8]

In our previous paper, we reported the preparation of solid super acids which exhibited catalytic activity for the skeletal isomerizations of butane and 2-methylpropane at room temperature.[9] The solid super acids were prepared by treatment of various types of metal oxides with SbF_5. Over these catalysts, pentane underwent skeletal isomerization to 2-methylbutane.[10] The selectivity to 2-methylbutane was 100% in the initial stage of the reaction, but lowered in the final stage of the reaction, which was caused by successive production of 2-methylpropane. As a result, there appeared a maximum conversion to 2-methylbutane in the course of the reaction. In this paper, several factors which might affect the maximum value of the conversion to 2-methylbutane are examined, and the reasons for appearance of the maximum are discussed. The variable factors examined are the type of base metal oxide, the temperature of treatment of base metal oxide with SbF_5, the number of treatment with SbF_5, the pretreatment temperature of base metal oxide, the reaction phase, and the presence of H_2.

Experimental

Preparation of Catalyst. Solid super acids were prepared by exposure of various metal oxides to SbF_5 vapor followed by evacuation of excess SbF_5. The base metal oxides used in this study were SiO_2, TiO_2, ZrO_2, Al_2O_3, SiO_2–Al_2O_3, and TiO_2–ZrO_2. Silica, TiO_2, and ZrO_2 were prepared by hydrolysis of aqueous solutions of ethyl orthosilicate, titanium tetrachloride, and zirconium dichloride oxide, respectively, with aqueous ammonia, followed by washing with deionized water and calcination at 500 °C in air. Alumina was AE-11 γ-Al_2O_3 purchased from Nishio Ind. Co. Ltd. Silica–alumina was N 631L obtained from Nikki Chemicals Co. Ltd. Titanium dioxide–zirconium dioxide was prepared by hydrolysis of aqueous solution of a mixture of $TiCl_4$ and $ZrOCl_2$ with aqueous ammonia, followed by washing and calcination at 500 °C in air. The composition was 63% TiO_2 and 37% ZrO_2 by mole.

Prior to exposure to the vapor of SbF_5, all base metal oxides were outgassed at 500 °C for 2 h. Procedures of exposure to SbF_5 for 10 min and following evacuation for 10 min were carried out at different temperatures in the range of 0—100 °C, and were repeated different times.

Specific surface area was determined by applying the adsorption isotherm of N_2 at the boiling point to BET equation. The amount of SbF_5 remained in the resulting catalyst was determined by measuring the weight change of the sample on exposure to SbF_5.

The reaction was carried out primarily at 0 °C in a closed recirculation reactor having a volume of *ca.* 325 ml. The initial pressure of a reactant was about 50 Torr (1 Torr= 133 Pa), and the amount of catalyst was 0.1 g before exposure to SbF_5. The reaction was also carried out in liquid phase under the atmospheric pressure of N_2 or the 13.5 kg/cm^2 of H_2. The reaction products were analyzed by gas chromatography. A 6-m column packed with VZ-7 was operated at room temperature.

Results

As shown in Table 1, the amount of SbF_5 remained in the catalysts after treatmetn with SbF_5 at different temperatures decreased with increase in the pretreatment temperature. Generally, the amount of SbF_5 was smaller for single component metal oxides than for binary ones. The specific surface areas of the catalysts decreased to a considerable extent on treatment with SbF_5. The areas became smaller as the treatment temperature was lower. For example, the area (445 m^2/g) of SiO_2–Al_2O_3 became 205 when SbF_5 was adsorbed at 30 °C and evacuated at 50 °C and 86 when SbF_5 was adsorbed at 0 °C and evacuated at 0 °C.

The product distributions in the reaction of pentane in 60 min (or 70 min) over the different types of base metal oxides treated with SbF_5 are summarized in

Table 1. Amount of SbF_5 remained in catalyst, wt %

Catalyst[a]	SbF_5 ads. temp/°C	Evacuation temp 0 °C	30 °C	50 °C	100 °C
SbF_5-SiO_2-Al_2O_3	0	49.7	37.6	27.7	
	10	53.2	40.9	34.5	30.7
	30		34.1	32.2	
	100				17.2
SbF_5-TiO_2-ZrO_2	0	49.9	30.0	32.8	
	10		33.5	27.2	
	30			29.8	
	100				30.9
SbF_5-SiO_2	0	33.1	18.8	12.8	
	10			18.2	
	30			17.2	
SbF_5-Al_2O_3	0	37.1			
SbF_5-TiO_2	0	23.1			
SbF_5-ZrO_2	0	24.8			

a) Adsorption-desorption cycle in SbF_5 treatment was repeated four times.

Table 2. Treatment with SbF_5 was done at 0 °C both for adsorption and for desorption, and repeated four times. Among the catalysts examined, the SbF_5–TiO_2–ZrO_2 catalyst showed the highest activity. The SbF_5–SiO_2–Al_2O_3 catalyst and the SbF_5–SiO_2 also exhibited high activity.

The time courses of the reactions of pentane and 2-methylbutane over the SbF_5–SiO_2–Al_2O_3 catalyst which was prepared by exposure of SiO_2–Al_2O_3 to SbF_5 at 10 °C followed by evacuation at 30 °C and repeating four times (hereafter represented by SbF_5–SiO_2–Al_2O_3 (10-30) IV) are shown in Figs. 1 and 2. Pressure changes during the reactions were negligible. In the reaction of pentane, only 2-methylbutane was produced in the initial stage of the reaction. In 30 min, 2-methylpropane began to be produced and became a predominant product in 90 min. The maximum conversion to 2-methylbutane was observed in about 60 min. The formation of hexanes was very small compared with that of 2-methylpropane. In the reaction of 2-methylbutane, pentane was produced in the initial period of the reaction in a small amount, and 2-methylpropane began to be formed in 30 min and became the main product.

The features of the time courses in these reactions were commonly observed for all catalysts prepared from different base metal oxides. However, the maximum conversion to 2-methylbutane from pentane

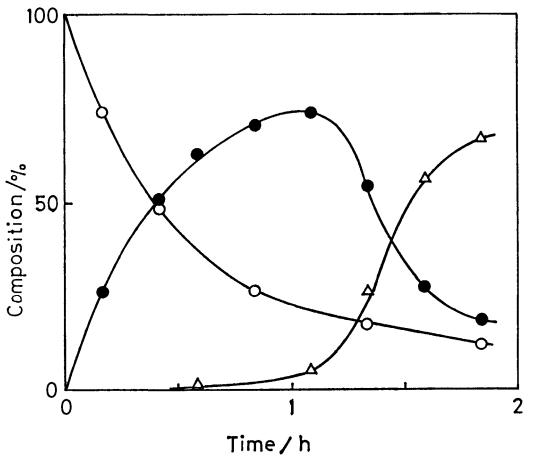

Fig. 1. Time course of reaction of pentane over SbF_5–SiO_2–Al_2O_3(10-30) IV catalyst at 0 °C.
○: Pentane, ●: 2-methylbutane, △: 2-methylpropane.

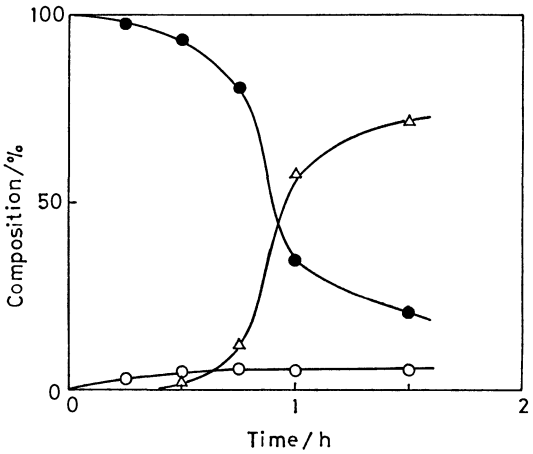

Fig. 2. Time course of reaction of 2-methylbutane over SbF_5–SiO_2–Al_2O_3(10-30) IV catalyst at 0 °C.
○: Pentane, ●: 2-methylbutane, △: 2-methylpropane.

varied with the treatment temperature with SbF_5. The maximum conversions to 2-methylbutane are given in Table 3, and the reaction times to give the maximum conversion are also included in Table 3 in parentheses. As the treatment temperature, especially the evacuation temperature, became higher, the value of the maximum conversion was decreased, and

Table 2. Reaction of pentane over solid super acid at 0 °C

Catalyst	Time/min	Product distribution/% 2-MP[a]	Pentane	2-MB[b]	2,2-DMB	Other hexanes
SbF_5-SiO_2-Al_2O_3	60	0.2	48.0	51.6		
SbF_5-TiO_2-ZrO_2	60	0.2	37.4	62.0	0.3	0.1
SbF_5-SiO_2	60	0.2	42.2	57.3		
SbF_5-Al_2O_3	70		71.1	28.5		
SbF_5-TiO_2	60	0.1	89.8	9.5		
SbF_5-ZrO_2	60	12.6	76.5	10.1	0.1	0.7

a) 2-Methylpropane. b) 2-Methylbutane. c) 2,2-Dimethylbutane.

Table 3. Maximum conversion to 2-methylbutane in reaction of pentane, %

Catalyst	SbF_5 ads. temp/°C	Evacuation temp 0 °C	30 °C	50 °C	100 °C
SbF_5–SiO_2–Al_2O_3	0	80 (210) a)	73 (60)	34 (15)	
	10	78 (180)	73 (65)	60 (35)	10 (25)
	30		58 (30)	24 (20)	
	100				5 (10)
SbF_5–TiO_2–ZrO_2	0	87 (210)	32 (15)	15 (15)	
	10		43 (30)	14 (15)	
	30			20 (20)	
	100				20 (20)
SbF_5–SiO_2	0	83 (210)	43 (60)	20 (30)	
	10			53 (60)	
	30			39 (60)	

a) Numbers in parentheses denote reaction time in minute.

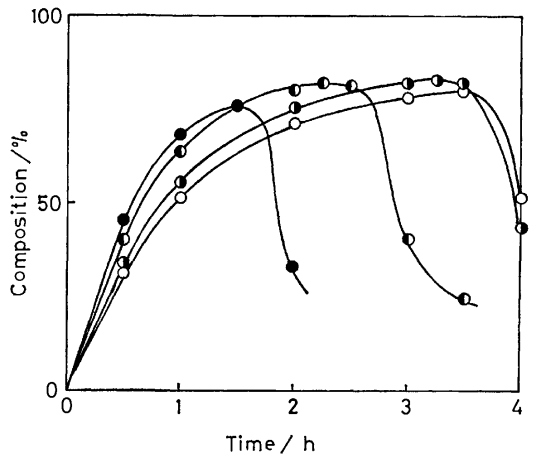

Fig. 3. Time courses of formation of 2-methylbutane from pentane over SbF_5–SiO_2–Al_2O_3(0-0) I—IV catalysts at 0 °C.
●: SbF_5–SiO_2–Al_2O_3 (0-0) I, ◐: II, ◑: III, ○: IV.

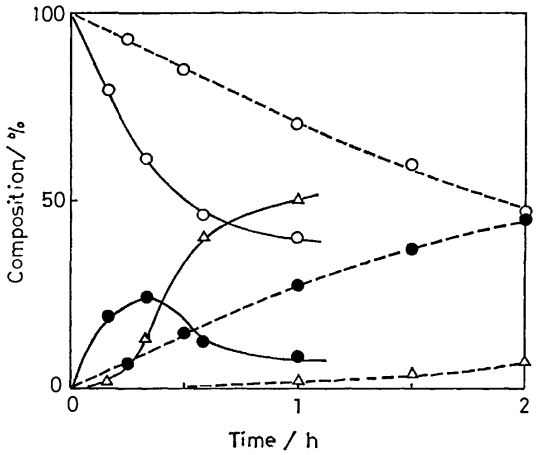

Fig. 4. Effect of reaction temperature in reaction of pentane over SbF_5–SiO_2–Al_2O_3(30-50) IV catalyst.
——: At 0 °C, – – –: at −20 °C, ○: pentane, ●: 2-methylbutane, △: 2-methylpropane.

the reaction time to give the maximum was shortened. Among three different types of catalysts, the SbF_5–SiO_2–Al_2O_3 catalyst exhibited a high maximum conversion over a wide range of the pretreatment temperature, while the SbF_5–TiO_2–ZrO_2 was most easily affected by the treatment temperature, the maximum conversion being lowered from 87% to *ca.* 15% by raising the temperature of evacuation from 0 °C to 50 °C.

The number of repetition of adsorption-desorption cycle in treatment of base metal oxide with SbF_5 also affected the reaction time to reach the maximum conversion to 2-methylbutane. The time courses of the formation of 2-methylbutane from pentane over the SbF_5–SiO_2–Al_2O_3 catalysts which were prepared with different number of repetition of adsorption-desorption cycle at 0 °C are shown in Fig. 3. Although the maximum conversions to 2-methylbutane were almost the same, the initial conversion rates decreased and the reaction times to reach the manixmum conversion was prolonged as the number of repetition increased. The SbF_5–SiO_2–Al_2O_3(0-0) I catalyst and the SbF_5–SiO_2–Al_2O_3(0-0) IV catalyst had the surface areas of 120 and 86 m^2/g, respectively, and contained 49.3 and 49.7 wt % of SbF_5, respectively.

In Fig. 4, the time courses of the reaction of pentane over the SbF_5–SiO_2–Al_2O_3(30-50) IV catalyst at 0 °C and at −20 °C are shown. The maximum conversion to 2-methylbutane was higher when the reaction was carried out at lower temperature, though the initial conversion rate was lower.

When the reaction mixture was briefly evacuated at a certain reaction time and the fresh reactant was introduced, both the conversion rate of pentane and that of 2-methylbutane in the subsequent runs were quite dependent on the reaction time in the previous runs. The time courses of the previous reaction of pentane and the subsequent reaction are shown in Figs. 5 and 6 in which the subsequent reactant was pentane and 2-methylbutane, respectively. When the previous reaction was stopped before the conversion to 2-methylbutane reached the maximum, the isomerization of pentane to 2-methylbutane was faster than the formation of 2-methylpropane from 2-methylbutane in the subsequent runs. On the contrary, when the previous reaction was run to such an extent that the conversion to 2-methylbutane had passed the maximum and the formation of 2-methylpropane had

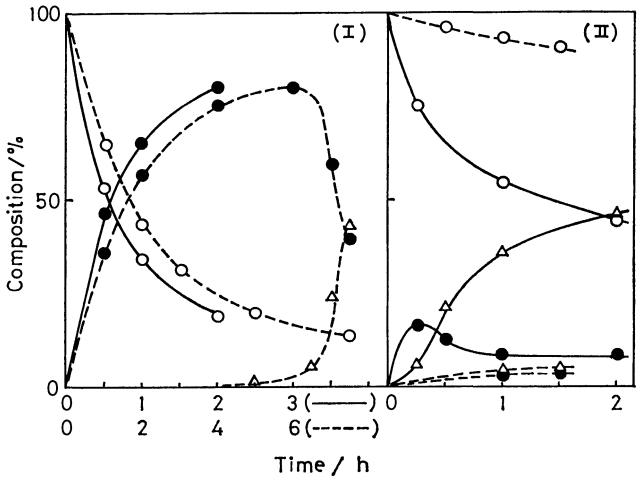

Fig. 5. Time courses of reaction of pentane in the first run (I) and in the second run (II) over SbF_5–SiO_2–Al_2O_3(0-0) IV catalyst at 0 °C.
○: Pentane, ●: 2-methylbutane, △: 2-methylpropane.

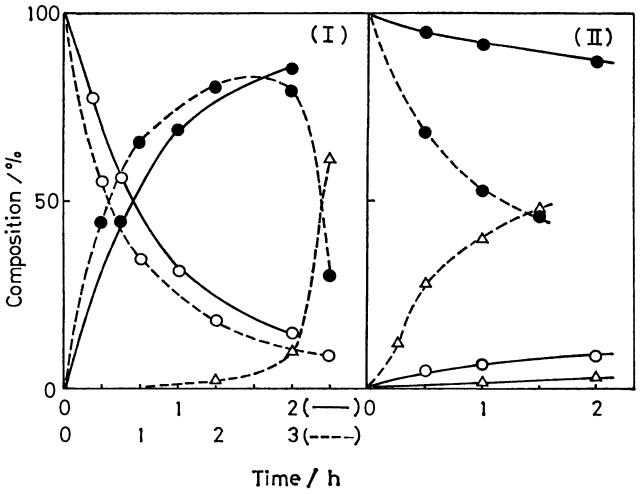

Fig. 6. Time courses of reaction of pentane in the first run (I) and of 2-methylbutane in the second run (II) over SbF_5–SiO_2–Al_2O_3(0-0) IV catalyst at 0 °C.
○: Pentane, ●: 2-methylbutane, △: 2-methylpropane.

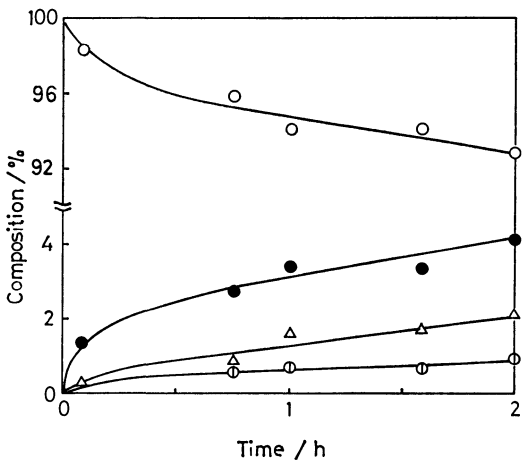

Fig. 7. Liquid phase reaction of pentane over SbF_5–TiO_2–ZrO_2(30-50) IV catalyst at 0 °C under atmolspheric pressure of N_2. Amount of catalyst: 0.269 g, amount of pentane: 10 ml.
○: Pentane, ●: 2-methylbutane, ⓘ: hexanes, △: butane.

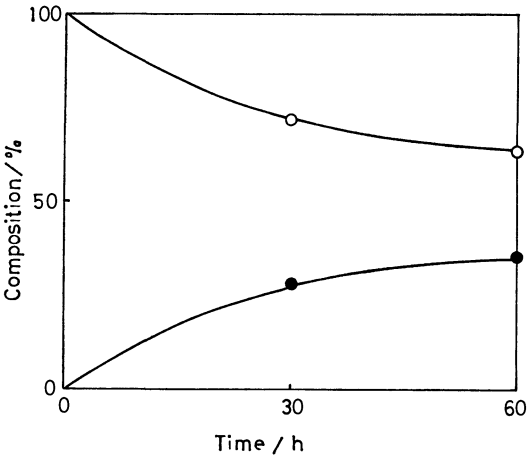

Fig. 8. Liquid phase reaction of pentane over SbF_5–TiO_2–ZrO_2(0-0) IV catalyst at 15 °C under 13.5 kg/cm² of H_2. Amount of catalyst: 0.200 g, amount of pentane: 2 ml.
○: Pentane, ●: 2-methylbutane.

been considerable, the formation of 2-methylpropane from 2-methylbutane became much faster than the isomerization of pentane to 2-methylbutane in the subsequent runs. If the nature of active sites were unchanged throughout the reaction, the reaction features in the subsequent runs would be independent of the reaction time in the previous runs. Therefore, the nature of active sites should gradually change as the reaction proceeds.

The pretreatment temperature of the base metal oxide also affected the catalytic activity. The SbF_5–SiO_2–Al_2O_3(0-0) IV catalyst whose SiO_2–Al_2O_3 had been outgassed at 100 °C prior to treatment with SbF_5 exhibited twice as high conversion rate of pentane as the standard catalyst. The catalytic activity of the SbF_5–SiO_2–Al_2O_3(0-0) IV catalyst whose SiO_2–Al_2O_3 had been outgassed at 1000 °C was negligibly small.

The liquid phase reaction of pentane was carried out over the SbF_5–TiO_2–ZrO_2(30-50) IV catalyst under the atmosphere of N_2. The main product was 2-methylbutane as shown in Fig. 7. 2-Methylpropane was produced from the initial period of the reaction, but not increased to be a main product even in 120 min. Presence of H_2 (13.5 kg/cm²) greatly enhanced the catalytic activity of the SbF_5–TiO_2–ZrO_2(0-0) IV catalyst and the products consisted primarily of 2-methylbutane as shown in Fig. 8. In Fig. 9, the time course of the reaction of 2-methylbutane over the SbF_5–SiO_2–Al_2O_3(30-50) IV catalyst is shown. The conversion rate of 2-methylbutane remained constant until the conversion level of 50%. The main products were hexanes; mostly 2,3-dimethylbutane and 2-methylpentane. To check the elusion of Sb into liquid phase, the liquid products after the reaction

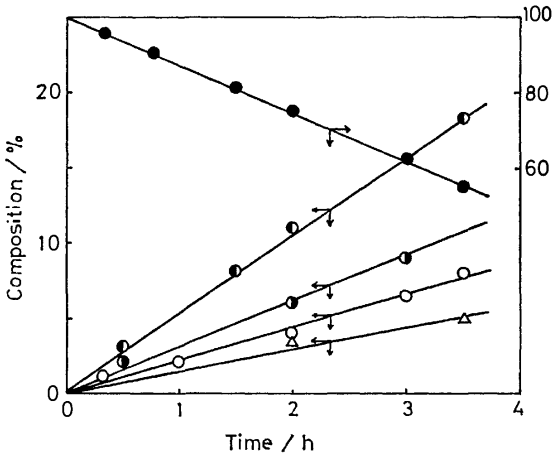

Fig. 9. Liquid phase reaction of 2-methylbutane over SbF_5–SiO_2–Al_2O_3(30-50) IV catalyst at 20 °C under atmospheric pressure of N_2. Amount of catalyst: 0.269 g, amount of pentane: 10 ml.
○: Pentane, ●: 2-methylbutane, △: 2-methylpropane, ◐: 2,3-dimethylbutane+2-methylpentane, ◑: 2,2-dimethylbutane+3-methylpentane.

were subjected to atomic absorption spectroscopic analysis. No Sb could be detected.

In order to check whether SbF_3 which may be formed by reduction of SbF_5 is active or not, the reaction of pentane over SbF_3–SiO_2–Al_2O_3 was carried out at 0 °C in a gas phase. The catalyst was found to be completely inactive.

Discussion

The skeletal isomerization of pentane to 2-methylbutane is important, since 2-methylbutane is known to be a harmless sbustance which raises the octane value of gasoline. In the present work, the maximum conversion of pentane to 2-methylbutane was found to be affected by various factors which appeared in preparation of the SbF_5–oxide catalysts. Out of the factors examined in this study, the temperature at which the base metal oxide was treated with SbF_5 exhibited the greatest effect. To obtain a high maximum conversion to 2-methylbutane, the treatment temperature is desirable to be low. Comparison of Table 3 with Table 1 reveals that the maximum conversion increases with the increase of the amount of SbF_5 remained in the catalysts, though the surface areas of the catalysts decreases with the increase of the amount of SbF_5.

The decrease in the conversion to 2-methylbutane as the reaction proceeds is caused by the formation of 2-methylpropane from 2-methylbutane.

Since the catalyst that had been used for the reaction to a considerable extent became not so active for the skeletal isomerization of pentane but active for the formation of 2-methylpropane from 2-methylbutane, the nature of active sites on the catalyst should gradually change as the reaction proceeds.

On the freshly prepared catalyst, only the active sites for the skeletal isomerization of pentane, I-sites, may exist, and I-sites are gradually transformed to the sites which are active for the formation of 2-methylpropane from 2-methylbutane, C-sites, during the skeletal isomerization. An alternative explanation could be this. Both I-sites and C-sites exist on the fresh catalyst, and only I-sites are gradually poisoned as the reaction proceeds. The I-sites are considered to act as Lewis acid sites which abstract hydride ions from pentane to form the carbenium ions, since the existence of Lewis acid sites on SbF_5–SiO_2–Al_2O_3 has been evidenced by infrared spectra of adsorbed pyridine.[11]

According to the deuterium tracer study,[12] 2-methylpropane is not produced by a simple cracking of 2-methylbutane. Two different mechanisms can be proposed for the formation of 2-methylpropane from 2-methylbutane. One of them is the recombination of four methyl and/or methylene groups on the catalyst surface (Eq. 1),[12] and the other is the disproportionation of 2-methylbutane, that is, the dimerization-decomposition mechanism (Eq. 2).[13,14]

$$\text{2-methylbutane} \xrightarrow{\text{cracking}} \text{methyl and/or methylene groups} \xrightarrow{\text{recombination}} \text{2-methylpropane} \quad (1)$$

$$\text{2-methylbutane} \xrightarrow{\text{dimerization}} C_{10}\ \text{species} \xrightarrow{\text{decomp.}} \text{2-methylpropane} + \text{a hexane} \quad (2)$$

In the Eq. 1, 2-methylbutane was formed from pentane over the I-sites at first and it cracked to the methyl and/or methylene groups over the C-sites. The methyl and/or methylene groups accumulate on the surface as the reaction proceeds. When the accumulation becomes saturated, four methyl and/or methylene groups recombine to produce 2-methylpropane and it desorbs into the gas phase. Since the formation of hexanes are very small compared with that of 2-methylpropane in the gas phase reactions, 2-methylpropane may be produced mainly by the Eq. 1.

In the liquid phase reactions, however, not so large difference exists between the formation of 2-methylpropane and that of hexanes. Therefore, in the liquid phase reactions, the contribution of the Eq. 2 may be much larger than that of the Eq. 1 to the formation of 2-methylpropane. The effect of hydrogen is considered to prevent the carbonization of hydrocarbons or to retard the reduction of SbF_5.

Since the catalytic activity became smaller when the base metal oxide had been previously outgassed at higher temperature, the presence of OH groups on the base metal oxide seems to be necessary to form the active sites by treatment with SbF_5. In the catalyst, SbF_5 may not be simply adsorbed on the surface but may be reacted with surface, propably with surface OH groups. The existence of Brönsted acid sites, besides Lewis acid sites, is also evidenced by infrared study on adsorbed pyridine.[11] The speculative structure of acid sites on SbF_5–SiO_2–Al_2O_3 may be drawn as follows.

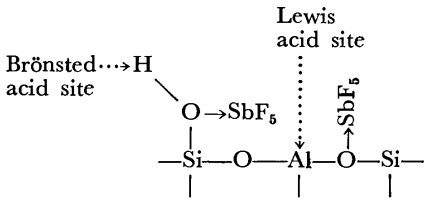

SbF_5 adsorbs on oxygen atoms of Al–O–Si and O–H to attract the electron pairs of the oxygen atoms and by the inductive effects, both Lewis and Brönsted acid sites are considered to increase their acid strengths. A small amount of SbF_5 may be reduced to SbF_3 which is inactive for the reaction of pentane.

References

1) V. L. Magnotta, B. C. Gates, and G. C. A. Schuit, *J. Chem. Soc., Chem. Comm.*, **1976**, 342.
2) V. L. Magnotta and B. C. Gates, *J. Catal.*, **46**, 266 (1977).
3) G. A. Olah, J. Kaspi, and J. Bukala, *J. Org. Chem.*, **42**, 4187 (1977).
4) J. Kaspi and G. A. Olah, *J. Org. Chem.*, **43**, 3142 (1978).
5) J. Kaspi, D. D. Montgomery, and G. A. Olah, *J. Org. Chem.*, **43**, 3147 (1978).
6) Y. Ono, T. Tanabe, and N. Kitajima, *Chem. Lett.*, **1978**, 625.
7) Y. Ono, S. Sakuma, T. Tanabe, and N. Kitajima, *Chem. Lett.*, **1978**, 1061.
8) Y. Ono, T. Tanabe, and N. Kitajima, *J. Catal.*, **56**, 47 (1979).
9) K. Tanabe, and H. Hattori, *Chem. Lett.*, **1976**, 625.
10) O. Takahashi, H. Hattori, and K. Tanabe, submitted for publication in *J. Catal.*
11) O. Takahashi, H. Hattori, and K. Tanabe, *Shokubai*, **20**, 28 (1978).
12) O. Takahashi and H. Hattori, submitted for publication in *J. Catal.*
13) A. Schneider and R. M. Kennedy, *J. Am. Chem. Soc.*, **73**, 5017 (1951).
14) D. A. McCaulay, *J. Am. Chem. Soc.*, **81**, 6437 (1959).

The Energy Dependence of Selective Hydrogen Atom Abstraction by H(D) Atoms in the Photolysis of Neopentane–Ethane Mixtures at 77 K

Tetsuo MIYAZAKI,* Selma Matheus Loureiro GUEDES, and Kenji FUEKI

Department of Synthetic Chemistry, Faculty of Engineering, Nagoya University, Chikusa-ku, Nagoya 464

(Received October 9, 1979)

Selective hydrogen-atom-abstraction reaction by an H or D atom has been studied in a *neo*-C_5H_{12}–C_2H_6 (less than 1 mol%) mixture at 77 K by ESR spectroscopy. The H (or D) atom produced by the photolysis of HI (or DI) reacts with *neo*-C_5H_{12} and C_2H_6 to form *neo*-C_5H_{11} and C_2H_5 radicals. In order to obtain H atoms with different kinetic energies, the photolysis was performed with different lights of 313, 254, and 229 nm. The selective formation of the C_2H_5 radical by the reaction of the H (or D) atom with C_2H_6 becomes more effective with the decrease in the energy of the H (or D) atom. The formation of the *neo*-C_5H_{11} radical by the reaction of the H (or D) atom with *neo*-C_5H_{12} becomes more effective with the increase in the energy of the H (or D) atom.

The reaction of the H atom is quite important in chemical kinetics as well as in the radiation chemistry of organic compounds. Though extensive results on the reaction of hot H atom have been reported in the gas phase,[1] information on the solid phase at low temperatures is quite scanty at present.

Recently Miyazaki *et al.* found interesting phenomena concerning hydrogen-atom abstraction reactions by the H atom in the solid neopentane-alkane mixtures at 77 K.[2] When the H atom is produced at 77 K by the radiolysis of neopentane or by the UV-photolysis of hydrogen halide, the H atom reacts selectively with the solute, resulting in the formation of the solute radical. The H atom produced by the radiolysis or the photolysis has excess kinetic energy. When the wavelength of light is changed in the photolysis of HI, an H atom with a different kinetic energy is produced.

In order to obtain information on the reactivity of an H atom with a differential initial kinetic energy in the solid alkane, the reactions of the H atoms produced by the photolysis of HI in neopentane–ethane mixture are studied here.

Experimental

The D content of deuterium iodide, supplied by Merk Sharp and Dohm, Canada, Ltd., is more than 98%. The other reagents used in this study are the same as those used before.[2c]

UV illumination was provided by a medium-pressure mercury lamp with a UV-29 filter, a low-pressure mercury lamp with a UV-25 filter, and a home-made cadmium lamp. The cadmium lamp was made of quartz and kept in an electric furnace at 533 K.[3] The emission spectra of the light from the lamps used in the experiment were measured with an emission spectrometer. The emission spectra are shown in Fig. 1. In order to determine the light absorbed by HI, the extinction coefficient (ε) of HI was measured. Since neopentane is polycrystalline at 77 K, the extinction coefficient of HI was measured in 3-methylpentane glass at 77 K. ε at 254 nm, for example, is 95 $mol^{-1}\,dm^3\,cm^{-1}$, nearly equal to the reported values of 95 $mol^{-1}\,dm^3\,cm^{-1}$ in the gas phase[4] and 127 $mol^{-1}\,dm^3\,cm^{-1}$ in the liquid solvent.[5] The absorption spectrum of 0.5 mol% HI is shown in Fig. 1 by the unit of absorbance percentage, where the pass length of light is 0.3 cm.

The free radical formed in the photolysis was measured at 77 K with a JES-3BX ESR spectrometer. The microwave power levels used did not result in the saturation of the signal of the alkyl radicals.

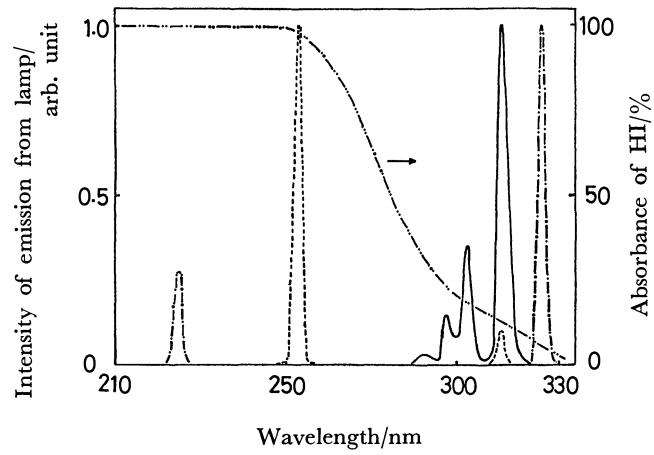

Fig. 1. Emission spectra from lamp and absorbance of HI. Maximum intensity of light from each lamp is normalized to 1.
——: Medium-pressure mercury lamp with UV-29 filter; ----: low pressure mercury lamp with UV-25 filter; —·—: cadmium lamp; —··—: absorbance of HI(0.5 mol %) in 3-methylpentane glass at 77 K, where a pass length of light is 0.3 cm.

Results

The emission intensity multiplied by the absorbance of HI in Fig. 1 corresponds to the light absorbed by HI in the photolysis. The most effective lights for the photolysis of HI are 313 nm from the medium-pressure mercury lamp with a UV-29 filter, 254 nm from the low-pressure mercury lamp with a UV-25 filter, and 229 nm from the cadmium lamp. In fact, the photolysis of HI does not occur upon the irradiation with the cadmium lamp with a UV-29 filter, which cuts off the light of 229 nm and transmits only 326 nm.

Figure 2 shows the yield of the C_2H_5 radical in the photolysis of *neo*-C_5H_{12}–HI(0.5 mol %)–C_2H_6 mixtures at 77 K. The relative yield of the C_2H_5 radical was estimated from the peak height of the C_2H_5 radical in the ESR spectrum. In the present work, the peaks which do not overlap with those of other radicals were used for the measurement of the relative yield of the C_2H_5 radical. The yield of the C_2H_5 radical

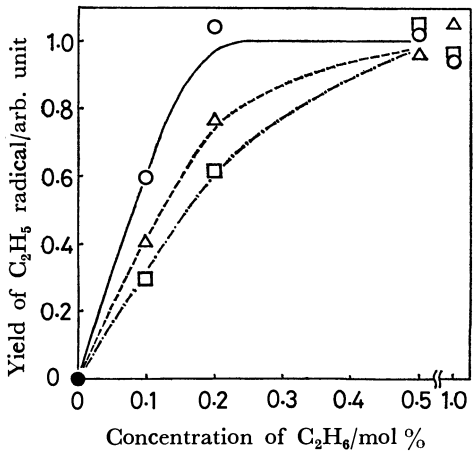

Fig. 2. Yield of C_2H_5 radical against concentration of C_2H_6 in the photolysis of *neo*-C_5H_{12}–HI(0.5 mol %)–C_2H_6 at 77 K. The plateau yield at high concentration of C_2H_6 is normalized to 1.
○: Photolysis at 313 nm; △: photolysis at 254 nm; □: photolysis at 229 nm.

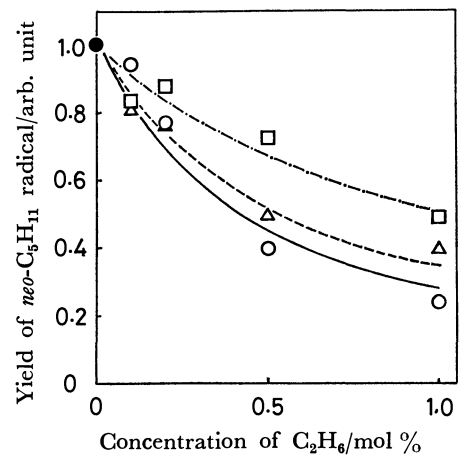

Fig. 3. Yield of *neo*-C_5H_{11} radical against concentration of C_2H_6 in the photolysis of *neo*-C_5H_{12}–HI(0.5 mol %)–C_2H_6 at 77 K. The yield in the absence of C_2H_6 is normalized to 1.
○: Photolysis at 313 nm; △: photolysis at 254 nm; □: photolysis at 229 nm.

increases with the increase in the C_2H_6 concentration and reaches a plateau at a high concentration of C_2H_6. The plateau yield is taken as 1.0.

Figure 3 shows the yield of the *neo*-C_5H_{11} radical in the photolysis of *neo*-C_5H_{12}–HI(0.5 mol %)–C_2H_6 mixtures at 77 K. The relative yield of the *neo*-C_5H_{11} radical was estimated also from the peak height of the *neo*-C_5H_{11} radical in the ESR spectrum. The peak which does not overlap with those of the other radicals was used for the measurement of the yield of the *neo*-C_5H_{11} radical. The yield in the absence of C_2H_6 is taken as 1.0.

Figures 4 and 5 show the yields of the C_2H_5 and *neo*-C_5H_{11} radicals respectively in the photolysis of *neo*-C_5H_{12}–DI(0.5 mol %)–C_2H_6 mixtures at 77 K.

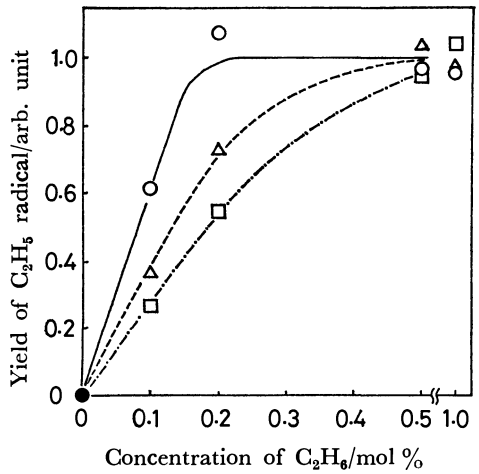

Fig. 4. Yield of C_2H_5 radical against concentration of C_2H_6 in the photolysis of *neo*-C_5H_{12}–DI(0.5 mol %)–C_2H_6 at 77 K. The plateau yield at high concentration is normalized to 1.
○: Photolysis at 311 nm; △: photolysis at 254 nm; □: photolysis at 229 nm.

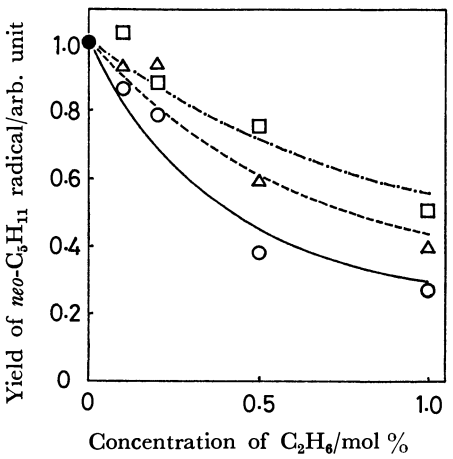

Fig. 5. Yield of *neo*-C_5H_{11} radical against concentration of C_2H_6 in the photolysis of *neo*-C_5H_{12}–DI(0.5 mol %)–C_2H_6 at 77 K. The yield in the absence of C_2H_6 is normalized to 1.
○: Photolysis at 313 nm; △: photolysis at 254 nm; □: photolysis at 229 nm.

Discussion

Formation of the C_2H_5 Radical. When *neo*-C_5H_{12}–HI–alkane mixtures are UV-irradiated or *neo*-C_5H_{12}–alkane mixtures are γ-irradiated at 77 K, the alkyl radical from the solute, such as *i*-C_4H_{10}, C_3H_8, *c*-C_6H_{12}, and C_2H_6, is produced in a much higher yield than would be expected from the concentration of the solute. The reaction mechanism for the selective formation of the alkyl radical has been reported in detail in previous papers,[2a-d,2h] The formation of the alkyl radical by the radical site migration (Reaction 1) can be neglected for the following reasons:

$$\textit{neo}\text{-}C_5H_{11} + RH \longrightarrow \textit{neo}\text{-}C_5H_{12} + R \quad (1)$$

where RH represents the solute, such as *i*-C_4H_{10} and C_2H_6. First, when the *neo*-C_5H_{12}–*i*-C_4H_{10} mixture is

γ-irradiated at 4 K, only the *neo*-C_5H_{11} radical is produced. The selective formation of the C_4H_9 radical is not observed when the irradiated sample is warmed from 4 K to 77 K, though the C_4H_9 radical is formed in the γ-irradiation at 77 K.[2e] Second, when the *neo*-C_5H_{12}–*i*-C_4H_9D-2-d_1–HI mixture is irradiated with UV light at 77 K, the selective formation of the HD molecule and the *t*-C_4H_9 radical is observed, though the H_2 molecule and the *t*-C_4H_9 radical should be formed by the mechanism of the radical-site migration. Thus, the formation of the *t*-C_4H_9 radical is not due to the radical-site migration, but to the selective hydrogen-atom abstraction by the H atom. The other experimental evidence for the selective reaction of the H atoms has been presented in the previous papers.[2b,d] When *neo*-C_5H_{12}–C_2H_6–*i*-C_4H_{10}–HI mixtures are UV-irradiated at 77 K, the yield of the C_2H_5 radical decreases upon the addition of *i*-C_4H_{10}, resulting in the complementary formation of the *t*-C_4H_9 radical.[2h] Therefore, the C_2H_5 radical is also formed by the selective reaction of the H atom.

Figure 2 shows that the yield of the C_2H_5 radical in the photolysis of *neo*-C_5H_{12}–HI(0.5 mol %)–C_2H_6 mixtures increases with the increase in C_2H_6 and reaches a plateau at high concentrations. Since the plateau value is normalized to 1 in Fig. 2, the amounts of the reactive H atoms produced by the photolysis of HI with three different lights are normalized to the same value. The reaction mechanism for the formation of the C_2H_5 radical can be represented as follows:

$$HI + h\nu \xrightarrow{I_2} H + I \quad (2)$$

$$H + C_2H_6 \xrightarrow{k_3} H_2 + C_2H_5 \quad (3)$$

$$H + P \xrightarrow{k_4} \text{product}, \quad (4)$$

where I_2 is the rate of the production of the reactive H atom which reacts with C_2H_6 at high concentrations of C_2H_6. k is a rate constant. Reaction 4 represents some reaction which competes with Reaction 3. P may be *neo*-C_5H_{12} and HI. Since I_2 is normalized to 1,

$$k_3/\{k_4[P]\} = [C_2H_5]/\{[C_2H_6](1-[C_2H_5])\}. \quad (5)$$

Since [P] is constant in the present experiment, $k_3/\{k_4[P]\}$ represents the relative reactivity of Reaction 3 and is summarized in the third column in Table 1. When hydrogen iodide absorbs ultraviolet light, the H atom produced by the photolysis obtains excess kinetic energy. The energetics of the dissociation process is a little complicated by the possibility that iodine atoms can be formed in two electronic states, the ground or the first-excited state.[6] It is assumed here, however, that most of the iodine atoms are in the ground state and that the average initial energy of the hydrogen atom is the difference between the energy of light and the bond energy of HI. The average excess energy is shown in the second column in Table 1. The relative reactivity of the selective hydrogen-atom abstraction reaction increases with the decrease in the kinetic energy of the H atom. If the reactive H atom is a thermal H atom, $k_3/\{k_4[P]\}$ should be independent of the light sources in the evolution of H from HI.

Table 1. Rate constant for hydrogen-atom abstraction reaction by the H(D) atom at 77 K

Wave length of photolysis / nm	Excess energy of the hydrogen atom / kcal/mol	$k_3/\{k_4[P]\}$ [a]	k_8/k_7
neo-C_5H_{12}–HI(0.5 mol%)–C_2H_6			
313	20	1500	250
254	41	1100	190
229	54	600	100
neo-C_5H_{12}–DI(0.5 mol%)–C_2H_6			
313	20	1600	250
254	41	900	130
229	54	500	80

a) The unit of concentration is the mole fraction. See text.

The yield of the C_2H_5 radical in the photolysis of *neo*-C_5H_{12}–DI(0.5 mol %)–C_2H_6 mixtures is shown in Fig. 4. The amount of the C_2H_5 radical increases with the increase in the C_2H_6 concentration and reaches a plateau at a high concentration. The same mechanism as in Reactions 2, 3, and 4 can be applied to the formation of the C_2H_5 radical in the photolysis of DI. The $k_3/\{k_4[P]\}$ value for the D atom, as estimated from Eq. 5, is shown in Table 1. The relative reactivity of the selective hydrogen-atom abstraction by the D atom increases with the decrease in the kinetic energy of the D atom. It is noted that the $k_3/\{k_4[P]\}$ value and its energy dependence for the D atom are similar to those for the H atom.

Formation of the neo-C_5H_{11} *Radical.* Figure 3 shows that the yield of the *neo*-C_5H_{11} radical in the photolysis of *neo*-C_5H_{12}–HI(0.5 mol %)–C_2H_6 mixtures decreases upon the addition of C_2H_6, while that of the C_2H_5 radical increases (Fig. 2). Since the *neo*-C_5H_{11} radical does not react with C_2H_6 in the solid phase at 77 K,[2e] the dependence of the *neo*-C_5H_{11}-radical yield upon C_2H_6 may be due to a competitive reaction between *neo*-C_5H_{12} and C_2H_6 for the H atom.

$$HI + h\nu \xrightarrow{I_6} H' + I \quad (6)$$

$$H' + \textit{neo}\text{-}C_5H_{12} \xrightarrow{k_7} H_2 + \textit{neo}\text{-}C_5H_{11} \quad (7)$$

$$H' + C_2H_6 \xrightarrow{k_8} H_2 + C_2H_5, \quad (8)$$

where I_6 is the rate of the production of the reactive H atom, which produces the *neo*-C_5H_{11} radical in the absence of C_2H_6. The two reactive hydrogen atoms in Reactions 2 and 6 will be compared below. Since I_6 is normalized to 1 in Fig. 3, the following equation is obtained:

$$\frac{1}{[\textit{neo}\text{-}C_5H_{11}]} = 1 + \frac{k_8[C_2H_6]}{k_7[\textit{neo}\text{-}C_5H_{12}]} \quad (9)$$

The average values of k_8/k_7, obtained from the kinetic plots of $1/[\textit{neo}\text{-}C_5H_{11}]$ and $[C_2H_6]/[\textit{neo}\text{-}C_5H_{12}]$, are shown in the last column in Table 1. k_8/k_7 decreases with the increase in the energy of the H atom. Thus, the formation of the *neo*-C_5H_{11} radical becomes more favorable with the increase in the energy of the H atom.

Figure 5 shows the dependence of the *neo*-C_5H_{11} radical yield upon C_2H_6 in the photolysis of *neo*-C_5H_{12}–DI(0.5 mol %)–C_2H_6 mixtures. The yield decreases upon the addition of C_2H_6, while that of the C_2H_5 radical increases (Fig. 4). The same kinetics as in Reactions 6—8 and Eq. 9 can be applied to the formation of the *neo*-C_5H_{11} radical by the D atom. The k_8/k_7 ratio for the D atom is shown in Table 1. k_8/k_7 decreases with the increase in the energy of the D atom.

Now, Reactions 8 and 7 will be compared with Reactions 3 and 4. Since the concentration of P in $k_3/\{k_4[P]\}$ is represented by a mole fraction, $[P]=1$ if P corresponds only to *neo*-C_5H_{12}. In this case, however, the experimental values of k_3/k_4 for the H and D atoms are not equal to k_8/k_7, but about 6 times as large as k_8/k_7 (Table 1). Thus, Reaction 4 must contain some reaction other than Reaction 7.

The ratio of the decrement in the *neo*-C_5H_{11}-radical yield ($-\Delta C_5H_{11}$) to the increment in the C_2H_5-radical yield (ΔC_2H_5) is shown in Fig. 6 as a function of the C_2H_6 concentration. Since the reliability of the $-\Delta C_5H_{11}$ value at 0.1 mol % is low, the value at 0.1 mol % is omitted in the figure. If Reaction 4 represents only a reaction between H (or D) and *neo*-C_5H_{12}, the $-\Delta C_5H_{11}/\Delta C_2H_5$ ratio should be constant at all concentrations of C_2H_6. Figure 6 shows, however, that the ratio is not constant. In fact, this ratio changes more remarkably with the decrease in the energy of the H (or D) atom. Some of the reactive H (or D) atoms which react with C_2H_6 do not react with *neo*-C_5H_{12}, and the role of these H (or D) atoms increases with the decrease in the energy of the H (or D) atom. Therefore, the H atoms in Reaction 2 represent all the hydrogen atoms which react with C_2H_6, while the H′ atoms in Reaction 6 represent only the hydrogen atoms which can react with *neo*-C_5H_{12}.

It is concluded from the energy dependence of the formation of the C_2H_5 radical that H (or D) atoms with different excess energies play an important role in the selective hydrogen-atom abstraction reaction and that the selective reaction occurs more easily with the decrease in the excess energy of the H (or D) atom. The hydrogen atoms with small excess energies migrate through the neopentane matrix at 77 K. The atoms neither react with neopentane nor are deactivated during their migration. These results seem to contradict a kinetic theory of a hot-atom reaction in the gas phase. The reactions in the solid phase, however, may be different from those in the gas phase. Further studies of the reaction and the deactivation process of the hot H atom in the solid phase are now under way.

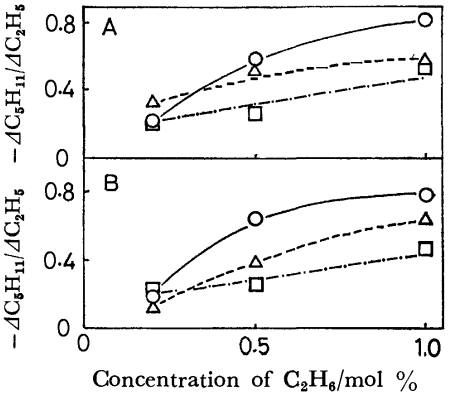

Fig. 6. The ratio of decrement of *neo*-C_5H_{11} radical yield ($-\Delta C_5H_{11}$) to increment of C_2H_5 radical yield (ΔC_2H_5) against concentration of C_2H_6. Figures A and B are *neo*-C_5H_{12}–HI(0.5 mol %)–C_2H_6 system and *neo*-C_5H_{12}–DI(0.5 mol %)–C_2H_6 system respectively.
○: Photolysis at 313 nm; △: photolysis at 254 nm; □: photolysis at 229 nm.

The authors wish to thank Professor Shin Sato of the Tokyo Institute of Technology for his fruitful advice with regard to making a cadmiun lamp.

References

1) J. Dubrin, *Ann. Rev. Phys. Chem.*, **24**, 97 (1973), and the references cited therein.
2) a) T. Wakayama, T. Miyazaki, K. Fueki, and Z. Kuri, *J. Phys. Chem.*, **77**, 2365 (1973); b) T. Miyazaki and T. Hirayama, *ibid.*, **79**, 566 (1975); c) T. Miyazaki, K. Kinugawa, M. Eguchi, and S. M. L. Guedes, *Bull. Chem. Soc. Jpn.*, **49**, 2970 (1976); d) T. Miyazaki, K. Kinugawa, and J. Kasugai, *Radiat. Phys. Chem.*, **10**, 155 (1977); e) K. Kinugawa, T. Miyazaki, and H. Hase, *ibid.*, **10**, 341 (1977); f) T. Miyazaki, J. Kasugai, M. Wada, and K. Kinugawa, *Bull. Chem. Soc. Jpn.*, **51**, 1676 (1978); g) K. Kinugawa, T. Miyazaki, and H. Hase, *J. Phys. Chem.*, **82**, 1697 (1978); h) T. Miyazaki, N. Goshima, K. Fueki, Y. Aratono, and E. Tachikawa, *Radiat. Phys. Chem.*, **15**, 561 (1980).
3) S. Tsunashima, T. Toyono, and S. Sato, *Bull. Chem. Soc. Jpn.*, **46**, 2654 (1973).
4) C. F. Goodeve and A. W. C. Taylor, *Proc. R. Soc. London, Ser. A*, **154**, 181 (1936).
5) L. Perkey and J. E. Willard, *J. Chem. Phys.*, **60**, 2732 (1974).
6) R. D. Clear, S. J. Riley, and K. R. Wilson, *J. Chem. Phys.*, **63**, 1340 (1975).

 © 1980 The Chemical Society of Japan Bull. Chem. Soc. Jpn., 53, 1817—1824 (1980)

The Absorption Spectra of Monolayers of Fat-soluble Vitamins and the Orientations of Their Chromophores

Kazunori MATSUKI,* Yukio NAGAHIRA,† and Hideo FUKUTOME
Department of Physics, Faculty of Science, Kyoto University, Kyoto 606
(Received October 11, 1979)

The UV absorption spectra at normal incidence and the polarized spectra at 45° incidence of monolayers of vitamin K_1, α-tocopherylquinone, vitamin E, ergosterol, and vitamin D_2 were measured. The absorption peaks of the monolayers of vitamin K_1, α-tocopherylquinone, and vitamin D_2 shifted to wavelengths longer than those in a hexane solution, while vitamin E and ergosterol showed little shift. The orientations of their chromophores in the monolayers were investigated by means of the dichroic ratios obtained from their polarized spectra. The molecular axes of vitamin K_1, α-tocopherylquinone, and vitamin E were found to be oriented in the range from 0° to about 30° against the normals of their monolayer planes. The molecular axis of ergosterol was found to tilt about 24° against the normal of the monolayer plane. For vitamin D_2, no reliable conclusion could be obtained as to its orientation.

Fat-soluble vitamins and their related compounds used in this study, vitamin K_1, α-tocopherylquinone(α-TQ), vitamin E, ergosterol, and vitamin D_2, have a quinone or a linear polyene moiety as their chromophores and form stable monolayers at air-water interfaces. These compounds exist in biological membranes and are involved in some biochemical processes. Vitamin K_1, α-TQ, and vitamin E are contained in chloroplasts and are thought to play a part in the electron-transfer system. Vitamin D_2 and ergosterol, which are steroid hormones, are known to have strong affinities for biological membranes. Their chromophores are thought to be important in their biological functions.

The states and the interactions of chromophores of these molecules and other fat-soluble vitamins in monolayers are interesting from both biological and physical points of view, but they have not been well studied except for the vitamin A group,[1] although the surface pressure-area curves, surface potentials, and other properties of their monolayers have been investigated by several workers.[2-7] The main difficulty in such a study is that the intensities of the absorption spectra of chromophores in monolayers are generally very small. Several methods of measuring the absorption spectra of monolayers were devised by Jacob *et al.*,[8] Trurnit and Colmano,[9] and Tweet.[10] These methods, however, are all more or less troublesome. More recently, Kuhn *et al.*[11] designed a high-sensitivity spectrophotometer for thin layers and investigated the absorption spectra of monolayers of ionic cyanine dyes substituted with long hydrocarbon chaines. We constructed in our laboratory a spectrophotometer similar to theirs because the absorption spectra of monolayers can be measured more easily with it than with any other methods. We have then measured the polarized absorption spectra of monolayers of vitamin K_1, α-TQ, vitamin E, vitamin D_2, and ergosterol in order to get information about the interactions and the orientations of their chromophores in monolayers.

Experimental

Materials. Guaranteed-reagent-grade vitamin K_1, vitamin D_2, ergosterol, and β-cholestanol were purchased from Nakarai Chemicals, Ltd. The vitamin E (Wako first grade) and phytol were obtained from Wako Pure Chemical Industries, Ltd., and the α-TQ, from the Nutritional Biochemicals Corporation. The absorption spectra of the fat-soluble vitamins in organic solutions were identical with the reported values in peak positions and extinction coefficients as follows: Vitamin K_1 (in hexane): within 1 nm and 4% compared with the values reported for petroleum ether[12] and isooctane(2,2,4-trimethylpentane)[13] solutions; α-TQ (in ethanol): within 1 nm and 5% compared with the values reported for an ethanol solution;[14] vitamin E (in hexane): within 1 nm and 3% compared with the values reported for a cyclohexane solution;[15] vitamin D_2 (in hexane): within 0.5 nm and 2% compared with the values reported for a hexane solution;[16] ergosterol (in ethanol): within 0.5 nm and 3% compared with the values reported for an ethanol solution.[17] All the above chemicals were stored in the dark at about −20 °C in a reduced-pressure desiccator in which air had been replaced with nitrogen. Guaranteed-reagent-grade Na_2HPO_4, KH_2PO_4, and spectroscopic-grade hexane were purchased from Nakarai Chemicals, Ltd. All the chemicals were used without further purification. Twice-distilled water (pH=5.6—5.9) was used in all the experiments. Optically flat quartz slides ($50\times24\times0.8$ mm^3) were obtained from the Takahashi Giken Co.

Methods. The UV-absorption spectra of the above compounds in a hexane solution were recorded on an MPS-5000 spectrophotometer (Shimadzu Co.). The absorption spectra of monolayers were measured with a high-sensitivity spectrophotometer using the single-beam and sample in-sample out technique developed by Kuhn *et al.*[11] The apparatus constructed in our laboratory was the same as theirs in fundamental design. It consists of an automatic scanning monochromator, a self-exciting oscillator system, a light-detecting system (a photomultiplier and a preamplifier), a high-tension control system which feeds a highly negative voltage to the photomultiplier, a lock-in amplifier, and an X-Y recorder. The self-exciting oscillator system consists of a mechanical oscillator made of a long, thin iron plate ($95\times16\times1$ mm^3) which is fixed vertically on a rigid frame made of iron and attached at its top with a holder to mount a quartz slide vertically against the iron plate, two electro-magnets to drive the oscillation of the oscillator, a coil to detect the frequency and the amplitude of the oscillation, and a negative-feedback electric circuit fed with the signal from the coil to provide the magnets with the a.c. current with the resonance frequency of the oscillator and a constant amplitude. The oscillator, with a quartz slide

† Present address: Osaka University of Economics and Law, Gakuonji, Yao City, Osaka 581.

mounted in it, was oscillated at a resonance frequency of about 40 Hz and with a constant amplitude (measured at the center of the quartz slide) of about 10 mm. In measurements of the absorption spectra of monolayers, one half of the quartz slide was covered with a monolayer. Then the sample area of the slide (covered with the monolayer) and the reference area (not covered with it) passed the light beam alternately. The transmitted and modulated light was directed to the photomultiplier. The a.c. signal from the pre-amplifier was amplified by the lock-in amplifier, and the absorbance was recorded. The reference signal for the lock-in amplifier was taken from the self-exciting oscillator system. The following minor modifications were made in our apparatus: The light from the exit slit of the monochromator was focused on the quartz slide not with lenses, but with two mirrors, in order to eliminate the chromatic aberration. The integrated signal from the pre-amplifier was used to regulate the high tension fed into the photomultiplier, because the absorptions of the monolayers are very small.

The a.c. signal from the pre-amplifier was assumed to be a rectangular wave. This assumption is plausible because the boundary between the sample area and the reference area most quickly passes the light beam. The peak-to-peak value of the rectangular wave is proportional to the absorbance because the absorptions of monolayers are very small. The conversion factor from absorption(%) to absorbance is $\log_{10}(e/100)$. The high tension fed into the photomultiplier was adjusted to make the output from the pre-amplifier 50 mV for the case of a 5% absorption. In the lock-in amplifier, the first term of the Fourier series of the rectangular wave is synchronously rectified in the full wave and the rms value of the rectified wave is obtained. The conversion factor from the rms value of the rectified wave to the peak-to-peak value of the rectangular wave is $\pi/\sqrt{2}$. Therefore, the absorbance is obtained by multiplying the output of the lock-in amplifier (volt) by $(\pi/\sqrt{2})\log_{10}e(=0.9647)$. The absorbance measured with our apparatus agreed with that measured with usual spectrophotometers within a 4% error in the range of optical density (OD) of $(3—4)\times10^{-2}$.

The sensitivity of our apparatus was limited by noises which could not be synchronized by the lock-in amplifier. The noise level was 1×10^{-4} OD/layer. The systematic noises caused by the magnetic field and the mechanical vibration from the oscillator system could, however, be suppressed to a level which did not exceed the above random noise level by making a magnetic shielding of the photomultiplier and a mechanical insulation of the oscillator to prevent dissipation of the vibration energy to other parts of the apparatus. Therefore, measurements were possible up to the range of the 2.5×10^{-3} OD/layer on a full scale with a noise level below 4%.

In the measurements of the polarized absorption spectra at 45° incidence, a polarizer (a Glan-Thomson prism made of calcite) was set just before the slide. The polarizer was set in such a manner as to make the plane of polarization parallel to the plane of incidence (p-spectrum) or perpendicular to it (s-spectrum).

The Blodgett method[18] was used for preparing spectroscopic samples of monolayers. A monolayer was spread on twice-distilled water or a 10^{-3} mol/dm^3 phosphate buffer (pH=7.8—8.0) at 20±1 °C by dropping a fresh solution in hexane (5—10 mg/10 cm^3). A clean quartz slide held vertically was moved slowly into the water until the lower half of it sank below the air-water interface. At this time the monolayer was not transferred because the slide was hydrophilic. Then surface pressure was applied to the monolayer by using oleic acid (30 mN/m) or a mixture of ethyl myristate and liquid paraffin (6.3- or 16.3-mN/m)[19] as the piston oil, and the slide was raised slowly from the water. One monolayer was thereby transferred on each side of the lower half of the slide. The absorption spectra were recorded on the high-sensitivity spectrophotometer described above as soon as the slide became dry. All the operations handling monolayers were performed under dim red lights to avoid photochemical decomposition.

The quartz slide was cleaned by immersing it in a hot chromic acid mixture for about one hour. The slide was then washed with a great quantity of city water and immersed in a NaOH solution (pH=*ca.* 12) for about one hour. It was then taken out and washed first with much city water and then with distilled water. Finally, it was rinsed sufficiently with twice-distilled water and dried in an electric dryer. Its cleanliness was checked by light scattering in the dark.

Results and Discussion

In the spectrophotometer with the single-beam and sample in-sample out technique, a transparent plate, half of which is covered with a monolayer, is oscillated at a constant frequency so that the sample area (covered with the monolayer) and the reference area (not covered with it) pass the light beam alternately. The transmitted and modulated light is directed into a photomultiplier. The a.c. signal from it is amplified by a lock-in amplifier, and the absorbance of the monolayer is recorded. Therefore, the measured absorption includes the apparent absorption due to the difference in reflectivity between the monolayer and the plate when their reflectivities do not coincide. The difference between the two reflectivities can be expected to become larger at shorter wavelengths in the UV region because the dispersions of their refractive indices become larger there. Because of the high sensitivity of the apparatus, a very small difference in the reflectivities and even an inhomogeneousness in the quartz slide which can not be detected by usual optical techniques may produce detectable apparent absorptions.

The apparent absorption of a phytol monolayer was subtracted from the apparent absorptions of the monolayers of vitamin K_1, α-TQ, and vitamin E, which have a phytol chain or a phytol-like chain, and the apparent absorption of a β-cholestanol monolayer was subtracted from the apparent absorptions of the monolayers of vitamin D_2 and ergosterol, which have skeletons similar to it, as a correction to cancel out the apparent absorption due to the differences in reflectivity between the monolayers and the quartz slide and to the inhomogeneousness in the slide. Most peculiarities observed in the apparent absorptions of monolayers were eliminated by this correction. For instance, the difference between the apparent p- and s-spectra in the order of the 4×10^{-4} OD/layer, which almost all the monolayers showed in the region of wavelengths longer than 400 nm, were eliminated by this correction. The negative absorption in the order of the 1×10^{-3} OD/layer, which the spectra of the α-TQ and ergosterol monolayers showed in the wavelength region of 220—240 nm, also became positive in ergosterol after this

correction. However, the α-TQ monolayer still showed a small negative absorption at wavelengths shorter than 235 nm (Fig. 2) even after this correction. This seems to be due to the smaller refractive index of the α-TQ monolayer than that of the phytol monolayer in this wavelength region because the long chain of α-TQ does not have the double bond which phytol has. The error due to the difference in the refractive index, which is attributed to the difference in the structure of the long-chain moiety or the skeleton from phytol or β-cholestanol, may become significant in the wavelength region shorter than 250 nm, but its effect does not seem serious in the longer-wavelength region, where the absorption peaks of the chromophores exist.

The polarized absorption spectra at normal and 45° incidences were measured in order to investigate the anisotropy of the monolayers. In the case of the normal incidence, the spectra of monolayers were examined with the plane of polarization set at the angles 0°, ±45°, and 90° against the direction of the withdrawal of the slide from the monolayer on the air-water interface. All the monolayers examined showed no significant difference in the polarized spectra at normal incidence, indicating that no anisotropy in the layer plane existed. In the case of the 45° incidence, however, remarkable differences between the p- and s-spectra were observed, indicating that the molecules in all the monolayers were oriented uniaxially. The apparent dichroic ratio, $R_{app}=A_s/A_p$, was obtained from A_s and A_p, the absorbances of the s- and p-spectra, which were corrected for the apparent absorption as has been described above. We calculated the true dichroic ratio corrected for the interference effect as follows.

The refractive indices of the long-chain moieties of the monolayers, which are almost identical with those of phytol or β-cholestanol, can be assumed to be equal to that of quartz at wavelengths longer than 250 nm, because the apparent absorptions of the phytol and β-cholestanol monolayers due to the differences in their reflectivities from that of the quartz slide were below 4×10^{-4} OD/layer and about one order smaller than the absorption of the chromophores, which amounted to $(1.5—5.0)\times10^{-3}$ OD/layer. Therefore, we can use the equations of correction for the interference at the substrate-air interface proposed by Kuhn *et al.*[11] In the case of a monolayer with a thickness much smaller than the wavelength of the measuring light, the true absorbances are given by:

$$\bar{A}_s = \frac{A_s}{1+r_s} \tag{1}$$

$$\bar{A}_p = \frac{A_p}{1+r_p}, \tag{2}$$

where r_s and r_p are the reflection coefficients for the s- and p-polarized lights respectively at a 45° incidence. We will assume hereafter that the refractive indices of the monolayers are isotropic and coincide with that of quartz. According to Fresnel's equations, r_s and r_p are given by:

$$r_s = \frac{n\cdot\cos\beta-\cos\alpha}{n\cdot\cos\beta+\cos\alpha} \tag{3}$$

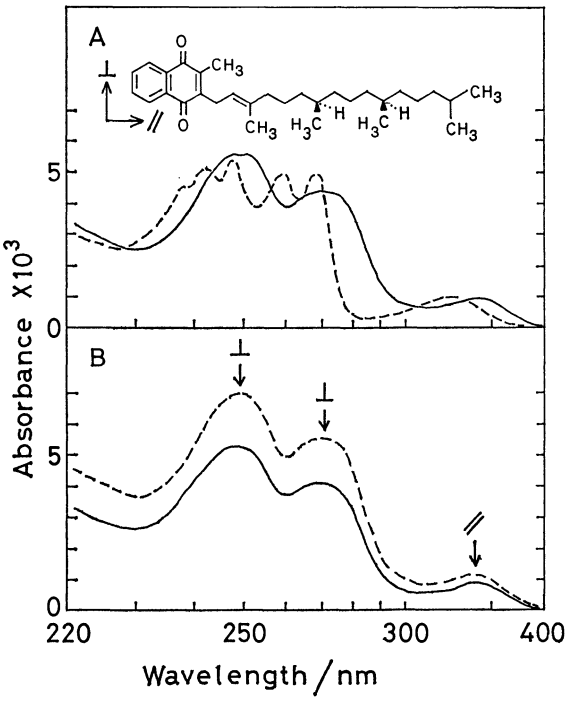

Fig. 1. Absorption spectra of vitamin K_1 monolayer spread on 10^{-3} mol/dm³ phosphate buffer pH 7.8—8.0 and transferred to quartz slide under the surface pressure of 6.3 mN/m.
(A) ——: Absorption of the monolayer at normal incidence (n-spectrum), ----: absorption of the hexane solution in an arbitrarily chosen scale. (B) Polarized spectra of the monolayer at 45° incidence. ——: The plane of polarization is parallel to the plane of incidence (p-spectrum), ----: the plane of polarization is perpendicular to it (s-spectrum). The symbols ⊥ and // indicate the directions of the transition moments.

$$r_p = \frac{n\cdot\cos\alpha-\cos\beta}{n\cdot\cos\alpha+\cos\beta}, \tag{4}$$

where n is the refractive index of quartz; $\alpha(=45°)$, the angle of incidence, and β, the angle of refraction. The refractive index of air is assumed to be unity. Finally, the true dichroic ratio is obtained by:

$$R = \frac{\bar{A}_s}{\bar{A}_p} = \frac{R_{app}(1+r_p)}{1+r_s}. \tag{5}$$

The values of n at the absorption peaks of the monolayers are obtained from the data of Jerrard and Turpin[20] and Malitson[21] for the dispersion of the refractive index of quartz. For instance, n is 1.507 at 250 nm and 1.478 at 340 nm.

We show in Figs. 1 to 5 the observed absorption spectra of the monolayers which are corrected for the apparent absorption. We summarize in Table 1 the positions of the absorption peaks in the hexane solution and in the monolayers and the shifts of the peaks between monolayer and solution.

The spectra of vitamin K_1 and α-TQ monolayers were red-shifted compared with those of their solutions, and the vibronic structures seen in solution disappeared (Figs. 1 and 2). The spectra of the vitamin E mono-

TABLE 1. SPECTRAL DATA AND ORIENTATION ANGLES OF THE MONOLAYERS

Compound	λ_{max}/nm		Shift	R_{app}[a]	R[a]	γ	θ
	Solution	Monolayer	cm^{-1}				
Vitamin K_1	239, 242, 248	250	820	1.34±0.02	1.12±0.02	0—38°	64—90°
	260, 269	270	840	1.35±0.02	1.13±0.02		
	326	340	1260	1.35±0.03	1.13±0.02		
α-TQ	250, 260, 268	270	840	1.39±0.04	1.16±0.03	0—34°	67—90°
Vitamin E	291, 298	292	—	1.42±0.01	1.19±0.01	0—30°	69—90°
Ergosterol	262	262	—	0.33±0.02	0.28±0.02	21.7±0.7°	0°
	271	270	—	0.35±0.02	0.30±0.02	22.5±0.8°	
	282	282	—	0.42±0.02	0.35±0.02	25.1±0.6°	
	294	294	—	0.46±0.04	0.39±0.03	26.6±1.1°	
Vitamin D_2	265	267	280	1.28±0.02	1.07±0.01	—	56°

a) The average of the results for two samples prepared independently.

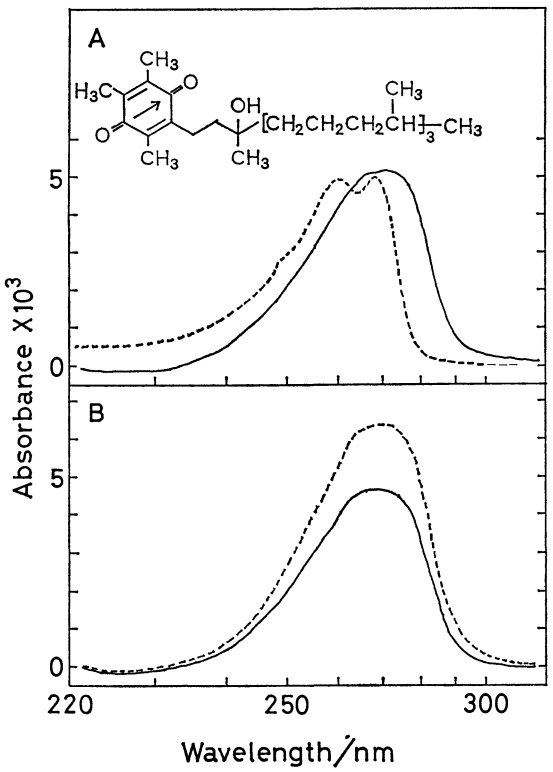

Fig. 2. Absorption spectra of α-tocopherylquinone monolayer spread on 10^{-3} mol/dm³ phosphate buffer pH 7.8—8.0 and transferred to quartz slide under the surface pressure of 16.3 mN/m. The arrow indicates the direction of the transition moment.
(A) ——: The n-spectrum of the monolayer, ----: the spectrum in hexane solution in an arbitrarily chosen scale. (B) Polarized spectra of the monolayer at 45° incidence. ——: The p-spectrum, ----: the s-spectrum.

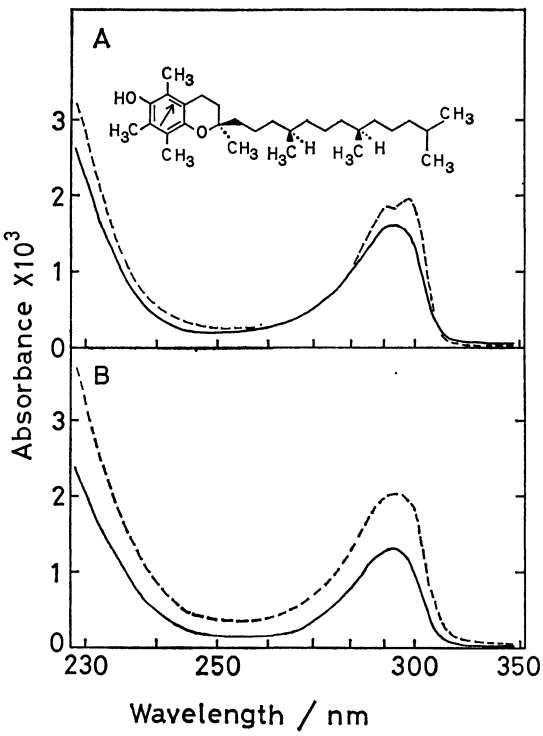

Fig. 3. Absorption spectra of vitamin E monolayer spread on 10^{-3} mol/dm³ phosphate buffer pH 7.8—8.0 and transferred to quartz slide under the surface pressure of 16.3 mN/m. The arrow indicates the direction of the transition moment.
(A) ——: The n-spectrum of the monolayer, ----: the spectrum in hexane solution in an arbitrarily chosen scale. (B) Polarized spectra of the monolayer at 45° incidence. ——: The p-spectrum, ----: the s-spectrum.

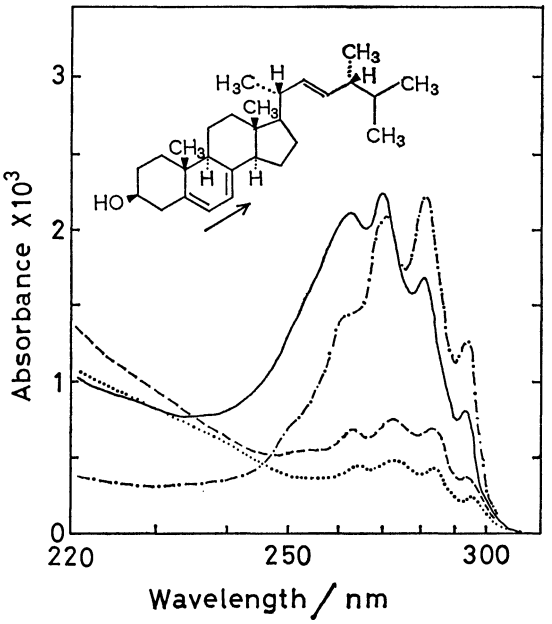

Fig. 4. Absorption spectra of ergosterol monolayer spread on twice distilled water and transferred to quartz slide under the surface pressure of 30 mN/m. ·····: Absorption at normal incidence (n-spectrum), ——: polarized p-spectrum at 45° incidence, ----: polarized s-spectrum at 45° incidence, —·—: the spectrum in hexane solution in an arbitrarily chosen scale. The arrow indicates the direction of the transition moment.

layers (Fig. 3) showed little shift, but the vibronic structure disappeared. The spectra of the ergosterol monolayers (Fig. 4) also showed little shift, but the relative intensities of the vibronic peaks changed greatly compared with those in solution. The spectra of the vitamin D_2 monolayers were slightly red-shifted (Fig. 5).

Concerning the polarized spectra at a 45° incidence, the strengths of the s-spectra were larger than those of the p-spectra in the vitamin K_1, α-TQ, vitamin E, and vitamin D_2 monolayers. On the other hand, the strength of the p-spectrum is about three times as large as that of the s-spectrum in the ergosterol monolayers. The strength of the non-polarized spectrum at a normal incidence (n-spectrum) is smaller than that of the s-spectrum. This indicates that the transition moment of ergosterol tilts only a little against the normal of the layer plane.

The apparent dichroic ratios, R_{app}'s, and the true ones, R's, at the absorption peaks of the monolayers are listed in Table 1. The listed values are the averages of the results for two samples prepared independently.

We calculated the orientation angles of the molecules by assuming a model (Fig. 6A) the same as that of Akutsu *et al.*,[22] because the transition moments in the monolayers were found to be oriented uniaxially. In Fig. 6A, the x-y plane is the layer plane and the y-z plane is the plane of light incidence. Now we assume that the molecules are rigid and have principal axes fixed to them (the 2nd rotation axes). As to the orientation of the whole molecule, it is assumed

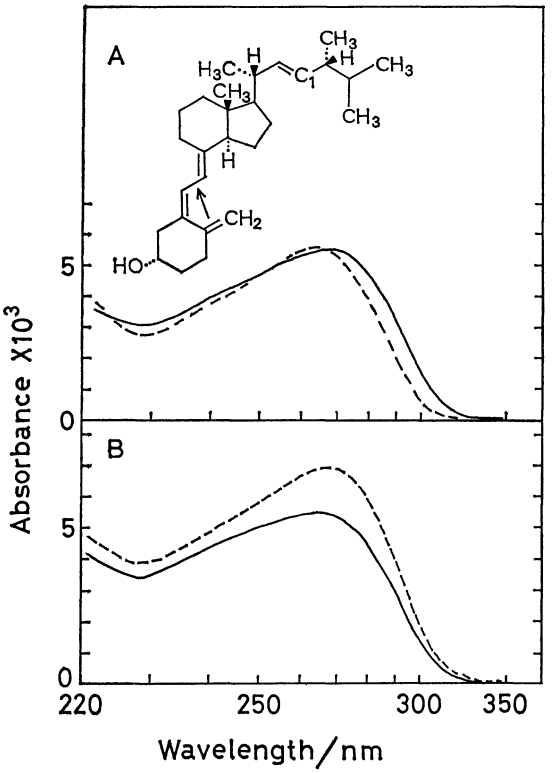

Fig. 5. Absorption spectra of vitamin D_2 monolayer spread on twice distilled water and transferred to quartz slide under the surface pressure of 30 mN/m. (A) ——: The n-spectrum of the monolayer, ----: the spectrum in hexane solution in an arbitrarily chosen scale. (B) Polarized spectra at 45° incidence. ——: The p-spectrum, ----: the s-spectrum. The arrow indicates the direction of the transition moment.

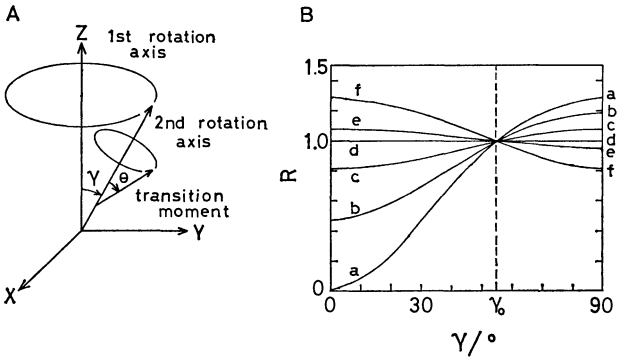

Fig. 6. (A) The model of uniaxial orientation of transition moments in a monolayer. The x-y plane is the monolayer plane and the y-z plane is the plane of light incidence. (B) The true dichroic ratio R as functions of the orientation angle γ at different θ's, where n is 1.50 and α is 45°.
Curve a: $\theta=0°$, b: 30°, c: 45°, d: $\arcsin\sqrt{2/3}(=54.7°)$, e: 60°, f: 90°. The angle γ_0 is $\arcsin\sqrt{2/3}$.

that the 2nd rotation axis tilts against the normal of the layer plane (the 1st rotation axis) by a fixed angle, γ, and is distributed uniformly around it. The transition moment in the chromophore is assumed to tilt against the 2nd rotation axis by a fixed angle,

θ, and to be distributed uniformly around it. Then the dichroic ratio is given by:

$$R=\frac{B}{(1-3\sin^2\beta)B+4\sin^2\beta}, \quad (6)$$

where:

$$B = 2\sin^2\theta + 2\sin^2\gamma - 3\sin^2\theta\sin^2\gamma. \quad (7)$$

We show in Fig. 6B how the dichroic ratio, R, depends on γ at different θ's when α is 45° and n is 1.50. As can be seen in Fig. 6B, the relation between R and γ is sensitively dependent on θ. We may note that there is a special value of θ, 54.7°, independently of n, where R equals unity independently of γ. Therefore, if θ is near 54.7°, it is impossible to make a reliable determination of γ from the observation of R. When θ has a definite value not close to 54.7°, we can determine γ from the observed value of R. However, if there is any uncertainty in the value of θ, a unique determination of γ is not possible and we can determine it only in a certain range. There is an ambiguity in the definition of the θ angle in vitamin K_1, α-TQ, and vitamin E because their chromophores may make an internal rotation against the long chain moiety and θ may depend on the conformation of the molecules. On the other hand, in ergosterol and vitamin D_2, the chromophores are fixed to rigid molecular skeletons, and so we can determine θ by quantum mechanical calculations for the directions of the transition moments.

The directions of the transition moments in the chromophore of vitamin K_1 were assumed to be parallel to the O–O direction for the bands at 250- and 270-nm and to be perpendicular to it for the band at 340 nm, as is shown in Fig. 1, according to Kuboyama's calculation of 1,4-naphthoquinone by the simple MO method.[23] The dichroic ratios obtained by us were nearly equal for these two groups of transition (Table 1), where the directions of the transition moments are perpendicular to each other. The γ angle must have the same value for all the transitions. Therefore, the θ's for these transition moments must be nearly equal in order for their R's to be nearly equal. This shows that the 2nd rotation axis must lie on the plane which is perpendicular to the naphthoquinone plane and which bisects the orthogonal angle formed with the two groups of the transition moments. Then, the θ angle may have a value within the range from 45° to 90°. The δ angle between the 2nd rotation axis and the naphthoquinone plane is then given by:

$$\cos\delta = \sqrt{2}\cdot\cos\theta. \quad (8)$$

By curves a and a' in Fig. 7 we show the relations between the θ and γ angles which give the observed values of 1.12 and 1.13 of the R's for the transitions at 250- and 270-nm respectively. Because of the slight difference in n for these transitions, the two curves are not identical, but the difference between them is small. The curve corresponding to the transition at 340 nm is almost identical with the a' curve, and so it is not shown in Fig. 7. The dependence of δ on θ is also shown in Fig. 7. We can see in Fig. 7 that the θ and γ angles consistent with the observed value of R range from 64° to 90° and from 0° to 38° respectively. The tilt angle of the naphthoquinone plane

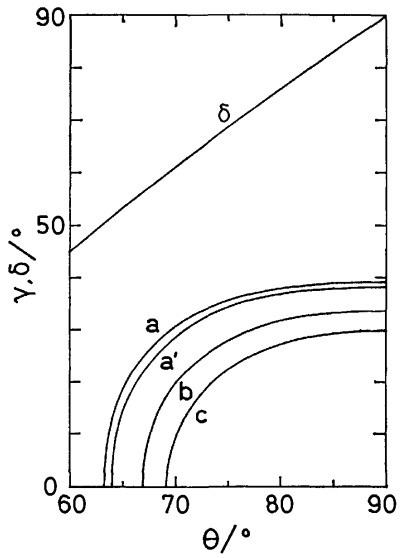

Fig. 7. The trajectories of the angles γ and θ to give the observed values of the dichroic ratio R.
Curve a: R=1.12 and n=1.507 for the 250 nm band of vitamin K_1, a': R=1.13 and n=1.498 for the 270 nm band of vitamin K_1, b: R=1.16 and n=1.498 for the 270 nm band of α-TQ, c: R=1.19 and n=1.491 for the 292 nm band of vitamin E. The θ dependence of the tilt angle δ of naphthoquinone plane against the 2nd rotation axis in vitamin K_1 monolayer is also shown in the upper side.

against the normal of the layer plane (the 1st rotation axis) is distributed in the range from $\delta-\gamma$ to $\delta+\gamma$. If γ has a value not near 0°, then the tilt angle of the naphthoquinone moiety is distributed over a wide range, for instance, from 32° to 92° for γ=30° and from 52° to 128° for γ=38°. As a result, the hydrophilic naphthoquinone moieties in a vitamin K_1 monolayer have to make contacts with the water surface with contact angles distributed over a wide range. Considering the structure of naphthoquinone, it seems to be unnatural that naphthoquinone moieties can make contacts with the water surface with widely distributed contact angles without any meaningful effect on the interaction energy of the monolayer with water. Therefore, it seems likely that γ has a value near the lower boundary, 0°, of its admissible range. When γ is near 0°, θ and δ nearly equal 64° and 51° respectively, and the naphthoquinone plane contacts with the water surface at an almost constant angle of about 51°. As can be seen from Fig. 7, θ is limited in a narrow range from 64° to 71°, even if γ varies from 0° to 30°. Hence, it seems reasonable to guess that γ is smaller than 30° and that θ is close to 64°.

The spectral shifts in vitamin K_1 monolayers can be explained qualitatively by the molecular exciton theory by assuming $\gamma\approx0°$. McRae and Kasha[24] showed that a linear-stacked array of chromophores has a spectrum with a blue shift compared with its monomer spectrum when $\eta<\arcsin\sqrt{1/3}=35.3°$ (η is the complementary angle between the transition moment and the direction of the linear arrangement) and one with a red shift when $\eta>\arcsin\sqrt{1/3}$. The red shift in the spectrum of the vitamin K_1 monolayers can be

explained by this theory, because the η angle is near 64° if the naphthoquinone moieties make stacked linear arrays with their orientation angle, γ, near 0°. Thus, the naphthoquinone moieties in a vitamin K_1 monolayer appear to be stacked at least in a short range.

In α-TQ, the direction of the transition moment was assumed to be parallel to the O–O direction, as is shown in Fig. 2, according to Kuboyama's calculation of benzoquinone.[23] The θ and γ values, which give the observed R value of 1.16, are in the following two ranges: $\theta=0$—34° and $\gamma=67$—90°, and $\theta=67$—90° and $\gamma=0$—34°. Because of the symmetry of Eq. 6 for θ and γ, there are always two sets of solutions in which θ and γ are exchanged when only an R for a transition is available for the determination of γ. Since the 2nd rotation axis should agree roughly with the axis of the long-chain moiety, the former set of solutions is inadequate because it implies that the long chains of some molecules are almost parallel to the water surface. Therefore, we adopt the latter set. The shape of the admissible θ-γ curve for this case is shown by Curve b in Fig. 7. The orientation angle of the plane of the hydrophilic group of α-TQ can not be determined because at least two observable transitions with different directions of the transition moments are necessary for its determination. However, if γ is not near 0°, then the O–O direction of the α-TQ chromophore should make contact angles with the water surface over a wide range from $\theta-\gamma$ to $\theta+\gamma$, for instance, from 56° to 124° for $\gamma=34°$. This also seems to be unnatural, and so we may guess that the value of γ is perhaps on the side near 0° in its admissible range. The red shift in the spectrum of the α-TQ monolayers can be explained in the same manner as in vitamin K_1 if γ is near 0° and if the chromophores of α-TQ are stacked at least in a short range. The η angle then becomes about 67°, which yields a red shift in the spectrum.

The direction of the transition moment in the chromophore of vitamin E was assumed to be perpendicular to the O–OH direction for the band at 292 nm, as is shown in Fig. 3, according to Nishimoto and Fujishiro's calculation of hydroquinone by the ASMO method.[25] The θ and γ angles which give the observed R value of 1.19 are in the following two ranges: $\theta=0$—30° and $\gamma=69$—90°, and $\theta=69$—90° and $\gamma=0$—30°. The former set seems to be inadequate for the same reason as in the case of α-TQ. Similarly, we may guess that γ has a value near 0° in its admissible range, shown by Curve c in Fig. 7. The spectrum of the vitamin E monolayers showed little shift in contrast with those of vitamin K_1 and α-TQ. The spectrum must show a red shift if γ is near 0° and if the chromophores are stacked in a short range, for η becomes about 69° when $\gamma\approx0°$. This suggests that the chromophores in a monolayer of vitamin E are not stacked even in a short range.

In ergosterol, the chromophore for the band from 262 nm to 294 nm is an *s-cis*-butadiene structure. The direction of its transition moment, calculated by the HMO method, roughly agrees with the direction of the molecular axis, as is shown in Fig. 4. We assume for this molecule that $\theta=0°$. From the observed values of R for the vibronic peaks at 262-, 270-, 282-, and 294-nm (Table 1), their γ's are determined to be 22°, 23°, 25°, and 27° respectively. The obtained values of γ agree nicely within an error of 5°. These values are also in good agreement with the tilt angle, 25°, suggested by Langmuir *et al.*[26] from a comparison of the thickness of the built-up film of ergosterol with the X-ray data of its crystal. This provides evidence in support of our method for the determination of the orientation angles. In ergosterol with $\theta=0°$, the η angle is equal to γ. The fact that the spectrum of the ergosterol monolayers showed little shift may be explained by the closeness of the orientation angle, $\gamma\approx24°$, to the critical angle, $\eta=35.3°$, where the molecular exciton theory predicts no-shift. The observed change in the relative absorption intensities at the three vibronic peaks suggests that the coupling between electrons and nuclear vibrations in the excited state suffers a change upon the formation of a monolayer.

The chromophore of vitamin D_2 for the band at 267 nm has a hexatriene structure. We calculated the direction of the transition moment by the HMO method. The chromophore moiety was regarded as plane, and the angles between the adjacent carbon atoms were assumed to be 120°. The result is shown by the arrow in Fig. 5. If the straight line joining the oxygen atom with the carbon atom, C_1, in Fig. 5 is regarded as the 2nd rotation axis, θ is about 56°. This θ value is very close to the angle, 54.7°, at which R equals unity independently of γ, and it is difficult to determine γ from R unless R is measured with a very high accuracy. If we put $\theta=56°$, we can not find the γ angle, which gives the observed value, 1.07 of R. This seems to be due to the insufficient accuracy of the measurement of R. Therefore, we can not get any information about the orientation of the vitamin D_2 molecule from the dichroic ratio. Vitamin D_2 in a monolayer, however, might have an orientation angle, γ, roughly as large as that of ergosterol, because its monolayer area is only slightly larger than that of ergosterol, according to the data of Langmuir *et al.*[26]

We summarize in Table 1 the orientation angles, γ and θ, or their admissible ranges, as determined from the dichroic ratio. The orientation angle, γ, of the principal axis of the ergosterol molecule was determined precisely as 24° (the average of the four values) within an error of 5°. This value is in good agreement with the value, 25°, suggested by Langmuir *et al.* For vitamin K_1, α-TQ, and vitamin E, only the admissible ranges for the orientation angles, γ and θ, were determined. The determined ranges for γ are similar for these three molecules. This suggests that they have a similar arrangement of the molecular axis in their monolayers, perhaps because of the similarity of their molecular structures. However, the shifts in their monolayer spectra suggest that the chromophores of vitamin K_1 and α-TQ are stacked at least in a short range, while those of vitamin E are not even in a short range. In vitamin D_2, no con-

clusion about the orientation of the molecules in its monolayer could be obtained because the value of θ is close to the angle, 54.7°, where the dichroic ratio, R, is independent of γ.

We would like to thank Professor Hans Kuhn for kindly sending us information about the electric circuit of the high-sensitivity spectrophotometer made in his laboratory.

References

1) S. Hotchandani, R. M. Leblanc, and F. Boucher, *Vision Res.* **15**, 605 (1975).
2) G. L. Gaines, Jr., *J. Colloid Interface Sci.*, **28**, 334 (1968).
3) G. L. Gaines, Jr., A. G. Tweet, and W. D. Bellamy, *J. Chem. Phys.*, **42**, 2193 (1965).
4) S. M. B. Costa, J. R. Froines, J. M. Harris, R. M. Leblanc, B. H. Orger, and G. Porter, *Proc. R. Soc. London, Ser. A*, **326**, 563 (1972).
5) N. K. Adam, F. A. Askew, and J. F. Danielli, *Biochem. J.*, **29**, 1786 (1935).
6) O. Rosenheim and N. K. Adam, *Proc. R. Soc. London, Ser. B*, **105**, 422 (1930).
7) G. Weitzel, A.-M. Fretzdorff, and S. Heller, *Hoppe-Seyler's Z. Physiol. Chem.*, **303**, 14 (1956).
8) E. E. Jacobs, A. S. Holt, and E. Rabinowitch, *J. Chem. Phys.*, **22**, 142 (1954).
9) H. J. Trurnit and G. Colmano, *Biochem. Biophys. Acta*, **31**, 434 (1959).
10) A. G. Tweet, *Rev. Sci. Instrum.*, **34**, 1412 (1963).
11) H. Kuhn, D. Möbius, and H. Bücher, "Physical Methods of Chemistry," ed by A. Weissberger and B. W. Rossiter, Wiley-Interscience, New York (1972), Vol. I, Pt.III B, Chap.VII.
12) O. Isler, *Angew. Chem.*, **71**, 7 (1959).
13) R. Hirschmann, R. Miller, and N. L. Wendler, *J. Am. Chem. Soc.*, **76**, 4592 (1954).
14) "Biochemistry of Quinones," ed by R. A. Morton, Academic Press, London and New York (1965), p.39.
15) J. F. Pennock, G. Neiss, and H. R. Mahler, *Biochem. J.*, **85**, 530 (1962).
16) "The Merck Index," 9th ed, ed by M. Windholz, Merck & Co., U. S. A. (1976), Monogragh Number 9678.
17) T. R. Hogness, A. E. Sidwell, Jr., and F. P. Zcheile, Jr., *J. Biol. Chem.*, **120**, 239 (1937).
18) K. B. Blodgett, *J. Am. Chem. Soc.*, **56**, 495 (1934); **57**, 1007 (1935).
19) A. Norris and J. W. J. Taylor, *J. Chem. Soc.*, **1938**, 1719.
20) H. G. Jerrard and J. Turpin, *J. Opt. Soc. Am.*, **55**, 453 (1965).
21) I. H. Malitson, *J. Opt. Soc. Am.*, **55**, 1205 (1965).
22) H. Akutsu, Y. Kyogoku, H. Nakahara, and K. Fukuda, *Chem. Phys. Lipids*, **15**, 222 (1975).
23) A. Kuboyama, *Bull. Chem. Soc. Jpn.*, **31**, 752 (1958).
24) E. G. McRae and M. Kasha, "Physical Process in Radiation Biology," ed by L. Augenstein, Academic Press Inc., New York and London (1964), pp. 23—42.
25) K. Nishimoto and R. Fujishiro, *Bull. Chem. Soc. Jpn.*, **35**, 905 (1962).
26) I. Langmuir, V. J. Schaefer, and H. Sobotka, *J. Am. Chem. Soc.*, **59**, 1751 (1937).

 © 1980 The Chemical Society of Japan Bull. Chem. Soc. Jpn., 53, 1825—1831 (1980)

Raman Study of Aqueous Solutions of Tetraalkylammonium and Bis(tetraalkylammonio) Electrolytes

Hiroyasu NOMURA,* Yoshiaki TSUKAMOTO, Ronald Ernest VERRALL,† and Yutaka MIYAHARA

Department of Chemical Engineering, Faculty of Engineering, Nagoya University, Chikusa-ku, Nagoya 464

† *Department of Chemistry and Chemical Engineering, University of Saskatchewan, Saskatoon, Saskatchewan, S7N, OWO, Canada*

(Received October 11, 1979)

The Raman and infrared spectra of 1,4-bis(triethylammonio)butane dibromide (J4), 1,10-bis(triethylammonio)decane dibromide (J10), and tetraethylammonium bromide (TEABr) were measured in the solid and dissolved states. The Raman spectra of these salts in the solid and solution states were roughly similar to those of normal paraffins having the same number of skeletal atoms, but some minor differences were found. It was confirmed that molecular conformations of these ions in the solid and solution states are somewhat similar and take the all-trans form, but in main chain of J4 and J10, the gauche form is also observed. In addition, the effects of hydrophobic interaction of these salts in aqueous solution are discussed by comparison of the Raman spectra of OH stretching vibration region of water.

A number of nonspectroscopic studies of aqueous solutions of bolaform type electrolytes[1-4] have been reported with the object of investigating their effect on water structure and the ability of the bolaform cation to act as a model for cation-cation pairing in R_4NX systems. Unlike thermodynamic properties, spectroscopic investigations of aqueous solutions of these salts can provide additional information on the conformation of the hydrocarbon chains of these cations in solution.

In a previous paper,[5] it was confirmed by means of Raman spectroscopy that the molecular structure of the tetraalkylammonium ion in aqueous solution is an extended one, *i.e.*, the $-CH_2-$ groups assume an all-trans conformation, much the same as the lower members of the normal paraffin series of molecules.

In this study the Raman and infrared spectra of several bis(tetraalkylammonio) electrolytes and tetraethylammonium bromide were measured in the solid and dissolved states. In this paper emphasis is placed on obtaining information about molecular conformations of the hydrocarbon chains in aqueous solutions from a comparison of the analysis of the Raman spectra in both the solid and solution states. In addition, the effects of hydrophobic interaction of these salts in aqueous solution are discussed by comparison of the Raman spectra of the OH stretching vibration region of water with that for the pure solvent.

Experimental

Materials. Tetraethylammonium bromide, hereafter abbreviated as TEABr was of extra-pure reagent grade supplied by Nakarai Chemical Co., Ltd. The Bis(tetraalkylammonio)salts, 1,4-bis(triethylammonio)butane dibromide and 1,10-bis(triethylammonio)decane dibromide, abbreviated J4 and J10, respectively, were prepared and purified as described elsewhere.[4] Water used was deionized by ion-exchange-regin and distilled by means of usual laboratory techniques.

Apparatus. The apparatus used for Raman spectroscopy measurements consisted of an argon ion laser source manufactured by Coherent Radiation Co., Ltd. and the scattered light was analyzed with a JRS-Ul Laser Raman spectrometer from Japan Electron Optics Laboratory Co., Ltd. An A-2 IR spectrometer manufactured by Japan Spectroscopic Co., Ltd. was used to obtaine IR spectra.

Procedures. Solutions used for Raman measurements were prepared so as to contain 2 M** of bromide ion and $^+NEt_4$ unit, ($^+NEt_3-(CH_2)_2$ for the case of the bolaform cation). All measurements were carried out at room temperature.

The experiments were done using 90° scattering. The horizontal ($I_\parallel$) and vertical ($I_\perp$) components of the scattered light were measured with a polaroid analyzer.

The Raman spectra of water in the OH stretching region were obtained in aqueous solutions of TEABr, J4, and J10. The intensities were corrected for photomultiplier sensitivity. In the case of J10 it was impossible to correct the spectra owing to the existence of luminescence and consequently this salt was excluded from the analysis of salt effect on the OH vibrational spectra. The observed spectra were divided into their isotropic (I_{isot}) and anisotropic (I_{anis}) components.

$$I_{isot} = I_\parallel - 4/3\, I_\perp$$

$$I_{anis} = 4/3\, I_\perp$$

In the case of the infrared measurements, the solid sample was mixed with Nujol and measured at room temperature.

Results and Band Assignments

The Raman and infrared bands observed in the solid state and aqueous solutions are summarized in Table 1. The vibrational assignment of these bands was carried out on the basis of previous assignments made for normal paraffins,[6-9] and tetramethylammonium halides,[10-12] in the solid state.

At low frequencies (below 300 cm^{-1}), lattice modes, which are not observed in aqueous solutions, are found in the solid state for all compounds investigated. Commonly, the $C-N^+$ symmetric and asymmetric stretching bands are observed at about 700 cm^{-1} and 800 cm^{-1}, respectively. These bands are assigned on the basis of the following criteria: (1) The $C-N^+$ symmetric and asymmetric bands must be observed below 752 cm^{-1} and 955 cm^{-1}, respectively, since the corresponding bands for $(CH_3)_4N^+$ are centered at 752 cm^{-1} and 955 cm^{-1}, respectively and, for all compounds investigated in this work the mass of the substitutional groups on the N atom is heavier than that of $(CH_3)_4N^+$.

** 1M=1 mol dm^{-1}.

TABLE 1. OBSERVED RAMAN AND IR FREQUENCIES (cm^{-1}) OF Et_4NBr, $Et_3N(CH_2)_4NEt_3Br_2$, $Et_3N(CH_2)_{10}NEt_3Br_2$

Et_4NBr				$Et_3N(CH_2)_4NEt_3Br_2$				$Et_3N(CH_2)_{10}NEt_3Br_2$				
Solid		Solution		Solid		Solution		Solid		Solution		
IR	Raman	Raman	ρ	IR	Raman	Raman	ρ	IR	Raman	Raman	ρ	Assignments
					60 vw							
	66 m											
					72 m							
									81 w			Lattice
									88 w			
					105 m							
	112 w											
									122 vw			LA(J10)
	128 m											
					138 m							
					201 m	195 w	0.23					LA(J4)
		200 w	0.75									
	217 w								216 w	200 vw		CH_2–CH_3 torsion
										222 vw		
					265 vw				271 w			
		312 vw								300 vw	0.3	
	372 m	360 vw	0.75		369 m	360 w	0.7		360 w	361 vw	0.7	
		391 m	0.11			395 m	0.14		396 w	391 m	0.11	N–C–C bend
418 w	424 vs	418 vs	0.21		418 s	423 s	0.17		420 s	420 vs	0.18	LA(Et_4N^+)
		467 w	0.75		458 m	466 w	0.75		467 vw	456 vw	0.75	
515 vw						504 vw	0.75	488 vw	485 vw	494 vw	0.55	
		559 vw	0.54	560 vw	542 vw	552 w	0.36		532 w	552 w	0.15	
									572 w	572 w	0.29	
						582 vw	0.75					
	663 vs											
673 vw	683 vs	673 vs		700 vs	704 s	708 vs	0.01	700 w	702 s	702 vs	0.01	C–N sym. stretch
								742 m				$C–H_2$ rock-twist
				746 m								$C–H_2$ rock-twist
785 s				785 m	782 w			785 s	788 w			
		790 m	0.71			792 vw	0.75			800 w	0.65	$C–N^+$ asym. stretch
798 s	792 w			798 m	792 w			800 s	804 w			
				815 m	810 w	810 w	0.56	817 w	820 w			C–H rock-twist
	838 w											
								850 vw	851 w	847 vw	0.43	
						871 vw	0.75			874 vw	0.5	
895 m	900 w	900 w	0.75	893 vw	893 m			894 w	897 m	893 w	0.6	
						900 m	0.72					C–H rock
	913 s	905 m	0.75		899 m				909 w	908 vw	0.75	
948 w				942 m	948 m	951 m	0.72	938 w	942 w	938 w	0.63	
								954 m	954 m	954 w	0.67	
				968 w								C–C stretch
									983 w			C–C stretch

1006 s	1007 s	1005 m	0.75	1009 m	1007 s	1010 m	0.75	1003 s	1004 m	1006 w	0.74	$C-H_3$ rock
						1017 m	0.75	1017 m	1014 m	1011 m	0.74	
	1028 sh	1033 sh	0.75									C–C stretch
								1036 w	1033 w	1030 w		C–C stretch
				1040 vw	1040 w	1047 w	0.59					C–C stretch
1052 m				1054 w				1055 m				C–C stretch
1070 w	1073 s	1073 s	0.16	1075 w	1068 w	1077 m	0.23	1075 w	1088 w	1078 w	0.31	C–C stretch
	1107 sh			1105 w				1097 vw	1103 vw	1093 w	0.75	
				1115 vw		1116 m	0.08	1113 m	1116 m	1114 m	0.03	C–C stretch
	1120 s	1120 s	0.06		1120 s	1119 s	0.08	1128 vw	1129 m	1124 m	0.11	C–C stretch
	1157 vw	1154 vw	0.33	1158 m	1159 m	1155 vw	0.4	1142 vw	1153 vw	1154 vw		C–C stretch
1173 s								1163 s				
	1182 m	1177 w	0.75		1173 m	1172 m	0.75		1166 m	1165 w	0.75	$C-H_2$ twist-rock
1188 m		1187 vw	0.5	1193 w				1192 m		1187 vw	0.75	
									1234 w			
				1235 vw								
								1261 vw				
	1269 m			1267 w	1269 w			1277 w	1280 m			$C-H_2$ wag
									1295 m			
	1308 s	1304 m	0.75	1302 w	1292 s	1306 m	0.75		1303 m	1307 m	0.72	$C-H_2$ twist-rock
								1320 vw	1317 w			
					1323 w							
1334 m	1335 vw			1334 w	1338 w	1336 w	0.72	1336 vw				$C-H_2$ wag
		1355 vw	0.75		1353 w	1363 vw	0.64	1347 m		1355 vw	0.53	
1377 s	1379 vw	1379 vw	0.75	1376 s	1379 w			1378 m	1376 vw			$C-H_2$ sym. bend
								1386 m	1385 vw			
1398 m	1397 m	1393 m	0.5	1397 m	1398 m	1399 w	0.45	1400 s	1400 w	1394 w	0.38	$C-H_2$ wag
1407 m	1408 vw	1408 vw	0.75									
				1418 w					1417 w			
1442 s	1445 m	1449 m	0.75	1449 m	1443 m	1455 m	0.75	1443 s	1448 s	1448 m	0.72	$C-H_3$ asym. bend
1475 m	1472 s	1466 s	0.75	1467 s	1471 m	1471 s	0.75	1456 m	1456 s	1466 s	0.75	$C-H_3$ asym. bend
1495 s	1499 w	1494 w	0.63	1488 m	1492 w	1495 w	0.32	1496 s	1496 m	1488 m	0.67	$C-H_2$ bend
				2728 vw					2731 w			
	2744 w	2754 w			2747 w				2755 vw	2751 vw		
2760 w						2767 vw						combination
	2774 w	2774 w			2777 w	2788 vw				2778 vw		
									2792 vw			
2852 s	2852 w			2860 s				2860 s	2852 s	2861 m	0.06	$C-H_2$ sym. stretch
2900 w	2905 m	2900 m		2904 w	2887 m	2905 m			2892 s	2900 s	0.17	$C-H_3$ sym. stretch
2920 s	2928 w			2930 w	2925 m			2920 s	2918 w			$C-H_2$ asym. stretch
	2946 s	2951 s	0.03		2937 s	2960 s	0.06		2933 vs	2950 s	0.07	
2952 m	2970 s				2946 s							
									2963 w			
					2960 s	2972 s			2979 s			
2988 m	2997 s	2997 s	0.34		2986 s	3001 s	0.27	2980 s	2985 s	2994 s	0.32	$C-H_3$ asym. stretch
	3003 w				3005 m				2996 w			

ρ: Depolarization ratio

(2) The C–N$^+$ symmetric stretching mode gives rise to the strong, polarized, Raman bands usually observed. (3) The asymmetric stretching mode gives rise to the depolarized Raman line and strong infrared band commonly observed. Above 900 cm^{-1}, the Raman and infrared spectra of all compounds investigated are roughly similar to those of normal paraffins having the same number of skeletal atoms.

The band assignments were made from consideration of those criteria and are summarized in the last column of Table 1. A careful comparison of the Raman spectra of solid state and aqueous solution shows that some minor differences exist for the compounds investigated. Therefore it appears that the molecular conformations in the solid and solution states are somewhat similar.

Discussion

Low Frequency Regions (below 500 cm^{-1}). The Raman spectra for each compound in the frequency range below 500 cm^{-1} are shown in Fig. 1. In the solid state, several lattice modes are observed, but in aqueous solutions, these lattice modes disappear. Also, some longitudinal accoustic vibrational modes (LA mode) are observed in both the solid phase and aqueous solution, X-ray crystallographic studies have shown[13,14] that the chain conformation of $-CH_2-$ groups in normal paraffins and in tetraalkylammonium ions are in all-trans form. By analogy with these results, the chain conformations in the Bis(tetraalkylammonio) salts in the solid state can be considered to be in all-trans form.

The LA mode is regarded as a symmetric accordion-type longitudinal vibration of a string of beads with antinodes at the chain ends. Therefore, this band is ascribed to the molecules taking an all-trans form. In the previous paper,[5] studies were reported on the LA band of tetraalkylammonium ions. From the existence of the LA band, it was confirmed that the tetraalkylammonium ions in the solid and aqueous solution are in an extended form, such as the all-trans form of the $-CH_2-$ chain.

For TEA ion, the LA bands were observed at 424 cm^{-1} in the solid and 420 cm^{-1} in aqueous solution.[5] A strong peak is observed at about 420 cm^{-1} in the Raman spectra of J4 and J10 in both states. This band corresponds to the LA band of TEA ion and is ascribed to the LA band in the Et–N–Et structure of the bolaform ion. Therefore, the Et–N–Et structure is mostly in the all-trans form in both states.

In solid J4 and J10, the LA bands of the main chain were also observed, although they were weak. These were identified by the criterion that the frequency of the band decreases as the length of the carbon chain (involving nitrogen atom) increases. The relationship between the frequency of the LA band and the reciprocal carbon number shown in Fig. 2 along with the corresponding relationship for tetraalkylammonium ions.[5] The existence of this band indicates the molecules take an all-trans form in main chain in the solid state. This band is observed weakly in aqueous solution of J4, but not in aqueous solution of J10. Therefore, it appears that in aqueous solution the J4 ions assume an all-trans conformation to some extent but less in those of the J10 ion. This result may be rationalized on the basis that random conformation in the main chain increases as the distance between the two charged nitrogen atoms increases and hence the repulsive force decreases.

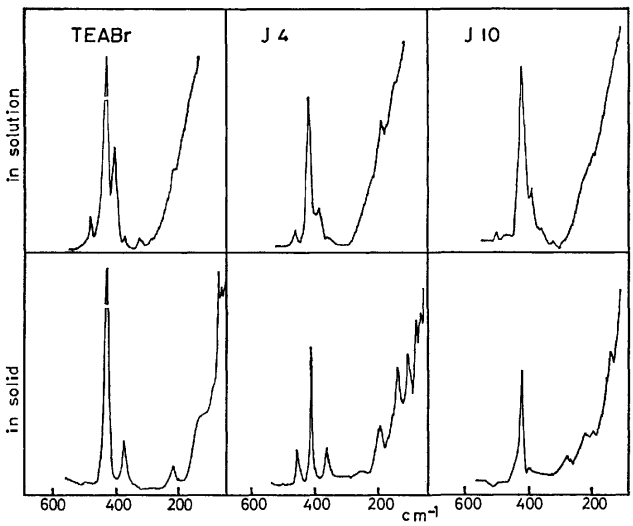

Fig. 1. Raman spectra for TEABr, J4, and J10 in the frequency range below 500 cm^{-1} in the solid and solution states.

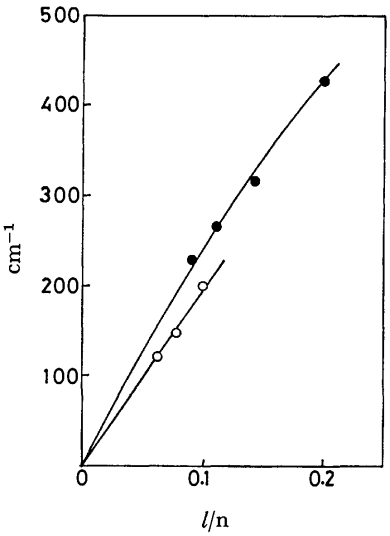

Fig. 2. Relationship between the frequencies of the LA mode and the reciprocal carbon number (involving nitrogen atom); (○) bolaform ions, (●) tetraalkylammonium ions.

Intermediate Frequency Regions (500 cm^{-1}—1400 cm^{-1}). The solution and solid state Raman spectra of TEABr, J4, and J10 are shown in Figs. 3, 4, and 5, respectively. Some minor differences are observed between the two phases. In the case of TEABr, Raman lines observed in aqueous solution at 467 cm^{-1} and 559 cm^{-1} are not seen in the solid state. These lines are ascribed to the rotational conformations around the $-CH_2-CH_2-$ bonds.

In the Raman spectra of J4, the two bands at 466

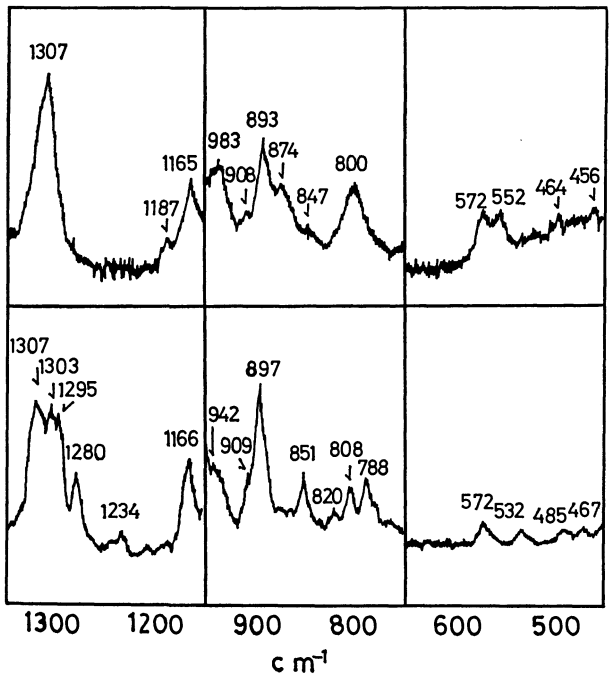

Fig. 3. Raman spectra of TEABr in the solid and solution states in the frequency range from 500 cm^{-1} to 1400 cm^{-1}.

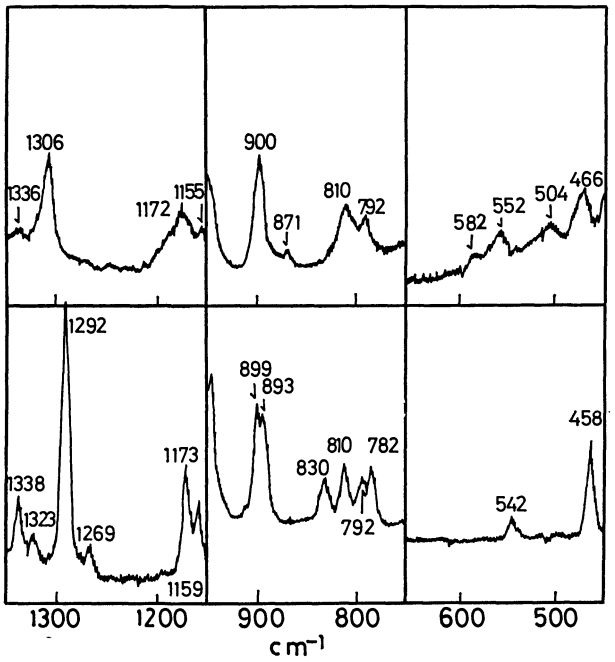

Fig. 4. Raman spectra of J4 in the solid and solution states in the frequency range from 500 cm^{-1} to 1400 cm^{-1}.

cm^{-1} and 552 cm^{-1} in aqueous solution are also observed in the solid state. These lines correspond closely to the Raman bands of TEABr at 467 cm^{-1} and 559 cm^{-1} in aqueous solution, which have been attributed to the *gauche* conformation around the $-CH_2-CH_2-$ bonds. Accordingly, the molecular structures taking a *gauche* conformation in the Et–N structure of J4 exist both in aqueous solution and in the solid state. Further, since the two Raman lines at 504 cm^{-1} and

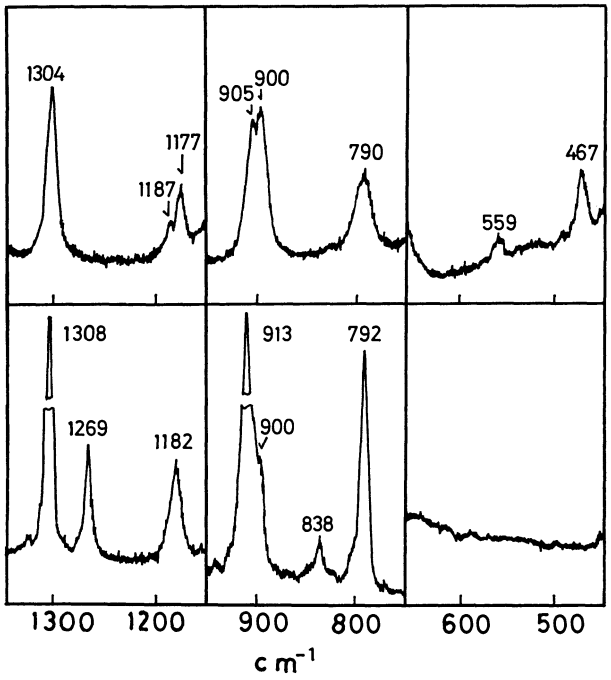

Fig. 5. Raman spectra of J10 in the solid and solution states in the frequency range from 500 cm^{-1} to 1400 cm^{-1}.

582 cm^{-1} in aqueous solution are not observed in the solid state, these may indicate that they are the *gauche* isomers that relate to the main chain of the J4 ions.

For the J10 salt, the two Raman lines observed in solution at 456 cm^{-1} and 552 cm^{-1} are also observed in the solid state. They correspond to those of TEABr at 467 cm^{-1} and 559 cm^{-1} in aqueous solution and have been ascribed to gauche conformation. Therefore, the molecular units taking a gauche conformation in the Et–N chain of J10 exist in both aqueous solution and solid phases. The two Raman lines at 494 cm^{-1} and 572 cm^{-1} in aqueous solution are also found in the solid state. These lines correspond to those of J4 at 504 cm^{-1} and 582 cm^{-1} in aqueous solution, which have been ascribed to the gauche isomers in the main chain. Accordingly, the molecules taking *gauche* form in main chain exist in both states.

The bands located at 1269 cm^{-1} for J4 and 1234 cm^{-1}, 1230 cm^{-1}, 1295 cm^{-1}, and 1303 cm^{-1} for J10 are observed only in the solid state. These bands can be assigned to the twisting-rocking mode of $-CH_2-CH_2-$ groups in the molecular chains. The fact that these bands are not observed in solution indicates that the motion of the $-CH_2-CH_2-$ groups in the main chains of the ions are less constrained. The bands located at 838 cm^{-1} for TEABr, 830 cm^{-1} for J4, and 820 cm^{-1} for J10 are observed in the solid state, but not in solution. Also, the bands located at 782 cm^{-1} for J4 and 788 cm^{-1} for J10 are not observed in solution. Although at this stage we can not assign these bands to the internal motions of these molecules, one may speculate that these bands are related to the terminal $-CH_2-CH_3$ rocking-twisting vibrational modes.

C–H Stretching Vibration Regions (2850 cm^{-1}*—3000*

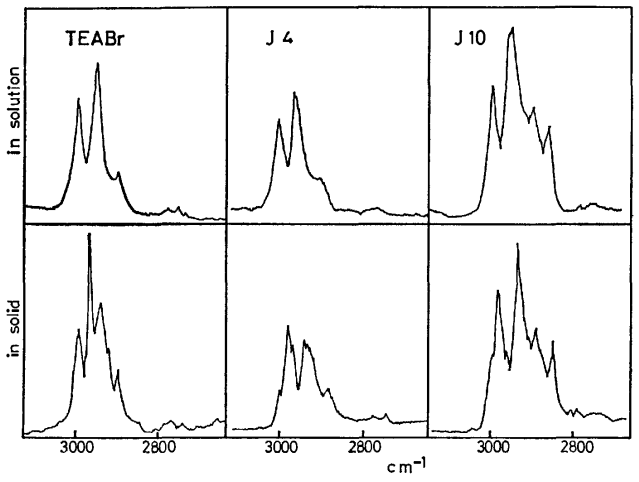

Fig. 6. Raman spectra for TEABr, J4, and J10 in the frequency range from 2850 cm^{-1} to 3000 cm^{-1} in the solid and solution states.

cm^{-1}). The vibrational C–H stretching modes can be classified into two groups; one from the methyl end group and the other arising from the methylene group vibrations. The symmetric and asymmetric methyl C–H stretching vibrations located at 2884 cm^{-1} and 2967 cm^{-1} are independent of the chain length in normal paraffins.[7] On the other hand, the methylene symmetric and asymmetric vibrations located at 2849 cm^{-1}—2861 cm^{-1} and 2912 cm^{-1}—2929 cm^{-1} are slightly dependent on the chain length.[7]

The Raman spectra for each compound in this frequency range are shown in Fig. 6. As can be seen, there are many bands which can be assigned to the methylene group vibration in the solid state. On the other hand in solution, only three bands are observed in each compound, located at about 2900 cm^{-1}, 2951 cm^{-1}, and 2997 cm^{-1} and these frequencies are almost independent of the chain length. In the case of the J10 ion in solution, one additional band at 2861 cm^{-1} is observed. This band can be assigned to the methylene symmetric stretching band. As J10 has 16 $-CH_2-$ units in an ion, this weak band is likely to be observed in the case of J10.[11] The reason that only three bands are observed in the solution state may be due to the fact that, since in the solution state the C–C bond of the main chain and branched chains are rotating or tumbling, then the C–H stretching vibration mode of the methylene groups will be strongly coupled to each other and leads to a reduction in the number of observed bands.

Raman Spectra of Water, OH Stretching Region. The isotropic (I_{isot}) and anisotropic (I_{anis}) Raman spectra of water and aqueous solutions of TEABr and J4 are shown in Fig. 7. The main effect of the salts on the water spectra is to change the spectral line shape. The opposing results are clearly evident for the I_{isot} and I_{anis} spectra; intensities in the lower frequency region (3000 cm^{-1}—3350 cm^{-1}) decrease while intensities in the higher frequency region (3350 cm^{-1}—3550 cm^{-1}) increase, in comparison with the spectrum of water. The effect of salt addition to water is similar to the effects produced by increasing

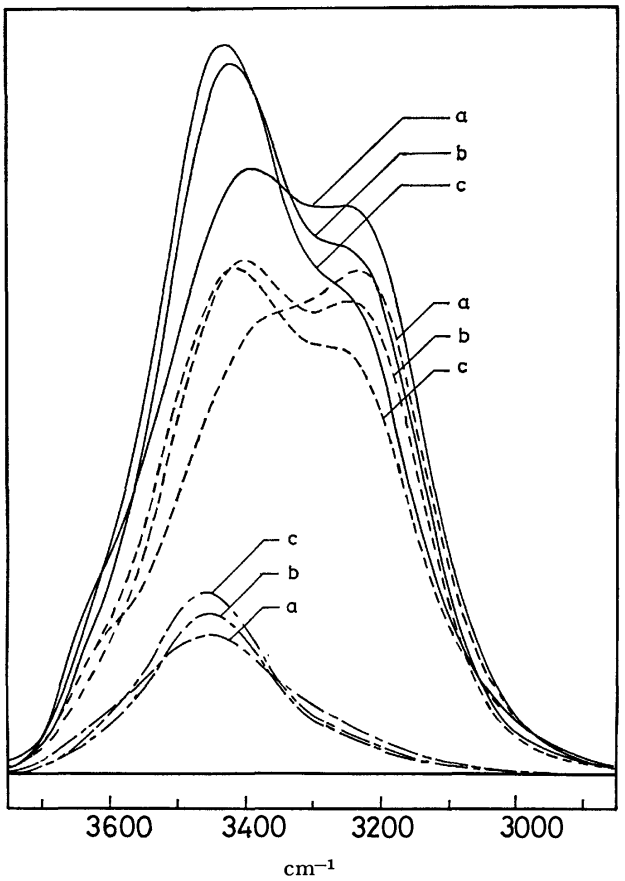

Fig. 7. Effects of added salts on the OH stretching vibration regions; —— observed, —-- isotropic parts, and —•— anisotropic ones.
(a) Water, (b) aqueous solution of TEABr, and (c) aqueous solution of J4.

temperature.[15–17] Therefore these salts, at least superficially seem to have a structure breaking effect on water at these high concentration and this is contrary to their structure-enforcing effect at dilute concentration. The influence of the TEA ion on the OH stretching region is greater than that of the J4 ion. The main effects of these salts on the water structure are of an electrostatic and hydrophobic nature.

Since the molecular conformations of the TEA and J4 ions are both observed to be of the extended form in aqueous solutions and the salt concentrations have been prepared so as to normalize the hydrophobic effect (approximately same hydrocarbon concentration for each ion in solution), it would appear that the difference in line shape for the OH stretching vibration in aqueous solutions of these salts is caused by the electrostatic atmosphere of the ion. The presence of two charged sites in a single ion and the incompatibility of several "type" of water around the solute to "interface" readily indicate the J4 ions are more complex in their influence on solvent interactions.

References

1) T. L. Broadwater and D. F. Evans, *J. Phys. Chem.*, **73**, 3985, 164 (1969).
2) S. Lindenbaum, *J. Phys. Chem.*, **73**, 4334 (1969).

3) C. V. Krishnan and H. L. Firdman, *J. Phys. Chem.*, **74**, 2356 (1970).
4) J. A. Burns and R. E. Verrall, *J. Solution Chem.*, **2**, 489 (1973); **4**, 369 (1975).
5) H. Nomura, S. Koda, F. Kawaizumi, and Y. Miyahara, *J. Phys. Chem.*, **81**, 2261 (1977).
6) R. G. Snyder and J. H. Schatschneider, *Spectrochim. Acta*, **19**, 85 (1963).
7) J. H. Schatschneider and R. G. Snyder, *Spectrochim. Acta*, **19**, 117 (1963).
8) R. Faiman and K. Laesson, *J. Raman Spectrosc.*, **4**, 387 (1976).
9) I. Harada, H. Takeuchi, M. Sakakibara, H. Matsuura, and T. Shimanouchi, *Bull. Chem. Soc. Jpn.*, **50**, 102 (1977).
10) N. Krishnamirphy, *Proc. Ind. Acad. Sci., A*, **61**, 164 (1965).
11) S. J. Anhouse and M. C. Tobin, *Spectrochim. Acta*, **28A**, 2141 (1972).
12) R. W. Berg, *Spectrochim. Acta*, **34A**, 655 (1978).
13) N. C. Stephenaon, *Acta Crystallogr., Sect. B*, **17**, 587 (1964).
14) A. Zalkin, *Acta Crystallogr., Sect. B*, **10**, 557 (1957).
15) G. E. Walrafen, *J. Chem. Phys.*, **47**, 114 (1967).
16) J. R. Sherer, M. K. Go, and S. Kint, *J. Phys. Chem.*, **78**, 1304 (1974).
17) S. Koda, H. Nomura, and Y. Miyahara, to be published.

The Adsorption of Dodecyldimethylammonium Chloride on Aqueous Surfaces of Concentrated NaCl Solutions

Sumio Ozeki and Shoichi Ikeda*

Department of Chemistry, Faculty of Science, Nagoya University, Chikusa, Nagoya 464

(Received October 18, 1979)

Surface tension of aqueous NaCl solutions of dodecyldimethylammonium chloride has been measured at high NaCl concentrations. Surface excesses of surfactant cation, Na^+ and Cl^- are derived by means of the Gibbs adsorption isotherm from the derivatives of surface tension with respect to surfactant concentration and NaCl concentration. The rational mean activity coefficients of surfactant and NaCl are both approximated by a common expression satisfying the Brönsted principle for mixed electrolytes but including the ionic strength as a variable. Saturated value of surface excess of surfactant cation remains constant at low NaCl concentrations up to 0.10 M, while it increases as the NaCl concentration exceeds 0.50 M. The adsorption of Na^+ is negative at low NaCl concentrations, but it increases rapidly and is positive above 0.50 M NaCl. Surfactant and NaCl are subject to the strong salting-out effect when the NaCl concentration is higher than 0.50 M. The Corrin-Harkins plot of the critical micelle concentration at high NaCl concentrations deviates from the straight line.

Recently[1,2] we have developed a general method for applying the Gibbs adsorption isotherm to aqueous solutions of electrolytes and elucidated implication of the Gibbs convention for the dividing surface and distinction of chemical species from components in the multicomponent system. The method enables us to derive the surface excesses of surfactant ion, coion and counterion from surface tension data, when it is applied to aqueous solutions containing an ionic surfactant and a simple salt, having a common counterion, but without forming any micelle yet.

In a previous paper[3] we have published some results of surface tension measurements on aqueous NaCl solutions of dodecyldimethylammonium chloride and derived the surface excesses of surfactant cation (D^+), Na^+, and Cl^- by means of the Gibbs adsorption isotherm. The previous work was restricted to the region of NaCl concentrations less than 0.50 M, and the mean activity coefficients of surfactant and NaCl were both approximated by the limiting expression of the Debye-Hückel equation. Then we obtained a strongly positive adsorption of surfactant cation at the saturation. However, we also found a small positive adsorption for Na^+ or coion, which would not necessarily be reasonable in the presence of dilute NaCl, because coions should be repelled from the surface dominantly occupied by surfactant cations.

In the present work we will extend the surface tension measurements on the same solutions up to the region of higher NaCl concentrations and examine how the surface excesses of ions are influenced by the salting-out effect. In this paper we will present the experimental results obtained in the present work and also include the previous data together. We will develop a treatment based on more exact expressions for the mean activity coefficients of electrolytes and apply it to obtain surface excesses of surfactant cation, Na^+ and Cl^-.

Experimental

Dodecyldimethylammonium chloride was prepared from *N,N*-dimethyldodecylamine by passing dry HCl gas, as previously described.[3] Commercial dimethyldodecylamine was purchased from Tokyo Kasei Kogyo Co., Inc., and purified by fractional distillation.

Surface tension of aqueous solutions was determined at 25±0.01 °C by means of the drop weight method, in the same way as previously performed.[3]

Results

Figure 1 shows the relation of surface tension, γ, with logarithm of molar concentration of surfactant, log C, at different NaCl concentrations, C_s. Surface tension decreases with increasing surfactant concentration and also with increasing NaCl concentration. At concentrations higher than the critical micelle concentration, C_0, surface tension always remains constant. The lowering of surface tension is formally represented by

$$-\mathrm{d}\gamma = RT\{\Gamma_2'\mathrm{d}\ln C + \Gamma_3'\mathrm{d}\ln C_s\} \quad (1)$$

where R is the gas constant and T is the temperature. The apparent surface excesses are defined by

$$\Gamma_2' = -\frac{1}{RT}\left(\frac{\partial\gamma}{\partial\ln C}\right)_{C_s} \quad (2)$$

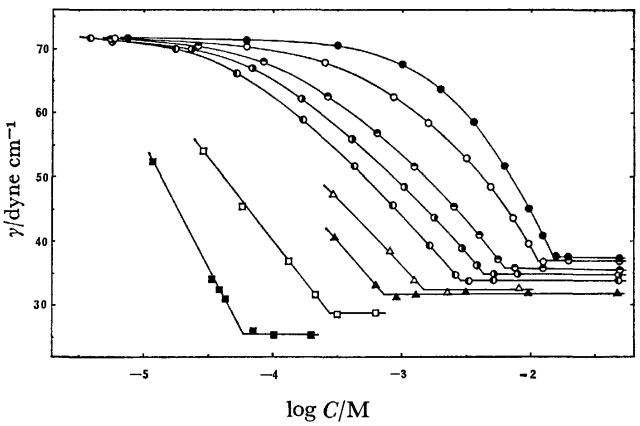

Fig. 1. Variation of surface tension with logarithm of surfactant concentration at different NaCl concentrations.
C_s (M): ●; 0, ○; 0.01, ◓; 0.05, ◑; 0.10, ◐; 0.20, △; 0.50, ▲; 0.94, □; 2.00, ■; 4.00.

† 1 M=1 mol dm^{-3}, 1 dyne cm^{-1}=1 mN m^{-1}.

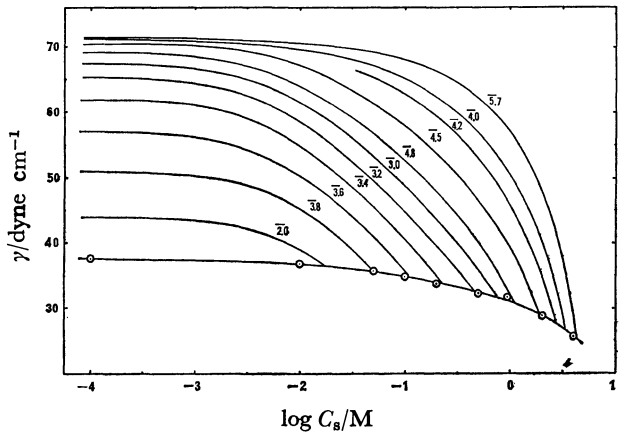

Fig. 2. Variation of surface tension with logarithm of NaCl concentration at different surfactant concentrations. Values of log C are given for the curves obtained by interpolation. ○, Constant surface tension at a given NaCl concentration, obtained at surfactant concentrations higher than the critical micelle concentration.

Table 1. Critical micelle concentration, apparent surface excess and surface tension associated with aqueous NaCl solutions of dodecyldimethylammonium chloride

C_s (M)	C_0 (10^{-3} M)	Γ_2' at C_0 (10^{-10} mol cm^{-2})	γ at C_0 (dyne cm^{-1})
0	14.7	7.66	37.6
10^{-4}	14.6	6.90	37.6
0.01	11.4	6.34	36.9
0.05	6.27	4.64	35.8
0.10	4.29	4.39	34.8
0.20	2.84	4.13	33.9
0.50	1.48	4.02	32.4
0.94	0.725	4.03	31.8
2.00	0.276	4.52	28.8
4.00	0.059	6.74	25.6

$$\Gamma_2' = -\frac{1}{RT}\left(\frac{\partial \gamma}{\partial \ln C_s}\right)_C. \tag{3}$$

As can be seen in Fig. 1, it is clear that $\Gamma_2'=0$ for $C>C_0$.

In Fig. 2 surface tension is plotted against log C_s at different surfactant concentrations. The lowest curve gives dependence of the constant surface tension on NaCl concentration, the constancy being observed at concentrations higher than the critical micelle concentration.

Table 1 summarizes related numerical data derived from Figs. 1 and 2, together with those previously obtained. With increasing NaCl concentration, the value of Γ_2' decreases in the range of NaCl concentrations up to 0.50 M, and then it increases rapidly at higher NaCl concentrations. In addition, the constant value of surface tension observed above C_0 is lowered with increasing NaCl concentration. The critical micelle concentration decreases with increasing NaCl concentration.

Discussion

The Gibbs Adsorption Isotherm. We will be mainly concerned with the adsorption of ions in the region of concentrations lower than the critical micelle concentration. It was shown[1] that the Gibbs adsorption isotherm for aqueous solutions containing DCl (dodecyldimethylammonium chloride) and NaCl can be expressed by either

$$-d\gamma = \Gamma_{D^+}d\mu_{D^+} + \Gamma_{Na^+}d\mu_{Na^+} + \Gamma_{Cl^-}d\mu_{Cl^-} \tag{4}$$

or

$$-d\gamma = \Gamma_{D^+}d\mu_{DCl} + \Gamma_{Na^+}d\mu_{NaCl} \tag{5}$$

provided that no micelle is formed yet. Here Γ_i is the surface excess of species or component, i, and μ_i is its chemical potential. Equation 4 is subject to an electroneutrality condition

$$\Gamma_{D^+} + \Gamma_{Na^+} = \Gamma_{Cl^-} \tag{6}$$

while Eq. 5 is free from such a subsidiary condition.

The chemical potentials of DCl and NaCl are given by

$$\mu_{DCl} = \mu^\circ_{DCl} + RT \ln y_\pm^2 C_{D^+}C_{Cl^-} \tag{7}$$

$$\mu_{NaCl} = \mu^\circ_{NaCl} + RT \ln y_{s\pm}^2 C_{Na^+}C_{Cl^-} \tag{8}$$

where the superfix ° means the standard states assigned to 1 M DCl and 1 M NaCl, respectively, in the ideal state, and $y_\pm$ and $y_{s\pm}$ are the mean activity coefficients of DCl and NaCl. The molar concentrations of ions are expressed by

$$C_{D^+} = C,\ C_{Na^+} = C_s, \text{ and } C_{Cl^-} = C + C_s. \tag{9}$$

The molar mean activity coefficients of DCl and NaCl, $y_\pm$ and $y_{s\pm}$, can be related to their rational mean activity coefficients, $f_\pm$ and $f_{s\pm}$, by[5a]

$$\frac{y_\pm}{f_\pm} = \frac{y_{s\pm}}{f_{s\pm}} = \frac{\rho_w}{\rho - \dfrac{M-2M_w}{1000}C - \dfrac{M_s-2M_w}{1000}C_s} \tag{10}$$

where M_w, M, and M_s are the molecular weights of water, DCl, and NaCl, respectively, and ρ_w and ρ are the densities of water and the solution respectively.

It will be demonstrated below that the rational mean activity coefficients of DCl and NaCl can be approximately represented by an identical expression as a function of ionic strength, $C+C_s$. Then we have identities and introduce abbreviations as follows:

$$\eta = \left(\frac{\partial \ln y_\pm^2}{\partial C}\right)_{C_s} = \left(\frac{\partial \ln y_{s\pm}^2}{\partial C}\right)_{C_s} \tag{11}$$

$$\eta_s = \left(\frac{\partial \ln y_\pm^2}{\partial C_s}\right)_{C} = \left(\frac{\partial \ln y_{s\pm}^2}{\partial C_s}\right)_{C} \tag{12}$$

Introducing these approximations we arrive at the expression of Gibbs adsorption isotherm in the form of Eq. 1, in which the apparent surface excesses are given by

$$\Gamma_2' = \left(1+\frac{C}{C+C_s}+\eta C\right)\Gamma_{D^+} + \left(\frac{C}{C+C_s}+\eta C\right)\Gamma_{Na^+} \tag{13}$$

$$\Gamma_3' = \left(\frac{C_s}{C+C_s}+\eta_s C_s\right)\Gamma_{D^+} + \left(1+\frac{C_s}{C+C_s}+\eta_s C_s\right)\Gamma_{Na^+}. \tag{14}$$

By solving Eqs. 13 and 14 we obtain the surface excesses of D^+ and Na^+, and also, together with Eq. 6 we have the surface excess of Cl^-.

$$\Gamma_{D^+} = \frac{1}{2+\eta C+\eta_s C_s}\left\{\left(1+\frac{C_s}{C+C_s}+\eta_s C_s\right)\Gamma_2' - \left(\frac{C}{C+C_s}+\eta C\right)\Gamma_3'\right\} \quad (15)$$

$$\Gamma_{Na^+} = \frac{1}{2+\eta C+\eta_s C_s}\left\{-\left(\frac{C_s}{C+C_s}+\eta_s C_s\right)\Gamma_2' + \left(1+\frac{C}{C+C_s}+\eta C\right)\Gamma_3'\right\}, \quad (16)$$

and

$$\Gamma_{Cl^-} = \frac{1}{2+\eta C+\eta_s C_s}(\Gamma_2'+\Gamma_3'). \quad (17)$$

It can be readily seen from Eq. 15 that

$$\Gamma_{D^+} = \Gamma_2' \quad (18)$$

provided that C_s is very high or much higher than C. That is, the value of Γ_{D^+} is independent of the choice of activity coefficients of DCl and NaCl, if the NaCl concentration is sufficiently high.

The Mean Activity Coefficients and Their Derivatives. The molar mean activity coefficients of DCl and NaCl are related to their rational mean activity coefficients by means of Eq. 10. We will derive the approximate forms of rational mean activity coefficients of DCl and NaCl in their mixed solutions as follows.

According to Brönsted's principle of specific interaction of ions,[4,5d] the rational mean activity coefficients can be written

$$\log f_\pm = -\frac{P\sqrt{C+C_s}}{1+Qa\sqrt{C+C_s}} + BC + B_{Cl\text{-}C_s} \quad (19)$$

$$\log f_{s\pm} = -\frac{P\sqrt{C+C_s}}{1+Qa\sqrt{C+C_s}} + B_s C_s + B_{Cl\text{-}C} \quad (20)$$

where the constants, P and Q, of the Debye-Hückel electrostatic term are determined by temperature and dielectric constant, and the ionic radius, a, serves as an adjustable parameter.[5b] The salting-out constants, B and B_s, are characteristic of DCl and NaCl, respectively, and the specific ion interaction constant, B_{Cl^-}, represents the averaged specific interaction of Cl^- with D^+ and Na^+. Our experimental range covers 0—10^{-2} M for C and 0—4.00 M for C_s.

In a recent work Cutler, Meares, and Hall[6] measured the activity coefficients of sodium dodecyl sulfate in NaCl solutions and found that the mean activity coefficient obeys the Debye-Hückel equation of Guggenheim type, that is, P=0.5115 and Qa=1.000 in Eq. 19, when the NaCl concentration is in the range of 0—0.2 M and the surfactant concentration is lower than the critical micelle concentration. This means that an ionic surfactant behaves like a simple salt such as NaCl unless micelles are formed. Then we may anticipate that the activity coefficient of dilute surfactant obeys Eq. 19, in which the salting-out term is negligibly small.

Robinson and Stokes[5c] published following values of parameters in Eq. 20 which fit well the observed values of $\log f_{s\pm}$ for NaCl solutions up to 2.00 M at 25 °C.

$$P = 0.5115, \quad Qa = 1.316, \quad B_s = 0.055 \quad (21)$$

In Eq. 19 we will also be able to use the identical value of Qa, because of thermodynamic requirement and of small contribution of the ionic-size term. In addition, since the value of C is small, it will not introduce serious errors even if we put $B=B_s$.

We have scarce information about the value of B_{Cl^-}. The result of Cutler *et al.*[6] suggests that the last term of Eq. 19 is negligibly small when C_s is lower than 0.2 M. We may expect that the value of B_{Cl^-} is not very large. Then the last term of Eq. 20 would have a small magnitude as compared to the other two terms: if C_s is as low as 0.01 M, the term will be negligible in comparison with the former, and if C_s is higher, the term will be much smaller than the salting-out term. Considering such a small contribution of this term and also the principle of ionic strength, we may include it in a single term without serious errors by putting $B_{Cl^-}=B$.

In this approximation we have a common expression for the molar mean activity coefficients of DCl and NaCl:

$$\log f_\pm = \log f_{s\pm} = -\frac{P\sqrt{C+C_s}}{1+Qa\sqrt{C+C_s}} + B_s(C+C_s) \quad (22)$$

together with Eqs. 21. Then we obtain

$$\eta = \eta_0 + \frac{2\left[\left(\frac{\partial\rho}{\partial C}\right)_{C_s} - \frac{M-2M_w}{1000}\right]}{\rho - \frac{M-2M_w}{1000}C - \frac{M_s-2M_w}{1000}C_s} \quad (23)$$

$$\eta_s = \eta_0 + \frac{2\left[\left(\frac{\partial\rho}{\partial C_s}\right)_{C} - \frac{M_s-2M_w}{1000}\right]}{\rho - \frac{M-2M_w}{1000}C - \frac{M_s-2M_w}{1000}C_s} \quad (24)$$

where

$$\eta_0 = -\frac{2.303P}{(1+Qa\sqrt{C+C_s})^2\sqrt{C+C_s}} + 4.606B_s. \quad (25)$$

For actual calculations of ρ and $(\partial\rho/\partial C_s)_C$ we may use the literature values of density of NaCl solutions.[7] The density of aqueous electrolyte solutions can be represented by a quadratic form of molal concentration, m_s, up to 4.00 M, which is equivalent to write

$$\frac{C_s}{m_s} = \rho_w - \alpha m_s \quad (26)$$

where α is a constant. For NaCl solutions at 25 °C, ρ_w=0.9970 g cm^{-3} and α=0.0183. It is found alternatively that

$$\rho = \rho_w + 0.00387\sqrt{C_s} + 0.0362C_s. \quad (27)$$

For the calculation of $(\partial\rho/\partial C)_{C_s}$, which is given by

$$\left(\frac{\partial\rho}{\partial C}\right)_{C_s} = \frac{M(1-\bar{v}\rho_0)}{1000} \quad (28)$$

at low C values, we have used the value of partial specific volume of DCl, $\bar{v}$, in water, 1.06,[8] where ρ_0 is the density of water or NaCl solutions.

Surface Excesses of Ions. Figure 3 shows the surface excesses of D^+, Na^+, and Cl^- as functions of surfactant concentration. It is seen in Fig. 3 (a)

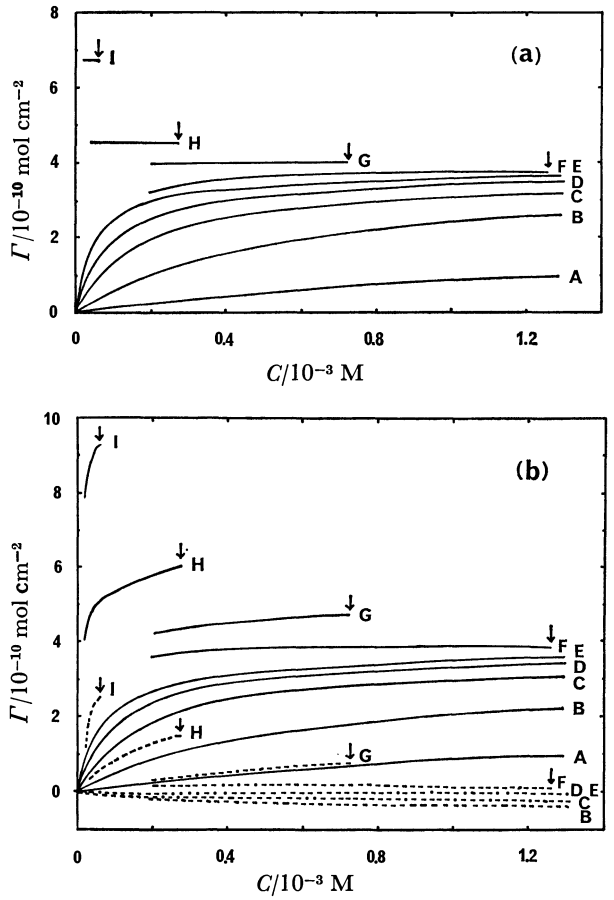

Fig. 3. Adsorption isotherms of ions on aqueous surfaces of different NaCl concentrations. (a) Γ_{D^+} *vs.* C; (b) Γ_{Na^+} (----) and Γ_{Cl^-} (——) *vs.* *C*. Arrows indicate the location of critical micelle concentrations. C_s (M): A; 0, B; 0.01, C; 0.05, D; 0.10, E; 0.20, F; 0.50, G; 0.94, H; 2.00, I; 4.00.

that the value of Γ_{D^+} increases more rapidly and reaches the saturated value at a lower concentration, as the NaCl concentration is higher. This is caused by the electrostatic shielding effect of added NaCl on the charged layer of adsorbed surfactant. When the NaCl concentration exceeds 0.20 M, the value of Γ_{D^+} has already reached the saturated value and is constant at the concentration range in concern. Table 2 gives the saturated values of Γ_{D^+} at different NaCl concentrations, which are obtained as the values of Γ_{D^+} at the critical micelle concentration. Figure 4 shows the saturated value of Γ_{D^+} as a function of NaCl concentration. With increasing NaCl concentration, the saturated adsorption of surfactant cation is at first almost constant and then slightly decreases. When the NaCl concentration exceeds 0.50 M, the adsorption increases at higher NaCl concentrations. This increase in adsorption must be ascribed to the salting-out effect of NaCl. The observed behavior of saturated adsorption of dodecyldimethylammonium ion is different from that of dodecyl sulfate ion, since it was reported for aqueous solutions of sodium dodecyl sulfate[9–11] that the adsorption of dodecyl sulfate ion is strongly promoted by the addition of NaCl up to 0.1 M. The difference in adsorption behavior between

Table 2. Surface excesses of surfactant cation, Na^+ and Cl^- at the critical micelle concentration

C_s (M)	Γ_{D^+} at C_0 (10^{-10} mol cm^{-2})	Γ_{Na^+} at C_0 (10^{-10} mol cm^{-2})	Γ_{Cl^-} at C_0 (10^{-10} mol cm^{-2})
0	4.13[a)]	—	4.13[a)]
0.01	4.27	−0.36	3.91
0.05	4.26	−0.23	4.03
0.10	4.25	−0.16	4.09
0.20	4.08	−0.01	4.07
0.50	4.01	0.09	4.10
0.94	4.03	0.67	4.70
2.00	4.52	1.49	6.01
4.00	6.74	2.51	9.25

a) These values were calculated by using the limiting expression of Debye-Hückel equation for the mean activity coefficient of surfactant.

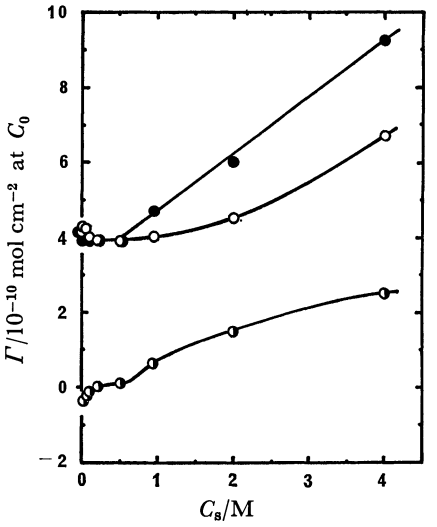

Fig. 4. Surface excesses of ions at the critical micelle concentration plotted against NaCl concentration. ○; Γ_{D^+}, ◑; Γ_{Na^+}, ●; Γ_{Cl^-}.

these surfactants must be elucidated in future work.

It is seen in Fig. 3 (b) that the adsorption of Na^+ and Cl^- is still increasing without reaching their saturation even at the critical micelle concentration, if the NaCl concentration is higher than 0.50 M. Values of Γ_{Na^+} and Γ_{Cl^-} at the critical micelle concentration are also listed in Table 2, and they are plotted as functions of NaCl concentration in Fig. 4. Previously,[3] the value of Γ_{Na^+} was calculated at low NaCl concentrations, by assuming the limiting expression of Debye-Hückel equation for activity coefficients, and it was found to be positive. In the present treatment assuming a more exact equation for the activity coefficients, the value of Γ_{Na^+} at the critical micelle concentration is negative at low NaCl concentrations, and then it turns to be positive at NaCl concentrations higher than 0.10 M. The negative adsorption of coion, Na^+, at low NaCl concentrations seems to be more reasonable. The initial negative adsorption of Na^+ decreases with increasing NaCl concentration, which numerically comes from the contribution of the effect

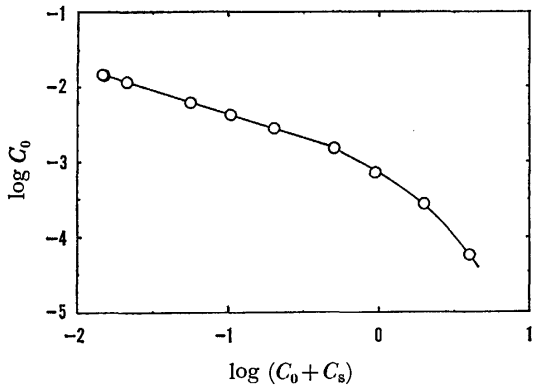

Fig. 5. The Corrin-Harkins plot. Relation of logarithm of critical micelle concentration with logarithm of chloride ion concentration.

of ionic size represented by the term, Qa, in Eq. 22. In the Gouy theory of diffuse double layer an increase in negative adsorption of coion should occur when the NaCl concentration increases. The marked increase in positive adsorption of Na^+ observed at NaCl concentrations higher than 0.50 M is caused by the salting-out term, B_s, of Eq. 22.

In the above treatment we have made some simplification to express the two rational activity coefficients in the common form, Eq. 22. In Eq. 19 we could also set $B=B_{Cl^-}=0$, as was found by Cutler *et al.*,[6] but this would not be applicable for the region of higher NaCl concentrations. If we assume $B=B_{Cl^-}=0$, however, Eq. 16 leads to much larger values of Γ_{Na^+} at higher NaCl concentrations. We may then conclude that the approximate form of activity coefficients, Eq. 22, is effective in the Gibbs adsorption isotherm for mixed solutions of an ionic surfactant and a simple salt, as far as the surfactant does not form micelles.

The Corrin-Harkins Relation. Previously[3] we have demonstrated that the Corrin-Harkins plot of the critical micelle concentration is linear up to 0.20 M NaCl. As can be seen in Fig. 5, however, such a linear relation no longer holds between logarithm of critical micelle concentration and logarithm of ionic strength, when the plot is extended to higher NaCl concentrations. It seems likely that the linear Corrin-Harkins relation is closely connected with the electrostatic shielding effect of simple salt but is disrupted by the other effects such as counterion binding and salting-out.

In a current paper[12] we are reporting the same results on the critical micelle concentration determined by light scattering. According to the results of light-scattering measurement, the Corrin-Harkins plot is linear as far as the spherical micelles are formed, but it deviates from the straight line when the rod-like micelles become more stable. It is inferred that the sphere-rod transition of ionic micelles would be caused by the difference in electrostatic effect of added salt, or, more directly, in the degree of counterion binding.

References

1) S. Ikeda, *Bull. Chem. Soc. Jpn.*, **50**, 1403 (1977).
2) S. Ikeda, *Hyomen*, **15**, 592 (1977).
3) S. Ozeki, M. Tsunoda, and S. Ikeda, *J. Colloid Interface Sci.*, **64**, 28 (1978).
4) K. S. Pitzer and L. Brewer, "Thermodynamics," McGraw-Hill Book Co., Inc., New York (1961) pp. 343 and 567.
5) R. A. Robinson and R. H. Stokes, "Electrolyte Solutions," 2nd ed, Butterworths Scientific Publications, Lodon (1959), (a) p. 32; (b) p. 235; (c) p. 236; (d) p. 435.
6) S. G. Cutler, P. Meares, and D. G. Hall, *J. Chem. Soc., Faraday Trans. 1*, **1978**, 1758.
7) H. S. Harned and B. B. Owens, "The Physical Chemistry of Electrolytic Solutions," Reinhold Publishing Corporation, New York (1949), p. 556.
8) S. Ozeki and S. Ikeda, *J. Colloid Interface Sci.*, in press.
9) K. Tajima, M. Muramatsu, and T. Sasaki, *Bull. Chem. Soc. Jpn.*, **43**, 1991 (1970).
10) K. Tajima, *Bull. Chem. Soc. Jpn.*, **44**, 1767 (1971).
11) K. Tajima, *Bull. Chem. Soc. Jpn.*, **43**, 3063 (1970).
12) S. Ikeda, S. Ozeki, and M. Tsunoda, *J. Colloid Interface Sci.*, **73**, 27 (1980).

The Gibbs Adsorption Equation for Aqueous Solutions Containing a Weak Base

Shoichi IKEDA* and Sumio OZEKI

Department of Chemistry, Faculty of Science, Nagoya University, Chikusa, Nagoya 464

(Received October 18, 1979)

The Gibbs adsorption isotherm for quaternary systems of water, weak base, HCl or NaOH, and NaCl including a vapor-solution interface is expressed in terms of variations of chemical potentials of neutral components added to make up the solution. Four systems are treated, and the Gibbs convention is introduced in such a way that the surface excess of added water is zero and the surface excesses of solute components are defined. Assuming that the activity coefficients of solute components are unity, the lowering of surface tension is given in terms of variations of total molar concentrations of weak base or its hydrochloride, HCl or NaOH, and NaCl, or of pH of the solution.

Recently[1,2] we have established a general method for applying the Gibbs adsorption isotherm to aqueous solutions containing two or three electrolytic solutes, either strong or weak. So far there has been no clear cognizance for an electrolyte solution containing two kinds of electrolytic solutes to be a multicomponent system, and, when the Gibbs adsorption isotherm has been applied to an aqueous solution of an ionic surfactant and a simple salt, the lowering of surface tension of the solution has been exclusively connected with the variation of surfactant concentration alone.[3–6] We have pointed out[1,2] that such an aqueous solution must be treated as a ternary system and the lowering of surface tension should be represented as a function of variations of concentration of simple salt as well as of surfactant concentration. The application of this method to aqueous solutions of a cationic surfactant has been exemplified previously[7,8] to derive the surface excesses of various ions on the solution.

When we are concerned with aqueous solution of a weak electrolyte such as an ionic-nonionic surfactant, in the presence of a strong acid or base and a simple salt, we have to treat the solution as a quaternary system, and the lowering of its surface tension should be related to the variations of concentrations of surfactant, acid or base, and simple salt. In a previous paper[9] we have applied the method to aqueous solution of a cationic-nonionic surfactant in the presence of HCl and NaCl, in which the lowering of surface tension is expressed as a function of variations of concentrations of surfactant and NaCl, as well as of degree of neutralization instead of concentration of HCl.

In the present paper we will give a general treatment of the Gibbs adsorption isotherm applied to aqueous solution containing a weak base, HCl or NaOH, and NaCl. Following four systems of added components are considered: (I) H_2O+D+HCl+NaCl, (II) H_2O+D+NaOH+NaCl, (III) H_2O+DHCl+HCl+NaCl, and (IV) H_2O+DHCl+NaOH+NaCl, where D is a weak base capable of combining with H^+ to form a cation DH^+. Final results will be given in the form as a function of variations of molar concentrations of added components, D or DHCl, HCl or NaOH, and NaCl, or alternatively, of molar concentrations of two components, D or DHCl, and NaCl, and pH of the solution. These equations enable us to derive the surface excesses of total base (D+DH^+), added HCl or NaOH, and NaCl from the derivatives of surface tension with respect to concentrations of added base (D) or its hydrochloride (DHCl), and of NaCl, as well as to concentration of added HCl or NaOH, or, alternatively, to pH of the solution.

Expressions in Terms of Chemical Potentials

A plane surface of aqueous solution formed by dissolving a weak base D or its hydrochloride DHCl, strong acid HCl or alkali NaOH, and NaCl into water will be treated with reference to its surface tension at constant temperature. The plane surface forms a vapor-solution interface. Since the weak base D combines with H^+ to form a cation DH^+ in water, or DH^+ dissociates into D and H^+ in water, and water itself consists of H_2O, H^+, and OH^-, the Gibbs adsorption isotherm for the vapor-solution interface can be written in terms of chemical potentials of species

$$-d\gamma = \Gamma_{H_2O}d\mu_{H_2O} + \Gamma_D d\mu_D + \Gamma_{H^+}d\mu_{H^+} + \Gamma_{DH^+}d\mu_{DH^+} + \Gamma_{Na^+}d\mu_{Na^+} + \Gamma_{OH^-}d\mu_{OH^-} + \Gamma_{Cl^-}d\mu_{Cl^-}, \quad (1)$$

where γ is the surface tension of solution, Γ_i and μ_i are the surface excess and chemical potential of species, i. Equation 1 is subject to several conditions of equilibrium and stoichiometry. Among them, water and the weak base are in ionization equilibrium, respectively, respresented by

$$\mu_{H_2O} = \mu_{H^+} + \mu_{OH^-}, \quad (2)$$

$$\mu_{DH^+} = \mu_D + \mu_{H^+}. \quad (3)$$

Furthermore, stoichiometric relations hold for strong electrolytes:

$$\mu_{DHCl} = \mu_{DH^+} + \mu_{Cl^-}, \quad (4)$$

$$\mu_{HCl} = \mu_{H^+} + \mu_{Cl^-}, \quad (5a)$$

$$\mu_{NaOH} = \mu_{Na^+} + \mu_{OH^-}, \quad (5b)$$

$$\mu_{NaCl} = \mu_{Na^+} + \mu_{Cl^-}. \quad (6)$$

Equations 2 and 3, together with the electroneutrality condition among surface excesses of ionic species

$$\Gamma_{H^+} + \Gamma_{DH^+} + \Gamma_{Na^+} = \Gamma_{OH^-} + \Gamma_{Cl^-}, \quad (7)$$

reduce the number of variables in Eq. 1 from 7 to 4. Individual cases will be demonstrated below, and Eq. 1 may be represented in terms of variations of chemical potentials of four added components, *i.e.*, H_2O, D or DHCl, HCl or NaOH, and NaCl.

Since the number of variances should be 3 for the

quaternary system including an interface or two phases at constant temperature, the Gibbs convention must be introduced, so that the surface excess of solvent, *i.e.*, water, may vanish. The expression of the Gibbs convention for the individual cases is not necessarily given in a comprehensive form, but it proves to represent that the total surface excess of added water counted as moles of H_2O is zero.[10]

Thus, Eq. 1 can be completely converted into a form consisting of independent variables alone, and the lowering of surface tension is given by variations of chemical potentials of added solute components.

Expressions in Terms of Solute Concentrations

When we express the chemical potentials of added components in terms of their molar concentrations, we can obtain the Gibbs adsorption isotherm in the form given by the variations of molar concentrations of added solutes. To do this in a tractable form, we make an assumption that the solution is ideal and the activity coefficients of added solute components are unity. Let the molar concentration of added D or DHCl be C, that of added HCl or NaOH be C_A or C_B, and that of NaCl be C_S, respectively. Then the chemical potentials are given by

$$\mu_D = \mu_D^\circ + RT \ln C_D \tag{8a}$$

$$\mu_{DHCl} = \mu_{DHCl}^\circ + RT \ln C_{DH^+} C_{Cl^-} \tag{8b}$$

$$\mu_{HCl} = \mu_{HCl}^\circ + RT \ln C_{H^+} C_{Cl^-} \tag{9a}$$

$$\mu_{NaOH} = \mu_{NaOH}^\circ + RT \ln C_{Na^+} C_{OH^-} \tag{9b}$$

$$\mu_{NaCl} = \mu_{NaCl}^\circ + RT \ln C_{Na^+} C_{Cl^-}, \tag{10}$$

where the superfix $\circ$ refers to the standard states.

There are several restrictions among the molar concentrations of species present in the solution, C_D, C_{DH^+}, C_{H^+}, C_{Na^+}, C_{OH^-}, and C_{Cl^-}. Concentrations of counter ion, C_{Cl^-} and coion, C_{Na^+}, for the surfactant ion are given by C_A or C_B and C_S. If the ionic product of water is defined by K_w, the molar concentrations of H^+ and OH^- are mutually dependent by means of Eq. 2, *i.e.*,

$$C_{H^+} C_{OH^-} = K_W. \tag{11}$$

If the degree of ionization or protonation is α, the molar concentrations of base, in unionized and ionized forms, are given by

$$C_D = (1-\alpha)C \text{ and } C_{DH^+} = \alpha C, \tag{12}$$

and the ionization equilibrium, Eq. 3, is defined by the ionization constant

$$\frac{1-\alpha}{\alpha} C_{H^+} = K. \tag{13}$$

There is the condition of electroneutrality in bulk

$$C_{H^+} + C_{DH^+} + C_{Na^+} = C_{OH^-} + C_{Cl^-}. \tag{14}$$

Then we can obtain C_{H^+} or α as a function of C and C_A or C_B for individual cases. For this purpose, however, we have to solve a cubic equation with respect to C_{H^+} or α, which is derived by substituting Eqs. 11, 12, and 13 into Eq. 14. For the derivation of the Gibbs adsorption equation it is not necessary to have C_{H^+} or α itself but to evaluate dC_{H^+} or $d\alpha$, and, consequently, we differentiate the cubic equation with respect to C and C_A or C_B and obtain dC_{H^+} or $d\alpha$ as a function of dC and dC_A or dC_B. The function includes α explicitly, and for numerical evaluation we have to calculate it from C, C_A, or C_B, and K and K_w by solving the cubic equation.

The final form of the Gibbs adsorption isotherm is written

$$-d\gamma = RT\{\Gamma_2 d \ln C + \Gamma_X d \ln C_X + \Gamma_3 d \ln C_S\}, \tag{15}$$

where X is A for HCl and B for NaOH. It should be noted, however, that values of Γ_A and Γ_B do not imply the surface excesses of HCl and NaOH, respectively. Values of Γ_2, Γ_X, and Γ_3 can be evaluated from the derivatives of surface tension with respect to molar concentrations of added components.

Alternatively, we are often interested in assigning pH of a solution rather than giving molar concentration of HCl or NaOH added. In such cases we must express α in terms of C_{H^+} from Eq. 13 and then C_A or C_B in terms of C_{H^+} and C from the cubic equation of C_{H^+} as mentioned above.

The lowering of surface tension is then given by

$$-d\gamma = RT\{\Gamma_c d \ln C + \Gamma_h d \ln C_{H^+} + \Gamma_3 d \ln C_S\}, \tag{16}$$

where Γ_c can be obtained from the derivative of surface tension at constant pH with respect to molar concentration of the weak base or its hydrochloride, and Γ_h can be evaluated from the variation of surface tension with pH. Γ_3 is identical with that in Eq. 15.

(I) $H_2O+D+HCl+NaCl$. This system was treated previously,[9] and a modification of the derived equations was applied to surface tension of aqueous solutions of a nonionic-cationic surfactant at different degrees of neutralization. The Gibbs convention has the form

$$\Gamma_{H_2O} + \Gamma_{OH^-} = 0, \tag{17}$$

and the Gibbs adsorption isotherm can be written as

$$-d\gamma = (\Gamma_D + \Gamma_{DH^+}) d\mu_D + (\Gamma_{Cl^-} - \Gamma_{Na^+}) d\mu_{HCl} + \Gamma_{Na^+} d\mu_{NaCl}. \tag{18}$$

Concentrations of counterion and coion are given by

$$C_{Cl^-} = C_A + C_S \text{ and } C_{Na^+} = C_S. \tag{19}$$

For Eq. 15 we have

$$\Gamma_2 = \left(1 + \frac{\alpha^2 C}{Q_A}\right)(\Gamma_D + \Gamma_{DH^+}) - \frac{\alpha C}{Q_A}(\Gamma_{Cl^-} - \Gamma_{Na^+}), \tag{20a}$$

$$\Gamma_A = -\frac{\alpha C_A}{Q_A}(\Gamma_D + \Gamma_{DH^+}) + \left(\frac{C_A}{Q_A} + \frac{C_A}{C_A + C_S}\right)\Gamma_{Cl^-} - \frac{C_A}{Q_A}\Gamma_{Na^+}, \tag{20b}$$

$$\Gamma_3 = \frac{C_S}{C_A + C_S}\Gamma_{Cl^-} + \Gamma_{Na^+}, \tag{20c}$$

where

$$Q_A = \alpha(2-\alpha)C - C_A + 2C_{H^+} \tag{20d}$$

$$= -\alpha^2 C + C_A + 2C_{OH^-}. \tag{20e}$$

Solving Eqs. 20a,b,c we have

$$\Gamma_D + \Gamma_{DH^+} = \frac{1}{H_A}\left\{(H_A - \alpha^2 C)\Gamma_2 + \frac{\alpha C}{C_A}(C_A + 2C_S)\Gamma_A - \alpha C \Gamma_3\right\}, \tag{21a}$$

$$\Gamma_{Cl^-} = \frac{C_A+C_S}{H_A}\left\{\alpha\Gamma_2 + \frac{1}{C_A}(H_A-C_A-2C_S)\Gamma_A + \Gamma_3\right\}, \quad (21b)$$

$$\Gamma_{Na^+} = \frac{1}{H_A}\left\{-\alpha C_S\Gamma_2 - \frac{C_S}{C_A}(H_A-C_A-2C_S)\Gamma_A + (H_A-C_S)\Gamma_3\right\}, \quad (21c)$$

where

$$H_A = 2\alpha C + 2C_S + 2C_{H^+} \quad (21d)$$

$$= 2C_A + 2C_S + 2C_{OH^-}. \quad (21e)$$

Similarly, for Eq. 16 we have

$$\Gamma_c = \Gamma_D + \Gamma_{DH^+} + \frac{\alpha C}{C_A+C_S}\Gamma_{Cl^-} \quad (22a)$$

$$\Gamma_h = -\alpha(\Gamma_D+\Gamma_{DH^+}) + \left(1+\frac{Q_A}{C_A+C_S}\right)\Gamma_{Cl^-} - \Gamma_{Na^+} \quad (22b)$$

and, solving Eqs. 22 and 20c, we have

$$\Gamma_D + \Gamma_{DH^+} = \frac{1}{H_A}\left\{(H_A-\alpha^2C)\Gamma_c - \alpha C(\Gamma_h+\Gamma_3)\right\} \quad (23a)$$

$$\Gamma_{Cl^-} = \frac{C_A+C_S}{H_A}\{\alpha\Gamma_c+\Gamma_h+\Gamma_3\}, \quad (23b)$$

$$\Gamma_{Na^+} = \frac{1}{H_A}\{-\alpha C_S\Gamma_c - C_S\Gamma_h + (H_A-C_S)\Gamma_3\}. \quad (23c)$$

(II) $H_2O+D+NaOH+NaCl$. In order to suppress possible ionization of weak base dissolved in water, NaOH is added to the solution. In this case the Gibbs convention for the dividing surface is expressed by

$$\Gamma_{H_2O} + \Gamma_{H^+} + \Gamma_{DH^+} = 0, \quad (24)$$

and the Gibbs adsorption isotherm has the form

$$-d\gamma = (\Gamma_D+\Gamma_{DH^+})d\mu_D + (\Gamma_{Na^+}-\Gamma_{Cl^-})d\mu_{NaOH} + \Gamma_{Cl^-}d\mu_{NaCl}. \quad (25)$$

Concentrations of counterion and coion are given by

$$C_{Cl^-} = C_S \text{ and } C_{Na^+} = C_B + C_S. \quad (26)$$

For Eq. 15 we have

$$\Gamma_2 = \left(1+\frac{\alpha^2C}{Q_B}\right)(\Gamma_D+\Gamma_{DH^+}) - \frac{\alpha C}{Q_B}(\Gamma_{Cl^-}-\Gamma_{Na^+}), \quad (27a)$$

$$\Gamma_B = \frac{\alpha C_B}{Q_B}(\Gamma_D+\Gamma_{DH^+}) - \frac{C_B}{Q_B}\Gamma_{Cl^-} + \left(\frac{C_B}{Q_B}+\frac{C_B}{C_B+C_S}\right)\Gamma_{Na^+}, \quad (27b)$$

$$\Gamma_3 = \Gamma_{Cl^-} + \frac{C_S}{C_B+C_S}\Gamma_{Na^+}, \quad (27c)$$

where

$$Q_B = \alpha(2-\alpha)C + C_B + 2C_{H^+}, \quad (27d)$$

$$= -\alpha^2C - C_B + 2C_{OH^-}. \quad (27e)$$

Solving Eqs. 27a,b,c we have

$$\Gamma_D + \Gamma_{DH^+} = \frac{1}{H_B}\left\{(H_B-\alpha^2C)\Gamma_2 - \frac{\alpha C}{C_B}(C_B+2C_S)\Gamma_B + \alpha C\Gamma_3\right\}, \quad (28a)$$

$$\Gamma_{Cl^-} = \frac{1}{H_B}\left\{\alpha C_S\Gamma_2 - \frac{C_S}{C_B}(H_B-\alpha^2C-C_B)\Gamma_B + (H_B-C_S)\Gamma_3\right\}, \quad (28b)$$

$$\Gamma_{Na^+} = \frac{C_B+C_S}{H_B}\left\{-\alpha\Gamma_2+\frac{1}{C_B}(H_B-\alpha^2C-C_B)\Gamma_B+\Gamma_3\right\}, \quad (28c)$$

where

$$H_B = 2\alpha C + 2C_B + 2C_S + 2C_{H^+} \quad (28d)$$

$$= 2C_S + 2C_{OH^-}. \quad (28e)$$

Similarly, for Eq. 16 we have

$$\Gamma_c = \Gamma_D + \Gamma_{DH^+} - \frac{\alpha C}{C_B+C_S}\Gamma_{Na^+}, \quad (29a)$$

$$\Gamma_h = -\alpha(\Gamma_D+\Gamma_{DH^+}) + \Gamma_{Cl^-} - \left(1+\frac{Q_B}{C_B+C_S}\right)\Gamma_{Na^+}, \quad (29b)$$

and, solving Eqs. 29 and 27c, we have

$$\Gamma_D + \Gamma_{DH^+} = \frac{1}{H_B}\{(H_B-\alpha^2C)\Gamma_c - \alpha C(\Gamma_h+\Gamma_3)\}, \quad (30a)$$

$$\Gamma_{Cl^-} = \frac{1}{H_B}\{\alpha C_S\Gamma_c + C_S\Gamma_h + (H_B-C_S)\Gamma_3\}, \quad (30b)$$

$$\Gamma_{Na^+} = \frac{C_B+C_S}{H_B}\{-\alpha\Gamma_c-\Gamma_h+\Gamma_3\}. \quad (30c)$$

(III) $H_2O+DHCl+HCl+NaCl$. In order to suppress possible hydrolysis of hydrochloride of weak base, HCl is added to the solution. In this case the Gibbs convention is written as

$$\Gamma_{H_2O} + \Gamma_{OH^-} = 0, \quad (31)$$

and the Gibbs adsorption isotherm is given by

$$-d\gamma = (\Gamma_D+\Gamma_{DH^+})d\mu_{DHCl} + (\Gamma_{Cl^-}-\Gamma_D-\Gamma_{DH^+} - \Gamma_{Na^+})d\mu_{HCl} + \Gamma_{Na^+}d\mu_{NaCl}. \quad (32)$$

Concentrations of counterion and coion are

$$C_{Cl^-} = C + C_A + C_S \text{ and } C_{Na^+} = C_S. \quad (33)$$

For Eq. 15 we have

$$\Gamma_2 = \left(1-\frac{\alpha(1-\alpha)C}{P_A}\right)(\Gamma_D+\Gamma_{DH^+}) + \left(\frac{(1-\alpha)C}{P_A}+\frac{C}{C+C_A+C_S}\right)\Gamma_{Cl^-} - \frac{(1-\alpha)C}{P_A}\Gamma_{Na^+}, \quad (34a)$$

$$\Gamma_A = -\frac{\alpha C_A}{P_A}(\Gamma_D+\Gamma_{DH^+}) + \left(\frac{C_A}{P_A}+\frac{C_A}{C+C_A+C_S}\right)\Gamma_{Cl^-} - \frac{C_A}{P_A}\Gamma_{Na^+}, \quad (34b)$$

$$\Gamma_3 = \frac{C_S}{C+C_A+C_S}\Gamma_{Cl^-} + \Gamma_{Na^+}, \quad (34c)$$

where

$$P_A = -(1-\alpha)^2C - C_A + 2C_{H^+}, \quad (34d)$$

$$= (1-\alpha^2)C + C_A + 2C_{OH^-}. \quad (34e)$$

Solving Eqs. 34a,b,c, we have

$$\Gamma_D + \Gamma_{DH^+} = \frac{1}{Z_A}\left\{(Z_A-\alpha^2C)\Gamma_2 - \frac{C}{C_A}[Z_A-(1+\alpha)(\alpha C+C_S)-\alpha C_A]\Gamma_A - \alpha C\Gamma_3\right\}, \quad (35a)$$

$$\Gamma_{Cl^-} = \frac{C+C_A+C_S}{Z_A}\left\{\alpha\Gamma_2 + \frac{1}{C_A} \times [Z_A-(1+\alpha)C-C_A-2C_S]\Gamma_A + \Gamma_3\right\}, \quad (35b)$$

$$\Gamma_{Na^+} = \frac{1}{Z_A}\left\{-\alpha C_S\Gamma_2 - \frac{C_S}{C_A}[Z_A-(1+\alpha)C-C_A -2C_S]\Gamma_A+(Z_A-C_S)\Gamma_3\right\}, \quad (35c)$$

where

$$Z_A = 2\alpha C + 2C_S + 2C_{H^+} \quad (35d)$$

$$= 2C + 2C_A + 2C_S + 2C_{OH^-}. \quad (35e)$$

Similarly, for Eq. 16 we have

$$\Gamma_e = \Gamma_D + \Gamma_{DH^+} + \frac{\alpha C}{C+C_A+C_S}\Gamma_{Cl^-}, \quad (36a)$$

$$\Gamma_h = -\alpha(\Gamma_D+\Gamma_{DH^+}) + \left(1+\frac{P_A}{C+C_A+C_S}\right)\Gamma_{Cl^-} - \Gamma_{Na^+}, \quad (36b)$$

and, solving Eqs. 36 and 35c, we have

$$\Gamma_D + \Gamma_{DH^+} = \frac{1}{Z_A}\{(Z_A-\alpha^2C)\Gamma_e - \alpha C(\Gamma_h+\Gamma_3)\}, \quad (37a)$$

$$\Gamma_{Cl^-} = \frac{C+C_A+C_S}{Z_A}(\alpha\Gamma_e+\Gamma_h+\Gamma_3), \quad (37b)$$

$$\Gamma_{Na^+} = \frac{1}{Z_A}\{-\alpha C_S\Gamma_e - C_S\Gamma_h + (Z_A-C_S)\Gamma_3\}. \quad (37c)$$

(IV) $H_2O+DHCl+NaOH+NaCl$. The Gibbs dividing surface is set in such a way that

$$\Gamma_{H_2O} + \Gamma_{H^+} - \Gamma_D = 0, \quad (38)$$

and the Gibbs adsorption isotherm is written as

$$-d\gamma = (\Gamma_D+\Gamma_{DH^+})d\mu_{DHCl} + (\Gamma_D+\Gamma_{DH^+}+\Gamma_{Na^+} -\Gamma_{Cl^-})d\mu_{NaOH} + (\Gamma_{Cl^-}-\Gamma_D-\Gamma_{DH^+})d\mu_{NaCl}. \quad (39)$$

Concentrations of counterion and coion are given by

$$C_{Cl^-} = C + C_S \text{ and } C_{Na^+} = C_B + C_S. \quad (40)$$

For Eq. 15 we have

$$\Gamma_2 = \left(1-\frac{\alpha(1-\alpha)C}{P_B}\right)(\Gamma_D+\Gamma_{DH^+}) + \left(\frac{(1-\alpha)C}{P_B}+\frac{C}{C+C_S}\right)\Gamma_{Cl^-} - \frac{(1-\alpha)C}{P_B}\Gamma_{Na^+}, \quad (41a)$$

$$\Gamma_B = \frac{\alpha C_B}{P_B}(\Gamma_D+\Gamma_{DH^+}) - \frac{C_B}{P_B}\Gamma_{Cl^-} + \left(\frac{C_B}{P_B}+\frac{C_B}{C_B+C_S}\right)\Gamma_{Na^+}, \quad (41b)$$

$$\Gamma_3 = \frac{C_S}{C+C_S}\Gamma_{Cl^-} + \frac{C_S}{C_B+C_S}\Gamma_{Na^+}, \quad (41c)$$

where

$$P_B = -(1-\alpha)^2C + C_B + 2C_{H^+} \quad (41d)$$

$$= (1-\alpha^2)C - C_B + 2C_{OH^-}. \quad (41e)$$

Solving Eqs. 41a,b,c we have

$$\Gamma_D + \Gamma_{DH^+} = \frac{1}{Z_B}\left\{(Z_B-\alpha^2C)\Gamma_2 + \frac{C}{C_B}[Z_B-(1+\alpha^2)C-\alpha C_B-(1+\alpha)C_S]\Gamma_B - \frac{C}{C_S}[Z_B-\alpha(1+\alpha)C-\alpha C_S]\Gamma_3\right\}, \quad (42a)$$

$$\Gamma_{Cl^-} = \frac{C+C_S}{Z_B}\left\{\alpha\Gamma_2 - \frac{1}{C_B}[Z_B-(1+\alpha)C-C_B-2C_S]\Gamma_B + \frac{1}{C_S}[Z_B-(1+\alpha)C+C_S]\Gamma_3\right\}, \quad (42b)$$

$$\Gamma_{Na^+} = \frac{C_B+C_S}{Z_B}\left\{-\alpha\Gamma_2 + \frac{1}{C_B}[Z_B-(1+\alpha)C-C_B-2C_S]\Gamma_B + \frac{1}{C_S}[(1+\alpha)C+C_S]\Gamma_3\right\}, \quad (42c)$$

where

$$Z_B = 2\alpha C + 2C_B + 2C_S + 2C_{H^+}, \quad (42d)$$

$$= 2C + 2C_S + 2C_{OH^-}. \quad (42e)$$

Similarly, for Eq. 16 we have

$$\Gamma_e = \Gamma_D + \Gamma_{DH^+} + \frac{C}{C+C_S}\Gamma_{Cl^-} + \frac{(1-\alpha)C}{C_B+C_S}\Gamma_{Na^+}, \quad (43a)$$

$$\Gamma_h = -\alpha(\Gamma_D+\Gamma_{DH^+}) + \Gamma_{Cl^-} - \left(1+\frac{P_B}{C_B+C_S}\right)\Gamma_{Na^+} \quad (43b)$$

and, solving Eqs. 43 and 41c, we have

$$\Gamma_D + \Gamma_{DH^+} = \frac{1}{Z_B}\left\{(Z_B-\alpha^2C)\Gamma_e - \alpha C\Gamma_h - \frac{C}{C_S}[Z_B-\alpha(1+\alpha)C-\alpha C_S]\Gamma_3\right\}, \quad (44a)$$

$$\Gamma_{Cl^-} = \frac{C+C_S}{Z_B}\left\{\alpha\Gamma_e + \Gamma_h + \frac{1}{C_S}[Z_B-(1+\alpha)C-C_B]\Gamma_3\right\}, \quad (44b)$$

$$\Gamma_{Na^+} = \frac{C_B+C_S}{Z_B}\left\{-\alpha\Gamma_e - \Gamma_h + \frac{1}{C_S}[(1+\alpha)C+C_S]\Gamma_3\right\}. \quad (44c)$$

Discussion

As was pointed out previously,[1,2] it has been shown that the Gibbs adsorption isotherm can be expressed in either of two forms, *i.e.*, in terms of variations of chemical potentials of constituents of two types, for an electrolyte solution. One is based on the ionic and nonionic species present in the solution, as given by Eq. 1, and the other is based on the neutral components added to make up the solution. The former expression is subject to various restrictions such as the ionic equilibria, Eqs. 2 and 3, and the stoichiometry, Eqs. 4—7, among different species, while the latter is free from such restrictions, except for setting the position of dividing surface. It was demonstrated that both expressions are equivalent and the dividing surface should be carefully drawn only after the latter expression has been obtained. The Gibbs convention is then expressed by Eq. 17, 24, 31, or 38, as is also illustrated in the expression for the Gibbs-Duhem equation.[10] As a result, the Gibbs adsorption isotherm is expressed in the form of Eqs. 18, 25, 32, or 39 by

the variations of chemical potentials of all the solute components added and their surface excesses can be defined uniquely.

There has been a prevailing superstition that the Gibbs adsorption isotherm should be written down in terms of chemical potentials of ionic and nonionic species present in the solution, since Guggenheim[11] gave it exclusively in this expression. Furthermore, this expression has often lead to an erroneous expression for the Gibbs convention in the cases containing weak electrolytes or attending hydrolysis of salts, because the ionization of water itself has been overlooked.[3,11,12]

After introducing the correct Gibbs convention, we can proceed to convert the chemical potentials of solute components into their (molar) concentrations, by relying on some approximations. In the present work we have made an approximation that the activity coefficients of all the solute components are unity. Even in this approximation, the calculation is intricate. After a straightforward calculation, the lowering of surface tension is expressed in terms of variations of concentrations of added components, or of pH of solution, as given by Eq. 15 or 16. Then we can readily derive the surface excesses of three species, *i.e.*, $D+DH^+$, Cl^-, and Na^+, as functions of three experimentally measurable quantities, Γ_2, Γ_X, and Γ_3, or Γ_e, Γ_h, and Γ_3. For the actual calculation we may usually neglect C_{H^+} or C_{OH^-} in the final equations.

It is not possible to separate the surface excess of DH^+ from that of D, nor to derive the surface excesses of H^+ and OH^-, as far as only measurements of surface tension are performed.

As special cases we will now derive expressions for ternary systems without added HCl or NaOH. Two systems, (I) and (II), reduce to $H_2O+D+NaCl$, and we put $C_X=0$ and $\Gamma_{Cl^-}=\Gamma_{Na^+}$. Then we have

$$\Gamma_D + \Gamma_{DH^+} = \left(1-\frac{\alpha^2 C}{2C_{OH^-}}\right)\Gamma_2, \tag{45a}$$

$$\Gamma_{Cl^-} = \Gamma_{Na^+} = \frac{1}{2}\Gamma_3. \tag{45b}$$

Similarly, two other systems, (III) and (IV), reduce to $H_2O+DHCl+NaCl$, and we put $C_X=0$. Since the surface excess of total added hydrochloride should be equal to that of Cl^- not originating from added NaCl, we have $\Gamma_D+\Gamma_{DH^+}=\Gamma_{Cl^-}-\Gamma_{Na^+}$. Then we obtain

$$\Gamma_D + \Gamma_{DH^+} = \frac{P}{Y}\{(C+2C_S)\Gamma_2 - C\Gamma_3\} \tag{46a}$$

$$\Gamma_{Cl^-} = \frac{C+C_S}{Y}\{P\Gamma_2 + 2C_{H^+}\Gamma_3\} \tag{46b}$$

$$\Gamma_{Na^+} = \frac{1}{Y}\{C_S P\Gamma_2 + 2(C+C_S)C_{H^+}\Gamma_3\}, \tag{46c}$$

where

$$P = -(1-\alpha)^2 C + 2C_{H^+} = (1-\alpha^2)C + 2C_{OH^-} \tag{46d}$$

$$Y = -(1-\alpha)^2 C^2 + 4(C+C_S)C_{H^+}$$
$$= 2(1-\alpha^2)C(C+2C_S) + 4(C+C_S)C_{OH^-}. \tag{46e}$$

Finally we will suggest that formal conversion is possible from the quaternary systems containing a weak base treated in this paper to those of a weak acid treated in a previous paper,[1] when $\Gamma_{HD}+\Gamma_{D^-}$ is substituted for $\Gamma_D+\Gamma_{DH^+}$, and Γ_{Cl^-} and Γ_{Na^+} are exchanged, in the equations cited below.

Equations, 20a,b,c, 21a,b,c, 22, and 23 hold for (I') $H_2O+HD+NaOH+NaCl$, if C_A and C_{H^+} in Eqs. 20d and 21d are replaced by C_B and C_{OH^-}, respectively. Similarly, Eqs. 27a,b,c, 28a, b, c, 29, and 30 are valid for (II') $H_2O+HD+HCl+NaCl$, if C_B and C_{H^+} in Eqs. 27d and 28d are replaced by C_A and C_{OH^-}, respectively.

Equations 34a,b,c, 35a,b,c 36, and 37 hold for (III') $H_2O+NaD+NaOH+NaCl$, if C_A and C_{OH^-} in Eqs. 34e and 35e are replaced by C_B and C_{H^+}, respectively. Similarly, Eqs. 41a,b,c, 42a,b,c, 43, and 44 are valid for (IV') $H_2O+NaD+HCl+NaCl$, if C_B and C_{OH^-} in Eqs. 41e and 42e are replaced by C_A and C_{H^+}, respectively.

References

1) S. Ikeda, *Bull. Chem. Soc. Jpn.*, **50**, 1403 (1977).
2) S. Ikeda, *Hyomen*, **15**, 592 (1977).
3) B. A. Pethica, *Trans. Faraday Soc.*, **50**, 412 (1954).
4) J. T. Davies, cited in E. Matijević and B. A. Pethica, *Trans. Faraday Soc.*, **54**, 1382 (1958).
5) D. K. Chattoraj, *J. Colloid Interface Sci.*, **26**, 379 (1968).
6) J. B. Rijnbout, *J. Colloid Interface Sci.*, **62**, 82 (1977).
7) S. Ozeki, M. Tsunoda, and S. Ikeda, *J. Colloid Interface Sci.*, **64**, 28 (1978).
8) S. Ozeki and S. Ikeda, *Bull. Chem. Soc. Jpn.*, **53**, 1832 (1980).
9) S. Ikeda, M. Tsunoda, and H. Maeda, *J. Colloid Interface Sci.*, **67**, 336 (1978).
10) S. Ikeda, unpublished.
11) E. A. Guggenheim, "Thermodynamics," North Holland, Amsterdam (1967), Chap. 7, p. 293f.
12) J. T. Davies and E. K. Rideal, "Interfacial Phenomena," Academic, New York and London (1961), Chap. 4, p. 197f.

Catalysis by Alkaline Earth Metal Oxides. I. The Mechanism of Ethylene Hydrogenation on Calcium Oxide

Kaname Kasama, Yasunobu Inoue,* and Iwao Yasumori

Department of Chemistry, Tokyo Institute of Technology, Ookayama, Meguro-ku, Tokyo 152

(Received October 26, 1979)

The mechanism of ethylene hydrogenation on a thermally activated CaO was studied in the overall temperature range of 197—623 K. The maximum in the reaction rate was observed around 320 K, while the activation energy was found to vary with the range of reaction temperatures, *i.e.*, 12.6 kJ/mol (197—273 K) and −16.7 kJ/mol (373—623 K). The partial pressure dependence of the rate was also different in these ranges; the reaction orders with respect to the hydrogen and ethylene pressures were 0.7 and nearly zero at 273 K respectively, whereas the orders shifted to 1.0 and 0.9 at 523 K in the pressure range from 6 to 40 Torr (1 Torr= 133.3 Pa). The reaction with deuterium at 523 K produced ethane containing widely distributed deuterium and was accompanied by the formation of highly-exchanged ethylene, HD, and H_2 molecules in the gas phase. On the contrary, the reaction at 273 K formed ethane [D_2] (>60%) selectively, and the hydrogen-deuterium exchange occurred to a lesser extent in both ethylene and deuterium. By the proposed associative mechanism, the variation in the kinetic behavior with the temperature was explained in terms of the change in the slow step from the reaction between the adsorbed hydrogen and surface ethylene to the hydrogenation of the ethyl radical. The poisoning of the hydrogenation by preadsorbed CO indicated that only 0.5% of the total surface atoms contributed actively to the reaction. On the basis of these results, the structures of active sites are briefly discussed.

Alkaline earth metal oxides have been known to become catalytically active in the H_2–D_2 equilibration reaction after irradiation with γ-rays.[1] Recently, however, Boudart *et al.* found that the thermal treatment *in vacuo* at temperatures as high as 873 K can activate MgO to catalyze the same reaction.[2] This finding has turned attention to the possibility of alkaline earth metal oxides as effective catalysts for other reactions. Tanabe and his co-workers found that the hydrogenation[3a,3b] as well as the isomerization[4] of olefins was catalyzed by BaO, MgO, CaO, and SrO when these oxides were evacuated at definite ranges of high temperatures. The mechanisms of such a generation of high activity and of the hydrogenation are of particular interest, but no precise information about them has so far been obtained.

In our series of work, we first studied the catalytic activity of calcium oxide in ethylene hydrogenation, since the reaction on CaO had not been investigated in detail, though extensive data on reactions over transition metals[5] and their oxides[6] had been accumulated. For a better understanding of the reaction mechanism, the kinetic study was carried out over a wide range of reaction temperatures and was supplemented by an analysis of deuterium distributions in the reaction of ethylene with deuterium. It is known that catalyses by transition metals and their oxides contrast remarkably with each other in terms of the deuterium distributions in the produced ethane;[6] metal surfaces provide a wide distribution of ethane from [D_0] to [D_6], whereas such oxides as Cr_2O_3[7] or ZnO[8] are characterized by the selective formation of ethane [D_2]. These features are apparently attributable to the nature of the active sites on the catalysts; in this regard, an examination of the deuterium distributions in the reaction on CaO is interesting.

It is necessary to determine the portion of the surface which participates in the catalytic reaction. The poisoning by preadsorbed CO was, therefore, examined, and the quantitative relationship between the increased amount of surface CO and the extent of activity fall was obtained. On the basis of these results, we can provide a brief description of the structure of the active sites, the details of which will appear in a following paper.

Experimental

The calcium oxide used as a catalyst was prepared by decomposing calcium hydroxide of an extra pure grade, purchased from the Junsei Kagaku Co., Ltd., *in vacuo*. The oxide thus obtained was evacuated ($<1\times10^{-6}$ Torr) for 2 h at temperatures between 873 and 1273 K. Emission spectral analysis showed that CaO contained Mg (<3 ppm), Si (<80), Fe (<0.1), Cu (<0.5), and Mn (<10). Ethylene hydrogenation was studied at temperatures between 197 and 623 K over a pressure range from 6 to 40 Torr by using a closed circulating system with a volume of 610 ml which was directly connected to a gas chromatograph for the analysis of C_2-hydrocarbons. About 0.2 g of CaO was used for the kinetic runs. Since ethane was the only product under the present experimental conditions, the initial rate of ethane formation was employed as the measure of catalytic activity throughout the study. In the reaction of ethylene with deuterium, the product and reactants were separated gas chromatographically and analyzed on a Hitachi RMU-7M mass spectrometer at an ionization voltage of 70 V. Hydrogen, hydrogen deuteride, and deuterium were analysed by means of a gas chromatograph.[9] The adsorption of CO on CaO activated at various temperatures was measured at room temperature and under pressures up to 40 Torr.

The hydrogen (99.99% pure), deuterium (containing less than 0.5% HD), carbon monoxide (99.5%), and ethylene (99.8%) were obtained from the Takachiho Chemical Co., Ltd., and were used without further purification.

Results

Figure 1 shows the variation in the surface area and the catalytic activity, V_e, represented by the ethane molecules produced per min and per m^2 of CaO as a function of the evacuation temperature. With an increase in the temperature, the surface area decreased monotonously, whereas V_e exhibited a max-

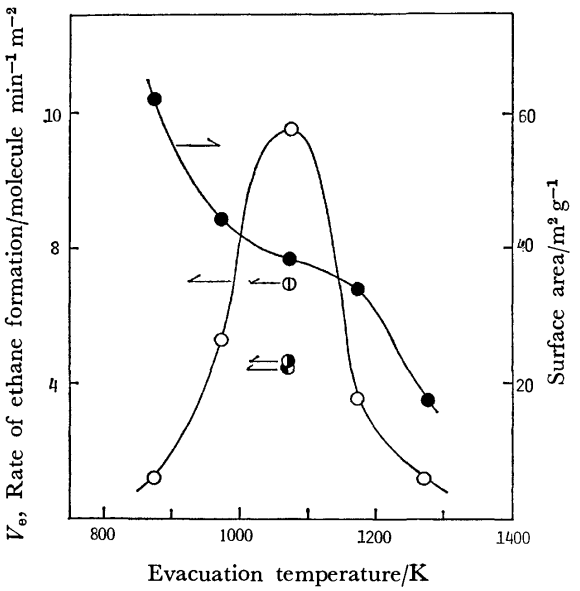

Fig. 1. Changes in surface area and catalytic activity of ethylene hydrogenation with evacuation temperature.
Reaction temp=573 K; P_h=20 Torr; P_e=10 Torr; ○; $Ca(OH)_2$ was decomposed *in vacuo*, followed by evacuation at respective temperatures, ⓘ; $Ca(OH)_2$ was calcined in air at 873 K before evacuation at 1073 K. ◑; Calcined at 973 K, ◐; calcined at 1073 K.

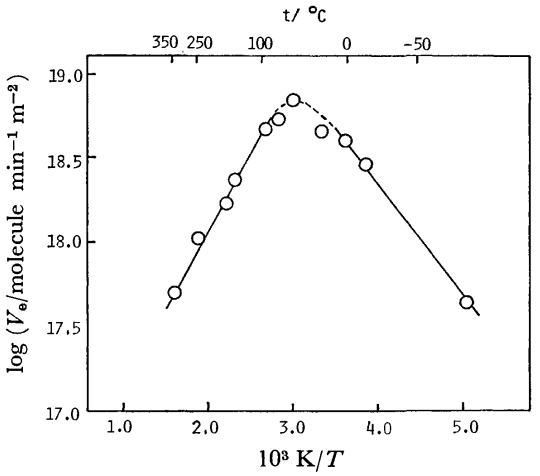

Fig. 2. Arrhenius plots of ethylene hydrogenation. P_h=20 Torr; P_e=10 Torr.

imum at 1073 K, which is larger by approximately one order of magnitude than the activity of the catalysts treated at 873 or 1273 K. This variation in the activity is similar to that previously reported by Hattori *et al.*,[3a] although their results involved no correction for the change in the surface area. Figure 1 also shows V_e for the oxides which were prepared by calcining $Ca(OH)_2$ in air at 873, 973, or 1073 K for 2 h, followed by evacuation at 1073 K for 2 h. In this case the V_e's were smaller by 40 to 60% than those for the catalysts prepared by the decomposition *in vacuo*.

Since the CaO surface activated at 1073 K exhibited not only the maximum activity, but also the typical

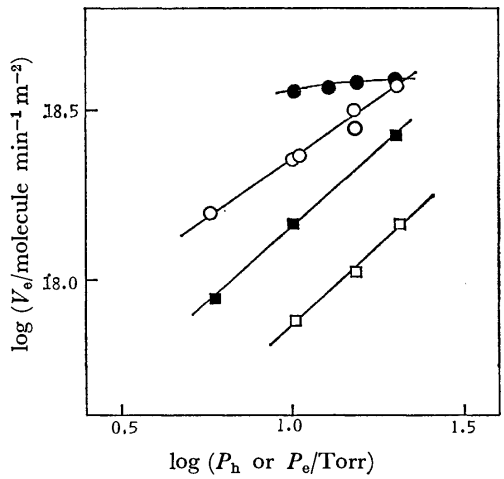

Fig. 3. Partial pressure dependence at 273 and 523 K. ○; $5.8<P_h<20$ Torr, P_e=10 Torr at 273 K, ●; $10<P_e<20$ Torr, P_h=20 Torr at 273 K, □; $10<P_h<20$ Torr, P_e=10 Torr at 523 K, ■; $6<P_e<20$ Torr, P_h=20 Torr at 523 K.

features of the catalysis, the kinetic study was carried out on the surface, unless otherwise stated. A gradual decay in the activity occurred during the course of the reaction at 533 K; the original activity was attenuated to almost 40% in the second run and to 10% in the third run. The activity thus reduced was, however, restored almost completely to the initial level after evacuation at 1073 K; hence, prior to each kinetic run, the catalyst was evacuated at that temperature for 30 min.

Figure 2 illustrates the Arrhenius plots of the hydrogenation in the temperature range between 197 and 623 K. The maximum in the rate appeared at around 340 K; the values of the apparent activation energy were determined to be 12.6 kJ mol^{-1} below 340 K and −16.7 kJ mol^{-1} above it. Such a complicated behavior suggests that the kinetics of the reaction is different in these regions. Thus, the reactions at 273 and 523 K were investigated as typical of the two regions. Figure 3 shows the partial pressure dependence of the rate. For the hydrogenation at 273 K, the reaction orders with respect to the hydrogen pressure, P_h, and the ethylene pressure, P_e, were, respectively, 0.7 and nearly zero, whereas at 523 K these orders shifted to 1.0 and 0.9. The deuterium distributions in ethylene and ethane at conversions of from 10 to 80% are summarized in Tables 1 and 2, together with the isotopic compositions of hydrogen in the gas phase. It should be noted that the differences in the distributions as well as the reaction orders between the reactions at these temperatures are striking. No isotopic exchange between D_2 and C_2H_6 occurred on CaO at reaction temperatures up to 523 K.

The adsorption of CO on CaO was examined at room temperature and in the pressure range up to 40 Torr. The amount CO adsorbed increased with the CO pressure and attained an almost saturation at the highest pressure employed. After the first run of adsorption the CO-covered surface was evacuated

TABLE 1. DEUTERIUM DISTRIBUTIONS IN THE REACTANT AND PRODUCT MOLECULES AT 273 K

Conv. (%)	Ethylene (%)					Ethane (%)							H_2	HD	D_2
	d_0	d_1	d_2	d_3	d_4	d_0	d_1	d_2	d_3	d_4	d_5	d_6		(%)	
12	97.7	0.5	1.5	0.2	0.1	0.6	16.0	72.3	9.9	1.2	0	0	0	5.7	94.3
26	94.6	0.9	4.0	0.4	0.1	1.3	18.5	62.8	11.7	5.0	0.7	0	0	12.9	87.1
52	88.6	1.6	9.2	0.5	0.1	2.5	20.4	58.3	15.5	2.9	0.4	0	1.0	17.6	81.4
74	69.9	8.7	17.2	3.9	0.3	1.0	20.8	54.4	19.8	3.4	0.6	0	1.1	23.0	75.9

P_D=20 Torr, P_e=10 Torr.

TABLE 2. DEUTERIUM DISTRIBUTIONS IN THE REACTANT AND PRODUCT MOLECULES AT 523 K

Conv. (%)	Ethylene (%)					Ethane (%)							H_2	HD	D_2
	d_0	d_1	d_2	d_3	d_4	d_0	d_1	d_2	d_3	d_4	d_5	d_6		(%)	
11	59.6	23.6	11.7	4.4	0.7	0	31.8	34.2	19.0	10.3	3.9	0.8	2.1	22.4	75.5
28													10.7	34.8	54.5
53	5.4	23.9	35.9	26.6	8.2	0	29.7	29.3	21.2	13.4	5.4	1.0	16.7	43.9	39.4
77													17.8	43.0	39.2
84	0	11.3	32.4	38.9	17.4	0	27.7	27.9	23.6	14.0	5.6	1.2	18.0	44.3	37.7

P_D=20 Torr, P_e=10 Torr.

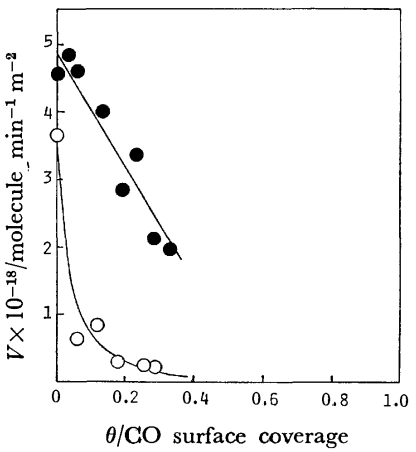

Fig. 4. Effect of preadsorbed CO on ethylene hydrogenation.
○; 273 K, ●; 373 K, P_h=20 Torr, P_e=10 Torr. CaO evacuated at 1073 K. The number of CO molecule at θ=1.0 is 1.48×10^{17} molecule m^{-2}.

at room temperature for 30 min and then exposed again to CO. In the second run, no significant adsorption occurred, indicating that the sites for the adsorption are saturated almost completely with the irreversibly bound CO. The amount at saturation was evaluated to be 1.6, 14.8, and 3.7×10^{16} molecules m^{-2} for CaO outgassed at 873, 1073, and 1273 K respectively. The evacuation temperature, after the first run of adsorption, was raised to 373 K, but the subsequent exposure to CO at room temperature gave rise to no detectable adsorption. Such a strong adsorption of CO accords with the preliminary results on thermal desorption; no gases were evolved from the surface with CO adsorbed on heating up to 423 K.

The effect of the irreversibly adsorbed CO upon the catalytic activity was examined at different reaction temperatures. Figure 4 indicates that the catalytic activity at 373 K decreased almost linearly with the increase in the coverage of CO, whereas the reaction at 273 K was characteristic in showing a drastic fall in the activity at the initial coverage of CO adsorption. The extrapolation of the plot showed that the activity is completely destroyed at the surface density of CO, 8×10^{16} molecules m^{-2}, which corresponds to about 0.5% of the total surface atoms.

Discussion

Reaction Pathway and Mechanism. The variation in the kinetic behavior of the reaction with the reaction temperature has been reported on the hydrogenation of ethylene[10] and 1-butene[11] over Ni metal catalysts. It is of interest that a similar phenomenon was observed in the present study of the reaction catalyzed by the calcium oxide surface. Such a similarity in the kinetic behavior is striking in the high-temperature region.

During the course of the reaction with deuterium in the high-temperature region, an equilibrium among the partial pressures of H_2, HD and D_2 in the gas phase was readily reached, and highly-exchanged ethylenes with deuterium were produced, even in a conversion as low as 11%. Thus, the following pathway of the reaction including the associative adsorption of ethylene can be proposed:

$$H_2(g) \rightleftharpoons 2H(a) \quad (1)$$

$$C_2H_4(g) \rightleftharpoons C_2H_4(a) \quad (2)$$

$$H(a) + C_2H_4(a) \rightleftharpoons C_2H_5(a) \quad (3)$$

$$H(a) + C_2H_5(a) \longrightarrow C_2H_6(g) \quad (4)$$

where (g) and (a) denotes, respectively, species in the gas phase and the adsorbed state. The observed deuterium distributions clearly indicate that Steps (1) and (2) are in a pseudo-equilibrium. The wide distributions of deuterium in the produced ethane further suggest that the forward and reverse processes of Step (3) are fast. Accordingly, the surface reaction (4)

is assumed to be the rate-determining step in the reaction at high temperatures, and we can obtain the following rate equation for ethane formation:

$$V_e^h = k_4\theta_h\theta_{el} = \frac{k_4K_hK_eK_3P_hP_e}{(1+\sqrt{K_hP_h}+K_eP_e+K_3K_eP_e\sqrt{K_hP_h})^2} \quad (5)$$

where θ_h and θ_{el} denote, respectively, the fractions of the hydrogen atom and the ethyl radical, which occupy the surface sites. The k_4, K_h, and K_e constants are the rate constant and the adsorption constants of hydrogen and ethylene respectively. K_3 is an equilibrium constant in Step (3). When $1 \gg \sqrt{K_hP_h}+K_eP_e+K_3K_eP_e\sqrt{K_hP_h}$, Eq. 5 is reduced to

$$V_e^h = k_4K_hK_eK_3P_hP_e = kP_hP_e \quad (6)$$

which agrees with the experimental pressure dependence. Equation 6 leads to the energy relationship, $E_a=E_t-Q_h-Q_e-Q_3$, where E_t is the activation energy of Reaction Step (4); Q_h is the heat of hydrogen adsorption; Q_e, the heat of ethylene adsorption, and Q_3, the heat of Reaction 3. The amounts of hydrogen and ethylene adsorbed on the CaO surface are so small that no reliable numerical data on the heat of adsorption are available at present, but the negative value of the apparent activation energy, $E_a=-16.7$ kJ mol^{-1}, is explicable if $E_t<Q_h+Q_e+Q_3$, as is seen in the case of Ni catalysts.

In the low-temperature range below 340 K, the characteristic features are the hydrogen order of 0.7, which was smaller than that, 1.0, for Ni and other transition metal catalysts, and also the selective formation of ethane[D_2] in the reaction with deuterium. Unlike Ni metal, no drastic rise in ethane[D_0] in the initial stage of the reaction was observed. The exchanged ethylene as well as hydrogen deuteride was produced in the gas phase, but their fractions were much smaller than those in the high-temperature range. These results predict that Step (3) is relatively slow compared to the other steps. In order to explain the kinetic order of 0.7 with respect to hydrogen, however, we have to introduce the assumption that a pair of dissociated hydrogen atoms on an isolated site is allowed to react with the adsorbed ethylene, because the contribution of hydrogen atoms in a randomly-mixed state to the reaction leads to a rate equation which cannot provide a kinetic order higher than 0.5. The assumption of an isolated site is supported by the results of CO posioning, which revealed that the fraction of the active site is less than 0.5% of the total surface. The selective formation of ethane-[D_2] is also well accounted for by the nearly irreversible addition of the paired deuterium atoms on the site. Thus, the rate of ethane formation, V_e^1, is given by the following equation:

$$V_e^1 = k_3^1\theta'_h\theta_e = \frac{k_3^1K_hK_eP_hP_e}{(1+K_hP_h+K_eP_e)^2} \quad (7)$$

where θ'_h and θ_e are the fractions of coverage for the adsorbed hydrogen atom pair and for the adsorbed ethylene respectively. k_3^1 is a rate constant. Equation 7 was then transformed into

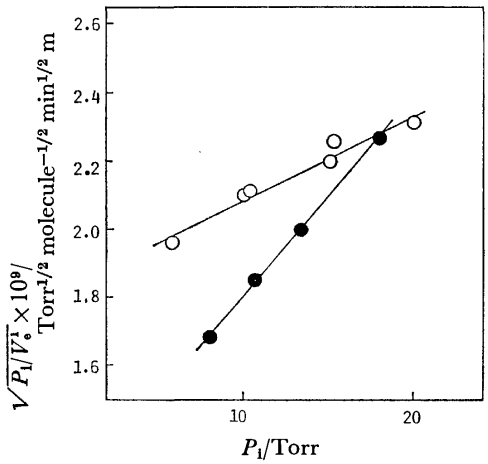

Fig. 5. Plots of $\sqrt{P_l/V_e^1}$ *vs.* P_l.
○; $P_l=P_h$ ($P_e=10$ Torr), ●; $P_l=P_e$ ($P_h=20$ Torr).

$$\sqrt{\frac{P_h}{V_e^1}} = \sqrt{\frac{1}{k_3^1K_hK_eP_e}}(1+K_eP_e+K_hP_h) \quad (8)$$

or

$$\sqrt{\frac{P_e}{V_e^1}} = \sqrt{\frac{1}{k_3^1K_hK_eP_h}}(1+K_eP_e+K_hP_h). \quad (9)$$

Figure 5 shows the plots of the $\sqrt{P_e/V_e^1}$ term against P_e (P_h=constant) and of the $\sqrt{P_h/V_e^1}$ term against P_h (P_e=constant). The linear relationships observed in the experimental results indicate the validity of the derived equation and, hence, the mechanism proposed.

It is of interest to compare the present data with those of others. The activation energy of 12.6 kJ mol^{-1} in the low-temperature range was smaller than those for such transition metal catalysts as Ni, Fe, and Pd,[5] 30—40 kJ mol^{-1}. This is due to the fact that the slow step of the hydrogenation on CaO is the addition of the dissociated hydrogen atom pair to the adsorbed ethylene, whereas that on the metals is the dissociative adsorption of hydrogen. Another difference was observed in the deuterium distributions in ethane; the selectivity of ethane[D_2] formation in the present case was considerably higher than the earlier-reported values, 20% for Ni[10] (363 K and 20% in conversion), 22% for Fe[12] (173 K and 100%), and 17% for Pd[13] (257 K and 5%). The selectivity, however, was much less than those, almost 100% for such oxides as Cr_2O_3[7] (273 K), ZrO[8] (298 K), and Co_3O_4[14] (296 K). The CaO surface is also different from these metals in the infeasibility of the isotopic exchange between D_2 and ethane. Since the catalytic properties are different from those of the transition metals or their oxides, one can rule out the possibility that the catalytic activity of CaO might be ascribable to a trace of such components exposed at the surface.

As for the density of the active sites, the amount of CO which caused zero activity enables us to determine the fraction of the active part at be about 0.5%, which corresponds to 8×10^{12} surface ions cm^{-2}, provided that a CO molecule adsorbs on a surface ion. This result also shows that only specific sites are able to contribute to the catalytic reaction. By the use of this value, the turn-over frequency, N_t, was determined to be 0.75 s^{-1} at 273 K (P_h=20 and P_e=10

Torr). For a comparison of N_t, the data of others were corrected to the conditions of our work. N_t is given as 0.7—1.3 s^{-1} for the silica-supported Pt[15] after calculation using the rate equation of $V_e=k'P_H^{1.0}P_e^{0.0}$. The value of N_t for the reaction on ZnO is evaluated to be 3×10^{-4}—6×10^{-4} s^{-1} by using the pressure dependence of a half-order with respect to the hydrogen pressure and by assuming that a reactive ethylene occupies an active site.[8,16] These comparisons clearly show that the activated CaO is able to catalyze the hydrogenation of ethylene effectively.

Structure of Active Sites. A detailed study of the active sites will be published in a subsequent paper;[17] thus, we will present here only a brief description of the plausible models of the structure of the sites and the pathway of the hydrogenation on them. The decomposition of $Ca(OH)_2$ caused the rearrangement of the structure from trigonal hydroxide to cubic oxide. A recent mass-spectrometric analysis of gases evolved during the thermal decomposition of $Mg(OH)_2$ to MgO showed that hydrogen is released together with H_2O by evacuation at high temperatures.[18] This suggests that the desorption of hydrogen leaves oxygen atoms which are coordinatively unsaturated and negatively charged. The same processes presumably take place on CaO, since the oxide tends to form the peroxide more readily than does MgO. Thus, the electron-donating species, $-O-\overset{O^{\delta-}}{\underset{|}{Ca}}-O-$, are likely to participate in the catalytic cycle of the hydrogenation. The importance of this species, O_s^-, adjacent to an isolated OH^- group has also been pointed out in the case of the H_2–D_2 equilibration reaction on MgO.[2] It is plausible that the active sites on CaO for the equilibration are analogous to those on MgO. It should be noted, however, that there existed a clear difference in the activation temperature of CaO for these reactions; CaO evacuated at 1273 K still possessed a high capability of catalyzing the equilibration reaction,[2] but lost its activity for the hydrogenation of ethylene. These facts indicate that the active sites for the reactions are not identical and predict that the hydrogenation requires a contribution from the exposed Ca cations. This view is supported by the preliminary results on the structural rearrangement of CaO upon heat treatment.[17] The fact that the active sites correspond to a small surface fraction, 0.5%, of the total surface atoms shows only a part of the surface in a specific conformation to be effective; thus, we tentatively propose a structure which is composed of the exposed Ca ion and the nearby O_s^- species. The hydrogenation of ethylene presumably proceeds as follows:

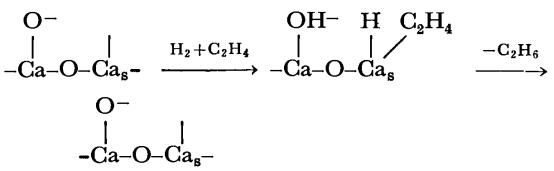

where Ca_s denotes the exposed Ca ion.

The poisoning effect of CO on the hydrogenation of ethylene varied with the reaction temperature. The catalytic activity for the reaction at a high temperature decreased almost proportionaly to the CO coverage as a consequence of the homogeneous occupation of the active sites. This homogeneous character in the distribution of the active sites is probably achieved by the migration of hydrogen atoms from site to site at high temperatures. The presence of the hydrogen atom is consistent with the proposed mechanism that the rate-determining step is the surface reaction of a hydrogen atom with an ethyl radical. On the contrary, the poisoning effect at low temperatures was characterized by a marked fall in the activity in the initial coverage of CO. The presence of hydrogen-pair atoms together with ethylene in the low-temperature reaction puts more restrictions on the conformation of the active sites available for their adsorption than those for the reaction at high temperatures.

The adsorbed state of CO on CaO is not clear at present, but information from an infrared spectroscopic study of CO adsorbed on MgO[19] is available; the exposure of MgO evacuated at 1273 K to CO at room temperature gave rise to two absorption peaks at 2100 cm^{-1}, in addition to complex bands in the region of 1450 cm^{-1}. The former absorption is characteristic of the stretching vibration of the CO molecule linked through the carbon atom to a single atom of the surface, whereas the latter might be associated with the CO molecule undergoing interaction with O^- and/or O^{2-} in the vicinity.[20] A CO adsorption of a similar type is plausible in the case of CaO, and it appears likely that CO exists as a linear form on the exposed $-Ca_s-$.

A study is now in progress by the aid of X-ray Photoelectron Spectroscopy and ESR to clarify further the details of the structure and nature of the active sites.

References

1) J. H. Lunsford, *J. Phys. Chem.*, **68**, 2321 (1964); C. G. Harkins, W. W. Shang, and T. W. Leland, *J. Phys. Chem.*, **73**, 130 (1969).

2) M. Boudart, A. Delbouille, E. G. Derouane, V. Indovina, and A. B. Walters, *J. Am. Chem. Soc.*, **94**, 6622 (1972).

3a) Y. Tanaka, H. Hattori, and K. Tanabe, *Chem. Lett.*, **1976**, 37.

3b) H. Hattori, Y. Tanaka, and K. Tanabe, *J. Am. Chem. Soc.*, **98**, 4652 (1976).

4) H. Hattori, Y. Tanaka, and K. Tanabe, *Chem. Lett.*, **1975**, 659; H. Hattori and A. Satoh, *J. Catal.*, **45**, 32 (1976).

5) G. C. Bond, "Catalysis by Metals," Acad. Press, New York (1962), p. 241.

6) A. Ozaki, "Isotopic Studies of Heterogeneous Catalysis," Kōdansha, Tokyo (1977), p. 92.

7) R. L. Burwell, Jr., A. B. Littlewood, M. Cardew, G. Pass, and C. T. H. Stoddart, *J. Am. Chem. Soc.*, **82**, 6272 (1960).

8) W. C. Corner, R. A. Innes, and R. J. Kokes, *J. Am. Chem. Soc.*, **90**, 6858 (1968).

9) S. Ohno and I. Yasumori, *Bull. Chem. Soc., Jpn.*, **41**, 2227 (1968).

10) G. I. Jenkins and E. K. Rideal, *J. Chem. Soc.*, **1955**,

2490; S. Sato and K. Miyahara, *J. Res. Inst. Catal. (Hokkaido Univ.)*, **13**, 10 (1965).
11) Y. Amenomiya, *J. Res. Inst. Catal. (Hokkaido Univ.)*, **9**, 1 (1961).
12) C. Kemball, *J. Chem. Soc.*, **1956**, 735.
13) G. C. Bond, J. J. Phillipson, P. B. Wells, and J. M. Winterbottom, *Trans. Faraday Soc.*, **62**, 443 (1966).
14) K. Tanaka, H. Nihira, and A. Ozaki, *J. Phys. Chem.* **74** 4510 (1970).
15) J. C. Schlatter and M. Boudart, *J. Catal.*, **24**, 482 (1972).
16) K. Tanaka and G. Blyholder, *J. Phys. Chem.*, **76**, 1394 (1972).
17) Y. Inoue and I. Yasumori, to be published.
18) R. Martens, H. Gentsch, and F. Freud, *J. Catal.*, **44**, 366 (1976).
19) H. Imai, H. Hattori, and K. Tanabe, 43th Meeting of the Catalysis Society, Nagoya, Japan (1978), Preprint(A), p. 168.
20) M. Courtois and S. J. Teichner, *J. Catal.*, **1**, 121 (1962).

Solvent Effect on the Partition Equilibrium of Normal Aliphatic β-Diketones between Heptane and Water–Dimethyl Sulfoxide Mixed Solvents. The Extended McDevit-Long Approach

Hitoshi WATARAI and Nobuo SUZUKI*

Department of Chemistry, Faculty of Science, Tohoku University, Sendai 980

(Received October 30, 1979)

The partition equilibria of 7 normal aliphatic (C_5-C_9) β-diketones were investigated in the two-phase systems of heptane/water–dimethyl sulfoxide (DMSO) mixed solvents at 25 °C. The partition coefficients, P, of the keto and enol forms of the β-diketones were determined, and the linear correlations between log P and the number of carbon atoms in the *n*-alkyl groups were observed. In general, an increase in the mole fraction of DMSO, X_S, in the mixed-solvent phase caused a lowering of the partition coefficient, while with smaller β-diketones, distinct maxima were observed at $X_S \simeq 0.2$. The solvent effect of the mixed-solvent phase was interpreted on the basis of the extended McDevit-Long theory previously proposed by the present authors.

The importance of the solvent effect of the aqueous phase on the liquid-liquid partition equilibrium is well recognized by workers engaged in extraction chemistry. For example, an increase in the electrolyte concentration in the aqueous phase improves the extraction of nickel(II) with acetylacetone[1] and the partition of 8-quinolinol[2] and β-diketones.[3] Recently, it has been reported that the introduction of a water-missible organic solvent, *e.g.*, acetone,[4] 2-propanol,[5] or DMSO,[6] into the aqueous phase also improves the extraction of inorganic substances, *e.g.*, uranium,[4] protactinium,[5] or hafnium.[6] However, no systematic investigation of the role of the aqueous phase has yet been reported.

Previously, we pointed out that the partition coefficient of acetylacetone in the heptane/water–DMSO system shows a distinct maximum at a mole fraction of DMSO of about 0.2.[7] Recently, we observed that the addition of an organic solvent to the aqueous phase produces an interesting effect like a salting-out on the partition of the nonpolar solute and that the variation in the partition coefficient at a different solvent composition can be interpreted semi-quantitatively by making use of the extended McDevit-Long theory.[8]

In the present study, the partition coefficients of a series of normal aliphatic β-diketones in the two-phase system of heptane/water–DMSO are determined, and the substituent effect and the solvent effect are discussed.

Experimental

Chemicals. The acetylacetone (Nakarai, G. R.) was purified by fractional distillation. The methods of synthesis and purification of the normal aliphatic β-diketones were described previously.[9] The β-diketones are listed in Table 1. The solvents used in this study were purified by a method described previously.[7] The mixed aqueous solvents were prepared by weight at desired mole fractions within ±0.0005.

Partition Experiment. Five ml of a heptane solution of β-diketone ($<10^{-2}$ M) and an equal volume of the mixed solvent were stirred by means of a magnetic stirrer in a water-jacketted partition vessel thermostated at 25±0.1 °C for 12 h. After standing for 2 h, the mixed-solvent phase was pipetted out into a quartz cell and the concentration of β-diketone in the solution was determined photometrically. The partition coefficient was calculated from the initial concentration and the concentration in the mixed-solvent phase. For larger β-diketones, a relatively concentrated solution (0.1 M) in heptane has to be used because of its large partition coefficient, but no concentration effect on the partition coefficient was observed up to 0.54 M. Partition measurements were repeated twice or more, and the relative standard deviation was within 3%.

Estimation of Enol Fraction. β-Diketones are present as enol and keto forms in both phases of the partition system. The NMR method is now considered to be the most reliable one for the determination of the enol fraction of β-diketone in solution.[10] In the present study, however, the NMR method is difficult to apply because of the low solubility of the β-diketones and the large solvent signals of water–DMSO mixed solvent, which make an accurate determination of the enol fraction impossible. Previously, we found, for acetylacetone, a linear relationship between the apparent molar absorptivity at the absorption maximum and the enol fraction as determined by the NMR method.[7,11] Therefore, the enol fractions of normal aliphatic β-diketones in the mixed solvents were estimated by making use of the empirical relationship, assuming that the substituent effect of the alkyl group on the molar absorptivity could be neglected. The error in the estimated enol fraction is less than 0.05. The enol fractions in heptane were determined by the NMR method. The enol fraction was calculated from the integrated signal intensities of the keto-methylene protons and the enol-methine proton, or from those of the methyl protons in both tautomers.

Results

The observed partition coefficients and the enol fractions in heptane and in mixed solvents are listed in Table 1. The partition coefficients for the keto and enol forms are calculated from the following equations:

$$P_K = \frac{1-f_o}{1-f}P \qquad P_E = \frac{f_o}{f}P. \tag{1}$$

In Fig. 1, log P_K and log P_E are shown as functions of the mole fraction of DMSO. The results show that the variation in the partition coefficient with X_S is more remarkable for the enol tautomer than for the keto tautomer and that a distinct maximum in the partition coefficient appeares at $X_S \simeq 0.2$ for smaller β-diketones.

Table 1. Observed partition coefficients, P, of normal aliphatic β-diketones in heptane/water–DMSO and enol fractions in the mixed solvent, f,[b] and in heptane, f_o[c]

Solute		Mole fraction of DMSO								
		0.000	0.100	0.200	0.300	0.400	0.500	0.600	0.800	1.000
Acetylacetone	P	0.887	1.06	1.10	0.920	0.675	0.470	0.33	0.21	0.156
	f	0.17[a]	0.23	0.30	0.38	0.44	0.48	0.51	0.54	0.55[c]
	f_o	0.97								
2,4-Hexane-dione	P	3.28	3.21	3.26	2.31	1.57	1.01	0.644	0.384	0.236
	f	0.12	0.18	0.24	0.30	0.36	0.39	0.42	0.46	0.51[c]
	f_o	0.96								
3,5-Heptane-dione	P	10.4	9.00	7.83	5.59	3.41	2.10	1.21	0.601	0.371
	f	0.10	0.15	0.20	0.26	0.30	0.35	0.37	0.41	0.44[c]
	f_o	0.95								
2,4-Heptane-dione	P	15.0	12.5	10.6	7.18	4.01	2.33	1.49	0.699	0.425
	f	0.16	0.24	0.32	0.39	0.45	0.50	0.52	0.57	0.60
	f_o	0.97								
3,5-Octane-dione	P	53.7	38.4	29.7	17.5	9.42	5.03	2.90	1.26	0.644
	f	0.13	0.19	0.26	0.33	0.39	0.43	0.46	0.51	0.52
	f_o	0.96								
2,4-Octane-dione	P	54.2	39.4	29.3	17.5	9.36	4.61	2.65	1.16	0.646
	f	0.17	0.24	0.32	0.39	0.46	0.49	0.53	0.57	0.61
	f_o	0.97								
4,6-Nonane-dione	P	269	171	113	56.9	26.2	12.3	5.92	2.32	1.18
	f	0.16	0.25	0.34	0.41	0.48	0.52	0.55	0.58	0.64
	f_o	0.97								

a) M. L. Eidinoff, *J. Am. Chem. Soc.*, **67**, 2073 (1945). b) Estimated from the relationship between f and ε_{max}. c) By the NMR method.

Discussion

Correlation between log P *and the Carbon Number.*

The plots of log P_K and log P_E against the number of carbon atoms in the *n*-alkyl substituent show a linear relationship in every partition system (Fig. 2); *i.e.*,

$$\log P = An + B, \tag{2}$$

where A corresponds to the logarithm of the partition coefficient of the methylene group, log P(–CH_2–), and B, to that of the enol or diketone skeleton, log P(–COCHCOH–) or log P(–$COCH_2CO$–). The values of A and B, obtained from the slope and intercept in Fig. 2, respectively, are illustrated in Fig. 3. This decreasing order of the partition coefficients: P(–CH_2–) > P(–COCHCOH–) > P(–$COCH_2CO$–) was observed in every partition system; it corresponds to the expected order of increase in the dipole moment of the groups. Log P(–CH_2–) decreases monotonously with the increases in X_s and gives an equal value for the two tautomers. Both log P(–COCHCOH–) and log P(–$COCH_2CO$–) show maxima in the water-rich region. From the results shown in Fig. 3, the maxima in log P_K and log P_E, which become remarkable in smaller β-diketones, as has been noted in Fig. 1, can be ascribed to those in log P(–$COCH_2CO$–) and log P(–COCHCOH–).

Composition Dependence of Partition Coefficient.

In a previous paper, the McDevit-Long theory has been extended to the estimation of the activity coefficient in a water–organic solvent mixture.[8] In this extended treatment, the activity coefficient of a nonelectrolyte infinitely diluted in an aqueous mixed solvent can be expressed by the following equation;

$$\ln f_n = -\frac{v_n^\infty}{RT}\frac{P_i}{\alpha T}\frac{v^E}{v}, \tag{3}$$

where f_n and v_n^∞ refer to the activity coefficient and the partial molar volume of the nonelectrolyte respectively; v and v^E to the mean molar volume of the ideal mixed solvent and the excess molar volume of the real mixed solvent, and P_i and α, to the internal pressure and the coefficient of the thermal expansion of the mixed solvent respectively. The activity coefficient given by Eq. 3 reflects the difference in the cavity-formation energy or the solvophobic interaction energy of the solute in different solvent systems, the ideal mixed solvent, and the real mixed solvent, because a direct interaction between the solute and the solvent molecules is left out of account in this treatment. When Eq. 3 is applied to an interpretation of the solvent effect, the contribution of the solvation should be eliminated by a reasonable treatment. For this purpose, we adopted the volume-fraction treatment, which is recommended for the calculation of the excess value when the molar volumes of the solute and the solvent differ considerably,:[12]

$$\Delta \ln P_x = \ln P_x - (1-\phi_s)\ln P_{x,0} - \phi_s \ln P_{x,1}, \tag{4}$$

where P_x refers to the partition coefficient in the mole-

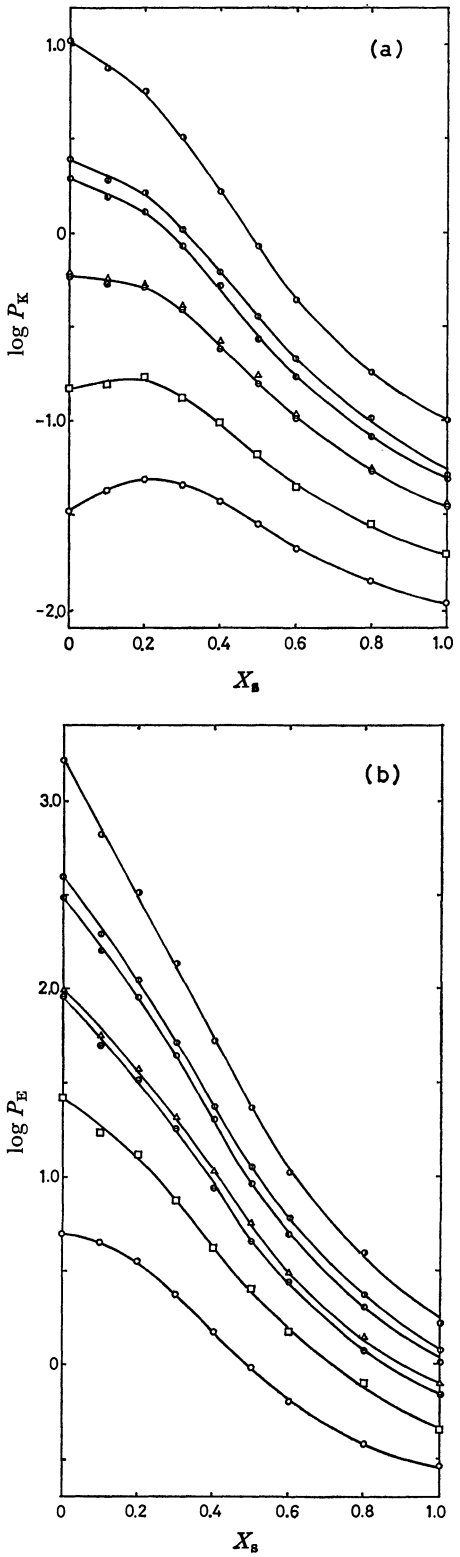

Fig. 1. Variation of partition coefficients of keto form (a) and enol form (b) of β-diketones with mole fraction of DMSO in mixed solvent phase.
○: Acetylacetone, □: 2,4-hexanedione, △: 3,5-hexanedione, ⓘ: 2,4-heptanedione, ⓘ: 3,5-octanedione, ◐: 2,4-octanedione, ◑: 4,6-nonanedione.

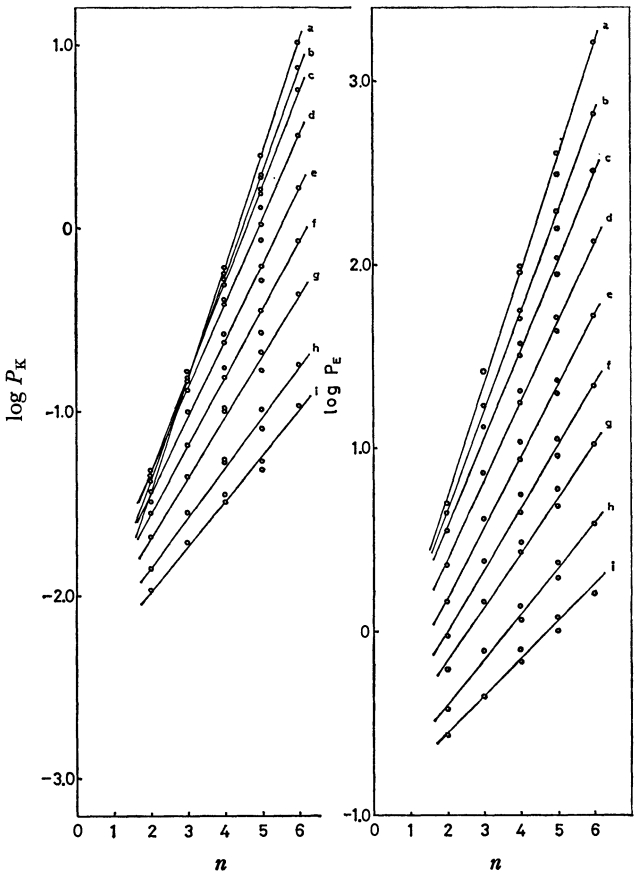

Fig. 2. Correlation between log P_K or log P_E and number of carbon atoms in substituent.
n: Mole fraction of DMSO; a: 0.0, b: 0.1, c: 0.2, d: 0.3, e: 0.4, f: 0.5, g: 0.6, h: 0.8, i: 1.0.

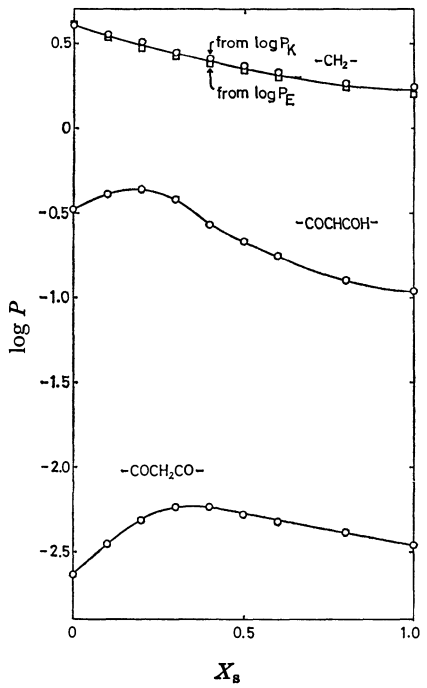

Fig. 3. Variation of group partition coefficients, log P(-CH_2-), log P(-COCHCOH-), and log P(-$COCH_2$-CO-), with X_S.

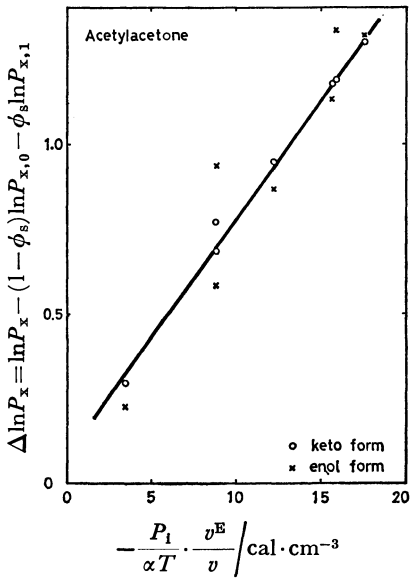

Fig. 4. Correlation between $\Delta \ln P_x$ of keto and enol forms of acetylacetone and the pressure factor.

fraction scale, ϕ_s to the volume fraction of DMSO, and the subscripts 0 and 1 to the heptane/water and heptane/DMSO systems. $\Delta \ln P_x$ in Eq. 4 corresponds to $\ln f_n$ in Eq. 3. From Eqs. 3 and 4, a linear correlation between $\Delta \ln P_x$ and the pressure factor, $-(P_1/\alpha T)(v^E/v)$, can be expected. In practice, for acetylacetone and other β-diketones the plots of $\Delta \ln P_x$ against $-(P_1/\alpha T)(v^E/v)$ show linear correlations both for the keto form and the enol form (Figs. 4 and 5). The slopes in these figures are expected to increase with increases in the molar volume or length of the alkyl chain (*cf.* Eq. 3). The slopes for keto forms were plotted against the molar volumes, v_n, calculated assuming that the molar volume of the acetylacetone-keto form is 110.99 cm^3 mol^{-1} [13] and the volume of methylene group is 22.2 cm^3 mol^{-1}.[14] Figure 6 shows clearly a proportionality between $\Delta \ln P_x$ and the molar volume. From these results, it may be concluded that the maximum observed in the partition coefficient is correlated to the increase in the pressure factor $-(P_1/\alpha T)(v^E/v)$, which reflects an increase in the solvent-solvent interaction. This situation is quite similar to a salting-out phenomenon induced by a structure-making electrolytes. The composition dependences of the group partition coefficient, P(–CH_2–), P(–$COCH_2CO$–) and P(–COCH-COH–), shown in Fig. 3, can also be understood from the present consideration.

A further discussion will be given to compare the slopes in Figs. 4 and 5 with the one expected from Eq. 3, but the observed slope is one half to one-third of the expected one. This is noted also by McDevit and Long in their original treatment of the salt effect;[15] they ascribed the discrepancy in their results to a disregard of the closest distance between electrolyte and nonelectrolyte and suggested the introduction of the correction term of $a/(a+b)$, where a and b correspond to the distances of the closest approach to the average "solvated" ion and to the nonelectrolyte molecule, respectively. Recently, Cross and McTigue

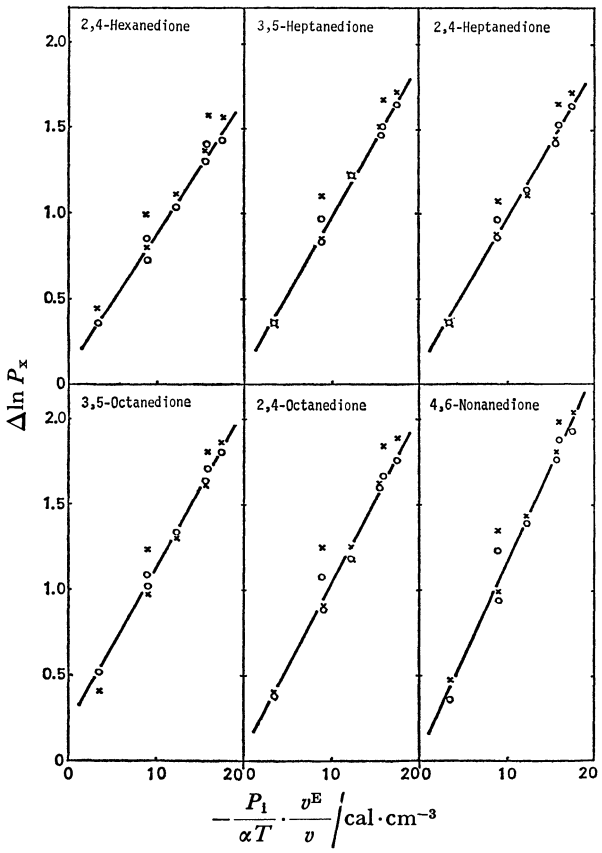

Fig. 5. Correlation between $\Delta \ln P_x$ and the pressure factor for normal aliphatic β-diketones.

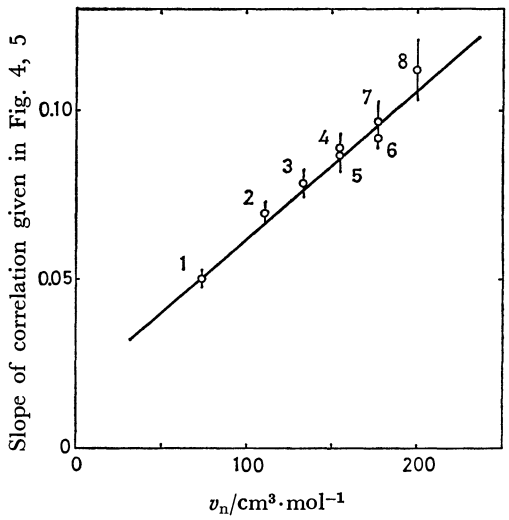

Fig. 6. Correlation between the slopes shown in Figs. 4 and 5 and the estimated molar volumes of the solutes. 1: Acetone (Ref. 8), 2: acetylacetone, 3: 2,4-hexanedione, 4: 3,5-heptanedione, 5: 2,4-heptanedione, 6: 3,5-octanedione, 7: 2,4-octanedione, 8: 4,6-nonanedione.

have reported a successful interpretation of the salting effect in a concentrated electrolyte solution by taking into account the correction term.[16] In the present study also, we introduce the term of $a'/(a'+b')$, where a' and b' correspond to the van der Waals radius of the mixed solvent and radius of the nonelectrolyte.

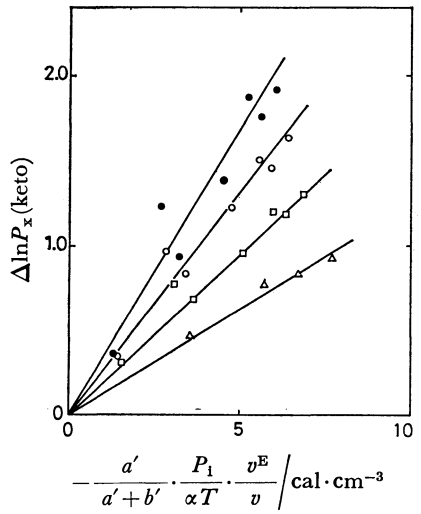

Fig. 7. Correlation between $\Delta \ln P_x$ of keto forms and $-\{a'/(a'+b')\}(P_1/\alpha T)(v^E/v)$.
The slopes of the solid lines are the expected one of v_n/RT; △: Acetone (Ref. 8), □: acetylacetone, ○: 3,5-heptanedione, ●: 4,6-nonanedione.

The values of a' and b' were calculated by

$$a' = \left(\frac{v - 593/P_1}{4.189}\right)^{1/3} \quad (5)$$

$$b' = \left(\frac{v_n}{4.189}\right)^{1/3}. \quad (6)$$

Equation 5 is based on the same idea as that proposed by Bagley et al. in which the occupied volume in a liquid is estimated from the internal pressure.[17] The slopes obtained from the plot of $\Delta \ln P_x$ against $-a'/(a'+b')\ (P_1/\alpha T)\ (v^E/v)$ were very close to the expected one of v_n/RT, as is shown in Fig. 7.

In conclusion, it is noteworthy that the solvent effect of a highly associated mixed solvent such as water–DMSO, could be interpreted by means of a new solvent parameter, *i.e.*, the pressure factor, which can be calculated from the available solvent parameters. The usefulness of the pressure factor as a measure of the solvent effect due to the solvent-solvent interaction was demonstrated. We believe that the solvophobic contribution to the solvent effect should be investigated in detail for a quantitative elucidation of the role of an aqueous solvent in solvent extraction and in reversed-phase chromatography.

The authors wish to express their gratitude to the Takeda Science Foundation for the financial support granted to this research.

References

1) H. Akaiwa, H. Kawamoto, and H. Kondo, *Bunseki Kagaku*, **24**, 12 (1975).
2) J. G. Mason and I. Lipschitz, *Talanta*, **13**, 1462 (1966).
3) Y. Yoshimura and N. Suzuki, *Anal. Chim. Acta*, **91**, 315 (1977).
4) R. Shabana and F. Hafez, *J. Radioanal. Chem.*, **26**, 63 (1975).
5) A. Alian, W. Sanad, and R. Shabana, *Talanta*, **15**, 639 (1968).
6) J. Příhoda and J. Hála, *J. Radioanal. Chem.*, **30**, 343 (1976).
7) H. Watarai and N. Suzuki, *J. Inorg. Nucl. Chem.*, **38**, 1683 (1976).
8) H. Watarai and N. Suzuki, *Chem. Lett.*, **1977**, 321.
9) H. Watarai and N. Suzuki, *J. Inorg. Nucl. Chem.*, **40**, 1909 (1978).
10) N. C. Sǿndergaad, P. E. Sǿrensen, and J. Ulstrup, *Acta. Chem. Scand.*, *A*, **29**, 709 (1975).
11) H. Watarai and N. Suzuki, *J. Inorg. Nucl. Chem.*, **36**, 1815 (1974).
12) J. H. Hildebrand, J. M. Prausnitz, and R. L. Scott, "Regular and Related Solutions," Van Nostrand Reinhold Company, New York (1970), p. 133.
13) M. Inoue, Doctoral thesis, Tohoku University (1975).
14) Le Bas, *Proc. Chem. Soc.*, **22**, 322 (1906).
15) W. F. McDevit and F. A. Long, *J. Am. Chem. Soc.*, **74**, 1773 (1952).
16) R. F. Cross, *J. Phys. Chem.*, **79**, 1822 (1975); R. F. Cross and P. T. McTigue, *J. Phys. Chem.*, **80**, 814 (1976).
17) E. B. Bagley, T. P. Nelson, and J. M. Scigliano, *J. Phys. Chem.*, **77**, 2794 (1973).

An ENDOR Study of the Hindered Internal Rotation of the Cyclopropyl Group in the 2,6-Di-*t*-butyl-4-cyclopropylphenoxyl Radical

Fumio SHIMODA*

Department of Chemistry, Faculty of Science, Hiroshima University, Higashisendamachi, Naka-ku, Hiroshima 730

(Received November 1, 1979)

The ESR and ENDOR spectra were observed for the 2,6-di-*t*-butyl-4-cyclopropylphenoxyl radical. The assignments of the proton hyperfine coupling constants were confirmed with reference to those of the 2,6-di-*t*-butyl-4-methyl- and 4-(1-deuteriocyclopropyl)phenoxyl radicals. The β-proton hyperfine coupling constant for the cyclopropyl group and its temperature dependence were precisely determined. Of particular interest is the fact that the observed cyclopropyl β-proton splitting is smaller than the γ-proton splittings (A_4^{β}: 0.72, $A_4^{\gamma^1}$: 0.83, $A_4^{\gamma^2}$: 1.44 G at -70 °C). Based on the modified $\cos^2\theta$ rule, $A_4^{\beta}=(1.85\langle\cos^2\theta\rangle-0.10)\times A_4^{Me}$, where the conjugative interaction between the π-system and the cyclopropyl pseudo π-orbital was incorporated, as proposed by Hudson and Bauld, the β-proton splitting was evaluated. The magnitude of the β-proton splitting and its temperature dependence were interpreted in terms of the restricted rotation of the cyclopropyl group in a two-fold potential; the stable conformation was the bisected one. The rotational barrier height, which corresponds to the difference in energy between the bisected and perpendicular conformations, was estimated to be 2.6 kcal/mol. The rotational barrier was attributed to the stabilization of the bisected conformation arising from the conjugative interaction of the aromatic and cyclopropyl moieties.

It has been well-known for a long time that a cyclopropyl group has a stronger π-conjugative ability than the other alkyl groups,[1] and so the behaviour of a cyclopropyl group in chemical reactions has been of interest. For example, accelerations by a cyclopropyl group have been observed in the reactions which proceed *via* a cationic intermediate.[2] The results have been explained in terms of the conjugative stabilization effect of a cyclopropyl group for the intermediate. This effect is greatly affected by the conformation of the cyclopropyl group.[3] On the other hand, the double-bond character of a cyclopropane ring and its electronic structure have been investigated in detail. Several models of the bond system in cyclopropane have been proposed by several authors.[4] The Walsh model of the chemical bonds in cyclopropane, which is a typical model, suggests that the conjugative interaction between the pseudo π-orbital of the cyclopropyl ring and the phenyl π-system is at its maximum when the molecule adopts the bisected conformation in which C_1–H_β bond of the cyclopropyl ring lies on the aromatic plane (Fig. 1). Indeed, the conformational investigations of the cyclopropylbenzene by using NMR spectroscopy support the above expectation.[5]

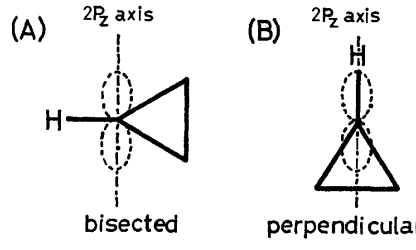

Fig. 1. Conformations of the cyclopropyl group in the 2,6-di-*t*-butyl-4-cyclopropylphenoxyl radical.
(A) Bisected conformation, (B) perpendicular conformation.

* Present address: Department of Applied Physics and Chemistry, Faculty of Engineering, Hiroshima University, Sendamachi, Naka-ku, Hiroshima 730.

It has been established that the internal rotation of an alkyl group can be studied for the various free radicals on the basis of the ESR and ENDOR techniques. For a number of aromatic radicals, the rotational barrier of an alkyl group has been estimated by the Heller-McConnell relationship[6] with the aid of some statistic procedures treating the observed β-proton splitting and its temperature dependence. Particularly, the hindered internal rotations of alkyl groups in the 4,4′-dialkylbiphenyl anion radicals[7] and the 2,6-di-*t*-butyl-4-alkylphenoxyl radicals[8] have been reported in previous papers.

In the present paper, from an analysis of the temperature dependence of the β-proton splitting on the basis of the modified $\cos^2\theta$ rule,[9] the hindered internal rotation of the cyclopropyl group in the 2,6-di-*t*-butyl-4-cyclopropylphenoxyl radical has been studied. The comparison of the results thus obtained with those for the other 2,6-di-*t*-butyl-4-alkylphenoxyl radicals[8] has been made with the purpose of examining the effect of the cyclopropyl group on the aromatic neutral radical. In this radical series, the spin density on the carbon atom of the phenoxyl moiety to which an alkyl group is attached is expected to be generally high. If this is so, the cyclopropyl β-proton splitting as well as its temperature dependence may be precisely determined. Therefore, this phenoxyl radical may be adequate for this study.

Results

ESR Spectra. The ESR spectra of the 2,6-di-*t*-butyl-4-cyclopropylphenoxyl radical (Radical-H) and the 2,6-di-*t*-butyl-4-(1-deuteriocyclopropyl)phenoxyl radical (Radical-D), generated by the lead-dioxide oxidation of the corresponding phenols,[10] in toluene were observed in the temperature range from -80 °C to 20 °C. As is shown in Fig. 2, the pattern of the ESR spectrum observed for the Radical-H varied with the change in the temperature, while that for the Radical-D remained unchanged. These results imply that the magnitude of the cyclopropyl β-proton hy-

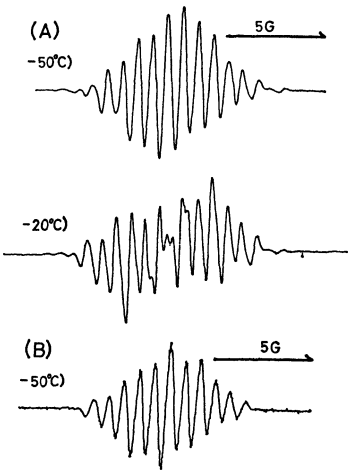

Fig. 2. ESR spectra of the Radical-H and Radical-D. (A) Radical-H, (B) Radical-D.

perfine coupling constant is strongly dependent on the temperature. The hyperfine coupling constants, however, could not be determined precisely because of the poorly resolved ESR spectrum.

ENDOR Spectra. The ENDOR spectrum of the Radical-H at −70 °C, shown in Fig. 3 (A), was composed of five signals in the upper half of the spectrum. With reference to the hyperfine splittings for the 2,6-di-*t*-butyl-4-alkylphenoxyl radicals,[8] the signals at 13.91 and 16.21 MHz could be assigned to the splittings due to the *t*-butyl protons and two protons at the 3-positions of the phenoxyl moiety respectively. The signal corresponding to the cyclopropyl β-proton splitting, at 14.84 MHz, was easily assigned with reference to the ENDOR spectrum of the Radical-D, as is shown in Fig. 3 (B). The other signals, at 15.01 and 15.81 MHz, were then assigned to those due to the non-equivalent pair of cyclopropyl γ-proton splittings. The analyzed hyperfine coupling constants of the Radical-H, Radical-D, and related phenoxyl radicals are summarized in Table 1. As may be seen in Fig. 3 (A), the β-proton splitting for the Radical-H showed a large positive temperature dependence. The temperature dependence of these hyperfine coupling constants for the Radical-H is depicted in Fig. 4.

In comparing the coupling constants for the Radical-H with those for the 2,6-di-*t*-butyl-4-alkylphenoxyl radicals,[8] the following interesting facts may be pointed out:

(1) The magnitude of the β-proton coupling constant for the cyclopropyl group was much smaller than those for the other alkyl groups, but its temperature dependence was considerably large.

(2) The magnitudes of the non-equivalent γ-proton coupling constants were several times as large as that for the 2,6-di-*t*-butyl-4-isopropylphenoxyl (isopropylphenoxyl) radical.

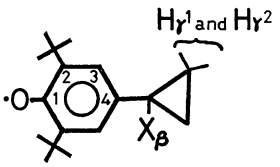

Radical-H (X_β=H)
Radical-D (X_β=D)

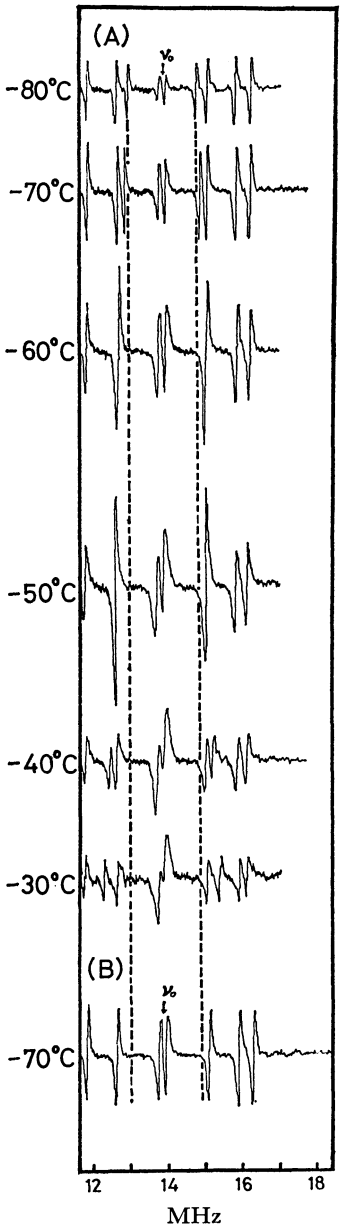

Fig. 3. ENDOR spectra of the Radical-H and Radical-D; the free proton frequency is designated with ν_0. The ENDOR signal arising from the β-proton is lost in the spectrum (B).

Discussion

Magnitude of the β-Proton Splitting. In the previous works on the 4,4′-dialkylbiphenyl radical anions and the 2,6-di-*t*-butyl-4-alkylphenoxyl (alkylphenoxyl) radicals, the magnitude of the β-proton splitting was interpreted in connection with the steric interaction between the aromatic ring protons and the rotating alkyl group.[7,8] From this point of view, the β-proton splitting for the Radical-H may resemble to that for the isopropylphenoxyl radical, because both the skeletal composition and the size of a cyclopropyl group seem to be similar to those of an isopropyl group. In fact, the β-proton splitting for the 4,4′-dicyclopropylbiphenyl anion was 3.31 G[11,12] (1 G=10^{-4} T) and that for the 4,4′-diisopropylbiphenyl anion was 2.78 G[7] at −90

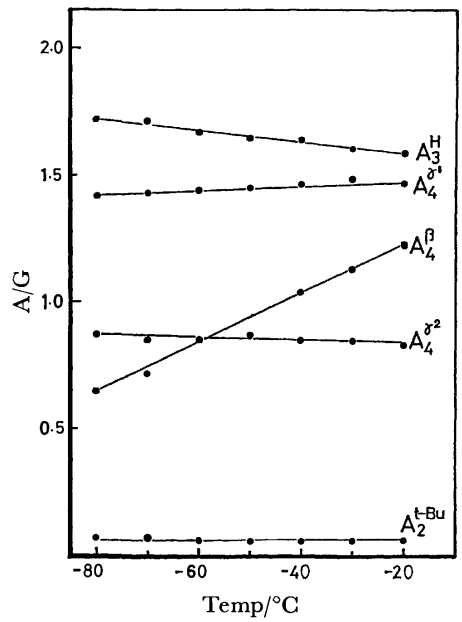

Fig. 4. Temperature dependence of the hyperfine coupling constants for the Radical-H.

°C. The results were in line with the above expectation. However, the observed β-proton splitting for the Radical-H deviated greatly from the expectation, as has been described in the previous section (see Table 1). This discrepancy could not be explained solely in terms of the steric interaction model.

The small value of the β-proton splitting, which is remarkably distinct from that for the 4,4'-dicyclopropylbiphenyl anion, suggests that the cyclopropyl group in the Radical-H strongly prefers the bisected conformation (Fig. 1-A). That may be attributed to the conjugative interaction between the aromatic and cyclopropyl moieties.

Similar observations have been reported in earlier works. In the semidiones, the β-proton splitting of the cyclopropyl group was one-tenth as large as that of the methyl group.[13] For the cyclopropylmethyl radicals, the β-proton splitting was much smaller than that for the methyl substituent.[14] In aromatic radicals, the β-proton splitting for the 4,4',4"-tricyclopropyltriphenylmethyl radical was one-sixth that of methyl-substituted analogue.[11] These observations were interpreted in terms of the propensity of the bisected conformation for the cyclopropyl group.

Temperature Dependence of the β-Proton Splitting. The magnitude of a β-proton splitting is often calculated using the following equations:

$$A^{\beta} = \langle Q(\theta) \rangle \rho^{\pi}, \quad (1)$$

and:

$$Q(\theta) = B_0 + B_2 \cos^2 \theta, \quad (2)$$

where B_0 and B_2 are empirical parameters, ρ^{π} is the spin density on the aromatic-ring carbon attached to an alkyl group, and θ is the angle between the axis of the $2p_z$ orbital and the C–H_{β} bond of the alkyl group, both projected on the plane perpendicular to the bond between the methine carbon of the alkyl group and the aromatic carbon. The term of $\langle \cos^2 \theta \rangle$ is the quantum mechanical average of $\cos^2 \theta$ over the appropriate rotational wave functions.

Table 1. Proton hyperfine coupling constants of the 2,6-di-*t*-butyl-4-alkylphenoxyl radicals (G)

Alkyl	$A_2^{t\text{-Bu}}$	A_3^H	A_4^{β}	$A_4^{\gamma^1}$	$A_4^{\gamma^2}$	A_4^{β}/A_4^{Me}	Ref.
Me	—	1.63	11.22	—	—	1.00	8
Et	0.06	1.60	8.21	—	—	0.73	8
i-Pr	0.07	1.66	4.05	0.38	—	0.36	8
c-He	0.08	1.60	4.09	0.60	0.47	0.36	8
c-Pr	0.07	1.70	0.83	1.44	0.83	0.07	
c-Pr-d_1	0.06	1.68	a)	1.43	0.86	—	

The Data at −60 °C.
a) The ENDOR signal disappeared.

For the cases of the alkylphenoxyl radicals (alkyl; Et, *i*-Pr, and *c*-He), Eq. 1 was successfully approximated to Eq. 3 on the basis of the following assumptions:[8] (1) The values of $A_2^{t\text{-Bu}}$ (*t*-butyl proton splitting) and A_3^H (phenoxyl-ring proton splitting) for the above phenoxyl radicals were nearly the same as that for the 2,6-di-*t*-butyl-4-methylphenoxyl (methylphenoxyl) radical; hence, each spin density on the 4-carbon of the phenoxyl ring among these alkylphenoxyl radicals was much like that for the methylphenoxyl. (2) If the methyl group in the methylphenoxyl radical is assumed to rotate freely, the value of the $\langle \cos^2 \theta \rangle$ is one-half it, since the methyl-proton splitting for this radical remains almost unchanged from −45 °C to 15 °C. Therefore, $B_2\rho_4^{\pi}$ was assumed to be $2 \times A_4^{Me}$. A_4^{Me} is the methyl-proton splitting for the methylphenoxyl radical. (3) The B_0 term being smaller than the $B_2\langle \cos^2 \theta \rangle$ term, the B_0 term was neglected in Eq. 2:

$$A_4^{\beta} = 2 \times A_4^{Me} \langle \cos^2 \theta \rangle. \quad (3)$$

Although the first assumption may be appropriate for the Radical-H, the latter two assumptions may be no longer valid for any cyclopropyl-substituted radicals. There are two difficulties with the above simple model:

(1) Because of the conjugative interaction between the aromatic π-system and the cyclopropyl pseudo π-orbital, the mechanism which induces spin density on the β-hydrogen atom may be different. Therefore, the B_0 and B_2 terms for the cyclopropyl-substituted radical systems may not be identical to those for the cases of the normal alkyl-substituted radicals.

(2) The propensity of the cyclopropyl group to take the bisected conformation makes the $\langle \cos^2 \theta \rangle$ value small in Eq. 2. When the $\langle \cos^2 \theta \rangle$ value is small, the contribution of the B_0 term is no longer negligible.[15] To avoid the above difficulties, Hudson and Bauld added a third term, one which resulted from the conjugative interaction between the cyclopropyl group and the π-system, to the conventional Heller-McConnell relationship.[6] They divided the third term into conformational-dependent and -independent parts, which they then added to the B_0 and B_2 terms respectively of the normal $\cos^2 \theta$ rule. From the comparative study of the 4-(2-cyclopropyl-1-ethynyl)nitrobenzene and the 4-(1-propynyl)nitrobenzene anion radicals, they sug-

gested that the conjugative effect produced a negative spin density at the β-hydrogen atom and proposed Eq. 4 for the conformational analysis of a cyclopropyl group in a radical system:[9]

$$A_4^{\beta} = [1.85\langle\cos^2\theta\rangle - 0.10] \times A_4^{Me}. \quad (4)$$

The β-proton splitting of the methylphenoxyl radical, A_4^{Me}, was 11.20 G.[8] With the aid of the Boltzmann statistics, the β-proton splitting of the Radical-H as a function of the temperature was calculated based on Eqs. 4 and 6.

$$\theta = \alpha + \theta_0 \quad (5)$$

$$\langle\cos^2\theta\rangle = \frac{\sum_{i=0} \langle\psi_i(\alpha)\,|\cos^2(\alpha+\theta_0)|\,\psi_i(\alpha)\rangle e^{-E_i/kT}}{\sum_{i=0} e^{-E_i/kT}} \quad (6)$$

Here, the wave functions, $\psi_i(\alpha)$, and the eigen values, E_i, are obtained by solving the following equation:

$$-\frac{\hbar^2}{2I}\left(\frac{d^2\psi_i}{d\alpha^2}\right) + [V_{(\alpha)} - E_i]\psi_i = 0. \quad (7)$$

In Eq. 7, the moment of inertia, I, of the molecular fragment aryl-cyclopropyl may be calculated to be 7.8×10^{-39} g cm^2 for the Radical-H, assuming that the preferred rotation of the residual group occurs about the long axis of this radical. In Eq. 7, $V_{(\alpha)}$ is the potential function to the internal rotation of the cyclopropyl group in this radical. In order to solve Eq. 7, the precise potential function must be assumed. Sorriso *et al.* and Collet *et al.*[16] theoretically calculated the angular dependence of the rotational barrier in the cyclopropylbenzene by means of the molecular orbital theory. By reference to these results, the potential function was approximated as follows:

$$V_{(\alpha)} = \frac{V_0}{2}(1-\cos 2\alpha). \quad (8)$$

In Eq. 8, V_0 is the difference in energy between the lowest energy state, the bisected conformation, and the highest one, the perpendicular. The α value is the dihedral angle between the β-proton and the aromatic plane, so it is equal to zero in the bisected conformation and $\pi/2$ in the perpendicular. The θ_0 value in Eq. 5 becomes equal to $\pi/2$. The Hamiltonian matrix, $\langle i|H|j\rangle$, was diagonalized by expanding the wave function in a Fourier series:

$$\psi_i(\alpha) = \sum_{j=0} (A_{ij}\cos j\alpha + B_{ij}\sin j\alpha). \quad (9)$$

The temperature dependences of $\langle\cos^2\theta\rangle$ as a function of V_0 for the Radical-H have also been calculated. The results calculated in the temperature range from −80 °C to 0 °C for the various values of V_0 are shown in Fig. 5. The best agreement between the calculated and the experimental temperature dependence, evaluated by means of Eq. 4, was obtained with V_0=2.6 kcal/mol (1 kcal=4.184 kJ). On the other hand, the magnitudes $\langle\cos^2\theta\rangle$ evaluated from Eq. 3 were very small. In this case, the potential barrier calculated was 5.0—7.5 kcal/mol, although the observed temperature dependence of the β-proton splitting could not be adequately explained. The latter value of the potential barrier, which corresponds to

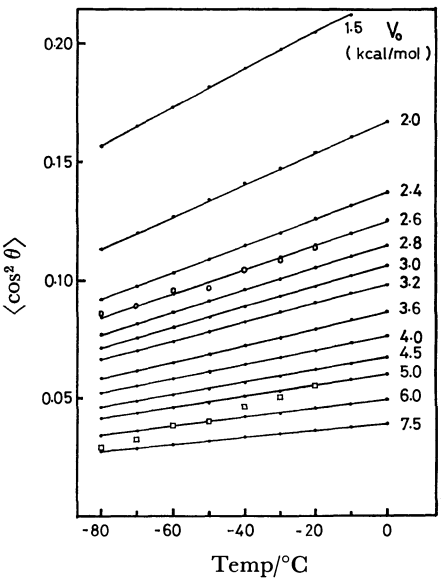

Fig. 5. The theoretically calculated and experimental temperature dependence of $\langle\cos^2\theta\rangle$ for the Radical-H. The numerical calculations were carried out with various values of V_0, which was the energy difference between the bisected and perpendicular conformation. —●—; Theoretically calculated values of $\langle\cos^2\theta\rangle$, ○; $\langle\cos^2\theta\rangle$ vaules evaluated from Eq. 4, □; $\langle\cos^2\theta\rangle$ values evaluated from Eq. 3.

the energy difference between the bisected and perpendicular conformation (Fig. 1), may be comparable to the conjugative energy between two phenyl rings for the biphenyl molecule when the molecule is coplanar (about 6 kcal/mol).[17] Then, the potential barrier of 5.0—7.5 kcal/mol may not be adequate for the internal rotation of the cyclopropyl group in the Radical-H. However, the former value, 2.6 kcal/mol, is more appropriate for this radical. This result is compatible with the results of other investigations of the cyclopropylbenzene made using several techniques. Parr and Schaefer have reported on the basis of their NMR measurements, that the rotational barrier of the cyclopropyl group in the cyclopropylbenzene (assuming a two-fold potential) was 2.0±0.3 kcal/mol.[5] Based on the molecular orbital calculations for the cyclopropylbenzene,[16] the energy difference between the bisected and perpendicular conformations was reported to be 11.7 kJ (2.8 kcal/mol; CNDO/2) or 3.67×10^{-2} au. (2.3 kcal/mol; INDO). The compatibility with the other results implies the validity of the adoption of Eq. 4 to estimate the $\langle\cos^2\theta\rangle$ for the Radical-H.

In previous papers, the potential barriers to the internal rotation of the alkyl group in the alkyl-substituted biphenyl anion and phenoxyl radicals have been reported. As is shown in Table 2, in the 4,4′-dialkylbiphenyl radical anion series[7] the rotational barriers were 1.0, 1.2, and 1.2 kcal/mol for the 4,4′-diethyl-, 4,4′-diisopropyl-, and 4,4′-dicyclohexylbiphenyl anions respectively. In the phenoxyl series,[8] those for the 2,6-di-*t*-butyl-4-ethyl-, -4-isopropyl-, and -4-cyclohexylphenoxyl radicals were 1.1, 1.6, and 1.6 kcal/mol respectively. In both cases, the rotational

Table 2. The values of the rotational barriers for the 2,6-di-*t*-butyl-4-alkylphenoxyl and 4,4-dialkylbiphenyl anion radicals (kcal/mol)

	Alkyl	$\langle\cos^2\theta\rangle$	V_0	V_m	Ref.
Phenoxyl	Et	0.37 (at −60 °C)	1.1		8
	i-Pr	0.18 (at −60 °C)	1.6	0.7	8
	c-He	0.18 (at −60 °C)	1.6	0.7	8
	c-Pr	0.09 (at −60 °C)[a]	2.6		
Biphenyl anion	Et	0.36 (at −90 °C)	1.0		7
	i-Pr	0.21 (at −85 °C)	1.2	0.5	7
	c-He	0.20 (at −85 °C)	1.2	0.6	7
	c-Pr	0.37 (at −80 °C)[a]	0.46		9

The V_0 values show the highest values for the two-fold potential (Et, *c*-Pr) or the double-well potential (*i*-Pr, *c*-He). The V_m values show the medium value for the double-well potential (*i*-Pr, *c*-He). For particulars, see Refs. 7 and 8. a) The $\langle\cos^2\theta\rangle$ values were estimated based on Eq. 4.

barriers obtained were very similar to each other for the same alkyl groups, and in both they were interpreted in terms of the steric repulsion between the rotating alkyl group and the aromatic protons. However, the rotational barrier of the cyclopropyl group in the Radical-H deviated remarkably from the above alkylphenoxyl radical series. Based on the magnitudes of $\langle\cos^2\theta\rangle$ at −90 °C as evaluated with Eq. 4, Hudson and Bauld estimated the rotational barrier of the cyclopropyl group in the 4,4′-dicyclopropylbiphenyl radical anion to be 0.46 kcal/mol, assuming a two-fold potential in which the bisected conformation was more stable than the perpendicular one.[9] The present conclusion that the rotational barrier of the cyclopropyl group in the Radical-H is 2.6 kcal/mol is not compatible with their result. Because the steric factors are nearly comparable with the two cases, the difference in the rotational barriers for these radicals may be mainly correlated to the proportion of the contribution of the conjugative interaction between the cyclopropyl and aromatic moieties. The difference may not be expected from the solvent effects or the difference in the moment of inertia.[15] Therefore, the conjugative interaction in the Radical-H may be anticipated to be considerably important.

The Conjugative Interaction. The conclusion obtained in the previous section indicates that the contribution of the π-type conjugation between the cyclopropyl group and the π-system is more significant in the Radical-H than in the 4,4′-dicyclopropylbiphenyl anion radical. This difference may be well understood in terms of the perturbational molecular orbital theory.[18]

On the basis of the perturbational molecular orbital theory, Hoffmann *et al.* have discussed the stabilization of the cyclopropyl carbinyl cation arising from the interaction of the cyclopropyl group and the vacant carbonium $2p_z$ orbital.[19] The stabilization energy, E_s, of a molecule arising from the conjugative interaction between the cyclopropyl pseudo-π-orbital and the aromatic π-system may be approximately comprehended in terms of the following equations and the energetic

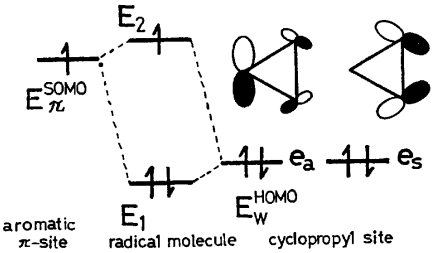

Fig. 6. Energy diagram: left-handed and right-handed are schemes of the cyclopropyl site and aromatic π-site respectively, before a perturbational interaction. The central one is the energy diagram after the interaction. E_π^{SOMO}; the energy level of the SOMO for the aromatic π-system, which contains unpaired electron, E_w^{HOMO}; the energy levels of the HOMO for the cyclopropyl system. E_1 and E_2; the energy levels of the radical molecule after the perturbational interaction between the aromatic and the cyclopropyl system. The right-handed pictures are the outline for the HOMO of the Walsh-type molecular orbitals for the cyclopropyl system, the symmetry labels refer to the C_s point group.

picture shown in Fig. 6:

$$E_s = \frac{|H_{ij}|^2}{\Delta E}, \qquad \Delta E = E_\pi^{SOMO} - E_W^{HOMO}, \tag{10}$$

$$|H_{ij}|^2 = (C_i^\pi)^2(C_j^W)^2\beta^2, \tag{11}$$

where H_{ij} is the matrix element of the perturbational interaction and where ΔE is the energy difference between the SOMO (Singly Occupied Molecular Orbital) of the π-system, E_π^{SOMO}, and the HOMO (Highest Occupied Molecular Orbital) of the cyclopropyl Walsh orbital, E_w^{HOMO} (see Fig. 6). The $|H_{ij}|^2$ term contains the square of the coefficients of the corresponding AO's (Atomic Orbitals) at the carbon atoms, attached to each other, for the HOMO of the cyclopropyl and the SOMO of the aromatic moieties; β is the resonance integral between the aromatic π-system and the cyclopropyl group. Only one orbital in the HOMO's of the cyclopropane which interacts with the π-system is denoted as e_a, because the Walsh-type orbital denoted e_s has a node on the plane of the three-membered ring at the cyclopropyl-1-carbon atom (Fig. 6). The resonance integral, β, should be dependent on the conformation of the cyclopropyl group, because the Walsh-type orbital denoted as e_a spreads on the plane of the three-membered ring. The terms of $(C_j^W)^2\beta^2$ in Eq. 11 for the Radical-H and the 4,4′-dicyclopropylbiphenyl anion being assumed to be equal, the stablization energy arising from the conjugative interaction, E_s, may be proportional to the square of the coefficient of the SOMO-AO on the aromatic carbon attached to the cyclopropyl group. On the other hand, the stabilization energy, E_s, is inversely proportional to the energetic separation between the SOMO of the π-system and the HOMO of the cyclopropyl group.

The results of the HMO calculation, summarised in Table 3, suggest that the contribution of the conjugative interaction in the Radical-H is larger than that of the 4,4′-dicyclopropylbiphenyl radical anion. When the molecule adopts the bisected conformation,

TABLE 3. THE CALCULATED SOMO ENERGIES AND COEFFICIENTS AT THE AROMATIC 4-POSITIONS[20]

	Biphenyl anion[a]	Phenoxyl[b]
Aromatic SOMO energy	$\alpha-0.705\beta$	$\alpha+0.894\beta$
Aromatic SOMO coefficient	0.398	0.545

a) Data from Ref. 20a. b) The values of the parameters, α_o as the Coulomb integral and β_{c-o} as the resonance integral, for the 2,6-di-*t*-butylphenoxyl radical were $\alpha+2\beta$ and 0.6β respectively.[20b] The HMO calculation was carried out by neglecting the contributions from the two *t*-butyl groups.

the overlapping between the π-orbital of the phenoxyl and the cyclopropyl pseudo-π-orbital is at its maximum, therefore, the stabilization effect is the most. On the contrary, the overlapping is at its minimum, and the effect is least in the perpendicular conformation. The large potential barrier estimated for the Radical-H can be understood from this point of view.

Experimental

General. All the melting points are uncorrected. The IR spectra were obtained on a Hitachi 215 spectrometer; the Mass spectra, on a Hitachi RMS-4 and RMU-6L spectrometer; the NMR spectra, on a Varian T-60 spectrometer, and the UV spectrum, on a Hitachi 124 spectrophotometer. The chemical shifts of the NMR spectra are given in ppm (δ), with tetramethylsilane as the internal standard.

The ESR spectra were measured on a JEOL-ME-3X spectrometer operating with a 100 kHz magnetic-field modulation. The ENDOR spectra were measured in the temperature range from -80 °C to -20 °C using a JEOL-EDX-1 spectrometer operating with a 80 Hz magnetic-field modulation. About 150 W of continuous radiowaves (frequency modulated at 6.5 kHz) were present in the cavity for NMR excitation.

Materials. *2,6-Di-t-butyl-4-acetylphenyl Acetate*: Into a cold mixture of anhydrous aluminum chloride (67 g, 0.5 mol) and acetyl chloride (31 ml, 0.4 mol) in carbon disulfide (150 ml), was added a solution of the commercial 2,6-di-*t*-butylphenol (31 g, 0.15 mol) in the same solvent (70 ml) below 5 °C[21] over a 2-h period. After being stirred for an hour at room temperature, the mixture was heated under reflux for 2 h. Then, the mixture was poured into an ice-cold 1 mol dm^{-3} HCl solution, the organic layer was separated, and the aqueous layer was extracted with a solvent. The combined organic layer was washed with water, an aqueous sodium hydrogencarbonate solution, and water, successively. The subsequent evaporation of the solvent, after being dried with anhydrous calcium chloride, gave a solid residue, which was then recrystallized from hexane to give colorless prisms (35 g) in an 80% yield.

Mp 100.5—101.2 °C. NMR (CCl_4) 7.83 (s, 2H), 2.50 (s, 3H), 2.29 (s, 3H), 1.37 (s, 18H). IR (nujol) 1765 cm^{-1} and 1680 cm^{-1}. Found: C, 74.60; H, 9.15%; M$^+$, 290. Calcd for $C_{18}H_{26}O_3$: C, 74.45; H, 9.02%; M, 290.

2,6-Di-t-butyl-4-(1-hydroxyethyl)phenyl Acetate: A solution of the above acetate (20 g, 0.07 mol) dissolved in 2-propanol (120 ml) was gradually stirred into a suspension of sodium borohydride (1.3 g, 0.03 mol) in 2-propanol (50 ml) at room temperature. After being stirred for 2 d at room temperature, the solvent was removed *in vacuo*. The residue was slowly poured into a cold 1 mol dm^{-3} HCl solution; then the aqueous layer was extracted with ether three times. The organic layer was washed with a saturated solution of sodium hydrogencarbonate and water. After the solution had been dried over anhydrous sodium sulfate, the concentration of the solution *in vacuo* gave a solid residue, which was subsequently recrystallized from cyclohexane to afford colorless plates (15 g, 74%).

Mp 103.4—104.0 °C, NMR (CCl_4) 7.25 (d, 1H, J= 2 Hz), 7.18 (d, 1H, J=2 Hz), 4.68 (q, 1H, J=6 Hz), 2.24 (s, 3H), 2.13 (s, 1H, OH), 1.40, 1.33 (d, J=6 Hz, s, 21H), IR (nujol) 3550 and 1740 cm^{-1}. Found: C, 74.12; H, 9.75%; M$^+$, 292. Calcd for $C_{18}H_{28}O_3$: C, 73.93; H, 9.65%; M, 292.

2,6-Di-t-butyl-4-ethenylphenyl Acetate: Into concd phosphoric acid (6 g) was added a solution of the above hydroxy ester (8.8 g, 0.03 mol) dissolved in benzene (60 ml). The mixture was heated under a gentle reflux of benzene for 3 h, until no more water was taken off as an azeotropic mixture. The organic layer was then washed with water and an aqueous sodium hydrogencarbonate solution. The evaporation of the solvent *in vacuo* left a colorless oil (7 g), which was employed as the reactant of the following experiment without any further purification. The NMR and IR data were as follows: NMR (CCl_4) 7.33 (s, 2H), 6.68 (dd, 1H, J= 11 Hz, 17 Hz), 5.64 (d, 1H, J=17 Hz), 5.16 (d, 1H, J= 11 Hz), 2.22 (s, 3H), 1.37 (s, *t*-Bu), and IR (nujol) 1775 cm^{-1}.

2,6-Di-t-butyl-4-cyclopropylphenyl Acetate: Into a mixture of palladium acetate (10 mg) and a solution of the above crude oil (7 g) dissolved in ether (30 ml) was added an ethereal solution of diazomethane,[22] prepared from 45 g of *N*-methyl-*N*-nitroso-*p*-toluenesulfonamide according to a previously reported method[23] in an ice–salt bath over a 3-h period. Since the yellow color which is indicative of the presence of diazomethane remained unchanged, additional palladium acetate (10 mg) was added. The mixture was stirred overnight at room temperature and then washed with cold 1 mol dm^{-3} HCl and water. After the mixture has been dried, the removal of the solvent *in vacuo* gave a pale yellow oil. If the olefinic absorptions (6.8—5.0 ppm) were found upon NMR observation, the above procedure was done over again. The product was purified by alumina-column chromatography, using cyclohexane and benzene as eluents. The product (5.9 g) was eluted in the fraction of the mixed solvent (5—10% benzene and 90—95% cyclohexane). The NMR and IR data were as follows: NMR (CCl_4) 6.93 (d, 2H), 2.24 (s, 3H), 1.35 (*t*-Bu), 0.55—0.98 (m, 4H), and IR (neat) 1770 cm^{-1}.

2,6-Di-t-butyl-4-cyclopropylphenol: To an ethereal suspension of lithium aluminum hydride (0.6 g, 0.02 mol), was added a solution of the above acetate (5.9 g, 0.02 mol) in ether (10 ml) below 10 °C over period of an hour. After the mixture had been stirred at room temperature for an hour, it was heated under reflux for 2 h. Then, cold water was added to the mixture and it was poured into an ice-cooled 1 mol dm^{-3} HCl solution, the organic layer was separated, and the aqueous layer was extracted with ether. The combined organic layer was washed with water, an aqueous sodium hydrogencarbonate solution, and water. After the organic layer had been dried, the solvent was removed off *in vacuo* to leave a yellow, crystalline substance. It was chromatographed on silica gel, using light petroleum ether as the eluent. The first fraction gave white crystals. Recrystallization from pentane gave 2.4 g of white plate crystals. The total yield of the product from the 2,6-di-*t*-butyl-4-(1-

hydroxyethyl)phenyl acetate was 32%.

Mp 63.5—65.0 °C, NMR (CCl_4) 6.80 (s, 2H), 4.82 (s, 1H), 1.52—1.80 (m, 1H), 1.43 (s, 18H), 0.46—0.88 (m, 4H). IR (nujol) 3660 cm^{-1}. Found: C, 82.72; H, 10.75%; M^+, 246. Calcd for $C_{17}H_{26}O$: C, 82.87; H, 10.64%; M, 246. UV_{max} (hexane) 224 nm (log ε: 3.6).

The desired deuterio compound was prepared from the 2,6-di-*t*-butyl-4-acetylphenyl acetate in a manner similar to that used in the preparation of the 2,6-di-*t*-butyl-4-cyclopropylphenol. Deuterium was introduced by means of sodium borodeuteride reduction.

2,6-Di-t-butyl-4-(1-deuterio-1-hydroxyethyl)phenyl Acetate: To a suspension of sodium borodeuteride (0.4 g, 0.01 mol) in 2-propanol (20 ml), a saturated solution of the 2,6-di-*t*-butyl-4-acetylphenyl acetate (5.6 g, 0.02 mol) in the same solvent was added. Thereafter, the procedure described above was employed. The spectral data of the product; mp 102.6—103.3 °C (4.5 g, 81% yield) are as follows: NMR (CCl_4) 7.23 (d, 1H, J=2 Hz), 7.18 (d, 1H, J=2 Hz), 2.23 (s, 3H), 2.17 (s, 1H, OH), 1.37, 1.33 (s, s, 21H); IR (nujol) 3530 and 1740 cm^{-1}; M^+ 293.

2,6-Di-t-butyl-4-(1-deuterioethenyl)phenyl Acetate: A solution of the above acetate (4 g, 0.01 mol) dissolved in benzene (30 ml) was added to a suspension of concd phosphoric acid (4 g) in benzene (20 ml). The further procedure, described above, gave an oily product. The NMR data were as follows: NMR (CCl_4) 7.25 (s), 5.59 (m), 5.15 (s), 2.26 (s), 1.36 (*t*-Bu).

2,6-Di-t-butyl-4-(1-deuteriocyclopropyl)phenyl Acetate: Into a mixture of palladium acetate (10 mg) and a solution of the above crude oil dissolved in ether (20 ml) was added an excess of an ethereal solution of diazomethane in an ice–salt bath over a 3-h period. The further procedure was as has been described above; it gave 3.5 g of an oily product. The NMR data were as follows: NMR (CCl_4) 6.96 (s), 2.23 (s), 1.32 (*t*-Bu), 0.56—0.93 (m).

2,6-Di-t-butyl-4-(1-deuteriocyclopropyl)phenol: Into a suspension of lithium aluminum hydride (0.5 g, 0.01 mol) in ether (10 ml), a solution of the above acetate (3.5 g) in the same solvent (10 ml) was added below 10 °C for 1 h. Subsequent treatment as above gave white crystalline plates (1.0 g, 0.004 mol).

The total yield of the product from the 2,6-di-*t*-butyl-4-(1-deuterio-1-hydroxyethyl)phenyl acetate was 28%. Mp 60.5—63.0 °C, NMR (CCl_4) 6.78 (s, 2H), 4.80 (s, 1H), 1.45 (s, 18H), 0.49—0.86 (m, 4H); IR (nujol) 3650 cm^{-1}; M^+, 247.

Preparation of the Radicals. *In vacuo*, both phenoxyl radicals were prepared by the oxidation of the corresponding phenols with lead dioxide (PbO_2) in toluene.[10] Both solutions of the radicals were slightly blue.[24]

Computations. The numerical computations were carried out on the HITAC 8700 system in the Hiroshima University Computing Center.

The author wishes to thank Professor Terukiyo Hanafusa for his valuable discussions and encouragement throughout the course of this work. The author is also grateful to Dr. Fujito Nemoto for his support in the ESR and ENDOR measurements, his gift of the computing programs, and his useful discussions. The author is also indebted to Professor Kazuhiko Ishizu and Dr. Kazuo Mukai for their helpful suggestions. The ESR and ENDOR observations were performed at the Chemistry Department of Ehime University.

References

1) The olefinic properties of the cyclopropyl groups are reviewed in M. Charton, "The Chemistry of Alkenes," ed by J. Zabicky, Vol. 2, Chap. 10 (1970) and the references therein.

2) H. Hart and P. A. Law, *J. Am. Chem. Soc.*, **86**, 1957 (1964).

3) H. C. Brown and J. D. Cleaveland, *J. Am. Chem. Soc.*, **88**, 2051 (1966); Y. E. Rhodes and V. G. Diffit, *ibid.*, **94**, 7589 (1972).

4) C. A. Coulson and W. E. Moffit, *Philos. Mag.*, **40**, 1 (1949); A. D. Walsh, *Trans. Faraday Soc.*, **45**, 179 (1949); W. A. Bernett, *J. Chem. Educ.*, **44**, 17 (1967).

5) G. L. Closs and H. B. Klinger, *J. Am. Chem. Soc.*, **87**, 3266 (1965); W. J. E. Parr and T. Schaefer, *ibid.*, **99**, 1033 (1977).

6) C. Heller and H. McConnell, *J. Chem. Phys.*, **32**, 1535 (1960).

7) F. Nemoto, F. Shimoda, and K. Ishizu, *Bull. Chem. Soc. Jpn.*, **48**, 2627 (1975); F. Nemoto and K. Ishizu, *J. Phys. Chem.*, **79**, 1730 (1975).

8) F. Shimoda, T. Hanafusa, F. Nemoto, K. Mukai, and K. Ishizu, *Bull. Chem. Soc. Jpn.*, **52**, 3743 (1979).

9) C. E. Hudson and N. L. Bauld, *J. Am. Chem. Soc.*, **94**, 1158 (1972).

10) J. K. Becconsall, S. Clough, and G. Scott, *Trans. Faraday Soc.*, **56**, 459 (1960).

11) N. L. Bauld, J. D. McDermed, C. E. Hudson, Y. S. Rim, J. Zoeller, Jr., R. D. Gordon, and J. S. Hyde, *J. Am. Chem. Soc.*, **91**, 6666 (1969).

12) The ENDOR measurement of the 4,4′-dicyclopropylbiphenyl radical anion in the temperature range from −120 °C to −90 °C was reexamined. A_4^{β}: 3.31 G, $A_4^{\gamma_1}$: 0.13 G, $A_4^{\gamma_2}$: 0.05 G, A_3^{H}: 0.40 G, A_2^{H}: 2.66 G at −90 °C in tetrahydrofuran.

13) G. A. Russell and H. Malkus, *J. Am. Chem. Soc.*, **89**, 160 (1967).

14) J. K. Kochi, P. J. Krusic, and D. R. Eaton, *J. Am. Chem. Soc.*, **91**, 1877, 1979 (1969).

15) E. W. Stone and A. H. Maki, *J. Chem. Phys.*, **37**, 1326 (1962).

16) S. Sorriso, F. Stefani, E. Semprini, and A. Flamini, *J. Chem. Soc., Perkin Trans.* 2, **1976**, 374. G. Collet and G. Leroy, *J. Chim. Phys.*, **71**, 1033 (1977).

17) I. Fischer-Hjalmars, *Tetrahedron*, **19**, 1805 (1963).

18) M. J. S. Dewar, "The Molecular Orbital Theory of Organic Chemistry," McGraw-Hill (1969), Chap. 6; R. Hoffmann, *Acc. Chem. Res.*, **4**, 1 (1971).

19) C. F. Wilcox, L. M. Loew, and R. Hoffmann, *J. Am. Chem. Soc.*, **95**, 8192 (1973).

20) a) E. Heilbronner and H. Bock, "Das HMO-Modell und Seine Anwendung," Verlag Chemie, Weinheim/Bergstr. (1968); b) Y. Shinagawa and Y. Shinagawa, *J. Am. Chem. Soc.*, **100**, 67 (1978).

21) N. V. Portnykl, A. A. Volodd'kin, and V. V. Ershou, *Izv. Akad. Nauk SSSR, Ser. Khim.*, **1966**, 2243; *Chem. Abstr.*, **66** 85580z.

22) R. Raulissen, J. Hubert, and Ph. Teyssie, *Tetrahedron Lett.*, **1972**, 1465.

23) *Org. Synth.*, Coll. Vol. **4**, 250.

24) The investigation of the fate of the radical is now in progress.

 © 1980 The Chemical Society of Japan Bull. Chem. Soc. Jpn., 53, 1860—1863 (1980) [Vol. 53, No. 7

Boron Isotope Separation by Ion Exchange Chromatography Using Weakly Basic Anion Exchange Resin

Yoichi SAKUMA,* Masao AIDA, Makoto OKAMOTO, and Hidetake KAKIHANA

Research Laboratory for Nuclear Reactors, Tokyo Institute of Technology, O-okayama, Meguro-ku, Tokyo 152

(Received November 2, 1979)

Isotopic plateau displacement chromatography, a useful method for isotope separation is presented. The boric acid band formed in a column of weakly basic anion exchange resin Diaion WA21 can be eluted with pure water. In order to obtain good accumulation of the isotope effect, a series of experiments with different migration length were carried out. The boron-10 enriched part of the boric acid absorbed band was always preceded by the isotopic plateau part, in which the atomic fraction of boron-10 was maintained at its original value. The atomic fraction of boron-10 at the end of the chromatogram increased with migration length, and in the case of 256-m migration, boron-10 was enriched from its original atomic fraction of 19.84 to 91.00%, the separation factor S being constant irrespective of migration length: $S=1.0100\pm0.0005$.

The following conditions have been found to be favorable for effective isotope separation in chromatographic systems.[1,2] (1) The single stage separation factor should be large. (2) The rates of the ion exchange and isotope exchange reactions should be as high as possible. (3) When the separation factor is not so large as in the case of hydrogen-deuterium isotope separation, sharp band boundary such as characteristic of displacement chromatogram should be maintained at the front or at the rear, if possible at both ends of the chromatographic band. (4) Chromatography should be carried out in such a way that an "isotopic plateau zone" in which the atomic fraction of isotopes remains at its original value, always exists somewhere within the chromatogram. (5) Column operation should be as simple as possible.

Kotaka *et al.* reported that a boric acid band formed in a column packed with weakly basic anion exchange resin (Diaion WA21) can be eluted with pure water, resulting in good isotope fractionation.[3] The result seems to satisfy the five conditions mentioned above. (1) The separation factor is comparatively large (about 1.01). (2) The rates of ion exchange and isotope exchange reaction are not very low. (3) Under suitable conditions, a sharp boundary can be formed at the rear of the boric acid band, where boron-10 would be enriched. (4) An isotopic plateau zone can be maintained if the boric acid band is sufficiently long. (5) The operation is easy. The boric acid band can be eluted with pure water, and the eluted column can be used again with no special regeneration process.

These prospects were realized and the optimum experimental conditions to maintain the isotopic plateau displacement chromatography were found.[2] In the present paper we will report the results obtained with various migration lengths under the optimum conditions.

Experimental

A boric acid saturated band formed in a column of weakly basic anion exchange resin Diaion WA21 can be eluted with pure water, keeping the isotopic plateau displacement chromatogram at the rear part under certain conditions.[2] The optimum conditions are: concentration of boric acid solution, 0.1 mol dm^{-3}; temperature, 40 °C; rate, 20 $cm^3\ h^{-1}\ cm^{-2}$. Experiments were carried out with migration lengths of boric acid band 1—256 m.

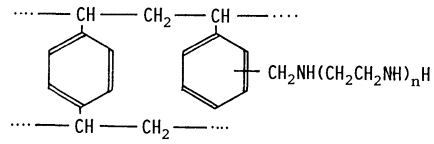

Fig. 1. Structure of Diaion WA21 resin.

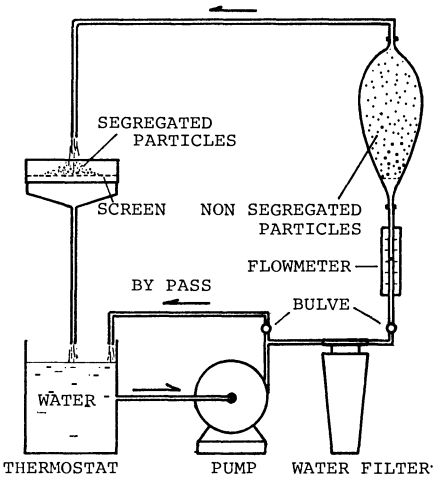

Fig. 2. An apparatus for segregating resin particle size.

Anion Exchange Resin. The structure of the weakly basic anion exchange resin Diaion WA21 is shown in Fig. 1. At first, the resin particles in chloride form were segregated by size (Fig. 2), and the particles between 80 and 100 mesh were packed into the column in chloride form.

Apparatus. The apparatus (Fig. 3) and method were the same as reported.[2] The height of the resin bed was 1 m and its diameter 21 mm. In order to detect the conductivity of the resin phase, a pair of platinum electrodes were inserted at the bottom of the resin bed. Since the conductivity of the boron band is much higher than that of the resin of free base form, the movement of boron band through column is effectively followed by the conductivity between the platinum electrodes.

Operation. A column packed with the Diaion WA21 resin in chloride form was converted into free base form by passing NaOH solution (Fig. 4-i), and was washed with pure water (Fig. 4-ii). To the column was fed excess (*ca.* 1.2 dm^3) 0.1 mol dm^{-3} H_3BO_3 solution to form a band saturated with boric acid and boron-10 depleted effluent from the column was discarded (Figs. 4-iii,iv); a few columns

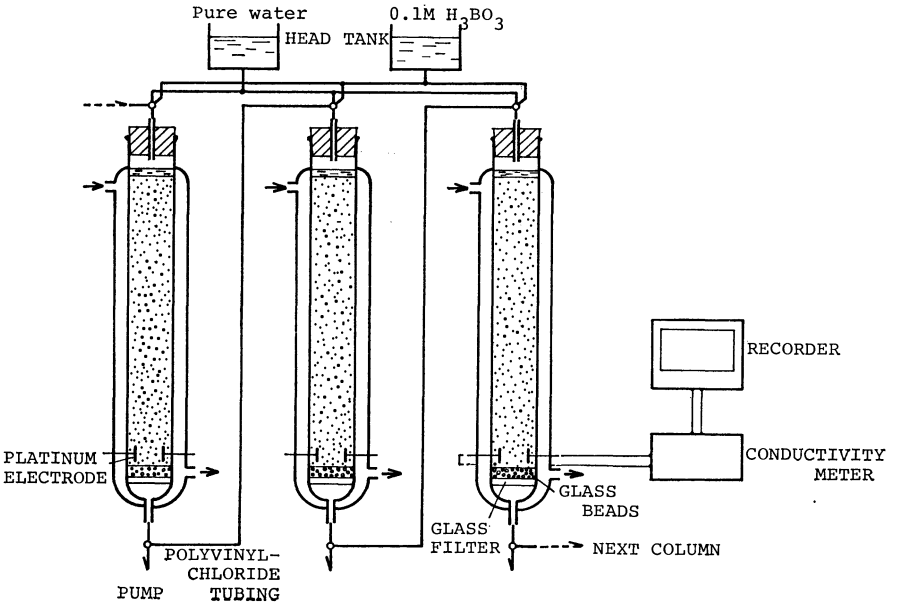

Fig. 3. Experimental apparatus.

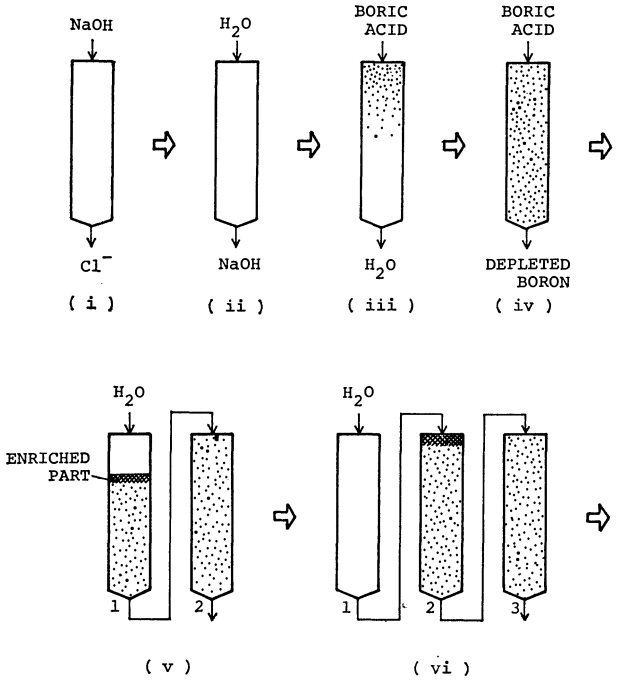

Fig. 4. Column operation.

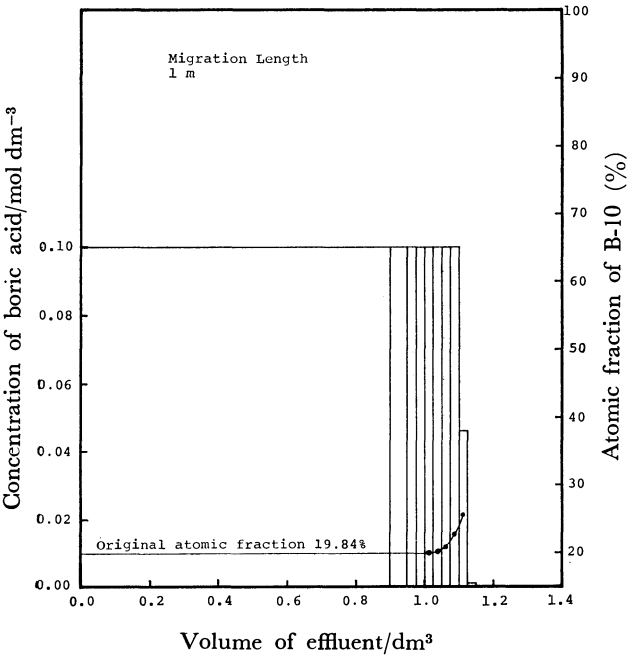

Fig. 5. Elution curve and isotope distribution curve of 1 m migration.

were treated in a similar way. The columns were equilibrated with boric acid aqueous solution having natural abundance ratio of boron isotopes (boron-10 content 19.84%); the columns were slightly enriched with boron-10. Two columns were connected in series by a thin polyvinyl chloride tubing.

Pure water was fed to the first column in order to elute the boric acid band, boron-10 being enriched at the rear boundary (Fig. 4-v). The effluent from the second column (the column holding isotopic plateau) was discarded. The third column was connected to the second column in series when the boric acid band of the first column had been completely transferred to the second column (Fig. 4-vi). The first column was again saturated with 0.1 mol dm^{-3} H_3BO_3 aqueous solution having natural abundance ratio of boron isotopes and used for another plateau holding column (the fourth column, Figs. 4-iii,iv). In the case of a longer migration length about 50 m, it was necessary to use three columns in series to hold the isotopic plateau region. In this way the chromatogram was migrated to the required length; 1, 2, 4, 8, 16, 32, 64, 128, and 256 m. The effluent of each experiment was collected in fraction.

Measurements. The samples were analyzed in a similar way to that reported.[1,2] The concentration of boric acid was determined by neutralization titration using mannitol and the atomic fraction of boron-10 by the surface ionization method using a Variant MAT CH-5 mass spectrometer.[4]

Reabents. All the chemicals used were of reagent grade.

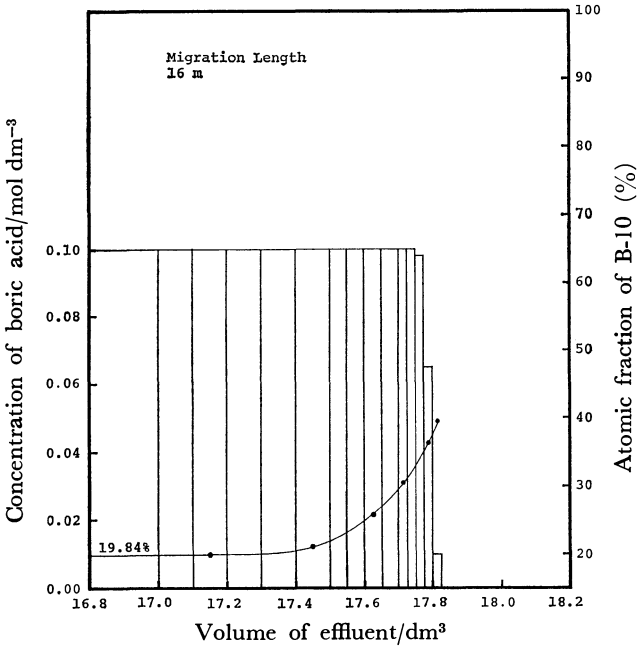

Fig. 6. Elution curve and isotope distribution curve of 32 m migration.

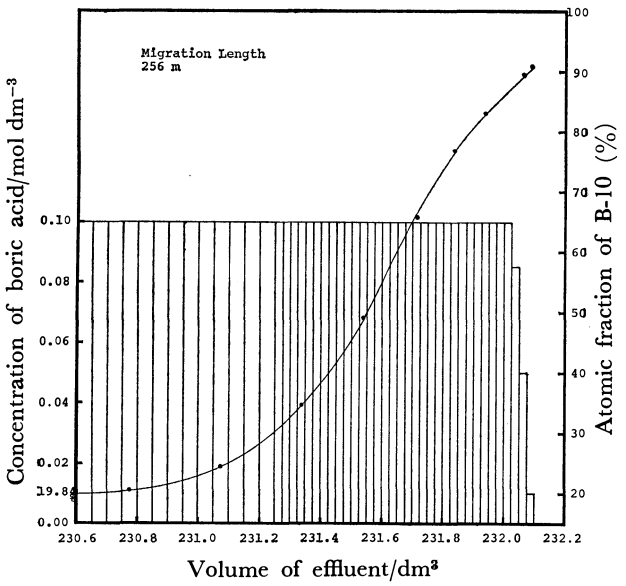

Fig. 7. Elution curve and isotope distribution curve of 256 m migration.

Results and Discussion

Three examples of the elution curve and isotope distribution curve of each run are shown in Figs. 5—7. The profiles of enriched zone of boron-10 are surveyed with regard to migration length in Fig. 8.

Migration Length and Extent of Boron-10 Enrichment. The most enriched boron-10 was always obtained at the most rear part of the chromatogram. The atomic fractions of boron-10 at the end of each chromatogram increased steadily with increase of migration length (Table 1). This indicates that an ideal chromatogram is accomplished in each run.

In the case of 256-m migration, boron-10 was enriched to 91.00% from its original atomic fraction of 19.84.

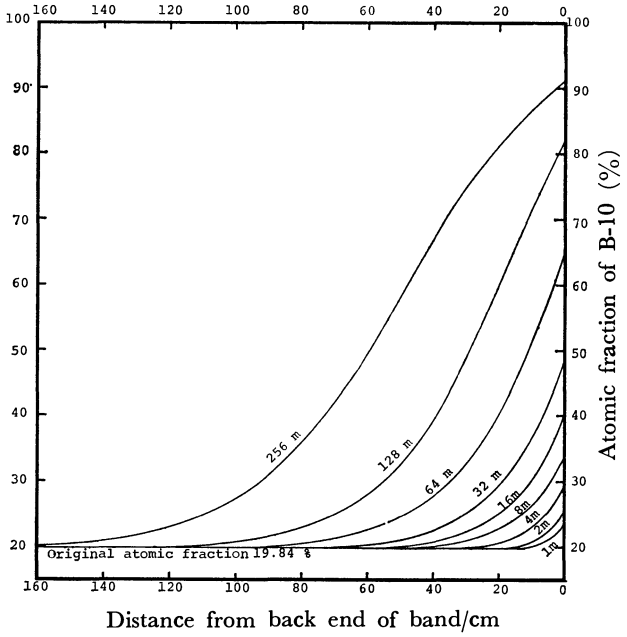

Fig. 8. Dependence of atomic fraction of boron-10 on migration length.

Table 1. Migration length *vs.* separation factor S and maximum atomic fraction of boron-10

L[a] / m	S[b]	R_m[c] / %
1	1.0096	25.62
2	1.0099	26.91
4	1.0095	27.76
8	1.0098	33.26
16	1.0105	39.62
32	1.0100	48.12
64	1.0101	62.43
128	1.0104	81.62
256	1.0105	91.00
S_a[d]	1.0100±0.0005	

a) Migration length of each run. b) Separation factor. c) Maximum atomic fraction of boron-10 obtained. d) Average value of S.

Migration Length and Separation Factor. The single stage separation factor S is defined by

$$S = \frac{[\overline{^{10}B}][^{11}B]}{[^{10}B][\overline{^{11}B}]} \quad (1)$$

where [ ] denotes the concentration of isotopes in the aqueous phase and [¯] the concentration of the isotopes in the resin phase. The value of separation factor S can be obtained from the data by means of

$$S = \frac{\Sigma f_i(R_i - R_0)}{QR_0(1-R_0)} + 1 \quad (2)$$

where f_i is the total amount of boron in the i-th fraction, R_0 the original atomic fraction of boron-10, R_i the atomic fraction of boron-10 in the i-th fraction and Q the total capacity of ion exchange column. The

calculated values are given in Table 1. The separation factor S is constant irrespective of migration length. This is quite different from the results obtained by Hagiwara *et al.* on lithium isotope separation[5] and by Aida *et al.* on boron isotope separation,[1] in which the separation factor decreases with increase of migration length. The experiments were carried out without holding the isotopic plateau part in the chromatogram, the depleted part being mixed with an enriched part during the course of migration, making it impossible to obtain a reliable value of separation factor. In the present study, an isotopic plateau region in which the atomic fraction of isotopes remains unchanged always existed, no mixing taking place. The value obtained by means of Eq. 2 gives a satisfactory separation factor.

Conclusion

(1) Boron-10 was enriched from its original atomic fraction of 19.84 to 91.00% by the simple process of eluting a boric acid band with pure water through columns of weakly basic anion exchange resin Diaion WA21.

(2) The steady increase in atomic fraction of boron-10 with migration length indicates the merit of isotopic plateau displacement chromatography.

(3) At 40 °C a constant value 1.010 was obtained for the separation factor irrespective of migration length 1—256 m.

References

1) M. Aida, Y. Sakuma, M. Nomura, and H. Kakihana, *Nippon Genshiryoku Gakkai Shi*, **19**, 614 (1977).
2) Y. Sakuma, M. Aida, and H. Kakihana, *Nippon Genshiryoku Gakkai Shi*, **19**, 782 (1977).
3) H. Kotaka, K. Murayama, and H. Kakihana, *Nippon Kagaku Kaishi*, **1973**, 1482.
4) M. Nomura, M. Okamoto, and H. Kakihana, *Shitsuryo Bunseki*, **21**, 277 (1973).
5) Z. Hagiwara and Y. Takakura, *J. Nucl. Sci. Technol.*, **1969**, 326.

Studies of the Interaction of Poly(ethylene oxide) with Sodium Dodecyl Sulfate by Gel Filtration

Tsunetaka SASAKI,* Kaoru KUSHIMA, Kazunori MATSUDA, and Hitoshi SUZUKI

Department of Chemistry, Faculty of Science, Tokai University, Hiratsuka 259-12

(Received November 8, 1979)

The interaction between poly(ethylene oxide) (PEO), with a molecular weight of 6000, and sodium dodecyl sulfate (SDS) was studied by the gel-filtration method. The elution curve of the PEO–SDS system showed a tail of the elution volume smaller than that of SDS micelles at a concentration larger than about 4 mmol dm^{-3}. This suggests that the PEO–SDS (PS) complex is formed in the system. The dissolution-state diagram in the presence of PEO was then constructed in which the fractions of SDS single ions, SDS micelles, and the PS complex were shown against the SDS concentration. For a constant concentration of PEO, the molecular weight of the PS complex increased with the increase in the concentration of SDS up to the CMC of the PEO–SDS system, beyond which it became constant. The molecular weight of the PS complex was estimated to decrease from 21000 at 0.025 wt% PEO to 15000 at 0.2 wt% PEO.

The interaction of poly(ethylene oxide) (PEO) with sodium dodecyl sulfate (SDS) has been studied by the measurements of: (1) the equilibrium dialysis,[1] (2) the electrical conductance,[2,3] (3) the surface tension,[2,3] (4) the viscosity,[2] and (5) the solubilization.[3] (1) is a direct method of detecting the change in molecular size; however, it requires a long time to attain an equilibrium and also needs a supporting electrolyte of a concentration sufficient to suppress the Donnan effect, while from (2) to (5) are indirect methods. The band-gel-filtration method adopted in the present study offers a simple and direct method of measuring PEO–SDS interaction free from any supporting electrolyte. Using this method, two of the present authors have previously reported the interaction between poly(vinyl acetate) and SDS.[4] The present paper reports the studies of the interaction between PEO and SDS.

Experimental

Materials. Commercial pure-grade SDS previously recrystallized from ethanol was refluxed with charcoal in ethanol, filtered, and recrystallized. The purified sample showed no minimum in the surface tension *vs.* concentration curve. The PEO used was a commercial pure-grade substance with the mean molecular weight of 6000; it was dissolved in methanol, precipitated by the addition of diethyl ether, filtered, and dried. The gel used for packing the column was Sephadex G 100 produced by Farmacia.

Apparatus and Measurement. Gel-filtration apparatus used is shown in Fig. 1. Gel column used was 30 cm in length and 1.2 cm in inner diameter. For the measurement, sample solution of 30 cm^3 was introduced in the gel column, eluted with water and the elution curve was obtained by the conductometry. The flow rate was about 0.5 cm^3 min^{-1}. The measurement was made in an air thermostat at 30±0.5 °C.

Results and Discussion

Figure 2 is the elution curve showing the conductance *vs.* elution volume for the SDS solution. In this figure, Curve 1 is the elution curve of the SDS solution below the CMC. The curve shows a single tail, S, and a conductance plateau, κ_s. The elution volume of the tail and the height of plateau, corresponds to the size and the concentration respectively, of SDS single ions. Curve 2 in Fig. 2 is the elution curve of the SDS solution above the CMC. Here, the elution tail consists of two steps, S′ and M, which correspond to the sizes of single ions and micelles, while the heights of the two plateaux, κ_{cmc} and κ_m, correspond to the concentrations of single ions at the CMC and micelles respectively.

Figure 3 shows the elution curve of the PEO–SDS system for constant PEO and various SDS concentrations. Here, Curve 1 indicates the elution curve of the solution containing SDS below 4 mmol dm^{-3}. The curve shows a tail of a single step, S, and a corresponding single conductance plateau κ_s. Above 4 mmol dm^{-3} up to a certain concentration which is later identified as the CMC of the PEO–SDS system, the type of elution curve as represented by Curve 2 with tail of two steps, S′ and C, and two conductance plateaux,

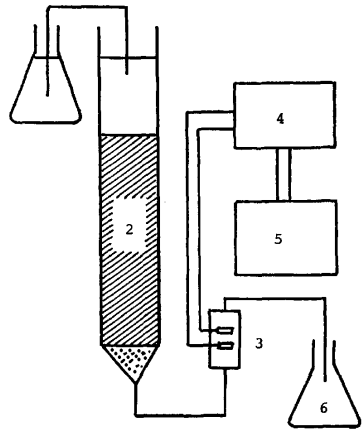

Fig. 1. Gel filtration apparatus.
1; Reservoir, 2; gel column, 3; conductance cell, 4; conductometer, 5; recorder, 6; weighing vessel.

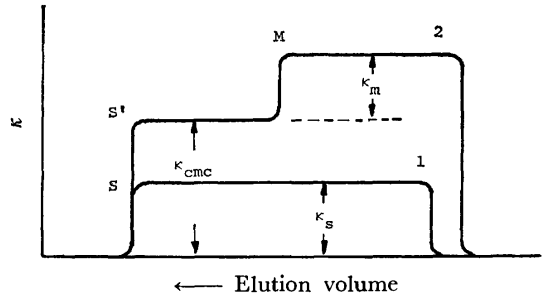

Fig. 2. Elution curve of SDS system.

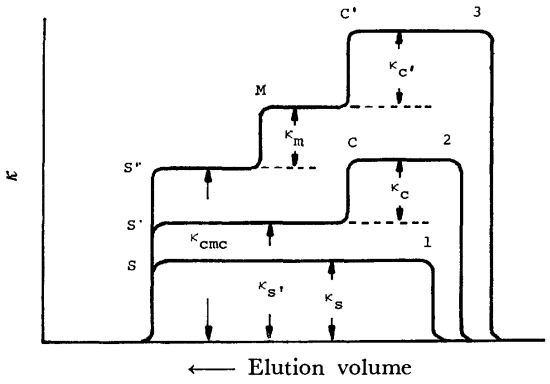

Fig. 3. Elution curve of PEO–SDS system.

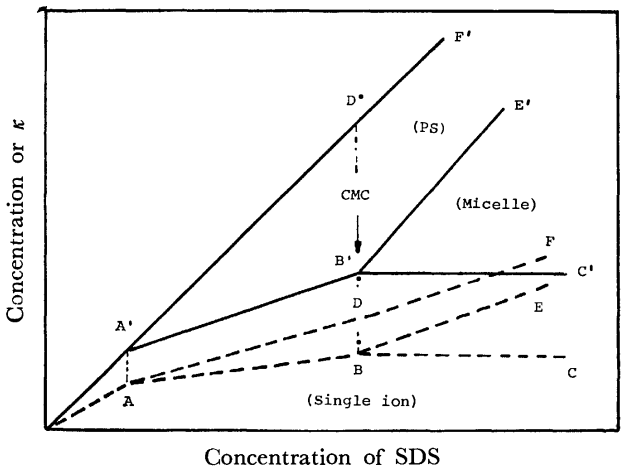

Fig. 4. Phase diagram of PEO–SDS system.
——; Concentration, ----; κ.

κ_s, and κ_c, was observed. At a higher concentration of SDS beyond the CMC, Elution Curve 3 was obtained. Here, the elution tail showed three steps, S", M, and C', and three conductance plateaux, κ_{cmc}, κ_m, and $\kappa_{c'}$.

Now, when we compare these three curves, 1, 2, and 3, with Fig. 2, it can be confirmed, that S, S', and S" correspond to the tails of SDS single ions, M to the tail of the SDS micelles, and C and C', to the tails of particles containing SDS and being larger than the SDS micelles. These particles can be regarded as forming the PEO–SDS complex (the PS complex). By plotting the conductances κ_s, κ_m, κ_c, *etc.*, against the total concentration of SDS, the lines in Fig. 4 were obtained. By transforming the conductances into the concentration, the solid lines in Fig. 4 were obtained.

The conductance *vs.* concentration relations for SDS single ions and SDS micelles, as obtained from Fig. 2, were used to convert the conductance values to the concentrations of the single ionic and micellar SDS. The concentration of the PS complex was obtained as the difference between the total concentration of SDS and the sum of the concentration of the SDS single ions and micelles.

The solid lines in Fig. 4 show the range of the regions of the SDS single ions the SDS micelles, and the PS complex; that is, the area below the OA'B'C' line

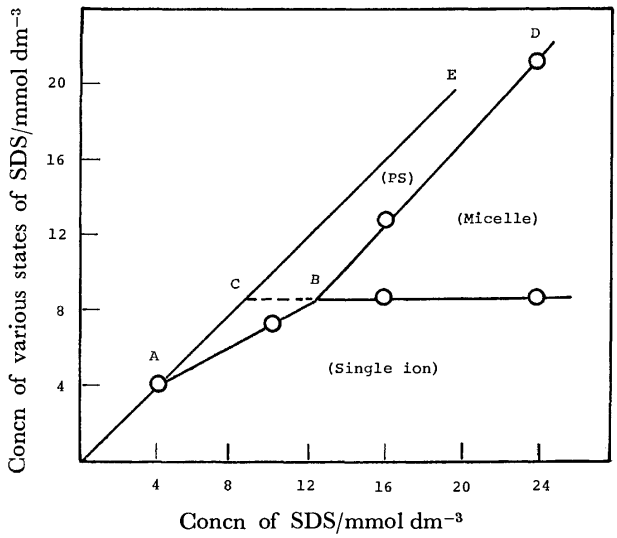

Fig. 5. Phase diagram of PEO–SDS system (0.05wt% PEO).

is the region of single SDS ions, the E'B'A'F' area the region of the PS complex, and the E'B'C', the region of the SDS micelles. Below the point A', the SDS is exclusively in the state of single ions not combined with PEO. Between A' and B', free SDS single ions and the SDS complex are in a mutual equilibrium. In the region above the point B', SDS micelles appear in the solution in addition to the PS complex and free SDS single ions. The concentration of SDS single ions was constant in this region and was equal to the CMC of the pure SDS solution. This suggests that the point B' is the CMC of the PEO–SDS system.

In such a manner, we can construct a diagram of the dissolution state of the SDS. Four such diagrams were obtained for SDS solutions containing 0.025, 0.05, 0.1, and 0.2 wt% of PEO. Figure 5 shows the results obtained for the SDS solution containing 0.05 wt% PEO. The concentration of SDS at point A is 4 mmol dm^{-3}. This concentration was almost independent of the concentration of PEO, except for the lowest concentration of 0.025 wt% PEO, where the point A shifted to 6 mmol dm^{-3}. This tendency is in accord with the results obtained by Jones.[2] The amount of SDS bound to PEO, which was estimated as the ordinate between lines AB and AC, increased from point A to B, which may suggest an increase in the size of the PS complex. This is in accord with the decrease in the elution volume from 23.0 cm^3 to 18 cm^3, for instance, for the 0.1 wt% PEO system. Beyond point B, the size of the PS complex became nearly constant, as judged from the constancies of the elution volume and the ordinate between BD and CE in this region in Fig. 5, although, according to Jones,[2] it is uncertain whether or not the size of the complex beyond point B continues to increase by the further binding of SDS.

The maximum amount of SDS bound to PEO can be calculated from the difference in the concentration of SDS between points B and C and the concentration of PEO. The calculated binding ratio de-

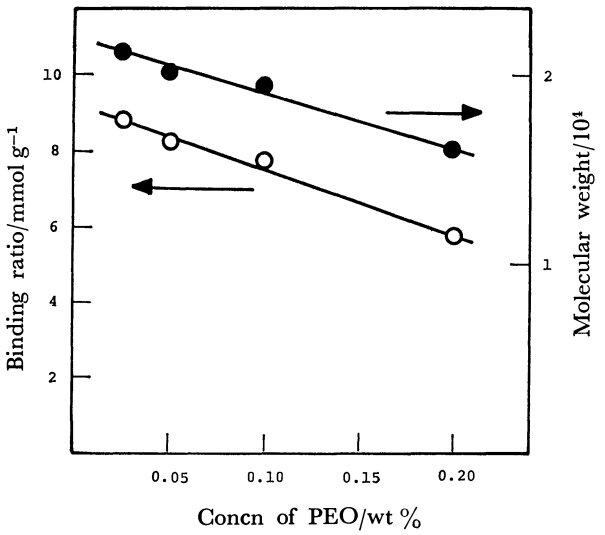

Fig. 6. Binding ratio and molecular weight of PEO–SDS complex.

creased with an increase in the PEO concentration, as is shown by the open circles in Fig. 6. The decrease in the SDS binding ratio agrees with the increase in the elution volume of the PS complex with the PEO concentration.

In Fig. 6, the maximum binding ratio at 0.1 wt% PEO is 7.7 mmol SDS/g PEO. This is comparable with the value of about 9 mmol SDS/g PEO in the presence of 1 mol dm^{-3} sodium chloride, as estimated from the equilibrium dialysis results obtained by Shirahama.[1)]

In the present study, the absolute size of the PS complex was not estimated by comparing the elution volume to that of the standard-molecular-weight substances. However, from the known weight ratio of SDS to PEO shown in Fig. 6 and the mean molecular weight 6000 of PEO, the molecular weight of the PS complex at CMC was calculated to be as shown by the solid circles. The molecular weight decreased from about 21000 at 0.025 wt% PEO to 15000 at 0.2 wt% PEO, as may be seen in the figure.

References

1) K. Shirahama, *Colloid Polym. Sci.*, **259**, 978 (1974).
2) M. N. Jones, *J. Colloid Interface Sci.*, **23**, 36 (1967).
3) M. J. Schwuger, *J. Colloid Interface Sci.*, **43**, 491 (1973).
4) T. Sasaki, K. Tanaka, and H. Suzuki, Proc. 6th International Congress on Surface Activity, Zürich, II 2, 849 (1972).

Adsorption of Dyes, Chromate, and Metallic Ions by Poly(ethyleneimine)

Tsunetaka Sasaki,* Osamu Asakawa, Kazuyo Kurosawa,
Minoru Mizushima, and Teruhiro Nakazono
Department of Chemistry, Faculty of Science, Tokai University, Hiratsuka 259-12

(Received January 21, 1980)

Ion exchange and chelate properties of poly(ethyleneimine) resin (PEI) were studied. Adsorption of neucoccin anions (NC^-) (maximum 1.7×10^{-4} mol/g) was greater than that of Crystal Violet cations (CV^+) (maximum 0.17×10^{-4} mol/g), indicating that PEI is an anion exchanger. CV^+ adsorption increased with the addition of sodium polyacrylate due to its bridging action between CV^+ ions and PEI. Adsorption of CrO_4^{2-} was confirmed to be much greater than that of NC^- ions amounting to 4×10^{-3} mol/g at a sufficiently concentrated solution of CrO_4^{2-}. The acid exchange capacity of PEI was found to be about the same as the maximum amount of adsorption of CrO_4^{2-}. Kinetics of adsorption of CrO_4^{2-} by PEI was studied at various temperatures. Adsorption followed a bimolecular reaction. Activation energy of 28.03×10^3 J/mol obtained is a right order of magnitude as an ion exchange adsorption. Chelating adsorption of Fe^{3+} and Cu^{2+} ions by PEI studied, the maximum amounts of adsorption being 3.1×10^{-3} mol/g and 3.3×10^{-3} mol/g, respectively. The values are greater than those for other synthetic polyethylene polyamine. PEI can be used as an anion and metallic cation adsorbent.

Poly(ethyleneimine) resin (PEI) is obtained in a large amount as a water insoluble by-product during the synthesis of polyethylene polyamine oligomers, causing trouble as an industrial waste. However, it is an effective anion exchanger as regards its chemical structure, and it would be worthwhile to study its behavior as both an anion exchanger and a cation chelating resin, like many synthetic polyamine reported.[1,2] It is noted that cheap anion exchangers can scarcely be found, while there exist abundant available cation exchangers such as clay minerals including bentonite and kaolinite.[3]

In the present experiment, adsorption of chromate, iron(III) and copper(II) ions as inorganic ions, and Crystal Violet and neucoccin as organic ions by PEI has been studied.

Experimental

Materials. PEI (Shunan Petroleum Co.) is a brown, fluffy, water insoluble powder. The sample for the measurement was prepared by removing impurities, washing with water and repeated decantation until the supernatant layer became clear after 10 min. The sample was then dried at 100 °C and kept in a desiccator.

Organic ions used were Crystal Violet cation (CV^+) and neucoccin anions (NC^-), inorganic ions being chromate anions (CrO_4^{2-}), iron(III) (Fe^{3+}), and copper(II) (Cu^{2+}) cations. For purification, Crystal Violet was precipitated from its ethanol solution by addition of diethyl ether. The precipitate was filtered and dried under reduced pressure. Neucoccin was recrystallized from its aqueous solution by addition of anhydrous sodium carbonate. Crystals deposited were filtered, washed with ethanol and dried under reduced pressure. Potassium chromate, iron(III) chloride, and copper(II) sulfate of guaranteed grade were used without further purification. Commercial sodium polyacrylate (NaPA) was used without further purification, the degree of polymerization being 22000—66000.

Measurement. The amounts of adsorption of CV^+ and NC^- were calculated from the difference in concentration of the solute before and after the adsorption by PEI. The concentration was determined with a spectronic colorimeter (Shimazu Spectronic 20) at wavelengths 480 nm and 580 nm for CV^+ and NC^-, respectively. The amounts of adsorption of CrO_4^{2-}, Fe^{3+}, and Cu^{2+} were calculated as in the cases of CV^+ and NC^-. The concentration was determined with a Hitachi atomic absorption spectrometer at wave lengths of 357.9, 248.5, and 324.7 nm, respectively. The experiments were carried out at room temperature, *ca.* 25 °C unless otherwise stated.

Results and Discussion

Adsorption of CV^+ and NC^-. Adsorption Isotherm: 0.1 g of PEI was put in a test tube containing 20 cm^3 solution of varying CV^+ and NC^- concentrations. The solutions were shaken frequently for 1 h and the amounts of adsorption determined. The results are shown in Fig. 1. We see that maximum adsorption of NC^- of 1.7×10^{-4} mol/g PEI is greater than that

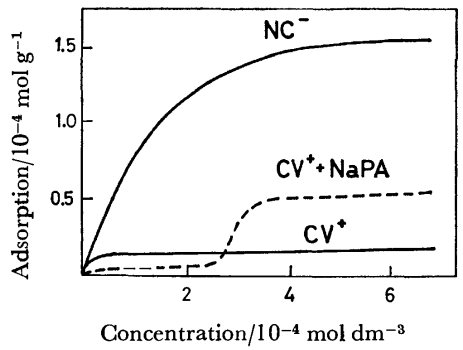

Fig. 1. Adsorption of dyes by PEI.

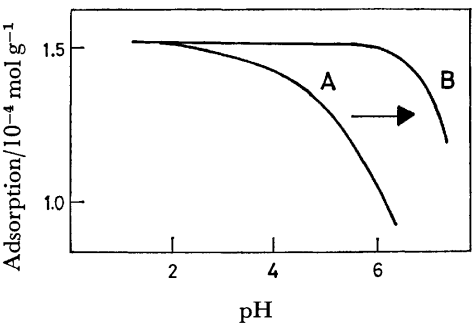

Fig. 2. Effect of pH on NC^- adsorption by PEI.

of CV^+ of 0.17×10^{-4} mol/g PEI. This confirms that PEI behaves as an anion exchanger as a whole. The slight adsorption exhibited by CV^+ might be due to the nonexchange adsorption.

Effect of pH *on* NC^- *Adsorption.* 0.1 g of PEI was added to a test tube containing 21 cm^3 of 7.88×10^{-4} mol/dm^3 NC^- solution of varying pH adjusted by the addition of HCl and NaOH, the solutions being shaken frequently for 1 h. The amount of adsorption calculated is plotted against pH before and after the adsorption in Fig. 2. The amount of adsorption increases with the decrease in pH, while pH increases with adsorption. These reactions can be explained by

$$RNH + NC^- + H^+ \longrightarrow RNH_2^+NC^-$$

where RNH denotes PEI. The equation indicates that PEI is an anion exchanger or an acid adsorbent.

Bridging Action of NaPA for the Adsorption of CV^+ *by PEI.* Because of the anion exchange property of PEI, adsorption of CV^+ was found to be small (Fig. 1). However, the adsorption of CV^+ might increase with the addition of a polymer anion such as NaPA. In the present experiment, 60 ppm of NaPA was added to the solution of CV^+ and the adsorption was measured under the same conditions as in the preceding experiments (broken line, Fig. 1). A marked increase took place in the amount of adsorption by the addition of NaPA in a higher concentration region of CV^+ as expected, but a slight decrease is seen in the lower concentration region. The increase of CV^+ adsorption by the addition of NaPA is explained by the bridging action of polyacrylate anions between PEI molecules and CV^+ cations. A similar bridging action has been reported in the case of EDTA.[4] The decrease of CV^+ adsorption at lower concentration is probably due to polyacrylate anions, not acting as a bridge but covering the sites on PEI available for the adsorption of CV^+ ions.

Adsorption of CrO_4^{2-}. *Adsorption Isotherm*: 0.2 g of PEI was added to 50 cm^3 of CrO_4^{2-} ion solutions of varying concentration in an Erlenmeyer flask, and the amount of adsorption was measured after stirring for 2 h. The result is shown in Fig. 3. The adsorption of CrO_4^{2-} ions is 4×10^{-3} mol/g PEI at 3×10^{-3} mol/dm^3 CrO_4^{2-} concentration. The amount is greater than that of NC^- ion which might be due to the smaller size of anions which can penetrate the inner surface of PEI.

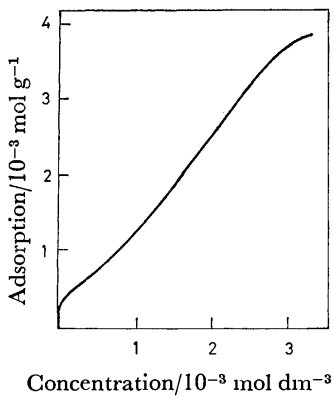

Fig. 3. Adsorption of CrO_4^{2-} by PEI.

Effect of pH *on* CrO_4^{2-} *Adsorption.* The effect of pH on CrO_4^{2-} adsorption was studied as in the case of NC^- adsorption. 0.2 g of PEI was added to 200 cm^3 of 0.84×10^{-3} mol/dm^3 CrO_4^{2-} solution, the pH of the solution being adjusted by addition of HCl. The amount of adsorption was measured after stirring at 25 °C for 1 h. The result is plotted against pH at equilibrium in Fig. 4. Adsorption of CrO_4^{2-} exhibits a maximum at pH 3, the behavior differing from the effect of pH on NC^- (Fig. 2). The increase of adsorption with the decrease of pH down to 3 can be explained by

$$2RNH + CrO_4^{2-} + 2H^+ \longrightarrow (RNH_2^+)_2CrO_4^{2-}$$

as in the case of NC^-. However, the decrease of adsorption of CrO_4^{2-} below pH 3 may be due to the following reaction:

$$(RNH_2^+)_2CrO_4^{2-} + 2HCl \longrightarrow 2RNH_2^+Cl^- + H_2CrO_4$$

The ion exchange of CrO_4^{2-} ions with Cl^- ions as well as the formation of weak acid H_2CrO_4 seem to favor the desorption of CrO_4^{2-} ions.

Rate of CrO_4^{2-} *Adsorption.* To 500 cm^3 of 0.85×10^{-3} mol/dm^3 K_2CrO_4 solution was added 0.5 g of PEI and the concentration of CrO_4^{2-} ions was measured at various intervals with stirring at constant temperatures in the range 9.5 °C—40.2 °C. Figure 5 shows plot of concentration C in 10^{-3} mol/dm^3 *vs.* time t in min at 19.8 °C. In most cases a rapid decrease in CrO_4^{2-} ion concentration took place during the first 10 or 20 min, equilibrium being attained after *ca.* 1 h.

A linear plot was obtained between $1/(C-C_\infty)$ and t (Fig. 6), which can be expressed as

$$1/(C-C_\infty) = Kt + L \qquad (1)$$

where C_∞, K, and L are constants, C_∞ being the equilibrium concentration after a sufficiently long time. Differentiating Eq. 1, we get

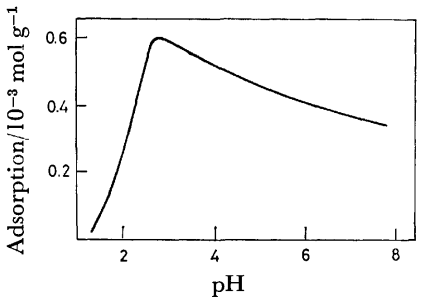

Fig. 4. Effect of pH on CrO_4^{2-} adsorption by PEI.

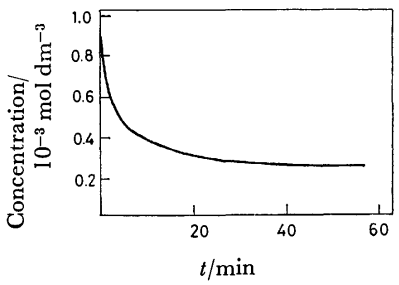

Fig. 5. Rate of CrO_4^{2-} adsorption by PEI.

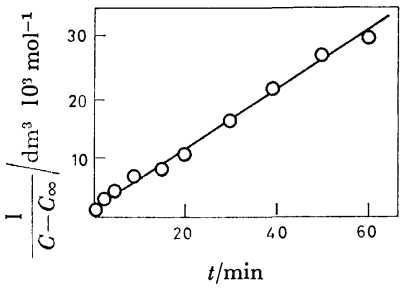

Fig. 6. $\frac{1}{C-C_\infty}$ *vs.* t plots.

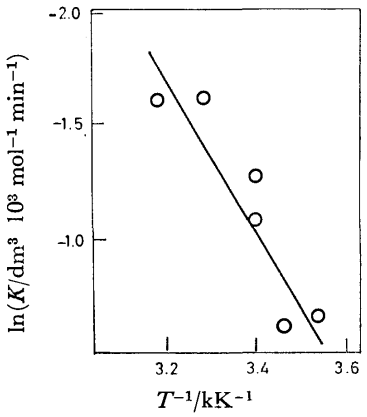

Fig. 7. Arrhenius plots.

$$-dC/dt = K(C-C_\infty)^2 \quad (2)$$

The precise physical meaning of Eq. 2 expressing a bimolecular reaction is not clear. Arrhenius plot was made between ln K and the reciprocal of the absolute temperature T (Fig. 7). From the straight line we get the activation energy 28.03×10^3 J/mol. This is considered to be reasonable as a value for the ion exchange reaction in an aqueous solution.[5]

Anion Exchange Capacity of PEI. Anion exchange capacity was measured for PEI by the method of Kunin and Myers.[6] A given amount of the chloride form of PEI prepared by treatment with HCl solution and washing with ethanol was first treated with ammonia and then with aqueous Na_2SO_4 solution. The chloride contents in ammonia and aqueous Na_2SO_4 solution were then determined by titration with aqueous $AgNO_3$ solution. Weak base, strong base and total exchange capacities were calculated from the chloride contents, and found to be 1.51, 8.23, and 9.73 meq/g PEI, respectively. The strong base exchange capacity can be compared with the saturation amount, *ca.* 8 meq/g PEI, of CrO_4^{2-} adsorption, as estimated from Fig. 3. It was also confirmed that the exchange capacity obtained for PEI is larger as compared with that for the polyethylene polyamine synthesized as an ion exchanger.[2]

Adsorption of Fe^{3+} and Cu^{2+}. Although the adsorption of dye cation, CV^+, by PEI is comparatively small, the adsorption of metallic cations such as Fe^{3+} and Cu^{2+} might be large due to the amine complex formation of these ions with PEI.[1]

Rate of Fe^{3+} and Cu^{2+} Adsorption. 0.1 g of PEI was added to 200 cm^3 of 1×10^{-4} mol/dm^3 (pH=8) and Cu^{2+} (pH=7) ion solutions and the resulting solutions were stirred. 5 cm^3 each was taken at different times from these solutions and the concentration decrease due to the adsorption measured, the result being plotted against time of adsorption (Fig. 8). Adsorption is rapid and is completed within 10 min.

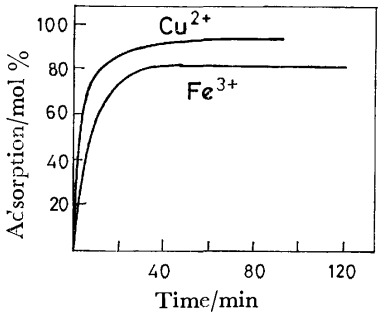

Fig. 8. Rate of adsorption of Fe^{3+} and Cu^{2+} by PEI.

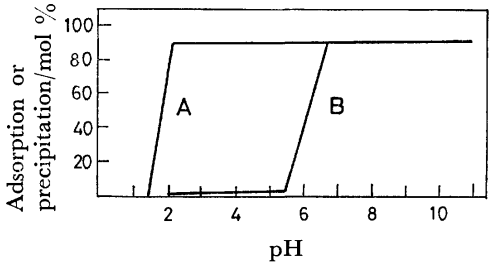

Fig. 9. Effect of pH of Fe^{3+} adsorption by PEI. A; Amount of adsorption, B; amount of precipitation.

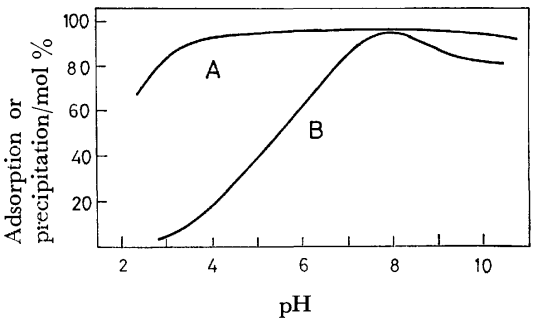

Fig. 10. Effect of pH on Cu^{2+} adsorption by PEI. A; Amount of adsorption, B; amount of precipitation.

Effect of pH on Fe^{3+} and Cu^{2+} Adsorption. The pH of 1×10^{-4} mol/dm^3 Fe^{3+} and Cu^{2+} ion solutions was adjusted by the addition of HCl and NaOH. To 50 cm^3 of these solutions was added 0.1 g of PEI and the amount of adsorption was calculated from the concentration decrease of the solution due to adsorption after stirring for 1 h. The amount of adsorption expressed in terms of the percentage of the initial amount of solute is plotted against the pH in Figs. 9 and 10; the amount of removed Fe^{3+} and Cu^{2+} ions due to precipitation by the addition of NaOH without PEI was measured and the results are also plotted against pH for comparison. We see a distinct adsorption effect of Fe^{3+} and Cu^{2+} by PEI below pH 7. However, the amount of adsorption and precipitation became equal for the systems with and without PEI above pH 7. Thus, from this graph alone we cannot

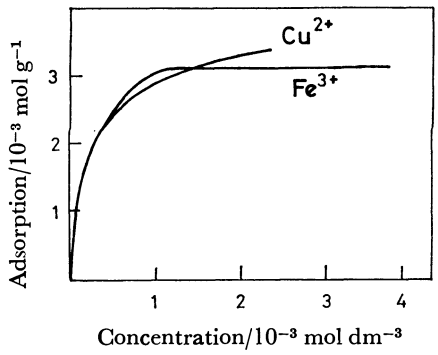

Fig. 11. Adsorption isotherm of Fe^{3+} and Cu^{2+} by PEI.

confirm whether adsorption or precipitation takes place above pH 7. However, we believe that the adsorption of Fe^{3+} and Cu^{2+} on PEI takes place even in this pH region, since these ions can be floated with PEI by shaking the suspension with the addition of polyacrylamide and cationic surfactant, while iron and copper hydroxides without PEI cannot be floated from its suspension by a similar treatment.

Adsorption Isotherms of Fe^{3+} and Cu^{2+}. To 50 cm^3 of Fe^{3+} and Cu^{2+} ion solutions of varying concentration was added 0.1 g of PEI at pH 5 and the solutions were continuously stirred. After 1 h the amount of adsorption was measured; the result is plotted against equilibrium concentration in Fig. 11. The maximum amounts of adsorption were found to be about 3.1×10^{-3} mol/g and 3.3×10^{-3} mol/g PEI for Fe^{3+} and Cu^{2+}, respectively. The maximum amount of adsorption for Cu^{2+} is larger in the order of magnitude than the amount of adsorption reported for synthetic polyethylene polyamine,[5] but smaller than the simple ion exchange adsorption of CrO_4^{2-} ions by PEI.

Conclusion. From the results obtained, PEI is considered as a good anion exchange adsorbent as well as a chelating agent for metallic cations. Such properties are conveniently and effectively utilized further in the operation of ion flotation.

References

1) T. Kuwamura, S. Yoshikawa, and T. Kubodera, *J. Ind. Chem., Jpn.*, **57**, 676 (1954); G. Izumi, M. Sato, S. Shoji, and K. Oikawa, *Bull. Chem. Soc. Jpn.*, **49**, 1727 (1976).
2) H. Egawa, *J. Ind. Chem. Jpn.*, **68**, 2499 (1965).
3) H. van Olphen, "An Introduction to Clay Colloid Chemistry," Interscience Pub., John Wiley & Sons Inc., New York, London (1963).
4) N. Aoki and T. Sasaki, *Bull. Chem. Soc. Jpn.*, **39**, 939 (1966).
5) R. L. Rich and H. Traube, *J. Phys. Chem.*, **58**, 1 (1954).
6) R. Kunin and R. J. Myers, "Ion Exchange Resin," John Wiley and Sons Inc., New York, London (1950), p. 341.

 © 1980 The Chemical Society of Japan Bull. Chem. Soc. Jpn., 53, 1871—1876 (1980)

X-Ray Photoelectron Spectroscopic Study of Tetrathiafulvalene-Tetracyanoquinodimethane (TTF·TCNQ) and Related High Conductive Organic Complexes

Isao Ikemoto, Masamichi Yamada, Tadashi Sugano, and Haruo Kuroda
Research Centre for Spectrochemistry and Department of Chemistry, Faculty of Science, The University of Tokyo, Hongo, Tokyo 113
(Received November 9, 1979)

Tetrathiafulvalene–tetracyanoquinodimethane (TTF·TCNQ) and related high conductive organic complexes were studied by X-ray photoelectron spectroscopy (XPS). The N 1s peak shape of TTF·TCNQ evaporated film was found to change by X-ray irradiation; the high-binding energy shoulder of the N 1s peak increased its intensity with X-ray irradiation time and finally showed a new peak separated by about 1.5 eV from the main peak. TTF·TCNQ was found to be 1:1 both in the surface and in the bulk. The amounts of charge transfer in TTF·TCNQ and other TTF complexes as well as those in 5,6:11,12-bis(dithio)naphthacene(tetrathiotetracene, TTT) complexes were determined from the analysis of the S 2p peak shape. The amount of charge transfer is 0.56 ± 0.05 in TTF·TCNQ and 0.55 ± 0.05 in TTF·TNAP (tetracyanonaphthoquinodimethane). The molecular ratio of $(donor)^+$ in donor molecules is 0.71 ± 0.05 in $TTF\cdot Br_{0.7}$, 0.52 ± 0.05 in $TTF\cdot I_{0.7}$, 0.65 ± 0.05 in $(TTF)_3(BF_4)_2$, 0.49 ± 0.05 in $(TTT)_2I_3$, and 0.93 ± 0.05 in $(TTT)(TCNQ)_2$, which correspond respectively to 100, 73, 100, 100, and 100% charge transfer between donors and acceptors. The N 1s peak shape of TTF·TCNQ is also discussed.

The charge-transfer salt, tetrathiafulvalene–tetracyanoquinodimethane (TTF·TCNQ), is a typical example of the organic solid that exhibits the behaviors as a quasi-one-dimensional conductor. The crystal of TTF·TCNQ was initially considered to be composed of TTF^+ and $TCNQ^-$ as a result of a complete charge transfer from TTF to TCNQ. However, several experimental evidences were accumulated later to indicate that the charge transfer between TTF and TCNQ is not complete.[1-10]

There are a variety of highly-conductive charge-tranfer salts which involve TTF or its analogs as the electron donor and/or TCNQ or its analogs as the electron acceptor. In almost all cases of these metal-like conductors, donor stacks and/or acceptor stacks are in a mixed-valence state as in TTF·TCNQ. It is now believed that this mixed-valence character has an important bearing on the metallic behaviors of these organic solids.

X-Ray photoelectron spectroscopy (XPS) could provide informations concerning the electronic state of a mixed-valence molecular stack. If holes in a donor stack (or electrons in an acceptor stack) are highly localized, each core electron peak in the XPS spectrum will be composed of the components corresponding to the neutral molecule and the ion, respectively. On the other hand, if holes in a donor stack (or electrons in an acceptor stack) are completely delocalized, the core electron peaks will be of single component corresponding to the partially ionized state of the molecule.[11]

Some years ago, we first reported the results of the XPS studies on a series of TCNQ salts.[12,13] As compared with the N ls peaks of TCNQ simple salts, the N ls peaks were found to be significantly broader in the XPS spectra of TCNQ complex salts, as if it is composed of the peaks due to the neutral molecule and ion of TCNQ. However, the observed peak shapes could not be satisfactorily reproduced by the simple superposition of the N ls peak of $TCNQ^0$ and that of $TCNQ^-$.[13] In the XPS spectra of TCNQ salts, the N ls peaks are always accompanied by a strong shake-up satellite, which seems to vary depending on the intermolecular charge-transfer interaction within a TCNQ stack. This introduces a considerable complexity into the analysis of the observed peak profile. In contrast, the S 2p peak of TTF is not accompanied by a strong satellite. Thus it seems worthwhile to see if the S 2p peak profiles in the XPS spectra of TTF salts can be well interpreted by the superposition of the components associated with TTF^0 and TTF^+.

There is another aspect which should be examined in order to establish the interpretation of the XPS spectra of TTF·TCNQ and related materials. The chemical composition in the surface region could be different from the bulk. In effect, it was pointed out by Ritsko *et al.*,[14] from the XPS studies of an evaporated film of TTF·TCNQ, that the surface of a TTF·TCNQ film prepared at room temperature was more nitrogen rich than the bulk. Thus we tried to know if there is actually any significant difference between the bulk and surface by means of the observation of the angular dependence of the XPS spectrum.

In the present paper, we will report the results of these XPS studies made on a series of TTF salts and related materials.

Experimental

Materials. The chemical formulae of the organic donors and acceptors used in the present study are given in Fig. 1.

TTF, TTT, and TNAP were synthesized according to the literatures.[15-19] Other compounds were commercially obtained.

The crystalline powders of the charge-transfer salts were prepared by the procedures described in the literatures.[18,20-22] In the cases of the bromide and iodide of TTF, the mole ratio of donor and acceptor is known to vary depending on the condition of preparation.[20,21] We obtained $TTF\cdot Br_{0.7}$ and $TTF\cdot I_{0.7}$ by the methods given in our previous paper.[15]

XPS Measurements. X-Ray photoelectron spectra were

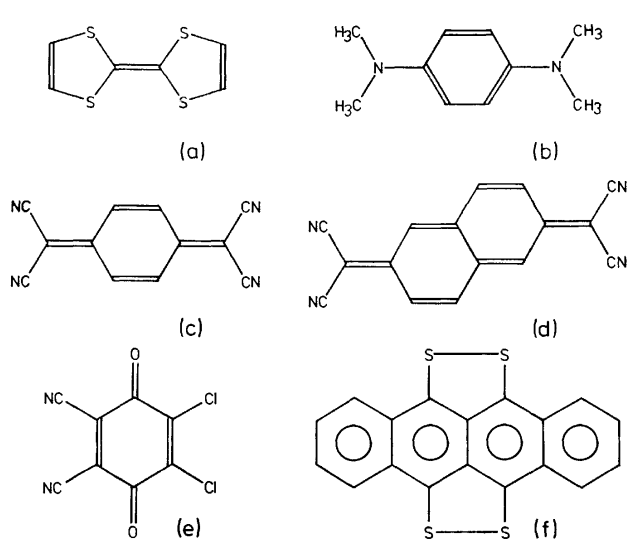

Fig. 1. (a) Tetrathiafulvalene (TTF), (b) *N,N,N',N'*-tetramethyl-*p*-phenylenediamine (TMPD), (c) tetracyanoquinodimethane (TCNQ), (d) tetracyanonaphthoquinodimethane (TNAP), (e) 2,3-dichloro-5,6-dicyano-*p*-benzoquinone (DDQ), (f) 5,6:11,12-bis(dithio)naphthacene (tetrathiotetracene, TTT).

measured with a McPherson ESCA 36 electron spectrometer using Mg $K\alpha$ (1253.6 eV) as the stimulating radiation. In all cases except K·TCNQ, TTF·TNAP and TTT salts, samples were deposited onto aluminum plates by the sublimation within the sample chamber of the spectrometer. XPS measurements were also done on powder samples pressed onto aluminum plates. The spectra thus obtained were almost the same as those obtained with evaporated films. To measure the spectrum of TTF solid, the sample was deposited onto an aluminum substrate cooled with a dry ice–ethanol mixture in order to reduce the evaporation of TTF.

The binding energies of photoelectron peaks were calibrated by using the Au $4f_{7/2}$ peak (83.8 eV) of a thin gold film deposited on the sample surface.

To vary the photoelectron take-off angle, an angle-variable sample holder was specially designed so as to be incorporated into our XPS spectrometer. The details of this sample holder will be reported elsewhere.[23]

Results and Discussion

Angular Dependence of XPS Spectrum of TTF·TCNQ and the Effects of X-Ray Irradiation. We measured the XPS spectrum of an evaporated film of TTF·TCNQ setting the photoelectron take-off angle θ, measured from the sample plane, at 10° and at 80°. We noted that the shape of N ls peak changed with time as we repeated XPS measurements on the same sample. Figure 2 shows the variation of the N ls peak shape with X-ray irradiation time, observed under the conditions that $\theta=80°$. The intensity at the high-binding energy shoulder of the N ls peak increased with irradiation time, and finally showed a new peak separated by about 1.5 eV from the main peak. The irradiation effect did not appear so clearly in the spectra measured at $\theta=10°$. In this case, the

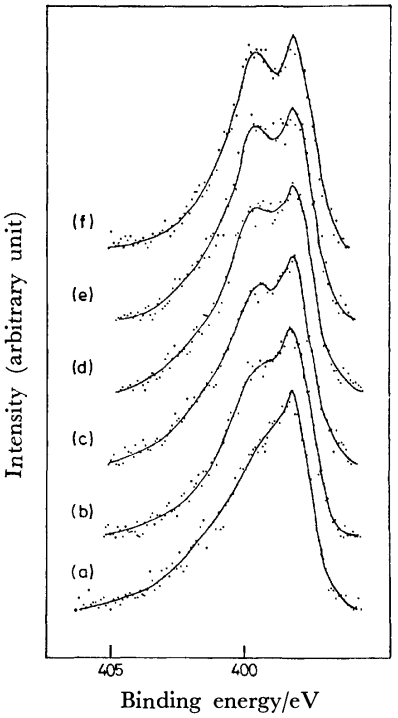

Fig. 2. The variation of the N ls peak shape of TTF·TCNQ evaporated film with X-ray irradiation time. (The photoelectron take-off angle is 80°.)
X-Ray irradiation time: (a) 0 min, (b) 200 min, (c) 465 min, (d) 630 min, (e) 795 min, and (f) 960 min.

change of the N ls peak shape was almost negligible after 400 min irradiation while a significant change was observable with the same film when $\theta=80°$.

It is well established that, when the angular distribution of XPS spectrum is measured on a very flat surface of a solid sample, the contribution of the surface relative to that of the bulk increases with the decrease of the photoelectron take-off angle. It was discussed by Fadley *et al.* that the same tendency can be also expected when the sample is an evaporated film with considerable surface roughness.[24] However, an opposite interpretation was taken by Ritsko *et al.*, in the case of the TTF·TCNQ evaporated film.[14] They observed by a scanning electron microscope that needle crystals of TTF·TCNQ are standing up on the substrate. From this structure of the film, they considered that the XPS spectrum obtained at a high take-off angle must reflect the surface state more strongly than the spectrum obtained at a low take-off angle. This interpretation seems to be consistent with our results concerned with the X-ray irradiation effect, since, in our experiments, the change of the N ls peak shape was markedly observed in the spectra measured at $\theta=80°$, not at $\theta=10°$, while the change by X-ray irradiation is naturally expected to take place rather in the surface region than in the bulk.

We found no appreciable change by X-ray irradiation in the S 2p peak shape, even if a marked change had already taken place in the N ls peak of the same sample.

We estimated the N/S atomic ratio from the in-

Table 1. Angular dependent XPS results of TTF·TCNQ evaporated films

	Run	Measured peaks	X-Ray irradiation time / min	Take-off angle/°	N/S atomic ratio
Exp. I	1	S 2p, N 1s	0	80	1.00 : 1
	2	S 2p, N 1s	100	10	0.96 : 1
	3	S 2p, N 1s	200	80	1.00 : 1
	4	S 2p, N 1s	300	10	0.90 : 1
	5	S 2p, N 1s	465	80	0.96 : 1
	6	S 2p, N 1s	630	80	0.96 : 1
Exp. II	1	S 2p, N 1s	0	10	0.94 : 1
	2	S 2p, N 1s	100	80	0.93 : 1
	3	S 2p, N 1s	200	10	0.89 : 1
Exp. III	1	S 2p, N 1s	0	10	0.94 : 1
	2	S 2p, N 1s	100	80	0.99 : 1
	3	S 2p, N 1s	200	10	0.98 : 1
	4	S 2p, N 1s	300	80	0.98 : 1
Exp. IV	1	S 2p, N 1s	0	80	0.96 : 1
	2	S 2p, N 1s	100	10	0.94 : 1
Exp. V	1	S 2p, N 1s	0	10	0.95 : 1
	2	S 2p, N 1s	100	80	0.99 : 1

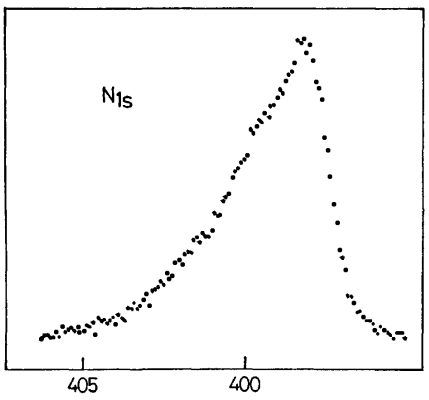

Fig. 3. The intrinsic N 1s peak of TTF·TCNQ. (Refer the text.)

tegrated intensities of the N 1s and S 2p peaks.[25] The results are given in Table 1. In each experiment, an evaporated film of TTF·TCNQ was freshly prepared, and the N 1s and S 2p peaks were repeatedly recorded by setting the take-off angle at either 10° or 80°. The results show that the N/S atomic ratio does not vary on X-ray irradiation in spite of the change of the N 1s peak shape. It should be noted also that the atomic ratio is the same within the experimental error between the cases $\theta=10°$ and 80°, the average value being 0.94 ± 0.03 for $\theta=10°$ and 0.96 ± 0.04 for $\theta=80°$. This fact may indicate that the mole ratio of TTF and TCNQ is not significantly different between the surface and the bulk, and does not vary with X-ray irradiation.

The mechanism that causes the change of the N 1s peak shape of TTF·TCNQ is not clear at present. The new peak which appeared at the high-binding energy side of the main peak after a long X-ray irradiation could correspond to the N 1s peak due to $TCNQ^0$.[9] If this is the case, we should consider that the ratio of TCNQ neutral molecule to $TCNQ^-$ ion increased in the surface region by X-ray irradiation. One could suspect that this change of the $TCNQ^0/TCNQ^-$ ratio is associated with a partial loss of TTF molecules from the surface region. But this is not likely to be the case since the N/S atomic ratio did not change with X-ray irradiation. If the new peak is attributable to $TCNQ^0$, a possible interpretation for the appearance of this peak could be that the electron transfer from $TCNQ^-$ to some adsorbed chemical species is enhanced by some way with X-ray irradiation. But we cannot exclude the possibility that the new peak is associated not with $TCNQ^0$, but with some product of an X-ray induced chemical reaction.

In any case, it is of vital importance to record the N 1s peak with a fresh film minimizing X-ray irradiation time in order to get the true peak shape. We summed up the data obtained within a short measuring time on several freshly-deposited TTF·TCNQ films, and obtained the N 1s peak shape which is shown in Fig. 3. This can be taken as the true N 1s peak shape without the deformation due to X-ray irradiation. It is very asymmetric with a long tail in the higher binding energy side. This is considerably different from the N 1s peak shapes which were reported by other authors.[6,14] The peak shapes hitherto reported seem to correspond to the state which has been already affected by X-ray irradiation.

Peak Shape and Degree of Charge Transfer. The S 2p spectra of TTF, $(TTF)^+\cdot(DDQ)^-$, TTT, and $(TTT)^+\cdot(ClO_4)^-$ are shown in Fig. 4. In each case, the observed spectrum shows a peak corresponding to S $2p_3/_2$ and a shoulder corresponding to S $2p_1/_2$. The overall fwhm (full width at half-maximum height) is 2.1 eV in the cases of TTF and TTT, and 2.5 eV in the cases of $(TTF)^+\cdot(DDQ)^-$ and $(TTT)^+\cdot$

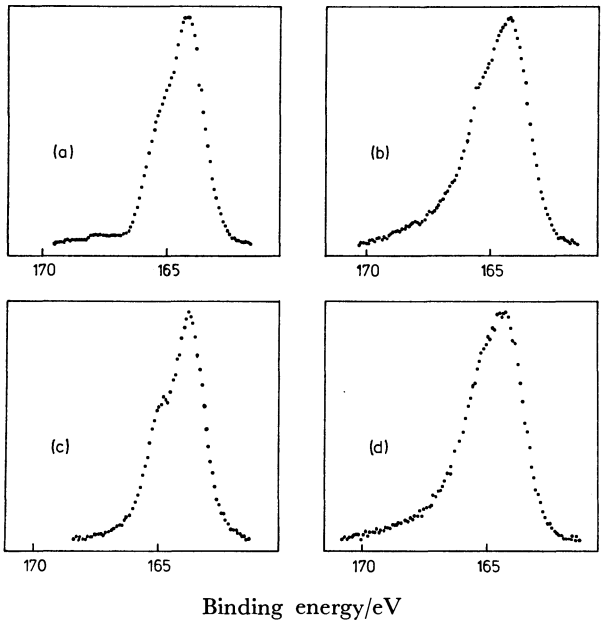

Fig. 4. S 2p peaks in the XPS spectra of (a) TTF, (b) TTF·DDQ, (c) TTT, and (d) TTT·(ClO_4).

$(ClO_4)^-$.[26] Any strong shake-up satellite does not appear in these S 2p spectra.

The S 2p spectra of TTF·$Br_{0.7}$, TTF·$I_{0.7}$, $(TTF)_3(BF_4)_2$, TTF·TCNQ, and TTF·TNAP are shown in Fig. 5. The peak profiles observed in these cases are significantly different from those shown in Fig. 4, showing a larger peak width; the fwhm is 2.7—3.1 eV in these cases. Obviously, TTF stacks in TTF·$Br_{0.7}$ and TTF·$I_{0.7}$ are in a mixed-valence state. From the chemical composition of TTF·$Br_{0.7}$, one can expect that about 70 percent of TTF molecules are in the state of TTF^+ and the remaining 30 percent are in the state of TTF^0, provided that all bromine atoms are in the state of Br^-. As shown in Fig. 5, the S 2p spectrum of TTF·TCNQ is similar to those of TTF·$Br_{0.7}$ and TTF·$I_{0.7}$, and distinctly different from those of $(TTF)^+\cdot(DDQ)^-$ and $(TTF)^+\cdot(ClO_4)^-$. This fact suggests that an incomplete charge transfer is taking place in TTF·TCNQ.

Assuming that the observed S 2p peak profile of $(TTF)^+\cdot(DDQ)^-$ is the one characteristic of TTF^+ and that of TTF is the one characteristic of TTF^0, we tried to reproduce the observed peak profiles of mixed-valence TTF salts by superimposing these two standard peak profiles, treating their separation and relative intensities as adjustable parameters. We defined the following error function:

$$R = \sum_i |I_{obsd}(E_i) - I_{calcd}(E_i)|/I_{obsd}(E_i)$$

where $I_{obsd}(E_i)$ is the observed intensity at the binding energy E_i and $I_{calcd}(E_i)$ is the calculated intensity of the superimposed peak profile at the same binding energy. We calculated the R value for each assumed parameter set and looked for the minimum point of the R map, which was taken to give the parameter set for the best fit between the observed and calculated peak profiles. All of these calculations were performed by use of a computer HITAC 8700/8800 at the Computer Center, University of Tokyo. The final results of the simulations for the mixed-valence TTF salts are shown in Fig. 5 with solid lines. The TTF^0 and TTF^+ components are shown in the same figure with broken lines. The results shown in Fig. 5 indicate that the S 2p peak profiles observed of the mixed-

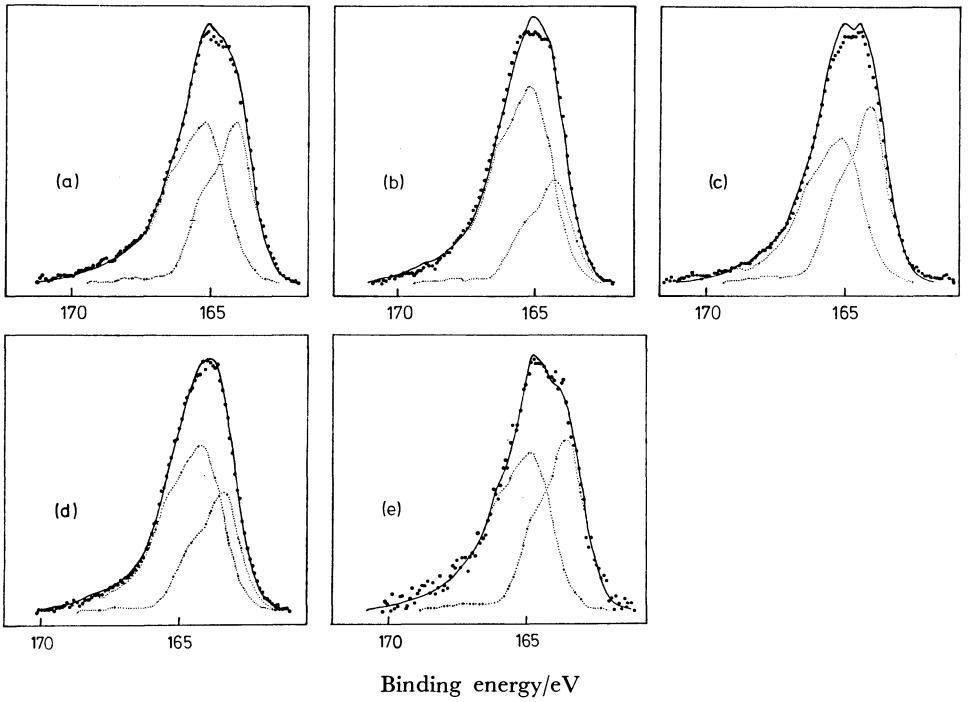

Fig. 5. S 2p peaks in the XPS spectra of (a) TTF·TCNQ, (b) TTF·$Br_{0.7}$, (c) TTF·$I_{0.7}$, (d) $(TTF)_3(BF_4)_2$, and (e) TTF·TNAP.
Observed peak (•••), simulated peak (——), and component peaks of simulation (···).

Table 2. Amount of (Donor)$^+$ and (Donor)^0 in the TTF and TTT complexes

	(Donor)$^+$ %	(Donor)^0 %
TTF·TCNQ	56±5	44±5
TTF·TNAP	55±5	45±5
TTF·$Br_{0.7}$	71±5	29±5
TTF·$I_{0.7}$	52±5	48±5
$(TTF)_3(BF_4)_2$	65±5	35±5
$(TTT)_2I_3$	49±5	51±5
(TTT)$(TCNQ)_2$	93±5	7±5

The errors were estimated from the *R*-maps obtained from the peak profile analysis.

valence TTF salts can be very satisfactorily reproduced by superimposing the S 2p peaks of TTF^+ and TTF^0.

From the intensity ratio of the component peaks which gives the best fit between the observed and calculated peak profiles ,we can estimate the relative amounts of TTF^+ and TTF^0 in each mixed-valence TTF salt. The results are listed in Table 2. In the case of TTF·$Br_{0.7}$, the relative amount of TTF^+ is determined to be 71 percent, which agrees well with the value that is expected from the chemical composition. The shape of the Br 3d peak of this salt coincides well with that of the Br 3d peak of KBr. Thus all XPS data consistently indicate that bromine atoms in TTF·$Br_{0.7}$ are completely in the state of Br^-. This is also consistent with the ESR data.[15] In the case of $(TTF)_3(BF_4)_2$, 67 percent of TTF molecules must be in the state of TTF^+ since each BF_4 group receives one electron from TTF. The relative amount of TTF^+ derived from the peak profile analysis is in good agreement with the above value. These examples do indicate the validity of our procedure of peak profile analysis. It is interesting to see that, in the case of TTF·$I_{0.7}$, the peak profile analysis gave the relative amount of TTF^+ significantly smaller than the value that is expected from the chemical composition. We noted also that the profile of the I $3d_{3/2}$ peak is appreciably different from that of KI, indicating that there are some iodine species which are different from I^-. Using the peak profile of I $3d_{3/2}$ of KI, we decomposed the I $3d_{3/2}$ peak observed of TTF·$I_{0.7}$ into the component corresponding to I^- and the one corresponding to the other iodine species which has less negative charge, possibly being in the state of I^0. The analysis of I $3d_{3/2}$ peak profile mentioned above gave the conclusion that about 79 percent of iodine atoms are in the state of I^-. If we assume that the remaining iodine atoms are in the neutral state, the relative amount of TTF^+ is expected to be 56 percent. This is in good agreement with the value obtained from the analysis of the S 2p peak profile. Seemingly an incomplete charge transfer is taking place in TTF·$I_{0.7}$. This conclusion is consistent also with the ESR data, which indicate that some unpaired spins are on iodine atoms.[15]

In the case of TTF·TCNQ, the analysis of the S 2p peak profile gave the relative amount of TTF^+ as 56 percent. From the analysis of the X-ray diffuse scattering, Comès *et al.*[5] and Kagoshima *et al.*[3] concluded that the degree of charge transfer from TTF to TCNQ is to be 59 percent. The relative amount of TTF^+ determined by the analysis of the S 2p peak profile is in good agreement with the above conclusion. The analysis of the S 2p peak profile gives almost same degree of charge transfer for TTF·TNAP.

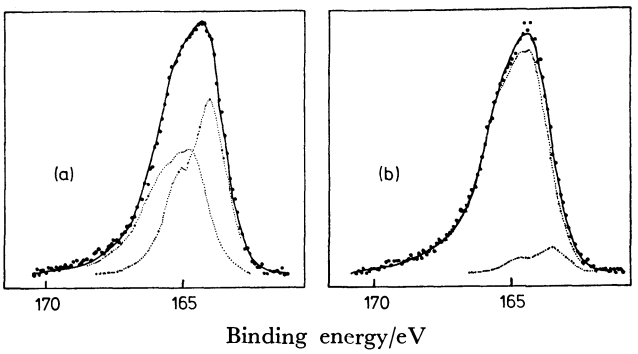

Fig. 6. S 2p peaks in the XPS spectra of (a) $(TTT)_2I_3$ and (b) (TTT)$(TCNQ)_2$.
Observed peak (•••), simulated peak (——), and component peaks of simulation (···).

The same procedure was taken for the analysis of S 2p peak profiles of TTT salts, using the S 2p peak profile of TTT and that of $(TTT)^+\cdot(ClO_4)^-$ as the standard peak profiles for TTT^0 and TTT^+ respectively. Results are shown in Fig. 6 and Table 2. In $(TTT)_2I_3$, iodine is known to exist as I_3^-.[27,28] Thus one should expect that a half of TTT molecules are in the ionized state. The result obtained by the analysis of the S 2p peak profile agrees with the above expectation. According to the analysis of the S 2p peak profile, almost all TTT molecules are in the ionized state in (TTT)$(TCNQ)_2$. If this is the case, a half of TCNQ molecules are in the state of $TCNQ^-$ and the remaining half are in the state of $TCNQ^0$. The shape of the N ls peak of this material is the same as those of the TCNQ complex salts where 50 percent of TCNQ molecules are in the ionized state, hence it is consistent with the conclusion obtained from the S 2p peak.

As we have mentioned, we treated the separation of the two component peaks as an adjustable parameter. This is because the shifts of the peaks associated with neutral molecules and ions are not necessarily the same for all TTF salts (or TTT salts), so that their separation could vary more or less from salt to salt. The relative separation of the component peaks obtained from the peak profile analysis was 0.9 eV for TTF·$Br_{0.7}$ and $(TTF)_3(BF_4)_2$, 1.0 eV for TTF·$I_{0.7}$, 1.2 eV for TTF·TCNQ, 1.4 eV for TTF·TNAP and 0.7 eV for the two TTT salts studied here. These values seem to be quite reasonable for the separation between the peaks due to TTF^0 and TTF^+ (or between those due to TTT^0 and TTT^+), but it is not possible to carry out at the present stage a quantitative discussion on the difference of the peak separation obtained for different salts.

The results described above show that observed S 2p peak profiles of TTF and TTT salts can be well reproduced by superimposing the standard peak profile characteristic of the neutral molecule and that of the

ion with an appropriate intensity ratio, and by this peak profile simulation, we can determine the ratio of neutral molecules and ions (or the degree of charge transfer).

As we have already mentioned, the situations are rather complicated in the case of the N ls peaks of TTF·TCNQ and TCNQ complex salts. The N ls peak profile of TTF·TCNQ, shown in Fig. 3, cannot be reproduced by superimposing the N ls peak profile observed of TCNQ and that of K·TCNQ with the intensity ratio that is expected from the degree of charge transfer. Almost same N ls peak profile is observed for $[(C_6H_5)_3PCH_3]^+(TCNQ)_2^-$ and other TCNQ complex salts which formally contain $TCNQ^-$ and $TCNQ^0$ with 1:1 mole ratio. In this respect, $Cu^+(TCNQ)_2^-$ is an exception. In this case, the observed N ls peak can be almost exactly reproduced by superimposing the N ls peak profile of $TCNQ^0$ and that of $TCNQ^-$ with the intensity ratio corresponding to the 1:1 mole ratio.[29] Unfortunately, the crystal structure of $Cu(TCNQ)_2$ is not known so far, but the arrangement of $TCNQ^0$ and $TCNQ^-$ in this salt is likely to be quite different from those in other TCNQ complex salts since $Cu(TCNQ)_2$ does not exhibit the absorption band which is characteristic of the charge transfer between $TCNQ^-$ and $TCNQ^0$.

TTF·TCNQ is a metal-like conductor, and conduction electrons (or holes) might be delocalized along the TTF stack as well as along the TCNQ stack. In spite of this delocalization of conduction electrons, the S 2p spectrum of TTF·TCNQ can be well explained as the superposition of the peak due to TTF neutral molecules and that due to TTF^+ ions. This fact may suggest that each TTF molecule in TTF·TCNQ can be regarded to be either in the state of TTF^+ or in the state of TTF^0 within the characteristic time scale of photoionization by X-ray. On the other hand, the N ls peak profile cannot be reproduced by the superposition of the peaks due to $TCNQ^0$ and $TCNQ^-$. The delocalization of conduction electrons along the TCNQ stack is not likely to be the origin of this phenomenon, since almost the same peak profile is observed also in many TCNQ complex salts which are not metal-like conductors, but are semiconductors of relatively low conductivity. Ritsko *et al.* suggested that the N ls peak profile of TTF·TCNQ could be understood in terms of the Hush's model[30] for the mixed-valence two-site system, by considering the local delocalization of valence electrons among neighboring TCNQ ions and molecules.[14] But, if this is the case, it is not easy to understand why the same mechanism does not work in the case of the S 2p spectra of TTF salts while a strong charge-transfer interaction is also taking place between TTF^0 and TTF^+.

As we have mentioned, in the N ls spectra of TCNQ salts, the relative intensity of the satellite band varies depending on the charge-transfer interaction between $TCNQ^-$ ions or between $TCNQ^0$ and $TCNQ^-$. Thus, one cannot expect anyway that the observed N ls peak profile of a TCNQ complex salt will be exactly reproduced by simply superimposing the N ls peaks of TCNQ and $K^+\cdot(TCNQ)^-$. Therefore, it is possible that each TCNQ molecule in a mixed-valence TCNQ stack can be regarded to be either in the state of $TCNQ^-$ or in that of $TCNQ^0$ as in the case of TTF molecules in a mixed-valence TTF stack, disregarding the delocalization of valence electrons, within the characteristic time scale of photoionization by X-ray, and the failure of the analysis of N ls peak profile is entirely due to the disturbing effect of the strong shake-up satellite.

References

1) T. J. Kistenmacher, T. E. Phillips, and D. O. Cowan, *Acta Crystallogr., Sect. B*, **30**, 763 (1974).
2) P. Coppens, *Phys. Rev. Lett.*, **35**, 98 (1975).
3) S. Kagoshima, T. Ishiguro, and H. Anzai, *J. Phys. Soc. Jpn.*, **41**, 2061 (1976).
4) F. Denoyer, R. Comès, A. F. Garito, and A. J. Heeger, *Phys. Rev. Lett.*, **35**, 445 (1975).
5) R. Comès, S. M. Shapiro, G. Shirane, A. F. Garito, and A. J. Heeger, *Phys. Rev. Lett.*, **35**, 1518 (1975).
6) W. D. Grobman, R. A. Pollak, D. E. Eastman, E. T. Maas, Jr., and B. A. Scott, *Phys. Rev. Lett.*, **32**, 534 (1974).
7) M. A. Butler, J. P. Ferraris, A. N. Bloch, and D. O. Cowan, *Chem. Phys. Lett.*, **24**, 600 (1974).
8) C. R. Ginnard, R. S. Swingle, II, and B. M. Monroe, *J. Electron Spectrosc. Relat. Phenom.*, **6**, 77 (1975).
9) R. S. Swingle, II, R. P. Groff, and B. M. Monroe, *Phys. Rev. Lett.*, **35**, 452 (1975).
10) W. D. Grobman and D. B. Silverman, *Solid State Commun.*, **19**, 319 (1976).
11) W. L. Jolly, *Coordination Chem. Rev.*, **13**, 47 (1974).
12) I. Ikemoto, J. M. Thomas, and H. Kuroda, *Mol. Cryst. Liq. Cryst.*, **18**, 87 (1972).
13) I. Ikemoto, J. M. Thomas, and H. Kuroda, *Faraday Discuss. Chem. Soc.*, **54**, 208 (1972).
14) J. J. Ritsko, A. J. Epstein, W. R. Salaneck, and D. J. Sandman, *Phys. Rev. B*, **17**, 1506 (1978).
15) T. Sugano and H. Kuroda, *Chem. Phys. Lett.*, **47**, 92 (1977).
16) E. P. Goodings, D. A. Mitchard, and G. Owen, *J. Chem. Soc., Perkin Trans. 1*, **1972**, 1310.
17) J. Diekmann, W. R. Hertler, and R. E. Benson, *J. Org. Chem.*, **28**, 2719 (1963).
18) D. J. Sandman and A. F. Garito, *J. Org. Chem.*, **39**, 1165 (1974).
19) G. R. Johnson, M. G. Miles, and J. D. Wilson, *Mol. Cryst. Liq. Cryst.*, **33**, 67 (1976).
20) S. J. La Placa, P. W. R. Corfield, R. Thomas, and B. A. Scott, *Solid State Commun.*, **17**, 635 (1975).
21) R. B. Somoano, A. Gupta, V. Hadek, T. Datta, M. Jones, R. Deck and A. M. Hermann, *J. Chem. Phys.*, **63**, 4970 (1975).
22) L. R. Melby, R. J. Harder, W. R. Hertler, W. Mahler, R. E. Benson and W. E. Mochel, *J. Am. Chem. Soc.*, **84**, 3374 (1962).
23) M. Yamada and H. Kuroda, *Bull. Chem. Soc. Jpn.*, in press.
24) C. S. Fadley, R. J. Baird, W. Siekhaus, T. Novakov, and S. Å. L. Bergström, *J. Electron Spectrosc. Relat. Phenom.*, **4**, 93 (1974).
25) The peak intensities of the N ls and S 2p peaks of CH_3SCN and thiourea were used as reference.
26) The infrared spectra show that TTF and TTT are in completely ionized states in these complexes.
27) D. L. Smith and H. R. Luss, *Acta Crystallogr., Sect. B*, **33**, 1744 (1977).
28) L. M. Kachapina, M. G. Kaplunov. E. B. Yagubskii and Yu. G. Borod'ko, *Chem. Phys. Lett.*, **58**, 394 (1978).
29) I. Ikemoto, J. M. Thomas, and H. Kuroda, *Bull. Chem. Soc. Jpn.*, **46**, 2237 (1973).
30) N. S. Hush, *Chem. Phys.*, **10**, 361 (1975).

The Light-driven Electron Transfer Reaction of Chlorophyll a–Lumiflavin in Micelle

Akio Yoshimura* and Shunji Kato

Institute of Chemistry, College of General Education, Osaka University, Toyonaka, Osaka 560

(Received November 9, 1979)

The light-driven electron transfer reaction for the system of chlorophyll a–lumiflavin in micelles was studied by means of flash photolysis. In the sodium dodecyl sulfate micellar solution, the chlorophyll a cation radical appeared on the flash excitation and then decayed by means of a second-order process under aerated conditions as well as under deaerated conditions (the radical was not observed in dioxane). The decay parameter in the aerated solution was smaller than that in the deaerated solution by a factor of twenty. The difference in the decay parameter was explained in terms of the function of the surface charge of micelles. In the deaerated solution, the chlorophyll a cation radical decays by means of a reaction with lumiflavin semiquinone of no charge; in the aerated solution, however, it decays by means of a reaction with the O_2^- produced by the electron transfer from lumiflavin semiquinone to oxygen. The latter decay reaction is retarded by the charge on the micelles.

In the photosynthesis, it is established that the electron is transferred from the excited chlorophyll a (Chl a) in P700 (the primary reaction center of the photosystem I of chloroplasts) to $NADP^+$-reductase, which has flavin adenine dinucleotide (FAD) as the prosthetic group, through ferredoxin (iron–sulfer protein). Wang *et al.* studied the complexes of Chl a derivatives, with flavins as model complexes for P700, and observed the light-induced electron-transfer reactions from the chlorophyll to the flavin.[1] The electron-transfer reactions from Chl a to *p*-benzoquinone[2] or to Chl a[3,4] were also examined under suitable homogeneous conditions, and it was concluded that the electron transfer proceeded from the singlet excited state of Chl a[3] or from the triplet state.[2,4]

In the chloroplast membrane, the specific environmetal effect must play an important role. Micellar systems have been examined[5] as models for membrane, especially in order to clarify the interfacial effects. In this work, kinetical studies have been made of Chl a–lumiflavin in aqueous micellar systems. Photolyses under different concentrations of dissolved oxygen were performed. Lumiflavin was used instead of riboflavin as an electron acceptor to avoid the interference of the reactive side chain, as in our previous studies of the sensitized photooxygenation.[6] Photolysis in dioxane was also examined in order to make a comparison with that in an ordinary solution.

Experimental

Materials. The chlorophyll a was extracted from spinach, purified chromatographically by the procedure of Strain and Svec,[7] and stored at −20 °C. The lumiflavin was synthesized as has been described by Hemmerich *et al.*[8] The sodium dodecyl sulfate (SDS) was recrystallized from ethanol, and the hexadecyltrimethylammonium bromide (CTAB) was recrystallized from ethanol–ether. The dioxane was freshly distilled after several days of refluxing over sodium.

Procedure. All the sample solutions were prepared just before their use. The Chl a–SDS solutions were prepared by the following procedure. The Chl a was first dissolved in ethanol, mixed with a concentrated SDS solution containing a buffer, and finally diluted with the buffer solution. The final solutions contained 2% ethanol by volume. In anionic micellar solutions such as SDS solutions, the local pH value around the micelles is lower than the bulk according to the electrostatic potential of the micellar surface. Therefore, the SDS solutions were required to be rather basic (pH 9.0) to avoid the elimination of Mg from Chl a. As the buffer, *N*-tris(hydroxymethyl)methyl-3-aminopropanesulfonic acid (TAPS, 0.05 M†) was used. The concentration of Chl a was adjusted to be not less than 7 μM, because it is less stable at lower concentrations. Chlorophyll a dissolved in this manner was stable for two hours, judging from the absorption spectrum.

The Chl a–CTAB solutions were prepared just as the Chl a–SDS solutions, but the solutions were adjusted to pH 7.2 with a sodium phosphate buffer. Unlike anionic micellar solutions, the local concentration of the hydroxide ion around the CTAB micelles is relatively high, and it tends to cause the allomerization (oxidative degradation) of Chl a.

The critical micelle concentration (CMC) values of the surfactants were determined by the use of a stalagmometer. The amounts of dissolved oxygen in aerated solutions were measured by means of Winkler's method.[9] The solutions with reduced concentrations of oxygen were prepared by purging with mixtures of nitrogen and oxygen of known compositions.

Flash photolysis was carried out in a 1-cm rectangular quartz cell or in a 10-cm cylindrical quartz cell, with exciting light from xenon flash lamps (9 μs half-maximum duration) through red glass filters (cut off at 580 nm) to avoid the excitation of lumiflavin. The fluorescence was measured with a Hitachi MPF-2A fluorescence spectrophotometer.

Partition of Reactants between SDS Micellar and Water Phases. In the SDS micellar solution, Chl a is exclusively present in the micellar phase, because Chl a is insoluble in water. On the other hand, lumiflavin is present in both micellar and water phases. The partition of lumiflavin into them was determined from the measurements of the change in the fluorescence intensity of lumiflavin with different concentrations of SDS. The fluorescence intensity ratio of micellar solutions to the solution without micelles was independent of the lumiflavin concentration in the range from 30 μM to 100 μM (the solubility limit in the bulk). Therefore, the distribution of lumiflavin can be treated as the partition equilibrium.

Putting the fluorescence yields in aqueous and micellar phases as ϕ_a and ϕ_m respectively ($\phi_m > \phi_a$ in this case), the intensity ratio of the fluorescence of the micellar solution to the aqueous solution for the same dye concentration is

† In this paper 1 M = 1 mol dm^{-3}.

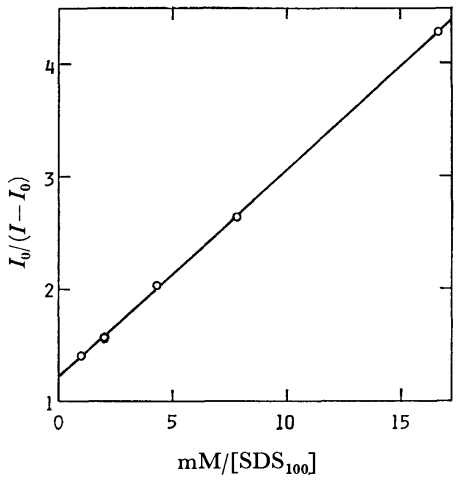

Fig. 1. The plots of $I_0/(I-I_0)$ *vs.* the inverse of the concentration of SDS micelle.
Lumiflavin, 30 μM; 0.05 M TAPS at pH 9.0 (27 °C); excitation at 440 nm; emission at 520 nm.

written as;

$$\frac{I}{I_0} = \frac{\phi_a[LF_a] + \phi_m[LF_m]}{\phi_a[LF_t]}, \quad (1)$$

where $[LF_m]$ is the partial apparent concentration of lumiflavin in the micellar phase relative to the total volume of the micellar solution, $[LF_a]$ is the concentration in the aqueous phase, and $[LF_t]=[LF_m]+[LF_a]$. On the other hand, the partition coefficient (K), which is the ratio of the local concentration of lumiflavin in the micellar phase to $[LF_a]$ (the volume of the micellar phase is negligibly small compared with the total volume), is written as;

$$K = \frac{[LF_m]/[N_a v_m[M])}{[LF_a]}, \quad (2)$$

where [M] is the molar concentration of micelle particles, v_m is the volume of a micelle, and N_a is the Avogadro constant. By combining Eqs. 1 and 2, Eq. 3 is obtained:

$$\frac{I_0}{I-I_0} = \left(\frac{\phi_a}{\phi_m-\phi_a}\right)\left(\frac{1}{KN_a v_m[M]}+1\right). \quad (3)$$

The micelle concentration [M] was estimated from the aggregation number (100)[10] and the CMC value (2.0 mM) under these conditions, assuming a constant concentration of the monomer surfactant above the CMC. Figure 1 shows that Eq. 3 holds, from which the partial concentration of lumiflavin present in the micellar phase is obtained for a given micelle concentration ($KN_a v_m = 7.0\times10^3$ M^{-1}, at 20 °C).

The highest concentration of lumiflavin examined was 270 μM under the SDS concentration of 27 mM (micelle concentration: 250 μM); then, the concentration of lumiflavin in the micelles was calculated to be 170 μM, and the concentration of lumiflavin in the bulk, to be 100 μM (nearly saturation).

Assuming the Poisson distribution of the lumiflavin molecules among the micelle particles, the fraction of micelles which contain no lumiflavin molecules is $e^{-\lambda}$, where λ is the ratio of the number of lumiflavin molecules in micelles to the number of micelle particles. Under the present conditions, where the concentration of micelles and the partial concentration of lumiflavin in the micellar phase are 250 μM and 170 μM respectively, the fraction of micelles with lumiflavin is calculated to be 0.53.

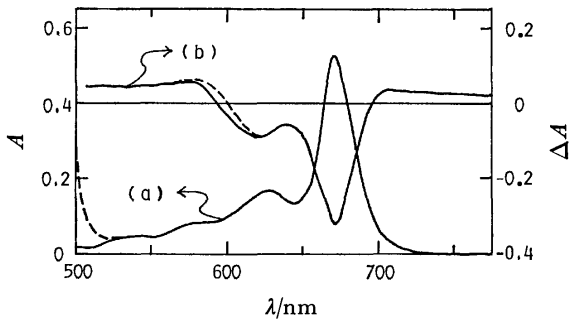

Fig. 2. The absorption spectra (a) and the transient difference spectra immediately after the flash excitation (b) of Chl a in the deaerated SDS micellar solutions with and without lumiflavin.
Chl a, 10 μM; lumiflavin, 0 mM (——) and 270 μM (- - -); SDS, 27 mM; 0.05 M TAPS at pH 9.0 by 200 J flash.

The local concentration of lumiflavin in the micelle particles is evaluated as 30 mM, assuming a spherical micelle with a radius of 1.8 nm, which is 300 times larger than the solubility in water and about 10 times larger than that in chloroform.

The oxygen concentration in the aerated solution with 27 mM SDS (250 μM in micelle concentration) and 50 mM TAPS at 30 °C was 233 μM, while that in the solution without SDS was 226 μM. The increase in the 7 μM oxygen content is attributable to the solubilization of oxygen in micelles. This means that only one-thirtieth of the micelles contain oxygen, on the average, although the local concentration of oxygen in micelles is calculated to be as high as 2 mM, which agrees with the solubility of oxygen in typical organic solvents.

Results and Discussion

Photolysis in Deaerated SDS Micellar Solutions. When a deaerated SDS micellar solution of Chl a without lumiflavin was irradiated by flashing light, only the triplet state of Chl a was observed as the transient species; it showed a broad absorption spectrum (Fig. 2) and decayed exponentially at the rate parameter of 1380 s^{-1}. The second-order component due to the T–T annihilation was not observed.

The addition of 270 μM lumiflavin had little effect on either the transient absorption spectrum or the initial absorbance change on the flash excitation (Fig. 2) and effected no permanent change at all. However, the kinetical behavior of the transient species was quite different; that is, the decay followed a second-order rate, as is shown in Fig. 3a. The value of $k_1/(\Delta\varepsilon d)$ is determined from the slope to be 1.0×10^4 s^{-1} at 670 nm for a 1-cm cell, where k_1 (M^{-1}S^{-1}) is the rate parameter of the second-order process, $\Delta\varepsilon$(M^{-1} cm^{-1}) is the difference in the molar absorption coefficients between the transient and final species at 670 nm, and d is the cell length in cm.

The transient absorbance change induced by the flash irradiation is considered to be due to the electron-transfer reaction from Chl a to lumiflavin in the initial stage, followed by the backward electron-transfer reaction between the Chl a cation radical and lumiflavin

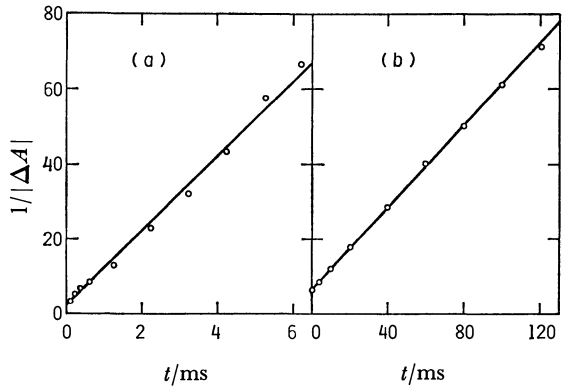

Fig. 3. Second order decay of the flash induced absorbance change of Chl a with lumiflavin in the deaerated (a) and aerated (b) SDS micellar solutions.
Chl a, 10 μM, lumiflavin, 270 μM; 0.05 M TAPS at pH 9.0 by 200 J flash, observed at 670 nm with 1-cm cell.

semiquinone, which are the products of the initial reaction. If both radicals remained in the same micelle after the initial stage, the back reaction should be first-order, contradicting the observation. Accordingly, the lumiflavin semiquinone anion radical must be immediately expelled to the bulk by the effect of the negative charge of the micelle. This second-order decay was also observed in the solution of Chl a with a lower concentration of lumiflavin (15 μM), where 97% of the Chl a molecules are in micelle particles free from lumiflavin. Therefore, the triplet state of Chl a in micelles (Chl a^T_m) can also react, within its lifetime, with the lumiflavin present in the bulk (LF_a):

$$\text{Chl } a^T_m + LF_a \longrightarrow \text{Chl } a^{+\cdot}_m + LF^{-\cdot}. \quad (4)$$

When the flash energy was increased, the initial absorbance change asymptotically reached 0.46 for 10 μM Chl a in the micellar solution with lumiflavin (270 μM). Under these limiting conditions, Chl a is completely converted to the cation radical. Therefore, $\Delta\varepsilon$ is calculated to be 4.6×10^4 M^{-1} cm^{-1}, and the rate parameter, (k_1) to be 4.6×10^8 M^{-1} s^{-1}.

The decay reaction was examined for different ionic strengths in the presence of 0-, 0.07-, and 0.13-M NaCl, and it was found that the decay was not altered. This shows that the species reacting with Chl a cation radicals in micelles is the protonated form (LFH·) of the lumiflavin semiquinone anion radical, with no charge:

$$\text{Chl } a^{+\cdot}_m + \text{LFH}\cdot \xrightarrow{k_1} \text{Chl } a_m + LF + H^+, \quad (5)$$

where k_1 is the rate parameter evaluated above. Under the present conditions (pH 9.0), it is natural that most of the lumiflavin semiquinone radicals exist in the acidic form, with no charge, in the close vicinity of micelle particles, because the pK_a value of LFH· has been reported to be 8.36[11] and the pH in the vicinity of SDS micelles is lower by 2 units than the value in the bulk.[12]

Photolysis in Aerated SDS Micellar Solutions. In an aerated SDS micellar solution, Chl a showed no absorbance change upon flash irradiation, but upon the addition of 270 μM lumiflavin, the following absorbance change was observed upon the flash excitation. The transient-difference spectrum was similar to those observed in the deaerated solutions, but the decay was much slower. The decay kinetics was also second-order as is shown in Fig. 3b, from which the slope is obtained as 540 s^{-1} at 670 nm with a 1-cm cell. The initial absorbance change for an infinite light intensity was obtained to be 0.23 at 670 nm with 10 μM Chl a and 270 μM lumiflavin, this is half of the value for the deaerated solution.

Table 1. Effect of NaCl on the decay parameter (k) of the Chl a cation radical in the aerated SDS micellar solutions

[NaCl] / M	k / 10^7 M^{-1} s^{-1}	k/k_0
0	2.5	(1)
0.055	3.5	1.41
0.104	4.7	1.88
0.179	5.4	2.16

Chl a, 10 μM; lumiflavin, 270 μM; SDS, 27 mM; 0.05 M TAPS pH 9.0.

Combining this with the finding that 53% of Chl a is present with lumiflavin in the same micelle, one may safely propose the following mechanism. The triplet Chl a in a micelle is rapidly quenched by oxygen in the aqueous phase without reacting with lumiflavin if lumiflavin is absent in the same micelle:

$$\text{Chl } a^T_m + O_2 \longrightarrow \text{Chl } a_m + O_2. \quad (6)$$

However, if present, Chl a is immediately oxidized to the cation radical and the lumiflavin semiquinone anion radical is expelled from the micelle. This anion radical will be rapidly oxidized back to lumiflavin as:

$$LF^{-\cdot} + O_2 \longrightarrow LF + O_2^{-\cdot}. \quad (7)$$

Since the pK_a value of $HO_2\cdot/O_2^{-\cdot}$ is 4.88,[13] the reduced oxygen exists exclusively as $O_2^{-\cdot}$, even in the vicinity of a micelle when the bulk pH value is 9:

$$\text{Chl } a^{+\cdot}_m + O_2^{-\cdot} \xrightarrow{k_2} \text{Chl } a_m + O_2. \quad (8)$$

Using the same $\Delta\varepsilon$ value as in the case of the deaerated solution, the rate parameter (k_2) is calculated to be 2.5×10^7 M^{-1} s^{-1}, about one-twentieth of the value for the deaerated solution. This slow back reaction of the Chl a cation radical can be explained by the repulsive action of the anionic micelle against $O_2^{-\cdot}$. This is supported by the fact that the decay parameter is increased with the concentration of sodium chloride, as is shown in Table 1.

When the dissolved oxygen concentration is reduced to below 30 μM, a fast process appears at the initial stage of the decay profile, and the initial absorbance change becomes larger (Fig. 4). The fraction of the slower component is obtained from the later stage of the decay curve; its change with the oxygen concentration is also shown in Fig. 4. In these low oxygen concentrations, the reactions in Eqs. 4 and 6 compete with each other, as do the reactions in Eqs. 5 and 7.

Photolysis in Dioxane. On the flash excitation

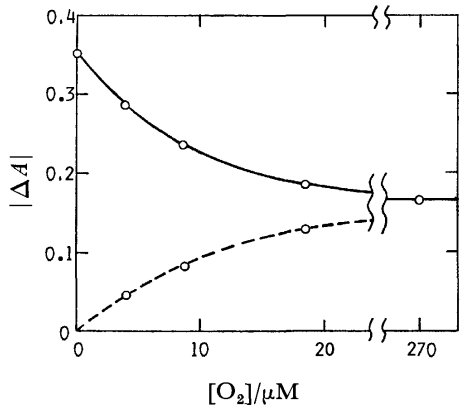

Fig. 4. Variation of the initial absorbance change of 10 μM Chl a in the presence of 270 μM lumiflavin by 200 J flash at 670 nm, with the concentration of oxygen.
Total (——); the component with the longer life time (----).

of Chl a in deaerated dioxane, the triplet state of Chl a was observed. It decayed at 700 s^{-1} at a low concentration of the triplet state, and the second-order component due to the T–T annihilation was overlapped at the early stage of the decay. (In the micellar solutions, the T–T reaction is blocked, because each Chl a is present statistically in a different micelle under the conditions examined.) On the flash photolysis of Chl a in the deaerated dioxane with 90 μM lumiflavin, the signal height and the decay were almost the same as those without lumiflavin. That is to say, neither the light-driven electron transfer reaction nor the quenching occurs in such a nonpolar solvent. In aerated solutions with and without lumiflavin, no absorbance change was observed after the flash excitation.

Photolysis in CTAB Micellar Solutions. When Chl a was irradiated by flashing light in a deaerated CTAB micellar solution, the triplet state of Chl a appeared as in the SDS solution and showed a first-order decay with 1600 s^{-1}. However, in the presence of 160 μM lumiflavin, the results were quite different from those in the SDS solutions; that is, the transient absorbance change in the deaerated solution was markedly small compared with the change in the SDS solution, and it was barely observed at all in the aerated solution. Under these conditions, lumiflavin acts mainly as quencher for the triplet state of Chl a. These results can be explained by saying that the escape of the lumiflavin semiquinone from the micelle is blocked by the positive charge of the cationic micelle.

The function of the surface charge of micelles is a dominant factor in both the formation and decay processes of the Chl a cation radical.

References

1) S.-I. Tu, Y. J. Tan, and J. H. Wang, *Bioinorg. Chem.*, **1**, 79 (1971); S.-I, Tu and J. H. Wang, *Briophys. Res. Commun.*, **36**, 79 (1969).
2) R. Raman and G. Tollin, *Photochem. Photobiol.*, **13**, 135 (1971); R. A. White and G. Tollin, *ibid.*, **14**, 15 (1971).
3) J. R. Harbour and G. Tollin, *Photochem. Photobiol.*, **19**, 69 (1974).
4) T. Imura, T. Furutsuka, and K. Kawabe, *Photochem. Photobiol.*, **22**, 129 (1975).
5) M. Grätzel and J. K. Thomas, *J. Phys. Chem.*, **78**, 2248 (1974); S. A. Alkaitis and M. Grätzel, *J. Am. Chem. Soc.*, **98**, 3549 (1976); A. J. Frank, M. Grätzel, and J. J. Kozak, *ibid.*, **98**, 3317 (1976).
6) A. Yoshimura and S. Kato, *Bull. Chem. Soc. Jpn.*, **46**, 1141 (1973); *ibid.*, **49**, 813 (1976).
7) H. H. Strain and W. A. Svec, "The Chlorophylls," ed by L. P. Vernon and G. R. Seely, Academic Press, New York (1966), p. 21.
8) P. Hemmerich, S. Fallab, and H. Erlenmeyer, *Helv. Chim. Acta*, **39**, 1242 (1956).
9) F. P. Treadwell, "Analytical Chemistry," John Wiley and Sons, New York (1930), Vol. II, p. 654.
10) J. N. Phillips, *Trans. Faraday Soc.*, **51**, 561 (1955).
11) S. P. Vaish and G. Tollin, *J. Bioenerg.*, **2**, 61 (1971).
12) M. S. Fernandez and P. Fromherz, *J. Phys. Chem.*, **81**, 1755 (1977); A. D. James and B. H. Robinson, *J. Chem. Soc., Faraday Trans. 1*, **74**, 10 (1978).
13) D. Behar, G. Czapski, J. Rabani, and H. A. Schwartz, *J. Phys. Chem.*, **74**, 3209 (1970).

A Spectroscopic Study of Hydrogen-bonds Involving the 2-Thiouracil Residue

Hidemi Todoriki,†† Yoshifumi Nishimura, Shigesada Higuchi,†
Akiko Y. Hirakawa, and Masamichi Tsuboi*

Faculty of Pharmaceutical Sciences, The University of Tokyo, Hongo, Bunkyo-ku, Tokyo 113
† *Mitsubishi-Kasei Institute of Life Sciences, Machida, Tokyo 194*

(Received November 17, 1979)

Infrared absorption spectra, ultraviolet absorption spectra, phosphorescence spectra, phosphorescence lifetimes, and phosphorescence excitation spectra have been examined of 1-propyl-2-thiouracil in various solvents, including CCl_4, CH_3OH, CCl_4+CH_3OH, and CCl_4+9-ethyladenine. For 1-cyclohexyluracil, and for 2-*S*-propyl-2-thiouracil, similar infrared spectroscopic examinations were also made. The results obtained are as follows: (1) In CCl_4, the 2-thiouracil residue forms a hydrogen-bond complex with the adenine residue, in which the C^4=O is involved in the hydrogen-bond. (2) The binding of 2-thiouracil and adenine is much stronger than that of 2-thiouracil and CH_3OH; the 2-thiouracil·methanol binding is stronger than the uracil·methanol binding. (3) The hydrogen-bonding of the 2-thiouracil residue (with CH_3OH or with adenine) causes an elevation of the lowest singlet excited state S_1, which is probably an $^1(n\pi^*)$, from 2.5×10^4 cm^{-1} to 2.6×10^4 cm^{-1}, and the lowest triplet excited state T_1, which is probably an $^3(n\pi^*)$, from 2.4×10^4 cm^{-1} to 2.6×10^4 cm^{-1}. (4) The hydrogen bonding of the 2-thiouracil residue causes a great enhancement of the phosphorescence intensity. On the basis of these observations, a discussion is given on the nature of the inter-base hydrogen-bonds involving 2-thiouracil residue.

2-Thiouracil is a modified base, closely related with a number of naturally occurring nucleic acid constituents. Yeast $tRNA_3^{Glu}$, for example, has 2-thiouridine-5-acetic acid methyl ester as the first letter of its anti-condon triplet.[1] The thymidine residue in the TψC sequence is partly replaced by 2-thiothymidine residue in the tRNAs of *Thermus thermophilus*, an extremely thermophilic bacterium.[2] In an attempt to characterize the hydrogen-bondings involving the 2-thiouracil residue, we have made a detailed spectroscopic examination of 1-propyl-2-thiouracil, which is soluble both in polar and nonpolar solvents.

Experimental

Materials and Methods. 1-Propyl-2-thiouracil was prepared by a direct alkylation of 2-thiouracil (from Tokyo-Kasei Co.) with propyl bromide, following the method previously given for N-1 alkylation of uracil.[3,4] 1 Mol of 2-thiouracil and 2/3 mol (or less) of propyl bromide were mixed together in a small amount of dry dimethyl sulfoxide with 1 mol of potassium carbonate, and the slurry was kept at room temperature for 48 h under vigorous stirring. After removing K_2CO_3 by filtration, the clear solution was concentrated *in vacuo*, and an excess of ethanol was added. The precipitates, unreacted 2-thiouracil, was discarded after filtration. This process was repeated three times or more until the 2-thiouracil is adequately removed from the solution. The final filtrate was subjected to a silica gel chromatography with CCl_4/*t*-BuOH(10:1) as the eluent. Two fractions corresponding to 1-propyl-2-thiouracil and to 2-*S*-propyl-2-thiouracil were obtained. The yields of the above products were about 3% and 20%, respectively. Both were purified by recrystallization from ethanol. No 3-propyl derivative was produced. The 1-propyl-2-thiouracil sample, thus obtained, gave a single spot in a thin layer chromatography: R_f 0.82 with $CHCl_3/C_2H_5OH$=9/1. Melting point, 187 °C.

The ultraviolet absorption spectrum of 1-propyl-2-thiouracil was found to be identical to 1-ethyl-2-thiouracil in neutral and pH 12 solutions. The 1-ethyl-2-thiouracil sample was provided by Professor D. Shugar of Department of Biophysics, Institute of Experimental Physics, University of Warsaw, Poland, to whom we are indebted. The product was also identified by its mass spectrum (M^+(*m/e*): Found 170, Calcd, 170) and elementary analysis. Found: C, 49.34; H, 6.09; N, 16.52; O, 9.37; S, 18.78%. Calcd for $C_7H_{10}N_2OS$: C, 49.39; H, 6.21; N, 16.46; O, 9.40; S, 18.83%.

2-*S*-Propyl-2-thiouracil obtained as described above was identified by infrared absorption spectrum,[5] ultraviolet absorption spectrum,[5] melting point (117 °C), and elementary analysis. Found: C, 49.24; H, 5.97; N, 16.50; O, 9.16; S, 18.59%. Calcd for $C_7H_{10}N_2OS$: C, 49.39; H, 6.21; N, 16.46; O, 9.40; S, 18.83%.

1-Cyclohexyluracil was prepared by Dr. T. Katsura, Research Institute for Polymer and Textiles, Tsukuba, and was kindly given us by him. Its infrared and ultraviolet absorption spectra were found to be identical with what are known.[6,7]

9-Ethyladenine is a gift of Professor T. Miyazawa, Department of Biochemistry and Biophysics, Faculty of Science, University of Tokyo. Its identification was made by the infrared and ultraviolet absorption spectra.[6,7]

All the solvents used were carefully purified by distillation and then mostly by an activated alumina column. Bases were dissolved in these solvents by the use of a sonicator and by heating at 40 °C with hot air. For phosphorescence measurements, the solutions were carefully degassed in a vacuum line.

Infrared absorption spectra were observed by the use of a Digilab FTS-14 Fourier transform spectrophotometer. The disturbance due to the atmospheric water vapour was removed by filling the inside of the instrument with dry air. Each of the absorption curves in Figs. 1, 2, and 4 was recorded with resolution=4 cm^{-1} and number of scans=240. Each of the sample solutions was placed in one of the following three sealed cells: one with KBr windows and with 1 mm path, another with CaF_2 windows and 1 mm path, and that with CaF_2 windows and 50 μm path. The actual optical path lengths of these cells were determined by examining interference patterns. Ultraviolet absorption spectra were examined by the use of a Hitachi 124 spectrophotometer. Phosphorescence was observed with a Hitachi MPF-4 fluorometer with a phosphoroscope. Spectral slit width was set at 10 nm. Phosphorescence decay curves were obtained by the use of a nitrogen laser of 20 kW in the peak power

†† Present address: National Center for Nervous, Mental, and Muscular Disorders, 2620, Ogawa-Higashi-Machi, Kodaira, Tokyo 187.

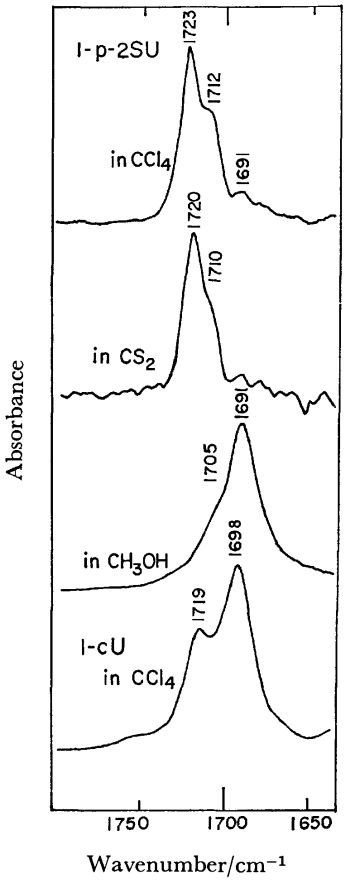

Fig. 1. Infrared absorption spectra of 1-propyl-2-thiouracil (1-p-2SU) in various solvents.
1.3×10^{-3} M in CCl_4; 9.2×10^{-4} M in CS_2, and 8.0×10^{-3} M in CH_3OH, and of 1-cyclohexyluracil (1-cU) 1.6×10^{-3} M in CCl_4.

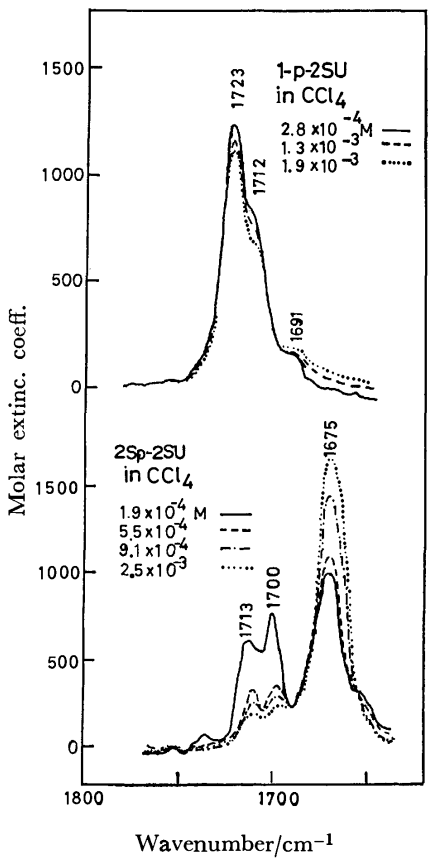

Fig. 2. Infrared absorption spectra of 1-propyl-2-thiouracil and 2-*S*-propyl-2-thiouracil (2Sp-2SU) in the solution of CCl_4 at various concentrations.

and 8 ns in duration time. This was combined with a monochromator, photomultiplier (HTV R106 UH) and Tektronix 465 (100 MHz) oscilloscope. Decay curves were also observed with another apparatus with two electromagnetic shutters placed before and after the light beam (313 nm from a Hg lamp) goes into the sample,[8] through the courtesy of Professor Minoru Kinoshita, Dr. Noriko Iwasaki and Dr. Nobuyuki Nishi, Institute for Solid State Physics, University of Tokyo.

Infrared Absorption Spectra

Carbonyl Bands of Free Base. As is shown in Fig. 1 (top), 1-propyl-2-thiouracil shows two absorption bands at 1723 and 1712 cm^{-1} in the carbonyl stretching region, in its dilute CCl_4 solution (concentration 1.3×10^{-3} M). In dilute CS_2 solution it shows two bands at 1720 and 1710 cm^{-1}. 1-Cyclohexyluracil, which has two carbonyl groups at 2- and 4- positions, shows also two bands in the 1700 cm^{-1} region, at 1719 and 1698 cm^{-1}.

The appearance of two (instead of one) carbonyl bands for 1-propyl-2-thiouracil, free from any hydrogen bonds, may be ascribed to a Fermi resonance, although there is no strong evidence established for supporting this idea.

Self-association. When the concentration of 1-propyl-2-thiouracil in CCl_4 is increased from 2.8×10^{-4} M to 1.9×10^{-3} M, a lowering of the absorption intensities of the 1723 and 1712 cm^{-1} bands takes place while their intensity ratio remains unchanged. In addition, a new band appears at 1691 cm^{-1} (see Fig. 2). These are considered to be caused by a formation of a hydrogen-bond dimer of two 2-thiouracil residues, such as Fig. 3 (d). The 1691 cm^{-1} band is assigned to such a dimer. On the basis of an intensity measurement of the 1723 and 1691 cm^{-1} bands, and by postulating only one form of dimer, the equilibrium constant of the dimerization has been estimated to be about 40 M^{-1} in CCl_4 at 34 °C.

2-*S*-Propyl-2-thiouracil shows three bands (at 1700, 1713, and 1675 cm^{-1}) in its dilute (1.9×10^{-4} M) CCl_4 solution (see Fig. 2, lower). The former two are assignable to the carbonyl bands of free base, while the last one is assignable to a dimer band. The equilibrium constant of dimerization of 2-*S*-propyl-2-thiouracil has been found to be about 100 times as great as that of 1-propyl-2-thiouracil (see Fig. 3 (f)).

Hydrogen-bond Complex with Methanol. When methanol is added to a dilute CCl_4 solution of 1-propyl-2-thiouracil, the 1723 and 1712 cm^{-1} bands become weaker and two new bands appear at 1708 and 1693 cm^{-1}, which become stronger with the methanol concentration (see Fig. 4, top). Both of the 1708 and 1693 cm^{-1} bands are attributed to a binary complex of 1-propyl-2-thiouracil and methanol bound through

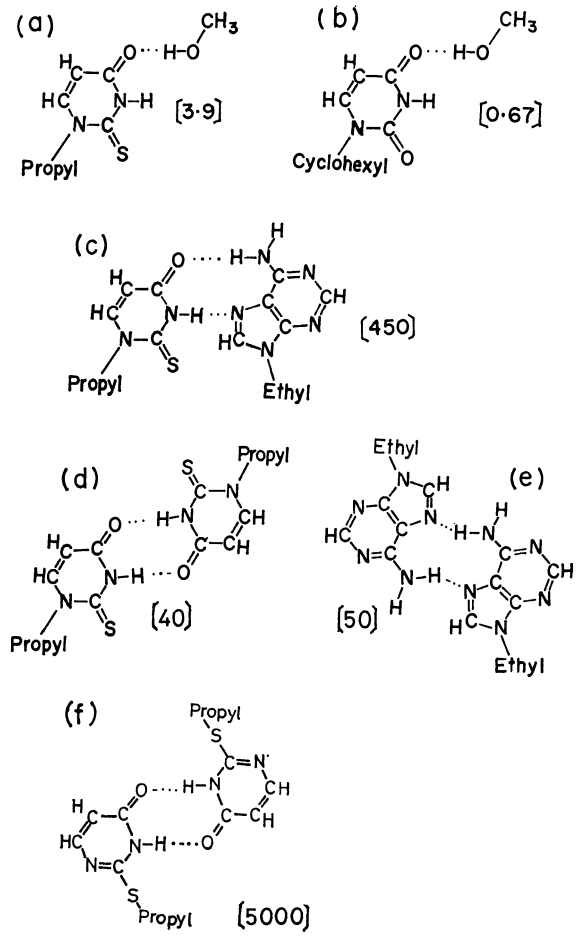

Fig. 3. Possible structures of hydrogen-bonded complexes involving uracil, 2-thiouracil, and/or adenine residues. The figure in bracket indicates the equilibrium constant in M^{-1} of the association reaction of each complex in CCl_4 at 34 °C. The equilibrium constants have been calculated by the method of Refs. 6 and 14.

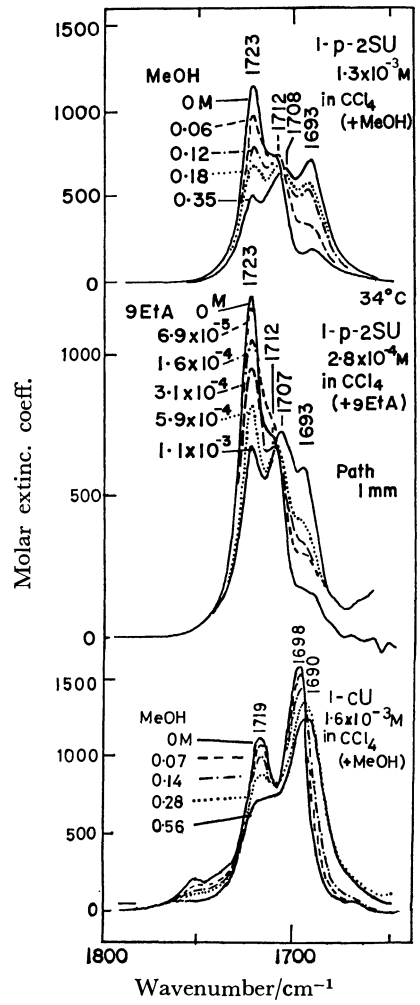

Fig. 4. Infrared absorption spectra of 1-propyl-2-thiouracil in the solutions of CCl_4+CH_3OH and in the solutions of CCl_4+9-ethyladenine and of 1-cyclohexyluracil in the solutions of CCl_4+CH_3OH.

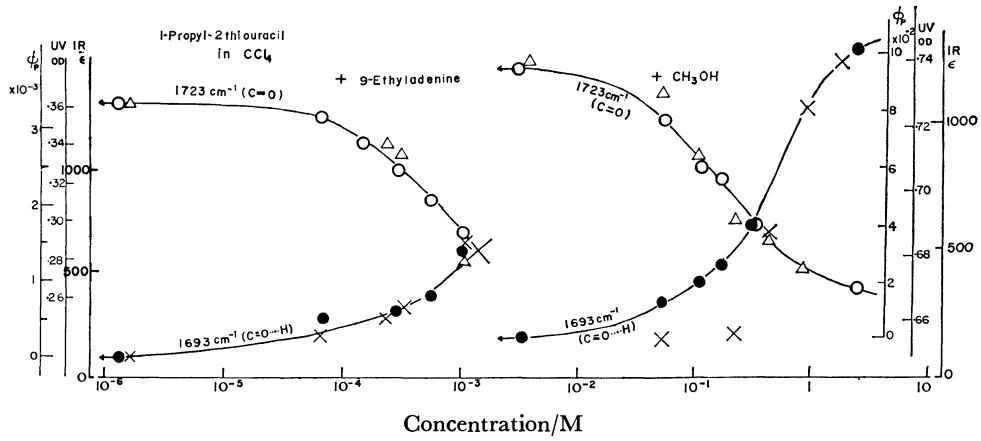

Fig. 5. The absorption- and phosphorescence-intensities of 1-propyl-2-thiouracil in CCl_4 plotted against the concentration of the proton-donor molecule (methanol or 9-ethyladenine) in the solvent.
(○ and ●): Infrared absorption intensities; concentration of 1-propyl-2-thiouracil, temperature of the solution, and optical path length are all what are given in Fig. 4, (△): ultraviolet absorption intensity at 302.5 nm, read from the curves given in Fig. 7, (×): phosphorescence intensity at 410 nm, read from the curves given in Fig. 8; the arrows in this figure show intensities of 1-propyl-2-thiouracil in pure CCl_4.

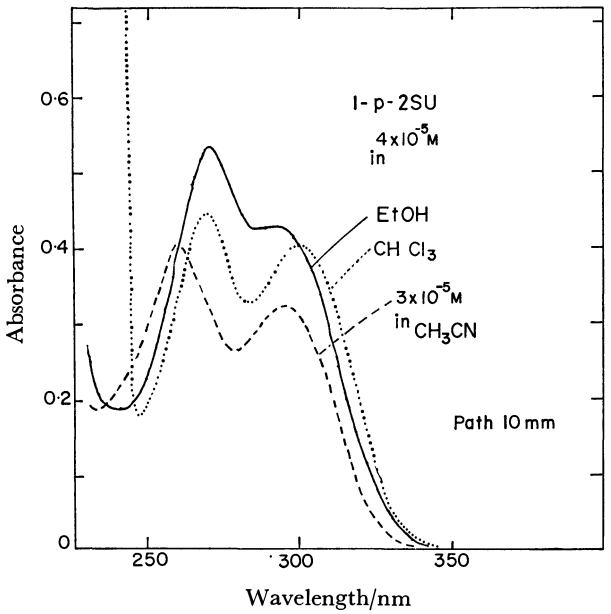

Fig. 6. Ultraviolet absorption spectra of 1-propyl-2-thiouracil in various solvents.

the O–H···O hydrogen bond between the methanol OH and position-4 carbonyl of the 2-thiouracil residue (see Fig. 3 (a)). By assuming that only one form of complex is involved in the methanol-2-thiouracil interaction, the equilibrium constant for that complex formation has been estimated from the intensity measurements of the carbonyl bands. This is found to be 3.9 M^{-1} in CCl_4 at 34 °C. This value is to be compared with the equilibrium constant, 0.67 M^{-1}, for the complex formation (Fig. 3 (b) and Fig. 4, bottom) between methanol and 1-cyclohexyluracil, which was determined in a similar way in dilute CCl_4 solution at 34 °C.

Association with Adenine. If 9-ethyladenine, instead of methanol, is added to the dilute CCl_4 solution of 1-propyl-2-thiouracil, the complex formation is caused more easily. As may be seen in Figs. 4 (middle) and 5, the lowering of the 1723 cm^{-1} band (free C=O) and the elevation of the 1693 cm^{-1} band (hydrogen-bonded C=O) take place for 9-ethyladenine at a concentration 100 times as low as that for methanol. This fact may be taken as indicating that a binding (such as Fig. 3 (c)) of 2-thiouracil and adenine residues is much greater than that of 2-thiouracil and methanol. The association constant of the former pair has been determined to be 450 M^{-1} in CCl_4 at 34 °C.

Ultraviolet Absorption Spectra

Solvent Effect. 1-Propyl-2-thiouracil shows two strong absorption peaks at 268 and 300 nm in $CHCl_3$, while in ethanol these two come closer, at 272 and 295 nm (Fig. 6).

Complex with Methanol. On adding methanol to a dilute (7×10^{-4} M) CCl_4 solution of 1-propyl-2-thiouracil, two absorption peaks (see Fig. 7 upper) at 269 and 301 nm (molar extinction coefficient are 12800 and 10400 respectively) are replaced by other

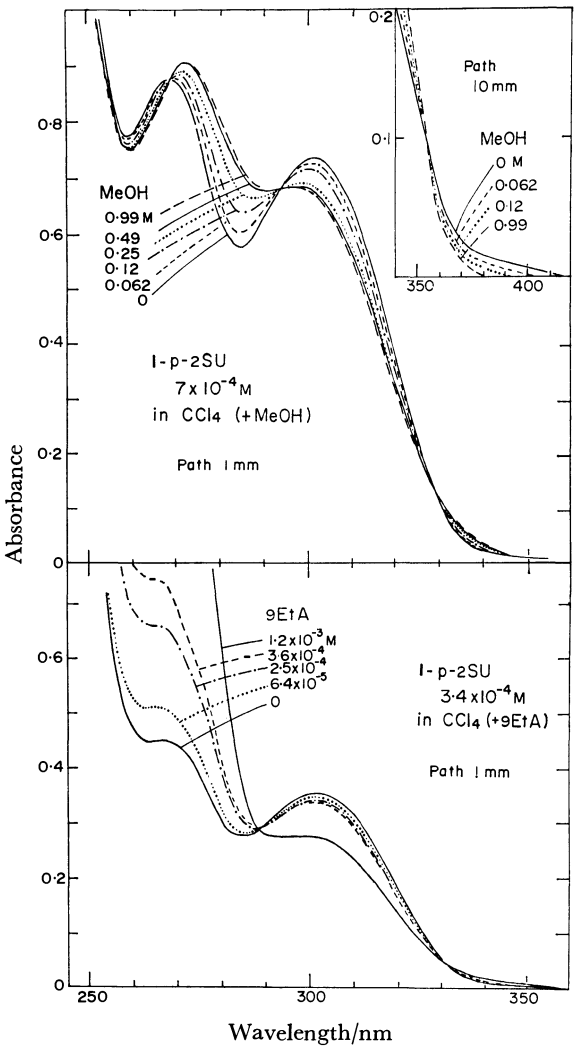

Fig. 7. Ultraviolet absorption spectra of 1-propyl-2-thiouracil in the solutions of CCl_4+CH_3OH (upper) and in the solutions of CCl_4+9-ethyladenine (lower).

two strong peaks at 272 and 298 nm. There appear isosbestic points not only at 268 and 294 nm, but also at 329 and 352 nm. Thus, there must be a very weak absorption band at about 400 nm in dilute CCl_4 solution, and this is shifted to a shorter wavelength on forming a complex with methanol. This weak band (molar extinction coefficient $\fallingdotseq 10^2$) is assignable to an n-π^* transition, and the two strong bands to π-π^* transitions.

The lowering of the 301 nm peak (or the elevation of the 269 nm peak) takes place on adding methanol in parallel with the lowering of the 1723 cm^{-1} band (see Figs. 4 and 5). Therefore, these ultraviolet spectral changes are attributed to the change from free 2-thiouracil base to the hydrogen-bonded complex which is the same as what was observed in our infrared spectroscopic examination. On the basis of a series of absorption intensity measurements, the association constant is calculated here to be 5.5 M^{-1} (which is comparable to 3.9 M^{-1}, obtained in the infrared absorption measurements).

By a similar experiment on a dilute methylcyclohexane solution of 1-propyl-2-thiouracil with ethanol,

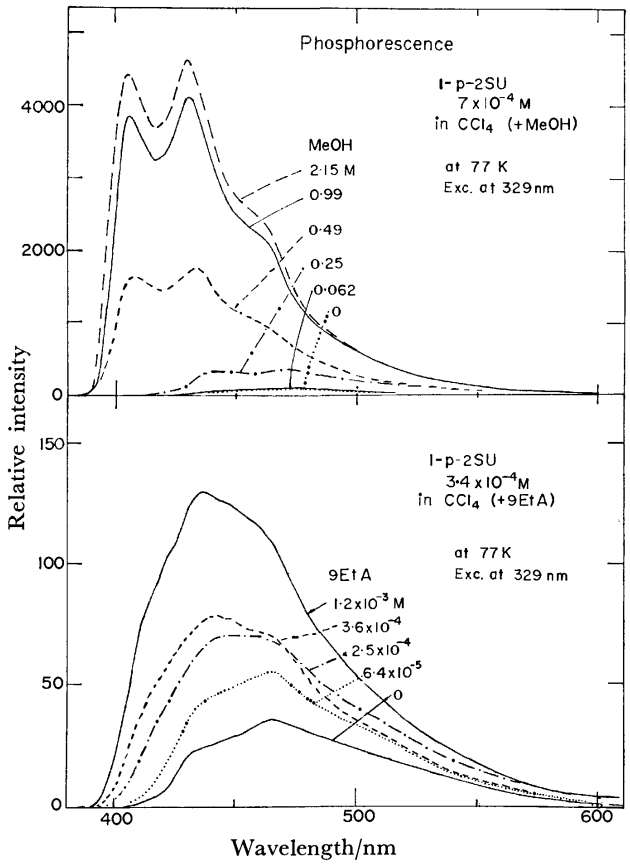

Fig. 8. Phosphorescence spectra of 1-propyl-2-thiouracil dissolved in the solutions of CCl_4+CH_3OH (upper) or dissolved in the solutions of CCl_4+9-ethyladenine (lower) and then cooled by liquid nitrogen. Sector: fast (about 10000 rpm).

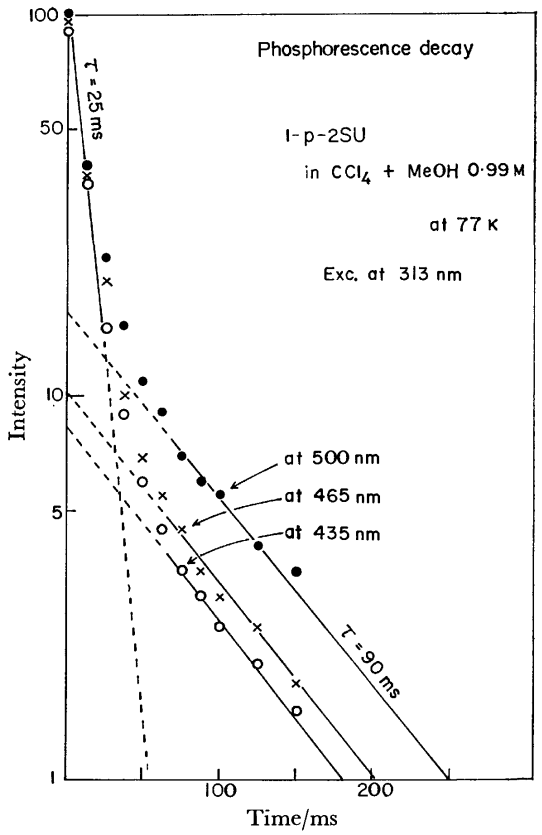

Fig. 9. Phosphorescence decay curves of 1-propyl-2-thiouracil dissolved in the solutions of CCl_4+CH_3OH and then cooled to the liquid nitrogen temperature. τ is the life time, which is the time required for bringing the intensity from 1 to 1/e.

the association constant of 1-propyl-2-thiouracil and ethanol is estimated to be 4.7 M^{-1}. When 2,2,2-trifluoroethanol, which is considered to be a stronger proton donor than ethanol (or methanol), is added to the dilute CCl_4 solution of 1-propyl-2-thiouracil, the complex bands appear at 270 and 291 nm. Here, the equilibrium constant for the complex formation is found to be 7.4 M^{-1}.

Complex with 9-Ethyladenine. Next 9-ethyladenine was added to the dilute CCl_4 solution of 1-propyl-2-thiouracil to observe ultraviolet absorption spectrum of the thiouracil–adenine complex examined in the infrared spectroscopy. Here a spectral change similar to that observed when CH_3OH was added instead of 9-ethyladenine was observed (see Fig. 7, lower). The isosbestic points appear at 289 and 331 nm. The decrease in the absorption intensity at 300 nm, which is considered to correspond to the decrease in the amount of free 2-thiouracil residue, goes in parallel with the lowering of the 1723 cm^{-1} band (see Figs. 4 and 5).

Phosphorescence

At liquid nitrogen temperature, 1-propyl-2-thiouracil shows only a weak phosphorescence (excited at 329 nm) with peaks at 445 and 465 nm in CCl_4. The phosphorescence is also very weak in 2-methylpentane and in methylcyclohexane. In all of these nonpolar solvents, the quantum yield ϕ_P was estimated to be 10^{-3}, on the basis of a comparison with the known phosphorescence of naphthalene.[9] While, in acetonitrile $\phi_P=0.02$, and in methanol and in ethanol $\phi_P=0.1$. In all of these three polar solvents, the phosphorescence maxima are found at 408 and 432 nm. When methanol is added stepwise into a dilute CCl_4 solution of 1-propyl-2-thiouracil, a stepwise increase in phosphorescence intensity is observed at 408 and 432 nm (Fig. 8, upper). When 9-ethyladenine is added, a similar increase in phosphorescence intensity at 408 nm (shoulder) and 432 nm (peak) is observed, except that it is observed at much lower concentration of 9-ethyladenine than that of methanol (Fig. 8, lower).

Phosphorescence lifetime of 1-propyl-2-thiouracil in pure CCl_4 was found to be 90 ms. Figure 9 shows phosphorescence decay curves at various wavelengths for 1-propyl-2-thiouracil in a mixed solvent CCl_4+0.99 M CH_3OH. On the basis of our infrared spectroscopic study, roughly 80% of the 1-propyl-2-thiouracil molecules in the solution are supposed to be involved in a hydrogen-bond complex (with CH_3OH) and remaining 20% are free. While, the phosphorescence decay curves indicate that the emission from this consists of two components: one with lifetime=25 ms at liquid N_2 temperature) which predominates at 435 nm and the other with lifetime=90 ms whose

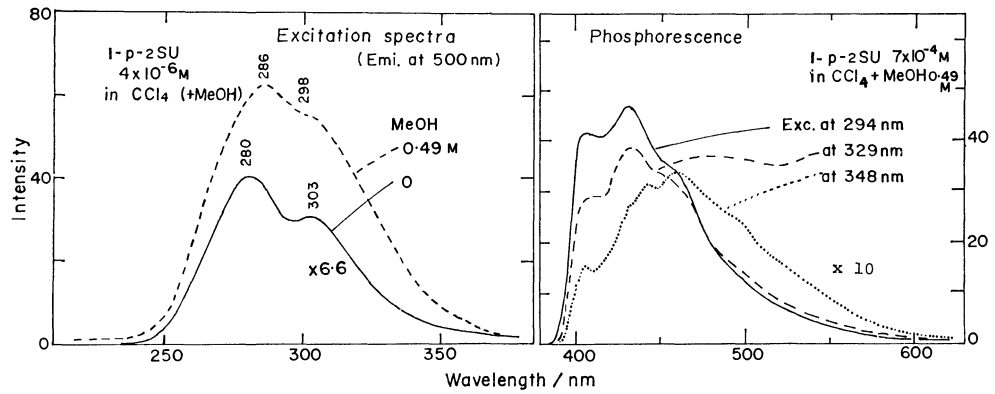

Fig. 10. (Left) Uncorrected excitation spectra of phosphorescence of 1-propyl-2-thiouracil dissolved in CCl_4 with and without CH_3OH. Sector: fast (about 10000 rpm). (Right) Phosphorescence spectra of 1-propyl-2-thiouracil in CCl_4+CH_3OH, where half of the thiouracil molecules are involved in a hydrogen-bond complex and the other half are free, with various excitation wavelengths. Sector: slow (about 1000 rpm).

contribution is only 17% (at zero time) at 500 nm and 8% at 435 nm.

The phosphorescence excitation spectrum of the free 1-propyl-2-thiouracil molecule has its maxima at 280 and 303 nm (Fig. 10, left). On going from a pure nonpolar solvent (CCl_4) to a mixed solvent ($CCl_4+0.49$ M CH_3OH) the excitation spectrum shows a change which is similar to the corresponding change in the ultraviolet absorption spectrum; *i.e.*, a blue shift of the longest wavelength peak and a red shift of the second longest wavelength peak. In the mixed solvent of $CCl_4+0.49$ M CH_3OH, about 50% of the 1-propyl-2-thiouracil molecules are involved in a hydrogen-bond complex (with CH_3OH) and 50% is free, on the basis of our infrared spectroscopic study. Figure 10 (right) shows phosphorescence spectra of 1-propyl-2-thiouracil in such a solvent with various excitation wavelengths (294, 329, and 348 nm). This figure indicates that the phosphorescence component with longer lifetime is located in the longer wavelength region ($\approx$500 nm), and that the longer wavelength excitation (348 nm) causes the longer lifetime component.

Discussion

It has been shown in our present study that, in an interaction of the 2-thiouracil residue with a residue having a proton-donating power, the position-4 carbonyl can act as a strong proton-acceptor.

Secondly, it has been found that the proton accepting power of the position-4 carbonyl of 2-thiouracil residue is greater than that of uracil residue. This is supported by an infrared spectroscopic study in the NH stretching region (3000 cm^{-1}) made by one of us, Higuchi.[10] This finding may be associated with some biological significance. Thus, it is in consistence with the fact[11] that a trinucleotide diphosphate codon $s^2U_pU_pU$ or $U_ps^2U_pU$ causes an *in-vitro* ribosome binding of *Escherichia coli* $tRNA^{Phe}$ (whose anticodon is G_pA_pA) more efficiently than a codon U_pU_pU. The finding may also be associated with the fact that a thermal stability of *Thermus thermophilus* HB8 tRNA is acquired by replacing the ribothymidine in its TψC loop by 2-thiothymidine.[2] It is true that an X-ray structure analysis for yeast $tRNA^{Phe}$ showed that the ribothymidine in TψC sequence binds to 1-methyladenosine with the position-2 carbonyl in the hydrogen bonding.[12] We suspect, however, that the position-4 carbonyl (instead of the position-2 carbonyl) is involved in the corresponding hydrogen bonding in the HB8 tRNA. We like to point out that, such a hydrogen bonding is quite possible if the 1-methyladenosine takes a *syn* conformer instead of *anti* (like in yeast $tRNA^{Phe}$), and that such a small variation in the bonding scheme is not improbable among different tRNA molecules.

It has been shown that the binding between 2-thiouracil residue and adenine residue is much stronger than the binding between 2-thiouracil residue and methanol. This fact indicates that there must be a second hydrogen bond between the 2-thiouracil and adenine residues in addition to the hydrogen bond between the position-4 carbonyl of the 2-thiouracil and the position-6 amino group of adenine. The second hydrogen bond may be formed between the position-3 imide of 2-thiouracil and position-7 nitrogen of adenine but it may also be formed between the position-3 imide of 2-thiouracil and position-1 nitrogen of adenine.

We have shown in the present work that hydrogen bonding of 2-thiouracil residue with alcohol or with adenine causes a marked enhancement of the phosphorescence. This fact suggests that phosphorescence may be a useful probe of the intramolecular environment of the 2-thiouracil residue in a biological system. In pursuing this line, however, it is desirable to discuss on the nature of the excited singlet and triplet states of this residue (especially these states with hydrogen bonding) slightly more in detail.

The ultraviolet absorption spectrum suggests (see Fig. 7) that 2-thiouracil residue in nonpolar solvent has an $n\rightarrow\pi^*$ level (S_1) at 2.5×10^4 cm^{-1} (its 0—0 transition is probably around 400 nm) and two $\pi\rightarrow\pi^*$ levels (S_2 and S_3) around 2.9×10^4 cm^{-1} (340 nm). When its position-4 carbonyl is brought into an intermolecular hydrogen bonding, S_1 is elevated by about 1300 cm^{-1}, S_2 is elevated by about 400 cm^{-1}, while

Table 1. A classification of phosphorescence of 2-thiouracil residue

	Transition frequency cm^{-1} (nm)	Intensity	Lifetime ms	Proposed assignment of the triplet state
I	24000 (410)	Weak	90	$^3(n\pi^*)$, free
II	26000 (385)	Strong	25	$^3(n\pi^*)$ with H-bonds

S_3 is lowered by about 300 cm^{-1}. On the basis of Strickler-Berg relation, [13] the radiative lifetime of S_1 is estimated to be 10^{-6} s (from the $S_1 \leftarrow S_0$ absorption intensity) and of S_2 10^{-8} s at room temperature. The fluorescence quantum yield ϕ_F is very low; it is less than 10^{-4}. Therefore, from the relation $\phi_F = k_F/(k_F + k_{nr}^F + k_{isc})$, k_{nr}^F and/or k_{isc} must be as high as 10^{10}, where k_F ($\fallingdotseq 10^6$) is the $S_1 \rightarrow S_0$ fluorescence rate constant, k_{nr}^F is the $S_1 \rightarrow S_0$ internal conversion rate constant, and k_{isc} is the $S_1 \rightarrow T_1$ intersystem crossing rate constant. Because phosphorescence is appreciable at liquid nitrogen temperature, k_{isc} is supposed to be high here.

In interpreting the observed phosphorescence spectra, we propose to classify them into two, as shown in Table I. The weak phosphorescence of 1-propyl-2-thiouracil residue in pure CCl_4 (see Fig. 8, upper) with lifetime 90 ms ($k_p \fallingdotseq 11$ s^{-1}) is spectrum I. When methanol is added to the CCl_4 solution, a stronger phosphorescence appears first at the slightly shorter wavelength with nearly the same lifetime. Its intensity becomes stronger with the methanol concentration. A further addition of methanol to the solution results in the appearance of a new phosphorescence, at about 1600 cm^{-1} higher frequency than spectrum I. This is spectrum II. The phosphorescence lifetime of spectrum II is shorter *i.e.*, 25 ms ($k_p = 40$ s^{-1}) at 77 K. There would be no problem to attribute spectrum I to the free 2-thiouracil residue. We speculate here that the intensity of spectrum I, which is due to the free molecule, becomes higher by a change of the environment, *i.e.*, from matrix without methanol to that with some amount of methanol. On the other hand, the fact that the spectrum II become stronger with methanol concentration is attributable to the increase of the amount of 2-thiouracil hydrogen-bonded to methanol. In other words, we postulated here a dynamic equilibrium among free triplet-state 2-thiouracil residue $^3(2SU)^*$, a hydrogen-bonded complex $^3(2SU)^* \cdot CH_3OH$ and the free CH_3OH molecules.

We wish to express our thanks to Dr. Junko Nakamura, the Institute of Physical and Chemical Research, and Professor Michiya Itoh, the Faculty of Pharmaceutical Sciences, Kanazawa University, for their kind help and valuable discussions. This work was partly supported by a grant from Ministry of Education.

References

1) S. Nishimura, *Prog. Nucleic Acid Res. Mol. Biol.*, **12**, 49 (1972).
2) K. Watanabe, T. Oshima, M. Saneyoshi, and S. Nishimura, *FEBS Lett.*, **43**, 59 (1974).
3) B. R. Baker and G. B. Chheda, *J. Pharm. Sci.*, **54**, 25 (1965).
4) D. T. Browne, J. Eisinger, and N. J. Leonard, *J. Am. Chem. Soc.*, **90**, 7302 (1968).
5) D. Shugar and J. J. Fox, *Bull. Soc. Chim. Belg.*, **61**, 293 (1952).
6) Y. Kyogoku, R. C. Lord, and A. Rich, *J. Am. Chem. Soc.*, **89**, 496 (1967).
7) C. C. Cheng and L. R. Lewis "Synthetic Procedures in Nucleic Acid Chemistry," ed by W. W. Zorbach and R. S. Tipson, John-Wiley & Sons (1968), Vol. I.
8) N. Nishi and M. Kinoshita, *Chem. Phys. Lett.*, **27**, 342 (1974).
9) E. H. Gilmore, G. E. Gibson, and D. C. McClure, *J. Chem. Phys.*, **20**, 829 (1952).
10) S. Higuchi, Sixth International Biophysics Congress, Paper IV-12-(501), September 3—9, 1978, Kyoto.
11) R. Vormbrock, R. Morawiesz, and H. G. Gassen, *Biochim. Biophys. Acta*, **340**, 348 (1974).
12) A. Jack, J. E. Ladner, and A. Klug, *J. Mol. Biol.*, **108**, 619 (1976).
13) S. Strickler and R. Berg, *J. Chem. Phys.*, **37**, 814 (1962).
14) E. Küchler and J. Derkosch, *Z. Naturforsch., Teil B*, **21**, 209 (1966).

Sound Velocity, Density, and Compressibility in Solutions of Hexamethylphosphoric Triamide in H_2O and D_2O

A. K. Lyashchenko, V. S. Goncharov, Toshiro Iijima,*,† Hisashi Uedaira,†† and Jiro Komiyama†

Institute of General and Inorganic Chemistry of the U.S.S.R. Academy of Science, Moscow, U.S.S.R.

† *Tokyo Institute of Technology, Department of Polymer Science, Meguro-ku, Ookayama, Tokyo 152*

†† *Research Institute for Polymers and Textiles, Tsukuba, Yatabe-Higashi, 1-1-4, Ibaraki 305*

(Received November 17, 1979)

Sound velocity and density measurements for H_2O and D_2O solutions of hexamethylphosphoric triamide (HMPT), $[(CH_3)_2N]_3PO$ at 25 °C have been carried out. The concentration dependence of the molar volumes and adiabatic compressibilities calculated therefrom are interpreted in terms of the water structure. The differences found between the H_2O and D_2O solutions are similarly explained.

Aqueous HMPT solutions are of interest in the study of hydrophobic interactions and structural variations of water. Recently, the large retarding action of HMPT on the rotational mobility of water molecules[1] has been observed. HMPT is miscible in all proportions with water, forming strong hydrogen bonds.[2] Having several nonpolar groups, HMPT can be regarded as a simplified model element of biopolymers that exhibit complex interactions with water. With this in mind, we have conducted a study of sound velocity, density and compressibility of HMPT solutions in H_2O and D_2O to elucidate the characteristics of the hydration of this molecule.

Experimental

The sound velocity, U, in aqueous HMPT solutions over the concentration range used was determined by two methods. For both H_2O and D_2O solutions, a sing-around ultrasonic velocimeter UVM-2 (Cho-onpa Kogyo) at 5 MHz was used. Deionized, distilled and deaerated water was used as a calibration liquid. The standard U values of water were taken from the work of Greenspan and Tschiegg.[4] The measurements were performed with an accuracy of ± 4 cm s^{-1} for each sample. A conventional ultrasonic interferometer method[4] at a frequency of 3 MHz was also used for H_2O solutions for comparison purposes. The accuracy of the measurements was within $\pm 0.2\%$.

The density of the aqueous HMPT solutions was determined at 25.00 °C with a digital precision densimeter, DMA 02C (Anton Paar). The instrument was placed in an air thermostat controlled at 25 ± 0.1 °C and the temperature of the sample solution was regulated by circulating water at a rate, *ca.* 6 dm^3 min^{-1} from an external thermostat with a stability of ± 0.001 °C. Reproducibility of the frequency for water was within $\pm 5 \times 10^{-7}$. The calibration was made with distilled mercury (Merck, Suprapur 13.5336 g cm^{-3}),[5] water (0.997045 g cm^{-3})[6] and distilled toluene (Eastman Kodak, Spectrograde), the density of which was determined as 0.862247 g cm^{-3}.[7,8] Calibration was repeated every day using water and the toluene.

HMPT (Aldrich, $n_D^{20\,°C} = 1.4579$, $d^{20\,°C} = 1.03$ g cm^{-3}, bp= 230 to 232 °C at 740 mmHg) was used as received. For the interferometric method, HMPT purified by the method given in Ref. 9 was used. D_2O had 99.75% deuterium content.

Results

The sound velocity (U) and the density (d) for HMPT solutions in H_2O and D_2O, and also for 0.5

Table 1. Density and sound velocity of HMPT solutions of H_2O and D_2O at 25 °C

Mol % HMPT		Density (g/cm³)	Sound velocity (m/s)
0	(H_2O)	0.997045	1497.33
0.9766		1.004443	—
1.0		—	1560[a]
1.9444		1.011610	1609.86
2.0		—	1605[a]
2.9853		1.018662	1647.37
3.0		—	1640[a]
4.9926		1.029508	1681.77
5.0		—	1676[a]
9.8211		1.042575	1662.74
10		—	1654[a]
14.9534		1.046143	1611.97
15		—	1610[a]
20		—	1557[a]
30		—	1488[a]
50		—	1416[a]
80		—	1358[a]
100		1.019[9]	1332[a]
0	(D_2O)	1.10406	1400.13
0.2525		1.10359	—
0.5202		1.10330	1441.57
0.9925		1.10299	1473.03
1.1587		1.10288	1484.18
1.6111		1.10288	—
2.1899		1.10314	1540.55
2.2188		1.10310	1542.01
3.2491		1.10344	1580.74
5.5882		1.10294	1620.415
9.7847		1.09764	1612.02
16.0006		1.08628	1565.52
22.1777		1.07523	1523.42
28.6169		1.06525	1481.34
48.2903		1.04439	1401.495
100	(HMPT)	1.019[9]	1336.62
0	$\left(\frac{0.5\text{ mol NaCl}}{55.5\text{ mol }D_2O}\right)$	1.12347	
0.5202	(mol% HMPT)	1.12175	
1.6111		1.12070	
3.2491		1.11812	
5.5882		1.11506	

a) Determined by ultrasonic interferometer.

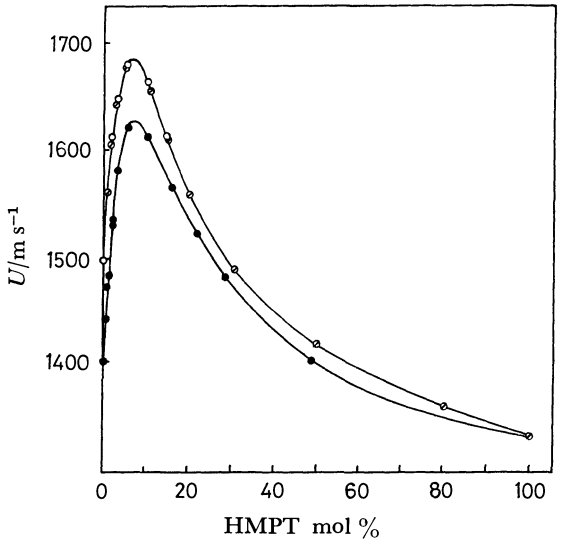

Fig. 1. Ultrasonic velocity in aqueous solutions of HMPT at 25 °C: in H_2O (⊘, ultrasonic interferometer method; ○, sing-around method) and in D_2O (●, sing-around method).

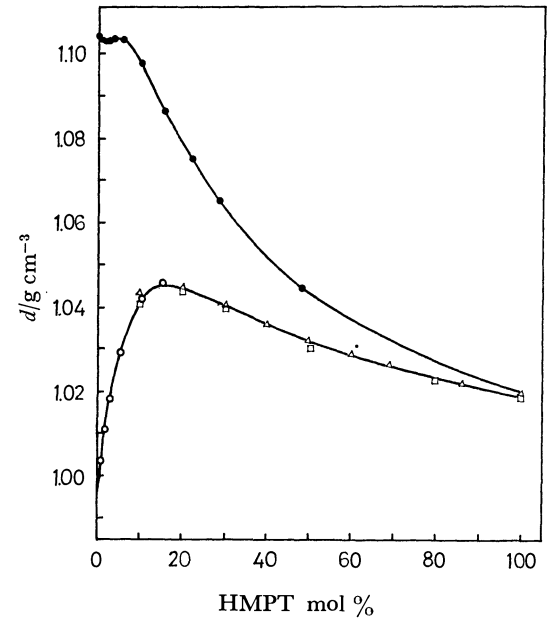

Fig. 2. Densities of aqueous solutions of HMPT in H_2O (○) and D_2O (●) at 25 °C. Data represented by △[12] and □[2] are taken from literatures.

mol dm^{-3} NaCl solution in D_2O at 25 °C are shown in Table 1. The value of the sound velocity for pure D_2O is consistent with reported values.[10,11] Figures 1 and 2 show the variations of U and d with HMPT concentration in H_2O and D_2O. In Fig. 2, the reported values[2,12] of the densities of HMPT solutions are also plotted. The sound velocity shows maxima at *ca.* 7 mol % HMPT in both H_2O and D_2O solutions.

The density of HMPT solutions in H_2O passes through a maximum at 15—20 mol % HMPT. On the other hand, the density of the solutions in D_2O shows a rather complicated variation with a minimum at 1.5% HMPT. The minimum in the D_2O solution disappears on addition of small amounts of NaCl.

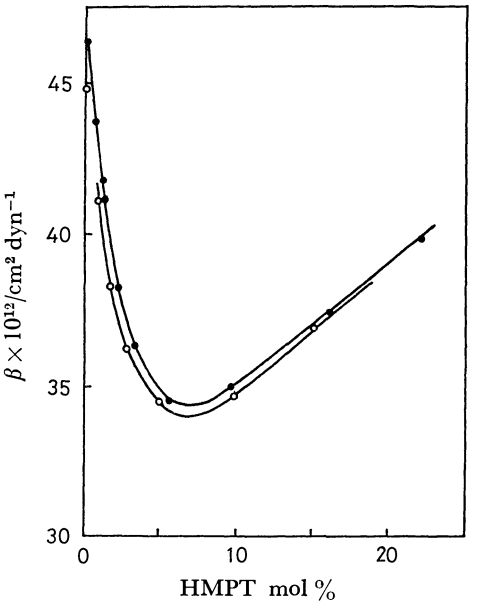

Fig. 3. Adiabatic compressibility of aqueous solutions of HMPT in H_2O (○) and D_2O (●) at 25 °C.

From the data of the sound velocity and the density for aqueous HMPT solutions, the adiabatic compressibility, β, was calculated. Figure 3 shows that β values for the H_2O and D_2O solutions pass minima at *ca.* 7 mol % HMPT. The variation of β is more pronounced in D_2O solutions than in H_2O solutions.

Discussion

The apparent molar volumes of HMPT calculated from the density data are presented in Fig. 4. A similar concentration dependence of apparent molar volumes is found for a number of hydrophobic molecules, *e.g.*, *t*-butanol, in aqueous solution.[13–15] The molecular mechanism of hydrophobic hydration can be described as a stabilization of water structure under action of nonpolar groups or molecules.[19–22] In the present case, the stabilization of water structure is ascribed to the filling of the cavities of the water structure with the nonpolar groups or molecules. As a consequence, the fraction of water molecules in the framework increases.[16,18] The concept of the inclusion of HMPT molecules in the cavities of water structure has been employed to explain some physicochemical properties of its aqueous solutions.[1,2,22] In terms of the structural model of nonelectrolytes in aqueous solution,[17,23,24] the volumetric changes on the introduction of HMPT molecules into water can be interpreted based on two effects; 1) the exclusion of free water molecules from the cavities caused by the occupation by HMPT molecules and the partial displacement of water molecules in the framework, and 2) the increase in the fraction of water molecules in the water tetrahedral structure outside the first coordination sphere of HMPT.

Given the similarity in the structures of light and heavy water[25,26] and the types of interaction between nonpolar groups of HMPT and H_2O and D_2O molecules in the cavities, there is a strong possibility that

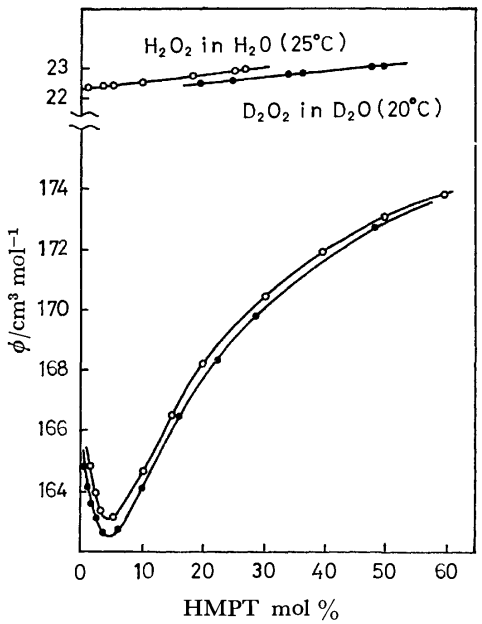

Fig. 4. Apparent molar volumes of HMPT at 25 °C and H_2O_2[27] in H_2O (○) and D_2O (●).

HMPT has a similar effect on the structures of light and heavy water. However, as the fraction of the cavities filled with free water molecules in the D_2O structure is smaller than in the H_2O structure, the fraction of free water molecules excluded by HMPT molecules from the cavities, mainly into the framework, must be greater for H_2O solutions. Accordingly, the apparent molar volume of HMPT (ϕ_{HMPT}) in H_2O is expected to be greater than in D_2O, which is actually found in Fig. 4.

We can explain the concentration dependence of ϕ_{HMPT} in H_2O and D_2O solutions along the same lines. The first of the above mentioned volumetric effects, associated with the introduction of nonelectrolyte molecules into water in the concentration range where the solution structure is based on the tetrahedral water structure, is the same for solutions of polar or nonpolar molecules. This effect does not undergo any serious change in solutions where cavities are available. The second effect is not found for a nonelectrolyte that undergo hydrophilic hydration.[23,24] The concentration dependence of the apparent molar volume of H_2O_2 in aqueous solution,[28] which is typical of a hydrophilic hydration, is shown in Fig. 4. The effect of increasing water structure outside the first hydration sphere around a hydrophobic molecule is such that, as the cavities become free of water molecules, each subsequent fraction of the molecule can eject from the cavities a smaller number of water molecules than the preceding one.

This process corresponds to a decrease in the apparent molar volume of HMPT with increasing concentration. It is expected to be observed up to the solution concentration corresponding to the complete or maximum possible filling of the water cavities with HMPT molecules. At higher concentrations, the durability of the water tetrahedral structure is exhausted and one can anticipate the initiation of transition to a different type of the spatial ordering of the system with the appearance of the contacts, HMPT–HMPT and HMPT–H_2O–HMPT. At these concentrations, the filling of the cavity volume by HMPT molecules becomes less and less important. This is connected with the significant increase in the values of ϕ_{HMPT} beyond the concentration range corresponding to a water-like ordering. The same type of structural ordering found in light and heavy water warrants the same number of cavities in their structures and hence the occurance of ϕ_{HMPT} minima at similar concentrations as actually observed in the experiments. The use of geometrical models to describe the introduction of HMPT molecules into the water structure with simultaneous substitution of the sites and cavity filling, enables one to estimate the concentration range where practically all water molecules bound to each other by a tetrahedral arrangement enter into the first surrounding sphere of HMPT molecules. At higher concentrations, the appearance of HMPT–HMPT contacts is observed by the X-ray method.[27]

The difference in the variations of the adiabatic compressibilities in H_2O and D_2O solutions (Fig. 3) can be explained using the same model for the solution structure. The sharper compressibility drop observed for D_2O solutions when changing from pure water to a solution is explained by a greater packing of D_2O structure when HMPT is added. This is due to the fact that the fraction of the cavities filled with water molecules is less for D_2O than for H_2O, and hence for D_2O, a smaller fraction of water molecules is excluded from the cavities into the sites on addition of HMPT. That the minimum values of β and of ϕ_{HMPT} in H_2O and D_2O solutions occur at approximately the same concentration follows from the similarity of the networks in H_2O and D_2O when all the molecules are located in the sites. The slight differences in the concentrations corresponding to the minimum ϕ_{HMPT} and β are likely to be related to the different structural states of the system at these concentrations. In the model under discussion, the first minimum corresponds to the maximum possible cavity filling when all the water molecules are distributed over the hydrate spheres, but a certain number of intermediate cavities may still exist. The minimum value of β can be related to a more complete cavity filling with simultaneous appearance of the contacts, HMPT–HMPT and HMPT–H_2O–HMPT.

One of us (A. K. L.) gratefully acknowledges the support of the Japan Society for the Promotion of Science through its Research Fellowship programme. The authors wish to thank Professor O. Ya. Samoilov for the discussion of the present work.

References

1) V. S. Goncharov, P. Ya. Yastremsky *et al.*, *Zh. Fiz. Khim.*, **54**, 789 (1977).
2) Yu. M. Kessler, V. P. Yemelin *et al.*, *Zh. Strukt. Khim.*, **16**, 797 (1977).
3) V. I. Stremousov, *Zh. Fiz. Khim.*, **36**, 380 (1962).
4) M. Greenspan and C. E. Tschiegg, *J. Res. Nat. Bureau*

Stand., **59**, 249 (1957).
5) "International Critical Tables of Numerical Data, Physics, Chemistry and Technology," ed by E. W. Washburn, McGraw-Hill (1926), II, p. 457.
6) G. S. Kell, *J. Chem. Eng. Data*, **20**, 97 (1975).
7) "Selected Values of Properties of Hydrocarbons and Related Compounds," American Petroleum College Section, Texas (loose-leaf sheet dated October 31, 1950).
8) O. Kiyohara and G. S. Benson, *J. Chem. Thermodyn.*, **9**, 691 (1977).
9) Yu. M. Kessler, M. G. Fomichyova, N. M. Alpatova, and B. P. Yemelin, *Zh. Strukt. Khim.*, **13**, 517 (1972).
10) O. Kiyohara, C. J. Hapin, and G. S. Benson, *Can. J. Chem.*, **55**, 3544 (1977).
11) R. N. Gupta, P. C. Jain, and V. S. Nanda, *J. Chem. Thermodyn.*, **8**, 627 (1976).
12) Jean-Yves Gal and F. Persin, *C. R. Acad. Sci., Ser. C*, 282 (1976).
13) F. Franks, "Water-a Comprehensive Treatise," ed by F. Franks, Plenum Press, N. Y. (1975), Vol. IV.
14) F. Franks, *Ann. N. Y. Acad. Sci.*, **125**, 277 (1965).
15) C. deVisser, G. Perron, and J. E. Desnoyers, *J. Am. Chem. Soc.*, **99**, 5894 (1977).
16) P. S. Yastremsky, G. V. Kokovina, A. K. Lyashchenko, O. Ya. Samoilov, and Yu. A. Mirgorod, *Zh. Fiz. Khim.*, **49**, 1442 (1975).
17) A. K. Lyashchenko, *J. Res. Inst. Catal., Hokkaido Univ.*, **25**, 129 (1978).
18) P. S. Yastremsky, G. V. Kokovina, A. K. Lyashchenko, and Yu. A. Mirgorod, *Zh. Strukt. Khim.*, **16**, 1002 (1975).
19) Z. I. Grigorovich and O. Ya. Samoilov, *Zh. Strukt. Khim.*, **3**, 404 (1962).
20) V. A. Mikhailov, *Zh. Strukt. Khim.*, **2**, 677 (1961).
21) G. G. Malenkov, *Zh. Strukt. Khim.*, **7**, 331 (1966).
22) O. Ya. Samoilov, P. S. Yastremsky, and V. S. Goncharov, *Zh. Strukt. Khim.*, **17**, 844 (1976).
23) A. K. Lyashchenko, V. S. Goncharov, and P. S. Yastremsky, *Zh. Strukt. Khim.*, **17**, 1020 (1976).
24) A. K. Lyashchenko and P. A. Stunjas, Preprints of the All-Union Conference on Calorimetry and Chemical Thermodynamics, Gvanovo, U.S.S.R., 1979.
25) I. B. Rabinovich, "The Effect of Isotope on the Physicochemical Properties of Liquids," ed by M. Nauka, 1968.
26) A. H. Harten and H. A. Levy, *Science*, **165**, 447 (1969).
27) V. I. Korsunsky and Yu. I. Naberukhin, *Zh. Strukt. Khim.*, **18**, 587 (1977).
28) P. A. Gigulze, O. Krop, and M. Falk, *Can. J. Chem.*, **36**, 883 (1958).

Electrochemical Study of Spectral Sensitization Using AgCl Sheet Crystal as a Window. Ag^+ Ion Effect

Seiichi SUMI,* Tadashi WATANABE, Akira FUJISHIMA, and Kenichi HONDA
Department of Synthetic Chemistry, Faculty of Engineering, The University of Tokyo, Hongo, Bunkyo-ku, Tokyo 113
(Received November 20, 1979)

With use of AgCl sheet crystal as a window, sensitized photocurrent was measured in an electrochemical cell with a lock-in amplifier. With five sensitizing dyes having different lowest vacant levels, it was found that the higher the level of the dye, the larger the sensitized photocurrent, the sensitized photocurrent increasing with decreasing pAg of the dye-bearing solution. The Ag^+ ion effect can be explained by a band edge shift of the AgCl electrode, which also explains the blue desensitization recovery by Ag^+ ions.

Recent studies on spectral sensitization have made it clear that the electron transfer mechanism is dominant.[1-3] On the basis of electron transfer, three processes of donation or acceptance between the dye and silver halide (AgX) can be considered (Fig. 1): (1) spectral sensitization, *i.e.*, electron transfer from excited dye to the conduction band of the AgX (Fig. 1a), (2) desensitization, *i.e.*, the transfer generated in AgX by intrinsic light absorption to the dye (Fig. 1b), (3) hole injection, *i.e.*, the transfer from the AgX valence band to oxidized dye (Fig. 1c). Ag^+ ion is known to influence these processes.

As regards (1), Gilman *et al.*[1,4] found that spectral sensitivity increases with decreasing pAg (pAg=$-\log[Ag^+]$) of photographic emulsions and explained this by a subconduction band event, a process in which Ag^+ ions at the AgX surface accept electrons from excited dyes to form silver atoms, with the result that the surface sensitivity of the photographic emulsion increases. Silver atoms are unstable, decomposing by thermal energy to Ag^+ ions and electrons, and the electrons go up the conduction band of the AgX. Iwasaki *et al.*[5] have utilized electrochemical techniques using AgCl sheet crystal as a membrane. They found that sensitized photocurrent (SPC) increases with decrease in the pAg of the solution containing dye, and explained the phenomenon by a band edge shift of AgCl.

As regards (2), Collier and Gilman[6] found the recovery of blue desensitization by Ag^+ ions in emulsion systems, and explained this by a subconduction band event.

As regards (3), Berriman and Gilman[7] reported a restraining action by Ag^+ ions in photographic emulsion systems, and explained it by change in the oxidation potential of silver by Ag^+ ions.

In connection with AgX/dye electron donation/acceptance, it is of great interest that Ag^+ ions can influence these three processes. In our experiment on the Ag^+ ion effect using electrochemical techniques, five sensitizing dyes were used, each having different lowest vacant levels. Constitutional formulas of the dyes and their energy levels[1] are shown in Figs. 2 and 3, respectively. Using these dyes, we measured SPC based on electron transfer from excited dyes to the AgCl conduction band[5,8] by an electrochemical method with use of a lock-in amplifier, AgCl sheet crystal being used as an electrochemical cell window.

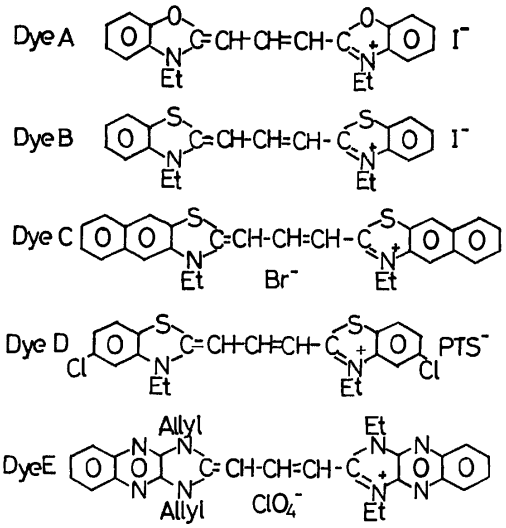

Fig. 2. Constitutional formula of sensitizing dyes.

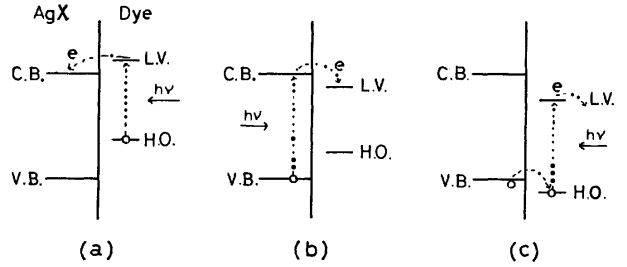

Fig. 1. A scheme of electorn transfer.
C.B.: Conduction band, V.B.: valence band, L.V.: lowest vacant level, H.O.: highest occupied level, e: electron, o: hole, a): spectral sensitization, b): desensitization, c): hole injection.

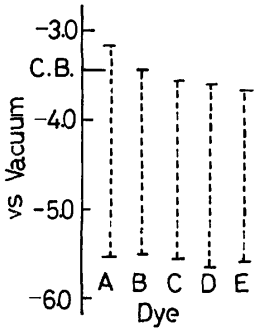

Fig. 3. Energy levels of sensitizing dyes reported by Gilman.[1]

Experimental

Preparation of AgCl Sheet Crystal. 2 M (1 M=1 mol dm^{-3}) $AgNO_3$ (Kojima Chemical Co., Ltd., reagent grade) and 5 M HCl (Sankyo Chemical Co., Ltd., reagent grade) were mixed, and the resulting precipitate was washed with distilled water and ground to powder in a mortar. The powder was packed into a quartz tube, and melted at 465 °C in a vacuum. When all the AgCl powder was melted, zone melting was carried out at a velocity of 1 cm/h. The upper (less pure) half of the transparent crystal produced was used in dye-adsorption experiments. The lower half was used to measure SPC. Cutting was done by a slicer (Maruto Co., Ltd.) to make crystals 0.5 mm thick, and the crystal surface was treated with 1 M KCN and polished with silk cloth to make it 80% transparent. All the crystals showed nearly the same behavior toward blank photocurrent which is due to intrinsic light absorption, as well as dark current which is based on interstitial silver ion.

Apparatus for Measurement. The apparatus is shown in Fig. 4. The exciting light from a 500 W Xe lamp (Ushio Electric Co.) illuminated the AgCl-dye interface through a light chopper, an interference filter (10 nm half-width), and transparent AgCl. AgCl electrode potential was adjusted to 0.4 V *vs.* a saturated calomel electrode (SCE) with dry cells. SPC was measured with a lock-in amplifier having a frequency of 125 Hz. During measurement, contact to the voltmeter was broken to exclude noise.

Measurement of Sensitized Photocurrent. The AgCl sheet crystal was held in contact with an electrochemical cell with epoxy resin. After *ca.* 10 h the crystal face not in contact with the electrolyte solution was attached to a lead wire with silver paste, while the opposite face was etched with 1 M KCN for 15 min and washed with distilled water. Dye solutions A, B, C, D, and E were prepared, methanol content being 5 vol % for A and B, 15% for C, 35% for D, and 25% for E. A dye solution with 0.04 M KNO_3 was put into the cell. SPC measurement was started 30 min after the addition of dye solution, and repeated every 10 min to check changes due to dye adsorption. If no change was observed, $AgNO_3$ solution was added to control pAg, SPC being measured after 5 min. After SPC measurement at pAg 1, dark currents were again measured to confirm that no large change have occurred in comparison with solutions without dye.

All experiments were carried out at room temperature in a dark room, the solution used not being deoxidized. The photon distribution of the light source was measured with a thermocouple.

Adsorption Experiments. The AgCl sheet crystal was immersed for 30 min in dye solutions of the same composition as those used in the SPC measurement (in this case dye adsorbed to both faces of AgCl crystal), and washed with hexane. The absorbance of this dyed crystal was measured as a reference of AgCl without dye using Shimadzu Model MPS-5000 recording spectrometer, after which the crystal was again immersed for 10 min in the same solution to check changes due to dye adsorption. The duration of immersion increased when such a change was found. The pAg of the dye solution was controlled by addition of $AgNO_3$ solution. The crystal was immersed in the solution for 5 min and washed with hexane, and its absorbance was measured. All the experiments were carried out at room temperature in a dark room.

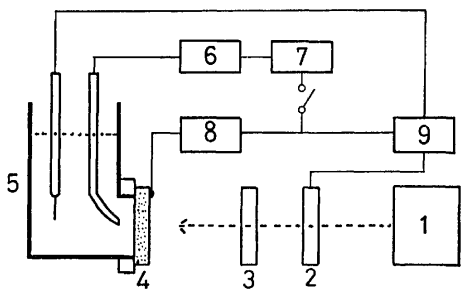

Fig. 4. Measurement apparatus.
1: Xe lamp, 2: light chopper, 3: interference filter, 4: AgCl, 5: Pt counter electrode, 6: SCE, 7: voltmeter, 8: dry cell, 9: lock-in amplifier.

Results

The characteristics of dye A are shown in Fig. 5. The insets in Fig. 5 a) and b) show the dependence of values of solid curve peaks on pAg. The adsorption of dye A decreases with the addition of Ag^+ ions, the absorption peak of the dye solution remaining unchanged. The dye solutions are diluted slightly by the addition of $AgNO_3$ solution. It was found that the 500 nm peak in the SPC action spectra is based on a dye monomer, and the 465 nm peak on a dimer. In the adsorption of dye A, the absorption peaks shifted to longer wavelength by an approximately 20 nm than that for the solution itself by stabilization, its SPC action spectra coinciding with its absorption spectrum when dye was adsorbed. The SPC increased, despite the decrease in adsorption of dye A with lowering pAg. The pAg ∞ shows the case without addition of $AgNO_3$.

The characteristics of dye B are shown in Fig. 6 a) and b). Adsorption was not influenced by Ag^+ ions, while SPC increased with lowering in pAg. The peak at 585 nm arose from a dye monomer, and the SPC of dimer could not be detected clearly.

Figure 7 shows the characteristics of dye C. Adsorption was not influenced by Ag^+ ions. No SPC could be detected at pAg 4 and above, but at 3 and below, SPC increased with fall in pAg. A 600 nm absorption peak arose from a dye monomer and 560 nm peak from a dimer. We could detect only the monomer peak in SPC. It is very interesting that SPC could be detected only at pAg 3 and below for dye C.

Figure 8 shows the characteristics of dye D. Adsorption was not influenced by Ag^+ ions, SPC increasing with decreasing pAg. An SPC peak was detected at 585 nm based on a monomer, but there was no clear peak on a dimer.

For dye E, no SPC could be detected down to pAg 1.

Though the methanol content of the various dye solutions was changed from 5% to 35%, the change in reference electrode (SCE) potential was less than 20 mV,[9] negligibly small. The redox potential of halide ions, which can act as electron donors,[15] shifted due to the change in methanol content. However, the amount contained as a counter ion to the cation dyes was very small, so that this effect can also be neglected. The NO_3^- ions contained in the 0.04 M electrolyte solution did not behave as electron donors.[15] The changes in methanol content influenced dye ad-

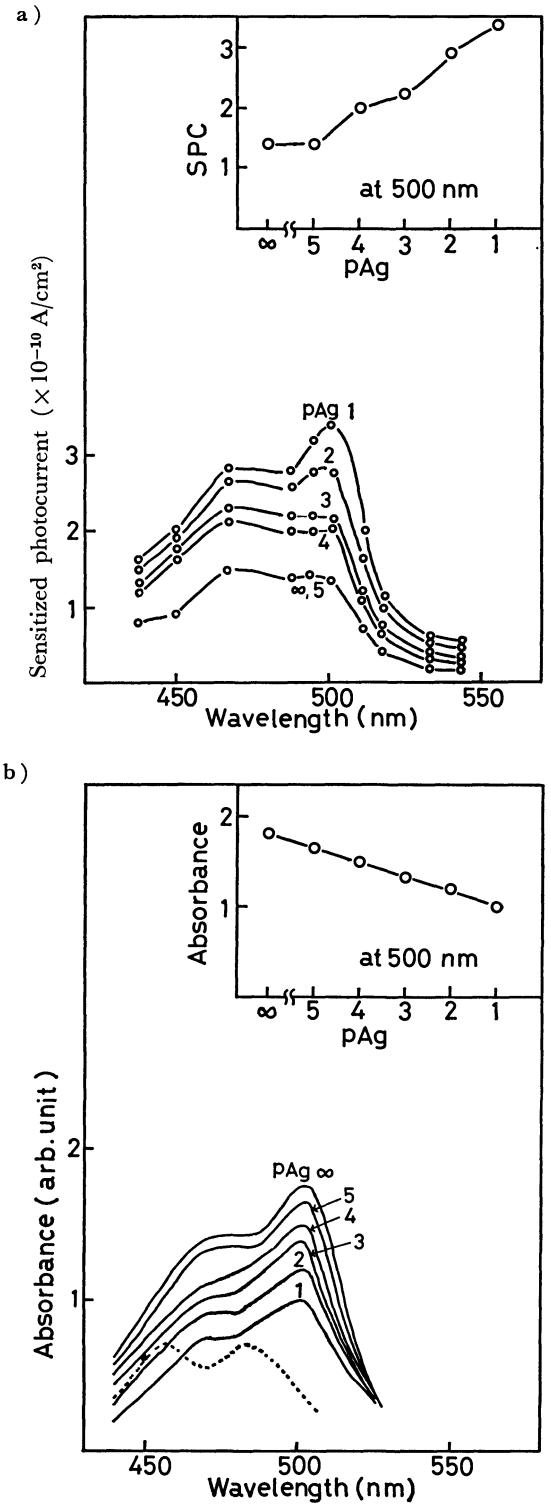

Fig. 5. Dye A characteristics (10^{-4} M dye in 0.04 M KNO_3 aqueous solution containing 5% methanol). a): pAg dependence of SPC, b): pAg dependence of absorption spectra, ——: adsorption to AgCl, ----: solution only.

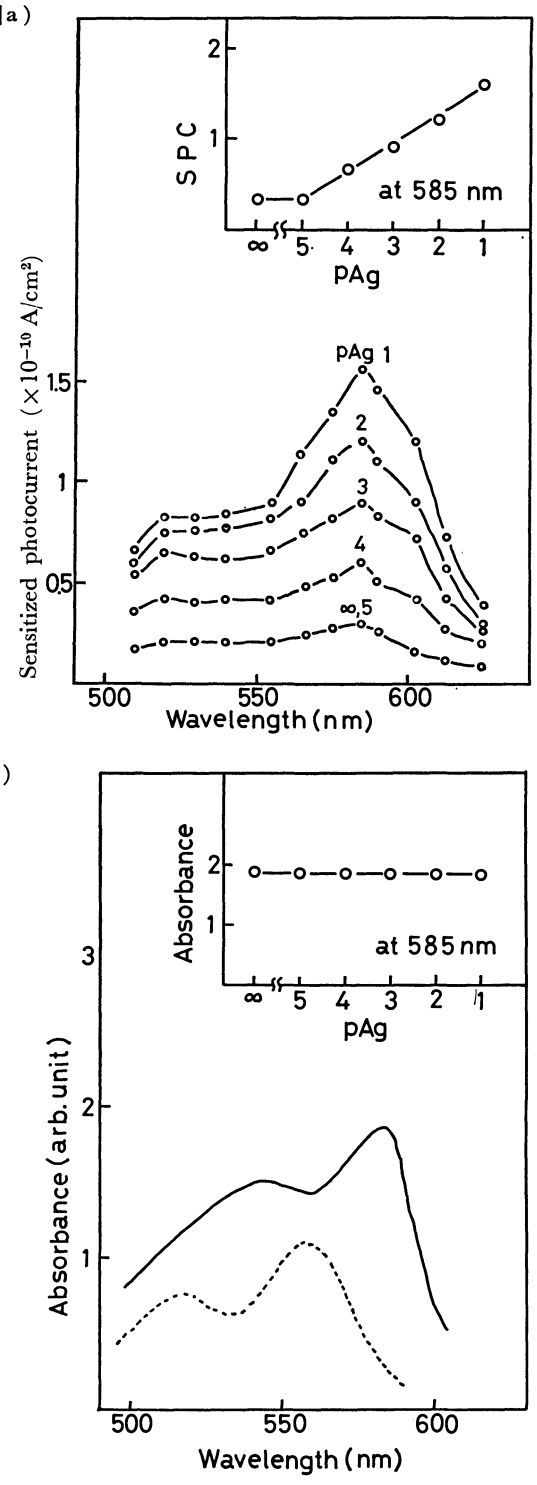

Fig. 6. Dye B characteristics (10^{-4} M dye in 0.04 M KNO_3 aqueous solution containing 5% methanol). a): pAg dependnence of SPC, b): pAg dependence of absorption spectra, ——: adsorption to AgCl, ----: solution only.

sorption only.

Levy[10] found that if AgX is brought into contact with silver, a print-out effect occurs, producing small silver specks absorbing light of *ca.* 585 nm wavelength. In our experiments, blank photocurrents were measured for 3 h, but almost no effect was detected at wavelengths of 500—700 nm. Thus it is concluded that the print-out effect due to silver paste does not influence SPC. The actual duration of SPC measurement including all processes was *ca.* 2 h.

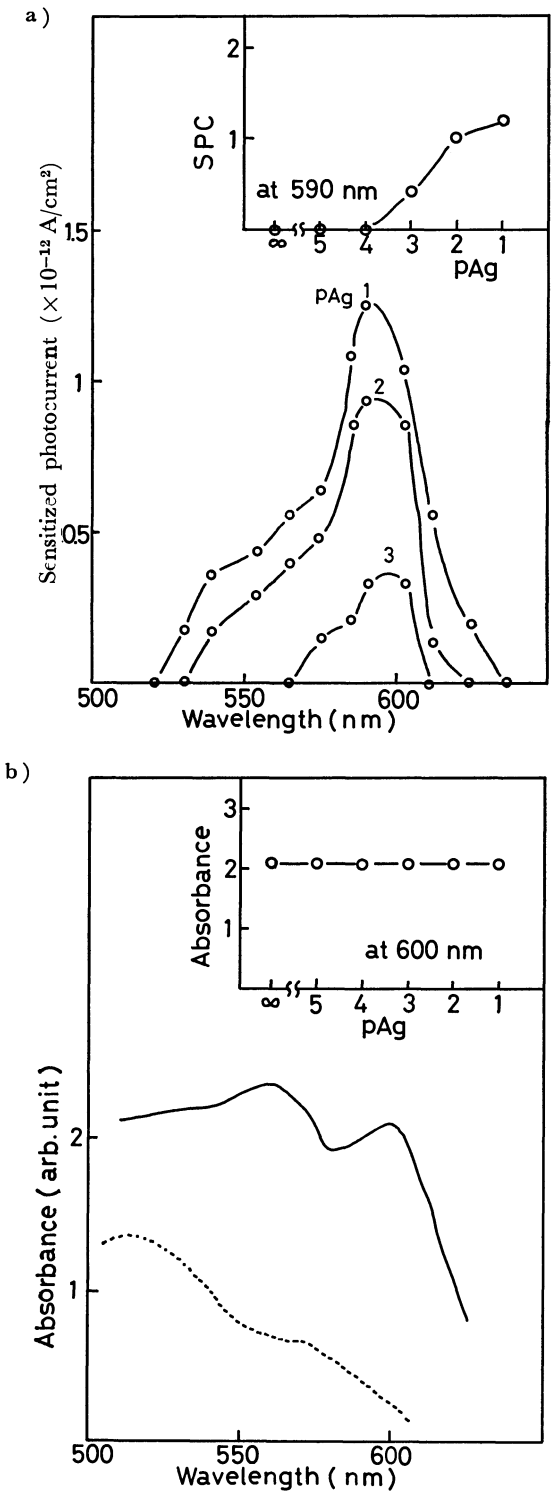

Fig. 7. Dye C characteristics (10^{-4} M dye in 0.04 M KNO_3 aqueous solution containing 15% methanol). a): pAg dependence of SPC, b): pAg dependence of absorption spectra ——: adsorption to AgCl, ----: solution only.

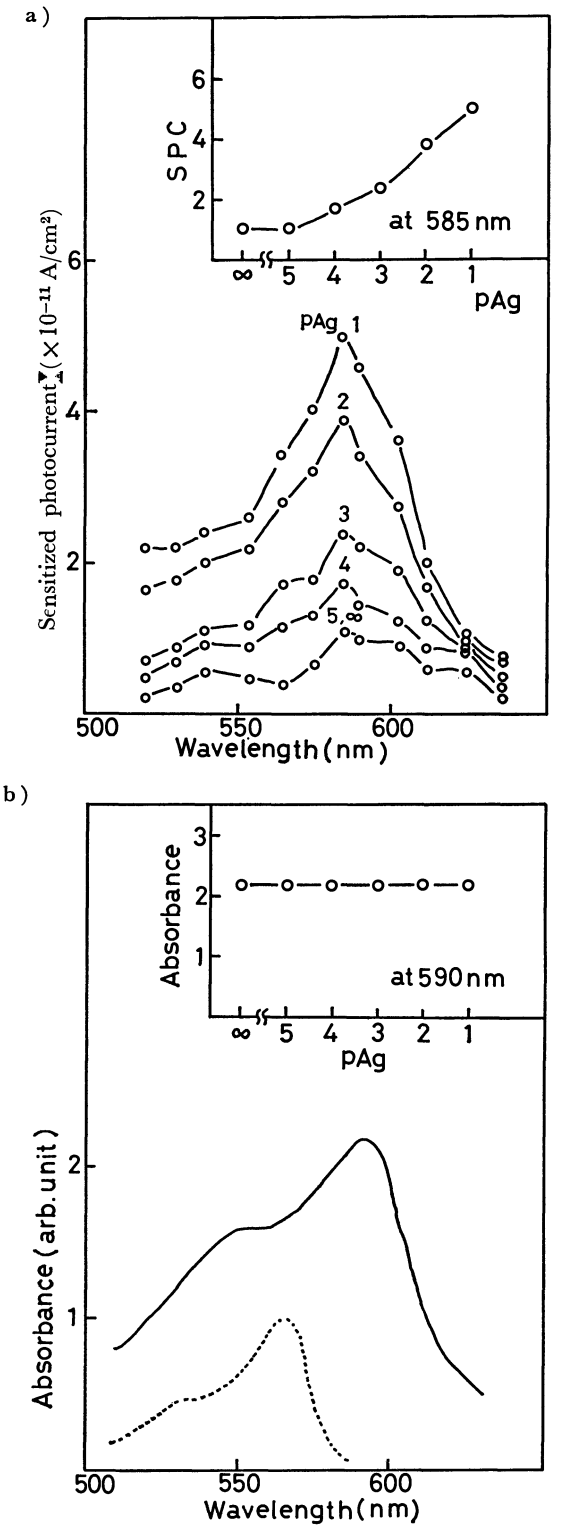

Fig. 8. Dye D characteristics (10^{-4} M dye in 0.04 M KNO_3 aqueous solution containing 35% methanol). a): pAg dependence of SPC, b): pAg dependence of absorption spectra ——: adsorption to AgCl, ----: solution only

Discussion

As shown in Figs. 5—8, the absorption spectra of dyes adsorbed to AgCl coincide with the SPC action spectra detected by the lock-in amplifier, showing that SPC indicates electron transfer from excited dyes to the conduction band of AgCl.[5,8] No dark currents based on interstitial Ag^+ ions could be detected with the lock-in amplifier at a light chopper frequency of 125 Hz.

However, in electrochemical studies using other semi-

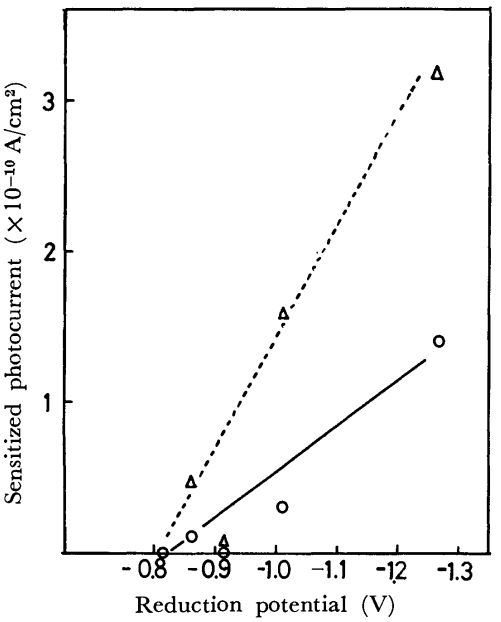

Fig. 9. Relation between SPC and reduction potential of sensitizing dyes.
----: at pAg 1, ——: at pAg ∞.

conductors such as ZnO,[2] and TiO_2,[3] SPC values exceeded 10^3 times of our values. This indicates that difficulty of movement of electrons from the excited dyes is due to resistance and electron traps in the AgCl. It is evident that this trait makes AgX most sensitive to light.

Since dye adsorption was restrained or not influenced by Ag^+ ions (Figs. 5—8) and the absorption peaks of adsorbed dyes did not change with lower pAg, the interaction between the dyes and Ag^+ ions can be neglected.[5] Ag^+ ions and NO_3^- ions can not donate electrons to oxidized dyes because of their redox potentials.[15] Therefore, the increase in SPC with lower pAg indicates a higher probability of electron transfer from excited dyes to the AgCl conduction band. Our results coincide qualitatively with those of the experiments of Gilman[1] on emulsion systems.

Increase in the spectral sensitivity of dye A was reported to be only slightly dependent on Ag^+ ions.[1] However, in our experiments, the SPC of dye A was greatly influenced by Ag^+ ions. Since the adsorption of dye A was reduced by Ag^+ ions even 5 min (Fig. 5b), it seems that the adsorption is reduced more in emulsion than in the electrochemical system so that the spectral sensitivity of the emulsion did not change.

Figure 9 shows the relationship between SPC and the reduction potential of sensitizing dyes;[1] the higher the reduction potential, the larger the SPC. This finding indicates that the electron transfer mechanism is dominant in this system. Adsorption experiments, however, showed that there is not much difference among dyes in terms of absorbance; we suppose that the quantum efficiency in spectral sensitization is proportional to the SPC.

We measured the current due to electrons going through the conduction band of the AgCl. If Ag^+ ions at the surface of AgCl trap the electrons, and the

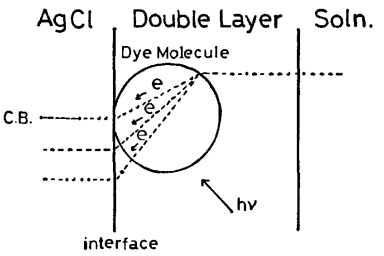

Fig. 10. Mechanism of Ag^+ ion effect.

electrons are excited to the conduction band by thermal energy, SPC should increase as pAg falls. At room temperature, however, thermal excitation energy is 20—30 mV, so we can neglect this thermal process. Since high-level electrons such as those in dye A can transfer smoothly to the conduction band, even temporary traps by Ag^+ ions bring about a decrease in SPC. Explanation of the Ag^+ ion effect by means of a subconduction band event does not seem feasible.

Yaenicke,[11] Leubner,[12] and Berriman and Gilman[7] considered that the Ag^+ ion effect arises from the potential shift of AgX. From the relationship between a potential shift of AgCl and SPC, Iwasaki *et al.*[5] postulated that the Ag^+ ion effect is due to a band edge shift of AgCl. Usually a potential shift of a semiconductor is measured by the flatband potential using the Mott-Schottky relationship, but if the present experiment is conducted using an AgCl electrode, Ag^+ ions in electrolyte solution are deposited as silver at the AgCl surface, making quantitative measurement impossible. However, this effect can also be measured by adding Cl^- ions.[14]

The flatband potential of AgCl was found to shift cathodically with an increase in Cl^- ions in the electrolyte solution. If Ag^+ ions were added, the flatband potential would shift anodically in contrast to Cl^- ions. Since potential distribution through the dye molecules becomes steeper with lower pAg, the rate of electron transfer from the excited dye increase, the probability of the transfer becoming higher (Fig. 10).

This provides a particularly satisfactory explanation in the case of dye C (Fig. 7a). There is no overlap between the excited level of this dye and the AgCl conduction band at pAg 4 and above. At pAg 3 and below, overlap begins to occur due to the anodic potential shift, SPC becoming detectable.

Studies on the SPC change in TiO_2–pH[3] and ZnO–pH[2] systems by a potential shift of a semiconductor show that SPC increases by several powers of ten with lower pH. In our experiments, however, the increase was only a few times. This can be attributed to the small shift of potential of AgCl. In a CdS–S^{2-}, Cd^{2+} system,[13] flatband potential shift differs according to the face index. However, since we have used no AgCl single crystal, it was impossible to determine its face index.

The recovery of blue desensitization[6] by Ag^+ ions can also be explained by the potential shift. It was deduced that the electron transfer from the conduction band of the AgX to the dyes occurs with lower prob-

ability as a result of band edge shift.

Conclusion

1. The use of AgCl sheet crystal as a window of an electrochemical cell is very effective in the study of spectral sensitization. 2. The Ag^+ ion effect arises from the potential shift of AgX. 3. The electron transfer is the dominant mechanism in AgX spectral sensitization.

We would like to thank Dr. Paul B. Gilman, Jr., the Kodak Research Laboratory, for valuable dyes, and Dr. Tamotsu Iwasaki and Dr. Kiminori Itoh of our laboratory for their useful suggestions.

References

1) P. B. Gilman, Jr., *Photogr. Sci. Eng.*, **18**, 475 (1974).
2) E. Daltrozzo and H. Tributsch, *Photogr. Sci. Eng.*, **19**, 303 (1975).
3) T. Watanabe, A. Fujishima, O. Tatsuoki, and K. Honda, *Bull. Chem. Soc. Jpn.*, **49**, 8 (1976).
4) P. B. Gilman, Jr., F. J. Evans, and T. D. Koszelak, *Photogr. Sci. Eng.*, **21**, 296 (1977).
5) T. Iwasaki, T. Abe, S. Sumi, A. Fujishima, and K. Honda, *Photogr. Sci. Eng.*, **24**, No. 3/4 (1980).
6) S. S. Collier and P. B. Gilman, Jr., *Photogr. Sci. Eng.*, **16**, 413 (1972).
7) R. W. Berriman and P. B. Gilman, Jr., *Photogr. Sci. Eng.*, **17**, 235 (1973).
8) T. Iwasaki, S. Sumi, A. Fujishima, and K. Honda, *Photogr. Sci. Eng.*, **23**, 17 (1979).
9) A. K. Convington and T. Dickinson, "Physical Chemistry of Organic Solvent Systems," Plenum Press, London and New York (1973), p. 190.
10) B. Levy, *Photogr. Sci. Eng.*, **15**, 279 (1971).
11) W. Yaenicke, "Advances in Electrochemistry and Electrochemical Engineering," ed by H. Gerischer and C. W. Tobias, Interscience Pub. Co., New York (1977), Vol. 10, p. 156.
12) I. H. Leubner, *Photogr. Sci. Eng.*, **18**, 175 (1974).
13) H. Minoura and T. Watanabe, *Jpn. J. Appl. Phys.*, **16**, 865 (1977).
14) S. Sumi, T. Watanabe, A. Fujishima, and K. Honda, *Bull. Chem. Soc. Jpn.*, in press.
15) K. H. Hauffe, *Photogr. Sci. Eng.*, **20**, 124 (1976).

Pressure and Solvent Shifts of Absorption Spectra. II. Intramolecular Charge Transfer Bands[1)]

Seiji SAWAMURA, Yoshihiro TANIGUCHI, and Keizo SUZUKI*

Department of Chemistry, Faculty of Science and Engineering, Ritsumeikan University, Kita-ku, Kyoto 603

(Received December 7, 1979)

Absorption spectra of intramolecular CT bands of nitrobenzene, *p*-nitrophenol, *p*-nitroaniline, acetophenone, *p*-hydroxyacetophenone, and *p*-aminoacetophenone are observed in several nonpolar solvents at 1 bar, and in heptane up to 4400 bar. The fact that all solvent shifts are linearly red for the function of refractive index (n) of solvents, $(n^2-1)/(2n^2+1)$, consists with the solvent shift theory. On the other hand, the pressure shifts are not straight but convex upward for $(n^2-1)/(2n^2+1)$ and the red shifts by pressure exceeds the solvent shifts. The similar convex pressure shifts are found in ^1L_b bands of several aromatic compounds by plotting the high pressure data of Robertson *et al.* in spite of the straight solvent shifts in these ^1L_b bands measured by us. Therefore the convex pressure shift may be regarded as a general tendency of the electronic spectrum, being ascribed to decrease in the distance between a solute and the surrounding solvents by compression. From comparison with the pressure shift of the intramolecular CT band, it is suggested that, in the pressure shift of the intermolecular CT band of the I_2 complexes shifted to red previously, the effect of decrease in the bond distance between a donor and an acceptor proposed by Offen and Nakashima contributes to not a red shift but a blue shift.

The pressure shifts of the intermolecular charge transfer (CT) bands have been observed to be red,[1-7)] blue,[1,8)] and red to blue.[1,3,4,6)] Offen and Nakashima ascribed these shifts to a sum of two effects of the increase in the dielectric constant (or refractive index) of solvent contributing to a red shift and the decrease in the bond distance between a donor and an acceptor contributing to a red or blue shift,[8)] and their interpretation was supported by us.[1)] Whether the decrease in the bond distance contributes to a red or blue shift in the observed pressure shift may be clarified by eliminating the effect of increase in the dielectric constant of solvent from the pressure shift.

As the binding energy of the covalent bond between a donor and an acceptor in the chromophore of intramolecular CT band is much larger than that of CT interaction of the chromophore of intermolecular CT band (*i.e.*, CT complex), the bond distance between a donor and an acceptor in the chromophore of intramolecular CT band is thought to be far less compressible than that of the CT complex. Therefore, from comparison of the pressure shift between intermolecular and intramolecular CT band, the effect of decrease in the bond distance of CT complex by compression may become clear. In the present study, the pressure and solvent shifts of the intramolecular CT bands were interpreted in comparison with those of π-π^* (^1L_b) band of aromatic compounds, and then compared with those of intermolecular CT bands. Used chromophores of the intramolecular CT band are nitrobenzene, *p*-nitrophenol, *p*-nitroaniline, acetophenone, *p*-hydroxyacetophenone, and *p*-aminoacetophenone. These have well-defined CT bands in the ultraviolet region. In these chromophores, $-NO_2$ and $-\overset{O}{\overset{\|}{C}}CH_3$ (-Ac) correspond to acceptors, and 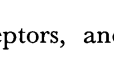 -, HO- -, and H_2N- - correspond to donors.

Experimental

Nitrobenzene and acetophenone were distilled under reduced pressure. *p*-Nitrophenol, *p*-nitroaniline, *p*-hydroxyacetophenone, and *p*-aminoacetophenone were recrystallized from aqueous ethanol. Benzene, toluene, chlorobenzene, phenol, and solvents (pentane, hexane, heptane, cyclohexane, and decalin) were purified by usual method.[9)] The method of measuring the absorption spectra under high pressure was reported.[10)] Refractive indices (n) of the solvents at high pressure were estimated from the dielectric constant (ε) of Refs. 11, 12, and 13 using the relation, $n^2=\varepsilon$.

Results and Discussion

Solvent Shift. Comparison between the solvent and pressure shifts of CT band is important in order to investigate the contribution of the refractive index of solvents to the pressure shifts. Ooshika[14)] and McRae[15)] theoretically proposed Eq. 1 for the estimation of solvent shift of electronic spectrum in nonpolar solvents.

$$\Delta\tilde{\nu} \equiv \tilde{\nu}_s - \tilde{\nu}_o = C_{solv}\frac{n^2-1}{2n^2+1}, \quad (1)$$

where $\tilde{\nu}_o$ and $\tilde{\nu}_s$ are wavenumber at absorption maxima in the vapor and the solvent whose refractive index is n, respectively. C_{solv} is a constant and consists of a sum of two terms: one is the dispersive interaction between a chromophore and the surrounding solvents, and the other is the electrostatic interaction between the chromophore permanent dipole and the solvent dipole thereby induced. The values of $\tilde{\nu}_s$ in nonpolar solvents are expected to depend linearly on $(n^2-1)/(2n^2+1)$ of the solvents. Solvent shifts of several intermolecular CT bands in nonpolar solvents have been linear for $(n^2-1)/(2n^2+1)$ of the solvents.[1,16)] In Fig. 1 absorption maxima of intramolecular CT bands are plotted against $(n^2-1)/(2n^2+1)$ of nonpolar solvents. All CT bands shift to red linearly with increase in $(n^2-1)/(2n^2+1)$. Values of the slopes (C_{solv}) in Fig. 1 are shown in Table 1, and are comparable with those of intermolecular CT bands ($C_{solv} \approx 10^4$ cm^{-1}).[1,16)]

Pressure Shift. Figure 2 shows absorption spectra of intramolecular CT band of *p*-nitroaniline in heptane at several pressures. The absorption maximum shifts to red with increasing pressure. Other

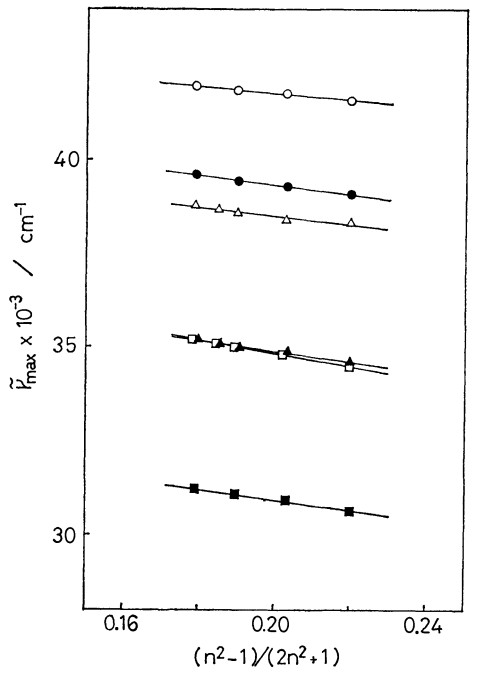

Fig. 1. Solvent shifts of several intramolecular CT bands.

○: 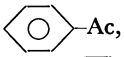 , △: ,

□: 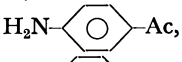 , ●: ,

▲: 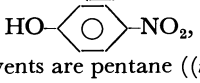 , ■: .

Solvents are pentane ($(n^2-1)/(2n^2+1)=0.179$), hexane (0.185), heptane (0.190), cyclohexane (0.203), and decalin (0.220).

Table 1. Slopes of solvent (C_{solv}) and pressure (C_{press}) shifts of several intramolecular CT bands

	C_{solv} / 10^3 cm^{-1}	C_{press}[a] / 10^3 cm^{-1}
(A) Nitro compounds		
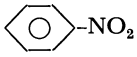	−13±2	−16±3
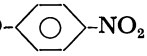	−14±2	−22±3
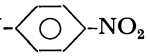	−15±2	−25±3
(B) Acetyl compounds		
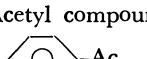	−9±2	−10±3
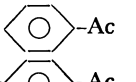	−11±2	−16±3
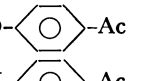	−15±2	−19±3

a) Estimated from the straight line through the two points at 1 and 1100 bar in Figs. 3 and 4.

intramolecular CT bands behave similarly. The observed shifts are plotted in Figs. 3 and 4 as a function of $\Delta[(n^2-1)/(2n^2+1)]$ of heptane. All of shifts are not straight for $\Delta[(n^2-1)/(2n^2+1)]$ but convex upward. Values of the initial slopes in Figs. 3 and 4 are shown in Table 1 as C_{press}. The red shift by pressure (C_{press}) exceeds the solvent shift (C_{solv}) in each chromophores.

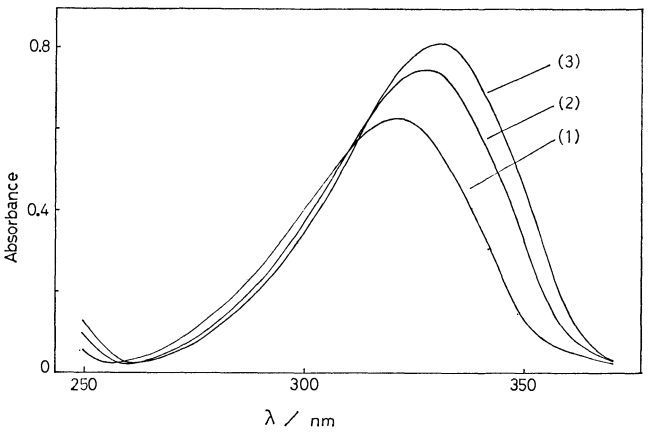

Fig. 2. Absorption spectra of intramolecular CT band of H_2N- 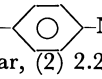 -NO_2 in heptane (2.7×10^{-5} mol dm^{-1}). (1) 1 bar, (2) 2.2 kbar, (3) 4.4 kbar. The absorptions are not corrected for compression.

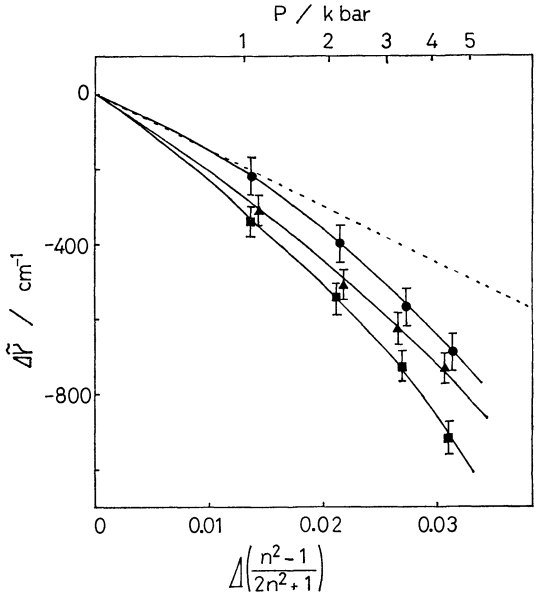

Fig. 3. Pressure shifts of intramolecular CT bands of nitro compounds in heptane.
The marks are the same as in Fig. 1. $\Delta\tilde{\nu}=\tilde{\nu}_P-\tilde{\nu}_1$, where $\tilde{\nu}_P$ and $\tilde{\nu}_1$ are wavenumber of absorption maxima at P and 1 bar. $\Delta[(n^2-1)/(2n^2+1)]=(n_P^2-1)/(2n_P^2+1)-(n_1^2-1)/(2n_1^2+1)$, where n_P and n_1 are refractive indices of solvent at 1 and P bar. Dotted line shows the solvent shift of H_2N- 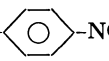 -NO_2 ($C_{solv}=-15\times10^3$ cm^{-1}).

In the serieses of (A) and (B) of Table 1, the chromophores of larger C_{solv} values have larger C_{press} values. This fact shows that there is a contribution from the refractive index of solvent for the pressure shift of intramolecular CT band. The similar relation between C_{press} and C_{solv} was observed in the intermolecular CT bands of the series of I_2 complexes and tetracyanoethylene (TCNE) complexes (CT complexes with I_2 and TCNE as acceptors, respectively).[1)]

Pressure shifts of the electronic absorption spectra of molecules, such as π-π^* band or intramolecular

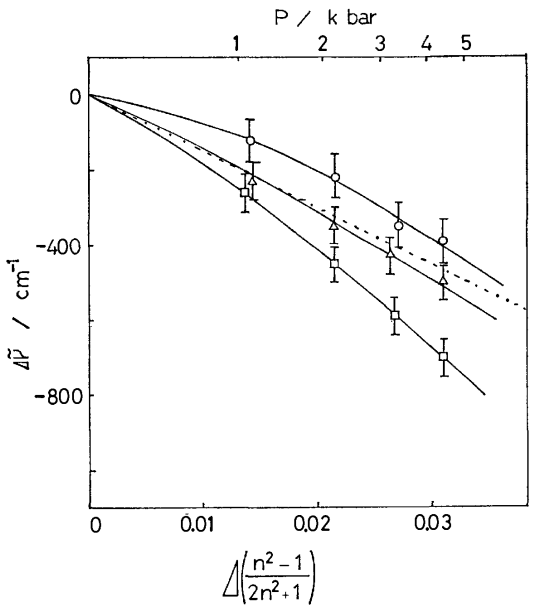

Fig. 4. Pressure shift of intramolecular CT band of acetyl compounds in heptane.
The marks are the same as in Fig. 1. $\Delta\tilde{\nu}$ and $\Delta[(n^2-1)/(2n^2+1)]$ are defined in Fig. 3. Dotted line shows the solvent shift of H_2N-⟨○⟩-Ac ($C_{solv}=-15\times10^3$ cm^{-1}).

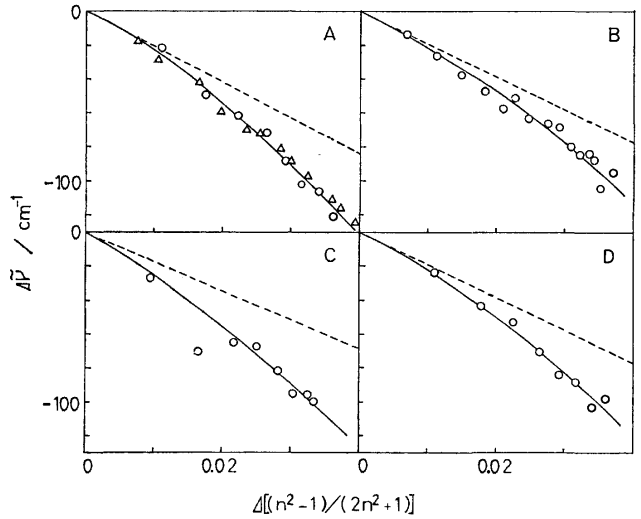

Fig. 5. Comparison between pressure and solvent shifts of ^1L_b band of several aromatic compounds.
A: Benzene at 261 nm, $C_{solv}=-2100$ cm^{-1}. B: Toluene at 271 nm, $C_{solv}=-1900$ cm^{-1}. C: Chlorobenzene at 271 nm, $C_{solv}=-1700$ cm^{-1}. D: Phenol at 277 nm, $C_{solv}=-1900$ cm^{-1}. Data of pressure shifts (—) in pentane (△) and hexane (○) were cited from Ref. 17 and solvent shifts (----) were estimated in present work as well as in Fig. 1.

CT band, have been studied without an attention whether the shift is convex or not for $(n^2-1)/(2n^2+1)$ of solvent. Then the previous data of pressure shifts should be reexamined. As such data, only the table of absorption maxima (λ_{max}) in π-π^* (^1L_b) bands of several aromatic compounds by Robertson *et al.*[17]

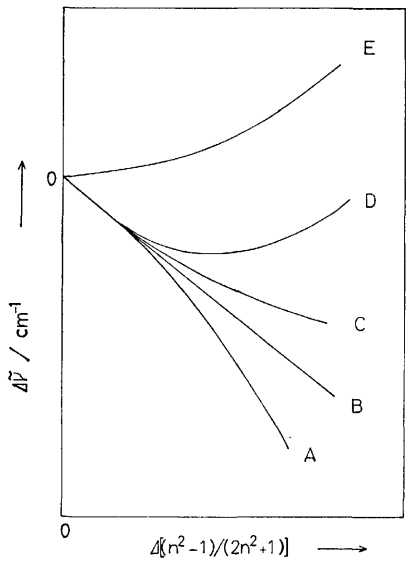

Fig. 6. Several patterns of pressure shift.
A: Convex red shift which should be normal for the pressure shift. Intramolecular CT bands in Figs. 3 and 4 and ^1L_b bands in Fig. 5. B: Straight red shift which is redder than the solvent shift. Benzene– and toluene–I_2 complexes. C: Concave red shift. Mesitylene– and Et_2O–I_2 complexes. D: Inversion shift from red to blue. Hexamethylbenzene–, Et_2S–, and Et_2Se–I_2 complexes. E: Blue shift. Et_3N–, *n*-Pr_3N–, and *n*-Bu_3N–I_2 complexes.

can be evaluated. The data is plotted in Fig. 5 as a function of $\Delta[(n^2-1)/(2n^2+1)]$ of solvent. All pressure shifts are not straight for $\Delta[(n^2-1)/(2n^2+1)]$ but convex upward as well as those of intramolecular CT bands in Figs. 3 and 4, though the solvent shifts (dotted lines in Fig. 5) measured by us as well as in Fig. 1 are straight for $(n^2-1)/(2n^2+1)$ of solvents. The deviation of pressure shift from the solvent shift is observed.

The solvent shift theory of Ooshika and McRae expressed by Eq. 1 considers the dispersive interaction and the electrostatic interaction between a chromophore and the surrounding solvents. Such interactions are a function of the distance between a chromophore and the solvents, and enhanced with decrease in the distance. Therefore, if the distance decreases by compression, pressure shift should deviate from the shift estimated by Eq. 1 and its deviation should become large with increasing $(n^2-1)/(2n^2+1)$ of solvent (or increasing pressure). The pressure shifts in Figs. 3, 4, and 5 deviated from the solvent shifts may be ascribed to such an effect.

Pressure shifts of intermolecular CT bands of I_2 complexes observed in the preceding paper[1] are not convex upward but concave or straight as shown in shifts B, C, D, and E of Fig. 6, where absolute values of the shifts are out of consideration and only the patterns of shifts (*i.e.*, straight, convex, or concave shift) are considered. In comparison with the convex shift (shift A) of the intramolecular CT band, there seems to be a blue shift contribution for the shifts of intermolecular CT bands, not only shifts D and E

but also shifts B and C. As such difference in the pressure shifts between the intermolecular and intramolecular CT bands seems to correspond to whether the bond distance between a donor and an acceptor is reducible or not by compression, the contribution to the pressure shift of the I_2 complexes from the decrease in the bond distance is thought to be a blue.

We wish to thank Mr. Mitsuharu Matsumoto and Mr. Kenji Matsuda for their assistance in the experiments.

References

1) Part I: S. Sawamura, Y. Taniguchi, and K. Suzuki, *Bull. Chem. Soc. Jpn.*, **52**, 3511 (1979).
2) J. Ham, *J. Am. Chem. Soc.*, **76**, 3881 (1954).
3) J. R. Gott and W. G. Maisch, *J. Chem. Phys.*, **39**, 2229 (1963).
4) A. H. Ewald, *Trans. Faraday Soc.*, **64**, 733 (1968).
5) Y. Torihashi, Y. Furutani, K. Yagii, N. Mataga, and A. Sawaoka, *Bull. Chem. Soc. Jpn.*, **44**, 2985 (1971).
6) T. Nakayama and J. Osugi, *Rev. Phys. Chem. Jpn.*, **45**, 79 (1975); T. Nakayama, M. Sasaki, and J. Osugi, *ibid.*, **46**, 57 (1976); T. Nakayama, *ibid.*, **49**, 25 (1979).
7) O. C. Kwun and H. Lentz, *Z. Phys. Chem. N. F.*, **96**, 177 (1979); O. C. Kwun, *Taehan Hwahak Hoechi*, **22**, 245 (1978).
8) H. W. Offen and T. T. Nakashima, *J. Chem. Phys.*, **47**, 4446 (1967).
9) "Thechniques of Chemistry," 3rd ed, ed by A. Weissberger, Wiley-Interscience, New York (1970), Vol. 2.
10) S. Sawamura, Y. Taniguchi, and K. Suzuki, *Chem. Lett.*, **1977**, 823.
11) W. G. S. Scaife, *J. Phys. A*, **4**, 413 (1971).
12) W. E. Danforth, Jr., *Phys. Rev.*, **38**, 1224 (1931).
13) F. I. Mopsik, *J. Res. Natl. Bur. Std.*, **71A**, 287 (1967).
14) Y. Ooshika, *J. Phys. Soc. Jpn.*, **9**, 594 (1954).
15) E. G. McRae, *J. Phys. Chem.*, **61**, 562 (1957).
16) J. Aihara, M. Tsuda, and H. Inokuchi, *Bull. Chem. Soc. Jpn.*, **42**, 1824 (1969); E. M. Voigt, *J. Phys. Chem.*, **61**, 562 (1957).
17) W. W. Robertson, S. E. Babb, Jr., and F. A. Matsen, *J. Chem. Phys.*, **26**, 367 (1957).

Photooxidation of 2-Hydroxy Acids by Copper(II) Species in Aqueous Solution

Ryoka MATSUSHIMA,* Yoshinori ICHIKAWA, and Katsuyuki KUWABARA
Department of Industrial Chemistry, Faculty of Engineering, Shizuoka University, Hamamatsu 432
(Received December 8, 1979)

Ultraviolet irradiation of aqueous lactic, glycolic, or 2-hydroxybutanoic acid in the presence of copper(II) leads to photoredox reaction to give corresponding α-keto acid, aldehyde with evolution of carbon dioxide, and the precipitate of copper(I). The mole ratio of the carbonyl products to the consumption of copper(II) is close to 0.5. Oxidative decarboxylation dominates at pH>1 while the formation of α-keto acids favors at lower pH. The formation of α-keto acids is selectively suppressed by the addition of free radical scavengers. Free radical oxidations of the acids with bromine atom or benzoyl radicals give exclusively α-keto acids. The reaction mechanism has been discussed.

Despite many publications and potential utility of the photoredox reactions of Cu(II)–organic substrate systems,[1] their mechanisms seem to have been less clarified, except for a few cases, *e.g.*, the Cu(II) complexes of malonate,[2] 2,9-dimethyl-1,10-phenanthroline,[3] and 2,2′-biquinoline derivatives.[4]

On the other hand, catalytic photoreactions of organic substrates with Cu(I)[5,6] and Cu(II)[7,8] species have received much attention in synthetic as well as in mechanistic photochemistry.

In several cases the apparent photocatalyses of Cu(II) species seem to be relevant to the reversible cycles leading to no final (apparent) reduction of Cu(II).

In this paper we deal with the photooxidation of 2-hydroxy acids by Cu(II) species whose results are comparable with those for the uranyl–lactic acid system.[9]

Experimental

Guaranteed grade reagents were used without further purification while water was used after deionization and distillation.

The acidity of solution was adjusted with dilute sodium hydroxide or perchloric acid solution using a pH meter (Toa Denpa). Each sample solution was deoxygenated by bubbling with oxygen-free nitrogen current for 30 min, after the upper surface of the solution had been covered with liquid paraffin to keep airtight in one of identical Pyrex test tubes. It was then irradiated with light from a 400 W high pressure mercury lamp by means of a merry-go-round irradiation apparatus thermostated at 20 °C.

The consumption of Cu(II) species during photolysis was followed either by measuring its 810 nm absorption, or by colorimetric determination of the Cu(I) precipitate formed. The carbonyl products (aldehydes and α-keto acids) were converted into the precipitate of 2,4-dinitrophenylhydrazone derivatives (2,4-DNP).

The 2,4-DNP derivatives were then separated from each other on PLC (silica gel–benzene) and were identified by comparing their IR and NMR spectra with those of authentic samples. The amounts of the aldehydes and the α-keto acids were determined by colorimetric measurements at 360 nm in chloroform and at 380 nm in aqueous 0.25 mol/dm^3 sodium carbonate solution respectively, after the mixture of the 2,4-DNP precipitates had been separated by extraction with chloroform/aqueous 0.25 mol/dm^3 sodium carbonate solution.[9] The formation of carbon dioxide was implied by white precipitate which was formed when the evolved gases from the photoreaction mixture were passed through an aqueous barium(II) solution. UV absorption was measured by means of a Hitachi 124-Type recording spectrophotometer.

Results

Photooxidation of Lactic Acid by Cu(II) Species. Aqueous acid solution containing 0.2—0.4 M† lactic acid and 0.1 M Cu(II) sulfate gave acetaldehyde with evolution of carbon dioxide, pyruvic acid, and Cu(I) precipitate, on irradiation with light of 313—366 nm at 20 °C. No carbonyl products were detected either by thermal reaction at 70—80 °C for 5 h or by photolysis in the absence of Cu(II) species. Aqueous pyruvic acid in the presence of Cu(II) species underwent no significant decomposition under the photolytic conditions.

Table 1 lists the mole of Cu(II) species consumed, ΔCu(II), and the sum of the carbonyl products, A+P, formed during photolysis in various pH regions. In the pH region of 1.5—3.5 the mole ratio (A+P)/ΔCu(II) is close to 0.5 in consistent with the redox

Table 1. Mole ratio's of the photochemical redox products of aqueous copper(II)–lactic acid solution[a]

pH	Atmosphere	ΔCu(II)[b] / mM	(A+P)[c] / mM	(A+P)/ΔCu(II)
0	air	0.0	0.98	
1.0	air	0.0	3.65	
1.5	air	12.6	6.40	0.51
1.5	N_2	9.6	7.63	0.80
2.0	air	11.3	8.23	0.73
2.5	air	16.2	8.50	0.53
2.5	N_2	15.6	10.9	0.70
3.0	air	16.5	8.50	0.52
3.0	N_2	22.6	12.5	0.55
3.5	air	19.8	9.88	0.50
3.5	N_2	23.5	11.5	0.49

a) Copper(II) sulfate: 0.1 M, lactic acid: 0.4 M, irradiation time: 5 h, temperature: 20 °C. b) Consumption of the copper(II) species. c) The sum of acetaldehyde and pyruvic acid concentrations.

† 1 M=1 mol/dm^3.

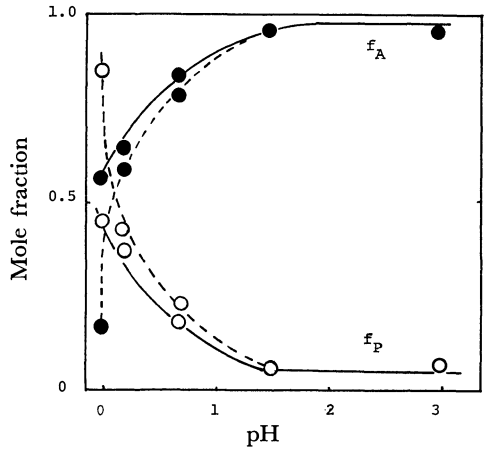

Fig. 1. Mole fractions of acetaldehyde (A) and pyruvic acid (P) formed in the photolysis of aqueous lactic acid–Cu(II) solution in Pyrex test tubes. (——): Deoxygenated, (----): not deoxygenated, before irradiation. Cu(II) sulfate: 0.1 M, lactic acid: 0.4 M, irradiation time: 5 h, f_A: A/(A+P), f_P: P/(A+P).

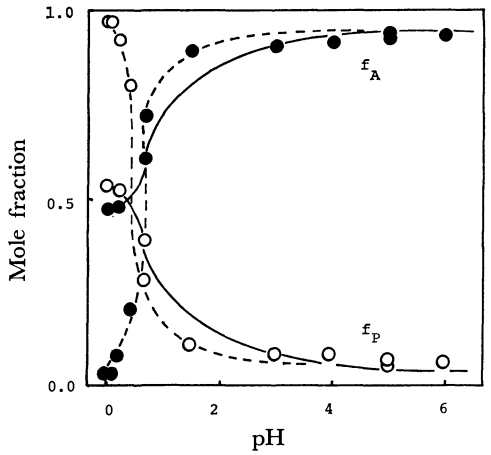

Fig. 2. Mole fractions of acetaldehyde (A) and pyruvic acid (P) formed in the photolysis of aqueous lactic acid–Cu(II) solution in glass ampuls. (——): Deoxygenated, (----): not deoxygenated, before irradiation. Other conditions and notations are the same as those in Fig. 1.

stoichiometry, both in the absence and presence of the dissolved oxygen. However, photolysis at pH≦1 in the presence of oxygen gives no final Cu(II)-reduction, implying reversible redox reaction of Cu(I) and Cu(II) species.

Figure 1 illustrates the pH-dependence of the mole fractions of acetaldehyde f_A and pyruvic acid f_P; f_A decreases and f_P increases with the decrease in pH. The broken lines in Fig. 1 show the effects of the dissolved oxygen which are significant in a lower pH region. Figure 2 illustrates the results obtained by irradiation in glass ampoules in the absence (solid lines) and presence (broken lines) of the dissolved oxygen, somewhat differing from those by irradiation in Pyrex test tubes. The present experiments have been carried out by the latter method because of its better reproducibility and simplicity, without further clarification of the discrepancy between the two methods.

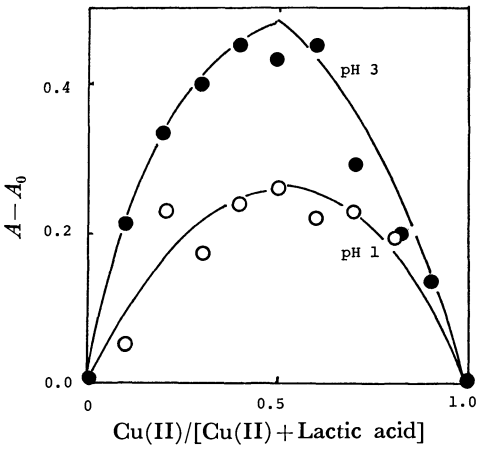

Fig. 3. Application of the continuous variation method to aqueous Cu(II)–lactic acid solution, as measured at 320 nm (pH 3) and at 290 nm (pH 1). Lactic acid+Cu(II)=0.20 M.

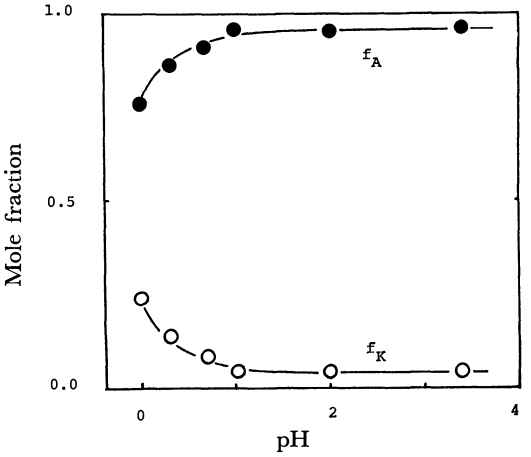

Fig. 4. Mole fractions of propanal (A) and 2-oxobutanoic acid (K) formed in the photolysis of deoxygenated aqueous 2-hydroxybutanoic acid–Cu(II) solution. Cu(II) sulfate: 0.1 M, 2-hydroxybutanoic acid: 0.2 M, f_P: A/(A+K), f_K: K/(A+K). Similar results were obtained for glycolic acid–Cu(II) solution.

The composition of aqueous Cu(II)–lactic acid solution in the ground state equilibrium was investigated, in relation to the pH-dependence of the photoproducts. Application of continuous variation method revealed the formation of a 1:1 Cu(II)–lactate complex in a higher pH region, while no such complex formation was observed at pH near zero (Fig. 3).

Photooxidation of Glycolic and 2-Hydroxybutanoic Acids by Cu(II) Species. On irradiation under conditions similar to those for the Cu(II)–lactic acid system, deoxygenated aqueous solution containing 0.2 M glycolic acid and 0.1 M Cu(II) sulfate gave glyoxylic acid, formaldehyde with evolution of carbon dioxide, and a small amount of unidentified carbonyl product, besides Cu(I) precipitate. Similar irradiation of 2-hydroxybutanoic acid–Cu(II) solution gave 2-oxobutanoic acid, propanal with evolution of carbon dioxide, and a small amount of unidentified carbonyl product, besides the Cu(I) precipitate. The pH-de-

TABLE 2. ADDITIVE EFFECTS OF SODIUM BROMIDE[a)]

[NaBr]/mM	[A]/mM	[P]/mM	f_A	f_P
0	34.7	3.68	0.90	0.10
2	35.0	1.74	0.95	0.05
20	34.7	0.70	0.98	0.02
200	17.0	0.03	1.00	0.00

a) Aerated aqueous solution containing 0.1 M copper(II) sulfate and 0.4 M lactic acid at pH 1.7, 20 °C, irradiation time: 5 h.

TABLE 3. ADDITIVE EFFECTS OF ACRYLONITRILE(AN) AT VARIOUS pH'S[a)]

pH	[AN]/mM	[A]/mM	[P]/mM	f_A	f_P
0	0	1.8	1.4	0.56	0.44
0	40	0.63	0.04	0.94	0.06
0.7	0	4.8	1.0	0.83	0.17
0.7	40	1.0	0.08	0.92	0.08
1.6	0	8.4	0.45	0.95	0.05
1.6	40	1.4	0.08	0.95	0.05
2.9	0	8.6	0.58	0.94	0.06
2.9	40	3.0	0.09	0.96	0.06

a) Copper(II) sulfate: 0.1 M, lactic acid: 0.4 M, irradiation time: 5 h, temperature: 20 °C.

TABLE 4. EFFECTS OF ACRYLONITRILE(AN) AT pH≒0[a)]

[AN]/mM	Irrd. time/h	[A]/mM	[P]/mM	f_A	f_P
0	5	1.60	1.43	0.53	0.47
1	5	1.05	0.80	0.57	0.43
2	5	0.95	0.45	0.68	0.32
3	5	0.73	0.01	0.88	0.12
4	5	0.83	0.06	0.94	0.06
0	8	0.70	1.20	0.37	0.63
8	8	1.15	0.03	0.91	0.03
16	8	0.95	0.03	0.97	0.03
24	8	0.95	0.02	0.97	0.03
32	8	1.00	0.05	0.96	0.04
40	8	1.05	0.03	0.98	0.02

a) Copper(II) sulfate: 0.1 M, lactic acid: 0.4 M, perchloric acid: 1.0 M.

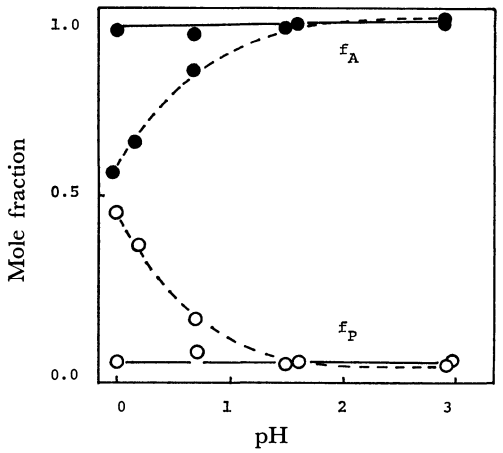

Fig. 5. Additive effects of acrylonitrile in the photolysis of deoxygenated aqueous lactic acid–Cu(II) solution. (——): In the presence of 40 mM acrylonitrile, (----): in the absence of acrylonitrile. Cu(II) sulfate: 0.1 M, lactic acid: 0.4 M.

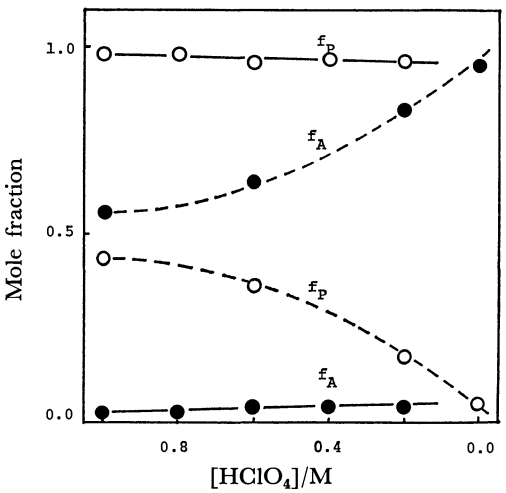

Fig. 6. Additive effects of maleic acid in the photolysis of deoxygenated aqueous lactic acid–Cu(II) solution, in the absence (----) and presence (——) of 0.1 M maleic acid. Cu(II) sulfate: 0.1 M, lactic acid: 0.4 M.

pendences of the mole fractions of the carbonyl products are shown in Fig. 4, which is comparable with those in Fig. 1.

Effects of Additives. In order to test the possible involvement of free radical intermediates, the effects of some free radical scavengers have been investigated for the photoredox reaction of the Cu(II)–lactic acid system. Table 2 lists the results with bromide ion, showing selective suppression toward the formation of pyruvic acid. Tables 3 and 4 are the effects of acrylonitrile in different pH regions and in different acrylonitrile concentrations at pH 0 respectively, which again reveal selective suppression toward the formation of pyruvic acid. For example, the yield of pyruvic acid is decreased to 1/25 (from 1.43 to 0.056 mM) while that of acetaldehyde to 1/2 (from 1.60 to 0.83 mM), by the addition of 4 mM acrylonitrile. Figure 5 is a plot of f_A and f_P as a function of pH in the presence and absence of acrylonitrile. The addition of *t*-butyl alcohol (20 v/v%) as a scavenger of hydroxyl radical[10] suppressed the formation of pyruvic acid almost completely without affecting the yield of acetaldehyde, in the photooxidation of lactic acid with Cu(II) chloride at pH 0, 1, and 1.5.

Figure 6 illustrates the effects of maleic acid, showing selective suppression toward acetaldehyde formation. Though maleic acid suppresses the formation of both acetaldehyde and pyruvic acid considerablly, the effect is much more pronounced toward the former.

Neither acetaldehyde nor pyruvic acid formation was suppressed by the addition of 1 mM sodium azide, an effective scavenger of singlet molecular oxygen, in the photolysis of the Cu(II)–lactic acid system at pH 0, 1, and 1.5.

Free Radical Oxidations of 2-Hydroxy Acids. Since the formation of α-keto acids has been assumed

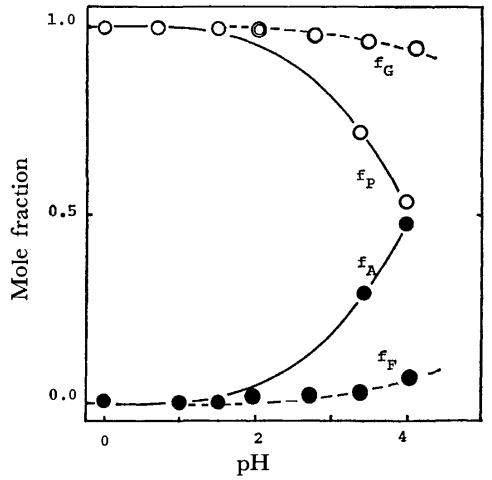

Fig. 7. Mole fractions of aldehydes (●) and α-keto acids (○) formed in the photolyses of aqueous lactic acid (——) and glycolic acid (——), in the presence of 0.5 M bromine. The results with 2-hydroxybutanoic acid were similar to those with lactic acid.

to involve free radical processes, it appeared of interest to investigate free radical oxidations for comparison with the Cu(II)-photooxidation. Reaction of 2-hydroxybutanoic acid with benzoyl peroxide at 80—90 °C in benzene for 20 min led, indeed, to the formation of 2-oxobutanoic acid without propanal formation. Photooxidation of lactic, glycolic, and 2-hydroxybutanoic acids by bromine water (without deoxygenation) gave corresponding α-keto acids with minor amounts of aldehydes. The pH-depencences of the two sets of the carbonyl products are shown in Fig. 7. The pH-dependences appear to be in sharp contrast to those of the Cu(II)-photooxidation.

These results seem to provide some evidence for the intermediacy of free radical processes in the formation of α-keto acids as will be discussed in the following section.

Reaction of lactic acid with Fenton's reagent, which generates hydroxyl and hydroperoxyl radicals,[11] gave no carbonyl products. Nor was formed 2-oxobutanoic acid by reaction of 2-hydroxybutanoic acid with singlet molecular oxygen generated by reaction of sodium hypochlorite with hydrogen peroxide.[12]

Discussion

The pH-dependences of the photooxidation of 2-hydroxy acids by Cu(II) species are apparently similar to those of the photolysis of the uranyl–lactic acid system under similar conditions.[9]

Because of the similarity it seems reasonable to refer to the outline of the latter photoreactions. It has been shown that pyruvic acid is formed at pH≦1 *via* electron or α-hydrogen atom abstraction by excited state uranyl ion on bimolecular collisions with lactic acid while the formation of acetaldehyde and carbon dioxide dominates in a higher pH region *via* unimolecular photodecomposition of uranyl–lactate complex, for the photolysis of aqueous uranyl–lactic acid solution. Later, ESR detection of free radical intermediates, such as $R\dot{C}(OH)R'$,[13] and kinetic isotope effects[14] have strongly supported the assumed mechanisms for the photooxidation of alcohols and acids by uranyl ion.

Similar mechanism seems to be applicable to the photooxidation of 2-hydroxy acids by Cu(II) species with a minor modification.

Equation 1 represents the ground state equilibrium between Cu(II), 2-hydroxy acid (HA), and a 1:1 chelate complex (CuX). Here, Cu(II) represents aquo complex ion which may be present far apart from or in the close proximity of HA without formation of chelate complex. Equations 2 and 3 represent the processes for the formation of α-keto acids and aldehydes, respectively.

The pH-dependence of the two carbonyl products may be interpreted as a reflection of the ground state equilibrium. Equations 1—3 may explain the fact that the formation of α-keto acids is favored by the decrease in pH while oxidative decarboxylation is favored by the increase in pH. UV excitation of CuA would lead to unimolecular redox, *i.e.*, electron transfer from the carboxyl group to the metal center (*d*), followed by oxidative decarboxylation to give aldehyde (*e*). On the other hand, Cu(II) is excited to its LMCT excited state, Cu(II)*, which then undergoes redox reaction with HA on bimolecular collision to produce radical intermediate, $R\dot{C}(OH)COOH$. This radical would be rapidly oxidized by Cu(II)[15] to give α-keto acid.

If the free radical $P\dot{C}(OH)COOH$ is actually the precursor of α-keto acids in the photooxidation by Cu(II) species, as suggested in Eq. 2, then α-hydrogen atom abstraction by other oxidants should also give α-keto acids. In fact, oxidation by free radicals generated in thermolysis of benzoyl peroxide or in photo-

$$\mathrm{Cu(II)} + \mathrm{RCH(OH)COOH} \overset{K}{\rightleftharpoons} \mathrm{RCH(O\cdots Cu(II))COO} + \mathrm{H^+} \quad (1)$$

$$\mathrm{Cu(II)} \xrightarrow[a]{h\nu} \mathrm{Cu(II)^*} \xrightarrow[b]{\mathrm{HA}} \mathrm{R\dot{C}(OH)COOH} + \mathrm{H^+} + \mathrm{Cu(I)}$$

$$\mathrm{R\dot{C}(OH)COOH} \xrightarrow[c]{\mathrm{Cu(II)}} \mathrm{RCOCOOH} + \mathrm{H^+} + \mathrm{Cu(I)} \quad (2)$$

$$\mathrm{CuA} \xrightarrow[d]{h\nu} \left(\mathrm{RCH(O\cdots Cu(I))COO}\right)^* \xrightarrow[e]{\mathrm{Cu(II)\ or\ CuA}} \mathrm{RCH{=}O} + \mathrm{H^+} + \mathrm{CO_2} + \mathrm{2Cu(I)} \quad (3)$$

Scheme 1.

$$\mathrm{Cu(II)^*_{aq}} \xrightarrow{\mathrm{HA}} \mathrm{Cu(I) + H^+ + R\dot{C}(OH)COOH} \quad (4)$$

$$\mathrm{Cu(II)^*_{aq}} \longrightarrow \mathrm{Cu(I) + H^+ + \dot{O}H} \xrightarrow{\mathrm{HA}} \mathrm{R\dot{C}(OH)COOH + H_2O} \quad (5)$$

$$\mathrm{Cu(II)^*_{aq}} \xrightarrow{\mathrm{HA}} \mathrm{Cu(I) + RCH(OH^+)COOH} \longrightarrow \mathrm{RCH(O\cdot)COOH + H^+}$$

$$\mathrm{RCH(O\cdot)COOH} \longrightarrow \mathrm{R\dot{C}(OH)COOH} \quad (6)$$

Scheme 2.

lysis with bromine water (where bromine atoms are formed as active species)[16] gave α-keto acids as the main carbonyl products, in consistent with our assumption.

The selective suppression toward the formation of α-keto acid by free radical scavengers (Tables 2—4) may be interpreted as follows. Because of its bareness the intermediate $\mathrm{R\dot{C}(OH)COOH}$ would be sensitive to the radical scavengers and be effectively scavenged, whereas the intermediate precursor for aldehyde is assumed to be less sensitive to the additives due to complexation or less bareness (Eq. 3). Studies on the flash photolysis of Cu(II)–malonate complex have demonstrated that the oxidized ligand remains bound to the reduced metal center until it undergoes further redox reaction.[2] The suppression of both acetaldehyde and pyruvic acid formation by maleic acid may be ascribable to the dual effects of maleic acid acting as both a masking agent toward complex formation and a radical scavenger.

No satisfactory explanation is available as yet for the effects of the dissolved oxygen. Singlet molecular oxygen is ruled out since its reaction with 2-hydroxybutanoic acid did not give 2-oxobutanoic acid and since sodium azide did not affect the yields of the carbonyl products in the Cu(II)-photooxidation of lactic acid. Nor is the role of the hydroperoxyl radical relevant since pyruvic acid was not produced by reaction of lactic acid with Fenton's reagent. Reoxidation of the Cu(I) species by the dissolved oxygen to Cu(II) species is considered to be relevant to the oxygen effects, at least partly. In aerated solution at pH near 0 no practical (final) reduction is observed, while in a higher pH region the ratio $(A+P)/\Delta Cu(II)$ is close to the value expected from Scheme 1. This in turn implies that cyclic (or catalytic) photooxidation by Cu(II) species can only be effective in a highly acidic ($pH \leqq 0$) solution in the presence of the dissolved oxygen.

As to the primary interactions of Cu(II)* with HA to give $\mathrm{R\dot{C}(OH)COOH}$, following processes may be considered; 1) direct H-atom abstraction, 2) oxidation of water by LMCT interaction to give $\dot{O}H$ radical, followed by H-atom abstraction by $\dot{O}H$ from HA, 3) electron transfer from HA to Cu(II)* giving radical cation, followed by deprotonation and radical rearrangement to the more stable radical (Scheme 2).

The $\dot{O}H$ radical mechanism (Eq. 5) might be supported by the selective suppression by *t*-butyl alcohol toward pyruvic acid formation. In fact, photoredox reaction of the labile Cu(II) complex of 2,9-dimethyl-1,10-phenanthroline has been shown to involve the $\dot{O}H$ radical process.[3] However, the failure to observe pyruvic acid formation by reaction of lactic acid with Fenton's reagent excludes this possibility. The direct H-atom abstraction (Eq. 4) is a likely process, and many thermal and photochemical oxidations of organic substrates by transition metal ions seem to involve this process. However, it seems more likely that electron transfer (Eq. 6) occurs as the primary act than the direct H-atom abstraction, because of the LMCT character of Cu(II)* and larger affinity of Cu(II) for the hydroxyl group than for the α-hydrogen atom of HA.

The primary bimolecular interactions between Cu(II)* and HA would only be effective in a short range. This is because Cu(II)* is assumed to be too short-lived to permit a long range bimolecular reaction, whereas the long lifetime of the excited state uranyl ion, 10^{-5}—10^{-4} s,[17] may permit it.

It may be notable that the pH-dependences of the carbonyl products in the Cu(II)-photooxidation appear to be contrast to those in thermal permanganate oxidation: permanganate oxidation of 2-hydroxy acids gives α-keto acids in basic solution but undergoes oxidative decarboxylation to give aldehydes in acidic solution.[18] Permanganate oxidation of 2-hydroxy acids may be assumed to occur by a similar process to that proposed for the permanganate oxidation of alcohols, *i.e.*, α-hydrogen abstraction as hydrogen atom or hydride ion.[19] The decarboxylation in the acid permanganate oxidation may be ascribable to the vigorousness of the oxidation conditions, whereas in the case of the Cu(II)-photooxidation the decarboxylation is relevant to the unimolecular LMCT interactions of the CuA complex.

References

1) H. R. Cooper and B. M. Talbot, *Trans. Faraday Soc.*, **61**, 506 (1965); V. Balzani and V. Carassiti, "Photochemistry of Coordination Compounds," Academic Press, London (1970), p. 270; P. Natarajan, K. Chandrasekaran, and M. Santappa, *J. Polym. Sci., Polym. Lett.*, **14**, 455 (1976).

2) J. Y. Morimoto and B. A. Degraff, *J. Phys. Chem.*, **76**, 1387 (1972); **79**, 326 (1975).

3) S. Sandararajan and E. L. Wehry, *J. Chem. Soc., Chem. Commun.*, **1970**, 267; *J. Inorg. Nucl. Chem.*, **34**, 3699 (1972); *J. Phys. Chem.*, **76**, 1528 (1972).

4) P. Thomas, H. Spindler, and D. Rehorek, *Z. Anorg. Chem.*, **401**, 165 (1973); *Z. Chem.*, **13**, 188, 258 (1973).

5) H. Nozaki, Y. Nishimoto, M. Kawanishi, and R. Noyori, *Tetrahedron*, **23**, 2173 (1967); G. M. Whitesides, G. L. Goe, and A. C. Cope, *J. Am. Chem. Soc.*, **91**, 2608 (1969);

J. A. Deyrup, M. J. Betkouski, *J. Org. Chem.*, **37**, 3561 (1972).

6) R. G. Salomon and J. K. Kochi, *J. Am. Chem. Soc.*, **96**, 1137 (1974); R. G. Salomon, K. Forting, W. E. Streib, and J. K. Kochi, *ibid.*, **96**, 1145 (1974); R. G. Salomon and M. F. Salomon, *ibid.*, **98**, 7454 (1976); D. P. Schwendiman and C. Kutal, *Inorg. Chem.*, **16**, 719 (1977); *J. Am. Chem. Soc.*, **99**, 5677 (1977).

7) M. Asai, H. Matsui, and S. Tazuke, *Bull. Chem. Soc. Jpn.*, **47**, 864 (1974); F. Bellamy, P. Marz, and J. Streith, *Heterocycles*, **3**, 395 (1975); G. H. Jones, D. W. Edwards, and D. Parr, *J. Chem. Soc., Chem. Commun.*, **1976**, 969.

8) T. Sato, *Yuki Gosei Kagaku*, **32**, 989 (1974); T. Sato, K. Tamura, K. Maruyama, O. Ogawa, and T. Imamura, *J. Chem. Soc., Perkin Trans. 1*, **1976**, 779, 783.

9) S. Sakuraba and R. Matsushima, *Bull. Chem. Soc. Jpn.*, **43**, 1950 (1970); **44**, 1278 (1971); D. B. Smith, "Photochemistry," The Chemical Society, Burlington House, London (1973), Vol. 4, pp. 419—421.

10) M. R. Pileni, R. Santus, and E. J. Land, *Photochem. Photobiol.*, **28**, 525 (1978); G. L. Greenstock and G. W. Ruddock, *ibid.*, **28**, 877 (1978); R. H. Bisby, R. B. Cundal, and A. K. Davies, *ibid.*, **28**, 825 (1978).

11) D. F. Sangster, "The Chemistry of the Hydroxyl Group," ed by S. Patai, Interscience Pub., London (1971), pp. 164—167.

12) A. U. Khan and M. Kasha, *J. Chem. Phys.*, **39**, 2105 (1963); R. J. Browne and E. A. Ogryzlo, *Can. J. Chem.*, **43**, 2915 (1965).

13) D. Gratorex, R. J. Hill, T. J. Kemp, and T. J. Stone, *J. Chem. Soc., Faraday Trans. 1*, **68**, 2059 (1972); **70**, 216 (1974); M. Ahmad, A. Cox, T. J. Kemp, and O. Sultana, *J. Chem. Soc., Perkin Trans. 2*, **1975**, 1867.

14) R. J. Hill, T. J. Kemp, D. M. Allen, and A. Cox, *J. Chem. Soc., Chem. Commun.*, **1973**, 59; *J. Chem. Soc., Faraday Trans. 1*, **70**, 847 (1974).

15) F. S. Dainton, G. A. Salmon, and P. Wardman, *Proc. R. Soc. London, Ser. A*, **313**, 1 (1969).

16) I. Ziderman and J. B. Ayche, *Carbohydr. Res.*, **27**, 341 (1973); O. Larm, E. Scholander, and O. Theander, *ibid.*, **49**, 69 (1976); A. Treinin and E. Hayon, *J. Am. Chem. Soc.*, **97**, 1716 (1975).

17) E. Rabinwitch and R. L. Belford, "Spectroscopy and Photochemistry of Uranyl Compounds," Pergamon Press, Oxford (1964), pp. 103—104, 346.

18) R. Stewart, "Oxidation in Organic Chemistry," ed by K. B. Wiberg, Academic Press, New York, N. Y. (1965), pp. 64—65.

19) R. Stewart, *J. Am. Chem. Soc.*, **79**, 3057 (1957); R. Stewart and R. V. Linden, *Discuss. Faraday Soc.*, **1960**, 211; J. L. Kurz, *J. Am. Chem. Soc.*, **86**, 2229 (1964).

Molecular Structures of Complexes of Trimethylamine with Boron Trichloride and Boron Tribromide as Determined by Gas Electron Diffraction

Kinya Iijima and Shuzo Shibata*

Department of Chemistry, Faculty of Science, Shizuoka University, Oya, Shizuoka 422

(Received December 8, 1979)

The molecular structures of trimethylamine-boron trichloride $(CH_3)_3N \cdot BCl_3$ and trimethylamine-boron tribromide $(CH_3)_3N \cdot BBr_3$ were determined from gas electron diffraction and vibrational-spectroscopic data. The molecular parameters and their uncertainties for $(CH_3)_3N \cdot BCl_3$ were r_g(B–Cl) = 1.836±0.002 Å, r_g(N–B) = 1.652±0.009 Å, r_g(C–N) = 1.497±0.003 Å, r_g(C–H) = 1.107±0.005 Å, ∠ClBCl = 110.9±0.2°, ∠CNC = 108.1±0.3°, while those for $(CH_3)_3N \cdot BBr_3$ were r_g(B–Br) = 2.001±0.003 Å, r_g(N–B) = 1.663±0.013 Å, r_g(C–N) = 1.500±0.005 Å, r_g(C–H) = 1.095±0.007 Å, ∠BrBBr = 110.3±0.3°, ∠CNC = 107.8±0.5°. The potential barriers around the N–B bonds in $(CH_3)_3N \cdot BCl_3$ and $(CH_3)_3N \cdot BBr_3$ were also estimated to be higher than 18 kcal mol^{-1} and about 12 kcal mol^{-1} respectively.

The molecular structures of several N–B and P–B donor-acceptor complexes have been determined recently in the gas phase[1–4] and in the solid phase;[5–8] it was found that the N–B bond length in trimethylamine-boron trifluoride is appreciably longer in the gas phase[3] than that in the solid phases,[5] while the P–B bond length in trimethylphosphine-boron trichloride is similar in the two phases.[4,8] It was also noted that, on the formation of the complex, the structural changes in trimethylamine are quite different from those in trimethylphosphine; that is, in both complexes the CNC angle decreases and the CN distance increases,[3] but the CPC angle increases and the CP distance decreases[4] in comparison with the molecular parameters of free molecules. In order to understand the complicated properties of these molecular complexes, it is necessary to determine the molecular structures of trimethylamine and trimethylphosphine complexes with various boron compounds, BX_3. The present study will report the molecular structures of trimethylamine-boron trichloride $(CH_3)_3N \cdot BCl_3$ and trimethylamine-boron tribromide $(CH_3)_3N \cdot BBr_3$, as determined by means of gas electron diffraction.

The molecular structures of gaseous trimethylamine-boron trifluoride $(CH_3)_3N \cdot BF_3$ and trimethylamine-boron trichloride $(CH_3)_3N \cdot BCl_3$ have been reported by several workers.[1–3] The molecular parameters of $(CH_3)_3N \cdot BF_3$ previously obtained by the present authors[3] were consistent with the microwave spectroscopic data,[1] but these parameters were systematically different from those obtained by Hargittai and Hargittai.[2] Thus, we tried to determine the molecular structure of $(CH_3)_3N \cdot BCl_3$ as well as that of $(CH_3)_3N \cdot BBr_3$ in order to compare its molecular parameters with those reported by them. The rotational barriers about the N–B bonds in $(CH_3)_3N \cdot BCl_3$ and $(CH_3)_3N \cdot BBr_3$ were also estimated from the electron-diffraction and vibrational-spectroscopic data in the present study.

Experimental

The trimethylamine was prepared by the method described in Ref. 9; it was allowed to react in dry benzene with boron trichloride and boron tribromide, which were commercially available from Wako Pure Chemical Industries, Ltd. The complexes were recrystallized from ethanol and then sublimed under a vacuum. Their infrared spectra revealed no impurities.[10]

The electron-diffraction photographs were recorded on Kodak Electron-Image plates using an r^3-sector. The accelerating voltage was 40 kV. Samples of $(CH_3)_3N \cdot BCl_3$ and $(CH_3)_3N \cdot BBr_3$ were vaporized at 192 °C and 212 °C respectively. The beam current was about 0.8 μA; the exposure time at a long camera distance of 294 mm was 20 s, and that at a short camera distance of 144 mm was 40 s. The pressure in the diffraction chamber was below 1×10^{-5} Torr during the experiment. The electron wavelength was measured from the diffraction patterns of thallium chloride.[11] The optical densities of the plates were measured at 0.4 mm intervals by means of a digital microphotometer. The electron-diffraction unit and the digital microphotometer have been described elsewhere.[12]

Analysis and Results

Molecular Intensity and Radial Distribution. The scattering intensities for both complexes were obtained in the ranges of s = 2.5—14.8 and 7.5—34.2 Å^{-1} from the photographic plates taken at the long and short camera distances respectively. They were leveled by theoretical backgrounds, and then the leveled intensities of several plates for each camera distance were averaged. The elastic and inelastic scattering factors were taken from the tables prepared by Schäfer *et al.*[13] and by Cromer and Mann[14] respectively. The inelastic scattering factor for the hydrogen atom was taken from the table prepared by Tavard *et al.*[15]

The experimental background curves were drawn smoothly; the experimental molecular intensities shown in Figs. 2 and 3 were thus obtained.[16] The radial distribution curves for $(CH_3)_3N \cdot BCl_3$ and $(CH_3)_3N \cdot$

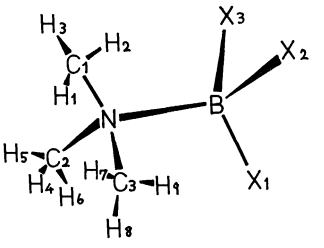

Fig. 1. Numbering of atoms in trimethylamine-boron trihalide (symmetry C_{3v}).

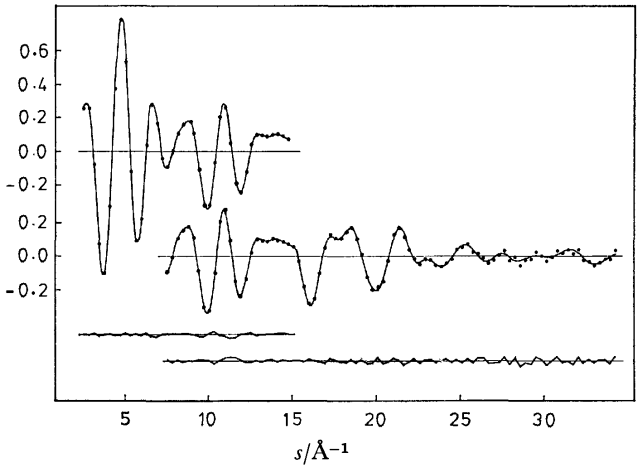

Fig. 2. Molecular intensities for trimethylamine-boron trichloride. The two upper curves are long and short camera-distance data, respectively. Dots represent observed ones, solid curves calculated ones, and the two lower curves the residuals.

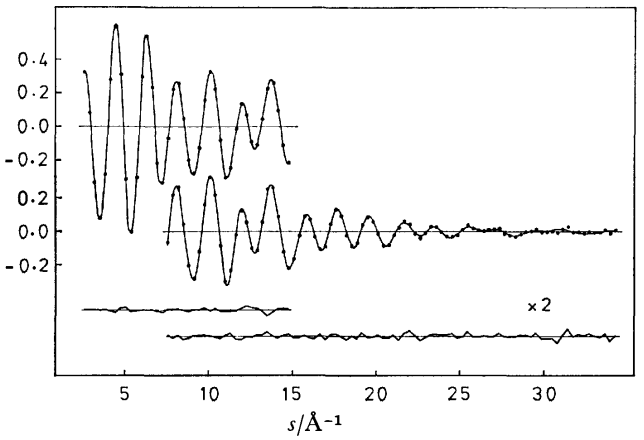

Fig. 3. Molecular intensities for trimethylamine-boron tribromide. The two upper curves are long and short camera-distance data, respectively. Dots represent observed ones, solid curves calculated ones, and the two lower curves two times the residuals.

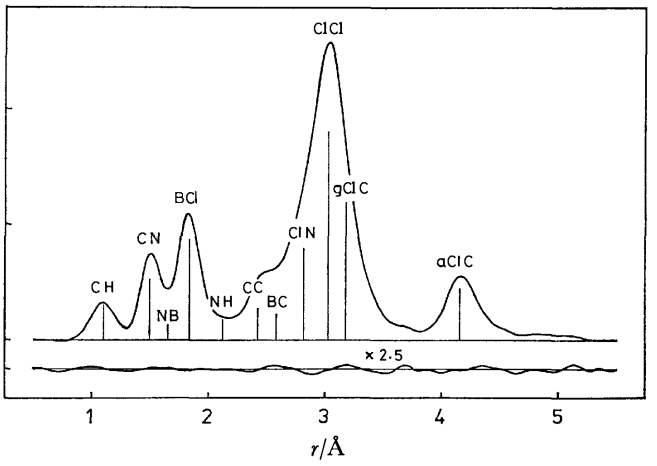

Fig. 4. Radial distribution curve for trimethylamine-boron trichloride.
Solid curve, experimental; lower curve, 2.5 times the residuals.

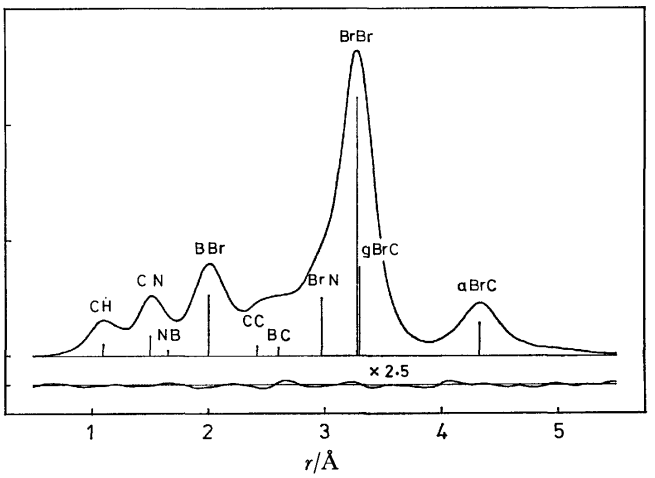

Fig. 5. Radial distribution curve for trimethylamine-boron tribromide.
Solid curve, experimental; lower curve, 2.5 times the residuals.

BBr_3, shown in Figs. 4 and 5 respectively, were calculated by using the molecular intensities in s=2.5—14.8 Å^{-1} from the long camera-distance data and those in s=15.1—34.2 Å^{-1} from the short camera-distance data.

Root-Mean-Square Amplitude of Vibration and Shrinkage Effect. The vibrational spectra for $(CH_3)_3N \cdot BCl_3$ and $(CH_3)_3N \cdot BBr_3$ were observed by Laswick and Taylor in the solid phase.[10] In the present study, the Urey-Bradley force field was adopted, and the vibrational wave numbers were calculated by using the values listed in Table 1. The σ's ($\sigma = [\sum(\tilde{\nu}_{obsd} - \tilde{\nu}_{calcd})^2 / \sum \nu_{obsd}^2]^{1/2}$) were 0.017 and 0.021 for $(CH_3)_3N \cdot BCl_3$ and $(CH_3)_3N \cdot BBr_3$ respectively. The root-mean-square amplitudes of the vibration and shrinkage effects,[17] $r_a - r_\alpha$, based on this force field were also calculated; they are listed in Table 2.

Torsional Vibration and Height of the Potential Barrier. The torsional vibration around the N–B bond cannot be observed directly in the vibrational spectra of these complexes. However, the potential barrier around the N–B bond, V_0, can be estimated from a comparison of the observed mean amplitude for the *gauche* halogen-carbon atomic pair, l(*gauche* X···C), with that calculated from the force field,[3] since this vibration contributes greatly to the l(*gauche* X···C) value.[18]

The l(*gauche* Br···C) value of $(CH_3)_3N \cdot BBr_3$ was found to be 0.164±0.018 Å from the least-squares analysis of the electron-diffraction data. This value corresponds to the V_0 value of 12 kcal mol^{-1}. The lower and upper limits of the V_0 values were estimated to be about 6 kcal mol^{-1} and about 40 kcal mol^{-1} respectively from the error in the observed mean amplitude. The V_0 value in $(CH_3)_3N \cdot BCl_3$ was also estimated to be higher than 18 kcal mol^{-1} from the observed l(*gauche* Cl···C) value of 0.140±0.008 Å.

The force constant of the torsional vibration around the C–N bonds was 0.14×10^{-18} N m in both of the

present complexes. This value corresponds to the V_0 value of 4.4 kcal mol^{-1}, in good agreement with that in the trimethylamine molecule, 4.41 kcal mol^{-1}.[19]

Analysis of the Electron-diffraction Intensities. The molecular parameters of $(CH_3)_3N\cdot BCl_3$ and $(CH_3)_3N\cdot BBr_3$ were determined from the least-squares analysis of the molecular intensities. It was assumed that these molecules have a staggered form with C_{3v} symmetry in the gas phase and that the methyl groups also have C_{3v} symmetry in a staggered form with respect to the C–N bonds. The shrinkage effects for the bonds in the complexes were fixed to the values listed in Table 2. The asymmetry parameters, κ, for the C–H, C–N, N–B, and B–Cl bonds in $(CH_3)_3N\cdot BCl_3$ were estimated to be 12, 2.5, 6.6, and 8.3×10^{-6} Å^3 respectively by means of a diatomic approximation.[20] The κ parameters for the C–H, C–N, N–B, and B–Br bonds in $(CH_3)_3N\cdot BBr_3$ were estimated to be 12, 2.6, 7.1, and 12×10^{-6} Å^3 respectively, while those for the other bonds were assumed to be zero in both the present complexes.

The geometrical parameters, r_α, refined by the least-squares analysis were as follows: r(B–X), r(X···X), r(N–B), r(C–N), r(C···C), r(C–H), and ∠NCH. The r_g parameters were calculated from the r_α parameters obtained in the least-squares calculations;[17] they are

Table 1. Urey-Bradley force field for $(CH_3)_3N\cdot BCl_3$ and $(CH_3)_3N\cdot BBr_3$

	$(CH_3)_3N\cdot BCl_3$	$(CH_3)_3N\cdot BBr_3$		$(CH_3)_3N\cdot BCl_3$	$(CH_3)_3N\cdot BBr_3$
K(NB)	1.1	1.2	F(XX)	0.65	0.75
K(BX)	1.1	0.9	F(XN)	0.7	0.7
K(CN)	2.1	2.1	F(CC)	0.3	0.3
K(CH)	4.4	4.4	F(CB)	0.15	0.15
H(XBX)	0.1	0.1	F(HH)	0.1	0.1
H(XBN)	0.35	0.2	F(NH)	0.6	0.6
H(CNC)	0.45	0.45	Y(NB)	—	0.35
H(CNB)	0.3	0.3	Y(CN)	0.14	0.14
H(HCH)	0.4	0.4	p	−0.05	−0.05
H(NCH)	0.3	0.3			

The torsional force constants, Y, and the internal tension of the methyl carbon, p, are in 10^{-18} N m, while the others are in 10^2 N m^{-1}.

Table 2. Mean amplitudes and shrinkage effects for $(CH_3)_3N\cdot BCl_3$ and $(CH_3)_3N\cdot BBr_3$ (in 10^{-4} Å)

	$(CH_3)_3N\cdot BCl_3$		$(CH_3)_3N\cdot BBr_3$	
	l	r_a-r_α	l	r_a-r_α
B–X_1	667	14	699	11
B–N	655	−5	654	4
B···C_1	937	0	932	75
B···H_1	1139	118	1139	186
B···H_2	1827	25	1811	173
X_1···X_2	846	0	812	0
X_1···N	765	0	798	−1
X_1···C_1	892	−2	902	27
X_1···C_2	1312	−31	1643	−13
X_1···H_1	1231	66	1275	95
X_1···H_2	1656	31	1709	93
X_1···H_4	1738	35	1935	64
X_1···H_5	2414	−76	2863	−59
X_1···H_6	2379	−77	2665	9
N–C_1	548	37	551	144
N···H_1	1033	200	1035	283
C_1···C_2	811	31	824	225
C_1–H_1	784	332	784	351
C_1···H_4	1758	64	1781	236
C_1···H_5	1769	55	1811	267
C_1···H_6	1060	138	1068	417
H_1···H_2	1286	489	1287	569
H_1···H_4	2590	17	2605	192
H_1···H_5	2843	−41	2894	142
H_1···H_6	1875	159	1916	412
H_2···H_5	1848	152	1879	460
H_2···H_6	1349	194	1352	552
H_2···H_9	2639	4	2718	188

The numbering of the atoms is shown in Fig. 1.

Table 3. Molecular parameters obtained from least-squares analysis for $(CH_3)_3N\cdot BCl_3$ and $(CH_3)_3N\cdot BBr_3$

	$(CH_3)_3N\cdot BCl_3$				$(CH_3)_3N\cdot BBr_3$		
	Present study			H and H[a]	Present study		
	r_α	r_g	σ	r_g	r_α	r_g	σ
B–X	1.833	1.836	0.002	1.841 (4)	1.997	2.001	0.003
N–B	1.650	1.652	0.009	1.663 (6)	1.656	1.663	0.013
C–N	1.491	1.497	0.003	1.497 (4)	1.483	1.500	0.005
C–H	1.067	1.107	0.005	1.118 (4)	1.054	1.095	0.007
X···X	3.022	3.025	0.005	3.030 (6)	3.280	3.283	0.003
C···C	2.417	2.423	0.006	2.433 (8)	2.398	2.424	0.010
∠NCH	108.9		1.0	107.0 (7)	109.2		1.7
∠XBX[b]	111.1	110.9	0.2	110.8 (3)	110.4	110.3	0.3
∠CNC[b]	108.3	108.1	0.3	108.7 (5)	107.9	107.8	0.5

Bond distance: Å unit; bond angle: degree unit.

a) Results reported by Hargittai and Hargittai.[2] The r_a parameters given by them are transformed to r_g parameters by the $r_g=r_a+l^2/r_a$ relation. The numbers in parentheses represent the limits of error. b) Calculated from independent parameters.

Table 4. Root-mean-square amplitudes for $(CH_3)_3N \cdot BCl_3$ and $(CH_3)_3N \cdot BBr_3$ (in Å unit)

	$(CH_3)_3N \cdot BCl_3$		$(CH_3)_3N \cdot BBr_3$	
	Obsd	Calcd	Obsd	Calcd
B–X	0.060(4)	0.067	0.065(7)	0.070
N–B	0.070(26)	0.066	0.101(43)	0.065
C–N	0.056(5)	0.055	0.058(6)	0.055
C–H	0.083(6)	0.078	0.075(8)	0.078
X···X	0.092(3)	0.085	0.101(2)	0.081
C···C	0.075(7)	0.081	0.0824 (assumed)	
anti X···C	0.091(6)	0.089	0.092(8)	0.090
gauche X···C	0.140(8)	0.131	0.164(18)	0.164
X···N	0.090(5)	0.077	0.092(8)	0.080

listed in Table 3, together with their limits of error. The errors were estimated from random errors in the least-squares calculations and systematic errors originating from the measurements of the camera distance and the electron wavelength. The mean amplitudes obtained by the least-squares analysis are listed in Table 4. The other mean amplitudes were fixed to the values listed in Table 2 throughout the analysis. The best-fit theoretical intensity curves are shown in Figs. 2 and 3, while the correlation matrices are listed in Tables 5 and 6. The calculations of the mean amplitudes and the shrinkage effects and the least-squares analysis were carried out on a HITAC 8800/8700 computer in the Computer Center of the University of Tokyo.

The observed l(N–B) and l(Br···Br) values in $(CH_3)_3N \cdot BBr_3$ are found to be larger than their calculated values. This disagreement may be due to the fact that the calculation was based on the force field estimated in the solid phase. A large l(N–B) value has also been observed in the analysis of gaseous $(CH_3)_3N \cdot BF_3$;[3] therefore, it may be suggested that the N–B bond is strengthened in the solid phase in comparison with that in the gas phase.

The bond distances of $(CH_3)_3N \cdot BCl_3$ obtained in the present study are shorter by about 0.3% than those obtained by Hargittai and Hargittai.[2] This value is greater than the systematic error in the present study (0.1%), but if random errors are taken into account, the molecular parameters obtained in these independent studies are in essential agreement with each other.

Discussion

The molecular parameters for gaseous trimethylamine-boron trihalide complexes are listed in Table 7 in comparison with those for the complexes in the solid phase and those for the free molecules. When a trimethylamine molecule and a boron trihalide molecule form a complex, the distances of the B–X and C–N bonds increase, while the XBX and CNC angles decrease. The experimental results show that such structural changes are greater in the acceptor molecule than in the donor molecule, and that the magnitude of the changes on the complex formation

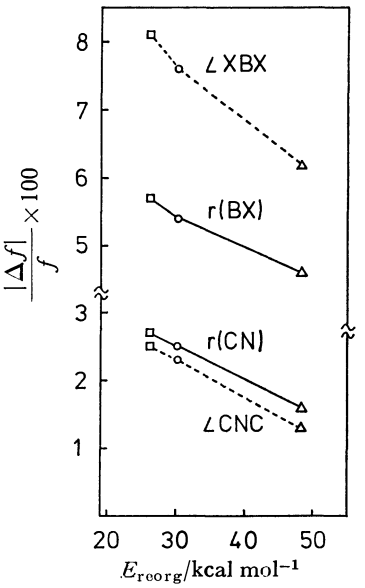

Fig. 6. Parameter changes on complex formation *versus* reorganization energies for acceptor molecules.
Solid curves represent positive Δf and dashed curves negative Δf.
△: $(CH_3)_3N \cdot BF_3$, ○: $(CH_3)_3N \cdot BCl_3$, □: $(CH_3)_3N \cdot BBr_3$. The reorganization energies for BF_3, BCl_3, and BBr_3 are 48.4, 30.3, and 26.2 kcal mol^{-1}, respectively.[25]

is in the order of $(CH_3)_3N \cdot BBr_3 > (CH_3)_3N \cdot BCl_3 > (CH_3)_3N \cdot BF_3$. The fractional difference, $\Delta f/f$, between the parameter in the complex and that in the corresponding free molecule[21–24] is plotted in Fig. 6 against the reorganization energies calculated by Cotton and Leto[25] for boron trihalides. The figure shows a correlation of the structural changes in the donor and acceptor molecules with the reorganization energy of the acceptor molecule. However, no systematic relation can be observed with respect to the N–B bond distance.

In the solid phase,[5–7] the B–X and C–N distances are larger and the XBX angles are smaller than the corresponding values in the gas phase. Furthermore, the N–B dative bonds are much shorter in the solid phase than in the gas phase. These facts indicate that, in the solid phase, the charge transfer occurs to a larger extent, thereby enhancing the dative bonding. This trend is also in accord with our foregoing remarks with regard to its mean amplitude.

The rotational barrier around the N–B bond, V_0, is considerably larger in $(CH_3)_3N \cdot BCl_3$ and $(CH_3)_3N \cdot BBr_3$ than in $(CH_3)_3N \cdot BF_3$, 4.3 ± 0.3 kcal mol^{-1}.[3] As has been described above, the potential barrier for $(CH_3)_3N \cdot BCl_3$ seems to be larger than that for $(CH_3)_3N \cdot BBr_3$, though these barriers could not be determined very accurately in the present study. Thus, the magnitudes of the potential barriers about the N–B bonds are in the order of $(CH_3)_3N \cdot BCl_3 \geq (CH_3)_3N \cdot BBr_3 > (CH_3)_3N \cdot BF_3$, in agreement with that obtained from an NMR study.[26] This order seems to be consistent with the inverse order of the observed N–B bond lengths in the gas phase.

Table 5. Correlation matrix of $(CH_3)_3N \cdot BCl_3$

	r(BCl)	r(NB)	r(CN)	r(CH)	r(ClCl)	r(CC)	∠NCH	l(BCl)	l(CN)	l(aClC)	l(gClC)	l(CC)	l(CH)	l(ClCl)	l(ClN)	l(NB)	R_1[a]	R_2[a]
r(BCl)	1.0																	
r(NB)	−0.13	1.0																
r(CN)	0.03	−0.13	1.0															
r(CH)	−0.07	−0.10	0.01	1.0														
r(ClCl)	0.55	0.59	−0.09	−0.07	1.0													
r(CC)	0.13	0.39	0.59	−0.11	0.26	1.0												
∠NCH	0.54	0.07	0.18	−0.30	0.40	0.30	1.0											
l(BCl)	0.04	−0.20	0.28	0.02	−0.02	−0.04	0.14	1.0										
l(CN)	0.12	−0.36	0.35	−0.11	−0.14	−0.01	0.18	0.68	1.0									
l(aClC)	−0.07	−0.13	−0.03	0.13	−0.07	−0.19	−0.21	0.24	0.17	1.0								
l(gClC)	0.42	0.34	−0.16	−0.01	0.83	0.04	0.26	0.10	−0.02	0.08	1.0							
l(CC)	−0.11	−0.18	−0.20	0.05	−0.28	−0.20	−0.41	0.00	0.02	0.13	−0.18	1.0						
l(CH)	−0.08	−0.04	0.08	0.02	−0.03	−0.06	−0.14	0.21	0.12	0.17	0.08	0.09	1.0					
l(ClCl)	0.24	0.04	−0.11	0.08	0.38	0.05	0.24	0.33	0.21	0.21	0.61	−0.09	0.20	1.0				
l(ClN)	0.30	0.04	−0.04	−0.01	0.35	0.02	0.46	0.18	0.12	0.02	0.54	−0.26	0.04	0.73	1.0			
l(NB)	0.12	−0.22	0.52	−0.15	−0.06	0.25	0.37	0.64	0.74	−0.02	−0.07	−0.16	−0.07	0.04	0.12	1.0		
R_1	0.08	−0.23	−0.05	0.24	0.11	−0.39	−0.17	0.36	0.25	0.35	0.39	0.11	0.24	0.46	0.28	0.02	1.0	
R_2	−0.06	−0.21	0.00	0.14	−0.07	−0.30	−0.20	0.59	0.46	0.43	0.16	0.26	0.43	0.47	0.12	0.07	0.54	1.0

a) R_1 and R_2 are the indices of resolution for the long and short camera distance data respectively. The indices of resolution and their uncertainties are $R_1 = 0.93 \pm 0.02$ and $R_2 = 0.93 \pm 0.04$.

Table 6. Correlation matrix of $(CH_3)_3N \cdot BBr_3$

	r(BBr)	r(NB)	r(CN)	r(CH)	r(BrBr)	r(CC)	∠NCH	l(BBr)	l(CN)	l(CH)	l(BrN)	l(aBrC)	l(gBrC)	l(BrBr)	l(NB)	R_1[a]	R_2[a]
r(BBr)	1.0																
r(NB)	−0.58	1.0															
r(CN)	0.11	−0.35	1.0														
r(CH)	−0.17	0.06	0.00	1.0													
r(BrBr)	0.12	0.52	−0.42	−0.03	1.0												
r(CC)	0.17	0.22	0.59	0.00	0.32	1.0											
∠NCH	0.02	0.34	0.16	−0.14	0.17	0.42	1.0										
l(BBr)	0.10	−0.23	−0.23	0.02	0.11	−0.29	−0.69	1.0									
l(CN)	0.35	−0.36	0.28	−0.16	−0.09	0.13	0.08	0.06	1.0								
l(CH)	0.00	−0.03	−0.04	−0.03	0.07	−0.06	−0.17	0.21	0.02	1.0							
l(BrN)	0.17	0.21	−0.35	0.01	0.67	0.11	0.01	0.26	0.03	0.13	1.0						
l(aBrC)	0.02	−0.06	−0.16	0.09	0.14	−0.15	−0.32	0.38	0.05	0.13	0.23	1.0					
l(gBrC)	0.14	0.13	−0.42	0.03	0.55	−0.11	−0.33	0.58	0.06	0.23	0.73	0.43	1.0				
l(BrBr)	−0.11	−0.42	0.09	0.10	−0.39	−0.33	−0.24	0.23	0.13	0.09	−0.17	0.09	−0.20	1.0			
l(NB)	0.33	−0.30	0.66	−0.16	−0.21	0.48	0.36	−0.25	0.51	−0.17	−0.23	−0.19	−0.36	−0.02	1.0		
R_1	0.08	−0.10	−0.29	0.11	0.30	−0.24	−0.45	0.68	0.14	0.27	0.55	0.48	0.87	0.16	−0.32	1.0	
R_2	0.05	−0.09	−0.29	0.12	0.20	−0.29	−0.34	0.63	0.18	0.27	0.43	0.40	0.71	0.37	−0.29	0.82	1.0

a) R_1 and R_2 are the indices of resolution for the long and short camera distance data respectively. The indices of resolution and their uncertainties are $R_1 = 0.91 \pm 0.03$ and $R_2 = 0.92 \pm 0.03$.

Table 7. Comparison of molecular parameters

	$(CH_3)_3N \cdot BF_3$		$(CH_3)_3N \cdot BCl_3$		$(CH_3)_3N \cdot BBr_3$		BF_3,[c] $(CH_3)_3N$[d]	BCl_3[e]	BBr_3[f]
	Gas	Solid[a]	Gas	Solid[b]	Gas	Solid[b]			
r(N-B)	1.674(4)	1.585	1.652(9)	1.609(6)	1.663(13)	1.60 (2)			
r(B-X)	1.374(2)	1.39	1.836(2)	1.864(4)	2.001(3)	2.04 (2)	1.313(1)	1.742(4)	1.893(5)
r(C-N)	1.485(2)	1.50	1.497(3)	1.52 (1)	1.500(5)	1.52 (1)	1.461(2)		
∠XBX	112.6(3)	107	110.9(2)	109.5(2)	110.3(3)	108.3(7)	120	120	120
∠CNC	109.2(4)	114	108.1(3)	108.6(14)	107.8(5)	107.7(7)	110.6(6)		

Bond distance: Å unit; bond angle: degree unit. The values in the gas phase represent r_g parameters.
a) Ref. 5. Limits of error are not clear. b) Ref. 7. c) Ref. 22. d) Ref. 21. e) Ref. 23. f) Ref. 24.

References

1) P. Cassoux, R. L. Kuczkowski, and A. Serafini, *Inorg. Chem.*, **16**, 3005 (1977).
2) M. Hargittai and I. Hargittai, *J. Mol. Struct.*, **39**, 79 (1977).
3) K. Iijima and S. Shibata, *Bull. Chem. Soc. Jpn.*, **52**, 711 (1979).
4) K. Iijima and S. Shibata, *Bull. Chem. Soc. Jpn.*, **52**, 3204 (1979).
5) S. Geller and J. L. Hoard, *Acta Crystallogr.*, **4**, 399 (1951).
6) H. Hess, *Acta Crystallogr., Sect. B*, **25**, 2338 (1969).
7) P. H. Clippard, J. C. Hanson, and R. C. Taylor, *J. Cryst. Mol. Struct.*, **1**, 363 (1971).
8) D. L. Black and R. C. Taylor, *Acta Crystallogr., Sect. B*, **31**, 116 (1975).
9) R. Adams and B. K. Brown, *Org. Synth.*, Coll. Vol. I, 528 (1941).
10) P. H. Laswick and R. C. Taylor, *J. Mol. Struct.*, **34**, 197 (1976).
11) W. Witt, *Z. Naturforsch., Teil A*, **19**, 1363 (1964).
12) S. Shibata, K. Iijima, R. Tani, and I. Nakamura, *Rep. Fac. Sci. Shizuoka Univ.*, **9**, 33 (1974).
13) L. Schäfer, A. C. Yates, and R. A. Bonham, *J. Chem. Phys.*, **55**, 3055 (1971).
14) D. T. Cromer and J. B. Mann, *J. Chem. Phys.*, **47**, 1892 (1967); D. T. Cromer, *ibid.*, **50**, 4857 (1969).
15) C. Tavard, D. Nicolas, and M. Rouault, *J. Chim. Phys.*, **64**, 540 (1967).
16) The numerical experimental data of the leveled total intensity and background have been deposited with the Chemical Society of Japan (Document No. 8019).
17) K. Kuchitsu and S. J. Cyvin, "Molecular Structures and Vibrations," ed by S. J. Cyvin, Elsevier, Amsterdam (1972), Chap. 12.
18) Y. Morino and E. Hirota, *J. Chem. Phys.*, **28**, 185 (1958).
19) W. G. Fateley and F. A. Miller, *Spectrochim. Acta*, **17**, 857 (1961); **18**, 977 (1962).
20) K. Kuchitsu, *Bull. Chem. Soc. Jpn.*, **40**, 505 (1967).
21) B. Beagley and A. R. Medwid, *J. Mol. Struct.*, **38**, 229 (1977).
22) K. Kuchitsu and S. Konaka, *J. Chem. Phys.*, **45**, 4342 (1966).
23) S. Konaka, Y. Murata, K. Kuchitsu, and Y. Morino, *Bull. Chem. Soc. Jpn.*, **39**, 1134 (1966).
24) S. Konaka, T. Ito, and Y. Morino, *Bull. Chem. Soc. Jpn.*, **39**, 1146 (1966).
25) F. A. Cotton and J. R. Leto, *J. Chem. Phys.*, **30**, 993 (1959).
26) C. T. Yim and D. F. R. Gilson, *Can. J. Chem.*, **48**, 515 (1970).

Effect of the Phase Transition in Liposomes on the Fluorescence of Amphiphilic Cyanine Dyes

Kaoru Onuki, Kazue Kurihara, Yoshinori Toyoshima,† and Mitsunori Sukigara*
Institute of Industrial Science, The University of Tokyo, 7—22—1, Roppongi, Minato-ku, Tokyo 106
(Received December 20, 1979)

The dependence of fluorescence intensity of amphiphilic cyanine dyes on the thermotropic fluid-solid phase transition of lipid bilayer membranes has been investigated. *N,N'*-dioctadecyl oxacarbocyanine iodide or *N,N'*-dioctadecyl thiacarbocyanine bromide was incorporated into single lamellar liposomes, and the fluorescence intensity of each dye was observed to be modified considerably by the phase transition of the lipid bilayers. An amphiphilic cyanine dye with single long alkyl chain, *N*-octadecyl-*N'*-methyl thiacarbocyanine bromide was also incorporated in the lipid bilayers, but in this case, the phase transition showed little effect on the fluorescence intensity. These results were interpreted in terms of the effect of the bilayer membrane fluidity and rigidity on the rotational motion of the incorporated cyanine dyes. The phase transition parameters were obtained by applying those amphiphilic dyes as the fluorescence probe of the phase transition of the liposomes.

The fluidity of the hydrocarbon chain in a lipid bilayer membrane has been known to play an important role in the functions of the biological membrane[1,2]. The fluid-solid phase transitions observed in many kinds of lipid membranes are associated with an abrupt change in the membrane characteristics, such as NMR relaxation time[3,4] and permeability,[5] and many methods have been applied for detecting the phase transition, *e.g.* the calorimetry which directly measures the enthalpy change of transition,[6—8] ESR spin label method by which the solubility or the mobility change of the probes in a membrane is detected,[9,10] and light scattering method.[11] Fluorescence probes were also used widely.[12] Fluorescence probes so far used are mainly lyophobic fluorescent materials such as 1,6-diphenyl-1,3,5-hexatriene (DPH) which are localized in the hydrocarbon chain region of the membrane, and its fluorescence anisotropy reflects the microviscosity of that region.[13] Also, the 5-(dimethylamino)-1-naphthylsulfonyl group or 9-anthracenecarbonyl group which covalently binds to the alkyl chain of lipid was used for detecting the microviscosity of the chains[14,15].

A cyanine dye, composed of two long *N*-alkyl chains and a chromophore, has an amphiphilic molecular structure and can be incorporated into a bilayer membrane as a constituent.[16] We reported previously the effect of the phase transition on the aggregation of the dye in the vesicle.[17] Calzaferry *et al.*[18] reported that twisting around the conjugated hydrocarbon bond plays an important role in the nonradiative relaxation of excitation energy. So it is expected that a change in the fluorescence intensity of a cyanine dye incorporated into a lipid bilayer will reflect the difference of the microviscosity of the bilayer. We examined the temperature dependence of the fluorescence intensity of cyanine dyes, such as *N,N'*-dioctadecyl oxacarbocyanine iodide (DSOCC), *N,N'*-dioctadecyl thiacarbocyanine bromide (DSSCC), and *N*-octadecyl-*N'*-methyl thiacarbocyanine bromide (MSSCC) incorporated into a single bilayer vesicle composed of dimyristoyl phosphatidylcholine (DMPC) or dipalmitoyl phosphatidylcholine (DPPC).

† Permanent address: Faculty of Integrated Arts and Sciences, Hiroshima University, Higashisendamachi, Hiroshima 730.

Experimental

DMPC and DPPC were purchased from Sigma Chem. Co. and the cyanine dyes were purchased from the Japanese Research Institute for Photosensitizing Dyes Co. Ltd. and used without further purification. The purity of the reagents was checked by thin layer chromatography. KCl and tris-(hydroxymethyl)aminomethane (tris) of analytical grade were used.

Phosphatidylcholine colyophilized under vacuum with a dye of a desired composition from a benzene solution was suspended in 10 ml of buffered 0.1 M KCl aqueous solution (0.1 M KCl in 0.01 M tris–HCl at pH 7.5). The electrolyte concentrations in the dispersion were kept constant throughout the experiments. The suspension was ultrasonically irradiated (Otake Seisakusho OT-5202 Sonicator) for 20 min at 20 kHz under an argon atmosphere. The sonication temperature was kept about 5 °C above the phase transition temperature of the lipid. After sonication the sample was centrifuged at 13000 r.p.m. for 10 min to remove undispersed reagents.

The phosphatidylcholine concentration in the vesicle dispersion was checked by the Fiske-Subbarow method.[19] The lipid concentration was 1—3 mg/dm^3 throughout the experiments. Concentration of DSOCC, DSSCC, and MSSCC in the vesicle dispersion were estimated from the absorbances at 492 nm, 560 nm, and 560 nm respectively attributed to the monomer bands, using the molecular extinction coefficients determined in methanol. The dye concentration in the dispersion was below 7×10^{-7} mol/dm^3 throughout the experiments. Thus the molar ratio of lipid to dye was 4600—7000, or the local concentration of the dye was less than 1 molecule/vesicle throughout the experiments.

Absorption measurements were carried out using a spectrophotometer, Beckman 25. Fluorescence measurements were performed on a spectrofluorophotometer, Hitachi MPF-2A under argon atmosphere. The temperature was monitored with a thermocouple dipped in the sample cell. The decrease of excitation light intensity caused by the light scattering by the vesicles had little effect on the fluorescence measurement.

Results and Discussion

The fluorescence spectra of the dyes, DSOCC, DSSCC, and MSSCC, in vesicles were respectively quite similar to those in methanol solutions. The fluorescence intensity of DSOCC and that of DSSCC

in the vesicles were two to six times as large as those of the dyes in methanol at 20 °C while the fluorescence intensity of MSSCC was twice the intensity of the same dye in methanol. These facts are interpreted qualitatively in terms of the difference of effective viscosity of the media affecting the freedom of motion of the dyes. The fluorescence of DSOCC and that of DSSCC in vesicles were enhanced as the temperature was lowered, and there are two points, T_1 and T_2 ($T_1 > T_2$), where the increment of the fluorescence intensity changes. Those temperatures are in good agreement with the upper and the lower limits of the phase transition temperature range of each vesicle, suggesting that the temperature dependence of the fluorescence intensity reflects the phase transition of the vesicles. On the other hand, the same measurement of MSSCC did not show any inflection point in the experimental temperature range. If we know the equation which gives the temperature dependence of fluorescence intensity in each phase, we may estimate the fraction of phase transition at any temperature in the region of phase separation.

The fluorescence quantum yield, Φ, is given in the following form.

$$\Phi = \frac{k_f}{k_f + k_1 + k_2 \exp(-E/kT)} \tag{1}$$

where k_f is the rate constant of the fluorescent process, $[k_1 + k_2 \exp(-E/kT)]$reflects the rate constants of the nonradiative processes, and E is the activation energy of a temperature dependent nonradiative porcess. Eq. 1 is rewritten into the following form.

$$\ln\left[\frac{1}{\Phi} - \left(1 + \frac{k_1}{k_f}\right)\right] = \ln\frac{k_2}{k_f} - \frac{E}{kT} \tag{2}$$

We cannot directly apply this equation to our experimental results, because we cannot determine the quantity k_1/k_f at present. The fluorescence quantum yields of oxacarbocyanine and thiacarbocyanine in methanol were respectively reported to be 0.053 and 0.048 at room temperature,[20] and we assume the following temperature dependence of the fluorescence intensity, I_f,

$$\ln I_f = A + \frac{B}{T} \tag{3}$$

where A and B are constants. The above approximation means that the temperature dependent nonradiative process is the dominant path for dissipation of excitation energy. We tested the applicability of Eq. 3 by plotting the temperature dependence of fluorescence intensity of SOCC in methanol in the range, 10—50 °C, showing a good linear relationship between $\ln I_f$ and $1/T$. The plots according to Eq. 3 for DSOCC and DSSCC are shown in Figs. 1 and 2, respectively. These plots clearly show that each $\ln I_f$ *vs.* $1/T$ curve is divided into three parts, *i.e.*, low temperature part, high temperature part, and middle part. The low temperature part and the high temperature part correspond to the monophase regions, and the Arrhenius relation holds as expected. The temperature dependence of the fluorescence intensity of MSSCC incorporated into the DPPC vesicle is shown in Fig. 3. In this case, the fluorescence intensity of MSSCC does not reflect the phase transition. This result suggests that the temperature dependent nonradiative process is the twisting motion of the

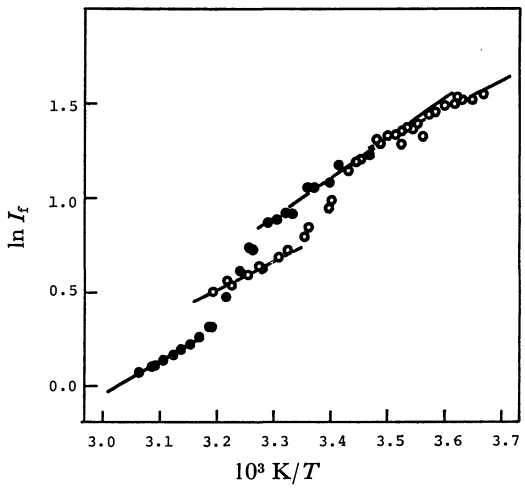

Fig. 1. Logarithm of the fluorescence intensity of DSOCC *vs.* reciprocal of temperature. (○); DMPC vesicles, (●); DPPC vesicles.

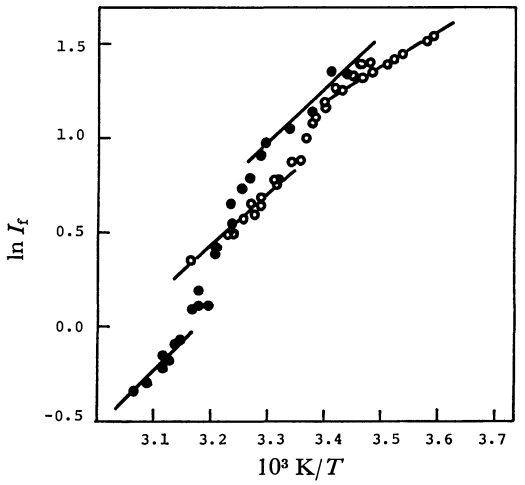

Fig. 2. Logarithm of the fluorescence intensity of DSSCC *vs.* reciprocal of temperature. Notation is the same as in Fig. 1.

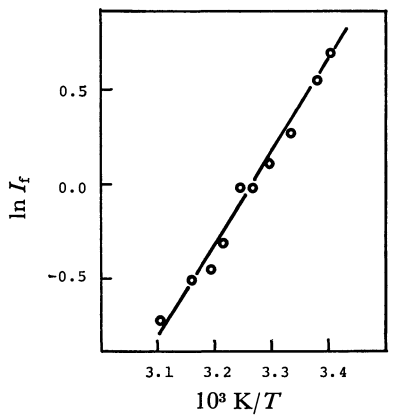

Fig. 3. Logarithm of the fluorescence intensity of MSSCC in DPPC vesicles *vs.* reciprocal of temperature.

chromophore around the bridging bond in the excited singlet state and the suppression of this motion by the membrane lipid moiety will increase the fluorescence intensity of dioctadecyl carbocyanines incorporated into the membrane. Thus, the fluorescence intensity of dioctadecyl cyanines will reflect the phase transition of the lipid bilayers. The observed fluorescence intensity, I_f, in the region of a phase transition may be given in the following form,

$$I_f(T) = I_s(T)\cdot\theta + I_{fl}(T)\cdot(1-\theta) \quad (4)$$

where $I_{fl}(T)$ and $I_s(T)$ are the fluorescence intensity of the dye in the fluid phase region and the solid phase region, respectively, at temperature T, and θ is the fraction of the solid phase region at T. From Eq. 4 we get the following expression for θ.

$$\theta = \frac{I_f(T)-I_{fl}(T)}{I_s(T)-I_{fl}(T)} \quad (5)$$

Temperature dependence of θ is shown in Figs. 4 and 5.

It is possible to calculate the cluster size of cooperative transition from the data in Figs. 4 and 5, if we assume that the solubility of the amphiphilic cyanine dye in the lipid bilayer is not affected by the physical state of the bilayer. The phase transition phenomenon can be regarded as a quasi-first-order reaction with the equilibrium constant, K.

$$K = \frac{\theta}{1-\theta} \quad (6)$$

Combining Eq. 6 with van't Hoff equation, the following equation is obtained.[21]

$$\left(\frac{d\theta}{dT}\right)_{T_m} = \frac{\Delta H_{v.H.}}{4RT_m}, \quad (7)$$

where T_m is the temperature at the center of the transition and $\Delta H_{v.H.}$ is the so-called van't Hoff enthalpy of the transition. Thus, we can calculate the van't Hoff enthalpy from the slope of the curve in Figs. 4 and 5 at $\theta=0.5$. The values of the van't Hoff enthalpy obtained with DSOCC fluorescence were 66.8 kcal/mol and 90.7 kcal/mol for DMPC and DPPC vesicles, respectively. The calorimetrically obtained enthalpy of transition has not been reported for single bilayer vesicles, though the values for multilamellar liposomes have been reported as listed in Table 1. Assuming that those values are also applicable to the phase transition of single bilayer vesicles, the cluster size of the cooperative transition was estimated. The phase transition parameters obtained in the present study are listed in Table 2 together with those obtained by other methods, *e.g.* ESR, fluorescence depolarization, and the differential scanning calorimetry (DSC). The centers of the transition temperatures obtained in the present study are in good agreement with those of the other methods, although values of the cooperativity obtained in this work are smaller than those reported previously. Although the reason for such differences is not clear at the present stage, we may conclude that the fluorescence intensity of the amphiphilic cyanine dyes with two long alkyl chains which are incorporated in bilayer liposomes is significantly modified by the phase transition of the bilayers through the suppression of twisting motion of the chromophores around the bridging chain in the excited singlet state.

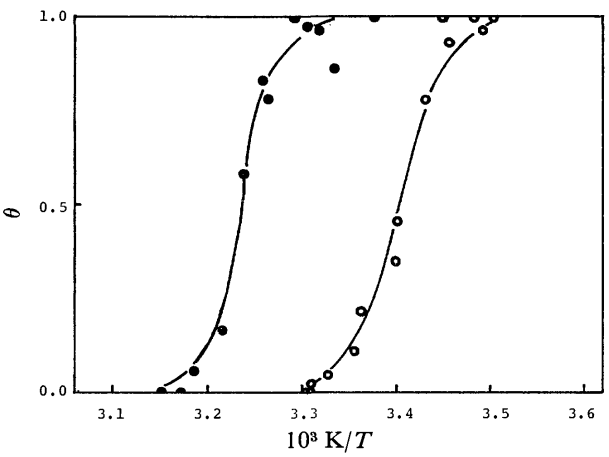

Fig. 4. Mole fraction of solid phase obtained with the DSOCC fluorescence *vs.* reciprocal of temperature. Notation is the same as in Fig. 1.

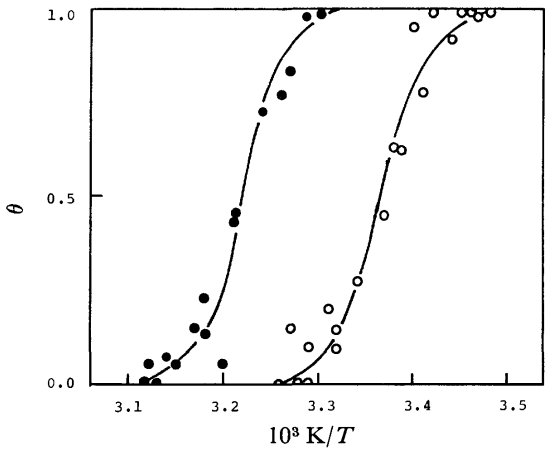

Fig. 5. Mole fraction of solid phase obtained with the DSSCC fluorescence *vs.* reciprocal of temperature. Notation is the same as in Fig. 1.

Table 1. Heat of transition of multilamellar liposomes of DMPC and DPPC

Lipid	Heat of transition ΔH_{cal} (kcal/mol)	
DMPC	6.64[a]	6.26[b]
DPPC	8.66[a]	9.69[b]

a) Phillips *et al.*[6] b) Hintz *et al.*[7]

References

1) D. Marsh, "Essays in Biochemistry," ed by P. N. Champbell and W. N. Aldridge, Academic Press, London (1975), Vol. 11.
2) A. G. Lee, *Prog. Biophys. Mol. Biol.*, **29**, 3 (1975).
3) D. Chapman, R. M. Williams, and B. D. Ladbrooke, *Chem. Phys. Lipids*, **1**, 445 (1967).
4) A. G. Lee, N. J. M. Birdsall, Y. K. Levine, and J. C. Metcaffe, *Biochim. Biophys. Acta*, **255**, 43 (1972).
5) D. Papahadjopoulos, K. Jacobson, S. Nir, and T.

Table 2. Phase transition parameters of DMPC and DPPC

Method	Lipid	Transition temperature		$\frac{\Delta H_{v.H.}}{\Delta H_{cal}}$	Reference
		T_m (°C)	Range[a] (°C)		
DSOCC fluorescence	DMPC	20.3	16.0—30.0	12	This work
	DPPC	36.0	27.3—42.2	12	
DSSCC fluorescence	DMPC	23.5	16.1—30.9	11	This work
	DPPC	37.6	30.0—45.4	11	
DPH[b] fluorescence depolarization	DMPC	20.9±0.5	14.3—27.4		Lenz *et al.*[13]
	DPPC	36.4±0.5	29.4—40.6		
ESR (Tempo 1)[c]	DMPC	22.4		21	Marsh *et al.*[10]
	DPPC	36.4		23	
ESR (Tempo 2)[d]	DMPC	19.7		14	Marsh *et al.*[10]
	DPPC	36.0		35	
Differential scanning calorimetry	DPPC	36.9±0.1			Suurkuusk *et al.*[8]

a) Temperature range of the transition. b) 1,6-Diphenyl-1,3,5-hexatriene.

c) 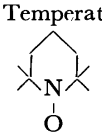

d) 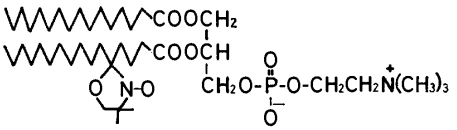

Isac, *Biochim. Biophys. Acta*, **311**, 330 (1973).
6) M. C. Phillips, R. M. Williams, and D. Chapman, *Chem. Phys. Lipids*, **3**, 234 (1969).
7) H. J. Hinz and J. M. Sturtevant, *J. Biol. Chem.*, **247**, 6071 (1972).
8) J. Suurkuusk, B. R. Lentz, Y. Barenholz, R. L. Biltonen, and T. E. Thompson, *Biochemistry*, **15**, 1393 (1976).
9) E. Sackmann and H. Träuble, *J. Am. Chem. Soc.*, **94**, 4482 (1972).
10) D. Marsh, A. Watts, and P. F. Knowless, *Biochim. Biophys. Acta*, **465**, 500 (1977).
11) N. Ostrowsky and Ch. Hesse-Bezot, *Chem. Phys. Lett.*, **52** 141 (1977).
12) W. W. Mantulin and H. J. Pownall, *Photochem. Photobiol.*, **26**, 69 (1977).
13) B. R. Lentz, Y. Barenholz, and T. E. Thompson, *Biochemistry*, **15**, 4521 (1976).
14) D. A. Cadenhead, B. M. J. Kellner, K. Jacobson, and D. Papahadjopoulos, *Biochemistry*, **16**, 5386 (1977).
15) J. F. Faucon and C. Lussan, *Biochim. Biophys. Acta*, **307** 459 (1973).
16) J. Yguerabide and L. Stryer, *Proc. Natl. Acad. Sci. U.S.A.*, **68**, 1217 (1971).
17) K. Kurihara, Y. Toyoshima, and M. Sukigara, *J. Phys. Chem.*, **81**, 1833 (1977).
18) G. Calzaferri, H. Geiger, and S. Lentwyler, *Helv. Chim. Acta*, **59**, 1969 (1976).
19) C. H. Fiske and Y. Subbarow, *J. Biol. Chem.*, **66**, 375 (1925).
20) N. T. L. Roth and A. C. Craig, *J. Phys. Chem.*, **78**, 1154 (1974).
21) H. Trauble, *Naturwissenschaften*, **58**, 277 (1971).

Interaction of Water with the Surface of Calcite

Tetsuo MORIMOTO,* Jiro KISHI,† Osamu OKADA, and Toshie KADOTA

Department of Chemistry, Faculty of Science, Okayama University, Tsushima, Okayama 700

† *Research Center for Industry in Okayama Prefecture, Ifuku-cho, Okayama 700*

(Received December 26, 1979)

The interaction of water with the surface of ground calcite was investigated by measuring the water adsorption isotherm and the amount of thermally desorbed molecules *in vacuo*. The results showed that the surface of ground calcite has chemisorbed water at room temperature which can be completely desorbed by evacuation up to 600 °C, and on which water can be physisorbed in a H_2O:OH ratio between 1:2 and 1:1, depending on the conditions of the pretreatment. The isosteric heat of the physisorption of water on the hydroxyls showed that the activity of the adsorption sites for water is reduced by treating the sample at higher temperatures or by washing with water. Moreover, it was found that the surface of the calcite sample starts to release CO_2 molecules by heat treatment at relatively low temperatures below 300 °C *in vacuo*, and that the amount of CO_2 increases exponentially with an increase in the temperature.

It has previously been shown that metal oxide, when preserved in the atmosphere, chemisorbs water to form surface hydroxyls, on which water is further physisorbed, resulting in the alteration of the surface properties.[1-4] The studies of surface properties, especially those of the interaction with water, of inorganic materials provide important information concerning their technical use. We ourselves have reported that $BaSO_4$ only physisorbs, but does not chemisorb, water.[5] Calcite is one of the most important natural resources used as pulverized filler materials. Gammage and Gregg[6] have reported the effect of grinding Iceland Spar on its adsorbability for water. Recently, Goujon and Mutaftschiev[7] have investigated the dependence of the surface properties of ground calcite upon the calcination temperature by means of pH-measurements, heat of immersion, and mass spectrometry, and have concluded that about 30% of the surface carbonate ions are decomposed by calcination up to 450 °C. Hackerman and Hall[8] measured the water adsorption isotherm on calcite, but did not evaluate the effect of the calcination temperature on the adsorbability of water. The purpose of the present work is to study the interaction of water with the calcite surface in various stages of heat treatment, especially the existence and behavior of surface hydroxyls, by measuring the adsorption isotherms of water and the amounts of thermally desorbed water and CO_2.

Experimental

Natural calcite, from the Niimi district in Okayama Prefecture, was ground by using an impact pulverizer; a portion of the finest grade was then collected. The main impurities involved in the original material were SiO_2 0.06, Fe_2O_3 0.07, Al_2O_3 0.04, MgO 0.016, and P 0.01%. Part of the powdered sample was washed with water until the electric conductivity of the supernatant liquid became constant. X-Ray analysis showed the sample to be of the calcite type and not to contain aragonite. Electron-microscopic observation, using a scanning electron microscope (Hitachi S310), of the washed and unwashed samples did not show any characteristic difference between them and any evidence of sharp cleavage along the rhombohedral faces.

A sample of the 12—15 m^2 surface area was first pretreated at 150, 300, or 500 °C for 4 h in a vacuum of 1×10^{-3} Pa, followed by measurement of the water-adsorption isotherm in a volumetric adsorption apparatus equipped with an oil manometer. After measuring the first adsorption isotherm at 25 °C, the sample was exposed to saturated water vapor for 12 h at 25 °C to ensure surface hydration, evacuated at 1×10^{-3} Pa for 4 h at the same temperature to remove physisorbed water, and subjected to the measurement of the second adsorption isotherm of water at the same temperature as before. For the determination of the isosteric heat of adsorption, the second adsorption isotherms were also measured at 15 and 20 °C. The adsorption equilibrium of water was established within a short time, *i.e.*, within 10—20 min, for the whole measurement. The surface area was obtained by means of the BET N_2-adsorption.

The surface water content was determined by the successive ignition-loss method.[9] As it was found from mass analysis that the gas evolved during the course of this measurement is composed of H_2O and/or CO_2, the mixed gas was analysed by separating it into individual components in the following way. The sample treated at room temperature *in vacuo* was heated at 100 °C for 4 h, and the gas expelled was once trapped in a vessel cooled at −196 °C; its amount was determined volumetrically after evaporation at room temperature. Next, the gas was condensed at the temperature of a solid CO_2–ethanol mixture and outgassed to remove the CO_2 thoroughly; then the remaining condensed gas was determined volumetrically after reevaporation as before. The same procedure was repeated after every treatment of the same sample at increasingly elevated temperatures.

Results and Discussion

Figure 1 shows the surface water content and the amount of CO_2 on $CaCO_3$, which were obtained by the successive ignition-loss method. Assuming a water molecule to come from two hydroxyls through the condensation dehydration at higher temperatures, the water content is expressed by the number of OH groups per nm^2 remaining on the surface after the treatment at the temperature indicated, while the amount of CO_2 is the number of total CO_2 molecules evolved when the sample is heated up to the temperature. As is shown in Fig. 1, the surface water content decreases exponentially with a rise in the temperature of the treatment, and vanishes at 600 °C; the absolute values at relatively lower temperatures are comparable to those of metal oxides, but decrease more rapidly

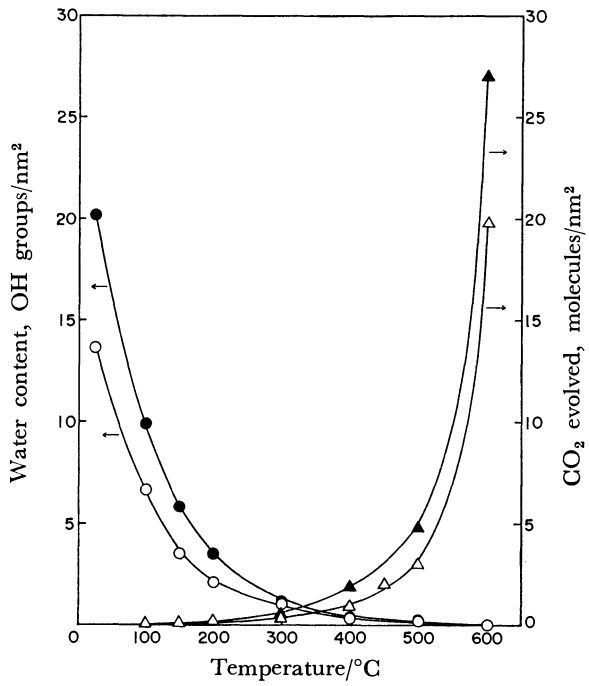

Fig. 1. Surface water content and the amount of evolved CO_2 on calcite as a function of evacuation temperature.
○△, Washed sample; ●▲, unwashed sample.

with a rise in the temperature compared to the cases of metal oxides.[1-4] It should be noticed that the evolution of CO_2 *in vacuo* starts at a very low temperature and increases exponentially with a rise in the temperature up to 600 °C; this result is entirely different from that found by Goujon and Mutaftschiev,[7] *i.e.*, that a constant amount of about 30% of CO_3^{2-} ions on the ground calcite surface was decomposed by outgassing the sample up to 420 °C.

The cleavage of the calcite crystal is known to be perfect on the $(10\bar{1}1)$ plane.[10] Assuming the actual surface of powdered calcite to be composed of this plane, the surface density of each of the Ca^{2+} and CO_3^{2-} ions can be computed to be 4.97 ions/nm². The surface water content of the washed calcite sample, after outgassing at room temperature, was found to be larger than the surface density of the Ca^{2+} ions. However, part of the surface water content survives even after the evacuation at 300 or 400 °C, which leads us to the conclusion that there is a great possibility of the chemisorption of water on the calcite surface.

In the present procedure for measuring water content, a part of the surface CO_3^{2-} ions are dissociated to evolve CO_2 molecules, as is shown in Fig. 1; the amount of CO_2 evolved when the sample is heated at 500 °C *in vacuo* is nearly equal to the number of CO_3^{2-} ions on the crystal surface, as calculated above. Admittedly, the chemisorbed water should have CO_3^{2-} ions beneath it, as is evident from the fact that it is

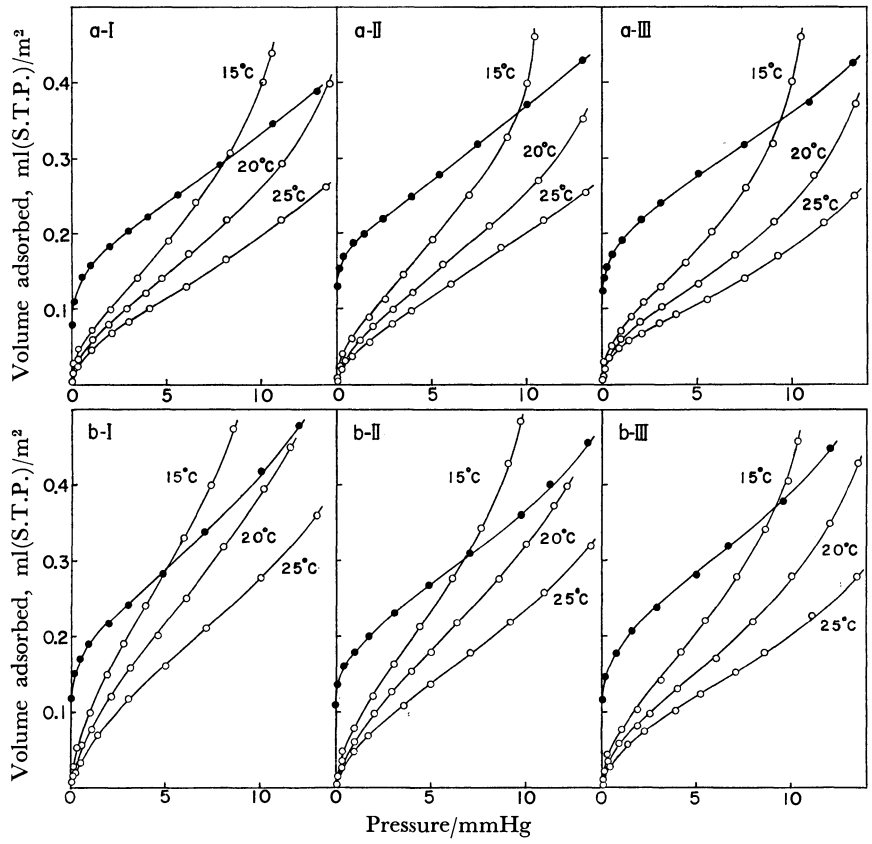

Fig. 2. Adsorption isotherms of water on (a) washed and (b) unwashed calcite treated at various temperatures: I, 150 °C; II, 300 °C; III, 500 °C.
●, First adsorption at 25 °C; ○, second adsorption.

Table 1. Relation between the amounts of physisorbed and chemisorbed water on the $CaCO_3$ surface (25 °C)

Sample	Pretreatment temperature (°C)	Specific surface area (m^2/g)	V_m (ml/m^2)	V_p ($H_2O's/nm^2$)	V_c ($OH's/nm^2$)	V_h ($OH's/nm^2$)	V_c+V_h ($OH's/nm^2$)	$V_p/(V_c+V_h)$
Washed	150	6.91	0.219	3.98	3.82	3.43	7.25	0.549
	300	6.80	0.236	3.93	4.83	1.17	6.00	0.655
	500	5.70	0.238	3.66	5.48	0.19	5.67	0.646
Unwashed	150	7.72	0.257	5.46	2.90	5.95	8.85	0.617
	300	7.67	0.242	4.65	3.72	1.33	5.05	0.921
	500	5.96	0.247	4.12	5.01	0.14	5.15	0.800

depleted at 500 °C, at which temperature the monolayer of CO_3^{2-} is decomposed completely. This circumstance may be one of the reasons why the desorbability of chemisorbed water from calcite is greater than that from metal oxides.

It is interesting to note that the calcite surface which has never experienced washing with water has a larger amount of chemisorbed water than the sample which was washed. This makes it possible to infer that water can be chemisorbed on the active sites like surface defects as soon as they are formed by grinding the sample in air and that they can be removed by washing the sample with water.

Figure 2 illustrates the adsorption isotherms of water on calcite powders pretreated *in vacuo* at 150, 300, and 500 °C. The adsorption isotherms obtained are all Type II isotherms, according to Brunauer's classification. In addition, the amount of adsorbed water for the first adsorption, measured just after the pretreatment at a higher temperature, is larger than that for the second adsorption obtained after evacuating the sample at room temperature after the first adsorption measurement has been completed; the two isotherms are parallel to each other. The water adsorption isotherm measured by Gammage and Gregg on a precipitated calcite sample is similar to the first adsorption isotherm in the present samples.[6] The parallelism between the first and second adsorption isotherms in the present study is quite similar to the cases of water adsorption on metal oxides.[1,2,11] On the basis of previous discussions concerning the parallelism of the first and second isotherms for most metal oxides,[1,2] we can conclude that the chemisorpion of water occurs on the surface of calcite, the difference between the two isotherms being the amount of chemisorbed water.

Table 1 gives the numerical data analysed from both water adsorption isotherms and water contents on calcite samples. The specific surface area of the samples was measured before the first and second water adsorption measurements, and the two values thus obtained were found to be equal to each other within an experimental error of ±1.5%. V_m and V_p are the monolayer capacities obtained by applying the BET equation to the first and second adsorption isotherms respectively, the latter involving only the amount of physisorbed water and being expressed by the number of water molecules per nm^2. V_m contains both physisorbed and chemisorbed water, expressed as the gaseous volume adsorbed on a unit of the surface area. The amount of chemisorbed water V_c, can, therfore, be obtained by subtracting V_p from V_m after changing the unit of V_m to the number of molecules of H_2O per nm^2; the difference (V_m-V_p) is then expressed as the number of OH groups per nm^2 by assuming a water molecule to be chemisorbed dissociatively on calcite to form two hydroxyls, as in the case of metal oxides. Another quantity of chemisorbed water is the water content, V_h, remaining on the surface after pretreatment at indicated temperatures, as obtained from Fig. 1.

It may be seen from Table 1 that the total amount of chemisorbed water falls within the range of 5 to 9 $OH's/nm^2$, regardless of whether the sample was washed with water or not. This indicates that the surface state of calcite is almost the same after the water adsorption measurement. These values are likely if we consider that a considerable portion of the surface CO_3^{2-} ions have been converted to OH^- ions.

From the above considerations, we may conclude that the real surface of calcite contains chemisorbed water molecules, irrespective of whether the sample was washed with water or not. Here, we may reasonably expect that the surface of calcite has been hydrolysed when washed with water,[7] which results in the formation of a hydroxylated surface according to this reaction:

$$CaCO_3 + 2H_2O \rightleftharpoons Ca(OH)_2 + H_2CO_3 \quad (1)$$

If the outermost monolayer of the calcite surface is altered to a hydroxide layer by this reaction during the course of washing, the resulting sample should release a maximum amount of water molecules or 4.97 H_2O/nm^2 upon heating *in vacuo*; reversely, the dehydrated surface can chemisorb the same number of water molecules. The experimental values, *i.e.*, 5—9 $OH's/nm^2$, of the total amount of chemisorbed water, V_c+V_h, are within this limit.

The evolution of CO_2 from the calcite surface takes place (Fig. 1) through the following reaction upon heat treatment *in vacuo*:

$$CaCO_3 \longrightarrow CaO + CO_2 \quad (2)$$

The CaO layer thus formed will chemisorb water molecules during the adsorption process according to this reaction:

$$CaO + H_2O \rightleftharpoons Ca(OH)_2 \quad (3)$$

Here also, surface hydroxyls are produced and will behave similarly to those formed by the hydrolysis of the calcite surface, as has been described above.

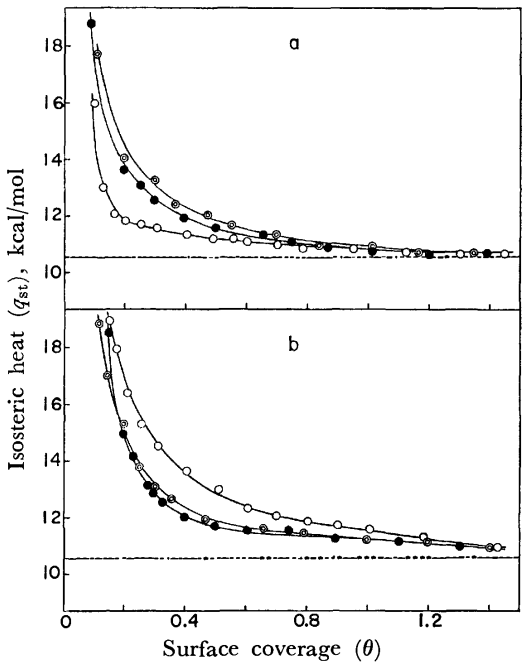

Fig. 3. Isosteric heat of adsorption of water on (a) washed and (b) unwashed calcite.
○, 150 °C; ●, 300 °C; ◎, 500 °C. Broken line represents the heat of liquefaction of water.

Indeed, it is interesting to realize that the total number of chemisorbed water molecules is 5—9 OH's/nm^2, despite the fact that at least two layers of CaO should be formed on the 500 °C-treated samples due to the decarbonation of $CaCO_3$ and the dehydration of $Ca(OH)_2$. In other words, only the outermost layer of the two CaO layers is considered to be partially hydroxylated during the water-adsorption process.

As may be seen from Table 1, the ratio, $V_p/(V_c+V_h)$, of the number of physisorbed water molecules in the first monolayer to that of the underlying hydroxyls is between 1:2 and 1:1. This indicates that a water molecule is physisorbed on one hydroxyl group or on two hydroxyls.

The isosteric heat of the physical adsorption of water, q_{st}, on the fully hydroxylated surface of calcite can be obtained by applying the Clausius-Clapeyron equation to the water-adsorption data in Fig. 2; it is illustrated in Fig. 3. The q_{st} value reveals a decreasing curve with an increase in the coverage of water, θ, and approaches the heat of the liquefaction of water at $\theta=1$, which indicates a characteristic surface heterogeneity in the samples used. Hackerman and Hall reported the q_{st}-curve of water on the 100 °C-treated powdered calcite, which is similar to that obtained on the washed and 150 °C-treated sample in the present study; it is not clear, however, whether their measurement was carried out on a fully hydroxylated surface.[8] With the washed sample in the present study, treatment at 300 or 500 °C gives higher q_{st} values than that at 150 °C, whereas with the unwashed sample the 150 °C-treatment provides the highest value among the three treatments; the q_{st} curves of the 300 °C- and 500 °C-treated samples are similar to each other regardless of whether the sample is washed or unwashed. If the sample is unwashed, the surface will involve a variety of active sites, such as corners, edges, and other kinds of surface defects, and washing will remove some of these stronger adsorption sites; a partial removal of active sites will more or less also take place when the sample is subjected to heat treatment at higher temperatures. Thus, both the washing and the heating of the original sample may produce a similar surface activity. Finally, the washed and 150 °C-treated sample seems to give too small activity for water adsorption. This may be due to the fact that the fully washed surface of calcite could have lost active sites through dissolution and hydrolysis, resulting in the establishment of a less active surface; however, the succeeding treatment at higher temperatures (300 or 500 °C) produces more active surfaces.

The authors are indebted to Dr. Shigeharu Kittaka in Okayama College of Science and Dr. Mahiko Nagao in Okayama University for their helpful discussions.

References

1) T. Morimoto, M. Nagao, and F. Tokuda, *Bull. Chem. Soc. Jpn.*, **41**, 1533 (1968).
2) T. Morimoto, M. Nagao, and F. Tokuda, *J. Phys. Chem.*, **73**, 243 (1969).
3) T. Morimoto, M. Nagao, and J. Imai, *Bull. Chem. Soc. Jpn.*, **44**, 1282 (1971).
4) S. Kittaka, S. Kanemoto, and T. Morimoto, *J. Chem. Soc., Faraday Trans., 1*, **74**, 676 (1978).
5) T. Morimoto, T. Takeshita, and M. Nagao, *Rep. Res. Lab. Surface Sci. Okayama Univ.*, **4**, 45 (1973).
6) R. B. Gammage and S. J. Gregg, *J. Colloid Interface Sci.*, **38**, 118 (1972).
7) G. Goujon and B. Mutaftschiev, *J. Colloid Interface Sci.*, **57**, 148 (1976).
8) N. Hackerman and A. C. Hall, *J. Phys. Chem.*, **62**, 1212 (1958).
9) T. Morimoto and H. Naono, *Bull. Chem. Soc. Jpn.*, **46**, 2000 (1973).
10) S. Dana and W. E. Ford, "A Textbook of Mineralogy," Wiley New York (1960), p. 513.
11) T. Morimoto and M. Nagao, *J. Phys. Chem.*, **78**, 1116 (1974).

Quantitative Study of Metachromasy. The Analysis of the Dye–Polyphosphate Multiequilibrium System by the Principal Component Analysis Method

Mineo TAKATSUKI

Faculty of Science, Hiroshima University, Higashisenda-machi, Hiroshima 730

(Received December 26, 1979)

The absorption spectra of three dyes, 9-aminoacridine (AA), Crystal Violet (CV), and Trypaflavine (TF), were measured in the presence of sodium polyphosphate (NaPP). The optical titrations were performed at phosphate residue-to-dye ratios between 26.6 and 2130 for AA, between 42.6 and 788 for CV, and between 53.9 and 1120 for TF. Using a model in which the condensation of dyes to a polyelectrolyte and the bound monomer⇌bound aggregate equilibrium in the vicinity of the polymer are assumed, the extended principal component analysis was applied to the observed spectra of each dye–NaPP system. The equilibrium constants and the pure spectra of bound dye species were determined. Both the bound monomer and the bound dimer were present in the AA–NaPP system, while the bound monomer, bound dimer, and bound tetramer were present in both CV– and TF–NaPP systems. In all the cases, the absorption spectrum of the bound monomer showed a slight bathochromic shift. The absorption spectrum of the bound dimer of AA showed a considerable bathochromic shift without any new band, while the spectrum of the bound dimer and bound tetramer of CV and TF showed metachromasy bands in wavelength ranges both shorter and longer than the peak wavelength of free CV and TF.

An aqueous solution of several dyes in the presence of a polyelectrolyte shows a color change, namely metachromasy, which is affected in various ways by the combination of dyes and polymers.[1–22] Many papers have been published on the interaction between metachromatic dyes and biological polymers including DNA,[4,6,14–22] because most metachromatic dyes show mutagenic effects. In order to investigate the interactions between the dyes and polymers, the measurement of the absorption spectra is a useful method. However, the absorption spectra of a dye-polyelectrolyte solution are generally composed of some absorbing species, whose fractions vary with the change in the molar ratio of the polymer residue to the dye (P/D). Therefore, in order to study the nature of metachromasy quantitatively, the number of absorbing species and the 'pure' spectrum of the species in an equilibrium system of dye and polymer have to be determined.

The method of principal component analysis (the PCA method) was extended to determine not only the number of absorbing species in an equilibrium system, but also the equilibrium scheme among the species and their pure absorption spectra.[23] The PCA method was successfully applied to the equilibrium systems of cationic dyes and various polyanions in the low-P/D region between 0 and 1.[4,5] The presence of two dye species, namely a free and a bound dye, in the low-P/D region was ascertained for those systems. Furthermore, it was predicted that two or more bound dye species are present in the high-P/D region.[5]

The main purpose of this work is to determine the number of bound dye species over a wide P/D region and to determine the equilibrium scheme of the dye–polymer system and the absorption spectrum of the bound-dye species by using the PCA method. It is also interesting to study the effect of the structure of the dye on the metachromasy. Therefore, three different dyes 9-aminoacridine (AA, monoaminoacridine dye), Crystal Violet (CV, triphenylmethane dye), and Trypaflavine (TF, diaminoacridine dye), all of which interact with DNA and show metachromasy,[4,20,21] were chosen as sample dyes. Sodium polyphosphate (NaPP), which can be thought of as a model of the DNA backbone, was chosen as the polymer, because the pure spectrum of the dye species bound to NaPP will give information about distinguishing the interaction between the dye and the ionized group of DNA from that between the dye and the base pair of DNA.

The application of the PCA method to the spectra observed over a wide P/D region revealed that only two bound-dye species are present in the AA–NaPP system and that only three are present in the CV– and TF–NaPP systems. Such results do not agree with the cooperative binding model, which has been used for metachromasy, because that model implies that a large number of bound-dye species are present over a wide P/D region.[9,10,24,25] Hence, a new model was proposed for the metachromasy. In the present model, it was assumed that the dyes are condensed near the polyelectrolyte and aggregate in its vicinity. Then, the equilibrium constants among the bound-dye species and their pure spectra were determined by the extended PCA method.

Experimental

Materials. The preparation of AA was reported elsewhere.[26] The dyes of CV and TF are the same samples as were reported previously.[4] The NaPP samples (with number-average degrees of polymerization, $\bar{n}$, of 154 and 158) used in this work are the same refractionated preparations as have been described elsewhere.[2] The difference in the degree of polymerization of the two NaPP's did not affect the metachromasy for CV and TF.[2,3]

Procedure. A series of absorption spectra of a dye solution were measured by titrating it with an NaPP solution delivered through a micrometer buret (Gilmont). The volume change in the titrate was made smaller than 10% so as not to shift the binding equilibrium. The concentration of the dye solution was optically determined immediately before the addition of the NaPP solution from the molar absorption coefficient: 1.03×10^4 at 401 nm for AA, 9.20×10^4 at 592 nm for CV, and 4.67×10^4 at 452 nm for TF. The initial concentrations of AA, CV, and TF were 44.3 μM (1 μM = 1×10^{-6} mol dm^{-3}), 8.37 μM, and 9.58 μM re-

spectively. The residue concentrations of the titrant NaPP were 0.847 M ($\bar{n}=158$) for AA and 0.301 M ($\bar{n}=154$) for CV and TF. The absorbances of NaPP in the UV range were subtracted from the observed absorbance of the AA–NaPP system.

Measurements. A Hitachi EPS-3T recording spectrophotometer was used together with matched pair of 1-, 2-, and 5-cm long quartz cells. The temperature of the solution was kept at 25 °C. Other precautions for measurements were described in Ref. 4.

The Extended Principal Component Analysis Method

The PCA method, which is applicable to the family of spectrophotometric data including absorption, CD, and ORD spectra for the determination of the number of components involved in a chemical equilibrium system, was extended to determine the equilibrium scheme, equilibrium constant, and the pure spectrum of components in an equilibrium system.[23,27] A specific application to the multiequilibrium system will be described here, because the description of the general method has been given previously.[4,23,27]

Assume that m observed absorption spectra are measured at n selected wavelengths, λ_j, $j=1\cdots n$. The observed data can be represented as an $m\times n$ matrix, $\boldsymbol{D}$:

$$\boldsymbol{D}=\begin{pmatrix} D_1(\lambda_1)\cdots D_1(\lambda_n) \\ \cdots\cdots\cdots\cdots \\ D_m(\lambda_1)\cdots D_m(\lambda_n) \end{pmatrix}. \tag{1}$$

The number of absorbing species, which are assumed to vary independently, can be determined by the variation in the eigenvalue of the second-moment matrix, $\boldsymbol{A}$, which is constructed by the product of the data matrix, $\boldsymbol{D}$, and its transposed matrix, ${}^t\boldsymbol{D}$: $\boldsymbol{A}={}^t\boldsymbol{D}\boldsymbol{D}$. The eigenvalues and eigenvectors can be calculated by the diagonalization of the $\boldsymbol{A}$ matrix. The magnitude of the eigenvalue represents the contribution of the corresponding eigenvector to the $\boldsymbol{D}$ matrix. In view of the reading error of the observed spectra, if the ratio of a given eigenvalue to the maximum eigenvalue is greater than 10^{-5}, the corresponding eigenvector is thought to be significant. If p eigenvalues satisfy such a condition, one can conclude that the data matrix is composed of p independent principal components. The data matrix can be reconstructed by a linear combination of the p eigenvectors as follows:

$$\boldsymbol{D}=\boldsymbol{f}\boldsymbol{e}=\begin{pmatrix} f_{11}\cdots f_{1p} \\ \cdots\cdots \\ f_{m1}\cdots f_{mp} \end{pmatrix}\begin{pmatrix} e_{11}\cdots e_{1n} \\ \cdots\cdots \\ e_{p1}\cdots e_{pn} \end{pmatrix}, \tag{2}$$

where $\boldsymbol{f}$ is the linear combination coefficient matrix and $\boldsymbol{e}$ is the eigenvector matrix. Furthermore, the molar absorption coefficient matrix, $\boldsymbol{\varepsilon}$, which represents the pure spectrum of the p absorbing species, can also be transformed from the p eigenvectors by means of the transformation matrix, $\boldsymbol{t}$: $\boldsymbol{\varepsilon}=\boldsymbol{t}\,\boldsymbol{e}$.[23] The evaluation of the ε's is reduced to the problem of evaluating the $\boldsymbol{t}$ matrix.

According to Beer's law, a $\boldsymbol{D}$ matrix can also be represented by the product of a concentration matrix, $\boldsymbol{C}$, and an $\boldsymbol{\varepsilon}$ matrix: $\boldsymbol{D}=\boldsymbol{C}\,\boldsymbol{\varepsilon}$. Thus, the $\boldsymbol{C}$ matrix is given by the product of an $\boldsymbol{f}$ matrix and an inverse matrix of $\boldsymbol{t}$: $\boldsymbol{C}=\boldsymbol{f}\,\boldsymbol{t}^{-1}$.[23] The $\boldsymbol{f}$ matrix can be calculated from Eq. 2 by the least-squares method. Thus, the $\boldsymbol{C}$ matrix can also be evaluated if the $\boldsymbol{t}$ matrix is given.

The PCA method was extended to evaluate the most probable $\boldsymbol{t}$ matrix by successive examinations of the probable equilibrium equation for an unknown equilibrium system. A general expression for the equilibrium constant among the p absorbing species is:

$$K=\prod_{i=1}^{p}[X_i]^{\nu_i}, \tag{3}$$

where X_i is the ith absorbing component and ν_i is the stoichiometric coefficient of X_i, whose equilibrium concentration is denoted by the brackets. The substitution of the elements of the $\boldsymbol{C}$ matrix into the right-hand side of Eq. 3 yields m different values for K unless the elements of the $\boldsymbol{t}$ matrix and the assumed equilibrium expression are correct. In order to discriminate the most probable $\boldsymbol{t}$ matrix and the equilibrium expression from the remainder, the coefficient of the variation, S, of K is defined by Eq. 4 and used as a criterion:

$$S=\left(\frac{1}{m}\sum_{j=1}^{m}(K_j-\bar{K})^2\right)^{1/2}\Big/\bar{K}, \tag{4}$$

where $\bar{K}$ denotes the mean value of K_j. The elements of the $\boldsymbol{t}$ matrix and the equilibrium expression which yields the minimum S value can be determined by iterative calculations.

In the multiequilibrium system, the values of S are calculated for individual equilibrium constants, and then the mean value of the S's for the equilibrium constants is used as a criterion. In the iterative calculations, the $\boldsymbol{t}$ matrix sometimes gave as the S values some minima where the calculated concentrations and/or ε of absorbing species were negative. Therefore, the most probable $\boldsymbol{t}$ matrix was selected to yield the positive value for the concentrations and to minimize the value of S. In this work, an acceptable upper limit of 0.10 was preset for the minimized value of S in view of the experimental errors.[23] All the calculations were carried out with a HITAC-8700 computer in FORTRAN language.

Results

Absorption Spectra of AA–, CV–, and TF–NaPP Systems. The absorption spectra of dye–NaPP systems over a wide P/D region were measured in order to obtain significant information on the metachromasy by the use of the extended PCA method. The absorption spectra of AA were measured in both visible and UV wavelength ranges, because the ^1L_a and ^1L_b bands of free AA are located in visible and UV ranges separately.[21,28] As is shown in Fig. 1(a), the ε's of the four bands of AA in the visible range increase and their positions shift toward shorter wavelengths with the increase in P/D. A few UV absorption spectra of AA are shown in Fig. 1(b). The intensities of the two bands in the UV range also increase, and

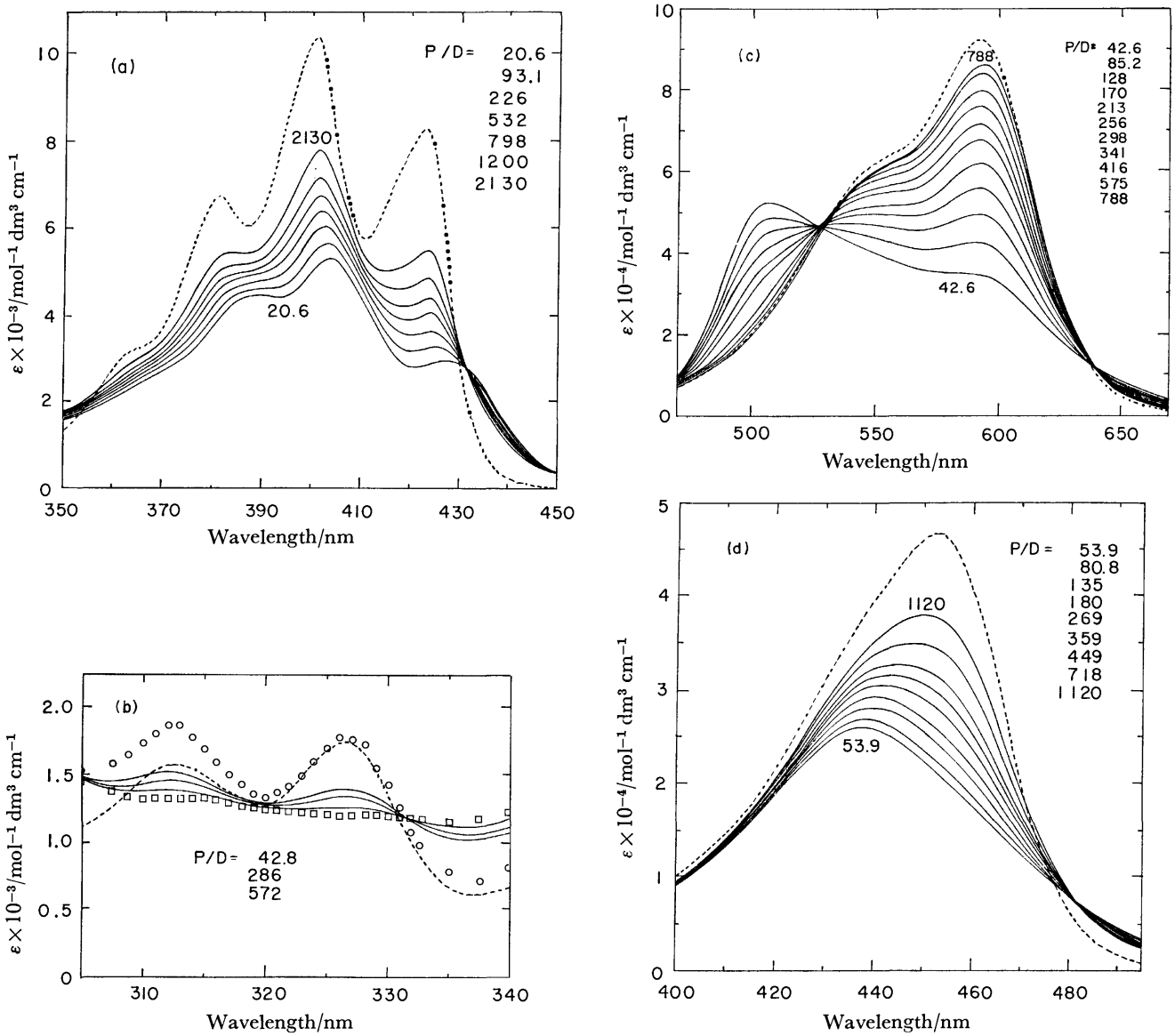

Fig. 1. Visible (a) and UV (b) absorption spectra of AA and visible absorption spectra of CV (c) and TF (d) in the high P/D region.
The concentrations of dyes are: (a) 44.3 μM, (b) 44.3 μM, (c) 8.37 μM, and (d) 9.58 μM. The concentrations of NaPP are listed in each figure in terms of P/D, the order of which corresponds to the order of the increase in the maximum absorbance. Spectrum of free dye is shown by dashed curve in each figure for comparison. Pure spectra of bound monomer (○) and dimer (□) are shown in (b).

TABLE 1. THE POSITIONS OF ISOSBESTIC POINTS

Dye	P/D	Wavelength/nm			
AA	0—1[a]	306	331	352	428
	26.6—2130	—	—	350	431
CV	0—1[b]	460	529	639	
	40—150	452	526	636	
TF	0—1[b]	371	476		
	50—130	374	479		

a) Ref. 29. b) Ref. 4.

their positions shift toward shorter wavelengths with the increase in P/D. Figure 1(c) shows that a remarkable metachromasy band of CV observed at 510 nm gradually disappears and that the ε at the peak position of the free dye spectrum increases with the increase in P/D. In the TF–NaPP system, as is shown in Fig. 1(d), the ε at the absorption peak increases and its position shifts toward longer wavelengths with the increase in P/D.

The positions of the observed isosbestic points and P/D regions, in which the isosbestic points were observed, are listed in Table 1 for each system. In the CV- and TF–NaPP systems, the isosbestic points were observed within a high-P/D region, while those in the AA–NaPP system were observed over a wide P/D region. It is noteworthy that the isosbestic points observed in the high-P/D region differ from those in the low-P/D region in all the cases shown in Table 1. This means that more than two absorbing components are present throughout the P/D region.

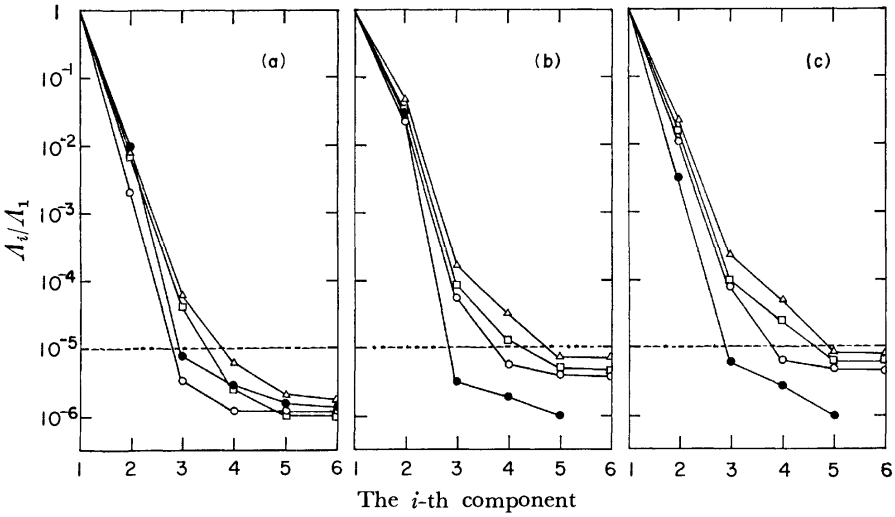

Fig. 2. Variation in eigenvalue Λ_i with the i-th absorbing component for various combinations of observed spectra in the systems of NaPP and AA (a), CV (b), and TF (c). P/D regions of spectra applied the PCA method are; ○: high P/D region ((a) P/D=26.6—2130, (b) 42.6—788, and (c) 53.9—1120), ●: low P/D region ((a) P/D=0—1.02, (b) 0—1.21, and (c) 0—1.25), □: high P/D region and free dye, △: high P/D region and low P/D region. The dashed line indicates the lower limit of the magnitude of eigenvalue for principal component. Selected wavelengths are (a) 48 points from 356 to 450 nm, (b) 50 points from 470 to 666 nm, and (c) 48 points from 400 to 494 nm.

Table 2. The variation in the number of absorbing species with the combination of spectra

Dye	Low P/D	High P/D	Low and high P/D	Free dye and high P/D
AA	2[a)]	2	3	3
CV	2[b)]	3	4	4
TF	2[b)]	3	4	4

a) Ref. 29. b) Ref. 4.

The Number of Absorption Species in AA–, CV–, and TF–NaPP Systems. In order to determine the number of absorbing species in each system, the PCA method was applied to the observed spectra. In each system, four data matrices were analyzed: 1) a set of spectra observed in the high-P/D region, 2) a set of spectra observed in the low-P/D region,[4,29)] 3) a set of spectra observed in both the low- and high-P/D region, and 4) a set of spectra observed in the high-P/D region and the spectrum of a free dye. The variations in the eigenvalues, Λ_i, with the ith component are shown in Figs. 2(a)—(c). The number of absorbing species in each set was determined by the use of the criterion mentioned in the previous section. The results listed in Table 2 show that three absorbing species of AA and four of CV and TF are present in the entire P/D region. In all the systems, the sum of the number of species in the low-P/D region and the number of species in the high-P/D region is greater by one than the number of species in the entire P/D region. That is, there is a common species in the low- and high-P/D regions. Furthermore, the results show that the absorbing species present in the high-P/D region differ from the free dye, because the number of species is increased by the addition of the spectrum of the free dye to the spectra observed in the high-P/D region. Thus, it can be said that two bound-dye species of AA and three of CV and TF are present in the high-P/D region. It can also be said that the amount of free dye in the high-P/D region is negligibly small. Therefore, the presence of the free dye can be neglected in the analysis of the observed data in the high-P/D region.

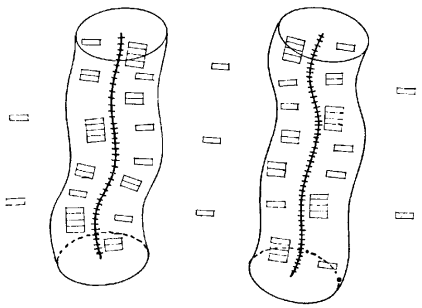

Fig. 3. Schematic model of dye–polyelectrolyte solution.

Equilibrium Scheme among the Bound-dye Species and Their Absorption Spectra. The number of bound-dye species determined in the preceding section is contrary to the number of those expected by the cooperative binding model, which has previously been used for Metachromasy,[9,10,24,25)] as will be discussed later. In this work, a model is used for the distribution of dyes in a polyelectrolyte solution on the basis of the theory for the condensation of the counter ion of a polymer.[30)] As is shown in Fig. 3, dyes in a polyelectrolyte solution are classified into two categories: dyes freely moving outside the region occupied by macroions, and those condensed as bound but mobile ions in the vicinity of the polymer. Assume that the equilibrium of aggregation among the bound

TABLE 3. VALUES OF S FOR EQUILIBRIUM SCHEMES EXAMINED

AA		CV				TF		
n	S	Scheme	S	Concn	Spectrum	S	Concn	Spectrum
2	0.075	I	—	posi.	neg.	—	posi.	neg.
3	0.22	II	0.21	posi.	neg.	0.22	posi.	neg.
4	0.52	III	0.09	posi.	posi.	0.09	posi.	posi.
		IV	—	posi.	posi.	—	posi.	neg.

—: $S>1$.

dyes is established inside the region occupied by macroions. Generally, the equilibrium equation for the aggregation can be expressed as follows:

$$n\mathrm{D}_1^b \rightleftharpoons \mathrm{D}_n^b, \tag{5}$$

where D_1^b is the bound monomer dye and D_n^b is the bound n-mer dye. In the vicinity of the polymer, the concentration of the respective bound-dye species may be proportional to the ratio of the amount of dyes to that of the polymer residues. Therefore, the equilibrium constant in the vicinity of the polymer can be represented as:

$$K = \frac{[\mathrm{D}_n^b]/C_p}{([\mathrm{D}_1^b]/C_p)^n} \tag{6}$$

where C_p denotes the total concentration of the polymer residues. In the application of the extended PCA method to the multiequilibrium system, such an expression for the equilibrium constant of the individual equilibrium is convenient for finding the most probable combination of equilibrium equations.

The presence of two bound-dye species in the high-P/D region of the AA–NaPP system was confirmed. Hence, the equations for the aggregation numbers, n, of 2, 3, and 4 were examined on the assumption that a bound-dye species is the bound monomer dye. The values of S, minimized for each n, are listed in Table 3. The minimized value of S for $n=2$ is smaller than the preset upper limit of S and is the smallest in the three cases of $n=2$, 3, and 4. The minimized values of S for $n=3$ and 4 exceed the preset upper limit; therefore, the aggregation number in the AA–NaPP system is two.

In both CV– and TF–NaPP systems, there are three bound-dye species, one of which may be the bound monomer. The following four equilibrium scheme were considered for those systems. As Scheme I, the simplest growth process of aggregation was adopted. The equilibrium equations and equilibrium constants can be expressed as follows:

$$2\mathrm{D}_1^b \rightleftharpoons \mathrm{D}_2^b, \quad K_1 = \frac{[\mathrm{D}_2^b]/C_p}{([\mathrm{D}_1^b]/C_p)^2}, \tag{7}$$

$$\mathrm{D}_1^b + \mathrm{D}_2^b \rightleftharpoons \mathrm{D}_3^b, \quad K_2 = \frac{[\mathrm{D}_3^b]/C_p}{([\mathrm{D}_1^b]/C_p)([\mathrm{D}_2^b]/C_p)}. \tag{8}$$

In Scheme II, the formation of the bound tetramer from two bound dimers was assumed to be as follows:

$$2\mathrm{D}_1^b \rightleftharpoons \mathrm{D}_2^b, \quad K_1 = \frac{[\mathrm{D}_2^b]/C_p}{([\mathrm{D}_1^b]/C_p)^2}, \tag{9}$$

$$2\mathrm{D}_2^b \rightleftharpoons \mathrm{D}_4^b, \quad K_2 = \frac{[\mathrm{D}_4^b]/C_p}{([\mathrm{D}_2^b]/C_p)^2}. \tag{10}$$

TABLE 4. EQUILIBRIUM CONSTANTS OF AGGREGATION AMONG THE BOND-DYE SPECIES AT 25 °C

Dye	K	K_1	K_2
AA	2.2×10^3		
CV		6.6×10^1	2.8×10^6
TF		2.8×10^2	2.8×10^7

The formation of a bound dimer from two bound monomers and the direct formation of a bound tetramer from four bound monomers were assumed to proceed as in Scheme III:

$$2\mathrm{D}_1^b \rightleftharpoons \mathrm{D}_2^b, \quad K_1 = \frac{[\mathrm{D}_2^b]/C_p}{([\mathrm{D}_1^b]/C_p)^2} \tag{11}$$

$$4\mathrm{D}_1^b \rightleftharpoons \mathrm{D}_4^b, \quad K_2 = \frac{[\mathrm{D}_4^b]/C_p}{([\mathrm{D}_1^b]/C_p)^4} \tag{12}$$

As Scheme IV, the formation of a bound trimer from three bound monomers and the formation of a bound hexamer from two trimers were assumed to proceed as follows:

$$3\mathrm{D}_1^b \rightleftharpoons \mathrm{D}_3^b, \quad K_1 = \frac{[\mathrm{D}_3^b]/C_p}{([\mathrm{D}_1^b]/C_p)^3} \tag{13}$$

$$2\mathrm{D}_3^b \rightleftharpoons \mathrm{D}_6^b, \quad K_2 = \frac{[\mathrm{D}_6^b]/C_p}{([\mathrm{D}_3^b]/C_p)^2} \tag{14}$$

The minimized S value for each scheme is listed in Table 3. In both CV– and TF–NaPP systems, the S value for Scheme III is the smallest among the four schemes and smaller than the preset upper limit of S, and all the corresponding concentrations and ε values are positive. The values of S for the formation of the trimer and the hexamer were extremely large whenever the $\boldsymbol{t}$ matrix gave positive values to the elements of the concentration matrix, $\boldsymbol{C}$.

The fractions of the bound monomer, f_1^b, and the bound dimer, f_2^b, of AA and the fractions of the bound monomer, the bound dimer, and the bound tetramer, f_4^b, of CV and TF obtained from $\boldsymbol{C}$ matrix are plotted as functions of P/D in Figs. 4(a)—(c). The equilibrium constants are listed in Table 4. In Fig. 4, the solid curves show the value of the fractions which were obtained by the Newton method with the values of K for AA or K_1 and K_2 for CV and TF by solving Eq. 6 ($n=2$ for AA) and Eqs. 11 and 12 (for CV and TF) at a given P/D ratio for the concentrations. In the AA–NaPP system, the fraction of the bound monomer increases and that of the bound dimer decreases with the increase in the P/D value. In both the CV– and TF–NaPP systems, the fraction of the bound monomer increases with the increase in P/D and that

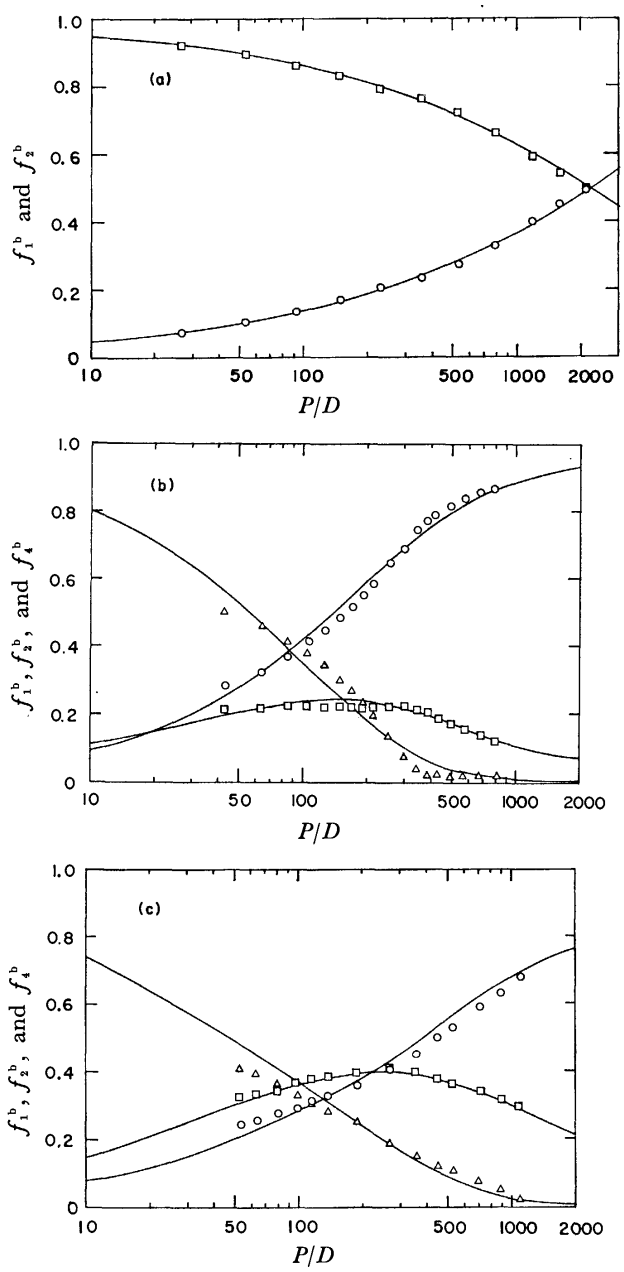

Fig. 4. Variation in the fraction of bound dye species with P/D for (a) AA–, (b) CV–, and (c) TF–NaPP systems.
○: Bound monomer, □: bound dimer, and △: bound tetramer.

of the bound dimer shows a maximum at a P/D value of *ca.* 200. The fraction of the bound tetramer tends to increase with the decrease in P/D.

The pure absorption spectra of bound-dye species of AA, CV, and TF thus obtained are shown in Figs. 5(a)—(c). In all the systems, a slight bathochromic shift is observed in the spectrum of the bound monomer. The absorption spectrum of the bound dimer of AA shows hypochromism and a bathochromic shift, while that of the bound dimer and tetramer of CV and TF has absorption bands at both shorter and longer wavelengths than the position of the main band of the free dye. It is noteworthy that the absorption spectrum of the bound dimer of AA and the bound tetramers of CV and TF excellently fits that of the bound-dye species obtained in the low-P/D region.[4,29]

The UV absorption spectrum of the bound monomer and dimer of AA shown in Fig. 1(b) was calculated from three observed spectra, while the fractions of the bound monomer and dimer were obtained from Fig. 4(a) by the least-squares method using the following equation:

$$\varepsilon_\lambda = f_1^b \varepsilon_\lambda^1 + f_2^b \varepsilon_\lambda^2, \tag{15}$$

where ε_λ^1 and ε_λ^2 denote the molar absorption coefficients of the monomer and the dimer respectively and where ε_λ denotes the apparent molar absorption coefficient of the observed spectrum at the λ wavelength. In the UV range, the absorption spectrum of the bound monomer shows a slight bathochromic shift, while that of the bound dimer shows hypochromism and a bathochromic shift, as is observed in the visible-wavelength range.

Discussion

The Number of Bound-dye Species over a Wide P/D *Region.* In order to interpret the metachromasy, a model in which the dyes are bound cooperatively to polyelectrolyte has been used. According to the model, the spectral changes of the dye-polymer solution are attributed to the change in the distribution of dyes on the polymer. Several quantitative expressions[10,24,25] have been used for the distribution of dyes on the polymer chain, assuming that the aggregated dyes interact with the nearest neighbor bound dye. The cooperative binding model implies that the mean aggregation number depends on the P/D (*cf.* Eq. 22 in Ref. 10 and Eq. 22 in Ref. 25), so that a large number of bound-dye species are expected in the wide P/D region. Hence, in order to examine whether or not the cooperative-binding model expresses the metachromatic phenomena correctly, the number of bound-dye species has to be ascertained over a wide P/D region.

The application of the PCA method to the absorption spectra observed over a wide P/D region clearly revealed that there are only two bound-dye species for AA and only three for CV and TF. These results contradict the results expected from the cooperative-binding model.

Equilibrium Scheme of the Binding of Dye to NaPP. In this study, the bound dyes were assumed to be condensed near the polyelectrolyte. Therefore, the equilibrium scheme of the bound monomer⇌bound aggregate in the vicinity of the polymer molecule was examined by the extended PCA method. As is shown in Fig. 4, the agreement between the experimental and calculated data for the fraction of the respective bound-dye species is reasonably good. This means that the simple equilibrium equation expressed by Eq. 5 can be adopted to represent the metachromatic phenomena observed in the high-P/D region.

In a previous report,[4] the equilibrium constant for the binding of a dye to a polyelectrolyte in the low-P/D region less than unity was expressed as follows:

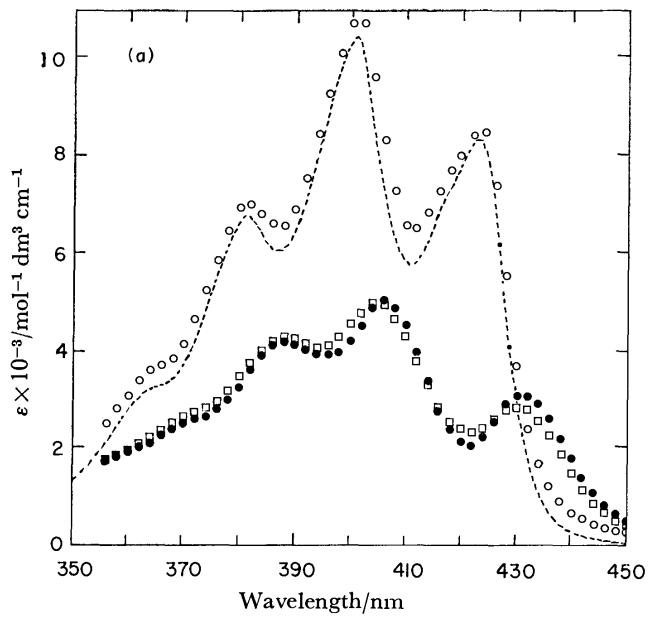

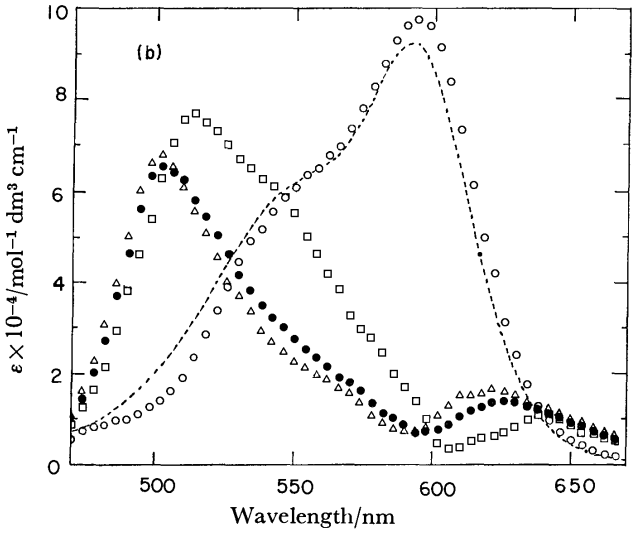

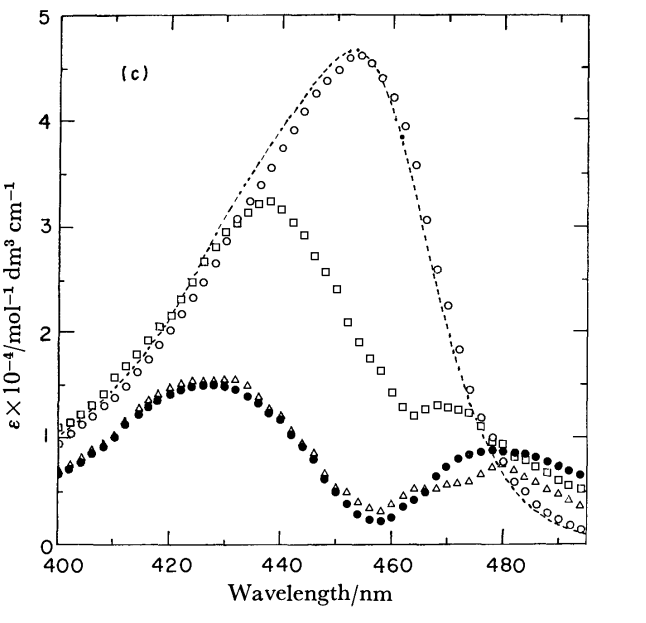

Fig. 5. Pure absorption spectra of bound dyes of AA (a), CV (b), and TF (c).
○: Bound monomer, □: bound dimer, and △: bound tetramer. The absorption spectrum of free dye and bound dye spectrum obtained in the low P/D region are shown by dashed curve and closed circles respectively.

$$K = \frac{[\text{complex}]}{[\text{free dye}][\text{unoccupied binding site}]^{\alpha}}, \tag{16}$$

where α is an empirical parameter. This equation may represent the distribution of the free dye and the total condensed dye in a solution; then the equilibrium constant for the formation of an aggregate in the vicinity of the polymer may be expressed by Eq. 6. Therefore, the amount of dye molecules represented as a complex in Eq. 16 is equal to the sum of the dye molecules of the respective bound-dye species. The fraction of the bound dimer of AA and that of the bound tetramers of CV and TF tends to increase up to unity in the low-P/D region, as is shown in Fig. 4. Hence, the amount of the dye molecules of the complex in Eq. 16 is nearly equal to that of the bound dimer for AA and that of the bound tetramers for CV and TF in the low-P/D region. This is consistent with the fact that the spectrum of the bound dimer of AA and that of the bound tetramers of CV and TF fits into the spectrum of the bound-dye species obtained in the low-P/D region. That is, the bound dimer of AA and the bound tetramers of CV and TF may be primarily present in the low-P/D region. Pal and Mandel[31] also suggested, for the pynacyanol–poly(L-glutamic acid) system, that dyes bound to a long polymer chain may form several small stacks, primarily tetra- and pentamer.

Equation 6 can be express another equilibrium scheme when the equation is rewritten with attention to the counter ion of the polyelectrolyte. In the polyelectrolyte solution without any added salt, the concentration of counter ions, for example, that of Na of NaPP, is equal to that of the polymer residues, so that Eq. 6 can be rewritten as follows:

$$K = \frac{[\mathrm{D}_n^b][\mathrm{Na}]^n}{[\mathrm{D}_1^b]^n[\mathrm{Na}]} = \frac{[\mathrm{D}_n^b][\mathrm{Na}]^{n-1}}{[\mathrm{D}_1^b]^n}. \tag{17}$$

In a previous report,[5] it was clarified that the fraction of bound CV and TF at a P/D, for example, $P/D=1$, increases with an increase in the chain length of NaPP. It was also reported that the amount of bound Na increases with an increase in the chain length of NaPP.[32] These facts suggest that the polyelectrolyte condenses not only the dyes, but also the counter ions, near it and that complexes are formed with the polymer residues, the dyes and the counter ions. Therefore, if it can be assumed that the dyes are bound to the polymer by the Na, Eq. 17 can be rewritten as follows:

$$K = \frac{[\mathrm{NaD}_n^b][\mathrm{Na}]^{n-1}}{[\mathrm{NaD}_1^b]^n}. \tag{18}$$

That is, this equation represents the following scheme:

$$n\mathrm{NaD}_1^b \rightleftharpoons \mathrm{NaD}_n^b + (n-1)\mathrm{Na} \tag{19}$$

where n bound monomers, which are bound to the

polymer by an Na, form the n-mer bound to the polymer by an Na. The participation of sodium in the formation of the dye–polyelectrolyte complex might be represented by the empirical parameter, α, introduced into Eq. 16, as has previously been mentioned.[4,5] The participation of sodium in the metachromasy could not be examined by the PCA method; however, it may be examined by means of electrochemical measurements, such as electrophoretic, potentiometric, and conductometric measurements.[2,3,33]

The Pure Spectrum and Structure of Bound-dye Species. The pure spectra of bound-dye species could be obtained for AA, CV, and TF by the application of the extended PCA method to a set of absorption spectra observed over a wide P/D region. It was revealed that the absorption spectra of the bound monomers of AA, CV, and TF show a slight bathochromic shift. The visible and UV absorption bands of AA, CV, and TF are attributable to the π-π^* transition.[34,35] The bathochromic shift of the π-π^* transition is generally induced by interaction with the polar solvent or the formation of a hydrogen bond.[36] Therefore, the bathochromic shift observed for the bound monomer may be due to the interaction between the dye and the ionized group of NaPP. The observed bathochromic shift is very small, so that it may be thought that the dye in monomeric form is loosely bound to NaPP and moves in its vicinity. Yamaoka and Noji[37] reported a sharp triplet line in the ESR spectrum of the spin-labeled proflavine–NaPP system at $P/D=200$; this also suggests that a bound-dye species rotates or moves rapidly.

The absorption spectrum of the bound dimer of AA shows a bathochromic shift, while those of the bound dimer and tetramer of CV and TF have absorption bands at wavelengths both shorter and longer than the position of the main band of the free dye. According to the exciton theory for metachromasy,[38] the relations between the position of the metachromasy bands and the orientation of the transition moments in a dye oligomer have been classified into three categories: (i) a parallel side-by-side orientation of the particular transition moments gives rise to the band on the shorter-wavelength side of the transition characterizing the monomer, (ii) an asymmetric oblique orientation gives rise to two bands, on both shorter- and longer-wavelength side, and (iii) a head-to-tail orientation gives rise to a band on the longer-wavelength side. Both the visible and UV absorption spectra of the bound dimer of AA show a bathochromic shift. The visible and UV transition moments of the monomer-free AA are at right angles.[21,28] If a pair of transition moments of AA is oriented head-to-tail in a dimer so as to have a band on the longer-wavelength side, the other pair of transition moments must be oriented side-by-side so as to have a band on the shorter-wavelength side. That is, the relation between the position of the metachromasy bands and the orientation of the transition moment in the dimer of AA is not classified into any category.

The position and number of metachromasy bands may be related to the symmetry of the dye structure, because the absorption spectrum of spin-labeled proflavine, in which the two-fold symmetry of proflavine is distorted by the spin-labeling to an amino group, has two bands, at wavelengths both shorter and longer than the position of the main band of proflavine,[29] while that of doubly spin-labeled proflavine, which is labeled at two aminogroups and which has a two-fold symmetry, has a band on the shorter-wavelength side.[39] Therefore, the absorption spectrum of a dye may have bands at wavelengths both shorter and longer than the position of the original band when the symmetry of the dye is sufficiently distorted. On the other hand, when the symmetry characterizing the monomer dye is not distorted sufficiently by the interaction between the dye and another substance, the absorption spectrum may show only a shift, without any new band. Therefore, the model of the bound dimer shown in Fig. 6 was considered for AA, CV, and TF. In the model, it was assumed that two dye molecules are combined not only by hydrophobic interaction, but also by the interaction between positively charged nitrogen and amino or dimethylamino nitrogen. Then, each of the two dyes has a two-fold symmetry in AA, while the symmetry of the monomer dye is distorted in the dimers of CV and TF.

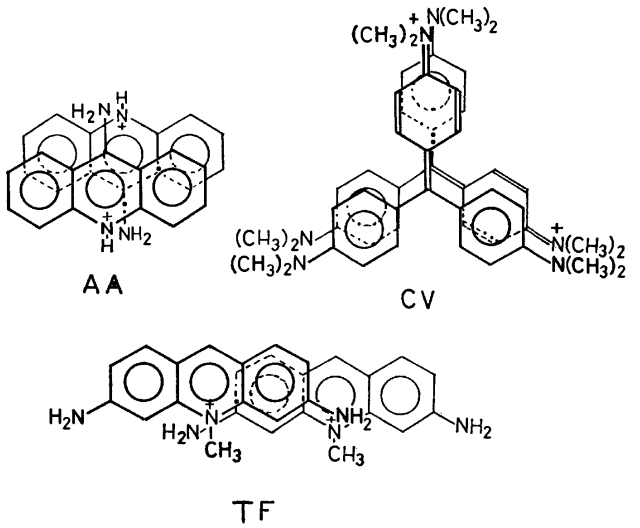

Fig. 6. Schematic model of bound dimer.

The symmetry in the bound tetramer may be more heavily distorted than that in the dimer, because the absorption band located on the shorter-wavelength side shows a larger hypsochromic shift in the bound tetramer than in the bound dimer, as is shown in Figs. 5(b) and (c). The bound tetramers of CV and TF may be more attracted than the monomer by the NaPP because of the four postively charged nitrogen atoms. Therefore, the conformation of the bound aggregate may depend on the backbone structure of the polymer, such as the mean distance between the functional groups of the polymer. Hence, the position and intensity of the absorption bands of the bound-dye species may depend on the polymers, as has previously been mentioned.[4]

For a quantitative discussion of the position of metachromasy bands, however, information is necessary on the electronic states and transition moments of the

aggregated dyes. The LCAO calculation may provide such information. Since the extended PCA method is powerful in a multicomponent system, its application to a series of absorption spectra of dye–polyelectrolyte systems at various temperatures or ionic strenghts should yield information leading to a fuller understanding of metachromasy.

Conclusion

The number of bound-dye species was determined to be two for the AA–NaPP system and three for the CV– and TF–NaPP systems. Using a simple model, in which the condensation of dyes near the polymer is assumed, the equilibrium constant, aggregation number, and pure absorption spectra of the bound-dye species were determined by the extended PCA method. The spectrum of the bound monomer shows a slight bathochromic shift in all cases. The absorption spectrum of the bound dimer of AA shows a considerable bathochromic shift. On the other hand, the absorption spectra of the bound dimer and tetramer of CV and TF have absorption bands at wavelengths both shorter and longer than the position of the main bands of free CV and TF.

The author wishes to express his hearty gratitude to Assistant Professor Kiwamu Yamaoka of Hiroshima University for his helpful discussions and continuous encouragement in the course of this study.

References

1) K. Yamaoka, T. Suenaga, A. Fujita, and M. Miura, *J. Sci., Hiroshima Univ., Ser. A*-II, **34**, 1 (1970).
2) K. Yamaoka, M. Takatsuki, K. Yaguchi, and M. Miura, *Bull. Chem. Soc. Jpn.*, **47**, 611 (1974).
3) K. Yamaoka, M. Takatsuki, and M. Miura, *Bull. Chem. Soc. Jpn.*, **48**, 2739 (1975).
4) K. Yamaoka and M. Takatsuki, *Bull. Chem. Soc. Jpn.*, **51**, 3182 (1978).
5) M. Takatsuki and K. Yamaoka, *Bull. Chem. Soc. Jpn.*, **52**, 1003 (1979).
6) K. Yamaoka and M. Masujima, *Biopolymers*, **17**, 2485 (1978).
7) T. Soda and K. Yoshioka, *Nippon Kagaku Zasshi*, **87**, 22 (1966).
8) G. Schwarz, S. Klose, and W. Balthasar, *Eur. J. Biochem.*, **12**, 454 (1970).
9) V. Vitagliano and L. Costantino, *J. Phys. Chem.*, **74**, 194 (1970).
10) V. Vitagliano, L. Costantino, and A. Zagari, *J. Phys. Chem.*, **77**, 204 (1973).
11) V. Vitagliano, L. Costantino, and R. Sartorio, *J. Phys. Chem.*, **80**, 959 (1976).
12) W. H. J. Stork, P. L. de Hasseth, W. B. Shippers, C. M. Kormeling, and M. Mandel, *J. Phys. Chem.*, **77**, 1772 (1973).
13) M. Shirai, T. Nagatsuka, and M. Tanaka, *Makromol. Chem.* **178**, 37 (1977).
14) G. Weill and M. Calvin, *Biopolymers*, **1**, 401 (1963).
15) V. Kleinwächter and J. Koudelka, *Biophysik*, **5**, 119 (1968).
16) G. Löber, J. Koudelka, and E. Smékal. *Biophys. Chem.*, **2**, 158 (1974).
17) Z. Balcarova, V. Kleinwächter, J. Koudelka, R. Klarner, and G. Löber, *Biophys. Chem.*, **8**, 17 (1978).
18) G. Löber and G. Achtert, *Biopolymers*, **8**, 595 (1969).
19) R. K. Tubbs, W. E. Ditmars, Jr., and Q. Van Winkle, *J. Mol. Biol.*, **9**, 545 (1964).
20) K. Yamaoka, *Biopolymers*, **11**, 2537 (1972).
21) K. Jakson and S. F. Mason, *Trans. Faraday Soc.*, **69**, 966 (1971).
22) R. W. Armstrong, T. Kurucsev, and U. P. Strauss, *J. Am. Chem. Soc.*, **92**, 3174 (1970).
23) M. Takatsuki and K. Yamaoka, *J. Sci. Hiroshima Univ., Ser. A*, **40**, 387 (1976).
24) D. F. Bradley and M. K. Wolf, *Proc. Natl. Acad. Sci., U. S. A.*, **45**, 944 (1959).
25) G. Schwarz, *Eur. J. Biochem.*, **12**, 442 (1970).
26) K. Yamaoka and R. A. Resnik, *Biopolymers*, **8**, 289 (1969).
27) K. Yamaoka, T. Matsuda, and M. Takatsuki, *Bull. Chem. Soc. Jpn.*, **53**, 968 (1980).
28) W. Seiffert, V. Zanker, M. Mantsch, and B. Schneider, *Tetrahedoron Lett.*, **54**, 5655 (1968).
29) K. Yamaoka, M. Takatsuki, and K. Nakata, unpublished.
30) F. Oosawa, "Polyelectrolytes," Marcel Dekker, New York (1971), Chap. 2.
31) M. K. Pal and M. Mandel, *Biopolymers*, **18**, 2267 (1979).
32) U. Schindewolf, *Z. Phys. Chem.*, **1**, 134 (1954).
33) F. Watanabe, *Bull. Chem. Soc. Jpn.*, **49** 1465 (1976).
34) Y. Matsuoka and K. Yamaoka, *Bull. Chem. Soc. Jpn.*, **52**, 2244 (1979).
35) Y. Matsuoka and K. Yamaoka, *Bull. Chem. Soc. Jpn.*, **52**, 3163 (1979).
36) H. H. Jaffé and M. Orchin, "Theory and Applications of Ultraviolet Spectroscopy," John Wiley and Sons, Inc., New York (1966), p. 186.
37) K. Yamaoka and S. Noji, *Chem. Lett.*, **1976**, 1355.
38) D. F. Bradley, I. Tinoco, Jr., and R. W. Woody, *Biopolymers*, **1**, 239 (1963).
39) K. Yamaoka and S. Noji, *Chem. Lett.*, **1979**, 1123.

 © 1980 The Chemical Society of Japan Bull. Chem. Soc. Jpn., 53, 1931—1936 (1980)

Shapes of the ν_1 Band of Liquid Chloroform and Intermolecular Interaction

Tetsuo SUZUKI, Yumiko K. TSUTSUI, and Tsunetake FUJIYAMA*,†

Department of Chemistry, Faculty of Science, Tokyo Metropolitan University, Setagaya-ku, Tokyo 158

† *Institute for Molecular Science, Myodaiji, Okazaki 444*

(Received January 5, 1980)

The infrared absorption spectrum for the ν_1 fundamental of chloroform or chloroform-*d* shows strong asymmetry, with a remarkable tailing on the high-frequency side. The observed band-width of the ν_1 fundamental of chloroform-*d* is significantly narrower than that of chloroform. These asymmetric band profiles of the ν_1 bands of chloroform and chloroform-*d* can be interpreted in terms of the existence of two different types of chloroform molecules. One is a molecule which interacts with another molecule, and the other is a non-interacting molecule. The isotope effect on the band-width can be explained in terms of the difference in the reduced mass for chloroform and chloroform-*d*.

It has been well established, that the absorption maximum of the infrared absorption spectrum for the ν_1 band of chloroform decreases from 3033 to 3018 cm^{-1}, and that the intensity increases from 11 to 198 $cm^2\ mol^{-1}$, on passing from the gas to the liquid phase.[1,2] These spectral changes have been interpreted in terms of the formation of hydrogen bonding in the liquid phase.[3] However, Rothschild *et al.* have studied the band shapes of the Raman scattering spectra and the infrared absorption spectra for the ν_1 band of chloroform and have concluded that the vibrational relaxation processes for the ν_1 band of chloroform do not support the presence of hydrogen bonding in the pure liquid.[4] Thereafter, several studies of the line-shape of the ν_1 band of chloroform and chloroform-*d* in the liquid phase have been reported.[5—9] All these reports have concluded that the shape of the ν_1 band may not be affected by the existence of hydrogen bonding. In other words, the observed width of the ν_1 band has been regarded as a homogeneous width. However, as will be shown in the present report, the observed infrared absorption spectrum for the ν_1 fundamental of chloroform or chloroform-*d* shows strong asymmetry, with a remarkable tailing on the high-frequency side. Therefore, the observed band-width can not be analyzed on the basis of the homogeneous width.

It has also been established that the band-width of the ν_1 fundamental of chloroform-*d* is significantly narrower than that of chloroform. Moradi-Araghi *et al.* have considered that the increased vibrational relaxation rate in chloroform, in comparison with that in chloroform-*d*, is ascribable to the stronger coupling between the ν_1 vibration and the molecular motions in the liquid, which itself arises from the anharmonic terms in the vibrational Hamiltonian.[8]

We will show in the present report that the observed asymmetric band profiles of the infrared-absorption spectra for the ν_1 bands of chloroform and chloroform-*d* can be interpreted in terms of the existence of a hydrogen-bonding-like interaction in the liquid phase. It will also be shown that the isotope effect on the band-width can be explained in terms of the difference in the reduced mass for chloroform and chloroform-*d* instead of the anharmonicity in the vibrational Hamiltonian.

Experimental

All the chemicals used in this work were commercially available reagents. The chloroform was passed through a chromatographic column packed with alumina to remove the ethanol used as a stabilizer. The eluent was fractionally distilled. The elimination of water and ethanol from the sample solution was confirmed by observing the infrared-absorption spectra. The chloroform-*d* was purchased from E. Merck Co., Ltd., and was dried over zeorite A-3. The carbon tetrachloride was purified by fractional distillation. The solutions were prepared gravimetrically.

The absorption spectra were recorded with a Perkin-Elmer 180 infrared spectrometer at the temperature of 22± 1 °C. A sample cell with NaCl windows was used, and the thickness of a sample was determined by the interference-fringe method. The absorption spectra of the ν_1 bands of chloroform and chloroform-*d* were measured under resolutions of 0.7 cm^{-1} and 0.5 cm^{-1} respectively and at the scanning speed of 4 $cm^{-1}\ min^{-1}$.

The observed spectra were then reduced to:

$$\frac{1}{lv}\ln\left(\frac{I_0}{I}\right)$$

where v is the wave number in cm^{-1}; l, the thickness of the sample; I_0 the intensity of the incident light, and I, the intensity of the transmitted light. The relative intensities, I^c, were defined as:

$$I^c = \frac{f_d}{l}\int_{band}\frac{1}{v}\ln\left(\frac{I_0}{I}\right)dv \qquad (1)$$

where f_d is the correction factor for the dielectric-field effect. Since the intensities of the observed bands were weak, Polo-Wilson's scheme[10] was applied to the dielectric-field correction; that is, the correction factor, f_d, was expressed as:

$$f_d = \frac{9n_D}{(n_D^2+2)^2} \qquad (2)$$

where n_D is the refractive index of the solution.

Results and Discussion

Observed Spectra. The observed spectra of the ν_1 band of pure liquid chloroform are shown in Fig. 1 (see the circles). The peak frequency and the full width at the half maximum are found to be 3018 cm^{-1} and 12.8 cm^{-1} respectively. It is apparent from the figure that the part of the half-intensity band-width which falls on the high-frequency side of the

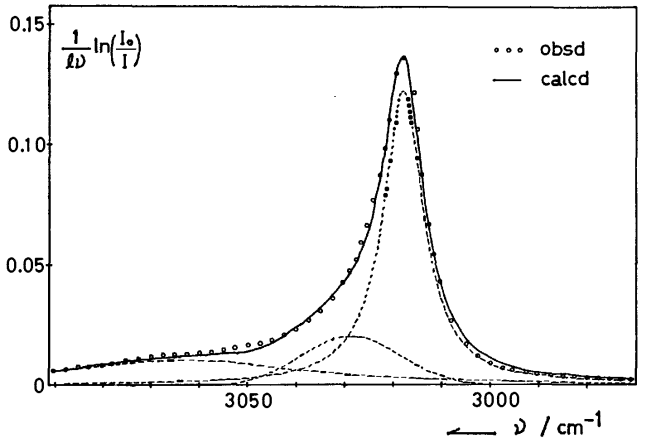

Fig. 1. Observed (circles) and calculated (real line) spectra for the ν_1 band of $CHCl_3$.

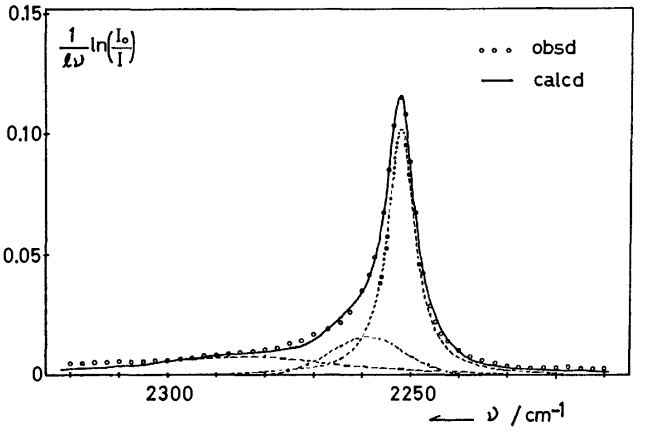

Fig. 2. Observed (circles) and calculated (real line) spectra for the ν_1 band of $CDCl_3$.

band maximum is broader than the corresponding part on the low-frequency side. The observed spectrum of the ν_1 band of pure liquid chloroform-*d* is shown in Fig. 2 (see the circles). The peak frequency and the full width at half the maximum are found to be 2252 cm^{-1} and 8.0 cm^{-1} respectively. The observed band profile of chloroform-*d* is similar to that of chloroform. However, there appears a remarkable isotope effect on the vibrational band-width.

Separation of the Observed Band into Symmetry Band Profiles. First, our attention was focused on the asymmetry of the band profile observed for the ν_1 band of chloroform. It can easily be ascertained that the asymmetry does not originate from any hot bands or any bands originating from isotopic species. Also, the asymmetry cannot be ascribed to any overlapping of summation bands, because the asymmetric band profiles are closely analogous both for pure liquid chloroform and chloroform-*d*.

An attempt was made, therefore, to resolve the observed asymmetric band profile into some symmetric intensity distribution functions in order to understand the origin of the asymmetry. First, we used two Lorentzian functions which correspond to the peaks at 3060 and 3018 cm^{-1} for pure chloroform (see Fig. 1). The agreement between the calculated and observed profiles was poor until we added another band between the 3060 and 3018 cm^{-1} bands. The best fit between the observed and calculated profiles has been obtained by considering two Lorentzian functions near 3060 and 3018 cm^{-1} and one Gaussian function near 3030 cm^{-1}. The explicit expression of the linear combination is given by:

$$F(\nu) = \frac{h_1\gamma_1^2}{(\nu-\nu_1)^2+\gamma_1^2} + h_2\exp\left\{-\frac{\ln 2}{\gamma_2^2}(\nu-\nu_2)^2\right\} + \frac{h_3\gamma_3^2}{(\nu-\nu_3)^2+\gamma_3^2}. \quad (3)$$

The observed and calculated spectra of the ν_1 band of chloroform are shown in Fig. 1. The best-fit parameter values of these functions are summarized in Table 1. Hereafter, we will call the broader Lorentzian at the highest frequency "the band 3," the narrower Lorentzian at the lowest frequency "the band 1," and the Gaussian "the band 2."

Table 1. Best-fit parameters of the ν_1 bands of $CHCl_3$ and $CDCl_3$

		Band 1	Band 2	Band 3
$CHCl_3$	γ/cm^{-1}	5.1	12	28
	h	0.1220	0.0204	0.0106
	ν/cm^{-1}	3017.5	3028	3062
	I^c/cm^{-1}	1.522	0.406	
$CDCl_3$	γ/cm^{-1}	3.4	9	22
	h	0.1025	0.0160	0.00799
	ν/cm^{-1}	2252	2259	2284
	I^c/cm^{-1}	0.853	0.239	

For chloroform-*d*, the observed intensity distribution was also expressed by a linear combination of two Lorentzian functions and one Gaussian function, as is shown in Fig. 2. The best-fit parameter values of the functions for chloroform-*d* are also listed in Table 1.

Assignment of the Resolved Bands. In order to assign the resolved bands, the spectra of the ν_1 band observed in the liquid phase are compared with those observed in the gas and solid phases in Table 2. The ν_1 band is observed at 3033 and 3007 cm^{-1} in the gas and solid phases respectively. The intensity of the ν_1 band, on the other hand, increases from 11 to 400 cm^2 mol^{-1} on passing from the gas to the solid phase. As is seen in Table 2, the frequency and intensity observed in the liquid phase take values intermediate between those of the gas and solid phases. These spectral changes have been interpreted in terms of the hydrogen-bond formation between chloroform molecules.[3] Therefore, it is reasonable to expect the existence of the two kinds of chloroform molecules in the liquid phase. One is a molecule which forms a hydrogen bonding with another chloroform molecule; the other is a molecule which behaves rather like a free molecule. We call these two kind of chloroform molecules a "strongly interacting molecule" and a "weakly interacting molecule" respectively.

Based upon these ideas, we assign the band 1 at the lowest frequency to the ν_1 vibration of the strongly

Table 2. Observed intensities and frequencies for the ν_1 bands of $CHCl_3$ and $CDCl_3$ in the gas, liquid, and solid phases

	Frequency, ν_0/cm^{-1}			Intensity, Γ/cm^2 mol^{-1}		
	Gas	Liquid	Solid[d]	Gas[a]	Liquid[c]	Solid[d]
$CHCl_3(\nu_1)$	3032.9[b]	3018	3007	11	198	400
$CDCl_3(\nu_1)$	2265[a]	2252	2250	3	127	133

a) See Ref. 1. b) See Ref. 2. c) The direct integration of the unresolved band. d) See Ref. 16.

Table 3. Concentration dependence of band parameters and intensities

	mol % ($CHCl_3$)	100	80	50	40	20
Band 1	ν_0/cm^{-1}	3017.5	3017.5	3017.5	3017.5	3017.5
	$\Delta\nu_{1/2}$/cm^{-1}	10.2	10.2	10.2	10.2	10.2
	I^c/cm^{-1}	1.552	1.078	0.758	0.495	0.216
	I^*/cm^{-1}	1.552	1.347	1.264	1.238	1.081
Band 2	ν_0/cm^{-1}	3028	3027	3027	3027	3026
	$\Delta\nu_{1/2}$/cm^{-1}	24	24	24	24	24
	I^c/cm^{-1}	0.406	0.336	0.270	0.186	0.0972
	I^*/cm^{-1}	0.406	0.421	0.450	0.466	0.486

interacting molecule. The band 2, on the other hand, is assigned to the ν_1 vibration related to the weakly interacting molecule.

The assignment of the band 3 has not yet been established. Its band maximum is observed 40 cm^{-1} higher than that of the band 1 and its half-width is much broader than that of the band 1. Therefore, we can safely conclude that the band 3 is not related to any fundamental vibrations. As no absorption band is observed in this wavenumber region for the gas sample,[2] it may arise from the combination tone of the ν_1 fundamental and the pseudo-lattice vibrations.[11]

If the assignments of the bands 1 and 2 are correct, the relative intensities, I_2/I_1, of the bands 1 and 2 should be equal for liquid chloroform and chloroform-*d*. It may be seen from Table 1 that the relative intensity, I_2^c/I_1^c, was observed to be 0.27 in chloroform and 0.28 in chloroform-*d*. These results partially support the validity of the present assignment of the bands 1 and 2.

Concentration Dependence of the Relative Intensities of the Band 1 and the Band 2. In order to confirm the validity of the assignment of the band 1 and the band 2, the concentration dependence of the intensities of the band 1 and the band 2 were observed in the binary solutions of chloroform–carbon tetrachloride. Since excess enthalpy is positive in a chloroform–carbon tetrachloride mixture,[12] the existence of a hydrogen-bonding-like interaction can be expected between chloroform molecules. This interaction is assumed to be broken down in the carbon tetrachloride solution. With the increase in the carbon tetrachloride concentration, therefore, it is expected that the number of the strongly interacting molecules will decrease while the number of the weakly interacting molecules will increase. In other words, the intensity of the band 1 is expected to decrease, while that of the band 2 is expected to increase.

The intensity change due to dilution is listed in Table 3. The quantities, I_1^* and I_2^*, of the table are defined as:

$$I_1^* \equiv \frac{c_0 f_d}{cl}\int_{\text{band 1}} \frac{1}{\nu}\ln\left(\frac{I_0}{I}\right)d\nu \simeq \frac{c_0 f_d}{cl}\int \frac{h_1\gamma_1^2}{(\nu-\nu_1)^2+\gamma_1^2}d\nu \quad (4)$$

$$I_2^* \equiv \frac{c_0 f_d}{cl}\int_{\text{band 2}} \frac{1}{\nu}\ln\left(\frac{I_0}{I}\right)d\nu \simeq \frac{c_0 f_d}{cl}\int h_2 \exp\left\{-\frac{\ln 2}{\gamma_2^2}(\nu-\nu_2)^2\right\}d\nu, \quad (5)$$

in cm^{-1}, where c_0 is the molar concentration of chloroform in pure liquid and c, the molar concentration of chloroform in solution. Table 3 shows that, as the concentration of carbon tetrachloride increases, I_1^* decreases, while I_2^* increases. These results support the validity of the assignments for the band 1 and the band 2.

Based upon these results, an attempt was made to obtain the absolute intensities of the band 1 and the band 2. The absolute intensities, Γ_1 and Γ_2, are given by:

$$I_1^* = c_0\frac{c_1}{c}\Gamma_1 \quad (6)$$

$$I_2^* = c_0\frac{c_2}{c}\Gamma_2 \quad (7)$$

where c_1 and c_2 are the molar concentrations of the chloroform molecules corresponding to the band 1 and the band 2 respectively. The $c=c_1+c_2$ relation and Eqs. 6 and 7 give the relation:

$$\frac{I_1^*}{\Gamma_1}+\frac{I_2^*}{\Gamma_2} = c_0$$

or:

$$I_1^* = -(\Gamma_1/\Gamma_2)I_2^* + \Gamma_1 c_0. \quad (8)$$

By plotting I_1^* against I_2^* at a series of concentrations, a straight line with a slope of $-(\Gamma_1/\Gamma_2)$ is generated so long as the absolute intensities, Γ_1 and Γ_2, are independent of the concentration. The values of Γ_1 and Γ_2 are obtained from the extrapolated I_1^* value at $I_2^*=0$ and the (Γ_1/Γ_2) value.[13]

TABLE 4. INTENSITIES AND FREQUENCIES OF THE BAND 1 AND BAND 2, AND THE ν_1 BANDS IN THE GAS AND SOLID PHASES

	Gas	Liquid		Solid[c]
		Band 1	Band 2	
Γ/cm^2 mol^{-1}	11[b]	250—300	45—60	400
ν_0/cm^{-1}	3032.9[a]	3017.5	3028	3007

a) See Ref. 2. b) See Ref. 1. c) See Ref. 16.

The values of the peak frequencies and the absolute intensities for the band 1 and the band 2 are listed in Table 4, together with those values for pure chloroform in the gas and solid phases. It may be seen from the table that the peak frequency and the absolute intensity of the band 1 are rather close to those values for the solid chloroform. On the other hand, the peak frequency and the absolute intensity of the band 2 are closer to those values for the gas chloroform. These results are consistent with the idea that there exist two kinds for chloroform molecules in the liquid phase. One is a strongly interacting molecule which causes the band 1 to appear, while the other is a rather weakly interacting molecule which causes the band 2 to appear.

Incidentally, the relative population of the strongly interacting molecules to the weakly interacting molecules in liquid chloroform was estimated to be 44% using the values of Γ_1 and Γ_2 and also Eqs. 6 and 7.

Isotope Effect on the Band-width. It is of much interest to consider the isotope effect on the band-width of the ν_1 fundamental. The band-widths of the ν_1 fundamentals are observed to be quite different for liquid chloroform and chloroform-*d* (see Table 1). This result is rather strange because of the following reason.

If the coupling between the vibrational and rotational motions of a molecule is negligible, the observed band-width, $\Delta\nu_{1/2}$, of an infrared spectrum may be expressed as:

$$\Delta\nu_{1/2} = \delta_v + \delta_r \tag{9}$$

where δ_v is the width originating from the vibrational relaxation and δ_r, the width originating from the reorientational relaxation. Since the moments of inertia and viscosity are almost equal for chloroform and chloroform-*d*, the values of δ_r for chloroform and chloroform-*d* should be almost equal also. It is ascertained that the effect of the vibrational relaxation of the resonace type is negligibly small for the ν_1 band because of the weak absorption intensity.[14] Therefore, we tried to explain the isotope effect on the band-width by considering the random modulation of vibration frequencies due to the surrounding molecules.

In order to elucidate the isotope effect on the vibrational relaxation due to the random-frequency modulation, we consider a harmonic oscillator whose vibrational frequency is modulated by a stochastic potential, $V(t)$, arising from the neighbouring molecules. In the present case, it can reasonably be assumed that the dissipation process of the vibrational energy is negligible, because the correlation time of $V(t)$ is much longer than the inverse of the harmonic frequency of the unperturbed oscillator. The vibrational relaxation function is, then, characterized by two parameters: the mean-square magnitude of the frequency shift, Δ, and the correlation time of the stochastic potential, τ_c, which are defined as:

$$\Delta^2 \equiv \langle(\Delta\omega)^2\rangle \tag{10}$$

$$\tau_c \equiv \frac{1}{\Delta^2}\int_0^\infty \langle\Delta\omega(0)\Delta\omega(t')\rangle dt' \tag{11}$$

where $\Delta\omega$ is the vibrational frequency shift due to the stochastic potential and where $<\ >$ indicates an average over the ensemble.[15]

If the condition

$$\Delta\cdot\tau_c \gg 1 \tag{12}$$

is fulfilled, the frequency modulation is very slow. Therefore, a line shape is a direct reflection of the random distribution of $\Delta\omega$. If the random distribution of $\Delta\omega$ is Gaussian, the vibrational relaxation function, $\psi_v(t)$, is also Gaussian, as is expressed by:

$$\psi_v(t) = \exp(i\omega_0 t)\exp\left(-\frac{\Delta^2}{2}t^2\right) \tag{13}$$

where ω_0 is the harmonic frequency of the unperturbed oscillator. Therefore, the corresponding line shape function, $I(\omega)$, is:

$$I(\omega) = \frac{1}{\sqrt{2\pi}\Delta}\exp\left\{-\frac{(\omega-\omega_0)^2}{2\Delta^2}\right\} \tag{14}$$

and the half-width due to the vibrational relaxation, δ_v, becomes:

$$\delta_v = 2\sqrt{2\ln 2}\,\Delta. \tag{15}$$

On the other hand, if the condition

$$\Delta\cdot\tau_c \ll 1 \tag{16}$$

is fulfilled, the frequency modulation is fast and the spectrum shows the phenomenon of motional narrowing. The vibrational relaxation function, $\psi_v(t)$, is expressed as:

$$\psi_v(t) = \exp(i\omega_0 t)\exp(-\Delta^2\tau_c|t|). \tag{17}$$

The line-shape function, $I(\omega)$, is expressed as:

$$I(\omega) = \frac{1}{\pi}\frac{\Delta^2\tau_c}{(\omega-\omega_0)^2+(\Delta^2\tau_c)^2}. \tag{18}$$

Therefore, the half-band width is:

$$\delta_v = 2\Delta^2\tau_c. \tag{19}$$

Since the correlation time, τ_c, of $V(t)$ is rather similar for the two isotope species, the isotope effect on the band-width may be ascribed to the mean-square magnitude, Δ, of the frequency shift. For the fundamental band, the frequency shift, $\Delta\omega$, originating from the intermolecular potential, V, is given by:

$$\Delta\omega = \frac{1}{2\omega_0}\left(\frac{\partial^2 V}{\partial Q^2}\right)_0 \tag{20}$$

where Q is the normal coordinate corresponding to the harmonic vibration. As Q is expressed as:

$$Q = \sqrt{\mu}\,\Delta r \tag{21}$$

where μ is the reduced mass of the oscillator, and Δr, the displacement from equilibrium, $(\partial^2 V/\partial Q^2)_0$ is given by:

Table 5. Calculated values of δ_r and δ_v

Modulation		Band 1		Band 2	
		δ_v/cm^{-1}	δ_r/cm^{-1}	δ_v/cm^{-1}	δ_r/cm^{-1}
Slow	$CHCl_3$	13.4	−3.2	23.6	0.4
	$CDCl_3$	10.0	−3.2	17.6	0.4
Fast	$CHCl_3$	7.7	2.5	13.5	10.5
	$CDCl_3$	4.3	2.5	7.5	10.5

$$\left(\frac{\partial^2 V}{\partial Q^2}\right)_0 = \frac{1}{\mu}\left(\frac{\partial^2 V}{\partial(\Delta r)^2}\right)_0. \quad (22)$$

A straightforward calculation using Eqs. 10, 20, and 22 leads to:

$$\Delta = \frac{1}{2\omega_0\mu}\sqrt{\left\langle\left(\frac{\partial^2 V}{\partial(\Delta r)^2}\right)_0^2\right\rangle}. \quad (23)$$

Since $\langle(\partial^2 V/\partial(\Delta r)^2)_0^2\rangle$ seems to be unchangeable on isotope substitution, Δ_H/Δ_D may be expressed by:

$$\Delta_H/\Delta_D = (\omega_{0D}\mu_D)/(\omega_{0H}\mu_H). \quad (24)$$

In Eq. 24, all the symbols suffixed by H and D correspond to chloroform and chloroform-*d* respectively. The force constant also seems to be unchageable on isotope substitution.

Therefore, the ratio of μ_H and μ_D is:

$$\mu_D/\mu_H = (\omega_{0H}/\omega_{0D})^2. \quad (25)$$

Equations 24 and 25 give this relation:

$$\Delta_H/\Delta_D = \omega_{0H}/\omega_{0D}. \quad (26)$$

Consequently, in the case of a slow modulation, the ratio of the half-widths for chloroform and chloroform-*d* is:

$$\delta_{vH}/\delta_{vD} = \omega_{0H}/\omega_{0D}. \quad (27)$$

In the case of a fast modulation, on the other hand, δ_{vH}/δ_{vD} is given by:

$$\delta_{vH}/\delta_{vD} = (\omega_{0H}/\omega_{0D})^2. \quad (28)$$

Since the δ_r value is considered to be almost equal for the two isotope species, the δ_r and δ_v values can be calculated from Eqs. 9, 27, and 28; the results are summarized in Table 5.

It may be concluded from the results shown in Table 5, first of all, that the present experimental results do not correspond to the case of a slow modulation, because the δ_r is calculated to be negative for the band 1 if we apply the slow-modulation limit to the present system.

In the fast-modulation limit, however, the δ_r values are calculated to be positive for both the band 1 and the band 2. Moreover, the δ_r of the band 2 is much larger than that of the band 1. This seems quite reasonable if we consider that the rotational motion of the molecule corresponding to the band 1 is hindered by the interaction from the surrounding molecules much more strongly than that of the molecule corresponding to the band 2. It is interesting to add that the δ_r for chloroform is calculated to be about 22.4 cm^{-1} if we apply the free-rotation model. This δ_r value of 22.4 cm^{-1} is closer to the δ_r value of the band 2 than to that of the band 1. These results support the idea that the fast-modulation limit is a more appropriate model to explain the observed isotope effect on the band-width than is the slow modulation limit. It has also been concluded that the isotope effect on the band-width of the ν_1 fundamental of chloroform arises mainly from the difference in the vibrational relaxation width. These conclusions are quite consistent with the assignment of the bands 1 and 2 to the two different types of chemical species existing in the liquid phase of chloroform, *i.e.*, the existence of the strongly and the weakly interacting molecules.

Concluding Discussion. The main results of the present work may be summarized as follows:

(1) There exist two different types of chloroform molecules in pure liquid chloroform. One is a molecule which interacts with another molecule, and the other is a non-interacting molecule.

(2) Although the infrared absorption spectrum for the ν_1 band of chloroform shows a single peak, the observed spectrum consists of two bands, which correspond to the two different types of chloroform molecules in the pure liquid. Both the peak frequency and the absorption intensity are different for these two bands in liquid chloroform; the observed band profile for the ν_1 vibration is asymmetric.

(3) The isotope effect on the width of the ν_1 band can be explained in terms of the difference in the reduced mass.

(4) Incidentally, the present results reveal the real difficulty of the intensity study of condensed phases. The intensities of the vibration spectra observed for the condensed systems have been used mainly for the study of intermolecular interactions. This can be done by comparing the intensities observed for the gas and condensed phases. It has been shown in the present work that a vibration spectrum of a condensed phase is, in principle, composed of many different bands with different band maxima and intensities. These different bands should correspond to different chemical species or different types of intermolecular interactions. In order to override this difficulty, the detailed study of the band shapes of the vibration spectra should be strongly pushed forward, together with the intensity measurements of condensed systems.

References

1) K. Tanabe and S. Saeki, *Spectrochim. Acta, Part A*, **26**, 1469 (1970). The intensity in this report is expressed in the units of $A/cm^{-2}\,mol^{-1}\,dm^3$. For convenience, we converted the value of it to the units of $\Gamma/cm^2\,mol^{-1}$ by the use of the relation: $\Gamma = 1000\,\nu_0^{-1}\,A$, where ν_0 is the wavenumber of the band origin.

2) I. Rossi, Nguyen-Van-Thanh, and C. Haeusler, *Can. J. Chem.*, **47**, 3319 (1969).

3) G. C. Pimentel and A. L. McClellan, "The Hydrogen Bond," W. H. Freeman and Company, San Francisco (1960).

4) W. G. Rothschild, G. J. Rosasco, and R. C. Livingston, *J. Chem. Phys.*, **62**, 1253 (1975).

5) L. C. Rosenthal and H. L. Strauss, *J. Chem. Phys.*, **64**, 282 (1976).

6) C. Brodbeck, I. Rossi, Nguyen-Van-Thanh, and A. Ruoff, *Mol. Phys.*, **32**, 71 (1976).

7) J. Schroeder, V. H. Schiemann, and J. Jonas, *Mol. Phys.*, **34**, 519 (1977).

8) A. Moradi-Araghi and M. Schwartz, *J. Chem. Phys.*, **68**, 5548 (1978).
9) J. Schroeder, V. H. Schiemann, and J. Jonas, *J. Chem. Phys.*, **69**, 5479 (1978).
10) S. R. Polo and M. K. Wilson, *J. Chem. Phys.*, **23**, 2376 (1955).
11) According to the private communication of S. Ikawa of Hokkaido University, the pseudo-lattice vibration has been observed to be: $CHCl_3$, $\nu=34$ cm^{-1}, $\Delta\nu_{1/2}=68$ cm^{-1}; $CDCl_3$, $\nu=34$ cm^{-1}, $\Delta\nu_{1/2}=68$ cm^{-1}.
12) "International Critical Tables of Numerical Data, Physics, Chemistry and Technology," National Research Council, McGraw-Hill, New York (1929), Vol. V.
13) M. Okazaki, I. Hara, and T. Fujiyama, *J. Phys. Chem.*, **80**, 64 (1976).
14) M. Kakimoto and T. Fujiyama, *Bull. Chem. Soc. Jpn.*, **45**, 2970 (1972); **47**, 1883 (1974).
15) R. Kubo, *Adv. Chem. Phys.*, **15**, 105 (1969).
16) A. Kimoto and H. Yamada, *Bull. Chem. Soc. Jpn.*, **41**, 1096 (1968).

 © 1980 The Chemical Society of Japan Bull. Chem. Soc. Jpn., 53, 1937—1941 (1980)

Excess Volumes of Ternary Mixtures

Masanao KATO

Department of Chemistry, Faculty of Science, Tohoku University, Sendai 980

(Received January 11, 1980)

An expression for excess volumes of multi-component mixtures was derived, and its applicability to the experimental values of ternary mixtures was demonstrated. It was found, in 1,2-dichloroethane+benzene+cyclohexane, ethanol+benzene+cyclohexane and ethanol+acetone+cyclohexane mixtures, that the agreements between the calculated and the experimental values were satisfactory.

Many expressions and models for the thermodynamic properties of a liquid mixture have been proposed by many workers in the past two decades. Of these theories, some semi-empirical equations, such as the Wilson equation[1,2] and the UNIFAC equation,[3] have successfully interpreted the experimental values in many liquid mixtures. These theories can be extended to the calculation of the thermodynamic quantities observed in the multi-component mixtures,[1-4] despite some ambiguity in the physical meaning of the parameters involved. However, these theories are useless for the expression of the excess volume of the mixtures.

From this point of view, the present author recently proposed a new semi-empirical expression for the excess volume of binary mixtures based on the local composition in the mixture, and demonstrated that the results calculated by means of the equation are in good agreement with the experimental values.[5] This expression contains only two semi-empirical parameters for molecular arrangement in a binary mixture and can be expected to be extended to ternary mixtures in a simple manner. In this study, the expression for multi-component mixtures was derived, after which we examined its applicability to the experimental values obtained in three different ternary mixtures, 1,2-dichloroethane+benzene+cyclohexane, ethanol+benzene+cyclohexane, and ethanol+acetone+cyclohexane mixtures, selected as typical mixtures.

Theoretical

In multi-component mixtures consisting of n species, consider the n kinds of cells, each of them including an i-th ($1 \leqq i \leqq n$) component at the center. In this situation, if molecular association can be neglected, the volume occupied by one mol of the central molecule i, v_i, is expressed as follows:[5]

$$v_i = v_{1i}x_{1i} + v_{2i}x_{2i} + \cdots + v_{ii}x_{ii} + \cdots + v_{ni}x_{ni}, \quad (1)$$

where v_{ji} is the volume of the i-th component surrounded by the j-th component, and where x_{ji} denotes a local mole fraction of the j-th component in the vicinity of the i-th component. From Eq. 1, the volume of the mixture, v_{mix}, is represented as follows:

$$v_{mix} = \sum_{i=1}^{n} x_i \left(\sum_{j=1}^{n} v_{ji}x_{ji} \right). \quad (2)$$

Since the volume of an ideal mixture, v_{ideal}, is:

$$v_{ideal} = \sum_{i=1}^{n} x_i v_i^* = \sum_{i=1}^{n} x_i v_{ii}, \quad (3)$$

where v_i^* denotes the molar volume of the pure i-th component, the excess volume, v^E, is represented as follows:

$$v^E = \sum_{i=1}^{n} x_i \left(\sum_{j=1}^{n} (v_{ji} - v_{ii})x_{ji} \right). \quad (4)$$

In Eq. 4, the $\sum_{j=1}^{n} x_{ji} = 1$ relation was used. If the non-randomness factor, Λ_{ji}, is defined as:[5]

$$\frac{x_{ji}}{x_{ii}} = \Lambda_{ji}\frac{x_j}{x_i}, \quad (5)$$

the local mole fraction, x_{ji}, is represented as follows:

$$x_{ji} = \frac{\Lambda_{ji}x_j}{\sum_{k=1}^{n} \Lambda_{ki}x_k}. \quad (6)$$

From Eqs. 4 and 6, the expression for the excess volume of a multi-component mixture is obtained as follows:

$$v^E = \sum_{i=1}^{n} x_i \left(\frac{\sum_{j=1}^{n} (v_{ji} - v_{ii})\Lambda_{ji}x_j}{\sum_{k=1}^{n} \Lambda_{ki}x_k} \right). \quad (7)$$

The parameters $(v_{ji} - v_{ii})$ and Λ_{ji} can be obtained from the data of binary mixtures by a method previously described.[5]

Experimental

1,2-Dichloroethane, benzene, cyclohexane, acetone (Wako Pure Chemical Industries, Ltd.; G.R. grade) and ethanol (Kanto Chemical Co., Ltd.; G.R. grade) were used. Each of them was purified by means of fractional distillation on an apparatus with a 1.5-meter condenser under a reflux ratio of 3:1; a middle portion was collected at a constant condensation temperature. The purified reagents showed no signal due to any impurity on G.L.C. The densities and vapor pressures at 298.15 K agree well with the literature values.[6]

The excess volumes were obtained from density measurements made by using pycnometers with contents of 1.9 cm^3, 6 cm^3, and 9 cm^3 and immersed in a thermostat controlled at (298.15±0.001) K.

Results and Discussion

In this study, the excess volumes of binary and ternary mixtures were measured since only a few literature data on the excess volume of a ternary mixture are available.[7,8] The applicability of Eq. 7 was examined in the following sequence.

Binary Mixtures. The observed excess volumes of seven binary mixtures, *i.e.*, 1,2-dichloroethane+benzene, benzene+cyclohexane, 1,2-dichloroethane+cyclohexane, acetone+cyclohexane, ethanol+acetone,

TABLE 1. EXCESS VOLUMES v^E OF SEVEN BINARY MIXTURES AT 298.15K

x_1	v^E / cm^3 mol^{-1}	x_1	v^E / cm^3 mol^{-1}	x_1	v^E / cm^3 mol^{-1}
1,2-Dichloroethane(1) + benzene(2)		Benzene(1) + cyclohexane(2)		1,2-Dichloroethane(1) + cyclohexane(2)	
0.07120	0.1081	0.06079	0.2003	0.06588	0.3372
0.10135	0.1200	0.14356	0.3722	0.06958	0.3779
0.14697	0.1557	0.18165	0.4524	0.10138	0.5191
0.19028	0.1731	0.23076	0.5185	0.15762	0.6811
0.22435	0.2030	0.24060	0.5170	0.15879	0.6831
0.28366	0.2237	0.29127	0.6260	0.23505	0.8846
0.33058	0.2471	0.29313	0.5932	0.23586	0.8909
0.35393	0.2507	0.38093	0.7011	0.31166	0.9980
0.38791	0.2502	0.38643	0.7074	0.36840	1.0745
0.47153	0.2621	0.41625	0.7250	0.46430	1.0739
0.47828	0.2372	0.45588	0.6971	0.47928	1.0876
0.56491	0.2381	0.51291	0.7114	0.53750	1.0431
0.58035	0.2455	0.57722	0.7064	0.56165	1.0224
0.64277	0.2202	0.59442	0.6634	0.64041	0.8872
0.67581	0.2077	0.65144	0.6471	0.65305	0.8999
0.74666	0.1863	0.68664	0.6241	0.70900	0.8054
0.76017	0.1795	0.74889	0.5246	0.81384	0.5500
0.86542	0.1036	0.76753	0.5040	0.82661	0.5389
0.86850	0.0978	0.77438	0.4857	0.83954	0.5059
0.93796	0.0504	0.85142	0.3645	0.92938	0.2338
0.94712	0.0416	0.85738	0.3682	0.93417	0.2255
		0.92058	0.2318		
		0.94684	0.1672		
Acetone(1) + cyclohexane(2)		Ethanol(1) + benzene(2)		Ethanol(1) + cyclohexane(2)	
0.06944	0.3595	0.03181	0.0472	0.03778	0.1260
0.17215	0.7183	0.04746	0.0671	0.08566	0.2393
0.25602	0.9083	0.09497	0.0930	0.09387	0.2511
0.39779	1.0857	0.13980	0.0923	0.15896	0.3434
0.51404	1.1271	0.20116	0.0937	0.19412	0.3902
0.61379	1.0716	0.26573	0.0775	0.23602	0.4386
0.70018	0.9549	0.27633	0.0848	0.33095	0.5085
0.80288	0.7337	0.31006	0.0808	0.40925	0.5383
0.88628	0.4648	0.40830	0.0610	0.49511	0.5540
0.95246	0.2142	0.50169	0.0366	0.55255	0.5432
		0.55738	0.0126	0.60901	0.5317
Ethanol(1) + acetone(2)		0.63807	−0.0055	0.68480	0.5153
0.05530	−0.0064	0.66235	−0.0040	0.74540	0.4709
0.15373	−0.0236	0.72272	−0.0225	0.81722	0.3989
0.30963	−0.0411	0.77333	−0.0334	0.87048	0.3124
0.40671	−0.0548	0.82111	−0.0352	0.92440	0.2034
0.50854	−0.0587	0.86939	−0.0318	0.97483	0.0778
0.57634	−0.0702	0.92857	−0.0198		
0.59389	−0.0622	0.95126	−0.0179		
0.70507	−0.0614				
0.80208	−0.0562				
0.90075	−0.0331				
0.94251	−0.0249				

ethanol+benzene, and ethanol+cyclohexane mixtures, are listed in Table 1. These mixtures were selected because they are strongly non-ideal mixtures and because they possess a sufficient magnitude of excess volumes to be measured from density with sufficient accuracy. The data obtained were smoothed by the method of least squares to the following polynomial equation:

$$v^E = x(1-x)\sum_{i=0}^{4} A_i\,(1-2x)^i. \qquad (8)$$

TABLE 2. THE VALUES OF COEFFICIENTS FOR THE POLYNOMIAL EQUATION (Eq. 8) AT 298.15K

Mixtures	A_0	A_1	A_2	A_3	A_4	$\sigma(v^E)$ / cm^3 mol^{-1}
1,2-Dichloroethane(1)+benzene(2)	1.0077	0.1291	0.1322	0.2546	0.0560	0.0072
Benzene(1)+cyclohexane(2)	2.8772	0.1674	−0.2828	−0.1473	1.0377	0.0158
1,2-Dichloroethane(1)+cyclohexane(2)	4.2462	1.1368	0.1794	−0.0789	0.5340	0.0175
Acetone(1)+cyclohexane(2)	4.5015	0.0283	0.6692	0.6683	0.2233	0.0023
Ethanol(1)+acetone(2)	−0.2438	0.1250	−0.0341	0.0354	−0.0281	0.0026
Ethanol(1)+benzene(2)	0.1431	0.4873	−0.1413	0.5359	0.7410	0.0043
Ethanol(1)+cyclohexane(2)	2.2039	−0.1407	0.8225	0.2304	0.4036	0.0120

The obtained parameters, A_i, and standard deviation, σ, are summarized in Table 2. The partial molar volumes at an infinite dilution, v_i^∞ (as $v_i^\infty - v_i^*$), non-randomness factors, Λ_{ji}, and volume parameters, $v_{ji}-v_{ii}$ are also listed in Table 3. The volume parameters were calculated from $v_i^\infty - v_i^*$ by the use of the following equation:

$$v_{ji} - v_{ii} = \frac{(v_i^\infty - v_i^*) - \Lambda_{ij}(v_j^\infty - v_j^*)}{1 - \Lambda_{ij}\Lambda_{ji}}. \quad (9)$$

From Eq. 9, the volume change in the central molecule, i, surrounded by an unlike molecule, j, can be estimated. In the mixtures which show a positive deviation, the $v_{21}-v_{11}$ and $v_{12}-v_{22}$ values are smaller than the values of the corresponding $v_1^\infty - v_1^*$ and $v_2^\infty - v_2^*$ respectively. The $v_i^\infty - v_i^*$ values contain the volume changes of both the central and the surrounding molecules. On the other hand, the $v_{ij}-v_{jj}$ values consist of only the volume change of the central molecule. In the ethanol+acetone mixture, which shows a negative excess volume, the small $v_{12}-v_{22}$ value of acetone shows little volume change upon interaction with ethanol molecules, while the negative value of $v_{21}-v_{11}$ for ethanol shows a decrease in the volume upon interaction with acetone. In the ethanol+benzene mixture, the negative value of the volume change of benzene indicates the OH-π interaction and the positive value of ethanol molecule results from the destruction of the hydrogen-bonding interaction of the ethanol molecules.

The excess volumes calculated from Eq. 7 are in good agreement with the experimental values, shown by solid lines in Fig. 1. The solid lines were drawn on the basis of Eq. 7.

Ternary Mixtures. The excess volumes of three ternary mixtures, the 1,2-dichloroethane+benzene+cyclohexane, ethanol+benzene+cyclohexane, and ethanol+acetone+cyclohexane mixtures, were measured and compared with the values calculated from Eq. 7. In the 1,2-dichloroethane+benzene+cyclohexane mixture, all binary mixtures composed of the three components show positive excess volumes. In the ethanol+benzene+cyclohexane mixture, the ethanol+benzene binary mixture shows an S-shaped excess-volume curve. The ethanol+acetone mixture in the ethanol+acetone+cyclohexane mixture shows a negative excess volume. These three ternary mixtures are typical systems which show representative excess-volume curves. When two binary mixtures composed of the components of the ternary mixtures show negative excess volumes, the calculated and observed excess volumes are considered to have a tendency similar to that when two binary mixtures show positive excess volumes, if the signs of the values of the excess volume and the volume parameters are changed.

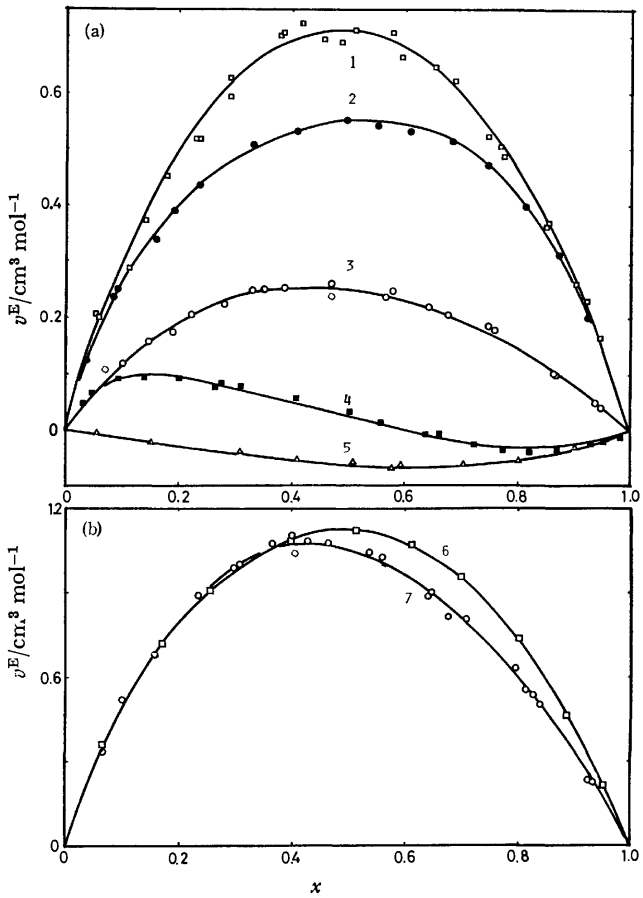

Fig. 1. Observed and calculated excess volumes of seven binary mixtures at 298.15 K.
The solid lines indicate the calculated curves from Eq. 7 using the values of parameters in Table 3. 1; Benzene+cyclohexane, 2; ethanol+cyclohexane, 3; 1,2-dichloroethane+benzene, 4; ethanol+benzene, 5; ethanol+acetone mixtures, which are shown in Fig. 1a, and 6, acetone+cyclohexane; 7, 1,2-dichloroethane+cyclohexane mixtures are shown in Fig. 1(b).

The observed and calculated excess volumes of the

TABLE 3. THE DERIVED QUANTITIES FROM THE COEFFICIENTS A_i IN Eq. 8 AND THE APPLICABILITY OF Eq. 7

Mixtures	$v_1^\infty - v_1^*$ / cm³ mol⁻¹	$v_2^\infty - v_2^*$ / cm³ mol⁻¹	A_{21}	A_{12}	$v_{21} - v_{11}$ / cm³ mol⁻¹	$v_{12} - v_{22}$ / cm³ mol⁻¹	$\sigma(v^E)$ / cm³ mol⁻¹
1,2-Dichloroethane(1) + benzene(2)	1.5795	0.8122	0.4786[a)]	0.1812[a)]	1.4385	0.2233	0.0096
Benzene(1) + cyclohexane(2)	3.6522	3.6121	3.7543	2.4504	0.6342	1.2317	0.0231
1,2-Dichloroethane(1) + cyclohexane(2)	6.0775	3.9617	6.3452	2.0276	0.1648	2.9161	0.0192
Acetone(1) + cyclohexane(2)	6.0906	4.6973	0.1406	0.8253	2.5045	4.3452	0.0089
Ethanol(1) + acetone(2)	−0.1457	−0.4664	2.7140	3.0170	−0.1755	0.0099	0.0026
Ethanol(1) + benzene(2)	1.7661	−0.2803	0.1594	0.7006	2.2092	−0.6325	0.0125
Ethanol(1) + cyclohexane(2)	3.5196	3.3403	0.1991	0.3125	2.6404	2.8150	0.0064

a) Calculated from the following values of the coefficients in Eq. 8; $A_0=0.9918$, $A_1=0.2836$, and $A_2=0.2036$.

TABLE 4. OBSERVED EXCESS VOLUMES, v^E_{obsd}, OF TERNARY MIXTURES AT 298.15K, AND THE CALCULATED VALUES, v^E_{calcd}, FROM Eq. 7

x_1	x_2	v^E_{obsd} / cm³ mol⁻¹	v^E_{calcd} / cm³ mol⁻¹	x_1	x_2	v^E_{obsd} / cm³ mol⁻¹	v^E_{calcd} / cm³ mol⁻¹
1,2-Dichloroethane(1) + benzene(2) + cyclohexane(3)							
0.16181	0.10822	0.8315	0.8015	0.37619	0.54744	0.4351	0.4083
0.15592	0.21786	0.8157	0.8252	0.45702	0.09156	1.0273	0.9653
0.14390	0.37338	0.8273	0.7925	0.43892	0.18588	0.9461	0.8673
0.13755	0.47434	0.7918	0.7373	0.41082	0.31482	0.8013	0.7319
0.13277	0.56359	0.7193	0.6641	0.56022	0.08152	0.9615	0.8833
0.11488	0.80393	0.3625	0.3235	0.55097	0.17551	0.8206	0.7543
0.29002	0.09498	0.9836	0.9628	0.50679	0.29440	0.6726	0.6339
0.27667	0.21334	0.9823	0.9016	0.56591	0.36310	0.4285	0.3989
0.25582	0.34827	0.8407	0.8075	0.66078	0.07835	0.7828	0.7378
0.24893	0.45729	0.7750	0.7051	0.63407	0.16175	0.6916	0.6407
0.24202	0.62002	0.4896	0.4873	0.65913	0.27086	0.4052	0.3784
0.22318	0.69970	0.3564	0.3686	0.71173	0.15909	0.5088	0.4862
0.38916	0.40256	0.7039	0.6344	0.82163	0.06866	0.4246	0.4038
0.38602	0.47876	0.5567	0.5174	0.86941	0.06419	0.2869	0.2794
Ethanol(1) + acetone(2) + cyclohexane(3)							
0.13745	0.12130	0.6836	0.5907	0.47672	0.13572	0.6534	0.6261
0.14842	0.25582	0.9083	0.8309	0.45854	0.35078	0.5087	0.5031
0.14338	0.41722	0.9673	0.9366	0.47704	0.44319	0.2248	0.2319
0.13677	0.57478	0.8414	0.8307	0.53882	0.10430	0.6109	0.5868
0.12985	0.75011	0.4483	0.4442	0.52280	0.23803	0.5571	0.5427
0.25102	0.39847	0.8991	0.8054	0.54100	0.38390	0.1779	0.2076
0.39128	0.06770	0.6438	0.5968	0.65937	0.16991	0.4060	0.4041
0.36529	0.30142	0.7405	0.7073	0.81402	0.08978	0.2365	0.2432
0.38048	0.43502	0.5380	0.5222				
Ethanol(1) + benzene(2) + cyclohexane(3)							
0.14628	0.14040	0.5768	0.6360	0.42111	0.20990	0.6265	0.6558
0.15294	0.31744	0.7299	0.7773	0.40934	0.32452	0.5651	0.5935
0.13411	0.42651	0.7239	0.7751	0.44806	0.39016	0.4087	0.4415
0.14881	0.55405	0.6448	0.6919	0.46057	0.45622	0.2535	0.2790
0.12821	0.57810	0.6308	0.6861	0.54359	0.09818	0.5727	0.5864
0.14142	0.77175	0.3020	0.3576	0.57801	0.28090	0.3356	0.3617
0.25864	0.45372	0.6269	0.6685	0.62485	0.13932	0.4693	0.4793
0.39986	0.33098	0.5707	0.6003	0.80450	0.05251	0.3209	0.3258
0.45345	0.07094	0.5974	0.6222	0.84905	0.11362	0.0792	0.0895

ternary mixtures are summarized in Table 4. As is shown in this table, the calculated excess volumes of all the ternary mixtures are in good agreement with the experimental values. The maximum difference between the calculated and the observed values is about 0.09 cm^3 mol^{-1}, most of the differences are within 0.05 cm^3 mol^{-1}.

As has been described above, the present expression for the excess volumes of multi-component mixtures is considered to be successful in reproducing the experimental values. As Eq. 7 shows, the excess volume can be determined in terms of the molecular arrangement in a mixture, the intermolecular interaction assessed by non-randomness factors, and the molecular size as measured from the $v_{ij}-v_{jj}$ values.

From these results and this discussion, it should be noticed that the excess volumes of ternary mixtures can be represented without ternary terms of molecular-size parameters and three-body interaction in a given mixture, as was shown in the derivation of Eq. 7. The effect of three-body interaction is considered to be small, and the degree of correction required for the three-body terms can be assumed to be of the same magnitude as the difference between the observed and the calculated values in Table 4, *i.e.*, about 0.05 cm^3 mol^{-1}.

References

1) G. M. Wilson and G. Scatchard, *J. Am. Chem. Soc.*, **86**, 127 (1964).

2) J. M. Prausnitz, "Molecular Thermodynamics of Fluid-phase Equilibria," Prentice-Hall, Englewood Clifs, New Jersey (1969).

3) H. Renon and J. M. Prausnitz, *AIChE J.*, **14**, 135 (1968).

4) D. S. Abrams and J. M. Prausnitz, *AIChE J.*, **21**, 116 (1975).

5) M. Kato and N. Suzuki, *Bull. Chem. Soc. Jpn.*, **51**, 1020 (1978).

6) J. A. Riddick and W. B. Bunger, "Organic Solvents," John Wiley and Sons, New York (1970), 3rd Edition.

7) A. N. Campbell, E. M. Karzmark, and R. M. Chatterjee, *Can. J. Chem.*, **44**, 1183 (1966).

8) R. P. Rastogi, J. Nath, and M. L. Yadava, *J. Chem. Thermodyn.*, **6**, 1197 (1974).

Theory of A.c. Polarization and A.c. Polarography and Voltammetry of Two-step Surface Redox Reactions

Tadaaki KAKUTANI* and Mitsugi SENDA

Department of Agricultural Chemistry, Faculty of Agriculture, Kyoto University, Kyoto 606

(Received January 14, 1980)

Theoretical expressions are presented of the a.c. polarization and of the a.c. polarography and voltammetry for a two-step surface redox reaction ($O_{ad}+n_1e\rightleftharpoons S_{ad}$, $S_{ad}+n_2e\rightleftharpoons R_{ad}$) in which the charge transfer reactions take place exclusively between the adsorbed reactants O_{ad}, S_{ad}, and R_{ad}, and all the reactants are adsorbed so strongly that the amount of O, S, or R brought to or removed from the electrode surface can be neglected. The interaction between the adsorbed reactants is assumed to be expressed by Frumkin's a-parameters. The effect of the double layer impedance is taken into account. Several simplified cases are discussed in detail.

There have been recently increasing studies on redox modified electrodes, which are prepared by attaching irreversibly redox species to the surface of an electrode material (*via* irreversible adsorption, coating, or chemical binding *etc.*), in prospect of their applications to electroanalysis and electrocatalysis (for reviews, see Refs. 1 and 2). Information on the electrochemical characteristics of surface redox reactions is very important in the applications of the redox modified electrodes. For this purpose cyclic voltammetry has been widely used. In a previous paper[3] we have presented a theory of the faradaic impedance and of a.c. polarography and voltammetry for surface redox reaction ($O_{ad}+ne\rightleftharpoons R_{ad}$) in which the interaction between the adsorbed reactants and the correction for the double layer impedance are taken into account. This theory has been applied to the electrode processes of ferredoxins irreversibly adsorbed on the mercury electrode surface.[4,5] The results indicated that a.c. polarography and voltammetry are powerful techniques, in particular, for elucidating the kinetic aspect of the electrode processes.

Two-step charge transfer mechanism is an important mechanistic category in biochemical as well as chemical redox reactions. Numerous studies have been devoted to this type of electrode reaction (EE mechanism) and theoretical treatments of the EE mechanism have been presented for d.c.[6-13] and a.c.[14-18] polarography and other electrochemical techniques.[19-25] To our knowledge, however, no theoretical treatment of a.c. polarization has been presented for the two-step surface redox reaction (*surface EE mechanism*).

In this study we present a theory of the faradaic impedance and of a.c. polarography and voltammetry for the two-step surface redox reaction. In this theory the interaction between the adsorbed reactants is taken into account. Also the effect of the double layer impedance is considered.

Derivation of the General Expressions

Let us consider a two-step surface redox reaction,

$$\text{1st Step: } O_{ad} + n_1e \rightleftharpoons S_{ad} \tag{1a}$$

$$\text{2nd Step: } S_{ad} + n_2e \rightleftharpoons R_{ad}. \tag{1b}$$

In the following we shall make the same assumptions as made in the previous work:[3] (a) the charge transfer reactions take place exclusively between the adsorbed reactants, (b) all the electroactive species (O, S, and R) are adsorbed so strongly (irreversibly) that the amount of O, S, or R brought to or removed from the electrode surface by mass transfer can be neglected in comparison with the amount which remains adsorbed, and (c) the interaction between the adsorbed reactants can be expressed by Frumkin's a-parameters.[26]

Since the surface redox reaction proceeds exclusively between the adsorbed reactants (assumption (a)), the faradaic current-density, I_F, is a function of the electrode potential, E, and the surface concentration of the reactants, Γ_O, Γ_S, and Γ_R;

$$I_F = I_F(1) + I_F(2) \tag{2a}$$

$$I_F(1) = g_1(E, \Gamma_O, \Gamma_S) \tag{2b}$$

$$I_F(2) = g_2(E, \Gamma_S, \Gamma_R), \tag{2c}$$

where Γ_i (i=O, S, or R) is the amount of the adsorbed reactant i per unit electrode surface area, $I_F(1)$ and $I_F(2)$ are the faradaic current-densities of the first and second step, respectively.

For a small variation of the potential, δE, superimposed on the "d.c." potential, E_{dc}, ($E=E_{dc}+\delta E$), the surface concentration Γ_i will change around the mean ("d.c.") value, $\overline{\Gamma}_i$, with a small variation, $\delta\Gamma_i$, ($\Gamma_i=\overline{\Gamma}_i+\delta\Gamma_i$) and the faradaic current-density will be given by

$$I_F = I_{dc} + \delta I_F. \tag{3}$$

Thus we have for the first harmonic of faradaic current,[27] $\delta_1 I_F$,

$$\delta_1 I_F = \delta_1 I_F(1) + \delta_1 I_F(2), \tag{4a}$$

$$\delta_1 I_F(1) = (\partial I(1)/\delta E)\delta_1 E + (\partial I(1)/\partial\Gamma_O)\delta_1\Gamma_O + (\partial I(1)/\partial\Gamma_S)\delta_1\Gamma_S, \tag{4b}$$

$$\delta_1 I_F(2) = (\partial I(2)/\partial E)\delta_1 E + (\partial I(2)/\partial\Gamma_S)\delta_1\Gamma_S + (\partial I(2)/\partial\Gamma_R)\delta_1\Gamma_R, \tag{4c}$$

where $\delta_1 E$ and $\delta_1\Gamma_i$'s are the first harmonic variations of E and Γ_i's, respectively. From assumption (b) we further have

$$d(\delta_1\Gamma_O)/dt = j\omega\delta_1\Gamma_O = \delta_1 I_F(1)/n_1F, \tag{5a}$$

$$d(\delta_1\Gamma_S)/dt = j\omega\delta_1\Gamma_S = -(\delta_1 I_F(1)/n_1F) + (\delta_1 I_F(2)/n_2F), \tag{5b}$$

$$d(\delta_1\Gamma_R)/dt = j\omega\delta_1\Gamma_R = -\delta_1 I_F(2)/n_2F, \tag{5c}$$

where j is the operator $(-1)^{1/2}$, and ω the angular frequency of sinusoidal variations.

By combining Eqs. 4a to 5c we obtain the *I-E* characteristic for sinusoidal variation of small amplitude,

$$\delta_1 I_F = \delta_1 I_F^{real} + j\delta_1 I_F^{imag} = \frac{(r_1+r_2)-j[y_1+y_2+(n_1/n_2)x_1-(n_2/n_1)x_2]}{(r_1r_2-y_1y_2-x_1x_2)-j(r_2y_1+r_1y_2)}\delta_1 E, \tag{6a}$$

$$\delta_1 I_F^{real} = \frac{(r_1+r_2)(r_1r_2-y_1y_2-x_1x_2)+(r_1y_2+r_2y_1)[y_1+y_2+(n_1/n_2)x_1-(n_2/n_1)x_2]}{(r_1r_2-y_1y_2-x_1x_2)^2+(r_1y_2+r_2y_1)^2}\delta_1 E, \tag{6b}$$

$$\delta_1 I_F^{imag} = \frac{(r_1+r_2)(r_1y_2+r_2y_1)-(r_1r_2-y_1y_2-x_1x_2)[y_1+y_2+(n_1/n_2)x_1-(n_2/n_1)x_2]}{(r_1r_2-y_1y_2-x_1x_2)^2+(r_1y_2+r_2y_1)^2}\delta_1 E, \tag{6c}$$

where $\delta_1 I_F^{real}$ and $\delta_1 I_F^{imag}$ are the real and imaginary component of the faradaic a.c. current-density, respectively, and r_1, r_2, y_1, y_2, x_1, and x_2 are given by

$$r_1 = 1/(\partial I(1)/\partial E), \tag{7a}$$

$$r_2 = 1/(\partial I(2)/\partial E), \tag{7b}$$

$$y_1 = (1/\omega n_1 F)[-(\partial I(1)/\partial \Gamma_O) + (\partial I(1)/\partial \Gamma_S)]/(\partial I(1)/\partial E), \tag{7c}$$

$$y_2 = (1/\omega n_2 F)[-(\partial I(2)/\partial \Gamma_S) + (\partial I(2)/\partial \Gamma_R)]/(\partial I(2)/\partial E), \tag{7d}$$

$$x_1 = (1/\omega n_1 F)(\partial I(1)/\partial \Gamma_S)/(\partial I(1)/\partial E), \tag{7e}$$

$$x_2 = (1/\omega n_2 F)(\partial I(2)/\partial \Gamma_S)/(\partial I(2)/\partial E). \tag{7f}$$

Because of the specific adsorption of the reactants, the non-faradaic impedance may differ from that observed in the absence of the electroactive species. In this case we can assume that the surface charge density on the electrode, q, is a function of E, Γ_O, Γ_S, and Γ_R only. Thus for sinusoidal variation of the nonfaradaic current-density we have for the first harmonic,[27]

$$\begin{aligned}\delta_1 I_{NF} &= (dq/dt)_{ac} \\ &= j\omega[(\partial q/\partial E)\delta_1 E + (\partial q/\partial \Gamma_O)\delta_1 \Gamma_O + (\partial q/\partial \Gamma_S)\delta_1 \Gamma_S \\ &\quad + (\partial q/\partial \Gamma_R)\delta_1 \Gamma_R].\end{aligned} \tag{8}$$

From Eqs. 5a, 5b, 5c, and 8 we obtain for the non-faradaic a.c. current-density,

$$\begin{aligned}\delta_1 I_{NF} &= [(m_1-n_1)/n_1]\delta_1 I_F(1) + [(m_2-n_2)/n_2]\delta_1 I_F(2) \\ &\quad + j\omega(\partial q/\partial E)\delta_1 E\end{aligned} \tag{9}$$

where $(m_1-n_1)/n_1$ and $(m_2-n_2)/n_2$ are given by

$$(m_1-n_1)/n_1 = (1/n_1F)[(\partial q/\partial \Gamma_O)-(\partial q/\partial \Gamma_S)], \tag{10a}$$

$$(m_2-n_2)/n_2 = (1/n_2F)[(\partial q/\partial \Gamma_S)-(\partial q/\partial \Gamma_R)], \tag{10b}$$

Thus for the total (faradaic and non-faradaic) a.c. current-density we obtain

$$\begin{aligned}\delta_1 I_t &= \delta_1 I_F + \delta_1 I_{NF} \\ &= (m_1/n_1)\delta_1 I_F(1) + (m_2/n_2)\delta_1 I_F(2) + j\omega(\partial q/\partial E)\delta_1 E,\end{aligned} \tag{11}$$

and the real and imaginary component of the total a.c. current are

$$\delta_1 I_t^{real} = (m_1/n_1)\delta_1 I_F^{real}(1) + (m_2/n_2)\delta_1 I_F^{real}(2), \tag{12a}$$

$$\begin{aligned}\delta_1 I_t^{imag} &= (m_1/n_1)\delta_1 I_t^{imag}(1) + (m_2/n_2)\delta_1 I_F^{imag}(2) \\ &\quad + \omega(\partial q/\partial E)\delta_1 E,\end{aligned} \tag{12b}$$

where $\delta_1 I_F^{real}(i)$ and $\delta_1 I_F^{imag}(i)$ are the real and imaginary component of $\delta_1 I_F(i)$, respectively, and are given by

$$\delta_1 I_F^{real}(1) = \frac{r_2(r_1r_2-y_1y_2-x_1x_2)+(r_1y_2+r_2y_1)[y_2+(n_1/n_2)x_1]}{(r_1r_2-y_1y_2-x_1x_2)^2+(r_1y_2+r_2y_1)^2}\times \delta_1 E, \tag{13a}$$

$$\delta_1 I_F^{real}(2) = \frac{r_1(r_1r_2-y_1y_2-x_1x_2)+(r_1y_2+r_2y_1)[y_1-(n_2/n_1)x_2]}{(r_1r_2-y_1y_2-x_1x_2)^2+(r_1y_2+r_2y_1)^2}\times \delta_1 E, \tag{13b}$$

$$\delta_1 I_F^{imag}(1) = \frac{r_2(r_1y_2+r_2y_1)-(r_1r_2-y_1y_2-x_1x_2)[y_2+(n_1/n_2)x_1]}{(r_1r_2-y_1y_2-x_1x_2)^2+(r_1y_2+r_2y_1)^2}\times \delta_1 E, \tag{13c}$$

$$\delta_1 I_F^{imag}(2) = \frac{r_1(r_1y_2+r_2y_1)-(r_1r_2-y_1y_2-x_1x_2)[y_1-(n_2/n_1)x_2]}{(r_1r_2-y_1y_2-x_1x_2)^2+(r_1y_2+r_2y_1)^2}\times \delta_1 E. \tag{13d}$$

As pointed out previously,[3] the term $\omega(\partial q/\partial E)\delta_1 E$ on the right-hand side of Eq. 12b can be estimated from double-layer capacity measurements employing very high frequencies and for practical purpose can be eliminated approximately by the conventional method of correction for a.c. base current as usually used in a.c. polarographic technique:

$$\begin{aligned}\delta_1 I_{corr}^{imag} &= \delta_1 I_t^{imag} - \omega(\partial q/\partial E)\delta_1 E \\ &= (m_1/n_1)\delta_1 I_F^{imag}(1) + (m_2/n_2)\delta_1 I_F^{imag}(2).\end{aligned} \tag{12c}$$

On the other hand it is very difficult to estimate the terms (m_1/n_1) and (m_2/n_2) experimentally. However, since the potential range in which the faradaic current of each step appears does not exceed a few tenths of a volt, it would be reasonable to assume that these terms are practically constant within the range studied.

In a similar manner as has been done in the previous work,[3] we assume that the current-potential-concentration characteristic can be expressed as

$$I_F = I_F(1) + I_F(2) \tag{14a}$$

$$I_F(1) = n_1F(\overleftarrow{V}(1)-\vec{V}(1)) \tag{14b}$$

$$I_F(2) = n_2F(\overleftarrow{V}(2)-\vec{V}(2)) \tag{14c}$$

$$\overleftarrow{V}(1) = k_s'(1)f_2\theta_t B_S(1)^{-1}\exp[\beta_1(n_1F/RT)(E-E_{o1})] \times \exp[-a_{SS}f_2\theta_t - a_{SO}f_1\theta_t - a_{SR}(1-f_1-f_2)\theta_t] \tag{14d}$$

$$\vec{V}(1) = k_s'(1)f_1\theta_t B_O(1)^{-1}\exp[-\alpha_1(n_1F/RT)(E-E_{o1})] \times \exp[-a_{OO}f_1\theta_t - a_{OS}f_2\theta_t - a_{OR}(1-f_1-f_2)\theta_t] \tag{14e}$$

$$\overleftarrow{V}(2) = k_s'(2)(1-f_1-f_2)\theta_t B_R(2)^{-1}\exp[\beta_2(n_2F/RT)(E-E_{o2})] \times \exp[-a_{RR}(1-f_1-f_2)\theta_t - a_{RO}f_1\theta_t - a_{RS}f_2\theta_t] \tag{14f}$$

$$\vec{V}(2) = k_s'(2)f_2\theta_t B_S(2)^{-1}\exp[-\alpha_2(n_2F/RT)(E-E_{o2})] \times \exp[-a_{SS}f_2\theta_t - a_{SO}f_1\theta_t - a_{SR}(1-f_1-f_2)\theta_t]. \tag{14g}$$

In these equations $B_i(1)$ and $B_i(2)$ are constants related to the molar adsorption energies of species i on the electrode surface at $E=E_{o1}$ and $E=E_{o2}$, respectively; a_{ij} is the Frumkin's a-parameter of interaction between

the adsorbed molecules i and j (a_{ij} is positive for attraction and negative for repulsion); θ_t is the total coverage defined by $\theta_t=\Gamma_t/\Gamma_m=\theta_O+\theta_S+\theta_R$ with $\theta_O=\Gamma_O/\Gamma_m$, $\theta_S=\Gamma_S/\Gamma_m$, $\theta_R=\Gamma_R/\Gamma_m$, and $\Gamma_t=\Gamma_O+\Gamma_S+\Gamma_R=\overline{\Gamma}_O+\overline{\Gamma}_S+\overline{\Gamma}_R$, Γ_m being the maximum value of the total surface concentration; $f_1=\theta_O/\theta_t$, $f_2=\theta_S/\theta_t$; $k'_s(1)=k_s(1)\Gamma_m$; $k'_s(2)=k_s(2)\Gamma_m$; $k_s(1)$ and $k_s(2)$ are respectively the rate constants of the first and second charge transfer step at the formal standard potentials of the surface redox reactions, E'_{o1} and E'_{o2}, which are defined by

$$E'_{o1}=E_{o1}+[RT/(\alpha_1+\beta_1)n_1F][\ln(B_S(1)/B_O(1))-(1/3)(a_{OO}-a_{SS}+a_{OS}-a_{SO}+a_{OR}-a_{RS})\theta_t] \quad (15a)$$

$$E'_{o2}=E_{o2}+[RT/(\alpha_2+\beta_2)n_1F][\ln(B_R(2)/(B_S(2))-(1/3)(a_{SS}-a_{RR}+a_{SR}-a_{RS}+a_{SO}-a_{RO})\theta_t] \quad (15b)$$

α_i and β_i (i=1 and 2) are the transfer coefficients for cathodic and anodic charge transfer of the i-th redox step, respectively. E_{o1} and E_{o2} correspond to the standard potentials of the redox couples O/S and S/R in the bulk of solution, respectively. Here we shall make the following two assumptions: (1) α_i's and β_i's are independent of the potential, and (2) the a_{ij}-parameters are independent of the potential. These assumptions will be reasonable as the first approximation, because the potential range in which the faradaic a.c. current appears does not exceed a few tenths of a volt.

From Eqs. 7a to 7f and 14a to 14g we obtain

$$r_1=(1/n_1F)[\beta_1(n_1F/RT)\overleftarrow{V}_{dc}(1)+\alpha_1(n_1F/RT)\vec{V}_{dc}(1)]^{-1} \quad (16a)$$

$$r_2=(1/n_2F)[\beta_2(n_2F/RT)\overleftarrow{V}_{dc}(2)+\alpha_2(n_2F/RT)\vec{V}_{dc}(2)]^{-1} \quad (16b)$$

$$y_1=(r_1/\omega)\{\vec{V}_{dc}(1)[(1/\overline{\Gamma}_O)-(a_{OO}-a_{OS})(\theta_t/\Gamma_t)]+\overleftarrow{V}_{dc}(1)[(1/\overline{\Gamma}_S)-(a_{SS}-a_{SO})(\theta_t/\Gamma_t)]\} \quad (16c)$$

$$y_2=(r_2/\omega)\{\vec{V}_{dc}(2)[(1/\overline{\Gamma}_S)-(a_{SS}-a_{SR})(\theta_t/\Gamma_t)]+\overleftarrow{V}_{dc}(2)[(1/\overline{\Gamma}_R)-(a_{RR}-a_{RS})(\theta_t/\Gamma_t)]\} \quad (16d)$$

$$x_1=(r_1/\omega)[\overleftarrow{V}_{dc}(1)(1/\overline{\Gamma}_S)-(\overleftarrow{V}_{dc}(1)a_{SS}-\vec{V}_{dc}(1)a_{OS})(\theta_t/\Gamma_t)] \quad (16e)$$

$$x_2=-(r_2/\omega)[\vec{V}_{dc}(2)(1/\overline{\Gamma}_S)-(\vec{V}_{dc}(2)a_{SS}-\overleftarrow{V}_{dc}(2)a_{RS})(\theta_t/\Gamma_t)]. \quad (16f)$$

Here $\overleftarrow{V}_{dc}(1)=\overleftarrow{V}(1)[E=E_{dc}, f_1=\overline{f_1}, f_2=\overline{f_2}]$, $\vec{V}_{dc}(1)=\vec{V}(1)[E=E_{dc}, f_1=\overline{f_1}, f_2=\overline{f_2}]$, $\overleftarrow{V}_{dc}(2)=\overleftarrow{V}(2)[E=E_{dc}, f_1=\overline{f_1}, f_2=\overline{f_2}]$, and $\vec{V}_{dc}(2)=\vec{V}(2)[E=E_{dc}, f_1=\overline{f_1}, f_2=\overline{f_2}]$ with $\overline{f_1}=\overline{\Gamma}_O/\Gamma_t$ and $\overline{f_2}=\overline{\Gamma}_S/\Gamma_t$, and these are related to the faradaic d.c. current-densities by

$$(I_F(1))_{dc}/n_1F=\overleftarrow{V}_{dc}(1)-\vec{V}_{dc}(1), \quad (17a)$$

$$(I_F(2))_{dc}/n_2F=\overleftarrow{V}_{dc}(2)-\vec{V}_{dc}(2). \quad (17b)$$

(i) A.c. Polarization with Negligible Rectification[27] *at D.c. Equiliblium Potential*: In this case

$$(\overleftarrow{V}_{dc}(1)-\vec{V}_{dc}(1))_{equilibrium}=0 \quad (18a)$$

$$(\overleftarrow{V}_{dc}(2)-\vec{V}_{dc}(2))_{equilibrium}=0 \quad (18b)$$

and the mean surface-coverage fractions $\overline{f_1}=\overline{\Gamma}_O/\Gamma_t$ and $\overline{f_2}=\overline{\Gamma}_S/\Gamma_t$ are given by

$$E_{dc}=E_{o1}+[RT/(\alpha_1+\beta_1)n_1F][\ln(B_S(1)/B_O(1))-(1/3)(a_{OO}-a_{SS}+a_{OS}-a_{SO}+a_{OR}-a_{SR})\theta_t+\ln(\bar{f}_1/\bar{f}_2)+(1/3)(1-3\bar{f}_1)G_1\theta_t+(1/3)(1-3\bar{f}_2)H_1\theta_t] \quad (19a)$$

$$E_{dc}=E_{o2}+[RT/(\alpha_2+\beta_2)n_2F][\ln(B_R(2)/B_S(2))-(1/3)(a_{SS}-a_{RR}+a_{SR}-a_{RS}+a_{SO}-a_{RO})\theta_t+\ln(\bar{f}_2/(1-\bar{f}_1-\bar{f}_2))+(1/3)(1-3\bar{f}_1)G_2\theta_t+(1/3)(1-3\bar{f}_2)H_2\theta_t] \quad (19b)$$

with

$$G_1=a_{OO}-a_{OR}-a_{SO}+a_{SR} \quad (20a)$$

$$H_1=a_{OS}-a_{OR}-a_{SS}+a_{SR} \quad (20b)$$

$$G_2=a_{SO}-a_{SR}-a_{RO}+a_{RR} \quad (20c)$$

$$H_2=a_{SS}-a_{SR}-a_{RS}+a_{RR} \quad (20d)$$

In this case r_1, r_2, y_1, y_2, x_1, and x_2 are given by

$$r_1=[(\alpha_1+\beta_1)(n_1F/RT)I_o(1)]^{-1} \quad (21a)$$

$$r_2=[(\alpha_2+\beta_2)(n_2F/RT)I_o(2)]^{-1} \quad (21b)$$

$$y_1=[(\alpha_1+\beta_1)(n_1^2F^2/RT)\omega\Gamma_t]^{-1}\times[(1/\bar{f}_1)+(1/\bar{f}_2)-(G_1-H_1)\theta_t] \quad (21c)$$

$$y_2=[(\alpha_2+\beta_2)(n_2^2F^2/RT)\omega\Gamma_t]^{-1}\times[(1/\bar{f}_2)+(1/(1-\bar{f}_1-\bar{f}_2))-H_2\theta_t] \quad (21d)$$

$$x_1=[(\alpha_1+\beta_1)(n_1^2F^2/RT)\omega\Gamma_t]^{-1}[(1/\bar{f}_2)-(a_{SS}-a_{OS})\theta_t] \quad (21e)$$

$$x_2=-[(\alpha_2+\beta_2)(n_2^2F^2/RT)\omega\Gamma_t]^{-1}[(1/\bar{f}_2)-(a_{SS}-a_{RS})\theta_t] \quad (21f)$$

where $I_o(1)$ and $I_o(2)$ are respectively the exchange current densities of the first and second step at $E=E_{eq}$, and are given by

$$I_o(1)=n_1F\Gamma_tk_s(1)(\bar{f}_1B_O(1)^{-1}\gamma_O)^{\beta_1/(\alpha_1+\beta_1)}\times(\bar{f}_2B_S(1)^{-1}\gamma_S)^{\alpha_1/(\alpha_1+\beta_1)} \quad (22a)$$

$$I_o(2)=n_2F\Gamma_tk_s(2)(\bar{f}_2B_S(2)^{-1}\gamma_S)^{\beta_2/(\alpha_2+\beta_2)}\times((1-\bar{f}_1-\bar{f}_2)B_R(2)^{-1}\gamma_R)^{\alpha_2/(\alpha_2+\beta_2)} \quad (22b)$$

with

$$\gamma_O=\exp\{-[a_{OO}\bar{f}_1+a_{OS}\bar{f}_2+a_{OR}(1-\bar{f}_1-\bar{f}_2)]\theta_t\} \quad (23a)$$

$$\gamma_S=\exp\{-[a_{SS}\bar{f}_2+a_{SO}\bar{f}_1+a_{SR}(1-\bar{f}_1-\bar{f}_2)]\theta_t\} \quad (23b)$$

$$\gamma_R=\exp\{-[a_{RR}(1-\bar{f}_1-\bar{f}_2)+a_{RO}\bar{f}_1+a_{RS}\bar{f}_2]\theta_t\} \quad (23c)$$

The phase angle, ψ, is given by

$$\cot\psi=(\delta_1I_F^{real}/\delta_1I_F^{imag})=\frac{(r_1r_2-y_1y_2-x_1x_2)(r_1+r_2)+(r_1y_2+r_2y_1)[y_1+y_2+(n_1/n_2)x_1-(n_2/n_1)x_2]}{(r_1y_2+r_2y_1)(r_1+r_2)-(r_1r_2-y_1y_2-x_1x_2)[y_1+y_2+(n_1/n_2)x_1-(n_2/n_1)x_2]} \quad (24)$$

(ii) A.c. Polarography and Voltammetry for D.c. Reversible Steps: Equations 19a, 19b, 21a to 21f, and 24 are applicable without alteration to a.c. polarography and a.c. cyclic voltammetry of the two-step surface redox reaction, when both the steps (1a) and (1b) are d.c. reversible (d.c. Nernstian), that is, when $k_s(1)\tau\gg1$ and $k_s(2)\tau\gg1$ in a.c. polarography with a d.m.e. whose drop time is τ or when $4RTk_s(1)/n_1Fv\gg1$ and

$4RTk_s(2)/n_2Fv \gg 1$ in a.c. voltammetry with the potential sweep rate of v;

$$(\overleftarrow{V}_{dc}(1)-\overrightarrow{V}_{dc}(1))_{dc\ reversible} \approx 0 \tag{25a}$$

and

$$(\overleftarrow{V}_{dc}(2)-\overrightarrow{V}_{dc}(2))_{dc\ reversible} \approx 0. \tag{25b}$$

Simplified Cases

In the following we shall consider several simplified cases, in which both the redox steps (1a) and (1b) are d.c. reversible, and $n_1=n_2=n$, $\alpha_1=\alpha_2=\alpha$, and $\beta_1=\beta_2=\beta$.

Case (I): $a=a_{OO}=a_{OS}=a_{OR}=a_{SS}=a_{SO}=a_{SR}=a_{RR}=a_{RO}=a_{RS}$. When all the interaction parameters a_{ij}'s are of the same value, a, the effect of the interaction between the adsorbed reactants on a.c. waves is characterized implicitly by the parameter a in Eqs. 27a and 27b; that is, the terms r_1, r_2, y_1, y_2, x_1, and x_2 are reduced to

$$r_1 = \left[(\alpha+\beta)nF(nF/RT)k_{sap}(1)\Gamma_t\frac{(\sqrt{K})^{\alpha/(\alpha+\beta)}\rho^{\beta/(\alpha+\beta)}\rho}{(1+\sqrt{K}\rho+\rho^2)}\right]^{-1} \tag{26a}$$

$$r_2 = \left[(\alpha+\beta)nF(nF/RT)k_{sap}(2)\Gamma_t\frac{(\sqrt{K})^{\beta/(\alpha+\beta)}\rho^{\beta/(\alpha+\beta)}}{(1+\sqrt{K}\rho+\rho^2)}\right]^{-1} \tag{26b}$$

$$y_1 = \left[(\alpha+\beta)nF(nF/RT)\omega\Gamma_t\frac{\sqrt{K}\rho^2}{(1+\sqrt{K}\rho+\rho^2)(\sqrt{K}+\rho)}\right]^{-1} \tag{26c}$$

$$y_2 = \left[(\alpha+\beta)nF(nF/RT)\omega\Gamma_t\frac{\sqrt{K}\rho}{(1+\sqrt{K}\rho+\rho^2)(\sqrt{K}\rho+1)}\right]^{-1} \tag{26d}$$

$$x_1 = -x_2 = \left[(\alpha+\beta)nF(nF/RT)\omega\Gamma_t\frac{\sqrt{K}\rho}{(1+\sqrt{K}\rho+\rho^2)}\right]^{-1} \tag{26e}$$

where

$$k_{sap}(1) = k_s(1)B_O(1)^{-\beta/(\alpha+\beta)}B_S(1)^{-\alpha/(\alpha+\beta)}\exp(-a\theta_t) \tag{27a}$$

$$k_{sap}(2) = k_s(2)B_S(2)^{-\beta/(\alpha+\beta)}B_R(2)^{-\alpha/(\alpha+\beta)}\exp(-a\theta_t) \tag{27b}$$

$$K = \exp[(\alpha+\beta)(nF/RT)(E'_{o1}-E'_{o2})] \tag{28}$$

$$\rho = \exp[(\alpha+\beta)(nF/RT)(E_{dc}-E'_o)] \tag{29}$$

with

$$E'_{o1} = E_{o1} + [RT/(\alpha+\beta)nF]\ln[B_S(1)/B_O(1)] \tag{30}$$

$$E'_{o2} = E_{o2} + [RT/(\alpha+\beta)nF]\ln[B_R(2)/B_S(2)] \tag{31}$$

$$E'_o = (E'_{o1}+E'_{o2})/2. \tag{32}$$

In these equations K corresponds to the formation constant of the adsorbed intermediate S_{ad} defined by

$$K = [S_{ad}]^2/[O_{ad}][R_{ad}] \tag{33}$$

and E'_o to the formal standard potential of the adsorbed redox couple O_{ad}/R_{ad}.

From Eqs. 6b, 6c, and 26a to 26e, $\delta_1 I_F^{real}$ and $\delta_1 I_F^{imag}$ are given by

$$\delta_1 I_F^{real} = (\alpha+\beta)nF(nF/RT)\omega\Gamma_t\frac{\sqrt{K}\rho\rho^{\alpha/(\alpha+\beta)}}{(1+\sqrt{K}\rho+\rho^2)} \times \frac{\{\sqrt{K}[\lambda_1\lambda_2\rho^{2\alpha/(\alpha+\beta)}-(1+\sqrt{K}\rho+\rho^2)][\lambda_1(\sqrt{K})^{\beta/(\alpha+\beta)}+\lambda_2(\sqrt{K})^{\alpha/(\alpha+\beta)}\rho]+(\sqrt{K}+4\rho+\sqrt{K}\rho^2)[\lambda_1(\sqrt{K})^{\beta/(\alpha+\beta)}(1+\sqrt{K}\rho)+\lambda_2(\sqrt{K})^{\alpha/(\alpha+\beta)}(\sqrt{K}+\rho)]\}\delta_1 E}{\{K[\lambda_1\lambda_2\rho^{2\alpha/(\alpha+\beta)}-(1+\sqrt{K}\rho+\rho^2)]^2+[\lambda_1(\sqrt{K})^{\beta/(\alpha+\beta)}(1+\sqrt{K}\rho)+\lambda_2(\sqrt{K})^{\alpha/(\alpha+\beta)}(\sqrt{K}+\rho)]^2\rho^{2\alpha/(\alpha+\beta)}\}} \tag{34a}$$

$$\delta_1 I_F^{imag} = (\alpha+\beta)nF(nF/RT)\omega\Gamma_t\frac{\sqrt{K}\rho}{(1+\sqrt{K}\rho+\rho^2)} \times \frac{\{\rho^{2\alpha/(\alpha+\beta)}[\lambda_1(\sqrt{K})^{\beta/(\alpha+\beta)}+\lambda_2(\sqrt{K})^{\alpha/(\alpha+\beta)}\rho][\lambda_1(\sqrt{K})^{\beta/(\alpha+\beta)}(1+\sqrt{K}\rho)+\lambda_2(\sqrt{K})^{\alpha/(\alpha+\beta)}(\sqrt{K}+\rho)]-\sqrt{K}[\lambda_1\lambda_2\rho^{2\alpha/(\alpha+\beta)}-(1+\sqrt{K}\rho+\rho^2)][\sqrt{K}+4\rho+\sqrt{K}\rho^2]\}\delta_1 E}{\{K[\lambda_1\lambda_2\rho^{2\alpha/(\alpha+\beta)}-(1+\sqrt{K}\rho+\rho^2)]^2+[\lambda_1(\sqrt{K})^{\beta/(\alpha+\beta)}(1+\sqrt{K}\rho)+\lambda_2(\sqrt{K})^{\alpha/(\alpha+\beta)}(\sqrt{K}+\rho)]^2\rho^{2\alpha/(\alpha+\beta)}\}} \tag{34b}$$

with

$$\lambda_1 = \omega/k_{sap}(1) \tag{35a}$$

$$\lambda_2 = \omega/k_{sap}(2). \tag{35b}$$

For the phase angle we obtain

$$\cot\psi = \delta_1 I_F^{real}/\delta_1 I_F^{imag} = \frac{\{\sqrt{K}[\lambda_1\lambda_2\rho^{2\alpha/(\alpha+\beta)}-(1+\sqrt{K}\rho+\rho^2)][\lambda_1(\sqrt{K})^{\beta/(\alpha+\beta)}+\lambda_2(\sqrt{K})^{\alpha/(\alpha+\beta)}\rho]+(\sqrt{K}+4\rho+\sqrt{K}\rho^2)[\lambda_1(\sqrt{K})^{\beta/(\alpha+\beta)}(1+\sqrt{K}\rho)+\lambda_2(\sqrt{K})^{\alpha/(\alpha+\beta)}(\sqrt{K}+\rho)]\}\rho^{\alpha/(\alpha+\beta)}}{\{\rho^{2\alpha/(\alpha+\beta)}[\lambda_1(\sqrt{K})^{\beta/(\alpha+\beta)}+\lambda_2(\sqrt{K})^{\alpha/(\alpha+\beta)}\rho][\lambda_1(\sqrt{K})^{\beta/(\alpha+\beta)}(1+\sqrt{K}\rho)+\lambda_2(\sqrt{K})^{\alpha/(\alpha+\beta)}(\sqrt{K}+\rho)]-\sqrt{K}[\lambda_1\lambda_2\rho^{2\alpha/(\alpha+\beta)}-(1+\sqrt{K}\rho+\rho^2)][\sqrt{K}+4\rho+\sqrt{K}\rho^2]\}}. \tag{36}$$

Case (I)-(i): *A.c. Wave (I).* When $k_{sap}(1)=k_{sap}(2)=k_{sap}$ and $\alpha=\beta$, it can easily be shown from Eqs. 34a, 34b, and 36 that both components of the a.c. wave as well as the $\cot\psi$ *versus* E_{dc} curve are symmetrical with respect to the E'_o-axis and that the value of $\cot\psi$ at $E_{dc}=E'_o$, $[\cot\psi]_{E_{dc}=E'_o}$, is given by

$$[\cot\psi]_{E_{dc}=E'_o} = \lambda/(K)^{1/4} \tag{37}$$

with $\lambda=\omega/k_{sap}$. Thus in this simplified case a plot of $[\cot\psi]_{E_{dc}=E_o}$ against angular frequency yields a straight line passing through the origin with a slope of $k_{sap}^{-1}(K)^{-1/4}$. Since the thermodynamic parameter K can, if n and $(\alpha+\beta)$ are known, be determined from the reversible linear sweep (d.c.) voltammograms as will be described in *Case (I)-(iii)*, we can determine the apparent rate constant, k_{sap}, from this plot.

Case (I)-(ii): *Reversible A.c. Wave(I).* When

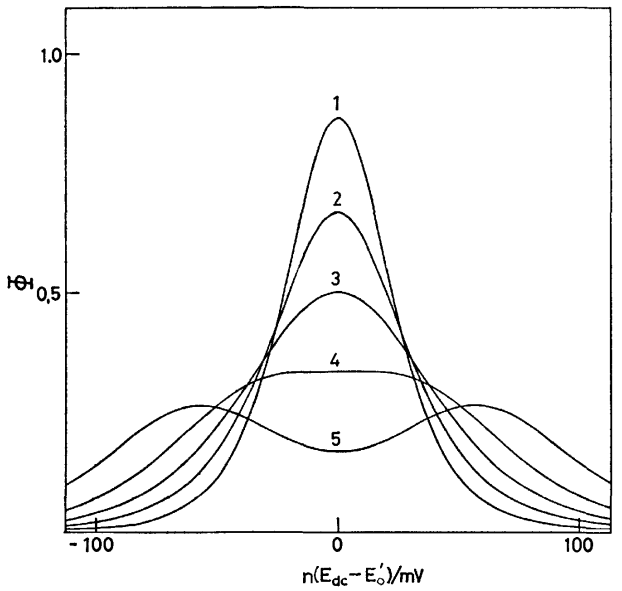

Fig. 1. Normalized reversible a.c. wave(I) calculated by Eq. 38 with $\alpha+\beta=1$.
K: (1); 0.1, (2); 1, (3); 4, (4); 16, (5); 100.

both the rate constants $k_{sap}(1)$ and $k_{sap}(2)$ are so large (*i.e.*, $\omega/k_{sap}(1)\ll 1$ and $\omega/k_{sap}(2)\ll 1$) that the conditions $(r_1/y_1)\ll 1$ and $(r_2/y_2)\ll 1$ are satisfied, Eq. 6 is reduced to

$$(\delta_1 I_F)_{rev} = (\delta_1 I_F^{imag})_{rev} = \frac{y_1+y_2+x_1-x_2}{y_1y_2+x_1x_2}\delta_1 E$$
$$= (\alpha+\beta)nF(nF/RT)\omega\Gamma_t \times \frac{\rho[\rho(\sqrt{K}\rho+2)+(\sqrt{K}+2\rho)]}{(1+\sqrt{K}\rho+\rho^2)^2}\delta_1 E \quad (38)$$

and

$$\cot\psi \to 0.$$

Namely, $\delta_1 I_F^{real}$ becomes vanishingly small and ψ approaches 90°. In Eq. 38 ρ and K are given by Eqs. 29 and 28, respectively. This equation predicts that the reversible a.c. wave (voltammograms with stationary electrode as well as polarograms with d.m.e.) is symmetrical with respect to the potential $E_{dc}=E_o'$. The normalized a.c. waves, $\Phi\equiv(\delta_1 I_F)_{rev}/nF(nF/RT)\omega\Gamma_t\delta_1 E$, are shown in Fig. 1 for different values of K at $(\alpha+\beta)=1$.

When $K\ll 16$, there is only one peak, of which the peak potential E_p^{rev} is equal to E_o'. The peak current, $(\delta_1 I_F^p)_{rev}$, and the half-peak width, $\Delta E_{p/2}^{rev}$, are given by

$$(\delta_1 I_F^p)_{rev} = (\alpha+\beta)nF(nF/RT)\omega\Gamma_t\frac{2}{(2+\sqrt{K})}\delta_1 E \quad (39)$$

$$\Delta E_{p/2}^{rev} = [2RT/(\alpha+\beta)nF]\,|\ln\xi| \quad (40)$$

where ξ is the solution of the equation: $\xi^4-K\xi^3+(K-4\sqrt{K}-6)\xi^2-K\xi+1=0$.

On the other hand, there are two peaks for $K>16$. Their peak potentials E_{p1}^{rev} and E_{p2}^{rev} are given by

$$E_{p1}^{rev} = E_o' + [RT/(\alpha+\beta)nF] \times \ln[(K-8)+\sqrt{(K-4)(K-16)}]/2\sqrt{K} \quad (41a)$$

$$E_{p2}^{rev} = E_o' + [RT/(\alpha+\beta)nF] \times \ln[(K-8)-\sqrt{(K-4)(K-16)}]/2\sqrt{K}. \quad (41b)$$

Thus the thermodynamic parameter K can be determined from the half-peak width, $\Delta E_{p/2}^{rev}$, for $K\leqslant 16$, or from the peak separation, $|E_{p1}^{rev}-E_{p2}^{rev}|$, for $K>16$, if $(\alpha+\beta)$ and n are known.

Case (I)-(iii): *Reversible D.c. Wave.* Furthermore it can be shown that the theoretical expression of the reversible linear sweep (d.c.) voltammogram is the same as that of the reversible a.c. wave if the term $\omega\delta_1 E$ is replaced by the potential sweep rate v. That is, the shape of the reversible linear sweep (d.c.) voltammogram is the same as that of the reversible a.c. wave, and the peak potential of the reversible linear sweep (d.c.) voltammogram, E_p^{dc}, coincides with the peak potential of the reversible a.c. wave, E_p^{rev}; $E_p^{dc}=E_p^{rev}=E_o'$, and the same discussion as described in *Case (I)-(ii)* is applicable to the reversible linear sweep (d.c.) voltammograms.

Application of these simplified equations given in *Case (I)-(i)* through *(I)-(iii)* to the electrode processes of flavins irreversibly adsorbed on mercury electrode surface will be reported in a succeeding paper.

Case (II): $a_{OO}+a_{SO}=a_{OS}+a_{SS}=a_{OR}+a_{SR}=a_{SO}+a_{RO}=a_{SS}+a_{RS}=a_{SR}+a_{RR}$, $a_{ij}=a_{ji}$ *(i,j=O, S, or R) and* $\alpha=\beta$. In this simplified case, the effects of the interaction between the adsorbed reactants on a.c. waves can be characterized explicitly by an interaction parameter $G=2(a_1-a_2)$ (Eq. 44) and implicitly by (a_1+a_2) (Eq. 43). That is, the terms r_1, r_2, y_1, y_2, x_1, and x_2 are reduced to

$$r_1 = [2\alpha nF(nF/RT)k_{sap}(1)\Gamma_t(\bar{f}_1\bar{f}_2)^{1/2}]^{-1} \quad (42a)$$

$$r_2 = [2\alpha nF(nF/RT)k_{sap}(2)\Gamma_t\bar{f}_2^{1/2}(1-\bar{f}_1-\bar{f}_2)^{1/2}]^{-1} \quad (42b)$$

$$y_1 = [2\alpha nF(nF/RT)\omega\Gamma_t]^{-1}[(1/\bar{f}_1)+(1/\bar{f}_2)-G\theta_t] \quad (42c)$$

$$y_2 = [2\alpha nF(nF/RT)\omega\Gamma_t]^{-1}[(1/\bar{f}_2)+(1/(1-\bar{f}_1-\bar{f}_2))-G\theta_t] \quad (42d)$$

$$x_1 = -x_2 = [2\alpha nF(nF/RT)\omega\Gamma_t]^{-1}[(1/\bar{f}_2)-(1/2)G\theta_t] \quad (42e)$$

where

$$k_{sap}(1) = k_s(1)(B_O(1)B_S(1))^{-1/2}\exp[-(1/2)(a_1+a_2)\theta_t] \quad (43a)$$

$$k_{sap}(2) = k_s(2)(B_S(2)B_R(2))^{-1/2}\exp[-(1/2)(a_1+a_2)\theta_t] \quad (43b)$$

and G is given by

$$G = 2(a_1-a_2) \quad (44)$$

with

$$a_1 = a_{OO} = a_{SS} = a_{RR} = a_{OR} = a_{RO} \quad (45a)$$

$$a_2 = a_{OS} = a_{SO} = a_{SR} = a_{RS}. \quad (45b)$$

The mean fractions of the surface coverages $\bar{f}_1$ and $\bar{f}_2$ are related to the d.c. potential E_{dc} by

$$E_{dc} = E_o' + [RT/2\alpha nF][\ln\sqrt{K}+\ln(\bar{f}_1/\bar{f}_2) - (1/2)(1-2\bar{f}_2)G\theta_t] \quad (46a)$$

$$E_{dc} = E_o' + [RT/2\alpha nF][-\ln\sqrt{K}+\ln(\bar{f}_2/(1-\bar{f}_1-f_2)) + (1/2)(1-2\bar{f}_2)G_t] \quad (46b)$$

where E_o' and K are respectively defined as

$$E_o' = (E_{o1}'+E_{o2}')/2 \quad (47)$$

$$K = \exp[(2\alpha nF/RT)(E'_{o1}-E'_{o2})] \quad (48)$$

with $E'_{o1}=E_{o1}+[RT/2\alpha nF]\ln[B_S(1)/B_O(1)]$ and $E'_{o2}=E_{o2}+[RT/2\alpha nF]\ln[B_R(2)/B_S(2)]$.

The a.c. wave is expressed by Eq. 6 with Eqs. 42a to 48, and the phase angle by Eq. 24 with Eqs. 42a to 48, which are, when $G=0$, reduced to the same equations as given in *Case (I)*.

Case (II)-(i): A.c. Wave(II). When it is further assumed that $k_{sap}(1)=k_{sap}(2)=k_{sap}$, it can easily be shown from these equations that both components of the a.c. wave as well as the cot ψ *versus* E_{dc} curve are symmetrical with respect to the E'_o-axis. Furthermore the value of cot ψ at $E_{dc}=E'_o$, $[\cot\psi]_{E_{dc}=E'_o}$, is given by

$$[\cot\psi]_{E_{dc}=E'_o} = (\omega/k_{sap})[2A/(2B-C-G\theta_t)] \quad (49)$$

with

$$A = [2/\eta(1-\eta)]^{1/2} \quad (50a)$$

$$B = (1+\eta)/\eta(1-\eta) \quad (50b)$$

$$C = 2/\eta \quad (50c)$$

$$\eta = \{1+(2/\sqrt{K})\exp[(1/2)(1-2\eta)G\theta_t]\}^{-1}. \quad (50d)$$

That is, $[\cot\psi]_{E_{dc}=E'_o}$ is proportional to angular frequency but in this case the slope of a plot of $[\cot\psi]_{E_{dc}=E'_o}$ *versus* ω depends on the interaction parameter $G\theta_t$ as well as K and k_{sap}. Since K and $G\theta_t$ can, if n and α are given, be determined from the reversible linear sweep (d.c.) voltammograms as will be described in *Case (II)-(iii)*, these three parameters, *i.e.*, k_{sap}, $G\theta_t$, and K, can be determined by combination of the a.c. and d.c. measurements.

Application of these simplified equations to the electrode processes of a ferredoxin irreversibly adsorbed on the surface of the dropping mercury electrode has been reported in another article.[5]

Case (II)-(ii): Reversible A.c. Wave(II). When the rate constant k_{sap} is so large compared to ω that $(r_1/y_1)\ll 1$ and $(r_2/y_2)\ll 1$, then, the a.c. wave(II) is reduced to the reversible a.c. wave(II), $\delta_1 I_F^{rev}$, which is expressed by

$$\delta_1 I_F^{rev} = (\delta_1 I_F^{imag})_{rev} = \frac{y_1+y_2+x_1-x_2}{y_1y_2+x_1x_2}\delta_1 E \quad (51)$$

and the phase angle approaches 90°. In this equation the terms y_1, y_2, and $x_1=-x_2$ are given by Eqs. 42c, 42d, and 42e, respectively. The mean fractions of the surface coverages $\overline{f_1}$ and $\overline{f_2}$ are related to the d.c. potential E_{dc} by Eqs. 46a and 46b.

These equations predict that the a.c. wave is also symmetrical with respect to the E'_o-axis. However, in contrast to *Case (I)-(ii)*, the wave shape will change with changing the total surface coverage θ_t. That is, with increasing $G\theta_t$, the normalized peak current, $\Phi_p\equiv(\delta_1 I_F^{rev})_p/nF(nF/RT)\omega\Gamma_t$, becomes larger and the half-peak width, $\Delta E_{p/2}^{rev}$, smaller, as shown, for example, for the case of $K=1$ in Fig. 2. Thus the two parameters K and G can be determined from the reversible a.c. waves measured at various values of θ_t if n and α are given.

Case (II)-(iii): Reversible D.c. Wave. It can easily be shown that the theoretical equations of the reversible linear sweep (d.c.) voltammogram are the same as those of the reversible a.c. wave if the term $\omega\delta_1 E$ is replaced by the potential sweep rate v. Thus the same discussion as described in *Case (II)-(ii)* is applicable to the reversible linear sweep (d.c.) voltammograms.

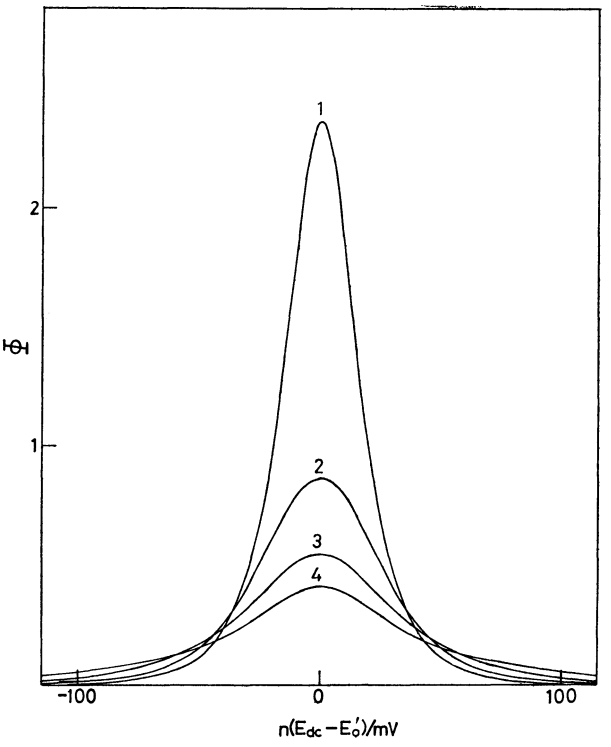

Fig. 2. Normalized reversible a.c. wave(II) calculated by Eqs. 51, 42c, 42d, 42e, 46a, and 46b with $\alpha=\beta=0.5$ and $K=1$.
$G\theta_t$: (1); 3, (2); 1, (3); −1, (4); −3.

References

1) W. R. Heineman and P. T. Kissinger, *Anal. Chem.*, **50**, 166R (1978).
2) D. K. Roe, *Anal. Chen.*, **50**, 9R (1978).
3) T. Kakutani and M. Senda, *Bull. Chem. Soc. Jpn.*, **52**, 3236 (1979).
4) T. Ikeda, K. Toriyama, and M. Senda, *Bull. Chem. Soc. Jpn.*, **52**, 1937 (1979).
5) T. Kakutani, K. Toriyama, T. Ikeda, and M. Senda, *Bull. Chem. Soc. Jpn.*, **53**, 947 (1980).
6) R. Brdička, *Z. Elektrochem.*, **47**, 319 (1941).
7) O. H. Müller, *Ann. N.Y. Acad. Sci.*, **40**, 91 (1940).
8) K. J. Vetter, *Z. Naturforsch., Teil A*, **7**, 328 (1952); **8**, 823 (1953).
9) T. Berzins and P. Delahay, *J. Am. Chem. Soc.*, **75**, 5716 (1953).
10) A. A. Vlček, *Collect. Czech. Chem. Commun.*, **22**, 1736 (1957).
11) M. Suzuki and P. J. Elving, *Collect. Czech. Chem. Commun.*, **25**, 3202 (1960).
12) J. M. Hale, *J. Electroanal. Chem. Interfacial Chem.*, **8**, 181 (1964).
13) I. Ružić, *J. Electroanal. Chem. Interfacial Chem.*, **52**, 331 (1974).
14) M. Senda, M. Senda, and I. Tachi, *Rev. Polarogr. (Kyoto)*, **10**, 142 (1962).
15) H. L. Hung and D. E. Smith, *J. Electroanal. Chem.*

Interfacial Chem., **11**, 236, 425 (1966).
16) I. Ružić and D. E. Smith, *J. Electroanal. Chem. Interfacial Chem.*, **58**, 145 (1975).
17) J. M. Hale, *J. Electroanal. Chem. Interfacial Chem.*, **8**, 408 (1964).
18) S. K. Rangarajan, *J. Electroanal. Chem. Interfacial Chem.*, **55**, 337, 363 (1974).
19) K. J. Bachmann and U. Bertocci, *Electrochim. Acta*, **15**, 1877 (1970).
20) K. J. Bachmann, *J. Electrochem. Soc.*, **118**, 226 (1971).
21) R. Kruse, *Electrochim. Acta*, **21**, 85 (1976).
22) H. Schweickert, A. A. El Miligy, A. Melendez, and W. J. Lorenz, *J. Electroanal. Chem. Interfacial Chem.*, **68**, 19 (1976).
23) M. D. Ryan, *J. Electrochem. Soc.*, **125**, 547 (1978).
24) R. K. Jain, H. C. Gaur, and B. J. Welch, *J. Electroanal. Chem. Interfacial Chem.*, **79**, 211 (1977).
25) V. Plichon and E. Laviron, *J. Electroanal. Chem. Interfacial Chem.*, **71**, 143 (1976).
26) B. B. Damaskin, O. A. Petrii, and V. V. Batrakov, "Adsorption of Organic Compounds on Electrodes," Plenum, New York (1971).
27) M. Senda and P. Delahay, *J. Phys. Chem.*, **65**, 1580 (1961).

A Study of Electronic Structure of 1,2,4,5-Tetracyanobenzene Anion Radical by Resonance Raman Effect

Kenji YOKOYAMA* and Shiro MAEDA

Research Laboratory of Resources Utilization, Tokyo Institute of Technology, Nagatsuta, Midori-ku, Yokohama 227

(Received February 8, 1980)

Resonance Raman spectrum of 1,2,4,5-tetracyanobenzene anion radical ($TCNB^-$) was measured and compared with that of the neutral molecule (TCNB). Particularly, a Raman line assigned to C_1C_2 stretching vibration decreased its frequency remarkably when TCNB was converted to $TCNB^-$. This decrease indicated that the lowest unoccupied molecular orbital (LUMO) of TCNB had a node on C_1C_2 bonding, showing that the LUMO belonged to an a_u species. Furthermore vibrational analyses of TCNB and $TCNB^-$ were carried out and the assignment of their Raman lines was confirmed.

1,2,4,5-Tetracyanobenzene (TCNB, see Fig. 1) is a familiar molecule as an electron acceptor and many spectroscopic studies have been carried out in connection with its charge transfer interaction. However, the symmetry of the lowest unoccupied molecular orbital (LUMO) of TCNB has not been certified clearly. A simple theory such as linear combination of molecular orbital (LCMO) method shows only that both of an a_u and a b_{1u} MO can become the LUMO but does not indicate which MO really is the LUMO. ESR studies do not lead to a clear conclusion, either.[1]

Recently, Takahashi and Maeda reported resonance Raman spectra of some aromatic anion radicals and found the striking resonance enhancement of their skeletal stretching vibrations.[2] They studied the change of frequency of the respective Raman lines when a neutral molecule was converted to an anion radical and showed that the change was closely related to the distribution of nodes of the LUMO which is occupied by an unpaired electron.

Therefore, in the present study, resonance Raman spectrum of TCNB anion radical ($TCNB^-$) was measured and compared with that of TCNB in order to certify the assignment of the LUMO more clearly. Furthermore $TCNB^-$ has a pseudo degeneracy in the ground electronic state, which is an interesting case among the complicated vibronic potentials. Consequently vibrational analyses were carried out taking a vibronic effect into account.

Experimental

Commercially available TCNB (Frinton Laboratories) was used after sublimation, together with one offered by Dr. M. Tahara, our laboratory. TCNB-d_2 was offered by Prof. T. Takenaka, Kyoto University. Tetracyanoethylene (TCNE), tetracyanoquinodimethane (TCNQ) and hexamethylbenzene (HMB) (Tokyo Kasei) were used after sublimation and recrystallization. Tetrahydrofuran (THF), 1,2-dimethoxyethane (DME), and *N,N*-dimethylformamide (DMF) (Wako, Special Grade) were degassed and dehydrated repeatedly *in vacuo* after distillation and used as solvents for anion radicals. Acetonitrile and dichloromethane (Wako, Spectroscopic Grade) were used without further purification.

$TCNB^-$ was prepared by reduction with alkali metals *in vacuo* as usual.[3]

Raman spectra were obtained with a JEOL 400D spectrometer equipped with a HTV 649 photomultiplier, using a CR 52G Ar^+ laser as a continuous exciting source.

All measurements were carried out at room temperature.

Results and Discussion

Resonance Raman Spectra and Their Assignment. $TCNB^-$ showed an intense absorption band at 463 nm, as shown in Fig. 2, which is in good agreement with the result by Ishitani and Nagakura.[3] Figure 3 shows the resonance Raman spectrum of $TCNB^-$ by 457.9 nm excitation in THF solution, together with the Raman spectrum of TCNB in acetonitrile solution. The observed values of Raman shift and depolariza-

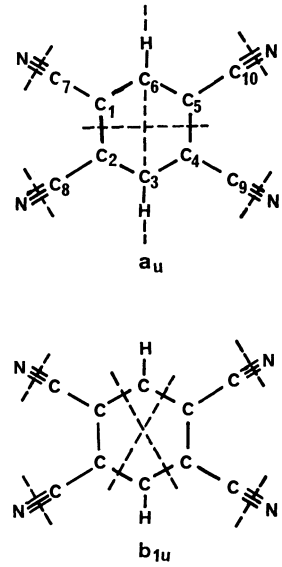

Fig. 1. The a_u MO and the b_{1u} MO of TCNB.

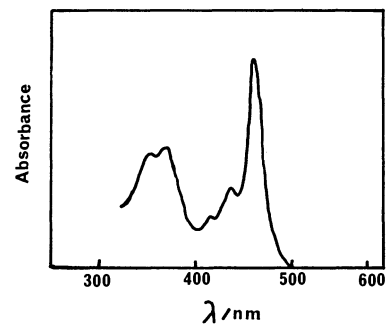

Fig. 2. Absorption spectrum of K^+TCNB^- in THF solution.

TABLE 1. OBSERVED RAMAN FREQUENCIES, DEPOLARIZATION RATIOS AND THEIR ASSIGNMENT FOR $TCNB^-$ AND $TCNB\text{-}d_2^-$

	ν (cm^{-1})		ρ_l	Assignment
K^+TCNB^-	408	m	0.22	a_g ring bend. (402 cm^{-1})
	522	s	0.27	a_g CN bend.
	679	w	0.34	a_g ring bend. (725 cm^{-1})
	792	w	0.25	
	928	s	0.34[a]	
	991	w	+	
	1039	m	0.26[b]	$522\times2=1044$
	1279	m	0.25	a_g C_1C_6 and C_1C_7 str. (1260 cm^{-1})
	1456	s	0.29	a_g C_1C_2 str. (1546 cm^{-1})
	1791	w	+	$1279+522=1801$
	1858	m	0.22	$928\times2=1856$ or $1456+408=1864$
	1976	m	0.26	$1456+522=1978$
	2198	m	0.19	a_g CN str. (2237 cm^{-1})
	2283	w	0.31	$1456+928=2384$
$K^+TCNB\text{-}d_2^-$	409	w	0.35	a_g ring bend. (403 cm^{-1})
	520	s	0.38	a_g CN bend.
	917	s	0.32[a]	
	980	w	0.33	
	1043	m	0.31[b]	$520\times2=1040$
	1266	m	0.35	a_g C_1C_6 and C_1C_7 str. (1250 cm^{-1})
	1446	s	0.27	a_g C_1C_2 str. (1539 cm^{-1})
	1792	w	0.36	$1266+520=1786$
	1844	w	0.25	$917\times2=1834$ or $1446+409=1855$
	1967	w	0.37	$1446+520=1966$
	2198	w	0.33	a_g CN str. (2243 cm^{-1})
	2362	w	0.36	$1446+917=2363$

a) In DME. b) In DMF. s; Strong, m; medium, w; week. +; Polarized but cannot be presented numerically. ( ); Observed frequencies of corresponding lines of TCNB.

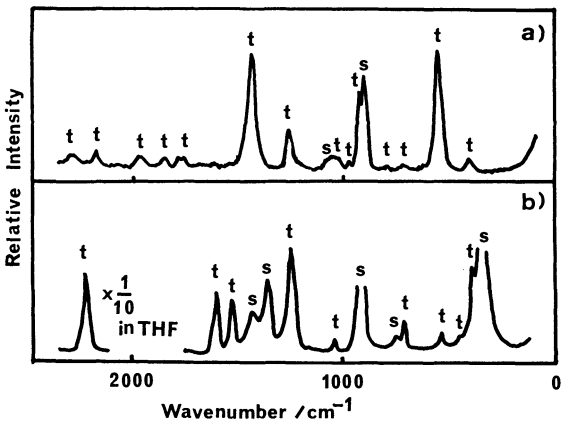

Fig. 3. Raman spectrum of $TCNB^-$ and TCNB.
a) Resonance Raman spectrum of K^+TCNB^- in THF solution (1.8×10^{-3} mol·dm^{-3}) by 457.9 nm excitation. s) Lines of solvent, t) Lines of $TCNB^-$.
b) Raman spectrum of TCNB in acetonitrile solution (2.8 mol·dm^{-3}) by 488.0 nm excitation. s) Lines of solvent, t) Lines of TCNB. A 2237 cm^{-1} line was measured in THF solution.

tion ratio of $TCNB^-$ are shown in Table 1. All of the observed lines are totally symmetric because they were strongly polarized. The spectrum is not affected by varying solvents (THF, DME, and DMF) and cations (Na^+ and K^+).

The assignment of the observed Raman lines of $TCNB^-$ was carried out by referring to the assignment of Raman lines of TCNB. Table 1 shows the assignment for $TCNB^-$ and TCNB. TCNB has three totally symmetric lines, 1260, 1546, and 2237 cm^{-1} in the region of their skeletal stretching vibrations. Takenaka *et al.* assigned these lines to a mixing mode of C_1C_6 stretching and C_1C_7 stretching, a C_1C_2 stretching and a CN stretching vibration, respectively.[4] The three lines of $TCNB^-$, 1279, 1456, and 2198 cm^{-1}, should correspond to the fundamental vibrations of TCNB, 1260, 1546, and 2237 cm^{-1}, respectively. A 725 cm^{-1} line of TCNB may correspond to one of a few weak lines of $TCNB^-$ observed in 600—700 cm^{-1} region. A 402 cm^{-1} line of TCNB corresponds to a 408 cm^{-1} line of $TCNB^-$.

The present correspondence of the three Raman lines assigned to the skeletal stretching vibrations between TCNB and $TCNB^-$, which is essential in the later discussion, was confirmed by the resonance Raman study of CT complex of TCNB. Kaya *et al.*

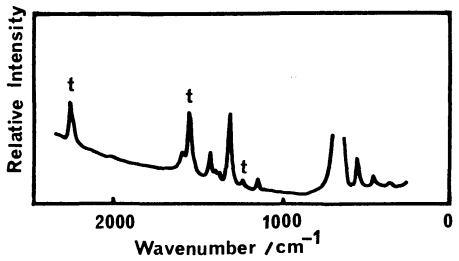

Fig. 4. Resonance Raman spectrum of HMB–TCNB in dichloromethane solution (TCNB; 0.17 mol·dm^{-3}, HMB; 0.58 mol·dm^{-3}) by 457.9 nm excitation. t) Lines of TCNB moiety.

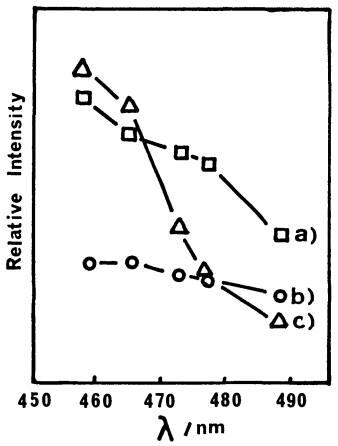

Fig. 5. Excitation profiles of the three Raman lines of HMB–TCNB.
a) 2237 cm^{-1} line, b) 1260 cm^{-1} line, c) 1546 cm^{-1} line.

reported the resonance Raman effect of weak CT complex[5] and obtained an interesting result where the degree of resonance enhancement of Raman lines of an acceptor moiety by the excitation at CT absorption band was closely related to the change in frequency of the acceptor molecule when it was converted to the anion radical. In a weak CT complex, an acceptor moiety in an excited CT state can be regarded as an anion radical. According to the Franck-Condon mechanism of Raman intensity, when a deviation of molecular geometry of an acceptor from neutral molecule to anion radical is large along a vibrational coordinate, the Raman lines of the acceptor moiety which relate to the vibrational coordinate show resonance enhancement by the excitation at CT absorption band.

TCNB forms CT complex with HMB and the complex has an absorption band of CT character at 426 nm. Figure 4 shows the observed resonance Raman spectrum of HMB–TCNB by the excitation with 457.9 nm line. The change of intensity by complex formation was observed for the three skeletal stretching vibrations of TCNB but any frequency changes were not observed. A striking enhancement was observed to take place for 1546 cm^{-1} line and a mild enhancement for 2237 cm^{-1} line, while 1260 cm^{-1} line showed an inappreciable change of intensity, as shown in Fig. 5. On the other hand, when TCNB is converted to TCNB$^-$, the above mentioned three lines of TCNB

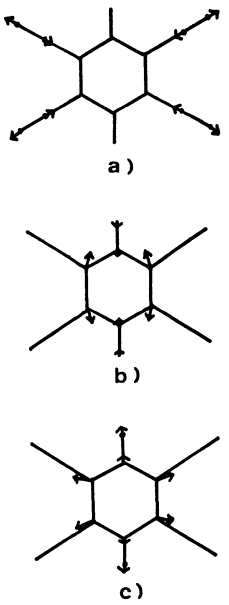

Fig. 6. The Cartesian displacements of normal vibrations of TCNB$^-$.
a) a_g 2215 cm^{-1}, b) a_g 1466 cm^{-1}, c) a_g 1259 cm^{-1}.

show the frequency changes, 1546−1456=90, 2237−2198=37, and 1260−1279=−19 cm^{-1}, respectively. These values correspond to the change of force constants, −11.6, −3.3, and +3.0%, respectively. These imply, in turn, the changes of bond order, that is, bond length of the relating CC and CN bondings. Therefore it is reasonably supported that the change of bond length from TCNB to TCNB$^-$ is striking for C_1C_2, mild for CN and C_1C_7 bondings. This inclination is parallel to that of resonance enhancement of the Raman intensity for the CT complex by the excitation at CT absorption band. Consequently, it is confirmed that the present relations of the three Raman lines between TCNB and TCNB$^-$ are reasonable.

Assignment of the LUMO of TCNB. The present analysis of Raman spectra of TCNB$^-$ led to a clearcut assignment of the LUMO of TCNB, as follows. As TCNB has four substituents on 1,2,4, and 5 positions, the two components of e_{2u} MO of benzene (one a_u MO, the other b_{1u} MO) are able to form bonding MO's with orbitals of substituents (see Fig. 1). When TCNB is reduced to TCNB$^-$, an unpaired electron occupies the LUMO of TCNB. If the a_u MO is occupied, C_1C_2 and CN bondings become to have more antibonding character, while C_1C_7 bonding becomes to have more bonding character. Therefore the force constants of the former bondings decrease, but that of the latter bonding increases. Consequently, the Raman lines assigned to C_1C_2 and CN stretching vibrations decrease their frequencies, while the line assigned to C_1C_7 stretching vibration increases its frequency. If the b_{1u} MO is occupied, the Raman lines assigned to C_1C_6 and CN stretching vibrations decrease their frequency, while the lines assigned to C_1C_7 and C_1C_2 stretching vibrations increase their frequency.

The present result shows the large decrease in fre-

Table 2. Observed and calculated fundamental frequencies of TCNE

Species	ν_{obsd}[a)]	ν_{calcd}	Assignment
a_g	2235 cm^{-1}	2243 cm^{-1}	CN str.
	1569	1561	C_1C_2 str.
	595	610	C_1C_3 str.
	535	512	($C_3C_1C_4$+CCN) bend.
		126	$C_3C_1C_4$ bend.
b_{1g}	2247	2238	CN str.
	1282	1287	C_1C_3 str. + $C_2C_1C_3$ bend.
		498	(CCN+$C_2C_1C_3$) bend.
	254	271	CCN bend.
b_{2u}	2230	2224	CN str.
	1155	1138	C_1C_3 str.
	429	428	CCN bend.
		102	$C_2C_1C_3$ bend.
b_{3u}	2262	2249	CN str.
	959	975	C_1C_3 str.
	579	576	$C_3C_1C_4$ bend.
		168	CCN bend.

a) For b_{2u} and b_{3u} species, the values reported by Takenaka and Hayashi[7] were used. For a_g and b_{1g} species, the values observed in the present work were used, based on the assignment by Michaelian *et al.*[8]

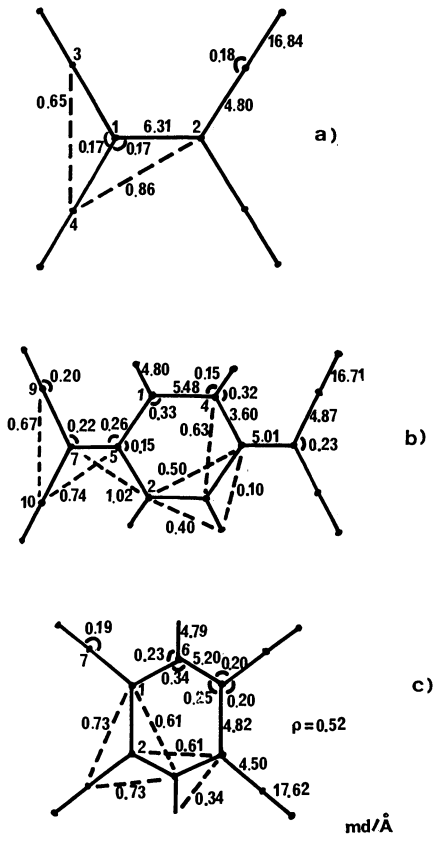

Fig. 7. The force constants of TCNE, TCNQ, and TCNB.
a) TCNE, b) TCNQ, c) TCNB,

Table 3. Observed and calculated fundamental frequencies of TCNQ

Species	ν_{obsd}[a)]	ν_{calcd}	Assignment
a_g	3048 cm^{-1}	3050 cm^{-1}	CH str.
	2229	2228	CN str.
	1602	1608	(C_1C_4+C_5C_7) str.
	1454	1451	C_5C_7 str.
	1207	1207	CH bend.
	948	960	(C_1C_5+C_7C_9) str. + ($C_9C_7C_{10}$+ring) bend.
	711	724	C_1C_5 str. + ring bend.
	602	600	($C_9C_7C_{10}$+CCN) bend.
	334	330	($C_9C_7C_{10}$+CCN+ring) bend.
	114	130	$C_9C_7C_{10}$ bend.
b_{1g}	3030	3053	CH str.
	2223	2226	CN str.
	1451	1454	CH bend.
	1323	1342	(C_1C_5+C_7C_9) str. + ($C_1C_5C_7$+$C_5C_7C_9$) bend.
	1187	1182	
	609	620	ring bend.
	519	529	(ring+$C_1C_5C_7$) bend.
		407	CCN bend.
		127	$C_5C_7C_9$ bend.
b_{2u}	3053	3048	CH str.
	2228	2226	CN str.
	1540	1538	C_1C_4 str.
	1354	1344	(C_7C_9+C_1C_5) str. + ($C_1C_5C_7$+$C_5C_7C_9$) bend.
		1231	CH bend.
	1125	1108	(C_7C_9+C_1C_5) str.
	498	496	(CCN+$C_5C_7C_9$) bend.
		321	
		77	CCN bend.
b_{3u}	3065	3055	CH str.
	2228	2227	CN str.
	1545	1540	C_5C_7 str. + CH bend.
	1405	1413	
	998	999	(C_1C_5+C_7C_9) str. + ($C_9C_7C_{10}$+ring) bend.
	962	952	C_1C_5 str. + ring bend.
	600	605	C_7C_9 str. + $C_9C_7C_{10}$ bend.
	549	542	(ring+CCN) bend.
	146	160	CCN bend.

a) The values reported by Girando and Pecile.[9] The observed values in the present study were in good agreement with them.

quency from 1546 cm^{-1} for TCNB to 1456 cm^{-1} for $TCNB^-$, as shown in Table 1. The line at 1456 cm^{-1} for $TCNB^-$ has the character of C_1C_2 stretching vibration according to our calculation, as shown in Fig. 6. The Cartesian displacement of this mode was almost unchanged for TCNB. Therefore, this result asserts that an additional electron does occupy the a_u MO but not the b_{1u} MO. This is also supported by the moderate decrease of CN stretching vibration fre-

TABLE 4. OBSERVED AND CALCULATED FUNDAMENTAL FREQUENCIES OF TCNB AND TCNB-d_2

Species	TCNB		TCNB-d_2		Assignment
	ν_{obsd}[a]	ν_{calcd}	ν_{obsd}[a]	ν_{calcd}	
a_g	3087 cm^{-1}	3083 cm^{-1}	2298 cm^{-1}	2274 cm^{-1}	CH(D) str.
	2251	2249	2251	2249	CN str.
	1541	1529	1535	1534	C_1C_2 str.
	1259	1240	1256	1234	($C_1C_6+C_1C_7$) str.
	726	749	711	728	ring bend.
		491		491	($C_2C_1C_7+CCN$) bend.
	407	421	405	420	ring bend.
	143	119	143	119	CCN bend.
b_{1g}	2247	2250	2247	2250	CN str.
	1605	1596	1590	1576	C_1C_6 str.
	1256	1254	970	978	CH(D) bend.
	1041	1045	1040	1045	C_1C_7 str.
	707	702	655	656	$C_2C_1C_7$ bend.
	350	352	350	352	ring bend.
	224	254	220	250	CCN bend.
b_{2u}	3087	3084	2292	2276	CH(D) str.
	2249	2251	2249	2250	CN str.
	1388	1409	1379	1402	C_1C_6 str.
		1221		1202	(ring+$C_2C_1C_7$) bend.
	628	608	620	601	(ring+CCN) bend.
	466	472	466	472	($C_2C_1C_7+CCN$) bend.
	152	145	151	145	CCN bend.
b_{3u}	2252	2248	2251	2249	CN str.
	1485	1506	1427	1440	CH(D) bend. + C_1C_6 str.
	1278	1282	1272	1281	C_1C_2 str.
	1181	1142	945	929	CH(D) str.
	762	801	710	734	C_1C_7 str.
	498	486	497	486	($CCN+C_2C_1C_7$) bend.
	128	127	127	127	CCN bend.

a) The values reported by Takenaka *et al.*[4] are adopted as ν_{obsd}, except for a doubtful line. The observed values for a_g species in the present study were in good agreement with them.

quency and the slight increase in frequency of the mixing mode of C_1C_6 and C_1C_7 stretching vibrations. These Cartesian displacements are also shown in Fig. 6. Thus it is concluded clearly that the LUMO of TCNB is the a_u MO. This conclusion agrees with the result of PPP-SCF-MO calculation of TCNB by Iwata *et al.*[6]

Vibrational Analyses of In-plane Vibrations of TCNB and TCNB$^-$. A normal coordinate calculation based on Urey-Bradley force field with Kekulé potential was carried out for TCNB and TCNB$^-$. In this calculation, the library programs, BGLZ and LSMB, of the computer center, the University of Tokyo, were used.

First, normal vibrations of TCNE and TCNQ were investigated in order to get an initial set of force constants for TCNB. The observed frequencies of TCNE and TCNQ are shown in Tables 2 and 3.[7-9] Their molecular parameters are the same as previously reported.[7,9] A more reasonable and transferable set of force constants was obtained by a trial and error method for TCNE and TCNQ as shown in Fig. 7. The calculated frequencies show good agreements with the observed values as shown in Tables 2 and 3.

An initial set of force constants of TCNB was derived from those of benzene,[10] 1,2,4,5-tetrachlorobenzene,[11] TCNE, and TCNQ. Table 4 shows the observed frequencies of TCNB reported by Takenaka *et al.*[4] The values of molecular parameters reported by Niimura *et al.* were used.[12] The distribution pattern of the Kekulé potential function of TCNB has been estimated from bond-bond polarizability, $\pi_{rs,tu}$, using PPP-SCF-MO of TCNB[6,13] under the approximation that $d\beta/dr$=constant for various bonds, as shown in Fig. 8 (β; resonance integral). Kekulé constant has been taken zero, initially. An adjustment by a trial and error method was carried out for the skeletal stretching force constants and the Kekulé constant. The final set of force constants of TCNB is shown in Fig. 7. Their values were reasonable in view of the bond orders of the corresponding bondings.[6] The calculated frequencies agree with the observed values as shown in Table 4.

For TCNB$^-$, the skeletal stretching force constants were changed according to the following equation, (bond order)$\propto$[(stretching force constant)$-$(Kekulé constant)$\times$(self bond-bond polarizability)].

Table 5. Observed and calculated fundamental frequencies of TCNB$^-$ and TCNB-d_2^-

Species	TCNB$^-$		TCNB-d_2^-		Assignment
	ν_{obsd}	ν_{calcd}	ν_{obsd}	ν_{calcd}	
a_g	cm^{-1}	3083 cm^{-1}	cm^{-1}	2274 cm^{-1}	CH(D) str.
	2198	2215	2198	2216	CN str.
	1456	1466	1446	1456	C_1C_2 str.
	1279	1259	1266	1254	($C_1C_6+C_1C_7$) str.
		732		712	ring bend.
	522	490	520	490	($C_2C_1C_7$+CCN) bend.
	408	422	409	422	ring bend.
		119		119	CCN bend.
b_{1g}		2149		2148	CN str.
		1312		1016	CH(D) bend.
		1060		1062	C_1C_7 str.
		810		810	C_1C_6 str.
		644		599	ring bend.
		263		257	(CCN+ring) bend.
		234		234	($C_2C_1C_7$+ring) bend.
b_{2u}		3084		2276	CH(D) str.
		2176		2176	CN str.
		1415		1408	C_1C_6 str.
		1226		1206	C_1C_7 str. + ring bend.
		611		603	C_1C_7 str. + (ring+CCN) bend.
		473		473	(CCN+$C_2C_1C_7$) bend.
		145		145	CCN bend.
b_{3u}		2157		2158	CN str.
		1418		1343	C_1C_6 str. + CH(D) bend.
		1305		1250	($C_1C_6+C_1C_2+C_1C_7$) str.
		1048		904	C_1C_6 str. + ring bend.
		798		727	C_1C_7 str.
		482		482	($C_2C_1C_7$+CCN) bend.
		127		127	CCN bend.

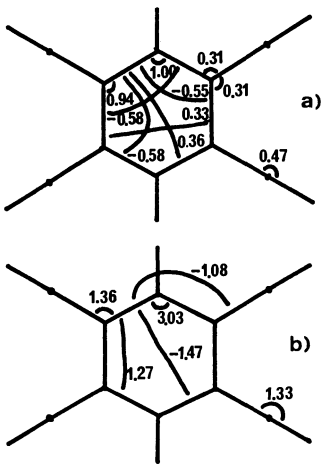

Fig. 8. Distribution patterns of $\pi_{rs,tu}$ of TCNB and TCNB$^-$. a) TCNB, b) TCNB$^-$.
The values are normalized as $\pi_{16,65}$ of TCNB=1.00.

The distribution pattern of Kekulé potential function of TCNB$^-$ is considerably changed from that of TCNB as shown in Fig. 8. As previously mentioned, the vacant b_{1u} MO of TCNB$^-$ must be located close to the a_u MO. Therefore, the denominator $E_{a_u}-E_{b_{1u}}$ in the formula of $\pi_{rs,tu}$ is fairly small, resulting in a large change in the Kekulé potential function. The pattern of the Kekulé potential of TCNB$^-$ (Fig. 8 b)) is similar to the pattern of the symmetry coordinate of C_1C_6 stretching vibration belonging to b_{1g} species, that is to say, there is a strong vibronic interaction between the a_u and the b_{1u} MO through this vibrational mode.

The calculated frequencies of TCNB$^-$ and their assignment based on L_x matrix and potential energy distribution are shown in Table 5. They agree with the observed values. Figure 6 shows the Cartesian displacements of the totally symmetric skeletal stretching vibrations derived from the L_x matrix. A Raman line of TCNB$^-$ at 520 cm^{-1} was assigned to C_1C_7N bending vibration of a_g species on the basis of this calculation. The C_1C_6 stretching vibration belonging to b_{1g} species shows remarkable decrease in frequency from 1605 cm^{-1} for TCNB to 810 cm^{-1} for TCNB$^-$, as shown in Tables 4 and 5. This decrease is due to the vibronic interaction between the a_u and the b_{1u} MO. A Raman line of TCNB$^-$ at 928 cm^{-1} cannot be assigned so far. This totally symmetric line is strong and has a combination line at

$2383 \approx 928 + 1456\ cm^{-1}$. So it may be assigned to a totally symmetric fundamental, but TCNB has not such a line in 750—1200 cm^{-1} region, nor other 1,2,4,5-tetrasubstituted benzene, for example 1,2,4,5-tetrachlorobenzene.[11] The assignment of this line has not been resolved rigorously and will be a further problem whereas it is guessed that this line may originate from the vibronic interaction.

The authots thank Prof. Tohru Takenaka, Kyoto University, and Dr. Masao Tahara, our laboratory, for offering of TCNB-d_2 and TCNB, respectively.

References

1) A. Zweig, J. E. Lehnsen, W. G. Hodgson, and W. H. Jura, *J. Am. Chem. Soc.*, **85**, 3937 (1963).
2) C. Takahashi and S. Maeda, *Chem. Phys. Lett.*, **22**, 364 (1973); **24**, 584 (1974); **28**, 22 (1974).
3) A. Ishitani and S. Nagakura, *Theoret. Chim. Acta*, **4**, 236 (1966).
4) J. Umemura and T. Takenaka, *Bull. Inst. Chem. Res., Kyoto Univ.*, **51**, 206 (1973); T. Takenaka, J. Umemura, and S. Tadokoro, The Symposium on Molecular Structure, Kyoto, 1971, Abstr. No. 1A05; J. Umemura, T. Takenaka, and S. Oka, The Symposium on Molecular Structure, Sendai, 1972, Abstr. No. 6C09; T. Takenaka, Private Communication.
5) K. Kaya, A. Nakatsuka, N. Kubota, and M. Ito, *J. Raman Spectrosc.*, **1**, 595 (1973).
6) S. Iwata, J. Tanaka, and S. Nagakura, *J. Am. Chem. Soc.*, **88**, 894 (1966).
7) T. Takenaka and S. Hayashi, *Bull. Chem. Soc. Jpn.*, **37**, 1216 (1964).
8) K. H. Michaelian, K. E. Rieckhoff, and E. M. Voigt, *Spectrosc. Lett.*, **10**, 99 (1977).
9) A. Girando and C. Pecile, *Spectrochim. Acta, Part A*, **29**, 1859 (1973).
10) J. R. Scherer and J. Overend, *Spectrochim. Acta*, **17**, 719 (1961).
11) J. R. Scherer and J. C. Evans, *Spectrochim. Acta*, **19**, 1739 (1963).
12) N. Niimura, Y. Ohashi, and Y. Saito, *Bull. Chem. Soc. Jpn.*, **41**, 1815 (1968).
13) C. A. Coulson and H. C. Longuet-Higgins, *Proc. R. Soc. London, Ser. A*, **191**, 39 (1947).

The Crystal and Molecular Structure of Grayanotoxin II

Akio FURUSAKI,* Nobuyuki HAMANAKA, and Takeshi MATSUMOTO
Department of Chemistry, Faculty of Science, Hokkaido University, Sapporo 060

(Received October 16, 1979)

The detailed molecular geometry of grayanotoxin II has been examined by means of X-ray crystallographic analysis. The crystals are orthorhombic, with four molecules in a unit cell with dimensions of $a=10.040$, $b=26.517$, and $c=6.672$ Å; the space group is $P2_12_12_1$. 1908 unique intensity data were collected on a four-circle diffractometer with LiF-monochromated Cu $K\alpha$ radiation. The structure was solved by the Monte Carlo direct method, using the 20 strongest reflections as the starting set; the 3rd random phase set led to the correct solution. The R value reached 3.8% by repeated block-diagonal least-squares refinements. The A, B, C, and D rings take envelope, twist-chair, chair, and half-chair conformations respectively. The conformation of the B ring closely resembles the preferred one of cycloheptane itself. The crystal consists of hydrogen-bonded double molecular layers piled parallel to the (010) plane.

A number of grayanane diterpenoids have been isolated from *Leucothoe grayana Max.*, *Pieris japonica* D. Don, *Rhododendron japonicum* Suringer, *etc.*, and their structures have been extensively investigated.[1-3] Since these diterpenoids contain four rings, especially a flexible seven-membered ring, their chemical reactivities are closely related to the ring conformations. Although one of the grayanoids, grayanotoxin (hereafter G) I, was subjected to X-ray crystallographic analysis, details of the molecular geometry have not yet been published.[4] In the present paper, we wish to report on the X-ray structure determination and molecular geometry of another grayanoid, G II (**1**).

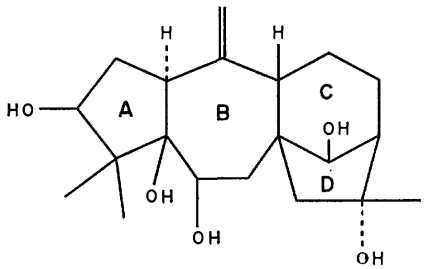

1

Experimental

A colorless, single crystal with dimensions of about $0.3\times0.4\times0.6$ mm^3 was used for the X-ray measurement. The crystal data are summarized in Table 1. The cell dimensions and reflection intensities were measured on a Rigaku four-circle diffractometer using Cu $K\alpha$ radiation ($\lambda=1.5418$ Å) monochromatized with an LiF crystal. The intensity measurement was made by the θ-2θ continuous-scan technique at a 2θ scan rate of 2° min^{-1}; the background was measured for 30—60 s at each end of the scan range. Three standard reflections, measured at intervals of every 62 reflections, showed no significant decrease in intensity during the course of data collection. The intensities were corrected for the Lorentz and polarization factors, but not for the absorption or the extinction effect. In the range of 2θ values up to 140°, 1908 unique structure factor magnitudes above the $2\sigma(F)$ level were selected for the structure determination.

Table 1. The crystal data

Mol. formula	$C_{20}H_{32}O_5$
Mol. weight	352.5
Crystal system	Orthorhombic
Space group	$P2_12_12_1$
Cell dimensions	$a=10.040(3)$ Å
	$b=26.517(5)$
	$c=6.672(2)$
V	1776.3 Å^3
Z	4
D_x	1.318 g cm^{-3}
μ(Cu $K\alpha$)	7.14 cm^{-1}

Structure Determination

In the early stage of the structure determination, attempts were made to solve the structure by the symbolic-addition method,[5] but all such attempts were unsuccessful. The structure was finally elucidated by the Monte Carlo direct method.[6] The 20 strongest reflections were chosen as members of the starting set. Tentative phase values for the starting reflections were derived from successively-generated random numbers. In order to extend this tentative phase set, 10 cycles of the tangent procedure were performed using 421 $|E|$ values above 1.30; during the first 5 cycles, the phases of the starting reflections were kept constant. The 3rd phase set, which showed a low R_K value of 24.6% ($R_K=\Sigma||E_o|-k|E_c||/\Sigma|E_o|$), led to the correct solution. An E-map calculated with 407 phases clearly revealed the locations of all 25 non-hydrogen atoms.

The structure thus obtained was refined by the block-diagonal-matrix least-squares method, first with isotropic and then with anisotropic temperature factors. After all the 32 hydrogen atoms had been located in a difference Fourier map, further least-squares refinement was repeated including these hydrogen atoms with isotropic temperature factors. For this refinement, the following weighting scheme was used:

$$W = 1/\{\sigma(F)^2\exp(AX^2+BY^2+CXY+DX+EY)\},$$

where $X=|F_o|$ and $Y=\sin\theta/\lambda$. The coefficients, A, B, C, D, and E, are constants which were determined from the $(\Delta F)^2$ values. The final value of $R=\Sigma||F_o|-k|F_c||/\Sigma|F_o|$ was 3.8%. The atomic parameters thus obtained are listed in Table 2. The tables of the observed and calculated structure factors are kept at the Chemical Society of Japan (Document No. 8025).

TABLE 2. THE FINAL ATOMIC PARAMETERS AND ESTIMATED STANDARD DEVIATIONS

(1) The non-hydrogen atoms.

The temperature factors are defined as $\exp[-(\beta_{11}h^2+\beta_{22}k^2+\beta_{33}l^2+\beta_{12}hk+\beta_{13}hl+\beta_{23}kl)]$.

Atom	$x(\times 10^4)$	$y(\times 10^5)$	$z(\times 10^4)$	$\beta_{11}(\times 10^4)$	$\beta_{22}(\times 10^5)$	$\beta_{33}(\times 10^4)$	$\beta_{12}(\times 10^5)$	$\beta_{13}(\times 10^4)$	$\beta_{23}(\times 10^4)$
O (1)	3228 (2)	14147 (8)	8918 (4)	84 (2)	170 (3)	303 (6)	−61 (11)	148 (6)	−47 (2)
O (2)	5990 (1)	12968 (5)	8326 (2)	56 (1)	96 (2)	111 (2)	−44 (7)	10 (3)	−20 (1)
O (3)	7065 (2)	2594 (5)	7829 (2)	69 (1)	66 (1)	139 (3)	−24 (7)	−30 (3)	12 (1)
O (4)	8604 (2)	7031 (5)	1494 (2)	82 (1)	60 (1)	141 (3)	14 (7)	57 (3)	−6 (1)
O (5)	11011 (2)	12035 (6)	1501 (3)	58 (1)	97 (2)	216 (4)	68 (8)	81 (4)	3 (1)
C (1)	5032 (2)	12248 (6)	4938 (3)	39 (1)	75 (2)	115 (3)	31 (9)	−5 (4)	−5 (1)
C (2)	3530 (2)	13215 (9)	5385 (4)	43 (2)	125 (3)	244 (5)	92 (11)	18 (5)	21 (2)
C (3)	3202 (2)	10507 (8)	7342 (4)	46 (2)	108 (2)	233 (5)	−6 (10)	57 (5)	1 (2)
C (4)	4306 (2)	6487 (7)	7580 (3)	44 (2)	99 (2)	173 (4)	−84 (9)	10 (4)	8 (2)
C (5)	5560 (2)	9491 (6)	6820 (3)	40 (1)	68 (2)	103 (3)	−40 (8)	10 (3)	−5 (1)
C (6)	6757 (2)	6181 (6)	6276 (3)	47 (1)	62 (2)	104 (3)	14 (8)	−12 (4)	1 (1)
C (7)	8047 (2)	9031 (6)	5848 (3)	41 (1)	72 (2)	101 (3)	51 (8)	3 (3)	4 (1)
C (8)	8186 (2)	13220 (5)	4275 (2)	37 (1)	58 (2)	99 (3)	14 (8)	4 (3)	−1 (1)
C (9)	7239 (2)	17876 (6)	4618 (3)	50 (2)	56 (2)	117 (3)	15 (8)	8 (4)	−3 (1)
C (10)	5762 (2)	16910 (6)	4163 (3)	47 (1)	74 (2)	131 (3)	79 (9)	14 (4)	1 (2)
C (11)	7781 (2)	22354 (6)	3398 (3)	62 (2)	56 (2)	177 (4)	13 (9)	18 (5)	0 (2)
C (12)	8058 (2)	20983 (6)	1209 (3)	61 (2)	69 (2)	153 (4)	10 (9)	−8 (4)	18 (2)
C (13)	8833 (2)	16005 (6)	1019 (3)	58 (2)	71 (2)	100 (3)	−17 (9)	6 (4)	5 (1)
C (14)	8024 (2)	11809 (6)	2040 (3)	50 (1)	58 (2)	105 (3)	5 (8)	2 (3)	−1 (1)
C (15)	9680 (2)	14919 (7)	4381 (3)	42 (1)	93 (2)	115 (3)	−30 (9)	−11 (4)	5 (2)
C (16)	10147 (2)	16061 (6)	2213 (3)	48 (1)	72 (2)	138 (4)	3 (9)	25 (4)	4 (2)
C (17)	10987 (2)	20809 (8)	1986 (4)	57 (2)	97 (2)	210 (5)	−91 (10)	23 (5)	15 (2)
C (18)	4410 (3)	4625 (13)	9743 (5)	80 (2)	203 (4)	215 (6)	−163 (17)	53 (6)	51 (3)
C (19)	3961 (2)	2071 (8)	6195 (5)	65 (2)	87 (2)	309 (7)	−158 (11)	−21 (6)	−9 (2)
C (20)	5059 (2)	20031 (9)	2999 (4)	55 (2)	132 (3)	267 (6)	117 (12)	20 (6)	51 (2)

(2) The hydrogen atoms.

The positional and thermal parameters are multiplied by 10^3 and 10 respectively.

Atom[a)]	x	y	z	B/Å^2	Atom	x	y	z	B/Å^2
H (1)	510 (3)	100 (1)	386 (5)	24 (5)	H (17a)	1181 (4)	204 (1)	268 (6)	34 (6)
H (2a)	304 (5)	120 (2)	422 (7)	48 (8)	H (17b)	1053 (4)	237 (1)	242 (6)	36 (6)
H (2b)	333 (5)	170 (2)	566 (7)	49 (8)	H (17c)	1123 (4)	213 (2)	67 (7)	45 (8)
H (3)	231 (3)	87 (1)	732 (5)	27 (5)	H (18a)	486 (6)	17 (2)	1003 (9)	66 (11)
H (6)	650 (3)	42 (1)	510 (4)	17 (4)	H (18b)	355 (6)	35 (2)	1015 (9)	70 (12)
H (7a)	868 (3)	65 (1)	557 (4)	19 (4)	H (18c)	481 (6)	71 (2)	1083 (9)	61 (11)
H (7b)	829 (3)	104 (1)	715 (5)	23 (5)	H (19a)	321 (5)	4 (2)	683 (7)	46 (8)
H (9)	728 (3)	187 (1)	599 (5)	25 (5)	H (19b)	466 (4)	−5 (2)	622 (7)	43 (7)
H (11a)	714 (3)	250 (1)	342 (5)	29 (5)	H (19c)	379 (5)	30 (2)	485 (7)	46 (8)
H (11b)	859 (3)	234 (1)	394 (5)	30 (5)	H (20a)	542 (4)	230 (1)	245 (7)	40 (7)
H (12a)	723 (4)	206 (1)	62 (5)	33 (6)	H (20b)	413 (3)	193 (1)	265 (5)	31 (6)
H (12b)	855 (3)	238 (1)	64 (4)	21 (4)	H (O1)	266 (4)	133 (2)	977 (7)	46 (8)
H (13)	900 (3)	152 (1)	−35 (5)	31 (6)	H (O2)	538 (4)	143 (1)	877 (6)	35 (6)
H (14)	713 (2)	119 (1)	164 (4)	15 (4)	H (O3)	741 (4)	39 (1)	863 (5)	33 (6)
H (15a)	1014 (4)	123 (1)	494 (5)	34 (6)	H (O4)	825 (3)	47 (1)	216 (5)	26 (5)
H (15b)	979 (4)	177 (2)	527 (7)	44 (8)	H (O5)	1055 (5)	96 (2)	151 (8)	52 (9)

a) The hydrogen atoms are denoted by the number of the carbon atom to which they are attached, suffixed by a, b, or c where necessary.

All the calculations were performed on a FACOM 230-75 computer at the Hokkaido University Computing Center, using our own programs. Random numbers were generated by calling a function RANDOM which existed in the program library of the Computing Center. The atomic scattering factors were taken from the International Tables.[7)]

Results and Discussion

Molecular Structure. The molecular structure of G II is illustrated in Fig. 1, where each atom is represented as a thermal ellipsoid enclosing a 50%

Table 3. The bond distances (l/Å) and angles (ϕ/°), with their standard deviations

The standard deviations given in parentheses refer to the last decimal position.

C (1) - C (2)	1.559 (3)	C (16) - C (17)	1.523 (3)	C (7) - C (8) - C (14)	118.4 (1)
C (1) - C (5)	1.547 (2)	C (16) - O (5)	1.455 (2)	C (7) - C (8) - C (15)	105.3 (1)
C (1) - C (10)	1.527 (2)	C (2) - C (1) - C (5)	104.7 (2)	C (9) - C (8) - C (14)	105.5 (1)
C (2) - C (3)	1.526 (4)	C (2) - C (1) - C (10)	113.3 (2)	C (9) - C (8) - C (15)	110.2 (1)
C (3) - C (4)	1.546 (3)	C (5) - C (1) - C (10)	119.5 (1)	C (14) - C (8) - C (15)	102.3 (1)
C (3) - O (1)	1.428 (3)	C (1) - C (2) - C (3)	107.1 (2)	C (8) - C (9) - C (10)	115.1 (1)
C (4) - C (5)	1.574 (3)	C (2) - C (3) - C (4)	105.0 (2)	C (8) - C (9) - C (11)	108.3 (1)
C (4) - C (18)	1.528 (4)	C (2) - C (3) - O (1)	108.0 (2)	C (10) - C (9) - C (11)	111.5 (1)
C (4) - C (19)	1.532 (3)	C (4) - C (3) - O (1)	112.2 (2)	C (1) - C (10) - C (9)	122.1 (1)
C (5) - C (6)	1.531 (2)	C (3) - C (4) - C (5)	101.0 (2)	C (1) - C (10) - C (20)	116.4 (2)
C (5) - O (2)	1.430 (2)	C (3) - C (4) - C (18)	111.6 (2)	C (9) - C (10) - C (20)	121.4 (2)
C (6) - C (7)	1.527 (2)	C (3) - C (4) - C (19)	107.7 (2)	C (9) - C (11) - C (12)	112.7 (1)
C (6) - O (3)	1.440 (2)	C (5) - C (4) - C (18)	114.4 (2)	C (11) - C (12) - C (13)	112.0 (2)
C (7) - C (8)	1.535 (2)	C (5) - C (4) - C (19)	111.9 (2)	C (12) - C (13) - C (14)	108.6 (1)
C (8) - C (9)	1.575 (2)	C (18) - C (4) - C (19)	109.8 (2)	C (12) - C (13) - C (16)	112.5 (1)
C (8) - C (14)	1.545 (2)	C (1) - C (5) - C (4)	103.1 (1)	C (14) - C (13) - C (16)	103.3 (1)
C (8) - C (15)	1.568 (2)	C (1) - C (5) - C (6)	110.3 (1)	C (8) - C (14) - C (13)	101.4 (1)
C (9) - C (10)	1.535 (3)	C (1) - C (5) - O (2)	111.7 (1)	C (8) - C (14) - O (4)	114.5 (1)
C (9) - C (11)	1.539 (2)	C (4) - C (5) - C (6)	114.5 (1)	C (13) - C (14) - O (4)	108.1 (1)
C (10) - C (20)	1.336 (3)	C (4) - C (5) - O (2)	109.9 (1)	C (8) - C (15) - C (16)	107.1 (1)
C (11) - C (12)	1.531 (3)	C (6) - C (5) - O (2)	107.4 (1)	C (13) - C (16) - C (15)	102.8 (1)
C (12) - C (13)	1.537 (2)	C (5) - C (6) - C (7)	115.2 (1)	C (13) - C (16) - C (17)	115.5 (2)
C (13) - C (14)	1.536 (2)	C (5) - C (6) - O (3)	112.1 (1)	C (13) - C (16) - O (5)	109.6 (1)
C (13) - C (16)	1.542 (3)	C (7) - C (6) - O (3)	106.2 (1)	C (15) - C (16) - C (17)	114.9 (2)
C (14) - O (4)	1.441 (2)	C (6) - C (7) - C (8)	124.3 (1)	C (15) - C (16) - O (5)	110.0 (1)
C (15) - C (16)	1.551 (3)	C (7) - C (8) - C (9)	114.4 (1)	C (17) - C (16) - O (5)	104.1 (2)

Table 4. The dihedral angles (ϕ/°)

The A-B-C-D angle is positive if, when looking along B to C, A has to be rotated clockwise to eclipse D.

C (5) - C (1) - C (2) - C (3)	−6.6	C (7) - C (8) - C (9) - C (10)	−72.5
C (10) - C (1) - C (2) - C (3)	−138.5	C (7 (- C (8) - C (9) - C (11)	162.0
C (2) - C (1) - C (5) - C (4)	30.7	C (14) - C (8) - C (9) - C (11)	−66.1
C (2) - C (1) - C (5) - C (6)	153.3	C (15) - C (8) - C (9) - C (11)	43.6
C (2) - C (1) - C (5) - O (2)	−87.3	C (7) - C (8) - C (14) - C (13)	−155.0
C (10) - C (1) - C (5) - C (6)	−78.4	C (9) - C (8) - C (14) - C (13)	75.5
C (2) - C (1) - C (10) - C (20)	−34.5	C (15) - C (8) - C (14) - C (13)	−39.9
C (5) - C (1) - C (10) - C (9)	23.7	C (15) - C (8) - C (14) - O (4)	76.3
C (5) - C (1) - C (10) - C (20)	−158.7	C (7) - C (8) - C (15) - C (16)	142.3
C (1) - C (2) - C (3) - C (4)	−20.7	C (9) - C (8) - C (15) - C (16)	−93.9
C (1) - C (2) - C (3) - O (1)	99.1	C (14) - C (8) - C (15) - C (16)	18.0
C (2) - C (3) - C (4) - C (5)	39.1	C (8) - C (9) - C (10) - C (1)	47.3
C (2) - C (3) - C (4) - C (18)	161.1	C (11) - C (9) - C (10) - C (1)	171.1
C (2) - C (3) - C (4) - C (19)	−78.3	C (11) - C (9) - C (10) - C (20)	−6.4
O (1) - C (3) - C (4) - C (5)	−77.8	C (8) - C (9) - C (11) - C (12)	50.6
C (3) - C (4) - C (5) - C (1)	−43.1	C (10) - C (9) - C (11) - C (12)	−76.9
C (18) - C (4) - C (5) - C (1)	−163.1	C (9) - C (11) - C (12) - C (13)	−46.9
C (19) - C (4) - C (5) - C (1)	71.2	C (11) - C (12) - C (13) - C (14)	58.0
C (18) - C (4) - C (5) - C (6)	77.0	C (11) - C (12) - C (13) - C (16)	−55.7
C (18) - C (4) - C (5) - O (2)	−44.0	C (12) - C (13) - C (14) - C (8)	−71.4
C (1) - C (5) - C (6) - C (7)	73.4	C (16) - C (13) - C (14) - C (8)	48.2
C (1) - C (5) - C (6) - O (3)	−165.0	C (16) - C (13) - C (14) - O (4)	−72.5
C (4) - C (5) - C (6) - O (3)	−49.3	C (12) - C (13) - C (16) - C (15)	80.6
O (2) - C (5) - C (6) - O (3)	73.1	C (12) - C (13) - C (16) - C (17)	−45.3
C (5) - C (6) - C (7) - C (8)	−55.7	C (12) - C (13) - C (16) - O (5)	−162.5
O (3) - C (6) - C (7) - C (8)	179.6	C (14) - C (13) - C (16) - C (15)	−36.2
C (6) - C (7) - C (8) - C (9)	59.3	C (8) - C (15) - C (16) - C (13)	11.0
C (6) - C (7) - C (8) - C (14)	−66.0	C (8) - C (15) - C (16) - C (17)	137.3
C (6) - C (7) - C (8) - C (15)	−179.5	C (8) - C (15) - C (16) - O (5)	−105.6

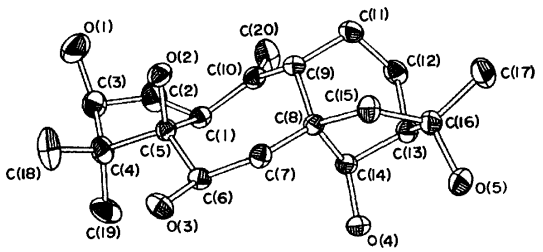

Fig. 1. A perspective view of the G II molecule. For the sake of clarity, hydrogen atoms are omitted.

probability. As can be seen in Fig. 1, the molecular framework obtained corresponds precisely to Structure **1** based on the chemical evidence.[1] The bond distances and angles and the dihedral angles are listed in Tables 3 and 4 respectively.

The five-membered A ring takes a deformed envelope conformation, with the C(4) atom deviating remarkably from the mean plane for the other four atoms in this ring. The O(1)H and O(2)H hydroxyl groups occupy the 1,3-diaxial positions in the A ring and form an intramolecular hydrogen bond, O(2)–H··· O(1), with each other (see Table 5). The equatorial methyl carbon, C(18), is only 3.004(3) Å distant from the O(3) atom. Because of this close contact, the C(5)–C(4)–C(18) and C(5)–C(6)–O(3) angles, 114.4 and 112.1°, may become somewhat greater than the standard tetrahedral angle.

The seven-membered B ring has a somewhat complicated conformation an approximate two-fold rotation axis running through the C(10) atom and the middle point of the C(6)–C(7) bond. This conformation corresponds almost exactly to the most stable twist-chair form of cycloheptane itself.[8] It is an interesting fact that, notwithstanding its incorporation in the complicated ring-system, the B ring keeps such a flexible conformation. All the sp^3-valency angles in the B ring are greater than 109.5°. Especially the C(6)–C(7)–C(8) and C(5)–C(1)–C(10) angles, 124.3 and 119.5°, are quite within the range of the normal sp^2-valency angle. The exocyclic methylene group, $C(20)H_2$, nearly eclipses the $C(11)H_2$ group around the C(9)–C(10) bond. As a result, the distance between the H(20a) and H(11a) atoms is only 1.92(5) Å. The difference of 5° between the C(1)–C(10)–C(20) and C(9)–C(10)–C(20) angles is probably due to this steric repulsion.

Table 5. The hydrogen bonds, X–H···Y

X	Y	X···Y (l/Å)	H···Y (l/Å)	X–H···Y (ϕ/°)
(1) Intramolecular				
O(2)	O(1)	2.818(2)	2.17(4)	144(4)
O(5)	O(4)	2.757(2)	2.07(5)	144(5)
(2) Intermolecular				
O(1)	O(5)[a]	2.871(3)	2.04(4)	169(4)
O(3)	O(4)[b]	3.122(2)	2.41(4)	173(3)
O(4)	O(3)[c]	2.785(2)	2.02(3)	152(3)

Symmetry codes are: a) $-1+x$, y, $1+z$; b) x, y, $1+z$; c) $3/2-x$, $-y$, $-1/2+z$.

The six-membered C ring in G II adopts a chair conformation, although it has recently been found that, in some other grayanoids, the C ring takes a boat conformation.[9] Since the seven-membered ring composed of the C(8), C(9), C(11), C(12), C(13), C(15), and C(16) atoms takes a boat conformation, the axial hydrogen, H(11b), is close to the H(15b) and H(17b) atoms; the distances are 2.12(5) and 2.20(5) Å respectively.

The five-membered D ring has a half-chair conformation, with an approximate two-fold rotation axis running through the C(15) atom. Since this conformation gives the 1,3-diaxial positions to the O(4)H

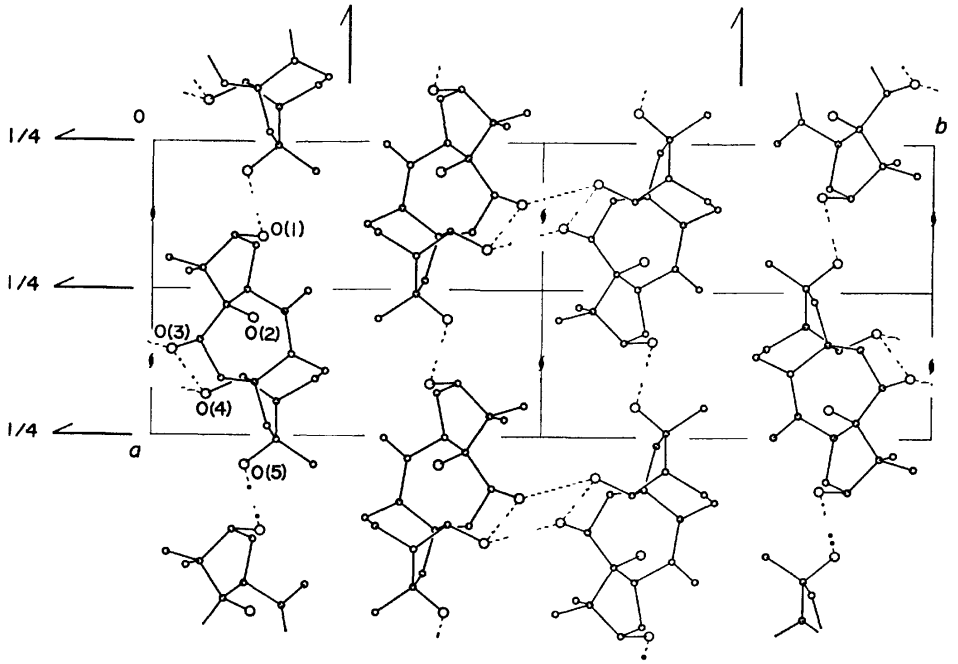

Fig. 2. The crystal structure viewed along the c axis.

and O(5)H hydroxyl groups, a stable intramolecular hydrogen bond, O(5)–H···O(4), is formed. The C(17)H_3 group, like the other two methyl groups, takes a stable staggered conformation.

Crystal Structure. The crystal structure viewed along the c axis is drawn in Fig. 2. The details of hydrogen bonding are given in Table 5. The molecules are connected by three kinds of intermolecular hydrogen bonds, forming a double molecular layer about the two-fold screw axes along the c axis. These molecular layers parallel to the (010) plane are further held together mainly by the van der Waals interactions.

References

1) S. Miyajima and S. Takei, *J. Agric. Chem. Jpn*, **10**, 1093 (1934); H. Kakisawa, M. Kurono, S. Takahashi, and H. Hirata, *ibid.*, **1961**, 59; J. Iwasa and Y. Nakamura, *Tetrahedron Lett.*, **1969**, 3937; H. Hikino, M. Ogura, T. Ohta, and T. Takemoto, *Chem. Pharm. Bull.*, **18**, 1072 (1970).

2) T. Okuno, N. Hamanaka, H. Miyakoshi, and T. Matsumoto, *Tetrahedron*, **26**, 4765 (1970); N. Hamanaka, H. Miyakoshi, A. Furusaki, and T. Matsumoto, *Chem. Lett.*, **1972**, 779; S. Gasa, R. Ikeda, N. Hamanaka, and T. Matsumoto, *Bull. Chem. Soc. Jpn.*, **49**, 835 (1976).

3) M. Yasue, Y. Kato, T. Kishida, and H. Ohta, *Chem. Pharm. Bull.*, **9**, 171 (1961); H. Hikino, K. Ito, and T. Takemoto, *ibid.*, **17**, 854 (1969); H. Hikino, M. Ogura, T. Ohta, and T. Takemoto, *ibid.*, **18**, 1071 (1970).

4) P. Narayanan, M. Rohl, K. Zechmeister, and W. Hoppe, *Tetrahedron Lett.*, **1970**, 3943.

5) J. Karle and I. L. Karle, *Acta Crystallogr.*, **21**, 849 (1966).

6) A. Furusaki, *Acta Crystallogr., Sect. A*, **35**, 220 (1979).

7) "International Tables for X-Ray Crystallography," The Kynoch Press, Birmingham (1974), Vol. IV.

8) J. B. Hendrickson, *J. Am. Chem. Soc.*, **83**, 4537 (1961).

9) A. Furusaki, S. Gasa, R. Ikeda, T. Matsumoto, N. Yasuoka, and Y. Matsuura, unpublished.

Copper(I) and Copper(II) Complexes of Tripod Ligands, Tris(2-alkylthioethyl)amine

Masatatsu Suzuki,* Hajime Kanatomi, Hiroyuki Koyama, and Ichiro Murase

Laboratory of Chemistry, College of General Education, Kyushu University, Ropponmatsu, Chuo-ku, Fukuoka 810

(Received July 26, 1979)

A series of five-coordinate copper(II) complexes with tripod ligands, tris(2-alkylthioethyl)amines (NS_3–R, R=CH_3, C_2H_5, *n*-C_3H_7, *i*-C_3H_7, and *t*-C_4H_9), $[Cu(NS_3–R)L](ClO_4)_n$, where L represents Cl^-, Br^-, I^-, NCS^-, im(imidazole), py(pyridine) and H_2O, $n=1$ or 2 were prepared and characterized. The electronic, infrared and ESR spectral data suggest that $[Cu(NS_3–Me)im](ClO_4)_2$ and $[Cu(NS_3–Me)OH_2](ClO_4)_2$ have a five-coordinate square pyramidal geometry, the other complexes having distorted trigonal bipyramidal or trigonal bipyramidal geometry. The copper(I) complexes with NS_3–Me, $[Cu(NS_3–Me)]ClO_4$ and [Cu(NS_3–Me)NCS] were also prepared and characterized.

The stereochemistry of various cobalt(II) and nickel(II) complexes with tripod ligands, tris(2-alkylthioethyl)amine (NS_3–R), has been extensively studied, the bulkiness of the terminal donor groups being found to exhibit a marked influence on the geometry of the complexes.[1,2] In general, tripod ligands (L) such as tris(2-aminoethyl)amine and tris(2-dimethylaminoethyl)amine form penta-coordinated copper(II) complexes, $[CuLX]^+$ with additional monodentate anionic ligands (X) and the ligands (L) carrying bulky substituents bound to terminal donor atoms tend to form trigonal bipyramidal complexes.[3,4] For similar type ligands (NS_3–R) containing sulfur, however, only a little information is available on the stereochemistry of their copper(II) complexes, only the Cu(II) complex of tris(2-methylthioethyl)amine, [Cu(NS_3–Me)Br]Br being known to take a trigonal bipyramidal geometry.[1]

In the present work, copper(II and I) complexes with tripod ligands, NS_3–R (I) have been studied by varying the terminal alkyl groups R with additional monodentate ligands. The stereochemistry of the complexes is discussed in terms of IR, ESR, and electronic spectra. A study of this kind of copper complex containing sulfur would give useful information on the chemistry of so-called copper proteins which sometimes exhibit unusual behavior as copper complexes.[5-8]

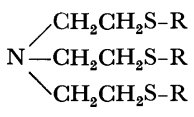

(I)

R=Me, Et, *n*-Pr, *i*-Pr, or *t*-Bu

Experimental

Ligands. Tris(2-alkylthioethyl)amine (NS_3–R), where R refers to methyl, ethyl, *n*-propyl, isopropyl, and *t*-butyl, were prepared according to the procedure of Ciampolini *et al.*[1]

Complexes. $[Cu(NS_3–R)X]ClO_4$ (R=Me, Et, *n*-Pr, *i*-Pr, and *t*-Bu; X=Cl^- and Br^-) A methanol solution of copper(II) halide (1 mmol) was mixed with NS_3–R (1 mmol) in methanol. To this mixture (20 cm^3) was added a methanol solution (20 cm^3) of sodium perchlorate (2 mmol). Green crystals were immediately precipitated. In the case of the bromo complexes of NS_3-*i*-Pr and NS_3-*t*-Bu, ether was added to the reaction mixture to promote crystallization.

[Cu(NS$_3$–R)NCS]ClO$_4$ (R=Me or Et). NH_4NCS (1 mmol) in methanol (10 cm^3) was added to a methanol solution (20 cm^3) of $Cu(ClO_4)_2·6H_2O$ (1 mmol) and NS_3–R (1 mmol). The complex soon precipitated as dark green crystals.

[Cu(NS$_3$–R)OH$_2$](ClO$_4$)$_2$ (R=Me or Et). A methanol solution (20 cm^3) of NS_3–R (1 mmol) was mixed with $Cu(ClO_4)_2·6H_2O$ (1 mmol) in methanol (20 cm^3). Addition of ether gave green crystals.

[Cu(NS$_3$–Me)I]ClO$_4$. A cold methanol solution (20 cm^3) of NaI (1 mmol) was added to an ice-cold solution of $Cu(ClO_4)_2·6H_2O$ (1 mmol) and NS_3–Me (1 mmol) in methanol (20 cm^3) and the mixture was left to stand in a refrigerator overnight. The complex was obtained as a dark green powder.

[Cu(NS$_3$–R)Y](ClO$_4$)$_2$ [R=Me or Et; Y=Pyridine (py) or Imidazole (im)]. A methanol solution (20 cm^3) of NS_3–R (1 mmol) was mixed with $Cu(ClO_4)_2·6H_2O$ (1 mmol) in methanol (20 cm^3). To the mixture was added 1 mmol of pyridine or imidazole in methanol (10 cm^3). Green (Y=py) or dark blue (Y=im) crystals were obtained upon cooling.

[Cu(NS$_3$–Me)]ClO$_4$. $[Cu(CH_3CN)_4]ClO_4$ (1 mmol)[9] was added to a methanol solution (20 cm^3) of NS_3–Me (1 mmol) and the mixture was heated on a water bath for few minutes. A small amount of insoluble material was filtered off and the filtrate was cooled in a refrigerator. The complex was obtained as colorless crystals.

[Cu(NS$_3$–Me)NCS]. $[Cu(NS_3–Me)]ClO_4$ (1 mmol) was dissolved in warm methanol (30 cm^3). NH_4NCS (1 mmol) in methanol (10 cm^3) was added to the solution. Colorless crystals were immediately precipitated.

All complexes were air-dried at room temperature. The results of elemental analyses are given in Table 1.

Measurements. Electronic spectra in solid state and in solution were obtained with a Hitachi EPS-3T recording spectrophotometer, and infrared spectra with a Hitachi 295 infrared spectrophotometer by means of a KBr disk. Electrolytic conductivities were measured with a Yokogawa·Hewlett·Packard 4261A LCR meter in approximately 10^{-3} mol/dm^3 *N,N*-dimethylformamide (DMF) solution at 25 °C. Molecular weights were determined in DMF at 53 °C with a Hitachi Osmometer Type-115, calibrated with benzil. The concentration of each sample was approximately 10^{-2} mol/dm^3, the results being reproducible in ±3%.

Results and Discussion

Pyridine or imidazole reacted with equimolar $[Cu(NS_3–R)OH_2]^{2+}$ to form $[Cu(NS_3–R)py]^{2+}$ or $[Cu(NS_3–R)im]^{2+}$. However, addition of pyridine or imidazole in great excess resulted in displacement of

Table 1. Elemental analyses

Complex	Found(Calcd), %		
	C	H	N
$[Cu(NS_3\text{-}Me)Cl]ClO_4$	24.64(24.69)	4.78(4.83)	3.36(3.20)
$[Cu(NS_3\text{-}Me)Br]ClO_4$	22.31(22.41)	4.25(4.39)	2.95(2.90)
$[Cu(NS_3\text{-}Me)I]ClO_4$	20.31(20.42)	3.98(4.00)	2.67(2.65)
$[Cu(NS_3\text{-}Me)NCS]ClO_4$	25.48(26.08)	4.46(4.60)	6.24(6.08)
$[Cu(NS_3\text{-}Me)OH_2](ClO_4)_2$	20.63(20.79)	4.46(4.46)	2.67(2.67)
$[Cu(NS_3\text{-}Me)im](ClO_4)_2$	25.03(25.29)	4.37(4.42)	7.00(7.37)
$[Cu(NS_3\text{-}Me)py](ClO_4)_2$	28.76(28.94)	4.35(4.51)	4.77(4.82)
$[Cu(NS_3\text{-}Et)Cl]ClO_4\cdot H_2O$	28.96(28.94)	5.49(5.86)	2.80(2.81)
$[Cu(NS_3\text{-}Et)Br]ClO_4$	27.34(27.48)	5.11(5.19)	2.66(2.61)
$[Cu(NS_3\text{-}Et)NCS]ClO_4$	31.00(31.07)	5.38(5.41)	5.54(5.57)
$[Cu[NS_3\text{-}Et)OH_2](ClO_4)_2$	25.49(25.65)	5.15(5.20)	2.43(2.49)
$[Cu(NS_3\text{-}Et)py](ClO_4)_2\cdot H_2O$	31.83(31.85)	5.10(5.35)	4.41(4.37)
$[Cu(NS_3\text{-}n\text{-}Pr)Cl]ClO_4$	34.04(34.51)	6.32(6.37)	2.64(2.68)
$[Cu(NS_3\text{-}n\text{-}Pr)Br]ClO_4$	31.57(31.80)	5.90(5.87)	2.51(2.47)
$[Cu(NS_3\text{-}i\text{-}Pr)Cl]ClO_4$	34.46(34.51)	6.47(6.37)	2.71(2.68)
$[Cu(NS_3\text{-}i\text{-}Pr)Br]ClO_4$	31.77(31.80)	5.88(5.87)	2.48(2.47)
$[Cu(NS_3\text{-}t\text{-}Bu)Cl]ClO_4$	37.87(38.32)	6.83(6.97)	2.51(2.48)
$[Cu(NS_3\text{-}t\text{-}Bu)Br]ClO_4$	35.26(35.52)	6.55(6.46)	2.38(2.30)
$[Cu(NS_3\text{-}Me)]ClO_4$	26.88(26.86)	5.25(5.26)	3.58(3.48)
$[Cu(NS_3\text{-}Me)NCS]$	33.03(33.26)	5.77(5.86)	7.77(7.76)
$[Cu(NS_3\text{-}Me)]I_3$	15.74(15.81)	3.06(3.10)	2.08(2.05)
$H(NS_3\text{-}Me)[CuCl_3]$	26.27(26.34)	5.32(5.40)	3.47(3.41)
$H(NS_3\text{-}Me)[CuBr_3]$	19.84(19.88)	4.07(4.08)	2.54(2.58)

Table 2. Powder ESR and reflectance spectral data of complexes

Group	Complex	g_1	$g_\parallel$	g_2	g_3	$g_\perp$	$\nu/10^3$ cm^{-1}			
c	$[Cu(NS_3\text{-}Me)Cl]ClO_4$	2.037		2.096	2.129		11.56	15.04		27.55
d	$[Cu(NS_3\text{-}Me)Br]ClO_4$						11.43	15.15	24^s	a)
d	$[Cu(NS_3\text{-}Me)I]ClO_4$						11.05	15.08	20^s	a)
c	$[Cu(NS_3\text{-}Me)NCS]ClO_4$	2.015		2·109	2.162		12.99	16.15^s	22^s	a)
a	$[Cu(NS_3\text{-}Me)OH_2](ClO_4)_2$		2.130			2.086	12.69		24^s	a)
a	$[Cu(NS_3\text{-}Me)im](ClO_4)_2$		2.142			2.064	14.08	17.24^s		27.10
c	$[Cu(NS_3\text{-}Me)py](ClO_4)_2$	2.006		2.090	2.136		12.58	16.67^s		26.74
b	$[Cu(NS_3\text{-}Et)Cl]ClO_4\cdot H_2O$		2.005			2.128	11.63	15.06		27.03
b	$[Cu(NS_3\text{-}Et)Br]ClO_4$		2.006			2.094	11.24	15.02	23^s	a)
b	$[Cu(NS_3\text{-}Et)OH_2](ClO_4)_2$		2.034			2.133	11.72			26.95
b	$[Cu(NS_3\text{-}Et)py](ClO_4)_2\cdot H_2O$		2.012			2.117	12.82	16.66^s		26.32
d	$[Cu(NS_3\text{-}Et)NCS]ClO_4$						12.42	15.15^s	22^s	a)
c	$[Cu(NS_3\text{-}n\text{-}Pr)Cl]ClO_4$	2.026		2.107	2.138		11.70	15.11	26.5—28.0	
d	$[Cu(NS_3\text{-}n\text{-}Pr)Br]ClO_4$						11.11	14.95	23^s	a)
b	$[Cu(NS_3\text{-}i\text{-}Pr)Cl]ClO_4$		2.012			2.117	11.63	15.08	26.5—28.0	
c	$[Cu(NS_3\text{-}i\text{-}Pr)Br]ClO_4$	2.031		2.065	2.124		11.49	15.06	23^s	
b	$[Cu(NS_3\text{-}t\text{-}Bu)Cl]ClO_4$		2.043			2.116	11.11	14.71	26.5—28.0	
b	$[Cu(NS_3\text{-}t\text{-}Bu)Br]ClO_4$		2.036			2.092	10.70	14.43	23^s	a)

s: Shoulder. a) No peak observed up to 29,000 cm^{-1}.

the ligand NS_3–R to form $[Cu(py)_4]^{2+}$ or $[Cu(im)_4]^{2+}$. A similar displacement was observed with various bidentate ligands such as ethylenediamine, 2,2′-bipyridine, and glycine. This tendency suggests that the thioether group in the NS_3–R ligands has poor affinity to a copper(II) ion.

The chloro, bromo, and aquo complexes were considerably stable in acidic solution. For example, $[Cu(NS_3\text{–}Me)Cl]ClO_4$ could be recrystallized from hot 6 mol dm^{-3} hydrochloric acid, though NS_3–Me was replaced by chloride anions to give $[CuCl_3]$ $[H(NS_3\text{–}Me)]$ in hot concd hydrochloric acid.

The coloration of NS_3–R complexes in solution gradually fades on standing, this being attributable to the reduction of Cu(II) to Cu(I). When a basic aqueous solution of $[Cu(NS_3\text{–}Me)OH_2](ClO_4)_2$ was heated for a few minutes, a small amount of a monovalent copper complex $[Cu(NS_3\text{–}Me)]ClO_4$ was ob-

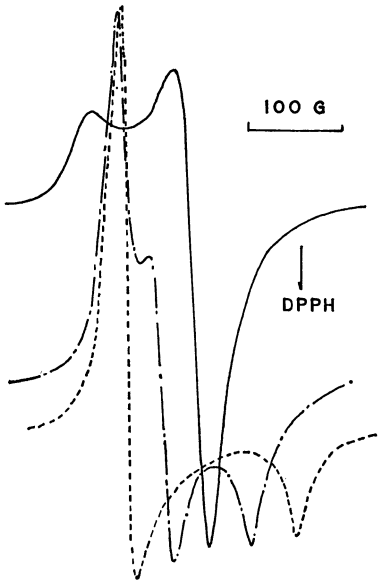

Fig. 1. The powder ESR spectra of $[Cu(NS_3–Me)im](ClO_4)_2$ (—), $[Cu(NS_3–Me)Cl]ClO_4$ (—·—), and $[Cu(NS_3–Et)Cl]ClO_4$ (----).

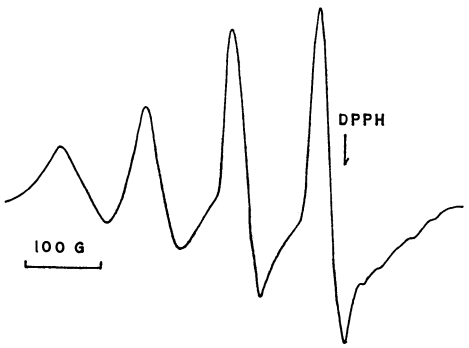

Fig. 2. ESR spectrum of $[Cu(NS_3–Et)Cl]ClO_4$ in DMF at liquid nitrogen temperature.

tained as colorless crystals.

$[Cu(NS_3–R)I]ClO_4$ is extremely unstable, reddish brown $[Cu(NS_3–Me)]I_3$ being isolated from the aqueous solution. This is due to the reduction of the Cu(II) ion by the coordinated iodide ion.

The powder ESR data are summarized in Table 2. The powder technique provides only crystal g-values rather than molecular g-values, the results sometimes causing misinterpretation.[10–12] However, the technique was useful for a rough estimation of the electronic ground state of the copper(II) complexes we studied. The results are supported by the electronic spectra as well as by the frozen solution ESR spectra.

The complexes are classified into four groups (a—d) from their ESR patterns (Table 2). The representative spectra of each group are given in Fig. 1 except for that of (d). The group (a) complex, $[Cu(NS_3–Me)im](ClO_4)_2$ shows an axial spectrum with $g_{\parallel} > g_{\perp}$, suggesting a $d_{x^2-y^2}$ electronic ground state.[12] Thus, a penta-coordinated square pyramid or a hexa-coordinated octahedron can be considered as a possible geometry. For the octahedron, coordination of one perchlorate anion is essential. However, the coordinated perchlorate anion was absent since no splitting of the ν(Cl–O) was observed in the infrared spectrum.[13] It can be assumed that group (a) complexes should have the penta-coordinated square pyramidal geometry. Group (b) complexes show axial spectra with $g_{\parallel} < g_{\perp}$ and group (c) complexes rhombic ones in which one of the g-values is less than 2.04. It is reasonable to suppose that group (b) and (c) complexes have a d_{z^2} or $ad_{z^2}+bd_{x^2-y^2}$ ($a \gg b$) ground state in trigonal bipyramidal or distorted trigonal bipyramidal geometry.[12] Group (d) complexes showed broad ESR spectra and could not be characterized.

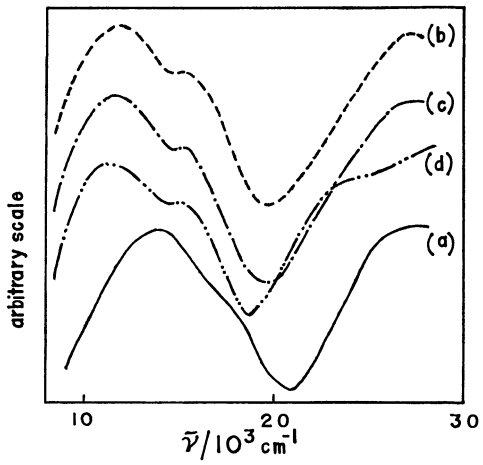

Fig. 3. Reflectance spectra of $[Cu(NS_3–Me)im](ClO_4)_2$ (——), $[Cu(NS_3–Me)Cl]ClO_4$ (—·—), $[Cu(NS_3–Me)Br]ClO_4$ (—··—), and $[Cu(NS_3–Et)Cl]ClO_4$ (----).

The ESR spectra were also measured in DMF and nitromethane at room temperature and at liquid nitrogen temperature. Only three complexes, $[Cu(NS_3–Me)Cl]ClO_4$, $[Cu(NS_3–Et)Cl]ClO_4$, and $[Cu(NS_3–t\text{-}Bu)Cl]ClO_4$ exhibited relatively simple spectra at liquid nitrogen temperature.[14] The spectrum of $[Cu(NS_3–Et)Cl]ClO_4$ (Fig. 2) is a typical one for trigonal bipyramidal copper(II) complexes.[15–17]

Since the frozen solution spectra of these complexes were unresolved in high field region, $g_{\parallel}$-values were calculated using $<g>$ values $[<g>=(g_{\parallel}+2g_{\perp})/3]$ from the room temperature spectra with $g_{\perp}$-values from the frozen solution spectra with the following results: $g_{\parallel}=2.015$, $g_{\perp}=2.122$ for $[Cu(NS_3–Me)Cl]ClO_4$; $g_{\parallel}=2.023$, $g_{\perp}=2.120$ for $[Cu(NS_3–Et)Cl]ClO_4$; $g_{\parallel}=2.023$, $g_{\perp}=2.128$ for $[Cu(NS_3–t\text{-}Bu)Cl]ClO_4$. The $g_{\parallel}$-values suggest that the complexes have a geometry of trigonal bipyramid or distorted trigonal bipyramid in DMF as well as in solid state.

The reflectance spectral data are also given in Table 2. The complexes $[Cu(NS_3–R)X]ClO_4$ ($X=Cl^-$, Br^-, I^-, and NCS^-) belonging to group (b), (c), or (d) show an intense band at lower energy side and a less intense band at higher energy side (Fig. 3). These spectra are closely similar to those of trigonal bipyramidal complexes, $[Cu(NS_3–Me)Br]Br$[1] and $[Cu(Me_6–tren)Br]Br$[18] where Me_6–tren represents tris(2-dimethylaminoethyl)amine. The energy shift of the d-d bands can be correlated with the position of the coordinated anion X in the spectrochemical series. The spectral similarity suggests that $[Cu(NS_3–R)X]$-

ClO_4 in groups (b), (c), and (d) have similar geometry, *i.e.*, trigonal bipyramidal or distorted trigonal bipyramidal. Ciampolini *et al.*[1] assigned two bands at 11400 and 15200 cm^{-1} observed for [Cu(NS_3–Me)Br]Br to the electronic transitions of $d_{x^2-y^2}$, $d_{xy} \rightarrow d_{z^2}$, and d_{xz}, $d_{yz} \rightarrow d_{z^2}$, respectively. Their assignment seems to be valid for the present [Cu(NS_3–R)X]ClO_4 type complexes. It should be noted that these complexes have extremely high intensities (ε=700—1000) of the d-d bands at the lower energy side as compared with that of [Cu(Me_6-tren)Br]Br (ε=450).[18] It is probably due to the lower symmetry of the complexes. The molar extinction coefficients were reported to be 390 at 11400 cm^{-1} in nitromethane for [Cu(NS_3–Me)Br]Br,[1] but *ca.* 900 for freshly prepared solution for [Cu(NS_3–Me)Br]ClO_4. This discrepancy is attributed to the instability of these complexes in solution. They exhibit some bands in the near ultraviolet and ultraviolet region (Table 2), and probably contain electronic transitions of X (σ and π) and S (σ and/or π) to Cu(II), since the free ligands showed no absorption in this region.

It should be noted that [Cu(NS_3–Me)im]$(ClO_4)_2$ of group (a) has a d-d band maximum at 14080 cm^{-1} whereas [Cu(NS_3–Me)py]$(ClO_4)_2$ of group (c) has one at 12580 cm^{-1}. Since imidazole and pyridine have similar ligand field strength, the large difference in the d-d transition energy should be attributed to the difference in their geometry. This is in line with the grouping by powder ESR spectra. The grouping of [Cu(NS_3–Me)OH_2]$(ClO_4)_2$ to (a) and [Cu(NS_3–Et)OH_2]$(ClO_4)_2$ to (b) is also supported by the electronic spectral data.

Although no principle controlling the stereochemistry of the tripod ligand copper(II) complexes could be found in the present investigation, the combination of the bulkiness of the terminal alkyl groups and the ligand field strength of the fifth monodentate ligands may have some influence on the geometry of the complexes.

Copper(I) Complexes. The copper(II) complexes undergo self reduction to the copper(I) complexes in solution. In fact, the copper(I) complexes isolated are very stable towards molecular oxygen even in solution. Although direct evidence for structure determination is lacking, it could be assumed from the steric requirement of the tripod ligands that [Cu(NS_3–Me)]ClO_4 is trigonal pyramidal and [Cu(NS_3–Me)-NCS] trigonal bipyramidal or square pyramidal.

The infrared spectrum of [Cu(NS_3–Me)NCS] showed the CN stretching vibration of NCS^- at 2080 cm^{-1} which indicates the coordination of NCS^- in the solid state.[19] On the other hand, the conductivity measurement in DMF reveals that the complex is an 1:1 electrolyte which could be formulated as [Cu(NS_3–Me)]NCS or [Cu_2(NS_3–Me)$_2$NCS]NCS. The molar conductance based on the former was 43 Ω^{-1} cm^2 mol^{-1}, being typical for an uni-univalent electrolyte.[20] Molecular weight determination[18] revealed that the van't Hoff factor i values are 1.3 for the former and 2.6 for the latter. These values suggest that the complex is monomeric in DMF. The low conductance value based on the monomeric form seems to be attributable to the following equilibrium in DMF:

$$[Cu(NS_3\text{-}Me)NCS] \rightleftharpoons [Cu(NS_3\text{-}Me)]^+ + NCS^-$$

The conductivity of [Cu(NS_3–Me)]ClO_4 in DMF suggests that the complex can be formulated as [Cu_n(NS_3–Me)$_n$]$(ClO_4)_n$ (Λ=79 Ω^{-1} cm^2 mol^{-1} for n=1, Λ=158 Ω^{-1} cm^2 mol^{-1} for n=2 *etc.*). The van't Hoff factor i values were $1.7 \times n$. It is probable that the complex is monomeric with the formula, [Cu(NS_3–Me)]ClO_4 in DMF.

Our thanks are due to Prof. S. Kida, and Prof. H. Okawa, Dr. Y. Nishida and Mr. Y. Nonaka for helpful discussions and valuable comments, and to Mr. Y. Nonaka for the ESR measurement and Prof. A. Matsubara and Mr. K. Nomura for the conductivity measurement.

References

1) M. Ciampolini, J. Gelsomini, and N. Nardi, *Inorg. Chim. Acta*, **2**, 343 (1968).
2) G. Fallani, R. Morassi, and F. Zanobini, *Inorg. Chim. Acta*, **12**, 147 (1975).
3) M. S. Haddad and D. N. Hendrickson, *Inorg. Chem.*, **17**, 2622 (1978) and references therein.
4) R. Morrasi, I. Bertini, and L. Sacconi, *Coord. Chem. Rev.*, **11**, 343 (1973).
5) T. E. Jones, D. B. Rorabacher, and L. A. Ochrymowycz, *J. Am. Chem. Soc.*, **97**, 7485 (1975).
6) E. R. Dockal, T. E. Jones, W. F. Sokol, R. J. Engerer, D. B. Rorabacher, and L. A. Ochrymowycz, *J. Am. Chem. Soc.*, **98**, 4322 (1976).
7) A. R. Amundsen, J. Whelan, and B. Bosnich, *J. Am. Chem. Soc.*, **99**, 6730 (1977).
8) U. Sakaguchi and A. W. Addison, *J. Chem. Soc., Dalton trans.*, **1979**, 600.
9) P. Hemmerich and C. Sigwart, *Experientia*, **19**, 488 (1963).
10) I. M. Orocter, B. J. Hathaway, and P. Nicholls, *J. Chem. Soc., A*, **1968**, 168.
11) R. C. Slade, A. A. G. Tomlinson, B. J. Hathaway, and D. E. Billing, *J. Chem. Soc., A*, **1968**, 61.
12) B. J. Hathaway, *Coord. Chem. Rev.*, **5**, 143 (1970).
13) B. J. Hathaway and A. E. Underhill, *J. Chem. Soc.*, **1961**, 3091.
14) Under investigation.
15) H. A. Senyukova, I. D. Mikheikin, and K. I. Zamaraev, *Russ. J. Struc. Chem.*, **11**, 18 (1970).
16) R. Barbucci and M. J. Campbell, *Inorg. Chim. Acta*, L15 (1975).
17) R. Barbucci, A. Bencini, and D. Gatteschi, *Inorg. Chem.*, **16**, 217 (1977).
18) M. Ciampolini and N. Nardi, *Inorg. Chem.*, **5**, 41 (1966).
19) K. Nakamoto, "Infrared Spectra of Inorganic and Coordination Compound," John Wiley and Sons, Inc., New York, N. Y. (1970), p. 187.
20) W. J. Geary, *Coord. Chem. Rev.*, **7**, 81 (1971).

 © 1980 The Chemical Society of Japan Bull. Chem. Soc. Jpn., 53, 1965—1967 (1980)

A Quantum Chemical Study on the Ion Influence on Linear Water Polymer

Bernd M. Rode,† Ryo Fujikura, and Shizuo Fujiwara*

Department of Chemistry, Faculty of Science, The University of Tokyo, Hongo, Bunkyo-ku, Tokyo 113

(Received October 26, 1979)

Quantum chemical model calculations have been performed using an STO-3G basis set for linear water polymers under the influence of electrostatically approximated cations and anions. It is found that the influence of the cations on the ligand chains can be described properly as a purely electrostatic interaction from the third water molecule on. The mutual influencing of cation and anion in ion pairs separated by more than one solvent molecule seems to be also a merely electrostatic one. An estimation of the range of these electrostatic forces is given.

Recently, one of the present authors (S.F.) has shown experimentally that any simple ion or molecule in aqueous solution requires a certain volume of solution for the maintenance of the free motion and named the latter "molecular space."[1] This raised several questions concerning the nature and the extent of the ion-solvent interactions being responsible for this phenomenon.

Due to technical and computational limitations, usual quantum chemical calculations concerning the interactions of ions with solvent molecules can take into account only a few solvent molecules and represent, therefore, a rather poor approximation to the reality of solutions. Several attempts have been made, therefore, to take into account the conditions of the solution by means of perturbation terms or electrostatic approximations.[2-4] Large computations of some examples of solvated ions[5] and a study on the interaction of a cation with an anion through 2—3 water molecules[6] allow a limited comparison of the results obtained by the approximations with those of full *ab initio* calculations.

Recent calculations of hydrated ions by the MESQUAC-MO-method[4,7] allowed to obtain ion-solvent interaction energies up to the third shell and proved to form a good basis for the discussion of the structural influence of the ion on the surrounding water layers and hence for the phenomenon of the "molecular space."

In the work presented here, we have carried out model calculations on the nature of ion/solvent interactions as a function of the distance between the ion and the water molecules. A molecular model consisting of cation and/or anion bonded to a linear water chain was used for this purpose. It was to be expected that this model would indicate something about the relevant contributions to the binding of solvent molecules even at larger distances and hence form a useful basis for the construction of larger theoretical models for hydrated ions.

Experimental

General Remarks. The idea to reduce the computational problem by means of a partial electrostatic treatment is based on general considerations on importance and range of the contributions to the chemical bond. For ions with ns^2np^6 valence electron configuration, the description as electrostatic point charges seems to be reasonable within certain limitations, as it has been shown already in an analogous example.[3] The interaction between two solute entities, either ions or molecules, which are separated over a larger distance, may be interpreted in terms of the typical "quantum effect" of interference,[7] which is proportional to the overlap integral and hence decreasing exponentially with the distance r, whereas the electrostatic terms, decreasing with r^{-1}, will be effective even at a larger distance and hence can be a dominant factor of interaction over such distances. One of the main scopes of this work was to find out at what distance electrostatic effects will dominate the quantum effects. If one attempts to describe a model for the interaction of an ion with a "chain" of water molecules applying an electrostatic approximation for the central ion, the description of the ion interaction with the first water molecule will be somewhat less satisfactory. For the ion-binding to the first water molecule, however, accurate MO-HF-SCF calculations have been performed,[8] and including the consideration of the experimental gas phase interaction energies, the results of our simplified model calculation can be controled easily.

Performance of the Calculations. The cations were taken into account by means of the point charges of +1 and +2 for alkali and alkaline earth metal ions, respectively, sited at the *ab initio* SCF energy optimized distances from the oxygen of the water molecule (C_{2v} symmetry). The procedures taken here are same as that shown in a previous paper[3] for the case of ion-amide interactions. The corresponding values are given in Table 1.

The water molecule(s), linked to a chain of increasing length ($n=1,2,\cdots 8$) were considered by a nonempirical all-electron (*ab initio*) LCAO-MO-SCF treatment using an STO-3G basis set.[9] In order to evaluate the effect of the ion species, the energy of the chain was calculated with and without the "perturbation" by the point charges representing the ions. Subtracting both energy values the ion solvent interaction energy is obtained. Dividing this value by the number of water molecules building up the chain, one obtains the stabilization energy per water molecule,

Table 1. The distance between the point charge of the metal ion and the coordinative center of the water molecule

Bond	Distance/Å	Bond	Distance/Å
Li-O	1.85	Mg-O	1.85
Na-O	2.10	Ca-O	2.10
K-O	2.63	Ba-O	2.46
Cs-O	2.80	I-H	1.87
Be-O	1.46		

† On leave from Institut für Anorganische und Analytische Chemie, Universität Innsbruck, Innrain 52a, A-6020 Innsbruck, Austria.

Table 2. Stabilization energies per water molecule for chain lengths of 1—8 and experimental (10) and full *ab initio* results (8) for the monohydrates (n-1), all values in kcal/mol

n	Li	Na	K	Cs	Be	Mg	Ca	Ba	I
1	34.1	26.4	16.6	14.8	122.3	74.2	56.7	40.6	5.8
exp.	34.0	24.0	17.9	—	—	—	—	—	—
SCF(9)	36.0	23.9	16.6	—	—	80.0	53.0	—	—
2	22.2	17.7	11.6	10.5	74.8	47.7	37.5	27.9	5.0
3	16.2	13.1	8.9	8.1	53.1	34.7	27.7	21.0	3.6
4	12.6	10.2	7.0	6.4	40.8	26.8	21.5	16.4	2.8
5	10.4	8.5	5.9	5.4	33.3	22.1	17.9	13.7	2.7
6	8.8	7.2	5.0	4.6	28.1	18.7	15.1	11.7	2.5
7	7.7	6.3	4.4	4.1	24.3	16.3	13.2	10.2	2.1
8	6.7	5.5	3.9	3.6	21.4	14.3	11.6	9.9	2.0

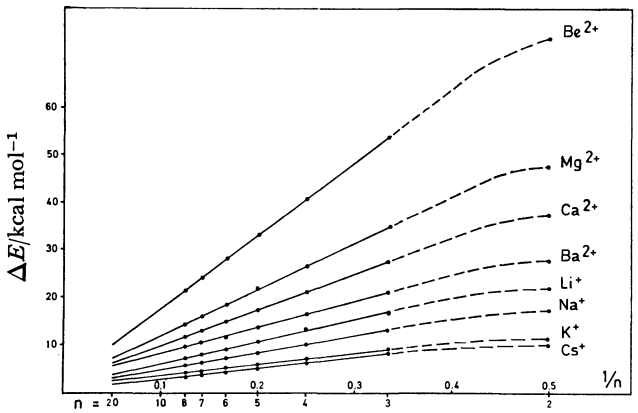

Fig. 1. Stabilization energy per water molecule for varying chain lengths and ions *versus* the inverse number of water molecules in the polymer.

which will be the basis for further discussion.

The geometry of the chain was based on the following values: O–H=0.96 Å, O/H/O=104.5°, O···H–O=2.75 Å. Furthermore, we have performed some calculations on ion pair interactions, *i.e.*, the interaction between the cation and the anion separated from each other by solvent molecules. For this purpose, iodide ion was taken as the counter anion which was linked to the other end of the water chain.

All calculations have been performed using a modified GAUSSIAN 70 program at the FACOM 230-60/75 computer of the Institute of Physical and Chemical Research at Wako City.

Results and Discussion

Applicability of the Method. The use of the electrostatic approximation for the ions is somewhat problematic due to the neglect of some binding effects and the charge transfer. In the case of the main group metal ions, however, these effects could be shown to be of rather minor magnitude.[4,7] The energies calculated within our model approach here prove this once more being in quite satisfactory agreement with the binding energies obtained by either full *ab initio* calculations or gas phase experiments (*cf.* Table 2). We can expect, therefore, that the electrostatic approach for the ions is justified and would not influence the reliability of the results to a serious extent.

Binding of Single Ions to the Water Chain. In Table 2 the binding energies per water molecule in a chain containing 1 to 8 molecules are listed. As can be seen from Fig. 1, they decrease linearly with $1/n$ from the third water molecule on, which actually means a decrease following the law of Coulomb interactions decreasing with $1/r$. We can conclude, therefore, that for a correct description of the ion-solvent interaction concerning the first and second water molecules, we need the formalism of quantum theory allowing to reflect redistribution of electron density within the solvent molecules upon ion influence. For the more far located water molecules (*i.e.* the third and all further molecules), a purely electrostatic interaction of ion and solvent molecules seems to exist. It will be sufficient, therefore, to use an electrostatic approximation for these solvent molecules when discussing their interaction with the ion. This gives a further proof for the applicability of the MESQUAC-MO method to such systems.[4,7] This statement is expected to hold even for ions not having the noble gas electron configuration, as the stronger quantum effects appearing in the ion-solvent binding of such ions should be restricted mainly to the interaction with the first solvation layer. The absolute value for the interaction energy calculated for the iodide ion with water is also in good agreement with the corresponding *ab initio* value and the widely discussed effect of this low binding energy on the phenomenon of "negative" hydration.[11] For Cs^+, however, which also shows negative hydration, this phenomenon cannot be predicted from the present calculation. The reasons for the latter fact are to be seen mainly in the uncertainity of the ion-ligand distance chosen according to the ionic radii only, and in an artificial stabilization for larger cations due to the merely electrostatic description. For iodide ion, this failure could be avoided partially using the distances obtained in previous full *ab initio* calculations.

Solvent Separated Ion Pairs. The stabilization energies per water molecule in chains separating cations and anion are listed in Table 3. As can be shown from Fig. 2, the mutual interaction of the ions through the water chain seems to follow the $1/n$ (*i.e.*, the $1/r$) Coulomb law for any case where more than one solvent

Table 3. Stabilization energies per water molecule for solvent separated ion pairs of alkali iodides, for chain lengths 1—8 (in kcal/mol)

n	Li(water)I	Na(water)I	K(water)I	Cs(water)I
1	101.2	91.1	76.7	73.8
2	48.5	43.3	35.9	34.5
3	32.5	29.0	24.0	23.1
4	22.9	20.3	16.8	16.1
5	18.1	16.1	13.3	12.7
6	14.6	13.0	10.7	10.3
7	12.5	11.1	9.1	8.5
8	10.7	9.5	7.8	7.5

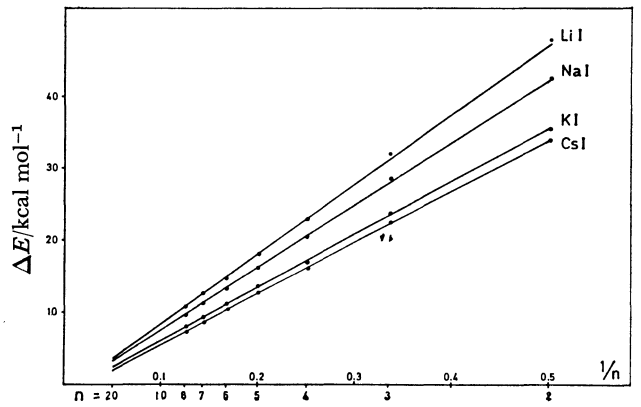

Fig. 2. Stabilization energy per water molecule for varying chain length and ion pairs *versus* the inverse number of water molecules in the polymer.

molecule is present. We can expect therefore also for larger solvent separated ion pairs that an electrostatic description of the cation/anion interaction will be quite satisfactory and sufficient.

The Range of Interactions. The level of 7.1 kcal/mol, being the hydrogen bond energy within the STO-3G *ab initio* framework, actually represents the "critical level" down to which ion-solvent binding energy might have some influence on the solvent structure. The linear chain model, however, is insufficient for the description of the solution reality, since it is an idealized structure, not taking into account effects of 3-dimensional solvates, thermal motions and entropic contributions, which all will lead to a faster decrease of structural influence of the ions. It is, however, useful for a rough estimation of a theoretical upper limit of the range of interaction under "optimal" conditions, *i.e.*, in a well ordered solvent matrix. For such a case, we have to expect, according to the values of Tables 2 and 3, rather far reaching effects of binding. This seems to be in agreement with some recent discussions within the framework of an extended donor-acceptor theory.[12]

Besides representing an estimation of the possible upper limit of interaction ranges, these data might get some practical importance in systems, where a peculiar ordering of the solvent molecules can take place, as for example in quick frozen solutions or in gel matrices.

Summarizing thus the results of our model calculations, we can assume that the application of mixed electrostatic-quantum chemical calculation procedures, taking into account far reaching binding effects by purely electrostatic terms, seem to be justified. The same can be expected for the theoretical investigation of solvent separated ion pairs containing more than one water molecule as a dielectric between the ions. The range of these electrostatic effects will depend very strongly on the degree of ordering of these solvent molecules and hence be influenced strongly by thermal and entropy effects. Finally, a construction of theoretical models describing well ordered solvent matrices will have to consider rather large unities in order to describe all interactions possible in such a system.

Thanks are due to Dr. S. Iwata for his kind support with the computing facilities at the Institute of Physical and Chemical Research at Wako City. Thanks are due also to the Funds zur Förderung der Wissenschaftlichen Forschung (Vienna, Austria, Project Nr. 3725) and the government of Tyrol for financial support.

References

1) S. Fujiwara, K. Nagashima, H. Morita, and Y. Kanaoka *Bull. Chem. Soc. Jpn.*, **50**, 2851 (1977).
2) J. O. Noell and K. Morokuma, *Chem. Phys. Lett.*, **36**, 465 (1975).
3) B. M. Rode and R. Fussenegger, *Monatsh. Chem.*, **108**, 703 (1977).
4) B. M. Rode and G. J. Reibnegger, *J. Chem. Soc. Faraday Trans. 2*, **1979**, 178.
5) G. H. F. Diercksen and W. P. Kraemer, *Theor. Chim. Acta*, **23**, 387 (1972).
6) A. Pullman, B. Pullman, and H. Berthod, *Theor. Chim. Acta*, **47**, 175 (1978).
7) W. Kutzelnigg, *Angew. Chem.*, **85**, 551 (1973).
8) H. Kistenmacher, H. Popkie, and E. Clementi, *J. Chem. Phys.*, **61**, 799 (1974); **58**, 1689 (1973); P. A. Kollman and I. D. Kuntz, *J. Am. Chem. Soc.*, **94**, 9236 (1972).
9) GAUSSIAN 70 Program, QCPE Bloomington, Indiana/USA.
10) I. Dzidzic and P. Kebarle, *J. Chem. Phys.*, **74**, 1466 (1970).
11) B. M. Rode, *Z. Naturforsch., Teil A*, **31**, 1081 (1976).
12) V. Gutmann, "The Donor-Acceptor Approach to Molecular Interactions," Plenum Press, N. Y./London (1978).

The Reaction of *cyclo*-Triphosphate with L-Valine

Mitsutomo Tsuhako,* Naoko Fujita, Akiko Nakahama, Tsuneo Matsuo, Masamitsu Kobayashi, and Shigeru Ohashi**

Kobe Women's College of Pharmacy, Kitamachi, Motoyama, Higashinada-ku, Kobe 658

***Department of Chemistry, Faculty of Science, Kyushu University 33, Hakozaki, Higashi-ku, Fukuoka 812*

(Received November 8, 1979)

The reaction of *cyclo*-triphosphate(P_{3m}) with L-valine in an aqueous solution was studied by means of anion-exchange chromatography, paper chromatography, chemical analysis for phosphorus and valine, IR spectroscopy, and ninhydrin reaction. 1) P_{3m} reacted with L-valine at pH 10—12 to form an unknown compound, the amount of which reached about 22% at pH 12 and about 9% at pH 10. This compound decomposed into orthophosphate-(P_1) and valine at a lower pH. 2) The unknown compound was proved to be a P_1-derivative of valine, 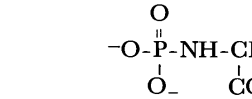 , which has a P–N bond in its molecule. 3) In the reaction of P_{3m} with L-valine at pH 10, in addition to the unknown compound, small amounts of tetra(P_4) and pentaphosphate(P_5) were produced. 4) The disappearance rate of P_{3m} in this reaction was first-order, and its rate constants were 0.317 and 0.138 d^{-1} at pH 12 and 10 respectively at room temperature. 5) Short-chain phosphates, such as P_1, pyro (P_2), and triphosphate(P_3), did not react with L-valine at all. 6) The mechanism of the reaction of P_{3m} with L-valine was discussed.

It was first reported in 1958 by Quimby and Flautt[1] that P_{3m} easily underwent ring cleavage by ammonia to give amidotriphosphate. After that, the reactions of various alkylamines with P_{3m} and *cyclo*-tetraphosphate(P_{4m}) have been studied by Feldmann.[2–5] Furthermore, the application of condensed phosphates as inhibitors to the formation of *N*-nitrosodimethylamine, which is a well known carcinogenic substance and which is easily formed by the reaction of dimethylamine with nitrous acid or nitrite, has recently been reported.[6] That is, when a condensed phosphate is added to an aqueous solution of dimethylamine, they react with each other and the reaction of dimethylamine with nitrous acid or nitrite is inhibited. On the other hand, Rabinowitz,[7–9] applying various phosphates as condensing agents for the polymerization of glycine or alanine, has obtained the corresponding dimers (glycylglycine and alanylalanine) and trimers (glycylgylcylglycine and alanylalanylalanine).

As has been described above, the reactions of cyclic phosphates with ammonia and its derivatives have attracted notice from various points of view. However, up to the present, little attention has been paid to the phosphorus-containing products in the reaction between cyclic phosphates and amino acids or to the mechanisms of the formation of these products. The present investigation was undertaken to see what products, especially phosphorus-containing products, are formed in the reaction of P_{3m} with L-valine, an α-amino acid. The reaction products were examined by means of anion-exchange chromatography, paper chromatography, chemical analysis for phosphorus and valine, IR spectroscopy, and ninhydrin reaction. For the sake of comparison, the reactions of L-valine with P_1, P_2, and P_3 were also tested. From the data obtained, the mechanism of the reaction of P_{3m} with L-valine was discussed.

Experimental

Chemicals. Sodium *cyclo*-triphosphate hexahydrate,[10] $Na_3P_3O_9 \cdot 6H_2O$, was prepared by heating sodium dihydrogenorthophosphate dihydrate at 530 °C for 5 h, cooling it slowly to room temperature, and then crystallizing from an aqueous solution. The $Na_3P_3O_9 \cdot 6H_2O$ thus obtained was identified by paper chromatography and X-ray diffractometry. Reagent-grade L-valine was used without purification. Unless otherwise stated, guaranteed reagents from Wako Chemical Industries, Ltd., were used without further purification.

Reaction between cyclo-*Triphosphate and* L-*Valine.* Two aqueous solutions, 0.4 mol dm^{-3} sodium *cyclo*-triphosphate hexahydrate and 0.4 mol dm^{-3} L-valine, were mixed in a volume ratio of 1:1. The pH of the mixture was about 5.8. The solution was then adjusted with a 6 mol dm^{-3} sodium hydroxide solution to the prescribed pH (10 and 12) and allowed to stand at room temperature. With the progress of the reaction, the pH of the solution was gradually lowered, and then the sodium hydroxide solution was added to maintain the prescribed pH. It was also observed that, at pH values below 9, the solution became moldly.

Anion-exchange Chromatography.[11,12] A chromatographic column of 64×1.5 cm I. D. packed with an anion-exchange resin, Bio-Rad AG 1-X8 (chloride form) of 100—200 mesh, was used. The gradient-elution technique was employed. Sodium chloride solutions of 0.32 mol dm^{-3} and 0.12 mol dm^{-3} were stored in a reservoir (3000 cm^3) and a mixing bottle (750 cm^3) respectively. 150 and 40 cm^3 of a mixture (2:1) of the 0.1 mol dm^{-3} tetrasodium ethylenediaminetetraacetate (EDTA-4Na) and 0.1 mol dm^{-3} disodium ethylenediaminetetraacetate (EDTA-2Na) solutions were added to the sodium chloride solutions in the reservoir and the mixing bottle. The pH of the eluent was about 10. The sample solution was diluted 20 times, and 1 cm^3 of it was injected into a column. The effluent was collected in 10-g fractions with a fraction collector of the weight type.

Determination of Phosphorus.[11,13] The phosphorus in the effluent was determined by the orthophosphoric heteropoly-blue method. To 10-g of the fractionated effluent, 2 cm^3 of the molybdenum(V)–molybdenum(VI) reagent[14] and about 5 cm^3 of distilled water were added. The mixture was heated in a water bath at 95 °C for 1 h. After cooling, the solution was made up to 25 cm^3 with distilled water. The absorbance was measured at 830 nm by means of a Hitachi Spectrophotometer, 100-20 type.

Determination of Valine. A Hitachi Amino-acid An-

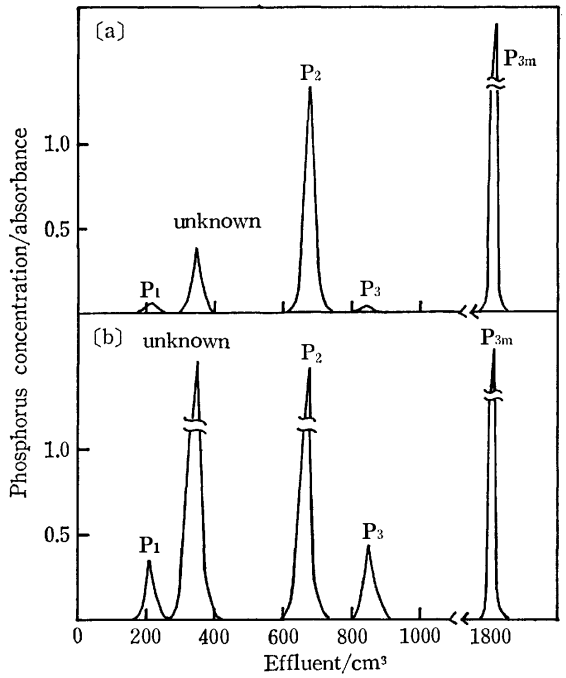

Fig. 1. Elution patterns for the reaction products of P_{3m} with L-valine at pH 12.
(a): After 1 d, (b): after 14 d.

alyzer, KLA-5 type, was used for the determination of valine in the reaction products.

Paper Chromatography. Using Toyo Roshi No. 51A filter paper and acidic and basic solvents,[15-17] the phosphate species in the reaction products were paper-chromatographed by an ascending technique at 5 °C and at room temperature for about 20 h.

Ninhydrin Reaction. To 5 cm³ of the fractionated effluent we added a few drops of a 5% ninhydrin solution, after which the mixture was boiled and then cooled. The reddish purple coloration indicates the presence of valine.

IR Spectroscopy. After the fractionated effluent had been dehydrated under reduced pressure, it was submitted to IR spectroscopy. Since, in the sample, sodium chloride was present in a large amount, a direct measurement was possible without any dilution with potassium bromide. A Hitachi Infrared Spectrophotometer, EPI-S2 type, was used.

Results and Discussion

Reaction of cyclo-*Triphosphate with* L-*Valine.* The aqueous solutions of P_{3m} and L-valine were mixed at a molar ratio of 1:1 and adjusted to pH 10 and 12 with a sodium hydroxide solution. When the mixture was allowed to stand at room temperature, the pH of this solution gradually lowered. This may suggest the formation of chain phosphates and/or their derivatives by the reaction of P_{3m} with water and/or L-valine. During the progress of the reaction, the sodium hydroxide solution was added to maintain the prescribed pH. The reaction products of P_{3m} with L-valine were separated by anion-exchange chromatography. As examples, the elution patterns for the reaction mixture at pH 12 after 1 d and after 14 d are shown in Fig. 1. Between the elution peaks of P_1 and P_2, a peak of an unknown compound appeared. P_2 began

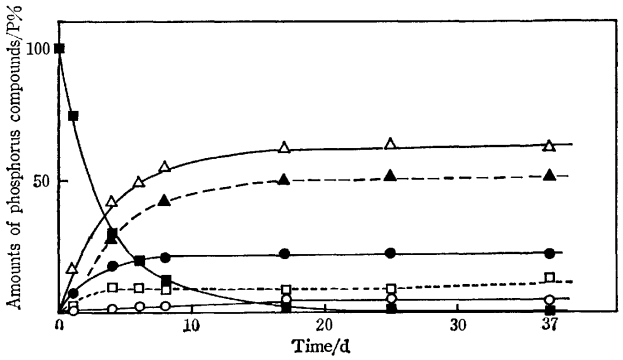

Fig. 2. Change of the amounts of phosphorus compounds in the reaction of P_{3m} with L-valine at pH 12.
—●—: Unknown compound, —○—: P_1, —△—: P_2 (total), --▲--: P_2 (precipitated), --□--: P_3, —■—: P_{3m}.

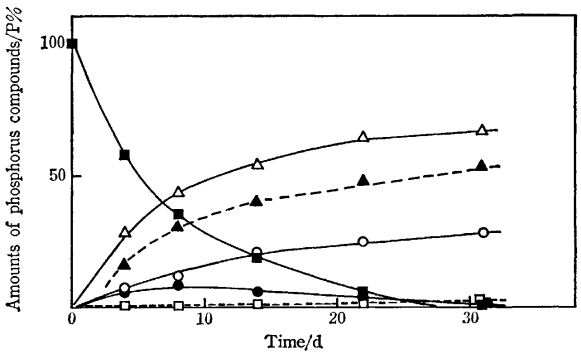

Fig. 3. Change of the amounts of phosphorus compounds in the reaction of P_{3m} with L-valine at pH 10.
—●—: Unknown compound, —○—: P_1, —△—: P_2 (total), --▲--: P_2 (precipitated), —□—: P_3, —■—: P_{3m}.

to precipitate as crystals of tetrasodium pyrophosphate decahydrate on the 2nd day. Figure 2 shows the changes in the amounts of P_1, P_2, P_3, P_{3m}, and the unknown compound during the progress of the reaction. As can be seen from Fig. 2, the amount of the starting material, P_{3m}, rapidly decreased with time and became nearly zero within four weeks. On the contrary, the amounts of P_2 and the unknown compound gradually increased with time, reached about 62 and 22% respectively after 2 weeks, and after that were almost constant. Although the amounts of P_1 and P_3 were less than those of P_2 and the unknown compound, they gradually increased with time.

The products obtained by the reaction of P_{3m} with L-valine at pH 10 were somewhat different from those obtained at pH 12 and consisted of six kinds of phosphates, *i.e.*, the unknown compound, P_1, P_2, P_3, P_4, and P_5. The changes in the amounts of the unknown compound, P_1, P_2, P_3, and P_{3m} with time are shown in Fig. 3. The data for P_4 and P_5 are omitted, because their amounts are very small. Unlike the results in the case of pH 12, the yield of the unknown compound at pH 10 reached a maximum, about 9%, after 7—8 d, and after that gradually decreased. It was only about 2.6% after 31 d. The amounts of P_4 and P_5 formed at pH 10 were about 0.7 and 0.5% respectively after

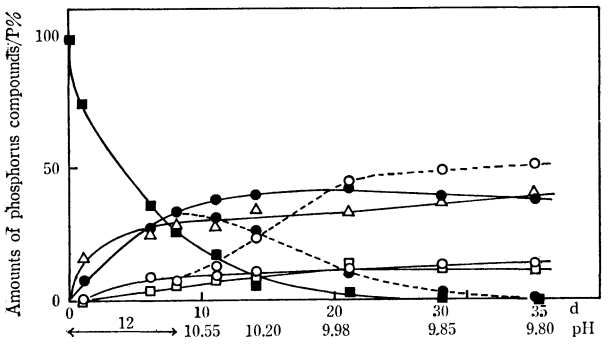

Fig. 4. Change of the amounts of phosphorus compounds in the reaction of P_{3m} with L-valine at pH 12 and when pH was not controlled.
——: pH 12, ……: pH not controlled, —●—: unknown compound, —○—: P_1, —△—: P_2, —□—: P_3, —■—: P_{3m}.

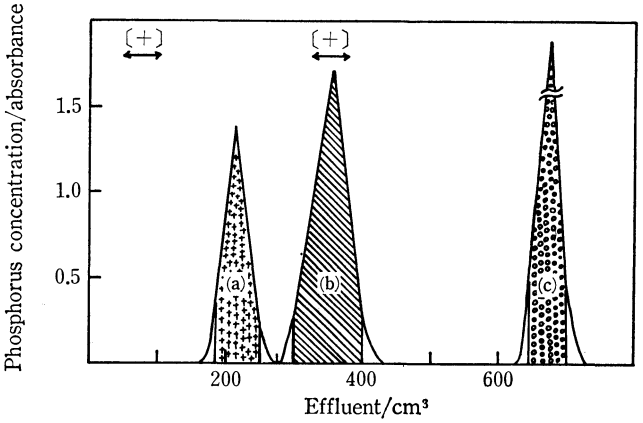

Fig. 5. An elution pattern for the reaction products of P_{3m} with L-valine at pH 12 and the tests by ninhydrin reaction and IR spectroscopy.
Ninhydrin reaction; (+) positive. IRS: (a): orthophosphate, (b): unknown compound, (c): pyrophosphate.

31 d. It is an interesting phenomenon that, at pH 10, P_4 and P_5 are produced. The mechanism of their formation has not yet been definitely proved, but will be discussed later.

The above experimental results indicate that the yield of the unknown compound was higher at pH 12 than that at pH 10. In order to confirm this fact, the reaction of P_{3m} and L-valine was tried at a lower pH. A mixture of P_{3m} and L-valine solutions at a molar ratio of 1:1 was allowed to react at pH 12 for a week. After that, this sample solution was divided into two portions, one being set at pH 12 and the other being allowed to stand without any adjustment of the pH. The yields of the products in these two series of experiments are shown in Fig. 4, in which the amount of precipitated P_2 has been omitted. The variations in the pH are indicated below the abscissa. The amounts of P_2, P_3, and P_{3m}, when the pH was not controlled, are also omitted, because they are almost the same as those when the pH was controlled at 12. When the pH was not controlled, the pH of the solution gradually decreased with the progress of the reaction, and the yield of the unknown compound decreased and became nearly zero at pH 9.8. On the contrary, the yield of P_1 was found to increase sharply. The curve of the formation of the unknown compound has a tendency reverse-symmetric to that of P_1. This suggests that the unknown compound, initially formed in a large quantity at pH 12, decomposed into P_1 as the pH of the solution was lowered. This means, in turn, that the unknown compound may be a P_1-derivative of valine.

The disappearance rates of P_{3m} in the reactions with L-valine at pH 12 and 10 at room temperature were found to be first-order. The rate constants were 0.317 and 0.138 d^{-1} at pH 12 and 10 respectively.

The reactions of P_{3m} with L-valine at molar ratios of 0.1:1, 0.5:1, 5:1, and 10:1 were also studied at pH 12, but it was found that the products were completely the same kinds as those at the molar ratio of 1:1. By the reactions of P_{3m} with L-valine in neutral and acidic solutions, no unknown compound was obtained at all.

Molecular Structure of the Unknown Compound. As has been described in the preceding section, it was concluded that the unknown compound may be a P_1-derivative of valine. In order to get more information on the molecular structure of this compound various methods were employed. A solution of the unknown compound, separated by ion-exchange chromatography, was paper-chromatographed with an acidic solvent. The unknown compound gave a spot with a strong coloration at the position corresponding to P_1 and another spot with a weak coloration at a position between those of P_1 and P_2. The latter may be due to the unknown compound. The former may be due to the P_1 produced by the hydrolysis of the unknown compound in the acidic solvent. This fact also supports the idea that the unknown compound is a P_1-derivative of valine.

The amounts of phosphorus and valine in the unknown compound separated by ion-exchange chromatography were determined by chemical analysis. It was found that the ratio of phosphorus to valine in the unknown compound is unity, suggesting that this unknown compound is a P_1-derivative of valine containing P_1 and valine in the molar ratio of 1:1.

Each solution fractionated by ion-exchange chromatography was dehydrated under reduced pressure to obtain the respective components in a solid state and tested by ninhydrin reaction and IR spectroscopy. The results are shown in Fig. 5. In this elution, an eluent containing no EDTA was employed, because EDTA disturbs the ninhydrin reaction. The components in the fractions of 50—100 and 300—400 cm^3 are ninhydrin-reaction positive. The component in the former fractions is attributable to the unreacted valine. The component in the latter fractions is attributable to the unknown compound. These results also support the idea that the unknown compound is a P_1-derivative of valine. Furthermore, from the IR spectra, the components in the fractions of 180—250 and 630—700 cm^3 were proved to be P_1 and P_2 respectively. Figure 6 shows the IR spectrum of the component in the fraction with an elution peak at

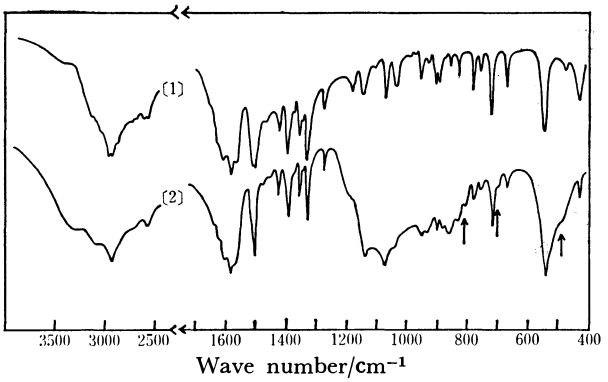

Fig. 6. IR spectra of L-valine and the unknown compound.
Arrow (↑): absorption due to the P-N bond, (1): L-valine, (2): unknown compound.

about 350 cm[3] (the unknown compound). The unknown compound indicates absorptions at about 2950, 1610—1560, 1500, 1420, 1390, 1350, 1330, 1270, 780, 720, and 540 cm^{-1} attributed to valine. In addition, at about 1150—1050, 1000—950, and 860 cm^{-1} absorptions attributable to P_1 [18,19] are found. Further, at about 810—800 (ν_{P-N}), 700 (ν_{P-N}), and 490 cm^{-1} (δ_{P-N}) weak absorptions, which may be due to the P–N bond,[20-23] are found. Also, strong absorptions caused by the carboxylato group of valine are observed at about 1610—1550 and 1400 cm^{-1}. Therefore, this unknown compound probably has the P–N bond and the COO^- group in its molecule.

From all the results presented above, it was concluded that the unknown compound is a P_1-derivative of valine, an anion of *N*-(1-carboxy-2-methylpropyl)phosphoramidic acid,

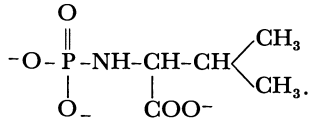

Reaction of Short-chain Phosphates with L-*Valine.*
A solution of trisodium orthophosphate, tetrasodium pyrophosphate, or pentasodium triphosphate was mixed with the L-valine solution in a molar ratio of 1:1, and then the mixed solution was adjusted with a sodium hydroxide solution to pH 12 and allowed to react at room temperature. No reaction products were observed at all in the reactions of L-valine with P_1 and P_2. Only in the reaction of P_3 was a slight amount of P_2, produced by the hydrolysis of P_3, observed. Therefore, it may be concluded that, from short-chain phosphates, such as P_1, P_2, and P_3, no phosphate derivatives of valine can be formed.

Mechanism of the Reaction of cyclo-*Triphosphate with* L-*Valine.* The mechanism of the reaction of P_{3m} with L-valine at pH 10—12 is summarized in Fig. 7. At pH 10—12, P_{3m} is easily attacked by an amino group of L-valine to produce a P_3-derivative of valine;

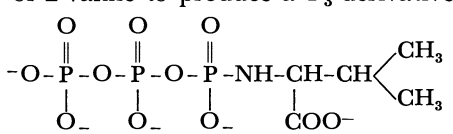

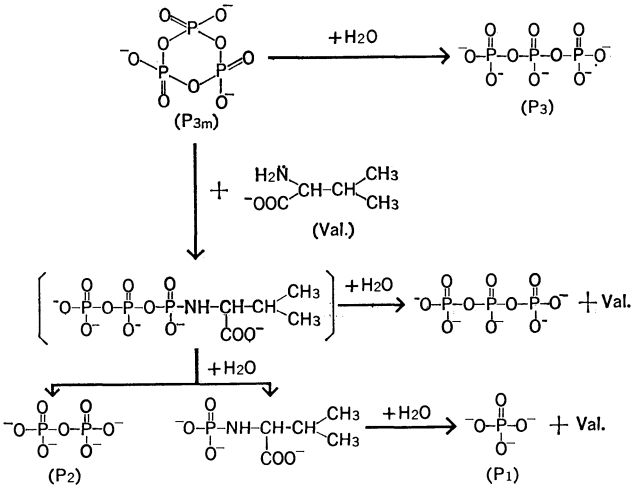

Fig. 7. Mechanism of the reaction of P_{3m} with L-valine.

(P_3-(N)Val). However, since P_3-(N)Val can not be detected at all by means of either ion-exchange chromatography or paper chromatography, this compound may be extremely unstable and immediately hydrolyzed to P_2 and a P_1-derivative of valine, P_1-(N)Val, as well as to P_3 and valine. The latter route of hydrolysis is suggested because the yield of P_3 is much higher than that to be expected from only the hydrolysis of P_{3m}. As has been described before, small amounts of P_4 and P_5 were produced in the reaction of P_{3m} with L-valine at pH 10. This phenomenon may have some connection with Quimby's finding that the amidotriphosphate produced by the reaction of P_{3m} with ammonia in an alkaline solution returns to being P_{3m}, accompanying the abstraction of ammonia, when the solution is acidified. In the present reaction, the following mechanism may be one of the possibilities; P_3-(N)Val reacts with P_1 or P_2 to form P_4 or P_5, accompanying the abstraction of valine. A similar phenomenon has been reported by Feldmann and Thilo,[3] who found that, when a solution of amidotriphosphate is acidified, small amounts of P_4, P_5, and P_6 are produced. On the other hand, in the reaction of P_{3m} with L-valine, divaline and trivaline can not be detected by thin-layer chromatography.

References

1) O. T. Quimby and T. J. Flautt, *Z, Anorg. Allg. Chem.*, **296**, 220 (1958).
2) W. Feldmann and E. Thilo, *Z. Anorg. Allg. Chem.*, **327**, 159 (1964).
3) W. Feldmann and E. Thilo, *Z, Anorg. Allg. Chem.*, **328**, 113 (1964).
4) W. Feldmann, *Z. Chem.*, **1**, 26 (1965).
5) W. Feldmann, *Z. Chem.*, **4**, 154 (1969).
6) M. Kobayashi, Japan 53—072768.
7) J. Rabinowitz, *Helv. Chim. Acta*, **52**, 2663 (1969); **53**, 1350 (1970); **54**, 1483 (1971).
8) J. Rabinowitz, *Nature*, **224**, 795 (1969).
9) N. M. Chung, R. Lohrmann, L. E. Orgel, and J. Rabinowitz, *Tetrahedron*, **27**, 1205 (1971).
10) L. F. Audrieth, *Inorg. Synth.* Vol. III, 104 (1950).

11) M. Tsuhako, C. Oyama, T. Matsuo, I. Motooka, and M. Kobayashi, *Yakugaku Zasshi*, **98**, 1349 (1978).
12) T. Nakamura, T. Yano, A. Fujita, and S. Ohashi, *J. Chromatogr.*, **130**, 384 (1977).
13) N. Yoza and S. Ohashi, *Bull. Chem. Soc. Jpn.*, **37**, 33 (1964).
14) N. Yoza, K. Ishibashi, and S. Ohashi, *J. Chromatogr.*, **134**, 497 (1977).
15) G. Biberacher, *Z. Anorg. Allg. Chem.*, **285**, 86 (1956).
16) S. Utsumi and M. Shima, *Nippon Kagaku Zasshi*, **81**, 138 (1960).
17) I. Motooka, M. Ishizaki, H. Nozu, and M. Kobayashi, *Kogyo Kagaku Zasshi*, **69**, 2071 (1966).
18) D. E. C. Corbridge and E. J. Lowe, *J. Chem. Soc.*, **1954**, 493.
19) D. E. C. Corbridge, *J. Appl. Chem.*, **6**, 456 (1956).
20) E. Steger, *Z. Anorg. Allg. Chem.*, **309**, 305 (1961).
21) E. Steger and G. Mildner, *Z. Anorg. Allg. Chem.*, **332**, 314 (1964).
22) E. Kobayashi, *Nippon Kagaku Kaishi*, **1972**, 38; **1973**, 1437.
23) N. Kumagai and H. Mase, *Nippon Kagaku Kaishi*, **1976**, 1831; **1978**, 46.

Kinetics of the Formation and Transformation of Alkoxy-derived Strontium Metaborate

Osamu YAMAGUCHI,* Muneaki KAMATA, and Kiyoshi SHIMIZU*

Department of Applied Chemistry, Faculty of Engineering, Doshisha University, Karasuma Imadegawa, Kamigyo-ku, Kyoto 602

(Received November 26, 1979)

A new metastable SrB_2O_4 was formed by heating amorphous material prepared by the simultaneous hydrolysis of strontium and boron alkoxides. Crystallization isotherms were obtained by means of the Avrami equation $\ln(1-\alpha)=-kt^n$ with $n=2$, the activation energy being determined to be 351 kJ/mol. The kinetics of transformation of metastable into stable SrB_2O_4 is interpreted by the first-order equation $-\ln(1-\alpha)=kt$. Activation energies are 498 kJ/mol and 343 kJ/mol for initial and final stages, respectively.

Crystalline strontium metaborate (SrB_2O_4) has been known only in orthorhombic modification.[1,2] In a previous paper[3] dealing with the heating process of mixed powder prepared by the simultaneous hydrolysis of strontium and boron alkoxides, it was reported that metastable SrB_2O_4, similar in structure to low-temperature form of ZnB_2O_4,[4,5] is formed at 650—690 °C. The present study deals with the kinetics of the formation of metastable SrB_2O_4 and the transformation of metastable into stable SrB_2O_4. The kinetic data were analyzed with use of available solid state models.

Experimental

Materials and Procedure. Boron triethoxide was of guaranteed purity. Strontium methoxide was synthesized by heating strontium metal (purity 99.9%) in an excess amount of dehydrated methanol at 64 °C for 5 h. A mixture of boron and strontium alkoxides in the mole ratio $Sr^{2+}/B^{3+}=1:2$ was poured into aqueous ammonia solution at 25 °C. The temperature was slowly raised up to 60 °C while being stirred. The resulting mixed powder (starting powder, average particle size *ca.* 550 Å) was washed repeatedly with hot water and dried at 60 °C under reduced pressure.

Measurement. Thermal analyses (TG, DTA) were carried out in the air at the heating rate 10 °C/min. Alpha-alumina was used as a standard material in DTA. On the basis of DTA data, the specimens heated at the rate 10 °C/min were examined by means of X-ray diffraction using nickel filtered copper K_α. The scanning speed 1/4°/min of the goniometer was selected to satisfy the accuracy of *d*-spacing. Kinetic studies of the formation of metastable SrB_2O_4 and its transformation into stable SrB_2O_4 have been made by means of X-ray diffraction. The starting powder was pre-heated; the specimens were placed in an electric furnace equipped with a temperature regulator, heated for the desired time, and then cooled repidly to room temperature.

Results and Discussion

Thermal Analysis. TG analysis of the starting powder showed that the weight loss is 16.7% due to the loss of ammonia, absorbed water, hydrated water, and organic residue from the parent alcohol up to 560 °C. On the other hand, two exothermic reactions in DTA were observed at 650—690 °C and 715—780 °C. X-Ray diffraction analysis confirmed that the first exothermic peak (650—690 °C) is due to the crystallization of metastable SrB_2O_4 from an amorphous phase, the second (715—780 °C) to the transformation of metastable phase into stable SrB_2O_4.

X-Ray Analysis. The starting powder was amorphous, no significant change being observed up to 600 °C. The peaks corresponding to metastable SrB_2O_4[3] appeared after heating at 620 °C for 5 min, and the intensity increased rapidly up to 670 °C. Table 1 gives the X-ray powder diffraction data of metastable SrB_2O_4. The observed *d*-values of the compound were similar to those of ZnB_2O_4 of low-temperature form, the structure of which has not been determined. Both compounds disagree in relative intensities of main peaks.[3] The peaks of stable SrB_2O_4 (orthorhombic)[1,2] appear when heated at 710 °C, the specimen heated at 780 °C showing characteristic X-ray diffraction pattern of stable SrB_2O_4.

Kinetics of the Formation of Metastable SrB_2O_4. Figure 1 shows the fraction of the crystallized metastable SrB_2O_4 at 620, 640, and 660 °C. The starting powder was pre-heated at 580 °C. The fractional crystallization of each specimen was determined from

Table 1. X-Ray powder diffraction data of metastable SrB_2O_4

d/Å	I/I_1	*d*/Å	I/I_1
5.97	32	2.675	2
5.56	2	2.607	7
5.25	8	2.550	2
4.26	2	2.501	3
4.17	3	2.417	41
4.12	2	2.411	43
4.01	3	2.338	5
3.952	6	2.304	2
3.731	6	2.268	36
3.693	2	2.225	7
3.569	3	2.219	8
3.548	5	2.166	2
3.460	100	2.137	3
3.363	84	2.083	4
3.238	3	2.062	5
3.159	5	2.029	20
3.131	3	1.991	42
3.105	2	1.979	53
2.998	42	1.941	31
2.921	52	1.907	7
2.871	5	1.873	8
2.853	5	1.845	10
2.801	19		

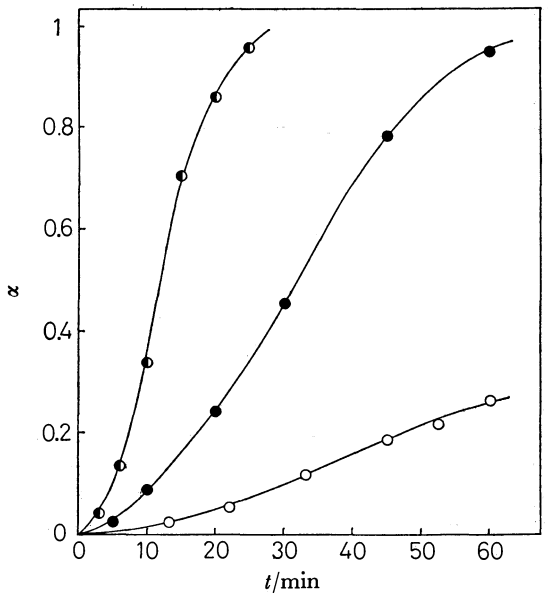

Fig. 1. Formation of metastable SrB_2O_4 as a function of time at different temperatures.
○: 620 °C, ●: 640 °C, ◐: 660 °C.

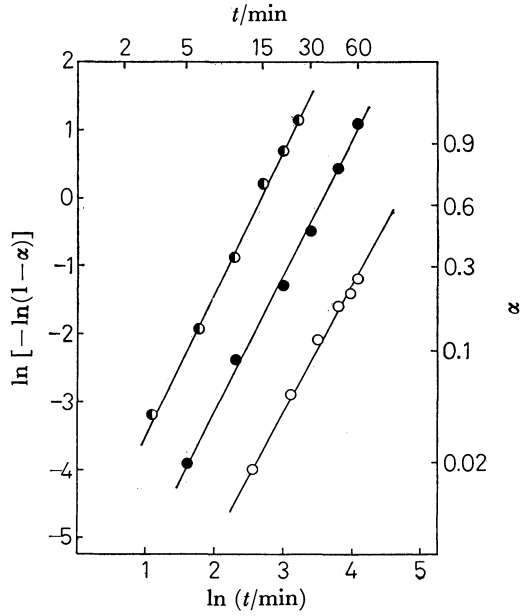

Fig. 2. Plots of $\ln(1-\alpha)$ *vs.* time t of the data shown in Fig. 1.
○: 620 °C, ●: 640 °C, ◐: 660 °C.

the height of $d=3.36$ Å, the main characteristic peak. A well-crystallized specimen was obtained by heating at 670 °C for 30 min. Magnesium oxide (MgO) was used as an internal standard. Crystallization isotherms were characterized by sigmoidal shape (Fig. 1), the kinetics being best described by the Avrami equation (Fig. 2),[6]

$$\ln(1-\alpha) = -kt^n \qquad (n=1.9-2\fallingdotseq 2) \qquad (1)$$

where α, t, k, and n are the fractional crystallization, time, rate constant, and a constant related to the reaction mechanism, respectively. The metastable SrB_2O_4 powder consists of plate-like particles. From the result and the fact that the Avrami equation with $n=2$

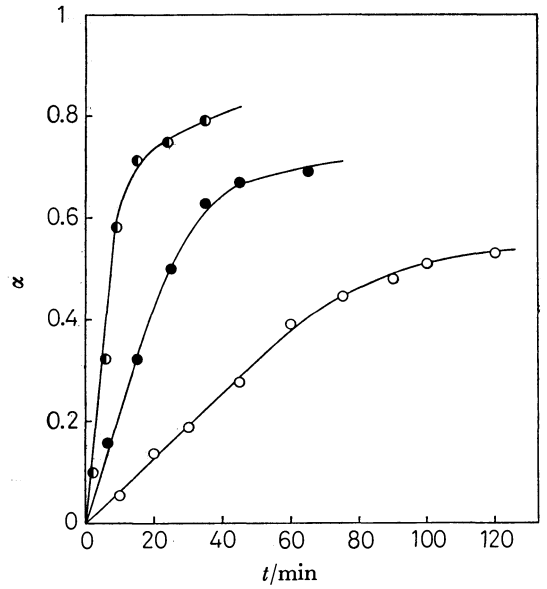

Fig. 3. Phase transformation from metastable into stable SrB_2O_4 as a function of time at different temperatures.
○: 710 °C, ●: 730 °C, ◐: 750 °C.

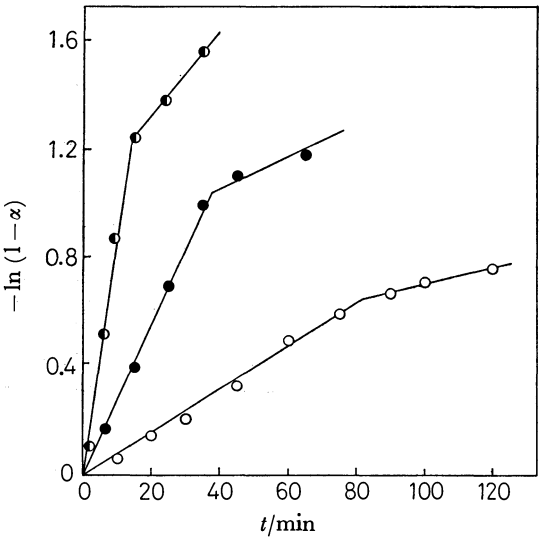

Fig. 4. First-order plots of the data shown in Fig. 3.
○: 710 °C, ●: 730 °C, ◐: 750 °C.

fits crystallization curves over the whole range, two dimensional growth of metastable SrB_2O_4 with site-saturation for nucleation seems to be the rate-determining step. The activation energy calculated from the Arrhenius plot is 351 kJ/mol.

Kinetics of the Transformation. The fractional transformation of metastable into stable SrB_2O_4 was determined as a function of time at different temperatures (Fig. 3). Metastable SrB_2O_4 obtained by heating the starting powder at 670 °C for 30 min was used as a starting material. The fractional transformation was determined from the heights of the main characteristic peaks of metastable ($d=3.36$ Å) and stable SrB_2O_4 ($d=2.69$ Å), using the calibration curve prepared with known compositions. No line broadening was observed during the course of transformation.

Attempts were made to fit the results to kinetic laws. As shown in Fig. 4, transformation isotherms are best described by the first-order equation,[7]

$$-\ln(1-\alpha) = kt \quad (2)$$

where α is the fractional transformation and t time. There are linear portions in each of the plots. The rate constants were determined from the slopes of the straight lines. Activation energies are 498 kJ/mol and 343 kJ/mol for initial and final stages, respectively. They might represent activation energies for nucleation process and propagation process, respectively.[8]

References

1) C. E. Weir and R. A. Schroeder, *J. Res. Nat. Bur. Stand.*, **68A**, 465 (1964).
2) X-Ray powder data file (ASTM card 15—779).
3) O. Yamaguchi, M. Kamata, and K. Shimizu, *Chem. Lett.*, **1979**, 1341.
4) D. E. Harrison and F. A. Hummel, *J. Electrochem. Soc.*, **103**, 491 (1956).
5) X-Ray powder data file (ASTM card 9—107).
6) M. Avrami, *J. Chem. Phys.*, **7**, 1103 (1939); **8**, 212 (1940).
7) For example, R. W. Grimshaw, J. Hargreaves, and A. L. Roberts, *Trans. Brit. Ceram. Soc.*, **55**, 36 (1956).
8) For example, Y. Kotera and Y. Yonemura, *Trans. Faraday Soc.*, **59**, 147 (1963).

Reactions of Halogeno-bridged Organopalladium(II) Complexes with an Electron-rich Olefin. New Cyclopalladated Carbene Complexes, and (Carbene)chloropalladium(II) Complexes Containing a σ,π-Methallyl Group or a π-Coordinated-chelating Alkyl-Palladium σ-Bond

Katsuma HIRAKI,* Keiichi SUGINO, and Masayoshi ONISHI*

Department of Industrial Chemistry, Faculty of Engineering, Nagasaki University, Bunkyo-machi, Nagasaki 852

(Received November, 30, 1979)

A chloro-bridged organopalladium(II) complex, di-μ-chloro-bis(3-*t*-butylthio-2-methoxy-2-methylpropyl-1-*C*,*S*)dipalladium(II) reacted with an electron-rich olefin, bis(1,3-diphenyl-2-imidazolidinylidene) (L_2) to yield a new dinuclear carbene complex, di-μ-chloro-bis(1,3-diphenyl-2-imidazolidinylidenato-2-*C*,2′-*C*)dipalladium(II) (**4**). Complex **4** was treated with thallium acetylacetonate, triisopropyl phosphite, 4-picoline, silver acetate, and L_2, affording the corresponding new carbene complexes. On the basis of spectroscopic properties, these complexes were ascribed to new complexes containing cyclopalladated chelate structure in the carbene ligand. Di-μ-chloro-bis(1-3-η^3-methallyl)dipalladium(II) and di-μ-chloro-bis(6-*exo*-methoxy-3a,4,7,7a-tetrahydro-*endo*-4,7-methanoindene-*endo*-5σ, 2π)dipalladium(II) reacted with L_2 to give new mononuclear (carbene)chloropalladium(II) complexes possessing a σ,π-methallyl group and a π-coordinated-chelating alkyl-palladium σ-bond, respectively.

Recently, some aryl(carbene)palladium(II) complexes were prepared from reactions of chloro-bridged cyclopalladated complexes towards an electron-rich olefin, bis(1,3-diphenyl-2-imidazolidinylidene) [=CN(Ph)-CH_2CH_2N(Ph)]$_2$ (L_2).[1] However, few works have been reported as regards isolation and characterization of alkyl- and vinyl(carbene)palladium(II) complexes,[2] while several alkyl-,[3-6] aryl-,[7] and ethynyl(carbene)-platinum[8] complexes have been reported.

It is interesting to compare the reactivities of chloro-bridged alkyl-, π-allyl-, and 1-alkenylpalladium(II) complexes towards L_2 with that of the cyclopalladated complexes. The present paper deals with the reactions of the chloro-bridged alkyl- or π-methallylpalladium(II) complexes towards L_2, and with the resulting new types of (carbene)organopalladium(II) complexes, *i.e.* cyclopalladated carbene complexes, and (carbene)-chloropalladium(II) ones containing a σ,π-methallyl group or a π-coordinated-chelating alkyl-palladium σ-bond. A preliminary communication of this work has been published recently.[9]

Experimental

General Procedures. Melting points, molecular weight, molar conductivity, and IR and ^{1}H-NMR spectra were determined according to the previous paper.[1] ^{13}C-NMR spectra were measured on a JEOL model FT-100 spectrometer, using tetramethylsilane as an internal standard.

The electron-rich olefin L_2,[10] thallium(I) acetylacetonate,[11] and the chloro-bridged organopalladium(II) complexes, di-μ-chloro-bis(3-*t*-butylthio-2-methoxy-2-methylpropyl-1-*C*,*S*)-dipalladium(II) (**1**),[12] di-μ-chloro-bis(1-3-η^3-methallyl)dipalladium(II) (**2**),[13] and di-μ-chloro-bis(6-*exo*-methoxy-3a,4,7,7a-tetrahydro-*endo*-4,7-methanoindene-*endo*-5σ,2π)dipalladium(II) [{Pd(6-MeO-themi)Cl}$_2$] (themi=3a,4,7,7a-tetrahydro-*endo*-4,7-methanoindene-*endo*-5σ,2π) (**3**)[14] were prepared according to the respective literature.

*Reaction of **1** with L_2.* A mixture of **1** (1.42 mmol) and L_2 (1.44 mmol) in 27.5 ml of *m*-xylene was heated under reflux for 40 min. Resulting black precipitates were collected and extracted with boiling acetonitrile for 10 h. The extracted solid was washed with dichloromethane to afford microcrystals, di-μ-chloro-bis(1,3-diphenyl-2-imidazolidinyl-idenato-2-*C*,2′-*C*)dipalladium(II) [{Pd(dpim)Cl}$_2$] (dpim= 1,3-diphenyl-2-imidazolidinylidenato-2-*C*,2′-*C*) (**4**).

*Reaction of **4** with Tl(acac).* A benzene suspension of **4** (0.11 mmol) and Tl(acac) (0.23 mmol) was heated at reflux for 2 h. After benzene was removed, the residue was extracted with dichloromethane. Addition of diethyl ether to the extract yielded a pale yellow white needle, [Pd-(dpim)(acac)] (**5**).

*Reaction of **4** with Triisopropyl Phosphite.* A tetrahydrofuran (THF) suspension of **4** (0.14 mmol) and triisopropyl phosphite (1.74 mmol) was heated at reflux for 30 min to yield a brown solution. The solution was concentrated at reduced pressure and diluted with hexane to afford a pale yellow solid. The solid was recrystallized from dichloromethane-hexane to give a pale yellow needle, [Pd(dpim)Cl-{P(OCHMe$_2$)$_3$}] (**6**).

*Reaction of **4** with 4-Picoline.* A THF suspension (10 ml) of **4** (0.18 mmol) and 4-picoline (pic) (0.37 mmol) was heated under reflux for 2.5 h. After the solvent was evaporated at reduced pressure, the residue was extracted with dichloromethane. Addition of diethyl ether to the extract gave a pale yellow-white needle, [Pd(dpim)Cl(pic)] (**7**).

Halogen metathesis of **7** with lithium bromide took place in acetone at room temperature, followed by the similar procedures to the preparation of **7**, to afford [PdBr(dpim)-(pic)] (**8**).

*Reaction of **4** with Silver Acetate.* An acetone suspension (12.5 ml) containing **4** (0.14 mmol) and silver acetate (0.30 mmol) was heated at reflux for 2 h. The solvent was removed, and the resulting residue was recrystallized from dichloromethane and hexane to yield an acetato-bridged complex, [{Pd(dpim)(O$_2$CMe)}$_2$] (**9**).

A methanol suspension (10 ml) involving **9** (0.10 mmol) and lithium bromide (0.70 mmol) was heated under reflux for 6 h, and then stirred at room temperature for 1 d. The resulting solids were collected and washed with methanol and diethyl ether to give a bromo-bridged complex, [{PdBr-(dpim)}$_2$] (**10**).

*Reactions of **4** and **10** with L_2.* A *m*-xylene suspension (15 ml) containing **4** (0.28 mmol) and L_2 (0.34 mmol) was refluxed for 2 h. After the solvent was removed with a rotary evaporator, the residue was recrystallized from dichloromethane-hexane to afford a dicarbene complex, [Pd-(dpim)ClL]·1/2CH_2Cl_2 (**11**).

An acetone suspension (12.5 ml) involving **11** (0.19 mmol),

Table 1. Yields and properties of the carbene complexes

Complex		Yield[a] %	Mp[b] °C	Color	C% Found	C% Calcd	H% Found	H% Calcd	N% Found	N% Calcd
[{Pd(dpim)Cl}$_2$]	**4**	46.2[c]	>300	Pale yellow	49.61	49.61	3.58	3.61	7.79	7.71
[Pd(dpim)(acac)]	**5**	64.1	225	Off white	56.12	56.29	4.74	4.72	6.58	6.56
[Pd(dpim)Cl{P(OCHMe$_2$)$_3$}]	**6**	76.3	180	Yellow	50.48	50.45	6.02	6.00	4.89	4.90
[Pd(dpim)Cl(pic)]	**7**	24.5	212	Off white	55.27	55.28	4.41	4.42	9.10	9.21
[PdBr(dpim)(pic)]	**8**	54.7[d]	223	Off white	50.15	50.37	3.89	4.03	8.31	8.39
[{Pd(dpim)(O$_2$CMe)}$_2$]	**9**	75.1	189—202	Yellow	53.39	52.80	4.29	4.17	7.05	7.24
[{PdBr(dpim)}$_2$]	**10**	100[e]	246—254	Pale yellow	43.93	44.20	3.02	3.22	6.69	6.87
[Pd(dpim)ClL]·½CH$_2$Cl$_2$	**11**	70.9	240—260	White	58.24	58.34	4.61	4.50	8.80	8.92
[Pd(dpim)L(pic)]ClO$_4$	**12**	56.4[f]	158—168	Pale yellow	57.88	58.23	4.66	4.62	9.31	9.31
[PdBr(dpim)L]	**13**	25.9[g]	220—260	Pale yellow	56.64	57.21	4.36	4.32	8.65	8.89
[Pd(σ,π-CH$_2$CMe=CH$_2$)ClL]	**14**	65.8[h]	150—163	Cream	54.62	54.43	5.13	5.05	6.64	6.68
[Pd(6-MeO-themi)ClL]	**15**	71.3[i]	153—157	Off white	58.57	59.21	5.58	5.54	5.25	5.35

a) Based on **4**, unless noted elsewhere. b) With decomposition. c) Based on **1**. d) Based on **7**. e) Based on **9**. f) Based on **11**. g) Based on **10**. h) Based on **2**. i) Based on **3**.

Table 2. Characteristic IR bands of the carbene complexes

Complex	ν(C$_{carbene}$–N)	ν(C$_\phi$–N)[b]	ν(Pd–Cl)	Others
4	1480, 1495	1280	239, 258	—
5	1475, 1495	1275	—	1510+1580{ν(C=C)+ν(C=O)}
6	1485, 1500	1280	280	1100{(ν(C–O)}
7	1480, 1495	1280	305	1568+1620{ν(C=N)+ν(C=C)}[c]
8	1495	1275	—	1565+1615{ν(C=N)+ν(C=C)}[c]
9	1480	1275	—	1405{ν_s(OCO)}, 1580{ν_a(OCO)}
10	1485	1280	—	—
11	1465, 1490	1275	246	—
12	1485	1270	—	1570+1610{ν(C=N)+ν(C=C)}[c] 1100{ν(Cl–O)}
13	1485	1270	—	—
14	1485	1270	272	—
15	1485	1275	274	1075{ν(C–O)}

a) In cm^{-1}, in KBr disk. b) ν(C(aromatic)–N)}. c) For the pyridine ring.

4-picoline (0.54 mmol), and sodium perchlorate–water(1/1) {Na[ClO$_4$]·H$_2$O} (0.21 mmol) was heated under reflux for 1.5 h. After acetone had been evaporated, the resulting residue was recrystallized from acetonitrile–diethyl ether to give an ionic complex, [Pd(dpim)L(pic)]ClO$_4$ (**12**).

Complex **10** (0.10 mmol) reacted with L_2 (0.10 mmol) in refluxing *m*-xylene (10 ml) for 2 h, followed by the similar treatment to **11**, to yield [PdBr(dpim)L] (**13**).

Reaction of 2 with L_2. The electron-rich olefin L_2 (0.27 mmol) was added to a toluene solution (10 ml) of **2** (0.25 mmol). The mixture was heated under reflux for 10 min. Addition of hexane to the resulting solution afforded cream needles, [Pd(σ,π-CH$_2$CMe=CH$_2$)ClL] (**14**).

Reaction of 3 with L_2. A toluene suspension (12.5 ml) containing **3** (0.16 mmol) and L_2 (0.17 mmol) was heated under reflux for 30 min. Addition of petroleum ether to the resulting solution gave an off-white needle, [Pd(6-MeO-themi)ClL] (**15**).

Reactions of 14 and 15 with L_2. A benzene–*m*-xylene mixture (1:1, 12 ml) involving **14** (0.25 mmol) and L_2 (0.24 mmol) was heated under reflux for 2.7 h. After the solvents were evaporated at a reduced pressure, the resulting solid was recrystallized from dichloromethane and hexane to give **11** in 23.4% yield.

Similarly, **15** (0.19 mmol) reacted with L_2 (0.20 mmol) in *m*-xylene (10 ml) under reflux for 11 h to afford **11** in 25.2% yield.

Results and Discussion

General Properties. Yields, analytical data, and some physical properties of the new (carbene)palladium(II) complexes are summarized in Table 1. All these complexes are air-stable in the solid state. Mononuclear complexes, **5**—**8** and **12**—**15** are fairly soluble in dichloromethane and chloroform, whereas the halogeno-bridged dinuclear complexes, **4** and **10** are sparingly soluble in usual oragnic solvents. The IR spectra of the twelve complexes showed a strong band near 1280 cm^{-1}, characteristic of ν(C(aromatic)–N} and a medium band at *ca.* 1490 cm^{-1} for ν(C-(carbene)–N} (Table 2).

Cyclopalladated Carbene Complexes, 4—10. The sulfur-chelated alkylpalladium(II) complex, **1** reacted with L_2 in refluxing xylene to afford the cyclopalladated complex, **4**. In the IR spectrum of **4**, two bridging ν(Pd–Cl) bands were observed at 258 and 239 cm^{-1}. The chlorobridged complex, **4** reacted with Tl(acac), triisopropyl phosphite, 4-picoline, and silver acetate,

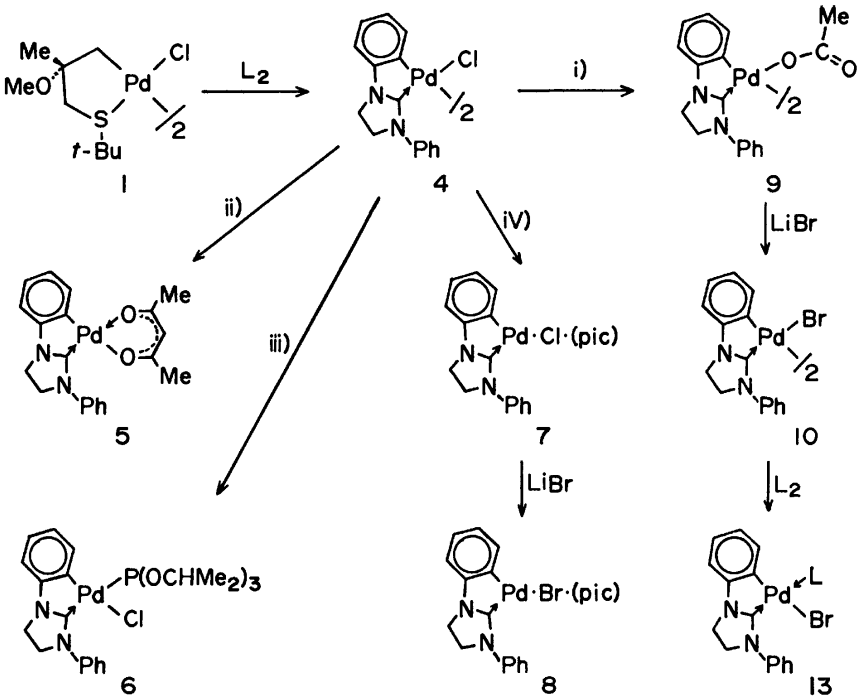

Scheme 1. i) AgO_2CMe; ii) Tl(acac); iii) $P(OCHMe_2)_3$; iv) 4-picoline.

Table 3. Characteristic ^{1}H-NMR data of the carbene complexes[a]

Complex	dpim or L (NCH_2CH_2N)	The other groups: CH_3	The other groups: The other protons[b]
5	3.9—4.5(m)	1.36(s), 1.96(s)	5.20(s, 1H, acac-CH)
6[c]	3.9—4.5(m)	1.33(d)[d]	5.0(c, 1H, $OCHMe_2$)[d]
7	3.9—4.5(m)	2.15(s)	6.51(d, 2H, H_β),[d] 8.16(d, 2H, H_α)[d]
8	3.9—4.3(m)	2.17(s)	8.18(d, 2H, H_α)[d,e]
9[c]	3.0—4.0(c)	1.27(s)	—
11[b,f]	3.2—3.45(c, 2H)	—	5.71(s, 1H, $\frac{1}{2}CH_2Cl_2$)
	3.6—3.95(c, 6H)		
12[b]	3.3—4.0(c, 4H)	2.16(s, 0.9H)	6.23(d, 0.6H, H_β)[d]
	4.05(s, 2.8H)	2.34(s, 2.1H)	6.63(d, 1.4H, H_β)[d]
	4.36(s, 1.2H)		8.97(d, 2H, H_α)[d]
13[b]	3.2—4.2(c, 4H)	—	—
	3.92(s, 4H)		
14	4.1—4.5(m)	1.44(s)	1.91(s, 1H, H_a), 2.91(d, 1H, H_b)[g]
			2.95(s, 1H, H_c), 3.95(d, 1H, H_d)[g]
15[c]	4.0—4.6(m)	2.64(s)	6.37(s, 2H, CH=CH)
			0.97(d, 1H, 8-H_a), 1.21(d, 1H, 8-H_b)[h,i]

a) δ value (ppm) from TMS. In CD_2Cl_2, unless noted elsewhere. Abbreviations used; c=complicated, d=doublet, m=an AA'BB' type multiplet, s=singlet, phenyl and phenylene protons are omitted. b) Approximate proton numbers are given in parentheses. c) In $CDCl_3$. d) $^3J_{HH}$=*ca.* 7 Hz. e) H_β was not distinguished. f) In DMSO-d_6. g) $^4J_{HH}$=2.5 Hz. h) $^2J_{H_aH_b}$=8 Hz. i) 1-Methylene and the other methine resonances are not distinguished.

and resulted in the splitting of the chloro-bridged bonds to yield the corresponding complexes, **5**, **6**, **7**, and **9**, respectively (Scheme 1). Bridging acetato ligands of **9** in Nujol mull showed two bands at 1560 and 1420 cm^{-1}. Complexes **7** and **9** were treated with lithium bromide to give the corresponding bromo complexes, **8** and **10**, respectively.

The $^{13}C\{^1H\}$-NMR spectrum of **5** in CD_2Cl_2 exhibited a resonance at δ 192.1 from TMS, characteristic of the carbene carbon (2-C). Three quarternary carbon resonances at δ 149.2, 139.2, and 140.3 are ascribed to a palladium-bonded carbon (2'-C), an *N*-substituted carbon (1'-C) of an *o*-phenylene group, and an *N*-substituted carbon (1''-C) of the uncoordinated phenyl group, respectively,[15] by comparison with the cases of **6** and its related complexes.[1,16] Two oxygen-bonding carbons of acetylacetonato ligand resonated at δ 187.5 and 186.5, and two methyl carbons did

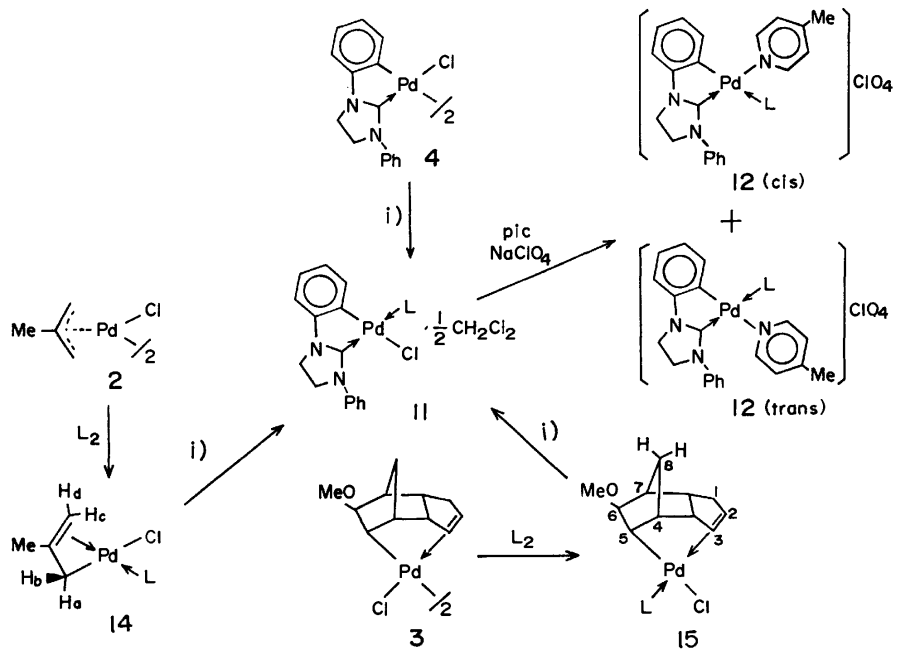

Scheme 2. i) With L_2 in refluxing *m*-xylene or xylene–benzene mixture, followed by recrystallization from dichloromethane–hexane.

at δ 28.0 and 27.3, indicating the non-equivalence of two coordination sites of the acetylacetonato ligand, due to the cyclopalladation of the carbene ligand. In addition, a mass spectrum of **5** exhibited a parent-ion isotope pattern centered at 426 of *m/e* in accord with the proposed structure. Complex **5** showed C=O and C=C stretching bands characteristic of the enolate chelate.

The $^{13}C\{^1H\}$-NMR spectrum of **6** was observed in $CDCl_3$, and gave a doublet at δ 200.6 (^2J=205.1 Hz), attributable to a carbene carbon. This large coupling constant indicates unambiguously that the triisopropyl phosphite ligand is situated *trans* to the carbene carbon.[16] Two doublets at δ 44.6 [^4J(CP)= 3.9 Hz] and 53.8 [^4J(CP)=8.8 Hz] were assigned to two methylene carbons of the 2-imidazolidinylidene ring. Remaining two doublets at δ 121.9 [^4J(CP)= 4.9 Hz] and 138.5 [^3J(CP)=10.7 Hz] were tentatively assignable to 6'-C and 1'-C of the cyclopalladated phenylene group, respectively.[17] These splittings of the carbon resonances were attributable to a long range phosphorus-carbon coupling.[16] Two singlets at δ 140.7 and 150.2 were ascribed to the *N*-substituted aromatic carbon (1"-C) of the unmetallated phenyl group and a palladium-bonded carbon (2'-C), respectively.[17] It is worth noting that a palladium-substituted phenylene carbon in the cyclopalladated complexes resonates in the range of δ 146—151.[1,18]

The ^{1}H-NMR spectra of **5**—**8** showed complicated signals in the range of δ 6.4—8.6, which were attributed to both the cyclopalladated *o*-phenylene group and the unmetallated phenyl one. Moreover, the spectra gave an AA'BB' type multiplet for the ethylene group of the dpim moiety in the region of δ 3.9 to 4.5 (Table 3). Complex **9** exhibited complicated signals in the range of δ 3.0—4.0, which were assignable to the ethylene protons of the dpim moiety.[19]

On the basis of these facts, **4**—**10** were ascribed to new complexes containing cyclopalladated chelate structure within the carbene ligand. It seems likely that the halogeno-bridge splitting reaction of **1** with L_2 afforded an intermediate of a carbene complex retaining the 3-*t*-butylthio-2-methoxy-2-methylpropyl moiety, and that the moiety then abstracted immediately an *ortho*-proton from a phenyl ring attached to the 2-imidazolidinylidene ligand to be eliminated. The presence of such the intermediate is readily inferred from the isolation of (carbene)(π-coorinated chelating alkyl)palladium(II) complex **15**, as stated later. Similar cyclometallated structures have been reported concerning {(alkylamino)(phenylamino)methylenato-1-*C*,2'-*C*}platinum(IV) complexes,[20] {bis(*p*-tolylamino)-methylenato-1-*C*,2'-*C*}platinum(II) ones,[21] and (1,3-di-*p*-tolyl-2-imidazolidinylidenato-2-*C*,2'-*C*)ruthenium-(II) ones.[22]

Di(carbene)palladium(II) Complexes. The halogeno-bridged cyclopalladated complexes, **4** and **10** reacted with L_2 in refluxing xylene to yield the di-carbene complexes, **11** and **13**, respectively. The ^{1}H-NMR spectrum of **11** in DMSO-d_6 showed a singlet at δ 5.7 (1H, 1/2 CH_2Cl_2, as solvent of crystallization) and complicated signals near δ 3.3 (2H) and 3.8 (6H), which were ascribed to the ethylene protons of the cyclopalladated and unmetallated 1,3-diphenyl-2-imidazolidinylidene groups.

Complex **11** reacted with both 4-picoline and Na-[ClO_4]·H_2O in refluxing acetone to afford **12**. Molar conductivity of **12** for 1.0×10^{-3} M acetone solution at 25 °C was 132 Ω^{-1} cm^2/mol, implying a 1:1 electrolyte. Its ^{1}H-NMR spectrum in CD_2Cl_2 exhibited two 4-picoline-methyl singlets at δ 2.16 (*ca.* 0.9H) and 2.34 (*ca.* 2.1H), and three kinds of the 2-imidazolidinylidene-ethylene protons; one at δ 3.3—4.0 (4H, complicated), the second at δ 4.05 (*ca.* 2.8H, singlet),

Table 4. The reactivities of the chloro-bridged dinuclear organopalladium(II) complexes with L_2

Bond type	Complex	Mp/°C	Reaction temp/°C	Main product
Pd-σ-aryl	$[Pd_2\{C_6H_4$-CMe(N=OH)-1-$C,N\}_2Cl_2]$	>210[29]	139	$[Pd\{C_6H_4$-CMe(N=OH)-1-$C,N\}ClL]$[1]
Pd-σ-aryl	$[Pd_2(C_6H_4$-CH_2NMe_2-1-$C,N)_2Cl_2]$	185—187[28]	139	$[Pd(C_6H_4$-CH_2NMe_2-1-$C,N)ClL]$[1]
Pd-σ-aryl	$[Pd_2\{C_6H_4$-CPh(N=OH)-1-$C,N\}_2Cl_2]$	150—152[29]	139	$[Pd\{C_6H_4$-CPh(N=OH)-1-$C,N\}ClL]$[1]
Pd-π-methallyl	$[\{Pd(\eta^3$-$CH_2CMe{=}CH_2)Cl\}_2]$ **2**	166—168[13]	110	$[Pd(\sigma,\pi$-$CH_2CMe{=}CH_2)ClL]$ **14**
Pd-σ,π-methallyl	$[Pd$-σ,π-$CH_2CMe{=}CH_2)ClL]$ **14**	150—168	97	[Pd(dpim)ClL] **11**
Pd-σ-alkyl	$[Pd_2\{CH_2CMe(OMe)CH_2S$-^{t}Bu$\}_2Cl_2]$ **1**	178—184[12]	139	$[\{Pd(dpim)Cl\}_2]$ **4**
Pd-σ-alkyl	$[\{Pd$(6-MeO-themi)$Cl\}_2]$ **3**	166—170[14]	110	[Pd(6-MeO-themi)ClL] **15**
Pd-σ-alkyl	[Pd(6-MeO-themi)ClL] **15**	153—157	139	[Pd(dpim)ClL] **11**
Pd-σ-alkyl	$[\{Pd(8$-MeO-C_8H_{12}-1σ, 4π)$Cl\}_2]$	130—135[14]	45	"The pale yellow powder"[a]
Pd-σ-alkyl	$[\{Pd(6$-MeO-C_7H_8-5σ, 2π)$Cl\}_2]$	108—110[30]	80	Pd black and black oil.[a]
Pd-σ-1-alkenyl	$[\{Pd(CH{=}CCl$-CMe_2NMe_2-1-$C,N)Cl\}_2]$	172—175[31]	139	"The pale olive powder" [a]

a) See the text.

and the third at δ 4.36 (*ca.* 1.2H, singlet) (Table 3). The data indicate unambiguously that **12** involves two kinds of both the picoline-methyl groups and of the unmetallated 2-imidazolidinylidene moieties in the same ratio of about 7:3. On the basis of these facts, the elemental analyses, and the conductivity data, **12** was ascribed to a mixture of *cis* and *trans* isomeric cationic di(carbene)palladium(II) complexes, each of which contains the cyclopalladated and the unmetallated 1,3-diphenyl-2-imidazolidinylidene moieties. The population ratio of the *cis*: *trans* isomers was about 7:3. The ethylene resonances of the dpim moieties in these isomers overlapped with each other. In consideration of the relative electron-deficient effect of the carbene ligand,[16,23] the lower-field methyl resonance at δ 2.34 and the higher-field ethylene singlet at δ 4.05 were assigned to the major *cis* isomer. The two ethylene singlets of the unmetallated 2-imidazolidinylidene moieties were possibly due to an accidental coincidence, since the signals did not changed actually on cooling to −35 °C.

Carbenepalladium(II) Complexes Containing a σ,π-Methallyl Group or a π-Coordinated-chelating Alkyl-palladium σ-Bond. Complex **2** and **3** reacted with L_2 in refluxing toluene to give **14** and **15**, respectively. The ^{1}H-NMR spectrum of **14** in $CDCl_3$ showed three singlets at δ 1.44 (3H, Me), 1.91 (1H, H_a), and 2.95 (1H, H_c), and two doublets at δ 2.91 [1H, H_b, $^4J(H_bH_d)$=2.5 Hz] and 3.95 (1H, H_d). The doublets of the H_b and H_d were ascribed to a long range coupling through the allylic double bond.[24] This pattern of the methallyl proton resonances indicates that the π-methallyl group in **2** was converted into a σ,π-methallyl one with the displacement of one of the two bridging chlorine atoms by L, similarly to the case of chloro(σ,π-methallyl)(neutral Lewis base)palladium(II).[25] Moreover, **14** exhibited the AA'BB' type resonance for the ethylene protons of L, in the range of δ 4.1 to 4.5.

^{1}H-NMR spectrum of the 6-MeO-themi moiety in **15** showed a methyl resonance at δ 2.64 (3H, singlet), bridge-head methylene ones at δ 0.97 and 1.21 (2H, an AB type quartet), and olefinic one at δ 6.37 (2H, virtually singlet), besides complicated signals in the region of δ 1.6—3.0. In addition, **15** gave AA'BB' type resonances for the ethylene protons of L near δ 4.3 and aromatic resonances in the range of δ 7.2 to 8.4. On the basis of these data, elemental analyses, and IR spectrum, **15** was assigned to a new carbenepalladium(II) complex, which contains the 6-MeO-themi moiety coordinated to the central metal.

It is significantly noteworthy that **14** and **15** involve three kinds of carbon-palladium bond; the carbene-, the alkyl σ-, and the π-olefin-palladium bonds, and that they are regarded as model compounds of the active species in catalytic olefin metathesis reactions.[26] Only four papers have ever been published as concerns isolation of stable complexes which contain both a carbene- and a π-olefin-metal bonds.[27] Complexes **14** and **15** reacted with L_2 in a more severe condition, namely in refluxing xylene, and afforded the dicarbene complex **11** in about 25% yield after recrystallization from dichloromethane–hexane.

Reactivities of the Chloro-bridged Organopalladium(II) Complexes towards L_2. In conclusion, the reactivities of the σ-aryl-, π-methallyl-, σ,π-methallyl-, σ-alkyl-, and σ-1-alkenylpalladium(II) complexes towards L_2 are summarized in Table 4. The cyclopalladated σ-aryl complexes retained the palladium-aryl σ-bond unchanged during the reaction with L_2.[1] The π-methallyl complex, **2** reacted with L_2 in refluxing toluene to give **14**, retaining the palladium-σ,π-methallyl bond, which was furthermore converted into the palladium-aryl σ-bond of the dpim moiety through the reaction with additional L_2 at 97 °C.

The π-coordinated-chelating σ-alkylpalladium(II) complex, **3** and **15** reacted with L_2 in similar manners to the π-methallyl complex, **2** and to the σ,π-methallyl one, **14**, respectively. However, an analogous complex, di-μ-chloro-bis(8-*exo*-methoxycyclooct-4-enyl-*endo*-1σ,4π)dipalladium(II)[14] was treated with L_2 at 45 °C to afford a small amount of a pale yellow powder, which showed two IR bands assignable to the carbene ligand but could not be characterized in details owing to the low yield. Di-μ-chloro-bis(6-*exo*-methoxybicyclo-[2,2,1]hept-2-ene-*endo*-5σ,2π)dipalladium(II), having a relatively low melting point,[30] reacted with L_2 in refluxing benzene for 10 min to yield *ca.* 70%

of palladium black and a small amount of black oil, which was impossible to be characterized. The sulfur-chelated σ-alkylpalladium bond in **1** was converted into the palladium-aryl σ-one of the dpim moiety in the reaction with L_2, not only in refluxing *m*-xylene, but also in refluxing toluene.

A 1-alkenylpalladium(II) complex, di-μ-chloro-bis(2-chloro-3-dimethylamino-3-methyl-1-butenyl-1-*C*,*N*)dipalladium(II)[31] yield only a small amount of a pale olive powder, which exhibited two bands at 1490 and 1275 cm^{-1}, characteristic of the carbene ligand, but could not be full characterized because of the low yield.

It is noteworthy that the carbene ligands studied in the present paper do not insert into the carbon-palladium σ-bond. The innertness of the carbene ligands is probably due to the electron-donating character of two nitrogen atoms attached to the carbene carbon. This shows sharp contrasts with hexafluoro-3-propylidene which inserts into a hydrido-platinum bond,[32] and with alkyl isocyanide which does into an alkyl-palladium σ-bond.[33]

We wish to express our gratitude to Mrs. Hisako Mazume and Miss Yumi Kojima, Nagasaki University, for their technical assistence.

References

1) K. Hiraki, M. Onishi, K. Sewaki, and K. Sugino, *Bull. Chem. Soc. Jpn.*, **51**, 2548 (1978).
2) C. H. Davies, C. H. Game, M. Green, and F. G. A. Stone, *J. Chem. Soc., Dalton Trans.*, **1974**, 357.
3) M. H. Chisholm and H. C. Clark, *J. Am. Chem. Soc.*, **94**, 1532 (1972).
4) R. F. Stepaniak and N. C. Payne, *J. Organomet. Chem.*, **57**, 213 (1973); **72**, 453 (1974).
5) B. Cetinkaya, E. Cetinkaya, and M. F. Lappert, *J. Chem. Soc., Dalton Trans.*, **1973**, 906; B. Cetinkaya, P. Dixneuf, and M. F. Lappert, *ibid*, **1974**, 1827.
6) M. H. Chisholm and H. C. Clark, *Inorg. Chem.*, **10**, 1711 (1971); M. H. Chisholm, H. C. Clark, W. S. Johns, J. E. H. Ward, and K. Yasufuku, *ibid*, **14**, 900 (1975).
7) H. C. Clark and J. E. H. Ward, *J. Am. Chem. Soc.*, **96**, 1741 (1974).
8) M. H. Chisholm and D. A. Couch, *J. Chem. Soc., Chem. Commun.*, **1974**, 42.
9) K. Hiraki, M. Onishi, and K. Sugino, *J. Organomet. Chem.*, **171**, C50 (1979).
10) H. W. Wanzlick, *Org. Synth.*, **47**, 14 (1967).
11) W. H. Nelson, W. J. Randall, and D. F. Martin, *Inorg. Synth.*, **9**, 53 (1971).
12) Y. Takahashi, A. Tokuda, S. Sakai, and Y. Ishii, *J. Organomet. Chem.*, **35**, 415 (1972).
13) W. T. Dent, R. Long, and A. J. Wilkinson, *J. Chem. Soc.*, **1964**, 1585.
14) J. Chatt, L. M. Vallarino, and L. M. Vananzi, *J. Chem. Soc.*, **1957**, 3413.
15) It was erroneous that three quarternary carbon resonances at δ 149.2, 139.2, and 140.3 were ascribed to the *N*-substituted carbon (1″-C) of the unmetallated phenyl group, the palladium-bonded carbon (2′-C), and the *N*-substituted carbon (1′-C) of the *o*-phenylene group, respectively, in Ref. 9.
16) D. J. Cardin, B. Cetinkaya, E. Cetinkaya, M. F. Lappert, E. W. Randal, and E. Rosenberg, *J. Chem. Soc., Dalton Trans.*, **1973**, 1982.
17) It was erroneous that the doublet at δ 138.5 was assigned to the palladium-substituted carbon (2′-C), and that the singlet at 150.2 was done to one of the two *N*-substituted aromatic carbons, in Ref. 9.
18) A. R. Garber, P. E. Garrou, G. E. Hartwell, M. J. Smas, J. R. Wilkinson, and L. J. Todd, *J. Organomet. Chem.*, **86**, 219 (1975).
19) It was erroneous that [{Pd(dpim)(OAc)}$_2$] showed a multiplet in the range of δ 4.3—4.2 for the ethylene group, in Ref. 9.
20) K. W. Muir, R. Walker, J. Chatt, R. L. Richards, and G. H. D. Royston, *J. Organomet. Chem.*, **56**, C-30 (1973).
21) D. F. Christian, D. A. Clark, H. C. Clark, D. H. Farrar, and N. C. Payne, *Can. J. Chem.*, **56**, 2516 (1978).
22) P. B. Hitchcock, M. F. Lappert, and P. L. Pye, *J. Chem. Soc., Chem. Commun.*, **1977**, 196.
23) D. J. Cardin, B. Cetinkaya, and M. F. Lappert, *Chem. Rev.*, **72**, 545 (1972).
24) F. A. Bovey, "Nuclear Magnetic Resonance Spectroscopy," Academic Press, New York (1969), Chap. 5.
25) K. Vrieze, P. Cossee, C. Maclean, and C. W. Hilbers, *J. Organomet. Chem.*, **6**, 676 (1966).
26) N. Calderon, E. A. Ofstead, and W. A. Judy, *Angew. Chem. Int. Ed. Engl.*, **15**, 401, (1976).
27) a) T. Mitsudo, Y. Watanabe, H. Nakanishi, I. Morishima, T. Inubushi, and Y. Takegami, *J. Chem. Soc., Dalton Trans.*, **1978**, 1298; b) W. Priester and M. Rosenblum, *J. Chem. Soc., Chem. Commun.*, **1978**, 26; c) A. N. Nesmeyanov, J. N. Sal'nikova, Yu. T. Struchkov, V. G. Andrianov, A. A. Poprebnyak, L. V. Rybin, and M. I. Rybinskaya, *J. Organomet. Chem.*, **117**, C16 (1976); d) M. F. Lappert, *ibid*, **100**, 139 (1975).
28) A. C. Cope and E. C. Friedlich, *J. Am. Chem. Soc.*, **90**, 909 (1968).
29) H. Onoue, K. Minami, and K. Nakagawa, *Bull. Chem. Soc. Jpn.*, **43**, 3480 (1970).
30) M. Green and R. L. Hancock, *J. Chem. Soc., A*, **1967**, 2054.
31) T. Yukawa and S. Tsutsumi, *Inorg. Chem.*, **7**, 1458 (1968).
32) J. Cook, W. R. Cullen, M. Green, and F. G. A. Stone, *J. Chem. Soc., Chem. Commun.*, **1968**, 170.
33) Y. Yamamoto and H. Yamazaki, *Bull. Chem. Soc. Jpn.*, **43**, 2653, (1970).

The Reductive Acylation of Organic Disulfides with Aldehydes under Photochemical and Radical Conditions[1)]

Makoto TAKAGI,* Setsuo GOTO, Masato TAZAKI, and Tsutomu MATSUDA*

Department of Organic Synthesis, Faculty of Engineering, Kyushu University, Hakozaki, Higashi-ku, Fukuoka 812

(Received September 6, 1979)

The irradiation of organic disulfides in aldehyde solvents resulted in the reductive fission of the S–S linkage, giving an equimolar mixture of the corresponding thiol and the thiol acylate in a good yield. The cyclic disulfides gave mono *S*-acylated dithiols. The reaction proceeded by means of the photo-initiated radical chain mechanism, and AIBN (azobisisobutyronitrile) effected the same reaction under thermal conditions.

In previous communications, a photochemical reductive acylation of organic disulfides with aldehydes has been described, with particular emphasis on the synthesis and the reaction of the 8-*S*-acylated derivative of coenzyme lipoic acid.[2-4)] The present report includes some of the experimental details. In addition, the reactions under radical conditions are described; these data, combined with those of other photochemical studies, suggest that the photo-reaction of organic disulfides with aldehydes proceeds by means of a photo-initiated radical chain mechanism.

Results

Photo-reactions. Reactions were carried out for $0.5—1\times10^{-2}$ M (1 M=1 mol dm^{-3}) solutions of the disulfide in aldehyde at ≤5 °C under nitrogen or argon, using liquid-filtered ($\lambda<330$ nm removed) radiation from a 100-W immersion-type high-pressure mercury lamp. A radiation through a Pyrex filter ($\lambda<300$ nm removed) may be used with a slight decrease in the yields of the products. The concentration of the disulfides may be increased to 0.2—0.7 M (see the reaction under radical conditions), but the reaction is cleaner when the concentration is lower. The reaction could be followed by TLC or GLC. For 1,2-dithiolane compounds, the color (yellow) disappearance indicated the completion of the reaction. After 1—2 h of irradiation, followed by concentration under reduced pressure, the residue was purified by distillation or column chromatography on silica gel. The experimental procedure has been described in detail elsewhere.[3)] The colorless liquid obtained was identified by elemental and spectral analyses.

TABLE 1. PHOTO-REACTION OF SYMMETRICAL CYCLIC DISULFIDES WITH ALIPHATIC ALDEHYDES

Disulfide	Aldehyde	Irradiation time/min	Product	Yield[a)] %
1	CH_3CHO	90	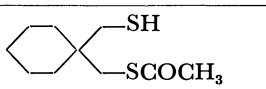	**5** (71)
2	CH_3CHO	50	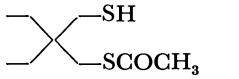	**6** (73)
2	C_2H_5CHO	90	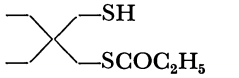	**7** (68)
2	$CH_3(CH_2)_2CHO$	25	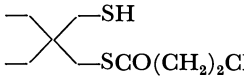	**8** (89)
2	$(CH_3)_2CHCHO$	90	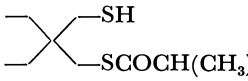	**9** (85)
2	$(CH_3)_3CCHO$	60	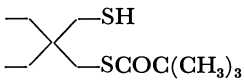	**10** (71)
3	C_2H_5CHO	80	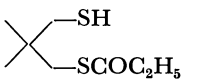	**11** (42[b)])
4	C_2H_5CHO	90	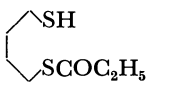	**12** (90)
1	C_6H_5CHO	75	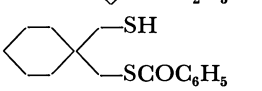	**13** (59)
2	C_6H_5CHO	110	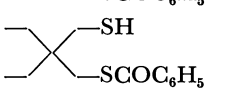	**14** (69)

a) Isolated yields. b) The lower yield is due to the polymerization of the starting disulfide before irradiation.

Table 2. Photo-reaction of symmetrical linear disulfides with propionaldehyde

Disulfide	Irradiation time/min	Product, yield/%	
		R'COSR	RSH
$(n\text{-}C_4H_9S)_2$	150	$C_2H_5COSC_4H_9$ (97)	C_4H_9SH (87)
$(C_6H_5S)_2$	150	$C_2H_5COSC_6H_5$ (54)	C_6H_5SH (58)
$(i\text{-}C_3H_7S)_2$	240	$C_2H_5COSC_3H_7$ ($\leq$40)	C_3H_7SH ($\leq$40)
$(t\text{-}C_4H_9S)_2$	360	a)	a)

a) No reaction; $(t\text{-}C_4H_9S)_2$ recovered.

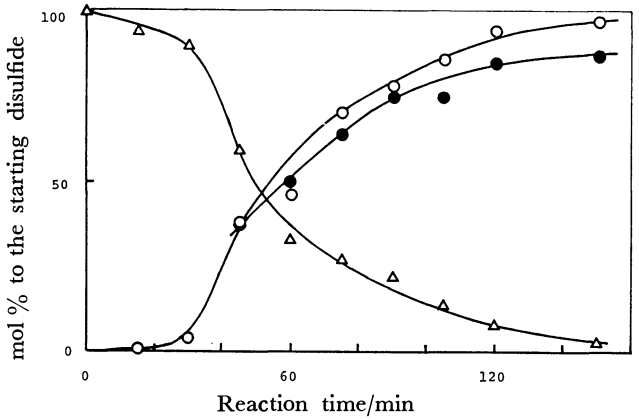

Fig. 1. Photo-reaction of dibutyl disulfide with propionaldehyde.
△, $(n\text{-}C_4H_9S)_2$; ●, $n\text{-}C_4H_9SH$; ○, $n\text{-}C_4H_9SCOC_2H_5$.
GLC: column Apiezon L (2%); internal standard, $n\text{-}C_{12}H_{26}$; column temperature, 50→150 °C.

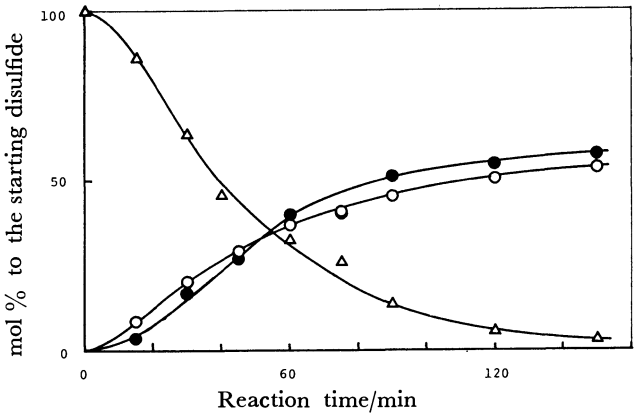

Fig. 2. Photo-reaction of diphenyl disulfide with propionaldehyde.
△, $(C_6H_5S)_2$; ●, C_6H_5SH; ○, $C_6H_5SCOC_2H_5$.
GLC: column Apiezon L (2%); internal standard, $n\text{-}C_8H_{18}$; column temperature, 60→150 °C.

Reaction of Symmetrical Disulfides: The results with cyclic disulfides and aliphatic aldehydes are summarized in Table 1.

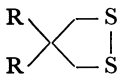

1, (R, R) = $(CH_2)_5$
2, R = C_2H_5
3, R = CH_3

4

All the aliphatic aldehydes reacted with similar ease, and the effect on the reactivity of branching on the α-carbon of the aldehyde is unimportant. The effect of the disulfide-ring size, whether five- or six-membered, is also trivial. The reactivities of cyclic disulfides and linear disulfides are similar insofar as the carbons bound to sulfur are not branched (see below). No by-products were detected by either TLC or GLC. Thus, the reaction may be formulated simply by Eq. 1:

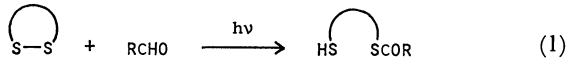

(1)

The reactions with aromatic aldehydes were not straightforward. The isolation of the reaction products was not easy, since the benzoins were formed in a considerable amount, along with other unidentifiable, high-boiling by-products. In the reaction of *p*-anisaldehyde with **2**, the formation of the thioester was suggested by the results of spectral analysis, but the isolation was not successful due to the overwhelming side reactions. In view of the complexity of the reaction and the unavailability of the liquid aromatic aldehydes, the photo-reaction with disulfides would not have practical value. Pyruvic acid and formate esters did not react under the conditions of Table 1.

The reaction of symmetrical linear disulfides is shown in Table 2 and Eq. 2.

$$RSSR + R'CHO \xrightarrow{h\nu} RSH + RSCOR' \quad (2)$$

The reaction of dibutyl disulfide with propionaldehyde was monitored by a direct GLC analysis of the reaction mixture, the results are shown in Fig. 1. The reaction of diphenyl disulfide with propionaldehyde is similarly illustrated in Fig. 2. The reaction in Fig. 1 was intentionally chosen from among several similar experiments, since it happened to show an "induction period." The induction period does not appear when the reactants are carefully purified. Aldehydes have to be distilled just before use. For dibutyl disulfide, the reaction approached a theoretical completion (Fig. 1), but for diphenyl disulfide the yields of the products leveled off at 50—60% of the theoretical yield, while the starting disulfide was almost 100% consumed. The fate of the unbalanced sulfur compound is not clear. The decrease in reactivity of aliphatic disulfides as the carbon bound to sulfur becomes branched is obvious in Table 2, suggesting the steric influence on the ease of the reaction.

Reaction of Unsymmetrical Disulfides: Unsymmetrical disulfides were allowed to react with aliphatic aldehyde to clarify the selectivity of *S*-acylation among different thiyl groups. The disulfides used were butyl isopropyl disulfide, *t*-butyl ethyl disulfide, and

Table 3. Radical reaction of symmetrical disulfide with butyraldehyde[a)]

Disulfide mmol		Aldehyde ml	AIBN mmol	Reaction time/h	Product yield/%[b)]	
$(n\text{-}C_4H_9S)_2$	10	50	1.2	2	$n\text{-}C_4H_9SCO\text{-}n\text{-}C_3H_7$	79
$(n\text{-}C_4H_9S)_2$	2.0	10	0	32	c)	
$(n\text{-}C_4H_9S)_2$	25	10[d)]	0.3	13	c)	
$(i\text{-}C_3H_7S)_2$	6.7	10	1.5	4	$i\text{-}C_3H_7SCO\text{-}n\text{-}C_3H_7$	71
$(t\text{-}C_4H_9S)_2$	5.6	10	1.2	12	c)	
	3.1	10	0.6	2	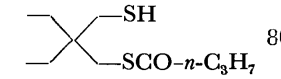	80

a) Reaction temperature, 76 °C (refluxing). b) Isolated yield. c) No reaction, starting disulfide being recovered. d) Propionaldehyde was used. Reaction temperature, 48 °C.

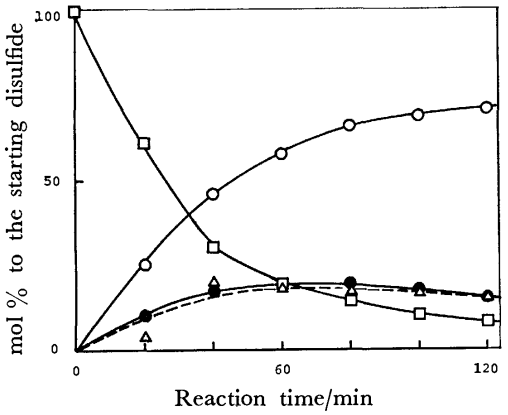

Fig. 3. Photo-reaction of butyl isopropyl disulfide with propionaldehyde.
□, $n\text{-}C_4H_9SS\text{-}i\text{-}C_3H_7$; ○, $C_2H_5COS\text{-}n\text{-}C_4H_9$; ●, $C_2H_5COS\text{-}i\text{-}C_3H_7$; △, $n\text{-}C_4H_9SH$; $i\text{-}C_3H_7SH$, not determined. GLC: column, Apiezon L (2%); internal standard, $n\text{-}C_{11}H_{24}$; column temperature, 40—150 °C.

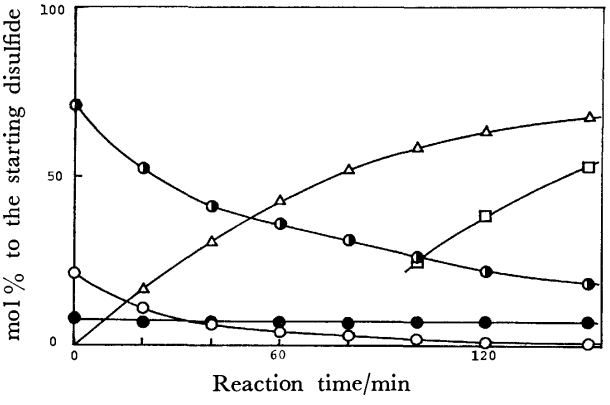

Fig. 4. Photo-reaction of *t*-butyl ethyl disulfide with acetaldehyde. The starting disulfide contained diethyl disulfide (21%) and di-*t*-butyl disulfide (8%).
◑, $t\text{-}C_4H_9SSC_2H_5$; ○, $(C_2H_5S)_2$; ●, $(t\text{-}C_4H_9S)_2$; △, $C_2H_5SCOCH_3$; □, $t\text{-}C_4H_9SH$; no formation of $t\text{-}C_4H_9SCOCH_3$. GLC: column, Apiezon L (2%); internal standard, $n\text{-}C_8H_{18}$; column temperature, 20→160 °C.

butyl phenyl disulfide. The progress of the reaction was monitored by means of GLC analysis of the reaction mixture (Figs. 3, 4, and 5). The reaction is formulated by Eq. 3;

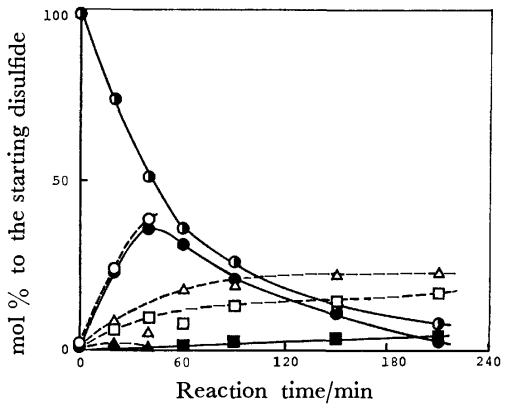

Fig. 5. Photo-reaction of butyl phenyl disulfide with propionaldehyde.
◑, $n\text{-}C_4H_9SSC_6H_5$; ●, $(C_6H_5S)_2$; ○, $(n\text{-}C_4H_9S)_2$; △, $n\text{-}C_4H_9SCOC_2H_5$; ▲, $C_6H_5SCOC_2H_5$; □, $n\text{-}C_4H_9SH$; ■, C_6H_5SH. GLC: column, Silicone SE 30 (10%); internal standard, $n\text{-}C_{14}H_{30}$; column temperature, 20→180 °C.

$$RSSR' + R''CHO \xrightarrow{h\nu} RSH + R'SH + RSCOR'' + R'SCOR'' \quad (3)$$

Butyl isopropyl disulfide gave *S*-*n*-butyl propionate and *S*-isopropyl propionate in a ratio of more than 7:2 in favor of the former at the completion of the reaction (Fig. 3), indicating that the sulfur bound to primary (butyl) carbon is more than three times as reactive as that bound to secondary (isopropyl) carbon. Even more pronounced is the reaction of *t*-butyl ethyl disulfide (Fig. 4). Only *S*-ethyl acetate was formed, no *S*-*t*-butyl acetate at all being detected. These results are in harmony with those in Table 2, where diisopropyl disulfide is less reactive than dibutyl disulfide, and where di-*t*-butyl disulfide is entirely unreactive. The reactivity difference between aliphatic and aromatic sulfur could not be assessed clearly, because the disproportionation of the unsymmetrical disulfide to symmetrical disulfides took place rapidly (Fig. 5). However, Fig. 5 indicates that the aliphatic sulfur (butylthio group) is more reactive toward the acyl group than the aromatic. The disproportionation did not occur without light, suggesting the introduction of radical species under photo-conditions.

As an unsymmetrical cyclic disulfide, 3-methyl-1,2-dithiane (**15**) was allowed to react with acetaldehyde;

it was found to give the dithiol monoacetate, **16**, in a 96% yield, where the primary thiol was selectively acetylated and the isomeric product could not be detected. The same reactivity has been observed with lipoic acid.[2,3] Thus, the selectivity of acylation among primary and secondary thiyl groups is much more strict in cyclic disulfides than in linear disulfides.

Reactions under Radical Conditions. The disulfides were dissolved in a 0.2—0.7 M concentration in an aldehyde solvent, followed by the addition of AIBN in a 10 mol % concentration of the disulfides. The atmosphere was then replaced with nitrogen, and the mixture was heated to initiate the radical reaction. The products were isolated and identified in a manner similar to that above. The results are summarized in Table 3. Some of the reactions were followed by GLC analysis; the results showed that the progress of the reaction was strikingly similar to those for the photo-reactions, including the appearance of the induction period and the disproportionation of unsymmetrical disulfides.

That the reaction proceeds by means of radical chain mechanism is obvious from the facts that it required only a catalytic amount of AIBN and that it did not take place in the absence of AIBN. Peroxides failed to initiate the reaction, and so the RSH–Fe(III) combination failed. Peroxides probably reacted with thiol or thiol acylate and were deactivated. At present, AIBN is the sole radical initiator effective in this reaction.

Discussion

The resemblance between the photo- and the radical reactions suggests that the former is, in fact, a photo-induced radical reaction. The fact that the photo-reaction occurs with non-light-absorbing aliphatic linear disulfides as well indicates that the disulfide is not responsible for the primary photo-act; *i.e.*, it is not the disulfide molecule which is photo-activated and produces radicals. Aliphatic aldehydes have weak absorption maxima in the 290—300 nm region, and since the compounds are used as reaction solvents, the effective absorption extends up over 365 nm, where the major radiation from the high-pressure mercury lamp falls. A radical formation from aldehydes according to Eq. 4 is well documented in the literature.[5]

$$\mathrm{RCHO} \longrightarrow \mathrm{R}\cdot + \cdot\mathrm{CHO} \qquad (4)$$

1,2-Dithiolanes have absorption maxima around 334 nm (ε, 150—200),[6,7] and the possibility could not be excluded that these disulfides accepted the radiation to form radicals, thus initiating the reaction with aldehydes. The formation of the thiyl radical from the cyclic disulfides under photo-irradiation has been shown by Calvin *et al.*[8,9] in their early works on 1,2-dithiolane as well as by other investigators.[10,11] In this context, the photochemical behavior of **1** and **2** was studied. A 1×10^{-3} M solution of **1** or **2** in pentane was irradiated by means of a high-pressure mercury lamp in the usual manner for 100 min. The reaction was followed by GLC and UV spectroscopy (λ_{max}, 334 nm). The subsequent work-up of the mixture gave **17** (19% yield from **1**) and **18** (8% from **2**) along with the recovery of the starting disulfide (50%) and a polymeric material (Eqs. 5 and 6). The polymeric material gave two dithiol compounds, **19** and **20**, upon reduction with lithium aluminium hydride. However, an appreciable amount of the polymer yet remained unconverted to the dithiols, suggesting

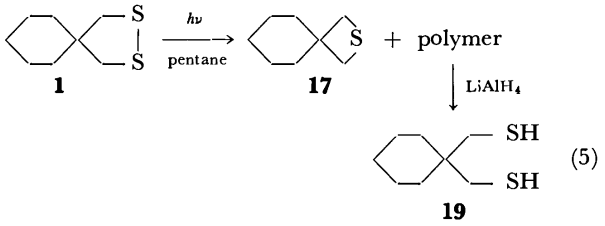

1 **17** **19** (5)

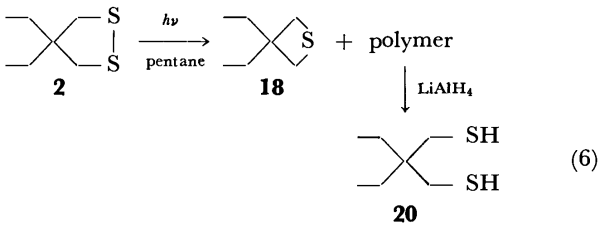

2 **18** **20** (6)

that the polymer chain was not composed of mere S–S linkages. Thus, the photo-activated 1,2-dithiolanes seem to perform a complicated series of radical reactions, including a desulfurization to thietanes. The formation of radicals under photo-irradiation was readily indicated by the polymerization of such added vinyl monomers as styrene, butyl vinyl ether, and acrylonitrile. To the authors' knowledge, a photo-desulfurization with ring contraction has not been documented in the literature, and it is quite possible that the unknown photo-products from lipoic acid reported by Brown *et al.*[11] involved a similar structure.

It is also possible that the above-mentioned photo-desulfurization was a result of the particular reaction conditions, where good hydrogen donors to the thiyl radicals were not available. When 2-propanol instead of pentane was used as a solvent, two 1,3-dithiols, **19** and **20** (as determined by iodometry), were formed, and the yield of the thietanes, **17** and **18** was greatly reduced (<1%). It should be stressed, however, that the desulfurized products were formed even in a good hydrogen-donating solvent such as 2-propanol when the disulfide was photo-activated.

As has been noted earlier,[3] the photo-reaction of 1,2-dithiolanes in aldehydes is less clean when the concentration of the disulfide is high. At a concentration below 1×10^{-2} M, the fraction of radiation absorbed by the sulfur compound is unimportant because of the overwhelming absorption by the aldehyde solvent. As the concentration increases, more of the light is absorbed by the sulfur compound, leading to the introduction of side reactions. Thus, the activation of 1,2-dithiolane is not a necessity for the reductive acylation to take place.

The reaction most probably involves the following sequence of events:

(initiation)

$$\text{initiator} \xrightarrow{\Delta} \text{In}\cdot$$

$$(\text{or RCHO} \xrightarrow{h\nu} \text{R}\cdot + \cdot\text{CHO})$$

$$\text{In}\cdot(\text{or R}\cdot) + \text{RCHO} \longrightarrow \text{InH (or RH)} + \text{R}\dot{\text{C}}{=}\text{O} \quad (7)$$

$$\text{In}\cdot(\text{or R}\cdot) + \text{R'SSR'} \longrightarrow \text{In}-\text{SR'} \text{ (or RSR')} + \text{R'S}\cdot \quad (7')$$

(propagation)

$$\text{R}\dot{\text{C}}{=}\text{O} + \text{R'SSR'} \longrightarrow \text{R'S}\cdot + \text{R'SCOR} \quad (8)$$

$$\text{R'S}\cdot + \text{RCHO} \longrightarrow \text{R'SH} + \text{R}\dot{\text{C}}{=}\text{O} \quad (9)$$

A selectivity in acylation appears when the acyl radical attacks the disulfide on a sterically less hindered sulfur. An electronic factor is not responsible for the selectivity, since the electron density on sulfur would not be much different among primary, secondary, and tertiary disulfides in view of the small variation in the acid-dissociation constants of the corresponding thiols.[12] Moreover, an electronegative acyl radical should show a preferred reactivity for the electropositive tertiary thiyl sulfur if the electronic factor were indeed controlling.

Mechanistically related to the present reaction is the photochemical decarbonylation of aliphatic aldehydes at elevated temperatures. The reaction is strongly accelerated by the presence of a catalytic amount of either disulfides or thiols (Eq. 10).[13] An induction period has been reported for the catalysis of disulfides, but not for that of thiols. It is very probable that the reductive acylation of the disulfide first took place to afford the thiol and the thiol acylate, though the formation of the latter had not been studied. After most of the disulfides were consumed, the unimolecular decomposition of the acyl radical became predominant under high-temperature conditions (>140 °C), thus giving carbon monoxide and alkyl radical (decarbonylation, Eq. 11). The alkyl radical then abstracts hydrogen either from thiol or aldehyde to form an alkane molecule (RH) and a chain-propagating radical (either R'S· or R$\dot{\text{C}}$=O). The decarbonylation from the acyl radical is obviously not important at lower temperatures (76 °C, Table 3).

$$\text{RCHO} \xrightarrow[\text{R'SH or (R'S)}_2]{h\nu,\ >140\,^\circ\text{C}} \text{RH} + \text{CO} \quad (10)$$

$$\text{R}\dot{\text{C}}{=}\text{O} \xrightarrow{>140\,^\circ\text{C}} \text{R}\cdot + \text{CO} \quad (11)$$

Experimental

Materials. The cyclic disulfides, **1**,[14] **2**,[14] **3**,[14] **4**,[8] and **15**,[8] were prepared according to the reported procedures. Butyl isopropyl disulfide, butyl phenyl disulfide, and *t*-butyl ethyl disulfide were prepared by oxidizing the corresponding thiol mixtures.[15] Compound **2**, prepared according to the previously reported procedure,[14] showed a small absorption peak at 330 nm in addition to the normal absorption at 334 nm. The former absorption was eliminated by reduction with lithium aluminum hydride, followed by reoxidation with iodine. No differences in reactivity or other spectral characteristics (NMR and IR) were observed between the two methods of preparation. A very minute impurity seems to be responsible for the 330 nm absorption.

Photo-reactions. High-pressure mercury lamps, UVL-100HA (100 W output) and UVL-400HA (400 W) (Riko Kagaku Co.), fitted with Pyrex glass-made double jackets, were used as light sources. The sample solutions, 100—200 ml in volume, were internally irradiated by a liquid-filtered light ($\lambda \leq 330$ nm removed) under nitrogen or argon at ≤ 5 °C. The reaction mixture was analyzed by GLC, using appropriate straight-chain alkanes as internal standards (Figs. 1—5). The reaction product was isolated either by distillation or by column chromatography. The detailed experimental procedure has been described elsewhere.[3]

Radical Reactions. In 10—50 ml of freshly distilled aldehyde we dissolved an appropriate amount of the organic disulfide to give a 0.2—0.7 M solution. AIBN was then added in a 10 mol% concentration of the disulfide, and the mixture was heated under nitrogen or argon to reflex. The reaction was monitored by GLC. The work-up of the reaction mixture was similar to that used in the photo-reactions.

Reaction Products. The simple thiocarboxylates and thiols were identified by comparisons on GLC with authentic samples. The dithiol monocarboxylates were isolated and identified by the spectral method (IR, NMR, and MS) as well as by elemental analysis.

5: Isolated by distillation; 91—92 °C/1 mmHg (1 mmHg=133 Pa); IR (neat) 2580 (SH) and 1695 cm^{-1} (CO); NMR (CCl_4) δ=1.02 (1H, t, J=8.8 Hz, SH), 1.40 (10H, m, cyclic CH_2), 2.28 (3H, s, $COCH_3$), 2.42 (2H, d, CH_2SH), 3.01 (2H, s, CH_2SCO). Found: C, 54.88; H, 8.28%. Calcd for $C_{10}H_{18}OS_2$: C, 55.00; H, 8.30%.

6: Isolated by distillation; 95 °C/2.5 mmHg; IR (neat) 2580 (SH) and 1695 cm^{-1} (CO); NMR (CCl_4) δ=0.78 (6H, t, J=7.1 Hz, CH_3CH_2), 1.07 (1H, t, J=8.8 Hz, SH), 1.36 (4H, q, CH_3CH_2), 2.29 (3H, s, $COCH_3$), 2.37 (2H, d, CH_2SH), 2.92 (2H, s, CH_2SCO). Found: C, 52.36; H, 8.80%. Calcd for $C_9H_{18}OS_2$: C, 52.38; H, 8.79%.

7: Isolated by chromatography (silicagel, benzene); colorless liquid; IR (neat) 2580 (SH) and 1695 cm^{-1} (CO); NMR (CCl_4) δ=0.79 (6H, t, J=7.0 Hz, $CH_3CH_2C\leqslant$), 1.10 (1H, t, J=8.5 Hz, SH), 1.17 (3H, t, J=7.5 Hz, CH_3CH_2CO), 1.36 (4H, q, $CH_3CH_2C\leqslant$), 2.38 (2H, d, CH_2SH), 2.55 (2H, q, CH_3CH_2CO), 2.93 (2H, s, CH_2SCO); MS (*m/e*), 220 (M^+), 163 ($M^+-C_2H_5CO$), 57 (C_2H_5CO). Found: C, 54.78; H, 9.20%. Calcd for $C_{10}H_{20}OS_2$: C, 54.50; H, 9.15%.

8: Isolated by chromatography (silica gel, hexane containing 1% ether); colorless liquid; IR (neat) 2580 (SH) and 1695 cm^{-1} (CO); NMR (CCl_4) δ=0.79 (6H, t, J=7.0 Hz, $CH_3CH_2C\leqslant$), 0.95 (3H, t, J=7.0 Hz, $CH_3CH_2CH_2CO$), 1.07 (1H, t, J=8.6 Hz, SH), 1.36 (4H, q, $CH_3CH_2C\leqslant$), 1.58 (2H, sex, J=7.0, 7.6, $CH_3CH_2CH_2CO$), 2.38 (2H, d, CH_2SH), 2.49 (2H, t, $CH_3CH_2CH_2CO$), 2.92 (2H, s, CH_2SCO). Found: C, 57.03; H, 9.45%. Calcd for $C_{11}H_{22}OS_2$: C, 56.36; H, 9.46%.

9: Isolated by chromatography (silica gel, hexane); colorless liquid; IR (neat) 2580 (SH) and 1695 cm^{-1} CO); NMR (CCl_4) δ=0.78 (6H, t, $CH_3CH_2C\leqslant$), 1.03 (1H, t, J=7.0 Hz, SH), 1.17 (6H, d, J=6.8 Hz, $CH(CH_3)_2$), 1.35 (4H, q, $CH_3CH_2C\leqslant$), 2.37 (2H, d, CH_2SH), 2.72 (1H, sep, $CH(CH_3)_2$), 2.89 (2H, s, CH_2SCO). Found: C, 56.27; H, 9.42%. Calcd for $C_{11}H_{22}OS_2$: C, 56.36; H, 9.46%.

10: Isolated by chromatography (silica gel, hexane containing 5% ether); colorless liquid; IR (neat) 2580 (SH) and 1695 cm^{-1} (CO); NMR (CCl_4) δ=0.79 (6H, t, J=7.0 Hz, $CH_3CH_2C\leqslant$), 1.03 (1H, t, J=8.5 Hz, SH), 1.21

(9H, s, $C(CH_3)_3$), 1.36 (4H, q, $CH_3\underline{CH_2}C\lessgtr$), 2.37 (2H, d, $\underline{CH_2}SH$), 2.87 (2H, s, CH_2SCO). Found: C, 58.22; H, 9.75%. Calcd for $C_{12}H_{24}OS_2$: C, 58.01; H, 9.73%.

13: Isolated by chromatography (silica gel, hexane containing 5% ether); colorless liquid; IR (neat) 3060 (aromatic CH), 2580 (SH), and 1665 cm^{-1} (CO); NMR (CCl_4) δ= 1.09 (1H, t, J=8.5 Hz, SH), 1.46 (10H, m, cyclic CH_2), 2.50 (2H, d, $\underline{CH_2}SH$), 3.22 (2H, s, CH_2SCO), 7.2—7.5 (3H, m, aromatic *m*- and *p*-H), 7.8—8.0 (2H, m, aromatic *o*-H). Found: C, 64.82; H, 7.21%. Calcd for $C_{15}H_{20}OS_2$: C, 64.24; H, 7.18%. a contamination from by-products.

14: Isolated by chromatography (silica gel, hexane containing 2% ether); colorless liquid; IR (neat) 3060 (aromatic CH), 2580 (SH), and 1665 cm^{-1} (CO); NMR (CCl_4) δ= 0.81 (6H, t, J=7.0 Hz, $\underline{CH_3}CH_2$), 1.10 (1H, t, J=8.5 Hz, SH), 1.39 (4H, q, $CH_3\underline{CH_2}$), 2.41 (2H, d, $\underline{CH_2}SH$), 3.10 (2H, s, CH_2SCO), 7.2—7.5 (3H, m, aromatic *m*- and *p*-H), 7.8—8.0 (2H, m, aromatic *o*-H); MS (*m/e*), 268 (M^+), 163 ($M^+-C_6H_5CO$), 105 (C_6H_5CO). Found: C, 63.87; H, 7.34%. Calcd for $C_{14}H_{20}OS_2$: C, 62.64; H, 7.51%. a contamination from by-products.

16: Isolated by distillation, 95 °C/3 mmHg; IR (neat) 2580 (SH) and 1695 cm^{-1} (CO); NMR (CCl_4) δ=1.32 (3H, d, J=6.5 Hz, $\underline{CH_3}CH(SH)CH_2$), 1.37 (1H, d, J= 6.3 Hz, SH), 1.5—1.9 (4H, m, $CH_3CH(SH)\underline{CH_2}\underline{CH_2}CH_2S$), 2.28 (3H, s, CH_3CO), 2.6—3.0 (3H, m, $CH_3\underline{CH}(SH)CH_2$-$CH_2\underline{CH_2}S$). Found: C, 47.24; H, 7.98%. Calcd for $C_7H_{14}OS_2$: C, 47.15; H, 7.91%.

17: Isolated by distillation, 80 °C/1.3 mmHg; IR (neat) 2925, 2850 (CH), and 1452 cm^{-1} (CH); UV (pentane) λ_{max} 266 nm, ε 70; NMR (CCl_4) δ=1.50 (10H, m, 6-membered cyclic CH_2), 2.81 (4H, s, CH_2S). Found: C, 67.73; H, 9.93%. Calcd for $C_8H_{14}S$: C, 67.54; H, 9.92%.

18: Isolated by distillation, 53 °C/10 mmHg; IR (neat) 2925, 2850 (CH), and 1450 cm^{-1} (CH); NMR (CCl_4) δ= 0.83 (6H, t, J=7.5 Hz, CH_3), 1.63 (4H, q, $CH_3\underline{CH_2}$), 2.79 (4H, s, CH_2S). Found: C, 65.45; H, 11.07%. Calcd for $C_7H_{14}S$: C, 64.55; H, 10.83%.

References

1) Presented at the 5th Symposium on Organo-sulfur and -phosphorus Chemistry, Tsukuba University, February 9—10, 1977.

2) M. Takagi, S. Goto, and T. Matsuda, *J. Chem. Soc., Chem. Commun.*, **1976**, 92.

3) M. Takagi, "Methods in Enzymology," ed by D. B. McCormick and L. D. Wright, Academic Press, New York (1979), Vol. 62, p. 145.

4) M. Takagi, S. Goto, R. Ishihara, and T. Matsuda, *J. Chem. Soc., Chem. Commun.*, **1976**, 993.

5) J. G. Calvert and J. N. Pitts, "Photochemistry," John Wiley and Sons, New York (1966), p. 368.

6) L. Schotte, *Arkiv Kemi*, **8**, 580 (1955); **9**, 441 (1956).

7) G. Bergson, G. Claeson, and L. Schotte, *Acta Chem. Scand.*, **16**, 1159 (1962).

8) J. A. Barltop, P. M. Hayes, and M. Calvin, *J. Am. Chem. Soc.*, **76**, 4348 (1954).

9) R. Whitney and M. Calvin, *J. Chem. Phys.*, **23**, 1750 (1955).

10) E. E. Smissman and J. R. Sorenson, *J. Org. Chem.*, **30** 4008 (1965).

11) P. Brown and J. Edwards, *J. Org. Chem.*, **34**, 3131 (1969).

12) M. R. Crampton, "The Chemistry of Functional Groups, The Chemistry of the Thiol Group, Part 1," ed by S. Patai, John Wiley and Sons, New York (1974), p. 398.

13) I. D. Berman, J. H. Stanley, W. V. Sherman, and S. G. Cohen, *J. Am. Chem. Soc.*, **85**, 4010 (1963).

14) G. Bergson and A. Biezais, *Arkiv Kemi*, **22**, 475 (1964); *Chem. Abstr.*, **63**, 6996f (1965).

15) D. T. McAllen, T. V. Cullum, R. A. Dean, and F. A. Fidler, *J. Am. Chem. Soc.*, **73**, 3627 (1951).

Solvent-induced Conformational Changes of Arylazo-substituted Polyaspartates

Akihiko Ueno,* Keiko Takahashi, Jun-ichi Anzai, and Tetsuo Osa
Pharmaceutical Institute, Tohoku University, Aobayama, Sendai 980
(Received September 20, 1979)

Copolymers of β-benzyl L-aspartate and β-[*p*-(phenylazo)phenethyl] L-aspartate were prepared and their conformations studied by circular dichroism (CD) spectroscopy. The copolymers with less than 40% azo amino acid residues were found to be left-handed (LH) helical, those with more azo amino acid residues right-handed (RH) helical in 1,2-dichloroethane (DCE) solution. The former undergo LH helix→random coil transition on addition of hexafluoro-2-propanol (HFIP) to their DCE solutions, the latter RH helix→LH helix→random coil transition on addition of HFIP. All polymers in DCE exhibit a negative CD band in the side-chain n-π* transition region. The side-chain π-π* CD band was observed only for the copolymers with the highest azo amino acid residues (67%). Its absolute ellipticity decreases with increasing HFIP content, finally disappearing at 10% HFIP. The sign of the n-π* CD band of the copolymer remains negative irrespective of the helix reversion, its absolute ellipticity being unchanged below 10% HFIP and decreasing on further increase in HFIP content. The results suggest solvent-induced changes in orientation or mobility of the side-chain phenylazo moieties.

Circular dichroism (CD) measurements have been extensively used to evaluate the conformation of polypeptides in solution, the evaluation being based on the peptide CD bands. However, it is very difficult to assign the conformation of polypeptides with aromatic side chains since the usually very useful indications are made useless by the presence of additional side-chain CD bands in the same spectral region.[1] In spite of this unfavorable effect, the side-chain CD might provide information of main-chain conformation as well as orientation, mobility and arrangement of side chains themselves. As examples of polypeptides with aromatic side chains, some arylazo polypeptides have been prepared, and their chiroptical properties investigated.[1–10] Goodman *et al.* prepared polypeptides composed of (phenylazo)phenylalanine and its analogues,[2–6] and observed that the peptide CD bands of their α-helices are significantly perturbed by the presence of the aromatic side chains. There is no such complication for the arylazo polyaspartates[7–9] and azo-modified poly(L-glutamic acid).[1,10] The use of these polypeptides would establish a relationship between side-chain CD and main-chain conformation. Various conformations are needed in order to gain insight into the relationship. Arylazo polyaspartates seem to be suitable since polyaspartates often exhibit conformational versatility.[11] Light-induced conformational changes, such as left-handed (LH) helix→right-handed (RH) helix and LH helix→random coil transitions have been observed on some arylazo polyaspartates.[7–9] We have prepared a new series of arylazo polyaspartates composed of β-[*p*-(phenylazo)-phenethyl] L-aspartate and β-benzyl L-aspartate,

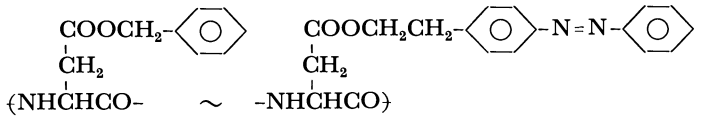

and found that their conformations are very sensitive to solvent. Several reports have appeared on solvent-induced conformational changes of polypeptides: helix reversion for polyaspartates[11d,12] and poly[L-β-[3,4-bis(benzyloxycarbonyloxy)phenyl]-α-alanine],[13] transformations between single and double stranded helices for poly(γ-benzyl D-L-glutamate).[14] The present paper deals with the solvent-induced conformational changes of the arylazo copolymers among LH helix, RH helix, and random coil. The behavior of the side-chain CD during the course of conformational change was investigated in order to elucidate the relationship between the side-chain CD and the main-chain conformation.

Results and Discussion

The CD spectra in the region below 260 nm measured for the copolymers dissolved in 1,2-dichloroethane (DCE) are shown in Fig. 1. The spectra of copolymers with less phenylazo residues (azo amino acid residues< 40%) exhibit a positive CD band around 222 nm,

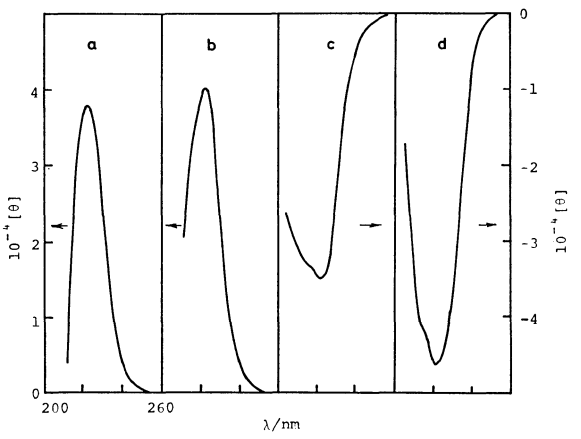

Fig. 1. CD spectra of the copolymers with different contents of phenylazo residues in DCE solution. Phenylazo content: 11% (a); 26% (b); 46% (c); 67% (d).

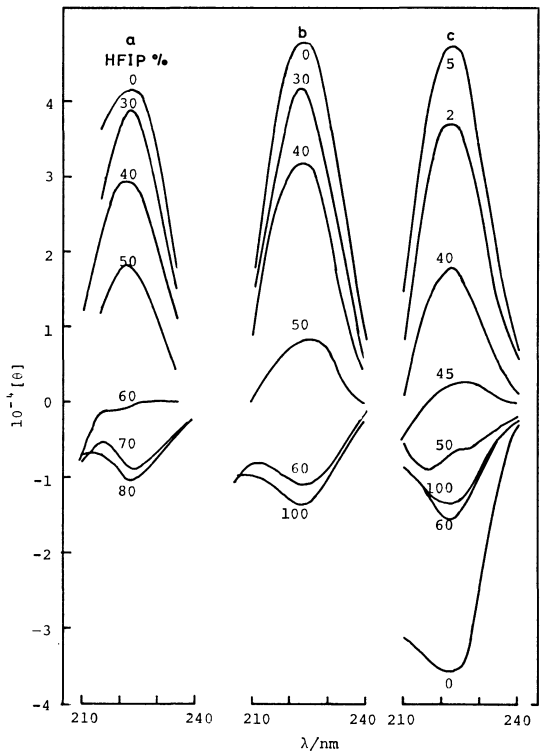

Fig. 2. CD spectra of the copolymers with phenylazo residues of 11% (a), 26% (b), and 46% (c) in mixed solutions of DCE and HFIP.

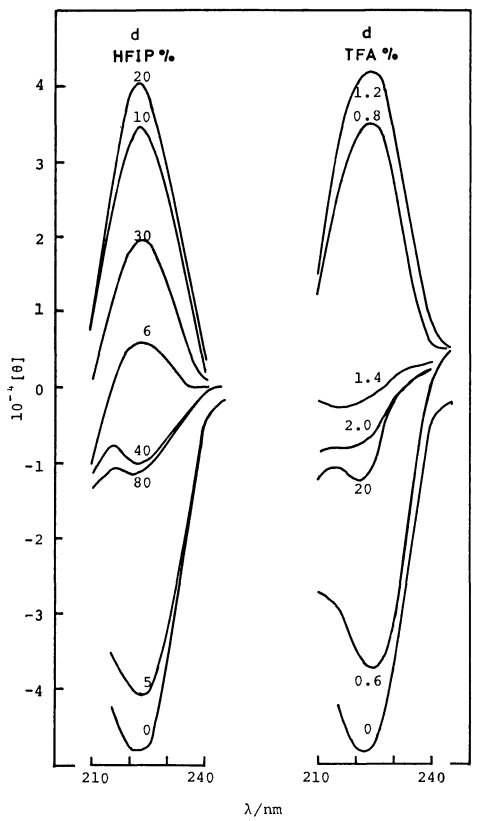

Fig. 3. CD spectra of the copolymer with 67% phenylazo residues in DCE–HFIP and DCE–TFA solvent systems.

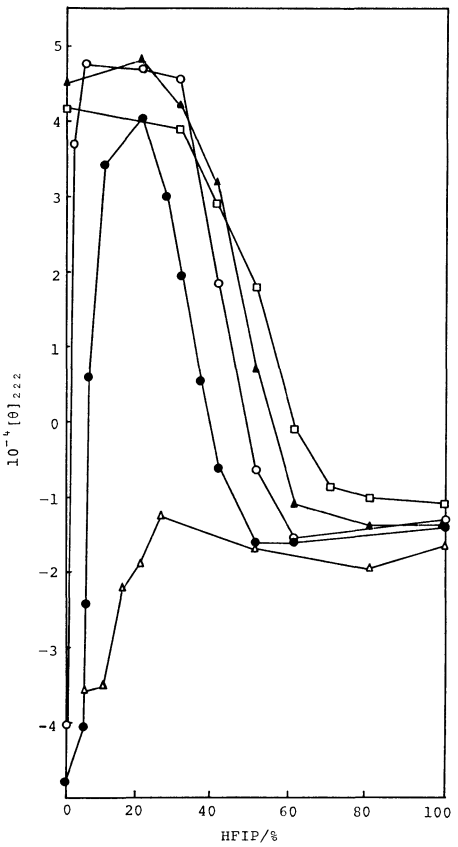

Fig. 4. Dependence of the ellipticity at 222 nm on HFIP content.
Phenylazo content: 11% (□); 26% (▲); 46% (○); 67% (●); 100% (△).

characteristic of the LH helix, those with more phenylazo residues (>40%) a negative CD band around 222 nm, characteristic of the RH helix. The homopolymer with 100% azo residues being insoluble in DCE, no spectral measurement was carried out in this solvent.

The CD spectra of the polymers were found to change on addition of hexafluoro-2-propanol (HFIP) to their DCE solutions (Figs. 2, 3, and 4). The molecular ellipticities $[\theta]$ for the copolymers with more than 40% phenylazo residues change from negative to positive on increasing HFIP content (up to 20%), confirming the conformational transition from RH helix to LH helix. Further increase in HFIP content causes another change in the $[\theta]$ values from positive to negative, which may correspond to the conformational transition from LH helix to random coil; increase in HFIP content above 50% causes no significant change. The following transition process is thus established.

$$\text{RH helix} \xrightarrow{\text{HFIP}} \text{LH helix} \xrightarrow{\text{HFIP}} \text{random coil} \quad (1)$$

The anomalous $[\theta]$ values for the random coil suggest that the conformation of these copolymers is not entirely random, possibly due to side chain - side chain steric interactions. Bradbury *et al.* reported a similar phenomenon, the conformational transitions in their case being induced by addition of trifluoroacetic acid

Table 1. Elemental analyses and viscosities of copolymers of β-benzyl L-aspartate and β-[p-(phenylazo)phenethyl] L-aspartate

Mol % phenylazo residues	Found (%)			Calcd (%)			η_{sp}/c
	C	H	N	C	H	N	
10.53	64.24	5.41	7.63	64.69	5.40	7.63	1.41
25.92	64.87	5.42	9.02	65.25	5.38	9.02	3.97
45.79	65.20	5.35	10.35	65.79	5.35	10.35	2.36
67.24	65.72	5.42	11.54	66.26	5.33	11.54	2.50
100	65.81	5.51	12.47	66.85	5.31	13.00	—

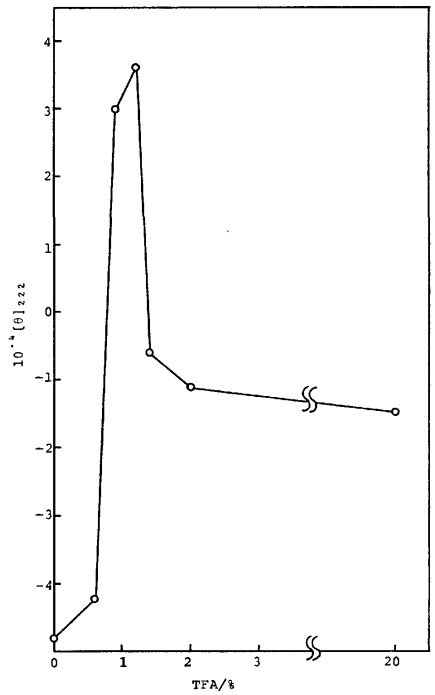

Fig. 5. Dependence of the ellipticity at 222 nm on TFA content for the copolymer with 67% phenylazo residues.

(TFA) or dichloroacetic acid to chloroform solutions of copolymers of β-ethyl L-aspartate and β-benzyl L-aspartate.[12a] RH Helix→LH helix transition for the arylazo polyaspartates we studied was also induced by TFA addition, in agreement with their results (Fig. 5). The helix reversal for arylazo polyaspartates occurs on addition of a very small amount of TFA (<2%). The resulting LH helix readily turns into the random form on further addition of TFA, in line with the behavior of TFA as a random-coil promoting solvent.

In contrast to the copolymers with more than 40% phenylazo residues, the copolymers with less phenylazo residues are LH helical in pure DCE, undergoing only LH helix→random coil transition on addition of HFIP.

$$\text{LH helix} \xrightarrow{\text{HFIP}} \text{random coil} \qquad (2)$$

The homopolymer with 100% phenylazo residues is insoluble in DCE but soluble in HFIP. Its CD spectra at different HFIP contents were therefore measured on solutions prepared by adding DCE to the HFIP solution. The spectrum of the polymer in 100% HFIP exhibits a negative band around 222 nm at-

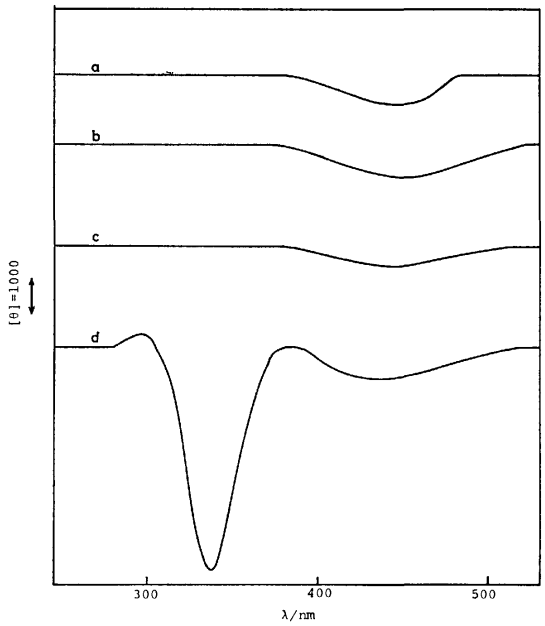

Fig. 6. CD spectra associated with the side-chain n-π* and π-π* transitions in DCE.
Phenylazo content: 11% (a); 26% (b); 46% (c); 67% (d).

tributable to the random-coil form. No positive band appears on increasing the DCE content, the spectrum attributable to a RH helix being finally attained (Fig. 4). Thus, the following process should occur if HFIP is added to the DCE solution.

$$\text{RH helix} \xrightarrow{\text{HFIP}} \text{random coil} \qquad (3)$$

Processes (1), (2), and (3) might arise from an alteration of the energy balance as a consequence of hydrogen bonding of HFIP to the side-chain ester groups, or to the main-chain amide groups.

The CD spectra associated with the side-chain n-π* and π-π* transitions were obtained for the polymers in DCE solution (Fig. 6). Molar ellipticities of the side-chain CD bands were calculated using the molar concentration of phenylazo residues. Among the four copolymers used, only one with 67% phenylazo residues exhibits the π-π* CD band, suggesting that the π-π* CD arises from electronic interactions between the side-chain azobenzene moieties. On the other hand, the n-π* CD band appears for all copolymers, the sign being the same regardless of the conformational differences. The minimum ellipticities around 440 nm are similar irrespective of copolymer composition. The results suggest that side chain-main

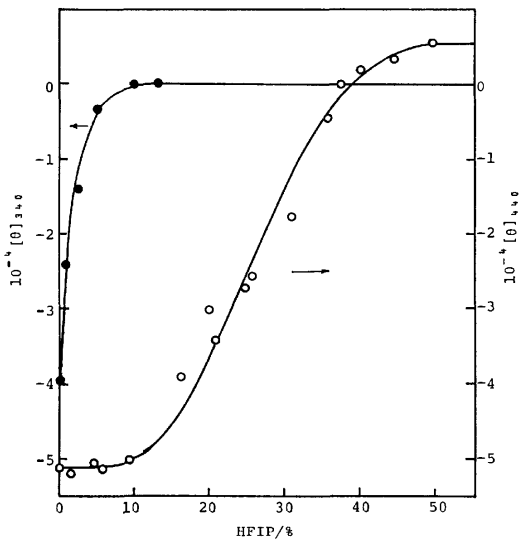

Fig. 7. Dependence of the ellipticities of the side-chain n-π^* and π-π^* CD bands on HFIP content for the copolymer with 67% phenylazo residues.
○: n-π^* CD band around 440 nm, ●: π-π^* CD band around 340 nm.

chain electronic interactions give rise to the band. Addition of HFIP to a DCE solution of the copolymer with 67% phenylazo residues alters both side-chain CD bands. The π-π^* CD band decreases in intensity with increasing HFIP content, finally disappearing at 10% HFIP where the conformation of the polymer is LH helical (Fig. 7). This indicates that the side chain - side chain electronic interactions, which are origin of the π-π^* CD band, become impossible, probably due to the disordered arrangement of the side-chain chromophores in the HFIP-solvated LH helix. The n-π^* CD band of the copolymer with 67% phenylazo residues shows no change up to 10% HFIP in spite of the observed RH helix→LH helix transition in this solvent range, confirming the insensitivity of this band to helix nature. Further increase in the HFIP content causes a decrease in the absolute ellipticity, even in the solvent range where the main-chain conformation remains LH helical. The absolute ellipticity continues to decrease over the HFIP concentration range in which LH helix→random coil transition occurs, the $[\theta]$ value becoming constant with a positive sign for the random-coil form. This behavior of the n-π^* CD band indicates that helical structures are necessary for its appearance. In the helical structures the side chains might be limited in mobility, adopting certain geometric positions in relation to the asymmetric centers of the main-chain backbone.

Experimental

CD spectra were recorded on a JASCO J-20 circular dichrograph apparatus at 25 °C using 0.3—1 g/l solutions. "Dotite Spectrosol" grade DCE and "Merck Urasol" grade HFIP were used without further purification. Due to the absorption of DCE, no spectra could be obtained below 210 nm. Molecular ellipticities for the band around 222 nm were calculated by means of the molar concentration of the amide group. Ellipticities for the side-chain CD bands were calculated by means of the molar concentration of the phenylazo residues. Polymers used for the CD measurements were synthesized as described below.

p-*(Phenylazo)phenethyl Alcohol (1).* The alcohol was prepared from *p*-aminophenethyl alcohol (25 g) and nitrosobenzene (19.5 g) by the method reported previously.[8] Yield, 30.5 g (74%); mp 90—91 °C. Found: C, 74.04; H, 6.22; N, 12.33%. Calcd for $C_{14}H_{14}N_2O$: C, 74.30; H, 6.25; N, 12.38%.

β-[p-*(Phenylazo)phenethyl*] L-*Aspartate (2).* Amino acid **2** was prepared from alcohol **1** (13.3 g) and L-aspartic acid (7.83 g) by the method reported previously.[15] Yield, 15.8 g (79%); mp 199—200 °C. IR (KBr): 1740, 1600, 1240 cm^{-1}. Found: C, 63.09; H, 5.56; N, 12.23%. Calcd for $C_{18}H_{19}N_3O_4$: C, 63.32; H, 5.62; N, 12.31%.

β-[p-*(Phenylazo)phenethyl*] L-*Aspartate* N-*Carboxy Anhydride (3).* *N*-Carboxy anhydride (NCA) was prepared from **2** (4 g) and trichloromethyl chloroformate (2.36 g).[16] The crude product was recrystallized twice from ethyl acetate and hexane. Yield, 0.93 g (22%); mp 160—161 °C. IR (KBr): 1858, 1800, 1766, 1740, 1180 cm^{-1}. Found: C, 62.33; H, 4.80; N, 11.64%. Calcd for $C_{19}H_{17}N_3O_5$: C, 62.11; H, 4.67; N, 11.44%.

Polymers. Polymers with different azo amino acid contents were prepared from **3** and *β*-benzyl L-aspartate NCA by varying the ratio of the two NCAs. Polymerization was carried out in dioxane at room temperature for 5 d using triethylamine as an initiator (monomer/initiator ratio 50:1). The reaction mixture was added to ethanol stirred vigorously. The precipitate was collected by filtration, washed with several portions of ethanol and dried *in vacuo* at 40 °C. Mole percentage of azo amino acid residues in the copolymers was estimated from the nitrogen content obtained by elemental analysis. The reduced specific viscosity, η_{sp}/c, for each polymer was measured for a 0.1% DCE solution at 25 °C. Viscosity measurement for the polymer composed of 100% azo amino acid residues could not be carried out due to its insolubility in DCE. Data for the polymers are sammarized in Table 1.

References

1) F. Ciardelli, E. Chiellini, C. Carlini, O. Pieroni, P. Salvadori, and R. Menicagli, *J. Polym. Sci., Polym. Symp.*, **62**, 143 (1978).
2) M. Goodman and A. Kossoy, *J. Am. Chem. Soc.*, **88**, 5010 (1966).
3) M. Goodman and M. L. Falxa, *J. Am. Chem. Soc.*, **89**, 3863 (1967).
4) M. Goodman and E. Benedetti, *Biochemistry*, **7**, 4226 (1968).
5) E. Benedetti, A. Kossoy, M. L. Falxa, and M. Goodman, *Biochemistry*, **7**, 4234 (1968).
6) E. Benedetti and M. Goodman, *Biochemistry*, **7**, 4242 (1968).
7) A. Ueno, J. Anzai, T. Osa, and Y. Kadoma, *J. Polym. Sci., Polym. Lett. Ed.*, **15**, 407 (1977).
8) A. Ueno, J. Anzai, T. Osa, and Y. Kadoma, *Bull. Chem. Soc. Jpn.*, **50**, 2995 (1977).
9) A. Ueno, J. Anzai, T. Osa, and Y. Kadoma, *Bull. Chem. Soc. Jpn.*, **52**, 549 (1979).
10) J. L. Houben, O. Pieroni, A. Fissi, and F. Ciardelli, *Biopolymers*, **17**, 799 (1978).
11) (a) E. M. Bradbury, A. R. Downie, A. Elliott, and W. E. Hanby, *Proc. R. Soc. London, Ser. A*, **259**, 110 (1960);

(b) R. H. Karlson, K. S. Norland, G. D. Fasman, and E. R. Blout, *J. Am. Chem. Soc.*, **82**, 2268 (1960); (c) M. Hashimoto and J. Aritomi, *Bull. Chem. Soc. Jpn.*, **39**, 2713 (1966); (d) M. Hashimoto, *ibid.*, **39**, 2713 (1966); (e) M. Hashimoto and S. Arakawa, *ibid.*, **40**, 1698 (1967); (f) C. Toniolo, M. L. Falxa, and M. Goodman, *Biopolymers*, **6**, 1579 (1968); (g) M. Goodman, C. M. Deber, and A. M. Felix, *J. Am. Chem. Soc.*, **84**, 3773 (1962); (h) J. B. Aragao and M. H. Loucheux, *J. Chim. Phys.*, 1578 (1974); (i) D. F. Bradley, M. Goodman, A. Felix, and R. Records, *Biopolymers*, **4**, 607 (1966); (j) M. Goodman, A. M. Felix, C. M. Deber, A. R. Brause, and G. Schwartz, *ibid.*, **1**, 371 (1963); (k) M. L. Loucheux and C. Duflot, *ibid.*, **14**, 469 (1975); (l) E. H. Erenrich, R. H. Andreatta, and H. A. Sheraga, *J. Am. Chem. Soc.*, **92**, 1116 (1970).

12) (a) E. M. Bradbury, B. G. Carpenter, C. Crane-Robinson, H. Goldman, *Macromolecules*, **4**, 557 (1971); (b) V. Giancotti, F. Quadrifoglio, and V. Crescenzi, *J. Am. Chem. Soc.*, **94**, 297 (1972).

13) H. Yamamoto and T. Hayakawa, *Biopolymers*, **16**, 1593 (1977).

14) (a) F. Heitz and G. Spach, *Macromolecules*, **10**, 520 (1977); (b) F. Heitz, P. D. Cary, and C. Crane-Robinson, *ibid.*, **10**, 526 (1977).

15) Y. Kadoma, A. Ueno, K. Takeda, K. Uno, and Y. Iwakura, *J. Polym. Sci., Polym. Lett. Ed.*, **12**, 715 (1974).

16) Y. Koiwa, K. Tatsukawa, A. Miike, M. Teranishi, and Y. Fujimoto, *Yuki Gosei Kagaku Kyokai Shi*, **33**, 628 (1975).

 © 1980 The Chemical Society of Japan Bull. Chem. Soc. Jpn., 53, 1993—2001 (1980)

Electronic Structures and Conformations of *N*-Benzylideneanilines. I. Electronic Absorption Spectral Study Combined with CNDO/S CI Calculations

Ryoichi Akaba, Katsumi Tokumaru,* and Tsunetoshi Kobayashi*,†

Department of Chemistry, The University of Tsukuba, Sakura-mura, Ibaraki 305

† *The Institute of Physical and Chemical Research, Wako, Saitama 351*

(Received October 8, 1979)

The electronic structures and molecular conformations of *N*-benzylideneaniline and its several derivatives bearing 2-methyl, 2,6-dimethyl, and/or 4-nitro groups on the anilino benzene ring (ring A) have been investigated by electronic absorption spectroscopy combined with CNDO/S CI calculations. The lower energy bands are assigned and the molecular conformations are estimated. The results show that the 4-nitro derivatives as well as the 2,6-dimethyl derivatives take considerably twisted conformations.

It is well known that the UV absorption spectral pattern of *N*-benzylideneaniline is remarkably different from those of π-isoelectronic *trans*-stilbene and *trans*-azobenzene,[1] and it has been reasonably understood in terms that *N*-benzylideneaniline takes a nonplanar conformation[1b,1c,2] in which the anilino benzene ring (ring A) twists from the rest part of the molecule considerably (see Fig. 1) whereas *trans*-stilbene[1c,3] and *trans*-azobenzene[1c,4] do not take drastically twisted conformations.

The molecular conformations of *N*-benzylideneanilines have been investigated by several methods. A recent gas phase electron diffraction study has indicated that the twist angle θ_N of *N*-benzylideneaniline **1** is about 52°.[5] The PCILO[6] and NDDO[7] calculations also supported the twisted conformation of **1**.

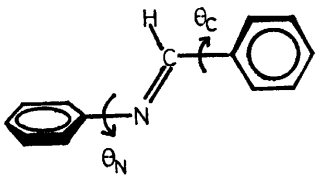

Fig. 1. Twisted conformation of *N*-benzylideneaniline.

In crystalline states, the molecular structures of *N*-benzylideneaniline and some of its derivatives have been determined by X-ray crystallography.[8-14] For example, it was reported that *N*-benzylideneaniline,[8] the 4-carboxy derivative,[8] and the 4-dimethylamino-4′-nitro derivative[9] take nonplanar conformations with the twist angle θ_N of 55.2, 41.1, and 9.1°, respectively. The 4,4′-dichloro derivative crystallizes in two modifications, and in one modification the molecule has the twist angle θ_N of about 25° and in another modification it takes a planar conformation.[10] Similar phenomenon is also found for the 4,4′-dimethyl derivative.[12,13] These facts clearly show that the twist angles θ_N of these compounds in crystals are controlled by the way of molecular packing,[15] and that it is not suitable for estimating the twist angles θ_N of the molecules dissolved in solutions from those determined in crystalline states.

In solution, the electronic absorption spectra of various *N*-bezylideneanilines have already been reported.[1b,1c,2,9,16,17] Historically, Wiegand and Merkel[16] examined for the first time the UV absorption spectrum of *N*-benzylideneaniline and proposed the linear planar model as its structure. Ebara analyzed UV spectra of various substituted *N*-benzylideneanilines including nitro derivatives and postulated that in these compounds the ring A is perpendicular to the rest part of the molecule, the imino nitrogen taking sp hybridization.[2b] This model was taken later by El-Bayoumi and coworkers also in their extensive study of UV absorption spectra of various substituted *N*-benzylideneanilines.[2g] On the other hand, Brocklehurst[1b] and Smith[2c] proposed the model in which the ring A is rather twisted around the C–N bond by the examination of the UV absorption spectra of *N*-benzylideneaniline and related compounds. And nowadays, this model is reasonable, judging from the results for the other phases mentioned above.

Skrabal and his coworkers compared the UV spectra of several substituted *N*-benzylideneanilines with those of their corresponding 5-substituted 2-aryl-3,3-dimethyl-3*H*-indoles, and suggested that substitution of 4-dimethylamino group will reduce the twist angle θ_N, that 4-nitro group would not change the angle, and that the 4-dimethylamino-4′-nitro derivative takes a nearly planar conformation.[2h] Ezumi *et al.* reported that the 4-dimethylamino-4′-nitro derivative takes a nearly planar conformation on the basis of the comparison of its UV spectrum with that of 4-dimethylamino-4′-nitro-*trans*-stilbene together with calculations of the transition energies and intensities of their absorptions, and the planarity of the molecule was attributed to the favourable π-delocalization throughout the molecule by intramolecular charge transfer interaction between the substituents.[9] These results indicate that the substitution on the ring A is quite important in determining the twist angle θ_N.

In order to get deeper insight into the substituent effect on the twist angles θ_N of *N*-benzylideneanilines, an attempt has been made to investigate the effect of 4-nitro group as well as 2-methyl and 2,6-dimethyl groups on the electronic absorption spectra. The electronic absorption spectra of six *N*-benzylideneanilines, that is, *N*-benzylideneaniline **1**, *N*-benzylidene-2-methylaniline **2**, *N*-benzylidene-2,6-dimethylaniline **3**, *N*-benzylidene-4-nitroaniline **4**, *N*-benzylidene-2-methyl-4-nitroaniline **5**, and *N*-benzylidene-2,6-dimethyl-4-nitroaniline **6**, have been measured, and their transition properties have been calculated to interpret the observed spectra.

Table 1. Electronic absorption spectral data for **1**—**6** in cyclohexane[a)]

Compound	λ_{max}/nm	E_{max}/eV	ε_{max} 10^{-4}/dm^3 mol^{-1} cm^{-1}	f
N-Benzylideneaniline (**1**)	210		1.78	
	222		1.37	
	(236)		1.03	
	264	4.70	1.72	0.36
	315	3.94	0.70	0.18
N-Benzylidene-2-methyl-aniline (**2**)	212		1.81	
	227.5		1.18	
	(237)		1.24	
	(247.5)		1.41	
	263	4.71	1.71	0.43
	330	3.76	0.59	0.13
N-Benzylidene-2,6-dimethylaniline (**3**)	212.5		2.13	
	253	4.90	2.23	0.42
	340	3.65	0.18	0.04
N-Benzylidene-4-nitroaniline (**4**)	210		1.62	
	223.5		1.47	
	298	4.38	1.65	0.18
	321	3.86	1.47	0.38
N-Benzylidene-2-methyl-4-nitroaniline (**5**)	209		2.18	
	225		1.62	
	(268)		1.20	
	295	4.37	1.69	0.25
	327	3.79	1.34	0.37
N-Benzylidene-2,6-dimethyl-4-nitroaniline (**6**)	207.5		2.81	
	233		1.27	
	254	5.05	1.28	0.29
	(296)	4.13	1.32	0.42

a) λ_{max} and ε_{max} are for the apparent band maxima and E_{max} and f are for the deconvoluted bands.

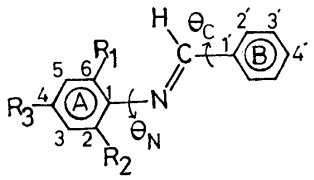

1: $R_1=R_2=R_3=H$
2: $R_1=H$, $R_2=CH_3$, $R_3=H$
3: $R_1=R_2=CH_3$, $R_3=H$
4: $R_1=R_2=H$, $R_3=NO_2$
5: $R_1=H$, $R_2=CH_3$, $R_3=NO_2$
6: $R_1=R_2=CH_3$, $R_3=NO_2$

Method and Results

The electronic absorption spectra of six *N*-benzylideneanilines **1**—**6** are shown in Figs. 2—7, respectively. The observed absorption spectral data are listed in Table 1. The long wavelength regions of the observed spectra were approximately deconvoluted into the first and second main component bands to estimate their transition energies and oscillator strengths which are also included in Table 1. The intensity ratios of the first bands to the second ones are shown in Table 2.

In order to reproduce the observed spectral patterns, the transition energies and the oscillator strengths have been calculated by the CNDO/S[18)] CI calculations including interactions between sixty-four singly-excited configurations for varying degrees of the twist angle θ_N. In the calculations of **1**, **2**, and **3**, the

Table 2. Calculated and observed intensity ratio, f_1/f_2[a)]

Compound	f_1/f_2	
	Calcd(θ_N/°)	Obsd
N-Benzylideneaniline (**1**)	0.70 (30)	0.50
	0.42 (35)	
	0.29 (40)	
	0.12 (55.2)	
N-Benzylidene-2-methyl-aniline (**2**)	0.40 (40)	0.30
	0.26 (45)	
	0.20 (48.16)	
	0.17 (50)	
	0.12 (55.2)	
	0.04 (76.84)	
N-Benzylidene-2,6-dimethylaniline (**3**)	0.29 (40)	0.10
	0.24 (70)	
	0.14 (75)	
	0.05 (76.84)	
	0.008 (90)	
N-Benzylidene-4-nitro-aniline (**4**)	9.70 (50.2)	2.11
	6.87 (60)	
	3.56 (80)	
	2.89 (90)	
N-Benzylidene-2-methyl-4-nitroaniline (**5**)	7.44 (50.2)	1.48
	5.73 (60)	
	2.96 (80)	
	1.96 (90)	
N-Benzylidene-2,6-dimethyl-4-nitroaniline (**6**)	3.48 (60)	1.45
	2.57 (76.73)	
	2.31 (80)	
	1.70 (90)	

a) f_1 and f_2 correspond to the oscillator strengths for the observed first and second bands, respectively.

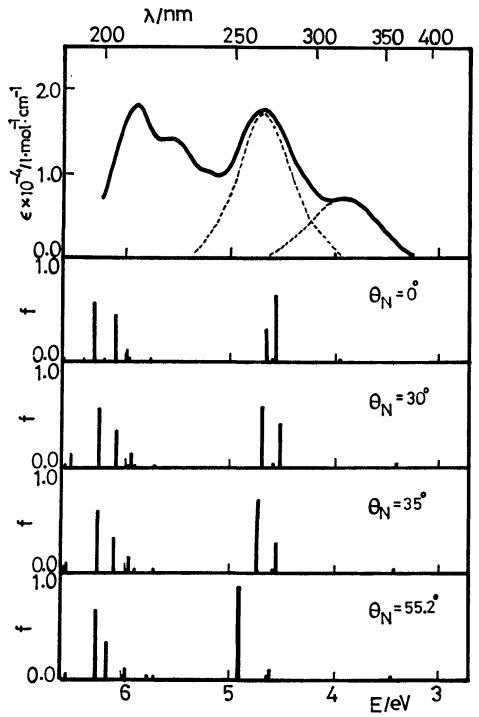

Fig. 2. Observed absorption spectrum and calculated spectral patterns of *N*-benzylideneaniline **1**.

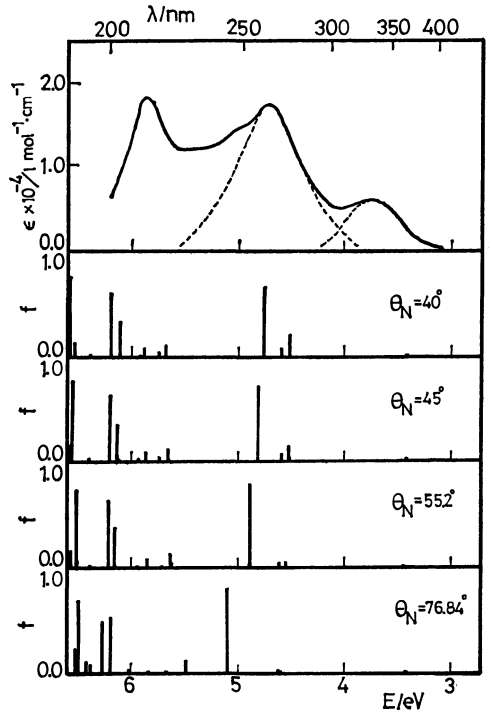

Fig. 3. Observed absorption spectrum and calculated spectral patterns of *N*-benzylidene-2-methylaniline **2**.

twist angles θ_C were kept at the same angle as for crystalline **1**, 10.3°,[8] since, in the preliminary calculations, the spectral pattern was not appreciably changed with its variation from 0° to 10.3°. Likewise, the angles θ_C for **4**, **5**, and **6** were fixed at the same angle as reported for crystalline *N*-(4-methylbenzylidene)-4-nitroaniline, 8.1°.[8]

The calculated results for the spectral patterns at

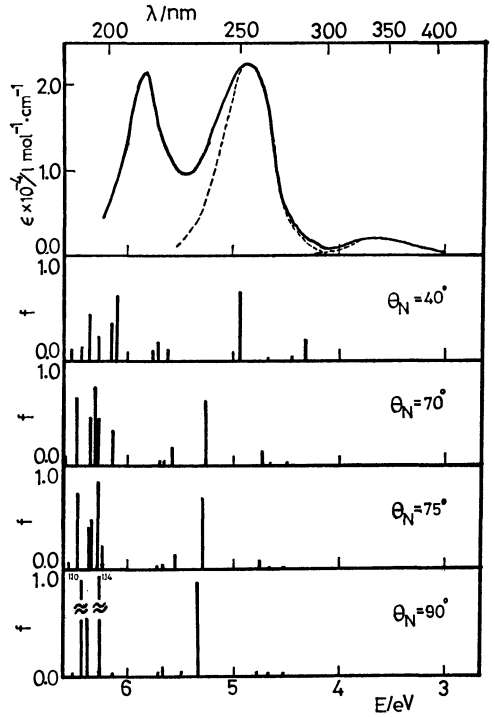

Fig. 4. Observed absorption spectrum and calculated spectral patterns of *N*-benzylidene-2,6-dimethylaniline **3**.

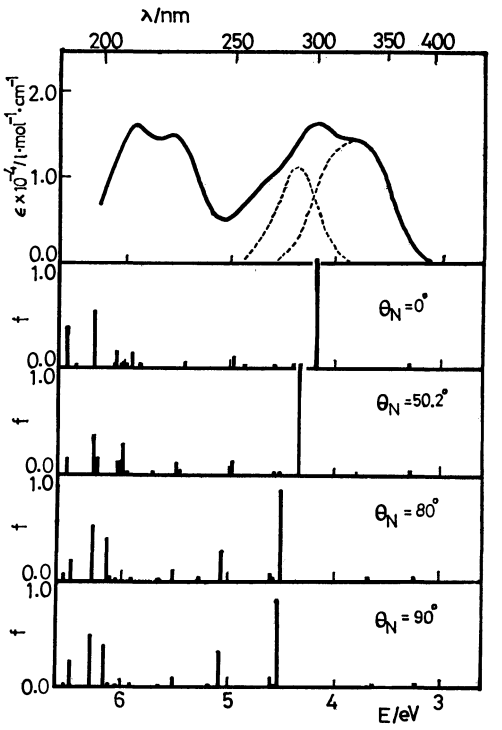

Fig. 5. Observed absorption spectrum and calculated spectral patterns of *N*-benzylidene-4-nitroaniline **4**.

various θ_N are also schematically illustrated in Figs. 2—7, and the ratios of the calculated oscillator strengths of the two strong transitions in the longer wavelength region at the various θ_N are shown in Table 2. Comparison of these calculated ratios with those of the observed ones has enabled us to estimate the twist

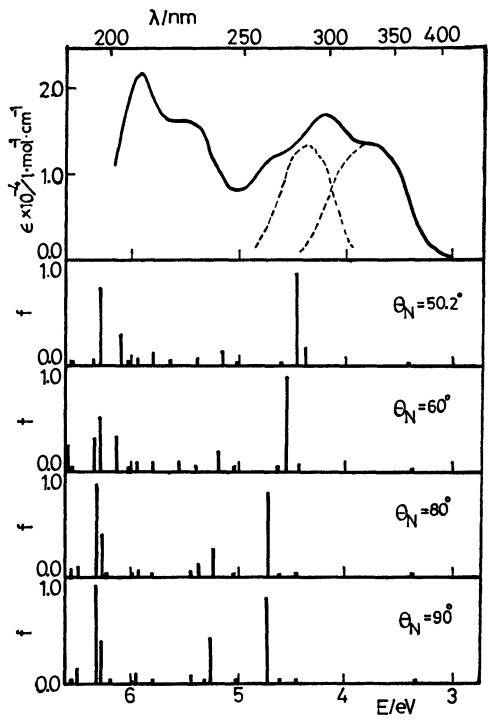

Fig. 6. Observed absorption spectrum and calculated spectral patterns of *N*-benzylidene-2-methyl-4-nitroaniline **5**.

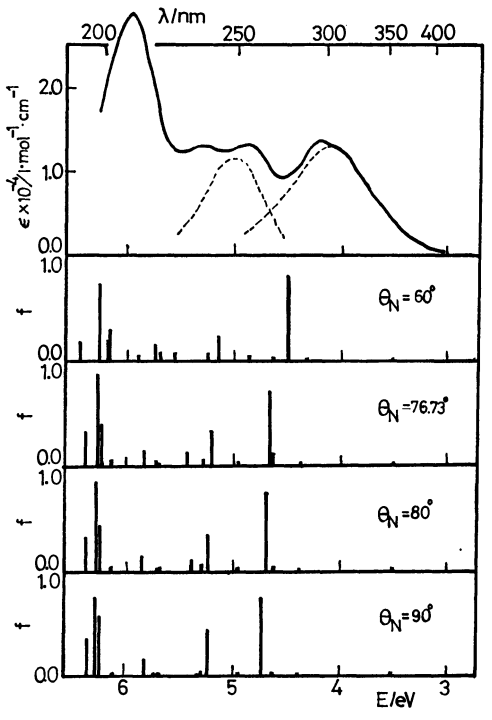

Fig. 7. Observed absorption spectrum and calculated spectral patterns of *N*-benzylidene-2,6-dimethyl-4-nitroaniline **6**.

angle θ_N which can reproduce well the observed results. The twist angles θ_N thus estimated are 30—35, 40—45, 70—80, 90, 90, and 90° for **1**, **2**, **3**, **4**, **5**, and **6**, respectively. Tables 3 and 4 respectively list the calculated transition energies and oscillator strengths for **1** and **4** at the above estimated angles θ_N=35° and 90°, respectively, together with the CI compositions and types of excitations. Figures 8 and 9 show schematic illustrations of the molecular orbitals calculated for **1** and **4** at the above twist angles, respectively.

Discussion

Compound ***1***. As Fig. 2 and Table 1 indicate, **1** shows the first absorption band at 315 nm (3.94 eV) and the intense second band at 264 nm (4.70 eV) in cyclohexane. The calculated transitions at 4.56 and 4.75 eV are regarded to correspond to these observed bands. The observed first band can be assigned mainly to the π-π^* transition with predominant configurations of 34—32, 34—33, and 36—33 (Table 3). Although the calculations predict the existence of an n-π^* transition with low intensity in the long wavelength region, this band was not identified probably owing to its low intensity and overlapping with the strong 315 nm band. The higher energy bands may tentatively be assigned as shown in Table 3.

As Fig. 2 indicates, with the increase in the twist angle θ_N, the first band is expected to decrease in intensity, and on the contrary, the second band is to increase in intensity. As Table 2 and Fig. 2 indicate, the calculation with the twist angle θ_N of 30—35° can well reproduce the observed spectral pattern. This estimated twist angle θ_N is smaller than that observed in the gas phase (θ_N=52±5°[5]); however, the present result may be taken to show that the twist angle θ_N of **1** in a solution is far from 90°, and may be in qualitative agreement with that estimated from photoelectron spectroscopy as described in a subsequent paper.[19]

The method used in this study seems more suitable for estimating approximately the twist angle θ_N than the previous work by Minkin *et al.*[2f] employing the ASMO PPP CI method which was not successful in reproducing the observed intensity ratio of the first to the second band.

Compound ***2***. On introduction of an ortho-methyl group on the ring A (in going from **1** to **2**), the first band undergoes bathochromic shift by 15 nm; however, the second band remains unchanged in position (see Table 1). The intensity of the first band (f=0.13) is moderately reduced compared with **1** (f=0.18), and the intensity ratio of the first to the second band is decreased from 0.50 for **1** to 0.30 for **2**. The results of the calculations (Table 2) show that the twist angle θ_N of **2** may be 40—45° slightly larger than that evaluated for **1**. Accordingly, an ortho-methyl group on the ring A seems to exhibit not so pronounced effect on the twist angle θ_N. The first band is assigned mainly to the π-π^* transition with predominant configurations of 37—33, 37—36, and 38—34. The second band is also assigned mainly to the π-π^* transition with predominant cofiguration of 37—36. Here, molecular orbitals 32—42 of **2** correspond to orbitals 29—39 of **1**, respectively.

Compound ***3***. For compound **3**, its first band, as compared with **2**, shows bathochromic shift by 10 nm and reduces in intensity. The intensity ratio of the first to the second band is much smaller than

TABLE 3. CALCULATED TRANSITION ENERGIES AND OSCILLATOR STRENGTHS FOR *N*-BENZYLIDENEANILINE **1** ($\theta_N = 35°$)

Calcd					Obsd	
		CI Composition[a]				
E/eV	*f*	Excitation	Coefficient	Type	*E*/eV	*f*
3.460	0.010	38—29	−0.477	n-π^*		
		38—33	−0.671	n-π^*		
4.563	0.291	34—32	0.338	π-π^*	3.94	0.18
		34—33	0.537	π-π^*		
		36—33	0.406	π-π^*		
4.610	0.001	34—30	0.469	π-π^*		
		34—32	0.306	π-π^*		
		35—31	−0.389	π-π^*		
		35—33	−0.414	π-π^*		
4.748	0.692	34—32	−0.311	π-π^*	4.70	0.36
		34—33	0.751	π-π^*		
5.738	0.001	34—31	0.634	π-π^*		
		35—30	0.315	π-π^*		
		36—33	−0.375	π-π^*		
		37—33	−0.324	π-π^*		
5.905	0.034	34—31	0.445	π-π^*		
		36—33	0.532	π-π^*		
		37—33	0.310	π-π^*		
		38—33	−0.386	n-π^*		
5.955	0.146	34—30	0.434	π-π^*	5.25[b]	
		35—33	0.797	π-π^*		
5.967	0.001	36—31	0.371	π-π^*		
		38—31	0.599	n-π^*		
6.109	0.336	34—32	0.607	π-π^*	5.59[b]	
		36—33	−0.337	π-π^*		
		37—33	0.588	π-π^*		
6.256	0.580	34—29	−0.403	π-π^*	5.90[b]	
		35—30	0.553	π-π^*		
		36—32	−0.319	π-π^*		
		37—32	0.410	π-π^*		
6.555	0.106	34—29	−0.429	π-π^*		
		38—30	0.325	n-π^*		
		39—33	0.554	σ-π^*		
6.557	0.079	34—30	0.328	π-π^*		
		36—30	0.360	π-π^*		
		38—30	0.533	n-π^*		
		39—33	−0.360	σ-π^*		
6.656	0.621	34—30	−0.455	π-π^*		
		35—29	0.323	π-π^*		
		35—31	−0.609	π-π^*		
		38—30	0.309	n-π^*		
6.715	0.015	34—32	0.442	π-π^*		
		36—29	0.307	π-π^*		
		37—32	−0.309	π-π^*		
		36—32	−0.462	π-π^*		
6.748	0.100	36—32	−0.402	π-π^*		
		39—31	0.359	σ-π^*		
		39—33	0.342	σ-π^*		
6.810	0.206	34—29	0.465	π-π^*		
		35—30	0.582	π-π^*		

a) The transition, indicated *i*-*j*, refers to a one-electron excitation from orbital *i* to virtual orbital *j*. The second column gives the CI coefficient of the configuration *i*-*j*. Orbitals 33 and 34 are the LUMO and HOMO, respectively. b) The apparent band maximum.

Table 4. Calculated transition energies and oscillator strengths for *N*-benzylidene-4-nitroaniline **4** ($\theta_N=90°$)

Calcd					Obsd	
		CI composition[a]				
E/eV	*f*	Excitation	Coefficient	Type	*E*/eV	*f*
3.257	0.000	44—32	0.385	n(NO_2)-π^*		
		44—36	0.919	n(NO_2)-π^*		
3.660	0.000	38—31	−0.319	π-π^*		
		38—35	−0.609	π-π^*		
		41—31	0.361	n-π^*		
		41—35	0·617	n-π^*		
4.520	0.816	37—35	−0.427	π-π^*	3.86	0.38
		38—36	−0.825	π-π^*		
4.573	0.000	38—34	−0.653	π-π^*		
		40—32	−0.331	π-π^*		
		40—36	0.670	π-π^*		
4.586	0.081	37—33	−0.644	π-π^*		
		38—36	0.361	π-π^*		
		39—35	−0.611	π-π^*		
5.076	0.310	37—35	0.843	π-π^*	4.38	0.18
		38—36	−0.396	π-π^*		
5.229	0.001	37—32	−0.415	π-π^*		
		37—36	0.813	π-π^*		
5.514	0.087	38—34	0.509	π-π^*		
		40—32	0.350	π-π^*		
		40—36	0.703	π-π^*		
5.651	0.005	38—35	0.662	π-π^*		
		41—35	0.587	n-π^*		
5.893	0.005	38—32	−0.739	π-π^*		
		40—34	0.316	π-π^*		
		41—36	−0.320	n-π^*		
6.030	0.004	37—34	−0.897	π-π^*		
		43—34	−0.366	π-π^*		
6.109	0.027	40—35	0.931	π-π^*		
6.149	0.381	37—33	0.554	π-π^*	5.55[b]	
		39—35	−0.698	π-π^*		
6.260	0.478	37—31	−0.376	π-π^*	5.90[b]	
		39—33	−0.502	π-π^*		
		40—34	0.542	π-π^*		
6.470	0.236	39—33	0.503	π-π^*		
		41—32	−0.391	n-π^*		
		41—36	0.579	n-π^*		
6.515	0.038	37—32	−0.483	π-π^*		
		37—36	−0.379	π-π^*		
		40—32	−0.511	π-π^*		
		42—36	−0.387	π(NO_2)-π^*		
6.586	0.007	37—32	0.503	π-π^*		
		37—36	0.387	π-π^*		
		40—32	−0.454	π-π^*		
		42—36	−0.466	π(NO_2)-π^*		
6.650	0.000	39—36	0.966	π-π^*		
6.743	0.569	37—31	0.741	π-π^*		
		39—33	−0.402	π-π^*		
		43—35	−0.420	π-π^*		
6.882	0.006	38—33	−0.963	π-π^*		
6.893	0.756	40—32	0.377	π-π^*		
		41—34	0.442	n-π^*		
		42—36	−0.723	π(NO_2)-π^*		
6.921	0.200	38—32	0.490	π-π^*		
		39—33	0.331	π-π^*		
		40—34	0.657	π-π^*		
		41—36	−0.345	n-π^*		

a) The transition, indicated *i*-*j*, refers to a one-electron excitation from orbital *i* to virtual orbital *j*. The second column gives the CI coefficient of the configuration *i*-*j*. Orbitals 36 and 37 are the LUMO and HOMO, respectively. b) The apparent band maximum.

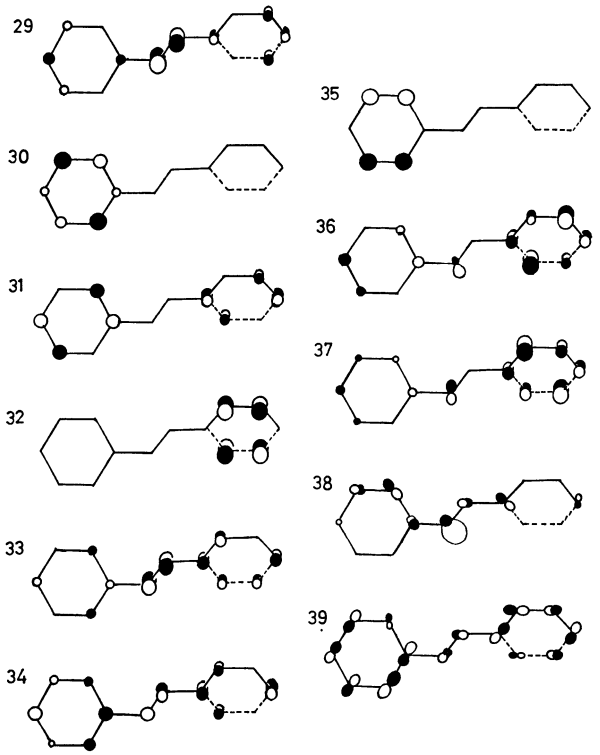

Fig. 8. Molecular orbitals of *N*-benzylideneaniline **1** (θ_N=35° and θ_C=10.3°).

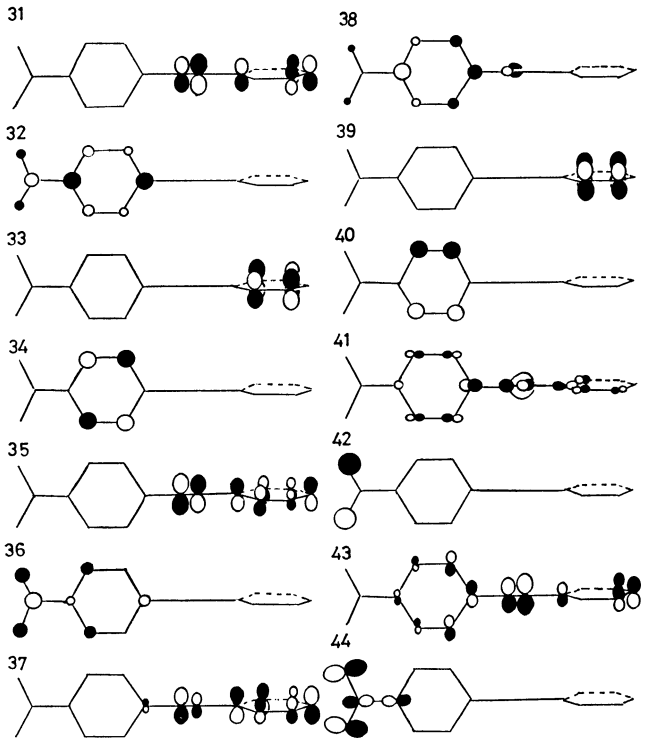

Fig. 9. Molecular orbitals of *N*-benzylidene-4-nitroaniline **4** (θ_N=90° and θ_C=8.1°).

those of **1** and **2**. The present calculations indicate that the first band is assigned mainly to the π-π^* transition with a slight n-π^* character. The π-π^* transition is mainly caused by charge transfer from the ring A to the PhCH=N– group. The second band at 253 nm is also assigned mainly to the π-π^* transition with a slight n-π^* character in which a local excitation in the PhCH=N– group is the main configuration. The most probable twist angle θ_N is estimated to be 70—80° (see Table 2 and Fig. 4). This value corresponds well to that estimated on the basis of the van der Waals radii, $\gtrsim$77°.

It is worth noting that the present calculations provide a quantitative interpretation for the previous UV absorption data by Smith[2c] which show that the consecutive introduction of ortho-methyl groups on the ring A successively lowers the intensity of the first band.

Compound ***4***. Compounds **4**, **5**, and **6** carrying 4-nitro group exhibit characteristic absorption bands in the long wavelength region different from those of **1**, **2**, and **3** which do not carry 4-nitro group. Deconvolution of the observed spectra reveals that, in **4**, **5**, and **6**, the first main bands are stronger in intensity than the second bands in contrast with **1**, **2**, and **3** in which the first bands are weaker in intensity than the second bands (see Figs. 2—7).

For **4**, Fig. 5 and Table 2 indicate that the calculated ratio of the oscillator strengths of the first to the second main transition decreases with the increase in the twist angle θ_N, but the observed ratio is still lower than the calculated one even at the perpendicular conformation (θ_N=90°). This suggests that, within the limitation of the CNDO/S CI calculations employed, **4** assumes a considerably twisted conformation in solution. As Table 4 indicates, the first band can be mainly assigned to the charge transfer excitation from the aniline-like group to the nitro group mixed with the local excitation in the PhCH=N– group.

The present result is in contrast with that by Skrabal and his coworkers who reported, without deconvolution of the spectra, that **4** would have a similar twist angle θ_N to that of **1** on comparsion of the apparent spectral patterns between **4**, **1**, and their corresponding 3*H*-indoles which can be regarded to take planar conformations.[2h] However, as described above, the transition characters of the first and second bands, particularly their intensity ratios, are remarkably different from each other between **1** and **4**. Their postulation, therefore, seems not fully satisfactory.

Compound ***5***. In the case of **5**, similar trend on the twist angle θ_N was observed (Fig. 6 and Table 2). The observed intensity ratio of the first to the second band (f_1/f_2) is 1.48. The twist angle θ_N predicted by the present calculations to reproduce best this intensity ratio is 90°.

The observed first band can be assigned mainly to the π-π^* transition. The main configurations are the so-called charge transfer ones from the toluidine-like group to the nitro group. The second band is also assigned mainly to the π-π^* transition. The main configuration is a local excitation in the PhCH=N– group.

Compound ***6***. Comparison of the observed spectrum of **6** with those calculated at various twist angles θ_N (Table 2 and Fig. 7) leads to conclusion that **6** also takes a considerably twisted conformation like

TABLE 5. ELECTRONIC ABSORPTION SPECTRAL DATA OF *N*-BENZYLIDENEANILINE **1**, *N*-BENZYLIDENE-4-NITROANILINE **4**, AND THE CORRESPONDING 3*H*-INDOLES **7** AND **8**[a]

Compound	λ_{max}/nm	E_{max}/eV	ε_{max} 10^{-4}/dm^3 mol^{-1} cm^{-1}
N-Benzylideneaniline (**1**)	236	5.25	1.030
	262	4.73	1.710
	313	3.96	0.686
3,3-Dimethyl-2-phenyl-3*H*-indole (**7**)	228	5.44	1.530
	235	5.28	1.580
	245	5.06	1.250
	309	4.01	1.660
N-Benzylidene-4-nitroaniline (**4**)	220	5.64	1.650
	295	4.20	1.770
	(325)	3.81	1.540
3,3-Dimethyl-5-nitro-2-phenyl-3*H*-indole (**8**)	229	5.41	1.460
	(234)	5.30	(1.420)
	335	3.70	2.460

a) Taken from Ref. 2h. λ_{max}, E_{max}, and ε_{max} in this table are all for the apparent band maxima.

those of **4** and **5**. The first band can be mainly assigned to the π-π^* charge transfer transition from the benzylideneaniline group to the nitro group. The second band is assigned mainly to the π-π^* transition. The main configurations are the excitations to the PhCH=N– group π from the delocalized π-orbitals.

*Consideration on the Electronic Absorption Spectra of 2-Phenyl-3,3-dimethyl-3*H*-indoles.* Finally, it is worth noting that the present CNDO S CI method can well reproduce the reported UV spectral patterns[2h] of 3,3-dimethyl-2-phenyl-3*H*-indole **7** and 3,3-dimethyl-5-nitro-2-phenyl-3*H*-indole **8** regarded as the model compounds for the planar forms of *N*-benzylideneaniline **1** and *N*-benzylidene-4-nitroaniline **4**, respectively. Their spectral data are shown in Table 5. The spectral patterns calculated by the CNDO/S CI method for planar conformations (θ_N=0°) for **1** and **4** are shown in Figs. 2 and 5, respectively. As shown in Table 5, the planarization in each case (from **1** to **7** and from **4** to **8**) is accompanied by increase in the intensity of the first band, and this trend can be well reproduced by the present calculations (see Figs. 2 and 5).

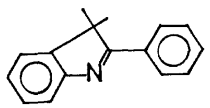

7

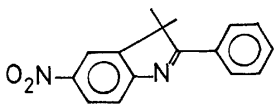

8

This finding may suggest that the CNDO/S CI method employed here is suitable for estimating the twist angles θ_N of *N*-benzylideneanilines in solutions.

In summary, it is concluded from the present results that the twist angle θ_N for *N*-benzylideneaniline **1** may be far from 90° and the introduction of 4-nitro group (compound **4**) remarkably increases the twist angle θ_N in the liquid phase.

Experimental

Materials. *N*-Benzylideneanilines **1**—**6** were prepared by refluxing equimolar amounts of appropriate amine and aldehyde in ethanol or benzene in the presence of molecular sieve (Wako synthetic zeolite; 8—12 mesh). For the preparation of **6**, refluxing in xylene for 3 d was required. The new compounds **5**, mp 119—120 °C, and **6**, mp 108—109 °C, gave satisfactory results of elemental analyses and spectroscopic data.

Spectral Measurements. Electronic absorption spectra were recorded with a JASCO UVIDEC-1 double-beam spectrophotometer in cyclohexane at room temperature.

Theoretical Calculations

The CNDO/S[18] CI calculations were carried out with a FACOM 230-75 computer at the Institute of Physical and Chemical Research. All the necessary atomic integrals and parameters were taken from or estimated according to Ref. 18. In the configuration interactions all the singly-excited configurations concerning the eight highest occupied and eight lowest unoccupied molecular orbitals were taken into account. In the evaluation of the oscillator strengths also the ZDO approximation was used. The geometrical structures were properly assumed on the basis of the appropriate data given in Ref. 8.

References

1) (a) See, for example, as a review: C. Sandorfy, "General and Theoretical Aspects," in "The Chemistry of the Carbon–Nitrogen Double Bond," ed by S. Patai, John Wiley, New York (1970), Chap. 1, pp. 1—60. See also, for example: (b) P. Brocklehurst, *Tetrahedron*, **18**, 299 (1962); (c) E. Haselbach and E. Heilbronner, *Helv. Chim. Acta*, **51**, 16 (1968).

2) See, for example: (a) V. A. Izmail'skii and E. A. Smirnov, *Zh. Obsch. Khim.*, **26**, 3042 (1956); (b) N. Ebara, *Bull. Chem. Soc. Jpn.*, **33**, 534 (1960); (c) W. F. Smith, *Tetrahedron*, **19**, 445 (1963); (d) G. Favini and A. Gamba, *J. Chim. Phys.*, **62**, 995 (1965); (e) G. Favini, D. Pitea, and F. Zuccarello, *ibid.*, **69**, 9 (1972); (f) V. I. Minkin, Yu. A. Zhdanov, E. A. Medyantzeva, and Yu. A. Ostroumov, *Tetrahedron*, **23**, 3651 (1967); (g) M. A. El-Bayoumi, M. El-Aasser, and F. Abdel-Halim, *J. Am. Chem. Soc.*, **93**, 586 (1971); (h) P. Skrabal, J. Steiger, and H. Zollinger, *Helv. Chim. Acta*, **58**, 800 (1975); (i) T. Bally, E. Haselbach, S. Lanyiova, F. Marschner, and M. Rossi, *ibid.*, **59**, 486 (1976); (j) M. Kobayashi, M. Yoshida, and H. Minato, *Chem. Lett.*, **1976**, 185.

3) (a) J. M. Robertson and I. Woodward, *Proc. R.*

Soc. London, Ser. A, **162**, 568 (1937). See also (b) M. Traetteberg, E. B. Frantsen, F. C. Mijlhoff, and A. Hoekstra, *J. Mol. Struct.*, **26**, 57 (1975).
4) (a) J. J. de Lange, J. M. Robertson, and I. Woodward, *Proc. R. Soc. London, Ser. A*, **171**, 398 (1939); (b) C. J. Brown, *Acta Crystallogr.*, **21**, 146 (1966). See also (c) M. Traetteberg, I. Hilmo, and K. Hagen, *J. Mol. Struct.*, **39**, 231 (1977).
5) M. Traetteberg, I. Hilmo, R. J. Abraham, and S. Ljunggren, *J. Mol. Struct.*, **48**, 395 (1978).
6) P. Jacques and J. Faure, *Theor. Chim. Acta*, **46**, 307 (1977).
7) H.-J. Hofmann and F. Birnstock, *J. Mol. Struct.*, **44**, 231 (1978).
8) H. B. Bürgi and J. D. Dunitz, *Helv. Chim. Acta*, **53**, 1747 (1970).
9) K. Ezumi, H. Nakai, S. Sakata, K. Nishikida, M. Shiro, and T. Kubota, *Chem. Lett.*, **1974**, 1393.
10) J. Bernstein and I. Izak, *J. Chem. Soc., Perkin Trans. 2*, **1976**, 429.
11) J. Bernstein, *J. Chem. Soc., Perkin Trans. 2*, **1972**, 946.
12) J. Bernstein and G. M. J. Schmidt, *J. Chem. Soc., Perkin Trans. 2*, **1972**, 951.
13) J. Bernstein, I. Bar, and A. Christensen, *Acta. Crystallogr., Sect. B*, **32**, 1609 (1976).
14) I. Bar and J. Bernstein, *Acta Crystallogr., Sect. B*, **33**, 1738 (1977).
15) J. Bernstein and A. T. Hagler, *J. Am. Chem. Soc.*, **100**, 673 (1978).
16) C. Wiegand and E. Merkel, *Liebigs Ann. Chem.*, **550**, 175 (1942).
17) S. A. Houlden and I. G. Csizmadia, *Tetrahedron*, **25**, 1137 (1969).
18) R. L. Ellis, G. Kuehnlenz, and H. H. Jaffé, *Theor. Chim. Acta*, **26**, 131 (1972).
19) R. Akaba, K. Tokumaru, T. Kobayashi, and C. Utsunomiya, *Bull. Chem. Soc. Jpn.*, **53**, 2002 (1980).

Electronic Structures and Conformations of *N*-Benzylideneanilines. II. Photoelectron Spectral Study

Ryoichi Akaba, Katsumi Tokumaru,* Tsunetoshi Kobayashi,*,† and Chikatoshi Utsunomiya††

Department of Chemistry, The University of Tsukuba, Sakura-mura, Ibaraki 305

† *The Institute of Physical and Chemical Research, Wako, Saitama 351*

†† *The Institute for Solid State Physics, The University of Tokyo, Roppongi, Minato, Tokyo 106*

(Received October 8, 1979)

Electronic structures and molecular conformations have been studied for *N*-benzylideneaniline and its 2-methyl, 2,6-dimethyl, and their 4-nitro derivatives by photoelectron spectroscopy. The lower energy bands are analyzed in detail, and the twist angles θ_N of the anilino benzene rings (ring A) about the carbon-nitrogen bonds are estimated by examining the effect caused by a methyl substitution. It is concluded that *N*-benzylidene-4-nitroaniline takes a more twisted conformation than *N*-benzylideneaniline.

In a preceding paper,[1] the electronic structures and the molecular conformations of *N*-benzylideneaniline and its derivatives bearing 2-methyl, 2,6-dimethyl, and/or 4-nitro groups on the aromatic nuclei on the nitrogen atoms (ring A) (compounds **1**—**6**) have been investigated by electronic absorption spectroscopy.

Concerning the photoelectron spectra (PES)[2] of *N*-benzylideneanilines, four reports have been published, but there has been some controversy on the PES band assignment and the molecular conformations estimated by this method.[3-6]

As regards to the twist angle θ_N (see the formula shown below) of *N*-benzylideneanilines, Bally *et al.* have recently estimated the twist angle θ_N to be approximately 36° by PES.[5] Gas phase electron diffraction study has determined the twist angle θ_N to be about 52°.[7] The calculations by the PCILO method with geometry optimization,[8] and by the NDDO method[9] have indicated that *N*-benzylideneaniline is twisted in θ_N by 36° and 65°, respectively. Concerning the PES of substituted *N*-benzylideneanilines, Klasinc *et al.* have investigated *N*-benzylideneaniline and some of its derivatives bearing methoxyl and/or nitro groups *etc.* as ring substituents and tried the HMO calculations.[6] They explained the results on the ground that these compounds take twisted conformations but on the assumption that the twist angle θ_N would be the same among the compounds examined. However, this assumption seems not to be adequate as has been described in the preceding paper.[1]

In order to get deeper insight into these problems, PES of *N*-benzylideneanilines **1**—**6** have been investigated. An attempt has been made to assign the PES bands precisely, and to estimate the molecular conformations of these compounds. The present results support our conclusion in the preceding paper that *N*-benzylidene-4-nitroaniline **4** is more twisted than *N*-benzylideneaniline **1**.

Results and Discussion

Photoelectron spectra have been measured for **1**—**6** and their 3′-methyl derivatives **7**—**12**; the latters are employed to assist the band assignments of the formers. Figures 1 and 2 show the PES of **1**—**6**. Table 1 summarizes the vertical ionization energies, E_{iv}, of **1**—**12**

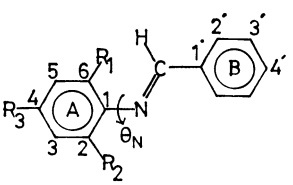

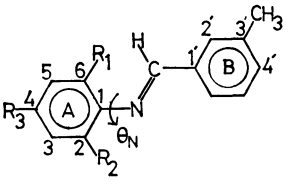

1: $R_1=R_2=R_3=H$
2: $R_1=H$, $R_2=CH_3$, $R_3=H$
3: $R_1=R_2=CH_3$, $R_3=H$
4: $R_1=R_2=H$, $R_3=NO_2$
5: $R_1=H$, $R_2=CH_3$, $R_3=NO_2$
6: $R_1=R_2=CH_3$, $R_3=NO_2$
7: $R_1=R_2=R_3=H$
8: $R_1=H$, $R_2=CH_3$, $R_3=H$
9: $R_1=R_2=CH_3$, $R_3=H$
10: $R_1=R_2=H$, $R_3=NO_2$
11: $R_1=H$, $R_2=CH_3$, $R_3=NO_2$
12: $R_1=R_2=CH_3$, $R_3=NO_2$

together with those of some related compounds for the sake of comparison.

In the present work, in order to assign the PES bands precisely and to estimate the twist angles, θ_N, the effect of methyl substitution on the ionization energy has been extensively employed, which has been successfully applied to analyze the PES of styrenes,[10] for example.

Band Assignments. As shown in Fig. 1 and Table 1, *N*-benzylideneaniline **1** shows three groups of bands in the range of 8—10.5 eV. In this region, *trans*-stilbene has five π-bands.[11]

The first band of **1** has previously been assigned to the π-orbital corresponding to the highest occupied π-orbital of *trans*-stilbene delocalized over the entire molecular framework.[4] The first bands of the other *N*-benzylideneanilines studied can be reasonably correlated with the first band of **1**.

Compounds **1**, **2**, and **3** exhibit bands at nearly the same ionization energies, E_{iv}, 9.47 (shoulder), 9.49 (shoulder), and 9.47 eV, respectively, irrespective of 2-methyl, and 2,6-dimethyl substitution on the ring A. This fact suggests that these bands do not correspond to the π-orbital localized on the ring A. On the other hand, on 3′-methyl substitution on the benzylidene benzene ring (ring B), these bands are sensitively shifted to the low energy side by 0.34, 0.36, and 0.48 eV, respectively, as shown in Table 1. Accordingly, it is reasonable to correlate these bands with the 9.38 eV π-orbital band of *N*-benzylidenemethylamine.[5] Likewise, the 9.51 eV band of **4** and one of the 9.50 eV

TABLE 1. VERTICAL IONIZATION ENERGIES, E_{iv}, OF *N*-BENZYLIDENEANILINES **1**—**12** AND RELATED COMPOUNDS

Compound	E_{iv}/eV					
	Band 1	2	3	4	5	6
N-Benzylideneaniline **1**	8.25	9.17	9.47[sh]	9.97	11.3	
N-Benzylidene-2-methylaniline **2**	8.06	8.80[sh]	9.04	9.49[sh]	9.88	11.0[3]
N-Benzylidene-2,6-dimethylaniline **3**	8.00	8.54	8.94	9.47	9.86	10.9[6]
N-Benzylidene-4-nitroaniline **4**	8.76	9.51	9.73	10.48	10.71	11.6[3]
N-Benzylidene-2-methyl-4-nitroaniline **5**	8.66	9.50	9.78[sh]	10.61	11.6[0]	
N-Benzylidene-2,6-dimethyl-4-nitroaniline **6**	8.51	9.23	9.74	10.50	11.2[8]	
N-(3-Methylbenzylidene)aniline **7**	8.07	8.92[sh]	9.13	9.90	11.1[5]	
N-(3-Methylbenzylidene)-2-methylaniline **8**	8.00	8.74	9.13[sh]	9.78	10.94	
N-(3-Methylbenzylidene)-2,6-dimethylaniline **9**	7.90	8.47[sh]	8.73	8.99	9.80	10.73
N-(3-Methylbenzylidene)-4-nitroaniline **10**	8.58	9.14	9.72	10.67		
N-(3-Methylbenzylidene)-2-methyl-4-nitroaniline **11**	(8.49) [a]	(9.14[sh])	(10.43)	(11.6)		
N-(3-Methylbenzylidene)-2,6-dimethyl-4-nitroaniline **12**	8.43	8.98[sh]	9.44[sh]	10.21	10.55	11.2[0]
trans-Stilbene[b]	7.87	9.08	9.50	10.51	11.3	
trans-Azobenzene[c]	8.46	8.77	9.30	9.77	11.6	
Benzene[d]	9.23	11.67	12.32	13.97		
Nitrobenzene[d]	9.88	10.29	10.97	11.15	12.56	
m-Xylene[d]	8.71	9.03	11.24			
N-Benzylidenemethylamine[e]	8.77	9.38	10.87	11.71		

a) No well-resolved spectrum was observed. b) Ref. 11. c) Ref. 4. d) Ref. 13. e) Ref. 5.

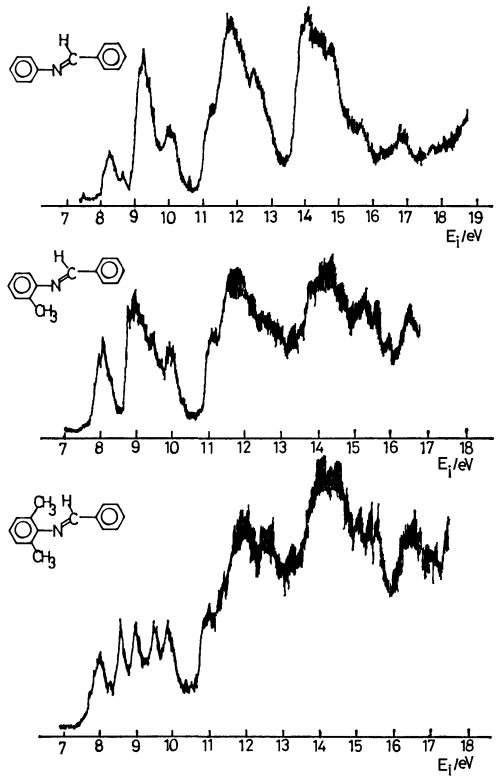

Fig. 1. Photoelectron spectra of **1**—**3**.

bands of **5** can be correlated with the same type of π-orbital since these bands are not sensitive to 2-methyl substitution on the ring A but sensitive to 3'-methyl substitution on the ring B (ΔE_{iv}=0.37 and 0.36 eV in going from **4** to **10** and **5** to **11**, respectively).

In the nitro derivative **4**, one can expect that π-orbitals mainly localized on the ring B should be lower in ionization energy than those on the ring A since the nitro group should increase the ionization energies of orbitals mainly localized on the ring A. This consideration suggests that one of the doubly degenerate 9.73 eV bands of **4** is correlated with the first π-band of nitrobenzene at 9.93 eV.[12,13]

The second band of **3** at 8.54 eV is insensitive to 3'-methyl substitution on the ring B (ΔE_{iv}=0.07 eV in going from **3** to **9**), and is closely located to the 8.71 eV $a_2\pi$ band of *m*-xylene.[12,13] So, it may be reasonably assigned to the π-orbital corresponding to the first $a_2\pi$ band of *m*-xylene. The ionization energy of the first $a_2\pi$ band of *m*-xylene is smaller than that of the $e_{1g}\pi$ band of benzene by 0.52 eV due to the destabilization of the $a_2\pi$ type orbital of the benzene ring by meta-dimethylation. Therefore, the bands corresponding to the 8.54 eV band of **3** are expected to appear around 9.06 eV for **1** and 8.80 eV for **2**. Thus, one of the degenerate 9.17 eV bands of **1** and the 8.80 eV band of **2** may safely be correlated with the 8.54 eV band of **3**. This assignment is supported by the fact that the 8.80 eV band of **2** is not sensitive to 3'-methyl substitution (ΔE_{iv}=0.06 eV in going from

2 to **8**). Similarly, one of the degenerate 9.50 eV bands of **5** and the 9.23 eV band of **6** can be correlated with the 9.73 eV band of **4** corresponding to the first π-band of nitrobenzene.

Assignment of the N-lone pair orbital is now considered by inspecting the well-resolved PES of **3**. As mentioned before, its 8.54 and 9.47 eV bands correspond to the π-orbitals mainly localized on the ring A and the ring B, respectively. The CNDO/S[14] calculations suggest that its 8.94 eV band corresponds to the 8.77 eV π-band of *N*-benzylidenemethylamine and the 9.86 eV band corresponds to the N-lone pair orbital, and, in fact, the 9.86 eV band is not so sensitive to 3'-methyl substitution (ΔE_{1v}=0.06 eV in going from **3** to **9**) as the 8.94 eV band (ΔE_{1v}=0.21 eV in going from **3** to **9**). However, as shown in the preceding paper,[1] *N*-benzylideneanilines examined take, more or less, twisted conformations so that the N-lone pair orbital will interact with π-orbitals to some extent. Therefore, it is not adequate to assign a specific band to the pure N-lone pair orbital, and the 9.86 eV band of **3** has to be considered as "delocalized" N-lone pair orbital. This interpretation seems in keeping with recent postulation by Klasinc *et al.*[6]

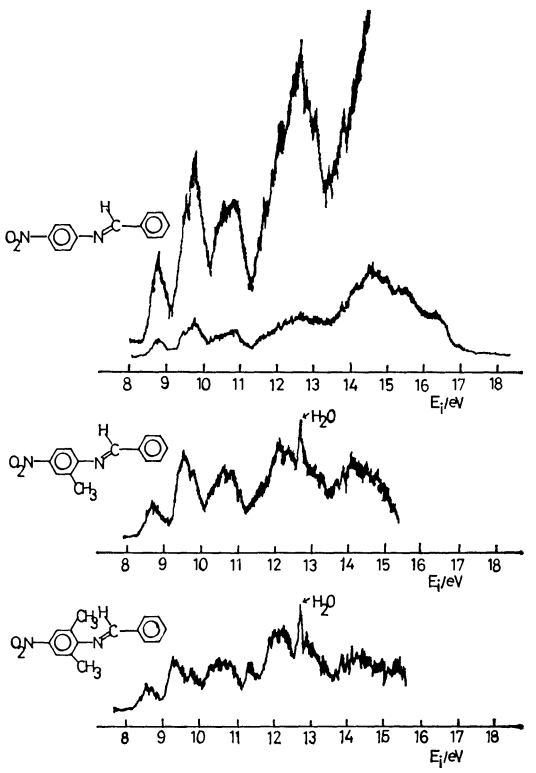

Fig. 2. Photoelectron spectra of **4**—**6**.

The above considerations have enabled us to draw the band correlation diagram as shown in Fig. 3.

Estimation of the Twist Angles, θ_N. We now wish to report an approach to estimate the twist angles θ_N in *N*-benzylideneanilines and present the evidence that the twist angle θ_N is significantly changed by the introduction of 4-nitro group on the ring A.

In the present method, one considers the first band energy difference ΔE_{1v} between **1** and **2** and that between the corresponding 4-nitro derivatives **4** and **5** as the perturbation caused by the substitution of a methyl group for 2-hydrogen on the ring A. Then, the ΔE_{1v} is calculated with changing the twist angle θ_N to find out a value which coincides with the observed ΔE_{1v} value. In the calcualtions, the ΔE_{1v} is estimated by the following equation derived on the basis of the first order perturbation treatment,[15]

$$\Delta E_{1v} = 0.0528 + 1.0110 a_J$$

$$a_J = \sum_{\xi} (3C_{J\xi}^2 + C_{J\tau}^2 + C_{J\tau'}^2)/3,$$

where ξ denotes the position of the methyl substitution and τ and τ' denote the ortho-positions to that

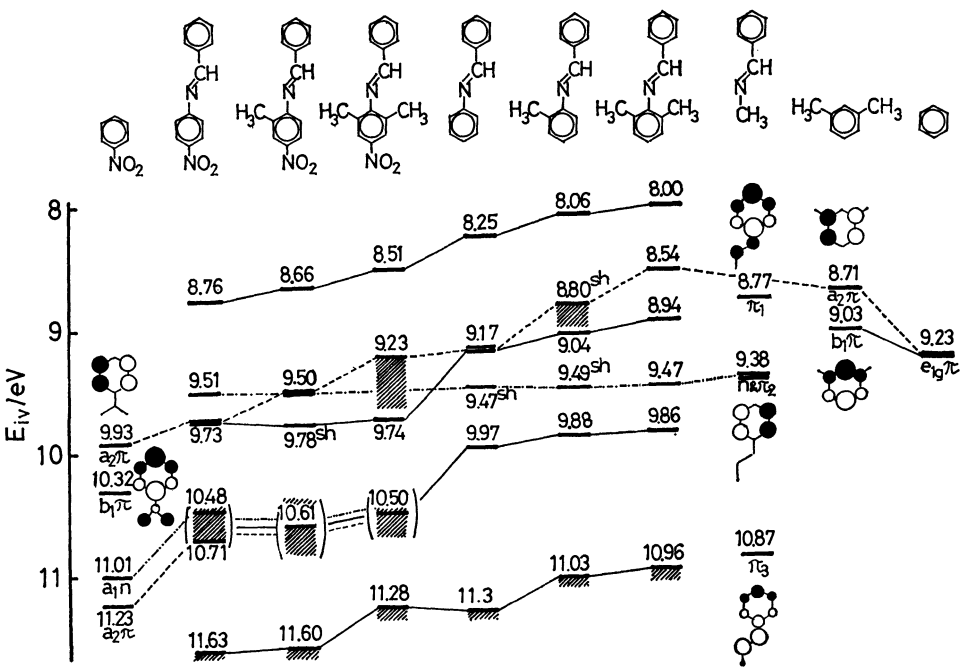

Fig. 3. The observed band correlation diagram for **1**—**6**.

of the methyl substitution. C_{JK} is the coefficient of the K-th AO in the J-th MO. C_{JK}'s were calculated for **1** and **4** by the CNDO/S[14] method at various twist angles θ_N. Then, the corresponding ΔE_{iv} values were calculated by the above equation and plotted in Fig. 4 against θ_N.

As is evident in Fig. 4, the calculated ΔE_{iv}'s become closer to the observed one in the range of smaller twist angle θ_N for **1** and of larger twist angle θ_N for **4**. Estimation of the twist angle θ_N by using the van der Waals radius of a hydrogen atom indicates that the twist angle θ_N for **1** is larger than 48°. Therefore, on taking into account of the probable error (0.02[6] eV **) accompanying the PES measurements and the calculations of ΔE_{iv}, the twist angle θ_N for **1** is estimated to be $48° \lesssim \theta_N \lesssim 55°$. The present result accords with that recently determined by the gas phase electron diffraction (ED) method, 52°.[7]

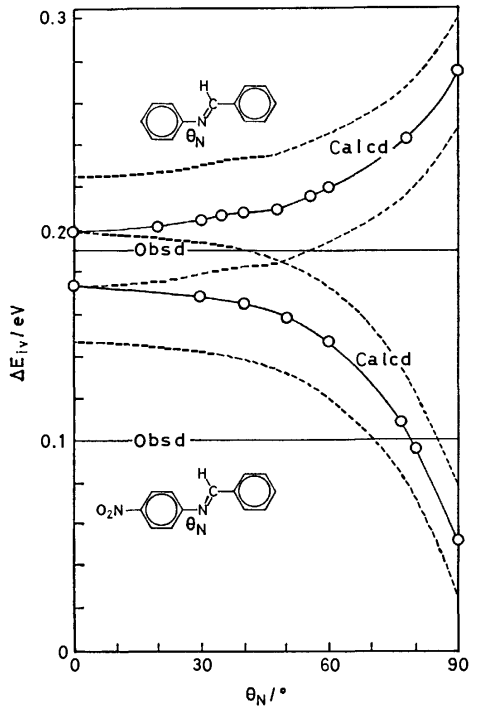

Fig. 4. Variations of the calculated ΔE_{iv} as a function of θ_N.
The broken lines indicate probable error.

Similarly, the twist angle θ_N for **4** can be estimated to be $70° \lesssim \theta_N \lesssim 85°$. These results, to our knowledge, for the first time by PES, indicate that **4** takes a more twisted conformation than **1**. The significant increase in the twist angle θ_N caused by the introduction of 4-nitro group on the ring A can be rationalized in terms of enhancement of conjugation between the N-lone pair and the aromatic π-system due to the strong electron-withdrawing property of the nitro group.

In the case of **1**, the present result on the twist angle θ_N is in qualitative agreement with that given by Bally *et al.*[5] Concerning the first band of **1**, 2-methyl substitution on the ring A shifts the band to lower energy side by 0.19 eV; however, additional 6-methyl substitution (from **2** to **3**) further causes the shift to lower energy side but by only 0.06 eV. Thus, in the series of **1**—**3**, the methyl substituent effect is not additive. The band shape of **1** in the range of 7.8—10.5 eV is very similar to that of **2**. However, it is drastically changed by the introduction of 2,6-dimethyl groups (see Fig. 1). These facts suggest that the twist angle θ_N is significantly increased by the introduction of the two methyl groups because of their steric effect. The twist angle θ_N for **3** can thus be estimated to be $\gtrsim 77°$ by taking into account of the van der Waals repulsion between the imidoyl hydrogen atom and the 2-methyl group of the ring A.

On the other hand, the introduction of 4-nitro group on the ring A increases the ionization energy by 0.51 eV and the successive methyl substitutions (in going from **4** to **5**, and to **6**) decrease the ionization energy by 0.10 and 0.15 eV in each step. In this case, the methyl substituent effect appears to be roughly additive. This fact suggests that the twist angle θ_N is not changed drastically even by the 2,6-dimethyl substitution of **4**. These results are consistent with our results by electronic absorption spectroscopy.[1]

Table 2. Comparison of the twist angle, θ_N

Compound	Method (state)					
	PES (gas)	ED (gas)	UV[a] (solution)	XD (solid)	MO	v.d.W.[b]
N-Bezylideneaniline **1**	(48)[b] −55° 36°[c]	52°[d]	30—35°	55.2°[e]	36°[f] 65°[g]	≳48°
N-Benzylidene-2-methylaniline **2**	(48)[b] −55°		40—45°			≳48°
N-Benzylidene-2,6-dimethyl-aniline **3**	≳(77°)[b]		70—80°			≳77°
N-Benzylidene-4-nitroaniline **4**	70—85°		not far from 90°	50.2°[e,h]		≳48°
N-Benzylidene-2-methyl-4-nitroaniline **5**	70—85°					≳48°
N-Benzylidene-2,6-dimethyl-4-nitroaniline **6**	≳(77°)[b]					≳77°

a) Ref. 1. b) Estimated using the van der Waals radii for a methyl group and a hydrogen atom. c) Ref. 5. d) Ref. 7. e) Ref. 16. f) The PCILO method, Ref. 8. g) The NDDO method, Ref. 9. h) Value observed for *N*-(4-methylbenzylidene)-4-nitroaniline.

** The probable error was calculated by using the data in Table 3 of Ref. 15.

In Table 2 are summarized the twist angles θ_N for **1**—**6** estimated by various methods. It seems to be of interest, that at least in solutions and in the gas phase, the electronic effect of a nitro group as well as the steric effect by bulky 2,6-dimethyl groups may result in considerable twisting of the ring A from the azomethine skeletal plane. It is worth pointing out that in this class of compounds their molecular conformations may be sensitively changed by the electronic effect of a substituent introduced in the aromatic ring on the nitrogen atom.

Experimental

Materials. *N*-benzylideneanilines **1**—**6** were prepared as described in the preceding paper,[1] and other *N*-benzylideneanilines employed were similarly prepared. The new compounds **8**, bp 142—143 °C/7 mmHg, **9**, bp 152—153 °C/2 mmHg, **10**, mp 72—73 °C, **11**, mp 101—102 °C, and **12**, mp 104—105.5 °C, gave the satisfactory results of elemental analyses.

Spectral Measurements. Photoelectron spectra were recorded on the instrument reported previously using the He I resonance line (21.22 eV) as the excitation source, and were calibrated using Xe as an internal standard.[10] The sample inlet and target chamber system was heated up to *ca.* 110—140 °C to obtain sufficient vapor pressure.

Theoretical Calculations

The CNDO/S calculations were carried out with a FACOM 230-75 computer at the Institute of Physical and Chemical Research. The geometrical structures were properly assumed on the basis of appropriate data given in Ref. 16 just as in Ref. 1.

References

1) R. Akaba, K. Tokumaru, and T. Kobayashi, *Bull. Chem. Soc. Jpn.*, **53**, 1993 (1980).
2) D. W. Turner, C. Baker, A. D. Baker, and C. R. Brundle, "Molecular Photoelectron Spectroscopy," John Wiley, London (1970).
3) H. Goetz, F. Marschner, and H. Juds, *Tetrahedron*, **30**, 1133 (1974).
4) T. Kobayashi, K. Yokota, and S. Nagakura, *J. Electron Spectrosc. Relat. Phenom.*, **6**, 167 (1975).
5) T. Bally, E. Haselbach, S. Lanyiova, F. Marschner, and M. Rossi, *Helv. Chim. Acta*, **59**, 486 (1976).
6) L. Klasinc, B. Ruščić, G. Heinrich, and H. Güsten, *Z. Naturforsch., Teil B*, **32**, 1291 (1978).
7) M. Traetteberg, I. Hilmo, R. J. Abraham, and S. Ljunggren, *J. Mol. Struct.*, **48**, 395 (1978).
8) P. Jacque and J. Faure, *Theor. Chim. Acta*, **46**, 307 (1977).
9) H. J. Hofmann and F. Birnstock, *J. Mol. Struct.*, **44**, 231 (1978).
10) T. Kobayashi, K. Yokota, and S. Nagakura, *J. Electron Spectrosc. Relat. Phenom.*, **2**, 449 (1973).
11) T. Kobayashi, K. Yokota, and S. Nagakura, *Bull. Chem. Soc. Jpn.*, **48**, 412 (1975).
12) T. Kobayashi and S. Nagakura, *Chem. Lett.*, **1972**, 903.
13) T. Kobayashi and S. Nagakura, *Bull. Chem. Soc. Jpn.*, **47**, 2563 (1974).
14) R. L. Ellis, G. Kuehnlentz, and H. H. Jaffé, *Theor. Chim. Acta*, **26**, 131 (1972).
15) E. Heilbronner, V. Hornung, F. H. Pinkerton, and S. F. Thames, *Helv. Chim. Acta*, **55**, 289 (1972).
16) H. B. Bürgi and J. D. Dunitz, *Helv. Chim. Acta*, **53**, 1747 (1970).

The Preparation of 3-Phenyl[1,2,4]triazolo[4,3-*a*]pyridines and Their Benzologs from *N*-(Phenylsulfonyl)benzohydrazonoyl Chloride and Pyridines[1)]

Suketaka Ito,* Akikazu Kakehi, Toshiyuki Matsuno, and Jun-ichi Yoshida
Department of Industrial Chemistry, Faculty of Engineering, Shinshu University, Wakasato, Nagano 380

(Received September 5, 1979)

3-Phenyl[1,2,4]triazolo[4,3-*a*]pyridines were obtained in good yields from *N'*-[α-(1-pyridinio)benzylidene]-benzenesulfonohydrazidates, generated from 2-unsubstituted pyridines and *N*-(phenylsulfonyl)benzohydrazonoyl chloride (**2**), by oxidation with chloranil. The reaction of quinoline and isoquinoline with **2** gave 1-phenyl-3-phenylsulfonyl-3,3a-dihydro[1,2,4]triazolo[4,3-*a*]quinoline and 3-phenyl-1-phenylsulfonyl-1,10b-dihydro[1,2,4]-triazolo[3,4-*a*]isoquinoline respectively, both in good yields; they aromatized to the corresponding triazoles by the 1,2-elimination of benzenesulfinic acid on heating.

[1,2,4]Triazolo[4,3-*a*]pyridines, -quinolines, and [1,2,4]triazolo[3,4-*a*]isoquinolines[2)] are generally prepared by the ring closure of 2-hydrazinopyridines, -quinolines, or 1-hydrazinoisoquinolines with acidic-type cyclodehydration agents.[3)] A variation of this method involving the oxidative cyclization of 2-pyridylhydrazones and their homologs is also available.[4)]

In the present paper, we wish to describe an alternative route for preparing the title triazolopyridines (**4**) *via* the oxidative cyclization of *N'*-[α-(1-pyridinio)-benzylidene]benzenesulfonohydrazidates (**3**), obtained from *N*-(phenylsulfonyl)benzohydrazonoyl chloride (**2**) and pyridines (**1**), and also a simple method for obtaining [1,2,4]triazoloquinoline (**8a**) and -isoquinoline (**8b**) from quinoline (**5a**) and isoquinoline (**5b**) by the reaction with **2** *via* dihydrotriazoloquinoline (**7a**) and -isoquinoline (**7b**) respectively as the intermediates. A specific feature of **2** lies in the electrophilicity of the imidoyl carbon and the acidity of the amino proton (and hence the stability of the resulting anion), which are enhanced by the phenylsulfonyl group. The sulfonyl group serves not only as the activating group in **2**, but also as the leaving group in a cationic or an anionic mode in the elimination step, leading to the triazoles, **4** and **8**.

Results and Discussion

Reaction of Hydrazonoyl Chloride (2) with Pyridines (1), Quinoline (5a), and Isoquinoline (5b). The reaction of *N*-(2,4-dichlorophenyl)pyruvohydrazonoyl chloride with excess pyridine (**1a**) under refluxing gave *N'*-[α-(1-pyridinio)acetonylidene]-2,4-dichlorophenylhydrazidate.[5)] Analogously, *N*-(phenylsulfonyl)benzohydrazonoyl chloride (**2**) reacted with **1a** and alkyl-substituted pyridines (**1b**—**e**) at room temperature to afford the corresponding, bright-yellow colored pyridinium betaines, *N'*-[α-(1-pyridinio)benzylidene]benzenesulfonohydrazidates (**3**). However, the reaction of **2** with quinoline (**5a**) and isoquinoline (**5b**) yielded 1-phenyl-3-phenylsulfonyl-3,3a-dihydro[1,2,4]triazolo-[4,3-*a*]quinoline (**7a**) and 3-phenyl-1-phenylsulfonyl-1,10b-dihydro[1,2,4]triazolo[3,4-*a*]isoquinoline (**7b**) respectively, both in good yields (Scheme 1, Table 1).

In the reaction of **1** with **2**, the use of a solvent such as dichloromethane and THF resulted in the formation of 3,6-diphenyl-1,4-bis(phenylsulfonyl)-1,4-dihydro-1,2,4,5-tetrazine as a by-product; such a by-product may be formed *via* the mutual nucleophilic process

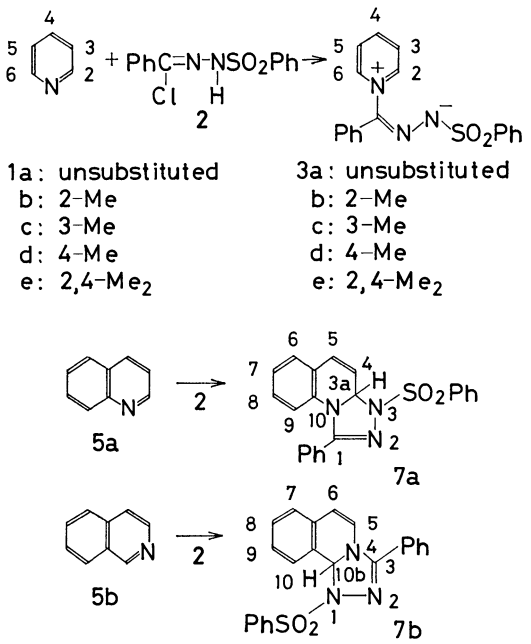

Scheme 1.

of **3** generated: compounds **3a**—**e** changed into the dihydrotetrazine when dissolved in such solvents.

The IR and NMR spectral data for these compounds are summarized in Table 2. The sulfonyl absorptions near 1275 and near 1135 cm^{-1} in the IR spectra were diagnostic for the characterization of **3a**—**e** and were consistent with those observed at lower frequencies (1270—1285 and 1130—1140 cm^{-1}) with *N*-(1-pyridinio)benzenesulfonamidates.[6,7)] Furthermore, a gross similarity can be seen in the NMR patterns of the pyridine ring between **3a**—**e** and the *N*-(1-pyridinio)-benzenesulfonamidates. The normal sulfonyl-absorption frequencies and the chemical shifts at δ 5.90—6.61 ppm with compounds **7a**, **b** support the cyclized structures.

The mass spectra of **3** (ionizing energy: 75 eV) did not exhibit the M^+ ions: the main fragment ions with the betaine **3a**, for example, are *m/e* 250 (15%), 141 (10%, $PhSO_2^+$), 125 (21%, $PhSO^+$), 105 (23%, $PhC{\equiv}O^+$), 79 (100%, $C_5H_5N^{+\cdot}$), 77 (35%, Ph^+), 52 (60%, $[C_5H_5N\text{–}HCN]^{+\cdot}$), and 51 (34%, $[Ph\text{–}C_2H_2]^+$). The signal at *m/e* 250 is compatible with the $[PhSO_2\text{-}SPh]^{+\cdot}$ ion, probably arising from thermal processes.[8)] The occurrence of the $PhC{\equiv}O^+$ ion can be explained as is illustrated below:

Table 1. Pyridinium betaines, dihydrotriazoloquinoline, and -isoquinoline

Compound	Yield/%[a)]	Mp/°C	Formula	Calcd (%)			Found (%)		
				C	H	N	C	H	N
3a	89	153—155 (dec)	$C_{18}H_{15}N_3O_2S$	64.08	4.48	12.45	63.87	4.45	12.57
3b	58	116—120	$C_{19}H_{17}N_3O_2S$	64.94	4.88	11.96	64.45	5.01	11.76
3c	83	150—153 (dec)	$C_{19}H_{17}N_3O_2S$	64.94	4.88	11.96	64.81	4.86	11.87
3d	82	153—156 (dec)	$C_{19}H_{17}N_3O_2S$	64.94	4.88	11.96	65.12	4.92	11.85
3e	26	107—109	$C_{20}H_{19}N_3O_2S$	65.73	5.24	11.50	65.33	5.29	11.16
7a	91	114—116 (dec)	$C_{22}H_{17}N_3O_2S$	68.20	4.42	10.85	68.05	4.40	10.84
7b	96	128—130 (dec)	$C_{22}H_{17}N_3O_2S$	68.20	4.42	10.85	68.00	4.47	10.79

a) Yield (isolated) as mole per cent based on **2**.

Table 2. Spectral data of compounds **3** and **7**

Compound	IR (νSO_2, cm^{-1}, KBr)	^{1}H-NMR (δ, ppm, $CDCl_3$)
3a	1274 1138	7.07—8.03 (m, 13H; 2 Ph, 3,4,5-H), 8.62 (dd, 2H; J=5 Hz, J=1 Hz; 2,6-H)
3b	1279 1139	2.55 (s, 3H; 2-Me), 6.91—7.99 (m, 13H; 2 Ph, 3,4,5-H), 8.49 (dd, 1 H; J=5 Hz, J=1.5 Hz; 6-H)
3c	1274 1135	2.33 (s, 3H; 3-Me), 7.03—8.00 (m, 12H; 2 Ph, 4,5-H), 8.43 (br s, 2 H; 2,6-H)
3d	1273 1132	2.35 (s, 3H; 4-Me), 7.02—7.99 (m, 12H; 2 Ph, 3,5-H), 8.47 (dd, 2H; J=5 Hz, J=2 Hz; 2,6-H)
3e	1276 1134	2.26 (s, 3H; 4-Me), 2.45 (s, 3H; 2-Me), 6.80—8.07 (m, 12H; 2 Ph, 3,5-H), 8.33 (d, 1H; J=5 Hz; 6-H)
7a	1364 1176	6.07 (s, 1H; 3a-H), 6.12 (d, 1H; J=8.8 Hz; 4-H), 6.61 (d, 1H; J=8.8 Hz; 5-H), 6.76—8.17 (m, 14 H; 2 Ph, 6,7,8,9-H)
7b	1359 1170	5.90 (d, 1H; J=7.5 Hz; 5-H), 6.29 (d, 1H; J=7.5 Hz; 6-H), 6.42 (s, 1H; 10b-H), 6.93—8.17 (m, 14H; 2 Ph, 7,8,9,10-H)

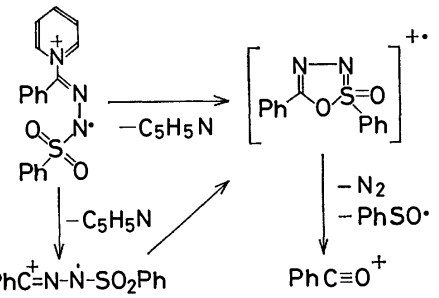

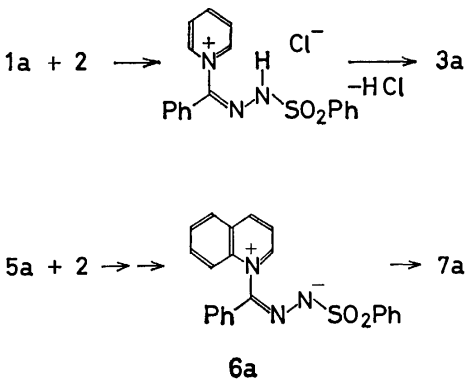

Scheme 2.

As has previously been reported,[9] **2** does not afford *N*-(phenylsulfonyl)benzonitrilimine, a 1,3-dipole, on treatment with triethylamine, but is subjected to nucleophilic attack on the imidoyl carbon by the hydrazonoyl chloride *N*-anion generated from another molecule of **2** *via* deprotonation, which results in the formation of 3,6-diphenyl-1,4-bis(phenylsulfonyl)-1,4-dihydro-1,2,4,5-tetrazine. Thus, the formation of **3** and **7** probably proceeds *via* the step-by-step mechanism given in Scheme 2. Compound **7a** (and **7b**) should be formed by the 1,5-dipolar cyclization of the betaine intermediate.

The behavior in quinoline and isoquinoline systems different from that in the pyridine series can be explained in terms of the mesomeric effect of the fused benzene ring; that is, the electron deficiency attributable to this effect at the α-carbon (2-C of quinoline, and 1-C of isoquinoline skeleton) in the betaine structure (**6a**, **b**) and that at the amino nitrogen (10-N in **7a** and 4-N in **7b**) may contribute to the ready cyclization of **6a**, **b** and the stabilization of **7a**, **b** respectively. On the other hand, the corresponding pyridine derivatives are lacking in such an effect, and so the aromatic stabilization of the pyridine ring is lost when **3** cyclize to dihydrotriazolopyridines. Consequently, the products from **1** prefer the betaine structure.

*Oxidation of Pyridinium Betaines (**3**) and Dihydrotriazoles (**7**) with Chloranil.* When the betaine **3a** was treated with chloranil (2,3,5,6-tetrachloro-*p*-benzoquinone) in benzene or dioxane at room temperature, 3-phenyl[1,2,4]triazolo[4,3-*a*]pyridine (**4a**) was obtained in a comparable yield, together with a small amount of 3,6-diphenyl-1,4-bis(phenylsulfonyl)-1,4-dihydro-1,2,4,5-tetrazine. 2,3-Dichloro-5,6-dicyano-

Table 3. Oxidation of the betaine **3a**

Oxidizing agent	Solvent	Reaction time/h[a]	Yield/%[b] of **4a**[c]
Chloranil	Benzene	3	61
DDQ	Benzene	2	38
Chloranil	Dioxane	2	51
DDQ	Dioxane	1	37
HgO	Dioxane	6	5

a) The progress of reaction was checked by means of TLC. b) Isolated yield. c) Mp 173—175 °C (lit,[3b] mp 173—174 °C).

Table 4. Triazolopyridines, -quinoline, and -isoquinoline obtained by the oxidation of **3** and **7**

Reactant[a]	Reaction time/h	Product (Yield[b]/%)
3b	2	**4b** (0)
3c	2.5	**4c**+**4c**′ (25+2)[c,d]
3d	2	**4d** (39)[e]
3e	2	**4e** (0)
7a	1	**8a** (94)[f]
7b	9	**8b** (35)[g]

a) Oxidizing agent and solvent: chloranil-benzene. The progress of reaction was checked by means of TLC. b) Isolated yield. c) **4c** and **4c**′ were obtained as a mixture; the ratio was determined by means of NMR. d) Recrystallization gave no uncontaminated **4c** or **4c**′, and further purification was not attempted. Mp of the mixture: 156—160 °C (**4c**: lit,[3a] mp 187—188 °C; **4c**′: lit,[3a] mp 115 °C). e) Mp 128—130 °C (lit,[3a] mp 127—128 °C). f) Mp 114—115 °C (lit,[4b] mp 89 °C; lit,[4e] mp 136—137 °C). g) Mp 186—188 °C (lit,[4d] mp 186—187 °C; lit,[4e] 182 °C).

p-benzoquinone (DDQ) or mercury(II) oxide (yellow) also gave **4a** in a diminished yield. The results are summarized in Table 3. 2,3-Dichloro-5,6-dicyano-4-hydroxyphenyl benzenesulfonate generated from DDQ could be isolated. In the case of chloranil, 2,3,5,6-tetrachloro-1,4-phenylene bis(benzenesulfonate) and 2,3,5,6-tetrachlorohydroquinone, disproportionated products of the 2,3,5,6-tetrachloro-4-hydroxyphenyl benzenesulfonate which should be primarily formed, were obtained.

On the same treatment (chloranil–benzene), the betaines **3c**, **d** and the dihydrotriazoles **7a**, **b** afforded the corresponding triazolo compounds, **4c**, **4d**, **8a**, and **8b**, and also **4c**′ which was detected by means of NMR as a minor component in the production of **4c** (Table 4). However, the betaines **4b**, **e** yielded no triazolopyridines; this may be the result of spatial interference between the *C*-phenyl and the α-methyl group of the pyridine ring. UV and NMR spectroscopic studies[10] have revealed the steric interaction between 3-phenyl and 5-methyl group in the 3-phenyl-[1,2,4]triazolo[4,3-*a*]pyridine systems and have led to the conclusion that the 3-phenyl group is coplanar with the bicyclic nucleus in the 5-unsubstituted derivatives, but with a 5-methyl substituent the steric requirement can only be satisfied by the phenyl group adopting a conformation skew to the nucleus. Thus, in the betaines **3b**, **e**, the coplanarity of the *C*-phenyl group with the hydrazidate moiety, if conserved, should prevent the formation of **4b**, **e**.

Table 5. Aromatization of dihydrotriazoloquinoline and -isoquinoline by the elimination of benzenesulfinic acid

Method[a]	Solvent	Refluxing time/h	Yield/% of **8**	
A	CCl_4	3	67	(**8a**)
A	Dioxane	5	82	
B	CCl_4	5	64	
B	Dioxane	5	24	
A	CCl_4	2	68	(**8b**)
A	Dioxane	6	60	
B	CCl_4	8	48	
B	Dioxane	5	10	

a) A: Thermolysis of **7** isolated. B: Direct method from **2** and **5**.

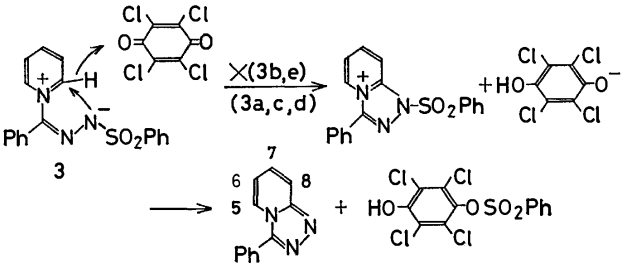

4a: unsubstituted
c: 6-Me
c′: 8-Me
d: 7-Me

Scheme 3.

*Aromatization of Dihydrotriazoloquinoline (**7a**) and -isoquinoline (**7b**) by the Thermally Induced Elimination of Benzenesulfinic Acid.* The dihydrotriazolo compounds **7a**, **b** gave aromatized compounds, **8a**, **b** respectively, in good yields, along with *S*-phenyl benzenethiosulfonate (**9**), when refluxed in dioxane or carbon tetrachloride. Compound **9** is probably generated from benzenesulfinic acid[11] (Scheme 4).

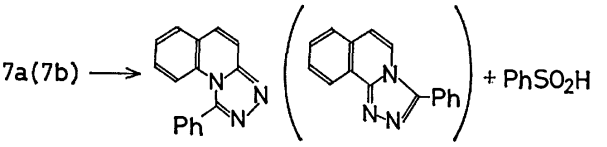

8a 8b

Scheme 4.

A direct method in which **2** was treated with **5** in a boiling solvent also gave **8** in a diminished yield. Table 5 summarizes these results. The good leaving ability of the arenesulfinato group has been revealed in aromatization reactions[12] and other reactions, such as a cyclization reaction,[13] and it is probably the driving force for the present reaction.

Experimental

The melting points were determined with a Yanagimoto micromelting point apparatus, Model MP-S3, and are

uncorrected. The microanalysis was performed on a Perkin-Elmer elemental analyzer, Model, 240. The IR, NMR, and mass spectra were recorded with a Hitachi 260, a Varian EM-360A, and a JEOL JMS-013G-2 spectrometer respectively. *N*-(Phenylsulfonyl)benzohydrazonoyl chloride (**2**) was prepared by the method previously reported.[13a]

Preparation of **3**. *General Procedure*: A ground 2.95-g (10 mmol) portion of **2** was dissolved in pyridine (15 ml) at room temperature with stirring. A few minutes after dissolution, the product was separated by adding water, collected by filtration, and then washed with water, followed by small amounts of dilute ethanol. Further purification was achieved by repeated washings with ethanol. The results are summarized in Table 1.

Reaction of **5** *with* **2**. A solution of **5a** (1.42 g, 11 mmol) in dichloromethane (3 ml) was added, drop by drop, to a solution of **2** (1.47 g, 5 mmol) in dichloromethane (5 ml) at room temperature. The reaction mixture was allowed to stand for 10 min. After the subsequent removal of the solvent *in vacuo*, a small portion of water was added to the oily residue. Crystallization was induced by scratching the flask, and the resulting precipitates were filtered. 1-Phenyl-3-phenylsulfonyl-3,3a-dihydro[1,2,4]triazolo[4,3-*a*]-quinoline (**7a**; 1.87 g; 92%) was obtained in a fairly pure state by washing the precipitates with water and then with small amounts of cold ethanol. A further purified specimen could be prepared by repeated washings with ethanol. 3-Phenyl-1-phenylsulfonyl-1,10b-dihydro[1,2,4]triazolo[3,4-*a*]-isoquinoline (**7b**; 1.84 g; 95%) was also obtained from **5b** and **2** in a similar manner. For the preparation of **7**, the procedure for **3** described above can also be used, but the present method may be more convenient. Table 1 shows the results obtained by the former procedure.

Oxdation of **3** *and* **7**. *(A) With Chloranil or DDQ. General Procedure*: A mixture of 2 mmol of **3** (or **7**) and 2 mmol of chloranil (or DDQ) in a 15-ml portion of a solvent (benzene or dioxane) was stirred at room temperature for the period given in Tables 3 and 4. After the removal of the solvent *in vacuo*, the residue was chromatographed on a silica-gel column (100—200 mesh, 2.0×15 cm). Elution with benzene gave traces of 3,6-diphenyl-1,2,4,5-tetrazine and 3,6-diphenyl-1,4-bis(phenylsulfonyl)-1,4-dihydro-1,2,4,5-tetrazine (mp 151—156 °C(dec), 6—30%).[14] Elution with benzene–ether (19:1, and then 9:1, v/v) gave 2,3,5,6-tetrasubstituted 4-hydroxyphenyl benzenesulfonate (from DDQ) or its disproportionated products (from chloranil),[15] 1,4-phenylene bis(benzenesulfonate), and free hydroquinone (total yield in one run: 13—65%).

2,3-Dichloro-5,6-dicyano-4-hydroxyphenyl Benzenesulfonate. Mp 202—204 °C, IR (KBr, cm^{-1}): 1384, 1186 (νSO_2). Found: C, 45.38; H, 1.65; N, 7.17%. Calcd for $C_{14}H_6Cl_2N_2O_4S$: C, 45.55; H, 1.64; N, 7.59%.

2,3,5,6-Tetrachloro-1,4-phenylene Bis(benzenesulfonate). Mp 237—238 °C, IR (KBr, cm^{-1}): 1385, 1191 (νSO_2). Found: C, 40.88; H, 1.73%. Calcd for $C_{18}H_{10}Cl_4O_6S_2$: C, 40.93; H, 1.91%.

2,3,5,6-Tetrachlorohydroquinone. Mp 228—230 °C (lit,[16] mp 230—231 °C). Found: C, 28.96; H, 0.71%.

Elution with benzene–ethanol (19:1, v/v) gave the corresponding triazolo compound, which was then purified by crystallization from benzene or carbon tetrachloride. The results are summarized in Tables 3 and 4. Each triazolo compound gave satisfactory C, H, and N analyses (±0.4%), and all were found to be spectroscopically identical with authentic specimens.

(B) With Mercury(II) Oxide (Yellow). A mixture of **3a** (1.685 g, 5 mmol), HgO (1.62 g, 7.5 mmol), K_2CO_3 (2 g, 15 mmol), $CaSO_4$ (2 g, 15 mmol), and dioxane (50 ml) was stirred for 6 h at room temperature. The reaction mixture was then filtered and washed with dioxane. The filtrate combined with washings was concentrated and then chromatographed to give **4a** (51 mg, 5%). Table 1 shows the results.

Thermolysis of **7**. A 775-mg (2 mmol) portion of **7a** (or **7b**) was refluxed in a 30-ml portion of a solvent (CCl_4 or dioxane) for a period required. After the removal of the solvent, the reaction mixture was chromatographed (silica gel, benzene–ethanol), giving the corresponding triazoloquinoline, **8a** (or -isoquinoline, **8b**), along with *S*-phenyl benzenethiosulfonate, **9** (mp 42—43 °C, lit,[17] mp 45 °C, yield: 20—25%) (Table 5: Method A).

One-flask Preparation of **8** *from* **2** *and* **5**. A mixture of **2** (590 mg, 2 mmol) and **5a** or **5b** (775 mg, 6 mmol) in a solvent (30 ml) was refluxed. The reaction mixture was extracted with chloroform and washed with dilute hydrochloric acid, followed by water. The subsequent chromatographic treatment of the chloroform extract gave **8a** or **8b** (Table 5: Method B).

The present work was partially supported by a Grant-in-Aid for Scientific Research from the Ministry of Education (Grant No. 355369).

References

1) Presented in part at the 38th National Meeting of the Chemical Society of Japan, Nagoya, October, 1978.

2) These classes of compounds are known to be effective agricultural fungicides and bactericides or valuable pharmaceuticals because of their cardiovascular and antiinflammatory characteristics.

3) a) K. T. Potts and H. R. Burton, *J. Org. Chem.*, **31**, 251 (1966), and the references cited therein. b) S. Takase and T. Demura, *Kogyo Kagaku Zasshi*, **69**, 1417 (1966); c) J. R. Geigy, Neth. Patent 6614979; *Chem. Abstr.*, **68**, 69003z (1968); d) H. K. Reimlinger and J. M. Vandewalle, Fr. Patent 1573135; *Chem. Abstr.*, **72**, 100714r (1970); e) S. Yurugi, A. Miyake, and T. Fushimi, *Yakugaku Zasshi*, **93**, 642 (1973); f) E. Braye, F. Eloy, C. Hoogzand, and R. Lenaers, *Eur. J. Med. Chem.-chim. Ther.*, **9**, 197 (1974); *Chem. Abstr.*, **81**, 91434f (1974); g) H. D. Tam, J. Igolen, J. P. Marquet, E. Bisagni, and J. M. Lhoste, *J. Org. Chem.*, **41**, 3124 (1976); h) B. A. Dreikorn and K. E. Kramer, Ger. Patent 2239892, *Chem. Abstr.*, **78**, 136304v (1973); Fr. Patent (applied for) 2149467, *Chem. Abstr.*, **79**, 78814u (1973); Fr. Patent (applied for) 2135295, *Chem. Abstr.*, **79**, 96989j (1973); U. S. Patent 3953457, *Chem. Abstr.*, **85**, 29564c (1976).

4) a) J. D. Bower and F. P. Doyle, *J. Chem. Soc.*, **1957**, 727. b) G. A. Reynolds and J. A. van Allan, *J. Org. Chem.*, **24**, 1478 (1959). c) S. Naqui and V. R. Srinivasan, *J. Sci. Ind. Res.*, **B21**, 456 (1962); *Chem. Abstr.*, **58**, 2448b (1963). d) M. S. Gibson, *Tetrahedron*, **19**, 1587 (1963). e) S. Naqui and V. R. Srinivasan, *Indian J. Chem.*, **3**, 162 (1965).

5) a) C. Bülow and F. Seidel, *Ber.*, **57B**, 629 (1924). b) P. W. Neber and H. Wörner, *Ann.*, **526**, 173 (1936).

6) R. A. Abramovitch and T. Takaya, *J. Org. Chem.*, **37**, 2022 (1972).

7) This type of bathochromic shift has also been observed with respect to the carbonyl absorptions of various *N*-(1-pyridinio)carboxamidates: T. Okamoto, M. Hirobe, and A. Ohsawa, *Chem. Pharm. Bull.*, **14**, 518 (1966); T, Sasaki, K. Kanematsu, A. Kakehi, I. Ichikawa, and K. Hayakawa, *J. Org. Chem.*, **35**, 426 (1970); A. Balasubramanian, *J. M.* McIntosh, and V. Snieckus, *J. Org. Chem.*, **35**, 433 (1970);

A. Kakehi, S. Ito, Y. Kon-no, and T. Maeda, *Bull. Chem. Soc. Jpn.*, **51**, 251 (1978).

8) For example, the $[ArSO_2SAr]^{+\cdot}$ ion has been observed in the mass spectrums of 1-(*p*-tolylsulfonylmethyl)pyridinium salt[12a] and 3,6-diphenyl-1,4(and 1,2)-bis(phenylsulfonyl)-1,4-(and 1,2)-dihydro-1,2,4,5-tetrazine.[12b]

9) S. Ito, Y. Tanaka, A. Kakehi, and H. Miyazawa, *Bull. Chem. Soc. Jpn.*, **50**, 2969 (1977).

10) K. T. Potts, H. R. Burton, T. H. Crawford, and S. W. Thomas, *J. Org. Chem.*, **31**, 3522 (1966).

11) J. L. Kice and K. W. Bowers, *J. Am. Chem. Soc.*, **84**, 605 (1962).

12) a) R. A. Abramovitch and V. Alexanian, *J. Org. Chem.*, **41**, 2144 (1976); b) S. Ito, A. Kakehi, Y. Tanaka, K. Yoshida, and T. Matsuno, *Bull. Chem. Soc. Jpn.*, **52**, 483 (1979).

13) a) S. Ito, Y. Tanaka, and A. Kakehi, *Bull. Chem. Soc. Jpn.*, **49**, 762 (1976); b) S. Ito, Y. Tanaka, A. Kakehi, and K. Kondo, *Bull. Chem. Soc. Jpn.*, **49**, 1920 (1976).

14) In general, the yield of dihydrotetrazine was low when the triazolo compound was formed in a high yield.

15) Chromatographic treatment and recrystallization induced the disproportionation: no undisproportionated compound could be isolated in a pure state from the chloranil–oxidation reaction.

16) J. B. Conant and L. F. Fieser, *J. Am. Chem. Soc.*, **45**, 2194 (1923).

17) E. Knoevenagel and A. Römer, *Ber.*, **56B**, 215 (1923).

The Asymmetric Homogeneous Hydrogenation of Olefins with the Rhodium Complexes of (1*S*,2*S*)-1,2-Bis(diphenylphosphinamino)cyclohexane and (2*S*,3*S*)-2,3-Bis(diphenylphosphinamino)butane

Ken-ichi Onuma,* Tomiyasu Ito, and Asao Nakamura

Central Research Laboratories, Ajinomoto Co., Inc., 1-1 Suzuki-cho, Kawasaki 210

(Received September 22, 1979)

The effect of triethylamine on asymmetric hydrogenation has been studied using the cationic rhodium complex of (1*S*,2*S*)-1,2-bis(diphenylphosphinamino)cyclohexane or (2*S*,3*S*)-2,3-bis(diphenylphosphinamino)butane as a catalyst. By the addition of triethylamine, higher optical yields are achieved in the hydrogenation of (*Z*)-α-acetamidocinnamic acid and itaconic acid and higher conversion rates are obtained in the hydrogenation of (*E*)-2-methylcinnamic acid, mesaconic acid, and citraconic acid. The specific effect of triethylamine on the substrates with a carboxyl group may be explained by the ionization of the carboxyl group, which coordinates the catalytic rhodium complex firmly.

In recent years, the asymmetric hydrogenation of olefins has been successfully carried out with chiral phosphine–rhodium complexes.[1] It has been often observed that the addition of triethylamine improves the reactivity or the stereoselectivity of the asymmetric hydrogenation of olefins,[2] for which several explanations have been attempted. We would like to describe here the effect of triethylamine on the asymmetric hydrogenation of olefins with the rhodium complexes of (1*S*,2*S*)-1,2-bis(diphenylphosphinamino)cyclohexane, [(*S*,*S*)-I][3] and (2*S*,3*S*)-2,3-bis(diphenylphosphinamino)-butane, [(*S*,*S*)-II].[3b] The six olefins listed in Table 1 are adopted as the substrates. As the substrates have different substituents on the olefinic group, the effects of triethylamine on the hydrogenation of these compounds have been interpreted in terms of the structures of the substituents.

Results and Discussion

Either (*S*,*S*)-I or (*S*,*S*)-II was used as a chiral bisphosphine ligand in the catalytic precursor, [Rh(1,5-cyclooctadiene)(bisphosphine)]$^+ClO_4^-$.[4] The six olefins were hydrogenated with each of the rhodium complexes as shown below (Scheme 1). The product

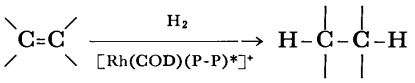

Scheme 1.

was then isolated carefully, and the optical purity was determined. The results are shown in Table 1, together with some results obtained from a neutral *in situ* catalyst. As can be seen there, the cationic catalyst gave better results in both reactivity and stereoselectivity than the neutral catalyst. Therefore, the hydrogenation has been studied with the cationic catalyst.

Effect of Triethylamine. In the absence of triethylamine, (*Z*)-α-acetamidocinnamic acid (III) and itaconic acid (V) were hydrogenated quantitatively. *N*-(1-Phenyl-1-propenyl)acetamide (VIII) was hydrogenated with a conversion of 50%. The other substrates were hydrogenated with lower conversions. Therefore, as for the substituent on the ethylenic bond in the substrate, the acetamido and carboxymethyl groups are considered to play an important role in the hydrogenation. Recent studies[9] on the substrate structures show that an efficient asymmetric hydrogenation depends on the ability of the substrate to form a bidentate complex in the transition state and that the β-carbonyl group in the substituent of an olefin, –C=C–X–C(=O)– (X=NH, CH_2, O), is favorable for the chelate formation. The high conversion rate and optical yield for the hydrogenation of III and V support the importance of the presence of the β-carbonyl group.

The effect of the addition of triethylamine varies, depending on the substrate structures, as follows:

For the substrate with free carboxyl, but no β-carbonyl group of an olefin, *e.g.*, (*E*)-2-methylcinnamic acid (IV), mesaconic acid (VI), and citraconic acid (VII), the conversion rate increases upon the addition of triethylamine, to a particularly remarkable extent in VII. However, the optical yield is low in the presence of triethylamine. The optical yields could not be measured in the absence of triethylamine because of the low conversion rate. Therefore, the effect of triethylamine on the optical yield could not be examined.

For a substrate with both free carboxyl and β-carbonyl groups, *e.g.*, III and V, the hydrogenation proceeds quantitatively irrespective of the presence of triethylamine. As far as the optical yield is concerned, the addition of triethylamine seems to have some favorable effect.

For the substrate with no free carboxyl but with a β-carbonyl group, VIII, the conversion rate rather decreases and the optical yield is not affected.

As has been mentioned above, the addition of triethylamine affects the conversion or the optical yield only in the hydrogenation of a substrate with a free carboxyl group. This implies that triethylamine may interact with the carboxyl group to ionize it and that the substrate may coordinate the catalytic rhodium complex more firmly.

On the addition of triethylamine, the optical yield increases in the hydrogenation of III and V. In the hydrogenation of IV, VI, and VII, however, the optical yield is low even if triethylamine is added. In the former cases, triethylamine is considered to make a chelating substrate–rhodium complex more rigid. In

TABLE 1. ASYMMETRIC HYDROGENATIONS[a] OF OLEFINS WITH CHIRAL AMINOPHOSPHINE–RHODIUM COMPLEXES

	Substrate	Et_3N[b]	(*S*,*S*)-I complex[c]			(*S*,*S*)-II complex[c]		
			S/Rh[d]	Conv.[e]	O.Y.[f]	S/Rh	Conv.	O.Y.
III	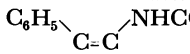	—	550	100%	72(*S*)%e.e.	540	100%	62(*S*)%e.e.
		+	550	100	83(*S*)			
	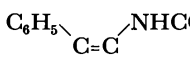	g) —	90	100	48(*S*)			
IV	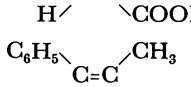	—	140	12	h)	140	7	h)
		+	140	73	29(*S*)	150	49	14(*S*)
V	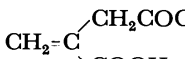	—	860	100	76(*R*)	860	100	48(*R*)
		+	850	100	85(*R*)	840	100	82(*R*)
	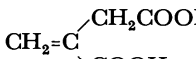	g) —	150	100	55(*R*)			
VI	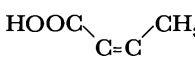	—	170	5	h)			
		+	170	32	3(*S*)			
VII	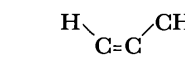	—	430	0	h)	200	0	h)
		+	160	90	3(*S*)	190	95	1(*S*)
VIII	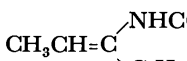	—	320	50	19(*S*)			
		+	320	24	20(*S*)			

a) Hydrogenation was carried out with 1 g of a substrate and a cationic rhodium complex in benzene/ethanol (v/v=1/1). b) The triethylamine-to-substrate molar ratio was 1.15. c) Catalytic precursor. (*S*,*S*)-I complex: [Rh(COD)(*S*,*S*)-I]$^+ClO_4^-$. (*S*,*S*)-II complex: [Rh(COD)(*S*,*S*)-II]$^+ClO_4^-$. d) Molar ratio of the substrate to the complex. e) Estimated by NMR analysis. f) Calculated on the basis of the reported value for the optically pure enantiomer as follows: (*S*)-2-methyl-3-phenylpropionic acid; $[\alpha]_D^{20}=+27.02°$ ($c=11.59$, C_6H_6).[5] (*R*)-methylsuccinic acid; $[\alpha]_D^{20}=+16.88°$ ($c=2.16$, EtOH).[6] (*S*)-*N*-(1-phenylpropyl)acetamide; $[\alpha]_D^{20}=-137.8°$ ($c=2.4$, MeOH).[7] *N*-acetyl-(*S*)-phenylalanine; $[\alpha]_D^{20}=+46.0$ ($c=1.0$, EtOH).[8] The predominant configuration of the product is shown in parentheses. g) Hydrogenations were carried out with an *in situ* catalyst. h) The optical rotation was not measured.

the latter cases, the lack of steric control may be caused by the non-rigid conformation of the substrate–rhodium complex because of the absence of the β-carbonyl group. The very low optical yield in VI and VII especially may be caused by the approximately symmetrical structure of the substrates, in which the deviation from the symmetry originates only from the difference in the substituents between the hydrogen and methyl groups.

Catalyst Studies. The (*S*,*S*)-I complex was expected to give a higher optical yield than the (*S*,*S*)-II complex, as the former had a more rigid conformation, restricted by the cyclohexane ring. However, the (*S*,*S*)-I complex gave a conversion rate and/or optical yields similar to those of the (*S*,*S*)-II complex for any of the substrate, as is shown in Table 1. Therefore, it may be concluded that the two complexes have similar reactivities and stereoselectivities.

The stereoselectivity of the catalytic rhodium complexes of (*S*,*S*)-I and (*S*,*S*)-II was compared with that of the other chiral rhodium catalysts, which make a similar seven-membered chelate ring with rhodium, as is shown in Fig. 1. The optical yields and the predominant configurations of the product of the asymmetric hydrogenation of (*Z*)-α-acetamidocinnamic acid

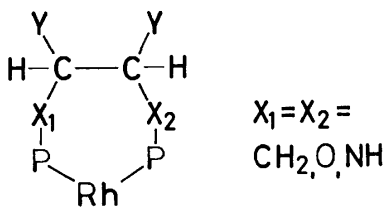

Fig. 1. The seven-membered chelate ring.

are as follows: 72% e.e. (*S*) for (*S*,*S*)-I, 70% e.e. (*R*) for (*R*,*R*)-I,[3b] 62% e.e. (*S*) for (*S*,*S*)-II, 94% e.e. (*S*) for (1*S*,2*S*)-1,2-bis(diphenylphosphinamino)-1,2-diphenylethane,[3a] 82% e.e. (*R*) for (*R*,*R*)-DIOP,[10] 68.5% e.e. (*S*) for (1*S*,2*S*)-1,2-bis(diphenylphosphinoxy)-cyclohexane,[11] 35% e.e. (*S*) for (1*S*,2*S*)-1,2-bis(diphenylphosphinomethyl)cyclohexane,[12] and 36% e.e. (*R*) for (1*R*,2*R*)-1,2-bis(diphenylphosphinomethyl)cyclohexane.[13] Thus the predominant configuration of the product may be supposed to be governed by the configuration arround the asymmetric carbons in the seven-membered ring for any of these eight complexes. That is, the complex with X_1 on the upper side and X_2 on the down side of the plane described in this paper would always give *N*-acetyl-(*S*)-phenylalanine

and the complex with X_1 on the down side and X_2 on the upper side would always give *N*-acetyl-(*R*)-phenylalanine. Therefore, the rhodium complexes with any one of the eight chiral ligands are considered to have essentially the same conformation, even if X is CH_2, NH, or O.

Experimental

General. The melting points were determined with a Yanagimoto melting-point-measuring apparatus, MP-S2. The NMR spectra were recorded on a Varian high-resolution NMR spectrometer, EM-390. The optical rotations were measured with a JASCO J-20 recording spectropolarimeter. The hydrogenations were carried out in a glass autoclave, EM-U-300, of Taiatsu Glass Industry.

Substrates and Solvents. The (*E*)-2-methylcinnamic acid (mp 80—81 °C) was obtained from Nakarai Chemicals. The itaconic acid (mp 162—164 °C dec), mesaconic acid (mp 204—205 °C), and citraconic acid (mp 98—99 °C) were obtained from Tokyo Kasei Industry. The *N*-(1-phenyl-1-propenyl)acetamide was prepared according to the procedure in the literature.[14] The α-acetamidocinnamic acid[15] was prepared by a standard Erlenmeyer procedure. The solvents for hydrogenation were purified as follows: the benzene was distilled, dried over sodium metal, degassed by means of the vacuum technique, and stored under argon; the ethanol was distilled, dried over a molecular sieve, degassed, and stored similarly.

Preparation of (S,S)-*I.* (1*S*,2*S*)-1,2-Cyclohexanediamine was prepared from D-(−)-tartaric acid according to the method of Asperger and Liu:[16] bp 79—81 °C (15 mmHg), $[\alpha]_D^{24}=+40.1°$ ($c=4.9$, C_6H_6). (1*S*,2*S*)-1,2-Cyclohexanediame (6.8 g) was dissolved in dry benzene (180 ml) and dried over NaOH pellets for several days. The benzene solution was transferred into the reaction flask, to which dry triethylamine (16.6 ml) was then added. Chlorodiphenylphosphine (26.4 g) was then added dropwise to the stirred solution at 10 °C. After the addition was complete, the resulting solution was stirred for 30 min at 20 °C. The solution was filtered and concentrated under reduced pressure. (*S*,*S*)-I was separated as crystals, which were recrystallized twice from benzene. 10.0 g. Mp 130—132 °C. $[\alpha]_D^{15}=+4.48°$ ($c=1.0$, C_6H_6). Found: C, 74.60; H, 6.68; N, 5.75; P, 12.50%. Calcd for $C_{30}H_{32}N_2P_2$: C, 74.67; H, 6.68; N, 5.81; P, 12.84%.

Preparation of (S,S)-*II.* (2*S*,3*S*)-2,3-Butanediamine was prepared according to the procedure of Dickey and his co-workers.[17] $[\alpha]_D^{29}=+29.0°$ ($c=3.23$, C_6H_6). (*S*,*S*)-II was prepared by the reaction of chlorodiphenylphosphine and (2*S*,3*S*)-2,3-butanediamine, much like (*S*,*S*)-I. Mp 83—85 °C. $[\alpha]_D^{15}=+2.98°$($c=0.5$, C_6H_6). Found: C, 73.44; H, 6.58; N, 6.09; P, 13.28%. Calcd for $C_{28}H_{30}N_2P_2$: C, 73.67; H, 6.62; N, 6.14; P, 13.57%.

Catalytic Precursors. The cationic rhodium complexes $[Rh(COD)(P\text{-}P)]^+ClO_4^-$ were prepared according to the method of Schrock and Osborn.[4] $[Rh(COD)Cl]_2$ (576 mg) and sodium perchlorate (400 mg) were placed in acetone (4 ml). (*S*,*S*)-I (1.13 g) was then slowly stirred in. Stirring was continued for 5 min, and then dichloromethane (20 ml) was added. The suspension was filtered and washed with dichloromethane. The filtrate was concentrated to *ca.* 5 ml under reduced pressure and then left at room temperature. The wine-red crystals were filtered off, washed with diethyl ether, and air-dried. The yield of the product was 1.46 g. The crystals were solvated with dichloromethane as detected by NMR (δ 5.30 ppm). $[Rh(COD)(S,S)\text{-}I]^+ClO_4^-\cdot 1/2CH_2Cl_2$; mp 142—145 °C (dec); Found: C, 55.38; H, 5.55; N, 3.21%. Calcd for $RhC_{38}H_{44}N_2P_2ClO_4\cdot 1/2CH_2Cl_2$: C, 55.34; H, 5.43; N, 3.35%. The rhodium complex of (*S*,*S*)-II was prepared by the same procedure. The crystals were also solvated with dichloromethane. $[Rh(COD)(S,S)\text{-}II]^+ClO_4^-\cdot 1/2CH_2Cl_2$; mp 143—144 °C (dec); Found: C, 54.02; H, 5.45; N, 3.38%. Calcd for $RhC_{36}H_{42}N_2P_2ClO_4\cdot 1/2CH_2Cl_2$: C, 54.15; H, 5.35; N, 3.46%. These rhodium complexes were stored in an ampoule under argon.

Hydrogenation Procedure. A substrate (1 g), one of the cationic rhodium complexes, ethanol, and benzene were placed in the glass autoclave under argon. The rhodium complex was dissolved completely. In the case of the addition of triethylamine, triethylamine was added at this stage. Hydrogen was then admitted into the autoclave. After the hydrogenation was complete, the solution was filtered and evaporated to dryness. The conversion rate of the substrate was determined by NMR at this stage. For the isolation of the hydrogenation product, either one of the following methods was applied. Method 1: For α-methylsuccinic acid in the absence of triethylamine and *N*-(1-phenylpropyl)acetamide, the product was separated from the insoluble catalyst by extraction with water and by concentration. Method 2: For other cases, the product was dissolved in 0.5 mol dm^{-3} NaOH. The resulting solution was acidified with dilute HCl and repeatedly extracted with a mixed solvent of ether and dichloromethane (v/v= 1/4). The organic layer was dried over anhydrous sodium sulfate and evaporated to dryness.

References

1) D. Valentine, Jr., and J. W. Scott, *Synthesis*, **5**, 329 (1978), and the references cited therein.

2) a) W. S. Knowles, M. J. Sabacky, and B. D. Vineyard, *Ann. N. Y. Acad. Sci.*, **172**, 232 (1970); G. Descotes, D. Lafont, and D. Sinou, *J. Organometal. Chem.*, **150** (1978) c14; b) K. Achiwa, *J. Am. Chem. Soc.*, **98**, 8265 (1976); c) I. Ojima, and T. Kogure, *Chem. Lett.*, **1978**, 567.

3) a) M. Fiorini and G. M. Giongo, *J. Mol. Catal.*, **5**, 303 (1979); b) K. Onuma, T. Ito, and A. Nakamura, *Chem. Lett.*, **1979**, 905; c) K. Hanaki, K. Kashiwabara, and J. Fujita, 28th Symposium on Coordination Chemistry, Japan (Matsuyama), 1978, Abstracts 2A07.

4) R. R. Schrock and J. A. Osborn, *J. Am. Chem. Soc.*, **93**, 2397 (1971).

5) A. M. Aguiar, C. J. Morrow, J. D. Morrison, R. E. Burnett, and W. F. Masler, *J. Org. Chem.*, **41**, 1545 (1976).

6) E. Berner and R. Leonardsen, *Ann.* **538** 1 (1939).

7) A. La Manna, V. Chislande, O. B. Hulbert, and O. M. Scope, *Farmaco Ed., Sci.*, **22**, 1037 (1967).

8) M. D. Fryzuk and B. Bosnich, *J. Am. Chem. Soc.*, **99**, 6262 (1977).

9) a) J. Halpern, Symposium on Rhodium in Homogeneous Catalysis, Veszprem Hungary (1978), p. 30; b) W. C. Christopfel and B. D. Vineyard, *J. Am. Chem. Soc.*, **101**, 4406 (1979); c) J. M. Brown and P. A. Chaloner, *Tetrahedron Lett.*, **1978**, 1877; d) G. Gelbard and H. B. Kagan, *Tetrahedron*, **32**, 233 (1976).

10) H. B. Kagan and T. P. Dang, *J. Am. Chem. Soc.*, **94**, 6249 (1972).

11) M. Tanaka and I. Ogata, *J. Chem. Soc., Chem. Commun.*, **1975**, 735.

12) R. Glaser, M. Twaik, S. Geresh, and J. Blumenfeld,

Tetrahedron Lett., **1977**, 4635.
13) P. Aviron-Violet, Y. Colleuille, and J. Varagnat, *J. Mol. Catal.*, **5**, 41 (1979).
14) Y. H. Suen, A. Horeau, and H. B. Kagan, *Bull. Soc. Chim. Fr.*, **1965**, 1454.
15) R. M. Herbst and D. Shemin, *Org. Synth.*, Coll. Vol. 2, 1 (1943).
16) R. G. Asperger and C. F. Liu, *Inorg. Chem.*, **4**, 1493 (1965).
17) F. H. Dickey, W. Fickett, and H. J. Lucas, *J. Am. Chem. Soc.*, **74**, 944 (1952).

Asymmetric Hydrogenation with Chiral Aminophosphine–Rhodium Complexes[1] and Chiral Recognition by Bisphosphine–Rhodium Complexes in the Asymmetric Hydrogenation of Olefins through the Chiral Helical Conformation of Phenyl Groups on the Phosphorus Atom

Ken-ichi Onuma,* Tomiyasu Ito, and Asao Nakamura
Central Research Laboratories, Ajinomoto Co., Inc., 1-1 Suzuki-cho, Kawasaki 210
(Received September 22, 1979)

The asymmetric hydrogenation of α-acylaminocinnamic acids with the rhodium complex of (1*R*,2*R*)-1,2-bis(*N*-diphenylphosphino-*N*-methylamino)cyclohexane has been reported to give preferentially (*S*)-amino acids. On the contrary, it has been found that the enantiomeric (*R*)-amino acids are obtained by hydrogenation with the rhodium complex of (1*R*,2*R*)-1,2-bis(diphenylphosphinamino)cyclohexane. The study of the inversion of the stereoselectivity of the rhodium complex of (1*R*,2*R*)-1,2-bis(diphenylphosphinamino)cyclohexane by the *N*-methylation of the ligand in asymmetric hydrogenation has been described. From stereochemical considerations, the chiral helical conformation of the phenyl groups attached on the phosphorus in bisphosphine–rhodium complexes may be responsible for the induced chirality of the product of the hydrogenation. A complex with a left-handed helicity would give (*R*)-amino acid, and a complex with a right-handed helicity would give (*S*)-amino acid. The effects of the solvents and substrate structures on the optical yields are also discussed.

In recent years, the catalytic asymmetric hydrogenation of α-acylaminocinnamic acid has been investigated in order to obtain chiral α-amino acid. Considerable efforts have been devoted not only to developing new chiral ligands,[2] but also to studying the mechanism of asymmetric hydrogenations.[3] Only a few papers have been reported,[2a] however, about the correlation of the ligand structure to the chirality of the products.

The stereochemistry of the produced acylamino acids is reversed by the *N*-methylation of the ligand in the hydrogenation with the rhodium complex of the bis-aminophosphine, which has a 1,2-bis(diphenylphosphinamino)ethane skeleton.[4] For example, (1*R*,2*R*)-1,2-bis(diphenylphosphinamino)cyclohexane, (*R*,*R*)-I, has been found to be an effective ligand for the rhodium-catalyzed asymmetric hydrogenation of α-acylaminocinnamic acids to give preferentially (*R*)-amino acids. On the contrary, its *N*,*N*′-dimethyl derivative, (1*R*,2*R*)-1,2-bis(*N*-diphenylphosphino-*N*-methylamino)cyclohexane, (*R*,*R*)-II, has been reported to give preferentially (*S*)-amino acids under similar reaction conditions. In view of the subtlety of the structural divergence between these two ligands, the origin of this marked difference in stereoselectivity should be further explored. The stereochemical consideration suggests that the chiral inversion may be caused by the difference in the configuration of the nitrogen atom, by which the four phenyl groups are caused to be arranged in a reverse helical orientation in each (*R*,*R*)-I and (*R*,*R*)-II complex.

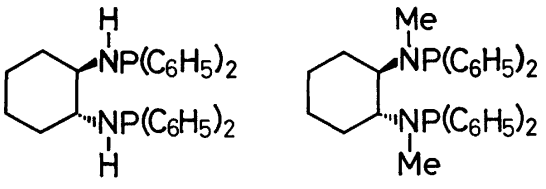

Fig. 1. Chiral aminophosphines, (*R*,*R*)-I (left) and (*R*,*R*)-II (right).

Results and Discussion

The α-acylaminocinnamic acids were hydrogenated with the cationic rhodium complexes of (*R*,*R*)-I, (*S*,*S*)-I, and (2*S*,3*S*)-2,3-bis(diphenylphosphinamino)butane, [(*S*,*S*)-III]. The results are summarized in Table 1.

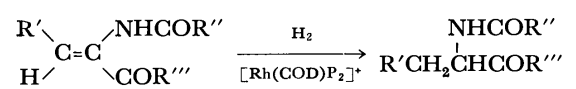

Scheme 1.

Stereochemical Studies. As can be seen in Table 1, acylamino acids with an *R*-configuration were always obtained preferentially by the hydrogenation using the rhodium complex of (*R*,*R*)-I. On the other hand, the products with an *S*-configuration were preferentially obtained using either (*S*,*S*)-I or (*S*,*S*)-III as the chiral ligand. The most noticeable result is that *N*-acyl-(*S*)-amino acids were always obtained by using the (*R*,*R*)-II complex, contrary to the result obtained with the (*R*,*R*)-I complex. Moreover, it has previously been reported that the chiral inversion of the stereoselectivity by the *N*-methylation of the ligand is also observed in the rhodium complexes of (1*S*,2*S*)-1,2-bis(diphenylphosphinamino)-1,2-diphenylethane[4b] and (*R*)-1,2-bis(diphenylphosphinamino)propane.[4c] Therefore, the inversion may be an essential feature of these aminophosphine–rhodium complexes. The chiral inversion may be deduced as having the same origin, as the complex of (*S*,*S*)-I or (*S*,*S*)-III gives similar results in the hydrogenation, as has been described in the preceding paper.[1] In order to clarify the origin of the chiral inversion, the stereochemistry of these complexes has been considered.

As is shown in Fig. 2, the seven-membered chelate ring, consisting of the rhodium atom and two phosphorus atoms, may be considered to take predominantly a twist-chair conformation,[6] for the repulsion between the phenyl groups and the cyclohexane ring is reduced. By deduction by analogy, with the preferred conforma-

Table 1. Asymmetric hydrogenation[a] with chiral aminophosphine-rhodium complexes

Substrate			Solvent[b]	Optical yield[c]				
R′	R″	R‴		(*R*,*R*)-I	(*S*,*S*)-I	(*S*,*S*)-III	(*R*,*R*)-II[d]	
C_6H_5	CH_3	OH	Methanol	32(*R*)	30(*S*)			
C_6H_5	CH_3	OH	Ethanol	41(*R*)	41(*S*)	45(*S*)	89(*S*)	92(*S*)
C_6H_5	CH_3	OH	2-Propanol	70(*R*)	71(*S*)	80(*S*)		
C_6H_5	CH_3	OH	Methanol/benzene	50(*R*)	50(*S*)			
C_6H_5	CH_3	OH	Ethanol/benzene	70(*R*)	72(*S*)	62(*S*)		
C_6H_5	CH_3	OH	2-Propanol/benzene	64(*R*)	63(*S*)	94(*S*)		
C_6H_5	C_6H_5	OH	Ethanol	43(*R*)	43(*S*)	32(*S*)	92(*S*)	
C_6H_5	C_6H_5	OH	2-Propanol	70(*R*)	70(*S*)	80(*S*)		
C_6H_5	C_6H_5	OH	Ethanol/benzene	62(*R*)	60(*S*)	69(*S*)		
C_6H_5	C_6H_5	OH	2-Propanol/benzene	49(*R*)	48(*S*)	93(*S*)		

a) Hydrogenation was carried out with 1 g of a substrate and 7 mg of a cationic rhodium complex. b) The ratio of the mixed solvent was 1:1 (v/v). c) Calculated on the basis of the following reported values for optically pure enantiomers: *N*-acetyl-(*S*)-phenylalanine $[\alpha]_D^{26}=+46.0°$ ($c=1.0$, C_2H_5OH),[5] *N*-benzoyl-(*S*)-phenylalanine $[\alpha]_D^{26}=-40.3°$ ($c=1.0$, CH_3OH).[5] The predominant configuration of the product is shown in parentheses. d) Quoted from Refs. 4b, c.

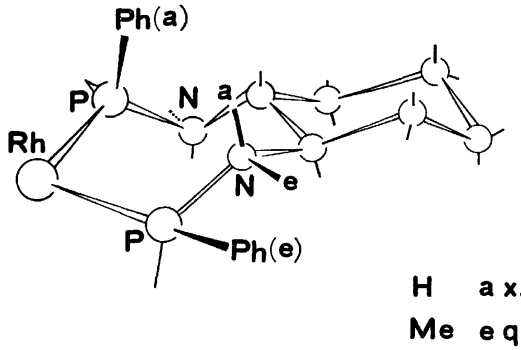

Fig. 2. The conformation of seven-membered chelate ring. The letters of a and ax. mean a *quasi*-axial position. The letters of e and eq. mean a *quasi*-equatorial position.

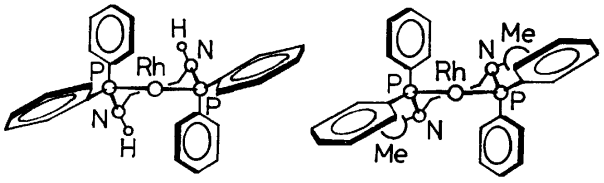

Fig. 3. Chiral skew conformation of four phenyl groups in the rhodium complex of (*R*,*R*)-I and (*R*,*R*)-II. The skeleton of the cycleohexane ring is omitted for simplicity.
Left: (*R*,*R*)-I complex, left-handed helicity; Right: (*R*,*R*)-II complex, right-handed helicity.

tion of piperazine derivatives,[7] the hydrogen atom on the nitrogen atoms in the (*R*,*R*)-I complex may occupy a *quasi*-axial position and so be $(R)_N$, and the methyl group in the (*R*,*R*)-II may occupy a *quasi*-equatorial position and so be $(S)_N$, in the twist-chair conformation. This inversion of the configuration around the nitrogen atoms, despite having the same configuration of $(R)_C$, may exert significant effects on the orientation of the *quasi*-equatorial phenyl groups. Affected by the substituent (H or CH_3) on the nitrogen atoms, the rotation of the *quasi*-equatorial phenyl groups in (*R*,*R*)-I complex and (*R*,*R*)-II complex may be restricted in a reverse direction, and the correlated rotation of the *quasi*-axial phenyl groups may give reverse helical conformations, as is shown in Fig. 3. That is, the four phenyl groups may be twisted in a left-handed orientation in the (*R*,*R*)-I complex and in a right-handed orientation in the (*R*,*R*)-II complex. These preferred conformations can also be satisfactorily understood in terms of the CPK molecular models.

The inversion of stereoselectivity in the asymmetric hydrogenation may be caused mainly by the difference in the helical conformation; the complex with left-handed helicity would give (*R*)-amino acids, while the complex with right-handed helicity would give (*S*)-amino acids. The hypothesis concerning the structural correlation between the helical conformation of phenyl groups and the chirality of the products may also be adopted in treating other results previously reported.[2a,b] The structure of the rhodium complex of (2*S*,3*S*)-2,3-bis(diphenylphosphino)butane has been determined by X-ray analysis.[8] This complex has the left-handed helicity and has been reported surely to give (*R*)-amino acids.[2b] The phenyl groups are skewed in a right-handed orientation in the rhodium complex of (*R*,*R*)-1,2-bis(*P*-phenyl-*o*-methoxyphenylphosphino)ethane,[2a] which has been reported certainly to give (*S*)-amino acids.

Solvent Effect. As is shown in Table 1, the optical yield of the products is dependent on the solvent used in the reaction. For the reaction carried out in an alcohol, such as methanol, ethanol, or 2-propanol, as well as in a mixed solvent of alcohol and benzene, the optical yield generally increases in this order: methanol<ethanol<2-propanol, and is higher in the mixed solvent than in alcohol, with the exception of the hydrogenation in the mixed solvent of 2-propanol and benzene with the (*S*,*S*)-I complex. The solvent may be supposed to play an important role in making a specific conformation of the catalyst more predominant. Thus, a solvent may be considered to contribute to fixing the specific conformation of the transition

TABLE 2. ASYMMETRIC HYDROGENATION OF α-ACYLAMINOCINNAMIC ACID DERIVATIVES

Substrate			Optical yield[a]	
R′	R″	R‴	[Rh(COD)(*S,S*)-I]$^+$	[Rh(COD)(*S,S*)-III]$^+$
C_6H_5	CH_3	OH	72(*S*)	62(*S*)
C_6H_5	CH_3	NH_2	92(*S*)	94(*S*)
C_6H_5	C_6H_5	OH	60(*S*)	69(*S*)
C_6H_5	C_6H_5	NH_2	70(*S*)	80(*S*)
HO- 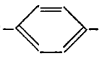	CH_3	OH	53(*S*)	43(*S*)
AcO- 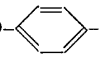	CH_3	OH	56(*S*)	53(*S*)
CH_3O CH_3O- 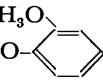	CH_3	OH	56(*S*)	42(*S*)
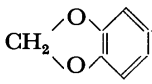	CH_3	OH	49(*S*)	34(*S*)
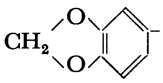	C_6H_5	OH	28(*S*)	13(*S*)
CH_3O AcO- 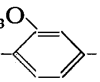	CH_3	OH	48(*S*)	

a) Calculated on the basis of the following reported values for optically pure enantiomers: *N*-acetyl-(*S*)-tyrosine $[\alpha]_D^{27}=+51.5°$ ($c=1.0$, MeOH),[5] *O,N*-diacetyl-(*S*)-tyrosine $[\alpha]_D^{27}=+45.4°$ ($c=1.0$, MeOH),[5] *N*-acetyl-β-(3,4-dimethoxyphenyl)-(*S*)-alanine $[\alpha]_D=+46.2°$ ($c=5.0$, MeOH),[9] *N*-acetyl-β-(3,4-methylenedioxyphenyl)-(*S*)-alanine $[\alpha]_D^{18}=+53.4°$ ($c=1.8$, EtOH),[10] *N*-benzoyl-β-(3,4-methylenedioxyphenyl)-(*S*)-alanine $[\alpha]_D=-11.0°$ ($c=2.0$, *N*-NaOH),[11] *N*-acetyl-β-(4-acetoxy-3-methoxyphenyl)-(*S*)-alanine $[\alpha]_D^{20}=+40.7°$ ($c=1.0$, MeOH).[5]

state in a degree dependent upon its ability of coordination and its bulkiness.

Substrate Studies. Further studies were carried out on the hydrogenation of α-acylaminocinnamic acid derivatives with the rhodium complexes of (*S,S*)-I and (*S,S*)-III. The results are shown in Table 2.

As can be seen in Table 2, the optical yield depends greatly on the substrate structures. For the effects of substituents of α-acylaminocinnamic acid on the optical yield of the reaction, a tendency to obtain a higher optical yield is generally observed: 1) As for the phenyl group, the unsubstituted one is more advantageous than one with a substituent, such as a hydroxyl, alkoxyl, or acetoxyl group. 2) As for the carboxylic acid moiety, the carbamoyl derivative is more favorable compared with the parent carboxylic acid. Any substituent on the phenyl groups may prevent the substrate from approaching the catalytic rhodium complex. The hydrogenation of α-acetamidocinnamic acid and its amide with the (−)-DIOP–rhodium complex has been reported to give the corresponding product, with 82%e.e. and 71%e.e. respectively.[12] Therefore, the advantage of the carbamoyl group over the carboxyl group may be characteristic of this system.

Experimental

General. The measurements of the melting points, the ^{1}H-NMR, the optical rotations, and the apparatus used for hydrogenation were the same as those described in the preceding paper.[1] The liquid chromatograms were recorded on a Hitachi KLA-5 amino-acid analyzer.

Substrates and Solvents. The α-acetamidocinnamic acid,[13] α-benzamidocinnamic acid,[14] α-acetamido-3,4-dimethoxycinnamic acid,[15] α-acetamido-3,4-methylenedioxycinnamic acid,[13] α-benzamido-3,4-methylenedioxycinnamic acid,[16] α-acetamido-4-hydroxycinnamic acid,[17] α-acetamido-4-acetoxycinnamic acid,[18] and α-acetamido-4-acetoxy-3-methoxycinnamic acid[19] were prepared by standard Erlenmeyer procedures, sometimes with minor modifications of the published directions. The α-benzamidocinnamamide was prepared as follows: 2-phenyl-4-benzylidene-5-oxazolone (15.3 g) was allowed to react with liquid ammonia (20 ml) in a sealed tube at room temperature for one night. The ammonia was then removed by breaking the seal, and the residual crystals were recrystallized from methanol; 10.9 g; mp 165—166 °C, Found: C, 71.99; H, 5.34; N, 10.57%. Calcd for $C_{16}H_{14}N_2O_2$: C, 72.16; H, 5.30; N, 10.52%. The α-acetamidocinnamamide was prepared by a similar procedure; mp 197—198 °C. Found: C, 64.51; H, 5.92; N, 13.59%. Calcd for $C_{11}H_{12}O_2N_2$: C, 64.99; H, 5.92; N, 13.72%.

The solvents for hydrogenation were purified as has been described in the preceding paper.

Preparation of (R,R)-I and Its Rhodium Complex. (1*R*,2*R*)-1,2-Cyclohexanediamine was prepared according to the method of Asperger and Liu;[20] bp 76—78 °C (13 mmHg), $[\alpha]_D^{24}=-41.6°$ ($c=4.9$, C_6H_6). (*R,R*)-I and its cationic rhodium complex were prepared much like (*S,S*)-I, described in the preceding paper; mp 130—132 °C, $[\alpha]_D^{15}=-4.51°$ ($c=1.0$, C_6H_6). Found: C, 74.47; H, 6.65; N, 5.79; P, 12.81%. Calcd for $C_{30}H_{32}N_2P_2$: C, 74,67; H, 6.68; N, 5.81; P, 12.84%. [Rh(COD)(*R,R*)-I]$^+$$ClO_4^-$·1/2$CH_2Cl_2$; mp 142—145 °C (dec), Found: C, 55.87; H, 5.90; N, 3.30%. Calcd for $RhC_{38}H_{44}N_2P_2ClO_4$·1/2$CH_2Cl_2$:

C, 55.34; H, 5.43; N, 3.53%. The rhodium complex was stored in an ampoule under argon.

Hydrogenation Procedure. Hydrogenation was carried out by the method described in the preceding paper. Three methods for the isolation of the hydrogenation product were used, depending on the substrate, as follows: Method 1. For *N*-acetyltyrosine, *O*,*N*-diacetyltyrosine, and *N*-acetyl-*β*-(4-acetoxy-3-methoxylphenyl)alanine, the hydrogenation product was separated from the insoluble catalyst by extraction with water followed by concentration. Method 2. For *N*-acetylphenylalaninamide and *N*-benzoylphenylalaninamide, the product was hydrolyzed with concd hydrochloric acid by refluxing for 1 h. The solution was then filtered, and the filtrate was evaporated to dryness. The optical purity of the phenylalanine thus obtained was determined by means of a liquid chromatogram according to the Manning and Moore method.[21] Method 3. For the other compounds, the product was extracted with 0.5 mol dm^{-3} NaOH. The filtrate was acidified with dilute HCl and then repeatedly extracted with the mixed solvent of ether (5 ml) and dichloromethane (20 ml). The organic layer was dried over sodium sulfate and then evaporated to dryness.

References

1) K. Onuma, T. Ito, and A. Nakamura, *Bull. Chem. Soc. Jpn.*, to be published.

2) a) B. D. Vineyard, W. S. Knowles, M. J. Sabacky, G. L. Bachman, and D. J. Weinkauff, *J. Am. Chem. Soc.*, **99**, 5946 (1977); b) M. D. Fryzuk and B. Bosnich, *J. Am. Chem. Soc.*, **99**, 6262 (1977); c) M. D. Fryzuk and B. Bosnich, *J. Am. Chem. Soc.*, **100**, 5491 (1978), and the references therein.

3) a) J. Halpern, D. P. Riley, A. S. C. Chan, and J. J. Pluth, *J. Am. Chem. Soc.*, **99**, 8055 (1977); b) C. Detellier, G. Gelbard, and H. B. Kagan, *J. Am. Chem. Soc.*, **100**, 7556 (1978); c) K. B. Koenig and W. S. Knowles, *J. Am. Chem. Soc.*, **100**, 7561 (1978); d) J. M. Brown and P. A. Chaloner, *Tetrahedron Lett.*, **1978**, 1887; e) W. C. Christopfel and B. D. Vineyard, *J. Am. Chem. Soc.*, **101**, 4406 (1979); f) I. Ojima, T. Kogure, and N. Yoda, *Chem. Lett.*, **1979**, 495; g) J. Halpern, Symposium on Rhodium in Homogeneous Catalysis, Veszprem Hungary (1978), p. 30.

4) a) K. Onuma T. Ito, and A. Nakamura, *Tetrahedron Lett.*, **1979**, 3163; *Chem. Lett.*, **1979**, 905; Japanese Patent Application (Oct. 18, 1977); b) M. Fiorini and G. M. Giongo, *J. Mol. Catal.*, **5**, 303 (1979); c) K. Hanaki, K. Kashiwabara, and J. Fujita, *Chem. Lett.*, **1978**, 489; K. Hanaki, K. Kashiwabara, and J. Fujita, 28th Symposium on Coordination Chemistry, Japan (Matsuyama) (1978), Abstract 2A07.

5) The values of specific rotations of pure enantiomers were taken from Ref. 2b.

6) a) N. L. Allinger, J. G. D. Carpenter, and F. M. Karkowski, *J. Am. Chem. Soc.*, **81**, 232 (1959); b) M. Hanack "Conformation Theory," Academic Press, New York and London (1965), pp. 158—162.

7) N. L. Allinger, J. G. D. Carpenter, and F. M. Karkowski, *J. Am. Chem. Soc.*, **87**, 1322 (1965).

8) R. G. Ball and N. C. Payne, *Inorg. Chem.*, **16**, 1187 (1977).

9) H. Nakamoto, M. Aburatani, and M. Inagaki, *J. Med. Chem.*, **41**, 1021 (1971).

10) S. Yamada, T. Fujii, and T. Shioiri, *Chem. Pharm. Bull.*, **10**, 680 (1962).

11) E. Toyoura, *Chem. Pharm. Bull.*, **7**, 787 (1959).

12) H. B. Kagan and T. P. Dang, *J. Am. Chem. Soc.*, **94**, 6249 (1972).

13) R. M. Herbst and D. Shemin, *Org. Synth.*, Coll. Vol. 2, 1 (1943).

14) H. B. Gilespie and H. R. Spyder, *Org. Synth.*, Coll. Vol. 1, 489 (1941).

15) Prepared by a procedure similar to that given in Ref. 13, using the appropriate aldehyde and recrystallizing the acid from methanol.

16) Prepared as in Ref. 13. The acid was recrystallized from ethanol.

17) H. D. Dalkin, *J. Biol. Chem.*, **92**, 439 (1929).

18) Prepared as in Ref. 13. The acid was recrystallized from ethanol.

19) Prepared as in Ref. 13. The acid was recrystallized from methanol.

20) R. G. Asperger and C. F. Liu, *Inorg. Chem.*, **4**, 1493 (1965).

21) J. M. Manning and S. Moore, *J. Biol. Chem.*, **243**, 5591 (1968).

A New Bromophenol from the Red Alga *Polysiphonia urceolata*[1)]

Kazuya KURATA* and Takashi AMIYA†

Department of Industrial Chemistry, Hakodate Technical College, Tokura-cho, Hakodate 042

†*Hokkaido Institute of Pharmaceutical Sciences, Katsuraoka-cho, Otaru 047-02*

(Received November 2, 1979)

The investigation of the red alga *Polysiphonia urceolata* afforded a new bromophenol, 3,3′-dibromo-4,4′,5,5′-tetrahydroxybibenzyl. The structure was elucidated by a combination of spectroscopic methods and chemical transformations. Besides this compound, seven known bromophenols were isolated.

Many bromophenols have been previously obtained from the red marine algae, Rhodomelaceae,[1-18)] with the *Polysiphonia*, *Rhodomela*, *Odonthalia*, and *Symphyocladia* species being especially rich in bromine-containing compounds. Bromophenols of *Polysiphonia* species have been extensively investigated.[1,3,4,8,9,15,17)] In the course of the investigation of the constituents of the red marine algae, we obtained a new bromophenol, 3,3′-dibromo-4,4′5,5′-tetrahydroxybibenzyl (**1**), together with seven known bromophenols, from *Polysiphonia urceolata*. In this paper the isolation and structural elucidation of these compounds will be described.

An acidic fraction obtained from the dried alga collected at Matsumae Bay by extraction with methanol was chromatographed on silica gel. A benzene eluate gave 3,5-dibromo-4-hydroxybenzyl methyl ether (**2**)[8)] and 3-bromo-4,5-dihydroxybenzyl methyl ether (**3**).[8,9,16)] Their structures were deduced from the chemical and spectral properties, and confirmed by direct comparison with an authentic sample and by conversion to the dimethyl derivative (**3m**) respectively. Compounds **2** and **3** could be artifacts derived by the methylation of the corresponding alcohols or bromophenol precursors during the extraction procedure.[11)] A benzene–ether (19:1) eluate gave 3-bromo-4,5-dihydroxybenzaldehyde (**4**)[3,9)] as the main constituent and 3,3′-dibromo-4,4′,5,5′-tetrahydroxybibenzyl (**1**) as the minor constituent. Compound **1** was a colorless crystalline substance (mp 205—206 °C); elemental analysis established it to be $C_{14}H_{12}O_4Br_2$. It developed an intense green color with iron(III) chloride and precipitated easily on the addition of lead acetate. The mass spectrum showed the presence of 406, 404, and 402 (M^+). The UV spectrum in EtOH exhibited a maximum at 287 nm. The IR spectrum showed bands due to OH groups at 3550, 3470, and 3250 cm^{-1}, and benzene rings at 1595, 1520, and 845 cm^{-1}. The ^{1}H-NMR spectrum showed a signal of methylene protons at δ 2.58 (4H, s), signals of two aromatic protons at δ 6.54 (2H, d, J=2 Hz) and 6.73 (2H, d, J=2 Hz), and signals of phenolic protons at δ 8.72 (2H, bs), and 9.49 (2H, bs). Two finely split doublets at δ 6.54 and 6.73 in the ^{1}H-NMR spectrum indicated a 1,2,3,5-tetrasubstituted benzene ring. The oxidation of tetramethyl ether (**1m**) derived from **1** with potassium permanganate in acetone yielded 3-bromo-4,5-dimethoxybenzoic acid (**5**), which was confirmed by comparison with a synthetic sample of **5**. All of these results helped to elucidate the structure of Compound **1**.

An ethanol extract of the dried alga collected at Hakodate Bay was chromatographed on silica gel.

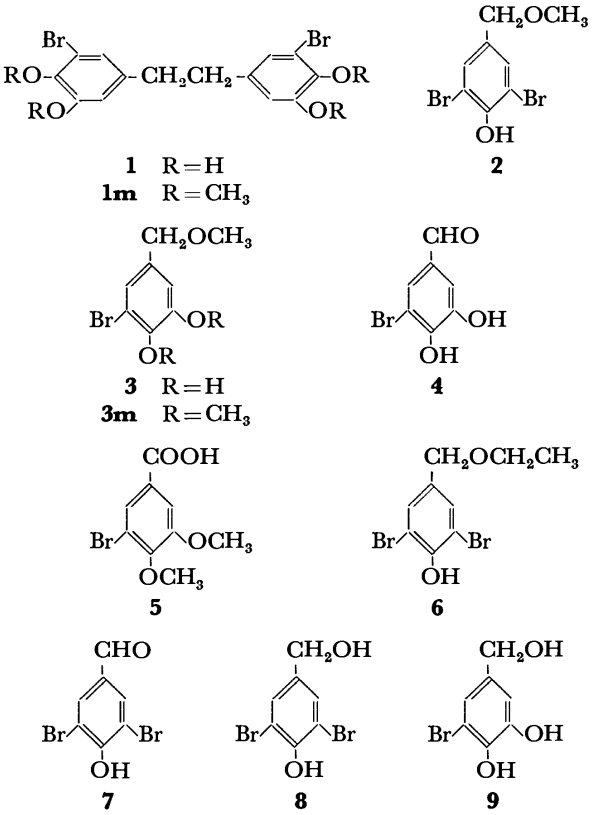

The TLC separation of a benzene eluate gave 3,5-dibromo-4-hydroxybenzyl ethyl ether (**6**)[8)] and the corresponding benzaldehyde (**7**), which has also been obtained from other marine sources. Compound **4** was also isolated from the benzene–ether (19:1) eluate. Compounds **6** and **7** were identified by comparison with the respective authentic samples. The presence of the benzyl methyl ethers (**2** and **3**) and ethyl ether (**6**) in the methanol and ethanol extracts respectively suggested the existence of a bromophenol precursor similar to lanosol sulfate in *P. lanosa* and *R. larix*. Therefore, we extracted the frozen alga collected at Hakodate Bay with 80% acetone. An acetone-soluble fraction was chromatographed on silica gel. Early-eluted fractions of the benzene–ether (19:1) eluate gave 3,5-dibromo-4-hydroxybenzyl alcohol (**8**),[8,9,15)] which was confirmed by comparison with an authentic sample, whereas later-eluted fractions gave **4** and 3-bromo-4,5-dihydroxybenzyl alcohol (**9**).[8,9,16)] Compound **9** was identified by comparison with a synthetic sample. The dried and frozen alga from Hakodate Bay was lacking in Compound **1**, which is present in the dried alga from Matsumae Bay.

Experimental

All the melting points were determined on a micro hot stage and are uncorrected. The IR spectra were taken on a Hitachi EPI-G2 spectrophotometer, and the UV spectra, on a Hitachi 124 spectrophotometer. The mass spectra were measured on a Hitachi RMO-4E spectrometer, and the ^{1}H-NMR spectra, on a JEOL PMX-60 or Hitachi R-20B spectrometer, using TMS as the internal standard. The column chromatography was carried out over silica gel (Wakogel C-100 or C-200). The TLC was performed on silica gel (Merck silica gel 60 F_{254}) and polyamide (Carl Chleicher & Chüll), with benzene–methanol–acetic acid (45:8:4 v/v) as the eluent.

Extraction and Isolation. *Methanol Extraction*: *P. urceolata* was collected at Matsumae Bay in May, 1974. A methanol extract of the air-dried alga (2.5 kg) gave a syrup, which was then treated with ether. The ether solution was treated with 5% aqueous KOH. The alkaline aqueous solution was acidified with hydrochloric acid and extracted with ether. The acidic fraction (75 g) from the ether extract was chromatographed on a silica-gel column. The column was then eluted, yielding 17 fractions, 4 l each; Fractions 1—13 with benzene and Fractions 14—17 with benzene–ether (19:1). Fractions 1—2 and 7—12 afforded Compounds **2** (650 mg) and **3** (460 mg) respectively. The recrystallization of a solid residue of Fractions 15—17 from benzene–methanol gave Compound **4** (2 g), while Compound **1** (400 mg) was obtained on the recrystallization of the mother liquor.

Ethanol Extraction: The dried alga (2.0 kg) collected at Hakodate Bay in May, 1976, was immersed in ethanol. The subsequent removal of the solvent from the ethanol solution gave an ethanol extract, which was treated with ether. The ether extract (3.2 g) was subjected to chromatography on a silica-gel column. The column was eluted with benzene as has been described above. On separation by TLC (polyamide), the eluate gave Compounds **7** (43 mg; R_f 0.69) and **6** (25 mg; R_f 0.94). The further elution of the column with benzene–ether (19:1) afforded Compound **4** (78 mg).

80% Acetone Extraction: The alga (14 kg) collected at Hakodate Bay in May, 1978, was immersed in 80% acetone. The acetone solution was then evaporated to dryness and treated with dry acetone. The acetone extract (70 g) was chromatographed on a silica-gel column. The column was then eluted with the series of solvents mentioned above. Early-eluted fractions of a benzene–ether (19:1) eluate afforded Compound **8** (1.8 g). Later-eluted fractions contained two components which gave spots with R_f 0.65 and 0.16 on TLC (silica gel). A mixture (3.1 g) of these components was rechromatographed on a silica gel column with benzene–ether (19:1) to give Compounds **4** (670 mg) and **9** (190 mg).

3,3′-Dibromo-4,4′5,5′-tetrahydroxybibenzyl (1). Compound **1** was recrystallized from benzene–methanol to yield colorless needles (120 mg); mp 205—206 °C; λ_{max} (EtOH) 287 nm; IR(KBr) ν 3550, 3470, 3250, 2930, 2860, 1630, 1610, 1595, 1520, 1430, 1340, 1295, 1190, 1000, 905, and 845 cm^{-1}; ^{1}H-NMR (DMSO-d_6) δ 2.58 (4H, s, methylene protons), 6.54 (2H, d, J=2 Hz, aromatic protons), 6.73 (2H, d, J=2 Hz, aromatic protons), 8.72 (2H, bs, phenolic protons), and 9.49 (2H, bs, phenolic protons); MS *m/e* 406, 404, 402 (M^+), 203, 201 ($M^+-C_7H_6O_2Br$), and 185, 183 ($M^+-C_7H_6O_2Br-H_2O$). Compound **1** gave an intense green color with iron(III) chloride and was precipitated easily on the addition of lead acetate.

Found: C, 41.38; H, 2.92%. Calcd for $C_{14}H_{12}O_4Br_2$: C, 41.62; H, 2.99%.

Identification of 1. *a*): The phenol **1** (20 mg), dissolved in ether, was treated with diazomethane, thus yielding a tetramethyl derivative (**1m**) (13 mg) as colorless needles; mp 92—95 °C; IR(KBr) ν 2900, 1600, 1455, 1410, 1365, 1210, 1085, 975, 835, and 770 cm^{-1}.

b): A solution of **1m** (10 mg) in acetone (3 ml) was added to a solution of potassium permanganate (30 mg) in acetone (10 ml). The mixture was refluxed. The resulting precipitates were filtered and extracted with water. The water solution, after acidification with dilute hydrochloric acid, was extracted with ether. The subsequent removal of the solvent from the ether extract gave crystals, which were recrystallized from hexane–ethanol to yield 3-bromo-4,5-dimethoxybenzoic acid (**5**) (2.8 mg); mp 195—198 °C; IR(KBr) ν 2950, 1690, 1595, 1575, 1410, 1290, 1115, 1045, and 990 cm^{-1}. Compound **5** was shown to be identical with a synthetic sample by a comparison of the IR spectrum and TLC.

Synthesis of 5. 3-Bromo-4,5-dimethoxybenzaldehyde was oxidized by the procedure described for the oxidation of **1m**. The recrystallization of the oxidation product from hexane–ethanol furnished **5** as colorless needles; mp 197—198 °C.

Found: C, 41.55; H, 3.28; Br, 30.28%.

3,5-Dibromo-4-hydroxybenzyl Methyl Ether (2). Compound **2** was recrystallized from hexane to yield colorless crystals; mp and mixed mp 70—71 °C; λ_{max} (EtOH) 290 nm (log ε 3.46); IR(KBr) ν 3240, 2990, 2920, 2810, 1590, 1550, 1475, 1280, 1140, 1080, and 860 cm^{-1}; ^{1}H-NMR($CDCl_3$) δ 3.31 (3H, s, $-CH_2O\underline{CH_3}$), 4.28 (2H, s, $-\underline{CH_2}OCH_3$), 5.93 (1H, bs, phenolic proton), and 7.38 (2H, s, aromatic protons); MS *m/e* 298, 296, 294 (M^+), 267, 265, 263 (M^+-OCH_3), 217, 215 (M^+-Br).

3-Bromo-4,5-dihydroxybenzyl Methyl Ether (3). Compound **3** was recrystallized from benzene–methanol to afford colorless needles; mp 98—99 °C; λ_{max} (EtOH) 287 nm; IR(KBr) ν 3450, 3075, 3050, 2950, 2925, 2860, 2830, 1610, 1590, 1525, 1425, 1065, 855, and 840 cm^{-1}; ^{1}H-NMR($CDCl_3$) δ 3.37 (3H, s, $-CH_2O\underline{CH_3}$), 4.33 (2H, s, $-\underline{CH_2}OCH_3$), 5.98 (2H, bs, phenolic protons), 6.79 (1H, d, J=2 Hz, aromatic proton), and 6.98 (1H, d, J=2 Hz, aromatic proton); MS *m/e* 234, 232 (M^+), 203, 201 (M^+-OCH_3), and 153 (M^+-Br).

3-Bromo-4,5-dimethoxybenzyl Methyl Ether (3m). Compound **3** (100 mg), dissolved in ether, was treated with diazomethane, yielding a dimethyl ether (80 mg) as a colorless oil; bp 262 °C; n_D^{20}=1.5474; IR (neat) ν 2930, 2825, 1595, 1570, 1490, 1410, 1100, 1045, 1005, 845, and 815 cm^{-1}; ^{1}H-NMR($CDCl_3$) δ 3.47 (3H, s, $-CH_2O\underline{CH_3}$), 3.95 (6H, s, ϕ-$O\underline{CH_3}$), 4.44 (2H, s, $-\underline{CH_2}OCH_3$), 6.93 (1H, d, J=2 Hz, aromatic proton), and 7.16 (1H, d, J=2 Hz, aromatic proton). This compound was identified with the synthetic **3m** by a comparison of their IR and ^{1}H-NMR spectra.

3-Bromo-4,5-dihydroxybenzaldehyde (4). Compound **4** was recrystallized from benzene–methanol to yield colorless needles; mp and mixed mp 230 °C; λ_{max} (EtOH) 288 nm; IR (KBr) ν 3425, 1650, 1580, 1440, 1310, 1185, 860, and 845 cm^{-1}; ^{1}H-NMR(DMSO-d_6) δ 7.24 (1H, d, J=2 Hz, aromatic proton), 7.53 (1H, d, J=2 Hz, aromatic proton), 9.68 (1H, s, formyl proton), and 10.29 (2H, bs, phenolic protons); MS *m/e* 218, 216 (M^+), 217, 215 (M^+-1), 189, 187 (M^+-CHO), and 137 (M^+-Br).

3,5-Dibromo-4-hydroxybenzyl Ethyl Ether (6). Compound **6** was recrystallized from hexane to yield colorless needles; mp and mixed mp 93—94 °C; λ_{max} (EtOH) 290

nm; IR (KBr) ν 3210, 2970, 2860, 1595, 1555, 1478, 1403, 1305, 1265, 1145, 1075, 1010, 875, and 730 cm^{-1}; ^{1}H-NMR ($CDCl_3$) δ 1.24 (3H, t, J=7 Hz, $-CH_2\underline{CH_3}$), 3.53 (2H, q, J=7 Hz, $-\underline{CH_2}CH_3$), 5.94 (1H, bs, phenolic proton), and 7.42 (2H, s, aromatic protons).

3,5-Dibromo-4-hydroxybenzaldehyde (7). Compound **7** was recyrstallized from hexane, yielding colorless needles; mp and mixed mp 189—190 °C; λ_{max} (EtOH) 277 and 346 nm; IR(KBr) ν 3180, 2860, 1670, 1580, 1550, 1480, 1415, 1305, 1245, 1205, 1055, 875, 740, and 660 cm^{-1}; ^{1}H-NMR ($CDCl_3$) δ 7.87 (1H, bs, phenolic proton), 8.10 (2H, s, aromatic protons), and 9.87 (1H, s, formyl proton).

3,5-Dibromo-4-hydroxybenzyl Alcohol (8). Compound **8** was recrystallized from benzene, yielding colorless crystals; mp and mixed mp 119—120 °C; λ_{max} (EtOH) 291 nm; ^{1}H-NMR ($CDCl_3$+DMSO-d_6) δ 4.12 (1H, t, J=4 Hz, $-CH_2O\underline{H}$), 4.60 (2H, d, J=4 Hz, $-\underline{CH_2}OH$), 7.50 (2H, s, aromatic protons), and 7.65 (1H, bs, phenolic proton). The ^{1}H-NMR spectrum of this compound has partially been reported previously.[19]

3-Bromo-4,5-dihydroxybenzyl Alcohol (9). Compound **9** was recrystallized from benzene–acetone yielding colorless needles; mp and mixed mp 104—105 °C; λ_{max} (EtOH) 287 nm; IR (KBr) ν 3410, 2960, 1595, 1425, 1340, 1290, 1185, 1120, 960, 860, and 840 cm^{-1}; ^{1}H-NMR (acetone-d_6) δ 4.48 (2H, s, $-\underline{CH_2}OH$), 4.3—4.7 (1H, bs, $-CH_2O\underline{H}$), 6.85 (1H, d, J=2 Hz, aromatic proton), 6.97 (1H, d, J=2 Hz, aromatic proton), and 8.02 (2H, bs, phenolic protons); MS *m/e* 220, 218 (M^+), 219, 217 (M^+-1), 203, 201 (M^+-H_2O+1), 202, 200 (M^+-H_2O), and 139 (M^+-Br).

We wish to thank Dr. Isao Sekikawa, Hokkaido University, for providing the ^{1}H-NMR and MS and much helpful advice.

References

1) For a preliminary account of this work, see K. Kurata, T. Amiya, and N. Nakano, *Chem. Lett.*, **1976**, 821.
2) D. J. Faulkner, *Tetrahedron*, **33**, 1421 (1977).
3) T. Saito and Y. Ando, *Nippon Kagaku Zasshi*, **76**, 478 (1955).
4) J. H. Hodgikin, J. S. Craigie, and A. G. McInnes *Can. J. Chem.*, **44**, 74 (1966).
5) J. S. Craigie and D. E. Gruenig, *Science*, **1967**, 1058.
6) N. Katsui, Y. Suzuki, S. Kitamura, and T. Irie, *Tetrahedron*, **23**, 1185 (1967).
7) J. M. Chantraine, G. Combaut, and J. Teste, *Phytochemistry*, **12**, 1793 (1973).
8) M. Pedersén, P. Seanger, and L. Fries *Phytochemistry*, **13**, 2273 (1974).
9) K. W. Glombitza and H. Stoffelen, *Planta Med.*, **22**, 391 (1972); H. Stoffelen, K. W. Glombitza, U. Murawski, U. Bielaczek, and H. Egge, *ibid.*, **22**, 396 (1972); K. W. Glombitza, H. Stoffelen, U. Murawski, U. Bielaczek, and H. Egge, *ibid.*, **25**, 104 (1974).
10) M. Pedersén and L. Fries, *Z. Pflanzenphysiol.*, **74**, 272 (1975).
11) B. Weinstein, T. D. Rold, C. E. Harrel Jr., M. W. Burns III and J. B. Waaland, *Phytochemistry*, **14**, 2667 (1975).
12) K. Kurata, T. Amiya, and K. Yabe, *Bull. Jap. Soc. Sci. Fish.*, **39**, 973 (1973); K. Kurata and T. Amiya, *ibid.*, **41**, 657 (1975).
13) K. Kurata and T. Amiya, *Chem. Lett.*, **1977**, 1134.
14) A. M. C. Magueur, A. C. P. Potier, J. Teste, A. Chiaroni, and C. Roche, *Phytochemistry*, **15**, 767 (1976).
15) M. Pedersén, *Phytochemistry*, **17**, 291 (1978).
16) G. Combaut, J. M. Chantraine, J. Teste, and K. W. Glombitza, *Phytochemistry*, **17**, 1791 (1978).
17) L. Lundgren, K. Olsson, and O. Threander, *Acta Chem. Scand.*, **33**, 105 (1979).
18) K. Kurata and T. Amiya, *Phytochemistry*, in press.
19) T. Higa and P. J. Scheuer, *Tetrahedron*, **31**, 2379 (1975).

Direct Conversion of Arylamines to the Corresponding Halides, Biphenyls, and Sulfides with *t*-Butyl Thionitrate

Shigeru OAE,* Kōichi SHINHAMA, and Yong Hae KIM
Department of Chemistry, The University of Tsukuba, Niiharigun, Ibaraki 305

(Received November 10, 1979)

t-Butyl thionitrate have been found to be an excellent diazotizing reagent of arylamines in aprotic nonpolar media, affording eventually such products as aryl chlorides, aryl bromides, aryl iodides, biphenyls, and aryl methyl sulfides in the presence of CCl_4, $CHBr_3$, I_2, benzene, and dimethyl disulfide, respectively, *via* extrusion of N_2.

In the course of our studies on the synthetic applications of thionitrites or thionitrates, we now have found that *t*-butyl thionitrate (**2**)[1] was an excellent diazotizing reagent in neutral, aprotic, and homogeneous media to convert various arylamines (**1**) in the presence of carbon tetrachloride, bromoform, iodine in benzene, benzene alone, and dimethyl disulfide to afford the corresponding aryl chloride (**4**), aryl bromide (**5**), aryl iodide (**6**), biphenyls (**3**), and methyl aryl sulfides (**7**), respectively, in good yields.

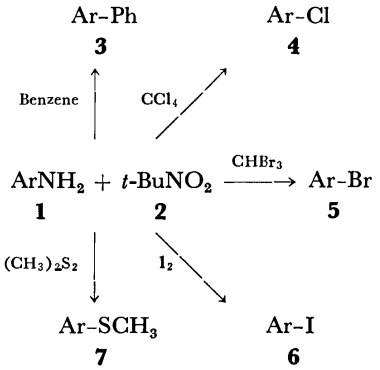

Although alkyl nitrites have been used for the same purposes,[2] thionitrites and thionitrates are considered to be better reagents for deamination of arylamines **1** due to the relatively weak S–N bonds of thionitrites and thionitrates. Indeed, the thionitrate **2** was found to be a remarkably effective reagent for deamination. Although *t*-butyl thionitrite is also an effective deaminating reagent which can afford aryl halides in the reaction with arylamines in the presence of copper(II) halides in acetonitrile at room temperature,[3] it is not thermally stable as compared to the thionitrate **2** and decomposes readily in boiling benzene or carbon tetrachloride, and hence it was not used for these uncatalyzed reactions.

Reactions of various arylamines (**1a—i**) with **2** in benzene gave the corresponding biphenyls (**3a—i**) in good yields (Table 1). The reaction was found to proceed in a short time when *p*-methoxyaniline (**1c**), which possesses an electron-donating methoxyl group, was treated with thionitrate **2**. However, the yield of 4-methoxybiphenyl (**3c**) was relatively low because of the formation of a large amount of dark uncharacterized substance. On the contrary, *p*-nitroaniline (**1d**) was found to react rather slowly but converted to the corresponding 4-nitrobiphenyl (**3d**) in a good yields in several hours.

$$\underset{\mathbf{1}}{ArNH_2} + \underset{\mathbf{2}}{t\text{-}BuSNO_2} \xrightarrow[80\ ^\circ C]{\text{Benzene}} \underset{\mathbf{3}}{Ar\text{-}Ph}$$

1a, 3a: Ar=Ph
1b, 3b: Ar=*p*-Cl-C_6H_4
1c, 3c: Ar=*p*-MeO-C_6H_4
1d, 3d: Ar=*p*-NO_2-C_6H_4
1e, 3e: Ar=*o*-NO_2-C_6H_4
1f, 3f: Ar=*p*-Br-C_6H_4
1g, 3g: Ar=*p*-CH_3-C_6H_4
1h, 3h: Ar=*m*-CH_3-C_6H_4
1i, 3i: Ar=*o*-CH_3-C_6H_4

Meanwhile, when isopentyl nitrate (**8**) was treated in a similar way with *p*-chloroaniline (**1b**), no reaction took place due undoubtedly to the relatively strong O–N bond of **8**.

$$\mathbf{1b} + \underset{\mathbf{8}}{(CH_3)_2CH(CH_2)_2ONO_2} \xrightarrow{\text{Benzene}} \not\rightarrow \mathbf{3b}$$

When aniline (**1a**) was treated with **2** in toluene, methylbiphenyl (**3j**) was obtained as a mixture of its positional isomers. GLC and ^{1}H-NMR analyses of this reaction mixture showed that the ortho, meta, and para isomers are formed in the ratio of *ca.* 4:2:1.

Table 1. Reactions of arylamines **1a—i** with thionitrate **2** in benzene

Compound	[2][a]/[1]	Reaction temp/°C[b]	Reaction time/h	Product	Yield/% c)	Yield/% d)	Mp/°C or Bp/°C/mmHg of the product
1a	1.4	80	2	**3a**	62	47	69—70 (lit,[2b] 68)
1b	1.4	80	6	**3b**	67	60	75—76 (lit,[2b] 76)
1c	1.4	80	0.2	**3c**	28	26	88—90 (lit,[2b] 90)
1d	1.4	80	19	**3d**	75	67	113—115 (lit,[2a] 111—113)
1e	1.4	80	14	**3e**	39	33	142—147/2[e] (lit,[2a] 180—82/20)
1f	1.4	80	7	**3f**	76	58	85—87 (lit,[5] 89.5—90)
1g	1.4	80	8	**3g**	39	38	46—47 (lit,[2a] 49—50)
1h	1.4	80	6	**3h**		35	110—115/2[e] (lit,[2a] 265—269/714)
1i	1.4	80	6	**3i**		27	114—120/2[e] (lit,[2a] 250—253/716)

a) Mol ratio. b) Refluxed in benzene. c) GLC yield. d) Isolated yield. e) Bath temperature.

Table 2. Reactions of arylamines **1** with thionitrate **2** in several aromatic solvents

Compound	Solvent	[2]/[1] [a]	Reaction temp/°C	Reaction time/h	Product	Isolated yield/% [b]
1a	Toluene	1.4	110 [c]	2	**3j**	30
1d	Toluene	1.4	110 [c]	2	**3k**	47
1d	Chlorobenzene	1.4	110 [c]	1	**3l**	58
1e	Toluene	1.4	110 [c]	2	**3m**	45
1g	Nitrobenzene	1.4	100	1	**3n**	42

a) Mol ratio. b) Mixture of isomers. c) Refluxed in solvents.

Table 3. Reactions of arylamines **1** with thionitrate **2** in halides

Compound	Solvent	[2]/[1] [a]	Reaction temp/°C	Reaction time/min	Product	Yield/% c)	Yield/% d)
1b	CCl_4	1.4	76 [b]	60	**4a**	46	40
1c	CCl_4	1.4	76 [b]	60	**4b**	37	28
1c	$CHBr_3$	1.4	25	5	**5a**	48	34
1d	$CHBr_3$	1.4	120	40	**5b**	80	75
1e	$CHBr_3$	1.4	76 [b]	30	**4c**	38	25
1f	$CHBr_3$	1.4	100	20	**5d**	65	60

a) Mol ratio. b) Refluxed in CCl_4. c) GLC yield. d) Isolated yield.

Table 4. Reactions of arylamines **1** with thionitrate **2** in the presence of iodine

Compound	[2]/[1] [a]	Reaction temp/°C	Reaction time/h	Product	Yield/% c)	Yield/% d)
1b	1.0	80 [b]	0.7	**6a**	35	32
1c	1.0	25	0.2	**6b**	51	48
1d	1.0	80 [b]	15	**6c**	80	71
1e	1.0	80 [b]	16	**6d**	64	53
1f	1.0	80 [b]	1.5	**6e**	79	64
1g	1.0	80 [b]	0.3	**6f**	79	74

a) Mol ratio. b) Refluxed in benzene. c) GLC yield. d) Isolated yield.

$$\underset{\mathbf{1a}}{PhNH_2} + \underset{\mathbf{2}}{t\text{-}BuSNO_2} \xrightarrow[2\,h]{\text{Toluene}} Ph\text{-}C_6H_4\text{-}CH_3 \quad (\mathbf{3j})$$

Steric hindrace of methyl group seems to have little effect in this reaction. Similar treatment of *p*-nitroaniline (**1d**), *o*-nitroaniline (**1e**), and *p*-toluidine (**1g**) in several solvents such as toluene, nitrobenzene, and chlorobenzene gave corresponding biphenyls (**3j**—**n**) as the mixture of ortho, meta, and para isomers. The results are listed in Table 2.

$$\underset{\mathbf{1}}{ArNH_2} + \underset{\mathbf{2}}{t\text{-}BuSNO_2} \xrightarrow{\text{Ph-Y}} Ph\text{-}C_6H_4\text{-}Y \quad (\mathbf{3})$$

3j: Ar=Ph, Y=CH_3
3k: Ar=*p*-NO_2-C_6H_4, Y=CH_3
3l: Ar=*p*-NO_2-C_6H_4, Y=Cl
3m: Ar=*o*-NO_2-C_6H_4, Y=CH_3
3n: Ar=*p*-CH_3-C_6H_4, Y=NO_2

Reaction of *p*-bromoaniline (**1f**) with **2** in pyridine did not give any deaminated product, since **2** rapidly decomposed in pyridine to give *S*-*t*-butyl 2-methyl-2-propanethiosulfonate (**9**).

$$\underset{\mathbf{1f}}{p\text{-}Br\text{-}C_6H_4NH_2} + \mathbf{2} \xrightarrow{\text{Pyridine}} \underset{\mathbf{9}}{t\text{-}BuSO_2S\text{-}Bu\text{-}t} + \mathbf{1f}$$

Various aryl chlorides **4** and aryl bromides **5** were also obtained by treating the corresponding arylamines **1** with **2** in carbon tetrachloride and bromoform, respectively. The results are listed in Table 3.

$$\underset{\mathbf{1}}{ArNH_2} + \underset{\mathbf{2}}{t\text{-}BuSNO_2} \xrightarrow{CCl_4} \underset{\mathbf{4}}{ArCl} \qquad \xrightarrow[CHBr_3]{} \underset{\mathbf{5}}{ArBr}$$

4a: Ar=*p*-Cl-C_6H_4
4b, **5a**: Ar=*p*-CH_3O-C_6H_4
5b: Ar=*p*-NO_2-C_6H_4
4c, **5d**: Ar=*p*-Br-C_6H_4
5c: Ar=*o*-NO_2-C_6H_4

The thionitrate **2** was found to be far better than alkyl nitrite in the syntheses of iodides **6** from the arylamines **1**. Upon treatment of **1** with **2** in the presence of iodine (half mol of amine) in refluxing benzene, the corresponding aryl iodides **6** were obtained in good yields as shown in Table 4. *p*-Toluidine (**1g**) was found to be converted to *p*-iodotoluene with isopentyl nitrite in the presence of iodine after a long reaction time (4 h) in a lower yield (40%).[2d] In

Table 5. Reactions of arylamines **1** with thionitrate **2** in dimethyl disulfide

Compound	[2][a] / [1]	Reaction temp/°C	Reaction time/min	Product	Isolated yield/%	Mp/°C or Bp/°C/mmHg of the product
1c	1.5	110	10	**7a**	47	90—95/2[b] (lit,[6] 104—106/7.1)
1d	1.5	110	10	**7b**	79	65—67 (lit,[4] 67)
1e	1.7	110	10	**7c**	77	58—60 (lit,[7] 60)
1f	1.1	110	10	**7d**	88	35—36 (lit,[8] 38—39)
1g	1.5	110	10	**7e**	62	90—93/53[b] (lit,[9] 94/31)

a) Mol ratio. b) Bath temperature.

the reaction of **1** and **2** in benzene, the yields of the corresponding biphenyls **3** were found to be very low due mainly to the superior reactivity of iodine over benzene to result in the rapid formation of **6**.

$$\underset{\mathbf{1}}{ArNH_2} + \underset{\mathbf{2}}{t\text{-}BuSNO_2} + I_2 \xrightarrow{\text{Benzene}} \underset{\mathbf{6}}{Ar\text{-}I}$$

6a: Ar=*p*-Cl-C_6H_4 **6d**: Ar=*o*-NO_2-C_6H_4
6b: Ar=*p*-MeO-C_6H_4 **6e**: Ar=*p*-Br-C_6H_4
6c: Ar=*p*-NO_2-C_6H_4 **6f**: Ar=*p*-CH_3-C_6H_4

Reactions of various arylamines **1** and **2** in dimethyl disulfide gave the corresponding aryl methyl sulfide (**7**) in good yields in a short reaction time and the results are listed in Table 5. Heating the solution prior to the addition of **2** is essential for the reaction. When the reaction was carried out at room temperature, deamination of arylamines **1** was slow and **2** was consumed by the reaction with dimethyl disulfide and the yields of the aryl methyl sulfides were low.

$$\underset{\mathbf{1}}{ArNH_2} + \underset{\mathbf{2}}{t\text{-}BuSNO_2} \xrightarrow{(CH_3)_2S_2} \underset{\mathbf{7}}{ArSCH_3}$$

7a: Ar=*p*-MeO-C_6H_4 **7d**: Ar=*p*-Br-C_6H_4
7b: Ar=*p*-NO_2-C_6H_4 **7e**: Ar=*p*-CH_3-C_6H_4
7c: Ar=*o*-NO_2-C_6H_4

Formation of nitrogen gas was clearly observed by mass spectrum, divulging the reaction to proceed *via* the $ArN_2^+OH^-$ that rapidly decomposes forming an aryl radical (**10**) which then reacts with the solvent or I_2 to afford the corresponding substitution product. Thiosulfonic *S*-ester **9** was also isolated in this reaction.

$$t\text{-}BuSNO_2 \underset{\mathbf{2}}{\rightleftharpoons} t\text{-}BuSONO \xrightarrow{\overset{Ar}{:NH_2\ 1}}$$

$$t\text{-}BuSO^- + ArN^+H_2NO \rightarrow t\text{-}BuSOH + ArN_2^+OH^- \rightarrow$$

$$\underset{\mathbf{10}}{Ar\cdot} + N_2 + H_2O + 1/2\ \underset{\mathbf{9}}{t\text{-}BuSO_2S\text{-}Bu\text{-}t}$$

When octylamine **11** was treated with **2** under similar conditions, no formation of deaminated product was observed, but *N*-(*t*-butylthio)octylamine (**12**) was obtained in a good yield.

$$\underset{\mathbf{11}}{n\text{-}C_8H_{17}NH_2} + \underset{\mathbf{2}}{t\text{-}BuSNO} \xrightarrow[81\%]{} \underset{\mathbf{12}}{n\text{-}C_8H_{17}NHS\text{-}Bu\text{-}t}$$

Experimental

All the melting points and boiling points were uncorrected. Elemental analyses were carried out by the Chemical Analysis Center at our University. Analytical determinations by GLC were performed on a Hitachi 163 gas chromatograph fitted with the following column (3 mm o.d.× 3 m): 10% SE-30 on Chromosorb W. ^{1}H-NMR spectra were taken at 60 MHz on a Hitachi R-24 A apparatus. IR spectra were recorded with a Hitachi 215 spectrometer. Mass spectra were recorded with a Hitachi RMU-6M spectrometer. The starting arylamines are all commercial products. Thionitrate **2** was prepared from the corresponding thiol with dinitrogen tetroxide.[1] Purely isolated deaminated products were used for GLC analyses.

Reactions of Arylamines (1) with Thionitrate (2) in Aromatic Compounds. The following is a typical procedure. *p*-Chloroaniline (**1b**) (637 mg, 5 mmol) and **2** (875 mg, 7 mmol) were refluxed in dry benzene (20 ml) for 6 h. The reaction mixture was concentrated by removing benzene *in vacuo*, and purified by TLC (silica gel, hexane:ether=10:1), affording 569 mg (60%) of 4-chlorobiphenyl (**3b**): mp 75—76 °C (recrystallized from ethanol), (lit,[2b] 76 °C).

Structures of **3a**—**n** were identified by IR, NMR, and mass spectroscopic data. Melting or boiling points of **3a**—**i** were identical with those of literatures as shown in Table 1. Physical and elemental analytical data of **3j**—**n** are listed in Table 6.

Reaction of Arylamines (1) with Thionitrate (2) in CCl_4 or $CHBr_3$. The following is a typical procedure. The thionitrate **2** (845 mg, 7 mmol) was added for a few minutes to a stirred solution of *p*-nitroaniline (**1d**) (690 mg, 5 mmol) in bromoform (10 ml) at 120 °C. After several minutes, vigorous evolution of nitrogen gas was observed. The solution was further stirred for 40 min at 120 °C. The solution was cooled and the solvent was evaporated *in vacuo*. TLC (silica gel, hexane:ether=10:1) gave 752 mg (75%) of pure *p*-bromonitrobenzene (**5b**).

IR spectra of all the halides in Table 3 were identical with those of commercial authentic samples.

Reactions of Arylamines (1) with Thionitrate (2) in the Presence of Iodine. The following is a typical procedure. *p*-Toluidine (**1g**) (535 mg, 5 mmol) and **2** (675 mg, 5 mmol) were added to a stirred solution of iodine (635 mg, 5 mmol) in dry benzene (20 ml). The solution was refluxed for 17 min. After the solution was cooled, diethyl ether was added to the solution and washed with aq sodium thiosulfate solution to remove iodine. The solution was dried ($MgSO_4$), concentrated, and purified by TLC (silica gel, hexane:ether=10:1) to give 812 mg (74%) of pure *p*-iodotoluene (**6f**).

IR spectra of all the iodides in Table 4 were identical with those of commercial authentic samples.

Reactions of Arylamines (1) with Thionitrate (2) in Dimethyl Disulfide. The following is a typical procedure. The solution of *p*-nitroaniline (**1d**) (690 mg, 5 mmol) in dimethyl disulfide (5 ml) was heated (*ca.* 100 °C) in advance. Then, **2** (1.01 g, 7.5 mmol) was added to the stirred solution

Table 6. Physical and analytical data of compounds **3j**—**n**[a]

Compound	Physical and analytical data
3j	IR (neat): 1472, 842, 750, and 687 cm^{-1}. NMR (CCl_4): δ 2.23 (s, 1.5H, $C\underline{H}_3$-),[b] 2.40 (br, s, 1.5H, $C\underline{H}_3$-),[c] and 7.00—7.60 (m, 9H, ring protons). Found: C, 92.55; H, 7.12%. Calcd for $C_{13}H_{12}$: C, 92.81; H, 7.19%.
3k	IR (neat): 1590, 1510, 1340, 848, 740, and 693 cm^{-1}. NMR (CCl_4): δ 2.23 (s, 1.7H, $C\underline{H}_3$-), 2.40 (s, 1.3H, $C\underline{H}_3$-), 7.00—7.73 (m, 6H, ring protons), and 7.73—8.20 (m, 2H, ring protons). Found: C, 72.93; H, 5.17; N, 6.75%. Calcd for $C_{13}H_{11}O_2N$: C, 73.23; H, 5.20; N, 6.57%.
3l	IR (neat): 1512, 1348, 1103, 850, 745, and 690 cm^{-1}. NMR (CCl_4): δ 7.14—7.70 (m, 6H), and 7.70—8.17 (m, 2H). Found: C, 61.42; H, 3.80; N, 5.95%. Calcd for $C_{12}H_8ClO_2N$: C, 61.69, H, 3.45, N, 5.99%.
3m	IR (neat): 1510, 1350, 843, 780, 743, and 700 cm^{-1}. NMR (CCl_4): δ 2.03 (s, 1.6H, $C\underline{H}_3$-), 2.28 (s, 1.4H, $C\underline{H}_3$-), and 7.4—8.0 (m, 8H, ring protons). Found: C, 72.85; H, 5.22; N, 6.82%. Calcd for $C_{13}H_{11}O_2N$: C, 73.23; H, 5.20; N, 6.57%.
3n	IR (neat): 1508, 1345, 812, 742, 700 cm^{-1}. NMR (CCl_4): δ 2.30 (s, 3H, $C\underline{H}_3$-), and 6.45—8.10 (m, 8H, ring protons). Found: C, 72.99; H, 5.25; N, 6.90%. Calcd for $C_{13}H_{11}O_2N$: C, 73.23; H, 5.20; N, 6.57%.

a) A mixture of its positional isomers. b) Ortho isomer. c) Meta and para isomers.

in a few minutes. The solution was stirred further for 10 min, then cooled and the solvent was evapolated *in vacuo*. Purification by TLC (silica gel, hexane:ether=20:1) gave 664 mg (79%) of methyl *p*-nitrophenyl sulfide (**7b**): mp 65—67 °C (recrystallized from ethanol), (lit,[4] 67 °C).

Structures of **7a**—**e** were identified by IR, NMR and mass spectroscopic data. Melting or boiling points of **7a**—**e** were identical with those of literatures as shown in Table 5.

N-*(t-Butylthio)octylamine (12)*. Thionitrate **2** (875 mg, 7 mmol) was added in a few minutes to a stirred solution of amine **11** (648 mg, 5 mmol) in benzene (10 ml). The solution was refluxed for 10 min, cooled, and then concentrated *in vacuo*. The mixture was purified by TLC (silica gel, hexane), to give 885 mg (81%) of **12** as a colorless oil, bp (bath temp) 85—95 °C/533 Pa. IR (neat): 1460, 1135, and 910 cm^{-1}. NMR (CCl_4): δ=0.6—2.0 (m, 15H, $C\underline{H}_3$-$(C\underline{H}_2)_6$-), 1.17 (s, 9H, *t*-Bu), 2.36 (br, 1H, N$\underline{H}$), and 2.86 (br, 2H, -$C\underline{H}_2$-NH). MS (70 eV), *m/e* (rel intensity), 217 (36, M^+), 160 (39, *n*-$C_8H_{17}NHS^+$), 128 (16, *n*-$C_8H_{17}NH^+$), and 57 (100, *t*-Bu^+).

Found: C, 65.95, H, 12.41; N, 6.32%. Calcd for $C_{12}H_{17}NS$: C, 66.29; H, 12.52; N, 6.44%.

References

1) a) R. S. George, U. S. Patent 2307624 (1943). *Chem. Abstr.*, **37**, p3588[9] (1943); b) S. Oae, K. Shinhama, and Y. H. Kim, *Chem. Lett.*, **1979**, 1077; c) S. Oae, K. Shinhama, K. Fujimori, and Y. H. Kim, *Bull. Chem. Soc. Jpn.*, **53**, 775 (1980).

2) a) S. Huang, *Hua Hsüeh Hsüeh Pao*, **25**, 171 (1959). *Chem. Abstr.*, **54**, 4489h (1960); b) J. I. G. Cadogan, *J. Chem. Soc.*, 4257 (1962); c) J. I. G. Cadogan, D. A. Roy, and D. M. Smith, *J. Chem. Soc., C*, **1966**, 1249; d) L. Friedamn and J. F. Chlebowski, *J. Org. Chem.*, **33**, 1636 (1968).

3) Y. H. Kim, K. Shinhama, and S. Oae, *Tetrahedron Lett.*, **1978**, 4519.

4) F. Mayer, *Ber.*, **42**, 3050 (1909).

5) M. Gomberg and W. E. Bachmann, *Org. Synth.* Coll. Vol. I, 113 (1956).

6) N. C. Cutress, T. B. Grindley, A. R. Katritzky, and R. R. Topson, *J. Chem. Soc., Perkin Trans. 2*, **1974**, 263.

7) D. G. Foster and E. E. Reid, *J. Am. Chem. Soc.*, **46**, 1936 (1924).

8) J. B. Hyne and J. W. Greidanus, *Can. J. Chem.*, **47**, 803 (1969).

9) K. Auwers and F. Arndt, *Ber.*, **42**, 2714 (1909).

Synthetic Photochemistry. XVII.[1] The Singlet-oxygen Oxidation of Vinylcyclopropane in the Presence of Diphenyl Sulfide. The Chemical Reduction of a Dioxetane to a *cis*-1,2-Glycol

Toshihide HATSUI and Hitoshi TAKESHITA*

Research Institute of Industrial Science, 86, Kyushu University, Hakozaki, Fukuoka 812

(Received November 14, 1979)

The singlet-oxygen oxidation of a spirocyclic vinylcyclopropane in the presence of diphenyl sulfide, a reducing agent, was shown to form a *cis*-glycol by the O–O cleavage of dioxetane. The determination of the stereochemistry of isomeric glycols obtained by chemical derivation led to a revision of the structure of the azido alcohol formed during the photosensitized oxygenation in a presence of the azide ion to the *trans*-derivative.

Previously, we have reported[2] a *cis*-glycol formation by a photoreductive O–O cleavage of the dioxetane (**A**) in the Rose Bengal (RB)-sensitized photooxidation of **1**, dispiro[cyclopropane-1,3′-tricyclo[5.2.1.$0^{2,6}$]deca-4′,8′-diene-10′,1″-cyclopropane], a spirocyclic vinylcyclopropane, which is a typical dioxetane-forming alicyclic olefin in the singlet-oxygen oxygenation. This new process has been verified by low-temperature experiments monitored by NMR spectroscopy,[13] and its generality has been demonstrated by experiments with indene[2] and thujopsene.[4] From a comparative point of view, it will be worthwhile to examine the chemical reduction of **A**. The results have in fact verified the O–O cleavage to give the *cis*-glycol (**2**) by the thioether-reduction which will be a subject of this paper. In literature, several investigations along the same line of a singlet-oxygen oxidation with a reducing agent are recorded; Kaneko *et al.*[5] used thiourea to reduce the endo-peroxide from cyclopentadiene, and Wassermann and Saito[6] showed the results of the thioether-reduction of a series of photooxygenation products. In this paper we will describe the reaction in a system of diphenyl sulfide (**3**) and Methylene Blue (MB) in chloroform. This selection was made out of consideration of the solubility as well as the moderate reactivity of **3** toward singlet oxygen compared with that of dialkyl sulfides.

When a chloroform solution of **1**, **3**, and MB was irradiated by means of a tungsten lamp under an oxygen atmosphere, a considerable rate retardation was recognized; the reaction was still not completed after 32 h. From the reaction mixture, **2**,[7] **4**, **5**, **6**, and **7** were isolated, along with large amounts of diphenyl sulfoxide and diphenyl sulfone, by silica-gel chromatography. The major product, **4** (41%), and another product, **5** (31%), were identified as the dioxetane-derived dialdehyde and the known vinyloxirane respectively.[8] In addition, a glycol, **2** (19%), was identical with the authentic sample of *cis*-glycol prepared by the RB-sensitized photooxidation of **1**[2] in respect to the NMR spectral analysis and the easy formation of the dioxolane derivative, **8**. **6** (3%) and **7** (3%) were a pair of isomeric ketones, and the NMR and IR spectra of **6** [δ:[9] 0.45 (4H, m), 0.75—1.35 (4H, m), 2.03 (1H, dd, J=19.5, −0.1 Hz*), 2.17 (1H, m), 2.42 (1H, dd, J=19.5, 13.5 Hz*), 2.53 (1H, m), 2.77—3.02 (2H, m), and 6.16 (2H, m). $\nu_{C=O}$: 1730 cm^{-1}] and of **7**[δ: 0.3—0.7 (8H, m), 1.95 (1H, dd, J=19.7, 1.5 Hz), 2.25 (1H, d, J=19.7 Hz),

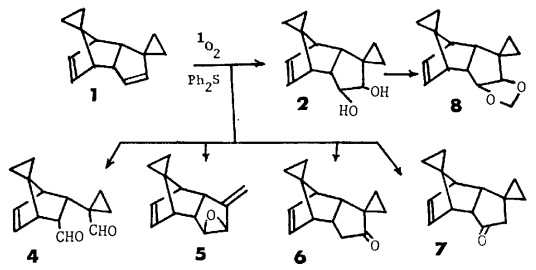

Chart 1.

2.27 (1H, m), 2.58 (1H, m), 2.68 (1H, dd, J=8.5, 4 Hz), 3.25 (1H, ddm, J=8.5, 4.5 Hz), 6.12 (1H, ddd, J=6, 3, 1 Hz), and 6.25 (1H, J=6, 3, 1 Hz . $\nu_{C=O}$: 1740 cm^{-1}] were consistent with the depicted structures (Chart 1), which were themselves supported chemically by the selective derivation of **6** from a monotosylate of **2**.

It is noteworthy that the concomitant formation of **6** and **7** strongly suggests that an epoxide, **9**, is not likely to be their precursor. This can be checked experimentally: The epoxidation of **1** with *m*-chloroperbenzoic acid (MCPA) in dichloromethane yielded no **9**; alternatively, we obtained were isomeric epoxide (**10**), the cyclopropyl ketone (**7**), and two glycol mono-*m*-chlorobenzoates (**11a** and **12**). The **10** was identical with the sample obtained in the sensitized photooxygenation of **1** in the presence of sodium azide[10] or in the RB-sensitized photooxygenation.[1] On the basis of the NMR analysis, **12** was demonstrated to be a *m*-chlorobenzoate of the primary alcohol; it is probably formed by the solvolysis of the cyclopropane. On the other hand, **11a** was convertible to an isomer (**11b**) by prolonged standing at room temperature. The coupling patterns of the NMR spectra of **11a** and **11b** were quite similar and suggested an intact stereochemistry on the oxygen functions. Therefore, **11a** and **11b** must be derivatives of **2**, **11**, and **12** are secondary products of an intermediate epoxide, **9**. **11a** was indeed saponified to **2** in methanol, and **11b** was converted to **2** by an LAH reduction. The spontaneous formation of the *cis*-glycol derivatives during the epoxidation is remarkable, but not surprising; it can be explained in terms of an orbital asistance form the norbornene double bond of **1**.

Meanwhile, the MCPA-oxidation of **1** in a solvent containing methanol yielded predominantly methoxy derivatives, **13**, and its further epoxidized product, **14**, together with **10** and **7**. Again, the ionic cleavage of the cyclopropane ring is characteristic. Therefore,

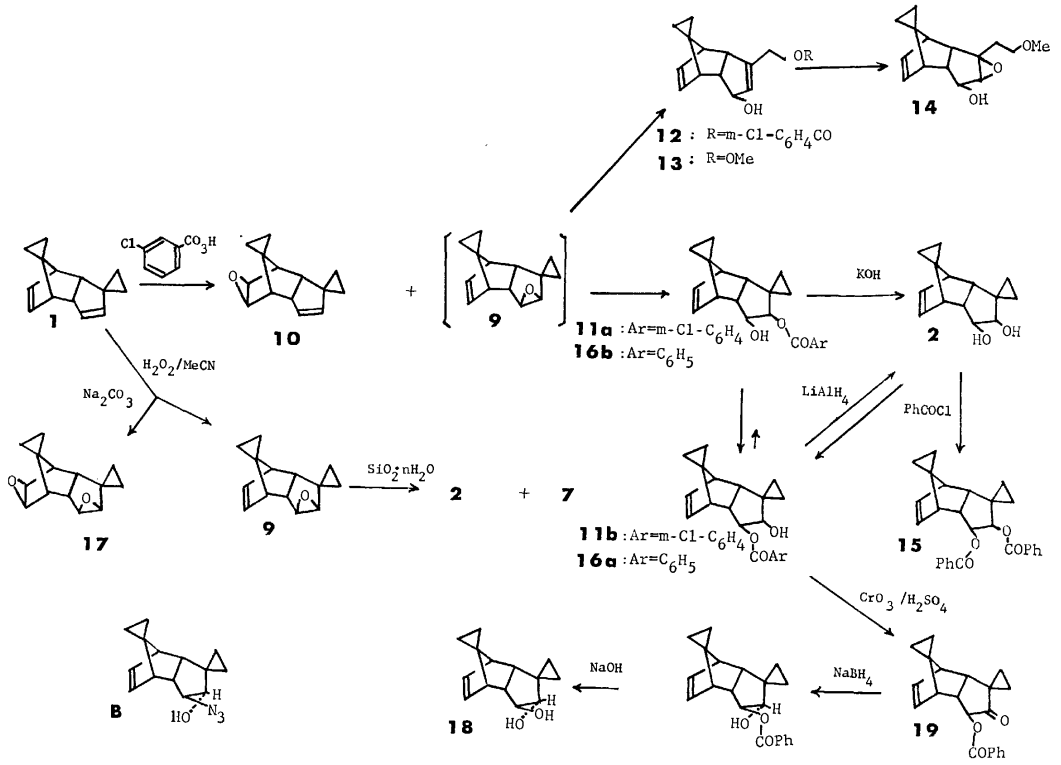

Chart 2.

the absence of the ketone (**6**) in the chemical oxidation is clear evidence of the involvement of independent precursors in chemical and photochemical oxidations.

In this regard, the benzoylation products of **2** were a dibenzoate (**15**) and a monobenzoate (**16**) [δ: 0.40 (7H, m), 0.90 (1H, m), 1.83 (1H, br., OH), 2.04 (1H, m), 2.40 (1H, m), 2.82 (1H, dd, J=9.5, 4 Hz), 3.07 (1H, ddd, J=9.5, 4.5, 3.5 Hz), 3.90 (1H, d, J=4.5 Hz), 5.03 (1H, dd, J=4.5, 3.5 Hz), 6.35 (2H, m), 7.28—7.55 (3H, m), and 7.99 (2H, m) for the **a**-isomer; 4.06 (1H, dd, J=4.5, 4 Hz), and 4.98 (d, J=4 Hz) for the **b**-isomer (**a**:**b**=85:15)]. Again, the monobenzoate showed acyl-migration.

After extensive investigations, we have found a method to obtain this acid-sensitive epoxide, **9**. By the mild oxidation of **1** with the acetonitrile–hydrogen peroxide adduct under weakly basic conditions,[11,12] two epoxides, **9** and **17**, were obtained; they were subsequently purified by fractional recrystallization. **9** (colorless needles, from methanol) was highly reactive, as expected; *i.e.*, a brief treatment with silica gel in chloroform caused a facile conversion into **2** and **7**, but not to **6**. On the other hand, crystalline bisepoxide (**17**), lacking the norbornene C–C bond, was relatively stable.

These findings have established that the precursor of **2** in the photooxygenation must be the dioxetane, **A**. The following points are particularly important: i) There is a difference in the selectivity of the reaction site between the chemical epoxidation and the photooxygenation, ii) there is no incorporation of the solvent nucleophile into the photooxygenation products, iii) there is no cleavage product of the cyclopropane ring in the photooxygenation, and iv) the compositions of the ketones formed in the different reactions differ. Should **2** be derived by the oxidation of **1** by some active species like a complex of diphenyl sulfide and oxygen, the observed reactivity, an overwhelming oxidation at the spiroheptene moiety, must be rather controversial.[10]

At the same time, we wish to make an additional point as to the effect of the reducing agent on the relative yields of **4** and **5** in this sensitized photooxygenation. Upon the addition of **3**, although the yield of **5** was almost unaffected, the yield of **4** decreased considerably, from 85 to 41%. This certainly suggests that the precursor of **5** is not interconvertible with the dioxetane, being parallel to the previous results on the solvent and temperature dependences for the occurrence of **5**.[2,3] Therefore, the precursor of **5**, if any, must be very short-lived to be trapped by a bimolecular process.

Furthermore, since the formation of **6** can not be explained in terms of a simple hydrolysis of **9**, an alternative pathway should be provided. To explain the reaction of the diphenyl-sulfide reduction of dioxetanes, the involvement of dipolar S–O-linked intermediate has been suggested by Wassermann and Saito.[6] In fact, they have identified a *trans*-glycol *via* an epoxide, which is shown to be derived by complicated rearrangements, but have failed to detect a *cis*-glycol. The present study can well be explained also in terms of an S–O-intermediate; otherwise, the direct isolation of **2**, a *cis*-glycol, together with **6** and **7**, isomeric ketones, is difficult to explain. Thus, Chart 3 is provided to interpret all the results.

The coupling patterns in the NMR spectra of the *cis*-glycol derivatives disclosed a discrepancy from those

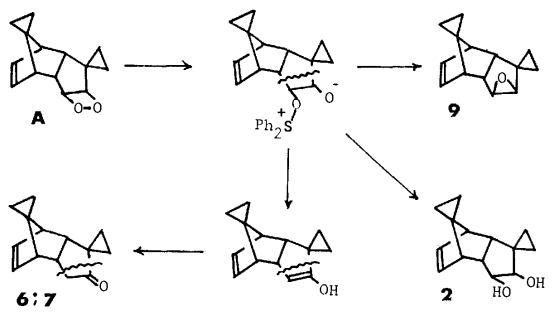

Chart 3.

of the azido alcohol (**B**), which was formed in the sensitized photooxidation of **1** in the presence of sodium azide.[10] The stereochemistry of **17** was identified as *cis* on the basis of the observed $^3J_{CH-OH}$ splittings due to a slow exchange of the hydroxyl proton, and this phenomenon was interpreted in terms of the hydrogen-bonding of the hydroxyl group to the azido group. To solve the problem, we should take the isomeric *trans*-glycol (**18**) for an NMR comparison. Thus, **15** was converted into a keto ester (**19**) by chromium(VI) oxide oxidation; the subsequent reduction of **19** with sodium borohydride yielded another glycol, which must be **18**. Indeed, the spin-spin splitting patterns of the NMR spectrum of **18** were similar to those of **B**. Therefore, the orginal assignment, a *cis*-orientation for the substituents of **B**, must be revised to *trans*.[13] Nevertheless, the conclusion of our previous work, *i.e.*, that the dioxetanes or peroxiranes are not responsible for the formation of azido alcohols, is still valid.

Experimental

*MB-Sensitized Photooxygenation of **1** in the Presence of Diphenyl Sulfide (**3**).* A chloroform solution (15 cm³) of **1** (460 mg), MB (60 mg), and **3** (3.73 g) was irradiated by means of a 500-W tungsten lamp under an oxygen stream at room temperature for 110 h. Subsequent silica gel column chromatography of the mixture gave recovered **1** (170 mg, 37%) and **3** (3.3 g) from the hexane fractions. Subsequently, a vinyloxirane (**5**, 90 mg, 31%), a ketone (**6**, 9 mg, 3%), a colorless oil [Found: M. W., 200.1170. Calcd for $C_{14}H_{16}O$: 200.1201], another ketone (**7**, 8 mg, 3%; colorless prisms; mp 76—77 °C [Found: M. W., 200.1170]), a dialdehyde (**4**, 109 mg, 41%), and a glycol (**2**, 54 mg, 19%; colorless needles, mp 56—57 °C)[7] were eluted from hexane–ether (4:1). From the most polar fractions (hexane–ether=1:1), considerable amounts of diphenyl sulfoxide and diphenyl sulfone were obtained.

*Preparation of a Dioxolane Derivative (**8**).* A benzene solution (1 cm³) of **2** (11.6 mg) and dimethoxymethane (0.5 cm³) containing TsOH (1 mg) was kept at room temperature for 18 h. The mixture was then extracted with benzene, and the extracts were purified on a silica-gel column to give **8** (a colorless oil, 56 mg (45%) [Found: M.W., 230.1334. Calcd for $C_{15}H_{18}O_2$: 230.1307. δ: 0.08—0.75 (7H, m), 0.90 (1H, m), 2.05 (1H, m), 2.36 (1H, m), 2.74 (1H, dd, J=9, 5 Hz), 3.07 (1H, dd, J=9, 5 Hz), 4.08 (2H, s), 4.88 (1H, s), 4.90 (1H, s), 6.22 (1H, ddd, J=6, 3, 1 Hz), and 6.32 (1H, ddd, J=6, 3, 1 Hz). ν: 2950, 1090 cm⁻¹]).

*MCPA-Oxidation of **1** in Dichloromethane: Formation of **7**, **10**, **11**, and **12**.* **1** (900 mg) was dissolved in dichloromethane (15 cm³), after with MCPA (500 mg) was added in portions. After 1 h, an aqueous sodium carbonate was added and then extracted into dichloromethane. Silica gel column chromatography of the extracts gave recovered **1** (440 mg, from hexane–ethyl acetate (98:2)), **10**[2] (130 mg, 26%, from hexane–ethyl acetate (95:5)), **7** (14 mg, 3%, from hexane–ethyl acetate (9:1)), **11** (438 mg, 49%, from hexane–ethyl acetate (8:2 to 7:3) [Found: M.W., 356.1143. Calcd for $C_{21}H_{21}O_3Cl$: 356.1179. δ: 0.28—0.7 (7H, m), 0.88 (1H, m), 2.00 (1H, OH), 2.0 (1H, m), 2.36 (1H, m), 4.04 (1H, t, J=4.5 Hz), 4.95 (1H, d, J=4.5 Hz), 6.33 (2H, m), 7.2—7.6 (2H, m), and 7.7—8.0 (2H, m). ν: 3600, 3480, 1730, 1260 cm⁻¹], a colorless oil), and **12** (174 mg, 20%, from hexane–ethyl acetate (6:4)) [Found: M.W., 356.1184. δ: 0.43 (4H, s), 1.69 (1H, br., OH), 2.25 (1H, m), 2.44 (3H, m), 2.74 (1H, ddd, J=8, 5, 2 Hz), 3.48 (1H, m), 4.12 (1H, br., s), 4.44 (2H, t, J=7 Hz), 5.41 (1H, br., s), 5.99 (2H, m), 7.25—7.55 (2H, m), and 7.8—8.0 (2H, m). ν: 3430, 1735, 1260 cm⁻¹].

*MCPA-Oxidation of **1** in Methanol and Dichloromethane.* **1** (1010 mg) was dissolved in a mixture of methanol (30 cm³) and dichloromethane (8 cm³) and was then oxidized by MCPA (420 mg) at room temperature for 2.5 h. The mixture was treated with $NaHCO_3$ and extracted with dichloromethane. Silica gel chromatography of the extracts afforded, at first, recovered **1** (700 mg), and then **10** (92 mg (28%)), **7** (8 mg (2%)), and a mixture of methoxy derivatives (265 mg (**13**, *ca.* 44%, and **14**, *ca.* 20%)), which were later fractionated by the use of a pre-packed silica gel column (Merck) to give two colorless oils, **13** [Found: M.W., 232.1481. Calcd for $C_{15}H_{20}O_2$: 232.1463. δ: 0.41 (4H, br. s), 1.71 (1H, br., OH), 2.20 (1H, m), 2.24 (2H, t, J=7 Hz), 2.40 (1H, m), 2.69 (1H, ddd, J=7.5, 4.5, 2 Hz), 3.32 (3H, s), 3.4 (1H, m), 3.50 (2H, t, J=7 Hz), 4.08 (1H, m), 5.32 (1H, m), 5.91 (1H, ddd, J=6, 3, 1 Hz), and 6.01 (1H, ddd, J=6, 3, 1 Hz). ν: 3400 cm⁻¹] and **14** [Found: M. W., 248.1381. Calcd for $C_{15}H_{20}O_3$: 248.1413. δ: 0.39 (4H, br. s), 1.75 (1H, dt, J=15, 7 Hz), 2.05 (1H, dt, J=15, 7 Hz), 2.24 (1H, m), 2.32 (1H, br. s, OH), 2.4 (2H, m), 3.12 (1H, m), 3.31 (3H, s), 3.34 (1H, dm, J=2 Hz), 3.43 (2H, tm, J=7 Hz), 3.81 (1H, t, J=2 Hz), and 6.22 (2H, m). ν: 3610, 3500 cm⁻¹].

*Isomerization of **11a** to **11b**.* **11a** (neat liquid, 45 mg) was kept at room temperature for a month. The NMR analysis disclosed the formation of **11b** [δ: 0.42 (4H, m), 0.88 (4H, m), 1.94 (1H, OH), 2.04 (1H, m), 2.38 (1H, m), 2.92 (1H, dd, J=9.5, 4 Hz), 3.08 (1H, dt, J=9.5, 4 Hz), 3.89 (1H, d, J=4.5 Hz), 5.00 (1H, dd, J=4.5, 4 Hz), 6.34 (2H, m), 7.2—7.6 (2H, m), and 7.8—8.0 (2H, m). ν: 3620, 3500, 1728, 1255 cm⁻¹] (**a**:**b**=15:85).

*Saponification of **11a**: Formation of **2**.* **11a** (42 mg) was dissolved in a methanolic KOH solution (0.2 M (1 M= 1 mol dm⁻³), 10 cm³) and then kept at room temperature for 24 h. The mixture was subsequently acidified by dil HCl, and extracted with ether. Silica gel chromatography of the extracts gave a colorless oil, **2** (15 mg, 58%).

*LAH Reduction of **11b** to **2**.* An anhydrous ether solution (3 cm³) of **11b** (77 mg), containing *ca.* 13 mg of **11a**, was treated with LAH (30 mg) for 15 h. The mixture was then chromatographed on a silica gel column to give **2**, 28 mg (51%).

*Benzoylation of **2**: Formation of a Dibenzoate (**15**) and a Monobenzoate (**16**).* A benzene solution (8 cm³) of **2** (290 mg) was treated with benzoyl chloride (262 mg) and pyridine (0.4 cm³) for 48 h. Extractions by dichloromethane and water and subsequent silica gel column chromatography of the extracts gave **15** (colorless prisms, mp 155—156 °C

(from ethanol)) [Found: C, 78.67; H, 6.08%. Calcd for $C_{28}H_{26}O_4$: C, 78.85; H, 6.14%. δ: 0.44 (4H, m), 0.55—0.75 (3H, m), 0.95 (1H, m), 2.06 (1H, m), 2.44 (1H, m), 3.18 (2H, m), 5.20 (2H, m), 6.48 (1H, m), 7.1—7.6 (6H, m), and 7.8—8.0 (2H, m). ν: 1725 cm^{-1}], 42 mg (11%) and **16** (a colorless oil, 236 mg (80%), which consisted of an inseparable mixture (**15a**:**15b**=85:15) [Found: C, 78.07; H, 6.95%. Calcd for $C_{21}H_{22}O_3$: C, 78.23; H, 6.88%]).

*Epoxidation of **1** under Weakly Basic Conditions: Formation of a Bisepoxide (**17**) and a Monoepoxide (**9**).* To an acetonitrile solution (10 cm^3) of **1** (320 mg) and one drop of aqueous 1 M KOH, hydrogen peroxide (30%, 0.7 cm^3) was added under ice-cooling. At once, an evolution of oxygen gas occurred, after which an aqueous 10% sodium carbonate solution was added, drop by drop, until the gas evolution ceased. The mixture was then warmed to 40 °C. After 1 h, the mixture was extracted with dichloromethane and water, and dried on magnesium sulfate. The subsequent evaporation of the solvent *in vacuo* left a crystalline solid (258 mg), which was indicated to be a mixture of **9** and **17** (4:3 according to the NMR spectrometry). Upon fractional recrystallizations from hexane, it gave **17** (colorless prisms, mp 121—122 °C [Found: C, 77.85; H, 7.38%. Calcd for $C_{14}H_{16}O_2$: C, 77.75; H, 7.46%. δ: −0.05—0.25 (2H, m), 0.4—0.75 (4H, m), 0.8—1.05 (2H, m), 1.70 (1H, d, J= 4.5 Hz), 2.08 (1H, d, J=4.6 Hz), 2.40 (1H, dd, J=8.5, 4.5 Hz), 2.94 (1H, dd, J=8.5, 4.6 Hz), 2.99 (1H, d, J= 2.7 Hz), 3.42 (1H, dd, J=3.7, 1 Hz), 3.52 (1H, d, J=2.7 Hz), and 3.59 (1H, dd, J=3.7, 1 Hz)]). Then, recrystallizations of the residue from methanol gave **9** (colorless prisms, mp 80.5—82 °C [Found: M. W., 200.1182. Calcd for $C_{14}H_{16}O$: 200.1201. δ: 0.3—0.8 (8H, m), 2.01 (1H, m), 2.32 (1H, m), 2.50 (1H, dd, J=7.7, 4.2 Hz), 2.79 (1H, d, J=2.4 Hz), 3.17 (1H, dd, J=7.7, 4.3 Hz), 3.28 (1H, d, J=2.4 Hz), and 6.20 (2H, m)]).

*Treatment of **9** with Silica Gel.* A dichloromethane solution (2 cm^3) of **9** was mixed with a silica gel (Merck, Kieselgel 60). The products, as characterized on thin-layer plates, were **7** and **2**.

*Chromium(VI) Oxide Oxidation of **16**: Formation of a Keto Ester (**19**).* An acetone solution (10 cm^3) of **16** (90 mg) was oxidized by chromium(VI) oxide and sulfuric acid for 5 min. A colorless oil, **19** (86 mg, 96%) [Found: C, 78.72; H, 6.29%. Calcd for $C_{21}H_{20}O_3$: C, 78.72; H, 6.29%. δ: 0.45 (4H, m), 0.90—1.55 (4H, m), 2.18 (1H, m), 2.68 (1H, m), 3.05 (2H, m), 4.83 (1H, d, J=3.7 Hz), 6.33 (2H, m), 7.3—7.6 (3H, m), and 8.00 (2H, m). ν: 1740, 1730, 1265 cm^{-1}] was obtained after silica gel chromatography.

*Sodium Borohydride Reduction of **19**: Formation of a* trans*-Glycol (**18**).* A methanol solution (5 cm^3) of **19** (81 mg) was reduced by $NaBH_4$ (52 mg) for 4 h. An aqueous alkaline solution was then added to the mixture, and it was hydrolyzed for 24 h. By silica gel column chromatography of the mixture, the desired glycol (**18**), as a single product, was isolated as colorless crystals (mp 85—86 °C, 42 mg (76%) [Found: M. W., 218.1297. Calcd for $C_{14}H_{18}O_2$: 218.1307. δ: 0.0—0.7 (8H, m), 1.8 (2H, OH), 1.95 (1H, m), 2.32 (1H, m), 2.70 (1H, ddd, J=10, 7, 4 Hz), 2.88 (1H, dd, J=10, 4 Hz), 3.43 (1H, dd, J=8, 7 Hz), 3.86 (1H, d, J=8 Hz), and 6.27 (2H, m). ν: 3320, 1100 cm^{-1}]).

*Conversion of **2** into **6**.* An anhydrous benzene solution (3 cm^3) of **2** (135 mg) was treated with TsCl (150 mg) at room temperature for 15 h and subsequently at 80 °C for 4 h. The mixture was then diluted with dil HCl and extracted with ether, and the extract was purified on a silica-gel column to give a colorless oil, **6** (30 mg, 52%), and some recovered **2** (70 mg, 52%).

References

1) Part XVI: H. Takeshita, T. Hatsui and T. Masuda, *Kyushu Daigaku Sogo Rikogaku Kenkyuka Hokoku*, **1**, 35 (1979).
2) H. Takeshita and T. Hatsui, *J. Org. Chem.*, **43**, 3080 (1978).
3) H. Takeshita, T. Hatsui, and H. Mametsuka, *Heterocycles*, **11**, 323 (1978).
4) H. Takeshita, T. Hatsui, and I. Shimooda, *Tetrahedron Lett.*, **1978**, 2889.
5) C. Kaneko, A. Sugimoto, and S. Tanaka, *Synthesis*, **12**, 876 (1974).
6) H. H. Wassermann and I. Saito, *J. Am. Chem. Soc.*, **97**, 905 (1975).
7) In a preliminary report,[2] we have described **2** as an oil.
8) H. Takeshita, T. Hatsui, and H. Kanamori, *Tetrahedron Lett.*, **1973**, 1697.
9) The NMR spectra were measured in $CDCl_3$ solutions by means of an FX 100 Model apparatus, JEOL Co., and the chemical shifts were expressed in the δ scale from the internal standard, TMS. The coupling constants cited were obtained by the first order analysis except for the asterisked figures, which were obtained by the *ABX* treatment. The IR spectra were measured either as KBr disks or in CCl_4 solutions.
10) T. Hatsui and H. Takeshita, *Chem. Lett.*, **1977**, 603.
11) G. B. Payne, P. H. Deming, and P. H. Williams, *J. Org. Chem.*, **26**, 659 (1961).
12) R. Shankaranarayan, S. Krishnappa, and S. Dev, *Tetrahedron*, **33**, 885 (1977).
13) Previously, we have isolated three *vic*-azidoalcohols, two of which carry the functional groups on the norbornane moiety, and there was no problem in deducing the orientation. The third isomer (**17**) now turned out to be *trans*, rather surprisingly revealing a spin-spin splitting of the hydroxyl proton, ^3J=8 Hz, which is probably attributable to a sterical reason.

Synthesis of 2,11-Dehydrohomoadamantane (Tetracyclo[5.3.1.$0^{2,4}$.$0^{3,9}$]undecane) and 2,11-Dehydrohomoadamant-4-ene (Tetracyclo[5.3.1.$0^{2,4}$.$0^{3,9}$]undec-5-ene)[1,2]

Takeo KATSUSHIMA, Ken'ichiro MAKI, Ryohei YAMAGUCHI, and Mituyosi KAWANISI*

Department of Industrial Chemistry, Faculty of Engineering, Kyoto University, Yoshida, Sakyo-ku, Kyoto 606

(Received November 30, 1979)

Bromination of tricyclo[5.3.1.$0^{4,9}$]undeca-2,5-diene gave *endo*-2,*endo*-6- and *endo*-2,*exo*-6-dibromotetracyclo-[5.3.1.$0^{3,5}$.$0^{4,9}$]undecanes along with *syn*-11,*endo*-2-dibromotricyclo[4.3.1.$1^{3,8}$]undec-4-ene (**10a**) in a ratio of 3:3:1. A thermal treatment of the mixture of these dibromides at 140—150 °C induced a skeletal rearrangement to afford **10a** and *syn*-11,*exo*-2-dibromotricyclo[4.3.1.$1^{3,8}$]undec-4-ene (**10b**) in 87% yield (**10a**:**10b**=2:5). The new "non-bridgehead" 2,11-dehydrohomoadamantane was obtained by the hydrogenation of **10a** and **10b** followed by Wurtz type reductive cyclization. The unsaturated analogue, 2,11-dehydrohomoadamant-4-ene was also synthesized from **10a** and **10b** by the similar cyclization reaction.

The chemistry of strained organic molecules has attracted a considerable attention of many chemists and is still actively being explored.[3] Strained cage compounds which usually contain a cyclopropane and/or cyclobutane ring in their frameworks have demonstrated a number of interesting and unusual chemical properties of carbon-carbon σ-bond.[4] Out of five possible "non-bridgehead" mono-dehydrohomoadamantanes, the strained cage compounds which incorporate a cyclopropane or cyclobutane ring in their cage structures (**1**—**5**), three (**2**, **3**, and **4**) of them have been synthesized and characterized so far.[5-7] As a consequence of our continuing interest in the strained cage compounds,[5b,8] we have investigated a synthetic pathway to 2,11-dehydrohomoadamantane (**1**), a new entry to the "non-bridgehead" dehydrohomoadamantanes. We have recently prepared an interesting diene, tricyclo[5.3.1.$0^{4,9}$]undeca-2,5-diene (**7**),[8c] which is a potential precursor to some substituted homoadamantane (tricyclo[4.3.1.$1^{3,8}$]undecane) derivatives. For example, the homoallylic carbocation (**8**) generated by electrophilic reaction of **7** may produce homoadamantane system *via* homoallyl-cyclopropylcarbinyl-cyclobutyl rearrangement as is shown in Fig. 2.[9] We now wish to report here the synthesis of new "non-bridgehead" dehydrohomoadamantane, 2,11-dehydrohomoadamantane (**1**) as well as 2,11-dehydrohomoadamant-4-ene (**6**) *via* the above mentioned rearrangement.[10]

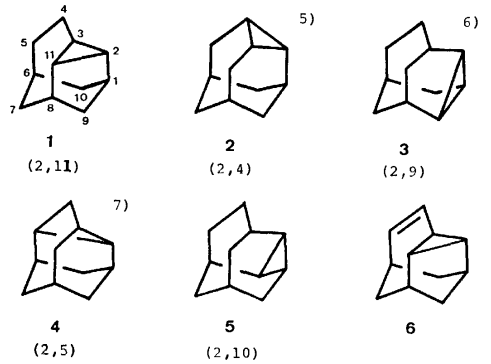

Fig. 1. "Non-bridgehead" dehydrohomoadamantanes.

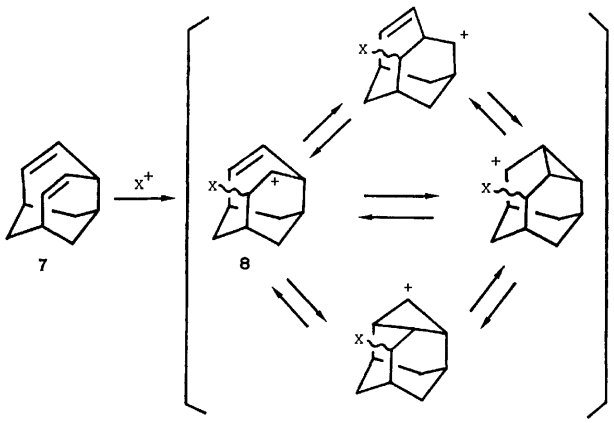

Fig. 2. Homoallyl-cyclopropylcarbinyl-cyclobutyl rearrangement.

Results and Discussion

When the diene (**7**) was treated with bromine in dichloromethane at 0 °C, three dibromides, *endo*-2,*endo*-6- and *endo*-2,*exo*-6-dibromotetracyclo[5.3.1.-$0^{3,5}$.$0^{4,9}$]undecanes (**9a** and **9b**) and *syn*-11,*endo*-2-dibromotricyclo[4.3.1.$1^{3,8}$]undec-4-ene (**10a**), were obtained in 96% yield (**9a**:**9b**:**10a**=3:3:1 by PMR analysis). Although their complete separation was difficult because of their instabilities toward chromatographic treatment, low temperature recrystallizations made it possible to obtain **9a**, and **9b** in pure forms, respectively. The dibromides, **9a** and **9b**, showed no olefinic proton in their PMR spectra and a absorption band at 3010 cm^{-1} indicative of a cyclopropane ring in their IR spectra. The presence of a plane of symmetry in **9a** was indicated by only one kind of carbinyl protons on the bromine substituted carbons at 4.48 ppm as a singlet shown in its PMR spectrum; this was also confirmed by CMR which demonstrated only seven kinds of carbons. On the other hand, the PMR spectrum of **9b** showed two kinds of carbinyl protons at 4.88 ppm as a triplet (J=6 Hz) and 4.83 ppm as a singlet. It has been already known that the *endo*-carbinyl proton on C_2 (or C_6) of tetracyclo[5.3.1.$0^{3,5}$.$0^{4,9}$]undecane deriva-

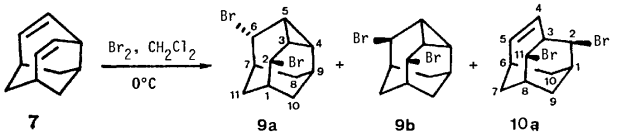

Scheme 1.

tives couples with the adjacent protons as a triplet with coupling constant of *ca.* 6 Hz but the *exo*-one does not in their PMR spectra.[8a,11] Accordingly, the structures of **9a** and **9b** were determined to be *endo*-2,*endo*-6- and *endo*-2,*exo*-6-dibromotetracyclo[5.3.1-$0^{3,5}.0^{4,9}$]undecanes, respectively. The above determination was further supported by the fact that reduction [12,13] of a mixture of the three dibromides by Raney-Ni gave tricyclo[5.3.1.$0^{4,9}$]undecane (**11**)[8] and homoadamantane (**12**) (**11**:**12**=7:1).

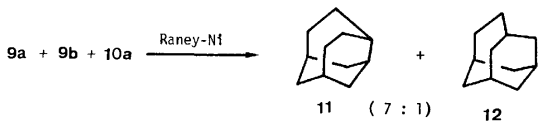

Scheme 2.

When the mixture of the dibromides (**9a**, **9b**, and **10a**) was heated under the reduced pressure (140—150 °C/533 Pa), an intriguing skeletal rearrangement took place to give **10a** and *syn*-11,*exo*-2-dibromotricyclo[4.3.1.$1^{3,8}$]undec-4-ene (**10b**) in 87% yield (**10a**:**10b**=2:5 by PMR analysis). It was also observed that a prolonged heating converted **10a** into **10b**; this result implies that **10b** is more thermodynamically stable than **10a**. Catalytic hydrogenation of this mixture over PtO_2 gave the saturated dibromides, *syn*-11,*endo*-2- and *syn*-11,*exo*-2-dibromotricyclo[4.3.1.-$1^{3,8}$]undecanes (**13a** and **13b**) in 26 and 53% yields, respectively. Since the saturated dibromides, **13a** and **13b**, were stable toward chromatographic treatment,

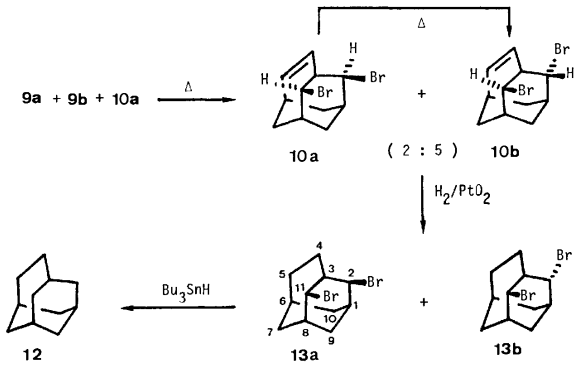

Scheme 3.

each of them was easily isolated by column chromatography on silica gel and could be completely characterized. Reduction of **13a** and **13b** with Bu_3SnH gave **12** in high yield, confirming the parent skeleton. The CMR and PMR spectra of **13a** showed only eight kinds of carbons and one kind of carbinyl protons on the bromine substituted carbons at 4.17 ppm as a singlet, respectively. Only *syn*-11,*endo*-2-dibromotricyclo[4.3.1.$1^{3,8}$]undecane can be responsible for the above spectra.[14] Consequently, **13b** was determined to be *syn*-11,*exo*-2-dibromotricyclo[4.3.1.$1^{3,8}$]undecane, because its PMR spectrum demonstrated two kinds of carbinyl protons at 5.10 ppm as a triplet (J=4.2 Hz) and 4.45 ppm as a singlet. Since the structures of **13a** and **13b** were established, those of the unsaturated dibromides, **10a** and **10b**, were deduced to be *syn*-11,*endo*-2- and *syn*-11,*exo*-2-dibromotricyclo-[4.3.1.$1^{3,8}$]undec-4-enes, respectively, on the basis of their CMR and PMR spectra. This deduction was confirmed by further chemical transformations (*vide infra*).

The following mechanistic pathway can well rationalize the formation of **9a**, **9b**, and **10a** in the bromination reaction of the diene **7**. The intervention of the homoallylic cations (A and B) may control the

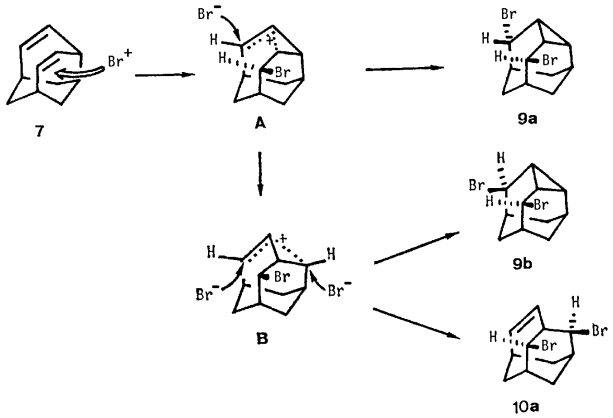

Scheme 4.

stereochemistry of the bromine addition. The analogous homoallylic cations were quoted in the bromination reactions of bicyclo[2.2.1]heptadiene[15] and bicyclo[2.2.2]octadiene.[13]

Since the thermal rearrangement of **9a** and **9b** seems interesting, the pure **9a** was heated under the same conditions as above in order to obtain further insight about the stereochemical outcome of the bromine substituents. Unfortunately, it was observed by PMR that **9a** was easily isomerized to **9b** under the rection conditions. For example, after 10 min, the mixture consisted of **9a**, **9b**, **10a**, and **10b** in a ratio of 47:31:14:8. Although the stereochemical course of this rearrangement could not be established, this process was much easier than the thermal isomerization of 2,4-dehydrohomoadamantane itself (**2**) to homoadamant-4-ene (tricyclo[4.3.1.$1^{3,8}$]undec-4-ene) (**14**) at 400 °C.[16]

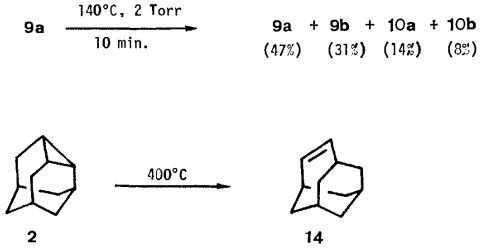

Scheme 5.

Now that 2,11-dibromotricyclo[4.3.1.$1^{3,8}$]undecanes (**13a** and **13b**) have become in our hands, the next step is reductive cyclization to 2,11-dehydrohomoadamantane (**1**). When **13b** was treated with lithium in dry THF at room temperature for 3.5 h, **1** was obtained in 94% yield along with a slight amount of homoadamantane (**12**) (**1**:**12**=15:1 by GLC analysis).

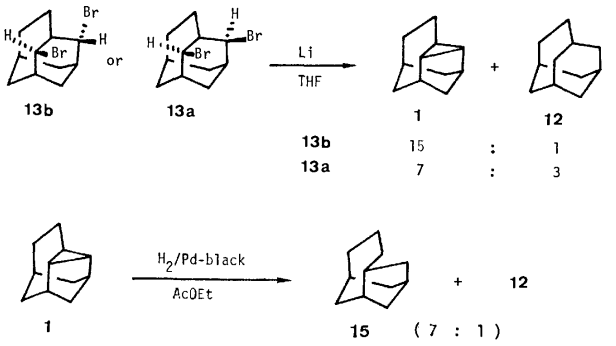

Scheme 6.

The similar treatment of **13a** with lithium gave the same products in 81% yield (**1**:**12**=7:3). The structure of **1** was confirmed by elemental analysis and spectroscopic data including its CMR spectrum which showed eight kinds of carbons due to its symmetry. Furthermore, hydrogenation of **1** over Pd-black gave 4-homoprotoadamantane (tricyclo[5.3.1.$0^{3,9}$]undecane) (**15**)[17] and **12** in 78% yield (**15**:**12**=7:1 by GLC analysis). This is a marked contrast with the fact that **2** is hydrogenated to give only **12**.[5a]

Whereas **13b** gave predominantly the cyclized product, the similar reaction of the unsaturated dibromide **10b** with lithium afforded a mixture of 2,11-dehydrohomoadamant-4-ene (**6**), the diene **7**, and **14** in 80% yield (**6**:**7**:**14**=9:3:1 by GLC analysis). The same treatment of a mixture of **10a** and **10b** gave **6**, **7**, and **14** in a ratio of 6:6:1 in 89% yield. The structure of **6** was particularly reflected in its CMR spectrum (eight kinds of carbons due to its symmetry) and further acertained by the hydrogenation to **1**.

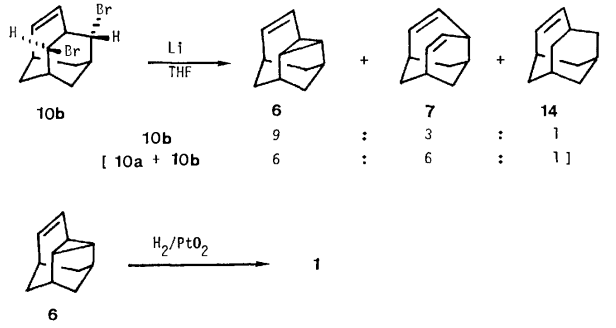

Scheme 7.

Finally, it should be mentioned that the new "non-bridgehead" dehydrohomoadamantane **1** may be a possible precursor hitherto unknown 2,4-disubstituted 4-homoprotoadamantanes, considering that the C_2–C_3 bond of **1** is easily cleaved upon hydrogenation as is described above.[18] In addition, **6** is an interesting cage molecule because it incorporates a vinylcyclopropane moiety which has long been known as a reactive grouping.[19]

Experimental

All the temperatures were uncorrected. Melting points were measured in sealed capillaries. The IR spectra were recorded on a Shimadzu IR-27 spectrometer. The mass spectra were taken by using a Hitachi RMS-4 mass spectrometer. The exact mass spectrum was obtained on a Hitachi RMU-8GN mass spectrometer. The PMR and CMR spectra were obtained on Varian EM-390 or EM-360 and CFT-20 spectrometers, tetramethylsilane being chosen as the internal standard. Microanalyses were performed in Kyoto University Elemental Analysis Center.

The Reaction of Tricyclo[5.3.1.$0^{4,9}$]undeca-2,5-diene (7) with Bromine. To a solution of **7** (400 mg; 2.70 mmol) in dichloromethane (20 ml) was added dropwise bromine (480 mg; 3.00 mmol) at 0 °C. Then, the reaction mixture was washed with 10% $Na_2S_2O_3$ aq and brine, and dried (Na_2SO_4). After filtration, the solvent was evaporated to give a colorless oil, which contained *endo*-2,*endo*-6-dibromotetracyclo[5.3.1.-$0^{3,5}$.$0^{4,9}$]undecane (**9a**), *endo*-2,*exo*-6-dibromotetracyclo[5.3.1.-$0^{3,5}$.$0^{4,9}$]undecane (**9b**), and *syn*-11,*endo*-2-dibromotricyclo-[4.3.1.$1^{3,8}$]undec-4-ene (**10a**) in a ratio of 3:3:1 (PMR analysis) (808 mg; 96%). When this oil was stored in a refrigerator, colorless crystals appeared. After a small amount of pentane was added, the crystals were collected by filtration and washed with cold pentane to give pure **9a** (197 mg). The filtrate was condensed under reduced pressure and amorphous solids appeared. The solids were collected by filtration, recrystallized from a small amount of pentane at low temperature, and then kept in a refrigerator for a few days to afford pure **9b** (40 mg). **9a**: mp 79—83 °C (dec). MS *m/e* (rel intensity): 308, 306, 304 (M^+, 5, 9, 5), 227 (96), 225 (100), 145 (59). IR (KBr): 3010 (weak), 2925, 1170, 940, 775, 690 cm^{-1}. PMR δ ($CDCl_3$): 4.48 (2H, s), 2.50—0.90 (12H, br. complex m). CMR δ ($CDCl_3$): 55.3 (2CH), 36.1 (2CH), 35.1 (CH_2), 27.2 ($2CH_2$), 23.0 (2CH), 20.9 (CH), 15.3 (CH). Found: C, 43.07; H, 4.90%. Calcd for $C_{11}H_{14}Br_2$: C, 43.16; H, 4.61%. **9b**: mp 57—61 °C (dec). MS *m/e* (rel intensity): 308, 306, 304 (M^+, 6, 12, 6), 227 (96), 225 (100), 145 (63). IR (KBr): 3010 (weak), 2925, 905, 735, 710 cm^{-1}. PMR δ (CCl_4): 4.88 (1H, t, J=6.0 Hz), 4.83 (1H, s), 2.40—1.00 (12H, br. complex m). CMR δ ($CDCl_3$): 61.0 (CH), 53.7 (CH), 36.0 (CH), 35.6 (CH_2), 35.0 (CH), 30.7 (CH_2), 27.3 (CH_2), 24.6 (CH), 22.9 (CH), 21.7 (CH), 20.6 (CH). Found: C, 43.08; H, 4.77%. Calcd for $C_{11}H_{14}Br_2$: C, 43.16; H, 4.61%. The dibromide (**10a**) could not be isolated in a pure form because of its unstability toward thermal and chromatographic treatments. Its spectral data were deduced from the mixture and described below.

*Reduction of **9a**, **9b**, and **10a** with Raney-Ni.* A solution of the dibromides, **9a**, **9b**, and **10a** (139 mg; 0.45 mmol), triethylamine (91 mg; 0.90 mmol), and excess Raney-Ni-W_2 (*ca.* 0.5 g) in cyclohexane was vigorously stirred under hydrogen for 24 h. The reaction mixture was filtered and washed with 5% HCl aq and brine and dried (Na_2SO_4). After being passed through a silica-gel column, the solvent was evaporated to give two hydrocarbons [46 mg; 68%, **11**:**12**=7:1 (GLC analysis, PEG 20 M, 90 °C)]. Each of the products was isolated by preparative GLC and shown to be completely identical with the authentic sample in GLC retention time and PMR.

*Reduction of the Dibromides, **9a**, **9b**, and **10a**.* (1) A mixture of the dibromides (243 mg; 0.79 mmol) and Bu_3SnH (433 mg; 1.49 mmol) in ether (30 ml) was refluxed for 30 h under nitrogen. After the solvent was evaporated, the residue was chromatographed on silica gel. Elution by hexane gave **7** (87 mg; 71%). (2) To a suspension of $LiAlH_4$ (75 mg; 1.97 mmol) in ether (10 ml) was added dropwise a solution of the dibromides (93 mg; 0.30 mmol) in ether (10 ml) and the mixture was stirred at room temperature for 24 h. After a small amount of saturated Na_2SO_4

aq was added to the mixture, the ether layer was separated by decantation and washed with brine, and dried (Na_2SO_4). Filtration followed by evaporation of the solvent gave **7** as a sole product (38 mg; 86%). (3) To a mixture of the dibromides (141 mg; 0.48 mmol), magnesium (35 mg; 1.46 mmol) in dry THF (5 ml) was added a few drops of methyl iodide. The reaction mixture was refluxed overnight under nitrogen, poured onto water, and extracted with ether. The extract was shown to contain only **7** by GLC analysis.

*Thermal Rearrangement of **9a**, **9b**, and **10a** to **10a** and **10b**.* Distillation of a mixture of **9a**, **9b**, and **10a** (1041 mg; 3.40 mmol) at 140—150 °C (533 Pa) by means of Kugelrohr gave **10a** and **10b** (903 mg; 87%) in a ratio of 2:5 (PMR analysis). When the mixture (450 mg) was heated at 150 °C for 3 h under atmospheric pressure and then distilled (140—150 °C/267 Pa), only **10b** was obtained (385 mg; 85%). *syn*-11,*exo*-2-Dibromotricyclo[4.3.1.$1^{3,8}$]undec-4-ene (**10b**): mp 123—1255 °C. MS *m/e* (rel intensity): 308, 306, 304 (M^+, 9, 16, 9), 227 (98), 225 (100), 145 (76). IR (KBr): 3025 (weak), 2925, 950, 730, 710, 670 cm^{-1}. PMR δ (CCl_4): 6.20 (1H, t, J=9.0 Hz), 5.70 (1H, t, J=9.0 Hz), 4.90 (1H, t, J=4.5 Hz), 4.67 (1H, s), 3.03 (1H, t, J=7.5 Hz), 2.90—1.40 (9H, br. complex m). CMR δ ($CDCl_3$): 140.5 (CH), 130.2 (CH), 58.6 (CH), 53.0 (CH), 49.6 (CH), 37.9 (CH), 37.5 (CH), 35.5 (CH_2), 32.4 (CH_2), 30.3 (CH), 27.3 (CH_2). Found: C, 43.43; H, 4.90%. Calcd for $C_{11}H_{14}Br_2$: C, 43.16; H, 4.61%. The following spectroscopic data for **10a** were deduced from those of the mixture of **10a** and **10b**. *syn*-11,*endo*-2-Dibromotricyclo[4.3.1.$1^{3,8}$]undec-4-ene (**10a**): PMR δ (CCl_4): 6.05 (2H, m), 4.55 (2H, s), 3.30—1.10 (10H, br. complex m). CMR δ ($CDCl_3$): 140.5 (CH), 132.1 (CH), 53.1 (2CH), 47.6 (CH), 38.1 ($2CH_2$), 35.5 (2CH), 30.3 (CH), 24.7 (CH_2).

syn-11, endo-*2- and* syn-*11*, exo-*2-Dibromotricyclo[4.3.1.$1^{3,8}$]-undecanes (**13a** and **13b**).* A mixture of **10a** and **10b** (915 mg; 2.99 mmol) and PtO_2 (40 mg) in methanol (50 ml) was vigorously stirred under hydrogen. After one equivalent of hydrogen had been absorbed, the catalyst was removed by filtration and the solvent was evaporated to give a crude mixture (886 mg), which was chromatographed on silica gel. Elution by hexane afforded **13b** (599 mg; 53%) and, subsequently, **13a** (240 mg; 26%). **13a**: mp 158—159 °C. MS *m/e* (rel intensity): 229, 227 (M^+—Br, 20, 20), 147 (100), 119 (42), 105 (33), 91 (51). IR (KBr): 2925, 1455, 1215, 1180, 940, 700 cm^{-1}. PMR δ (CCl_4): 4.17 (2H, s), 3.20—1.06 (14H, br. complex m). CMR δ ($CDCl_3$): 56.9 (2CH), 48.5 (CH), 36.8 ($2CH_2$), 35.6 (2CH), 31.9 (CH_2), 30.8 (CH_2), 29.6 (CH), 24.2 (CH_2). Found: C, 42.90; H, 5.18%. Calcd for $C_{11}H_{16}Br_2$: C, 42.88; H, 5.23%. **13b**: mp 162—163 °C. MS *m/e* (rel intensity): 229, 227 (M^+—Br, 29, 30), 147 (100), 119 (29), 91 (44). IR (KBr): 2925, 1455, 665 cm^{-1}. PMR δ (CCl_4): 5.10 (1H, t, J=4.2 Hz), 4.45 (1H, s), 2.93—1.15 (14H, br. complex m). CMR δ ($CDCl_3$): 62.9 (CH), 59.2 (CH), 49.4 (CH), 36.4 (CH), 35.7 (CH_2), 35.0 (CH), 33.8 (CH_2), 32.4 (CH_2), 32.2 (CH_2), 29.9 (CH), 27.8 (CH_2). Found: C, 42.95; H, 5.26%. Calcd for $C_{11}H_{16}Br_2$: C, 42.88; H, 5.23%.

*Reduction of **13a** or **13b** with Bu_3SnH.* A solution of **13b** (140 mg; 0.45 mmol) and Bu_3SnH (610 mg, 2.10 mmol) in benzene (10 ml) was refluxed under nitrogen for 3 h. The reaction mixture was washed with brine and dried (Na_2SO_4). After filtration, the solvent was evaporated to give a crude mixture, which was shown to contain only one hydrocarbon product by GLC analysis (PEG 20 M, 100 °C). The product was collected by preparative GLC and shown to be identical with authentic homoadamantane (tricyclo-[4.3.1.$1^{3,8}$]undecane) (**12**) in GLC retention time and PMR. The similar treatment of **13a** (68 mg; 0.22 mmol) with Bu_3SnH (175 mg; 0.60 mmol) to above also gave **12** as a sole product.

*2,11-Dehydrohomoadamantane (**1**).* A mixture of **13b** (596 mg; 1.94 mmol) and small pieces of lithium (458 mg; 65.00 mmol) in dry THF was stirred at room temperature under nitrogen for 3.5 h and poured onto ice-water. Organic materials were extracted with ether and washed with brine (three times), and dried (Na_2SO_4). After filtration, the solvent was evaporated to give **1** along with a slight amount of **12** (268 mg; 94%, **1**:**12**=15:1 by GLC analysis; PEG 20 M, 100 °C). The analytical sample was obtained by preparative GLC. Similarly, the reaction of **13a** (197 mg; 0.58 mmol) with lithium also afforded **1** and **12** in a ratio of 7:3 (70 mg; 81%). **1**: mp 124—127 °C. MS *m/e* (rel intensity): 148 (M^+, 27), 79 (100). IR (CCl_4): 3030, 2930, 1450 cm^{-1}. PMR δ (CCl_4): 3.00—1.05 (16H, br. complex m). CMR δ ($CDCl_3$): 54.0 (CH_2), 36.7 ($2CH_2$), 36.2 (CH_2), 34.7 (CH), 34.6 (2CH), 28.5 (CH), 28.4 (2CH), 23.6 (CH_2). Found: C, 88.89; H, 10.95%. Calcd for $C_{11}H_{16}$: C, 89.12; H, 10.88%.

*Hydrogenation of **1**.* A suspension of **1** (45 mg; 0.30 mmol) and Pd-black (25 mg) in ethyl acetate (4 ml) was vigorously stirred under hydrogen until **1** disappeared. After removal of the catalyst by filtration, the solvent was evaporated to give a mixture of 4-homoprotoadamantane (**15**) and **12** (36 mg; 78%) in a ratio of 7:1 (GLC analysis; PEG 20 M' 100 °C). Pure **15** was obtained by preparative GLC and shown to be identical with the authentic sample.[17]

*2,11-Dehydrohomoadamant-4-ene (**6**).* A mixture of **10b** (602 mg; 1.97 mmol) and small pieces of lithium (543 mg; 77.6 mmol) in dry THF (30 ml) was stirred for 20 h at room temperature under argon and poured onto ice-water. After filtration, organic materials were extracted with dichloromethane and washed with brine, and dried (Na_2SO_4). After filtration, the solvent was evaporated to give a mixture of three hydrocarbons, **6**, **7**, and **14** (230 mg; 80%), in a ratio of 9:3:1 (GLC analysis; PEG 20 M, 100 °C). Pure **6** (144 mg, 50%) was secured by preparative GLC. **6**: mp 109—110 °C. MS *m/e* (rel intensity): 146 (M^+, 52), 80 (100). IR (KBr): 3020, 2925, 2875, 1670, 1465, 1445, 1350, 1050, 960, 790, 750, 705 cm^{-1}. PMR δ (CCl_4): 5.97 (1H, d.d, J=10.5 and 8.0 Hz), 5.67 (1H, d, J=10.5 Hz), 2.90—1.20 (12H, br. complex m). CMR δ ($CDCl_3$): 139.6 (CH), 126.3 (CH), 54.4 (CH_2), 37.9 (2CH), 33.7 (CH), 30.8 ($2CH_2$), 29.7 (CH), 25.6 (2CH). Found: *m/e* 146.1098. Calcd for $C_{11}H_{14}$: M, 146.1095.

*Hydrogenation of **6** to **1**.* A suspension of **6** (20 mg; 0.13 mmol) and PtO_2 (2 mg) in methanol (2 ml) was vigorously stirred under hydrogen. After one equivalent of hydrogen was absorbed, the mixture was filtered and the solvent was evaporated to give almost pure **1** (13 mg; 64%).

We thank Dr. Ryusei Konaka of Shionogi Phamaceutical Co. Ltd., for obtaining the exact mass spectrum of **6**.

References

1) Part of this work has been presented in the 36th annual meeting of Chemical Society of Japan held in Osaka, 3S16, (1977).

2) Provided that there is no ambiguity, we use trivial nomenclature for simplicity.

3) A. Greenberg and J. F. Liebman, "Strained Organic Molecules," Academic Press, New York (1978).

4) *inter alia*, (a) P. G. Gassman, *Acc. Chem. Res.*, **4**, 128

(1971); (b) L. A. Paquette, *ibid.*, **4**, 280 (1971); (c) J. F. Liebman and A. Greenberg, *Chem. Rev.*, **76**, 311 (1976); (d) K. J. Bishop III, *ibid.*, **76**, 461 (1976).

5) For 2,4-dehydrohomoadamantane (**2**): (a) Z. Majerski, S. H. Liggero, and P. v. R. Schleyer, *J. Chem. Soc., Chem. Commun.*, **1970**, 949; (b) R. Yamaguchi, T. Katsushima, T. Imagawa, and M. Kawanisi, *Synth. Commun.*, **1974**, 83; R. Yamaguchi, T. Katsushima, and M. Kawanisi, *Bull. Chem. Soc. Jpn.*, **47**, 2830 (1974).

6) For 2,9-dehydrohomoadamantane (**3**): R. K. Murray, Jr., D. L. Goff, and R. E. Ratych, *Tetrahedron Lett.*, **1974**, 763.

7) For 2,5-dehydrohomoadamantane (**4**): T. Sasaki, S. Eguchi, and Y. Hirako, *J. Org. Chem.*, **42**, 2981 (1977). We could also synthesize **4** by an independent route. The result will be published in due course.

8) (a) R. Yamaguchi, T. Katsushima, and M. Kawanishi, *Bull. Chem. Soc. Jpn.*, **48**, 2328 (1975); (b) R. Yamaguchi and M. Kawanisi, *Chem. Lett.*, **1975**, 649; (c) T. Katsushima, R. Yamaguchi, and M. Kawanisi, *J. Chem. Soc., Chem. Commun.*, **1975**, 692; (d) T. Katsushima, R. Yamaguchi, M. Kawanisi, and E. Ōsawa, *ibid.*, **1976**, 39.

9) For this rearrangement under the stable conditions, see G. A. Olah, G. Liang, K. A. Babiak, T. K. Morgan, Jr., and R. K. Murray, Jr., *J. Am. Chem. Soc.*, **98**, 576 (1976).

10) During a preparation of this manuscript, Murray and coworker reported the synthesis of **1** and **6** in a completely different route [R. K. Murray, Jr., and T. M. Ford, *J. Org. Chem.*, **44**, 3504 (1979)].

11) D. P. G. Hamon, G. F. Taylor, and R. N. Young, *Tetrahedron Lett.*, **1975**, 1623.

12) The reduction with Bu_3SnH, LAH, and Mg regenerated the starting diene (**7**) in all cases. See Experimental Section.

13) For reduction of the similar dibromide of tricyclo-[3.2.1.$0^{2,7}$]octane system, see C. A. Grob and J. Hostynek, *Helv. Chim. Acta*, **46**, 1676 (1963).

14) It has been already known that the *exo*-proton on C_2 position of tricyclo[4.3.1.$1^{3,8}$]undecane (homoadamantane) system appears as a singlet in PMR and that the *endo*-one does as a triplet with a coupling constant of 4.5 Hz. See Ref. 8a and H. Langhals and C. Ruchardt, *Chem. Ber.*, **107**, 1245 (1974).

15) S. Winstein and M. Shatavsky, *Chem. Ind. (London)*, **1956**, 56.

16) J. E. Baldwin and M. W. Greyston, *J. Am. Chem. Soc.*, **96**, 1629 (1974).

17) N. Takaishi, Y. Inamoto, K. Aigami, Y. Fujikura, E. Ōsawa, M. Kawanisi, and T. Katsushima, *J. Org. Chem.*, **42**, 2041 (1977).

18) For the synthesis of 2,4-disubstituted homoadamantanes from 2,4-dehydrohomoadamantane, see Ref. 8a.

19) For example, see S. Sarel, *Acc. Chem. Res.*, **11**, 204 (1978).

The Chemistry of Phenalenium Systems. XXXI.[1] The Synthesis, Dimerization, and Trapping of 6-Methylenebenzo[*cd*]pyrene

Osamu Hara, Kagetoshi Yamamoto, and Ichiro Murata*
Department of Chemistry, Faculty of Science, Osaka University, Toyonaka, Osaka 560
(Received December 6, 1979)

The acetolysis of 6-mesyloxymethyl-6*H*-benzo[*cd*]pyrene (**6**) gave 7,7a-dihydrospiro[benzo[*ghi*]perylene-5(6*H*),6′-[6*H*]benzo[*cd*]pyrene] (**13**), whereas, on formolysis, **6** gave spiro[benzo[*ghi*]perylene-5(6*H*),6′-[6*H*]benzo[*cd*]pyrene], 6-hydroxymethyl-6*H*-benzo[*cd*]pyrene, and 6-methyl-6*H*-benzo[*cd*]pyrene as well as **13**. It might reasonably be supposed that the formation of **13** proceeds in a process involving four steps: (i) the formation of the intermediate 6*H*-6-benzo[*cd*]pyren-6-ylmethyl cation (**8**); (ii) the conversion of **8** into the reactive 6-methylenebenzo[*cd*]pyrene (**5**) by the loss of a proton; (iii) the head-to-head self-Diels-Alder dimerization of **5** to the initial dimer, 6,7-dihydrospiro[benzo[*ghi*]perylene-5(4a*H*),6′-[6*H*]benzo[*cd*]pyrene], and (iv) a 1,3-hydrogen shift to form **13**. When 6-methylbenzo[*cd*]pyren-6-yl tetrafluoroborate (**7**) was treated with triethylamine in chloroform, the spiro-dimer, **13**, was also obtained. The reaction of **7** with triethylamine in the presence of dimethyl acetylenedicarboxylate resulted in the formation of dimethyl benzo[*ghi*]perylene-5,6-dicarboxylate. These results strongly suggest the intermediate formation of **5** as a reactive compound.

In connection with our current interest in the chemistry of phenafulvenes (1-methylenephenalene) (**1**)[2,3] we have recently reported the formation of the parent phenafulvene (**1**: X=Y=H) as a reactive intermediate through the transition-metal-promoted isomerization of naphtho[1,8]tricyclo[4.1.0.0^{2,7}]heptene (**2**).[4] The formation of (**1**: X=Y=H) in this reaction has been confirmed by the isolation of its dimer, **3**, and by means of a trapping experiment with dimethyl acetylenedicarboxylate to give dimethyl 1,2-pyrenedicarboxylate (**4**).[4]

In order to learn how the stability of the parent phenafulvene changes with the annelation of benzene rings, we have tried to synthesize 6-methylenebenzo[*cd*]pyrene (**5**) as a higher benzolog of **1**. By analogy with the parent phenafulvene, the compound **5** could not be isolated because of its pronounced reactivity. In the study reported herein, the synthesis of **5** as well as various types of evidence for the intermediate existence of **5** are reported.

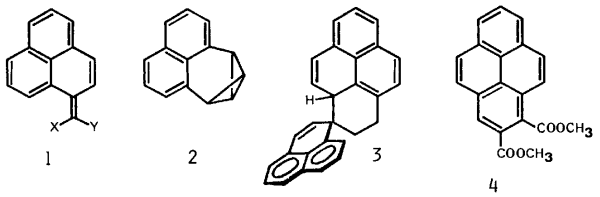

1 2 3 4

Results and Discussion

As is shown in Scheme 1, either the solvolysis of the mesylate **6**, or the proton abstraction of the 6-methylbenzo[*cd*]pyren-6-yl cation (**7**) appears to be an attractive route leading to **5**.

The synthesis of **6** was accomplished by the sequence of reactions shown in Scheme 2. The treatment of 6*H*-benzo[*cd*]pyrene (**9**) in tetrahydrofuran with butyllithium at −60 °C, followed by carboxylation with carbon dioxide, gave 6*H*-benzo[*cd*]pyrene-6-carboxylic acid (**10**) as the sole product. The exclusive formation of **10** is in good accordance with the highest Hückel charge density[6] at C-6 in the anion derived from **9**. The acid was converted into the methyl ester, **11**, with diazomethane under a nitrogen atmosphere,[7]

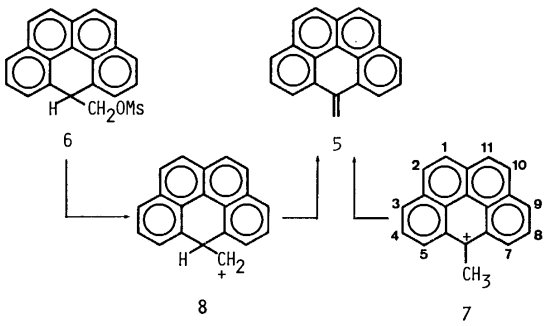

Scheme 1.

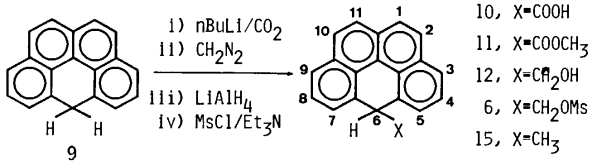

Scheme 2.

The ester, **11**, was reduced with lithium aluminium hydride to the alcohol, **12**, which, on treatment with mesyl chloride in the usual manner, then gave **6**.[8] The strucutres of **11**, **12**, and **6** were unambiguously confirmed by the respective spectroscopic properties given in the Experimental Section.

The acetolysis of **6** in gently refluxing glacial acetic acid led to 7,7a-dihydrospiro[benzo[*ghi*]perylene-5(6*H*),6′-[6*H*]benzo[*cd*]pyrene] (**13**), a dimer of the desired **5**, in a 50% yield, whereas the formolysis of **6** at 50 °C gave **13** in only a 15% yield, along with a trace amount of the corresponding dehydrogenated dimer, spiro[benzo[*ghi*]perylene-5(6*H*),6′-[6*H*]benzo[*cd*]pyrene] (**14**), in addition to **12** (26%) and 6-methyl-6*H*-benzo[*cd*]pyrene (**15**), as is shown in Scheme 3. On the other hand, the formolysis of **6** at 80 °C gave **14** (15%), along with **12** and **15**, in yields similar to those of the above experiment. The elemental analysis and the molecular-weight determination of **13** clearly indicated it to be a dimer of **5**. The final structural proof of **13** was obtained from its ^{1}H-NMR spectrum, which showed one proton triplet at δ 5.01 (H-7a, J= 7.5 Hz), a four-proton multiplet at δ 2.38—2.68, and

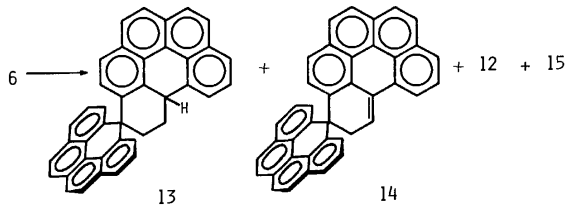

Scheme 3.

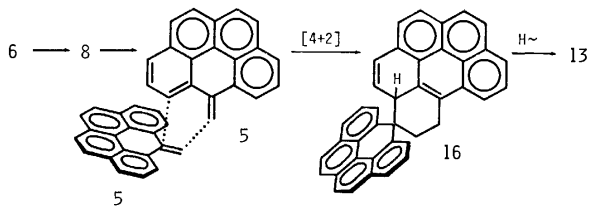

Scheme 4.

aromatic-proton multiplets at δ 7.00—7.94. The relation between the adjacent protons in the alicyclic moiety was confirmed by the aid of spin-decoupling experiments. Irradiation at about δ 2.6 changed the broad triplet at 5.01 into a broad singlet; conversely, irradiation at 5.01 changed the multiplet at 2.38—2.68 into the pseudo-symmetrical pattern of an AA'-BB'-like system. Furthermore, the electronic spectrum of **13** is very similar to that of **15**, indicating the existence of a benzo[*a*]phenanthrene chromophore in **13**. Although attempts to make an elemental analysis and mass-spectral measurement of **14** were unsuccessful because of its pronounced sensitivity to heat and air, the structure of **14** was established by means of the ^{1}H-NMR and electronic spectra and chemical evidence. The ^{1}H-NMR spectrum of **14** showed signals at δ 3.18 (H-6,6, d, 2H, J=5.0 Hz), 6.47 (H-7, t, 1H, J=5.0 Hz), and 7.03—7.93 (m, 19H). On the irradiation of the signals at δ 6.47, the doublet at δ 3.18 was converted into a clean singlet. A comparison of the electronic spectrum of **14** with that of **13** reflects the bathochromic shift anticipated for the introduction of an exo methylene double bond into the 6*H*-benzo[*cd*]pyrene π-system. An examination of the spectra of several 6-methylenebenzo[*cd*]pyrene derivatives[9] has shown the existence of the same chromophore in **14**. Furthermore, **14** could easily be obtained from **13** by treatment with iodine in benzene. The structure of **15** was established through an independent synthesis (*vide infra*).

The difference in the product distributions between the acetolysis and the formolysis of **6** was explained by the fact that formic acid, as is generally known, gradually decomposes into water and carbon monoxide, even at room temperature.[10] Thus, the intermediate carbonium ion, **8**, partly collapsed into an alcohol, **12**, upon the nucleophilic attack of water. The formation of **15** was closely parallel to the precedent in which triphenylmethanol is reduced to triphenylmethane by formic acid.[11]

A possible explanation for the formation of **13** from **6** might be that the reaction proceeds in a process involving four steps: (i) the initial formation of the intermediate carbonium ion, **8**; (ii) the conversion of **8** into the reactive hydrocarbon, **5**, by the loss of the proton; (iii) the head-to-head self-Diels-Alder dimerization of **5** to the initial dimer, **16**, and (iv) a 1,3-hydrogen shift to form the observed dimer, **13** (Scheme 4). The ease of the hydrogen shift in the final step may be attributed to the difference in π-energy between the 1-vinylpyrene and benzo[*a*]phenanthrene π-moieties in **16** and **13** respectively.[12]

The second synthetic route, which consists of proton abstraction from the 6-methylbenzo[*cd*]pyren-6-yl cation, **7**, would be a more favorable synthetic method for the labile **5**. To this end, 6-methyl-6*H*-benzo[*cd*]pyrene, **15**, readily accessible from **9** through lithiation with butyllithium, followed by methylation with excess methyl iodide, was treated with trityl tetrafluoroborate in chloroform to give a 83% yield of **7**. The structure of **7** was evident from its ^{1}H-NMR spectrum in trifluoroacetic acid, which exhibited signals at δ 3.87 (s, $-CH_3$), 8.33 (d, J=8.6 Hz, H-1,11), 8.57 (d, J=8.6 Hz, H-2,10), 8.41 (dd, J=7.0, 6.5 Hz, H-4,8), 9.12 (d, J=6.5 Hz, H-3,9), and 9.51 (d, J=7.0 Hz, H-5,7).

When the cation, **7**, was treated with triethylamine in chloroform at 0 °C, the spiro dimer, **13**, was obtained in a 42% yield. On the other hand, when the reaction was carried out at −10——15 °C, which is the practical lower limit for the reaction, the only product obtained was **13**, and no hydrocarbon corresponding to **5** could be detected by TLC monitoring. The formation of **13** even at low temperatures, suggested the pronounced reactivity of the initial product, **5**, for the self-Diels-Alder reaction as both 4π and 2π components. In order to confirm the transient existence of **5**, we carried out a trapping experiment. The reaction of **7** with triethylamine in chloroform in the presence of two mole equivalents of dimethyl acetylenedicarboxylate at 0 °C resulted in the formation of the product in a 20% isolated yield; to this product we assigned the structure of dimethyl 5,6-benzo[*ghi*]perylenedicarboxylate (**17**) on the basis of its mass spectrum [*m/e* 392 (M^+, 100%), 361 (M^+-OCH_3, 28%), 274 ($M^+-2COOCH_3$, 28%)], ^{1}H-NMR spectrum [δ 4.10 (s, $-OCH_3$), 4.17 (s, $-OCH_3$), 8.92 (dd, $J_{8,9}$=7.5 Hz, $J_{8,10}$=1.5 Hz, H-8), 9.41 (s, H-7), 7.87—8.28 (m, other aromatic protons)] and its electronic spectrum, which is closely similar to that of the parent benzo[*ghi*]perylene.[13]

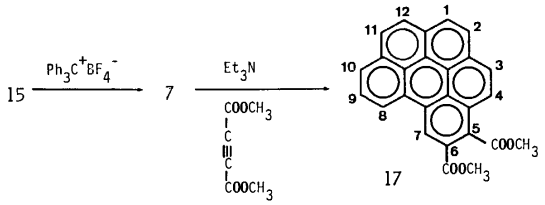

Scheme 5.

In conclusion, as in the case of the parent phenafulvene **1**: X=Y=H, all attempts to isolate 6-methylenebenzo[*cd*]pyrene **5** have thus far been unsuccessful, though it can be generated and trapped. Although it is well documented that nonalternant fulvenes, such

as tria-,[14] penta-,[15] and hepta-fulvenes,[16] belong to an extremely reactive group of substances, unsubstituted *exo*-cyclic methylene compounds with odd-alternant polycyclic benzenoid moieties, *e.g.*, **1** and **5**, also not have enough stability to permit isolation.[17]

Experimental

All the melting points were determined on a micro hot stage and are uncorrected. The mass spectra were obtained on a Hitachi RM-50 spectrometer operating at 20 or 70 eV. The electronic spectra were taken on a Hitachi 124 double-beam spectrometer. The NMR spectra were recorded with a Varian XL-100 (100 MHz) spectrometer and are given in δ-values with respect to tetramethylsilane as the internal standard.

6-Methoxycarbonyl-6H-benzo[cd]*pyrene (**11**).* To a stirred solution of 6*H*-benzo[*cd*]pyrene (**9**) (4.2 g, 175 mmol) in 30 ml of dry THF, we added a hexane solution containing 17.5 mmol of butyllithium at −60 °C under nitrogen. The mixture was then stirred for 30 min at this temperature, and dry carbon dioxide gas was bubbled through the solution. The resulting mixture was warmed to 0 °C with a continuous bubbling of carbon dioxide. After having been acidified with dil hydrochloric acid, the reaction mixture was extracted with ether. The ether layer was washed with water and extracted with a saturated aqueous solution of sodium hydrogencarbonate. After having been washed with ether, the aqueous layer was acidified with concd hydrochloric acid to give colorless precipitates which, after filtration and methylation with diazomethane under nitrogen, yielded a crude ester, **11**. The product was chromatographed on alumina, eluted with hexane–benzene (1:1), and recrystallized from hexane–benzene to give pure **11** as pale yellow needles; mp 149—150 °C. MS: *m/e* 298 (M^+, 12%), 239 ($M^+-COOCH_3$, 100%); IR (KBr): 1725 cm^{-1}; NMR ($CDCl_3$): 3.51 (s, 3H, $-CH_3$), 5.81 (bs, 1H, H-6), 7.41—7.81 (m, 10H, other protons).

Found: C, 84.32; H, 4.72%. Calcd for $C_{21}H_{40}O_2$: C, 84.54; H, 4.73%.

6-Hydroxymethyl-6H-benzo[cd]*pyrene (**12**).* A solution of **11** (1.19 g, 4.0 mmol) in 120 ml of dry ether was added, drop by drop, to a suspension of lithium aluminium hydride (152 mg) in 20 ml of dry ether at −20 °C over a 2-h period under nitrogen. After stirring for 3 h at this temperature, the reaction mixture was quenched with ether saturated with water and extracted with benzene. The combined organic layer was washed successively with dil hydrochloric acid, an aqueous solution of sodium hydrogencarbonate, and water, dried (Na_2SO_4), and evaporated under reduced pressure. The residue was recrystallized from hexane–benzene (2:3) under nitrogen to give 870 mg (80%) of **12** as brown prisms; mp 119.5—122 °C. MS: *m/e* 270 (M^+, 3.2%), 239 (M^+-CH_2OH, 100%); NMR ($CDCl_3$): 1.6 (bs, 1H, -OH), 3.60 (d, 2H, J=6.5 Hz, $-CH_2-O$), 4.67 (t, 1H, J=6.5 Hz, H-6), 7.49—7.91 (m, 10H, aromatic protons).

Found: C, 89.15; H, 5.39%. Calcd for $C_{20}H_{14}$: C, 88.86; H, 5.22%.

6-Mesyloxymethyl-6H-benzo[cd]*pyrene (**6**).* To a stirred solution of **12** (270 mg, 1.0 mmol) in 6 ml of dry dichloromethane containing 1.6 mmol of triethylamine, we added, drop by drop, 1.3 mmol of methanesulfonyl chloride in 7 ml of dry dichloromethane at −10 °C over a 30-min period under nitrogen. After stirring for 2 h at this temperature, the solution was poured into ice water and the layers were separated. The organic layer and the combined dichloromethane extracts were washed successively with cold dil hydrochloric acid, an aqueous solution of sodium hydrogencarbonate, and water, and then dried ($MgSO_4$). The solvent was evaporated under reduced pressure, leaving 277 mg (80%) of crude **6**, which was subsequently dissolved in 5 ml of dichloromethane and 5 ml of hexane at the ambient temperature under nitrogen, while the solution was concentrated to a volume of 4 ml. The solution was cooled gradually to −40 °C, giving 172 mg of the analytically pure **6** as pale yellow needles; mp 120—122 °C. MS: *m/e* 348 (M^+, 3%), 252 (M^+-OMs, 33%), 239 (M^+-CH_2OMs, 100%); NMR ($CDCl_3$): 2.39 (s, 3H, $-SO_2CH_3$), 4.28 (d, 2H, J=6.5 Hz, $-CH_2-SO_2-$), 5.04 (bt, 1H, J=6.5 Hz, H-6), 7.57—7.97 (m, 10H, aromatic protons).

Found: C, 72.13; H, 4.61; S, 9.05%. Calcd for $C_{21}H_{16}O_3S$: C, 72.39; H, 4.63; S, 9.20%.

*Acetolysis of **6**.* A solution of **6** (140 mg, 0.4 mmol) in 15 ml of dry acetic acid, containing 96 mg of anhydrous sodium dihydrogenphosphate as a buffer, was refluxed for 1 h under nitrogen. The reaction mixture was then poured into water and extracted with benzene. The extracts were washed with an aqueous solution of sodium hydrogencarbonate and water, and then dried, and the solvent was removed under reduced pressure. The residue was chromatographed on alumina containing 3% of water, eluting with hexane–benzene (9:1), to give 50 mg (50%) of the spiro-dimer, **13**, as pale yellow crystals; mp 158—162 °C (dec). MS: *m/e* 504 (M^+, 25%), 276 (benzo[*ghi*]perylene ion, 100%); UV λ_{max} nm (log ε) (hexane): 219 (4.74), 233 (4.63), 249 (4.19), 256 (4.24), 258 sh (4.22), 262 sh (4.43), 282 (4.67), 293 (4.63), 323 (4.13), 338 (4.00); NMR: see text.

Found: C, 94.98; H, 4.73%. Calcd for $C_{40}H_{20}$: C, 95.21; H, 4.79%.

*Formolysis of **6**.* A solution of **6** (140 mg, 0.4 mmol) in 14 ml of 99% formic acid containing 96 mg of anhydrous sodium dihydrogenphosphate was heated to 40—50 °C over a 4-h period under nitrogen. After workup in the same manner as the acetolysis just described, the crude products were chromatographed on alumina containing 3% of water, eluting gradually with hexane, hexane–benzene (9:1), and benzene. The solvent of each fraction was then evaporated, leaving 4 mg of **15**, 15 mg (15%) of **13**, and 26 mg (26%) of **12**. The structures of **12** and **15** were confirmed from the NMR spectra to be identical with those of the respective authentic compounds.

*Formolysis of **6** at High Temperatures.* A solution of **6** (140 mg, 0.4 mmol) in 14 ml of 99% formic acid containing 96 mg of anhydrous sodium dihydrogenphosphate was heated from room temperature to 80 °C over a 15-min period and then maintained at this temperature for 10 min under nitrogen. The solution was subsequently worked up, and the products were separated by the same procedures as above to give 8 mg of **15**, 15 mg (15%) of the dehydro spiro-dimer, **14**, as yellow crystals, and 23 mg (23%) of **12**. The dimer **14** is gradually decomposed around 80 °C. UV λ_{max} nm (log ε) (hexane): 216 (4.96), 232 (4.82), 265 sh (4.61), 279 (4.66), 320 (4.44), 334 (4.47), 390 (3.91), 413 (3.92); NMR: see text.

*Dehydrogenation of **13**.* A solution of 55 mg (0.11 mmol) of the spiro-dimer, **13**, in 6 ml of benzene was treated with 38 mg (0.3 mmol) of iodine at room temperature for 30 min under nitrogen. The products were chromatographed on alumina containing 2.5% of water, eluting with benzene, and again on the same deactivated alumina with hexane–benzene (9:1), to give 20 mg (45%) of pure **14**, which was identical in every respect with the authentic sample.

6-Methyl-6H-benzo[cd]*pyrene (**15**).* To a stirred solu-

tion of 6*H*-benzo[*cd*]pyrene (**9**) (1.56 g, 6.5 mmol) in 70 ml of dry THF, we added 6.5 mmol of butyllithium in hexane at −60 °C under nitrogen. After having been stirred for 30 min at this temperature, the reaction mixture was quenched by the addition of a large excess of methyl iodide. The mixture was stirred for 1 h at −50 °C, warmed to room temperature, and extracted with benzene. The extracts were washed successively with 2 mol dm^{-3} hydrochloric acid, a saturated aqueous solution of sodium hydrogencarbonate, and water, dried ($MgSO_4$), and evaporated. The residue was chromatographed on alumina with hexane–benzene (1:1). The solvent was evaporated, leaving a yellow solid which was recrystallized from cyclohexane under nitrogen to give pure **15** (1.51 g, 92%) as yellow crystals; mp 122—124 °C. MS: *m/e* 254 (M^+, 17%), 239 (M^+-CH_3, 100%); UV λ_{max} nm (log ε) (hexane): 268.5 (4.39), 278 (4.64), 289 (4.75), 312 (3.95), 325 (3.97), 338 (3.77); NMR: see text.

Found: C, 94.24; H, 5.55%. Calcd for $C_{20}H_{14}$: C, 94.45; H, 5.55%.

6-Methylbenzo[cd]*pyren-6-yl Tetrafluoroborate (7).* To a stirred solution of **15** (1.5 g, 6.0 mmol) in 40 ml of dry chloroform, we added finely powdered trityl tetrafluoroborate (2.05 g, 6.5 mmol) at room temperature. Black solids precipitated at once, after which the mixture was warmed at 50 °C for 2 h. After cooling, the black solid mass was collected by filtration and washed several times with dry chloroform in a dry box. The product was dried *in vacuo* to give 1.7 g (83%) of **7**; mp >350 °C. NMR: see text.

Dimerization of 6-Methylenebenzo[cd]*pyrene (5).* To a suspension of the cation, **7** (340 mg, 1.0 mmol), in 20 ml of dry chloroform, we added, drop by drop, 150 mg (3.0 mmol) of dry triethylamine in 5 ml of dry chloroform at 0 °C over a 15-min period under nitrogen. After stirring for an additional hour, the reaction mixture was poured into 2 mol dm^{-3} hydrochloric acid and the organic layer was washed successively with an aqueous solution of sodium hydrogencarbonate and water, dried ($MgSO_4$), and evaporated at reduced pressure to give a residue which was subsequently chromatographed on alumina containing 2.5% of water with hexane–benzene (9:1) to give 105 mg (42%) of the pure dimer, **13**, as pale yellow crystals, which were identical in every respect with the product of the acetolysis of **6**.

Trapping of 5 by Dimethyl Acetylenedicarboxylate. To a suspension of **7** (170 mg, 0.5 mmol) in 15 ml of dry chloroform containing dimethyl acetylenedicarboxylate (120 mg, 1.0 mmol), we added, drop by drop, triethylamine (75 mg, 1.50 mmol) in 10 ml of dry chloroform at room temperature under nitrogen. After additional stirring for 3 h, the reaction mixture was poured into water. The organic layer was washed successively with water, 2 mol dm^{-3} hydrochloric acid, an aqueous solution of sodium hydrogencarbonate, and water, dried ($MgSO_4$), and evaporated. The residue was chromatographed on alumina with benzene to give 39 mg (20%) of crude **17**. Pure **17** was obtained by recrystallization from hexane–benzene as reddish brown crystals; mp 239—240 °C. IR (KBr): 1725 cm^{-1}; MS and NMR: see text.

Found: C, 80.10; H, 4.19%. Calcd for $C_{26}H_{16}O_4$: C, 79.58; H, 4.11%.

References

1) Part XXX of this series; Y. Nesumi, T. Nakazawa, and I. Murata, *Chem. Lett.*, **1979**, 771.

2) H. Prinzbach, V. Freudenberger, and U. Scheidegger, *Helv. Chim. Acta*, **50**, 1087 (1967).

3) I. Murata, "Topics in Nonbenzenoid Aromatic Chemistry," ed by T. Nozoe *et al.*, Hirokawa Pub. Co., Tokyo (1973), Vol. 1, p. 159, and the references cited therein.

4) I. Murata, K. Nakasuji, and H. Kume, *Tetrahedron Lett.*, **1973**, 3401, 3405.

5) *Cf.* I. Murata, K. Yamamoto, and O. Hara, *Tetrahedron Lett.*, **1974**, 2047.

6) D. H. Reid and W. Bonthrone, *J. Chem. Soc.*, **1965**, 5920.

7) Compound **11** is very sensitive to air. When a solution of **11** was exposed to air, methyl 3-oxo-3*H*-benzo[*cd*]pyrene-6-carboxylate was obtained in a high yield.

8) R. K. Crossland and K. L. Servis, *J. Org. Chem.*, **35**, 3195 (1970).

9) O. Hara, K. Yamamoto, and I. Murata, unpublished results. *Cf.* O. Hara, Doctoral thesis, Osaka University, Osaka, Japan, 1976.

10) J. A. Riddick and W. B. Bunger, "Organic Solvents," in "Techniques of Chemistry," 3rd ed, Wiley-Interscience, New York (1970), Vol. II, p. 732.

11) H. Kauffmann and P. Pannwitz, *Ber.*, **45** 766 (1912); A. Kovache, *Ann. Chim.*, **10**, 184 (1918).

12) Variable β-SCF MO calculations revealed that benzo[*a*]phenanthrene is more stable than 1-vinylpyrene by 11 kcal/mol.

13) E. Clar, "Polycyclic Hydrocarbons," Academic Press, London (1964), Vol. 2 p. 60.

14) P. J. Stang and M. G. Mangum, *J. Am. Chem. Soc.*, **97**, 3854 (1975), and the references cited therein.

15) D. Meuche, M. Neuenschwander, H. Schaltegger, and H. U. Schlunegger, *Helv. Chim. Acta*, **48**, 955 (1965), and the references cited therein.

16) W. von E. Doering and D. W. Wiley, *Tetrahedron*, **11**, 183 (1960); H. E. Zimmerman and L. R. Sousa, *J. Am. Chem. Soc.*, **94**, 834 (1972); M. Neuenschwander and W. K. Schenck, *Chimia*, **26**, 194 (1972).

17) Recently, a quite similar dimerization of 10-methyleneanthrone has been reported: K. Hirakawa and S. Nakazawa, *J. Org. Chem.*, **43**, 1804 (1978).

Electrochemical Generation of Unstable Nitrogen Species. Part 4.[1] Electrochemical and Chemical Oxidation of Cyclic and Open-chain Diamines. The Formation of Cyclic Hydrazine Derivatives

Toshio FUCHIGAMI,* Tomoyasu IWAOKA, Tsutomu NONAKA, and Taro SEKINE

Department of Electronic Chemistry, The Graduate School at Nagatsuta, Tokyo Institute of Technology, Nagatsuta-machi, Midori-ku, Yokohama 227

(Received December 7, 1979)

Intramolecular N,N-coupling by the electrochemical oxidation of cyclic and open-chain diamines such as 3,3,7,7-tetraethylperhydro-1,5-diazocine (**1**) and *N,N*-dimethyl-2,2-diethyl-1,3-diaminopropane (**2**) was investigated with the use of platinum, silver, nickel, and carbon anodes. In the case of **1**, cyclic hydrazine derivatives, 3,3,7,7-tetraethyl-1,5-diazabicyclo[3.3.0]octane and 1-(2-ethyl-2-formylbutyl)-4,4-diethyl-4,5-dihydropyrazole, were formed in high current efficiency. In the case of **2**, the corresponding hydrazines, 1,2-dimethyl-4,4-diethylpyrazolidine and 1-methyl-3,3-diethyl-4,5-dihydropyrazole, were obtained in low current efficiency, because C–N bond cleavage took place before N,N-coupling. A carbon anode was found to be effective for N,N-coupling of such diamines. Chemical oxidative N,N-coupling of **1** and **2** was studied by using sodium peroxodisulfate and lead tetraacetate.

A number of studies have been carried out on the electrochemical oxidation of amines from both electrochemical and organic synthetic viewpoints.[2] However, only a few papers deal with electrooxidative N,N-coupling reaction. N,N-Coupling is known only in the case of aromatic amines,[3–6] *e.g.*, the formation of azobenzenes from aniline derivatives.

The initial electrode process of the oxidation of amines is supposed to be one electron transfer from a lone pair of electrons of a nitrogen atom to form a cation radical. In the case of aromatic amines, the life time of the cation radical intermediate thus produced is so long that it can give rise to various intermolecular coupling products.

In the case of aliphatic amines, the cation radical and radical intermediate is so unstable that N,N-coupling is difficult, C–N bond cleavage and/or nucleophilic substitution on an α-carbon supposedly taking place. In their work dealing with anodic N,N-coupling of aliphatic amines, Blackham *et al.*[7] found that 2,2′-dimethyl-2,2′-azopropane and 2,2′-dimethyl-2,2′-azoxypropane, with a total current efficiency 46%, are formed from *t*-butylamine. Recently, Bauer and Wendt[8] and Fuchigami *et al.*[9] found that secondary amines such as dibutylamine and piperidine give the corresponding hydrazine compounds in current efficiency lower than 50%.

In the case of chemical oxidation, no paper dealing with N,N-coupling of aliphatic amines seems to have appeared except for the formation of 1,1′-bipiperidines from piperidines reported by Nomura *et al.*[10]

We have investigated the intramolecular oxidative N,N-coupling of a cyclic diamine and an open-chain diamine such as **1** and **2**. Intramolecular N,N-coupling seems to occur more easily than intermolecular coupling, since reaction sites in the intramolecular N,N-coupling would be closer to each other. Neither electrochemical nor chemical oxidation of such aliphatic diamines seems to have been carried out so far. The chemical oxidative N,N-coupling of **1** and **2** was studied by using sodium peroxodisulfate and lead tetraacetate as an oxidizing reagent.

Results and Discussion

Electrochemical Oxidation of 1 and 2. Electrolysis of **1** was carried out in acetonitrile at a constant potential using various anode materials. In order to prevent **1** from becoming inert to oxidation due to the formation of salt during the course of electrolysis,

TABLE 1. RESULTS OF THE ELECTROCHEMICAL OXIDATION OF 3,3,7,7-TETRAETHYLPERHYDRO-1,5-DIAZOCINE (**1**)

Entry	Anode material	Anode potential (V *vs.* SCE)	Temp °C	Molar ratio of LiOH/**1**	Amount of electricity ($\times 10^4$ C/mol)	Yields of products[a] **3**	Yields of products[a] **4**	Recovery of **1** %
1	Pt	0.8	25	2	7.72	9 (23)	7 (53)	75
2	Pt	1.1	25	2	7.72	7 (18)	8 (60)	83
3	Pt	1.5	25	2	7.72	8 (20)	6 (45)	80
4	Pt	1.1	3	2	8.30	10 (23)	11 (76)	62
5	Pt	1.1	−12	2	7.33	9 (24)	9 (71)	56
6	Pt	1.1	25	0	7.72	4 (10)	10 (75)	89
7	Pt	1.1	25	10	18.14	12 (13)	21 (67)	40
8[b]	Pt	1.1	25	2	7.91	57[c]	13 (63)	—
9	C	0.3	25	2	9.07	14 (30)	10 (64)	51
10	Ni	0.7	25	2	8.30	12 (28)	8 (56)	69
11	Ag	0.3	25	2	9.46	trace	11 (67)	66

a) Values in parentheses show current efficiency (%). b) Electrolysis of **3**. c) Recovery of **3**.

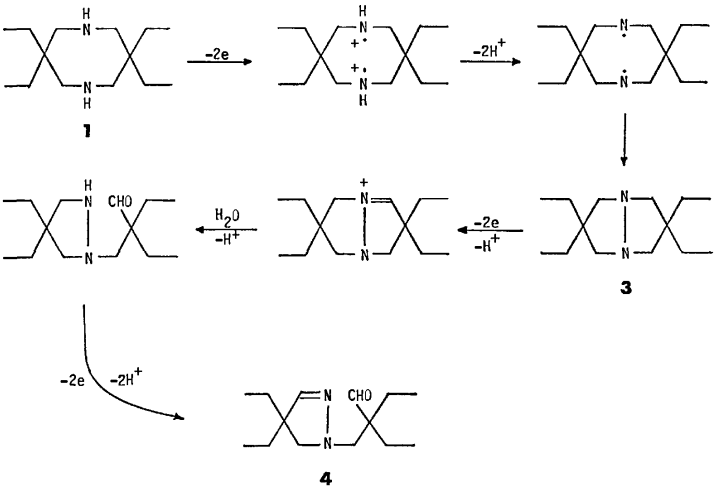

Scheme 1.

lithium hydroxide powder was suspended in the anolyte. The electrolytic conditions and results are summarized in Table 1.

Two products were detected by gas chromatography. One was identified as 3,3,7,7-tetraethyl-1,5-diazabicyclo[3.3.0]octane (**3**) by comparison of the mass fragmentation† and retention time with those of an authentic sample synthesized separately.[11] The other, isolated by column chromatography on almina with dichloromethane, was identified as 1-(2-ethyl-2-formylbutyl)-4,4-diethyl-4,5-dihydropyrazole (**4**), its structure being confirmed by the following results:

a) The compound shows a positive Tollens test.

b) In the IR spectrum, the characteristic strong absorption of a carbonyl group was observed at 1740 cm^{-1}.

c) In the NMR spectrum measured in CCl_4 with TMS as the internal standard, the characteristic signal of an aldehydic proton was observed at 9.30 ppm, the other signals being explained in terms of the structure of **4**.

d) In the mass spectrum, the molecular ion (*m/e* 238) was observed together with appropriate fragment peaks such as *m/e* 209 (M^+-CHO and/or M^+-Et) and 139 (M^+-Et_2CCHO).

e) The results of elemental analyses of the free base and the 2,4-dinitrophenylhydrazone of **4** agree with the calculated values within normal errors.

The compound thus isolated is neutral colorless oily material; such a 1-substituted dihydropyrazole derivative is unknown so far.

As shown in Table 1, N,N-coupling products were formed as expected, their current efficiency being generally good.

In the case of a platinum anode, both **3** and **4** were formed in approximately equal yields. A change in the anode potential caused no appreciable change in yield. However, the total current efficiency changed with anode potential and electrolytic temperature. N,N-Coupling proceeded efficiently at lower temperature. In the absence of lithium hydroxide, the current decreased more rapidly than in its presence, the yield of **3** being reduced to about one half, while that of **4** increased. The reason for this has not been clarified yet. In the presence of 10 equivalents of lithium hydroxide, *ca.* 193000 C/mol of electricity was consumed and the ratio of **4**/**3** doubled, suggesting that the more the electricity passes, the higher the yield of **4**. Carbon and nickel anodes gave **3** in slightly higher yields than **4**.

The electrochemical oxidation of **1** proceeded at extremely low potentials in the cases of carbon and silver anodes, the latter giving only **4**, though the current efficiency was relatively low. In the case of a silver anode, the initial electrochemical reaction gives an oxide coating on the electrode surface. This seems to effect the oxidation of **1**. The low current efficiency of **4** in the case of the silver anode can be attributed to the formation of silver oxide, since the corrosion of the silver anode surface was observed during the course of electrolysis. Hampson *et al.*[12–14] also found that platinum and silver anodes give different products in the oxidation of aliphatic monoamines in an alkaline solution. A nickel anode[15] behaves like a silver one, but no such tendency was observed in the present work.

Since **3** can be oxidized at a lower potential than **1**†† and **4** is formed by electrochemical oxidation of **3**, **4** seems to be formed by further oxidation of **3** produced in the course of the electrochemical oxidation of **1**.

Formation of **3** and **4** might proceed as shown in Scheme 1.

Intramolecular N,N-coupling of the open-chain diamine (**2**) was investigated. Electrochemical oxidation of **2** was carried out at a constant potential in 1 M NaOH solution instead of acetonitrile in the case of **1**, since the anode was passivated in the acetonitrile solution.

Three basic products were detected in the electrolyte by gas chromatography. 1,2-Dimethyl-4,4-diethyl-

† The mass spectrum of **3** was measured with a gas chromatograph-mass spectrometer.

†† This was shown by current density *vs.* anode potential curves of **1** and **3**. Such bicyclic diamines have extremely low oxidation potentials.[16]

pyrazolidine (**5**) was identified to be the authentic sample synthesized separately by gas chromatography and mass spectrometry. 1-Methyl-3,3-diethyl-4,5-dihydropyrazole (**6**) and 1,3-dimethyl-5,5-diethylperhydropyrimidine (**7**) were isolated by column chromatography and preparative gas chromatography, respectively. Their structures were confirmed by means of elemental analyses and spectral studies.

Table 2. NMR spectral data

	Compound	NMR (δ ppm)[a]
1	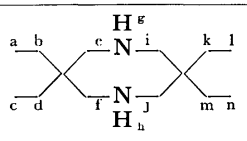	0.80 (12H, t, H^a, H^c, H^l, H^n) 1.20 (8H, q, H^b, H^d, H^k, H^m) 1.75 (2H, s, H^g, H^h) 2.53 (s) and 3.36 (s) (8H, H^e, H^f, H^i, H^j)
2	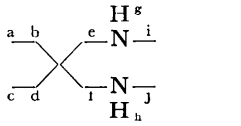	0.78 (6H, t, H^a, H^c) 0.88 (2H, s, H^g, H^h) 1.25 (4H, q, H^b, H^d) 2.30 (4H, s, H^e, H^f) 2.35 (6H, s, H^i, H^j)
3	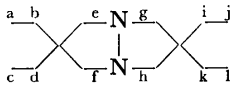	0.80 (12H, t, H^a, H^c, H^j, H^l) 1.45 (8H, q, H^b, H^f, H^i, H^k) 2.47 (8H, s, H^e, H^f, H^g, H^h)
4	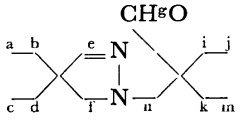	0.80 (6H, t, H^a, H^c) 0.82 (6H, t, H^j, H^l) 1.50 (8H, m, H^b, H^i, H^k) 2.78 (2H, s, H^f), 2.96 (2H, s, H^h) 6.24 (1H, s, H^e), 9.30 (1H, s, H^g)
5	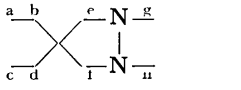	0.80 (6H, t, H^a, H^c) 1.40 (4H, q, H^b, H^d) 2.21 (6H, s, H^g, H^h) 2.38 (4H, s, H^e, H^f)
6	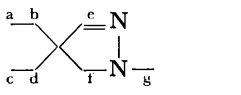	0.80 (6H, t, H^a, H^c) 1.40 (4H, q, H^b, H^d) 2.70 (5H, s, H^f, H^g) 6.25 (1H, s, H^e)
7	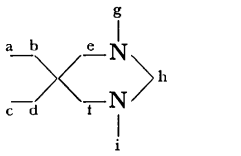	0.74 (6H, t, H^a, H^c) 1.32 (4H, q, H^b, H^d) 1.90 (4H, s, H^e, H^f) 2.11 (6H, s, H^g, H^i) 2.62 (2H, s, H^h)

a) Measured in CCl_4 with TMS as an internal standard. s: Singlet, t: triplet, q: qartet, m: multiplet.

In the NMR spectrum of **6**, the characteristic signal of an imino proton was observed at a low magnetic field such as 6.25 ppm; in that of **7**, the signal of N–H protons disappeared and that of singlet methylene protons appeared newly at 2.62 ppm. The compound was further identified by a mixed-melting-point test with a sample prepared from **2** and formaldehyde in an alkaline solution.

The basic products obtained are new. Their NMR spectral data together with those of the starting diamines, **1** and **2**, are summarized in Table 2.

When a large amount of electricity was passed in the electrolysis, a large amount of acidic substances were formed in addition to the basic products, but their structures could not be established.

The results of electrolysis of **2** are summarized in Table 3.

The N,N-coupling product, **5**, expected in this reaction, was scarcely formed; it was detected in a very small amount only in the case of using a carbon anode. In addition to **5**, a highly oxidized product, **6**, having a N–N bond was formed in a low yield. **6** was formed at the highest current efficiency 16% at a carbon anode, but scarcely formed at all at platinum and silver anodes. **7** was formed in a considerable yield at anodes other than nickel.

2 as well as **1** can be oxidized at a low potential at a carbon anode.

Since the oxidation of **5** was much easier than that of **2** (Fig. 1)††† and **6** was also formed by electrochem-

††† At a carbon anode, a negative shift of current *vs.* potential curve was induced in the presence of diamine, **2** (Fig. 1), no shift being observed at a platinum anode. Such a tendency was also observed in the case of **1**.

Table 3. Results of the electrochemical oxidation of *N,N'*-dimethyl-2,2-diethyl-1,3-propanediamine (**2**)[a]

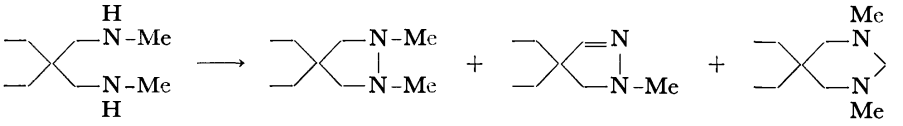

2 **5** **6** **7**

Entry	Anode material	Anode potential (V *vs.* SCE)	Amount of electricity ($\times 10^4$ C/mol)	Yields of products[b]/%			Recovery of **2**	Others[c]
				5	**6**	**7**	%	mg
12	Pt	1.2	9.65	0	trace	10	58	—
13	Pt	1.2	38.60	0	trace	26	13	60
14	C	0.5	9.65	trace	4(16)	8	65	—
15	C	0.5	38.60	trace	4(4)	23	17	55
16	Ag	0.7	9.65	0	1(4)	4	77	—
17	Ag	0.9	9.65	0	trace	3	80	—
18	Ag	0.9	62.73	0	4(3)	10	51	—
19	Ni	0.55	62.73	0	0	0	80	—
20[d]	C	0.4	9.65	29[e]	19(76)	—	—	41

a) **2**: 1 mmol (158 mg). b) Values in parentheses show current efficiency (%). c) Acidic products. d) Electrolysis of **5**. e) Recovery of **5**.

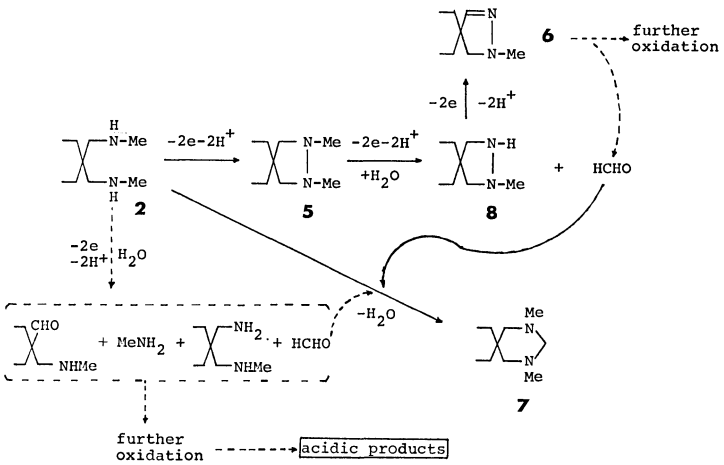

Scheme 2.

Table 4. Results of chemical oxidation of 1 and 2

Diamine	Oxidizing reagent	Yields of products/%					Recovery of 1 or 2
		3	4	5	6	7	%
1	$Na_2S_2O_8/Ag^+$ (1 eq./mol)	46	trace	—	—	—	24
1	$Pb(OAc)_4$ (1 eq./mol)	5	24	—	—	—	65
1	$Pb(OAc)_4$ (3 eq./mol)	4	89	—	—	—	0
2	$Na_2S_2O_8/Ag^+$ (1 eq./mol)	—	—	11	14	26	36

ical oxidation of **5** at a lower potential than the oxidation potential of **2**, **6** seems to be formed by further oxidation of **5** produced in the course of the electrochemical oxidation of **2**. Since **7** was formed in a good yield by the reaction of **2** with excess formaldehyde under the same conditions as the electrolysis of **2**, **7** seems to be formed by the reaction of **2** with formaldehyde produced in the course of the electrolysis.

From the results and the formation of 1-methyl-4,4-diethylpyrazolidine (**8**),†††† detected by a gas chromatography-mass spectrometer, electrochemical oxidation of **2** might proceed as in Scheme 2.

Chemical Oxidation of 1 and 2. Nomura *et al.* found that sodium peroxodisulfate is effective for N,N-coupling of piperidines in the presence of silver ions.[10] We investigated chemical oxidation of **1** and **2** with sodium peroxodisulfate and also lead tetraacetate in order to compare the results with those of electrochemical oxidation. The results are summarized in Table 4.

In the oxidation of **1** with sodium peroxodisulfate, the reaction stopped at the initial step of N,N-coupling, **3** being formed as the sole product. On the other hand, oxidation with lead tetraacetate afforded a highly oxidized product, **4**, far exceeding **3** in amount, though one equivalent of the oxidation reagent was employed. **4** was also formed in an excellent yield with use of three equivalents of the reagent.

In the oxidation of **2** with sodium peroxodisulfate, **5**, which could scarcely be obtained by electrolysis, was formed in *ca.* 10% yield. However, the highly oxidized product **6** was formed in a greater amount than **5**, though a large amount of the starting material remained. In the case of an open-chain diamine such as **2**, the oxidation reaction did not stop at the initial step of N,N-coupling, differing entirely from that of a cyclic diamine such as **1**. In the oxidation using lead tetraacetate, the analysis of products was difficult because of the formation of a large amount of polymer. Daniels and Martin[17] found that *N,N'*-

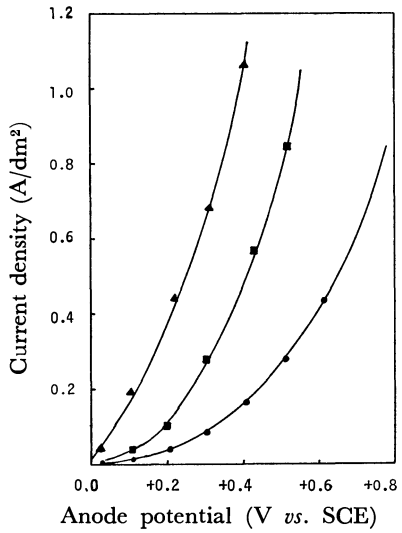

Fig. 1. Current density *vs.* anode potential curves of **2** and **5** in 1M NaOH at a carbon electrode.
—●—: 1 M NaOH (50 ml), —■—: 1 M NaOH (50 ml)+**2** (1 mmol), —▲—: 1 M NaOH (50 ml)+**5** (1 mmol).

†††† Its structure was tentatively determined by a study of the MS fragmentation: *m/e* 142 (M^+), 127 (M^+—Me), 126 (M^+—Me—H), 113 (M^+—Et).

Table 5. Efficiencies of electrochemical and chemical oxidative N,N-coupling

Anode material or oxidizing reagent	Efficiency of N,N-coupling (Current efficiency or yield %)		
	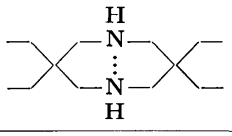	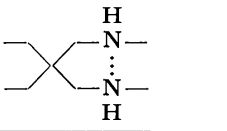	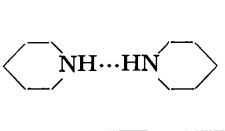
C	94	16	low
Pt	99	4	low
Ag	67	3	low
Ni	84	0	0
$Na_2S_2O_8/Ag^+$ (1 eq.)	46	25	61[10]
$Pb(OAc)_4$ (1 eq.)	29	—	5

diakyl-1,3-propanediamines affords only unchanged diamines, though the *N,N'*-diaryl derivatives give N,N-coupling products by the oxidation using manganese dioxide.

Comparison of Electrochemical and Chemical Oxidation. Efficiencies of electrochemical and chemical oxidative N,N-coupling of **1** and **2** together with piperidine[10] are summarized in Table 5.

A precise comparison of N,N-coupling efficiencies can not be made because of different reaction conditions. However, points to be noted are as follows. The intramolecular N,N-coupling took place more easily in electrochemical oxidation than in intermolecular oxidation. In the former reaction, N,N-coupling of the cyclic diamine proceeded more readily than that of the open-chain diamine. In the case of the cyclic diamine, current efficiency of the N,N-coupling was good, regardless of anode material. In the case of the open-chain diamine, efficiency changes a great deal with anode material, a carbon anode being most effective for N,N-coupling. A nickel anode was very effective for the oxidation of **1**, but not for **2** and piperidine.

In contrast, the structures of amines did not cause such a large difference in the results in chemical oxidation. Selectivities for the oxidation products differ a great deal in chemical and electrochemical oxidation; *e.g.*, **3** and **4** were formed in higher selectivity by oxidation with sodium peroxodisulfate and lead tetraacetate, respectively, than that in the electrochemical oxidation, selectivity for **7** being higher in the electrochemical oxidation.

Experimental

Materials. 3,3,7,7-Tetraethylperhydro-1,5-diazocine (1) and 3,3,7,7-Tetraethyl-1,5-diazabicyclo[3.3.0]octane (3): **1** and **3** were prepared according to a modification of Kemp's procedure.[11] To a stirred solution of 3,3,7,7-tetraethylperhydro-1,5-diazocine-2,4,6,8-tetrone (0.097 mol) in dry THF was gradually added a solution of diborane hexahydride (0.36 mol) in THF at 0—5 °C. Stirring was carried out at 0—5 °C for 1 h and then at room temperature for 1 h. The mixture was refluxed for 24 h. After cooling, 3 M HCl (1 M=1 mol·dm^{-3}) (200 ml) was added and THF was removed under reduced pressure. The residual solution was refluxed for 1 h. After cooling, the solution was made alkaline and was extracted repeatedly with ether. The extracts were dried over Na_2SO_4 and filtered. Hydrogen chloride gas was passed through the ether solution and the precipitates were collected by filtration. The crystals were treated with methanol at room temperature and insoluble parts were collected by filtration. Recrystallization of the matter from methanol–water (9:1, vol. ratio) gave pure hydrochloride of **1**: mp 231—233 °C (Ref.[11] 219—220 °C). From this salt, the free base of **1** was obtained by treatment with sodium hydroxide and extraction with ether: Yield 36%; mp 31—31.5 °C; *m/e* 226 (M^+). Found: C, 73.78; H, 13.67; N, 12.14%. Calcd for $C_{14}H_{30}N_2$: C, 74.27; H, 13.36; N, 12.37%. The methanolic solution of the filtrate was concentrated to dryness under reduced pressure. The residue was mixed with aqueous sodium hydroxide solution and the solution then extracted with ether. After drying of the ethereal extracts and concentration under reduced pressure, the residual oily substance was distilled under reduced pressure to give a fraction (**3**): Yield 7%, bp 115—116 °C/3 Torr; *m/e* 224 (M^+).

N,N'-Dimethyl-2,2-diethyl-1,3-propanediamine (2): The compound was prepared as a dihydrochloride by reduction of *N,N'*-dimethyl-α,α-diethylmalonamide with diborane by a procedure approximately the same as in the preparation of **1**. Recrystallization from methanol–ethanol (10:1, vol. ratio) gave pure dihydrochloride: Yield 45%; mp 265—267 °C. Found: C, 46.45; H, 10.94; N, 12.18%. Calcd for $C_9H_{24}N_2Cl_2$: C, 46.75; H, 10.46; N, 12.18%. The free base of **2** was obtained as an oil substance from the dihydrochloride: *m/e* 158 (M^+).

1,2-Dimethyl-4,4-diethylpyrazolidine (5): Using approximately the same procedure as above, **5** was prepared from 1,2-dimethyl-4,4-diethylpyrazolidine-3,5-dione.[18] Purification by column chromatography on alumina with hexane–ether (3:1, vol. ratio) gave **5** as an oily substance: *m/e* 156 (M^+), 141 (M^+-Me). Monohydrochloride of **5**: mp 165.5—167.5 °C (from hexane). Found: C, 56.31; H, 11.36; N, 14.54%. Calcd for $C_9H_{21}N_2Cl$: C, 56.08; H, 10.99; N, 14.53%.

1,3-Dimethyl-5,5-diethylperhydropyrimidine (7): The dihydrochloride of **2** (0.5 mmol) was dissolved in 20 ml of 1 M sodium hydroxide, and then 1 ml of 37% aq formaldehyde was added. After stirring for 2 h, the solution was extracted repeatedly with ether. Thorough evaporation of the ethereal extract, dried over anhydrous sodium sulfate under reduced pressure gave **7** as an oily substance: Yield 86%; *m/e* 170 (M^+), 155 (M^+-Me), 126 ($M^+-Me-Et$). Dihydrochloride of **7**: mp 217—218 °C (from isopropyl alcohol).

General Electrolytic Procedures. Electrolysis was carried

out at a constant potential as follows. An H type cell divided with a sintered glass diaphragm was used. Platinum, carbon, nickel, and silver plates (2×4 cm) were used as an anode. A platinum anode was treated with concd nitric acid and the others were carefully polished with an emery paper No. 3000 before electrolysis. 0.1 M Et_4NOTs acetonitrile solution (50 ml) suspending lithium hydroxide powder and 1 M NaOH (50 ml) were used as an anolyte for electrolysis of **1** and **2**, respectively. To the anolyte was added 1 mmol of diamine (**1** and **2**) and then a current was applied.

Analysis of Products. *Electrolysis of 1*: After electrolysis, the anolyte was acidified with hydrochloric acid. Acetonitrile was evaporated under reduced pressure, the residual aqueous solution being made strongly alkaline with sodium hydroxide. The alkaline solution was extracted repeatedly with ether and the ethereal extracts were subjected to gas chromatography (column packing, PEG 20 M, column temperature, 186 °C).

1-(2-Ethyl-2-formylbutyl)-4,4-diethyl-4,5-dihydropyrazole (**4**) was isolated as an oily substance by column chromatography on almina with dichloromethane: *m/e* 209 (M^+). Found: C, 70.44; H, 11.35; N, 11.71%. Calcd for $C_{14}H_{26}N_2O$: C, 70.54; H, 11.00; N, 11.75%.

Electrolysis of 2: After salting-out with sodium chloride, the anolyte was extracted repeatedly with ether and the ethereal extracts were subjected to gas chromatography. Analysis for **5**, **6**, and **7** was carried out on a PEG 20 M column and that for **2** on Chromosorb 103.

In the case of a low material balance between the starting diamine and the products, the above alkaline solution, which was extracted with ether, was acidified with hydrochloric acid. After the acidic solution had been extracted repeatedly with ether, the ethereal extracts were concentrated, the acidic polymer obtained being weighed.

1-Methyl-3,3-diethyl-4,5-dihydropyrazole (**6**) was isolated by column chromatography on almina with dichloromethane: *m/e* 140 (M^+), 111 (M^+-Et). Picrate of **6**: mp 129—130 °C. Found: C, 45.37; H, 5.07; N, 18.91%. Calcd for $C_{14}H_{19}N_5O_7$: C, 45.53; H, 5.18; N, 18.96%. 1,3-Dimethyl-5,5-diethylperhydropyrimidine (**7**) was isolated by preparative gas chromatography: *m/e* 170 (M^+). Dihydrochloride of **7**: mp 217—218 °C. Found: C, 50.05; H, 10.11; N, 11.33%. Calcd for $C_{10}H_{24}N_2Cl_2$: C, 49.39; H, 9.95; N, 11.52%.

Chemical Oxidation. *Oxidation of 1 and 2 with Sodium Peroxodisulfate*: To a stirred mixture of **1** (1 mmol), 0.5 M NaOH–acetone (8—10 ml), and a catalytic amount of silver nitrate (0.02 mmol), was added dropwise a solution of sodium peroxodisulfate (2 mmol) in water (2 ml) at 0 °C. After stirring at 0 °C for 2 h, a small amount of silver oxide was filtered off and the filtrate was extracted repeatedly with ether. The ethereal extracts were subjected to gas chromatography.

Oxidation of **2** with sodium peroxodisulfate was carried out without acetone as a co-solvent in a similar way to that above.

Oxidation of 1 with Lead Tetraacetate: To a stirred solution of **1** (1 mmol) in dry benzene (15 ml) was added lead tetraacetate (1 mmol) in a nitrogen atmosphere. After stirring at room temperature for 1 h, the precipitated lead acetate was filtered off. The filtrate of benzene was washed with 1 M NaOH, dried over Na_2SO_4, and then filtered. The filtrate was subjected to gas chromatography.

Oxidation of Piperidine with Lead Tetraacetate: Piperidine was oxidized in a similar way to that above. Analysis of the product, 1,1′-bipiperidine, was carried out in a similar manner to that described previously.[9]

This work was supported by a grant from the Kawakami Memorial Foundation.

References

1) Part 3: T. Fuchigami, T. Iwaoka, T. Nonaka, and T. Sekine, *Chem. Lett.*, **1978**, 1437.
2) a) V. D. Parker, "Organic Electrochemistry," ed by M. M. Baizer, Marcel Dekker, Inc., New York (1973), p. 315; b) C. K. Mann and K. K. Barnes, "Electrochemical Reactions in Nonaqueous Systems," Marcel Dekker, Inc., New York (1970), p. 259.
3) S. Wawzonek and T. W. McIntyre, *J. Electrochem. Soc.*, **114**, 1025 (1967).
4) A. G. Hudson, A. E. Pedler, and J. C. Tatlow, *Tetrahedron Lett.*, **1968**, 2143.
5) G. Cauquis, J. P. Cognard, and D. Serve, *Tetrahedron Lett.*, **1971**, 4645.
6) G. Cauquis, J. P. Coquand, and J. Rigaudy, *C. R. Acad. Sci., Paris, Ser. C*, **268**, 2265 (1969).
7) A. U. Blackham, S. Kwah, and J. L. Palmer, *J. Electrochem. Soc.*, **122**, 1081 (1975).
8) R. Bauer and H. Wendt, *Angew. Chem.*, **90**, 214 (1978).
9) T. Fuchigami, T. Toki, T. Iwaoka, and T. Nonaka, *J. Electrochem. Soc. Jpn.*, **47**, 627 (1979).
10) Y. Nomura, K. Ogawa, Y. Takeuchi, and S. Tomoda, *Chem. Lett.*, **1978**, 271.
11) D. S. Kemp, J. P. Chabala, and S. A. Marson, *Tetrahedron Lett.*, **1978**, 543.
12) N. A. Hampson, J. B. Lee, J. R. Morley, and B. Scanlon, *Can. J. Chem.*, **47**, 3729 (1969).
13) N. A. Hampson, J. B. Lee, J. R. Morley, K. I. MacDonald, and B. Scanlon, *Tetrahedron*, **26**, 1109 (1970).
14) N. A. Hampson, J. B. Lee, and K. I. MacDonald, *Electrochim. Acta*, **17**, 921 (1972).
15) B. Fleishmann, K. Korinek, and D. Pletcher, *J. Chem. Soc., Perkin Trans. 2*, **1972**, 1396.
16) S. F. Nelsen and P. J. Hinz, *J. Am. Chem. Soc.*, **94**, 7108 (1972).
17) R. Daniels and B. D. Martin, *J. Org. Chem.*, **27**, 178 (1962).
18) H. H. Hatt, *Org. Synth.*, Coll. Vol. II, 208.

Syntheses of 2*H*-1-Benzothiopyran-2-ones (Thiocoumarins) and Related Compounds from Benzenethiols and Diketene

Hiroyuki NAKAZUMI,* Akira ASADA, and Teijiro KITAO
Department of Applied Chemistry, College of Engineering, University of Osaka Prefecture, Sakai, Osaka 591

(Received December 14, 1979)

The products formed by the reaction of benzenethiols with diketene in the presence of H_2SO_4 are (*E*)-β-(arylthio)crotonic acids (**2**) and/or isomeric (*Z*)-β-(arylthio)crotonic acids and not, as has been reported, *S*-phenyl 3-oxobutanethioates (**1**). Compounds **1a**—**k**, as the precursor of thiocoumarins, were prepared from benzenethiols and diketene in the presence of triethylamine. The reaction of **1** with various condensing agents has been examined to prepare 2*H*-1-benzothiopyran-2-ones (thiocoumarins). It is found that 4-methyl(thiocoumarins) were conveniently prepared by the reaction of **1** with anhydrous aluminium chloride in yields of 16—48%. When **1** was treated with PPA, isomeric 2-methyl(thiochromones) were preferentially obtained in yields of 5—66%, and compound **2** was isolated as an intermediate. The spectral characteristics of 4-methyl(thiocoumarins) have also been described.

It is well known that 2*H*-1-benzothiopyran-2-ones (thiocoumarins) can not be obtained by the Pechmann reaction of benzenethiols.[1] Thiocoumarins are generally prepared from the unstable 2-mercaptobenzaldehydes which require multistage processes from benzenethiols.[2] Although Konishi *et al.* reported the convenient method to prepare thiocoumarins by the cyclization of *S*-phenyl 3-oxobutanethioates with PPA,[3] the products are mostly not thiocoumarins, but isomeric thiochromones (4*H*-1-benzothiopyran-4-ones).[4] Furthermore, recently we found that the *S*-phenyl 3-oxobutanethioates, described in our previous paper,[4] were really isomeric (*E*)-β-(arylthio)crotonic acids (**2**) and/or (*Z*)-β-(arylthio)crotonic acids (**3**).

We have now prepared a number of *S*-(substituted phenyl) 3-oxobutanethioates (**1**) from benzenethiols and diketene, and studied the cyclization of **1** with various condensing agents to prepare thiocoumarin derivatives. These works were reported in a preliminary form,[5] but in this paper we wish to report further details of these reactions. We also wish to report the spectral characteristics of 4-methyl(thiocoumarins), compared with those of isomeric 2-methyl(thiochromones).

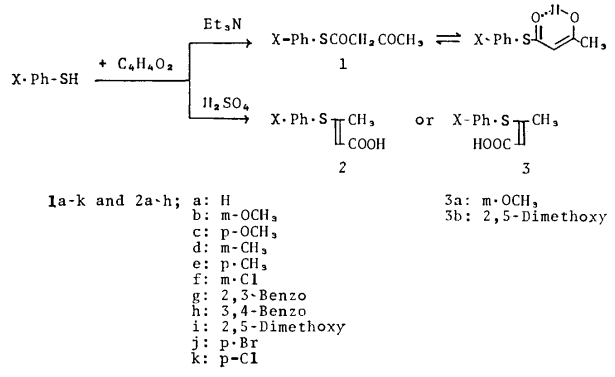

Scheme 1.

Results and Discussion

Preparation of S-*Phenyl 3-Oxobutanethioates.* Recently Yaggi and Douglas reported that the product obtained from the reaction between benzenethiols and diketene in the presence of sulfuric acid was (*E*)-β-(arylthio)crotonic acid **2** (X=H or *p*-Cl).[6] A number of authentic (*E*)-β-(arylthio)crotonic acids (**2**) were prepared from sodium (*E*)-β-chlorocrotonate and sodium benzenethiolates by a similar method to that for **2a**.[7] The IR spectra and mp's of previously reported products, obtained by the reaction of benzenethiols with diketene in the presence of H_2SO_4, were in agreement with those of authentic samples (**2**, except for *m*-methoxy (**3a**) and 2,5-dimethoxy (**3b**) derivatives. No depression in melting point was observed in admixture of any pair of those samples. However, the melting points and IR spectra of *m*-methoxy and 2,5-dimethoxy derivatives are quite different from those of authentic samples. These compounds were assigned to (*Z*)-β-(arylthio)crotonic acid derivatives (**3**), as isomers of **2**, on the basis of NMR spectra of (*Z*)- and (*E*)-β-thio-substituted crotonates.[8] That is, the chemical shifts for the vinylic methyl group and vinylic proton for **3a** and **3b** showed upfield chemical shift of *ca.* 0.5 ppm for vinylic methyl group and downfield chemical shift of *ca.* 0.65 ppm for vinylic proton, compared to the corresponding values for authentic samples. From the results, the products obtained from the reaction of benzenethiols with diketene in the presence of H_2SO_4 are not **1**, described in previous paper, but the isomeric **2** and/

Table 1. The NMR spectra of *S*-phenyl 3-oxobutanethioates (**1**)

Compound No.	X	NMR in CCl_4 (ppm)
1f	*m*-Cl	1.95 and 2.25 (total 3H, each s), 3.65 and 5.50 (total *ca.* 1.2H, each s), 7.20—7.60 (4H, m), 12.20 (broad)
1g	2,3-Benzo	1.90 and 2.15 (total 3H, each s), 3.68 and 5.45 (total *ca.* 1.4H, each s), 7.20—8.20 (7H, m)
1i	2,5-Dimethoxy	1.90 and 2.18 (total 3H, each s), 3.73(3H, s), 3.75(3H, s), 3.52 and 5.36 (total *ca.* 1.2H, each s), 6.50—7.00 (3H, m)
1j	*p*-Br	1.92 and 2.20 (total 3H, each s), 3.58 and 5.32 (total *ca.* 1.3H, each s), 7.00—7.55 (4H, m) 12.50 (broad)

See Ref. 5 for **1a**—**e** and **1h**.

Table 2. Spectral data of 4-methyl(thiocoumarins) (**8**)

Compound	X	NMR (ppm) in CDCl	ν_{CO} (cm^{-1})	UV λ_{max} ($\varepsilon \times 10^{-4}$) (nm) in EtOH	*m/e* (rel. intensity)
8a	H	2.58 (3H, s) 6.62 (1H, s) 7.45—7.56 (3H, m) 7.95 (1H, m)	1635	235 (2.5), 241 (2.5) 289 (0.7), 298 (0.7) 342 (0.29)	176 (M, 46), 148 (M−28, 76) 147 (M−29, 100)
8d	7-CH_3	2.44 (3H, s) 2.52 (3H, s) 6.53 (1H, s) 7.20—7.30 (2H, m) 7.78 (1H, d, J=10 Hz)	1645	230 (2.4), 239 (2.4) 295 (0.8), 303 (0.9) 343 (0.4)	190 (M, 45), 162 (M−28, 100) 161 (M−29, 100)
8e	6-CH_3	2.50 (3H, s) 2.54 (3H, s) 6.62 (1H, s) 7.44 (2H, s) 7.78 (1H, s)	1635	237 (2.8), 243 (3.0) 290 (0.8), 298 (0.8) 350 (0.3)	190 (M, 48) 162 (M−28, 95) 161 (M−29, 100)
8f	7-Cl	2.54 (3H, s) 6.57 (1H, s) 7.20—7.50 (2H, m) 7.80 (1H, d, J=10 Hz)	1645	233 (2.8), 241 (2.9) 266 (1.1), 290 (1.2) 301 (1.0), 337 (0.3)	212 (M+2, 9), 210 (M, 24) 184 (40), 183 (47) 182 (M−28, 100), 181 (M−29, 90)
8g	7,8-Benzo	2.65 (3H, s) 6.68 (1H, s) 7.48—8.37 (6H, m)	1650 1630	275 (2.6), 286 (2.5) 319 (0.6), 333 (0.6) 373 (0.24), 390 s (0.19)	226 (M, 43), 198 (M−28, 100) 197 (M−29, 79)
8h	5,6-Benzo	2.60 (3H, s) 6.48 (1H, s) 7.25—8.30 (6H, m)	1650 s 1630	246 (5.4), 281 (2.2) 295 (2.3), 333 (1.2) 380 b (0.2)	226 (M, 64), 198 (M−28, 100) 197 (M−29, 57)
8j	6-Br	2.50 (3H, s) 6.50 (1H, s) 7.30—7.65 (2H, m) 7.88 (1H, d, J=2 Hz)	1625	248 (4.5), 287 (0.65) 298 (0.60), 351 (0.28)	256 (M+2, 71), 254 (M, 68), 228 (100), 227 (83), 226 (M−28, 98), 225 (M−29, 72)
8k	6-Cl	2.50 (3H, s) 6.50 (1H, s) 7.35 (2H, s) 7.74 (1H, s)	1625	246 (4.5), 287 (0.65), 298 (0.60), 350 (0.29)	212 (M+2, 28), 210 (M, 73) 184 (38), 183 (45), 182 (M−28, 100), 181 (M−29, 96)

or **3**.

S-Phenyl 3-oxobutanethioates (**1**), precursor of thiocoumarins, were quantitatively prepared by the reaction of benzenethiols with diketene in the presence of triethylamine for 5—20 h at room temperature, and existed in a mixture of the keto-enol tautomeric forms, NMR spectra of which were shown in Table 1.

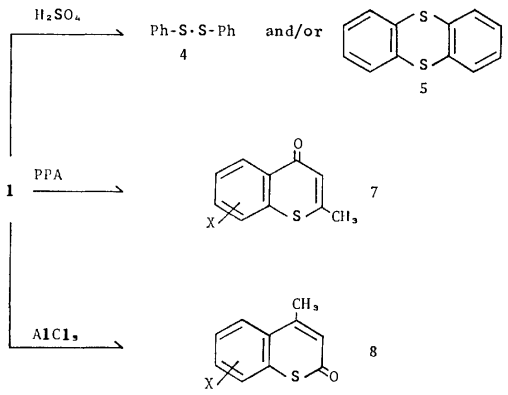

Scheme 2.

The Reaction of S-*Phenyl 3-Oxobutanethioates (**1**) with Various Condensing Agents.* The reaction of **1a** with sulfuric acid gave diphenyl disulfide (**4**) which was formed by decomposition of **1a**, and/or thianthrene derivatives (**5** and thianthrene 5,10-bis(dioxide) **6**) as oxidized products of **4**.

2-Methyl(thiochromone) derivatives (**7**), as the isomeric product of thiocoumarin, were preferentially obtained by treating **1** with polyphosphoric acid (PPA) at 70 °C. In the case of *m*-methoxy derivative (**1b**), only thiocoumarin **8b** was obtained. Compound **8b** also could be obtained from **2b** (X=*m*-OCH_3) and PPA. However, the other *S*-phenyl 3-oxobutanethioates, even with substituents such as methoxyl group(s) (**1c** and **1i**) gave the thiochromone **7** in yields of 10—79%. At lower temperatures of 5—10 °C, the same reaction of **1** afforded (*E*)-*β*-(arylthio)crotonic acid **2** (X=H, *m*-CH_3, or *p*-CH_3) in a low yield (4—10%). It is also known that the reaction of **1a** or **1d** with concd H_2SO_4 (1 equivalent) in Et_2O gave **2** (X=H or *m*-CH_3) in a yield of 21%.[9] It is concluded that compound **2** will be an intermediate to give **7**.

In the case of the use of anhydrous aluminium chloride as a condensing agent, some of 4-methyl(thiocoumarins) (**8**) were conveniently obtained in yields of 10—48% and no 2-methyl(thiochromones) (**7**) were obtained. However, the reaction of all methoxy derivatives of **1** with $AlCl_3$ gave only an oily undetermined material, and none of thiocoumarins was isolated. As the direct reaction of **1** with $AlCl_3$, without solvent, was favorable as regards to yield.[5] some of **8** were prepared by this method. In the cases of reaction of **1a**, **1j**, and **1k** with the suspension

of $AlCl_3$, carbon disulfide or benzene was used as the solvent.

When $ZnCl_2$ was used as a condensing agents for **1a**, **4** was obtained in 11% yield. In the cases of other condensing agents such as PCl_5, P_2O_5, and Ac_2O, oily undetermined materials were obtained.

Spectral Characteristics. The NMR, IR, UV, and mass spectra of **8** are summarized in Table 2. In the mass spectra, the major fragmentation was initial loss of carbon monoxide from the molecular ion, followed by the loss of a hydrogen atom leading to the formation of the ring-expanded thianaphthalenium ion as shown in Scheme 3. There was not the M−40 fragment ion, which was found characteristically in the mass spectra of 2-methyl(thiochromones) (**7**).[4] The base peak of **8** was the M−28 or M−29 fragment ion (Table 2).

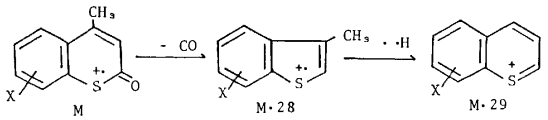

Scheme 3.

In the NMR spectra, the benzenoid proton at the 5-position of **8** showed the chemical shift in the range of 7.78—8.00 ppm. The difference between the proton at the 5-position and other aromatic protons was 0.34 —0.53 ppm, whereas that of **7** was *ca.* 1.00 ppm.

In the IR spectra, the carbonyl bands of **8** were found in the range 1635—1650 cm^{-1} and higher by 10—35 cm^{-1} than those of the corresponding thiochromones, except for **8j** and **8k**.

The fluorescent spectra of **8** and **7** were generally very weak, compared to those of the corresponding coumarins.

Experimental

All the melting points are uncorrected. IR spectra were recorded on a Hitachi ESI-S2 spectrophotometer using KBr pellts. ^{1}H-NMR spectra were taken on a Hitachi R-24A spectrometer with tetramethylsilane as an internal standard. Mass spectra were recorded on a Hitachi RMU-6E mass spectrometer operating at 80 eV. The fluorescent spectra were recorded on a Hitachi MPF-2A fluorescent spectrophotometer. Elemental analyses were recorded on a Yanaco CHN recorder MT-2.

(E)-*β*-*(Arylthio)crotonic Acid Derivatives (2).* *Method A*: Concd H_2SO_4 (9.0 g) was added dropwise to Et_2O (50 ml) solution of benzenethiol (5.0 g) at 30 °C. Diketene (5.0 g) was then added to this mixture. After 2 h, ether was removed *in vacuo* at 20 °C, and the residue was poured into an ice–water solution. White solid was separated, collected by filtration and recrystallized from EtOH to give **2a** (5.3 g). Other compounds **2** were prepared by a similar method. **2a**: 60%, mp 174.5—175.5 °C; **2c**: 5%, mp 172—175 °C; **2d**: 65%, mp 165—166 °C; **2e**: 60%, mp 204—205 °C; **2f**: 29%, mp 154—155 °C; **2g**: 10%, mp 198—202 °C; **2h**: 65%, mp 191—195 °C.

The NMR and IR spectra of these compounds corresponded to data of Table 3 described in previous paper.[4]

Method B: NaOH (1.2 g) was added to a solution of (*E*)-*β*-chlorocrotonic acid (2.0 g) in EtOH (10 ml). To the mixture, a solution of sodium *m*-methoxybenzenethiolate (*m*-methoxybenzenethiol (2.0 g)+NaOH (1.6 g)) in EtOH (5 ml) was added dropwise at 50 °C and stirred for 2 h. After cooling, dilute HCl was added to this solution until the pH was 1. The resulting solid was separated, and recrystallized from EtOH to give **2b** (X=*m*-OCH_3), yield 62%, mp 119—121 °C; NMR ($CDCl_3$): δ=2.40 (3H, s), 3.80 (3H, s), 5.28 (1H, s), 6.90—7.30 (4H, m), and 10.2 (1H, b); ν_{CO}: 1680 cm^{-1}. Found: C, 58.76; H, 5.48%. Calcd for $C_{11}H_{12}O_3S$: C, 58.93; H, 5.36%. **2i** (X=2,5-Dimethoxy): yield 50%, mp 126—128 °C; NMR ($CDCl_3$): δ=2.40 (3H, s), 3.80 (3H, s), 3.83 (3H, s), 5.23 (1H, s), 6.95—7.10 (3H, m), and 10.80 (1H, b); ν_{CO}: 1680 cm^{-1}. Found: C, 56.53; H, 5.59%. Calcd for $C_{12}H_{14}O_4S$: C, 56.69; H, 5.51%. Other compounds **2a** and **2c—h** were also prepared by a similar method in yields of 10—51%.

(Z)-*β*-*(Arylthio)crotonic Acid Derivatives (3).* Compound **3b** (X=2,5-dimethoxy) was prepared by the method A for **2a**: yield 22%, mp 169—171 °C; NMR ($CDCl_3$): δ=1.90 (3H, s), 3.78 (3H, s), 3.83 (3H, s), 5.90 (1H, s), and 6.90—7.10 (3H, m); ν_{CO}: 1675 cm^{-1}. Compound **3a** (X=*m*-OCH_3) was prepared by a similar method and isolated from the isomer mixture (**2b** and **3a**) by repeated recrystallization from EtOH. **3a**: mp 170—171 °C; NMR ($CDCl_3$): δ=1.90 (3H, s), 3.80 (3H, s), 5.90 (1H, s), and 7.00—7.30 (4H, m).

S-*Phenyl 3-Oxobutanethioates (1).* Compound **1a** was quantitatively obtained from benzenethiol and diketene in the presence of Et_3N in dichloromethane at room temperature for 20 h.[6] Other compounds **1b—k** were prepared similarly. All of compounds **1a—i** were colorless liquid, and **1j** and **1k** were recrystallized from Et_2O; **1j**: mp 51—53 °C; **1k**: mp 45 °C (lit,[6] 45—46 °C). Liquid **1** was used without purification for the cyclization with condensing agents.

The Reaction of 1 with Concd H_2SO_4. *Method I*: The mixed acid of 30% fuming H_2SO_4 (1.0 g) and concd H_2SO_4 (10 g) was added dropwise to **1a** (5.5 g) under stirring at 0 °C. The mixture was stirred at room temperature for 5 h, and was poured into an ice–water solution. The resulting solid was separated and recrystallized from EtOH to give diphenyl disulfide **4** (1.9 g): yield 61%, mp 58—59 °C.

Method II: Compound **1a** (5.0 g) was added dropwise to concd H_2SO_4 (20 ml) at 15 °C. The mixture was stirred for 5 h at 15 °C and was poured into an ice–water solution. The resulting solid was separated, washed with EtOH and acetone, and purified by acid-pasting to give thianthrene

Table 3. Elemental analyses of 4-methyl-(thiocoumarins) (**8**)

Compound	Formula (MW)	Analysis (%) Calcd (Found) C	H
8f	$C_{10}H_7OSCl$ (210.5)	57.01 (56.76)	3.33 (3.28)
8g	$C_{14}H_{10}OS$ (226)	74.34 (74.96)	4.42 (4.51)
8h	$C_{14}H_{10}OS$ (226)	74.34 (74.30)	4.42 (4.49)
8j	$C_{10}H_7OSBr$ (254.9)	47.08 (47.07)	2.75 (2.69)
8k	$C_{10}H_7OSCl$ (210.5)	57.01 (57.25)	3.33 (3.40)

5,10-bis(dioxide) **6** in 56% yield (mp>320 °C, lit,[10]> 360 °C). Found: C, 51.67; H, 2.97%. From the first filtrate in EtOH, thianthrene **5** was isolated in 4% yield; mp 152—154 °C (lit,[11] 157—159 °C).

The Reaction of 1 with PPA. Compound **1a** (3.0 g) was added to PPA (60 g) at 70 °C and stirred for 1—2 h. After cooling, the mixture was poured into an ice–water solution. The resulting solid was separated and recrystallized from EtOH–water mixture to give **7a** (1.8 g, 66%). Other **7** were similarly prepared. **7c**: X=6-OCH_3, 10%, mp 102—103 °C; **7d**: X=7-CH_3, 23%, mp 98—100 °C; **7e**: X=6-CH_3, 53%, mp 120 °C; **7f**: X=7-Cl, 25%, mp 165—166 °C; **7g**: X=7,8-benzo, 25%, mp 194—195 °C; **7h**: X=5,6-benzo, 15%, mp 126—128 °C; **7i**: X=5,8-dimethoxy, 79%, mp 146—148 °C; **7j**: X=6-Br, 23%, mp 181—182 °C (lit,[12] 176 °C); NMR ($CDCl_3$): δ=2.43 (3H, s), 6.79 (1H, s), 7.23—7.70 (2H, m), and 8.55 (1H, d, J=2 Hz); ν_{co}: 1623 cm^{-1}, Found: C, 46.87; H, 2.81%. λ_{max} (EtOH): 224 (ε 1.8×10^4), 252 (2.5×10^4), 281 (0.3×10^4), 292 (0.3×10^4), and 342b nm (0.8×10^4); **7k**: X=6-Cl, 34%, mp 164—166 °C (lit,[12] 170 °C); NMR ($CDCl_3$): δ=2.46 (3H, s), 6.81 (1H, s), 7.48 (2H, s), and 8.43 (1H, s); ν_{co}: 1628 cm^{-1}. Found: C, 57.13; H, 3.46%. λ_{max} (EtOH): 223 (ε 1.7×10^4), 250 (2.4×10^4), 280 (0.5×10^4), 291 (0.4×10^4), and 342b nm (0.9×10^4).

From the same reaction of **1a**, **1d**, and **1e** at 5—10 °C, **2a** (yield, 4%), **2d** (4%), and **2e** (10%) were isolated, respectively. Under the same conditions at 70 °C, **8b** (X=7-OCH_3) was obtained in 54% yield from **1b**.

The Reaction of 1 with Aluminium Chloride. *Method (i)*: Compound **1a** (3.0 g, 15 mmol) was added to a suspension of $AlCl_3$ (20 g) in CS_2 (20 ml). After reflux for 5 h, the mixture was poured into cold water. The resulting solid was separated and recrystallized from EtOH to give **8a** (1.0 g) in 38% yield, mp 126—127 °C (lit,[2] 124 °C). When benzene was used in the place of CS_2, **8j** and **8k** were obtained; **8j**: 27%, mp 184—185 °C; **8k**: 23%, mp 177—179 °C.

Method (ii): Compound **1a** (3.0 g, 15 mmol) was added to $AlCl_3$ (20 g), and stirred at 80—90 °C for 2 h. After cooling, the mixture was poured into cold water. The resulting solid was separated and recrystallized from EtOH to give **8a** in 48% yield. The others of **8** were similarly obtained by the method (ii); **8d**: 42%, mp 108—109 °C (lit,[2] 110 °C); **8e**: 31%, mp 114—115 °C (lit,[2] 120 °C); **8f**: 22%, mp 157—158 °C; **8g**: 16%, mp 169—171 °C; **8h**: trace, mp 133—134 °C.

The elemental analyses of those compounds were shown in Table 3.

The Fluorescent Spectra. **8b**: F_{max} (EtOH): 402 nm (rel. intensity based on **8b** as a standard); **8g**: F_{max}: 467 nm (1.5); **8h**: F_{max}: 405 (0.74) and 435 nm (0.66); **7b**[4] (X=7-OCH_3): F_{max}: 382 nm (2.0); **7g**: F_{max}: 398 nm (0.73); **7h**: F_{max}: 402 nm (0.6); **7i**; F_{max}: 494 nm (2.9×10); 7-MeO-4-methylcoumarin: F_{max}: 410 nm (2.7×10^2); 7,8-benzo-4-methylcoumarin:[3] F_{max}: 418 nm (9.1×10); 5,6-benzo-4-methylcoumarin:[3] F_{max}: 403 nm (9.6×10^2). The other thiocoumarins and thiochromones which were prepared herein showed no detectable fluorescence.

This work was supported in part by the Grant-in-Aid for Scientific Research from the Ministry of Education (No. 475675).

References

1) R. C. Elderfield, "Heterocyclic Compounds," John-Wiley & Sons, New York (1951), Vol. 2, p. 542.
2) A. Ruwet and M. Renson, *Bull. Soc. Chim. Belg.*, **78**, 449 (1969).
3) K. Konishi, H. Umemoto, M. Yamamoto, and T. Kitao, *Nippon Kagaku Kaishi*, **1973**, 118.
4) H. Nakazumi and T. Kitao, *Bull. Chem. Soc. Jpn.*, **50**, 939 (1977).
5) H. Nakazumi and T. Kitao, *Chem. Lett.*, **1978**, 929; H. Nakazumi, A. Asada, and T. Kitao, *ibid.*, **1979**, 387.
6) N. F. Yaggi and K. T. Douglas, *J. Chem. Soc., Chem. Commun.*, **1977**, 609.
7) W. Autenrienth, *Justus Liebigs Ann. Chem.*, **254**, 234 (1889).
8) E. Campaigne and Y. Abe, *Bull. Chem. Soc. Jpn.*, **49**, 559 (1976).
9) M. Sato of Tohoku University, private communication, 1977 (We also followed these results).
10) M. P. Genevresse, *Bull. Soc. Chim. Fr.*, **17**, 601 (1898).
11) Krafft and Lyons, *Ber.*, **29**, 436 (1896).
12) F. Bossert, *Justus Liebigs Ann. Chem.*, **680**, 40 (1964).

Carbocyclic Ring Formation by the Intramolecular Reaction between Enol Silyl Ether and Allylic Acetate Moieties

Akira Itoh, Koichiro Oshima,* Hisashi Yamamoto,** and Hitosi Nozaki

Department of Industrial Chemistry, Faculty of Engineering, Kyoto University, Yoshida, Kyoto 606

(Received January 12, 1980)

The title reaction of *trans*-3-acetoxy-4-(4-methyl-3-trimethylsiloxy-3-pentenyl)cyclohexene proceeds in the presence of Et_2AlOAr, where Ar=2,6-di-*t*-butyl-4-methylphenyl, affording stereospecifically the *cis* isomer of 2,2-dimethylbicyclo[4.4.0]dec-9-en-3-one. In contrast, the *cis*-disubstituted cyclohexene compound reacts only sluggishly to produce a mixture of the *cis*- and *trans*-fused octalones. Similar stereospecific effect of the allylic double bond configuration on the ease of cyclization has been observed in the synthesis of karahanaenone from 3,7-dimethyl-6-trimethylsiloxy-2,6-octadienyl acetate and related reactions.

We report a remarkable case of stereochemically controlled cyclization reaction proceeding intramolecularly among trimethylsiloxyethenyl group and allylic acetate moiety as shown in Eqs. 1 and 2.

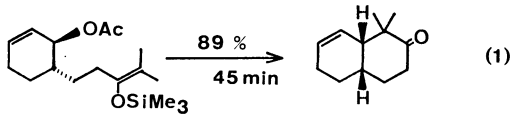

1 2 (1)

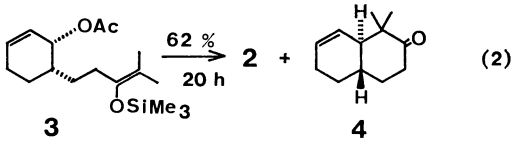

3 4 (2)

66 : 34

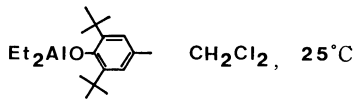

Obviously, the *trans*-substituted cyclohexenyl acetate (**1**) reacts smoothly in the presence of diethylaluminum 2,6-di-*t*-butyl-4-methylphenoxide as prepared from diethylaluminum chloride and the sterically hindered sodium phenoxide.[1] The resulting product is isomerically homogeneous *cis*-octalone (**2**). In sharp contrast, however, the *cis*-substituted cyclohexene (**3**) is transformed very sluggishly into a mixture of *cis*- and *trans*-octalone (**2** and **4**) only with inferior yields. This observation clearly excludes anticipated, possible intermediacy of the same, "free", allylic carbonium ion from both **1** and **3** which should be further cyclized into the trimethylsiloxy-stabilized cation presumably.

This type of cyclization has originally been described as a means of constructing the skeleton of karahanaenone (**6**) biomimetically (Eq. 3)[2] in the sense that neryl cation "equivalent" cyclizes in the *anti*-Markovnikov manner[3] to form a seven-membered ring. Extention of the same reaction to an isomeric system is shown in Eqs. 4, 5, and 6.

These equations impressively indicate that the (*E*), (*Z*) stereochemistry of the allylic double bond determines the rates of cyclization as well as the yields and distributions of the resulting products. Here again

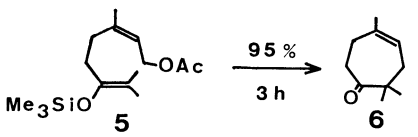

5 6 (3)

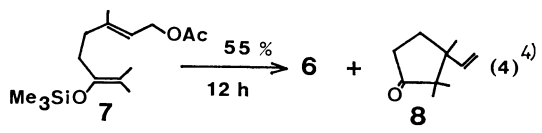

7 8

82 : 18

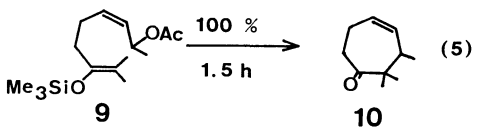

9 10

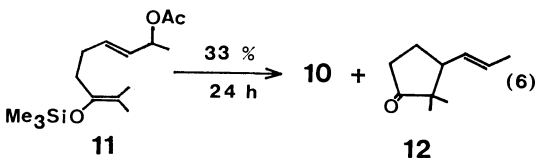

11 12

53 : 47

$MeAl(OCOCF_3)_2$, hexane-CH_2Cl_2, 25°C

the "free" allylic cation does not account for the observed dependence of the reaction on the allylic olefinic bond configuration of the substrates. Under comparable reaction conditions, diethyl geranyl phosphate does react quite analogously as the neryl isomer to afford limonene and terpinolene mixture in the presence of $(Bu^i_2Al)_2O$ in tetrahydrofuran (THF).[5,6] The $(Bu^i_2Al)_2O$–THF combination might increase the life-time of allylic carbonium ion so that (*E*)-allylic carbonium ion can be converted into (*Z*)-isomer which cyclizes with ease.[9]

The aluminum reagent in Eq. 3 through 6, methylaluminum bis(trifluoroacetate) or dimethylaluminum trifluoroacetate, was prepared from trimethylaluminum and calculated amount of trifluoroacetic acid in hexane and was used *in situ*. These proved to give less satisfactory results in the reaction of Eqs. 1 and 2.

Further examples of analogous cyclization are given in Eqs. 7, 8, and 9. For the allylic acetate unequally substituted at α and γ position, the silyl enol ether attacks the less substituted end of the allylic system

** Present address: Faculty of Engineering, Nagoya University, Furo-cho, Chikusa-ku, Nagoya 464.

preferentially.

The preparation of cyclization substrates merits brief descriptions. The acetates **1** and **3** are obtained through the sequence in Scheme 1.

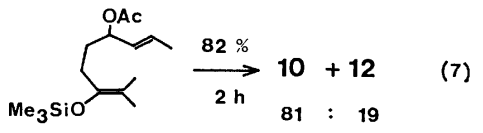

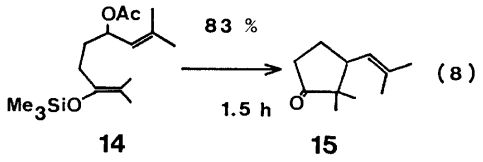

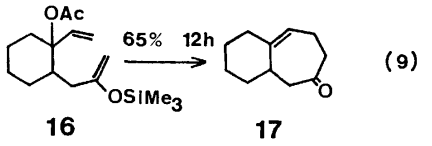

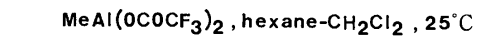

Scheme 1.

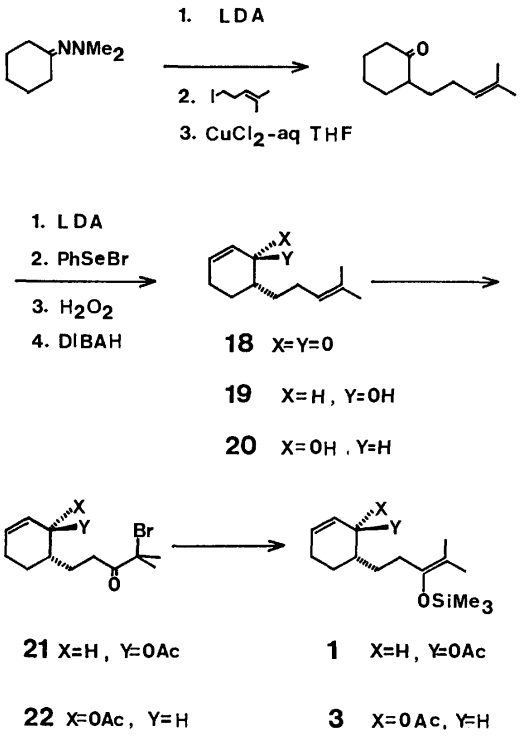

Experimental

The infrared spectra were determined on a Shimadzu IR-27-G spectrometer; the mass spectra on a Hitachi RMU-6L machine; the GLPC analyses on a Yanagimoto GCG-550F; and the NMR spectra on a JNM-PMX 60 or Varian EM-390H spectrometer. The chemical shifts are given in δ in ppm with TMS as the internal standard. Splitting patterns are designated as s, singlet; d, doublet; t, triplet; q, quartet; m, multiplet. The microanalyses were carried out by the staffs at the Elemental Analyses Center of Kyoto University. All experiments were carried under an atmosphere of dry argon. Tetrahydrofuran was dried by distillation from sodium-benzophenone. Thin layer or thick layer plates were made of E. Merck PF-254, and preparative column chromatography on silica gel E. Merck Art. 7734.

cis-2,2-Dimethylbicyclo[4.4.0]dec-9-en-3-one (2). A mixture of sodium hydride (50%, 50 mg, 1.0 mmol) and 2,6-di-*t*-butyl-4-methylphenol (0.22 g, 1.0 mmol) in hexane (5.0 ml) was stirred for 5 min at 0 °C. After stirring for an additional 15 min at 25 °C, a hexane solution of diethylaluminum chloride (1.0 M, 1.0 ml) was added. After 10 min, the solvent was removed *in vacuo* and the residue was diluted with dichloromethane (7.0 ml). A solution of **1** (157 mg, 0.51 mmol) in dichloromethane (3.0 ml) was added at −23 °C. After 3 h at −23 °C and 45 min at 25 °C, the mixture was poured into 1 mol dm^{-3} HCl and extracted with ethyl acetate (2×20 ml). The combined organic layers were washed with water and saturated aqueous sodium chloride solution and dried over anhydrous sodium sulfate. Removal of solvent *in vacuo* gave an oil which was purified by column chromatography on silica gel (5:1 hexane–ether) to give **2** (80 mg, 89%): IR (neat) 1710, 1382, 1070, 1010, 860, 755, 690 cm^{-1}; NMR (CCl_4) δ 1.06 (s, 3H), 1.24 (s, 3H), 5.63 (bs, 2H); MS *m/e* (%) 179 (9), 178 (M^+, 46), 93 (92), 92 (100), 79 (85). Hydrogenation (PtO_2) of **2** gave *cis*-2,2-dimethylbicyclo[4.4.0]decan-3-one which was spectrometrically identical with an authentic sample.[10]

trans-2,2-Dimethylbicyclo[4.4.0]dec-9-en-3-one (4). A solution of **3** (154 mg, 0.50 mmol) in dichloromethane (3.0 ml) was treated with the aluminum reagent (1.0 mmol) prepared as described above at 25 °C for 20 h. Purification by column chromatography afforded a mixture of **2** and **4** in 62% yield in a ratio of 66:34 as determined by GLPC (10% PEG, 2 m, 122 °C). Careful purification by preparative thick layer chromatography (PLC) on silica gel (5:1 hexane–ether) gave pure sample of **4**: IR (neat) 1708, 1180, 1110 cm^{-1}; NMR (CCl_4) δ 0.97 (s, 3H), 1.09 (s, 3H), 5.62 (m, 2H); MS *m/e* (%) 179 (11), 178 (M^+, 66), 79 (100). The compound **4** was hydrogenated to provide *trans*-2,2-dimethylbicyclo[4.4.0]decan-3-one.[10]

Karahanaenone (6). A solution of trifluoroacetic acid (0.91 g, 8.0 mmol) in hexane (4.0 ml) was added slowly at 0 °C to a solution of trimethylaluminum in hexane (1.0 M, 4.0 ml, 4.0 mmol) to give a white slurry. The mixture was stirred at 25 °C for 15 min and cooled to 0 °C. A solution of **5** (0.28 g, 1.0 mmol) in dichloromethane (8.0 ml) was added and stirring continued at 0 °C for 10 min and 25 °C for 3 h. After the usual workup, PLC (10:1 hexane–ether) gave **6** (130 mg, 85%): bp 160 °C (760 Torr); IR (neat) 1698, 1660, 1398, 1358 cm^{-1}; NMR (CCl_4) δ 1.05 (s, 6H), 1.70 (s, 3H), 2.03—2.30 (m, 4H), 2.55—2.80 (m, 2H), 5.42 (t, 1H, J=5.8 Hz); MS *m/e* (%) 152 (M^+, 100), 109 (66), 95 (94). The compound was identical with the authentic sample.[11] The yield determined by GLPC using 4-*t*-butylcyclohexanone as an internal standard was 95%.

2,2,3-Trimethyl-3-vinylcyclopentanone (8). The above procedure using **7** (142 mg, 0.5 mmol) and dimethylaluminum trifluoroacetate derived from trimethylaluminum (2.0 mmol) and trifluoroacetic acid (2.2 mmol) in dichloromethane (4.0 ml) afforded after usual workup and purification by PLC (10:1 hexane–ether) a mixture of **6** and **8** in 55% (42 mg) yield in a ratio of 82:18 as determined by GLPC (5% PEG 20 M, 1.5 m, 130 °C). Pure sample of **8** was obtained by preparative GLPC and its identity with an authentic sample[12] was established by IR and NMR. **8**: bp 110 °C (bath temp,

50 Torr); IR (neat) 1735, 1640, 1380, 1275, 1000, 915 cm^{-1}; NMR ($CDCl_3$) δ 0.88 (s, 3H), 0.93 (s, 3H), 1.06 (s, 3H), 1.80—2.05 (m, 2H), 2.32 (bd, 2H), 4.87—5.17 (m, 2H), 5.90 (dd, 1H, J=16, 12 Hz); MS *m/e* (%) 152 (M^+, 38), 137 (28), 109 (44), 96 (66), 81 (56), 70 (44), 67 (62), 55 (44), 43 (100), 41 (90).

*2,2,3-Trimethyl-3-cycloheptenone (**10**).* Following the procedure for the preparation of **6**, a solution of **9** (22 mg, 0.08 mmol) was treated with methylaluminum bis(trifluoroacetate) (0.5 mmol) in hexane (0.5 ml) to give **10** (12 mg, 100%): bp 80 °C (bath temp, 20 Torr); IR (neat) 1704, 1655, 1084, 780, 730 cm^{-1}; NMR (CCl_4) δ 1.01 (s, 3H), 1.05 (d, 3H, J=9 Hz), 1.10 (s, 3H), 5.45 (m, 2H); MS *m/e* (%), 153 (11), 152 (M^+, 73), 137 (18), 124 (16), 109 (60), 95 (100), 84 (60); Found: C, 78.97; H, 10.75%. Calcd for $C_{10}H_{16}O$: C, 78.90; H, 10.59%.

*2,2-Dimethyl-3-(1-propenyl)cyclopentanone (**12**)*: IR (neat) 1740, 1090, 1056, 975 cm^{-1}; NMR (CCl_4) δ 0.81 (s, 3H), 0.98 (s, 3H), 1.70 (d, 3H, J=5 Hz), 5.40 (m, 2H); MS *m/e* (%) 153 (12), 152 (M^+, 69), 137 (18), 109 (40), 95 (47), 81 (100); Found: *m/e* 152.1208. Calcd for $C_{10}H_{16}O$: M, 152.1202.

*2,2-Dimethyl-3-(2-methyl-1-propenyl)cyclopentanone (**15**)*: Bp 96 °C (bath temp, 19 Torr); IR (neat) 1745, 1671, 1090, 848, 802 cm^{-1}; NMR (CCl_4) δ 0.82 (s, 3H), 0.94 (s, 3H), 1.60 (s, 3H), 1.70 (s, 3H), 4.87 (bd, 1H, J=9 Hz); MS *m/e* (%) 167 (25), 166 (M^+, 48), 151 (34), 133 (21), 123 (99), 95 (69), 82 (100); Found: C, 79.23; H, 10.62%. Calcd for $C_{11}H_{18}O$: C, 79.47; H, 10.91%.

*Bicyclo[5.4.0]undec-5-en-2-one (**17**)*: IR (neat) 1707, 1225, 1150, 825 cm^{-1}; NMR (CCl_4) δ 2.40 (m, 2H), 2.67 (d, 1H, J=5.3 Hz), 2.70 (d, 1H, J=8.1 Hz), 5.50 (t, 1H, J=4.5 Hz); MS *m/e* (%) 164 (M^+, 61), 108 (52), 107 (52), 93 (71), 79 (100); Found: *m/e* 164.1189. Calcd for $C_{11}H_{16}O$: M, 164.1199.

*6-(4-Methyl-3-pentenyl)-2-cyclohexenone (**18**).* The title compound was prepared from 2-(4-methyl-3-pentenyl)cyclohexanone[13] as described by Reich[14] in 54% yield.

trans- *and* cis-*6-(4-Methyl-3-pentenyl)-2-cyclohexenol (**19** and **20**).* A solution of **18** (2.6 g, 14.6 mmol) and diisobutylaluminum hydride (0.5 M solution in hexane, 35 ml, 17.5 mmol) in benzene (50 ml) was stirred at 0 °C for 1.5 h. The resulting mixture was poured into 1 mol dm^{-3} HCl and extracted with ethyl acetate (2×100 ml). The combined extracts were washed with saturated sodium hydrogencarbonate and water, dried, and concentrated *in vacuo*. Trimethylsilylation (Et_3N, Me_3SiCl) of the crude mixture of **19** and **20** gave separable two bands by PLC (5:1 hexane–benzene). Hydrolysis of the slower moving band (R_f= 0.17) with 1 mol dm^{-3} HCl in tetrahydrofuran afforded **19**: IR (neat) 3330, 1650 cm^{-1}; NMR (CCl_4) δ 0.8—2.2 (m, 10H), 1.60 (s, 3H), 1.67 (s, 3H), 3.71 (m, 1H), 5.06 (t, 1H, J=7.5 Hz), 5.47—5.76 (m, 2H). Faster moving band (R_f= 0.37) gave **20**: IR (neat) 3350, 1650 cm^{-1}; NMR (CCl_4) δ 0.8—2.2 (m, 10H), 1.60 (s, 3H), 1.67 (s, 3H), 3.90 (bs, 1H), 5.07 (t, 1H, J=7.5 Hz), 5.74—5.82 (m, 2H). Hydrogenation of **19** or **20** provided *trans*- or *cis*-2-(4-methylpentyl)cyclohexanol, respectively, whose IR and NMR spectra agree with the published data.[15]

trans-*3-Acetoxy-4-(4-methyl-3-trimethylsiloxy-3-pentenyl)cyclohexene (**1**).* *m*-Chloroperbenzoic acid (70%, 1.47 g, 6.0 mmol) was added portionwise over a period of 30 min at 0 °C to a solution of *trans*-acetate (1.2 g, 5.4 mmol) derived from **19** in dichloromethane (25 ml). After 30 min, the reaction mixture was filtered through a pad of Celite 545 and the filtrate was washed with saturated sodium hydrogencarbonate, dried, and concentrated *in vacuo*. The crude epoxide (1.1 g) was dissolved in toluene (20 ml) and treated with 47% HBr (2.7 ml) at −78 °C. After 2 h, the mixture was poured into water and extracted with ether (2×20 ml). The combined ether layers were washed with brine and dried, and freed of the solvent. Purification of the residual oil by column chromatography on silica gel (10:1 benzene–ethyl acetate) gave *trans*-3-acetoxy-4-(4-bromo-4-methyl-3-hydroxypentyl)cyclohexene (1.1 g) as a pale yellow oil. Oxidation of bromohydrin by the method of Corey and Kim[16] afforded **21** (0.80 g, 74%). A solution of **21** (0.80 g, 2.5 mmol) in THF (5.5 ml) was added to a mixture of zinc–silver couple (0.51 g), chlorotrimethylsilane (0.97 ml, 7.7 mmol), and THF (10 ml) over a period of 30 min at 25 °C.[17] After 30 min, pyridine (2.1 ml, 25 mmol) was added[18] and the reaction mixture was poured into saturated sodium hydrogencarbonate and extracted with ether. After removal of solvent *in vacuo*, the resultant oil was purified by precooled (below 0 °C) silica gel column chromatography (10:1 hexane–ether) to give **1** (0.64 g, 82%): bp 145 °C (bath temp, 3 Torr); IR (neat) 1735, 1680, 1240, 750, 685 cm^{-1}; NMR (CCl_4) δ 0.13 (s, 9H), 1.52 (s, 3H), 1.55 (s, 3H), 1.96 (s, 3H), 4.96 (bs, 1H), 5.65 (m, 2H); MS *m/e* (%) 312 (1), 311 (3), 310 (M^+, 10), 251 (3), 250 (8), 249 (4), 207 (14), 171 (78), 170 (57), 73 (100); Found: C, 66.06; H, 9.97%. Calcd for $C_{17}H_{30}O_3Si$: C, 65.76; H, 9.74%.

cis-*3-Acetoxy-4-(4-methyl-3-trimethylsiloxy-3-pentenyl)cyclohexene (**3**).* In similar fashion, **20** was converted to **3** in 36% overall yield. **3**: bp 145 °C (bath temp, 3 Torr); IR (neat) 1733, 1680, 1248, 750, 682 cm^{-1}; NMR (CCl_4) δ 0.15 (s, 9H), 1.53 (s, 3H), 1.56 (s, 3H), 1.92 (s, 3H), 5.12 (bs, 1H), 5.80 (m, 2H); MS *m/e* (%) 312 (2), 311 (3), 310 (M^+, 11), 251 (4), 250 (10), 249 (4), 207 (16), 171 (54), 170 (88), 73 (100); Found: C, 65.54; H, 9.86%. Calcd for $C_{17}H_{30}O_3Si$: C, 65.76; H, 9.74%.

*6-Trimethylsiloxyneryl Acetate (**5**) and 6-Trimethylsiloxygeranyl Acetate (**7**).* As outlined for the preparation of **1**, the title acetates were obtained from neryl and geranyl acetate, respectively. **5**: bp 130 °C (bath temp, 0.5 Torr); IR (neat) 1740, 1682, 1374, 1250—1225, 1020, 950, 860—840 cm^{-1}; NMR (CCl_4) δ 0.17 (s, 9H), 1.53 (s, 3H), 1.58 (s, 3H), 1.74 (s, 3H), 1.95 (s, 3H), 2.17 (bs, 4H), 4.30 (d, 2H, J=7 Hz); MS *m/e* (%) 284 (3), 220 (6), 206 (4), 180 (17), 157 (35), 116 (23), 90 (69), 75 (72), 73 (100), 43 (59); Found: C, 63.33; H, 10.10%. Calcd for $C_{15}H_{28}O_3Si$: C, 63.33; H, 9.92%. **7**: bp 125 °C (bath temp, 0.5 Torr); IR (neat) 1740, 1677, 1380, 1362, 1240, 1190—1160, 1020, 965, 865, 840, 750 cm^{-1}; NMR ($CDCl_3$) δ 0.16 (s, 9H), 1.53 (s, 3H), 1.59 (s, 3H), 1.72 (s, 3H), 1.97 (s, 3H), 2.16 (bs, 4H), 4.48 (d, 2H, J=7 Hz), 5.31 (t, 1H, J=7 Hz); MS *m/e* (%) 284 (6), 181 (20), 158 (46), 117 (24), 91 (94), 75 (68), 73 (100), 43 (56); Found: C, 63.15; H, 10.06%. Calcd for $C_{15}H_{28}O_3Si$: C, 63.33; H, 9.92%.

*(3Z)-2-Acetoxy-8-methyl-7-trimethylsiloxy-3,7-nonadiene (**9**).* A solution of 6-methyl-5-hepten-2-one (21.4 g, 0.17 mol) in 2,6-lutidine (172 ml, 1.48 mol) was added at 0 °C over 40 min to a suspension of phosphorus pentachloride (89.6 g, 0.42 mol). The precipitate was removed by filtration through a pad of Celite 545 and the filtrate was washed with water, dried, and concentrated *in vacuo*. The crude product and lithium diisopropylamide, prepared from diisopropylamine (42.5 ml, 0.30 mol) and butyllithium (1.6 M hexane solution, 174 ml, 0.28 mol) in THF (300 ml) were reacted at 0 °C for 10 min and acetaldehyde (11.6 ml, 0.21 mol) was added. After usual workup, 8-methyl-7-nonen-3-yn-2-ol (4.7 g, 31 mmol) was obtained in 18% yield based on the heptenone. A mixture of the alcohol (3.1 g, 20.5 mmol), sodium borohydride (0.33 g, 8.5 mmol), and nickel acetate (1.8 g, 7.3

mmol) in ethanol (190 ml) was stirred at 25 °C for 1 h under hydrogen atmosphere. The black precipitate was removed by filtration and the filtrate was concentrated *in vacuo*. Acetylation followed by distillation under reduced pressure (bp 72—73 °C, 0.5 Torr) gave (3*Z*)-2-acetoxy-8-methyl-3,7-nonadiene (2.86 g, 47%). According to the procedure described for the preparation of **1**, the acetate was converted to **9**: IR (neat) 1735, 1678, 1240, 693 cm^{-1}; NMR (CCl_4) δ 0.16 (s, 9H), 1.23 (d, 3H, J=5.8 Hz), 1.56 (s, 3H), 1.58 (s, 3H), 1.96 (s, 3H), 2.16 (m, 4H), 5.2—5.7 (m, 3H); MS *m/e* (%) 286 (5), 285 (3), 284 (M^+, 12), 225 (15), 224 (10), 209 (9), 195 (4), 181 (10), 169 (9), 158 (20), 141 (34), 91 (69), 75 (61), 73 (100); Found: *m/e* 284.1805. Calcd for $C_{15}H_{28}O_3Si$: M, 284.1806.

*(3E)-2-Acetoxy-8-methyl-7-trimethylsiloxy-3,7-nonadiene (**11**).* Reduction of 8-methyl-7-nonen-3-yn-2-ol with lithium aluminum hydride in ether gave (3*E*)-8-methyl-3,7-nonadien-2-ol in 80% yield. As described previously, the alcohol was transformed to **11**: bp 118 °C (bath temp, 2 Torr); IR (neat) 1735, 1677, 1240, 965 cm^{-1}; NMR (CCl_4) δ 0.15 (s, 9H), 1.23 (d, 3H, J=6.3 Hz), 1.52 (s, 3H), 1.56 (s, 3H), 1.92 (s, 3H), 2.13 (m, 4H), 5.1—5.6 (m, 3H); MS *m/e* (%) 286 (2), 285 (5), 284 (M^+, 17), 225 (21), 224 (13), 209 (10), 195 (6), 181 (12), 156 (24), 141 (47), 91 (87), 75 (63), 73 (100); Found: C, 63.18; H, 10.21%. Calcd for $C_{15}H_{28}O_3Si$: C, 63.33; H, 9.92%.

*(2E)-4-Acetoxy-8-methyl-7-trimethylsiloxy-2,7-nonadiene (**13**).* Bp 100 °C (bath temp, 2.5 Torr); IR (neat) 1735, 1678, 1240, 962 cm^{-1}; NMR (CCl_4) δ 0.14 (s, 9H), 1.53 (s, 6H), 1.65 (d, 3H, J=6.3 Hz), 1.7 (m, 2H), 1.90 (s, 3H), 2.0 (m, 2H), 5.07 (m, 1H), 5.27 (dd, 1H, J=15, 7.5 Hz), 5.69 (dq, 1H, J=15, 6.3 Hz); MS *m/e* (%) 286 (2), 285 (2), 284 (M^+, 6), 224 (11), 209 (11), 181 (24), 158 (34), 143 (26), 141 (24), 119 (13), 117 (17), 75 (56), 73 (100); Found: C, 63.46; H, 9.75%. Calcd for $C_{15}H_{28}O_3Si$: C, 63.33; H, 9.92%.

*4-Acetoxy-2,8-dimethyl-7-trimethylsiloxy-2,7-nonadiene (**14**).* A solution of 6-methyl-5-hepten-2-one (6.0 g, 48 mmol) in THF (20 ml) was added at −78 °C over a period of 1 h by means of mechanically driven syringe to a solution of lithium diisopropylamide (53 mmol) generated from diisopropylamine and butyllithium in THF (100 ml). After 20 min, acetone (39 ml, 0.53 mol) was added in one portion and the mixture was stirred for an additional 20 min. The reaction was quenched by addition of acetic acid (3.6 ml, 63 mmol) and the resulting mixture was poured into water and extracted with ethyl acetate. The combined extracts were washed with saturated sodium hydrogencarbonate and brine, dried and concentrated *in vacuo*. The resultant crude oil was purified by column chromatography on silica gel to give 2,8-dimethyl-2-hydroxy-7-nonen-4-one (8.5 g, 97%). A mixture of this β-hydroxy ketone (8.5 g, 46 mmol) triethylamine (32 ml, 0.23 mol), and methanesulfonyl chloride (8.0 ml, 0.10 mol) in dichloromethane (200 ml) was stirred at 25 °C for 15 h. The suspension was diluted with ether and water. After extracting with ether and drying (Na_2SO_4), distillation (bp 49—52 °C, 0.5 Torr) gave 2,8-dimethyl-2,7-nonadien-4-one (7.1 g, 93%). The dienone (5.8 g, 35 mmol) was reduced with sodium borohydride (1.35 g, 35 mmol) in ethanol (35 ml) at 25 °C for 17 h to give an alcohol which was converted to 4-acetoxy-2,8-dimethyl-2,7-nonadiene (bp 75—76 °C, 10.5 Torr, 6.0 g, 82%) by the successive treatment with pyridine (20 ml) and acetic anhydride (20 ml) at 0 °C. Following the procedure for the preparation of **1**, the acetate gave **14** (30% overall yield): bp 139 °C (bath temp, 2 Torr); IR (neat) 1736, 1680, 1252 cm^{-1}; NMR (CCl_4) δ 0.15 (s, 9H), 1.53 (s, 6H), 1.68 (s, 6H), 1.94 (s, 3H), 4.93 (d, 1H, J=8.6 Hz), 5.28 (td, 1H, J=5.8, 8.6 Hz); MS *m/e* (%) 299 (3), 298 (M^+, 9), 239 (11), 238 (32), 223 (26), 195 (27), 158 (26), 141 (33), 91 (29), 75 (52), 73 (100); Found: *m/e* 298.1957. Calcd for $C_{16}H_{30}O_3Si$: M, 298.1963.

*1-Acetoxy-2-(2-trimethylsiloxy-2-propenyl)-1-vinylcyclohexane (**16**).* Vinylmagnesium bromide (0.27 mol) and 2-allylcyclohexanone (14.4 g, 104 mmol) were stirred in THF (200 ml) at 25 °C for 30 min. The reaction mixture was poured into aqueous ammonium chloride and extracted with ether. Distillation under reduced pressure (bp 95—105 °C, 10 Torr) afforded 2-allyl-1-vinylcyclohexanol (14.5 g, 87.7 mmol) in 84% yield. A mixture of this alcohol (6.2 g, 37.5 mmol) and sodium hydride (37.5 mmol) in benzene was refluxed for 1.5 h and diethylene glycol diacetate (6.5 g, 37.5 mmol) was added.[19] The mixture was stirred at 25 °C for 16 h, poured into water, and extracted with ether. Purification by column chromatography on silica gel gave 1-acetoxy-2-allyl-1-vinylcyclohexane (4.0 g, 52%) which was further converted in similar way to silyl enol ether **16** (2.5 g, 65% overall yield): IR (neat) 1736, 1678, 1671, 1010, 908 cm^{-1}; NMR (CCl_4) δ 0.18 (s, 9H), 1.95 (s, 3H), 3.90 (s, 2H), 4.89 (d, 1H, J=17 Hz), 5.03 (d, 1H, J=11 Hz), 5.94 (dd, 1H, J=11, 17 Hz); MS *m/e* (%) 253 (8), 237 (14), 236 (28), 223 (5), 222 (8), 221 (28), 195 (8), 193 (8), 182 (16), 147 (34), 117 (33), 91 (36), 75 (43), 73 (100); Found: *m/e* 296.1810. Calcd for $C_{16}H_{28}O_3Si$: M, 296.1808.

The authors wish to thank the Ministry of Education, Science and Culture, Japan, for the Grant-in-Aid (110309, 203014, 303023, 335042, 403022).

References

1) M. S. Ptasinska, K. B. Starowieyski, S. Pasynkiewicz, and M. Carewska, *J. Organomet. Chem.*, **160**, 403 (1978); A. Itoh, H. Nozaki, and H. Yamamoto, *Tetrahedron Lett.*, **1978**, 2903.

2) S. Hashimoto, A. Itoh, Y. Kitagawa, H. Yamamoto, and H. Nozaki, *J. Am. Chem. Soc.*, **99**, 4192 (1977).

3) Enzymic formations of humulene, dollabella carifornica, and lanosterol (C-ring) are the other examples of *anti*-Markovnikov cyclization in terpene biosynthesis.

4) $Me_2Al(OCOCF_3)$ was used instead of $MeAl(OCOCF_3)_2$. See experimental part.

5) Y. Kitagawa, S. Hashimoto, S. Iemura, H. Yamamoto, and H. Nozaki, *J. Am. Chem. Soc.*, **98**, 5030 (1976).

6) The most economical assumption to account for the observations as mentioned here would be as follows. Coordination of the aluminum reagent R_2AlX on the allyl acetate moiety of the substrate **1** in Eq. 1 produces the adduct **A**:

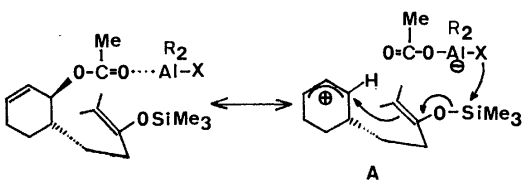

A

The very tight ion-pair lying slightly above the level of such an adduct may experience the attack on silicon atom either by X or by acetoxyl oxygen. This will result in "almost concerted" cyclization proceeding in the stereospecific manner as observed to afford completely homogeneous *cis*-octalone (**2**). Molecular models show such a process can not be expected with the *cis*-substrate (**3**). Similar explanation applies to Eq. 3 through 6. The importance of this kind of combined acid-base attack in the reactions of R_2AlX

reagents has been mentioned, see Refs. 7 and 8.
7) H. Nozaki, *LIFECHEM* (Kagaku-to-Yakugaku-no-Kyoshitsu, Bekkan) **2**, 1 (1979) (Hirokawa-Shoten).
8) K. Oshima and H. Nozaki, *Yuki Gosei Kagaku Kyokai Shi*, **38**, 460 (1980).
9) For similar solvent effect, see C. A. Bunton, J. P. Leresche, and D. Hachey, *Tetrahedron Lett.*, **1972**, 2431; S. Ozawa, A. Itoh, K. Oshima, and H. Nozaki, *ibid.*, **1979**, 2909.
10) J. A. Marshall and N. H. Anderson, *J. Org. Chem.*, **31**, 667 (1966).
11) Y. Naya and M. Kotake, *Tetrahedron Lett.*, **1968**, 1645; E. Demole and P. Enggist, *J. Chem. Soc., Chem. Commun.*, **1969**, 264; *Helv. Chim. Acta*, **54**, 456 (1971); N. Shimizu and Y. Tsuno, *Chem. Lett.*, **1979**, 103; H. Sakurai, A. Shirahata, and A. Hosomi, *Angew. Chem.*, **91**, 178 (1979).
12) H. M. R. Hoffmann, *Angew. Chem.*, **85**, 893 (1973).
13) E. J. Corey and D. Enders, *Chem. Ber.*, **111**, 1337, 1362 (1978).
14) H. J. Reich, I. L. Reich, and J. M. Renga, *J. Am. Chem. Soc.*, **95**, 5813 (1973).
15) E. L. Eliel, M. H. Gianni, Th. H. Williams, and J. B. Stothers, *Tetrahedron Lett.*, **1962**, 741.
16) E. J. Corey and C. U. Kim, *J. Am. Chem. Soc.*, **94**, 7586 (1972).
17) G. C. Joshi and L. M. Pande, *Synthesis*, **1975**, 450.
18) Because of the acid sensitivity of the product, pyridine should be added to quench the reaction; for the similar example, see J. M. Denis, C. Girard, and J. M. Conia, *Synthesis*, **1972**, 549.
19) E. Jirát and F. Vonášek, *Chem. Abstr.*, **55**, 6378b (1961).

The Substituent Effect. 15.[1] The LSFE Treatment of Substituent Effects on Basicities of Pyridines[2]

Masami SAWADA, Masaharu ICHIHARA, Yasuhide YUKAWA, Takeshi NAKACHI,† and Yuho TSUNO*,†

The Institute of Scientific and Industrial Research, Osaka University, Suita, Osaka 565

† *Department of Chemistry, Faculty of Science, Kyushu University, Hakozaki, Fukuoka 812*

(Received January 21, 1980)

The relative dissociation constants of meta and para substituted pyridinium ions in H_2O at 25 °C were collected from a number of sources. To understand the actual substituent effects with a combination of inductive(I) and pi-electronic(Pi) effect components, the LSFE equation has been employed statistically for each of the meta and para series.

$$\Delta pK_a = \rho_i\sigma_i + \rho_\pi^+\sigma_\pi^+ + \rho_\pi^-\sigma_\pi^-$$

The results illustrate (1) the I effect from the meta position is 1.2 times more effective than that from the para position, (2) the Pi effects from the para position have clearly different sensitivities for pi-donor($-R$) and pi-acceptor($+R$) classes of substituents; more exalted and more reduced Pi effects than that involved in σ_p° constants for $-R$ and $+R$ groups, respectively. Compared with earlier results from the Taft's DSP and relevant treatments, the soundness of the dual ρ_π approach and, further, the superiority of the LSFE treatment have been demonstrated for the description of substituent effects on basicity changes in pyridines.

Substituent effects on benzene reactivities have been most widely handled with a combination of two components, polar (inductive, I) and resonance (pi-electronic, Pi) effects, each of which is given as a $\rho\sigma$ product.[1,3,4] In an attempt to justify this treatment, the analysis of substituent effects in the extended pi-electron system of naphthalene has been discussed previously.[1,4f] The same treatment should be applicable to reactivities in heteroaromatic pi-electron systems.

Meta and para substituted pyridines are an interesting system for an application of the separation analysis in heteroaromatic reactivities. For basicities of pyridines, certain contradictions have recently appeared in the rationalization of the substituent effects obtained from different equations.[5,6] The validity of an equation may be tested most critically by establishing whether or not the substituent effects on reactivities in pyridines can be treated successfully. In this sense, Taft and coworkers have stressed the power of the DSP treatment[4a] mainly on the basis of the following two facts:[5] (i) the σ_R^+ parameter gives the best-fit DSP correlation, as anticipated from a structural point of view; (ii) the resultant ρ_I is essentially identical with the ρ_I for the corresponding saturated system, the 4-substituted quinuclidines.[7]

$$(\Delta pK_a)_{py}^{p} = 5.15\sigma_I + 2.69\sigma_R^+ \quad (1)$$

$$(\Delta pK_a)_{py}^{p} - (\Delta pK_a)_{qu}^{4} = 2.87\sigma_R^+ \quad (2)$$

The latter point is particularly notable, since it is in line with the relationship between benzoic acid and bicyclo[2.2.2]octane-1-carboxylic acid.[8]

Johnson *et al.* have interpreted the pi-donor para substituent effects using Eq. 3, based on the assumption that substituent effects of para pi-acceptors are exclusively inductive.[6,9]

$$(\Delta pK_a)_{py}^{p} = 5.66\sigma \text{ (for pi-donors) and } 5.66\sigma_I \text{ (for pi-acceptors)};$$

$$(\Delta pK_a)_{py}^{p} - 1.19\ (\Delta pK_a)_{qu}^{4} = 5.66\sigma_R \text{ (for pi-donors)} \quad (3)$$

They argued that the correlation with σ_R parameters (instead of σ_R^+) cast doubt on the validity of the DSP and, generally, of multiple substituent parameter treatments,[6] including our LArSR treatment. Thus, using the same data sets for pyridines and quinuclidines, different authors have reached conflicting conclusions on the significance of the DSP treatment.

We have demonstrated the applicability and the validity of the LSFE Eq. 4 through appropriate separation of substituent effects in various aromatic hydrocarbon systems as well as in the ordinary benzene system.[1]

$$\log k/k_o = \rho_i\sigma_i + \rho_\pi^+\sigma_\pi^+ + \rho_\pi^-\sigma_\pi^- \quad (4)$$

In the present study, we apply Eq. 4 to the analysis of substituent effects on the basicity of pyridines and provide evidence for the significance of the dual ρ_π approach for pi-donor and pi-acceptor substituents characteristic of our LSFE treatment, Eq. 4. The results provide a solution to the above controversial problem on the DSP treatment and characterize the LSFE treatment as a precise and useful equation for the separation analysis of actual substituent effects.

Results and Discussion

A number of reliable ΔpK_a values have been collected from various sources (Table 1). The ΔpK_a values were defined by $pK_H - pK_X$, where both data were determined by the same authors and under the same experimental conditions, unless otherwise noted. From examination of earlier compilations, together with some additional fragmentary data, best values were selected and are listed in the last column of Table 1. The data set consists mostly of Fischer's results, but for alkyl and nitro substituents, Brown's and Bellobono's data were employed, since, for the alkyl substituents, meta and para data were available as a pair, and, for the nitro substituent, Fischer's value was much lower than that reported by the other two authors. A full set of basicity data has been constructed for a total of 52 meta and para substituents.[20]

The present data set for the basicities of pyridines

TABLE 1. DATA OF ΔpK_a OF SUBSTITUTED PYRIDINIUM IONS IN H_2O AT 25 °C[a)]

Subst	Brown[10)] Bryson[11)]	Jaffe[12)]	Schofield[15)]	Fischer[9b)]	Bellobono[16)]	Taft[5a,17)]	Arnett[18)] others	Best selected[b)]
H	0.00	0.00	0.00	0.00	0.00	0.00	0.00	0.00
3-Me	(−0.53)	−0.53	−0.51	−0.46		(−0.46)	−0.51	−0.46
	0.41	(−0.51)					−0.45	
	−0.51[10)]							
	−0.34							
4-Me	−0.85[10)]	(−0.85)		−0.82		(−0.82)	−0.85	−0.82
							−0.79	
3-Et	−0.53[10)]	(−0.53)	−0.51					−0.53
4-Et	−0.85[10)]	(−0.85)		−0.82		(−0.85)		−0.85
3-*i*-Pr	−0.55[10)]	(−0.55)	−0.59					−0.55
4-*i*-Pr	−0.85[10)]	(−0.85)		−0.83		(−0.85)		−0.85
3-*t*-Bu	−0.65[10)]	(−0.65)						−0.65
4-*t*-Bu	−0.82[10)]	(−0.82)				(−0.82)		−0.82
3,5-Me_2	−0.93		−0.94	−0.93			−1.01	−0.93
3,4-Me_2				−1.27				−1.27
4-*n*-Pr				−0.84				−0.84
3-F	2.20[10)]	(2.20)				2.24		2.20
3-Cl	2.33[10)]	(2.33)		2.40		(2.40)		2.40
4-Cl		1.45		1.38		(1.38)		1.38
3-Br	2.33[10)]	(2.33)	2.33	2.36	2.49	(2.36)		2.36
4-Br				1.46	1.53	(1.46)		1.46
3-I	1.92[10)]	(1.92)				1.96		1.92
4-I						*ca.* 1.19*		*ca.* 1.2
3,5-Cl_2				4.54				4.54
3,5-Br_2				4.39				4.39
3-OMe	0.27	0.35*		0.43		0.30		0.43
4-OMe		−1.39*		−1.37		(−1.37)		−1.37
3-OH	(0.43)	0.43				0.41		*ca.* 0.4
3-SMe		0.78*[14)]				(0.78*)		0.78*
4-SMe		−0.74*[14)]				(−0.74*)		−0.74*
3-NH_2	(−0.80)[12)]	(−0.86*)[10)]		−0.83	−0.82	(−0.83)		−0.83
					−0.80			
4-NH_2		−3.94*	−3.93	−3.91	−3.94	(−3.91)		−3.91
3-NMe_2							−1.16[19)]	−1.16
4-NMe_2			−4.36			(*ca.* −4.49*)		−4.36
3-NHAc		0.77*				0.84		0.77*
4-NHAc		−0.64*				*ca.* −0.66		−0.64*
3-NHCOPh		1.43*						1.43*
4-NHCOPh		−0.09*						−0.09*
3-Ph						*ca.* 0.41		*ca.* 0.4
4-Ph				−0.14		(−0.14)		−0.14
4-$PhCH_2$				−0.38		(−0.38)		−0.38
3-COPh				2.03		(2.03)		2.03
4-COPh				1.86		(1.86)		1.86
3-CN	(3.84)	3.84		3.86	4.04	(3.86)		3.86
4-CN				3.35	3.73	(3.35)		3.35
3-NO_2	4.36	(4.42)[11,13)]		4.03	4.42	(4.03)		4.42
4-NO_2			3.62	3.82	3.98	(3.82)		3.98
3-COMe	1.99[10)]	(1.99)				2.03	1.95	1.95
4-COMe				1.70		(1.70)	1.70	1.70
3-$CONH_2$		*ca.* 1.72*						*ca.* 1.7*
4-$CONH_2$		*ca.* 1.51*						*ca.* 1.5*
3-COOMe				2.12		(2.12)		2.12
4-COOMe				1.72		(1.72)		1.72
4-CF_3						2.58		2.58
3-COO^-	0.45	*ca.* 0.52		0.45				0.45
4-COO^-		*ca.* 0.39		0.31				0.31

a) Values in brackets are from another column. b) An underlined value is chosen as the best selected value.
*) Data at 20 °C.

Table 2. Apparent σ and related values

Subst	$\bar{\sigma}_{py}$ [a]	σ° [b]
H	0.000	0.000
3-Me	−0.063	−0.069
4-Me	−0.120	−0.124
3-Et	−0.074	−0.07
4-Et	−0.125	−0.131
3-*i*-Pr	−0.077	−0.07
4-*i*-Pr	−0.125	−0.156
3-*t*-Bu	−0.093	−0.10
4-*t*-Bu	−0.120	−0.174
3-F	0.364	0.337
3-Cl	0.396	0.373
4-Cl	0.232	0.281
3-Br	0.389	0.391
4-Br	0.245	0.296
3-I	0.319	0.352
4-I	*ca.* 0.20	0.26
3-OMe	0.080	0.115
4-OMe	−0.208	−0.100
3-OH	*ca.* 0.08	0.12
3-SMe	0.136*	0.12
4-SMe	−0.107*	0.07
3-NH_2	−0.122	−0.15
4-NH_2	−0.615	−0.36
3-NMe_2	−0.175	−0.15
4-NMe_2	−0.688	−0.43
3-NHCOMe	0.135*	0.12
4-NHCOMe	−0.091*	0.00
3-NHCOPh	0.240*	0.22
4-NHCOPh	−0.003*	0.08
3-Ph	*ca.* 0.08	
4-Ph	−0.011	0.039
3-COMe	0.324	0.376
4-COMe	0.284	0.491
3-$CONH_2$	*ca.* 0.28*	0.32
4-$CONH_2$	*ca.* 0.25*	0.38
3-COOMe	0.351	0.36
4-COOMe	0.287	0.46
4-CF_3	0.425	0.505
3-COPh	0.336	0.35
4-COPh	0.309	0.49
3-CN	0.630	0.615
4-CN	0.548	0.653
3-NO_2	0.719	0.710
4-NO_2	0.649	0.800

*) Data at 20 °C. a) Calcd by using ρ_m=6.24 (see text). b) Taken from Ref. 3b: original references cited therein.

is comparable in size with that of ΔpK_a for benzoic acids, and shows large substituent effects ($\rho \simeq 6$)[9b] particularly useful for analysis of the substituent effects in detail. Since the solvent is water, it is not necessary to consider solvent modification of substituent constants.[3b]

A least squares calculation gives a linear relation of ΔpK_a with σ_m for meta substituents (n=20) with high precision.[21]

Table 3. Substituent constants used in the LSFE analysis[a]

Subst	σ_I	σ_R^+	σ_R^-
H	0.000	0.000	0.00
Me	−0.045	−0.078	0.00
Et	−0.045	−0.069	0.00
i-Pr	(−0.053) [b]	(−0.051) [b]	0.00
t-Bu	(−0.060) [b]	(−0.034) [b]	0.00
F	0.363	−0.118	0.00
Cl	0.348	−0.070	0.00
Br	0.337	−0.061 [c]	0.00
I	(0.289) [b]	(−0.068) [b]	0.00
OMe	0.185	−0.281	0.00
OH	0.19	−0.34	0.00
SMe	(0.17) [b]	(−0.285) [b]	0.00
NH_2	0.10 [c]	−0.46 [c]	0.00
NMe_2	0.11 [c]	−0.54	0.00
Ph	0.110	−0.090	0.12
COPh	0.20	0.000	0.28
$CONH_2$	*ca.* 0.20	0.000	0.175
COOMe	0.23	0.000	0.22
COMe	0.214	0.000	0.266
CF_3	0.34	0.000	0.143
CN	0.42	0.000	0.226
NO_2	0.46	0.000	0.332

a) Data taken from Refs. 22 and 23. b) Not confirmed yet. See Ref. 3b. c) Calcd by 0.415 $\Delta\bar{\sigma}_R^+$. The $\Delta\bar{\sigma}_R^+$ value of *p*-NH_2 was redetermined most recently as −1.10.[24]

$$(\Delta pK_a)_{py}^{m} = 6.240\sigma_m - 0.070 \quad (5)$$

Based on this correlation, apparent $\bar{\sigma}$ values for the pyridine system ($\bar{\sigma}_{py}$) are evaluated as (ΔpK_a+0.07)/6.24 in the same way as in the benzene reactivities (Table 2). In order to shed further light on the substituent effects in the pyridine system, it is appropriate to examine the application of LSFE Eq. 4 to the same data set.

As suggested by Taft, the reliability of any multiparameter correlation depends upon the spread of the values of substituent constants as well as on the non-linearity between the two sets of substituent constants.[4a] The present set covers a sufficiently wide range of substituents whose σ_I and σ_R values, given in Table 3, are scattered widely in an independent manner. In the present analysis, SMe, I, and $NHCOC_6H_5$ substituents were not included, since the substituent constants have not yet been well established. For alkyl groups, only methyl and ethyl groups were included as representative alkyls to prevent too much weight being attached to this class of substituents.

Table 4 summarizes the results of the LSFE analysis,[1,3,22-25] together with those of the relevant Taft DSP[4a,5] and of Johnson's[6] treatments. Examination of the LSFE correlation results reveals the following important facts.

(1) The LSFE Eq. 4 applies both for para and meta series in the present system with excellent precision comparable to that for correlations in the benzene system.

TABLE 4. CORRELATION PARAMETERS BY MEANS OF LSFE AND DSP TREATMENTS

Treatment	Position	Correlation parameters with substituent constants[a)]	Corr. coeff.	SD	Substituents included
LSFE	para	$6.49\sigma_I+9.50\sigma_R^+ +2.20\sigma_R^- -0.03$	0.9972	0.175	Me, Et, Cl, Br, OMe, NH_2, NMe_2, Ph, H, CF_3, COMe, CN, NO_2, COPh, COOMe.
LSFE	meta	$7.67\sigma_I+3.62\sigma_R^+ +2.03\sigma_R^- +0.01$	0.9974	0.123	Me, Et, F, Cl, Br, OMe, NH_2, NMe_2, H, COMe, CN, NO_2, COPh, COOMe.
DSP	para	$5.28\sigma_I+2.71\sigma_R^+ -0.03$	0.9987	0.120	Me, Cl, Br, OMe, NH_2, NMe_2, Ph, H, CF_3, COMe, CN, NO_2, COOMe.
DSP	para	$5.45\sigma_I+4.92\sigma_R(BA)-0.26$	0.9944	0.259	Me, Cl, Br, OMe, NH_2, NMe_2, Ph, H, CF_3, COMe, CN, NO_2, COOMe.
DSP	meta	$6.40\sigma_I+2.69\sigma_R^\circ -0.09$	0.9975	0.124	Me, F, Cl, Br, OMe, NH_2, NMe_2, H, COMe, CN, NO_2, COOMe.
Johnson's[b)]	para	$5.69\sigma_X+0.10$	0.9979	0.172	Me, Cl, Br, OMe, NH_2, NMe_2, Ph, H, CF_3, COMe, CN, NO_2, COOMe.

a) The numerical values for the DSP treatment are taken from Ref. 4a. b) $\sigma_X=\sigma_I+\sigma_R$(BA) for pi-donor substituents and $\sigma_X=\sigma_I$ for pi-acceptors.

(2) In the para correlation, the ρ_R^+ value differs from the ρ_R^-; the ρ_R^+ is higher than, but the ρ_R^- is significantly lower than, the ρ_I value. Note that in our LSFE Eq. 4, $\rho_I=\rho_R^+=\rho_R^-$ or $\rho_R^+/\rho_I=\rho_R^-/\rho_I=1.00$ refers by definition to the benzene σ_p° set.[1,3,22-25)] Neither the ratio ρ_R^+/ρ_I nor ρ_R^-/ρ_I is equal to unity in the present case, but the former (=1.5) is comparable to that of 1.6 for the σ_p constant,[26)] and the latter is much lower than that of 1.0 for the σ_p° constant. The ratio of ρ_R^+/ρ_R^- (=4) is comparable to that for the σ_p^+ constant.[26)]

(3) In the meta series, $\rho_R^+\simeq\rho_R^-$ is approximately satisfied and both ρ_R^+/ρ_I and ρ_R^-/ρ_I give essentially the same value of 0.4, which is comparable to the ratio in the benzene σ_m constant.[26)] It is worthy of note that the ρ_R^- value for the para pi-acceptor series is comparable to either ρ_R^- or ρ_R^+ for the meta series.

(4) The ratio of the inductive components in the meta and para substituent effects, ρ_I^m/ρ_I^p, is found to be 1.18, which is virtually identical with the corresponding ratio 1.17 in the benzene system. Based on $\sigma_I^m=1.17\sigma_I^p$ as in the benzene reactivity, the ρ_m value can be given as 6.5. This lends some support to the basic assumption of Hammett-type treatments; $\rho_m=\rho_p$ is as valid for the pyridine system as for the benzene system.

It is clear from (2) that the effect of pi-donor substituents at the para position is not significantly exalted relative to σ_p° and that the effect of pi-acceptors consists of a minor *Pi* effect. This is further suggested by the LArSR correlation for the present system (corr. coeff., 0.996 and standard deviation, ±0.21):

$$(\Delta pK_a)_{py} = 6.27\ (\sigma^\circ+0.20\Delta\bar{\sigma}_R^+ -0.48\Delta\bar{\sigma}_R^-).$$

The small r^+ and large negative r^- are in good accord with Johnson's conclusion rather than with the conclusion from the best-fit DSP correlation.

As far as the inductive contribution is concerned, all of the characteristic features of the LSFE treatment of the benzene system are found in the pyridine system, (4). In the benzene system, a bi-linear pi-electronic free energy relationship has been shown generally to result from combined meta and para substituent effects based on the inductive contribution factor of 0.85 (=1/1.17):[1,3,22-25)]

$$(\Delta pK_a)^p - 0.85(\Delta pK_a)^m = C_R^+\sigma_R^+ + C_R^-\sigma_R^-.$$

Here, the C_R^+ and C_R^- are coefficients[27)] describing pi-electronic contributions for pi-donor and pi-acceptor substituents, respectively, and are referred to as a simple function of ρ_R^+ or ρ_R^- parameter. As shown in Fig. 1, a good bi-linear relationship intersecting at the unsubstituted point is obtained without the aid of any inductive constants, suggesting the importance of different susceptibilities (duality) to the pi-electronic effect for pi-donor and pi-acceptor substituents in the present pyridine system. The slope for the acceptor groups is close to zero, providing evidence for the small *Pi* contribution from these groups.

The actual substituent effects on the basicities of pyridines are reasonably understood by the LSFE results, characterized by the dual pi-electronic effects. Unit positive charge in the conjugate acid of pyridine probably causes a moderately exalted pi-delocalization with para pi-donor substituents as compared with the *Pi* effect in the σ_p° constant, whereas it also causes the pi-delocalization interaction with para pi-acceptor groups to be lower than that in the σ_p° (repulsive acceptor-acceptor pi-interaction). For electrophilic reactivities in the benzene system, one could observe an exalted pi-delocalization with pi-donors, but scarcely detect such a repulsive saturation in *Pi* effect with pi-acceptor substituents. The present LSFE results for the pyridine system provide further evidence sub-

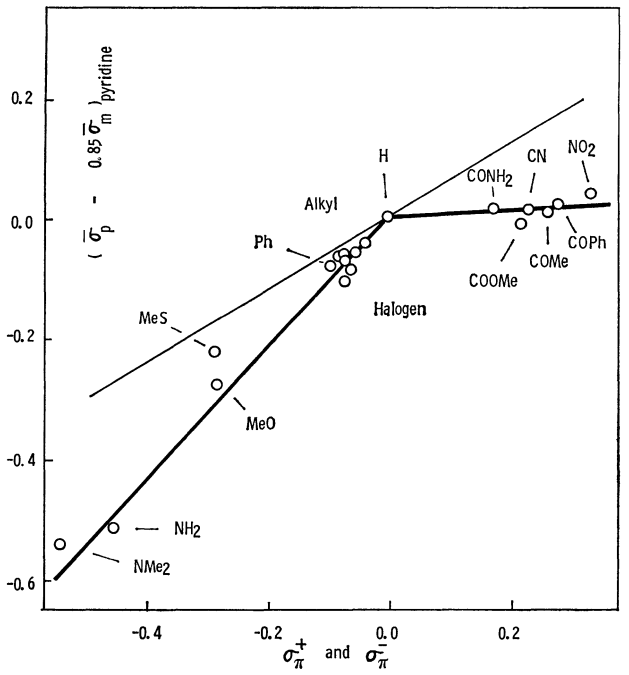

Fig. 1. The quantity of $\bar{\sigma}_p - 0.85\bar{\sigma}_m$ in the pyridine basicity against σ_π^+ and σ_π^-.
A thin line represents the corresponding plot of $\sigma_p^\circ - 0.85\sigma_m$ *vs.* $\sigma_\pi^\pm$.

stantiating the dual *Pi* effects for the analysis of substituent effects on general reactivities.

The DSP treatment,[4,8] using one of the four distinct resonance substituent constants, also results in good correlations of comparable precision for meta and para series by means of σ_R° and σ_R^+ constants, respectively (Table 4). However, significantly different inductive effects were obtained for meta and para derivatives; $\rho_I^m=6.40$, $\rho_I^p=5.28$ (Table 4). From the comparison with ρ_m value, the ρ_I value for the meta correlation appears to be more reasonable. The higher ratio, $\rho_I^m/\rho_I^p=1.2$, may indicate a breakdown of the original Taft assumption,[4a,e] $\rho_I^m=\rho_I^p$. It is interesting to note that the ρ_I in Johnson's correlation is nearly equal to the ρ_I derived from the DSP treatment with σ_R resonance constant (Table 4).

The LSFE treatment essentially stands on the concept that there exists a universal set of pi-electronic effect constants, σ_π^+ and σ_π^-, and that the pi-electronic contributions are expressed as a linear (or bilinear) function of σ_π using dual susceptibilities of ρ_π^+ and ρ_π^- for pi-donor and pi-acceptor substituents, respectively. The relative importance of the pi-electronic contribution from pi-acceptor/pi-donor substituents in any given system is generally accounted for by the ratio of both ρ_π values, whereas in the DSP treatment with a single ρ_R parameter, the relative importance of pi-donor/pi-acceptor resonance must be judged only by the best-fitting $\bar{\sigma}_R$ set. Continuous spectrum of ρ_π^+/ρ_π^- ratio with reaction systems must be characterized by four specific $\bar{\sigma}_R$ classes in the DSP treatment. This duality for the pi-electronic contributions is the most important feature of the LSFE treatment. Johnson's treatment is an extreme case of the dual ρ_π treatment, that is $\rho_\pi^-/\rho_\pi^+\to 0$. The requirement for the σ_R^+ set for the best-fit DSP correlation of the present system is due simply to the high ratio of pi-donor/pi-acceptor resonance contributions; *i.e.*, $\rho_\pi^+/\rho_\pi^-=4$.

Even though the requirement for the σ_R^+ set might imply the enhancement of pi-donor relative to pi-acceptor resonance, the enhancement of resonance relative to inductive effect is found to be quite low; $\rho_R/\rho_I\simeq 0.5$ in the pyridine para series (DSP, Table 4). Accordingly, the actual resonance contribution in this system is not so large as σ_R^+ in the σ_p^+, but is comparable with σ_R in the σ_p constant (since $\sigma_R^+\simeq 1.9\sigma_R$ roughly holds for pi-donors) and the *Pi* contribution of pi-acceptors is as low as that involved in the σ_m constant. Thus, the actual resonance effect evaluated by the best-fit DSP correlation with σ_R^+ is in fact at least qualitatively identical to that evaluated by Johnson's treatment as well as ours. Further, it is worthy of note that the σ_R^+ correlation gives excellent results with precision comparable to ours (Table 4). Johnson argued that the resonance contribution from para pi-acceptors is unreasonable, based on the observed insensitivity to steric twisting of the para nitro derivative. However, the minor resonance contribution of para pi-acceptors, comparable to that from the meta series suggested by DSP analysis, does not appear to be unreasonable, since not all the *Pi* contribution may be eliminated by means of steric twisting of the substituent. Likewise in the LSFE treatment, the *Pi* contribution estimated by the $\rho_\pi\sigma_\pi$ term should not all be referred to as the pi-delocalization effect, but may involve appreciable *I*-π interaction, which is insensitive to the loss of coplanarity.

The point of controversy between Johnson and Taft and coworkers arises from their interpretation of the correlation results. The difference is due essentially to the basic tenet of the DSP approximation.

General reactivities are classified into four distinctly different classes, σ°, σ, σ^+, and σ^-, depending on the mode of resonance interactions. The DSP treatment assumes that each class of substituent effects should be described only by a particularly suited one of four sets of resonance substituent constants, σ_R°, σ_R, σ_R^+, and σ_R^-, characteristic of the corresponding reactivity classes.[4a] In the present case, the requirement of σ_R^+ for the best-fit leads to the conclusion that the system belongs to the σ^+-class reactivity. The Johnson's σ_R-correlation, then, had to be a matter of controversy, since he also adheres to this traditional tenet. The above LSFE analysis provides a key to the solution of the controversy. Brownlee and Topsom put too much importance on the requirement of the σ_R^+ set in their interpretation,[5b] whereas the LSFE results put importance rather more on the resulting $\lambda(=\rho_R/\rho_I)$ value in the DSP treatment, in line with Johnson's criticism. The best-fit $\bar{\sigma}_R$ does not unequivocally indicate the class of resonance demand of the system.

A closely related system, the basicities of pyridine *N*-oxides, is an instructive example in this connection. The substituent effect on the basicities was proposed

to be roughly treated with the σ^+ constants for pi-donor substituents and the σ^- constants for pi-acceptor ones.[28] For this reactivity set, the DSP treatment has been found to give excellent best-fit correlations with either the σ_R or the $\sigma_R^\pm$ set.[29] Thus, the classification based on the best-fit $\bar{\sigma}_R$ set does not have any significance in this system. Further, the Johnson's treatment by no means applies to this system.

Finally, the ΔpK_a data of quinuclidines[7] can be directly incorporated into the regression analysis as an inductive measure instead of using σ_i constants.[30]

$$(\Delta pK_a)^p_{py} = 0.93\ (\Delta pK_a)_{qu} + 9.7\sigma_\pi^+ + 2.4\sigma_\pi^- \quad (6)$$

$$(\Delta pK_a)^m_{py} = 1.12\ (\Delta pK_a)_{qu} + 3.9\sigma_\pi^+ + 2.1\sigma_\pi^- \quad (7)$$

The result again verifies our basic assumption of the duality of *Pi* contributions and the unique position dependency of the *I* contribution, $I_m/I_p=1.17$. The effective scale of the *I* effect relative to that of quinuclidine is found to be 0.93 for the para series. This value differs appreciably from either 1.00 assumed by Taft (Eq. 2) or 1.19 employed by Johnson (Eq. 3). The problem is associated with the scaling of the inductive effects between the aromatic and the equivalent saturated systems, which will be discussed in a separate paper.

References

1) For part 14, Y. Tsuno, M. Sawada, T. Fujii, and Y. Yukawa, *Bull. Chem. Soc. Jpn.*, **52**, 3033 (1979).

2) This paper is taken to be "Reactivities of Nitrogen-Containing Heteroaromatics. 1." Part of this work was presented in 7th International Congress of Heterocyclic Chemistry, held at Tampa, Florida (Aug, 1979), Abstracts, p. 78.

3) a) Y. Tsuno, M. Fujio, M. Mishima, Y. Yukawa, and Y. Takai, unpublished; b) Y. Tsuno, M. Sawada, M. Fujio, N. Shimizu, T. Uemura, M. Ichihara, T. Nakachi, and Y. Yukawa, to be published.

4) a) S. Ehrenson, R. T. C. Brownlee, and R. W. Taft, "Progress in Physical Organic Chemistry," **10**, 1 (1973); b) R. D. Topsom, *ibid.*, **12**, 1 (1976); c) P. Tomasik and C. D. Johnson, *Adv. Heterocyclic Chem.*, **20**, 1 (1976); d) A. Zoltewicz and L. W. Deady, *ibid.*, **22**, 71 (1978); e) J. Shorter, "Correlation Analysis in Chemistry," ed by N. B. Chapman and J. Shorter, Plenum Press (1978), Chap. 4, p. 119; f) P. R. Wells, S. Ehrenson, and R. W. Taft, "Progress in Physical Organic Chemistry," **6**, 147 (1968).

5) a) C. A. Grob and R. W. Taft, *J. Am. Chem. Soc.*, **96**, 1236 (1974); b) R. T. C. Brownlee and R. D. Topsom, *Tetrahedron Lett.*, **1972**, 5187; c) M. Charton, *J. Org. Chem.*, **44**, 2097 (1979).

6) C. D. Johnson, I. Roberts, and P. G. Taylor, *J. Chem. Soc., Chem. Commun.*, **1977**, 897.

7) a) C. A. Grob and M. G. Schlageter, *Helv. Chim. Acta*, **59**, 264 (1976); b) C. A. Grob, *Angew. Chem. Int. Ed. Engl.*, **15**, 569 (1976).

8) For example, O. Exner, "Advances in Linear Free Energy Relationship," Plenum Press (1972), Chap. 1, p. 1.

9) a) J. M. Essery and K. Schofield, *J. Chem. Soc.*, **1963**, 2225; b) A. Fischer, W. J. Galloway, and J. Vaughan, *J. Chem. Soc.*, **1964**, 3591; the pK_a of unsubstituted pyridine (pK_H)=5.21.

10) H. C. Brown and S. R. Mihm, *J. Am. Chem. Soc.*, **77**, 1723 (1955); H. C. Brown and D. H. McDaniel, *ibid.*, **77**, 3752 (1955); H. C. Brown, D. H. McDaniel, and O. Hafligen, "Determination of Organic Structures by Physical Methods," Academic Press (1955), Chap. 14; pK_H=5.17.

11) A. Bryson, *J. Am. Chem. Soc.*, **82**, 4871 (1960), pK_H=5.18 References cited therein.

12) a) H. H. Jaffe and G. O. Doak, *J. Am. Chem. Soc.*, **77**, 4441 (1955); b) H. H. Jaffe and H. L. Jones, *Adv. Heterocyclic Chem.*, **3**, 209 (1964), references cited therein; c) A. Albert and J. N. Phillips, *J. Chem. Soc.*, **1956**, 1294.

13) The value of $\Delta pK_{3\text{-}NO_2}=3.42$ in the above book (Ref. 12b, p. 224, Table 4) should be read to 4.42.

14) A. Albert and G. B. Barlin, *J. Chem. Soc.*, **1959**, 2384; A. Albert, R. Goldacre, and J. Phillips, *ibid.*, **1948**, 2240; pK_H=5.23 at 20 °C.

15) J. M. Essery and K. Schofield, *J. Chem. Soc.*, **1961**, 3939; **1963**, 2225; their data were interpolated to those at 25 °C; pK_H=5.22.

16) I. R. Bellobono and P. Boltrame, *J. Chem. Soc., B*, **1969**, 620; I. R. Bellobono and G. Farini, *ibid.*, **1971**, 2034; I. R. Bellobono and E. Diani, *J. Chem. Soc., Perkin Trans. 2*, **1972**, 1707; I. R. Bellobono and M. A. Monetti, *ibid.*, **1973**, 790; pK_H=5.21.

17) a) Ref. 4f; b) M. Taagepera, W. G. Henderson, R. T. C. Brownlee, J. L. Beauchamp, D. Holts, and R. W. Taft, *J. Am. Chem. Soc.*, **94**, 1369 (1972); the pK_H=5.21 was employed to recalculate ΔpK's with the data taken from D. D. Perrin, "Dissociation Constants of Organic Bases in Aqueous Solution," Butterworths (1965).

18) E. M. Arnett and G. Scorrano, "Advances in Physical Organic Chemistry," **13**, 84 (1976).

19) P. Forsythe, R. Frampton, C. D. Johnson, and A. R. Katritzky, *J. Chem. Soc., Perkin Trans. 2*, **1972**, 671; pK_H=5.21.

20) The ΔpK_a values of *m*-NMe_2 and *p*-CF_3 were calculated by using pK_H=5.21.

21) r=0.9959, $s=\pm0.15$. If *m*-SMe, *m*-NHAc, and *m*-NHCOPh are excluded because of the data being for 20 °C, the correlation results are almost the same: ρ_m=6.250, r=0.9967, n=17.

22) a) Y. Tsuno, M. Fujio, and Y. Yukawa, *Bull. Chem. Soc. Jpn.*, **48**, 3324 (1975); b) Y. Tsuno, Y. Kusuyama, M. Sawada, T. Fujii, and Y. Yukawa, *ibid.*, **48**, 3337 (1975).

23) a) Y. Yukawa and Y. Tsuno, *Nippon Kagaku Zasshi*, **86**, 873 (1965); b) Y. Yukawa and Y. Tsuno, *Memoir, ISIR, Osaka Univ.*, **23**, 71 (1966).

24) Y. Tsuno, *et al.*, unpublished.

25) Y. Tsuno, M. Fujio, Y. Takai, and Y. Yukawa, *Bull. Chem. Soc. Jpn.*, **45**, 1519 (1972).

26) According to our LSFE analysis,

$\sigma_p^\circ=1.00\sigma_i+1.00\sigma_\pi^+ +1.00\sigma_\pi^-$

$\sigma_p=1.00\sigma_i+1.65\sigma_\pi^+ +1.00\sigma_\pi^-$

$\sigma_p^+=1.00\sigma_i+3.41\sigma_\pi^+ +1.00\sigma_\pi^-$

$\sigma_p^-=1.00\sigma_i+1.00\sigma_\pi^+ +2.37\sigma_\pi^-$

$\sigma_m=1.17\sigma_i+0.50\sigma_\pi^+ +0.50\sigma_\pi^-$

27) The C_π^+ corresponds to the quantity of $(\rho_\pi^+)_p-0.85(\rho_\pi^+)_m$ and the C_π^- to $(\rho_\pi^-)_p-0.85(\rho_\pi^-)_m$. Further, since $(\rho_\pi^+)_m=(\rho_\pi^-)_m=0.50(\rho_i)_p$, then $C_\pi^+=(\rho_\pi^+)_p-0.43(\rho_i)_p$ and $C_\pi^-=(\rho_\pi^-)_p-0.43(\rho_i)_p$.

28) H. H. Jaffe, *J. Org. Chem.*, **23**, 1790 (1958).

29) M. Sawada, Y. Tsuno, *et al.*, unpublished.

30) For the para series, R=0.9974, $s=\pm0.170$, n=13. For the meta series, R=0.9962, $s=\pm0.152$, n=13.

 © 1980 The Chemical Society of Japan Bull. Chem. Soc. Jpn., 53, 2061—2063 (1980)

New Application of Crown Ethers. III.[1] Synthesis of 4′-Hydroxybenzocrown Ethers and Their Bis(benzocrown ether)s Linked by Poly(oxyethylene) Chain

Fumio WADA,* Ryozo ARATA, Tokio GOTO, Kiyoshi KIKUKAWA, and Tsutomu MATSUDA

Department of Organic Synthesis, Faculty of Engineering, Kyushu University, Hakozaki, Higashi-ku, Fukuoka 812

(Received January 24, 1980)

Baeyer-Villiger oxidation of 4′-acetylbenzocrown ethers followed by alkaline hydrolysis was proved to be a convenient route to 4′-hydroxybenzo-15-crown-5 and -18-crown-6, which formed air-stable hydrated crystals containing three and one mole of water, respectively, on crystallization from the solvent containing a small amount of water. New bis(benzocrown ether)s, connected by poly(oxyethylene) chain, were obtained in good yields by the reaction of the sodium salts with the ditosylates of di-, tri-, tetra-, and pentaethylene glycol.

Various substituted benzocrown ethers have been synthesized by either electrophilic substitution to benzocrown ethers or crown ring forming cyclization of substituted catechols. The substituents of the compounds not only serve to modify the nature of complexation with cations, but also have been successfully utilized for preparing other functionalized benzocrown ethers, such as 4′-vinylbenzocrown ethers[2] and several bis(benzocrown ether)s.[3,4] Hydroxybenzocrown ethers are thought to be interesting starting materials for the latter purpose because of the reactive aromatic ring and of the utility of the phenolic hydroxyl group. Thus, various bis(benzocrown ether)s and long-chain substitued benzocrown ethers could be obtained by the reaction of the sodium salts with α,ω-di-, and monotosylates of polymethylene or poly(oxyethylene) chain, respectively. This paper describes the synthesis of 4′-hydroxybenzocrown ethers and the bis(benzocrown ether)s being linked with tri-, tetra-, penta-, and hexa(oxyethylene) chain.

Results and Discussion

4′-Hydroxybenzocrown Ethers. Successful preparation of 4′-hydroxybenzo-15-crown-5 (**4a**) and -18-crown-6 (**4b**) were achieved by the following route (Eq. 1). Hydrolysis of the diazonium salts of 4′-aminobenzocrown ethers in aqueous acid or in the presence of copper catalyst[5] afforded the mixture being too complex to allow isolation, and oxidation of benzocrown ethers with $Tl(OCOCF_3)$[6] led to decomposition of the starting materials.

4′-Acetylbenzocrown ethers (**2**) were prepared by acetylation of the corresponding benzocrown ethers (**1a** and **1b**) with acetic anhydride–polyphosphoric acid in acetic acid at 45 °C for 3 h. Yields of **2a** and **2b** under the optimized reaction conditions were 83% and 80%, respectively.[7] Use of aluminium chloride as the catalyst was proved to be unpractical because of deactivation of the catalyst, and in the reaction of **1a**, **1a**–aluminium chloride (1:1) complex, stable in protic solvent, could be isolated.[7]

Baeyer-Villiger oxidation[8] of **2** with peracetic acid at 30—32 °C for 5 h affords 4′-acetoxybenzocrown ethers (**3**) in high yields. The crude products were purified by either extraction with hot heptane or chromatography on a short alumina-silica gel column (THF or $CHCl_3$) to give white crystals.

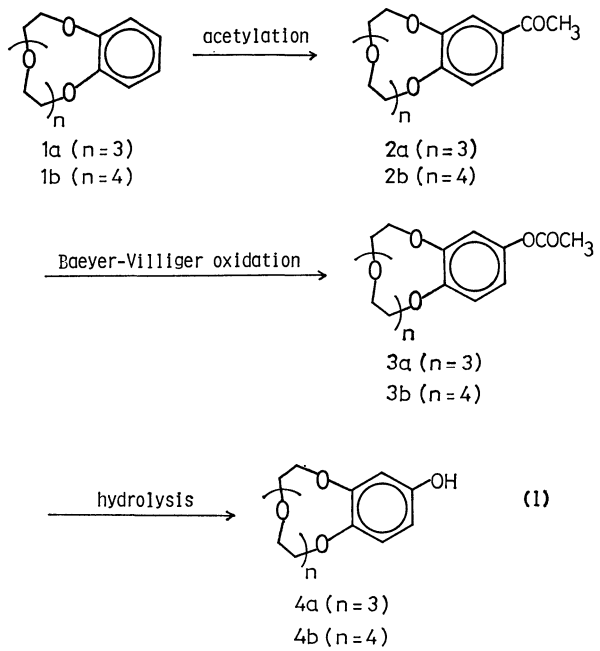

Hydrolysis of **3** to 4′-hydroxybenzocrown ethers (**4**) was carried out with aqueous sodium hydroxide at 40—50 °C for 3 h under nitrogen atmosphere. The crude product (**4a**) from **3a** was immediately precipitated as fine needles when the reaction mixture was acidified. In cases where the precipitation did not occur due to inadequate concentration of the product in the acidified solution, the product could be collected by extraction with chloroform. The crude product was further purified by recrystallization from a mixed solvent (THF–$CHCl_3$) containing a small amount of water to give white needles. The crystals were shown to contain three moles of water by measurement of loss of weight under vacuum at 110 °C for 3 h, and also by elemental analysis. Since **4b** did not separate as precipitate under the similar treatment, the product was taken up with chloroform and recrystallized from wet diethyl ether to give flat plates containing one mole of water. The monohydrated crystals showed a single melting point, 52.3—52.6 °C, without any visual transition of the crystal form,

TABLE 1. PREPARATION OF α,ω-BIS(4′-BENZOCROWN ETHER)POLYETHYLENEOXYETHERS

Crown	n	m	Yield/%	Mp/°C	Found C	Found H	Calcd (%) C	Calcd (%) H	
5a	3	1	67	73.0—74.5	60.01	7.27	60.18	7.26	($C_{32}H_{46}O_{13}$)
5b	3	2	83	88.9—92.2	59.64	7.49	59.81	7.38	($C_{34}H_{50}O_{14}$)
5c	3	3	21[a)]	73.0—74.0	59.42	7.51	59.49	7.49	($C_{36}H_{54}O_{15}$)
5d	3	4	63	liquid	58.93	7.60	59.21	7.58	($C_{38}H_{58}O_{16}$)
6a	4	1	52	74.6—77.5	58.97	7.48	59.49	7.49	($C_{36}H_{54}O_{15}$)
6b	4	2	78	69.5—72.0	58.82	7.56	59.21	7.58	($C_{38}H_{58}O_{16}$)
6c	4	3	50	52.0—54.5	58.67	7.65	58.96	7.67	($C_{40}H_{62}O_{17}$)
6d	4	4	58	liquid	58.34	7.64	58.73	7.74	($C_{42}H_{66}O_{18}$)

a) 1,8-Dichloro-3,6-dioxaoctane (triethylene glycol dichloride) was used in 1-butanol. The bis(benzocrown ether) was separated by HPLC since the recation product contained butyl ether of 4′-(9-hydroxy-1,4,7-trioxanonyl)-benzo-15-crown-5.

and were easily dehydrated under vacuum at room temperature for a few hours to afford a white solid. On the other hand, the hydrated crystals of **4a** showed two stage of transition of the crystal form at 43—47 °C and 75—78 °C, and completely melted at 100—103.0 °C (mp of the dehydrated crystals). Since, when being dehydrated, both **4a** and **4b** are liable to oxidized by air and readily impart a brown color, it is preferable to store in their hydrated forms and under nitrogen atmosphere. Although Cram and his coworkers[9)] recently described a monohydrated crown ether (a complex), such a trihydrated crown ether has not been reported.

Bis(benzocrown ether)s. Bis(benzocrown ether)s containing crown ether moieties at the two ends of a polymethylene or poly(oxyethylene) chain are known to have increased tendency of loose ion pair formation, and thus are expected to be effective in enhancing the reactivity of anionic species.[3)] Bis(benzocrown ether)s linked by ether linkages with poly(oxyethylene) chain are expected to be more resistant to the action of base (or acid)[4b)] than the known bis(benzocrown ether)s bridged by ester linkages,[3,4a)] and could be favorably utilized to various crown ether assisted reactions. Preparation of the bis(benzocrown ether)s were readily performed by the reaction of *in-situ* prepared sodium salts of **4a** or **4b** (from their dehydrated forms) with two molar equivalents of ditosylates of di-, tri-, tetra-, and pentaethylene glycol in THF (or dioxane–DMSO (10%)) (Eq. 2).

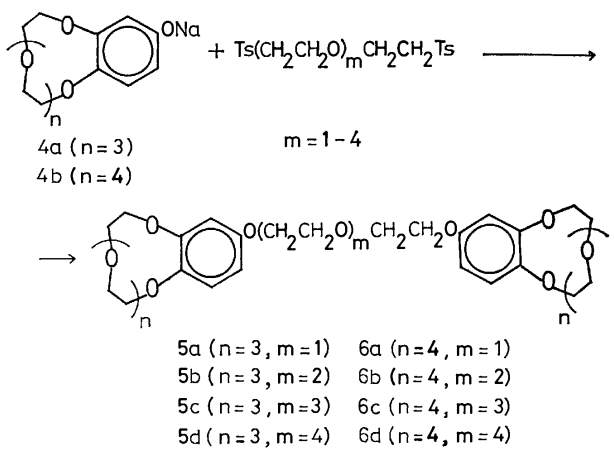

The crude products were chromatographed through an alumina column ($CHCl_3$), and recrystallized from ether–methanol (40:1). The purity and the structures of the products were confirmed by HPLC, IR, NMR, and elemental analysis. The results are summarized in Table 1, but the optimization of the yields has not been carried out.

Features of complex formation with cations and in S_N2 type reactions of these compounds are being investigated.

Experimental

Materials. Benzocrown ethers[10)] (**1a** and **1b**) and the ditosylate[11)] of di-, tri-, tetra-, and pentaethylene glycol were prepared according to the published procedures, respectively. Peracetic acid (9%) in acetic acid was prepared according to the published procedure.[12)]

4′-Acetoxybenzocrown Ethers (3a and 3b). Typical procedure was as follows. To the acetic acid solution of **2** (4.8 mmol), 8.0 g (9.5 mmol) of 9% peracetic acid was added dropwise over a 30 min period at 30—32 °C, and further stirred for 5 h. Longer reaction time caused a decrease of product yield. After aq sodium thiosulfate was added to the reaction mixture to decompose the excess peracetic acid, the solution was neutralized to pH 6 by the addition of Na_2CO_3, and extracted with chloroform. The chloroform layer was dried ($MgSO_4$), and the solvent was removed under vacuum. The residue was purified as mentioned above. 4′-Acetoxybenzo-15-crown-5 (**3a**): 82%; mp 57.0—58.2 °C; M^+: 326; ^{1}H-NMR (δ, $CDCl_3$): 2.25 (CH_3, 3H, singlet), 3.10—4.20 (-OCH_2CH_2O-, 16H, multiplet), 6.30—6.95 (aromatic protons, 3H, multiplet); Found: C, 58.60; H, 6.78%. Calcd for $C_{16}H_{22}O_7$: C, 58.89; H, 6.78%. 4′-Acetoxybenzo-18-crown-6 (**3b**): 65%; mp 48.5—50.0 °C; ^{1}H-NMR (δ, $CDCl_3$): 2.25 (CH_3, 3H, singlet), 3.30—4.30 (-OCH_2CH_2O-, 20H, multiplet); Found: C, 58.16; H 7.08%. Calcd for $C_{18}H_{26}O_8$: C, 58.37; H 7.07%.

4′-Hydroxybenzocrown Ethers (4a and 4b). To a suspension of 4′-acetoxybenzo-15-crown-5 (**3a**) (40 mmol) in water was added aq NaOH at 40—50 °C and the reaction mixture was stirred for 3 h under nitrogen atmosphere. Acidification of the reaction mixture to pH 2 with concd H_2SO_4 gave **4a** (trihydrated form) as fine needles. The precipitate was purified by recrystallization from THF–$CHCl_3$ (1:5) containing a small amount of water. Since **4b** did not formed from the mixture as precipitate under the similar treatment, the product was extracted with chloro-

form and the chloroform layer was dried ($MgSO_4$). After evaporation of solvent, the residual oily product was purified by chromatography (alumina, $CHCl_3$) and following recrystallization from wet diethyl ether. 4′-Hydroxybenzocrown ether (**4a**); 93% mp 100.9—103.0 °C (dehydrated crystal); ^{1}H-NMR (δ, CD_3CN): 2.39 (H_2O, 6H, singlet), 3.55—4.30 (–OCH_2CH_2O–, 16H, multiplet), 6.10—6.82 (aromatic protons, 3H, multiplet), 6.93 (–OH, 1H, broad singlet); Found: C, 49.62; H, 7.62%. Calcd for $C_{14}H_{20}O_6 \cdot 3H_2O$: C, 49.70; H, 7.74%. 4′-Hydroxybenzocrown ether (**4b**): 82%; mp 52.3—52.6 °C; ^{1}H-NMR (δ, CD_3CN): 2.27 (H_2O, 2H, singlet), 3.52—4.34 (–OCH_2CH_2O–, 20H, multiplet), 6.06—7.04 (aromatic protons and –OH, 4H, multiplet and broad singlet were overlapped); Found: C, 55.58; H 7.63%. Calcd for $C_{16}H_{24}O_7 \cdot H_2O$: C, 55.48; H, 7.54%.

*Bis(benzocrown ether)s (**5** and **6**).* General procedure. Triethylene glycol ditosylate or dihalide (1.5 mmol) in THF (or dioxane) was added dropwise to the mixture of 4′-hydroxybenzocrown ether (**3a**) (3 mmol) and sodium hydroxide (5.5 mmol) in THF (or dioxane–DMSO (10%)) under nitrogen atmosphere over a period of 2—3 h and then refluxed for 16—20 h. The reaction mixture was filtered and the filtrate was concentrated under vacuum. The residual oily product was chromatographed through an alumina column ($CHCl_3$) and purified by recrystallization from ether-methanol (40:1). The purity and structures of the product was confirmed by IR, NMR, HPLC, and EA. ^{1}H-NMR (δ, $CDCl_3$); **5a**: 3.46—4.35 (–OCH_2CH_2O–, 40H, multiplet), 6.15—6.94 (aromatic protons, 6H, multiplet). ^{1}H-NMR of other bis(benzocrown ether)s were closely resemble to that of **5a**.

References

1) Part I, F. Wada, R. Ishihara, Y. Kamohara, and T. Matsuda, *Bull. Chem. Soc. Jpn.*, **52**, 2959 (1979).
2) S. Kopolow, T. E. Hogen Esch, and J. Smid, *Macromolecules*, **6**, 133 (1973).
3) M. Bourgoin, K. H. Wong, J. Y. Hui, and J. Smid, *J. Am. Chem. Soc.*, **97**, 3462 (1975).
4) a) K. Kimura, H. Tamura, T. Tsuchida, and T. Shono, *Chem. Lett.*, **1979**, 611; b) K. H. Wong, and H. L. Ng, *Tetrahedron Lett.*, **1979**, 4295.
5) T. Cohen, A. G. Diety, Jr., and J. R. Miser, *J. Org. Chem.*, **42**, 2053 (1977).
6) S. W. Breuer, G. M. Pickles, J. C. Podesta, and F. G. Thorpe, *J. Chem. Soc., Chem. Commun.*, **1975**, 36.
7) F. Wada, and T. Matsuda, *Bull. Chem. Soc. Jpn.*, **53**, 421 (1980).
8) J. Boeseken and J. Greup, *Recl. Trav. Chim. Pays-Bas*, **58**, 528 (1939).
9) R. C. Helgeson, T. L. Tarnowski, and D. J. Cram, *J. Org. Chem.*, **44**, 2538 (1979).
10) C. J. Pedersen, *J. Am. Chem. Soc.*, **89**, 2495 (1967).
11) J. Dale, and P. O. Kristiansen, *Acta Chem. Scand.*, **26**, 1471 (1972).
12) F. P. Greenspan, *J. Am. Chem. Soc.*, **68**, 907 (1946).

Novel Synthetic Reactions Using Bis(2,2,2-trifluoroethoxy)diorganosulfuranes

Tomoya KITAZUME and Nobuo ISHIKAWA*

Department of Chemical Technology, Tokyo Institute of Technology, Ookayama, Meguro-ku, Tokyo 152

(Received November 24, 1979)

Alkoxy- or acyloxysulfuranes prepared *in situ* by the ligand exchange of bis(2,2,2-trifluoroethoxy)diorganosulfuranes with alcohols or carboxylic acids were found to behave as a potential alkylating or acylating reagent for the preparation of unsymmetrical sulfides, ketones, and esters.

Many studies have been made on the use of sulfuranes[1-18] but only a very few report on their application to organic synthesis, *viz.*, sulfilimines,[7,8,16] epoxides,[6] and olefins.[6,18]

Recently we reported the preparation of bis(2,2,2-trifluoroethoxy)diorganosulfuranes (**1**) in CH_2Cl_2–Et_2O system, and its reactions with alcohols, aldehydes, and carboxylic acids, affording olefins, 2,2,2-trifluoroethylated acetals, respectively.[1]

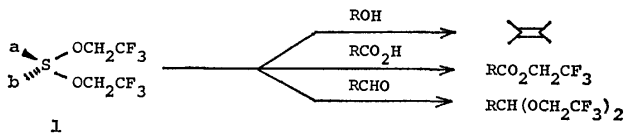

1

1A (a=b=Ph), 1B (a=Me, b=Ph)

The rapid ligand exchange of one of 2,2,2-trifluoroethoxyl groups of **1** with alcohol or carboxylic acid, giving (2,2,2-trifluoroethoxy)(alkoxy)diorganosulfurane (**2**) or (2,2,2-trifluoroethoxy)(acyloxy)diorganosulfurane (**3**) which affords a positive alkyl or acyl group, has a marked effect on the use of sulfuranes in organic synthesis.

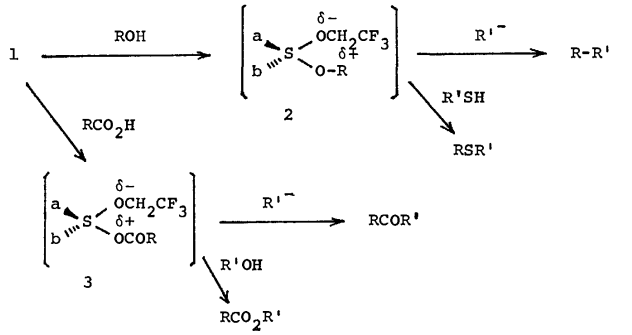

In a continuation of our research on the reactivity of **1**, we report on the formation of unsymmetrical sulfides, ketones, and esters.

Results and Discussion

Extensive investigations have been carried out on carbon–carbon bond formation, but only a few reports have appeared on *C*-alkylation by alcohols.[19-22]

We postulated the presence of (2,2,2-trifluoroethoxy)-(alkoxy)diorganosulfurane (**2**) with a positive alkyl group,[1] and have attempted to establish the carbon chain lengthening using **2**.

The reaction between **2** and Grignard or organolithium reagents was carried out first. However, 2,2,2-trifluoroethyl alcohol released in these systems reacts readily with magnesium or organolithium reagents, and the yields of the expected products were poor.

In contrast, an enolate anion, **5**, generated from trimethylsilyl ether–potassium fluoride system[23-27] readily attacked a positive carbon atom in alkoxysulfurane **2** to form a C–C bond compound (**6**).

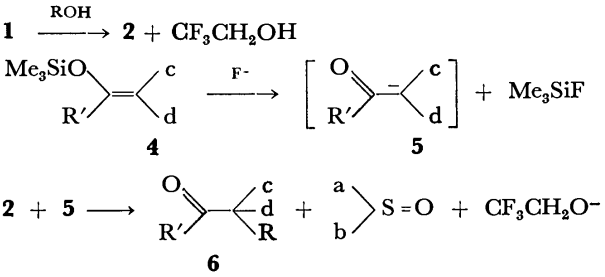

The results showing that no reaction occurs without an alcohol, olefins being obtained from alcohols in the absence of potassium fluoride, support the mechanism in which the ligand exchange of one of 2,2,2-trifluoroethoxyl groups for an alkoxyl group takes place first, the resulting **2** affording a positive alkyl group. A fluoride ion from potassium fluoride would aid formation of the carbanion (**5**) from the silyl enol ether (**3**), and the carbanion would attack the positive carbon atom of **2** to give a product **6**. The procedure seems to be effective for regioselective C–C coupling together with retention of configuration. No allylic rearrangement was observed in the reaction with allyl alcohols (Table 1).

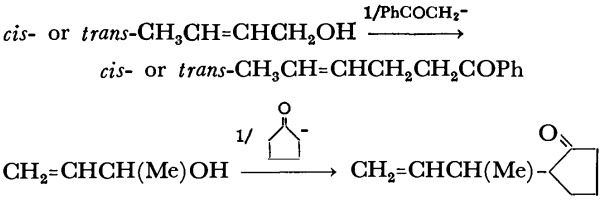

Synthetic application of **1** has been examined as regards the conversion of alcohols into sulfides.[28-30] The high dehydrating ability of the sulfurane made possible the one-pot regioselective synthesis of unsymmetrical alkyl aryl and aryl aryl sulfides (Table 2).

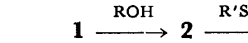

The formation of 2,2,2-trifluoroethyl esters (**7**) by the reaction of sulfurane **1** with carboxylic acids[1] leads to various applications of the intermediate sulfurane **3**.

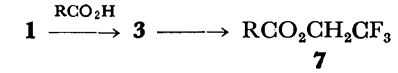

In fact, the enolated anion **5** and other nucleophiles such as alcohols attacked the positive carbon atom of **3** at −78 °C.

Table 1. Preparation

ROH or RCO_2H	Reagent	Product[a]	Sulfurane	Bp °C/mmHg [Mp °C]	Yield %
i-PrOH	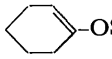	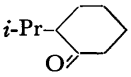	1 A	80—82/16 (83/17)[c]	62
$CH_3COCH_2CH(Me)OH$	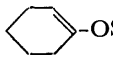	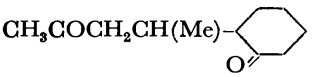	1 B	103—105/56[d]	53
trans-$CH_3CH{=}CHCH_2OH$	PhMgBr	*trans*-$CH_3CH{=}CHCH_2Ph$	1 A	101—102/15	28
trans-$CH_3CH{=}CHCH_2OH$	$PhC(OSiMe_3){=}CH_2$	*trans*-$CH_3CH{=}CHCH_2CH_2COPh$	1 A	98-99/5[b]	51
cis-$CH_3CH{=}CHCH_2OH$	$PhC(OSiMe_3){=}CH_2$	*cis*-$CH_3CH{=}CHCH_2CH_2COPh$	1 A	101—102/6[b]	62
$CH_2{=}CHCH(Me)OH$	PhMgBr	$CH_2{=}CHCH(Me)Ph$	1 A	132—135	36
$CH_2{=}CHCH(Me)OH$	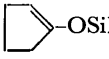	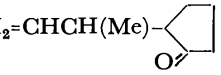	1 A	96—97/31	81
trans-$CH_3CH{=}CHCO_2H$	$PhC(OSiMe_3){=}CH_2$	*trans*-$CH_3CH{=}CHCOCH_2COPh$	1 A	153—154/1[b]	54
$PhCO_2H$	CH_3MgBr	$PhCOCH_3$	1 A	80/11 (79/10)[e]	20
CH_3CO_2H	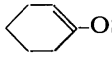	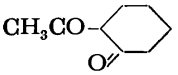	1 B	121—123/21 (111—112/18)[e]	71
$PhCO_2H$	$PhC(OSiMe_3){=}CH_2$	$PhCOCH_2COPh$	1 A	[80—81][81][e]	81
$PhCO_2H$	CH_3OH	$PhCO_2CH_3$	1 A	94—96/25 (96—98/24)[e]	81
$PhCO_2H$	C_2H_5OH	$PhCO_2C_2H_5$	1 B	84—86/10	76
trans-$CH_3CH{=}CHCO_2H$	C_2H_5OH	*trans*-$CH_3CH{=}CHCO_2C_2H_5$	1 A	97—98/18	79

a) Structures were confirmed by means of IR and NMR spectral data. b) New compound: The results of microanalysis agreed satisfactorily with the calculated value. c) "Dictionary of Organic Compounds," 4th ed, Eyre and Spottiswoode Pub. Ltd., (1965), Vol. 3. p. 1936. d) K. Narasaka, K. Soai, and T. Mukaiyama, *Chem. Lett.*, **1974**, 1223. e) "Spectral data and Physical Constants for Organic Compounds," ed by W. M. Ritchey, C. R. C. Press. Inc., (1975).

Table 2. Preparation of unsymmetrical sulfides

ROH	R'SH	Product[a]	Bp °C/mmHg	Yield %
C_2H_5OH	PhSH	C_2H_5SPh	72—74/6 (206)[b]	62
C_2H_5OH	$PhCH_2SH$	$C_2H_5SCH_2Ph$	78—80/5 (229)[b]	51
i-PrOH	PhSH	*i*-PrSPh	96—98/10 (102—104/14)[b]	86
$C_8H_{17}OH$	PhSH	$C_8H_{17}SPh$	107—109/2 (147/18)[b]	92
trans-$CH_3CH{=}CHCH_2OH$	PhSH	*trans*-$CH_3CH{=}CHCH_2SPh$	104—106/12 (70/1.3)[c]	89
trans-$CH_3CH{=}CHCH_2OH$	$PhCH_2SH$	*trans*-$CH_3CH{=}CHCH_2SCH_2Ph$	102—104/5 (86/0.5)[d]	78
cis-$CH_3CH{=}CHCH_2OH$	PhSH	*cis*-$CH_3CH{=}CHCH_2SPh$	102—105/12[e]	72
$CH_2{=}CHCH(Me)OH$	PhSH	$CH_2{=}CHCH(Me)SPh$	101—103/10[e]	76
$CH_2{=}CHCH(Me)OH$	$PhCH_2SH$	$CH_2{=}CHCH(Me)SCH_2Ph$	118—120/9[e]	72

a) Structures were confirmed by means of IR and NMR spectral data. b) H. H. Anderson, *J. Chem. Eng. Data*, **9**, 272 (1964). c) C. Cope, D. E. Morrison, and C. Field, *J. Am. Chem. Soc.*, **72**, 59 (1950). d) J. J. Bryan and D. W. Hysert, *Can. J. Chem.*, **49**, 325 (1971). e) T. Kubota, S. Miyashita, T. Kitazume, and N. Ishikawa, *Chem. Lett.*, **1979**, 845.

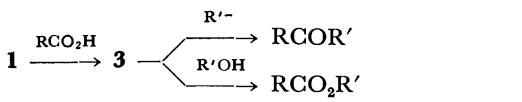

In each case, inhibition of the pseudorotation to produce 2,2,2-trifluoroethyl esters seems advantageous for producing ketones and esters.

In conclusion, the sulfurane **1** is a useful precursor through **2** or **3** for organic synthesis.

Experimental

General procedures are described.

2-Isopropylcyclohexanone. A mixture of bis(2,2,2-trifluoroethoxy)diphenylsulfurane (12 mmol) prepared from chlorodiphenylsulfonium chloride (14 mmol) and sodium 2,2,2-trifluoroethoxide (28 mmol) *in situ*,[1] and isopropyl alcohol (10 mmol) in freshly dried tetrahydrofuran (10 ml) was stirred at room temperature for 5 min. Into the mixture, were added successively 2-cyclohexenyl trimethylsilyl ether (10 mmol) and calcined potassium fluoride (10 mmol). After being stirred for 24 h, the reaction mixture was poured into water and the resulting oily substance was extracted

with diethyl ether. On removing the solvent, the residue was subjected to distillation *in vacuo*. Final purification was performed by preparative gas chromatography through a column containing 25% Silicone DC 550 on Shimalite. The product, 2-isopropylcyclohexanone, was obtained in a 62% yield, bp 80—82 °C/16 mmHg.**

2-Acetylcyclohexanone. A mixture of bis(2,2,2-trifluoroethoxy)methylphenylsulfurane (12 mmol) prepared from chloromethylphenylsulfonium chloride (14 mmol) and sodium 2,2,2-trifluoroethoxide (28 mmol) *in situ*,[1] acetic acid (10 mmol) and freshly dried tetrahydrofuran (10 ml) was stirred at −78 °C for 10 min. After successive addition of 2-cyclohexenyl trimethylsilyl ether (10 mmol) and calcined potassium fluoride (10 mmol), the mixture was stirred for 10 h. The resulting mixture was then poured into water, and subjected to the usual work-up. Distillation gave 2-acetylcyclohexanone in 71% yield, bp 121—123 °C/21 mmHg.

Ethyl Benzoate. A mixture of bis(2,2,2-trifluoroethoxy)methylphenylsulfurane (12 mmol),[1] benzoic acid (10 mmol) and freshly dried tetrahydrofuran (10 ml) was stirred at −78 °C for 10 min. Ethyl alcohol (10 mmol) was added to the reaction mixture, which was then stirred at −78 °C for 10 h. The mixture was poured into water, and the oily substance extracted with diethyl ether. After removal of the solvent, distillation gave ethyl benzoate in 76% yield, by 84—86 °C/10 mmHg.

Ethyl Phenyl Sulfide. A mixture of bis(2,2,2-trifluoroethoxy)diphenylsulfurane (12 mmol),[1] ethyl alcohol (10 mmol), thiophenol (11 mmol) and freshly dried diethyl ether (10 ml) was stirred at room temperature for 24 h. The reaction mixture was poured into water and the oily layer extracted with diethyl ether. The ethereal extract was washed with 5% aq sodium hydroxide solution and dried over magnesium sulfate. After removal of the solvent, the residual oily material was distilled in a vacuum yielding ethyl phenyl sulfide in 62% yield, bp 72—74 °C/6 mmHg.

** 1 mmHg=133.3 Pa.

References

1) T. Kitazume and N. Ishikawa, *Yuki Gosei Kagaku Kyokai Shi*, **37**, 81 (1979).
2) J. I. Darragh and D. W. A. Sharp, *Angew. Chem. Int. Ed. Engl.*, **9**, 73 (1970).
3) I. Kapovits and A. Kalman, *J. Chem. Soc., Chem. Commun.*, **1971**, 649.
4) W. A. Sheppard, *J. Am. Chem. Soc.*, **93**, 5597 (1971).
5) R. J. Arhart and J. C. Martin, *J. Am. Chem. Soc.*, **94**, 4997 (1972).
6) J. C. Martin, J. A. Franz, and R. J. Arhart, *J. Am. Chem. Soc.*, **96**, 4604 (1974).
7) J. A. Franz and J. C. Martin, *J. Am. Chem. Soc.*, **97**, 583 (1975).
8) J. C. Martin and J. A. Franz, *J. Am. Chem. Soc.*, **97**, 6137 (1975).
9) J. C. Martin and E. F. Perozzi, *Science*, **191**, 154 (1976).
10) L. J. Adzima, C. C. Chiang, I. C. Paul, and J. C. Martin, *J. Am. Chem. Soc.*, **100**, 953 (1978), and references cited therein.
11) D. S. Ross and D. W. A. Sharp, *J. Chem. Soc., Dalton Trans.*, **1972**, 34.
12) B. S. Campbell, D. B. Denney, D. Z. Denney, and L. Shih, *J. Am. Chem. Soc.*, **97**, 3850 (1975).
13) K. C. Hodgls, D. Schomburg, J. V. Weiss, and R. Schmutzler, *J. Am. Chem. Soc.*, **98**, 6096 (1977).
14) B. A. Arbuzov, N. N. Zubova, and O. V. Sofronova, *Izv. Akad. Nauk SSSR, Ser. khim.*, **1975**, 1206.
15) P. Huszthy, I. Kapovits, A. Kucsman, and L. Radlcs, *Tetrahedron Lett.*, **1978**, 1853.
16) T. Kitazume and J. M. Shreeve, *J. Am. Chem. Soc.*, **99**, 4194 (1977).
17) T. Kitazume and J. M. Shreeve, *J. Am. Chem. Soc.*, **100**, 985 (1978).
18) T. Kitazume and J. M. Shreeve, *Inorg. Chem.*, **17**, 2173 (1978).
19) H. Felkin and G. Swierczewski, *Tetrahedron Lett.*, **1972**, 1433.
20) H. Felkin and G. Swierczewski, *Tetrahedron*, **31**, 2735 (1975).
21) T. Mukaiyama, M. Imaoka, and T. Izawa, *Chem. Lett.*, **1977**, 1257.
22) Y. Tanigawa, H. Kanamaru, A. Sonoda, and S. Murahashi, *J. Am. Chem. Soc.*, **99**, 2361 (1977).
23) K. Kuroda and N. Ishikawa, *Kogyo Kagaku Zasshi*, **74**, 495 (1971).
24) N. Ishikawa and K. Isobe, *Chem. Lett.*, **1972**, 435.
25) N. Ishikawa, *Kagaku Kogyo*, **1972**, 638.
26) I. Kuwajima, *Yuki Gosei Kagaku Kyokaishi*, **37**, 107 (1979), and references cited therein,
27) I. Kuwajima, *Yuki Gosei Kagaku Kyokaishi*, **34**, 964 (1976).
28) Y. Tanigawa, H. Kanamaru, and S. Murahashi, *Tetrahedron Lett.*, **1975**, 4655.
29) T. Mukaiyama, T. Masui, and T. Izawa, *Chem. Lett.*, **1976**, 1177.
30) T. Kubota, S. Miyashita, T. Kitazume, and N. Ishikawa, *Chem. Lett.*, **1979**, 845.

 © 1980 The Chemical Society of Japan Bull. Chem. Soc. Jpn., 53, 2067—2073 (1980)

Studies of Zone Melting. V. The Solid-Liquid Equilibrium and Zone Melting of the Bibenzyl–Diphenylacetylene System

Hidemoto NOJIMA* and Seigou AKEHI

Department of Industrial Chemistry, Faculty of Engineering, Meiji University, Ikuta, Tama-ku, Kawasaki 214

(Received January 17, 1979)

The phase diagram of the bibenzyl–diphenylacetylene system was determined in detail from DSC by using the following equation:

$$T = \alpha\sqrt{F'} + \beta,$$

where T is the temperature; F', the corrected fraction melted, calculated by the use of the area for the vertex of the peak instead of the total peak area and α and β, the constants. Then, the melting and freezing temperatures were obtained from a plot of T *vs.* $\sqrt{F'}$ by the use of the values of β and $\alpha+\beta$ respectively. The results show the formation of solid solutions with a minimum melting point, at which difficulty in determining the composition often arises from the fact that the slopes of both the solidus and liquidus curves are zero. This could be overcome by multipass zone melting for two samples containing 20 and 30 wt % of diphenylacetylene; after 45 zone passes, the composition of the minimum melting point was found to be 26.4% at the end. Also, by Herington's theory, it has been revealed that zone-melting experiments were attained almost at equilibrium.

The behavior of a solute during the zone melting of binary mixtures can be interpreted to some extent by the phase diagrams of these mixtures. Conversely, it follows that a type of phase diagram may be shown from the results of zone-melting experiments. Herington[1] has theoretically described the relation between the zone-melting behavior and the phase diagrams of binary mixtures. However, few applications of zone melting to the study of the phase diagrams of organic compounds have been reported. By the combined use of zone melting and the differential thermal analysis, Jonchich *et al.*[2] have reconstructed the phase diagram of the phenanthrene–anthracene system, which had previously been reported by Bradley and Marsh,[3] and Kofler.[4]

It has also been reported[5] that the bibenzyl–diphenylacetylene system forms a continuous series of solid solutions with Roozeboom's Type I:[6] the freezing points of all mixtures lie between those of the pure components. The present authors, however, have argued against the above conclusion on the basis of the difference between the crystal structures and the molecular sizes of these two compounds.[7] The present work has been carried out in order to prove our argument against the formation of the phase diagram of Roozeboom's Type I; the solid-liquid equilibrium for this system is investigated in detail by means of both zone melting and DSC (differential scanning calorimetry) in the search for a useful equation for determining the melting and freezing temperatures from the relation between the temperature and the corrected fraction melted in DSC. It has thus been verified that this system does not form a continuous series of solid solutions, as has reported previously,[5] but forms solid solutions with a minimum melting point: Roozeboom's Type III.[6] In this case, the solidus and liquidus curves meet at a minimum temperature, at which the phases existing in equilibrium have the same composition. The slopes of both the solidus and liquidus curves at the minimum melting point are zero, in accordance with the Gibbs-Konovalow rule, and the difference between the melting and freezing temperatures on both sides in the vicinity of the minimum melting point is usually slight. Hence, it is often difficult for the composition at the minimum melting point to be determined precisely by ordinary thermal analysis. In this work, the composition of the minimum melting point was determined precisely by multipass zone-melting experiments for two specimens with initial concentrations at both sides near the composition of the minimum melting ponit, which has roughly been predetermined by DSC.

Moreover, the evaluation of the deviation from equilibrium in the multipass zone-melting experiments is discussed by means of Herington's theory.

No zone-melting experiments have previously been reported for this system.

Theoretical

Determination of the Solidus and Liquidus Curves by DSC. A typical DSC peak for a binary mixture forming a solid solution is shown in Fig. 1, in which the fraction melted, F, at a definite temperature, *e.g.*, T_n, is given in the following way:[11,13]

$$F = \frac{\text{area ACHA}}{\text{area AEFA}}. \tag{1}$$

Strictly speaking, Eq. 1 is valid only when the heats of fusion of the constituents are nearly equal and when the heat of mixing can be neglected in comparison with them. From Fig. 1, Eq. 1 may be rewritten as follows:

$$F = \frac{\text{area BCHB}+\text{area ABJA}}{\text{area BDGB}+\text{area DEFD}+\Delta a}, \tag{2}$$

where Δa denotes the difference between the area ABJA and the area FGIF. Equation 2 may further be rewritten as follows:

$$F = \frac{\text{area BCHB}+\text{area ABJA}}{\text{area BDGB}} \cdot \frac{\text{area BDGB}}{\text{area BDGB}+\text{area DEFD}+\Delta a}. \tag{3}$$

Assuming that the area ABJA is small and can be

neglected in comparison with the area BCHB, the following equation is obtained:

$$F = \frac{\text{area BCHB}}{\text{area BDGB}} \cdot \frac{\text{area BDGB}}{\text{area BDGB}+\text{area DEFD}+\Delta a}. \tag{4}$$

In Eq. 4 it is convenient to put as

$$F' = \frac{\text{area BCHB}}{\text{area BDGB}}, \tag{5}$$

$$K = \frac{\text{area BDGB}}{\text{area BDGB}+\text{area DEFD}+\Delta a}. \tag{6}$$

Hence, the following equation is obtained:

$$F = F'K \tag{7}$$

where F' is the fraction melted as calculated by the use of the areas of the ΔBDG and ΔBCH triangles instead of by the calculation of the total peak area and the area ACHA, as represented by Eq. 1, and where K is the constant, depending upon the samples. It follows that the relation between F and F' is represented by Eq. 7. We will term F' the corrected fraction melted. As will be described below the experimental results are better interpreted experientially by F' than by F.

Furthermore, the conclusion presented below may be made for the corrected fraction melted, F'. From Fig. 1, the following equations are obtained:

$$\text{area ADFA} = \text{area BDFB} + \text{area ABJA}, \tag{8}$$

$$\text{area BDGB} = \text{area BDFB} + \text{area IFGI}. \tag{9}$$

From Eqs. 8 and 9, the following equation is then obtained:

$$\text{area ADFA} = \text{area BDGB} + \text{area ABJA} - \text{area IFGI}. \tag{10}$$

Putting the second and third terms on the right-hand side of Eq. 10 as

$$\Delta b = \text{area ABJA} - \text{area IFGI}, \tag{11}$$

Eq. 10 is rewritten as follows:

$$\text{area ADFA} = \text{area BDGB} + \Delta b. \tag{12}$$

Assuming that Δb is small and can be neglected in comparison with the area BDGB, Eq. 13 is obtained:

$$\text{area ADFA} = \text{area BDGB}. \tag{13}$$

The following relation for F' is obtained, together with the assumption described previously; *i.e.*, the area ABJA can be neglected in comparison with the area BCHB:

$$F' = \frac{\text{area BCHB}}{\text{area BDGB}} = \frac{\text{area ACHA}}{\text{area ADFA}}. \tag{14}$$

In the DSC curve, the abscissa indicates the temperature, while the ordinate indicates the millicalories per second. Moreover, in the DSC chart, the time and the temperature can be read off from the abscissa and the ordinate respectively. Therefore, the assumption presented below and Fig. 1 seems to be true. Since the temperature, T, in the DSC chart is the linear function of time, t, for the line $\overline{BH}$ in Fig. 1, the following equation is obtained:

$$T = kt + l, \tag{15}$$

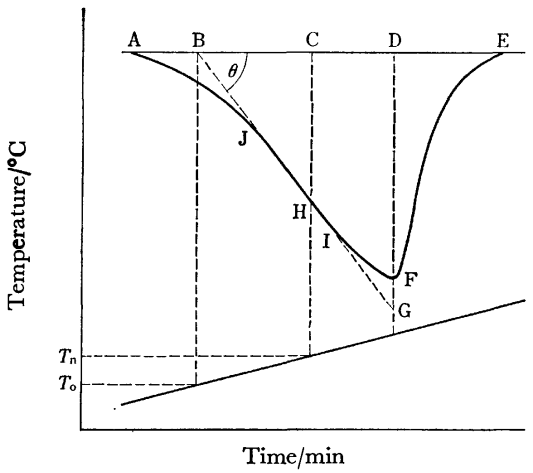

Fig. 1. Schematic diagram for the derivation of Eq. 32.

where k and l are constants. Much as in Eq. 15, for the line $\overline{BC}$ in Fig. 1, Eq. 16 is obtained:

$$T = mt + n, \tag{16}$$

where m and n are constants. Let v denote the chart speed; Eqs. 15 and 16 can then be rearranged as follows:

$$T = \frac{\overline{BH}}{v}k + l, \tag{17}$$

$$T = \frac{\overline{BC}}{v}m + n. \tag{18}$$

Rewrite Eqs. 17 and 18 as follows:

$$\overline{BH} = \frac{v}{k}T - \frac{lv}{k}, \tag{19}$$

$$\overline{BC} = \frac{v}{m}T - \frac{nv}{m}, \tag{20}$$

where it is convenient to put $(v/k)\equiv a$, $(-lv/k)\equiv b$, $(v/m)\equiv c$, and $(-nv/m)\equiv d$. Therefore, Eqs. 21 and 22 are obtained:

$$\overline{BH} = aT + b, \tag{21}$$

$$\overline{BC} = cT + d. \tag{22}$$

As is obvious from Fig. 1, when $\overline{BH}$ is zero; $\overline{BC}$ is also to be zero, and let T_0 be the temperature. Substituting the above conditions into Eqs. 21 and 22 yields Eqs. 23 and 24:

$$T_0 = -\frac{b}{a}, \tag{23}$$

$$T_0 = -\frac{d}{c}. \tag{24}$$

Therefore,

$$ad = bc. \tag{25}$$

The area, S, of the triangle ΔBCH is

$$S = \frac{1}{2} \times \overline{BC} \times \overline{CH} = \frac{1}{2}(aT+b)(cT+d)\sin\theta. \tag{26}$$

Equation 26 is rewritten by Eq. 25 as follows:

$$S = \frac{1}{2}(acT^2+2bcT+bd)\sin\theta. \tag{27}$$

Then, Eq. 28 is obtained:

$$S = \frac{1}{2}ac\left(T+\frac{b}{a}\right)^2 \sin\theta. \quad (28)$$

The area, S_0, of the triangle ΔBDG is represented by

$$S_0 = \frac{1}{2} \times \overline{BD} \times \overline{DG} = \frac{1}{2} \times \overline{BD} \times \overline{BG} \sin\theta. \quad (29)$$

From Eqs. 28 and 29, the corrected fraction melted, F', is obtained by

$$F' = \frac{S}{S_0} = \frac{ac}{\overline{BD} \times \overline{BG}}\left(T+\frac{b}{a}\right)^2, \quad (30)$$

by solving Eq. 30 for T, and from Eq. 23 the following equation is obtained:

$$T = \sqrt{\frac{\overline{BD} \times \overline{BG}}{ac}}\sqrt{F'} + T_0. \quad (31)$$

Since both $\sqrt{(\overline{BD} \times \overline{BG})/ac}$ and T_0 are constants, it is convenient to put these constants as α and β respectively. Then, we obtain Eq. 32:

$$T = \alpha\sqrt{F'} + \beta. \quad (32)$$

The DSC curve is the same in nature as the differential thermal analysis curve,[10] and the vertex of the peak (Point F in Fig. 1) most accurately reflects the melting point,[11] *i.e.*, the conclusion of the melting. Furthermore, in a binary system the melting temperature is signified by the first departure of the base line from the normal (Point A in Fig. 1), while the freezing temperature is signified by the vertex of the peak,[12] at which F'=(area ADFA/area ADFA)=1, as may be seen in Fig. 1.

From the above description, the melting temperature, corresponding to the solidus temperature, may be given by the intercept, β, of Eq. 32 when F' is zero, and the freezing temperature, corresponding to the liquidus temperature, may be obtained from the value of $\alpha+\beta$ when F' is unity, while the melting range is indicated by the slope, α.

Multipass Zone Melting. An equation for the solute distribution resulting from an infinite number of zone passes has been derived by Pfann.[8] This equation is, however, applicable only to a system with constant distribution coefficient. Pfann's equation for the ultimate distribution is as follows:

$$C(Z) = A\exp(BZ) \quad (33)$$

where $C(Z)$ is the solute concentration at the point Z from the top of the sample after the ultimate distribution has been reached and where A and B are constants obtainable from Eqs. 34 and 35:

$$k = \frac{B}{e^B-1}, \quad (34)$$

$$A = \frac{C_0BL}{e^{BL}-1}, \quad (35)$$

where C_0 is the initial concentration of the solute; L, the length of the sample, and k, the constant distribution coefficient. Rewrite Eq. 33 as follows:

$$\ln C(Z) = BZ + \ln A. \quad (36)$$

Moreover, from Eq. 36, the solute distribution at a small distance, dZ, further along the sample is give by

$$\ln C(Z+dZ) = B(Z+dZ) + \ln A. \quad (37)$$

The following equation is derived by subtracting Eq. 36 from 37:

$$\ln\frac{C(Z+dZ)}{C(Z)} = B dZ. \quad (38)$$

Equation 38 is rewritten as follows:

$$C(Z+dZ) = C(Z)\exp(BdZ). \quad (39)$$

Although Eq. 39 is applicable strictly to a system with a constant distribution coefficient, as has already been described, this equation is also approximately applicable to a system with a slight variation in the concentration near the end of the phase diagram. When the distribution coefficient, however, varies appreciably, Eq. 39 fails to be useful.

Herington[1] has extended Pfann's theory to binary systems when the distribution coefficients are dependent on the concentration.

For what follows, it is necessary to summarize his method for calculating the ultimate distribution curve, which should be calculated by the following procedures:

1. Depict a plot of the equilibrium distribution coefficient, k_1, against the concentration, C, of the solute in the solid phase with the aid of the phase diagram.

2. Obtain the values of B_1 from Eq. 40 with the values of k_1 from this plot. The subscript i is used to designate the concentration dependence of these values; the values of B_1 can be obtained essentially from the table of the Einstein function,

$$k_1 = \frac{B_1}{e^{B_1}-1}. \quad (40)$$

Plot the function B_1 against C from the resulting values.

3. Choose, near one end of the phase diagram, an arbitrary value of $C(Z)$. This value must, however, be chosen in the part of the phase diagram applicable to the initial uniform composition of the charge.

4. Read the value of B_1 corresponding to the solid composition $C(Z)$ from the graph obtained in Section 2; let this value be $B_1(Z)$.

5. Calculate, by means of Eq. 41, the value of $C(Z+1/d)$, applicable to the composition at a distance, $1/d$, of a zone length further along the specimen,

$$C\left(Z+\frac{1}{d}\right) = C(Z)\exp\left\{\frac{B_1(Z)}{d}\right\}. \quad (41)$$

6. Using this value for $C(Z+1/d)$, repeat the calculation discussed in Sections 4 and 5 to obtain a new value of B_1, that is, the value of $B_1(Z+1/d)$, and then calculate $C(Z+2/d)$ by means of Eq. 42:

$$C\left(Z+\frac{2}{d}\right) = C\left(Z+\frac{1}{d}\right)\exp\left\{\frac{B_1\left(Z+\frac{1}{d}\right)}{d}\right\}. \quad (42)$$

The calculations should similarly be iterated until the composition asymptotically approaches that of a pure component or the composition of the minimum melting point.

Equations 41 and 42 are rearranged in the following general form:

$$C\left(Z+\frac{n+1}{d}\right) = C\left(Z+\frac{n}{d}\right)\exp\left\{\frac{B_1\left(Z+\frac{n}{d}\right)}{d}\right\}, \quad (43)$$

n=0,1,2,3,……

Experimental

Materials. The bibenzyl and diphenylacetylene used for the determination of the phase diagram were purified by zone refining, followed by recrystallization once from ethanol.

For the multipass zone-melting experiments, a larger quantity of the bibenzyl as the solvent was used than that of the diphenylacetylene used as the solute. However, the zone-refining apparatus** which we employed for refining the chemicals cannot treat a large quantity of chemicals; hence, bibenzyl purified only by recrystallization once from ethanol was used, while the diphenylacetylene was purified by zone refining, followed by recrystallization once from ethanol.

For the determination of the phase diagram, ten specimens of the bibenzyl–diphenylacetylene mixtures (containing 5, 10, 20, 30, 40, 50, 60, 70, 80, and 90 wt % of diphenylacetylene) were prepared by melting in Pyrex ampoules under a dry nitrogen atmosphere and by grinding to powder after the ampoules had been taken out.

For multipass zone-melting experiments, two bibenzyl–diphenylacetylene mixtures containing 20 and 30 wt % of diphenylacetylene were prepared by melting in Pyrex ampoules under a dry nitrogen atmosphere and by grinding to powder after the ampoules had been taken out.

These mixtures were charged in a length of 30 cm in Pyrex tubes with an inner diameter of 0.7 cm and outer diameter of 0.9 cm. Then the tubes were sealed off under a dry nitrogen atmosphere of about 0.9 atm.

Apparatus and Procedures. The melting and freezing temperatures were determied with a Shimadzu differential scanning calorimeter, SC-20, under the following conditions: heating rate, 1 °C/min; chart speed, 40 mm/min; range, ±5 mcal/s.

The multipass zone-melting experiments were carried out with the apparatus described in a previous paper[9] and under the following conditions: zone travel rate, 0.73 cm/h; zone length, 3 cm; zone temperature, 61±1 °C; the number of zone passages, 45.

The samples after zone melting were cut into 3-cm-long divisions. The concentration of diphenylacetylene in each division was determined spectrophotometrically in an ethanol solution by the use of a Hitachi 101 spectrophotometer at a wavelength of 305 nm.

Results and Discussion

The Phase Diagram of the Bibenzyl–Diphenylacetylene System. With the results of DSC, the temperature, T, was plotted against the square root of the corrected fraction melted, $\sqrt{F'}$, as is shown in Fig. 2. From the resulting straight lines, the melting and freezing temperatures were calculated by means of Eq. 32.

As may be seen in Fig. 2, for pure components, that is, bibenzyl or diphenylacetylene, it is in conflict with the phase rule that the relation between T and $\sqrt{F'}$ obeys Eq. 32, like a mixture. Such behavior observed in pure components is probably due to the impossibility of obtaining an absolutely pure substance and a time lag caused mainly by the finite thermal conductivity in the samples during fusion.

Therefore, the value of α in Eq. 32 for a pure component, which may correspond to the apparent melting range caused by the above reasons, should be added to all the observed melting temperatures of the bibenzyl–diphenylacetylene mixtures for the corrections of the temperatures. These corrections were made by using the value, 1 °C, of pure bibenzyl for the specimens with 5 to 20% of diphenylacetylene, and by using the value, 0.8 °C, of pure diphenylacetylene for the specimens with 30 to 90% of diphenylacetylene. The results obtained are presented in Table 1 and Fig. 3; the old data reported by Pascal *et al.*[5] are also shown, represented by the broken lines in Fig. 3.

Indeed, such systems as the azobenzene–stilbene and diphenylacetylene–stilbene form a continuous series of solid solutions because of the close resemblances

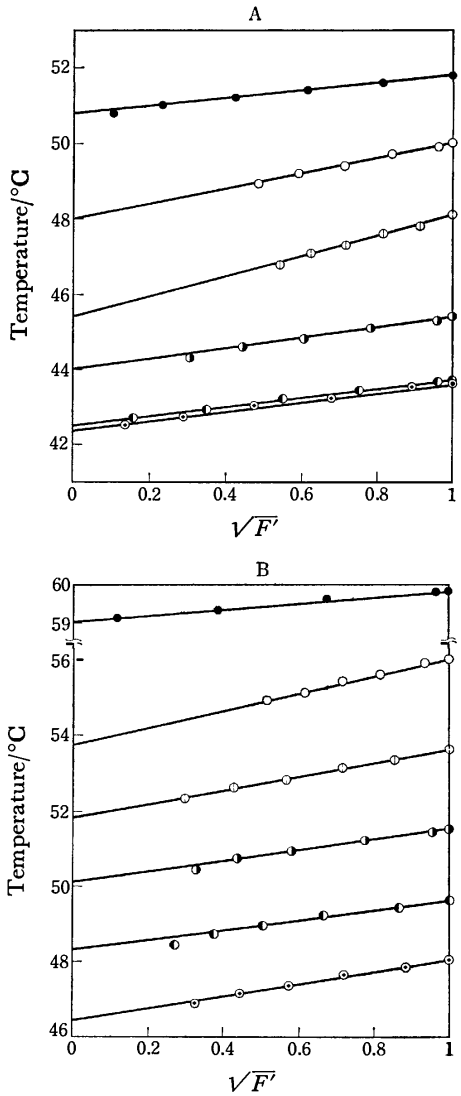

Fig. 2. Relation between the temperature and square root of the corrected fraction melted.
A: ●; 100% of bibenzyl, ○; 5% of diphenylacetylene, ◫; 10% of diphenylacetylene, ◐; 20% of diphenylacetylene, ⊙; 30% of diphenylacetylene, ◑; 40% of diphenylacetylene. B: ●; 100% of diphenylacetylene, ○; 90% of diphenylacetylene, ◫; 80% of diphenylacetylene, ◑; 70% of diphenylacetylene, ◐; 60% of diphenylacetylene, ⊙; 50% of diphenylacetylene.

** Shimadzu cryogenic zone-refiner, CZ-1.

Table 1. The melting and freezing temperatures for the bibenzyl-diphenylacetylene system

Concentration of diphenylacetylene wt%	Melting temp °C	Freezing temp °C
0	51.8	51.8
5	49.0	50.0
10	46.4	48.1
20	43.5	43.7
30	43.2	43.6
40	44.8	45.4
50	47.2	48.0
60	49.1	49.6
70	50.9	51.5
80	52.6	53.6
90	54.5	56.0
100	59.8	59.8

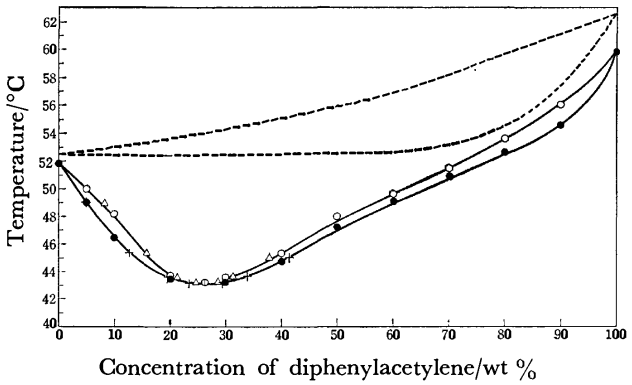

Fig. 3. Phase diagram of the bibenzyl–diphenylacetylene system.
○: Freezing temperature determined by DSC, ●: meting temperature determined by DSC, △: composition of liquid phase calculated by the Herington's theory, +: composition of solid phase calculated by the Herington's theory, ⓘ: composition of minimum melting point determined by multipass zone-melting experiments, ----: solidus and liquidus curves reported by Pascal *et al.*[5]

of the crystal structures and molecular sizes among these compounds,[7] but bibenzyl is somewhat different in these factors[7] from the above three compounds.

In consequence of these differences in the crystal structure and molecular size, the bibenzyl–diphenylacetylene system may deviate from an ideal solution and may form solid solutions with a minimum melting point, as has previously been predicted.

The Determination of the Composition of the Minimum Melting Point by Multipass Zone-melting Experiments. Figure 4 and Table 2 show the relation between the concentration of diphenylacetylene and the distance in zone lengths along the specimens after 45 zone passes for two specimens containing initially 20 and 30 wt % of diphenylacetylene respectively.

As is obvious from Fig. 3, the distribution coefficient of diphenylacetylene in bibenzyl for 20% of diphenylacetylene is less than unity, whereas, in the case of 30% of diphenylacetylene, the distribution coefficient

Table 2. Distribution of diphenylacetylene in bibenzyl after 45 zone passes

Distance in zone length $\left(\frac{x}{l}\equiv Z\right)$	Concentration of diphenylacetylene (wt %); initial concentration 20 wt % of diphenylacetylene	Concentration of diphenylacetylene (wt %); initial concentration, 30 wt % of diphenylacetylene
0.5	1.1	56.8
1.5	3.7	42.6
2.5	14.1	34.5
3.5	17.0	29.4
4.5	25.0	28.0
5.5	26.1	27.0
6.5	25.2	27.2
7.5	25.7	27.3
8.5	26.4	26.4
9.5	26.3	26.4
10.5	25.6	27.8

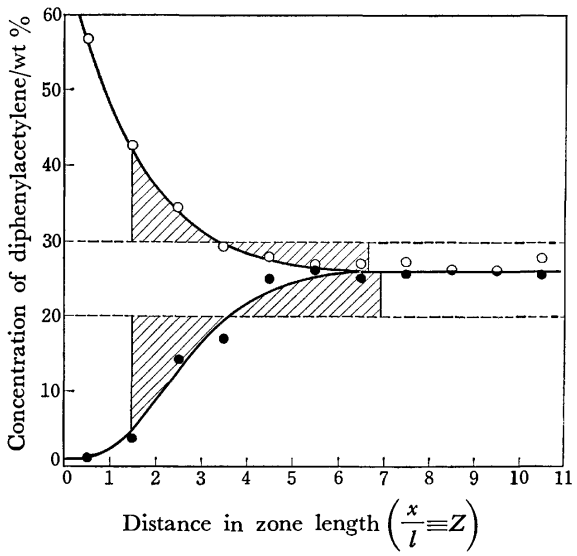

Fig. 4. Distrbution of diphenylacetylene in two samples after 45 zone passes.
●: Initial concentration: 20% of diphenylacetylene,
○: initial concentration: 30% of diphenylacetylene,
▨: the areas for calculating material balance after 45 zone passes.

is greater than unity. Such a difference in the distribution coefficients is reflected in the two distribution curves of diphenylacetylene shown in Fig. 4.

The two curves are each observed to approach a constant value gradually; this value may correspond to the composition of the minimum melting point. This phenomenon is analogous to that occurring with the fractional distillation of the azeotropic mixtures with a minimum boiling point.

A mixture with the composition of the minimum melting point must be, in principle, obtained at the end of the specimen. However, other impurities tend to concentrate at the end of the specimen; hence, the values at eight fractions from the top of the samples are adopted as the composition of the minimum melting point in both samples. Thus, we obtained the value

of 26.4% at the temperature of 43.2 °C.

The Evaluation of the Extent of Deviation from Equilibrium in the Multipass Zone Melting. Although the composition at the near end of the specimen gradually approaches the composition of the minimum melting point as a result of repeated zone passes, the compositions at the upper regions of the specimens (left part in Fig. 4) seem to become not necessarily equal to the compositions estimated from the phase diagram, depending upon the extent of devaition from equilibrium, which mainly varies with the zone-travel rate.

As is well known, the solute distribution between the solid and liquid phases in a non-equilibrium state is indicated by the effective distribution coefficient. Hence, the extent of the deviation from equilibrium in multipass zone-melting experiments will be discussed by estimating the effective distribution coefficients by means of Herington's method, which will, in the present case, be employed in the reverse of its original purpose so as to calculate the distribution coefficients from the observed distribution curve.

The boundary condition in Eq. 43 must be determined from the viewpoint of the material balance. The values of the Z and $n+1$ in Eq. 43 should be chosen so as to equalize the shaded areas divided into two portions across the lines indicating the initial concentrations for the two curves in Fig. 4. In the present case, the value of d is determined for convenience as unity, for the samples were cut into fractions equal to one zone length. Then, Eq. 43 is rewritten as follows:

$$C\{Z+(n+1)\} = C(Z+n)\exp\{B_1(Z+n)\}. \quad (44)$$

It is obvious from Fig. 4 that the numerical value of Z was defined as 1.5 for both curves. Therefore, $(n+1)$ equals 6 for both the lower and upper curves in Fig. 4. By substituting successively into Eq. 44 the values obtained from the curves in Fig. 4, the respective value of B_1 is calculated. The effective distribution coefficient is calculated by substituting the value obtained above into B_1 in Eq. 40; of course, the k_1 in Eq. 40 should be replaced by the k_e, symbolizing the effective distribution coefficient.

From the resulting effective distribution coefficient, the solute concentration in the liquid phase, C_1, is obtained by the definition of the distribution coefficient, *i.e.*, $k_e=C_s/C_1$, in which C_s is identical with $C(Z+n)$ in Eq. 44.

The results thus obtained are presented in Table 3. The relation between the solid and liquid phases is also shown, together with the results from DSC in Fig. 3, so as to indicate clearly the deviation from equilibrium.

It is revealed that the magnitude of deviation from equilibrium is fairly slight. This is, of course, a fact that does not commonly appear, but it is valid for this experiment. As one reason for such a slight departure from equilibrium, it may be considered that the difference between the melting and freezing temperatures is quite small in this system, as is shown in Fig. 3. Indeed, in the naphthalene–2-naphthol system, the difference between the melting and freezing temperatures is larger than that in the bibenzyl–diphenylacetylene system. Hence, it is shown by Herington's theory that the deviation from equilibrium is fairly great†, in contrast to the result in this work.

Table 3. The effective distribution coefficient and composition of diphenylacetylene in the liquid phase, as obtained by Herington's theory

Distance in zone length $\left(\frac{x}{l}\equiv Z\right)$	Composition of the solid phase (wt %)	Effective distribution coefficient	Composition of the liquid phase (wt %)
Initial concentration, 20 wt % of diphenylacetylene			
1.5	5	0.61	8.2
2.5	12.7	0.81	15.7
3.5	19.5	0.91	21.4
4.5	23.5	0.96	24.5
5.5	25.4	0.99	25.7
Initial concentration, 30 wt % of diphenylacetylene			
Distance in zone length $\left(\frac{x}{l}\equiv Z\right)$	Composition of the solid phase (wt %)	Effective distribution coefficient	Composition of the liquid phase (wt %)
1.5	41.4	1.10	37.6
2.5	33.8	1.07	31.5
3.5	29.7	1.04	28.5
4.5	27.4	1.04	26.3
5.5	26.4	1.01	26.1

Although, in the calculation of the corrected fraction melted, the theoretical ground is still obscure for replacing the total peak area by the area for the vertex of the peak, Eq. 20 has proved of great value as a means of determining precisely the melting and freezing temperatures in DSC, especially in the case of a peak too broad or even a noisy one.

The determination of the composition of the minimum melting point through the multipass zone-melting experiments would be applicable not only to organic systems, but also to inorganic and metallic systems, though an analytical technique must be utilized for determining the components precisely.

Conclusion

The behavior of diphenylacetylene in bibenzyl during zone melting can be well related to the phase diagram with the aid of Herington's theory. This, in other words, suggests the validity of the obtained phase diagram.

The authors wish to thank Professor Masaru Inagaki, of Meiji University, and Professor Sohachiro Hayakawa, of the Tokyo Institute of Technology, for their valuable advice.

References

1) E. F. G. Herington, "Zone Melting of Organic Compounds," Blackwell Scientific Publications, Oxford (1963),

† Evaluated by the use of the data in a previous paper.[9]

pp. 100—125.
2) M. J. Joncich and D. R. Bailey, *Anal. Chem.*, **32**, 1578 (1960).
3) G. Bradley and J. K. Marsh, *J. Chem. Soc.*, **1933**, 650.
4) A. Kofler, *Monatsh. Chem.*, **86**, 301 (1955).
5) "International Critical Tables," McGraw-Hill Book Co., New York (1928), Vol. 4, p. 163.
6) H. Schildknecht, "Zone Melting," Academic Press, New York (1966), pp. 4—12.
7) A. I. Kitaigorodskii, "Organic Chemical Crystallography," Consultants Bureau Enterprises, New York (1961), pp. 231—240.
8) W. G. Pfann, "Zone Melting," John Wiley & Sons, New York (1959), pp. 40—45.
9) H. Nojima, *Nippon Kagaku Zasshi*, **91**, 810 (1970).
10) T. Ozawa, *Netsusokutei*, **4**, 45 (1977).
11) E. M. Barrall, II, and J. F. Johonson, "Purification of Inorganic and Organic Materials," ed by M. Zief, Marcel Dekker, New York (1969), pp. 77—100.
12) Y. Otsubo, *Netsusokutei*, **1**, 107 (1974).
13) C. Plato and A. R. Glasgow, Jr., *Anal. Chem.*, **41**, 330 (1969).

Kinetic Studies of Co(II)-Malonate, Malate, and Glycolate Complex-formation Reactions in Aqueous Solutions by the Pressure-shock Method

Shoji HARADA, Masuo KAWASAWA, and Tatsuya YASUNAGA*

Department of Chemistry, Faculty of Science, Hiroshima University, 1-1 Higashisenda-machi, Hiroshima 730

(Received August 14, 1979)

A pressure-shock apparatus applicable for the kinetic studies of rapid reactions in solution was constructed and used to study Co(II)–carboxylate complex-formation reactions. The chelate complex-formation reaction was interpreted in terms of a step-by-step mechanism, and the rate constants were obtained. The chelate-ring closing-and-opening process was revealed to be the rate-determining step.

For the model of the complex formation of bidentate ligands, a step-by-step mechanism has been proposed. When the complex is stable as a chelate complex, the rate-determining step has been assigned to either the first-bond formation-and-dissociation process[1–6] or the chelate-ring closing-and-opening process.[7–9] The purpose of the present work is to examine these assignments for the Co(II)–bidentate carboxylate complex-formation reactions. Although the equilibrium properties of the cobalt(II) carboxylates have been well studied,[10] few kinetic studies have been carried out.[11] The reason may be that the reaction of cobalt(II) ion with ligand is too fast to be studied by conventional techniques.

Another purpose is to test the applicabilities of our newly constructed pressure-shock apparatus. Even though the pressure-jump method[12] is one of the most useful techniques for the kinetic studies of very rapid reactions in solution, applications of this method have been limited to reactions with relaxation times greater than 100 μs. This disadvantageous time constant has been improved by at least one order of magnitude by the pressure-shock method.[13–15]

Experimental

Apparatus. The pressure-shock apparatus constructed was a modification of that described by Platz and Hoffmann.[15] A schematic diagram is shown in Fig. 1. The experimental procedure is as follows. Nitrogen gas of 20 atm is introduced into the low pressure chamber (G). Next, the high-pressure N_2 gas is introduced into chamber (D). The increase of the pressure in chamber (D) bursts or shears out the metal diaphragm (E) at a definite pressure. The pressure-change takes at least 50 μs. While the pressure wave propagates in the low-pressure gas in (G) and in the transmitting liquid (ethanol) (H), the wave front is sharpened and becomes a shock wave.[16] The shock wave is reflected at the bottom of the sample cell (K) and propagates back through the liquid, and an expansion wave is generated at the surface of the liquid; the latter wave cancels the exerted pressure. As a result, the pressure in the sample cell continues to be high until the shock-front returns to the sample cell. The duration of the high-pressure pulse can be varied by changing the liquid level. The relaxation effect was detected conductometrically by a high-frequency bridge of 1.2 MHz. From the pressure-shock trace obtained for a $MnSO_4$ solution, which exhibits a relaxation effect faster than 1 μs (Fig. 2a), the time constant of the present apparatus was determined to be less than 4 μs. The features of the pressure pulses for the $MnSO_4$ solution and the Co(II)–malonate system are shown in Figs. 2b and 2c respectively. The temperature of the cell was controlled at 25.0±0.3 °C by circulating thermostated water through a copper tube spiraled around the shock tube and the cell.

Higher-pressure shock waves can be obtained by increasing the burst pressure by using a thicker metal diaphragm or by the use of lower-molecular-weight gas in the high-pressure chamber and higher-molecular-weight gas in the low-pressure chamber.[16] Following the latter idea, we tried H_2 gas in the high-pressure chamber and obtained a pressure pulse several times larger than that obtained when N_2 gas was used. In the present experiments, however, N_2 gas was used throughout the measurements since H_2 gas is explosive and the advantage was not so remarkable.

Materials. Wako reagent-grade chemicals were used. Stock solutions of cobalt(II) carboxylates were prepared in the same way as those of nickel(II) carboxylates.[4–6] By

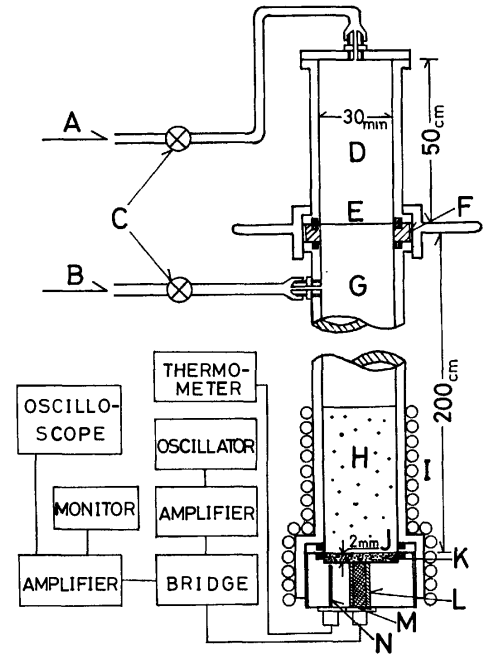

Fig. 1. The schematic diagram of the pressure-shock apparatus.
(A): High-pressure gas inlet, (B): low-pressure gas inlet, (C): electric solenoid valve, (D): high-pressure gas chamber, (E): metal diaphragm, (F): cutter, (G): low-pressure gas chamber, (H): transmitting liquid (ethanol), (I): thermostat tube, (J): polyethylene membrane, (K): sample cell, (L): insulator, (M): electrode, (N): thermistor.

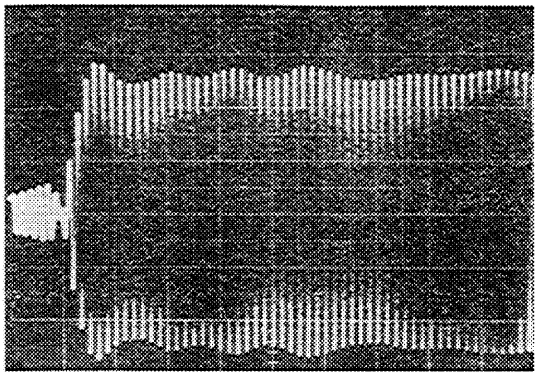

Fig. 2a. Pressure-shock trace obtained for 5×10^{-3} M $MnSO_4$ solution.
Sweep: 5 μs/div.

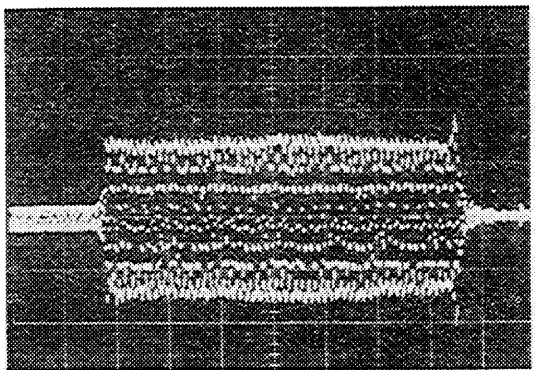

Fig. 2b. Whole features of the pressure-shock pulse.
Sample: 5×10^{-3} M $MnSO_4$, sweep: 200 μs/div.

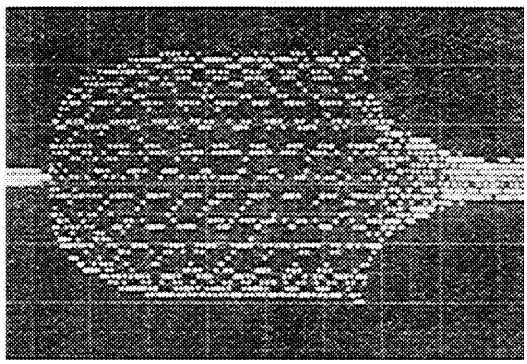

Fig. 2c. The relaxation spectra of Co(II)–malonate system.
Concentration; 1×10^{-3} M, sweep: 50 μs/div at 25 °C.

considering the hydrolysis of the cobalt(II) ion and the acid dissociation of the ligand, the proper value of the pH was determined; the pH was adjusted by the drop-by-drop addition of dilute nitric acid solution.

Results

The experimental conditions and the reciprocal relaxation times observed are shown in Table 1. The concentration dependence of the relaxation time is best explained by the following equilibria.

$$Co^{2+} + L^{n-} \underset{k_b}{\overset{K\ (k_f)}{\rightleftharpoons}} CoL^{2-n} \quad (1)$$

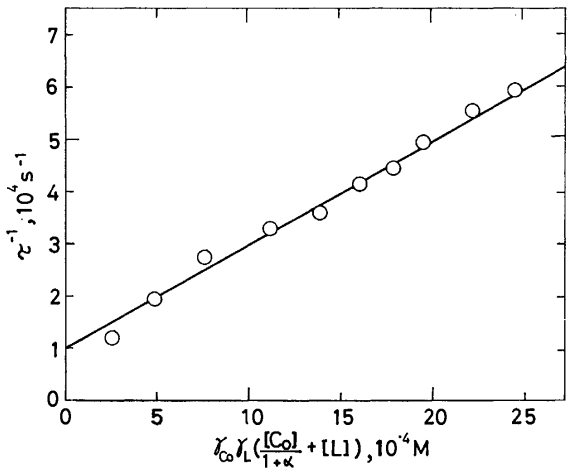

Fig. 3. τ^{-1} *vs.* $\gamma_{Co}\gamma_L\left(\frac{[Co]}{1+\alpha}+[L]\right)$ plot of Co(II)–malate system at 25 °C.

$$HL^{1-n} \rightleftharpoons H^+ + L^{n-} \quad (2)$$

($n=2$ for malonate and malate systems and 1 for glycolate system)

where L^{n-} is a dissociated ligand, HL^{1-n} is a monoprotonated ligand, CoL^{2-n} is a 1:1 complex, k_f and k_b are the rate constants, and $K(=k_f/k_b)$ is the stability constant. In the present pH ranges, the contributions of the complex formation with the monoprotonated ligand (Eq. 3):

$$Co^{2+} + HL^{1-n} \rightleftharpoons CoL^{2-n} + H^+ \quad (3)$$

to the present relaxation phenomenon was neglected. Since the protonation of the carboxyl group (Eq. 2) is much faster than the complex formation reaction (Eq. 1), the relaxation time, τ, of Eq. 1 is expressed by the equation:

$$\tau^{-1} = k_f \cdot \frac{\gamma_{Co}\cdot\gamma_L}{\gamma_{CoL^*}} \cdot \left(\frac{[Co]}{1+\alpha}+[L]\right) + k_b \frac{\gamma_{CoL}}{\gamma_{CoL^*}} \quad (4)$$

with

$$\alpha = \frac{[H]}{K_a+[L]} \quad (5)$$

where γ_i is the activity coefficient of the i-th species, the brackets indicate the concentration, the superscript $\neq$ means the activated complex, K_a is the acid dissociation constant of the (second) carboxyl group, and charges are omitted for the sake of convenience. On the assumptions that the activity coefficient of a noncharged complex is unity, $\gamma_{CoL}=\gamma_{CoL^*}$, and $\gamma_{CoL^*}=\gamma_{L^-}$, Eq. 4 is rewritten in the form:

$$\tau^{-1} = F(C)\cdot k_f + k_b \quad (6)$$

where $F(C)$ is the concentration term including the activity coefficient term. Calculations of the activity cofficients were performed using the Davies equation.[17]

Evaluation of the rate parameters was carried out as follows. First, the concentrations of the species in solution were calucalted from the stability constant, K, which is available in the literature. Then, the τ^{-1} values were plotted against $F(C)$ to give k_f and k_b from the slope and the intercept of the straight line respectively. The ratio of k_f and k_b gives a so-called kinetical-

TABLE 1. EXPERIMENTAL CONDITIONS AND τ^{-1} VALUES OF THE COBALT(II) CARBOXYLATES AT 25.0 °C

Malonate			Malate			Glycolate		
$\sum C$ a) (10^{-4} M)	pH	τ^{-1} b) (10^4 s^{-1})	$\sum C$ a) (10^{-4} M)	pH	τ^{-1} b) (10^4 s^{-1})	$\sum C$ a) (10^{-4} M)	pH	τ^{-1} b) (10^4 s^{-1})
1.5	6.43	0.9±0.3	2.0	6.56	1.2±0.1	5.0	5.75	5.4±0.2
2.0	6.49	0.9±0.1	5.0	6.55	2.0±0.1	10	5.87	5.7±0.8
5.0	6.57	2.0±0.4	10	6.49	2.7±0.2	20	5.97	7.2±0.3
7.5	6.59	2.0±0.2	20	6.39	3.3±0.2	40	6.07	8.1±0.6
10	6.60	2.5±0.2	30	6.54	3.6±0.3	60	6.14	9.0±0.7
20	6.60	3.3±0.3	40	6.50	4.2±0.4	80	6.16	10.3±0.7
40	6.51	4.4±0.9	50	6.59	4.4±0.3	100	6.17	11.5±0.9
60	6.45	4.6±0.2	60	6.56	5.0±0.3			
80	6.39	5.2±0.6	80	6.29	5.6±0.2			
100	6.37	6.0±1.6	100	6.40	6.0±0.4			

a) Overall concentration of the Cobalt(II) carboxylates. b) Mean value of at least seven experiments.

TABLE 2. RATE AND EQUILIBRIUM CONSTANTS OF Co(II) COMPLEX-FORMATION REACTION (I) AT 25 °C AND $\mu \to 0$

Ligand	Molonate	Malate	Glycolate
k_f, M^{-1} s^{-1}	$2.7(\pm0.1)\times10^7$	$2.1(\pm0.1)\times10^7$	$6.0(\pm0.3)\times10^6$
k_b, s^{-1}	$6.1(\pm2.5)\times10^3$	$8.9(\pm1.5)\times10^3$	$4.6(\pm0.3)\times10^4$
log K	3.6(±0.3)	3.4(±0.1)	2.1(±0.1)
log K a)	3.60[18]	3.00[18]	1.96[19]

a) Literature value.

ly determined K which should coincide with the foregoing K value used for the calculation of $F(C)$. If they did not coincide, the kinetically obtained K was used for the calculation of $F(C)$ and the τ^{-1} *vs.* $F(C)$ plot was again drawn. The above procedures were repeated until a self-consistent K value was obtained. The final plot of the Co(II)–malate system is shown in Fig. 3 as an example. The values of k_f, k_b, and K are listed in Table 2, along with the literature value of K.[18,19] The values of K obtained kinetically are in satisfactory agreement with those in the literature.

Discussion

The ligands used in the present experiment are known to make stable chelate complexes with cobalt(II) ion. The chelate complex-formation reaction is represented by the following step-by-step mechanism,

$$\underset{\text{(I)}}{\text{Co} + \text{L}} \underset{k_{-0}}{\overset{K_0}{\rightleftharpoons}} \underset{\text{(II)}}{\text{Co}\,\text{O}^{\text{H}}_{\text{H}}\,\text{L}} \underset{k_{-1}}{\overset{K_1}{\rightleftharpoons}} \underset{\text{(III)}}{\text{Co-L}} \underset{k_{-2}}{\overset{K_2}{\rightleftharpoons}} \underset{\text{(IV)}}{\text{Co=L}} \qquad (7)$$

where (I) represents free ions; (II), an ion-pair; (III), a monodentate complex; and (IV), a chelate complex.

Kinetic studies of the chelate-complex formation of bidentate carboxylates have been widely carried out for the nickel(II) complexes. In these studies, the rate-determining step of the complex formation has been ascribed to either the first-bond formation-and-dissociation process, (II)⇌(III),[1–6] or the chelate-ring closing-and-opening process, (III)⇌(IV).[7–9] In the former concept, the following problems remain unsolved. The values of k_1 obtained from the assumed equation $k_f = k_0 \cdot k_1$, have been regarded as equal to the water-exchange rate constant of the metal ion, k_{H_2O}.[20] However, the consistency has not been necessarily satisfactory, and the k_1's have occasionally been one order of magnitude smaller than k_{H_2O}. Also, even if $k_1 = k_{H_2O}$ could be satisfied, the assumption that $k_2 \gg k_1$ is dubious, because the water-substitution process is also involved in the chelate-ring-closing step, and k_2 cannot exceed k_{H_2O} ($=k_1$). The above reasons led us to adopt the second concept in the present study.

On the assumption that the intermediate species, (II) and (III), are in a steady state, the rate constants in Eq. 7 are related to the overall rate constants, k_f and k_b, by the following equations:

$$k_f = K_0 k_1 \left(\frac{k_2}{k_2 + k_{-1}}\right) \qquad (8)$$

$$k_b = k_{-2}\left(\frac{k_{-1}}{k_2 + k_{-1}}\right). \qquad (9)$$

The equilibrium and kinetic parameters in these equations were evaluated as follows.

K_0 was estimated theoretically by the Fuoss equation:[21]

$$K_0 = \frac{4\pi N a^3}{3000} \cdot e^{-U(a)/kT} \qquad (10)$$

were N is Avogadro's number, a is the distance of the closest approach of two ions, which was assumed to be 8 Å,[22] and $U(a)$ is a Coulomb-energy term. K_0 at $\mu \to 0$ was calculated to be 46 M^{-1} for the malonate and malate systems and 7.7 M^{-1} for the glycolate system.

The value of k_1 was assumed to be equal to that of the k_{H_2O} of the cobalt(II) ion, *i.e.*, $k_{H_2O} = 2.6 \times 10^6$

s^{-1}.[23] This assumption may be made because, in many monodentate complex-formation reactions, the rate-determining step has been revealed to be a water-dissociation process from the coordination site of the metal ion, irrespective of the entering ligand.

The value of k_{-1} was estimated from the pK_a value of the ligand. In the kinetic studies of the complex formation reactions of nickel(II) dicarboxylates, Hoffmann has estimated the k_{-1} value from the following experimental relationship between log k_{-1} and pK_a for each of the ligands:[7-9]

$$\log k_{-1} = -0.22\,pK_a + A \quad (A=\text{constant}). \tag{11}$$

Unfortunately, however, the same relationship has not been established for the cobalt(II) complexes because of the lack of the kinetic data. Thus, in the present case, the k_{-1} of the Co(II)–acetate system was estimated first. Since acetate makes only monodentate complexes, and a reliable stability constant is given in the literature, the k_{-1} can be estimated. First, the stability constant, K, of the acetate complex is related to the equilibrium and rate constants of each step by the equation:

$$K = K_0\,(1+K_1) = K_0\left(1+\frac{k_1}{k_{-1}}\right) \tag{12}$$

where K_0, K_1, k_1, and k_{-1} are the same as in Eq. 7. By employing the values of $K=10^{1.29}\,M^{-1}$,[19] $K_0=7.7\,M^{-1}$, and $k_1=2.6\times10^6\,s^{-1}$, the k_{-1} of the acetate system ($pK_a=4.75$) was calculated to be $1.7\times10^6\,s^{-1}$. Then, applying Eq. 11 to the Co(II)–carboxylate system, the k_{-1} value of each system was estimated from the value of the pK_a of the ligand; *i.e.*, by the use of the values for the acetate system, we obtain:

$$\log (k_{-1}/1.7\times10^6) = -0.22\,(pK_a-4.75). \tag{13}$$

The calculated values of k_{-1} and $K_1(=k_1/k_{-1})$ are listed in Table 3, together with the pK_a values. By the use of the values of K_0, k_1, k_{-1}, k_f, and k_b, the values of k_2 and k_{-2} were calculated by Eqs. 8 and 9; these results are also listed in Table 3.

By comparing the values of the equilibrium and the rate parameters in Tables 2 and 3, we can deduce the following:

(1) The complex is stable as a chelate complex rather than as a monodentate complex or an ion-pair.

(2) The chelate-ring closing and opening reactions are the rate-determining processes of the complex formation and dissociation reactions respectively.

(3) The stability of the malonate complex relative to the others is due to the fact that it has the slowest rate of chelate-ring opening (k_{-2}). The malonate system has once been studied kinetically by the temperature-jump method.[11] Compared with the temperature-jump data, the k_f value of the present work is three times larger, while the k_b value is two times smaller. These inconsistencies may be ascribed to the differences in either the experimental conditions, *e.g.*, the ionic strength, or the stability constants used for the caluclations.

(4) The glycolate complex is one order of magnitude less stable than the others. This is explained by the natures of the ligands, *i.e.*, the electrostatic charge (reflected by K_0), the acidity of the carboxyl group (K_1), and the chelating groups (K_2). From the kinetic standpoint, the fastest chelate-ring-closing rate indicates that a five-membered chelate complex is preferable to the complex formation, while the very rapid chelate-ring-opening rate is due to a weak coordination of a hydroxyl group in comparison with the carboxyl group.

In the malate system, both the equilibrium and the kinetic parameters were close to the corresponding values of the malonate system, even though some differences had been expected from the structural differences of these ligands. Further details of the malate complex formation may be revealed by additional experiments on analogous ligand systems, *e.g.*, β-hydroxypropionate or succinate systems.

Table 3. Equilibrium and rate constants of the step-by-step complex-formation reaction (7) of Co(II) carboxylate at 25 °C and $\mu\to0$

Ligand	Malonate	Malate	Glycolate
pK_a of acid[a]	5.69	5.11	3.83
K_0, M^{-1}	46	46	7.7
K_1	2.4	1.8	1.0
K_2	40	28	17
k_1, s^{-1}	2.6×10^6	2.6×10^6	2.6×10^6
k_{-1}, s^{-1}	1.1×10^6	1.4×10^6	2.7×10^6
k_2, s^{-1}	3.2×10^5	3.0×10^5	1.2×10^6
k_{-2}, s^{-1}	7.9×10^3	1.1×10^4	6.6×10^4

a) Ref. 24.

References

1) G. H. Nancollas and N. Sutin, *Inorg. Chem.*, **3**, 360 (1964).
2) F. P. Cavasino, *J. Phys. Chem.*, **69**, 4380 (1965).
3) J. L. Bear and C. T. Lin, *J. Phys. Chem.*, **72**, 2026 (1968).
4) S. Harada, K. Amidaiji, and T. Yasunaga, *Bull. Chem. Soc. Jpn.*, **45**, 1752 (1972).
5) S. Harada, H. Tanabe, and T. Yasunaga, *Bull. Chem. Soc. Jpn.*, **46**, 3125 (1973).
6) S. Harada, Y. Okuue, H. Kan, and T. Yasunaga, *Bull. Chem. Soc. Jpn.*, **47**, 769 (1974).
7) H. Hoffman and U. Nickel, *Ber. Bunsenges. Phys. Chem.*, **72**, 1096 (1968).
8) H. Hoffmann, *Ber. Bunsenges. Phys. Chem.*, **73**, 432 (1969).
9) U. Nickel, H. Hoffmann, and W. Jaenicke, *Ber. Bunsenges. Phys. Chem.*, **72**, 526 (1968).
10) "Stability Constants of Metal-Ion Complexes," Supplement No. 1, Special Publication No. 25, ed by L. G. Sillen and A. E. Martell, The Chemical Society, London (1971).
11) F. P. Cavasino, *Rec. Sci. Rend.*, **8**, 1120 (1965).
12) W. Knoche, "Pressure-Jump Methods," in "Investigation of Rates and Mechanisms of Reactions," Third ed, ed by G. G. Hammes, Wiley-Interscience, New York (1973). ("Techniques of Chemistry," Vol. 6), Part I, Chap. 5, pp. 187—211.
13) A. Jost, *Ber. Bunsenges. Phys. Chem.*, **70**, 1057 (1966).
14) H. Hoffmann and E. Yeager, *Rev. Sci. Instrum.*, **39**, 1151 (1968).
15) V. G. Platz and H. Hoffmann, *Ber. Bunsenges. Phys.*

Chem., **76**, 491 (1972).
16) A. G. Gaydon and I. R. Hurle, "The Shock Tube in High-Temperature Chemical Physics," Chapman and Hall, London (1963), Chap. 2, p. 9.
17) C. W. Davies, "Ion Association," Butterworths, London (1962).
18) P. G. Manning and C. B. Monk, *Trans. Faraday. Soc.*, **57**, 1996 (1961).
19) R. G. Seys and C. B. Monk, *J. Chem. Soc.*, **1965**, 2452.
20) D. J. Hewkin and R. H. Prince, *Coord. Chem. Rev.*, **5**, 45 (1970).
21) R. M. Fuoss, *J. Am. Chem. Soc.*, **80**, 5059 (1958).
22) K. Kustin and J. L. McClean, *J. Phys. Chem.*, **82**, 2549 (1978).
23) A. H. Zeltmann, N. A. Matwiyoff, and L. O. Morgan, *J. Phys. Chem.*, **73**, 2689 (1969).
24) "Stability Constants of Metal-Ion Complexes," Special Publication No. 17, ed by L. G. Sillen and A. E. Martell, The Chemical Society, London (1964).

© The Chemical Society of Japan NOTES Bull. Chem. Soc. Jpn., 53, 2079—2080 (1980)

Isotope Effect of the Glass Transition Temperature of Aqueous Solution. LiCl and $ZnCl_2$ Solutions in Water and D_2O

Hitoshi KANNO,* Ichimin SHIROTANI,† and Shigeru MINOMURA†

Department of Chemistry, Meisei University, Hino, Tokyo 191

† *The Institute for Solid State Physics, The University of Tokyo, Roppongi, Minatoku, Tokyo 106*

(Received November 19, 1979)

Synopsis. Glass transition temperatures of the LiCl and $ZnCl_2$ solutions in both water and D_2O were measured as a function of the concentration of the salt. The composition dependence of isotope effect is briefly discussed for these solutions.

In recent years, the glass formation of binary solution systems have been extensively studied.[1–5] It is clear from these studies that glass transition temperature (T_g) is a good parameter such as melting and boiling points to represent the thermodynamic properties of liquid systems, though it is not a fixed point and varies a little with experimental conditions (*e.g.*, cooling and heating rates) and the method by which T_g is determined. To maximize the glass transition temperature as a diagnostic tool for clearifying thermodynamic properties of supercooled liquid systems and their glassy states, it is of importance to investigate the effects of various factors affecting the magnitude of T_g.

In this note, we report the study of the T_g measurements of aqueous LiCl and $ZnCl_2$ solutions in both water and D_2O. Aqueous solutions of LiCl and $ZnCl_2$ were prepared by dissolving anhydrous LiCl and $ZnCl_2$ in either water or D_2O (E. Darmstadt, 99.8% atom D). A conventional, simple DTA system was used for the T_g measurements. The experimental arrangements were essentially the same as used by Angell and Sare[2] in their T_g measurements. Overall cooling rate during quenching a sample solution was about 2×10^3 K/min. The T_g value was obtained at a heating rate of about 5 K/min in the warmup DTA trace from liquid nitrogen temperature with using benzene as a reference material. A Teflon-covered chromel-alumel thermocouple system was used for the differential emf and temperature measurements. The accuracy of the T_g values was estimated to be ±1 °C by determinations of the melting points of ethylether, acetone and other low melting organic compounds. However, the reproducibility of T_g is better than ±0.2 °C.

The results are shown in Figs. 1 and 2. From these figures, we see that ΔT_g ($=T_g$ in D_2O-T_g in H_2O) increases almost linearly with the increase in R (=mol of water/mol of salt) in the concentration region where the T_g measurements were carried out. As there is, to authors' knowledge, no reported T_g value for glassy bulk water and D_2O, it is difficult to estimate how much ΔT_g will be in more diluted concentration region where no glass-forming is observed. However, we expect that homogeneous nucleation temperatures (T_H) of water and D_2O can be a guide for this purpose. The T_H values of water and D_2O are reported to be -38 and -33 °C at normal pressure, respectively.[6] Another possible canditate for estimating ΔT_g between glassy bulk water and D_2O is the glass transition temperatures of glassy crystals $SnCl_2\cdot2H_2O$ and $SnCl_2\cdot2D_2O$ (150 and 155 K, respectively).[7] From these results, the maximum of ΔT_g is estimated to be 5 °C

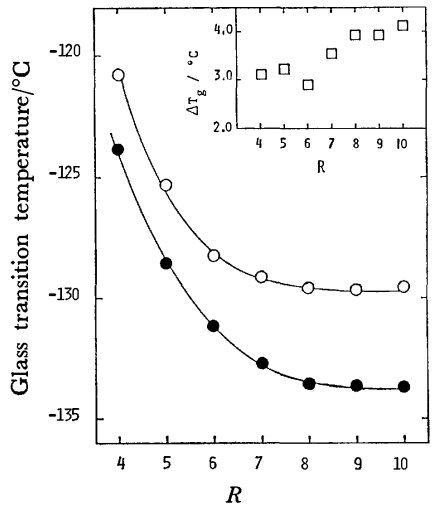

Fig. 1. Glass transition temperatures of the LiCl solutions in H_2O and D_2O.
●: T_g of the solutions in H_2O, ○: T_g of the solutions in D_2O, □: ΔT_g ($=T_g$ in D_2O-T_g in H_2O). The inset shows the variation of ΔT_g as a function of R.

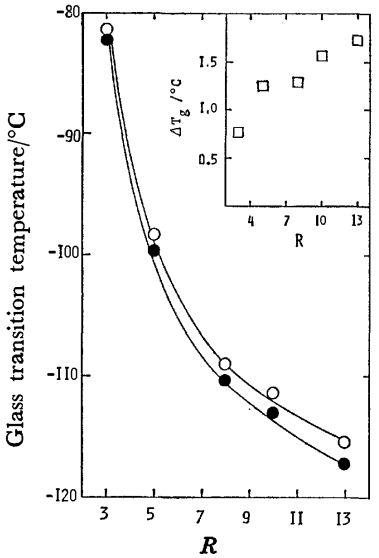

Fig. 2. Glass transition temperatures of the $ZnCl_2$ solutions in H_2O and D_2O.
●: T_g of the solutions in H_2O, ○: T_g of the solutions in D_2O, □: ΔT_g. The inset shows the variation of ΔT_g as a function of R.

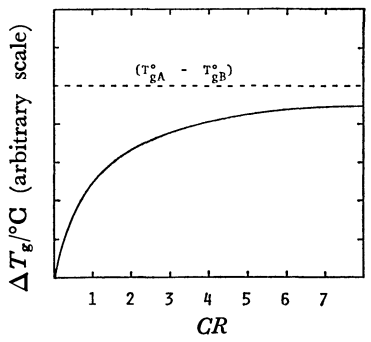

Fig. 3. Variation of ΔT_g as a function of CR.

for these aqueous solutions.

Aqueous solution is a typical non-ideal solution for which no applicable theory exists to interpret isotope effect. However, it is of interest to consider what relation exists between ΔT_g and R in a simple binary solution. An empirical equation which has proven successful in the fitting of experimental T_g data of a binary mixture is[8]

$$T_{gA}(x) = \frac{xT^0_{g1} + C(1-x)T^0_{gA}}{x + C(1-x)} \quad (1)$$

where T^0_{g1} and T^0_{gA} are the glass transition temperatures of pure components 1 and A, respectively, C is the adjustable parameter and x is the mole fraction of the component 1. If component A is replaced by the isotopic species B, we get the following relation under the assumption that C would not change for the isotopic substitution;

$$T_{gB}(x) = \frac{xT^0_{g1} + C(1-x)T^0_{gB}}{x + C(1-x)}. \quad (2)$$

From these two equations, the difference of the glass transition temperatures of the two solutions will be

$$\Delta T_g(x) = T_{gA}(x) - T_{gB}(x) = \frac{(1-x)C(T^0_{gA} - T^0_{gB})}{x + (1-x)C}$$

$$= \frac{CR(T^0_{gA} - T^0_{gB})}{1 + CR}. \quad (3)$$

When $CR \ll 1$, Eq. 3 can be approximated to be

$$\Delta T_g(R) \simeq CR(T^0_{gA} - T^0_{gB}) \quad (4)$$

and when $CR \gg 1$, we get

$$\Delta T_g(R) \simeq (T^0_{gA} - T^0_{gB}). \quad (5)$$

The variation of $\Delta T_g(R)$ is shown in Fig. 3 as a function of the variable CR. It is interesting to apply Eq. 3 to the LiCl and $ZnCl_2$ solutions, though there is some ambiguity about the applicability of Eq. 3 to aqueous solutions. Assuming that $(T^0_{gA} - T^0_{gB})$ is 5 °C, the calculations give $C = 0.4 \pm 0.1$ for the LiCl solution and $C = 0.05 \pm 0.01$ for the $ZnCl_2$ solution. The C value should be 1 in an ideal solution. From these values, it may be said that the non-ideality of the solution is larger for the $ZnCl_2$ solution than for the LiCl solution.

This work was supported by a Research Assistantship (to H. K.) from the Nishina Memorial Foundation.

References

1) E. Thilo, C. Wiecker, and W. Wiecker, *Silikattechnik*, **15**, 109 (1964).
2) C. A. Angell and E. J. Sare, *J. Chem. Phys.*, **52**, 1058 (1970).
3) A. V. Lesikar, *Phys. Chem. Glasses*, **16**, 83 (1975).
4) A. V. Lesikar, *J. Chem. Phys.*, **63**, 2297 (1975); **66**, 4263 (1977); **68**, 3323 (1978).
5) C. A. Angell, J. M. Sare, and E. J. Sare, *J. Phys. Chem.*, **82**, 2622 (1978).
6) D. H. Rasmussen, A. P. MacKenzie, C. A. Angell, and J. C. Tucker, *Science*, **181**, 342 (1973); C. A. Angell and H. Kanno, unpublished data (−33 °C for D_2O emulsion).
7) H. Suga and S. Seki, *J. Non-Cryst. Solids*, **16**, 171 (1974).
8) J. M. Gordon, G. B. Rouse, J. H. Gibbs, and W. M. Risen, *J. Chem. Phys.*, **66**, 4971 (1977).

The Fifth Overtone Spectra of Aryl C–H Stretching Vibrations in $C_6H_5CH_{3-n}Cl_n$

Yoshihiro MIZUGAI and Mikio KATAYAMA*

Department of Pure and Applied Sciences, College of General Education, The University of Tokyo, Meguro-ku, Tokyo 153

(Received December 11, 1979)

Synopsis. The fifth overtone frequencies of the aryl C–H vibration of $C_6H_5CH_{3-n}Cl_n$ were observed by means of the thermal-lens technique. The shifts of their vibrational frequencies from that of benzene were found to be proportional to the inductive contribution of the Hammett σ, thus supplying information on the reactivity of the chemical bond.

Since the development of dye lasers, the opto-acoustic and thermal-lens techniques have been powerful methods for studying overtone spectroscopy in polyatomic molecules, where high vibrational levels are excited by means of very weak single photon absorption rather than by multiphoton absorption.[1,2] The experimental study of highly excited vibrational transitions in the ground electronic state offers valuable information on the photodissociation and radiationless transitions of molecules.

In the present article we wish to report our observation of the fifth ($\Delta v_{CH}=6$) overtones of the aryl C–H stretching vibrations of toluene and its chlorinated derivatives, $C_6H_5CH_{3-n}Cl_n$ ($n=0,1,2,3$), in the liquid state. The spectra of the fundamental vibrations, which are mainly attributable to the oscillation of the aryl C–H bond, show relatively complicated structures, and it is difficult to deduce the properties of their C–H bonds from the differences in the fundamental vibrational spectra. However, in their fifth C–H overtone spectra, single broad bands with a bandwidth of about 300 cm^{-1} are observed. The frequencies of their band centers exhibit systematic differences, demonstrating that the change in the electronic properties of $CH_{3-n}Cl_n$ ($n=0,1,2,3$) groups gives rise to the variation in the nature of the aromatic C–H bonds.

The measurements of the C–H overtone spectra were performed by means of the thermal-lens technique. A flashlamp pumped dye laser (Chromatix CMX-4) was used for the exciting light source, and a He–Ne laser with an average power output of 5 mW was operated in the TEM_{00} mode. We can measure the absorption of the exciting laser by observing the decrease in the transmission of the He–Ne laser through the pinhole which is put after the absorption cell. The thermal blooming of the He–Ne laser was observed by means of photodiode.

TABLE 1. THE FIFTH OVERTONE SPECTRA OF ARYL C–H STRETCHING VIBRATIONS IN $C_6H_5CH_{3-n}Cl_n$ ($n=0,1,2,3$) MOLECULES; THE FREQUENCIES, THE SHIFTS FROM THAT OF BENZENE, AND THE LINE WIDTHS

Molecule	Frequency	Shift	Width(fwhm)
$C_6H_5CH_3$	16460 cm^{-1}	−15 cm^{-1}	275 cm^{-1}
C_6H_6	16475	0	235
$C_6H_5CH_2Cl$	16490	+15	270
$C_6H_5CHCl_2$	16520	+45	280
$C_6H_5CCl_3$	16555	+80	310

The observed results for $C_6H_5CH_{3-n}Cl_n$ ($n=0,1,2,3$) and benzene are listed in Table 1. As is shown in this table, the frequencies of the fifth C–H overtone increase with the number of substituted chlorine atoms in the CH_3 group. The aryl C–H overtone of toluene is on the lower side of benzene, while those of the chlorine substituted molecules are at higher frequencies than that of benzene.

It has been found that the frequencies of the overtone spectra are represented quite adequately by this simple two-parameter equation:

$$G_{v,0} = v(A+vB) \quad (1)$$

where A and B are the constants and where v is the vibrational quantum number. At least for high-frequency modes, the experimental results can well be described as corresponding to the excitation of localized modes of vibration rather than a set of symmetry-allowed combination of anharmonic normal modes.[3-5] Thus, it can be understood that the frequencies of the higher overtone of molecular vibrations can give information on the nature of individual isolated chemical bonds.

The overtone spectra of the aryl C–H stretching vibrations of $\Delta v=2$—5 for toluene and α,α,α-trichlorotoluene could be observed by means of a Cary 14 spectrophotometer, but not those of their fifth overtone spectra ($\Delta v=6$). Both the frequencies of the fifth overtone as measured by the thermal-lens technique and the overtone spectra of $\Delta v=2$—5 obtained by the conventional method can be well expressed by the following equations:

$$G_{v,0} = 3094v - 59v^2 \quad \text{for toluene} \quad (2)$$

$$G_{v,0} = 3113v - 58.5v^2 \quad \text{for } \alpha,\alpha,\alpha\text{-trichlorotoluene} \quad (3)$$

where $G_{v,0}$ is expressed in cm^{-1}. On the other hand, the overtone spectra of benzene are represented by:[5]

$$G_{v,0} = 3095v - 58.4v^2. \quad (4)$$

The second terms in these equations, *i.e.*, the B constants in the above three equations, are almost the same. Therefore, it would be reasonable to assume that the B constants in Eq. 1 are the same in benzene and $C_6H_5CH_{3-n}Cl_n$ ($n=0,1,2,3$). Thus, the increase in the number of the substituted Cl atoms in the CH_3 group gives rise to a slight increase in the A constant of Eq. 1, indicating that the strength of the aryl C–H bonds increases with the number of substituted Cl atoms. The experimental results show that the fifth-overtone frequency of $C_6H_5CCl_3$ is the highest and that of $C_6H_5CH_3$ is the lowest, demonstrating that the strength of the local mode of the aryl C–H stretching

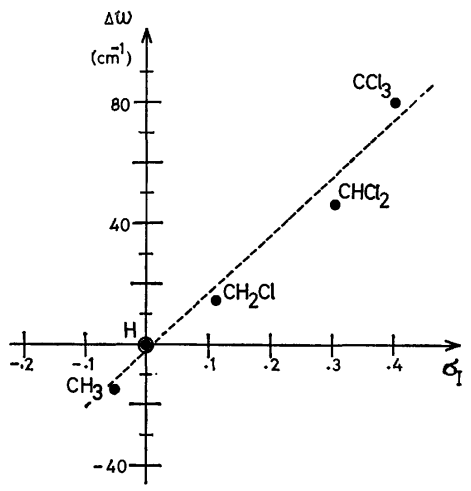

Fig. 1. The relation between the frequencies of the fifth overtone spectra of aryl C–H stretching vibration and the values of σ_I, the inductive contribution in Hammett σ, in $C_6H_5CH_{3-n}Cl_n$(n=0,1,2,3) molecules.

vibration in $C_6H_5CCl_3$ is the strongest among the four molecules of $C_6H_5CH_{3-n}Cl_n$ (n=0,1,2,3) and the benzene molecule. It was also found that the shifts of the fifth-overtone frequencies from that of benzene are proportional to the σ_I values of Hammett, as is shown in Fig. 1.[6] Therefore, the shifts of the frequencies of the higher-overtone spectra provide quantitative measures of the inductive contribution of the Hammett σ, supplying information on the chemical reactivity of a certain bond. This is because the highly excited vibration is well represented by the local mode, *i.e.*, the vibrational mode of an individual isolated bond. Therefore, the nature of its chemical bond is appropriately represented by the frequency of its higher-overtone vibration.

It should be noted that the linewidths of the fifth C–H overtone of $C_6H_5CH_{3-n}Cl_n$ are wider than that of benzene. This is brought about by the fact that the $C_6H_5CH_{3-n}Cl_n$ molecules have non-equivalent aryl C–H local modes with slightly different vibrational frequencies. Although it is desirable to observe the overtone frequencies in the gas phase for the more accurate measurement of their center frequencies, the power output of our laser is not large enough for us to obtain a good signal for the gas phase. Nevertheless, the liquid-state spectra may be expected to provide reliable information on the band center of the overtones.

This work was partly supported by a Grant-in-Aid from the Ministry of Education, Science and Culture. The authors would like to thank Dr. Hiroshi Morita, who allowed us to use the Cary 14 spectrophotometer.

References

1) C. K. N. Patel and A. C. Tam, *Chem. Phys. Lett.*, **62**, 511 (1979).
2) M. E. Long, R. L. Swofford, and A. C. Albrecht, *Science*, **191**, 183 (1976).
3) B. R. Henry and W. Siebrand, *J. Chem. Phys.*, **49**, 5369 (1968).
4) R. J. Hayward and B. R. Henry, *J. Mol. Spectrsc.*, **57**, 221 (1975).
5) R. L. Swofford, M. E. Long, and A. C. Albrecht, *J. Chem. Phys.*, **65**, 179 (1976).
6) O. Exner, "Advances in Linear Free Energy Relationship," Plenum, New York (1972), p. 37.

ESR Spectra of Mn(II) Ions in Reversed Micellar Systems

Manabu Senō,* Kiyoshi Sawada, Koji Araki, Hideo Kise, and Kazutoshi Iwamoto

Institute of Industrial Science, The University of Tokyo, 7-22 Roppongi, Minato-ku, Tokyo 106

(Received January 12, 1980)

Synopsis. ESR spectra of hexaaqua complex of Mn(II) in a hexadecyltrimethylammonium bromide (HTAB)/chloroform reversed micellar system are studied. The structure of the Mn(II) complex is distorted at low water concentrations because of the dehydration due to the lack of water molecules available for the complexes. The effect of dehydration of metal ions on their catalysis for ATP hydrolysis is discussed.

In our previous papers,[1,2] we have attempted to characterize the water in reversed micellar systems primarily by near infrared spectra and nuclear magnetic resonance spectra. The water in micelle cores is less polar[1] and more strongly immobilized[2] than the ordinary bulk water. A great deal of investigation has been made on the catalytic effects of reversed micellar systems.[3] For instance, the hydrolysis of adenosine 5′-triphosphate (ATP) is greatly enhanced with metal ions in a dodecylammonium propionate (DAP)–water–hexane system.[1] In this paper, we intend to clarify the relationship between the nature of water in and the catalytic effect of reversed micelles by the ESR measurement of Mn(II) ions.

The ESR line width of Mn(II) ions in aqueous solutions has been studied by several workers. The relaxation of the ESR spectrum has been interpreted in terms of several mechanisms; Garrett and Morgan[4] proposed that the relaxation is principally due to solvent fluctuation around the solvated ions, and that at high temperatures the solvent-ligand exchange effect is not negligible in determining the ESR line width. The relaxation due to the spin-spin interaction is neglected in Mn(II) solutions of concentrations lower than 0.01 mol dm^{-3}.[5] Therefore, if suitable conditions are chosen, the effect of spin-spin interaction and solvent-ligand exchange could be neglected in order to examine exclusively the effect of distortion of the solvent coordinated to metal ions. Thus, the ESR spectra of Mn(II) ions solubilized in the water pools of reversed micelles are expected to give valuable information on the nature of the water.

Experimental

ESR spectra at X band (9.4 GHz) were measured on a JEOL model JES-ME 3X spectrometer at a room temperature (22 °C±1 °C). Analytical grade $MnCl_2 \cdot 4H_2O$ was used without further purification. The purification of hexadecyltrimethylammonium bromide (HTAB), hexadecyltrimethylammonium chloride (HTAC), and chloroform was described previously.[2] Reversed micellar solutions were prepared according to the procedure in the literature.[6]

Results and Discussion

The forth line ($m_I=+1/2$) of the ESR spectrum of Mn(II), which has six hyperfine lines, is the most suitable for line width measurements, since it is least affected by imhomogeneous broadening.[7] Figure 1 shows the line widths of Mn(II) in aqueous solutions and HTAB/chloroform reversed micellar solutions as a function of concentration of $MnCl_2$. As the Mn(II) ions hardly exist in the chloroform phase, the line widths for both systems are reasonably compared to each other at the same ratio of $[Mn(II)]/[H_2O]$. It is estimated in these systems that 0.2 mol dm^{-3} of $MnCl_2$ corresponds to 125 of the ratio of [HTAB]/[Mn(II)] and at most one Mn(II) ion per micelle by considering the aggregation number of HTAB. Therefore, the broadening arising from the spin-spin interaction is almost negligible below this concentration. The observed ESR parametres of hyperfine coupling constant (A) and line width (ΔH) in the reversed micellar system (A=9.2 mT and ΔH=4.0 mT) are similar to those of $[Mn(H_2O)_6]^{2+}$ (A=9.2 mT and ΔH=3.07 mT)[8] and not to those of $[MnCl_4]^{2-}$ (A=7.9 mT and ΔH=0.96 mT) nor $[MnBr_4]^{2-}$ (A=7.5 mT and ΔH=8.0 mT).[8] Moreover, no spectral change was observed in HTAC compared to HTAB system, excluding the possible halogen coordination. Consequently, the ESR line broadening of hexaaquamanganese(II) complex in the reversed micellar system under consideration is thought to be attributable to fluctuations in arrangement of six water molecules in the solvation sphere.

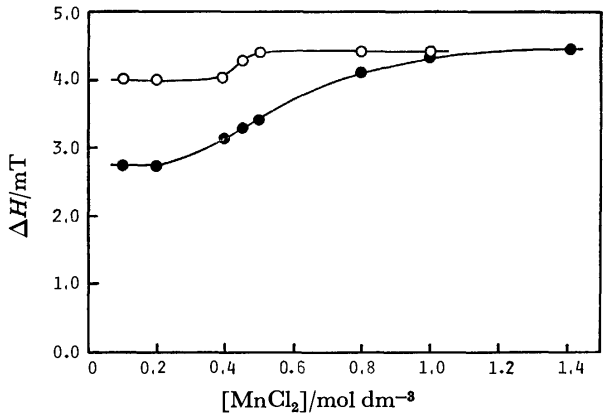

Fig. 1. Line width of Mn(II) as a function of $MnCl_2$ concentration in HTAB/$CHCl_3$ (○) and in aqueous (●) system.
[HTAB]=0.20 mol dm^{-3} and $[H_2O]$=0.444 mol dm^{-3}.

With an increase in water concentration resulting in larger water pools in the micellar cores, the line width of the ESR spectra decreases, gradually approaching to that in aqueous solution (ΔH=2.7 mT in Fig. 2). Figure 3 represents the water concentration dependence of ESR signal intensity, which is proportional to the product of height of the derivative curve and square of its width.[8] It is interesting to

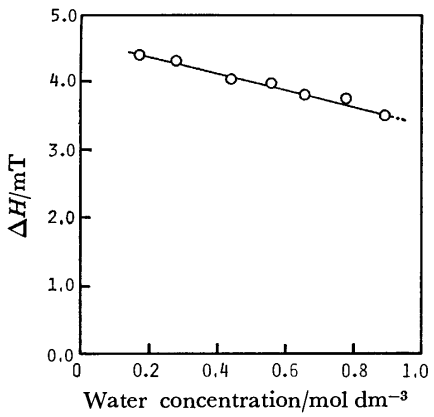

Fig. 2. Effect of water concentration on the line width of Mn(II) at a constant [Mn(II)]/[H_2O] ratio. [Mn(II)]=0.20 mol dm^{-3} of water and [HTAB]=0.20 mol dm^{-3}.

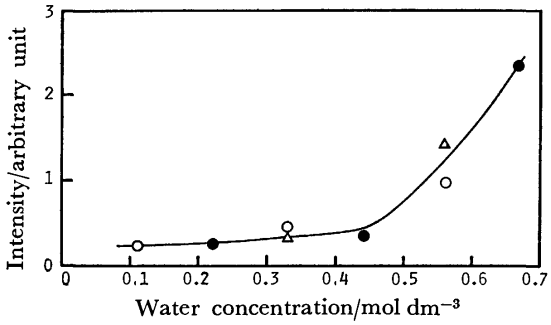

Fig. 3. Effect of water concentration of the ESR intensity of Mn(II).
[HTAB]=0.20 mol dm^{-3}, [Mn(II)]=4.4×10^{-4} mol dm^{-3} (○), 8.8×10^{-4} mol dm^{-3} (●), and 13.2×10^{-4} mol dm^{-3} (△).

note that the intensity remains nearly constant below 0.4 mol dm^{-3} of water concentration irrespectively of the Mn(II) concentration. This indicates that the water of these lower concentrations interacts exclusively with polar head group of HTAB and does not participate in the solvation of Mn(II) ions. As the water concentration increases above 0.4 mol dm^{-3}, the ESR intensity increases even though the ratio of [Mn(II)]/[H_2O] decreases. These results indicate that after completion of the hydration shell of the polar head groups of HTAB molecules, water molecules begin to coordinate to Mn(II) ions. Similar results were obtained by Sunamoto and Hamada[6] and Wells[9] by visible spectra of $CoCl_2$ in the reversed micellar system.

It was reported in the previous paper[1] that the polarity of water estimated from the λ_{max} value of pyridine 1-oxide in the DAP/hexane reversed micellar system decreases with a decrease in [H_2O]/[DAP] ratio, and attains the value between ethanol and chloroform at low water concentrations. The apparent decrease in the polarity is considered to be attributed to the lower degree of hydration of pyridine 1-oxide. This conclusion is supported by the present result that Mn(II) ions are dehydrated in small water pools of reversed micellar cores. The rate enhancement of ATP hydrolysis in the presence of metal ions such as Mg(II) or Mn(II)[10] in the reversed micellar system mentioned above may be accounted as the result of dehydration of metal cations. This could promote the formation of metal–ATP complexes in the reversed micellar system, enhancing the nucleophilic attack of water at condensed phosphate group of ATP.

References

1) M. Senō, S. Shiraishi, K. Araki, and H. Kise, *Bull. Chem. Soc. Jpn.*, **48**, 3678 (1975).
2) M. Senō, K. Sawada, K. Araki, K. Iwamoto, and H. Kise, *J. Colloid Interface Sci.*, in press.
3) J. H. Fendler, *Acc. Chem. Res.*, **9**, 153 (1976).
4) B. B. Garrett and L. O. Morgan, *J. Chem. Phys.*, **44**, 890 (1966).
5) C. C. Hinckley and L. O. Morgan, *J. Chem. Phys.*, **44**, 898 (1966).
6) J. Sunamoto and T. Hamada, *Bull. Chem. Soc. Jpn.*, **51**, 3130 (1978).
7) R. G. Hyes and R. J. Myers, *J. Chem. Phys.*, **40**, 877 (1964).
8) S. I. Chan, B. M. Fung, and H. Lütje, *J. Chem. Phys.*, **47**, 2121 (1967).
9) M. A. Wells, *Biochemistry*, **13**, 4937 (1974).
10) M. Senō, K. Sawada, K. Araki, and H. Kise, *Nippon Kagaku Kaishi*, **1980**, 469.

The Crystal Structure of Tetra-μ-acetato-diruthenium Chloride

Tadashi TOGANO,† Masao MUKAIDA,†† and Terunosuke NOMURA*

Department of Chemistry, Faculty of Science and Technology, Sophia University, Kioicho, Chiyoda-ku, Tokyo 102

(Received October 9, 1979)

Synopsis. The crystal structure of $Ru_2(OCOCH_3)_4Cl$ has been determined from visually estimated Cu $K\alpha$ data. The crystal is composed of the dinuclear, carboxylato-bridged species $Ru_2(OCOCH_3)_4^+$ and the bridging chloride anions. The molecular structure is almost identical with that of the analogous butyrato complex, but the chloride-bridged chains run parallel with the c axis only.

Carboxylato ruthenium complexes of the $Ru_2(OCOR)_4Cl$ type (R=Me, Et, *n*-Pr) were first reported by Stephenson and Wilkinson.[1] The structure determination of the analogous butyrato complex was accomplished by Bennett *et al.*, who revealed that the complex contains a dinuclear carboxylato-bridged species, $Ru_2(OCOC_3H_7)_4^+$, with a very short Ru–Ru distance.[2] It has also been indicated that the Ru atoms of the complex exist in the common nonintegral oxidation state of +2.5.

The present authors prepared the complexes of the $Ru_2(OCOR)_4X$ type (R=H, Me, Ph.; X=Cl, Br, I, SCN, NO_3, CH_3COO) independently[3,4] and presumed that these complexes have structures similar to that of the butyrato complex. The present work was undertaken in order to verify this prediction and to obtain more information about the properties of a series of carboxylato complexes.

Experimental

The crystals of $Ru_2(OCOCH_3)_4Cl$ were prepared as has been described previously;[3] they were recrystallized from a 5 mol dm^{-3} acetic-acid solution by means of slow evaporation at room temperature.

The cell constants were determined using Cu $K\alpha$ radiation by the least-squares refinement of the data from 150 reflections of h 0 l and h k 0 Weissenberg photographs, on which copper-powder lines were superimposed for calibration. The density was measured by flotation in a tetrachloromethane–methyl iodide mixture. The crystal data are as follows: $Ru_2(OCOCH_3)_4Cl$, $F.W.$=437.3, monoclinic, space group C2/c, a=14.869(3), b=7.735(1), c=12.868(3) Å, β=109.56(2)°, V=1393 Å^3, D_m=2.25 g cm^{-3}, D_c=2.26 g cm^{-3} (for Z=4), μ=207.5 cm^{-1} (for Cu $K\alpha$ radiation). The intensity data were collected by multiple-film equi-inclination Weissenberg photographs for the layer lines from 0 to 5 on the b axis and for 0 on the c axis. The two crystals were then re-formed into spheres with average diameters of 0.14 and 0.16 mm respectively. The intensities of 1116 independent reflections were corrected for Lorentz-polarization and absorption effects; 87 of them were, however, too weak to be measured and so were assumed to be zero.

Structure Determination

The positions of the ruthenium and chlorine atoms were determined from a three-dimensional Patterson map. Fourier synthesis, phased with the Ru atoms and Cl atoms, revealed all the carbon and oxygen atoms. The structures was refined by the block-diagonal least-squares method. The atomic scattering factors were taken from the International Tables for X-Ray Crystallography.[5] The refinement of the positional and thermal parameters, at first isotropic and subsequently anisotropic for all the Ru, Cl, C, and O atoms, but not the H atoms, reduced the discrepancy factor $R=\Sigma(w||F_o|-|F_c||)/\Sigma w|F_o|$ to 0.09, excluding non-observed reflections (R=0.10 for all 1116 reflections). The final atomic coordinates and thermal parameters are listed in Table 1, and the observed and calculated structure factors in Table 2.†††

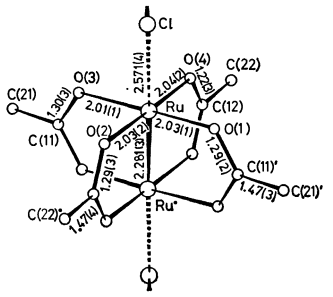

Fig. 1. Molecular structure with the numbering scheme of atoms and bond lengths (/Å) with e.s.d's in parentheses.

The computations were carried out on HITAC 8800/8700 computer at the Tokyo University Computer Center. The computer program used were UNICS by T. Sakurai *et al.* and HBLS IV by T. Ashida. In HBLS IV, the weighting scheme used was $w=(160.0/F_o)^2$ when $F_o>160.0$ and $w=1$ when $F_o\leqq 160.0$.

Results and Discussion

Bennett *et al.* have revealed that the tetra-*n*-butyrato complex contains dinuclear units consisting of two Ru atoms bridged by four *n*-butyrato groups. These dinuclear units, in crystal form, are linked by bridging chlorine atoms into infinite zigzag chains. The molecular structure of the acetato complex is almost identical with that of the butyrato complex. These dinuclear units have virtual D_{4h} symmetry if the alkyl chains are neglected in the case of the butyrato complex.

The geometry of, and bond distances in, the dinuclear cation and chlorine atoms are shown in Fig. 1. The bond angles and planes are given in Tables 3 and 4 respectively. The six nearest neighbors of a ruthenium atom are four oxygen atoms belonging to four different acetato groups, a ruthenium atom, and a chlorine atom. Six such atoms form distorted octahedral configuration about each of the two ruthenium

† Present address: Toho Girls' High School, 1-41-1 Wakabacho Chofu-shi, Tokyo 182.

†† Present address: Dept. of Chemistry, University of New Brunswick, Fredericton, N. B. Canada E3B 5A3.

††† The complete F_o–F_c data are deposited as document No. 8022 at the Office of the Editor of the Bulletin of the Chemical Society of Japan.

Table 1. Atomic parameters ($\times 10^4$) and their estimated standard deviations
The anisotropic thermal factors are of the form: $\exp[-(h^2B_{11}+k^2B_{22}+l^2B_{33}+hkB_{12}+hlB_{13}+klB_{23})]$.

Atom	x	y	z	B_{11}	B_{22}	B_{33}	B_{12}	B_{13}	B_{23}
Ru	0018(1)	0698(2)	0787(1)	31(1)	95(4)	28(1)	2(2)	35(1)	9(2)
Cl	0000	2392(10)	2500	40(3)	70(17)	31(3)	0	44(5)	0
O(1)	−1200(9)	1938(21)	−0079(10)	36(6)	157(39)	40(8)	34(24)	33(12)	−11(27)
O(2)	0792(9)	2603(21)	0414(11)	51(8)	136(40)	54(10)	−17(26)	61(14)	−10(29)
O(3)	1240(9)	−0522(21)	1614(10)	41(7)	167(40)	41(9)	38(25)	37(12)	1(27)
O(4)	−0759(9)	−1268(21)	1111(10)	44(7)	153(39)	44(8)	−22(25)	59(13)	−2(27)
C(11)	1602(13)	−1651(31)	1123(14)	37(9)	131(57)	38(11)	−2(33)	35(16)	−17(36)
C(12)	−0979(13)	−2519(29)	0493(15)	44(10)	72(54)	49(12)	−27(33)	54(18)	−11(36)
C(21)	2426(15)	−2711(36)	1764(17)	48(11)	238(73)	54(14)	71(44)	54(21)	13(48)
C(22)	−1505(19)	−3960(35)	0772(20)	85(17)	106(67)	82(19)	−66(50)	105(30)	−21(51)

Table 3. Bond angles and their e.s.d.'s

Atoms	Angle(/°)	Atoms	Angle(/°)
Ru'-Ru-O(1)	89.1(4)	Ru-O(1)-C(11)'	121(1)
Ru'-Ru-O(2)	88.8(5)	Ru-O(2)-C(12)'	120(1)
Ru'-Ru-O(3)	89.7(5)	Ru-O(3)-C(11)	121(1)
Ru'-Ru-O(4)	88.8(4)	Ru-O(4)-C(12)	121(2)
O(1)-Ru-O(2)	90.5(6)	O(1)'-C(11)-O(3)	120(2)
O(2)-Ru-O(3)	88.6(6)	O(2)'-C(12)-O(4)	122(2)
O(3)-Ru-O(4)	91.3(6)	O(1)'-C(11)-C(21)	120(2)
O(4)-Ru-O(1)	89.6(6)	O(2)'-C(12)-C(22)	118(2)
Cl-Ru-O(1)	88.1(4)	O(3)-C(11)-C(21)	118(2)
Cl-Ru-O(2)	90.2(5)	O(4)-C(12)-C(22)	120(2)
Cl-Ru-O(3)	93.1(5)	Ru'-Ru-Cl	177.0(1)
Cl-Ru-O(4)	92.2(5)		

Table 4. Best planes

Equations of planes[a)]
1. Ru, Ru', O(1), O(3)', C(11)';
$6.42x+7.36y-4.18z-0.015=0$
2. Ru, Ru', O(2), O(4)', C(12)';
$-7.23x+4.73y-2.32z-0.027=0$
3. Ru, O(1), O(2), O(3), O(4);
$-2.81x+4.78y+8.78z+11.15=0$

Dihedral angles

planes (1) and (2)	90.5°
planes (1) and (3)	90.4°
planes (2) and (3)	89.4°

a) The monoclinic-coordinate system (x, y, z) corresponds to the crystal (a, b, c) axes.

atoms. The mean values of the four different Ru–O bond lengths, all four O–Ru–O angles, the O–O' distances (2.22 Å) in the carboxylato groups, and the Ru–Cl distance were not significantly different from those of the butyrato complex. The very short Ru–Ru distance (2.281 Å), which was identical with that of the butyrato complex, implies that the interaction between the two metal ions is strong. The oxidation state of the Ru atoms in these complexes is thought to be +2.5, since the two metal atoms of a dinuclear cation are structurally equivalent. The abnormally high magnetic moments (2.90 BM (293 K) for the acetato complex[4)] and 3.37 BM (294 K) for the butyrato complex[1)]) and the electronic spectrum of the $Ru_2(OCOR)_4Cl$ species have been interpreted on the basis of a partial molecular orbital diagram of the M_2X_8 species.[2)]

The only difference between the acetato and butyrato complexes was found in their crystal structures. In both complexes, chloride ions bridged adjacent di-

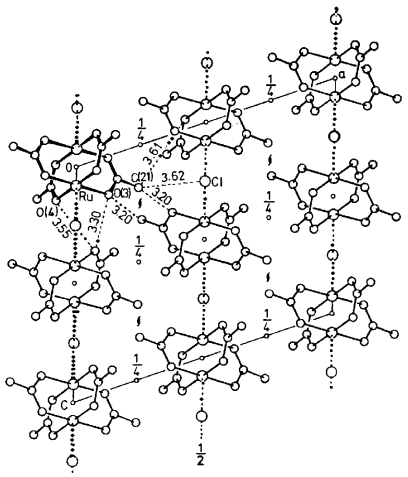

Fig. 2. Projection of the $Ru_2(OCOCH_3)_4Cl$ onto the (0 1 0) plane.

nuclear cations to form infinite zigzag chains. In the butyrato complex (tetragonal, space group I42d), there are alternating chains parallel to the a axis and the b axis. However as is shown in Fig. 2, the chains of the acetato complex (monoclinic, space group C2/c) lie along the c axis only. This finding is thought to reflect a substitution effect of R groups in the complexes.

While this manuscript was being prepared, structural studies of similar dinuclear carboxylato complexes of ruthenium were reported by Bino *et al.*[6)] However, there are some differences between the two acetato complexes, $Ru_2(O_2CCH_3)_4Cl\cdot 2H_2O$, in their article and the $Ru_2(O_2CCH_3)_4Cl$ in our article. In the former complex, the Cl bridges are perfectly linear, but in the latter complex the Cl bridges form zigzag chains, with an angle of 127.6° at the Cl atom.

The authors wish to thank Dr. Teruo Nomura of St. Paul's (Rikkyo) University for his help and advice.

References

1) T. A. Stephenson and G. Wilkinson, *J. Inorg. Nucl. Chem.*, **28**, 2285 (1966).
2) M. J. Bennett, K. G. Caulton, and F. A. Cotton, *Inorg. Chem.*, **8**, 1 (1969).
3) M. Mukaida, T. Nomura, and T. Ishimori, *Bull. Chem. Soc. Jpn.*, **40**, 2462 (1967).
4) M. Mukaida, T. Nomura, and T. Ishimori, *Bull. Chem. Soc. Jpn.*, **45**, 2143 (1972).
5) "International Tables for X-Ray Crystallography," Kynoch Press, Birmingham (1968), Vol. III, p. 201.
6) A. Bino, F. A. Cotton, and T. R. Felthouse, *Inorg. Chem.*, **18**, 2599 (1979).

Studies on the Solvent Extraction of Metal Perchlorates. II. Extraction of Alkali Metal Perchlorates with Trioctylphosphine Oxide

Satoshi KUSAKABE and Tatsuya SEKINE*

Departemnt of Chemistry, Science University of Tokyo, Kagurazaka, Shinjuku-ku, Tokyo 162

(Received December 12, 1979)

Synopsis. Solvent extraction of alkali metal ions in 1 mol dm^{-3} sodium perchlorate ionic media with trioctylphosphine oxide (TOPO) in hexane was measured. The extraction improved in the order Li(I)>Na(I)>K(I)>Rb(I)>Cs(I). This was explained in terms of the higher ability of solvation with TOPO of the smaller ions. The chemical form of the extracted species was $M(TOPO)_n^+(ClO_4)^-$, where n is three for Li(I), Na(I), and K(I) and three and four for Rb(I) and Cs(I).

Sodium perchlorate in aqueous solution is extractable with trioctylphosphine oxide (TOPO) in hexane but extraction was not effective.[1] In the present investigation, the extraction of other alkali metal perchlorates with TOPO was measured under identical conditions. Factors affecting the extractions are discussed.

Experimental

Hexane solution of TOPO and aqueous sodium perchlorate solution were prepared as reported previously.[1] Lithium hydroxide of reagent grade was dissolved in water and the concentration was measured by titration with a standard acid solution. It was neutralized by perchloric acid, a standard sodium perchlorate solution being added in order to obtain 1.0 mol dm^{-3} (Na, Li)ClO_4. Potassium, rubidium, and caesium chlorides each of reagent grade were dissolved in water and the concentration was measured by titration with a standard silver nitrate solution. One mol dm^{-3} (Na, M)ClO_4 solutions (where M^+ is the alkali metal ion) were prepared from a standard sodium perchlorate solution and the metal chloride solution. The concentration of potassium(I) was 0.025 mol dm^{-3}, that of the other metal ions being 0.01 mol dm^{-3}. The solutions except for that of lithium(I) thus contained a small amount of chloride but its effect on the extraction equilibrium was found to be negligible. The other reagents and procedures were the same as those in the previous work.[1] The distribution experiments were carried out at 25±0.3 °C. An aqueous perchlorate solution and an organic TOPO solution were placed in a glass stoppered tube, agitated vigorously and centrifuged. The metal in the organic phase was back-extracted with 1 mol dm^{-3} nitric acid containing 0.1 mol dm^{-3} of sodium nitrate which was added in order to reduce the error caused by back-extracted sodium perchlorate in flame photometry. The aqueous metal concentration was calculated from the initial aqueous and equilibrium organic concentrations.

Results and Discussion

The distribution ratio of an alkali metal ion is defined by

$$D = [M(I)]_{org}/[M(I)] \quad (1)$$

where the subscript "org" denotes chemical species in the organic phase. Its extraction with TOPO can be written as

$$M^+ + ClO_4^- + n\text{TOPO(org)} \rightleftarrows M(TOPO)_n^+(ClO_4)^-\text{(org)}, \quad (2)$$

$$K_{exn(M)} = [M(TOPO)_n^+(ClO_4)^-]_{org}/[M^+][ClO_4^-][TOPO]_{org}^n. \quad (3)$$

Dissociation of ion-pairs is negligible in solvents essentially nonpolar. The aqueous phase in the present study is neutral and therefore the extraction of perchloric acid should be negligible for statistical treatment. Since the solvation number of sodium perchlorate with TOPO is three,[1] the following equations can be obtained.

$$[TOPO]_{org,total} = [TOPO]_{org} + 3[Na(TOPO)_3^+(ClO_4)^-]_{org} + \sum n[M(TOPO)_n^+(ClO_4)^-]_{org} \quad (4)$$

$$= [TOPO]_{org} + 3K_{ex3(Na)}[Na^+][ClO_4^-][TOPO]_{org}^3 + \sum nK_{exn(M)}[M^+][ClO_4^-][TOPO]_{org}^n. \quad (5)$$

Thus the distribution ratio is given by

$$D = \sum [M(TOPO)_n^+(ClO_4)^-]_{org}/[M^+] = \sum K_{ex(M)}[ClO_4^-][TOPO]_{org}^n. \quad (6)$$

By use of a least squares computer program and the value of extraction constant of sodium(I),[1] $K_{ex3(Na)} = 10^{1.01}$, a successive approximation procedure was carried out by means of Eqs. 3—6, the "free" TOPO concentrations, $[TOPO]_{org}$, and the best-fit extraction constants of metal ion, $K_{exn(M)}$, being obtained. The "best-fit" with the data was obtained when extraction of only trisolvate was assumed for lithium(I) and potassium(I), as well as when extraction of both tri- and tetrasolvate was assumed for rubidium(I) and caesium(I). The extraction constants are given in Table 1. Figure 1 shows the log D *vs.* free TOPO concentration plot (the data of sodium(I) are taken from Ref. 1), the solid curves being calculated by introducing the values of constants in Table 1 into Eq. 6.

It is most probable that the interactions between the TOPO solvated metal ion and the perchlorate ion in the organic phase are electrostatic, *viz.*, the extracted species are ion-pairs. The present results differ from those of extraction into polar solvents in

Table 1. Summary of extraction constants of alkali metal perchlorates with TOPO in hexane[a]

	log K_{ex3}	log K_{ex4}
Li(I)	2.29±0.13	nil
Na(I)[b]	1.01±0.14	nil
K(I)	0.57±0.22	nil
Rb(I)	0.06±0.10	0.99±0.17
Cs(I)	−0.17±0.21	0.95±0.18

a) Aq phase 1 mol dm^{-3} ($NaClO_4$), temp 25 °C. Limit of error is 3σ. b) Value taken from Ref. 1.

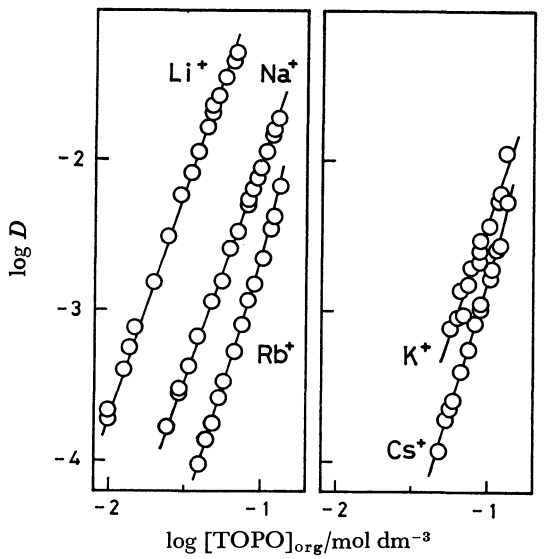

Fig. 1. The distribution ratio of alkali metal as a function of "free" TOPO concentration. The data of sodium(I) are taken from Ref. 1.
Org. phase: hexane containing TOPO. Aq phase: Li(I); 0.010 mol dm^{-3} $LiClO_4$+0.99 mol dm^{-3} $NaClO_4$, Na(I); 1.0 mol dm^{-3} $NaClO_4$, K(I); 0.025 mol dm^{-3} KCl+0.975 mol dm^{-3} $NaClO_4$, Rb(I) and Cs(I); 0.01 mol dm^{-3} of chloride+0.99 mol dm^{-3} $NaClO_4$. The solid curves are calculated by means of Eq. 6 and the values in Table 1.

which the solvation of metal ions is weaker than that with TOPO and in which at least a partial dissociation of the extracted ion-pairs is expected. For example, the extraction of sodium(I), potassium(I), rubidium(I), and caesium(I) as ion-pairs with tetraphenylborate ion into nitrobenzene was found to be better in the increasing order of the ionic size of the metal ion.[2] This type of extraction order often found in many other similar ion-pair extraction systems[3] is explained in terms of lower hydration and higher hydrofobic tendencies of large metal ions and in some cases also of their higher tendency to dissociate in the organic phase. The opposit extraction order in the present system can be explained in terms of the order of the formation of TOPO solvates. Although the size of the central metal ions in the TOPO solvates differs, the overall molar size of the solvated cations in the ion-pairs should be similar when the solvation number is the same, the effect of the molar size on the extraction (or the hydrofobic tendencies) should thus be similar. For this reason, best extraction of lithium(I) should be due to its highest tendency to be solvated with TOPO. Even though it is hydrated most strongly among these alkali metal ions in the aqueous phase, its small ionic size is also favorable for solvation with TOPO. The hydration interferes with extraction while TOPO solvation enhances it. However, the fact that the smaller the ionic size, the better the extraction indicates that the stronger solvation with TOPO overcomes the unfavorable stronger hydration. Thus although the metal ions are extracted as ion-pairs, the order of extraction is similar to that with β-diketones reported by Healy.[4] It seems reasonable that the less strongly solvated larger ions, rubidium(I) and caesium(I), have space to accept one more TOPO molecule and are extracted also as tetrasolvates.

No quantitative work seems to have been carried out on the extraction equilibria of these metal perchlorates with solvating type solvents such as TOPO in nonpolar solvents.

The authors are grateful to Messrs. Yuichi Ishida and Kenji Ohira for their assistance in experiments.

References

1) S. Kusakabe and T. Sekine, *Bull. Chem. Soc. Jpn.*, **53**, 1759 (1980).
2) T. Sekine and D. Dyrssen, *Anal. Chim. Acta*, **45**, 433 (1969).
3) T. Sekine and Y. Hasegawa, "Solvent Extraction Chemistry," Marcel Dekker, New York (1977), p. 500.
4) T. V. Healy, *J. Inorg. Nucl. Chem.*, **30**, 1025 (1968); **31**, 499 (1969).

Catalysis by 12-Heteropolymolybdic Acid. II. Friedel-Crafts-type Reaction of Aromatic Compounds

Kenji NOMIYA, Yoshio SUGAYA, Sadayoshi SASA, and Makoto MIWA*

Depertment of Industrial Chemistry, Faculty of Engineering, Seikei University, Musashino-shi, Tokyo 180

(Received November 14, 1979)

Synopsis. 12-Heteropolymolybdic acid, a heteropolyacid of Keggin-structure, behaves as an effective catalyst of the Friedel-Crafts-type reactions for aromatic compounds, such as alkylation by benzyl chloride and *t*-butyl chloride, acylation by acetyl chloride, and sulfonylation by tosyl chloride. The catalyst mainly gives para-substituted products for phenol and anisole. The reactions proceed *via* carbocation-generation mechanism brought about by the strong Brønsted acid.

Except for the catalytic alkylation of benzene with 1-dodecene by silicotungstic acid supported on silica gel,[1] no typical reaction catalyzed by heteropolyacid, recognized as a solid-acid, has been demonstrated in spite of advanced studies on its structure.[2-10]

Nomiya *et al.* have shown the catalytic polycondensation of benzyl alcohol and its derivatives by heteropolyacids of Keggin-structure such as $H_4SiM_{12}O_{40}$ and $H_3PM_{12}O_{40}$ (M=Mo and W).[11] These acids also give the same polybenzyl from benzyl chloride by dehydrohalogenation as that obtained from benzyl alcohol in comparably high yields. We wish to report that these heteropolymolybdic acids are active catalysts in substitution reactions such as alkylation, acylation, and sulfonylation of aromatic systems as well as polymerization reactions. The reaction scheme is as follows.

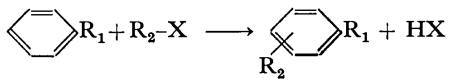

The reactions were performed by refluxing a mixture of reactants A and B in the presence of the heteropolyacid. The results of typical experiments are given in Table 1. The heteropolyacid homogeneously catalyzes all reactions. The reaction products were identified by IR and ^{1}H-NMR spectra. No poly-branched product was detected. The substituent groups are oriented mainly to the para-position of six-membered aromatic rings of phenol and anisole, and the 2-position of five-membered ring of thiophene. In the former case, only a slight ortho-substitution was detected in the products; no meta-substituted product was observed, indicating that the reaction proceeds by an ionic mechanism. On the benzyl chloride–benzene system the alkylation takes place sparingly, albeit catalytically, whereas on the benzyl alcohol–benzene system, instead of such a reaction, condensation-etherization and polymerization of benzyl alcohol take place. In the acylation of toluene by acetyl chloride, only a trace of the product was obtained.

In all polymerization and alkylation reactions, the catalyst undergoes color change corresponding to the reduced stages of molybdenum ions from original yellow to green and finally to blue.[12] However, the reduction of catalyst would not be essential in the coupling reaction since the initial activity of catalyst and the selectivity and yields of products were not influenced by the recharge of excess amount of reactants to the blue acid obtained. The blue acid appears to be an active catalyst.

In the acylation and sulfonylation reactions the catalyst partly decomposes, producing an unidentified black solid. This might be caused by a specific reaction between the acetyl chloride or the tosyl chloride and the catalyst. No typical color change of yellow-green-blue was observed.

In the reaction of six-membered aromatic substrates, the ease of coupling decreases in the order, alkylation> acylation>sulfonylation. However, in the five-membered substrate such as thiophene, alkylation scarcely takes place by *t*-butyl chloride. Thus, in the case of five-membered substrate, acylation by acetyl chloride takes place more easily than alkylation under the same conditions.

Since the tetrabutylammonium salts of both the unreduced yellow and the reduced blue heteropolyanions show no catalytic activity, the remarkable strong acidity of catalyst would be important.

The catalytic activity of the acid appears to be comparable to that of $Mo(CO)_6$ and Arene–$Mo(CO)_3$ previously reported as "Friedel-Crafts" like catalysts, with respect to the coupling reaction concerned.[13,14] Although typical Friedel-Crafts catalysts, whether homogeneous or heterogeneous, are all Lewis acids and are capable of promoting carbonium ion formation from certain organic molecules, the heteropolyacid and the "Friedel-Crafts" like catalysts would show no Lewis acid property; particularly the former behaves as Brønsted acid. $Mo(CO)_6$ is coordinatively saturated molecules. However, the complex added in the aromatic solvent is easily converted into Arene–$Mo(CO)_3$ prior to the coupling reaction.[13] In the present work, no evidence has been obtained for the direct coordination of arene rings of reactants to the molybdenum ions in the blue heteropolyacid during the course of reaction. The type of reactions studied here appears to be a carbonium-ion generation mechanism brought about by the strong Brønsted acid.

The essential feature of the heteropolymolybdic acid is the stability of catalyst, appearing in particular in the polymerization and alkylation, and the yielding of products with high selectivity in the case of phenol and anisole.

Although the heteropolyacid contains twelve molybdenums, all of them would not play a direct role as active site as in the case of solid-surface catalyst. Thus the turn-over numbers of catalyst have been simply calculated as the molar ratio of catalyst to product. The turn-over number per unit hour (Table 1) shows that (1) all reactions proceed catalytically, not stoichiometrically, and (2) the ease of carbocation forma-

Table 1. Examples of reactions catalyzed by $H_4SiMo_{12}O_{40}$

Reactant A (mol)	Reactant B (mol)	Amount of catalyst (mol)	Reflux time (h)	Remarks	Turn-over number per hour: This work	$Mo(CO)_6$ catalyst[b]	Friedel-Crafs catalyst[c]
——	Benzyl chloride (0.1)	4.81×10^{-5}	0.1	100% polybenzyl[a]			
——	Benzyl alcohol (0.1)	4.81×10^{-5}	0.1	100% polybenzyl[a]			
Benzene (0.1)	Benzyl chloride (0.1)	4.00×10^{-5}	3	5% alkylation	42		2.5×10^{-3}
Toluene (1.0)	Benzyl chloride (0.05)	9.90×10^{-5}	8	74% alkylation	47	66	
Toluene (0.3)	Benzyl alcohol (0.1)	7.68×10^{-5}	16	74% alkylation	60		
Toluene (0.05)	*t*-Butyl chloride (0.1)	2.63×10^{-4}	5	87% alkylation	33	32	
Phenol (0.05)	*t*-Butyl chloride (0.05)	8.01×10^{-5}	8.5	40% alkylation	29		$2.4\times10^{-}$
Anisole (0.3)	*t*-Butyl chloride (0.1)	8.23×10^{-5}	23	49% alkylation	26	21	
Toluene (0.24)	Tosyl chloride (0.01)	2.75×10^{-5}	20	23% sulfonylation	4	3	
Anisole (0.23)	Tosyl chloride (0.026)	5.49×10^{-5}	23	14% sulfonylation	3	2	
Anisole (0.23)	Acetyl chloride (0.1)	5.49×10^{-5}	20	19% acylation	17	25	
Thiophene (0.06)	Acetyl chloride (0.1)	5.49×10^{-5}	30	44% acylation	16		

a) Ref. 11. b) Ref. 13. c) Ref. 15.

tion may be related to the electronic structure of the halides, decreasing in the order

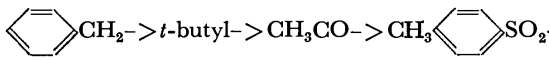

This tendency corresponds to that in the reactions catalyzed by $AlCl_3$, $Mo(CO)_6$.

The parameters on the corresponding reactions by $Mo(CO)_6$ catalyst and Friedel-Crafts catalyst have been conveniently calculated by the data of Farona and White,[13] and reported data,[15] respectively. The parameters reflect the catalytic efficiency of catalysts, indicating that the former reactions, including the case of the 12-heteropolyacid, are catalytic, and the latter reaction stoichiometric.

References

1) R. T. Sebulsky and A. M. Henke, *Am. Chem. Soc., Div. Petrol. Chem.*, **14**, A115 (1969); U. S. Patent 3346657 (*Chem. Abstr.*, **68**, P77941u).
2) M. Filowitz, R. K. C. Ho, W. G. Klemperer, and W. Shum, *Inorg. Chem.*, **18**, 93 (1979).
3) W. H. Knoth, *J. Am. Chem. Soc.*, **101**, 759, 2211 (1979).
4) F. Zonnevijlle and M. T. Pope, *J. Am. Chem. Soc.*, **101**, 2731 (1979).
5) K. Y. Matsumoto, A. Kobayashi, and Y. Sasaki, *Bull. Chem. Soc. Jpn.*, **48**, 3146 (1975).
6) A. Kobayashi and Y. Sasaki, *Bull. Chem. Soc. Jpn.*, **48**, 885 (1975).
7) M. T. Pope, *Inorg. Chem.*, **15**, 2008 (1976).
8) J. F. Garvey and M. T. Pope, *Inorg. Chem.*, **17**, 1115 (1978).
9) R. Strandberg, *Acta. Chem. Scand.*, **A**, **29**, 350, 359 (1975).
10) R. Acerete, C. F. Hammer, and L. C. W. Baker, *J. Am. Chem. Soc.*, **101**, 267 (1979).
11) K. Nomiya, T. Ueno, and M. Miwa, *Bull. Chem. Soc. Jpn.*, **53**, 827 (1980).
12) J. D. H. Strickland, *J. Am. Chem. Soc.*, **74**, 862, 868, 872 (1952).
13) M. F. Farona and J. F. White, *J. Am. Chem. Soc.*, **93**, 2826 (1971); *J. Organomet. Chem.*, **63**, 329 (1973).
14) C. P. Tsonis and M. F. Farona, *J. Organomet. Chem.*, **114**, 293 (1976).
15) C. C. Price, *Org. React.*, Vol. III, 1 (1959).

Telomerization of Isoprene with Dialkylamine Catalyzed by Palladium Complexes

Masanobu Hidai,* Haruyoshi Mizuta, Kiyomiki Hirai, and Yasuzo Uchida
Department of Industrial Chemistry, Faculty of Engineering, The University of Tokyo, Bunkyo-ku, Hongo, Tokyo 113
(Received November 28, 1979)

Synopsis. Telomerization of isoprene with diethylamine in the presence of catalytic amounts of palladium chloride and triphenylphosphine under carbon dioxide and/or using methanol as solvent gave three kinds of 2:1 adducts in good yields, one of which was found to be an adduct of new type.

Many transition metal complexes have been shown to catalyze the reaction of 1,3-butadiene with alcohols,[1] carboxylic acids,[2] amines,[3] water,[4] and active methylene and methylidyne compounds[5] yielding mainly 2,7-octadienyl derivatives (2:1 adducts). However, the analogous reactions of isoprene have not been well studied. The reaction of morpholine with isoprene by nickel complexes was reported to give mainly 1:1 adducts along with a small amount of 2:1 adducts.[3] This is in sharp contrast to the ready formation of 2:1 adducts from butadiene and amines with a variety of transition metal complexes. Recently Tanaka *et al.*[6] reported that butyllithium catalyzed telomerization of isoprene which led to formation of (2*Z*)-*N*,*N*-dialkyl-3,7-dimethyl-2,6-octadienylamine in a good yield.

We reported in a previous paper the synthesis of citronellol starting from isoprene through a 2:1 adduct with methanol.[7] We wish here to describe the reaction of isoprene with diethylamine catalyzed by palladium complexes, where carbon dioxide and methanol showed a remarkable effect on the product distribution.

Results and Discussion

Treatment of isoprene with diethylamine in the presence of $PdCl_2$ and triphenylphosphine under carbon dioxide and/or using methanol as solvent gave 2:1 adducts of isoprene and the amine, together with a small amount of 1:1 adducts and isoprene dimers. The 2:1 adducts were found to be a mixture of three octadienyl derivatives **1**, **2**, and **3**. Their structures

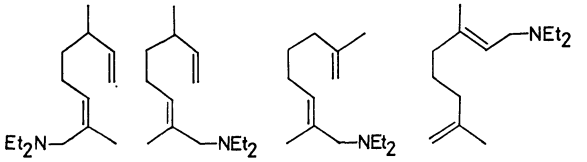

1 **2** **3**

have been determined on the basis of the infrared and NMR spectra after their separation by preparative GLC (Table 1). The product **1** gives rise to two quartets at 2.38 and 2.40 ppm in the NMR spectrum assignable to the methylene protons of the diethylamino group, indicating that the product **1** is a mixture of *E*- and *Z*-isomers around the trisubstituted C=C bond. On the other hand, measurement of the nuclear Overhauser effect in the 270 MHz ^1H NMR spectra of the products **2** and **3** clearly showed that they have an *E*-configuration around the trisubstituted C=C bond. Thus, the integrated intensity of the olefinic proton ($-CH_2-C\underline{H}=$) of **2** at 5.35 ppm increased *ca.* 16% by irradiating the methylene protons between the C=C bond and the nitrogen atom, whereas the intensity increased only *ca.* 1.8% by irradiating the methyl protons attached to the C=C bond at 1.71 ppm.

A standard procedure was adopted to study the effect of a number of parameters on the conversion of isoprene and the product ratio (Table 2). The reaction at 100 °C for 24 h under nitrogen without solvent gave only a 14% conversion into a mixture of 1:1 adducts, the adduct **2**, and isoprene dimers. However, the same reaction under carbon dioxide gave a 85% conversion to yield products comprising *ca.* 60% of the 2:1 adducts. The striking feature of this reaction is a large amount of the 2:1 adducts formed under nitrogen when alcohols such as methanol and ethanol were used as solvent. Methanol is especially effective among them and the reaction proceeds smoothly even at room temperature.

Carbon dioxide is effective not only in accelerating the reaction rate, but also in changing the product ratio. When the reaction was run in methanol at 100 °C under nitrogen, the ratio of the adducts **1**, **2**, and **3** was 20:44:28. However, the reaction under carbon dioxide changed the ratio into 40:32:13. The product ratio is also dependent upon the reaction temperature. The high temperature seems to favor the formation of the adducts **2** and **3**, and disfavor the formation of **1** when the reaction was run in methanol.

Among the 2:1 adducts obtained here, the compound **3** is an adduct of new type. The adducts with methanol corresponding to the compounds **1** and **2** are readily produced by using zero-valent palladium complexes as catalyst.[8] Use of a zero-valent palladium complex, $Pd(DBA)_2$ (DBA=dibenzylideneacetone), instead of $PdCl_2$ in the above amination reaction in methanol gave the 2:1 adducts of both diethylamine and methanol in low yields. On the other hand, in the early stage of the reaction in the presence of $PdCl_2$ and triphenylphosphine in methanol at room temperature, the adducts with the amine were only produced, while the adducts with methanol were not obtained at all. These results strongly suggest that a zero-valent complex may not be involved as an active species and that the adducts with the amine are not formed *via* the adducts with methanol, although Hata *et al.*[9] previously reported the exchange reaction of the allylic groups of ethers with a variety of active hydrogen compounds including secondary amines by using palladium complexes. It is of great interest to note that $Pd(DBA)_2$ coupled with diethyl ammonium chloride repressed the formation of the adducts with

Table 1. IR and NMR data of the products **1**, **2**, and **3**

Products	IR (cm^{-1})	NMR (δ values from TMS)
1	1640 ($\nu_{C=C}$), 905, 1000 (δ_{C-H} of the vinyl group)	0.94 (3H, d, J=7.0 Hz, $\underline{CH_3}$-CH$\langle$), 0.96 (6H, t, J=7.5 Hz, $\underline{CH_3}$-CH_2-N), 1.30 (2H, q, J=7.5 Hz, $\rangle$CH-$\underline{CH_2}$-), 1.70 and 1.84 (3H, 2×s, =C($\underline{CH_3}$)-), 1.85—2.20 (3H, m, =$\underline{CH}$-$\underline{CH}\langle$ and -$\underline{CH_2}$-CH=), 2.38 and 2.40 (4H, 2×q, J=7.5 Hz, CH_3-$\underline{CH_2}$-N), 2.86 and 2.91 (2H, 2×s, $\rangle$N-$\underline{CH_2}$-C=), 4.7—5.1 (2H, m, $\underline{CH_2}$=CH-), 5.1—5.9 (2H, m, =$\underline{CH}$-).
2	1640 ($\nu_{C=C}$), 895 (δ_{C-H} of the terminal methylene)	0.96 (6H, t, J=7.5 Hz, $\underline{CH_3}$-CH_2-N), 1.25—2.70 (2H, m, -CH_2-$\underline{CH_2}$-CH_2-), 1.63 (3H, s, $\underline{CH_2}$=C($\underline{CH_3}$)-), 1.71 (3H, s, -CH=C($\underline{CH_3}$)-), 1.7—2.2 (4H, m, -$\underline{CH_2}$-CH_2-$\underline{CH_2}$-), 2.41 (4H, q, J=7.5 Hz, CH_3-$\underline{CH_2}$-N), 2.87 (2H, s, =C-$\underline{CH_2}$-N$\langle$), 4.74, (2H, s, $\underline{CH_2}$=C$\langle$), 5.35 (1H, t, J=7.5 Hz, -$\underline{CH}$=).
3	1645 ($\nu_{C=C}$), 895 (δ_{C-H} of the terminal methylene)	0.99 (6H, t, J=7.5 Hz, $\underline{CH_3}$-CH_2-N), 1.1—1.5 (2H, m, -CH_2-$\underline{CH_2}$-CH_2-), 1.56 (3H, s, -$\underline{CH}$=C(-$\underline{CH_3}$)-), 1.62 (3H, s, CH_2=C($\underline{CH_3}$)-), 1.7—2.2 (4H, m, -$\underline{CH_2}$-CH_2-$\underline{CH_2}$-), 2.44 (4H, q, J=7.5 Hz, CH_3-$\underline{CH_2}$-N), 3.00 (2H, d, J=7.0 Hz, $\rangle$N-$\underline{CH_2}$-CH=), 4.72 (2H, m, $\underline{CH_2}$=), 5.34 (1H, t, J=7.0 Hz, -$\underline{CH}$=).

Table 2. Telomerization of isoprene with diethylamine

Catalyst[a]	Atmosphere	Solvent (Temp)	Conv. (%) of Isoprene	Product (%) 1	2	3	1 : 1[b] adducts	Isoprene[c] dimers	Methanol adducts
$PdCl_2$	N_2	none (100)	14	tr	25	—	40	34	0
$PdCl_2$	CO_2	none (100)	85	10	48	7	8	26	0
$PdCl_2$	N_2	MeOH (100)	100	20	44	28	4	4	0
$PdCl_2$	CO_2	MeOH (100)	100	40	32	13	15	tr	0
$PdCl_2$	N_2	EtOH (100)	100	11	65	16	1	6	0
$PdCl_2$	N_2	MeOH (28)	100	53	33	11	3	tr	0
$Pd(DBA)_2$	N_2	MeOH (28)	43	17	28	tr	tr	28	27[d]
$Pd(DBA)_2$ -$Et_2N^+H_2Cl^-$	N_2	MeOH (28)	46	69	31	—	tr	tr	0
$Pd(DBA)_2$ -$Me_4N^+I^-$	N_2	MeOH (28)	26	29	36	—	—	23	11[e]

a) In all cases, an equimolar amount of triphenylphosphine was added to the palladium complexes. b) The 1 : 1 adducts were mainly composed of *N*,*N*-diethyl-2-methyl-2-butenylamine and *N*,*N*-diethyl-3-methyl-2-butenylamine. c) The isoprene dimers predominantly contained 2,7-dimethyl-1,3,7-octatriene. d) The adducts were 1-methoxy-2,6-dimethyl-2,7-octadiene (9%) and 1-methoxy-2,7-dimethyl-2,7-octadiene (18%). e) The adducts were the same as above d), 4 and 9% respectively.

methanol. This may suggest intervention of proton in the above amination reaction, which may originally come from methanol or diethylcarbamic acid formed from the amine and carbon dioxide, and formation of a positively charged π-allyl intermediate similar to that proposed by Åkermark *et al.*[10]

Experimental

All reactions were performed under oxygen-free conditions. Alcohols and isoprene were dried and distilled over anhydrous $CaSO_4$. Diethylamine was purified by distillation over potassium or sodium hydroxide pellets. Bis(benzylideneacetone)palladium $Pd(DBA)_2$ was prepared according to the procedure reported by Ishii *et al.*[11]

Analysis was carried out with a Hitachi K23 gas chromatograph (He carrier gas through 2 m×3 mm in stainless-steal column, 10% Silicone DC 550) and a Shimadzu GC-5A chromatograph for all preparative GLC (He carrier gas through 2.1 m×10 mm in stainless-steal column, 10% Silicone DC 550). NMR spectra were obtained with a Hitachi Perkin-Elmer 90 MHz instrument using tetramethylsilane (TMS) as internal standard and C_6D_6 as solvent. IR spectra were recorded on a Hitachi 215 instrument.

General Procedure at 28 °C. In a 100 ml two neck flask or a 75 ml Pyrex glass ampule, in which palladium chloride (88.7 mg, 0.5 mmol) and triphenylphosphine (131.1 mg, 0.5 mmol) were placed, isoprene (15 ml, 150 mmol), diethylamine (15 ml, 144 mmol), and methanol (15 ml, 370 mmol) were added in this order. After stirring for 24 h at 28 °C, the reaction gave a 100% conversion into **1** 53%, **2** 33%, **3** 11%, and 1:1 adducts (3%). A mixture of **1**, **2**, and **3** was obtained by distillation (103—105 °C/933 Pa) and separated by preparative GLC at 150 °C. Found: C, 80.52; H, 13.40; N, 6.71% for **1**; C, 80.32; H, 13.16; N, 6.80% for **2**; C, 80.56; H, 13.24; N, 6.51% for **3**. Calcd for $C_{14}H_{27}N$: C, 80.31; H, 13.00; N, 6.69%. IR and NMR spectra are summarized in Table 1.

This general procedure was used for the series of experiments with changes in conditions as summarized in Table 2. The reactions at 100 °C and/or under carbon dioxide were achieved in a 100 ml stainless-steal autoclave for 24 h.

References

1) S. Takahashi, T. Shibano, and N. Hagihara, *Bull. Chem. Soc. Jpn.*, **41**, 454 (1968); S. Takahashi, H. Yamazaki, and H. Hagihara, *ibid.*, **41**, 254 (1968); E. J. Smutny, *J. Am. Chem. Soc.*, **89**, 6793 (1967).

2) M. Green, G. Scholes, and F. G. Stone, *J. Chem. Soc., Dalton Trans.*, **1978**, 309.

3) K. Takahashi, A. Miyake, and G. Hata, *Bull. Chem. Soc. Jpn.*, **45**, 1183 (1972); R. Baker, A. Onions, R. J. Popplestone, and T. N. Smith, *J. Chem. Soc., Perkin Trans. 2*, **1975**, 1133; R. Baker, A. H. Cook, D. E. Halliday, and T. N. Smith, *ibid.*, **1974**, 1151.

4) K. E. Atkins, W. E. Walker, and R. M. Manyik, *J. Chem. Soc., Chem. Commun.*, **1971**, 330.

5) R. Baker, A. H. Cook, and T. N. Smith, *J. Chem. Soc., Perkin Trans. 2*, **1974**, 1517; K. Takahashi, A. Miyake, and G. Hata, *J. Org. Chem.*, **36**, 2116 (1971).

6) K. Takabe, T. Katagiri, and J. Tanaka, *Tetrahedron Lett.*, **1972**, 4009.

7) M. Hidai, H. Ishiwatari, H. Yagi, E. Tanaka, K. Onozawa, and Y. Uchida, *J. Chem. Soc., Chem. Commun.*, **1975**, 170.

8) Japan Patent (Kokai) 73-23707.

9) G. Hata, K. Takahashi, and A. Miyake, *J. Chem. Soc., Chem. Commun.*, **1970**, 1392; *Bull. Chem. Soc. Jpn.*, **45**, 230 (1972).

10) B. Åkermark, G. Åkermark, and C. Moberg, *J. Organomet. Chem.*, **164**, 97 (1979).

11) T. Ukai, H. Kawahara, and Y. Ishii, *J. Organomet. Chem.*, **65**, 253 (1974).

The Photochemical Behavior of 3,3-Dimethyl-1,2-indanedione toward Aromatic Aldehydes

Kazuhiro MARUYAMA, Yoshinori NARUTA, Atsuhiro OSUKA,*,† and Hitomi SUZUKI†

Department of Chemistry, Faculty of Science, Kyoto University, Kyoto 606

† *Department of Chemistry, Faculty of Science, Ehime University, Matsuyama 790*

(Received December 3, 1979)

Synopsis. The photochemical reaction of 3,3-dimethyl-1,2-indanedione with aromatic aldehydes in benzene was found to give a mixture of two diastereoisomeric 2:2 adducts, a 1:1 adduct, a 2:1 adduct, and pinacol.

When photolyzed together with aldehydes, cyclic α-diketones in both aliphatic[1] and aromatic systems[2] abstract the formyl hydrogen atom to give in-cage combination products predominantly. In contrast, open chain α-diketones yield out-of-cage products mainly.[3] In the present work, we have investigated the photochemical reaction of 3,3-dimethyl-1,2-indanedione (**1**) (DMID) with several aromatic aldehydes and found a rather unexpected behavior of DMID toward these aldehydes.

After a benzene solution of DMID and *p*-anisaldehyde **2a** had been irradiated in a Pyrex tube for 2 h, the separation of the products by TLC gave two diastereoisomeric 2:2 adducts, **3a** (11%) and **4a** (10%), a 1:1 adduct, **5a** (4%), and a 2:1 adduct, **6a** (7%). In addition, the ^{1}H-NMR spectrum of this reaction mixture showed the presence of pinacol, **7** (15%).[4] The molecular weights of **3a** and **4a**, as determined by the vapor-pressure method, are 598±30 and 620±30 (Calcd, 618.25) respectively. The 2:2 adducts, **3a** and **4a**, show characteristic IR bands due to the unconjugated five-membered cyclic ketone and the aromatic ester at 1777 and 1729 cm^{-1} and at 1768 and 1720 cm^{-1}, respectively. The ^{1}H-NMR spectra show signals at 1.52 (s, 3H), 1.55 (s, 3H), and 3.76 (s, 3H), and at 0.82 (s, 3H), 1.52 (s, 3H), and 3.82 (s, 3H), respectively. The ^{13}C-NMR spectrum of **4a** shows peaks at 213.2 (ketone), 164.1 (ester), 86.1 (s), 55.5 (q, CH_3O–), and 48.9 (s) ppm, besides two methyl carbons and twelve sp^2 carbons. These spectral data and the results of elemental analyses are consistent only with the formulation of **3a** and **4a** as two diastereoisomers of 1,1′-bis(4-methoxybenzoyloxy)-3,3,3′,3′-tetramethyl-1,1′-biindane-2,2′-dione. The molecular weight of **6a**, as determined by the vapor-pressure method, is 430±30 (Calcd, 456.6). The IR spectrum shows characteristic bands at 1757 (unconjugated five-membered cyclic ketone), 1716 (aromatic ester), and 1695 (conjugated ketone). The ^{1}H-NMR and ^{13}C-NMR spectra reveal that the framework of **6a** consists of a half-unit of the 2:2 adduct and the 2-isopropylbenzoyl group. Thus **6a** was identified as 1-(4-methoxybenzoyloxy)-1-(2-isopropylbenzoyl)-3,3-dimethyl-2-indanone. In similar reactions with other aromatic aldehydes, **2b—d**, the products were **3b—d**, **4b—d**, **5b**, **6b—d**, and **7**. The yields and physical properties of the products are summarized in Tables 1 and 2.

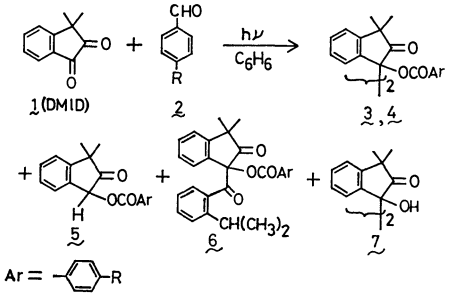

Scheme 1.

A plausible mechanism to account for the formation of the photoproducts, **3**, **4**, **5**, **6**, and **7**, is outlined in Scheme 2. The photoexcitation of DMID and the subsequent formyl hydrogen abstraction afford two radicals, **8** and **9**, a large portion of which escape from the solvent cage. The escaped radical, **8**, has earlier been shown to dimerize to yield pinacol **7**.[4] The aroyl radical, **9**, out of the cage attacks the oxygen atom of C-1 carbonyl group of DMID, leading to the formation of the **10** radical; the two radicals then couple with each other to give **3** and **4**. This reaction path is in agreement with the fact that the anisoyl radical, **9a**, generated by the thermal decomposition of di-*t*-butyl diperoxyoxalate,[5] reacted with DMID to give **3a** and **4a**, but neither **5a** nor **6a**. Hydrogen transfer from **8** to **10** will result in the formation of

Table 1. Photochemical reaction of DMID with aromatic aldehydes

Aromatic aldehydes	Isolated yields of photoadducts (%)[a),b)]				
	3	**4**	**5**	**6**	**7**
R-⟨⟩-CHO					
2a, R=MeO-	11	10	4	7	(15)
2b, R=Me-	12	6	6	trace	(17)
2c, R=H-	9	9	—	8	(19)
2d, R=Cl-	8	13	—	trace	(20)

a) Based on unrecovered DMID. b) Numerals in parentheses refer to the yields determined by ^{1}H-NMR analysis.

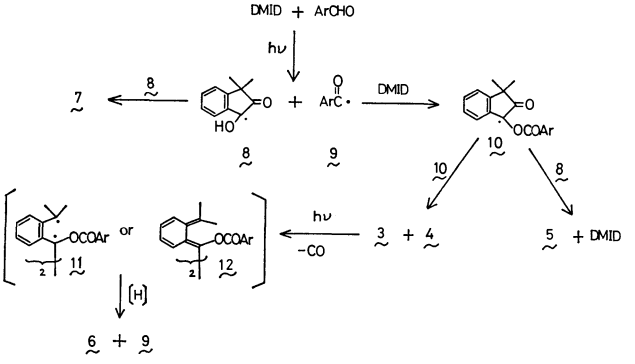

Scheme 2.

Table 2. Some physical properties of the photoproducts obtained

Photo-adducts	Molecular formula		Found (%)	Calcd (%)	Mp/°C	IR spectra (C=O) cm^{-1}		^{1}H-NMR spectra (CCl_4; ppm)
3a	$C_{38}H_{34}O_8$	C;	73.02	73.77	232—233	1724	1777	1.52(s, -Me), 1.55(s, -Me), 3.76(s, -OMe), 6.5—6.7(m, $2H_{arom.}$) 7.1—7.2(m, $2H_{arom.}$), 7.2—7.6(m, $4H_{arom.}$).
		H;	5.87	5.54				
4a[a]	$C_{38}H_{34}O_8$	C;	73.41	73.77	214—215	1720	1768	0.82(s, -Me), 1.52(s, -Me), 3.82 (s, -OMe), 6.8—6.9(m, $2H_{arom.}$), 6.9—7.4(m, $4H_{arom.}$), 8.0—8.1(m, $2H_{arom.}$).
		H;	5.81	5.54				
3b	$C_{38}H_{34}O_6$	C;	77.79	77.79	231—232	1723	1773	1.56(s, -Me), 1.60(s, -Me), 2.30(s, Ar-Me), 7.0(m, $4H_{arom.}$), 7.3—7.7(m, $4H_{arom.}$).
		H;	6.02	5.84				
4b	$C_{38}H_{34}O_6$	C;	77.39	77.79	250—251	1727	1763	0.76(s, -Me), 1.52(s, -Me), 2.41(s, Ar-Me), 6.8—7.4(m, $4H_{arom.}$), 7.1—7.2(m, $2H_{arom.}$), 7.9—8.0(m, $2H_{arom.}$).
		H;	5.87	5.84				
3c	$C_{36}H_{30}O_6$	C;	76.79	77.40	229—231	1727	1767	1.52(s, -Me), 1.57(s, -Me), 7.1—7.7 (m, $4H_{arom.}$), 7.16(m, $5H_{arom.}$).
		H;	5.59	5.41				
4c	$C_{36}H_{30}O_6$	C;	77.12	77.40	235—236	1728	1774	0.75(s, -Me), 1.60(s, -Me), 7.3—7.8 (m, $4H_{arom.}$), 7.1—7.3(m, $5H_{arom.}$)
		H;	5.62	5.41				
3d	$C_{36}H_{28}O_6Cl_2$	C;	68.42	68.91	223—224	1736	1775	1.50(s, -Me), 1.55(s, -Me), 6.5—6.9 (m, $4H_{arom.}$), 7.1—7.4(m, $4H_{arom.}$)
		H;	4.62	4.50				
		Cl;	11.27	11.30				
4d	$C_{36}H_{28}O_6Cl_2$	C;	68.99	68.91	223—224	1722	1767	1.21(s, -Me), 1.58(s, -Me), 7.1—7.8 (m, $4H_{arom.}$), 7.4—8.0(m, $4H_{arom.}$)
		H;	4.50	4.50				
		Cl;	11.26	11.30				
6a[b]	$C_{29}H_{28}O_5$	C;	76.45	76.29	129—130	1695	1716	1.22(d, -Me, J=7 Hz), 1.25(d, -Me, J= 7 Hz), 1.48(s, -Me), 1.63(s, -Me), 3.00(m, 1H), 3.76(s, -OMe), 7.2—7.5(m, $8H_{arom.}$), 6.7(m, $2H_{arom.}$), 7.6—7.7(m, $2H_{arom.}$)
		H;	6.18	6.18		1757		
6c	$C_{28}H_{26}O_4$	C;	78.80	78.85	111	1692	1720	1.20(d, -Me, J=7 Hz), 1.24(d, -Me, J=7 Hz), 1.48(s, -Me), 1.47(s, -Me), 1.65(s, -Me), 7.1—7.5(m, $8H_{arom.}$), 7.4(m, $5H_{arom.}$), 2.99(m, 1H).
		H;	6.14	6.14		1750		

a) ^{13}C-NMR of **4a**($CDCl_3$); 24.41(q), 28.32(q), 48.99(s), 55.50(q), 86.10(s), 114.09(d), 122.23(d), 123.37(d), 125.97(s), 127.44(d), 131.18(d), 132.48(d), 134.44(s), 149.57(s), 164.06(s), 163.00(s), and 213.22(s). b) ^{13}C-NMR of **6a** ($CDCl_3$); 24.08(q), 24.41(q), 26.04(q), 27.34(q), 30.76(d), 50.61(s), 55.00(q), 91.30(s), 113.90(d), 121.09(d), 123.04(d), 125.32(s), 126.46(d), 128.25(d), 130.69(d), 132.32(s), 137.04(d), 138.18(d), 147.13(s), 149.73(s), 163.57(s), 164.22(s), 201.66(s), and 213.22(s).

5. The 2:1 adduct, **6**, is apparently the secondary photoproduct derived from **3** and **4**, since it was not formed upon irradiation with light of wavelength above 400 nm, to which **3** and **4** were transparent. The facile photodecarbonylation of 2-indanone derivatives is a well-known process.[6] Hydrogen transfer to a possible intermediate, the diradical, **11** or *o*-xylylene, **12**, will lead to the formation of **6**. In accord with this, the photochemical conversion of **3** and **4** to **6** occurs in the presence of aromatic aldehydes.

Noteworthy is the finding that the out-of-cage products are formed exclusively in the photochemical reaction of DMID with aldehydes, in spite of the DMID's cyclic structure.

Experimental

The apparatus and equipment used in this study were described in a preceding paper.[4]

A degassed benzene solution of DMID[7] (33 mM) and aldehyde (33 mM) was irradiated for 2 h in a Pyrex tube, using a 300 W high-pressure Hg lamp. After the removal of the solvent, the products were separated by preparative TLC, developing three times with benzene/dichloromethane. The 2:1 adduct, **6**, developed at $R_f \approx 0.7$, the 1:1 adduct, **5**, at ≈ 0.5, and the 2:2 adducts, **3** and **4**, at ≈ 0.2—0.3. The 2:1 adduct, **6**, was purified once more by preparative TLC, developing with benzene, and by recrystallization from dichloromethane/hexane. The 2:2 adducts, **3** and **4**, were recrystallized from chloroform.

References

1) a) G. E. Gream, J. C. Paice, and C. C. R. Ramsey, *Aust. J. Chem.*, **20**, 1671 (1967); b) K. Maruyama and T. Takahashi, *Bull. Chem. Soc. Jpn.*, **49**, 3132 (1976).

2) K. Maruyama and A. Takuwa, *Bull. Chem. Soc. Jpn.*, **49**, 2760 (1976).

3) D. L. Bunbury and C. T. Wang, *Can. J. Chem.*, **46**, 1473 (1968).

4) K. Maruyama, A. Osuka, and Y. Naruta, *Bull. Chem. Soc. Jpn.*, **51**, 3047 (1978).

5) P. O. Bartlett, E. P. Benzing, and R. E. Pincok, *J. Am. Chem. Soc.*, **82**, 1762 (1960).

6) a) C. R. Starr and R. H. Eastman, *J. Org. Chem.*, **31**, 1393 (1966); b) K. K. de Fonseka, J. J. McCullongh, and A. Yarwood, *J. Am. Chem. Soc.*, **101**, 3277 (1979).

7) C. F. Koelsh and C. D. Le Claire, *J. Org. Chem.*, **6**, 516 (1941).

Restricted Rotation Involving the Tetrahedral Carbon. XXXI. Barriers to Rotation in 2,3-Dichloro-9-(1-cyano or 1-methoxycarbonyl-1-methylethyl)triptycenes[1]

Soichi Otsuka, Gaku Yamamoto, Tsutomu Mitsuhashi, and Michinori Ōki*
Department of Chemistry, Faculty of Science, The University of Tokyo, Tokyo 113
(Received December 8, 1979)

Synopsis. The title compounds were prepared to see the effects of substituents in 1-position on the barriers to rotation about the C_9–C_{subst} bond. The barrier was found to be higher for the cyano compound than those for the corresponding compounds carrying a substituent in 1-position, whereas the methoxycarbonyl compound gave almost the same barrier irrespective of the substituent.

In one of the preceding papers, we have shown that the barriers to rotation in 1-substituted 9-(1-cyano-1-methylethyl)triptycenes are always lower than that of 9,10-bis(1-cyano-1-methylethyl)triptycene[2] and have suggested that 9-(1-cyano-1-methylethyl)triptycenes which do not carry a substiuent in 1-position should demonstrate a higher barrier to rotation due to the enhanced stability of the ground state of the rotamers.[3] We wish to report in this paper that 2,3-dichloro-9-(1-cyano-1-methylethyl)triptycene (**1**), which lacks a substituent in 1-position, has shown a higher barrier than those with a substitutent in 1-position. Incidentally, the barrier to rotation of 2,3-dichloro-9-(1-methoxycarbonyl-1-methylethyl)-triptycene (**2**) is almost the same with those carrying a substituent in 1-position.

The syntheses of the compounds in question were carried out as was reported in the previous paper. Usually the ±*sc* form was obtained preferentially and the ±*sc* form (or a ±*sc*-form-rich mixture) was heated to obtain a ±*sc*-*ap* mixture. Chromatography of the ±*sc*-*ap* mixture gave the *ap* form.

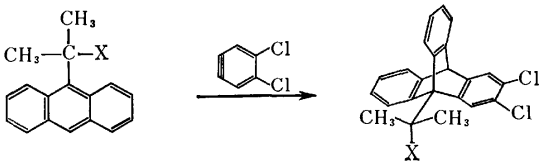

1: X=CN
2: X=COOCH$_3$

Experimental

Spectral Measurement. ^{1}H NMR spectra were recorded on a Hitachi R-20B spectrometer operating at 60 MHz. Infrared spectra were obtained with a Hitachi 260-30 infrared spectrometer.

Materials. Syntheses and isomerization were carried out as follows.

2,3-Dichloro-9-(1-cyano-1-methylethyl)triptycene (1). To a refluxing solution of 1.00 g (4.08 mmol) of 9-(1-cyano-1-methylethyl)anthracene and 1.0 ml of isopentyl nitrite in 35 ml of 1,2-dimethoxyethane, was slowly added 1.10 g (5.34 mmol) of 4,5-dichloroanthranilic acid[4] in 15 ml of 1,2-dimethoxyethane under a nitrogen atmosphere. The mixture was heated for further 40 min and filtered. The solution was evaporated and the residue was chromatographed on alumina to give 727 mg of ±*sc*-**1**, mp 283—284 °C. Found: C, 73.65; H, 4.39; N, 3.56; Cl, 18.19%. Calcd for $C_{27}H_{17}Cl_2N$: C, 73.85; H, 4.39; N, 3.59; Cl, 18.17%. ^{1}H NMR ($CDCl_3$, δ): 2.43 (6H, s), 5.26 (1H, s), 7.0—7.2 (4H, m), 7.3—7.6 (3H, m), 7.45 (1H, s), 7.8—8.0 (1H, m), 7.95 (1H, s). IR (KBr): 2235 cm^{-1}.

Refluxing a solution of 337 mg of ±*sc*-**1** in 20 ml of *o*-dichlorobenzene overnight and subsequent chromatography on alumina gave 116 mg of *ap*-**1**, mp 233—235 °C. Found C, 73.56; H, 4.19; N, 3.76; Cl, 17.74%. Calcd for $C_{27}H_{17}Cl_2N$: C, 73.85; H, 4.39; N, 3.59; Cl, 18.17%. ^{1}H NMR ($CDCl_3$, δ): 2.43 (6H, s), 5.26 (1H, s), 7.0—7.2 (4H, m), 7.3—7.5 (2H, m), 7.54 (1H, s), 7.60 (1H, s), 7.8—8.1 (2H, m). IR (KBr): 2240 cm^{-1}.

2,3-Dichloro-9-(1-methoxycarbonyl-1-methylethyl)triptycene (2) was prepared similarly from 9-(1-methoxycarbonyl-1-methylethyl)anthracene and 4,5-dichlorobenzyne. The reaction gave a 6:1 ±*sc* and *ap* mixture in 38% yield after rough chromatography. ±*sc*-**2** was obtained in pure form by chromatography since this form was eluted first: mp 211—213 °C. Found: C, 71.11; H, 4.61; Cl, 16.48%. Calcd for $C_{25}H_{20}Cl_2O_2$: C, 70.93; H, 4.76; Cl, 16.75%. ^{1}H NMR ($CDCl_3$, δ): 2.27 (6H, s), 3.78 (3H, s), 5.20 (1H, s), 6.9—7.5 (7H, m), 7.39 (2H, s), 7.6—7.8 (1H, m). IR (KBr): 1735, 1715 cm^{-1}.

ap-**2**, mp 244—245 °C, was obtained similarly by isomerization of ±*sc*-**2** followed by chromatography. Found: C, 71.19; H, 4.70%. Calcd for $C_{25}H_{20}Cl_2O_2$: C, 70.93; H, 4.76%. ^{1}H NMR ($CDCl_3$, δ): 2.28 (6H, s), 3.77 (3H, s), 5.22 (1H, s), 6.9—7.1 (4H, m), 7.2—7.5 (4H, m), 7.47 (1H, s), 7.72 (1H, s). IR (KBr): 1740 cm^{-1}.

Kinetic Measurement. Solutions of compound **1** or **2** in 1-chloronaphthalene were heated by immersing the samples in appropriate boiling baths. The details were reported elsewhere.[3]

Results and Discussion

Assignment of the ±*sc* structures was not straightforward, since both forms, ±*sc* and *ap*, gave a singlet signal for the methyl groups in ^{1}H NMR spectra. We took advantage of the method of syntheses and an aspect of ^{1}H NMR spectra for the structural assignments. Firstly, the formation of triptycenes from anthracenes and benzynes are known to be stereoselective to a large extent:[4] the incoming benzynes prefer the antiperiplanar position of the largest group. It will be reasonable to assume that the ±*sc*-form is produced preferentially in this case as well as the similar cases reported elsewhere.[3] Secondly, close examination of the NMR spectra in the aromatic region discloses that there are two singlets which are assignable to 1 and 4 protons. It may be reasonable to assume that the protons in 4-position give signals at almost the same chemical shift: a signal at δ 7.45 for the major product of **1** and that at δ 7.54 for the minor are due to 4-protons. Consideration of anisotropy effects of the cyano group[5] leads to the conclusion

Table 1. Rates of isomerization, equilibrium constants and thermodynamic parameters for the processes $\pm sc \rightleftharpoons ap$ of compounds **1** and **2**

X	T / °C	k ($\pm sc \rightarrow ap$) / s^{-1}	k ($ap \rightarrow \pm sc$) / s^{-1}	K ($\pm sc/ap$)	ΔH / kJ mol^{-1}	ΔS / J K^{-1} mol^{-1}
CN	189	5.99×10^{-5}	1.34×10^{-4}	2.24	−7.5	−22.6
	179	1.88×10^{-5}	3.81×10^{-5}	2.02		
	162	4.47×10^{-6}	9.11×10^{-6}	2.04		
	152	1.14×10^{-6}	2.07×10^{-6}	1.82		
$COOCH_3$	189	3.57×10^{-4}	1.00×10^{-3}	2.80	−1.3	−11.3
	179	1.88×10^{-4}	5.22×10^{-4}	2.78		
	162	3.54×10^{-5}	8.92×10^{-5}	2.52		
	152	1.44×10^{-5}	4.06×10^{-5}	2.82		

Table 2. Kinetic parameters for the internal rotation of compounds **1** and **2**

X	Process	ΔH^* / kJ mol^{-1}	ΔS^* / J K^{-1} mol^{-1}	E_a / kJ mol^{-1}	log A
CN	$\pm sc \rightarrow ap$	164.8	27.2	168.6	14.8
	$ap \rightarrow \pm sc$	172.4	49.8	176.0	16.0
$COOCH_3$	$\pm sc \rightarrow ap$	141.4	−7.5	145.0	13.0
	$ap \rightarrow \pm sc$	142.7	3.8	146.4	13.6

that the 1-proton in $\pm sc$-**1** should give a signal at a lower field than *ap*-**1**. This supports the conclusion that the major product is $\pm sc$-**1**. Similarly, of the two signals due to 1-protons of $\pm sc$-**2** and *ap*-**2**, the signal due to 1-proton of $\pm sc$-**2** should be at a higher field than that of *ap*-**2**. The signals at δ 7.39 for the major product is an overlap of those due to 1- and 4-protons and is at a higher field than the signal at δ 7.72 for the minor product. Thus the major product is again the $\pm sc$ form of **2**.

The equilibrium constants and the rates of isomerization obtained at various temperatures are listed in Table 1. From these values thermodynamic parameters were obtained as also shown in Table 1. Kinetic parameters were obtained by both Eyring plot and Arrhenius plot and are shown in Table 2.

Since the Arrhenius activation energy for rotation of 9-(1-cyano-1-methylethyl)triptycenes which carry a chloro or a methyl group in 1-position is about 150 kJ mol^{-1},[3] those of compound **1** are at least 12 kJ mol^{-1} higher than the former. Thus the barrier to rotation, being the difference in energies between the transition state and the ground state, is high for compound **1** because of the stability of the ground state, although the energy of the transition state for rotation is expected to be lower than that for the corresponding compounds carrying a peri-substituent.

It is interesting to note that the free energy of activation for rotation in compound **2** at 177 °C (143.1 kJ mol^{-1}) is about the same with the corresponding compounds carrying a substituent in 1-position, although in the latter two processes, $\pm sc \rightarrow ap$ and $ap \rightarrow \pm sc$, a fairly large difference has been seen because of the instability of the *ap* form. This phenomenon may to attributed to the raise of the ground state relative to the cyano compound (**1**) because the methoxycarbonyl group is a large group in a plane which causes severe interaction with the triptycyl moiety.

We wish to acknowledge the receipt of a Grant-in-Aid for Scientific Research of the Ministry of Education which supported this work.

References

1) Part XXX: G. Yamamoto and M. Ōki, *Chem. Lett.*, **1979**, 1255.
2) H. Iwamura, *J. Chem. Soc., Chem. Commun.*, **1973**, 232.
3) S. Otsuka, T. Mitsuhashi, and M. Ōki, *Bull. Chem. Soc. Jpn.*, **52**, 3663 (1979).
4) G. Yamamoto and M. Ōki, *Bull. Chem. Soc. Jpn.*, **48**, 3686 (1975).
5) G. S. Reddy and J. H. Goldstein, *J. Chem. Phys.*, **39**, 3509 (1963).

Formation of C–S Bond by the Elimination of Perfluorocarboxylic Acid

Hajimu KAWA and Nobuo ISHIKAWA*

Department of Chemical Technology, Tokyo Institute of Technology, Ookayama, Meguro-ku, Tokyo 152

(Received December 28, 1979)

Synopsis. Thiirane was readily generated from 2-mercaptoethyl trifluoroacetate or pentafluoropropionate by the intramolecular elimination of the perfluorocarboxylic acid with triethylamine. Alkyl benzyl sulfides were also prepared from benzyl trifluoroacetate or pentafluoropropionate and alkanethiols by the intermolecular elimination of the perfluorocarboxylic acid

In a course of our studies on pentafluoropropionylation of various 1,2-bifunctional ethanes with hexafluoro-1,2-epoxypropane(**1**)–triethylamine system,[1] it was found that a considerable amount of thiirane was formed from 2-mercaptoethanol.

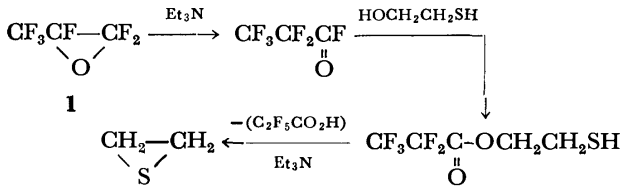

The reaction route shown above was supported by the experimental fact that pentafluoropropionic acid was eliminated very easily from 2-mercaptoethyl pentafluoropropionate (**2**) and thiirane was obtained in a yield of 60%. The formation of thiirane by decarboxylic acid reaction is not of novelty, because Miles and his co-workers have reported that thiirane was formed[2] when they examined the hydrolysis of 2-mercaptoethyl acetate with aqueous sodium hydroxide. However, the yield of thiirane in their reaction is very poor, as a mild base such as triethylamine is not strong enough for the formation of thiirane and this unstable compound easily polymerizes in the presence of aqueous sodium hydroxide.

In our process, the reaction in diglyme proceeded smoothly at room temperature, in a short period such as 30 min, and the resulting thiirane was separated by only distillation under a reduced pressure (≈30 mmHg). Thus the perfluorocarboxylate seemed to be a much more convenient intermediate compound for the generation of thiiranes from 2-mercaptoethanols rather than a usual fluorine-free carboxylate.

Further we confirmed that thiirane can also be prepared by treating 2-mercaptoethanol with trifluoroacetic anhydride and two equivalents of triethylamine.

In the extention of the C–S bond formation by

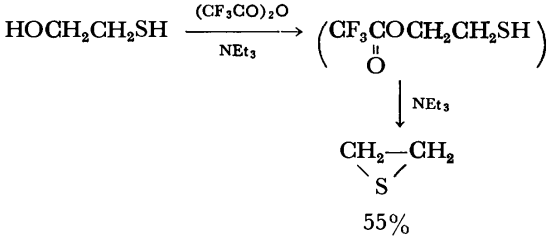

the intramolecular elimination of perfluorocarboxylic acid described above, a similar intermolecular elimination was examined. We chose benzyl alcohol as an active alcohol and reactions of benzyl trifluoroacetate or pentafluoropropionate with several alkanethiols were tried. Several results of the preparation

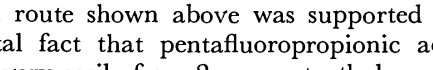

of benzyl sulfides by this procedure are shown in Table 1. For these intermolecular condensations, it was necessary to apply more polar solvents and higher temperatures.

Table 1. Yields of $PhCH_2SR$ (%)

R	Yield (%) R_f		$PhCH_2SR$	
	CF_3[a]	CF_3CF_2[b]	Bp °C/mmHg [Mp/°C]	(lit)
n-Pr	15	55	88—89/10	(112/14)[c]
n-Bu	20	71	113—114/8	(123/13)[c]
$PhCH_2$	33	76	[48—49]	([49—50])[d]

a) GLC yield. b) Isolated yield. c) I. J. Buchi, M. Prost, H. Eichenberger, and R. Lieberherr, *Helv. Chim. Acta.*, **35**, 1527 (1952). d) "Handbook of Chemistry and Physics," 55th ed, CRC Press, Inc., Cleveland, Ohio (1974—1975), p. C498.

Thus, benzyl perfluorocarboxylate and an alkanethiol were allowed to react in *N*,*N*-dimethylformamide at ≈120 °C in the presence of triethylamine. Pentafluoropropionate gave much higher yields of sulfides than trifluoroacetate did and this should be due to the fact that a pentafluoropropionyloxyl group is a better leaving group compared with a trifluoroacetoxyl group. As the electronegativities of trifluoromethyl and pentafluoroethyl groups are almost similar,[3] the difference should be due to the bulkiness of these leaving groups. Thus in comparison with a trifluoroacetyl group, the bulkier pentafluoropropionyl group should make the ester less stable thermodynamically.

Perfluorocarboxylates of other alcohols, such as cyclohexyl-, allyl-, and *t*-butyl alcohol, were tried for this reaction, but none of good results were obtained.

Experimental

2-Mercaptoethyl Pentafluoropropionate. In a sealed glass vessel, 2-mercaptoethanol (1.56 g, 20 mmol) was treated with hexafluoro-1,2-epoxypropane (bp −27 °C, 3.32 g, 20 mmol) and a catalytic amount of triethylamine (≈0.1 g) in acetonitrile (20 ml) for 30 min at room temperature. The reaction mixture was poured into water and the lower oily layer was separated. It was washed with water, dried ($MgSO_4$) and distilled to give 2-mercaptoethyl pentafluoropropionate (3.23 g, 72%). Bp 67—68 °C/77 mmHg (1 mmHg=133.322 Pa) (lit,[1] 68 °C/77 mmHg).

2-Mercaptoethyl trimethylsilyl ether and diethyl ether

were used instead of 2-mercaptoethanol and acetonitrile in the previous experiment. 2-Mercaptoethyl pentafluoropropionate was obtained in 85% yield.

Thiirane 2-Mercaptoethanol (1.56 g, 20 mmol), triethylamine (2.02 g, 20 mmol), and diglyme (10 ml) were placed in a sealed glass tube, and the mixture was cooled to −70 °C. Liquefied hexafluoro-1,2-epoxypropane (3.32 g, 20 mmol) was introduced into this vessel and the whole was brought to room temperature with stirring. After the reaction was continued for 30 min at this temperature, the pressure was reduced to about 30 mmHg, and the gas evolved was trapped in a Dry Ice–acetone bath. The trapped material was identified to thiirane (0.72 g, 60%). Bp 53—54° C (lit,[4] bp 54.0—54.5 °C).

Triethylamine (2.02 g, 20 mmol) was added to a solution of 2-mercaptoethyl pentafluoropropionate (4.48 g, 20 mmol) in diglyme (10 ml) in an ice bath. The mixture was stirred for 30 min at room temperature. The pressure was then gradually reduced to ≈30 mmHg and evolved thiirane was collected in a Dry Ice–acetone bath (0.84 g, 70%).

To a solution of 2-mercaptoethanol (1.56 g, 20 mmol) and triethylamine (4.04 g, 40 mmol) in diglyme (10 ml), trifluoroacetic anhydride (4.20 g, 20 mmol) was added slowly in an ice bath. After 1 h of stirring at room temperature, thiirane was obtained by a similar treatment (0.60 g, 50%).

Alkyl Benzyl Sulfides. A typical procedure is as follows. The benzyl perfluorocarboxylate (10 mmol) was mixed with a thiol (12 mmol) and triethylamine (15 mmol) in *N,N*-dimethylformamide (5 ml). The mixture was heated at 120 °C for 3 h with stirring and the resulting mixture was subjected to distillation *in vacuo* to give the corresponding sulfide.

References

1) H. Kawa and N. Ishikawa, *Bull. Chem. Soc. Jpn.*, **53**, 1694 (1980).

2) L. W. C. Miles and L. N. Owen, *J. Chem. Soc.*, **1952**, 817.

3) W. A. Sheppard and C. M. Sharts, "Organic Fluorine Chemistry," Benjamine Inc, New York (1969), p. 37.

4) S. Searles, E. F. Lutz, H. R. Hays, and H. E. Mortensen, *Org. Synth.*, Coll. Vol. V, 562 (1973).

Bromophenols from the Red Alga *Rhodomela larix*[1]

Minoru Suzuki, Nobuhiko Kowata, and Etsuro Kurosawa*
Department of Chemistry, Faculty of Science, Hokkaido University, Sapporo 060
(Received January 14, 1980)

Synopsis. Two new bromophenols, 3-bromo-4-hydroxybenzaldehyde and a brominated dibenzyl ether derivative, were isolated from the red alga *Rhodomela larix*, along with several known bromophenols which have previously been isolated from *R. larix* and other species.

In connection with our interest in the halogenated secondary metabolites of the marine red algae, especially Rhodomelaceae, we have investigated the neutral and acidic constituents of the red alga *Rhodomela larix* (Turner) C. Agardh, which was collected at Oshoro Bay, Hokkaido. Several bromophenols have previously been obtained from this algae, collected in different locations.[2-4] Our specimen displayed no halogenated compound in the neutral constituents, and instead yielded two new bromophenols, 3-bromo-4-hydroxybenzaldehyde (**6a**) and a brominated dibenzyl ether derivative (**8a**), along with known bromophenols, **1a**, **2a**, **3a**, **4a**, **5a**, and **7a**, from the acidic constituents. We wish to report herein the isolation and structures of these brominated phenols.

Half-dried algae were extracted with MeOH, and the neutral and acidic fractions were obtained from the MeOH extracts by the usual method. The neutral fraction gave no halogenated compound except for a sterol and a mixture of fatty acid esters. The acidic fraction was subjected to separation by a combination of column and thin-layer chromatography on silica gel to give several bromophenols. The isolation, purification, and identification of these bromophenols were carried out more conveniently *via* their acetates (**1b**—**8b**) (see Experimental section).

The major compound, **1b**, was identified as the acetate of 2,3-dibromo-4,5-dihydroxybenzyl methyl ether (**1a**)[2-4] by comparison of the spectral data with those of an authentic sample.[2] One of the minor compounds, **2b**, was found to be identical with the acetate of 3,5-dibromo-4-hydroxybenzaldehyde (**2a**), which has previously been isolated from the marine annelid *Thelepus setosus*[5] and recently from the red alga *Polysiphonia urceolata*.[6] Compounds **3b** and **4b** were found to be identical with the acetate of 3,5-dibromo-4-hydroxybenzyl methyl ether (**3a**) from *P. urceolata*[7] and *Odonthalia dentata*,[8] and the acetate of 3,5-dibromo-4-hydroxybenzyl alcohol (**4a**) from *O. dentata*,[8-10] *R. confervoides*,[8-10] *P. urceolata*,[6] and other species,[8,10] respectively. Furthermore, **5b** was identified as the acetate of 3-bromo-4-hydroxybenzyl methyl ether (**5a**) from *O. dentata*.[8] The structures of **2b**, **3b**, **4b**, and **5b** were confirmed by syntheses.

Compound **6b**, $C_9H_7O_3Br$, mp 60—62 °C, showed in its NMR spectrum the presence of an aryl acetate group at 2.34 (3H, s), a 1,3,4-trisubstituted aromatic ring at δ 7.26 (1H, d, J=8 Hz), 7.78 (1H, dd, J=8, 2 Hz), and 8.05 (1H, d, J=2 Hz), and an aldehyde group at 9.85 (1H, s). The spectral data of **6b** suggested that **6b** would be the acetate of 3-bromo-4-hydroxybenzaldehyde (**6a**), the structure of which was confirmed by comparison of the physical properties with those of the synthetic sample. To our knowledge, the isolation of 3-bromo-4-hydroxybenzaldehyde (**6a**) is the first example of the natural product.

One of the two other compounds, **7b**, was identified as the acetate of the brominated diphenylmethane derivative (**7a**), which has previously been isolated from *R. larix* together with **9**,[4] by comparison of the spectral data. The other compound, **8b**, $C_{22}H_{18}O_9Br_4$, mp 176—177 °C, revealed in its IR spectrum the absence of hydroxyl and carbonyl groups except for the acetoxyl groups at ν_{max} 1781 cm^{-1}. The NMR spectrum of **8b** showed four signals (each singlet) at δ 2.30 (6H) and 2.36 (6H) due to four acetoxyl groups, 4.70 (4H) due to two Ar–CH_2–(O) moieties, and 7.39 (2H) due to two aromatic protons. Hence, one of nine oxygen atoms in **8b** must form a straight chain ether linkage. The NMR spectrum of **8b** was very similar to that of **1b**, except for the signal of the methoxyl group in **1b**. Therefore, the structure of **8b** would be represented by formula **8b**, which will also be explicable well from the standpoint of biogenesis.

2,3-Dibromo-4,5-dihydroxybenzaldehyde has previously been isolated from *R. larix*.[2-4] However, we could not detect this aldehyde during our examination.[11] The result of our present study seems to be different from those of the previous studies[2-4] on account of the differences of the locations and seasons of the algal collections and/or the extraction procedures.

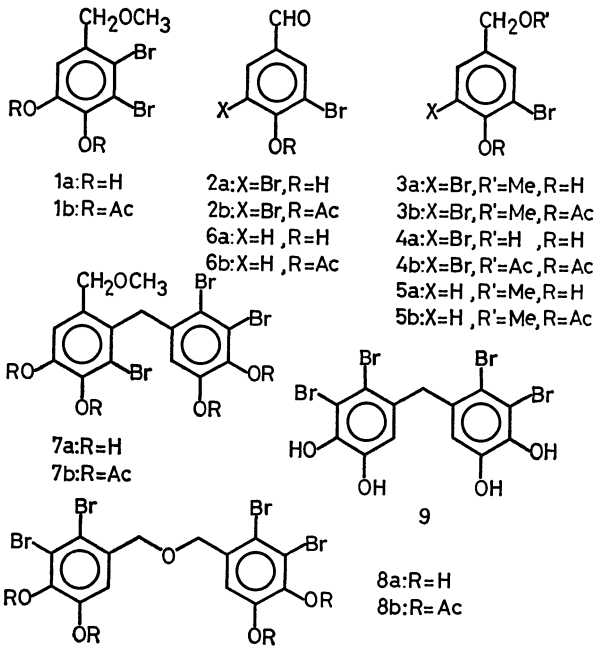

Experimental

All the mps were uncorrected. The IR spectra were measured on a Nihon-Bunko A-102 spectrometer. The NMR spectra were recorded on a JEOL JNM-PS-100 spectrophotometer, TMS being used as the internal reference. Coupling constants are given in Hz. Silica gel (Merck, Kieselgel 60, 70—230 mesh) was used for the column chromatography, and silica gel (Merck, Kieselgel GF_{254} (Type 60)) was used for the preparative thin-layer chromatography (PTLC).

Isolation. *Rhodomela larix* was collected in September 22, 1978, at Oshoro Bay, Hokkaido. The half-dried algae (1.3 kg) were extracted with MeOH, and the MeOH soln was concentrated under reduced pressure. The residue was percolated with ether, and the ether soln was shaken with 1 M KOH. The ether layer was washed with water, dried over Na_2SO_4, and then evaporated to give a neutral fraction (8 g). The KOH layer was cautiously acidified with dilute HCl and extracted with ether. The ether soln was washed with water, dried over Na_2SO_4, and then evaporated to give an acidic fraction (8 g). Repeated column chromatography of the neutral fraction gave only a sterol (probably cholesterol) and a mixture of fatty acid esters. The acidic fraction was fractionated by column chromatography as follows.

A Benzene-eluted Fraction: This fraction consisted of a mixture of **2a** and **3a**, which was subjected to repeated column chromatography and PTLC to yield **2a** (0.1% of the acidic constituents) and **3a** (0.8%). Acetylation of **2a** and **3a** was carried out with acetic anhydride in pyridine at room temp in the usual manner to yield **2b** and **3b**, respectively.

A Benzene/ether (10:1)-eluted Fraction: This fraction was further chromatographed on PTLC to yield **4a** (0.3%), **5a** (0.6%), **6a** (0.2%), and **1a** (6%). These phenols were acetylated by the usual method to yield **4b**, **5b**, **6b**, and **1b**.

A Benzene/ether (1:1)-eluted Fraction: This fraction consisted of a mixture of **7a** (1%) and **8a** (0.2%), which, following acetylation, was purified by PTLC to yield **7b** and **8b**.

1b: The mp and the spectral data were consistent with those of an authentic specimen.[2]

2b: Mp 110—111 °C (EtOH): IR, ν_{max} ($CHCl_3$): 1790, 1775, 1710, 1565, 1370, 1245, 1190, 1175, 1010, 925, and 890 cm^{-1}; NMR, δ (CCl_4): 2.39 (3H, s), 7.99 (2H, s), and 9.81 (1H, s); MS, *m/e* 324, 322, 320 (M^+). Found: C, 33.50; H, 1.86%. Calcd for $C_9H_6O_3Br_2$: C, 33.57; H, 1.88%.

3b: Colorless oil; IR, ν_{max} (film): 1785, 1775, 1595, 1560, 1405, 1370, 1245, 1205, 1180, 1110, 1010, 890, 805, and 740 cm^{-1}; NMR, δ ($CDCl_3$): 2.40 (3H, s), 3.40 (3H, s), 4.41 (2H, s), and 7.53 (2H, s); MS, *m/e* 340, 338, 336 (M^+).

4b: The mp and the NMR spectrum were consistent with those reported.[9]

5b: Colorless oil; IR, ν_{max} (film): 1770, 1600, 1490, 1370, 1205, 1190, 1105, 1045, 1010, 910, 870, and 825 cm^{-1}; NMR, δ ($CDCl_3$): 2.35 (3H, s), 3.39 (3H, s), 4.43 (2H, s), 7.11 (1H, d, J=8), 7.30 (1H, dd, J=8, 2), and 7.58 (1H, d, J=2); MS, *m/e* 260, 258 (M^+).

6b: Mp 60—62 °C (EtOH–hexane); IR, ν_{max} ($CHCl_3$): 1775, 1705, 1597, 1485, 1375, 1185, 1045, 1010, 915, 890, and 835 cm^{-1}; NMR, δ (CCl_4): 2.34 (3H, s), 7.26 (1H, d, J=8), 7.78 (1H, dd, J=8, 2), 8.05 (1H, d, J=2), and 9.85 (1H, s); MS, *m/e* 244, 242 (M^+). Found: C, 44.44; H, 2.98%. Calcd for $C_9H_7O_3Br$: C, 44.47; H, 2.90%.

7b: Mp 175—177 °C (C_6H_6); IR, ν_{max} ($CHCl_3$): 1777, 1371, 1193, 1141, 1011, 916, and 889 cm^{-1}; NMR, δ ($CDCl_3$): 2.20, 2.30, 2.32, 2.34, 3.31 (each 3H, s), 4.28 (4H, br s), 6.38 (1H, s), and 7.31 (1H, s).

8b: Mp 176—177 °C (chloroform–ether); IR, ν_{max} ($CHCl_3$): 1781, 1372, 1196, 1181, 1141, 1011, 917, and 898 cm^{-1}; NMR, δ ($CDCl_3$): 2.30 (6H, s), 2.36 (6H, s), 4.70 (4H, s), and 7.39 (2H, s); MS, *m/e* 708, 706, 704, 702, 700 ($M^+ - CH_2=C=O$). Found: C, 35.28; H, 2.37%. Calcd for $C_{22}H_{18}O_9Br_4$: C, 35.42; H, 2.43%.

Syntheses of 2b—6b. Bromination of *p*-hydroxybenzaldehyde with Br_2 (1 eq) in AcOH gave a mixture of **2a** and **6a** (1:3), which, following acetylation, was purified by PTLC to give **2b** and **6b**. Treatment of the acetates, **2b** and **6b**, with $NaBH_4$ in EtOH afforded dibromo-*p*-acetoxybenzyl alcohol, and monobromo-*p*-acetoxybenzyl alcohol, respectively. The latter benzyl alcohol was refluxed with MeOH and H_2SO_4 to yield **5a**, which was converted to **5b** by acetylation. The former benzyl alcohol gave **3b** in the same way as has been described above. Moreover, acetylation of the dibromobenzyl alcohol yielded **4b**. These synthetic compounds were identical with the natural bromophenols and their acetates in all respects.

The authors are grateful to Dr. Kazuya Kurata, Department of Industrial Chemistry, Hakodate Technical College, for valuable discussions and for providing the IR and NMR spectra of the acetates of several bromophenols.

References

1) Part XXXIX of "Constituents of Marine Plants." Part XXXVIII: A. Fukuzawa and E. Kurosawa, *Tetrahedron Lett.*, in press.

2) N. Katsui, Y. Suzuki, S. Kitamura, and T. Irie, *Tetrahedron*, **23**, 1185 (1967).

3) B. Weinstein, T. L. Rold, C. E. Harrell, Jr., M. W. Burns III, and J. R. Waaland, *Phytochemistry*, **14**, 2667 (1975).

4) K. Kurata and T. Amiya, *Chem. Lett.*, **1977**, 1435.

5) T. Higa and P. J. Scheuer, *Tetrahedron*, **31**, 2379 (1975).

6) Personal communication from Dr. K. Kurata.

7) K. Kurata, T. Amiya, and N. Nakano, *Chem. Lett.*, **1976**, 821.

8) M. Pedersen, P. Saenger, and L. Fries, *Phytochemistry*, **13**, 2273 (1974).

9) J. S. Craigie and D. E. Gruenig, *Science*, **157**, 1058 (1967).

10) M. Pedersen, *Phytochemistry*, **17**, 291 (1978).

11) *Rhodomela subfusca*,[12] collected in June, 1979, at Bakkai near Wakkanai, Hokkaido, contained only **1a** together with unusual 2,6-di-*t*-butyl-*p*-cresol.

12) K. Kurata and T. Amiya, *Bull. Jpn. Soc. Sci. Fish.*, **41**, 657 (1975).

Study on V_2O_5–Al_2O_3 Catalyst by Means of XPS for the Reduction of Nitric Oxide with Ammonia

Akio Nishijima,* Yoshimichi Kiyozumi, Akifumi Ueno, Minoru Kurita, Hiroyuki Hagiwara, Toshio Sato, and Naoyuki Todo

National Chemical Laboratory for Industry, Higashi, Yatabe-machi, Tsukuba-gun, Ibaraki 305

(Received June 22, 1979)

Synopsis. The V_2O_5–Al_2O_3 catalyst used for the NO reduction in flue gas from a sintering furnace was studied by means of X-ray photoeloctron spectroscopy and X-ray microanalysis. Effects of dust components accumulated on the catalyst and of electronic states of vanadium ions on catalytic activities were discussed.

Of various methods for the removal of nitrogen monoxide in flue gas emitted from stationary combustion equipments, the catalytic reduction of NO with ammonia seems to be most effective.[1–3] Supported V_2O_5 catalysts have been used for industrial gases. It is desirable to know the influence of dust components (Fe, Si, K, Ca, Na, C, S) in flue gas on the life of the catalysts. A pilot plant test using flue gas from a boiler or a coke oven showed that sulfur oxides (SO_x) reduce the activities of the catalysts.[4,5] However, it was observed that K in the flue gas from a sintering furnace lowers the catalytic activities to a greater extent than SO_x.[6,7] In this study, characterization of the V_2O_5–Al_2O_3 catalyst used in the flue gas from a sintering furnace was made by means of X-ray photoelectron spectrometer and X-ray microanalyzer.

Experimental

The catalyst was prepared by impregnating γ-Al_2O_3 (diam. 6 mm, surface area 210 m^2/g, average pore radius 60 Å) with an aqueous solution of vanadium(IV) oxalate.[6] A life test was carried out with a moving bed type reactor (1000 Nm^3/h) at a space velocity of 10000 h^{-1}. The composition of the dust in the flue gas was Fe 28 wt %, SO_4 25 wt %, K 1.5 wt %, Na 0.6 wt %, that of the flue gas from the sintering furnace being NO 170—280 ppm, SO_2 130—260 ppm, O_2 13—15 vol %, H_2O 10—15 vol %, CO_2 10 vol %, and dust 30—120 mg/Nm^3. 200 ml of catalyst taken from the reactor every 100 h of the reaction time was subjected to examination of the change in catalytic properties. The line profile of each element in the catalyst was obtained with a X-ray microanalyzer (Shimadzu). Dust components on catalyst particles and electronic states of the elements in the catalyst were measured with a X-ray photoelectron spectrometer (Dupont 650 B). The values of the binding energies were referred to C 1s photoelectron spectra of contaminant carbon (285.0).

Results and Discussion

Figure 1 shows line profiles of dust components accumulated on the catalyst. S, Si, and Ca were found in inner parts of the catalyst, K and Fe being restricted to surface layers of catalyst particles (Fig. 1 A). On Fe_2O_3–Al_2O_3 catalysts, K permeated into the catalyst particles to form a complex of $[K_2Fe(SO_4)_2]$. The difference in the behavior of K remains unclarified.

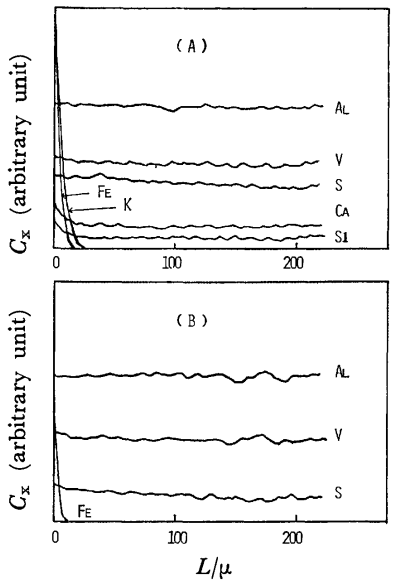

Fig. 1. Distribution analysis of each component in V_2O_5–Al_2O_3 catalyst confirmed by X-ray microanalyzer.
The sample was prepared in a form of hemi-sphere particle to obtain the depth profile. (A): Used for 2000 h, (B): regenerated (heating, washing, and treating with SO_2), L: depth from the surface, C_x: concentration of each component in the catalyst.

The amount of S increased with the reaction time, becoming constant after a certain time. Increase in the concentrations of K, Fe, Ca, and Si continued even after 1000 h.[7] Dust components except S and Fe were removed from the catalyst after regeneration (heating at 550 °C for 2 h and washing at 80 °C for 2 h and subsequent treatment with 500 ppm of SO_2 at 300 °C for 15 h). From the fact that the activity recovered after the regeneration, the effects of S and Fe on the activity are considered to be less than those of the other components.

Figure 2 shows the changes in photoelectron spectra of some dust components on the catalyst. Binding energies of K 2p spectra show that K exists in the form of K_2SO_4. Intensities of these photoelectron spectra, especially those of K and Fe, increased with reaction time. As regards S 2p spectra, the intensity was saturated after 800 h of the reaction. Changes of V $2p_{3/2}$ and Al 2p photoelectron spectra of the catalyst are shown in Fig. 3. The intensity of V $2p_{3/2}$ spectrum decreased more rapidly than that of Al 2p spectrum. This indicates that K sticks predominently on V, the active component, rather than on the carrier, causing a decrease of catalytic activity. The electronic states of vanadium and aluminium ions turned electronegative with reaction time (Fig. 3). The change of elec-

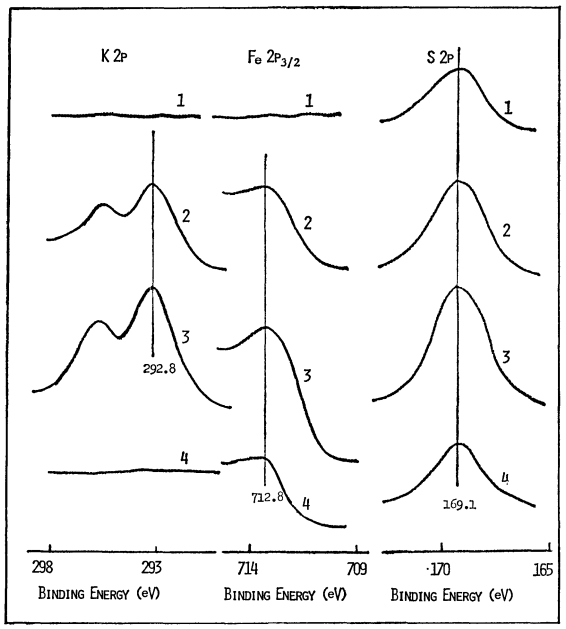

Fig. 2. Change in photoelectron spectra of dust component on V_2O_5–Al_2O_3 catalyst.
1: Fresh (treating with SO_2), 2: used for 600 h, 3: used for 2000 h, 4: regenerated (heating, washing, and treating with SO_2).

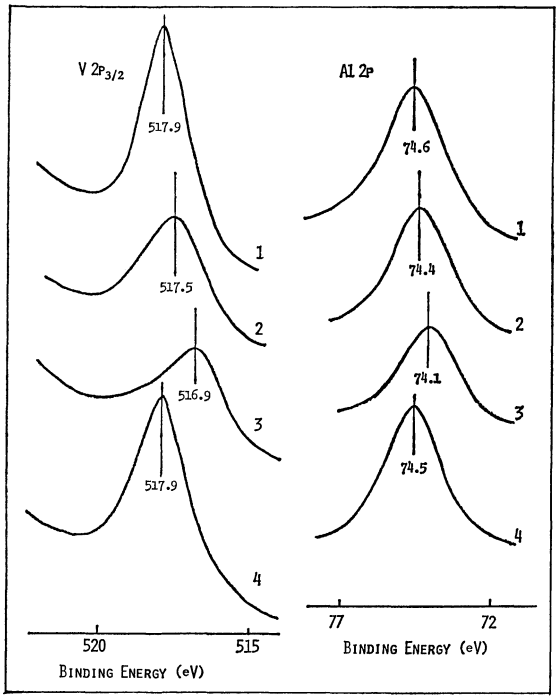

Fig. 3. Change in photoelectron spectra of active component and carrier on V_2O_5–Al_2O_3 catalyst.
1: Fresh (treating with SO_2), 2: used for 600 h, 3: used for 2000 h, 4: regenerated (heating, washing, and treating with SO_2).

tronic state of aluminium ions is due to the formation of $Al_2(SO_4)_3$.[4] The binding energy of vanadium ions of the catalyst subjected to the reaction using the flue gas from the sintering furnace decreased by 1.0 eV, while the value obtained for the catalyst used for a gas without dust components decreased only by 0.5 eV. The difference would be ascribed to the effects of K adhered on V. The optimum electronic state of the cation in the active component shows high activity, the catalytic activity decreasing when the electronic state of the cation deviates from the optimum state to electronegative or electropositive state.[8] Changes in electronic states of vanadium ions would affect the activity of the catalyst for NO reduction. A large decrease in the binding energy would give the result[6] in which the catalytic activity decreases much more rapidly when the catalyst is used in the flue gases containing dust components. The ratio of intensities between V $2p_{3/2}$ and Al 2p spectra and the electronic state of vanadium ions returns to the original one by the regeneration.

References

1) S. Jarros and J. Krizek, *Int. Chem. Eng.*, **8**, 216 (1968).
2) G. Chakrabarti and C. Chu, *Atom. Environ.*, **6**, 297 (1972).
3) P. L. Klimisch and K. C. Taylor, *Env. Sci. Technol.*, **7**, 127 (1973).
4) N. Todo, M. Kurita, H. Hagiwara, A. Ueno, and T. Sato, The Japan-U.S.A. Seminar on Catalytic NO_x Reaction, November (1975), Preprints 3-1.
5) S. Aramaki, M. Atsukawa, Y. Nishimoto, K. Yokoyama, The Japan-U.S.A. Seminar on Catalytic NO_x Reaction, November (1975), Preprints 4-1.
6) A. Nishijima, M. Kurita, T. Sato, Y. Kiyozumi, H. Hagiwara, A. Ueno, and N. Todo, *Nippon Kagaku Kaishi*, **1978**, 893.
7) A. Nishijima, M. Kurita, T. Sato, Y. Kiyozumi, H. Hagiwara, A. Ueno, and N. Todo, *Nippon Kagaku Kaishi*, **1979**, 276.
8) A. Nishijima, Y. Kiyozumi, A. Ueno, M. Kurita, H. Hagiwara, T. Sato, and N. Todo, *Bull. Chem. Soc. Jpn.*, **52**, 3724 (1979).

Heterogeneous Catalysis in the Liquid-phase Oxidation of Olefins. IV. The Activity of a Supported Vanadium or Chromium Oxide Catalyst in the Decomposition of *t*-Butyl Hydroperoxide

Katsuomi TAKEHIRA,* Takashi HAYAKAWA, and Toshio ISHIKAWA

Catalysis Division, National Chemical Laboratory for Industry, Tsukuba Research Center, Yatabe, Ibaraki 305

(Received March 17, 1979)

The liquid-phase decomposition of *t*-butyl hydroperoxide (*t*-BuOOH) has been carried out in benzene under an N_2 atmosphere using a vanadium or chromium oxide, supported on γ-Al_2O_3 or SiO_2 as the catalyst, for the purpose of clarifying the reaction mechanism of the cyclohexene oxidation. The decomposition of *t*-BuOOH on the supported oxide catalyst was a first-order reaction; the main products were *t*-butyl alcohol, di-*t*-butyl peroxide, and acetone, suggesting that *t*-BuOOH is decomposed homolytically on the catalyst by the Haber-Weiss mechanism. The effect of the vanadium–chromium binary system formation was small, but the interaction between metal oxides and the supports appeared to be important in the *t*-BuOOH decomposition. Tetrahedrally co-ordinated vanadium species were formed on SiO_2 and showed the highest activity, followed by the chromium co-ordinated tetrahedrally on SiO_2 or on γ-Al_2O_3, while an octahedrally co-ordinated vanadium or chromium showed low activity. Such order of the activity was in good agreement with that obtained in the liquid-phase oxidation of cyclohexene. We observed a relatively good correlation between the catalytic activity and the acidity of the supported binary metal oxides. The V_2O_5–SiO_2 system showed an especially large acidity; here *t*-butyl alcohol was dehydrated into di-*t*-butyl ether and 2-methyl propene.

The liquid-phase oxidation of cyclohexene with a heterogeneous catalyst, *i.e.*, vanadium–chromium binary oxides (V–Cr), has been studied in terms of the relationship between its structure and the catalytic activity.[1-3] When the binary system was supported on γ-Al_2O_3 or SiO_2, its activity varied greatly depending on the nature of the carrier.[1] It was suggested that the activity of the supported binary system is mainly due to the interactions between the metal oxides and the carrier; a tetrahedral co-ordination is favored on SiO_2, resulting in the increase in its activity. It was also suspected that the supported binary system catalyzes the autoxidation of cyclohexene by accelerating the decomposition of 1-cyclohexenyl hydroperoxide.[1] To confirm the validity of this mechanism, the decomposition of *t*-butyl hydroperoxide (*t*-BuOOH) on a supported binary oxide catalyst has been studied in the present work. *t*-BuOOH has been frequently used as a model compound in studying the mechanism of the catalytic decomposition of hydroperoxides because complicating reactions, such as hydration and rearrangement, can be minimized with tertially alkyl hydroperoxide.[4-12] Also, a direct comparison can be made with the other investigations where *t*-BuOOH was used.[4-12] A further study of the structure of the supported binary system has concurrently been carried out by measuring the electron-spin resonance and the surface acidity so as to clarify their roles in the oxidation of cyclohexene.

Experimental

Catalysts. The metal acetylacetonates ($Me(acac)_n$) were used as received (Tokyo Chemical Industry Co.). The supported binary system catalysts were prepared by the kneading method reported in a preceding paper.[1] The symbols, concentrations (calculated as $V_2O_5+Cr_2O_3$(wt %)) and compositions (in terms of atomic % of Cr/(V+Cr)) of the supported metal oxides, and the specific surface area (S_s), are shown in Tables 1 and 2 respectively.

Procedure of Reaction. The decomposition of *t*-BuOOH was performed in 10-ml reaction tubes with a joint which fitted into a smoothtapered joint provided with a stopcock. The same amount of catalyst (25 mg of the binary catalyst or 5×10^{-6} mol of $Me(acac)_n$) was added to a series of reaction tubes, in each of which the reaction was allowed to proceed for a different time interval. A reactor tube containing the weighed catalyst was placed in an ethanol-solid carbon dioxide mixture, and a 5-ml portion of a previously prepared benzene solution of *t*-BuOOH (0.1 M) was slowly added to the reactor to avoid the suspension of the catalyst. The reactor was then joined to a vacuum system, and the gas phase was replaced with dry nitrogen. The stopcock was then closed to isolate the system. The reactor was attached to a wrist-action shaker to achieve vigorous agitation and then plunged into an oil bath, the temperature of which could be controlled to within ±0.2 °C. The time was recorded from the moment the tube was immersed in the oil bath. Once the desired reaction-time interval had elapsed, the tube was quickly put back into the

TABLE 1. CONCENTRATIONS OF SUPPORTED METAL OXIDES, SYMBOLS, AND SPECIFIC SURFACE AREAS OF CATALYSTS

Concentration $V_2O_5+Cr_2O_3$ (wt %)	γ-Al_2O_3-series[a]		SiO_2-series[b]	
	Symbol	S_s(m^2/g)	Symbol	S_s(m^2/g)
0	γ-Al_2O_3	220	SiO_2	210
1	V–Cr–γ-Al_2O_3-(1)	246	V–Cr–SiO_2-(1)	202
5	V–Cr–γ-Al_2O_3-(5)	277	V–Cr–SiO_2-(5)	181
10	V–Cr–γ-Al_2O_3-(10)	293	V–Cr–SiO_2-(10)	160
20	V–Cr–γ-Al_2O_3-(20)	270	V–Cr–SiO_2-(20)	142

a) Cr/(V+Cr): 50 atom %. b) Cr/(V+Cr): 70 atom %. Both series were prepared from NH_4VO_3 and $Cr(NO_3)_3\cdot9H_2O$.

Table 2. Compositions of supported metal oxides, symbols, and specific surface areas of catalysts

Composition Cr/(V+Cr) (atom %)	G-series[a]		H-series[b]		I-series[c]	
	Symbol	S_s(m²/g)	Symbol	S_s(m²/g)	Symbol	S_s(m²/g)
0	G-0	261	H-0	255	I-0	109
20	G-2	274			I-2	105
30			H-3	268		
40	G-4	282			I-4	124
50	G-5	265	H-5	249		
60	G-6	260			I-6	132
70			H-7	232	I-7	138
80	G-8	252			I-8	131
100	G-10	244	H-10	212	I-10	136

a) Prepared from NH_4VO_3, $Cr(NO_3)_3 \cdot 9H_2O$, and alumina hydrate. b) Prepared from NH_4VO_3, $(NH_4)_2CrO_4$, and alumina hydrate. c) Prepared from NH_4VO_3, $Cr(NO_3)_3 \cdot 9H_2O$, and silica sol. The concentration of metal oxides (calculated as $V_2O_5+Cr_2O_3$) was 20 wt % in each series.

ethanol–solid carbon dioxide mixture to stop any further reaction, and the catalyst was allowed to settle. The clear liquid phase was then removed from the reactor for analysis.

Materials. The *t*-BuOOH was purified by vacuum distillation (40.0 °C/25 mmHg). The di-*t*-butyl peroxide (*t*-Bu_2O_2) obtained from the Nippon Kayaku Co. was shown to be pure by gas chromatography. The di-*t*-butyl ether (*t*-Bu_2O) was prepared by the method of West *et al.*[13] The other materials, *t*-butyl alcohol (*t*-BuOH), acetone, and 2-methyl propene were commercial products and were used without further purification. The benzene used as a solvent was purified by distillation.

Analytical Procedures. The decomposition products, *t*-BuOH, *t*-Bu_2O_2, acetone, 2-methyl propene, and *t*-Bu_2O, were identified by gas chromatography-mass spectrometry, using a Shimadzu LKB 9000 apparatus and using a 2-m column of PEG 6000 at an ionization voltage of 70 eV. The products were determined as follows. Part of the liquid sample was titrated for unconverted *t*-BuOOH by the iodometric method[12] using a mixture of 20 ml of 90:10 isopropyl alcohol–acetic acid and 1 g of NaI. *t*-Bu_2O_2 gave no titer in this method. The rest was treated with sufficient triphenylphosphine for the quantitative conversion of the *t*-BuOOH into *t*-BuOH,[14] and then analyzed for products by gas chromatography using a column of PEG 6000. The benzene used as a solvent was used as the internal standard. Part of the 2-methyl propene formed was detected in the gas phase and was determined by gas chromatography using a column of DMS.

The analytical results of the supported V–Cr catalysts obtained by means of X-ray diffraction, X-ray photoelectron spectroscopy (XPS), and infrared absorption were reported in the preceding paper.[1] The surface area has been determined by the BET method.[1] In the present work, we measured the electron-spin resonance (ESR) and the surface acidity of the catalyst. The ESR spectra of the catalyst evacuated at 400 °C for 2 h were recorded with a JEOL-JES-ME3X spectrometer at 25 °C and at −196 °C. The acid strength and acidity of the catalyst were measured by a butylamine titration method using 4-(phenylazo)-diphenylamine ($pK_a=1.5$) and Methyl Red ($pK_a=4.8$) as Hamett indicators. Silica–alumina, the acidity of which was 0.44 and 0.14 mmol/g in the ranges of $pK_a \leqq 1.5$ and $1.5 < pK_a \leqq 4.8$ respectively, was used as the internal standard because nearly all of the catalysts are strongly coloured.[15]

Results and Discussion

Decomposition of t-*BuOOH with the* $Me(acac)_n$ *Catalyst.*

Table 3. Rate constants and products distributions for the acetylacetonato-catalyzed decomposition of *t*-BuOOH[a]

Catalyst	k_1/s^{-1} [b]	*t*-BuOOH conversion (%)	Product selectivity				Reaction time (min)
			t-BuOH (%)[c]	*t*-Bu_2O_2 (%)[c]	Acetone (%)[c]	2-Methyl-propene (%)[c]	
$Co(acac)_2$	7.68×10^{-3}	98.6	81.0	12.3	3.3	—	120
$Mn(acac)_3$	1.92×10^{-4}	93.2	84.0	9.5	2.0	0.7	240
$Cr(acac)_3$[d]	1.59×10^{-4}	96.5	78.9	12.5	2.9	—	300
$Mn(acac)_2$	1.48×10^{-4}	90.1	79.8	13.7	4.1	0.5	240
$VO(acac)_2$	1.41×10^{-4}	85.0	81.1	10.5	3.2	3.0	300
$Co(acac)_3$	8.42×10^{-5}	72.0	82.1	11.3	4.0	—	300
$Cu(acac)_2$	1.07×10^{-5}	13.2	82.1	5.7	1.6	—	300
$MoO_2(acac)_2$	9.1×10^{-6}	7.4	72.9	8.3	4.5	5.3	300
$Ni(acac)_2$	4.5×10^{-6}	2.3	—	—	—	—	300
$TiO(acac)_2$	4.0×10^{-6}	2.5	—	—	—	—	300
$Fe(acac)_3$	3.7×10^{-6}	3.0	—	—	—	—	300

a) The concentrations of *t*-BuOOH and $Me(acac)_n$ were 10^{-1} and 10^{-5} mol/l respectively in benzene. The reaction temperature was 60 °C. b) First-order rate constants. c) Mol % based on *t*-BuO groups found. d) $Cr(acac)_3$ showed an induction period of about 30 min.

Table 3 shows the results of the decomposition of *t*-BuOOH with various metal acetylacetonate catalysts. In the absence of a catalyst, no reaction was observed. The decrease in the concentration of *t*-BuOOH obeyed good first-order kinetics in all reactions; accordingly, the activity of the metal ion is expressed by the first-order rate constant (k_1). Only $Cr(acac)_3$ showed an induction period (about 30 min), probably because of the stability of its chelate structure. Similar product distributions were observed for nearly all reactions; *i.e.*, the selectivities of the products were as follows: *t*-BuOH, 80%; *t*-Bu_2O_2, 10%, and acetone, 5%. When the reactions gave a sufficiently high conversion, *i.e.*, in the use of the chelates of Co, Mn, or Cr, the gas chromatography indicated the formation of a small amount of formaldehyde (not estimated quantitatively). The results can be interpreted by the following reaction scheme, which was been proposed in the literature:[4-12]

$$2t\text{-BuOOH} \xrightarrow{M^{n+}/M^{(n+1)+}} t\text{-BuOO}\cdot + t\text{-BuO}\cdot + H_2O \quad (1)$$

$$t\text{-BuO}\cdot + t\text{-BuOOH} \longrightarrow t\text{-BuOH} + t\text{-BuOO}\cdot \quad (2)$$

$$2t\text{-BuOO}\cdot \longrightarrow 2t\text{-BuO}\cdot + O_2 \quad (3)$$

$$2t\text{-BuOO}\cdot \longrightarrow t\text{-Bu}_2O_2 + O_2 \quad (4)$$

$$t\text{-BuO}\cdot \longrightarrow CH_3COCH_3 + CH_3\cdot \quad (5)$$

$$CH_3\cdot + O_2 \longrightarrow CH_3OO\cdot \quad (6)$$

$$CH_3OO\cdot + t\text{-BuOO}\cdot \longrightarrow CH_2O + t\text{-BuOH} + O_2 \quad (7)$$

The *t*-BuOOH is decomposed homolytically into peroxy and alkoxy radicals by the Haber-Weiss mechanism (1), followed by the induced decomposition (2) and the competitive reactions of peroxy radicals (3 and 4). Some of *t*-butoxyl radicals are separated into acetones and methyl radicals (5);[5,6,12] the latter products are then converted into formaldehyde (6 and 7).[10-12] Generally speaking, the choice of the metal ion, as long as it can undergo a facile one-electron redox reaction, seems to have little influence on the products. It is worth noting that the chelates of vanadium and chromium showed sufficiently high activities compared with cobalt and manganese chelates.

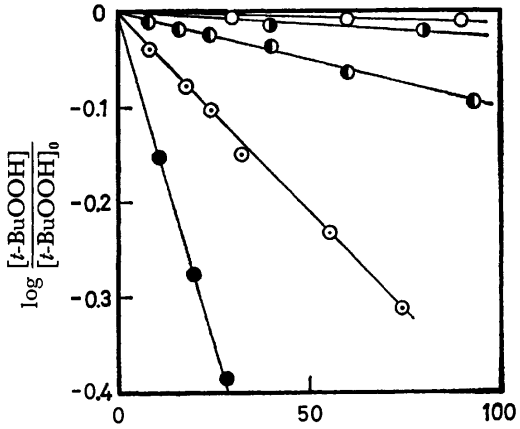

Fig. 1. Decomposition of *t*-BuOOH with V–Cr–γ-Al_2O_3.
The concentration of *t*-BuOOH and the catalyst were 10^{-1} mol/l and 5 g/l respectively in benzene. The raction temperature was 60°C. Cr/(V+Cr)=0.5.
○: γ-Al_2O_3, ◑: V–Cr–γ-Al_2O_3 (1), ◐: V–Cr–γ-Al_2O_3 (5), ⊙: V–Cr–γ-Al_2O_3 (10), ●: V–Cr–γ-Al_2O_3 (20).

Effect of the Amount of Metal Oxides Supported. As is shown in the results of the decomposition of *t*-BuOOH with the V–Cr–γ-Al_2O_3 catalyst (Fig. 1), good first-order rate plots were obtained up a conversion of 40% with the heterogeneous catalysts also. The first-order rate constants thus obtained are shown in Table 4, together with the product distribution when the amount of supported metal oxides varied. Both systems, *i.e.*, V–Cr–γ-Al_2O_3 and V–Cr–SiO_2, showed product distributions similar to that obtained with $Me(acac)_n$ catalysts, except that the V–Cr–SiO_2 system gave small amounts of 2-methyl propene and *t*-Bu_2O. Therefore, it may reasonably be considered that the decomposition of *t*-BuOOH on the present heterogeneous catalysts is initiated by the redox reaction 1 and that it then proceeds mainly by means of the radical chain reactions 2—7.

Table 4. Rate constants and product distributions for the V–Cr–γ-Al_2O_3 or –SiO_2-catalyzed decomposition of *t*-BuOOH[a]

Catalyst	k_1/s^{-1} [b]	*t*-BuOOH conversion (%)	Product selectivity[c]					Reaction time (min)
			t-BuOH (%)	*t*-Bu_2O_2 (%)	Acetone (%)	2-Methyl-propene (%)	*t*-Bu_2O (%)	
γ-Al_2O_3	3.8×10^{-6}	1.5	—	—	—	—	—	300
V–Cr–γ-Al_2O_3(1)	8.8×10^{-6}	9.0	67.0	13.1	2.3	—	—	300
V–Cr–γ-Al_2O_3(5)	3.7×10^{-5}	64.7	85.4	9.0	3.0	—	—	300
V–Cr–γ-Al_2O_3(10)	1.65×10^{-4}	91.5	84.7	12.8	2.1	—	—	240
V–Cr–γ-Al_2O_3(20)	5.37×10^{-4}	96.1	82.3	14.9	2.1	—	—	180
SiO_2	1.3×10^{-5}	2.6	—	—	—	—	—	300
V–Cr–SiO_2(1)	3.99×10^{-3}	99.5	79.4	15.3	2.6	tr	—	180
V–Cr–SiO_2(5)	4.42×10^{-3}	99.8	84.9	9.8	4.1	0.1	tr	120
V–Cr–SiO_2(10)	4.65×10^{-3}	99.8	84.1	10.0	4.8	0.1	tr	120
V–Cr–SiO_2(20)	4.24×10^{-3}	98.9	82.9	11.6	4.4	0.2	tr	120

a) The concentrations of *t*-BuOH and the catalyst were 10^{-1} mol/l and 5 g/l respectively in benzene. The reaction temperature was 60 °C. b) First-order rate constants. c) Mol % based on *t*-BuO groups found.

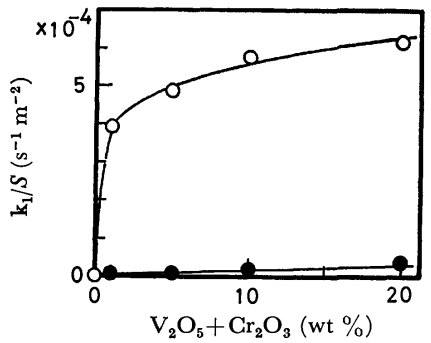

Fig. 2. Specific activity of V–Cr–γ-Al_2O_3 or –SiO_2 series catalyst for the decomposition of *t*-BuOOH.
●: V–Cr–γ-Al_2O_3 (Cr/(V+Cr)=0.5), ○: V–Cr–SiO_2 (Cr/(V+Cr)=0.7).

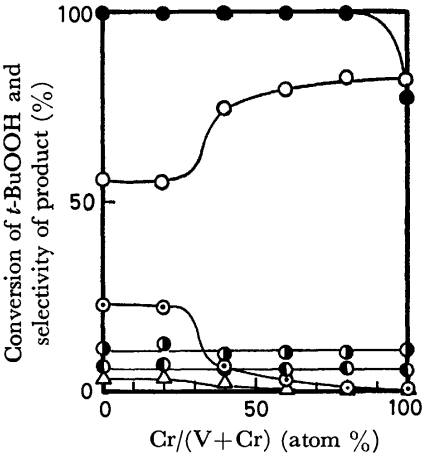

Fig. 3. Product distribution in the 4 h decomposition of *t*-BuOOH with I-series catalysts.
The concentration of *t*-BuOOH and the catalyst were 10^{-1} mol/l and 5 g/l respectively in benzene. The reaction temperature was 60 °C.
●: Conversion of *t*-BuOOH, Selectivity; ○: *t*-BuOH, ◑: *t*-Bu_2O_2, ◐: acetone, ⊙: 2-methyl propene, △: *t*-Bu_2O.

The decomposition proceeds rapidly on the V–Cr–SiO_2 system; this is more clearly observed in Fig. 2, which shows the specific activity of each system. It is noteworthy that the activity increased rapidly when a small amount of metal oxides was supported on SiO_2; on the contrary, no such rapid increase was observed on γ-Al_2O_3. A similar tendency of the activity was also observed when the binary catalysts were used in the oxidation of cyclohexene (see Fig. 4 in the preceding paper[1]).

Effects of Composition and Raw Materials of Metal Oxides. The systems supported on γ-Al_2O_3, *i.e.*, G- and H-series, gave product distributions similar to those obtained with a soluble Co or Mn chelate catalyst, while a different distribution was observed with the I-series, especially those with a high vanadium content, on SiO_2 (Table 5). That is, the I-series gave 2-methyl propene and *t*-Bu_2O, too, and the higher vanadium content increased the selectivity of the two products while decreasing that of *t*-BuOH. Such a tendency was observed more clearly after decomposition for 4 h (Fig. 3); the selectivities of 2-methyl propene and *t*-Bu_2O increased at the expense of that of *t*-BuOH when the I-0, I-2, and I-4 catalysts were used. The selectivity of *t*-Bu_2O_2 or acetone did not change over all the compositions of the I-series catalysts. The I-series

TABLE 5. RATE CONSTANTS AND PRODUCT DISTRIBUTIONS FOR THE G-, H-, OR I- SERIES CATALYZED DECOMPOSITION OF *t*-BuOOH[a]

Catalyst	k_1/s^{-1} [b]	*t*-BuOOH conversion (%)	Product selectivity[c]					Reaction time (min)
			t-BuOH (%)	*t*-Bu_2O_2 (%)	Acetone (%)	2-Methyl-propene (%)	*t*-Bu_2O (%)	
G-0	2.07×10^{-4}	90.2	83.9	10.5	4.8	0.2	—	240
G-2	2.79×10^{-4}	89.7	84.1	13.0	2.3	0.1	—	180
G-4	4.27×10^{-4}	93.1	84.1	12.1	2.8	0.2	—	180
G-5	5.37×10^{-4}	96.1	82.3	14.9	2.1	—	—	180
G-6	4.96×10^{-4}	96.3	81.3	14.0	2.8	—	—	180
G-8	4.13×10^{-4}	90.0	85.9	10.0	3.2	—	—	180
G-10	9.5×10^{-6}	17.8	70.3	12.5	5.0	—	—	240
H-0	1.91×10^{-4}	87.3	85.3	12.1	3.2	0.2	—	240
H-3	3.67×10^{-4}	84.4	83.6	10.7	4.4	—	—	180
H-5	5.35×10^{-4}	94.2	82.4	11.8	4.7	—	—	180
H-7	5.59×10^{-4}	97.1	83.8	10.6	5.1	—	—	180
H-10	7.42×10^{-4}	98.6	83.6	10.0	5.0	—	—	180
I-0	5.64×10^{-3}	99.2	75.6	10.5	5.8	7.2	0.6	120
I-2	5.28×10^{-3}	99.0	75.8	10.9	5.9	6.5	0.8	120
I-4	4.56×10^{-3}	98.5	79.7	11.9	5.8	1.3	0.3	120
I-6	4.16×10^{-3}	97.6	82.0	11.8	5.3	0.5	tr	120
I-8	3.41×10^{-3}	98.2	82.7	11.0	4.4	0.2	tr	120
I-10	1.26×10^{-3}	78.6	83.0	11.8	4.9	0.2	tr	240

a) The concentrations of *t*-BuOOH and the catalyst were 10^{-1} mol/l and 5 g/l respectively in benzene. The reaction temperature was 60 °C. b) First-order rate constants. c) Mol % based upon *t*-BuO groups found.

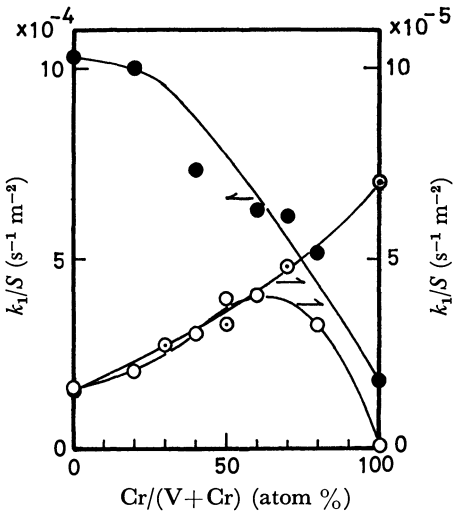

Fig. 4. Specific activity of G-, H-, and I-series catalyst for the decomposition of *t*-BuOOH.
The concentration of *t*-BuOOH and the catalyst were 10^{-1} mol/l and 5 g/l respectively in benzene. The reaction temperature was 60 °C.
○: G-series, ⊙: H-series, ●: I-series.

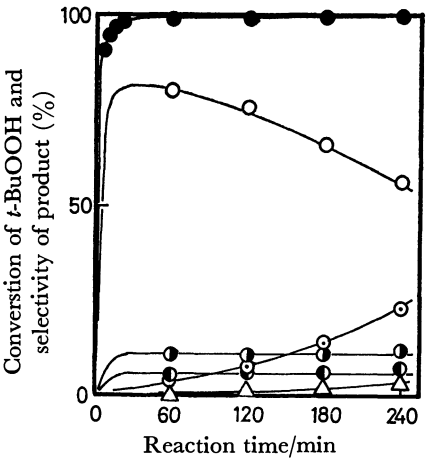

Fig. 5. Decomposition of *t*-BuOOH with I-0 catalyst.
The concentration of *t*-BuOOH and the catalyst were 10^{-1} mol/l and 5 g/l respectively in benzene. The reaction temperature was 60 °C.
●: Conversion of *t*-BuOOH. Selectivity; ○: *t*-BuOH, ◑: *t*-Bu_2O_2, ◐: acetone ⊙: 2-methyl propene, △: *t*-Bu_2O.

catalysts gave higher decomposition rates than the G- or H-series catalysts. The specific activities are shown in Fig. 4 in terms of k_1/S. When supported on SiO_2, a higher vanadium content resulted in a higher specific activity. Concerning the systems supported on γ-Al_2O_3, the use of $(NH_4)_2CrO_4$ (Cr^{6+}), *i.e.*, the H-series, instead of $Cr(NO_3)_3 \cdot 9H_2O$ (Cr^{3+}), *i.e.*, the G-series, as the raw material caused a markedly high activity at a high chromium content, while both series with low chromium contents showed similar activities. The fact that the H-series contains a higher valence state of chromium ions than the G-series has already been noted.[1] The binary system in the G-series clearly showed an increase in the activity, an increase which may be attributed to the formation of chromium isopolyvanadates, as has already been reported,[3] though the effect of the binary-system formation was not obvious in the I- and H-series.

The order of the activity mentioned above is well correlated with that observed in the oxidation of cyclohexene with the same catalyst systems[1] when the initial rate, R_{max}-A, is adopted as the activity of the I-series (Fig. 5 in the preceding paper[1]). That is, though the O_2 absorption rate shown by I-0 or I-2 in the steady state of cyclohexene oxidation, R_{max}-B, was much lower than would be expected from the *t*-BuOOH decomposition, the initial rate, R_{max}-A, was sufficiently high, in agreement with the decomposition rate. Thus, it may reasonably be considered that the main role of the binary catalyst in the oxidation of cyclohexene is in the acceleration of the homolysis of hydroperoxide.

Dehydration of t-*BuOH on the* V_2O_5–SiO_2 *Catalyst.* Tables 4 and 5 and Fig. 3 reveal that 2-methyl propene and *t*-Bu_2O were formed, together with the radical-reaction products, when the SiO_2-supported catalysts with a higher vanadium content were used. The amounts of 2-methyl propene and *t*-Bu_2O increased at the expense of *t*-BuOH; the amount of 2-methyl propene was, further, about 10 times that of *t*-Bu_2O. In order to clarify the mechanism of the formation of the two products, the variation in their selectivities during the reaction was examined by using the I-0 catalyst (Fig. 5). The decomposition of *t*-BuOOH was finished within about 30 min after the beginning of the reaction. The selectivity of *t*-BuOH reached its maximum value and then decreased gradually during 4 h of reaction; 2-methyl propene and *t*-Bu_2O took the place of *t*-BuOH. In contrast, no change was observed in the selectivities of *t*-Bu_2O_2 and acetone. The I-2 catalyst also showed a similar behavior. Thus, the dehydration of *t*-BuOH is suggested on the I-0 or I-2 catalyst. For the purpose of confirming this possibility, a solution of *t*-BuOH in benzene was treated at 60 °C with the I-2 catalyst in an N_2 atmosphere (Fig. 6). The dehydration of *t*-BuOH into 2-methyl propene was clearly observed, though *t*-Bu_2O was not detected; a similar phenomenon was also observed with

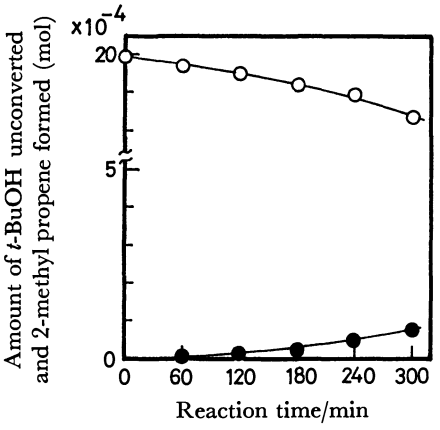

Fig. 6. Dehydration of *t*-BuOH with I-2 catalyst.
The concentration of *t*-BuOOH and the catalyst were 2×10^{-1} mol/l and 5 g/l respectively in benzene. The reaction was carried out under N_2 atmosphere at 60 °C.
○: *t*-BuOH, ●: 2-methyl propene.

the I-0 catalyst. It can, therefore, be concluded that the following dehydrations were catalyzed on the SiO_2-supported system with a high vanadium content:

$$t\text{-BuOH} \longrightarrow CH_3\text{–}C(CH_3)\text{=}CH_2 + H_2O \quad (8)$$

$$2t\text{-BuOH} \longrightarrow t\text{-}Bu_2O + H_2O \quad (9)$$

The probability of the intramolecular dehydration (8) may reasonably be larger than that of the intermolecular one (9), resulting in the higher selectivity of 2-methyl propene (Fig. 5). I-0 showed the X-ray diffraction lines of V_2O_5 crystals; I-2, on the contrary, showed no line,[1] and both the systems catalyzed the dehydration. Therefore, the active species for the dehydration on the catalysts seems to be composed of the vanadium oxide–SiO_2 system.

Co-ordination State of a Metal on a Catalyst. The analytical results of X-ray diffraction, infrared absorption, and XPS have been reported in the preceding paper.[1] The XPS analysis revealed that several valence states of chromium, *i.e.*, Cr^{6+}, Cr^{5+}, and Cr^{3+}, exist on the supported catalysts. On γ-Al_2O_3, the H-series prepared from $(NH_4)_3CrO_4(Cr^{6+})$ includes chromium ions of a higher valence state than the G-series from $Cr(NO_3)_3\cdot 9H_2O$ (Cr^{3+}) at a high chromium content, though the valence state of vanadium was not clearly assigned. Such valence states of metal contributed considerably to the activity for the cyclohexene oxidation[1] and also for the *t*-BuOOH decomposition (Fig. 4); the configuration of metal complexes on the catalyst surface seemed, however, to play a more important role.[1] In order to obtain information about the metal-complex configurations, the ESR spectra were measured.

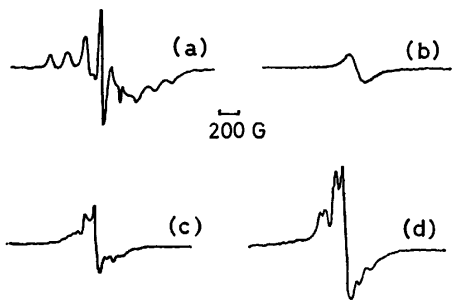

Fig. 7. ESR spectra of the supported vanadia systems.
(a) G-0 at 25 °C, (b) I-0 at 25 °C, (c) I-0 at 25 °C after an exposure to atmosphere at room temperature, (d) I-0 at −196 °C.

The spectra of the supported vanadia systems are shown in Fig. 7. At 25 °C, V_2O_5–γ-Al_2O_3 (G-0) exhibited a characteristic spectrum (a) with hfs due to ^{51}V(IV) in the octahedral (or distorted square pyramidal) co-ordination (VO_5),[16-21] whereas V_2O_5–SiO_2 (I-0) gave a very weak singlet spectrum (b), the line shape of which was nearly Lorentzian. At room temperature, the tetrahedrally co-ordinated V(IV) ions (VO_4) could not be detected by ESR.[16,20,22] Moreover, I-0 showed a clear X-ray diffraction pattern of the V_2O_5 crystal.[1] The (b) spectrum may, therefore, be assigned to V(IV) ions attributable to lattice defects in the V_2O_5 crystal. I-0 showed a spectrum (d) at the temperature of −196 °C; its line shape differed from (a) and (b), probably indicating the (VO_4) formation, as was suggested in the preceding paper.[1] Suzuki *et al.*[20] and Van Reijen *et al.*[16] also detected tetrahedrally co-ordinated V(IV) ions on the V_2O_5–SiO_2 system by ESR at low temperatures. The (b) spectrum became slightly strong and simultaneously anisotropic (c) when the evacuated I-0 was exposed to atmosphere at room temperature. Van Reijen reported that (VO_4) is very sensitive to atmosphere; for example, after the admission of water vapor at room temperature, (VO_4) changes probably to (VO_5), which is sufficiently stable and is detected at room temperature.[16] The (c) spectrum may be of V(IV) ions both in the V_2O_5 lattice defects and in (VO_5). Thus, two types of configurations of vanadium complexes, *i.e.*, (VO_5) on γ-Al_2O_3 and (VO_4) on SiO_2, are recognized.

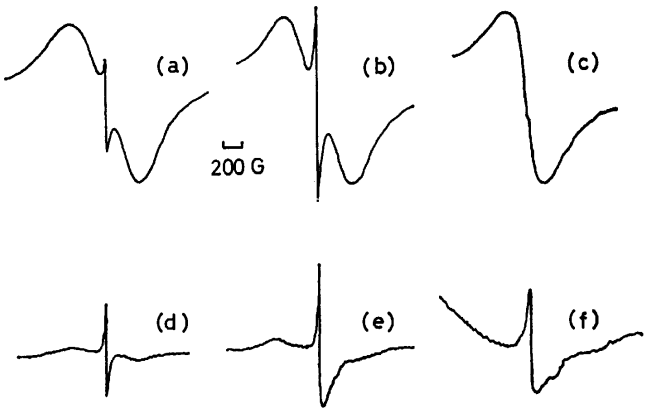

Fig. 8. ESR spectra of the supported chromia systems.
(a): G-10 at 25 °C, (b): H-10 at 25°C, (c): I-10 at 25 °C, (d): G-10 at −196 °C, (e): H-10 at −196 °C, (f): I-10 at −196 °C.

Figure 8 shows the spectra of the supported chromia systems. According to the analytical results obtained by the use of XPS,[1] these systems contained Cr^{5+} and Cr^{3+} ions which can be detected by ESR. X-Ray diffraction measurements showed that the Cr_2O_3 crystal grew on SiO_2, but not on γ-Al_2O_3.[1] Therefore, we can presume that, on γ-Al_2O_3, most of the Cr^{3+} is present in solution in the γ-Al_2O_3 lattice; on SiO_2, though, it is present mainly in a separate chromia phase. At room temperature, the ESR spectra of the Cr_2O_3–γ-Al_2O_3 systems (G-10 and H-10) showed a very broad band and another, relatively sharp peak, characterized by a *g*-factor of 1.97 and a linewidth of approximately 50 G, superimposed on it (a and b). The ratio of the intensities of the two bands varied considerably. The narrow signal may be assigned to the Cr^{5+} ions (the so-called γ-phase), whereas the broad one may be assigned to the Cr^{3+} ions (the β-phase).[24,25] The intensity of the γ-phase was as follows: H-10>G-10; the Cr^{5+} ions are more abundant on the Cr_2O_3–γ-Al_2O_3 system prepared from $(NH_4)_2CrO_4$ than on that prepared from $Cr(NO_3)_3\cdot 9H_2O$. This was in good agreement with the result obtained by the XPS measure-

ment.[1] The Cr_2O_3–SiO_2 (I-10) showed a spectrum similar to those of the Cr_2O_3–γ-Al_2O_3, though the intensity of the narrow band was very weak (c). The broad band may be assigned to the separate phase of the Cr_2O_3 crystals, which was detected by the X-ray analysis.[1] When the sample was cooled to −196 °C. The form of the spectrum changed appreciably; the intensity of the broad band was weakened. Moreover, the narrow signal of I-0 became stronger, accompanied by a marked anisotropy of its *g*-factor (f). The anisotropic signal may be assigned to the Cr^{5+} ions tetrahedrally co-ordinated (CrO_4), which are characterized by a small spin-lattice relaxation time and which are, accordingly, observed only at low temperatures.[16,23] The anisotropy was also observed in the narrow signal of the H-10 catalyst (e). However, G-10 gave a strong, narrow signal of the Cr^{5+} ions co-ordinated octahedrally (d).[23,26] These results can be summarized as follows: the Cr^{5+} ions are mainly co-ordinated tetrahedrally (CrO_4) on SiO_2 and octahedrally (or square-pyramidally) (CrO_5) on γ-Al_2O_3. In the latter case, however, the tetrahedral co-ordination may also occur on the H-series with a high chromium content, because the anisotropy was observed with H-10 at −196 °C, as has been mentioned above. This is supported by the fact that the tetrahedral $(CrO_4)^{3-}$ ions are preferentially found in a highly alkaline solution;[27] an H-series with a high chromium content was prepared from $(NH_4)_2CrO_4$, *i.e.*, in alkaline media. It may also be reasonable to assume that the (CrO_4) tetrahedron is linked to the SiO_2 network by sharing corners or edges with the SiO_4 tetrahedron, because the SiO_2 crystal has a tetrahedral structure.[16,23]

Acidity of Catalyst. The acidities of the supported catalysts obtained by means of the butylamine titration method are shown in Fig. 9; they are classified into two kinds of acid strengths, *i.e.*, $pK_a \leqq 1.5$ and $1.5 < pK_a \leqq 4.8$. γ-Al_2O_3 itself showed a strong acidity, whereas a weak acidity alone was observed on SiO_2. It is noteworthy that, when a small amount of V–Cr binary oxide was added to SiO_2, a remarkable increase in the strong acid sites was observed. On γ-Al_2O_3, the acidity

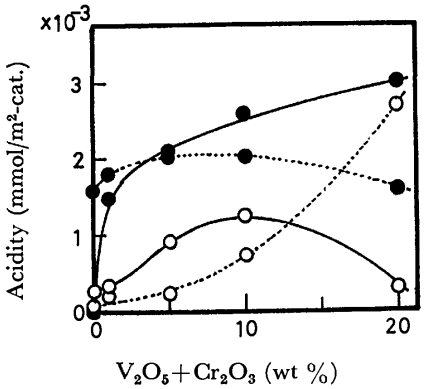

Fig. 9. Acidity on V–Cr–γ-Al_2O_3 or –SiO_2 system catalyst.
●: $pK_a \leqq 1.5$, ○: $1.5 < pK_a \leqq 4.8$.
——: V–Cr–SiO_2, (Cr/(V+Cr)=0.7), -----: V–Cr–γ-Al_2O_3, (Cr/(V+Cr)=0.5).

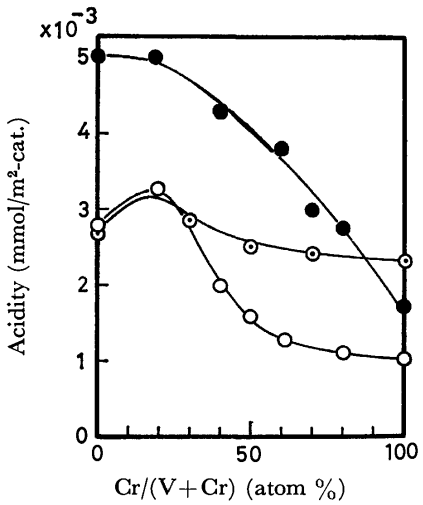

Fig. 10. Acidity of $pK_a \leqq 1.5$ on G-, H-, and I-series catalysts.
○: G-series, ⊙: H-series, ●: I-series.

of $pK_a \leqq 1.5$ did not vary upon the addition of the binary oxide; that of $1.5 < pK_a \leqq 4.8$, however, enhanced by its addition in sufficient amount. The strong acidities ($pK_a \leqq 1.5$) of the three series of catalysts, *i.e.*, the I-, H-, and G-series, are shown in Fig. 10 as the function of the chromium content. The largest acidity was given on SiO_2, whereas, on γ-Al_2O_3, the system prepared from $(NH_4)_2CrO_4$ showed a larger acidity than that prepared from $Cr(NO_3)_3 \cdot 9H_2O$, especially at high chromium contents. When the activities in Figs. 2 and 4 are compared to the acidities in Figs. 9 and 10 respectively, it seems that the activity for the decomposition of *t*-BuOOH is related to the acidity on the supported catalyst. A clear-cut correlation was observed particularly with the V–Cr–SiO_2 series (Fig. 2) and the I-series (Fig. 4), which are both supported on SiO_2. Both the activity and the acidity were at a maximum on the V_2O_5–SiO_2 system (I-0), in which the tetrahedral configuration was detected by ESR. The strength of the acidity of (VO_4) may be sufficiently large to dehydrate *t*-BuOH, as has been described already. The acidity observed on the Cr_2O_3–SiO_2 catalyst may be related to the tetrahedral (CrO_4) configuration, which is formed newly, because SiO_2 showed no acidity ($pK_a \leqq 1.5$) itself.

When supported on γ-Al_2O_3, which itself showed acidity, the correlation was not so clear as on SiO_2, but at a high chromium content the catalyst of the H-series, on which the (CrO_4) configuration was observed, showed both a higher activity and a higher acidity compared to the G-series catalysts. Thus, this higher acidity seems also to be related to the tetrahedral (CrO_4) configuration.

Though the details of the mechanism by which the acidic sites contribute to the autoxidation are not yet clear, it may be suggested that the tetrahedral complexes work both as acidic sites and as active sites for the homolytic decomposition of hydroperoxide, through which process the autoxidation is accelerated. The homolytic decomposition may proceed *via* the co-ordination of hydroperoxide to a vacant site in the

complex; the vacant site is also suspected to behave as an acidic site.

In conclusion, the activity for the cyclohexene oxidation (Fig. 5 in the preceding paper[1]) correlates fairly well with that for the *t*-BuOOH decomposition, supporting the theory of the oxidation mechanism which proceeds *via* the radical decomposition of hydroperoxide. The effects of the V–Cr binary-system formation was not so clear in the *t*-BuOOH decomposition as in the cyclohexene oxidation, but the interaction between the metal oxides and the supports strongly affected the activity for the *t*-BuOOH decomposition. The oxidation activity of the I-series (Fig. 5 in the preceding paper[1]), when compared with those of other series, was considerably lower than would be expected from the *t*-BuOOH decomposition (Fig. 4); such a lowering was most clearly observed at a high vanadium content. This may be due to the instability of the (VO_4) structure: this effect was not clearly observed in the *t*-BuOOH decomposition, which proceeded rapidly, but was recognized in a relatively slow reaction such as the cyclohexene oxidation.

References

1) K. Takehira, T. Hayakawa, and T. Ishikawa, *Bull. Chem. Soc. Jpn.*, **52**, 697 (1979).
2) K. Takehira and T. Ishikawa, *Bull. Chem. Soc. Jpn.*, **49**, 2351 (1976).
3) K. Takehira, T. Hayakawa, and T. Ishikawa, *Bull. Chem. Soc. Jpn.*, **51**, 1685 (1978).
4) R. Hiatt, K. C. Irwin, and C. W. Gould, *J. Org. Chem.*, **33**, 1430 (1968).
5) R. Hiatt, T. Mill, and F. R. Mayo, *J. Org. Chem.*, **33**, 1416 (1968).
6) W. H. Richardson, *J. Am. Chem. Soc.*, **87**, 247 (1965).
7) W. H. Richardson, *J. Am. Chem. Soc.*, **87**, 1096 (1965).
8) P. D. Bartlett and T. G. Traylor, *J. Am. Chem. Soc.*, **85**, 2407 (1963).
9) C. Walling and A. Padwa, *J. Am. Chem. Soc.*, **85**, 1593 (1963).
10) M. H. Dean and G. Skirrow, *Trans. Faraday Soc.*, **54**, 849 (1958).
11) F. H. Seubold, F. F. Rust, and W. E. Vaughan, *J. Am. Chem. Soc.*, **73**, 18 (1951).
12) R. Hiatt, T. Mill, K. C. Irwin, and J. K. Castleman, *J. Org. Chem.*, **33**, 1421 (1968).
13) R. West, D. L. Powell, M. K. T. Lee, and L. S. Whatley, *J. Am. Chem. Soc.*, **86**, 3228 (1968).
14) L. Horner and W. Jurgleit, *Ann. Chem.*, **591**, 139 (1955).
15) T. Sukeno and T. Shirasaki, *Nippon Kagaku Kaishi*, **1973**, 2229.
16) L. L. Van Reijen and P. Cossee, *Discuss. Faraday Soc.*, **41**, 277 (1966).
17) H. Takahashi, M. Shiotani, H. Kobayashi, and J. Sohma, *J. Catal.*, **14**, 134 (1969).
18) M. Akimoto, M. Usami, and E. Echigoya, *Bull. Chem. Soc. Jpn.*, **51**, 2195 (1978).
19) S. Yoshida, T. Iguchi, S. Ishida, and K. Tarama, *Bull. Chem. Soc. Jpn.*, **45**, 376 (1972).
20) T. Suzuki, S. Yoshida, and K. Tarama, presented at the 37th National Meeting of the Chemical Society of Japan, Tokyo, April 1978.
21) C. J. Ballhausen and H. B. Gray, *Inorg. Chem.*, **1**, 111 (1962).
22) L. L. Van Reijen, P. Cossee, and H. J. Van Haren, *J. Chem. Phys.*, **38**, 572 (1963).
23) V. B. Kazanskii, *Kinet. Katal.*, **11**, 455 (1970).
24) C. P. Poole, Jr., W. L. Kehl, and D. S. MacIber, *J. Catal.*, **1**, 407 (1962).
25) D. E. O'Reilly and D. S. MacIber, *J. Phys. Chem.*, **66**, 276 (1962).
26) V. V. Voevodskii, *Proc. Int. Congr. Catal., 3rd* 1964, **1**, 88 (1965).
27) N. Bailey and M. C. R. Symos, *J. Chem. Soc.*, **1957**, 203.

 © 1980 The Chemical Society of Japan Bull. Chem. Soc. Jpn., 53, 2111—2113 (1980)

The Crystal Structure of the A′-form of Tridecanoic Acid

Midori Goto* and Eiichi Asada

National Chemical Laboratory for Industry, 1-1, Higashi, Yatabe, Ibaraki 305

(Received July 6, 1979)

The A′-form of tridecanoic acid is triclinic, with the space group $P\bar{1}$ and with $a=4.273(1)$, $b=4.972(1)$, $c=37.69(1)$ Å, $\alpha=90.36(2)$, $\beta=109.44(2)$, and $\gamma=112.43(2)°$. The structure was determined by the Patterson method. Refinement by block-diagonal least-squares methods gave a final R factor of 0.071.

Odd-numbered fatty acids are known to crystallize in three polymorphic forms, named A′, B′, and C′.[1] Their crystal structures have been studied by von Sydow in only one projection (the A′-form[2] and the B′-form[3] of pentadecanoic acid; the C′-form[4] of undecanoic acid). We have now been able to obtain fairly good single crystals of the A′-form of tridecanoic acid; we also investigated its crystal structure.

Experimental

The tridecanoic acid was prepared by the Ajinomoto Co., Ltd. The A′-form crystal was obtained by crystallization in a 2,2,4-trimethylpentane solution. The crystal data and the diffraction intensities were measured on a Rigaku-Denki four-circle diffractometer by using graphite monochromated Cu $K\alpha$ radiation at room temperature (about 20 °C).

Table 1. Crystal data

n-Tridecanoic acid		A′-form	
Molecular formula:		$C_{13}H_{26}O_2$	
Molecular weight:		214	
Transition point:		34 °C	
Triclinic;		$P\bar{1}$	
$z=2$			
a(/Å)	4.273(1)	α(/°)	90.36(2)
b	4.972(1)	β	109.44(2)
c	37.686(8)	γ	112.43(2)

The crystal data are listed in Table 1. The total number of observed reflections was 533 out of 1415 possible reflections within the 2θ angle of 120 °.

Structure Determination

The positions of the carbon atoms were obtained by taking into account the three-dimensional Patterson maps. The positions of the oxygen atoms were obtained by difference synthesis. The positions of the hydrogen atoms, with the exception of the carboxyl hydrogen atom, were calculated by assuming C–H distances of 1.10 Å and a tetrahedral arrangement. The structure was refined by the block-diagonal least-squares method using the HBLS program (ashida).[5]

The R-value was reduced to 0.071. The final atomic parameters obtained are listed in Table 2. The large temperature factors, especially at the end carboxyl groups, may be caused by the proximity of the experimental temperature to the transition point of the acid.

Results and Discussion

The structure of the A′-form of tridecanoic acid reveals a layer characteristic and is not significantly different from that of the A′-form[2] of pentadecanoic acid.

The bond lengths, bond angles, and internal rotation angles are shown in Table 3. Figure 1 is an ORTEP drawing.[7] Table 4 reveals that the molecule may be slightly bowed. The dihedral angle between the plane of the carbon main chain and the plane containing the carboxyl group is calculated to be 15°, nearly the same as that in the A_1-form[8] or the A-super form[9] of lauric acid.

Table 2(a). Fractional atomic coordinates and anisotropic temperature factors for C and O atoms

	$x(\times10^4)$	$y(\times10^4)$	$z(\times10^4)$	$B_{11}(\times10^4)$	$B_{22}(\times10^4)$	$B_{33}(\times10^4)$	$B_{12}(\times10^4)$	$B_{13}(\times10^4)$	$B_{23}(\times10^4)$
C1	−618(35)	3317(22)	447(3)	2363(192)	578(75)	17(2)	764(103)	86(15)	23(9)
C2	−1440(27)	1914(20)	772(3)	975(124)	463(63)	11(1)	83(75)	34(12)	19(7)
C3	−405(27)	4060(21)	1124(3)	937(115)	734(73)	7(1)	467(79)	26(10)	13(7)
C4	−926(29)	2521(20)	1459(3)	1532(148)	478(65)	10(1)	334(83)	70(12)	14(7)
C5	37(27)	4597(21)	1806(3)	934(119)	658(69)	16(2)	532(79)	76(12)	41(8)
C6	−488(29)	3116(22)	2141(3)	1332(136)	729(76)	10(1)	484(87)	57(12)	19(8)
C7	623(29)	5161(21)	2508(3)	1125(133)	646(74)	13(1)	293(85)	41(12)	20(8)
C8	57(30)	3686(21)	2841(3)	1360(143)	513(68)	17(2)	362(87)	82(13)	30(9)
C9	1265(31)	5763(21)	3200(3)	1511(148)	501(70)	12(2)	191(88)	57(13)	12(8)
C10	740(30)	4282(22)	3536(3)	1237(143)	694(77)	10(1)	290(89)	33(12)	19(8)
C11	1977(32)	6348(23)	3895(3)	1690(163)	677(77)	14(2)	341(97)	77(14)	11(9)
C12	1608(36)	5000(27)	4232(3)	2137(195)	1157(104)	16(2)	795(121)	109(16)	50(11)
C13	2739(40)	7088(31)	4589(3)	2657(225)	1750(137)	12(2)	1289(152)	93(11)	40(12)
O1	−559(41)	2008(23)	194(3)	8323(329)	1779(101)	33(2)	3234(158)	416(24)	158(12)
O2	−537(31)	5709(18)	404(3)	4477(114)	910(61)	22(1)	1205(93)	227(14)	59(7)

Table 2(b). Fractional atomic coordinates and isotropic temperature factors for H atoms

	$x(\times 10^3)$	$y(\times 10^3)$	$z(\times 10^4)$	B(/Å^2)
H(C 2)	14(27)	59(21)	881(27)	11.8(3.2)
H(C′ 2)	−436(25)	46(19)	664(25)	9.9(2.8)
H(C 3)	−227(22)	515(17)	1061(23)	8.0(2.4)
H(C′ 3)	270(23)	550(18)	1204(24)	8.9(2.6)
H(C 4)	84(22)	134(17)	1527(23)	8.1(2.5)
H(C′ 4)	−368(22)	95(17)	1376(23)	8.1(2.4)
H(C 5)	−183(18)	572(14)	1729(19)	4.4(1.8)
H(C′ 5)	292(24)	601(19)	1891(24)	9.4(2.7)
H(C 6)	107(24)	178(19)	2197(24)	9.4(2.7)
H(C′ 6)	−333(23)	171(18)	2053(24)	8.8(2.6)
H(C 7)	−75(24)	646(19)	2440(25)	9.3(2.7)
H(C′ 7)	354(20)	658(16)	2604(21)	6.5(2.2)
H(C 8)	165(20)	233(16)	2902(21)	6.5(2.2)
H(C′ 8)	−282(24)	224(19)	2751(24)	9.5(2.7)
H(C 9)	−30(21)	704(17)	3147(22)	7.5(2.4)
H(C′ 9)	415(20)	727(16)	3279(21)	6.5(2.2)
H(C 10)	225(23)	299(18)	3592(23)	8.1(2.4)
H(C′ 10)	−225(22)	276(17)	3443(23)	7.5(2.3)
H(C 11)	29(22)	769(17)	3824(23)	8.1(2.4)
H(C′ 11)	477(22)	785(17)	3970(23)	8.2(2.5)
H(C 12)	299(23)	361(18)	4300(24)	9.1(2.6)
H(C′ 12)	−130(21)	352(16)	4147(21)	6.9(2.3)
H(C 13)	251(23)	600(18)	4682(26)	10.7(3.0)
H(C′ 13)	575(23)	845(20)	4682(26)	10.7(3.0)
H(C″ 13)	126(27)	844(22)	4554(28)	12.4(3.3)

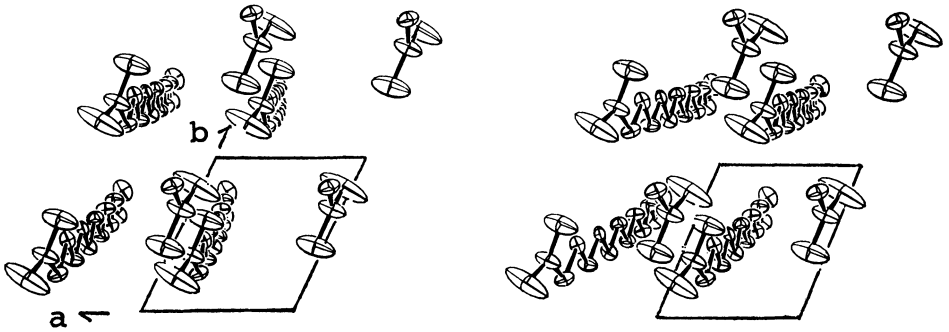

Fig. 1. A perspective view along the c-direction drawn by ORETP.
Only C2, C1, O1, O2 atoms were shown in the one molecule of the pair joined by the hydrogen bond.

Table 3. Bond lengths, angles and internal rotation angles

Bond lengths (/Å)			
C1–C2	1.49(2)	C 6–C 7	1.53(2)
C1–O1	1.16(2)	C 7–C 8	1.50(2)
C1–O2	1.19(2)	C 8–C 9	1.51(2)
C2–C3	1.53(1)	C 9–C10	1.51(2)
C3–C4	1.52(2)	C10–C11	1.50(2)
C4–C5	1.50(2)	C11–C12	1.47(2)
C5–C6	1.51(2)	C12–C13	1.51(2)
Bond angles (/°)			
C2–C1–O1	122(1)	C 7–C 6–C 5	116(1)
C2–C1–O2	121(1)	C 8–C 7–C 6	116(1)
O1–C2–O2	116(1)	C 9–C 8–C 7	115(1)
C3–C2–C1	115(1)	C10–C 9–C 8	115(1)
C4–C3–C2	113(1)	C11–C10–C 9	115(1)
C5–C4–C3	113(1)	C12–C11–C10	117(1)
C6–C5–C4	113(1)	C13–C12–C11	116(1)
Internal rotation angles (/°)			
C 3–C 2–C 1–O2	−28		
C 4–C 3–C 2–C1	−174		
C 6–C 5–C 4–C3	179		
C 8–C 7–C 6–C5	179		
C10–C 9–C 8–C7	−179		
C12–C11–C10–C9	−179		
C 3–C 2–C 1–O1	164		
C 5–C 4–C 3–C2	−179		
C 7–C 6–C 5–C4	177		
C 9–C 8–C 7–C6	178		
C11–C10–C 9–C8	179		

Table 4. Least-squares planes and displacements of atoms from the planes

Carbon chain	Carboxyl group
$Lx+My+Nz=D$	$Lx+My+Nz=D$
$L=0.88$	$L=0.87$
$M=-0.37$	$M=-0.06$
$N=0.35$	$N=0.50$
$D=-1.77$	$D=-0.14$

The equation expressed in the orthogonal Cartesian system:

Atom	Deviation(/Å)	Atom	Deviation(/Å)
C 2	0.07	C 2	−0.02
C 3	0.02	C 1	0.05
C 4	0.03	O 1	−0.02
C 5	−0.03	O 2	−0.02
C 6	−0.04		
C 7	−0.04		
C 8	−0.06		
C 9	−0.03		
C10	−0.03		
C11	0.02		
C12	0.05		
C13	0.05		
C 1[a)]	0.21		
O 1[a)]	0.53		
O 2[a)]	−0.20		

a) These atoms are not included in the least-squares calculation.

Table 5. Dimensions of the triclinic subcell[a)]

	a_s(/Å)	b_s(/Å)	c_s(/Å)	α(/°)	β(/°)	γ(/°)	V(/Å^3)
Tridecanoic acid A'-form	4.27	5.20	2.51	79	109	118	46.4
Lauric acid A-super form[8)]	4.33	5.42	2.52	76	109	122	47.1
Lauric acid A_1-form[7)]	4.25	5.41	2.45	75	108	122	47.4
Trilaurin[11)]	4.27	5.40	2.45	75	108	117	47.4

a) The triclinic packing was found in the branched-chain fatty acids. In these compounds, the subcell data vary considerably and show a distorted packing; the structures were studied in only one projection and could not be discussed in detail.

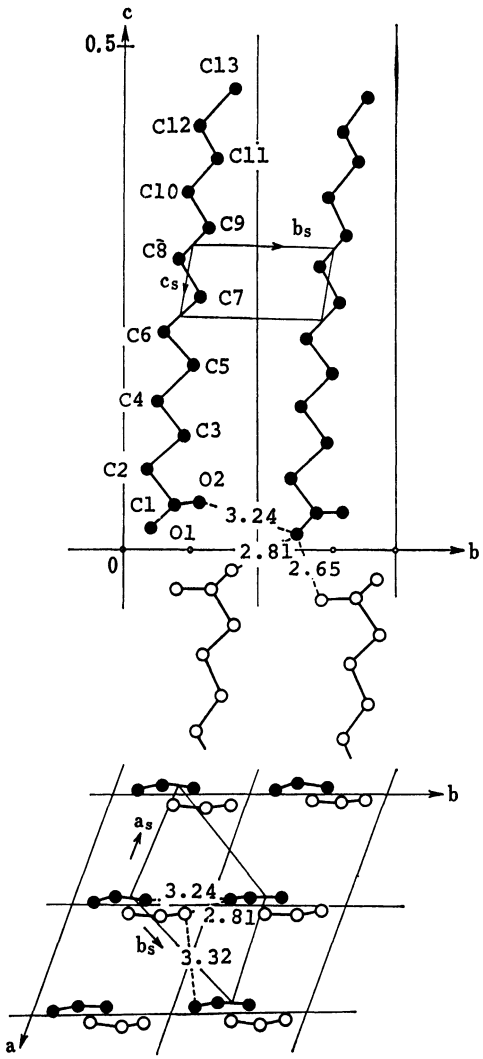

Fig. 2. The crystal structure.
a): Projection along the a*-axis, b): carboxyl groups projected along the c*-axis.

The arrangement of the chain and the end carboxyl group is shown in Fig. 2. The hydrogen bond length is 2.65 Å, and the second closest oxygen contact distance (except for the hydrogen bond) is 2.81 Å. This distance appears to be short compared with that of the other fatty acid,[9,10)] 3.13 Å.

The packing of the zig-zag chains of the carbon atoms is triclinic ($T_{//}$). The dimensions of the subcell are given in Table 5, together with the dimensions in other compounds with triclinic packing.

The structures of the B[10)] and C[11)] forms of the fatty acids reveal a typical layer structure, one in which the carboxyl groups and the methyl groups respectively are situated in alternate layers (parallel to 001). A-forms with the triclinic packing, both A_1[8)]- and A-super[9)] forms of lauric acid, have a structure in which the carboxyl and methyl groups appear mixed in the same layers in the crystal. However, the A'-form of tridecanoic acid has the typical layer structure, just as B-[10)] or C-[11)] forms.

We wish to thank Professor Yoichi Iitaka of the University of Tokyo for his encouragement and helpful discussions; we are also indebted to the Ajinomoto Co., Ltd., for providing the compound.

References

1) E. V. Sydow, *Arkiv Kemi*, **9**, 231 (1956).
2) E. V. Sydow, *Acta Crystallogr.*, **7**, 529 (1954); **8**, 845 (1955).
3) E. V. Sydow, *Acta Crystallogr.*, **7**, 823 (1954).
4) E. V. Sydow, *Acta Crystallogr.*, **8**, 810 (1955).
5) T. Ashida, HBLS(IV), The Universal Crystallographic Computing System (I), The Crystallographic Society of Japan (1967), p. 65.
6) The table of the observed and calculated structure factors has been deposited with the Office of the Chemical Society of Japan, 1–5, Kanda-Surugadai, Chiyoda-ku, Tokyo 101 (Document No. 8023).
7) C. K. Johnson, Oak Ridge National Laboratory ORNL-3794.
8) T. R. Lomer, *Acta Crystallogr.*, **16**, 984 (1963).
9) M. Goto and E. Asada, *Bull. Chem. Soc. Jpn.*, **51**, 70 (1978).
10) M. Goto and E. Asada, *Bull. Chem. Soc. Jpn.*, **51**, 2456 (1978).
11) V. Vand, W. H. Morley, and T. R. Lomer, *Acta Crystallogr.*, **4**, 324 (1951).
12) V. Vand and I. P. Bell, *Acta Crystallogr.*, **4**, 513 (1951).

 © 1980 The Chemical Society of Japan Bull. Chem. Soc. Jpn., 53, 2114—2119 (1980)

Solubility of Some Organic Mercury(II) Halides in Water[1]

Kooji TAJIMA,** Fumiaki KAI,* and Tetsuo KAWAHARA

Department of Chemistry, Faculty of Science, Kumamoto University, 2-39-1 Kurokami, Kumamoto 860
***Kumamoto Municipal Institute of Public Health, 1-13-16 Kuhonji, Kumamoto 862*

(Received August 30, 1979)

The solubilities of methylmercury(II) chloride (MMC), methylmercury(II) bromide (MMB), methylmercury(II) iodide (MMI), ethylmercury(II) chloride (EMC), and ethylmercury(II) bromide (EMB) in water have been determined over the temperature range of 10—55 °C (20—40 °C for MMC and EMC). The temperature dependence of the solubilities expressed as mole fractions x_2 was given by the following equations:

$$\log x_{2(\mathrm{MMC})} = -1059/T + 0.176 \quad (20—40\,^\circ\mathrm{C})$$
$$\log x_{2(\mathrm{MMB})} = -1094/T - 0.263 \quad (10—55\,^\circ\mathrm{C})$$
$$\log x_{2(\mathrm{MMI})} = -463/T - 3.246 \quad (10—25\,^\circ\mathrm{C})$$
$$\log x_{2(\mathrm{MMI})} = 5.498 \times 10^6(1/T)^2 - 3.711 \times 10^4(1/T) + 57.814 \quad (25—55\,^\circ\mathrm{C})$$
$$\log x_{2(\mathrm{EMC})} = -1048/T - 0.612 \quad (20—40\,^\circ\mathrm{C})$$
$$\log x_{2(\mathrm{EMB})} = -179/T - 4.293 \quad (10—25\,^\circ\mathrm{C})$$
$$\log x_{2(\mathrm{EMB})} = 5.389 \times 10^6(1/T)^2 - 3.603 \times 10^4(1/T) + 55.322 \quad (25—55\,^\circ\mathrm{C})$$

The thermodynamic parameters for the transfer process from solid to saturated aqueous solution were also determined.

Few papers have been published on the study of the organic mercury(II) compounds from the standpoint of pure chemistry. Waugh *et al.*[2] obtained the solubility product of MMC only at 25 °C from the dissociation constant and solubility in water. Schwarzenbach and Schellenberg[3] reported formation constants and the thermodynamic values of CH_3Hg^+ with several ligands, and Budevsky *et al.*[4] studied an interaction of CH_3Hg^+ with Cl^-. Hepler and Olofsson[5] also reviewed the thermodynamic properties, chemical equilibria, and standard potentials of the organic mercury(II) compounds. However, neither detailed solubility data with water over a wide temperature range nor thermodynamic parameters have been found in the literature.

As pointed out in the preliminary communication,[1] the determination of the solubility of the organic mercury(II) compounds in water is considered to be an urgent need. Accordingly, the present paper describes the solubilities of five organic mercury(II) compounds in water and the partial molal enthalpy and entropy of these compounds for the dissolution process, in which MMC is confirmed as the causal agent of the so-called "Minamata Disease".[6-8] The heat of fusion, one of the very important fundamental properties, was also measured.

Experimental

Materials. MMC, MMB, MMI, EMB, and ethylmercury(II) iodide (EMI)[9] were obtained from Wako Co., Ltd., and EMC from Tokyo Kasei Co., Ltd. They were recrystallized from hot ethanol. Before recrystallization, inorganic mercury(II) as an impurity was detected by spot test of TLC with dithizone. After recrystallization, no color spot due to inorganic mercury(II) was observed. Other impurities were measured quantitatively by a gas chromatograph equipped with an electron capture detector (Yanagimoto, G-80), and then the degree of purity was evaluated. The results are listed in Table 1, together with the melting points. Water was carefully purified twice by distillation with potassium permanganate.

Table 1. Purity and Mp

Substance	Purity / %	Mp[a] / °C
MMC	99.1	168 (ref. values; 167,[10] 168,[10] 174[8])
MMB	99.0	160 (ref. values; 160,[11] 160—161[12])
MMI	93.9	148 (ref. values; 148,[11] 150[10])
EMC	99.3	192 (ref. value; 192[13])
EMB	98.9	192 (ref. value; 192[11])

a) Different melting points have been reported in the literature, and it is our belief that some of these substances may have impurities.

Solubility Measurement. The solubility was determined by density measurements of the saturated aqueous solutions at a given temperature. The saturated aqueous solutions were prepared using two thermostated baths for all experiments. The temperature of the first bath was maintained higher by 3 °C than the desired temperature by continuous stirring, a saturated solution at higher temperature was thus primarily

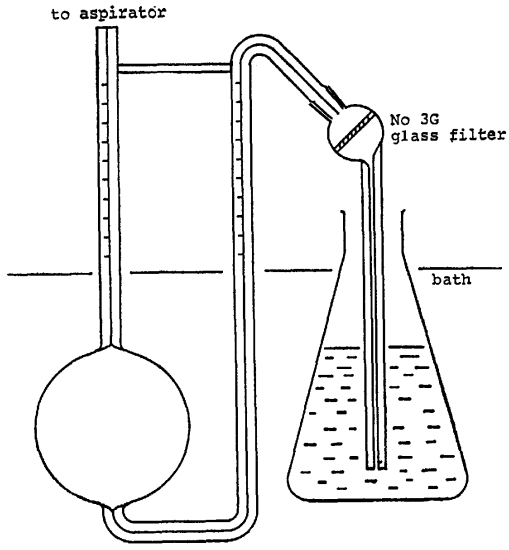

Fig. 1. Handling of solution.

obtained. The constant temperature of this first bath was controlled by a Pt–Hg regulator with ±0.05 °C accuracy. This solution was then immersed in the second bath controlled at the desired temperature with a Pt–toluene–Hg regulator having an accuracy of ±0.01 °C. Great care must be paid to deposition of the solutes with decreasing temperature of the solution and to the handling of such vigorous toxicant. Therefore, the apparatus in Fig. 1 was used to lead the saturated solution directly into the pycnometer (*ca.* 20 ml capacity for MMC and EMC, 45 ml for MMB, MMI, and EMB) without taking out the sample solution from the bath. The pycnometer was joined *via* a glass filter (G-4, 5—10 μ) to the flask containing the thermostated solution and then filled with the solution by aspiration.

Measurement of Heat of Fusion. TG-DTA analysis (Rigakudenki, 8076 E1) was carried out in order to obtain the heat of fusion. For determining the instrumental constant, benzoic acid (mp=122.28 °C, heat of fusion=17.3 kJ mol^{-1}), indium (mp=156.84 °C, heat of fusion=3.3 kJ mol^{-1}), and stannum (mp=231.94 °C, heat of fusion=7.07 kJ mol^{-1}) were used as the standard substances, because the melting points of the organic mercury(II) compounds studied (from 148 °C (MMI) to 192 °C (EMC and EMB) were included in the range of these three standard substances, and these standard substances have no solid-solid phase transition near their melting points. The mean value of the instrumental constant was estimated using $k=M\Delta H/A$ (M: sample weight, ΔH: heat of fusion, A: endothermic peak area) as 2.12.

Results and Discussion

The concentration of a solute is often determined by spectrophotometry. The present solutes, however, have no absorption maxima in the 200—300 nm region. Direct gravimetry could not be applied because of the volatility and high toxicity of the solutes studied. Therefore, the determination of the concentration was performed in this experiment by density measurements of the solutions at a given temperature. The error in density, mainly due to the weighing error of the pycnometer, was ±0.00005 g/cm^3. The relations between the mole fraction x_2 and the density of solution are illustrated in Figs. 2—6. All the figures showed good linearity, with a correlation coefficient of 0.999 at every experimental temperature. Table 2 shows the experimental solubility data expressed as mole fractions at various temperatures. The logarithm of the solubility against the reciprocal temperature is given in Fig. 7, which shows that all the solubilities increased with increasing temperature. From these data, the following solubilities

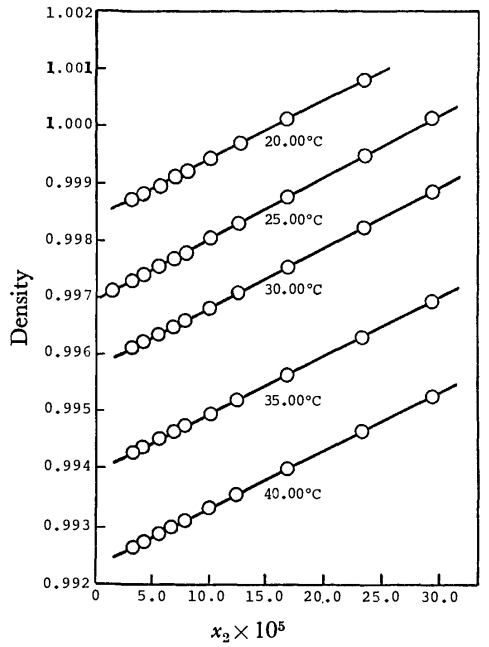

Fig. 2. Relation between mole fraction and density of MMC.

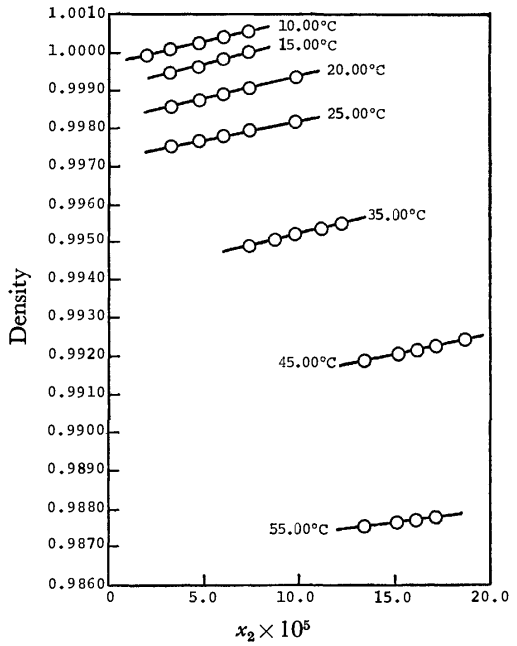

Fig. 3. Relation between mole fraction and density of MMB.

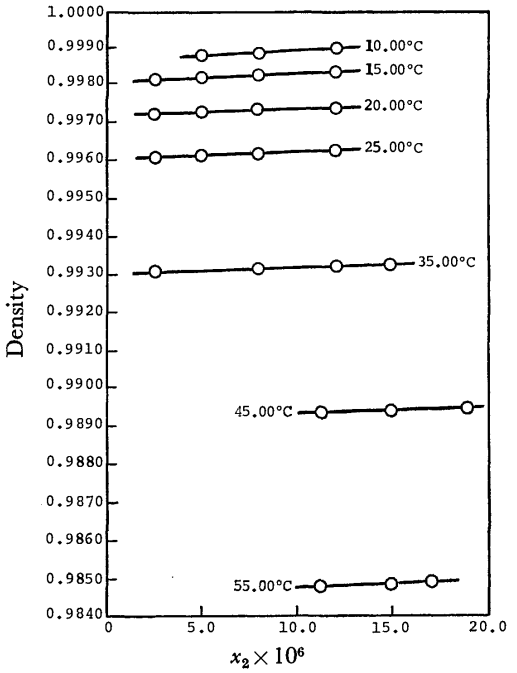

Fig. 4. Relation between mole fraction and density of MMI.

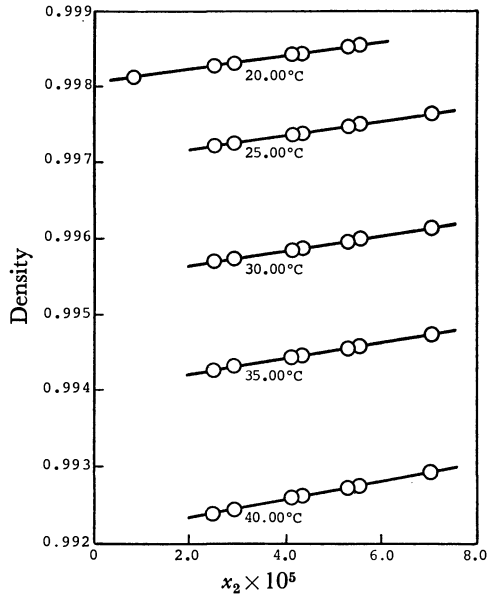

Fig. 5. Relation between mole fraction and density of EMC.

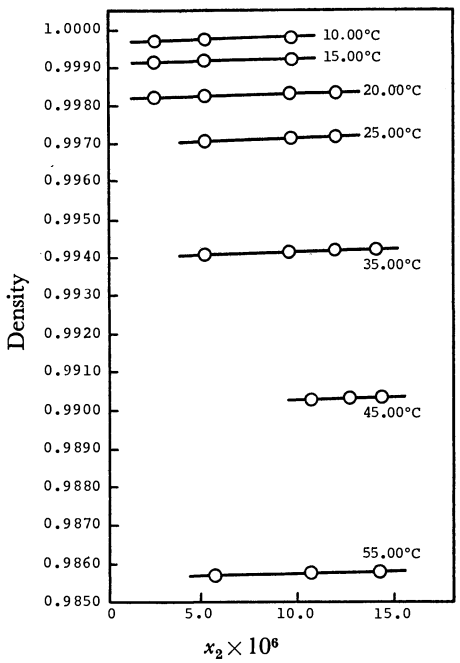

Fig. 6. Relation between mole fraction and density of EMB.

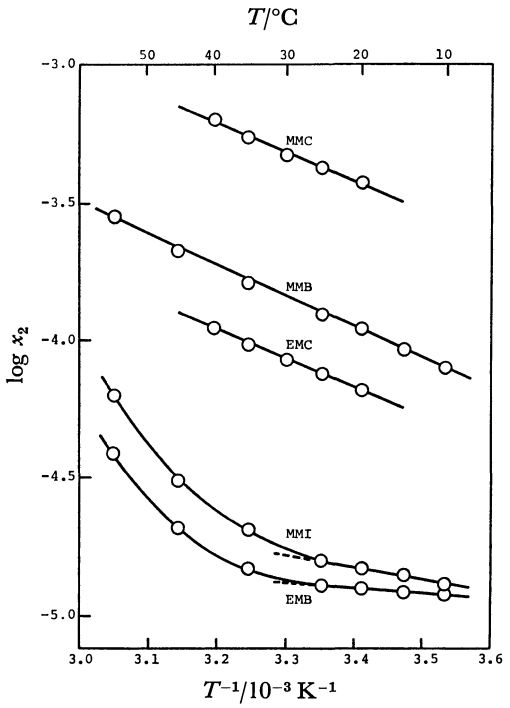

Fig. 7. Temperature dependence of solubility.

were obtained from the least squares fits:

$$\log x_{2(\mathrm{MMC})} = -1059/T + 0.176 \quad (20—40\,°C)$$

$$\log x_{2(\mathrm{MMB})} = -1094/T - 0.263 \quad (10-55\,°C)$$

$$\log x_{2(\mathrm{MMI})} = -463/T - 3.246 \quad (10-25\,°C)$$

$$\log x_{2(\mathrm{MMI})} = 5.498 \times 10^6(1/T)^2 - 3.711 \times 10^4(1/T) + 57.814 \quad (25—55\,°C)$$

$$\log x_{2(\mathrm{EMC})} = -1048/T - 0.612 \quad (20—40\,°C)$$

$$\log x_{2(\mathrm{EMB})} = -179/T - 4.293 \quad (10—25\,°C)$$

$$\log x_{2(\mathrm{EMB})} = 5.389 \times 10^6(1/T)^2 - 3.603 \times 10^4(1/T) + 55.322 \quad (25-55\,°C)$$

As can be seen from Fig. 7, the solubility features of MMI and EMB are different from those of MMC, MMB, and EMC: the former exhibits an abrupt curvature above 25 °C, while the latter shows linearity over the temperature range studied.

For a discussion of the thermodynamic behavior of the dissolution process of the solute, the heat of fusion of the solute was determined. As a typical example, the TG–DTA curve of MMI is shown in Fig. 8. As can be

Table 2. Temperature dependence of solubility

T/K	MMC $x_2 \times 10^5$	MMB $x_2 \times 10^5$	MMI $x_2 \times 10^5$	EMC $x_2 \times 10^5$	EMB $x_2 \times 10^5$
283.16		8.16±0.01	1.31±0.04		1.19±0.01
288.16		9.22±0.04	1.40±0.01		1.22±0.06
293.16	37.3±0.5	10.95±0.01	1.50±0.15	6.5±0.2	1.26±0.05
298.16	42.4±0.5	12.14±0.13	1.58±0.01	7.6±0.3	1.28±0.03
303.16	46.8±0.1			8.5±0.1	
308.16	54.8±0.1	15.80±0.02	2.03±0.01	9.4±0.2	1.49±0.03
313.16	63.4±0.1			11.2±0.2	
318.16		20.65±0.05	3.02±0.01		2.05±0.01
328.16		28.16±0.03	6.24±0.01		3.84±0.03

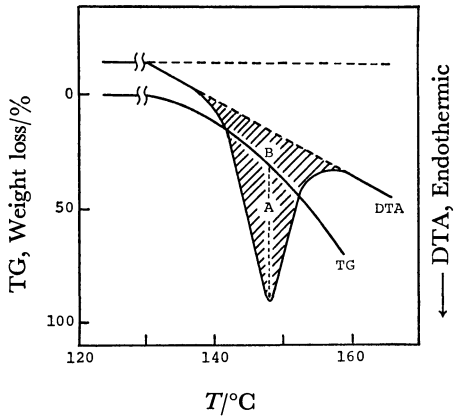

Fig. 8. TG–DTA curve of MMI.

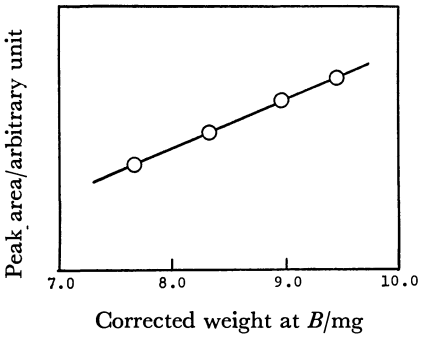

Fig. 9. Plot of corrected weight at B in Fig. 8 *vs.* peak area.

Table 3. Enthalpy and entropy of fusion

Substance	$H_2^\circ - H_2^s$ cal mol^{-1}	$S_2^\circ - S_2^s$ cal K^{-1} mol^{-1}
MMC	2300	5.1
MMB	2900	6.6
MMI	3500	8.3
EMC	2500	5.5
EMB	3000	6.5
EMI[9]	3200	6.9

seen from this TG curve, in general, the organic mercury(II) compounds sublime gradually before melting. Accordingly, it was required in this experiment to determine a heat purely due to fusion and not to sublimation. The relation between a sample weight corrected by the TG curve at the melting point (B) and an endothermic peak area (A) was examined repeatedly. The results gave a fine linear relation, as illustrated in Fig. 9. The values of the enthalpy and entropy of fusion, thus obtained, are listed in Table 3, where H_2° and H_2^s (S_2° and S_2^s) denote the enthalpy (entropy) of solution of supercooled liquid and solid, respectively, of the 2nd component.

For the transfer process from solid to saturated solution, the values of partial molal enthalpy and entropy of solution are estimated from the data of the temperature dependence of the solubility by using the following equation,

$$(\bar{H}_2 - H_2^s)/T = \bar{S}_2 - S_2^s \cong R(\partial \ln x_2/\partial \ln T)_{sat}$$

where $\bar{H}_2$ ($\bar{S}_2$) represents the enthalpy (entropy) of a solute in a solution. The thermodynamic parameters calculated from the data of the solubility and fusion are summarized in Table 4. Here the values of $(\bar{H}_2 - H_2^\circ)$ and $(\bar{S}_2 - S_2^\circ)$ mean the enthalpy and entropy changes for mixing of the solute in supercooled liquid and water, and they are related as:

$$(\bar{H}_2 - H_2^\circ) = (\bar{H}_2 - H_2^s) - (H_2^\circ - H_2^s)$$
$$(\bar{S}_2 - S_2^\circ) = (\bar{S}_2 - S_2^s) - (S_2^\circ - S_2^s)$$

The values in Table 4 were calculated by assuming that a molal heat capacity of a supercooled liquid (C_P^l) and that of a solid (C_P^s) are equal at a constant pressure, namely, $\Delta C_P = C_P^l - C_P^s = 0$.

The above discussion was made with the assumption that these solutes are non-electrolytes. Schwarzenbach and Schellenberg,[3] however, reported in detail the interactions of CH_3Hg^+ with Cl^-, Br^-, and I^- in water at 25 °C ($[CH_3Hg^+][Cl^-]/[CH_3HgCl] = 5.62 \times 10^{-6}$ mol dm^{-3}; $[CH_3Hg^+][Br^-]/[CH_3HgBr] = 2.40 \times 10^{-7}$ mol dm^{-3}; $[CH_3Hg^+][I^-]/[CH_3HgI] = 2.51 \times 10^{-9}$ mol dm^{-3}). MMC, MMB, and MMI thus seem to be very weak electrolytes. In order to estimate the effect of these slight dissociations, the thermodynamic values for the dissociation process were calculated by using the above constants. However, no influence was observed on the values of $(\bar{H}_2 - H_2^s)$ and $(\bar{S}_2 - S_2^s)$ in Table 4. Although the values of dissociation of EMC and EMB were not found in the literature, it can be assumed that

Table 4. Thermodynamic parameters

Substance	Temperature (°C)	$\bar{S}_2 - S_2^s$ (cal K^{-1} mol^{-1})	$\bar{H}_2 - H_2^s$ (cal mol^{-1})	$\bar{S}_2 - S_2^\circ$ (cal K^{-1} mol^{-1})	$-R \ln x_2$[a] (cal K^{-1} mol^{-1})	$\bar{H}_2 - H_2^\circ$ (cal mol^{-1})
MMC	20—40	15.8	4700	10.7	15.4	2400
MMB	10—55	16.5	4900	9.9	17.9	2000
MMI	10—25	7.3	2200	−1.0	22.0	−1300
	35	20.7	6400	12.4	21.5	2900
	45	36.3	11500	28.0	20.7	8000
	55	51.5	16900	43.2	19.2	13400
EMC	20—40	15.6	4600	10.1	18.8	2100
EMB	10—25	2.9	900	−3.6	22.4	−2100
	35	15.2	4700	8.7	22.1	1700
	45	30.6	9700	24.1	21.4	6700
	55	45.6	15000	39.1	20.2	12000

a) x_2 at 25 °C.

dissociations of EMC and EMB are less effective than those of MMC, MMB, and MMI. Further, it should be discussed whether the association of the solute can be neglected or not. However, no presence of, for example, an aggregate has been reported in the literature.

When the solubility behavior of these organic mercury(II) compounds in water is argued, the characteristics of "water" as a solvent should be considered necessarily. Frank and Evans[14] showed that, in spite of the small solubility of hydrocarbons such as higher alcohols in water, the heat of solution was small and the entropy of solution was negative. In order to rationalize this rather unusual situation, they postulated the formation of an "ice" which surrounds dissolved hydrocarbon molecules and they proposed to call this phenomenon an "iceberg" formation. In water, these phenomena are now considered to be usual.[15] This argument will show that, by dissolution of some kind of solute in water, the freedom of the water molecules surrounding the solute is restricted to some extent in the solution, compared with that of pure water.

In this study, the solubility behaviors could be classified into two groups according to the resemblances of the solubility features. In the first, the solubility increased abruptly above 25 °C (MMI and EMB). A behavior similar to this group was reported in the literature for the dissolution of aromatic hydrocarbons[16] such as benzene, toluene, *m*- and *p*-xylene, and ethylbenzene into water. In the cases of the solutes of MMI and EMB, the solubility curve could be divided into two parts: one was that in the 10—25 °C range and the other was that above 25 °C. In the range of 10—25 °C, because of negligibly weak interactions between solvent and solute, water molecules surrounding the solute were ice-like in structure. The tendency toward the formation of this ice-like structure in the 10—25 °C range, however, was considered to be relatively weak, because, as tabulated in Table 4, both the entropy and enthalpy changes for mixing were very small and negative as -1.0——-3.6 cal K^{-1} mol^{-1} and 1—2 kcal mol^{-1} (exothermic) respectively. Upon increasing the temperature above 25 °C, the ice-like structure of the water molecules surrounding the solute was obstructed, and thus the solutes could move more freely in the solution than could those in the 10—25 °C range. This breaking of the ice-like structure, that is, the abrupt increasing of the solubility above 25 °C, can be recognized by the large positive entropy and large endothermic enthalpy changes in Table 4.

In the cases of the solutes of MMC, MMB, and EMC as the second group, the formation of an ice-like structure may have been obstructed owing to the solvent-solute interaction, which was, however, considered to be weak. This interpretation seems to be consistent with the large positive entropy and endothermic enthalpy changes in Table 4. Similar behavios to this second group were reported for iodine,[17] naphthalene and biphenyl.[16] After all, the difference of the solubility features above 25 °C was considered to be mainly due to a delicate variance of the solvent-solute interactions. Although an interpretation for the different solubility features with respect to the kinds of alkyl group and halogen was attempted, it failed because the solubility of a solute having propyl or butyl group could not be measured in our experimental conditions owing to their small solubilities in water.

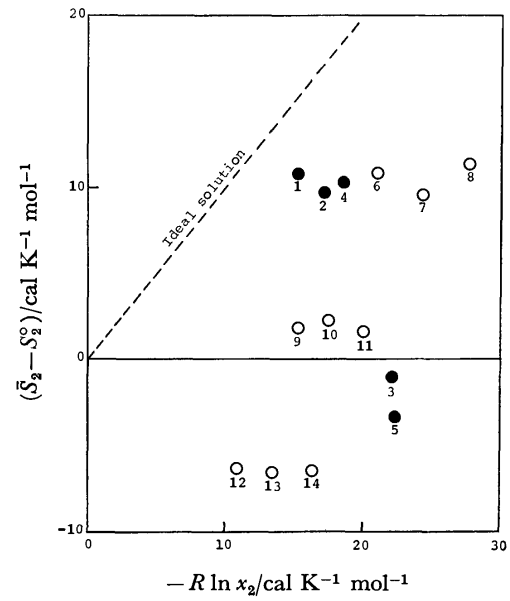

Fig. 10. Plot of $-R \ln x_2$ *vs.* $(\bar{S}_2-S_2^\circ)$.
1: MMC, 2: MMB, 3: MMI, 4: EMC, 5: EMB, 6: iodine,[19] 7: naphthalene,[16] 8: biphenyl,[16] 9: benzene,[16] 10: toluene,[15] 11: ethylbenzene,[16] 12: methane,[15] 13: ethane,[15] 14: propane.[15]

On the basis of the above discussion, so far as a non-polar solute is concerned, an argument of iceberg "making" or "breaking" should not be made as if it were a basic property possessed by a solute itself, but should be done in relation to the temperature studied.

Figure 10 shows the relation of the values of $(\bar{S}_2-S_2^\circ)$ against $-R \ln x_2$. If the solution is an ideal one, both values are identical as dotted line in the figure. For the comparison, besides the organic mercury(II) compounds studied, we plot the thermodynamic values of aromatic hydrocarbons[16] and of alkanes in the liquid state[15] obtained after converting the values in the gaseous state.[18] All the values of $-R \ln x_2$ are adopted as those at 25 °C. The solutes including the reference ones could be roughly classified. That is, the first group contained the solutes having the large positive values of $(\bar{S}_2-S_2^\circ)$, and their temperature dependence of the solubilities was shown to be linear (MMC, MMB, EMC, iodine, naphthalene, and biphenyl). Accordingly, the solutes having almost no ability to form an ice-like structure at the temperature studied were positioned in the vicinity of the ideal line. The second group (MMI, EMB, benzene, toluene, ethylbenzene, methane, ethan, and propane) largely deviated from the ideal line, showing nearly zero or negative $(\bar{S}_2-S_2^\circ)$ values, and the temperature dependence of the solubilities was curved.

The authors wish to thank Drs. M. Nakamizo and S. Sakagami of Goverment Industrial Research Institute, Kyushu, for their help with the TG–DTA measurements. One of the authors (K. T.) wishes to express his thanks

to Mr. S. Kitaoka, Chief of the Institute, for his encouragement throughout the work.

References

1) The solubilities of MMC and EMC were reported in a preliminary form: K. Tajima and F. Kai, *Chem. Lett.*, **1978**, 201.
2) T. D. Waugh, H. F. Walton, and J. A. Laswick, *J. Phys. Chem.*, **59**, 395 (1955).
3) G. Schwarzenbach and M. Schellenberg, *Helv. Chim. Acta*, **48**, 28 (1965).
4) O. Budevsky, F. Ingman, and D. H. Liem, *Acta Chem. Scand.*, **27**, 1277 (1973).
5) L. G. Hepler and G. Olofsson, *Chem. Rev.*, **75**, 585 (1975).
6) K. Irukayama, F. Kai, T. Kondo, and M. Fujiki, *Kumamoto Med. J.*, **14**, 157 (1961).
7) K. Irukayama, T. Kondo, F. Kai, and M. Fujiki, *Kumamoto Med. J.*, **15**, 1 (1962).
8) K. Irukayama, F. Kai, M. Fujiki, and T. Kondo, *Kumamoto Med. J.*, **15**, 57 (1962).
9) For EMI, because of lower solubility in water, only the heat of fusion was measured in this experiment.
10) P. L. Goggin and L. A. Woodward, *Trans. Faraday Soc.*, **62**, 1423 (1966).
11) J. H. S. Green, *Spectrochim. Acta, Part A*, **24**, 863 (1968).
12) Z. Meic and M. Randic, *Trans. Faraday Soc.*, **64**, 1438 (1968).
13) M. M. Kreevoy and R. L. Hansen, *J. Am. Chem. Soc.*, **83**, 626 (1961).
14) H. S. Frank and M. W. Evans, *J. Chem. Phys.*, **13**, 507 (1945).
15) K. Shinoda, *J. Phys. Chem.*, **81**, 1300 (1977).
16) R. L. Bohon and W. F. Claussen, *J. Am. Chem. Soc.*, **73**, 1571 (1951).
17) J. H. Hildebrand and R. L. Scott, "The Solubility of Nonelectrolytes," Reinhold (1950).
18) W. F. Claussen and M. F. Polglase, *J. Am. Chem. Scc.*, **74**, 4817 (1952).
19) J. H. Hildebrand and D. N. Glew, *J. Phys. Chem.*, **60**, 618 (1956).

Kinetic and Spectrophotometric Studies of Rhodamine 6G Dimerization in Aqueous Solution

Wataru INAOKA, Shoji HARADA, and Tatsuya YASUNAGA*

Department of Chemistry, Faculty of Science, Hiroshima University, Higashisenda-machi, Hiroshima 730

(Received September 3, 1979)

The dimerization reaction of dye, Rhodamine 6G, in aqueous solution was studied spectrophotometrically and kinetically: the equilibrium constant and the rate constants were found to be $K=1.6\times10^3$ M^{-1}, $k_f=1.1\times10^9$ M^{-1} s^{-1}, and $k_b=7.0\times10^5$ s^{-1}, respectively, at 15 °C. These rate constants, and those of other dyes are discussed. The effect of the ionic strength was also studied.

The aggregation of dye in solution has been of interest as a model system of the self-organization of sub-units into large structures of biological activity. The dimerization reaction of dye has been extensively investigated spectrophotometrically and kinetically. By the spectrophotometric experiments,[1-5] the equilibrium constant was obtained and the effect of additives has been studied. The kinetic experiments,[6-14] showed the rate constants to be very large. The rate constants of these dyes seem to be divided into two groups. Among them, Rhodamine B and 3B have been found to have relatively slow reaction rates, while the reaction of Rhodamine 6G was too fast to be observed by a conventional method.[12,13] Two purposes of the present work are to obtain the kinetic parameters of the dimerization of Rhodamine 6G and to discuss the difference in the rate constants of the two groups.

The increase of the ionic strength is known to promote the dimerization of dye.[3,15] Since the equilibrium constant is the ratio of the association and the dissociation rate constants, the ionic strength effect is also expected to be reflected in the rate constants. Another purpose is to investigate the effect of the ionic strength on this reaction.

Experimental

Rhodamine 6G hydrochloride (Tokyo Kasei) was recrystallized three times from water and dried under vacuum at 110 °C for 12 h. Distilled and deionized water was used throughout the experiment. The ionic strength was adjusted by the addition of NaCl.

The equilibrium constant was determined spectrophotometrically with a Union Giken SM 401 spectrophotometer. The kinetic experiment was performed with a stimulated Raman laser temperature-jump apparatus; the details of the apparatus were described elsewhere.[9] The measurement was carried out at 15 °C.

Results

Rhodamine 6G is known to aggregate in aqueous solution and this monomer-dimer equilibrium is established:

$$2M \underset{k_b}{\overset{k_f}{\rightleftarrows}} D \qquad (1)$$

where M is the monomer, D is the dimer, and k_f and k_b are the association and dissociation rate constants, respectively. The equilibrium constant K is related to the molar extinction coefficient and the concentration of dye as follows:[15]

$$\{(\varepsilon_M-\varepsilon)/C_0\}^{1/2} = (2K/\Delta\varepsilon)^{1/2}\{\Delta\varepsilon-(\varepsilon_M-\varepsilon)\} \qquad (2)$$

where

ε_M: the molar extinction coefficient of the monomer.
ε: the apparent molar extinction coefficient of dye.
$\Delta\varepsilon$: the difference between the molar extinction coefficient of the monomer and that of the dimer *per monomer unit.*
C_0: the initial concentration of dye.

According to Eq. 2, a plot of $\{(\varepsilon_M-\varepsilon)/C_0\}^{1/2}$ *vs.* $(\varepsilon_M-\varepsilon)$ will give a straight line with the intercept $(2K\Delta\varepsilon)^{1/2}$ on the ordinate and $\Delta\varepsilon$ on the abscissa. On this basis, ε_M was evaluated to give the best straight line with the measured values of ε and C_0. The plot is shown in Fig. 1. The equilibrium constant obtained, $K=1.6\times10^3$ M^{-1} at 15 °C, seems to be satisfactory compared with the previously reported values.[4,5,13] Furthermore, the equilibrium constants at various ionic strengths were obtained in the same way; they are listed in Table 1. As shown in the table, with the increase of the ionic strength, the equilibrium constant increases, *i.e.*, the formation of dimer is promoted.

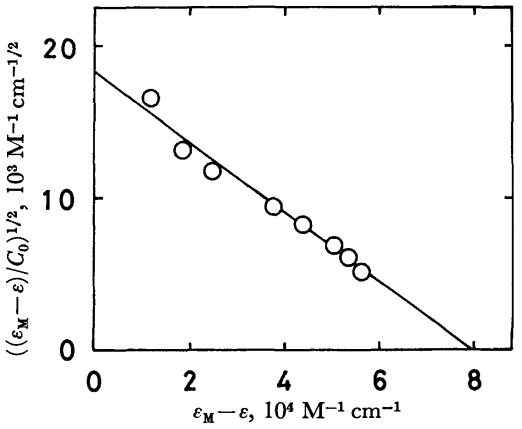

Fig. 1. Plots to determine the equilibrium constant K for Rhodamine 6G dimerization at $\mu=0$ M, 15°C.

TABLE 1. THE RATE CONSTANTS AND THE EQUILIBRIUM CONSTANT FOR RHODAMINE 6G DIMERIZATION AT VARIOUS IONIC STRENGTHS (15 °C)

Ionic strength (M)	k_f (10^9 M^{-1} s^{-1})	k_b (10^5 s^{-1})	K (10^3 M^{-1})
0.00	1.1	7.0	1.6
0.05	1.2	6.6	1.8
0.10	1.3	5.9	2.2
0.15	1.4	5.4	2.5

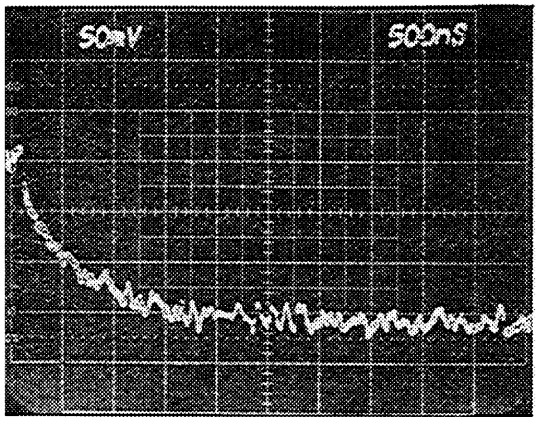

Fig. 2. Typical relaxation curve in 1.0×10^{-3} M Rhodamine 6G at $\mu=0$ M, 15°C, wavelength 525 nm, sweep 500 ns/div.

The kinetic experiment of the dimerization reaction of dye was performed in the concentration range of $(0.5—4.0)\times10^{-3}$ M. The relaxation phenomenon was detected spectrophotometrically at the monomer band (525 nm). A typical relaxation curve is shown in Fig. 2. The relaxation was also observed at the dimer band (500 nm) in the same time range but the change of the relaxation was in the opposite direction; this relaxation curve was not used because of its small relaxation amplitude. Each relaxation curve was characterized by a single relaxation time. Relaxation times were reproducible to $\pm10\%$.

The relaxation time τ is related to the rate constants as follows:

$$\tau^{-1} = 4k_f\bar{C}_M + k_b \qquad (3)$$

where $\bar{C}_M$ is the equilibrium concentration of the monomer, which is calculated from the equilibrium constant and the initial concentration. The plots of τ^{-1} against $\bar{C}_M$ are shown in Fig. 3, where every point of τ^{-1} is the mean value of at least 10 measurements. The good linear relationship indicates that the observed relaxation phenomenon is based on the monomer-dimer equilibrium of dye molecules. The value of k_f was

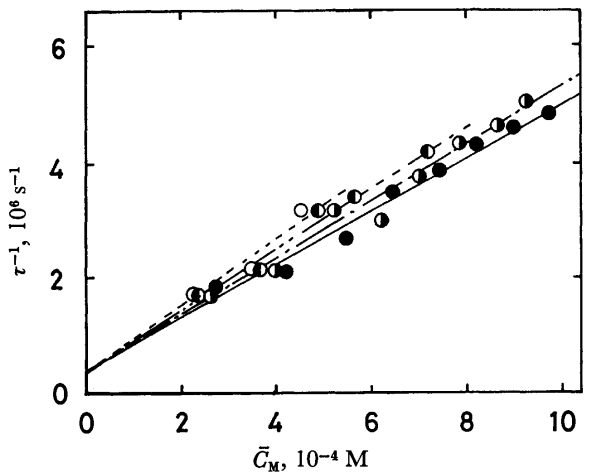

Fig. 3. Plots of τ^{-1} *vs.* $\bar{C}_M$ at various ionic strengths.
(●): $\mu=0$ M, (◑): $\mu=0.05$ M, (◐); $\mu=0.10$ M, (○): $\mu=0.15$ M.

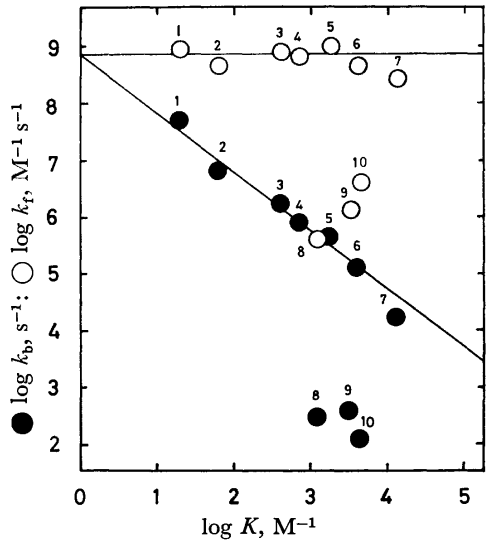

Fig. 4. Plots of log k_f and log k_b *vs.* log K for various dyes.
1: Dimethyladenine (5), 2: Ethidium Bromide (6), 3: Proflavine (7), 4: Thionine (8), 5: Rhodamine 6G (this work), 6: Methylene Blue (10), 7: Acridine Orange (11), 8: Rhodamine B (12), 9: Rhodamine 3B (13), 10: Congo Red (14).
(The number in parenthesis means the reference number).

obtained from the slope of the straight line. Since the value of k_b was small, it was calculated from k_f and K $(=k_f/k_b)$. The values of k_f and k_b obtained are listed in Table 1.

In order to compare the rate constants of dimerization of Rhodamine 6G with those of other dyes, log k_f and log k_b were plotted against log K in Fig. 4. From the kinetic standpoint of view, dyes in this figure seem to be divided into two groups. In group I, the values of k_f fall in the same order of magnitude and are close to that of the diffusion-controlled rate constant, and the linear relationship between log k_b and log K is recognized. On the other hand, in group II, the values of k_f and k_b are a few orders of magnitude smaller than the corresponding values in group I.

The effect of the ionic strength μ on the rate constants was studied under the conditions of $\mu=0.05$, 0.10, 0.15 M. At $\mu=0.15$ M, the measurement was limited to low concentrations since the dye precipitated at higher concentrations. The plots of τ^{-1} *vs.* $\bar{C}_M$ at different μ are also shown in Fig. 3. The rate constants obtained are listed in Table 1. As shown in the table, the increase of μ induces an increase of K, a small increase of k_f, and a small decrease of k_b.

Discussion

The dimerization reaction 1 may be divided into the following two processes:

$$M + M \underset{k_{-1}}{\overset{k_1}{\rightleftarrows}} (M, M) \underset{k_{-2}}{\overset{k_2}{\rightleftarrows}} D \qquad (4)$$

where the first process is the diffusion-controlled reaction to form the encounter complex (M,M) and the second process is the intramolecular reaction to form the stable

dimer D. Using the steady-state assumption for the encounter complex, the association and the dissociation rate constants are expressed as follows:

$$k_f = \frac{k_1 k_2}{k_{-1}+k_2} \quad (5)$$

$$k_b = \frac{k_{-1}k_{-2}}{k_{-1}+k_2} \quad (6)$$

The diffusion-controlled rate constants k_1 and k_{-1} can be theoretically estimated to be $k_1 = 1.8\times10^9\ M^{-1}\ s^{-1}$ and $k_{-1} = 3.0\times10^9\ s^{-1}$.[16] These values are in the same order of magnitude as those of other dyes; the difference of dyes is not reflected in the first step of Reaction 4. Inserting the values of k_1, k_{-1}, k_f, and k_b into Eqs. 5 and 6, k_2 and k_{-2} were calculated to be $4.7\times10^9\ s^{-1}$ and $1.8\times10^6\ s^{-1}$, respectively. Since the value of k_2 is very large and is nearly equal to k_1 and k_{-1}, the activation energy should be as small as that of the diffusion-controlled process. In the same way, the rate constants k_1, k_{-1}, and k_2 of other dyes in group I fall in the order of 10^9. Accordingly the difference in the equilibrium constant of the dyes in group I, including Rhodamine 6G, is attributed to that of k_{-2}.

Schelly *et al.*[12,13] have investigated kinetically the dimerization reaction of Rhodamine dyes (B, 3B, and 6G) by the stopped-flow method; the reaction of Rhodamine 6G, however, was too fast to be observed. With use of the reported values of k_f and k_b, the values for k_2 and k_{-2} of both Rhodamine B and 3B were estimated to be of the order of 10^6 and $10^{2.5}$, respectively. These rate constants are much smaller than the corresponding values of Rhodamine 6G, while the equilibrium constants of the dimerization of Rhodamine dyes are of the same order. These results can also be interpreted from the standpoint of free energy: the activation free energy of Rhodamine B and 3B is much higher than that of Rhodamine 6G, though the free energy differences are all of the same order (−4.1——4.7 kcal/mol); the free energy diagram is schematically shown in Fig. 5. Taking into account the structure of these dyes, we see that the existence of two methyl groups in the xanthene plane of Rhodamine 6G does not affect the free energy difference, but does affect the activation free energy between the encounter complex and the stable dimer states. The fact that Rhodamine 6G reacts through a different pathway from Rhodamine B may also be suggested by the μ dependence of the rate constants: the μ dependence of the rate constant of Rhodamine B has been reported to be very large,[12] while that of Rhodamine 6G was found to be small.

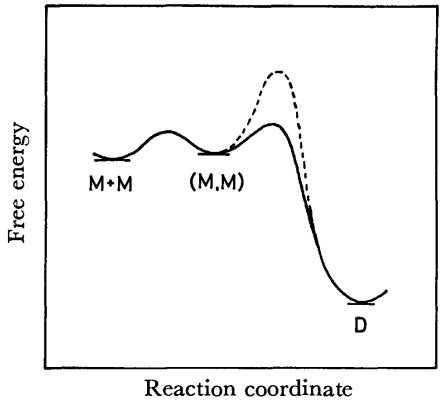

Fig. 5. Schematic diagram of the free energy of Rhodamine dyes.
(------): Rhodamine B and 3B, (——): Rhodamine 6G.

The ionic strength dependency of k_f and k_b given in Table 1 is realized in relation to Reaction 4. Since the dimerization is the reaction between the positive charges, the increase of the counter ion in solution decreases the electrostatic repulsion between dyes and promotes the dimerization, *i.e.*, k_1 increases with the increase of μ, while k_{-1} is unaffected.[18] Since the second step of Reaction 4 is the intramolecular process, the dependence of k_2 on μ may be small. Accordingly, with Eq. 5, the increase of k_f with the increase of μ is interpreted by that of k_1. From the above considerations on the rate constants (k_{-1} and k_2) with Eq. 6, the decrease of k_b with the increase of μ is ascribed to that of k_{-2}. The decrease of k_{-2} with the increase of μ may be understood by the contribution of the counter ion Cl^- to the stabilization of the dimer.

The authors gratefully acknowledge the support of the Toray Science Foundation for the establishment of the stimulated Raman laser temperature-jump apparatus.

References

1) K. K. Rohatigi and G. S. Singhal, *J. Phys. Chem.*, **70**, 1695 (1966).
2) V. Zanker, *Z. Phys. Chem.*, **199**, 225 (1952).
3) B. H. Robinson, A. Löffler, and G. Schwarz, *J. Chem. Soc., Faraday Trans. 1*, **69**, 56 (1973).
4) M. Hida and T. Sanuki, *Bull. Chem. Soc. Jpn.*, **43**, 2291 (1970).
5) J. E. Selwyn and J. I. Steinfeld, *J. Phys. Chem.*, **76**, 762 (1972).
6) D. Pörschke and F. Eggers, *Eur. J. Biochem.*, **26**, 490 (1972).
7) D. H. Turner, R. Yuan, G. W. Flynn, and N. Sutin, *Biophys. Chem.*, **2**, 385 (1974).
8) D. H. Turner, G. W. Flynn, S. K. Lundberg, L. D. Faller, and N. Sutin, *Nature*, **239**, 215 (1972).
9) W. Inaoka, S. Harada, and T. Yasunaga, *Bull. Chem. Soc. Jpn.*, **51**, 1701 (1978).
10) W. Spencer and J. R. Sutter, *J. Phys. Chem.*, **83**, 1573 (1979).
11) G. G. Hammes and C. D. Hubbard, *J, Phys. Chem.*, **70**, 1615 (1966).
12) M. M. Wong, R. A. Heckman, and Z. A. Schelly, *J. Phys. Chem.*, **77**, 1317 (1973).
13) M. M. Wong and Z. A. Schelly, *J. Phys. Chem.*, **78**, 1891 (1974).
14) T. Yasunaga and S. Nishikawa, *Bull. Chem. Soc. Jpn.*, **45**, 1262 (1972).
15) G. Schwarz, S. Klose, and W. Balthasar, *Eur. J. Biochem.*, **12**, 454 (1970).
16) k_1 and k_{-1} were calculated following Ref. 17 and 18, respectively; the diffusion coefficient of $3.5\times10^6\ cm^2\ s^{-1}$ (Ref. 19) and an encounter distance of 10 Å were used.
17) P. Debye, *Trans. Electrochem. Soc.*, **82**, 265 (1942).
18) M. Eigen, *Z. Phys. Chem. N. F. 1*, **1**, 176 (1954).
19) D. Magde, E. L. Elson, and W. W. Webb, *Biopolymers*, **13**, 29 (1974).

Thermal Desorption of Hydrogen Adsorbed on Copper Surface

Isao KOJIMA,* Makoto KIYOMIYA, and Iwao YASUMORI
Department of Chemistry, Tokyo Institute of Technology, Meguro-ku, O-okayama, Tokyo 152
(Received October 6, 1979)

The thermal desorption of hydrogen adsorbed on a clean surface of polycrystalline copper foil was studied under ultra high vacuum conditions. The presence of chemisorbed hydrogen in a dissociated state was verified in a temperature range between 193 and 573 K. During the desorption process, the adsorbed hydrogen atoms recombined into molecules; this follows second order kinetics. The activation energy for desorption was 68.6±8.0 kJ mol^{-1} and remained nearly constant in the range of surface coverage up to 1.6×10^{14} atom cm^{-2}. The isotope effect on the desorption of deuterium was found to be straightforward. These findings showed a good agreement with the results obtained from the analysis of H_2–D_2 equilibration on copper powder catalyst. In addition, the necessary conditions to obtain the exact desorption spectra were inspected with the aid of computer simulation.

Studies on the elementary processes of adsorption and desorption are important in understanding the catalytic reaction on solid surfaces. Although there have been many investigations of the adsorption of hydrogen on copper surfaces,[1–7] the mechanism has not been well established. An activated process for adsorption is the consensus in most of reports,[2,5,6] but they do not give concordant values for the activation energy and the heat of adsorption.

In our previous study,[8] it was shown that H_2–D_2 equilibration on reduced copper powder can be interpreted in terms of the Bonhoeffer-Farkas mechanism, which involves the dissociative adsorption of hydrogen and the surface recombination of adsorbed hydrogen atoms in the reaction pathway. From the analysis of the reaction time course, kinetic parameters of adsorption and desorption were evaluated. In a subsequent work,[9] these results were found to accord well with those of the classical trajectory calculations for the dissociative adsorption on a model (100) copper surface.

Thermal desorption (TD) gives direct information on the adsorbed states, the fraction of coverage, and the kinetics of desorption. A TD measurement, using a conventional high vacuum system, was applied to the hydrogen adsorbed on copper powder and the formation of HD together with H_2 and D_2 was successfully observed by heating the surface covered with hydrogen and deuterium. The estimated value for the activation energy of desorption was, however, about a half of that obtained from the analysis of the reaction kinetics.[10] Accordingly, the present study aimed to solve this contradiction between these experimental results and, further, to make clear the adsorbed state of hydrogen on a copper surface. To attain this purpose, we paid special attention to finding the optimum situation for pursuing the desorption process and designed a desorption system which is operated with high pumping speed in the range of ultra high vacuum (UHV). The desorption spectra obtained by using the system were analyzed in detail. The adsorbed state of hydrogen, the activation energy of desorption, and its dependence on the coverage of adsorbed hydrogen were determined, and the isotope effect on desorption was also inspected. Further, the obtained results were compared with those derived from the study of H_2–D_2 equilibration on copper catalyst.

Experimental

A schematic representation of the apparatus employed is shown in Fig. 1. The experiments were performed in a pyrex glass UHV system. The adsorption–desorption system with a volume of 410 cm^3 consisted of a desorption cell, a pressure gauge, a greaseless glass valve, and an ion getter pump. A 3-stage mercury diffusion pump was connected to the system through a liquid nitrogen cold trap and a bakeable metal valve and used for initial pumpdown to about 10^{-6} Torr (1 Torr= 133.3 Pa). After the bakeout of the system at 530 K for 24 h, a vacuum of about 5×10^{-10} Torr was readily attained by using the ion getter pump.

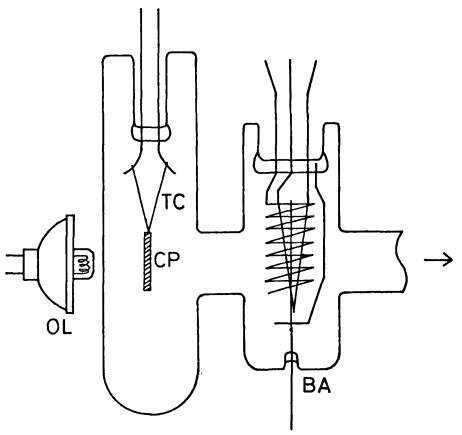

Fig. 1. A schematic representation of desorption system. BA: Bayard-Alpert gauge, CP: copper plate, OL: halogen lamp, TC: Pt–Pt/Rh13% thermocouple.

The desorption spectra were recorded by means of a Bayard-Alpert gauge, through which the desorbed gas was evacuated. This allowed us to measure directly the density of desorbed molecules related to the desorption rate. A polycrystalline plate of copper with a surface area of 4.2 cm^2 was used as the adsorbent. The sample was spot-welded to the junction point of Pt–Pt/Rh13% thermocouple wire, 0.05 mm in diameter, and was hung down in the desorption cell by the wire so as to minimize the temperature fluctuation and the desorption from the thermocouple. The sample after the bakeout was reduced in a flow of hydrogen of pressures between 10^{-3}—10^{-4} Torr at 570—670 K for 48 h and then outgassed at 773 K until no further gas evolution could be detected. The surface cleanliness was judged by the reproducibility of measurements after the reduction-outgas cycle. The surface with a constant

activity could then be obtained by reducing and outgassing several times at 773 K *in vacuo* better than 5×10^{-10} Torr. To avoid the wall effect, the sample was heated directly by infrared irradiation supplied from a halogen reflector lamp, Osram Model 15V 150W. The infrared light beam was dispersed on the copper plate. The heating rate was adjusted in a range 0.2—4 K s^{-1} using a constant-current power supply. Hydrogen pressures measured by the ion gauge were calibrated with nitrogen of equivalent pressures using the published value of the sensitivity ratio, $S_{H_2}/S_{N_2}=0.44$.[11] After the copper surface was exposed to hydrogen of 1×10^{-5}—1×10^{-8} Torr for 45 minutes at room temperature and was evacuated to 5—10×10^{-10} Torr at 193 K, the surface temperature was raised linearly with time up to 570 K.

Results

Since the detailed discussions on the basis for determining kinetic parameters from desorption spectra have already been given,[12,13] only the salient features will be outlined here.

An accurate knowledge of the effective pumping speed is necessary to determine the absolute values of kinetic parameters for desorption. From the following procedure, the pumping speed, S (cm^3 s^{-1}), was determined for hydrogen. The mass balance of gases present in a vacuum system requires the following equation to hold:

$$V\frac{dP}{dt} = Q - S\Delta P \qquad (1)$$

$$\text{and} \quad \Delta P = P - P_0,$$

where P and P_0 are the operating and background pressures in the system, respectively, V is the volume of the system, and Q is the external influx of gases (in Torr cm^{-3} s^{-1}). Accordingly, by introducing hydrogen gas into the closed vacuum system at a constant rate, the influx was evaluated from the increasing rate of pressure:

$$Q = V\frac{dP}{dt}. \qquad (2)$$

Then the system was evacuated and after the pressure attained an equilibrium value, P_{eq}, S was determined by using the relation

$$S = (P_{eq}-P_0)/Q. \qquad (3)$$

From the measurements stated above, S was evaluated to be 2.3×10^3 cm^3 s^{-1} in a pressure range between 10^{-8} and 10^{-6} Torr.

Figure 2 illustrates the typical desorption spectra of hydrogen and deuterium adsorbed at the same fraction of coverage on a surface. Only one peak was observed in each spectrum; the peak of D_2 appeared at the temperature higher than that of H_2 by about 10 K. The temperature at peak maximum shifted to the lower temperature side with increased amount of adsorption under a constant rate of temperature increase and showed the same trend of shift with a decrease of the rate of temperature rise under a constant amount of adsorption. The increase of surface coverage, for example from 1.4×10^{13} to 2.0×10^{14} atom cm^{-2} of hydrogen, shifted the peak maximum from 355 to 327 K at the rate of temperature rise of 1.2 K s^{-1}, and the

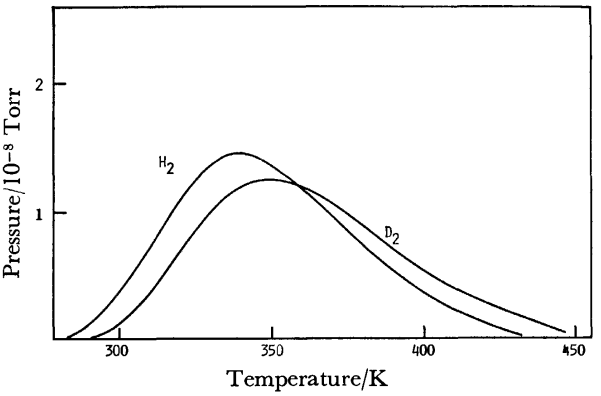

Fig. 2. Thermal desorption spectra of hydrogen and deuterium on copper surface.

increase in the rate from 0.17 to 3.2 K s^{-1} brought about the increase in the peak temperature from 330 to 368 K at the constant coverage of 1.8×10^{13} H-atom cm^{-2}.

Mass balance during the desorption requires that Q in Eq. 1 is replaced by the rate of desorption from the surface:

$$V\frac{dP}{dt} = \frac{A}{C}\frac{dN}{dt} - S\Delta P, \qquad (4)$$

where N is the number of desorbing molecules per unit area, A is the surface area and, C is a conversion factor in a unit of molecule K $Torr^{-1}$ cm^{-3}, which is equal to 3.2×10^{16} at 300 K. In the normal UHV system with large pumping speed, the ratio V/S is negligibly small and therefore the desorption rate becomes approximately proportional to the pressure increase:

$$\frac{dN}{dt} = \frac{C}{A}S\Delta P. \qquad (5)$$

The amount of adsorbed hydrogen, N_0 (molecule cm^{-2}) is given by

$$N_0 = \frac{CS}{A}\int_0^\infty \Delta P\, dt. \qquad (6)$$

The value of the integral in the right hand side of Eq. 6 is proportional to the area of the desorption peak.

The desorption rate per unit surface area is expressed as

$$R_d = \frac{dN}{dt} = \nu \exp(-E_d/RT)n^x, \qquad (7)$$

where ν is the pre-exponential factor, E_d is the activation energy of desorption, n is the number of adsorbed atoms per unit area, and x is the reaction order with respect to the adsorbed species. The desorption was operated in a linear temperature rise with time, *i.e.*, $T=T_0+\beta t$, where β is a coefficient of temperature rise. The differentiation of Eq. 7 with temperature shows that the temperature, T_m, at which the desorption spectrum gives a peak maximum can be correlated with the factors ν, E_d, β, and x by the following equation:

$$E_d/RT_m^2 = (x\, n_m^{x-1}\nu/\beta)\exp(-E_d/RT_m) \qquad (8)$$

where n_m is the number of adsorbed particles remaining at T_m. Then, it is found that

$$\log(T_m^2/\beta) = \frac{E_d}{2.303RT_m} + \log\frac{E_d}{R\nu x n_m^{x-1}}. \qquad (9)$$

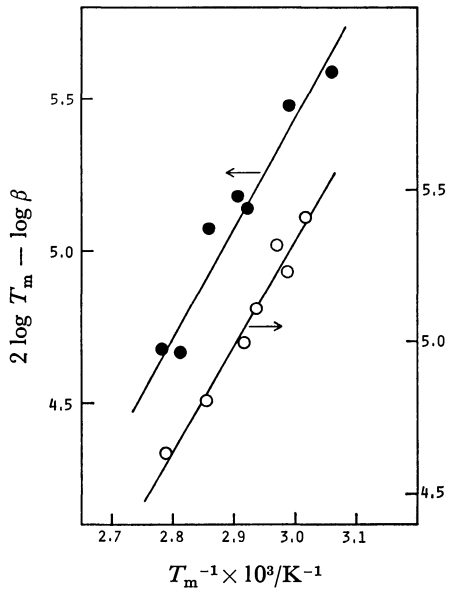

Fig. 3. Plots of (2 log T_m − log β) *vs.* T_m^{-1}.
○: H_2, ●: D_2.

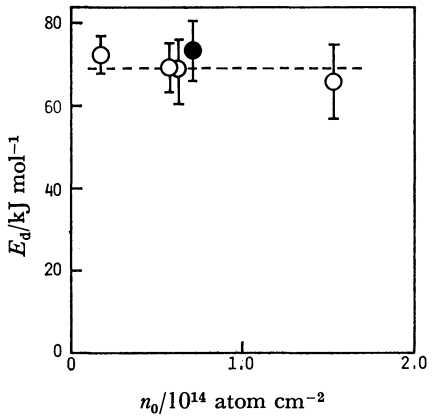

Fig. 4. Invariance of activation energy of desorption with surface concentration.
○: H_2, ●: D_2.

For a constant initial coverage, E_d and n_m would be unchanged even if β is varied. A plot of log (T_m^2/β) *versus* $1/T_m$ gives a straight line with slope of $E_d/2.303\,R$. This relationship is shown in Fig. 3 for adsorbed hydrogen and deuterium at the initial coverages of $6.4\pm0.2\times10^{13}$ H-atom cm^{-2} and $7.2\pm0.3\times10^{13}$ D-atom cm^{-2}, respectively. Figure 4 summarizes the activation energy of desorption as a function of the amount of desorption: Values of E_d for H_2, as shown by open circles, were constant at 68.6 ± 8.0 kJ mol^{-1} up to a surface concentration of 1.6×10^{14} atom cm^{-2}. The filled circle in Fig. 4 shows the activation energy of desorption for D_2. The obtained value of the energy was 73.6 ± 8.0 kJ mol^{-1}, which is slightly greater than that for H_2.

When the thermal desorption is carried out at constant β, the shifts of T_m shown in Fig. 2 lead to the determination of reaction order. Equation 8 can be rearranged to

$$2\log T_m - \frac{E_d}{2.303\,RT_m} = (1-x)\log n_m + \log\frac{\beta E_d}{x\nu R}. \quad (10)$$

Because E_d is constant with coverage, as seen from Fig. 4, a plot of $(2\log T_m - E_d/2.303\,RT_m)$ *versus* log n_m gives a straight line with a slope of $1-x$, where n_m is given by

$$n_m = \frac{CS}{A}\int_{t(T_m)}^{\infty}\Delta P\,dt. \quad (11)$$

The results are shown in Fig. 5. From the slope, the desorption order , x was evaluated to be 2.0 ± 0.2.

The values of E_d and x permitted us to calculate the frequency factor of desorption from the intercept of Fig. 2. This value of ν was found to be $1.0\pm0.5\times10^{-4}$.

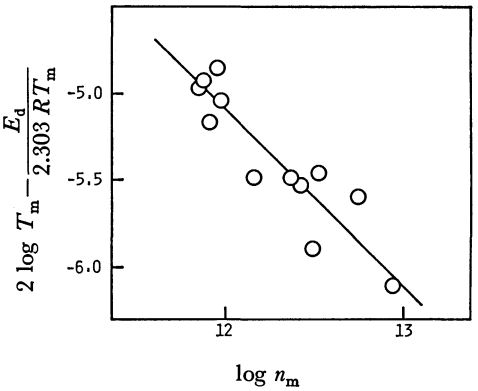

Fig. 5. A plot of $\left(2\log T_m - \frac{E_d}{2.303\,RT_m}\right)$ *vs.* log n_m.

Discussion

The present study proves that the thermal desorption is a useful method for determining the desorption kinetics. However, in typical adsorption systems many complicated situations occur;[14] there may be several different adsorbed states even for a single adsorbed species. In addition, the activation energy of desorption may depend on the concentration of adsorbed species and on the structures of surfaces. Transition metals such as W, Ni, Pt *etc.* have been found to show complicated desorption spectra of hydrogen because of superposed peaks.[14,15] It is, therefore, desirable to use more simple systems in order to perform the precise analysis of the desorption mechanism. In the present study, the desorption spectra on copper showed a single peak which shifted to the higher temperature side with the decreased coverage of surface. The activation energy of desorption was unchanged up to the surface concentration of 1.6×10^{14} atom cm^{-2} or $\theta_H=0.6$ when the saturated amount was estimated at 2.8×10^{14} atom cm^{-2} [8] (Fig. 4) and the desorption order was given by integer number as 2 (Fig. 5). All of these findings lead us to conclude that the chemisorption of hydrogen takes place dissociatively on a copper surface and that the interaction among adsorbed hydrogen atoms is quite weak.

In the previous studies of hydrogen adsorption and H_2–D_2 equilibration, it was found that the isothermal adsorption of hydrogen on a copper surface can be

interpreted in terms of the Langmuir equation for dissociative adsorption.[8,9] This behavior of adsorption was also verified by TD measurements. The activation energy of desorption evaluated by TD agreed well with that obtained from the kinetic measurement, 71 ± 4 kJ mol^{-1}. Further, the desorption rate constant at 287 K was evaluated by using the values of activation energy and the frequency factor as $3.3 \pm 2.0 \times 10^{-17}$ cm^2 molecule^{-1} s^{-1}, which is also consistent with the value $7.9 \pm 6.0 \times 10^{-17}$ obtained in the previous study. In the desorption of deuterium, T_m was higher than that of H_2 for the same fraction of coverage and E_d was also greater than that for H_2, indicating the presence of a normal isotope effect on desorption. The value of E_d for D_2 agreed with the previously obtained value within the experimental error.

In the analysis of the desorption spectrum, the magnitude of the evolution rate, relative to the changing rate of the accumulation in the system, takes an essential role is determining whether Eq. 5 exactly reflects the desorption process or not. When the difference between these two rates is not so large, Eq. 5 is not valid and its use would result in a lower value for the activation energy of desorption than the true one. In order to make the above situation clear, an exact simulation of Eqs. 4 and 7 for the second order desorption was performed by using a computer. As is seen from Figs. 6 and 7, the position of peak maximum shifted to the higher temperature side with the decrease of the pumping speed. The analysis of desorption spectra by using Eq. 9 resulted in the decrease of the apparent activation energy to 40.5 kJ mol^{-1} at 10 cm^3 s^{-1}. Such a depression of the energy seems to be the main reason why an incorrect energy value was obtained by using the usual high vacuum system with low evacuation conductance.[10] The desorption spectrum simulated at the speed of

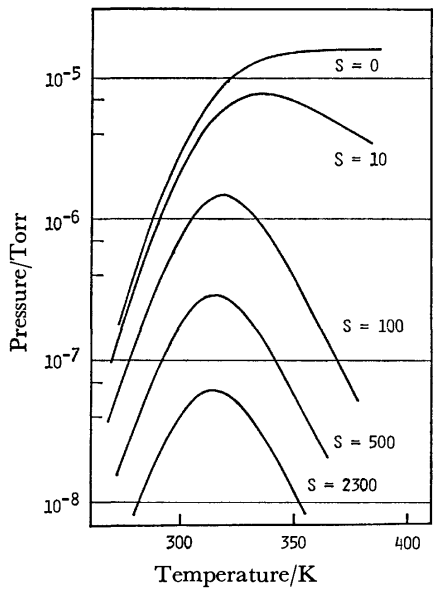

Fig. 6. Effect of pumping speed on desorption spectra. The spectra were simulated for different pumping speed, S (cm^3 s^{-1}) by using Eqs. 4 and 7 in the text. E_d: 68.6 kJ mol^{-1}, ν: 1×10^{-4}, β: 1 K s^{-1}, n_0: 1×10^{14} atom cm^{-2}, A: 4.2 cm^2, V: 410 cm^3.

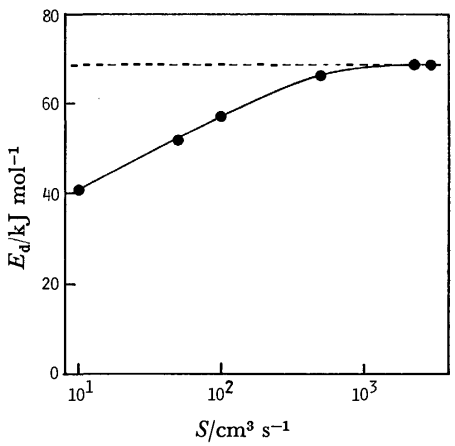

Fig. 7. Calculated activation energy of desorption as a function of pumping speed. Parameters used in the calculation were the same as those of Fig. 6 except that β is changed from 0.2 to 2 K s^{-1}. A dashed line shows the true value of activation energy of desorption.

2300 cm^3 s^{-1} accorded with that calculated from Eq. 5 within 0.1 K. This large difference of the two rates in the present study permitted us to determine exactly the kinetic parameters and mechanism of the desorption. In addition, the pressure gauge was located directly in front of the source of gas evolution; thus the pressure inside the cell and its change on heating was accurately followed and recorded by the gauge. It is to be noted that the same caution should be used for the gas chromatographic TD measurement with respect to the magnitude of the flow rate of the carrier.

Balooch *et al.* found that the activation energy for the adsorption of hydrogen on a copper surface depends on the crystallographic planes, as shown in the sequence $E_a(111) \gtrsim E_a(100) > E_a(113)$.[6] The present study cannot tell whether the desorption rate depends on the lattice planes or not. However, a single adsorbed state was observed on the polycrystalline copper used, and it is likely that the annealed surface exposed preferentially the (100) plane on which hydrogen is mainly adsorbed.

Classical trajectory calculations were applied to the adsorption of hydrogen on copper[9,16] and made possible the microscopic analysis of the process of dissociative adsorption. The desorption of the molecule from the surface is also interesting in view of the energy transfer from the lattice vibration to the vibration of adsorbed atoms and to the motion of molecules released from the surface. The results obtained here will be available for such microscopic descriptions of the behavior of adsorbed atoms. Trajectory calculation studies for the desorption of hydrogen from a copper surface are now in progress and will be published elsewhere.

References

1) D. O. Hayward and B. M. W. Trapnell, "Chemisorption," Butterworths, London (1964).
2) T. Kwan, *Adv. Catal.*, **6**, 67 (1954).
3) D. D. Eley and D. R. Rossington, "Chemisorption,"

Butterworths, London (1957).
4) J. Pritchard and F. C. Tompkins, *Trans. Faraday Soc.*, **56**, 540 (1960).
5) C. S. Alexander and J. Pritchard, *J. Chem. Soc., Faraday Trans.* 1, **68**, 202 (1972).
6) M. Balooch and R. E. Stickney, *Surf. Sci.*, **44**, 310 (1974).
7) D. A. Cadenhead and N. J. Wagner, *J. Catal.*, **21**, 312 (1971).
8) M. Kiyomiya, N. Momma, and I. Yasumori, *Bull. Chem. Soc. Jpn.*, **47**, 1852 (1974).
9) I. Yasumori, N. Momma, and M. Kiyomiya, *Jpn. J. Appl. Phys. Suppl.* 2, *Pt. 2*, 485 (1974).
10) N. Momma, Ph. D. Thesis, Tokyo Institute of Technology, 1972.
11) Z. Oda, *Shinku*, **3**, 240 (1960).
12) G. Ehrlich, *J. Appl. Phys.*, **32**, 4 (1961).
13) P. A. Redhead, *Vacuum*, **12**, 203 (1962).
14) D. Menzel, "Interactions of Metal Surfaces," Springer-Verlag, New York (1975).
15) I. Toyoshima and G. A. Somorjai, *Catal. Rev. -Sci. Eng.*, **19**, 105 (1979).
16) A. Gelb and M. Cardillo, *Surf. Sci.*, **59**, 128 (1976); **64**, 197 (1977).

The Thermal Desorption of Surface Hydroxyls on Tin(IV) Oxide

Kunimistu MORISHIGE,* Shigeharu KITTAKA, and Tetsuo MORIMOTO**

Department of Chemistry, Faculty of Science, Okayama College of Science, 1-1 Ridaicho, Okayama 700
***Department of Chemistry, Faculty of Science, Okayama University, Tsushima, Okayama 700*

(Received November 19, 1979)

The structure of the adsorbed layer of water on SnO_2 was investigated by means of thermal desorption, water physisorption, and electron diffraction, using four kinds of SnO_2 samples which differ in method of preparation. Two distinct peaks appear around 513 and 573 K in the thermal-desorption spectra. The peak around 513 K is due to the condensation dehydration of hydroxyls on the (100) plane of SnO_2, on which the two-dimensional condensation of water occurs. The peak around 573 K is associated with that on the (101) plane, on which the physisorption of water is strong and the two-dimensional condensation of water does not occur. The portion of the (100) plane occupied by water molecules is relatively small, and the 1 : 4 ratio (H_2O : OH) holds also on the surfaces on which the two-dimensional condensation of water does not occur. In conclusion, the fully hydroxylated surfaces of SnO_2 are hydrophobic in the sense that they sparsely adsorb water molecules.

In a series of studies[1-4] of the interaction between SnO_2 surfaces and water molecules, we have reported that a two-dimensional condensation of water occurs on the hydrated surface of the SnO_2 obtained from the calcination of stannic acid in air. The electron diffraction of SnO_2 particles and a crystallographic consideration of the hydroxylated surface structure lead to the conclusion that this phenomenon takes place on the surface hydroxyls formed on the (100) plane of SnO_2 with a rutile structure. Furthermore, the ratio of the number of physisorbed water molecules in the monolayer to that of the underlying surface hydroxyls was found to be about 1 : 3—4, indicating a very sparse packing of water molecules in the first physisorbed layer. Since the occurrence of two-dimensional condensation suggests the formation of a close-packed phase of the adsorbate at the monolayer coverage, the fact that water molecules condense two-dimensionally is apparently in conflict with the idea that water molecules are sparsely packed on the same surface.

It may reasonably be expected that there exist crystal planes other than (100), the relative area of which depends on the method of preparation, and that the formation or desorption energy of surface hydroxyls differs on different crystal planes. Therefore, it is interesting to investigate the dependence of the chemisorption or desorption energy of surface hydroxyls upon the nature of the crystal plane. Yamazoe *et al.*[5] reported on the desorbability of chemisorbed water on SnO_2 effected by means of a conventional temperature-programmed desorption technique, as a basis for the development of gas detectors. The aim of the present work is to correlate the peaks in the thermal-desorption spectra of surface hydroxyls to the crystal planes on SnO_2, and also to investigate the above-mentioned contradiction concerning the packing of water molecules on the hydroxylated SnO_2 surfaces.

Experimental

Materials. Tin (IV) oxide of a high purity (99.95%) was obtained from Mitsuwa Pure Chemicals, Ltd. (SnO_2-I). It was prepared by the same method as the sample which we had employed previously,[1-4] *i. e.*, by calcining β-stannic acid formed by oxidizing metallic tin with concd HNO_3. SnO_2-II was obtained by calcining α-stannic acid at 1073 K for 5 h in air, the latter having been prepared by the hydrolysis of $SnCl_4$ with ammonia water.[3] SnO_2-III was prepared by a gas-phase reaction.[6] A mixture of Sn and SnO_2 was heated in a quartz reaction tube at *ca.* 1473 K in a stream of N_2, and the resulting SnO gas was allowed to react with O_2 at the same temperature to give microcrystalline SnO_2 (SnO_2-III). SnO_2-IV was tin (IV) oxide (99.0%) prepared by Wako-Pure Chemicals, Ltd. O_2 and H_2 from a commercial gas cylinder were purified by passing them through a molecular sieve-5A cooled at 195 and 75 K respectively. D_2O (99.75%, Merck) was used without further purification.

Thermal Desorption. As has been described previously,[7] the measurement of the thermal desorption was carried out on a Sartorius vacuum-microbalance. SnO_2 can be readily reduced by evacuation at moderate temperature,[8] and the activity for water adsorption decreased upon reduction.[1,2,4] The surface cleaning of the sample, therefore, was carried out by the following procedure. The sample was evacuated at 773 K for 2 h under a vacuum of 1.3×10^{-2} Pa, heated in O_2 of 13.3 kPa at 773 K for 1 h, cooled room temperature in the O_2 atmosphere, and then evacuated briefly. The reduction of the samples was carried out by exposing the oxygenated sample to H_2 of 6.7 kPa at 433 or 473 K for 2 h. Then, the samples were exposed to saturated water vapor at room temperature for 15 h to ensure a full rehydroxylation of the surface. The thermal-desorption spectra were measured at a heating rate of 5/6 K min^{-1}. The amount of chemisorbed water was determined by the D_2O-exchange method:[9] a fully hydroxylated surface was subjected to three cycles of D_2O vapor exposure (2.0 kPa) at 313 K for 30 min and a subsequent brief evacuation. The number of surface hydroxyls was evaluated from the resulting weight increase in the sample.

Measurement of Water-physisorption Isotherms. The water-physisorption isotherms were measured by using a Sartorius microbalance, except for the case of the measurement of the isosteric heat of physisorption. The sample, rehydrated by the same pretreatment as in the thermal desorption experiments, was evacuated at 313 K for 4 h to remove the physisorbed water, after which the water adsorption was measured at 298 K. The adsorption equilibrium could be usually attained within 10 min, and the resulting isotherm was reversible. The isosteric heat of water physisorption was obtained by applying the Clausius-Clapeyron equation to seven isotherms, which were volumetrically measured in the range from 293 to 308 K. The specific surface area of the samples was determined by applying the BET method to the N_2 adsorption at the temperature of liquid nitrogen.

Residual Gas Analysis during Thermal Desorption. The sample was set into a vacuum line which was essentially

identical with that of the thermal-desorption apparatus, and then the temperature was raised at a constant rate of 10/6 K min^{-1} under evacuation. The change in the residual gas pressures was monitored continuously by means of a mass spectrometer, Hitachi RM-50.

Electron-diffraction Analysis. The electron diffraction was used to identify the exposed crystal surfaces of SnO_2. The measurement was made at an accelerating voltage of 200 kV in an electron microscope, Hitachi HU-200E.

Results and Discussion

Thermal-desorption Spectra of Surface Hydroxyls. The thermal-desorption spectra of surface hydroxyls on SnO_2 are shown in Fig. 1, where the desorption rate ($-dw/dT$) has been obtained by the graphical differentiation of the original thermal-gravimetrical-analysis curve. Oxygenated samples gave two distinct peaks, around 513 (Peak 1) and 573 K (Peak 2), together with the neighboring shallow peaks, which indicate a complex surface heterogeneity, common to all three samples, SnO_2-I, -II, and -III. Peak 1 is the greatest in SnO_2-I and the smallest in SnO_2-III. On the contrary, Peak 2 is very large in SnO_2-III and smaller in SnO_2-I and -II. These two peaks are united in oxygenated SnO_2-IV, indicating that the desorption energy of surface hydroxyls on this sample is heterogeneous. The H_2 treatment of every sample considerably reduced the height of these peaks or caused the disappearance of the peaks in the thermal-desorption spectra. These results indicate that the H_2 treatment of a sample increases the surface heterogeneity, which is consistent with the results[4] obtained from the heat of immersion, and that it suppresses the formation of surface hydroxyls.

Since the overlapping of Peak 2 with the others is smaller for SnO_2-III, a conventional line-shape

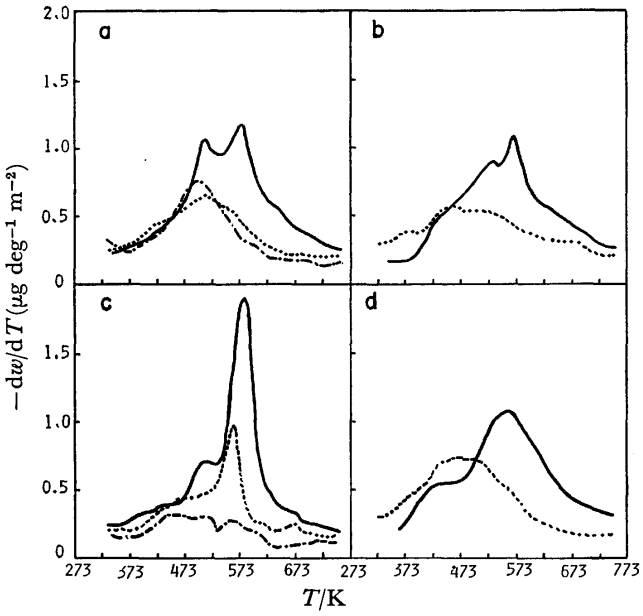

Fig. 1. Thermal desorption spectra of chemisorbed water on SnO_2.
a; SnO_2-I, b; SnO_2-II, c; SnO_2-III, d; SnO_2-IV.
Full line: oxygenated at 773 K, broken line: H_2-reduced at 433 K, dotted broken line: H_2-reduced at 473 K.

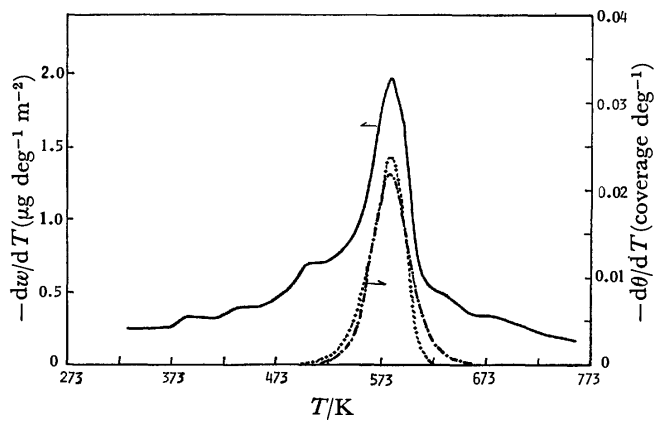

Fig. 2. Line shape analysis of thermal desorption spectrum of chemisorbed water on SnO_2-III.
Full line: experimental, broken line: first order, $E=174$ kJ mol^{-1}, $\nu=3\times10^{12}$ s^{-1}, dotted broken line: second order, $E=238$ kJ mol^{-1}, $\nu=3\times10^{18}$ s^{-1}.

analysis[10] of this peak allows us to estimate the parameters of the desorption kinetics. In the present study, the activation energy (E) and the frequency factor (ν) of the desorption, which give a peak maximum temperature and a peak half-width similar to those of the observed spectrum, were determined using the Polanyi-Wigner desorption-rate equation:[10]

$$-d\theta/dT = (\nu/\beta)\theta^n \exp(-E/RT) \quad (1)$$

where β is the heating rate; θ, the surface coverage of the adsorbed species, and n, the order of the desorption reaction. As is shown in Fig. 2, we could obtain the reasonable values of $E=174$ kJ mol^{-1} and $\nu=3\times10^{12}$ s^{-1} with the assumption of a first order or of $E=238$ kJ mol^{-1} and $\nu=3\times10^{18}$ s^{-1} with the assumption of a second order. In any case, it is evident that the surface hydroxyls which gave rise to Peak 2 are uniform in character, in the sense that an observed desorption peak can be approximated by that calculated with a constant value of the desorption-activation energy, E. The maximum temperature of Peak 1 is independent of the preparation method; from its value, the desorption activation energy was calculated to be 153 kJ mol^{-1} at $\nu=3\times10^{12}$ s^{-1} assuming the first-order kinetics.

In the present work, the gravimetric method was adopted for the measurement of the thermal-desorption spectra of surface hydroxyls. Therefore, it is necessary to check whether or not surface species other than the surface hydroxyls are removed, since SnO_2 is readily reduced when it is heated *in vacuo*. The partial pressure of water in the residual gas during thermal-desorption measurements was found to change similarly to the thermal-desorption spectra shown in Fig. 1. The removal of the surface oxygen of SnO_2 by reduction was monitored by measuring the change in the partial pressures of CO, O_2, and CO_2 in the residual gas. The results revealed that the reduction of the sample took place above *ca.* 473 K, and that its influence on the shape of the peaks in the thermal-desorption spectra was insignificant.

Correlation between the Peaks in Thermal-desorption Spectra and the Jump in the Water-adsorption Isotherm. The

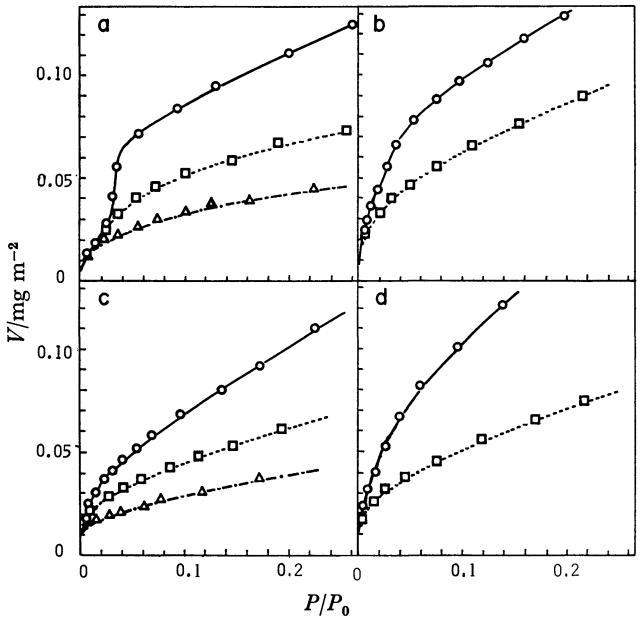

Fig. 3. Adsorption isotherms of water on SnO_2.
a; SnO_2-I, b; SnO_2-II, c; SnO_2-III, d; SnO_2-IV.
(○): Oxygenated at 773 K, (□): H_2-reduced at 433 K, (△): H_2-reduced at 473 K.

water-physisorption isotherms obtained on the oxygenated and reduced samples are illustrated in Fig. 3. It may be seen from Fig. 3 that the shapes of the isotherm vary drastically with the method of preparation and the pretreatment of the sample. The oxygenated SnO_2-I exhibits a clear jump, which arises from the two-dimensional condensation of water,[1] in the range of relative pressures of 0.02—0.04. This jump can be observed slightly on SnO_2-II, but not on SnO_2-III and -IV. The height of Peak 1 in the thermal-desorption spectra decreases in the same order: SnO_2-I>SnO_2-II> SnO_2-III≃SnO_2-IV, and becomes negligible in SnO_2-III and IV, as has been stated above. Therefore, it is reasonable to consider that the surface hydroxyls of Peak 1 are closely related to the two-dimensional condensation of water. As was demonstrated in the case of SnO_2-III, the surface hydroxyls of Peak 2 are evidently irrelevant to this phenomenon. H_2-treatment caused a marked decrease in the adsorbed amount and, at the same time, a disappearance of the jump in the isotherms for SnO_2-I and -II.

The relation between the amounts of physisorbed and chemisorbed water on SnO_2 are listed in Table 1. V_p is the monolayer capacity obtained by the B-point method from the adsorption isotherms. V_c is the amount of water chemisorbed expressed by OH groups nm^{-2}, which is obtained from the H-D exchange capacity with D_2O vapor. V_r is the reduced amount of SnO_2 samples, expressed by O atoms nm^{-2}, which was calculated from the weight decrease after H_2 reduction. The last column of Table 1 shows the ratio of the number of physisorbed water molecules in the monolayer to that of the underlying surface hydroxyls. The ratio, which is independent of both the method of preparation and the pretreatment conditions, was found to be about 1:4 (H_2O: OH), as has been reported previously.[1,2] Here, it is interesting to note that H_2-treatment reduces the amounts of both the physisorption and chemisorption of water, and that the ratio remains almost unchanged. This suggests that the ratio of about 1:4 (H_2O: OH) holds on the surfaces which are independent of the occurrence of the jump in the adsorption isotherm.

On the same sample as SnO_2-I which had a clear jump in the isotherm in a previous paper,[2] the isosteric heat (q_{st}-θ) curve exhibited a plateau at the same coverage as the jump appeared, indicating a strong lateral interaction between physisorbed water molecules.[1,2] Fig. 4 shows the q_{st}-θ curves of SnO_2-III and -IV, which have no jump in the adsorption isotherm, together with that of the same sample as SnO_2-I which has been reported in the previous paper.[2] The q_{st} curve of SnO_2-III, whose surface was covered with surface hydroxyls with almost the same desorption energy (Peak 2), has a pronounced plateau in the range of coverage of 0.3—0.7. However, this does not reflect a lateral interaction of physisorbed molecules, which leads to the occurrence of the jump, because no jump appeared in the isotherm. It may be a simple indication of surface homogeneity for water physisorption. As the ratio of V_p to V_c on SnO_2-III as well as

Table 1. Relation between the amounts of physisorbed and chemisorbed water on Oxygenated and Hydrogen-reduced SnO_2 surfaces

	Pretreatment condition	S (m^2/g)	Physisorbed amount V_p (H_2Os/nm^2)	Chemisorbed amount V_c (OHs/nm^2)	Amount of reduction V_r (O atoms/nm^2)	V_p/V_c (H_2O/OH)
SnO_2-I	O_2-773	10.78	2.61	10.40		0.25
	H_2-433		1.61[a]	6.81[a]	1.06[a]	0.24
	H_2-473	10.69	0.97	5.53	3.22	0.18
SnO_2-II	O_2-773	14.17	2.91	10.20		0.29
	H_2-433	12.29	1.81	7.05	1.08	0.26
SnO_2-III	O_2-773	10.87	2.21	10.61		0.21
	H_2-433		1.27[a]	7.23[a]	1.29[a]	0.18
	H_2-473	10.34	0.84	3.03	4.12	0.28
SnO_2-IV	O_2-773	44.44	3.11	12.01		0.26
	H_2-433	45.06	1.44	8.24	0.87	0.17

a) These quantities were evaluated using the surface area of H_2-473.

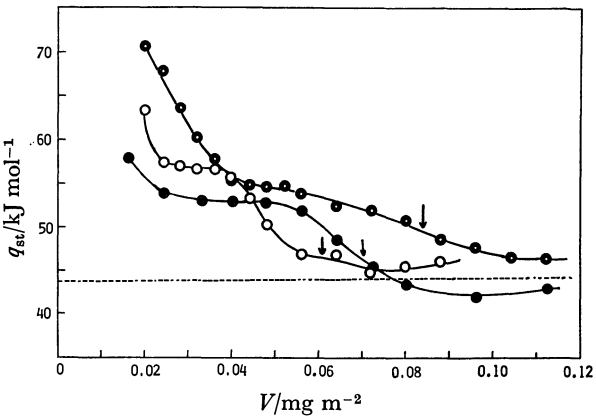

Fig. 4. Isosteric heat of adsorption, q_{st}, of water on SnO_2 as a function of the amount of adsorbed water.
Sample was as follows: SnO_2-III (○); SnO_2-IV (⊙); SnO_2-I (●).
A broken line represents the heat of liquefaction of water. Arrows indicate the monolayer coverage of water molecules.

on the other three samples was about 1 : 4, it may be considered that the surface hydroxyls of Peak 2 offer adsorption sites which are homogeneous and separated to such an extent that physisorbed water molecules can not interact with each other. SnO_2-IV, whose surface was covered with surface hydroxyls with a heterogeneous desorption energy, as can be understood from the shallow peak in Fig. 1, gave a q_{st} curve indicating a surface heterogeneity (Fig. 4). The ratio of V_p to V_c on this sample was about 1 : 4, as in the samples with homogeneous surfaces.

The amount of surface hydroxyls giving rise to the two desorption peaks, 1 and 2, in SnO_2-I, which exhibits a clear jump in the physisorption isotherm of water, were estimated roughly from the integrated peak area of the thermal-desorption spectrum. The surface hydroxyls of Peak 1 were only about 7—10% of the total surface hydroxyls, and those of Peak 2, about 13—18%, while the remaining part was occupied by heterogeneous surface hydroxyls. The following conclusion can be drawn from these results: the small ratios of V_p to V_c observed on the SnO_2 sample, where the two-dimensional condensation of water takes place, originated from a simple comparison of the number of the physisorbed water molecules with that of the underlying surface hydroxyls over the whole surface. Thus, it has been found that SnO_2 surfaces, except for the particular ones which are relevant to the two-dimensional condensation of water, are hydrophobic in the sence that they sparsely adsorb water molecules.

Morphological Considerations. Morphological studies[11,12] of the SnO_2 single crystal have shown that the (100), (110), and (101) were well-developed crystal planes, independent of the growing conditions. It was previously inferred[3] from the electron diffraction that SnO_2-I was composed of microcrystals with well-developed (110) and (100) crystal planes. A crystallographic consideration led to the conclusion[2] that the (100) plane of the rutile structure of SnO_2 is responsible for the occurrence of the two-dimensional condensation

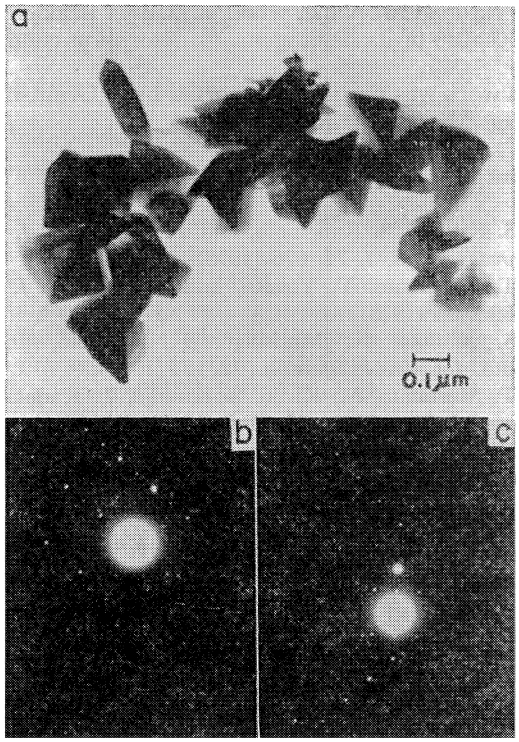

Fig. 5. Electron micrograph (a) and diffraction patterns (b, c) of SnO_2-III. b; N pattern of (101), c; N pattern of (001).

of water. The electron micrograph of Fig. 5 showed that SnO_2-III was composed of particles with a well-defined shape and with an acute angle; their electron diffraction gave two typical types of diffraction patterns, as is depicted in Fig. 5. The crystallographic analysis proved that these are N patterns of the (101) and (001) planes respectively of the rutile structure of SnO_2. The appearance of the former pattern was more frequent, *i.e.*, more than twice as frequent, than that of the latter. Further, the SnO_2-III sample, which has no jump in the water isotherm, did not give the N pattern of the (100) plane of SnO_2. This provides strong support for the idea that the (100) plane of SnO_2 is responsible for the occurrence of the two-dimensional condensation of water, as was proposed earlier.[2,4]

A crystallographic consideration showed that the surface hydroxyls on the (101) plane as well as on the (110) and (111) planes can not form closed hydrogen bonds.[2] Therefore, it may be concluded that the surface hydroxyls on the (101) plane, which give rise to a desorption peak, 2, around 573 K, interact strongly with water molecules through hydrogen bonding, whereas those on the (100) plane, which give rise to a desorption peak, 1, around 513 K, interact with water weakly to cause the two-dimensional condensation on the surfaces. Jones and Hockey[13] suggested that the desorption energy of the surface hydroxyls on the rutile (110) plane changed with the progress of desorption, according to Peri's model,[14] which explains why even uniformly chemisorbed water gives heterogeneous desorption energy on its successive removal. It might be considered that the surface hydroxyls on the (110) plane of SnO_2 desorb *via* a mechanism similar to that

on the rutile (110) plane, where a distinct peak can not arise because of its heterogeneous desorption energy.

This work was partially supported by a Grant-in-Aid from the Ministry of Education.

References

1) S. Kittaka, S. Kanemoto, and T. Morimoto, *J. Chem. Soc., Faraday Trans. 1*, **74**, 676 (1978).
2) T. Morimoto, Y. Yokota, and S. Kittaka, *J. Phys. Chem.*, **82** 1996 (1978).
3) S. Kittaka, K. Morishige, T. Fujimoto, and T. Morimoto, *J. Colloid Interface Sci.*, **72**, 191 (1979).
4) T. Morimoto, M. Kiriki, S. Kittaka, T. Kadota, and M. Nagao, *J. Phys. Chem.*, **83**, 2768 (1979).
5) N. Yamazoe, J. Fuchigami, M. Kishikawa, and T. Seiyama, *Surf. Sci.*, **86**, 335 (1979).
6) T. Matsushita and I. Yamai, *Nippon Kagaku Kaishi*, **1974**, 1893.
7) K. Morishige, S. Kittaka, T. Moriyasu, and T. Morimoto, *J. Chem. Soc., Faraday Trans. 1*, **76**, 728 (1980).
8) E. W. Thornton and P. G. Harrison, *J. Chem. Soc., Faraday Trans. 1.*, **71**, 461 (1975).
9) H. P. Boehm and R. Sappok, "Progress in Vacuum Microbalance Techniques," ed by Th. Gast and E. Robens, Heydon Son, London (1972) vol. 1, p. 247.
10) D. A. King, *Surf. Sci.*, **47**, 384 (1975).
11) M. L. Harvill and Rustum Roy, "Proc. Int. Conf. Crystal Growth," ed by H. S. Peiser, Pergamon, London (1966), p. 563.
12) Y. Fujiki and Y. Suzuki, *J. Jpn. Assoc. Min. Petr. Econ. Geol.*, **68**, 277 (1973).
13) P. Jones and J. A. Hockey, *Trans. Faraday Soc.*, **67**, 2679 (1971).
14) J. B. Peri, *J. Phys. Chem.*, **69**, 220 (1965).

 © 1980 The Chemical Society of Japan Bull. Chem. Soc. Jpn., 53, 2133—2140 (1980)

The Thermal Unimolecular Decomposition of Methyl Chloride behind Shock Waves

Osamu KONDO, Ko SAITO,* and Ichiro MURAKAMI

Department of Chemistry, Faculty of Science, Hiroshima University, Hiroshima 730

(Received November 22, 1979)

The thermal decomposition of methyl chloride diluted in Ar has been studied behind shock waves over the temperature range between 1680 and 2430 K and the total density range of 2.0×10^{-6}—3.5×10^{-5} mol cm^{-3}. The decomposition rate was monitored by means of the UV absorption of the CH_3 radical produced. The initiation reaction was found to be the C–Cl bond fission; the process proceeded in the fall-off region under the present experimental conditions. From the fall-off data, low- and high-pressure rate constants (k_0/[Ar] and k_∞) were obtained by the application of a refined RRKM theory involving a weak collision effect. Thus, the Arrhenius expressions were given as:

$$k_0/[\mathrm{Ar}] = 10^{15.56}\exp(-247\ \mathrm{kJ\ mol^{-1}}/RT)\ \mathrm{cm^3\ mol^{-1}\ s^{-1}},$$
$$k_\infty = 10^{13.86}\exp(-383\ \mathrm{kJ\ mol^{-1}}/RT)\ \mathrm{s^{-1}}.$$

The collision efficiency factor, β_c, was obtained as 0.02 at the mean temperature of the experiment by comparing the low-pressure rate constant with the strong collision-rate constant. The high-pressure rate constant was well explained by the maximum free-energy criterion presented by Quack and Troe.

The thermal unimolecular decompositions of halomethanes are very interesting in the following points: 1) They are important test cases for the theories of unimolecular reactions; 2) There are two possible reaction channels as the initiation reaction (*i.e.*, simple bond fission and molecular elimination); 3) The pressure dependence of the unimolecular reaction varies depending on the channel and halogen. The thermal decompositions were previously investigated behind shock waves for CHF_3,[1–4] CH_3F,[5] $CHClF_2$,[4] $CHCl_3$,[4,6] and CH_3I.[7] It was found that the decompositions of these molecules are initiated *via* the molecular elimination except for the case of CH_3I. A common feature of these reactions is that the heats of reaction, ΔH°_r, for the molecular eliminations are always substantially lower than that of the simple bond fissions. In most cases, the unimolecular processes of the molecular elimination were in the high- or falloff-pressure regions under the usual shock-wave conditions.[8] According to the experimental results obtained hitherto, the molecular eliminations which have three-center activated complexes have potential barriers above, but not more than 40 kJ mol^{-1}, the heats of reaction. However, for the case of CH_3I, the value of ΔH°_r for the C–I bond fission is rather lower than that of the HI elimination by about 159 kJ mol^{-1}. Moreover, the unimolecular process of this reaction was found in the low-pressure region. The energy-transfer efficiency in the CH_3I–Ar system was found to be very small.

For the case of CH_3Cl, the heats of reaction of the two channels are very close to each other (the ΔH°_r for the C–Cl bond fission is less than that for the HCl elimination by about 25 kJ mol^{-1}). It can, therefore, be expected that the decomposition occurs mainly *via* the C–Cl bond fission, as has been proposed by Shilov and Sabirova,[9] who investigated the pyrolysis in a flow system. If the experimental data for a unimolecular reaction are obtained in a pressure region, it is, in principle, possible to evaluate the rate constants over the whole pressure region involving low- and high-pressure limits by using currently proposed unimolecular theories. Thus, we can discuss, in the high-pressure region, the intramolecular energy distribution and the form of the activated complex, and, in the low-pressure region, the intermolecular energy transfer.

The present paper will report the thermal decomposition of methyl chloride behind shock waves by monitoring the CH_3 behavior. In this work, we could determine high- and low-pressure rate constants from the fall-off data for the primary unimolecular reaction.

Experimental

The experiments have been performed in a shock tube 5 cm in internal diameter. A detailed description of the procedure was given in a previous paper.[10] The UV-absorption system in this work consisted of a deuterium lamp (HTV, L544) as a light source, a monochromator (Jarrell-Ash, 0.25 M), and a photomultiplier (HTV, R106UH). Output signals from the photomultiplier were fed into a pre-amplifier (Iwatsu DA-2A) and then recorded with a transient recorder (Kawasaki Electronica, TM-1410). The resultant rise time of the signal was about 5 μs, enough for the present purposes. The physical properties of the shock-heated gas were calculated from the incident-shock velocity assuming non-reaction conditions. Although relatively high CH_3Cl mixtures (3—5 mol %) were used occasionally, it was considered that the effect of the enthalpy change during the reaction was negligibly small in the early stage of the reaction, from which the rate data were determined.

Methyl chloride (with a 99.5% stated minimum purity) and Ar (99.998%) were used without further purification. Mixtures (0.2—5.0 mol % CH_3Cl in Ar) were prepared in 10-l glass flasks and were allowed to stand for more than 12 h before use. The experimental conditions behind shock waves were as follows: temperature = 1680—2430 K and total density = 2.0×10^{-6}—3.5×10^{-5} mol cm^{-3}.

The methyl radical has an absorption band due to the $^2A_1\leftarrow{}^2A_2$ electronic transition which has a maximum at 216 nm.[11] Recent high-temperature measurements of the absorption coefficient at two laboratories have shown a good agreement, within the range of experimental error.[12,13] Glänzer *et al.*[12] determined the absorption coefficient of CH_3 produced from shock-heated azomethane at 216 nm (FWHM = 1.6 nm) in the temperature range of 1200—1800 K. Tsuboi[13] also

measured the absorption coefficient at 216 nm (FWHM= 1.4 nm) in a system of ethane–Ar mixtures in the range of 1500—2300 K. Since, in the present study, the absorption measurements were performed at much the same wavelength (FWHM=1.65 nm), it was considered that the absorption coefficient and its temperature dependence reported by the above investigators could be applied to the present analysis of the absorption data without any corrections.

Results

Figure 1 shows a typical absorption record behind reflected shock waves. The absorption intensity begins to increase just behind the reflected shock front and seems to approach a steady value as the reaction proceeds. At the observed wavelength, there is no absorption by the reactant. The products which are considered to have absorptions around 216 nm are C_2H_2, C_2H_3Cl, and HCl, besides the CH_3 radical. The absorption coefficient of C_2H_2 at this wavelength is known to be as small as 1/15 that of CH_3.[13] From the data of the absorption coefficient of C_2H_3Cl at 230 nm ($\varepsilon \simeq 2\times10^5$ cm^2 mol^{-1} at 1600 K),[14] we could estimate that the value at 216 nm is about one-third that of CH_3 at 2000 K. However, since C_2H_3Cl is not the main product, as will be seen later in the computer simulation, its contribution to the absorption profile is negligible. HCl has an absorption band in the vacuum UV region with a maximum at 150—160 nm (ε (160.8 nm)= 1.8×10^6 cm^2 mol^{-1} at 2000 K),[15] while around 200 nm it has a weak absorption which is less than one-tenth the maximum intensity at room temperature.[16] Therefore, the contribution of the HCl absorption to the CH_3 measurement at 216 nm is thought to be negligibly small.

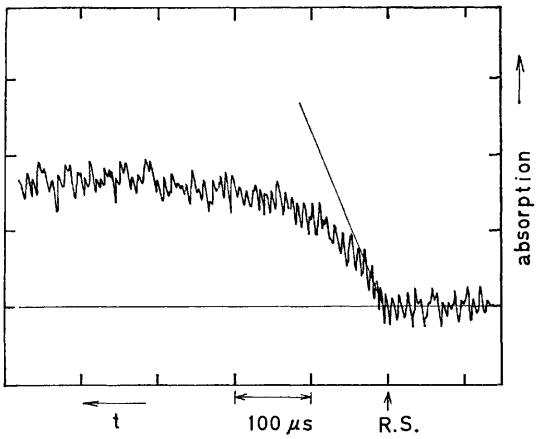

Fig. 1. Typical CH_3 absorption trace at 216 nm during decomposition of CH_3Cl.
T_5=2007 K, $\rho_5=3.52\times10^{-5}$ mol cm^{-3}, 0.5 mol % $CHCl_3$ in Ar. R. S. denotes the reflected shock front.

The initial rate of the CH_3 production was determined by the following relation:

$$\text{Rate} = \{\mathrm{d}[CH_3]/\mathrm{d}t\}_{t=0} = r_0/\varepsilon l$$

$$r_0 = \{\mathrm{d}\ln(I_0/I)/\mathrm{d}t\}_{t=0}$$

where ε is the absorption coefficient; l, the optical path length; I_0, the light intensity of 100% transmission, and

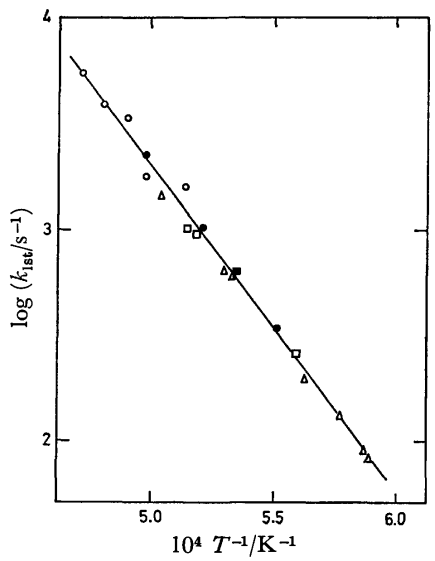

Fig. 2. Arrhenius plot of k_{1st} (initial rate constant of CH_3 production) for different mixtures and at a constant pressure of 5.0 atm (1 atm=101325 Pa).
○: 0.2%, ●: 0.5%, ■: 1.0%, △: 2.0%, □: 2.5%.

I, the intensity of the light that has transmitted the sample gas. In practice, the initial gradient was determined from the initial portion corresponding to the region within about 20% of the steady value. To ascertain the order of the CH_3 production rate with respect to the reactant concentration, the Arrhenius plots of the first-order rate constant, k_{1st}=Rate/$[CH_3Cl]_0$, obtained for various mixtures and at a constant total pressure were made; they are shown in Fig. 2. From this figure it may be seen that k_{1st} does not show any systematic departure from a straight line

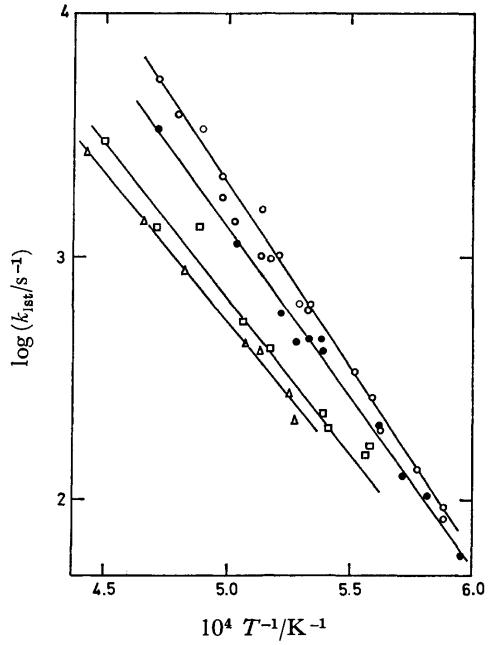

Fig. 3. Arrhenius plots of k_{1st} at different pressures.
Total densities in mol cm^{-3}, averaged over a series of experiments, ○: 3.7×10^{-5}, ●: 1.35×10^{-5}, □: 3.54×10^{-6}, △: 1.99×10^{-6} (incident shock waves).

Table 1. Arrhenius parameters of k_{1st}

Total density / mol cm^{-3}	T / K	A / s^{-1}	E / kJ mol^{-1}
2.0×10^{-6}	1892—2253	8.1×10^{8}	236 ± 4
3.5×10^{-6}	1790—2428	1.9×10^{9}	247 ± 8
1.4×10^{-5}	1678—2119	1.5×10^{10}	269 ± 10
3.7×10^{-5}	1700—2117	8.5×10^{10}	292 ± 14

as the initial concentration of CH_3Cl changes by 12.5-fold. The same results were obtained under the other total pressures adopted. Figure 3 shows a total density dependence of k_{1st}. Also in Table 1 the values of the Arrhenius parameters of k_{1st} are listed for each total density. From Fig. 3 and Table 1 it appears that the apparent first-order rate constants of the CH_3 production are in the fall-off region under the present experimental conditions. In the fall-off region, both the intermolecular energy transfer process and the intramolecular behavior are important equivalently. Thus, it is necessary to evaluate the limiting rate constants for the discussion based on kinetic theories.

Discussion

Reaction Mechanism of the CH_3Cl Decomposition. In the case of methyl chloride, the following two channels are probable for the initiation reactions:

(1) $CH_3Cl\,(+M) \longrightarrow CH_3 + Cl\,(+M)$
$\Delta H^\circ_{r0} = 347$ kJ mol^{-1}

(1a) $CH_3Cl\,(+M) \longrightarrow CH_2 + HCl\,(+M)$
$\Delta H^\circ_{r0} = 372$ kJ mol^{-1}.

Channel 1 has no barrier above the heat of reaction along the reaction coordinate if the potential barrier due to the centrifugal force is neglected. On the other hand, Channel 1a has an activation energy higher than ΔH°_{r0} because, in this channel, a three-center activated complex may be formed during the course of the reaction. Thus, the difference in the activation energies between the two channels becomes larger than the difference in the heats of reaction. Assuming that the values of the preexponential factor are equal, a rough estimation shows that the rate constant, k_{1a}, is smaller than k_1 by several hundredths at 2000 K. Furthermore, in Channel 1a the CH_2 radical produced is the $^3B_1$ state (a spin-forbidden reaction is known to have a small A factor).

A mechanism of the thermal decomposition of methyl chloride has been proposed by Shilov and Sabirova,[9] who investigated the decomposition at around 1100 K and at pressures of 10—15 Torr (1 Torr=133.322 Pa) in a flow system. From the concentration ratios of the products (HCl, CH_4, and C_2H_2), they proposed the following mechanism:

(1) $CH_3Cl \longrightarrow CH_3 + Cl$
(2) $CH_3Cl + Cl \longrightarrow CH_2Cl + HCl$
(3) $CH_3Cl + CH_3 \longrightarrow CH_2Cl + CH_4$
(4) $CH_3Cl + CH_2Cl \longrightarrow CH_2Cl_2 + CH_3$
(7) $2CH_2Cl \longrightarrow C_2H_4Cl_2$
(8) $C_2H_4Cl_2 \longrightarrow C_2H_3Cl + HCl$
(9) $C_2H_3Cl \longrightarrow C_2H_2 + HCl$

To consider the reaction process in further detail, several reactions including reverse reactions must be added to the above mechanism. Thus, we selected the following as probable reactions:

(1) $CH_3Cl\,(+M) \rightleftharpoons CH_3 + Cl\,(+M)$
(2) $CH_3Cl + Cl \rightleftharpoons CH_2Cl + HCl$
(3) $CH_3Cl + CH_3 \rightleftharpoons CH_2Cl + CH_4$
(4) $CH_3Cl + CH_2Cl \rightleftharpoons CH_3 + CH_2Cl_2$
(5) $C_2H_6\,(+M) \rightleftharpoons 2CH_3\,(+M)$
(6) $Cl_2 + M \rightleftharpoons 2Cl + M$

Table 2. Elementary reactions

Reaction	ΔH°_{r298} / kJ mol^{-1}	ΔG°_T / kJ mol^{-1}	Rate constant / cm^3 mol^{-1} s^{-1}	Reference of rate constant
1	347	$-1.381T+358.817$		This work
2	-5.0	$-0.0288T-5.581$	$k_2=10^{13.53}\exp(-14/RT)$	a)
3	-9.2	$17.231\times10^{-4}T-8.7316$	$k_3=10^{10.4}T^{1/2}\exp(-39/RT)$	b)
4	14	$6.887\times10^{-3}T+13.23$		See text
5	369	$-0.164T+372.396$	$k_5=10^{17.11}\exp(-375/RT)$	c)
6	242	$-0.1160T+242.534$	$k_6=10^{13.66}\exp(-190/RT)$	d)
7	-372			See text
8	62.8		$k_8=10^{13.5}\exp(-224/RT)$	e)
9	92.0		$k_9=10^{12.57}\exp(-257/RT)$	f)
10	-376			See text
11	72.0		$k_{11}=10^{13.16}\exp(-236.2/RT)$	g)
12	72.8		$k_{12}=10^{17.41}\exp(-331.7/RT)$	h)

a) T. Fueno, "Chemical Reaction Theory," Asakura-Shoten, (1975). b) F. A. Raal and E. W. R. Steacie, *J. Chem. Phys.*, **19**, 578 (1952). c) J. Troe, "Fifteenth Symposium (Int.) on Combustion," The Combustion Institute, Pittsburgh (1975), p. 667. d) M. van Thiel, D. J. Seery, and D. Britton, *J. Phys. Chem.*, **69**, 834 (1965). e) S. W. Benson and H. E. O'Neal, "Kinetic Data on Gas Phase Unimolecular Reactions," Washington, D.C. (1970). f) F. Zabel, *Int. J. Chem. Kinet.*, **9**, 651 (1977). g) W. Tsang, *J. Chem. Phys.*, **41**, 2487 (1964). h) T. Just, P. Roth, and R. Dumm, "Sixteenth Symposium (Int.) on Combustion," The Combustion Institute, Pittsburgh (1977), p. 961.

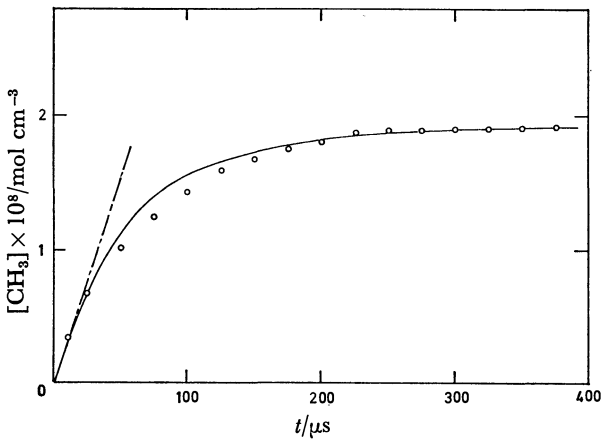

Fig. 4. Comparison of the CH_3 concentration profiles between the calculation (——) and the experiment (○).
T_5=2007 K, $\rho_5=3.52\times10^{-5}$ mol cm^{-3}, 0.5 mol % CH_3Cl in Ar.

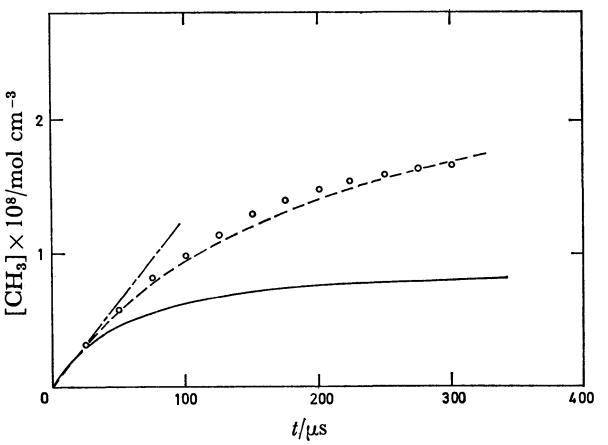

Fig. 5. Comparison of the CH_3 concentration profiles between the calculations (—— and --- , see text) and the experiment (○).
T_5=1730 K, $\rho_5=3.85\times10^{-5}$ mol cm^{-3}, 2.0 mol % CH_3Cl in Ar.

(7) $2CH_2Cl \longrightarrow C_2H_4Cl_2$

(8) $C_2H_4Cl_2 \longrightarrow C_2H_3Cl + HCl$

(9) $C_2H_3Cl\,(+M) \longrightarrow C_2H_2 + HCl\,(+M)$

(10) $CH_2Cl + CH_3 \longrightarrow C_2H_5Cl$

(11) $C_2H_5Cl \longrightarrow C_2H_4 + HCl$

(12) $C_2H_4 + M \longrightarrow C_2H_2 + H_2 + M$

The values of ΔH°_{f298} and ΔG°_T and the rate constants are listed in Table 2. For the present purposes, we need to know how the CH_3 production rate is affected by the secondary reactions. This is important, particularly because we base the decomposition-rate measurement on the initial slope of the CH_3 absorption records. Since there are no available kinetic data for Reactions 4, 7, and 10, we first assumed that Reaction 4 was negligible and that the values of k_7 and k_{10} were equal to the rate constant for the CH_3 recombination. The k_{1st} value corresponding to the total density considered was used as the rate constant of Reaction 1. At 2007 K, a good agreement is seen between the calculation and the observation over the whole range of reaction times, as is shown in Fig. 4. At 1730 K, however, the CH_3 concentration profiles show that the calculation gives a lower steady value, within a shorter reaction time, compared with the observed profile, as is shown in Fig. 5. It was, therefore, necessary to check the rate constants of the reactions which were connected with the CH_3 production. If the alternative reaction channel of the initiation, *i.e.*, Reaction 1a, is considered, a secondary reaction such as (b) $CH_3Cl + CH_2 \rightarrow CH_3 + CH_2Cl$ is needed for the production of the CH_3 radical. An Arrhenius expression of k_b was assumed by the use of the BEBO method[17] and the transition state theory as:

$$k_b = 10^{11.5}\exp\{-(41.8\text{ kJ mol}^{-1})/RT\}\text{ cm}^3\text{ mol}^{-1}\text{ s}^{-1}.$$

It was ascertained by simulations that the concentration of CH_3 produced by the above reaction was quite low compared with the observed value. Also, it was found that Reaction 5 does not affect the overall reaction profile of CH_3. Thus, it is likely that the computed low values of the steady concentration of CH_3 at lower temperatures are ascribable to the assumption for the k_4, k_7, and k_{10} values. Tentatively, if we use $k_4=10^{11.3}$ cm^3 mol^{-1} s^{-1} and $k_7=k_{10}=10^{11.5}$ cm^3 mol^{-1} s^{-1} at 1730 K, the calculation shows a good agreement with the observed profile (the dotted line in Fig. 5). However, we could not determine a unique set of rate constants which agrees with the profiles obtained over the temperature range and the concentration range employed in this work. Consequently, from the simulation study we found the following facts: (a) At lower temperatures Reaction 4 affects the CH_3 profile seriously, so that it cannot be neglected in considering the reaction mechanism. (b) The recombination reactions 7 and 10 could not be replaced by the recombination rate of CH_3; therefore, they should be evaluated independently. In this respect, it seems unreasonable to use the collision number as the recombination rate constant as in the case of C_2H_5.[18] (c) It was ascertained that the initial slope of the CH_3 production corresponds fairly well to the initiation reaction, *i.e.*, Reaction 1.

Evaluation of Low- and High-pressure Rate Constants.

a. Strong Collision Assumption: In order to evaluate the low- and high-pressure limit rate constants, we first treat the fall-off data on the basis of the strong collision assumption. Figure 6 shows fall-off curves of k_{1st}, with the temperature as a parameter. The solid lines in the figure were calculated by the reduced-form Kassel theory proposed by Troe and Wagner.[19] For the Kassel parameters, S_k and B_k, the definitions as suggested by Troe[20] have been adopted ($S_k=U_{vib}/RT+1=5.4$, 5.5, 5.7, 5.8 and $B_k=B_k(E_0, T, S_k, \nu_i)=15$, 14.5, 14, 13 at 1800, 1900, 2000, and 2100 K respectively, where U_{vib} is the vibrational energy content of CH_3Cl; E_0, the zero temperature activation energy, and ν_i, the vibrational frequencies of CH_3Cl, as taken from Ref. 11. The reduced fall-off curves were obtained using the Kassel integral tables[20] and fitted to the experimental data points in such a way as to meet the following requirements at the same time: (a) The calculated

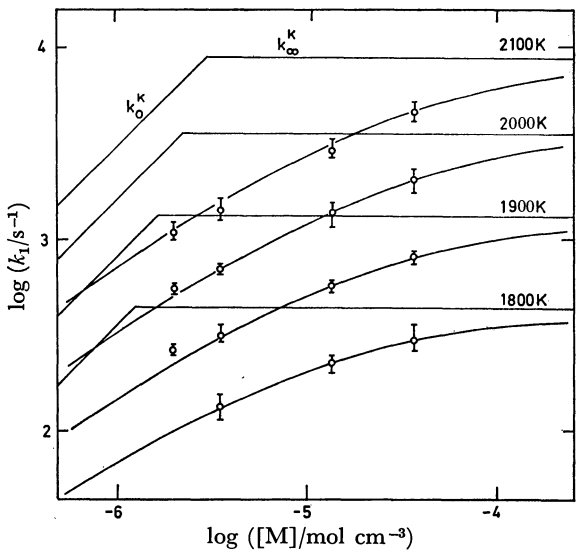

Fig. 6. Pressure dependences of k_{1st} at different temperatures. Full curves are calculated fall-off curves.

curves fit the experimental data points reasonably well, (b) the low- and high-pressure rate constants give temperature-independent activation energies, E_{a0} and $E_{a\infty}$, in the experimental region, and (c) the difference between E_{a0} and $E_{a\infty}$ values obtained is represented approximately by this relation:

$$E_{a\infty} - E_{a0} = (S_{eff}+0.5)R\bar{T},$$

where $S_{eff}=U_{vib}/RT$ and $\bar{T}$ is the mean temperature of the experiments.

The rate constants for the high-pressure limit, k_∞^K, and for the low-pressure limit, k_0^K/[Ar], were then determined at the four temperatures indicated in Fig. 6. Thus, these respective Arrhenius expressions were obtained:

$$k_\infty^K = 10^{11.78}\exp(-315\,\text{kJ mol}^{-1}/RT)\ \text{s}^{-1},$$

$$k_0^K/[\text{Ar}] = 10^{15.08}\exp(-224\,\text{kJ mol}^{-1}/RT)\ \text{cm}^3\ \text{mol}^{-1}\ \text{s}^{-1}.$$

The values of the rate constants evaluated by the above procedure are considered to have an error factor of *ca.* 2.

At first sight, it is likely that the activation energies, $E_{a\infty}$ and E_{a0}, are somewhat lower than those to be expected from the bond-dissociation energy. Also, the preexponential factor of the high-pressure rate constant is considered to be lower than the usual values for the single-bond fission reaction, *i.e.*, $A=10^{13.5\pm1.5}\ \text{s}^{-1}$. In the literature there are experimental results which show somewhat low values for the high-pressure-limit A factor, *e.g.*, $A=10^{11.79}\ \text{s}^{-1}$ for $COF_2\rightarrow COF+F$[21] and $A=10^{12.95}\ \text{s}^{-1}$ for $SF_6\rightarrow SF_5+F$.[22] It is noticable that these experiments were performed in the fall-off region and that the values of the high-pressure rate constant were evaluated by the extrapolation of fall-off curves based on the strong collision assumption. Later Rabinovitch *et al.*[23] corrected the small A factor for the above SF_6 dissociation by considering the weak collision effect to obtain a reasonable value, such as $A=10^{14.11}\ \text{s}^{-1}$. Thus, the above unexpectedly low value of the A factor for $CH_3Cl\rightarrow CH_3+Cl$ may be considered to be the result of the strong collision assumption.

b. Weak Collision Effect on Fall-off Curves: Recently, Luther and Troe[24] published an easy method to obtain a reduced fall-off curve including the weak collision effect. According to this method, the reduced-form rate constant, k/k_∞, is written by the product of three factors as:

$$k/k_\infty = F^{LH}(k_0/k_\infty)F^{SC}(k_0/k_\infty)F^{WC}(k_0/k_\infty) \qquad (I)$$

where $F^{LH}(k_0/k_\infty)$ is a simple Lindemann-Hinshelwood-type fall-off curve, in which the rate constant of the spontaneous reaction, $k(E)$, is independent of the energy,[25a] $F^{SC}(k_0/k_\infty)$ is a factor which includes an energy dependence of $k(E)$,[25b] and $F^{WC}(k_0/k_\infty)$ is a factor pertaining to the weak collision effect.[25c] The parameters used in the calculation of Eq. I are listed in Table 3. Figure 7 shows reduced fall-off curves calculated on the basis of Eq. I. Comparing the two types of fall-off curves in Figs. 6 and 7, it appears that, in the latter, the fall-off region is broad and that the data points fit better than in the former. From the revised fall-off curves in Fig. 7, the high- and low-pressure rate constants are evaluated again, as respectively:

Table 3. Evaluated parameters used for the calculation of k_∞

$\frac{T}{\text{K}}$	S_K	B_K	F^{SC}_{center}	N^{SC}	F^{WC}_{center} a)	N^{WC} a)
1800	5.4	16.1	0.34	1.363	0.63	1.96
1900	5.5	15.6	0.34	1.368	0.62	1.98
2000	5.7	15.5	0.33	1.383	0.62	2.04
2100	5.8	15.1	0.33	1.387	0.62	2.06

a) In the calculations of F^{WC}_{center} and N^{WC}, β_C was taken to be 0.037 at 1800 K (which was the experimental value evaluated from the fall-off curve based on the strong collision assumption) and to have a temperature dependence of $T^{-1.5}$.

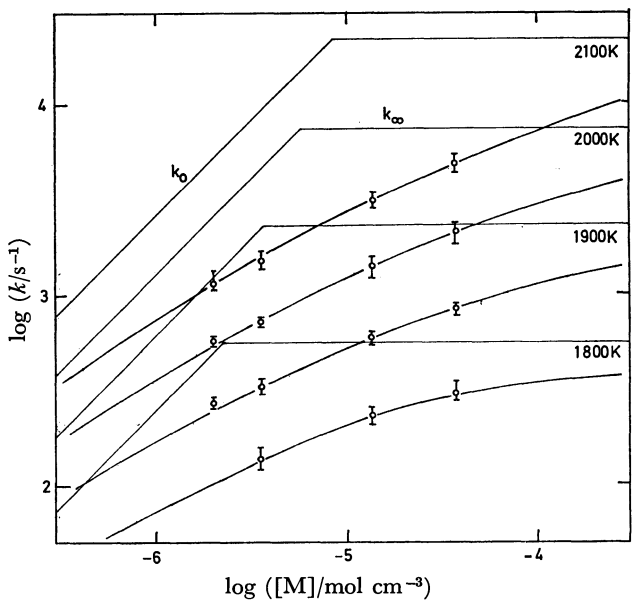

Fig. 7. Fall-off curves computed by considering the weak collision effect.
Data points are the same as in Fig. 6.

$k_\infty = 10^{13.86} \exp(-383 \text{ kJ mol}^{-1}/RT) \text{ s}^{-1}$,

$k_0/[\text{Ar}] = 10^{15.56} \exp(-247 \text{ kJ mol}^{-1}/RT) \text{ cm}^3 \text{ mol}^{-1} \text{ s}^{-1}$.

The error limits involved in these rate constants are considered to be less than a factor of two. It appears that the values of the activation energies and the preexponential factors appearing in the above results are not unexpected when compared with those of other, similar reactions for the single-bond fission.

Calculation of the Unimolecular Rate Constants. In order to ascertain the validity of the high- and low-pressure limit rate constants determined above, it is nescessary to calculate the rate constants theoretically by using currently useful methods. Thus, we will first perform RRKM calculations for the low-pressure rate constant and discuss the intermolecular energy transfer efficiency at high temperatures. Next, we will calculate high-pressure-limit rate constants by evaluating the maximum free energy in the course of the reaction path for the simple bond-fission process.

a. Low-pressure-limit Rate Constant: The theoretical calculation of the low-pressure rate constant was performed by using the appropriate RRKM strong-collision formulation given by Troe:[26,27]

$$k_0^{\text{SC}} = [\text{M}] Z_{\text{LJ}} \rho_{\text{vib}}(E_0) RT Q_{\text{vib}}^{-1} \exp(-E_0/RT) F_{\text{E}} F_{\text{rot}} F_{\text{anh}} \quad \text{(II)}$$

where Z_{LJ} is the Lennard-Jones collision frequency; $\rho_{\text{vib}}(E_0)$, the vibrational energy level density at E_0; E_0, the threshold energy of the reaction; Q_{vib}, the vibrational partition function; F_{E}, the energy dependence of the density of states; F_{rot}, the centrifugal correction factor, and F_{anh}, the anharmonicity factor.[28] The calculation of Eq. II was performed at four different temperatures. The calculated results are listed in Table 4. The molecular constants used in the calculation are shown in the footnote of Table 4.

Actually, at high temperatures the strong collision assumption is not considered to hold; that is, the average energy, $\langle \Delta E \rangle$, which is transferred during collisions between the reactant and the diluent molecule is much lower than RT, the thermal energy of the system. This effect, the weak collision effect, causes a reduction in the apparent reaction rate at high temperatures. The parameter expressing the weak collision effect is defined as the collision efficiency, β_{c}:

$$\beta_{\text{c}} \equiv k_0^{\text{obsd}}/k_0^{\text{SC}} \quad \text{(III)}$$

and:

$$\beta_{\text{c}}/(1-\sqrt{\beta_{\text{c}}}) \simeq -\langle \Delta E \rangle / F_{\text{E}} kT, \quad \text{(IV)}$$

where k_0^{obsd} is the low-pressure-limit rate constant obtained experimentally. The values of β_{c}, F_{E}, and $-\langle \Delta E \rangle / RT$ are also listed in Table 4. The absolute values of β_{c} range between 0.019 and 0.026 in the temperature range studied; this is considered to be reasonable compared with other, similar reactions in Ar (β_{c}=0.015 for CH_3I at 1400 K[7] and β_{c}=0.02 for CH_4 at 2000 K[29]). The temperature dependence of β_{c}, *i.e.*, $\beta_{\text{c}} \propto T^{-2.0}$, is also reasonable when it is compared with theoretical predictions.[30]

It is interesting to compare the value of $-\langle \Delta E \rangle$ evaluated from the experimental data for different reactions in the same diluent gas. For the CH_3I–Ar system, for instance, $-\langle \Delta E \rangle$ ranges from 0.043 to 0.023 in the temperature range of 1100—1500 K.[7] Although the temperature ranges of these systems do not overlap, it appears that the value of $-\langle \Delta E \rangle$ for the CH_3Cl–Ar system is larger than that for the CH_3I–Ar system by a factor of more than two. For the CH_4–Ar system, a value which is comparable to that of the CH_3I–Ar system can be estimated from the data in Ref. 26 ($-\langle \Delta E \rangle / RT$=0.019 at 2000 K). It may be seen that, in the case of the collinear collision of two rigid spheres, the energy-transfer efficiency per collision is largest when the masses of the two spheres are equal.[31] The relative differences in $-\langle \Delta E \rangle$ for the above three systems (*i.e.*, CH_3Cl–Ar > CH_3I–Ar ≅ CH_4–Ar) may be explained, in part, by the relative differences in mass between the reactant and Ar. In this respect, it is also interesting to observe the $-\langle \Delta E \rangle$ values for a given reaction in various diluent gases.

b. High-pressure-limit Rate Constant: A conventional method of estimating the preexponential factor, A, is by the use of the following relation:

$$A = (e\,kT/h) \exp(\Delta S^*/R)$$

ΔS^*, the entropy change of the activation, was evaluated to be 6.7 G mol^{-1}.[32] Consequently, $A = 10^{15.52}$ s^{-1} at 2000 K.

A theoretical prediction of the rate constant for the high-pressure limit may be given by the transition-state formula:[33]

$$k_\infty = (kT/h)(Q^*/Q)$$

where Q and Q^* are the partition functions of the reactant and the activated complex respectively. It is difficult to predict the form of the activated complex precisely although, in a simple bond fission, it does not take so limited a form as a three- or four-center reaction. In this situation, it is considered to be most suitable to apply the method of the maximum free-energy criterion (MFC method) proposed by Quack and Troe[34] for the calculation of Q^*. This method is based on the statistical adiabatic channel model for the activated complex.[35] Strictly speaking, the rate constant calculated with the

TABLE 4. VALUES OF k_0^{SC}, F_{E}, β_{c}, AND $-\langle \Delta E \rangle / RT$

T/K	F_{E}	k_0^{SC} a) / cm^3 mol^{-1} s^{-1}	β_{C}	$\beta_{\text{C}}^{\text{SC}}$ d)	$-\langle \Delta E \rangle / RT$
1800	1.35	9.94×10^9	0.026	0.037	0.042
1900	1.38	2.71×10^{10}	0.023	0.030	0.037
2000	1.41	6.59×10^{10}	0.020	0.025	0.033
2100	1.43	1.44×10^{11}	0.019	0.022	0.032

a) Input data for the calculation of k_0^{SC}: threshold energy, E_0=347 kJ mol^{-1}; Lennard-Jones collision diameter, $\sigma(CH_3Cl\text{–Ar})$=2.847 Å;[b] Lennard-Jones well depths, $\varepsilon(CH_3Cl)/k$=355 K, $\varepsilon(Ar)/k$=119 K;[b] vibrational frequencies of CH_3Cl, ν/cm^{-1}=732, 2928, 1355, 3047 (2), 1460 (2), 1020 (2).[c] b) J. O. Hirschfelder, C. F. Curtiss, and R. B. Bird, "Molecular Theory of Gases and Liquids," 2nd ed, Wiley, London (1963). c) "JANAF Thermochemical Tables," 2nd ed, Natl. Bur. Stand., (1971). d) $\beta_{\text{C}}^{\text{SC}}$ corresponds to the $k_0^{\text{K}}/k_0^{\text{SC}}$ ratio, where k_0^{K} is the rate constant evaluated by the fall-off curve uncorrected for the weak collision effect.

Table 5. Calculated k_∞^{MFC} values

T/K	γ/Å^{-1}			$q^{*a)}$/Å
	0	0.75	100	
1800		480[b)]		4.5
1900	40.7	2252	3749.8	4.5
2000	173.7	9059	15200	4.4
2200		98305		4.4

a) q^* is the C–Cl bond distance of the activated complex. b) In s^{-1}.

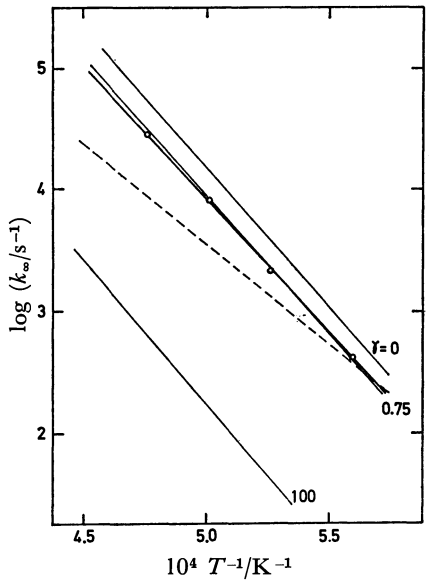

Fig. 8. Comparisons of the high-pressure rate constants. (-○-): k_∞, (------): k_∞^K, (——): k_∞^{MFC}.

MFC method, k_∞^{MFC}, corresponds to the upper limit of the true rate constant.[34] Moreover, the activated complex is defined by the molecular constants of the reactant molecule with only one unknown parameter, γ. Therefore, one could easily calculate the value of Q^* without any large error by using an appropriate γ value. In our calculation, the molecular constants of CH_3Cl and CH_3 were taken from Ref. 11. The C–Cl bond axis was taken as the reaction coordinate. The parameter γ(Å^{-1}) appearing in the equation of the MFC method has the following characteristics: $\gamma=0$ corresponds to the limit of the tight activated complex, and $\gamma=100$, to the limit of the loose activated complex. For many reactions, the calculated values of k_∞^{MFC} are in good agreement with the experimental values when $\gamma=0.75$.[34] In Table 5, the calculated results are listed for $\gamma=0$, 0.75, and 100. In Fig. 8, a comparison is shown between the observed rate constants, k_∞, and k_∞^{MFC}, showing a good agreement when $\gamma=0.75$.

Holbrook[36] analyzed Silov and Sabirova's data and evaluated the rate constants for Reaction 1 as:

$$k_0/[M] = 1.86\times10^4 \text{ cm}^3 \text{ mol}^{-1} \text{ s}^{-1}$$

and:

$$k_\infty = 1.5\times10^{-2} \text{ s}^{-1} \text{ at } 1116.7 \text{ K}.$$

Since the experimental data were near the low-pressure limit, and since he evaluated the limiting values by means of the Hinshelwood plot (*i.e.*, the plot of $1/k$ against $1/P$), the high-pressure value is considered to involve a large error. The extrapolation of the low-pressure rate constant determined in this work leads to $k_0/[Ar]=9.2\times10^3$ cm^3 mol^{-1} s^{-1} at 1116.7 K. Considering that the collision efficiency is large in Shilov and Sabirova's system (M=CH_3Cl), these two experimental values are in good agreement with each other. The value calculated by Forst and St. Laurent[37] is also close to these experimental values.

It was found, in the present study, that the evaluation of the high- and low-pressure-limit rate constants from the fall-off data tends to lead to erroneous results when, especially at high temperatures, the fall-off curve is used without correction for the weak collision effect.

References

1) E. Tschuikow-Roux and J. E. Marte, *J. Chem. Phys.*, **42**, 2049 (1965).
2) E. Tschuikow-Roux, *J. Chem. Phys.*, **42**, 3639 (1965).
3) A. P. Modica and J. E. LaGraff, *J. Chem. Phys.*, **44**, 3375 (1966).
4) K. P. Schug, H. G. Wagner, and F. Zabel, *Ber. Bunsenges. Phys. Chem.*, **83**, 167 (1979).
5) K. P. Schug and H. G. Wagner, *Z. Phys. Chem., N. F.*, **86**, 59 (1973).
6) T. Yano, *Bull. Chem. Soc. Jpn.*, **50**, 1272 (1977).
7) K. Saito, H. Tahara, O. Kondo, T. Yokubo, T. Higashihara, and I. Murakami, *Bull. Chem. Soc. Jpn.*, **53**, 1335 (1980).
8) Exceptionally, in the study of the CHF_3–Ar system by Tschuikow-Roux[2] the unimolecular decomposition to produce CF_2 and HF was found in the low-pressure region under these conditions: 1200 K$\leq T\leq$1800 K, $P\leq$18.7 atm (1 atm=101325 Pa).
9) A. E. Shilov and R. D. Sabirova, *Z. Fiz. Kim.*, **33**, 1365 (1959).
10) T. Higashihara, K. Saito, and H. Yamamura, *Bull. Chem. Soc. Jpn.*, **49**, 965 (1976).
11) G. Herzberg, "Molecular Spectra and Molecular Structure," D. Van Nostrand Co., Princeton, N. J. (1967), Vol. 3.
12) K. Glänzer, M. Quack, and J. Troe, "Sixteenth Symposium (International) on Combustion," The Combustion Institute, Pittsburgh (1977), p. 949.
13) T. Tsuboi, *Jpn. J. Appl. Phys.*, **17**, 709 (1978).
14) F. Zabel, *Int. J. Chem. Kinet.*, **9**, 651 (1977).
15) D. J. Seery and C. T. Bowman, *J. Chem. Phys.*, **48**, 4314 (1968).
16) J. M. Myer and J. A. R. Samson, *J. Chem. Phys.*, **52**, 266 (1970).
17) H. S. Johnston and C. Parr, *J. Am. Chem. Soc.*, **85**, 2544 (1963).
18) A. Lifshitz and M. Frenklach, *J. Phys. Chem.*, **79**, 686 (1975).
19) J. Troe and H. G. Wagner, *Ber. Bunsenges. Phys. Chem.*, **71**, 937 (1967).
20) J. Troe, *Ber. Bunsenges. Phys. Chem.*, **78**, 478 (1974).
21) A. P. Modica, *J. Phys. Chem.*, **74**, 1194 (1970).
22) J. F. Bott and T. A. Jacobs, *J. Chem. Phys.*, **50**, 3850 (1969).
23) B. S. Rabinovitch, D. G. Keil, J. F. Burkhalter, and G. B. Skinner, "Proceedings of the Tenth (International) Shock Tube Symposium," ed by G. Kamimoto, Kyoto (1975),

p. 579.

24) K. Luther and J. Troe, "Seventeenth Symposium (International) on Combustion," The Combustion Institute, Pittsburgh (1979), p. 535.

25) a) The Lindemann-Hinshelwood factor is given by:

$$F^{\mathrm{LH}}(k_0/k_\infty) = (k_0/k_\infty)/(1+k_0/k_\infty).$$

b) According to Ref. 24, $F^{\mathrm{SC}}(k_0/k_\infty)$ is expressed as:

$$\log F^{\mathrm{SC}}(k_0/k_\infty) \frac{\log F^{\mathrm{WC}}_{\mathrm{center}}}{1+\left\{\frac{\log(k_0/k_\infty)}{N^{\mathrm{WC}}}\right\}^2},$$

where $F^{\mathrm{SC}}_{\mathrm{center}}$, the broadening factor at the center of the fall-off curve, and the width, N^{SC}, depend on S_{K} and B_{K} as:

$$\log F^{\mathrm{SC}}_{\mathrm{center}} \simeq \frac{0.137(S_{\mathrm{K}}-1)B_{\mathrm{K}}}{1.10(S_{\mathrm{K}}-1)+B_{\mathrm{K}}}$$

and: $N^{\mathrm{SC}} \simeq 0.9 - \log F^{\mathrm{SC}}_{\mathrm{center}}$.

c) $F^{\mathrm{WC}}(k_0/k_\infty)$ is expressed as:

$$\log F^{\mathrm{WC}}(k_0/k_\infty) \simeq \frac{\log F^{\mathrm{WC}}_{\mathrm{center}}}{1+\left\{\frac{\log(k_0/k_\infty)}{N^{\mathrm{WC}}}\right\}^2},$$

where $F^{\mathrm{WC}}_{\mathrm{center}}$, the weak-collision broadening factor at the center of the fall-off curve, depends on β_{c}, and where the width, N^{WC}, depends on S_{K} and β_{c}.

26) J. Troe, *J. Chem. Phys.*, **66**, 4745 (1977).

27) J. Troe, *J. Chem. Phys.*, **66**, 4858 (1977).

28) F_{E}, F_{anh}, and F_{rot} were calculated by using the approximated equations, (9.9)—(9.12), appearing in Ref. 27.

29) P. Roth and T. Just, *Ber. Bunsenges. Phys. Chem.*, **79**, 682 (1975).

30) There are two opinions regarding the temperature dependence of β_{c}. Luther and Troe[24] stated that, at the limit of the weak collision, *i.e.*, $-\langle\Delta E\rangle \ll F_{\mathrm{E}}RT$, $\langle\Delta E\rangle$ is constant regardless of the temperature, and that, thus, $\beta_{\mathrm{c}} \propto T^{-1}$. On the other hand Tardy and Rabinovitch (*Chem. Rev.*, **77**, 359 (1977)) proposed $\beta_{\mathrm{c}} \propto T^{-2}$ on the basis of the temperature-independent behavior of $\langle\Delta E\rangle_{\mathrm{down}}$, where $\langle\Delta E\rangle_{\mathrm{down}}$, the average energy transferred per deactivating collision, is related to $\langle\Delta E\rangle$ as:

$$\langle\Delta E\rangle = -\langle\Delta E\rangle^2_{\mathrm{down}}/(\langle\Delta E\rangle_{\mathrm{down}}+F_{\mathrm{E}}RT).$$

If $\langle\Delta E\rangle_{\mathrm{down}}$ is assumed to be independent of the temperature, the above relation leads to a large drop in β_{c} at high temperatures.

31) In a collinear collision of the two rigid spheres A and B, the probability of the energy loss of A, R_{A}, is given by the conservation rules of energy and momentum as:

$$R_{\mathrm{A}} = \frac{4m_{\mathrm{A}}m_{\mathrm{B}}}{(m_{\mathrm{A}}+m_{\mathrm{B}})^2}\left(1-\frac{v_{\mathrm{B}}}{v_{\mathrm{A}}}\right)\left(1+\frac{m_{\mathrm{B}}v_{\mathrm{B}}}{m_{\mathrm{A}}v_{\mathrm{A}}}\right),$$

where m and v are the mass and the velocity along the collinear axis before collision respectively. It appears from this equation that R_{A} reaches its maximum when $m_{\mathrm{A}}=m_{\mathrm{B}}$.

32) ΔS^* for each mode is estimated as: ΔS^*(translation)=0; ΔS^*(rotation)=3.6; ΔS^*(symmetry)=0; ΔS^*(internal vibration)=−3.2 (C–Cl stretch)+6.3 (two H–C–Cl bends).

33) S. Glasstone, K. J. Laidler, and H. Eyring, "The Theory of Rate Processes," McGraw-Hill, New York (1941).

34) M. Quack and J. Troe, *Ber. Bunsenges. Phys. Chem.*, **81**, 329 (1977).

35) M. Quack and J. Troe, *Ber. Bunsenges. Phys. Chem.*, **78**, 240 (1974).

36) K. A. Holbrook, *Trans. Faraday Soc.*, **57**, 2152 (1961).

37) W. Forst and P. St. Laurent, *Can. J. Chem.*, **43**, 3052 (1965); **45**, 3169 (1967).

 © 1980 The Chemical Society of Japan Bull. Chem. Soc. Jpn., 53, 2141—2145 (1980)

Requirements for an "Organic Metal"

Gunzi SAITO* and John P. FERRARIS**

Institute for Molecular Science, Okazaki 444

***Chemistry, The University of Texas at Dallas, Richardson, Texas 75080, U.S.A.*

(Received December 3, 1979)

Current theories on the origin of high electrical conductivity in TCNQ-based materials emphasize the need for incomplete charge transfer as well as segregated stacks of donor and acceptor molecules and uniform spacing within the stacks. The requirements for an "organic metal" are discussed in terms of partial charge transfer. An examination of 61 structurally related TTF–TCNQ based complexes suggests that the combinations with the redox potential $-0.02 \leq E_1(\mathrm{D}) - E_1(\mathrm{A}) \leq 0.34$ V have a high possibility of being "organic metals." A method to arrange the complex by the difference between the electrochemical half-wave potentials of the donor and the acceptor molecule is proposed to predict electrical properties of the complex.

Since the discovery of highly electrically conducting charge transfer (CT) complexes[1,2] and anion-radical salts[3,4] of tetracyano-*p*-quinodimethane (TCNQ), several proposals have been forwarded to design new "organic metals." As early as five years after the first report of the electrical properties of TCNQ salts by the Dupont group,[5] LeBlanc proposed the importance of cation polarizability as a criterion for high conductivity.[6] Prior to this, Little[7] suggested a design for a high temperature organic superconductor by incorporation of high polarizability through suitable molecules pendant on a conjugated polymeric backbone. The efforts of organic chemists in the several years following to prepare "organic metals" solely on the basis of polarizability considerations met with little success.[8] Prior to 1973 only three anion radical salts of TCNQ displayed "metallic" behavior over a limited temperature range. The discovery of the TCNQ complex of tetrathiafulvalene (TTF) in 1973 and the demonstration of its metallic properties over a relatively wide temperature range reinstilled interest in the search for organic conductors. To date over 70 "organic metals" have been prepared and subjected to a battery of physical measurements. In general, these "organic metals" may be placed into one of four categories. An estimate of the number of known complexes for each classification is given in brackets.

1. Charge transfer complexes which are ionic at 300 K, with such notables as TTF–TCNQ, TTT (tetrathiatetracene)$_2$–TCNQ, Δ4,4′-bithiopyran–TCNQ and their derivatives and analogs. [>50]

2. Anion radical salts of TCNQ[3,4,9] with formally closed shell cations represented by quinolinium–(TCNQ)$_2$, acridinium–(TCNQ)$_2$ and *N*-methylphenazinium(NMP)–TCNQ. [≈7]

3. Cation radical salts[10] with formally closed shell anions typically halide (or related) salts of TTF, TTT, nickel phthalocyanine or perylene. [≈7]

4. Ternary salts[11] consisting of an amine complexed with TCNQ and iodide or water in varying proportions. [7]

In 1965, McConnel *et al.*[12] classified the alternating CT complexes in the solid state into two distinct categories —those with ionic ground states and those without on the basis of the magnitude of the molecular field energy, $E = \mathrm{N}[(I-A)\rho - M\rho^2/2]$ where I, A, M, and ρ are the ionization potential of the donor, electron affinity of the acceptor, electrostatic energy per DA pair, and the average charge density ($0 \leq \rho \leq 1$) per molecule, respectively, in N DA pairs in the crystal. Matsunaga[13] has pointed out the utility of IR spectra to distinguish the nature of the ground state as applied to a number of CT complexes including aromatic hydrocarbons, aromatic diamines and phenothiazines as donors with *p*-quinones, TCNQ, *etc.* as acceptors. He was able on the basis of IR and electronic spectra to place the alternating CT complexes into groupings similar to McConnell's classifications. In general, ionic complexes were more conducting than nonionic complexes.[14] It was also suggested that the *size* and *shape* of the component molecules were critical factors defining the ionic to nonionic boundary.[14a] It is in the borderline region between these phases that one may expect CT complexes or ion radical salts to display interesting properties like metallic conductivity due to incomplete charge transfer[15] or complex isomerism.[16–18]

Prerequisites to High Conductivity

The search for new materials and an understanding of those already in hand generated numerous criteria for achievement of the metallic state in these systems.[19–22] Some have yet to be fully tested. As a matter of convenience, we choose to divide these criteria into two categories but recognize that they are strongly correlated.

A. *Requirements for Molecular and Crystal Structure.*

1. The component molecule which is responsible for electron transport should be flat in the neutral and ionic state.[3]

2. The donor and/or acceptor should be highly symmetric to avoid strong random potentials which can drive the system insulating (Ref. 1 and references cited therein). The presence of weak electronic or structural disorder need not, in general, destroy the metallic state and may even be the source of stabilization for the uniform chain structure.[17,19,20]

3. The cation (or anion) should be of relatively small size to facilitate polarization effects.[1,2]

4. The geometry of the acceptor should be such that electron withdrawing functional groups are located at diametrically distant points on the molecule to enhance its electron affinity and minimize Coulombic repulsion of electrons in the doubly ionized state.[19]

5. Closely matched physical dimensions for the donor

and acceptor which facilitate packing in the crystal.[22] This militates against bulky substituents.

6. The donor and acceptor moieties must form segregated stacks.[3]

7. The spacing between component molecules in the donor and acceptor stacks must be uniform to delocalize electrons into a single metallic band[19] or into partially filled and partially empty bands which overlap (semimetal).

B. *Requirements for Electronic Structure of Component Molecules and Complexes.*

8. Unpaired electrons on the donor and/or acceptor molecules must be present in the complex.[3,19]

9. Incomplete charge transfer[15] (as will be seen later, this criterion is satisfied by moderately strong donors in combination with moderately strong acceptors such that their redox potential differences are closely matched.).

10. Minimal on site Coulomb repulsive energies to destabilize transitions to a Mott insulator.[19]

11. Enhanced polarizability derived from the introduction of heteroatoms or heavy atoms.[6,22]

12. Formation of a new aromatic sextet upon one electron oxidation or reduction with this aromaticity capable of migrating through the crystal.[21]

13. The dipole moment of the ions should be small.[9b,c]

The achievement of the metallic state in these systems is obviously a complicated interplay of many factors, some of which lend themselves to variability and control. Requirements 1 and 6—8 are fundamental. Unfortunately we are unable to predict *a priori* which systems will necessarily meet criteria 6 and 7. In addition, Torrance[15] has recently demonstrated the necessity of requirement 9. The degree of ionicity (or charge transfer) for several "organic metals" has been estimated by diffuse X-ray scattering measurements, thermopower studies or NMR experiments. Some examples are 0.91—0.94,[23a-c] *ca.* 0.5,[23d] or 0.66,[23e] 0.74,[24] 0.63,[24] and 0.48—0.67[25] for NMP-, HMTSF (hexamethylene-tetraselenafulvalene)-, TSF(tetraselenafulvalene)-, and TTF-TCNQ respectively. Systems with complete charge transfer[12,22a] such as TTF-TCNQF$_4$ and TTT-TCNQF$_4$ are invariably insulators. The lower limit of the degree of ionicity for the appearance of metallic behavior has yet to be determined.

Discussion

In this paper we examine 61 of the complexes based on TTF (or TTT) and TCNQ together with their various derivatives and analogs in an attempt to predict other systems which are likely to yield highly conducting complexes. The choice of this series is two-fold. First, by far the largest number of "organic metals" are related to TTF-TCNQ and the physical properties of many of these have been extensively investigated. Second, the size and shape of the component molecules will affect their mode of packing the magnitude of the polarization energies and Madelung energies in the solid complexes and the repulsive Coulomb energies in the ionized molecules. Therefore, only

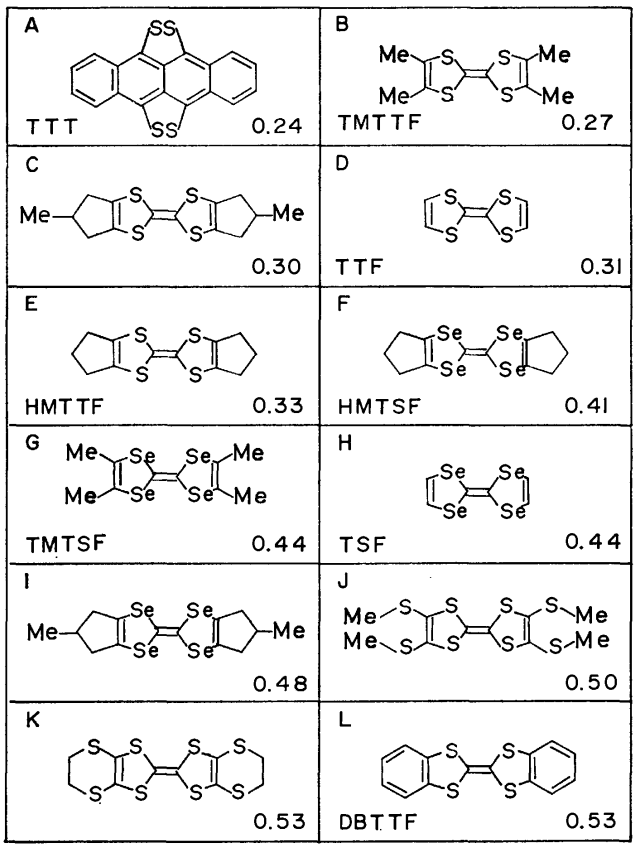

Fig. 1. Electron donors with corresponding electrochemical half-wave potentials.

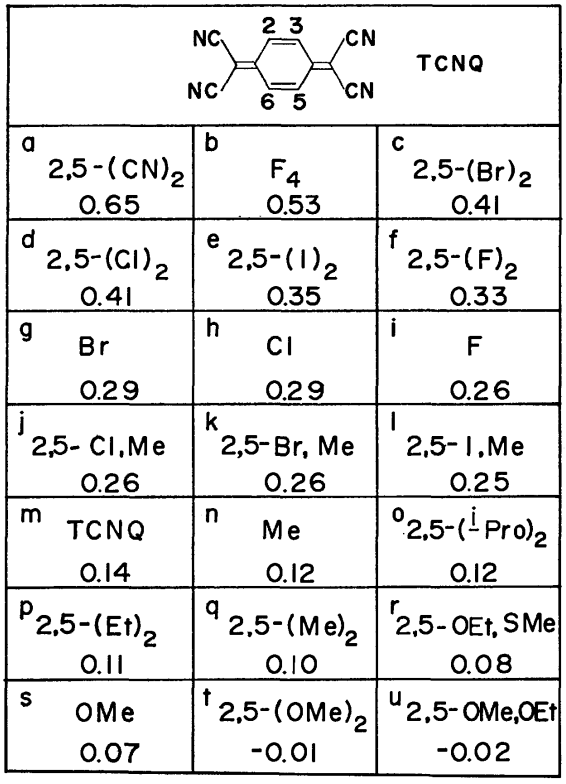

Fig. 2. Electron acceptors with corresponding electrochemical half-wave potentials.

an examination of a series with similar molecular structure can minimize the so called size and shape effect considerably. By this way one may discuss the certain parameter which controls the electric property of the complexes. In this meaning, Torrance's examination which includes a variety of structurally different donors such as Na, NMP, TTF, pyrene, *etc.* may have ambiguity.[15]

In a broad sense these systems should meet all the requirements for high conductivity except number 9, which we may then abstract exclusively. In Figs. 1 and 2 respectively are tabulated the structures of the donor and acceptor molecules considered here along with their first electrochemical half-wave potentials ($D \rightarrow D^+ + e$; $A + e \rightarrow A^-$). We have avoided asymmetric donors intentionally to minimize disorder effects. Since the TTF derivatives form an incomplete set we have also included several TTT complexes in this study. It is apparent that size and shape differences cannot be totally neglected but the differences in on-site Coulomb repulsive energies on the dications should be minimal across the series B-L. We have already shown there is virtually no enhanced on-site Coulomb repulsion present along the series, $TCNQF_n$ (n=0, 1, 2, 4).[26] The lattice energies are expected to be substantially different for the TTT and TTF complexes, but Madelung energies are relatively constant for donors of *similar size* when complexed with TCNQ, *e.g.* −4.6 to −5.3 eV for Na, Rb, NH_4,[27] and −2.3 to −2.4 eV for NMP- and TTF-TCNQ.[28] Therefore as a first approximation we take the Madelung energies as almost constant across the series.

Conductivity results are plotted in Fig. 3.[29] The

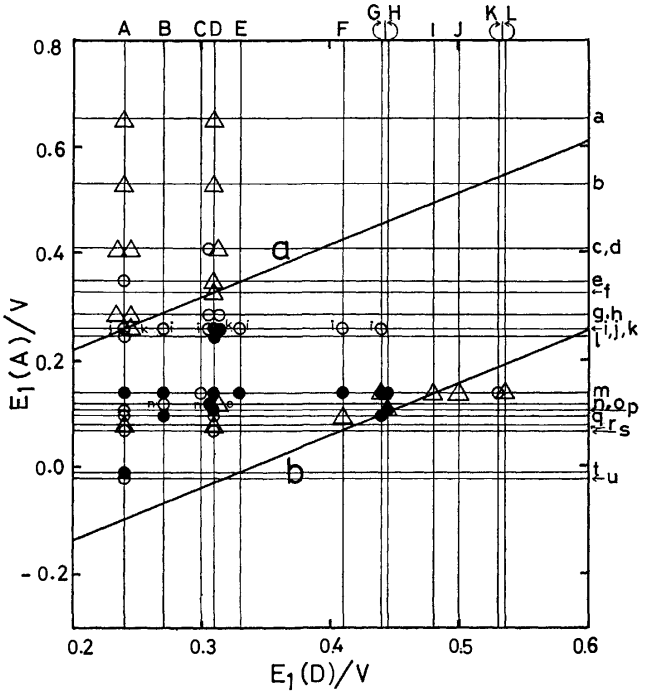

Fig. 3. Conductivity of complexes plotted as E_1 (A) *vs.* E_1 (D).
△=insulators or semiconductors; ○=highly conducting in compaction studies; ●="organic metals."

complexes have been arranged here by placing the ionization potentials of the donors on the abscissa and electron affinities of the acceptors on the ordinate. We have approximated these two quantities by the solution electrochemical half-wave potentials E_1(D) and E_1(A) respectively.[30] Similar treatments have been done by Wheland[22b] and by Torrance,[15] comparing the electric properties of the solid complexes with the solution electrochemical properties of the component molecules. Our treatment is, however, attempts to predict the properties of solid complexes from the solution electrochemical properties of the component molecules solely.

Those complexes in the upper left of the figure have small (I-A) values and favor the completely charge transferred ionic state. Those on the lower right favor the nonionic state. Those complexes which are insulators or semiconductors are represented by triangles whereas open circles designate highly conducting complexes based on compaction studies and closed circles are "organic metals." In general, complexes displaying substantial electrical conductivity fall between the two lines on the graph. The few exceptions are due to several factors. Complexes A–e and D–c are highly conducting due to heavy atom induced enhanced polarizability. Acceptors o and r are too bulky. It is uncertain why complex K–m is conducting. Some combinations yield complexes of variable stoichiometry: A–m (1:2), B–m (1:1), C–m (1:1), and D–l (1:1) are highly conductive but other compositions A–m (1:1),[31] B–m (1.3:2),[32] C–m (2:1)[29g] and D–l (2:1)[33] are semiconductors. There are two modifications of H–p[17] and of G–m,[18] a black "organic metal" and a red insulator. The structure of the latter for H–p has been assigned an alternating structure based on its optical spectrum.[17] The proximity of these complexes to the lower boundary in the absence of heavy-atom effects may place them at the minimum for degree of charge transfer with retention of metallic behavior.

The two boundaries shown are defined by the upper line (a): $E_1(A) = E_1(D) + 0.02$ and the lower line (b): $E_1(A) = E_1(D) - 0.34$ V respectively. Therefore, to the degree our approximation is accurate, *related combinations with the redox potential* $-0.02 \leq E_1(D) - E_1(A) \leq 0.34$ V *have a high probability of being "organic metals," where* $0.24 \leq E_1(D) \leq 0.53$ V *and* $-0.02 \leq E_1(A) \leq 0.65$ V. This result is compared well with those of Wheland[22b] ($|E_1(A) - E_1(D)| \leq 0.25$ V) and of Torrance[15] ($-0.19 \leq E_1(D) - E_1(A) \leq 0.31$ V). Those above line (a) would be completely ionic, those below line (b), nonionic. The idea that CT complexes display a whole spectrum of ionicity is not novel. As early as 1961 Kommandeur classified crystalline organic compounds into five areas based on the magnitude of ($I - A - P_+ - P_- - Q = E^*$) where P_+ and P_- are the polarization energies of the cation and anion and Q the electrostatic Coulomb energy.[34] Recently, Torrance *et al.*[28] have emphasized that in cases where the net electrostatic binding energy $E_B = (I - A) - M/2$ is small (≈ 2 eV), partial charge transfer may be energetically favored. Those complexes falling between lines (a) and (b) satisfy Torrance's criterion with $1.5 \leq (I - A) - M/2 \leq 1.9$ eV (using I=

6.85 eV for TTF,[35] A=2.84 eV for TCNQ[36] and $M/2$= ≈2.3 eV for these complexes.[28] The question still remains what degree of ionicity is necessary for metallic behavior? Investigation of complexes near the boundaries such as D–f, t, u, and D with Me_3TCNQ and Me_4TCNQ should provide the answer.[37] The latter two acceptors are still under construction but their E_1(A) values are estimated to be 0.02—0.03 and −0.01 to 0.00 V respectively. Figure 3 is far from complete and further studies of complexes of B, E—H and L with other known acceptors and weaker TCNQ's are required.

Some of the usages of the diagram are as follows. 1: The electrical property of an unknown TTF–TCNQ based complex can be easily predicted with the aid of the diagram. If the electrochemical potential were obtained for a TTF based donor or a TCNQ based acceptor, the other component molecules can be selected to give metallic complexes baring steric and/or some unforeseen effects. 2: A new TCNQ derivative which gives complexes with metallic behavior can be designed. Metallic complexes with *weak* partial charge transfer, *i.e.* in the proximate region of the lower line, may well be worth synthetic efforts. 3: In the course of the synthesis of TTF derivatives and analogs, the electrical properties of their TCNQ complexes have been compared with that of TTF–TCNQ. Considering the importance of partial charge transfer, this comparison should be made between the complexes belonging to the metallic region in the diagram.

One may extrapolate (with some danger) this treatment to the *p*-quinone acceptors, assuming values for Madelung energies, polarization energies and intermolecular spacings in segregated stacks are similar to their TCNQ counterparts though the *p*-quinones have larger disproportionation energies (*ca.* 0.3 eV)[38] when compared to the TCNQ series with the same E_1(A). Then *p*-chloranil (E_1(A)=0.01 V), *p*-bromanil (0.00 V) and *p*-fluoranil (−0.04 V) complexes with TTF and TMTTF[39] locate just above line(b)while 2,3-dichloro-5,6-dicyano-*p*-benzoquinone (0.51 V) complex with DBTTF[40] locates just below line (a).

We thank the Robert A. Welch Foundation and Research Corporation for support of this work.

Note added in proof: A recent paper by J-M Fabre, M. Vigroux, E. Torreilles, and L. Giral (*Tetrahedron Lett.* **1980**, 607) examined TMTTF–Et_2TCNQ (B-p) and found unusual stoichiometry (3 : 2) and structure. The electrical conductivity is metallic: $\sigma_{300K} \simeq 130\Omega^{-1}$ cm^{-1}.

References

1) J. P. Ferraris, D. O. Cowan, V. V. Walatka, Jr., and J. H. Perlstein, *J. Am. Chem. Soc.*, **95**, 948 (1973).

2) L. B. Coleman, M. J. Cohen, D. J. Sandman, F. G. Yamagishi, A. F. Garito, and A. J. Heeger, *Solid State Commun.*, **12**, 1225 (1973).

3) (a) L. R. Melby, R. J. Harder, W. R. Hertler, W. Mahler, R. E. Benson, and W. E. Mochel, *J. Am. Chem. Soc.*, **84**, 3374 (1962); (b) W. J. Siemons, P. E. Bierstedt, and R. G. Kepler, *J. Chem. Phys.*, **39**, 3523 (1963); (c) L. R. Melby, *Can. J. Chem.*, **43**, 1448 (1965).

4) (a) L. I. Buravov, D. N. Fedutin, and I. F. Shchegolev, *Sov. Phys. JETP*, **32**, 612 (1971); (b) I. F. Shchegolev, *Phys. Status Solidi A*, **12**, 9 (1972).

5) R. G. Kepler, P. E. Bierstadt, and R. E. Merrifield, *Phys. Rev. Lett.*, **5**, 503 (1960).

6) O. H. LeBlanc, *J. Chem. Phys.*, **42**, 4307 (1965).

7) W. A. Little, *Phys. Rev. A*, **134**, 1416 (1964).

8) B. H. Klanderman and D. C. Hoesterey, *J. Chem. Phys.*, **51**, 377 (1969).

9) (a) A. A. Gogolin, S. P. Zolotukhin, V. I. Melńikov, É. I. Rashba, and I. F. Shchegolev, *JETP Lett.*, **22**, 278 (1975); (b) G. Mihály, K Ritvay-Emandity, and G. Grüner, "Organic Conductors and Semiconductors. Lecture Notes in Physics 65," ed by L. Pal *et al.*, Springer-Verlag, Berlin (1977), pp. 535—551; (c) K. Holczer, G. Mihály ,A. Jánossy, G. Grüner, and M. Kertész, *J. Phys. C., Solid State Phys.*, **11**, 4707 (1978).

10) (a) F. Wudl, *J. Am. Chem. Soc.*, **97**, 1962 (1975); (b) L. C. Isett and E. A. Perez-Albuerne, *Solid State Commun.*, **21**, 433 (1977); (c) C. J. Schramm, D. R. Stojakovic, B. M. Hoffman, and T. J. Marks, *Science*, **200** No. 4337, 47 (1978); (d) H. C. I. Kao, M. Jones, and M. M. Labes, *J. Chem. Soc., Chem. Commun.*, **1979**, 329.

11) (a) G. J. Ashwell, D. D. Eley, and M. R. Willis, *Nature* **259**, 201 (1976); (b) G. J. Ashwell, *Phys. Status. Solidi B*, **86**, 705 (1978); (c) P. Dupuis, S. Flandrois, P. Delhaes, and C. Coulon, *J. Chem. Soc., Chem. Commun.*, **1978**, 337.

12) H. M. McConnel, B. M. Hoffman, and R. M. Metzger, *Proc. Natl. Acad. Sci., U. S. A.*, **53**, 46 (1965).

13) Y. Matsunaga, *J. Chem. Phys.*, **41**, 1609 (1964).

14) (a) Y. Matsunaga, *Bull. Chem. Soc. Jpn.*, **42**, 2490 (1969); (b) Y. Matsunaga and G. Saito, *Bull. Chem. Soc. Jpn.*, **44**, 958 (1971).

15) J. B. Torrence, *Acc. Chem. Res.*, **12**, 79 (1979).

16) Y. Matsunaga, *Bull. Chem. Soc. Jpn.*, **51**, 3071 (1978).

17) J. R. Andersen, R. A. Craven, J. E. Weidenborner, and E. M. Engler, *J. Chem. Soc., Chem. Commun.*, **1977**, 526.

18) K. Bechgaard, D. O. Cowan, and A. N. Bloch, *J. Chem. Soc., Chem. Commun.*, **1974**, 937.

19) A. F. Garito and A. J. Heeger, *Acc. Chem. Res.*, **7**, 232 (1974).

20) (a) A. N. Bloch, "Energy and Charge Transfer in Organic Semiconductors," ed by K. Masuda and M. Silver, Plenum Press, New York (1974), p. 159; (b) A. N. Bloch, D. O. Cowan, and T. O. Poehler, *ibid*, p. 167; (c) D. O. Cowan, P. Shu, C. Hu, W. Krug, T. Carruthers, T. O. Poehler, and A. N. Bloch, "Chemistry and Physics of One-dimensional Metals," ed by H. J. Keller, Plenum Press, New York (1976), p. 25.

21) J. H. Perlstein, *Angew. Chem. Int. Ed. Engl.*, **16**, 519 (1977).

22) (a) R. C. Wheland and J. L. Gillson, *J. Am. Chem. Soc.*, **98**, 3916 (1976); (b) R. C. Wheland, *ibid.*, **98**, 3926 (1976).

23) (a) M. A. Butler, F. Wudl, and Z. G. Soos, *Phys. Rev. B*, **12**, 4708 (1976); (b) J. F. Kwak, G. Beni, and P. M. Chaikin, *ibid.*, **13**, 641 (1976); (c) K. Ukei and I. Shirotani, *Commun. Phys.*, **2**, 159 (1977); (d) J. Tanaka, M. Tanaka, C. Tanaka, T. Ohno, T. Takabe, and H. Anzai, *Proc. New York Acad. Sci.*, **313**, 256 (1978); (e) R. Comes and A. J. Epstein, *Phys. Rev. B*, (in press).

24) C. Weyl, E. M. Engler, K. Bechgaard, G. Jehanno, and S. Etemad, *Solid State Commun.*, **19**, 925 (1976).

25) (a) R. Comes, S. M. Shapiro, G. Shirane, A. F. Garito, and A. J. Heeger, *Phys. Rev. Lett.*, **35**, 1518 (1973); (b) P. Coppens, *ibid.*, **35**, 98 (1975); (c) W. D. Grobman and B. D. Silverman, *Solid State Commun.*, **19**, 319 (1976).

26) G. Saito and J. P. Ferraris. *J. Chem. Soc., Chem. Commun.*, **1979**, 1027.

27) R. M. Metzger *J. Chem. Phys.*, **63**, 5090 (1975).

28) J. B. Torrance and B. D. Silverman, *Phys. Rev. B*, **15**, 788 (1977).

29) The conductivity data were taken from the following references. Complexes A–a,b,c,d,e,g,h,j,k,l,p,q,r,s,t,u, Ref. 22a. (a) Complex A–m; L. I. Buravov, O. N. Eremenko, R. B. Lyubouskii, L. P. Rozenberg, M. L. Khidekel, R. P. Shibaeva, I. F. Shchegolev, and E. B. Yagubskii, *JETP Lett.*, **20**, 208 (1974); (b) Complex B–i; J. P. Ferraris and G. Saito, *J. Chem, Soc., Chem. Commun.*, **1978**, 992; (c) Complex B–m; J. P. Ferraris, T. O. Poehler, A. N. Bloch, and D. O. Cowan, *Tetrahedron Lett.* **1973**, 2553 and A. N. Bloch, T. F. Carruthers, T. O. Poehler, and D. O. Cowan, "The Chemistry and Physics of One-dimensional Metals," ed by H. J. Keller, Plenum Press, New York (1977), p. 47; (d) Complex B–n; C. S. Jacobsen, J. R. Andersen, K. Bechgaard, and C. Berg, *Solid State Commun.*, **19**, 1209 (1976); (e) Complex B–q; C. S. Jacobsen, K. Mortensen, J. R. Andersen, and K. Bechgaard, *Phys. Rev. B*, **18**, 905 (1978); (f) Complex C–m; E. M. Engler, V. V. Patel, J. R. Andersen, R. R. Schumaker, and A. A. Fukushima, *J. Am. Chem. Soc.*, **100**, 3769 (1978); Complexes D–a,b,c,d,e, g,h,j,k,l,o,p,q,r,s; Ref. 22a, Complex D–f; Ref. 26, Complex D–i; Ref. 29b, Complex D–m; Refs. 1 and 2, Complex D–n; Ref. 29d, Complex E–i; Ref. 29b; (g) Complex E–m; E. M. Engler and V. V. Patel, IBM Research RC 5162, Dec. 6, 1974; Complex F–i; Ref. 29b; (h) Complex F–m; Ref. 18, and A. N. Bloch, D. O. Cowan, K. Bechgaard, R. E. Pyle, R. H. Banks, and T. O. Poehler, *Phys. Rev. Lett.*, **34**, 1561 (1975); (i) Complex F–q; J. R. Andersen, C. S. Jacobsen, G. Rindorf, H. Soling, and K. Bechgaard, *J. Chem. Soc., Chem. Commun.*, **1975**, 883; Complex G–i; Ref. 29b, Complex G–m; Ref. 29h, Complex G–q; Ref. 29i; (j) Complex H–m; E. M. Engler and V. V. Patel, *J. Am. Chem. Soc.*, **96**, 7376 (1974); Complex H–p; Ref. 17, Complex I–m; Ref. 29f; (k) Complex J–m; M. Mizuno, A. F. Garito, and M. P. Cava, *J. Chem. Soc., Chem. Commun.*, **1978**, 18; Complex K–m; Ref. 29k; (l) Complex L–m; H. K. Spencer, M. V. Lakshmikantham, M. P. Cava, and A. F. Garito, *J. Chem. Soc., Chem. Commun.*, **1975**, 867.

30) E_1 (D) and E_1 (A) values obtained from several literatures are tabulated under their respective compounds in Figs. 1 and 2.

31) J. H. Perlstein, J. P. Ferraris, V. Walatka, Jr., D. O. Cowan, and G. A. Candela, AIP Conference Proceedings (Magnetism and Magnetic Materials) 1972, p. 1494,

32) T. J. Kistenmacher, T. E. Phillips, D. O. Cowan, J. P. Ferraris, and A. N. Bloch, *Acta Crystallogr., Sect. B*, **32**, 539 (1976).

33) R. C. Wheland, *J. Am. Chem. Soc.*, **99**, 291 (1977).

34) J. Kommandeur, Am. Chem. Soc. Meeting, 1961 (St. Louis) and *U. S. Govt. Res. Develop. Rep.*, **68**, 170 (1968).

35) R. Gleiter, E. Schmidt, D. O. Cowan, and J. P. Ferraris, *J. Electron Spectrosc.*, **2**, 207 (1973).

36) E. C. M. Chen and W. E. Wentworth, *J. Chem. Phys.*, **63**, 3183 (1975).

37) A. Andrieux, C. Duroure, D. Jerome, and K. Bechgaard *J. Phys. Lett.*, **40**, L-381 (1979), $\rho=0.5$ for TMTSF–Me_2TCNQ (G–q).

38) G. Saito, unpublished results.

39) J. B. Torrance, J. J. Mayerle, V. Y. Lee, and K. Bechgaard, *J. Am. Chem. Soc.*, **101**, 4747 (1979).

40) H. Kobayashi, T. Yamamoto, T. Danno, and J. Nakayama, Paper presented at The Symposium on Molecular Structure, Tokyo, Japan (1979), p. 22. $\sigma_{R.T.}=ca.$ 70 Ω^{-1} cm^{-1}.

Film Dichroism. V. Linear Dichroism Study of Acridine Dyes in Films with Emphasis on the Electronic Transitions Involved in the Long-wavelength Band of the Absorption Spectrum

Yukio MATSUOKA and Kiwamu YAMAOKA*

Faculty of Science, Hiroshima University, Higashisenda-machi, Hiroshima 730

(Received December 10, 1979)

The long-wavelength bands of the absorption spectra of 10-methylacridinium (MeAcr), Acridine Orange (AO), and Acridine Yellow (AY) in the poly(vinyl alcohol) film were investigated by the linear dichroism method. The parallel- and perpendicular-dichroic spectra of each dye were resolved into the long-axis and short-axis polarized absorption components. From these component bands the isotropic spectrum was reconstituted and the reduced dichroism spectrum was simulated by computer with a new technique which utilizes a general expression for the reduced dichroism of planar molecules with the multiple band structure. A weak absorption band (or bands) hidden in a strong one could be revealed by reproducing the observed isotropic and linear-dichroic spectra. The vibrational sub-bands of MeAcr were shown to have the average intervals of *ca.* 1.5×10^3 cm^{-1} for the short-axis polarized ^1L_a band and of *ca.* 0.7×10^3 cm^{-1} for the long-axis polarized ^1L_b band. In the visible region of the isotropic spectrum, the weak ^1L_a band of AO was clearly shown to consist of the fine structure with a regular energy separation, although it is overlapped with the intense ^1L_b band which is also composed of a vibrational structure. The same spectral feature was observed for AY. The dichroic results are discussed under considerations of (1) the overlap of the mutually orthogonal transition moments, whose angles were determined relative to the long axis of the C_{2v}-symmetric dye molecule, (2) the angle between the orientation axis and the long axis of the molecular plane, and (3) the average degree of orientation of dye molecules in the film.

The unambiguous interpretation of the optical rotatory dispersion or the circular-dichroic spectrum of an acridine dye bound to an optically active biopolymer is often hampered because of the overlap of several electronic transitions in the absorption spectrum.[1-6] Acridine may be considered as the mother compound for a large number of the acridine dyes, such as 10-methylacridinium (MeAcr), Acridine Yellow (AY), and Acridine Orange (AO). A thorough understanding of the electronic transitions of acridine should facilitate the precise assignment of the electronic transitions involved in the absorption spectra of those more complicated derivatives of acridine.

The apparent location and the polarization of two electronic transitions of acridine (*i.e.*, the ^1L_a and ^1L_b bands) have been determined from the linear dichroism in the stretched film,[7,8] the polarized fluorescence in solution,[9,10] and the absorption spectrum in polymer matrix.[11] The linearly-polarized absorption spectra of acridine and other related acridine dyes were reported in a previous paper,[8] in which the overlapping ^1L_a and ^1L_b bands were separated with a *reduction procedure*.[12] The fine structure of each electronic band was not analyzed in detail, because a general expression for the linear dichroism of planar molecules was not yet available. The results clearly showed that the 3,6-diamino- or 3,6-bis(dimethylamino)-derivatives of acridine also possess the two electronic transitions in the long-wavelength region of the absorption spectrum.[8] However, the exact wavelength position and the fine structure of the ^1L_a band could not be determined unequivocally because of the weak absorption intensity of the unmasked ^1L_a band, which was overwhelmed by the strong ^1L_b band.[8]

The objective of this paper is to draw a clear conclusion on the controversy over the electronic transitions involved in the long-wavelength region of the absorption spectra of AO and AY on the basis of the detailed spectral data of acridine and MeAcr. For this purpose, the expression for the reduced dichroism of planar molecules[13,14] was extended to cover the absorption spectrum composed of numerous overlapping transitions. With the aid of this general expression, the observed isotropic and reduced dichroic spectra were analyzed by assuming the appropriate Gaussian band shape for the individual absorption bands. Both the ^1L_a and ^1L_b bands of MeAcr, AO, and AY were clearly shown to consist of a series of vibrational sub-bands. The energy separation of the sub-bands was also estimated. The present results have finally clarified the enigmatic character of the absorption spectra of the 3,6-disubstituted acridine dyes.

Experimental

Materials. Acridine dyes used in this work were monocationic 10-methylacridinium (MeAcr), Acridine Orange (AO), and Acridine Yellow (AY),[8] each of which was assumed to be a planar molecule with the negligible out-of-plane transition in the wavelength region between 220 and 550 nm. Poly(vinyl alcohol), (PVA), was used as the film matrix. Preparations of sample and reference films were described before.[8]

Measurements and Analytical Method. Measurements of the dichroic absorption spectra of each dye and the determination of the long- and short-axis polarized absorption spectra were reported previously.[8] For a single absorption band lying in the molecular plane of a given planar molecule, the reduced dichroism ($\Delta A/A$) can be expressed as [13,14]

$$\frac{\Delta A}{A}=\frac{3}{2}\{3(2M_z-1)\cos^2\theta-(3M_z-2)\}\Phi \qquad (1)$$

where Φ is the orientation function and θ is the angle between the transition moment of the absorption band and the molecular z-axis, as defined in Fig. 1. The constant M_z is given by $M_z=\cos^2\phi_z$, where ϕ_z is the angle between the z-axis and the direction of the molecular orientation axis (*cf.* Fig. 1).

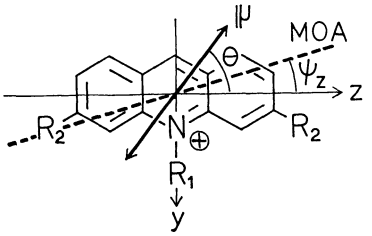

Fig. 1. Molecular coordinate system of acridine nucleus. Transition moment (μ) and molecular orientation axis (MOA) are measured from the molecular z-axis by the angles θ and ϕ_z, respectively.

Equation 1 indicates that the observed quantity $\Delta A/A$ for the single absorption band should be constant over the wavelength region concerned.

If an apparent absorption band is multiple and actually consists of n component bands (i=1, n), the total reduced dichroism should be an appropriate sum from each band and may be rewritten as

$$\frac{\Delta A}{A} = \frac{\sum_{i=1}^{n}\Delta A_i}{\sum_{i=1}^{n} A_i} = \frac{\sum_{i=1}^{n}\frac{3}{2}\{3(2M_z-1)\cos^2\theta_i-(3M_z-2)\}A_i}{\sum_{i=1}^{n} A_i}\,\phi \qquad (2)$$

where A_i is the absorption intensity, expressed with the absorbance, of the ith band. This expression reduces to the one previously derived for the rod-like molecule which may be assumed as the unit vector (Eq. 20 in Ref. 15 where $M_z=1$). Equation 2 indicates that the reduced dichroism can be expressed by the quantities θ_i and A_i, which are dependent on the wavelenth λ, and by M_z and ϕ, which are independent of λ and are characteristic of a particular planar molecule. The value of M_z is independent of the stretch ratio S of the film, while ϕ varies with S and approaches unity as the film is stretched infinitely.[13,14] A computer simulation of an experimental reduced dichroism spectrum by the use of Eq. 2 shows the presence of weak absorption bands overlapped with strong ones.

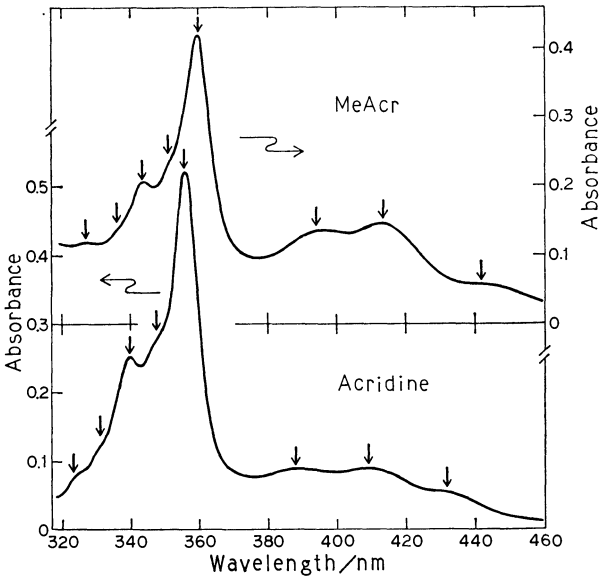

Fig. 2. Isotropic spectra of acridine and MeAcr in the nonstreched PVA film.

Results

Apparent Band Positions of Acridine and MeAcr. Figure 2 shows the isotropic spectra of acridine and MeAcr in the nonstretched (S=1) PVA film. In the spectrum of acridine, two peaks and three shoulders are observed in the 320—370 nm region and three humps in the 370—460 nm region. 10-Methylacridinium shows a similar spectrum, retaining most of these features, except for the 320—370 nm bands which are slightly diffused. From the studies of linear dichroism in the stretched polymer film[7,8] and the polarized fluorescence,[9,10] the short-wavelength band structure has been assigned to the ^1L_b transition and the long-wavelength one to the ^1L_a transition. It should be noted that the spectrum of AO differs from those in Fig. 2 in that it shows a deceptively simple absorption peak at 502 nm.[8] A similar change was always observed in the isotropic spectra of other 3,6-disubstituted acridine dyes: Proflavine, Trypaflavine, Acridine Yellow, and 10-Methyl Acridine Orange.[8] Although three shoulders are noticeable in the 400—490 nm region, the assignment of the polarization of AO was not so straightforward as in the case of acridine.[6,9,16] The isotropic spectrum of AO will be constituted from the individual component bands of the A_y- and A_z-spectra, in order to make the assignment of the polarization direction.

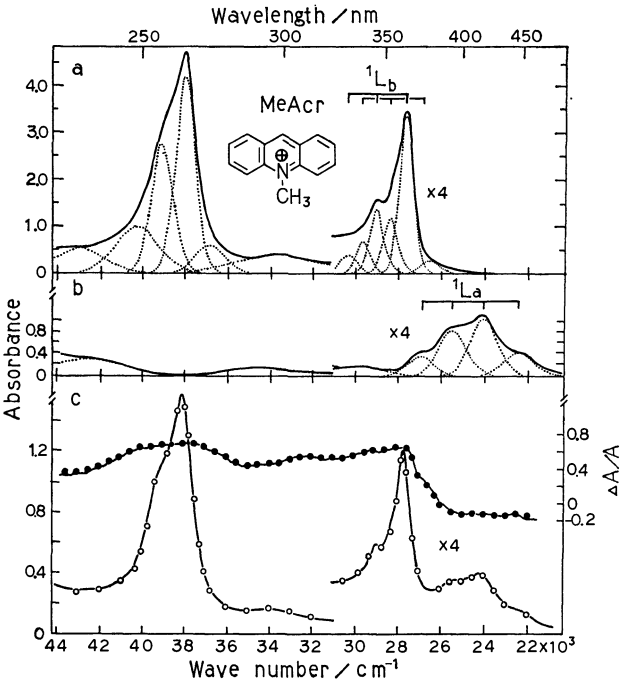

Fig. 3. Computer simulation of the dichroic data of MeAcr at ϕ=0.368. (a) Resolution of the A_z-spectrum (solid curve) into the component curves (dotted). (b) Resolution of the A_y-spectrum (solid curve) into the component curves (dotted). The absorbance scale of the ^1L_b and ^1L_a bands is four-fold expanded. (c) The results of the calculated (closed circles) and experimental (solid line) reduced dichroism in the upper half, and the reconstituted (open circles) and observed (solid line) isotropic spectrum. The numerical values for the resolution are given in Table 2.

For this purpose, the dichroic spectra of MeAcr as the base data will be analyzed with Eq. 2 in some detail below.

Computer Simulation of the Isotropic and Reduced Dichroism Spectra of MeAcr. The isotropic spectrum and the long-axis and short-axis polarized spectra (*i.e.*, the A_z- and A_y-spectra) of MeAcr are shown in Fig. 3, together with the wavelength dependence of the reduced dichroism (the RD-spectrum).[8] The A_z- and A_y-spectra of MeAcr [(a) and (b) of Fig. 3] are at first divided into the respective component bands. Then, the isotropic spectrum [(c) of Fig. 3] is reconstructed from all of those component bands by a computer synthesis, in which the band envelope, $A_i(\tilde{\nu})$, of the ith component band was conventionally assumed to be the Gaussian error function at a given wave number $\tilde{\nu}$ (Eq. 3):[17,18]

$$A_i(\tilde{\nu}) = A_{i,\max} \exp\left\{-\left(\frac{\tilde{\nu}-\tilde{\nu}_{i,\max}}{\delta_i}\right)^2\right\} \qquad (3)$$

where $\tilde{\nu}_{i,\max}$, $A_{i,\max}$, and δ_i are the peak position, the maximum intensity (absorbance) at $\tilde{\nu}_{i,\max}$, and the corresponding half-width of the ith band, respectively. The half-width is the band width in wave numbers measured at 1/2.718 of the maximum height.

The resolution of the A_z-spectrum (and also the A_y-spectrum) into the component bands was carried out with a HITAC-8700 computer according to the following procedure.[15] Both $A_{i,\max}$ and δ_i were taken as adjustable parameters. Since most of the peaks and shoulders in the A_z-spectrum (and the A_y-spectrum) are easily discernible (Fig. 3), the center of each component band, $\tilde{\nu}_{i,\max}$, was treated as a pre-determined constant and was read from the respective spectra. For the sub-bands whose peak positions were not visually clear, the following guide was observed:[19] The spacing of the sub-bands is characteristic of a particular electronic transition, but each sub-band in the transition is separated more or less evenly with an average spacing $(\Delta\tilde{\nu})_{avg}$. With the pre-determined values of $\tilde{\nu}_{i,\max}$, the values of $A_{i,\max}$ and δ_i were adjusted until a reasonable agreement was obtained between the observed and simulated A_z-spectra (and A_y-spectra). This iteration procedure was repeated with a new set of $\tilde{\nu}_{i,\max}$-values in case the agreement was poor. The value of δ_i was assumed to be constant for successive sub-bands belonging to a particular electronic transition.

Figure 3 shows the resolved component bands (dotted lines) of the A_z-spectrum (a) and the A_y-spectrum (b). With the relation $3A=A_y+A_z$,[13,20] the isotropic spectrum of MeAcr can be synthesized directly by the use of those component bands. The resultant isotropic spectrum [open circles in (c)] agrees well with the observed one (solid curve). This agreement assures the correctness of the Gaussian approximation for the profile of each component band and the assumption for the spacing of the peak positions for the component bands of a particular electronic transition.

The resolution of the A_z- and A_y-spectra into the component bands is verified by the construction of the RD-spectrum. This spectrum can be simulated by using the resolved component bands with the aid of Eq. 2, in which the transition moment angles θ_i of the component bands of the A_z-spectrum are all equal to 0° and those of the component bands of the A_y-spectrum are 90° under consideration of the C_{2v} symmetry of MeAcr.[8] The values of the orientation function Φ and the constant M_z in Eq. 2 were evaluated at the same stretch ratio of 4.3 as in a previous work: $\Phi=0.368$ and $M_z=0.75$.[13] (These values may be calculated from the values of the experimental reduced dichroism with Eq. 1, if the y-axis and the z-axis polarized transitions are well separated in an absorption spectrum, as in the case of MeAcr.[14])

The result is shown in Fig. 3c, where the simulated RD-spectrum (closed circles) agrees well with the experimental one (solid curve) in the 220—460 nm region. This agreement should be considered as a strong support for the set of all A_i, θ_i, Φ, and M_z values employed in the present simulation. Thus it is obvious that the ^1L_a transition centered at 412 nm consists of four component bands with an equal spacing of *ca.* 1.5×10^3 cm^{-1}, while the ^1L_b transition centered at 360 nm consists of about six component bands with an equal spacing of *ca.* 0.7×10^3 cm^{-1}. The UV band peaked at 263 nm was resolved into four component bands. The remaining absorption region (270—340 nm) was tentatively divided into the broad component bands.

Computer Simulation of the Isotropic and Reduced Dichroism Spectra of AO and AY. In the case of AO and AY, the energy gap between the ^1L_a and ^1L_b transitions is

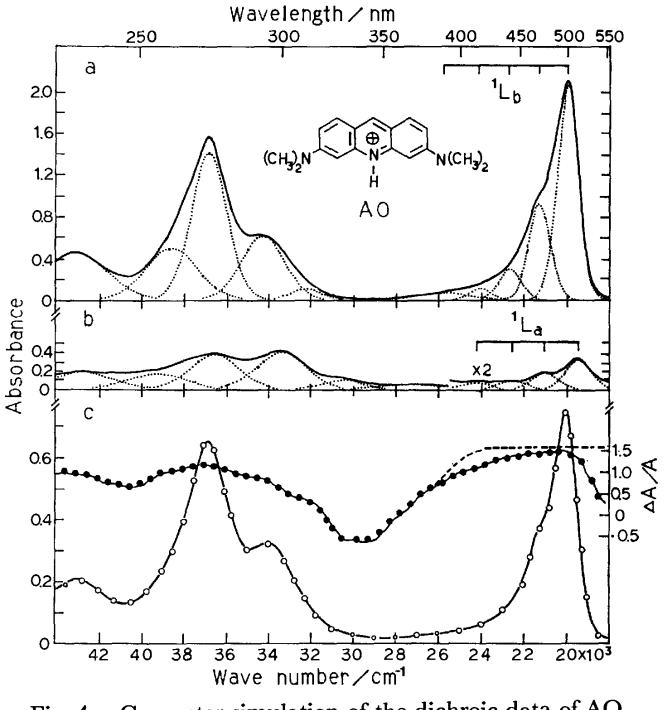

Fig. 4. Computer simulation of the dichroic data of AO at $\Phi=0.61$. Symbols are the same as in Fig. 3. The absorbance of the ^1L_a band is two-fold expanded. The thick dashed line in the visible region (c) indicates the resultant reduced dichroism under no consideration of the ^1L_a band. The presence of this band is essential to the correct reproduction of the experimental RD-spectrum.

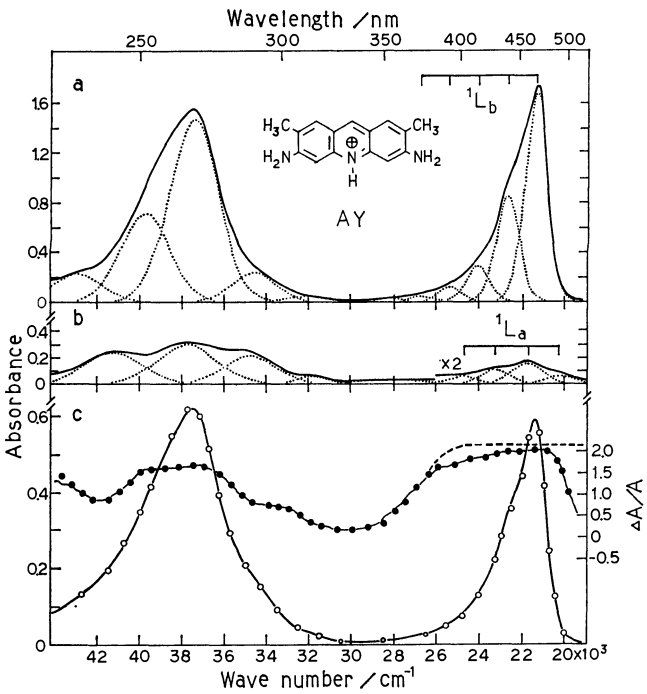

Fig. 5. Computer simulation of the dichroic data of AY at $\phi=0.72$. Symbols are the same as in Fig. 3. The absorbance of the ^1L_a band is two-fold expanded. The thick dashed line in the visible region (c) indicates the calculated reduced dichroism without the consideration of the ^1L_a band.

narrower, while the absorption intensity of the ^1L_a transition is much weaker than that of the ^1L_b transition.[8] The A_z- and A_y-spectra of AO were analyzed by the same method as used for MeAcr. The results are shown in Fig. 4, where the A_y-spectrum (b) is the average of four A_y-spectra which were obtained at four different stretch ratios. Thus the experimental error associated with the weak intensity of the A_y-spectrum was minimized. Both the A_z- and A_y-spectra of AO (a and b) were resolved into the respective component bands in the visible and UV regions. The A_z- and A_y-spectra of AY were analyzed in a manner similar to the case of AO. The results are shown in Fig. 5, which indicates that the spectral feature of AY is closely related to that of AO.

The vibrational progressions of the ^1L_a and ^1L_b bands of AY in the visible region were similar to those of AO. The A_z-spectra of AO and AY in the UV region could be divided into five component bands.[21] The highest-intensity bands at 272 nm for AO and at 266 nm for AY belong to ^1B_b transition.[9,16] However, the assignments of other bands were difficult to make. They may be either the vibrational sub-bands of the ^1B_b transition or other electronic transitions. The A_y-spectra of AO and AY in the UV region were resolved into the individual component bands. The assignments of these bands were also difficult to make. The isotropic spectra of AO and AY are finally reconstructed from those resolved bands as shown by open circles, which agree well with the observed spectra (solid curves), in Figs. 4c and 5c. The resolution of the A_z- and A_y-spectra into those component bands will be further justified by simulating the observed RD-spectrum.

The values of ϕ and M_z necessary for the simulation have already been evaluated:[13] $\phi=0.61$ (at $S=4.3$) and $M_z=0.90$ for AO, and $\phi=0.72$ (at $S=4.3$) and $M_z=1.0$ for AY. The transition moment angle θ_i is 0° for the component bands of the A_z-spectrum and 90° for the component bands of the A_y-spectrum under consideration of the molecular symmetry. The results of the simulation of the RD-spectrum are shown by closed circles for AO in Fig. 4c and for AY in Fig. 5c. The agreement between the simulated (closed circles) and the experimental (solid curve) RD-spectra is excellent over an entire wavelength region for AO and AY, which is a strong justification of both the procedure for the resolution of the A_z- and A_y-spectra into the component bands and the values of ϕ and M_z used in the simulation.

Discussion

Transition Moment Direction of an Overlapping Band and Expressions for Reduced Dichroism. If the y- and z-axis polarized electronic transitions of a molecule are isolated in the spectrum, the angle θ between either transition moment and the molecular z-axis can be determined with the aid of Eq. 1, together with the given values of M_z and ϕ. Hence, this equation yields a value of 0° for a z-axis polarized absorption band at 263 nm and 90° for a y-axis polarized band at 412 nm of MeAcr, in which these orthogonal bands are widely separated (Fig. 3). However, this is not true for the case in which two or more electronic bands are overlapped. Equation 1 is written for AO ($M_z=0.90$ and $\phi=0.61$) as

$$\frac{\Delta A}{A} = 0.915(2.4\cos^2\theta - 0.7). \qquad (4)$$

This equation yields the apparent θ-values of *ca.* 25° and 82°, which differ from 0° or 90°, for the overlapping 272 nm ($\Delta A/A=1.15$) and 330 nm ($\Delta A/A=-0.60$) bands respectively (Fig. 4). Other examples are given for the representative bands of MeAcr, AO, and AY in Table 1. Molecular orbital calculations[7,22,23] prescribe that the transition moment vector of an absorption band of the acridine dyes, which belong to the C_{2v} point symmetry group, should be polarized along the long- or short-axis in the molecular plane. Accordingly, the angle θ for the overlapping bands gives only the apparent direction of a resultant vector

Table 1. The angle of transition moment, θ_λ, for some apparent bands of MeAcr, AO, and AY calculated from Eq. 1

Dyes	θ_λ[a]		
MeAcr	$\theta_{412}=90\pm3$	$\theta_{360}=12\pm3$	$\theta_{263}=0\pm3$
AO	$\theta_{502}=13\pm2$	$\theta_{330}=82\pm3$	$\theta_{272}=25\pm2$
AY	$\theta_{467}=9\pm2$	$\theta_{295}=41\pm3$	$\theta_{266}=22\pm2$

a) θ_λ is the angle in degrees measured from the z-axis of the acridine nucleus (Fig. 1), and λ in nm indicates the observed apparent band position.

Table 2. Classification on the long-wavelength absorption bands of MeAcr, AO, and AY in the PVA film

Dyes	Bands							
	^1L_a				^1L_b			
	$A_{i,max}$	δ_i / 10^3 cm^{-1}	$\tilde{\nu}_{i,max}$ / 10^3 cm^{-1}	$\Delta\tilde{\nu}$ / 10^3 cm^{-1}	$A_{i,max}$	δ_i / 10^3 cm^{-1}	$\tilde{\nu}_{i,max}$ / 10^3 cm^{-1}	$\Delta\tilde{\nu}$ / 10^3 cm^{-1}
MeAcr	0.106	0.85	22.50	1.54				
	0.255	0.85	24.04	1.47				
	0.202	0.85	25.51	1.44				
	0.086	0.85	26.95		0.068	0.46	26.90	0.75
					0.827	0.46	27.65	0.72
					0.284	0.46	28.37	0.65
					0.322	0.46	29.02	0.66
					0.169	0.46	29.68	0.71
					0.096	0.46	30.39	
AO	0.157	0.85	19.50	1.60				
	0.095	0.85	21.10	1.55	2.053	0.72	19.97	1.33
	0.049	0.85	22.65	1.54	0.925	0.72	21.30	1.37
	0.035	0.85	24.19		0.305	0.72	22.67	1.37
					0.102	0.72	24.04	
AY	0.031	1.05	20.35	1.44				
	0.075	1.05	21.79	1.47	1.667	0.75	21.41	1.32
	0.054	1.05	23.26	1.49	0.842	0.75	22.73	1.35
	0.029	1.05	24.75		0.283	0.75	24.08	1.33
					0.116	0.75	25.41	1.30
					0.035	0.75	26.71	

of some differently polarized transitions. Neglect of this fact may cause some confusion in the assignment of the direction of transition moments.

The above difficulty may be avoided by the use of Eq. 2, which is written for AO as

$$\frac{\Delta A}{A} = 0.915\left(2.4\frac{A_y\cos^2\theta_y + A_z\cos^2\theta_z}{A_y + A_z} - 0.7\right). \quad (5)$$

In this equation the correct angles of transition moments, θ_y and θ_z, can be calculated to be 90° and 0° at any wavelength, provided that both A_y- and A_z-spectra are available from the reduction procedure, together with the values of M_z and ϕ. It should be emphasized here that Eq. 2 is the general expression which describes the dichroic property of any planar, light-absorbing molecules with no out-of-plane transition and will be employed for the analysis of the observed $A_{//}$- and $A_{\perp}$-spectra, each of which contains some overlapping bands. In order to utilize Eq. 2 fully, the values of M_z, ϕ, and $A_i(=A_y$ or $A_z)$ must be available without recourse to the reduction procedure. Both M_z and ϕ may be estimated experimentally by measuring the reduced dichroism at several stretch ratios, while A_i may be obtained by equating θ_y and θ_z to 90° and 0° in Eq. 5 (or 2) for the C_{2v}-symmetric molecules.

Identification of the ^1L_a and ^1L_b Transitions of MeAcr, AO, and AY. The spectral profile of the short-axis polarized transition (^1L_a) of MeAcr could be resolved into a series of the vibrational sub-bands. The energy separation $\Delta\tilde{\nu}$ of the successive sub-bands is (1.4—1.5) × 10^3 cm^{-1} (Table 2). This spacing is very close to the previously reported values for the ^1L_a transitions of acridine[7] and some polyacenes.[24,25] The spacing of the vibrational sub-bands of the ^1L_b transition of MeAcr is (0.7—0.8) × 10^3 cm^{-1} (Table 2), as obtained from the resolution of the long-axis polarized spectrum. This energy separation is also very close to the values for the vibrational sub-bands of the ^1L_b transition of the polyacene derivatives.[25] The band profiles of the individual vibrational sub-bands associated with the electronic ^1L_b transition strongly support the notions that two different vibrational progressions are involved and that their average energy spacings are both about 1.4×10^3 cm^{-1}, as indicated in Fig. 3a. It is interesting to note that the intense, solitary peak at 360 nm is actually the second of the vibrational sub-bands. If it were the first, the RD-spectrum in Fig. 3c should ascend much more sharply from −0.2 to 0.7 in the 360—380 nm region.

From Figs, 4 and 5, it is obvious that the ^1L_a transition of AO (and AY) also consists of several vibrational sub-bands which are overlapped by the intense ^1L_b transition. If the vibrational structure were due to an error in the trial-and-error reduction search,[8,12] there would be no short-axis polarized transition (^1L_a) involved in the visible region. In this case, the calculated wavelength dependence of the reduced dichroism should differ from the experimental curve, behaving like the curve of thick dashed lines in Figs. 4c and 5c, and, hence, the experimental reduced dichroism could never be reproduced. Therefore, the short-axis polarized band must be present in the visible region of AO (and AY). The spacing of the sub-bands of the ^1L_a transition of AO (and AY) is (1.4—1.6) × 10^3 cm^{-1} (*cf.* Table 2 and Figs. 4b and 5b). This energy separation is again in good agreement with the values

for the ^1L_a transitions of MeAcr and other aromatic compounds.[25] The vibrational spacing of the ^1L_b transition of AO (and AY) is $(1.3—1.4)\times10^3$ cm^{-1} (*cf.* Table 2 and Figs. 4a and 5a) and agrees with a reported value of 1.3×10^3 cm^{-1}.[26] It is now clear from the present work why the experimental verification of the ^1L_a transition for the 3,6-disubstituted acridine dyes has long been unsuccessful. It is because the ^1L_a band is weak and completely hidden by the intense ^1L_b band.

The ^1L_a and ^1L_b bands of AO and AY are distributed over a wide wavelength region. This wide progression of the ^1L_a band of AO (and AY) may be responsible for a variety of reports on the different wavelength positions of the ^1L_a band, *i.e.*, the short-wavelength side of the principal peak (Ballard *et al.*[16] and Ito and I'Haya[23]) or the long-wavelength side of the principal peak (Wittwer *et al.*[9] and Lang and Löber[22]). The classification of the long-wavelength absorption bands of MeAcr, AO, and AY has now been completed in this work. With this result, optical studies of the interaction between acridine dyes and natural or synthetic polymers should be facilitated. The geometrical studies of the complexes between 10-Methyl Acridine Orange and deoxyribonucleic acid and sodium polyphosphate will be reported shortly.

Conclusion

The isotropic spectra of MeAcr, AO, and AY were reconstituted from the component bands obtained by resolving the long- and short-axis polarized absorption spectra (A_y and A_z). The existence of a weak absorption band (the ^1L_a band) of AO and AY could be confirmed by reproducing the experimental reduced dichroism reasonably well with the aid of a new expression for the reduced dichroism of the multiple band system. The weak ^1L_a band of both AO and AY was shown to consist of the vibrational structure with regular energy intervals. The average spacing of the successive subbands for the ^1L_a and ^1L_b transitions of MeAcr, AO, and AY could be estimated from the resolved peak positions. The general expression for the reduced dichroism of a planar molecule (Eq. 2) has proved to be useful for analyzing the linear dichroism with overlapping absorption bands in the dichroic spectra of acridine dyes of C_{2v} point symmetry.

References

1) K. Yamaoka, *Biopolymers*, **11**, 2537 (1972).
2) K. Yamaoka and S. Noji, *Chem. Lett.*, **1979**, 1123.
3) M. Zama and S. Ichimura, *Biopolymers*, **9**, 53 (1970).
4) S. Ikeda and T. Imae, *Biopolymers*, **10**, 1743 (1971).
5) E. Fredericq and C. Houssier, *Biopolymers*, **11**, 2281 (1972).
6) A. Gafni, J. Schlessinger, and I. Z. Steinberg, *Israel J. Chem.*, **11**, 423 (1973).
7) J. Yoshino, T. Hoshi, T. Masamoto, H. Inoue, and K. Ota, *Nippon Kagaku Kaishi*, **1972**, 2227.
8) Y. Matsuoka and K. Yamaoka, *Bull. Chem. Soc. Jpn.*, **52**, 3163 (1979).
9) A. Wittwer and V. Zanker, *Z. Phys. Chem. (Frankfurt am Main)*, **22**, 417 (1959).
10) W. Seiffert, H. H. Limbach, V. Zanker, and H. Mantsch, *Histochemie*, **23**, 220 (1970).
11) E. H. Park, A. H. Kadhim, and H. W. Offen, *Photochem. Photobiol.*, **8**, 261 (1968).
12) E. W. Thulstrup, J. Michl, and J. H. Eggers, *J. Phys. Chem.*, **74**, 3868 (1970).
13) Y. Matsuoka, *J. Phys. Chem.*, **84**, 1361 (1980).
14) This was presented at the annual Meetings of Molecular Structures (Bunshikozosogotoronkai) of the Chemical Society of Japan held at Tokyo in October, 1979, Abstr. p. 540, and at Hiroshima in October, 1978, Abstr. p. 590.
15) K. Yamaoka and Y. Matsuoka, *J. Sci. Hiroshima Univ., Ser. A*, **40**, 105 (1976).
16) R. E. Ballard, A. J. McCaffery, and S. F. Mason, *Biopolymers*, **4**, 97 (1966).
17) L. M. Schwartz, *Anal. Chem.*, **43**, 1336 (1971).
18) T. Nakamura and Y. J. I'Haya, *Bull. Chem. Soc. Jpn.*, **45**, 2720 (1972).
19) H. H. Jaffé and M. Orchin, "Theory and Applications of Ultraviolet Spectroscopy," John Willey and Sons, Inc., New York, N. Y. (1966), pp. 302—303.
20) B. Nordén, G. Lindblom, and I. Jonáš, *J. Phys. Chem.*, **81**, 2086 (1977).
21) H. Jakobi and H. Kuhn, *Z. Elektrochem.*, **66**, 46 (1962).
22) H. Lang and G. Löber, *Tetrahedron Lett.*, **46**, 4043 (1969).
23) H. Ito and Y. J. I'Haya, *Int. J. Quantum Chem.*, **2**, 5 (1968).
24) H. Inoue, T. Hoshi, T. Masamoto, J. Shiraishi, and Y. Tanizaki, *Ber. Bunsenges. Phys. Chem.*, **75**, 441 (1971).
25) N. D. Coggeshall and A. Pozefsky, *J. Chem. Phys.*, **19**, 980 (1951).
26) T. Kurucsev and U. P. Strauss, *J. Phys. Chem.*, **74**, 3081 (1970).

Partner Orbitals in Hartree-Fock Theory

Kimihiko HIRAO

Department of Chemistry, College of General Education, Nagoya University, Chikusa-ku, Nagoya 464

(Received December 12, 1979)

The orbital ambiguity in the Hartree-Fock theory is removed in such a way as to improve the convergence property of the configuration interaction calculation. A practical proposal is made to obtain efficient orbitals for use in construction of wavefunctions. These orbitals are called the zeroth-order natural orbitals and their partner orbitals. It is also demonstrated by an illustrative calculation that use of partner orbitals rather than SCF orbitals gives much more rapid convergence and greater physical insight.

The variational condition in the Hartree-Fock (HF) theory determines the occupied and virtual manifolds, but it does not completely determine the individual orbitals belonging to each manifold.[1] This orbital ambiguity yields the possibility of obtaining a new set of orbitals within unitary transformations which may be more effective for the investigation of a particular physical problem than the SCF orbitals. Several attempts[2] were made to exploit this arbitrariness to produce physically meaningful virtual orbitals for some specific purposes. These methods, however, usually resolve the orbital ambiguity according to the criterion that the orbitals should change as little as possible under an excitation of a single electron. These orbitals are suitable to describe the singly excited states but do not help to improve the convergence in the perturbation theory and the configuration interaction (CI) calculation based on the HF equation.

The present discussion differs from these at some points in philosophy. We will consider that the orbital ambiguity should be resolved in such a way that the convergence may be improved in the CI calculation based on the HF equation. The orbitals obtained in such a way should be the zeroth-order approximation to the natural orbitals,[3] since they reduce the number of determinants required for any fixed accuracy in the wavefunction compared with most other techniques for selecting orbitals. Perturbation comparison of HF orbitals and natural orbitals indicates that the coupling of HF occupied and virtual manifolds occurs only in second order due to the Brillouin theorem.[4] This suggests the possibility that we can define zeroth-order natural orbitals by taking advantage of the arbitrariness of the manifolds. In the present study, we will define 2n zeroth-order natural orbitals for 2n-electron systems. The first n natural orbitals are determined by a unitary transformation of the HF manifold.[5] The remaining n natural orbitals are determined by a transformation of the virtual manifold involving pairing of first n zeroth-order natural orbitals with virtual orbitals. The virtual orbitals are, therefore, transformed so that each virtual orbital is largely localized in the same region as its occupied counterpart. There is no resemblance at all between any one of the SCF virtual orbitals and these transformed ones. We call these virtual orbitals as partner orbitals.

The existence of these partner orbitals is predicted in our previous study[6] of the orbital theories with the formalism of the cluster expansion method. The same kind of orbitals as partner orbitals play an important role in constructing wavefunctions of various orbital theories including electron correlation effects. Also the same kind of orbitals appear and help the HF orbitals when the HF state is unstable, that is, when the HF approximation fails to describe the system. However, when the HF solution is stable, as is usually the case, partner orbitals are embedded in the virtual manifold.

We will show how to resolve the orbital ambiguity to obtain the zeroth-order natural orbitals and their partner orbitals. We will also demonstrate that the use of partner orbitals rather than the SCF orbitals gives much more rapid convergence and greater physical insight.

Definition of Partner Orbitals

We consider the case of a determinatal wavefunction of 2n electrons with n doubly occupied orbitals

$$\Phi_0 = \|\phi_1\bar{\phi}_1 \cdots \phi_k\bar{\phi}_k \cdots \phi_n\bar{\phi}_n\| \quad (1)$$

as determined by an SCF calculation. Since we usually obtain these occupied orbitals from some kind of eigenvalue equations which give us more orbitals than needed, we have the so-called virtual orbitals. The virtual orbitals are mere mathematical by-products, so there are an infinitive number of possible choices of the virtual orbitals, the only requiring to be met being that they should be orthogonal to the HF orbitals. For a set of m orbitals (we assume $m \geq 2n$), of which n are occupied, choose pair orbital of the (m−n) virtual orbitals with each of the n occupied orbitals. Then define the Slater determinants Φ_k obtained by exciting a pair of electrons from occupied ϕ_k to its virtual counterpart orbital ϕ_{k^*},

$$\Phi_k = \|\phi_1\bar{\phi}_1 \cdots \phi_{k^*}\bar{\phi}_{k^*} \cdots \phi_n\bar{\phi}_n\|. \quad (2)$$

Throughout the paper, the indices k, l refer to the occupied orbitals, k*, l* to their virtual counterparts, u, v to the remaining virtual orbitals and i, j to general orbitals. Now consider the total wavefunction expressed as a linear combination of these determinants,

$$\Psi = C_0\Phi_0 + \sum_{k=1}^{n} C_k\Phi_k. \quad (3)$$

We assume Ψ is normalized to unity. Namely, the configuration expansion coefficients satisfy

$$C_0^2 + \sum_{k=1}^{n} C_k^2 = 1. \quad (4)$$

This expansion is different from the so-called complete MC-SCF (CMC-SCF) expansion of Clementi and

Veillard,[7] in which all possible pair excitations $\phi_k \rightarrow \phi_i$ are included for a finite set. We call this particluar expansion (3) the Selected Paired Excitational (SPE) expansion to distinguish this from other possible paired excitational expansions. The first order reduced density matrix for Φ is written

$$\rho(1|2) = 2\sum_{k=1}^{n}[(1-C_k^2)\phi_k^*(1)\phi_k(2)+C_k^2\phi_{k^*}^*(1)\phi_{k^*}(2)]. \quad (5)$$

These orbitals ϕ_k, ϕ_{k^*} constitute, therefore, the natural orbitals for Φ. The $(1-C_k^2)$ is the fractional occupation probability for ϕ_k and C_k^2 is that for ϕ_{k^*}. The configuration expansion coefficients are obtained by solving the conventional CI eigenvalue problem,

$$\boldsymbol{HC} = \boldsymbol{EC} \quad (6)$$

with $\boldsymbol{E}$ the diagonal energy matrix and $\boldsymbol{H}$ defined by the Hamiltonian matrix elements with respect to the SPE configurations.

The idea of the present method is to arrive at equations for the determination of the "best" HF occupied and virtual orbitals to be used in the SPE expansion of the wavefunction. "Best" is used here in the sense that the "best" occupied and virtual orbitals determined by a unitary transformation on each manifold will yield the lowest possible eigenvalue of (6). Thus, we predict that "best" orbitals are presumably close to the first 2n natural orbitals in the space spanned by the m orthonormal basis functions. Thus, we call the "best" occupied orbitals as the first n zeroth-order natural orbitals and the "best" virtual orbitals as partner orbitals to these occupied orbitals. The CI calculation with these "best" orbitals is called the CI with partner orbitals (CIP).

The energy expectation for Φ is given by

$$\begin{aligned} E = E_0 &- 2\sum_k C_k^2(h_{kk}-h_{k^*k^*}+G_{kk}-G_{k^*k^*}) \\ &-4\sum_{k>l}\sum[C_k^2(G_{kl}-G_{k^*l}) + C_l^2(G_{kl}-G_{kl^*}]) \\ &-2C_0\sum_k C_k K_{kk^*}, \end{aligned} \quad (7)$$

where E_0 is the HF energy

$$E_0 = 2\sum_k(h_{kk}+G_{kk}) + 4\sum_{k>l}\sum G_{kl}. \quad (8)$$

Here we set

$$G_{ij} = J_{ij} - \frac{1}{2}K_{ij}, \quad (9)$$

where J_{ij} and K_{ij} are the familiar Coulomb and exchange integrals. We use $\sum_k$ to mean summation over the occupied orbitals k and/or the partner orbitals k*. Variation of E with respect to the orbitals, subject to the condition that the occupied and virtual manifolds are kept fixed, gives

$$\langle\phi_k|(1-C_k^2)F_k-(1-C_l^2)F_l|\phi_l\rangle = 0 \quad (10a)$$

$$\langle\phi_{k^*}|C_k^2F_{k^*}-C_l^2F_{l^*}|\phi_{l^*}\rangle = 0 \quad (10b)$$

$$\langle\phi_v|F_{k^*}|\phi_{k^*}\rangle = 0, \quad (10c)$$

where

$$F_k = F_0 + (1-C_k^2)^{-1}[2\sum_{l(\neq k)} C_l^2(G_{l^*}-G_l)+C_0C_kK_{k^*}]$$

$$F_{k^*} = F_0 + 2(G_{k^*}-G_k) + C_0C_k^{-1}K_k. \quad (11)$$

Here the F_0 is the Fock operator

$$F_0 = h + 2\sum_k G_k \quad (12)$$

and

$$G_i = J_i - \frac{1}{2}K_i, \quad (13)$$

where J_i and K_i are the usual Coulomb and exchange operators. The variational conditions (10a), (10b), and (10c) determine the transformations between HF occupied orbitals, between partner orbitals, and between partner and unpaired virtual orbitals, respectively. These conditions can easily be decoupled with the use of projection operators and transformed into a pseudo-eigenvalue problem.[8]

Now let us examine the physical meaning of these variational conditions. For C_0 near unity and the rest close to zero in magnitude, the F_k can be conceptually approximated by Fock operator F_0. Hence the occupied orbitals are, to the first approximation, just the SCF orbitals. From the secular equation in (6), we have

$$E = E_0 - \sum_k(K_{kk^*})^2/(E_k-E) \quad (14)$$

and

$$C_k = -C_0K_{kk^*}/(E_k-E), \quad (15)$$

where E_k are the energies of Φ_k. Now we see C_k are negative. Hence the partner orbital ϕ_{k^*} determined by F_{k^*} is bound not only by the nuclear potential in F_0 but also by the very negative exchange potential, $C_0C_k^{-1}K_k$. As a consequence, the partner orbital ϕ_{k^*} remains strongly localized in the region of space occupied by its HF counterpart orbital ϕ_k. Thus, the partner orbitals have no resemblance to the eigenfunctions of F_0, that is, the SCF virtual orbitals. The general appearance of the partner orbitals can also be understood from the variational theorem. From (14), we see that $\delta E=0$ corresponds to finding "best" orbitals which maximize

$$\sum_k(K_{kk^*})^2/(E_k-E_0)$$

to first order approximation. This maximum property, especially maximization of $\sum_k(K_{kk^*})^2$ suggests that virtual orbitals should be transformed so that the partner orbitals are as close as possible to their HF occupied counterpart orbitals. Note here that the partner orbitals are not the localized orbitals but symmetry orbitals.

Numerical Examples

As an illustration we shall treat the He and Be atoms and HF molecule in the HF-Roothaan approximation. Optimizing Φ is carried out in a cyclic way varying C_0, C_k in accordance with the CI method and orbitals in accordance with the SCF scheme. The most important practical question is, will an SCF procedure based on (10) converge? At present it is well known that the program based on MC-SCF theory has convergence problems, so we expect that our program will have the same problems. In the present study, the orbital optimization was carried out by a two-by-two rotation technique and it presents no convergence difficulties.[9,10] Good first approximation, especially for the partner orbitals, is necessary to overcome the convergence

TABLE 1. WAVEFUNCTION FOR He

Basis function[a)]	HF	CIP	SPEMC SCF	CMC SCF[b)]
1s orbital				
1s(3.3)	0.12059	0.12059	0.14969	0.14505
2s(3.3)	0.01554	0.01554	0.03295	0.03221
4s(3.3)	0.00559	0.00559	0.00770	0.00826
1s(1.433)	0.96446	0.96446	0.87469	0.82599
2s(1.433)	−0.13474	−0.13474	−0.06105	−0.07289
3s(1.433)	0.05943	0.05943	0.03604	0.04408
4s(1.433)	−0.01065	−0.01065	−0.00496	−0.00671
1s*(2s) orbital				
1s(3.3)		−1.2597	−1.2426	−0.87615
2s(3.3)		−0.99455	−0.98522	−0.75327
4s(3.3)		0.15559	0.13957	0.15869
1s(1.433)		2.2981	2.2471	1.0651
2s(1.433)		−0.84574	−0.79441	0.22336
3s(1.433)		0.60263	0.59184	0.19390
4s(1.433)		−0.15903	−0.15425	−0.07708
CI coefficients				
$1s^2$		0.997987	0.997929	0.997799
$1s^2 \rightarrow 1s^{*2}(2s^2)$		−0.063415	−0.064318	−0.065666
$1s^2 \rightarrow 3s^2$				−0.008846
$1s^2 \rightarrow 4s^2$				−0.002370
$1s^2 \rightarrow 5s^2$				−0.000651
$1s^2 \rightarrow 6s^2$				0.000243
$1s^2 \rightarrow 7s^2$				−0.000052

a) Orbital exponents are given in parentheses.
b) Only 1s and 2s orbitals are listed for comparison.

TABLE 2. WAVEFUNCTION FOR Be

Basis function[a)]	HF	CIP	SPEMC SCF	CMC SCF[b)]
1s orbital				
1s(5.6858)	0.20816	0.20920	0.21092	0.21104
1s(2.9479)	0.89086	0.90740	0.90449	0.90573
3s(3.6747)	−0.10624	−0.10230	−0.09872	−0.09800
2s(1.3767)	−0.00655	−0.04422	−0.04890	−0.05248
2s(0.8441)	0.00250	−0.06903	−0.07274	−0.07963
2s orbital				
1s(5.6858)	0.02071	−0.00023	−0.00192	−0.00386
1s(2.9479)	0.21003	0.11984	0.11358	0.10494
3s(3.6747)	0.03412	0.04458	0.04392	0.04494
2s(1.3767)	−0.37676	−0.37421	−0.36843	−0.36824
2s(0.8441)	−0.71473	−0.71139	−0.71527	−0.71431
2s*(3s) orbital				
1s(5.6858)		−0.01099	−0.01076	0.01996
1s(2.9479)		−0.14353	−0.12951	0.09332
3s(3.6747)		−0.78212	−0.81523	0.87586
2s(1.3767)		2.9814	3.0081	3.0515
2s(0.8441)		−2.3402	−2.3501	−2.3687
1s*(4s) orbital				
1s(5.6858)		1.8853	1.8646	1.5771
1s(2.9479)		−1.7880	−1.7526	−1.2947
3s(3.6747)		−0.43786	−0.45474	−0.79337
2s(1.3767)		1.0425	1.0200	1.1372
2s(0.8441)		−0.42954	−0.40784	−0.44322
CI coefficients				
$1s^2 2s^2$		0.99871	0.99879	0.99887
$2s^2 \rightarrow 2s^{*2}(3s^2)$		−0.04592	−0.04405	−0.04120
$1s^2 \rightarrow 1s^{*2}(4s^2)$		−0.02174	−0.02198	−0.02327
$1s^2 \rightarrow 5s^2$				−0.00395
$2s^2 \rightarrow 3s^2$				−0.00124
$1s^2 \rightarrow 4s^2$				−0.00092
$2s^2 \rightarrow 5s^2$				−0.00023

a) Orbital exponents are given in parentheses.
b) The 5s orbital is not listed.

problems. The simple initial guess can be found on the structual analogy to the natural orbitals used in the beyond HF theories. We discussed in Appendix how to get initial orbitals.

We first perform ordinary HF-Roothaan calculation on the ground state of He and Be with STO basis functions and then transformed as above. The results can be seen in Tables 1—3 and Figs. 1—3. For He, the HF orbital ϕ_{1s} is kept fixed during the optimization of its partner orbitals ϕ_{1s^*}. The CIP covers 38.4% correlation energy for He and 14.9% for Be. Especially for He the CIP energy is 99.96% of the radial limit (−2.8790 au) and accounts for 93.5% of the radial correlation energy as defined with respect to the HF energy. The CIP results were compared with a more extensive calculations such as SPEMC-SCF (The variation that mixes occupied and virtual orbitals is considered) and CMC-SCF results. The orbital ambiguity provides 93.6 and 95.0% of the energy improvement of the CMC-SCF calculations over the HF values for He and Be, respectively, indicating the effectiveness of the partner orbital transformation. Comparison with the SPEMC-SCF method indicates that the coupling of the HF occupied and virtual manifolds makes little contribution to the energy improvement. Figures 1—3 illustrate radial dependence of each occupied and its partner orbitals for He and Be. These show the localization of each partner orbital in the region where its occupied counterpart is largest. There is no resemblance at all between any one of the SCF virtual orbitals and these partner orbitals. In view of the nodal property, the 2s* orbital of Be corresponds to the 3s Rydberg orbital and the 1s* to the 4s orbital.

We also applied the method to HF molecule. The basis set used here is Dunning's[11] (9s, 5p/4s) GTO set contracted to (4s, 3p/2s) centered on F and H. Experimental equilibrium geometry, $R=1.7328$ au is used in the present calculation of the ground state of HF. In Table 4 and 5 are presented the transformation matrices which take the SCF occupied and virtual orbitals into zeroth-order natural orbitals and their partner orbitals. The effect of zeroth-order transformation in Table 4 is surprizingly large, suggesting that the correct zeroth-order natural orbitals are not the SCF orbitals. Figure 4 shows controur maps for the zeroth-order natural orbitals and the partner orbitals in case of $R=1.7328$ au. These also illustrate that each partner orbital is localized in the region where the occupied counterpart has a high density.

Table 6 is adiabatic potentials by HF, unrestricted HF (UHF) and CIP methods for HF molecule. The HF method is inadequate for the description of the

Table 3. Calculated energies for He and Be[a)]

	He	Be	in au
HF	−2.861680	−14.57292	
CIP	−2.877866 (38.4)	−14.58702 (14.9)	
SPEMC-SCF	−2.877996 (38.5)	−14.58721 (15.1)	
CMC-SCF	−2.878972 (41.1)	−14.58776 (15.7)	
Experiment[b)]	−2.90378	−14.6674	

a) Recovered correlation energies in percent are given in parentheses. b) E. Clementi, *J. Chem. Phys.*, **38**, 2248 (1963).

Table 4. Unitary matrix for obtaining zeroth-order natural orbitals from HF occupied orbitals; HF molecule $R=1.7328$ au[a)]

i \ j	1σ	2σ	3σ	1π	$1\bar{\pi}$
1σ	0.99646	−0.08401	−0.00400		
2σ	0.07613	0.88078	0.46737		
3σ	−0.03574	−0.46602	0.88405		
1π				1.0	
$1\bar{\pi}$					1.0

a) The index i refers to HF orbitals, the index j to zeroth-order natural orbitals.

dissociation process since it does not give the correct dissociation limit. The usual SCF procedure of the HF method does not converge at large internuclear separations. In this region, the HF solution becomes unstable and another solution, having lower energy than the HF solution, must exist. The study of the instability problems of the HF solution tells us that the real triplet instability precedes other types of instability and the UHF solution appears when the HF solution is real triplet unstable.[6)] Thus, we can define 2n UHF natural orbitals[12)] when the HF solution is unstable. From the definition of the partner orbitals, these 2n UHF natural orbitals are similar to what we call zeroth-order natural orbitals and their partner orbitals. The determinant using the first n UHF natural orbitals is approximated as the HF determinant. Of course, they will not be identical, but this determinant differs only in second order from the HF determinant. So we employed the space spanned by these first n UHF natural orbitals as the occupied manifold when the HF solution is unstable.

Figure 5 shows the contour maps for the most important 3σ and $3\sigma^*$ orbitals at several H–F bond distances. At infinite distances of H–F bond, the wavefunction can be reduced asymptotically to the form

$$\begin{aligned}\Phi &= (1/\sqrt{2})\|\cdots(3\sigma\overline{3\sigma}-3\sigma^*\overline{3\sigma^*})\cdots\| \\ &= \|\cdots(3\sigma+3\sigma^*)/\sqrt{2}\cdot(3\sigma-3\sigma^*)/\sqrt{2}\cdot(\alpha\beta-\beta\alpha)/\sqrt{2}\cdots\| \end{aligned} \quad (16)$$

Figure 5 illustrates $(3\sigma\pm3\sigma^*)/\sqrt{2}$ orbitals at large nuclear separations converge to 1s orbital of H and 2p orbital of F, respectively. Thus, the dissociation process of the H–F bond was reproduced by the present method as most chemists had assumed.

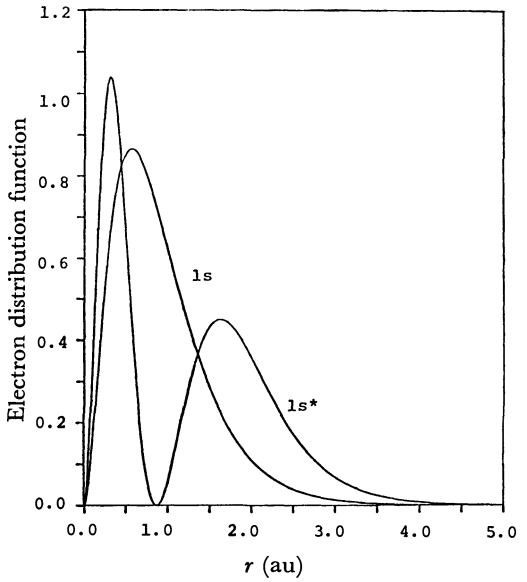

Fig. 1. Radial dependence of the ls and ls* orbitals of He.

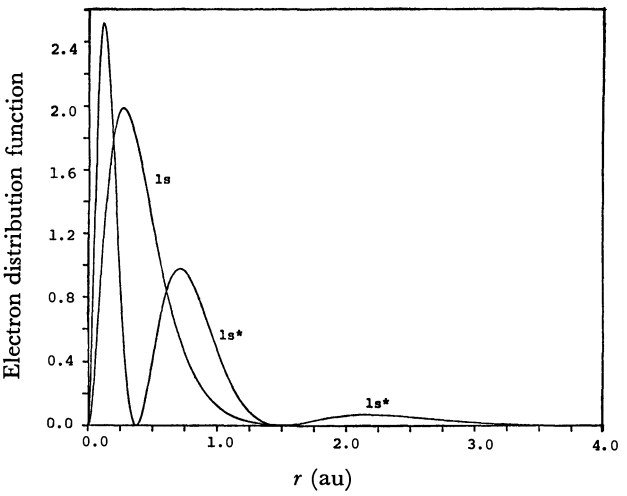

Fig. 2. Radial dependence of the ls and ls* orbitals of Be.

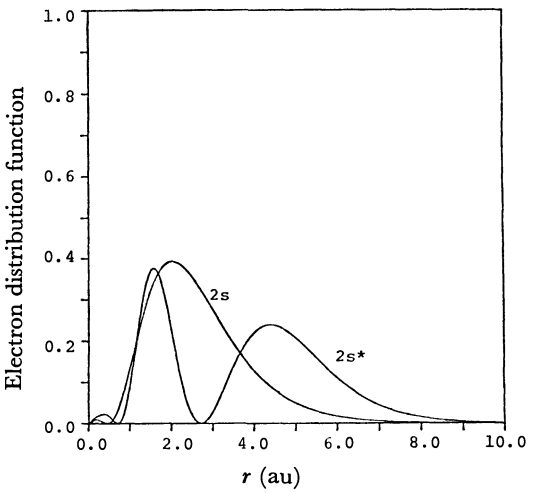

Fig. 3. Radial dependence of the 2s and 2s* orbitals of Be.

TABLE 5. UNITARY MATRIX FOR OBTAINING PARTNER ORBITALS FROM HF VIRTUAL ORBITALS; HF MOLECULE $R=1.7328$ au[a)]

i	j				
	$1\sigma^*$	$2\sigma^*$	$3\sigma^*$	$1\pi^*$	$1\bar{\pi}^*$
4σ	0.05607	−0.23052	−0.58540		
5σ	0.01585	0.08438	−0.75117		
6σ	0.06465	−0.65456	0.22430		
7σ	0.14818	0.66139	0.16474		
8σ	−0.05127	0.27000	−0.12487		
9σ	−0.98379	0.03075	0.00059		
2π				0.92666	
3π				−0.37589	
$2\bar{\pi}$					0.92666
$3\bar{\pi}$					−0.37589

a) The index i referers to HF virtual orbitals, the index j to partner orbitals.

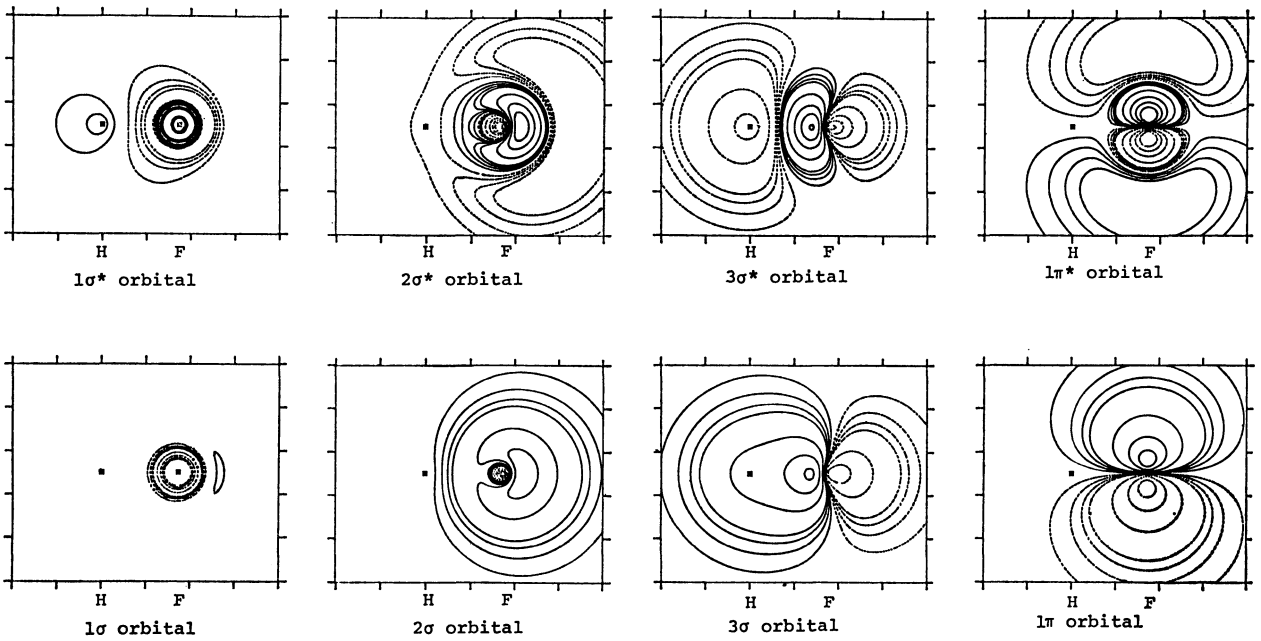

Fig. 4. Contour maps for zeroth-order natural orbitals and their partner orbitals of HF molecule; $R=1.7328$ au.

TABLE 6. ENERGIES OF HF MOLECULE AT SEVERAL BOND DISTANCES

	H–F bond distances in au				
	1.7328	2.0	3.0	5.0	10.0
Energy in au					
HF	−100.01795	−100.00460	−99.87084	−99.64488	−99.55020
UHF	—	—	−99.90784	−99.89457	−99.89434
CIP	−100.07912	−100.07219	−99.97815	−99.91576	−99.91063
CI coefficients					
$1\sigma^2 2\sigma^2 3\sigma^2 1\pi^2 1\bar{\pi}^2$	0.99116	0.98756	0.94385	0.78358	0.72401
$1\sigma^2 \rightarrow 1\sigma^{*2}$	−0.00827	−0.00840	−0.00841	−0.00723	−0.00667
$2\sigma^2 \rightarrow 2\sigma^{*2}$	−0.02548	−0.02064	−0.01021	−0.00473	−0.00432
$3\sigma^2 \rightarrow 3\sigma^{*2}$	−0.10137	−0.13264	−0.32173	−0.61862	−0.68786
$1\pi^2 \rightarrow 1\pi^{*2}$	−0.05750	−0.05757	−0.05221	−0.04020	−0.03605
$1\bar{\pi}^2 \rightarrow 1\bar{\pi}^{*2}$	−0.05750	−0.05757	−0.05221	−0.04020	−0.03605

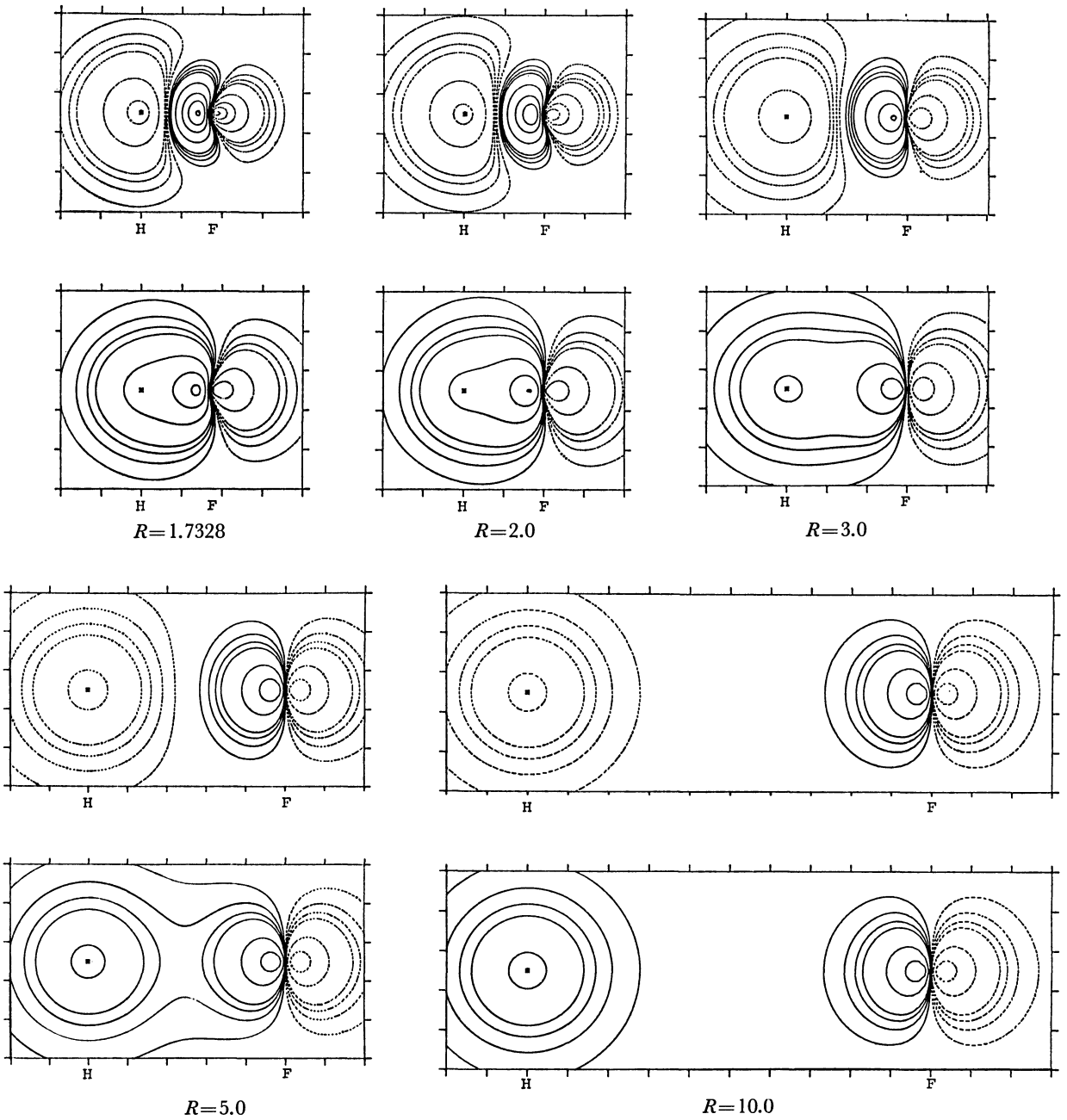

Fig. 5. Contour maps for the 3σ and $3\sigma^*$ orbitals of HF at several distances of H–F bond.

Summary

By taking advantage of the orbital ambiguity of the HF theory, we define the zeroth-order natural orbitals and their partner orbitals. The set of HF natural orbitals which is easy to construct, is fairly good enough to give the desired accuracy and facilitates physical interpretation of the results.

The CI with partner orbitals accounts for only intrapair correlation effect of the electron correlation. A theory can be developed which involves interpair correlation effect as well as intrapair correlation, if we choose an approximate CI expansion in (3) instead of the SPE expansion. In such a theory, however, the simplicity and ease of interpretation found in the present theory may be no longer preserved.

The author would like to express his sincere gratitude to Professor A. Imamura, Professor H. Kato and Dr. H. Nakatsuji for many valuable discussions. He is also indebted to Dr. S. Yamabe for his extensive assistance in computational work. Part of this work has been supported by the Scientific Research Grants from the Ministry of Education.

Appendix (How to Get the Initial Orbitals)

The initial orthonormal orbitals are generated by the corresponding orbital transformation procedure.

Let $\hat{a}_k$ and $\hat{b}_k$ be an approximated solution and its cor-

rection to the HF solution, respectively. Then the HF natural orbitals $\hat{c}_k$ and partner orbitals $\hat{c}_k^*$ are expressed in the form[6]

$$\hat{c}_k = (\hat{a}_k + \xi_k \hat{b}_k)/(1+\xi_k^2)^{1/2}$$
$$\hat{c}_{k^*} = (\hat{b}_k - \xi_k \hat{a}_k)/(1+\xi_k^2)^{1/2}$$

where the $\hat{a}_k$ and $\hat{b}_k$ are orthonormal and ξ_k are real coefficients.

Assume that the HF solution c_k is known and we have its approximate solution a_k. Given any two sets of orbitals c_k and a_k, there exist equivalent sets $\hat{c}_k$ and $\hat{a}_k$ such that their overlap matrix is diagonal $\langle \hat{c}_{k1} | \hat{a}_1 \rangle = \delta_{k1} T_k$ through the so-called corresponding orbital transformation. Then, we can construct $\hat{c}_k^*$ using the above relations. The problem is the choice of the approximate HF solution sicne the resultant resultant $\hat{c}_k$ and $\hat{c}_k^*$ depend on the approximate solution employed. In the practical application, we used the approximate solution generated by diagonalizing the core matrix. The method is simple and relatively accurate.

When the HF solution is unstable, the UHF natural orbitals are, of course, good initial orbitals to the partner orbitals.

References

1) T. L. Gilbert, *Phys. Rev. A*, **6**, 580 (1972); K. Hirao, *J. Chem. Phys.*, **60**, 3215 (1974).

2) H. J. Silverstone and M. L. Yin, *J. Chem. Phys.*, **49**, 2126 (1968); S. Huzinaga and C. Arnau, *Phys. Rev. A*, **1**, 1285 (1970); *J. Chem. Phys.* **54**, 1948 (1971); W. J. Hunt and W. A. Goddard, *Chem. Phys. Lett.*, **3**, 414 (1969); K. Morokuma and S. Iwata, *ibid.*, **16**, 192 (1972); K. Hirao, *J. Chem Phys.*, **61**, 3247 (1974); R. McWeeny, *Chem. Phys. Lett.*, **35**, 13 (1975).

3) P. O. Löwdin, *Phys. Rev.*, **97**, 1474 (1955).

4) E. R. Davidson, *Rev. Mod. Phys.*, **44**, 451 (1972).

5) The correct zeroth-order natural ortural orbitals are not the HF orbitals even if we do perturbation starting with the HF wavefunction as the zeroth-order approximation.

6) K. Hirao and H. Nakatsuji, *J. Chem. Phys.*, **68**, 4516, 4548 (1978).

7) E. Clementi and A. Veillard, *Theor. Chim. Acta*, **7**, 133 (1967); D. B. Cook, *Mol. Phys.*, **30**, 733 (1975).

8) K. Hirao and H. Nakatsuji, *J. Chem. Phys.*, **59**, 1457 (1973).

9) J. Hinze, *J. Chem. Phys.*, **59**, 6424 (1973).

10) The MC-SCF program originally written by Dr. K. Ishida is modified by the author for the present purpose.

11) T. H. Dunning, Jr., *J. Chem. Phys.*, **53**, 2823 (1970).

12) A. T. Amos and G. G. Hall, *Proc. R. Soc. London, Ser. A*, **263**, 483 (1961).

Thickness Measurement of Surface Layer by the Angular Dependent X-Ray Photoelectron Spectroscopy

Masamichi YAMADA and Haruo KURODA*

Department of Chemistry, Faculty of Science, The University of Tokyo, Hongo, Tokyo 113

(Received December 19, 1979)

A sample-holding device to study the photoelectron take-off angle dependence of XPS spectrum is described. The take-off angle dependence was studied on a silicon surface covered with an oxide layer and a contamination carbon layer, and the (thickness)/(electron attenuation length) ratio of each layer was determined from the analysis of the angular dependence of the Si2p, O1s, and C1s peak intensities.

An ordinary solid surface is often covered with an oxide layer, adsorbed materials, and so on. It is well known that the contribution from the surface layer to the XPS spectrum is enhanced while that from the substrate is depressed as the photoelectron take-off angle θ measured from the specimen surface is decreased, provided that the specimen has an atomically flat surface.[1,2] This method is useful to distinguish the photoelectron peaks due to the surface layer from those due to the substrate. Furthermore, the thickness of the surface layer t or the electron attenuation length Λ can be determined from the quantitative analysis of the angular dependent peak intensities.[1,2]

For such an analysis, it is necessary to measure signal intensities at various different photoelectron take-off angles ranging from nearly zero degree to about ninety degrees. As described later, it is predicted that the angular variation of the absolute peak intensity is determined by the (thickness)/(electron attenuation length) ratio t/Λ under the idealized experimental conditions.[1] However, this prediction has been experimentally verified only in few cases.[1,3] In most of angular dependent XPS studies performed so far, the angular variation of peak intensity was largely modified by instrumental factors such as an inhomogeneous X-ray flux,[4] a finite sample size and the misalignment of a sample, and consequently the observed total signal intensity decreased markedly at low take-off angles.[4,5] In such a case, instead of the absolute intensities, the angular dependence of the intensity ratios between photoelectron peaks of the same specimen had to be used in the analysis in order to cancell out the effect of the angular dependent instrumental factors.[2]

In this report, we describe a rather simple sample rotation device which is incorporated into a McPherson ESCA 36 photoelectron spectrometer. The utility of the device is verified by the results obtained on a silicon surface covered with oxide and contamination carbon layers. Further, the results show that, in a measurement carried out with the device, the angular variation of signal intensities can be analyzed to determine t/Λ values without any correction and without resort to intensity ratios.

Variable-angle Sample Holder

The electron energy analyzer of a McPherson ESCA 36 spectrometer is composed of two concentric spherical sectors of 360 mm mean radius, without any retarding lens system. The X-ray source and sample-treatment devices are incorporated into the sample chamber.

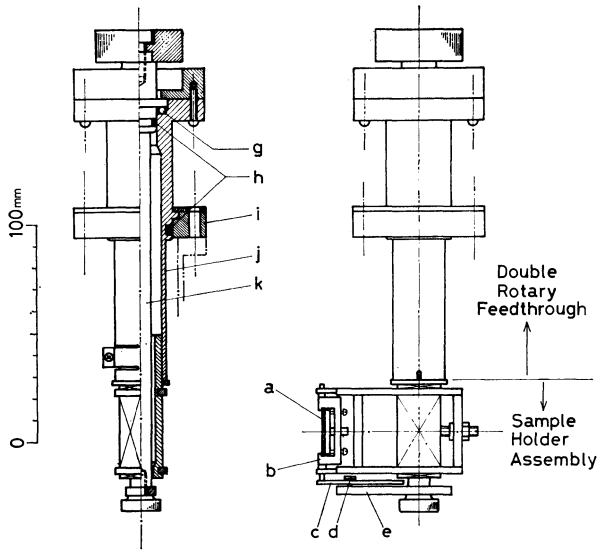

Fig. 1. Variable-angle sample-holding device. (a): Sample, (b): sample holder, (c): "tail" of sample holder, (d): pin, (e): arm, (g): stainless steel balls, (h): O-rings, (i): flange, (j): outer tube, (k): central shaft. (In the left drawing, the sample holder is omitted for brevity.)

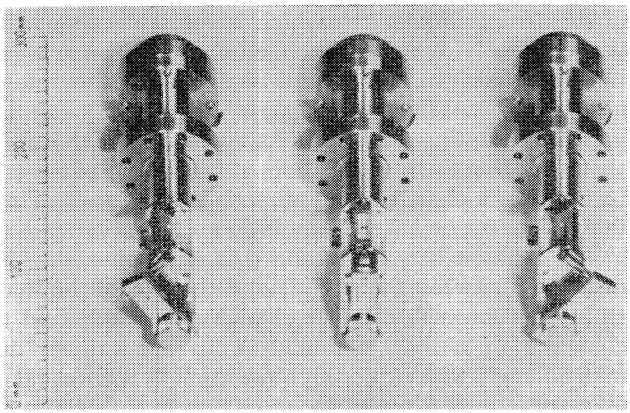

Fig. 2. Photographs showing the sample-holding device at three different sample orientations. From left to right, the photoelectron take-off angle θ is set to be *ca.* 10°, 45°, and *ca.* 80°, respectively.

Figure 1 illustrates full details of the variable-angle sample holding device. Its photographs are shown in Fig. 2. The device consists of two parts; a sample holder assembly and an O-ring-sealed double rotary

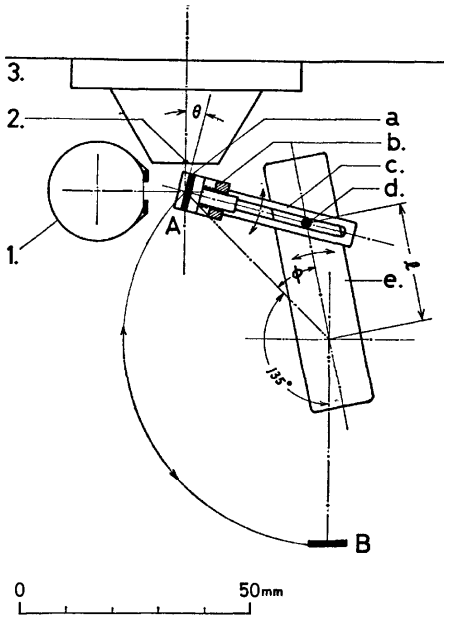

Fig. 3. Working principle of the variable-angle sample holder.
A: XPS measurement position, B: sample-treatment position, 1: X-ray source, 2: entrance slit, 3: analyzer chamber wall,
(a): sample, (b): sample holder, (c): "tail" of sample holder, (d): pin, (e): arm. (Each corresponding part is designated by the same letter as in Fig. 1.)

feedthrough which is composed of an outer tube (j) and a central shaft (k). The sample holder assembly is clamped to the outer tube (j), and can be rotated within the sample chamber by rotating the outer tube (j) from the outside. By this motion, the sample can be transferred between the measuring position (A) and the position (B) for sample deposition, argon-ion etching, and other sample treatments (see Fig. 3). In the sample holder assembly, a tail (c) is attached to the bottom of the sample holder (b) which is rotatable about the vertical axis lying in the specimen surface. The arm (e) is firmly fixed to the central shaft (k) of the rotary feedthrough so that the angle ϕ (in Fig. 3) can be varied by rotating the latter. As the angle ϕ is changed, the pin (d) on the arm (e) slides along the slit of the tail (c) causing a change of the direction of the tail. Thus the photoelectron take-off angle θ can be varied.

The relation between θ and ϕ is determined by the distance l between the pin (d) and the axis of the shaft (k). At a lower θ, a larger change of ϕ is required to change θ by a fixed amount. Thus one can set the take-off angle with rather high precision at a lower take-off angle. This is one of the great merits of this sample rotation mechanism. The pin (d) can be placed at one of the three positions on the arm (e) depending on the range of θ to be studied. Because of the narrow width (0.25 mm) of the entrance slit of the analyzer, the mispositioning of a specimen results in the large decrease of signal intensity at low θ. In the case of this device, monitoring the counting rate, we can set the specimen in the optimum position by adjusting the rotation of the outer tube (j), and thus prevent the deformation of the angular dependence. This is another merit of this device.

Angular Deapendent XPS Spectrum of a Silicon Wafer

We examined the angular dependence of the XPS spectrum of a silicon wafer with a polished (100) face. The wafer had been kept for a long time in the ordinary atmosphere without any oxidation treatment. The sample of the size 8 mm×21 mm was cut out from the wafer, and ultrasonically washed in organic solvents, distilled water, and finally trichloroethylene. After air-dried, the sample was transferred into the sample chamber of the McPherson ESCA 36 spectrometer. The XPS measurements were performed with Mg $K\alpha$ (1253.6 eV) radiation (7.4—7.5 kV, 25—27 mA) under the vacuum better than 10^{-4}Pa produced by a turbo-molecular pump. The take-off angle was varied successively from the highest (78°) to the lowest (3°) and finally again set at 78°. As compared with the initial measurement at 78°, the intensity obtained by the final measurement at the same angle was found to be slightly higher for all photoelectron peaks, which was probably due to the slight increase of the X-ray flux.

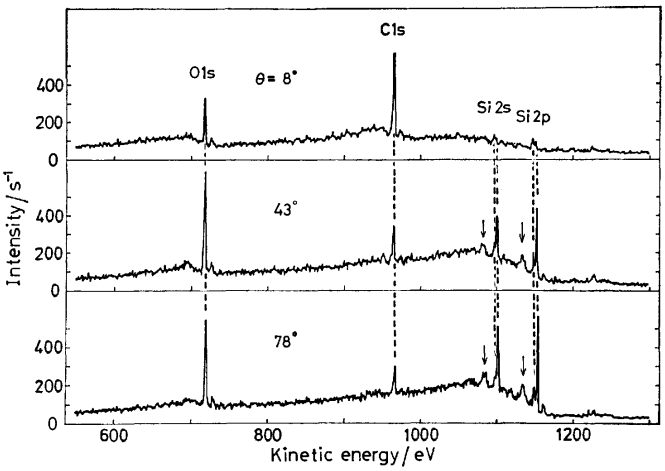

Fig. 4. Wide-scan spectra of a silicon wafer. The spectra were measured at the take-off angles, 78°, 43°, and 8°. Both Si2p and Si2s peaks are accompanied by loss peaks due to plasmon excitation (indicated by arrows).

Figure 4 shows the wide-scan spectra obtained at three different take-off angles, 8°, 43°, and 78°. The spectrum at θ=78° shows strong peaks attributable to Si2p, Si2s, and O1s, and a weak peak attributable to C1s. Both the Si2p and Si2s peaks are accompanied by energy-loss peaks. On decreasing θ, the intensities of the Si2p and Si2s peaks decrease, but that of the C1s peak increases. As can be seen in Fig. 4, the angular variation of the O1s peak intensity is different from the others. The narrow-scan spectra of the Si2p region are shown in Fig. 5, in which the higher kinetic energy peaks are due to elemental silicon and the lower kinetic energy ones are due to oxidized silicon.[6] Note that the angular dependence is different between these two components.

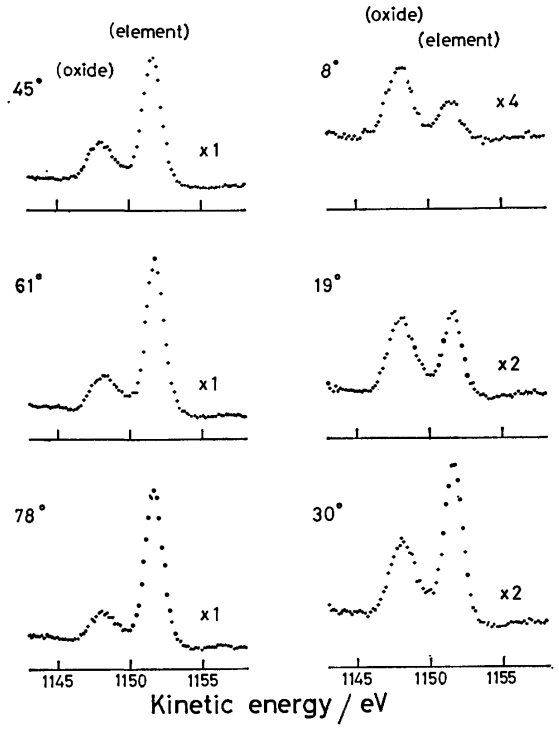

Fig. 5. Variation of the Si2p spectrum as the take-off angle changes from 78° to 8°. The higher kinetic energy peaks are due to elemental silicon and the lower kinetic energy ones are due to oxidized silicon.

Net intensities (peak height above background) of the Si2p(element), Si2p(oxide), Ols, and Cls peaks are plotted in Fig. 6 as a function of θ. We can clearly see that the θ dependences of the Si2p(oxide) and Ols peak intensities are very similar to each other, indicating that the observed Ols peak is entirely due to the silicon oxide. Thus we take the model that the silicon surface is covered with an oxide layer of the uniform thickness t_2

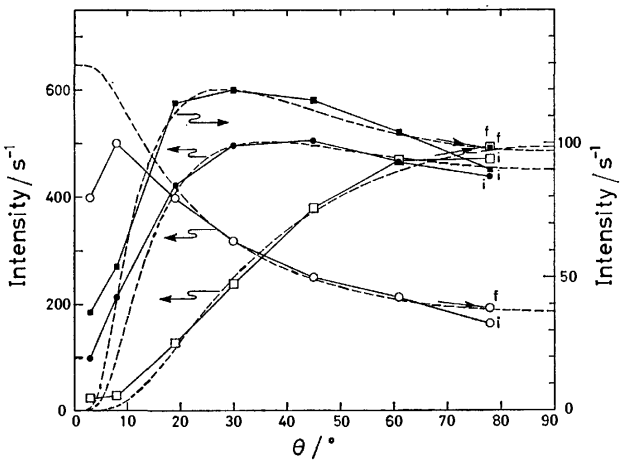

Fig. 6. Angular dependence of Cls (○), Ols (●), Si2p (oxide) (■), and Si2p (element) (□) peak intensilties (by net peak height).
At $\theta=78°$, the points designated by "i" and "f" represent the intensities obtained by the initial and final measurements, respectively. Broken lines represent the angular variations calculated for the model illustrated in Fig. 7 by using the t/Λ values in Table 1.

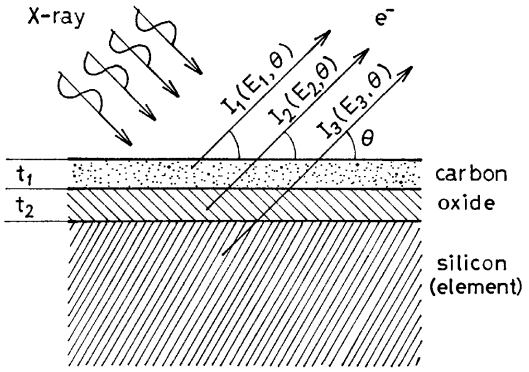

Fig. 7. Model for the surface region of the silicon wafer. $I_1(E_1, \theta)$, $I_2(E_2, \theta)$, and I_3 (E_3, θ) are the contributions from the top-most contamination carbon layer, from the silicon oxide layer, and from the elemental silicon substrate, respectively.

and a contamination carbon layer of the thickness t_1, as illustrated in Fig. 7.[7] We will assume also that no oxygen-containing species is included in the contamination carbon layer. As discussed by Fadley *et al.*,[1] on the assumptions that (a) the specimen surface is atomically flat, (b) the X-ray flux is uniformly distributed over the whole sample area, and (c) the specimen volume included in the acceptance area of the analyzer contributes uniformly to the spectrum and the portion outside the acceptance area does not contribute, the following expressions are derived for the intensity $I(E,\theta)$ of the peak (at the kinetic energy E) measured at the take-off angle θ:

$$I_1(E_1, \theta) = I_1^0[1-\exp\{-t_1/\Lambda_1(E_1)\sin\theta\}] \quad (1)$$

for the Cls peak (E_1=966 eV) due to the top-most layer,

$$I_2(E_2, \theta) = I_2^0[1-\exp\{-t_2/\Lambda_2(E_2)\sin\theta\}] \times\exp\{-t_1/\Lambda_1(E_2)\sin\theta\} \quad (2)$$

for the Si2p(oxide) (E_2=1150 eV) and Ols (E_2=718 eV) peaks due to the oxide layer, and

$$I_3(E_3, \theta) = I_3^0\exp\{-t_2/\Lambda_2(E_3)\sin\theta\} \times\exp\{-t_1/\Lambda_1(E_3)\sin\theta\} \quad (3)$$

for the Si2p(element) peak (E_3=1150 eV) due to the bulk. $\Lambda_1(E)$ and $\Lambda_2(E)$ are the electron attenuation lengths of the photoelectrons with kinetic energy E in the carbon and oxide layers respectively, and I_1^0, I_2^0, and I_3^0 are constants independent of θ. Equation 3 can be rewritten as follows:

$$I_3(E_3, \theta) = I_3^0\exp\left[-\left\{\frac{t_1}{\Lambda_1(E_3)}+\frac{t_2}{\Lambda_2(E_3)}\right\}\frac{1}{\sin\theta}\right]. \quad (3')$$

Thus $I_3(E_3,\theta)$ is expected to be exponentially dependent on $1/\sin\theta$. The observed angular dependence of the Si2p(element) peak intensity was found to be well described by Eq. 3' by using the following value:

$$\frac{t_1}{\Lambda_1(E_3)}+\frac{t_2}{\Lambda_2(E_3)} = 0.68 \quad (E_3=1150\,\text{eV}).$$

In the photoelectron kinetic energy range concerned here, $\Lambda(E)$ can be considered to be nearly proportional to $E^{1/2}$.[8] If we adopt the relation that $\Lambda(E)=\Lambda(E_3)\cdot(E/E_3)^{1/2}$, we can treat either $t_1/\Lambda_1(E_3)$ or $t_2/\Lambda_2(E_3)$ as the only one adjustable parameter, and determine its

TABLE 1. t/Λ VALUES DERIVED FROM THE ANALYSIS OF THE EXPERIMENTAL ANGULAR DEPENDENCE

	E/eV[a]	$t_1/\Lambda_1(E)$[b]	$t_2/\Lambda_2(E)$[c]
C1s	966	0.34	——
O1s	718	0.39	0.47
Si2p	1150	0.31	0.37

a) Approximate kinetic energy. b) The (thickness)/(electron attenuation length) ratio for the top-most contamination carbon layer. The relation $\Lambda_1(E) \propto E^{1/2}$ is assumed. c) The (thickness)/(electron attenuation length) ratio for the oxide layer. The relation $\Lambda_2(E) \propto E^{1/2}$ is assumed.

value so that the observed take-off angle dependences of other photoelectron peak intensities can be well reproduced by using Eq. 1 or Eq. 2. The t/Λ values thus obtained are listed in Table 1, and the angular dependence which is calculated for each peak by using these t/Λ values is shown in Fig. 6 with a broken line. The agreement between the observed and calculated angular dependences is very satisfactory for all peaks, except at angles below 10°. The above discrepancy at low angles may be attributed to the effect of small roughness of the surface.[9]

As described above, the angular-dependent XPS spectrum of a silicon wafer surface obtained with our variable-angle sample holder can be very satisfactorily explained by using Eqs. 1—3 on the model shown in Fig. 7. The Λ value at $E=1382$ eV (Si2p photoelectrons excited by Al $K\alpha$) in SiO_2 was reported to be 3.7 ± 0.4 nm.[7] If we take this value, the thickness of the oxide layer of the present sample is estimated to be about 1.2 nm from the value $t_2/\Lambda_2(1150\text{ eV})=0.37$.[10] Since we have not given any special oxidation treatment, this value may be considered as the typical thickness of the oxide layer that exists on the polished surface of a silicon wafer after prolonged exposure to the air, and it is in good agreement with the value <1.4 nm reported by Raider *et al.*[11] from fixed-angle XPS experiments. We do not know the materials contained in the contamination carbon layer, but most of them are likely to be hydrocarbons since the assumption that photoelectrons from the top-most layer does not contribute to the O1s peak intensity is supported by the above analysis of the angular dependent data. The electron attenuation length in a hydrocarbon layer was derived to be about 3.6 nm at $E=1117$ eV.[12] Thus from the value t_1/Λ_1 (1150 eV) $=0.31$, the thickness of the contamination carbon layer is estimated to be about 1.1 nm.

The authors wish to express their thanks to Dr. Katsuro Sugawara of Hitachi Ltd. for kindly supplying the silicon wafer used in the present study. We also would like to thank Dr. Isao Ikemoto, the University of Tokyo, for his helpful discussions.

References

1) C. S. Fadley, R. J. Baird, W. Siekhaus, T. Novakov, and S. Å. L. Bergström, *J. Electron Spectrosc. Relat. Phenom.*, **4**, 93 (1974).

2) C. S. Fadley, *Prog. Solid State Chem.*, **11**, 265 (1976), and references therein.

3) W. A. Fraser, J. V. Florio, W. N. Delgass, and W. D. Robertson, *Surf. Sci.*, **36**, 661 (1973).

4) R. J. Baird and C. S. Fadley, *J. Electron Spectrosc. Relat. Phenom.*, **11**, 39 (1977).

5) For example, R. O. Ansell, T. Dickinson, A. F. Povey, and P. M. A. Sherwood, *J. Electron Spectrosc. Relat. Phenom.*, **11**, 301 (1977).

6) It is claimed that thin oxide films (<2.0 nm) on silicon substrates are not stoichiometric SiO_2 but of nonstoichiometric nature containing silicon atoms in lower oxidation states. (See for example: S. I. Raider and R. Flitsch, *IBM J. Res. Develop.*, **22**, 294 (1978); D. E. Aspnes and J. B. Theeten, *Phys. Rev. Lett.*, **43**, 1046 (1979).) Also in this study, a Si2p-(oxide) peak is broader than a Si2p(element) peak, and exhibits tailing towards higher kinetic energies (Fig. 5, $\theta=19°$).

7) An angular-dependent XPS study on oxidized silicon wafers has been performed by Hill *et al.* with a modified Hewlett-Packard 5950A spectrometer. (J. M. Hill, D. G. Royce, C. S. Fadley, L. F. Wagner, and F. J. Grunthaner, *Chem. Phys. Lett.*, **44**, 225 (1976).) Based on the same model as shown in Fig. 7, they analyzed the angular variation of the Si2p(oxide)/Si2p(element) intensity ratio.

8) C. J. Powell, *Surf. Sci.*, **44**, 29 (1974).

9) The observed C1s signal intensity at $\theta=3°$ does not lie on the smoothly extrapolated line . At $\theta=3°$, the specimen stands nearly perpendicularly in front of the entrance slit. Therefore, when viewed from the entrance slit, the area occupied by the specimen surface becomes smaller than the acceptance area of the analyzer. This is likely to be the reason for the deviation from the curve at $\theta=3°$ (see Ref. 1).

10) It is necessary to take into account the difference between the kinetic energies of photoelectrons excited by Mg $K\alpha$ and Al $K\alpha$. The Λ value at $E=1150$ eV in SiO_2 is estimated to be 3.4 nm from the $E^{1/2}$ dependence.

11) S. I. Raider, R. Flitsch, and M. J. Palmer, *J. Electrochem. Soc.*, **122**, 413 (1975).

12) C. R. Brundle, H. Hopster, and J. D. Swalen, *J. Chem. Phys.*, **70**, 5190 (1979).

 © 1980 The Chemical Society of Japan Bull. Chem. Soc. Jpn., 53, 2163—2166 (1980)

MO Calculation of Some Aromatic Radicals. Geometry and Spin Density of Benzyl Radical

Toshihiro AMANO, Yoshihiro OSAMURA, Eiko KAI, and Kichisuke NISHIMOTO*

Department of Chemistry, Faculty of Science, Osaka City University, Sumiyoshi-ku, Osaka 558

(Received January 5, 1980)

The geometry of benzyl radical, nitrobenzene anion-, benzaldehyde anion-, aniline cation-, and phenol cation-radicals is optimized by means of the energy gradient method in the framework of the CNDO/2 method, and used for the calculation of spin densities by the INDO-UHF method. The geometrical change from a neutral molecule to the ion radical can be understood by considering the shape of particular MO's. It was found that the molecular structure of benzyl radical is not a regular hexagon, the contraction of C_1–C_7 bond being remarkable. The correct order of the spin densities on ortho(ρ_2)- and para (ρ_4)-positions is obtained by the full geometry optimization. The structure of the deformed ring of benzyl radical is discussed in terms of the orbital mixing rule.

It is difficult to determine the molecular structures of radicals experimentally in most cases, because of their low stability and high reactivity. Thus, it is significant to predict the structure of unstable radicals by means of a quantum chemical method. The spin densities are determined accurately. The spin density distribution in a π radical depends considerably on its geometry.[1] Theoretical studies have been made on the spin density of benzyl radical.[2-7] However, the calculated results have not been correlated with the experimental data[8,9] (ρ_4 being greater than ρ_2) except for a few cases.[10,11] Beveridge and Guth[1] reported that the geometrical change of benzyl radical affects its spin density. Physico-chemical properties of molecules should be calculated on the basis of the most stable structure. Theoretical consideration of the geometrical distortion of benzyl radical from the regular hexagonal geometry would be applicable to the examination of that of other radical species.

In the cases of ion radicals, the structural change by electron removal from or electron attachment to neutral molecule can be explained readily in terms of the shape of the highest occupied or the lowest unoccupied MO's. However, it is difficult to expect a stable molecular structure for a neutral radical. This report describes the semi-empirical MO calculation for benzyl radical, nitrobenzene anion-, benzaldehyde anion-, aniline cation-, and phenol cation-radicals. The geometry is optimized by the energy gradient method in the framework of CNDO scheme.[12-16] Spin desities are calculated by means of the INDO-UHF method.[17]

Results and Discussion

Geometries and Spin Densities. The optimized geometry of benzyl radical is given in Table 1. The numbering of atoms is as follows.

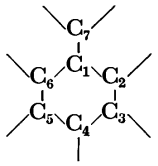

The geometry of benzyl ring differs a great deal from that of benzene. The calculated and experimental spin densities of benzyl radical are given in Table 2. The experimental spin density of ortho-carbon, ρ_2, is less than that of para-carbon, ρ_4. However, the calculation by means of regular hexagonal geometry shows that ρ_2 is greater than ρ_4. This problem is solved by calculation with use of optimized geometry. The calculated spin density by means of fully optimized geometry is in good accordance with the experimental data. Calculation with the optimized geometry shows that the spin density of C_7 flows somewhat into the ortho-, and para-carbons in comparison with the calculated value by means of the regular hexagonal geometry.

Table 1. Optimized geometry of benzyl radical

Bond length/Å		Bond angle/°	
C_1–C_2, C_1–C_6	1.424	$\angle C_2C_1C_6$	115.8
C_2–C_3, C_5–C_6	1.371	$\angle C_1C_2C_3$, $\angle C_1C_6C_5$	122.1
C_3–C_4, C_4–C_5	1.392	$\angle C_2C_3C_4$, $\angle C_4C_5C_6$	120.0
C_1–C_7	1.365	$\angle C_3C_4C_5$	120.0
C_2–H, C_6–H	1.118	$\angle C_1C_2H$, $\angle C_1C_6H$	118.0
C_3–H, C_5–H	1.117	$\angle C_2C_3H$, $\angle C_6H_5H$	120.0
C_4–H	1.117	$\angle C_3C_4H$	120.0
C_7–H	1.112	$\angle C_1C_7H$	124.0
		$\angle HC_7H$	112.0

Since the geometry of ion radicals is not well established experimentally, it is of interest to determine the geometrical changes from their neutral molecules and

Table 2. Spin densities of benzyl radical

	C_1	C_2	C_3	C_4	C_7
With standard geometry[a]	−0.171	0.247	−0.148	0.230	0.740
With optimized geometry	−0.188	0.275	−0.156	0.283	0.667
Expt[b]		0.189	−0.059	0.230	0.607

a) Calculated by assuming a regular geometry: l_{C-C}=1.40 Å, l_{C-H}=1.08 Å. b) Ref. 9.

TABLE 3. SPIN DENSITIES OF THE ANION RADICALS OF NITROBENZENE AND BENZALDEHYDE

Anion radical of nitrobenzene	C_1	C_2	C_3	C_4	N	O
With standard geometry[a)]	−0.034	0.175	−0.101	0.226	0.219	0.187
With optimized geometry	−0.018	0.151	−0.088	0.197	0.287	0.204
Expt		0.122[b)]	−0.041[b)]	0.148[b)]	0.359[c)]	0.326[c)]
Anion radical of benzaldehyde	C_1	C_2 C_6	C_3 C_5	C_4	C_7	O
With standard geometry[a)]	0.088	0.168	−0.092	0.257	0.016	0.441
		0.167	−0.093			
With optimized geometry	0.068	0.158	−0.086	0.255	0.042	0.497
		0.168	−0.091			

a) The spin densities of two anion radicals are calculated with use of the standard bond lengths and bond angles obtained by Pople *et al.* b) Ref. 18. c) Ref. 19.

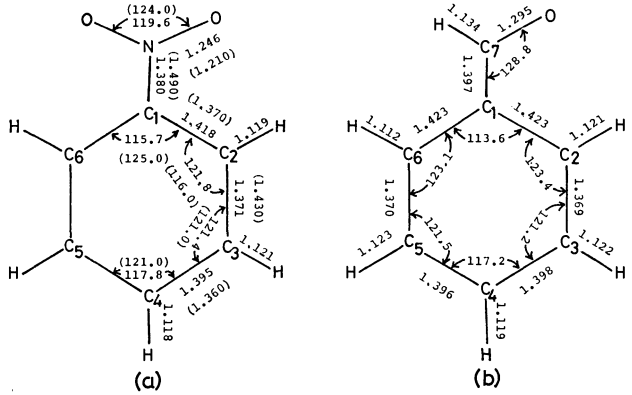

Fig. 1. The optimized geometries of the anion radicals of (a) nitrobenzene and (b) benzaldehyde. The bond lengths and bond angles are in the unit of Å and degree. The experimental values of neutral molecule, nitrobenzene, are also shown in parentheses.[21)]

their spin densities theoretically. Figure 1 and Table 3 show the geometry and spin densities of anion radicals of nitrobenzene, and benzaldehyde. The experimental value[18,19)] of spin densities of nitrobenzene anion radical is also given in Table 3. By a comparison of these values we see that the spin density calculated by means of optimized geometry is better than that by means of neutral geometry. Since the stabilization owing to the conjugation is maximum in a neutral molecule, the radical center of anion radical tends to localize on the substituent in order to minimize the destabilization due to an extra electron. The calculated results of cation radicals of aniline and phenol are summarized in Fig. 2 and Table 4. In the cation radical its geometrical distortion from that of neutral molecule is small. The spin densities of these cation radicals increase at the ortho- and para-positions.

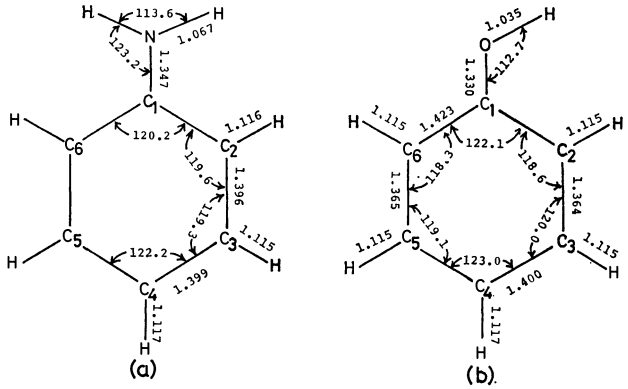

Fig. 2. The optimized geometries of the cation radicals of (a) aniline and (b) phenol. The bond lengths and bond angles are in the unit of Å and dergee.

TABLE 4. SPIN DENSITIES OF THE CATION RADICALS OF ANILINE AND PHENOL

Cation radical of aniline	C_1	C_2	C_3	C_4	N
With standard geometry[a)]	−0.032	0.185	−0.104	0.229	0.642
With optimized geometry	−0.021	0.195	−0.105	0.279	0.562
Cation radical of phenol	C_1	C_2 C_6	C_3 C_5	C_4	O
With standard geometry[b)]	0.048	0.162	−0.083	0.257	0.537
		0.172	−0.092		
With optimized geometry	0.082	0.159	−0.076	0.307	0.440
		0.169	−0.087		
Expt[c)]		0.196	−0.030	0.396	
		0.196	−0.030		

a), b) The spin densities of two cation radicals are calculated with use of the standard bond lengths and bond angles obtained by Pople *et al.* c) Ref. 21.

Consideration of Geometrical Change. Since the highest occupied and the lowest unoccupied MO's are responsible for the electron donation and the electron acceptance of the neutral molecule, respectively, the geometrical change in the ion radical may be predicted by consideration of the shape of these particular orbitals. Figure 3 shows the orbitals of neutral molecules. For example, LUMO of nitrobenzene has the bonding character at C_1–N, O–O, and C_2–C_3. The distances between these atoms decrease on accepting an electron. On the other hand, the distances associated with C_1–C_2 C_3–C_4 bonds increase.

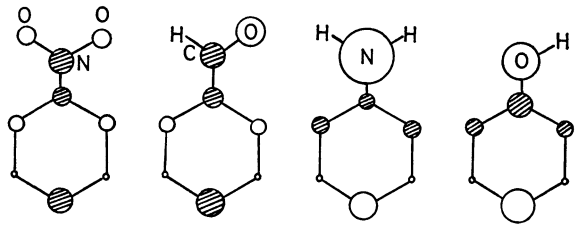

Fig. 3. The shapes of the particular orbitals of nitrobenzene, benzaldehyde, aniline, and phenol.

In cation radical, the distances between atoms being in-phase overlap increase and those in out-of-phase overlap decrease because of a loss of an electron in HOMO. However, the geometrical change is not so remarkable as that in the anion radical.

Let us explain the bond lengths of benzyl radical being neutral in view of the orbital mixing[20] of phenyl ring with CH_2 part. The distortion from one and half bond is visualized as follows.

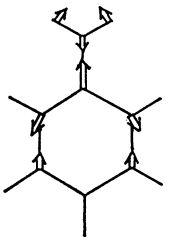

The π type orbital of benzene and CH_2 part and the mode of orbital interaction are shown in Fig. 4. The p_π orbital of C_7 mixes with the symmetric orbitals about the molecular axis of benzene, π_1, π_3, π_5, and π_6. Since the energy of p orbital of carbon is located in the middle of those of the HOMO and LUMO of benzene, the singly occupied MO is formed by the following orbital phase combination.

$$\text{SOMO} = p_\pi - \pi_3 + \pi_5.$$

Thus, the amplitude of C_1 atom is very small since π_3 is combined with π_5 out-of-phase with equal weight, whereas the in-phase orbital, ϕ_2, formed by π_3 and p_π of C_7 contains the large bonding overlap at C_1–C_7 bond. This is the origin of the shortening of C_1–C_7 bond length. Since the out-of-phase orbital SOMO formed by π_3 and π_5 has the large bonding overlap between C_2 and C_6, angle C_2–C_1–C_6 becomes smaller. The shortening of C_2–C_3 bond length and the lengthening of C_1–C_2 bond length are caused by the decrease in the antibonding overlap at C_2–C_3 and the decrease in the bonding overlap at C_1–C_2, respectively. The same consideration can be applied to the expectation of geometrical changes in phenol- and aniline-cations.

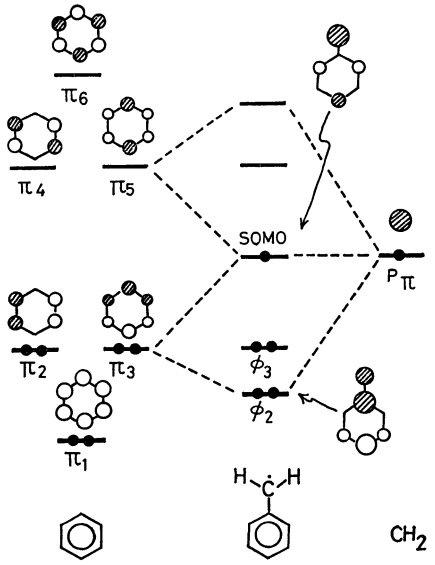

Fig. 4. The mode of the orbital interaction of benzyl radical.

The authors would like to thank Professor R. Zahradnik, Czechoslovak Academy of Sciences, for supplying the energy gradient program "DERIV" by the CNDO/2 method. Permission to use the HITAC-180 computer at the Institute for Molecular Science is gratefully acknowledged.

References

1) D. L. Beveridge and E. Guth, *J. Chem. Phys.*, **55**, 458 (1971).
2) A. T. Amos and B. L. Burrows, *J. Chem. Phys.*, **52**, 3072 (1970).
3) J. E. Harriman and K. M. Sando, *J. Chem. Phys.*, **48**, 5138 (1968).
4) J. A. Pople, D. L. Beveridge, and P. A. Dobosh, *J. Am. Chem. Soc.*, **90**, 4201 (1968).
5) L. C. Snyder and T. A. Amos, *J. Chem. Phys.*, **42**, 3670 (1965).
6) G. Vincow and P. M. Johnson, *J. Chem. Phys.*, **39**, 1143 (1963).
7) A. Hinchliffe, *Chem. Phys. Lett.*, **13**, 594 (1972).
8) A. Carrington and I. C. P. Smith, *Mol. Phys.*, **9**, 137 (1965).
9) W. T. Dixon and R. O. C. Norman, *J. Chem. Soc.*, **1964**, 4857.
10) N. Trinajstic, *Chem. Phys. Lett.*, **10**, 172 (1971).
11) H. H. Dearman and H. M. McConnell, *J. Chem. Phys.*, **33**, 1877 (1960).

12) J. Gerratt and I. M. Mills, *J. Chem. Phys.*, **49**, 1730 (1968).
13) P. Pulay, *Mol. Phys.*, **17**, 197 (1969).
14) P. Pulay and F. Torok, *Mol. Phys.*, **25**, 1153 (1973).
15) J. W. McIver, Jr., and A. Komornicki, *J. Am. Chem. Soc.*, **94**, 2625 (1972); *Chem. Phys. Lett.*, **10**, 303 (1971).
16) J. Pancir, *Theor. Chim. Acta*, **29**, 21 (1973).
17) J. A. Pople, D. L. Beveridge, and P. A. Dobosh, *J. Chem. Phys.*, **47**, 2026 (1967).
18) P. Ludwing, T. Layoff, and R. N. Adams, *J. Am. Chem. Soc.*, **86**, 4568 (1964).
19) W. M. Jr. Gulick and D. H. Geske, *J. Am. Chem. Soc.*, **87**, 4049 (1965).
20) S. Inagaki, H. Fujimoto, and K. Fukui, *J. Am. Chem. Soc.*, **98**, 4045 (1967).
21) J. Troffer, *Acta Crystallogr.*, **12**, 884 (1959).

 © 1980 The Chemical Society of Japan Bull. Chem. Soc. Jpn., 53, 2167—2172 (1980)

Light Scattering Study of Local Structures in Solutions. Cooperative Translational Motion of Alcohol Molecules in Carbon Tetrachloride Solutions

Tadashi KATO,* Nobuyuki ITO, and Tsunetake FUJIYAMA*,†

Department of Chemistry, Faculty of Science, Tokyo Metropolitan University, Setagaya-ku, Tokyo 158

† *Institute for Molecular Science, Myodaiji, Okazaki 444*

(Received January 5, 1980)

The concept of a "moving unit"—a group of molecules which move together for the time much longer than the velocity auto-correlation time, τ—was introduced in order to obtain information about cooperative translational motions of molecules in associated solution. The mutual diffusion coefficient was theoretically expressed in terms of the self diffusion coefficients and the number of moving units. The theoretical results were applied to the study of the mutual diffusion coefficients for methanol–carbon tetrachloride and ethanol–carbon tetrachloride solutions measured by Rayleigh scattering. It was shown that the mean number of alcohol molecules which constitute a moving unit is much smaller than the mean association number of alcohol, especially in the high concentration range of alcohol. This indicates that the hydrogen-bonded polymer of alcohol molecules cannot move without changing the polymer shape within the time τ.

Local fluctuations of concentration afford information which is useful for understanding the mixing of liquids from a molecular viewpoint. As the mean-square amplitude of concentration fluctuations is related to the spatial correlation between the positions of different molecules, it affords information about the local structure formation in solution. In the previous reports, we have discussed the local structures in various solutions on the basis of the quantitative analysis of the mean-square concentration fluctuation obtained from the Rayleigh scattering intensities.[1–8] The local structures were expressed in terms of the ordinary mean association number.

In order to discuss the state of mixing from a dynamical standpoint, however, the life-time of local structures should be taken into account in addition to the mean association number. Here, we define the "life-time" as the time during which the relative positions of molecules in a local structure change very little. The correlation time of concentration fluctuations, which is specified by a mutual diffusion coefficient, is considered to afford information about the life-time of the local structure. It is not possible, however, to obtain the life-time of the local structure directly from the mutual diffusion coefficient because too many parameters are necessary for the description of collective motions of molecules.

In the present report, we propose the existence of a group of molecules which move together for the time much longer than the velocity auto-correlation time of component molecules. We call this group of molecules a "moving unit." The mutual diffusion coefficient, which is obtained from the analysis of the Rayleigh scattering spectrum, can be expressed in terms of the number of moving units.

Binary solutions of methanol–carbon tetrachloride and ethanol–carbon tetrachloride were chosen as appropriate systems in which to determine the existence of such moving units. In these systems, the mean association numbers of hydrogen-bonded alcohol molecules increase with increasing alcohol concentration. Our main interest is to know whether these hydrogen-bonded alcohol molecules can be a moving unit particularly in the high concentration range of alcohols.

Theoretical

Mutual Diffusion Coefficient and Molecular Velocity Correlation. The spectrum of the Rayleigh light isotropically scattered by a binary solution can be approximated by two Lorentzian curves.[9] One of these corresponds to the scattering arising from the entropy fluctuations and the other to that from concentration fluctuations. Since the half-width of the latter spectrum is narrower than that of the former by a factor of about a hundred, these two curves can be identified separately, even though the band centers are overlapped. The spectrum for concentration fluctuations is expressed as[9]

$$I_c(k,\omega) \propto \frac{|k|^2 D}{\omega^2 + (|k|^2 D)^2} \tag{1}$$

where k is the scattering vector and D is the mutual diffusion coefficient. The time correlation function for concentration fluctuations is related to D:

$$\frac{\langle \Delta c(k,t)\Delta c(k,0)\rangle}{\langle |\Delta c(k)|^2\rangle} = \exp(-|k|^2 Dt) \tag{2}$$

$$\Delta c(k,t) \equiv \int_v [c(r,t) - \langle c\rangle] e^{ik\cdot r} d^3r \tag{3}$$

when temperature and pressure fluctuations are disregarded.[10] In Eqs. 2 and 3, $c(r,t)$ is the concentration at the point r at time t in the scattering volume V and the pointed brackets indicate an equilibrium ensemble average.

D is expressed in terms of the time derivative of $\Delta c(k,t)$:[11]

$$D = \lim_{s\to 0}\lim_{k\to 0} \frac{1}{|k|^2}\frac{1}{\langle |\Delta c(k)|^2\rangle}\int_0^\infty \langle \Delta\dot{c}(k,t)\Delta\dot{c}(k,0)\rangle e^{-st} dt. \tag{4}$$

We now consider a binary solution whose components are molecules A and B. If the concentration is expressed in the mole fraction of A, $\Delta X_A(r,t)$ can be approximately expressed as

$$\Delta X_A(k,t) = -\frac{i}{\rho} k\cdot[X_B J_A(k,t) - X_A J_B(k,t)] \tag{5}$$

with

$$\boldsymbol{J}_{\mathrm{A}}(\boldsymbol{k},t)=\sum_{\mathrm{a}}^{n_{\mathrm{A}}}\boldsymbol{v}_{\mathrm{a}}(t)\mathrm{e}^{\mathrm{i}\boldsymbol{k}\cdot\boldsymbol{r}_{\mathrm{a}}(t)}$$

$$\boldsymbol{J}_{\mathrm{B}}(\boldsymbol{k},t)=\sum_{\mathrm{b}}^{n_{\mathrm{B}}}\boldsymbol{v}_{\mathrm{b}}(t)\mathrm{e}^{\mathrm{i}\boldsymbol{k}\cdot\boldsymbol{r}_{\mathrm{b}}(t)} \tag{6}$$

where ρ is the number density, X_{A} and X_{B} are the mean mole fractions of A and B, respectively, and n_{A} and n_{B} are the mean numbers of molecules A and B in V, respectively. $\boldsymbol{v}_{\mathrm{a}}(t)$ is the velocity of an a-th molecule of A, and $\boldsymbol{v}_{\mathrm{b}}(t)$ that of a b-th molecule of B at time t. In the limit of small $|\boldsymbol{k}|$, $\langle|\Delta X_{\mathrm{A}}(\boldsymbol{k})|^2\rangle$ can be written as

$$\lim_{\mathrm{k}\to 0}\langle|\Delta X_{\mathrm{A}}(\boldsymbol{k})|^2\rangle=\frac{V}{\rho}N\langle(\Delta X_{\mathrm{A}})^2\rangle \tag{7}$$

where N is the mean number of total molecules in a region which is very large compared to the distances between molecules and X_{A} is the concentration fluctuation in the region. Substituing Eqs. 5—7 into Eq. 4, we can obtain

$$D=Q[X_{\mathrm{B}}\{V_{\mathrm{aa}}+(n_{\mathrm{A}}-1)V_{\mathrm{aa'}}\}+X_{\mathrm{A}}\{V_{\mathrm{bb}}+(n_{\mathrm{B}}-1)V_{\mathrm{bb'}}\}-2(n_{\mathrm{A}}+n_{\mathrm{B}})X_{\mathrm{A}}X_{\mathrm{B}}V_{\mathrm{ab}}] \qquad (\mathrm{a}\neq\mathrm{a'}\ \ \mathrm{b}\neq\mathrm{b'}) \tag{8}$$

with

$$Q=\frac{X_{\mathrm{A}}X_{\mathrm{B}}}{N\langle(\Delta X_{\mathrm{A}})^2\rangle} \tag{9}$$

$$V_{\mathrm{ij}}=\frac{1}{3}\int_0^\infty\langle\boldsymbol{v}_{\mathrm{i}}(t)\cdot\boldsymbol{v}_{\mathrm{j}}(0)\rangle\mathrm{d}t \tag{10}$$

where i and j represent a, a', b, or b'. Q is a so-called thermodynamic factor expessed in terms of mean-square concentration fluctuations, $N\langle(\Delta X_{\mathrm{A}})^2\rangle$, which can be obtained by analyzing integrated intensities of Rayleigh scattering spectra.[1] $(X_{\mathrm{A}}X_{\mathrm{B}})$ is the magnitude of $N\langle(\Delta X_{\mathrm{A}})^2\rangle$ expected for an ideal binary solution. It can be seen from Eq. 10 that V_{aa} and V_{bb} correspond to the self diffusion coefficients of A and B, respectively;

$$V_{\mathrm{aa}}=D_{\mathrm{A}}\qquad V_{\mathrm{bb}}=D_{\mathrm{B}} \tag{11}$$

$V_{\mathrm{aa'}}$, $V_{\mathrm{bb'}}$, and V_{ab} are related to the velocity correlations between different molecules. In the case where these pair-correlations are negligible, D can be written as

$$D=Q(X_{\mathrm{B}}D_{\mathrm{A}}+X_{\mathrm{A}}D_{\mathrm{B}}). \tag{12}$$

Moving Unit and Diffusion Coefficient. We consider a solution in which strong intermolecular interactions such as hydrogen bonding exist. In such a solution, the velocities of these interacting molecules are expected to be strongly correlated, that is, $V_{\mathrm{aa'}}$, $V_{\mathrm{bb'}}$ and V_{ab} can not be neglected. It is very difficult to express these quantities in terms of microscopic parameters such as intermolecular forces. Instead of studying the details of these dynamical interactions, we assume that some numbers of molecules move together as a group for a time much longer than the velocity auto-correlation time. We call this group of molecules a "moving unit." In the binary solution of A and B molecules, moving units can be represented by A_l, B_m, and $\mathrm{A}_l\mathrm{B}_m$ where l or m is the number of molecules A or B which constitutes a moving unit. We further assume that the velocity correlation between molecules belonging to different moving units can be neglected, because it is much smaller than the velocity correlation between molecules belonging to the same moving unit. Then, the velocity correlation function can be written as

$$\langle\boldsymbol{v}_{\mathrm{i}}(t)\cdot\boldsymbol{v}_{\mathrm{i}}(0)\rangle=\sum_\alpha P_{\mathrm{i}}^\alpha\langle\boldsymbol{v}_{\mathrm{i}}^\alpha(t)\cdot\boldsymbol{v}_{\mathrm{i}}^\alpha(0)\rangle \tag{13}$$

$$\langle\boldsymbol{v}_{\mathrm{i}}(t)\cdot\boldsymbol{v}_{\mathrm{j}}(0)\rangle=\sum_\alpha P_{\mathrm{ij}}^\alpha\langle\boldsymbol{v}_{\mathrm{i}}^\alpha(t)\cdot\boldsymbol{v}_{\mathrm{j}}^\alpha(0)\rangle=\sum_\alpha P_{\mathrm{ij}}^\alpha\langle\boldsymbol{v}_{\mathrm{i}}^\alpha(t)\cdot\boldsymbol{v}_{\mathrm{i}}^\alpha(0)\rangle \tag{14}$$

(i, j=a, a', b, or b')

where P_{i}^α is the probability of finding an i-th molecule in a moving unit α ($\alpha=\mathrm{A}_l$ *etc.*), P_{ij}^α the probability of finding both the i-th and the j-th molecule belonging to α, and v_{i}^α is the velocity of an i-th molecule belonging to α. Under these assumptions, V_{ij} in Eq. 8 is expressed as

$$\begin{aligned}
V_{\mathrm{aa}}&=D_{\mathrm{A}}=\sum_l P_{\mathrm{a}}^{\mathrm{A}l}D_{\mathrm{A}l}+\sum_l\sum_m P_{\mathrm{a}}^{\mathrm{A}l\mathrm{B}m}D_{\mathrm{A}l\mathrm{B}m}\\
V_{\mathrm{bb}}&=D_{\mathrm{B}}=\sum_l P_{\mathrm{b}}^{\mathrm{B}l}D_{\mathrm{B}l}+\sum_l\sum_m P_{\mathrm{b}}^{\mathrm{A}l\mathrm{B}m}D_{\mathrm{A}l\mathrm{B}m}\\
V_{\mathrm{aa'}}&=\sum_l P_{\mathrm{aa'}}^{\mathrm{A}l}D_{\mathrm{A}l}+\sum_l\sum_m P_{\mathrm{aa'}}^{\mathrm{A}l\mathrm{B}m}D_{\mathrm{A}l\mathrm{B}m}\\
V_{\mathrm{bb'}}&=\sum_l P_{\mathrm{bb'}}^{\mathrm{B}l}D_{\mathrm{B}l}+\sum_l\sum_m P_{\mathrm{bb'}}^{\mathrm{A}l\mathrm{B}m}D_{\mathrm{A}l\mathrm{B}m}\\
V_{\mathrm{ab}}&=\sum_l\sum_m P_{\mathrm{ab}}^{\mathrm{A}l\mathrm{B}m}D_{\mathrm{A}l\mathrm{B}m}
\end{aligned} \tag{15}$$

with

$$D_\alpha=\frac{1}{3}\int_0^\infty\langle\boldsymbol{v}_{\mathrm{i}}^\alpha(t)\cdot\boldsymbol{v}_{\mathrm{i}}^\alpha(0)\rangle\mathrm{d}t \tag{16}$$

$$\begin{aligned}
P_{\mathrm{a}}^{\mathrm{A}l}&=n_{\mathrm{A}l}\frac{l}{n_{\mathrm{A}}}\qquad P_{\mathrm{aa'}}^{\mathrm{A}l}=n_{\mathrm{A}l}\frac{l}{n_{\mathrm{A}}}\frac{l-1}{n_{\mathrm{A}}-1}\\
P_{\mathrm{b}}^{\mathrm{B}l}&=n_{\mathrm{B}l}\frac{l}{n_{\mathrm{B}}}\qquad P_{\mathrm{bb'}}^{\mathrm{B}l}=n_{\mathrm{B}l}\frac{l}{n_{\mathrm{B}}}\frac{l-1}{n_{\mathrm{B}}-1}\\
P_{\mathrm{aa'}}^{\mathrm{A}l\mathrm{B}m}&=n_{\mathrm{A}l\mathrm{B}m}\frac{l}{n_{\mathrm{A}}}\frac{l-1}{n_{\mathrm{A}}-1}\\
P_{\mathrm{bb'}}^{\mathrm{A}l\mathrm{B}m}&=n_{\mathrm{A}l\mathrm{B}m}\frac{m}{n_{\mathrm{B}}}\frac{m-1}{n_{\mathrm{B}}-1}\\
P_{\mathrm{ab}}^{\mathrm{A}l\mathrm{B}m}&=n_{\mathrm{A}l\mathrm{B}m}\frac{l}{n_{\mathrm{A}}}\frac{m}{n_{\mathrm{B}}}.
\end{aligned} \tag{17}$$

Substitution of Eqs. 15—17 into Eq. 8 yields the following equation:

$$D=Q\left[\frac{X_{\mathrm{B}}}{n_{\mathrm{A}}}\left(\sum_l l^2n_{\mathrm{A}l}D_{\mathrm{A}l}+\sum_l\sum_m l^2n_{\mathrm{A}l\mathrm{B}m}D_{\mathrm{A}l\mathrm{B}m}\right)+\frac{X_{\mathrm{A}}}{n_{\mathrm{B}}}\left(\sum_l l^2n_{\mathrm{B}l}D_{\mathrm{B}l}+\sum_l\sum_m m^2n_{\mathrm{A}l\mathrm{B}m}D_{\mathrm{A}l\mathrm{B}m}\right)-\frac{2}{n_{\mathrm{A}}+n_{\mathrm{B}}}\sum_l\sum_m lmn_{\mathrm{A}l\mathrm{B}m}D_{\mathrm{A}l\mathrm{B}m}\right] \tag{18}$$

and

$$\begin{aligned}
D_{\mathrm{A}}&=\frac{1}{n_{\mathrm{A}}}\left(\sum_l ln_{\mathrm{A}l}D_{\mathrm{A}l}+\sum_l\sum_m ln_{\mathrm{A}l\mathrm{B}m}D_{\mathrm{A}l\mathrm{B}m}\right)\\
D_{\mathrm{B}}&=\frac{1}{n_{\mathrm{B}}}\left(\sum_l ln_{\mathrm{B}l}D_{\mathrm{B}l}+\sum_l\sum_m mn_{\mathrm{A}l\mathrm{B}m}D_{\mathrm{A}l\mathrm{B}m}\right).
\end{aligned} \tag{19}$$

Moving Units in Alcohol–Carbon Tetrachloride System. In the binary solutions of methanol(A)–carbon tetrachloride(B) and ethanol(A)–carbon tetrachloride(B), the existence of the moving unit of A_l-type is expected. In this case, Eq. 18 is reduced to

$$D=Q(X_{\mathrm{B}}D'_{\mathrm{A}}+X_{\mathrm{A}}D_{\mathrm{B}}) \tag{20}$$

with

$$D'_{\mathrm{A}} \equiv \frac{\sum_l l^2 n_{\mathrm{A}l} D_{\mathrm{A}l}}{\sum_l l n_{\mathrm{A}l}} = \frac{\sum_l l^2 n_{\mathrm{A}l} D_{\mathrm{A}l}}{\sum_l l n_{\mathrm{A}l} D_{\mathrm{A}l}} D_{\mathrm{A}}. \quad (21)$$

$D_{\mathrm{A}l}$ is written as

$$D_{\mathrm{A}l} = \frac{1}{3}\langle|\boldsymbol{v}_{\mathrm{A}l}|^2\rangle\tau_{\mathrm{A}l} \quad (22)$$

with

$$\tau_{\mathrm{A}l} = \int_0^\infty \frac{\langle \boldsymbol{v}_{\mathrm{A}l}(t)\cdot\boldsymbol{v}_{\mathrm{A}l}(0)\rangle}{\langle|\boldsymbol{v}_{\mathrm{A}l}|^2\rangle}\mathrm{d}t. \quad (23)$$

In the above equations, $\langle|\boldsymbol{v}_{\mathrm{A}l}{}^2|\rangle$ is expected to be inversely proportional to l at constant temperature, because this relation holds:

$$\frac{1}{2}M_{\mathrm{A}l}\langle|\boldsymbol{v}_{\mathrm{A}l}|^2\rangle \propto T \quad (24)$$

where $M_{\mathrm{A}l}$ is the mass of the moving unit A_l ($\propto l$) and T is the temperature. If we assume $\tau_{\mathrm{A}l}$ is independent of l, we have

$$D_{\mathrm{A}l} \propto \frac{1}{l}. \quad (25)$$

Substituting Eq. 25 into Eq. 21, we obtain

$$D = Q[X_{\mathrm{B}}D_{\mathrm{A}}\langle l\rangle_{\mathrm{n}}^{\mathrm{d}} + X_{\mathrm{A}}D_{\mathrm{B}}] \quad (26)$$

$$\langle l\rangle_{\mathrm{n}}^{\mathrm{d}} \equiv \frac{\sum_l l n_{\mathrm{A}l}}{\sum_l n_{\mathrm{A}l}} \quad (27)$$

where $\langle l\rangle_{\mathrm{n}}^{\mathrm{d}}$ is the mean number of A molecules which constitute one moving unit. By substituting the experimentally observed values for D, Q, D_{A}, and D_{B} into Eq. 26, we can obtain the $\langle l\rangle_{\mathrm{n}}^{\mathrm{d}}$ value at each concentration.

Experimental

The light scattering spectrometer (heterodyne detection) used in the present study was designed and constructed in our laboratory.[12] The light source was an Argon ion laser (Spectra-Physics model 165-09) which produced 100-800 mW power at 488 nm. The scattering angle, θ, was defined by two pinholes approximately 50 cm apart and 0.5 mm in diameter. The laser beam was focused into a rectangular scattering cell. Scattered light and a local oscillator beam (scattered from the cell walls) were collected onto the surface of a photomultiplier tube (HTV R-374). The photocurrent was amplified and then fed to a spectrum analyzer (Takeda-Riken TR 4120S). This analyzer is designed for the analysis of the spectral region 50 Hz-30 MHz. Details of the spectrometer have been reported elsewhere along with the reliability of the observed data.[12]

Light scattering spectra were observed by using this spectrometer at the temperature of 24 ± 0.5 °C in the scattering angle range of $6°\leq\theta\leq11°$.

All the chemicals were commerical products. The sample solutions were made dust-free by the use of a millipore filter FG of 0.2 μm pore size.

Results and Discussion

Light Beating Spectra and Mutual Diffusion Coefficients. Figure 1 shows a typical example of an observed spectrum. All spectra were found to fit a Lorentzian. By plotting the observed half-widths against $|\boldsymbol{k}|^2$, the theoretical prediction of linear dependence of a half-width on $|\boldsymbol{k}|^2$ was confirmed. A mutual diffusion coefficient was obtained from the slope of the linear plot. The mutual diffusion coefficients thus obtained are plotted against the mole fractions of methanol and ethanol, respectively, in Figs. 2 and 3 (see the circles). The dashed lines in these figures indicate the mutual diffusion coefficients calculated for Eq. 12, where Q is obtained from the observed values of $N\langle(\Delta X_{\mathrm{A}})^2\rangle$ reported elsewhere.[8] Literature values were used for D_{A} and D_{B}.[13,14] It is seen from these figures that the observed values of diffusion coefficients are larger than those predicted from Eq. 12. This disagreement between the observed and theoretical values shows that velocity pair-correlation between different molecules cannot be neglected. As the observed values are larger than the

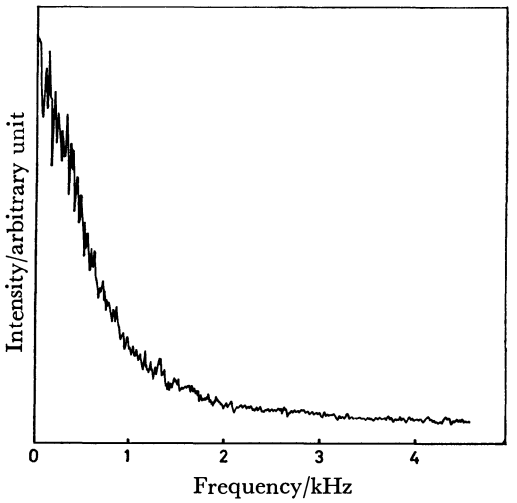

Fig. 1. Heterodyne beating spectrum of light scattered by methanol–carbon tetrachloride solution (0.3 mole fraction of methanol). Scattering angle is 7.25°.

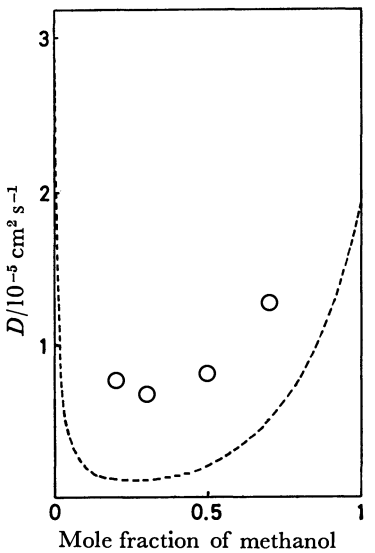

Fig. 2. Observed mutual diffusion coefficients for methanol–carbon tetrachloride system (○).
The dashed line corresponds to mutual diffusion coefficients calculated from Eq. 12.

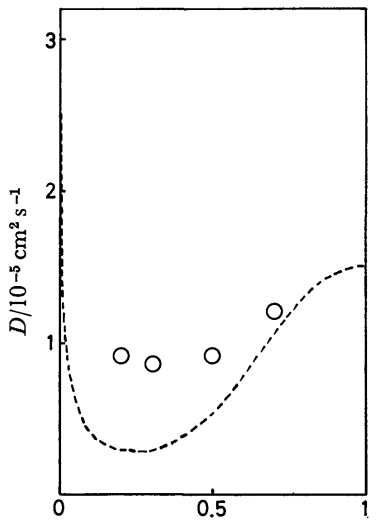

Fig. 3. Observed mutual diffusion coefficients for ethanol–carbon tetrachloride system (○). The dashed line corresponds to mutual diffusion coefficients calculated from Eq. 12.

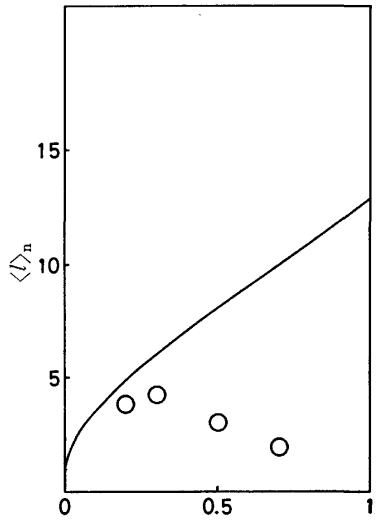

Fig. 5. Comparison of $\langle l \rangle_n^d$ (○) with $\langle l \rangle_n^p$ (——) for ethanol–carbon tetrachloride system.

theoretical ones, it can also be concluded that the velocity correlations between the molecules of the same species are stronger than between those of different species.

Moving Units and Mean Association Numbers in Alcohol–Carbon Tetrachloride System. The mean numbers, $\langle l \rangle_n^d$, were obtained from Eq. 26 using the observed mutual diffusion coefficients, D, the observed diffusion coefficients, D_A and D_B, and the observed mean-square concentration fluctuations, $N\langle(\Delta X_A)^2\rangle$. In Figs. 4 and 5 the mean numbers, $\langle l \rangle_n^d$, thus obtained are plotted against the mole fraction of alcohol for the methanol–carbon tetrachloride and ethanol–carbon tetrachloride systems, respectively.

In a previous paper,[8] we have analyzed the observed mean-square concentration fluctuations, $N\langle(\Delta X_A)^2\rangle$, by using the polymer chain model. In this model, a group of hydrogen-bonded alcohol molecules is treated as a polymer chain whose length is proportional to the association number of alcohol molecules. The solid lines in Figs. 4 and 5 shows the mean association numbers[15]

$$\langle l \rangle_n^p = \sum_l l n_{Al}^p / \sum_l n_{Al}^p$$

obtained from the above analysis, where n_{Al} is the mean number of alcohol l-mers (A_l). An "l-mer" is defined here as a group of l number of alcohol molecules which are linked by $(l-1)$ hydrogen bonds. We cannot obtain information about the life-time of local structures from $\langle l \rangle_n^p$ because the definition of an "l-mer" does not include the concept of life-time. On the other hand, $\langle l \rangle_n^d$ is the mean number of alcohol molecules which can move together for a time much longer than the velocity auto-correlation time. Therefore, $\langle l \rangle_n^d$ may be called a "dynamical mean association number." These two quantities, $\langle l \rangle_n^d$ and $\langle l \rangle_n^p$, are not necessarily equal in magnitude, as can be understood from their definitions.

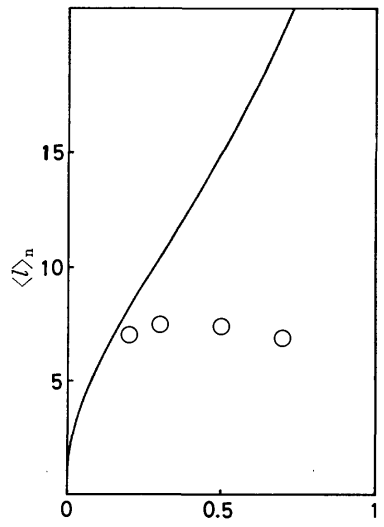

Fig. 4. Comparison of $\langle l \rangle_n^d$ (○) with $\langle l \rangle_n^p$ (——) for methanol–carbon tetrachloride system.

It is seen from Figs. 4 and 5 that $\langle l \rangle_n^d$ is only slightly smaller than $\langle l \rangle_n^p$ in the low concentration range of alcohol. As the alcohol concentration increases, however, the difference becomes very large. If all the hydrogen-bonded polymers of alcohol molecules can move for a time much longer than the velocity auto-correlation time without changing the polymer shape, each polymer can be regarded as a moving unit. Then, $\langle l \rangle_n^d$ is expected to be equal to $\langle l \rangle_n^p$. The above results indicate that a linear hydrogen-bonded polymer of alcohol molecules cannot always be a moving unit, especially in the high concentration range of alcohol. The difference between $\langle l \rangle_n^d$ and $\langle l \rangle_n^p$ may be explained as follows. Consider the velocity correlation between two alcohol molecules which form a polymer. If these two molecules are adjacent to each other, the

velocity correlation between them is expected to be strong. If these two molecules are not adjacent to each other, on the other hand, the velocity correlation between them becomes relatively weak. Therefore, it is expected that $\langle l\rangle_n^d$ cannot exceed a certain number, no matter how large the mean association number, $\langle l\rangle_n^p$.

From these results, the following picture may be drawn for the cooperative translational motion of alcohol molecules. In the low concentration range of alcohol, several alcohol molecules form a hydrogen-bonded polymer. The polymer can move for a time much longer than the velocity auto-correlation time without changing the polymer shape. The number of alcohol molecules moving together increases with the increase of the alcohol concentration in this concentration range. In the high concentration range, however, the polymer can no longer move without changing its shape as long as it could in the low concentration range. In other words, the number of molecules which can move together is much smaller than the mean association number.

Comparison with the Mean Association Number Obtained by Using an Ideal Associated Complex Model. In our previous paper,[8] the observed values of $N\langle(\Delta X_A)^2\rangle$ have been analyzed by using the ideal associated complex model. The model includes an assumption that alcohol molecules form an associated complex. The solution is regarded to be an ideal solution whose components are free molecules and the associated complexes. In other words, all the associated complexes are the same size as the carbon tetrachloride molecule and the internal degrees of the complexes are mutually independent. Under these assumptions, $N\langle(\Delta X_A)^2\rangle$ is expressed as

$$N\langle(\Delta X_A)^2\rangle = X_A(1-X_A)\{X_A+\langle l\rangle_w^c(1-X_A)\}$$
$$\langle l\rangle_w^c \equiv \sum_l l^2 n_{Al}^c / \sum_l l n_{Al}^c \qquad (28)$$

where n_{Al}^c is the mean number of associated complexes which are made up of l numbers of alcohol molecules. In the previous paper, it has been shown that this model cannot be applied to the present system (carbon tetrachloride solution of alcohols) especially in the high concentration range because the configurations of linear hydrogen-bonded polymers are not mutually independent. However, it has been also shown that $\langle l\rangle_w^c$ obtained from Eq. 28 is still a useful quantity, because the following expression can be obtained from the relation between $N\langle(\Delta X_A)^2\rangle$ and the spatial correlation of microscopic density:

$$\langle l\rangle_w^c - 1 = \int_{V^*} \rho_A g_{AA}(r)\mathrm{d}^3r - \int_{V^*} \rho_A g_{AB}(r)\,\mathrm{d}^3r$$

where A and B denote the alcohol and carbon tetrachloride molecules, respectively, ρ_A is the number density of alcohol, and $g_{\alpha\beta}(r)$ is the radial distribution function of α and β molecules (α, β=A or B). $\rho_\alpha g_{\alpha\beta}(r)\mathrm{d}^3r$ is the mean number of α molecules in a volume element d^3r, at a distance r from the center of a β molecule. Thus, $(\langle l\rangle_w^c - 1)$ represents the difference between the mean number of alcohol molecules in the neighborhood of a carbon tetrachloride molecule and that in a neighborhood of the same volume of an alcohol molecule. If the correlations between the positions of different alcohol molecules are rather strong in comparison with those between alcohol and carbon tetrachloride molecules, $\langle l\rangle_w^c$ takes larger values than unity according to the extent of the correlation. Therefore, $\langle l\rangle_w^c$ represents the number of alcohol molecules whose positions are strongly correlated.

In the case where the shape of each hydrogen-bonded species is spherical and their sizes are the same as the solvent molecules, $\langle l\rangle_w^c$ is expected to be equal to $\langle l\rangle_w^p$:[8]

$$\langle l\rangle_w^p \equiv \frac{\sum_l l^2 n_{Al}^p}{\sum_l l n_{Al}^p}.$$

This can be understood by considering that the positions of molecules which form a hydrogen-bonded species are strongly correlated in this case. In the case where the shape of each hydrogen-bonded species is like a polymer chain and various configurations are possible for the polymer chain, on the other hand, the correlation between positions of molecules which form an hydrogen-bonded species becomes relatively weak. Then, $\langle l\rangle_w^c$ is expected to be smaller than $\langle l\rangle_w^p$.

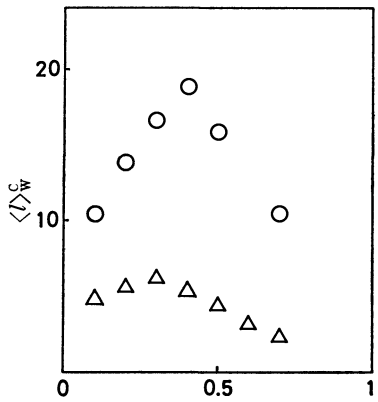

Fig. 6. Mean association numbers obtained from mean-square concentration fluctuation by using an associated complex model.
○: Methanol–carbon tetrachloride system, △: ethanol–carbon tetrachloride system.

Figure 6 shows the concentration dependences of $\langle l\rangle_w^c$ obtained from the observed $N\langle(\Delta X_A)^2\rangle$ values and Eq. 28. Comparison of $\langle l\rangle_n^d$ with $\langle l\rangle_n^p$ and $\langle l\rangle_w^c$ shows that the concentration dependence of $\langle l\rangle_n^d$ is more similar to that of $\langle l\rangle_w^c$ than to that of $\langle l\rangle_n^p$. These results can be understood by considering that the velocity time correlation between different molecules depends on the correlations of positions between these molecules.

Concluding Discussion. We have introduced the concept of a moving unit in order to obtain information about cooperative molecular motions. For the binary solutions of methanol–carbon tetrachloride and ethanol–carbon tetrachloride, we have compared the mean number of molecules which constitute an moving unit

(dynamical mean association number), $\langle l\rangle_n^d$, with two kinds of mean association number, $\langle l\rangle_n^p$ and $\langle l\rangle_w^c$. $\langle l\rangle_n^p$, the ordinary mean association number, is the mean number of molecules which are linked by hydrogen bonds. $\langle l\rangle_n^d$ is the number of molecules whose positions are strongly correlated. These parameters describe the local structure from different standpoints. We have shown that the concentration dependence of $\langle l\rangle_n^d$ is different from that of $\langle l\rangle_n^p$ for the present systems. This difference may be distinct for the solutions in which associated species of short life-time (the life-time is not much longer than the velocity auto-correlation time (10^{-12}—10^{-13} s)) exist. For the solutions in which associated species of long life-time exist, $\langle l\rangle_n^d$ is expected to approach $\langle l\rangle_n^d$. Incidentally, if all the associated species are spherical in shape and of the same size in addition to having long life-times, the relation that $\langle l\rangle_n^d \simeq \langle l\rangle_n^p \simeq \langle l\rangle_w^p \simeq \langle l\rangle_w^c$ is expected.

Although various techniques are available for studying statical structures of liquids or single molecular motions, there are few experimental methods which yield information about collective molecular motions. The measurement of mutual diffusion coefficients is useful for such study. In most of the reports on the mutual diffusion in associated solutions, however, little attention has been paid to the life-time of associated species. The observed mutual diffusion coefficients have usually been explained by using the mean association numbers such as $\langle l\rangle_n^p$ instead of $\langle l\rangle_n^d$.[18,19]

We have shown that the magnitude of the mutual diffusion coefficients depends on the life-time of the local structures formed in the solution. Though the moving unit is a fictitious concept at this stage, it is an important quantity for drawing pictures of the cooperative translational motions in associated solutions.

The present work was supported by a Grant-in-Aid for Scientific Research from the Ministry of Education.

References

1) K. Iwasaki, M. Tanaka, and T. Fujiyama, *Bull. Chem. Soc. Jpn.*, **49**, 2719 (1976).
2) K. Iwasaki, Y. Katayanagi, and T. Fujiyama, *Bull. Chem. Soc. Jpn.*, **49**, 2988 (1976).
3) T. Kato and T. Fujiyama, *J. Phys. Chem.*, **81**, 1560 (1977).
4) T. Kato and T. Fujiyama, *Bull. Chem. Soc. Jpn.*, **51**, 1328 (1978).
5) T. Kato, S. Hyodo, and T. Fujiyama, *J. Phys. Chem.*, **82**, 1010 (1978).
6) T. Fujiyama and M. Tanaka, *Bull. Chem. Soc. Jpn.*, **51**, 1655 (1978).
7) K. Iwasaki and T. Fujiyama, *J. Phys. Chem.*, **81**, 1908 (1977); **83**, 463 (1979).
8) T. Kato, T. Nakanishi, and T. Fujiyama, to be published.
9) R. D. Mountain and J. M. Deutch, *J. Chem. Phys.*, **50**, 1103 (1969).
10) As the correlation times for the temperature and pressure fluctuations are usually much shorter than that for concentration fluctuation, Eq. 3 is almost correct.
11) See for an example, R. Zwanzig, *J. Chem. Phys.*, **40**, 2527 (1964).
12) N. Ito, T. Kato, and T. Fujiyama, *Bunko Kenkyu*, **29**, 106 (1980).
13) A. P. Hardt, D. K. Anderson, R. Rathbun, B. W. Mar, and A. L. Bubb, *J. Phys. Chem.*, **63**, 2059 (1959).
14) Y. Oishi, Y. Kamei, and H. Sumie, *J. Chem. Phys.*, **61**, 2227 (1974).
15) In Ref. 8, the mean association number is expressed as
$$\langle l\rangle_w^p = \sum_l l^2 n_{Al}^p / \sum_l l n_{Al}^p.$$
Under the assumption of association equilibria described in Ref. 8, $\langle l\rangle_w^p$ is related to $\langle l\rangle_n^p$ by this relation: $\langle l\rangle_n^p = (\langle l\rangle_w^p + 1)/2$.
16) We cannot obtain information about the life-time of hydrogen bonds, because other molecular motions than the translational one may also break hydrogen bonds.
17) N. Ito, T. Kato, and T. Fujiyama, to be published.
18) Y. Oishi and M. Nanba, *J. Chem. Phys.*, **70**, 2205 (1979).
19) P. C. Carman, *J. Phys. Chem.*, **71**, 2565 (1967).

 © 1980 The Chemical Society of Japan Bull. Chem. Soc. Jpn., 53, 2173—2180 (1980)

Light Scattering Study of Local Structures in Solutions. Mean Association Numbers and Concentration Fluctuations for Alcohol–Carbon Tetrachloride Systems

Tadashi KATO,* Toru NAKANISHI, and Tsunetake FUJIYAMA*,†

Department of Chemistry, Faculty of Science, Tokyo Metropolitan University, Setagaya-ku, Tokyo 158

† *Institute for Molecular Science, Okazaki 444*

(Received January 5, 1980)

Light scattering spectra were observed for carbon tetrachloride solutions of methanol, ethanol, and 1-propanol. The Rayleigh intensities were reduced to concentration fluctuations. The observed concentration dependence of the concentration fluctuation was analyzed by using two distinct models: an ideal associated complex (IAC) model and a polymer chain (PC) model. In the IAC model, a group of hydrogen-bonded alcohol molecules is treated as a complex whose size is independent of the association number, l. In the PC model, on the other hand, the group of hydrogen-bonded molecules is treated as a linear polymer whose length is proportional to l. It was shown that the PC model can explain both the concentration fluctuation and the heat of mixing data, while the IAC model cannot be applied to the present systems. The mean association number obtained by the IAC model was discussed on the basis of the relation between the concentration fluctuation and the spatial correlation of microscopic density.

Local fluctuations of concentration afford information which is useful in understanding the mixing of a liquid from a molecular viewpoint. Thus we have carried out a series of studies to determine temperature and concentration dependences of concentration fluctuations through observation of light scattering spectra.

The relationship between the mean-square amplitude of concentration fluctuations and Rayleigh intensities has been theoretically established.[1] A method has been proposed for determining local structures in associated solutions from the observed concentration fluctuations at various concentrations and various temperatures,[2,3] and this method has been applied successfully for the studies of local structures in a few kinds of binary solutions.[4–9]

In the study of local structures which formed in the ethanol–carbon tetrachloride solution, it was found that the mean association number of ethanol increases up to about 7 with the increase of ethanol mole fraction up to 0.3 and then gradually decreases with the successive increases in ethanol concentration. On the other hand, the heats of mixing for this system have positive values at almost all the concentrations[10,11] (See Fig. 14). This suggests that the mean association number increases monotonously with the increase of alcohol concentration, because the heat of mixing can be approximately related to the change of the number of hydrogen bonds on mixing. A similar conclusion has been suggested by the studies by spectroscopic methods.[12–15] These results certainly suggest that our previous analysis of the concentration fluctuation values must be modified to some extent in the case of such associative solutions as the ethanol–carbon tetrachloride system.

In the present study, we will analyze the observed concentration fluctuations for the methanol–carbon tetrachloride and 1-propanol–carbon tetrachloride systems, in addition to the ethanol–carbon tetrachloride system, by using a model which can explain both the concentration fluctuations and the heat of mixing data. Then, the mean association number obtained by our previous analysis will be discussed on the basis of the relation between the concentration fluctuation and the spatial correlation of the microscopic density.

Experimental

The samples used in the present study were commercially available reagents. Methanol and 1-propanol were treated with zeorite A-3 in order to eliminate water. The binary solutions of methanol–carbon tetrachloride and 1-propanol–carbon tetrachloride were made dust-free by means of an Atago Abbe refractometer.

Light scattering spectra were observed at 24 ± 1 °C by using a spectrometer which is composed of He–Ne gas laser source (NEC, GLG 108, 60 mW) and a pressure-scanning Fabry-Perot interferometer.[16]

Results and Discussion

Concentration Fluctuations. The procedure for obtaining the concentration fluctuation values from the observed light scattering spectra is the same as that described in the previous reports. In Fig. 1, the observed mean-square concentration fluctuations, $N\langle(\Delta X_A)^2\rangle$, are plotted against the mole fraction, x_A, of the alcohol for the carbon tetrachloride solutions of methanol, ethanol, and 1-propanol where N is the total number of molecules included in the field within which the concentration fluctuation is considered. The dashed line in the figure corresponds to $N\langle(\Delta X_A)^2\rangle$ expected for an ideal binary solution. It is seen from the figure that observed concentration fluctuations are larger than that of an ideal solution and take maximum values at $X_A=0.3$—0.4.

Analysis of $N\langle(\Delta X_A)^2\rangle$ by Using an Ideal Associated Complex Model. In our previous reports, a method has been presented for determining local structures from the observed $N\langle(\Delta X_A)^2\rangle$.[2,3] In this method, we employed an ideal associated complex model[17] (IAC model, hereafter). This model includes an assumption that the local structure can be treated as an associated complex; the solution is regarded as an ideal solution whose components are free molecules and associated complex molecules.

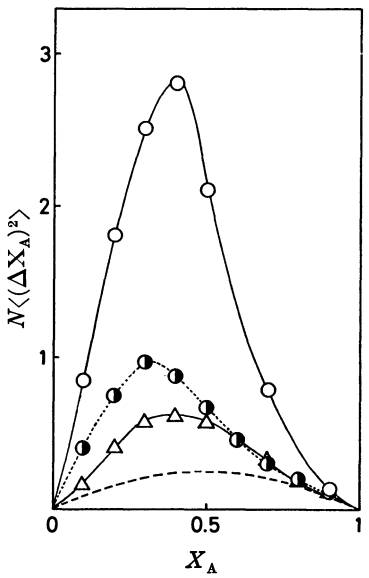

Fig. 1. Observed concentration fluctuation for methanol–carbon tetrachloride system (○), ethanol–carbon tetrachloride system (◑), and 1-propanol–carbon tetrachloride system (△).
The dashed line corresponds to the concentration fluctuation expected for an ideal binary solution.

In the present systems, we assume that associated molecules of the A_l type exist in the solution, where A represents the alcohol molecule and l is an association number. Then, $N\langle(\Delta X_A)^2\rangle$ is expressed as[7,9]

$$N\langle(\Delta X_A)^2\rangle = X_A(1-X_A)\{X_A+\langle l\rangle_w^c(1-X_A)\}$$
$$\langle l\rangle_w^c \equiv \sum_l l^2 n_{Al}^c / \sum_l l n_{Al}^c \qquad (1)$$

where n_{Al}^c is the mean number of A_l molecules. Thus, the mean association number of the alcohol, $\langle l\rangle_w^c$, can be obtained from the observed values of $N\langle(\Delta X_A)^2\rangle$ at each concentration. The results for the carbon tetrachloride solutions of methanol, ethanol, and 1-propanol are shown in Fig. 2. It is seen from the

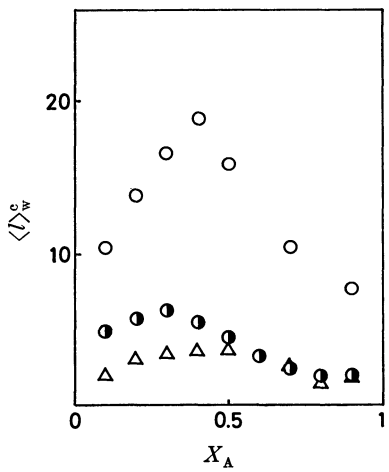

Fig. 2. Mean association numbers of methanol (○), ethanol (◑), and 1-propanol (△) in carbon tetrachloride solutions calculated from Eq. 1 and observed values of concentration flucutuation.

figures that $\langle l\rangle_w^c$ increases with the increase of alcohol mole fraction up to 0.3—0.4 and then decreases with the successive increases in alcohol concentration.

The heat of mixing per molecule, Δh^M, is expressed as

$$\Delta h^M = \frac{1}{n_A+n_B}\{\sum_l (l-1)n_{Al}^c \Delta h^c - \sum_l (l-1)n_{Al}^{c^\circ}\Delta h^c\}$$
$$= X_A \Delta h^c \left(\frac{1}{\langle l\rangle_n^{c^\circ}} - \frac{1}{\langle l\rangle_n^c}\right) \qquad (2)$$
$$\langle l\rangle_n^c \equiv \sum_l l n_{Al}^c / \sum_l n_{Al}^c$$

by using the same model, where n_A and n_B are the numbers of the alcohol and carbon tetrachloride, respectively, Δh^c is the enthalpy change for the reaction

$$A_l + A_1 \longrightarrow A_{l+1}$$

and $n_{Al}^{c^\circ}$ is the mean number of A_l molecules for the pure state. In Eq. 2, Δh^d is assumed to be independent of l. $\langle l\rangle_n^c$ and $\langle l\rangle_n^{c^\circ}$ are the mean association numbers of the alcohol for the solution and the pure state, respectively. Although $\langle l\rangle_n^c$ may differ from $\langle l\rangle_w^c$ in magnitude, they will show, in principle, the same concentration dependences. The results in Fig. 2 suggest that $\langle l\rangle_n^c$ is larger than $\langle l\rangle_n^{c^\circ}$ in magnitude over almost all the concentration range and, therefore, Δh^M will take negative values. However, the experimental values of Δh^M in the literature[10,11,18] are positive (see Fig. 14), which indicates that the IAC model cannot be applied to the present systems.

Analysis of $N\langle(\Delta X_A)^2\rangle$ by Using Polymer Chain Model. In the IAC model, it is assumed that the configurations of associated complexes are mutually independent. However, this assumption may not be appropriate for the present systems because the shapes of the complexes may be chain-like in the high concentration range of the alcohol. So we make the following assumptions in this section for a binary solution composed of alcohol(A) and carbon tetrachloride(B) molecules:

(1) Alcohol molecules form linear, hydrogen-bonded polymers A_l(l=1, 2,....), where l is an association number.

(2) The solution structure is treated by the quasi-lattice model.

(3) An alcohol l-mer, A_l, occupies the l numbers of cells in the lattice and a carbon tetrachloride molecule occupies one cell. The monomeric unit of the alcohol polymer can be exchanged with a carbon tetrachloride molecule in the lattice cells.

(4) The number of distinguishable ways of arranging the $(\sum_l n_{Al})$ numbers of polymers and n_B numbers of carbon tetrachloride molecules on the $(\sum_l n_{Al}+n_B)$ numbers of cells is given by Flory's equation for polymer solutions:[19]

$$W = \frac{(\sum_l l n_{Al}+n_B)!}{\prod_l (n_{Al}!)n_B!} \frac{1}{2^{\sum_l n_{Al}}} \left(\frac{z-1}{\sum_l l n_{Al}+n_B}\right)^{\sum_l (l-1)n_{Al}} \qquad (3)$$

where n_{Al} and n_B are the number of l-mers and carbon tetrachloride molecules, respectively, and z is the coordination number of the lattice.

(5) The internal motions of molecules belonging to different chemical species (*i.e.*, A_l and $A_{l'}$, A_l and B,

etc.) are mutually independent.

Under these assumptions, the free energy for (n_A+n_B) molecules, F, in the present system is expressed as

$$F = n_A f_A^\circ + n_B f_B^\circ + \sum_l n_{Al} f_{Al}^E + kT \ln W \quad (4)$$

$$f_{Al}^E \equiv f_{Al} - l f_A^\circ$$

where f_A° and f_A° are the free energy per molecule for the hypothetical pure states of an alcohol and carbon tetrachloride, respectively. The hypothetical pure state is defined as the state where only monomers exist and molecules are arranged on the same lattice as that of the solution. f_{Al} is the free energy for l numbers of alcohol molecules forming an l-mer.

If association equilibria are assumed, the distribution of an association number can be determined by the equilibrium conditions:

$$\mu_{Al} = l\mu_{A1} \text{ or } \mu_{Al+1} = \mu_{Al} + \mu_{A1} \quad (5)$$

where

$$\mu_{Al} = \partial F/\partial n_{Al}.$$

Combination of Eqs. 4 and 5 gives the relation

$$\frac{X_{Al+1}}{X_{Al}X_{A1}} = 2(z-1)\exp(-\Delta f_l/kT) \equiv K_l \quad (6)$$

$$\Delta f_l \equiv f_{Al+1}^E - f_{Al}^E$$

$$X_{Al} \equiv \frac{n_{Al}}{\sum_l l n_{Al} + n_B} \quad (7)$$

where Δf_l is the change of free energy due to the hydro gen bond formation:[20] $A_l + A_1 \rightarrow A_{l+1}$. For simplicity, we assume that Δf_l is independent of l, that is

$$K_1 = K_2 = \cdots \equiv K. \quad (8)$$

Then, the X_{Al} can be expressed as

$$X_{Al} = K^{l-1} X_{A1}^l. \quad (9)$$

The chemical potential of the alcohol is

$$\frac{\mu_A}{kT} = \frac{f_A^\circ}{kT} + \ln X_{A1} + KX_A X_{A1}. \quad (10)$$

Concentration fluctuations, $N\langle(\Delta X_A)^2\rangle$, are related to μ_A as

$$N\langle(\Delta X_A)^2\rangle = \left(\frac{X_B}{N}\right)^2 \langle(\Delta n_A)^2\rangle \quad (11)$$

$$\langle(\Delta n_A)^2\rangle = \frac{kT}{(\partial\mu_A/\partial n_A)_{n_B}} \quad (12)$$

where Δn_A is the fluctuation of n_A in the region which contains a constant number of B molecules. Combination of Eqs. 10, 11, and 12 gives the equation

$$N\langle(\Delta X_A)^2\rangle = \frac{X_A(1-X_A)}{X_A + (1-X_A)/\langle l\rangle_w^p} \quad (13)$$

$$\langle l\rangle_w^p \equiv \frac{\sum_l l^2 n_{Al}}{\sum_l l n_{Al}} = \frac{1+KX_{A1}}{1-KX_{A1}}. \quad (14)$$

In order to compare the present model (the polymer chain model: PC model, hereafter) with the IAC model, the theoretical values of $N\langle(\Delta X_A)^2\rangle$ calculated for various $\langle l\rangle_w^c$ or $\langle l\rangle_w^p$ values are illustrated in Figs. 3 and 4. Apparently $N\langle(\Delta X_A)^2\rangle$ increases in magnitude as $\langle l\rangle_w^c$ or $\langle l\rangle_w^p$ increases in either model. However, the rate of increase in $N\langle(\Delta X_A)^2\rangle$ for the PC model is smaller than that for the IAC model especially in the

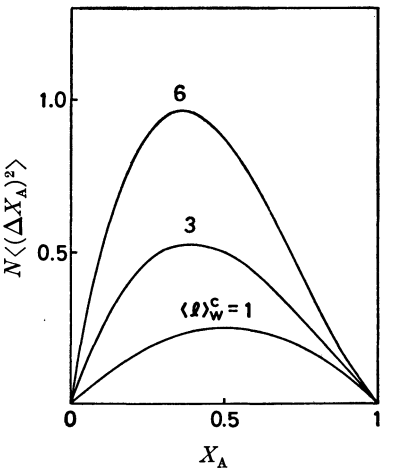

Fig. 3. Theoretical values of concentration fluctuation calculated from Eq. 1 for $\langle l\rangle_w^c = 1$, 3, and 6.

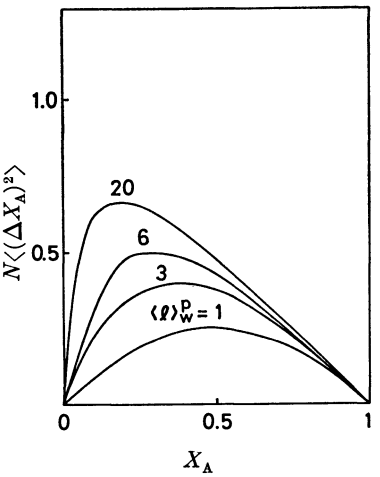

Fig. 4. Theoretical values of concentration fluctuation calculated from Eq. 13 for $\langle l\rangle_w^p = 1$, 3, 6, and 20.

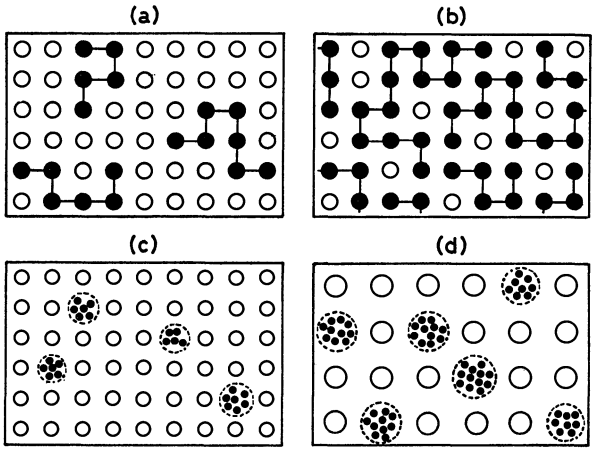

Fig. 5. Schematic representations of the ideal associated complex (IAC) model and the polymer chain (PC) model.
(a): PC model for $X_A \approx 0.3$, (b): PC model for $X_A \approx 0.8$, (c): IAC model for $X_A \approx 0.3$, (d): IAC model for $X_A \approx 0.8$. ● and ○ correspond to the alcohol molecule and the carbon tetrachloride molecule, respectively.

alcohol-rich solutions. The basic differences between the two models are schematically illustrated in Fig. 5. It may be seen from the figure that the two components mix with each other more homogeneously in the PC model than in the IAC model. Concentration fluctuations reflect sensitively the homogeneity of mixing, as can be seen from Figs. 3 and 4.

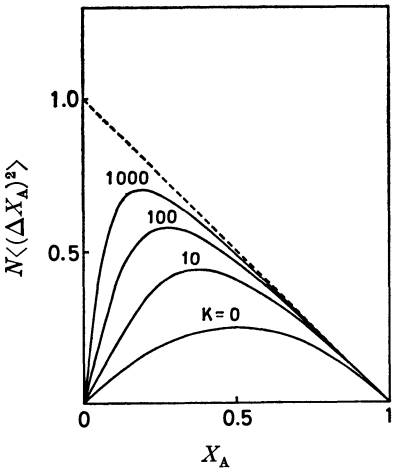

Fig. 6. Theoretical values of concentration fluctuation calculated from Eqs. 13 and 14 for $K=0$, 10, 100, and 1000.

Figure 6 shows the concentration dependences of concentration fluctuations calculated from Eq. 13 for various K values. Comparing the calculated results with the observed concentration fluctuation in Fig. 1, we can see that the PC model can explain the observed values of $N\langle(\Delta X_A)^2\rangle$ in the sense that $N\langle(\Delta X_A)^2\rangle$ takes maximum values at a mole fraction smaller than 0.5. However, the theoretical values of $N\langle(\Delta X_A)^2\rangle$ cannot exceed the values of $(1-X_A)$ even if $K=0$, which shows that the present model is still imperfect for explaining the alcohol solutions.

Modification of the PC Model. In the PC model, it is assumed that an alcohol l-mer occupies l cells in the lattice and, therefore, the number of different configurations of an l-mer is $Z(Z-1)^{l-1}$. In the IAC model, on the other hand, the sizes of associated complexes are all equal to that of a carbon tetrachloride molecule, regardless of their association numbers. It does not seem realistic to assume the ideal mixing of large linear polymers and small monomers, because the configurations of polymers are not mutually independent. In the previous calculation by using the PC model, however, these effects seem to be overemphasized because the hydrogen-bonded polymers are not entirely flexible, as we have assumed. Moreover, the sizes of an alcohol monomer and a carbon tetrachloride molecule are different. So we thought it better to assume that an alcohol l-mer occupies l/ρ cells. Then, the number of distinguishable ways of arranging molecules on the lattice becomes, instead of Eq. 3,

$$W=\frac{\{\sum_l (l/\rho)n_{Al}+n_B\}!}{\prod_l (n_{Al}!)n_B!}\frac{1}{2^{\sum_l n_{Al}}}\left(\frac{z-1}{\sum_l (l/\rho)n_{Al}+n_B}\right)^{\sum_l (l/\rho-1)n_{Al}} \quad (15)$$

and the relation among the mean number of polymers is

$$\frac{X'_{Al+1}}{X'_{Al}X'_{A1}}=2(z-1)\exp(-\Delta f_l/kT)\equiv K \quad (16)$$

$$X'_{Al}\equiv\frac{n_{Al}}{\sum_l (l/\rho)n_{Al}+n_B}. \quad (17)$$

Thus, $N\langle(\Delta X_A)^2\rangle$ is

$$N\langle(\Delta X_A)^2\rangle=\frac{X_A(1-X_A)\{X_A+\rho(1-X_A)\}^2}{X_A+(\rho/\langle l\rangle_w^p)(1-X_A)} \quad (18)$$

$$\langle l\rangle_w^p=\frac{\sum_l l^2 n_{Al}}{\sum_l l n_{Al}}=\frac{1+KX'_{Al}}{1-KX'_{Al}}. \quad (19)$$

In the case where $\rho=\langle l\rangle_w^p$, Eq. 18 is identical with the expression of $N\langle(\Delta X_A)^2\rangle$ in the IAC model, that is, $\langle l\rangle_w^p=\langle l\rangle_w^c$.

Figures 7 and 8 show the concentration dependences of $\langle l\rangle_w^p$ and $N\langle(\Delta X_A)^2\rangle$, respectively, for $K=100$ and various ρ values. Figure 8 demonstrates that the maximum position of the curve moves to the larger-mole-fraction side as ρ increases. Now we can choose the sets of K and ρ values determined for the three systems. These are summarized in Table 1 and the theoretical values of $N\langle(\Delta X_A)^2\rangle$ calculated for the typical sets of parameter in Table 1 are illustrated in Figs. 9—11. Though the agreement between theoretical and observed values was not complete, we were satisfied with the present results and did not modified the model further. The concentration dependences of $\langle l\rangle_w^p$ calculated for these K and ρ values are illustrated in Fig. 12.

The magnitudes of ρ for the three systems studied are in the order methanol>ethanol>1-propanol, as can be seen from Table 1. As ρ has been defined as the number of alcohol molecules which occupy one cell in the lattice, its magnitude is expected to increase with decreasing

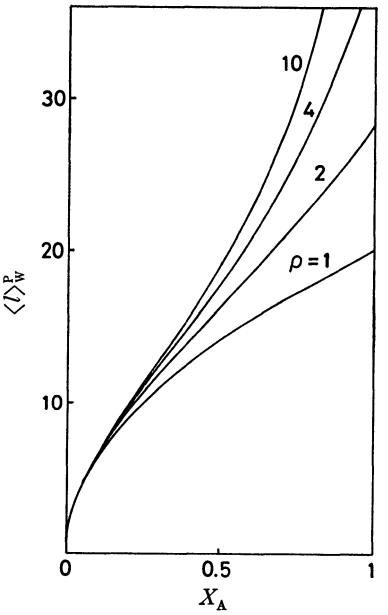

Fig. 7. Theoretical values of mean association numbers calculated from Eq. 19 for $K=100$ and $\rho=1$, 2, 4, and 10.

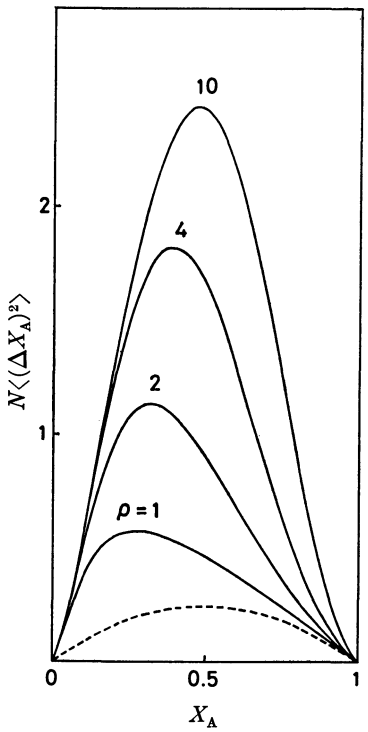

Fig. 8. Theoretical values of concentration fluctuation calculated from Eqs. 18 and 19 for $K=100$ and $\rho=1$, 2, 4, and 10.

Table 1. K and ρ values obtained in the present study for alcohol–carbon tetrachloride systems

	MeOH–CCl_4	EtOH–CCl_4	n-PrOH–CCl_4
K	200—300	50—150	10—20
ρ	5—6	1.6—2	1.3—1.6

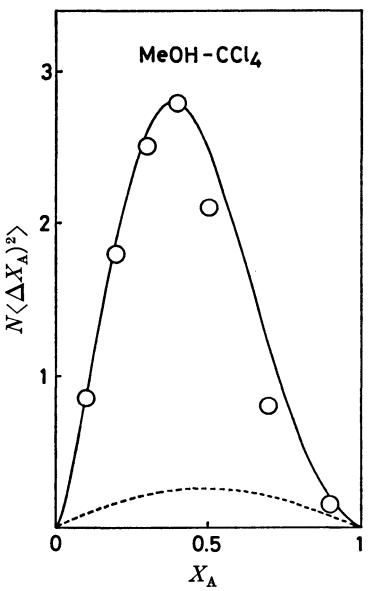

Fig. 9. Concentration fluctuation for methanol–carbon tetrachloride system.
○: Observed values, ——: calculated from Eqs. 18 and 19 for $K=250$ and $\rho=4.2$.

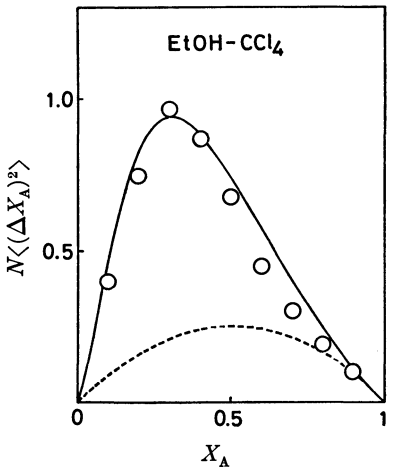

Fig. 10. Concentration fluctuation for ethanol–carbon tetrachloride system.
○: Observed values, ——: calculated from Eqs. 18 and 19 for $K=90$ and $\rho=1.7$.

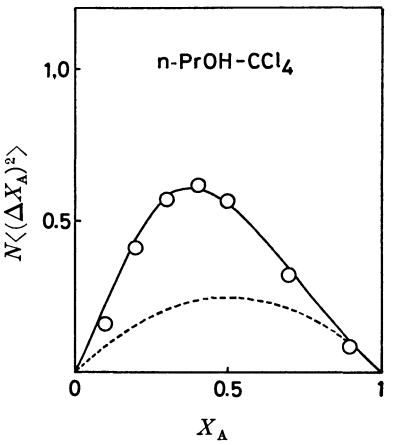

Fig. 11. Concentration fluctuation for 1-propanol–carbon tetrachloride system.
○: Observed values, ——: calculated from Eqs. 18 and 19 for $K=15$ and $\rho=1.45$.

the ratio of the molecular size of the alcohol to that of carbon tetrachloride.[21] The molecular sizes are in the order: carbon tetrachloride>1-propanol>ethanol>methanol. Therefore, the present results are consistent with the above expectation.

So far, ρ has been assumed to be independent of concentration. However, if its magnitude is influenced by the existence of carbon tetrachloride molecules, ρ should decrease its magnitude as the concentration of carbon tetrachloride decreases. Then, the theoretical values of $N\langle(\Delta X_A)^2\rangle$ in the high alcohol concentration range are expected to approach to the observed values, if the concentration dependence of ρ is taken into account.

Calculation of Heat of Mixing. The enthalpy for the (n_A+n_B) numbers of molecules, H, for the present system is expressed by using the PC model as

$$H = n_A h_A^\circ + n_B h_B^\circ + \sum_l n_{Al} h_{Al}^E \qquad (20)$$

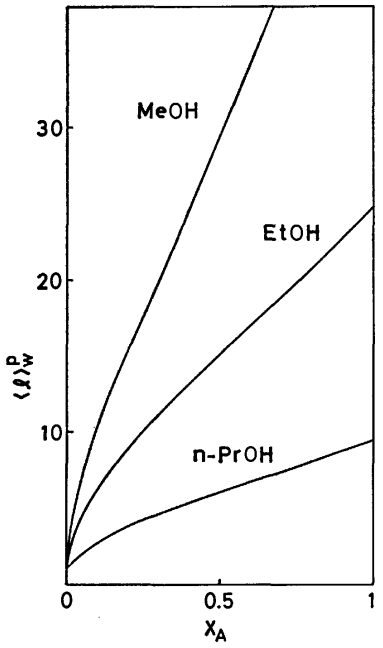

Fig. 12. Mean association numbers of methanol, ethanol, and 1-propanol in carbon tetrachloride solutions calculated from Eq. 19 for the parameters used in calculation of $N\langle(\Delta X_A)^2\rangle$ in Figs. 9—11.

$$h_\alpha^\circ \equiv kT^2\frac{\partial(f_\alpha^\circ/kT)}{\partial T} \quad (\alpha=\text{A or B})$$
$$h_{Al}^E \equiv kT^2\frac{\partial(f_{Al}^E/kT)}{\partial T}. \tag{21}$$

As we have assumed that Δf_{Al} of Eqs. 6 and 16 is independent of l, $\Delta h_l(\equiv h_{Al+1}^E - h_{Al}^E)$ is also independent of l, that is

$$\Delta h_1 = \Delta h_2 = \cdots \equiv \Delta h.$$

Then,

$$\sum_l n_{Al}h_{Al}^E = \sum_l n_{Al}(l-1)\Delta h$$
$$= \Delta h n_A\left(1-\frac{1}{\langle l\rangle_n^p}\right) \tag{22}$$

where

$$\langle l\rangle_n^p = \frac{\sum_l l n_{Al}}{\sum_l n_{Al}} = \frac{1}{1-KX_{A1}'}. \tag{23}$$

Thus the heat of mixing per molecule, Δh^M, is

$$\Delta h^M = \Delta h X_A\left(\frac{1}{\langle l\rangle_n^{p^\circ}} - \frac{1}{\langle l\rangle_n^p}\right) \tag{24}$$

where $\langle l\rangle_n^{p^\circ}$ is the mean association number in the pure alcohol. Figure 13 shows the values of $(\Delta h^M/\Delta h)$ calculated for the parameters used in the calculation of $N\langle(\Delta X_A)^2\rangle$ in Figs. 9—11. Observed values of Δh^M at 20 °C are shown in Fig. 14 in the form of $\Delta h^M/kT$. Comparing Fig. 13 with Fig. 14, we can see that the calculated values explain the experimental results in the senses that Δh^M takes positive values and that its magnitude is in the order: 1-propanol>ethanol> methanol.[22]

The calculation of $\Delta h^M/\Delta h$ in Fig. 13 is done by assuming that ρ is independent of concentration. We have also calculated $\Delta h^M/\Delta h$ for the ρ values which give the best fit between calculated and observed values of

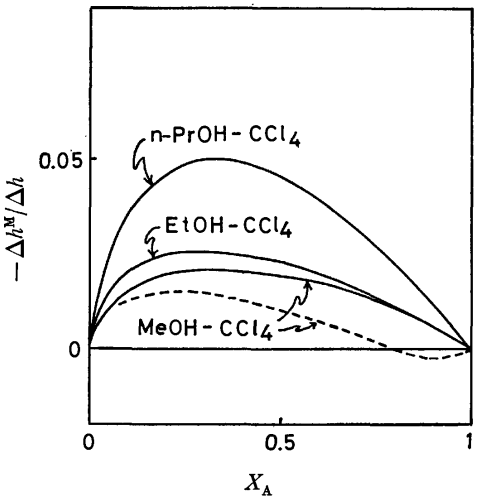

Fig. 13. Theoretical values of $-\Delta h^M/\Delta h$ calculated from Eq. 24 for the parameters used in calculation of $N\langle(\Delta X_A)^2\rangle$ in Figs. 9—11.

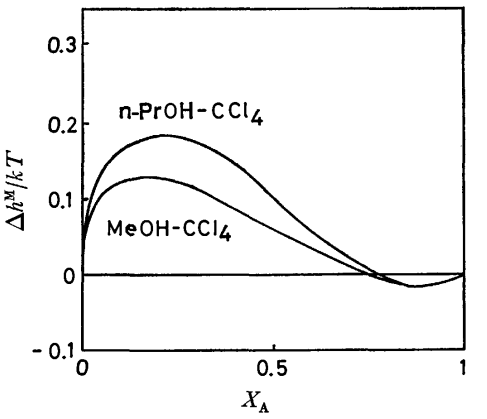

Fig. 14. Experimental values of $\Delta h^M/kT$ for methanol–carbon tetrachloride and ethanol–carbon tetrachloride systems at 20°C.[11]

$N\langle(\Delta X_A)^2\rangle$ without chaging the K value. For an example, the results for the methanol–carbon tetrachloride system are illustrated by the dashed line in Fig. 13.[23] The observed concentration dependences of Δh^M seem to be explained well by the dashed line rather than the solid line in Fig. 13. By comparing the observed values of $\Delta h^M/\Delta h$ and the observed values of Δh^M, the value of Δh has been roughly obtained as 5 kcal mol^{-1} for methanol.

Interpretation for $\langle l\rangle_w^c$. As previously described, the IAC model cannot be applied to the present systems. However, the concentration dependences of $\langle l\rangle_w^c$ seem to reflect a certain aspect of the mixing state. In this paragraph, $\langle l\rangle_w^c$ is interpreted based on the relation between $N\langle(\Delta X_A)^2\rangle$ and the spatial correlation of the microscopic density.

The fluctuation of mole fraction ΔX_A in the constant volume V^* is expressed in terms of the number fluctuation of component molecules as

$$\Delta X_A = \left(\frac{\partial X_A}{\partial n_A}\right)\Delta n_A + \left(\frac{\partial X_A}{\partial n_B}\right)\Delta n_B. \tag{25}$$

Noting that

$$\Delta n_\alpha = \int_{V^*} \rho_\alpha(\boldsymbol{r}) \mathrm{d}^3 r \qquad \Delta\rho_\alpha(\boldsymbol{r}) = \rho_\alpha(\boldsymbol{r}) - \rho_\alpha \tag{26}$$

where $\rho_\alpha(\boldsymbol{r})$ is the number density of α (α=A or B) at the point $\boldsymbol{r}$ and ρ_α the mean value of $\rho_\alpha(\boldsymbol{r})$, then $N\langle(\Delta X_\mathrm{A})^2\rangle$ is[24]

$$N\langle(\Delta X_\mathrm{A})^2\rangle = X_\mathrm{A}X_\mathrm{B}\{1+\rho X_\mathrm{A}X_\mathrm{B}(G_{\mathrm{AA}}+G_{\mathrm{BB}}-2G_{\mathrm{AB}})\} \tag{27}$$

$$G_{\alpha\beta} = \int_{V^*} [g_{\alpha\beta}(r)-1]\mathrm{d}^3 r \tag{28}$$

where ρ is the mean number density and $g_{\alpha\beta}(r)$ is the pair-distribution function of species α and β:

$$g_{\alpha\beta}(r) = \frac{\langle\rho_\alpha(0)\rho_\beta(r)\rangle - \langle\rho_\alpha\rangle\langle\rho_\beta\rangle\delta(r)\delta_{\alpha\beta}}{\langle\rho_\alpha\rangle\langle\rho_\beta\rangle}. \tag{29}$$

In our previously described treatment, the interactions between B molecules and between A and B molecules are neglected. This assumption corresponds to the relation

$$G_{\mathrm{BB}} = G_{\mathrm{AB}}. \tag{30}$$

Then, Eq. 27 is

$$N\langle\Delta X_\mathrm{A})^2\rangle = X_\mathrm{A}X_\mathrm{B}\{1+\rho X_\mathrm{A}X_\mathrm{B}(G_{\mathrm{AA}}-G_{\mathrm{AB}})\}. \tag{31}$$

On the other hand, Eq. 1 can be rewritten as

$$N\langle\Delta X_\mathrm{A})^2\rangle = X_\mathrm{A}X_\mathrm{B}\{1+(\langle l\rangle_\mathrm{w}^\mathrm{c}-1)X_\mathrm{B}\}. \tag{32}$$

By comparing Eq. 31 with Eq. 32, we obtain

$$\langle l\rangle_\mathrm{w}^\mathrm{c} - 1 = \rho_\mathrm{A}(G_{\mathrm{AA}}-G_{\mathrm{AB}})$$

$$= \int_{V^*} \rho_\mathrm{A} g_{\mathrm{AA}}(r)\mathrm{d}^3 r - \int_{V^*} \rho_\mathrm{A} g_{\mathrm{AB}}(r)\mathrm{d}^3 r. \tag{33}$$

$\rho_\alpha g_{\alpha\beta}(r)\ \mathrm{d}^3 r$ is the mean number of α molecules in a volume element $\mathrm{d}^3 r$ at a distance r from the center of a β molecule. Thus, $\rho_\mathrm{A}(G_{\mathrm{AA}}-G_{\mathrm{AB}})$ is the difference between the mean number of alcohol molecules in the entire surrounding of a carbon tetrachloride molecule and that in the entire surrounding of an alcohol molecule. If the correlations between the positions of different alcohol molecules are rather strong in comparison with those between the positions of alcohol and carbon tetrachloride molecules, $\langle l\rangle_\mathrm{w}^\mathrm{c}$ takes larger values than unity according to the extent of the correlation. Therefore, $\langle l\rangle_\mathrm{w}^\mathrm{c}$ is considered to represent the number of alcohol molecules whose positions are strongly correlated.

In the case where the shapes of the hydrogen-bonded species are spherical and their sizes are the same as that of the solvent molecule, $\langle l\rangle_\mathrm{w}^\mathrm{c}$ becomes equal to $\langle l\rangle_\mathrm{w}^\mathrm{p}$. This can be understood by considering that the positions of molecules which form a hydrogen-bonded species are strongly correlated in this case. In the case where the shape of hydrogen-bonded species is like a polymer chain and various configurations are possible for the polymer chain (*i.e.*, the polymer chain is flexible), on the other hand, the correlation between positions of molecules which form an hydrogen-bonded species becomes relatively weak. Then $\langle l\rangle_\mathrm{w}^\mathrm{c}$ is expected to be smaller than $\langle l\rangle_\mathrm{w}^\mathrm{p}$.

The concentration dependences of $\langle l\rangle_\mathrm{w}^\mathrm{c}$ and $\langle l\rangle_\mathrm{w}^\mathrm{p}$ may be interpreted as follows. In the low concentration range of alcohol, the hydrogen-bonded alcohols are isolated by carbon tetrachloride molecules. The correlation between positions of alcohol molecules increase with the increase of $\langle l\rangle_\mathrm{w}^\mathrm{p}$. In the high concentration range, however, the highly-associated alcohol molecules form a continuous medium. Then the correlation between positions of alcohol molecules becomes weak because of the decrease in the number of carbon tetrachloride molecules which perform the task of isolating the associated alcohol molecules.

Conclusion. We have analyzed the concentration dependences of the mean-square concentration fluctuations observed for carbon tetrachloride solutions of three kinds of alcohols by using two distinct models. In the IAC model, the mean association number, $\langle l\rangle_\mathrm{w}^\mathrm{c}$, can be obtained directly from the observed concentration fluctuation. However, the experimental values of heats of mixing cannot be explained by this model. On the other hand, the PC model can explain both the concentration fluctuation and the heat of mixing.

In previous reports, we have studied the local structures formed in various solutions by using the IAC model. The present study shows that this model cannot be applied to those solutions in which associative components form long chain-like local structures. For such solutions, the PC model should be used for obtaining the mean association numbers. It must be emphasized, however, that the mean association number, $\langle l\rangle_\mathrm{w}^\mathrm{c}$, obtained from the IAC model is still a useful quantity, because it represents the extent of correlations between the positions of different associative molecules and because it can be easily and uniquely obtained by measuring the mean-square concentration fluctuation.

References

1) K. Iwasaki, M. Tanaka, and T. Fujiyama, *Bull. Chem. Soc. Jpn.*, **49**, 2719 (1976).
2) K. Iwasaki, Y. Katayanagi, and T. Fujiyama, *Bull. Chem. Soc. Jpn.*, **49**, 2988 (1976).
3) T. Kato and T. Fujiyama, *J. Phys. Chem.*, **80**, 2771 (1976).
4) T. Kato and T. Fujiyama, *J. Phys. Chem.*, **81**, 1560 (1977).
5) T. Kato and T. Fujiyama, *Bull. Chem. Soc. Jpn.*, **51**, 1328 (1978).
6) K. Iwasaki and T. Fujiyama, *J. Phys. Chem.*, **81**, 1908 (1977), **83**, 463 (1979).
7) T. Kato, S. Hyodo, and T. Fujiyama, *J. Phys. Chem.*, **82**, 1010 (1978).
8) T. Fujiyama and M. Tanaka, *Bull. Chem. Soc. Jpn.*, **51**, 1655 (1978).
9) T. Kato, K. Yano, and T. Fujiyama, *Bull. Chem. Soc. Jpn.*, **53**, 53 (1980).
10) J. A. Barker, I. Brown, and F. Smith, *Discuss. Faraday Soc.*, **15**, 142 (1953).
11) J.-E. A. Otterstedt and R. W. Missen, *Trans. Faraday Soc.*, **58**, 879 (1962).
12) E. D. Becker and U. Liddel, *J. Mol. Spectroscopy*, **2**, 1 (1958).
13) J. C. Davis, Jr., K. S. Pitzer, and C. N. Rao, *J. Phys. Chem.*, **64**, 1744 (1960).
14) A. B. Littlewood and F. W. Willmott, *Trans. Faraday Soc.*, **62**, 3287 (1966).
15) H. Fujiwara and T. Ikenoue, *J. Chem. Soc., Faraday Trans. 2*, **72**, 2375 (1976).
16) K. Iwasaki, M. Tanaka, and T. Fujiyama, *Bunko Kenkyu*, **25**, 134 (1976).

17) I. Prigogine and R. Defay, "Chemical Thermodynamics," Longmans Green and Co., London (1954), Chap. 26.

18) E. A. Moelwyn-Hughes and R. W. Missen, *J. Phys. Chem.*, **61**, 518 (1957).

19) P. J. Flory, *J. Chem. Phys.*, **10**, 51 (1942); **12**, 425 (1944).

20) The change of free energy related with the polymer configuration is $\ln 2(z-1)$ and is excluded from Δf_l.

21) If ρ is replaced by v_B/v_A, where v_A and v_B are the molar volumes of alcohol and carbon tetrachloride, K is expressed in terms of the molarity, C_{Al} (mol dm^{-1}) and the volume fraction, ϕ_{Al}, as

$$K = \frac{1}{v_B}\frac{c_{Al+1}}{c_{Al}c_{A_1}} = \frac{v_A}{v_B}\frac{l}{l+1}\frac{\phi_{Al+1}}{\phi_{Al}\phi_{A_1}}.$$

22) No observed values of $\Delta h^M/kT$ at 20 °C for ethanol–carbon tetrachloride could be found in the literature. However, observed values at 35 °C for the three systems presently studied are in the order: 1-propanol>ethanol>methanol.

23) The ρ value for pure methanol is about 1.8.

24) $G_{\alpha\beta}$ in Eq. 28 is identical with $G_{\alpha\beta}$ defined by Kirkwood and Buff. See J. G. Kirkwood and F. P. Buff, *J. Chem. Phys.*, **19**, 774 (1951).

 © 1980 The Chemical Society of Japan Bull. Chem. Soc. Jpn., 53, 2181—2184 (1980)

Fluorescence Quenching Process of Anthracene by Maleic Anhydride

Hiroshi YESAKA,† Takayoshi KOBAYASHI, Kaoru SUZUKI,† and Saburo NAGAKURA*,†

The Institute of Physical and Chemical Research, Wako, Saitama 351

† *The Institute for Solid State Physics, The University of Tokyo, Roppongi, Minato-ku, Tokyo 106*

(Received January, 9, 1980)

The time dependence of fluorescence intensity after picosecond laser excitation and the steady-state fluorescence intensity were measured in order to study the mechanism of fluorescence quenching of anthracene by maleic anhydride in 1,4-dioxane. The nonlinear relationship between the reciprocal of steady-state fluorescence intensity and quencher concentration was observed for this system and interpreted in terms of the transient effect in the quenching process. The kinetic study by picosecond laser photolysis supports this interpretation. The reaction radius (R) and the sum of diffusion constants of both reactants (D) at various temperatures were determined by applying the diffusion model of Andre *et al.* The observed values are $R=7.2$ Å, $D=1.46\times10^{-5}$ cm^2 s^{-1} (22 °C), 1.87×10^{-5} cm^2 s^{-1} (50 °C), 2.42×10^{-5} cm^2 s^{-1} (75 °C). Studies of the main path in the quenching process by nanosecond laser photolysis suggest the existence of an extra path in the quenching process which overwhelms the fluorescent exciplex formation, the photoionization, the triplet anthracene formation, and the adduct formation.

Anthracene–maleic anhydride is one of the typical systems which undergo the photochemical Diels-Alder reaction.[1] In connection with the reaction mechanism, the fluorescence quenching process is also of interest. So far, however, only a few studies have been reported on the quenching and reaction mechanisms.[1–3]

Livingston *et al.* reported that the fluorescence quenching process of anthracene by maleic anhydride in 1,4-dioxane is controlled by diffusion and that the fluorescence quenching does not result appreciably in the formation of the triplet state of anthracene.[2]

Concerning the reaction intermediate Kaupp proposed that the biradical intermediate should exist in the photochemical reaction between anthracence and maleic anhydride, from an analogy of the mechanism of the photochemical reaction between anthracene and dimethyl maleate.[3]

Anthracene and maleic anhydride form a charge-transfer complex. In some cases an excited charge-transfer complex[4] or an exciplex[5] is the intermediate of photocycloaddition reaction. So it is probable that the fluorescence quenching due to charge-transfer interaction is related to the mechanism of the photoaddition reactions. Hence we studied the fluorescence quenching process of anthracene by maleic anhydride in the present paper.

Experimental

Measurements. Steady-state fluorescence quenching experiments were carried out with a spectrophotofluorometer (Shimadzu; model 502) which has two double monochromators for excitation and emission. The 1,4-dioxane solution of anthracene (7.5×10^{-5} mol dm^{-3}) in a 1 cm square quartz cell was excited at 370 nm and the emission was measured at right angle with the excitation light. The measurements were made at room temperature (20±2 °C).

A block diagram of our picosecond emission spectroscopy apparatus was shown in Fig. 1. The excitation light pulse was the second harmonic (347.2 nm, 20 ps fwhm) of an amplified single pulse which was selected from a pulse train generated by a mode-locked ruby laser. The detection system for fluorescence from the sample was composed of a 50 cm grating monochromator, an image-converter streak camera (John Hadland; IMACON 600) coupled to a three-stage image intensifier (EMI; model 9914), and an optical multichannel analyzer (abbreviated hereafter as OMA) (PAR 1205). Fluorescence decay curves were displayed on an oscilloscope coupled to OMA. The digitized data by OMA were accumulated and processed by a desk-top computer. The fluorescence intensity of anthracene was observed at 402.5 nm. The concentration of anthracene was 7×10^{-3} mol dm^{-3} for the observation of the time profile of the fluorescence intensity.

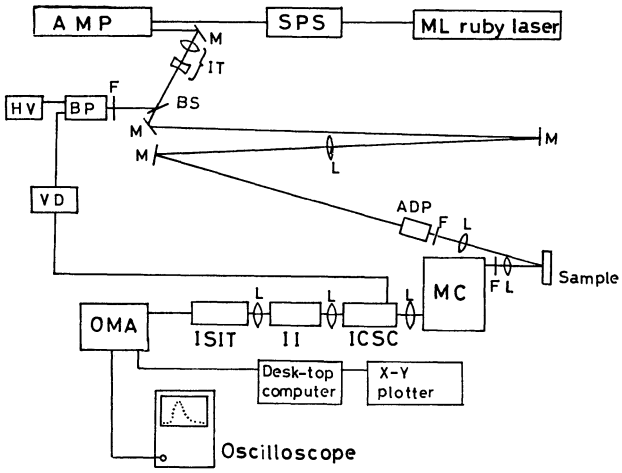

Fig. 1. Block diagram of the picosecond emission spectroscopy apparatus.
The excitation light generation system is composed of a mode-locked (ML) ruby laser, a single pulse selector (SPS), an amplifier (AMP), and an ADP crystal. The detection system is composed of a monochromator (MC), an image-converter streak camera (ICSC), an image intensifier (II), an intensified silicon intensified target tube (ISIT), an optical multichannel analyzer (OMA), an oscilloscope, a desk-top computer, and an X-Y plotter. The trigger system for ICSC is composed of a biplanar phototube (BP), a high-voltage power supply (HV), and a variable delay circuit (VD). L, M, BS, and IT represent lens, mirror, filter, beam splitter, and inverted telescop, respectively.

In the study of nanosecond laser photolysis a commercial nitrogen laser (337.1 nm, 10 ns fwhm, Molectron; model UV24) or a home-made nitrogen laser (3.7 ns fwhm) was used as an excitation light source and a Xe flash lamp with 40 μs duration was used as a monitoring light source.

The absorption spectrum measurements were carried out with a Cary 14 spectrophotometer.

Deoxygenation was done by bubbling dry nitrogen gas through the solution for 5 min.

Materials. The highly pure anthracene was a kind gift from Prof. Iwashima of Meisei University. Guaranteed reagent grade maleic anhydride (abbreviated to MA; Tokyo Kasei) and phthalic anhydride (Wako Pure Chemical) were sublimed *in vacuo* before use. Reagent grade pyromellitic dianhydride (Tokyo Kasei) was recrystallized twice from 1,4-dioxane and sublimed *in vacuo*. Acetonitrile (Wako Pure Chemical; spectrosol grade) was used without further purification. 1,4-Dioxane (Wako Pure Chemical) was let stand over iron (II) sulfate for several days. It was refluxed for 8 h with hydrochloric acid and water under nitrogen. Potassium hydroxide was added to the solution and the water layer was discarded. It was refluxed for 12 h with sodium under nitrogen, then distilled into flask and stoppered.

Results and Discussion

Steady-state Experiment. Plot of I_0/I *vs.* concentration of MA([MA]) is shown in Fig. 2 by open circles. I_0 and I are the fluorescence intensities without and with quencher, respectively. As can be seen in the figure, the plot is nonlinear. Five possible mechanisms to explain the nonlinear relation between I_0/I and [MA] are listed below: 1) (1: 1) charge-transfer complex formation in the ground state between anthracene and maleic anhydride, 2) photochemical and/or thermal reactions between anthracene and maleic anhydride, 3) internal filter effect, 4) dipole-dipole energy transfer from excited anthracene to maleic anhydride, 5) the transient effect in diffusion-controlled fluorescence quenching reaction. All but the fifth mechanism are concluded to be minor by the following considerations.

Anthracene and maleic anhydride in 1,4-dioxane form a (1: 1) ground state charge-transfer (CT) complex and its equilibrium constant is reported to be 0.05 mol^{-1} dm^3.[1] At the excitation wavelength (370 nm), not only anthracene but also the CT complex can absorb light to some extent. On the assumption that light absorption by the CT complex does not contribute to fluorescence intensity at all, I_0/I is represented as follows:

$$\frac{I_0}{I} = \frac{(1-10^{-C_0\varepsilon_A y})(1+K[\mathrm{MA}]\varepsilon_C/\varepsilon_A)(1+\tau k[\mathrm{MA}])}{1-10^{-C_0 y(K[\mathrm{MA}]\varepsilon_C+\varepsilon_A)/(1+K[\mathrm{MA}])}} \quad (1)$$

where ε_C and ε_A are the molar extinction coefficients of the complex and anthracene at the excitation wavelength, respectively. K is the equilibrium constant between free anthracene and maleic anhydride and their complex. The fluorescence lifetime of anthracene without quencher is given by τ and the quenching rate constant is represented by k. C_0 is the total concentration of anthracene and y is the optical path length of the cell.

The absorbance, A, of anthracene solution containing maleic anhydride of the concentration [MA] at the excitation wavelength (370 nm) and the absorbance, A_0, of anthracene solution without quencher at the same wavelength have the following relationship.

$$A/A_0 = \left(1+K\frac{\varepsilon_C}{\varepsilon_A}[\mathrm{MA}]\right)\Big/(1+K[\mathrm{MA}]) \quad (2)$$

Here $K=0.05$ mol^{-1} dm^3. Then we can estimate $\varepsilon_C/\varepsilon_A$ from the observed A/A_0, which is 3.4. Furthermore, from the data in the low quencher concentration region (below 0.074 mol dm^{-3}) in Fig. 2, τk is estimated to be 61.4 mol^{-1} dm^3. Combining the respective values of $\varepsilon_A(2.7\times10^6$ mol^{-1} cm^2), $C_0(7.5\times10^{-5}$ mol dm^{-3}) and y (1 cm) with K, $\varepsilon_C/\varepsilon_A$ and τk, the I_0/I values represented by Eq. 1 can be calculated as the function of [MA]. The results are shown by a dashed curve in Fig. 2. We can see from this figure that the values calculated by Eq. 1 are much smaller than the observed ones. Therefore we conclude that the ground state complex formation (mechanism 1) is a minor contributing factor in the nonlinear relationship between I_0/I and [MA].

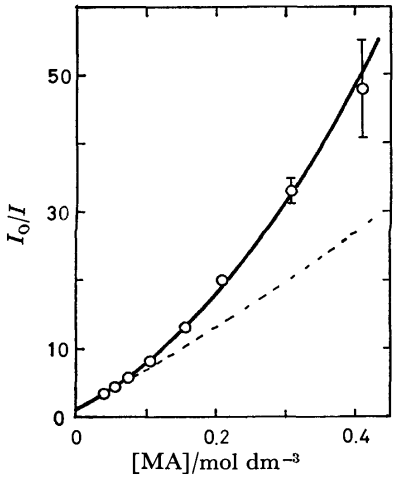

Fig. 2. Results of the steady-state intensity measurement of fluorescence from anthracene quenched by maleic anhydride in 1,4-dioxane at 20°C.
Open circles, experimental values; solid curve, calculated values for I_0/I from Eq. 3 with parameters from Table 1; dashed curve, calculated values for I_0/I from Eq. 1.

The decrease in the anthracene concentration by photochemical and/or thermal reactions with maleic anhydride during the measurement may decrease the fluorescence intensity of anthracene. The decrease was determined to be 1.6% at [MA]=0.42 mol dm^{-3} by the absorption spectrum measurement. Mechanism 2, thus, contributes little to the nonlinearity of I_0/I-[MA] plot.

The internal filter effect (mechanism 3) is estimated from the increase in absorbance brought about by the addition of maleic anhydride in the wavelength region of fluorescence. The maximum quencher concentration in the steady-state experiment is 0.42 mol dm^{-3}, and the maximum increase in absorbance in the fluorescence spectral region was 0.01 (388 nm). This means that the fluorescence intensity is reduced by this effect by 2.3%. The decrease of 2.3% in the intensity is much less than the observed decrease of 44%. Consequently mechanism 3 can be ruled out.

According to Förster's theory the rate constant for the dipole-dipole energy transfer depends on the overlap of the fluorescence spectrum of an energy donor and the absorption spectrum of an energy

acceptor. In the present case there is no overlap between the fluorescence spectrum of anthracene and the absorption spectrum of maleic anhydride. So we can rule out mechanism 4.

According to the modified theory by Andre *et al.* on the diffusion-controlled fluorescence quenching process, I_0/I is expressed by the following equation.[6]

$$I_0/I = \exp(NV[\mathrm{MA}])\ (1+4\pi RDN\tau[\mathrm{MA}])\ Y^{-1} \quad (3)$$

where R is a reaction distance. D represents the sum of diffusion constants of a fluorophor and a quencher, and N is Avogadro's number devided by 1000. Y and V are represented as follows:

$$Y = 1 - (b/a^{1/2})\pi^{1/2} \exp(b^2/a)\ \mathrm{erfc}\ (b/a^{1/2}),$$

$$\mathrm{erfc}\ (x) = \frac{2}{\sqrt{\pi}}\int_x^\infty \exp(-u^2)\mathrm{d}u, \quad V = \frac{4\pi}{3}(R^3 - R'^3),$$

$$a = \frac{1}{\tau} + 4\pi RDN[\mathrm{MA}], \quad b = 4R^2(\pi D)^{1/2}N[\mathrm{MA}]$$

where R' is a collisional distance which is taken as the sum of molecular radius of anthracene (3.51 Å) and that of maleic anhydride (2.63 Å). The molecular radii were determined from Lebas volume.[7]

R and D were determined by fitting the above theoretical expression to the observed dependence of I_0/I on [MA] shown in Fig. 2. In actuality the least-squares method was used for the determination. The values best fitted to the observed I_0/I-[MA] curve are listed in Table 1.

Table 1. The reaction distances (R's) and the sums of diffusion constants (D's)

	R/Å	$D/10^{-5}$ cm^2 s^{-1}	Temp/°C
From steady-state experiment	7.4	1.3	20±2
From decay curves			
[MA]/mol dm^{-3}			
0.214	7.2±1.4	1.56±0.4	22±1
0.428	7.2±0.7	1.36±0.2	22±1
0.208	7.2±0.7	1.87±0.2	50±1
0.202	7.2±0.7	2.42±0.2	75±1

Picosecond Emission Spectroscopy. The transient effect in the diffusion-controlled fluorescence quenching process can be observed directly by the picosecond laser photolysis technique. We can ascertain the applicability of the diffusion model to this system by comparing R and D values obtained by the picosecond photolysis technique with those obtained from the steady-state experiment.

The observed decay curves at various conditions are shown in Fig. 3 by open circles. In order to analyze these curves one must take into account the time profile of excitation pulse, $P(t)$, and the response function of the detection system, $G(t)$. The output from the detection system, $H(t)$, is given by the convolution integral as follows:

$$H(t) = \int_{-\infty}^{\infty}\int_{-\infty}^{t'} G(t-t')P(s)F(t'-s)\mathrm{d}s\mathrm{d}t', \quad (4)$$

where $F(t)$ is the undistorted response function of the fluorescent system. $P(t)$ is assumed to be a Gaussian

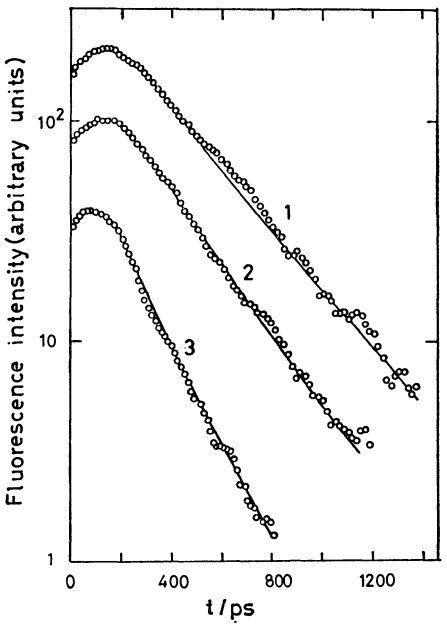

Fig. 3. Time dependence of anthracene fluorescence intensity quenched by MA in 1,4-dioxane.
Curve 1, [MA]=0.208 mol dm^{-3} at 50°C; curve 2, [MA]=0.202 mol dm^{-3} at 75°C; curve 3, [MA]=0.428 mol dm^{-3} at 22°C. Open circles are the observed values and solid lines the best fitted curves calculated by using the parameters in Table 1 and the corresponding MA concentration.

function with a parameter determined by the laser pulse width which was measured by two-photon fluorescence technique. $G(t)$ is also assumed to be a Gaussian function whose parameter is determined by the observed width of the excitation light pulse. If the fluorescent systems (anthracene molecules in the case of the present experiment) are quenched by the other molecules (maleic anhydride molecules) by the diffusion-controlled process, $F(t)$ is expressed in terms of $\exp(-at-2bt^{1/2})$. $H(t)$ was obtained numerically by computer calculation with various sets of R and D values. R and D were then estimated from the curve best fitted to the observed time profile of the fluorescence intensity.

The solid curves in Fig. 3 are the calculated curves of $H(t)$ that best fitted for the observed values. R and D values determined from these decay curves are listed in Table 1. The errors were estimated by comparing the caculated $H(t)$'s with the observed decay curves. R and D obtained from the decay curves at 22 °C agree well with those obtained from the steady-state experiment. This agreement justifies the application of the diffusion model to the fluorescence quenching process of anthracene by maleic anhydride in 1,4-dioxane.

The temperature dependence of D can be estimated by using the Stokes-Einstein equation:

$$D = \frac{k_B T}{6\pi\eta}(r_{An}^{-1} + r_{MA}^{-1}) \quad (5)$$

where k_B and T have ordinary meanings. η is the viscosity of the solvent. r_{An} and r_{MA} are the radii of anthracene and maleic anhydride, respectively. Anthracene and maleic anhydride molecules are, in fact, not

spherical. However, for the sake of simplicity we applied the above equation, and the radii of anthracene and maleic anhydride were determined by using Lebas volume.[7] The calculated D's are 1.18×10^{-5} cm^2 s^{-1} (22 °C), 2.03×10^{-5} cm^2 s^{-1} (50 °C), and 2.97×10^{-5} cm^2 s^{-1} (75 °C). A fairly good agreement is obtained with the D's obtained from the picosecond photolysis experiment.

The Main Path in Fluorescence Quenching Process. Following four possibilities for the main path in fluorescence quenching by the quencher were examined; 1) the formation of fluorescent exciplex, 2) photochemical Diels-Alder reaction, 3) the enhancement of intersystem crossing by charge-transfer interaction,[8] 4) photoionization. The possibility of formation of fluorescent exciplex was denied, because no detectable fluorescence appeared in the range from 375 nm to 750 nm by the addition of maleic anhydride to the 1,4-dioxane solution of anthracene. The adduct formation is not the main path in fluorescence quenching process because the quantum yield of the adduct formation was reported to be 0.026 at 26 °C with [MA]=0.5 mol dm^{-3}.[1]

TABLE 2. THE DEPENDENCE OF ABSORBANCE OF THE $T_n\leftarrow T_1$ TRANSITION OF ANTHRACENE IMMEDIATELY AFTER EXCITATION ON MALEIC ANHYDRIDE CONCENTRATION

[MA]/mol dm^{-3}	Absorbance of $T_n\leftarrow T_1$ transition
0	0.309
0.116	0.058
0.290	0.024
0.580	too weak to be observed

The absorbance was monitored at 425 nm. The concentration of anthracene is 3.9×10^{-3} mol dm^{-3}.

The dependence of absorbance of the $T_n\leftarrow T_1$ transition immediately after excitation on quencher concentration was studied by nanosecond laser photolysis. The results are shown in Table 2. The absorbance decreases remarkably as the quencher concentration increases. Maleic anhydride absorbs excitation light at 337.1 nm. However, the effect of this absorption upon the absorbance of the $T_n\leftarrow T_1$ transition is negligibly small, because the molar extinction coefficient at 337.1 nm is 1260 times smaller for maleic anhydride than for anthracene. Furthermore, the first excited triplet state (T_1) of anthracene was not drastically quenched by maleic anhydride, since at [MA]=0.32 mol dm^{-3} the lifetime of T_1 of anthracene was longer than 2 μs. Therefore we conclude that the intersystem crossing of anthracene cannot be enhanced by maleic anhydride.

The possibility of photoionization was examined by the nanosecond laser photolysis techniques. The anthracene cation radical, whose absorption maximum was near 720 nm,[9,10] was not observed at [anthracene]=10^{-2} mol dm^{-3} and [MA]=1 mol dm^{-3} in either 1,4-dioxane or acetonitrile. In the cases of anthracene (2.7×10^{-3} mol dm^{-3}) and pyromellitic dianhydride (2.2×10^{-2} mol dm^{-3}), and anthracene (2.4×10^{-3} mol dm^{-3}) and phthalic anhydride (1.9×10^{-2} mol dm^{-3}) in acetonitrile, the anthracene cation radical was observed by using the same experimental equipment. The quantum yield of photoionization is expected to increase with the increase in electron affinity of the acceptor. The electron affinities of pyromellitic dianhydride, maleic anhydride, and phthalic anhydride are 0.85 eV, 0.57 eV, and 0.15 eV, respectively.[11] The quantum yield of photoionization is very small for the system containing anthracene and maleic anhydride in acetonitrile compared with the others. This means that an extra channel which overwhelms the photoionization process should exist in the quenching process of excited singlet state anthracene by maleic anhydride. The process may be, for example, a formation of the biradical intermediate proposed by Kaupp,[3] or a formation of a very short-lived ion-pair whose main decay path is neither fluorescent exciplex formation, free ion formation, triplet anthracene formation, nor adduct formation.

The authors wish to express their gratitude to Mr. Hiroyuki Ohtani, The University of Tokyo, for his technical assistance in the picosecond laser photolysis experiment.

References

1) J. P. Simons, *Trans. Faraday Soc.*, **56**, 391 (1960).
2) R. Livingston, R. M. Go, and T. G. Truscott, *J. Phys. Chem.*, **70**, 1312 (1966).
3) G. Kaupp, *Angew. Chem.*, **84**, 259 (1972).
4) D. Bryce-Smith, *Pure Appl. Chem.*, **34**, 203 (1974).
5) R. A. Caldwell and L. Smith, *J. Am. Chem. Soc.*, **96**, 2994 (1974).
6) J. C. Andre, M. Niclause, and W. R. Ware, *Chem. Phys.*, **28**, 371 (1978).
7) J. H. Gorrell Jr., and J. T. Dubois, *Trans. Faraday Soc.*, **63**, 347 (1967).
8) N. Christodouleas and S. P. McGlynn, *J. Chem. Phys.*, **40**, 166 (1964).
9) T. Shida and S. Iwata, *J. Am. Chem. Soc.*, **95**, 3473 (1973).
10) T. Shida, S. Iwata, and M. Imamura, *J. Phys. Chem.*, **78**, 741 (1974).
11) G. Briegleb, *Angew. Chem.*, **76**, 326 (1964).

 © 1980 The Chemical Society of Japan Bull. Chem. Soc. Jpn., 53, 2185—2187 (1980)

Photodissociation Spectroscopy and Photoreactions in *t*-Butylbenzene Cation and Its Daughter Cations

Yoshiya TAKENOSHITA*,† and Robert C. DUNBAR††

Department of Chemistry, Case Western Reserve University, Cleveland, Ohio 44106, U.S.A.

(Received January 21, 1980)

Photodissociation spectra were observed for *t*-butylbenzene cation (*m/e* 134) and its daughter ion (*m/e* 119). Photoproduction spectra of the ions at *m/e* 119 and *m/e* 91 were observed in the visible region. It was shown that the photodissociation of *m/e* 134 yields *m/e* 119 almost 100% at wavelengths above 450 nm. Below 450 nm *m/e* 91 and *m/e* 57 appear as light-produced species. From pressure dependence and double resonance results, it was concluded that *m/e* 91 is a direct photoproduct from *m/e* 119, and that *m/e* 57 is produced in an ion-molecule reaction of *m/e* 91 with neutral *t*-butylbenzene. The photodissociation spectrum of *m/e* 119 is very similar to that of *m/e* 105 obtained by protonation of styrene, and it is reasonable to assume that *m/e* 119 has the protonated methylstyrene structure.

The photochemistry of gas-phase ions is conveniently studied using techniques of ion cyclotron resonance.[1-4] Aromatic radical ions have been particularly well explored, and many aspects of their spectroscopy and photochemical reactions have begun to be clarified, leaving a rich variety of unresolved and interesting questions.

The photodissociation spectrum of *t*-butylbenzene ion(I) was measured by Dymerski *et al.*[5] using steady-state ICR technqiues, showing, as is typical of alkylbenzene ions,[6] a broad photodissociation feature in the visible, and a peak near 270 nm. At wavelengths above about 400 nm, the only observed product was *m/e* 119, corresponding to loss of CH_3 (Eq. 1):

$$\underset{\text{I}}{C_6H_5C(CH_3)_3^+} \xrightarrow{h\nu} \underset{\text{II}}{C_9H_{11}^+} + CH_3\cdot \qquad (1)$$

(*m/e* 134) (*m/e* 119)

However, at shorter wavelengths another product ion was observed at *m/e* 57 ($C_4H_9^+$). The possibility of this being a direct photodissociation product, formed in competition with the less energetic *m/e* 119 product channel, is an interesting one. The 57^+ product channel is about 7 kcal more endothermic than the 119^+ channel;[7] competitive fragmentation to both products would be interesting, and might turn out to be indicative of non-statistical (non-RRKM) dissociation. However, the steady-state ICR technique is well known to have difficulty in distinguishing between direct photoproducts and subsequent ion-molecule reaction products,[3] and it seemed desirable to reexamine this photodissociation chemistry using the more powerful methods of pulsed ICR spectroscopy.

Experimental

The application of ion cyclotron resonance (ICR) spectroscopic techniques to studying photodissociation spectroscopy and ion photochemistry has often been described.[1-4] For one-photon photodissociations, the photodissociation cross section is obtained in the pulsed ICR technique from the extent of ion disappearance following illumination for a time τ:

$$\sigma = -[1/(I\tau)]\cdot\ln[(M_0^+ - M^+)/M_0^+] \qquad (2)$$

where M_0^+ and M^+ are the signal intensities of parent ions respectively without and with light, and I is the photon flux. Equivalent information can be obtained by observing the appearance of photoproduct ions under illumination.[8] The instrument and techniques used have been described.[2,3]

Commercial *t*-butylbenzene was used without further purification with a sample pressure ranging from 8×10^{-9} to 4×10^{-8} Torr, ionizing electron energy of 12 eV, and trapping times in the range 1—3 s. The detection radio frequency was 137.4 kHz, and the magnetic field varied from 3 to 11 kG to observe mass numbers from 41 to 134. Light from a 2.5 kW Hg–Xe arc lamp was wavelength-selected with a Schoeffel GM-250 monochromator at a resolution (FWHM) of 14 nm.

The ratio of signal intensities [119+]/[134+] was found very sensitive to electron beam parameters in the low-energy region used in this work, and varied from day to from about 1.2 to 1.8. The sum of [119+] and [134+] signal intensities was, however, kept constant within 20% in order to maintain constant ion density conditions in the cell. Representative photodissociation results are displayed in Fig. 1. All of the curves plotted in Figs. 2, 3, and 4 were obtained by measuring the extent of light-induced increase or decrease of the ap-

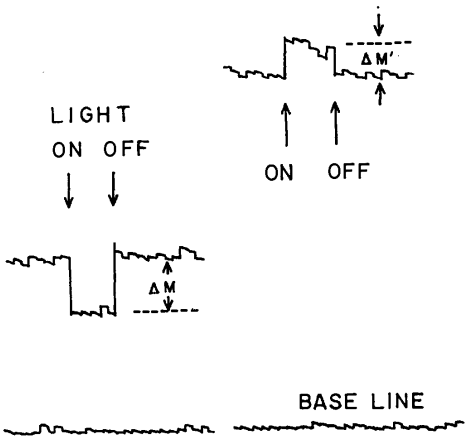

Fig. 1. Change under illumination of ICR signal intensities of *m/e* 134 (left) and *m/e* 119 for light at 440 nm. Neutral pressure was 3×10^{-8} Torr and reaction time τ was 3.0 s. ΔM denotes the signal decrease of *m/e* 134, and $\Delta M'$ denotes the signal increase of *m/e* 119.

† On leave from Kitakyushu University, Kitagata, Kokuraminami-ku, Kitakyushu 802.

†† John Simon Guggenheim Memorial Fellow, 1978—1979.

propriate ion, and dividing by (I) for photoproduction curves, or applying Eq. 2 for photodisappearance curves.

Results and Discussion

The visible-region photodissociation (photodisappearance) spectrum of the t-butylbenzene cation (m/e 134) is shown in Fig. 2, along with the photoproduction spectra of the ions at m/e 119 and m/e 91, whose abundance increases when the light is turned on. Above 450 nm m/e 119 is the only observed photoproduct under any conditions, and accounts quantitatively for all of the photolyzed parent ion, indicating that Eq. 1 is the only photodissociation process, and that the m/e 119 ion is stable against both photodissociation and ion-molecule reaction processes.

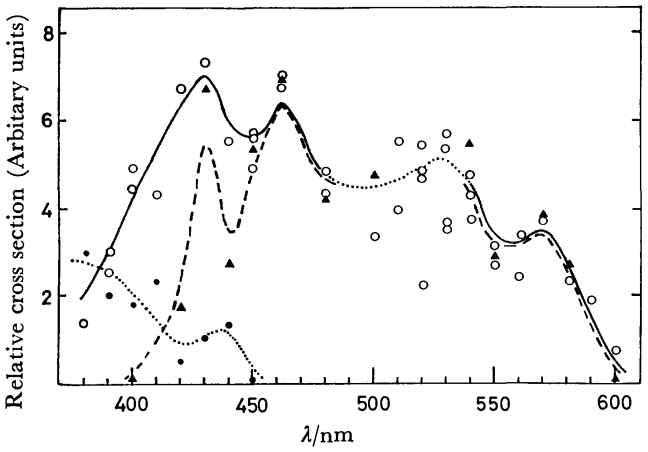

Fig. 2. Photodissociation spectrum of t-butylbenzene cation (m/e 134) (—○—), and the photoproduction spectra of its daughter ions m/e 119 (---▲---) and m/e 91 (···●···). While not absolute, the units for the three curves are consistent, so that the extent of parent-ion destruction and product-ion production may be directly compared. The pressure was 4×10^{-8} Torr, the reaction time τ was 3.0 s, and the errors of wave length are almost ±7 nm.

However, at shorter wavelengths the photochemistry becomes more complex, and ions at m/e 91 and m/e 57 become prominent as light-produced species. Figure 3 shows the complete photodisappearence spectrum of m/e 134, and shows that at shorter wavelengths, m/e 119 also decreases under illumination. Figure 4a shows that m/e 91 and m/e 57 increase under illumination parallel to the decrease in m/e 119.

The ion m/e 91 is evidently a direct photoproduct from m/e 119, but m/e 57 is not: at shorter times and lower pressure, as indicated in Fig. 4b, m/e 57 virtually disappears, and is apparently an ion-molecule reaction product from m/e 91. The photochemistry in this system is thus governed by three processes, Eqs. 1, 3, and 4.

$$\underset{(m/e\ 119)}{C_9H_{11}^+} \xrightarrow{h\nu} \underset{(m/e\ 91)}{C_7H_7^+} + C_2H_4 \qquad (3)$$

$$\underset{(m/e\ 91)}{C_7H_7^+} \xrightarrow{C_{10}H_{14}} \underset{(m/e\ 57)}{C_4H_9^+} + \text{Neutral products} \qquad (4)$$

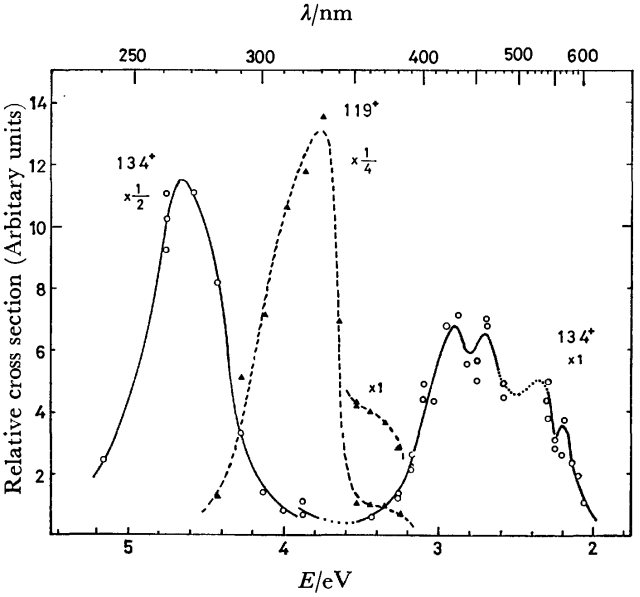

Fig. 3. Photodisappearance spectra of m/e 134 (—○—) and m/e 119 (---▲---). The intensity units are consistent for the two curves, and are also consistent with those of Fig. 2, (but note that this figure plots photodisappearance of m/e 119, while Fig. 2 plotted photoproduction of m/e 119 at the longer wavelengths involved). Pressure and τ as in Fig. 2.

Further confirmation of this sequence is provided by the double resonance results shown in Fig. 4b: the ejection of m/e 119 results in a large decrease in m/e 91, supporting the assignment of Eq. 3 as the immediate source of m/e 91. Ejection of m/e 134 gives a lesser, but still significant decrease in m/e 91, reflecting the two-reaction sequence connecting these two ions.

Under the conditions of Fig. 4a, about half of the m/e 91 ions are converted to m/e 57 over most of the wavelength range; the sharp increase in the [57]/[91] ratio near 320 nm (where both the photon flux and the m/e 119 photodissociation cross section are large) apparently reflects the extremely rapid conversion of m/e 119 to m/e 91 at this wavelength, giving, Eq. 4 more time to move further toward completion.

The photodissociation spectrum of the m/e 119 ion reflected in Fig. 3, while subject to some distortion by photoproduction of 119 by Eq. 1, is probably reasonably faithful from 3.3 to 4.3 eV. This spectrum, with a strong peak at 3.8 eV and a small peak around 3.4 eV, is very similar to the photodissociation spectrum of m/e 105 obtained by protonation of styrene[9] (showing a strong peak at 3.9 eV, and a weaker one near 3.1 eV). It is thus reasonable to assume that the m/e 119 ion produced by electron impact from t-butylbenzene has the protonated methylstyrene structure II. Since the

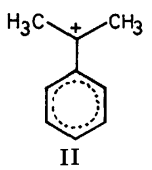

II

background of electron-impact-produced m/e 119 ions

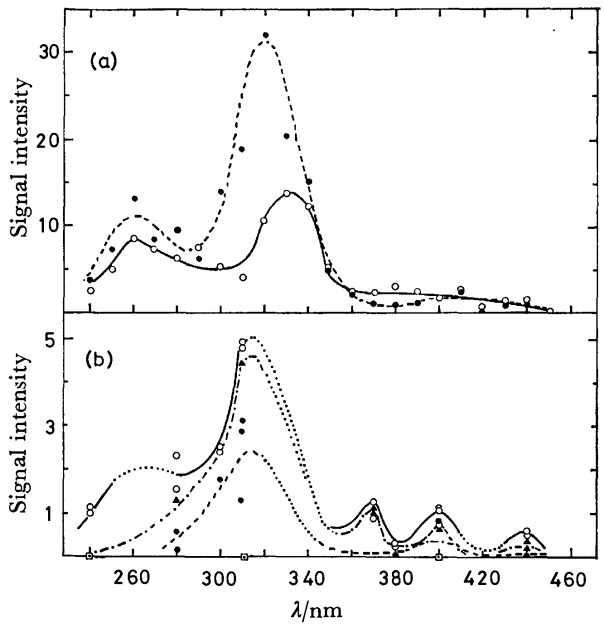

Fig. 4. a): Photoproduction curves for *m/e* 91 (—○—) and *m/e* 57 (---●---). Pressure and τ as in Fig. 2.
b): Photoproduction of *m/e* 91 using double resonance ejection of possible precursors: (—○—) shows *m/e* 91 production without double resonance; (---▲---) shows *m/e* 91 production with ejection of *m/e* 134, and (---●---) shows *m/e* 91 production with ejection of *m/e* 119. The pressure was 2.4×10^{-8} Torr, and τ was 1.0 s. Under these conditions of lower pressure and shorter τ, there was no observable signal for *m/e* (⊡).

was larger than the photoproduced *m/e* 119 ion, it was not possible to analyze separately the photoproduct ions of Eq. 1.

Reaction 4 can be visualized as a simple displacement of the *t*-butyl group by C_7H_7 on the neutral *t*-butylbenzene, although of course the present results give no information about the actual mechanism. Assuming the neutral product of this reaction to be diphenylmethane, the reaction is calculated to be exothermic by a few kcal/mol.

Conclusion

Considerable complexity has been found in the photochemistry of *t*-butylbenzene ions at shorter wavelengths, with the final product ion, *m/e* 57, terminating a sequence of two successive photodissociations and an ion-molecule reaction. No evidence was found for competitive dissociation of I into two different product channels, however, and the observed chemistry seems to be satisfactorily accounted for within the assumption that Reaction (1) is the only photoreaction of the parent ion I.

The support of the donors of the Petroleum Research Fund, administered by the American Chemical Society, the U. S. National science Foundation, and the U. S. Air Force Geophysics Laboratory is gratefully acknowledged. One of the authors, Yoshiya Takenoshita, thanks the Kitakyushu Mayor for the Kitakyushu Abroad Fellowship and Dr. Myung Soo Kim for his help at the beginning of this work.

References

1) E. W. Fu, P. P. Dymerski, and R. C. Dunbar, *J. Am. Chem. Soc.*, **98**, 377 (1976); R. C. Dunbar, *Anal. Chem.*, **48**, 723 (1976).
2) R. C. Dunbar and R. Klein, *J. Am. Chem. Soc.*, **99**, 3744 (1977).
3) M. S. Kim, R. C. Dunbar, and F. W. McLafferty, *J. Am. Chem. Soc.*, **100**, 4600 (1978).
4) R. C. Dunbar, "Ion Photodissociation," in "Gas-Phase Ion Chemistry," ed by M. T. Bowers, Academic Press (1979), Vol. 2.
5) P. P. Dymerski, E. Fu, and R. C. Dunbar, *J. Am. Chem. Soc.*, **96**, 4109 (1974).
6) R. C. Dunbar, *J. Phys. Chem.*, **83**, 2376 (1979).
7) J. L. Franklin, J. G. Dilland, H. M. Rosenstock, J. T. Herron, K. Draxl, and F. H. Field, "Ionization Potentials, Appearance Potentials and Heats of Formation of Gaseous Positive Cations," National Bureau of Standards, U. S. Government Printing Office, Washington, DC (1969).
8) J. H. Richardson, L. M. Stephenson, and J. I. Brauman, *J. Am. Chem. Soc.*, **96**, 3671 (1974).
9) R. C. Dunbar, M. S. Kim, and G. A. Olah, *J. Am. Chem. Soc.*, **101**, 1368 (1979).

Reaction of Halogenonitrobenzenes with Electro-generated Superoxide Ion

Hiromitsu SAGAE, Masamichi FUJIHIRA, Katsutaro KOMAZAWA,**
Henning LUND,† and Tetsuo OSA*
Pharmaceutical Institute, Tohoku University, Aobayama, Sendai 980
***Tokyo Metropolitan College of Aeronautical Engineering, Minamisenju, Arakawa-ku, Tokyo 116*
(Received January 9, 1980)

The reaction of halogenonitrobenzenes (XNBs) with electrogenerated superoxide ion in *N,N*-dimethylformamide was studied electrochemically using cyclic voltammetry (CV) and controlled potential macro-electrolysis. It was shown in the CV that electro-generated superoxide ion reacts with all of the *o*- and *p*-isomers of iodo-, bromo-, and chloronitrobenzene in the dissolved oxygen medium. However the superoxide ion did not react with the other XNBs during CV. Controlled potential macro-electrolysis of oxygen in the presence of *o*- and *p*-bromonitrobenzene yielded the corresponding nitrophenols as the main products. The reaction mechanism *via* nucleophilic attack of the superoxide ion on the XNB, in the preference to an electron-transfer mechanism, is proposed.

Electrochemical reduction of oxygen dissolved in non-aqueous organic solvents,[1-4] such as pyridine, acetonitrile, and *N,N*-dimethylformamide (DMF), occurs at *ca.* −0.85 V *vs.* silver–silver chloride (Ag/AgCl) and yields, reversibly, superoxide ion as shown in Eq. 1:[5-7]

$$O_2 + e \rightleftharpoons O_2^{\cdot-} \quad (1)$$

Recently, several studies regarding chemical reactions of electro-generated superoxide ion with organic compounds have been reported. Dietz *et al.*[8] suggested that superoxide ion in nonaqueous solvents possesses various reactivities, namely characteristics of a strong base, nucleophile, oxidant, reductant, and free radical. During the past several years we have studied the reactivity of electro-generated superoxide ion with alkylbenzenes,[9,10] methylpyridines and methylpyridine *N*-oxides.[11] Simultaneously we have studied the reaction of electro-generated superoxide ion with halogenonitrobenzenes (XNBs), expecting to observe the electron transfer reaction of superoxide ion. At the almost same time as this work was presented,[12] Rosenthal and Frimer also reported that superoxide ion solubilized in benzene by crown ether reacts rapidly with electron acceptors such as nitro substituted hydrocarbons and halides.[13]

There are several reports on the electrochemical reaction of XNBs in nonaqueous solvents, using electrochemical methods such as cyclic voltammetry and polarography.[14-17] However, electrochemical studies in the presence of oxygen have not previously been published. The cyclic voltammetric behavior of oxygen in the presence of some XNBs seemed to be interpretable in terms of the same mechanism as for catalytic reduction of aromatic halides, *via* electron transfer from the electro-generated radical anion to aromatic halides, as reported Lund *et al.*[18]

However, after detailed investigation using macro-electrolysis and cyclic voltammetry in DMF, we have concluded that the reaction mechanism of the system should be considered more in terms of a nucleophilic reaction of electro-generated superoxide ion[19-23] with XNBs than in terms of the electron transfer reaction of electro-generated superoxide ion to XNBs followed merely by elimination of halide ion. We report here the reaction of electro-generated superoxide ion with XNBs using macro-electrolysis and cyclic voltammetry in DMF solution, and discuss the results in terms of the nucleophilicity and reductant properties of superoxide ion.

† On leave from Department of Organic Chemistry, University of Aarhus, DK-8000, Aarhus C, Denmark.

Experimental

Materials. DMF was dried over anhydrous $CuSO_4$ for 24 h and then distilled under reduced pressure. Further purification was achieved by passage through a column of molecular sieve (4A 1/16) and activated alumina (both pretreated by heating at 400 °C). Tetraethylammonium perchlorate (TEAP) was synthesized and purified in the usual manner.[24] Iodonitrobenzenes (INBs), bromonitrobenzenes (BNBs), chloronitrobenzenes (CNBs), and fluoronitrobenzenes (FNBs) of E. P. grade were purchased commerically (Wako Pure Chemical Industries) and were recrystallized or distilled before use.

Cyclic Voltammetry. Cyclic voltammetry was carried out in DMF solution containing 0.1 M (1 M=1 mol dm^{-3}) TEAP as a supporting electrolyte on a hanging mercury drop electrode (HMDE). The cathode potential was referred to Ag/AgCl, aq 1 M KCl. Cyclic potential sweeps were generated by an NF Circuit Desigh Block FG-100AD function generator in connection with a potentionstat which was self-made according to the literature.[25]

Controlled Potential Macro-electrolysis. For controlled potential macro-electrolysis, a three compartment cell was employed in which the cathodic and anodic chambers were separated by two porous glass disks and a reference electrode with a Luggin capillary was put near the cathode. A mercury pool with a surface area of 16 cm^2 was used as the cathode, and platinum gauze as the anode. The electrolyte solution (0.1 M TEAP) of 60 cm^3 containing 0.06 M substrate was placed in the cathodic chamber, 40 cm^3 of electrolyte solution in the anodic chamber, and 10 cm^3 of electrolyte solution in the middle chamber. Oxygen was bubbled through the catholyte. The cathode potential was controlled with a Yanagimoto VE-8 controlled potential electrolyzer.

Separation of Products and Determination of the Yields. The main products of the electrolyses, nitrophenols, were separated and identified by the following procedure. The catholyte was poured into 200 cm^3 of 10% aqueous $NaHCO_3$ solution. Starting material and products other than nitrophenols were removed by extraction with CH_2Cl_2. The aqueous layer was evaporated to dryness *in vacuo* to remove DMF. The resulting solid was dissolved in water and acidified with 5% aqueous

HCl. The liberated nitrophenol was extracted with ether and purified by recrystallization from ethanol and weighed. The crystalline nitrophenol was identified by comparing its melting point and infrared spectrum (IR) with those of an authentic sample. The by-products of electrolysis, such as nitrobenzene and dinitrobiphenyls, were detected by using a Shimadzu gas chromatograph Model GC-6A equipped with 2 m×3ϕ SUS column packed with Silicone OV-1, and identified by comparing their retention times with those of authentic samples. Yields of products were also determined by gas chromatographic analysis.

Results and Discussion

Controlled Potential Macro-electrolysis. The reduction peak potentials of cyclic voltammograms of XNBs, together with those for oxygen, nitophenols, and nitrobenzene, are listed in Table 1. The controlled potential macro-electrolysis of oxygen in the presence of *p*-bromonitrobenzene (*p*-BNB) was carried out at −0.9 V in DMF solution. At −0.9 V, oxygen was reduced to superoxide ion while *p*-BNB was not reduced. The results of electrolysis are collected in Table 2. *p*-BNB reacted with electro-generated superoxide ion to yield *p*-nitrophenol as the main product. Trace amounts of nitrobenzene and 4,4′-dinitrobiphenyl were detected as by-prodects. In order to investigate the positional effect of the nitro group attached to the benzene ring, macro-electrolyses of oxygen in the presence of *o*- and *m*-BNB were also carried out. *o*-BNB reacted with electro-generated superoxide ion to yield *o*-nitrophenol as the main product. Trace amounts of nitrobenzene and 2,2′-dinitrobiphenyl were detected as by-products. *m*-BNB did not react with electro-generated superoxide ion and starting material was recovered.

Table 1. Reduction peak potentials of halogenonitrobenzenes by cyclic voltammetry

Compound	E_p^1	E_p^2	E_p^3
o-Fluoronitrobenzene	−1.09	−2.01	
m-Fluoronitrobenzene	−1.00	−1.90	
p-Fluoronitrobenzene	−1.12	−2.07	
o-Chloronitrobenzene	−1.10	−1.85	
m-Chloronitrobenzene	−1.00	−1.86	
p-Chloronitrobenzene	−1.04	−1.91	
o-Bromonitrobenzene	−1.12	−1.85	
m-Bromonitrobenzene	−0.94	−1.78	
p-Bromonitrobenzene	−1.02	−1.86	
o-Iodonitrobenzene	−0.96	−1.05	−1.77
m-Iodonitrobenzene	−0.96	−1.05	−1.90
p-Iodonitrobenzene	−1.02	−1.15	−1.92
o-Nitrophenol	−0.89	−1.85	
m-Nitrophenol	−1.19	−1.52	
p-Nitrophenol	−1.30	−1.95	
Nitrobenzene	−1.10	−1.95	
Cf. Oxygen	−0.85	−1.75	

E/V *vs.* Ag/AgCl, electrolyte: 0.1 M TEAP/DMF, electrode: HMDE.

Table 2. Controlled potential macro-electrolysis of oxygen in the presence of bromonitrobenzenes

Starting material	Product	Yield/%
o-Bromonitrobenzene	*o*-Nitrophenol	39
	Nitrobenzene	2—3
	2,2′-Dinitrobiphenyl	1—2
m-Bromonitrobenzene	—	—
p-Bromonitrobenzene	*p*-Nitrophenol	52
	Nitrobenzene	1—2
	4,4′-Dinitrobiphenyl	1

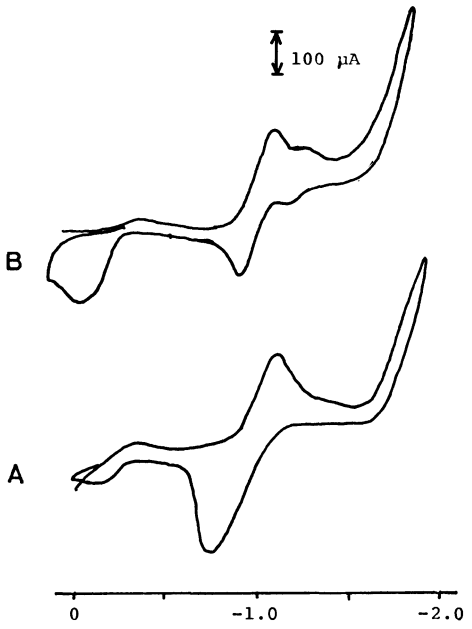

Fig. 1. Cyclic voltammograms of the catholyte in the course of the electrolysis at −0.9 V in the presence of *p*-bromonitrobenzene (oxygen is removed from the solution).
Electrolyte: 0.1 M TEAP/DMF, electrode: HMDE, sweep rate: 0.1 V s^{-1}, A: after 1 h, B: after 6 h.

Cyclic Voltammetry of the Catholyte. In the course of macro-electrolysis of oxygen at −0.9 V in the presence of *p*-BNB, cyclic voltammetry of the catholyte was carried out. The result is shown in Fig. 1. A and B are the cyclic voltammograms of the catholyte after 1 h and 6 h respectively from commencement of macro-electrolysis. During these cyclic voltammetric experiments, oxygen was removed by bubbling nitrogen. Since *p*-BNB remained as a major substrate in the solution, two large reduction waves observed at *ca.* −1.1 V and −1.8 V are attributed to *p*-BNB. The oxidation wave at *ca.* −0.13 V results from bromide ion as is described later. While no reduction wave other than that for *p*-BNB is appreciable on curve A, a new reduction wave is apparent at *ca.* −1.3 V on curve B. On curve B, the oxidation peak height of bromide ion is greater in comparison with that on curve A.

Cyclic Voltammetry of Bromonitrobenzenes (BNBs). In order to clarify the reaction mechanism of the reaction of electro-generated superoxide ion with XNBs,

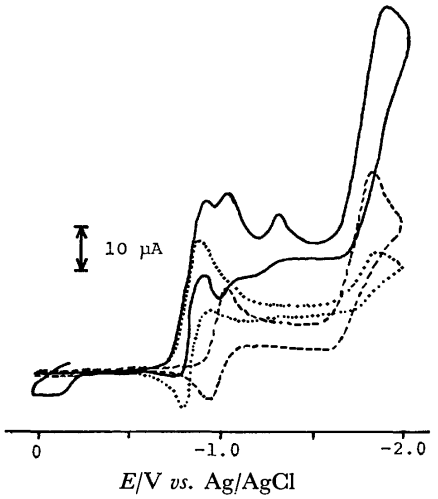

Fig. 2. Cyclic voltammograms of *p*-bromonitrobenzene. Concentration of *p*-bromonitrobenzene: *ca.* 1 mM, electrolyte: 0.1 M TEAP/DMF, electrode: HMDE, sweep rate: 0.1 V s^{-1}, ——: in the presence of air-saturated oxygen, ------: in the absence of oxygen, *cf.* ·····: cyclic voltammogram of air-saturated oxygen.

cyclic voltammetry of *o*-, *m*-, and *p*-BNB was carried out under air-saturation and under a nitrogen atmosphere. The cyclic voltammetric behaviors of *p*-BNB are shown in Fig. 2. The broken line represents the cyclic voltammogram of *p*-BNB under a nitrogen atmosphere and the solid line that under air-saturation. The dotted line represents the cyclic voltammogram of air-saturated oxygen. For *p*-BNB under a nitrogen atmosphere, only a reversible reduction wave at −1.0 V and an irreversible reduction wave at *ca.* −1.8 V were observed. On the other hand, under air saturation, a new reduction wave at *ca.* −1.3 V appeared on the first cathodic sweep, and another new wave was seen at *ca.* −0.13 V on the anodic sweep, in addition to the waves observed for oxygen alone and for *p*-BNB under nitrogen. On the subsequent cathodic sweep, a new wave, corresponding to the reduction of the oxidation product at −0.13 V, appeared at *ca.* −0.17 V. The peak potential of the new wave at −1.3 V corresponds accidentally to the first reduction peak potential of *p*-nitrophenol as is shown in Fig. 3. The first reduction wave of *p*-nitrophenol is the phenoxide formation from phenol.[26] Consequently the new reduction wave may not be that of *p*-nitrophenol because *p*-nitrophenol exists as phenoxide in such an aprotic medium as DMF even if *p*-nitrophenol is formed during cyclic voltammetry. The product showing this new reduction wave seemed to be dinitrophenyl peroxide as described later. Since the peak height of the redox wave near −0.15 V increased on addition of NaBr, this redox wave is attributed to the redox reaction of bromide ion at the mercury electrode. Consequently these additional wave of bromide and the product, observed only in the case of the simultaneous electro-reduction of oxygen, suggest the following. (1) The electro-generated superoxide ion reacted with *p*-BNB to release bromide ion and to give the redox wave during cyclic voltammetry. (2) A compound probably assigned dinitrophenyl peroxide was produced during cyclic voltammetry by the reaction of electro-generated superoxide ion with *p*-BNB.

In the cyclic voltammogram of *p*-BNB under air-saturation, the first reduction peak height of oxygen at *ca.* −0.85 V increased, and the reoxidation peak height of superoxide ion at −0.80 V diminished, in comparison with those of air-saturated oxygen in the absence of *p*-BNB (dotted line in Fig. 2). These behaviors depended on the concentration of *p*-BNB. In order to clarify the dependence of the increase of the reduction peak height of oxygen on the concentration of *p*-BNB, cyclic voltammetry of oxygen in the presence of increasing concentrations of *p*-BNB was carried out in the potential region

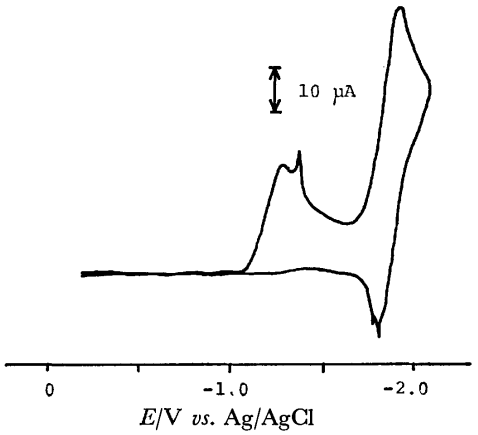

Fig. 3. Cyclic voltammogram of *p*-nitrophenol under nitrogen atmosphere.
Concentration of *p*-nitrophenol: *ca.* 10 mM, electrolyte: 0.1 M TEAP/DMF, electrode: HMDE, sweep rate: 0.1 V s^{-1}.

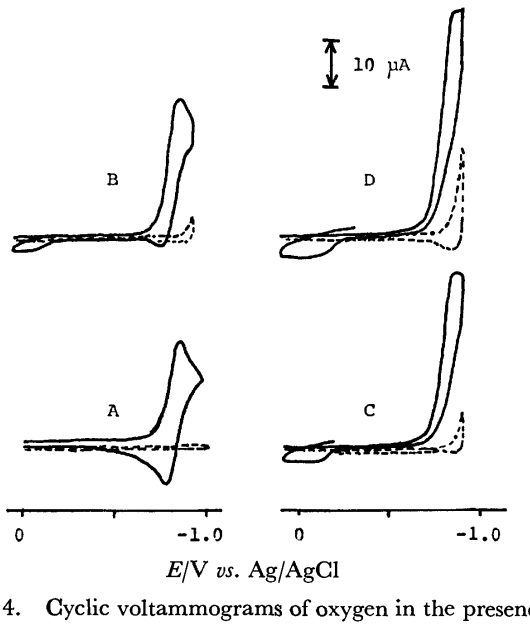

Fig. 4. Cyclic voltammograms of oxygen in the presence of increasing concentration of *p*-bromonitrobenzene. A: 0 mM, B: *ca.* 1 mM, C: *ca.* 4 mM, D: *ca.* 8 mM, electrolyte: 0.1 M TEAP/DMF, electrode: HMDE, sweep rate: 0.1 V s^{-1}, ——: air-saturation, ------: under nitrogen atmosphere.

from 0 to −1.0 V. The results are shown in Fig. 4. A is the cyclic voltammogram of air-saturated oxygen in the absence of *p*-BNB. Cyclic voltammograms of oxygen in the presence of increasing concentrations of *p*-BNB are shown in Figs. 4B, C, and D, in the order of increasing concentrations of *p*-BNB. Increasing concentration of *p*-BNB resulted in a corresponding increase in the reduction peak height of oxygen. This increase in height with increasing concentration of *p*-BNB did not continue infinitely but reached a limit. The maximum value of the ratio, i_c/i_p, for *p*-BNB is *ca.* 2, where i_c is the reduction peak height of oxygen in the presence of XNB and i_p is the peak height in the absence of XNB. Under a nitrogen atmosphere no oxidation wave corresponding to that of bromide ion appeared, as shown in Fig. 4A, while in the presence of air-saturated oxygen the oxidation wave of bromide ion was observed and the peak height increased with increasing concentration of *p*-BNB. Disappearance of the oxidation wave of superoxide ion indicates that the electro-generated superoxide ion was consumed by subsequent chemical reaction during cyclic voltammetry in the presence of a high concentration of *p*-BNB.

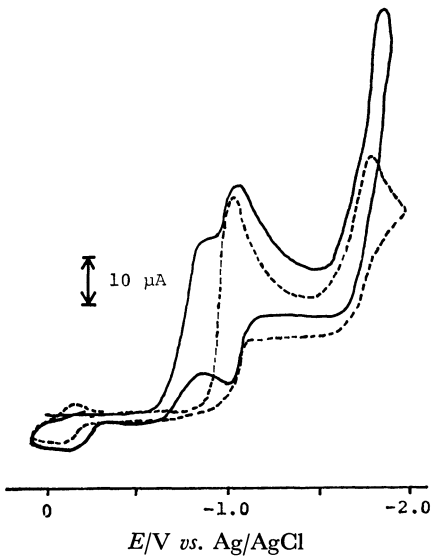

Fig. 5. Cyclic voltammograms of *o*-bromonitrobenzene. Concentration of *o*-bromonitrobenzene: *ca.* 10 mM, electrolyte: 0.1 M TEAP/DMF, electrode: HMDE, sweep rate: 0.1 V s^{-1}, ——: in the presence of air-saturated oxygen, ------: in the absence of oxygen.

In order to investigate the positional effect of the nitro group attached to the benzene ring, cyclic voltammetry of oxygen in the presence of increasing concentrations of *o*- and *m*-BNB was also carried out. The reduction peak height of oxygen increased in the presence of increasing concentration of *o*-BNB. This increase did not continue infinitly and the maximum of the i_c/i_p ratio for *o*-BNB is also *ca.* 2. Cyclic voltammetric behaviors of *o*-BNB in the presence and in the absence of oxygen are shown in Fig. 5. Under nitrogen atmosphere, the first reduction wave of *o*-BNB on the first cathodic sweep is irreversible, while that of *p*-BNB is reversible, and a redox wave corresponding to that of bromide ion appeared on the anodic sweep and on the subsequent cathodic sweep in spite of the absence of oxygen. In the presence of oxygen, the oxidation peak height of bromide ion also increased compared with that observed under a nitrogen atmosphere though the new reduction wave corresponding to the reduction of a product are not recognized. It is concluded from these results that bromide ion is released from *o*-BNB by an electrochemical reaction of *o*-BNB itself, but the reaction of electro-generated superoxide ion with *o*-BNB accelerates this release of bromide ion.

In the cyclic voltammogram of *m*-BNB in the presence of oxygen, no reduction wave appeared other than those for oxygen and *m*-BNB. An increased concentration of *m*-BNB did not results in a corresponding increase in the reduction peak height of oxygen, or in diminution of the reoxidation peak height of superoxide ion, in these cyclic voltammograms of oxygen in the presence of *m*-BNB. These results indicate that the electro-generated superoxide ion does not react with *m*-BNB during their cyclic voltammetry.

In order to investigate the difference in reactivity of electro-generated superoxide ion towards XNBs, dependent on the nature of substituted halogen, cyclic voltammetry of INBs, CNBs, and FNBs in the presence and in the absence of oxygen was carried out and is described in the following sections.

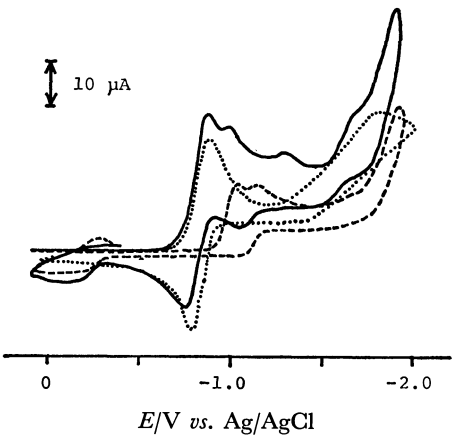

Fig. 6. Cyclic voltammograms of *p*-iodonitrobenzene. Concentration of *p*-iodonitrobenzene: *ca.* 1 mM, electrolyte: 0.1 M TEAP/DMF, electrode: HMDE, sweep rate: 0.1 V s^{-1}, ——: in the presence of air-saturated oxygen, ------: in the absence of oxygen, *cf.* ·····: cyclic voltammogram of air-saturated oxygen.

Cyclic Voltammetry of Iodonitrobenzenes (INBs). The cyclic voltammetric behavior of *p*-INB in the presence and in the absence of air-saturated oxygen is shown in Fig. 6, together with that of oxygen in the absence of *p*-INB. For *p*-INB under nitrogen, there are well-defined reduction waves near −1.0, −1.15, and −1.90 V on the cathodic sweep, and an oxidation wave near −0.2 V on the anodic sweep.[16b] On the subsequent cathodic sweep, a new reduction wave corresponding to reduction of the oxidation product apperaed at *ca.* −0.25 V. Since the oxidation peak height at −0.2 V increased on addition of NaI as

for the bromide peak described above, this oxidation wave is assigned to that of iodide ion. Under air-saturation, two new reduction waves at *ca.* −1.30 V and −1.75 V appeared as well as those for oxygen and *p*-INB, and the peak height of the oxidation wave at *ca.* −0.2 V was increased in comparison with that under a nitrogen atmosphere. The first reduction peak height of oxygen increased and the reoxidation peak height of superoxide ion diminished as compared with that for air-saturated oxygen in the absence of *p*-INB (dotted line in Fig. 6).

The cyclic voltammetric behavior of *o*-INB in the presence and in the absence of oxygen is almost identical to that of *p*-INB except absence of the new reduction wave of the product in the presence of oxygen corresponding to that appeared at −1.3 V for *p*-INB. An increase in the concentration of *o*- and *p*-INB resulted in a corresponding increase in the reduction peak height of oxygen in the cyclic voltammograms. Maximum values of the ratio, i_c/i_p, for both *o*- and *p*-INB are also *ca.* 2. In the cyclic voltammogram of *m*-INB in the presence of oxygen, no reduction wave appeared other than those for oxygen and *m*-INB as for *m*-BNB. The reduction peak height of oxygen in the presence of *m*-INB did not increase in comparison with that of air-saturated oxygen in the absence of *m*-INB.

Cyclic Voltammetry of Chloronitrobenzenes (CNBs). The cyclic voltammetric behavior of *o*-, *m*-, and *p*-CNB in the presence and in the absence of oxygen are almost identical to those of *o*-, *m*-, and *p*-BNB, respectively. Namely, *o*- and *p*-CNB readily react with electro-generated superoxide ion while *m*-CNB dose not. The ratio, i_c/i_p, for *o*- and *p*-CNB also reached a limit with increase in the concentration of *o*- and *p*-CNB, and their maximum values were *ca.* 2.

Cyclic Voltammetry of Fluoronitrobenzenes (FNBs). Reversible and irreversible reduction waves appeared near −1.1 and −2.0 V in the cyclic voltammograms of *o*-, *m*-, and *p*-FNB under a nitrogen atmosphere. In the cyclic voltammograms of *o*-, *m*-, and *p*-FNB in the presence of oxygen, no reduction waves other than those for oxygen and FNB appeared. The electro-generated superoxide ion did not therefore react with FNBs during their cyclic voltammetry. Although an increase in the reduction peak height of oxygen was observed in the presence of *o*- and *p*-FNB, the maximum values of the ratio, i_c/i_p, are close to unity, *ca.* 1.1, compared with *ca.* 2 in the presence of *o*- and *p*-isomers of other XNBs. In the presence of *m*-FNB, this increase in the reduction peak height of oxygen was not observed.

Reaction Mechanism for the Reaction of Superoxide Ion with Halogenonitrobenzenes (XNBs). A mechanism for the reaction of electro-generated superoxide ion with XNBs can be proposed as shown in Schemes 1 and 2. Scheme 1 represents S_N2 type reaction mechanism. This S_N2 type reaction of superoxide ion is well known with alkyl halides and alkyl sulfonate esters.[22,23] Electrochemically produced superoxide ion at −0.85 V attacks the carbon atom bearing halogen on the XNB to release halide ion (Eq. 2). The resulting peroxyl radical is readily reduced, by superoxide ion or at the electrode, to peroxide anion $ArOO^-$ (Eq. 3). Scheme 2 represents the electron-transfer mechanism. Electron transfer reactions between superoxide ion and aromatic nitro compounds have been reported.[13] An electron is transferred from electro-generated superoxide ion to XNB to give an anion radical $[ArX]^{\cdot}$ and oxygen is regenerated (Eq. 5). Halide ion is released from the anion radical $[ArX]^{\cdot}$ to yield phenyl radical Ar· (Eq. 6). Peroxide anion $ArOO^-$ is then produced according to Eqs. 7 and 3. In both mechanisms two electrons per molecule of oxygen are necessary to finally obtain the peroxide anion.

$$O_2 + e \rightleftarrows O_2^{\cdot} \quad (1)$$
$$O_2^{\cdot} + ArX \longrightarrow ArOO\cdot + X^- \quad (2)$$
$$ArOO\cdot + O_2^{\cdot} \longrightarrow ArOO^- + O_2 \quad (3)$$
overall: (1)×2+(2)+(3)
$$O_2 + ArX + 2e \longrightarrow ArOO^- + X^- \quad (4)$$

Scheme 1.

$$O_2 + e \rightleftarrows O_2^{\cdot} \quad (1)$$
$$O_2^{\cdot} + ArX \longrightarrow [ArX]^{\cdot} + O_2 \quad (5)$$
$$[ArX]^{\cdot} \longrightarrow Ar\cdot + X^- \quad (6)$$
$$Ar\cdot + O_2 \longrightarrow ArOO\cdot \quad (7)$$
$$ArOO\cdot + O_2^{\cdot} \longrightarrow ArOO^- + O_2 \quad (3)$$
overall: (1)×2+(5)+(6)+(7)+(3)
$$O_2 + ArX + 2e \longrightarrow ArOO^- + X^- \quad (4)$$

Scheme 2.

Since in the cyclic voltammograms of *p*-BNB and *p*-CNB under a nitrogen atmosphere the oxidation wave of halide ion did not appear, the formed anion radicals $[ArX]^{\cdot}$ are stable so that the elimination reaction as described in Eq. 6 could not occur during the period of cyclic voltammetry. In the presence of oxygen as shown in Fig. 2, the oxidation wave of halide ion appeared. These results support nucleophilic attack of superoxide ion on *p*-BNB and *p*-CNB as described in Eq. 2. In the cyclic voltammograms of INBs, *o*-BNB, and *o*-CNB, the oxidation wave of halide ion appeared even under a nitrogen atmosphere, and in the presence of oxygen these halide peaks increased further. These results indicate that these anion radicals $[ArX]^{\cdot}$ are unstable compared with those of *p*-BNB and *p*-CNB, and that the electron transfer reaction of superoxide ion to XNB (Eq. 5) proceeds forwards to some extent. If the superoxide ion reacts with XNB *via* an electron transfer mechanism, then the yield of nitrobenzene and dinitrobiphenyls should be great because of the production of radical Ar· (Eq. 6). However, as the main products of the macro-electrolysis of oxygen in the presence of *o*- and *p*-BNB were *o*- and *p*-nitrophenol respectively (Table 2), the contribution of the electron transfer reaction mechanism operating in these case is considered to be slight.

The difference in reactivity of electro-generated superoxide ion towards XNBs dependent on the nature of substituted halogen and on the position of the nitro group attached to benzene ring is discussed next. The maximum values of the ratio, i_c/i_p, of the reduction peak heights of oxygen in the presence of *o*- and *p*-

isomers of INB, BNB, and CNB are *ca.* 2. This result corresponds well with the fact that two electrons are necessary to produce peroxide anion $ArOO^-$ from XNB in Scheme 1, but disagrees with usual EC catalytic mechanism.[27] In the cyclic voltammograms of the *m*-isomers of INB, BNB, and CNB, the reduction peak heights of oxygen did not increase in the presence of high concentrations of XNB. In the case of FNBs, the reduction peak heights of oxygen did not increase even in the presence of *o*- and *p*-FNB. It has been reported that potassium superoxide reacted with some nitrophenyl halides[13] as electro-generated superoxide reacted with XNBs in this work but did not react with phenyl halides.[22] The difference in reactivity between nitrophenyl halides and phenyl halides is interpretable in terms of activation by the nitro group on the benzene ring. In the cyclic voltammograms of XNBs in the presence of oxygen, the high reactivities of *o*- and *p*-isomers of XNB, other than FNB, to superoxide ion are manifest, but the reactivity of *m*-isomers of XNB is seen to be very low.

The wave corresponding to the oxidation of peroxide anion $ArOO^-$ did not appear in Figs. 2, 5, and 6. This is probably due to the fact that its oxidation potential may be more positive than the measured potential region, as for alkylperoxide anion,[19] and also due to its reaction with XNB to yield bis(nitrophenyl) peroxides,[19] ArOOAr (Eq. 8). In general, the reduction peaks of dialkylperoxides appear at more negative potentials than −2.0 V *vs.* SCE (Et_2O_2; −2.15 V, Bu_2O_2; −2.19 V, $Bu^t{}_2O_2$; −2.4 V *vs.* SCE).[19] Since the bis(nitrophenyl) peroxides formed in this study have two nitro groups, their reduction peak potential should be more positive than those of dialkyl compounds. The first reduction potentials of organic nitro compounds between −1.0 and −1.2 V *vs.* SCE. The reduction of bis(nitrophenyl) peroxides by electrogenerated superoxide ion cannot occur because the maximum value of the i_c/i_p ratio is not over two. Consequently the reduction potentials of bis(nitrophenyl) peroxides lie at more negative potential than that of oxygen. The reduction wave of the bis(*p*-nitrophenyl) peroxide may correspond to the new reduction wave at *ca.* −1.3 V in Figs. 2 and 6, and that of the bis(*o*-nitrophenyl) peroxide may overlap with those of *o*-XNBs, and thus the new wave are not appreciable in Fig. 5.

As probable mechanisms for formation of phenols, two mechanisms can be proposed in the same manner as

$$ArOO^- + ArX \longrightarrow ArOOAr + X^- \quad (8)$$

$$ArOOAr + O_2^{\cdot-} \longrightarrow ArO_3\cdot + ArO^- \quad (9)$$
$$\longrightarrow ArOOAr, ArO^-, O_2$$

$$ArOOAr + O_2^{\cdot-} \longrightarrow ArO\cdot + ArO^- + O_2 \quad (10)$$

$$ArO\cdot + O_2^{\cdot-} \longrightarrow ArO^- + O_2 \quad (11)$$

Scheme 3.

$$ArOO^- + CH_3\overset{\overset{O}{\|}}{S}CH_3 \longrightarrow ArO^- + CH_3\overset{\overset{O}{\|}}{S}CH_3 \quad (12)$$

Scheme 4.

for the reaction of superoxide ion with alkyl halides[28,29] as shown in Schemes 3 and 4. If Reaction 9 or 10 and 11 proceed rapidly, the ratio i_c/i_p will exceed two due to the regeneration of oxygen *via* these reactions. Since the observed ratios were *ca.* 2, these reactions might be too slow to occure in the period of cyclic voltammetry.[19] On the other hand, nitrophenols can be formed without further consumption of electron *via* reaction 12 shown in Scheme 4. However this reaction is characteristic of dimethyl sulfoxide, and it is hardly applicable to the reaction in DMF.[29] Thus in the present system nitrophenols may be formed *via* the mechanism shown in Scheme 3 rather than the mechanism in Scheme 4. However, as shown in Fig. 1B, the appearance of the new reduction peak at *ca.* −1.3 V attributed to ArOOAr are clear, while the wave corresponding to the reduction of phenoxide is difficult to appreciate due to overlapping of the expected wave to that of the abundant starting material. From these results, therefore, it is not clear yet whether phenol obtained was produced during the macro-electrolysis according to the mechanism described in Scheme 3 or it was produced during the procedure for separation and purification. However it is difficult to determine the more probable mechanism for formation of nitrophenols between the reaction path of Reaction 9 and that of Reactions 10 and 11 from our present results.

We thank the Japan Society for the Promotion of Science for the Provision of Funds during the period (Feb—April 1976) when one of us (H.L.) was a Visiting Professor at Tohoku University. The present work was partially supported by a Grant-in-Aid for Scientific Reseach No. 47017 from the Ministry of Education, Science and Culture.

References

1) D. L. Maricle and W. G. Hodgson, *Anal. Chem.*, **37**, 1562 (1965).
2) M. E. Peover and B. S. White, *Electrochim. Acta*, **11**, 1061 (1966).
3) D. T. Sawyer and J. L. Roberts, Jr., *J. Electroanal. Chem.*, **12**, 90 (1966).
4) E. J. Johnson, K. H. Pool, and R. E. Hamm, *Anal. Chem.*, **38**, 183 (1966).
5) A. D. Goolsby and D. T. Sawyer, *Anal. Chem.*, **40**, 83 (1968).
6) D. Bauer and J. P. Beck, *J. Electroanal. Chem.*, **40**, 233 (1972).
7) T. Osa and M. Tezuka, *Denki Kagaku*, **44**, 2 (1976).
8) R. Dietz, M. E. Peover, and P. Rothbaum, *Chem. -Ing. -Tech.*, **42**, 185 (1970).
9) H. Sagae. M. Fujihira, T. Osa, and H. Lund, *Chem. Lett.*, **1977**, 793.
10) H. Sagae, M. Fujihira, H. Lund, and T. Osa, *Bull. Chem. Soc. Jpn.*, **53**, 1537 (1980).
11) H. Sagae, M. Fujihira, H. Lund, and T. Osa, *Heterocycles*, **13**, 321 (1979).
12) Parts of this work were presented at the 35 th National Meeting of the Chemical Society of Japan, Sapporo, August 1976, Abstr. III, p. 807.
13) A. Frimer and I. Rosenthal, *Tetrahedron Lett.*, **1976**, 2809.
14) a) T. Fujinaga, Y. Deguchi, and K. Umemoto, *Bull.*

Chem. Soc. Jpn., **37**, 822 (1963); b) T. Fujinaga, T. Arai, and C. Kitazawa, *Nippon Kagaku Zasshi*, **85**, 811 (1964).
15) T. Kitagawa, T. P. Layloff, and R. N. Adams, *Anal. Chem.*, **35**, 1086 (1963).
16) a) J. G. Lawless, D. E. Bartak, and M. D. Hawley, *J. Am. Chem. Soc.*, **91**, 7121 (1969); b) J. G. Lawless and M. D. Hawley, *J. Electroanal. Chem.*, **21**, 365 (1969).
17) A. H. Maki and D. H. Geske, *J. Am. Chem. Soc.*, **83**, 1852 (1961).
18) H. Lund, M. -A. Michel, and J. Simonet, *Acta Chem. Scand.*, **B28**, 900 (1974).
19) R. Dietz, A. E. J. Forno, B. E. Larcombe, and M. E. Peover, *J. Chem. Soc., B*, **1970**, 816.
20) M. V. Merritt and D. T. Sawyer, *J. Org. Chem.*, **35**, 2157 (1970).
21) F. Magno, R. Seeber, and S. Valcher, *J. Electroanal. Chem.*, **83**, 131 (1971).
22) J. San Filippo, Jr., C.-I. Chern, and J. S. Valentine, *J. Org. Chem.*, **40**, 1678 (1975).
23) R. A. Johnson and E. G. Nidy, *J. Org. Chem.*, **40**, 1679 (1975).
24) T. Fujinaga, K. Izutsu, and K. Takaoka, *J. Electroanal. Chem.*, **12**, 203 (1966).
25) T. Kuwana and J. W. Strojec, *Discuss. Faraday Soc.*, **45**, 134 (1968).
26) Polarography of *p*-nitrophenol in dimethyl sulfoxide shows two reduction waves at the half-wave potentials of −1.0 and −1.5 V *vs.* SCE. M. R. Lindbeck and H. Freund, *Anal. Chim. Acta*, **35**, 74 (1966). The first reduction wave seems to be the phenoxide formation from phenol, because the polarography of sodium *p*-nitrophenolate dose not show the wave. The first reduction peak potential in DMF, −1.3 V *vs.* Ag/AgCl in this work corresponds probably to the first reduction wave observed by Lindbeck and Freund by reason of different solvent used.
27) If EC catalytic mechanism is applicable to the present system the ratio, i_c/i_p, should increase infinitely with increasing concentration of XNBs.[18]
28) R. A. Johnson, E. G. Nidy, and M. V. Merritt, *J. Am. Chem. Soc.*, **100**, 7960 (1968).
29) M. J. Gibian and T. Ungermann, *J. Org. Chem.*, **41**, 2500 (1976).

 © 1980 The Chemical Society of Japan Bull. Chem. Soc. Jpn., 53, 2195—2200 (1980)

Electrochemical and Spectroscopic Studies of α,β,γ,δ-Tetrakis-[1-(2-hydroxyethyl)pyridinium-4-yl]porphine and Its Metal Complexes

Nagao KOBAYASHI, Masamichi FUJIHIRA, Tetsuo OSA,* and Theodore KUWANA**

Pharmaceutical Institute, Tohoku University, Aobayama, Sendai 980

***Department of Chemistry, The Ohio State University, Columbus, Ohio 43210, U.S.A.*

(Received January 29, 1980)

The preparation and properties of a water soluble porphyrin having functional groups, α,β,γ,δ-tetrakis[1-(2-hydroxyethyl)pyridinium-4-yl]porphine, are described. This porphyrin is water soluble from below pH 0 to above pH 14. Acid-base titration revealed the diprotonated diacid-monocation equilibrium ($pK_4=1.0$) and the monocation-free base equilibrium ($pK_3=1.9$) in the acidic range and the free base-monoanion equilibrium ($pK_2=13.0\pm0.2$) in the basic region. The zinc, iron, and cobalt derivatives of the porphyrin were also synthesized and purified. Catalytic properties of the iron and cobalt complexes for reduction of molecular oxygen in water are reported in terms of cyclic voltammetry. The electrochemical reduction utilizing these complexes was interpreted to proceed *via* electrochemical catalytic regeneration mechanism as had been observed for tetrakis(1-methylpyridinium-4-yl)porphinatoiron(III). The apparent rate constants for electron transfer from the iron and cobalt porphyrins to oxygen were estimated to be $3—4\times10^7$ and 1×10^7 dm^3 mol^{-1} s^{-1}, respectively.

Since its magnificent achievement[1] by Hans Fischer as long as a half century ago, porphyrin synthesis has been constantly of primary importance among many investigators. Hitherto various porphyrin skeltons occurring naturally have been synthesized, and the use of modified or newly prepared porphyrins with simpler structure has accumulated ample information for various purposes.[2] Especially recent advent of water soluble porphyrins accelerated a new field to open in their chemistry. Their demand is expanding not only as model compounds related to living body but also from industrial point of view. Recently, in relation to the study to find effective energy conversion/storage systems such as fuel cells, an eminent catalytic capability of α,β,γ,δ-tetrakis(1-methylpyridinium-4-yl)porphinatoiron(III) (Abbr; $Fe^{III}TmP$) has attracted attention[3,4] for the reduction of molecular oxygen to hydrogen peroxide.

In this paper, preparation and spectroscopic properties of a new water soluble porphyrin having hydroxyl groups, α,β,γ,δ-tetrakis[1-(2-hydroxyethyl)pyridinium-4-yl]porphine (Abbr; ThoepyP), and its zinc, iron and cobalt derivatives (Abbr; Zn^{II}ThoepyP, Fe^{III}-ThoepyP, and Co^{III}ThoepyP, respectively) are reported. Catalytic aspects of Fe^{III}ThoepyP and Co^{III}ThoepyP for the reduction of molecular oxygen to hydrogen peroxide are also presented in terms of cyclic voltammetry, in comparison mainly with the results reported for $Fe^{III}TmP$[3] and iron and cobalt tetrakis-(*o*-aminophenyl)porphines (Abbr; Fe^{III}TapP and Co^{III}TapP, respectively).[5]

Experimental

Materials. Most of the chemicals were commercially available guaranteed reagents and used without further purification. 2-iodoethanol was prepared from 2-chloroethanol and excess sodium iodate in dry acetone under reflux. 0.05 M Sulfuric acid (abbr; H_2SO_4) for cyclic voltammetric experiments was obtained from H_2SO_4 and doubly distilled water. Glassy carbon electrodes (area 0.785 cm^2) were purchased from Tokai Carbon Co. Ltd. and polished to a bright surface with alumina powder (final polish using 0.05 μm particle size), washed with 0.05 M H_2SO_4 and distilled water.

α,β,γ,δ-Tetrakis[1-(2-hydroxyethyl)pyridinium-4-yl]-porphinatozinc(II) Tetraiodide, Zn^{II}ThoepyP. α,β,γ,δ-Tetra-4-pyridylporphinatozinc (II), Zn^{II}TpyP, was prepared by the method of Fleischer.[6] *N*-Hydroxyethylation was accomplished accoriding to the same method of *N*-methylation[7] using *ca.* 300 molar excess of 2-iodoethanol, although reaction time was 2 d rather than 10 h.[8] Yield 54%. Found: C, 41.91; H, 3.39; N, 7.91%. Calcd for $Zn_1C_{48}H_{44}N_8O_4I_4$: C, 42.09; H, 3.24; N, 8.18%.

α,β,γ,δ-Tetrakis[1-(2-hydroxyethyl)pyridinium-4-yl]porphine Hexachloride, ThoepyP. The *N*-hydroxyethylated diacid was prepared by stirring 2.36 g of Zn^{II}ThoepyP in 600 cm^3 of 1.5 M H_2SO_4. When the dark blue solid dissolved to form a green solution, 190 g of sodium perchlorate was added, immediately producing a green precipitate of perchlorate salt. The mixture was refrigerated for 12 h and the precipitate was isolated by filtration, half dried in air, and acetone was added to the still moist product to wash away extra sodium perchlorate. The residue was dissolved in distilled water and imposed on an anion–exchange resin (Dowex 2X-8, Cl form) to get chloride salt solution, which was evaporated to dryness. The crude solid was recrystallized from water–methanol–ether. Drying at 110 °C for 14 h left 1.12 g (69%) of a solid. Found: C, 56.21; H, 4.61; N, 10.37%. Calcd for $C_{48}H_{48}N_8O_4Cl_6$: C, 56.99; H, 4.59; N, 11.08%.

α,β,γ,δ-Tetrakis[1-(2-hydroxyethyl)pyridinium-4-yl]-porphinatodiaquairon(III) Pentachloride, Fe^{III}ThoepyP. ThoepyP 400 mg (0.425 mmol) and *ca.* 600 mg of $FeCl_2\cdot nH_2O$ were heated at reflux in water (50 cm^3) for 0.5 h, when metal incorporation was ascertained from absorption spectra in 450—700 nm region. The addition of 30 g of $NaClO_4$ caused dark brownish solution of the perchlorate salt of the aiming compound. The solution was chilled in a refregirator for 12 h and the product was collected on a funnel and washed with acetone containing 10 (v/v) percent ether to remove $FeCl_2\cdot nH_2O$ and $NaClO_4$. To further separate those concomitant inorganic salts more perferctly from the porphyrin, the crude solid was dissolved in a distilled water and imposed on a Sephadex LH-20 column. The elute was then passed through ion-exchange resin (Dowex 2X-8, Cl form) to get chloride salt. After evaporation of water, drying at 110 °C

for 12 h left 211 mg (48.3%) of the dark bluish solid. Found: C, 53.63; H, 4.65; N, 10.27%. Calcd for $Fe_1C_{48}H_{44}N_8O_4Cl_5(H_2O)_2$: C, 54.08; H, 4.54; N, 10.51%.

α,β,γ,δ-Tetrakis[1-(2-hydroxyethyl)pyridinium-4-yl]porphinatodiaquacobalt(III) Pentachloride, Co^{III}ThoepyP. Cobalt was incorporated into the porphyrin ring by refluxing water solution containing *ca.* 500 mg of $CoCl_2 \cdot 6H_2O$ and 300 mg (0.319 mmol) of ThoepyP for 2 h. Then the solution was treated in a manner described for Fe^{III}ThoepyP. Drying at 110 °C for 15 h in a reduced pressure left 119 mg (35%) of a bluish purple solid. Found: C, 52.44; H, 4.71; N, 10.10%. Calcd for $Co_1C_{48}H_{44}N_8O_4Cl_5(H_2O)_2$: C, 53.92; H, 4.53; N, 10.48%.

Measurement. Absorption spectra were measured with a JASCO UVIDEC-1 spectrophotometer. Cyclic potential sweeps were generated by an NF Circuit Design Block FG-100AD function generator in conjunction with a potentiostat which was home-made according to the literature.[9] Nitrogen 99.9% pure was used for dearation of all solutions, and 5 min of air bubbling was conducted in order to saturate a solution with oxygen. Potentials were referred to a saturated calomel electrode (SCE). pH values were measured with a Hitachi-Horiba M-7 pH meter.

Results and Discussion

Spectroscopy. Because of the presence of four hydroxyl groups and four quaternary ammonium groups, ThoepyP is highly water soluble from pH 0 to above 14 and slightly soluble even in methanol or ethanol. Spectrophotometric titrations were used to determine the acid-base equilibria present.

Equilibria at pH *0—7*: Table 1 lists the main absorption maxima and extinction coefficients of ThoepyP at various pH values, as well as those of some metallated

Table 1. Absorption maxima and extinction coefficients of ThoepyPs and some of its complexes in water

Compound	pH of medium	Absorption maxima/nm	Extinction coefficient (10^{-3})
Free base	5.64	422	202
		519	12.9
		557	7.0
		583	6.9
		641	2.7
Diacid	0.0	447	101
		593	8.2
		642	9.9
Monoanion	14.0	448	53.5
		578	8.3
		622	6.3
Zn^{II}ThoepyP	5.64	439	159
		563	15.2
		606	5.3
Fe^{III}ThoepyP	5.64	422	84.4
		519	9.3
		580(shoulder)	4.4
		638	3.5
Co^{III}ThoepyP	5.64	435	184
		548	16.9

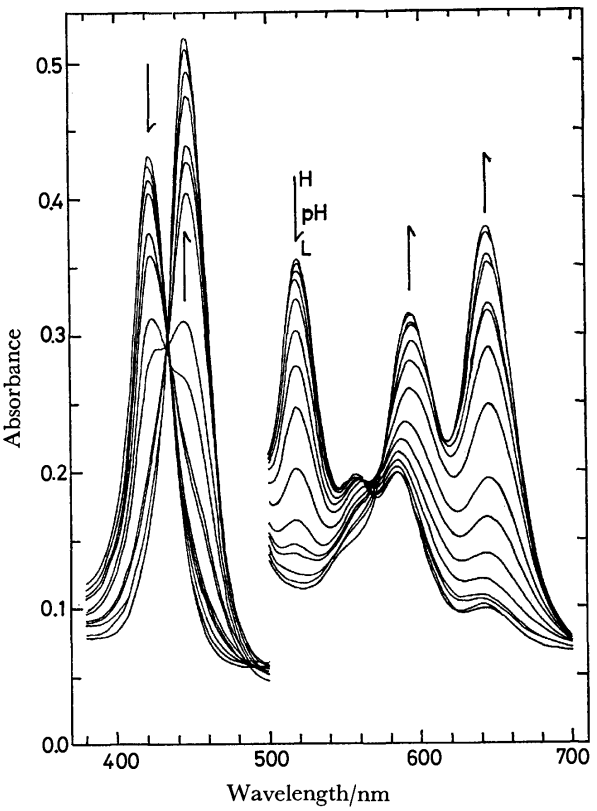

Fig. 1. Absorption spectra of ThoepyP when titrated with HNO_3 at $\mu=2.0$ ($NaNO_3$). The spectra are from pH 4.3 to 0.3. The Soret was run in 1 mm cells and visible in 10 mm cells, at the same concentration of ThoepyP (2.13×10^{-5} M). Temperature=21 °C

derivatives at neutral pH value. The four bands in the visible region from pH 4 to 7 were independent of pH value. Beer's law experiments (2×10^{-4}—3.7×10^{-6} M (1 M=1 mol dm^{-3})) conducted using the 447 and 422 nm bands at pH 0 and 7, respectively, gave linear plots at both wavelength maxima, indicating that the diacid and free base forms of the *N*-hydroxyethylated porphine are probably monomeric. Figure 1 shows spectrophotometric titrations from 380 to 700 nm of ThoepyP with nitric acid at ionic strength 2.0 ($NaNO_3$) at 21 °C. Seemingly one isosbestic point (435 nm) appeared in the Soret region, however, two isosbestic points were observed in the visible region at 562 and 575 nm corresponding to pH 4.3 to 1.6 and 1.5 to 0.3, respectively. Accordingly more than two protonated porphyrin species must be present between pH 0.3 and 4. Assuming that these species are to be diprotonated diacid (H_4P^{2+}), monocation (H_3P^+) and free base (H_2P), and that diacid-monocation, and monocation-free base equilibria

$$H_4P^{2+} = H_3P^+ + H^+ \qquad K_4 \qquad (1)$$

$$H_3P^+ = H_2P + H^+ \qquad K_3 \qquad (2)$$

are present and neglecting deviation of activity coefficients from unity, K_3 and K_4 were calculated from the visible region spectra, owing to the method by Baker *et al.*[10] That is, using the absorbance changes at high pH at 519 nm, K_3 could be obtained from the following

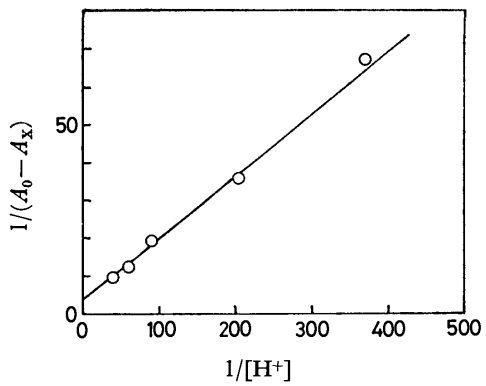

Fig. 2. Plot of $1/(A_0-A_x)$ *vs.* $1/[H^+]$ from the data in Fig. 1 to determine K_3 from Eq. 3. The wavelength is 517 nm for $\mu=2.0$. Temperature=21 °C

equation.[11]

$$\frac{1}{A_0-A_x}=\frac{K_3}{A_0-A_\infty}\frac{1}{[H^+]}+\frac{1}{A_0-A_\infty}, \qquad (3)$$

where A_0 and A_∞ are the absorbances of the free base and monocation forms of the porphyrin, and A_x is that of a mixture of H_3P^+ and H_2P at a constant wavelength. K_3 was calculated from the linear relationship between $1/(A_0-A_x)$ and $1/[H^+]$ to be *ca.* 1.3×10^{-2} (Fig. 2). K_4 was obtained from the low pH absorbances appeared at 562 nm to be *ca.* 10^{-1}. Therefore pK_4 and pK_3 of the equilibrium (1) and (2) are about 1.0 and 1.9, respectively. In agreement with the case for $\alpha,\beta,\gamma,\delta$-tetrakis(1-methylpyridinium-4-yl)porphine, TmpyP, pK_3 and pK_4 values were found to increase with ionic strength ($pK_4=1.2$, $pK_3=2.2$ at $\mu=5.0$).[10]

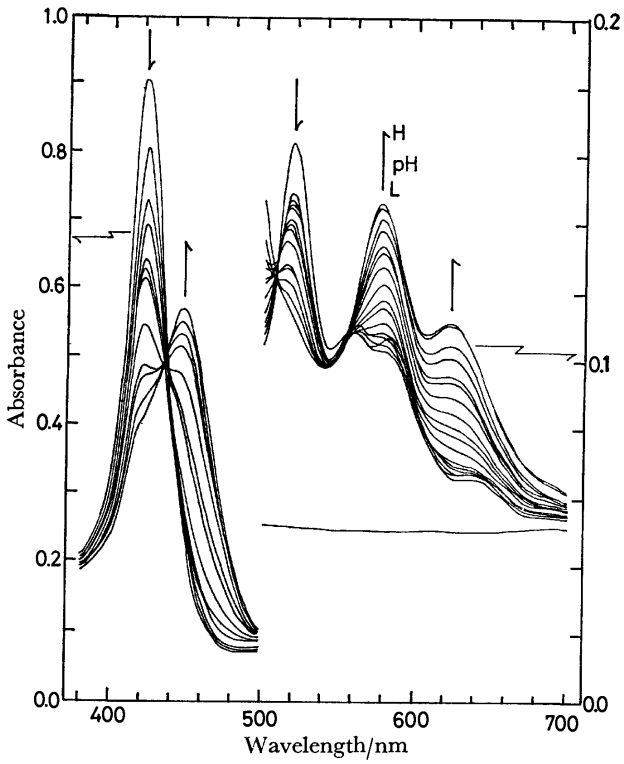

Fig. 3. Spectrophotometric titration of H_2P with NaOH forming HP^-.

Equilibria at pH *7—14*: To investigate the acidity of the free base, a spectrophotometric titration from pH 7 to 14 was performed with sodium hydroxide. Figure 3 shows the resulting titration of H_2P with sodium hydroxide and the isosbestic points at 556, 504, and 418 nm. Assuming that H_2P and monoanion, HP^-, are absorbing species, and that free base-monoanion equilibrium

$$OH^- + H_2P = HP^- + H_2O \qquad K_b \qquad (4)$$

is present, Eq. 5 is obtained.

$$\log [HP^-]/[H_2P] = \log K_b - p(OH) \qquad (5)$$

Thus the plots of the left-hand side of Eq. 5 *vs.* p(OH) should be linear with a slope of −1. The log ($[HP^-]/[H_2P]$) *vs.* p(OH) plots at 422, 578, and 622 nm (Fig. 4) showed a linear relation with an average slope of 1.0 ± 0.2 and a log K_b of 1.0 ± 0.2. Hence the dissociation constant, K_2, of the free base to monoanion and proton at 21 °C is 13.0 ± 0.2 in close accordance with the result for TmpyP (12.9 ± 0.2).[7]

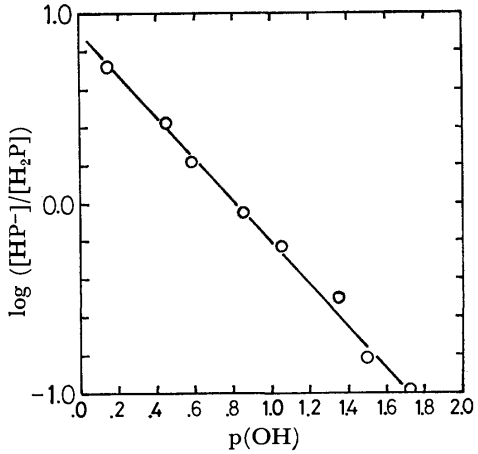

Fig. 4. Plots of log ($[HP^-]/[H_2P]$) *vs.* p(OH) at 578 nm to determine K_2 in Eq. 4.

As so far mentioned, ThoepyP as well as TmpyP[7] was found to exist from pH 0 to 7 as monomers of diacid, monocation, and free base forms in contrast to the trend that most porphyrins are apt to exist as dimers or polymers in solution, with formation constants large enough such that in the usual spectrophotometric concentration range (10^{-4} to 10^{-6} M), appreciable association occures.[12] Acid-base titmetric data were analyzed at a fixed ionic strength and temperature using Q bands because of their multiplicity. Results indicated that ThoepyP behaves apparently in the same fashion as TmpyP. The relatively low basicity and high acidity compared with other porphyrins[13] seem common aspects of porphyrins having quaternary ammonium ion and are not much influenced by the alkyl groups attached to nitrogen. A slight difference owing to side group was, however, reflected on the position of redox potential of its iron complex, a 0.020 V negative shift of ThoepyP (−0.048 V) from that of TmpyP (−0.028 V).

Cyclic Voltammetry. The cyclic voltammogram illustrated in Fig. 5 for Fe^{III}ThoepyP indicated an

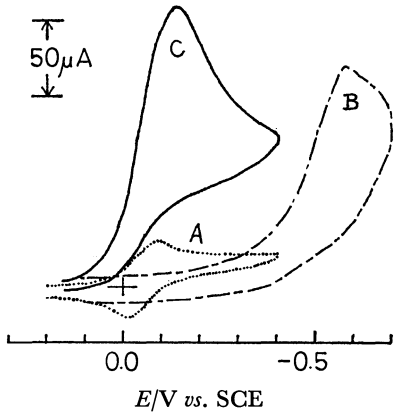

Fig. 5. Cyclic voltammetric current-potential curves at glassy carbon electrode in 0.05 M H_2SO_4. (A) 2.4×10^{-4} M Fe^{III}ThoepyP, saturated with N_2, scan rate= 64 mV s^{-1}: (B) only O_2 (air-saturated), scan rate=110 mV s^{-1}, replotted from Ref. 3; (C) 2.4×10^{-4} M Fe^{III} ThoepyP and O_2 (air-saturated), scan rate=64 mV s^{-1}.

electrochemical (*ec*) catalytic regeneration as for Fe^{III}TmP.[3]

$$Fe^{III}ThoepyP + e^- = Fe^{II}ThoepyP, \quad E_1 \qquad (6)$$

$$Fe^{II}ThoepyP + 1/2O_2 + H^+ \xrightarrow{k} Fe^{III}ThoepyP + 1/2H_2O_2, \qquad (7)$$

where Fe^{III}ThoepyP was reduced on the glassy carbon electrode and the generated Fe^{II}ThoepyP transferred its electron to oxygen, O_2, to return to the iron(III) porphyrin. The catalytic aspects of the O_2 electroreduction was recognized by comparing the cyclic voltammetric current-potential (*i-E*) curves, curve A to C in Fig. 5, (A) for a 0.05 M sulfuric acid solution containing 2.4×10^{-4} M Fe^{III}ThoepyP, (B) saturated with O_2 from the air, and (C) containing the iron porphyrin and saturated with O_2 from air, respectively. Although the O_2 reduction occurred at the peak potential, E_p, of *ca.* −0.057 V *vs.* SCE in the absence of Fe^{III}ThoepyP, the addition of the iron porphyrin shifted the reduction potential to −0.08 V which is close to redox potential of $Fe^{III/II}$ThoepyP (−0.06 V). The redox potential of $Fe^{III/II}$ThoepyP couple, trace A, was independent of scan rate, *v*, from 0.016 to 0.256 V s^{-1} and the separation between the cathodic and anodic potentials, ΔE_p, was 60—70 mV, which indicated that Reaction 6 was a diffusion controlled one-electron transfer reaction.

If the two-electron reduction of O_2 to form H_2O_2 in proton donating media is taken place rapidly, the theoretically calculated value[14,15] of the peak current versus square root of scan rate (i_p *vs.* $v^{1/2}$) would be 880 $\mu A(V/s)^{-1/2}$, assuming an O_2 concentration of 2.9×10^{-4} M[16] and a diffusion coefficient, D_{O_2}, value of 2.6×10^{-5} cm^2 s^{-1}.[17] At low concentration of the porphyrin (10^{-6}—10^{-5} M), the catalytic O_2 wave appeared as a prewave to the main O_2 wave and at potentials approximately corresponding to Reaction 6. With the increase of concentration of the iron porphyrin, the wave height dramatically increased, and at or above *ca.* 2×10^{-4} M, the i_p for the catalyzed wave became diffusion controlled in O_2. When this latter condition was satisfied, the slope of the i_p *vs.* $v^{1/2}$ approached to *ca.* 800 $\mu A(V/s)^{-1/2}$ which is close to that expected for a two-electron, diffusion controlled reduction of O_2 to hydrogen peroxide, H_2O_2, under reversible conditions. In alkaline pH solution (above *ca.* pH 11) the slope of the i_p *vs.* $v^{1/2}$ plot attained to the ideal value (880 $\mu A(V/s)^{-1/2}$). When the iron porphyrin concentration was much lower (*ca.* 10^{-6} M) than that of oxygen, the apparent rate constant for Reaction 7 was calculated using Eq. 8[18] from the height of the catalytic O_2 wave under the approximation of the pseudo first order *ec* catalytic mechanism with Reaction 7 being irreversible.

$$i_k = nFAC_{por}D_{por}^{1/2}k^{1/2}C_{O_2}^{1/2}, \qquad (8)$$

where i_k is the catalytic current observed in A, *F*; Faraday constant in C mol^{-1}, *A*; area of electrode in cm^2, C_{por}; concentration of porphyrin in mol cm^{-3}, D_{por}; diffusion coefficient of porphyrin in cm^2 s^{-1}, *k*; apparent rate constant in mol^{-1} cm^3 s^{-1} and C_{O_2}; concentration of oxygen in mol cm^{-3}. Taking the average of three independent experiments, the rate constant was calculated to be *ca.* $3—4\times10^{-7}$ dm^3 mol^{-1} s^{-1} for the 10^{-6} M iron porphyrin in air-saturated O_2 solutions (0.05 M H_2SO_4). This rate constant answers for why the catalytic wave becomes diffusion controlled in O_2 when the iron porphyrin concentration exceeds that of O_2.

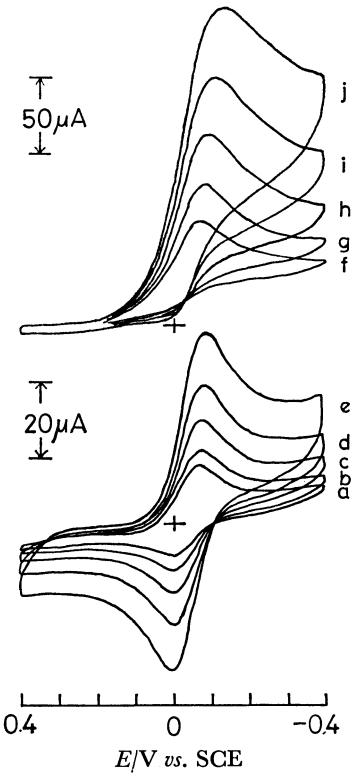

Fig. 6. Cyclic *i-E* curves of 2.4×10^{-4} M Co^{III}ThoepyP in 0.05 M H_2SO_4 at 16, 32, 64, 128, and 256 mV s^{-1}, N_2 saturated solution (a to e) and O_2 (air-saturated) solution (f to j).

Typical cyclic *i-E* curves are shown in Fig. 6 for 2.4×10^{-4} M Co(III)ThoepyP in 0.05 M H_2SO_4. In the potential range of +0.40 to −0.40 V under nitrogen, a well-defined voltammetric wave of a diffusion controlled electrode reaction was observed (line a to e). The $Co^{III/II}$ThoepyP redox potential was −0.035 V and their peak potentials (E_P = −0.07—−0.08 V) were almost independent of scan rate in the range from 0.016 to 0.256 V s^{-1}. When oxygen was introduced into the above solution (line f to j), a cathodic current increased at the peak potential of this cobalt complex and its peak height was linearly proportional to O_2 concentration at a constant scan rate. When this solution was fully saturated with air, the peak current increased at its potential with the increase of scan rate as seen for Fe^{III}ThoepyP. But the most distinct difference was the rate of increase. If we plot this peak current against $v^{1/2}$, its slope attains 490 $\mu A(V/s)^{-1/2}$ which is 56% of that theoretically expected for a two-electron, diffusion controlled reduction of O_2 under reversible conditions (880 $\mu A(V/s)^{-1/2}$). At low concentrations of the cobalt complex (10^{-6}—10^{-5} M), the catalytic O_2 wave appeared as a prewave to the main O_2 wave. As the concentration of the cobalt porphyrin increased, the wave height increased dramatically, and at or above 2.4×10^{-4} M, the i_p for the catalytic wave became saturated. Thus the above mentioned electrochemical behavior was similar in many points to that of Fe^{III}ThoepyP. So by applying *ec* catalytic regeneration mechanism, we evaluated the apparent rate constant for this system (which corresponds to k in Eq. 7) from the catalytic current when Co^{III}ThoepyP concentration is quite low. If we again assume the pseudo first order *ec* catalytic mechanism, the calculated rate constant was *ca.* 1×10^7 dm^3 mol^{-1} s^{-1} for the 10^{-6} M cobalt porphyrin in air-saturated solution (0.05 M H_2SO_4).

In the course of studies on various water soluble iron porpyrins such as Fe^{III}TpyP,[19] Fe^{III}TmP,[3] Fe^{III}-ThoepyP, and Fe^{III}TapP,[5] we could extract some electrochemically interesting features for those iron complexes as follows. (1) The redox potentials ranged between 0 and −0.06 V in 0.05 M H_2SO_4 solution and when cyclic voltammetric experiments were carried out in deaerated solution, they revealed *i-E* curves characteristic of a reversible diffusion controlled electrode reaction. (2) They could be good catalysts for the reduction of molecular oxygen and the potentials for the *ec* catalysis were governed by the $Fe^{III/II}$porphyrin redox couples which also depended on pH values; shifted to negative direction with the rise of pH value. (3) Electron transfer from electrode to oxygen by these complexes was so swift that if the porphyrin concentrations were enriched to some extent, then catalytic current became diffusion controlled in O_2, and the slope of the i_p *vs.* $v^{1/2}$ plot increased to that expected for a two-electron, diffusion controlled reduction of O_2 to H_2O_2 under "reversible conditions." (4) The apparent rate constants of the iron porphyrins to transfer electron(s) to oxygen were dissimilar among species used. For example that of Fe^{III}ThoepyP was estimated to be around 1/3—1/4 of that of Fe^{III}TmP (1.2×10^8 dm^3 mol^{-1} s^{-1}).[3]

In contrast to the case of iron porphyrins, only a few electrochemical studies[5,20] have been reported on the reduction of molecular oxygen with the cobalt incorporated water soluble porphyrins. Although we are still, in the present stage, in want of basic data if we dared to pick up what differed electrochemically from those of the corresponding iron porphyrins, they would be as follows. (1) The redox potentials were always more positive than those of corresponding iron porphyrins. (2) In common with the case of Co^{III}TapP[5] the slope of i_p vs. $v^{1/2}$ plots of O_2 reduction with Co^{III}-ThoepyP was approximately 60% of that of the corresponding iron porphyrin. Phenomenon (1) is easily understandable from the trend that potentials of metal(III/II) redox couple in the first transition metal period in the periodic table parallel to the 3rd ionic potentials, *i.e.*, metals which have less tendency to produce trivalent ions indicate more positive redox potentials.[21]

In order to estimate the apparent rate constant in Eq. 7, the assumptions have been made that these reactions proceeded *via ec* catalytic regeneration mechanism and that reactions were pseudo first order. However, we confronted the fact that these values depended on scan rates, though their degree was not so striking. For such a fact following three reasons may be casted. (1) Though reactions proceed *via ec* catalytic regeneration mechanism, O_2 concentration might be still too low compared with that of the porphyrins (10^{-6}—10^{-5} M) to postulate pseudo first order reaction. (2) Reaction in Eq. 7 *per se* may not simply be a pseudo first order. (3) Adosorption of porphyrins might be occurred. Within these possibilities, however, (3) is eliminated by the finding of the linearity of the i_p *vs.* $v^{1/2}$ plot from Fig. 6, curve a to e (not shown), because if adsorption occurred the slope would be increased with increment of scan rate.

Conclusion

It was indicated that ThoepyP behaves mostly in the same fashion as for TmpyP in water. Catalytic properties of its iron and cobalt complexes for reduction of molecular oxygen in water were recognized and interpreted to proceed *via ec* catalytic regeneration mechanism. The apparent rate constants for electron transfer from porphyrin to oxygen were calculated, assuming pseudo first order reaction, to be 3—4×10^7, and 1×10^7 dm^3 mol^{-1} s^{-1} for its iron and cobalt complexes, respectively. Simultaneously, the doubt was casted whether the above reactions were actually pseudo first order or not.

This research was partially supported by a Grant-in-Aid for Scientific Research No. 355346 from the Ministry of Education, Science and Culture and by the Japan-U.S. cooperative science program from the Japan Society for the Promotion of Science.

References

1) H. Fischer and K. Zeile, *Justus Liebigs Ann. Chem.*,

468, 98 (1929).
2) K. M. Smith, "Porphyrins and Metalloporphyrins," Elsevier, New York, N. Y. (1975).
3) T. Kuwana, M. Fujihira, K. Sunakawa, and T. Osa, *J. Electroanal. Chem.*, **88**, 299 (1978).
4) N. Kobayashi, M. Fujihira, K. Sunakawa, and T. Osa, *J. Electroanal. Chem.*, **101**, 269 (1979).
5) N. Kobayashi, T. Matsue, M. Fujihira, and T. Osa, *J. Electroanal. Chem.*, **103**, 427 (1979).
6) E. B. Fleischer, *Inorg. Chem.*, **1**, 493, (1962).
7) P. Hambright and E. B. Fleischer, *Inorg. Chem.*, **9**, 1757 (1970).
8) F. L. Harris and D. L. Toppen., *Inorg. Chem.*, **17**, 71 (1978).
9) T. Kuwana and J. W. Strojek, *Discuss. Faraday Soc.*, **45**, 134, (1968).
10) H. Baker, P. Hambright, and L. Wagner, *J. Am. Chem. Soc.*, **95**, 5942 (1973).
11) Since $[H_2P]=[A_0-A_\infty]-[A_0-A_x]$, it is readily shown from Eq. 2 that

$$\frac{[H_2P]}{[H_3P^+]}=\frac{[A_x-A_\infty]}{[A_0-A_x]}=\frac{K_3}{[H^+]}$$

$$\therefore \quad \frac{1}{[A_0-A_x]}=\frac{K_3}{[H^+][A_x-A_\infty]}$$

Removal of brackets by expansion and rearrangements of this equation afford Eq. 3.
12) R. F. Pasternack, P. R. Huber, P. Boyd, G. Engasser, L. Francesoconi, E. Giggs, P. Fasella, G. C. Venturo, and L. Hinds, *J. Am. Chem. Soc.*, **94**, 4511 (1972).
13) K. M. Smith, "Porphyrin and Metalloporphyrins," Elesevier, New York, N. Y. (1975), p. 24.
14) R. N. Adams, "Electrochemistry at Solid Electrode," Marcel Dekker, New York (1969), p. 135.
15) R. S. Nicholson and I. Shain, *Anal. Chem.*, **36**, 706 (1964).
16) W. F. Linke, "Solubilities of Inorganic and Metal Organic Compounds," 4th ed, Am. Chem. Soc., Washington, D. C. (1965), Vol. II, p. 1228.
17) I. M. Kolthoff and C. S. Miller, *J. Am. Chem. Soc.*, **63**, 1013 (1941).
18) Z. Galus, "Fundamentals of Electrochemical Analysis," Halsted, New York, N. Y. (1976), p. 316.
19) N. Kobayashi, M. Fujihira, and T. Osa, unpublished data.
20) A. Battelheim, R. Chan, and T. Kuwana, *J. Electroanal. Chem.*, **99**, 391 (1979).
21) S. Otsuka, *Kagaku*, **34**, 27 (1979).

 © 1980 The Chemical Society of Japan Bull. Chem. Soc. Jpn., 53, 2201—2204 (1980)

Direct Observation of the 1,4-Biradical of Benzophenone with *cis*-3-Methyl-2-pentene Excited by the Fourth Harmonic of a Nd:YAG Laser

Hisaharu HAYASHI

The Institute of Physical and Chemical Research, Wako, Saitama 351

(Received March 18, 1980)

Intermolecular biradical formation between the benzophenone triplet state with *cis*-3-methyl-2-pentene was studied by a ns laser-photolysis technique, the fourth harmonic (266 nm) of a *Q*-switched Nd : YAG laser being used as an exciting light source. We succeeded for the first time in observing the transient absorption due to the 1,4-biradical in the 380—300 nm region. Its lifetime was determined to be 25 ± 4 μs (in acetonitrile), 15 ± 4 μs (in methanol), and 6 ± 2 μs (in cyclohexane). Quenching experiments with methyl viologen dication were also carried out in order to assign the observed transient absorptions.

Photochemical reactions of benzophenone have been studied extensively as typical examples for those of carbonyl compounds.[1] Their primary processes are composed of: (1) triplet-triplet energy transfer, (2) hydrogen-abstraction reaction, and (3) biradical formation. Many studies on the processes (1) and (2) have been carried out with the aid of the time-resolved spectroscopy technique, their reaction intermediates being detected directly.[2-4] On the other hand, studies on the process (3) with the transient method are scanty.

Biradicals play important roles in photochemical reactions of carbonyl compounds.[1,5] Transient absorptions due to biradicals produced by the intramolecular hydrogen-abstraction reactions of valerophenones were recently found with the aid of the laser-photolysis technique.[6,7] Their spectra were found to resemble those of the triplet state and ketyl radical of acetophenone. The situation may be the same for the spectra of 1,4-biradicals formed from the triplet state of benzophenone with olefins.[5] Thus they may be expected to resemble the spectra of its triplet state and ketyl radical which have a strong peak at about 320 nm. However, no transient absorption due to the biradicals has ever been observed by the laser-photolysis technique using a *Q*-switched frequency doubled ruby laser (347.2 nm) or an N_2 laser (337.1 nm) as an exciting light source.[8] This is because it is very difficult to measure transient absorptions in the wavelength region shorter or slightly longer than that of the exciting light source.

Under these circumstances, we have undertaken to extend the measurement region to 300 nm by exciting samples by the fourth harmonic (266 nm) of a Nd: YAG laser and to detect the biradicals. Quenching experiments with methyl viologen dication (MV^{2+})[9] have also been carried out in order to confirm the assignment of the observed transient absorptions.

Experimental

Benzophenone (**1**) and methyl viologen hydrated were purified by repeated recrystallizations from ethanol and methanol–acetone (1 : 1) mixed solvent, respectively. *cis*-3-Methyl-2-pentene (*cis*-**2**) purified by vacuum distillation was used as olefin. Spectrograde acetonitrile, methanol, and cyclohexane were used as solvents without further purification.

Laser-photolysis measurements were made for degassed solutions at room temperature by using a Molectron UV-24 N_2 laser or the fourth harmonic of a Quanta-Ray DCR-1 Nd : YAG laser as an exciting light source. The laser pulse widths were 10 ns for the former and 5 ns for the latter. The details of the laser-photolysis apparatus have been published elesewhere.[7]

Results and Discussion

After exciting a ternary solution containing **1** and *cis*-**2** in acetonitrile with the fourth harmonic of the Nd : YAG laser, we have measured the time-dependence of its transient absorption, $I(t)$, in the 300—600 nm region. As examples the $I(t)$ curves observed at 520 and 330 nm for the solution containing **1** of 8.8×10^{-4} mol dm^{-3} and *cis*-**2** of 0.266 mol dm^{-3} are shown in Figs. 1 (a) and (b). We can see from Fig. 1(a) that the decay curve at 520 nm can be represented by a single exponential function with the lifetime (τ_1) of 15 ± 2 ns as follows:

$$I(t) = I_1 \exp(-t/\tau_1). \quad (1)$$

The decay curves at the different wavelength in the 380—600 nm region can also be represented by Eq. 1 with the same lifetime as that observed at 520 nm.

On the other hand, the decay curve at 330 nm is represented as follows:

$$I(t) = I_1 \exp(-t/\tau_1) + I_2 \exp(-t/\tau_2) + I_3. \quad (2)$$

Here τ_1 and τ_2 denote the fast and slow lifetimes, respectively, and they were determined to be 15 ± 2 ns and 25 ± 4 μs from Figs. 1(a) and (b), respectively. The fast lifetime is equal to that obtained at 520 nm. The third term on the right side of Eq. 2 is a constant component in the observed time range (shorter than 140 μs).[10] The decay curves at the different wavelength in the 300—380 nm region can also be represented by Eq. 2 with the same lifetimes as those observed at 330 nm.

It is well known that the primary photochemical processes of **1** with *cis*-**2** and MV^{2+} are shown by the following scheme:[1,5,9,11]

$$\mathbf{1} \xrightarrow{h\nu} S_1 \quad (3)$$

$$S_1 \xrightarrow{k_{ISC}} T_1 \quad (4)$$

$$T_1 \xrightarrow{k_T} \mathbf{1} \quad (5)$$

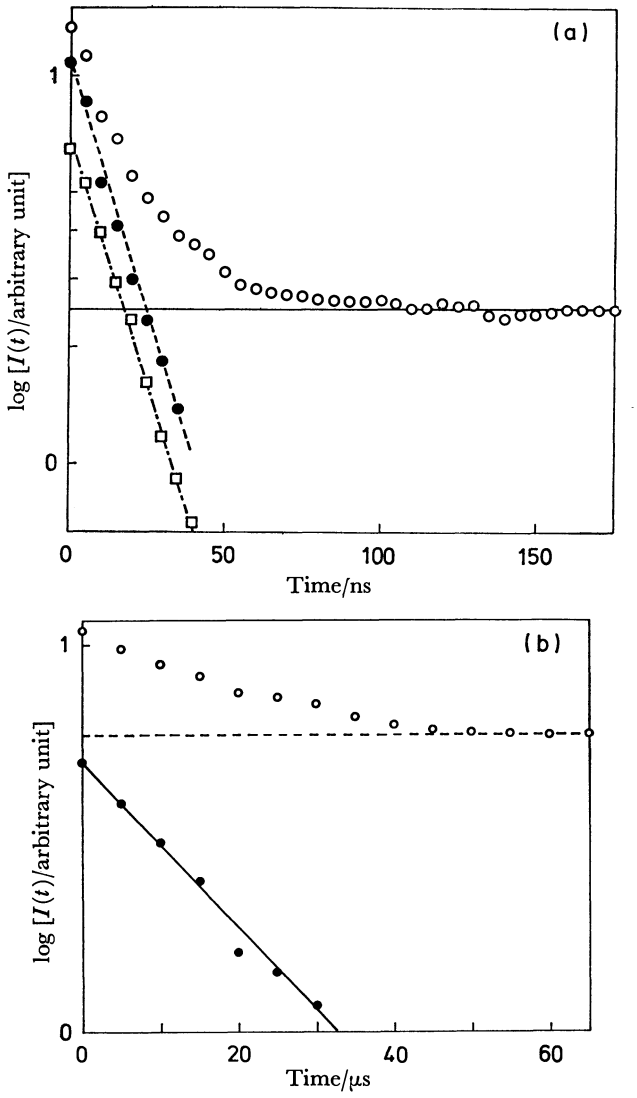

Fig. 1. Decay curves, I (t), of the transient absorption observed for the ternary solution containing benzophenone (8.8×10^{-4} mol dm^{-3}) and *cis*-3-methyl-2-pentene (0.266 mol dm^{-3}) in acetonitrile.
(a) ns region. ○: The total decay curve observed at 330 nm, ——: the constant component in this time region observed at 330 nm, ●: the difference between the total decay curve and the constant component observed at 330 nm, □: the total decay curve observed at 520 nm. (b) μs region observed at 330 nm. ○: The total decay curve ------: the constant component in this time region, ●: the difference between the total decay curve and the constant component.

$$T_1 + RH \xrightarrow{k_H[RH]} K\cdot + R\cdot \quad (6)$$

$$T_1 + \textit{cis}\text{-}\mathbf{2} \xrightarrow{k_q[\textit{cis}\text{-}2]} Ph_2C(O\text{—}CHCH_3)\cdot \cdot C(CH_3)(C_2H_5) \quad (7)$$
(B)

$$B \xrightarrow{k_B} \mathbf{1} + \textit{cis}\text{-}\mathbf{2},\ \mathbf{1} + \textit{trans}\text{-}\mathbf{2},\ \text{oxetane} \quad (8)$$

$$T_1 + MV^{2+} \xrightarrow{k_a[MV^{2+}]} \mathbf{1}\cdot^+ + MV\cdot^+ \quad (9)$$

$$K\cdot(R\cdot) + MV^{2+} \xrightarrow{k_b[MV^{2+}]} K^+(R^+) + MV\cdot^+ \quad (10)$$

$$B + MV^{2+} \xrightarrow{k_c[MV^{2+}]} B\cdot^+ + MV\cdot^+ \quad (11)$$

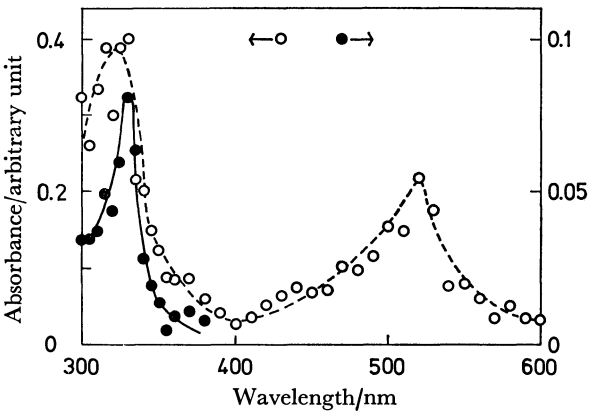

Fig. 2. Transient absorption spectra observed for the acetonitrile solution containing **1** (8.8×10^{-4} mol dm^{-3}) and *cis*-**2** (0.266 mol dm^{-3}) excited with the fourth harmonic of the Nd : YAG laser.
○: Observed immediately after excitation (Spectrum I), ●: observed 800 ns after excitation (Spectrum II).

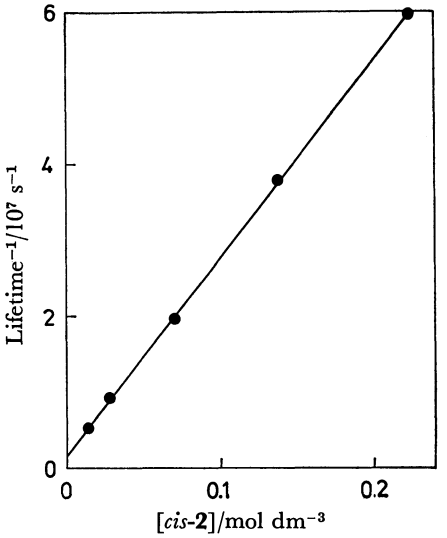

Fig. 3. Stern-Volmer relation between the inverse of the lifetime ($1/\tau_1$) observed at 520 nm and [*cis*-**2**] for the ternary solution containing **1** (8.8×10^{-4} mol dm^{-3}) and *cis*-**2** in acetonitrile

Here S_1 and T_1 are the lowest excited singlet and triplet states of **1**, respectively. RH is a hydrogen donor and K· is the benzophenone ketyl radical. The rate constants of the respective processes are represented by k_{ISC}, k_T, k_H, k_q, k_B, k_a, k_b, and k_c.

Time-resolved absorption spectra were measured before and after quenching of T_1 by *cis*-**2** with the result shown in Fig. 2. Spectrum I measured immediately after excitation of the acetonitrile solution containing **1** and *cis*-**2** is identical with that of the triplet-triplet (T_n—T_1) absorption of **1**[4] and corresponds to the spectrum before quenching of T_1, while Spectrum II measured 800 ns after excitation of the solution is a new one observed for the photochemical reaction of **1**. Thus the observed short lifetime (τ_1) corresponds to the quenching process of T_1 by *cis*-**2** and, as is shown in Fig. 3, the following Stern-Volmer relation was proved

to be fulfilled for this process:[12]

$$1/\tau_1 = k_T + k_{sv}[cis\text{-}2]. \quad (12)$$

Here k_{sv} is the slope of the $1/\tau_1$—[*cis*-**2**] plot in Fig. 3 and corresponds to either k_H or k_q. From the observed straight line in Fig. 3, the k_T and k_{sv} values were determined to be 1.4×10^6 s^{-1} and 2.7×10^8 s^{-1} mol^{-1} dm^3, respectively.

Spectrum II is not due to the triplet state of *cis*-**2** from the following reasons: (1) Upon exciting the acetonitrile solution of *cis*-**2** (0.32 mol dm^{-3}) with the fourth harmonic of the Nd : YAG laser, no transient absorption could be observed in the 300—600 nm region. (2) The energy level of its lowest triplet state is considered to be higher than that of T_1.[5] Furthermore, Spectrum II is not due to the ketyl radical of **1** from the following reasons: (1) The ratio of the absorbance of the peak at 530 nm (P_L) to that at 320 nm (P_S) for the ketyl radical was observed to be 0.25.[4] On the other hand, the P_L/P_S value for Spectrum II was observed to be nearly zero. (2) The k_{sv} value for this system is larger than the k_H one for the reaction of T_1 with cyclohexene in benzene (5.1×10^7 s^{-1} mol^{-1} dm^3),[12] in spite of the fact that the hydrogen-donating ability of cyclohexene is much larger than that of *cis*-**2**.[13] This means that Spectrum II is due to a product other than the ketyl radical. Therefore, the remaining possible assignment of Spectrum II is either due to the biradical or oxetane. But no electronic transition has been observed for 2,2-diphenyloxetanes at the wavelength longer than 300 nm.[14] Thus Spectrum II and the observed k_{sv} may be assigned to the 1,4-biradical and k_q, respectively.

In order to obtain further support to this assignment, the electron transfer experiments with MV^{2+} were carried out. Since MV^{2+} is almost insoluble in acetonitrile, wet acetonitrile was used as a solvent. The volume ratio of water to acetonitrile was 3.5×10^{-2}. The behavior of the transient absorption observed for the wet acetonitrile solution containing **1** and *cis*-**2** excited with the fourth harmonic of the Nd : YAG laser was proved to be actually the same as that in acetonitrile solution. The decay curve of the transient absorption observed at 330 nm for the ternary solution containing **1** of 8.0×10^{-4} mol dm^{-3} and *cis*-**2** of 0.29 mol dm^{-3} in wet acetonitrile is represented by Eq. 2 with the lifetimes of 14 ± 1 ns and 26 ± 5 μs. The slow decay curve is shown in Fig. 4(a).

For the laser-photolysis of solutions containing MV^{2+}, the N_2 laser was used as an exciting light source to avoid direct excitation of MV^{2+} which has a strong absorption at 266 nm but not at 337.1 nm, transient absorption being measured in the 380—650 nm region. MV^{2+} withdraws an electron from T_1, $K^{\cdot}$, or the biradical forming its radical cation ($MV^{\cdot+}$) (see Eqs. 9, 10, and 11).[9,11] $MV^{\cdot+}$ is stable in degassed solvents and has a broad absorption band at about 600 nm and a sharp one at about 390 nm.[15]

The transient absorption was measured for the ternary solution containing **1** of 2.77×10^{-2} mol dm^{-3} and MV^{2+} of 2.4×10^{-4} mol dm^{-3} in wet acetonitrile. The T_n—T_1 absorption of **1** was found to be quenched by MV^{2+} forming $MV^{\cdot+}$ The $I(t)$ curve observed at 530 nm is shown in Fig. 4(b). It is represented by the superposition of an exponential function with the lifetime of 570 ± 50 ns and a constant component in this time region. The decay part is due to the combination of the processes shown by Eqs. 5 and 9 and the constant corresponds to the absorption of $MV^{\cdot+}$.

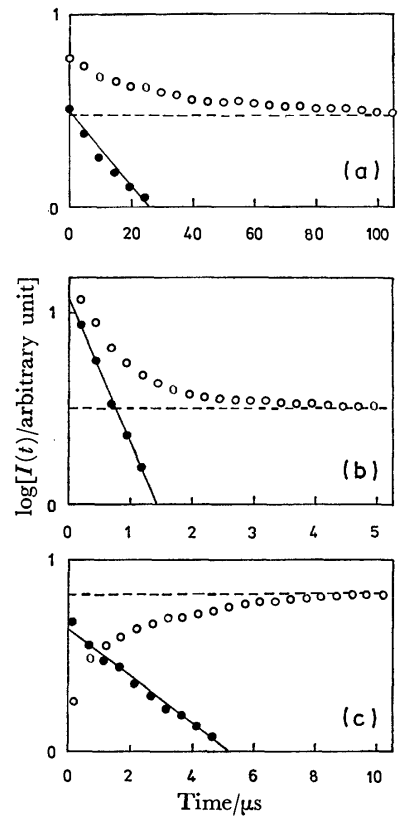

Fig. 4. Time dependence of transient absorption intensities, I (t), observed for wet acetonitrile solutions. ○: The total decay curve, ------: the constant component in this time region, ●: the difference between the total decay curve and the constant component.
(a) Decay curve observed at 330 nm for the ternary solution containing benzophenone (8.8×10^{-4} mol dm^{-3}) and *cis*-3-methyl-2-pentene (0.29 mol dm^{-3}) in wet acetonitrile. (b) Decay curve observed at 530 nm for the ternary solution containing benzophenone (2.77×10^{-2} mol dm^{-3}) and MV^{2+} (2.4×10^{-4} mol dm^{-3}) in wet acetonitrile. (c) Growth curve observed at 600 nm for the quaternary solution containing benzophenone (2.77×10^{-2} mol dm^{-3}), *cis*-3-methyl-2-pentene (0.32 mol dm^{-3}), and MV^{2+} (2.4×10^{-4} mol dm^{-3}) in wet acetonitrile.

The transient absorption was measured for the quaternary solution containing **1** of 2.77×10^{-2} mol dm^{-3}, *cis*-**2** of 0.32 mol dm^{-3}, and MV^{2+} of 2.4×10^{-4} mol dm^{-3} in wet acetonitrile. After fast quenching of the T_n—T_1 absorption of **1** by *cis*-**2** with the lifetime of 11 ns, the absorption of $MV^{\cdot+}$ appears slowly. As an example, the growth curve observed at 600 nm is shown in Fig. 4(c). It is represented by the following equation:

$$I(t) = I_4(1-\exp(-t/\tau_4)). \quad (13)$$

The growth time (τ_4) which is determined to be 3.6 ± 0.5

μs from the curve in Fig. 4(c) corresponds to the appearance time of the transient absorption of $MV^{\cdot+}$.

From the above-mentioned experimental results obtained with the wet acetonitrile solutions we conclude that, in the quaternary solution under study, *cis*-**2** quenches T_1 more effectively than MV^{2+} and an intermediate formed by the interaction between T_1 and *cis*-**2** transfers an electron to MV^{2+}. Generally speaking, either the ketyl radical or the biradical is the possible intermediate acting as an electron donor to MV^{2+}.[9,11] The spectrum of the intermediate (Spectrum II) is different from that of the ketyl radical as mentioned before. Thus it can be seen that the observed growth of $MV^{\cdot+}$ in Fig. 4(c) is brought about by the process represented by Eq. 11 and that Spectrum II is due to the 1,4-biradical.

From the above discussion, the obtained τ_2 value, 25 ± 4 μs, in acetonitrile can also be considered to be the lifetime of the biradical. Similar results were also obtained for the methanol and cyclohexane solutions containing **1** and *cis*-**2** with the laser-photolysis technique using the Nd : YAG laser. The lifetime of the biradical was determined to be 15 ± 4 μs in methanol and 6 ± 2 μs in cyclohexane. The lifetime in the polar solvents was observed to be longer than that in the nonpolar solvent. This tendency agrees well with that observed for the biradicals formed from the intramolecular hydrogen-abstraction reaction of valerophenones.[6,7]

This is the first direct observation of the transient absorption due to the biradical as a precursor of the reactions of oxetane formation and isomerization through the Yang mechanism,[5] although it has already been observed for the biradicals produced by the intramolecular hydrogen-abstraction reactions.[6,7] The reason for failure of the previous attempts to observe it[8] may be due to the fact that its strong band locates in the wavelength region shorter than 380 nm. In fact the following relation seems to hold for the absorption intensity ratio between the longer and shorter wavelength bands observed for the triplet state of **1**, its ketyl radical, and its biradical:

$$P_L/P_S(T_1) > P_L/P_S(K\cdot) \gg P_L/P_S(B). \quad (14)$$

Theoretical interpretation for this is a future problem. The constant component represented by the third term in Eq. 2 (I_3) was observed in all the solvents used in the present study. Its spectrum is similar to Spectrum II, but its origin is not yet clarified.

The author wishes to express his thanks to Professor Saburo Nagakura of The University of Tokyo for his continuous encouragement and fruitful discussion and Dr. Masao Kaneko of The Institute of Physical and Chemical Research for his kindness in informing the author of the purification method of methyl viologen hydrate. The present work was partially supported by a Grant-in-Aid for Scientific Research No. 454135 from the Ministry of Education, Science and Culture.

References

1) for example, N. J. Turro, "Modern Molecular Photochemistry," Benjamine, Menlo Park, California (1978), pp. 296—472.
2) G. Porter and F. Wilkinson, *Trans. Faraday Soc.*, **57**, 1686 (1961).
3) G. Porter and F. Wilkinson, *Proc. R. Soc. London. Ser. A*, **264**, 1 (1961).
4) T. S. Godfrey, J. W. Hilpern, and G. Porter, *Chem. Phys. Lett.*, **1**, 490 (1967).
5) N. C. Yang, J. I. Cohen, and A. Shani, *J. Am. Chem. Soc.*, **90**, 3264 (1968); J. Salitiel, K. R. Neuberger, and M. Wrighton, *ibid.*, **91**, 3658 (1969).
6) R. D. Small, Jr., and J. C. Scaiano, *Chem. Phys. Lett.*, **50**, 431 (1977).
7) H. Hayashi and S. Nagakura, *Bull. Chem. Soc. Jpn.*, **53**, 1519 (1980).
8) R. Caldwell and H. Masuhara, private communications.
9) R. D. Small, Jr., and J. C. Scaiano, *J. Phys. Chem.*, **81**, 829 (1977).
10) Very weak and constant components with long lifetimes were also observed at about 520 nm when the intensity of the exciting light increased. It is difficult, however, to distinguish them from a thermal lensing signal.
11) P. Hyde and A. Ledwith, *J. Chem. Soc., Perkin Trans. 2*, **1974**, 1768.
12) H. Hayashi, S. Nagakura, Y. Kubo, and K. Maruyama, *Chem. Phys. Lett.*, **72**, 291 (1980).
13) K. U. Ingold, "International Symposium on Free Radical in Solution," Butterworths, London (1966), p. 61.
14) J. G. Atkinson, D. E. Ayer, G. Büchi, and E. W. Robb, *J. Am. Chem. Soc.*, **85**, 2257 (1963).
15) E. M. Kosower and J. L. Cotter, *J. Am. Chem. Soc.*, **86**, 5524 (1964).

Analysis of the Short-range Force Including the r^{-s}-type Functional Force

Mitiko MIURA,*,† Yuji SHIRO, and Hiromu MURATA

Department of Chemistry, Faculty of Science, Hiroshima University, Higashisenda-machi, Hiroshima 730
†*Faculty of the School of Education, Hiroshima University, Shinonome-3-chome, Hiroshima 734*

(Received November 26, 1979)

In treating the lattice dynamics strictly, it is important to separate the short-range forces into various kinds according to their characters: covalent-bond, characteristic repulsive, and van der Waals. The purpose of this paper is to describe a method of separation and an appropriate treatment which is applicable to any crystal with any properties. For the repulsive and the van der Waals interactions, we apply the Jones-type potential function, varying as an inverse power of the distance. The results indicate that the repulsive force serves to emphasize the ionicity in the crystal-force field and that the covalent-bond force cannot be represented reasonably by the use of the valence force to such a crystal as the wurtzite structure, forming a coordination lattice.

We have studied the lattice dynamics of the wurtzite-type structure on the basis of the polarizable-ion model (PIM). A force-field model including the Coulomb force, where ions are assumed to be point-charge, is termed the rigid-ion model (RIM) regardless of the kind of short-range force. On the other hand, a model including the interaction of the induced electronic polarization is termed PIM. Though this model includes the effect of the electronic extension, we pay no heed to it in this paper, having submitted our ideas in an earlier paper.[1] In another earlier paper[2] the short-range force constants were estimated so as to reproduce the observed macroscopic quantities, such as, the Γ-point optical-mode frequencies, the elastic constants, and the piezoelectric constants, by the use of the effective ionic charge and the electronic polarizability, evaluated separately.[3]

In general, a crystal has two characteristics, ionicity and covalency, at the same time; this is not, however, true of the NaCl-type and the Diamond-type crystals. The atomic interaction in a partial ionic crystal will be treated as consisting of three parts, aside from the polarization part: electric Coulomb (long-range), overlap, and van der Waals.[4] By the overlap part, we mean the covalent attractive term and the characteristic repulsive term. Thus, three kinds of forces are contained in the short-range force: covalent-bond, characteristic repulsive, and van der Waals. In spite of this circumstance, they were previously not distinguished, but were treated collectively.[2] The purpose of this paper is thus to describe a method of separation and an appropriate treatment which is applicable to any crystal with any properties.

The Born-type functional form[5a] is available for use for the repulsive and the van der Waals forces, which are assumed to be expressed by a function varying as an inverse power of the atomic or ionic distance. From a formal point of view, the covalency of crystals differs from the ionicity in the greater complexity of representing explicitly the potential function. The formal theory of lattice vibrations has been described in terms of the interaction of the electrons and the nuclei involved in a solid.[6] As a phenomenological model, the shell model has been widely used in valency crystals.[7] A fornal justification of the shell model shows a rather large amount of arbitrariness possible in defining the parameters, because the number of parameters to be definde is too great. The valence-force-field model, taken from the theory of molecular vibration, describes the covalent-bond force directly.[8] While consisting of merely the nearest neighbor interaction, this is known to reproduce observed macroscopic quantities fairly well. For the covalent-bond force, therefore, we apply the valence-force-field model.

Method

Dynamical Matrix. The dynamical matrix, $\boldsymbol{D}$, for PIM is written as:

$$\boldsymbol{D} = \boldsymbol{D}^{\mathrm{N}} + \boldsymbol{D}^{\mathrm{C}} + \boldsymbol{D}^{\mathrm{P}}, \tag{1}$$

with three constituents:[5b] $\boldsymbol{D}^{\mathrm{N}}$, a short-range non-Coulomb contribution; $\boldsymbol{D}^{\mathrm{C}}$, a long-range Coulomb contribution; and $\boldsymbol{D}^{\mathrm{P}}$, a long-range electronic polarization contribution. $\boldsymbol{D}$ is the $(3n\times 3n)$ matrix, where n is the number of atoms per unit cell; it is a continuous function within the limits of the vanishing vector ($\boldsymbol{q}=0$) of the reciprocal space. It can be expanded into a MacLaurin series. The macroscopic quantities can be expressed by the use of coefficients of various orders of this series.[2]

For the short-range force, we used the valence-force-field (VFF) method in our preceding paper;[2] this method can be represented in terms of a function dependent on several force constants. Though VFF contains coupling terms between forces, we omitted these less important terms in order to simplify the procedure.[9] We have distinguished the following force constants: K_1 (parallel to the **c** axis) and K_2 (not parallel to it) for first-neighbor bond stretching, H for bending (without distinction between two sorts: cation-anion-cation and anion-cation-anion), and K_3 for second-neighbor stretching; *cf.* Fig. 1.

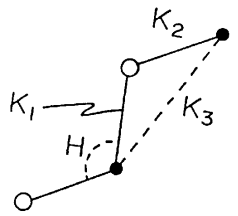

Fig. 1. The explanation of force constants used in this paper.

In this paper, the repulsive force (RF), whose role is known, together with the Coulomb force, for ionic crystals, and the van der Waals force are given separately in addition to the valence force (VF). After this separation is accomplished, the force analogous to RF and the van der Waals force are separated from VF. Accordingly, VF will denote the covalent-bond force more strictly than before. After the short-range force is separated into forces, the dynamical matrix is written as:

$$\boldsymbol{D} = \boldsymbol{D}^{\mathrm{V}} + \boldsymbol{D}^{\mathrm{R}} + \boldsymbol{D}^{\mathrm{W}} + \boldsymbol{D}^{\mathrm{C}} + \boldsymbol{D}^{\mathrm{P}}. \tag{2}$$

The van der Waals force, $\boldsymbol{D}^{\mathrm{W}}$, will not be treated separately because of its small contribution. Our new attempt is applied to the well-examined wurtzite-type structure in this paper. Though only one example, that of BeO, is treated, any other material may be treated similarly.

The repulsive force is assumed to be written as the sum of the two-body repulsive interaction. This is only approximately true. As the covalency is increased, the interactions of atoms with their different neighbors become more interdependent. Thus, the many-body interaction begins to take on an important role. As many authors have noted,[10] indeed, the many-body interaction is not negligibly small; in spite of this evidence, the interaction of the two bodies is large in comparison with it. The force, represented as a function of a force constant, H, denoting an angular rigidity, is, in a sense, the three-body force. Thus, the many-body interaction is considered to be included collectively in VF as a function of H. For the repulsive interaction, we apply the Jones-type potential function following Born's first assumption,[5a] where atoms or ions were pictured as rigid spheres mutually attracted by a force varying as an inverse power of the distance, r:

$$\beta \times r^{-s}, \tag{3}$$

where β is a strength parameter and s is a hardness parameter. s is independent of the species of ions in a given crystal. Another function of the repulsive interaction is assumed to have a form exponential with the distance; this is suited to the quantum-mechanical results more than the inverse power form. Since the exponential form is virtually equal to the inverse power form, we will employ the latter form, whose function is simple and which has been well examined mathematically.

Pauling[11] has studied the effect of relative ionic sizes on the properties of the alkali halides and has given an approximate formula providing a quantitative theory of the anion-contact and double-repulsive effect:

$$\beta_{\mathrm{AB}} B_0 e^2 (r_{\mathrm{A}} + r_{\mathrm{B}})^{s-1} r_{\mathrm{AB}}{}^{-s}, \tag{4}$$

where r_{AB} is the distance between the A and B ions, where r_{A} and r_{B} are constants representing their radii (which Pauling calls standard radii), where B_0 is a characteristic repulsive coefficient (whose value can be determined conveniently), and where β_{AB} is a constant obtained from a quantum-mechanical treatment.[11]

Characteristic Repulsive Force. The method for the calculation of RF will now be shown briefly. An expansion of the potential energy with respect to the nuclear displacement gives various orders of coefficients, which are denoted by various orders of derivatives with respect to the displacement. Among them, the second-order coefficient approximately gives the force field described by matrix elements.[5a] The definite expressions for evaluating these coefficients have scarcely been given. Now those will be given: the formula for the second-order coefficient of Eq. 4, those for the first- and second-order coefficients, given by the expansion of the second-order coefficient with repsect to the wave vector, and the method for checking the resulting values evaluated with the use of these formulas. The potential, ϕ, at a point $\boldsymbol{r}$ in a lattice space is given by summing up the influence from all lattice sites, $\boldsymbol{r}_l$:

$$\phi = \sum_l' |\boldsymbol{r} - \boldsymbol{r}_l|^{-s}. \tag{5}$$

In order to gain a rapid convergence of the summation, various methods of treatments have been given.[12] We have employed Tosi's method,[13] which is applicable to any value of s except for $s \leqq m$ (=dimension of lattice space).

The lattice summation of Eq. 5 is rewritten by Tosi[13] for the m-dimensional space as:

$$\begin{aligned} S^{(m,s)}(\boldsymbol{q}, kk') &= \sum_l' |\boldsymbol{r} - \boldsymbol{r}_l|^{-s} \\ &= \frac{1}{\Gamma(\sigma)} \left\{ \frac{2\pi^\tau \omega^{\sigma-\tau}}{v(s-m)} + \frac{\pi^\tau}{v} \sum_h' \exp\left[2\pi i (\boldsymbol{k}_h + \boldsymbol{q}) \cdot \boldsymbol{r}\right] \right. \\ &\quad \times \frac{\Gamma[\tau - \sigma, \pi^2 (\boldsymbol{k}_h + \boldsymbol{q})^2 / \omega]}{(\pi |\boldsymbol{k}_h - \boldsymbol{q}|)^{m-s}} - \frac{2}{s} \omega^\sigma \\ &\quad \left. + \sum_l' \exp\left(2\pi i \boldsymbol{q} \cdot \boldsymbol{r}_l\right) \frac{\Gamma[\sigma, (\boldsymbol{r} - \boldsymbol{r}_l)^2 \omega]}{|\boldsymbol{r} - \boldsymbol{r}_l|^s} \right\}, \end{aligned} \tag{6}$$

where $\boldsymbol{r} = \boldsymbol{x}\binom{0}{k'} - \boldsymbol{x}\binom{0}{k}$ and $\boldsymbol{r}_l = \boldsymbol{x}\binom{l}{k} - \boldsymbol{x}\binom{0}{k}$, where $\sigma = s/2$ and $\tau = m/2$, where the subindices l and h indicate, respectively, the direct-space and the reciprocal-space lattice points, where $\boldsymbol{q}$ is the wave vector, and where v is the unit-cell volume. $\Gamma(\mathrm{x})$ is the complete gamma function, and $\Gamma(\nu, \mathrm{x})$ is the incomplete gamma function. The second-order derivative of Eq. 6 with respect to the displacement comes out to:

$$\begin{aligned} S^{m,s}_{\alpha\beta}(\boldsymbol{q}, kk') &= \frac{1}{\Gamma(\sigma)} \left\{ \frac{\pi^\tau}{v} (-4\pi^2) \sum_h' (k_{h\alpha} + q_\alpha)(k_{h\beta} + q_\beta) \right. \\ &\quad \times \exp\left[2\pi i (\boldsymbol{k}_h + \boldsymbol{q}) \cdot \boldsymbol{r}\right] \frac{\Gamma[\tau - \sigma, \pi^2 (\boldsymbol{k}_h + \boldsymbol{q})^2 / \omega]}{(\pi |\boldsymbol{k}_h + \boldsymbol{q}|)^{m-s}} \\ &\quad + \sum_l' \exp\left(2\pi i\, \boldsymbol{q} \cdot \boldsymbol{r}_l\right) 4 (r_\alpha - r_{l\alpha})(r_\beta - r_{l\beta}) \\ &\quad \times \frac{\Gamma[\sigma + 2, \omega (\boldsymbol{r} - \boldsymbol{r}_l)^2]}{|\boldsymbol{r} - \boldsymbol{r}_l|^{s+4}} - 2\delta_{\alpha\beta} \sum_l' \exp\left(2\pi i \boldsymbol{q} \cdot \boldsymbol{r}_l\right) \\ &\quad \left. \times \frac{\Gamma[\sigma + 1, \omega (\boldsymbol{r} - \boldsymbol{r}_l)^2]}{|\boldsymbol{r} - \boldsymbol{r}_l|^s} + \delta_{\alpha\beta} \delta_{kk'} \frac{4}{s+2} \omega^{\sigma+1} \right\}. \end{aligned} \tag{7}$$

Though Eq. 6 is valid for $s > m$, it can be generalized for any real value of s.[12] Equation 7 is, hence, valid for any real value of s. Values evaluated according to Eq. 7 may be checked with the use of this relation:

$$\sum_{\alpha=1}^{m} S^{(m,s)}_{\alpha\alpha}(\boldsymbol{q}, kk') = s(s-1) S^{(m,s+2)}(\boldsymbol{q}, kk'). \tag{8}$$

If $s=1$ and $m=3$, there holds the well-known equation given by Born:

$$\sum_\alpha S^{(3,1)}_{\alpha\alpha}(\boldsymbol{q}, kk') = \frac{4\pi}{v}. \tag{9}$$

Moreover, the first- and the second-order derivatives with respect to the wave vector are given as:

$$S^{(m,s)}_{\alpha\beta,\gamma}(\boldsymbol{q}, kk') = \frac{2\pi i}{\Gamma(\sigma)}(A+B),$$

$$A = \frac{\pi^\tau}{v}(-2\pi i)\sum{}'_h\left\{[\delta_{\alpha\gamma}(k_{h\beta}+q_\beta)+\delta_{\beta\gamma}(k_{h\alpha}+q_\alpha)]\right.$$
$$\times\frac{\Gamma[\tau-\sigma, \pi^2(\boldsymbol{k}_h+\boldsymbol{q})^2/\omega]}{(\pi|\boldsymbol{k}_h+\boldsymbol{q}|)^{m-s}} - 2\pi^2(k_{h\alpha}+q_\alpha)(k_{h\beta}+q_\beta)(k_{h\gamma}+q_\gamma)$$
$$\left.\times\frac{\Gamma[\tau-\sigma+1, \pi^2(\boldsymbol{k}_h+\boldsymbol{q})^2/\omega]}{(\pi|\boldsymbol{k}_h+\boldsymbol{q}|)^{m-s+2}}\right\}\exp[2\pi i(\boldsymbol{k}_h+\boldsymbol{q})\cdot\boldsymbol{r}],$$

$$B = \sum{}'_l r_{l\gamma}\left\{4(r_\alpha-r_{l\alpha})(r_\beta-r_{l\beta})\frac{\Gamma[\sigma+2, \omega(\boldsymbol{r}-\boldsymbol{r}_l)^2]}{|\boldsymbol{r}-\boldsymbol{r}_l|^{s+4}}\right.$$
$$\left.-2\delta_{\alpha\beta}\frac{\Gamma[\sigma+1, \omega(\boldsymbol{r}-\boldsymbol{r}_l)^2]}{|\boldsymbol{r}-\boldsymbol{r}_l|^{s+2}}\right\}\exp(2\pi i\boldsymbol{q}\cdot\boldsymbol{r}_l), \qquad (10)$$

$$S^{(m,s)}_{\alpha\beta,\gamma\nu}(\boldsymbol{q}, kk') = \frac{-4\pi^2}{\Gamma(\sigma)}(C+D),$$

$$C = \frac{\pi^\tau}{v}\left\{(\delta_{\alpha\gamma}\delta_{\beta\nu}+\delta_{\beta\gamma}\delta_{\alpha\nu})\frac{\Gamma[\tau-\sigma, \pi^2(\boldsymbol{k}_h+\boldsymbol{q})^2/\omega]}{(\pi|\boldsymbol{k}_h+\boldsymbol{q}|)^{m-s}}\right.$$
$$-2\pi^2[\delta_{\alpha\nu}(k_{h\beta}+q_\beta)(k_{h\gamma}+q_\gamma)+\delta_{\beta\nu}(k_{h\alpha}+q_\alpha)(k_{h\gamma}+q_\gamma)$$
$$+\delta_{\gamma\nu}(k_{h\alpha}+q_\alpha)(k_{h\beta}+q_\beta)+\delta_{\alpha\gamma}(k_{h\beta}+q_\beta)(k_{h\nu}+q_\nu)$$
$$+\delta_{\beta\gamma}(k_{h\alpha}+q_\alpha)(k_{h\nu}+q_\nu)]\frac{\Gamma[\tau-\sigma+1, \pi^2(\boldsymbol{k}_h+\boldsymbol{q})^2/\omega]}{(\pi|\boldsymbol{k}_h+\boldsymbol{q}|)^{m-s+2}}$$
$$+4\pi^4(k_{h\alpha}+q_\alpha)(k_{h\beta}+q_\beta)(k_{h\gamma}+q_\gamma)(k_{h\nu}+q_\nu)$$
$$\left.\times\frac{\Gamma[\tau-\sigma+2, \pi^2(\boldsymbol{k}_h+\boldsymbol{q})^2/\omega]}{(\pi|\boldsymbol{k}_h+\boldsymbol{q}|)^{m-s+4}}\right\}\exp[2\pi i(\boldsymbol{k}_h+\boldsymbol{q})\cdot\boldsymbol{r}],$$

$$D = \sum{}'_l r_{l\gamma}r_{l\nu}\left\{4(r_\alpha-r_{l\alpha})(r_\beta-r_{l\beta})\frac{\Gamma[\sigma+2, \omega(\boldsymbol{r}-\boldsymbol{r}_l)^2]}{|\boldsymbol{r}-\boldsymbol{r}_l|^{s+4}}\right.$$
$$\left.-2\delta_{\alpha\beta}\frac{\Gamma[\sigma+1, \omega(\boldsymbol{r}-\boldsymbol{r}_l)^2]}{|\boldsymbol{r}-\boldsymbol{r}_l|^{s+2}}\right\}\exp(2\pi i\boldsymbol{q}\cdot\boldsymbol{r}_l). \qquad (11)$$

Values evaluated according to Eq. 11 may be checked by the use of this relation:

$$\sum_{kk'}z(k)z(k')S^{(m,s)}(\boldsymbol{q}, kk') =$$
$$\{s(s+1)\}^{-1}\sum_{\alpha\beta}\sum_{kk'}z(k)z(k')S^{(m,s)}_{\alpha\beta,\alpha\beta}(\boldsymbol{q}, kk'), \qquad (12)$$

which is a generalization of the equation given by Keffer *et al.*[14] for $s=1$ and $m=3$. The symbol $z(k)$ is the effective ionic charge of the kth ion. The left-hand side of Eq. 12 corresponds to the well-known Madelung constant, A, if $s=1$:

$$A = (2n)^{-1}\sum_{kk'}z(k)z(k')S^{(m,s)}(\boldsymbol{q}, kk'). \qquad (13)$$

Result

Before the evaluation of the repulsive interaction by means of Eq. 4 is made, the definite values of the repulsive parameters, B_0, ρ and s, and the ionic radii have to be given. Except for ρ, these parameters in a family of salts were determined by a simultaneous fit of the assumed expression of the lattice energy to the equation of the state and its volume derivative for the alkali halides with the NaCl structure, where the number of salts sizably exceeds the number of component ion species. ρ is independently determined by the use of the valence charge and the number of outer electrons of the pth ion following Pauling's equation:

$$\rho_{pp'} = 1 + (z_p/n_p) + (z_{p'}/n_{p'}). \qquad (14)$$

By means of the fact that the attractive forces and the repulsive forces are balanced in ionic crystals, Pauling determined B_0. The repulsive parameters for a wurtzite structure, however, can not be determined by a simultaneous fit because, in this case, the number of salts scarcely exceeds the number of component ion species. Therefore, the results for the NaCl structure are approximately applied here after converting them into the wurtzite structure.

The ionic radii for Be and O in the wurtzite-type structure are 0.293 and 1.32 Å respectively, after the values derived by Pauling in the NaCl-type structure had been modified as:[14]

$$r_{\text{Wurtzite}} = r_{\text{NaCl}} \times c,$$
$$c = [(B_{\text{W}}/B_{\text{N}})(A_{\text{N}}/A_{\text{W}})]^{1/(s-1)} = 0.944, \qquad (15)$$

where A is the Madelung constant and B is the coordination number. BeO is of the same ionic type as LiF. However, the value of the observed compressibility of BeO is not similar to that of LiF; rather, it is similar to that of MgO.[15] In spite of this evidence, $s=6$, which is the value for LiF on the average, is used so as to keep consistency with other parameters.

For a BeO compound with an ionic structure, ρ_{++}, ρ_{+-}, and ρ_{--} are taken as 3.0, 1.75, and 0.5 respectively by means of Eq. 14. If BeO has such a structure as wurtzite, the ionicity is weakened and the valence charge is deprived of its meaning. At this stage, the effective ionic charge seems to take the place of the valence charge in Eq. 14. The results are 3.0, 1.71, and 0.43—the effective ionic charge is nearly 1.0.[3] The values of the B_{AB} $[=\rho_{\text{AB}}(r_{\text{A}}+r_{\text{B}})^{s-1}]$ coefficient between like or unlike ions, then, are in this ratio:

$$B_{++}:B_{+-}:B_{--} = 1:94:276. \qquad (15)$$

The wurtzite-type structure has two "molecules," with two cations and two anions, in a unit cell (see Fig. 2).

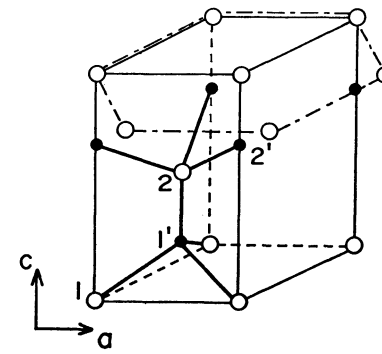

Fig. 2. Crystal structure of wurtzite type.

Since these four ions, displacing in one one and the same direction and amount, do not cause any relative displacement, that is, since the acoustic mode of frequency at the Γ point is kept at zero, the three coefficients, B_{AB}'s, should satisfy this relation:

$$B_{++}\times B_{--}/B_{+-}{}^2 = c_{\text{B}} = 1.^{\dagger\dagger} \qquad (17)$$

†† Fowler[16] has obtained the value of $B_{\text{AB}}{}^0$ $(=B_{\text{AB}}\times B_0)$ for alkali halides with the use of thermodynamical data. The approximate relation (Ref. 19, Eq. 922) suggested upon examination of the results of the study of an inert-gas mixture
$$(B_{+-}{}^0)^{1/s} = \{(B_{++}{}^0)^{1/s} + (B_{--}{}^0)^{1/s}\}/2,$$
has been used in order to estimate the ratio. Here, $(B_{+-}{}^0)^{1/s}$ is the arithmetic mean of $(B_{++}{}^0)^{1/s}$ and $(B_{--}{}^0)^{1/s}$.

That is, B_{+-} is the geometrical mean of B_{++} and B_{--}. As the ratio given in Eq. 16 does not satisfy Eq. 17 ($c_B=0.031\neq 1.$), the values of B_{AB} given in Eq. 16 seem to be unreliable; the $\beta_{++}\times\beta_{--}>\beta_{+-}^2$ relation has to be maintained, at least in order to satisfy Eq. 17. On the other hand, the ionic radii estimated by Born[13] reproduce the experimental ones quite well. It is known that the difference in ionic radius between a cation and an anion given by Pauling is too large in comparison with that derived from experiments.[13,17] The ionic radii for CsCl-type crystals derived by Hollinger *et al.*[18] with the use of observed elastic constants also show this tendency. Consequently, it is reasonable at present to treat B_{AB} as an adjustable parameter to be fitted empirically, keeping the relation in Eq. 17, just as the force constant is. After B_{AB} is estimated for compounds of salts, it can be divided into parameters, B_{AB} and β_{AB}, in a family of salts. This treatment is as follows: first, an arbitrary ratio of B_{AB} between like or unlike ions is chosen, and then the force constants of the covalent-bond force are estimated so as to reproduce the observed marcoscopic quantities. The results will be shown for four kinds of ratio:

$$B_{++}\quad B_{+-}\quad B_{--} \qquad (18.N)$$
$$=0.25\quad :0.5\quad :1.0, \qquad (18.1)$$
$$=0.01\quad :0.1\quad :1.0, \qquad (18.2)$$
$$=0.0025:0.05:1.0, \qquad (18.3)$$
$$=0.0001:0.01:1.0. \qquad (18.4)$$

If the short-range force is represented only by the use of RF, one of the calculated e_2-mode frequencies becomes a imaginary number. As the most characteristic feature of the covalent bonds is their directional nature, the force constant, H, in VF, representing an angular rigidity, is taken into account as a temporary expedient so that the imaginary number can be done away with. The effect of the ratio (B_{++}: B_{+-}: B_{--}) on the calculated macroscopic quantities is then examined. Table 1 shows the value of H, which is the limiting value to make the calculated results real, and the other parameters used here. The set of $B_0\times B_{+-}=1.6$ and $H=0.04$ ($B_0\times B_{+-}$ and H take constant values, regardless of the variable B_{+-}) are the limiting values when the imaginary number is done away with. $B_0\times B_{+-}$ being a constant value independent of the value of B_{+-} means that only the proportion of the two kinds of repulsive forces between like ions is varied, while the repulsive force between unlike ions is kept intact. The calculated results are shown in Table 2 for frequencies and elastic constants. (Since the short-range non-Coulomb contribution is not important with regard to piezoelectric constants, the results for them are omitted.) The results in the fourth column show the case where the characteristic repulsive force is not taken into account.

Table 1. The physical quantities used in this paper

Polarizability	$\alpha_+(1/\text{Å}^3)$	0.04
	$\alpha''(1/\text{Å}^3)$	1.269
	$\alpha^{\perp}(1/\text{Å}^3)$	1.259
Effective ionic charge	z(esu)	1.105
Force constant	H (mdyn/Å)	0.04
Structural parameter[a]	a(Å)	2.6979
	c(Å)	4.3772
	u	0.3786

a) Ref. 19.

The variation in the ratio of B_{AB} is remarkable in macroscopic quantities, as can be seen in Table 2. Let us first examine the frequencies. At the Γ point, the lattice vibration can be classified, by factor-group analysis, into the $2a_1+2b_1+2e_1+2e_2$ modes. Among these, though the a_1 and e_1 modes are independent of the ratio, the two frequencies belonging to b_1 and e_2

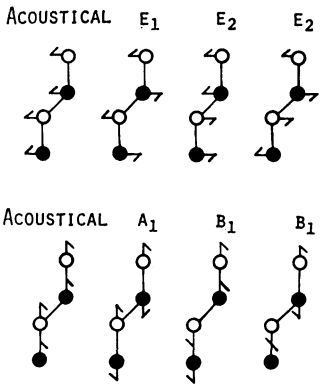

Fig. 3. The vibrational modes of wurtzite-type structure.

Table 2. The calculated macroscopic quantities against the variety of B_{+-}

		Obsd	Calcd				
B_{+-}			0.0	0.5	0.1	0.05	0.01
Wavenumber[a] (cm^{-1})	a_1	678	680.3	690.7	690.7	690.6	690.7
	b_1	—	894.9	769.8	950.5	1165.4	2255.5
		—	784.7	597.2	621.7	628.7	634.8
	e_1	722	725.4	738.3	738.3	738.3	738.3
	e_2	684	642.8	638.9	655.7	679.3	886.7
		338	378.0	47.6	131.8	189.1	337.4
Elast. const.[b] (10^{11} dyn/cm^2)	c_{11}	47.0	48.9	−48.0	33.3	66.0	289.3
	c_{12}	16.8	21.4	105.5	59.2	72.5	218.1
	c_{13}	11.9	20.9	29.6	40.8	55.4	172.6
	c_{33}	49.3	44.7	25.2	49.4	81.0	335.2
	c_{44}	15.3	15.9	1.9	5.1	9.2	42.0

a) Ref. 20. b) Ref. 21.

modes are particularly interesting. Each vibrational mode is shown in Fig. 3. In the a_1 and e_1 modes, the interatomic distance remains unchanged between like ions, but is changed between unlike ions. As the repulsive force between unlike ions is kept intact, the calculated results do not vary in spite of the variety of the ratio. The variety of the ratio denotes the relation between cation-cation and anion-anion repulsive forces: as the ratio decreases, the cation-cation repulsive force is decreased and the anion-anion repulsive force is increased. As the interatomic distance between like ions is changed, on the contrary, the calculated results vary remarkably with the ratio. The case where RF makes the main contribution as the short-range force causes a large splitting of the e_2- and b_1-mode frequencies. This splitting becomes rather too large in comparison with the observed values.

Let us next discuss the elastic constants. In this case, the variation in the ratio is more remarkable. Comparing the calculated c_{11} and c_{12} species with each other, c_{12} is larger than c_{11}, in contrast with the observed values. This difference varies remarkably depending on the value of the ratio; c_{11} becomes equal to c_{12} at nearly $B_{+-}=0.04$. In Fig. 4 the contribution of RF is shown for several species of elastic constants against the ratio. As the ratio becomes smaller, RF makes a large contribution and causes a large repulsion. This tendency can also be observed in the induced internal strain of the c_{11} and c_{12} species; the contribution of the internal strain of other species is small enough to be negligible. Reflecting the variation in the calculated frequencies, the contribution of the induced internal strain of the c_{11} and c_{12} species does not approach zero, but increases as the ratio increases. It is worthy of notice that the sign of the contribution is different between these two species. The fact that the calculated c_{12} species is larger than that of c_{11} is a result of this.

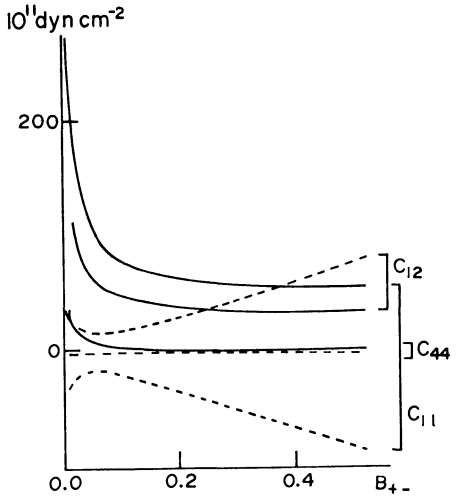

Fig. 4. The contribution of the repulsive force to elastic constants as a function of B_{+-}.

Thus far the characteristic effect of RF on calculated macroscopic quantities has been examined and only the covalent-bond force has been considered, so that the imaginary number has been done away with. Let us now take the covalency strictly into account. Before we do so, however, we must fix the value of B_{+-} by reference to the preceding results. Fortunately, the features appearing in the reproduction of e_2-mode frequencies and the relation between c_{11} and c_{12} are very specific; hence, the ratio can be roughly fixed. If we dare to estimate the approximate value for Be compounds by the use of Fowler's data,[16] in spite of the difference in the relation of B_{AB} (see footnote), the values are reduced to nearly zero except for B_{--}. This suggests that our conclusion derived from the reproduction of the macroscopic quantities is reasonable. Hence, we fix the ratio at:

$$B_{++}:B_{+-}:B_{--} = 0.01:0.1:1.0. \quad (19)$$

This result can be explained as follows: since the radius ratio is quite different from unity, the repulsion between anions is much larger than that between cations. The $B_{+-}=1.0$ ratio corresponds to the case when the ionic radii of cation and anion are nearly equal to each other. The way of treating the consideration of RF separately

Table 3. The calculated macroscopic quantities against B_0

B_0			0.0	3.53	5.0	10.0
K_1			2.22	1.79	1.61	1.00
K_2			2.39	1.92	1.72	1.07
H			0.0	0.0	0.0	0.0
K_3			0.269	0.200	0.177	0.110
		Obsd		Calcd		
Wave number (cm^{-1})	a_1	678	680.3	679.3	678.4	678.0
	b_1	—	894.9	837.6	847.8	912.2
		—	784.4	819.1	801.5	721.0
	e_1	722	725.4	724.7	723.2	726.4
	e_2	684	642.8	649.4	651.8	671.3
		338	378.0	327.4	305.0	219.5
Elast. const. (10^{11} dyn/cm^2)	c_{11}	47.0	48.9	48.8	48.7	48.6
	c_{12}	16.8	21.4	27.1	29.8	40.8
	c_{13}	11.9	20.9	25.0	27.0	35.1
	c_{33}	49.3	44.7	46.7	47.7	50.9
	c_{44}	15.3	15.9	13.0	11.9	8.1

is thus advantageous because it brings the effect of the radius ratio into operation.

Table 3 gives the results obtained against several values of B_0 at $B_{+-}=0.1$. If we assume that the Coulomb force and the repulsive force are balanced at the equilibrium (because the covalent-bond force is not regarded as such a force as to take part in an ionic balance), $B_0=3.53$ is obtained. If we assume that the lattice energy can be represented as the sum of the Coulomb and the repulsive energies, the result is too small in comparison with the observation for the wurtzite structure. In the case of NaCl, on the contrary, the reproduction is very good. We regard the difference between the calculated and the observed values as the covalency.

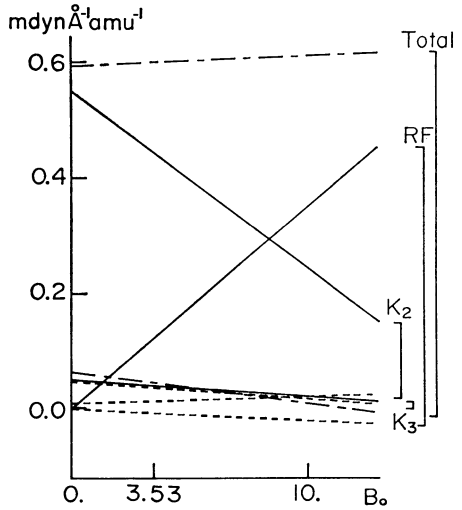

Fig. 5. The contribution of each short-range force to e_2-mode frequencies.

The increased B_0 value causes the contribution of RF to increase and the value of the force constants to decrease. The calculated results also vary appreciably in reproduction in terms of the increase. This evidence indicates that the manner of the contribution of RF is peculiar to itself. The contribution of RF and each force constant in VF to the e_2-mode frequencies is shown in Fig. 5, as examples. As can also be seen in it, RF makes a contribution not only so as to compensate VF, but also so as to give a peculiar feature.

Discussion

The short-range force was separated into the covalent-bond force and the repulsive force in the preceding chapter. On this occation, the Born-type central-force model was employed for the repulsive force. As for the covalent-bond force, on the other hand, the valence force was employed. On Born's notation, the force field occurring between the two particles of k and k' is described by the matrix elements α and β, $\phi_{\alpha\beta}(kk')$, denoting the coefficients of the derivatives with respect to the direction of the displacement, α and $\beta=x, y$, and z; the coefficients of the matrix elements are force constants. Accordingly, 3×3 kinds of force constants with respect to α and β are distinguished against each pair of atoms, k and k', —the number of them is reduced through symmetry operations. Among them, we distinguished the constants connected with the difference in the pair of particles, but identified those with a difference in the direction: as the most characteristic feature of the covalent-bond forces is their directional nature, a characteristic of this kind, expected to be involved in Born's notation in terms of the α and β elements, was considered to be put into the covalent-bond force collectively.

As can be seen in Table 3, the increased RF caused the VF to decrease; this resulted in a split of the e_2-mode frequencies and in an increase in the c_{12} and c_{13} species. Thus, the ionicity in the crystal-force field was emphasized according to the increase in RF. Even without RF, a lack of the covalent-bond force, that is, a lack of the rigidity in direction, can be observed in the calculated results, as shown in the fourth column in Table 3. However the value of H, which has been expected to represent an angular rigidity, became zero; this result reproduced the calculated results satisfactorily, but this matter seems strange. This evidence seems to indicate that each force constant in VF, which reasonably been defined by means of molecular spectroscopy, does not give the same meaning in such a crystal as a wurtzite structure forming a coordination lattice. The increase in RF causing a decrease of VF also indicates that the VF used here involves not only the covalent-bond force, but also a force similar to RF. VF is thus an inclusive force including not only the covalent-bond force, but also several other kinds of forces. Hence, we can scarcely make any progress in separating the short-range forces as long as we use an ambigous valence-force-field model. It may be supposed that we had better distinguish constants in terms of their α and β elements rather than use those defined on the basis of the molecular theory.

Conclusion

We have separated the short-range forces into various kinds of forces according to their characteristics in order to establish a suitable treatment which is applicable to any crystal with any character. By the use of an inclusive valence force, we can scarcely make any progress in separation.

The authors wish to express their thanks to Prof. Yosio Sakamoto, Hiroshima University, for his indispensable suggestions and help in the preparation of this paper.

References

1) J. Birman, *Phys. Rev.*, **97**, 897 (1955); M. Miura, T. Sato, H. Murata, and Y. Shiro, *J. Phys. Chem. Solids*, **41**, 189 (1980).

2) M. Miura, H. Murata, and Y. Shiro, *J. Phys. Chem. Solids*, **39**, 669 (1978).

3) M. Miura, H. Murata, and Y. Shiro, *J. Phys. Chem. Solids*, **38**, 1071 (1977).

4) Y. Sakamoto, *J. Sci. Hiroshima Univ., Ser. A*, **17**, 387 (1954).
5) a) M. Born and K. Huang, "Dynamical Theory of Crystal Lattices," Clarendon Press, Oxford (1954), Chap. 1; b) M. Born and K. Huang, *ibid.*, Chap. 5.
6) G. K. Horton and A. A. Maradudin, "Dynamical Properties of Solids," North-Holland Pub. Comp., Amsterdam, Vol. 1, Chap. 10.
7) R. A. Cowley and W. Cochran, *Phys. Rev.*, **131**, 1030 (1963); H. Kaplan and J. Sullivan, *Phys. Rev.*, **130**, 120 (1963); J. R. Hardy and A. M. Karo, *Phil. Mag.*, **5**, 859 (1060).
8) M. J. Musgrave and J. A. Pople, *Proc. R. Soc. London, Ser. A*, **268**, 474 (1962); R. Ramani, K. K. Mani, and R. P. Singh, *Phys. Rev. B*, **14**, 2659 (1976).
9) M. A. Nusimovici and M. Balkanski, *Phys. Rev. B*, **1**, 595 (1970); M. A. Nusimovici and J. Birman, *Phys. Rev.*, **156**, 925 (1967).
10) I. J. Zucker and D. Paik, *J. Phys. C*, **12**, 771 (1979).
11) L. Pauling, "The Nature of the Chemical Bond," 3rd ed, Clarendon Press, Cornell (1960), Chap. 13.
12) An article treating this problem will soon be published by Sakamoto and the present authors.
13) M. P. Tosi, *Solid State Phys.*, **16**, 1 (1960).
14) F. Keffer and A. M. Portis, *J. Chem. Phys.*, **27**, 675 (1957).
15) C. F. Cline and D. R. Stephens, *J. Appl. Phys.*, **36**, 2869 (1965); C. Kittel, "Introduction to Solid State Physics," John Wiley and Sons, New York (1953).
16) R. H. Fowler, "Statistical Mechanics," 2nd ed, Clarendon Press, Cambridge (1936), Chap. 10.
17) S. C. Agrawal, G. G. Agrawal, and J. Shanker, *J. Inorg. Nucl. Chem.*, **40**, 1735 (1978); A. K. Ghosh, A. Manna, and S. K. Deb, *J. Phys. Chem. Solids*, **38**, 701 (1977).
18) R. C. Hollinger and G. R. Barsch, *J. Phys. Chem. Solids*, **37**, 845 (1976).
19) S. L. Mair and Z. Bernea, *Acta Crystallogr., Sect. A*, **31**, 201 (1975).
20) C. A. Arguello, D. L. Rousseau, and S. P. Port, *Phys. Rev.*, **181**, 750 (1969).
21) G. G. Bentle, *J. Am. Ceram. Soc.*, **49**, 125 (1966).

Studies on the Aqueous Solutions of Guanidinium Salts. XIII. NMR Study of the Interactions between Guanidinium Salt and Tetraalkylammonium Salts in Water

Koichiro MIYAJIMA,* Hiromitsu YOSHIDA, Yoshihiro KURODA, and MASAYUKI NAKAGAKI

Faculty of Pharmaceutical Sciences, Kyoto University, Yoshida-shimoadachi-cho, Sakyo-ku, Kyoto 606

(Received September 14, 1979)

The quadrupole relaxation of ^{14}N nucleus of guanidinium bromide has been measured in aqueous ternary solutions containing symmetrical tetraalkylammonium salts by the ^1H NMR method. By means of Pople's line shape analysis and the Debye-Einstein equation, it has been confirmed that no complex formation takes place in the aqueous ternary solution containing symmetrical tetraalkylammonium salts. The rotational correlation time of the guanidinium ion is linearly related to the absolute viscosity of the solutions containing the homologous series of alkylammonium salts. A similar relationship was obtained for the ternary solutions with sugars or polyethylene glycols. This suggests that the correlation time depends on the microviscosity around the guanidinium ion.

In a previous work, the free energy change on mixing aqueous guanidinium bromide [GuBr] and tetrabutylammonium bromide [$(n$-Bu$)_4$NBr] solutions was determined and the mutual salting-in effect was observed.[1] The result has been interpreted in terms of the following: (a) complex formation between two kinds of solutes even in an aqueous ternary solution, and (b) alteration of the water structure, *viz.* structural salting-in. (a) is based on the fact that the guanidinium halides form crystalline complexes with symmetrical tetraalkylammonium halides in concentrated ternary solutions,[2] and (b) on the data of enthalpy of mixing of Bu_4NBr and guanidinium chloride in aqueous solution reported by Chawla *et al.*[3] The transfer of Bu_4NBr from water to guanidinium chloride solution is accompanied by a decrease in the excess partial molar heat capacity, indicating that the hydrophobic hydration around tetraalkylammonium ion is reduced in the aqueous guanidinium salt solution. Recent investigation of the volume of mixing of GuBr–Bu_4NBr–H_2O system has revealed that the reduction of the hydrophobic hydration caused by the structural breaking action of the guanidinium ion gives rise to increase in solution volume.[4] It seemed of interest to confirm whether the large salting-in effect is due to the complex formation or the structural change of water. For this purpose we measured the ^1H NMR spectra of GuBr in the aqueous ternary solution with various alkylammonium bromides, sugars or polyethylene glycol, with attention focussed on the change of shapes of amino proton signals. The results analyzed by means of Pople's theory[5] and the Debye-Einstein equation[6] support interpretation (b), the mutual salting-in effect due to the structural change of water.

Experimental

Materials. Symmetrical tetraalkylammonium bromides (Wako Chemical Co., Ltd.) were recrystallized at least twice from an appropriate solvent.[7] The other alkylammonium salts $C_iH_{2i+1}N(CH_3)_3Br$, (i=2—5), $C_6H_5N(CH_3)_3Br$, $C_6H_5N(C_2H_5)_3Cl$ (reagent grade, Tokyo Kasei Chemical Co., Ltd.) were recrystallized from ethanol several times. Sucrose, D-glucose and D-fructose of reagent grade were used without further purification. Polyethylene glycols (EG) with molecular weight 200 and 300 (Nakarai Chemical Co., Ltd.) were used without further purification. The solid solutes were dried *in vacuo* over phosphorus pentoxide before use. All solutes were dissolved in redistilled and deionized water. GuBr used was the same compound as reported previously.[8] The concentration of GuBr was 2 mol/kg·water throughout the experiments. All samples were not degassed. The pH values of these solutions were maintained in the range 4.2—4.6 with 0.01 mol dm^{-3} hydrobromic acid solution.

Method for NMR Measurement. The ^1H NMR spectra were measured on a Varian HA-100 D NMR spectrometer operating at 100 MHz. Cyclosilane-d_{18} sealed in a co-axial capillary tube was used for an internal lock signal and as an external reference for chemical shift. The temperature variation was made with a temperature variable accessory unit (V-6040) calibrated by ethylene glycol. Regulation of temperature was accurate to ± 2 °C throughout the NMR measurement.

Viscosity Measurement. The absolute viscosity of these ternary solutions, η, was measured with an Ostwald type viscometer. Temperature of the thermostat bath was controlled within ± 0.03 °C. The kinetic energy correction was made for determination of viscosity by the equation,

$$\eta/d = At - B/t,\ A = 2.628\times10^{-3}\ (\mathrm{cm^2/s^2}),$$
$$B = 15.00\ (\mathrm{cm^2}),$$

where t is the flow time and d the density of the solution, measured with Seiko SDM 421 and 422 vibration densimeters.[4]

Results and Discussion

Figure 1 shows the ^1H NMR spectra of a 2 mol/kg·water GuBr solution and a mixed aqueous solution of GuBr and R_4NBr molalities of which are 2 mol/kg·water, respectively. The broad signal at *ca.* 7—7.5 ppm is due to the NH absorption of the guanidinium ion, the sharp signal at about 5.15 ppm to the absorption of water proton. The chemical shifts are given in Table 1. The NH resonance shows a narrowing and slight shift to down field on addition of R_4NBr, the resonance of water proton remaining almost unchanged. The extent of the narrowing and shift progresses with increase in the chain lengths of the alkyl group. The sharpening accompanied by the addition of Bu_4NBr also depends on the concentration of the added salt. The down field shift seems to arise from the increase in the hydrogen bond of the guanidinium ion with water molecules. However, the absolute values of

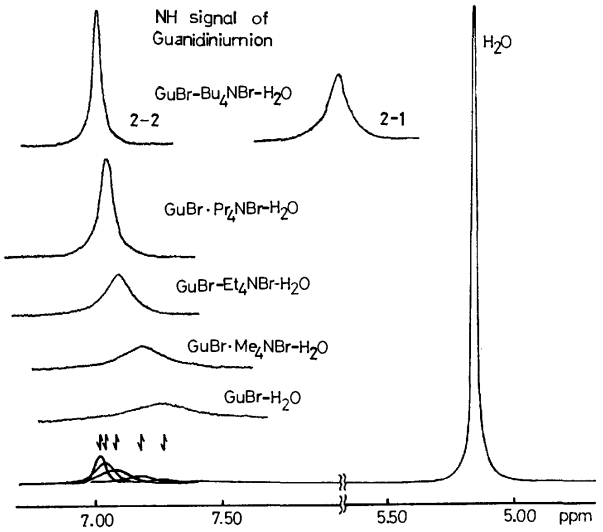

Fig. 1. ^{1}H NMR spectra of 2 mol/kg·water GuBr solution and the mixed aqueous solutions of GuBr and R_4NBr.

the shift could not be estimated since correction of the bulk susceptibility was not available. Two explanations can be considered for the narrowing: (a) change of the exchange rate of NH protons with the water proton, and (b) change of the extent of broadening by quadrupole relaxation of the ^{14}N nucleus. NMR studies of the aqueous guanidinium solutions show that the NH proton signals change depending on the pH of the solutions, the corresponding water proton signal varying simultaneously.[9] However, in the present case, the line width of the water proton is little affected in spite of the sharpening of NH signal of the guanidinium ion. Thus (a) can be eliminated and we will further consider explanation (b). The narrowing phenomenon can be treated by the equations derived by Pople for the NMR line shape of spin 1/2 nucleus relaxing by quadrupole mechanism.[5] In the following, we will discuss the change of line shapes by means of this theory.

The theoretical line shape $I(x)$ for the spectra of nuclei of spin 1/2 (^{1}H) coupled to a nucleus of spin 1 (^{14}N) is expressed by the parameter λ which is a product of spin-lattice relaxation time T_1 of the ^{14}N nucleus and the NH coupling constant $^1J_{NH}$:

$$I(x) = D\frac{45+\lambda^2(5x^2+1)}{225x^2+\lambda^2(34x^4-2x^2+4)+\lambda^4(x^6-2x^4+x^2)} \quad (1)$$

$$x = \Delta\nu/{}^1J_{NH} \quad (2)$$

$$\lambda = 10T_1\,{}^1J_{NH}, \quad (3)$$

where $\Delta\nu$ is the frequency relative to the center and D is a constant concerning the peak area. When we determine the parameter which can reproduce the best fit curve to the observed line shape, we simply take into account the half height width $\Delta\nu_{1/2}$, instead of the total line shape of the observed signal. Thus we get from Eqs. 1—3

$$I(x_0) = I(0)/2 = (45+\lambda^2)/8\lambda^2, \quad (4)$$

where x_0 is $\Delta\nu_{1/2}/2\cdot{}^1J_{NH}$. Thus λ can be so determined as to satisfy Eq. 4. This simplified treatment may be justified since the observed NH resonance is simply a single peak, suggesting that the parameter λ is approximately less than 5 (Fig. 1). In analyzing the observed line width by Eq. 4, the "natural" line width at half height in the absence of quadrupole relaxation should be substracted.[10] However, this approximation would cause no large error to the results. The theoretical curve of NH proton resonance for the GuBr–H_2O and GuBr–Bu_4NBr–H_2O systems were calculated by assuming the $^1J_{NH}$ value for both systems as 63 Hz, calculated from ^{15}NH coupling constant of urea by taking into account the difference of gyromagnetic ratio between ^{14}N and ^{15}N. The theoretical curves are shown in Fig. 2

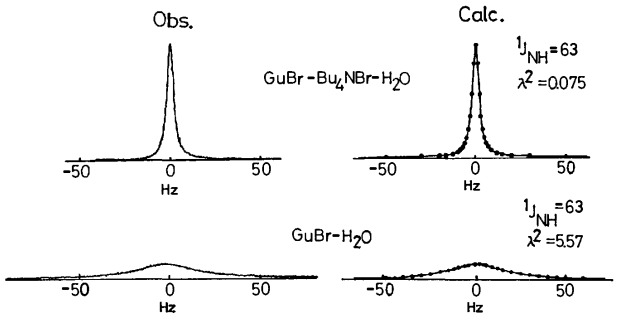

Fig. 2. Observed and calculated line shape of NH signals for the GuBr–Bu_4NBr–H_2O and GuBr–H_2O systems.

together with the observed ones. The peak height and area of the calculated signal largely depend on the assumed magnitude of λ. Accordingly, the peak height for the GuBr–Bu_4NBr–H_2O system was adjusted to that of the observed one, and the peak height for the GuBr–H_2O system was so determined as to give the same area of signal as that of the GuBr–Bu_4NBr–H_2O system. In spite of the assumption of the $^1J_{NH}$ value and approximate treatment for the line shape analysis, the calculated curve almost entirely fits the observed one.

From the adjusted parameters λ and by assuming $^1J_{NH}$ as 63 Hz, the remaining physical constant T_1, spin-lattice relaxation time of the ^{14}N nucleus can be calculated by means of Eq. 3. In the case of extreme narrowing condition ($w_0\tau_C \ll 1$, where w_0 is the Larmor frequency of ^{14}N nucleus), usually satisfied in our cases, the spin-lattice relaxation time is also related to the molecular rotational correlation time τ_C by means of the relation[11]

$$\frac{1}{T_1} = \frac{3}{2}\pi^2\left(1+\frac{\theta^2}{3}\right)\left(\frac{e^2qQ}{h}\right)^2\tau_c, \quad (5)$$

where θ is the asymmetry parameter of the field gradient tensor and e^2qQ/h the quadrupole coupling constant. T_1 and τ_C calculated for each system from the values of $^1J_{NH}$ are given in Table 1, θ and e^2qQ/h being given in the footnote. The value of T_1 obtained for the GuBr–H_2O system is comparable with those obtained by a different method, *i.e.* 0.932 ms for guanidine and 1.44 ms for urea,[13] which indicates that our assumption is reasonable. The spin-lattice relaxation times of mixed solutions are shortened with the increase of alkyl chain length of the added tetraalkylammonium bromide, *e.g.*,

TABLE 1. THE NMR DATA OF GUANIDINIUM SALT SOLUTIONS CONTAINING TETRAALKYLAMMONIUM SALTS

System	Chemical shift (ppm)	$\Delta\nu_{1/2}$ (Hz)	λ^2	T_1 (ms)	$\tau_c \times 10^{12}$ (s)
GuBr	7.21	39.0±1.0	5.57±0.33	1.19±0.03	4.38
GuBr–Me_4NBr	7.29	26.0±1.0	2.38±0.20	0.78±0.03	6.69
GuBr–Et_4NBr	7.38	15.6±0.5	0.86±0.06	0.47±0.02	11.1
GuBr–Pr_4NBr	7.41	7.6±0.2	0.20±0.01	0.23±0.01	22.7
GuBr–(n-Bu)$_4$NBr	7.44	4.6±0.2	0.07±0.01	0.14±0.01	37.3

$^1J_{NH}$=63 Hz, θ=0.412, e^2gQ/h=3500(kHz).[12]

even an order of magnitude in the case of R=$-C_4H_9$. Since the quadrupole coupling constant would not be much influenced by the addition of R_4NBr, the relation in Eq. 5 indicates that this shortening is attributable to the increase of the rotational correlation time, τ_C, *i.e.*, slowing down of the rotational motion of the guanidinium ion. The relationship between diffusing particle size and correlation time can be expressed by the Debye-Einstein equation[6]

$$\tau_c = \frac{4\pi a^3}{3kT}\cdot\eta, \qquad (6)$$

where k is the Boltzmam constant, T absolute temperature, η the viscosity of the solution, and a the radius of the solute molecule.

In the ternary system tetraalkylammonium bromide–GuBr–H_2O, the crystalline complexes with various mole ratios were isolated from highly concentrated solutions. The excess free energy of mixing obtained from the ternary system GuBr–Bu_4NBr–H_2O at relatively high concentration where the crystalline complexes were not isolated, were negative and large in magnitude. Considerably large salting-in effect was observed in the same system even at low concentration regions. It is of interest to confirm whether the complexes with the same composition as the crystalline complexes actually exist in the ternary solution or not. If no water soluble complexes exist in aqueous ternary solution, the complex formation is not the cause of large salting-in. Equation 6 is useful for our purpose. In order to calculate the correlation time τ_C by means of this equation, we should determine the radii of the solutes, a. By assuming that the 1-1 complexes are formed between GuBr and R_4NBr in aqueous solution, the radii of complex, a', were obtained by spherical approximation of the sum of the partial molar volumes of infinite dilution, and by using these radii and the observed viscosities of the solutions, the correlation times, $\tau_C^{calc}(a')$ at 30 °C were calculated. The results are given in Table 2, together with values of a calculated from observed τ_C and η. Disagreement of the τ_C values with the corresponding observed values is remarkable. The volume ratio of guanidinium ion in water and aqueous tetrabutylammonium bromide solution obtained from the a values is 1.87. On the assumption that a 1 to 1 complex is formed between GuBr and Bu_4NBr, the ratio is calculated to be 9.52 with the a' values. This indicates that no complex between guanidinium bromide and tetraalkylammonium bromide would be formed in ternary aqueous solution.

From the thermodynamic studies of the aqueous solutions of guanidinium salts and urea, it has been shown that guanidinium halides and urea have very similar physicochemical properties in aqueous solutions.[14] The NH resonance of aqueous urea solutions

TABLE 2. COMPARISON BETWEEN THE OBSERVED AND CALCULATED VALUES OF τ_c

System	$\tau_c^{obsd}\times 10^{12}$ (s)	a' (Å)	$\tau_c^{calcd}(a')\times 10^{12}$ [a] (s)	a (Å)	η (c.p.)
GuBr	4.38	2.51	13.4	1.73	0.848
GuBr–Me_4NBr	6.69	4.22	81.0	1.84	1.077
GuBr–Et_4NBr	11.1	4.63	154.0	1.93	1.551
GuBr–Pr_4NBr	22.7	5.00	322.0	2.06	2.570
GuBr–(n-Bu)$_4$NBr	37.3	5.32	579.1	2.13	3.863
Urea	2.88[b]	2.61	15.6[b]	1.54	0.784
Urea–Me_4NBr	6.30	3.99	70.1	1.79	1.101
Urea–Et_4NBr	10.3	4.44	139.0	1.86	1.585
Urea–Pr_4NBr	16.2	4.84	295.0	1.84	2.597
Urea–(n-Bu)$_4$NBr	26.4	5.17	540.0	1.89	3.900

a) $\tau_c^{calcd}(a')$ is calculated by means of Eq. 6 with a' value on the assumption that a 1 to 1 complex is formed between tetraalkylammonium bromides and GuBr or Urea. b) The calculation of the observed τ_c in urea solution was carried out using the following values: $^1J_{NH}$=63 Hz, e^2qQ/h=3510 kHz, θ=0,323.[13]

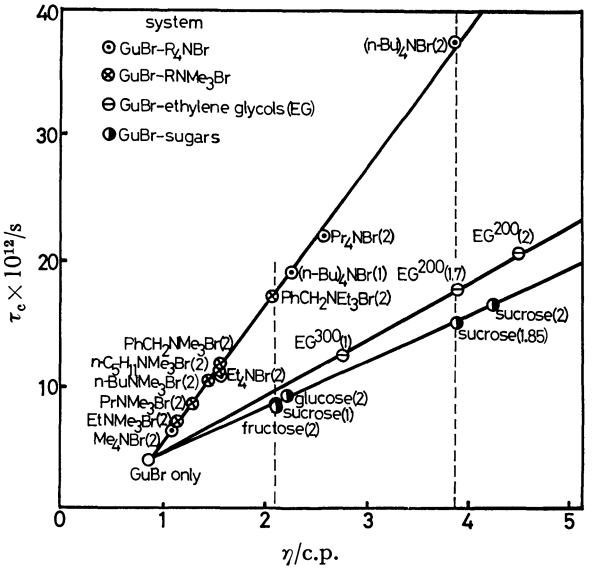

Fig. 3. Realtionships between the observed τ_c's and η's. The molalities of the second solutes are shown in parentheses.

might therefore be also expected to show narorwing to an extent similar to that of the GuBr solutions on addition of R_4NBr. This was actually observed. In the case of urea (Table 2), complex formation with tetra-alkylammonium salts in the aqueous solution[15] should be excluded as above.

With regard to the viscosity dependence of τ_C, it has been argued that microviscosity should be employed instead of macroviscosity.[16-19] The relationship between the observed τ_C of the guanidinium ion and the measured viscosity of the ternary solutions has been investigated. τ_C values are plotted against η of various ternary solutions containing alkylammonium salts, sugars or polyethylene glycols as the second solute in Fig. 3. We see that linear relationship exists between τ_C's and η values of the ternary solutions of the homologous series, irrespective of the concentration of the second solutes. The effect of the second solute on solution viscosity immediately influences τ_C. However, the τ_C values of the guanidinium ion have different values in the ternary solutions, even when the macroviscosity of the solutions is the same. This seems to indicate that τ_C is related to the quantity proportional to microviscosity around the guanidinium ion. The τ_C values seem to depend closely on the microstructure of the solution surrounding the guanidinium ion. The type of hydration of a series of alkylammonium salts was assumed to be of cage-like structure and that of a series of sugars to be purely hydrogen bonding with a definite orientation.[20] The type of hydration of polyethylene glycols is considered to be a mixed one in view of the chemical structure. Since the influence of the second solute on the water structure differs and each effect is reflected in the microviscosity surrounding the guanidinium ion, τ_C may have different values in the solutions where the macroviscosity is the same. Thus we might expect that τ_C would also influence the activation energy for the rotational motion of the guanidinium ion, E_{τ_c}. The values of τ_C at various temperatures were calculated from the line shape of NH proton (Fig. 4). E_{τ_c} values for various ternary solutions with the same viscosity (3.86 c.p.), and binary guanidinium bromide solution were determined by the temperature dependence of τ_C by means of the equation

$$\tau_c = \tau_c^0 \exp(E_{\tau_c}/RT). \quad (7)$$

The slope of $\ln \tau_C$ *vs.* $1/T$ curves determined by least squares fit gives the following activation energies: 5.3 ± 0.3 kcal/mol for GuBr–H_2O system, 7.9 ± 0.2 kcal/mol for GuBr–Bu_4NBr–H_2O system, 7.1 ± 0.2 kcal/mol for GuBr–EO_{200}–H_2O system and 7.0 ± 0.2 kcal/mol for GuBr–sucrose–H_2O system.

The activation energy of viscous flow E_η was also obtained by means of

$$E_\eta = \frac{RT\, d\ln \eta}{d\left(\frac{1}{T}\right)}. \quad (8)$$

Linear relationship holds between E_{τ_c} and E_η, indicating that the activation energy of macroviscous flow is proportional to the activation energy of the microviscous flow on the assumption that τ_C is another expression of microviscosity (Fig. 5).

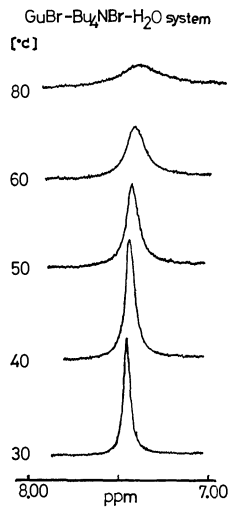

Fig. 4. Temperature dependence of the line shape of the NH proton for the ternary system GuBr–Bu_4NBr–H_2O.

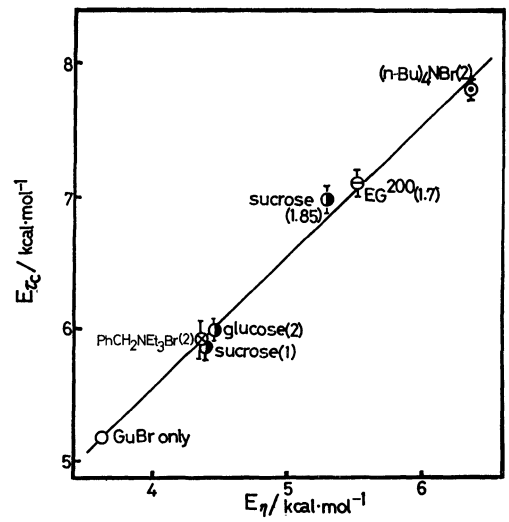

Fig. 5. Relationship between E_{τ_c} and E_η.
The molalities of the second solutes are shown in parentheses.

References

1) K. Miyajima, H. Yoshida, and M. Nakagaki, *Bull. Chem. Soc. Jpn.*, **51**, 2826 (1978).
2) K. Miyajima, H. Yoshida, and M. Nakagaki, *Bull. Chem. Soc. Jpn.*, **50**, 2854 (1977).
3) B. Chawla, S. Sunder, and J. C. Ahluwalia, *J. Phys. Chem.*, **77**, 2335 (1973).
4) K. Miyajima, H. Yoshida, and M. Nakagaki, *Bull. Chem. Soc. Jpn.*, **52**, 2880 (1979).
5) J. A. Pople, *Mol. Phys.*, **1**, 168 (1958).
6) A. Carrington and A. D. Maclachlan, "Introduction to Magnetic Resonance," Happer International, London (1967), p. 189.
7) B. E. Conway, R. E. Verrall, and J. E. Desnoyers, *Trans. Faraday Soc.*, **62**, 2738 (1966).
8) K. Miyajima, H. Yoshida, and M. Nakagaki, *Nippon Kagaku Kaishi*, **1976**, 366.

9) K. Miyajima, K. Kitamura, K. Inari, and M. Nakagaki, *Nippon Kagaku Kaishi*, **1975**, 2060.
10) J. P. Kinzinger, J. M. Lehn, and R. L. Williams, *Mol. Phys.*, **17**, 135 (1969).
11) A. Abragam, "The Principles of Nuclear Magnerism," Oxford Univ. Press, London (1961), p. 314.
12) C-H. Chen and H. W. Dodgen, *J. Magn. Reson.*, **22**, 139 (1976).
13) R. E. Richards and N. A. Thomas, *J. Chem. Soc., Perkin Trans. 2*, **1974**, 368.
14) D. B. Wetlaufer, S. K. Malik, L. Stoller, and R. F. Coffin, *J. Am. Chem. Soc.*, **86**, 509 (1964); M. J. Shick and A. H. Gilbert, *J. Colloid Sci.*, **20**, 464 (1965); S. Subramanian, T. S. Sarma, D. Barasubramanian, and J. C. Ahluwalia, *J. Phys. Chem.*, **75**, 815 (1971).
15) S. Saito, M. Lee, and W-Y. Wen, *J. Am. Chem. Soc.*, **88**, 5107 (1966).
16) A. Gierer and K. Wirtz, *Z. Naturforsch*, **A8**, 532 (1953).
17) R. J. Meakins, *Trans. Faraday Soc.*, **54**, 1160 (1958).
18) O. F. Kalman and C. P. Smyth, *J. Am. Chem. Soc.*, **82**, 783 (1960).
19) S. Hoshino, T. Oike, and H. Yakura, *Kagaku Kogaku*, **36**, 433 (1972).
20) F. Frank, "Water, A Comprehensive Treatise," ed by F. Frank, Prenum Press, New York, London (1975), Vol. 4, p. 1.

 © 1980 The Chemical Society of Japan Bull. Chem. Soc. Jpn., 53, 2217—2220 (1980)

Negative Azeotropic Transformation in Mixed Monolayers of Octadecylammonium Chloride and Tetradecanoic Acid

Kinsi MOTOMURA,* Masaki IKEMATSU, Yoshiteru HAYAMI,
Hirosi MATUO, and Ryohei MATUURA
Department of Chemistry, Faculty of Science, Kyushu University 33, Fukuoka 812
(Received December 7, 1979)

The surface pressure of mixed monolayers of octadecylammonium chloride and tetradecanoic acid has been measured as a function of mean area per film molecule at various compositions and temperatures. It has been observed that the transition pressure from expanded to condensed state of either constituent decreases with the addition of the other one. This behavior has been called a negative azeotropy in the two-dimensional state in contrast to the positive azeotropy observed for the ethyl heptadecanoate–tetradecanoic acid system. By applying the thermodynamic treatment, the phase diagram has been constructed and the apparent molar entropy and energy associated with the phase transition have been calculated. The results support the view that the negative azeotropic transformation in the mixed monolayer is brought about by the mutual interaction between octadecylammonium chloride and tetradecanoic acid molecules which is stronger than that between the same kind of molecules.

It has been found useful in clarifying the interaction between film-forming molecules in the monolayer state to analyze the phase transition of mixed monolayers from expanded to condensed states thermodynamically.[1-8] Recently we have shown that a positive azeotropic transformation is observed for the mixed monolayer of slightly different molecules between which the mutual interaction is weaker than that between the same kind of molecules.[6,7] It is now expected for a mixed monolayer of which the constituent molecules interact strongly with each other to exhibit a negative azeotropic transformation. Actually it has been found by Harkins *et al.*[9,10] that the equimolar mixed monolayer of fatty acid and alkylamine has the minimum area per film molecule at a given surface pressure, which can be explained in terms of the decrease of transition pressure by mixing the monolayers.

The object of this paper is to make clear the thermodynamic behavior of the mixed monolayer of tetradecanoic acid and octadecylammonium chloride by measuring the surface pressure as a function of composi tion and temperature.

Experimental

Tetradecanoic acid was purified by vacuum distillation and recrystallization from ether. Octadecylammonium chloride was synthesized from octadecylamine, which was fractionated by vacuum distillation, by the reaction with hydrochloric acid and then recrystallized from ethanol. As a spreading solvent, a mixture of benzene and ethanol (9 to 1 in volume) each purified by ordinary procedures was used. Monolayers were spread on 0.1 M sodium chloride solution which was prepared from twice distilled water and sodium chloride (Wako special grade).

Surface pressure was measured by a Wilhelmy-type surface balance. Temperature was kept constant within 0.1K by circulating thermostated water.

Results and Discussion

The surface pressure, π, of mixed monolayers consisting of octadecylammonium chloride and tetradecanoic acid was measured as a function of the mean area per film molecule, A, at various compositions at a constant temperature. The results at 298.2 K are illustrated in Fig. 1. It is observed that the break point pressure of π *vs.* A curve of either constituent decreases with the addition of the other one and becomes gradually obscure. In Fig. 2, the surface pressure of the break point, referred to as the transition pressure π^{eq}, is plotted against the mole fraction of tetradecanoic acid defined by

$$x_2^{\pi} = n_2/(n_1+n_2), \quad (1)$$

where n_i is the number of moles of film-forming component i. It is clearly seen that the value of π^{eq} of mixed monolayer deviates negatively from a straight line connecting that of the pure monolayers and have a minimum in the vicinity of $x_2^{\pi}=0.5$. This fact indicates that the mixed monolayer is homogeneous in both expanded and condensed states. Such a behavior may be called a negative azeotropic transformation in contrast with the positive azeotropic transformation

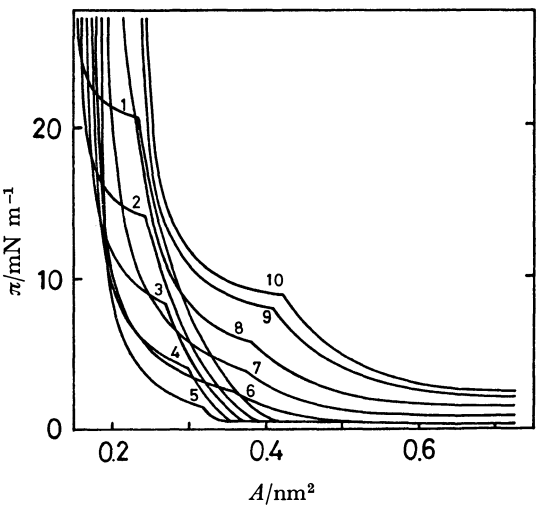

Fig. 1. Surface pressure π *vs.* mean area A curves of octadecylammonium chloride–tetradecanoic acid monolayers at 298.2 K.
(1) $x_2^{\pi}=1$, (2) 0.95, (3) 0.90, (4) 0.85, (5) 0.75, (6) 0.25, (7) 0.20, (8) 0.15, (9) 0.05, (10) 0.

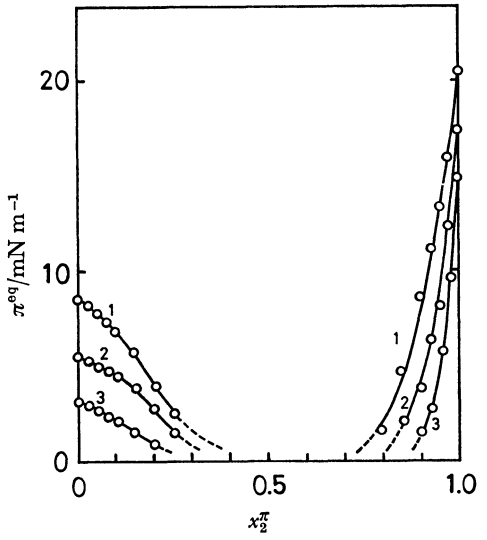

Fig. 2. Transition pressure π^{eq} *vs.* mole fraction of tetradecanoic acid x_2^{π} curves at constant temperature. (1) 298.2 K, (2) 295.7 K, (3) 293.2 K.

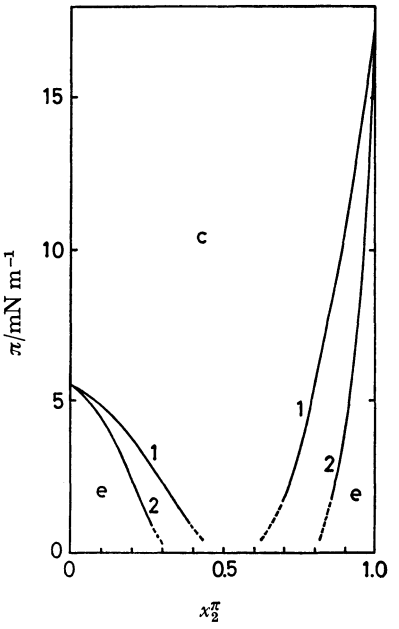

Fig. 3. Phase diagram of octadecylammonium chloride–tetradecanoic acid system at 295.7 K. (1) π^{eq} *vs.* $x_2^{\pi,c}$ curve, (2) π^{eq}*vs.* $x_2^{\pi,e}$ curve, (c) region of condensed phase, (e) region of expanded phase.

observed for the system of ethyl heptadecanoate and tetradecanoic acid of which the π^{eq} *vs.* x_2^{π} curve has a maximum.[6] There is a possibility that octadecylammonium chloride and tetradecanoic acid form the one-to-one addition compound in the condensed state. However, this possibility is denied by the fact that each π *vs.* A curves in Fig. 1 does not have more than one break point and the π^{eq} *vs.* x_2^{π} curves in Fig. 2 behave smoothly.

Measurements were made likewise at 295.7 and 293.2 K. The π^{eq} *vs.* x_2^{π} curves at these temperatures are shown in Fig. 2. It is found that these curves are similar in shape to each other and shift downward with decreasing temperature. Since the phase transition takes place from the expanded monolayer, of which the concentration is x_2^{π}, to the condensed monolayer, these curves are referred to as the π^{eq} *vs.* $x_2^{\pi,e}$ curves. Now let us consider to evaluate the composition of condensed monolayer in equilibrium with the expanded monolayer thermodynamically.

According to the thermodynamic treatment,[1,11] the mole fraction of tetradecanoic acid in the condensed monolayer $x_2^{\pi,c}$ is related to $x_2^{\pi,e}$ by the expression

$$x_2^{\pi,c} = x_2^{\pi,e} + (a^c - a^e)(\partial\pi^{eq}/\partial x_2^{\pi,e})_{T,p}/\{RT/x_1^{\pi,e}x_2^{\pi,e} + (\partial a^e/\partial x_2^{\pi,e})_{T,p,\pi}(\partial\pi^{eq}/\partial x_2^{\pi,e})_{T,p}\int_0^{\pi}[\partial^2 a^e/(\partial x_2^{\pi,e})^2]_{T,p,\pi}d\pi\}, \quad (2)$$

where a is the mean area per mole of film-forming components and the superscripts e and c represent expanded and condensed states, respectively. By applying Eq. 2 to the experimental results given in Figs. 1 and 2 on the assumption that the value of a^c may be replaced by the corresponding one of octadecanoic acid, the value of $x_2^{\pi,c}$ can be calculated numerically. The π^{eq} *vs.* $x_2^{\pi,c}$ curve obtained at 295.7 K is drawn in Fig. 3 as the curve 1, in which the corresponding π^{eq} *vs.* $x_2^{\pi,e}$ curve taken from Fig. 2 is also depicted as the curve 2. It is found that the areas denoted by the letters e and c are regions in which the expanded and condensed monolayers are stable, respectively, and the area between the curves 1 and 2 is a region in which the expanded and condensed monolayers coexist. Therefore, we may say that Fig. 3 is the phase diagram describing the equilibrium between expanded and condensed monolayers of octadecylammonium chloride–tetradecanoic acid system at 295.7 K.

Now we shall consider an apparent molar thermodynamic quantity change Δy^{γ} associated with the phase transition from expanded to condensed monolayer:

$$\Delta y^{\gamma} = x_1^{\pi,e}(\bar{y}_1^{\gamma,e} - \bar{y}_1^{\gamma,e}) + x_2^{\pi,c}(\bar{y}_2^{\gamma,c} - \bar{y}_2^{\gamma,e}). \quad (3)$$

On the right-hand side of Eq. 3, $\bar{y}_i^{\gamma}$ is the apparent partial molar quantity defined by

$$\bar{y}_i^{\gamma} = (\partial Y/\partial n_i)_{T,p,\gamma,n_{j\neq i}} \quad i = 1, 2\ (j \neq i), \quad (4)$$

where Y is the thermodynamic quantity inherent in the monolayer and γ the surface tension.[6,12]

The apparent entropy change Δs^{γ} is related to the derivative of π^{eq} with respect to T at constant $x_2^{\pi,e}$ under atmospheric pressure by

$$\Delta s^{\gamma} = [a^c - a^e - (x_2^{\pi,e} - x_2^{\pi,e})(\partial a^e/\partial x_2^{\pi,e})_{T,p,\pi}] \times [(\partial\pi^{eq}/\partial T)_{p,x_2^{\pi,e}} - (\partial\gamma^{\circ}/\partial T)_p], \quad (5)$$

where γ° is the surface tension of 0.1 M sodium chloride solution.[6,12] Since $\partial\pi^{eq}/\partial T$ is estimated on the basis of the experimental results shown in Fig. 2 and $\partial\gamma^{\circ}/\partial T$ on the basis of the value of γ° approximated by that of pure water,[13] we can calculate Δs^{γ}. In Fig. 4, the value of Δs^{γ} at 295.7 K is plotted against the mole fraction of tetradecanoic acid in the condensed monolayer. The Δs^{γ} *vs.* $x_2^{\pi,c}$ curve seems to be approximately linear over the whole range. Taking Eq. 3 into account, therefore, the apparent partial molar entropy

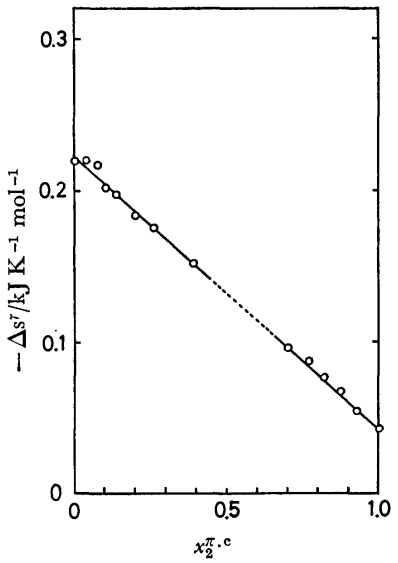

Fig. 4. Apparent molar entropy change Δs^{γ} *vs.* mole fraction of tetradecanoic acid in condensed monolayer $x_2^{\pi\cdot c}$ curve for octadecylammonium chloride–tetradecanoic acid system at 295.7 K.

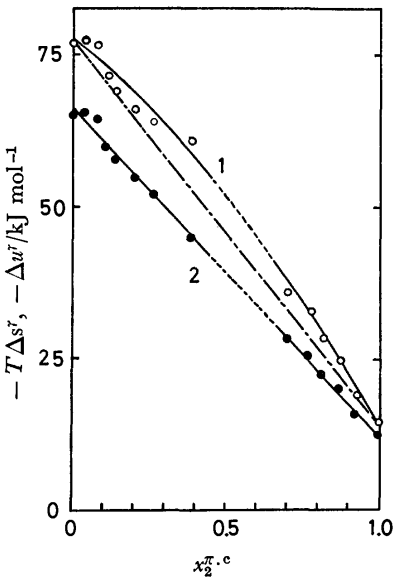

Fig. 5. Δu^{γ} *vs.* $x_2^{\pi\cdot c}$ curve (1) and $T\Delta s^{\gamma}$ *vs.* $x_2^{\pi\cdot c}$ curve (2) at 295.7 K for octadecylammonium chloride–tetradecanoic acid system.

changes of octadecylammonium chloride and tetradecanoic acid are given by intercepts of the straight line on the ordinates. This dependence of Δs^{γ} on $x_2^{\pi\cdot c}$ is quite similar to that of the system of pentadecanoic and tetradecanoic acids which is known to form an ideal mixed monolayer.[2] Furthermore, an analogous Δs^{γ} *vs.* $x_2^{\pi\cdot c}$ curve is observed for the mixed monolayer of ethyl heptadecanoate and tetradecanoic acid which exhibits the positive azeotropic transformation.[6] This fact indicates that the apparent molar entropy change associated with the phase transition has an ideal value even when the mixed monolayer behaves nonideally. This means that the apparent molar entropy change is of limited significance in the azeotropic transformation. Therefore, the azeotropic behavior of octadecylammonium chloride–tetradecanoic acid system should be explained in terms of other thermodynamic quantity changes.

Next let us consider the apparent molar internal energy change associated with the phase transition Δu^{γ} which is given by the relation

$$\Delta u^{\gamma} = -(\pi^{eq}-\gamma^{o})[a^{c}-a^{e}-(x_2^{\pi\cdot e}-x_2^{\pi\cdot e})(\partial a^{e}/\partial x_2^{\pi\cdot e})_{T,p,\pi}] - p\Delta v^{\gamma} - T\Delta s^{\gamma}, \quad (6)$$

where Δv^{γ} is the apparent molar volume change.[6] Taking into account that the $p\Delta v^{\gamma}$ term on the right-hand side of Eq. 6 is negligibly small compared with other terms under atmospheric pressure,[6,14] the value of Δu^{γ} can be evaluated by making use of the above experimental results. In Fig. 5, the Δu^{γ} *vs.* $x_2^{\pi\cdot c}$ curve is drawn. The curve is found to show a remarkable deviation from the straight line connecting the value of Δu^{γ} for the pure components as compared with the $T\Delta s^{\gamma}$ *vs.* $x_2^{\pi\cdot c}$ curve also depicted in Fig. 5. Here we notice that the value of Δu^{γ} is smaller than an ideal one for the system of octadecylammonium chloride and tetradecanoic acid, while it was larger for the system of ethyl heptadecanoate and tetradecanoic acid.[6]

In order to examine the connection of the azeotropic transformation with the interaction between film-forming molecules, it is appropriate to look closely at partial molar energies of the film-forming components. Taking account of Eq. 3, the apparent partial molar energy of component i is given by the intercept of tangent to the Δu^{γ} *vs.* $x_2^{\pi\cdot c}$ curve on the ordinate specified by $x_1^{\pi\cdot c}=1$. As seen in the previous paper,[6] the positive azeotropy of ethyl heptadecanoate–tetradecanoic acid system is characterized by the decrease of $\bar{u}_i^{\gamma\cdot c}-\bar{u}_i^{\gamma\cdot e}$ with increase in $x_1^{\pi\cdot c}$. For the octadecylammonium chloride–tetradecanoic acid system, however, we can see from Fig. 5 that the value of $\bar{u}_i^{\gamma\cdot c}-\bar{u}_i^{\gamma\cdot e}$ increases with increasing $x_1^{\pi\cdot c}$. This fact indicates that the mutual interaction between octadecylammonium chloride and tetradecanoic acid molecules in the mixed monolayer is stronger than the interactions between the same kind of constituent molecules. This finding is very reasonable.

References

1) K. Motomura, K. Sekita, and R. Matuura, *J. Colloid Interface Sci.*, **48**, 319 (1974).
2) K. Sekita, M. Nakamura, K. Motomura, and R. Matuura, *Mem. Fac. Sci. Kyushu Univ., Ser. C*, **10**, 51 (1976).
3) K. Motomura, T. Terazono, H. Matuo, and R. Matuura, *J. Colloid Interface Sci.*, **57**, 52 (1976).
4) H. Matuo, K. Hiromoto, K. Motomura, and R. Matuura, *Bull. Chem. Soc. Jpn.*, **51**, 690 (1978).
5) H. Matuo, K. Motomura, and R. Matuura, *J. Colloid Interface Sci.*, **69**, 192 (1979).
6) K. Motomura, T. Yano, M. Ikematsu, H. Matuo, and R. Matuura, *J. Colloid Interface Sci.*, **69**, 209 (1979).
7) H. Matuo, N. Yosida, K. Motomura, and R. Matuura, *Bull. Chem. Soc. Jpn.*, **52**, 667 (1979).

8) H. Matuo, K. Motomura, and R. Matuura, *Bull. Chem. Soc. Jpn.*, **52**, 673 (1979).
9) W. D. Harkins and R. T. Florence, *J. Chem. Phys.*, **6**, 847 (1938).
10) W. D. Harkins, "Physical Chemistry of Surface Films," Reinhold, New York (1952), p. 154.
11) K. Motomura, *J. Colloid Interface Sci.*, **48**, 307 (1974).
12) K. Motomura, *Adv. Colloid Interface Sci.*, **12**, 1 (1980).
13) J. J. Jasper, *J. Phys. Chem. Ref. Data*, **1**, 841 (1972).
14) N. Matubayasi, K. Motomura, M. Aratono, and R. Matuura, *Bull. Chem. Soc. Jpn.*, **51**, 2800 (1978).

A Thermodynamic Study on Hydrolytic Reactions of Lead(II) Ion in an Aqueous Solution and Dioxane-Water Mixtures. I. A Potentiometric Study

Takayoshi KAWAI, Shin-ichi ISHIGURO, and Hitoshi OHTAKI*

Department of Electronic Chemistry, Tokyo Institute of Technology, Nagatsuta, Midori-ku, Yokohama 227

(Received February 5, 1980)

The hydrolytic reactions of lead(II) ions were studied at 25 °C by means of potentiometric titrations by using a glass electrode in water and dioxane–water mixture (dioxane contents: 0.1 and 0.2 mol fractions) containing 3 mol dm^{-3} $LiClO_4$ as a constant ionic medium. Four complexes, $Pb_3(OH)_3^{3+}$, $Pb_4(OH)_4^{4+}$, $Pb_3(OH)_4^{2+}$, and $Pb_6(OH)_8^{4+}$ were found in the solvent systems examined at $pH \lesssim 8$, and the formation constant $*\beta_{pq}$ for the reaction, $qPb^{2+}+pH_2O=Pb_q(OH)_p^{(2q-p)+}+pH^+$, was determined. The autoprotolysis constants K_1 in the same solvent systems were also obtained by use of a hydrogen electrode. The formation constant $\beta_{pq}(=*\beta_{pq}/K_1^p)$ for the reaction, $qPb^{2+}+pOH^-=Pb_q(OH)_p^{(2q-p)+}$ was evaluated by combining the formation constants $*\beta_{pq}$ and the autoprotolysis constants obtained. The free energy change of transfer from water to a dioxane–water mixture for the reaction could be estimates as $\Delta G_{pq}^t=-RT\ln\{\beta_{pq}(\text{mix})/\beta_{pq}(\text{aq})\}$. The values $(1/p)\Delta G_{pq}^t$ of hydroxo complexes of various metal ions such as lead(II), copper(II), nickel(II), beryllium(II), and cadmium(II) ions were approximately independent of the complexes at a given concentration of dioxane. This result suggested that the formal charge per metal ion of the complex, z' $(=z-p/q$; z: charge of a metal ion), rather than the total charge of the complex, $zq-p$, is essential for the interactions between the hydroxo complexes and solvent molecules.

The hydrolytic reactions of lead(II) ion have so far been studied in aqueous solution containing various ionic media.[1-3] Recently, Olin has reported formation of four hydrolytic species, *i.e.*, the $PbOH^+$ and $Pb_4(OH)_4^{4+}$ complexes in the relatively low pH region ($5<pH<7$) and the $Pb_3(OH)_4^{2+}$ and $Pb_6(OH)_8^{4+}$ complexes at a higher pH ($6<pH<8$).[4] The $Pb_4(OH)_4^{4+}$ and $Pb_6(OH)_8^{4+}$ complexes are predominant species and most of lead(II) ions exist as the hydroxo complexes at $pH>6$. The structures of the $Pb_4(OH)_4^{4+}$ and $Pb_6(OH)_8^{4+}$ complexes have been studied by means of X-ray diffraction.[5,6] Raman spectroscopic studies on the complexes have also been reported.[7]

We have previously reported the medium effect on the hydrolytic reactions of various divalent metal ions such as beryllium,[8] copper,[9] nickel,[10] and cadmium[11] in dioxane–water mixtures. It has been found that the composition of the hydrolytic species and the formation constant $*\beta_{pq}$ for the reaction, $qM^{z+}+pH_2O=M_q(OH)_p^{(zq-p)+}+pH^+$ are generally little affected by the solvent composition up to 0.5 mole fraction (*ca.* 88 w/w %) of dioxane in the medium.

In the present study, the hydrolytic reactions of lead(II) ions were studied in water and dioxane–water mixtures. The autoprotolysis reaction of solvent was also investigated in the same solvent systems. On the basis of the formation constants of the hydroxo complexes of lead(II) ions, together with those of other metal ions previously obtained, the medium effect for the hydrolytic reactions of divalent metal ions is discussed.

Experimental

All measurements were carried out at (25.00±0.02) °C in a liquid paraffin bath set in a room thermostated at (25±0.5)°C. Lithium perchlorate was used as an ionic medium to keep the concentration of perchlorate ions at 3 mol dm^{-3}. Total concentrations of lead(II) ions examined were changed from 0.001 to 0.08 mol dm^{-3}. The total concentration of lead(II) ions was kept constant throughout a series of potentiometric titrations. The cell used for the emf measurements of the autoprotolysis reaction of the solvent was as follows:

$$\text{Ref}\,|\,\text{Test Solution}\,|\,H_2(Pt) \qquad \text{(A)}$$

$$\text{Ref} = \left|\begin{array}{l}3\text{ mol dm}^{-3}\\LiClO_4\\\text{in Mixture}\end{array}\right|\left|\begin{array}{l}3\text{ mol dm}^{-3}\\LiClO_4\\\text{in aqueous}\\\text{solution}\end{array}\right|\left|\begin{array}{l}0.01\text{ mol dm}^{-3}\\AgClO_4\\2.99\text{ mol dm}^{-3}\\LiClO_4\\\text{aqueous}\\\text{solution}\end{array}\right|\text{AgCl–Ag} \qquad \text{(B)}$$

The emf differences between the two hydrogen electrodes immersed in the same test solution were within 0.1 mV. The emf reached a constant value within 15—20 min after the addition of $HClO_4$ solution and remained unchanged within ±0.05 mV for at least 5—6 h. The cells used for emf measurements of free-hydrogen and free-lead(II) ions were, respectively, as follows:

$$\text{Ref}\,|\,\text{Test Solution}\,|\,\text{GE} \qquad \text{(C)}$$

$$\text{Ref}\,|\,\text{Test Solution}\,|\,\text{Pb(Hg)}. \qquad \text{(D)}$$

The emfs of both glass electrode (GE) and lead amalgam electrode reached a constant values within a minute and remained unchanged within ±0.1 mV for at least 5—6 h.

Reagents and Analysis. Lead(II) Perchlorate. A stock solution of lead(II) perchlorate was prepared as follows: First, reagent grade lead(II) nitrate was recrystallized twice from water. The lead nitrate crystals thus prepared were dissolved in perchloric acid of super special grade diluted with water. Lead perchlorate was crystallized from the solution by evaporating under vacuum and crystals thus obtained were recrystallized from perchloric acid solution by repeating the above procedure. Finally, lead perchlorate thus obtained was recrystallized twice from water. The concentration of lead(II) ions in the stock solution was gravimetrically determined in the form of lead sulfate.

Lithium Perchlorate and Lithium Hydroxide were prepared by the procedures as described in the previous paper.[12]

Dioxane was purified by an ordinary method.[12]

Apparatus. Beckman (No. 40495 and 40498) glass electrodes were used in combination with an Orion Digital pH Meter Model 801. Hydrogen electrodes used were prepared according to Feltham and Spiro.[13] The hydrogen electrodes

were stored in a 0.1 mol dm^{-3} H_2SO_4 solution and were electrolyzed about 30 min in the solution before measurements. Lead amalgam electrodes were prepared as described in Ref. 14 and the electrode cell design used was described in a previous paper.[15] The Ag–AgCl electrodes used as references were prepared according to Brown.[16] The emfs of hydrogen and lead amalgam electrodes were measured by using Takeda Riken Digital Voltmeter (TR-6515). For studying hydrolytic reactions of lead(II) ions, glass electrodes were used, while lead amalgam electrodes were used for measurements of potential changes with varying concentrations of dioxane in an acidic solution containing a constant total concentration of lead(II) ions where no hydrolysis occurs.

Results

The Autoprotolysis Constant of Solvent. An H_0 mol dm^{-3} $HClO_4$ ($H_0 \simeq 0.07$) solution containing $(3-H_0)$ mol dm^{-3} $LiClO_4$ was titrated with an LiOH solution containing 3 mol dm^{-3} $LiClO_4$, the concentration of LiOH in the titrant is about 0.03 mol dm^{-3}. The emf E at equilibrium is written by the following equation:

$$\begin{aligned} E &= E_{0,H} + 59.154 \log [H^+] + 59.154 \log y_H \\ &\quad + E_j - \Delta E_p \\ &= E^*_{0,H} + 59.154 \log [H^+] + E_j - \Delta E_p \end{aligned} \quad (1)$$

where

$$\Delta E_p = 29.577 \log (P_H/P_{0,H}) \quad (2)$$

and $E_{0,H}$ is a constant and P_H and $P_{0,H}$ stand for partial pressures of hydrogen gas at each point and initial point of the emf measurements, respectively. The value log $(P_H/P_{0,H})$ was so small in a course of one series of titrations that it was neglected. E_j is the liquid junction potential between the reference electrode and the test solution. y_H denotes the activity coefficient of hydrogen ion in the solution. Equation 1 is rewritten by using the autoprotolysis constant $K_i(=[H^+][OH^-])$ as follows:

$$\begin{aligned} E &= E^*_{0,H} + 59.154 \log (K_i/[OH^-]) \\ &= E^*_{0,A} - 59.154 \log [OH^-]. \end{aligned} \quad (3)$$

Since $E^*_{0,H}$ and $E^*_{0,A}$ are constant in a constant ionic medium with a constant composition of solvent, the autoprotolysis constant was estimated by using the $E^*_{0,H}$ and $E^*_{0,A}$ values obtained by Gran's plots in relatively low acidic and basic regions of the solution, where the liquid junction potentials were negligible.

$$\log K_i = \frac{E^*_{0,A} - E^*_{0,H}}{59.154} \quad (4)$$

The autoprotolysis constants obtained in various solutions by using hydrogen electrodes are summarized in Table 1.

Formation Constants of Hydroxo Complexes of Lead(II) Ions. The hydrolytic reactions of metal ions may be written as follows:

$$qM^{z+} + pH_2O = M_q(OH)_p^{(zp-q)+} + pH^+. \quad (5)$$

The average number of hydrogen ion set free per metal ion, Z, is an experimentally determinable quantity as given by the following equation:

$$Z = \frac{[H^+] - \boldsymbol{H}}{B} = \sum_p \sum_q p {}^*\beta_{pq} [M^{z+}]^q [H^+]^{-p}/B \quad (6)$$

where ${}^*\beta_{pq}$ is the formation constant of the $M_q(OH)_p^{(zq-p)+}$ complex given by Eq. 7;

$${}^*\beta_{pq} = [M_q(OH)_p^{(zq-p)+}][H^+]^p/[M^{z+}]^q \quad (7)$$

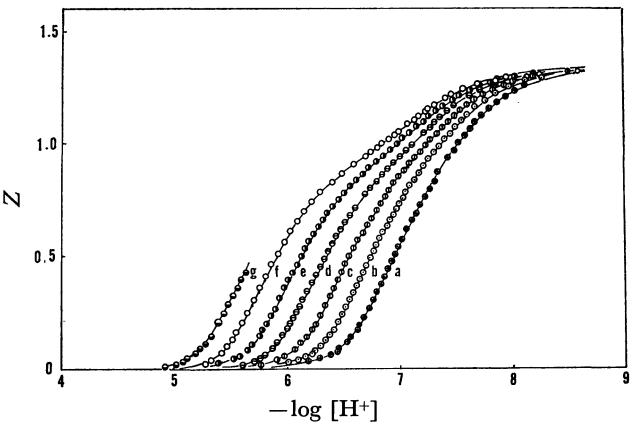

Fig. 1. Formation curves of the hydroxo complexes of lead (II) ions plotted as Z *vs.* −log [H$^+$] in aqueous solution.
Solid lines show calculated curves of Z with the formation constants listed in Table 3. The total concentrations of lead(II) ions in the solutions are (in mol dm^{-3}); a: 0.001251, b: 0.002521, c: 0.005055, d: 0.01001, e: 0.02000, f: 0.04001, g: 0.08008.

Table 1. Determination of pK_i in various aqueous organic mixtures containing 3 mol dm^{-3} $LiClO_4$[a]

	Aqueous solution		0.1 mole fraction (35.2 w/w %) Dioxane–water		0.2 mole fraction (55.0 w/w %) Dioxane–water		0.2 mole fraction (30.8 w/w %) Methanol–water		0.2 mole fraction (39.0 w/w %) Ethanol–water	
	$E^*_{0,H}$	$E^*_{0,A}$	$E^*_{0,H}$	$E^*_{0,A}$	$E^*_{0,H}$	$E^*_{0,A}$	$E^*_{0,H}$	$E^*_{0,A}$	$E^*_{0,H}$	$E^*_{0,A}$
1	616.19	−203.43	645.15	−219.19	664.69	−245.77	627.31	−208.29	625.75	−225.02
2	616.35	−203.54	644.72	−219.33	664.10	−246.11	627.39	−208.22	625.98	−225.11
3	617.06	−203.56	644.85	−219.47	663.31	−246.24	627.38	−208.27	626.46	−225.14
4	616.73	−203.63	644.86	−219.42	663.57	−246.30	627.33	−208.32	626.40	−225.37
5	616.73	−203.45	644.90	−219.16	663.40	−245.95	627.37	−208.30	626.42	−225.33
6	616.75	−203.53							626.39	−225.31
Mean	616.73	−203.51	644.90	−219.31	663.42	−246.07	627.36	−208.29	626.42	−225.13
Dev.	±0.37	±0.13	±0.25	±0.16	±0.15	±0.24	±0.06	±0.03	±0.30	±0.25
pK_i	13.87±0.01		14.61±0.01		15.38±0.01		14.13±0.01		14.40±0.01	

a) The values of emf are given by mV units.

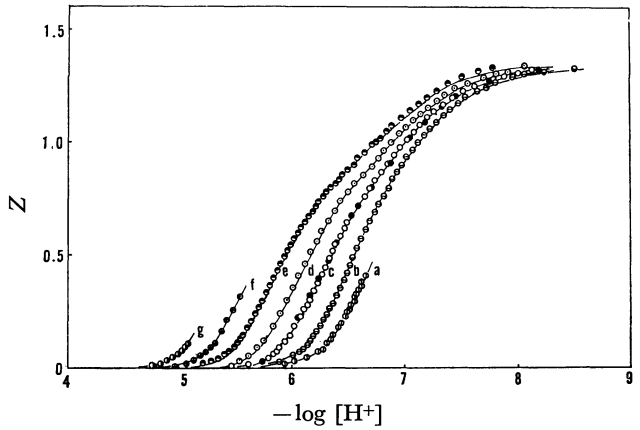

Fig. 2. Formation curves of the hydroxo complexes of lead(II) ions plotted as Z *vs.* $-\log [H^+]$ in 0.1 mole fraction dioxane–water mixture.
Solid lines show calculated curves of Z with the formation constants listed in Table 3. The total concentrations of lead(II) ions in the solutions are (in mol dm^{-3}); a: 0.01253, b: 0.002501, c: 0.005001, solid circles denote measured points by back titrations, d: 0.01001, e: 0.02002, f: 0.04001, g: 0.08000.

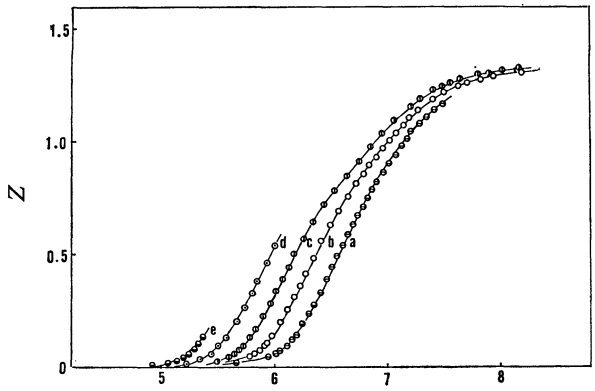

Fig. 3. Formation curves of the hydroxo complexes of lead(II) ions plotted as Z *vs.* $-\log [H^+]$ in 0.2 mole fraction dioxane–water mixture.
Solid lines show calculated curves of Z with the formation constants listed in Table 3. The total concentrations of lead(II) ions in the solutions are (in mol dm^{-3}); a: 0.002414, b: 0.005055, c: 0.01009, d: 0.02017, e: 0.03988.

and $\boldsymbol{H}$ denotes an analytical excess of hydrogen ions, B the total concentration of metal ion, $[M^{z+}]$ and $[H^+]$ the concentrations of free M^{z+} and H^+ ions, respectively. The results obtained are summarized in Figs. 1—3 as Z *vs.* $-\log [H^+]$ plots. The formation curves were analyzed by means of a graphical method at the first step of calculation, as has been used in previous papers.[8–11] However, we met with difficulties to

Table 2. Determination of the formation constants $*\beta_{pq}$ for the hydroxo complexes of lead(II) ion by the least-squares method

	Aqueous solution			0.1 mole fraction Dioxane–water			0.2 mole fraction Dioxane–water		
	Initial	Final	Fixed	Initial	Final	Fixed	Initial	Final	Fixed
PbOH	−8.80	(−8.314)	−7.65	−7.20	—	−7.41	−7.27	—	−7.21
$Pb_2(OH)_2$	−11.89	—		−11.52	(−11.581)		−11.52	(−11.310)	
$Pb_3(OH)_3$	−15.62	−15.286		−15.29	−14.982		−15.29	−14.813	
$Pb_4(OH)_4$	−19.25	−19.423	−19.14	−18.61	−18.598	−18.44	−18.57	−19.171	−18.63
$Pb_5(OH)_5$	−22.93	(−24.877)							
$Pb_6(OH)_6$	−26.61	—							
$Pb_7(OH)_7$	−30.29	—							
$Pb_8(OH)_8$	−33.97	—							
$Pb_9(OH)_9$	−37.65	—							
$Pb_3(OH)_4$	−22.75	−22.782	−22.75	−21.79	−21.788	−21.79	−21.75	−21.738	−22.73
$Pb_6(OH)_8$	−42.32	−42.329	−42.32	−40.92	−40.751	−40.75	−41.17	−41.122	−41.18
$Pb_9(OH)_{12}$	−61.89	—							
Pb_2OH	−6.48	—							
$Pb(OH)_2$	−15.00	(−16.372)		−4.96	—		−4.96	—	
$Pb_3(OH)_2$	−10.16	—							
$Pb_2(OH)_3$	−19.02	—							
$Pb_4(OH)_3$	−13.84	—							
$Pb_5(OH)_4$	−17.52	—					−25.61	—	
$Pb_4(OH)_5$				−25.61	—				
$Pb_6(OH)_5$	−20.90	—							
$Pb_5(OH)_6$				−29.37	—		−29.37	—	
$Pb_6(OH)_7$	−36.40	(−36.186)		−33.14	—		−33.14	—	
U	11.46	0.0219	0.0307	0.533	0.0537	0.0562	0.369	0.0208	0.0280

Initial: Formation constants initially assumed. Final: Formation constants finally obtained. Fixed: The set of the complexes is fixed at that proposed by Olin, but the formation constants of the complexes are floated.
( ): Minor species and uncertain. —: Unreasonable species which is rejected in the course of the calculation.

estimate the composition of complexes formed in a relatively low pH region if there exists either $Pb_4(OH)_4^{4+}$ or $Pb_3(OH)_3^{3+}$, or both. Therefore, the composition of the complexes formed and their formation constants were determined by the least-squares method using an electronic computer (HITAC 8700). As a first guess, a number of possible species were assumed to be present in the systems, and then unreasonable species were rejected in the course of the least-squares optimization. The method used was essentially based on the principle of the LETAGROP program developed by Sillén.[17] The minimum value of the error square sum $U=\sum(Z_{obsd}-Z_{calcd})^2$ for a given system was searched by choosing the best set of the composition (p and q) and the formation constants of the complexes in the system. As is shown in Table 2, the only four complexes, $Pb_3(OH)_3^{3+}$, $Pb_4(OH)_4^{4+}$, $Pb_3(OH)_4^{2+}$, and $Pb_6(OH)_8^{4+}$ were finally obtained as possible species in all the solvent systems examined. Formation of the $PbOH^+$ complex proposed by Olin[4] was rather uncertain in our measurements (see Table 2). An examination of the least-squares calculation by assuming a set of complexes, $PbOH^+$, $Pb_4(OH)_4^{4+}$, $Pb_3(OH)_4^{2+}$, and $Pb_6(OH)_8^{4+}$, which had been proposed by Olin, gave a larger error square sum than that for a set of the complexes, $Pb_3(OH)_3^{3+}$, $Pb_4(OH)_4^{4+}$, $Pb_3(OH)_4^{2+}$, and $Pb_6(OH)_8^{4+}$, and the $PbOH^+$ complex was excluded in the course of the refinement. In Table 2, columns "Initial" and "Final" show the initially assumed and finally obtained composition and stability constants of the complexes, respectively. Lack of number in the column "Final" means that the relevant complex is rejected as an unreasonable one during the course of the refinement. "Fixed" denotes that the set of the complexes is fixed at the proposed one by Olin, and the formation constants of the complexes are allowed to change to reach the minimum error square sum. Since the Z values never exceed 1.5, possible combinations of $p/q<1.5$ are assumed as the inital sets of complexes. Values in parentheses are uncertain ones. The final results obtained for the formation constants of the hydroxo complexes of lead(II) ions are summarized in Table 3, together with the autoprotolysis constants of the solvents.

TABLE 3. AUTOPROTOLYSIS CONSTANT $K_1(=[H^+][OH^-])$ AND FORMATION CONSTANTS OF HYDROXO COMPLEXES OF LEAD(II) ION IN AQUEOUS AND DIOXANE–WATER MIXTURES CONTAINING 3 mol dm^{-3} $LiClO_4$

$qPb^{2+}+pH_2O=Pb_q(OH)_p^{(2q-p)}+pH^+$

$*\beta_{pq}=[Pb_q(OH)_p^{(2q-p+)}][H^+]^p/[Pb^{2+}]^q$

	Mole fraction of dioxane		
	0.0	0.1	0.2
pK_1	13.87 (0.01)	14.61 (0.01)	15.38 (0.01)
$-\log*\beta_{33}$	−15.29 (0.03)	−14.98 (0.03)	−14.81 (0.03)
$-\log*\beta_{44}$	−19.42 (0.02)	−18.60 (0.02)	−19.17 (0.02)
$-\log*\beta_{43}$	−22.78 (0.05)	−21.79 (0.05)	−21.74 (0.05)
$-\log*\beta_{86}$	−42.33 (0.02)	−40.75 (0.02)	−41.12 (0.02)

Uncertainties of the formation constants were estimated as 3σ where σ denotes the standard deviation.

Discussion

As seen in Table 3, the formation constants of all of the lead(II) hydroxo complexes, $\log*\beta_{pq}$, were only slightly changed by the addition of dioxane in an aqueous solution, the fact having been found for other divalent metal ions so far examined.[8–11] Combination of the formation constant $*\beta_{pq}$ with the autoprotolysis constant of solvent K_1 leads to the formation constant β_{pq} for the hydrolytic reaction as follows:

$$qM^{z+} + pOH^- = M_q(OH)_p^{(zq-p)+} \quad (8)$$

$$\beta_{pq} = [M_q(OH)_p^{(zq-p)+}]/[M^{z+}]^q[OH^-]^p = *\beta_{pq}/K_1^p. \quad (9)$$

Thus, the free energy change of transfer for Reaction 8 from the aqueous solution to a dioxane–water mixture is obtained as follows:

$$\Delta G^t_{pq} = \Delta G^\circ_{pq}(\text{mix}) - \Delta G^\circ_{pq}(\text{aq}) = -RT\ln\{\beta_{pq}(\text{mix})/\beta_{pq}(\text{aq})\}. \quad (10)$$

The free energy changes of transfer ΔG^t_{pq} against the mole fraction of dioxane in the mixtures are represented in Fig. 4. The values ΔG^t_{pq} were negative for all of the hydrolytic species, as well as metal and hydrogen ions, and became more negative with an increase in the concentration of dioxane. However, no clear correlation was found between ΔG^t_{pq} and the composition or the total charge of the hydroxo complexes. ΔG^t_{pq} may be expressed in terms of the partial molar free energy change of transfer of a species i, Δg^t_i, as follows:

$$\Delta G^t_{pq} = \Delta g^t_{pq} - q\Delta g^t_M - p\Delta g^t_{OH}. \quad (11)$$

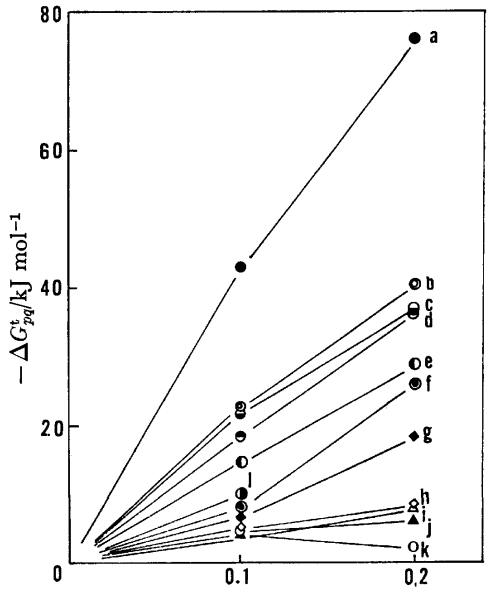

Fig. 4. Free energy changes of transfer of hydroxo complexes of divalent metal ions against the mole fraction of dioxane in mixed solvents.
a: $Pb_6(OH)_8^{4+}$, b: $Pb_3(OH)_4^{2+}$, c: $Pb_4(OH)_4^{4+}$, d: $Ni_4(OH)_4^{4+}$, e: $Pb_3(OH)_3^{3+}$, f: $Be_3(OH)_3^{3+}$, g: $Cu_2(OH)_2^{2+}$, h: $CuOH^+$, i: Cd_2OH^{3+}, j: Be_2OH^{3+}, k: Cu_2OH^{3+}, l: $Cu_3(OH)_2^{4+}$.

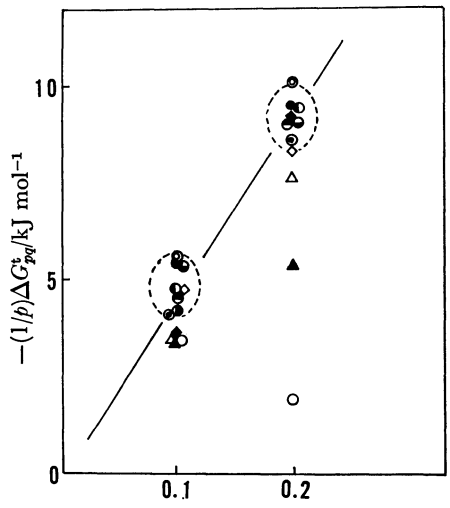

Fig. 5. Free energy changes of transfer per hydroxide ion of hydroxo complexes of divalent metal ions against the mole fraction of dioxane in mixed solvents.
Symbols are the same as those in Fig. 4.

Since the number of OH^- ion involved in a hydroxo complex depends on its composition, the values, $(1/p)\Delta G^t_{pq}$, were subsequently compared in Fig. 5 instead of ΔG^t_{pq} in Fig. 4. The values $(1/p)\Delta G^t_{pq}$ were approximately independent of the complexes examined at a given solvent composition, except for some complexes such as Cd_2OH^{3+}, Cu_2OH^{3+}, and Be_2OH^{3+}, which are all minor species in their systems. For the partial molar free energy change of transfer Δg^t_i from an aqueous solution to a dioxane–water mixture, it has been reported that Δg^t_i of a cation is usually negative and the value becomes more negative for ions with small ionic radius and that the reverse is the case for anions.[18]

In order to estimate the value of Δg^t_{pq}, the changes of the activity coefficients of lead(II) and hydrogen ions were measured at a constant total concentration of a relevant ion with varying solvent compositions by measuring emfs of cells (C) and (D). Emfs of the cells may be written as follows: for cell (C)

$$E_H = E_{0,H} + 59.154 \log [H^+] + 59.154 \log y_H + E_j \quad (12)$$

and for cell (D)

$$E_{Pb} = E_{0,Pb} + 29.577 \log [Pb^{2+}] + 29.577 \log y_{Pb} + E_j. \quad (13)$$

Since we used glass electrodes, ΔE_p equals zero. y_i denotes the activity coefficient of a species i in the solution. An activity coefficient of a species i in a given solvent may be described as follows:

$$y_i = y_i(aq) \cdot y_i(solvent) = y_i(mix) \quad (14)$$

where $y_i(aq)$ represents the activity coefficient of species i in an aqueous medium in which y_i approaches unity at infinite dilution. y_i may be reasonably assumed to be constant in a constant ionic medium of a given solvent. y_i(solvent) is a function of solvent composition in a given ionic medium and is unity in an aqueous solution.

Since $E_{0,H}$ is a constant independent of solvent composition, changes in E_H with changing solvent compositions at a constant $[H^+]$ is given as

$$\begin{aligned}\Delta E_H &= E_H(mix) - E_H(aq) \\ &= 59.154 \log \{y_H(mix)/y_H(aq)\} + \{E_j(mix) - E_j(aq)\} \\ &= 59.154 \log y_H(solvent) + \{E_j(mix) - E_j(aq)\}. \quad (15)\end{aligned}$$

Thus, ΔE_H may be independent of $[H^+]$, but depends on the solvent composition of 3 mol dm^{-3} $LiClO_4$ solution, as far as the term $\{E_j(mix) - E_j(aq)\}$ is negligibly small. Similar measurements were carried out for ΔE_{pq} by using lead amalgam lelectrodes.

The emf changes of cells (C) and (D), ΔE_H and ΔE_{Pb}, respectively, were measured at constant $[H^+]$ and $[Pb^{2+}]$. Since the measurements were carried out in an acidic solution where no hydrolysis of metal ion occurs, $[H^+]$ is equal to the total concentration of the acid in the solution, and $[Pb^{2+}]$ is equal to the total concentration of the metal ion, B.

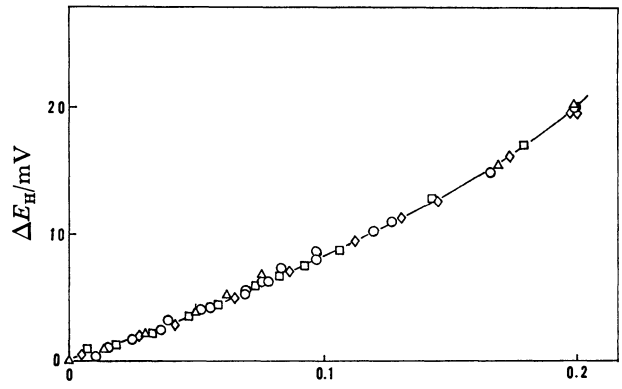

Fig. 6. Emf changes of cell (C) with varying solvent compositions.
The concentrations of hydrogen ions (in mol dm^{-3}); are; △: 0.00 (extrapolated by Gran's plot), (Ref_1), ○: 0.010 (Ref_1), □: 0.020 (Ref_1), ◇: 0.020 (Ref_2). Ref_1 and Ref_2 indicate the reference cells (E) and (F), respectively, used in the measurements.

The emf for cell (C) was measured by using two different reference electrodes in order to check the effect of the different liquid junction on potentials.

$$Ref_1 = \left| \begin{array}{l} 3 \text{ mol dm}^{-3} \\ LiClO_4 \\ \text{in aqueous} \\ \text{solution} \end{array} \right| \left| \begin{array}{l} 0.01 \text{ mol dm}^{-3} \\ AgClO_4 \\ 2.99 \text{ mol dm}^{-3} \\ LiClO_4 \\ \text{in aqueous} \\ \text{solution} \end{array} \right| AgCl\text{–}Ag \quad (E)$$

$$Ref_2 = \left| \begin{array}{l} 3 \text{ mol dm}^{-3} \\ LiClO_4 \\ \text{in 0.2 mole} \\ \text{fraction} \\ \text{dioxane–water} \\ \text{mixture} \end{array} \right| \left| \begin{array}{l} 0.01 \text{ mol dm}^{-3} \\ AgClO_4 \\ 2.99 \text{ mol dm}^{-3} \\ LiClO_4 \\ \text{in aqueous} \\ \text{solution} \end{array} \right| AgCl\text{–}Ag \quad (F)$$

As is seen from Fig. 6, ΔE_H obtained fell on one curve. Therefore, the liquid junction potentials of the cells were found to be negligible.

In these measurements, the changes of the activity coefficients or the partial molar free energy changes of transfer, Δg^t, of hydrogen and lead(II) ion in a 3 mol dm^{-3} $LiClO_4$ can be described with a good approximation as follows:

$$\Delta g_{\mathrm{H}}^{\mathrm{t}} = -RT\ln\{y_{\mathrm{H}}(\mathrm{mix})/y_{\mathrm{H}}(\mathrm{aq})\} = -F\Delta E_{\mathrm{H}} \quad (16)$$

$$\Delta g_{\mathrm{Pb}}^{\mathrm{t}} = -RT\ln\{y_{\mathrm{Pb}}(\mathrm{mix})/y_{\mathrm{Pb}}(\mathrm{aq})\} = -2F\Delta E_{\mathrm{Pb}} \quad (17)$$

where F stands for Faraday constant. The $\Delta g_{\mathrm{H}}^{\mathrm{t}}$ and $\Delta g_{\mathrm{Pb}}^{\mathrm{t}}$ values with varying mole fractions of dioxane are shown in Fig. 7.

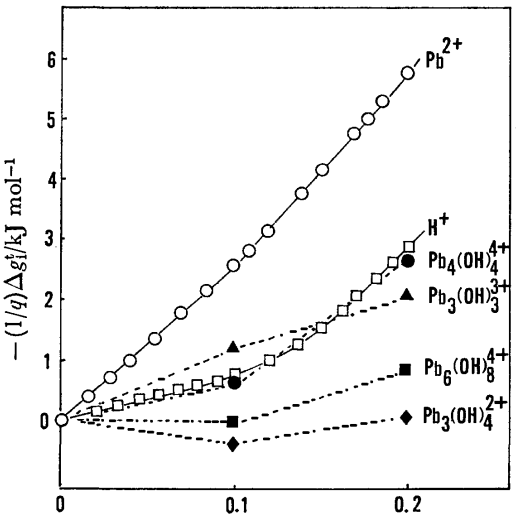

Fig. 7. Partial molar free energy changes of transfer of H^+, Pb^{2+}, and $Pb_q(OH)_p^{(2q-p)+}$ with varying solvent compositions.

The thermodynamic formation constant of the $M_q(OH)_p^{(zq-p)+}$ complex is given in terms of activities as follows:

$$*\beta_{pq}^{\circ} = (a_{pq}\cdot a_{\mathrm{H}}{}^{p})/(a_{\mathrm{M}}{}^{q}\cdot a_{\mathrm{H_2O}}{}^{p}) = \frac{[\mathrm{M}_q(\mathrm{OH})_p{}^{(zq-p)+}][\mathrm{H}^+]^p}{[\mathrm{M}^{z+}]^q}\cdot\frac{1}{[\mathrm{H_2O}]^p}\cdot\frac{y_{pq}y_{\mathrm{H}}{}^{p}}{y_{\mathrm{M}}{}^{q}f_{\mathrm{H_2O}}{}^{p}}. \quad (18)$$

$f_{\mathrm{H_2O}}$ represents the activity coefficient of water in a mixed solvent expressed by the mole fraction scale of the solvent component. If the standard state of any reacting species is so chosen that the activity coefficient of the species appraoches unity when the composition of the solution approaches 3 mol dm^{-3} $LiClO_4$ aqueous solution, $*\beta_{pq}$ obtained in the aqueous solution is given as the formation constant at the standard state ($=*\beta_{pq}^{0}$), and is independent of the solvent composition at a given temperature. The activity coefficient y is defined in terms of molarity and is independent of the concentration of the relevant species in a given constant ionic medium, but is dependent on the solvent composition, as is shown in Eq. 14.

Since the value $[\mathrm{M}_q(\mathrm{OH})_p{}^{(zq-p)+}][\mathrm{H}^+]^p/[\mathrm{M}^{z+}]^q = *\beta_{pq}$ is experimentally determinable for the complex $M_q(OH)_p^{(zq-p)+}$ in a given solvent and $*\beta_{pq}^{0}$ is defined as the formation constant of the complex in the aqueous solution, the difference between the formation constants obtained in a mixed solvent and an aqueous solution is given as follows:

$$\Delta\ln *\beta_{pq} = \ln *\beta_{pq}(\mathrm{mix}) - \ln *\beta_{pq}(\mathrm{aq}) = p\ln[\mathrm{H_2O}] + \ln(y_{\mathrm{M}}{}^{q}/y_{\mathrm{H}}{}^{p}) - \ln(y_{pq}/f_{\mathrm{H_2O}}{}^{p}). \quad (19)$$

The first two terms of the right hand side of Eq. 19 are experimentally determined, and thus, the value $\ln(y_{pq}/f_{\mathrm{H_2O}}{}^{p})$ is estimated. If we assume that $f_{\mathrm{H_2O}}=1$ as a first approach over the range of the solvent composition examined here, the values may represent the variations of the activity coefficient of the $M_q(OH)_p^{(zq-p)+}$ complex in the dioxane–water mixtures containing 3 mol dm^{-3} $LiClO_4$ at 25 °C. The partial molar free energy change of transfer of the $M_q(OH)_p^{(zq-p)+}$ complex may thus be calculated as follows:

$$\Delta g_{pq}^{\mathrm{t}} = -RT\ln[\mathrm{H_2O}]^p + q\Delta g_{\mathrm{M}}^{\mathrm{t}} - p\Delta g_{\mathrm{H}}^{\mathrm{t}} + RT\Delta\ln *\beta_{pq}. \quad (20)$$

$(1/q)\Delta g_{pq}^{\mathrm{t}}$ with varying mole fractions of dioxane are shown in Fig. 7.

As is seen from Fig. 7, $\Delta g_{\mathrm{H}}^{\mathrm{t}}$ and $\Delta g_{\mathrm{Pb}}^{\mathrm{t}}$ are both negative and become more negative with an increase in the mole fraction of dioxane. $(1/q)\Delta g_{pq}^{\mathrm{t}}$ seems to vary with a similar trend to $\Delta g_{\mathrm{H}}^{\mathrm{t}}$ and $\Delta g_{pq}^{\mathrm{t}}$. At a given mole fraction of dioxane, the $(1/q)\Delta g_{pq}^{\mathrm{t}}$ values are smaller than $\Delta g_{pq}^{\mathrm{t}}$, and the smaller the formal charge, $(zq-p)/q$, of a hydroxo complex is, the smaller $(1/q)\Delta g_{pq}^{\mathrm{t}}$ may become. The same results have previously been obtained for the hydroxo complex of cadmium.[11]

Equation 4 is rewritten as follows:

$$\frac{1}{p}\Delta G_{pq}^{\mathrm{t}} = \frac{q}{p}\left(\frac{1}{q}\Delta g_{pq}^{\mathrm{t}} - \Delta g_{\mathrm{M}}^{\mathrm{t}}\right) - \Delta g_{\mathrm{OH}}^{\mathrm{t}}. \quad (21)$$

The values $(1/p)\Delta G_{pq}^{\mathrm{t}}$ of formation of hydroxo complexes of divalent metal ions examined are approximately independent of the complexes at a given solvent composition. Since the contribution of $\Delta g_{\mathrm{OH}}^{\mathrm{t}}$ to $(1/p)\Delta G_{pq}^{\mathrm{t}}$ is the same for all the hydroxo complexes and $(1/q)\Delta g_{pq}^{\mathrm{t}}$ may vary with the formal charge of the complexes, the term $(q/p)\{(1/q)\Delta g_{pq}^{\mathrm{t}} - \Delta g_{\mathrm{M}}^{\mathrm{t}})\}$ may be independent of the complexes but dependent on the composition of solvents. Thus, at a given solvent composition,

$$\frac{q}{p}\left(\frac{1}{q}\Delta g_{pq}^{\mathrm{t}} - \Delta g_{\mathrm{M}}^{\mathrm{t}}\right) \approx k(\mathrm{constant}). \quad (22)$$

The formal charge z' per metal ion of the complex is defined as follows:

$$z' = \frac{1}{q}(zq-p) = z - p/q. \quad (23)$$

Thus, replacing $z-z'$ to p/q in Eq. 22, we rewrite the equation for free energy change of transfer of an $M_q(OH)_p^{(zq-p)+}$ complex in terms of the formal charge of the complex as follows:

$$\frac{1}{q}\Delta g_{pq}^{\mathrm{t}} \approx \Delta g_{\mathrm{M}}^{\mathrm{t}} + k(z-z'). \quad (24)$$

Since $(1/q)\Delta g_{pq}^{\mathrm{t}}$ may be less negative than $\Delta g_{\mathrm{M}}^{\mathrm{t}}$ (see Fig. 7), the value k may be positive at a given solvent composition. Thus, Eq. 24 indicates that the value $(1/q)\Delta g_{pq}^{\mathrm{t}}$ of a hydroxo complex approaches the value of $\Delta g_{\mathrm{M}}^{\mathrm{t}}$ when the formal charge z' of the complex approaches z, the charge of the free metal ion.

Medium effects on the thermodynamic parameters of the hydrolytic reactions of metal ions may be mainly due to changes in solvation structures of the species involved.[18-20] Ion-solvent interactions of the hydroxo complexes of beryllium ions in dioxane–water mixtures

were discussed in a previous paper.[20] The enthalpy changes of transfer per hydroxide ion $(1/p)\Delta H^{t}_{pq}$ $[=(q/p)\{(1/q)\Delta h^{t}_{pq}-\Delta h^{t}_{M}\}-\Delta h^{t}_{OH}$, where Δh^{t}_{i} denotes the partial molar enthalpy change of transfer of species i] strongly depended on metals.[20,21] Consequently, the value $(1/q)\Delta h^{t}_{pq}$ depends on both p/q and Δh^{t}_{M} at a given solvent composition.

The different features of the solvent effects between ΔG^{t}_{pq} and ΔH^{t}_{pq} of hydroxo complexes of divalent metal ions may be explained as follows: For a strongly solvated metal ion (*i.e.*, $(1/p)\Delta H^{t}_{pq}$ may be largely negative for such an ion), the ion may have a large ordering effect for the solvent molecules even in the secondary solvation shell of the ion, and thus, $(1/p)\Delta S^{t}_{pq}$ may become less positive. Therefore, the effect due to $(1/p)\Delta H^{t}_{pq}$ on $(1/p)\Delta G^{t}_{pq}$ may be compensated by the effect due to $(1/p)\Delta S^{t}_{pq}$, and thus, the $(1/p)\Delta G^{t}_{pq}$ value becomes practically independent of metal ion.

The present work has been partially supported by a Grant-in-Aid for Scientific Research from the Ministry of Education, Science and Culture(No. 343011).

References

1) K. J. Pederson, *Kgl. Danske Videnskab. Selskab. Mat-fys. Medd.*, **22**, 10 (1945).
2) J. Faucherre, *Bull. Soc. Chim. Fr.*, **1954**, 128.
3) B. Carell and Å. Olin, *Acta Chem. Scand.*, **14**, 1999 (1960).
4) Å. Olin, *Acta Chem. Scand.*, **14**, 126 (1960).
5) G. Johansson and Å. Olin, *Acta Chem. Scand.*, **22**, 3197 (1968).
6) Å. Olin and R. Soderquist, *Acta Chem. Scand.*, **26**, 3505 (1972).
7) V. A. Maroni and T. G. Spiro, *J. Am. Chem. Soc.*, **89**, 45 (1967).
8) H. Tsukuda, T. Kawai, M. Maeda, and H. Ohtaki, *Bull. Chem. Soc. Jpn.*, **48**, 691 (1965).
9) H. Ohtaki and T. Kawai, *Bull. Chem. Soc. Jpn.*, **45**, 1735 (1972).
10) T. Kawai, H. Otsuka, and H. Ohtaki, *Bull. Chem. Soc. Jpn.*, **46**, 3753 (1973).
11) H. Matsui and H. Ohtaki, *Bull. Chem. Soc. Jpn.*, **50**, 1472 (1977).
12) H. Ohtaki, *Inorg. Chem.*, **6**, 808 (1967).
13) A. M. Feltham and M. Spiro, *Chem. Rev.*, **71**, 177 (1971).
14) H. P. Benneto and A. R. Willmot, *Quart. Rev.*, **25**, 501 (1971).
15) H. Ohtaki, M. Tsurumi, and T. Kawai, *Anal. Chem.*, **49**, 190 (1977).
16) A. S. Brown, *J. Am. Chem. Soc.*, **56**, 646 (1934).
17) L. G. Sillén, *Acta Chem. Scand.*, **16**, 159 (1962).
18) H. P. Bennetto and D. Feakins, "Hydrogen-bonded Solvent Systems," Taylor and Francis Ltd., London (1968), p. 235.
19) G. H. Parsons and C. H. Rochester, *J. Chem. Soc., Faraday Trans. 1*, **1972**, 523.
20) S. Ishiguro and H. Ohtaki, *Bull. Chem. Soc. Jpn.*, **52**, 3198 (1979).
21) S. Ishiguro and H. Ohtaki, unpublished data.

Equilibria of Complex Formation between Bivalent Metal Ions and 3,3′-Bis[*N*,*N*′-bis(carboxymethyl)aminomethyl]-*o*-cresolsulfonphthalein

Sadaaki Murakami,* Kotaro Ogura, and Takashi Yoshino

Department of Industrial Chemistry, Faculty of Engineering, Yamaguchi University, Tokiwadai, Ube 755

(Received August 27, 1979)

The complex formation equilibria between several bivalent metal ions and 3,3′-bis[*N*,*N*′-bis(carboxymethyl)-aminomethyl]-*o*-cresolsulfonphthalein (XO) have been investigated potentiometrically and spectrophotometrically. The metal ions studied here were Co(II), Ni(II), Cu(II), Zn(II), Pb(II), and Cd(II). The formation constants and visible-absorption-spectrum parameters of these metal complexes have been determined. It has been found that all these metal ions form 1: 1 and 2: 1 (metal: XO) complexes with XO. Moreover, the complex of each composition changes into one of several protonated ones depending on the pH of the solution. The probale structures of the complexes in solution are discussed.

Xylenol Orange (abbreviated as XO or H_6L; Formula I) forms stable and colored complexes with metal ions, and it has been widely used as an indicator in the chelatometric and spectrophotometric determinations of numerous metal ions.[1–5] However, despite many interesting findings concerning the solution chemistry of its metal complexes, serious discrepancies have often been noted among the data and/or conclutions reported by different authors. These discrepancies are primarily caused by the use of commercial or incompletely purified XO.[6] Recently, new methods for the purification of XO have been established,[6–9] pure XO has been used, in particular, in the investigation of the solution chemistry of XO. However, discrepancies among the data and conclusions reported seem to remain. The following two facts may be offered as explanations of this problem:

1) The metal complexes of XO have a visible absorption spectrum. The compositions and the stability constants of these complexes have, therefore, often been determined only by spectrophotometry.

2) The XO molecule has two chelating groups on each side of its large sulfonphthalein nucleus, and each chelating group reacts with metal ions independently of the other;[3] hence, several complex species have various ratios of metal and XO.[3,5] Moreover, the complex of each component changes into different types of protonated or hydroxo complexes, depending on the pH of the solution.[10–12] The complex formation equilibria between metal ions and XO must, therefore, be complicated.

The change in the visible absorption spectrum of XO accompanying its complex formation is smaller than that of 3,3′-bis[*N*,*N*′-bis(carboxymethyl)aminomethyl]-thymolsulfonphthalein,[12–14] MTB, similar sulfonphthalein indicator (Formula I), and the difference in color between XO and its complexes, especially in neutral and alkaline solutions, not clearly distinguishable except in the case of metal ions with valences of 3 or more.[1,3,12] This may be due to differences in electron-donation effects of the substituent groups, R_1 and R_2, on the sulfonphthalein nucleus, as seen in Formula I.[15] Moreover, no clearly visible change in the spectrum is obsevable in the metal complex formation with sulfonphthalein indicators when the metal ions combine with coordinating donors other than phenolic or quinolic oxygen (1 or 1′ in Formula I).[10,12,14–21] In such a case, no information can be obtained spectrophotometrically. Also, most of the measurements have been limited to the narrow pH range of the solution (pH 3 to 6) in which the spectrum change is remarkable. The following points may be made regarding on investigation of XO chemistry in solution:

i) Measurement over a wide pH range should be under taken.

ii) The results by spectrophotometry should be compared with those obtained by other instrumental methods.

The present work is a study of the complex formation equilibria of XO with several bivalent metal ions in aqueous solutions over the pH range of 1 to 14 by spectrophotometry and potentiometry, refering to the results of research by ESR[22] and electrochemical (polarography and potential sweep voltametry)[23] techniques. The metal ions examined were Co(II), Ni(II), Cu(II), Zn(II), Pb(II), and Cd(II). The results obtained were compared with those reported by other authors: Co(II),[24] Ni(II),[24] Cu(II),[11,24,25] Zn(II),[26,27] Pb(II),[28] and Cd(II).[29]

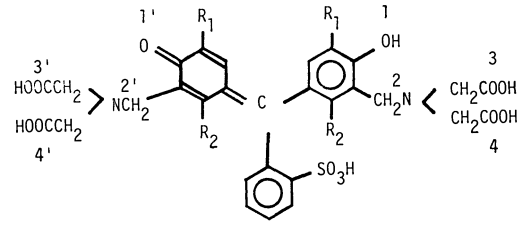

	R_1	R_2
XO	CH_3	H
MTB	$CH(CH_3)_2$	CH_3

I XO or MTB

Experimental

Xylenol Orange. XO was synthesized and purified by cellulose-column chromatography and by ion exchange using the batch method, as has been described previously.[8,16] The product was the free acid form of XO, and the purity was

nearly 100%, as measured by potentiometric titration with standard sodium hydroxide. This XO was weighed and dissolved in water in each experiment.

Metal Ion Solutions. The commercial perchlorate salt of each metal ion was dissolved in water without further purification. Each solution was standardized by EDTA titration.[1)]

The other reagents and apparatus for the potentiometric and spectrophotometric experiments were the same as have been described earlier.[14,16)] All the measurements were performed at 25±0.2 °C. The ionic strength of the solutions was maintained at 0.1 with sodium perchlorate. The pH values of the strongly acidic and alkaline media (pH<*ca.* 1.5 and pH>*ca.* 12) are difficult to measure by means of a pH meter using a glass electrode. The pH values of such media were determined directly from the concentrations of perchloric acid or sodium hydroxide, one of which was added to adjust the hydrogen ion concentrations, without account being taken of the activity coefficient.

Formation Constants. The formation constants of the complexes were calculated from the mass balances and the electroneutrality, utilizing the successive approximation method previously described in detail.[14-16)] The acid formation constants of XO used in the foregoing calculations were those determined previously[8)] ($\log k_i$: 12.23, 10.56, 6.74, 2.85, 2.32, and 1.5 from $i=1$ to 6 respectively).

Results

Complex Formation Equilibria. Potentiometric titrations of XO solutions containing 1: 1, 2: 1, and 3: 1 molar ratios of Co(II), Ni(II), Cu(II), Zn(II), Pb(II), and Cd(II) to XO were performed (the molar ratios of the metal ion to the ligand will be, hereinafter, referred to as "1/1", "2/1", and "3/1"). The visible absorption spectra of the 1/1 and 2/1 solutions for each metal ion at different pH values (pH 1—14) were measured between 350 and 700 nm, and the variation in the spectrum with the pH was investigated.

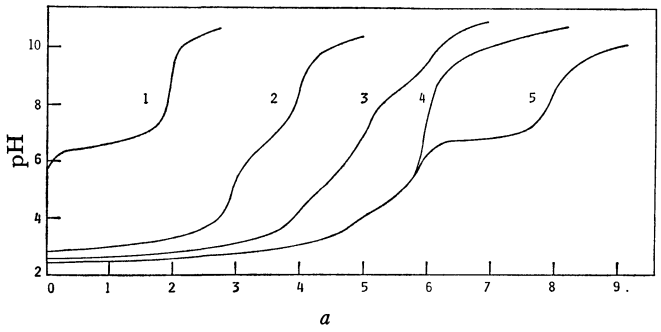

Fig. 1. Potentiomitric titration curves of Cu(II)–XO solutions.
1-Cu(II), 2-XO, 3, 4, and 5-1/1, 2/1, and 3/1 solutions, respectively. [XO]=about 1×10^{-3} mol/l and [Cu(II)] is varied.

Cu(II) Complexes. Figure 1 shows the foregoing titration curves for the Cu(II) complexes, together with the curves for the Cu(II) and XO solutions. The 1/1 Curve 3 exhibits three inflections at $a=4$, 5, and 6, indicating the formation of these three stable 1: 1 complex species: CuH_2L^{2-}, $CuHL^{3-}$, and CuL^{4-}, where a is the number of moles of base added per mole of XO. The 2/1 Curve 4 shows two inflections at $a=$ 5 and 6 (the first one is not well-defined), probably with the formation of two 2/1 complexes, $CuHL^{-}$ and Cu_2L^{2-}, at the respective a values. The 3/1 Curve 5 is quite identical with the 2/1 Curve up to $a=6$, but beyond this a value up to $a=8$ there is a buffer region in which copper(II) hydroxide is precipitated; this precipatation reaction of copper(II) hydroxide is in the same pH range as when the Cu(II) aquo ion is hydrolyzed ($a=0$ to 2 on Curve 1). The 3/1 solution may, therefore, contain the free Cu(II) ion. The extent of the buffer region over two unit of a indicates that there exists one mole of free Cu(II) ion per mol of ligand in the 3/1 solution, and that not more than two Cu(II) ions can combine with one XO molecule.[14,16)]

The absorption spectra of the 1/1 and 2/1 solutions for Cu(II) at various pH values are shown in Figs. 2 and 3 respectively. The absorbances of these spectra at a given wavelength are shown as a funtion of pH in Fig. 4. The 1/1 solutions below pH 10 show two steps of change in their absorbance (Plot 1 in Fig. 4). The first step in the pH region from 4 to 6, and the second step, from 7 to 10. Moreover, an isosbestic point for

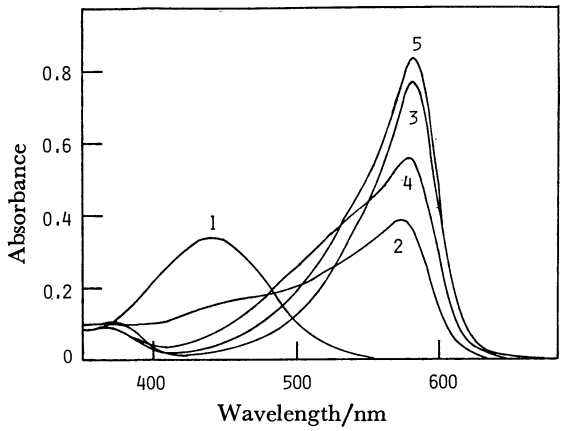

Fig. 2. Visible absorption spectra of 1/1 Cu(II)–XO solutions at various pH values.
pH: 1-2.75, 2-6.49, 3-11.20, 4-13.28, and 5-13.76.
[XO]=1.20×10^{-5} mol/l.

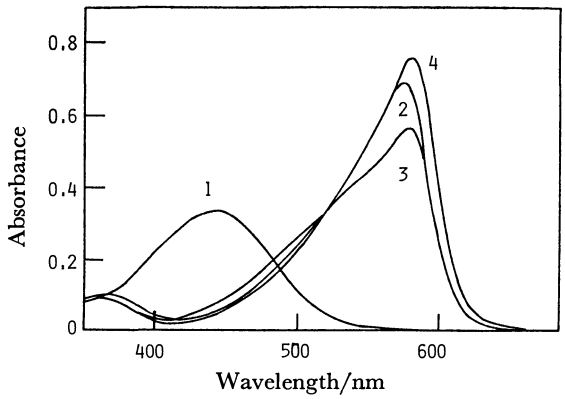

Fig. 3. Visible absorption spectra of 2/1 Cu(II)–XO solutions at various pH values.
pH: 1-2.62, 2-9.31, 3-13.42, and 4-13.57.
[XO]=1.20×10^{-5} mol/l.

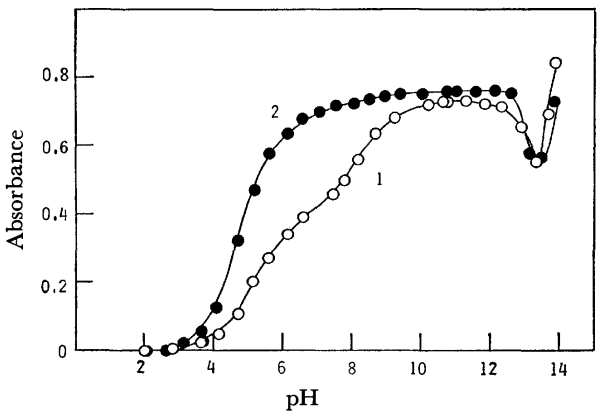

Fig. 4. Absorbances at 575 nm for Cu(II)–XO solutions as a function of pH.
1-1/1 and 2-2/1 solutions, respectively.
[XO]$=1.20\times10^{-5}$ mol/1.

the spectra in each pH range was observed at 483 and 533 nm respectively (the intercept points of Spectra 1 and 2, and of Spectra 2 and 3, respectively in Fig. 2). These pH regions are similar to those for the buffer regions of the titration curve (Fig. 1) from $a=4$ to 5 and from $a=5$ to 6 respectively. In addition, for the following reaction:

$$CuH_iL^{-4+i} \rightleftarrows CuH_{i-n}L^{-4+i-n} + nH^+$$

$$K^{nH}_{MH_iL} = \frac{[CuH_iL]}{[H]^n[CuH_{i-n}L]}.$$

The plot of $\log\{[CuH_iL]/[CuH_{i-n}L]\}$ *vs.* pH[30] gave a straight line with a slope of $n=1$ for each step of the absorbance change, as is seen in Fig. 5 for the proton dissociation from CuH_2L^{2-}. The value of each $K^{H}_{CuH_iL}$ for $i=1$ and 2 was evaluated from the pH value when the log term was equal to zero (Table 1). In the 1/1 solutions, the formation of the three complex species CuH_2L^{2-}, $CuHL^{3-}$, and CuL^{4-} may be complete around pH 3, 6.5, and 11 respectively, taking into account the change in their absorbance (Fig. 4). Spectra 1, 2, and 3 in Fig. 2, therefore, may correspond to the foregoing complex species. The wavelength, λ_{max}, and the absorptivity, ε, for the maximum absorbance of the spectrum attributed to each complex

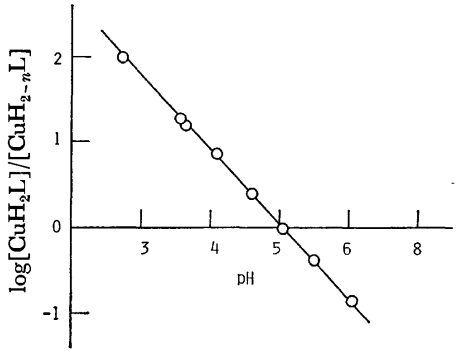

Fig. 5. Plot of $\log\{[CuH_2L]/[CuH_{2-n}L]\}$ *vs.* pH.
Wavelength: 575 nm.

species were also determined (Table 2).

The 2/1 solutions show a single step of change in their visible absorbance below pH 8 (Plot 2 in Fig. 4), and the isosbestic point was at 486 nm for the spectra in this pH range (the intercept point of Spectra 1 and 2 in Fig. 3). The plot of $\log\{[Cu_2H_iL]/[Cu_2H_{i-n}L]\}$ *vs.* pH showed a straight line, with a slope of $n=1$. The pH region for the change in this absorbance may correspond to that from $a=5$ up to 6 (Curve 4 in Fig. 1). These facts suggest that a mono-protonated complex, Cu_2HL^-, is almost complete around pH 3 (its corresponding spectrum may be seen in Curve 1 in Fig. 3). The change in the spectrum from pH 3 to 7 may be accompanied by a proton dissociation from Cu_2HL^-.

Below pH 3, no remarkable change in the spectrum as a function of pH is observed, and no observable inflections are seen on the titration curves. However, the spectra of both the 1/1 and 2/1 solutions at pH 2—3 are at slightly longer wavelengths than that of the XO solutions of the same pH (*i.e.*, λ_{max} and ε for the XO, 1/1 and 2/1 solutions are 439, 443, and 443 nm, and 2.62, 2.75, and 2.75×10^4 l mol^{-1} cm^{-1}, respectively). The results of the mole-ratio method at pH 2—3 showed the existence of the 1: 1 and 2: 1 complex species, as may be seen in Plots 1 and 2 in Fig. 9. (The results of the mole-ratio methods will be discussed below in more detail.) The ESR spectra of the 1/1 solutions indicated the existence of stable 1: 1 complex species down to around pH 1.[22] This fact suggests that more highly protonated complex species, *i.e.*, CuH_iL^{-4+i} ($i\geqslant3$), may be formed in such acidic solutions.[12,14] Around pH 1, the ESR spectra consisted of two overlapping lines attributed to the 1: 1 complex species and the Cu(II) aquo ion. Below pH 1, the spectra showed one line attributed to a Cu(II) aquo ion, indicating that the 1: 1 complex species CuH_iL^{-4+i} dissociates to a Cu(II) ion and H_6L in such strongly acidic solutions. The ESR spectra of the 2/1 solutions around pH 4 showed the existence of the 2: 1 complex species, but around pH 2—3 they consisted of three overlapping lines, attributed to the 2: 1 and 1: 1 complex species, and a Cu(II) aquo ion. Around pH 1 the ESR spectra consisted of two lines attributable to the 1: 1 complex species and Cu(II) aquo ion. These facts indicate that the 2: 1 complex species, Cu_2HL^-, begins to dissociate to CuH_iL^{-4+i} and the Cu(II) aquo ion as the pH decreases from 3, its dissociation being complete around pH 1.

Above pH 13, the visible absorbances for both 1/1 and 2/1 solutions decrease and exhibit their minimum value at almost the same pH value (*ca.* 13.2); they then increase beyond this pH value, as are seen of Spectra 3, 4, and 5 in Fig. 2 and Spectra 2, 3, and 4 in Fig. 3 for the 1/1 and 2/1 solutions respectively and in Plots 1 and 2 in Fig. 4. No precipitate of the copper(II) hydroxide was observed in the solutions. The spectra for both 1/1 and 2/1 solutions around pH 14 are quite identical with that of the XO solutions around this pH value. The ESR spectra of the 2/1 and 1/1 solutions around pH 13.2 suggested the existence of hydroxo complex species of Cu(II) with XO, while those around pH 14 were similar to that of the tetrahydroxocuprate-

(II) ion, $Cu(OH)_4^{2-}$. These findings suggest that both the 1:1 complex, CuL^{4-}, and the 2:1 complex, Cu_2L^{2-}, dissociate to $Cu(OH)_4^{2-}$ and L^{6-} through an intermediate hydroxo complex species,[12,14,15,17,19,21] such as $Cu(OH)L^{5-}$ and $[Cu(OH)]_2L^{4-}$.

Co(II), Ni(II), Zn(II), and Pb(II) Complexes. These metal complexes showed similar types of titration curves and changes in the spectra with pH value. Accordingly, the Zn(II) system will be discussed. The 2/1 and 3/1 solutions behaved similarly in their titration curves and their spectra to the Cu(II) system. However, two 1/1 titration curves for Zn(II) have the inflections, at $a=4$ and $a=5$, although the Cu(II) 1/1 curve has three inflections, at $a=4$, $a=5$, and $a=6$, as are seen in the 1/1 Curve 3 in Fig. 1. These facts suggest that the formations of their 1:1 complexes, MH_2L^{2-} and MHL^{3-}, are complete at the respective a values, but that the dissociation of a proton from MHL^{3-} occurs in more alkaline solutions at $a>5$. The 1/1 solution for Zn(II) showed only one step of change in the absorbance below pH 9. However, the absorbances decreased slightly from about pH 9 up to 11. This change may correspond to the dissociation of a proton from the MHL^{3-} complex. Both 1/1 and 2/1 solutions for the Zn(II) complexes showed a minimum absorbance at 12.5, as high as was observed in the Cu(II) system (Fig. 4).

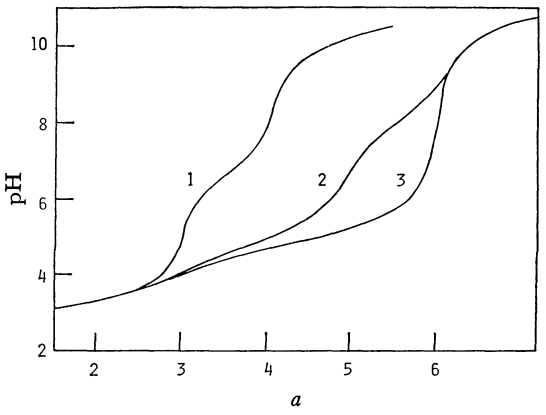

Fig. 6. Potentiometric titration curves of Cd(II)–XO solutions.
1-XO, 2-1/1, and 3-2/1 solutions, respectively.
[XO]=about 1×10^{-3} mol/l.

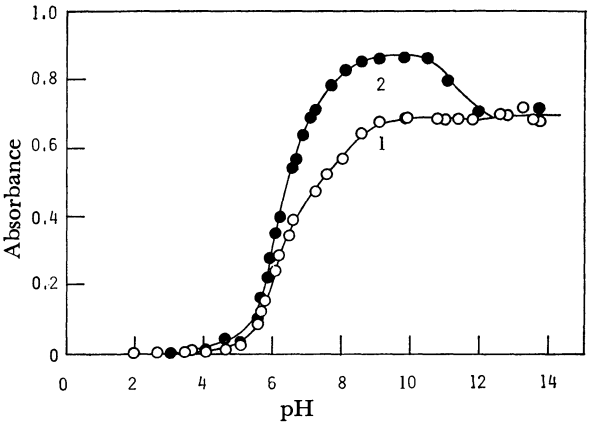

Fig. 7. Absorbances at 575 nm for Cd(II)–XO solutions.
1-1/1 and 2-2/1 solutions.
[XO]=1.20×10^{-5} mol/l.

These foregoing findings suggest that complex formation equilibria similar to those as found in the Cu(II) and XO system are also involved in both 1/1 and 2/1 (or 3/1) solutions of Co(II), Ni(II), Zn(II), and Pb(II), although the complex formation and proton dissociation reactions occur in different pH regions (see Table 1).

Cd(II) Complexes. Both the 1/1 and 2/1 titration curves for Cd(II) are identical to that for the XO solution up to around $a=3$ (Curves 1, 2, and 3 in Fig. 6). Cd(II), therefore, may not react with XO species, H_iL^{-6+i} ($i\geqslant3$),[8] in acidic media (pH 4). Beyond about $a=3$, these curves differ from that for XO and are terminated by an inflection at $a=5$ and $a=6$ for the 1/1 and 2/1 solutions respectively, indicating the formations of complex species, $CdHL^{3-}$ and Cd_2L^{2-}, at each a value. The 1/1 curve beyond $a=5$ is similar in type to that for Cu(II). The 1/1 solution showed two steps of change in the absorbance as a function of pH below 10, as is seen on Plot 1 in Fig. 7. The first step is from pH 4 to 7. The 1/1 curve shows the similar pH value between $a=3$ and 5. Accordingly, this change in absorbance may be ascribed to the complex formation of $CdHL^{3-}$. The plot of $\log\{[CdH_{3-n}L]/[H_3L]\}$ *vs.* pH gave a straight line with a slope of $n=2$ (XO exists as the H_3L^{3-} species in this pH region[8]), which suggests that a protonated complex, such as CdH_iL^{-4+i} ($i\geqslant2$), may not exist, and the complex formation reaction involved in the 1/1 solution from around $a=3$ to 5 may be as follows:

$$Cd^{2+} + H_3L^{3-} \rightleftarrows CdHL^{3-} + 2H^+.$$

The change in absorbance from pH 7 to 10 may correspond to the dissociation of a proton from $CdHL^{3-}$.

Up to about pH 6 the 2/1 solutions showed spectra almost identical with those of the 1/1 solutions (Fig. 7). In addition, the 2/1 titration curve is very similar in pH value to the 1/1 curve up to around $a=5$. These findings suggest that Cd(II) does not form the 2:1 complex until around pH 6. Beyond this pH value the 2/1 spectra differed from the 1/1 spectra. The change in the absorbance of the 2/1 solution from pH 4 to 6, therefore, may be accompanied by the formation of the 1:1 complex, $CdHL^{3-}$, while the change above pH 6 may be attributed to the formation of the 2:1 complex. The plot of $\log\{[CdH_iL]/[CdHL]\}$ *vs.* pH from 6 to 10 showed a straight line with a slope of $n=1$. Accordingly, the 1:1 protonated complex of Cd(II) does not exist until about pH 6, and the reaction involved in the 2/1 solution from pH 6 to 10 may be indicated as follows:

$$Cd^{2+} + CdHL^{3-} \rightleftarrows Cd_2L^{2-} + H^+.$$

Discussion

Problems in the Determination of the Complex Composition by Spectrophotometry. Otomo,[24,29] Hung *et al.*,[25] Studlar *et al.*,[26] Miyazima,[27] and Marchenko[28] have

Table 1. Formation constants of XO complexes at 25 °C and μ=0.1 ($NaClO_4$)

Reaction		log K					
		Co(II)	Ni(II)	Cu(II)	Zn(II)	Cd(II)	Pb(II)
$M^{2+}+L^{6-} \rightleftharpoons ML^{4-}$	K_{ML}	12.63	12.37	12.52	13.41	9.67	13.68
$M^{2+}+HL^{5-} \rightleftharpoons MHL^{3-}$	K_{MHL}	10.58	10.52	10.54	10.44	7.84	11.63
$M^{2+}+H_2L^{4-} \rightleftharpoons MH_2L^{2-}$	K_{MH_2L}	4.64	4.84	4.99	4.55		5.39
$H^{+}+ML^{4-} \rightleftharpoons MHL^{3-}$	K^{H}_{MHL}	10.18	10.38	8.15	9.27	8.03	10.08
				(8.21)		(7.96)	
$H^{+}+MHL^{3-} \rightleftharpoons MH_2L^{2-}$	$K^{H}_{MH_2L}$	4.62	4.88	5.01	4.56		4.32
		(4.76)	(4.61)	(5.05)	(5.21)		(4.36)
$M^{2+}+ML^{4-} \rightleftharpoons M_2L^{2-}$	K_{M_2L}	11.61	11.36	11.43	11.63	8.54	12.45
$M^{2+}+MHL^{3-} \rightleftharpoons M_2HL^{-}$	K_{M_2HL}	5.43	5.18	7.58	6.96		6.47
$H^{+}+M_2L^{2-} \rightleftharpoons M_2HL^{-}$	$K^{H}_{M_2HL}$	4.4	4.2	4.3	4.6		4.1
		(4.66)	(4.49)	(4.68)	(4.91)		(4.22)

Data in parentheses measured by spectrophotometry; the rest, by pH titration.

Table 2. The wavelength and absorptivity at the maximum absorbance of each complex species for bivalent metal complexes with XO

Complex species	λ_{max}/nm						$\varepsilon/10^4$ l mol^{-1} cm^{-1}					
	Co	Ni	Cu	Zn	Pb	Cd	Co	Ni	Cu	Zn	Pb	Cd
MH_iL^{-4+i}($i\geqq3$)	435	445	443	435	440							
MH_2L^{2-}	435	445	443	435	440		2.83	2.75	2.75	2.58	2.42	
MHL^{3-}	580	583	577	573	573	578	6.57	7.83	3.83	5.50	3.92	4.16
ML^{4-}	580	582	582	575	575	585	5.54	6.25	6.43	5.08	3.75	6.33
M_2HL^{-}	435	445	443	440	443		2.83	2.43	2.75	2.57	2.41	
M_2L^{2-}	587	585	578	574	578	578	8.75	9.58	6.42	7.58	7.50	7.42

concluded, from the results of the mole-ratio method and the continuous variation method, that Co(II),[24] Ni(II),[24] Zn(II),[26,27] Pb(II),[28] and Cd(II)[29] form only 1:1 complexes with XO in weakly acidic solutions (around pH 5.5—6.5). On the other hand, Yamada and Fujimoto[11] have concluded, from the results of the mole-ratio method using spectrophotometry, that Co(II) and Ni(II) form only 1:1 complexes at pH 3.5—4.5, but for Cu(II) only the 2:1 complexes are formed at pH 3.5—4.5. In the present work, it has been found that all these metal ions form both 1:1 and 2:1 complexes in all the solutions from acidic to alkaline pH. The same conclusions as offered here have been reported from the studies by ESR[22] and electrochemical[23] techniques. Thus, there are serious discrepancies among the results by different authors. Some authors[24–29] used commercial XO without further purification. However, Yamada and Fujimoto[11] used pure XO,[6,9] and so the different results might be caused not only by the purity of the XO used, but also by the experimental method.

The present results from the continuous variation method for Cu(II), Zn(II), and Cd(II) complexes in weakly acidic solutions are shown in Fig. 8. The individual plot at a given wavelength in the continuous variation method indicates the formation of either a 1:1 or 2:1 complex for each metal ion; that is, the plots at 574, 570, and 578 nm for Cu(II), Zn(II), and Cd(II) respectively in Fig. 8 exhibit an inflection at [M]/([M]+[XO])=2/3, but the plots at 498, 510, and 500 nm for these same metal ions show an inflection at 1/2. These facts indicate that the different conclusions are reached regarding the compositions of the complexes, depending on the wavelength used, in spite of testing the same metal ion at the same pH. The results of the mole-ratio method at various pH values for the Cu(II) system are shown in Fig. 9. The individual plot at a given pH exhibits either one inflection or two at [M]/[XO]=1 and/or 2, depending on the pH of the solution.

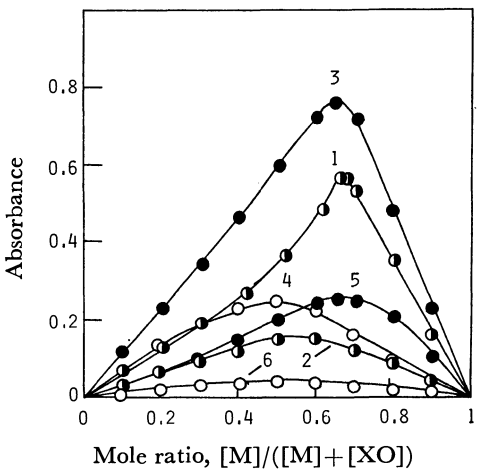

Fig. 8. Continuous variation method for Cu(II), Zn(II), and Cd(II) complexes with XO.
Cu(II): 1-574 and 2-498 nm at pH 5.86, Zn(II): 3-570 and 4-510 nm at pH 5.89, Cd(II): 5-578 and 6-500 nm at pH 6.20. [M]+[XO]=4.0×10^{-5} mol/l.

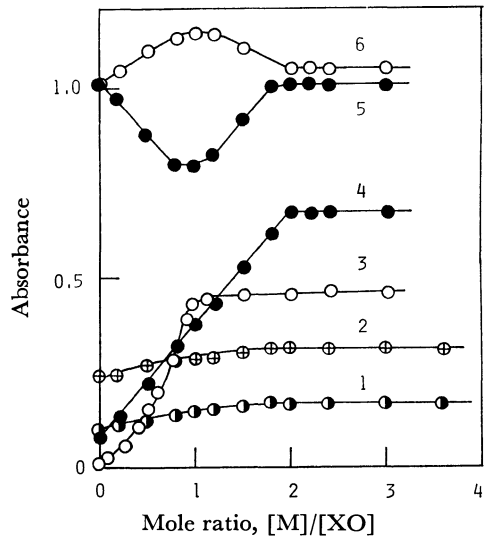

Fig. 9. Mole ratio method for Cu(II) complexes with XO at various pH values.
pH: 1-1.95, 2-3.12, 3-4.45, 4-5.58, 5-7.80, and 6-10.36.
Wavelength: 1-480, 2-500, 3-575, 4-540, 5-575, and 6-582 nm.

One of the explanations for this problem is that the 1: 1 and the 2: 1 complexes of XO formed in solutions of the same pH have absorption maxima at the same wavelength and differ only in absorptivity, as seen in Table 2. The complex of each component changes into a different type of protonated or hydroxo complex, therefore, the absorptivity, $\bar{\varepsilon}_1$ or $\bar{\varepsilon}_2$, is defined as $\bar{\varepsilon}=\sum\varepsilon_i x_i$ to express the apparent absorptivity of each component. ε_i and x_i are the absorptivity and the molar fraction of the complex species i, and the summation is performed on all the complex species of the same component which exist in the solution of a given pH. The subscript 1 or 2 indicates the 1: 1 or 2: 1 complex. The results of the mole-ratio method may be divided into the following three groups in terms of the relationship between $\bar{\varepsilon}$ and inflections on the plots:

(i) two inflections at [M]/[XO]=1 and 2 when $\bar{\varepsilon}_1 \neq \bar{\varepsilon}_2$.

(ii) one inflection at 1 when $\bar{\varepsilon}_1=\bar{\varepsilon}_2$.

(iii) one inflection at 2 when $2\bar{\varepsilon}_1=\bar{\varepsilon}_2$.

The 1, 2, 5, and 6 plots in Fig. 9 may be explained by (i), the 3 plot by (ii), the 4 plot by (iii). Accordingly, caution should be taken in determining the composition of the metal complexes with XO by spectrophotometry.

Arrangement of the Complex. The changes in the visible absorption spectrum of XO, accompanied by proton dissociation and/or complex formation, may be due to a change in the π-electron structure of its sulfonphthalein nucleus. Thus, the proton dissociation from the phenolic hydroxyl group (1 in Formula I) and the coordination of the phenolic (1) and/or quinolic oxygen (1′) lead to an important change in the absorption spectrum (the number in parentheses after the donor of the XO molecule, hereinafter, will refer to the donor, as indicated by its number in Formula I). Based on the visible absorption parameters, a discussion has been made of the coordination of the individual donor of XO, which is involved in the complex formation and/or in the proton dissociation from the acid group of the XO molecule of the protonated complex.

ML^{4-} dissociates all of the available protons; therefore, the arrangement of the complex may be presented as in Formula II. The mono-protonated complex, MHL^{3-}, dissociates its proton in alkaline solutions (with pH values of from 8 to 10.5, as seen in its acid dissociation constant in Table 1). In addition to this, the conversion from MHL^{3-} to ML^{4-} is accompanied by a slight change in ε, but almost no change in λ_{max} (Table 2). The protonated nitrogens (2 and 2′) of XO dissociate their protons in alkaline solutions, accompanied by a slight change in ε, but almost no change in λ_{max}.[8] Accordingly, the proton in MHL^{3-} may dissociate from the uncoordinating nitrogen (2′) in Formula II. The conversion from MH_2L^{2-} to MHL^{3-} accompanies the blue shift in the spectrum from around 440 to around 580 nm. This fact suggests that its proton dissociation is from phenolic oxygen (1) and that the coordinating donor involved in this reaction is the phenolic oxygen. MH_2L^{2-} exists in a weakly acidic medium. The uncoordinating phenolic oxygen (1) of XO in the MH_2L^{2-} complex would be protonated in such media, considering its pK value.[8] These considerations suggest the arrangement for the MH_2L^{2-} complex indicated in Formula III. The highly protonated complex species, H_iL^{-4+i} ($i \geqslant 3$), which are thought to exist in an acidic solution (pH 1—4), have λ_{max} around 440 nm. No remarkable change in the spectrum on its complex formation was observed, as has been mentioned above. In strongly acidic solutions with pH values from 1 to 2, carboxylic groups (3′ and 4′), which are not coordinated to metal ions, may be protonated based on their pK values.[8] Accordingly, the maximum value of i may be 4; that is, the four protons in MH_iL^{-4+i} ($i=4$) may be attached to two carboxylic oxygens (3′ and 4′) and the phenolic oxygen (1) and the amino nitrogen (2′)[12] in Formula III.

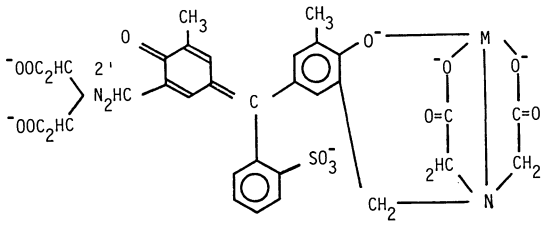

II ML^{4-}

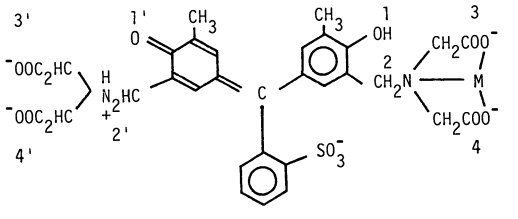

III MH_2L^{2-}

M_2L^{2-} dissociates all of the available protons; therefore, its arrangement may be offered as Formula IV. The spectra corresponding to the mono-protonated 2: 1

complex, M_2HL^-, for each metal ion have λ_{max} values of 435 to 445 nm and ε of 2.41 to 2.83×10^4 l mol^{-1} cm^{-1} respectively. There is not much difference in the spectra between this complex species and the XO species, H_iL^{-6+i} (i=3 to 6) the phenolic oxygen (1) of which is protonated, while its quinolic oxygen (1′) is not protonated (H_iL, i=3 to 6: λ_{max}=439—434 nm, $\varepsilon=2.62\times10^4$ l mol^{-1} cm^{-1}). These facts suggest that neither phenolic nor quinolic oxygens coordinate to metal ions; the arrangement indicated in Formula V is suggested for M_2HL^-.

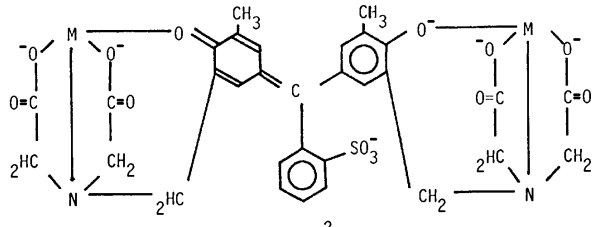

IV M_2L^{2-}

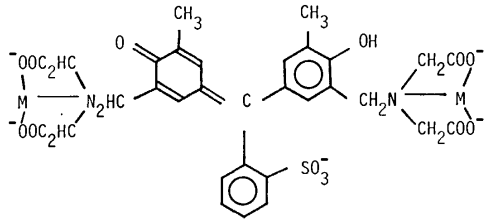

V M_2HL^-

Yamada *et al.*[11] have established the existence of the diprotonated 2:1 complex, Cu_2H_2L, at pH 3.5—5.5 from their spectrophotometric investigation. They have proposed that the phenolic and quinolic oxygens (1 and 1′) coordinate with Cu(II), but that the amino nitrogens (2 and 2′) do not coordinate and the nitrogens are protonated. Such a structure is, however, contradictory to the following two facts: i) If the Cu_2H_2L is formed at pH 3.5—5.5, the two protons might dissociate at a higher pH. However, the 2/1 titration curve indicates only one proton dissociation above pH 5.5. ii) Iminodiacetic acid, H_2L, forms ML with Cu(II) in weakly acidic media, and all the available protons in this ligand dissociate completely by pH about 5.[31] These facts suggest that all the donors of the bis(carboxymethyl)aminomethyl group in an XO molecule may coordinate to a Cu(II) ion in such weakly acidic solutions as are indicated in Formulas III and V for the MH_2L^{2-} and M_2HL^- complexes.

It is interesting to investigate whether the phenolic (or quinolic) oxygen (1 or 1′) coordinates to metal ions at a lower or higher pH than the amino nitrogen (2 or 2′). Among the metal complexes with SXO,[32] XO, SMTB,[33] MTB, and SGCR,[34] metal ions are, in general, divided into two groups in terms of the foregoing point: 1) Alkaline earth metal ions[10,18] and trivalent metal ions, such as Fe(III),[12] Cr(III),[21] and Al(III),[19] are coordinated by their phenolic oxygen at a lower pH than by their amino nitrogen. 2) Bivalent metal ions,[14–17,20] such as Co(II), Ni(II), Cu(II), Zn(II), Pb(II), and Cd(II), are coordinated by the amino nitrogen at lower pH and by the phenolic oxygen at higher pH. The metal ions of group (1) are hard metal ions, while those of group (2) are intermediate or soft metal ions, according to the hard and soft acid and base (HSAB) theory.[35,36] The phenolic oxygen, therefore, has more affinity to harder metal ions, and the amino nitrogen, to softer metal ions, in complexation in aqueous solutions.

Formation Constants. The formation constants were calculated utilizing the suceissive approximation method;[14,16] they are listed in Table 1. The formation constants of XO complexes with these metal ions have been determined by many authors. They have, however, assumed that only one reaction was involved in the solutions, as indicated in either of following equations:

i) $M^{2+} + L^{6-} \rightleftarrows ML^{4-}$: Refs. 24—29.

ii) $2M^{2+} + H_2L^{4-} \rightleftarrows Cu_2H_2L$: Ref. 11.

However, several reactions may be assumed to be involved, as has been determined above. This may be one reason why there are discrepancies among the formation constants calculated by the different authors. The present formation constants were calculated by taking all the probable reactions involved into account.[14,16]

The stabilities of the complexes in aqueous solutions frequently observed for the ligands, which coordinate to metal ions through oxygen and/or nitrogen donor atoms, follow this sequence: i) Co(II)<Ni(II)<Cu (II)> Zn(II) and ii) Pb(II)>Zn(II)> Cd(II). The stabilities of the XO complex species, ML^{4-}, MHL^{3-}, and M_2L^{2-}, do not follow this sequence, but that of MH_2L^{3-} does. The relative stabilities of the former three complex species for Cu(II) is considered to be lower than would be expected from the foregoing sequence. XO has two chelating groups on each side of the sulfonphthalein nucleus, consisting of phenolic (1) or quinolic (1′), amino (2 or 2′), and two carboxylic oxygens (3 and 4 or 3′ and 4′). In general, XO might act as a branched tetradentate ligand centered on the nitrogen atom. Such ligands prefer a regular octahedral or tetrahedral structure rather than a planar or tetragonal structure arising from elongation along an axis.[37] However, Cu(II) frequently forms complexes with the latter structure.[38,39] Accordingly, either of the following interpretations for the relative instabilities of the XO complexes for Cu(II) may be suggested: (i) If all of the four donor atoms of each chelating group were coordinated to such a structure, the complexes would be distorted into a lower symmetry or converted into a more regular octahedral one, resulting in the Jahn-Teller destabilization.[37,39] (ii) If the Cu(II) complexes keep a planar or tetragonal structure, it may be sterically impossible for one of the three branching donor atoms, *i.e.*, phenolic oxygen (1 and/or 1′), two carboxylic oxygens (3 and 4 and/or 3′ and 4′), to coordinate into a *trans* coordination site of the Cu(II) ion, in which another *trans* site is coordinated by the central nitrogen atom (2 and/or 2′), because it is too far away from it.[14,17] Therefore, each chelating group of XO would

act as a tridentate ligand, resulting in a decrease in the chelate effects.[39]

The relative instability of the Cu(II) complexes among the bivalent first transition metal ions has also been observed in other sulfonphthalein indicators, such as SXO,[15] MTB,[14] SMTB,[17] and SGCR.[20] Spectrophotometric and ESR studies of the Cu(II)-SXO complex[15] have suggested that the instability of this complex is explained by the foregoing interpretation (ii) and that the tetradentate ligand SXO acts as a tridentate one to Cu(II), to which one of the two carboxylic groups of SXO molecule remains uncoordinating. If the instabilities of the Cu(II)-XO complexes can be explained along the same lines as that for the Cu(II)-SXO complex, the sterical structure VI can be proposed for the $CuHL^{3-}$, CuL^{4-}, and Cu_2L^{2-} complex species. However, it still doubtful whether the explanation used for the SXO complex can also be applied to the XO complexes. The ESR study of the Cu(II)-complexes is being under taken: a valid discussion of these structure must await further investigation. The stabilities of the ML^{4-}, MHL^{3-}, and M_2L^{2-} complex species for Co(II), Zn(II), Cd(II), and Pb(II) exhibits the ordinary trend. This may be explained by the assumption that these metal ions probably take a regular octahedral or tetrahedral structure.[39] The Ni(II) complexes exhibit a property intermediate between Co(II) and Cu(II). Similar behavior of Ni(II) is encountered in connection with the other sulfonphthalein indicators.[14,15,17] The Ni(II) complexes frequently exhibit behavior similar in structure to that of the Cu(II) complexes as a result of the Jahn-Teller effect, although this effect is not so pronounced as that seen in the Cu(II) complexes.[40]

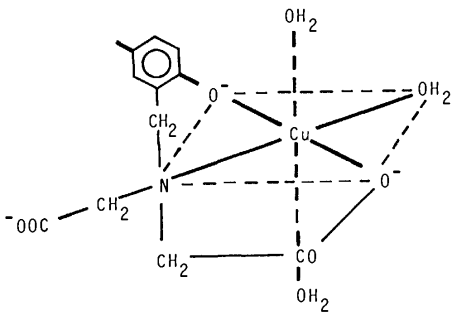

VI CuL^{4-}, $CuHL^{3-}$ and Cu_2L^{2-}

The stabilities of the MH_2L^{2-} and M_2HL^{-} complex species for all the metal ions exhibit the ordinary trend. The XO molecule in these complex species may act as a tridentate ligand; *i.e.*, the phenolic and/or quinolic oxygen may remain uncoordinated (Formulas III and V), so that its stability is not so much dependent on the coordination structures of the metal ions as the stabilities of ML^{4-}, MHL^{3-}, and M_2L^{2-} appear to be.

References

1) K. Ueno, "Kireito Tekiteiho," Nankodo, Tokyo (1960).
2) H. Flaschka, "Chelates in Analytical Chemistry," Marcel Dekker, New York (1967), Vol. 1, p. 15.
3) M. Otomo, *Jpn. Analyst*, **21**, 436 (1972).
4) S. P. Sangal, *Chim. Anal. (Paris)*, **47**, 239 (1965).
5) K. Tonosaki, *Dotite Newslett.*, **15**, No. 3, 2 (1967).
6) S. Nakada, M. Yamada, T. Ito, and M. Fujimoto, *Bull. Chem. Soc. Jpn.*, **50**, 1887 (1977).
7) D. C. Olson and D. W. Margerum, *Anal. Chem.*, **34**, 1299 (1962).
8) M. Murakami, T. Yoshino, and S. Harasawa, *Talanta*, **14**, 1293 (1967).
9) M. Yamada and M. Fujimoto, *Bull. Chem. Soc. Jpn.*, **49**, 693 (1976).
10) T. Yoshino, H. Okazaki, S. Murakami, and M. Kagawa, *Talanta*, **21**, 676 (1974).
11) M. Yamada, *Bull. Chem. Soc. Jpn.*, **49**, 1023 (1976).
12) T. Yoshino, S. Murakami, and K. Ogura, *J. Inorg. Nucl. Chem.*, **41**, 1011 (1979).
13) T. Yoshino, H. Imada, and T. Kuwano, *Talanta*, **16**, 151 (1969).
14) T. Yoshino, H. Imada, S. Murakami, and M. Kagawa, *Talanta*, **21**, 211 (1974).
15) S. Murakami, *J. Inorg Nucl. Chem.*, in press.
16) T. Yoshino, S. Murakami, M. Kagawa, and T. Araragi, *Talanta*, **21**, 79 (1974).
17) T. Yoshino, S. Murakami, and M. Kagawa, *Talanta*, **21**, 199 (1974).
18) T. Yoshino, H. Okazaki, S. Murakami, and M. Kagawa, *Talanta*, **21**, 673 (1974).
19) S. Murakami, *J. Inorg. Nucl. Chem.*, **41**, 209 (1979).
20) T. Yoshino, S. Murakami, and K. Arita, *Talanta*, **26**, 479 (1979).
21) T. Yoshino, S. Murakami, H. Takesue, and M. Ishihara, *J. Inorg. Nucl. Chem.*, **42**, 579 (1980).
22) T. Yoshino, S. Murakami, K. Arita, K. Ogura, and K. Ishizu, The 16th Annual Meeting of Discussion on ESR, Sendai, October 11—13, 1977, Abstract, p. 139.
23) K. Ogura, K. Seno, S. Ukita, S. Murakami, and T. Yoshino, The Annual Meeting of the Chugoku-Shikoku Branch of the Chemical Society of Japan, Tokushima, November 2-3, 1978, Abstract, p. 124.
24) M. Otomo, *Jpn. Analyst*, **14**, 45 (1965).
25) S. Hung and H. Chang, *Hua Hsuch Tung Pao*, **1964**, 46; [*Chem. Abstr.*, **61**, 2467 (1964)].
26) K. Studlar and I. Janousch, *Talanta*, **8**, 203 (1961).
27) T. Miyazima, *Jpn. Analyst*, **13**, 257 (1964).
28) P. V. Marchenko, *Ukr. Khim. Zh.*, **30**, 224 (1963).
29) M. Otomo, *Bull. Chem. Soc. Jpn.*, **37**, 504 (1964).
30) G. P. Hildebrand and C. N. Reilley, *Anal. Chem.*, **29**, 258 (1957).
31) S. Chaberek, Jr., and A. E. Martell, *J. Am. Chem. Soc.*, **74**, 5052 (1952).
32) 3-[*N*,*N*'-Bis(carboxymethyl) aminomethyl]-*o*-cresolsulfonphthalein.
33) 3-[*N*,*N*'-Bis (carboxymethyl) aminomethyl] thymolsulfonphthalein.
34) 3-[*N*-(Carboxymethyl) aminomethyl]-*o*-cresolsulfonphthalein.
35) R. G. Pearson, *J. Am. Chem. Soc.*, **85**, 3533 (1963).
36) G. Klopman, *J. Am. Chem. Soc.*, **90**, 223 (1968).
37) G. Schwarzenbach, *Helv. Chim. Acta*, **35**, 2344 (1952).
38) "Modern Coordination Chemistry," ed by J. Lewis and R. G. Willkins, Interscience, New York (1960), Chap. 1.
39) "Kireito Kagaku (3), Heiko To Hanno [I]," ed by K. Ueno, Nankodo, Tokyo (1977), Chap. 1.
40) F. A. Cotton and G. Wilkinson, "Advanced Inorganic Chemistry," Interscience, New York (1972), p. 893.

Three-dimensional Metal Complex Structures with Ambident Propylenediamine Ligands Serving as the Hosts of the Aromatic Guest Molecules. Hofmann-pn and pn-Td Type Clathrates

Shin-ichi NISHIKIORI, Toschitake IWAMOTO,* and Yukichi YOSHINO

Department of Chemistry, College of General Education, The University of Tokyo, Komaba, Meguro-ku, Tokyo 153

(Received September 29, 1979)

Novel clathrate compounds, Hofmann-pn type $Cd(pn)Ni(CN)_4 \cdot 3/2G$ (G=C_4H_5N, C_4H_4S, or C_6H_6) and pn-Td type $Cd(pn)Cd(or\ Hg)(CN)_4 \cdot 3/2C_6H_6$, have been prepared. Their host structures are analogous to those of the known Hofmann-en type $Cd(en)Ni(CN)_4 \cdot 2G$ and en-Td type $Cd(en)Cd(or\ Hg)(CN)_4 \cdot 2C_6H_6$. The propylenediamine (pn: 1,2-diaminopropane) molecule ambidently bridges six-coordinate Cd atoms, as the en (ethylenediamine) does in the latter types of clathrates. The guest molecules occupy at random three quarters of the cavities in the host structures: every remaining cavity contains two methyl groups of the pn molecules. The crystal structure of $Cd(l\text{-pn})Ni(CN)_4 \cdot 3/2C_4H_5N$ has been analyzed in order to demonstrate the structural features. The crystal is tetragonal with the space group P422, $a=7.575(2)$ and $c=7.742(2)$ Å, and $Z=1$. The degree of disorder is extremely high with regard to the arrangement and orientation of the *l*-pn molecule.

We have developed the synthetic and structural chemistry of the Hofmann type and the analogous clathrates with the general formula of $Cd(diam)M(CN)_4 \cdot 2G$ (diam=$(NH_3)_2$, en, or tn; M=square-planar Ni, Pd, or Pt, or tetrahedral Cd or Hg; G=C_4H_5N, C_4H_4S, C_6H_6, or $C_6H_5NH_2$), as has been summerized in a previous paper.[1] Among these clathrates, the Hofmann-en type (diam=en, M=Ni, Pd, or Pt), the en-Td type (diam=en, M=Cd or Hg), and the tn-Td type (diam=tn, M=Cd or Hg) have ambident α,ω-diamines bridging two six-coordinate Cd atoms in their host structures. In this paper we wish to add to them two novel series, the Hofmann-pn type $Cd(pn)Ni(CN)_4 \cdot 3/2G$ and the pn-Td type $Cd(pn)M(CN)_4 \cdot 3/2G$ (M=Cd or Hg), the hosts of which contain an ambident pn (propylenediamine) ligand as diam in the general formula of $Cd(diam)M(CN)_4 \cdot nG$ for the clathrates ($n=2$) reported previously.[1] However, the participation of the pn as a constituent of the host gives rise to a decrease in n from 2 to 3/2. Based on the present results of structural analysis, this decrement is interpreted in terms of the random distribution of a pair of pn-methyl groups with a 1/4 probability, and a guest molecule with a 3/4 probability, in the cavity formed in the metal-complex host structure. Our idea at the beginning of this investigation was to develop a stereospecific host structure using optically-active *l*-pn as one of the host constituents. Although this idea has not been realized, it has been suggested that the space volume of a cavity available for a guest molecule can be regulated by introducing bulky substituents into the ambident diamine ligand building up the three-dimensional host structure.

Experimental

Preparation. *Cd(*dl*-pn)Ni(CN)*$_4 \cdot 3/2C_4H_5N$: From a concentrated aqueous solution containing $CdCl_2$, $K_2[Ni(CN)_4]$, and racemic pn (*dl*-pn) in a 1:1:3 mole ratio, tris(*dl*-propylenediamine)cadmium tetracyanonickelate(II) $[Cd(dl\text{-pn})_3][Ni(CN)_4]$ was precipitated as pale yellow crystals. They were then recrystallized from hot water. Found: C, 30.9; H, 6.44; N, 28.2; Cd, 22.3; Ni, 11.7%. Calcd for $C_{13}H_{30}N_{10}CdNi$: C, 31.4; H, 6.08; N, 28.2; Cd, 22.6; Ni, 11.8%. The recrystallized complex was dissolved into water (0.2 g/50 cm^3) in a 300-cm^3 stoppered conical flask, and the solution was covered with an organic mixture of pyrrole and xylene (1:15 v/v). By leaving the flask in a refrigerator for a week, pale yellow plate-like crystals of the clathrate were obtained on the interface between the aqueous and the organic phases. Although the needle-like crystals of $[Cd(dl\text{-pn})_3][Ni(CN)_4]$ were occasionally mixed with those of the clathrate, it was easy to discriminate between the complex and the clathrate visually. The clathrate was filtered off on a sintered glass, washed with small amounts of water and ethanol successively, and preserved in a silica gel desiccator under the saturated vapor pressure of pyrrole.

*Cd(*dl*-pn)Ni(CN)*$_4 \cdot 3/2C_4H_4S$ and *Cd(*dl*-pn)Ni(CN)*$_4 \cdot 3/2C_6H_6$: These clathrates were prepared by procedures similar to the above one using a 1:1 thiophene–xylene mixture for the thiophene clathrate and a 1:2 benzene–xylene mixture for the benzene clathrate. They were obtained as coagulated polycrystals.

*Cd(*l*-pn)Ni(CN)*$_4 \cdot 3/2C_4H_5N$: *l*-Propylenediamine (*l*-pn) was obtained from racemic propylenediamine.[2] $[Cd(l\text{-pn})_3][Ni(CN)_4]$ and $Cd(l\text{-pn})Ni(CN)_4 \cdot 3/2C_4H_5N$ were prepared by a method similar to that used for the *dl*-pn compounds. Since $[Cd(l\text{-pn})_3][Ni(CN)_4]$ is less soluble in water than the *dl*-pn complex, an aqueous solution containing 0.1 g of the *l*-pn complex in 50 cm^3 of water was used for the preparation of the clathrate.

*Cd(*dl*-pn)Cd(CN)*$_4 \cdot 3/2C_6H_6$ and *Cd(*dl*-pn)Hg(CN)*$_4 \cdot 3/2C_6H_6$: To 25 cm^3 of a 0.2 M (1 M=1 mol dm^{-3}) $CdCl_2$ aqueous solution in a 300-cm^3 stoppered conical flask, 150 mmol of *dl*-pn and 25 cm^3 of 0.2 M $K_2[Cd(CN)_4]$ or $K_2[Hg(CN)_4]$ were added successively. After the pH had been adjusted to 8.0 by adding 6 M HCl drop by drop, the solution was covered with a benzene–xylene (1:1) mixture. After the flask had been left in a refrigerator for a week, colorless crystals of the clathrate were formed on the interface and at the bottom of the aqueous solution.

Powder X-Ray Diffraction. X-Ray diffraction patterns of powdered specimens were recorded on a JEOL DX diffractometer using Ni-filtered Cu $K\alpha$ radiation.

Structure Determination

Single crystals of $Cd(l\text{-pn})Ni(CN)_4 \cdot 3/2C_4H_5N$ (**1**) and $Cd(dl\text{-pn})Ni(CN)_4 \cdot 3/2C_4H_5N$ (**2**) were used for X-ray diffraction experiments to determine the crystal struc-

tures.

Data Collection. Each of the crystals of **1** and **2** cut into the cube with dimensions of *ca.* 0.3×0.3×0.3 mm was coated with epoxy resin in order to prevent the decomposition of the crystal under ambient conditions. Preliminary Weissenberg photographs showed 4/mmm symmetries for both **1** and **2** crystals; the lack of any systematic absences of reflections indicated that the possible space groups are P4/mmm, P422, P4mm, P$\bar{4}$2m, and P$\bar{4}$m2. As will be mentioned later, the P422 and P4/mmm space groups were adopted for **1** and **2** respectively. The precise determination of lattice parameters and the collection of the intensity data were carried out on a Philips automated four-circle diffractometer[3] for **1** and on a Rigaku automated four-circle diffractometer[4] for **2**. In both cases, the reflections with $2\theta \leq 60°$ were collected using Mo $K\alpha$ radiation. The intensities of three standard reflections recorded every fifty measurements showed no significant variations. The densities were measured by the flotation method using bromoform–xylene mixture. The crystal data are:

$C_{13}H_{17.5}N_{7.5}CdNi$,	F.W.=449.94, Tetragonal	
	1 (*l*-pn host)	**2** (*dl*-pn host)
Space group	P422	P4/mmm
$a(=b)$/Å	7.575±0.002	7.570±0.002
c/Å	7.742±0.002	7.741±0.004
Unit cell volume/Å^3	444.2±0.3	443.6±0.4
Z	1	1
D_m/g cm^{-3}	1.67	1.68
D_x/g cm^{-3}	1.68	1.68
Number of reflections used for refinement ($\|F_o\|>3\sigma(\|F_o\|)$)	414	425

Solution and Refinement of the Structures. The structures were solved by the heavy-atom method. The refinements were carried out by successive Fourier and difference Fourier syntheses and by the block-diagonal least-squares method on a HITAC 8800/8700 computer at the Computer Center of this University, using the programs in UNICS[5] and their local versions. The atomic scattering factors used were those in the International Tables.[6]

There is no significant difference in the unit cell dimensions between **1** and **2**. The Patterson maps of **1** and **2** showed that, in both structures, Cd and Ni atoms lie at 0,0,0 and 1/2,1/2,0, and that the cyanide group bridges these atoms. The two-dimensional extension of the metal cyanide sheet on the {001} plane is similar to those observed for Hofmann type and Hofmann-en type clathrates.[1] Therefore, the pn ligands were assumed to bridge two Cd atoms in adjacent metal cyanide sheets along the fourfold axis of crystal, as the en ligand does in Hofmann-en type clathrate.[7,8]

Because the *l*-pn molecule has no symmetry, the non-centrosymmetric space group P422 was assumed for **1**. As the *l*-pn molecule is located about a special position, 0,0,1/2 with the point symmetry 42, it should have an orientational disorder. The centrosymmetric space group P4/mmm was assumed for **2**. The other three space groups, P4mm, P$\bar{4}$2m, and P$\bar{4}$m2, giving the arrangement of pn-methyl groups with an unacceptable overlapping or the arrangements of pn and pyrrole molecules about the unacceptable $\bar{4}$ axis, were discarded.

For both **1** and **2**, the Fourier syntheses phased by the Cd and Ni atoms gave the positions of the C and N atoms of the cyanide group and the pyrrole molecule. The pyrrole molecule was found in the cavity between the metal cyanide sheets; like the pyrrole molecule in Hofmann-en type Cd(en)Ni(CN)$_4$·2C$_4$H$_5$N,[8] the molecular dipole axis is arranged with an equal probability parallel and antiparallel to the c axis of crystal.

At this stage, the atomic parameters for the Cd, Ni, and C and N atoms of the cyanide and pyrrole were refined by the block-diagonal least-squares procedure to minimize $\sum w(||F_o|-|F_c||)^2$; $w=1$ for $|F_o|<F_{max}$ and $w=(F_{max}/|F_o|)^2$ for $|F_o|\geq F_{max}$, $F_{max}=35.0$ for **1**, and 50.0 for **2**. After several cycles of the calculations by applying the anisotropic temperature factors to Cd and Ni atoms, and the isotropic ones to C and N atoms, the conventional reliability index, $R_1=\sum w(||F_o|-|F_c||)/\sum|F_o|$, became 0.088 for **1** and 0.128 for **2**. At this point a trial was made to find the positional parameters for the pn molecule, though the electron density due to the pn molecule was predicted to be very low because of the great extent of orientational disorder. The electron densities appearing on the difference Fourier map of **2** were so vague that we could hardly locate any atoms. In the case of **1** we could barely find two sets of the atomic coordinates forcibly assigned to the C and N atoms of the *l*-pn molecule. However, the positional and thermal parameters of a few atoms of *l*-pn obtained after several cycles of the least-squares calculations gave too large estimated standard deviations. Therefore, we ceased to refine the structures of **1** and **2** at this stage.[9] The atomic parameters determined for **1** are listed in Table 1, while an illustrative sketch of the structure is shown in Fig. 1.

Table 1. The atomic parameters of Cd(*l*-pn)Ni(CN)$_4$·3/2C$_4$H$_5$N and their estimated standard deviations (in parentheses)[a]

Atom[b]	x/a	y/b	z/c	B_{iso}
Cd	000	000	000	—[c]
Ni	500	500	000	—[c]
C(CN)	328 (1)	328	000	3.3 (2)
N(CN)	219 (2)	219	000	4.4 (2)
N(prl)[d]	500	000	335 (5)	5.4 (6)
C(prl)[d]	500	169 (5)	422 (4)	6.8 (6)
C(prl)[d]	500	087 (5)	598 (4)	6.7 (6)

a) The positional parameters have been multiplied by 10^3. b) The parameters of the C and N atoms of the *l*-pn molecule have not been determined accurately. c) The anisotropic thermal parameters have been obtained for Cd ($B_{11}=0.0063(1)=B_{22}$, $B_{33}=0.0144(2)$, and $B_{12}=B_{13}=B_{23}=0$) and Ni ($B_{11}=0.0060(2)=B_{22}$, $B_{33}=0.0179(4)$, and $B_{12}=B_{13}=B_{23}=0$) in the form of $\exp\{-(B_{11}h^2+B_{22}k^2+B_{33}l^2+2B_{12}hk+2B_{13}hl+2B_{23}kl)\}$. d) Each of the occupancy factors of the N and C atoms of the pyrrole molecule is 0.375.

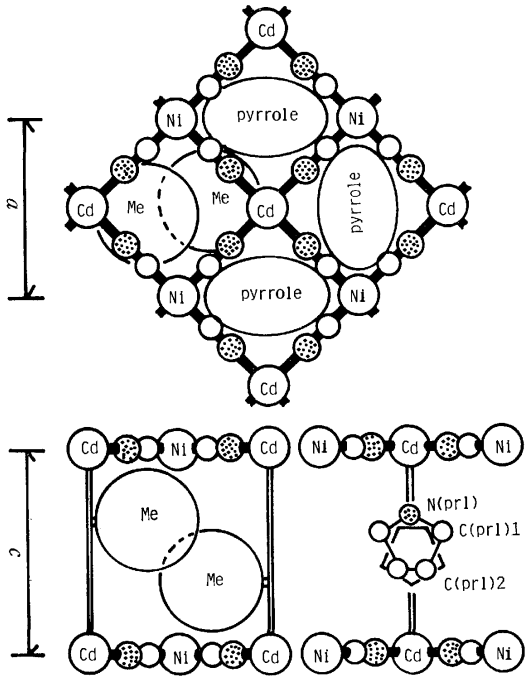

Fig. 1. Illustrative views of the structure of Cd(*l*-pn)-$Ni(CN)_4 \cdot 3/2C_4H_5N$.
Open circle: carbon atom; dotted cricle: nitrogen atom; doubled line: –N–C–C–N– skeleton of *l*-pn.

TABLE 2. THE HORMANN-pn AND pn-Td TYPE CLATHRATES AND THEIR ANALYTICAL RESULTS [FOUND/(CALCD)]

Hofmann-pn type:	C	H	N	Cd	Ni
Cd(*dl*-pn)$Ni(CN)_4 \cdot 3/2C_4H_5N$	34.2 (34.7)	3.94 (3.92)	23.3 (23.4)	25.2 (25.0)	12.7 (13.1)
Cd(*l*-pn)$Ni(CN)_4 \cdot 3/2C_4H_5N$	34.2 (34.7)	4.03 (3.92)	23.2 (23.4)	25.2 (25.0)	13.2 (13.1)
Cd(*dl*-pn)$Ni(CN)_4 \cdot 3/2C_4H_4S$	32.9 (32.8)	3.77 (3.39)	18.1 (18.0)	23.7 (23.6)	12.3 (12.3)
Cd(*dl*-pn)$Ni(CN)_4 \cdot 3/2C_6H_6$	41.0 (41.2)	4.18 (4.11)	18.2 (18.0)	24.5 (24.1)	12.4 (12.6)
pn-Td type:					
Cd(*dl*-pn)$Cd(CN)_4 \cdot 3/2C_6H_6$	37.5 (36.9)	3.81 (3.68)	16.5 (16.1)	43.1 (43.2)	
Cd(*dl*-pn)$Hg(CN)_4 \cdot 3/2C_6H_6$	31.7 (31.6)	3.29 (3.15)	14.0 (13.8)	18.1 (18.5)	

Results and Discussion

The clathrates prepared are listed in Table 2 along with their analytical results. In the earlier stage of the investigations of the Hofmann type clathrates, some clathrates were reported to have non-stoichiometric or substoichiometric compositions with regard to the number of guest molecules for a formula unit of the metal complex host, $M(NH_3)_2Ni(CN)_4$ (M=Ni, Cu, Zn, or Cd);[10–12] these observations were due to inadequate conditions in the preparation or to careless treatment of the prepared specimens.[13] It is well known that some hydrate clathrates and *p*-hydroxybenzene clathrates are non-stoichiometric.[14] However, in the novel clathrates the number of guest molecules can be counted as 3/2 for a formula unit of the metal complex host, within the limits of experimental error. As has been verified with regard to the crystal structures of **1** and **2**, the novel $Cd(pn)Ni(CN)_4$ host has linkages of the ambident CN and pn ligands substantially similar to those of the Hofmann-en type host; the structure of the Cd(pn)Cd(or Hg)$(CN)_4$ host is also concluded to be similar to that of the en-Td type, as will be discussed later. By analogy with the naming of the Hofmann-en type and the en-Td type, we can name the novel clathrates, $Cd(pn)Ni(CN)_4 \cdot 3/2G$ and Cd(pn)Cd(or Hg)$(CN)_4 \cdot 3/2G$, the "Hofmann-pn type" and the "pn-Td type" respectively.

Hofmann-pn Type Clathrates. The stoichiometry of the novel clathrates suggests that one of the four cavities is not occupied by a guest molecule. Since, in general, the crystal structure cannot be stable with vacant cavities, it is also suggested that the cavity unoccupied by a guest molecule should be occupied by another species instead of the guest. The crystal structures of **1** and **2** can be interpreted most plausibly in terms of the random distributions of the cavity occupied by a pyrrole molecule and that occupied by a pair of pn-methyl groups in a 3: 1 ratio throughout the crystal. As Fig. 1 shows, the square-planar metal cyanide sheet has a structure similar to those in the Hofmann type and the Hofmann-en type, with interatomic distances of Ni–C-(CN)=1.840(8) Å, C(CN)–N(CN)=1.17(2) Å, and Cd–N(CN)=2.35(2) Å in **1**. One of the four cavities formed between the metal cyanide sheets is occupied by a pair of methyl groups protruding from the confronting pair of pn molecules; each of the pn molecules bridges two Cd atoms in adjacent metal cyanide sheets. The other three cavities are occupied by pyrrole molecules oriented randomly upward and downward with regard to the molecular dipole axis. The apparent tetragonal symmetry of the crystal is derived from a random distribution of both kinds of cavities and from random orientations of the pn molecules.

The cause of disorder in this structure can be understood from the calculation of the void space of the cavity occupied by the methyl groups. According to Immirzi and Perini,[15] the volume of an organic molecule packed in a crystal can be approximated by a simple additivity rule within an error of *ca.* 3%. On the assumption that the pyrrole molecules have close packing in the Hofmann-en type pyrrole clathrate, $Cd(en)Ni(CN)_4 \cdot 2C_4H_5N$,[8] the volume of the Hofmann-en type host, $V_{en\text{-}host}$, is calculated to be 267.4 Å^3 by subtracting that of two pyrrole molecules, 2×95.1 Å^3, from that of the unit cell, 457.6 Å^3. By adding the volume of a methyl group, 31.7 Å^3, and that of 1.5 times pyrrole molecules, 1.5×95.1 Å^3, to, and subtracting that of a hydrogen, V_H 6.8 Å^3, from, $V_{en\text{-}host}$, we obtain the calculated unit cell volume of the Hofmann-pn type *l*-pn host clathrate **1** as 434.9 Å^3, nearly equal to the observed value, V_{cell} 444.2 Å^3. Since the approximation can be seen to be valid, we may calculate the volume of the cavity, V_{cav}, in **1** thus:

$$V_{cav} = [V_{cell} - (V_{en\text{-}host} - V_H)] \times 0.5 = 91.9 \text{ Å}^3$$

a value nearly equal to that of a pyrrole molecule. However, the volume of two methyl groups, 63.4 Å^3, is smaller by *ca.* 30 Å^3 than V_{cav}, the occupation ratio

TABLE 3. POWDER X-RAY DIFFRACTION DATA OF Cd(*dl*-pn)Cd(CN)$_4$·3/2C$_6$H$_6$ AND Cd(*dl*-pn)Hg(CN)$_4$·3/2C$_6$H$_6$

Ni-filtered Cu $K\alpha$ (λ=1.5418 Å), GM counter

Cd(*dl*-pn)Cd(CN)$_4$·3/2C$_6$H$_6$ Tetragonal a= 8.26 Å, b=15.31 Å					Cd(*dl*-pn)Hg(CN)$_4$·3/2C$_6$H$_6$ Tetragonal a= 8.23 Å, b=15.23 Å				
2θ	I	d_{obsd}/Å	hkl	d_{calcd}/Å	2θ	I	d_{obsd}/Å	hkl	d_{calcd}/Å
10.7_3	21	8.25	100	8.26	10.8_0	34	8.19	100	8.23
11.5_3	5	7.68	002	7.65_5					
12.1_7	69	7.27	101	7.27	12.2_5	34	7.23	101	7.24
					15.1_9	4	5.83	110	5.82
15.7_8	56	5.62	102	5.62	15.8_5	54	5.59	102	5.59
19.1_0	100	4.65	112	4.64	19.2_0	100	4.62	112	4.62
20.4_5	11	4.34	103	4.34	20.5_4	4	4.32	103	4.32
21.5_1	94	4.13	200	4.13	21.6_0	68	4.11	200	4.11_5
23.2_2	14	3.83	113	3.84_3	23.3_0	11	3.82	113	3.82_6
			004	3.82_7				004	3.80_8
24.5_3	4	3.63	202	3.63_5					
24.7_8	6	3.59	211	3.59_1	24.8_1	13	3.59	211	3.57_8
25.5_6	4	3.49	104	3.47_3	25.7_3	5	3.46	104	3.45_6
26.7_8	47	3.33	212	3.32_7	26.8_9	45	3.32	212	3.31_4
27.7_6	17	3.21	203	3.21_0	27.8_9	11	3.20	203	3.19_7
29.8_4	32	2.99	213	2.99_2	29.9_4	11	2.98	213	2.98_0
30.5_7	11	2.92	220	2.92_0	30.6_5	5	2.92	220	2.91_0
31.8_5	32	2.88	221	2.86_9	31.9_9	24	2.86	221	2.85_8
			105	2.87_1				105	2.85_7
32.5_0	19	2.76	300	2.75_3	32.6_3	21	2.74	300	2.74_3
32.9_8	14	2.72	301	2.71_0	33.1_7	11	2.70	301	2.70_0
			115	2.71_2				115	2.69_9
33.6_9	27	2.66	214	2.65_8	33.8_4	31	2.65	214	2.64_6
					34.4_2	4	2.61	310	2.60_3
34.5_7	6	2.59_5	302	2.59_1	34.7_8	6	2.57_9	302	2.58_1
36.3_1	39	2.47_4	312	2.47_2	36.4_8	25	2.46_3	312	2.46_3
					37.0_0	5	2.43_0	106	2.42_6
38.1_0	11	2.36_2	215	2.35_7	38.3_2	9	2.34_9	215	2.34_7
38.4_3	11	2.34_2	116	2.33_8	38.6_3	9	2.33_1	116	2.32_7
38.7_2	11	2.32_5	313	2.32_5	39.9_2	17	2.31_4	313	2.31_6
			224	2.32_2				224	2.31_2
39.3_0	4	2.29_2	320	2.29_1					
39.7_5	7	2.26_8	321	2.26_6					
					40.4_9	9	2.22_8	304	2.22_6

of the cavity being 69%. The void space may give much freedom of motion to the pn molecule.

pn-Td Type Clathrates. The powder X-ray diffraction patterns of pn-Td type benzene clathrates Cd(*dl*-pn)Cd(CN)$_4$·3/2C$_6$H$_6$ and Cd(*dl*-pn)Hg(CN)$_4$·3/2C$_6$H$_6$ were assigned to the tetragonal systems, as Table 3 shows. The unit cell dimensions of these clathrates are very close to those of the corresponding en-Td type benzene clathrates.[16] Since their diffraction patterns showed a close resemblance to those of the corresponding en-Td type clathrates, the substantial structure of the pn-Td type host can be thought of as being similar to that of the en-Td type host. One of the four cavities must be occupied at random by a pair of pn-methyl groups, too. The calculated volume (117 Å^3) of a cavity in the pn-Td type host gave a *ca.* 46% void space in the cavity occupied by the methyl groups. However, the three-dimensional framework, built of the tetrahedral Cd(CN)$_4$ or Hg(CN)$_4$ moieties and the ambident pn ligands, which are linked together at the six-coordinate Cd atoms, appears to be tight enough to keep the tetragonal crystal lattice, even with the considerably large void space in the cavity occupied by the methyl groups.

Conclusion. These observations suggest that the number of cavities available for the guest molecules can be regulated by introducing bulky substituents into the ambident diamine ligand building up the host structures of these types of clathrates. 2,3-Diaminobutane (bn) has two methyl groups. In the clathrate with the Cd(bn)M(CN)$_4$·nG formula, n can be expected to be one if such a clathrate is successfully prepared using bn in place of pn. The investigations are now in progress.

References

1) T. Iwamoto, M. Kiyoki, Y. Ohtsu, and Y. Takeshige-Kato, *Bull. Chem. Soc. Jpn.*, **51**, 488 (1978).
2) F. P. Dwyer, F. L. Garvan, and A. Schulman, *J. Am. Chem. Soc.*, **81**, 290 (1959).
3) The diffractometer was used by the courtesy of Professor Yoichi Iitaka of the Faculty of Pharmaceutical Science of this University.
4) The diffractometer was used by the courtesy of Professor Yukiyoshi Sasaki of the Department of Chemistry, Faculty of Science of this University.
5) "The Universal Crystallographic Computation Program System (UNICS)," ed by **T.** Sakurai, Crystallographic Society of Japan, Tokyo (1967).
6) "International Tables for X-Ray Crystallography," Kynoch Press, Birmingham (1974), Vol. IV.
7) T. Miyoshi, T. Iwamoto, and Y. Sasaki, *Inorg. Chim. Acta*, **6**, 59 (1972).
8) T. Iwamoto and M. Kiyoki, *Bull. Chem. Soc. Jpn.*, **48**, 2412 (1975).
9) The table of the structure factors for **1** is kept as Document No. 8026 at the Chemical Society of Japan.
10) K. A. Hofmann and H. Arnoldi, *Chem. Ber.*, **39**, 339 (1906).
11) R. S. Drago, J. T. Kwon, and R. D. Archer, *J. Am. Chem. Soc.*, **80**, 2667 (1958).
12) R. Baur and G. Schwarzenbach, *Helv. Chim. Acta*, **43**, 842 (1960).
13) T. Iwamoto, T. Miyoshi, T. Miyamoto, Y. Sasaki, and S. Fujiwara, *Bull. Chem. Soc. Jpn.*, **40**, 1174 (1967).
14) "Non-stoichiometric Compounds," ed by L. Mandelcorn, Academic Press, New York and London (1964).
15) A. Immirzi and B. Perini, *Acta Crystallogr., Sect. A*, **33**, 216 (1977).
16) T. Iwamoto and D. F. Shriver, *Inorg. Chem.*, **11**, 2570 (1972); T. Iwamoto, *Chem. Lett.*, **1973**, 723.

 © 1980 The Chemical Society of Japan Bull. Chem. Soc. Jpn., 53, 2241—2247 (1980)

Ion Pair Formation between Electro-generated 1,2-Naphtoquinone Anion Radicals and Alkali Metal Cations in Acetonitrile

Taitiro FUJINAGA, Satoshi OKAZAKI, and Tsutomu NAGAOKA*

Department of Chemistry, Faculty of Science, Kyoto University, Sakyo-ku, Kyoto 606

(Received December 24, 1979)

Ion association of 1,2-naphthosemiquinone with the alkali metal cations in acetonitrile has been comprehensively studied by the use of ESR, absorption spectroscopy, polarography and with MO calculation. A continuous flow electrolysis system with a glassy carbon column electrode has been developed for the rapid quantitative preparation of organic free radicals, whose ESR spectrum or absorption spectrum was observed *in situ*. The formation constants of the ion pair with K^+, Na^+, and Li^+ were estimated as $10^{3.2}$, $10^{4.5}$, and $10^{8.0}$, respectively. By the addition of alkali metal cations, the half-wave potentials shifted to more positive potential in the order of $K^+ < Na^+ < Li^+$. The proton hyperfine splitting constants in the ESR also varied in this order. This column electrolysis method is considered to be a powerful technique, particularly for the study of short lived free radicals, because the quantitative electrolysis is performed rapidly even in a solution of extremely diluted supporting electrolyte, such as 0.1 mM (mmol/dm^3).

In most of the studies of ion pair formation between organic free radicals and alkali metal cations by means of ESR and absorption spectroscopy, radical anions were usually obtained by chemical reactions with alkali metals using solvents, such as ether, having low dielectric constants.[1-3] Therefore, it is not particularly useful to carry out discussions of the comparisons of their characteristics with those obtained in polarography, in which dipolar aprotic solvents are generally used.

Fujinaga *et al.* have studied the electrolytic preparation of organic free radicals[4] and their electrochemical behavior in *N,N*-dimethylformamide by the use of ESR and polarography.[5] The effect of metal cations on the polarographic reduction of naphtoquinone in aprotic solvents have been investigated by Fujinaga *et al.*[6] and also recently, by Kalinowski *et al.*[7]

In the present paper, the authors employed a rapid flow electrolysis using a glassy carbon column electrode[8] in order to generate radical ions and studied the ion pair formation between 1,2-naphtoquinone radical anions (β-NPQ$^{-\cdot}$) and alkali metal cations of supporting electrolyte in acetonitrile by the comprehensive analysis of their ESR spectra and polarograms.

This column electrolysis method has the following advantages over the conventional constant potential electrolysis: 1) The objective depolarizers in the sample solution are completely electrolyzed immediately after flowing into the column; 2) The concentration of the electro-generated radical anion is determined by the simple monitoring of the electrolysis current instead of charge; 3) An ESR spectrum, or an absorption spectrum corresponding to the stepwise change of the electrode potentials can be observed *in situ*.

The formation constants of the ion pairs between β-NPQ$^{-\cdot}$ and alkali metal cations were inclined to increase with decreasing ionic radii of counterions, that is, $10^{3.2}$, $10^{4.5}$, and $10^{8.0}$ for K^+, Na^+, and Li^+, respectively. The proton hfs constants of their ESR spectra and half-wave potentials of their polarograms shifted significantly in the order of $K^+ < Na^+ < Li^+$. From these results, the complexes between β-NPQ anion and counter cations seem to be contact ion pairs.

Experimental

Reagents. Reagent grade β-NPQ from Wako Pure Chemicals, Ltd., Osaka was purified by the sublimation method. The concentration of β-NPQ used was 0.35 mM unless otherwise noted. Acetonitrile from the same supply was distilled over P_2O_5 after pretreated with calcium hydride. Propylene carbonate and *N,N*-dimethylformamid (DMF) were distilled under reduced pressure, after being dried with molecular sieves 4A. Tetraethylammonium perchlorate (TEAP) was prepared by the conventional method. All metal ions added were in their perchlorates. Other chemicals used were of analytical reagent grade.

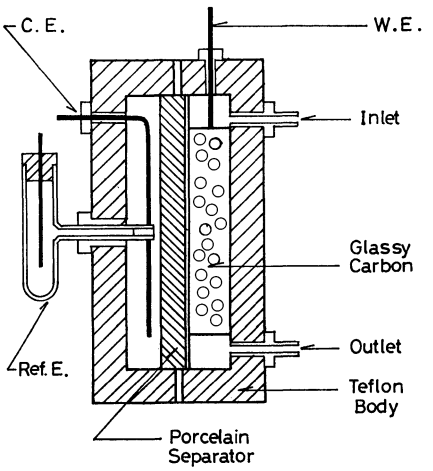

Fig. 1. Construction of flow-electrolysis cell.
(W. E.): Working electrode of carbon fibre, (C. E.): Pt wire counter electrode, and (Ref. E.): Ag/0.1 M $AgClO_4$ in acetonitrile (or DMF) reference electrode.

Apparatus. Figure 1 shows a vertical cross section of the column electrolysis cell made of a teflon body. Carbon fibres from Tokai Denkyoku Mfg. Co. Ltd., Nagoya were packed tightly and used as a working electrode. A platinum counter electrode and a reference electrode of Ag/0.1 M $AgClO_4$ in each solvent were used.

Figure 2 shows the block diagram of the flow cell system for ESR and absorption spectroscopic measurements. The parent quinone in the sample solution was electrolyzed immediately after flowing into the cell. Then electro-generated

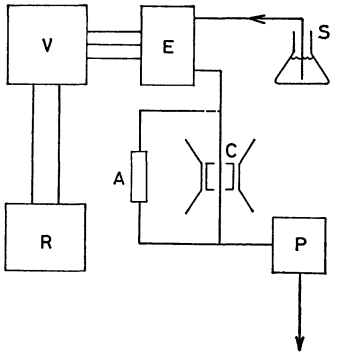

Fig. 2. Block diagram of flow system.
(E): Flow-electrolysis cell, (A): absorption cell, (C): ESR cavity, (S): sample reservoir, (V): potentiostat, (R): recorder, and (P): pump.

radical anion was sent into the cylindrical ESR cavity or the spectrophotometric flow-cell. The electrolysis current flowing through the cell was recorded by a National Pen Recorder Model VP 654-B. ESR spectra were measured with a JEOL JES-PE-3X, and the absorption spectra were measured with a Shimadzu UV 200 spectrophotometer. A PAR Model 174 Polarographic Analyzer was used for the measurements of polarograms. MO calculation was carried out by FACOM M-190 at the Data Processing Center of Kyoto University.

Results

Column Electrolysis and Absorption Spectroscopy. The fundamental examination of column electrolysis of β-NPQ were carried out by comparing the coulopotentiogram with its absorption spectrum. As a result, β-NPQ underwent two one-electron reductions in acetonitrile at glassy carbon electrode, and its electrolysis efficiency was 90—100% at the constant flow rate of 1.5 cm^3/min.

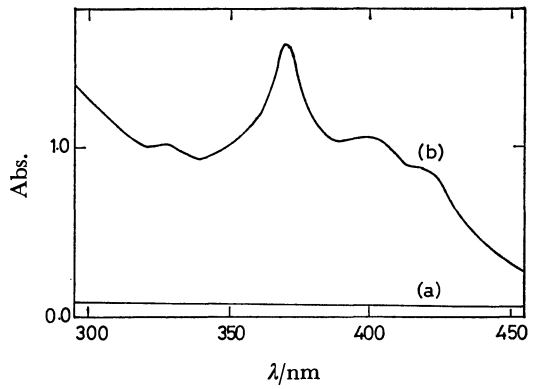

Fig. 3. UV absorption spectrum of β-$NPQ^{-\cdot}$ in acetonitrile with 0.1 M TEAP.
(a): Blank, and (b): 0.35 mM β-$NPQ^{-\cdot}$.

Figure 3 shows the absorption spectrum of electrogenerated β-$NPQ^{-\cdot}$ in acetonitrile with 0.1 M TEAP. The absorbance at 370 nm was proportional to the concentration of β-NPQ. By the addition of metal ion, the half-wave potentials of both waves shifted to more positive potentials owing to the ion pair formation effect. For the spectroscopic studies of ion pair formation of

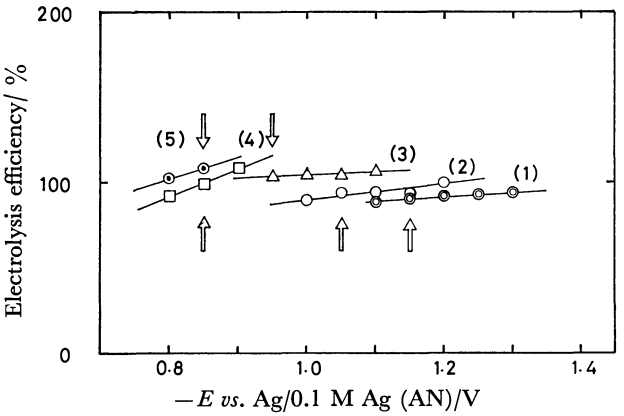

Fig. 4. Coulopotentiograms of β-$NPQ^{-\cdot}$ in acetonitrile with 0.1 M TEAP.
Concn of $LiClO_4$ in mM; (1): 0.0, (2): 0.06, (3): 0.15, (4): 0.3, and (5): 0.6.

monoanion radical, $M^+ \cdot$β-$NPQ^{-\cdot}$, the electrode potential was adjusted to maximize the absorption peak at 370 nm, which is inherent in the monoanion radical, β-$NPQ^{-\cdot}$. The same method was also adopted in ESR measurement.

Figure 4 illustrates the effect of lithium ions on the limiting current of the first wave, in which the arrow marks indicate the optimum potentials necessary to give the maximum intensity in the ESR spectra. As shown in the figure, the higher the lithium concentration, the narrower the available potential range to produce the monoanion radical alone became. With the addition of alkali metal, the absorption peak of β-$NPQ^{-\cdot}$ shifted to the shorter wave length, but within 10 nm.

ESR Spectroscopy. Figures 5-1 to 5-4 show the

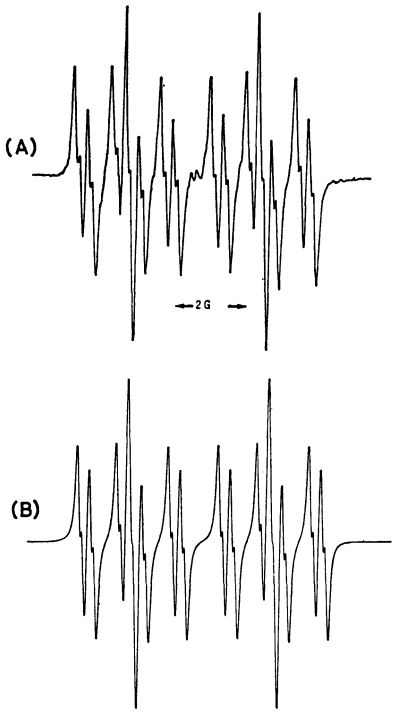

Fig. 5-1. Experimental (A) and simulated (B) ESR spectra of β-$NPQ^{-\cdot}$ in acetonitrile.
Concn of β-NPQ: 0.35 mM, 1 G=10^{-4} T.

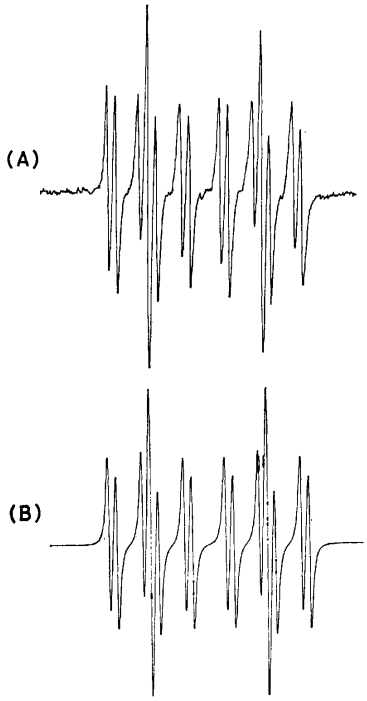

Fig. 5-2. Experimental (A) and simulated (B) ESR spectra of potassium ion pair in acetonitrile.
Concn of $KClO_4$: 3.0 mM.

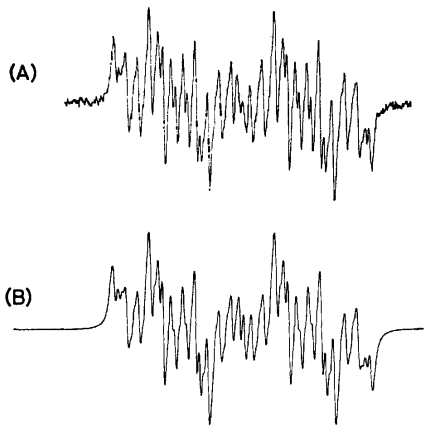

Fig. 5-3. Experimental (A) and simulated (B) ESR spectra of sodium ion pair in acetonitrile.
Concn of $NaClO_4$: 1.5 mM.

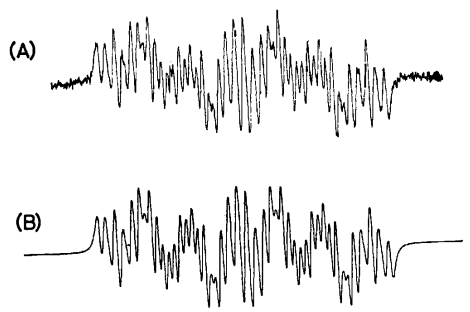

Fig. 5-4. Experimental (A) and simulated (B) ESR spectra of lithium ion pair in acetonitrile.
Concn of $LiClO_4$: 1.5 mM.

ESR spectra of β-$NPQ^{-\cdot}$ radical (5-1-A) and its potassium (5-2-A), sodium (5-3-A), and lithium (5-4-A) ion pairs together with their simulated spectra, from 5-1-B to 5-4-B, respectively. Good agreements were obtained between their observed spectra (A) and the corresponding simulated ones (B) within 20 mG (10^{-7} T). The fact that the spectrum of potassium ion pair (5-2-A) is similar to that of the free ion (5-1-A) suggests the weak association of β-NPQ radical anion with potassium cation. In the spectra of sodium and lithium ion pairs, however, each feature splits into four lines resulting from the coupling to ^{23}Na or ^{7}Li nuclei. The six ring-protons of the quinone are not equivalent, and these six proton hfs' are not all measurable. There were five protons with resolvable splittings for $Li^{+}\cdot\beta$-$NPQ^{-\cdot}$ and $Na^{+}\cdot\beta$-$NPQ^{-\cdot}$, whereas four for $K^{+}\cdot\beta$-$NPQ^{-\cdot}$.

When sodium or lithium perchlorate was added to the β-NPQ radical anion in acetonitrile, ESR signals due to both the free ion and its ion pair were observed simultaneously, as seen in Fig. 6-1-D. By the further addition of these cations, the intensity of the signal of the free anion was decreased, and only the spectrum of the ion pair was observed at the end. Figure 6-1-C shows the synthetic spectrum of β-$NPQ^{-\cdot}$ in the presence of 0.15 mM sodium ion, obtained by superimposing the simulated spectrum of the free ion (A) upon that of the sodium ion pair (B) on the assumption that the rate of the ion pair formation and dissociation of $Na^{+}\cdot\beta$-$NPQ^{-\cdot}$ is enough slow on the ESR time scale, *i.e.*, these two spectra can be simply superimposed upon each other.

In the case of the addition of potassium perchlorate, the ESR spectrum varied asymmetrically with respect

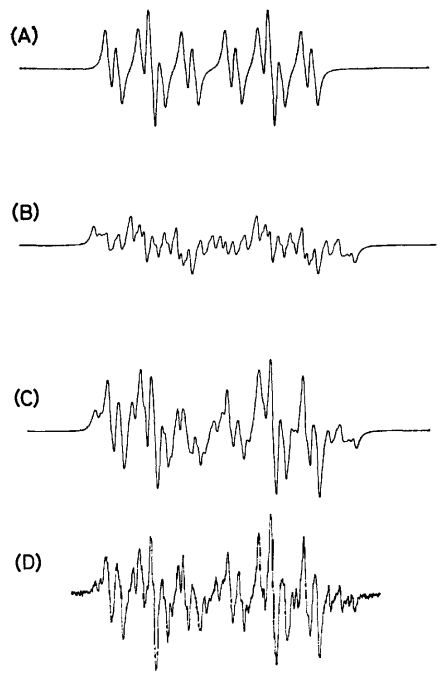

Fig. 6-1. Analysis of ESR spectrum of sodium ion pair. (A): Synthetic spectrum of free ion and (B): of sodium ion pair, (C): superimposed spectrum of (A) and (B), and (D): observed spectrum of sodium ion pair in the presence of 0.15 mM $NaClO_4$.

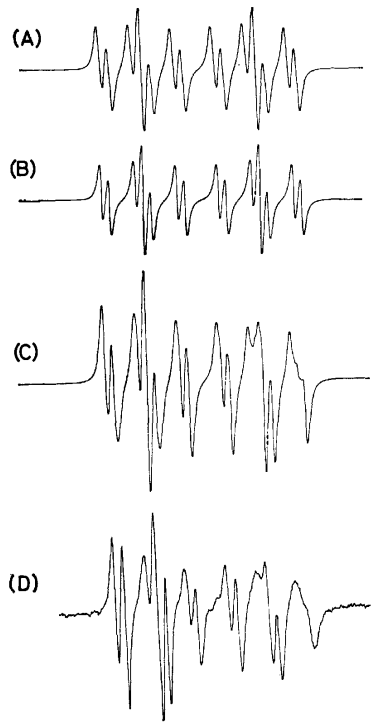

Fig. 6-2. Analysis of ESR spectrum of potassium ion pair. (A): Synthetic spectrum of free ion and (B): of potassium ion pair, (C): superimposed spectrum of (A) and (B), and (D): observed spectrum of potassium ion pair in the presence of 0.75 mM $KClO_4$.

to the line width. This asymmetry effect was most pronounced in the presence of about 0.75 mM potassium ions as seen in Fig. 6-2-D. This phenomenon suggests the coexistence of two radicals with slightly different coupling constants and *g*-values, *i.e.*, if the one having the smaller *g*-value possesses a larger coupling constant than the other, then the superposition of their ESR lines become loose at the region of high magnetic field. These two observed radicals were assigned to a free ion and an ion pair. Figure 6-2-C shows the synthetic spectrum of β-$NPQ^{-\cdot}$ in the presence of 0.75 mM potassium ion, obtained by the same method as in Fig. 6-1-C. Slight discordances were observed between the simulated (C) and observed (D) spectra owing to the line broadening at the region of high magnetic field. This fact suggests that the rate of the free ion–ion pair exchange kinetics of the potassium ion pair seems to be faster than those of the sodium and lithium ion pair, but still not to be so rapid as to give a time-averaged ESR spectrum.

MO Calculation. The proton hfs' in Table 1 were assigned by a HMO calculation adopting the McLachlan approximate configurational interaction. Table 2 summarizes the calculated results. The estimated value of the spin density of each carbon atom was very sensitive to given values of the coulomb integrals for two oxygen atoms (α_o). However, the spin density at position 6 defined in Fig. 7 was estimated still to be the largest even though the coulomb integral parameter (δ_o) was varied from 0.8 to 1.4. Therefore, the largest proton hfs constant in Table 1 is evidently assigned to the ring proton of position 6.

TABLE 1. PROTON HYPERFINE SPLITING CONSTANTS OF $M^+\cdot\beta$-$NPQ^{-\cdot}$ IN ACETONITRILE

Cation[a]	Proton hfsc (G)					Metal hfsc (G)
	a_6	a_5	a_7	a_9	a_{10}	a_M
TEA^+	4.05	1.49	1.12	0.34	0.11	0.00
K^+	4.16	1.49	1.20	0.29	≈0	≈0
Na^+	4.21	1.51	1.23	0.29	0.16	0.41
Li^+	4.43	1.57	1.40	0.24	0.35	0.59

a) Concentration of metal ions are 1.5 mM for lithium and sodium ion pairs and 3.0 mM for potassium ion pair.

TABLE 2. CALCULATED AND OBSERVED HYPERFINE SPLITTING CONSTANTS

Position	HMO[a]		Exptl[c]
	Spin density	$\lvert a_H\rvert$[b] (G)	$\lvert a_H\rvert$ (G)
5	−0.0584	1.36	1.49
6	0.1739	4.05	4.05
7	0.0313	0.73	1.12
8	0.0023	0.05	—
9	0.0239	0.56	0.34
10	0.0095	0.22	0.11

a) $\alpha_o=\alpha_c+\delta_o\cdot\beta(\delta_1=0.8,\ \delta_4=1.1)$, $\beta_{C=O}=\gamma_{C=O}\cdot\beta$ ($\gamma_{C=O}=0.8$). b) $Q=23.3$, $\lambda=1.2$. c) With 0.1 M TEAP in acetonitrile.

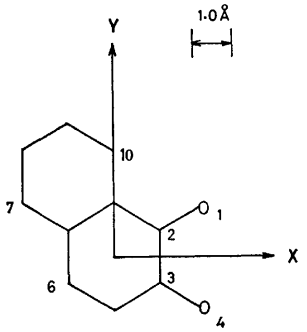

Fig. 7. Co-ordinate system for MO calculation of $M^+\cdot$ β-$NPQ^{-\cdot}$.
1 Å=10^{-10} m.

Variations of spin densities due to the ion pair formation can be discussed by means of the McClelland type MO calculation.[2,3,9] In this calculation, the effective Hamiltonian of the ion pair, H'_{eff} is defined by Eq. 1,

$$H'_{eff} = H_{eff} - \frac{Z\cdot e^2}{\varepsilon(r)\cdot r}, \qquad (1)$$

where, H_{eff} denotes the effective Hamiltonian in the absence of a cationic field, and $\varepsilon(r)$ is a screening factor introduced by Takeshita and Hirota[2] in order to explain the screening effect of solvent molecules on the anion. Figure 7 shows the co-ordinate system used in this calculation, in which a σ-type interaction was assumed and a positive point charge, $+e$ was approaching the anion along X-axis. Table 3 summarizes the results obtained by the use of this calculation, where $\varepsilon(r)$ was assumed to be constant, 10. The curves in Fig. 8 show the relationships between the calculated

Table 3. Variations of spin densities with the separation between cation and 1,2-naphtosemiquinone

Position	Å						
	∞	8.0	7.0	6.0	5.0	4.0	3.0
5	−0.0584	−0.0599	−0.0603	−0.0608	−0.0615	−0.0617	−0.0578
6	0.1739	0.1776	0.1789	0.1809	0.1844	0.1906	0.1995
7	0.0313	0.0337	0.0347	0.0362	0.0392	0.0455	0.0597
8	0.0023	0.0043	0.0049	0.0059	0.0077	0.0109	0.0162
9	0.0239	0.0231	0.0229	0.0226	0.0223	0.0221	0.0224
10	0.0095	0.0145	0.0162	0.0190	0.0240	0.0336	0.0521

$\varepsilon(r)=10.0$.

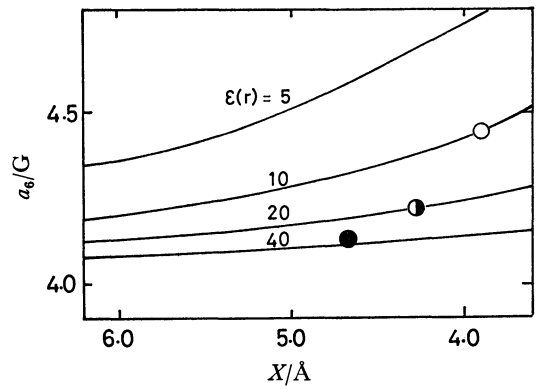

Fig. 8. Calculated and experimental proton hfs at position 6 as a function of interionic distance (X).
(○): Lithium, (◑): sodium and (●): potassium.

proton hfs at position 6 for each given value of $\varepsilon(r)$ and the interionic distance. In the figure, the experimental values are indicated by circles, the interionic distances of which were estimated on the assumption of a contact ion pair. From the results, it seems reasonable to consider $\varepsilon(r)$ for these ion pairs as an adjustable parameter being changed between 1 and the macroscopic dielectric constant of the solvent. This fact suggests the solvation tendency of acetonitrile toward these ion pairs. However, the quantitative discussions about $\varepsilon(r)$ are difficult owing to the rough approximation in the calculation.

Polarography. In acetonitrile, propylene carbonate, and DMF, β-NPQ undergoes two one-electron reductions corresponding to the formations of the stable monoanion and dianion. The polarographic characteristics for the reduction of the quinone are summarized in Table 4. The first wave was fairly reversible, but the second wave was less so in the solvents investigated, provided TEAP was used as the supporting electrolyte. When alkaline earth metals were used as the supporting electrolytes, both waves became less reversible than those with alkali metals. Both waves shifted to more positive potentials with increasing the concentration of the supporting electrolytes of metal salts, owing to their complex formation effects.

This potential shift was discussed according to Peover's method.[10] After the first one-electron reduction, the following complex formation equilibrium is assumed to be,

$$p\mathrm{M}^+ + \mathrm{Q}^{-\cdot} \overset{K}{\rightleftharpoons} \mathrm{M}_p\cdot\mathrm{Q}^{(p-1)+} \qquad (2)$$

Table 4. Polarographic data for the reduction of 1,2-naphtoquinone

Cation	$-E_{1/2}$ [b] / V	I_d / μA	Slope / mV	ΔE_p [c] / mV	I_c/I_a [d]
Acetonitrile					
Hex_4N^+	0.903	2.1	64	68	1.0
Pnt_4N^+	0.916	1.7	62	68	1.0
But_4N^+	0.903	1.9	61	70	1.0
Et_4N^+	0.908	1.9	60	68	1.0
Na^+	0.673	1.5	58	58	0.8
Li^+	0.492	1.7	54	82	0.5
Ba^{2+}	0.394	1.5	62	75	0.9
Mg^{2+}	0.083	2.0	77	85	1.3
Propylene carbonate					
Et_4N^+	1.323	0.62	64	68	1.0
Na^+	1.107	0.60	65	68	0.9
Li^+	0.985	0.60	83	75	0.6
N,N-Dimethylformamide					
Et_4N^+	0.955	1.60	63	73	1.1
K^+	0.886	1.65	65	68	1.3
Na^+	0.820	1.30	60	65	1.1
Li^+	0.758	1.30	60	68	1.0
Ba^{2+}	0.695	1.40	65	68	1.0
Sr^{2+}	0.650	1.68	62	88	≈1
Ca^{2+}	0.640	1.50	68	68	1.0
Mg^{2+}	0.576	1.20	76	190	1.0

a) Concn of β-NPQ: 0.35 mM in acetonitrile and propylene carbonate and 0.5 mM in DMF, concn of metal cation: 0.1 M. b) Potential was referred to Ag/0.1 M Ag^+ in each solvent. c) Potential difference between the anodic and cathodic peak of cyclic voltammmograms, sweep rate: 100 mV/s. d) Ratio of the cathodic (I_c) and anodic (I_a) peak current of cyclic voltammograms.

where, Q,$Q^{-\cdot}$ and $M_p\cdot Q^{(p-1)+}$ represent 1,2-naphthoquinone, its anion radical and ion pair, respectively, and p is a coordination number. The association constant K is given by Eq. 3,

$$K = \frac{[\mathrm{M}_p\cdot\mathrm{Q}^{(p-1)+}]}{[\mathrm{M}^+]^p\cdot[\mathrm{Q}^{-\cdot}]}. \qquad (3)$$

The shift of the half-wave potential, $\Delta E_{1/2}$ due to ion pair formation is given by Eq. 4,

$$\Delta E_{1/2} = -\frac{RT}{F}\ln\frac{[\mathrm{Q}^{-\cdot}]^\circ}{1/2[\mathrm{Q}]}, \qquad (4)$$

where $[Q^{-\cdot}]^\circ$ is the concentration of semiquinone at the electrode surface. When metal ions are in large excess,

$$\Delta E_{1/2} = \frac{RT}{F} \ln K + \frac{RT}{F} p \cdot \ln C_{M^+}. \quad (5)$$

A coordination number and an association constant are simply evaluated from the slope and intercept in the plot of the half-wave potential of β-NPQ *vs.* the logarithm of the concentration of metal ions, C_{M^+} as shown in Fig. 9.

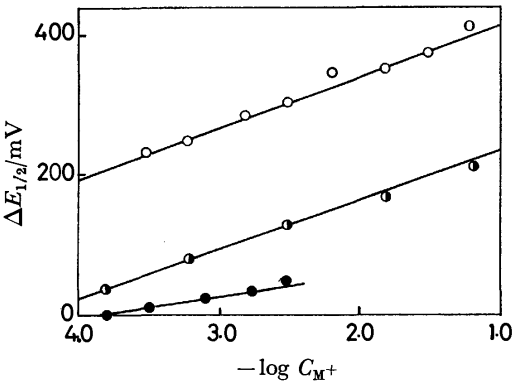

Fig. 9. Relationships between half-wave potentials of β-NPQ and concentrations of alkali metals.
Slopes in mV; 70 for Li^+ (○), 70 for Na^+ (◑) and 33 for K^+ (●).

Equation 5, however, cannot be used when a low soluble salt, *i.e.*, potassium perchlorate, is added in acetonitrile or when the coordination number varies at the low concentration of counterions. In these cases, the tentative association constant obtained from Eqs. 3 and 4, was converged by fitting p value so as to allow K to be nearly constant. This method could offer reliable association constants and coordination numbers even at a low concentration of counterions. These results are summarized in Table 5.

Table 5. Dependence of association constants of $M_p^{\ddagger} \cdot$β-NPQ$^{-\cdot}$ on metal concentrations
0.35 mM β-NPQ in acetonitrile with 0.1 M TEAP.

Concentration (mM)	log K		
	Li^+	Na^+	K^+
0.150		4.62	
0.300	8.15		3.19
0.600	7.88	4.38	
0.750			3.18
1.50	7.99		3.17
3.00	7.97	4.49	3.18
15.0	7.99	4.52	
30.0	8.00		
60.0		4.66	
Coordination number	1.10	0.90	0.93

Discussion

The ion pair formation effects of supporting electrolyte cations with β-NPQ$^{-\cdot}$ were observed to be in the order of $TEAP^+ < K^+ < Na^+ < Li^+ < Ba^{2+} < Sr^{2+} < Ca^{2+} < Mg^{2+}$ as shown in Tables 1 and 4. The observed changes of proton hfs of ESR spectra in acetonitrile were somewhat larger than those in 1,2-dimethoxyethane (DME) reported by Warhurst *et al.*[1] This distinction between these two solvents is explained by the fact that the solvation of acetonitrile toward the ion pair is not more significant than DME as expected from their donor number; 14 for acetonitrile and 24 for DME. An unusual tendency of β-NPQ$^{-\cdot}$ for the coupling to metal nuclei also appeared in acetonitrile as well as in DME. This fact suggests the strong tendency of β-NPQ$^{-\cdot}$ toward ion pair formation, because it is not generally observed in these polar solvents. The variation of the coupling constants of ESR spectra are qualitatively well explained using a McClelland-type MO calculation. Table 3 shows a slight decrease in the spin density at position 9 but little increase at the other positions when a positive point charge approaches the β-NPQ anion along X-axis as illustrated in Fig. 7.

Polarography provides also much helpful information about the ion association equilibrium. Table 5 indicates that the association constants and the coordination numbers can be looked upon as being constant over the experimental concentration range of counterions. Therefore, it can be concluded that 1: 1 type of ion pair is formed predominately between K^+ and β-NPQ$^{-\cdot}$, though 1: 2 association may be expected from the slope of the plot in Fig. 9. The association constant for the potassium ion pair ought to be sufficiently accurate judging from a good accordance between the results obtained in polarography and ESR. As mentioned previously, the observed ESR spectrum is most asymmetric in the presence of 0.75 mM potassium ion, in which the signal intensities due to both the free ion and ion pair become almost equivalent. It is ascertained by calculation that the concentration ratio of free ion to ion pair is closed to unity in the presence of 0.75 mM potassium ion.

The relationships between the half-wave potentials and the effective ionic potentials $[\phi = Z/(r_c + S)]$[11,12] give straight lines with positive slopes as shown in Fig. 10. Though it is known that the ion pair with a contact structure gives a positive slope in this relation, a few comments will be needed here. Ion pairs may not always be in a form either solvent separated or contact, but may be intermediate between them. In this figure, the steeper slope for acetonitrile than DMF shows clearly that the association energy in acetonitrile is fairly large when compared to that in DMF, and moreover the solvation of the ion pair is more remarkable in DMF than in acetonitrile. As a result, the interionic distance between the cation and β-NPQ$^{-\cdot}$ anion may be larger in DMF than in acetonitrile. In this case, solvent molecules seem to act as pegs to separate the ion pair. In this study, the solvent effects on the half-wave potentials can be explained in terms of the difference in the solvation energies of these cations, because the solvation tendencies of DMF and acetonitrile to anions are almost equivalent.

The effect of the ionic size of the cation on the ion pair formation tendency will be discussed next. Simple MO calculations lead to the conclusion that the larger

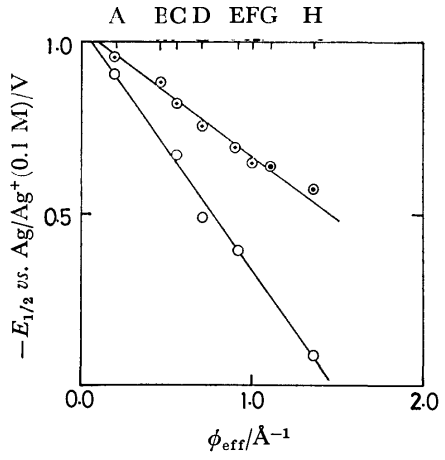

Fig. 10. Relationships between half-wave potentials of β-NPQ and effective ionic potentials of counterions.
(○): Acetonitrile, (⊙): DMF, correction parameter, S=0.8, (A): TEA$^+$, (B): K$^+$, (C): Na$^+$, (D): Li$^+$, (E): Ba^{2+}, (F): Sr^{2+}, (G): Ca^{2+}, (H): Mg^{2+}.

the radius of the counterion, the stronger the solvation of the ion pair become. That is to say, the structure of the potassium ion pair is looser than that of the lithium ion pair. As a result, the interionic distance of the potassium ion pair may be somewhat larger in fact than that given in Fig. 8. The structure of the potassium ion pair, however, is not a typical form of the solvent separated one, considering the contact structures of the ion pairs with sodium and lithium ions which have larger solvation energies than potassium.

The screening effects of the solvent molecules also seem to play an important role in this study. Toshima *et al.*[13] assume the $\varepsilon(r)$ value for the ion pair of nitrobenzene anion with alkali metal cations in DMF to be of the same order as the macroscopic dielectric constant of the solvent. In the ion pair considered here, however, $\varepsilon(r)$ should be regarded as an adjustable parameter.

It can be concluded that the smaller the ionic size of the counterion, the weaker the solvent separation of ion pairs becomes, *i.e.*, a so called contact ion pair is formed, and moreover the tendency of separation is dependent on the nature of the solvent used.

Recently, Chauhan *et al.*[14] reported on the weak association between nitromesitylene anion and tetraalkylammonium cation with the association constant of *ca.* 35. However, no complex formation effect of TEA$^+$ on the ESR spectrum of β-NPQ$^{-\cdot}$ was observed over the concentration range of TEAP from 10^{-4} M to 10^{-1} M.

It is also a great advantage of the column electrolysis that the electrolysis can be performed quantitatively even in the solution with a low concentration such as 10^{-4} M of the supporting electrolyte.

The present work was partially supported by a Grant-in-Aid for Scientific Research, No. 243010 from the Ministry of Education, Science and Culture.

References

1) E. Warhurst and A. M. Wilde, *Trans. Faraday Soc.*, **65**, 1413 (1969).
2) T. Takeshita and N. Hirota, *J. Am. Chem. Soc.*, **93**, 55 (1971).
3) "Ions and Ion Pairs in Organic Reactions," ed by M. Szwarc, John Weily and Sons, New York (1972), Vol. 1.
4) T. Fujinaga, Y. Deguchi, and K. Umemoto, *Bull. Chem. Soc. Jpn.*, **37**, 822 (1964).
5) T. Fujinaga, Y. Deguchi, and K. Umemoto, *Bull. Chem. Soc. Jpn.*, **46**, 2716 (1973).
6) T. Fujinaga, K. Izutsu, and T. Nomura, *J. Electroanal. Chem.*, **29**, 203 (1971).
7) J. S. Jaworski and M. K. Kalinowski, *J. Electroanal. Chem.*, **76**, 301 (1977).
8) T. Fujinaga, S. Okazaki, and T. Yamada, *Chem. Lett.*, **1972**, 836.
9) B. J. McClelland, *Trans. Faraday Soc.*, **57**, 1458 (1961).
10) M. E. Peover and J. D. Davies, *J. Electroanal. Chem.* **6**, 46 (1963).
11) M. K. Kalinowski, *Chem. Phys. Lett.*, **7**, 55 (1971).
12) T. M. Krygowski, M. Lipsztajn, and Z. Galus, *J. Electroanal. Chem.* **42**, 261 (1973).
13) S. Toshima, and K. Itaya, *Bull. Chem. Soc. Jpn.*, **49**, 957 (1976).
14) B. G. Chauhan, W. R. Fawcett, and A. Lasia, *J. Phys. Chem.*, **81**, 1476 (1977).

Non-covalent Interactions in Metal Complexes. II.[1] Induction of Asymmetry in Cobalt(III) Complexes with Amino Acid-Schiff Bases. Importance of CH···π-Interaction in Determining Configuration of Complexes

Hisashi Okawa,* Yoshihiko Numata, Ayako Mio, and Sigeo Kida
Department of Chemistry, Faculty of Science, Kyushu University, Hakozaki, Higashi-ku, Fukuoka 812
(Received December 20, 1979)

Cobalt(III) complexes, $[Co(l\text{-mop=aa})_2]^-$ and $[Co(cop=aa)_2]^-$ (aa=ala$^-$, val$^-$, leu$^-$, phe$^-$), where $H_2(l\text{-mop=aa})$ and $H_2(cop=aa)$ denote amino acid–Schiff bases of *l*-menthyl 3-(*o*-hydroxybenzoyl)propionate and cholesteryl 3-(*o*-hydroxybenzoyl)propionate, respectively, were prepared in solution. The intensity of the CD peak induced at 520 nm changes with the solvent used for preparation of the complex, decreasing in the order: ethanol, methanol, dimethyl sulfoxide, *N*,*N*-dimethylformamide and acetonitrile. Since the order corresponds to the increasing order of the CH..π-interaction between the solvent and benzene, it seems that the CH..π-interaction between the chiral group and the aromatic nucleus in the ligand plays an important role in determining the configuration of the complexes.

Asymmetric transformation of racemic amino acids into an optical isomer by the use of metal complexes is important in amino acid industry and of interest in connection with the model of transamination reaction in the biological system. Amino acid coordinated to an optically active cobalt(III) complex is epimerized in alkaline solution, whereby D- or L-amino acid is produced in excess in equilibrium.[2,3] Activation of the hydrogen at the α-carbon of amino acid coordinated to a metal is attained only under high pH conditions. On the other hand, when an amino acid is incorporated into the ligand system of a complex by Schiff base formation, the hydrogen at the α-carbon atom is easily labilized in the physiological pH range, an optical amino acid being isomerized.[4-6] This is thought to be a racemase model in the biological system. If a complex with amino acid–Schiff base is formed in an asymmetric environment, DL-amino acids might be transformed into an optical isomer. This type of reaction should operate in the transamination reaction of vitamine B_6.[7] However, only a few studies have been reported on asymmetric transformation of racemic amino acid into an optical isomer by the use of Schiff base complex.[1,8,9]

It was found that in the cobalt(III) complexes, $[Co(l\text{-mop=aa})_2]^-$ (Fig. 1a), with the Schiff base obtained from *l*-menthyl 3-(*o*-hydroxybenzoyl)propionate and DL-amino acid, asymmetry around the metal is induced and DL-amino acids are partially transformed into an optical isomer.[1] The *l*-menthyl group on the side chain exerts a vicinal effect but not a Pfeiffer effect on determining the configuration of the complex, since the group no longer affects the asymmetry induction when it is detached from the ligand. However, the origin of the vicinal effect has not been clarified yet. We intended to elucidate how the *l*-menthylg roup causes the asymmetry around the metal. For this purpose new cobalt(III) complexes, $[Co(cop=aa)_2]^-$, with the amino acid–Schiff bases of cholesteryl 3-(*o*-hydroxybenzoyl)propionate were also prepared in solutions (Fig. 1b) and the effect of the cholesteryl group on the asymmetry induction was examined.

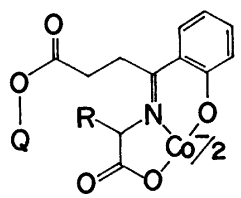

Fig. 1.
(a) Q=*l*-menthyl
(b) Q=cholesteryl

Experimental

Preparation. 3-(*o*-Hydroxybenzoyl)propionic acid was synthesized by the method of Fieser *et al.*[10] Synthesis of *l*-menthyl 3-(*o*-hydroxybenzoyl)propionate (H(*l*-mop)) was described in the preceding paper.[1]

Cholesteryl 3-(o-Hydroxybenzoyl)propionate (Hcop). 3-(*o*-Hydroxybenzoyl)propionic acid (7.2 g) and cholesterol (14.3 g) were dissolved in benzene (100 cm^3). To this was added a drop of concd sulfuric acid and the mixture was refluxed for 48 h. During the course of this reaction, water formed by esterification was eliminated as a benzene azeotrope. The solvent was evaporated and the pale brown precipitate obtained was recrystallized twice from a ethanol–benzene mixture to give colorless needles melting at 160—161 °C.

Found: C, 79.30; H, 9.81%. Calcd for $C_{37}H_{52}O_4$: C, 78.96; H, 9.67%.

Cobalt(III) Complexes. Preparation of the solutions of $[Co(l\text{-mop=aa})_2]^-$ is as follows. Racemic amino acid (5×10^{-4} mol), H(*l*-mop) (5×10^{-4} mol), cobalt(II) acetate tetrahydrate (2.5×10^{-4} mol) and triethylamine (*ca.* 60 mg) were placed in a 50 cm^3 volumemetric flask and the volume was adjusted with a solvent (ethanol, methanol, dimethyl sulfoxide, *N*,*N*-dimethylformamide, or acetonitrile). Synthesis of $[Co(cop=aa)_2]^-$ is nearly the same as that of $[Co(l\text{-mop=aa})_2]^-$ except for using a 1: 1 mixture of a solvent and carbon tetrachloride, because of low solubility of Hcop in ethanol and so on. Clear red solutions were obtained after 2 or 3 d.

Measurements. Electronic spectra and circular dichroism spectra were measured with a Shimazu multipurpose spectrophotometer Model MSP-5000 and a JASCO ORD/CD optical dispersion recorder, respectively. NMR spectra were measured with a Hitachi NMR spectrophotometer Model R-20-B in carbon tetrachloride and in benzene using tetramethylsilane as an internal standard.

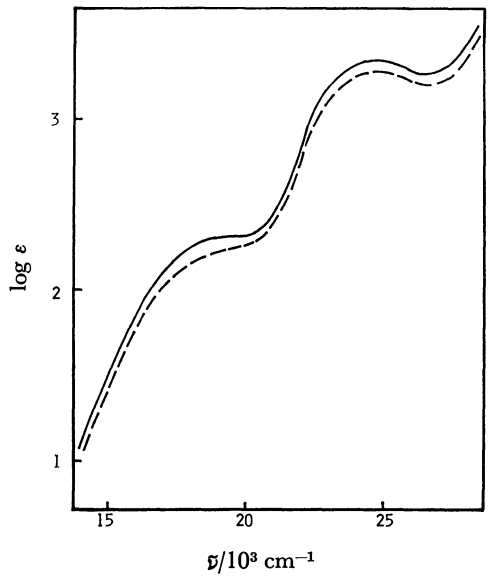

Fig. 2. Electronic spectra of (——) $[Co(l\text{-mop=ala})_2]^-$ (in methanol) and (– – –) $[Co(cop=ala)_2]^-$ (in methanol–carbon tetrachloride).

Results and Discussion

Electronic spectra of $[Co(l\text{-mop=aa})_2]^-$ and $[Co(cop=aa)_2]^-$ are similar to each other. Typical examples are shown in Fig. 2. Two absorption bands appeared near 19000 and 24500 cm^{-1}, whose extinction coefficients gradually increased and converged after 120 h to *ca.* 200 and 1500 $mol^{-1}\,dm^3\,cm^{-1}$, respectively. The frequencies and the extinction coefficients of these bands are almost independent of the amino acid and the solvent used for preparation of the complex. Although we were not successful in isolating the complexes, it seems reasonable to formulate the complexes as $[Co(l\text{-mop=aa})_2]^-$ and $[Co(cop=aa)_2]^-$.

CD spectra of $[Co(l\text{-mop=ala})_2]^-$ prepared in methanol and $[Co(cop=ala)_2]^-$ prepared in methanol–carbon tetrachloride (1 : 1) are given in Figs. 3 and 4,

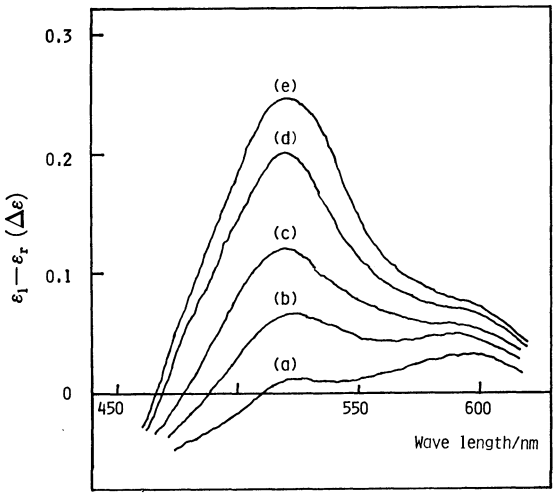

Fig. 3. CD spectra of $[Co(l\text{-mop=ala})_2]^-$ (in methanol) at various reaction times.
(a) 20, (b) 43, (c) 63, (d) 113, and (e) 230 h.

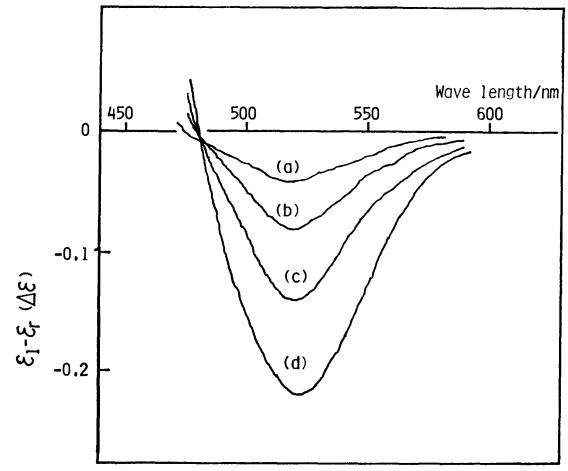

Fig. 4. CD spectra of $[Co(cop=ala)_2]^-$ (in methanol–carbon tetrachloride) at various reaction times.
(a) 20, (b) 60, (c) 120, and (d) 240 h.

respectively. In the spectrum of $[Co(l\text{-mop=ala})_2]^-$ a positive CD peak appeared near 520 nm, whose intensity gradually increased and converged after *ca.* 240 h. Similar CD spectra were observed for $[Co(l\text{-mop=val})_2]^-$ and $[Co(l\text{-mop=leu})_2]^-$. On the other hand, a negative CD peak was induced in $[Co(cop=ala)_2]^-$. A negative CD peak was also induced in $[Co(cop=val)_2]^-$ and $[Co(cop=leu)_2]^-$ prepared in methanol–carbon tetrachloride. It is likely that the cholesteryl group exerts an opposite vicinal effect to the *l*-menthyl group. Appearance of the CD band in the visible region indicates that an asymmetry around the metal is induced. We presumed that *l*-mop=aa^{2-} facially coordinates to the cobalt(III) ion form the view of Burrows and Bailar, Jr.,[11] that the *fac*-form is more stable than the *mer*-form. Belokon *et al.*[12] determined the structure of an optically active form (*Λ*(*SS*)) of potassium bis[*N*-(3-methylsalicylidene)threoninato]-cobaltate(III) and showed that the Schiff base meridionally coordinates to the metal. $[Co(l\text{-mop=aa})_2]^-$ and $[Co(cop=aa)_2]^-$ are thus presumed to also possess a *mer*-configuration. One set of optical isomers (*Δ* and *Λ*) is considered for these complexes. It seems that an isomer showing a positive CD peak at 520 nm is formed in excess for $[Co(l\text{-mop=aa})_2]^-$, while an isomer showing a negative CD peak at 520 nm for $[Co(cop=aa)_2]^-$, owing to the effect of the chiral group on the side chain.

On the basis of the Dreiding model, it is unlikely that the chiral group in the present complexes exerts any steric hindrance to the complex formation. In fact, no CD peak was detected for the copper(II) and the nickel(II) complexes with $H_2(l\text{-mop=aa})$ and $H_2(cop=aa)$. A hydrophobic interaction between the chiral group and the group attached to the α-carbon of the amino acid can not be the main effect, since the CD peak was induced in $[Co(l\text{-mop=gly})_2]^-$.[1] Thus, it is most probable that some non-covalent interaction between the chiral group and some part of the molecule or an asymmetric packing effect of the chiral group in the cavity of the molecule[13] causes the asymmetry around the metal.

Table 1. Intensities ($\Delta\varepsilon$) of CD band induced at 520 nm

	EtOH	MeOH	DMSO	DMF	AN
$[Co(l\text{-mop=ala})_2]^-$	0.40	0.24	0.14	0.12	0
$[Co(l\text{-mop=val})_2]^-$	0.21	0.20	0.06	0.05	0
$[Co(l\text{-mop=leu})_2]^-$	0.24	0.18	0.09	0.07	0
$[Co(l\text{-mop=phe})^2]^-$	0	0	0	0	0
$[Co(cop=ala)_2]^-$	−0.22	−0.11	0	0	0
$[Co(cop=val)_2]^-$	−0.04	−0.03	0	0	0
$[Co(cop=leu)_2]^-$	−0.03	−0.02	0	0	0
$[Co(cop=phe)_2]^-$	0	0	0	0	0

$[Co(cop=aa)_2]^-$ was prepared in a 1:1 mixture of a solvent and carbon tetrachloride. EtOH=ethanol, MeOH=methanol, DMSO=dimethyl sulfoxide, DMF=*N,N*-dimethylformamide, and AN=acetonitrile.

In order to elucidate the CD induction in the complexes, the complexes were prepared in various solvents (1:1 mixture of a solvent and CCl_4 in the case of $[Co(cop=aa)_2]^-$) and their CD spectra were compared. Despite the resemblance of absorption spectra of the complexes, the CD spectrum depends a great deal on the solvent used for preparation of the complex. CD intensities induced at 520 nm are summarized in Table 1. We see that the CD intensity of $[Co(l\text{-mop=aa})_2]^-$ except for $[Co(l\text{-mop=phe})_2]^-$ decreases in the order ethanol, methanol, dimethyl sulfoxide, *N,N*-dimethylformamide. No CD peak was induced in acetonitrile. On the other hand, the absolute CD intensity of $[Co(cop=aa)_2]^-$ except for $[Co(cop=phe)_2]^-$ decreases in the order: ethanol and methanol. No CD peak was induced in dimethyl sulfoxide, *N,N*-dimethylformamide and acetonitrile. Thus, the order of solvents in inducing the asymmetry around the metal is as follows: ethanol>methanol>dimethyl sulfoxide>*N,N*-dimethylformamide>acetonitrile. The solvent dependence of CD intensity indicates that the vicinal effect of the chiral group is greatly affected by the character of solvent. However, the order mentioned above can not be correlated with any property of solvent such as dielectric constant or dipole moment. From the fact that no CD induction takes place in $[Co(l\text{-mop=phe})_2]^-$ and $[Co(cop=phe)_2]^-$ even in ethanol, we presume that a certain interaction operates between the chiral group and the aromatic nucleus of the ligand. For the sake of confirmation, proton NMR spectra of ethanol, methanol, dimethyl sulfoxide, *N,N*-dimethylformamide and acetonitrile were measured in carbon tetrachloride and in benzene, and the chemical shifts of methyl proton were compared. The results are given in Table 2. Proton NMR signals are always observed at higher field in benzene as compared with in carbon tetrachloride. This can be interpreted in terms of the CH..π-interaction[14] between the methyl proton and benzene. As a measure of the CH..π-interaction we adopted the difference in methyl proton chemical shift between in carbon tetrachloride and in benzene ($\Delta\delta=\delta(CCl_4)-\delta(Bz)$). The small $\Delta\delta$ values of ethanol and methanol indicate that these molecules weakly interact with the aromatic nucleus. The $\Delta\delta$ values of dimethyl sulfoxide, *N,N*-dimethylformamide and acetonitrile are considerably large, indicating a strong CH..π-interaction with the aromatic nucleus. When we adopt the mean of the $\Delta\delta$ values for two inequivalent methyl groups of *N,N*-dimethylformamide, the increasing order in $\Delta\delta$ value (increasing order of the CH..π-interaction) of solvents is as follows: ethanol<methanol<dimethyl sulfoxide<*N,N*-dimethylformamide<acetonitrile. The decreasing order of the induced CD intensity agrees with the increasing order of the CH..π-interaction of solvents utilized for preparation of the complexes. A typical example of this correlation is given for $[Co(l\text{-mop=val})_2]^-$ in Fig. 5. It is likely that the chiral group at the side chain interacts with the aromatic nucleus of the ligand in ethanol or methanol, the CH..π-interaction causing the asymmetry of the configuration of the complex. On the other hand, in dimethyl sulfoxide, *N,N*-dimethylformamide or acetonitrile the CH..π-interaction between the solvent and the aromatic ring of the ligand is strong enough to supress the CH..π-interaction between the chiral group and the aromatic nucleus. $[Co(l\text{-mop=ala})_2]^-$ prepared in a chloroform-methanol (8:2) mixture showed a weak CD peak ($\Delta\varepsilon=0.113$) as compared with the complex prepared in methanol. This can be attributed to the fact that the CH..π-interaction between chloroform and benzene is so strong ($\Delta\delta=1.0$) as to reduce the CH..π-interaction between the chiral group and the aromatic nucleus of the ligand. The CD intensity induced in $[Co(cop=aa)_2]^-$ is much weaker than that induced in $[Co(l\text{-mop=aa})_2]^-$. It seems that the cholesteryl group is

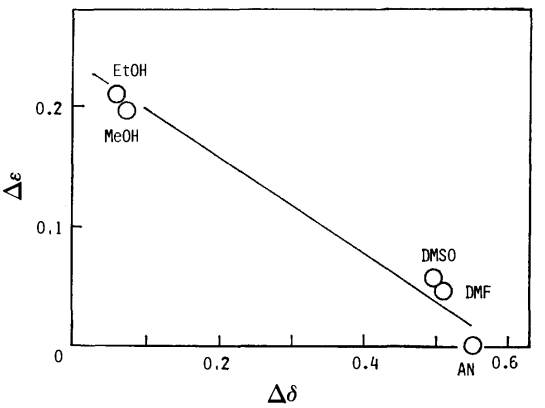

Fig. 5. Correlation between induced CD intensity ($\Delta\varepsilon$) and CH···π-interaction ($\Delta\delta$) of solvents used for preparation of $[Co(l\text{-mop=val})_2]^-$.

Table 2. Chemical shifts (ppm) of methyl proton of solvents in benzene and in carbon tetrachloride

	$\delta(CCl_4)$	δ(Bz)	$\Delta\delta$[a]
EtOH	1.20	1.14	0.06
MeOH	3.36	3.29	0.07
DMSO	2.52	2.02	0.50
DMF	2.96 2.82	2.51 2.25	0.51[b]
AN	1.96	1.41	0.55

a) $\Delta\delta=\delta(CCl_4)-\delta(Bz)$. b) Average value.

less effective than the *l*-menthyl group for introducing the asymmetry around the metal. So far we can not explain why no asymmetry was induced in $[Co(l\text{-}mop{=}phe)_2]^-$ and $[Co(cop{=}phe)_2]^-$. However, it is likely that the chiral group interacts with the phenylalanine nucleus rather than the phenolic nucleus, the interaction exerting no marked effect on asymmetry induction around the metal ions.

The authors are grateful to Assoc. Prof. T. Inazu and Dr. T. Shinmyozu for the measurement of NMR spectra and valuable discussions. The work was carried out with a Grant-in-Aid from the Ministry of Education for Scientific Research.

References

1) Part I: Y. Numata, H. Okawa, and S. Kida, *Chem. Lett.*, **1979**, 293.
2) D. A. Buckingham, L. G. Marzilli, and A. M. Sargeson, *J. Am. Chem. Soc.*, **89**, 5133 (1967).
3) S. Yoshikawa, M. Saburi, and M. Yamaguchi, *Pure Appl. Chem.*, **50**, 915 (1978).
4) P. Pfeiffer, W. Offermann, and H. Werner, *J. Prakt. Chem.*, **159**, 313 (1942).
5) K. Toi, Y. Izumi, and S. Akabori, *Bull. Chem. Soc. Jpn.*, **35**, 1422 (1962).
6) D. E. Metzler, M. Ikawa, and E. E. Snell, *J. Am. Chem. Soc.*, **76**, 648 (1954).
7) R. H. Holm, "Inorganic Biochemistry," ed by G. L. Eichhorn, Elsevier Scientific Publishing Co., New York (1973), Vol. 2, p. 1165.
8) H. Kuzuhara, T. Komatsu, and S. Emoto, *Tetrahedron Lett.*, **38**, 3563 (1978).
9) Yu. N. Belokon, I. E. Zel'tzer, N. M. Loim, V. A. Tsiryapkin, Z. N. Parnes, D. N. Kursanov, and V. M. Belikov, *J. Chem. Soc., Chem. Commun.*, **1979**, 789.
10) L. F. Fieser, M. D. Gates, Jr., and G. W. Kilmer, *J. Am. Chem. Soc.*, **62**, 2966 (1940).
11) R. C. Burrows and J. C. Bailar, Jr., *J. Am. Chem Soc.*, **88**, 4150 (1966).
12) Yu. N. Belokon, V. M. Belikov, S. V. Vitt, T. F. Savel'eva, V. M. Burbelo, V. I. Bakhmutov, G. G. Aleksandrov, and Yu. T. Struchkov, *Tetrahedron*, **33**, 2551 (1977).
13) B. Bosnich and D. W. Watts, *Inorg. Chem.*, **14**, 47 (1975).
14) M. Nishio, *Kagaku No Ryoiki*, **31**, 92 (1977).

Thermochromism of Metal Chelates with Triphenylmethane Complexons in Aqueous Solutions. III. Copper(II)–Methylthymol Blue and -Methylxylenol Blue Systems†

Shoji NAKADA, Mutsuo YAMADA, Tasuku ITO,†† and Masatoshi FUJIMOTO*

Department of Chemistry, Faculty of Science, Hokkaido University, Sapporo 060

(Received December 20, 1979)

Reversible thermochromisms of copper(II) complexes with 3,3′-bis[bis(carboxymethyl)aminomethyl]thymolsulfonphthalein (Methylthymol Blue; MTB) and 3,3′-bis[bis(carboxymethyl)aminomethyl]-*p*-xylenolsulfonphthalein (Methylxylenol Blue; MXB) were studied in aqueous solutions. The thermochromisms of these complexes were primarily ascribed to the temperature-dependence of the protolytic equilibria between a complex species AH having an uncoordinated free phenolic hydroxyl group and a complex species A having a coordinated phenolate group: $AH \rightleftarrows A + H$. The equilibrium constants K of the reactions at 25 °C were determined to be $p(K/\text{mol dm}^{-3}) = 4.66$ for Cu(II)–MTB and 4.78 for Cu(II)–MXB. The thermodynamic parameters ΔH and ΔS for the reactions were calculated to be 26 ± 2 kJ mol^{-1} and -6 ± 3 J K^{-1} mol^{-1} (298 K) for both complexes, respectively. The rate constants of the proton dissociation of the phenolic hydroxyl group in the complexes AH were estimated to be 1.6×10^5 and 1.8×10^5 s^{-1} for Cu(II)–MTB and Cu(II)–MXB, respectively. The thermodynamic and kinetic data are discussed in terms of the effects of the substituents in the ligand molecules on the thermochromism.

The complexes of the multidentate ligands of the triphenylmethane complexons with various bivalent metal ions were found to be thermochromic in aqueous media.[1] In the previous papers, the thermochromism observed for the Cu(II)–Xylenol Orange (XO) system was interpreted in terms of the temperature-dependence of a protolytic equilibrium between a complex species AH having an uncoordinated free phenolic hydroxyl group and a complex species A having a coordinated phenolate group:

$$AH \rightleftarrows A + H.^{1)} \quad (1)$$

In the present paper we study the thermochromisms observed for the Cu(II) complexes of the similar ligands MTB and MXB by means of a spectrophotometric and a temperature-jump method. The data obtained for the thermochromisms of Cu(II) complexes of the ligands will be compared with that for the Cu(II)–XO system in relation to the differences in alkyl substituents in the ligand molecules (see Fig. 1).

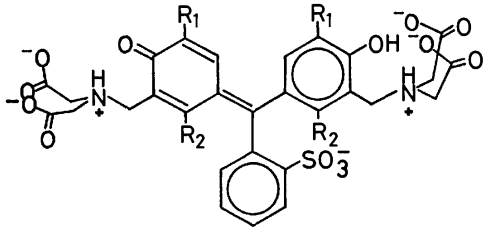

MTB : $R_1 = CH(CH_3)_2$, $R_2 = CH_3$

MXB : $R_1 = CH_3$, $R_2 = CH_3$

XO : $R_1 = CH_3$, $R_2 = H$

Fig. 1. The structural formulae of the ligands.

† Presented in part at the 29th Annual Meeting on Coordination Chemistry, Hamamatsu, October 1, 1979, Abstracts, p. 82.

†† Present address: Institute for Molecular Science, Okazaki 444.

Experimental

Materials. All chemicals used were of analytical grade, unless otherwise specified. Water was deionized and distilled.

Methylthymol Blue and Methylxylenol Blue were synthesized by Mannich condensation from Thymol Blue or *p*-Xylenol Blue, iminodiacetic acid (IDA), and formaldehyde, respectively.[2] The crude samples of the synthesized MTB and MXB purified beforehand by means of cellulose column chromatography were finally purified by means of high-performance liquid chromatography as in the case of XO.[3] The purity of the specimens of the ligands was confirmed by elemental analyses and melting point measurements. The purified ligands were used as a free acid form. Stock solutions of the ligands (1.0×10^{-3} mol dm^{-3}) were prepared by dissolving a desired amount of MTB and MXB in water. It should particularly be emphasized that for the quantitative studies the use of the highly purified specimens of the ligands was essential. In the pH range above 8.8, the color of the solutions of the ligands faded within one or two days because of the decomposition, whereas the solutions of the ligands were very stable in the acidic media.

Copper(II) perchlorate and sodium perchlorate were prepared and purified as described previously.[1] Acetate and phosphate buffer solutions were used for the Cu(II) complexes and the free ligands, respectively.

Measurements. The equilibria were measured with Hitachi recording spectrophotometers Model ESP-3T and Model 323 equipped with a cell thermostated at various temperatures. A 1 cm quartz cell was used. The kinetic measurements were carried out with a Union Giken co-axial-cable temperature-jump apparatus Model RA-105.[4] The pH values of the solutions were adjusted with the buffer solutions and measured with a Hitachi-Horiba pH-meter Model F-7SS. Temperature of the solution was measured with a copper-constantan thermocouple and a millivoltmeter within ± 0.2 °C. The ionic strength of the solution was adjusted to 0.1 mol dm^{-3} with sodium perchlorate.

Melting point was measured with a Rigaku Denki differential scanning calorimeter Model 8001 SL/C.

Results and Discussion

In the previous papers we ascribed the thermochromism observed for the Cu(II)–XO system primarily to the temperature-dependence of the protolytic equilibrium (1) based on the similarity of the temperature-dependence and the pH-dependence of the absorption spectra and on the results of molar-ratio method carried out at various temperatures.[1] Quite similar features were observed for the thermochromisms of the Cu(II) complexes of MTB and MXB.

As compared with XO these ligands contain two additional methyl groups R_2 and two isopropyl groups R_1 for MTB and two methyl groups R_1 for MXB (see Fig. 1). The effects of such structural factors in the ligand molecules on the phenomena of thermochromisms of their metal chelates are discussed in relation to the thermodynamic functions and the kinetic data.

Equilibria. Figures 2(a) and 2(b) show the typical examples of the temperature-dependence of the visible absorption spectra of the aqueous solution of Cu(II)–MTB at pH 4.36 and of Cu(II)–MXB at pH 4.57, respectively, the solutions containing 3.0×10^{-5} mol dm^{-3} ligand and 2.4×10^{-4} mol dm^{-3} Cu^{2+} ion.

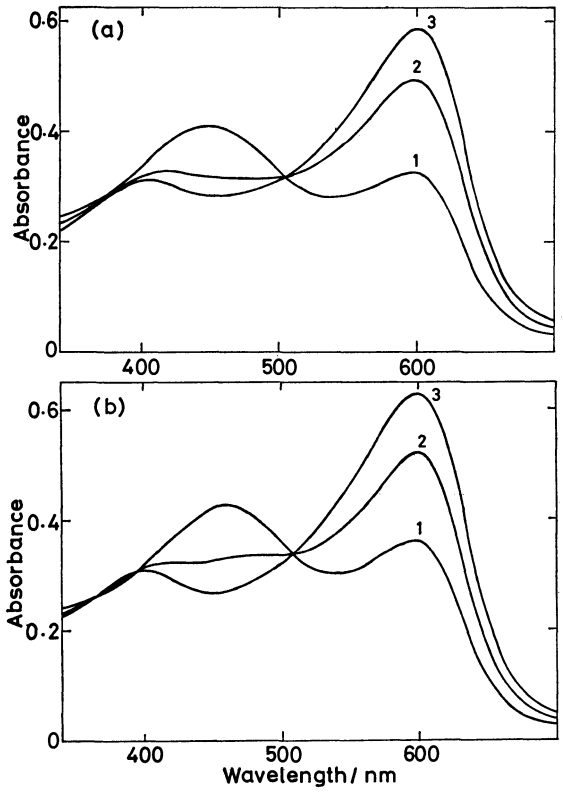

Fig. 2. Temperature-dependence of the absorption spectra of the Cu(II) complexes.
(a) Cu(II)–MTB. At 29 (1), 58 (2), and 77 °C (3). [Cu]$=2.4\times10^{-4}$ mol dm^{-3}; [MTB]$=3.0\times10^{-5}$ mol dm^{-3}. I=0.1 mol dm^{-3} ($NaClO_4$). At pH$=4.36\pm0.02$. (b) Cu(II)–MXB. At 28 (1), 54 (2), and 78 °C (3). [Cu]$=2.4\times10^{-4}$ mol dm^{-3}; [MXB]$=3.0\times10^{-5}$ mol dm^{-3}. I=0.1 mol dm^{-3} ($NaClO_4$). At pH$=4.57\pm0.02$.

The absorption spectra change reversibly with a distinct isosbestic point at 504 nm for Cu(II)–MTB and at 509 nm for Cu(II)–MXB. As the temperature rises the absorbances at 450 nm for Cu(II)–MTB and at 460 nm for Cu(II)–MXB decrease accompanied with a large increase in the absorbance at 600 nm for both systems. For the temperature-rise from 20 to 78 °C the absorbance at 600 nm increases about two-fold, the color changing from dark yellowish brown to dark blue for both systems. The increase of the absorbances at 600 nm was much the same as that of the Cu(II)–XO system at 574 nm under similar conditions. For the Cu(II) complexes of MTB and MXB the features of the temperature-dependences of the absorption spectra at a constant pH were all the same as those

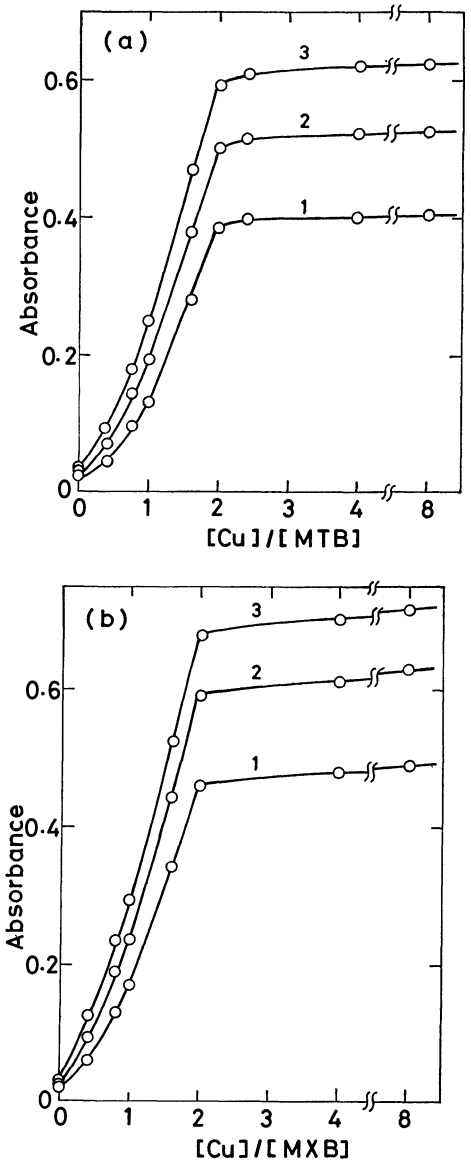

Fig. 3. Molar-ratio method at 600 nm for Cu(II) complexes at various temperatures.
(a) Cu(II)–MTB. At 25 (1), 50 (2), and 70 °C (3), [MTB]$=3.0\times10^{-5}$ mol dm^{-3}. pH$=4.57\pm0.02$. I=0.1 mol dm^{-3} ($NaClO_4$). (b) Cu(II)–MXB. At 25 (1), 50 (2), and 70 °C (3). [MXB]$=3.0\times10^{-5}$ mol dm^{-3}. pH$=4.88\pm0.02$. I=0.1 mol dm^{-3} ($NaClO_4$).

of the pH-dependences of the absorption spectra at a constant temperature.[5-9] The wavelengths of the absorption maxima and the isosbestic points observed for the two dependencies of the spectra were found to be all the same. Namely, also in the cases of the Cu(II) complexes of MTB and MXB the effect of heating the solutions essentially corresponds to the effect of the increase in pH of the same solutions.

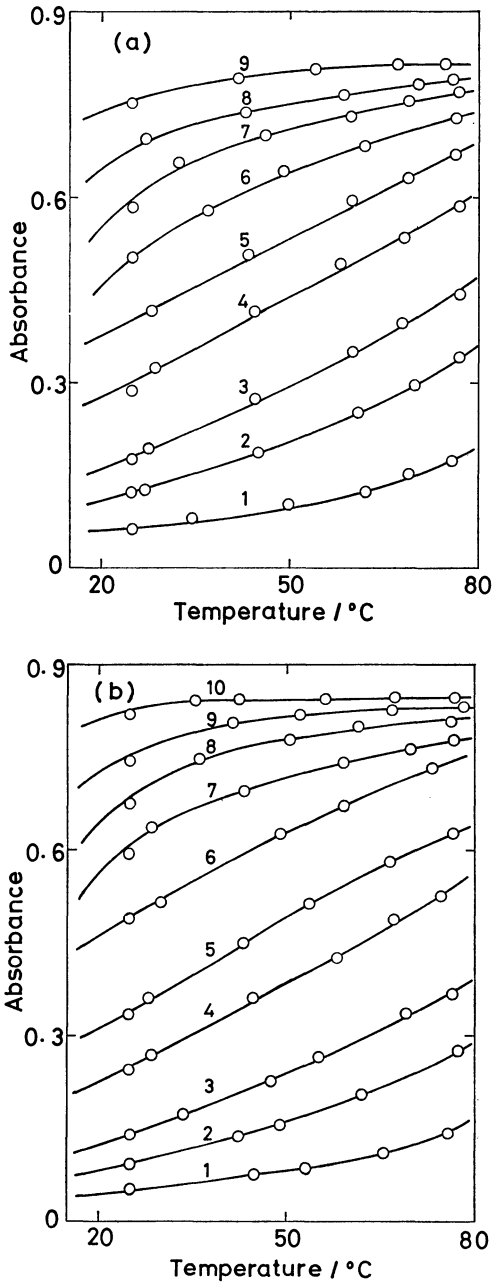

Fig. 4. The temperature-dependence of the absorbance at 600 nm of the Cu(II) complexes at various pH's.
(a) Cu(II)–MTB. At pH 3.26 (1), 3.71 (2), 3.99 (3), 4.36 (4), 4.59 (5), 4.90 (6), 5.20 (7), 5.47 (8), and 6.10 (9). [Cu]$=2.4\times10^{-4}$ mol dm^{-3}; [MTB]$=3.0\times10^{-5}$ mol dm^{-3}. I=0.1 mol dm^{-3} ($NaClO_4$). (b) Cu(II)–MXB. At 3.24 (1), 3.69 (2), 4.00 (3), 4.33 (4), 4.57 (5), 4.88 (6), 5.18 (7), 5.44 (8), 5.70 (9), and 6.08 (10). [Cu]$=2.4\times10^{-4}$ mol dm^{-3}; [MXB]$=3.0\times10^{-5}$ mol dm^{-3}. I=0.1 mol dm^{-3} ($NaClO_4$).

Figures 3(a) and 3(b) show the results of molar-ratio method measured at 600 nm, at various temperatures, and at pH 4.57 for Cu(II)–MTB and at 4.88 for Cu(II)–MXB, respectively. The metal-to-ligand ratio of the complex species formed in the solution for both systems was found to be invariably 2: 1 irrespective of the temperature.[1]

From the results described above, we concluded that the observed thermochromisms of Cu(II) complexes of MTB and MXB are also ascribed to the temperature-dependence of the protolytic equilibrium between two 2: 1 complex species, *i.e.*, between the low-temperature and the high-temperature form of a 2 : 1 complex species (see equilibrium (1)).

Figures 4(a) and 4(b) show the temperature-dependences of the absorbances at 600 nm of the solutions of the 2 : 1 Cu(II) complexes of MTB and MXB at various pH values. Upon heating the solutions at pH higher than 5.5 or lower than 3.7 the absorbances of both systems increase only slightly. The marked increase in the absorbance was observed for both systems only in a narrow pH range, *e.g.*, between pH 4.0 and 4.9 for Cu(II)–MTB and between pH 4.3 and 5.1 for Cu(II)–MXB (see Figs. 4(a) and 4(b)).

From the temperature-dependences of the absorbance the pH-dependences of the absorbance at various temperatures were derived as reproduced in Figs. 5(a) and 5(b). From these figures the pK values for the Eq. 1 were calculated at 25, 35, 50, and 70 °C. The

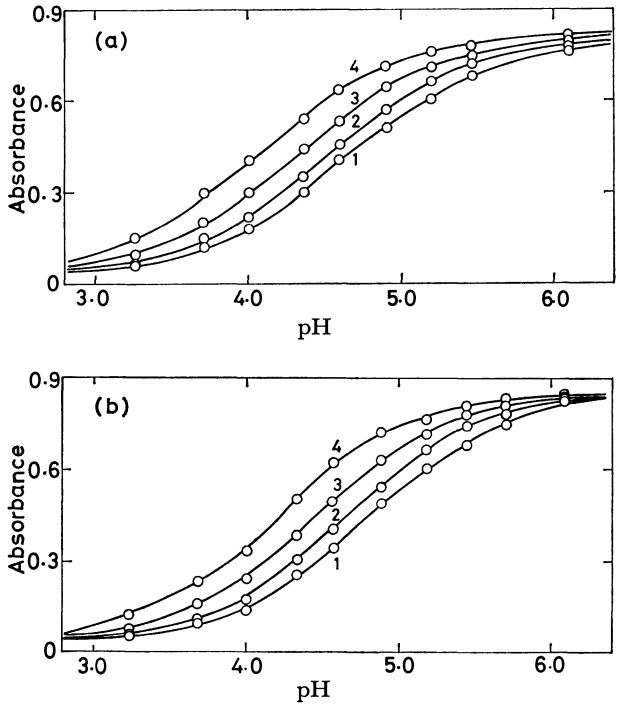

Fig. 5. The pH-dependence of the absorbance at 600 nm of the Cu(II) complexes at various temperatures.
(a) Cu(II)–MTB. At 25 (1), 35 (2), 50 (3), and 70 °C (4). [Cu]$=2.4\times10^{-4}$ mol dm^{-3}; [MTB]$=3.0\times10^{-5}$ mol dm^{-3}. I=0.1 mol dm^{-3} ($NaClO_4$). (b) Cu(II)–MXB. At 25 (1), 35 (2), 50 (3), and 70 °C (4). [Cu] $=2.4\times10^{-4}$ mol dm^{-3}; [MXB]$=3.0\times10^{-5}$ mol dm^{-3}. I=0.1 mol dm^{-3} ($NaClO_4$).

Table 1. Temperature-dependence of the acid-dissociation constants for the Cu(II) complexes and the free ligands at I=0.1 mol dm^{-3} ($NaClO_4$)[a]

T/°C	15	25	35	50	70
Cu(II)–MTB		4.66	4.54	4.34	4.10
Cu(II)–MXB		4.78	4.65	4.45	4.20
Cu(II)–XO[b]	4.62	4.40	4.27	4.11	3.83
MTB	6.94	6.87	6.81		
MXB	7.05	6.98	6.90		
XO[b]	6.66	6.57	6.50		

a) p(K/mol dm^{-3}) for the complexes. p(K_a/mol dm^{-3}) for the free ligands. b) See Ref. 1.

data were summarized in Table 1 together with those for Cu(II)–XO.

The pK_a values of the phenolic proton of the free ligands MTB and MXB also were obtained at various temperatures by the same procedure as in the case of XO[1] (Table 1).

The temperature-dependences of the absorption spectra of the free ligands in neutral region were smaller compared with those in the Cu(II) complexes in weakly acidic region. For the temperature-rise from 25 to 45 °C the absorbance at 600 nm of the free ligands MTB at pH 6.85 and MXB at pH 6.95, *viz.*, near the pK_a values of the phenol proton of the free ligands, increased only by 11% for MTB and 14% for MXB; the absorbance at 600 nm of Cu(II) complexes of MTB at pH 4.60 and MXB at pH 4.80 increased by so large as 28 and 37%, respectively.

Table 2. Thermodynamic functions for the protonation of the Cu(II) complexes and the free ligands

	ΔH	ΔS
	kJ mol^{-1}	J K^{-1} mol^{-1} (298 K)
Cu(II)–MTB	25±2	−6±3
Cu(II)–MXB	26±2	−6±3
Cu(II)–XO[a]	26±2	1±3
MTB	12±2	−92±3
MXB	13±2	−91±3
XO[a]	14±1	−78±1

a) See Ref. 1.

The thermodynamic parameters ΔH and ΔS for the Eq. 1 for Cu(II) complexes, and for the acid-dissociation of the phenol proton for the free ligands were graphically determined by plotting the values of log K and log K_a against $1/T$, respectively. The obtained values are listed in Table 2 together with the corresponding values for the Cu(II)–XO complex and the free ligand XO.

The positive values of ΔH show that the thermochromic changes of the Cu(II) complexes of MTB and MXB also are endothermic.

The values of ΔH for the Cu(II) complexes were about twice as large as that for the free ligands; the thermochromism was not observed for the free ligands.

A relationship is observed between the thermodynamic data and the position of alkyl substituents in the ligand molecule. Namely, the thermodynamic data for the three ligands, MTB, MXB, and XO, indicate that the effect of the substituents R_2 at meta position to the phenol group is reflected on the values of ΔS, but the effect of the substituents R_1 at ortho position is not (see Table 2). Similar relationship was also observed for the Cu(II) complexes of these ligands.

Bolton and co-workers reported the increase in values of pK_a and ΔS caused by the presence of meta-methyl substituents in phenols.[10]

The difference in the substituents R_1 at ortho position to the phenol group did not affect the thermodynamic functions.

As described in our previous report,[1] the data obtained in the present study also show that the values of ΔS for the equilibrium (1) differ much from those for the protolytic equilibrium in the free ligands. The small values of ΔS for the Cu(II) complexes would be ascribed to the compensation of the increase in the entropy by water molecules released from the coordination sphere of the metal ion upon coordination of the phenolate oxygen and the decrease in the entropy by the hydration of a dissociated proton.[1] Similar discussions have been reported by Desai and Milburn[11] for the complex formation of Fe(III) with phenols, and by Wright *et al.*[12] and Brunetti *et al.*[13] for the protonation of EDTA and its bivalent metal complexes.

Molar absorptivities of the ligands MTB and MXB were found to depend on the temperature. In the pH region between 3.5 and 3.9 corresponding to the pK_a of the carboxyl proton of the ligands[6,8,9] where the absorption spectra of the free ligands show no pH-dependency, a definite temperature-dependence of the spectra was clearly observed. This temperature-dependence of the absorbance would be attributed to the change in molar absorptivity of the ligands and might also contribute to the thermochromism of the Cu(II) complexes, though the effect is not so strong.

Kinetics. The temperature-jump studies were carried out for the Cu(II) complexes of MTB and MXB, and the free ligands, according to the procedure used in the case of Cu(II)–XO.[1] Only one relaxation signal of an increasing absorbance at 600 nm was observed in 5—10 μs region for the Cu(II) complexes in acidic solutions; the corresponding signal for the ligands in nearly neutral solutions was observed in 10—20 μs region. The relaxation times for the protolytic changes can be expressed by

$$\tau^{-1} = k_1 + k_{-1}([\bar{H}]+[\bar{A}]), \quad (2)$$

where k_1, k_{-1}, and [¯] denote the forward and the backward rate constants and equilibrium concentrations, respectively. The kinetic data were listed in Table 3 together with those for Cu(II)–XO and the ligand XO.

The values of k_1 and k_{-1} for the acid-dissociation of phenol proton of the free ligands differ from those of XO. The values of quotient, k_1/k_{-1}, for free ligands were determined to be $10^{-6.7}$ and $10^{-6.9}$ mol dm^{-3} for MTB and MXB, respectively. These values are in good agreement with the values of K_a determined by the equilibrium measurements, though the errors are arge. The kinetic data for the free ligands, MTB and

TABLE 3. THE PROTONATION-DEPROTONATION RATE CONSTANTS FOR THE Cu(II) COMPLEXES AND THE FREE LIGANDS, AT 25 °C AND I=0.1 mol dm^{-3} ($NaClO_4$)

	k_1 / 10^4 s^{-1}	k_{-1} / 10^{10} mol^{-1} dm^3 s^{-1}
Cu(II)–MTB	16	—
Cu(II)–MXB	18	—
Cu(II)–XO[a)]	20	—
MTB	0.2±0.8	0.9±0.5
MXB	0.2±0.8	1.5±0.5
XO[a)]	1.0±0.6	3.0±0.1

a) See Ref. 1. —: For the complexes the values of τ^{-1} did not depend on the sum of equilibrium concentrations, $[\bar{H}]+[\bar{A}]$.

MXB, would suggest that the differences in the values of $K_a=k_1/k_{-1}$ observed may primarily be ascribed to the differences in the values of k_{-1}. This indicates that isopropyl substituent R_1 at ortho position to the phenol group slows down the rate of the proton recombination to somewhat larger extent compared with the methyl substituent R_1 at the same position.

For the Cu(II) complexes of MTB and MXB the values of k_1 estimated for reaction (1) were found to be in the same order of magnitude as that for Cu(II)–XO, *i.e.*, *ca.* 2×10^5 s^{-1}. The values of τ^{-1}, reciprocal of the relaxation times, for the protonation-deprotonation of the Cu(II) complexes of MTB, MXB, and XO are essentially independent of the sum of the equilibrium concentrations of proton and the chelate species involved. These results may be attributed to (1) an instrumental problem that the values of τ derived from the exponential signals for the Cu(II) complexes would reflect the time constant τ_c for the temperature-rise of our apparatus; (2) a possibility of a mechanism involving a contribution of a sort of intramolecular rate-determining step to the recombination of the phenolate with a central Cu(II) ion. The problems on the ambiguity of these possibilities are still open and will be reported elsewhere.

For the kindness in the DSC measurements, the authors thank Professor Yoshio Matsunaga. They also thank Professor Mitsuo Shimoji and Professor Yoshio Nakamura for aid in the use of a spectrophotometer for the measurements at high temperatures.

References

1) S. Nakada, M. Yamada, T. Ito, and M. Fujimoto, *Chem. Lett.*, **1977**, 1243; *Bull. Chem. Soc. Jpn.*, **52**, 766 (1979).
2) J. Körbl and R. Přibil, *Chem. Ind. (London)*, **1957**, 233.
3) S. Nakada, M. Yamada, T. Ito, and M. Fujimoto, *Bull. Chem. Soc. Jpn.*, **50**, 1887 (1977).
4) N. Yoshida and M. Fujimoto, *Bull. Chem. Soc. Jpn.*, **50**, 1328 (1977).
5) The values of the molar absorptivity for Cu(II) complexes of MTB and MXB at 600 nm, and the free ligands at 610 nm were determined to be 2.7×10^4, 2.9×10^4, 2.0×10^4, and 2.3×10^4 mol^{-1} dm^3 cm^{-1}, respectively. These values were found to be reasonable by comparing with the corresponding values by other authors.[6-9]
6) B. Buděšínský, "Chelates in Analytical Chemistry," Vol. 1, ed by H. A. Flaschka and A. J. Barnard, Jr., Marcel Dekker, New York, N. Y. (1967), pp. 15—47.
7) T. Yoshino, H. Imada, T. Kuwano, and K. Iwasa, *Talanta*, **16**, 151 (1969).
8) M. Otomo, *Bunseki Kagaku*, **21**, 436 (1972).
9) T. Yoshino, H. Imada, S. Murakami, and M. Kagawa, *Talanta*, **21**, 211 (1974).
10) P. D. Bolton, F. M. Hall, and J. Kudrynski, *Austral. J. Chem.*, **21**, 1514 (1968); P. D. Bolton, J. Ellis, and F. M. Hall, *J. Chem. Soc., B*, **1970**, 1252.
11) A. G. Desai and R. M. Milburn, *J. Am. Chem. Soc.*, **91**, 1958 (1969).
12) D. L. Wright, J. H. Holloway, and C. N. Reilley, *Anal. Chem.*, **37**, 884 (1965).
13) A. P. Brunetti, G. H. Nancollas, and P. N. Smith, *J. Am. Chem. Soc.*, **91**, 4680 (1969).

 © 1980 The Chemical Society of Japan Bull. Chem. Soc. Jpn., 53, 2257—2261 (1980)

Stereochemistry of *Λ-uns*-(2*S*,2*S*′)-1,1′-Trimethylenedipyrrolidine-2,2′-dicarboxylato Cobalt(III) Complexes with *N*-Alkyl Substituted Amino or Cyclic Imino Acids

Minahiro Okabayashi, Ken-ichi Okamoto, and Jinsai Hidaka*

Department of Chemistry, University of Tsukuba, Ibaraki 305

(Received January 5, 1980)

((2*S*,2*S*′-1,1′-Trimethylenedipyrrolidine-2,2′-dicarboxylato)(α-amino carboxylato)cobalt(III) complexes were prepared and characterized, where the α-amino carboxylate ligand is glycinate, (*R*)- or (*S*)-alaninate, (*R*)- or (*S*)-valinate, sarcosinate, *N*-ethylglycinate, (*R*)-prolinate, or (*S*)-pipecolate((*S*)-2-piperidinecarboxylate). Of the three possible isomers, only the *Λ-uns-mer* form was prepared for each of the complexes except for the glycinato complex. The (*R*)-prolinato and (*S*)-pipecolato complexes were stereoselectively prepared by using (*RS*)-proline or (*RS*)-pipecolic acid. The pipecolate ion coordinated selectively was assigned to *S*(*C*) configuration on the basis of the CD measurement of the 2,4-dinitrophenyl-pipecolic acid. The nitrogen atom of the sarcosinate, *N*-ethylglycinate, (*R*)-prolinate, or (*S*)-pipecolate ion, which coordinated stereoselectively to Co(III) ion, took the *R*(*N*) configuration. The stereoselectivity in this work was discussed on the basis of the electronic absorption, CD, and PMR spectra.

When the ethylenediamine-*N*,*N*′-diacetate ion (edda) coordinated to Co(III) ion to form [Co(edda)(am)]-type complex (am: α-amino carboxylate ion), the edda preferred to take a symmetric coordination rather than an unsymmetric one,[1–3] while the trimethylenediamine-*N*,*N*′-diacetate ion (tmdda) preferred the unsymmetric one.[4–6] It was assumed that the preference depends mainly on the probable conformation of the backbone diamine chelate ring of the linear O–N–N–O-type ligand.[4] The linear quadridentate ligand in this work, the (2*S*,2*S*′)-1,1′-trimethylenedipyrrolidine-2,2′-dicarboxylate ion (*S*,*S*-tmpro), has two chiral centers, *S*(*C*)*S*(*C*), and two pyrrolidine rings. By coordination to Co(III) ion, therefore, the possible configurations are regulated to only two, *Δ*-symmetric and *Λ*-unsymmetric. This is useful for investigations of the stereochemical preference of the quadridentate ligand and of the selective coordination of the bidentate ligand, α-amino carboxylate, for the remaining two coordination sites.

In the present paper, some aspects of the stereochemistry of the [Co(*S*,*S*-tmpro)(am)]-type complexes are dealt with, where am denotes glycinate, (*S*)- or (*R*)-alaninate, (*S*)- or (*R*)-valinate, (*R*)-prolinate, (*S*)-pipecolate ((*S*)-2-pipelidinecarboxylate, *S*-pipec), sarcosinate (sar), and *N*-ethylglycinate (*N*-et-gly). The *S*,*S*-tmpro complexes obtained have been characterized from their electronic absorption, CD, and PMR spectra. The stereoselective coordination of the *S*,*S*-tmpro and bidentate ligands are discussed in relation to the conformational preference and their steric interaction. The absolute configurations of the coordinated pipecolate ion and of the coordinated nitrogen atoms of the sar, *N*-et-gly, *R*-pro, and *S*-pipec were assigned by means of their CD and PMR spectra.

Experimental

1) Preparation of Ligands. (2*S*,2*S*′)-1,1′-Trimethylenedipyrrolidine-2,2′-dicarboxylic acid was prepared from (*S*)-proline and 1,3-dibromopropane according to the method of Schoenberg *et al.*[7] The needle crystals obtained were recrystallized from ethanol. Found: C, 39.74; H, 6.05; N, 7.05%. Calcd for $C_{13}H_{22}N_2O_4 \cdot 2NaCl \cdot 0.5H_2O$: C, 39.40; H, 5.86; N, 7.07%.

N-Ethylglycine was prepared by the ethylation of glycine using ethyl iodie.[8] Found: C, 34.77; H, 7.24; N, 10.12%. Calcd for $C_4H_9NO_2 \cdot HCl$; C, 34.41; H, 7.17; N, 10.04%.

2) Λ-uns-*Ba*[*Co*(S,S-*tmpro*)*Cl*(*OH*)]$_2 \cdot H_2O$. To a solution containing 1.6 g of tmpro$H_2 \cdot 2NaCl \cdot 0.5H_2O$ and 1.0 g of $CoCl_2 \cdot 6H_2O$ in 20 cm^3 of water was gradually added 1.0 g of PbO_2 by means of vigorous stirring at 65 °C for 10 min. The color of the solution changed from pale red to blue. The solution was cooled to room temperature and then filtered. The filtrate was poured into an anion-exchange column (Dowex 1-X8, 200—400 mesh, Cl^- form, 5×15 cm). The absorbed band was eluted with an 1 mol dm^{-3} $BaCl_2$ aqueous solution, and the eluate was evaporated to dryness. The complex was extracted from the solid with methanol, and the blue complex was obtained by the addition of ether. The complex was recrystallized from methanol by adding a small amount of ether. The CD spectral pattern in the visible region suggested that the *S*,*S*-tmpro has a *Λ-uns* form, but the geometrical arrangement with respect to Cl^- and OH^- is still unknown.

3) Λ-uns-[*Co*(S,S-*tmpro*)(*gly*)]. To the solution of *Λ-uns*-[Co(*S*,*S*-tmpro)Cl(OH)]$^-$ in *2)* was added a solution containing 0.3 g of glycine in 10 cm^3 of water. The pH of the solution was then adjusted to 7.0 by the addition of an 1 mol dm^{-3} NaOH aqueous solution. After the addition of a small amount of activated charcoal, to the mixture was added 1.0 g of PbO_2 at 65 °C for 30 min. The reaction solution was cooled to room temperature and then filtered. The filtrate was passed through the anion-exchange column as in *2)* in order to remove the unreacted anion, *Λ-uns*-[Co(*S*,*S*-tmpro)Cl(OH)]$^-$. The eluate was evaporated to a small volume with a rotary evaporator and then chromatographed on an anion-exchange column (QAE-Sephadex A-25, (*R*,*R*)-tartrate form, 3.5×85 cm). The adsorbed band was separated into five bands: yellow, violet, violet, violet, and red, in the order of elution, by eluting with water. The first yellow band contained cationic compounds, because it was adsorbed by a cation-exchange resin (SP-Sephadex C-25, Na^+ form). It was found, from the absorption and CD spectra, that the second band contained *Λ-uns-mer*-[Co(*S*,*S*-tmpro)(gly)]; the third one, *mer*-[Co(gly)$_3$]; the fourth one, *Λ-uns-fac*-[Co(*S*,*S*-tmpro)(gly)], and the fifth one, *fac*-[Co(gly)$_3$] (the earlier-eluted part of the fifth band consists of the *Δ-fac* isomer, and the later-eluted part, the *Λ-fac* isomer). The fourth band contained a very small amount of the complex in comparison

with the second band.

4) *Λ*-uns-mer-[*Co*(S,S-*tmpro*)(*gly*)]·H_2O. The second eluted band in *3)* was evaported to a small volume, and to the concentrated solution was added ethanol and then acetone. The solution was kept in a refrigerator overnight. The needle crystals thus precipitated were collected and recrystallized from water by the addition of ethanol and acetone. The pure crystals were collected, washed with ethanol and then ether, and dried in the air. Yield: 0.125 g.

5) *Λ*-uns-fac-[*Co*(S,S-*tmpro*)(*gly*)]·$3H_2O$. The fourth eluate in *3)* was evaporated to dryness. The violet solid was suspended in ethanol and collected by filtration. The crude complex was purified as in *4)*. Yield: 0.01 g.

6) *Λ*-uns-mer-[*Co*(S,S-*tmpro*)(S-*ala*)]·H_2O, [*Co*(S,S-*tmpro*)(R-*ala*)]·H_2O, [*Co*(S,S-*tmpro*)(S-*val*)]·H_2O, *and* [*Co*(S,S-*tmpro*)(R-*val*)]·H_2O. These complexes were prepared and isolated in the same method as that used for *Λ-uns-mer*-[Co(*S*,*S*-tmpro)(gly)]. The *Λ-uns-fac* isomer was not detected in these complexes.

7) *Λ*-uns-mer-[*Co*(S,S-*tmpro*)(*sar*)]. The complex was prepared by the same procedure as that used for [Co(*S*,*S*-tmpro)(gly)] using 0.37 g of sarcosine. The reaction mixture being passed through the columns (Dowex 1-X8 and SP-Sephadex C-25) in order to remove the negative and positive charged compounds was chromatographed on a column (QAE-Sephadex A-25, Cl^- form, 3.5×85 cm). The only band was eluted with water and fractionated into eight parts. It was found from their absorption and CD spectra that all eight fractions contained *Λ-uns-mer*-[Co(*S*,*S*-tmpro)(sar)]. Yield: 0.15 g.

8) *Λ*-uns-mer-[*Co*(S,S-*tmpro*)(N-*et-gly*)]·$0.5H_2O$. The complex was prepared and isolated using the same procedure as had been used for *Λ-uns-mer*-[Co(*S*,*S*-tmpro)(sar)]. Yield: 0.10 g.

9) *Attempt to Prepare* [*Co*(S,S-*tmpro*)(S-*pro*)]. The preparation of the [Co(*S*,*S*-tmpro)(*S*-pro)] was attempted by a procedure similar to that used for the glycinato complex, but using (*S*)-proline instead of glycine. After the removal of the charged compounds as in *7)*, a small amount of the violet complex was obtained. Chromatography behavior and the absorption and CD spectra showed that the eluate contained *mer*- and *fac*-[Co(*S*-pro)$_3$], while the desired [Co(*S*,*S*-tmpro)-(*S*-pro)] was not detected.

10) *Λ*-uns-mer-[*Co*(S,S-*tmpro*)(R-*pro*)]·$2.5H_2O$. This complex was prepared by the same procedure as that used for [Co(*S*,*S*-tmpro)(gly)] using 1 g of (*RS*)-proline. The reaction mixture having been removed the negative and positive charged compounds as in *7)* was chromatographed on the column (QAE-Sephadex A-25, Cl^- form). The complex was separated into three bands: blue-violet, violet, and red, in the order of elution. The absorption and CD spectra showed that the first adsorbed band contained *Λ-uns-mer*-[Co(*S*,*S*-tmpro)(*R*-pro)], and the second and third bands, *mer*- and *fac*-[Co(*RS*-pro)$_3$] respectively. The needle crystals were isolated from the first eluate by a procedure similar to that used for *4)*. Yield: 0.15 g. The complex was recrystallized from ethanol by adding ether and dried in a vacuum desiccator.

11) *Λ*-uns-mer-[*Co*(S,S-*tmpro*)(S-*pipec*)]·$0.5H_2O$. This complex was prepared and isolated by the same procedure as in *10)* using 0.60 g of (*RS*)-pipecolic acid. The complex was chromatographed on the column (QAE-Sephadex A-25, (*R*,*R*)-tartrate form); the CD spectra of the eight fractionated eluates were identical. The crude complex was recrystallized twice from an ethanol–methanol (1:1) mixture by the addition of ether without any change in the CD spectrum. Yield: 0.14 g. The absolute configuration of the coordinated (*R*)- and/or (*S*)-pipecolate ion was determined by the following method.

A solution containing 0.033 g of [Co(*S*,*S*-tmpro)(pipec)]·$0.5H_2O$ in 20 cm^3 of a 0.6 mol dm^{-3} $NaHCO_3$ aqueous solution was warmed at 55 °C. To the solution was added 6 cm^3 of a 0.1 mol dm^{-3} NaOH solution, whereupon the color of the solution immediately changed from blue-violet to colorless. The colorless solution was cooled to room temperature as soon as possible, neutralized by the addition of 6 mol dm^{-3} HCl, and then evaporated to dryness with a rotary evaporator. The pipecolic acid thus released was dinitrophenylated by the method reported by Yonetani *et al.*[9] The resulting dinitrophenylated pipecolic acid (DNP-pipec) showed the same CD spectrum as that of DNP-pipecolic acid described in the literature.[10] Thus, it was determined that the coordinated pipecolate ion has *S* configuration.

12) uns-mer-[*Co*(*tmdda*)(*sar*)]·$0.5H_2O$. This complex was prepared by the method described in a previous paper.[4] Only the *uns-mer* isomer was obtained, without the *uns-fac* one being formed.

Analyses. The analytical results for the complexes obtained are summarized in Table 1.

Measurements. The electronic absorption spectra were recorded with a JASCO UVIDEC-1 spectrophotometer, and the CD spectra, with a JASCO J-20 spectropolarimeter. The PMR spectra were recorded on a JEOL JNM-MH-100 NMR spectrometer at the probe temperature in a D_2O solvent. Sodium 2,2-dimethyl-2-silapentanesulfonate (DSS) was used as the internal reference.

Table 1. Elemental analyses (%)

Complex	C		H		N	
	Found	Calcd	Found	Calcd	Found	Calcd
Λ-uns-Ba[Co(*S*,*S*-tmpro)Cl(OH)]$_2$·H_2O	33.96	34.13	4.64	4.86	5.88	6.13
Λ-uns-mer-[Co(*S*,*S*-tmpro)(gly)]·H_2O	42.78	42.96	6.22	6.26	10.24	10.02
Λ-uns-fac-[Co(*S*,*S*-tmpro)(gly)]·$3H_2O$	39.41	39.56	6.22	6.65	9.21	9.23
Λ-uns-mer-[Co(*S*,*S*-tmpro)(*S*-ala)]·H_2O	44.67	44.33	6.55	6.53	9.99	9.70
Λ-uns-mer-[Co(*S*,*S*-tmpro)(*R*-ala)]·H_2O	44.02	44.33	6.32	6.53	9.85	9.70
Λ-uns-mer-[Co(*S*,*S*-tmpro)(*S*-val)]·H_2O	46.72	46.85	6.98	7.00	9.05	9.11
Λ-uns-mer-[Co(*S*,*S*-tmpro)(*R*-val)]·H_2O	46.36	46.85	6.84	7.00	9.26	9.11
Λ-uns-mer-[Co(*S*,*S*-tmpro)(sar)]	45.93	46.26	6.29	6.32	10.26	10.12
Λ-uns-mer-[Co(*S*,*S*-tmpro)(*N*-et-gly)]·$0.5H_2O$	46.67	46.60	6.54	6.68	9.62	9.59
Λ-uns-mer-[Co(*S*,*S*-tmpro)(*R*-pro)]·$2.5H_2O$	44.74	44.44	6.73	6.85	8.33	8.64
Λ-uns-mer-[Co(*S*,*S*-tmpro)(*S*-pipec)]·$0.5H_2O$	49.64	49.13	6.65	6.52	9.04	9.05
uns-mer-[Co(tmdda)(sar)]·$0.5H_2O$	35.07	34.89	5.44	5.57	12.17	12.21

Results and Discussion

Structural Assignments. The (2S,2S')-1,1'-trimethylenedipyrrolidine-2,2'-dicarboxylate anion is an O–N–N–O-type ligand similar to the trimethylenediamine-*N,N'*-diacetate anion,[4-6] while the *S,S*-tmpro has two chiral centers, (*S*(*C*) and *S*(*C*)), and two pyrrolidine rings. Accordingly, only three chiral configurations, *Δ-s*, *Δ-uns-fac*, and *Δ-uns-mer*, are possible for the [Co(*S,S*-tmpro)(am)] complex (Fig. 1).

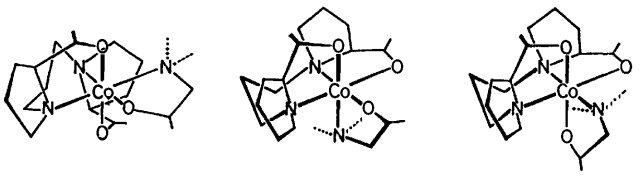

(a) (b) (c)

Fig. 1. Three possible isomers of [Co(*S,S*-tmpro)(am)] type complex, (a) *Δ-s*, (b) *Δ-uns-fac*, and (c) *Δ-uns-mer*.

The absorption and CD spectral data of the isolated *S,S*-tmpro complexes are summarized in Tables 2 and 3, while the representative curves are shown in Figs. 2 and 3. Of the nine complexes in this work, only the glycinato complex gave two kinds of isomers, though the later-eluted glycinato isomer formed a trace amount. The absorption curves of the nine complexes resemble each other remarkably except for the later-eluted glycinato isomer, and their CD curves all show a positive

Table 2. Absorption data of *Δ-uns*-[Co(*S,S*-tmpro)(am)], *Δ-uns*-[Co(*S,S*-tmpro)Cl(OH)]$^-$, and *uns*-[Co(tmdda)(sar)]

Complex	First band	Second band	Charge-transfer band
mer-[Co(*S,S*-tmpro)(gly)]	18.18(2.20)	25.64(2.31)	41.32(4.26)
fac-[Co(*S,S*-tmpro)(gly)]	17.99(2.26)	25.38(2.25)	40.82(3.99)
mer-[Co(*S,S*-tmpro)(*S*-ala)]	18.21(2.22)	25.71(2.33)	41.49(4.29)
mer-[Co(*S,S*-tmpro)(*R*-ala)]	18.25(2.23)	25.77(2.33)	41.32(4.35)
mer-[Co(*S,S*-tmpro)(*S*-val)]	18.08(2.22)	25.58(2.34)	40.98(4.30)
mer-[Co(*S,S*-tmpro)(*R*-val)]	18.18(2.24)	25.71(2.33)	41.32(4.29)
mer-[Co(*S,S*-tmpro)(sar)]	17.86(2.25)	25.38(2.34)	40.65(4.27)
mer-[Co(*S,S*-tmpro)(*N*-et-gly)]	17.70(2.26)	25.32(2.34)	40.16(4.27)
mer-[Co(*S,S*-tmpro)(*R*-pro)]	17.89(2.22)	25.38(2.29)	40.32(4.27)
mer-[Co(*S,S*-tmpro)(*S*-pipec)]	17.86(2.28)	25.25(2.41)	39.84(4.44)
mer-[Co(tmdda)(sar)]	18.87(2.03)	26.46(2.21)	44.25(4.32)
[Co(*S,S*-tmpro)Cl(OH)]$^-$	17.18(2.22)	24.69(2.24)	39.68(4.15)

The wave numbers and log ε values (in parentheses) are given in 10^3 cm^{-1} and mol^{-1} dm^3 cm^{-1} respectively.

Table 3. CD data of *Δ-uns*-[Co(*S,S*-tmpro)(am)] and *Δ-uns*-[Co(*S,S*-tmpro)Cl(OH)]$^-$

Complex	First-band region	Second-band region	Charge-transfer-band region
mer-[Co(*S,S*-tmpro)(gly)]	16.23(−1.05)	25.38(−1.80)	39.37(−16.49)
	18.38(+5.74)		42.02(sh)
fac-[Co(*S,S*-tmpro)(gly)]	18.12(+2.98)	25.38(−1.05)	40.98(−13.70)
mer-[Co(*S,S*-tmpro)(*S*-ala)]	16.23(−0.94)	25.38(−1.70)	39.06(−16.42)
	18.38(+6.01)		43.86(sh)
mer-[Co(*S,S*-tmpro)(*R*-ala)]	16.29(−1.05)	25.51(−1.90)	39.37(−15.34)
	18.52(+6.38)		43.86(sh)
mer-[Co(*S,S*-tmpro)(*S*-val)]	16.23(−1.43)	25.51(−1.88)	38.76(−18.22)
	18.32(+6.77)		44.64(− 9.76)
mer-[Co(*S,S*-tmpro)(*R*-val)]	16.10(−0.52)	25.51(−1.59)	41.32(−15.20)
	18.38(+6.40)		
mer-[Co(*S,S*-tmpro)(sar)]	16.18(−2.14)	25.13(−1.86)	38.17(−14.40)
	18.15(+5.40)		45.25(−12.52)
mer-[Co(*S,S*-tmpro)(*N*-et-gly)]	16.18(−2.31)	25.13(−1.67)	37.88(+12.58)
	18.12(+5.06)		45.25(−11.10)
mer-[Co(*S,S*-tmpro)(*R*-pro)]	16.16(−1.49)	25.13(−1.56)	37.88(−14.34)
	18.25(+4.37)		45.25(− 9.30)
mer-[Co(*S,S*-tmpro)(*S*-pipec)]	16.13(−1.94)	25.25(−1.80)	38.17(−13.36)
	18.12(+5.69)		45.05(−11.58)
[Co(*S,S*-tmpro)Cl(OH)]$^-$	15.63(−0.43)	24.27(−0.79)	39.68(−13.52)
	17.67(+4.18)		45.45(sh)

The wave numbers and $\Delta\varepsilon$ values (in parentheses) are given in 10^3 cm^{-1} and mol^{-1} dm^3 dm^{-1} respectively. Sh denotes the shoulder of the peak.

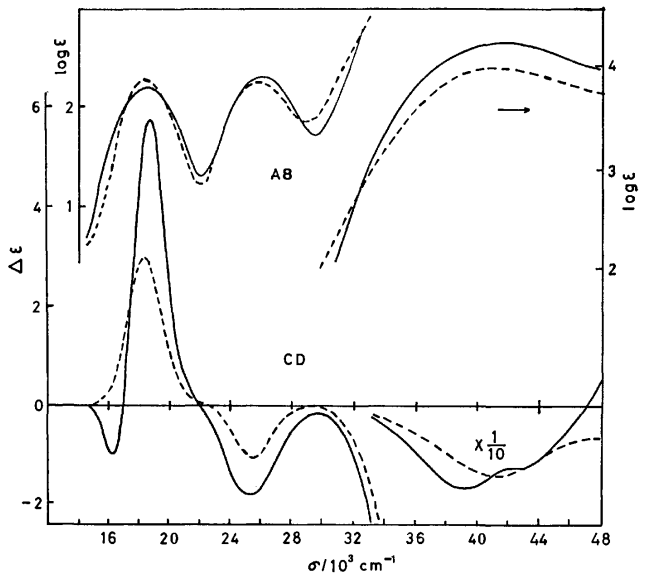

Fig 2. Absorption and CD spectra for the isomers of [Co(*S*,*S*-tmpro)(gly)], *Λ-uns-mer* (——) and *Λ-uns-fac* (----).

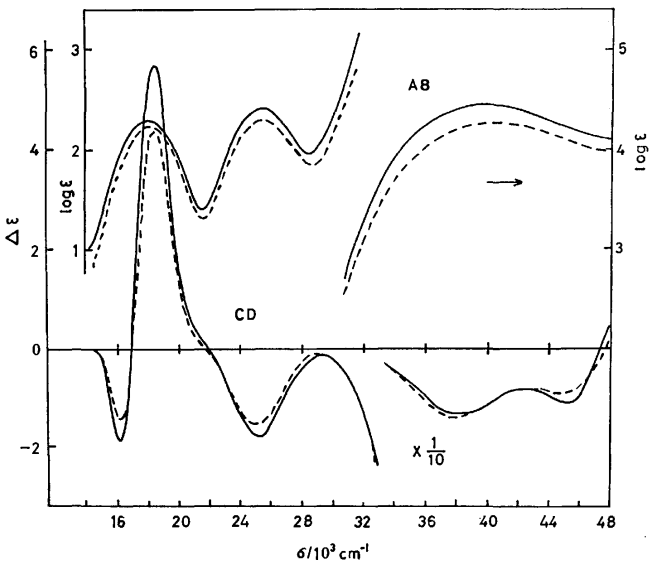

Fig. 3. Absorption and CD spectra of *Λ-uns-mer*-[Co(*S*,*S*-tmpro)(*R*-pro)] (——) and *Λ-uns-mer*-[Co(*S*,*S*-tmpro)(*S*-pipec)] (——).

dominant CD band in the first absorption band region, such as those of *Λ-uns-mer*-[Co(tmdda)(am)].[4] The later-eluted glycinato isomer, the absorption spectral pattern of which differs from those of the earlier-eluted isomer and the other eight complexes, also shows a positive dominant CD band in the corresponding region. This CD behavior suggests that all of the complexes isolated commonly take *Λ* configuration, namely, *Λ-uns-mer* or *Λ-uns-fac* (Fig. 1).

As is shown in Fig. 2, the first absorption band of the earlier-eluted glycinato isomer is broad, whereas that of the later one is sharp. These absorption spectral patterns indicate that the earlier-eluted isomer is *mer*(N_3O_3), and the later one, *fac*(N_3O_3).[11] The absorption spectra of the other complexes coincide with that of the earlier-eluted glycinato isomer (Figs. 2 and 3 and Table 2). Therefore, the later-eluted glycinato isomer is assigned to the *Λ-uns-fac* form, and the earlier-eluted isomer and the eight complexes, the *Λ-uns-mer* form.

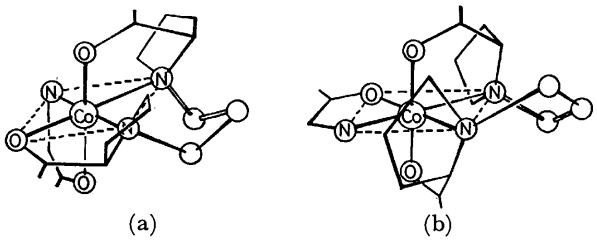

Fig. 4. Chair (a) and skew-boat (b) conformations for the trimethylenediamine chelate ring of *Λ-uns-mer-* and *Δ-s*-[Co(*S*,*S*-tmpro)(am)], respectively.

Stereospecificity. For all of the present complexes, the coordinated *S*,*S*-tmpro ligand takes the *Λ*-unsymmetric form. Furthermore, the CD spectrum of the starting complex, [Co(*S*,*S*-tmpro)Cl(OH)]$^-$, suggests that the chiral configuration is *Λ*-unsymmetric (Table 3). Molecular models reveal that the backbone trimethylenediamine ring of *S*,*S*-tmpro takes a symmetrical chair form for the *Λ*-unsymmetric coordination, while a skew-boat is most probable for the *Δ*-symmetric one (Fig. 4). From the present results, accordingly, it is possible to say that the *Λ*-unsymmetric preference of the *S*,*S*-tmpro depends mainly on the more stable conformation of the backbone trimethylenediamine ring.[12,13]

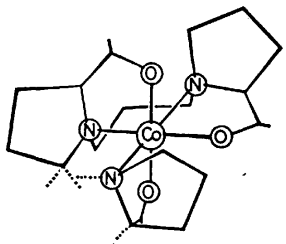

Fig. 5. Probable chiral configuration, *R*(*N*), of the (*R*)-prolinate ion in *Λ-uns-mer*-[Co(*S*,*S*-tmpro)(*R*-pro)].

The *Λ-uns-mer* and *Λ-uns-fac* isomers were obtained only for the glycinato complex. For both the sarcosinato and *N*-ethylglycinato complexes, however, the *mer* isomer was obtained, and no *fac* isomer was detected. It seems that this preference for the *Λ*-unsymmetric *mer* is attributable to the proximity between the *N*-alkyl group of the sarcosinate or *N*-ethylglycinate ring and the chair-conformed trimethylenediamine ring of the *S*,*S*-tmpro (Fig. 1). A similar trend was also observed for the [Co(tmdda)(sar)] complex (Tables 2 and 3). Another steric factor is found between the axial pyrrolidine ring of the *S*,*S*-tmpro and *N*-alkyl group of the bidentate ligand. A typical example of this interaction is found in the *Λ-uns-mer*-[Co(*S*,*S*-tmpro)(*S*-pro)] complex (Fig. 5). The prolinato complex could not be formed by using (*S*)-proline as the bidentate ligand, though the (*R*)-prolinato complex was selectively

formed, without the forming of the (*S*)-prolinato complex, by using (*RS*)-proline. This selectivity is due to the fact that the *N* atom of (*S*)-proline is regulated to the *S* configuration by coordinating to Co(III). That is, the *S*(*N*) coordination can not be realized in the *Λ-uns-mer S,S*-tmpro complex because of the proximity between the pyrrolidine rings of (*S*)-prolinate and *S,S*-tmpro (Fig. 5). In the *R*(*N*) coordination of (*R*)-prolinate, on the contrary, the pyrrolidine ring of the (*R*)-prolinate chelate avoids that of *S,S*-tmpro. A similar selectivity can also be expected for the pipecolato, sarcosinato, and *N*-ethylglycinato complexes of the *Λ*-unsymmetric configuration. The pipecolato complex, *Λ-uns-mer*-[Co(*S,S*-tmpro)(*S*-pipec)], was selectively prepared by using (*RS*)-pipecolic acid, as in the case of *Λ-uns-mer*-[Co(*S,S*-tmpro)(*R*-pro)]. The absolute configuration of the selected pipecolate ion was determined to be *S*(*C*) by the 2,4-dinitrophenyl (DNP) method.[9,10]

From model constructions, the order of the interligand crowd for the possible isomers of *Λ-uns-mer*-[Co(*S,S*-tmpro)(*R*- or *S*-pipec)] is $S(N)S(C) \gg S(N)R(C) > R(N)S(C) \approx R(N)R(C)$. Of the four isomers, the *R*(*N*)*S*(*C*) isomer is most probable for the pipecolato complex, since the *S*(*N*)*R*(*C*) and *R*(*N*)*R*(*C*) isomers are eliminated on the basis of the DNP method described above. In the $[Co(R\text{-pipec})(NH_3)_4]^+$ complex, the pipecolate ion coordinated to Co(III) with the *S*(*N*) configuration and the piperidine ring conformation took the chair form.[14] In the *Λ-uns-mer*-[Co(*S,S*-tmpro)(*S*-pipec)] complex, therefore, it is probable that the (*S*)-pipecolate ion coordinates to Co(III) to take the *R*(*N*) configuration. This suggests that the repulsion between the pyrrolidine ring and the chair-conformed piperidine one is relaxed by the *R*(*N*) preference of the pipecolate chelate.

The *R*(*N*) preference in the sarcosinato and *N*-ethylglycinato complexes is vague in comparison with that in the (*S*)-pipecolato one, and so their PMR spectra were measured in D_2O. The singlet (at 2.28 ppm) due to the *N*-methyl group is observed for the sarcosinato complex, and the triplet (at 1.32 ppm) due to the *N*-ethyl group for the *N*-ethylglycinato complex. These spectral patterns indicate that, for both of the complexes, the nitrogen atom of the bidentate ligand takes either the *R* or *S* configuration. However, no further information was obtained. In order to estimate the configuration of the nitrogen atoms of the complexes, the vicinal CD curves due to the nitrogen atom were estimated for the (*R*)-prolinato, (*S*)-pipecolato, sarcosinato, and *N*-ethylglycinato complexes, namely, $\Delta\varepsilon(R\text{-pro}) - \Delta\varepsilon(R\text{-val})$ for *R*-pro, $\Delta\varepsilon(S\text{-pipec}) - \Delta\varepsilon(S\text{-val})$ for *S*-pipec, $\Delta\varepsilon(\text{sar}) - \Delta\varepsilon(\text{gly})$ for sar, and $\Delta\varepsilon(N\text{-et-gly}) - \Delta\varepsilon(\text{gly})$ for *N*-et-gly (Fig. 6). The vicinal CD curves are quite similar to each other. These results suggest that the nitrogen atoms of the (*S*)-pipecolate, sarcosinate, and *N*-ethylglycinate ions of the *Λ-uns-mer* type

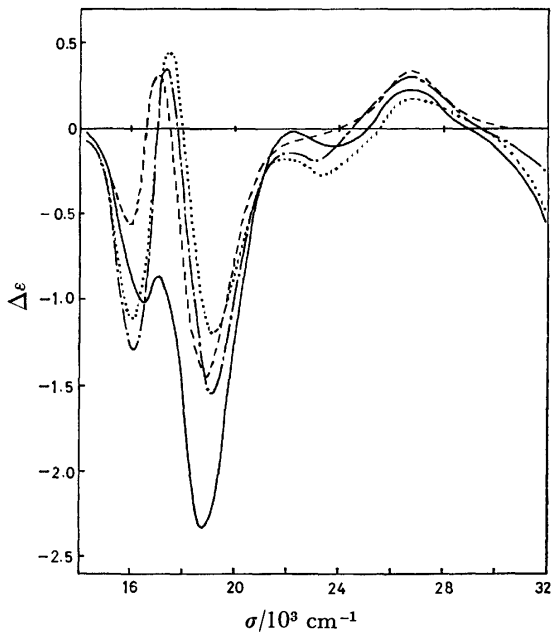

Fig. 6. Calculated vicinal CD curves of *Λ-uns-mer*-[Co(*S,S*-tmpro)(am)] complexes, *R*-pro (——), *S*-pipec (——) *N*-et-gly (-·-·-), and sar (------).

complexes coordinate selectively to Co(III) by means of the *R*(*N*) configuration.

References

1) J. I. Legg, D. W. Cooke, and B. E. Douglas, *Inorg. Chem.*, **6**, 700 (1967).
2) W. E. Keyes and J. I. Legg, *J. Am. Chem. Soc.*, **98**, 4970 (1976).
3) L. J. Halloran and J. I. Legg, *Inorg. Chem.*, **9**, 2193 (1974).
4) M. Okabayashi, K. Igi, and J. Hidaka, *Bull. Chem. Soc. Jpn.*, **52**, 753 (1979).
5) K. Igi and B. E. Douglas, *Inorg. Chem.*, **13**, 425 (1974).
6) K. Igi and B. E. Douglas, *Inorg. Chim. Acta*, **10**, 109 (1974).
7) L. N. Schoenberg, D. W. Cooke, and C. F. Liu, *Inorg. Chem.*, **7**, 2386 (1968).
8) J. P. Greenstein and M. Winitz, "Chemistry of the Amino Acids," John Wiley and Sons, New York (1961), Vol. 2, p. 2750.
9) K. Yonetani, Y. Hirotsu, and T. Shiba, *Bull. Chem. Soc. Jpn.*, **48**, 3302 (1975).
10) U. Nagai and Y. Kani, *Tetrahedron Lett.*, **1977**, 2333.
11) N. Matsuoka, J. Hidaka, and Y. Shimura, *Bull. Chem. Soc. Jpn.*, **40**, 1868 (1967).
12) C. J. Hawkins, "Absolute Configuration of Metal Complexes," Wiley-Interscience, New York, N. Y. (1971), p. 33.
13) J. R. Gollogly and C. J. Hawkins, *Inorg. Chem.*, **11**, 156 (1972).
14) M. Saburi and S. Yoshikawa, *Inorg. Chem.*, **7**, 1890 (1968).

Preparation and Spectral Properties of Oxovanadium(IV), Nickel(II), Copper(II), and Palladium(II) Complexes of Tetraaza[14]annulenes

Kazunori SAKATA,* Mamoru HASHIMOTO, Noriyoshi TAGAMI, and Yukito MURAKAMI*,†

Department of Chemistry, Kyushu Institute of Technology, Tobata-ku, Kitakyushu 804

†*Department of Organic Synthesis, Faculty of Engineering, Kyushu University, Hakozaki, Higashi-ku, Fukuoka 812*

(Received January 7, 1980)

The oxovanadium(IV), nickel(II), copper(II), and palladium(II) complexes of 5,14-dihydrodibenzo[*b,i*]-[1,4,8,11]tetraazacyclotetradecine and 7,8,15,16,17,18-hexahydrodibenzo[*b,j*][1,4,8,11]tetraazacyclotetradecine have been synthesized, and studied by electronic, vibrational, NMR, ESR, and ESCA spectroscopy. The absorption bands appearing in the energy region greater than 16800 cm^{-1} were attributed to $\pi \rightarrow \pi^*$ transitions within a ligand molecule and metal to ligand charge-transfer transitions. The ligand-field bands were not assigned for the present complexes, because all the ligand-field bands were obscured by the $\pi \rightarrow \pi^*$ and charge-transfer bands of high intensity. The metal complexes assume the square-planar configurations since no significant absorption band was detected in the region below 17000 cm^{-1}. A strong band appearing at *ca.* 1620 cm^{-1} was assigned to the C=N stretching mode, and this band was shifted to lower frequency upon metal coordination. A V=O streching band was observed at *ca.* 950 cm^{-1} for the oxovanadium complexes. The oxovanadium, nickel, copper, and palladium complexes showed a single nitrogen 1s peak by ESCA spectroscopy, whereas the metal-free ligand, 5,14-dihydrodibenzo[*b,i*][1,4,8,11]tetraazacyclotetradecine, revealed double nitrogen 1s peaks. ESR spectra were measured in xylene–benzene (2: 1 v/v) as well as in the corresponding ligand matrices at room temperature. Judging from *g* tensors, the copper complexes were confirmed to have D_{2h} coordination symmetry with an unpaired electron in the d_{xy} orbital. On the other hand, vanadium(IV) is in C_{4v} coordination symmetry with an unpaired electron in the $d_{x^2-y^2}$ orbital.

The naturally occurring macrocycles with N_4-donor atoms, porphyrins and corrins, may form metal complexes which involve four conjugated six-membered chelate rings (6^4 type) and three six- and one five-membered chelate rings (6^3-5 type), respectively. However, there are many N_4-macrocycles which can yield metal complexes having other combinations of chelate-ring sizes. The chemistry of metal porphyrins and metal corrins has been widely investigated up to the present time because of their biochemical interest.[1,2]

In the present work, we employed N_4-macrocycles which can form two six- and two five-membered chelate rings of 6-5-6-5 type; a 16 π-macrocyclic ligand, 5,14-dihydrodibenzo[*b,i*][1,4,8,11]tetraazacyclotetradecine (**1**), and a 12 π-macrocycle, 7,8,15,16,17,18-hexahydrodibenzo[*b,j*][1,4,8,11]tetraazacyclotetradecine (**2**). A number of π-electrons placed in the interior molecular skeleton of this type extends from none for the completely saturated system to 16 for complete conjugation.[3] Hiller *et al.*[4] and Green *et al.*[5] reported electronic and vibrational spectra of the nickel(II) and copper(II) of macrocyclic ligands **1** and **2** without assignments of characteristic bands. We characterized the spectral properties of the oxovanadium(IV), nickel(II), copper-(II), and palladium(II) complexes of the present macrocycles by means of electronic, vibrational, ESR, NMR, and ESCA spectroscopy. The characteristic coordination behavior of the present planar ligand has been discussed in reference to the ligand properties of porphyrins.

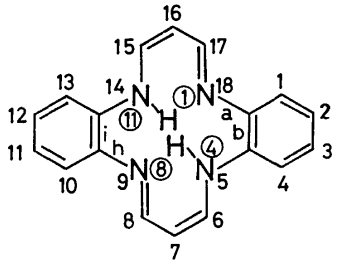

1

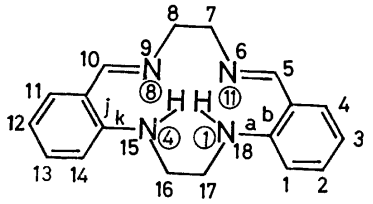

2

Experimental

5,14-Dihydrodibenzo[b,i][*1,4,8,11*]*tetraazacyclotetradecine(1).* Prepared after Hiller *et al.*[4] from 1,2-diaminobenzene (36.5 g) and 2-propynal (18.2 g)[6] in a mixed solvent composed of methanol (90 ml) and *N,N*-dimethylformamide (45 ml). The crystalline solid was washed with methanol (50 ml) and recrystallized from *N,N*-dimethylfomamide as glittering red needles; yield 11.0 g (23%). Found: C, 74.82; H, 5.57; N, 19.55%; M^+, 288.[7] Calcd for $C_{18}H_{16}N_4$: C, 74.98; H, 5.59; N, 19.43%; M, 288.35.

(Dibenzo[b,i][*1, 4, 8, 11*]*tetraazacyclotetradecinato) oxovanadium-(IV).* A mixture of **1** (0.50 g), vanadium (IV) chloride oxide (0.40 g), and *N,N*-dimethylformamide (80 ml) was heated under reflux for 5 h. To the filtrate of the hot mixture was added water (400 ml), and fine brown crystals were recovered; yield 0.47 g (77%). Found: C, 61.69; H, 4.09; N, 15.64%; M^+, 353.[7] Calcd for $C_{18}H_{14}N_4OV$: C, 61.20; H, 3.99; N, 15.86%; M, 353.28.

(Dibenzo[b,i][*1,4,8,11*]*tetraazacyclotetradecinato)nickel(II).* This complex was prepared from **1** (0.25 g) and nickel(II) acetate tetrahydrate (0.30 g) in the presence of sodium acetate trihydrate (0.50 g) and *N,N*-dimethylformamide (23 ml)

after Hiller *et al.*,[4] and recrystallized from *N,N*-dimethylformamide to give glittering violet plates; yield 0.28 g (94%). Found: C, 63.28; H, 4.11; N, 16.21%; M+, 344.[7] Calcd for $C_{18}H_{14}N_4Ni$: C, 62.66; H, 4.09; N, 16.24%; M, 345.05.

(Dibenzo[b,i]*[1,4,8,11]tetraazacyclotetradecinato)copper(II).* This was prepared from **1** (1.00 g) and copper(II) acetate monohydrate (2.25 g) in the presence of sodium acetate trihydrate (1.50 g) and *N,N*-dimethylformamide (100 ml) after Hiller *et al.*,[4] and recrystallized from *N,N*-dimethylformamide to give glittering dark red needles; yield 1.11 g (91%). Found: C, 61.85; H, 4.15; N, 15.98%; M+, 349.[7] Calcd for $C_{18}H_{14}N_4Cu$; C, 61.79; H, 4.03; N, 16.01%; M, 349.88.

(Dibenzo[b,i]*[1,4,8,11]tetraazacyclotetradecinato)palladium (II).* A mixture of **1** (0.50 g), palladium(II) chloride (0.40 g), and *N,N*-dimethylformamide (25 ml) was heated under reflux for 2 h. The hot mixture was filtered, and water (500 ml) was added to the filtrate. The precipitates were separated and washed with water (100 ml) and methanol (10 ml) to give pale brown needles; yield 0.24 g (35%). Found: C, 55.47; H, 3.91; N, 13.26%; M+, 392.[7] Calcd for $C_{18}H_{14}N_4Pd$; C, 55.05; H, 3.59; N, 14.27%; M, 392.74.

7,8,15,16,17,18-Hexahydrodibenzo[b,j]*[1,4,8,11]tetraazacyclotetradecine (2).* 1,2-Ethanediamine (1.2 ml) dissolved in methanol (100 ml) was added in 1.5 h to a mixture of zinc(II) acetate dihydrate (3.07 g), 2,2′-(ethylenediimino)dibenzaldehyde[8] (2.68 g), and methanol (300 ml) under reflux with stirring. The reaction mixture was refluxed for another 2 h with stirring. After the mixture was cooled down with ice–water, the precipitated crystalline solid was recrystallized from chloroform as colorless needles; yield 1.77 g (61%), mp 279—282 °C (dec). Found: C, 74.24; H, 6.90; N, 19.08%; M+, 292.[7] Calcd for $C_{18}H_{20}N_4$: C, 73.94; H, 6.89; N, 19.16%; M, 292.39.

(7,8,16,17-Tetrahydrodibenzo[b,j] [*1,4,8,11]tetraazacyclotetradecinato)oxovanadium(IV).* 1,2-Ethanediamine (1.07 ml) dissolved in methanol (50 ml) was added in 1 h to a mixture of vanadium (IV) chloride oxide (1.70 g), sodium acetate trihydrate (2.10 g), 2,2′-(ethylenediimino)dibenzaldehyde (1.07 g), and methanol (250 ml) under reflux with stirring. The reaction mixture was refluxed for another 1 h with stirring. After the solvent was evaporated off *in vacuo*, the residue was extracted with chloroform (300 ml), concentrated to *ca.* 10 ml *in vacuo*, and brown needles were obtained upon addition of methanol (35 ml); yield 0.08 g (6%). Found: C, 60.08; H, 5.09; N, 15.50%; M+, 357.[7] Calcd for $C_{18}H_{18}N_4OV$: C, 60.51; H, 5.08; N, 15.68%; M, 357.31.

(7,8,16,17-Tetrahydrodibenzo[b,j] [*1,4,8,11]tetraazacyclotetradecinato)nickel(II).* This was prepared from nickel(II) acetate tetrahydrate (2.49 g), 2,2′-(ethylenediimino) dibenzaldehyde (2.68 g), 1,2-ethanediamine (1.3 ml), and methanol (110 ml) after Green *et al.*,[5] and recrystallized from benzene–petroleum ether (3 : 1 v/v) as glittering dark brown needles; yield 2.38 g (68%). Found: C, 62.42; H, 5.05; N, 15.85%; M+, 348.[7] Calcd for $C_{18}H_{18}N_4Ni$: C, 61.93; H, 5.20; N, 16.05%; M, 349.08.

(7,8,16,17-Tetrahydrodibenzo [b,j][*1,4,8,11]tetraazacyclotetradecinato)copper(II).* This was prepared from copper(II) acetate monohydrate (1.00 g), 2,2′-(ethylenediimino)-dibenzaldehyde (1.34 g), 1,2-ethanediamine (0.67 ml), and methanol (40 ml) after Green *et al.*,[5] and recrystallized from benzene–petroleum ether (3 : 1 v/v) to give glittering dark brown plates; yield 0.75 g (42%). Found: C, 60.89; H, 5.09; N, 15.60%; M+, 353.[7] Calcd for $C_{18}H_{18}N_4Cu$: C, 61.09; H, 5.13; N, 15.83%; M, 353.91.

(7,8,16,17-Tetrahydrodibenzo[b,j][*1,4,8,11]tetraazacyclotetradecinato)palladium(II).* 1,2-Ethanediamine (0.33 ml) dissolved in methanol (10 ml) and sodium hydroxide (0.16 g in 0.5 ml H_2O) in methanol (10 ml) was added concurrently in 30 min to a mixture of palladium(II) chloride (0.36 g), 2,2′-(ethylenediimino)dibenzaldehyde (0.27 g), and methanol (20 ml) under reflux with stirring. The reaction mixture was refluxed for another 1 h with stirring, and cooled down with ice–water. The crystalline solid was recovered and extracted with chloroform (30 ml); upon addition of a 10-fold amount of methanol red needles were obtained; yield 0.09 g (23%). Found: C, 54.39; H, 4.49; N, 13.76%; M+, 396.[7] Calcd for $C_{18}H_{18}N_4Pd$: C, 54.49; H, 4.57; N, 14.12%, M, 396.77.

Spectral Measurements. Ultraviolet and visible spectra were recorded on a Shimadzu UV-200S double beam spectrophotometer at room temperature. Infrared spectra covering the 650—4000 cm^{-1} range were measured with a JASCO IRA-2 grating spectrophotometer at room temperature. A JEOL JNM-FX 60 spectrometer was used to obtain NMR spectra at room temperature and chemical shifts were reported in ppm from internal TMS. ESR spectra were recorded at room temperature on a JEOL JES-ME-1 X-band and a JEOL JES-ME-3 K-band spectrometer equipped with a 100 kHz field modulation unit. The copper(II) and oxovanadium(IV) complexes of **1** were doped in ($\approx$1 wt%) the isomorphous ligand, while the metal complexes of **2** were in ($\approx$1 wt%) the isomorphous nickel complex for measurements. All the ESR sensitive metal complexes were also measured in xylene–benzene (2 : 1 v/v) at room temperature. The manganese ion diffused into magnesium oxide was used to obtain standard reference signals for measurements. ESCA spectroscopy was performed on a Du Pont 650B spectrometer using a Mg $K\alpha$ irradiation unit. A signal due to Au $4f_{5/2.7/2}$ was used for calibration.

Results and Discussion

Electronic Spectra. Visible and ultraviolet spectra covering the 16000—32000 cm^{-1} region are shown in Figs. 1 and 2 for the metal chelates of 5,14-dihydrodibenzo[*b,i*][1,4,8,11]tetraazacyclotetradecine (**1**) and 7,8,15,16,17,18-hexahydrodibenzo[*b,j*][1,4,8,11]tetraazacyclotetradecine (**2**), respectively, and the absorption bands appearing in the energy region greater than 16800 cm^{-1} are reasonably attributed to $\pi \rightarrow \pi^*$ transitions within a ligand molecule and charge-transfer transitions from metal to ligand. General feature of the spectra for the 16π-macrocycle (**1**) system is similar to those observed for metal porphyrins.[9,10] An extremely intense absorption band observed in the 23000—26000 cm^{-1} region is assigned to the so-called Soret-type transition, and a pair of weaker bands in the 19000—24000 cm^{-1} region are to the α- and β-type transitions (Table 1). The α, β, and Soret bands for the metal chelates of **1** are located in a higher energy region than those for the corresponding metal porphyrins. The oxovanadium(IV), nickel(II), copper(II), and palladium(II) complexes do not show any significant absorption in the region lying below *ca.* 17000 cm^{-1}. The spectral behavior is consistent with the square-planar coordination.[11]

The spectral features for the metal complexes of 12π-macrocycle **2** are quite different from those for metal porphyrins. The nickel(II) complex shows a spectrum similar to those observed for the nickel(II)–amben complex (**3**).[5,12,13] It is rather difficult at present to make exact assignments of absorption bands observed

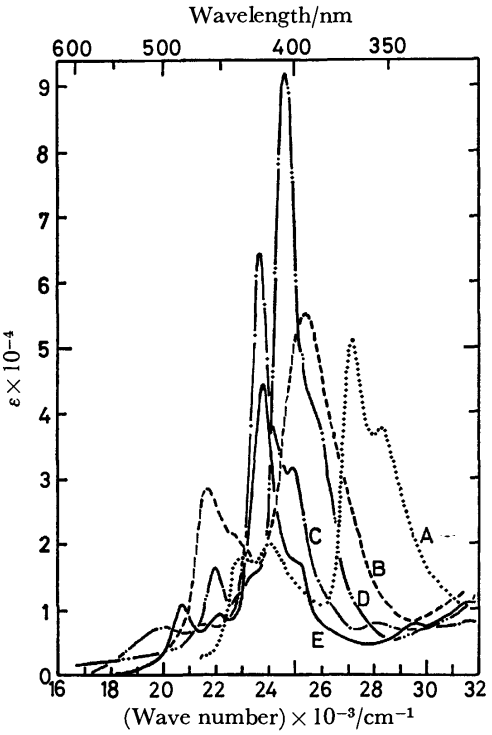

Fig. 1. Electronic absorption spectra of 5,14-dihydrodibenzo[*b*,*i*][1,4,8,11]tetraazacyclotetradecine chelates in *N*,*N*-dimethylformamide at room temperature.
A: Ligand, B: oxovanadium(IV), C: nickel(II), D: copper(II), E: palladium(II).

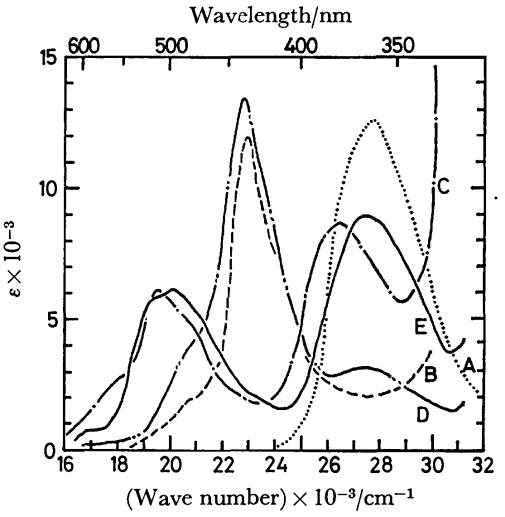

Fig. 2. Electronic absorption spectra of 7,8,15,16,17,18-hexahydrodibenzo[*b*,*j*][1, 4, 8, 11] tetraazacyclotetradecine chelates in benzene at room temperature.
A: Ligand, B: oxovanadium(II), C: nickel(II), D: copper(II), E: palladium(II).

in the visible and near UV regions, we tentatively assign intensive bands in the 18000—30000 cm^{-1} region

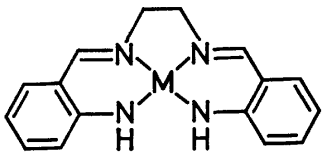

3

to charge-transfer and/or $\pi \rightarrow \pi^*$ transitions (Table 1). A low energy band, which is attributable to a ligand-field transition was observed only for the copper(II) and palladium(II) at 16900 (ε 700) and 15400 (ε 220) cm^{-1}, respectively.

Vibrational Spectra. The characteristic IR absorption bands for the present discussion are summarized in Table 2 together with those for Ni(amben)[13] and Ni(porphine).[14] The metal-free macrocycles show a weak band at *ca.* 3200 cm^{-1} which is associated with a N–H stretching mode in a manner as observed for the metal-free porphyrins.[15] This vibrational mode disappears upon complex formation.

A strong absorption band observed in the 1600 cm^{-1} region can be attributed to the stretching mode of C=N bond. This band is most sensitive to metal-coordination among the absorption peaks appearing in the NaCl region, and shifts significantly to lower frequency upon

Table 1. Characteristic absorption bands in the visible and near UV regions for the oxovanadium(IV), nickel(II), copper(II), and palladium(II) complexes of macrocycles **1** and **2**[a,b]

Metal	Transition energy in cm^{-1} (ε)			
	Macrocyclic ligand (**1**)[c]		Macrocyclic ligand (**2**)[d]	
	α-Band β-Band	Soret band	Charge-transfer/$\pi \rightarrow \pi^*$	
VO(IV)	21700 (28700) 22700sh (21600)	25400 (55600)	23000 (11900)	
Ni(II)	19900 (7200) 21600 (7620)	23600 (64400)	19600 (6110)	26500 (8680)
Cu(II)	22000 (16400) 23500sh (15740)	24700 (92100)	20800sh (4000) 27200 (3100)	22800 (13400)
Pd(II)	20700 (10900) 22100 (9570)	23800 (44600)	19600sh (5930) 20200 (6070)	27600 (8880)

a) **1**, 5,14-Dihydrodibenzo[*b*,*i*][1,4,8,11] tetraazacyclotetradecine; **2**,7,8,15,16,17,18-hexahydrodibenzo [*b*,*j*][1,4,8,11]tetraazacyclotetradecine. b) The most intense band observed for metal-free ligands: **1**, 27200 cm^{-1} (ε 51300); **2** 27800 cm^{-1} (ε 12700). c) Measured in *N*,*N*-dimethylformamide at room temperature. d) Measured in benzene at room temperature.

Table 2. Characteristic IR absorption bands for the oxovanadium(IV), nickel(II), copper(II), and palladium(II) complexes of macrocycles[a,b]

Ligand[c]	Metal	IR-band (cm^{-1})	Assignment	Ref.
1		1544(s)	$\nu_{C=C,C=N}$(macrocyclic skeletal)	
		1587(w)	$\nu_{C=C}$(conjugated ring)	
		1626(s)	$\nu_{C=N}$	
		3200(w)	ν_{N-H}	
1	VO^{IV}	967(s)	$\nu_{V=O}$	
		1448(s,br),1461(s,br)	$\nu_{C=C,C=N}$(macrocyclic skeletal)	
		1575(m)	$\nu_{C=N}$	
		1592(w)	$\nu_{C=C}$(conjugated ring)	
1	Ni^{II}	1460(s,br),1473(s,br)	$\nu_{C=C,C=N}$(macrocyclic skeletal)	
		1574(w)	$\nu_{C=N}$	
		1591(w)	$\nu_{C=C}$(conjugated ring)	
1	Cu^{II}	1452(m),1480(s,br)	$\nu_{C=C,C=N}$(macrocyclic skeletal)	
		1574(w)	$\nu_{C=N}$	
		1590(w)	$\nu_{C=C}$(conjugated ring)	
1	Pd^{II}	1440(s,br),1460(s,br)	$\nu_{C=C,C=N}$(macrocyclic skeletal)	
		1571(m)	$\nu_{C=N}$	
		1587(w)	$\nu_{C=C}$(conjugated ring)	
2		1581(s)	$\nu_{C=C,C=N}$(macrocyclic skeletal)	
		1623(s)	$\nu_{C=N}$	
		3260(w)	ν_{N-H}	
2	VO^{IV}	940(m)	$\nu_{V=O}$	
		1528(w)	$\nu_{C=C,C=N}$(macrocyclic skeletal)	
		1606(s)	$\nu_{C=N}$	
2	Ni^{II}	1509(w)	$\nu_{C=C,C=N}$(macrocyclic skeletal)	
		1606(s)	$\nu_{C=N}$	
2	Cu^{II}	1510(w)	$\nu_{C=C,C=N}$(macrocyclic skeletal)	
		1609(s)	$\nu_{C=N}$	
2	Pd^{II}	1510(w)	$\nu_{C=C,C=N}$(macrocyclic skeletal)	
		1601(s)	$\nu_{C=N}$	
Amben[d]	Ni^{II}	1537(s)	$\nu_{C=C}$(aromatic)	13
		1593(s)	$\nu_{C=N}$	
Porphine	Ni^{II}	1547(m)	$\nu_{C=C,C=N}$	14
		1547(m)	$\nu_{C=C}$	

a) Measured by KBr disk method at room temperature. b) Relative intensities: s, strong; m, medium; w, weak; br, broad. c) See Table 1 for numbering the ligands **1** and **2**. d) Amben, *N,N'*-ethylenebis(*o*-aminobenzylideneiminato).

metal-coordination. Such a spectral feature has been observed for Ni(amben),[13] but is not clear for metal porphyrins.[15] The magnitude of these frequency-shifts with respect to metal ions follows the sequence in an increasing order: Cu(II)≲VO(IV)≲Ni(II)≲Pd-(II). For the 5,14-dihydrodibenzo[*b,i*][1,4,8,11]tetra-azacyclotetradecine system, this characteristic band reduces its intensity to medium upon metal coordination. On the other hand, the C=N band observed for 12π-macrocyclic ligand **2** does not lose its intensity upon complex formation. The formation of a square-planar complex with higher conjugation system seems to be responsible for such reduction in IR activity.

A strong absorption band at around 950 cm^{-1} observed for the oxovanadium(IV) complexes is attributed to the V=O stretching mode.[16,17]

NMR Spectra. NMR data for macrocyclic ligands **1** and **2** and the nickel(II) and palladium(II) chelates of the latter ligand are listed in Table 3 along with the comparable data for Ni(II) ambtn,[13] zinc(II) dipyrromethene,[18] and nickel(II) porphyrin.[19,20] The complexes of macrocycle **1** are too insoluble to give satisfactory NMR spectra. The methine proton peak for **1** observed in the lower field region is shifted to down-field by *ca.* 1 ppm relative to that of dipyrromethenes (free base).[18] As the extent of down-field shift is smaller than that for porphyrins, the cyclic conjugation throughout the macrocyclic skeleton of **1** seems to be not so extensive as observed for porphyrins. In the case of **1**, the proton signals for methine groups (=CH–

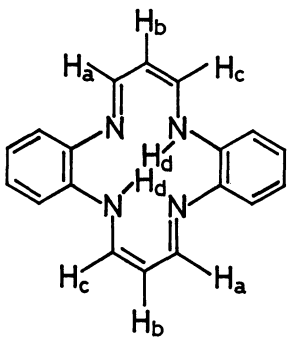

4

NH–, –CH=N–) of the 6-, 8-, 15-, and 17-positions were observed as a quintet. The H_a-methine proton (–CH=N–) shown by **4** couples with the H_b-methine proton (–CH=CH–), and the H_a-signal is split into a symmetrical doublet. On the other hand, the H_c-methine proton (–CH=NH–) couples both with H_b-(–CH=CH–) and H_d- (N–H), the H_c-signal being split into a triplet. Consequently, the quintet signal is referred to the overlap of a doublet and a triplet signal. The coupling of H_b- (–CH=CH–) with H_a- and H_c- seems to result in a triplet signal for H_b. A signal for the H_d-amine proton (N–H) was observed as a broad triplet with equal intensity due to coupling with the nitrogen nucleus ($I=1$).

The signal (9.27 ppm) for protons attached to the aniline-type nitrogen in **2** was found to disappear upon metal-coordination. The methine proton peak (8.32 ppm) observed for macrocycle **2** in the lowest field is shifted to up-field by 0.3 (palladium complex)—0.6 ppm (nickel complex) upon complex formation. This up-field shift is comparable to that observed for the meso-methine protons of nickel(II) porphyrin (Table 3).[19] This may be attributed to reduction of the ring current by incorporation of the nickel or the palladium. The shielding effect by nickel(II)-coordination is larger than that by palladium(II)-coordination. The metal-free macrocycle (**2**) showed the H_a-signal (refer to **5**) in the highest field (3.37 ppm) with some broadening. Upon substitution of the H_b proton on the nitrogen(–NH–) with deuterium(D), the H_a-signal at 3.37 ppm turned to be sharp. A similar spectral change was observed upon nickel(II)- and palladium(II)-coordination. Accordingly, the H_a protons(–CH_2–NH–) placed at the 16- and 17-positions must couple with the H_b protons(–CH_2–NH–) placed at the 15- and 18-positions, and the H_a protons absorption is observed as a broad signal owing to a small proton spin-coupling constant (J_{ab}). The H_a- and H_c-signals(=N–CH_2–, –CH_2–NH–) show down-field shift upon formation of the palladium chelate. These down-field shifts can be attributed to the deshielding effect provided by the positive charge on palladium-(II). The H_a- and H_c-(methylene protons) peaks are shifed to up-field upon formation of the nickel(II) complex. These up-field shifts can be attributed to the significant shielding effect provided by the chelate rings rather than the deshielding effect due to the positive charge on nickel(II). This seems to indicate that the methylene groups of the nickel(II) complex are placed in a conformational space different from that occupied by those of the palladium(II) complex, most likely due to the difference in ionic radius between Ni^{2+} and Pd^{2+}.

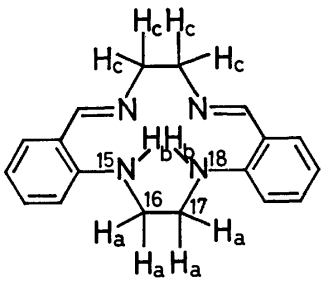

5

ESCA Spectra. For macrocyclic ligands **1** and **2** and their complexes, binding energies of carbon(C $1s_{1/2}$), nitrogen(N $1s_{1/2}$), vanadium(V $2p_{1/2}$, $2p_{3/2}$), oxygen(O $1s_{1/2}$), nickel(Ni $2p_{1/2}$, $2p_{3/2}$), copper(Cu $2p_{1/2}$, $2p_{3/2}$), and palladium(Pd $3p_{1/2}$, $3p_{3/2}$) are listed in Tables 4 and 5 together with those for 5,10,15,20-tetraphenylporphine, phthalocyanine, and their copper(II) complexes.[21] There are these possible structure as to the location of inner hydrogen atoms in macrocycles **1** and **2** (Fig. 3). Macrocyclic ligand **1** shows two N 1s peaks

TABLE 3. PROTON NMR DATA FOR NICKEL(II), AND PALLADIUM(II) COMPLEXES OF MACROCYCLES[a]

Ligand[b]	Sample	Amine –NH	Methine =CH–NH–	Methine –CH=N–	Methine –CH=C–	Aromatic	Methylene =N–CH_2–	Methylene –CH_2–NH–	Methylene –CH_2–C–	Ref.
1	ligand[c]	13.63(3)[e] (J=6.2Hz)	7.664(3)[e] (J=6.2Hz)	7.657(2)[e] (J=6.2Hz)	4.97(3)[e] (J=6.2Hz)	7.13—6.73(m)				
2	ligand[d]	9.27br		8.32		7.47—6.43(m)	3.76	3.37br		
2	Ni-chelate[d]			7.74		7.37—6.13(m)	3.49	3.36		
2	Pd-chelate[d]			7.99		7.53—6.20(m)	3.85	3.75		
MP	ligand[d]	−3.91			10.095					19,20
MP	Ni-chelate[d]				9.805					19
Ambtn	Ni-chelate[d]	6.06br		7.64		7.2—6.4(m)	3.53(3)[e] (J=6.0Hz)		1.85(5)[e] (J=6.0Hz)	13
DM	ligand				6.62					18
DM	Zn-chelate[d]				6.98					18

a) Chemical shifts are given in ppm for TMS. b) MP, mesoporphyrin IX dimethyl ester; Ambtn, *N,N'*-trimethylene-bis(*o*-aminobenzylideneiminato); DP, 3,3',4,4',5,5'-hexamethyldipyrromethene. c) Measured in dimethyl sulfoxide-d_6 with TMS as an internal reference. d) Measured in chloroform-*d* with TMS as an internal reference. e) Multiplicity of a proton signal is given in parentheses after δ-value.

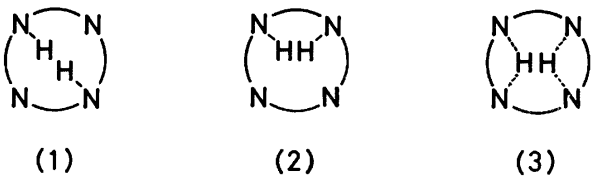

(1) (2) (3)

Fig. 3. Three possible structures arising from the location of inner hydrogen atoms of macrocycles.
(1) Two inner hydrogen atoms are directly bound to diagonally opposite nitrogen atoms.
(2) Two inner hydrogen atoms are fixed to adjacent nitrogen atoms.
(3) Two inner hydrogen atoms are shared by four equivalent central nitrogen atoms.

(396.0, 397.2 eV) (Table 4) with nearly equal intensity. The general feature of a nitrogen 1s peak is similar to those observed for porphyrins and phthalocyanine.[21,23-25] Moreover, the ^{1}H-NMR spectrum shows the presence of two kinds of nitrogen atoms as judged by the methine proton signal (Table 3). Consequently, there are two kinds of nitrogen atoms in macrocycle **1**; the one without hydrogen atom, and the other with hydrogen attached. Our result rules out any structure with hydrogen bridges, yielding equivalent nitrogens (Fig. 3-(3)), although the possibility of forming intramolecular hydrogen bonding is not eliminated. A structure of type(2) in Fig. 3 must be ruled out, since this destroys π-conjugation of the ligand. The most plausible molecular structure for macrocycle **1** is type(1) in Fig. 3; two inner hydrogen atoms are bound to nitrogen at diagonal positions.

Since macrocyclic ligand **2** shows only one N 1s peak at 397.5 eV as shown in Table 4, this feature is different from those observed for porphyrins, phthalocyanine, and macrocycle **1**. The tautomeric effect (refer to **6**) which provide only equivalent nitrogens seems to be responsible for the existance of one N 1s signal (type(3) in Fig. 3).

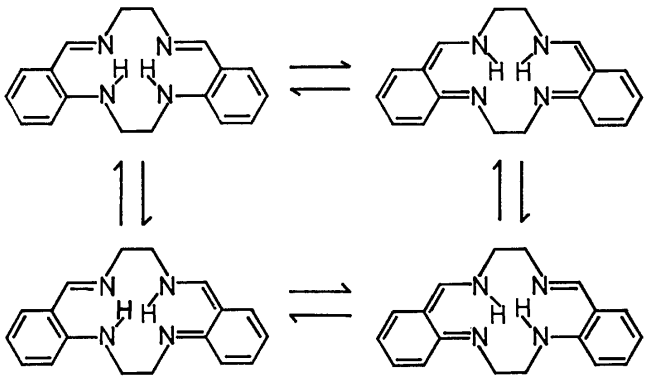

6

As shown in Table 4, only one N 1s peak was observed for the macrocyclic chelates; namely, the four nitrogens are chemically equivalent in these complexes. The nitrogen 1s peak observed in the 397—398 eV region for the bivalent metal chelates does not appreciably vary the peak position by changing metal species as

Table 4. Carbon and nitrogen core-electron binding energies for macrocyclic and their metal complexes[a]

Ligand[b]	Sample	Binding energy in eV		Ref.
		C $1s_{1/2}$	N $1s_{1/2}$	
1	ligand	282.7	396.0,397.2	
1	VO-chelate	283.5	397.3	
1	Ni-chelate	284.0	397.8	
1	Cu-chelate	284.0	397.7	
1	Pd-chelate	283.9	397.9	
2	ligand	283.8	397.5	
2	VO-chelate	284.0	397.8	
2	Ni-chelate	283.9	397.4	
2	Cu-chelate	283.4	396.8	
2	Pd-chelate	283.8	397.6	
TPP	ligand	284.8	398.2,400.2	21
TPP	Cu-chelate	284.8	398.9	21
PC	ligand	284.8,286.2	398.9,400.4	21
PC	Cu-chelate	284.8,286.2	399.2	21

a) Measured in the tablet state (5-mm diameter); for calibration, the signal of Au $4f_{5/2}$ and Au $4f_{7/2}$ was used.
b) See Table 1 for numbering the ligands **1** and **2**; TPP, 5,10,15,20-tetraphenylporphine; PC, phthalocyanine.

shown in Table 4. Our result is comparable to those obtained for porphyrins.[21,23-25] The N 1s peak for porphyrins and phthalocyanine is somewhat shifted to higher energy because of high π-conjugation.

ESR Spectra. Oxovanadium(IV) Complex: In the ESR spectra of macrocyclic oxovanadium(IV) complexes measured in xylene–benzene (2 : 1 v/v) at room temperature, a set of eight hyperfine lines were observed by the magnetic interaction between an unpaired electron and vanadium nucleus ($I=7/2$). The similar spectral features have been observed for (5,10,15,20-tetraphenylporphinato)oxovanadium(IV) complex.[26] Figure 4 shows the ESR spectrum recorded at room temperature for the powdered sample of (dibenzo[*b*,*i*]-[1,4,8,11]tetraazacyclotetradecinato)oxovanadium(IV) magnetically diluted with the corresponding ligand as an example. This spectrum is composed of two sets of vanadium hyperfine lines; $g_{//}$ and $g_{\perp}$ components.

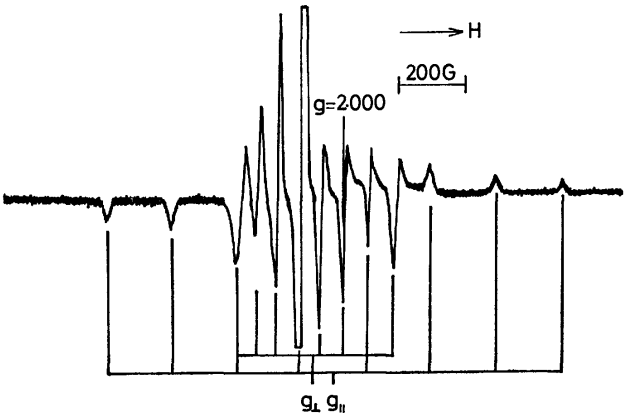

Fig. 4. ESR spectrum of (dibenzo[*b*, *i*][1, 4, 8, 11]tetraazacyclotetradecinato)oxovanadium(IV) complex magnetically diluted with the corresponding metal-free ligand at room temperature.

TABLE 5. METAL 2p, 3p, AND OXYGEN 1s BINDING ENERGIES FOR METAL-MACROCYCLIC COMPLEXES[a)]

Compound[b)]	Binding energy in eV								
	V $2p_{1/2}$	V $2p_{3/2}$	O $1s_{1/2}$	Ni $2p_{1/2}$	Ni $2p_{3/2}$	Cu $2p_{1/2}$	Cu $2p_{3/2}$	Pd $3p_{1/2}$	Pd $3p_{3/2}$
V-metal	520[c)]	513[c)]							
O			532[c)]						
1-VO-chelate	521.8	514.8	529.3						
2-VO-chelate	522.1	514.6	531.2						
Ni-metal				872[c)]	855[c)]				
1-Ni-chelate				871.0	853.5				
2-Ni-chelate				871.1	853.9				
Cu-metal						951[c)]	931[c)]		
1-Cu-chelate						953.0	933.1		
2-Cu-chelate						953.0	933.0		
Pd-metal								559[c)]	531[c)]
1-Pd-chelate								557.0	531.5
2-Pd-chelate								561.7	534.1

a) Measured in the tablet state (5-mm diameter); for calibration, the signal of Au $4f_{5/2}$ and Au $4f_{7/2}$ was used. b) See Table 1 for numbering the ligands. c) Values reported in Ref. 22.

The superhyperfine splitting, due to magnetic interaction between an unpaired electron in V(IV) and nitrogen nuclei($I=1$), has not been observed in the present oxovanadium(IV) complexes. Consequently, the oxovanadium(IV) complexes are of square-planar type with an unpaired electron in the $d_{x^2-y^2}$ orbital. The similar spectral features have also been observed for the complexes derived from porphyrins[26–28] and phthalocyanine.[29] A plausible structure around the coordination site for the oxovanadium(IV) complexes are illustrated schematically by (**7**) except for V=O on

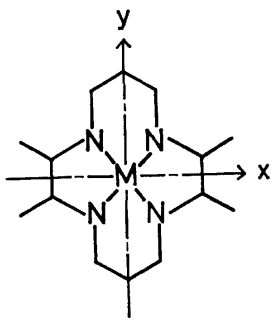

7

z-axis. Since the spin-orbit coupling constant is much smaller than the orbital excitation energies, the first-order perturbation can be applied to our system for evaluation of g values

$$g_z = g_0 - 8\lambda/\Delta_3 = g_{\parallel} \quad (1)$$

$$\left.\begin{aligned} g_x &= g_0 - 2\lambda/\Delta_2 \\ g_y &= g_0 - 2\lambda/\Delta_1 \end{aligned}\right\} = g_{\perp} \quad (2), (3)$$

where $\Delta_3=\Delta E(d_{xy}\leftarrow d_{x^2-y^2})$, $\Delta_2=\Delta E(d_{xz}\leftarrow d_{x^2-y^2})$, $\Delta_1=\Delta E(d_{yz}\leftarrow d_{x^2-y^2})$, and λ is the spin-orbit coupling constant of V^{4+} ion. The g ($g_{//}$ and $g_{\perp}$) and A ($A_{//}$ and $A_{\perp}$) values for the oxovanadium(IV) complex of macrocycle **1** are in agreement with those obtained for the complex of macrocycle **2** as shown in Table 6. The $g_{//}$ and $g_{\perp}$ values in this work are slightly larger in magnitude than those obtained for the complexes of 5,10,15,20-tetraphenylporphine and phthalocyanine, but the $A_{//}$ and $A_{\perp}$ values are smaller.[26,29] The $|g_0-g_{//}|$ values in this work are comparable to those obtained for the complexes of 5,10,15,20-tetraphenylporphine[26] and phthalocyanine.[29] This may be attributed to equivalent Δ_3 (refer to Eq. 1) value for the complexes of the present macrocycles, 5,10,15,20-tetraphenylporphine, and phthalocyanine. The $|g_0-g_{\perp}|$ values in this work are smaller in magnitude than those obtained for the complexes of 5,10,15,20-tetraphenylporphine and phthalocyanine (Table 6). On the basis of Eqs. 2 and 3, the Δ_1 and Δ_2 values obtained in this work are larger than those for the complexes of 5,10,15,20-tetraphenylporphine and phthalocyanine. Namely, the relative energy level of d_{xy}, d_{yz} is higher than those estimated for the 5,10,15,20-tetraphenylporphine and phthalocyanine complexes.

Copper(II) Complex. The ESR spectra of (dibenzo[*b*,*i*][1,4,8,11]tetraazacyclotetradecinato) copper(II) magnetically diluted with the corresponding metal-free ligand at room temperature are shown in Fig. 5 as an example. The general feature of spectra (A) and (B) is similar to that observed for the square-planar copper(II) complexes derived from porphyrins[26,30] and phthalocyanine.[31] In these two spectra, a set of four copper hyperfine lines on the parallel component of the g-tensor($g_{//}$), which lie in the low field region, are observed, while such hyperfine lines are not obvious on the perpendicular component of the g-tensor($g_{\perp}$) in the higher field region. The X- and K-band ESR spectra shown in Fig. 5 indicates that the $g_{\perp}$-tensor is of anisotropic nature; D_{2h} coordination symmetry. In addition, superhyperfine lines due to four chemically equivalent nitrogen donor atoms, appear on the perpendicular component of the g-tensor($g_{\perp}$, g_2, and g_3) at higher field, while such superhyperfine lines are not observed on the parallel component of the g-tensor($g_{//}$) at lower field. As judged from the general feature of superhyperfine lines, it may be concluded that an unpaired electron of the copper(II)

Table 6. Spin Hamiltonian parameters for oxovanadium(IV) and copper(II) complexes of macrocycles[a,b]

Ligand[c]	Metal	Medium	$\bar{g}$	$\lvert g_0-g_{//}\rvert$	$\lvert g_0-g_{\perp}\rvert$	$\bar{A}\times 10^4\mathrm{cm}^{-1}$	$A_{//}\times 10^4\mathrm{cm}^{-1}$	$A_{\perp}\times 10^4\mathrm{cm}^{-1}$	$A_{\perp}^{N}\times 10^4\mathrm{cm}^{-1}$	Ref.
1[f]	VO	xylene–benzene[d]	1.989			86.1				
1[f]	VO	ligand(**1**)[e]		0.035	0.004		150.0	52.8		
2[f]	VO	xylene–benzene[d]	1.989			86.3				
2[f]	VO	Ni(II)complex[e]		0.031	0.003		149.4	53.2		
H_2TPP[f]	VO	$CHCl_3$	1.9797			89.4				26
H_2TPP[f]	VO	H_2TPP[c]		0.036	0.017		161	55		26
1[f]	Cu	xylene–benzene[d]	2.089			96.4				
1[f]	Cu	ligand(**1**)		0.128	0.033,0.010		218.0		7.3	
1[g]	Cu	ligand(**1**)		0.126	0.029,0.009		219.0		7.1	
2[f]	Cu	xylene–benzene[d]	2.089			96.0				
2[f]	Cu	Ni(II)complex[e]		0.133	0.040,0.008		208.7		15.6	
H_2TPP[f]	Cu	$CHCl_3$	2.1073			97.7			15.9	26
H_2TPP[f]	Cu	H_2TPP[c]		0.191	0.069		202		14.5	26

a) Measured at room temperature. b) Maximum possible essors: g, ± 0.0005; $\bar{A}$,$A_{//}$, $\pm 0.5\times 10^{-4}$ cm^{-1}; $A_{\perp}$,$A_{\perp}^{N}$, $\pm 0.05\times 10^{-4}$cm^{-1}. c) See Table 1 for numbering the ligands **1** and **2**; H_2TPP, 5,10,15,20-tetraphenylporphine. d) Concentration of the complex, 10^{-3}—10^{-4} mol/l (xylene–benzene; 2: 1 v/v). e) (7,8,16,17-Tetrahydrodibenzo[*b*, *j*] [1,4,8,11] tetraazacyclotetradecinato)nickel(II)complex. f) X-Band microwave. g) K-Band microwave.

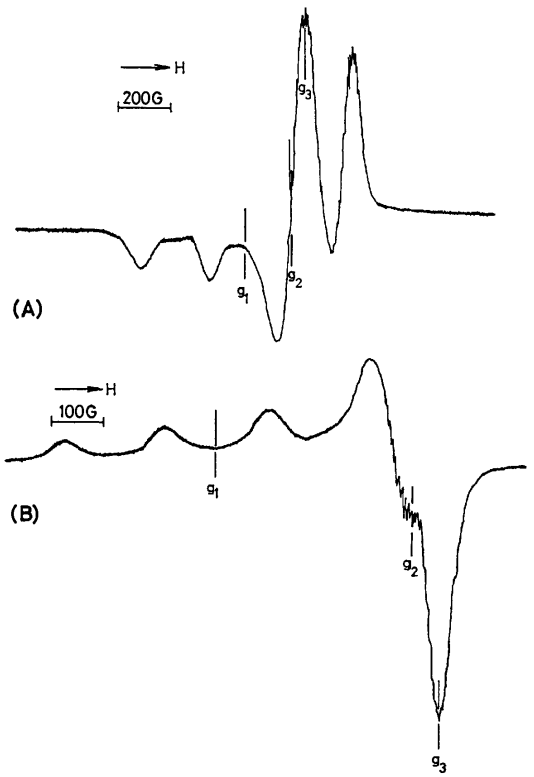

Fig. 5. ESR spectrum of (dibenzo[*b*,*i*][1,4,8,11]tetraazacyclotetradecinato)copper (II) complex magnetically diluted with the corresponding metal-free ligand at room temperature.
(A): X-Band microwave, (B): K-band microwave.

complex is placed in its d_{xy} orbital.

Although the $g_{//}$ and $g_{\perp}$ values are somewhat smaller in magnitude than those observed for the complexes derived from porphyrins[26,30] and phthalocyanine,[31] the Δg value ($\Delta g=g_{//}-g_{\perp}$) is approximately equal in magnitude to those of porphyrin complexes and phthalocyanine complex. Moreover, the $A_{//}$ value is somewhat larger in magnitude than those reported for porphyrin complexes[26,30] and phthalocyanine complex.[31] This is attributed to the greater electron density of the unpaired electron of copper(II) nucleus. The K-band ESR spectrum for the magnetically diluted powdered sample indicates the presence of three g values such as g_z, g_y, g_x as shown in Fig. 5-(B). If the coordination symmetry is D_{2h} (refer to **7**), these values are expected to be $g_z > g_y$, g_x ($g_x \neq g_y$). On this basis, the copper atom most plausibly assumes a distorted square-planar coordination of Cu–N_4 type due to the presence of five- and six-membered chelate rings. Furthermore, the five- and six-membered chelate rings are placed in the same plane, so that efficient π-conjugation is attained in the macrocyclic ligand moiety. The $A_{\perp}^{N}$ value for the complex of macrocycle **1** is about a half of the one observed for the complexes derived from porphyrins[26,31] and phthalocyanine,[31] but the $A_{\perp}^{N}$ value for the complex of macrocycle **2** is similar in magnitude to those for the porphyrins and phthalocyanine complexes. Consequently, the metal d-electrons in the copper(II) complex are more delocalized toward the ligand moiety through the coordinate bonds in a manner as expected for the corresponding complexes of **2**.

References

1) J. E. Falk, "Porphyrins and Metalloporphyrins," Elsevier Publishing Co., Amsterdam (1964).

2) For dehydrocorrins and corroles: (a) Y. Murakami, K. Sakata, Y. Tanaka, and T. Matsuo, *Bull. Chem. Soc. Jpn.*, **48**, 3622 (1975); (b) Y. Murakami and Y. Aoyama, *Bull. Chem. Soc. Jpn.*, **49**, 683 (1976); (c) Y. Murakami, S. Yamada, Y. Matsuda, and K. Sakata, *Bull. Chem. Soc. Jpn.*, **51**, 123 (1978); (d) N. S. Hush and I. S. Woolsey, *J. Am. Chem. Soc.*, **94**, 4107 (1972); (e) N. S. Hush and I. S. Woolsey, *J. Chem. Soc., Dalton Trans.*, **1972**, 24. For corrins: (f) J. M. Pratt, "Inorganic Chemistry of Vitamin B_{12}," Academic Press, London (1972).

3) T. J. Truex and R. H. Holm, *J. Am. Chem. Soc.*, **94**, 4529 (1972).

4) H. Hiller, P. Dimroth, and H. Pfitzner, *Liebigs Ann. Chem.*, **717**, 137 (1968).

5) M. Green and P. A. Tasker, *Inorg. Chim. Acta*, **5**, 65 (1971).
6) C. Sauer, *Org. Synth.*, Coll. Vol. IV, 813 (1963).
7) Mass spectral measurements were carried out with a GCMS-9000 gas chromatograph-mass spectrometer.
8) M. Green, J. Smith, and P. A. Tasker, *Inorg. Chim. Acta*, **5**, 17 (1971).
9) L. Edwards, D. H. Dolphin, and M. Gouterman, *J. Mol. Spectrosc.*, **35**, 90 (1970).
10) C. Weiss, H. Kobayashi, and M. Gouterman, *J. Mol. Spectrosc.*, **16**, 415 (1965).
11) A. B. P. Lever, "Inorganic Electronic Spectroscopy," Elsevier Publishing Co., Amsterdam (1968).
12) M. Green and P. A. Tasker, *Discuss. Faraday. Soc.*, **47**, 172 (1969).
13) M. Green and P. A. Tasker, *J. Chem. Soc., A*, **1970**, 2531.
14) H. Ogoshi, Y. Saito, and K. Nakamoto, *J. Chem. Phys.*, **57**, 4194 (1972).
15) L. J. Boucher and J. J. Katz, *J. Am. Chem. Soc.*, **89**, 1340 (1967).
16) K. Nakamoto, "Infrared Spectra of Inorganic and Coordination Compounds," John Wiley and Sons, Inc., New York (1970), p. 114.
17) J. G. Erdman, V. G. Ramsey, N. W. Kalenda, and W. E. Hanson, *J. Am. Chem. Soc.*, **78**, 5844 (1956).
18) Y. Murakami and K. Sakata, *Bull. Chem. Soc. Jpn.*, **47**, 3025 (1974).
19) D. A. Doughty and C. W. Dwiggins, Jr., *J. Phys. Chem.*, **73**, 423 (1969).
20) E. D. Becker, R. B. Bradley, and C. J. Watson, *J. Am. Chem. Soc.*, **83**, 3743 (1961).
21) Y. Niwa, H. Kobayashi, and T. Tsuchiya, *J. Chem. Phys.*, **60**, 799 (1974).
22) K. Siegbahn, C. Nordling, A. Fahlman, R. Nordberg, K. Hamrin, J. Hedman, G. Johansson, T. Bergmark, S. E. Karlsson, I. Lindgran, and B. Lindberg, "Electrion Spectroscopy for Chemical Analysis-Atomic, Molecular, and Solid State Structure Studies by Means of Electron Spectroscopy," Almqvist and Wiksell, Uppsala (1969).
23) M. V. Zeller and R. G. Hayes, *J. Am. Chem. Soc.*, **95**, 3855 (1973).
24) D. Karweik, N. Winograd, D. G. Davis, and K. M Kadish, *J. Am. Chem. Soc.*, **96**, 591 (1974).
25) J. P. Macquet, M. M. Millard, and T. Theophanides, *J. Am. Chem. Soc.*, **100**, 4741 (1978).
26) J. M. Assour, *J. Chem. Phys.*, **43**, 2477 (1965).
27) E. M. Roberts, W. S. Koski, and W. S. Caughey, *J. Chem. Phys.*, **34**, 591 (1961).
28) D. Kivelson and S. K. Lee, *J. Chem. Phys.*, **41**, 1896 (1964).
29) J. M. Assour, J. Goldmacher, and S. E. Harrison, *J. Chem. Phys.*, **43**, 159 (1965).
30) E. M. Roberts and W. S. Koski, *J. Am. Chem. Soc.*, **82**, 3006 (1960).
31) D. Kivelson and R. Neiman, *J. Chem Phys.*, **35**, 149 (1961).

 © 1980 The Chemical Society of Japan Bull. Chem. Soc. Jpn., 53, 2271—2274 (1980)

The Reaction Process between α-Iron(III) Oxide and Sulfur Dioxide in the Presence of Carbon

Hiromitsu Araki, Young Hong Ryoo,† Motonori Eguchi, Ryoko Matsuzaki, and Yuzo Saeki*

Research Laboratory of Resources Utilization, Tokyo Institute of Technology, Nagatsuta-cho, Midori-ku, Yokohama 227

(Received January 9, 1980)

The reaction products obtained by heating a mixture of α-Fe_2O_3 and carbon in a SO_2 stream at various temperatures were examined. The possible reactions during the above process were also examined. The solid products obtained by heating a mixture of α-Fe_2O_3 and carbon in a SO_2 stream were Fe_3O_4 at 500—700 °C, pyrrhotite and Fe_3O_4 at 750 °C, and pyrrhotite ($Fe_{0.88}S$) alone at 800 °C. Sulfur was obtained outside the heating zone throughout the temperature range. The process of the formation of pyrrhotite by the reaction between α-Fe_2O_3 and SO_2 in the presence of carbon can be represented as follows: The reaction between carbon and SO_2 occurs even at 350 °C to form sulfur, and the reaction proceeds markedly above *ca.* 700 °C. Above *ca.* 500 °C, the reductions of α-Fe_2O_3 with carbon and sulfur occur to form Fe_3O_4. Above *ca.* 750 °C, pyrrhotite is formed by the reaction between Fe_3O_4 and sulfur. These results were supported by the thermodynamical consideration based on the chemical potential diagram for the Fe–S–C–O system.

As sulfidizing agents for synthesizing the transition-metal sulfides, sulfur, hydrogen sulfide and carbon disulfide have been well known. It is not only interesting from the viewpoint of the synthesis of the transition-metal sulfide itself, but also important for the development of sulfur dioxide(SO_2) utilization, to obtain knowledge of the chemical process for synthesizing the sulfide from the oxide using SO_2 as a sulfidizing agent. In this work, the reaction process between α-iron(III) oxide(α-Fe_2O_3) and SO_2 in the presence of carbon was investigated in order to understand the above chemical process.

Pechkovskii[1] has reported that iron sulfide is formed at 650—800 °C by heating a mixture of Fe_2O_3 and carbon in a SO_2 stream and that 99.7% of the charged Fe_2O_3 is sulfidized at 800 °C by using a 8 : 1 mixture of carbon and Fe_2O_3 (molar ratio). Pechkovskii and Mal'tseva[2] have carried out a differential thermal analysis for the mixture of Fe_2O_3 and carbon (Fe_2O_3: C=1: 5 by molar ratio) in a SO_2 stream and have observed the formation of pyrrhotite($Fe_{1-x}S$) above 640 °C. Also, they have estimated that the pyrrhotite may be formed through the reaction between FeO and gaseous sulfur, both substances having been formed during the reaction between Fe_2O_3 and SO_2 in the presence of carbon. The composition of the pyrrhotite formed was not mentioned.

In this work, the reaction products between α-Fe_2O_3 and SO_2 in the presence of carbon were examined. The reactions between carbon and SO_2, α-Fe_2O_3 and carbon, α-Fe_2O_3 or Fe_3O_4 and sulfur in a SO_2 stream, and Fe_3O_4 and sulfur in the presence of carbon were examined in order to elucidate the reaction process between α-Fe_2O_3 and SO_2 in the presence of carbon. Some thermodynamical consideration were also made of the formation of pyrrhotite.

Experimental

Materials. The α-Fe_2O_3 used was prepared by the thermal decomposition of the guaranteed reagent, $Fe(NO_3)_3 \cdot 9H_2O$, and confirmed as α-Fe_2O_3[3] by X-ray analysis. The chemical analysis gave Fe, 70.0$_0$% (Calcd for Fe_2O_3; Fe, 69.94%). The Fe_3O_4 was synthesized by Harber's method[4] and confirmed as Fe_3O_4[5] by X-ray analysis. The chemical analysis gave Fe, 72.2$_6$% (Calcd for Fe_3O_4; Fe, 72.36%). The carbon was prepared by the thermal decomposition of the guaranteed reagent glucose. The above materials were used as powders under 150 mesh. Gaseous SO_2 was dried by passing it through concd H_2SO_4 and over P_2O_5.

Procedures. A mixture of α-Fe_2O_3 and carbon in a quartz boat (length: 72 mm, width: 16 mm, depth: 9 mm) was placed in a transparent quartz reaction tube (inner diameter: 28 mm, length: 1000 mm). Gaseous SO_2 was then introduced into the reaction tube. The sample part was positioned in the middle of a tubular electric furnace (heating length: 300 mm) maintained at a specified temperature for 1 h. The temperature of the sample part was controlled within ±2 °C. After heating, the sample was held at 100 °C for 1 h in an argon stream in order to release the adsorbed SO_2 on unreacted carbon. The reactions between carbon and SO_2, α-Fe_2O_3 and carbon in an argon stream, α-Fe_2O_3 or Fe_3O_4 and sulfur in a SO_2 stream, and Fe_3O_4 and sulfur in the presence of carbon in an argon stream were examined in a similar manner.

Analytical. The X-ray analysis of the sample was performed with an X-ray powder diffractometer equipped with a proportional counter using Mn filtered Fe radiation.

Concerning the chemical analysis of pyrrhotite, the sample was oxidatively decomposed in HNO_3 with $KClO_3$. The iron and sulfur contents were determined by the volumetric method with $KMnO_4$ and the gravimetric method as $BaSO_4$, respectively. In the case of a mixture of pyrrhotite, unreacted carbon, and sulfur adsorbed on the carbon, the sample was oxidatively decomposed and the contents of iron and total sulfur in the filtrate were determined by the above techniques. Then, after dissolving pyrrhotite in the sample selectively with dilute HCl, the undissolved residue, which consisted of unreacted carbon and sulfur adsorbed on it, was oxidatively decomposed in HNO_3 with $KClO_3$, and the amount of sulfur adsorbed on the carbon was gravimetrically determined. The

† Present address: College of Engineering, Korea University, 1, Anam-Dong, Sungbuk-ku, Seoul 132, Korea.

amount of sulfur due to pyrrhotite was calculated as the difference between the above total sulfur and the sulfur adsorbed on the carbon. From this value and the foregoing iron content, the composition of pyrrhotite was determined.

Results and Discussion

Reaction Products between α-Fe_2O_3 and SO_2 in the Presence of Carbon. The products obtained by heating the mixture of α-Fe_2O_3 (2.00 g) and carbon (1.20 g) (Fe_2O_3: C=1: 8 by molar ratio) at various temperatures for 1 h in a SO_2 stream at a flow-rate of 100 cm^3/min were examined. The results are shown in Table 1, together with the weight changes in the samples. The solid products were identified by X-ray analysis.[3,5,6]

Table 1. Products obtained by heating a mixture of α-Fe_2O_3 and carbon in a SO_2 stream at various temperatures

Temp/°C	Weight change/%	Sample in the boat	Amount of sulfur obtained outside the heating zone/g
350	+0.2	α-Fe_2O_3	Trace
400	+0.1	α-Fe_2O_3	Trace
450	+0.1	α-Fe_2O_3	Trace
500	+0.1	α-$Fe_2O_3 \gg Fe_3O_4$	Trace
550	−0.1	α-$Fe_2O_3 \gg Fe_3O_4$	0.01
600	−0.2	α-$Fe_2O_3 \approx Fe_3O_4$	0.01
650	−1.1	$Fe_3O_4 \gg$ α-Fe_2O_3	0.06
700	−2.2	Fe_3O_4	0.14
750	−12.3	$Fe_{1-x}S > Fe_3O_4$	0.39
800	−25.5	$Fe_{1-x}S$	1.11

The formation of Fe_3O_4 was observed above 500 °C, while the formation of pyrrhotite($Fe_{1-x}S$) in addition to Fe_3O_4 was observed above 750 °C. The only solid product obtained at 800 °C was pyrrhotite. Sulfur was obtained outside the heating zone throughout the temperature range in this experiment, and the amount of sulfur markedly increased above *ca.* 700 °C. Also, the sample weight markedly decreased above *ca.* 700 °C. The slight increase in the sample weight at 350—500 °C was due to the adsorption of the sulfur formed by the reaction on the unreacted carbon, as will be described later.

The composition of the pyrrhotite obtained at 800 °C was determined by chemical analysis. The analysis gave Fe, 59.1$_4$%; S, 38.6%. From the results, the composition of the pyrrhotite formed was determined to be $Fe_{0.88}S$.

Possible Reactions during the Reaction between α-Fe_2O_3 and SO_2 in the Presence of Carbon. To elucidate the reaction process between α-Fe_2O_3 and SO_2 in the presence of carbon, the following experiments were carried out under conditions similar to those described above.

Reaction between Carbon and SO_2: Carbon (1.20 g) was heated in a SO_2 stream (100 cm^3/min) for 1 h. Under such conditions as in this experiment, sulfur is formed at temperatures below *ca.* 1000 °C.[7] Hence, the amounts of sulfur formed at various reaction temperatures were determined. A part of the sulfur was deposited outside the heating zone, while the other part was adsorbed on the unreacted carbon in the boat. The amount of adsorbed sulfur was determined by chemical analysis. The amount of sulfur formed is shown in Fig. 1, together with the weight change in the sample.

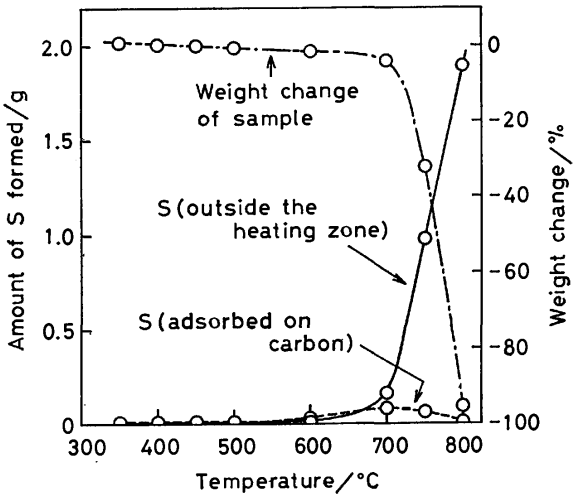

Fig. 1. Experimental results for the reaction between carbon and SO_2.

A slight amount of sulfur was formed even at *ca.* 350 °C, and the amount was markedly increased above *ca.* 700 °C. Also, the sample weight markedly decreased above *ca.* 700 °C. These facts indicate that the reaction between carbon and SO_2;

$$C(s) + SO_2(g) \longrightarrow S_n^{\dagger\dagger}(g) + CO_2(CO)(g) \quad (1)$$

occurs even at 350 °C and proceeds markedly above *ca.* 700 °C.

Reaction between α-Fe_2O_3 and Carbon: The products formed by heating a mixture of α-Fe_2O_3 (2.00 g) and carbon (1.20 g) in an argon stream (100 cm^3/min) for 1 h were examined by X-ray analysis. The results are shown in Table 2.

The results indicate that the following known reactions;

$$Fe_2O_3(s) + C(s) \longrightarrow Fe_3O_4(s) + CO(CO_2)(g) \quad (2)$$

Table 2. Reaction products between α-Fe_2O_3 and carbon at various temperatures

Temp/°C	Sample in the boat
350	α-Fe_2O_3
400	α-$Fe_2O_3 \gg Fe_3O_4$
450	α-$Fe_2O_3 \gg Fe_3O_4$
500	α-$Fe_2O_3 \gg Fe_3O_4$
550	α-$Fe_2O_3 \gg Fe_3O_4$
600	α-$Fe_2O_3 \approx Fe_3O_4$
650	$Fe_3O_4 >$ α-Fe_2O_3
700	Fe_3O_4
750	Fe_3O_4
800	$Fe_3O_4 \gg FeO$

†† Above 650 °C, the S_2 is dominant in all species. At lower temperatures the S_6, S_7, and S_8 species become important constituents.[8]

$$Fe_3O_4(s) + C(s) \longrightarrow FeO(s) + CO(CO_2)(g) \quad (3)$$

proceed above *ca.* 400 and *ca.* 800 °C respectively.

Reaction between α-Fe_2O_3 and Sulfur: The reaction between α-Fe_2O_3 and sulfur formed by the reaction of carbon with SO_2 was examined.

α-Fe_2O_3 (2.00 g) was heated in a stream of SO_2 containing a specified amount of gaseous sulfur at various temperatures for 1 h. The gaseous sulfur was formed by heating liquid sulfur and was carried by a stream of SO_2 (100 cm^3/min). The heating temperature of the sulfur was controlled so as to give the same amounts of gaseous sulfur as those obtained by the reaction between carbon and SO_2, described in the previous paragraph. The amounts of sulfur introduced were 0.01 g for the experiments at 400 and 500 °C and 0.03 g for the experiment at 600 °C.

X-Ray analyses of the samples in the boat showed them to be unreacted α-Fe_2O_3 alone at 400 °C, α-Fe_2O_3>Fe_3O_4 at 500 °C, and α-Fe_2O_3≈Fe_3O_4 at 600 °C.

These results show that, even in a SO_2 stream, the reaction between α-Fe_2O_3 and gaseous sulfur proceeds above *ca.* 500 °C to form Fe_3O_4, according to the reaction,

$$Fe_2O_3(s) + S_n(g) \longrightarrow Fe_3O_4(s) + SO_2(g). \quad (4)$$

From the above results, it could be explained that the sulfur and Fe_3O_4, formed by heating a mixture of α-Fe_2O_3 and carbon in a SO_2 stream (Table 1), were formed by Reaction 1 and by Reactions 2 and 4 respectively.

Formation Reaction of Pyrrhotite from Fe_3O_4: As has been mentioned before, when a mixture of α-Fe_2O_3 and carbon was heated in a SO_2 stream, pyrrhotite was formed above *ca.* 750 °C. Above this temperature, the amount of sulfur formed increased markedly and α-Fe_2O_3 was reduced to Fe_3O_4. Considering these results, the possible reactions giving the pyrrhotite were considered to be;

$$Fe_3O_4(s) + S_n(g) \longrightarrow Fe_{1-x}S(s) + SO_2(g), \quad (5)$$

and;

$$Fe_3O_4(s) + C(s) + S_n(g) \longrightarrow Fe_{1-x}S(s) + CO(CO_2)(g). \quad (6)$$

Therefore, Reaction 5 was examined in a SO_2 stream. Fe_3O_4 (2.00 g) was heated in a stream of SO_2 containing a specified amount of gaseous sulfur at 700—800 °C for 1 h. The amounts of sulfur introduced were controlled so as to be the same as those obtained by the reaction between carbon and SO_2, being 0.25 g for the experiment at 700 °C, 1.12 g at 750 °C, and 1.90 g at 800 °C.

X-Ray analyses of the samples in the boat showed them to be unreacted Fe_3O_4 alone at 700 °C, Fe_3O_4> Fe_{1-x}S at 750 °C, and Fe_{1-x}S>Fe_3O_4 at 800 °C. From these results, it is revealed that Reaction 5 proceeds above *ca.* 750 °C, even in a SO_2 stream.

The chemical analysis of the pyrrhotite free from unreacted Fe_3O_4, obtained at 800 °C for 2 h, gave Fe, 60.4$_5$%; S, 39.5%. From this result, the composition of the pyrrhotite formed by the reaction between Fe_3O_4 and sulfur was evaluated to be $Fe_{0.88}S$. This composition agreed with that of the pyrrhotite formed by heating a mixture of α-Fe_2O_3 and carbon in a SO_2 stream.

In order to examine Reaction 6, a mixture of Fe_3O_4 (2.00 g) and carbon (1.20 g) was heated in a stream of argon containing a specified amount of gaseous sulfur at 700—800 °C for 1 h. The amount of sulfur introduced was controlled so as to be the same (1.90 g) as that obtained by the reaction between carbon and SO_2 at 800 °C. The experimental results are shown in Table 3.

Table 3. Experimental results for the reaction between Fe_3O_4 and sulfur in the presence of carbon

Temp/°C	Sample in the boat	Amount of SO_2 formed/g
700	$Fe_{1-x}S \gg Fe_3O_4$	0.80
750	$Fe_{1-x}S \gg Fe_3O_4$	0.77
800	$Fe_{1-x}S$	0.34

Pyrrhotite and SO_2 were formed at all experimental temperatures.

From the results, it is found that the formation of pyrrhotite is due to Reaction 5, in which SO_2 is also formed. When 2.00 g of the Fe_3O_4 used is converted to $Fe_{0.88}S$ by Reaction 5, the formation of 1.11 g of SO_2 must be expected. However, the values of SO_2 formed, shown in Table 3, were less than the calculated value. This suggests that the SO_2 formed by Reaction 5 tends to react with carbon according to Reaction 1. For this reason, it is considered that carbon does not directly take part in the sulfidizing reaction, but contributes to sulfur formation by reacting with SO_2.

From the above-mentioned experimental results, the formation process of pyrrhotite by the reaction between α-Fe_2O_3 and SO_2 in the presence of carbon can be represented as follows: (i) Reaction 1 occurs even at 350 °C to form sulfur, and the reaction markedly proceeds above *ca.* 700 °C. (ii) Above *ca.* 500 °C, α-Fe_2O_3 is reduced to Fe_3O_4 by Reactions 2 and 4. (iii) Above *ca.* 750 °C, Reaction 5 occurs between Fe_3O_4 and sulfur, which are formed by the reactions mentioned above, to form $Fe_{0.88}S$.

This result disagrees with the above-mentioned estimation of Pechkovskii and Mal'tseva[2] that pyrrhotite is formed by the reaction between FeO and sulfur.

Thermodynamical Consideration. In order to discuss the present experimental results from the thermodynamical point of view, the chemical potential diagrams for the Fe–S–C–O system were constructed in a manner similar to that described by Yazawa[9] on the basis of the available thermodynamic data[10–13] and phase relations.[14] As an example, the diagram at 800 °C is shown in Fig. 2. N_S/N_{Fe} represents the atomic ratio of sulfur to iron in pyrrhotite. The broken line shows the oxygen and sulfur potentials in the gas phase formed by the reaction between carbon and SO_2, depending on the carbon content in the gas phase. The activity of carbon is unity at the dot mark. In these calculations, CO, CO_2, O_2, COS, CS_2, SO_2, SO_3, S_2, S_4, S_6, and S_8 were assumed to be gaseous products between carbon and SO_2.

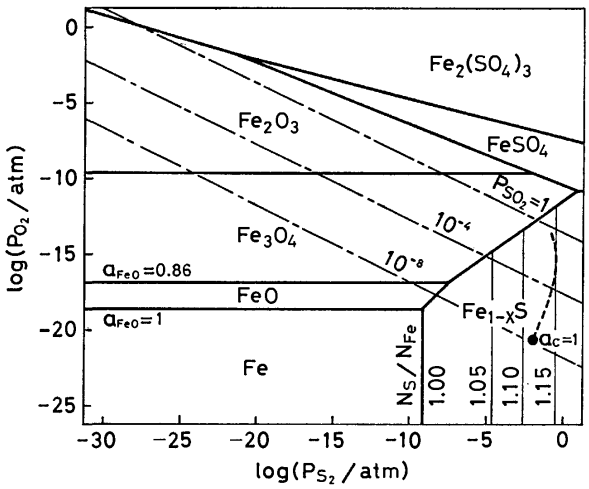

Fig. 2. Chemical potential diagram for the Fe–S–C–O system at 800 °C.

From the results shown in Fig. 2, it is clear that the reduction of Fe_2O_3 to Fe_3O_4 occurs at first when Fe_2O_3 is heated in the presence of carbon in a SO_2 stream. It is also shown that Fe_3O_4 is converted to pyrrhotite *via* FeO under a low pressure of SO_2 below *ca.* 10^{-7} atm, and that Fe_3O_4 is converted to pyrrhotite without FeO formation under a higher partial pressure of SO_2. Considering the experimental conditions in this work, the results in Fig. 2 support the above-mentioned estimation that pyrrhotite is formed through the $Fe_2O_3 \rightarrow Fe_3O_4 \rightarrow Fe_{1-x}S$ path without any FeO formation.

$Fe_{0.88}S$ ($N_S/N_{Fe} \approx 1.14$) was obtained in this work. This composition of pyrrhotite is in the range of values shown by the broken line in Fig. 2. From this fact, it can be said that pyrrhotite with nearly an equilibrium composition is formed in this experiment.

References

1) V. V. Pechkovskii, *J. Appl. Chem. USSR*, **30**, 873 (1957).
2) V. V. Pechkovskii and T. G. Mal'tseva, *J. Appl. Chem. USSR*, **38**, 1190 (1965).
3) JCPDS, Powder Diffraction File, 13-534.
4) "Mukikagōbutsu No Gōsei [I], Shin-Zikkenkagaku-Kōza 8," ed by the Chemical Society of Japan, Maruzen, Tokyo (1976), p. 297.
5) JCPDS, Powder Diffraction File, 11-614.
6) JCPDS, Powder Diffraction File, 17-201, 20-534, 22-358, 22-1120, 25-410.
7) K. I. Ushakov, O. V. Nadinskaya, I. G. Dobrochiver, and S. P. Zharova, "Fiziko-Khimicheskie Osnovy Metallurgicheskikh Protsessov," Metallugia, Moskva (1967), p. 168.
8) M. Wakihara, J. Nii, T. Uchida, and M. Taniguchi, *Chem. Lett.*, **1977**, 621.
9) A. Yazawa, *Metall. Trans.*, **10B**, 307 (1979).
10) O. Kubaschewski, E. Ll. Evans, and C. B. Alcock, "Metallurgical Thermochemistry," 4th ed, Pergamon Press (1967).
11) F. D. Richardson and J. H. E. Jeffes, *J. Iron Steel Inst.*, **171**, 165 (1952).
12) J. M. Skaeff and A. W. Espelund, *Can. Metall. Quart.*, **12**, 445 (1973).
13) L. S. Darken and R. W. Gurry, *J. Am. Chem. Soc.*, **67**, 1398 (1945).
14) E. M. Levin and H. F. McMurdie, "Phase Diagram for Ceramists, 1975 Supplement," *Am. Ceram. Soc.*, (1975), p. 412.

Chiral Recognition in Catalytic Hydrogenation of α-Acylaminoacrylic Acids by Cationic Rhodium(I) Complexes of Chiral Aminophosphines Derived from (*R,R*)-1,2-Cyclohexanediamine or (*R*)-1,2-Propanediamine[1]

Kazuo KASHIWABARA, Kazuhiro HANAKI, and Junnosuke FUJITA*

Department of Chemistry, Faculty of Science, Nagoya University, Chikusa-ku, Nagoya 464

(Received February 8, 1980)

Four chiral diphosphines, (*R,R*)-1,2-bis[*N*-methyl(diphenylphosphino)amino]cyclohexane, (*R,R*)-1,2-bis-[(diphenylphosphino)amino]cyclohexane, (*R*)-1,2-bis[*N*-methyl(diphenylphosphino)amino]propane, and (*R*)-1,2-bis[(diphenylphosphino)amino]propane have been prepared from the corresponding optically active diamines. The cationic 1,5-cyclooctadiene rhodium(I) complexes with these diphosphines act as effective homogeneous catalysts for the stereoselective hydrogenation of α-acylaminoacrylic acids. The optical yields and the absolute configurations of the products depend on the kind of diphosphine ligands. The (*R,R*)-1,2-bis[*N*-methyl(diphenylphosphino)amino]cyclohexane complex catalyst yields *N*-benzoyl-(*S*)-leucine, *N*-benzoyl-(*S*)-phenylalanine, and *N*-acetyl-(*S*)-phenylalanine in 94, 92, and 89% e.e., respectivcly. The other three catalysts are less effective (6—74% e.e.). The aminophosphine complexes with methyl groups on the nitrogen atoms always give (*S*)-amino acids, those with no methyl group (*R*)-amino acids. Such a difference in the chiral recognition has been discussed on the basis of circular dichroism spectra and Dreiding molecular models of the rhodium(I) complexes.

Reports have been given on the surprisingly high stereoselectivity for asymmetric hydrogenation of α-acylaminoacrylic acids catalyzed by chiral rhodium(I) diphosphine complexes.[2-4] The mechanism of the hydrogenation reactions has been found to involve oxidative addition of molecular hydrogen which takes place after the coordination of a substrate molecule to a catalyst.[5] Brown and Chaloner[6] confirmed the formation of a diastereomeric intermediate complex coordinated with a substrate molecule by ^{31}P NMR spectroscopy in solution. However, it is still not clear as to how chiral recognition operates in such asymmetric hydrogenation reactions.

Recently, three research groups reported that rhodium(I) complex catalysts of aminophosphines derived from (*R,R*)-1,2-diamines always give (*R*)-amino acid derivatives, and those from *N,N'*-dimethyl derivatives of these diamines (*S*)-amino acid derivatives.[1,7,8] The results seem to be useful for elucidating the mechanism of chiral recognition in catalytic hydrogenation reactions by rhodium(I) complexes, since a simple modification of a ligand affords an enantiomeric product. In this paper, we wish to report the results of catalytic hydrogenation reactions by rhodium(I) complexes with aminophosphines derived from chiral 1,2-diamines and to discuss factors of the chiral recognition in these reactions on the basis of circular dichroism spectra and Dreiding molecular models of the catalysts.

Experimental

NMR, absorption, and circular dichroism spectra were recorded on a JEOL JNM-PMX 60 spectrometer, a Hitachi 323 spectrophotometer, and a JASCO J-40 spectropolarimeter, respectively. Optical rotations were determined with a JASCO DIP-4 polarimeter. (*Z*)-α-Acetamidocinnamic acid,[9] (*Z*)-α-benzamidocinnamic acid,[10] and (*Z*)-β-isopropyl-α-benzamidoacrylic acid[11] were prepared according to the procedures reported.

Preparation of Ligands. *(R,R)-1,2-Bis[N-methyl(diphenylphosphino)amino]cyclohexane (1)*: To a vigorously stirred aqueous solution (40 cm^3) of sodium hydroxide (8.0 g, 0.2 mol) was added 5.0 g (0.044 mol) of (*R,R*)-1,2-cyclohexanediamine[12] ($[\alpha]_D^{22} = -36.0°$ (*c* 2.8, H_2O)) under cooling in an ice-cold bath. A solution of ethyl chloroformate (7.6 cm^3, 0.095 mol) in 40 cm^3 of benzene was then added dropwise over 30 min. The reaction mixture was allowed to stand at room temperature for 3 h. The resulting precipitate, (*R,R*)-1,2-bis(ethoxycarbonylamino)cyclohexane was filtered, washed with cold water, and dried *in vacuo*. The product was recrystallized from ethanol. Yield: 9.0 g (80%). 10 g (0.26 mol) of lithium tetrahydridoaluminate(III) and 150 cm^3 of dry tetrahydrofuran (THF) were placed in a 500-cm^3 three-necked, round-bottomed flask equipped with a mechanical stirrer and a reflux condenser with a soda lime tube. To this vigorously stirred mixture was added 9.0 g (0.035 mol) of (*R,R*)-1,2-bis(ethoxycarbonylamino)cyclohexane in small portions, the vessel being kept in an ice-cold bath. After the addition was completed, the mixture was allowed to stand at room temperature for 30 min and then refluxed overnight. The reaction mixture was cooled in an ice-bath and the unreacted hydride was carefully quenched by dropwise addition of water (30 cm^3). A white precipitate was filtered and washed three times with boiling THF (300 cm^3). The combined filtrate and washings were evaporated under reduced pressure to give an oily residue. This was neutralized with concd hydrochloric acid, mixed with acetone, and cooled in an ice bath. The resulting crystalline product, (*R,R*)-1,2-bis(methylamino)cyclohexane dihydrochloride was filtered and dried in a vacuum desiccator over diphosphorus pentaoxide. Yield: 5.0 g (67%). The product (6.6 g, 0.031 mol) and ethanol-free chloroform (200 cm^3) were placed in a 500-cm^3 three-necked, round-bottomed flask equipped with a serum cap and a nitrogen inlet. The flask was successively evacuated and filled with nitrogen while the contents were stirred. 12.5 g (0.124 mol) of triethylamine and 13.0 g (0.059 mol) of chlorodiphenylphosphine were then injected through the serum cap with syringes. The resulting solution was stirred overnight at room temperature. Chloroform was removed under reduced pressure and ether (300 cm^3) was added. The mixture was refluxed for 1 h and filtered in order to remove triethylamine hydrochloride. All the precedures were carried out under nitrogen atmosphere. The filtrate was evaporated under reduced pressure to yield

a pale yellow solid, which was recrystallized from acetone and water. Yield: 8.0 g (50%) (overall yield from the starting amine, 27%). Mp 137—139 °C, $[\alpha]_D^{22}=-7.3°$ (*c* 1.1, $CHCl_3$). Found: C, 75.09; H, 6.92; N, 5.33%. Calcd for $C_{32}H_{36}N_2P_2$: C, 75.26; H, 7.12; N, 5.49%. NMR ($CDCl_3$, TMS): δ(ppm)=1.0—2.1 (8p, CH_2), 2.63 (d, 6p, CH_3, $J_{H-P}=3.5$ Hz), 3.47 (m, 2p, CH), 7.4 (m, 20p, C_6H_5).

(R,R)-1,2-Bis[(diphenylphosphino)amino]cyclohexane (2): This ligand was prepared from (*R,R*)-1,2-cyclohexanediamine (4.0 g, 0.035 mol), triethylamine (7.1 g, 0.070 mol), and chlorodiphenylphosphine (15.4 g, 0.070 mol) by a method similar to that for aminophosphine **1**, dry benzene (100 cm^3) being used as solvent instead of chloroform. A white solid obtained was recrystallized from acetone and water. Yield: 4.25 g (25%). Mp 119—120 °C, $[\alpha]_D^{22}=-69.0°$ (*c* 1.3, $CHCl_3$). Found: C, 74.30; H, 6.92; N, 5.57%. Calcd for $C_{30}H_{32}N_2P_2$: C, 74.64; H, 6.70; N, 5.80%. NMR ($CDCl_3$, TMS): δ(ppm) =0.9—2.5 (m, 8p, CH_2), 2.7 (m, 2p, CH), 7.4 (m, 20p, C_6H_5).

(R)-1,2-Bis[N-methyl(diphenylphosphino)amino]propane (3): (*R*)-1,2-Bis(methylamino)propane dihydrochloride was prepared from (*R*)-1,2-propanediamine[13] ($[\alpha]_D^{22}=-33.8°$ (*c* 1.56, C_6H_6)) by a procedure similar to that for aminophosphine **1**. Yield: 79%. A solution of (*R*)-1,2-bis(methylamino)-propane dihydrochloride (4.0 g, 0.023 mol), triethylamine (9.3 g, 0.092 mol), and chlorodiphenylphosphine (10.1 g, 0.046 mol) in 100 cm^3 of ethanol-free chloroform was stirred overnight at room temperature under nitrogen atmosphere. Chloroform was evaporated under reduced pressure and the resulting residue was extracted with benzene (100 cm^3). The benzene solution was filtered in order to remove triethylamine hydrochloride, the filtrate being evaporated under reduced pressure to give an oily product. Yield: 7.4 g (69%) (overall yield from the starting amine, 54%). NMR ($CDCl_3$, TMS): δ(ppm)=1.18 (d, 3p, CH_3, $J_{H-H}=6.0$ Hz), 2.4 (d, 3p, NCH_3, $J_{P-H}=4.0$ Hz), 2.5 (d, 3p, NCH_3, $J_{P-H}=5.0$ Hz), 3.2 (m, 2p, CH_2), 3.8 (m, 1p, CH), 7.4 (s, 20p, C_6H_5).

(R)-1,2-Bis[(diphenylphosphino)amino]propane (4): (*R*)-1,2-propanediamine dihydrochloride (2.4 g, 0.016 mol) was added to an aqueous solution (20 cm^3) of sodium hydroxide (12.0 g). The amine was extracted with boiling benzene (100 cm^3) and the extract was dried over potassium hydroxide overnight. To the benzene solution were added triethylamine (2.3 g, 0.023 mol) and chlorodiphenylphosphine (5.1 g, 0.023 mol) with stirring under nitrogen atmosphere over a period of 30 min. The mixture was stirred at room temperature for 1 h and the triethylamine hydrochloride precipitated was removed by filtration. The filtrate was evaporated under reduced pressure to give an oily product. Yield: 3.0 g (60%). NMR ($CDCl_3$, TMS): δ(ppm)=1.11 (d, 3p, CH_3, $J_{H-H}=6.0$ Hz), 2.7—3.5 (m, 3p, CH and CH_2), 7.45 (s, 20p, C_6H_5).

Aminophosphines **3** and **4** were used for preparing rhodium (I) complexes without further purification.

Preparation of Rhodium(I) Complexes. *[Rh(cod)(1)]PF_6 (I)*: A dichloromethane solution (10 cm^3) of [Rh(cod)-Cl]$_2$[14] (0.5 g, 1 mmol, cod=1,5-cyclooctadiene) was mixed with an aqueous solution (10 cm^3) of sodium hexafluorophosphate (0.5 g, 3 mmol) with stirring under nitrogen atmosphere. To the mixture was added aminophosphine **1** (1.1 g, 2.2 mmol) and the solution was stirred vigorously for 20 min. The dichloromethane layer was washed three times with water (10 cm^3), its volume being reduced to *ca.* 5 cm^3 by passing nitrogen. On addition of ethanol (10 cm^3) and then diethyl ether (25 cm^3), the solution gave fine orange crystals which were filtered, washed with diethyl ether, and recrystallized from chloroform and diethyl ether. Yield: 1.14 g (66%). $[\alpha]_D^{25}=-79.1°$ (*c* 0.18, $CHCl_3$). Found: C, 54.78; H, 5.60; N, 3.19%. Calcd for $RhC_{40}H_{48}N_2P_3F_6$: C, 55.41; H, 5.59; N, 3.23%. NMR ($CDCl_3$, TMS): δ(ppm)= 0.8—1.9 (m, 8p, CH_2), 2.1 (m, 8p, CH_2 of cod), 2.48 (d, 6p, NCH_3, $J_{P-H}=8.0$ Hz), 4.0 and 4.6 (m, 4p, –CH=CH–), 5.0 (m, 2p, CH), 6.4—8.3 (m, 20p, C_6H_5).

The other aminophosphine complexes were prepared similarly.

[Rh(cod)(2)]$PF_6\cdot CHCl_3$ (II): Yield: 77%, orange blocks from chloroform/diethyl ether. $[\alpha]_D^{25}=-94.8°$ (*c* 0.13, $CHCl_3$). Found: C, 48.96; H, 4.68; N, 3.07%. Calcd for $RhC_{39}H_{45}N_2P_3F_6Cl_3$: C, 48.89; H, 4.74; N, 2.92%. NMR ($CDCl_3$, TMS): δ(ppm)=0.5—2.0 (m, 8p, CH_2), 2.3 (m, 8p, CH_2 of cod), 3.4 (m, 2p, CH), 4.4 and 4.9 (m, 4p, –CH=CH–), 6.9—8.2 (m, 20p, C_6H_5),

[Rh(cod)(3)]PF_6 (III): Yield: 35%, orange crystalline needles from chloroform/diethyl ether. $[\alpha]_D^{25}=-97.6°$ (*c* 0.17, $CHCl_3$). Found: C, 53.43; H, 5.66; N, 2.99%. Calcd for $RhC_{37}H_{44}N_2P_3F_6$: C, 53.74; H, 5.38; N, 3.39%. NMR ($CDCl_3$, TMS): δ(ppm)=1.24 (d, 3p, CH_3, $J_{H-H}=7.0$ Hz), 2.2 (m, 8p, CH_2 of cod), 2.34 (d, 3p, NCH_3, $J_{P-H}=9.0$ Hz), 2.51 (d, 3p, NCH_3, $J_{P-H}=7.0$ Hz), 4.4 and 5.0 (m, 4p, –CH=CH–), 7.2—8.0 (m, 20p, C_6H_5).

[Rh(cod)(4)]$PF_6\cdot CHCl_3$ (IV): Yield: 44%, orange blocks from chloroform/diethyl ether. $[\alpha]_D^{25}=-0.5°$ (*c* 0.20, $CHCl_3$). Found: C, 46.99; H, 4.29; N, 3.14%. Calcd for $RhC_{36}H_{41}N_2P_3F_6Cl_3$: C, 47.10; H, 4.51; N, 3.05%. NMR ($CDCl_3$, TMS): δ(ppm)=1.17 (d, 3p, CH_3, $J_{H-H}=7.0$ Hz), 2.3 (m, 8p, CH_2 of cod), 2.7 (m, 2p, CH_2), 2.9—3.5 (m, 1p, CH), 4.55 and 4.80 (m, 4p, –CH=CH–), 7.4—7.8 (m, 20p, C_6H_5).

Hydrogenation Procedures. Ethanol was dried overnight over molecular sieves 3A and purged with a stream of nitrogen for at least 30 min before use. In a Schlenk tube equipped with a serum cap were placed 6 mmol of a substrate and 0.03 mmol of a rhodium (I) complex. The tube was successively evacuated and filled with nitrogen. Ethanol (20—60 cm^3) was then injected. The mixture was stirred vigorously and the reaction vessel was connected to an atmospheric pressure hydrogenation apparatus. After hydrogen uptake ceased, reaction work-up and isolation of the products were carried out according to reported methods[2,15] in order to avoid undue optical enrichment. NMR spectra of all the products were measured to check the chemical conversions. Optical purities were determined by optical rotations of the products at 589 nm.

Results and Discussion

Catalysts and Hydrogenation. The optically pure aminophosphines **1**—**4** (Fig. 1) are easily obtained in a large scale since the parent 1,2-diamines can be resolved by a simple procedure with *d*-tartaric acid and the reactions proceed with full configurational retention. Aminophosphines **1** and **2** form stable white block and needle crystals, respectively, while **3** and **4** are viscous oily substances. These aminophosphines would form chelate rings with similar skeletal structures upon coordination. The absolute configurations of aminophosphines **1**—**4** are shown together with those prepared by Onuma *et al.*[7] and Fiorini and Giongo[8] (**5**—**7**), which were derived from (*S,S*)-2,3-butanediamine or (*S,S*)-1,2-diphenyl-1,2-ethanediamine (Fig. 1).

Hydrogenation was carried out with (*Z*)-α-acylamino-acrylic acid derivatives.

Table 1. Optical purity/%, and absolute configuration of products

Substrate	Catalyst (I)	(II)	(III)	(IV)	(V)[a]	(VI)[b]	(VII)[c]
(a) $R^1=C_6H_5$, $R^2=CH_3$	89(*S*)	49(*R*)	70(*S*)	28(*R*)	68(*R*)	93(*S*)	45(*S*)
(b) $R^1=C_6H_5$, $R^2=C_6H_5$	92(*S*)	41(*R*)	48(*S*)	21(*R*)	—	—	32(*S*)
(c) $R^1=(CH_3)_2CH$, $R^2=C_6H_5$	94(*S*)	9(*R*)	74(*S*)	6(*R*)	—	—	—
(d) $R^1=H$, $R^2=CH_3$	91(*S*)[d]	24(*R*)[d]	—	—	86(*R*)	89(*S*)	—

Solvent: Ethanol. P_{H_2}: 1.0 atm. Room temperature. Substrate/Rh=200. [Rh]: 0.5—1.5 mmol/dm^3. Hydrogenation time: 15—50 min. Chemical yield: 90—98%. Optical purity was determined based on the values given in Ref. 2. a) Rhodium (I) catalyst with aminophosphine **5** (Fig. 1) derived from (*S,S*)-1,2-diphenyl-1,2-ethanediamine, see Ref. 8. b) Rhodium(I) catalyst with aminophosphine **6** derived from (*S,S*)-1,2-diphenyl-1,2-ethane diamine, see Ref. 8. c) Rhodium(I) catalyst with aminophosphine **7** derived from (*S,S*)-2,3-butanediamine, see Ref. 7. d) Ref. 8.

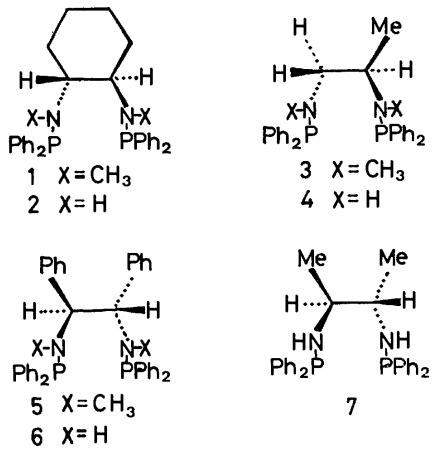

Fig. 1. Absolute configurations of chiral aminophosphines.

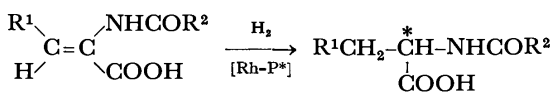

The optical purity and absolute configuration of the reaction products are summarized in Table 1 together with those reported by Onuma *et al.*[7] and Fiorini and Giongo.[8] The values were reproducible within ±2%. The addition of triethylamine did not improve the optical purity. The results can be summarized as follows, (1) The catalysts of (*R,R*)-aminophosphines with secondary amino groups, (II) *etc.*, show selectivity giving (*R*)-amino acid derivatives. Several rhodium(I) catalysts with other (*R,R*)-diphosphines[16] or -phosphites[17] whose skeletal structures are similar to those of catalysts (II) *etc.* also give the same (*R*)-amino acid derivatives. The *N*-methylation of the aminophosphines reverses the selectivity to afford (*S*)-amino acid derivatives. (2) The optical purity of the products depends on the bulkiness of substituents in a chelate ring, (I), (VI)>(V)>(III)>(II)>(VII)>(IV). (3) The products from substrate (c) show a big difference in optical purity between catalysts (I) and (II), and (III) and (IV), indicating the importance of fitness of the substrate to the catalysts. (4) The cationic catalyst (I) gives a product of higher optical purity than that obtained *in situ*,[18] suggesting that chloride ions have strong coordinating ability to the rhodium(I) ion to reduce the stereoselectivity in the hydrogenation. The cationic complexes work more effectively in asymmetric hydrogenation reactions.[19,20]

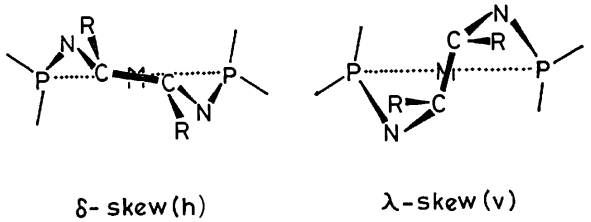

Fig. 2. Two skew conformations of a (1*R*, 2*R*)-aminophosphine chelate ring.

Chiral Recognition. Each of the aminophosphines (Fig. 1) coordinates to a rhodium(I) ion to form a seven-membered chelate ring. It will be more flexible than a five- and probably a six-membered one and can form a variety of conformations. Among the conformations, two skew forms, skew(h) and skew(v) appear to be stable (Fig. 2), since the forms would involve less intra- and inter-ligand steric interactions. The skew(h) and skew(v) imply "horizontal" and "vertical," respectively, named with reference to the direction of the central C–C bonds of the chelate rings. The skew(h) conformation was confirmed by X-ray analysis of $[Co(1,4\text{-butanediamine})_3]^{3+}$.[21] In *trans*-$[CoCl_2(1,4\text{-butanediamine})_2]^+$, one chelate ring is the skew(h), and the other the skew(v).[22] Thus, the two skew forms of a seven-membered chelate ring with no substituent group appear to have similar conformational stability.

Similar skew conformations of seven-membered chelate rings can be assumed for the aminophosphines in the rhodium(I) complexes. Aminophosphine **1** can form stereoselectively two types of chiral chelate rings, δ-skew(h) and λ-skew(v), owing to the chirality of the (*R,R*)-1,2-cyclohexanediamine moiety. However, molecular models show that the δ-skew(h) form is a less crowded

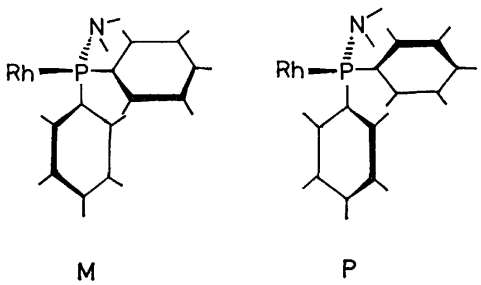

Fig. 3. Two helical orientations of two phenyl groups.

and a less strained structure than the other form. When the δ-skew(h) conformation is assumed for aminophosphine **1**, the two nitrogen atoms are forced to take (*S*)-configuration stereoselectively in order to reduce steric interactions with the phenyl groups. Furthermore the two phenyl groups on each phosphorus atom are prohibited to rotate freely around the phosphorus–carbon bonds and would be disposed in particular orientations to afford, in most cases, new helical chirality, left-handed helicity(*M*) or right-handed helicity(*P*)[23] such as seen in biaryls (Fig. 3). It is not clear from studies of molecular models which helicity is preferred for the δ-skew(h) conformation of aminophosphine **1**. However, according to X-ray analysis, the 1,2-bis-[(*R*)-(*o*-methoxyphenyl)phenylphosphino]ethane[3] and (+)-isopropylidene-2,3-dihydroxy-1,4-(diphenylphosphino)butane (diop)[24] complexes have *P* helicity and give products of (*S*)-amino acids, while the (*S*,*S*)-2,3-bis(diphenylphosphino)butane complex[25] with *M* helicity produces (*R*)-amino acids. Thus aminophosphine **1** is tentatively assumed to have *P* helicity.

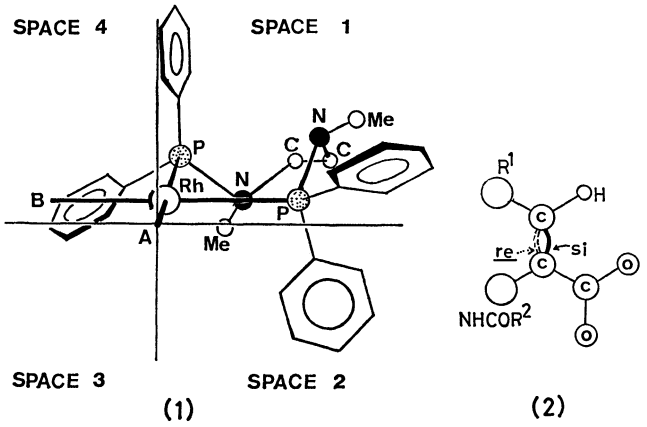

Fig. 4. (1): A schematic drawing of aminophosphine **1** coordinated to a rhodium(I) ion with the δ-skew conformation and the *P* helicity. (2): A substrate.

Figure 4 shows a schematic drawing of aminophosphine **1** coordinated to the rhodium(I) ion with the δ-skew form, viewed from the site (A) where a substrate would enter. The space 1 viewed from site (A) is occupied by the edge of one phenyl group and would be the most crowed. A substrate (Fig. 4(2)) would therefore preferentially coordinate to the rhodium(I) ion *via* the α-*re* face so that the most crowded site 1 is occupied by the small hydrogen atom on the olefinic carbon atom. The coordination through the α-*re* face of a substrate can lead to the formation of a bond between the rhodium(I) ion (site B) and the oxygen atom of the amido carbonyl of the substrate as shown by X-ray analysis on [Rh{1,2-bis(diphenylphosphino)ethane}-{methyl(*Z*)-α-acetamidocinnamate}]$^+$.[26] An (*S*)-*N*-acylamino acid is derived, when the substrate thus coordinated is hydrogenated stereoselectively from the olefinic face coordinated to the rhodium(I) ion. CH_2=C-(NHCOCH$_3$)COOH (substrate (d), Table 1) has two hydrogen atoms on one olefinic carbon atom, and hence the two coordination modes of this prochiral olefin may not be discriminated by the CH_2 group. However, the coordination through the same α-*re* face as the other olefins can similarly induce the coordination of the oxygen atom of the amido group, while that through the opposite α-*si* face introduces the bulky carboxyl group instead of the hydrogen to the most crowded space 1. Thus, substrate (d) would coordinate preferentially to the rhodium(I) ion through its α-*re* face to give (*S*)-*N*-acylalanine.

In contrast to catalyst (I), catalyst (II) gives products of (*R*)-*N*-acylamino acids, although the difference in the structure of these catalysts seems to be small. For such reverse chiral recognition, two explanations can be given. (a) The seven-membered chelate ring of aminophosphine **2** which would be less crowded and more flexible than aminophosphine **1** is in the λ-skew(v) conformation opposite to the δ-skew(h) conformation of aminophosphine **1**. (b) The stable orientation of the two phenyl groups has *M* helicity opposite to that for aminophosphine **1**, although the seven-membered chelate ring is fixed in the same δ-skew(h) form as aminophosphine **1**. Explanation (b) is more likely since molecular models indicate that the δ-skew(h) form of aminophosphine **2** is also less crowded than λ-skew(v) form, but the phenyl groups in the less crowded complex (II) can rotate more freely than those in the more crowded complex (I) and it is possible to form *M* helicity as the stable orientation. The circular dichroism (CD) spectra of the catalysts seem to support this explanation.

Figure 5 shows absorption and CD spectra of catalysts (I) and (II) in chloroform. Both catalysts exhibit similar absorption spectra over the whole region. On the other hand, the CD curves are nearly the same in the small wave number region to *ca.* 31000 cm^{-1}, but

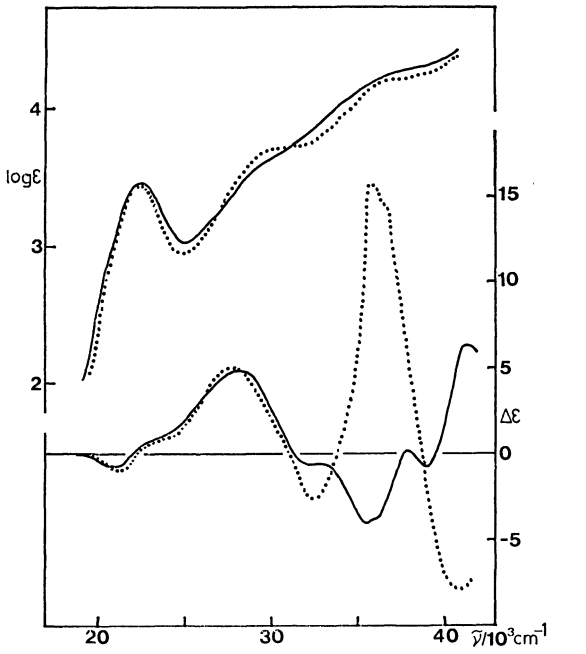

Fig. 5. Absorption and circular dichroism spectra of rhodium(I) complexes in chloroform.
——: [I], ·····: [II].

appreciably differ in the ultraviolet region. The absorption bands in the small wave number region might comprise d-d transitions in the rhodium(I) ion and charge transfer transitions from the metal ion to the ligands.[27] The CD spectra corresponding to these transitions should be affected by chiral conformation of the seven-membered aminophosphine chelate rings as observed in many cobalt(III) complexes with chiral chelate ligands.[28] The similarity in the CD spectra of catalysts (I) and (II) in this transition region suggests that the chiral aminophosphine ligands in both catalysts are in the same conformation, δ-skew(h). The CD spectra of the catalysts in the ultraviolet region differ considerably from each other. The CD bands may correspond to the intra-ligand transitions. In fact, the signs or patterns resemble those of the free ligands (Fig. 6). No definite information seems to be provided on the conformation of the chelate ligands.

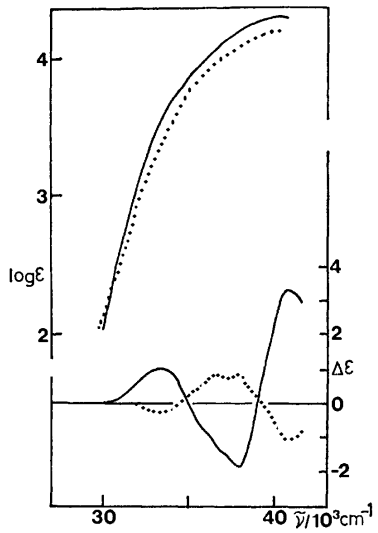

Fig. 6. Absorption and circular dichroism spectra of free aminophosphines in chloroform.
——: (**1**), ……: (**2**).

When catalyst (II) in the δ-skew(h) conformation has the phenyl groups of *M* helicity, the edge phenyl group occupies site 2. Thus site 2 is more crowded than site 1 and the substrate given in Fig. 4(2) would coordinate to the rhodium(I) ion *via* the α-*si* face to produce an (*R*)-amino acid by the same hydrogenation mechanism as that given for catalyst (I), although the optical yields are rather low. The low optical yields might be attributed to the instability of a conformer with the phenyl groups in a particular helicity resulting from the less crowded structure of catalyst (II) as compared with that of catalyst (I).

A similar chiral recognition would operate on the hydrogenation reactions with catalysts (III) and (IV) and their analogues (Table 1), since these catalysts give the same selectivity as that of catalysts (I) and (II) depending on the presence or absence of the methyl groups on the nitrogen atoms. The optical yields of catalysts (III) and (IV) are considerably lower than those of the corresponding catalysts (I) and (II), respectively, probably because of more flexible skeletones

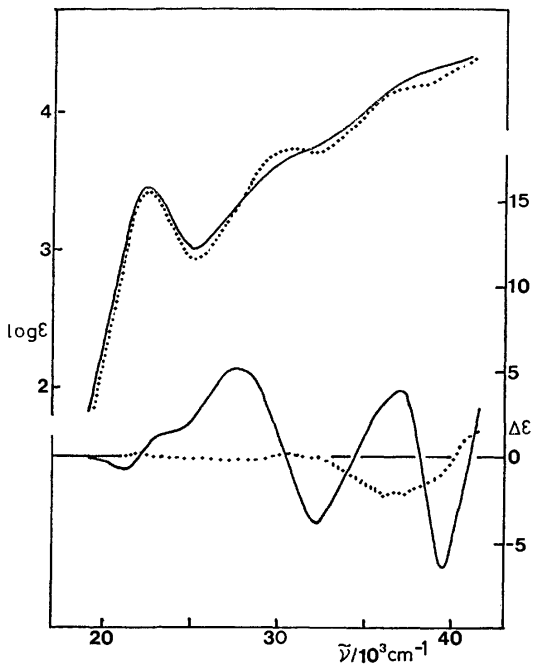

Fig. 7. Absorption and circular dichroism spectra of rhodium(I) complexes in chloroform.
——: [III], ……: [IV].

of the seven-membered chelate rings in the former catalysts. The absorption and CD spectra of catalysts (III) are similar to those of catalysts (I) and (II) in the small wave number region. On the other hand, catalyst (IV) shows very weak CD in this region, although the absorption spectrum is nearly the same as those of the other catalysts (Fig. 7). The very weak CD of catalyst (IV) suggests that the seven-membered aminophosphine **4** chelate ring is extremely flexible, existing in the two conformers of opposite chirality, δ-skew(h) and λ-skew(v), the amounts of which are almost equal at equilibrium. The conformational flexibility of catalyst (IV) is also suggested from ^{1}H NMR spectrum. The coordinated 1,5-cyclooctadiene ligand in each catalyst (I—IV) shows two kinds of vinyl proton signals probably because of the two nonequivalent phenyl groups disposed in different orientations on each phosphorus atom. The difference in chemical shift of such two vinyl proton signals would decrease with an increase in the flexibility of a diphosphine ligand.[2] The differences are 0.5—0.6 ppm for catalysts (I), (II), and (III), and only 0.25 ppm for catalyst (IV). The phenyl groups in such a flexible catalyst would hardly form a stable helical configuration, and thus the chiral recognition would not operate effectively on the hydrogenation if we assume the same mechanism as that given for catalyst (I). It seems that selectivity in the hydrogenation reactions catalyzed by rhodium(I) complexes with aminophosphines derived from chiral 1,2-diamines is most closely related with the helicity and stability of orientations of the phenyl groups on phosphorus atoms of the diphosphine ligands.

The discussion has been made on the basis of the mechanism proposed by Halpern *et al.*[5] and Brown and Chaloner[6] that a substrate coordinates to a catalyst

prior to the hydrogenation. It has also been made by assuming that the stereoselective coordination of a prochiral substrate to a vacant coordination site of a catalyst is controlled thermodynamically. In order to elucidate the selectivity of a complex catalyst, detailed kinetic studies will also be needed.[29]

This work was partially supported by Grant-in-Aid for Scientific Research from the Ministry of Education, (Nos. 243013 and 454194).

References

1) Presented at the 28th Symposium on Coordination Chemistry, Japan (Matsuyama), 1978, Abstracts 2A07.
2) M. D. Fryzuk and B. Bosnich, *J. Am. Chem. Soc.*, **100**, 5491 (1978); **99**, 6262 (1977).
3) B. D. Vineyard, W. S. Knowles, M. J. Sabacky, G. L. Bachman, and D. J. Weinkauff, *J. Am. Chem. Soc.*, **99**, 5946 (1977); W. S. Knowles, M. J. Sabacky, B. D. Vineyard, and D. J. Weinkauff, *ibid.*, **97**, 2567 (1975).
4) T. Hayashi, T. Mise, S. Mitachi, and K. Yamamoto, and M. Kumada, *Tetrahedron Lett.*, **1976**, 1133.
5) J. Halpern, D. P. Riley, A. S. C. Chan, and J. J. Pluth, *J. Am. Chem. Soc.*, **99**, 8055 (1977).
6) J. M. Brown and P. A. Chaloner, *J. Chem. Soc., Chem. Commun.*, **1978**, 321; *Tetrahedron Lett.*, **1978**, 1877.
7) K. Onuma, T. Ito, and A. Nakamura, *Chem. Lett.*, **1979**, 905; *Tetrahedron Lett.*, **1979**, 3163.
8) M. Fiorini and G. M. Giongo, *J. Mol. Catal.*, **5**, 303 (1979).
9) R. M. Herbst and D. Schemin, *Org. Synth.*, Coll. Vol. 2, 1 (1943).
10) H. B. Gillespie and H. R. Snyder, *Org. Synth.*, Coll. Vol. 1, 489, (1941).
11) E. Erlenmeyer and J. Kunlin, *Justus Liebigs Ann. Chem.*, **307**, 138 (1899).
12) F. Galsbøl, P. Steenbøl, and B. S. Sørensen, *Acta Chem. Scand.*, **26**, 3605 (1972).
13) F. P. Dwyer, F. L. Garvan, and A. Shulman, *J. Am. Chem. Soc.*, **81**, 290 (1959).
14) J. Chatt and L. M. Venanzi, *J. Chem. Soc., A*, **1957**, 4735.
15) H. B. Kagan and T. P. Dang, *J. Am. Chem. Soc.*, **94**, 6429 (1972).
16) R. Glaser, M. Twaik, S. Geresh, and J. Blumenfeld, *Tetrahedron Lett.*, **1977**, 4635.
17) M. Tanaka and I. Ogata, *J. Chem. Soc., Chem. Commun.*, **1975**, 735; T. Hayashi, M. Tanaka, and I. Ogata, *Tetrahedron Lett.*, **1977**, 295.
18) K. Hanaki, K. Kashiwabara, and J. Fujita, *Chem. Lett.*, **1978**, 489.
19) R. R. Schrock and J. A. Osborn, *J. Am. Chem. Soc.*, **93**, 2397 (1971).
20) D. Sinou and H. B. Kagan, *J. Organomet. Chem.*, **114**, 325 (1976).
21) S. Sato and Y. Saito, *Acta Crystallogr., Sect. B*, **31**, 1378 (1975).
22) Y. Nakayama, S. Ooi, and H. Kuroya, 30th National Meeting of the Chemical Society of Japan, Osaka, April 1974, Abstr. No. 3D36.
23) R. S. Cahn, C. K. Ingold, and V. Prelog, *Angew. Chem., Int. Ed. Engl.*, **5**, 385 (1966).
24) S. Brunie, J. Mazan, N. Langlois, and H. B. Kagan, *J. Organomet. Chem.*, **114**, 225 (1976).
25) R. G. Ball and N. C. Payne, *Inorg. Chem.*, **16**, 1187 (1977).
26) A. C. S. Chan, J. J. Pluth, and J. Halpern, *Inorg. Chim. Acta*, **37**, L477 (1979).
27) G. L. Geoffroy, M. S. Wrighton, G. S. Hammond, and H. B. Gray, *J. Am. Chem. Soc.*, **96**, 3105 (1974).
28) For example, C. J. Hawkins, "Absolute Configuration of Metal Complexes," Wiley-Interscience, New York (1970), Chap. 5.
29) Y. Terai, H. Kido, K. Kashiwabara, and K. Saito, *Bull. Chem. Soc. Jpn.*, **51**, 3245 (1978).

Thiocarbonyl Ylide Intermediates Generated by Deprotonation of 2-Phenacylthio- and 2-(*p*-Bromophenacylthio)-1,3-dithiolylium and 2-(*p*-Bromophenacylthio)-1,3-dithiolanylium Bromides

Juzo Nakayama,* Toshiro Takemasa,** and Masamatsu Hoshino

Department of Chemistry, Faculty of Science, Saitama University, Urawa, Saitama 338

***Department of Chemistry, College of Liberal Arts, Saitama University, Urawa, Saitama 338*

(Received October 4, 1979)

2-(*p*-Bromophenacylthio)-1,3-dithiolylium bromide, when treated with triethylamine, gave 2-(*p*-bromophenacylidene)-1,3-dithiole (17%) and bis[(*p*-bromobenzoyl)(1,3-dithiol-2-ylidene)methyl] disulfide (72%). Treatment of 2-phenacylthio-1,3-dithiolylium bromide with triethylamine also gave similar results. On the other hand, 2-(*p*-bromophenacylthio)-1,3-dithiolanylium bromide yielded 1-(*p*-bromophenyl)-2-(1,3-dithiolan-2-yl)-2-thioxoethanone (12%) in addition to 2-(*p*-bromophenacylidene)-1,3-dithiolane (49%) contrary to the reported results. These results can best be rationalized by 1,3-cyclization of thiocarbonyl ylide intermediates to the valence tautomeric episulfides.

Thiocarbonyl ylides are generally unstable transient intermediates and can not be isolated under normal conditions. One of exceptions is the ylide **1** which is a thermally stable crystalline compound.[1] Unusual stability of **1** must be, at least in part, due to an aromatic sextet retained in the five membered ring. In fact the ylide **2** in which positive charge is delocalized over only a three-atom center is an unstable transient intermediate.[2] Recent ^{13}C NMR study has shown that 1,3-dithiolylium ion belongs to a typical heteroaromatic cation whose positive charge is delocalized over the entire ring.[3] Keeping this background in mind we investigated the reactions of 2-phenacylthio- and 2-(*p*-bromophenacylthio)-1,3-dithiolylium bromides (**4a** and **4b**) with base with expectation of obtaining a new class of stable thiocarbonyl ylides **3**.

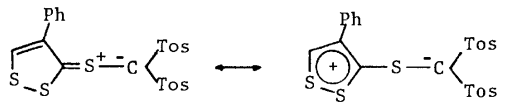

1

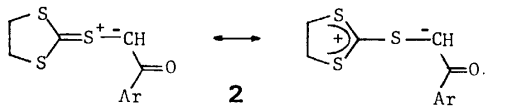

2

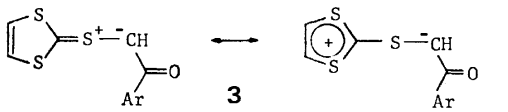

3

Dithiolylium salts **4a** and **4b** were conveniently prepared in good yields by treatment of 1,3-dithiole-2-thione (**5**) with phenacyl and *p*-bromophenacyl bromides, respectively.

An acetonitrile solution of **4b** was treated with a large excess of triethylamine at room temperature. Purification of products by column chromatography gave 2-(*p*-bromophenacylidene)-1,3-dithiole (**6b**) (18%),

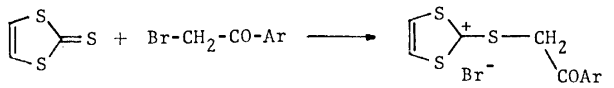

5 **4a**: Ar = C_6H_5; **b**: Ar = p-BrC_6H_4

bis[(*p*-bromobenzoyl)(1,3-dithiol-2-ylidene)methyl] disulfide (**7b**) (72%), and **5** (7%). The mass spectrum of **6b** has an M+2 peak which is almost equal in intensity to the molecular peak at *m/e* 298 because of the presence of the ^{81}Br isotope. The NMR spectrum showed a singlet of the exocyclic vinyl proton at δ 7.43 ppm, a singlet (with fine line structure) of dithiole ring protons at 6.89, and a multiplet of benzene ring protons at 7.5—8.0. The carbonyl stretching absorption appears abnormally low at 1585 cm^{-1} suggesting strong conjugation between carbonyl and 1,3-dithiol-2-ylidene groups. Campaigne and Haaf reported that the carbonyl absorptions of this type of compounds occur at 1590—1610 cm^{-1}.[4] Furthermore the structure of **6b** was confirmed by an independent synthesis; the condensation of the sodium salt of *p*-bromoacetophenone with the dithiolylium salt **11** gave **6b** in a 32% yield. The mass spectrum of **7b** has its molecular peak at *m/e* 658, M+2 peak at 660, and M+4 peak at 662 in intensity ratio of *ca.* 1:2:1 suggesting the presence of two bromine atoms. The base peak appears at *m/e* 329 which is exactly the half of the molecular peak. The NMR spectrum shows a singlet at δ 7.28 ppm and an $A'_2X'_2$ multiplet at 7.0—7.5. The UV spectrum closely resembles that of **6b** and the IR spectrum has a carbonyl absorption at 1565 cm^{-1}. These data are indicative of the symmetrical structure of **7b** with the same structural unit as **6b** and are in harmony with the presented structure. Further support for the structure of **7b** comes from its conversion to compound **10**; reduction of **7b** by sodium borohydride and methylation of the resulting product with methyl iodide gave **10** in a 61% yield.

Treatment of the dithiolylium salt **5a** with triethylamine gave results similar to those obtained with **5b**. Compounds **6a**, **7a**, and **5** were obtained in 17, 71, and 6% yields, respectively.

These results can best be explained in terms of thiocarbonyl ylide intermediate **3** produced by dehydrobromination of **4**. The ylide **3** is not so stable as was expected and cyclizes immediately to episulfide **8**, which either gives **6** with spontaneous extrusion of sulfur or isomerizes to **9**. The latter gives rise to disulfide **7** as the final product by air oxidation. Evidence for the intermediacy of **9** comes from the fact that treatment of **4b** with triethylamine in the presence of methyl iodide gives **10**, the product of methylation of **9**, in an 83% yield along with a 6% yield of **6b**.

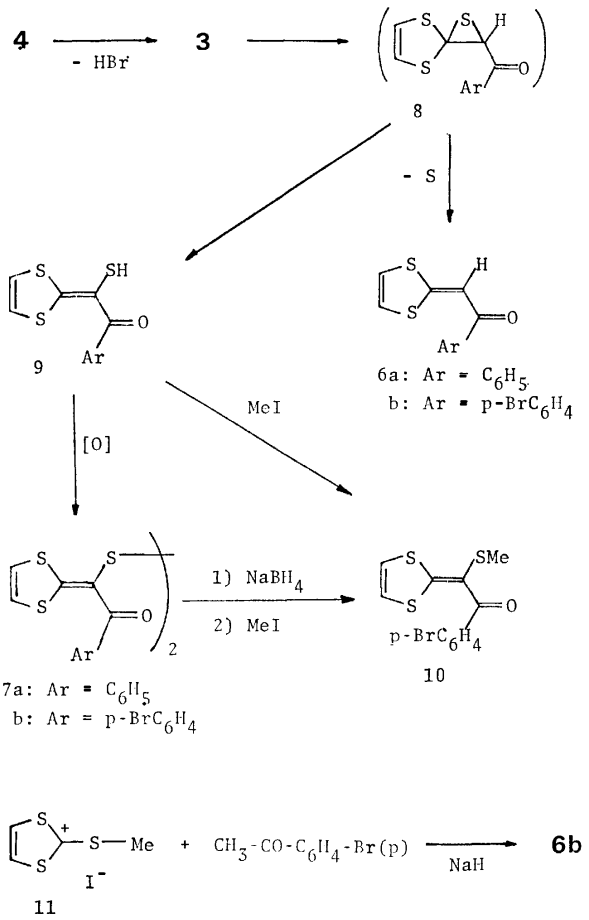

Ueno and Okawara reported that the ylide **2**, generated by deprotonation of the salt **12** with sodium hydride in acetonitrile, gives compound **13** in an excellent yield. The formation of **13** was explained as a result of 1,5-cyclization of **2**.[2] We now investigated the reaction of **12** with triethylamine in order to compare the properties of **2** and **3** under normalized conditions. Results were rather surprising. Treatment of **12** with excess triethylamine gave 1-(*p*-bromophenyl)-2-(1,3-dithiolan-2-yl)-2-thioxoethanone (**14**) (12%), 2-(*p*-bromophenacylidene)-1,3-dithiolane (**15**) (49%), and ethylene trithiocarbonate (27%). Compound **13** was not detected at all.[5] Compound **14** has its carbonyl absorption at 1560 cm^{-1}. The mass spectrum shows molecular and M+2 peaks of about equal intensity at *m/e* 332 and 334. The juncture of 1,3-dithiolan-2-yl group to thiocarbonyl group is supported by the occurence of an intense peak at *m/e* 149 (S–CH_2CH_2–S–CH–C=S).

The presence of *p*-bromobenzoyl group is evident from two peaks at *m/e* 183 and 185. The methylene protons signal appears at δ 3.38 ppm as singlet in harmony with the presented structure. The carbonyl absorption of compound **15** occurs at 1615 cm^{-1}. Reported carbonyl frequencies of this type of compounds are in the range of 1595—1630 cm^{-1}.[4] The NMR spectrum shows a multiplet of methylene protons at δ 3.36—3.62 ppm, a singlet of vinyl proton at 7.30, and a multiplet of benzene ring protons at 7.5—8.0.

The result can be explained as follows: The ylide **2** undergoes 1,3-cyclization to episulfide **16**, which either gives **15** with loss of sulfur or isomerizes to **17**. The latter further isomerizes to the final product **14**. The enol form of compound **9** may be stabilized by the contribution of the canonical structure like **18** as would be expected from unusually low carbonyl absorptions observed with compounds **6**, **7**, and **10**. As a result, compound **9** is easily methylated to give **10** or oxidized to disulfide **7**. However, such stabilization is not expected for the enol form of compound **14** and this accounts for the fact that **14** can be isolated as stable compound in the thiocarbonyl form.

We must thus conclude that (1) the ylides **3** can not be stabilized by the aromatic sextet retained in the five membered ring so that they can be isolated under usual conditions, (2) the ylides **3** undergo 1,3-cyclization to give the valence tautomeric episulfides, which is one of the characteristic reactions of thiocarbonyl ylides,[6] and (3) as far as judging from present evidence, the ylide **2** preferentially undergoes 1,3-cyclization rather than 1,5-cyclization contrary to the reported results.[2]

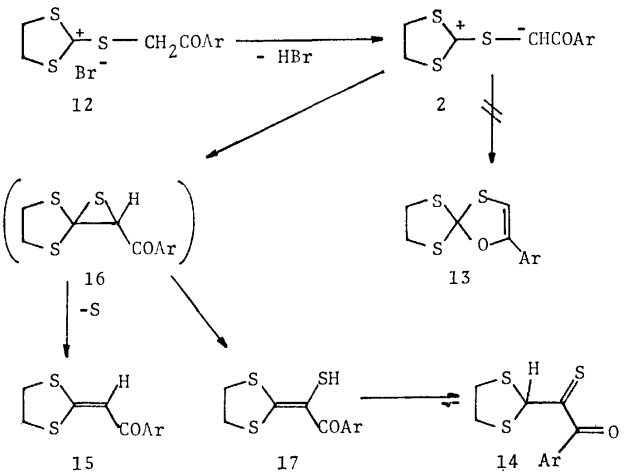

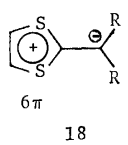

18

Experimental

General. All melting points were measured on a Mel-

temp capillary melting point apparatus and are uncorrected. NMR spectra were recorded on a Varian A-60 spectrometer or a Hitachi R 24B spectrometer with tetramethylsilane as internal reference. IR and UV spectra were determined with a JASCO IRA-2 spectrometer and a Hitachi EPS-3T spectrometer, respectively. Mass spectra were taken on a Japan Electron Optics Lab. Model JMS-OISJ instrument operating at 40 eV. Acetonitrile and tetrahydrofuran were refluxed over and distilled from calcium hydride and stored over molecular sieves. Merck Art 7734 (E. Merck, Darmstadt) was used for silica gel chromatography.

2-Phenacylthio- and 2-(p-Bromophenacylthio)-1,3-dithiolylium Bromides (4a and 4b). A mixture of 1.0 g (7.5 mmol) of 1,3-dithiole-2-thione[7] (**5**) and 7.2 g (36.3 mmol) of phenacyl bromide in 45 ml of anhydrous acetonitrile was stirred at room temperature. After 1.5 h of stirring, **4a** began to separate as yellowish brown crystals. The mixture was stirred for 2 d and diluted with 45 ml of anhydrous ether to complete the precipitation of **4a**. The resulting precipitate was collected and washed with ether to give **4a** in 66—71% yield. **4a**, on attempted recrystallization from hot acetonitrile or ethanol, suffered extensive decomposition to **5** and phenacyl bromide. It was therefore purified by reprecipitating it from an acetonitrile solution with ether as diluent. **4a**, thus obtained, melted at 114—115 °C.

NMR (CF_3CO_2H) δ 5.32 (2H, s, $-CH_2-$), 7.39—8.02 (5H, m, phenyl), and 8.33 (2H, s, dithiole ring); IR (KBr) $\nu_{C=O}$ 1676 cm^{-1}. Found: C, 39.52; H, 2.73; S, 28.85% Calcd for $C_{11}H_9OS_3Br$: C, 39.64; H, 2.72; S. 28.86%.

4b was prepared from **5** and *p*-bromophenacyl bromide in 65—70% yield as above; mp 138 °C (decomp), yellowish brown crystals. Although, judging from the NMR spectrum, the compound thus obtained was sufficiently pure, satisfactory elemental analysis could not be obtained (Found: C, 32.78; H, 2.18; S, 22.32%. Calcd for $C_{11}H_8OS_3Br$: C, 32.05; H, 1.96; S, 23.34%). NMR (CF_3CO_2H) δ 5.52 (2H, s, $-CH_2-$), 7.7—8.2 (4H, $A'_2X'_2m$, benzene ring), and 8.71 (2H, s, dithiole ring); IR (KBr) $\nu_{C=O}$ 1652 cm^{-1}; UV (EtOH) λ_{max} (log ε) 229 (4.02) (sh), 260.5 (4.00), and 465 nm (4.19).

Reaction of 4a with Triethylamine. Over a period of 10 min, 3 ml of triethylamine was added dropwise to a stirred suspension of 932 mg (2.8 mmol) of **4a** in 50 ml of anhydrous acetonitrile cooled at -10 °C. The mixture was warmed to room temperature and stirred for additional 2 h. The resulting red mixture was diluted with ice-water (150 ml) and extracted with 150 ml of chloroform. The extract was washed with water, dried (Na_2SO_4), and evaporated to give 813 mg of a red oil, which was subjected to column chromatography on silica gel (50 g). Elution with benzene gave 42 mg (6%) of **5**, 105 mg (17%) of 2-phenacylidene-1,3-dithiole (**6a**), and 503 mg (71%) of bis[benzoyl(1,3-dithiol-2-ylidene)methyl] disulfide (**7a**).

In a separate reaction carried out under similar conditions, **5**, **6a**, and **7a** were obtained in 7, 14, and 55% yields, respectively.

6a: Yellow needles (from hexane); mp 80—81 °C; NMR ($CDCl_3$) δ 6.82 (2H, s with fine structure, dithiole ring), 7.30—8.13 (5H, m, phenyl), and 7.47 (1H, s, vinyl); IR (KBr) $\nu_{C=O}$ 1587 and 1560 cm^{-1}. Found: C, 59.91; H, 3.69; S, 29.07%. Calcd for $C_{11}H_8OS_2$: C, 59.97; H, 3.66; S, 29.11%.

7a: Orange needles (from benzene); mp 115—116 °C. Compound recrystallized from benzene contained one molecule of benzene as solvent of crystallization. Found: C, 57.89; H, 3.45; S, 33.06%. Calcd for $C_{22}H_{14}O_2S_6 \cdot C_6H_6$: 57.94; H, 3.47; 33.08%. NMR ($CDCl_3$) δ 6.80—7.52 (14H, m); IR (KBr) $\nu_{C=O}$ 1580 and 1555 cm^{-1}.

Reaction of 4b with Triethylamine. Triethylamine (3 ml) was added dropwise during 10 min to a stirred suspension of 1.0 g 2.4 mmol) of **4b** in 40 ml of anhydrous acetonitrile cooled at -12 °C with an ice–salt bath. The bath was removed and stirring was continued for 2 h. During this period, crystals of the starting material disappered and orange crystals of product began to precipitate instead. The mixture was left overnight at room temperature and the resulting orange crystals were collected to give 485 mg of bis[(*p*-bromobenzoyl)(1,3-dithiol-2-ylidene)methyl] disulfide (**7b**). The filtrate was diluted with water and extracted with chloroform. The extract was washed with water, dried, and evaporated to leave 272 mg of a dark red oil, which was chromatographed on a column of silica gel (30 g). Elution with benzene gave 20 mg (7%) of **5**, 133 mg (18%) of 2-(*p*-bromophenacylidene)-1,3-dithiole (**6b**), and 87 mg (total yield; 72%) of **7b**.

The reaction was repeated three times. The yield of **6b** varied in the range of 18—20% and that of **7b** in the range of 65—72%.

6b: Yellowish brown crystals (from acetonitrile); mp 168 °C (decomp); NMR ($CDCl_3$) δ 6.89 (2H, s with fine line structure, dithiole ring), 7.43 (1H, s, vinyl), and 7.47—7.97 (4H, $A'_2X'_2m$, benzene ring); IR (KBr) $\nu_{C=O}$ 1585 cm^{-1}; UV (EtOH) λ_{max} (log ε) 226 (4.05), 234 (3.99) (sh), 270.5 (4.06) and 412 nm (4.49); MS *m/e* (%) 300 (M^++2, 98), 298 (M^+, 95), 185 ($^{81}BrC_6H_4CO$, 22), 183 ($^{79}BrC_6H_4CO$, 25), 157 ($^{81}BrC_6H_4$, 41), 155 ($^{79}BrC_6H_4$, 44), 149 (48), 143 (S–CH=CH–S–C=CH–C=O, 100), and 115 (S–CH=CH–S–C=CH, 18). Found: C, 44.13; H, 2.39; S, 21.41; Br, 26.79%. Calcd for $C_{11}H_7OS_2Br$: C, 44.15; H, 2.36; S, 21.43; Br, 26.71%.

7b: Orange prisms (from chloroform–hexane); mp 198—198.5 °C; NMR ($CDCl_3$) δ 7.28 (4H, s, dithiole ring) and 7.03—7.40 (8H, m, benzene ring); IR (KBr) $\nu_{C=O}$ 1565 cm^{-1}; UV (EtOH) λ_{max} (log ε) 225 4.26) (sh), 270 (3.98), 339.5 (3.78), and 425 nm (4.37); MS *m/e* 662 (M^++4), 660 (M^++2), 658 (M^+), 331, and 329. Found: C, 39.93; H, 1.84; S, 29.12%. Calcd for $C_{22}H_{12}O_2S_6Br_2$: C, 40.00; H, 1.83; S, 29.12%.

6b from 11 and p-*Bromoacetophenone.* A solution of 1.55 g (7.8 mmol) of *p*-bromoacetophenone in 20 ml of anhydrous tetrahydrofuran was added to a suspension of 0.52 g (10.9 mmol) of 50% sodium hydride dispersion in oil in 20 ml of anhydrous acetonitrile. The mixture was stirred for 1 h, and then 1.07 g (3.9 mmol) of **11**[7] was added all at once. The mixture was stirred for 1 h, poured into ice-water, and extracted with chloroform. The extract was washed with water, dried, and evaporated, The brown oily residue was purified by chromatography on a column of silica gel (40 g) with benzene as eluent to give 0.37 g (32%) of **6b**, mp 168 °C (decomp) (from acetonitrile). **6b**, thus obtained, agreed with a specimen obtained from **4b** and triethylamine in all respects.

Conversion of 7b to (p-Bromobenzoyl)(1,3-dithiol-2-ylidene)-methyl Methyl Sulfide (10). A solution of 0.50 g (0.75 mmol) of **7b** in 35 ml of tetrahydrofuran was added during 1 h to a stirred suspension of 104 mg (2.7 mmol) of sodium borohydride in 20 ml of tetrahydrofuran. After 2 h of stirring at room temperature, 0.37 g (2.6 mmol) of methyl iodide in 20 ml of tetrahydrofuran was added. The mixture was stirred for 1 h, poured into ice-water, and extracted with chloroform. The extract was washed with water, dried and evaporated to leave an orange oil. The crude product was separated by chromatography on silica gel (35 g) with chloroform as eluent to give 208 mg (61%) of **10** and 170 mg (34%) of the starting material.

10: Yellowish orange needles (from cyclohexane); mp 125—126 °C; NMR ($CDCl_3$) δ 2.09 (3H, s, Me), 6.94—7.24 (2H, m, dithiole ring), and 7.40—7.80 (4H, m, benzene ring); IR (KBr) $\nu_{C=O}$ 1564 cm^{-1}. Found: C, 41.77; H, 2.65; S, 27.77%. Calcd for $C_{12}H_9OS_3Br$; C, 41.74; H, 2.63; S, 27.86%.

*Reaction of **4b** with Triethylamine in the Presence of Methyl Iodide.* Over a period of 10 min, 3.3 ml of triethylamine was added to a stirred mixture of 1.19 g (2.9 mmol) of **4b** and 2.05 g (14.4 mmol) of methyl iodide in 30 ml of acetonitrile at −10 °C under nitrogen. The mixture was warmed to room temperature and stirred overnight. The resulting yellow crystalline precipitate was collected to give 224 mg of **10**. The filtrate was diluted with water and extracted with chloroform. The extract was washed, dried, and evaporated to leave an orange oil, which was chromatographed on silica gel (30 g). Elution with chloroform afforded 37 mg (10%) of **5**, 332 mg (total yield; 83%) of **10**, and 55 mg (6%) of **6b**. **10**, thus obtained and recrystallized from cyclohexane, melted at 128—128.5 °C and agreed in all respects with a specimen derived from **7b**.

*Reaction of 2-(p-Bromophenacylthio)-1,3-dithiolanylium Bromide[8] (**12**) with Triethylamine.* Triethylamine (4 ml) was added to a stirred solution of 828 mg (2 mmol) of **12** in 35 ml of anhydrous acetonitrile at 0 °C. The mixture was warmed to room temperature and stirred for 8 h, and then poured into ice–water and extracted with ether. The extract was washed with water, dried, and evaporated. The residue was chromatographed on silica gel (40 g). Elution with chloroform afforded 82 mg (12%) of 1-(*p*-bromophenyl)-2-(1,3-dithiolan-2-yl-)-2-thioxoethanone (**14**), 74 mg (27%) of ethylene trithiocarbonate, and 296 mg (49%) of 2-(*p*-bromophenacylidene)-1,3-dithiolane (**15**).

The reaction was repeated several times. The yield of **14** changed in the range of 7—24%, that of ethylene trithiocarbonate in the range of 20—40%, and that of **15** in the range of 49—57%.

14: Yellow prisms (from cyclohexane); mp 84.5—85 °C; NMR ($CDCl_3$) δ 3.38 (4H, s, dithiolane ring), 6.48 (1H, s, methine), and 7.52—8.00 (4H, $A'_2X'_2m$, benzene ring); IR (KBr) $\nu_{C=O}$ 1660 cm^{-1}; UV (EtOH) λ_{max} (log ε) 260 (4.31) and 350 nm (3.76); MS *m/e* (%) 334 (M^+ +2, 58), 332 (M^+, 53), 185 ($^{81}BrC_6H_4CO$, 96), 183 ($^{79}BrC_6H_4CO$, 95), 156 ($^{81}BrC_6H_4$, 91), 154 ($^{79}BrC_6H_4$, 100), 149 (S–CH_2CH_2–S–CH–C=S, 88), and 105 (S–CH_2CH_2–S–CH, 61). Found: C, 39.63; H, 2.75; S, 28.87%. Calcd for $C_{11}H_9OS_3Br$: C, 39.64; H, 2.72; S, 28.86%.

15: Yellow needles (from acetonitrile); mp 145 °C (decomp); NMR ($CDCl_3$) δ 3.36—3.62 (4H, m, dithiolane ring), 7.30 (1H, s, methine), and 7.49—7.99 (4H, $A'_2X'_2m$, benzene ring); (CF_3CO_2H) δ 3.90 (4H, s), 7.15 (1H, s), and 7.70 (4H, broad s); UV (EtOH) λ_{max} (log ε) 220 (3.89) (sh), 269 (4.00), and 349 nm (4.30). Found: C, 43.73; H, 2.99%. Calcd for $C_{11}H_9OS_2Br$: C, 43.86; H, 3.01%.

References

1) S. Tamagaki and S. Oae, *Tetrahedron Lett.*, **1972**, 1159.
2) Y. Ueno and M. Okawara, *Bull. Chem. Soc. Jpn.*, **45**, 1797 (1972).
3) K. Sakamoto, N. Nakamura, M. Ōki, J. Nakayama, and M. Hoshino, *Chem. Lett.*, **1977**, 1133.
4) E. Campaigne and F. Haaf, *J. Org. Chem.*, **30**, 732 (1965).
5) We examined the reaction of **12** with sodium hydride in acetonitrile. Chromatographic purification gave **14** (3%), **15** (29%), and ethylene trithiocarbonate (22%). The expected product **13** was not produced.
6) E. Block, "Reactions of Organosulfur Compounds," Academic Press, New York (1978), p. 97.
7) L. R. Melby, H. D. Hartzler, and W. A. Sheppard, *J. Org. Chem.*, **39**, 2456 (1974).
8) R. Mayer and K. Schafer, *J. Prakt. Chem.*, **26**, 279 (1964).

Synthesis and Photoreaction of *D*-Nor-5α-androstan-16-one Acetylhydrazone in the Presence of Oxygen[1)]

Hiroshi SUGINOME,*,** Tsutomu UCHIDA, Kazuhiko KIZUKA, and Tadashi MASAMUNE

Department of Chemistry, Faculty of Science, Hokkaido University, Sapporo 060

(Received October 13, 1979)

D-Nor-5α-androstan-16-one was prepared *via* seven steps from 16-diazo-3β-hydroxyandrost-5-en-17-one. The major products of the photolysis of its acetylhydrazone in dioxane containing oxygen were the parent ketone and 17-oxa-5α-androstan-16-one, accompanied by low yields of three isomeric lactams: 17-aza-5α-androstan-16-one, 16-aza-5α-androstan-17-one, and 17-aza-5α,13α-androstan-16-one. These three are the same lactams formed in the photo-Beckmann rearrangement of the corresponding oxime, *D*-nor-5α-androstan-16-one oxime. Their formation from the acetylhydrazone may have some mechanistic significance with regard to the path of the formation of lactams in the photolysis of 5α-androstan-17-one acetylhydrazone in the presence of oxygen reported previously. The mass spectrometric fragmentations of fifteen *D*-nor-5α-androstanes with functional groups at their C-16 positions are described.

In the previous paper,[2)] it was reported that *O*-acetylandrosterone acetylhydrazone and its analogue afforded a pair of lactams, 17-oxo-17a-aza-*D*-homosteroid and its 13α-isomer, in 32% yield, upon photolysis in the presence of oxygen; the corresponding hydrazone afforded no lactams and yielded the corresponding azine as the major product. To gain more insight into the pathway of the formation of lactams, we have undertaken the photolysis of *D*-nor-5α-androstan-16-one acetylhydrazone (**20**), a steroidal four-membered ring ketone acetylhydrazone. The study is described in this paper.

Results

Synthesis of D-*Nor-5α-androstan-16-one Hydrazone (18) and Its* N-*Acetyl Derivative 20.* The parent ketone, *D*-nor-5α-androstan-16-one (**16**) was synthesized by the method devised by Cava *et al.*,[3)] adopted for steroids first by Mateos,[4)] then by Meinwald *et al.*[5)] and Cava and Moroz,[6)] with some modifications. Thus, a 1 : 5.5 mixture of methyl 3β-hydroxy-*D*-norandrost-5-en-16α- and 16β-carboxylates **2** and **3** were directly obtained by photolysis of 16-diazo-3β-hydroxyandrost-5-en-17-one (**1**)[5)] in THF containing methanol in 89% yield. Recrystallization of the mixture from acetone readily afforded 16β-isomer **3** in 62% yield.

16β-Isomer **3** was hydrogenated in acetic acid in the presence of Adams' platinum catalyst to afford methyl 3β-hydroxy-*D*-nor-5α-androstane-16β-carboxylate (**5**),[7)] mp 141—142 °C, in 76% yield. Jones oxidation of **5** afforded methyl 3-oxo-*D*-nor-5α-androstane-16β-carboxylate (**7**), mp 157—158 °C, in 81% yield. This was subjected to Wolff-Kishner reduction to yield *D*-nor-5α-androstane-16β-carboxylic acid (**9**), mp 226—227 °C, in 90% yield. This sequence of the reaction was repeated on the mixture of methyl 16α- and 16β-carboxylates **2** and **3** to afford a mixture of *D*-nor-5α-androstane-16α-carboxylic acid (**8**) and the 16β-isomer **9**. These isomers could be separated by recrystallization and column chromatography.

Treatment of 16β-isomer **9** with methyllithium afforded *D*-norpregnan-20-one (**11**), mp 125—127 °C, in 90% yield. A similar treatment of 16α-isomer **8**, mp 208—209 °C, gave 16α-*D*-norpregnan-20-one (**10**), mp 135—137 °C, in 68% yield.

Baeyer-Villiger oxidations of 20-ones **10** and **11** afforded *D*-nor-5α-androstan-16α-yl acetate (**12**) and the 16β-isomer (**13**) respectively. Without purification, these were hydrolyzed with methanolic potassium hydroxide to afford 16α-hydroxy-*D*-nor-5α-androstane (**14**), mp 171—173 °C, and the 16β-isomer (**15**), mp 132—135 °C, in 21 and 84% yields.

The Sarret's oxidation of 16β-isomer **15** then afforded 16-oxo-*D*-nor-5α-androstane (**16**), mp 128—129 °C. On the other hand, the Jones oxidation of **15** resulted in the formation of 17-oxa-5α-androstan-16-one (**17**). Its structure was confirmed by spectral data and through its preparation by Baeyer-Villiger oxidation of ketone **16**.

D-Nor-5α-androstan-16-one hydrazone (**18**), mp 116 °C (dec), was readily prepared by the standard method. In this procedure, evaporation of solvent from the reaction mixture caused dimerization of hydrazone **18** to give rise to the corresponding azine (**19**). Hydrazone **18** was therefore isolated by the addition of water to the solution after the formation of the hydrazone was complete. On the basis of its NMR spectrum, hydrazone **18** in solution was concluded to be a mixture of *E* and *Z* isomers although one isomer predominated; as in the case of oximes,[8,9)] it is believed that protons attached to carbon α of the $-C=N-NH_2$ group generally resonate at a lower field when the proton is eclipsed by the C=N bond and the NH_2 group *syn* to it. The NMR spectrum of **18** exhibited a multiplet signal at τ 7.14—7.56 assignable to the C-16 methylene protons and a doublet signal centered at τ 6.49 (J=6.9 and 14.3). The combined integral area of these signals corresponded to two protons and the ratio of the area of the signal at the lower field to that of the signal at the higher field was approximately 5 : 1. A double doublet signal at the lower field is assignable to the 15α-H deshielded by the eclipsed $C=N-NH_2$ group, assuming that the conformation of the ring D of **18** and the coupling constants of the 15α-H are similar to those of the parent ketone **16**. On the basis of this integral ratio of signals, the ratio of *syn* and *anti* isomers with respect to the C-13–C-16 bond was calculated

** Present address: Organic Chemistry Laboratory, Department of Chemical process Engineering, Faculty of Engineering, Hokkaido University, Sapporo 060.

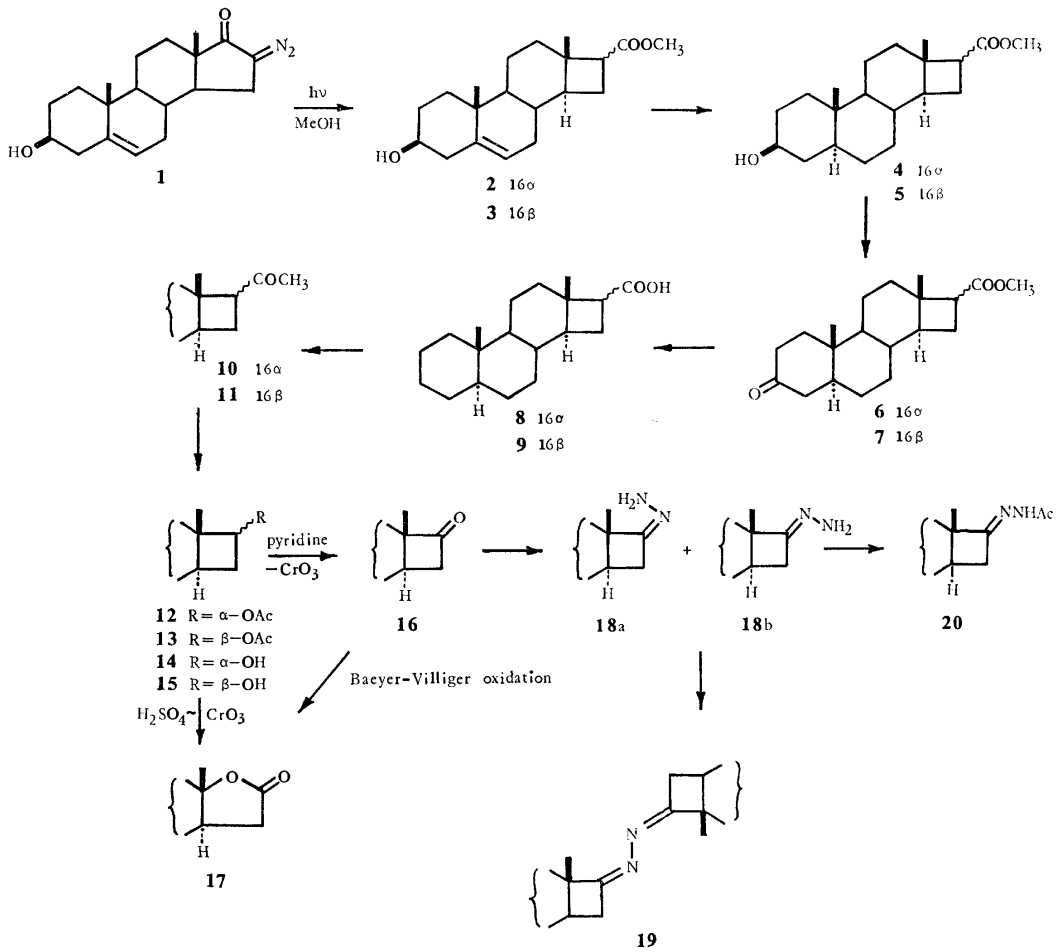

Scheme 1.

to be approximately 2 : 1.

Acetylation of the mixture of hydrazones **18a** and **18b** under controlled conditions afforded a mixture of *N*-acetyl- and *N*-diacetylhydrazones, from which *N*-acetyl derivative (**20**), mp 204—206 °C, was obtained by column chromatography in 61% yield.

Photolysis of Acetylhydrazone 20. The photolysis of acetylhydrazone **20** was carried out under the same procedure as described for the photo-rearrangement of androsterone acetylhydrazone in the previous paper.[2] Thus, acetylhydrazone **20** in dioxane was bubbled with oxygen and was irradiated with a 15-W low pressure mercury arc for 7 h. Extensive preparative TLC of the product mixture afforded lactone **17** (6%), parent ketone **16** (38%), and a mixture of lactams. The separation of the lactam mixture into its components was not possible by preparative TLC. However, the mixture could be separated into its three isomeric lactam components (**21**, **22**, and **23**) by high performance liquid chromatography. The yields of **21**, **22**, and **23** were 0.7, 1.1, and 0.7%. These lactams (**21**, **22**, and **23**) were identified as 17-aza-5α,13α-androstan-16-one by mass, IR, and NMR spectra and by direct comparisons with the authentic specimens obtained by the Beckmann and the Photo-Beckmann rearrangements of *D*-nor-5α-androstan-16-one oxime.[9] Thus, the major products in the present reaction were the parent ketone and 17-oxa-5α-androstan-16-one and the lactams were formed in only low yields. These results are in contrast to those in the photolysis of *O*-acetylandrosterone acetylhydrazone,[2] a fused cyclopentanone analogue of **20** obtained under similar conditions. In the photolysis of *O*-acetylandrosterone acetylhydrazone, 17-oxo-17α-aza-*D*-homosteroid and its 13α-isomer are formed in 32% yield.

In the previous paper,[2] some plausible paths of the formation of the lactams in the photo-reaction of the steroidal 17-one acetylhydrazone in the presence of oxygen were discussed on the basis of various available experimental results, including those of the photolysis of the corresponding hydrazone in the presence of oxygen. Thus, oxygen is required for the formation of the lactams.[2] One of the most probable paths suggested was the one involving intermediate(s) common with those involved in the formation of the lactams in the photorearrangement of the corresponding oxime, since the same lactams are formed in a comparable ratio in photo-reactions of both an oxime and the corresponding acetylhydrazone. The formation of three lactams **21**, **22**, and **23**, despite their low yields, may have a mechanistic significance. Not only two isomeric 17-azalactams, **21** and **23**, resulting from the migration of the more substituted carbon center were formed, but 16-aza-lactam **22** resulting from the migration of the less substituted carbon center was also obtained in the present reaction. These three (**21**, **22**, and **23**) are the

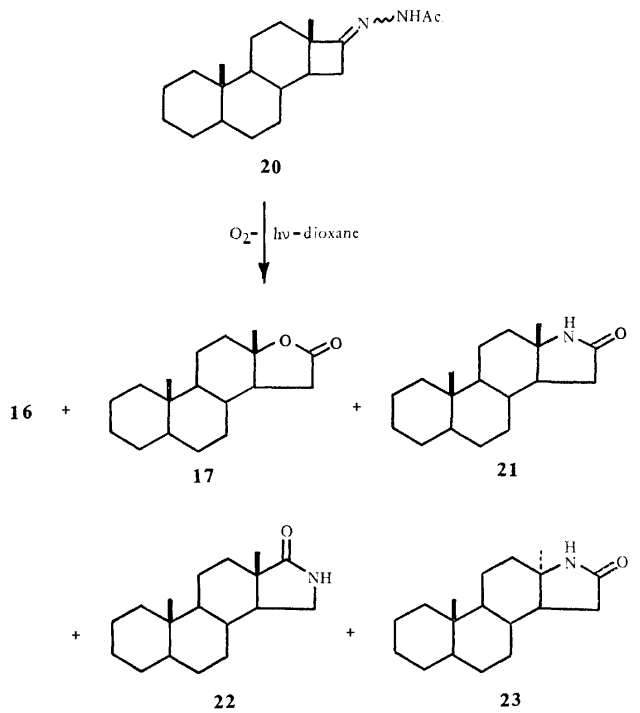

Scheme 2.

very lactams which arise from the photo-Beckmann rearrangement of *D*-nor-5α-androstan-16-one oxime.[9] Thus, the present results reinforce the validity of the pathway suggested in the previous paper.[2] The reason why the lactams are not major products in the fused cyclobutanone acetylhydrazone **20** is not clear at the present stage.

The formation of the parent ketone from the *N*-acetylhydrazones has been discussed in the previous paper.[2] It almost certainly involves the thermal decomposition of hydroperoxides which will be generated by either a radical-induced autoxidation, as was observed for benzaldehyde phenylhydrazones[11] and for some steroidal ketone phenylhydrazones,[12] or by the other pathway proposed for the photo-oxidation of some imines.[13] If the reaction proceeds through the autoxidation pathway, the initiator of the chain reaction can be a radical species generated by irradiation, since we found that no hydroperoxide nor any ketone derived from it was formed from steroidal ketone acetylhydrazone[2] under conditions similar to the formation of hydroperoxide of steroidal ketone phenylhydrazones[12] and that irradiation is necessary for the progress of the reaction. There is another possibility: the formation of the parent ketone by photo-oxidation with singlet oxygen, as was initially observed for acetone phenylhydrazone.[14] However, generation of singlet oxygen by sensitization with the substrate itself is not likely and this path may be excluded.

It is almost certain that 17-oxa-5α-androstan-16-one (**17**) is formed by the reaction of an oxocarbene,[15,16] generated photochemically from the ketone **16**, with molecular oxygen. Careful examination of the reaction mixture showed the absence of the 13-epimer of **17** in the product. This stereospecificity favors a concerted process for the formation of the oxocarbene from the ketone **17**, at least in this instance.[17]

Notes on the Mass Spectra of D-*Nor-5α-androstane Derivatives.* The mass spectra of 16-functionalized *D*-nor-5α-androstanes are of interest since they may give some information on the competition between the decomposition directed by their monofunctionalized cyclobutane ring and the fragmentation of the hydrocarbon framework. In Table 2, the intensities of some significant fragments are summarized. Some of the characteristic features of these results are the following:

a) Isomeric carboxylic acids **8** and **9**, isomeric methyl ketones **10** and **11**, hydrazone **18**, and azine **19** give strong molecular ion peaks.

b) In the mass spectra of isomeric carboxylic acids **8** and **9**, isomeric 16-ols **12** and **13**, isomeric acetates **14** and **15**, and ketone **16**, the M^+—ring D peak (*m/e* 218)[18] is either their base peak or the second most intense fragment; a peak at *m/e* 203, which probably arises from ejections of their 10β-CH_3 and ring D from the molecular ion, is prominent. Moreover, in the mass spectra of isomeric carboxylic acids **8** and **9**, isomeric methyl ketones **10** and **11**, and a lactone **17**, a peak at *m/e* 217, arising from cleavage of ring D involving hydrogen rearrangements,[18] is also prominent.

c) The mass spectra of a pair of methyl ketones **10** and **11** exhibit the base peak at *m/e* 230, which is attributable to $M^+-Ac-CH_3$.

d) No significant difference in their fragmentation and intensity between isomers was found in a pair of isomeric 16-carboxylic acids **8** and **9**, a pair of isomeric methyl ketones **10** and **11**, a pair of 16-ols **12** and **13** and a pair of 16-ol acetates.

e) Analogous to the 3β-methoxy derivative,[19] the base peak in the mass spectrum of lactone **17** was the one attributable to the ejection of 13β-CH_3 from the molecular ion.

f) The mass spectra of hydrazone **18** and acetylhydrazone **20** exhibited the base peaks at *m/e* 56 and 98, respectively, and M^+—ring D as well as M^+—ring D—CH_3 were appreciable only in the hydrazone. Apart from the base peak, no fragment ions which exceed 3% in their intensity were found in the spectrum of acetylhydrazone **20**. The ions at *m/e* 56 and 98 may be generated *via* the pathway depicted in Scheme 3.

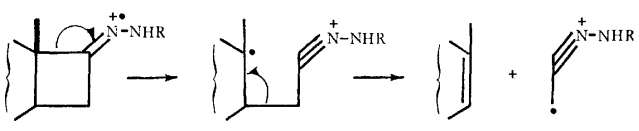

Scheme 3.

g) In all the *D*-nor-5α-androstanes **8**—**19** other than **20**, the mass spectra exhibited two very intense peaks at *m/e* 108 and 109 [the base peak in **14**] regardless of their 16-functional group.

Experimental

Instruments and general procedures are described in the preceding paper.[2] All the low resolution mass spectra were taken with a Hitachi RMU-6E spectrometer (ion-source temperature 200° and ionizing voltage 80 eV) in the Faculty of

TABLE 1. NMR PARAMETERS (100 MHz) FOR THE *D*-NOR-5α-ANDROSTANE DERIVATIVES
Chemical shifts (τ) and splittings (Hz; in parentheses).

Compound	18-H	19-H	16-H	$COOCH_3$ or $COCH_3$	Others
5	9.04(s)	9.17(s)	7.15 (dd) (7.2; 8.4)	6.35(s)	6.44 br (3-H)
7	8.99(s)	8.95(s)	7.24 (dd) (6.8; 8.6)	6.34(s)	
8	8.79(s)	9.20(s)	7.20 (dd) (1.4; 4.9)	—	
9	8.98(s)	9.20(s)	7.23 (dd) (7.2; 9.0)	—	
10	8.74(s)	9.20(s)	7.03 (dd) (0.7; 5.4)	7.92(s)	
11	9.11(s)	9.20(s)	7.18 (dd) (6.0; 9.6)	7.98(s)	
12	8.93(s)	9.20(s)	5.34 (d) (4.1)	7.90(s)	
13	9.05(s)	9.19(s)	5.51 (dd) (6.0; 8.0)	7.96(s)	
14	9.01(s)	9.18(s)	5.95 (d) (3.9)	—	
15	8.99(s)	9.17(s)	6.23 (dd) (5.5; 7.9)	—	
16	8.85(s)	9.18(s)	—	—	7.44 (15α-H) (dd) (7.8; 13.8) 6.89 (15β-H)(dd) (12.8; 13.8)
17	8.77(s)	9.20(s)	—	—	7.66 (dd) (10.0; 1.1)
18	8.86(s)	9.17(s)	—	—	5.82 (br) (NH_2), 7.14—7.56(m) 1.7H, 6.49 (dd), 0.3H(6.9; 14.3)
19	8.81(s)	9.17(s)	—	—	
20	8.83(s)	9.17(s)	—	7.82(s)	7.21—7.42(m) (15-H), 1.96(s)(NH)

TABLE 2. INTENSITY OF SOME IMPORTANT FRAGEMENTS IN THE MASS SPECTRA OF *D*-NOR-5α-ANDROSTANE DERIVATIVES

Compound	Intensity of fragments (%)								Others
	M^+	M^+-CH_3	M^+—ring-D—CH_3(*m/e* 203)	M^+—ring-D—H (*m/e* 217)	M^+—ring-D (*m/e* 218)	$M^+-Ac-CH_3$ (*m/e* 230)	*m/e* 108	*m/e* 109	
8	13	37	70	37	90	7	65	85	
9	15	38	71	32	100	7	59	13	
10	13	5	29	47	31	96	26	56	
11	12	9	36	59	39	100	47	78	
12	0.2	1	45	7	100	—	51	65	
13	1	5	46	8	100	—	53	65	
14	1	2	34	0	96	—	59	100	
15	4	5	54	5	100	—	60	85	
16	1	1	52	8	100	—	61	76	
17	7	100	9	48	12	—	33	39	
18	10	7	37	5	45	—	66	96	100 (*m/e* 56)
19	9	2	27	9	39	—	21	95	
20	0.2	0.4	0.6	0.3	0.5	—	1	2	100 (*m/e* 98)

Pharmaceutical Sciences, with the exceptions of compounds **18** and **20**, the spectra of which were taken with a Hitachi JMS-D 300 spectrometer. The high resolution mass spectrum of **19** was measured in the Faculty of Agriculture (ion-source temperature 220 °C and ionizing voltage 70 eV).

*Methyl 3β-Hydroxy-*D*-norandrost-3-ene-16α- and 16β-carboxylates, (2 and 3).* 16-Diazo-3β-hydroxyandrost-5-en-17-one (**1**)[7] (18 g) in dry tetrahydrofuran (720 ml) and absolute methanol (180 ml) was irradiated through a Pyrex filter with a 200-W high pressure mercury arc (Ushio UMB-200 H3) for 34 h, while nitrogen gas was bubbled slowly through the mixture. After removal of the solvent, the residue was recrystallized from acetone to yield methyl 3β-hydroxy-*D*-norandrost-5-ene-16β-carboxylate (11.29 g).[7] The residue from the filtrate (6.803 g) was subjected to column chromatography (Wakogel C-200, 90 g). Elutions with benzene afforded a 1 : 1 mixture of 16α- and 16β- carboxylates, (4.972 g).

*Catalytic Hydrogenations of Methyl 3β-Hydroxy-*D*-nor-5α-androstane-16β-carboxylate (3) and a Mixture of 16α- and 16β-Carboxylates (2 and 3).* (*a*): 16β-Carboxylate **3** (11 g), obtained as given above, in acetic acid (100 ml) in the presence

of Adams' platinum catalyst (300 mg) was hydrogenated under an atmosphere of hydrogen until absorption of hydrogen ceased (24 h). After removal of the catalyst and the solvent, the residue was dissolved in dichloromethane. The solution was washed with 5% sodium hydrogencarbonate, saturated sodium chloride solution, and water successively, and dried (Na_2SO_4). Removal of the solvent left a residue which was recrystallized from acetone to yield the hydrogenated product **5** (8.345 g), mp 141—142 °C. Found: C, 75.00; H, 10.19%. Calcd for $C_{20}H_{32}O_3$: C, 74.96; H, 10.06%. IR (Nujol): 3527 and 3438 (OH), 1736 and 1714 ($COOCH_3$), 1258, 1198, and 1049 cm^{-1}. For NMR see Table 1. MS *m/e* (rel intensity): 320 (M^+, 10%), 305 (M^+-CH_3, 14), 287 (9), 271 (8), 234 (M^+—ring-D, 39), 219 (28), 216 (M^+—ring-D—H_2O, 49), 201 (M^+—ring-D—H_2O—CH_3, 31), 190 (28), 173 (16), 147 (26), 108 (100), 107 (67), 95 (27), 93 (37), 91 (29), 81 (36), 67 (27), 55 (42), 41 (33), and 28 (87).

(*b*): A mixture of carboxylates **2** and **3** was similarly hydrogenated to afford a mixture of the dihydro derivatives of carboxylates **4** and **5** in 95% yield.

*Oxidations of Methyl 3β-Hydroxy-*D*-nor-5α-androstane-16β-carboxylate (5) and of a Mixture of 16α- and 16β-Carboxylates (4 and 5).* (*a*): To the 3β-ol **5** (8.345 g) in acetone (180 ml), there was added dropwise Jones reagent (20 ml) at 0 °C. After stirring for 1.5 h, a saturated sodium hydrogen sulfite solution was added until the color of the solution became blue. The solution was filtered and the filtrate was partly evaporated. The crystals of ketone **7** (4.622 g) was collected by filtration and the filtrate was extracted with diethyl ether. The diethyl ether solution was worked up in the usual way. The crude product was recrystallized from acetone to yield ketone **7** (1.243 g). The residue from the filtrates of this recrystallization was purified by column chromatography (Wakogel C-200) with benzene to afford a further amount of ketone **7** (0.750 g). The total yield of **7**, mp 157—158 °C, was 81%. Found: C, 75.27; H, 9.76%. Calcd for $C_{20}H_{30}O_3$: C, 75.43; H, 9.50%. IR (Nujol): 1731 (6-membered ring ketone), 1710 ($COOCH_3$), 1350, 1224, 1192, 1172, 1047 and 1028 cm^{-1}. For NMR see Table 1. MS *m/e* (rel intensity) 318 (M^+, 11%), 303 (5), 287 (6), 271 (9), 244 (11), 232 (M^+—ring-D, 50), 218 (75), 203 (6), 175 (11), 149 (17), 109 (27), 95 (18), 93 (18), 91 (15), 81 (25), 67 (17), 55 (36), 41 (25), and 28 (100).

(*b*): A mixture of carboxylates **4** and **5** was similarly oxidized to afford a mixture of ketones **6** and **7** in 70% yield.

Wolff-Kishner Reduction of Methyl D*-Nor-3-oxo-5α-androstane-16β-carboxylate (7) and of a Mixture of 16α- and 16β-Carboxylates (6 and 7).* (*a*): Ketone **7** (5.92 g), hydrazine (16 ml), and potassium hydroxide (16 g) were refluxed in triethylene glycol (160 ml) for 1 h. After removal of the excess of hydrazine and water, the solution was refluxed for 1.5 h. The cooled solution was poured into water–ice (200 ml). The pH of the solution was adjusted by the addition of 6 mol dm^{-3} hydrochloric acid and the solution was stirred for 0.5 h and set aside for 0.5 h. The crystals were collected by filtration and dissolved in dichloromethane. The solution was washed with water and dried (Na_2SO_4). The product was recrystallized from methanol to afford *D*-nor-5α-androstane-16β-carboxylic acid (3.16 g), mp 226—227 °C. (lit,[13] mp 207—209 °C). The residue from the filtrate afforded a further amount of the product (1.668 g) on column chromatography (Wakogel C-200, benzene). The total yield was 90%. Found: C, 78.53; H, 10.50%. Calcd for $C_{19}H_{30}O_2$: C, 78.57; H, 10.41%. IR (Nujol): 3200—2400 (COOH), 1692 (COOH), 1268 and 958 cm^{-1}. For NMR see Table. MS *m/e* (rel intensity): 290 (M^+, 15%), 275 (38), 230 (7), 218 (100), 217 (32), 203 (71), 189 (15), 175 (62), 161 (23), 148 (55), 109 (13), 108 (59), 95 (40), 93 (29), 91 (18), 81 (46), 79 (27), 67 (39), 55 (38), 41 (33), and 28 (72).

(*b*): A mixture of the 16α- and 16β-carboxylates (6.256 g) was similarly subjected to reduction to afford a mixture of 16α- and 16β-carboxylic acids **8** and **9**. This was recrystallized from methanol to afford 16β-carboxylic acid **9** (2.690 g). The residue (2.330 g) from the filtrate was subjected to column chromatography (Wakogel C-200) with benzene to afford three fractions: A, B, and C. The first fraction (0.988 g) was 16α-carboxylic acid **8**. An analytical specimen was obtained by recrystallizing it from methanol, mp 208—209 °C. Found: C, 78.48; H, 10.47%. Calcd for $C_{19}H_{30}O_2$: C, 78.57; H, 10.41%. IR (Nujol): 3600—2400 (COOH), 1695 (COOH), 1418, 1332, 1238, and 943 cm^{-1}; for NMR see Table 1. MS *m/e* (rel intensity); 290 (M^+, 13%), 275 (37), 230 (7), 218 (90), 217 (37), 203 (70), 189 (13), 175 (52), 161 (24), 148 (54), 109 (85), 108 (65), 95 (40), 93 (31), 91 (20), 81 (45), 79 (28), 67 (40), 55 (38), 41 (34), and 28 (100). The second fraction (0.3 g) was a mixture of carboxylic acids **8** and **9**. The third fraction (0.808 g) was a pure 16β-carboxylic acid **9**.

Preparation of D*-Norpregnan-20-one (11).* To 16β-carboxylic acid **9** (3.651 g) in benzene (300 ml) was added, dropwise with stirring, 1 M methyllithium (40 ml) in diethyl ether. The solution was stirred for 1 h at room temperature and was then poured into water–ice. The solution was extracted with diethyl ether and the solution was worked up as usual. After removal of the solvent, the residue was recrystallized from methanol to yield *D*-norpregnan-20-one (**11**) (3.254 g, 90%), mp 125—127 °C. (lit,[18] oil). Found: C, 83.22; H, 11.30%. Calcd for $C_{20}H_{32}O$: C, 83.27; H, 11.18%. IR (Nujol): 1715 (Ac), 1354, 1186, and 1161 cm^{-1}. For NMR see Table 1. MS *m/e* (rel intensity) 288 (M^+, 12%), 270 (12), 230 (100), 218 (39), 217 (59), 215 (35), 203 (36), 189 (11), 175 (32), 161 (26), 148 (32), 135 (28), 121 (37), 109 (78), 108 (47), 95 (40), 93 (30), 91 (19), 81 (50), 79 (29), 67 (37), 55 (40), 43 (50), and 28 (42).

Preparation of D*-Nor-16α-pregnan-20-one (10).* 16α-Carboxylic acid **8** was similarly transformed into *D*-nor-16α-pregnan-20-one (**10**), mp 135—137 °C, in 68% yield. Found: C, 83.08; H, 11.32%. Calcd for $C_{20}H_{32}O$: C, 83.27; H, 11.18%. IR (Nujol) 1697 (Ac), 1356, 1180, and 1108 cm^{-1}. For NMR see Table 1. MS *m/e* (rel intensity); 288 (M^+, 13%), 270 (11), 255 (14), 230 (96), 218 (31), 217 (47), 215 (29), 203 (29), 189 (9), 175 (25), 161 (21), 148 (28), 135 (18), 121 (26), 109 (56), 108 (26), 95 (22), 93 (19), 91 (14), 81 (28), 79 (15), 67 (22), 55 (23), 43 (21), 41 (17), and 28 (100).

The Baeyer-Villiger Oxidation of D*-Norpregnan-20-one (11).* *D*-Norpregnan-20-one (**11**) (3.408 g), *m*-chloroperbenzoic acid (3.5 g) and *p*-toluenesulfonic acid (60 mg) in dichloromethane (100 ml) in a vessel covered by an aluminium foil were stirred for 72 h at room temperature. Further amounts of the reagents [*m*-chloroperbenzoic acid (500 mg) and *p*-toluenesulfonic acid (100 mg)] were added after 26 h and 41 h. The excess peracid was decomposed by adding 5% sodium thiosulfite to the solution. The solution was washed first with 10% sodium hydrogencarbonate, then with water, and dried (Na_2SO_4). The crude acetate **13** in methanol (100 ml) was hydrolyzed by adding potassium hydroxide (3.0 g) and by stirring the solution for 2 h at room temperature. The solution was neutralized with 2 mol dm^{-3} hydrochloric acid and extracted with diethyl ether. The solution was worked up as usual. The crude product was recrystallized from acetone to yield *D*-nor-5α-androstan-16β-ol (**15**) (1.619 g), mp 132—135 °C (dec). (lit,[13] mp 103—105 °C). The residue from the filtrate was subjected to column chromatography (Wakogel C-200, benzene) to yield a further amount

of the product (0.993 g). The combined yield was 84%. Found: C, 82.38; H, 11.79%. Calcd for $C_{18}H_{30}O$: C, 82.38; H, 11.52%. IR (Nujol) 3600—3200 (OH), 1191, 1131, and 1062 cm^{-1}. For NMR see Table 1. MS *m/e* (rel intensity): 262 (M^+, 4%), 247 (5), 233 (8), 299 (5), 218 (100), 203 (54), 175 (51), 161 (27), 148 (52), 135 (17), 122 (17), 109 (85), 108 (60), 95 (30), 93 (25), 91 (13), 81 (30), 67 (30), 55 (32), and 41 (28). The acetate **13** was prepared by the standard method, mp 50—53 °C. Found: C, 78.87; H, 10.95%. Calcd for $C_{20}H_{32}O_2$: C, 78.89; H, 10.59%. IR (Nujol): 1745 (Ac), 1235 (C–O), and 1042 cm^{-1}. For NMR see Table 1. MS *m/e* (rel intensity) 304 (M^+, 1%), 289 (5), 262 (4), 244 (8), 299 (8), 218 (100), 203 (46), 175 (44), 161 (19), 148 (49), 135 (15), 121 (14), 109 (65), 108 (53), 95 (24), 93 (21), 91 (12), 81 (26), 67 (26), 55 (26), 43 (42), 41 (25), and 28 (55).

Baeyer-Villiger Oxidation of D-*Nor-16α-pregnan-20-one (**10**).* *D*-Nor-16α-pregnen-20-one (800 mg) was similarly oxidized and was hydrolyzed to yield *D*-nor-5α-androstan 16α-ol (**14**) (154 mg). This was recrystallized from acetone to yield a pure 16α-ol **14**, mp 171—173 °C (dec). Found: C, 82.43; H, 11.70%. Calcd for $C_{18}H_{30}O$: C, 82.38; H, 11.52%. IR (Nujol) 3237 (OH), 1174, 1030, 1037, 999 and 976 cm^{-1}. For NMR see Table. MS *m/e* (rel intensity): 262 (M^+, 4%), 247 (5), 233 (6), 299 (5), 218 (48), 203 (66), 175 (62), 161 (30), 148 (66), 135 (18), 122 (20), 109 (100), 108 (70), 95 (35), 93 (29), 91 (16), 81 (36), 67 (36), 55 (37), and 41 (31). The acetate **12** was prepared by the standard method, mp 56—57 °C. Found: C, 77.90; H, 10.51%. Calcd for $C_{20}H_{32}O_2$: C, 78.89; H, 10.59%. IR (Nujol): 1751 (OAc), 1239 (C–O), 1030, and 1019 cm^{-1}. For NMR see Table; MS *m/e* (rel intensity) 304 (M^+, 0.2%), 289 (1.4), 262 (3), 244 (7), 229 (7), 218 (100), 203 (45), 175 (41), 161 (17), 148 (48), 135 (14), 121 (17), 109 (65), 108 (51), 95 (21), 93 (18), 91 (10) 81 (24), 67 (25), 55 (25), 43 (42), 41 (20), and 28 (34).

Sarret's Oxidation of D-*Nor-5α-androstan-16β-ol (**15**).* *D*-Nor-5α-androstan-16β-ol (**15**) (320 mg) in pyridine (2 ml) was added dropwise to a solution of chromium trioxide (320 mg) in pyridine (2 ml) at room temperature and stirred for 48 h. The solution was then dissolved in dichloromethane and washed first with water, then with 2 mol dm^{-3} -hydrochloric acid, and again with water, and dried (Na_2SO_4). The crude product was purified by column chromatography (Wakogel C-200) with a 1: 1 mixture of hexane and benzene. The first fraction (178 mg) was a crude *D*-nor-5α-androstan-16-one (**16**) which was recrystallized from methanol to afford the pure ketone, mp 128—219 °C. Found: C, 83.15; H, 10.94%. Calcd for $C_{18}H_{28}O$: C, 83.02; H, 10.84%. IR (Nujol): 1775 (4-membered ring ketone), 1143, 1019, 987 and 973 cm^{-1}. For NMR see Table. MS *m/e* (rel intensity) 260 (M^+, 1%), 245 (1), 232 (3), 218 (100), 203 (52), 175 (50), 161 (21), 148 (26), 135 (13), 122 (17), 121 (15), 109 (76), 108 (61), 95 (21), 93 (23), 91 (11), 81 (26), 67 (26), 55 (20), and 41 (22).

The Baeyer-Villiger Oxidation of D-*Nor-5α-androstan-16-one (**16**).* The ketone **16** (50 mg), *m*-chloroperbenzoic acid (100 mg), and *p*-toluenesulfonic acid monohydrate (50 mg) in dichloromethane (5 ml) were stirred for 3.5 h at room temperature. The solution was washed with 5% sodium thiosulfite solution, sodium hydrogencarbonate solution and water successively, and dried (Na_2SO_4). After removal of the solvent, the residue (60 mg) was recrystallized from aq acetone (13 mg) to give lactone **17**, mp 185—187 °C. Found: C, 78.22; H, 10.33%. Calcd for $C_{18}H_{28}O_2$: C, 78.21; H, 10.21%. IR (Nujol): 1775 (lactonic C=O), 1210, 1161, 1050, 1003, 954, and 910 cm^{-1}. For NMR see Table. MS *m/e* (rel intensity) 276 (M^+, 7%), 261 (100), 232 (34), 217 (48), 149 (60), 109 (33), 108 (39), 95 (35), 81 (36), 67 (34), 55 (36), and 43 (38).

Jones Oxidation of D-*Nor-5α-androstan-16β-ol (**15**).* To *D*-nor-5α-androstan-16β-ol (**15**) (2.612 g) in acetone (50 ml), there was added Jones reagent (5 ml) dropwise at room temperature in the course of 1 h. After the addition of a saturated sodium hydrogensulfite solution until the color of the solution became blue, the solution was extracted with diethyl ether. The residue (2.72 g) was recrystallized from acetone to yield 17-oxa-5α-androstan-16-one (**17**), mp 185—187 °C, (400 mg). Column chromatography of the residue from the filtrate afforded a further amount (769 mg) of the lactone **17**.

Preparation of D-*Nor-5α-androstan-16-one Hydrazone (**18a** and **18b**).* Ketone **16** (500 mg) and hydrazine hydrate (5 ml) in ethanol (15 ml) were refluxed for 1.5 h. After a part of the solvent was removed, water was added to the solution. Crystals of hydrazones **18a** and **18b** were collected by filtration (302 mg). The filtrate afforded a further amount of crystals (214 mg), mp 116 °C (dec). The combined yield was 98%. Found: C, 78.93; H, 11.03; N, 9.93%. Calcd for $C_{18}H_{30}O_2$: C, 78.77; H, 11.02; N, 10.21%. IR (Nujol): 3345 (NH_2), 1162, 1112, 926, 910, and 896 cm^{-1}. For NMR see Table. MS *m/e* (rel intensity): 274 (M^+, 10%), 259 (M^+-CH_3, 7), 258 (M^+-NH_2, 5), 218 (45), 203 (35), 175 (37), 161 (8), 148 (49), 123 (9), 109 (96), 108 (66), 95 (24), 93 (22), 84 (23), 81 (26), 67 (41), 56 (100), 55 (39), and 41 (30). In this procedure, extraction of the hydrazone in aq ethanol with diethyl ether and evaporation of the solvent resulted in the formation of azine **19**, as described in the next procedure.

Preparation of D-*Nor-5α-androstan-16-one Azine (**19**).* Ketone **16** (50 mg) and hydrazine hydrate (0.5 ml) in ethanol (1.5 ml) were refluxed for 2 h. After a part of the solvent was removed by a rotary evaporator, the solution was extracted with diethyl ether. The diethyl ether solution was washed with water and dried (Na_2SO_4). Removal of the solvent left a residue which was recrystallized from methanol to yield azine **19** (5 mg), mp 220 °C (dec). Found: *m/e* 516.4460. Calcd for $C_{36}H_{56}N_2$ M^+ 516.4443. IR (Nujol): 1699 cm^{-1} (C=N–N=C). For NMR see Table. MS *m/e* (rel intensity): 516 (M^+. 8.5%), 501 (17), 314 (78), 258 (29), 218 (39), 203 (27), 175 (30), 148 (37), 109 (95), 95 (56), 93 (53), 91 (42), 81 (71), 79 (61), 67 (88), 55 (69), and 41 (100).

Preparation of D-*Nor-5α-androstan-16-one Acetylhydrazone (**20**)* Hydrazone **18** (516 mg) and acetic anhydride (2.5 ml) in pyridine (10 ml) were stirred for 16 h at room temperature. After the addition of methanol, a part of the solvent was removed. The solution was extracted with diethyl ether. The diethyl ether solution was washed with water, 5% acetic acid, and water again, and dried (Na_2SO_4). Removal of the solvent afforded a residue which was recrystallized from methanol (300 mg). The residue from the filtrate was subjected to column chromatography (Wakogel C-200) with benzene to afford two fractions. The first fraction (35 mg) was found to be *D*-nor-5α-androstan-16-one acetylhydrazone (**20**) by its NMR spectrum. The total yield was 61%. Recrystallization from methanol afforded an analytical specimen, mp 204—206 °C, Found: C, 75.79; H, 10.15; N, 8.73%. Calcd for $C_{20}H_{32}N_2O$: C, 75.90; H, 10.19; N, 8.85%. IR (Nujol): 3207 (NH), 1664 (NHCO), 1558, 1290, and 1079 cm^{-1}. For NMR see Table. MS *m/e* (rel intensity): 317 (M+1, 0.3%) 316 (M^+, 0.2), 301 (0.4), 290 (0.7), 275 (0.5), 258 (0.5), 218 (0.5), 203 (0.6), 175 (0.6), 161 (0.5), 125 (2.4), 112 (1.2), 109 (1.9), 98 (100), 67 (1.9), 55 (1.9), 43 (1.5), and 41 (1.7).

Photo-reaction of D-*Nor-5α-androstan-16-one Acetylhydrazone (**20**) in the Presence of Oxygen.* Acetylhydrazone **20** (350 mg) in dioxane (150 ml) was bubbled with oxygen. The solution

was irradiated with a 15-W low pressure mercury arc for 7 h under an atmosphere of oxygen. After removal of the solvent, the residue was dissolved in dichloromethane. The solution was washed with water and dried (Na_2SO_4). The product was subjected to preparative TLC with a 99: 1 mixture of diethyl ether and methanol to afford ten fractions (A to J) in the order of decreasing polarity. Fractions A (93 mg) and B(36 mg) were a mixture of the parent ketone and 17-oxa-5α-androstan-16-one (**17**). Fraction A was recrystallized from methanol to afford the parent ketone (47 mg). The residue from the filtrate and fraction B were combined and subjected to preparative TLC with benzene (Wako gel B-5F) to afford the parent ketone (61 mg) as the most mobile fraction (B_1). The second mobile fraction B_2 (54 mg) was subjected to preparative TLC with a 50: 1 mixture of benzene and diethyl ether to afford three fractions: B_{2a} (18 mg), B_{2b} (9 mg) and B_{2c} (1 mg). Fractions B_{2a} (5%) was 17-oxa-5α-androstan-16-one **17** and was recrystallized from acetone-water to afford 4 mg of lactone **17**, identical with the specimen prepared by the Baeyer-Villiger oxidation of ketone **16**. The third mobile fraction (171 mg) was subjected to preparative TLC with a 50 : 1 mixture of benzene and diethyl ether to afford five fractions: B_{3a} (7 mg), B_{3b} (6 mg), B_{3c} (6 mg), B_{3d} (21 mg), and B_{3e} (12 mg). The fractions B_{3d} was subjected to HPLC (column, μ-Bondapak CN; diethyl ether as the solvent; detector, JASCO UVIDEC-100; pump, Varian series 4100) to give two fractions. The fraction with a shorter retention time was evaporated to yield crystals of 16-aza-5α-androstan-17-one (**22**) (3.3 mg), mp 259—261 °C, identical with a specimen obtained by the Beckmann rearrangement of *D*-nor 5α-androstan-16-one oxime.[9] (lit,[10] mp 259—260 °C). The fraction (5.1 mg) with a longer retention time was still a mixture and this mixture was again subjected to preparative HPLC (column; μ-Bondapak NH_2, diethyl ether as the solvent). The fraction (2 mg) with the shorter retention time was 17-aza-5α-androstan-16-one (**21**),[10] identical with an authentic specimen obtained by the Beckmann rearrangement.[9] The fraction (2 mg) of a longer retention time was 17-aza-5α,13α-androstan-16-one (**23**), mp 154—157 °C(diethyl ether), identical with a specimen obtained by the photo-Beckmann rearrangement.[9]

We thank Mrs. Tomoko Okayama and Miss Hiroko Maki for the measurements of NMR spectra.

References

1) Photoinduced Transformations. Part 47. Part 46: H. Suginome and Chi-Ming Shea, *Synthesis*, **1980**, 229.
2) H. Suginome and T. Uchida, *J. Chem. Soc., Perkin Trans. 1*, in press.
3) M. P. Cava, R. L. Litle. and D. R. Napier, *J. Am. Chem. Soc.*, **80**, 2257 (1958).
4) J. L. Mateos and O. Chao, *Biol. Inst. Quim. Univ. Nat. Suton. Mex.*, **13**, 3 (1961).
5) J. Meinwald, G. G. Curtis, and P. G. Gassman, *J. Am. Chem. Soc.*. **84**, 116 (1962).
6) M. P. Cava and E. Moroz, *J. Am. Chem. Soc.*, **84**, 115 (1962).
7) J. Meinwald, L. L. Labana, and T. N, Wheeler, *J. Am. Chem. Soc.*, **92** ,1006 (1970).
8) H. Suginome and H. Takahashi, *Bull. Chem. Soc. Jpn.*, **48**, 582 (1975); H. Suginome and F. Yagihashi, *J. Chem. Soc., Perkin Trans. 1*, **1977**, 2488.
9) H. Suginome and T. Uchida, *Bull. Chem. Soc. Jpn*, **53**, 2292 (1980).
10) E. R. H. Jones, G. D. Meakins, and K. Z. Tuba, *J. Chem. Soc., C*, **1969**, 1597.
11) M. Busch and W. Dietz, *Ber.*, **47**, 3277 (1914); R. Criegee and B. Lohaus, *ibid.*, **84**, 219 (1951); H. C. Yao and P. Resnick, *J. Org. Chem.*, **30**, 2832 (1965).
12) J. Buckingham and R. O. Guthrie, *J. Chem. Soc., C*, **1968**, 1445.
13) N. Toshima and H. Hirai, *Tetrahedron Lett.*, **1970**, 434.
14) K. Gollnick, *Adv. Photochem.*, **6**, 1 (1968); C. S. Foots, *Acc. Chem. Res.*, **1**, 104 (1968); W. R. Adam, *Oxidation*, **2**, 65 (1971); J. Griffiths and H. Hawkins, *J. Chem. Soc., Perkin Trans. 2*, **1977**, 747.
15) P. Yates and L. Kilmurry, *Tetrahedron Lett.*, **1966**, 1739; for review see P. Yates and R. O. Loutfy, *Acc. Chem. Res.*, **8**, 209 (1975).
16) D. R. Morton, E. Lee-Ruff, R. M. Southam, and N. J. Turro, *J. Am. Chem. Soc.*, **92**, 4349 (1970); for review see D. R. Morton and N. J. Turro, *Adv. Photochem.* **9**, 197 (1974).
17) G. Quinkert, G. Cimballek, and G. Buhr, *Tetrahedron Lett.*, **1966**, 4573; G. Quinkert, D. Jacobs, and W. D. Stohrer, *Angew. Chem. Int. Ed.* **13**, 197 (1974); D. M. McDaniel and N. J. Turro, *Tetrahedron Lett.*, **1972**, 3035.
18) G. Eadon, S. Popov, and C. Djerassi, *J. Am. Chem. Soc.*, **94**, 1282 (1972).
19) H. Budzikiewicz, J. Buchler and G. Quinkert, *Monatsh. Chem.* **98**, 1115 (1967).

Photoreaction of *D*-Nor-5α-androstan-16-one Oxime, a Steroidal Cyclobutanone Oxime[1)]

Hiroshi SUGINOME*,** and Tsutomu UCHIDA

Department of Chemistry, Faculty of Science, Hokkaido University, Sapporo 060

(Received January 16, 1980)

Irradiation of *D*-nor-5α-androstan-16-one oxime in methanol leads to a mixture of seco-nitriles; *D*-nor-13,16-seco-5α-androst-13(18)-ene-16-nitrile (**3**), *D*-nor-13,16-seco-5α-androst-12-ene-16-nitrile (**7**), 13ξ-methoxy-*D*-nor-13,16-seco-5α-androstane-16-nitrile (**8**), and 15-hydroxy-*D*-nor-15,16-seco-5α-androstane-16-nitrile (**9**). These result from ionic α-fissions at either of the α-bonds. Low yields of three lactams, 17-aza-5α-androstan-16-one (**6**), 17-aza-5α,13α-androstan-16-one (**11**), and 16-aza-5α-androstan-17-one (**5**), resulting from photo-Beckmann rearrangement, are also formed. The formation of **11** is the second proven example of a photo-Beckmann rearrangement in which a chirality of the migrating carbon center is not retained in the product lactam and an intervention of a ring-opened intermediate must be involved. It was found that direction of the α-cleavage of this excited four-membered cyclic ketone oxime was not governed only by the stability of cleaved ions, since seco-nitrile **9** resulting from α-fission to a less stable primary carbonium ion was formed together with seco-nitriles **3**, **7**, and **8** from a more stable tertiary carbonium ion. The Beckmann rearrangement of the mixture of *syn* and *anti* oximes with thionyl chloride afforded the two expected lactams **5** and **6** together with the products of Beckmann fission **3** and *D*-nor-13,16-seco-5α-androst-13(14)-ene-16-nitrile resulting from a cleavage to tertiary carbonium ion.

In the photo-Beckmann rearrangement of steroidal saturated ketone oximes, the chirality of the migrating center of the oximes is generally retained in the product lactams.[2)] We have found one exception to this rule: irradiation of *O*-acetylandrosterone oxime afforded a pair of lactams epimeric at the C-13.[3)] This exception implies that another mechanism, in which lactams are formed *via* rebonding of species resulting from α-fission of the oximes or the corresponding species resulting from the breakdown of the intermediate oxaziridines, is involved in the lactam formation. In order to gain more insight into the mechanism of the photoreaction of oximes, the Beckmann and the photo-Beckmann rearrangements of a steroidal cyclobutanone oxime were investigated. The results are described in this paper.

Results

D-Nor-5α-androstan-16-one oxime (**2**), prepared by the standard method, was chosen as the substrate. NMR showed that the crude oxime, as well as the one recrystallized from aqueous ethanol, were mixtures of the (*Z*) and (*E*) isomers **2a** and **2b**. Thus, a signal due to the 18-H of the oxime before the recrystallization appeared as two singlets at τ 8.87 and 8.84 (19-H as a singlet at τ 9.22), indicating it to be a mixture of geometrical isomers. This was proved more clearly by an analysis of the signals in lower fields. In the spectrum, there were a triplet centered at τ 7.34 with J=11.3 Hz, a double doublet centered at τ 7.15 with J=7.8 and 11.3 Hz, and another double doublet centered at τ 6.54 with J=7.8 and 11.3 Hz. The integrated signal areas corresponded to 1 H, 0.8 H and 0.2 H. These signals were ascribable to the 15α(or β)-H of **2a** and **2b**, the 15β(or α)-H of **2a** and the 15β(or α)-H of **2b**. As we reported previously, protons of the hydroxyimino group, which is nearly eclipsed by the C=N bond of the oximes, are deshielded[2)] when the hydroxyl group is *syn* to them and appear at *ca.* τ 6.6. The α-oriented proton at the C-15 of **2b** falls in this category; from the ratio of the signal areas of the 15β(or α)-H of **2a** and the 15β(or α)-H of **2b**, the ratio of **2a** and **2b** is estimated to be approximately 4: 1. This ratio did not change significantly after its recrystallization from aq ethanol.

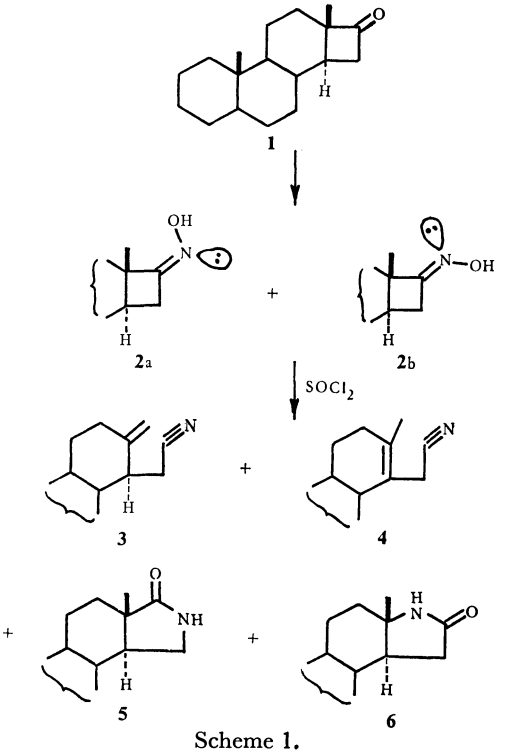

Scheme 1.

Scheme 1 shows the results of ordinary Beckmann rearrangement. Treatment of oxime mixture **2a** and **2b** with thionyl chloride at room temperature afforded a product mixture, much simpler than that from the photolysis (*vide infra*). The mixture was subjected to preparative TLC to afford a mixture of two seco-nitriles **3** and **4** and a mixture of two lactams **5** and **6**. The two seco-nitriles **3** and **4** were separated by preparative TLC with silica gel containing silver nitrate. The structure of the less mobile compound **3**, mp 66—70

** Present address: Organic Chemistry Laboratory, Department of Chemical Process Engineering, Faculty of Engineering, Hokkaido University, Sapporo 060.

°C, (35%) was confirmed to be *D*-nor-13,16-seco-5α-androst-13(18)-ene-16-nitrile (**3**) by IR, mass, and NMR spectroscopy. The molecular formula $C_{18}H_{27}N$ was confirmed by high resolution mass spectrometry. The IR spectrum exhibits a band due to the C≡N group at 2242 cm^{-1} and a series of bands due to the *exo*-methylene at 1647 and 894 cm^{-1}. The low resolution mass spectrum shows the molecular ion at *m/e* 257 (71.2%), M^+-CH_3 at *m/e* 242 (57.0%), the base peak at *m/e* 149, and the ion at *m/e* 109 (63.1%). The NMR spectrum has a singlet due to the 19-H at τ 9.28 and no signal due to the 13β-methyl group is found. Instead, the spectrum shows two broad one-proton singlets at τ 5.16 and 5.28($W_{1/2}$=4.5 Hz) and a two-proton doublet centered at τ 7.38 (J=5.3 Hz). These results are in agreement with the structure **3**; the two broad singlets are ascribed to the *exo*-methylene protons and the doublet to the C-15 methylene protons.

The spectral results of oily seco-nitrile **4** (8%) were in agreement with the structure of *D*-nor-13,16-seco-5α-androst-13(14)-ene-16-nitrile (**4**). The high resolution mass spectrometry proved that **4** has the molecular formula $C_{18}H_{27}N$. The low resolution mass spectrum of **4** exhibits the molecular ion at *m/e* 257 (15.7%), M^+-CH_3 peak at *m/e* 242 (5.6%), a fragment at *m/e* 149 (5.1%), and the base peak at *m/e* 109. The IR spectrum has a nitrile band at 2245 cm^{-1}. The NMR spectrum has two singlets (each 3H) at τ 9.28 and 8.32 and a two-proton singlet at τ 6.93. These signals are assignable to the 19-H, the 18-H, and the 15-H of **4**.

Lactams **5** and **6**, obtained from a less mobile fraction, were separated with the aid of HPLC. The molecular formula of lactam **5** (12%) which has a shorter retention time was confirmed to be $C_{18}H_{29}NO$ by high resolution mass spectrometry. The physical and the spectral properties were in agreement with 16-azaandrostan-17-one (**5**).[4] The molecular formula of lactam **6** (7%) which has a longer retention time, was also confirmed to be $C_{18}H_{29}NO$ by high resolution mass spectrometry. The physical and spectral properties were in accordance with 17-azaandrostan-16-one (**6**).[4]

The photo-Beckmann rearrangement of oxime **2** in methanol was carried out under the same procedure as we reported previously.[2] Irradiation of a solution of the mixture of oximes **2a** and **2b** afforded a complex mixture of the products, from which a mixture of seco-nitriles **3** and **7**, two other seco-nitriles **8** and **9**, and three lactams **5**, **6**, and **11** have been isolated by preparative TLC (Scheme 2). Although the separation of the mixture of seco-nitriles **3** and **7** to its components by means of preparative TLC was unsuccessful, spectrometry confirmed that it was a mixture of two seco-nitriles, **3** and *D*-nor-13,16-seco-5α-androst-12-ene-16-nitrile (**7**). Thus, the IR spectrum shows the molecular ion at *m/e* 257. The NMR shows all the signals due to seco-nitrile **3** obtained by the Beckmann rearrangement. Besides these signals it has two singlets at τ 9.29 and 8.34, and a broad singlet at τ 4.34. These signals are ascribed to the 19-H, the 18-H, and the 12-H of *D*-nor-13,16-seco-5α-androst-12-ene-16-nitrile (**7**). On the basis of the ratio of the integrated areas of the singlet at τ 4.34 due to the 12-H of **7** and the two singlets at τ 5.16 and 5.28 due to the *exo*-methylene protons of **3**, the ratio of **3** and **7** was estimated to be approximately 1.8 : 1.0 (2.8% and 1.5% yields). The structure of a less mobile amorphous compound (**8**) (1%) was proved to be 13ξ-methoxy-*D*-nor-13,16-seco-5α-androstane-16-nitrile by means of spectrometry. The IR spectrum shows a nitrile band at 2192 cm^{-1}. The high resolution mass spectrum of **8** proves that it has the molecular formula $C_{19}H_{31}NO$. The NMR exhibits three singlets (each 3H) at τ 9.23, 8.84, and 6.80, and a doublet (2H) centered at τ 7.84 (J=3.0 Hz). These signals are ascribable to the 19-H, the 18-H, the methoxyl group and the 15-H of **8**. The fragment ions in the mass spectrum supported this assignment. In the spectrum the base peak is present at *m/e* 85 and no other peak has an abundance of more than 7.9%. The formation of the base peak is rationalized in terms of structure **8** in a manner depicted in Scheme 3. The other crystalline compound (**9**) (2.7%) was also a seco-nitrile and its structure, 15-hydroxy-*D*-nor-15,16-seco-5α-androstane-16-nitrile (**9**), has been assigned from the analysis of the mass, IR, and NMR spectra. The molecular formula $C_{18}H_{29}NO$ was deduced from high resolution mass spectrometry. The IR spectrum exhibits a nitrile band at 2220 cm^{-1} and a hydroxyl band at 3571 cm^{-1}. The NMR shows two singlets (each 3H) at τ 9.27 and 8.24 and a doublet (2H) centered at τ 6.06 (J=2 Hz) which are ascribed to the 19-H, the 18-H, and the 15-H of **9**. The low resolution mass spectrum exhibits the parent

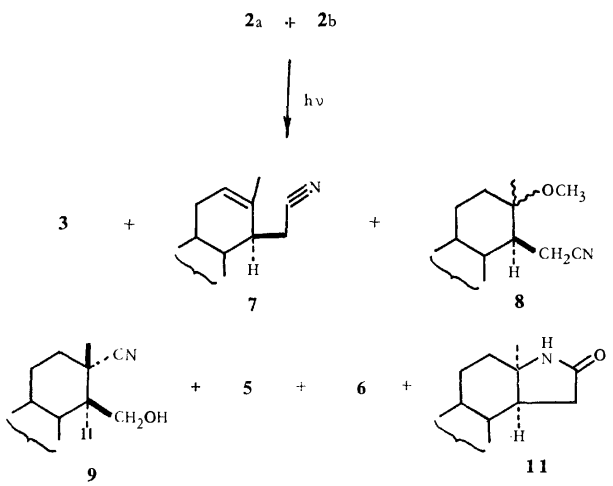

Scheme 2.

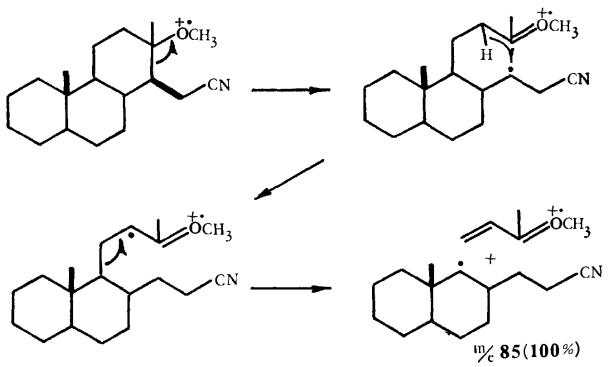

Scheme 3.

peak at *m/e* 275 (58.0%), M^+-CH_3 at *m/e* 260 (40.8%), M^+-H_2O at *m/e* 257 (25.6%), M^+-CH_2OH at *m/e* 244 (38.3%), and a base peak at *m/e* 218. Structure **10** is assigned to the last fragment ion.

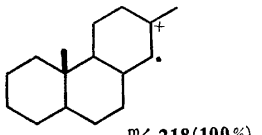

10

A mixture of lactams, which were again difficult to separate by means of preparative TLC, was obtained as a less mobile fraction. This mixture could be separated, however, to 16-aza-5α-androstan-17-one (**5**), 17-aza-5α-androstan-16-one (**6**), and a new lactam **11** by HPLC. Lactams **5** and **6** were identified by direct comparisons with the authentic specimens obtained by the Beckmann rearrangement. The new lactam **11** has the molecular formula $C_{18}H_{29}NO$, as shown by its high resolution mass spectrum, and the lactam carbonyl bands at 1701 and 1675 cm^{-1} and the NH band at 3240 cm^{-1} in the IR spectrum. The most diagnostic spectral property is the mass spectrum which shows a fragmentation pattern nearly identical to that of 17-aza-5α-androstan-16-one (**6**). Thus, the structure of the new lactam is clearly 17-aza-5α,13α-androstan-16-one (**11**).

Discussion

These results confirmed that the photo-reaction of fused cyclobutanone oxime **2** leads mostly to the products resulting from α-fissions and gives only a low yield of a mixture of lactams. Although the yield of lactams is very low, the present result is the second proven example of a photo-Beckmann rearrangement in which the chirality of the migrating center of the oximes is not retained in the product lactam. The formation of lactam **11** implies that, as we described in our previous papers,[2,3] a ring-opened intermediary species should be involved in the course of the photo-rearrangement and reinforces the possibility of the presence of an exceptional mechanistic pathway for the lactam formation from the excited saturated ketone oxime.

As we pointed out in our previous papers, the α-fission reaction is rare in the photo-reaction of oximes.[7] The oximes in which α-fissions in the photo-reaction are observed[8,9] appear to be those in which an increase of non-bonded interaction or strain in the molecule is expected by the formation of the corresponding oxaziridine intermediate.

The observed α-fission in the present case is attributable to the ring strain of the four-membered ring. The present α-fission is apparently ionic in nature since all the products which result from α-fission are those expected for an ionic mechanism. Another example of ionic α-fission was recently reported by Inamoto and his colleagues.[9]

A remarkable feature in the present photo-reaction is the formation of nitrile **9** which arises from a less stable primary carbonium ion generated by a cleavage of the C-15–C-16 bond. This is contrasted to the α-fission in the ground state reaction in which the products in α-fission are nitriles **3** and **4** resulting from a more stable carbonium ion, as would be expected. This result indicates clearly the difference in behaviour of the α-fission in the ground state reaction and in the excited state reaction. The selectivity in the site of the α-fission in excited cyclobutanone oxime **2** seems to be reduced. An analogous anomalous behaviour for the α-fission has been found in an excited steroidal cyclobutanone; 3β-methoxy-*D*-nor-5α-androstan-16-one gives 12% of the acetal derived from a less stable 1,4-biradical.[10,11] (Scheme 4).

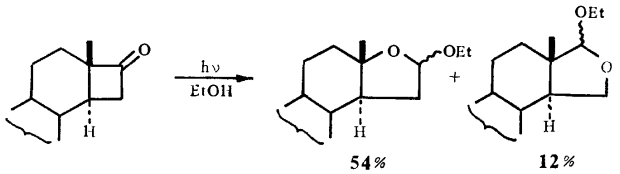

Scheme 4.

It is noted that while the photo-Beckmann rearrangement of *O*-acetylandrosterone oxime, a *trans* fused cyclopentanone oxime, afforded two isomeric lactams arising from the migration of the more-substituted carbon center and no accompanying lactams arising from the migration of the less-substituted carbon center,[3] the corresponding *trans* fused cyclobutanone oxime **2** afforded lactam **5** arising from the migration of the less substituted carbon center.

Experimental

Mps were determined with a Yanagimoto micro-melting point apparatus. IR spectra were determined for Nujol mulls with a JASCO IR-E spectrophotometer unless stated otherwise. 100 MHz ^1H NMR spectra were recorded with a JEOL PS 100 high-resolution spectrometer (solvent $CDCl_3$; Me_4Si as internal reference). Preparative TLC was carried out on Wakogel B-5F unless stated otherwise. Mass spectra were recorded in the Faculty of Pharmaceutical Sciences or the Faculty of Agriculture of this University with a Hitachi JMS-D 300 spectrometer using a direct inlet system. (Ion source temperatures: 175 °C for compounds **2**, **3**, and **8**; 180 °C for compounds **6** and **9**; 185 °C for compound **5** and 100 °C for compound **4**. Ionizing voltage, 70 eV). Only fragment peaks of relative intensities over 40% are mentioned. High resolution mass spectra were measured by Miss Y. Chiba in the Faculty of Agriculture. Dotite spectrosol methanol (Wako) was used as solvent for the photoreactions.

Preparation of D-*Nor-5α-androstan-16-one Oxime* **2a** *and* **2b**. *D*-Nor-5α-androstan-16-one (**1**) (50 mg), hydroxylamine hydrochloride (30 mg) and sodium acetate trihydrate (20 mg) in ethyl alcohol (1 ml) and water (0.2 ml) were stirred for 2 h at room temperature. After the usual work-up the product was recrystallized from aq ethanol to afford the oxime (15 mg), mp 87—90 °C, which was a mixture of geometrical isomers. Found: C, 78.31; H, 10.42; N, 5.30%. Calcd for $C_{18}H_{29}NO$: C, 78.49; H, 10.61; N, 5.09%. IR: 3260 (OH), 1705 (C=N), and 937 cm^{-1}. MS *m/e* (rel intensity) 275 (M^+, 11.7), 260 (M^+-CH_3, 39.8), 259 (M^+-16, 22.5), 258 (M^+-H_2O, 100), 109 (76.6), 95 (63.9), 81 (59.1), 67 (68.3), 55 (68.2), 41 (60.7); for NMR see text.

The Beckmann Rearrangement of D-*Nor-5α-androstan-16-one Oxime,* ***2a*** *and* ***2b***. To the amorphous oxime (41 mg) in dioxane (2 ml) was added thionyl chloride (0.5 ml) at room temperature. The solution was stirred for 20 min. The solution was extracted with dichloromethane. The organic layer was washed with water, 5% sodium hydrogencarbonate, and water again and then dried (Na_2SO_4). The residue(40 mg) was subjected to preparative TLC with a 2 : 1 mixture of dichloromethane and diethyl ether to afford two fractions (A and B). The more mobile fraction A (27 mg) was a mixture of the Beckmann fission products and was subjected to preparative TLC. The TLC plates were developed twice with hexane and benzene, once with a 9 : 1 mixture of hexane and benzene, and five times with a 99: 9 : 1 mixture of hexane, benzene, and dichloromethane to afford two fractions. The more mobile fraction A_1 (6 mg) was still a mixture of two nitriles **3** and **4**. This fraction was again subjected to preparative TLC (Wakogel B-5F containing 5% silver nitrate) with a 3: 1 mixture of benzene and diethyl ether to afford two fractions. The more mobile fraction (3 mg, 8%) was a colorless oil and was a 13,17-seco-nitrile **4**. Found: *m/e* 257.2124. Calcd for $C_{18}H_{27}N$: M, 257.2141; IR (Nujol): 2245 cm^{-1} (C≡N). For MS and NMR see text.

The less mobile crystalline fraction (2 mg) was the seco-nitrile **3**. The less mobile crystalline fraction A_2 (12 mg) was also nearly pure nitrile **3**, which gave crystals on addition of methanol, mp 66—70 °C. Found: *m/e* 257.2160. Calcd for $C_{18}H_{27}N$: M, 257.2141; IR (Nujol): 2242 (C≡N), 1773, 1647, and 894 cm^{-1} (C=CH_2); MS *m/e* (rel intensity) 257 (M^+, 71.2), 242 (M^+-CH_3, 57.0), 163 (46.6), 149 (100), 109 (63.1), 95 (60.4), 81 (68.3), 67 (59.7), 55 (64.5), and 41 (50.0). For NMR see text.

The fraction B (11 mg) was subjected to HPLC (μ Bondapak CN; JASCO UVIDEC-100 detector; pump, Varian Series 4100) with diethyl ether as the solvent. The fraction (7 mg) having the shorter retention time (7.5 min) was 16-azaandrostan-17-one (**5**). This was recrystallized from acetone to yield crystals (5 mg, 12%), mp 259—261 °C. (lit,[4] 259—260 °C). Found: *m/e* 275.2242. Calcd for $C_{18}H_{29}NO$: M,+ 275.2247; IR: 3306 (NH), 1716 and 1679 cm^{-1} (lactam carbonyl) (lit,[4] 3451, 3200, 1720, and 1700 cm^{-1}); MS *m/e* (rel intensity) (ion-source temp, 185 °C, 70 eV) 275 (M^+, 100), 260 (21.5), 230 (24.6), 218 (28.0), and 98 (33.8%) (lit,[4] *m/e* 275 (100), 260 (25), 230 (16), and 218 (26%)); NMR: τ 9.04 (3H, s, 18-H), 9.22 (3H, s, 19-H), 7.01 (1H, t, 15β-H), 6.08 (1H, dd, 15α-H) ($J_{15\alpha,15\beta}=J_{15\beta,14\alpha}=9.8$ Hz; $J_{15\alpha,14\alpha}=$ 4.5 Hz), and 3.41 (1H, br. s, $W_{1/2}$ 12 Hz, NH).

The fraction (3 mg, 7%) of longer retention time (11.5 min) was 17-azaandrostan-16-one (**6**). This was recrystallized from acetone to yield crystals (2 mg), mp 250—251 °C. (lit,[4] mp 256—257 °C). Found: *m/e* 275.2255. Calcd for $C_{18}H_{29}$-NO: M, 275.2247, IR: 3287 (NH), 1715 and 1677 cm^{-1} (lactam carbonyl) (lit,[4] 3420, 3200, 1720, and 1697 cm^{-1}); MS *m/e* (rel intensity) (ion-source temp 180 °C and ionizing voltage 70 eV) 275 (M^+, 1.2), and 260 (100%) (lit,[4] *m/e* 275 (2) and 260 (100); 8.94 (3H, s, 18-H), 9.24 (3H, s, 19-H), 7.89 (1H, d, 15α- or 15β-H), 7.91 (1-H, d, 15α- or 15β-H) ($J_{15\beta,14\alpha}=J_{15\alpha,14\alpha}=9.8$ Hz) 4.04 (1-H, br. s, $W_{1/2}$ 10 Hz).

The Photo-Beckmann Rearrangement of D-*Nor-5α-androstan-17-one Oxime.* The mixture of *syn* and *anti* oximes (300 mg) in methanol (300 ml) was irradiated for 48 h with a 15-W low pressure mercury arc. Argon was slowly bubbled during the irradiation. After the removal of the solvent, the residue was subjected to preparative TLC (Wakogel B-5F) with a 1: 4 mixture of diethyl ether and benzene to afford eight fractions A (53 mg), B (33 mg), C (21 mg), D (16 mg), E (15 mg), F (37 mg), G (24 mg), and H (80 mg) in the order of decreasing mobility. The fraction A was subjected again to preparative TLC with benzene to afford two fractions (A_1 and A_2). The fraction A_1 (34 mg) was further subjected to preparative TLC with a 5: 1 mixture of hexane and benzene. The plates were developed five times to afford a mixture of two seco-nitriles **3** and **7** (12 mg, 4.3%). Analysis of the NMR spectrum is described in the text. The fraction B was subjected to preparative TLC with benzene to afford a gummy compound (9 mg). This was again purified by preparative TLC (Merck silica gel 60 F_{254} with concentration zone) with a 4 : 1 mixture of hexane and diethyl ether to afford a colorless gum **8** (3 mg, 1%). Found: *m/e* 289.2391. Calcd for $C_{19}H_{31}NO$: M, 289.2404; IR (neat): 2192 (C≡N), 1468, 1451, 1436, 1378, 1135, and 1084 cm^{-1}; MS *m/e* (rel intensity) 289 (M^+, 3.6%), 274 (2.6), 257 (2.6), 242 (1.4), 85 (100), 72 (4.5), 67 (5.1), 55 (7.9), and 41 (5.1), for NMR see text. The fraction E was again purified by preparative TLC to afford the seco-nitrile **9** (8 mg) which was recrystallized from diethyl ether–hexane to afford crystals, mp 164—166 °C. Found: *m/e* 275.2241. Calcd for $C_{18}H_{29}NO$: M, 275.2248; IR (Nujol): 3571 (OH), 2220 (C≡N) and 1088 cm^{-1}. For NMR see text; MS *m/e* (rel intensity) (ion-source temp 180 °C, 70 eV) 275 (M^+, 58.0%), 260 (40.8), 257 (25.6), 247 (11.8), 244 (38.3), 242 (23.2), 218 (100), 200 (15.3), 190 (26.7), 175 (15.6), 149 (33.6), 135 (18.5), 121 (26.5), 110 (54.8), 109 (64.4), 95 (7.13), 81 (71.6), 67 (65.4), 55 (65.9), and 41 (62.1). The fraction F was again subjected to preparative TLC (Merck silica gel 60 F_{254} with concentration zone) with a 4 : 1 mixture of hexane and ethyl acetate. The plates were developed five times to afford two fractions (F_1 and F_2). The fraction F_1 (2 mg) was unidentified and a less mobile fraction F_2 (19 mg) was a mixture of other seco-nitriles. However, the separation to its components by preparative TLC was not successful. The fraction H was subjected to preparative HPLC, as with the case of the lactam mixture from the Beckmann rearrangement, to afford three fractions (H_1, H_2, and H_3) in the order of the retention times. The fraction H_1 (63 mg) with the shortest retention time was an unidentified gum. The second fraction H_2 (2 mg, 0.7%) was 16-aza-5α-androstan-17-one **5** identical with the specimen obtained by the Beckmann rearrangement. The fraction H_3 (8 mg, 2.7%) was a mixture of two lactams, 17-aza-5α-androstan-16-one (**6**) and 17-aza-5α,13α-androstan-16-one (**11**). This was subjected to preparative HPLC (μ Bondapak NH_2) with diethyl ether as the solvent to afford pure lactam **6** and its epimer **11** in a 3 : 1 ratio. Lactam **6** with the shorter retention time was identical with an authentic specimen of lactam **6** obtained by the Beckmann rearrangement. The new lactam **11** having a longer retention time was recrystallized from diethyl ether. It had mp 154—157 °C. Found: *m/e* 275.2249. Calcd for $C_{18}H_{29}NO$; M, 275.2249; for IR see text. NMR: τ 8.83 (3H, s, 18-H) and 9.36 (3H, s, 19-H), MS *m/e* 275 (rel intensity) (M^+, 3.9%), 260 (M^+-CH_3, 100), 136 (6.9), 109 (4.9), 81 (5.9), 79 (4.3), 67 (7.5), 55 (8.0), and 41 (8.6).

We thank Miss Hiroko Maki for the measurement of NMR spectra.

References

1) Photoinduced Transformations. Part 48. Part 47: H. Suginome, T. Uchida, K. Kizuka, and T. Masamune, *Bull. Chem. Soc. Jpn.*, **53**, 2285 (1980).

2) H. Suginome and H. Takahashi, *Tetrahedron Lett.*, **1970**, 5119; *Bull. Chem. Soc. Jpn.*, **48**, 582 (1975); H. Suginome

and F. Yagihashi, *J. Chem. Soc., Perkin Trans. 1*, **1977**, 2488.

3) H. Suginome and T. Uchida, *Tetrahedron Lett.*, **1973**, 2293; *Bull. Chem. Soc. Jpn.*, **47**, 687 (1974).

4) E. R. H. Jones, G. D. Meakins, and K. Z. Tuba, *J. Chem. Soc., C*, **1969**, 1597.

5) H. Budzikiewicz, F. Compernolle, K. V. Cauwenberghe K. Schulze, H. Wolf, and G. Quinkert, *Tetrahedron*, **24**, 6797 (1968).

6) R. T. Aplin, G. D. Meakins, K. Z. Tuba, and P. D. Woodgate, *J. Chem. Soc., C*, **1969**, 1602.

7) For a review of the Photo-Beckmann rearrangement see H. Suginome, *Kagaku No Ryoiki*, **30**, 10 (1976).

8) T. Sato and H. Obase, *Tetrahedron Lett.*, **1967**, 1633.

9) R. Okazaki, M. Watanabe, and N. Inamoto, *Tetrahedron Lett.*, **1977**, 4515.

10) F. Quinkert, G. Cimbollek, and G. Buhr, *Tetrahedron Lett.*, **1966**, 4573.

11) This anomaly in the direction of α-fission can not be taken as general for excited cyclobutanones, since all other monocyclic cyclobutanones and 3β-methoxy-*D*-nor-5α,13α-androstan-16-one show good selectivity with respect to the site of α-cleavage. [D. R. Morton, E. Lee-Ruff, R. M. Southam, and N. J. Turro, *J. Am. Chem. Soc.*, **92**, 4349 (1970)].

Preparation and Properties of Nitrosyl Complexes of Molybdenum[1]

Takashi TATSUMI,* Kazuhiko SEKIZAWA, and Hiroo TOMINAGA
Department of Synthetic Chemistry, Faculty of Engineering, The University of Tokyo, Hongo, Tokyo 113
(Received November 8, 1979)

Reactions of some dpe(dpe=$Ph_2PCH_2CH_2PPh_2$) complexes of molybdenum with nitrosyl hexafluorophosphate ($NOPF_6$) have been investigated. The reaction of $MoH_4(dpe)_2$ with $NOPF_6$ in benzene–methanol affords two types of complexes, a protonated species, *trans*-$[MoF(HNO)(dpe)_2]PF_6$ (**1a**) and a non-protonated species, *trans*-$MoF(NO)(dpe)_2\cdot 1/2C_6H_6$. From the nitroxyl complex **1a**, a series of nitrosyl complexes has been obtained. Some nitrosyl complexes exhibit *cis-trans* isomerism. Reactions of the nitrosyl complexes with protonic acids afford the corresponding nitroxyl complexes or the anion substitution products. Cationic nitrosyl complexes are obtained by the reactions of $Mo(CO)L(dpe)_2$ (L=N_2 or C_2H_4) and $Mo(C_2H_4)_2(dpe)_2$ with $NOPF_6$. Attempts were also made to prepare nitrosyl complexes of molybdenum by use of other nitrosylating agents.

Recently dinitrogen,[2] isonitriles,[3] thiocarbonyl,[4] and ethylene,[5] which are attached to the electron-rich site of $M(dpe)_2$ (M=Mo or W, dpe=$Ph_2PCH_2CH_2PPh_2$), have been shown to be susceptible to electrophilic attack. Such attack at coordinated dinitrogen has been extensively investigated, leading to the formation of nitrogen–hydrogen and nitrogen–carbon bonds.[2] This finding prompted us to prepare metal complexes containing nitrogen monoxide activated by coordination to this site. We describe below the nitrosylation of some dpe complexes of molybdenum by use of versatile nitrosylating agents[6,7] and the protonation of the nitrosyl complexes thus obtained. Chatt *et al.* briefly commented on the formation of $MoX(NO)(dpe)_2$ (X= F and Br) from $MoX(N_2H)(dpe)_2$ and nitrogen monoxide.[8] Very recently King and Leigh reported the preparation of a series of nitrosyl complexes of molybdenum and tungsten with only halide and tertiary phosphine as coligands.[9] The reactions of nitrosyl compleses with electrophiles such as HCl, HBr, $PhCH_2Br$, O_2, and NO have recently been reviewed.[10]

Results and Discussion

Reaction of Phosphine Complexes of Molybdenum with $NOPF_6$. The reaction of a hydride complex, $MoH_4(dpe)_2$, with $NOPF_6$ ($NOPF_6$/Mo=1.05) in benzene–methanol solution gives *trans*-$[MoF(HNO)(dpe)_2]PF_6$ (**1a**) and *trans*-$MoF(NO)(dpe)_2\cdot 1/2C_6H_6$ (**2a**). Complex (**1a**) is a purple crystalline diamagnetic solid. The ^{31}P NMR spectrum of **1a** exhibits a doublet (J_{P-F}=39 Hz) at −45 ppm (relative to PPh_3) assigned to the four equivalent phosphorus nuclei, suggesting a *trans* configuration. Complex **2a** is a yellow crystalline diamagnetic solid which also has a *trans* configuration since its ^{31}P NMR spectrum shows a doublet (J_{P-F}= 27 Hz) at −58 ppm. This complex appears to be identical with that prepared by an alternative route.[8] Without methanol as a cosolvent, the starting material was recovered almost quantitatively. Complex (**1a**) is apparently a protonation product of **2a** by HPF_6. Treatment of **2a** with a benzene–methanol solution of $NOPF_6$ gives **1a** in good yield. HPF_6 must have been formed *in situ* by Eq. 1.[7] Expectedly, reaction of **2a** with aqueous HPF_6 in benzene affords **1a**.

$$NOPF_6 + MeOH \rightleftarrows HPF_6 + MeONO \quad (1)$$

In the reactions of nitrosonium salts with transition metal complexes, three types of reaction products have been found;[7] *i.e.*, formation of cationic nitrosyl species, one-electron oxidation, and protonation affording metal hydrides (in methanol). The basic character of the NO ligand of **2a** (see below) results in its rapid protonation but prevents the selective preparation of its complex by addition of 1 mol eq. of $NOPF_6$ to the hydride. One might expect that as the $NOPF_6$/Mo ratio is increased, **1a** would be exclusively obtained. In fact, however, the yield of **1a** decreased, whereupon benzene-soluble unknown complexes were obtained.

Treatment of the dinitrogen complex, *trans*-$Mo(N_2)_2(dpe)_2$, with $NOPF_6$ afforded no nitrosyl complex; dark red crystals of $[MoF(N_2H_2)(dpe)_2]PF_6$ (**3a**) were obtained which show the antisymmetric and symmetric N–H stretching frequencies at 3350 and 3260 cm^{-1}, respectively. Presumably the ligating dinitrogen was protonated by the *in situ*-formed HPF_6. This complex seems to be analogous to the hydrazido(2−) complex $[MoF(NNH_2)(dpe)_2]BF_4$.[11] Complex **3a** is isoelectronic to **1a**. Chatt *et al.* isolated $MoF(N_2H)(dpe)_2$, which is isoelectronic to **2a** and can be protonated in a similar way with **2a** to afford N_2H_2 complexes.

In contrast, *trans*-$Mo(CO)(N_2)(dpe)_2\cdot 1/2C_6H_6$ reacted with $NOPF_6$ to yield the known $[Mo(CO)(NO)(dpe)_2]PF_6$ (**3b**).[12] In this reaction, we have also detected *cis*-$[Mo(CO)_2(dpe)_2]PF_6$ and *cis*-$Mo(CO)_2(dpe)_2$ by IR. $Mo(CO)(C_2H_4)(dpe)_2$ showed a similar behavior toward $NOPF_6$. It should be noted that **3b** cannot obtained from *cis*-$Mo(CO)_2(dpe)_2$ and $NOPF_6$.[13] In the reactions of *trans*-$Mo(CO)(N_2)(dpe)_2\cdot 1/2C_6H_6$ and $Mo(CO)(C_2H_4)(dpe)_2$, *cis*-$[Mo(CO)_2(dpe)_2]PF_6$ would be formed by way of *cis*-$Mo(CO)_2(dpe)_2$ since these monocarbonyl complexes slowly changed to the *cis*-dicarbonyl in the absence of $NOPF_6$. In the reaction of $Mo(C_2H_4)_2(dpe)_2$ with $NOPF_6$, $[Mo(C_2H_4)(NO)(dpe)_2]PF_6$ (**3c**) was obtained in very poor yield.

Reaction of trans-*$Mo(N_2)_2(dpe)_2$ and $MoH_4(dpe)_2$ with NO Gas and Some NO Sources* Treatment of *trans*-$Mo(N_2)_2(dpe)_2$ in benzene with NO at atmospheric pressure afforded an orange yellow solution, from which yellow crystals were obtained. Elemental analysis suggests the empirical formula $[Mo(NO)(dpe)]_2\cdot 2C_6H_6$ (**4**) for the complex. The complex $[Mo(NO)(dpe)_2]_2\cdot CH_2Cl_2$ has been prepared previously from $[Mo(CO)_3(NO)(dpe)]PF_6$ and dpe.[13] Since **4** reacts successively

TABLE 1. NITROSYL COMPLEXES OF MOLYBDENUM

	Complex	Found (Calcd), %				IR, cm^{-1} a)	Color
		C	H	N	Halogen	ν(NO)	
2a	*trans*-MoF(NO)(dpe)$_2$·1/2C_6H_6	68.0 (67.4)	5.4 (5.2)	1.2 (1.4)	1.5 (1.9)	1528	yellow
2b	*cis*-MoCl(NO)(dpe)$_2$	64.6 (65.2)	5.0 (5.0)	1.5 (1.5)	3.5 (3.7)	1567	yellow
2c	*cis*-MoBr(NO)(dpe)$_2$	61.7 (62.3)	5.0 (4.8)	1.1 (1.4)	8.3 (8.0)	1567	yellow
2d	MoI(NO)(dpe)$_2$	59.2 (59.5)	4.6 (4.6)	1.2 (1.3)		1570	yellow brown
2e	Mo(NCS)(NO)(dpe)$_2$	64.6 (64.9)	4.9 (4.9)	2.5 (2.9)		1570	yellow
2f	*trans*-MoCl(NO)(dpe)$_2$·1/2C_6H_6	67.1 (67.5)	5.1 (5.2)	1.4 (1.4)	3.5 (3.6)	1542	yellow
2g	Mo($OCOCF_3$)(NO)(dpe)$_2$	63.3 (63.6)	4.8 (4.7)	1.2 (1.4)		1570	yellow
3b	[Mo(CO)(NO)(dpe)$_2$]PF_6	58.5 (58.1)	4.4 (4.4)	1.1 (1.3)		1648	pink
3c	[Mo(C_2H_4)(NO)(dpe)$_2$]PF_6	58.6 (59.2)	4.7 (4.7)	1.1 (1.3)		1606	brown
4	[Mo(NO)(dpe)$_2$]$_2$·2C_6H_6	70.1 (69.6)	5.6 (5.4)	1.2 (1.4)		1516	yellow

a) Recorded in KBr.

with NO to afford a brown powder, contaminated with the phosphine oxide(IR), the yield of **4** is low, but it can be isolated under appropriate conditions. The reaction of MoH_4(dpe)$_2$ with NO under similar conditions gave no nitrosyl complexes; MoH_4(dpe)$_2$ being recovered unchanged. With *N*-methyl-*N*-nitroso-*p*-toluenesulfoamide, the reagent known to be capable of nitrosylating metal hydrides,[7] MoH_4(dpe)$_2$ was recovered quantitatively.

The reaction of *trans*-Mo(N_2)$_2$(dpe)$_2$ with NOCl (NOCl/Mo=10) was carried out in toluene giving a greenish yellow solid, the IR spectrum of which suggested that it was a mixture of two known complexes, $MoCl_3$(NO){Ph_2P(=O)$CH_2CH_2PPh_2$(=O)},[14] $MoCl_2$(NO)$_2${Ph_2P(=O)$CH_2CH_2PPh_2$(=O)},[15] and free phosphine oxide. In the case of NOCl/Mo=1, a yellow solid was obtained, whose IR spectrum shows the presence of **2f′** (see below), $MoCl_2$(NO)$_2${Ph_2P(=O)-$CH_2CH_2PPh_2$(=O)}, and the starting dinitrogen complex. In either case the components of these mixtures were inseparable by crystallization and thus as a nitrosylating agent NOCl is not suitable for the clean synthesis of nitrosyl complexes.

*Product Derived from the Nitroxyl Complex (**1a**).* The reaction of **1a** with appropriate alkali metal salts (MX) in acetone afforded MoX(NO)(dpe)$_2$ [X= Cl(**2b**), Br(**2c**), I(**2d**), and NCS(**2e**)] (Table 1). With NaN_3 and NaNCO, **1a** gives **2a**. From the position of the C–S frequencies at 840 cm^{-1}, it was concluded that in the complex (**2e**) the nitrogen of the thiocyanate group is coordinated to molybdenum. With $NaBH_4$, **1a** gives **4** in good yield.

In CH_2Cl_2 the ^{31}P NMR spectrum of **2b** shows a broad multiplet centered at −60 ppm, suggesting a *cis* configuration. Refluxed in benzene, **2b** is converted into yellow crystals analyzing as *trans*-MoCl(NO)(dpe)$_2$·1/2C_6H_6 (**2f**). The ^{31}P NMR spectrum of **2f** shows a sharp singlet at −58 ppm, suggesting a *trans* configuration. Preliminary X-ray data of **2f** also shows the presence of benzene as a crystal solvent, and essentially linear M–N–O system.[16] Dissolved in CH_2Cl_2, **2f** is slowly converted into **2b** (Eq. 2).

$$\underset{(\mathbf{2b})}{\textit{cis}\text{-MoCl(NO)(dpe)}_2} \underset{CH_2Cl_2}{\overset{C_6H_6\ \text{reflux}}{\rightleftharpoons}} \textit{trans}\text{-MoCl(NO)(dpe)}_2\cdot 1/2C_6H_6 \quad (2)$$
$$(\mathbf{2f})$$

In the *trans* compound ν(NO) is shifted to lower frequency by 20 cm^{-1}. These data are compatible with Feltham and Nyholm's interpretation.[17] They prepared a series of six-coordinate nitrosyl complexes [CoX(NO)(diars)$_2$]X (X=Cl, Br, I, and NCS; diars= *p*-$Me_2AsC_6H_4AsMe_2$) in which there were two NO frequencies present. On the basis of examination of bands in the 900 cm^{-1} region in their IR spectra, they suggested that these complexes were a mixture of *cis* and *trans* isomers. The isomer with lower NO frequency was assigned to the *trans* configuration, while the isomer with the higher frequency was assigned to the *cis* one. Since both the molybdenum nitrosyls and the cobalt nitrosyls are six-coordinate complexes having the ligands such as NO, halogen, and four group VB donors, it is natural that the ν(NO) frequencies are assumed to shift similarly on change of configuration. On refluxing in benzene the bromo analog (**2c**) was not converted into its *trans*-isomer. But we could find the presence of *trans*-MoBr(NO)(dpe)$_2$ (ν(NO)=1547 cm^{-1}) in a separate experiment (see below). The iodo (**2d**) and NCS (**2e**) analogs exhibit no such isomerism. Unfortunately the low solubility of the complexes in usual organic solvents precluded the direct determination of their molecular structure by NMR spectroscopy.

In the $[CoX(NO)(diars)_2]X$ complexes, Feltham and Nyholm observed an effect of the halogen ligand (X) on the preference of one configuration over the other. Their data are indicative of increasing stability of the *trans* configuration up the halogen group. The tendency observed holds in our $MoX(NO)(dpe)_2$ (X=F, Cl, and Br) series as well. Graham estimated the order of σ-inductive strength F>Cl>Br>I and π-donor strength F>Cl>Br>I.[18] Since the NO ligand has a strong π-acidity, we expect that the ligand which has a considerable π-donor ability may be preferred for the *trans* ligand to NO. We may conclud that is the reason why we can obtain only the *trans* isomer of the fluoro complex. The ν(NO) of the *trans* complexes are lowered with increasing π-donor strength of halogens.

Table 2. XPS data for some molybdenum nitrosyl complexes

Complex	N 1s(eV)	Mo 3p3/2(eV)
cis-$MoCl(NO)(dpe)_2$ (**2b**)	400.4	394.5
trans-$MoCl(NO)(dpe)_2 \cdot 1/2C_6H_6$ (**2f**)	400.0	394.4
$Mo(NO)_2Cl_2(PPh_3)_2$	401.6	396.5
$Mo(CO)_5(PPh_3)$		393.5
$MoCl_2(CO)_3(PPh_3)_2$		395.7

The XPS data of **2b**, **2f**, and related complexes are given in Table 2. Hughes and Baldwin have observed a linear relationship between 3d and 3p binding energies of molybdenum and a charge parameter q calculated as the sum of the partial ionic characters over the metal-ligand bonds.[19] The observed 3p3/2 binding energy for the complexes (**2b**) and (**2f**) corresponds to a q_{Mo} value nearly intermediate between $Mo(CO)_5(PPh_3)$ and $MoCl_2(CO)_3(PPh_3)_2$, indicating a substantial electroneutrality for the NO ligand. In terms of a formal oxidation state, the molybdenum would be closest to Mo(I). The nitrogen 1s binding energies for **2b** and **2f** are fairly low as expected from the low ν(NO) in their IR spectra. As stated above, however, the M–N–O system is found to be essentially linear. The low N 1s energy of these complexes is responsible for their reactivity to protonic acids, which will be described in the following section.

Reaction of Nitrosyl Complexes with Protonic Acids. As stated above, **1a** is prepared from the reaction of **2a** with aqueous HPF_6 in benzene. Similarly with HBF_4, **2a** gives $[MoF(HNO)(dpe)_2]BF_4$ (**1b**). $[MoF(HNO)(dpe)_2]I_3$ (**1c**) was obtained by the reaction of **1a** with I_2. It has been tried to prepare some cationic HNO (nitroxyl) complexes by using common protonic acids (Table 3). King and Leigh reported that in CH_2Cl_2, $MoCl(NO)(dpe)_2$ did not react with hydrogen chloride.[9] Treatment of **2b** with an excess of dry hydrogen chloride in benzene, however, gives the complex formulated as $MoCl_2(HNO)(dpe)_2$ (**1d**) as a violet precipitate. From **2f**, **1d** was also obtained similarly. We can not determine whether **1d** is a seven-coordinate 18-electron species or a cationic complex. So far suitable crystals for X-ray crystal structure determination have not been obtained. The one chlorine atom is labile and easily replaced by a non-coordinating anion, *i.e.*, PF_6 or BPh_4 to afford stable crystalline products, $[MoCl(HNO)(dpe)_2]X$ [X=PF_6(**1e**) and BPh_4(**1f**)]. In contrast with **1e** and **1f**, the protonic H of the HNO ligand of **1d** is very labile; dissolved in acetone, **1d** releases hydrogen chloride spontaneously to afford *trans*-$MoCl(NO)(dpe)_2$ (**2f'**).

With dry hydrogen bromide, **2c** gives $MoBr_2(HNO)(dpe)_2$ (**1g**) as a violet precipitate. Complex **1g** decomposed easily in acetone to afford a mixture of yellow and orange yellow crystals. The IR spectrum of the former indicated that it was the starting material (**2c**). That of the latter show ν(NO) at 1547 cm^{-1} and its elemental analysis suggests that it has the same composition as **2c**. We may conclude that it is the *trans* isomer of $MoBr(NO)(dpe)_2$ and that the isomer with higher NO

Table 3. HNO complexes of molybdenum

	Complex	Found(Calcd),% C	H	N	Halogen	IR, cm^{-1} a) ν(NO)	Color
1a	$[MoF(HNO)(dpe)_2]PF_6$	58.2 (57.4)	4.5 (4.5)	1.3 (1.3)	12.2 (12.2)	1624	dark red
1b	$[MoF(HNO)(dpe)_2]BF_4$	59.8 (60.6)	4.8 (4.8)	1.2 (1.4)		1631	violet
1c	$[MoF(HNO)(dpe)_2]I_3$	47.4 (47.2)	3.7 (3.7)	1.0 (1.1)	F, 1.4 (1.4)	1625	orange
1d	$MoCl_2(HNO)(dpe)_2$	61.8 (62.8)	4.9 (4.9)	1.2 (1.4)	7.5 (7.1)	1640	violet
1e	$[MoCl(HNO)(dpe)_2]PF_6$	57.0 (56.5)	4.3 (4.4)	1.0 (1.3)		1646	violet
1f	$[MoCl(HNO)(dpe)_2]BPh_4$	70.9 (71.4)	5.7 (5.4)	1.0 (1.1)		1645	light blue
1g	$MoBr_2(HNO)(dpe)_2$	56.5 (57.6)	4.5 (4.5)	1.1 (1.3)	15.8 (14.8)	1641	light blue
1h	$MoClBr(HNO)(dpe)_2$	59.5 (60.1)	4.7 (4.7)	1.1 (1.3)	Cl,2.8; Br,9.4 (3.4) (7.4)	1639	light blue
1i	$MoFBr(HNO)(dpe)_2$	59.6 (61.1)	4.7 (4.7)	1.0 (1.4)	Br,9.1 (7.8)	1610	blue

a) Recorded in KBr.

frequency (**2c**) is the *cis* one. The mixture was recrystallized from CH_2Cl_2 to give pure crstals of **2c**. The *trans* isomer could not be obtained free from the *cis* isomer.

Complex **2a** reacts similarly with dry hydrogen chloride or hydrogen bromide giving the complex consisting almost entirely of **1d** or **1g**, fluorine content being negligible. The reaction of **2f'** with dry hydrogen bromide affords a complex approximately formulated as $MoClBr(NO)(dpe)_2$ (**1h**). But chlorine seems to be partially replaced by bromine. In contrast, treatment of **2a** with an excess of aqueous hydrochloric or hydrobromic acid gives the neutral complex **2b** or **2c**. Complex **2a** was also treated with benzoyl chloride, with the aim of isolating compounds incorporating the organic moiety, but the formation of such derivatives was not observed, **2f** being the only product isolated. Protonation of N_2H, N_2R, or N_2COR ligands in the complexes formally isoelectronic to **2a** took place even with aqueous hydrochloric acid.[8,21,22] This means that the ligating NO is a weaker base than those ligands. Trifluoroacetic acid reacted with **2a** giving yellow crystals of $Mo(OCOCF_3)(NO)(dpe)_2$ (**2g**). IR bands for $\nu_{asym}(CO_2)=1700\ cm^{-1}$ and $\nu_{sym}(CO_2)=1410\ cm^{-1}$ are characteristic of those of the unidentate trifluoroacetate-complexes.[23]

Complex **4** also reacts with aqueous HPF_6 in toluene–methanol to yield **1a** and H_2. With aqueous hydrogen chloride, **4** gives the mixture of **2b** and **2f** with the evolution of H_2. In contrast with $MoX(NO)(dpe)_2$ (X=F, Cl, and Br) and **4**, the complexes such as **3b**, **3c**, and $MoCl_2(NO)_2(PPh_3)_2$ did not react with HPF_6. These results are consistent with the expectation that the protonation of the nitrosyl group leading to HNO derivatives is possible only in the case of nitrosyl complexes of particularly low ν(NO), *i.e.*, with a substantial negative charge localized on the NO ligand.[20] The nitrosyl complexes (**2a**—**g**) were unreactive to other electrophiles such as NO or O_2.

On treatment of **2a** with benzoyl bromide, a blue solid was obtained, which although slightly impure, proved to be $MoFBr(HNO)(dpe)_2$ (**1i**). The simple addition of hydrogen bromide, which was presumably provided by adventitious moisture, seems to have occurred.[22]

Characterization of Nitroxyl Complexes. Protonation of the NO ligand may occur at either the nitrogen or oxygen atom. The ^1H NMR spectrum of **1a** shows a doublet, integrating for one proton, centered at 10.1 ppm, which is assigned to the N–H proton. This assignment is consistent with the observation that the H atom attached to a nitrogen atom adjacent to a transition metal ion exhibits a ^1H NMR resonance at much lower field than δ 6 ppm.[24] This resonance disappared on addition of ^2H_2O. The HNO resonance of a previously reported cobalt complex is δ 7.9.[25] The anomalously large coupling constant ($J=130$ Hz) is tentatively assigned to the long-range coupling with the Mo–F fluorine atom. Unfortunately, the ^{19}F NMR spectrum of **1a** showed only a P–F signal and no Mo–F was observed possibly because of its multiplicity. The doublet pattern of ^{31}P NMR spectrum of the DPE ligands is ascribed to the coupling not with the N–H proton but with the Mo–F fluorine atom. The N–H proton NMR resonance was observed only for **1a**. In the other complexes the N–H proton resonance may coincide with other resonance or be very broad,[26] or the measurement was impossible due to their instability.

All the HNO complexes show a strong band at 1600—1650 cm^{-1} assigned to ν(NO) in their IR spectrum, in the ν(NO) region observed for $RhCl(HNO)(PPh_3)_3$.[27] The complex $RhCl(NOH)(PPh_3)_3$, which is the only one example of a proton attack at oxygen, was reported to have no band ascribable to ν(NO). It is noticiable that ν(NO) of the complexes containing fluorine ligands is lower than those containing chlorine or bromine. We were able to detect very weak N–H IR absorptions only in **1c** (2400 cm^{-1}) and **1i** (2386 cm^{-1}). In the other complexes, perhaps because of an electronic effect, the IR absorptions may be very weak and broad. Similar behavior was observed in the diazenido complexes of Mo and W,[8] and HNO complexes of Re.[26]

Based upon the ^1H NMR and IR data, we propose that the protonation of the NO ligand occurred at the nitrogen atom. Several examples of protonation of metals to give hydrides have been reported in reactions with NO^+ in the presence of methanol.[7] No signals, however, were observed in the hydride region. The presence of protonic H in **1a** was also supported by the reaction with triethylamine, which afforded $[NEt_3H]PF_6$ with the formation of Complex (**2a**) (Eq. 3).

$$\underset{(\mathbf{1a})}{trans\text{-}[MoF(HNO)(dpe)_2]PF_6} \underset{HPF_6}{\overset{NEt_3}{\rightleftharpoons}} trans\text{-}MoF(NO)(dpe)_2\cdot 1/2C_6H_6 \quad (3)$$
$$(\mathbf{2a})$$

Other complexes having a non-coordinating anion also react with the amine to afford the corresponding nitrosyl complex with concomitant formation of ammonium salts. As stated above, the others decompose spontaneously to the neutral nitrosyls in solution, whereas evolved hydrogen halides can be trapped as ammonium halides in the presence of triethylamine.

Reaction Pathways of the Interconversion of Nitrosyl and Nitroxyl Complexes. The reactions of the nitrosyl and nitroxyl complexes are summarized in Scheme 1. We observed the selective formation of *trans*-nitrosyl complex (**2f'**) by decomposition of **1d** in acetone,

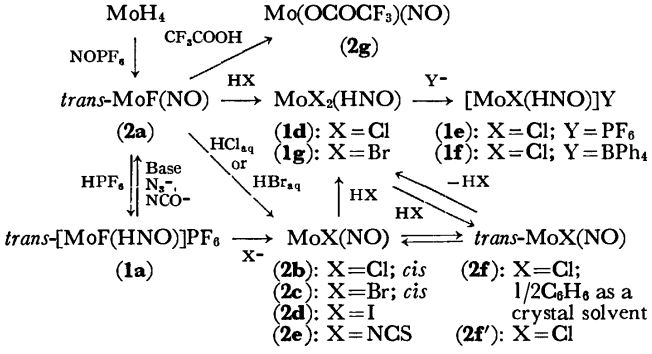

dpe ligands are omitted for clarity.

Scheme 1.

whereas *cis* isomer (**2b**) was exclusively obtained by the reaction of **1a** with LiCl. The stereochemistry of **1d** is unknown because of its instability. For the seven-coordinate polyhedra, geometrical isomers are not yet established by X-ray diffraction, as shown in a recent review.[28] If **1d** is seven-coordinate with both the chlorine atoms *trans* to the HNO ligand, loss of one chlorine with concomitant proton dissociation would result in the formation of *trans*-nitrosyl complex.

Preferential formation of *cis* isomer from **1a** and LiCl makes a marked contrast with the finding above. Two possible pathways are conceivable in the fluoride displacement reaction; a dissociative path and an associative path.[29] The simple case is that of a dissociative mechanism. If the intermediate is a square-pyramid having an open face where the leaving group was located, one would expect that the addition of a new group yields 100% *trans* product. The trigonal-bipyramidal intermediate is expected to yield a mixture of *cis* and *trans* product.

One possible elucidation of selective formation of *cis* isomer is that the entering group X attacks the complex by an associative mechanism and furthermore that Y attacks through any one of the edges of the octahedron *trans* to the leaving group, that is, from the back of the complex. If attack of X had been *cis* to the leaving group, 100% *trans* product would be obtained. We consider that the back side attack of X does occur since it is possible that X makes some hydrogen bond to H of the HNO ligand. That is, the entering group X is anchored to the back side of the complex, attack from the front side having been made impossible. In fact such hydrogen bonding of N_2H_2 ligand with BF_4^-,[11] and I^- [30] was observed from X-ray analysis.

Fluorine displacement was widely observed in the reactions in Scheme 1: simple anion exchange, **2a**→**2b**, **2c**; nitroxyl formation with anion exchange, **2a**→**1d**, **1g**; nitrosyl formation with anion exchange, **1a**→**2b**, **2c**, **2d**, **2e**. In these reactions a seven-coordinate complex must be included as the intermediate or at least in the transition state. In contrast, fluorine was retained in the reactions of **1a** with N_3^- or NCO^-. The product selectivity in these reactions may be apprehensible in terms of pK_a of the conjugated acid (HX) of the anion X. The pK_a of HX is as follows: HF, 3.14; HCl, −7, HBr, −9; HI, −10; HNCS, 0.85; HOCN, 3.46; HN_3, 4.72; CF_3COOH, <0.6. The anion X with pK_a(HX) lower than pK_a(HF) undergoes substitution of the fluorine ligand by X, whereas those with greater pK_a results in the retention of the fluorine, elimination of the weaker acid having occurred preferentially. That is, direct correlation was found between pK_a of various acids in water and the propensity to add to metal complexes.

Experimental

All operations were conducted under nitrogen at room temperature or as otherwise stated. $MoH_4(dpe)_2$, *trans*-$Mo(N_2)_2(dpe)_2$, *trans*-$Mo(CO)(N_2)(dpe)_2$, $Mo(CO)(C_2H_4)(dpe)_2$, $Mo(C_2H_4)_2(dpe)_2$, and *cis*-$Mo(CO)_2(dpe)_2$ were prepared accoding to the published methods. ^1H (100 MHz), ^{19}F (94.2 MHz), and ^{31}P (40.5 MHz) NMR spectra were recorded on a computer-assisted EOL PS-100 spectrometer. IR spectra were recorded on a JASCO IRA-2 spectrophotometer. X-ray photoelectron binding energies were recorded on a JASCO ESCA-1 electron spectrometer and were referenced to the carbon ls line (taken to be 285.0 eV) of each sample. The Mg K_α X-ray line (1253.6 eV) was used as a photoelectron excitation source.

Reaction of $MoH_4(dpe)_2$ with $NOPF_6$. To a suspension of $MoH_4(dpe)_2$ (4.4 g) in benzene (350 ml) was added a freshly prepared solution of $NOPF_6$ (0.9 g) in methanol (10 ml). The evolution of hydrogen was observed. The mixture was stirred at room temperature for 4 h. After the mixture turned dark brown, a dark red solid precipitated. Addition of hexane to the mixture deposited an additional quantity of the complex. The precipitate was filtered, washed with ether, recrystallized from acetone–ether and dried *in vacuo* to yield dark red crystals of **1a** (2.3 g, 43%). Further addition of hexane to the mother liquor precipitated yellow crystals. The crystals were filtered, washed with methanol, recrystallized from benzene–hexane and dried *in vacuo* to yield **2a** (0.70 g, 15%). The presence of benzene as the crystal solvent was confirmed by gas chromatography of a toluene solution of the complex.

Reaction of Diphosphine Complexes of Mo (0) with $NOPF_6$. To a solution of *trans*-$Mo(N_2)_2(dpe)_2$ (0.95 g) in benzene (50 ml) was added a freshly prepared solution of $NOPF_6$ (0.35 g) in methanol (5 ml). After the mixture was stirred at ambient temperature for 4 h, the mixture deposited dark red crystals, which were filtered, washed with hexane and dried *in vacuo* to yield 0.59 g (54%) of $[MoF(N_2H_2)(dpe)_2]PF_6$ (Found: C, 58.0; H, 4.7; N, 2.3%. Calcd for $C_{52}H_{50}N_2F_7P_5Mo$: C, 57.5; H, 4.6; N, 2.6%). Similarly, the reaction of *trans*-$Mo(CO)(N_2)(dpe)_2 \cdot 1/2C_6H_6$ with $NOPF_6$ afforded **3b** [ν(CO) = 1934 cm^{-1}] (17%) and a mixture of *cis*-$Mo(CO)_2(dpe)_2$ and *trans*-$[Mo(CO)_2(dpe)_2]PF_6$. The reaction of $Mo(CO)(C_2H_4)(dpe)_2$ afforded **3b** (16%) and a mixture of the dicarbonyl complexes. The reaction of $Mo(C_2H_4)(dpe)_2$ afforded **3c** (5%).

$[Mo(NO)(dpe)_2]_2 \cdot 2C_6H_6$. To a solution of *trans*-$Mo(N_2)_2(dpe)_2$ (200 mg) in benzene (30 ml) was bubbled NO_2-free NO. When the reaction was complete, as indicated by the color, the undissolved brown solid [IR ν(NO) = 1775 and 1665 cm^{-1}] were removed from the solution by filtration. Addition of hexane to the filtrate deposited yellow crystals, which were filtered, washed with hexane and dried *in vacuo* to yield 42 mg (20%) of **4**. The presence of benzene as the crystal solvent was checked by gas chromatographic analysis of a toluene solution of the complex. The undissolved brown solid increased with time; apparently it is a product of successive reaction of **4** with NO. Its purification, however, was unsuccessful.

Reaction of trans-$Mo(N_2)_2(dpe)_2$ with NOCl. To a solution of *trans*-$Mo(N_2)_2(dpe)_2$ (155 mg) in toluene (10 ml) was added 6% NOCl in toluene (2 ml) (NOCl/Mo = 10). The mixture was stirred for 40 min during which time dinitrogen was evolved. A greenish brown solid precipitated, which was filtered, washed with hexane and recrystallized from CH_2Cl_2–hexane, yield 80 mg. The IR spectrum of the product showed that it was a mixture of two complexes, $MoCl_3(NO)\{Ph_2P(=O)CH_2CH_2PPh_2(=O)\}$ [ν(NO) = 1690 cm^{-1}], and $MoCl_2(NO)_2\{Ph_2P(=O)CH_2CH_2PPh_2(=O)\}$ [ν(NO) = 1770 and 1660 cm^{-1}]. In the case of NOCl/Mo = 1, a mixture of three complexes, 2f′ [ν(NO) = 1543 cm^{-1}], $MoCl_2(NO)_2\{Ph_2P(=O)CH_2CH_2PPh_2(=O)\}$], and the starting material was obtained.

*Reaction of **1a** with Alkali Metal Salts.* Acetone (20 ml) was added to the mixture of **1a** (500 mg) and LiCl (240 mg).

The resulting orange brown suspension was quickly filtered. From the filtrate yellow crystals deposited on standing, which were filtered, washed with acetone and dried *in vacuo* to yield 221 mg (50%) of **2b**. Similar procedures using LiBr, LiI, NaSCN, NaNCO, and NaN_3 afforded **2c** (55%), **2d** (17%), **2e** (50%), **2a** (48%), and **2a** (41%), respectively.

Reaction of 1a with $NaBH_4$. Tetrahydrofuran (50 ml) was added to **1a** (385 mg) and $NaBH_4$ (43 mg), and the mixture was stirred for 8 h. Solvent was then evaporated off *in vacuo* to leave a brown solid, which was recrystallized from benzene–hexane to yield yellow crystals of **4** (156 mg, 44%) (Found: C, 70.1, H, 5.6; N, 1.1%. Calcd for $C_{116}H_{108}O_2N_2P_8Mo$: C, 69.6; H, 5.4; N, 1.4%).

Interconversion of 2b and 2f. The solution of **2b** (52 mg) in benzene (5 ml) was refluxed for 1 h. On addition of hexane, yellow crystals precipitated, which were filtered, washed with hexane and dried *in vacuo* to yield 34 mg (63%) of **2f**. Similarly, dissolved in CH_2Cl_2, **2f** was converted to **2b** (61%) after 1 d.

Reaction of 2a with Protonic Acids. To a solution of **2a** (30 mg) in benzene (3 ml) was added a 65% aqueous solution of HPF_6 (0.1 mg). The mixture, which turned orange brown immediately, was stirred for 1 h at room temperature. Solvent was then evaporated off *in vacuo* to leave a reddish brown powder, which was recrystallized from acetone–ether to yield dark red crystals of **1a** (23 mg, 70%). Similar procedures using $NOPF_6$–MeOH, HBF_4, and I_2 afforded **1a** (76%), **1b** (72%), and **1c** (24%), respectively.

$MoCl_2(HNO)(dpe)_2$. On bubbling HCl gas into a solution of **2a** (91 mg) in benzene (10 ml) for 30 min, a violet powder precipitated. The complex, which was too unstable for recrystallization, was filtered, washed with benzene and hexane, and dried *in vacuo*, to yield 74 mg (80%) of **1d**. The complex contained no fluorine and complete displacement by chlorine seems to have occurred (Found: Cl, 7.0; F, 0%. Calcd for $C_{52}H_{49}ONP_4Cl_2Mo$: Cl, 7.1; F, 0%). Similarly the reactions of **2b** and **2f** with HCl gas afforded **1d** in 87 and 85% yield, respectively. The reactions of **2a**, **2c**, and **2f′** with HBr gas afforded **1g** (70%), **1g** (82%), and **1h** (73%), respectively.

Conversion of 1d and 1g into Nitrosyl Complexes. Complex **1d** (122 mg) was dissolved in acetone (5 ml). The initial violet suspension became a yellow solution, from which a yellow precipitate was obtained and analyzed as **2f′** (91 mg-77%) (Found: C, 64.6; H, 4.9; N, 1.2%. Calcd for $C_{52}H_{48}ONP_4ClMo$: C, 65.2; H, 5.0; N, 1.5%). The IR spectrum shows ν(NO) at 1543 cm^{-1}. Recrystallization of **2f′** from benzene–hexane yielded yellow crystals containing 1/2 mol solvated benzene. Similarly, **1g** was converted into a mixture of yellow crystals[ν(NO) = 1567 cm^{-1}] and orange yellow crystals[ν(NO) = 1547 cm^{-1}]. The former was formulated as **2c**. The latter was also analyzed as $MoBr(NO)(dpe)_2$ and supposed to have the *trans* configuration (Found: C, 62.0; H, 5.0; N, 1.2; Br, 7.8%. Calcd for $C_{52}H_{48}ONP_4BrMo$: C, 62.3; H, 4.8; N, 1.4; Br, 8.0%). Recrystallization of the mixture from CH_2Cl_2–ether gave yellow crystals of **2c** (60%).

Reaction of 1d with Non-coordinating Anions. Acetone (10 ml) was added to the mixture of **1d** (124 mg) and KPF_6 (50 mg). After stirring for 10 min the mixture was filtered. The filtrate, a light-green solution was evaporated to dryness and the solid residue was recrystallized from acetone–ether to give 100 mg (73%) of **1e** as violet crystals. A similar procedure using $NaBPh_4$ afforded **1f** (79%).

Anion Substitution of 2a. Aqueous hydrogen chloride (0.5 ml, 35% solution) was added to **2a** (80 mg) in acetone (5 ml). After stirring for 1 h, the precipitate was filtered, recrystallized from CH_2Cl_2–ether to yield 47 mg (60%) of **2b**. Similar procedures using aqueous hydrogen bromide, benzoyl chloride, and trifluoroacetic acid afforded **2c** (54%), **2b** (83%), and **2g** (41%), respectively. The reaction of **2a** with benzoyl bromide afforded **1i** (39%), but no satisfactory analyses were obtained for the product (see Table 3), which was found to be contaminated with a small amount of **1g** (IR).

Reaction of 4 with Protonic Acids. On addition of 65% aqueous solution of HPF_6 (0.07 ml) to a solution of **4** (80 mg) in toluene (5 ml)–methanol (1 ml), an immediate reaction took place yielding a reddish brown solution. Evolution of hydrogen was confirmed by GLC. Addition of hexane deposited dark red crystals, which were filtered to yield 61 mg (70%) of **1a** (Found: C, 57.7; H, 4.8; N, 1.2%. Calcd for $C_{52}H_{49}ONF_7P_5Mo$: C, 57.4; H, 4.5; N, 1.3%). A similar procedure using aqueous hydrogen chloride afforded a mixture of **2b** and **2f**, which was recrystallized from CH_2Cl_2–ether to give **2b** (45%) (Found: C, 64.9; H, 5.2; N, 1.2%. Calcd for $C_{52}H_{48}ONP_4ClMo$: C, 65.2; H, 5.0; N, 1.5%).

Reaction of 1a with Triethylamine. To a solution of **1a** (99 mg) in acetone (5 ml) was added triethylamine (0.5 ml) in benzene (3 ml). On standing the resulting yellow solution, a yellow powder precipitated, which was filtered, washed with ether and dried *in vacuo* to yield 41 mg (46%) of **2a**. Addition of hexane to the filtrate deposited an additional quantity of **2a** contaminated with $[NEt_3H]Cl$ (IR) which was washed with methanol and dried. The combined yield amounted to 68%.

References

1) This work was presented at the 34 th National Meeting of the Chemical Society of Japan, Hiratsuka, April 1976.
2) J. Chatt, J. R. Dilworth, and R. L. Richards, *Chem. Rev.*, **78**, 589 (1978) and refs. therein.
3) J. Chatt, a. J. L. Pombeiro, R. L. Richards, G. H. D. Royston, K. W. Muir, and R. Walker, *J. Chem. Soc., Chem. Commun.*, **1975**, 708.
4) B. D. Dombek and R. J. Angelici, *J. Am. Chem. Soc.*, **97**, 1261 (1975).
5) J. W. Byrne, H. U. Blaser, and J. A. Osborn, *J. Am. Chem. Soc.*, **97**, 3871 (1975).
6) N. G. Connely, *Inorg. Chem. Acta Rev.*, **6**, 47 (1972).
7) K. G. Caulton, *Coord. Chem. Rev.*, **14**, 317 (1975).
8) J. Chatt A. J. Pearman, and R. L. Richards, *J. Chem. Soc., Dalton Trans.*, **1976**, 1520.
9) F. King and G. J. Leigh, *J. Chem. Soc., Dalton Trans.*, **1977**, 429.
10) J. A. McCleverty, *Chem. Rev.*, **79**, 53 (1979).
11) M. Hidai, T. Kodama, M. Sato, M. Harakawa, and Y. Uchida, *Inorg. Chem.*, **15**, 2694 (1976).
12) N. G. Connely, *J. Chem. Soc., Dalton Trans.*, **1973**, 2183.
13) R. H. Rieman and E. Singleton, *J. Organomet. Chem.*, **32**, C44. (1971); B. F. G. Johnson, S. Bhaduri, and N. G. Connelly, *ibid.*, **40**, C36 (1972).
14) R. Davies, B. F. G. Johnson, and K. H. Al-Obaidi, *J. Chem. Soc., Dalton Trans.*, **1971**, 508.
15) F. Canziani, U. Sartorelli, and F. Cartiani, *Ann. Chim. (Italy)*, **54**, 1354 (1964).
16) M. Sato, private communication.
17) R. D. Feltham and R. S. Nyholm, *Inorg. Chem.*, **4**, 1334 (1965).
18) W. A. G. Graham, *Inorg. Chem.*, **7**, 315 (1968).
19) W. B. Hughes and B. A. Baldwin, *Inorg. Chem.*, **13**, 1531 (1974).
20) P. Finn and W. L. Jolly, *Inorg. Chem.*, **11**, 893 (1972).
21) T. Tatsumi, M. Hidai, and Y. Uchida, *Inorg. Chem.*,

14, 2530 (1975).
22) A. A. Diamantis, J. Chatt, G. A. Heath, and G. J. Leigh, *J. Chem. Soc., Dalton Trans.*, **1977**, 688.
23) T. A. Stephenson, S. M. Morehouse, A. R. Powell, J. P. Heffer, and G. Wilkinson, *J. Chem. Soc.*, **1965**, 3632.
24) D. Sellman, *J. Organomet. Chem.*, **49**, C22 (1973).
25) J. H. Enemark, R. D. Feltham, J. Rikker-Nappier, and K. F. Bizot. *Inorg. Chem.*, **14**, 624 (1975).
26) G. LaMonica, M. Freni, and S. Cennini, *J. Organomet. Chem.*, **71**, 57 (1974).
27) J. P. Collman, N. W. Hoffman, and D. E. Moriis, *J. Am. Chem., Soc.*, **91** 5659 (1969).
28) M. G. B. Drew, *Progr. Inorg. Chem.*, **23**, 67 (1977).
29) C. H. Langford and H. B. Gray, "Ligand Substitution Processes," W. A. Benjamin, Reading, Massachusetts (1966), p. 55.
30) V. W. Day, T. A. George, S. D. A. Iske, and S. D. Wagner, *J. Organomet. Chem.*, **112**, C55 (1976).

Photochemistry of Host-Guest Complex. III.[1] Effect of Guest Cation on the Photoreactivity of Acetophenone Oxime Derivatives Having Crown Ether Moiety

Masaru TADA,* Hideki HIRANO, and Atsushi SUZUKI

Department of Chemistry, School of Science and Engineering, Waseda University, Shinjuku-ku, Tokyo 160

(Received November 12, 1979)

The *syn-anti* isomerization of acetylbenzocrown ether oximes was stimulated by the complex-formation with sodium ion. The photolysis of these oximes gave mother ketones and amides through an oxaziridine intermediate. The photolysis of the oximes was depressed by the formation of host–guest complexes. Reactivity in the photolysis of the crown ether oximes corresponds to that of 3,4-dimethoxyacetophenone oxime, whereas the reactivity of the complexed crown ether oxime with sodium ion corresponds to that of *p*-cyanoacetophenone oxime. Such behavior is explained by the change of the electronic properties of excited states of acetophenone oxime chromophore, which enhances the intersystem crossing.

Few photochemical reactions of crown ether and cryptand have been reported, though these classes of compounds are the targets of active current research.[2] Hautala and Hasting[3] observed the stimulated type II fission of monovalery-dibenzo-18-crown-6 by the formation of the complexes with alkali metal ions. In our earlier study,[4] the photochemical cross coupling between 18-crown-6 and alkyl aryl ketones was enhanced by the introduction of a cyano group or a potassium salt of carboxylato-group at the terminal position of the alkyl aryl ketone. These groups form complexes with crown ether and can hold radical pairs nearby by host–guest interaction or Coulomb interaction. Now we report the photochemical behavior of acetylbenzocrown ether oximes.

Experimental

Syntheses of Oximes. A mixture of benzo-15-crown-5 (930 mg, 3.5×10^{-3} mol), acetic acid (240 mg, 4.0×10^{-3} mol), and polyphosphoric acid (15 ml) was heated to 80 °C for 3 h under stirring. After cooling, the mixture was diluted with 30 ml of water under further cooling and stirred for 30 min to hydrolyse the polyphosphoric acid. The precipitate was combined with the chloroform extract and washed with saturated sodium hydrogencarbonate solution and water. Evaporation of chloroform after drying over magnesium sulfate gave a pale yellow solid. Recrystallization of the solid from ethanol gave acetylbenzo-15-crown-5 (**3b**) (40% yield). Mp, 93—95 °C: IR($CHCl_3$), 1665 cm^{-1}; NMR ($CDCl_3$) (δ), 2.50 (3H, s), 3.67—4.30 (crown ether), 6.78 (1H, d, J=9 Hz), and 7.51 (2H, m).

A mixture of acetylbenzo-15-crown-5 (**3b**) (200 mg, 6.5×10^{-4} mol), hydroxylamine hydrochloride (70 mg, 1.0×10^{-3} mol), and potassium acetate (100 mg, 1.5×10^{-3} mol) was heated under reflux for 2 h in a mixed solvent of ethanol, chloroform, and water (10: 3: 2). After cooling, the reaction mixture was diluted with 10 ml of water. Chloroform extraction (20 ml×3) of the mixture gave a pale yellow solid after conventional work-up. Recrystallization from methanol gave a colorless acetylbenzo-15-crown-5 oxime (**1b**) in 75% yield. Mp, 133—135 °C. Found: C, 58.75; H, 7.02; N, 4.38%. Calcd for $C_{16}H_{23}NO_6$: C, 59.06; H, 7.13; N, 4.31%. $\lambda_{max}^{CH_3CN}$ 263 (17300) and 294 nm (7050); IR ($CHCl_3$): 3560, 3450—3100, 1599, 1503, 1419, and 1130 cm^{-1}; NMR ($CDCl_3$) (δ): 2.21 (3H, s), 3.69—4.22 (crown ether), 6.78 (1H, d, J=9 Hz), 7.10 (1H, dd, J=9 and 1 Hz), 7.21 (1H, d, J=1 Hz), and 8.75 (1H, br, s).

The same procedure gave acetylbenzo-18-crown-6 oxime (**1c**). Mp, 106—107 °C. Found: C, 58.21; H, 7.67; N, 3.84%. Calcd for $C_{18}H_{27}NO_7$: C, 58.52; H,7.37; N, 3.79%. IR ($CHCl_3$): 3560, 3450—3100, 1602, 1510, 1432, and 1140 cm^{-1}; NMR ($CDCl_3$) (δ): 2.24 (3H, s) 3.68—4.34 (crown ether), 6.84 (1H, d, J=9 Hz), 7.12 (1H, dd, J=9 and 1 Hz), 7.23 (1H, d, J=1 Hz), and 9.20 (1H, br, s).

Acetophenone Oxime Derivatives. 3,4-Dimethoxyacetophenone oxime (**1a**), acetophenone oxime, *p*-chloroacetophenone oxime, *p*-methoxyacetophenone oxime, and *p*-cyanoacetophenone oxime were synthesized from the mother ketones in the manner used for the preparation of acetylbenzo-15-crown-5 oxime (**1b**); these oximes have the reported physical constants.

General Procedure of Photochemical Reaction. One of the oximes in 10 ml of appropriate solvent was placed in a Pyrex tube (unless otherwise mentioned) and irradiated externally by using a Rikosha rotary irradiation-apparatus equipped with a 450 W high pressure mercury lamp mounted in a quartz cooling jacket. The distance between tubes and the lamp was *ca.* 5 cm. The absorption spectra of the oximes (**1a**, **1b**, and **1c**) show large extinction coefficients around the emission lines of the lamp at 302.5 and 313 nm and no absorption is seen at 366 nm. The spectra were changed only slightly by addition of sodium, potassium, or tetramethylammonium salts. The concentration of the oximes for irradiation were arranged to absorb more than 99.9% of the emission-light from the lamp at 302.5 and 313 nm, so that all samples in the rotary irradiation-apparatus absorb essentially equal number of photons.

Geometrical Isomerization. A preparative scale experiment was carried out in acetonitrile by irradiation of one of the oximes (5.0×10^{-2} mol/dm^3, 10 ml) for 6 h. The reaction mixture was separated by chromatography on a silica gel plate eluted with chloroform–ethyl acetate (2: 1). The *syn*-isomer of 3,4-dimethoxyacetophenone oxime (**1a**) gave almost identical IR and NMR spectra to its *anti*-isomer, but the chemical shift of acetoxime methyl is slightly different. 3,4-Dimethoxyacetophenone oxime (**1a**): *anti*-isomer (δ,2.26); *syn*-isomer (δ, 2.19). Acetylbenzo-15-crown-5 oxime (1b) has a similar spectral property: *anti*-isomer (δ, 2.21); *syn*-isomer (δ, 2.19). Recrystallization of the *syn*-isomer formed photochemically gave original *anti*-isomer.

A solution (1.6×10^{-1} mol/dm^3) of one of the oximes (**1a** or **1b**) placed in an NMR sample tube was irradiated in the presence of sodium perchlorate, and the ratio of *syn*- and *anti*-oxime was determined by NMR analysis using the relative intensity of the acetoxime methyls.

Photolyses in Acetic Acid. One of the oximes (**1a** or **1b**)

in anhydrous acetic acid was irradiated until the starting material disappeared. Evaporation of the solvent *in vacuo* and chromatography on an alumina column eluted with chloroform gave the products. The products were further separated by chromatography on a silica gel plate. This was eluted with chloroform–ethyl acetate (2 : 1) for the products from dimethoxyacetophenone oxime (**1a**) and with chloroform–ethyl acetate–methanol (2: 1: 0.1) for the products from acetylbenzo-15-crown-5 oxime (**1b**). The mother ketones were obtained as major products (*ca.* 70%) and two types of amide (**4a**, **4b**), with arene migration and methyl migration respectively, were obtained in *ca.* 30% yield.

An acetic acid solution (6.25×10^{-2} mol/dm^3, 10 ml) of one of the oximes (**1a** or **1b**) combined with various amounts of sodium acetate was irradiated for only 10 min. Within this period less than 0.1% of the starting oxime was converted to oxaziridine. Immediately after irradiation the solution were combined with an aqueous solution of potassium iodide and starch under magnetic stirring; then the mixture was allowed to stand for 10 min. These solutions were titrated with aqueous sodium thiosulfate. The results are shown in Table 1.

Photolysis in Acetonitrile. One of the oximes (**1a**, **1b**, **1c**) (5.0×10^{-2} mol/dm^3) in acetonitrile–water (20 : 1) was irradiated until the starting oxime disappeared. Evaporation of the solvent and chromatography gave the mother ketone in quantitative yield.

Various amounts of sodium, potassium, or tetramethylammonium salts were added to an acetonitrile solution (5.0×10^{-2} mol/dm^3, 10 ml) of one of the oximes. The mixture was irradiated until 30—40% of the starting oxime disappeared (10—15 h), then the reaction mixture was condensed *in vacuo*. The residue was extracted three times with chloroform (20 ml×3). After drying over magnesium sulfate the combined extract was condensed to about 3 ml and the precipitated sodium perchlorate was removed. The filtrate was further condensed and analyzed by NMR spectroscopy in deuteriochloroform containing measured amount of tetrachloroethane as an internal reference. This procedure can extract both complexed and non-complexed acetylbenzo-15-crown-5 (**1b**) almost completely and hence the relative yield of **3** can be determined with reasonable accuracy. The results thus obtained for **1b** and **1c** are shown in Figs. 2 and 3.

Photolysis of Acetophenone Oxime Derivatives. An acetonitrile solution (5.0×10^{-2} mol/dm^3, 10 ml) of one of the oxime derivatives was irradiated for 16 h; less than 20% of the starting oximes were consumed within this period. The work-up used for the photolysis of the oximes (**1a**, **1b**, **1c**) and NMR analyses using tetrachloroethane as an internal reference gave the results shown in Fig. 4.

Results and Discussion

Irradiation of 3,4-dimethoxyacetophenone oxime (**1a**) caused *syn-anti* isomerization at the early stage. Further irardiation gave the mother ketone (**3a**) in quantitative yield in acetonitrile containing or not containing water. Prolonged irradiation of (**1a**) in glacial acetic acid gave two amides, formed by photochemical Beckmann rearrangement, as minor products (*ca.* 30%) in addition to the mother ketone (**3a**) (*ca.* 70%). In the same manner, acetylbenzo-15-crown-5 oxime (**1b**) and acetylbenzo-18-crown-6 oxime (**1c**) gave similar products to those obtained in the case of oxime (**1a**). One type of amide was identical to the authentic sample prepared by Beckmann rearrangement of the *anti*-oximes by the

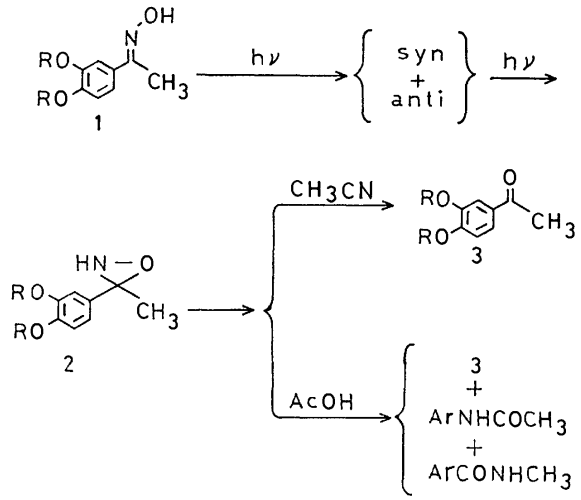

1a, 2a, 3a: R=CH_3
1b, 2b, 3b: R=$-(CH_2CH_2O)_3CH_2CH_2-$
1c, 2c, 3c: R=$-(CH_2CH_2O)_4CH_2CH_2-$

Scheme 1.

catalysis of sulfuric acid. This type of amide must be formed by migration of arene moiety. Though the structure of the other type of amide has not been studied in detail, its NMR spectra show clearly the existence of the *N*-methyl group (δ, 2.95), and hence the amide must be formed by methyl migration. The photoreactivity of oximes should be the same, whether or not they contain crown ether moiety.

Geometrical Isomerization. The effect of sodium perchlorate on *syn-anti* isomerization is changed by the introduction of crown ether moiety into the oxime. As shown in Fig. 1, the isomerization of acetylbenzo-15-crown-5 oxime (**1b**) in chloroform–methanol (3 : 4) was stimulated in the presence of sodium perchlorate. On the other hand, the isomerization of 3,4-dimethoxyacetophenone oxime (**1a**) was only slightly affected. These results clearly show that the complexation of

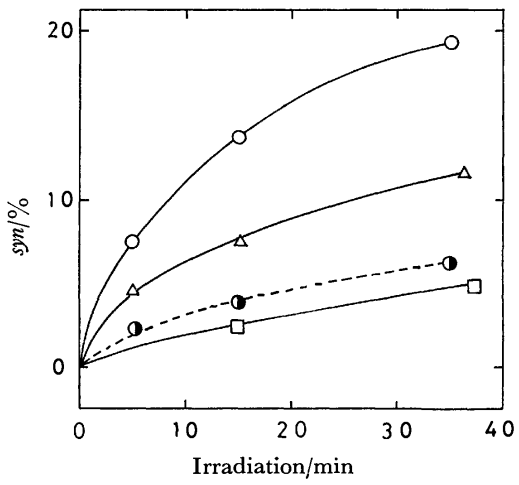

Fig. 1. Geometrical isomerization of **1a** and **1b** (1.6×10^{-1} mol dm^{-3}) in $CHCl_3$–CH_3OH (3: 4).
□—□: **1a** or **1b** without added salt, ◑···◑: **1a**+$NaClO_4$ (1.06 mol dm^{-3}), △—△: **1b**+$NaClO_4$ (0.16 mol dm^{-3}), ○—○: **1b**+$NaClO_4$ (1.06 mol dm^{-3}).

sodium cation stimulates the isomerization of crown ether oxime (**1b**). Geometrical isomerization of an oxime has been reported to take place from a triplet excited state.[5] The complexation of (**1b**) must therefore increase the quantum yield of this triplet state.

Oxaziridine Formation. A mother ketone and two amides are believed to form photochemically through an oxaziridine intermediate.[5,6] We analyzed the oxaziridine by iodometry[6] at the very early stage of photolysis (10 min) in glacial acetic acid. Only 0.1% of oxaziridine was formed within this period, so secondary photolysis to produce the mother ketone and amides shoud be negligible. Therefore, the values obtained by iodometry must be a good measure of relative quantum yield of the oxaziridine intermediate (**2**) in the presence of sodium acetate (see Table 1).

TABLE 1. RELATIVE QUANTUM YIELDS OF OXAZIRIDINE FORMATION FROM **1a** AND **1b** IN THE PRESENCE OF SODIUM ACETATE

Added NaOAc[a]	Starting oxime	
	1a[b]	**1b**[b]
0.0	1.00	1.00
5.0	0.76	0.82
10.0	0.60	0.68
15.0	0.53	0.48
20.0	0.51	0.29

a) Molecular equivalents of NaOAc to the oxime. b) 6.25×10^{-2} mol dm^{-3} solution of **1a** and **1b** in acetic acid was used.

The relative quantum yield of oxaziridine formation from acetylbenzo-15-crown-5 oxime (**1b**) deviates from those of 3,4-dimethoxyacetophenone oxime (**1a**) in somewhat higher concentrations of the added sodium acetate. The formation constant of the complex between **1b** and sodium acetate was determined by Benesi-Hildebrand method;[7] the value is very small (K=2—3 M^{-1}) in acetic acid. The small formation constant must be one of the major factors of the salt effect only in the higher concentration range.

The photochemical formation of oxaziridine from an oxime has been reported to occur from a singlet state.[5,6] Hence the complexation seems to retard the process involving a singlet excited state of crown ether oxime (**1b**). The similar decrease in the quantum yields for both **1a** and **1b** in the lower concentration range of the added salt must be due to the basic nature of sodium acetate. It has been established that a base inhibits the photolysis of an oxime.[8]

Formation of Mother Ketones. Prolonged irradiation of the oximes (**1a**, **1b**, and **1c**) in acetonitrile containing or not containing water gave only the mother ketones. Fig. 2 shows the effect of sodium salts on photolyses, The mother ketone must be derived from the oxaziridine intermediate by a photochemical or thermal process.[6] Since no other product than the mother ketone was obtained, the relative quantum yield of the ketone must be a reasonable reflection of the formation of oxaziridine intermediate, whatever the

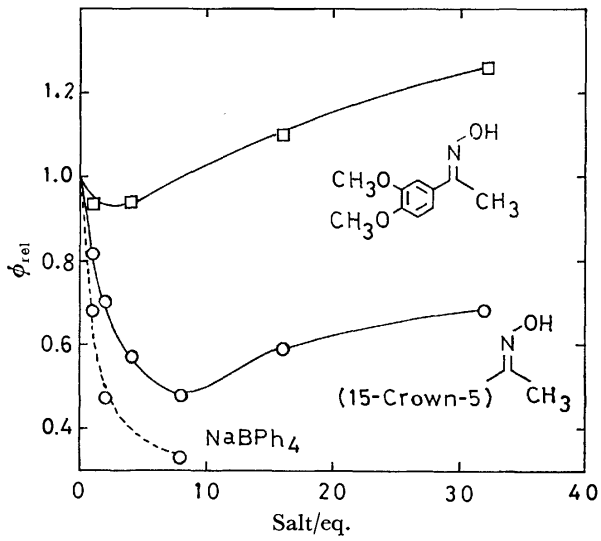

Fig. 2. Relative quantum yield of the mother ketone on photolysis of **1a** (1.3×10^{-1} mol dm^{-3}) and **1b** (5.0×10^{-2} mol dm^{-3}) in CH_3CN–H_2O (20: 1) in the presence of sodium salt.
□—□: **1a**+$NaClO_4$, ○—○: **1b**+$NaClO_4$, ○···○: **1b**+$NaBPh_4$.

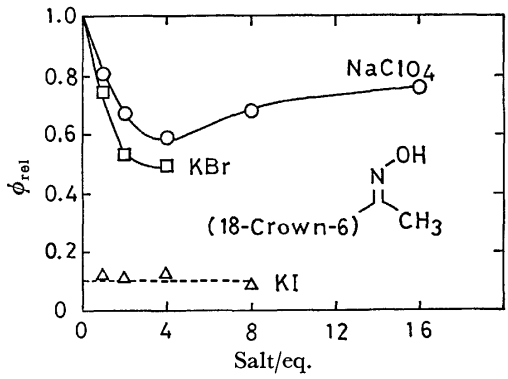

Fig. 3. Relative quantum yield of the mother ketone on photolysis of **1c** (5.0×10^{-2} mol dm^{-3}) in CH_3CN–H_2O (20: 1) in the presence of alkali metal salts.
○—○: $NaClO_4$, □—□: KBr, △···△: KI.

mechanism of formation is. The photolysis of acetyl-15-crown-5 oxime (**1b**) was depressed by sodium salts in the lower concentration range. By contrast, 3,4-dimethoxyacetophenone oxime (**1a**) showed only a slight effect. Recovery of the reactivity is seen in both types of oxime in higher concentration range of the added sodium perchlorate; this effect can be accounted for by the enhanced acidity or the polarity of the reaction media. It is well established that the photolysis of oxime is stimulated by acidic or polar conditions.[8-10] The effect of complex formation on the reactivity, therefore, must be limited to the lower concentration range of the added sodium perchlorate. The Benesi-Hildebrand method[7] gave the formation constant of *ca.* 5×10^2 M^{-1} for the complex between crown ether oxime (**1b**) and sodium ion from perchlorate in acetonitrile. Sodium tetraphenylborate depressed the photolysis strongly, though the effect in higher concentration could not be tested due to the insolubility of the

salt. A similar result was obtained with crown ether oxime (**1c**). Potassium salts were more effective. In the case of potassium iodide, however, a different mechanism must be operative to account for its powerful quenching. An electron transfer from iodide ion to the excited oxime is the most probable mechanism.[11]

Mechanism of Salt Effect. Hitherto discussed phenomena suggest that the effect of alkali metal salts on the photoreactivity of crown ether oximes differs to some extent according to the counter ion of the salts. So we can not deny the effect of perchlorate anion on the reactivity of crown ether oximes in the presence of sodium perchlorate, but the photolysis of 3,4-dimethoxyacetophenone oxime (**1a**) and acetylbenzo-15-crown-5 oxime (**1b**) were little affected by the addition of tetramethylammonium perchlorate. Therefore, it is clear that the difference in the effect of sodium perchlorate on **1a** and **1b** must be due to the formation of host–guest complexes between crown ether oxime and sodium cation. The slightly concave curve for oxime (**1a**) in Fig. 2 may indicate a weak chelation of sodium ion by the dimethoxybenzene moiety of **1a**.

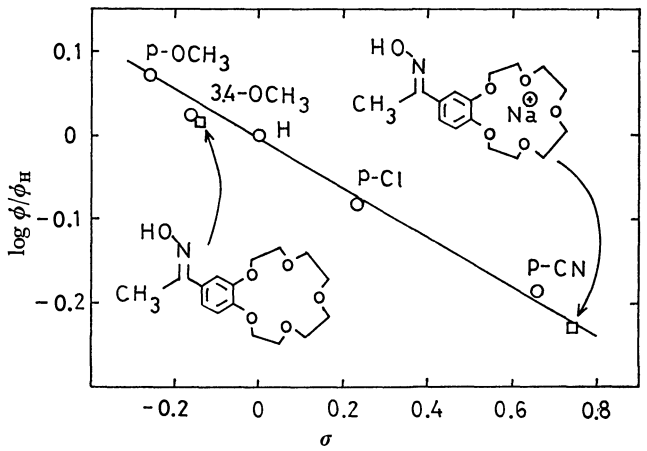

Fig. 4. Relative quantum yield of the mother ketones from acetophenone oxime derivatives (5.0×10^{-2} mol dm^{-3}) in CH_3CN.

Complexation of a cation in the cavity of crown ether must reduce the electron donating ability of alkoxyl groups. Such a change must affect the nature of both the excited state and the ground state of aromatic oximes. Actually the photoreactivity of acetophenone oxime derivatives varies depending on the electronic nature of the substituent on the benzene ring (see Fig. 4). The oxime having an electron donating substituent has higher reactivity than the oxime having an electron withdrawing substituent. Though we can not clarify the exact nature of the excited state responsible for the photolysis, the relative quantum yields of the ketone formation from acetophenone oxime derivatives in acetonitrile show a linear correlation with Hammet σ-constant. The photoreactivity of free crown ether oxime (**1b**) corresponds to that of oxime (**1a**), and the reactivity of the complexed **1b** with sodium ion, obtained by extrapolation of the curve in Fig. 2, corresponds to *p*-cyanoacetophenone oxime. The complexation of crown ether oxime (**1b**) with sodium ion induces a slight change in its electronic absorption spectrum, a small hypsochromic shift (*ca.* 3 nm) and a small decrease in extinction coefficient, but the complexation may affect the nature of the excited state more profoundly.

The photochemistry of oximes can be summarized by the scheme shown below, which was established by

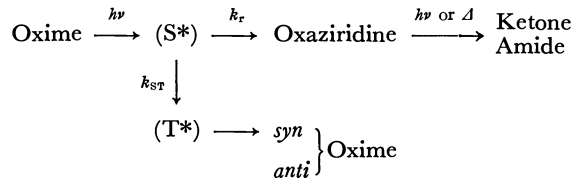

Mukai and Oine[6] and de Mayo *et al.*[5] A singlet state of oxime gives an oxaziridine, which affords a mother ketone and an amide on further photolysis or thermal process. A triplet excited state, on the other hand, causes geometrical isomerization. Our findings show that the formation of a host–guest complex stimulates the geometrical isomerization and depresses the formation of oxaziridine. The present results and the general scheme indicate that the ratio of the rate of intersystem crossing to the rate of oxaziridine formation (k_{ST}/k_r) becomes larger with the host–guest complex than with the free crown ether oxime. There are a several possible explanations of this behavior. First, the spin-orbital coupling may vary by complex formation due to a heavy atom effect and modify the rate of intersystem crossing (k_{ST}); but a light atom such as sodium usually does not show such a heavy atom effect.[12] Second, the difference in energy gap between a singlet and a triplet excited state (ΔE_{ST}) may alter the rate of intersystem crossing (k_{ST}). Unfortunately, these oximes are non-emissive, at least in the solvent system used for photoreaction, and no direct information on the excited state was available. However, the change in electronic absorption spectra was not remarkable by complex formation—a small hypsochromic shift of *ca.* 3 nm—and we do not consider this factor to be important. Third, any electronic property of the excited state must affect both k_r and k_{ST}. In analogy with alkyl aryl ketones,[13] the excited state of the acetophenone oxime derivatives must reduce the $n\pi^*$ character of the singlet state by introduction of an electron donating substituent such as alkoxyl group and diminish the rate of intersystem crossing, $(n\pi^*)^1\rightarrow(\pi\pi^*)^3$. On the other hand, an electron withdrawing substituent such as cyano group enhances an $n\pi^*$ nature of the singlet state and hence the rate of intersystem crossing. This concept is reasonable, since the intersystem crossing $(n\pi^*)^1\rightarrow(\pi\pi^*)^3$ is larger than the intersystem crossing $(\pi\pi^*)^1\rightarrow(\pi\pi^*)^3$.[14] This is the most reasonable explanation for the depression of the formation of oxaziridine which affords the mother ketone and amides, and the stimulated geometrical isomerization from $(\pi\pi^*)^3$. We believe the variation in the electronic property of the excited states is the most important factor in characterizing the photochemical behavior of the host–guest complex of acetylbenzocrown ether oximes.

References

1) Part II: M. Tada, A. Suzuki, and H. Hirano, *J. Chem. Soc., Chem. Commun.*, **1979**, 1004.
2) M. Hiraoka, "Crown Compound," (in Japanese), Kodansha Scientific, Tokyo (1978); "Synthentic Multidentate Macrocyclic Compounds," ed by R. M. Izatt and J. J. Christensen, Academic Press, New York (1978); "Chemistry of Crown Ether," (in Japanese), ed by R. Oda, T. Shono, and I. Tabushi, Kagakudojin, Kyoto (1978).
3) R. R. Hautala and R. H. Hasting, *J, Am. Chem. Soc.*, **100**, 648 (1978).
4) M. Tada and H. Hirano, *Tetrahedron Lett.*, **1978**, 5111.
5) H. Izawa, P. de Mayo, and T. Tabata, *Can. J. Chem.*, **47**, 51 (1969).
6) T. Oine and T. Mukai, *Tetrahedron Lett.*, **1969**, 157.
7) H. A. Benesi and J. H. Hildebrand, *J. Am. Chem. Soc.*. **71**, 2703 (1949).
8) B. Laurence and H. M. Rosenberg, *J. Chem. Soc., Chem. Commun.*, **1969**, 1115.
9) T. Sasaki, S. Eguchi, and T. Toru, *J. Chem. Soc., Chem. Commun.*, **1970**, 1239.
10) T. Sato, T. Inoue, and K. Yamamoto, *Bull. Chem. Soc, Jpn.*, **45**, 1176 (1972).
11) H. Shizuka, T. Saito, and T. Morita, *Chem. Phys. Lett.*, **56**, 519 (1978).
12) L. R. Sausa and J. M. Larson, *J. Am. Chem. Soc.*, **99**, 307 (1977).
13) "Energy Transfer and Organic Photochemistry," ed by A. A. Lamola and N. J. Turro, Interscience Publ., New York (1969), p. 215
14) N. J. Turro, "Modern Molecular Photochemistry," Benjamin/Cummings Publ., Menlo Park, Cal. (1978), p. 185.

The Thermal Decomposition of *N,O*-Diacyl-*N*-*t*-butylhydroxylamines

Yuzuru UCHIDA,* Yukinobu HASHIMOTO, and Seizi KOZUKA†

Department of Applied Chemistry, Osaka Institute of Technology, Asahi-ku, Osaka 535

†*Department of Applied Chemistry, Faculty of Engineering, Osaka City University, Sumiyoshi-ku, Osaka 558*

(Received November 12, 1979)

Several *N,O*-diacyl-*N*-*t*-butylhydroxylamines and *O*-acyl-*N*-*t*-butylhydroxylamines were prepared, and their thermal decompositions were studied. The thermal decompositions of *N,O*-diacyl-*N*-*t*-butylhydroxylamines in tetralin gave substituted *N*-*t*-butylbenzamides, carboxylic acids, 1,1′-bitetralyl, and 1,2-dihydronaphthalene as the major products, together with small amounts of carbon dioxide, *t*-butylamine, and benzanilides. In the thermal decompositions of *O*-acyl-*N*-*t*-butylhydroxylamines, the products were *t*-butylamine, carboxylic acids, substituted *N*-*t*-butylbenzamides, 1,1′-bitetralyl, and 1,2-dihydronaphthalene.

It is well known that such chemical bonds as the O–O bonds in diacyl peroxides are cleaved on heating in both homolytic and heterolytic manners.[1] Although a number of workers have investigated the thermal decomposition of diacyl peroxides, few surveys of the thermal properties of the acylated hydroxylamines have appeared in the literature.[2] *N,O*-Dibenzoylhydroxylamine decomposes thermally, giving mainly phenyl isocyanate and benzoic acid (Lossen rearrangement), and the decomposition initiates the polymerization of methyl methacrylate.[2a] Horner and Steppan examined the thermal decomposition of *N,O*-diacyl-*N*-arylhydroxylamines at 180—190 °C and found *N,O*-diacyl-*o*-aminophenols as the main products, together with 20—30% of carbon dioxide. They suggested that at least 20—30% of the decomposition underwent the homolytic cleavage of the N–O bond. On the other hand, the thermal decomposition of *N,O*-diacyl-*N*-*t*-alkylhydroxylamines has not yet been studied. The alkyl group on the nitrogen atom would suppress such reactions as the Lossen rearrangement and the migration of the acyloxyl group; hence, a different type of thermolysis would result. In order to obtain further information about the thermal properties of the N–O bond in hydroxylamine derivatives, we have studied the thermal decompositions of *N*-*O*-diacyl-*N*-*t*-butylhydroxylamines and *O*-acyl-*N*-*t*-butylhydroxylamines, with tetralin as the solvent.

Results and Discussion

Preparation of N,O-*Diacyl*-N-t-*butylhydroxylamines.* The *N,O*-diacyl-*N*-*t*-butylhydroxylamines (**1**) and *O*-acyl-*N*-*t*-butylhydroxylamines (**2**) were prepared by the reactions of *N*-*t*-butylhydroxylamine and the corresponding acyl chlorides in the presence of pyridine. The reactions of *N*-*t*-butylhydroxylamine with an excess of acyl chlorides gave **1a**—**d**; the results are summarized in Table 1. On the other hand, the reaction of *N*-*t*-butylhydroxylamine with an equivalent of acyl chloride afforded **2** as the main product. The results are summarized in Table 2. Under reduced pressure, *O*-benzoyl-*N*-*t*-butylhydroxylamine (**2a**) and *O*-*p*-toluoyl-*N*-*t*-butylhydroxylamine (**2b**) could be isolated by distillation, although the distillation was accompanied by a slight decomposition. The other hydroxylamines

TABLE 1. YIELDS AND PHYSICAL PROPERTIES OF *N,O*-DIACYL-*N*-*t*-BUTYLHYDROXYLAMINES

Compd	Yield/%	Mp/°C	IR/cm^{-1} (KBr) C=O	Found (Calcd) (%)		
				C	H	N
1a	69	98.0—99.0 (lit, 98—99)[10]	1750, 1645	72.79 (72.70)	6.40 (6.44)	4.77 (4.71)
1b	62	114.5—115.5	1745, 1650	73.83 (73.82)	7.12 (7.12)	4.38 (4.30)
1c	55	90.0—91.0	1750, 1625	67.11 (67.21)	6.34 (6.49)	3.97 (3.92)
1d	65	112.5—113.5	1760, 1665	58.90 (59.03)	4.52 (4.68)	3.82 (3.82)
1e	82	95.0—96.0	1750, 1650	73.19 (73.29)	6.84 (6.80)	4.55 (4.50)
1f	52	73.0—74.0	1745, 1660	69.74 (69.70)	6.45 (6.47)	4.30 (4.28)
1g	67	90.0—91.0	1755, 1650	65.11 (65.16)	5.31 (5.47)	4.21 (4.20)
1h	91	63.0—64.0	1790, 1650	66.37 (66.36)	7.20 (7.28)	5.95 (5.95)
1i	79	115.0—116.0	1755, 1635	73.18 (73.29)	6.88 (6.30)	4.36 (4.50)
1j	71	101.5—102.5	1760, 1640	69.79 (69.70)	6.48 (6.47)	4.26 (4.28)
1k	73	130.5—131.5	1750, 1655	65.12 (65.16)	5.40 (5.47)	4.29 (4.22)

Table 2. Yields and physical properties of *O*-acyl-*N*-*t*-butylhydroxylamines

Compd	Yield/%	Mp (bp)/°C	IR/cm^{-1} (neat)		Found (Calcd) (%)		
			N–H	C=O	C	H	N
2a	78	(101—104/3 mmHg) (lit, 73/0.5 mmHg)[10]	3220	1720	68.47 (68.37)	8.06 (7.82)	7.25 (7.25)
2b	32	(109/3 mmHg)	3220	1715	69.85 (69.54)	8.56 (8.27)	6.77 (6.76)
2c	52	27.0—28.0	3220	1710	64.55 (64.55)	7.87 (7.68)	6.18 (6.27)
2d	70	23.0—24.0	3210	1720	58.16 (58.03)	6.11 (6.20)	6.06 (6.15)

were isolated by recrystallization. The treatment of *N,O*-dibenzoyl-*N*-*t*-butylhydroxylamine (**1a**) with sodium hydroxide in methanol afforded *N*-benzoyl-*N*-*t*-butylhydroxylamine (**3a**) in a good yield. The *N,O*-diacyl-*N*-*t*-butylhydroxylamines (**1e—k**), bearing different acyl groups on the N and O aroms, were prepared by the acylation of **2a** and **3a**, as is shown in Scheme 1. The results are also given in Table 1.

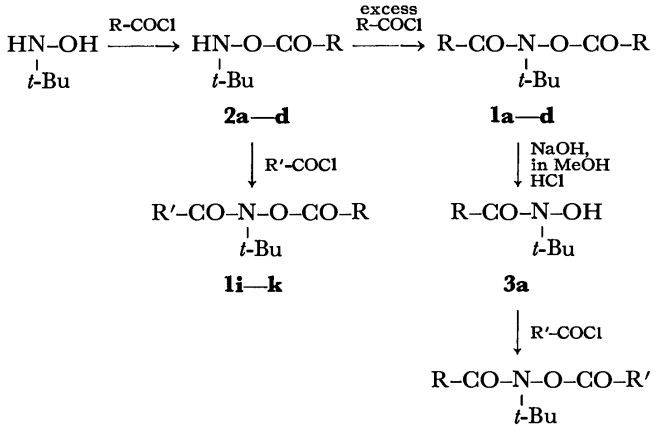

1a, **2a**, and **3a** R=Ph
1b and **2b** R=*p*-CH_3–C_6H_4
1c and **2c** R=*p*-CH_3O–C_6H_4
1d and **2d** R=*p*-Cl–C_6H_4
1e and **1i** R=Ph, R'=*p*-CH_3–C_6H_4
1f and **1j** R=Ph, R'=*p*-CH_3O–C_6H_4
1g and **1k** R=Ph, R'=*p*-Cl–C_6H_4
1h R=Ph, R'=CH_3

Scheme 1.

Thermal Decomposition of N,O-*Diacyl*-N-t-*butylhydroxylamines.* *N,O*-Diacyl-*N*-*t*-butylhydroxylamines (**1**) were quite stable in comparison with *N,O*-dibenzoylhydroxylamine[2a] or *N,O*-diacyl-*N*-arylhydroxylamines,[2b] and no detectable decomposition was observed below 180 °C. Therefore, the thermal decompositions of **1** were carried out in tetralin as the solvent above 205 °C. In the thermal decompositions of **1a—d**, bearing the same acyl groups on the N and O atoms, the corresponding substituted *N*-*t*-butylbenzamides (**4**) and carboxylic acids (**5**) were formed as the products in good yields. These products were isolated by extraction from the reaction mixture with an alkaline solution and by means of column chromatography, and then identified by comparing their properties with those of authentic samples. The yields of the products were estimated by means of GLC; the results are summarized in Table 3. A detailed product analysis was performed for the thermal decomposition of **1a**; *N*-*t*-butylbenzamide (**4a**) and benzoic acid (**5a**) were found along with minor amounts of *t*-butylamine as the salt of benzoic acid, benzanilide, and carbon dioxide. 1,1'-Bitetralyl (**6**) and 1,2-dihydronaphthalene (**7**) were also obtained as the products derived from tetralin. On the gas chromatogram of the reaction mixture, the stereoisomers of **6** showed two distinct peaks of approximately equal intensities, as had been reported by Williams.[3]

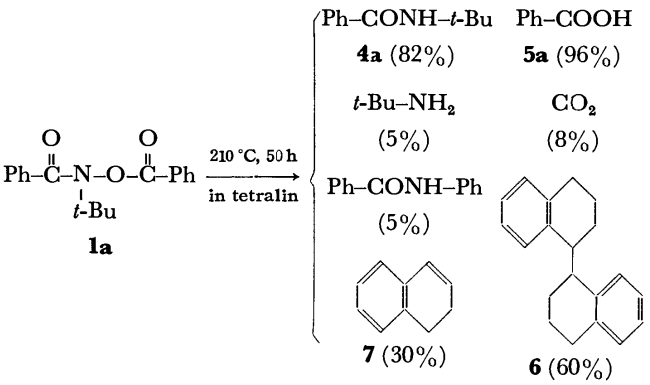

Scheme 2.

In each of the thermal decompositions of **1e—k**, bearing different acyl groups on the N and O atoms, two kinds of amides (**4**) and acids (**5**), originating from the two different acyl groups, were formed. These results are also given in Table 3. For example, on heating in tetralin at 210 °C for 26 h, **1e** was completely decomposed, giving *N*-*t*-butylbenzamide (**4a**) (82%) and *p*-toluic acid (**5b**) (82%) as the major products plus small amounts of *N*-*t*-butyl-*p*-toluamide (**4b**) (13%), benzoic acid (**5a**) (9%), and carbon dioxide (4%).

Oae and Sakurai studied the reaction of *N*-aroyl-*O*-3,5-dinitrobenzoyl-*N*-phenylhydroxylamines with sodium cyanide in dipolar aprotic solvents at room temperature.[4] The products were aroylanilides and a small amount of carbon dioxide. They suggested that the reaction proceeds *via* the decarboxylation of a Meisenheimer-type complex formed as an intermediate, as in the displacement reaction of polynitro aromatics. Although the formation of the anilides is quite comparable to the present results of thermal decompositions, the mechanisms of those two reactions must be quite

Table 3. Thermal decomposition of *N,O*-diacyl-*N*-*t*-butylhydroxylamines in tetralin (0.1 M) at 210 °C

Compd	Time/h	Yields/mol%										
		4[a]				5[b]				CO_2[c]	6[d]	7[d]
1a	50	**4a**	82			**5a**	96			8	60	30
1b	40	**4b**	92			**5b**	86			6	49	42
1c	40	**4c**	94			**5c**	99			3	38	43
1d	40	**4d**	97			**5d**	89			3	42	42
1e	26	**4a**	82	**4b**	13	**5b**	82	**5a**	9	4	33	52
1e	9[e]	**4a**	93	**4b**	3	**5b**	84	**5a**	1	f)	f)	f)
1f	26	**4a**	80	**4c**	16	**5c**	76	**5a**	16	5	36	41
1g	40	**4a**	70	**4d**	19	**5d**	76	**5a**	15	2	58	23
1h	36	**4a**	71	**4e**	18	**5e**	67[c]	**5a**	25	9	64	19
1i	40	**4b**	71	**4a**	21	**5a**	72	**5b**	22	f)	58	39
1j	24	**4c**	75	**4a**	21	**5a**	79	**5c**	20	f)	56	27
1k	36	**4d**	78	**4a**	21	**5a**	76	**5d**	21	f)	56	37

a) R–CONH–*t*-Bu **4a**; R=Ph, **4b**; R=*p*-CH_3–C_6H_4, **4c**; R=*p*-CH_3O–C_6H_4, **4d**; R=*p*-Cl–C_6H_4, **4e**; R=CH_3. b) Acids were estimated after methylation with diazomethane. R–CO_2H **5a**; R=Ph, **5b**; R=*p*-CH_3–C_6H_4, **5c**; R=*p*-CH_3O–C_6H_4, **5d**; R=*p*-Cl–C_6H_4, **5e**; R=CH_3. c) Estimated by titration. d) Based on **1**. e) In the presence of 10 mol% of *t*-butylammonium benzoate at 205 °C. f) Not determined.

different, since no efficient nucleophile is present and since a nonpolar solvent was used in the present reaction. Moreover, in the present case, the *O*-acetyl derivative (**1h**) can not form such a complex. It is also unlikely that the *O*-benzoyl, *O*-*p*-toluoyl, and *O*-*p*-methoxybenzoyl derivatives, without bearing such an electron-withdrawing substituent as a nitro group, would form a complex in tetralin. In addition, the product, **6**, derived from tetralin could not be explained in terms of such ionic mechanisms. The precursors of **6** are obviously the tetralyl radicals formed by the abstraction of a hydrogen atom from tetralin. Dihydronaphthalene (**7**) would also be formed from the tetralyl radicals by disproportionation. Thus, the formation of these products suggests a homolytic decomposition of **1**, giving the acylaminyl radical and the acyloxyl radical. However, the amount of carbon dioxide formed by the thermal decomposition is too small to be accounted for by the decarboxylation of the acyloxyl radical formed by the homolysis of the N–O bond of **1**.

In order to compare the yields of carbon dioxide, the thermal decomposition of benzoyl peroxide was carried out under the same conditions as in the thermolysis of **1a**. When benzoyl peroxide was heated in tetralin (0.05 M, 1 M=1 mol dm^{-3}) at 210 °C for 2 h, benzoic acid and carbon dioxide were formed in 37 and 60% yields respectively, based on benzoyl peroxide. These results indicate a facile decomposition of the benzoyloxyl radical at that temperature to give carbon dioxide rather than the abstraction of a hydrogen atom from the solvent to give benzoic acid. Moreover, no detectable amount of benzene was formed in the thermal decomposition of **1a**. It is also highly unlikely that the acetoxyl radical efficiently abstracts a hydrogen atom from tetralin to give acetic acid at this temperature, because the acetoxyl radical has been known to be unstable and more easily decarboxylates than the benzoyloxyl radical.[5] On the contraly, acetic acid was formed in a high yield by the decomposition of *N*-benzoyl-*O*-acetyl-*N*-*t*-butylhydroxylamine (**1h**). These results rule out the mechanism involving homolytic fission of the N–O bond of **1**, giving the acylaminyl radical and the acyloxyl radical, as the main process of the reaction.

A probable mechanism for the thermal decomposition of **1** which is in accordance with the present results is shown in Scheme 3. The thermal decomposition of **1** would be initiated by the attack of a nucleophile, which may consist of some trace impurities or the products formed by the thermal decomposition of the hydroxylamine itself. This is suggested on the basis of the facts that a certain induction period was observed in the thermal decomposition of **1e** at 205 °C, as is shown in Fig. 1. The addition of a small amount of *t*-butylammonium benzoate to the reaction solution obviously depressed the induction period and accelerated the rate

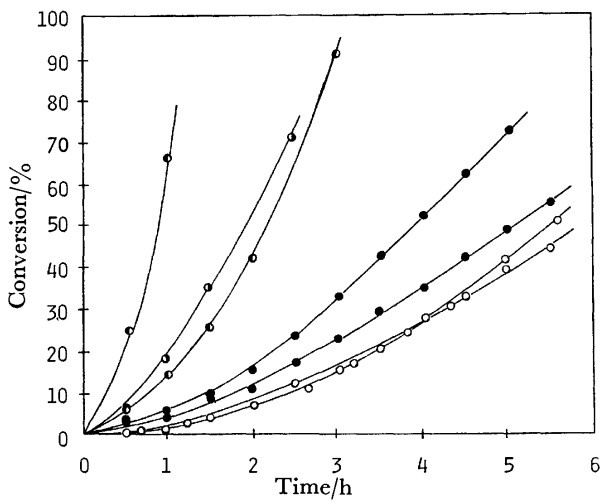

Fig. 1. Thermal decomposition of *N*-benzoyl-*O*-*p*-toluoyl-*N*-*t*-butylhydroxylamine in tetralin (0.1 M) at 205.0±0.2 °C.
○: No additive, ●: in the presence of an equilolar amount of benzoic acid, ◐: in the presence of 10 mol% of *t*-butylammonium benzoate, ◑: in the presence of 10 mol% of *N*-benzoyl-*N*-*t*-butylhydroxylamine (**3a**).

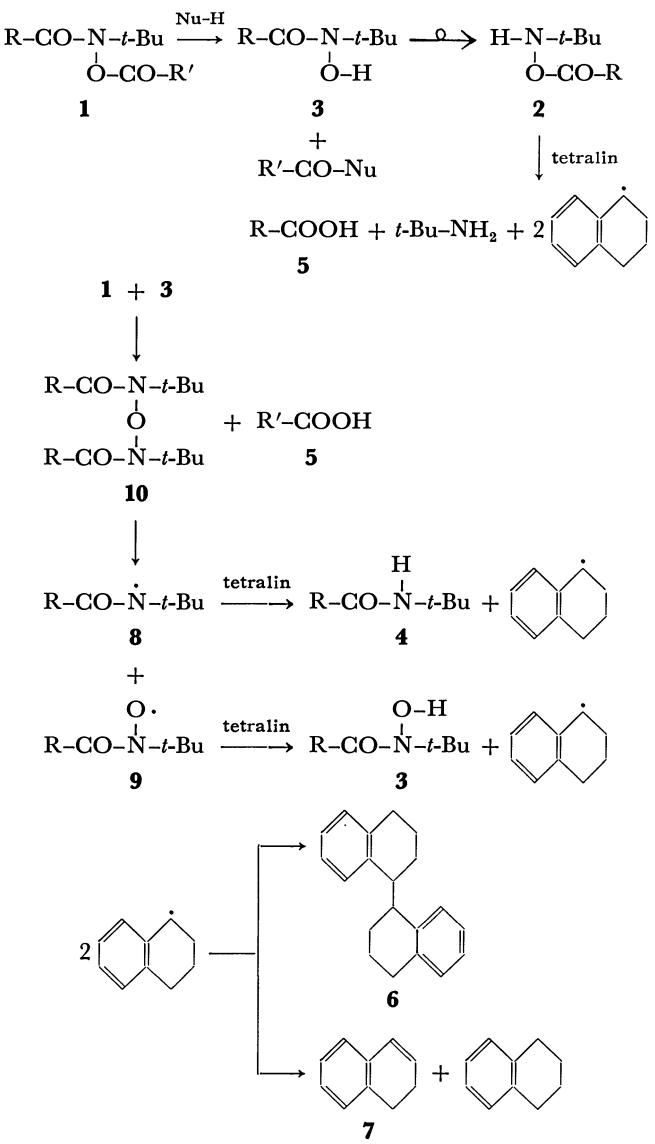

Scheme 3.

of the decomposition. The reactions of some *N,O*-diacylhydroxylamines with amines,[6] sodium methoxide, sodium azide, thiophenols, and sodium cyanide[4] have been studied. In those reactions, the nucleophiles attack the carboxylic carbonyl carbon atom of the reactant. By analogy, the nucleophile would attack the carboxylic carbonyl carbon atom of **1e** in the present reaction, giving *N*-benzoyl-*N*-*t*-butylhydroxylamine (**3a**) in the initiation reaction.

Although *t*-butylammonium benzoate accelerated the rate of the decomposition, the mechanism of the thermal decomposition of **1** requires the formation of radical species, because the hydrocarbons, **6** and **7**, are formed from the solvent. This can be explained by a mechanism in which the initial reaction gives *N*-acyl-*N*-*t*-butylhydroxylamine (**3**), which then reacts with **1** to give the acylaminyl radical (**8**), the acylaminoxyl radical (**9**), and carboxylic acid (**5**). These radicals and acid may be formed by the nucleophilic attack of **3** upon the N atom of **1**, thus forming **5** and the intermediate (**10**). This process was confirmed by the observation that the thermolysis of **1e** was apparently accelerated by the addition of a small amount of **3** as is shown in Fig. 1. The intermediate (**10**) probably collapses rapidly into the radicals (**8** and **9**) under the conditions used. The radicals (**8** and **9**) would then abstract hydrogen atoms from the solvent to form amide (**4**) and to regenerate **3** respectively. A similar substitution reaction on the nitrogen atom has been established in the reaction of *O*-acetyl-*N*-benzoyl-*N*-(*p*-methoxyphenyl)hydroxylamine with phenols, pyrrole, and indoles.[7]

The mechanism shown in Scheme 3 does not involve the formation of carbon dioxide. In detailed product studies of the thermal decomposition of **1a**, benzanilide was found (5%). This suggests that a part of the **1a** undergoes Lossen rearrangement to form benzoic acid, phenyl isocyanate, and 2-methylpropene. The isocyanate would rapidly react with benzoic acid, giving benzanilide and carbon dioxide as follows:[8]

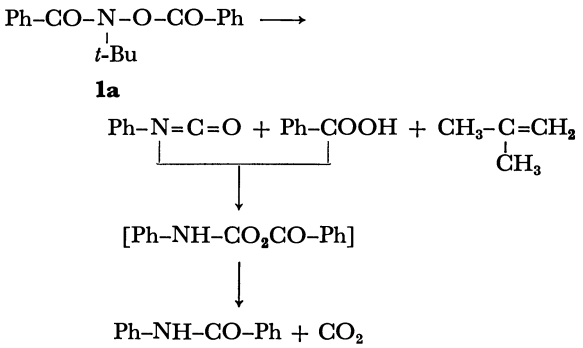

Under the same conditions, slow acyl-exchange reactions between the amides and acids were observed. That is, after the heating of **4a** with an equivalent of **5b** at 210 °C for 30 h, **4b** and **5a** were formed, both in 7% yields. On the other hand, the reaction of **4b** with **5a** under the same conditions gave **4a** and **5b** in 8 and 8% yields respectively. These results suggest that a route to give the minor amides (for instance, **4b** and **4c** from **1e** and **1f** respectively) and acids (for instance, **5a** and **5b** from **1e** and **1i** respectively) would be the subsequent acyl-exchange reaction between the major amide and the acid formed by the decompositions of **1e—k**.

In order to examine the prosess giving *t*-butylamine, which was found as a minor product in the thermal decomposition of **1a**, *N*-benzoyl-*N*-*t*-butylhydroxylamine (**3a**) was heated in tetralin. On heating **3a** in tetralin at 150 °C, a rearranged product (**2a**) was isolated and characterized. The further heating of the reaction mixture at 210 °C for 2 h gave *t*-butylammonium benzoate (50%). These results suggest that *t*-butylamine was derived from **3a** *via* **2a** during the thermal decomposition of **1a**. The same results also suggest an alternative route for the formation of minor amides (**4**) and minor acids (**5**) in the decomposition of **1e—k**, bearing different acyl groups on the N and O atoms. In the initiation reaction of the decomposition of **1**, the attack of *t*-butylamine upon the carboxylic carbonyl carbon atom of **1** gives the minor amide and **3**, which then subsequently decomposes to afford a minor acid and *t*-butylamine. The amounts of the minor amide and the minor acid, which appeared to be somewhat higher

Table 4. Thermal decomposition of *O*-acyl-*N*-*t*-butylhydroxylamines in tetralin (0.1 M) at 210 °C

Compd	Time/h	Yield/mol%					
		t-$BuNH_2$[a]	**4**		**5**[b]	**6**[c]	**7**[c]
2a	4	65	**4a**	12	**5a** 81	47	35
2b	4	68	**4b**	13	**5b** 83	43	38
2c	4	76	**4c**	15	**5c** 82	47	25
2d	4	71	**4d**	15	**5d** 76	34	38

a) Isolated as the salt of the acid (**5**). b) Estimated after methylation with diazomethane. c) Based on **2**.

than would be expected from the slow acyl-exchange reaction alone, may be explained by these two processes, *i.e.*, the acyl-exchange reaction and the rearrangement reaction.

Thermal Decomposition of O-*Acyl*-N-t-*butylhydroxylamines.* In order to study the thermal properties of *O*-acyl-*N*-*t*-butylhydroxylamines (**2**), and also to prove the intermediacy of **2** during the thermal decomposition of **1**, several **2** were prepared and subjected to thermal decomposition. On heating at 210 °C for 4 h in tetralin, **2** decomposed completely, giving *t*-butylamine and carboxylic acid as a salt in high yields, together with a small amount of the amide (**4**). The products derived from tetralin, **6** and **7**, were also obtained in substantial yields. These results are summarized in Table 4. No

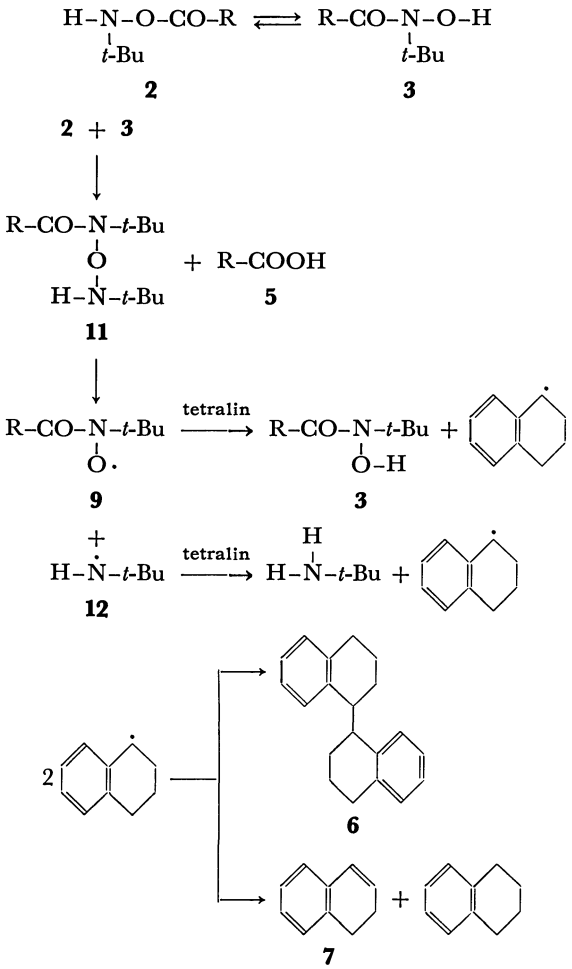

Scheme 4.

detectable amount of carbon dioxide was formed in the thermal decomposition of **2**. Thus, we can eliminate the possibility which involves the homolytic fission of the N–O bond of **2** to yield aminyl and acyloxyl radicals. The mechanism involving the nitrene intermediate is unlikely because *t*-butylnitrene does not afford *t*-butylamine in a good yield.[9] These results suggest that the decomposition of **2** involves the initial formation of *N*-acyl-*N*-*t*-butylhydroxylamine (**3**), which subsequently reacts with the starting material, resulting in the formation of an aminyl radical (**12**) and an acylaminoxyl radical (**9**), as is shown in Scheme 4. These radicals would abstract hydrogen atoms from tetralin to yield *t*-butylamine and to regenerate **3** respectively.

Experimental

All the melting points and the boiling points are uncorrected. The IR spectra were recorded on a Shimadzu IR-430 infrared spectrometer. The tetralin was washed succesively with concd H_2SO_4, aq NaOH, and water, dried over $CaCl_2$ and distilled under reduced pressure. The distillate was passed through a column of alumina and redistilled before use.

Preparation of N,O-*Diacy*-N-t-*butylhydroxylamines (1).* *(a)*: Benzoyl chloride (112.5 g, 0.800 mol) was added to a solution of *N*-*t*-butylhydroxylamine (30.0 g, 0.337 mol) and pyridine (63.3 g, 0.800 mol) in dry benzene (700 cm^3) at room temperature with stirring. The mixture was then heated at 60 °C for 15 h with stirring. The mixture was cooled, washed with aq NH_4OH, dil aq NaOH, dil HCl, and water, and dried over Na_2SO_4. The solvent was evaporated *in vacuo*, and the residue was recrystallized from CH_2Cl_2–petroleum ether, thus giving **1a** (69.3 g, 69%); mp 98.0—99.0 °C (lit, 98—99 °C).[10] By the reaction of *N*-*t*-butylhydroxylamine with the corresponding acyl chloride, **1b—d** were prepared similarly. The yields, physical properties, and elemental analyses are shown in Table 1.

(b): *p*-Toluoyl chloride (19.7 g, 0.127 mol), was added to a solution of **3a** (22.4 g, 0.116 mol) and pyridine (10.0 g, 0.127 mol) in dry benzene (200 cm^3), after which the whole mixture was stirred at 75 °C for 12 h. The reaction mixture was washed with aq NH_4OH, dil aq NaOH, dil HCl, and water, and dried over Na_2SO_4. The solvent was evaporated *in vacuo*, and the residue was recrystallized from CH_2Cl_2–petroleum ether, thus giving **1e** (29.5 g, 82%). By the same procedures, **1f**, **1g**, and **1h** were prepared by the reactions of **3a** with the corresponding acyl chlorides. The reactions of **2a** with the corresponding acyl chlorides gave **1i**, **1j**, and **1k**. The yields, physical properties, and elemental analyses are shown in Table 1.

Preparation of O-*Acyl*-N-t-*butylhydroxylamines (2).* Benzoyl chloride (127 g, 0.90 mol) was added to a solution of *N*-*t*-butylhydroxylamine (80 g, 0.90 mol) and pyridine (78 g, 1.0 mol) in dry ether (500 cm^3), after which the mixture was refluxed with stirring for 15 h. The reaction mixture was then washed with aq NH_4OH, dil aq NaOH, dil HCl, and water, and dried over Na_2SO_4. The solvent was evaporated, and the residue was distilled under reduced pressure to give *O*-benzoyl-*N*-*t*-butylhydroxylamine (**2a**) (135 g, 78%); bp 101—104 °C/3 mmHg** (lit, 73 °C/0.5 mmHg).[10] The distillate was then further purified by chromatography on silica gel, with CH_2Cl_2 as the eluent. By the same procedure

** Through this paper 1 mmHg=133.322 Pa.

as has been described above, **2b—d** were prepared. The yields, physical properties, and elemental analyses are shown in Table 2.

Preparation of N-*Benzoyl*-N-t-*butylhydroxylamine (3a).* A solution of NaOH (10.2 g, 0.255 mol) in water (40 cm³) was added to a stirred suspension of **1a** (43.7 g, 0.147 mol) in methanol (200 cm³). The mixture was then stirred at room temperature for 1.5 h. After the evaporation of the methanol under reduced pressure, water (200 cm³) and ether (50 cm³) were added to the residue. The separated water layer was acidified with HCl. The formed crystals were taken in ether, and the ethereal solution was washed with saturated $NaHCO_3$ and water, and dired over Na_2SO_4. The ether was then evaporated, and the residue was recrystallized from CH_2Cl_2–petroleum ether to give **3a** (23.4 g, 82%); mp 108—109 °C (lit, 109 °C).[10]

Thermal Decomposition of 1. A solution of **1** in tetralin (0.1 M, 20 cm³) was sealed in a degassed tube with break-off tips at both ends and then heated in a constant-temperature bath at 210 °C. The tube was opened in a vacuum system, and the carbon dioxide formed by the decomposition was introduced into an aq $Ba(OH)_2$ solution (0.1 M, 50 cm³) after having been passed through a cold trap by a nitrogen stream. The $Ba(OH)_2$ solution was filtered, and the filtrate (40 cm³) was titrated with HCl (0.1 M). An excess of an ethereal solution of diazomethane was added to the decomposition mixture, and the mixture was allowed to stand for 1 h. After the evaporation of the ether *in vacuo*, the reaction mixture was subjected to GLC analysis, with the addition of a known amount of biphenyl as an internal standard. The following three columns were used a 2-m column packed with Apiezon Grease L (30%) on Cerite 545 to analyze methyl benzoate; a 2-m column packed with Thermon 1000+H_3PO_4 (5+0.5%) on Chromosorb W to analyze the amides, bitetralyl, and methyl esters, and a 5-m column packed with polyethylene glycol 20 M (25%) on Shimalite 101 to analyze dihydronaphthalene. The results are summarized in Table 3.

Thermal Decomposition of 2. A solution of **2a** in tetralin (0.1 M, 20 cm³) sealed in a degassed ampule was heated in a constant-temperature bath at 210 °C for 4 h. After cooling, the precipitated *t*-butylammonium benzoate was collected by filtration, and washed with petroleum ether. The filtrate was subjected to GLC analysis after methylation with diazomethane.

Kinetic Procedure. A solution of **1e** (0.1 M, 25 cm³) in tetralin was placed in a reaction vessel fitted with a gas-inlet tube and a reflux condenser. It was heated in a constant-temperature bath (205.0±0.2 °C) after nitrogen had been bubbled into, for 30 min. Aliquots were withdrawn at scheduled intervals and quenched by chilling to 0 °C. The aliquot (100 mm³) and methanolic NaOH (0.25%, 10 cm³) were placed in a volumetric flask (25 cm³), and the mixture was heated in a water bath at 65 °C for 30 min. After a methanolic iron(III) chloride solution (10 cm³) had been added, the solution was diluted to the volume of the flask with methanol and the absorbance at 510 nm was measured. The iron(III) chloride solution was prepared by dissolving 5 g of $FeCl_3 \cdot 6H_2O$ in 1 dm³ of methanol containing HCl (0.0321 M) to prevent iron(III) hydroxide formation.[11]

References

1) a) D. B. Denny, *J. Am. Chem. Soc.*, **78**, 590 (1956); b) D. B. Denny and D. Z. Denny, *J. Am. Chem. Soc.*, **78**, 4290 (1956); c) F. D. Green, H. P. Syein, C. C. Chu, and F. M. Vans, *J. Am. Chem. Soc.*, **68**, 2081 (1964); d) T. Kashiwagi, S. Kozuka, and S. Oae, *Tetrahedron*, **26**, 3169 (1970); e) C. Walling, H. P. Waits, Milovanovic, and C. G. Pappiannou, *J. Am. Chem. Soc.*, **92**, 4927 (1970).

2) a) C. Walling and A. N. Naglieri, *J. Am. Chem. Soc.*, **82**, 1820 (1960); b) L. Horner and H. Steppan, *Ann.* **606**, 24 (1957); c) S. Oae and T. Sakurai, *Bull. Chem. Soc. Jpn.*, **48**, 3759 (1975); d) W. T. Bouma and Jan B. F. N. Engberts, *J. Org. Chem.*, **41**, 143 (1976); e) R. M. Coates and I. M. Said., *J. Am. Chem. Soc.*, **99**, 2355 (1977).

3) R. H. Williams, *J. Chem. Eng. Data*, **1964**, 567.

4) S. Oae and T. Sakurai, *Bull. Chem. Soc. Jpn.*, **48**, 1075 (1975).

5) C. Walling and R. B. Hodgdon, *J. Am. Chem. Soc.*, **80**, 228 (1959).

6) a) P. G. Sammes, *J. Chem. Soc.*, **1965** 6608; b) D. Sarantakis, J. K. Sutherlamd, C. Tortorella, and V. Tortorella, *J. Chem. Soc., C*, **1968**, 72.

7) T. Ohta, K. Shudo, and T. Okamoto, *Tetrahedron Lett.*, **1978**, 1983.

8) L. Ötvös, J. Marton, and J. M. Agoston, *Tetrahedron Lett.*, **1960**, 15.

9) W. Pritzkow and D. Timm, *J. Prakt. Chem.*, **32**, 178 (1966).

10) H. G. Aurich and J. Trosken, *Chem. Ber.*, **106**, 3483 (1973).

11) D. C. Berndt and R. L. Fuller, *J. Org. Chem.*, **31**, 3312 (1966).

The Confirmation of the Configuration of Ethyl 2-Bromo-3-nitro-2-alkenoate by ^{13}C NMR Spectroscopy

Chung-gi SHIN, Yasuchika YONEZAWA, Katsumi AJISAKA,† and Juji YOSHIMURA*,††

Laboratory of Organic Chemistry, Faculty of Technology, Kanagawa University, Rokkakubashi, Kanagawa-ku, Yokohama 221

††*Laboratory of Chemistry for Natural Products, Faculty of Science, Tokyo Institute of Technology, Nagatsuta, Midori-ku, Yokohama 227*

(Received November 26, 1979)

The configuration of the ethyl 2-bromo-3-nitro-2-alkenoate formed by the elimination of hydrogen bromide from ethyl 2,3-dibromo-3-nitroalkanoate was determined to be (*Z*) by the examination of the ^{13}C NMR spectra.

In a previous paper, it was found that the base-catalyzed elimination of hydrogen bromide from a *threo* and *erythro* mixture of ethyl 2,3-dibromo-3-nitroalkanoate (**1**) afforded only one kind of geometric isomer of ethyl 2-bromo-3-nitro-2-alkenoate (**2**).[1] The same phenomenon was also observed in the case of a *threo* and *erythro* mixture of ethyl 2-acetoxy-3-nitroalkanoate.[2] The configuration of **2** was deduced to be (*Z*) from the fact that the reduction of **2** with diethyl phosphonate gave ethyl 3-nitro-2-alkenoate (**3**) with the (*E*)-configuration,[3] the geometry of which was determined by ^1H NMR spectroscopy.[1]

In the present investigation, the authors measured the ^{13}C NMR spectra of **2** and related compounds in order to confirm the configuration of **2** and then discussed the reaction mechanism.

Results and Discussion

The ^{13}C NMR chemical shifts of Compounds **2** and **3** and of ethyl (*E*)- and (*Z*)-2-nitro-2-alkenoates [(*E*)-**4**, and (*Z*)-**4**] are presented in Table 1. It is noticeable that, in every (*E*), and (*Z*) isomeric pair of 3-nitro-2-alkanoate, **3**, each carbon at positions C-1, C-2, and C-3 (for numbering, see Table 1) of the (*Z*)-isomer always resonates at a higher field than does the corre-

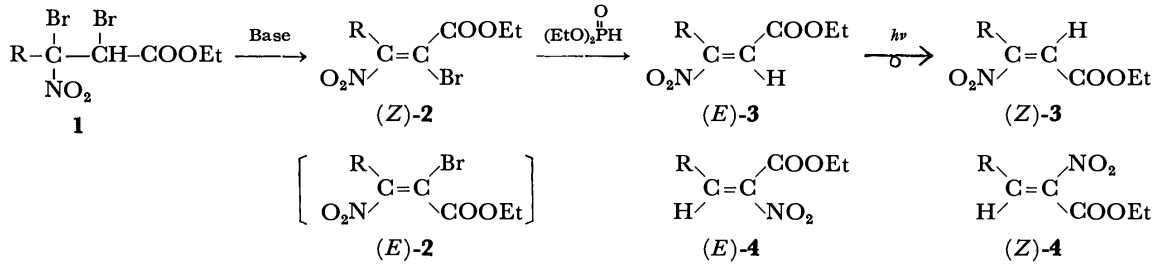

Scheme 1.

TABLE 1. ^{13}C CHEMICAL SHIFTS OF CARBONS[a] IN **2**, **3**, AND **4**

Compound	R		C-2′ δ/ppm	C-1′ δ/ppm	C-1 δ/ppm	C-2 δ/ppm	C-3 δ/ppm	C-4 δ/ppm	C-5 δ/ppm	C-6 δ/ppm
2	Et		13.6	63.5	161.7	118.9	155.9	25.9	10.6	
	n-Pr		13.7	63.5	161.8	119.6	155.0	33.9	20.1	13.4
	i-Pr		13.7	63.6	162.2	113.5	160.4	32.9	18.7	
3	Me	(*Z*)	14.0	61.9	163.0	116.7	155.9	18.9		
		(*E*)	14.0	62.0	164.4	121.5	160.4	14.2		
	Et	(*Z*)	14.1	61.9	162.8	113.9	162.4	26.8	11.0	
		(*E*)	14.2	61.9	165.6	120.9	164.1	21.4	12.5	
	i-Pr	(*Z*)	14.0	61.6	166.7	111.8	162.4	32.5	19.2	19.9
		(*E*)	14.2	61.8	169.4	118.9	164.1	28.2	19.7	
	n-Pr	(*Z*)	13.9	61.6	162.3	114.5	160.4	34.9	20.0	13.0
		(*E*)	14.3	62.0	164.3	121.4	164.3	29.4	21.8	13.8
4	Me	(*Z*)	14.1	63.0	159.0	146.1	136.1	13.5		
		(*E*)	14.1	62.9	160.1	146.1	140.0	13.5		
	Et	(*Z*)	14.1	62.9	159.3	145.0	141.5	21.9	12.3	
		(*E*)	14.1	62.8	160.1	145.0	141.5	21.8	12.5	
	n-Pr	(*Z*)	14.1	62.9	158.9	145.3	139.8	30.2	21.5	13.7
		(*E*)	14.1	62.7	160.1	145.3	143.3	30.0	21.8	13.7

a) The carbons were commonly numbered as follows: $\overset{6}{C}\text{–}\overset{5}{C}\text{–}\overset{4}{C}\text{–}\overset{3}{C}X{=}\overset{2}{C}Y\text{–}\overset{1}{C}OO\overset{1'}{C}H_2\overset{2'}{C}H_3$.

† Present address: Ajinomoto Co., Inc., Central Research Laboratories, 1-1 Suzuki-cho, Kawasaki-ku, Kawasaki 210.

sponding carbon of the (*E*)-isomer. This tendency is, however, less pronounced in the case of 2-nitro-2-alkenoate, **4**.

Savitsky *et al.*[4] reported that the chemical shift of olefinic carbons of 3-substituted alkenoate with two bulky substituents in a *cis* orientation deviates from the expected value due to the alteration in the electron density by the steric inhibition of the resonance. Consequently, the above facts are attributed to the diminished electron-withdrawing effect of the nitro and ethoxycarbonyl groups of (*Z*)-**3** in the *cis* orientation. This empirical fact is a useful clue for the determination of the configuration of the isomeric pair of **2**; however, it is not applicable when only one isomer is available, as in the present case. Therefore, the observed ^{13}C shifts of olefinic carbons in **2** were compared with those calculated from the results of (*E*)- and (*Z*)-**3** and the substituent effect. The substituent effects for a series of 2-alkenoates have been studied by Lippmaa *et al.*[5,6] and by Brower and Stothers,[7] and the substituent parameter of the bromine atom suggested by Lippmaa *et al.* was used for the calculation here; that is, the shifts of the C-2 and C-3 of **3** were corrected by 8.0 ppm to an upper field by the bromination of C-2. The results are presented in Table 2. The observed shifts agree well with the calculated values for the (*Z*)-isomer, but not with those of the (*E*)-isomer. This is in accordance with our previous deduction.[1] However, it should be noticed that the observed shifts of the C-2 of (*Z*)-**2** deviate comparatively much from the calculated shifts. This deviation might also be attributed to the *cis* configuration between the bromine atom and the nitro group in (*Z*)-**2**, because such crowded compounds were not used by Lippmaa *et al.*[5,6] in determining the substituent parameters.

An analogous tendency is found in the differences in the chemical shifts ($\Delta\delta$/ppm) of the olefinic carbons of **3** or **4** and the corresponding 2-alkenoates with no nitro group[7] (Table 3). In the case of **4** with a nitro group on C-2 both (*Z*)- and (*E*)-isomers showed a similar trend. That is, the substituent shifts for both isomers were 23—25 ppm lower for C-2, to which a nitro group is attached, and 10—13 ppm higher for C-3. On the other hand, in the case of **3**, where the nitro group is attached to C-3, the substituent shifts exhibited quite different profiles. For the (*E*)-isomer, C-2 showed field shifts higher by 6—7 ppm and C-3 field shifts lower by 4—10 ppm, as was observed in the case of **4**. In contrast, the C-2 and C-3 of the (*Z*)-isomer shifted to fields lower by 0.5—1.5 and 4—14 ppm respectively. These anomalous shifts may be attributed to the factor mentioned above.

In conclusion, it can be said that the substitution shifts are strongly affected by the configuration and the position of the substituent. If the stereoelectronic influence is taken into account in the estimation of the substituent shift of the bromine atom, a much better consistency will result than is found in Table 2.

Table 2. Calculated and observed ^{13}C chemical shifts of the olefinic carbons of **2**

R	Calcd and obsd	^{13}C shifts (δ/ppm) C-2	C-3
Et	Calcd (*Z*)	112.9	156.1
	Calcd (*E*)	105.9	154.4
	Obsd	118.9	155.9
i-Pr	Calcd (*Z*)	110.9	156.1
	Calcd (*E*)	103.8	154.4
	Obsd	113.5	160.4
n-Pr	Calcd (*Z*)	113.4	156.3
	Calcd (*E*)	106.5	152.4
	Obsd	119.6	155.0

Table 3. The substituent shift[a] of C-2 and C-3 caused by the nitro group on the C-3 of **3** and on the C-2 of **4**

Compound	R	(*Z*) C-3	(*Z*) C-2	(*E*) C-3	(*E*) C-2
3	Me	14.2	0.5	9.9	−6.1
	Et	8.9	1.2	8.7	−6.8
	i-Pr	4.6	1.3	4.2	−7.1
	n-Pr	11.2	1.5	8.2	−7.0
4	Me	−10.1	25.1	−9.9	23.3
	Et	−13.7	25.3	−12.2	24.3
	n-Pr	−9.8	25.4	−12.4	23.8

a) The differences in chemical shifts between **3** or **4** and the correspondlng 2-alkenoates are shown in δ/ppm. Consequently, the negative sign implies a higher field shift upon substitution with a nitro group.

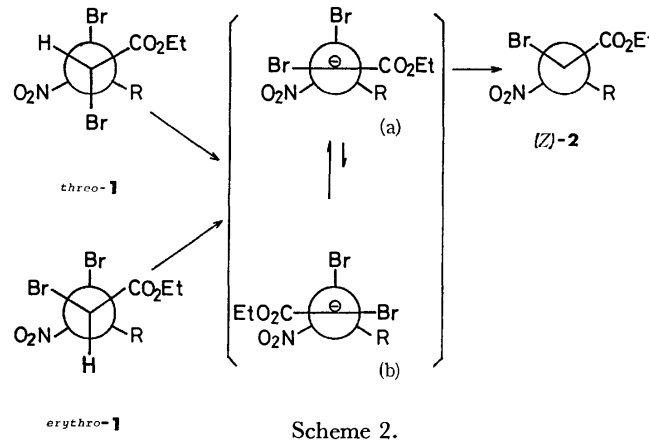

Scheme 2.

The above results show that both the *erythro* and *threo* isomers of **1** afforded only the (*Z*)-isomer of **2**. It means that the elimination from the two isomers proceeds *via* a common intermediate, analogous to the *E1cB* mechanisms proposed by Cummings and Kreuz[8] and by Kaplan *et al.*[9,10] As is shown in Scheme 2, the deprotonation of both diastereomers of **1** will result in the formation of a common, resonance-stabilized carbanion. Although two conformations, in which the leaving bromine atom is in a proper disposition for elimination, are possible for this anion, (a) will predominate over (b) because of the electrostatic repulsion between nitro and ethoxycarbonyl groups. Thus, the predominant formation of (*Z*)-**2** will result.

Experimental

The ^{13}C NMR spectra were recorded at 30 °C on a JEOL

JNM FX-100 spectrometer in the pulse Fourier transform mode at 25.15 MHz. Each spectrum was obtained after 1000 transients with a frequency range of 6250 Hz. The pulse angle of 45° was used, with an acquisition time of 0.8 s and a pulse delay of 0.7 s. All the measurements were carried out in a deuteriochloroform solution containing a drop of TMS as the internal standard. The chemical shifts were recorded in δ/ppm.

References

1) C. Shin, Y. Yonezawa, K. Suzuki, and J. Yoshimura, *Bull. Chem. Soc. Jpn.*, **51**, 2614 (1978).
2) C. Shin, Y. Yonezawa, and J. Yoshimura, *Nippon Kagaku Kaishi*, **1974**, 718.
3) The notations of (*Z*) and (*E*) are reversed in **2** and **3**.
4) G. B. Savitsky, P. D. Ellis, K. Namikawa, and G. M. Maciel, *J. Chem. Phys.*, **49**, 2391 (1968).
5) C. Rapper, E. Lippmaa, T. Pehk, and K. Andersson, *Acta Chem. Scand.*, **23**, 1447 (1969).
6) E. Lippmaa, T. Pehk, K. Andersson, and C. Rappe, *Org. Magn. Reson.*, **2**, 109 (1970).
7) H. Brower and J. B. Stothers, *Can. J. Chem.*, **50**, 601 (1972).
8) W. W. Cummings and K. L. Kreuz, *J. Org. Chem.*, **37**, 3929 (1972).
9) L. A. Kaplan and N. E. Burlington, *J. Org. Chem.*, **37**, 3932 (1972).
10) L. A. Kaplan and H. B. Pichard, *J. Am. Chem. Soc.*, **93**, 3447 (1971).

Enolate Anions. III. Substituent Effects of Sodium Diethyl Alkylmalonates in DMSO[1]

Syun-ichi KIYOOKA,* Tsukasa KODANI, and Kojiro SUZUKI
Department of Chemistry, Faculty of Science, Kochi University, Akebono-cho, Kochi 780
(Received November 30, 1979)

The conformations of sodium enolate anions, derived from diethyl malonate and diethyl alkylmalonates (alkyl=methyl, ethyl, propyl, isopropyl, butyl, isobutyl, and *s*-butyl), have been determined to be *Z,Z*-type by the analysis of their ^{1}H-NMR spectra in DMSO. In the case of diethyl *t*-butylmalonate, such a *Z,Z* type contributes to the lesser extent to the conformations of the sodium enolate anion because of repulsion between the *t*-butyl substituent and the two ethoxyl groups, which exist in three types (*Z,Z*, *Z,E*, *E,E*) of conformation, as is evident in the ^{1}H-NMR spectra. The IR spectra of sodium diethyl malonate in DMSO showed two characteristic absorption bands at 1679 and 1556 cm^{-1}. The IR isotope shifts upon the use of the enolates of diethyl malonate-2-^{13}C and diethyl malonate-1,3-$^{13}C_2$ suggested that these two bands are attributable to the C=O and C=C=C bonds. All sodium diethyl alkylmalonates except for the *t*-butyl derivative have two characteristic IR bands in the region of 1500—1700 cm^{-1}, the bands on the high-frequency side of which have nearly equal wave numbers, while those on the low-frequency side have a good correlation with the substituent constant, σ^*.

Since the reaction rates in the alkylation of enolate anions have been reported to be rapidly accelerated by the addition of dipolar aprotic solvents, such as DMSO and DMF,[2] the effect of the difference in the solvation state on the reactivity has been investigated for various reactions.[3] Because of the mutual electrostatic-interaction between a cation and an enolate anion, almost all enolate anions tend to be present as ion pairs.[4] Moreover, it is generally expected that the degree of this ion-pairing association would be altered by the extent of the solvation of the cation.

Recently, Raban *et al.* discussed the effect of the ion-pairing on the structures of the enolate anions of β-diketones on the basis of their ^{1}H- and ^{13}C-NMR spectra.[5] The relations between the reactivity of the enolate anions derived from β-diketones and the ion-pairing were reported in detail by DePalma *et al.*[6] In order to evaluate the reactivity of the enolate anions with ester groups, which are very important for organic synthesis, various spectral studies of them have been continued.[1]

The substituent effects on the electron density at the delocalized anionic moiety of the enolate anions and on the conformations of them in DMSO were examined using the sodium enolates of ethyl substituted-phenylacetates.[1b] The ^{13}C-NMR spectra of sodium diethyl alkylmalonates were shown to correspond to a single conformer except in the case of the *t*-butyl derivative.

This report deals with alkyl substituent effects on the electron density at the delocalized anionic moiety of sodium diethyl malonates and on their conformations by means of IR and ^{1}H-NMR measurements.

Results and Discussion

The enolate anions produced from acetylacetone were found to be 100% in the *Z,Z* conformation for lithium enolate and 34% in the *Z,Z* conformation for sodium enolate in methanol-d_4.[5a] Further, the enolate anions from acetoacetaldehyde and ethyl acetoacetate exist exclusively in the *Z,Z* conformation for lithium enolates in DMF, and in the latter enolate anion, a *Z,Z* conformer is predominant even for sodium and potassium enolates.[7] The sodium enolate of ethyl 2-methylacetoacetate in DMF was shown to exist 66% in the *Z,Z* conformation, which is slightly destabilized by the introduction of the α-methyl group.[7]

Three arrangements are possible for the structures of enolate anions derived from diethyl alkylmalonates. Compared with the stereomodels of other enolate anions, such as acetylacetonato-alkali metals, those of sodium diethyl alkylmalonates are so crowded that the most preferred conformation can not be presumed by the inspection of their stereomodels alone.

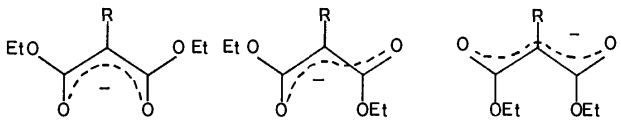

Z,Z *Z,E*(⇌*E,Z*) *E,E*

Table 1 shows the ^{1}H-NMR chemical shifts of diethyl alkylmalonates and their enolate anions in DMSO. The ^{1}H-NMR spectra of the enolates with the alkyl substituents other than the *t*-butyl group can be correlated to one conformation, as has been deduced from their ^{13}C-NMR spectra;[1a] the number of conformers existing in the enolate anion can be determined simply by the inspection of the spectra of the ethoxyl groups. Upon enolate-anion formation, the chemical shifts of the methylene and methyl protons of the ethoxyl groups are shifted to a higher field, $\Delta\delta$ being +0.25—+0.30 and +0.09—+0.15 ppm respectively, while down-field shifts ($\Delta\delta$ −0.31——0.81 ppm) are observed for the β-protons. The alkyl-substituent effects for these $\Delta\delta$ values can not, however, interpreted quantitatively.

On the other hand, the unusual chemical shifts of the enolate anion with a *t*-butyl substituent are very informative in estimating the structures of these enolate-anion series in DMSO. In this enolate anion, the chemical shifts of the methylene protons in ethoxyl groups are observed at 3.44 and 3.98 ppm, where the former is a quartet and the latter consists of two overlapping quartets. This result suggests the existence of three different conformers of the enolate anion in DMSO. In the case of the isopropyl substituent, the quartet

TABLE 1. ^{1}H-NMR CHEMICAL SHIFTS OF DIETHYL ALKYLMALONATES AND THEIR ENOLATES $(CH_3{}_b\text{–}CH_2{}_a\text{–}O\text{–}\overset{\overset{O}{\|}}{C}\text{–})_2\text{–}CH\text{–}R_{\alpha\ \beta.\gamma.\delta.\varepsilon}$

R	Chemical shifts (δ/ppm)						
	a	b	α	β	γ	δ	ε
Hydrogen	4.15[a]	1.20	3.45				
	3.85[b]	1.09	3.66				
	+0.30[c]	+0.11	−0.21				
Methy	4.11	1.19	3.52	1.25			
	3.86	1.10		1.61			
	+0.25	+0.09		−0.36			
Ethyl	4.11	1.20	3.33	1.81	0.90		
	3.86	1.07		2.11	0.82		
	+0.25	+0.13		−0.30	+0.08		
Propyl	4.11	1.19	3.39	1.77		0.89	
	3.85	1.05		2.10		0.75	
	+0.26	+0.14		−0.33		+0.14	
Isopropyl	4.13	1.20	3.36	2.26	0.95		
	3.86[d]	1.06		3.07	1.00		
	+0.27	+0.14		−0.81	−0.05		
Butyl	4.11	1.19	3.38				0.87
	3.85	1.04					0.82
	+0.26	+0.15					+0.05
Isobutyl	4.09	1.18	3.49	1.70		0.88	
	3.84	1.03		2.01		0.75	
	+0.25	+0.15		−0.31		+0.13	
s-Butyl	4.13	1.21	3.28			0.86	
	3.85	1.06				0.70	
	+0.28	+0.15				+0.16	
t-Butyl	4.10	1.16	3.27	1.05			
	3.44 3.98[e]	1.13		1.03			
	+0.66 +0.12	+0.03		+0.02			

a) Parent esters. b) Enolate anions. c) Differences (a—b); a minus sign denotes down-field shift. d) After 24 h, the quartet at 3.86 ppm separated into two signals, at 3.45 (q) and 3.90 (dq) ppm. The integral intensity of the signal at 3.45 ppm was about half of that at 3.90 ppm. e) The ratio of the integral intensity of the signal at 3.44 ppm to that at 3.98 was about 2/3. The signal at 3.98 ppm is a multiplet similar to that at 3.90 ppm of the isopropyl derivative.

signal of methylene protons in the ethoxyl groups appeared at 3.86 ppm immediately after the enolate-anion preparation, but separated into two signals at 3.45 (a quartet) and 3.90 ppm (a double-quartet) after 24 h. This spectral change also suggests a change in the conformational distribution from a single conformational entity to a mixture of three different conformations closely related to the case of the *t*-butyl derivative. The conformational change might be attributable to the bulkiness of an alkyl group at α-carbon, which induces repulsions between the alkyl substituent and the ethoxyl groups.

If the same phenomenon could be observed for the sodium dimethyl alkylmalonate system, more precise information would be obtained, since far more simplified spectra are obtained for methoxyl groups. In practice, the ester-methyl parts of the ^{1}H-NMR spectra of the enolates were found to be in circumstances similar to those of the diethyl-ester system, as is illustrated in Fig. 1. The methoxyl parts of the ^{1}H-NMR spectra of the enolates with isopropyl or *t*-butyl substituents consisted of three singlet peaks with different intensities,

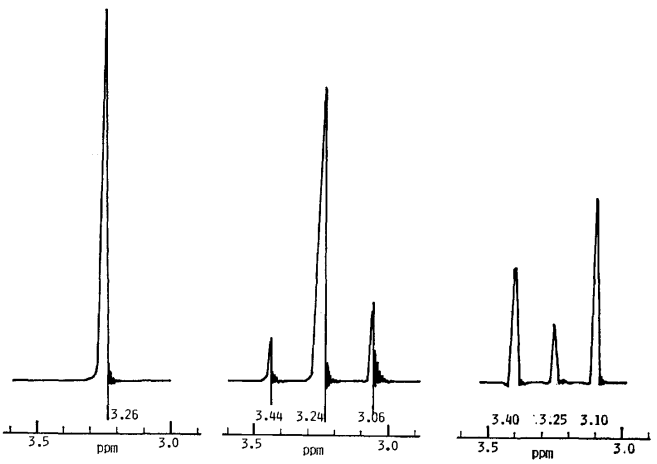

1) Ethyl derivative 2) Isopropyl derivative 3) *t*-Butyl derivative

Fig. 1. The methoxyl parts of the ^{1}H-NMR spectra of sodium enolates derived from dimethyl alkylmalonates in DMSO.

their chemical shifts closely corresponding to each other. On the other hand, only one singlet peak, corresponding to the central peaks of the three peaks described above, was observed in the enolate with an ethyl substituent. Again, in the case of the isopropyl derivative, methoxyl signals other than that at 3.24 ppm did not appear in the spectrum observed immediately after the enolate-anion preparation. The two signals at 3.44 and 3.06 ppm gradually appeared after the solution had been allowed to stand for 24 h at room temperature.

In order to determine the conformation to which the singlet peak in the case of ethyl derivative is to be ascribed, the spectral changes upon the addition of 18-crown-6 were investigated with the enolates of diethyl ethylmalonate, dimethyl isopropylmalonate, and dimethyl *t*-butylmalonate. Though the ^{1}H-NMR signal of 18-crown-6 and that of the lowest-field peak in the three singlet peaks of the enolates overlap each other, the integral intensities of the other two peaks could be measured and compared with those of the α-alkyl moieties. Thus, the intensities of the singlet peak in the ethyl derivative and of the central singlet peaks in the isopropyl and *t*-butyl derivatives were decreased by the addition of 18-crown-6. This spectral change caused by 18-crown-6 is a result of the dissociation of the ion pairs, facilitated by the ability of 18-crown-6 to capture the cation.[5a]

Among the three possible arrangements, the most stable conformation for the non-dissociated ion pairs is thought to be the *Z,Z* type. Zaugg *et al.* have discussed how *Z,E* and *E,E* types are more dissociated than the *Z,Z* type.[8] It has generally been accepted that, in the absence of compelling steric interactions, the *Z,Z* conformers exist only as ion pairs; chelation by the counter-cation is necessary to offset the coulombic repulsions between the two oxygen atoms.[7] The small central peak in the case of the *t*-butyl substituent can also be assigned to the *Z,Z* conformer, while the outer two peaks may be ascribed to the *Z,E* and *E,E* conformers, although their assignment remains to be definitely settled.

Vibrational spectroscopy is useful in estimating the electron density of bonds. Zook *et al.* found that the typical C=O stretching frequency (1710 cm^{-1}) of pinacolone shifts to a much lower region (1575 cm^{-1}) on conversion to its sodium derivative.[3a] A similar lower frequency shift, from 1724 to 1589 cm^{-1}, has also been observed when ethyl phenylacetate was converted to its sodium enolate.[1b]

Table 2 shows the IR absorption frequencies of diethyl alkylmalonates and their sodium enolates in DMSO in the region of 1800—1500 cm^{-1}. These enolate anions have two characteristic absorption bands, except that the *t*-butyl substituent, which has a broad absorption band at 1600 cm^{-1}, presumably because its complex conformational composition is different from those with the other substituents. The enolate anions of β-dicarbonyl compounds have been established to have two absorption bands in this region.[9] Acetylacetone forms a metal chelate, and the chelate ring (*Z,Z* conformation) is planar and symmetrical; the two C=O bonds are equivalent, as are the C=C bonds in the ring. The IR spectra of bis(acetylacetonato)copper(II) showed two bands (1578 and 1527 cm^{-1}) in the carbonyl region; they were assigned to the C=O stretching and C=C=C stretching modes of vibration respectively, on the basis of their ^{13}C isotope shifts; the original 1578 and 1527 cm^{-1} absorptions were found to shift to frequencies lower by 30 and 7 cm^{-1} respectively in the 2,4-$^{13}C_2$ derivative and by 3 and 1 cm^{-1} respectively in the 1,3,5-$^{13}C_3$ derivative.[10]

TABLE 2. IR SPECTRA OF DIETHYL ALKYLMALONATES AND THEIR SODIUM ENOLATES IN DMSO IN THE REGION OF 1800—1500 cm^{-1}

Alkyl	Wave numbers		
	Parent ester	Sodium enolate	
Hydrogen	1732	1679	1556
Methyl	1729	1677	1524
Ethyl	1731	1675	1521
Propyl	1729	1671	1519
Isopropyl	1728	1667	1512
Butyl	1727	1670	1517
Isobutyl	1728	1668	1516
s-Butyl	1732	1665	1509
t-Butyl	1731	1600	

a) The wave numbers were given as the mean values of two split absorptions, which were identified as symmetrically and *anti*-symmetrically coupled vibrations; R. A. Abramovitch, *Can. J. Chem.*, **36**, 151 (1958); **37**, 361 (1959).

TABLE 3. IR SPECTRA OF SODIUM DIETHYL MALONATES LABELED BY ^{13}C AND THE ISOTOPE-SHIFTS VALUES IN THE REGION OF 1700—1500 cm^{-1}

^{12}C Compound	1,3-^{13}C Compound	2-^{13}C Compound
1679	(1659 sh.)	1675 ($\Delta\delta$ 4)
	1640[a] ($\Delta\delta$ 39)	
	1630[a]	
(1564 sh.)		
1556	1519 ($\Delta\delta$ 37)	1552 ($\Delta\delta$ 4)

a) The intensity of the absorption at 1640 cm^{-1} is slightly smaller than that at 1640 cm^{-1}; this may be caused by combination vibrations.

Isotope-labeling experiments were employed to assign the two absorption bands of sodium diethyl malonate. In the IR spectrum of sodium diethyl malonate-1,3-$^{13}C_2$, the absorption bands at 1679 and 1556 cm^{-1} of the ^{12}C compound shifted to a frequency region lower by 39 and 37 cm^{-1} respectively, as is shown in Table 3. On the other hand, the sodium diethyl malonate-2-^{13}C gave only a small isotope shift ($\Delta\delta$ −4 cm^{-1}), which indicated that the C-2 carbon atom participates little in these two vibrations, such as in the case of the β-diketone system. Consequently, the two absorptions of sodium diethyl malonate at 1679 and 1556 cm^{-1} are assigned to vibrations of the C=O and C=C=C bonds respectively.[10] The assignment of the latter is further verified by the examination of the alkyl-substituent effect on the positions of the two absorptions of the sodium

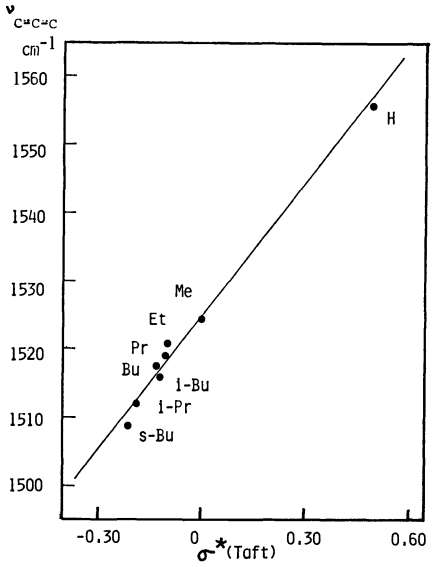

Fig. 2. Correlation of $\nu_{C=C=C}$ (cm^{-1}) in the IR spectra of sodium diethyl alkylmalonates in DMSO to Taft's σ*.

enolate of diethyl alkylmalonates. While the absorptions at higher frequencies of the two remain rather unaffected by the alkyl substituent, those at lower frequencies are nicely correlated ($r=0.994$) to the substituent constants, σ*, as is shown in Fig. 2. The inductive effect of α-alkyl substituents will affect the C=C=C group more intensely than the C=O group, a bond away from the α-carbon.

Experimental

The diethyl and dimethyl esters of alkylmalonic acids were synthesized according to the literature[12] and were identified by elementary analysis and by means of the ^{1}H-NMR spectra. Diethyl malonate-1,3-$^{13}C_2$ and diethyl malonate-2-^{13}C, from the British Oxygen Company, Limited, labeled with 93.0 and 92.0 atom% respectively, were used.

The preparation of enolate anions and the IR and ^{1}H-NMR measurements of them were carried out in a manner similar to that described in a previous report.[1b]

References

1) Previous papers in this series: a) Part 1, S. Kiyooka and K. Suzuki, *Chem. Lett.*, **1975**, 793; b) Part 2, S. Kiyooka, Y. Ueda, and K. Suzuki, *Bull. Chem. Soc. Jpn.*, **53**, 1656 (1980).

2) a) H. E. Zaugg, B. W. Horrom, and S. Borgwardt, *J. Am. Chem. Soc.*, **82**, 2895 (1960); b) G. H. Barlow and H. E. Zaugg, *J. Org. Chem.*, **37**, 2246 (1972).

3) a) H. D. Zook, T. J. Russo, E. F. Ferrand, and D. S. Stotz, *J. Org. Chem.*, **33**, 2223 (1968); b) C. Carvajal, K. J. Tölle, J. Smid, and M. Szwarc, *J. Am. Chem. Soc.*, **87**, 5548 (1965); c) L. L. Chan and J. Smid, *ibid.*, **89**, 4547 (1967); d) H. E. Zaugg, J. F. Ratajczyk, J. E. Leonard, and A. D. Schaefer, *J. Org. Chem.*, **37**, 2249 (1972).

4) "Ions and Ion Pairs in Organic Reactions," ed by M. Szwarc, Wiley, New York (1972), Vol. 1.

5) a) M. Raban, E. A. Noe, and G. Yamamoto, *J. Am. Chem. Soc.*, **99**, 6527 (1977); b) M. Raban and D. P. Haritos, *ibid.*, **101**, 5178 (1979).

6) V. M. DePalma and E. M. Arnett, *J. Am. Chem. Soc.*, **100**, 3514 (1978).

7) a) S. M. Esakov, A. A. Petrow, and B. A. Ershov, *J. Org. Chem., USSR (Eng.)* **11**, 679 (1975); b) A. A. Petrow, S. M. Esakov, and B. A. Ershov, *ibid.*, **12**, 774 (1976).

8) H. E. Zaugg and A. D. Schafer, *J. Am. Chem. Soc.*, **87**, 1857 (1965).

9) K. Nakamoto, "Infrared Spectra of Inorganic and Coordination Compounds," 2nd ed, John Wiley and Sons, (1963). p. 247.

10) H. Musso and H. Junge, *Tetrahedron Lett.*, **1966**, 4003, 4009.

11) a) R. W. Taft, Jr., "Steric Effects in Organic Chemistry," ed by M. S. Newman, John Wiley, New York (1956), p. 619; b) J. A. MacPhee and J. E. Dubois, *Tetrahedron Lett.*, **1978**, 2225; They showed a good correlation between Taft's σ* and the IR carbonyl-group frequency of aliphatic carboxylic acids.

12) a) N. Weiner, *Org. Synth.*, Coll. Vol. II, 279 (1943); b) E. L. Eliel, R. O. Hutchins, and Sr. M. Knoeber, *ibid.*, Vol. 50, 38 (1970); c) R. Adams and R. M. Kamm, *ibid.*, Coll. Vol. I, 250 (1932), p. 250.

Stereochemistry of Nucleophilic Addition Reactions. 10.[1] Preparation of 2-*C*-Diacetylmethyl and 2-*C*-Acetylmethyl Derivatives with the *Altro*, *Gluco*, and *Manno* Configuration from Methyl 4,6-*O*-Benzylidene-2,3-dideoxy-3-nitro-α-D-*erythro*-hex-2-enopyranoside

Tohru SAKAKIBARA,* Akinori SETA, Yoshifusa TACHIMORI, and Rokuro SUDOH

Department of Chemistry, Faculty of Science, Tokyo Institute of Technology, Ookayama, Meguro-ku, Tokyo 152

(Received December 11, 1979)

Reaction of the title compound with acetylacetone in the presence of a catalytic amount of sodium hydroxide afforded the 2-*C*-diacetylmethyl and 2-*C*-acetylmethyl derivatives having the *altro*, *gluco*, and *manno* configurations. The 2-*C*-diacetylmethyl derivative with the *altro* configuration exceptionally exists in a skew boat form. The product ratio depends on solvent and the amount of THF.

The reaction of an α-nitro olefin with active methylene compounds predominantly affords a thermodynamically more stable product, because of its reversible character.[2] However, it has been found that phase transfer catalyzed, heterogeneous reactions of methyl 4,6-*O*-benzylidene-2,3-dideoxy-3-nitro-α-D-*erythro*-hex-2-enopyranoside (**1**) with active methylene compounds give the thermodynamically less stable mannopyranoside in good yields.[3] These results prompted us to investigate a similar reaction in a homogeneous system. In a preliminary communication,[4] we reported the preparation of the altropyranoside **8** from **1** and acetylacetone; in spite of the high tendency of the nitro group to occupy an equatorial orientation in nitro sugars,[5] the nitro group of **8** is orientated axially. Studies have been carried out in order to clarify kinetically controlled protonation. In this paper, we report the preparation of 2-*C*-diacetylmethyl and 2-*C*-acetylmethyl derivatives having the *altro*, *gluco*, and *manno* configuration as well as solvent effects.

Results and Discussion

Treatment of **1** (0.1 mmol) with dimethyl malonate (0.11 mmol) in THF (2 ml) in the presence of 0.05 M (1 M=1 mol dm^{-3}) NaOH (0.2 ml) for 1 h at room temperature resulted in the recovery of **1**, while in the presence of 5.0 M NaOH (0.2 ml) it afforded a complex mixture, from which isolation of the adduct **2** or **3** was unsuccessful. A similar reaction, however, with 0.2 M NaOH (0.1 ml) predominantly afforded the mannopyranoside **2**; similar results were obtained in the reaction with diethyl malonate in the heterogeneous system.[3] A similar reaction of **1** with malononitrile afforded mannopyranoside **4** and glucopyranoside **5** in a 9 : 1 ratio, the highest ratio being 1 : 1.3 in the heterogeneous reaction.[3]

Although in the heterogeneous system the reaction of **1** with acetone resulted in the introduction of a hydroxyl group instead of an acetylmethyl group at the C-2 position, homogeneous reaction afforded the desired

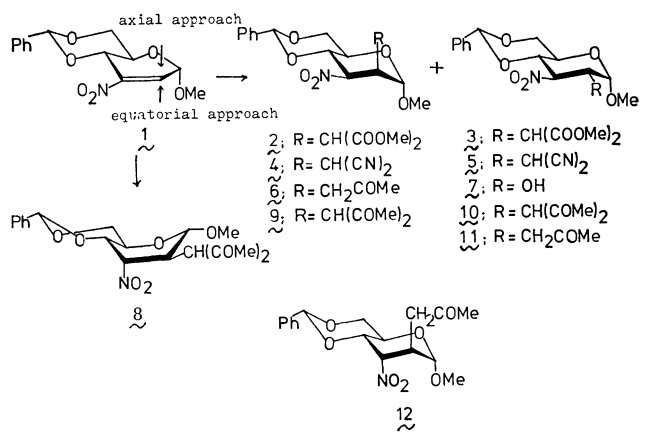

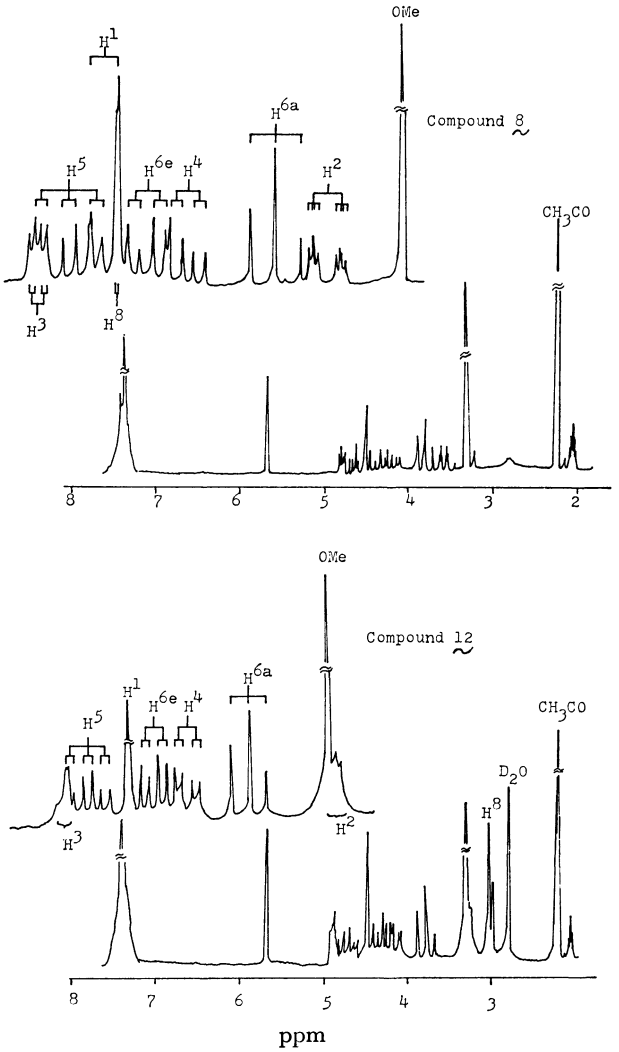

Fig. 1. The NMR spectra of the altropyranoside **8** and **12** (in acetone-d_6, 100 MHz).

TABLE 1. NMR SPECTRA IN $CDCl_3$ (Me_4Si AS INTERNAL STANDARD) AT 100 MHz

Compd	Chemical shifts, δ/ppm						First-order coupling constants, J/Hz				
	H^1	H^2	H^3	H^4	PhCH	H^{8} a)	$J_{1,2}$	$J_{2,3}$	$J_{3,4}$	$J_{4,5}$	$J_{2,8}$
2	4.87	3.56	5.23	?	5.64	~3.86	~1.0	5.2	10.9	?	5.2
3	5.21	3.18	5.27	?	5.56	3.46	3.0	11.0	9.3	?	3.7
8 b)	4.46	3.57	4.70	4.14	5.66	4.40	10.5	2.5	4.5	10.0	1.5
10	4.77	3.36	4.87	4.19	5.56	4.04	3.1	11.9	10.0	10.0	6.5
11	4.91	2.96	4.73	4.17	5.57	2.2—3.0	3.0	11.0	10.0	10.0	?
12	4.47	3.22	4.86	4.13	5.67	2.8—3.0	≤1.0	1.9	4.1	10.0	?

a) Methine or methylene proton(s) of the substituent at C-2. b) Recorded in acetone-d_6.

2-*C*-acetylmethyl derivative **6**, together with a small amount of the nitro alcohol **7**.

Reaction of **1** (0.1 mmol) with acetylacetone (0.15 mmol) in THF (2 ml) in the presence of 0.2 M NaOH (0.1 ml) at 21 °C for 1 h afforded a mixture consisting mainly of the altropyranoside **8** and mannopyranoside **9** in an approximately 4: 1 ratio. These compounds were separated by fractional crystallization. The *altro* configuration with a skew boat form was assigned to **8** by NMR data (Fig. 1). The assignment of signals, carried out by INDOR method, was confirmed by comparison with the spectrum of 3-deuterated derivative of **8**; i) $J_{1,2}$=10.5 Hz indicating the diaxial relationship between H-1 and H-2, ii) $J_{2,3}$=2.5 Hz and $J_{3,4}$=4.5 Hz the equatorial orientation of H-3, and iii) $J_{4,5}$=$J_{5,6a}$= 10 and $J_{5,6e}$=5.0 Hz the benzylidene acetal ring with normal chair conformation.

When dioxane (12 ml) was used as a solvent instead of THF (2 ml), a similar reaction of **1** (20 mg) with acetylacetone afforded predominantly the glucopyranoside **10**, the configuration of which was determined from the coupling constants; $J_{1,2}$=3.1, $J_{2,3}$=11.9, and $J_{3,4}$= 10 Hz.

Treatment of **1** (20 mg) with acetylacetone (10 mg) in THF (1.3 ml) in the presence of 1 M NaOH (0.1 ml) at 21 °C for 1 h afforded a deacetylated product, methyl 2-*C*-acetylmethyl-4,6-*O*-benzylidene-2,3-dideoxy-3-nitro-α-D-mannopyranoside (**6**), in 89% yield. When the reaction was stopped at 15 min, the nitro olefin **1**, mannopyranoside **6**, and altropyranoside **8** were detected in an approximate ratio of 1: 1.2: 14, but only a trace of diacetylmethyl derivative with *manno* configuration **9** was detected by NMR spectroscopy. Under the same conditions, deacetylation of **9** was slow; the ratios of **9** to **6** were 8: 1 and 2.5: 1 after 15 min and 1.5 h, respectively. On the other hand, the altropyranoside **8** was completely converted into **6** within 1.5 h. It is noteworthy that a small amount of **8** was detected during the course of deacetylation of **9**.

A similar treatment of the glucopyranoside **10** with 1 M NaOH for 15 h gave the glucopyranoside **11** in a high yield, structure of which was deduced by coupling constants; $J_{1,2}$=3.0, $J_{2,3}$=11, and $J_{3,4}$=10 Hz. Deacetylation of **10** occurred slowly; the ratios of **10** to **11** were 4: 1 and 1.3: 1 after 40 min and 1.5 h, respectively.

When the mixture of **8** and **9** (*ca.* 5: 1, 200 mg) in THF (2.3 ml) was treated with 0.2 M NaOH (0.7 ml) for 50 h, a complex mixture was formed, from which the mannopyranoside **9** and glucopyranoside **10** were isolated in 75 and 12.5% yield, respectively. In addition to these compounds, a small amount of a new compound **12** was isolated. Elemental analysis and the NMR spectrum show that it was a 2-*C*-acetylmethyl derivative. The possibility of **12** being *allo* configuration was chemically excluded; treatment of **12** with 0.2 M NaOD in acetone-d_6 exclusively afforded the C-3 deuterated derivative of the mannopyranoside **6**.[6] Thus, compound **12** should be the altropyranoside; appearance of the H-5 signal at a low field (δ 4.72) as that of **8** (δ 4.60)[7] supports the axial orientation of the nitro group. However, in contrast to the case of **8**, the NMR data strongly suggest that it has the chair conformation;[8] $J_{1,2}\leq$1.0, $J_{2,3}$=1.9, $J_{3,4}$=4.1, $J_{4,5}$=$J_{5,6a}$=10, and $J_{5,6e}$=5.0 Hz (Fig. 1). The reason why compound **8** has a skew boat conformation and compound **12** a chair conformation is not clear. If such assignments were correct, compound **12**, having unfavorable 1,3-diaxial interaction between the nitro and methoxyl group, should be less stable than compound **8**. In fact epimerization of **12** to the mannopyranoside **6** occurred more readily than that of **8** to **9**.

In these reactions no evidence for formation of the allopyranoside was obtained. Attempts for epimerization of the glucopyranoside **10** with 1 M NaOH or sodium hydride in THF failed, only glucopyranosides **10** and **11** being detected.

Re-examination of phase transfer catalyzed, heterogeneous reaction of **1** (benzene–0.2 M NaOH) with acetylacetone showed the formation of a trace of altropyranoside **8** besides the mannopyranoside **9** (main product). In the heterogeneous system, about half the amount of **8** epimerized to **9** within 2 min. In the homogeneous system the epimerization was much slower.

This seems to be the first example to isolate the kinetically controlled product of not only the addition of nucleophile but also the following protonation, in the Michael reaction of nitro olefin derivatives. Then we have studied the reaction in detail and found two remarkable solvent effects.

As seen from Table 2, the relative ratios of the altropyranoside **8** to the mannopyranoside **9** increase with an increase in the amount of THF or acetone. Nearly equal amounts of **8** and **9** are formed, when 0.3 ml of THF is used (Entry 1), whereas a 4.2: 1 ratio is obtained for 3 ml of THF (7). From the fact that all of **9** and most of **8** were recovered under the same conditions (2 and 3), the formation of nearly equal

TABLE 2. EFFECTS OF AMOUNT OF THF OR ACETONE IN THE REACTION OF **1** WITH ACETYLACETONE[a)]

Entry	Starting material	Solvent (ml)	Reaction time/min	Product ratio[b)] **1** : **8** : **9** : **10**
1	**1**	THF(0.3)	10	— : 1 : 1 : —
2	**8**[c)]	THF(0.3)	10	— : 9 : 1 : —
3	**9**[c)]	THF(0.3)	10	— : — : 1 : —
4	**1**	THF(0.8)	30	1.7 : 2.2 : 1 : —
5	**1**	THF(1.3)	10	2.3 : 3.4 : 1 : t
6	**1**	THF(2.0)	30	1 : 3.8 : 1 : t
7	**1**	THF(3.0)	30	0.8 : 4.2 : 1 : 0.8
8	**1**	THF(6.0)	60	0.8 : 3.1 : 1 : 1.5
9	**1**	THF(6.0)+H_2O(0.03)	40	3.2 : 5.7 : 1 : t
10	**1**	THF(6.0)+H_2O(0.03)	180	— : 2 : 1 : t
11	**8**[c,d)]	THF(6.0)	60	— : 5[e)] : 1[e)] : —
12	**9**[c,d)]	THF(6.0)	60	— : — : 1 : —
13	**1**	THF(12)	60	t : 3 : 1 : 3.3
14	**1**	THF(12)	140	t : 1.2 : 1 : 1.8
15	**1**[f)]	THF(12)	240	1 : 3 : 1 : 7
16	**1**	Acetone(0.3)	10	— : 1.3 : 1 : —
17	**1**	Acetone(1.3)	10	0.4 : 2.9 : 1 : —
18	**1**	Acetone(3.0)	10	0.7 : 3.2 : 1 : —

a) A solution of the nitro olefin **1** (20 mg, 0.068 mmol) in the solvent indicated was stirred at 21 °C with acetylacetone (10 mg, 0.1 mmol) in the presence of 0.2 M NaOH (0.1 ml). b) Determined by NMR spectroscopy: —, product not detected; t, trace. c) Twenty-six mg (0.066 mmol) of starting material used. The same results were obtained in the absence of acetylacetone. d) Instead of 0.2 M NaOH, 0.2 M NaOD used. e) The C-3 position completely deuterated. f) Amount of sodium hydroxide (0.2 M) reduced to 0.03 ml.

amounts of **8** and **9** reflected, at least mostly, kineticall controlled reaction. Treatment of **9** with 0.2 M NaOD for 1 h at 21 °C gave undeuterated **9**, whereas the same treatment of **8** afforded a mixture of **8** and **9** in a 5: 1 ratio, where the C-3 position of both compounds was completely deuterated. This suggests that the protonation at C-3 of the intermediary nitronate derived from **8** is more favorable from the face *cis* to the C-2 substituent, giving the altropyranoside **8**.

Epimerization of **8** to **9** in acetone-d_6 in the presence of 0.2 M NaOD was monitored by NMR spectroscopy. As shown in Fig. 2, epimerization of the mannopyranoside **9** to the altropyranoside **8** occurred more slowly than that of **8** to **9**.

The proportion of axial and equatorial approach of the nucleophile to the nitro olefin **1** varies with solvent. In such a polar solvent as DMSO and acetone, no glucopyranoside **10** was detected, whereas in a less polar solvent such as dioxane, **10** became the major product. Under the conditions for formation of **10** (23), epimerization of **8** or **9** to **10** was negligible as judged from NMR spectroscopy. When the amount of dioxane was decreased to 1.3 ml or a small amount of water was added, the ratio of **10** considerably decreased (Table 3).

A similar but not conspicuous trend was observed in

TABLE 3. REACTION OF **1** WITH ACETYLACETONE IN VARIOUS SOLVENTS[a)]

Entry	Solvent (ml)	Reaction time	Product ratio[b)] **1** : **8** : **9** : **10**
19	DMSO(12)	1h	— : 1 : 2.6 : —
20	Acetone(12)	1h	— : 1 : 1 : —
21	Acetone(12)	2h	— : 1 : 4 : —
22	THF(12)	1h	— : 3 : 1 : 3.3
23	Dioxane (12)	1h	— : 1 : 2 : 13
24	Dioxane (12)+H_2O(0.3)	3h 40 min	t : 1 : t : 1.4
25	Dioxane (1.3)	30 min	— : 4.2 : 1 : 1.2
26	Diethyl ether (12)	3h 20 min	2.5 : 2 : 1 : 3.7
27	Isopropyl alcohol(1.3)	10 min	8 : 2 : 1 : —
28	Benzene (6)[c)]	1h	2 : t : 3.5 : 1
29	Benzene (6)[d)]	10 min	— : 1 : 8 : t

a) The nitro olefin (20 mg, 0.068 mmol) was treated with acetylacetone (10 mg, 0.1 mmol) in the presence of 0.2 M NaOH (0.1 ml) at 21 °C with stirring. b) Determined by NMR spectro scopy: —, product not detected; t, trace. c) Powdered KOH (13 mg) used instead of 0.2 M NaOH. d) Crushed KOH (*ca.* 3 mg) used instead of 0.2 M NaOH in the presence of 18-crown-6 (5 mg).

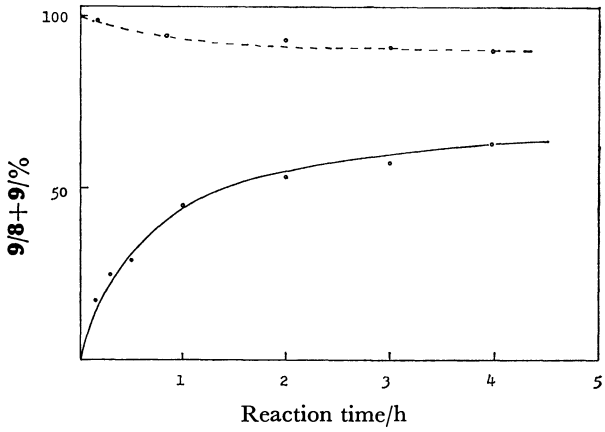

Fig. 2. Epimerization of **8** and **9**.
Compounds **8** and **9** (26 mg, each, 0.66 mmol) in acetone-d_6 (0.25 ml) were treated with 0.2 M NaOD (0.05 ml) in an NMR sample tube at *ca.* 21 °C, and the product ratios were calculated on the basis of integration of the signals due to the benzylidene methine proton at δ 5.78 (**9**) and 5.72 (**8**) and methoxyl group at δ 3.40 (**9**) and 3.30 (**8**). ——: from **8**, ------: from **9**.

Table 4. Reaction of **1** with dimethyl malonate in various solvents[a]

Solvent (ml)	Reaction time	Product ratio[b] 1 : 2 : 3
DMF(12)	2h 40 min	— : 1 : —
Acetone(12)	2h 40 min	— : 1 : —
THF(12)	2h 40 min	— : 10 : 1
THF(6.0)	2h 40 min	— : 15 : 1
THF(0.3)	45 min	— : 1 : —
Dioxane(12)	2h 40 min	1.1 : 1.5 : 1

a) A solution of **1** (20 mg, 0.068 mmol) in the solvent indicated was stirred at 21 °C with dimethyl malonate (13.2 mg, 0.1 mmol) in the presence of 0.2 M NaOH (0.1 ml). b) Determined by NMR spectroscopy; —, product not detected.

the reaction of **1** with dimethyl malonate (Table 4).

In the nucleophilic addition reaction to **1**, previous examples always showed a favorable axial approach under kinetically controlled conditions. This was explained in terms of steric hindrance and stereoelectronic control.[9] However, predominant equatorial approach in less polar medium is not explained in terms of these factors. Abramovitch and Struble found that such a bulky nucleophile as anion of diethyl malonate exceptionally approaches from the equatorial side of 4-*t*-butyl-1-cyanocyclohexene[10] and ethyl 4-*t*-butylcyclohexene-1-carboxylate.[11] They explained the results on the basis of 1,3-interaction between the axial hydrogen atom and an approaching nucleophile. The explanation is not applicable to the present reaction; steric hindrance due to the methoxyl group is apparently more serious than that due to the lone pair on the ring oxygen atom.

Experimental

Melting points were determined in capillaries and are uncorrected. IR spectra were recorded for KBr discs and NMR spectra were determined in chloroform-*d* and/or acetone-d_6 with tetramethylsilane as an internal standard on either a Varian XL-100-15 or a JEOL-PS-100 spectrometer. Column chromatography was carried out on silica gel (C-300, Wakogel). TLC was performed using Merck (Darmstadt) silica gel GF 254. Solutions were concentrated under reduced pressure.

Methyl 4,6-O-Benzylidene-2,3-dideoxy-2-C-[bis(methoxycarbonyl)-methyl]-3-nitro-α-D-mannopyranoside (2). To a solution of **1**[12] (29.3 mg, 0.1 mmol) and dimethyl malonate (13.8 mg, 0.11 mmol) in THF (2 ml) was added 0.2 M NaOH (0.1 ml) at 21 °C. The mixture was stirred for 2 h and then deionized with cation exchange resin (Amberlite IR-120, H^+). After removal of the resin, the filtrate was concentrated to yield a syrup (42 mg), its NMR spectrum showing it to be almost pure **2**. The syrup (42 +40 mg) was chromatographed on silica gel eluted with benzene–ethyl acetate (20 : 1, v/v) to afford 70 mg of **2** (82%), $[\alpha]_D^{31}$ −30.2° (*c* 1, $CHCl_3$); IR 1750, 1740 (COOMe), and 1560 cm^{-1} (NO_2).

Found: C, 54.02; H, 5.62; N, 3.01%. Calcd for $C_{19}H_{23}NO_{10}$: C, 53.64; H, 5.45; N, 3.29%.

Methyl 4,6-O-Benzylidene-2,3-dideoxy-2-C-[bis(methoxycarbonyl)-methyl]-3-nitro-α-D-glucopyranoside (3). To a solution of **1** (60 mg, *ca.* 0.2 mmol) and dimethyl malonate (42 mg, 0.32 mmol) in dioxane (36 ml) was added 0.2 M NaOH (0.3 ml) at 21 °C, and the mixture was stirred for 6 h. Similar work-up to that for **2** afforded a residue consisting of **2** and **3** in a 1.5: 1 ratio as shown by NMR spectroscopy. The residue (85 +87 mg) was chromatographed on silica gel eluted with benzene–ethyl acetate (20: 1, v/v). The fast running fraction was 83.5 mg of **2** (48%), which was found to be identical with an authentic sample by NMR spectroscopy. The slow running fraction was 57 mg of **3**, which was recrystallized from ethanol to give 52.2 mg of **3** (30%), mp 133—134 °C; $[\alpha]_D^{22}$ +126° (*c* 1, $CHCl_3$); IR 1742, 1722 (COOMe), and 1558 cm^{-1} (NO_2).

Found: C, 53.86; H, 5.50; N, 3.26%. Calcd for $C_{19}H_{23}NO_{10}$: C, 53.64; H, 5.45; N, 3.29%.

Methyl 4,6-O-Benzylidene-2-C-dicyanomethyl-2,3-dideoxy-3-nitro-α-D-mannopyranoside (4). To a solution of **1** (29.3 mg) and malononitrile (7.9 mg, 0.12 mmol) in THF (2 ml) was added 0.2 M NaOH (0.1 ml). The mixture was stirred for 2 h and deionized in a similar way to that for **2**. After removal of the resin, the filtrate was concentrated to give a syrup (34 mg), NMR spectrum of which revealed the presence of **4** and **5** in a ratio of 9 : 1. The same reaction was performed three more times and the combined residue was chromatographed on silica gel.[3] The mannopyranoside **4** and the glucopyranoside **5** isolated were identical with respective authentic samples in IR and NMR spectra.

Methyl 2-C-Acetylmethyl-4,6-O-benzylidene-2,3-dideoxy-3-nitro-α-D-mannopyranoside (6). To a solution of **1** (29.3 mg) in acetone (2 ml) was added 1 M NaOH (0.2 ml) at 21 °C. The mixture was stirred for 2 h and subjected to a similar work-up to that for **2**, giving a residue (32 mg). Recrystallization of the residue (32 +30 mg) from ethanol afforded 53 mg of **6** (75%), which was identical with an authentic sample by IR and NMR spectroscopy.[3]

The mother liquor mainly consists of **11** and 3-nitro alcohol **7**, as judged from NMR spectroscopy and TLC.

A similar reaction of **1** (20 mg, 0.068 mmol) with acetylacetone (10 mg, 0.1 mmol) in THF (1.3 ml) in the presence of 1 M NaOH (0.1 ml) at 21 °C for 1 h afforded a residue (24 mg). Recrystallization of the residue (24 +26 mg) from ethanol gave 47.7mg of **6** (89%).

Methyl 4,6-O-Benzylidene-2-C-diacetylmethyl-2,3-dideoxy-3-nitro-α-D-altropyranoside (8). To a solution of **1** (29.3

mg) and acetylacetone (15 mg, 0.15 mmol) in THF (2 ml) was added 0.2 M NaOH (0.1 ml) at 21 °C. The mixture was stirred for 20 min and then deionized with cation exchange resin. After removal of the resin, the filtrate was concentrated to give a white powder (36 mg). The powder (36 +35 mg) was recrystallized from isopropyl alcohol to give 55.8 mg of **8** (71%), mp 163—164 °C; $[\alpha]_D^{22}$ +26.8° (*c* 1, acetone); IR 1725, 1700 (CO), and 1555 cm^{-1} (NO_2).

Found: C, 57.91; H, 5.87; N, 3.62%. Calcd for $C_{19}H_{23}NO_8$: C, 58.01; H, 5.89; N, 3.56%.

The mother liquor mainly consists of the mannopyranoside **9**, which was isolated as a second crop (10.2 mg, 13%).

Methyl 4,6-O-Benzylidene-2-C-diacetylmethyl-2,3-dideoxy-3-nitro-α-D-glucopyranoside (10). To a solution of **1** (20 mg, 0.068 mmol) and acetylacetone (10 mg, 0.1 mmol) in dioxane (12 ml) was added 0.2 M NaOH (0.1 ml) at 21 °C. After the solution had been stirred for 1 h, the mixture was treated in a similar way to that for **8**, giving a crystalline residue. The same reaction was carried out two more times and the combined residues were recrystallized from ethanol to afford 60 mg of **10** (75%), mp 198—199 °C; $[\alpha]_D^{22}$ +30.2° (*c* 0.5, DMSO); IR 1730, 1700 (CO), and 1555 cm^{-1} (NO_2).

Found: C, 57.74; H, 5.88; N, 3.72%. Calcd for $C_{19}H_{23}NO_8$: C, 58.01; H, 5.89; N, 3.56%.

Methyl 2-C-Acetylmethyl-4,6-O-benzylidene-2,3-dideoxy-3-nitro-α-D-glucopyranoside (11). To a solution of **10** (26 mg, 0.066 mmol) in THF (1.3 ml) was added 1 M NaOH (0.1 ml) at 21 °C. The mixture was stirred for 15 h and deionized in a similar way to that for **8**. After removal of the resin, the filtrate was concentrated to give a pure powder by NMR spectroscopy. Recrystallization from ethanol afforded 21 mg of **11** (91%), mp 187—188 °C; $[\alpha]_D^{22}$ +84.3° (*c* 0.5, $CHCl_3$); IR 1710 (CO) and 1545 cm^{-1} (NO_2).

Found: C, 57.95; H, 6.00; N, 4.02%. Calcd for $C_{17}H_{21}NO_7$: C, 58.11; H, 6.02; N, 3.99%.

Methyl 2-C-Acetylmethyl-4,6-O-benzylidene-2,3-dideoxy-3-nitro-α-D-altropyranoside (12). A mixture of **8** and **9** (in a ratio of *ca.* 5: 1, 200 mg, 0.51 mmol) was dissolved in THF (2.3 ml). To this solution was added 0.2 M NaOH (0.7 ml). The resulting solution was stirred at 21 °C for 50 h and worked up in a similar way to that for **8**, affording a powder. Recrystallization from ethanol gave 150 mg (75%) of platelet crystals of **9** as the first crop, 25 mg (12.5%) of needles of **10** as the second crop, and 23 mg of granular crystals as the third crop. A small amount of chloroform was added to the last crystals and the insoluble material was filtered and recrystallized from ethanol to give 10 mg of **12** as needles (5.6%), mp 204—205 °C; $[\alpha]_D^{22}$ +15.4° (*c* 0.5, acetone); IR 1717 (CO) and 1560 cm^{-1} (NO_2).

Found: C, 58.39; H, 6.00; N, 4.05%. Calcd for $C_{17}H_{21}NO_7$: C, 58.11; H, 6.02; N, 3.99%.

Attempts for Epimerization of 10. To a solution of **10** (26 mg, 0.066 mmol) in THF (1.3 ml) was added *ca.* two equiv NaH (6.4 mg, purity *ca.* 50%) at 21 °C. The mixture was stirred for 1.5 h and worked up in a similar way used for **8** to give a residue, NMR spectrum of which showed the presence of **11** and **10** in a ratio of 2 : 1, but no evidence for formation of the allopyranoside.

A similar treatment of **10** (26 mg) with 1 M NaOH (0.1 ml) in THF (1.3 ml) at 21 °C for 1.5 h also gave a mixture of **11** and **10** in a 1: 1.3 ratio. No evidence was again obtained for formation of the allopyranoside.

Epimerization of 12 to 6. To an acetone-d_6 solution of **12** (13 mg, 0.033 mmol) was added 0.2 M NaOD (0.05 ml). Within 20 min, **12** was completely epimerized to give the 3-deuterated derivative of **6**, the C-2 position of which was not deuterated.

Under the same conditions, epimerization of the altropyranoside **8** was much slower; even after 45 min *ca.* 16% of **8** was epimerized to the mannopyranoside **9**, revealing that compound **12** is much less stable than **8**.

References

1) Part 9 of this series; T. Sakakibara and R. Sudoh, *Carbohydr. Res.*, in press.

2) In general, the Michael reaction is reversible, *e.g.*, H. O. House, "Modern Synthetic Reactions," 2nd ed, W. A. Benjamin, Inc., California (1972), pp. 595—623.

3) T. Sakakibara and R. Sudoh, *J. Org. Chem.*, **40**, 2823 (1975).

4) T. Sakakibara, A. Seta, Y. Tachimori, T. Takamoto, and R. Sudoh, *Chem. Lett.*, **1977**, 1365; presented in part, at the ACS/CSJ Chemical Congress, Honolulu, Hawaii, 1979. Abstract Carbohydr. 74.

5) T. Takamoto, T. Sakakibara, and R. Sudoh, *Yuuki Gosei Kagaku Kyokai Shi*, **36**, 277 (1978); H. H. Baer, *Adv. Carbohydr. Chem. Biochem.*, **24**, 67 (1969).

6) If the epimerization occurred *via* the nitro olefin intermediate, the possibility of **12** as being an allopyranoside was not excluded. However, this is not likely since no acetylmethyl group of the product was completely deuterated, *i.e.*, this group did not come from the solvent, and the nitro alcohol **7**, formed (**6** : **7**=3 : 1) by the reaction of the nitro olefin **1** with acetone-d_6 under the same conditions, was not detected by NMR spectroscopy.

7) The H-5 signal of 3-nitro sugar with the *gluco* and *manno* configuration resonated at around δ 3.6.

8) A strongly distorted chair conformation like $^4H_5$ form is also possible from the NMR data.

9) T. Sakakibara and R. Sudoh, *J. Org. Chem.*, **42**, 1746 (1977), and references cited therein.

10) R. A. Abranovitch and D. L. Struble, *Tetrahedron*, **24**, 357 (1968).

11) R. A. Abramovitch, S. S. Singer, M. M. Rogić, and D. L. Struble, *J. Org. Chem.*, **40**, 34 (1975).

12) H. H. Baer and F. Kienzle, *Can. J. Chem.*, **45**, 983 (1967).

Synthesis of *dl*-12,15-Ethylene-13,14-dihydro-prostaglandin-$F_{2\alpha}$ Methyl Ester

Nobuyuki HAMANAKA,* Hisao NAKAI, and Masayasu KURONO

Ono Pharmaceutical Co., Ltd., Research Institute, 3-1-1, Sakurai, Shimamoto-cho, Mishima-gun, Osaka 618

(Received January 10, 1980)

A report is given on the synthesis of a spiro prostaglandin analog *via* triketone obtained by the double Michael addition of 1,3-cyclopentanedione to 1,4-pentadien-3-one.

Prostaglandin (PG) is a highly active autacoid which might act as a mediator in many physiological activities.[1] The synthesis of 12-methyl[2] and that of 15-methyl PGs[3] have been described in investigations carried out to find stable PG analogs having higher biological activities than natural PG. In the present report we describe the synthesis of a spiro PG analog in which an ethylene linkage is introduced between the C-12 and C-15 positions, Δ^{13}-double bond being saturated.

The starting bicyclic triketone **3** was obtained as follows. The sodium salt of 1,3-cyclopentanedione was treated with 1,4-pentadien-3-one (1 equiv, −40 °C, 4 h, then −20 °C, 1.5 h) to afford the intermediate anion **2**. Cyclization of **2**, which rapidly polymerized during the course of isolation, was accomplished by treatment *in situ* with AcOH (5 equiv, −20 °C, 20 h) to give the bicyclic triketone **3**[4] in 56% yield on the basis of 1,3-cyclopentanedione. Selective protection of the C-8 carbonyl group in six-membered ring of **3** with ethylene glycol (1 equiv, TsOH, benzene, reflux, 30 min) afforded monoacetal **4** quantitatively. Dehydrogenation of **4** with SeO_2 in dioxane (92—93 °C, 20 h) gave 1,3-cyclopentanedione **5** in 88% yield. Addition of two carbon units (corresponding to C-6 and C-7 of PG) was achieved by treatment of **5** with $LiCH_2COOBu^t$[5] in benzene (1.2 equiv, 25 °C, 30 min) to give hydroxy ester **6** in 79% yield. Treatment of **6** with $SOCl_2$ (4.4 equiv)–pyridine (5.6 equiv) in CH_2Cl_2 at −40 °C for 30 min gave the deconjugated α-chloro ketone **7** quantitatively. Reductive dechlorination of **7** with Zn–CH_3OH (40—43 °C, 3.5 h) gave the conjugated ketone **9** in 84% yield. Treatment of **9** with TsOH in toluene gave unstable lactone **10** which was directly reduced with *i*-Bu_2AlH in toluene (−70 °C, 5 min) to give the hydroxy hemiacetal **11** in 77% yield on the basis of **9**. Condensation of **11** with $Ph_3P{=}CH(CH_2)_3COONa$ (9.5 equiv) in DMSO (34 °C, 75 h) followed by esterification with CH_2N_2 gave methyl ester **13** in 50% yield. Geometry of the two hydroxyl groups of **13** was confirmed by lanthanoid induced ^1H NMR shifts (Fig. 1). Since the proton signals at C-9 and C-11 of **13** showed the same gradient while two protons of C-10 showed different gradients, 9- and 11-hydroxyl groups of **13** are *cis* as expected from the synthetic route of **13**. Compound **13** was deprotected with TsOH–acetone (reflux, 2 h) to give **14** quantitatively. The α-chain was introduced by treatment of **14** with *n*-$C_5H_{11}MgBr$ to give the desired *dl*-12,15-ethylene-13,14-dihydro-$PGF_{2\alpha}$ methyl ester **1** in 60% yield. Treatment of **1** with AcOH (50 °C, 2 h) exclusively gave **15** possessing exocyclic double bond [*m/e* 378 (M^+), 335 ($M^+-C_3H_7$)]. *m/e* 321 ($M^+-C_4H_9$) was not observed among fragment ion peaks of **15**. This suggests that the hydroxyl group of C-15 occupies an equatorial position, and **18**

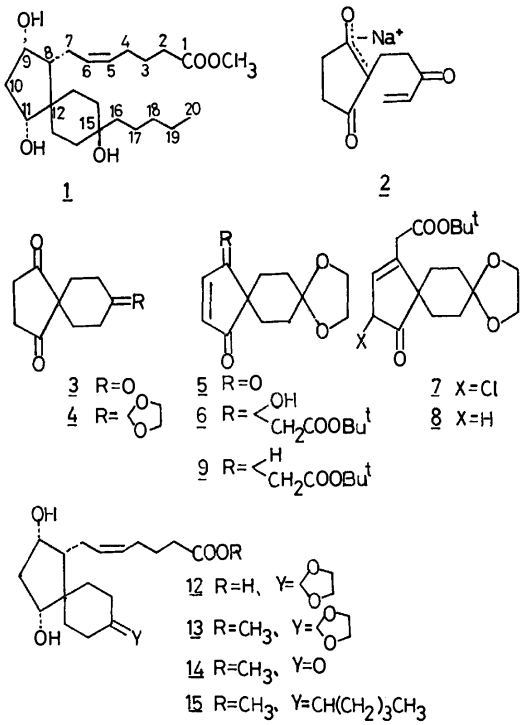

Scheme 1.

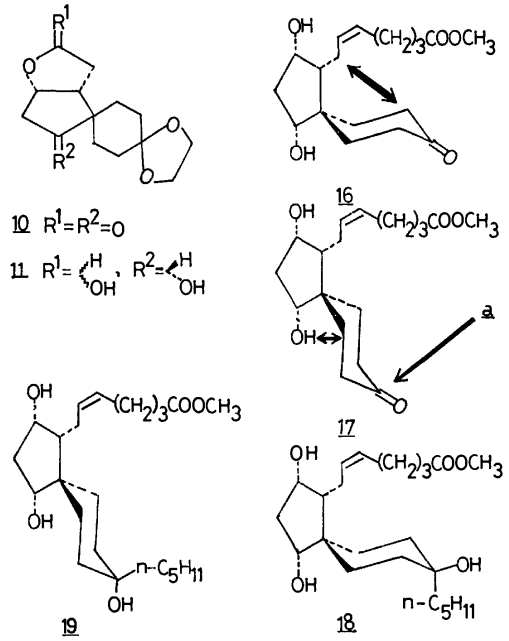

Scheme 2.

TABLE 1. SPECTRAL DATA OF NEW COMPOUNDS

Compound	Mp/°C	IR cm^{-1} ($CHCl_3$)	NMR δ ($CDCl_3$)
1	oil	3400, 1735	5.43(2H, m), 4.22(1H, m)
3	98—100(AcOEt-Et_2O)[a]	1755, 1720, 1715	2.01(4H, t, J=7.2Hz), 2.61(4H, t, J=7.2Hz)
4	100—101 (Et_2O)[a]	1760, 1721	1.84(8H, bs), 2.28(4H, s), 3.95(4H, s)
5	129—130 (Et_2O)[a]	1750, 1710	1.70—2.65(8H, A_2B_2), 3.97(4H, s),7.15(2H, s)
6	80—81.5 (i-Pr_2O)[a]	3480, 1725, 1600	2.34 and 2.69 (each 1H, AB, J=15 Hz), 6.09 and 7.39 (each 1H, d, J=5.0 Hz), 1.50(9H,bs)
7	oil	1755, 1725	6.14(1H, m), 4.70(1H, m), 3.06(2H, m), 1.50(9H, bs)
8	oil	1735	5.95(1H, m), 2.94(2H, m), 1.50(9H, bs)
9	81—83 (i-Pr_2O)[a]	1725, 1710, 1600	6.06(1H, quart, J=1.8, 6.0 Hz), 7.58(1H, quart, J=2.5, 6.0 Hz), 1.50 (9H, bs)
10	137—140 (i-Pr_2O)[a]	1780, 1735, 3500	5.18(1H, m)
11	oil	3500	5.02(1H, bt, J=5.0Hz), 4.65(1H, m)
12	oil	1710	
13	oil	3500, 1730	5.38(2H, m), 4.15(2H, m), 3.92(4H, s), 3.67(3H, s)
14	oil	3500, 1730, 1710	5.40(2H, m),4.20(2H, m) 3.70(3H, s)

a) Recrystallization solvents.

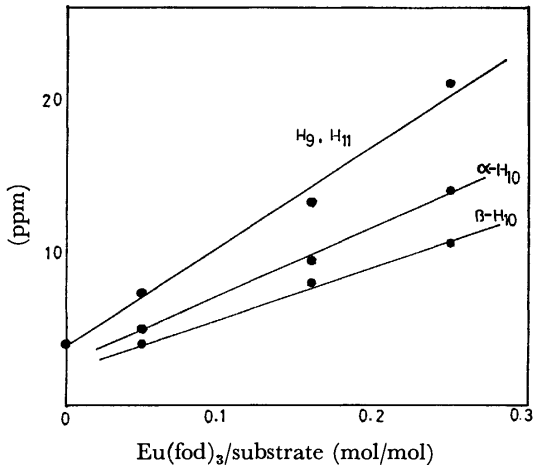

Fig. 1. Lanthanoid induced ^{1}H-NMR shifts of **13**.

or **19** are the possible stereoisomers of **1**. We tentatively assigned the stereochemistry of **1** to **19** on the basis of the following. i) Conformer **17** is more stable as compared with **16**, the steric repulsions between the C-11 OH and six-membered ring of **17** being less than those between α-chain carbons and the six-membered ring of **16**; ii) Axial attack of Grignard reagent to the six-membered cyclic ketone **17** favors approach from axis a.

After intravenous administration, PG analog **1** showed no effect on uterine contractile activity in a pregnant rat at a dose of 200 γ/kg or on blood pressure in rabbit and dog at a dose of 50 γ/kg.

Experimental

General. Melting and boiling points are uncorrected. ^{1}H-NMR spectra were recorded on a Varian XL-100 spectrometer with Me_4Si as an internal standard, and IR spectra on a Hitachi EPI-G2 spectrophotometer. MS data were obtained on a JEOL JMS-01 SG at 75 eV.

Spiro[4.5]decane-1,4,8-trione (3). To a suspension of 230 mg (10.0 mmol) of NaH in DMF (90 ml) was added 980 mg (10.0 mmol) of 1,3-cyclopentanedione at −35 °C over a period of 10 min. To the resulting mixture was added a solution of 820 mg (10.0 mmol) of 1,4-pentadien-3-one in DMF (10 ml) at −35 °C over a period of 5 min. The resulting solution was allowed to stand at −35 °C for 4 h, then at −20 °C for 1.5 h and then treated with AcOH (3 ml) at −20 °C for 20 h. The reaction mixture was poured into 1 mol dm^{-3} HCl (300 ml) and extracted with CH_2Cl_2. The organic layer was washed with H_2O and dried (Na_2SO_4). After removal of the solvent, the residue obtained was purified by column chromatography on silica gel using a mixture of benzene and AcOEt as an eluent to afford 1.01 g (56%) of **3** as colorless crystals; MS *m/e* 180 (M^+).

8,8-(Ethylenedioxy)spiro[4.5]decane-1,4-dione (4). A mixture of 100 mg (0.556 mmol) of triketone **3**, 34.5 mg (0.556 mmol) of ethylene glycol, 1 mg of TsOH and benzene (5 ml) was refluxed for 1 h. The resulting mixture was diluted with benzene (20 ml) and was shaken with saturated aqueous $NaHCO_3$ solution. The organic layer was dried ($MgSO_4$) and evaporated *in vacuo* to afford 125 mg (100%) of **4** as colorless crystals; MS *m/e* 224 (M^+).

8,8-(Ethylenedioxy)sprio[4.5]dec-2-ene-1,4-dione (5). A solution of 70 mg (0.312 mmol) of monoacetal **4** in dioxane (2 ml) was treated with 35 mg (0.315 mmol) of SeO_2 at 92—93 °C for 20 h. The resulting mixture was diluted with AcOEt (15 ml) and washed with H_2O and saturated aqueous $NaHCO_3$ solution. The organic layer was dried ($MgSO_4$) and evaporated under reduced pressure to afford 82 mg of oily residue which was purified by column chromatography on silica gel using Et_2O as an eluent to afford 61 mg (88%) of **5** as colorless crystals; MS *m/e* 222 (M^+).

1-(t-Butoxycarbonylmethyl)-1-hydroxy-8,8-(ethylenedioxy)spiro-[4.5]dec-2-en-4-one (6). To a stirred solution of 30 mg (0.135 mmol) of **5** in benzene (1 ml) was added dropwise a solution of 20 mg (0.164 mmol) of $LiCH_2COOBu^t$ in benzene (2 ml) at 0 °C over a period of 30 min. The resulting solution was diluted with benzene (20 ml) and washed with water and dried ($MgSO_4$). After removal of the solvent under reduced pressure, the residue obtained was purified by thin layer chromatography on silica gel using Et_2O as a developing solvent to afford 36 mg (79%) of **6** as colorless crystals; MS *m/e* 338.1707 (Calcd for $C_{18}H_{26}O_6$: 338.1729).

1-(t-Butoxycarbonylmethyl)-3-chloro-8,8-(ethylenedioxy)spiro[4.5]-dec-1-en-4-one (7). To a stirred solution of 150 mg (0.443 mmol) of **6** in CH_2Cl_2 (1 ml) were added dropwise a solution of 155 mg (1.96 mmol) of $SOCl_2$ in CH_2Cl_2 (7 ml)

and then a solution of 195 mg (2.45 mmol) of pyridine in CH_2Cl_2 (7 ml) at −40 °C over a period of 30 min. The resulting mixture was diluted with CH_2Cl_2 (20 ml) and washed with H_2O, dried (Na_2SO_4) and evaporated under reduced pressure to afford an oily residue which was purified by thin layer chromatography on silica gel using Et_2O as a developing solvent to give 151 mg (100%) of **7** as an oil; MS *m/e* 356.1376 (Calcd for $C_{13}H_{25}O_5Cl$: 356.1390).

1-(t-Butoxycarbonylmethyl)-8,8-(ethylenedioxy)spiro[4.5]dec-1-en-4-one (8). A solution of 580 mg (1.63 mmol) of **7** in MeOH (25 ml) was treated with 4.00 g (61.2 mmol) of Zn dust at 60 °C for 2 h. After removal of the Zn dust by filtration, the filtrate was evaporated. The resulting residue was extracted with CH_2Cl_2. The organic layer was washed with H_2O, dried (Na_2SO_4) and evaporated. Purification of the residue by column chromatography on silica gel using Et_2O as an eluent afforded 520 mg (100%) of **8** as an oil; MS *m/e* 322.1780 (Calcd for $C_{18}H_{26}O_5$: 322.1780).

1-(t-Butoxycarbonylmethyl)-8,8-(ethylenedioxy)spiro[4.5]dec-2-en-4-one (9). A solution of 50 mg (0.155 mmol) of **8** and 5.04 mg (0.0933 mmol) of NaOMe in MeOH (3 ml) was treated at 40—43 °C for 3.5 h. After removal of MeOH *in vacuo*, the residue was extracted with AcOEt. The organic layer was washed with H_2O, dried ($MgSO_4$) and evaporated. Purification of the residue by column chromatography on silica gel using a mixture of benzene and AcOEt as an eluent gave 42 mg (84%) of **9** as colorless crystals; MS *m/e* 322.1800 (Calcd for $C_{18}H_{26}O_5$: 322.1780).

(4S,8S)-4',4'-Ethylenedioxy-5-oxaspiro[bicyclo[3.3.0]octane-1,1'-cyclohexane]-2,6-dione (10). A solution of 120 mg (0.372 mmol) of **9** in benzene (10 ml) was treated with 2 mg of TsOH at 60 °C for 16 h. The resulting solution was diluted with benzene (30 ml), washed with H_2O and saturated aqueous $NaHCO_3$ solution and dried ($MgSO_4$). After removal of benzene *in vacuo*, the residue obtained was purified by column chromatography on silica gel using AcOEt as an eluent to afford 62 mg (63%) of **10** as colorless crystals; MS *m/e* 266.1130 (Calcd for $C_{14}H_{18}O_5$: 266.1154).

(4S,6R,8S,2R)- and/or (4S,6S,8S,2R)-4'4'-Ethylenedioxy-6-oxospiro[bicyclo[3.3.0]octane-1,1'-cyclohexane]-3,7-diol (11) Directly from (9). A solution of 100 mg (0.310 mmol) of **9** in toluene (3 ml) was treated with 64 mg (0.340 mmol) of TsOH at 40 °C for 3 h and then cooled to −70 °C. To the resulting solution was slowly added 4.80 mmol of *i*-Bu_2AlH in toluene (3 ml) over a period of 30 min. After the addition of MeOH (3 ml), the reaction mixture was treated with H_2O (9 ml) at 25 °C and stirred vigorously. After removal of the gel by filtration, the filtrate was dried ($MgSO_4$) and evaporated *in vacuo* to afford 65 mg (77% based on **9**) of **11** as an oil.

1-(cis-6-Methoxycarbonyl-2-hexenyl)-8,8-(ethylenedioxy)spiro-[4.5]decane-2,4-diol (13) Directly from (11). To a stirred solution of 2.5 g (5.65 mmol) of (4-carboxybutyl)triphenylphosphonium bromide in DMSO (3 ml) was added a solution of 2.0 mmol of sodium methylsulfinylmethide in DMSO (5 ml) at 10 °C. To the above solution was added a solution of 160 mg (0.592 mmol) of the crude hemiacetal **11** in DMSO (5 ml) at 25 °C. The resulting solution was allowed to stand at 34 °C for 45 h. The reaction mixture was quenched with H_2O (50 ml) and then extracted with a mixture of Et_2O and AcOEt (1: 1). The aqueous layer was acidified with oxalic acid (≈pH 5) and then extracted with a mixture of Et_2O and pentane (1: 1). The organic layer was dried ($MgSO_4$) and evaporated *in vacuo*. The residue was purified by thin layer chromatography on silica gel using a mixture of AcOEt and AcOH (98: 2) as a developing solvent to afford 120 mg of **12** which was treated with CH_2N_2 in MeOH and then evaporated *in vacuo* to afford 109 mg (50% based on **11**) of **13** as an oil after purification by column chromatography on silica gel using AcOEt as an eluent; MS *m/e* 368.2188 (Calcd for $C_{20}H_{32}O_6$: 368.2198).

1-(cis-6-Methoxycarbonyl-2-hexenyl)-2,4-dihydroxyspiro[4.5]-decan-8-one (14). A solution of 56 mg (0.152 mmol) of **13** and 1 mg of TsOH in acetone (5 ml) was refluxed for 5 h. The resulting solution was diluted with AcOEt and washed with saturated aqueous $NaHCO_3$ solution. The organic layer was dried ($MgSO_4$) and evaporated under reduced pressure to give 52 mg (100%) of **14** as an oil; MS *m/e* 324 (M^+).

dl-*12,15-Ethylene-13,14-dihydro-PGF$_{2\alpha}$ Methyl Ester (1).* To a stirred solution of 52 mg (0.160 mmol) of **14** in Et_2O (10 ml) was added dropwise a solution of 0.500 mmol of *n*-$C_5H_{11}MgBr$ in Et_2O (1 ml). After being left to stand at 25 °C for 30 min, the resulting mixture was diluted with AcOEt, washed with aqueous NH_4Cl solution and dried ($MgSO_4$). After removal of the solvent under reduced pressure, the residue obtained was purified by thin layer chromatography on silica gel using AcOEt as a developing solvent to afford 36 mg (60%) of **1** as an oil; MS *m/e* 396.2866 (Calcd for $C_{23}H_{40}O_5$: 396.2875).

References

1) J. W. Hinman, *Ann. Rev. Biochem.*, **41**, 161 (1972); J. R. Weeks, *Ann. Rev. Pharmacol.*, **12**, 317 (1972).

2) E. J. Corey, C. S. Shiner, R. P. Volante, and C. R. Cyr, *Tetrahedron Lett.*, **1975**, 1161.

3) E. W. Yankee, U. Axen, and G. L. Bundy, *J. Am. Chem. Soc.*, **96**, 5865 (1974).

4) H. A. P. de Jongh and H. Wynberg, *Recl. Trav. Chim.*, **82**, 202 (1963).

5) M. W. Rathke and D. F. Sullivan, *J. Am. Chem. Soc.*, **95**, 3050 (1973).

Retardation of the Cleavages of Nitrophenyl 1-Adamantanecarboxylates by Cyclodextrins

Makoto KOMIYAMA* and Shohei INOUE

Department of Synthetic Chemistry, Faculty of Engineering, The University of Tokyo, Bunkyo-ku, Tokyo 113

(Received January 21, 1980)

Cleavages of *p*- and *m*-nitrophenyl 1-adamantanecarboxylates (**1** and **2**) were carried out in the presence of α-, β-, and γ-cyclodextrins at 16 °C. The complex formation of **1** with α-, β-, and γ-cyclodextrins decelerated its cleavage by 3.2, 28, and 13 fold, respectively, in the 99 : 1 (v/v) mixture of 0.1 mol dm^{-3} NaOH aqueous solution and acetonitrile. All α-, β-, and γ-cyclodextrins showed decelerations of the cleavages of **1** and **2** also in the 66 : 34 mixture of 0.1 mol dm^{-3} NaOH aqueous solution and acetonitrile, although the magnitudes of the rate effects were smaller. The decelerations of the cleavages of **1** and **2** by cyclodextrins were markedly in contrast with the accelerations of the cleavages of other phenyl esters by cyclodextrins previously reported, and were ascribed to the formation of the complexes, in which **1** and **2** were protected sterically and/or electrostatically by cyclodextrins.

Cyclodextrins (CDs), cyclic oligosaccharides composed of 6—8 glucose units, have been used as an enzyme model, since they form complexes with substrates prior to their catalytic functions, resulting in many specificities exhibited by enzymes. The stereochemistry in the complex formation was shown to have quite important roles in the catalyses by CDs.[1]

Of many kinds of catalyses by CDs, hydrolyses of esters have been most widely and precisely studied, and much information has been obtained, especially on the effects of different leaving groups on the catalyses by CDs. Thus, CDs accelerated cleavages of phenyl esters of acetic acid,[2] benzoic acids,[2] and 3-carboxy-2,2,5,5-tetramethyl-1-pyrrolidinyloxyl.[3] The cleavages of trifluoroethyl benzoate[4] and *S*-ethyl thiobenzoate[5] were also accelerated by CDs, whereas the cleavages of ethyl and methyl esters of benzoic acids and cinnamic acids were retarded or totally inhibited by CDs.[2,6,7]

However, little is known about the role of the acyl portions of esters in the catalyses by CDs.

In this paper, the effects of α-, β-, and γ-cyclodextrins (α-, β-, and γ-CD) on the cleavages of *p*-nitrophenyl 1-adamantanecarboxylate (**1**) and *m*-nitrophenyl 1-adamantanecarboxylate (**2**) are described. The acyl portions of **1** and **2**, adamantanecarbonyl groups, are much more bulky and apolar than the acyl portions of any esters ever studied. Furthermore, a ^{13}C-NMR spectrometry on the CD–1-adamantanecarboxylate (**3**) system was carried out to shed light on the interactions of the adamantane moieties of **1** and **2** with CDs.

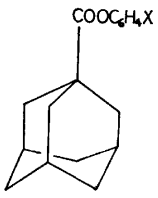

1 : X= p-NO_2
2 : X= m-NO_2

Experimental

Materials. **1** and **2** were synthesized from 1-adamantanecarbonyl chloride and the corresponding phenols and were recrystallized from ethanol. **1**: mp 132.5—132.8 °C (lit, 130—131 °C[8]). **2**: mp 137.8—138.3 °C. Found: C, 67.79; H, 6.37; N, 4.59%. Calcd for $C_{17}H_{19}NO_4$: C, 67.76; H, 6.36; N, 4.65%. α-CD and β-CD were recrystallized from water. γ-CD was purchased from Nakarai Chem. Co. and was used without further purification.

Kinetics. The cleavage of **1** was carried out at 16 °C in the 99 : 1 (v/v) mixture of 0.1 mol dm^{-3} NaOH aqueous solution and acetonitrile. The small amount of acetonitrile was due to the initiation of the reaction by the addition of the 30 μl stock solution of **1** in acetonitrile to 3 ml 0.1 mol dm^{-3} NaOH aqueous solution.

The attempt to examine the cleavage of **2** in the similar way, however, was not successful because of poor solubility of **2** in aqueous solution.

For the purpose of comparison, the cleavages of both **1** and **2** were carried out in the 66 : 34 (v/v) mixture of 0.1 mol dm^{-3} NaOH aqueous solution and acetonitrile. The reactions were also initiated by the addition of 30 μl stock solutions in acetonitrile to the mixture of 2 ml 0.1 mol dm^{-3} NaOH aqueous solution and 1 ml acetonitrile.

The initial concentrations of **1** and **2** were approximately 2×10^{-5} and 10^{-4} mol dm^{-3}, and their cleavages were followed by the release of the corresponding phenols at 410 and 390 nm, respectively. The rate constant of the cleavage, k_{obsd}, was determined by the usual first-order plot.

^{13}C-NMR Spectrometry. ^{13}C-NMR spectra were taken in D_2O solutions at pDs 9 and 13 at 60 °C on a JEOL PFT-100 spectrometer operating at 25.03 MHz by use of a deuterium lock. The chemical shifts were referenced to external benzene and the accuracy was within ±0.03 ppm.

Results

All α-, β-, and γ-CDs retarded the cleavages of both **1** and **2**. Figure 1 shows the dependence of k_{obsd} on the concentrations of CDs ($[CD]_0$) for the cleavage of **1** in the 99 : 1(v/v) mixture of 0.1 mol dm^{-3} NaOH aqueous solution and acetonitrile. Obviously, k_{obsd} asymptotically decreased with $[CD]_0$. Similar results were observed also in the cleavages of **1** and **2** in the 66 : 34(v/v) mixture of 0.1 mol dm^{-3} NaOH aqueous solution and acetonitrile.

These retardations of the cleavages of **1** and **2** by CDs are markedly in contrast with the accelerations of the cleavages of phenyl esters by CDs previously reported.[1-3]

The dependences of k_{obsd} on $[CD]_0$ were analyzed according to the Scheme 1 involving the complex

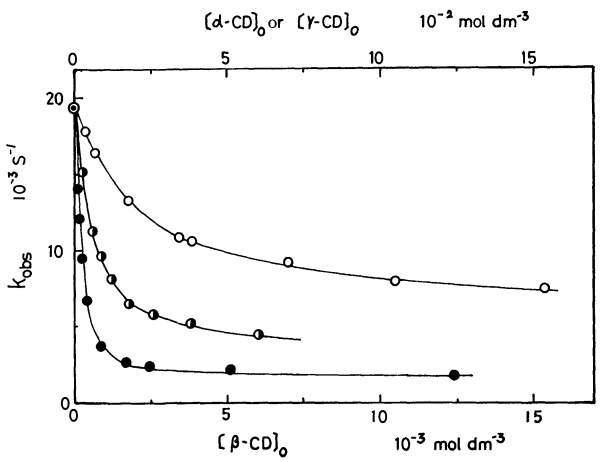

Fig. 1. Dependences of the rate constants of the cleavage of **1** (k_{obsd}) upon the initial concentrations of cyclodextrins ([CD]$_0$); in the 99 : 1 (v/v) mixture of 0.1 mol dm^{-3} NaOH aqueous solution and acetonitrile at 16 °C. ●: β-CD (the lower scale), ○: α-CD, ◑: γ-CD (the upper scale).

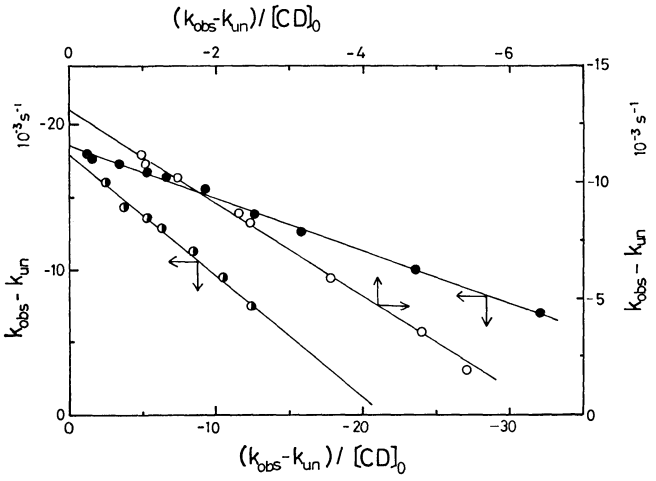

Fig. 2. Plots of $(k_{obsd}-k_{un})$ *vs.* $(k_{obsd}-k_{un})/[CD]_0$ in the cleavage of **1** in the presence of CDs. ○, ●, and ◑ refer to α-, β-, and γ-CDs, respectively; the data in Fig. 1 are used here.

formation of the substrate (S) with CD prior to the reaction:

$$S + C \underset{K_d}{\rightleftharpoons} S\cdot C \xrightarrow{k_c} \text{products}$$
$$\downarrow k_{un}$$
$$\text{products}$$

Scheme 1.

The rate constants of the cleavage of the substrate in the S·C complex, k_c, and the dissociation constant of the S·C complex, K_d, were determined by use of the Eadie-type plot Eq. 1:

$$(k_{obsd}-k_{un}) = -K_d(k_{obsd}-k_{un})/[CD]_0 + (k_c-k_{un}). \quad (1)$$

Table 1 lists the values of k_c and K_d, determined from the slope and intercept of the straight lines in the Eadie-type plots as shown in Fig. 2.

Table 1. Values of k_c, k_c/k_{un}, and K_d for the cleavages of *p*- and *m*-nitrophenyl 1-adamantanecarboxylates (**1** and **2**) in the presence of cyclodextrins (CDs)

Substrate	CD	k_c / 10^{-4} s^{-1}	k_c/k_{un}	K_d / 10^3 mol dm^{-3}
1[a]	α-CD	60±6	0.31	13±2
	β-CD	6.9±0.7	0.036	0.36±0.04
	γ-CD	15±2	0.078	0.82±0.06
1[b]	α-CD	39.2[c]	—	—
	β-CD	14±3	0.30	4.7±0.9
	γ-CD	35.3[c]	—	—
2[b]	α-CD	43.3[c]	—	—
	β-CD	28±5	0.60	2.2±0.5
	γ-CD	45.2[c]	—	—

a) In the 0.1 mol dm^{-3} NaOH aqueous solution–acetonitrile mixture (99 : 1 in volume), at 16 °C; k_{un} under these conditions was 1.93×10^{-2} s^{-1}. b) In the 0.1 mol dm^{-3} NaOH aqueous solution–acetonitrile mixture (66: 34 in volume) at 16 °C; k_{un}'s of **1** and **2** under these conditions were 4.75×10^{-3} and 4.65×10^{-3} s^{-1}, respectively. c) k_{obsd} in the presence of 3×10^{-2} mol dm^{-3} CD.

It was found that the complex formation of **1** with α-, β-, and γ-CDs decelerated its cleavage by 3.2, 28, and 13 fold, respectively, in the 99 : 1(v/v) mixture of 0.1 mol dm^{-3} NaOH aqueous solution and acetonitrile. Similarly, the cleavages of **1** and **2** were retarded by 3.3 and 1.7 fold, respectively, by the complex formations with β-CD in the 66 : 34 mixture of 0.1 mol dm^{-3} NaOH aqueous solution and acetonitrile.

Determinations of k_c and K_d for the cleavages of **1** and **2** by α- and γ-CDs in the 66 : 34 mixture by use of the Eadie-type plots were not successful because of small magnitudes of effects by CDs, although these CDs showed decelerations in these reactions.

The magnitudes of the deceleration of the cleavage of *p*-nitrophenyl ester **1** by CDs were similar to those of the cleavage of *m*-nitrophenyl ester **2** by CDs. These small effects of the positions of the phenyl substituents on the rate constants of their cleavages in the presence of CDs were also in contrast with the predominant roles of the positions of the phenyl substituents in the acceleration of the cleavages of phenyl acetates by CDs. For example, the cleavages of *p*- and *m*-nitrophenyl acetates were accelerated by α-CD by 3.4 and 300 fold, respectively.[6]

Table 2 shows the changes of the ^{13}C-NMR chemical shifts on the complex formation of CDs with **3** in D_2O. At pDs 9 and 13, the secondary hydroxyl groups of CDs are overwhelmingly in the unionized and ionized states, respectively, since their pK_a is around 11 at 60 °C.[9]

Furthermore, at pD 9, almost all of CD and **3** form complexes under the experimental conditions, in consideration of the previously determined dissociation constants of these complexes (for the α-CD–**3** complex, 1.1×10^{-3} mol dm^{-3} and for the β-CD–**3** complex, 1.4×10^{-3} mol dm^{-3} at 60 °C[10]).

On the complex formation of **3** with α-CD at pD 9, the C-4 atoms showed shifts toward the lower magnetic field, whereas the C-2 and C-3 atoms showed shifts

TABLE 2. CHANGES OF THE ^{13}C CHEMICAL SHIFTS ON THE COMPLEX FORMATION BETWEEN CYCLODEXTRINS (CDs) AND 1-ADAMANTANECARBOXYLATE (**3**)[a]

Carbons[b,c]	α-CD		β-CD	
	pD 9[d]	pD 13	pD 9	pD 13
1	0.00(0.00)	0.00	+0.12	+0.02
2	+0.09(+0.08)	+0.02	−0.15	−0.42
3	+0.12(+0.12)	+0.02	+0.34	+0.40
4	−0.20(−0.22)	0.00	−0.49	−0.61
1′	−0.13(−0.15)	0.00	−0.32	−0.36
2′	−0.03(−0.02)	+0.04	+0.06	−0.09
3′	−0.06(−0.06)	0.00	−0.06	−0.25
4′	−0.09(−0.09)	+0.04	−0.20	−0.55
5′	−0.03(0.00)	0.00	−0.25	−0.12
6′	+0.02(+0.01)	+0.02	+0.21	0.00

a) In ppm at 60 °C, and [CD]=[**3**]=5×10^{-2} mol dm^{-3} in D_2O; +signs refer to the shifts toward the higher field with reference to the chemical shifts of **3** (or CD) in the absence of CD (or **3**). b) The numbering systems are as follows;

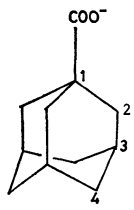

3

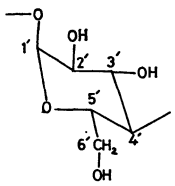

CD

c) Assignment following Ref. 11. d) The values in parentheses show the results of the duplicate experiments.

toward the higher magnetic field. The C-1 atom, however, exhibited little shift.

At pD 13, where virtually all of α-CD is in the anionic form, however, no changes of the chemical shifts for both α-CD and **3** were observed considering experimental error. This indicates that no complex is formed between α-CD and **3** at pD 13.

Larger changes of the chemical shifts of both the guest and host molecules were observed on the complex formation between β-CD and **3** at pDs 9 and 13.

Discussion

The retardation of the cleavages of **1** and **2** by CDs in spite of the acceleration of the cleavages of many other phenyl esters previously studied is attributable to the apolar and bulky properties of the adamantane moieties of **1** and **2**. These groups can be included in the cavity of β-CD (and also the cavity of γ-CD) as indicated by the considerable changes of the ^{13}C-NMR chemical shifts on the complex formation of **3** with β-CD. The adamantane moieties of **1** and **2**, however, can not be included in the small cavity of α-CD and only sit on the top of the cavity, as proposed by the study using the molecular models.[6] This is consistent with the small changes of the ^{13}C chemical shifts on the complex formation of **3** with α-CD. In the hydrolyses of phenyl esters accelerated by CDs, the phenyl portions are included in the cavity, followed by the nucleophilic attack of CDs at the substrates.[1]

Two Structures A and B are possible for the complex of **1** or **2** with β-CD or γ-CD, both of which are nonproductive or less productive. Structure A is formed by the inclusion of **1** and **2** in the cavity from the secondary hydroxyl side with their phenyl portions first, whereas Structure B is formed by the inclusion of **1** and **2** in the cavity from the same side with their adamantane portions first.[12] In Structure A, the carbonyl carbon atoms of the substrates should be located deeply in the cavity, since the apolar property of the adamantane portions require most of them as well as the phenyl portions to be included in the cavity. Consequently, nucleophilic attack of the secondary alcoholate anion of CDs at the carbonyl carbon atoms is sterically unfavorable. Furthermore, steric protection by the walls of CDs and electrostatic repulsion by the negative charges of CDs retard alkaline hydrolyses of **1** and **2**.

In Structure B, nucleophilic attack by the secondary alcoholate anions of CDs can not produce the acyl-CD (the intermediate) with the release of the phenols, since the acyl-CD with the acyl portion inside the cavity involves too drastic distortion(s) in bond(s). Furthermore, alkaline reactions are retarded sterically and electrostatically in the similar way as in Structure A.

The retardation of the cleavages of **1** and **2** by α-CD indicates that the phenyl portions of **1** and **2** are included in the cavity with the adamantane portions sitting on the top of the cavity. In this structure, nucleophilic attack both by the secondary alcoholate anion of CD and by hydroxide ion are prevented sterically and/or electrostatically. If the adamantane portions alone is located in the cavity and the phenyl portion is outside, any retardation by α-CD is unlikely.

Much smaller deceleration effects by CDs on the cleavages of **1** and **2** in the 66 : 34 mixture of 0.1 mol dm^{-3} NaOH aqueous solution and acetonitrile than in the 99: 1 mixture is attributable to shallower inclusions of the substrates in the cavities of CDs because of apolar properties of the adamantane portions. In this structure, any effect by CDs should be small. This interpretation is supported by the 13 fold large K_d of the β-CD–**1** complex (corresponding to less stable complex) in the 66: 34 mixture than that in the 99: 1 mixture.

In conclusion, the cleavages of **1** and **2** were retarded by CDs, which is in contrast with the acceleration of the cleavages of many other phenyl esters by CDs. The present results show that the acyl portions of the substrates can have a predominant effect on the catalyses by CDs.

We would like to thank Prof. Teiji Tsuruta at the University of Tokyo for his valuable comments.

References

1) M. L. Bender and M. Komiyama, "Cyclodextrin Chemistry," Springer-Verlag, Berlin (1978).
2) R. L. VanEtten, G. A. Clowes, J. F. Sebastian, and M. L. Bender, *J. Am. Chem. Soc.*, **89**, 3253 (1967).
3) K. Flohr, R. M. Paton, and E. T. Kaiser, *J. Am. Chem.*

Soc., **97**, 1209 (1975).
4) M. Komiyama and S. Inoue, *Chem. Lett.*, **1979**, 1101.
5) M. Komiyama and M. L. Bender, *Bull. Chem. Soc. Jpn.*, **53**, 1073 (1980).
6) R. L. VanEtten, J. F. Sebastian, G. A. Clowes, and M. L. Bender, *J. Am. Chem. Soc.*, **89**, 3242 (1967).
7) J. L. Lach and T. -F. Chin, *J. Pharm. Sci.*, **53**, 924 (1964).
8) D. S. Kristol, R. C. Parker, and H. D. Perlmutter, *J. Org. Chem.*, **41**, 3205 (1976).
9) M. Komiyama and M. L. Bender, *J. Am. Chem. Soc.*, **100**, 4576 (1978).
10) M. Komiyama and M. L. Bender, *J. Am. Chem. Soc.*, **100**, 2259 (1978).
11) P. Colson, H. J. Jennings, and C. P. Smith, *J. Am. Chem. Soc.*, **96**, 8081 (1974).
12) These descriptions do not mean that the inclusion of **1** and **2** in β- and γ-CDs should take place only from the secondary hydroxyl side of the cavities. Inclusion from the primary hydroxyl side can also form Structures A and B.

Reaction of 1,2-Dimethoxybiphenylene with Dichlorocarbene. Chemical Detection of the Bond Fixation in Biphenylene Derivatives

Masaru SATO, Keiko INABA, Seiji EBINE,* and Josuke TSUNETSUGU
Department of Chemistry, Saitama University, Urawa, Saitama 338
(Received January 26, 1980)

1,2-Dimethoxybiphenylene reacted with dichlorocarbene to give three chloro(methoxy)-6*H*-benzo[3,4]-cyclobuta[1,2]cyclohepten-6-one derivatives, two chloro(methoxy)fluorenones and two dimethoxyfluorenones. The reaction with dibromocarbene gave similar products. The formation of these products serves as unequivocal chemical evidence for bond fixation of 1,2-dimethoxybiphenylene. The chloro(methoxy)-6*H*-benzo[3,4]cyclobuta-[1,2]cyclohepten-6-one was led to 9-chloro-5-hydroxy-6*H*-benzo[3,4]cyclobuta[1,2]cyclohepten-6-one, the first tropolone analogue of biphenylene. This compound was shown to exist in only one of the two possible tautomers in contrast with general monocyclic tropolones.

Delocalization of π-electrons in benzene nucleus of aromatic compounds can be perturbed by some demands of an electronic environment or the incorporation of steric strain. The former is demonstrated in such molecules as naphthalene, phenanthrene, and other condensed-ring aromatic compounds, where some bond fixation in one benzene ring results from the fusion with the other benzene rings. The latter is illustrated in benzocyclobutene derivatives. Biphenylene provides the special case of double bond fixation in which both electronic and steric factors are participated: biphenylene prefers one canonical structure (**1a**) over the others, especially the structure (**1b**) carrying an anti-aromatic cyclobutadiene ring. Such a partial bond fixation of biphenylene was proved by electron diffraction[1] and X-ray analysis,[2] and suggested from the proton-proton coupling constant of the aromatic ring[3] and some chemical reactions.[4] It is also well-known that the carbene addition may be valuable as a chemical probe for the detection of bond fixation in aromatic molecules.[5] The carbene addition to naphthalenes, for example, takes place at C_1–C_2 and C_3–C_4 double bond but does not at C_2–C_3 double bond,[6] and methoxycarbonylcarbene reacts with biphenylene preferentially at the C_2–C_3 double bond.[7] In connection with our work on chemistry of small ring-annelated non-benzenoid aromatics, we are investigating the reaction of dichlorocarbene with methoxybiphenylenes, because the reaction can provide a convenient synthetic route to the troponoid analogues of biphenylene. The addition of dichlorocarbene to 1- (**2**) and 2-methoxybiphenylenes

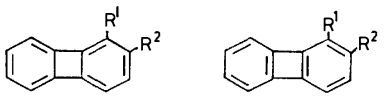

(1) $R^1=R^2=H$ (2) $R^1=OMe$, $R^2=H$ (3) $R^1=H$, $R^2=OMe$
(4) $R^1=R^2=OMe$

(**3**) takes place at C_2–C_3 and C_1–C_{8b}, or C_2–C_3 and C_4–C_{4a} double bonds, respectively, as previously reported.[8] We now wish to report the details about the addition of dihalocarbene to 1,2-dimethoxybiphenylene (**4**).[9]

Results and Discussion

2-Methoxybiphenylene (**3**)[10] was metalated with butyllithium and the lithio intermediate was allowed to react with tributyl borate, and the resulting 1-biphenylenylboronic acid was subsequently oxidized with hydrogen peroxide to give 1-hydroxy-2-methoxybiphenylene. This fact is parallel to the predominant α-metalation of biphenylene.[11] 1-Hydroxy-2-methoxybiphenylene was treated with dimethyl sulfate and alkali to afford 1,2-dimethoxybiphenylene (**4**) is a nearly quantitative yield.

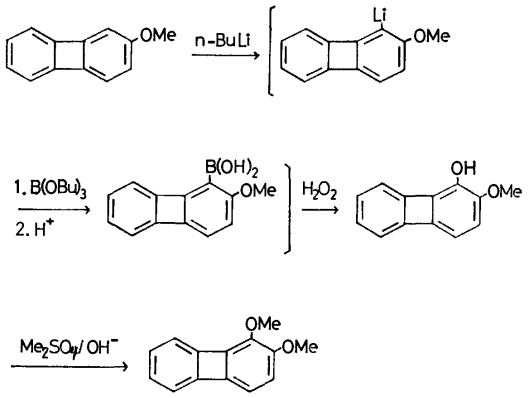

1,2-Dimethoxybiphenylene (**4**) reacted with dichlorocarbene, generated from chloroform (3 equiv.) and 33% aqueous sodium hydroxide in the presence of catalytic amount of hexadecyltrimethylammonium chloride,[12] to give three chloro(methoxy)-6*H*-benzo[3,4]cyclobuta-[1,2]cyclohepten-6-ones (**8a**, **9a**, and **10a**), two chloro-(methoxy)fluorenones (**11a** and **12a**), and two dimethoxyfluorenones (**13** and **14**), along with the recovered starting material (70.0%). The yields, IR, NMR, and electronic spectra of these compounds are summarized in Table 1. Similarly, the reaction of **4** with dibromocarbene generated by the Dehmlow's method[13] gave two bromo(methoxy)-6*H*-benzo[3,4]cyclobuta[1,2]-cyclohepten-6-ones (**9b**) and (**10b**), two bromo-(methoxy)fluorenones (**11b**) and (**12b**), and 3,4-dimethoxyfluorenone (**14**). The yields, IR, ^{1}H-NMR, and electronic spectra of those products are summarized

Table 1. Spectral data for the products from the reaction of **4** with dichlorocarbene

Compound	Yield (%)	IR (cm^{-1})	^{1}H-NMR (ppm, Hz)	UV (nm, log ε)
8a	1.3	1613	3.80(s, 3H), 6.29(s, 2H), 7.0—7.5 (m, 4H)	298(4.73), 364(3.95), 379(3.87)
9a	0.6	1608	4.07(s, 3H), 6.20(d, 1H, J=9.0), 7.05—7.45(m,4H), 7.42(d, 1H, J=9.0)	306(4.52), 336(4.06), 365(3.37)
10a	5.6	1602	4.08(s, 3H),6.37(d, 1H, J=13.2), 6.71(d, 1H, J=13.2), 7.12—7.4(m, 4H)	288(4.12), 312(4.54), 345(3.68), 387(3.92)
11a	4.7	1705	4.30(s, 3H), 7.18(d, 1H, J=7.8), 7.25—7.75(m, 5H)	264(4.85), 300(3.56), 328(3.50), 405(3.18)
12a	0.8	1706	3.95(s, 3H), 6.83(d, 1H, J=9.5), 7.56(d, 1H, J=9.5),7.25—7.8(m, 3H), 8.2(m, 1H)	254(4.72), 302(3.34), 370(3.65)
13[a]	0.9	1710	3.89(s, 3H), 4.12(s, 3H), 6.94(d, 1H, J=8.2), 7.19(d, 1H, J=8.2) 7.2—7.75(m, 4H)	
14[a]	1.9	1702	3.92(s, 3H), 3.96(s, 3H), 6.75 (d, 1H, J=8.3), 7.05—8.0 (m, H), 7.44(d, 1H, J=8.3)	

a) See Ref. 14.

Table 2. Spectral data for the products from the reaction of **4** with dibromocarbene

Compound	Yield (%)	IR (cm^{-1})	^{1}H-NMR (ppm, Hz)	UV (nm, log ε)
9b	0.4	1605	4.08(s,3H), 6.13(d, 1H, J=8.5), 7.10—7.33(m, 4H), 7.77(d, 1H, J=8.5)	284(4.39), 306(4.59), 337(4.22)
10b	6.2	1602	4.06(s, 3H), 6.28(d, 1H, J=13.2), 6.79(d, 1H, J=13.2), 7.17—7.37 (m, 4H)	273(4.28), 314(4.60)
11b	4.1	1708	4.15(s, 3H), 7.14(d, 1H, J=7.4), 7.18—7.82(m, 5H)	264(4.79), 295(3.44), 332(3.29), 407(3.04)
12b	1.2	1705	3.98(s, 3H), 6.75(d, 1H, J=8.8), 7.54(d, 1H, J=8.8), 7.19—7.82 (m, 3H), 8.28—8.49(m, 1H)	255(4.65), 302(3.22), 314(3.22), 376(3.53)
14[a]	5.0			

a) See Ref. 14.

in Table 2. Chloro(methoxy)-6*H*-benzo[3,4]cyclobuta-[1,2]cyclohepten-6-one derivatives (**8a**, **9a**, and **10a**) had the molecular ion at *m/e* 244, and the corresponding bromo derivatives **9b** and **10b** had the molecular ion at *m/e* 290 in their mass spectra. These tropone derivatives showed the strong absorption near 1600 cm^{-1} in their IR spectra. Their electronic spectra were closely similar to each other and moreover to those of other 6*H*-benzo[3,4]cyclobuta[1,2]cyclohepten-6-one derivatives reported previously.[8] In the NMR spectra, **10a** showed two olefinic doublets (AB type) at δ 6.37 and 6.71 ppm (J=13.2 Hz), and similarly **9a** at δ 6.20 and 7.42 ppm (J=9.0 Hz). The large coupling constant in the former and the small one in the latter mean the intervention of a double bond and a single bond, respectively, between the vicinal protons. Hence **10a** and **9a** can be assigned to 9- and 7-chloro-5-methoxy-6*H*-benzo[3,4]cyclobuta[1,2]cyclohepten-6-ones, respectively. The two olefinic protons in **8a** appeared accidentally as a singlet at δ 6.29 ppm but on addition of the shift reagent (Eu-fod) the singlet separated into two doublets (J=9.0 Hz), whereby **8a** is assigned to 5-chloro-7-methoxy-6*H*-benzo[3,4]cyclobuta[1,2]cyclohepten-6-one. The NMR spectra of **10b** and **9b** showed two doublets at δ 6.28 and 6.79 (J=13.2 Hz), and 6.13 and 7.77 (J=8.5 Hz), respectively. Therefore, in a similar manner, **10b** and **9b** were assigned to 9-bromo- and 7-bromo-5-methoxy-6*H*-benzo[3,4]cyclobuta[1,2]cyclohepten-6-ones, respectively. Two dimethoxyfluorenones (**13** and **14**), and two chloro(methoxy)-fluorenones (**11a** and **12a**) were identified as 1,2- and 3,4-dimethoxyfluorenones,[14] and 2- and 4-chloro-1-methoxyfluorenones, respectively, by the mixed mp and IR spectral coincidence with the authentci samples. The latter two authentic compounds were prepared by another route: 1-methoxyfluorenones[15] was chlorinated with sulfuryl chloride in the presence of azobis-(isobutyronitrile) to give 2- and 4-chloro-1-methoxyfluorenones in 23 and 57% yields, respectively. 2-Bromo- (**11b**) and 4-bromo-1-methoxyfluorenones (**12b**) were assigned by the close similarity of their IR, UV, and ^{1}H-NMR spectra to those of **11a** and **12a**, respectively.

The formation of these products seems to be elucidated best as proceeding through the reaction path shown in Scheme 1. Dichlorocarbene added to **4a** giving the intermediate adducts **5**, **6**, and **7**. The adduct **7** converted spontaneously to **10** and, on the other hand, was attacked by a hydroxide ion at C_{4a} and C_{8b} to give **12** and **14**, respectively. The path to fluorenone derivatives is similar to that in the reaction between 1-methoxybiphenylene and dichlorocarbene.[8] Similarly, the adduct **5** afforded **8** and **13**, and the adduct **6** did **9** and **11**. Thus, the addition of dichlorocarbene must have taken place at the fixed C_{8b}–C_1, C_2–C_3, and C_4–C_{4a} double bonds of the canonical structure **4a** of 1,2-dimethoxybiphenylene, although dibromocarbene cannot add to the corresponding C_{8b}–C_1 double bond. No adduct from another canonical structure **4b** was obtained. This is the first example in the reaction of

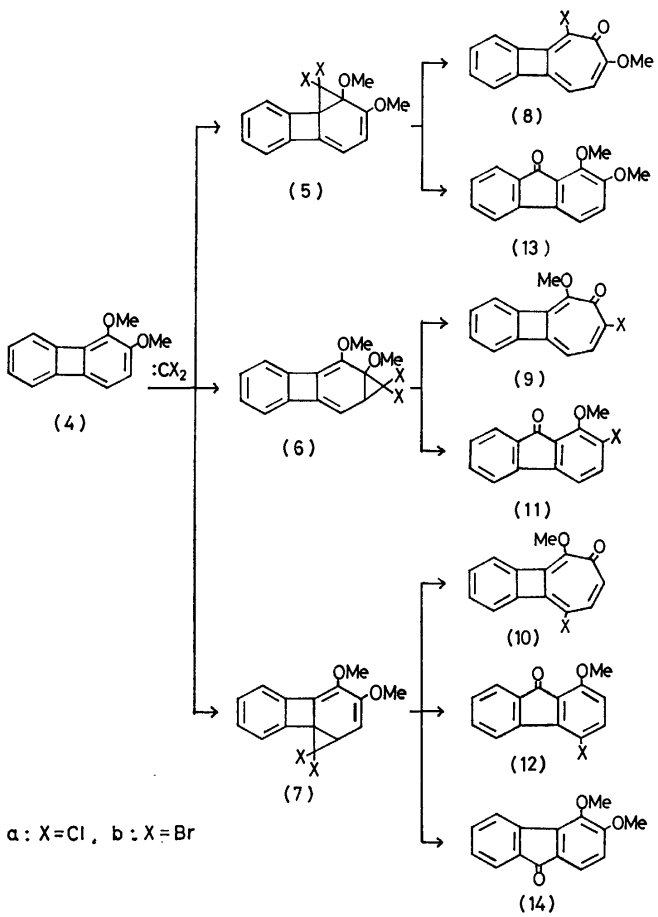

Scheme 1.

biphenylene series where all the possible products resulting from one of the Kekule's canonical structures are obtained, and this observation serves as unequivocal chemical evidence for the bond fixation of biphenylene system.

The addition of dichlorocarbene to C_{8b}–C_1, C_2–C_3, and C_4–C_{4a} double bonds of **4a** gave 2.2, 5.3, and 8.3% yields of the products, respectively, while the addition of dibromocarbene to the corresponding double bonds did in 0, 4.4, and 12.4% yields, respectively. In the reaction of **4** with dihalocarbene, the addition of the carbene to C_4–C_{4a} double bond was most favorable. The observation may be explained by the absence of steric hindrance in the approach of the carbene and by the best stabilization of the intermediate **7** in term of both conjugated methoxyl groups compared with others **5** and **6**. The predominant addition of dihalocarbene to C_4–C_{4a} double bond is also observed in the dichlorocarbene-addition to 2-methoxybiphenylene[8] but is in contrast with the exclusive addition of ethyl diazoacetate to the C_2–C_3 double bond of biphenylene itself.[7] In the latter, the addition of the carbene may be controlled by the electron-deficiency of C_{8b}–C_1 double bond induced with rehybridization of the junction carbon (C_{8b}).[16] The similar conjugative effect of methoxyl group was observed in the addition of dichlorocarbene to methoxynaphthalenes.[17,18] The less addition of dichlorocarbene to the C_{8b}–C_1 double bond than to the C_4–C_{4a} double bond seems to be in part due to the steric hindrance of the methoxyl group. Dibromocarbene added in the best yield to C_4–C_{4a} double bond and did not add to the most crowded double bond (C_{8b}–C_1). Therefore, the difference in yields between dichloro- and dibromocarbene addition to 1,2-dimethoxybiphenylene is probably due to the bulkiness of dibromocarbene compared with dichlorocarbene.

Attempted hydrolysis of the tropolone methyl ether **10a** with concentrated hydrochloric acid in boiling ethanol led to the hydroxyfluorenone derivative **15**. This facile rearrangement may be due to the release of the central four-membered ring strain, according to Scheme 2.

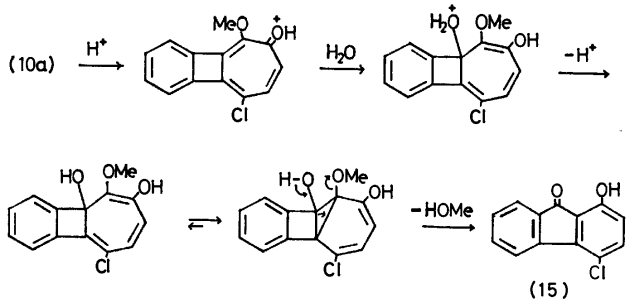

Scheme 2.

The tropolone methyl ether **10a** was treated with boron tribromide in dichloromethane at −65 °C and subsequently hydrolyzed to give 9-chloro-5-hydroxy-6*H*-benzo[3,4]cyclobuta[1,2]cyclohepten-6-one (**16a**), that is, the tropolone analogue of biphenylene in 93% yield. Similarly, bromo derivative **10b** was hydrolyzed to 9-bromo-5-hydroxy-6*H*-benzo[3,4]cyclobuta[1,2]-cyclohepten-6-one (**16b**) in 55% yield. Attempts to debrominate **10b** with tributyltin hydride[19] or zinc-copper couple in aqueous THF[20] in order to develope the route to the parent 5-hydroxy-6*H*-benzo[3,4]-cyclobuta[1,2]cyclohepten-6-one (benzo[3,4]cyclobuta-[1,2-*c*]tropolone) (**17**) were not successful. Catalytic hydrogenation of **16b** to **17** was also tried in vain.

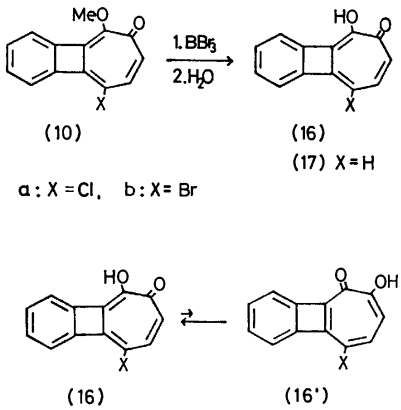

The tautomerism **16**⇄**16'**, like monocyclic tropolones, is potentially expected. The equilibrium, however, proved to be imposed predominantly or exclusively to the tautomer **16** by the following facts. The electronic spectrum of **16a** is closely similar to that of the methyl

ether **10a**. The NMR coupling constant $J_{7,8}=13.3$ Hz of **16a** is nearly the same as that of the corresponding protons of **10a** ($J=13.2$ Hz). If the rapid equilibrium **16**⇄**16′** exsists, the coupling constant $J_{7,8}$ in **16** should be reduced to the corresponding value ($J_{6,7}=10.9$ Hz) of tropolone.[21] If the tautomer **16′** exists, the high-field shift of the benzenoid protons would be expected due to the paramagnetic ring current of the central four-membered ring, but actually this was not observed in **16a**. The absence of the contribution of **16′** is probably due to the instability of anti-aromatic cyclobutadiene structure in the central four-membered ring. The tropolone derivative **16a** gave a red coloration in chloroform layer with aqueous iron(III) chloride, like monocyclic tropolones. The tropolone **16a** could not be extracted with aqueous sodium hydrogen carbonate but reacted with aqueous sodium carbonate to give a red precipitate from which **16a** was recovered by neutralization with hydrochloric acid (2 mol dm^{-3}). The acidic property of **16a** is also shown by the fact that **16a** reacted with diazomethane to give the methyl ether **10a**, an alternate tautomeric methyl ether of **16a′** not being detected after careful search of the reaction mixture.

Experimental

1-Hydroxy-2-methoxybiphenylene. To a solution of 2-methoxybiphenylene (9.10 g, 0.05 mol) in dry ether (100 ml) was added the solution of butyllithium prepared from lithium (1.29 g, 0.186 mol) and butyl bromide (10.3 g, 0.075 mol) in dry ether (10 ml) under nitrogen. After the mixture was stirred for 1 h at room temperature, it was refluxed for 20 h. The resulting mixture was dropwise added to a solution of tributyl borate (19.1 g, 0.083 mol) in dry ether (60 ml) at −78 °C under nitrogen. After the addition had been completed, the cooling bath was removed and the mixture was stirred for 1 h at room temperature. To the mixture was added 10% HCl (25 ml). The ethereal layer was separated and the aqueous layer was extracted with ether. The ethereal solution combined was washed with water and then transfered to a 2-necked round-bottomed flask equipped with a reflux condenser. To the ethereal solution was added 30% hydrogen peroxide (22 ml) dropwise at such a rate that mild reflux was maintained. After the addition had been completed, the mixture was stirred for 0.5 h. The ethereal layer was separated and the aqueous layer was extracted with ether. The ethereal solution combined was washed with water and dried over anhydrous magnesium sulfate. Evaporation of the ether gave yellow crystals, the silica gel chromatography of which gave the recovered starting material (0.81 g, 8.9%) and 1-hydroxy-2-methoxybiphenylene (yellow needles, mp 94—95 °C) (6.03 g, 60.9%). Found: C, 78.83; H, 5.27%. Calcd for $C_{13}H_{10}O_2$: C, 78.77; H, 5.09%. IR(KBr): 3380, 1498, 1438, 1138, and 739 cm^{-1}. NMR ($CDCl_3$): δ 3.77 (s, 3H), 5.6 (broad s, 1H), 6.08 (d, 1H, $J=7.6$ Hz), 6.25 (d, 1H, $J=7.6$ Hz), 6.42—6.83 (m, 4H). MS (75 eV): *m/e* 198 (M^+, 100%), 183 (M^+-CH_3, 75.5%), and 155 (M^+-CH_3-CO, 58%).

1,2-Dimethoxybiphenylene (4): To a solution of 1-hydroxy-2-methoxybiphenylene (5.94 g, 0.03 mol) and dimethyl sulfate (60.5 ml, 0.64 mol) in methanol (33 ml) was slowly added a solution of sodium hydroxide (54.9 g) in water (65 ml) under stirring at such a rate as the temperature of the solution was kept at 20—30 °C. After the addition had been completed, the mixture was warmed at 60 °C for 1 h. To the mixture was added water (465 ml). The crystals precipitated were collected by filtration and recrystallized from ethanol to give white-yellow leaflets (5.97 g, 94%), mp 132.5—133.5 °C. Found: C, 79.14; H, 5.74%. Calcd for $C_{14}H_{12}O_2$: C, 79.22; H, 5.70%. IR (KBr): 1488, 1407, 1292, 1240, 1228, 802, and 736 cm^{-1}. NMR($CDCl_3$): δ 3.77 (s, 3H), 3.98 (s, 3H), 6.13 (d, 1H, $J=7.5$ Hz), 6.88 (d, 1H, $J=7.5$ Hz), and 6.5—6.83 (m, 4H). MS(75 eV): *m/e* 212 (M^+ 100%), 197 (M^+-CH_3, 70%), and 169 (M^+-CH_3-CO, 59%).

Reaction of 1,2-Dimethoxybiphenylene (4) with Dichlorocarbene. A mixture of 1,2-dimethoxybiphenylene (**4**) (1.70 g, 8 mmol), chloroform (2 ml, 24 mmol), dichloromethane (5 ml), 33% aqueous sodium hydroxide (4 ml), and hexadecyltrimethylammonium chloride (25 mg) was stirred for 3 h at room temperature. The resulting red mixture was diluted with water and extracted with dichloromethane. The extract was washed twice with saturated aqueous sodium chloride and dried over sodium sulfate. After the solvent had been evaporated, the red-orange crystalline residue was chromatographed on silica gel with elution of benzene–ether. The following compounds were in turn eluted and purified with thin-layer chromatography and recrystallization. Their spectral data were summarized in Table 1. 2-Chloro-1-methoxyfluorenone (**11a**)(90 mg, 4.7%), yellow needles, mp 122—122.5 °C. Found: C, 68.84; H, 3.71%. Calcd for $C_{14}H_9ClO_2$: C, 68.72; H, 3.71%. 1,2-Dimethoxybiphenylene (**4**) (recovery 70.0%). 3,4-Dimethoxyfluorenone (**14**) (36 mg, 1.9%), mp 142.5 °C, yellow rods (lit,[14] 145.5 °C). 4-Chloro-1-methoxyfluorenone (**12a**) (16 mg, 0.8%), fine yellow needles, mp 152—152.5 °C. Found: C, 68.68; H, 3.74%. Calcd for $C_{14}H_9ClO_2$: C, 68.72; H, 3.71%. 1,2-Dimethoxyfluorenone (**13**) (17 mg, 0.9%), orange-yellow plates, mp 113—114 °C (lit,[14] 113 °C). 7-Chloro-5-methoxy-6*H*-benzo[3,4]cyclobuta[1,2]cyclohepten-6-one (**9a**) (12 mg, 0.6%), fine yellow needles, mp 142—143 °C. Found: C, 68.68; H, 3.89%. Calcd for $C_{14}H_9ClO_2$: C, 68.72; H, 3.71%. 9-Chloro-5-methoxy-6*H*-benzo[3,4]cyclobuta[1,2]-cyclohepten-6-one (**10a**) (110 mg, 5.6%), yellow needles, mp 135—136 °C. Found: C, 68.60; H, 3.79%. Calcd for $C_{14}H_9ClO_2$: C, 68.72; H, 3.71%. 5-Chloro-7-methoxy-6*H*-benzo[3,4]cyclobuta[1,2]cyclohepten-6-one (**8a**) (26 mg, 1.3%), yellow crystals, mp 150—151 °C. Found: C, 68.76; H, 3.76%. Calcd for $C_{14}H_9ClO_2$: C, 68.72; H, 3.71%.

Reaction of 1,2-Dimethoxybiphenylene (4) with Dibromocarbene. To a mixture of 1,2-dimethoxybiphenylene (**4**) (1.70 g 8 mmol), dichloromethane (3 ml), 33% aqueous sodium hydroxide (9 g), and hexadecyltrimethylammonium chloride (30 mg) was dropwise added bromoform (3.5 ml, 40 mmol) for a period of 15 min on an ice–water bath. After the mixture was stirred for 30 min, the ice–water bath was removed. The mixture was further stirred for 1.5 h at room temperature. The resulting mixture was treated in the same work-up as that in the reaction of **4** with dichlorocarbene described above. The following products were isolated: 2-Bromo-1-methoxyfluorenone (**11b**) (95 mg, 4.1%), yellow needles, mp 72.8—73.8 °C. Found: C, 58.33; H, 3.10%. Calcd for $C_{14}H_9BrO_2$: C, 58.16; H, 3.14%. 1,2-Dimethoxybiphenylene (**4**) (1.07 g, 70% recovery). 3,4-Dimethoxyfluorenone (**14**) (96 mg, 5.0%), yellow needles, mp 139.7—140.2 °C (lit,[14] 145.5 °C). Found: C, 74.74; H, 5.05%. Calcd for $C_{15}H_{12}O_2$: C, 74.79; H, 5.03%. 4-Bromo-1-methoxyfluorenone (**12b**) (27 mg, 1.2%), yellow needles, mp 134.8—135.8 °C. Found: C, 58.16; H, 3.15%. Calcd for $C_{14}H_9BrO_2$: C, 58.16; H, 3.14%. 7-Bromo-5-methoxy-6*H*-benzo[3,4]cyclobuta[1,2]cyclohepten-6-one (**9b**) (9 mg, 0.4%), yellow nee-

dles, mp 147—148 °C. Found: C, 58.00; H, 3.06%. Calcd for $C_{14}H_9BrO_2$: C, 58.16; H, 3.14%. 9-Bromo-5-methoxy-6*H*-benzo[3,4]cyclobuta[1,2]cyclohepten-6-one (**10b**) (143 mg, 6.2%), yellow needles, mp 144.3—144.8 °C. Found: C, 58.17; H, 3.45%. Calcd for $C_{14}H_9BrO_2$: C, 58.16; H, 3.14%. The spectral data were summarized in Table 2.

2- *(11a) and 4-Chloro-1-methoxyfluorenones (12a).* A solution of 1-methoxyfluorenone[16] (210 mg, 1 mmol), sulfuryl chloride (160 mg, 1.2 mmol), and azobis(isobutyronitrile) (small amount) in dichlormethane (10 ml) was stirred for 1.5 h. After the solvent was evaporated up, the residue was chromatographed on silica gel with elution of benzene–ether. The first elute gave pale yellow crystals (mp 191—192 °C, 11 mg). The second elute gave 2-chloro-1-methoxyfluorenone (56 mg, 23%) as yellow needles (mp 120—121 °C). Found: C, 68.73; H, 3.61%. Calcd for $C_{14}H_9ClO_2$: C, 68.72; H, 3.71%. The third fraction was 4-chloro-1-methoxyfluorenone (136 mg, 57%), as yellow needles, mp 152.5—153 °C. Found: C, 68.27; H, 3.67%. Calcd for $C_{14}H_9ClO_2$: C, 68.72; H, 3.71%.

4-Chloro-1-hydroxyfluorenone (15). *A*: To a solution of 4-chloro-1-methoxyfluorenone (**10a**) (65 mg) in dichloromethane was added boron tribromide (0.12 ml) at −65 °C under nitrogen. The red-brown solution was stirred for 45 min at the same temperature. The solution was warmed up to room temperature and poured into water. The mixture was extracted with dichloromethane. The extract was washed with water and dried over anhydrous sodium sulfate. After evaporation, the residue was sublimed under reduced pressure (110 °C/10 mmHg) to give a yellow crystalline product (55 mg, 90%), which was recrystallized from hexane, mp 158.5—159.5 °C. Found: C, 67.67; H, 2.99%. Calcd for $C_{13}H_7ClO_2$: C, 67.70; H, 3.06. UV (EtOH): 254 (log ε 4.76), 299 (3.35), 382 (3.61) nm. IR (KBr): 3387, 1699, 1614, 1297, 1183, and 741 cm^{-1}. NMR ($CDCl_3$): δ 6.74 (d, 1H, J=9.0 Hz), 7.29 (d, 1H, J=8.9 Hz), 7.3—7.8 (m, 3H), 8.13 (m, 1H), and 8.64 (broad s, 1H).

B: A mixture of 9-chloro-5-methoxy-6*H*-benzo[3,4]cyclobuta[1,2]cyclohepten-6-one (**10a**) (37 mg), concd HCl (2 ml), and ethanol (5 ml) was refluxed for 4 h. The solution was poured into water, and the resulting mixture was extracted with ether. The ethereal extract was washed with water and dried over anhydrous sodium sulfate. After evaporation, the residue was chromatographed on silica gel to give, along with the starting material (16 mg, 45%), 4-chloro-1-hydroxyfluorenone (**15**) (18 mg, 52%), yellow needles, mp 158—159 °C. Admixed mp 158—159 °C.

*9-Chloro-5-hydroxy-6*H*-benzo[3,4]cyclobuta[1,2]cyclohepten-6-one (16a).* To a solution of 9-chloro-5-methoxy-6*H*-benzo[3,4]cyclobuta[1,2]cyclohepten-6-one (**10a**) (105 mg, 0.43 mmol) in dichloromethane (15 ml) was added boron tribromide (0.2 ml) at −65 °C under nitrogen. After being stirred for 30 min at the same temperature, the solution was warmed gradually to room temperature and poured into water. The mixture was extracted with dichloromethane. The extract was dried over anhydrous sodium sulfate. After the solution had been evaporated up, the residue was sublimed at about 140 °C/2 mmHg to give yellow crystals (92 mg, 93% yield), which were recrystallized from ethanol to give bright-yellow needles, mp 207—208 °C. Found: C, 67.87; H, 2.98%. Calcd for $C_{13}H_9ClO_2$: C, 67.70; H, 3.06%. UV (EtOH): 278 (log ε 4.27), 312 (4.64), 348 (3.86), 386sh (3.40), and 419 (3.10) nm. IR (KBr): 3250, 1602, 1569, 1373, 1215, 833, and 729 cm^{-1}. NMR (DMSO-d_6): δ 6.49 (d, 1H, J=13.3 Hz), 7.02 (d, 1H, J=13.3 Hz), 7.2—7.45 (broad s, 4H), and 10.3 (1H). MS (60 eV): *m/e* 230 (M^+, 63%) and 202 (M^+−CO, 100%).

*9-Bromo-5-hydroxy-6*H*-benzo[3,4]cyclobuta[1,2]cyclohepten-6-one (16b).* To a solution of 9-bromo-5-methoxy-6*H*-benzo[3,4]cyclobuta[1,2]cyclohepten-6-one (**10b**) (118 mg, 0.41 mmol) in dichloromethane (15 ml) was added boron tribromide (0.4 ml) at −65 °C under nitrogen. After the solution had been stirred for 30 min at the same temperature and then poured into water. The mixture was extracted with dichloromethane. The extract was dried over anhydrous sodium sulfate and then evaporated up. The residue was sublimated under reduced pressure. The crystals obtained were recrystallized from ethanol to give yellow needles, mp 199—200 °C. Found: C, 56.61; H, 2.37%. Calcd for $C_{13}H_7BrO_2$: C, 56.76; H, 2.56%. UV (EtOH): 213 (log ε 4.47), 280 (4.27), 313 (4.63), 347 (4.01), and 392 (3.42) nm. IR (KBr): 3260, 1595, 1570, 1375, 1220, and 750 cm^{-1}. NMR ($CDCl_3$): δ 6.49 (d, 1H, J=13.5 Hz), 7.04 (d, 1H, J=13.5 Hz), and 7.20—7.42 (m, 4H).

Reaction of (16a) with Diazomethane. To a solution of diazomethane in ether (20 ml) prepared from *N*-nitrosomethylurea (103 mg, 1 mmol) was added 9-chloro-5-hydroxy-6*H*-benzo[3,4]cyclobuta[1,2]cyclohepten-6-one (**16a**) (40 mg, 0.17 mmol) on an ice-water bath. The solution was stirred for 6 h. The solution was extracted with aqueous sodium carbonate. The ethereal layer was dried over anhydrous sodium sulfate, and then evaporated up. The residue was chromatographed on silica gel with elution of dichloromethane to give the methyl ether **10a** as yellow crystals (38 mg, 90%). The aqueous layer was acidified with HCl (2 mol dm^{-3}) and then extracted with ether. From the ethereal extract the starting material was recovered (3 mg, 7%).

The auther thanks Prof. L. Horner (Universitat Mainz) for kindhearted offer of the authentic samples and their NMR spectra of dimethoxyfluorenones, and also Prof. K. Suzuki (Utsunomiya Univ.) for kindhearted offer of 1-methoxyfluorenone. The author is also grateful to Dr. K. Takahashi and Prof. K. Takase (Tohoku Univ.) for 100 MHz-NMR measurements.

References

1) A. Yokozeki, C. F. Wilcox, Jr., and S. H. Bauer, *J. Am. Chem. Soc.*, **96**, 1026 (1974) and the references therein.
2) J. K. Fawcett and J. Trotter, *Acta Crystallogr.*, **20**, 87 (1966).
3) G. Frankel, Y. Asahi, M. J. Mitchel, and M. P. Cava, *Tetrahedron*, **20**, 1179 (1964).
4) W. Baker, J. W. McOmie, D. R. Preston, and V. Rogers, *J. Chem. Soc.*, **1960**, 414.
5) W. Kirmse, "Carbene Chemistry," 2nd ed, Academic Press, New York and London (1971), pp. 381—395.
6) For example, R. Huisgen and G. Juppe, *Chem. Ber.*, **94**, 2332 (1961).
7) A. S. Kende and P. T. MacGregor, *J. Am. Chem. Soc.*, **86**, 2088 (1964).
8) M. Sato, S. Ebine, and J. Tsunetsugu, *J. Chem. Soc., Chem. Commun.*, **1974**, 846; *J. Chem. Soc., Perkin Trans. 1*, **1977**, 1282.
9) A preliminary communication: M. Sato, A. Uchida, J. Tsunetsugu, and S. Ebine, *Tetrahedron Lett.*, **1977**, 2151; M. Sato, S. Ebine, and J. Tsunetsugu, *ibid.*, **1977**, 855.
10) W. Baker, J. W. Barton, and J. F. W. McOmie, *J. Chem. Soc.*, **1958**, 2658.
11) A. J. Boulton, J. B. Chadwick, C. R. Harrison, and J. F. W. McOmie, *J. Chem. Soc., C*, **1968**, 328.
12) G. C. Joshi, N. Singh, and L. M. Pande, *Tetrahedron*

Lett., **1972**, 1461.
13) E. V. Dehmlow, *Angew. Chem. Int. Ed. Engl.*, **16**, 502 (1977).
14) L. Horner and D. W. Baston, *Ann. Chem.*, **1973**, 910.
15) G. Heyl, *J. Prakt. Chemm*, [2] **59**, 453 (1893).
16) A. Streitwieser, Jr., G. R. Ziegler, P. C. Mowery, A. Lewis, and R. G. Lawler, *J. Am. Chem. Soc.*, **90**, 1357 (1968).
17) W. E. Parham, D. A. Bolon, and E. E. Schweizer, *J. Am. Chem. Soc.*, **83**, 603 (1961).
18) M. Sato, J. Tsunetsugu, and S. Ebine, *Bull. Chem. Soc. Jpn.*, **49**, 2230 (1976).
19) H. G. Kuivila, *Synthesis*, **1970**, 499.
20) R. M. Blankenship, K. A. Burdett, and J. S. Swenton, *J. Org. Chem.*, **39**, 2300 (1974).
21) D. J. Bertelli, T. G. Andrews, Jr., and P. O. Crews, *J. Am. Chem. Soc.*, **91**, 5286 (1969).

Mechanism of Base Catalyzed Oxidation of 2-(1-Hydroxyalkyl)-thiazolium Ion with 3-Methyllumiflavin

Yumihiko YANO, Yoshiharu TAMURA, Yutaka HOSHINO, and Waichiro TAGAKI*

Department of Chemistry, Faculty of Engineering, Gunma University, Kiryu, Gunma 376

(Received January 30, 1980)

The oxidation of 2-(α-hydroxybenzyl)- and 2-(1-hydroxyethyl)thiazolium ions with 3-methyllumiflavin was studied kinetically in an aqueous buffer solution. The results indicate that the rate-determining step is carbanion formation followed by rapid oxidation. The carbanion formation was subjected to general base catalysis.

The mechanism of catalysis of thiamine coenzyme involves the formation of active aldehyde as a key intermediate[1] as shown in the following equation.

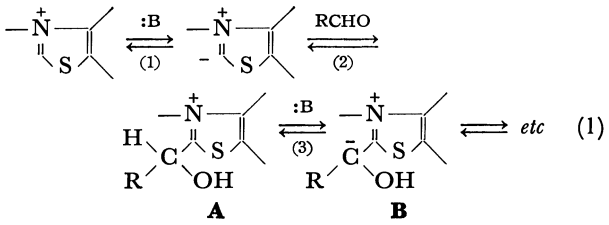

(1)

A **B**

The first step (1) of ionization of 2-hydrogen of thiazolium ring was thoroughly investigated.[2] However, the mechanism of the subsequent deprotonation of **A** (step 3) has remained unclarified, whether it is subjected to a general base or a specific base catalysis, although α-hydrogen exchange of 2-(1-hydroxyethyl)thiazolium ion (**A**, R=CH_3) had been confirmed by NMR.[3] Recently, it has been shown by NMR that carbanion formation from 2-(1-hydroxyethyl)- and 2-(α-hydroxybenzyl)thiazolium ions is subjected to general base catalysis in aqueous buffer solutions.[4]

Flavins are reduced by carbanions such as those generated from α-hydroxy ketones. Usually, the reduction is so fast that the rate limiting step is the formation of carbanion.[5] Namely, the rate of carbanion formation can be measured spectrophotometrically by observing oxidation-reduction of flavin. The method allows the use of a much lower concentration of substrate than that for NMR. In addition to such a merit, the use of flavin is of interest as a model reaction of flavin pyruvate oxidase. This enzyme catalyzes the oxidative decarboxylation of pyruvate to give acetate and CO_2,[6] the flavoprotein being reduced by 2-(1-hydroxyethyl)-thiamine diphosphate.[7]

As a part of studies on the model thiamine catalysis,[8] a kinetic study was carried out on the reaction of 2-(α-hydroxybenzyl)- and 2-(1-hydroxyethyl)thiazolium ions (**1** and **2**) with flavin (**3**), together with the H-D exchange reaction of **1** for comparison.

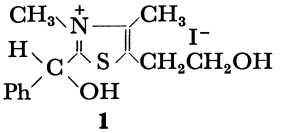

1

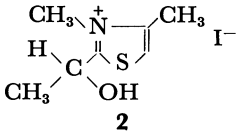

2

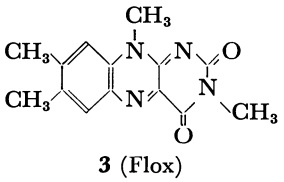

3 (Flox)

Results and Discussion

Carbanion Oxidation by Flavin. The reaction was followed by monitoring the decrease in absorption of **3** (Flox) at 443 nm under anaerobic conditions. The disappearance of Flox was found to be linear with the reaction time to 75% reaction. The reaction is of zero order with respect to flavin concentration as observed in the other α-hydroxy carbanion oxidations by flavins.[5] The bubbling of O_2 after the reaction regenerated more than 95% Flox in all the runs.

The results are in line with the mechanism of Eqs. 2 and 3, *i.e.* the rate limiting formation of carbanion (I^-) followed by a rapid oxidation. Thus, on the assumption of steady state with respect to (I^-), Eq. 4 can be derived resulting in the zero order dependency in [Flox] (Eq. 6) under the conditions of Eq. 5. The rates were also confirmed to be of first order with respect to (I) to give first order rate constant, k_a (Fig. 1).

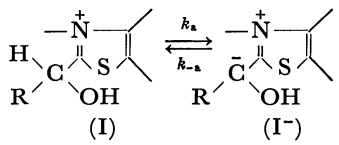

(2)

(I) (I^-)

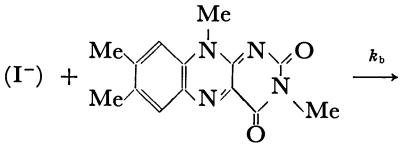

3 (Flox)

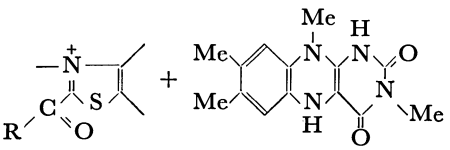

(3)[9]

$$-\frac{d[Flox]}{dt} = \frac{k_a k_b [I][Flox]}{k_{-a} + k_b[Flox]} \quad (4)$$

$$k_b[Flox] \gg k_{-a} \quad (5)$$

$$-\frac{d[Flox]}{dt} = k_a[I] \quad (6)$$

$$k_a = k_{OH^-}[OH^-] + k_B[B] \quad (7)$$

The k_a values obtained under various conditions are summarized in Table 1. The pH-log k_a plots for compound **1** give a straight line of slope=0.93 (Fig. 2). The buffer concentrations were changed for Tris and carbonate buffers. The rate increase is linear with the

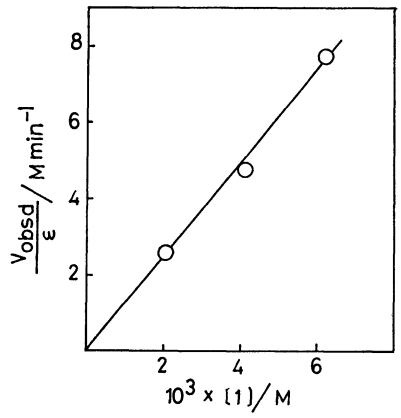

Fig. 1. Plots of V_{obsd} *vs.* [I].
pH=9.19 (0.1 M Borate), μ=0.5 (NaCl) at 30 °C, [Flox]=6.9×10^{-5} M.

Table 1. The first order rate constants of **3**(Flox) reduction at 30 °C

Compd	pH	[Buffer]/M	$10^4\times k_a$/min^{-1}
1	8.23[b]	0.1	1.69
	8.64[b]	0.1	3.86
	9.01[c]	0.1	9.63
		0.25	12.6
		0.4	13.8
		0.5	15.9
	9.23[b]	0.1	13.9
	9.45[d]	0.1	22.5
		0.2	24.5
		0.4	30.5
	9.53[b]	0.1	25.6
	9.78[b]	0.1	44.3
2	9.46[d]	0.1	0.392
		0.25	0.751
		0.5	1.14

a) [Flox]=6.9×10^{-5}M, [**1**]=[**2**]=2.07×10^{-3}M, μ=0.5 (NaCl). b) Borate buffer. c) Tris buffer. d) Carbonate buffer.

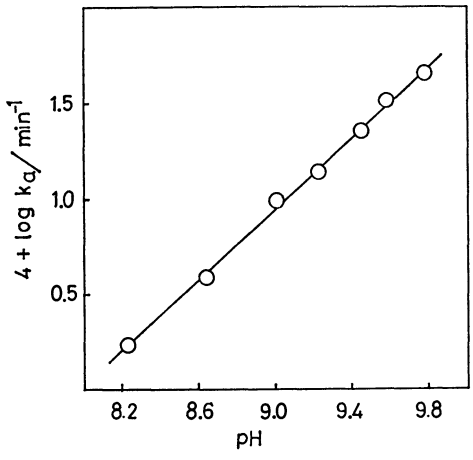

Fig. 2. pH-log k_a plots for **1** (see Table 1).

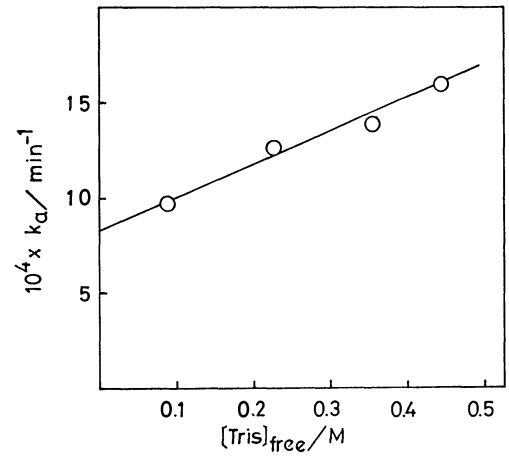

Fig. 3. Plots of k_a *vs.* Tris buffer concentration for **1** (pH=9.01, see Table 1).

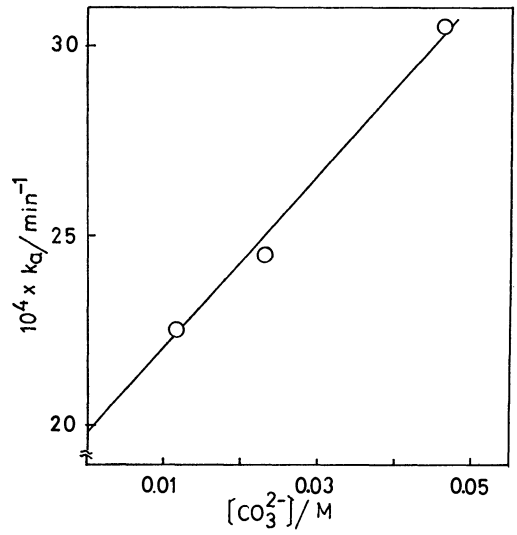

Fig. 4. Plots of k_a *vs.* carbonate buffer concentration for **1** (pH=9.45, see Table 1).

increase of buffer concentration in both cases (Figs. 3 and 4). Thus, k_a is represented by Eq. 7, where k_{OH^-} and k_B are the hydroxide ion and buffer (general base) catalyzed second order rate constants, respectively. The k_{OH^-} and k_{Tris} values for **1** are 91.3 and 1.66×10^{-3} M^{-1} min^{-1}, respectively in the Tris buffer (Fig. 3). For the carbonate buffer, k_{OH^-} and $k_{CO_3^{2-}}$ are 72 and 2.3×10^{-2} M^{-1} min^{-1}, respectively (Fig. 4). Since k_{OH^-} values should be the same, the average value, 82 M^{-1} min^{-1} can be used as the k_{OH^-} for **1**. In a similar way, k_{OH^-} and $k_{CO_3^{2-}}$ for **2** can be calculated to be 0.80 and 1.68×10^{-3} M^{-1} min^{-1}, respectively. The reactivities of **1** and **2** can then be compared by the ratio of k_{OH^-} (**1**)/k_{OH^-} (**2**)=10^2 and $k_{CO_3^{2-}}$ (**1**)/$k_{CO_3^{2-}}$ (**2**)=14, respectively. The ratios seem to be reasonable, since the carbanion formation should be much easier from **1** than from **2**.

The β value of the Brönsted plots could be regarded as a criterion to distinguish a general base from a specific base catalysis; the β value is close to unity in the case of specific base catalysis and *ca.* 0.5 for general base catalysis.[10] As shown in Fig. 5, the Brönsted plots of log k_a *vs.* pK_a of bases for **1** give a straigh line of slope=0.63 (β values). The β value for **2** can be calculated to be 0.5, from the available two data of k_{OH^-}

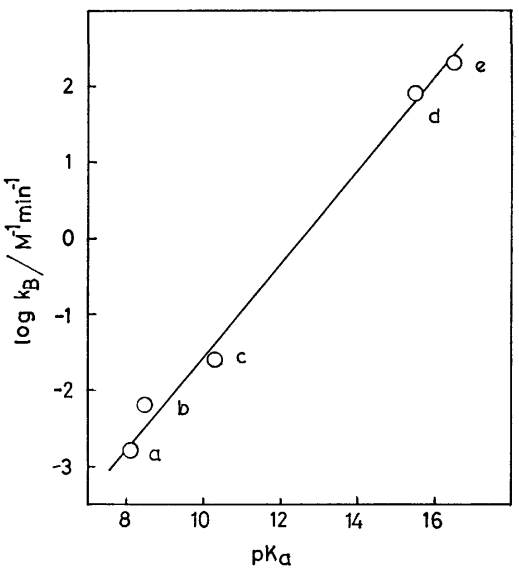

Fig. 5. The Brönsted plots for carbanion formation of **1**.
a) k_{Tris}, $pK_a=8.10$,[11] b) k_{Tris} (NMR), $pK_a=8.50$,[12] c) $k_{CO_3^{2-}}$, $pK_a=10.3$,[13] d) k_{OH^-}, $pk_a=15.6$,[14] e) k_{OD^-} (NMR), $pK_a=16.5$.[14]

and $k_{CO_3^{2-}}$. The β values indicate that the carbanion formation is a process of general base catalysis for both **1** and **2**.

H-D Exchange of 1. Since the carbanion formation is rate limiting in the above flavin reduction, the rates should be the same as those of H-D exchange of α-hydrogen of **1** and **2**. Thus, H-D exchange of **1** was also examined by means of NMR. The rate was followed by determining the relative intensities of the α-hydrogen and unexchangeable hydrogens of phenyl ring of **1**. First order kinetics was observed, although measurement of 1: 5 proton ratio involves large experimental error. The rate constants (k_{obsd}) thus obtained, however, were found to involve the rate term of decomposition of **1** to the corresponding thiazolium ion and benzaldehyde as shown by $k_{obsd}=k_{ex}+k_{dec}$. Therefore, in order to obtain k_{ex}, the rate of decomposition of **1** (k_{dec}) was determined spectrophotometrically by following the decrease of **1** at λ_{max} 267 nm ($\varepsilon=10{,}000$ $M^{-1}cm^{-1}$) under the same conditions as those of H-D exchange reaction. The results are given in Table 2. Although we have only two data, the k_{ex} values give $k_{OD^-}=2.0\times10^2$ $M^{-1}min^{-1}$ and $k_{Tris}=6.0\times10^{-3}$ M^{-1} min^{-1} on the basis of Eq. 7. These rate constants should involve considerable error. Nevertheless, they fit reasonably on the straight line of Fig. 5, when we consider the relationship, $pK_a(D_2O)=pK_a(H_2O)+0.4$.[12]

The results indicate that the deprotonation of active aldehyde such as **1** and **2** proceeds *via* general base catalysis. It should be noted that the present method is superior to the usual NMR method. The rate of carbanion formation can easily be determined by the spectrophotometric method. Substrate concentration required (2×10^{-3} M) is much lower than that (0.2 M) for NMR method. Furthermore, the time necessary for rate measurement can be reduced a great deal. For example, if the rate constant (k_a or k_{ex}) is 4×10^{-3} min^{-1}, the half-life is 170 min in the H-D exchange reaction, whereas, in the flavin reduction, zero order rate is $V_{obsd}=\Delta OD/\Delta t=k_a[I]\varepsilon=(4\times10^{-3})\times(2.07\times10^{-3})\times(1.2\times10^4)=0.099$, and when [Flox] is 6.9×10^{-5} M (OD=0.83), the half-life is only 4.6 min (=0.415/0.099). This makes the decomposition of **1** negligible during the course of rate determination.

Table 2. Rate constants of H-D exchange of **1**

pD[a]	[Tris]/M	$10^3\times k_{ex}/min^{-1}$[b]
9.20	0.1	1.4
9.20	0.4	2.9

a) $pD=pH_{obsd}+0.4$. b) $k_{ex}=k_{obsd}-k_{dec}$; $k_{dec}=4.76\times10^{-4}$ min^{-}, [**1**]=0.2 M, μ=0.5(NaCl) at 30 °C.

Experimental

Materials and Methods. All melting points were uncorrected. UV and visible spectra were recorded with a Shimadzu UV 200 spectrophotometer, and NMR spectra with a Varian A-60 spectrometer. pH was measured with a Hitachi-Horiba F-7DE pH meter. Water used for kinetics was purified by treating deionized water with potassium permanganate and by distillation twice. Buffer reagents were of commercial special grade.

3,4-Dimethyl-2-(α-hydroxybenzyl)-5-(2-hydroxyethyl)thiazolium iodide (**1**) was prepared by the method reported. Mp 113—115 °C (from ethanol-acetone) (lit,[15] mp 111—113 °C).

2-(1-Hydroxyethyl)-4-methylthiazolium iodide (**2**) was prepared from the corresponding thiazole and methyl iodide in ethanol. Mp 149—151 °C (from methanol-ether) (lit,[2a] mp 149—150 °C).

3-Methyllumiflavin (**3**) was prepared by the method reported. Mp 315 °C (from DMF) (lit,[16] mp 318 °C).

Kinetics. All kinetic measurements were carried out in an aqueous buffer solution containing 1% acetonitrile at 30 °C. 30 μl of the substrate (**1** or **2**) solution (1×10^{-1} M) was placed in the upper compartment of a Thunberg cuvette, and 3 ml of an aqueous buffer solution and 30 μl of Flox (6.9×10^{-3} M in acetonitrile) in the lower cell. Each solution was bubbled for 30 min with nitrogen which had been scrubbed with vanadous ion solution[17] and prehumidified with water. In the case of Tris buffer, nitrogen bubbling was performed in the dark to avoid the light-reduction of flavin. After equilibration at 30 °C for 15 min, the reaction was initiated by mixing the two solutions, the reaction being followed by observing the decrease of optical density at 443 nm. The slopes of optical density *vs.* time plots ($\Delta OD/\Delta t$) are plotted against substrate concentration (Fig. 1, 1 M=1 mol dm^{-3}).

Kinetics for H-D Exchange. The reaction mixtures for the kinetics were prepared as follows. The thiazolium salt (0.1 mmol) was weighed accurately in a microtube, and 0.5 ml of buffer solution added, the tube being capped with septum-rubber. Nitrogen was bubbled for 5 min through an injection needle. The solution was transfered to the NMR tube with syringe and capped quickly. The rate constants were determined by following the relative intensities of α-proton and phenyl ring protons in a similar manner to that reported.[18]

References

1) a) R. Breslow, *J. Am. Chem. Soc.*, **80**, 3719 (1958);

Ann. N. Y. Acad. Sci., **98**, 445 (1962); b) L. O. Krampitz, *Ann. Rev. Biochem.*, **38**, 213 (1969).

2) a) R. Breslow and E. McNelis, *J. Am. Chem. Soc.*, **81**, 3080 (1959); b) P. Haake, L. P. Bausher, and W. B. Miller, *ibid.*, **91**, 1113 (1969); c) D. S. Kemp and J. T. O'Brien, *ibid.*, **92**, 2554 (1970).

3) a) J. Ullrich and A. Mannschreck, *Eur. J. Biochem.*, **1**, 110 (1967); b) J. J. Mieyal, R. G. Votaw, L. O. Krampitz, and H. Z. Sable, *Biochem. Biophys. Acta*, **141**, 205 (1969); c) J. J. Mieyal, G. Bantle, R. G. Votaw, I. R. Rosner, and H. Z. Sable, *J. Biol. Chem.*, **246**, 5213 (1971).

4) a) A. A. Gallo and H. Z. Sable, *J. Biol. Chem.*, **251**, 2564 (1967); b) J. A. Zoltewicz and S. Sridharan, *J. Org. Chem.*, **43**, 3785 (1978).

5) a) L. Main, G. J. Kasperek, and T. C. Bruice, *Biochemistry*, **11**, 3991 (1972); b) S. Shinkai, T. Kunitake, and T. C. Bruice, *J. Am. Chem. Soc.*, **96**, 7140 (1974); c) T. C. Bruice and J. P. Taulane, *ibid.*, **98**, 7769 (1976); d) T. C. Bruice, "Progress in Bioorganic Chemistry," ed by E. T. Kaiser and F. J. Kezdy, John Wiley and Sons, New York (1976), Vol. 4, p. 1.

6) a) L. P. Hager, *J. Biol. Chem.*, **229**, 251 (1957); *Bacterial Proc.*, **1959**, 109; b) F. R. Williams and L. P. Hager, *J. Biol. Chem.*, **236**, 36 (1961).

7) L. P. Hager and L. O. Krampitz, *Federation Proc.*, **22**, 536 (1969).

8) a) W. Tagaki and H. Hara, *J. Chem. Soc., Chem. Commun.*, **1973**, 891; b) W. Tagaki, Y. Tamura, and Y. Yano, *Bull. Chem. Soc. Jpn.*, **53**, 478 (1980); c) Y. Yano, Y. Tamura, and W. Tagaki, *ibid.*, **53**, 740 (1980).

9) 2-Acylthiazolium ion is known to undergo rapid hydrolysis in an aqueous alkaline solution; T. C. Bruice and N. G. Kundu, *J. Am. Chem. Soc.*, **88**, 4097 (1966); G. E. Lienhard, *ibid.*, **88**, 5642 (1966).

10) W. P. Jencks, "Catalysis in Chemistry and Enzymology," MacGraw-Hill, New York (1969), p. 163.

11) T. C. Bruice and J. L. York, *J. Am. Chem. Soc.*, **83**, 1382 (1961).

12) a) P. K. Glosoe and F. A. Long, *J. Phys. Chem.*, **64**, 188 (1960); b) A. K. Covington, M. Paabo, R. A. Robinson, and R. G. Bates, *Anal. Chem.*, **40**, 700 (1968).

13) S. A. Khan and A. J. Kirby, *J. Chem. Soc.*, **1970**, 1172.

14) A. K. Covington, R. A. Robinson, and R. G. Bates, *J. Phys. Chem.*, **70**, 3820 (1966).

15) Y. Oka, S. Kishimoto, and H. Hirano, *Chem. Pharm. Bull.*, **18**, 527 (1970).

16) F. Yoneda, Y. Sakuma, M. Ichiba, and K. Shinomura, *J. Am. Chem. Soc.*, **98**, 830 (1976).

17) L. Meites and T. Meites, *Anal. Chem.*, **20**, 984 (1948).

18) Y. Yano, T. Okonogi, and W. Tagaki, *J. Org. Chem.*, **38**, 3912 (1973).

 © 1980 The Chemical Society of Japan Bull. Chem. Soc. Jpn., 53, 2344—2347 (1980)

Studies on Biologically Active Pteridines. IV.[1] Synthesis of Several Biopterin Derivatives as an Antigen in Radioimmunoassay for Biopterin

Takashi SUGIMOTO,* Sadao MATSUURA, and Toshiharu NAGATSU†

Department of Chemistry, College of General Education, Nagoya University, Chikusa-ku, Nagoya 464

† *Laboratory of Cell Physiology, Department of Life Chemistry, Graduate School at Nagatsuta, Tokyo Institute of Technology, Midori-ku, Yokohama 227*

(Received February 8, 1980)

The synthesis of biopterin, D(and L)-*erythro*-neopterins, and their derivatives having a substituent at the 2-amino group *via* the 2-methylthio analogues is described. The 2-(methylthio)pteridines were synthesized by condensation of 4,5-diamino-6-hydroxy-2-(methylthio)pyrimidine with 5-deoxy-L-arabinose and D(and L)-arabinose phenylhydrazones, followed by oxidation with $K_3[Fe(CN)_6]$ and O_2 in the presence of KI in an acidic solution, respectively. Aminolysis of these thioethers with ammonia and other amines in the presence of acetic acid gave the title compounds.

The aromatic amino acid hydroxylases, phenylalanine hydroxylase,[2] tyrosine hydroxylase,[3] and tryptophan hydroxylase,[4] play key roles in the biosynthesis of catecholamine neurotransmitters or indoleamine neurotransmitter. Since these hydroxylases require tetrahydrobiopterin as cofactor, defficiency of the biopterin cofactor causes serious neuropathological disorders. Indeed, hyperphenylalaninemia due to defficiency of biopterin has been reported as a variant form of phenylketonuria.[5,6] In order to diagnose such disease, assay of biopterin in serum or urine is required.

Recently we studied a radioimmunoassay for biopterin (**3a**) by employing 6-[[4-hydroxy-6-(L-*erythro*-1,2-dihydroxypropyl)-2-pteridinyl]amino]hexanoic acid–bovine serum albumin conjugate (**1a**) as the immunogen and *N*-[2-(4-hydroxy-3-[^{125}I]phenyl)ethyl]-6-[[4-hydroxy-6-(L-*erythro*-1,2-dihydroxypropyl)-2-pteridinyl]-amino]hexanamide (**1b**) as the radioactive antigen.[7] The antiserum produced by rabbits against **1a** showed high specificity toward biopterin and did not cross-react with other pteridines including D- and L-*erythro*-neopterins (**4a** and **5a**) and 6,7-dimethylpterin. During a preliminary experiment, we found that the sensitivity of the radioimmunoassay increased about ten-fold on preincubating the antiserum with 6-[(4-hydroxy-6,7-dimethyl-2-pteridinyl)amino]hexanoic acid (**2**); most probably, antibodies having specificity against the hexanoic acid moiety were removed by the preincubation.

This finding suggests that the sensitivity of the assay could be more increased even when the time-consuming preincubation procedure is omitted, if a radioactive antigen having no hexanoic acid moiety were used. In order to examine this possibility, we synthesized several biopterin and neopterin derivatives to be used as antigen carrying a hydroxyphenyl or methoxyphenyl group linked to the amino nitrogen of biopterin and neopterin directly or indirectly through a carbon chain smaller than a pentyl group.

In the present paper, we studied a synthetic route for such biopterin derivatives by a nucleophilic replacement of 4-hydroxy-6-(L-*erythro*-1,2-dihydroxypropyl)-2-(methylthio)pteridine (**3b**) with an appropriate amine to save reaction steps and time. The required common intermediate (**3b**) was synthesized by condensation of 4,5-diamino-6-hydroxy-2-(methylthio)pyrimidine and 5-deoxy-L-arabinose phenylhydrazone, followed by oxidation of the unstable condensate with potassium hexacyanoferrate(III) and oxygen in the presence of a small amount of potassium iodide.[8,9] Two blue fluorescent compounds were obtained in this reaction. The minor

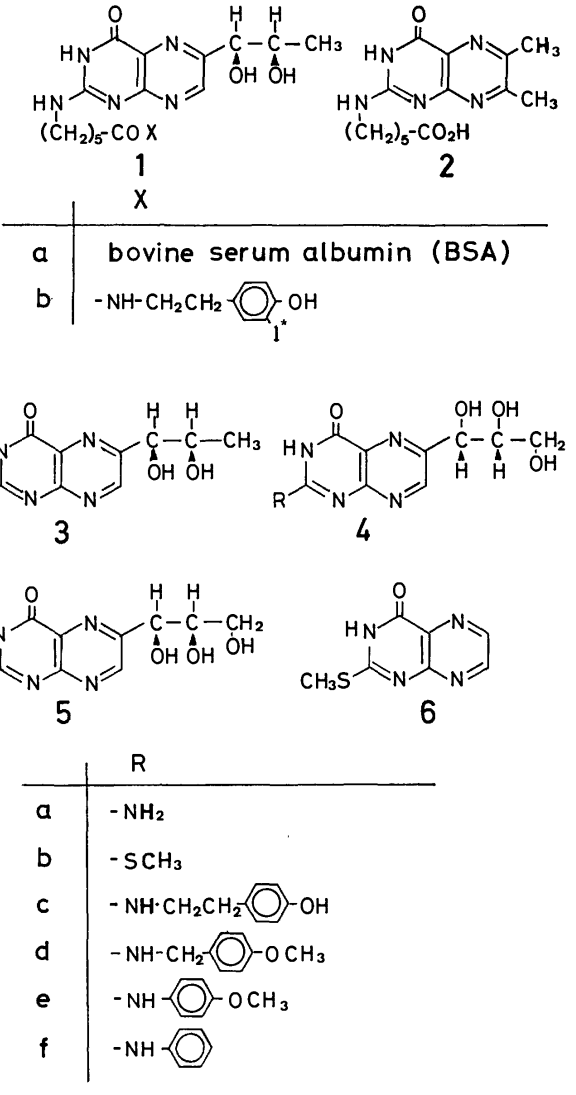

Table 1. The pK_a and UV spectra of 6-(dihydroxypropyl)- and 6-(trihydroxypropyl)pteridines

Compound	pK_a	pH of buffer[a]	λ_{max} (log ε)[b]	Ionic species[c]
3b	−1.01±0.05	−3.05	289(4.15), *300(4.11)*, 386(3.81)	+
	6.55±0.01	3.0	231(3.99), 282(4.21), 336(3.85)	○
		9.0	247(4.03), 269(4.32), 353(3.86)	−
4b	−1.10±0.06	−3.05	289(4.17), *300(4.13)*, 386(3.84)	+
	6.52±0.01	3.0	230(3.96), 282(4.24), 336(3.90)	○
		9.0	244(4.04), 270(4.35), 353(3.90)	−
5b	−1.04±0.05	−3.05	289(4.19), *300(4.15)*, 386(3.87)	+
	6.51±0.01	3.0	230(3.95), 282(4.22), 336(3.89)	○
		9.0	244(4.04), 270(4.36), 353(3.90)	−
3c	1.86±0.04	−0.5	240(4.18), *252(4.15)*, 325(3.86)	+
	8.02±0.02	5.0	224(4.20), 281(4.28), 354(3.75)	○
	10.2±0.5	9.0	222(4.21), 267(4.32), 370(3.80)	−
		12.0	241(4.24), 265(4.43), 372(3.86)	2−
4c	1.86±0.05	−0.5	241(4.22), *252(4.19)*, 325(3.88)	+
	7.94±0.03	5.0	224(4.27), 282(4.32), 353(3.78)	○
	9.5±0.5	9.0	222(4.25), 267(4.37), 370(3.85)	−
		12.0	240(4.27), 265(4.46), 373(3.90)	2−
5c	1.94±0.05	−0.5	241(4.21), *252(4.18)*, 325(3.88)	+
	7.84±0.03	5.0	224(4.25), 282(4.31), 354(3.78)	○
	9.6±0.5	9.0	221(4.25), 267(4.36), 370(3.84)	−
		12.0	240(4.27), 265(4.46), 373(3.89)	2−
3d	1.66±0.04	−0.5	226(4.33), *252(4.24)*, 324(3.70)	+
	7.95±0.05	5.0	226(4.29), 281(4.35), 352(3.80)	○
		10.0	*225(4.26)*, 265(4.44), 370(3.88)	−
4d	1.60±0.05	−0.5	226(4.35), *250(4.26)*, 324(3.90)	+
	7.92±0.07	5.0	226(4.30), 281(4.35), 352(3.80)	○
		10.0	222(4.25), 265(4.44), 370(3.88)	−
5d	1.63±0.05	−0.5	227(4.34), *250(4.26)*, 324(3.90)	+
	7.91±0.03	5.0	227(4.25), 281(4.35), 352(3.80)	○
		10.0	222(4.24), 265(4.43), 370(3.88)	−
3e	1.70±0.03	−1.0	228(4.26), 256(4.20), 325(3.94)	+
	7.40±0.04	4.5	236(4.16), 287(4.37), 354(3.81)	○
		9.5	*265(4.28)*, 287(4.38), 377(3.93)	−
4e	1.66±0.02	−1.0	228(4.27), 256(4.20), 325(3.94)	+
	7.35±0.05	4.5	233(4.17), 287(4.35), 353(3.79)	○
		9.5	*265(4.25)*, 287(4.35), 377(3.90)	−
5e	1.63±0.04	−1.0	228(4.26), 256(4.19), 325(3.92)	+
	7.31±0.05	4.5	235(4.16), 287(4.34), 354(3.78)	○
		9.5	*264(4.26)*, 287(4.35), 377(3.90)	−
3f	1.43±0.05	−1.0	255(4.20), 324(3.90)	+
	7.14±0.01	4.5	236(4.03), 289(4.32), 352(3.78)	○
		9.5	*243(4.05)*, 284(4.38), 374(3.91)	−
4f	1.43±0.03	−1.0	255(4.21), 324(3.91)	+
	7.21±0.04	4.5	237(4.05), 289(4.33), 353(3.80)	○
		9.5	*240(4.06)*, 284(4.39), 374(3.92)	−
5f	1.44±0.03	−1.0	255(4.21), 324(3.91)	+
	7.20±0.04	4.5	237(4.05), 289(4.34), 353(3.80)	○
		9.5	*240(4.06)*, 285(4.38), 375(3.92)	−
6	−1.01±0.05	−3.05	287(3.81), *296(3.77)*, 379(3.81)	+
	6.51±0.01	3.0	230(3.92), 278(4.15), 331(3.83)	○
		9.0	240(3.92), 268(4.27), 349(3.85)	−

a) Negative figures are H_0 values. b) Wave length in nm measured in aqueous buffer of given pH; shoulders or influexions in italics. c) Ionic species are shown by + (cation), ○ (neutral molecule), − (mono-anion), and 2 − (dianion).

product was found to be 4-hydroxy-2-(methylthio)-pteridine (**6**) which was unambiguously synthesized by condensation of 4,5-diamino-6-hydroxy-2-(methylthio)-pyrimidine and glyoxal. The structure of the main product was determined to be **3b** from the elemental analyses and UV spectra similar to those of **6** (Table 1). This conclusion was further confirmed by aminolysis of the main product into biopterin (**3a**). The 6-(D-*erythro*-1,2,3-trihydroxypropyl) and 6-(L-*erythro*-1,2,3-trihydroxypropyl) analogues (**4b** and **5b**) of **3b** were similarly synthesized by condensation of 4,5-diamino-6-hydroxy-2-(methylthio)pyrimidine with D- or L-arabinose phenylhydrazone and oxidation of the condensates with the above oxidizing agents; their structures were confirmed by aminolysis to the known D- or L-*erythro*-neopterin (**4a**, **5a**),[10] respectively. A considerable amount of the condensate again lost the trihydroxypropyl substituent during the oxidation. It is to be noted that an analogous condensate from 2,4,5-triamino-6-hydroxypyrimidine and D-arabinose phenylhydrazone did not loose the trihydroxypropyl group even when the condensate was oxidized by air in an alkaline solution;[10] under such conditions, the present condensate entirely lost the trihydroxypropyl group to give **6**.

The (methylthio)pteridine (**3b**) proved to be a good precursor for the synthesis of the present required biopterin derivatives carrying a substituent at the 2-amino group. When **3b** was heated with tyramine in 2-methoxyethanol or *N,N*-dimethylformamide in the presence of acetic acid, **3b** was easily converted into 4-hydroxy-2-[2-(*p*-hydroxyphenyl)ethylamino]-6-(L-*erythro*-1,2-dihydroxypropyl)pteridine (**3c**); in the absence of acetic acid, decomposition of **3b** into several unclarified substances took place to a fair extent. Analogous treatment of **3b** with *p*-methoxybenzylamine, *p*-anisidine, or aniline gave the biopterin derivatives (**3d**—**f**) possessing respectively a *p*-methoxybenzyl, *p*-methoxyphenyl, or phenyl group at the 2-amino nitrogen. The thioethers (**4b** and **5b**), on aminolysis with those amines, gave the corresponding derivatives of D-*erythro*-neopterin (**4c**—**f**) and L-*erythro*-neopterin (**5c**—**f**).

The (methylthio)pteridines (**3b**, **4b**, and **5b**) showed very weak basicity (pK_a −1.0) and a characteristic bathochromic shift on protonation (see Table 1). The aminolysis products exhibited two pK_a values at about 1.6 and 7.5: the former is attributed to the protonation of the pteridine ring to form cations and the latter to the ionization of the 4-hydroxyl group to form anions. Both values are slightly lower than those of biopterin (pK_a 2.23 and 7.89[9]). An additional pK_a value at 10 was observed with **3c**, **4c**, and **5c** owing to the ionization of the phenolic hydroxyl group. However, the ionization changed the UV spectra only slightly, because the hydroxyl group is not conjugated to the main pteridine chromophore.

A study of radioimmunoassay for biopterin and neopterin using the present synthesized compounds will be reported eleswhere.

Experimental

The elemental analyses were conducted at The Analytical Section, Meijo University, Nagoya. The pK_a values were determined by a spectroscopical method,[11] and the UV spectra in an appropriate buffer solution on a Shimadzu UV-300 spectrophotometer.

*4-Hydroxy-6-(*L-erythro-*1,2-dihydroxypropyl)-2-(methylthio)-pteridine (**3b**) and the Trihydroxypropyl Analogues (**4b** and **5b**).* 4-Amino-6-hydroxy-2-methylthio-5-nitrosopyrimidine[12] (18 g) was hydrogenated over 5% palladium on carbon (10 g) in 0.5 M KOH (500 ml) at room temperature and atmospheric pressure till the calculated amount of hydrogen was absorbed. The catalyst was removed by filtration and the filtrate was adjusted to pH 3—4 with formic acid. A considerable amount of colorless needles of the 5-aminopyrimidine deposited on neutralization. Without isolating the needles, the mixture was added to 5-deoxy-L-arabinose phenylhydrazone[9] (32 g) in methanol (400 ml). The resulting solution was stirred under nitrogen at 25 °C for 90 min, and then under reflux for 30 min. After chilling, it was added to a solution of potassium hexacyanoferrate(III) (100 g), potassium iodide (5 g), and formic acid (10 ml) in water (500 ml). The solution was stirred under bubbling oxygen at pH 3—4 and 25 °C for 20 h. The solution was concentrated to about 500 ml under reduced pressure and made alkaline (pH 9—10) with ammonia. The nonfluorescent precipitate was removed by filtration and the filtrate was fractionated on a Florisil column (5×60 cm) using water as the elution solvent to give two blue fluorescent fractions. The major fraction, after concentration to about 150 ml, was chromatographed again on Florisil in the same way as above. The eluate was evaporated to dryness under reduced pressure and the residue was extracted with hot methanol (500 ml). Concentration of the extract to about 50 ml and chilling gave colorless needles (5.5 g) of 4-hydroxy-6-(L-*erythro*-1,2-dihydroxypropyl)-2-(methylthio)pteridine (**3b**), which decomposed above 210 °C without melting (from water) (Found: C, 40.27; H, 4.45; N, 18.65%. Calcd for $C_{10}H_{12}N_4O_3S \cdot 2H_2O$: C, 39.46; H, 5.31; N, 18.41%). The minor fraction, after purification as above, yielded 1.9 g of 4-hydroxy-2-(methylthio)pteridine (**6**), mp 268—269 °C (dec) (from water) (Found: C, 43.59, H, 3.08; N, 28.72%. Calcd for $C_7H_6N_4OS$: C, 43.29; H, 3.11; N, 28.85%). This compound was synthesized alternatively by heating 4,5-diamino-6-hydroxy-2-(methylthio)pyrimidine and equimolar glyoxal in water under reflux for 30 min (68% yield).

By employing D- or L-arabinose phenylhydrazone in palce of 5-deoxy-L-arabinose phenylhydrazone in the above reaction, 4-hydroxy-6-(D-*erythro*-1,2,3-trihydroxypropyl)-2-(methylthio)-pteridine (**4b**) [70% yield, mp 156—158 °C (dec) (from water) (Found: C, 39.63; H, 4.68; N, 18.03%. Calcd for $C_{10}H_{12}N_4O_4S \cdot H_2O$: C, 39.72; H, 4.68; N, 18.54%)] and the L-isomer (**5b**) [62% yield, mp 156—158 °C (dec) (from water) (Found: C, 39.75; H, 4.63; N, 18.17%. Calcd for $C_{10}H_{12}N_4O_4S \cdot H_2O$: C, 39.72; H, 4.68; N, 18.54%)] were respectively obtained.

*Biopterin (**3a**) and* D *(and* L*)*-erythro-*Neopterins (**4a** and **5a**).* A solution of **3b** (200 mg), ammonium acetate (0.6 g), and 28% aqueous ammonia (5 ml) was heated under reflux for 4 h. The solution was adjusted to pH 2 with hydrochloric acid and fractionated on a Florisil column (3.5×20 cm) using water as the elution solvent. The eluate was evaporated to dryness under reduced pressure and the residue was extracted with 1% ammonia (50 ml). The extract was concentrated to about 10 ml, adjusted to pH 3, and chilled to give ivory needles (90 mg) of biopterin, which was identified with

the authentic sample.[9])

In a similar way, **4b** and **5b** were converted to D-*erythro*-neopterin (**4a**) (62% yield) and L-*erythro*-neopterin (**5a**) (72% yield), respectively.

*4-Hydroxy-2-[2-(p-hydroxyphenyl)ethylamino]-6-(*L-erythro-*1,2-dihydroxypropyl)pteridine (3c) and the Trihydroxypropyl Analogues (4c and 5c).* A solution of **3b** (1.0 g), tyramine (3 g), and acetic acid (0.8 g) in 50% aqueous 2-methoxyethanol (8 ml) was heated at 100—105 °C for 6 h. The solution was adjusted to pH 1—2 with hydrochloric acid and placed on a Florisil column (3.5×40 cm). The column was washed with 2 M formic acid (0.5 l) and water (0.5 l) to remove the excess tyramine and a small amount of **3b**. The column was then eluted gradiently with 0—2% ammonia (1 l). The eluate, after concentration to about 150 ml, was again chromatographed in the same way as above and the final eluate was evaporated to dryness. The residue was extracted with 2% ammonia (200 ml), which was concentrated to about 100 ml. The solution was adjusted to pH 3 with formic acid and chilled to give yellow needles (34% yield) of **3c**, which decomposed at 165 °C (from water) (Found: C, 54.56; H, 5.62; N, 18.38%. Calcd for $C_{17}H_{19}N_5O_4 \cdot H_2O$: C, 54.39; H, 5.64; N, 18.66%).

Similar treatnent of **4b** and **5b** with tyramine gave **4c** [30% yield, mp 180—182 °C (dec) (from water) (Found: C, 49.88; H, 5.05; N, 16.72%. Calcd for $C_{17}H_{19}N_5O_5 \cdot 2H_2O$: C, 49.87; H, 5.66; N, 17.11%)] and **5c** [32% yield, mp 180—182 °C (dec) (from water) (Found: C, 49.88; H, 5.23; N, 16.90%. Calcd for $C_{17}H_{19}N_5O_5 \cdot 2H_2O$: C, 49.87; H, 5.66; N, 17.11%)], respectively.

*4-Hydroxy-6-(*L-erythro-*1,2-dihydroxypropyl)-2-(*p-*methoxybenzylamino)pteridine (3d) and the Trihydroxypropyl Analogues (4d and 5d).* A mixture of **3b** (1.0 g), *p*-methoxybenzylamine (2 g), and acetic acid (0.6 g) was heated at 100—105 °C for 4 h. The solution was adjusted to pH 3 with 50% formic acid and placed on a Florisil column (3.5×30 cm). The column was washed with 2M formic acid (500 ml) and then eluted gradiently with 0—2% ammonia (2 l). The eluate was concentrated to about 100 ml, made acid with formic acid, and then evaporated to dryness. The residue was extracted with hot methanol (100 ml). Concentration of the extract to about 5 ml and dilution with water (5 ml) gave pale yellow needles (50% yield) of **3d**, mp 226—227 °C (dec) (from 50% aqueous methanol) (Found: C, 54.70; H, 5.35; N, 18.33%. Calcd for $C_{17}H_{19}N_5O_4 \cdot H_2O$: C, 54.39; H, 5.64; N, 18.66%).

A similar reaction of **4b** and **5b** with *p*-methoxybenzylamine gave respectively **4d** as pale yellow needles [26% yield, darkened above 230 °C without melting (from methanol) (Found: C, 54.60; H, 5.02; N, 18.56%. Calcd for $C_{17}H_{19}N_5O_5$: C, 54.68; H, 5.13; N, 18.76%)] and **5d**[50% yield, darkened above 230 °C without melting (Found: C, 54.57; H, 5.06; N, 18.44%. Calcd for $C_{17}H_{19}N_5O_5$: C, 54.68; H, 5.13; N, 18.76%)].

*4-Hydroxy-6-(*L-erythro-*1,2-dihydroxypropyl)-2-(*p-*methoxyphenylamino)pteridine (3e) and the Trihydroxypropyl Analogues (4e and 5e).* A solution of **3b** (1.0 g), *p*-anisidine (8 g), and acetic acid (3 g) in *N,N*-dimethylformamide (15 ml) was heated at 80 °C for 8 h. The solution was fractionated on Florisil as above to give pale yellow needles (78% yield) of **3e**, which decomposed at 273 °C (from water) (Found: C, 56.08; H, 4.86; N, 20.23%. Calcd for $C_{16}H_{17}N_5O_4$: C, 55.97; H, 4.99; N, 20.40%).

In a similar way, the D-trihydroxypropyl analogue (**4e**) [43% yield, decomposed above 250 °C without melting (Found: C, 53.43; H, 4.63; N, 19.28%. Calcd for $C_{16}H_{17}N_5O_5$: C, 53.48; H, 4.77; N, 19.49%)] and the L-trihydroxypropyl analogue (**5e**) [30% yield, decomposed above 250 °C without melting (Found: C, 53.30; H, 4.64; N, 19.24%. Calcd for $C_{16}H_{17}N_5O_5$: C, 53.48; H, 4.77; N, 19.49%)] were obtained from the respective 2-(methylthio)pteridines (**4b** and **5b**).

*4-Hydroxy-6-(*L-erthro-*1,2-dihydroxypropyl)-2-phenylaminopteridine (3f) and the Trihydroxypropyl Analogues (4f and 5f).* These compounds were synthesized from the corresponding 2-methylthio precursors (**3b**, **4b**, and **5b**) and aniline in a way similar to that for the *p*-methoxybenzylamino analogues. The (1,2-dihydroxypropyl)pteridine (**3f**) was obtained as pale yellow needles (22% yield), mp 270—271 °C (dec) (from methanol) (Found: C, 57.38; H, 4.77; N, 21.83%. Calcd for $C_{15}H_{15}N_5O_3$: C, 57.50; H, 4.83; N, 22.34%). The (D-*erythro*-trihydroxypropyl)pteridine (**4f**) was obtained in 57% yield as pale yellow needles which decomposed above 260 °C without melting (Found: C, 54.80; H, 4.37; N, 21.04%. Calcd for $C_{15}H_{15}N_5O_4$: C, 54.71; H, 4.59; N, 21.27%). The (L-*erythro*-trihydroxypropyl)pteridine (**5f**), obtained in 33% yield as pale yellow needles, decomposed above 260 °C without melting (Found: C, 54.82; H, 4.46; N, 21.12%. Calcd for $C_{15}H_{15}N_5O_4$: C, 54.71; H, 4.59; N, 21.27%).

The authors would like to thank Mrs. Noriko Nishioka for the measurement of pK_a values and UV spectra.

References

1) Part III: S. Matsuura, T. Sugimoto, H. Hasegawa, S. Imaizumi, and A. Ichiyama, *J. Biochem.* (*Tokyo*), **87**, 951 (1980).

2) S. Kaufman, *Proc. Natl. Acad. Sci. U.S.A.*, **50**, 1085 (1963).

3) T. Nagatsu, M. Levitt, and S. Underfield, *J. Biol. Chem.*, **239**, 2910 (1964).

4) A. Ichiyama, S. Nakamura, Y. Nishizuka, and O. Hayaishi, *J. Biol. Chem.*, **245**, 1699 (1970).

5) S. Kaufman, S. Berlow, G. K. Summer, S. Milstein, J. D. Schulman, S. Orloff, S. Spielberg, and S. Pueschel, *New Engl. J. Med.*, **299**, 673 (1978).

6) A. Neiderwieser, H. -Ch. Curtius, O. Bettoni, J. Beri, B. Schirks, M. Viscontini, and J. Schaub, *Lancet*, i, 131 (1979).

7) T. Nagatsu, T. Yamaguchi, T. Kato, T. Sugimoto, S. Matsuura, K. Kobayashi, M. Akino, S. Tsushima, N. Nakazawa, and H. Ogawa, *Proc. Jpn. Acad., Ser. B*, **55**, 317 (1979).

8) T. Sugimoto and S. Matsuura, *Bull. Chem. Soc. Jpn.*, **52**, 181 (1979).

9) T. Sugimoto and S. Matsuura, *Bull. Chem. Soc. Jpn.*, **48**, 3767 (1975).

10) M. Viscontini, R. Provenzale, S. Ohlgart, and J. Mallevialle, *Helv. Chim. Acta*, **53**, 1202 (1970).

11) A. Albert and E. P. Serjant, "Ionization Constants of Acids and Bases," Methuen, London (1962).

12) C. O. Johns and E. J. Baumann, *J. Biol. Chem.*, **14**, 381 (1913).

Neighboring Group Participation in Solvolysis. X. Dissection of Ar_1-5 and Ar_2-6 Pathways in Trifluoroacetolysis of 4-Arylbutyl 6-Methyl-2-naphthalenesulfonates[1]

Takashi Ando,* Junko Yamawaki, Yoshimasa Saito, Yoshio Takai, and Hiroshi Yamataka

The Institute of Scientific and Industrial Research, Osaka University, Yamadakami, Osaka 565

(Received February, 9, 1980)

Trifluoroacetolysis rates and products were determined for eleven 4-(*m*- and *p*-substituted phenyl)butyl 6-methyl-2-naphthalenesulfonates. Most substrates solvolyze predominantly or even exclusively with aryl assisted (k_Δ) pathway. Dissection of k_Δ into Ar_1-5 and Ar_2-6 components was performed by means of quantitative ^{13}C NMR study of suitably labeled *p*-methyl and *p*-fluoro derivatives; the results were 32.4% Ar_1-5 and 67.6% Ar_2-6 for the former and 43.3% Ar_1-5 and 56.7% Ar_2-6 for the latter. For other substrates the dissection was carried out by postulating two independent linear free energy relationships (LFER) for the two pathways determined by the above four partial rates. Ar_2-6 is much prefered over Ar_1-5 through the series; for the unsubstituted derivative 90.6% Ar_2-6 *vs.* 9.4% Ar_1-5 was determined. A completely different approach by means of non-linear regression analysis of k_Δ as a sum of two independent LFER gave fairly different and rather unsettled results, limitations of such an approach being suggested. The characteristics of remote aryl participation are discussed based on the above data.

Recent study in this laboratory has shown that participation of a remote phenyl group is much more enhanced in a solvent of low nucleophilicity and high ionizing power such as trifluoroacetic acid than in an ordinary solvent.[2] 4-Phenylbutyl 6-methyl-2-naphthalenesulfonate (menasylate; Mns)[3] was found to solvolyze exclusively *via* the phenyl assisted pathway with 26.2 times rate enhancement relative to the standard, butyl menasylate. Heck and Winstein, who studied remote aryl participation in solvolysis systematically for the first time, proposed that δ-aryl participation proceeds with two possible modes; participation by the phenyl-1 (ipso) carbon forming a five-membered ring (Ar_1-5) and that by the phenyl-2 (ortho) carbon forming a six-membered ring (Ar_2-6) (Scheme 1).[4]

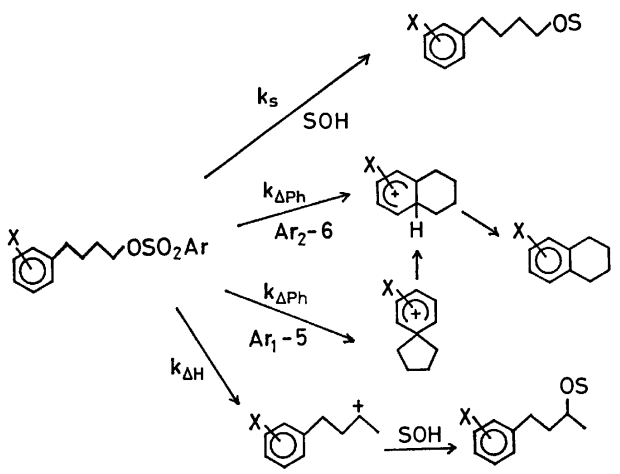

Scheme 1.

While anchimerically unassisted solvolysis gives a primary alkyl product, either mode of phenyl assisted solvolysis gives rise to 1,2,3,4-tetrahydronaphthalene (tetralin) as a final product. The rate constant of the former was designated k_s and that of the latter $k_{\Delta ph}$ as distinguished from $k_{\Delta H}$, the rate constant of neighboring hydrogen assisted solvolysis, which was found important in trifluoroacetic acid (Scheme 1, S= CF_3CO).[2,4] The identity of the products from the two modes of the $k_{\Delta ph}$ pathway makes its dissection difficult. The dissection is possible, however, by the double labeling technique, one lable on the phenyl ring and the other on the alkyl chain (Scheme 2).

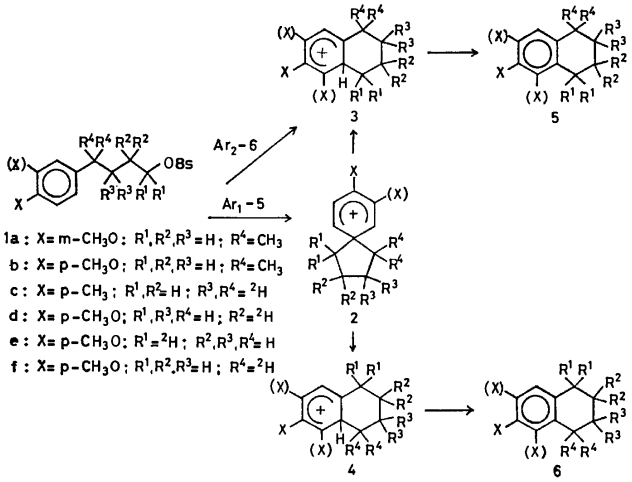

Scheme 2.

Two differently substituted tetralins will be produced from a *p*-substituted substrate, and four from a *m*-substituted one. If we can accurately analyze the composition of tetralin isomers and also if we can reasonably estimate the migration ratio of CR^1R^1 and CR^4R^4 groups from the Ar_1-5 intermediate (**2**) to two types of protonated tetralins (**3** and **4**), then the two modes of $k_{\Delta ph}$ can be dissected quantitatively. Thus, Winstein and Heck studied the formolysis of 4-(*m*- and *p*-methoxyphenyl)butyl *p*-bromobenzenesulfonates (brosylates; Bs) utilizing methyl groups as a label on the alkyl chain (**1a** and **b**).[5] They postulated that only the $C(CH_3)_2$ group could migrate to the ortho position and the CH_2 group could not in the spiro intermediate **2**. Thus, the product ratio of **5** *vs.* **6** was considered to

be equal to the path ratio of Ar_2-6 *vs.* Ar_1-5. Introduction of two methyl groups on the chain, however, allows the intervention of a tertiary cation produced by ring opening of **2**, making the product analysis rather complicated. Furthermore, substitution with methyl groups is too large to be regarded as a perturbation. It is risky to estimate the behavior of the unperturbed substrate from the results of the dimethylated ones.

Jackman and Haddon,[6] and Gates and his coworkers[7] studied this dissection problem by use of deuterium as a label on the chain (**1c**—**f**). Although their analyses seem reasonable and substitution by deuterium is small enough a perturbation, the produced tetralins had to suffer rather drastic reaction such as oxidation or reduction before isotope analysis by means of mass spectroscopy was performed. These operations are tedious and may cause serious errors.

Carbon-13 NMR spectroscopy has become a familiar technique for organic chemists in recent years. Although quantitative application of FT NMR has so far been little exploited because of the widespread belief that the peak area does not give any information about the number of nuclei, it is actually quite useful in the quantitative and nondestructive analysis if enough precautions are taken. The large chemical shift range of ^{13}C NMR becomes one of the principal advantages in the quantitative analysis too. In this paper we report our study of the dissection of $k_{\Delta ph}$ in the trifluoroacetolysis of 4-(*p*-methyl- and *p*-fluorophenyl)butyl brosylates into Ar_1-5 and Ar_2-6 pathways by applying ^{13}C NMR to the analysis of the tetralins produced from suitably isotope-labeled substrates.

Although the double labeling technique with ^{13}C on the chain and a substituent on the ring is a sound method for evaluating the two reaction pathways, preparation of all the substituted phenylbutyl derivatives labeled with ^{13}C is laborious and expensive. Furthermore, the technique is not generally applicable because the quantitative analysis is only possible when tetralin isomers give a sufficient chemical shift difference. Among others $k_{\Delta ph}$ of the unsubstituted substrate can never be dissected by this method. On the other hand, if the two pathways are discrete and the partial rates of the both pathways follow individual LFER, a study of the substituent effects on the rate constants $k_{\Delta ph}$, when combined with the results of the double labeling technique, must give a possibility of a new and general approach to the dissection problem. Thus, $k_{\Delta ph}$ of substituted and unsubstituted substrates can reasonably be dissected to the two partial rates in such a manner as they follow two Hammett-type relationships, which have been determined by the data obtained from the double labeling method utilizing ^{13}C NMR spectroscopy. Two LFER thus obtained may give further information on the characteristics of remote aryl participation.

If the two independent LFER hold for the individual partial rates as postulated above, $k_{\Delta ph}$ can be described as a sum of them. Then, a completely different approach by means of non-linear regression analysis of substituent effects on $k_{\Delta ph}$ may become another possibility. It is a pure kinetic approach in contrast to the combination of the kinetic and product analyses described above. The results of this computer-programmed analysis are compared with those from the above combinational one, and the soundness of the two approaches is discussed.

Results

Trifluoroacetolysis rates of eleven 4-(*m*- and *p*-substituted phenyl)butyl menasylates (**7a**—**k**) were determined by the spectrophotometric method as described earlier.[2,3] The observed rate constants together with the corresponding activation parameters are given in Table 1, in which the data of butyl menasylate (**8**)[2] are also included. Each reported rate constant is the average value of duplicate to quadruplicate runs. The individual runs gave linear first-order rate plots over two half-lives for all the compounds with correlation coefficients greater than 0.9995.

$X\text{-}C_6H_4(CH_2)_4OMns$ $CH_3(CH_2)_3OMns$

7a: X=*m*-CH_3 **g**: X=*p*-F **8**
b: X=*p*-CH_3 **h**: X=*m*-Cl
c: X=*m*-CH_3O **i**: X=*p*-Cl
d: X=*p*-CH_3O **j**: X=*p*-Br
e: X=H **k**: X=*m*-CF_3
f: X=*m*-F

Reaction products were analyzed by gas chromatography after more than six half-lives under the same conditions as those for the kinetic runs. Reaction solutions containing dodecane as an internal standard were injected directly into a gas chromatograph. The yields of the products corrected with their respective sensitivities are summarized in Table 2. Control experiments showed that typical tetralins (unsubstituted and 6-CH_3) and a primary trifluoroacetate (unsubstituted) were stable under the reaction conditions.[2]

In the trifluoroacetolysis of [1,1-$^2H_2$]-4-(*p*-methoxyphenyl)butyl menasylate (**7d**-1,1-$^2H_2$), no deuterium scrambling was detected in the recovered menasylate after one half-life. The same observation was already reported for **7e**-1,1-$^2H_2$.[2]

^{13}C NMR study was performed with 4-(*p*-methyl- and *p*-fluorophenyl)butyl brosylates (**9b** and **g**, respectively) instead of menasylates **7b** and **g**. Although the menasylate is an excellent leaving group for the rate study,

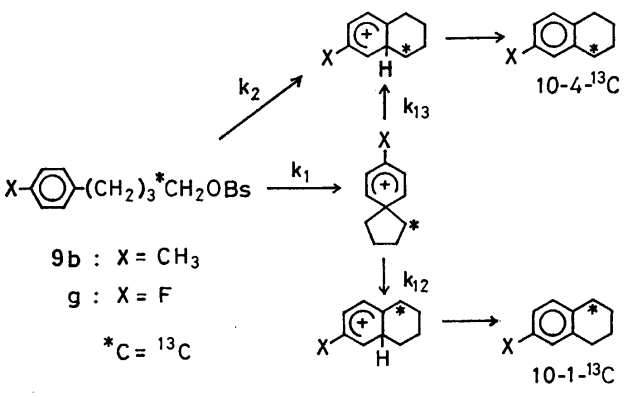

Scheme 3.

Table 1. Trifluoroacetolysis rates of 4-arylbutyl menasylates

Substituent	t/°C	$k_t \times 10^5$/s^{-1}	k_{rel}[a]	$\Delta H^{\neq}$/kcal mol^{-1} [b]	$\Delta S^{\neq}$/cal K^{-1} mol^{-1} [c]
m-CH_3 (**7a**)	50	4.19±0.02	117	19.9	−17.2
	65	17.3 ±0.1			
	70[d,e]	27.0			
p-CH_3 (**7b**)	50	3.64±0.03	106	20.3	−16.3
	60	9.58±0.03			
	70	24.3 ±0.1			
m-CH_3O (**7c**)	60	3.34±0.03	38.1	21.2	−15.5
	70	8.76±0.14			
p-CH_3O (**7d**)	60	2.93±0.02	34.2	22.1	−13.5
	70	7.86±0.04			
	80	20.6 ±0.1			
H (**7e**)[f]	70	7.46±0.02	32.4	21.2	−15.7
m-F (**7f**)	70[d]	1.02	4.43	21.3	−19.6
	85	3.95±0.02			
	105	20.3 ±0.1			
p-F (**7g**)	70[d]	1.24	5.39	21.3	−19.2
	85	4.79±0.06			
	105	24.6 ±0.3			
m-Cl (**7h**)	70[d]	0.832	3.62	21.5	−19.5
	90	4.98±0.02			
	110	24.8 ±0.1			
p-Cl (**7i**)	70[d]	0.615	2.67	22.5	−17.0
	90	3.98±0.01			
	100	9.65±0.03			
	110	21.4 ±0.1			
p-Br (**7j**)	70[d]	0.622	2.70	21.4	−20.2
	90	3.72±0.05			
	110	18.5 ±0.2			
m-CF_3 (**7k**)	70[d]	0.168	0.730	21.3	−23.2
	100	2.25±0.01			
	110	18.5 ±0.2			
$CH_3(CH_2)_3OMns$ (**8**)[f]	70[d]	0.230	1.00	23.1	−17.2

a) Relative rates to that of **8** at 70 °C. b) 1 kcal mol^{-1}=4.184 kJ mol^{-1}. c) 1 cal K^{-1} mol^{-1}=4.184 J K^{-1} mol^{-1}. d) Calculated from data at other temperatures. e) An observed rate constant of a single run was 27.4×10^{-5} s^{-1}. f) Ref. 2.

menasyl chloride is commercially unavailable. As the difference in the leaving group is reasonably expected to have no effect on the fractions of the two neighboring aryl assisted pathways, **9b** and **g** both labeled with 90% ^{13}C at 1-position as well as the unlabeled ones were prepared and solvolyzed. ^{13}C-Enriched and "natural abundance"[8] tetralins with a substituent on the 6-position (**10b** and **g**) were isolated from the reaction solutions after more than seven half-lives and then purified by column chromatography and molecular distillation (Scheme 3).

FT NMR spectra were taken with great care under the conditions adequate for quantitative analysis,[9,10] particularly with a long pulse interval and a small pulse flip angle (*cf.* Experimental Section). Under these conditions the peak area ratio of the two benzylic carbons, 1- to 4-position, of the 6-methyl "natural abundance" tetralin (**10b**) was 1/1.016, and that of the 6-fluorotetralin (**10g**) was 1/1.097. The inequality in the latter may be attributed to the peak splitting of the C_4 by the long-range coupling with the fluorine (1.6 Hz). The peak area ratio of the ^{13}C-enriched tetralin was 1/4.950 for the 6-CH_3 derivative and 1/3.817 for the 6-F one under the same conditions as above.

Discussion

Table 1 shows that the trifluoroacetolysis rates of 4-arylbutyl menasylates **7** vary more than 10^2 depending on the substituents of the phenyl ring. This large substituent effect of the aryl group remote from the reaction center clearly indicates the development of the direct interaction between these two groups in the transition state of the reaction. It is consistent with the fact that most substrates gave tetralins as principal products in the yields more than 90% (Table 2). Thus, it is concluded undoubtedly that the trifluoroacetolyses of most of 4-arylbutyl menasylates proceed predominantly or even exclusively with remote aryl group participation.

As being implied qualitatively in the above discussion, it is generally accepted that aryl assisted ($k_{\Delta ph}$) and aryl unassisted (k_s) reactions are discrete in 4-arylbutyl solvolysis just like as in 2-arylethyl solvo-

Table 2. Trifluoroacetolysis products of 4-arylbutyl menasylates[a]

Substituent	6-Tetralin[b]	5-Tetralin[c]	1-ROTFA[d]	2-R'OTFA[e]
m-CH_3 (**7a**)[f]	48.9	51.1	0	0
p-CH_3 (**7b**)	97.6	—	0	0
m-CH_3O (**7c**)[g]	56.6	24.6	0	0
H (**7e**)	99.8	—	0	0
m-F (**7f**)	91.2[h]		2.3	2.6
p-F (**7g**)	94.3	—	0.4	1.1
m-Cl (**7h**)	47.2	42.9	3.8	4.6
p-Cl (**7i**)	91.5	—	4.4	4.8
p-Br (**7j**)	91.1	—	4.5	5.4

a) Yields in %. No analysis was performed for the *p*-CH_3O derivative (**7d**). The *m*-CF_3 derivative (**7k**) did not give a clear-cut result. b) 6-Substituted tetralin. c) 5-Substituted tetralin. d) 4-Arylbutyl trifluoroacetate. e) 3-Aryl-1-methylpropyl trifluoroacetate. f) Only relative yields were determined, but methyltetralin was confirmed to be stable under the reaction conditions. g) An unknown compound (*ca.* 5%) was detected. h) The isomers could not be separated by gas chromatography. ^{13}C and ^{19}F NMR spectra showed that the mixture contained 75±1% 6-fluoro- and 25±1% 5-fluorotetralins.

lysis.[2,5,6,11] Thus, the yields of tetralins correspond to the fractions of $k_{\Delta ph}$ in k_t. Furthermore, the lack of deuterium scrambling in the samples of **7d-** and **e**-1,1-$^2H_2$ recovered from the reaction solutions revealed that ion-pair return from the spiro Ar_1-5 intermediate to the starting menasylate, either directly or *via* the Ar_2-6 intermediate, is prohibited. Friedlich and Winstein also reported their observation that ring expansion of the spiro Ar_1-5 intermediate was very much faster than ring opening or solvolysis.[12] These facts suggest that the two pathways of $k_{\Delta ph}$ are also discrete, and that the ratio of the two partial rate constants can be described as a function of the relative amounts of two isomeric tetralins. Thus, the two partial rate constants, k_1 and k_2 in Scheme 3, are able to be calculated from the combined data of the titrimetric rate constants k_t (Table 1), the yields of tetralins determined by gas chromatography (Table 2), and the fractions of the two pathways estimated quantitatively from the contents of isomeric tetralins.

From the two sets of the ^{13}C NMR data on **10b** and **g**, the ratio of the two pathways, k_1 *vs.* k_2, can be calculated for both **9b** and **g**. A "natural abundance" tetralin was obtained from **9** labeled with 1.1% each of 1-^{13}C and 4-^{13}C, and an enriched tetralin from **9** labeled with 90% 1-^{13}C and 1.1% 4-^{13}C. Since k_1/k_2 and k_{12}/k_{13} are common for each isotopic substrate, the rate ratio k_1/k_2 can be described as a function of k_{12}/k_{13} and the peak area ratios of the two benzylic carbons in the two types of tetralins, "natural abundance" and ^{13}C-enriched. By assuming no kinetic isotope effect at the migration step ($k_{12}/k_{13}=1.00$), the fractions of the two pathways were determined 32.4% Ar_1-5 and 67.6% Ar_2-6 for the *p*-CH_3 derivative and 43.3% Ar_1-5 and 56.7% Ar_2-6 for the *p*-F one. The isotope effect can reasonably be neglected because an effect of 5% ($k_{12}/k_{13}=1.05$) could alter the fractions of the pathways by only 0.3%. Then, by neglecting the difference in the leaving group, four partial rate constants, $k_1^{p\text{-}CH_3}$, $k_2^{p\text{-}CH_3}$, $k_1^{p\text{-}F}$, and $k_2^{p\text{-}F}$, in the trifluoroacetolysis of **7** can be obtained. The ^{13}C NMR measurement was repeated for **10g** with two other FT instruments and even with a CW one in order to confirm the above results. The fractions of the two pathways thus obtained agreed with each other within a range of ±1.0%.

It is interesting to compare the present results in the trifluoroacetolysis of **9b** with those in the formolysis of **1c** reported by Jackman and Haddon.[6] Their results, 30.6—33.6% Ar_1-5 and 69.4—66.4% Ar_2-6 varying with an assumed kinetic isotope effect in the migrating step of **2**, is in complete agreement with ours. It suggests the accuracy of their results in spite of the difficulty in their experiment as well as the absence of the solvent effect on the fractions of the two pathways. The latter conclusion is reasonable because the two pathways are both neighboring aryl assisted ones and the susceptibilities of the two transition states to the nature of the solvent must be similar. It is in contrast with the solvent effect on the ratio of k_Δ *vs.* k_s as we demonstrated already.[2]

It is well known that reactivities of *m*- and *p*-substituted benzene derivatives generally follow the Hammett-type LFER.[13] Substituent effects on the rates of the neighboring aryl assisted solvolysis of 2-arylethyl derivatives have also been treated successfully in this manner.[11] As a quite natural extension of 2-arylethyl solvolysis, the two pathways of remote aryl participation are expected to follow their individual LFER. The four partial rate constants of **7b** and **g** obtained above must give rise to two Hammett-type relationships for the two pathways, which then must hold for other substrates.[14] Thus, the rate constants $k_{\Delta ph}$ of other substrates can be divided into k_1 and k_2 in such a manner as their ratios hold the ones determined by the above two LFER.

Yukawa and Tsuno proposed the LArSR (linear aromatic substituent reactivity) relationship (Eq. 1)

$$\log k/k_0 = \rho(\sigma^0 + r\Delta\bar{\sigma}_R^+) \qquad (1)$$

as a generalized equation of the extended Hammett relationship for reactions with nucleophilic character.[15] According to Tsuno, most k_Δ pathways of 2-arylethyl and related substrates have *r* values (resonance parameters) about 0.5.[16] Schadt, Lancelot, and Schleyer reported that the substituent constants obtained from the acetolysis of substituted neophyl brosylates, σ(neophyl), are effective for all other related solvolyses; σ(neophyl) correspond to the substituent constants with $r=0.58$ in the Yukawa-Tsuno treatment, Eq. 1.[11] Thus, we assumed that similar substituent constants, $\sigma^0+0.5\Delta\bar{\sigma}_R^+$ ($\equiv\sigma^\Delta$), are also effective for the two remote aryl participation reactions, and carried out the kinetic dissection using these σ^Δ.

Contrast to the Ar_1-5 pathway, in which *m*- and *p*-substituents behave naturally as *m*- and *p*-ones, respectively, in the Ar_2-6 pathway *m*-substituents affect the reaction center as *o*- or *p*-ones, and *p*-substituents as *m*-ones, respectively (Scheme 2). As σ_o has not been

well established as σ_p, only σ_p was used for the Ar_2-6 pathway of the *m*-CH_3 and *m*-Cl derivatives, for which the reactivities of the *o*- and *p*-positions were estimated similar from the relative yields of 5- and 6-substituted tetralins (Table 2). The dissection of $k_{\Delta ph}$ of the *m*-F derivative, in which the reactivity of the *o*-position is apparently lower than that of the *p*-one[17] (*cf.* footnote h of Table 2), was carried out by modifying the σ_p value in order to reflect this decreased reactivity. Since the substituent constants of a methoxyl group are not clear in trifluoroacetic acid, which is a strongly acidic solvent prone to form a hydrogen bond with the methoxyl oxygen, the dissection was unable to be performed. In fact, the rate enhancement in **7c** and **d** was much smaller than that expected for substrates with a strongly electron-donating substituent. Furthermore, the product study of **7c** revealed that an unknown compound other than methoxytetralins was detected in the reaction solution. Methoxytetralins may be unstable under the reaction conditions. The dissection was also impossible for the *m*-CF_3 derivative **7k**, because its product analysis did not give a clear-cut result. Thus, the dissection by means of the combination of the product and kinetic analyses was carried out for **7a**, **b**, **e**, **f**, **g**, **h**, **i**, and **j**. The results are summarized in Table 3.

Table 3. Dissection of $k_{\Delta Ph}$ into Ar_1-5 and Ar_2-6 pathways

Substituent	$k^{70}_{\Delta Ph}\times 10^5/s^{-1}$	$k_1\times 10^5/s^{-1}$	$k_2\times 10^5/s^{-1}$	% Ar_1-5	% Ar_2-6
m-CH_3 (**7a**)	27.0	1.0	26.0	3.7	96.3
p-CH_3 (**7b**)	23.7	7.7	16.0	32.4[a]	67.6[a]
H (**7e**)	7.45	0.70	6.75	9.4	90.6
m-F (**7f**)	0.930	0.009	0.921	1.0	99.0
p-F (**7g**)	1.17	0.51	0.66	43.3[a]	56.7[a]
m-Cl (**7h**)	0.750	0.009	0.741	1.2	98.8
p-Cl (**7i**)	0.563	0.132	0.431	23.4	76.6
p-Br (**7j**)	0.567	0.122	0.445	21.5	78.5

a) Determined by NMR analysis.

The four partial rate constants of **7b** and **g** gave ρ values of -4.07 for Ar_1-5 and -3.29 for Ar_2-6. After the dissection for the other substrates were performed, the linear regression of the calculated partial rate constants of all the substrates except **7f** gave the two LFER, Eqs. 2 and 3, in which k_1^X and k_2^X represent the rate constants of the Ar_1-5 and Ar_2-6 pathways, respectively, of the X-substituted **7**, and k^H ($=k_1^H+k_2^H$) denotes the overall rate constant of **7e**. The two LFER are plotted in Fig. 1.

$$\log k_1^X/k^H = -4.42\sigma^\Delta - 0.99 \quad \text{(correlation coeff: 0.985)} \quad (2)$$

$$\log k_2^X/k^H = -3.05\sigma^\Delta - 0.07 \quad \text{(correlation coeff: 0.978)} \quad (3)$$

The successful dissection of the rate constants of the neighboring aryl assisted reaction, $k_{\Delta ph}$, into k_1 and k_2, which are described by the two independent LFER, suggests a possibility of completely different approach. Since the two LFER are represented as Eqs. 4 and 5,

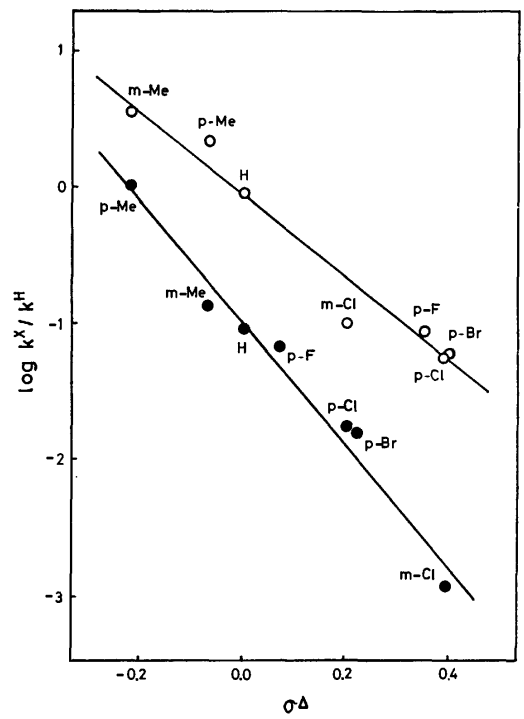

Fig. 1. LFER plots of dissected rate constants *vs.* σ^Δ.
●: k_1 (for Ar_1-5), ○: k_2 (for Ar_2-6).

the substituent effects on $k_{\Delta ph}$ ($\equiv k=k_1+k_2$) can be written as Eq. 6.

$$\log k_1^X/k_1^H = \rho_1\sigma_1^\Delta; \quad k_1^X = k_1^H\, 10^{\rho_1\sigma_1^\Delta} \quad (4)$$

$$\log k_2^X/k_2^H = \rho_2\sigma_2^\Delta; \quad k_2^X = k_2^H\, 10^{\rho_1\sigma_1^\Delta} \quad (5)$$

$$k^X/k^H = k_1^X/k^H + k_2^X/k^H = k_1^H\, 10^{\rho_1\sigma_1^\Delta}/k^H + k_2^H\, 10^{\rho_1\sigma_1^\Delta}/k^H \quad (6)$$

When the Ar_1-5 fraction of **7e**, k_1^H/k^H, is designated α, Eq. 6 can be substituted by Eq. 7.

$$k^X/k^H = \alpha 10^{\rho_1\sigma_1^\Delta} + (1-\alpha)10^{\rho_1\sigma_1^\Delta} \quad (7)$$

Non-linear regression analysis utilizing Eq. 7 was thus performed by putting in k^H and sets of k^X, σ_1^Δ, σ_2^Δ in order to determine the optimum values of α, ρ_1, and ρ_2. Computer-programmed calculations by means of the simplex[18] and Powell methods[19] gave a same answer, Eqs. 8 and 9.

$$\log k_1^X/k^H = -3.95\sigma^\Delta - 0.54 \quad \text{(correlation coeff: 0.996)} \quad (8)$$

$$\log k_2^X/k^H = -3.53\sigma^\Delta - 0.24 \quad \text{(correlation coeff: 0.997)} \quad (9)$$

Although the linearity of each LFER is excellent, fractions of the two pathways for all the substrates are quite different from those obtained by the combinational approach of product and kinetic analyses (Table 3). In particular, the calculated results for **7b** and **g**, 67% Ar_1-5 and 33% Ar_2-6 for **7b** and 83% Ar_1-5 and 17% Ar_2-6 for **7g**, did not coincide with the values determined directly by the NMR analysis at all.

Since the substituent constants are variable as shown in Eq. 1 and we are unaware how large the resonance parameter r should be in the two LFER, the non-linear regression analysis was extended to include the sets of

r_1 and r_2 both varied independently from 0 to 1 in Eq. 10.

$$k^X/k^H = \alpha 10^{\rho_1(\sigma_1^0 + r_1\Delta\bar{\sigma}_{R1}^+)} + (1-\alpha)10^{\rho_2(\sigma_2^0 + r_2\Delta\bar{\sigma}_{R2}^+)} \quad (10)$$

The results varied to a large extent depending on the r values used. However, any combination of r_1 and r_2 was unable to reproduce the observed data of the fractions of the two pathways for **7b** and **g** simultaneously. Furthermore, when the non-linear regression analysis by use of Eq. 10 was performed by treating r_1 and r_2 also as variables, it converged on an improbable point where r_1 was close to 0 and r_2 was larger than 1. The observed data for **7b** and **g** were again not reproduced at this point. Thus, the nonlinear regression analysis was unsuccessful in this case.

We do not regard the failure of the non-linear regression analysis in this case as the fundamental defect of the method. This type of analysis must be easier when the two reactions have different types of characters.[11,20,21] Unfortunately, ρ_1 and ρ_2 are both negative and similar in magnitude in this case. Strict accuracy of all the data used for the analysis, *i.e.*, $k_{\Delta ph}$ and σ, is an indispensable condition in such a case. However, $k_{\Delta ph}$ are estimated values from k_t and the product yields, and the identity of σ_o and σ_p was postulated in some cases. Such uncertainties in the data used, although they must be not large, may cause the analysis very difficult in the present case.

The idea of variable substituent constants (Eq. 10) is also applicable to the combinational approach of product and kinetic analyses. Calculations were thus performed using variable r values. Fractions of the two pathways obtained for each substrate certainly varied as expected according to the sets of the r values used. However, the extent of the variation was not so large as in the case of the non-linear regression analysis with variable r. The reason is obviously because the four partial rate constants were fixed to the experimental values throughout the calculations.

The above calculations with variable r revealed some characteristic features: (i) ρ_1 is always larger than ρ_2. (ii) The linearity of the two LFER is governed mostly by the value of r_2; the correlation coefficient becomes too small (<0.97) when r_2 larger than 0.5 is employed. (iii) There is a tendency that a better linearity is obtained when r_1 is larger than r_2. Further search for a point of best fit is apparently meaningless in the present case when the risk of statistical approach such as those encountered in the non-linear regression analysis is considered. We regard the results shown in Table 3 and Eqs. 2 and 3 as a reasonable answer to the dissection problem, although some uncertainties still remain.

It is apparent from Table 3 that the Ar_2-6 pathway is much favored than Ar_1-5. For the unsubstituted ester **7e** the former is 4.5 times more rapid than the latter after the statistical correction. Since the former pathway can be regarded as a kind of electrophilic aromatic substitution at the ortho position to the alkyl chain and the latter as the one at the ipso, the above result must reflect a difference in the reactivity of these positions toward a potential electrophile. A low π-electron density at the ipso position of toluene in comparison with the other positions was calculated by Libit and Hoffmann as an extended Hückel result.[22] Recently, *ab initio* STO-3G calculations of the relative energies of "late" and "early" transition state models for attack of a proton on benzene and the various positions of toluene were reported by Santiago *et al.*[23] The results show that the relative energies are para>ortho>H(benzene)>ipso for both the late and early transition state models. Our result indicating the unfavorable Ar_1-5 pathway is thus compatible with the theoretical calculations.

Santiago *et al.* also suggested that the ipso position is deactivated toward formation of an early transition state.[23] Thus, it is expected that the ipso substitution has a later transition state than the ortho substitution. Our conclusions that ρ_1 is larger than ρ_2 and, though not secured enough, r_1 may be larger than r_2 can be attributed to the development of a positive charge to a larger extent in the case of the ipso substitution, Ar_1-5. Another possible explanation that the lower electron density at the ipso position may cause a larger electron demand in the substitution reaction can also rationalize the larger substituent effect on Ar_1-5. A larger substituent effect on the chemical shifts of the ipso carbons in ^{13}C NMR spectra was reported in the case of *p*-substituted toluenes (**11**) compared with those of the para carbons of substituted benzenes (**12**).[24,25]

11 **12**

The relative ease of remote aryl participation is affected by the ring size of the transition state other than the electronic effect. The ring size effect can be discussed in two aspects, *i.e.*, entropy and strain energy.

According to Page, the standard entropy loss on cyclization of terminal olefins is larger for a six-membered ring than for a five-membered one by *ca.* 8 cal K^{-1} mol^{-1} (=33 J K^{-1} mol^{-1}) at 298 K.[26] The corresponding difference in the ring-size corrections in Benson's thermochemical analysis[27] is also 8.5 cal K^{-1} mol^{-1}. Thus, the activation entropy must be in favor of the five-membered transition state. On the other hand, the strain energy of cyclopentane is 6 kcal mol^{-1} larger than that of cyclohexane.[28] Thus, the activation enthalpy must be in favor of the six-membered transition state. The preponderance of the Ar_2-6 pathway may be the outcome of the relative importance of the ethalpy term, but the firm conclusion is difficult because of the simultaneous operation of the electronic effect described above.

In connection with the above discussion, it is interesting to compare the activation parameters of the pairs of the substrates with same substituents at the *m*- and *p*-positions, namely **7a**, **c**, **f**, and **h** *vs.* **7b**, **d**, **g**, and **i**, respectively (Table 1). Throughout the series of these pairs, the *m*-substituted esters have smaller enthalpies

and smaller (more negative) entropies of activation than the corresponding *p*-substituted isomers. The activation enthalpy of **7f** must be raised slightly because of the peculiar deactivation at the ortho position of the fluorine substituent (*vide supra*).[17] It is apparent from Table 3 that the *m*-substituted esters solvolyze almost exclusively *via* the Ar_2-6 pathway. This must be also true for the *m*-CH_3O ester **7c**.[5] On the contrary, the solvolyses of the *p*-isomers proceed considerably *via* the Ar_1-5 pathway. Thus, the differences in the activation parameters are in perfect harmony with the differences in the reaction pathways. Furthermore, these observations secure our first assumption that the two modes of remote aryl participation are discrete.

Finally, the magnitude of the ρ values should be discussed briefly. The value for the Ar_1-5 pathway, *ca.* −4, is well in the range of the ρ values for the k_Δ pathway of 2-phenylethyl solvolysis (Ar_1-3).[11] Ouellette *et al.* reported that the ρ^+ values of the acetolyses decreased in the order benzyl>2-phenylethyl>4-phenylbutyl systems.[21] However, in their analysis of the acetolysis rates of 4-arylbutylmercury(II) perchlorates, they regarded all the k_Δ pathway as Ar_1-5. Since it is not the case as revealed in the present study, their ρ^+ value, −1.2, must be in serious error. Similar magnitudes of the ρ values for the Ar_1-5 and Ar_1-3 pathways rather indicate that the electronic natures of the aromatic rings in these through-space interactions with the potential electrophiles are almost identical independently of the ring size.

Experimental

General. All melting points were determined on a Yanagimoto MP-S2 hot stage melting point apparatus and not corrected. ^1H NMR spectra were obtained on a Hitachi R-20 or R-24 instrument at 60 MHz using tetramethylsilane as an internal standard.

Preparation of 4-Aryl-1-butanols. All the 4-(*p*-substituted phenyl)-1-butanols were prepared by the Friedel-Crafts reaction of substituted benzenes with succinic anhydride and aluminum chloride,[29] followed by the Wolff-Kishner reduction,[30] esterification, and lithium aluminum hydride reduction, successively. All the 4-(*m*-substituted phenyl)-1-butanols except the *m*-CH_3 derivative were prepared from the corresponding 3-(*m*-substituted phenyl)-1-propanols *via* chlorides,[31] cyanides,[32] acids, and esters, successively. The propanols were prepared by the Knoevenagel reaction of the corresponding *m*-substituted benzaldehydes with malonic acid,[33] followed by esterification and lithium aluminum hydride reduction.[34] 4-(*m*-Tolyl)-1-butanol was prepared by the hydroboration-oxidation[35] of 4-(*m*-tolyl)-1-butene, which was obtained by the coupling reaction of *m*-tolylmethylmagnesium chloride with allyl bromide.[36,37]

4-(m-Tolyl)-1-butanol: Bp 130.5 °C/7.5 Torr (1 Torr= 133.322 Pa). Found: C, 80.17; H, 9.99%. Calcd for $C_{11}H_{16}O$: C, 80.44; H, 9.82%.

4-(m-Fluorophenyl)-1-butanol: Bp 90—92 °C/5.5 Torr. Found: C, 71.12; H, 7.87%. Calcd for $C_{10}H_{13}FO$: C, 71.40; H, 7.79%.

4-(p-Fluorophenyl)-1-butanol: Bp 138.5—139.5 °C/15 Torr. Found: C, 71.17; H, 7.97%. Calcd for $C_{10}H_{13}FO$: C, 71.40; H, 7.79%.

4-(m-Chlorophenyl)-1-butanol: Bp 133 °C/5.0 Torr. Found: C, 64.89; H, 7.32; Cl, 19.02%. Calcd for $C_{10}H_{13}ClO$: C, 65.04; H, 7.10; Cl, 19.20%.

4-(p-Chlorophenyl)-1-butanol: Bp 140—148 °C/4.5 Torr. Found: C, 65.16; H, 7.21; Cl, 19.11%. Calcd for $C_{10}H_{13}ClO$: C, 65.04; H, 7.10; Cl, 19.20%.

4-(p-Bromophenyl)-1-butanol: Bp 157—158 °C/5.0 Torr. Found: C, 52.26; H, 5.75; Br, 34.58%. Calcd for $C_{10}H_{13}BrO$: C, 52.42; H, 5.72; Br, 34.88%.

4-(m-Trifluoromethylphenyl)-1-butanol: Bp 119—120 °C/40 Torr. Found: C, 60.25; H, 5.89; F, 25.78%. Calcd for $C_{11}H_{13}F_3O$: C, 60.55; H, 6.01; F, 26.12%.

Preparation of Labeled Alcohols. Both [1-^{13}C]-4-(*p*-tolyl)-1-butanol and [1-^{13}C]-4-(*p*-fluorophenyl)-1-butanol were prepared by carbonation of the corresponding Grignard reagents with $^{13}CO_2$ gas,[38] followed by esterification and reduction. [1,1-$^2H_2$]-4-(*p*-Methoxyphenyl)-1-butanol was prepared by the reduction of ethyl 4-(*p*-methoxyphenyl)-butanoate with lithium aluminum deuteride.

Table 4. Physical properties and analytical data of 4-(*m*- and *p*-substituted phenyl)butyl menasylates (**7**) and brosylates (**9**)

Ester	Subst	Mp/°C	Solv[a]	Carbon Found(Calcd)	Hydrogen Found(Calcd)	Sulfur Found(Calcd)	Other Found(Calcd)
7a	*m*-CH_3	64.0—64.3	P–B	71.82(71.71)	6.54(6.57)	8.87(8.70)	
7b	*p*-CH_3	131.2—131.7	L	71.56(71.71)	6.46(6.57)	8.85(8.70)	
7c	*m*-CH_3O	54.8—55.4	Pe–B	68.65(68.72)	6.21(6.29)	8.28(8.34)	
7d	*p*-CH_3O	95.5—96.5	H–B	68.54(68.72)	6.14(6.29)	8.08(8.34)	
7f	*m*-F	79.5—80.5	H–B	67.45(67.72)	5.52(5.68)	8.63(8.61)	
7g	*p*-F	97.8—98.5	H–B	67.99(67.72)	5.37(5.68)	8.79(8.61)	
7h	*m*-Cl	71.8—72.0	Pe–B	65.06(64.86)	5.42(5.44)	8.31(8.24)	(Cl) 9.33(9.11)
7i	*p*-Cl	122.3—123.4	C	64.86(64.86)	5.25(5.44)	8.43(8.24)	(Cl) 9.33(9.11)
7j	*p*-Br	125.2—125.7	C	58.08(58.20)	4.83(4.88)	7.49(7.40)	(Br) 18.28(18.44)
7k	*m*-CF_3	72.8—73.5	H	62.62(62.55)	5.02(5.01)	7.68(7.59)	(F) 13.22(13.49)
7d-1,1-$^2H_2$	*p*-CH_3O	95.7—96.2	H–B	68.27(68.30)	6.19(6.23)	8.33(8.29)	
9b	*p*-CH_3	46.0—46.5[c]	Pe–E	53.18(53.27)	4.88(5.00)	8.39(8.37)	(Br) 20.87(20.85)
9b-1-^{13}C[b]	*p*-CH_3	45.0—45.4	Pe–E	53.03(53.15)	4.99(4.98)	8.41(8.35)	(Br) 20.54(20.80)
9g-1-^{13}C[b]	*p*-F	liquid[d]	P	49.34(49.51)	3.98(4.15)	8.58(8.26)	(Br) 20.31(20.59)

a) Solvent used for recrystallization: B, benzene; C, carbon tetrachloride; E, ether; H, hexane; P, pentane; Pe, petroleum ether. b) Calculated values are for 90% ^{13}C enrichment. c) Lit,[6] 45.5—46.5 °C. d) Recrystallized from pentane at low temperature.

[*1*-^{13}C]-*4*-(p-*Tolyl*)-*1*-*butanol*: Bp 102—103 °C/3.5 Torr. ^{13}C Enrichment was 89.4% as measured by ^{1}H NMR.

[*1*-^{13}C]-*4*-(p-*Fluorophenyl*)-*1*-*butanol*: Bp 127—128 °C/10 Torr. ^{13}C Enrichment was 90.4% as measured by ^{1}H NMR.

[*1,1*-$^{2}H_2$]-*4*-(p-*Methoxyphenyl*)-*1*-*butanol*: Bp 151—152 °C/7.0 Torr. Deuterium content was better than 99% as measured by ^{1}H NMR.

Preparation of 4-Arylbutyl Arenesulfonates. The menasylates and brosylates were prepared by the standard procedures from alcohols with menasyl chloride and brosyl chloride, respectively, at 0 °C in pyridine as a solvent.[3,39] Physical properties and analytical data of these esters are summarized in Table 4.

Preparation of Solvolysis Products. 4-(p-*Chlorophenyl*)-*butyl Trifluoroacetate*: Three molar equivalents of trifluoroacetic anhydride was added dropwise to 4-(*p*-chlorophenyl)-1-butanol under stirring at 0 °C. After stirring further 2 h at room temperature, the excess of the anhydride was removed under reduced pressure. Distillation of the residual oil gave the trifluoroacetate: bp 101—111 °C/5.0 Torr. Found: C, 51.27; H, 4.25%. Calcd for $C_{12}H_{12}ClF_3O_2$: C, 51.35; H, 4.31%.

3-(p-*Chlorophenyl*)-*1*-*methylpropyl Trifluoroacetate and 3-*(m-*Trifluoromethylphenyl*)-*1*-*methylpropyl Trifluoroacetate*: These secondary trifluoroacetates were prepared by heating 4-(*p*-chlorophenyl)-1-butene and 4-(*m*-trifluoromethylphenyl)-1-butene, respectively, in trifluoroacetic acid at 80 °C for 6 h.[37] After removing the excess of trifluoroacetic acid, these materials were used as the authentic samples for identification of solvolysis products by gas chromatography without further purification.

5-Methoxytetralin: The Wolff-Kishner reduction[30] of 25.0 g (0.142 mol) of 3,4-dihydro-5-methoxy-1(2*H*)-naphthalenone with 23.3 g of potassium hydroxide and 16.5 ml of 90% hydrazine hydrate in 200 ml of diethylene glycol gave 14.0 g of 5-methoxytetralin: bp 109.5 °C/10 Torr (lit,[40] 85—88 °C/3 Torr).

*6-Methyltetralin (**10b**)*: This material was isolated from the trifluoroacetolysis solution of **9b**. ^{13}C NMR (C_6D_6) δ (from external tetramethylsilane)=21.1 (Me), 23.8 (C_2 and C_3), 29.3 (C_1), 29.7 (C_4), 126.9 (C_7), 129.5 (C_8), 130.2 (C_5), 134.2 (C_6), 134.9 (C_9), and 137.0 (C_{10}); ^{1}H NMR ($CDCl_3$) δ=1.89 (4H, m, CH_2), 2.38 (3H, s, Me), 2.84 (4H, m, $ArCH_2$), and 7.04 (3H, br s, Ar). Found: C, 90.09; H, 9.52%. Calcd for $C_{11}H_{14}$: C, 90.35; H, 9.65%.

*6-Fluorotetralin (**10g**)*: This material was isolated from the trifluoroacetolysis solution of **7g**. ^{13}C NMR (C_6D_6) δ (from external tetramethylsilane)=23.1 (C_2 or C_3), 23.4 (C_3 or C_2), 28.9 (C_1), 29.6 (d, J_{CF}=1.6 Hz, C_4), 112.9 (d, J_{CF}=22.0 Hz, C_7), 115.7 (d, J_{CF}=20.7 Hz, C_5), 130.9 (d, J_{CF}=7.3 Hz, C_8), 132.8 (d, J_{CF}=3.6 Hz, C_9), 139.3 (d, J_{CF}=7.3 Hz, C_{10}), and 161.7 (d, J_{CF}=240.7 Hz, C_6); ^{1}H NMR ($CDCl_3$) δ=1.76 (4H, m, CH_2), 2.72 (4H, m, $ArCH_2$), and 6.67—7.05 (3H, m, Ar). Found: C, 79.72; H, 7.26%. Calcd for $C_{10}H_{11}F$: C, 79.97; H, 7.38%.

Trifluoroacetolysis Media. Trifluoroacetic acid containing 1 wt% of trifluoroacetic anhydride and 0.125 M (1M=1 mol dm^{-3}) of sodium trifluoroacetate was prepared according to the procedure described before.[3]

Kinetic Procedures. The usual ampule technique described before was employed.[3] Absorbance at about 326 nm was measured with a Hitachi Perkin-Elmer 139 or a Hitachi 100-30 UV-visible spectrophotometer. The absorbance after more than seven half-lives was used as that at "infinity."

Product Analyses. Reaction solutions containing 0.01 M of dodecane after more than six half-lives were directly injected into a Varian Aerograph Model 2850-30 gas chromatograph with a flame ionization detector and a Hewlett-Packard 3370B digital integrator. Columns packed with Silicone DC550 on Celite 545, Silicone OV-1 on Chromosorb W AW-DMCS, or PEG 20M on Chromosorb W NAW were used. Sensitivities were determined using authentic samples for tetralin, 6-methyltetralin, 5-methoxytetralin, and 4-(*p*-chlorophenyl)butyl trifluoroacetate. For other compounds sensitivities were calculated by the method described by Sternberg *et al.*[41] Accuracy of the calculated sensitivites were confirmed for the above authentic samples.

Trifluoroacetolyses of [*1*-^{13}C]-*4*-(p-*Tolyl and* p-*Fluorophenyl*)-*butyl Brosylates (**9b**-*1*-^{13}C *and* **9g**-*1*-^{13}C)* A reaction solution of 3.0 g **9b**-1-^{13}C in 100 ml of the same media as that for kinetic runs was heated at 70 °C for 14 h. The solvent was removed under reduced pressure, water being added to the residue. Extraction with ether gave a reaction product as an oil. Column chromatography through silica gel and molecular distillation gave 890 μl of a pure sample of [1,4-^{13}C]-6-methyltetralin (**10b**-1,4-^{13}C). Found: C, 89.82; H, 9.70%. Calcd for $C_{11}H_{14}$ containing 0.9 atom of ^{13}C: C, 89.80; H, 9.59 %. A similar reaction of **9g**-1-^{13}C at 85 °C for 22 h gave [1,4-^{13}C]-6-fluorotetralin (**10g**-1,4-^{13}C). Found: C, 79.28; H, 7.24% Calcd for $C_{10}H_{11}F$ containing 0.9 atom atom of ^{13}C: C, 79.50; H, 7.34%.

Trifluoroacetolysis of [*1,1*-$^{2}H_2$]-*4*-(p-*Methoxyphenyl*)*butyl Menasylate (**7d**-*1,1*-$^{2}H_2$)*. A solution of 970 mg of **7d**-1,1-$^{2}H_2$ in 50 ml of trifluoroacetic acid containg 1 wt% of trifluoroacetic anhydride was heated at 80 °C for 120 min. After the removal of the solvent under reduced pressure, the residue was poured into ice–water. Precipitates were recovered by filteration and purified by recrystallization. No scrambling of the deuterium in the recovered **7d**-1,1-$^{2}H_2$ was indicated by the absence of any signal due to the α-hydrogen.

Quantitative ^{13}C NMR Measurements. The measurements were performed on a JEOL JNM-FX 100 instrument at 25.05 MHz in normal FT mode. All spectra were run on 0.56 M (^{13}C-enriched) and 1.12 M (natural abundance) samples in perdeuteriobenzene solution contained in a 10-mm tube. The spectrometer was locked on the deuterium resonance of the solvent. Spectra were obtained at a spectral width of 1000 Hz with 16K data points using a normal pulse sequence (decoupling on at all the time). A pulse width was 4 μs, which corresponds to a flip angle of 30 °. A pulse repetition time was 25 s and an acquisition time was 8.192 s. Relaxation time of benzylic carbons is 5.1 s for both C_1 and C_4 of **10b**, and 5.4 and 5.5 s for C_1 and C_4, respectively, of **10g**. A longer pulse repetition time (60 s) did not alter the results. Number of pulses was 800 for the natural abundance samples and 100 for the ^{13}C-enriched ones. Relative peak areas integrated were described in the text.

Quantitative ^{13}C NMR spectra of **10g** were also obtained on another JEOL JNM-FX 100 instrument (25.05 MHz) and a Hitachi R22-FT one (22.633 MHz) both in FT mode, and on a Hitachi R20 instrument (15.085 MHz) in CW mode. Measurements were carried out using the same samples as above but in deuteriochloroform and under different conditions. All the results were identical to within a range of ±1.0%.

Non-linear Regression Analyses. The calculations were carried out using the ACOS 900 computer at the Computation Center of Osaka University.

We thank Professor Y. Tsuno of Kyushu University for his valuable discussion and Dr. K. Uozaki of Osaka University for his helpful suggestions on the statistical

analysis. We also thank Professors Y. Sasaki and Y. Kyogoku of Osaka University for making the NMR spectrometers available for the quantitative analysis. The present work was partially supported by a Grant-in-Aid (Nos. 747018, 964097, and 274154) for science research from the Ministry of Education.

References

1) For Part, 9, see T. Ando and H. Morisaki, *Tetrahedron Lett.*, **1979**, 121.
2) T. Ando, J. Yamawaki, and Y. Saito, *Bull. Chem. Soc. Jpn.*, **51**, 219 (1978).
3) T. Ando, Y. Saito, J. Yamawaki, H. Morisaki, M. Sawada, and Y. Yukawa, *J. Org. Chem.*, **39**, 2465 (1974).
4) R. Heck and S. Winstein, *J. Am. Chem. Soc.*, **79**, 3105, 3114 (1957).
5) S. Winstein and R. F. Heck, *J. Org. Chem.*, **37**, 825 (1972).
6) L. M. Jackman and V. R. Haddon, *J. Am. Chem. Soc.*, **96**, 5130 (1974).
7) M. Gates, D. L. Frank, and W. C. von Felten, *J. Am. Chem. Soc.*, **96**, 5138 (1974).
8) ^{13}C Contents of all the atoms of so-called "natural abundance" compounds are not necessarily the same according to their origin. The two benzylic carbons of the unlabeled tetralins prepared by this solvolysis may contain different amounts of ^{13}C when k_{12}/k_{13} in Scheme 3 is not unity.
9) F. W. Wehrli and T. Wirthlin, "Interpretation of Carbon-13 NMR Spectra," Heyden and Son LTD., London (1976), pp. 264—271.
10) R. S. Bly, R. K. Bly, J. B. Hamilton, J. N. C. Hsu, and P. K. Lillis, *J. Am. Chem. Soc.*, **99**, 216 (1977).
11) Among others see F. L. Schadt III, C. J. Lancelot, and P. v. R. Schleyer, *J. Am. Chem. Soc.*, **100**, 228 (1978).
12) E. C. Friedrich and S. Winstein, *Tetrahedron Lett.*, **1962**, 475.
13) a) L. P. Hammett, "Physical Organic Chemistry," 2nd ed, McGraw-Hill, New York (1970), Chap. 11; b) J. E. Leffler and E. Grunwald, "Rates and Equilibria of Organic Reactions," John Wiley and Sons, New York (1963), Chap. 7.
14) Determination of two lines with four points is insufficient for evaluating their reliability. Discussions described hereunder have limitations of unkown errors in the two Hammett-type relationships, although qualitative conclusions are not affected.
15) Y. Yukawa, Y. Tsuno, and M. Sawada, *Bull. Chem. Soc. Jpn.*, **39**, 2274 (1966).
16) Y. Tsuno, private communication.
17) R. W. Taft, "Steric Effects in Organic Chemistry," ed by M. S. Newman, Wiley, New York (1956), Chap. 13.
18) J. A. Nelder and R. Nead, *Computer J.*, **7**, 308 (1965).
19) M. J. D. Powell, *Computer J.*, **7**, 303 (1965).
20) J. M. Harris, F. L. Schadt, P. v. R. Schleyer, and C. J. Lancelot, *J. Am. Chem. Soc.*, **91**, 7508 (1969).
21) R. J. Ouellette, R. Papa, M. Attea, and C. Levin, *J. Am. Chem. Soc.*, **92**, 4893 (1970).
22) L. Libit and R. Hoffmann, *J. Am. Chem. Soc.*, **96**, 1370 (1974).
23) C. Santiago, K. N. Houk, and C. L. Perrin, *J. Am. Chem. Soc.*, **101**, 1337 (1979).
24) B. M. Lynch, *Can. J. Chem.*, **55**, 541 (1977).
25) M. Mishima, Ph. D. Thesis, Osaka University, Osaka, 1976.
26) M. I. Page, *Chem. Soc. Rev.*, **2**, 295 (1973).
27) S. W. Benson, "Thermochemical Kinetics," 2nd ed, John Wiley and Sons, New York (1976), p. 273.
28) A. S. Pell and G. Pilcher, *Trans. Faraday Soc.*, **61**, 71 (1965).
29) L. F. Somerville and C. F. H. Allen, *Org. Synth.*, Coll. Vol. II, 81 (1943).
30) D. Todd, *Org. React.*, **4**, 378 (1948).
31) H. Rapoport and J. E. Campion, *J. Am. Chem. Soc.*, **73**, 2239 (1951).
32) L. Friedman and H. Schechter, *J. Org. Chem.*, **25**, 877 (1960).
33) J. Koo, M. S. Fish, G. N. Walker, and J. Blake, *Org. Synth.*, Coll., Vol. IV, 327 (1963).
34) F. A. Hochstein and W. G. Brown, *J. Am. Chem. Soc.*, **70**, 3484 (1948).
35) G. Zweifel and H. C. Brown, *Org. React.*, **13**, 1 (1963).
36) E. B. Hershberg, *Helv. Chim. Acta*, **17**, 352 (1934).
37) P. E. Peterson, D. M. Chevli, and K. A. Sipp, *J. Org. Chem.*, **33**, 972 (1968).
38) a) A. Murray and D. L. Williams, "Organic Syntheses with Isotopes," Interscience, New York (1958), Part 1, pp. 87—102; b) K. -P. Zeller, *Chem. Ber.*, **108**, 3566 (1975).
39) L. F. Fieser and M. Fieser, "Reagents for Organic Synthesis," John Wiley and Sons, New York (1967), p. 1180.
40) D. M. Musser and H. Adkins, *J. Am. Chem. Soc.*, **60**, 664 (1938).
41) J. C. Sternberg, W. S. Gallaway, and D. T. L. Jones, *Gas Chromatogr. Intern. Symp., 1961*, **3**, 231 (1962).

Stereochemical Studies on the Nucleophilic Substitution in the Reaction of Allylic Phosphates with Organoaluminum Reagents

Akira Itoh, Shuji Ozawa, Koichiro Oshima,* Shizuka Sasaki, Hajime Yamamoto, Tamejiro Hiyama, and Hitosi Nozaki

Department of Industrial Chemistry, Faculty of Engineering, Kyoto University, Yoshida, Kyoto 606

(Received February 25, 1980)

The reaction of *cis*- or *trans*-5-isopropenyl-2-methyl-2-cyclohexenyl diethyl phosphate (**1**) with Me_2AlX (X= OPh, SPh, NHPh) in hexane results in substitution of the $-O-PO(OEt)_2$ group with X under predominant inversion. In contrast, treatment of *cis*- or *trans*-**1** with trialkylaluminum produces predominantly the allyl-nonallyl couplingproducts of the same (thermodynamically more stable) configuration. Similar alkylation of *endo*- and *exo*-2-acetoxynorcarane gave *endo*-2-methylnorcarane, exclusively.

The reaction of geranyl and neryl phosphates with R_2AlX type organoaluminum reagents[1] or trialkylaluminum compounds[2] results in nucleophilic substitution. The interest in stereoselectivity of these unique "ionic" reactions proceeding in nonpolar or less polar solvents has motivated the present studies on (1) the reaction of *cis*- or *trans*-5-isopropenyl-2-methyl-2-cyclohexenyl diethyl phosphate (**1**) with R_2AlX and (2) the reaction of *cis*- or *trans*-**1** with R_3Al.[3]

(1) Reaction of cis- *or* trans-*1 with R_2AlX.* Much attention has been paid to the conversion of esters to RCOX by means of R_2AlX (X=NR^1R^2,[4] SR,[5] SeR[6]). However, few examples are known for the nucleophilic substitution on a saturated carbon. The reaction of geranyl and neryl diethyl phosphates with R_2AlX (X=SPh, S^{t}Bu, OPh, NHPh) reagents results in the replacement of the $OPO(OEt)_2$ group by X group without affecting both olefinic bonds in any sense of the words. No allylic migration, no *E,Z*-isomerization, and no cyclization occur. Notably, this ionic reaction proceeds in *hexane*, which is a poor solvent of the reaction system and the whole forms a white suspension.

Further investigation of this kind of substitution with *cis*- and *trans*-**1** has clarified the steric course of the reaction. Treatment of *cis*- or *trans*-**1** with a heterogeneous white suspension of Me_2AlX (2 equiv) in hexane at 0 °C for 2 h gave substitution products **2** in good yields, as summarized in Table 1.

Invariably, substitution occurs under extensive configurational inversion and accompanies considerable allylic migration in contrast to the open chain geranyl and neryl diethyl phosphates. In order to determine the α/γ ratios, or S_N2/S_N2' ratios, products in the reaction of α-deuterio-*cis*-**1** or *trans*-**1** have been analyzed by NMR method.[7]

Solvent effect on the reaction between α-deuterio-*cis*-**1** and Me_2AlOPh is shown in Table 2. All the solvents except hexane gave clear solutions, in which ions should be much more free than in hexane. In the extreme tetrahydrofuran solvent, the retention product was predominant and the α/γ ratio was almost close to unity. Possibly an intimate ion-pair in a solvent cage could explain the findings. The similar solvent effect was observed in the reaction of *cis*-**1** with Me_2AlSPh or $Me_2AlNHPh$ (Table 3).

Assignments of the products were based on the examination of those NMR spectra. All the *trans* isomers, **2a**, **2b**, and **2c**, exhibited the narrow signals for the protons attached to carbon bearing X group at higher field than those for protons in *cis* isomers. The spectra are consistent with the postulated configuration

Table 1. Reaction of *cis*-**1** or *trans*-**1** with Me_2AlX in hexane[a]

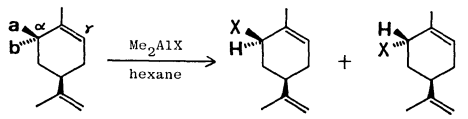

cis-**1**: **a**=O-PO(OEt)$_2$, **b**=H(D)
trans-**1**: **a**=H(D), **b**=O-PO(OEt)$_2$

cis-**2a,b,c** *trans*-**2a,b,c**
a: X=OPh, **b**: X=SPh, **c**: X=NHPh

Substrate	Reagent X	Ptoduct **2** Yield (%)[b]	*cis* (%)[c]	*trans* (%)[c]
cis-**1**	OPh	80	2	98 (84/16)
cis-**1**	SPh	92	3	97 (60/40)
cis-**1**	NHPh	70	12	88 (76/24)
trans-**1**	OPh	86	89 (90/10)	11
trans-**1**	SPh	94	90 (76/24)	10
trans-**1**	NHPh	87	99 (82/18)	1

a) These data are averages of at least three independent experiments. b) Isolated by chromatography on silica gel and adequately characterized by analytical and spectral data. The isolated yields refer to the isomeric mixtures. c) Isomeric compositions were determined by GLPC. The data in parentheses indicate α/γ ratios for the predominant isomer which were determined by NMR spectra of deuterium labelled products.

Table 2. Solvent effect on the substitution

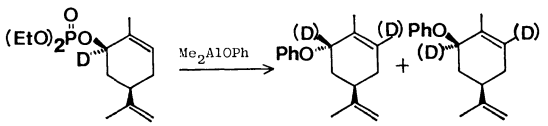

Solvent	Yield (%)[a]	*trans* (α/γ)	*cis* (α/γ)
Hexane	80	98 (84/16)	2
CH_2Cl_2	70	76 (74/26)	24 (71/29)
Et_2O	79	87 (75/25)	13 (77/23)
DME	82	57 (63/37)	43 (63/37)
THF	91	25 (60/40)	75 (63/37)

a) Isolated as mixtures of *trans* and *cis* isomers.

Table 3. Solvent effect on the substitution reaction of *cis*-**1** with Me_2AlSPh or $Me_2AlNHPh$

Solvent	Me_2AlSPh Yield (%)[a]	*trans*/*cis*	Solvent	$Me_2AlNHPh$ Yield (%)[a]	*trans*/*cis*
Hexane	92	97/ 3	Hexane	70	88/12
CH_2Cl_2	82	80/20	CH_2Cl_2	63	71/29
THF	79	58/42	THF	76	20/80

a) Isolated as mixtures of *trans* and *cis* isomers.

assuming those chair conformations in which the isopropenyl group is equatorial and the H–C–X protons therefore pseudo-equatorial. On the other hand, the much broader, lower field proton signals of *cis* isomers are ascribed to pseudo-axial ones.[8] Further support for the assignment has been given by the following transformation of *trans*-**2b** to *trans*-carveol (Scheme 1).

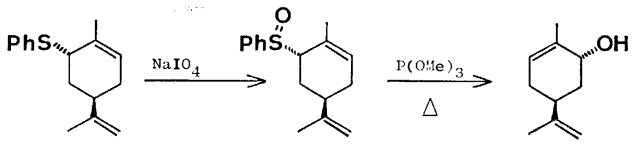

Scheme 1.

(*2*) *Reaction of* cis- *or* trans-*1 with* R_3Al. An investigation of the reaction of allylic phosphates with organoaluminum reagents has provided an exceptionally mild procedure to effect allyl-nonallyl coupling.[2] This C–C bond formation is now found to be characterized by carbocationic intermediates being produced from allylic phosphates in hexane.

Treatment of *cis*- or *trans*-**1** with trialkylaluminum (3 equiv) in hexane at 0 °C for 20 min gave a mixture of **4** and **5**. The results are summarized in Table 4, which indicates that the alkylation occurs predominantly from the side opposite to the isopropenyl group.

Table 4. Alkylation of *cis*-**1** or *trans*-**1** with R_3Al

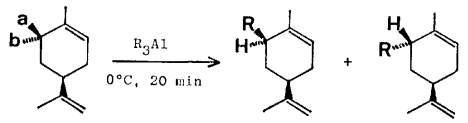

cis-**1**: **a**=OPO(OEt)$_2$, **b**=H
trans-**1**: **a**=H, **b**=OPO(OEt)$_2$
cis-**3**: **a**=$OCOCH_3$, **b**=H (D)
trans-**3**: **a**=H (D), **b**=$OCOCH_3$

4a,b,c **a**: R=Me **b**: R=Et **c**: R=^{t}Bu

5a,b,c

Run	Substrate	Reagent R	Solvent	Product Yield (%)[a]	Product **4**:**5**[b]
1	*trans*-**1**	Me	Hexane	85	4:96
2	*cis*-**1**	Me	Hexane	87	16:84
3	*trans*-**3**	Me	Hexane	78	4:96
4	*cis*-**3**	Me	Hexane	85	18:82
5	*trans*-**1**	Et	Hexane	89	6:94
6	*cis*-**1**	Et	Hexane	82	51:49
7	*trans*-**1**	^{t}Bu	Hexane	93	9:91
8	*cis*-**1**	^{t}Bu	Hexane	88	37:63
9	*cis*-**1**	Me	CH_2Cl_2	89	22:78
10	*cis*-**1**	Me	THF	63	8:92

a) Isolated yields refer to the epimeric mixtures. b) Isomeric ratios were determined by GLPC.

It is worth noting that this alkylation takes place also with carboxylic esters (runs 3 and 4) instead of the phosphate as a leaving group. A synthetically useful transformation of alcoholic substrates R^1OH into the coupling products R^1–R^2 [9] is thus based on the reaction of the corresponding esters R^1–OCOR with organometallic reagents R^2Mtl. No carbonyl attack[10] is observed with trialkylaluminum reagents.

The α-deuterio-*cis*-**3** and *trans*-**3** gave mainly *trans*-methylated products, **5** and its regioisomer **6** being produced in a ratio of 45: 55 and 40: 60 respectively. The product distribution of the alkylation was also independent of the solvent (runs 1, 9, and 10). The reaction of allylic phosphates with trialkylaluminum is in sharp contrast to the substitution reaction of those with Me_2AlX reagents described in section 1, where S_N2 type introduction of the X group predominates with inversion of the configuration.[11]

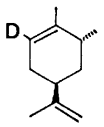

6

The structures of the products were unambiguously confirmed by the alternative synthesis of **4a** and **5a** according to Scheme 2.[12]

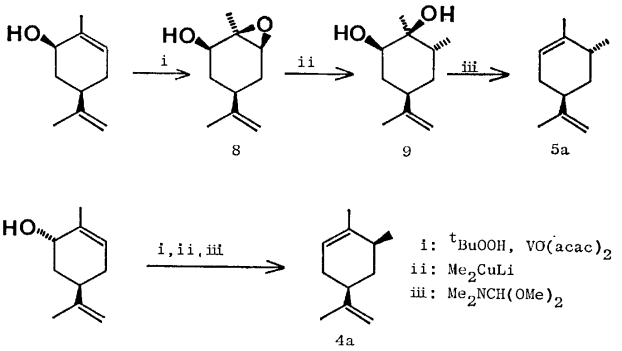

Scheme 2.

Similar stereochemistry was observed in the transformation of *endo*-2-acetoxynorcarane **10a** and its epimer **11a**. Subjection of the acetate **10a** to the action of trimethylaluminum in dichloromethane for 2 h at room temperature gave **12a** (contaminated with less than 7% of its epimer **13a**) in 80% yield. The exclusive product from **11a** was again **12a** (80%). As the deuterated acetates (**10b** and **11b**, a 22 : 78 mixture) gave

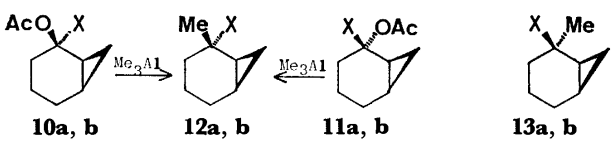

10a, b **12a, b** **11a, b** **13a, b**

a: X=H; **b**: X=D

Scheme 3.

12b (>93%), a mechanism involving rearrangement with ring opening can be rejected.[14]

Authentic samples of the products were prepared from 3-methylcyclohexene (Scheme 4). The stereochemical identities were established by hydrogenating this mixture (H_2, 1 atm, PtO_2, AcOH) to 1:5 mixture of *cis*- and *trans*-1,2-dimethylcyclohexane, each of which was separated by GLPC and compared spectrometrically with the corresponding authentic sample.[15]

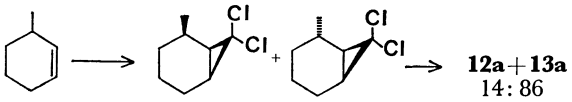

Scheme 4.

Experimental

The optical rotations were measured using a Yanaco-OR-50 polarimeter. The infrared spectra were determined on a Shimadzu IR-27-G spectrometer; the mass spectra on a Hitachi RMU-6L machine; the GLPC analyses on a Yanagimoto GCG-550F; and the NMR spectra on a JEOL-C-60H or Varian EM-390H spectrometer. The chemical shifts are given in δ in ppm with TMS as the internal standard. Splitting patterns are designated as s, singlet; d, doublet; t, triplet; q, quartet; m, multiplet. The microanalyses were carried out by the staffs at the Elemental Analyses Center of Kyoto University. All experiments were carried out under an atmosphere of dry argon. Tetrahydrofuran was dried by distillation from sodium–benzophenone. Thin layer or thick layer plates were made of E. Merck PF-254, and preparative column chromatography on silica gel E. Merck Art. 7734.

Preparation of cis-*Carveol.* (−)-Carvone (21.0 g, 140 mmol) was reduced by lithium aluminum hydride (2.66 g, 70 mmol) in THF (300 ml) at −15 °C.[16] The crude carveol (*cis*: *trans*=92:8, determined by GLPC, 10% PEG 20M on Celite 545, 2 m, 140 °C) was then treated with 3,5-dinitrobenzoyl chloride (37.8 g, 164 mmol) in pyridine (120 ml) at 25 °C. The mixture was stirred at the same temperature for 12 h, poured into precooled 1 M (1 mol dm^{-3}) HCl, and extracted with ethyl acetate twice. The organic phase was washed with 1 M HCl, and brine, dried, and concentrated. The crude product was passed through a short column of silica gel and the *cis*-benzoate was recrystallized from ethanol–ethyl acetate (3 : 1) twice (mp 92.5 °C). Hydrolysis (5% KOH in methanol, 100 ml, 20 min at reflux) followed by purification by column chromatography on silica gel (hexane: ethyl acetate=3 : 1) afforded *cis*-carveol (6.84 g, 32%) contaminated by <0.5% *trans* isomer.

Preparation of trans-*Carveol.* According to the reported procedure,[17] the title compound (>99.5% pure) was prepared from (−)-carvone by reduction with aluminum triisopropoxide in isopropyl alcohol and purification by recrystallization of 3,5-dinitrobenzoate (mp 111.5 °C) followed by hydrolysis.

*Preparation of α-Deuterio-*cis*-carveol.* (−)-Carvone (3.0 g, 20 mmol) was reduced by lithium aluminum deuteride (0.42 g, 10 mmol, Merck 98% d) in THF (25 ml) at −15 °C and the product was further purified by the method described above.

*Preparation of α-Deuterio-*trans*-carveol.* A solution of diethyl phosphate of α-deuterio-*cis*-carveol (1.15 g, 4.0 mmol) in 1,2-dimethoxyethane (3.0 ml) was added to a mixture of potassium superoxide (0.98 g, 13.8 mmol), 18-crown-6 (2.43 g, 9.2 mmol), dimethyl sulfoxide (10.0 ml), and 1,2-dimethoxyethane (10.0 ml) at 25 °C. After 16 h, the reaction mixture was poured into water and the organic phase was extracted with ethyl acetate three times. The combined extracts were washed with brine, dried, and freed of the solvent. Purification by column chromatography on silica gel afforded α-deuterio-*trans*-carveol (0.19 g, 1.3 mmol, contaminated by <5% *cis* isomer) in 32% yield. Absence of γ-deuterio-carveol was confirmed by the examination of its NMR spectrum.

cis-*5-Isopropenyl-2-methyl-2-cyclohexenyl Diethyl Phosphate* (cis-***1***). Butyllithium in hexane (1.5 M, 31.4 ml, 47.2 mmol) was added to a solution of *cis*-carveol (6.82 g, 44.9 mmol) in ether (40 ml) at −23 °C. After 20 min, a solution of diethyl phosphorochloridate (13.0 ml, 89.8 mmol) and triethylamine (12.5 ml, 89.8 mmol) in ether (30 ml) was added. The mixture was stirred for 2 h at the same temp, poured into ice–water, and extracted with ethyl acetate three times. The organic phase was washed with brine, dried, and freed of the solvent. Purification by column chromatography on silica gel (hexane: ethyl acetate=3: 1) afforded *cis*-**1** (9.54 g, 33.1 mmol) in 74% yield as a colorless oil: NMR (CCl_4) δ 1.33 (t, J=7.2 Hz, 6H), 1.74 (s, 6H), 1.6—2.3 (m, 5H), 4.03 (m, 4H), 4.69 (s, 2H), 4.85 (m, 1H), 5.49 (m, 1H).

trans-*5-Isopropenyl-2-methyl-2-cyclohexenyl Diethyl Phosphate* (trans-***1***): NMR (CCl_4) δ 1.33 (t, J=7.2 Hz, 6H), 1.74 (s, 6H), 1.6—2.3 (m, 5H), 4.03 (m, 4H), 4.57 (m, 1H), 4.69 (s, 2H), 5.60 (m, 1H).

General Procedure for the Reaction between Me_2AlX (X=OPh,[18] *SPh,*[19] *NHPh,*[20]*) and* ***1*** *in Hexane.* The substitution of *cis*-**1** with Me_2AlOPh is representative. Phenol (0.18 ml, 2.0 mmol) was added dropwise to a solution of trimethylaluminum (1.0 M solution in hexane, 2.0 ml, 2.0 mmol) in hexane (10 ml) at 0 °C. After stirring for 30 min, a solution of *cis*-**1** (0.29 g, 1.0 mmol) in hexane (3.0 ml) was added to the resulting white suspension at 0 °C and the mixture was held there for 2 h. Workup (1 M HCl and ether) followed by column chromatography on silica gel with ether–hexane (1: 50) afforded a mixture of *trans*-**2a** and *cis*-**2a** (0.18 g, 80% yield) in a ratio of 98 : 2 as determined by GLPC (PEG 20 M 10% on Celite 545, 2 m, 195 °C). Further purification by preparative TLC (hexane, three developments) gave pure *trans*-**2a**: bp 152 °C (bath temp, 2 Torr); IR (neat) 1645, 1600, 1590, 1495, 1235 cm^{-1}; NMR (CCl_4) δ 1.70 (s, 3H), 1.76 (s, 3H), 1.83—2.50 (m, 5H), 4.48 (m, 1H), 4.66 (s, 2H), 5.63 (m, 1H), 6.75—7.33 (m, 5H); MS *m/e* (%) 228 (M^+, 3), 185 (2), 135 (18), 134 (71), 119 (50), 107 (62), 93 (100).

Found: C, 83.94; H, 8.93%. Calcd for $C_{16}H_{20}O$: C, 84.16; H, 8.83%.

cis-*5-Isopropenyl-2-methyl-3-phenoxycyclohexene* (cis-***2a***): Bp 160 °C (bath temp, 2 Torr); IR (neat) 1645, 1595, 1585, 1492, 1238, 1030, 888 cm^{-1}; NMR (CCl_4) δ 1.71 (s, 3H), 1.76 (s, 3H), 1.9—2.4 (m, 5H), 4.67 (s, 2H), 4.76 (m, 1H), 5.53 (m, 1H), 6.72—7.23 (m, 5H); MS *m/e* (%) 228 (M^+, 3), 185 (3), 135 (17), 134 (51), 119 (47), 107 (78), 93 (100).

Found: C, 84.38; H, 8.96%. Calcd for $C_{16}H_{20}O$: C, 84.16; H, 8.83%.

trans-*5-Isopropenyl-2-methyl-3-(phenylthio)cyclohexene* (trans-***2b***): Bp 155 °C (bath temp, 2 Torr); IR (neat) 1645, 1583, 1479, 889 cm^{-1}; NMR (CCl_4) δ 1.7—2.6 (m, 5H), 1.73 (s, 3H), 1.90 (s, 3H), 3.56 (m, 1H), 4.67 (s, 2H), 5.53 (m, 1H), 7.1—7.5 (m, 5H); MS *m/e* (%) 245 (1), 244 (M^+, 4), 134 (62), 119 (28), 107 (64), 93 (100).

Found: C, 78.90; H, 8.51%. Calcd for $C_{16}H_{20}S$: C, 78.63; H, 8.25%.

cis-*5-Isopropenyl-2-methyl-3-(phenylthio)cyclohexene* (cis-***2b***):

Bp 155 °C (bath temp, 2 Torr); IR (neat) 1645, 1585, 1483, 889 cm^{-1}; NMR (CCl_4) δ 1.8—2.7 (m, 5H), 1.70 (s, 3H), 1.89 (s, 3H), 3.65 (m, 1H), 4.61 (s, 2H), 5.56 (m, 1H), 7.1—7.5 (m, 5H); MS *m/e* (%) 245 (5), 244 (M^+, 10), 134 (59), 119 (45), 107 (78), 93 (100).

Found: C, 78.54; H, 8.46%. Calcd for $C_{16}H_{20}S$: C, 78.63; H, 8.25%.

trans-*3-(Phenylamino)-5-isopropenyl-2-methylcyclohexene* (trans-**2c**): Bp 175 °C (bath temp, 2 Torr); IR (neat) 3420, 1645, 1600, 1506, 1313, 1250, 888 cm^{-1}; NMR (CCl_4) δ 1.70 (s, 3H), 1.78 (s, 3H), 1.6—2.4 (m, 5H), 3.43 (m, 1H), 3.80 (m, 1H), 4.76 (s, 2H), 5.53 (m, 1H), 6.4—7.2 (m, 5H); MS *m/e* (%) 228 (6), 227 (M^+, 29), 159 (29), 158 (13), 119 (26), 93 (100).

Found: C, 84.63; H, 9.55%. Calcd for $C_{16}H_{21}N$: C, 84.53; H, 9.31%.

cis-*3-(Phenylamino)-5-isopropenyl-2-methylcyclohexene* (cis-**2c**): Bp 175 °C (bath temp, 2 Torr); IR (neat) 3400, 1645, 1601, 1506, 1315, 1248, 890 cm^{-1}; NMR (CCl_4) δ 1.70 (s, 6H), 1.6—2.3 (m, 5H), 3.27 (m, 1H), 3.95 (s, 1H), 4.66 (s, 2H), 5.50 (m, 1H), 6.4—7.1 (m, 5H); MS *m/e* (%) 228 (7), 227 (M^+, 29), 159 (37), 158 (14), 119 (26), 93 (100).

Found: C, 84.56; H, 9.38%. Calcd for $C_{16}H_{21}N$: C, 84.53; H, 9.31%.

General Procedure for the Reaction between Me_2AlX *and* **1** *in Various Solvents.* Me_2AlX (2.0 mmol) was prepared in hexane and the solvent was removed *in vacuo* to leave a white solid. Dichloromethane (ether, DME, THF) (10 ml) was added and the mixture was stirred for 5 min at 25 °C. A solution of *cis*-**1** (0.29 g, 1.0 mmol) in the same solvent (3.0 ml) was added at 0 °C. After 2 h, the mixture was worked up as previously described.

Transformation of trans-**2b** *into* trans-*Carveol.* A solution of **2b** (*trans*: *cis*=97: 3, 1.54 g) in methanol (20 ml) was treated with sodium periodate (2.8 g, 13.1 mmol) at 25 °C for 2 d. The mixture was filtered and the filtrate was concentrated *in vacuo*. The residue was chromatographed on silica gel (hexane: ethyl acetate=5: 1) to give a diastereomeric mixture of the sulfoxide (0.91 g, 3.5 mmol) in 66% yield. A mixture of trimethyl phosphite (2.1 ml, 17.8 mmol, freshly distilled from sodium), the sulfoxide (0.91 g, 3.5 mmol), and methanol (3.3 ml) was heated to reflux for 1 h. The mixture was poured into saturated aqueous sodium hydrogencarbonate and extracted with ethyl acetate three times. The combined extracts were washed with brine, dried, and concentrated. Purification by column chromatography on silica gel (hexane: ethyl acetate=10 : 1) afforded *trans*-carveol (0.28 g, 1.9 mmol, contaminated by $<2\%$ *cis*-carveol) in 53% yield.

General Procedure for the Alkylation of **1** *or* **3** *with Trialkylaluminum.* Trialkylaluminum (1.0 M solution in hexane, 3.0 ml, 3.0 mmol) was added dropwise to a solution of **1** or **3** (1.0 mmol) in hexane, dichloromethane or tetrahydrofuran (7.0 ml) at 0 °C. After 20 min, ethanol (1.0 ml) was added to decompose the excess trialkylaluminum. The mixture was poured into 1 M HCl and extracted twice with pentane. The combined extracts were washed with brine, dried, and freed of the solvent. Purification by preparative TLC (hexane) afforded a mixture of **4** and **5** whose ratio was determined by GLPC (PEG 20 M 10% on Celite 545, 2 m, 72 °C (R=Me), 88 °C (R=Et), 114 °C (R=^{t}Bu)). Pure samples of **4** and **5** were obtained by preparative GLPC (PEG 20 M 30% on Celite 545, 3 m, 98 °C (R=Me), 110 °C (R=Et), 120 °C (R=^{t}Bu)).

cis-*2,3-Dimethyl-5-isopropenylcyclohexene* (**4a**): Bp 130 °C (bath temp, 20 Torr); IR (neat) 3185, 1645, 888, 800 cm^{-1}; NMR (CCl_4) δ 0.94 (d, J=6.9 Hz, 3H), 1.57 (s, 3H), 1.65 (s, 3H), 1.8—2.3 (m, 6H), 4.57 (s, 2H), 5.28 (m, 1H); MS *m/e* (%) 151 (3), 150 (M^+, 16), 135 (19), 121 (26), 108 (100), 107 (73), 93 (89), 82 (24), 67 (99).

Found: C, 88.17; H, 11.84%. Calcd for $C_{11}H_{18}$: C, 87.93; H, 12.07%.

trans-*2,3-Dimethyl-5-isopropenylcyclohexene* (**5a**): Bp 130 °C (bath temp, 20 Torr); IR (neat) 3185, 1645, 888, 800 cm^{-1}; NMR (CCl_4) δ 1.07 (d, J=6.9 Hz, 3H), 1.64 (s, 3H), 1.72 (s, 3H), 1.6—2.3 (m, 6H), 4.64 (s, 2H), 5.29 (m, 1H); MS *m/e* (%) 151 (4), 150 (M^+, 20), 135 (11), 121 (10), 107 (100), 93 (39), 82 (54), 67 (92).

Found: C, 87.72; H, 11.97%. Calcd for $C_{11}H_{18}$: C, 87.93; H, 12.07%.

cis-*3-Ethyl-5-isopropenyl-2-methylcyclohexene* (**4b**): Bp 188 °C (bath temp, 760 Torr); IR (neat) 3080, 1643, 887, 802 cm^{-1}; NMR (CCl_4) δ 0.94 (t, J=7.5 Hz, 3H), 1.67 (s, 3H), 1.74 (s, 3H), 1.2—2.3 (m, 8H), 4.64 (s, 2H), 5.30 (m, 1H); MS *m/e* (%) 165 (4), 164 (M^+, 22), 149 (8), 135 (14), 121 (65), 107 (32), 96 (28), 93 (99), 91 (28), 81 (100).

Found: C, 87.73; H, 11.99%. Calcd for $C_{12}H_{20}$: C, 87.73; H, 12.27%.

trans-*3-Ethyl-5-isopropenyl-2-methylcyclohexene* (**5b**): Bp 188 °C (bath temp, 760 Torr); IR (neat) 3080, 1645, 881, 800 cm^{-1}; NMR (CCl_4) δ 0.85 (t, J=7.5 Hz, 3H), 1.63 (s, 3H), 1.73 (s, 3H), 1.1—2.2 (m, 8H), 4.63 (s, 2H), 5.38 (m, 1H); MS *m/e* (%) 165 (2), 164 (M^+, 8), 135 (11), 122 (28), 121 (18), 107 (23), 96 (36), 93 (55), 81 (100), 80 (47).

Found: C, 88.00; H, 12.52%. Calcd for $C_{12}H_{20}$: C, 87.73; H, 12.27%.

cis-*3-Isobutyl-5-isopropenyl-2-methylcyclohexene* (**4c**): Bp 220 °C (bath temp, 760 Torr); IR (neat) 3100, 1646, 1381, 1377, 886, 800 cm^{-1}; NMR (CCl_4) δ 0.87 (d, J=4.5 Hz, 3H), 0.93 (d, J=4.5 Hz, 3H), 1.62 (s, 3H), 1.72 (s, 3H), 1.1—2.3 (m, 9H), 4.64 (s, 2H), 5.34 (m, 1H); MS *m/e* (%) 193 (5), 192 (M^+, 27), 149 (44), 107 (51), 93 (100), 81 (48), 80 (45), 68 (43), 57 (66).

Found: C, 86.70; H, 12.57%. Calcd for $C_{14}H_{24}$: C, 87.42; H, 12.58%.

trans-*3-Isobutyl-5-isopropenyl-2-methylcyclohexene* (**5c**): Bp 220 °C (bath temp, 760 Torr); IR (neat) 3060, 1643, 1376, 1364, 888, 800 cm^{-1}; NMR (CCl_4) δ 0.87 (d, J=3.0 Hz, 3H), 0.96 (d, J=3.0 Hz, 3H), 1.64 (s, 3H), 1.73 (s, 3H), 1.2—2.3 (m, 9H), 4.66 (s, 2H), 5.30 (m, 1H); MS *m/e* (%) 193 (5), 192 (M^+, 23), 150 (21), 149 (23), 109 (40), 107 (50), 93 (97), 81 (69), 80 (100), 68 (67), 57 (36).

Found: C, 87.65; H, 12.77%. Calcd for $C_{14}H_{24}$: C, 87.42; H, 12.58%.

Alternative Synthesis of **4a** *and* **5a**. Epoxidation of (−)-*cis*-carveol (0.61 g, 4.0 mmol) by the method of Sharpless afforded epoxy alcohol **8**[21] (0.42 g, 64% yield). A solution of **8** (0.10 g, 0.61 mmol) in ether (2.0 ml) was treated with lithium dimethylcuprate(I) (3.7 mmol) in ether (6.0 ml) at 0 °C.[22] After 1.3 h at 0 °C and 1 h at 25 °C, the mixture was poured into ice–water and filtered. The filtrate was washed with 1 M HCl, saturated sodium hydrogencarbonate, and brine, dried, and concentrated. The residue was submitted to column chromatography on silica gel to afford the diol **9** (0.11 g, 97% yield) as a colorless solid: mp 68 °C; IR (Nujol) 3340, 3080, 1645, 1130, 1077, 1043, 887 cm^{-1}; NMR (CCl_4) δ 0.95 (d, J=7.5 Hz, 3H), 1.22 (s, 3H), 1.70 (s, 3H), 1.3—2.2 (m, 6H), 2.88 (bs, 2H, –OH), 3.52 (dd, J=5.7 and 10.4 Hz, 1H), 4.65 (s, 2H); MS *m/e* (%) 184 (M^+, 6), 166 (26), 151 (22), 140 (29), 122 (58), 97 (65), 69 (100), 57 (65), 55 (67). A mixture of the diol **9** (70 mg, 0.38 mmol), *N,N*-dimethylformamide (1.0 ml), and *N,N*-dimethylformamide dimethyl acetal (0.5 ml) was heated at 150 °C for 1 h. Acetic anhydride (1.0 ml) was added and the

resulting mixture was heated for another 3.5 h.[23] Purification of the product by column chromatography on silica gel (pentane) afforded **5a** (20 mg, $[\alpha]_{25}^{D}$ +125° (*c* 0.84, MeOH)) in 36% yield.

In similar fashion, the authentic sample of **4a** ($[\alpha]_{25}^{D}$ +28° (*c* 0.78, MeOH)) was obtained from (−)-*trans*-carveol *via* a corresponding diol: mp 104 °C; IR (CCl_4) 3410, 3090, 1645, 1139, 1102, 1041, 886 cm^{-1}; NMR (CCl_4) δ 0.90 (d, J=7.1 Hz, 3H), 1.05 (s, 3H), 1.71 (s, 3H), 1.1—2.5 (m, 6H), 3.60 (m, 1H), 3.93 (bs, 2H, -OH), 4.62 (s, 2H); MS *m/e* (%) 184 (M^+, 3), 166 (30), 151 (11), 140 (13), 125 (15), 124 (20), 123 (21), 122 (23), 97 (26), 85 (100), 72 (79).

exo- *and* endo-*2-Norcaranol.* The title compounds were prepared from 2-cyclohexenol following the method reported by Dauben and Berezin.[24] Acetylation (acetic anhydride and pyridine) of these alcohols gave **10a** and **11a**.

2-Norcaranol-2-d. Lithium aluminum deuteride reduction of 2-norcaranone gave a mixture of *endo*-alcohol-2-*d* and *exo*-isomer (*endo* : *exo*=22 : 78).

Alkylation of ***10a*** *or* ***11a*** *with Trimethylaluminum.* A solution of trimethylaluminum in hexane (1.0 M, 3.0 ml, 3.0 mmol) was added to a solution of **10a** or **11a** (1.0 mmol) in dichloromethane (3.5 ml) at 0 °C. After 2 h at 25 °C, the mixture was worked up in a usual way. A ratio of **12a**: **13a** was determined by GLPC (Apiezone 10% on Celite 545, 3 m, 100 °C). Purification by preparative GLPC (PEG 20 M 20% on Celite 545, 2 m, 50 °C) gave pure samples of **12a** and **13a**: IR (neat) 3100, 3025, 2950, 2880, 1468, 1015 cm^{-1}; NMR (CCl_4) δ 0.33—0.59 (m, 2H), 0.60—2.13 (m, 9H), 0.94 (d, J=4.4 Hz, for **12a**) and 1.08 (d, J=4.4 Hz, for **13a**).

endo-*2-Methylnorcarane-2*-d (***12b***): NMR (CCl_4) δ 0.26—0.66 (m, 2H), 0.71—2.12 (m, 8H), 0.95 (d, J=0.6 Hz, 3H); MS *m/e* (%) 111 (M^+, 10), 110 (3), 96 (76), 82 (100), 69 (59), 68 (94), 67 (58), 54 (76), 41 (53).

Alternative Synthesis of a Mixture of ***12a*** *and* ***13a***.[25] A solution of 3-bromocyclohexene (8.1 g, 50 mmol) in ether (20 ml) was treated with lithium dimethylcuprate (I) (50 mmol) in ether (200 ml) at −20 °C for 1.5 h. A mixture of the resulting crude 3-methylcyclohexene, hexadecyltrimethylammonium bromide (0.5 g), and chloroform (30 ml) was treated with aqueous NaOH (50%, 30 g) at 50 °C. After stirring for additional 40 min, the mixture was diluted with ice-water and 10% HCl and extracted with dichloromethane. Distillation under reduced pressure (bp 95 °C, 20 Torr) afforded a mixture of 7,7-dichloro-*endo*-2-methylnorcarane and its 2-epimer (4.3 g, 48% yield). The mixture was reduced with sodium (0.91 g, 39 mg-atoms) in liquid ammonia(25 ml)-ethanol (0.24 g) to give *endo*-2-methylnorcarane **12a** and *exo*-epimer **13a** in 14: 86 ratio (0.22 g, 35% yield).

Stereochemical Assingnment of ***12a*** *and* ***13a***. A mixture of **12a** and **13a** (96 mg, 0.87 mmol, **12a**: **13a**=14: 86), platinum(IV) oxide (20 mg), and acetic acid (2.0 ml) was stirred at 25 °C for 12 h under hydrogen atmosphere to yield a mixture of *cis*- and *trans*-1,2-dimethylcyclohexane (*cis*: *trans*=17: 83). Both isomers were separated by preparative GLPC (Apiezone 5% on Celite 545, 3 m, 100 °C) and their IR spectra were compared with published data.

The authors wish to thank the Ministry of Education, Science, and Culture, Japan, for the Grant-in-Aid (203014, 303023, 335042, 403022).

References

1) Y. Kitagawa, S. Hashimoto, S. Iemura, H. Yamamoto, and H. Nozaki, *J. Am. Chem. Soc.*, **98**, 5030 (1976).

2) S. Hashimoto, Y. Kitagawa, S. Iemura, H. Yamamoto, and H. Nozaki, *Tetrahedron Lett.*, **1976**, 2615.

3) Preliminary accounts of this work have appeared: S. Ozawa, A. Itoh, K. Oshima, and H. Nozaki, *Tetrahedron Lett.*, **1979**, 2909; A. Itoh, K. Oshima, S. Sasaki, H. Yamamoto, T. Hiyama, and H. Nozaki, *ibid.*, **1979**, 4751.

4) R. B. Woodward, K. Hensler, J. Naegeli, W. Oppolzer, R. Ramage, S. Rangunathan, and H. Vorbriiggen, *J. Am. Chem. Soc.*, **88**, 852 (1966); T. Hirabayashi, K. Itoh, S. Sakai, and Y. Ishii, *J. Organomet. Chem.*, **25**, 33 (1970); A. Basha, M. Lipton, and S. M. Weinreb, *Tetrahedron Lett.*, **1977**, 4171.

5) R. R. Hatch and S. M. Weinreb, *J. Org. Chem.*, **42**, 3960 (1977), and references therein.

6) A. P. Kozikowski and A. Ames, *J. Org. Chem.*, **43**, 2735 (1978).

7) We are tempted to explain the observed results by assuming an aggregated complex in Scheme 5. Elastic collisions of hexane molecules can separate the ions to some extent and induce the intermolecular transfer of X under inversion.

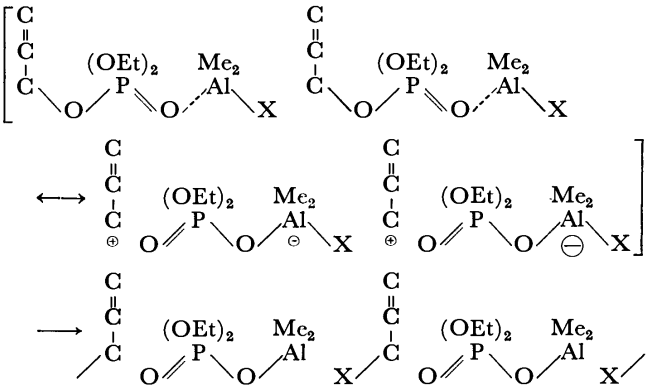

Scheme 5.

8) S. H. Schroeter and E. L. Eliel, *J. Org. Chem.*, **30**, 1 (1965).

9) H. O. House, "Modern Synthetic Reactions," 2nd ed, Benjamin (1972), p. 492; J. P. F. Normant, *Pure Appl. Chem.*, **50**, 709 (1978), and references cited therein.

10) Another example is a cuprate reaction with allylic, propargylic acetates. See G. H. Posner, *Org. React.*, **22**, 253 (1975).

11) The present alkylation is explained by assuming a symmetrical cationic intermediate of type **7**, the cyclohexenyl cation moiety of which is attacked by the methyl group from the side opposite to the isopropenyl group.

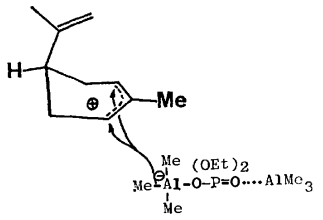

12) Treatment of *cis*-**3** and *trans*-**3** with lithium dimethylcuprate(I) according to the method of Goering (Ref. 13) afforded a mixture of **4a** and **5a** in low yields (20—30%) predominantly with inversion. A mixture of **4a** and **5a** (30: 70) was produced from *cis*-**3** and a 93: 7 mixture of the same products was produced from *trans*-**3**.

13) H. L. Goering and V. D. Singleton, Jr., *J. Am. Chem.*

Soc., **98**, 7854 (1976). See also C. Gallina and P. G. Ciattini, *ibid.*, **101**, 1035 (1979).

14) The data are all consistent with a common cationic intermediate **14**, to which methyl anion is delivered from the less hindered *cis* direction as indicated below.

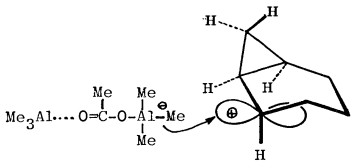

14

15) The Simmons-Smith reaction of 3-methylcyclohexene yields **13a** preferentially: P. A. Tardella and L. Pellacani, *Gazz. Chim. Ital.*, **107**, 107 (1977).

16) H. G. Kuivila and O. F. Beumel, Jr., *J. Am. Chem. Soc.*, **83**, 1246 (1961).

17) R. G. Johnston and J. Read, *J. Chem. Soc.*, **1934**, 233.

18) E. A. Jeffery and T. Mole, *Aust. J. Chem.*, **21**, 2683 (1968).

19) N. Davidson and H. C. Brown, *J. Am. Chem. Soc.*, **64**, 316 (1942).

20) J. I. Jones and W. S. McDonald, *Proc. Chem. Soc., London*, **1962**, 366.

21) A. Yasuda, H. Yamamoto, and H. Nozaki, *Bull. Chem. Soc. Jpn.*, **52**, 1757 (1979).

22) B. C. Hartman, T. Livinghouse, and B. Rickborn, *J. Org. Chem.*, **38**, 4346 (1973).

23) F. W. Eastwood, K. J. Harrington, J. S. Josan, and J. L. Pura, *Tetrahedron Lett.*, **1970**, 5223.

24) W. G. Dauben and G. H. Berezin, *J. Am. Chem. Soc.*, **85**, 468 (1963).

25) O. M. Nefedov, N. N. Novitskaya, and A. D. Petrov, *Dokl. Akad. Nauk SSSR*, **152**, 629 (1963).

 © 1980 The Chemical Society of Japan Bull. Chem. Soc. Jpn., 53, 2363—2365 (1980)

Preferential Solvation of Ag(I) Bromate and Iodate in Dimethyl Sulfoxide-Water Mixtures

Sivasankaran nair JANARDHANAN and Chatty KALIDAS*

Department of Chemistry, Indian Institute of Technology, Madras 600 036, India

(Received June 18, 1979)

The selective solvation of Ag(I) bromate and iodate was studied in dimethyl sulfoxide–water mixtures at 30 °C by solubility and EMF measurements. The solubility of silver bromate decreases down to $X_{DMSO}=0.2$ and thereafter increases with addition of dimethyl sulfoxide, the solubility of silver iodate continuously decreasing under the same conditions. The transfer free energy of silver cation decreases while that of halate ions increases with the addition of dimethyl sulfoxide. The solvent transport number, Δ, passes through a maximum around $X_{DMSO}=0.5$ in both cases. These results were interpreted in terms of a heteroselective solvation of both the salts, the silver ion being preferentially solvated by dimethyl sulfoxide and the halate ions selectively hydrated by water in the mixtures.

Investigations on ion solvation have largely been confined to aqueous[1] and pure non-aqueous solvents,[2] only few studies being carried out[3-5] in binary mixed solvents. In mixed solvents containing an electrolyte, there are two possibilities[6] depending on whether (a) both the ions of the electrolyte are solvated by the same solvent component, *i.e.*, a homoselective solvation or (b) one ion is bound more strongly by one solvent component while the other ion prefers the second solvent, *i.e.*, a heteroselective solvation. The present work deals with the selective solvation of two salts. The behavior of silver bromate and silver iodate in DMSO–water mixtures of varying composition was studied by means of electromotive force and solubility measurements in order to study the solvation of these salts and also the effect of solvent-solvent interactions on ion solvation.

Experimental

Materials. Dimethyl sulfoxide (BDH, LR Grade) was purified by the method of Maricle and Hodgson.[7] The middle fraction boiling at 60 °C under a pressure of 12 mm of Hg was collected and stored out of contact with air. Doubly distilled water was used in the preparation of DMSO–water mixtures. Ferrocene (E. Merck) was purified by sublimation in a vacuum. Silver bromate and silver iodate were prepared by the reaction of silver nitrate with the corresponding potassium salt. The precipitated silver halates were first thoroughly washed with water and then with acetone, and dried in a vacuum at 70—80 °C for several hours. The purity of the salts was checked by estimation of their silver content.

Solubility Measurements. The solubility measurements on the salts were performed at 30±0.1 °C in accordance with the general procedure.[4] The silver content of the saturated solution was determined by the addition of excess standard aqueous potassium iodide, the remaining potassium iodide being estimated by potentiometric titration with a standard solution of silver nitrate. A Metrohm Multidosimat (Type E 415) automatic titrator in conjunction with a Knick pH meter (for recording the EMF data) was employed. Oxidation of the iodide ion by iodate was found to be negligible.

Electromotive Force Measurements. The concentration cell was of the following type:[8]

$$\mathrm{Ag}\left|\begin{array}{l|l} x_1'\ \mathrm{H_2O} & x_1''\ \mathrm{H_2O} \\ x_2'\ \mathrm{DMSO} & x_2''\ \mathrm{DMSO} \\ \text{saturated with } \mathrm{AgXO_3} & \text{saturated with } \mathrm{AgXO_3} \end{array}\right|\mathrm{Ag} \qquad (1)$$

X=Br or I

EMF measurements were carried out over the complete range of DMSO–water mixtures keeping the mole fraction difference $x_2''-x_2'$ at 0.1. A U-type cell fitted with ground joints at the top and a G_3 frit in the middle to avoid direct contact of the solution was used in the EMF measurements. Silver electrodes freshly prepared according to the method of Carmody[9] were used. The EMF of cell 1 was measured at 30 °C with a Keithley (Model 602) Solid State Electrometer having an input impedence $>10^{14}$ Ω, reproducible with accuracy better than ±1 mV.

Results and Discussion

Solubility Measurements. The solubility and the transfer free energies of the salt (for transfer from water to DMSO–water mixtures) was calculated from the relation

$$\Delta G^{\circ}_{t(\mathrm{salt})} = 2.303RT\log\frac{K_{sp(\mathrm{water})}}{K_{sp(\mathrm{solvent})}} \qquad (2)$$

in different compositions of DMSO–water mixtures for both the salts. The results are given in Table 1, together with the free energy of transfer of silver ion in these mixtures.[11] The transfer free energy of the salts is related to that of the corresponding ions by

$$\Delta G^{\circ}_{t(\mathrm{AgXO_3})} = \Delta G^{\circ}_{t(\mathrm{Ag^+})} + \Delta G^{\circ}_{t(\mathrm{XO_3^-})}. \qquad (3)$$

The transfer free energies of the anions calculated from Eq. 3 are given in Table 1, the results being plotted in Fig. 1. K_{sp} in Eq. 2 represents the thermodynamic solubility product of the salt in water or the solvent mixtures and the mean activity coefficients required in these calculations were obtained from the extended Debye-Hückel equation with $a=6.5$ Å. The solubility of silver bromate decreases down to $X_{DMSO}=0.2$ and subsequently increases with the addition of DMSO, the solubility of silver iodate decreasing continuously under the same conditions. Thus $\Delta G^{\circ}_{t(\mathrm{salt})}$ increases up to $X_{DMSO}=0.2$ and thereafter decreases down to $X_{DMSO(\mathrm{pure})}$ in the case of silver bromate; it increases continuously in the case of silver iodate. However, the transfer free energy of silver ion (on the basis of ferrocene reference method, Table 1) shows a continuous decrease with the addition of DMSO, indicating that silver ion is preferentially solvated by DMSO. On the contrary, the transfer free energy of the anions is positive and continuously increases with the addition of DMSO indicating that they are selectively hydrated. Thus a

TABLE 1. SOLUBILITY AND TRANSFER FREE ENERGY DATA FOR $AgBrO_3$ AND $AgIO_3$ IN DMSO–WATER MIXTURES

Mole fraction of DMSO	Solubility of $AgBrO_3$ mol|kg^{-1} $\times 10^2$	Solubility of $AgIO_3$ mol kg^{-1} $\times 10^4$	$\Delta G^\circ_{t(AgBrO_3)}$ kcal mol^{-1}	$\Delta G^\circ_{t(AgIO_3)}$ kcal mol^{-1}	$\Delta G^\circ_{t(Ag^+)}$ kcal g-ion^{-1}	$\Delta G^\circ_{t(BrO_3^-)}$ kcal g-ion^{-1}	$\Delta G^\circ_{t(IO_3^-)}$ kcal g-ion^{-1}
0.0	0.98	3.3	0	0	0	0	0
0.1	0.80	3.0	0.24	0.08	−0.61	0.85	0.69
0.2	0.71	2.8	0.37	0.18	−2.52	2.89	2.70
0.3	0.87	2.4	0.15	0.34	−4.30	4.45	4.64
0.4	1.14	2.1	−0.13	0.53	−5.75	5.62	6.28
0.5	1.40	0.73	−0.38	1.78	−7.09	6.71	8.87
0.6	1.84	0.46	−0.68	2.33	−8.00	7.33	10.33
0.7	2.27	0.40	−0.89	2.51	−8.80	7.91	11.31
0.8	2.77	0.25	−1.09	3.05	−9.55	8.41	12.60
0.9	3.33	0.18	−1.27	3.49	−10.10	8.83	13.59
1.0	3.79	0.08	−1.36	4.36	−10.57	9.23	14.92

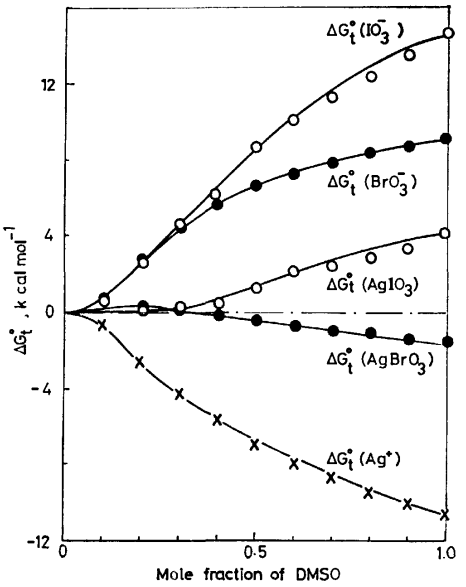

Fig. 1. Variation of ΔG_t° for silver bromate, silver iodate, Ag^+, BrO_3^-, and IO_3^- ions (from water to water–DMSO mixtures) with the mole fraction of DMSO at 30 °C.

heteroselective solvation of the salts in these mixtures may be inferred. Harakany and Schneider[8] arrived at a similar conclusion in the case of Ag_2SO_4–DMSO–water system.

We see from Table 1 that in aqueous solutions containing small amounts of DMSO ($X_{DMSO} \approx 0.1$), $\Delta G^\circ_{t(Ag^+)}$ is nearly equal to zero or slightly negative indicating that Ag^+ ion behaves as if it were in pure aqueous solution because of the strong interactions of DMSO with water molecules at low mole fractions of DMSO.[12,13] These strong solvent-solvent interactions result in a decrease of solubility of both salts at low mole fractions of DMSO. At higher mole fractions of DMSO, the relatively strong hydration of IO_3^- over that of BrO_3^- has a profound effect on the observed solubility of the two salts. The large positive ΔG_t° values of the bromate and iodate ions agree with earlier results,[14] the unusually strong hydration of these ions being attributed to their pyramidal structure with the halogen at the apex.

Solvent-transport Number Δ, from EMF Measurements. The emf data obtained from cell (1) utilised to calculate the solvent transport number, Δ of DMSO in these mixtures is expressed[12] by

$$E = \frac{-RT}{F} \frac{(x_2'' - x_2')\Delta}{X_2(1-X_2)} \left(1 + \frac{\partial \ln f_2}{\partial \ln X_2}\right), \qquad (4)$$

where $X_2 = (x_2'' + x_2')/2$ and $\partial \ln f_2 / \partial \ln X_2$ represents the variation of the activity coefficient of DMSO with the mole fraction in these mixtures, taken from the work of Cox and Mctigue[15] for the calculation of Δ. The other terms have their usual meanings. Δ may be defined as the net increase in the number of moles of DMSO in the cathode compartment, with the mean molar velocity of the solvent mixtures as a reference, when one faraday of electricity is passed through the cell during the course of electrolysis at the given solvent composition. The EMF data, values of $\partial \ln f_2 / \partial \ln X_2$ and the calculated Δ values of DMSO in the case of the two salts are given in Table 2 and Fig. 2. The values are positive throughout, passing through a maximum at $X_{DMSO} = 0.45$ ($\Delta = 1.6$) in the case of silver bromate and at $X_{DMSO} = 0.55$ ($\Delta = 2.1$) in the case of silver iodate. The Δ_{max} values provide direct information on ion solvation. The considerable positive values of Δ for both salts is in line with the conclusion arrived at from the transfer

TABLE 2. EMF DATA ON CELL (1) AND SOLVENT TRANSPORT NUMBER FOR $AgBrO_3$ AND $AgIO_3$ IN DMSO–WATER MIXTURES AT 30 °C

Mole fraction of DMSO (X_2)	$\frac{\partial \ln f_2}{\partial \ln X_2}$	Silver bromate		Silver iodate	
		$-E$(mV)	Δ	$-E$(mV)	Δ
0.05	1.175	5	0.08	17	0.26
0.15	1.245	20	0.78	20	0.78
0.25	1.365	22	1.16	18	0.95
0.35	1.515	24	1.38	23	1.32
0.45	1.705	29	1.61	30	1.70
0.55	1.920	15	0.74	43	2.12
0.65	2.155	14	0.57	41	1.66
0.75	2.235	9	0.30	36	1.16
0.85	2.235	8	0.18	26	0.57
0.95	2.235	5	0.04	20	0.16

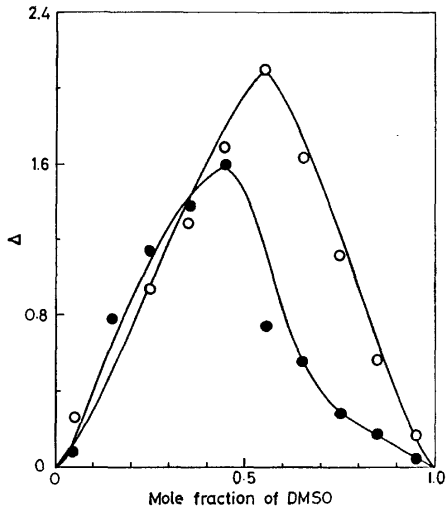

Fig. 2. Variation of solvent transport number, Δ for $AgBrO_3$ (●—●) and $AgIO_3$ (○—○) in water–DMSO mixtures at 30 °C.

free energy data of the two salts in the mixtures. The transport of DMSO into the cathode compartment occurs largely through the silver ion while the anions transport water into the anode compartment. The two effects are combined, characterising the heteroselective solvation with significantly large Δ.

References

1) H. L. Friedman and C. V. Krishnan, "Water, A comprehensive Treatise," ed by F. Franks, Plenum Press, New York (1973), Vol 3, pp. 2—118.
2) A. K. Covington and T. Dickinson, "Physical Chemistry of Organic solvent systems," Plenum Press, London (1973).
3) H. Schneider, *Electrochim. Acta*, **21**, 711 (1976).
4) C. Kalidas and P. Sivaprasad, *Indian J. Chem.* (accepted).
5) H. Schneider, "Solute-Solvent interaction," ed by J. F. Coetzee and C. D. Ritchie, New York (1976), p. 301.
6) H. Strehlow and H. Schneider, *Pure Appl. Chem.*, **25**, 327 (1971).
7) D. L. Maricle and W. G. Hodgson, *Anal. Chem.*, **37**, 1562 (1965).
8) A. A. El-Harakany and H. Schneider, *J. Electroanal. Chem.*, **46**, 255 (1973).
9) W. R. Carmody, *J. Am. Chem. Soc.*, **51**, 2901 (1928).
10) J. Courtot-Coupez *et al.*, *J. Electroanal. Chem.*, **29**, 21 (1971).
11) C. Wagner, "Advances in Electrochemistry and Electrochemical Engineering, Wiley-Interscience, New York (1966), Vol. 4, pp. 1—46.
12) D. Martin and H. G. Hauthal, "Dimethyl sulphoxide," Translated by E. S. Halberstaott, Van Nostrand Reinhold Company Ltd., Workingham, Berkshire, England (1975).
13) G. J. Safford *et al.*, *J. Chem. Phys.*, **50**, 2140 (1969).
14) I. M. Kolthoff and M. K. Chantooni, Jr., *J. Phy. Chem.*, **77**, 523 (1973).
15) B. G. Cox and P. T. McTigue, *Aust. J. Chem.*, **20**, 1815 (1967).

Oxidation Studies with Peroxomonophosphoric Acid. III. A Kinetic and Mechanistic Study of Oxidation of Dialkyl Sulfides

Ganesh Prasad PANIGRAHI* and Radhasyam PANDA
Department of Chemistry, Berhampur University, Berhampur 760 007, Orissa, India
(Received August 25, 1979)

The kinetics of oxidation of dialkyl sulfides by peroxomonophosphate in aqueous medium at 308 K and μ= 0.4 mol dm^{-3} follow the rate expressions (i) $-$d[peroxomonophosphate]/dt=$\{k_1[H_2PO_5^-]+k_2[HPO_5^{2-}]\}$[sulfide] in the pH region 6.8—8.7 where k_1 and k_2 values are 336.5 and 0.95, 69.7 and 0.254, and 27.5 and 0.126 dm^3 mol^{-1} s^{-1} for dimethyl, diethyl and dipropyl sulfides, respectively, (ii) $-$d[peroxomonophosphate]/dt=$k_2[HPO_5^{2-}]$·[sulfide] in the pH region 8.5—12.5, where the average k_2 values are 0.86, 0.247, and 0.128 dm^3 mol^{-1} s^{-1} for dimethyl, diethyl, and dipropyl sulfides, respectively, and (iii) $-$d[peroxomonophosphate]/dt=$\{k_2[HPO_5^{2-}]+k_3$·$[PO_5^{3-}]\}$[sulfide] in the pH region 12.5—13.7, the k_2 and k_3 values being 0.947 and 0.107, and 0.233 and 0.018 dm^3 mol^{-1} s^{-1} for dimethyl, and diethyl sulfides, respectively. The mechanism of the reaction is in line with a nucleophilic attack of the sulfide-sulfur on the peroxo oxygen, giving rise to S_N 2-type transition states which undergo oxygen–oxygen bond fission to give the corresponding sulfoxide and phosphate.

Organic sulfides have been oxidised[1–14] by various peroxo compounds. Howard and Levitt[6] pointed out that in the oxidation of diethyl sulfide by persulfate at pH 8 the reaction sequence should be sulfide→sulfoxide→sulfone, the second step of oxidation of the sulfoxide to sulfone being very slow. Electrophilic nature of the peroxo oxygen in this oxidation was suggested.

Curci and Modena[11,12] carried out studies on the steric and polar influences on peroxide oxidation rates of organic sulfides. In the oxidation of methyl phenyl sulfides and diphenyl sulfides by H_2O_2 in acidic ethanol solution,[8] the nucleophilic nature of the sulfide molecule was well established. Modena[9] observed the effects of alkyl group structure in alkyl phenyl sulfides, alkyl benzyl sulfides being predominantly steric.

Various reports have appeared on the oxidation of organic sulfides by peroxo compounds. However, no work seems to have been carried out on the oxidation of sulfides by peroxomonophosphoric acid. In continuation of our work[15,16] on the oxidation of organic substrates by peroxomonophosphoric acid in acid and alkaline pH, we are reporting the study on the oxidation of dialkyl sulfides by peroxomonophosphoric acid.

The oxidation was studied over the pH range 6—14, contribution of the various peroxomonophosphoric acid species being estimated. It is of interest that the pH dependence of the oxidation rate is quite contrary to that observed in the dimethyl sulfoxide oxidation.[16]

Experimental

All the chemicals were of AnalaR grade. Peroxomonophosphoric acid (PMPA) was prepared by the acid hydrolysis[17–20] of potassium peroxodiphosphate. Perchloric acid, used for hydrolysis, was neutralised by addition of a requisite amount of sodium hydroxide. The ionic strength of the medium was maintained with sodium perchlorate. The pH of the solution, adjusted with standard buffers or carbonate-free hydroxide, was determined with a Systronics digital pH-meter 335. Reactions were followed by measuring the rate of disappearance of peroxomonophosphoric acid, the estimation of which was made in an acetic acid–acetate buffer at a pH≈ 4—5 with a drop of ammonium molybdate solution (to avoid the diffused end point due to the presence of 2—3% of H_2O_2 formed during the course of hydrolysis) by the usual iodometric procedure. The self-decomposition of peroxomonophosphate (PMP), which occurs to some extent in the presence of higher [OH$^-$] due to

$$PO_5^{3-} \longrightarrow PO_4^{3-} + 1/2O_2$$

was found to be either nil or negligibly small. However, in a few cases, due allowance has been made to account for the self decomposition of the oxidant.

Results and Discussion

The kinetics of oxidation of dialkyl sulfides by PMP in alkaline pH have been investigated at 308 K. Kinetic runs with PMP in the range 2.91—9.26×10^{-4} mol dm^{-3} in the presence of excess [sulfide] at fixed pH and μ show a first-order disappearance of PMP. This follows from the constancy of the first-order rate constants (k_1') up to at least 60% completion of the reaction with respect to the disappearance of PMP in any single run when [sulfide]>[PMP].

The oxidation also exhibits a first order dependence on [sulfide] as seen from the constancy of the second-order rate constants k_2' (Table 1), calculated either by: $k_2'=k_1'$/[sulfide] (when [sulfide]>[PMP]) or from the usual second-order rate expression (when [sulfide]≈ [PMP]).

The variation of ionic strength using $NaClO_4$ was found to have negligible effect on the oxidation rate, indicating the rate determining slow step to involve at least one neutral molecule.[21] The oxidation rate is insensitive to the addition of acrylamide, indicating the absence of radicals in the reaction system.

Temperature dependence in the range 298—318 K for different dialkyl sulfides at pH 13.01 is given in Table 1. Activation parameters have been evaluated from the linear Arrhenius plots of log k_2' *vs.* T^{-1} (Table 2).

The influence of pH on oxidation rate has been studied in the pH ranges 7.36—13.7 for dimethyl sulfide, 6.76—13.7 for diethyl sulfide, and 6.87—13.0 for dipropyl sulfide. The results are interesting. Plots of pH *vs.* log k_{obsd}(=log k_2') for different dialkyl sulfides are shown in Fig. 1. The plots in sigmoid form suggest the participation of various species of PMP in the oxidation. The pH $-$log k_{obsd} plots can be

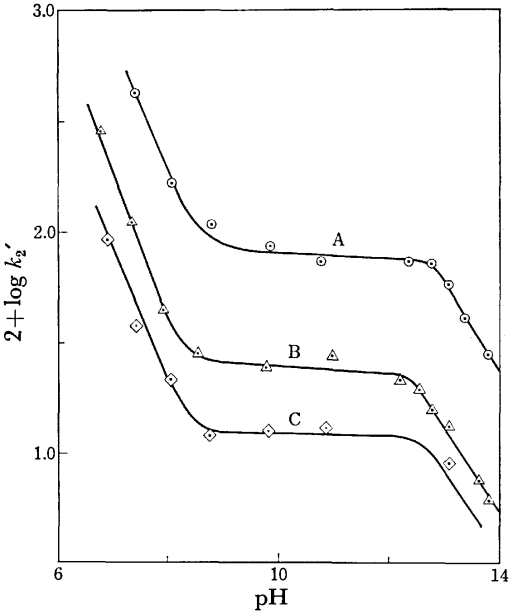

Fig. 1. Plots of log k_2' *vs.* pH (pH range 6.8 to 13.7).
A: Dimethyl sulfide, B: diethyl sulfide, C: dipropyl sulfide.

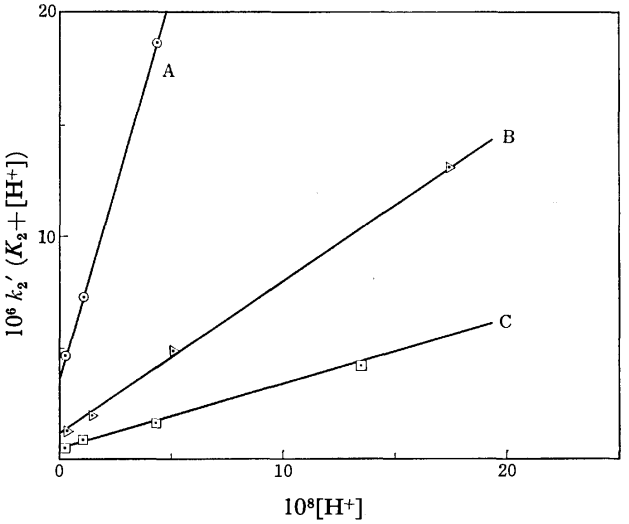

Fig. 2. Plots of k_2' ($K_2+[H^+]$) *vs.* $[H^+]$ (pH range 6.8 to 8.7).
A: Dimethyl sulfide, B: diethyl sulfide, C: dipropyl sulfide.

divided into three distinct pH regions 6.8—8.7, 8.7—12.5, and 12.5—13.7. The oxidation rate in the case of sulfides decreases with increasing $[OH^-]$, quite contrary to the oxidation of dimethyl sulfoxide by PMP where the rate increases with the increasing $[OH^-]$ (Table 3).[16]

Various equilibria[19] involving peroxomonophosphoric acid in solution are:

$$H_3PO_5 \overset{K_1}{\rightleftharpoons} H_2PO_5^- + H^+ \quad (1)$$

$$H_2PO_5^- \overset{K_2}{\rightleftharpoons} HPO_5^{2-} + H^+ \quad (2)$$

$$HPO_5^{2-} \overset{K_3}{\rightleftharpoons} PO_5^{3-} + H^+ \quad (3)$$

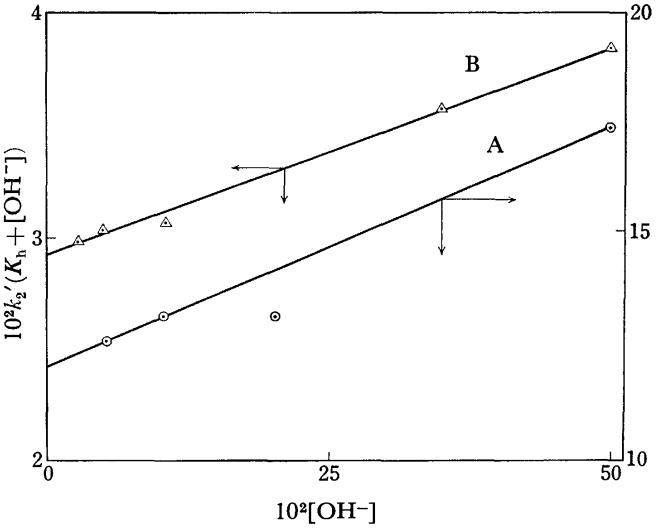

Fig. 3. Plots of k_2' ($K_h+[OH^-]$) *vs.* $[OH^-]$ (pH range 12.5 to 13.7).
A: Dimethyl sulfide, B: diethyl sulfide.

The dissociation constants, K_1, K_2, and K_3 are 8.0×10^{-2}, 4.2×10^{-6}, and 1.6×10^{-13}, respectively[19] at 298 K and $\mu=0.2$ mol dm^{-3}.

Since the species H_3PO_5, $H_2PO_5^-$, HPO_5^{2-}, and PO_5^{3-} become predominant with increasing pH in the order specified and the electrophilic character of these species decreases, it is evident from the pH dependence of the sulfide oxidation that the rate of oxidation decreases with decreasing electrophilic character of PMP species. A reverse trend has been observed in the case of DMSO oxidation[16] by PMP in the pH range 10—13.6; this has been rationalised on the basis of a nucleophilic attack of the PMP species on the sulfur of the sulfoxide.

The oxidation rate decreases in the order: dimethyl> diethyl>dipropyl sulfide. This could be attributed to the steric factor rather than to the polar effects which arises from the fact that in the oxidation[9] of alkyl phenyl sulfides and alkyl benzyl sulfides the effect of alkyl group structure is postulated to be predominantly steric. Although it is hard to sort out the polar and steric effects in the case of the dialkyl sulfides, the rate enhancement observed by the electron-releasing substituents on the aromatic rings of the alkyl phenyl sulfides is in the expected order of reactivity for the sulfide acting as a nucleophile.

On the other hand peroxides acting as electrophiles are not uncommon;[22,23] the observed second-order kinetics, the high negative entropies of activation and catalysis by acid support the electrophilic nature of the peroxide.

The sulfide molecule can be envisaged to participate in a nucleophilic attack on the peroxo oxygen, giving rise to the corresponding sulfoxide which does not undergo further oxidation. This arises from the fact that (i) TLC-analysis of the reaction mixture after about 80% completion of the reaction with respect to the consumption of PMP does not show the presence of any sulfone, and (ii) the rate of oxidation of dimethyl sulfoxide[16] is much lower than that of the dimethyl

TABLE 1.[a] OXIDATION OF DIALKYL SULFIDES BY PEROXOMONOPHOSPHATE

Sulfide	10^3 [sulfide] / mol dm^{-3}	10^4[PMP] / mol dm^{-3}	pH	$10^2k_2'$[b] / dm^3 mol^{-1} s^{-1}	$10^2k_2'$ Calcd / dm^3 mol^{-1} s^{-1}
Dimethyl sulfide	2.65	3.63	13.01	57.8	
	5.31	3.42	13.01	65.0	
	1.91	4.89	13.01	58.1	
	1.75	4.69	13.01	58.7[c]	
	2.09	4.69	13.01	29.7[d]	
	2.09	4.62	13.01	36.5[e]	
	1.54	4.26	13.01	74.1[f]	
	1.75	4.44	13.70	27.8[g]	27.4
	1.78	3.30	13.30	40.4	42.8
	1.91	4.89	13.01	58.1	56.7
	1.78	4.49	12.72	71.5	69.9
	1.46	3.64	12.30	73.0	
	2.15	3.80	10.71	73.8	
	2.15	4.00	9.77	87.8	
	2.12	4.63	8.74	111	110
	2.12	4.36	8.00	174	175
	2.18	4.29	7.36	441	440
Diethyl sulfide	1.67	9.26	13.01	14.6	
	1.67	2.91	13.01	14.9	
	1.77	4.54	13.01	13.3	
	0.59	4.54	13.01	13.4	
	1.06	3.76	13.01	12.9	
	2.12	3.76	13.01	13.5	
	1.43	3.99	13.01	17.2[h]	
	1.43	4.01	13.01	14.9[i]	
	1.75	5.13	13.01	9.6[d]	
	1.75	5.20	13.01	11.9[e]	
	1.93	4.80	13.01	18.9[f]	
	1.83	4.64	13.70	6.1[g]	6.1
	1.83	5.53	13.54	7.5	7.5
	1.77	4.54	13.02	13.3	13.5
	1.81	3.81	12.69	17.4	17.3
	1.63	4.49	12.45	19.4	19.3
	1.63	4.78	12.11	21.5	
	1.76	3.73	10.87	28.4	
	1.76	4.54	9.74	24.9	
	1.64	3.84	8.49	29.5	30.7
	1.64	4.36	7.84	46.1	49.2
	1.51	4.86	7.29	115	109
	1.51	4.67	6.76	300	301
Dipropyl sulfide	0.62	4.92	13.02	9.1	
	0.67	4.70	13.02	10.2[f]	
	0.67	4.27	13.02	11.6[j]	
	0.66	3.68	10.80	13.4	
	0.66	4.62	9.77	13.0	
	0.66	4.03	8.69	12.2	13.9
	0.67	3.09	7.97	22.3	19.6
	0.67	3.62	7.37	39.1	40.1
	0.67	4.01	6.87	97.9	97.7

a) In aqueous medium, at 308 K and $\mu=0.4$ mol dm^{-3}. b) Observed second-order rate constant. c) In the presence of acrylamide (1.50×10^{-3} mol dm^{-3}). d) At 298 K. e) At 303 K. f) At 313 K. g) $\mu=0.55$ mol dm^{-3}. h) $\mu=0.15$ mol dm^{-3}. i) $\mu=0.6$ mol dm^{-3}. j) At 318 K.

sulfide under similar conditions (Tables 1 and 3).

Since PMPA exists[19] as $H_2PO_5^-$ and HPO_5^{2-} in the pH range 4—7, the reaction sequence can be presented as

$$R_2S: + H_2PO_5^- \xrightarrow{k_1} R_2SO + H_2PO_4^- \quad (4)$$

$$R_2S: + HPO_5^{2-} \xrightarrow{k_2} R_2SO + HPO_4^{2-} \quad (5)$$

Table 2.[a] Oxidation of dialkyl sulfides by peroxomonophosphate (Thermodynamic parameters).

Sulfide	$\Delta H^{\neq}$/kJ mol^{-1}	$\Delta S^{\neq}$/J K^{-1} mol^{-1}
Dimethyl sulfide	44.6	−105
Diethyl sulfide	33.1	−153
Dipropyl sulfide	16.6	−211

a) Calculated at 308 K; in aqueous medium, at μ=0.4 mol dm^{-3} and pH 13.01.

Table 3.[a] Oxidation of dimethyl sulfoxide (DMSO) by peroxomonophosphate (PMP)

10^2 [DMSO] / mol dm^{-3}	10^4 [PMP] / mol dm^{-3}	pH	$10^3 k_2''$ [b] / dm^3 mol^{-1} s^{-1}
5.09	3.23	13.60	23.9[c]
5.09	4.13	13.30	17.9
5.20	2.66	13.03	12.7
5.20	3.45	12.78	8.2
5.09	3.11	12.28	3.7
20.4	4.14	11.55	1.4
20.4	4.06	11.36	0.74
20.4	4.15	11.17	0.59
20.3	4.25	10.88	0.58
20.5	4.29	10.84	0.53
20.3	4.41	10.65	0.40

a) Ref. 16, in aqueous medium at 308 K and μ=0.4 mol dm^{-3}. b) Observed second-order rate constant. c) At μ=0.45 mol dm^{-3}.

The reaction sequence in the pH range 12—14 in which PMP exists[19] as HPO_5^{2-} and PO_5^{3-} would be

$$HPO_5^{2-} + OH^- \overset{K_4}{\rightleftharpoons} PO_5^{3-} + H_2O \quad (6)$$

$$R_2S: + HPO_5^{2-} \xrightarrow{k_2} R_2SO + HPO_4^{2-} \quad (7)$$

$$R_2S: + PO_5^{3-} \xrightarrow{k_3} R_2SO + PO_4^{3-} \quad (8)$$

These equations suggest the rate laws corresponding to pH regions 6.8—8.7 and 12.5—13.7, respectively, as

$$-\text{d[peroxomonophosphate]}/dt = \{k_1[H_2PO_5^-] + k_2[HPO_5^{2-}]\}[\text{sulfide}] \quad (8a)$$

and

$$-\text{d[peroxomonophosphate]}/dt = \{k_2[HPO_5^{2-}] + k_3[PO_5^{3-}]\}[\text{sulfide}] \quad (8b)$$

from which we get:

$$-\frac{\text{d[PMPA]}}{dt} = \frac{k_1[H^+] + k_2K_2}{K_2 + [H^+]}[\text{PMPA}][\text{sulfide}] \quad (9)$$

where

$$k_2' = \frac{k_1[H^+] + k_2K_2}{K_2 + [H^+]}, \quad (9a)$$

$$-\frac{\text{d[PMP]}}{dt} = \frac{k_2K_h + k_3[OH^-]}{K_h + [OH^-]}[\text{PMP}][\text{sulfide}] \quad (10)$$

where

$$k_2' = \frac{k_2K_h + k_3[OH^-]}{K_h + [OH^-]} \quad (10a)$$

and

$$\frac{[H_2O]}{K_4} = K_h \quad (11)$$

Plots (Fig. 2) of $k_2'\{K_2 + [H^+]\}$ against $[H^+]$ (Eq. 9a) in the pH range 6.8—8.7 give straight lines (r=0.999, 0.999, and 0.998 for dimethyl, diethyl, and dipropyl sulfides respectively). From the intercepts and slopes of these least-square plots the values of k_1 and k_2 are respectively calculated to be 336.5 and 0.95 dm^3 mol^{-1} s^{-1} for dimethyl sulfide, 69.7 and 0.254 dm^3 mol^{-1} s^{-1} for diethyl sulfide, and 27.5 and 0.126 for dipropyl sulfide. The second-order rate constants (k_2' calcd) obtained from Eq. 9a with these k_1 and k_2 values, are given in Table 1.

Similarly from Eq. 10a, plots (Fig. 3) of $k_2'\{K_h + [OH^-]\}$ against $[OH^-]$ (with $K_h = K_w/K_3$, where K_w is the ionic product of water and K_3 is the dissociation constant of HPO_5^{2-}) for dimethyl and diethyl sulfides in the pH region 12.5—13.7 are found to be straight lines (r=0.97 and 0.99 respectively). The values of k_2 and k_3 as obtained from the intercepts and slopes of the above plots are respectively 0.947 and 0.107, and 0.233 and 0.018 dm^3 mol^{-1} s^{-1} for dimethyl and diethyl sulfides. With these k_2 and k_3 values, k_2' calcd values have been obtained from Eq. 10a (Table 1).

The k_2 values corresponding to the pH regions 6.8—8.7 and 12.5—13.7 agree excellently with the average k_2' values (0.86, 0.247, and 0.128 for dimethyl, diethyl, and dipropyl sulfides, respectively) in the pH region 8.5—12.5. This leads us to conclude that the PMP species predominantly exists as HPO_5^{2-} in the pH region 8.5—12.5. Thus the oxidation in this pH region can be expressed by

$$-\text{d[PMP]}/dt = k_2[HPO_5^{2-}][\text{sulfide}] \quad (12)$$

The oxidation of dialkyl sulfides by PMP in the pH range 6.8—13.7 can be visualised to involve a nucleophilic attack of the sulfide-sulfur atom on the peroxo-oxygen giving rise to S_N2-type transition states I, II, and III corresponding to steps (4), (5 and 7), and (8) respectively, which undergo oxygen-oxygen bond fission to form the products.

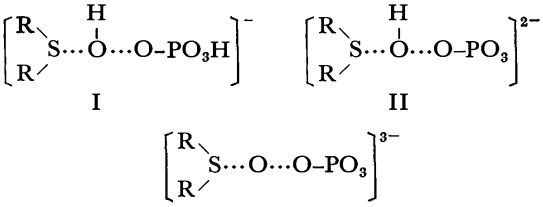

I II

III

This mechanism is in line with the thermodynamic parameters,[7] the magnitude of reactivity of different PMP species and the steric factor[9] involved in the sulfide.

The authors are thankful to Prof. P. S. Radhakrishna Murti, Dr. S. N. Mohapatro, and Dr. R. K. Panda of this department for helpful discussions and encouragement. One of the authors (R. S. P.) is grateful to C. S. I. R. (New Delhi) for the award of a Senior Research Fellowship.

References

1) L. Lewin, *J. Prakt. Chem.*, **118**, 282 (1928); **119**, 211 (1928); **127**, 77 (1930); **128**, 171 (1930).

2) J. Boeseken and E. Arrias, *Recl. Trav. Chim.*, **54**, 711 (1935).
3) J. Boeseken and A. T. H. Vander Meulen, *Recl. Trav. Chim.*, **56**, 925 (1936).
4) C. G. Overberger and R. W. Cummins, *J. Am. Chem. Soc.*, **75**, 4250 (1953).
5) C. G. Overberger and R. W. Cummins, *J. Am. Chem. Soc.*, **75**, 4783 (1953).
6) E. Howard, Jr., and L. S. Levitt, *J. Am. Chem. Soc.*, **75**, 6170 (1953).
7) L. Bateman and K. R. Hargrave, *Proc. R. Soc. London, Ser. A*, **224**, 389, 399 (1954).
8) G. Modena and L. Maioli, *Gazz. Chim. Ital.*, **87**, 1306 (1957).
9) G. Modena, *Gazz. Chim. Ital.*, **89**, 834 (1959).
10) I. P. Gragerov and A. F. Levitt, *Zh. Obshch. Khim.*, **33**, 543 (1963).
11) R. Curci and G. Modena, *Tetrahedron Lett.*, **25**, 1749 (1963).
12) R. Curci and G. Modena, *Tetrahedron Lett.*, **14**, 863 (1965).
13) R. Curci, F. D. Furia, R. Testi, and G. Modena, *J. Chem. Soc., Perkin Trans. 2*, **1974**, 752.
14) R. Curci, F. D. Furia, and G. Modena, *J. Chem. Soc., Perkin Trans. 2*, **1977**, 576.
15) G. P. Panigrahi and R. S. Panda, *Bull. Chem. Soc., Jpn.*, **52**, 3084 (1979).
16) G. P. Panigrahi and R. S. Panda, *Int. J. Chem. Kinet.*, (in press).
17) D. H. Fortnum, C. J. Battaglia, S. R. Cohen, and J. O. Edwards, *J. Am. Chem. Soc.*, **82**, 778 (1960).
18) C. J. Battaglia, Ph. D. Thesis, Brown University, 1962.
19) C. J. Battaglia and J. O. Edwards, *Inorg. Chem.*, **4**, 552 (1965).
20) F. Secco and M. Venturini, *J. Chem. Soc., Dalton Trans.*, **1976**, 1410.
21) K. J. Laidler, "Chemical Kinetics," Tata McGraw-Hill (1965), p. 229.
22) E. J. Behrman and J. O. Edwards, "Progress in Physical Organic Chemistry," ed by A. Streitwiesser and R. W. Taft, Interscience, New York (1967), Vol. 4, p. 94.
23) J. O. Edwards, "Peroxide reaction mechanisms," ed by J. O. Edwards, Interscience, New York (1962), p. 67.

Concentration Dependence of Flow Properties of Molten Salt Systems

Nurul Islam* and Anwar Ali
Department of Chemistry, Aligarh Muslim University, Aligarh 202001, India
(Received December 15, 1979)

The concentration dependence of fluidities and conductances of molten calcium nitrate tetrahydrate–MNCS ($M=Na^+$ or NH_4^+) systems was quantitatively explained by the isoenergetic and isoentropic equations essentially based on the Vogel-Tammann-Fulcher (VTF) and the Configurational Entropy Model (CEM) equations. The pre-exponential terms of the VTF and the Doolittle's equations were found to depend linearly on the values of the corresponding parameters, *i.e.*, T_0, the zero mobility temperature and those of V_0, the molar intrinsic volume at T_0, respectively. The linear interdependence of the two thermodynamic parameters, T_0 and V_0 on each other has been demonstrated. In addition to the linear dependence of the corrected energy of activation, E_{cor} on V_0, a physically meaningful linear dependence of E_{cor} on T_0 has also been demonstrated.

A solute experiences strong interionic effects due to the close proximity of charged species even in extremely dilute solutions of molten salts as is the case with very concentrated electrolytes. This renders such solutions to behave differently from those of the aqueous solutions. Attention has recently been drawn to the fact that the great majority of solutions which reach concentrations approaching their maximum solubility become very viscous on cooling to their melting temperatures and may readily supercool to the vitreous state.[1-4] This has led to the examination of relaxation processes in glass-forming melts in order to have greater insight into the nature of the transport behaviour in highly concentrated solutions and to provide new empirical description for the concentration dependence of such properties.

In order to achieve this aim Angell[2] transformed the Vogel-Tammann-Fulcher (VTF) equation[5] to an isothermal expression for the variation of transport properties with concentration by assuming the pre-exponential, A_Y, and the exponential, k_Y, parameters as concentration independent while taking only the T_0 as varying linearly with concentration. The resulting expression is of the form,

$$Y = A_Y T^{-1/2} \exp\left[-k_Y/Q_Y(N_0-N)\right], \quad (1)$$

where Y stands for the fluidity, $\phi=\eta^{-1}$, or the conductance, Λ, Q_Y (denoted by Q_{2Y} in Eq. 2) is the slope of the linear plot of T_0 *versus* N being in mol% and is given as,

$$T_0 = T_{0(0)} \pm Q_{2Y}N \quad (2)$$

The parameter N_0 is the characteristic concentration at which the isothermal temperature, T becomes the glass transition temperature T_g of the system, *i.e.*, the concentration at which the particle mobilities would fall to zero at the isothermal temperature. Recent studies on a large varieties of molten salt systems[6-8] have revealed that the parameter A_Y also varies linearly with concentration and may be expressed as,

$$A_Y = A_{0Y} \pm Q_{1Y}N, \quad (3)$$

in which Q_{1Y} represents the slope of the plot of A_Y *versus* N and A_{0Y} is the value of A_Y for the pure solvent. By accounting for such a dependence of A_Y Eq. 1 was modified[8] to

$$Y = (A_{0Y}\pm Q_{1Y}N)\,T^{-1/2} \exp\left[-k_Y/Q_{2Y}(N_0-N)\right]. \quad (4)$$

The above isothermal equation has been satisfactorily employed to explain the concentration dependence of transport properties of many molten salt mixtures. The limitations of this equation may, however, be pointed out. This equation has been found to be meaningfully applicable only within the T_0 values of the two components of the melts. If we try to go beyond this range of temperature the values of N_0 will be either less than zero or more than 100 mol% which are physically meaningless. For example, in the case of $Ca(NO_3)_2\cdot 4.09H_2O$–$Cd(NO_3)_2\cdot 4.07H_2O$[6] melts the T_0 values of the solvent and that of the solute range between 205 and 193 K. Therefore, the concentration dependence of transport properties obtained above 205 K cannot be explained by such an isothermal equation. Similar difficulties arise in applying the above isothermal equation to the mixtures of alkali metal nitrates in molten $Cd(NO_3)_2\cdot 4H_2O$[9] and $Ca(NO_3)_2\cdot 4H_2O$.[10] In view of such an inherent difficulty with Eq. 4 another expression based on the VTF equation was obtained[11] at equal values of T/T_0 $(=c)$. This results in an isoenergetic equation,

$$Y = (A_{0Y}\pm Q_{1Y}N)c^{-1/2}(T_{0(0)}\pm Q_{2Y}N)^{-1/2} \times \exp\left[-k_Y/(T_{0(0)}\pm Q_{2Y}N)(c-1)\right]. \quad (5)$$

Similarly, such behaviours may also be quantitatively explained in terms of the essentially configurational entropy model,[12]

$$Y = (A'_{0Y}\pm Q'_{1Y}N)\exp\left[-k'_Y/(T_{0(0)}\pm Q_{2Y}N)c\ln c\right]. \quad (6)$$

Some of the melts employed for this purpose have inherent glass-forming ability while others are induced by the presence of high concentrations of solute. In the latter category, the solubility of solutes, namely transition metal salts, in a given molten salt solvent depends upon several factors, *e.g.*, the ease of ionization, complex ion forming ability and their energetics, solvation, equilibria among several chemical species, *etc.* Furthermore, these molten salt mixtures could either be grouped as ideal with respect to the intrinsic volume, $V_{0,i}$ as well as to the zero mobility temperature, $T_{0,i}$ or as non-ideal. The former is marked by the absence of reactions involving complex-ion formation while the latter seems to have been caused by the presence of either tetrahedral or octahedral complex-ions as a result of pronounced interactions among the components of the melts.

The purpose of this paper is to examine the ability of generalized Eqs. 5 and 6 to explain the concentration dependence of the transport properties without being

restricted by the T_0 values of the two components and the role of the relevant parameters including the derived ones in understanding the successive variations in their behaviour with concentration.

The mixed molten salt systems, calcium nitrate tetrahydrate–ammonium thiocyanate and calcium nitrate tetrahydrate–sodium thiocyanate have been selected for the present investigation. In addition to these melts, reported[12,13] data on the concentration dependence of the flow processes in the cases of non-ideal melts containing either tetrahedral or octahedral complex-ions have also been analysed.

Experimental

Calcium nitrate tetrahydrate (BDH; mp 42.7 °C) was used as solvent in the molten state. Ammonium thiocyanate (BDH; mp 149.6 °C) and sodium thiocyanate (BDH; mp 287 °C, recrystallized twice from double distilled water) were used as solutes.

Samples were prepared in a thermostated paraffin bath at about 333 K. During the samples' preparation all the chemicals were handled with extra care in an atmosphere of pure and dry nitrogen. Several samples of different concentrations were prepared. Calcium nitrate tetrahydrate was found to dissolve approximately 60 mol% of ammonium thiocyanate, and 24 mol% of sodium thiocyanate.

Density measurements were made using a calibrated dilatometer of approximately 6.0 ml capacity with graduated stem of 0.01 ml divisions. The viscosities of the melts were determined with the help of a Cannon-Ubbelohde[14] type viscometer (viscometer constant, 6.26 cSt/s). The conductance measurements were made with conductivity bridge of Philips Model PR 9500 type. The cells used were of capillary-type[15,16] of cell constant values as 542 cm^{-1} and 730 cm^{-1} at 298 K.

Densities, viscosities, and conductivities were measured within $\pm 0.3\%$, $\pm 0.1\%$, and $\pm 1.5\%$ accuracy, respectively, in a thermostated paraffin bath of ± 0.1 °C thermal stability under dry nitrogen atmosphere.

Table 1. Equivalent conductance ($10^4\ \Lambda$, $Sm^2\ equiv^{-1}$) and fluidity ($10^{-1}\ \phi$, $N^{-1}\ m^2\ s^{-1}$) data as a function of temperature for molten (a) $Ca(NO_3)_2 \cdot 4.23H_2O$–$NH_4NCS$ and (b) $Ca(NO_3)_2 \cdot 4.1H_2O$–NaNCS systems

T/K	(a) NH_4^+/mol%						
	0.00	10.11	20.02	30.35	40.48	51.30	63.42
313.0	1.25 (1.246)	1.18 (1.110)	1.08 (1.201)	1.42 (1.338)	1.71 (1.413)	2.06 (1.814)	2.51 (2.477)
318.0	1.62 (1.600)	1.44 (1.394)	1.35 (1.587)	1.65 (1.724)	2.09 (1.789)	2.49 (2.330)	2.94 (3.063)
323.0	1.88 (2.005)	1.75 (1.761)	1.66 (1.976)	1.95 (2.164)	2.50 (2.200)	2.93 (2.841)	3.39 (3.696)
328.0	2.25 (2.454)	2.10 (2.200)	1.97 (2.484)	2.34 (2.699)	3.03 (2.950)	3.31 (3.408)	4.07 (4.425)
333.0	2.63 (2.974)	2.48 (2.599)	2.32 (3.030)	2.71 (3.154)	3.60 (3.415)	3.82 (4.132)	4.45 (5.218)
338.0	3.13 (3.570)	2.92 (3.154)	2.67 (3.634)	3.12 (3.777)	4.15 (3.926)	4.27 (4.814)	5.07 (6.099)
343.0	3.58 (4.370)	3.36 (3.766)	3.14 (4.273)	3.57 (4.466)	4.78 (5.004)	4.93 (5.660)	5.79 (7.018)
348.0	4.05 (4.907)	3.85 (4.388)	3.55 (4.977)	4.17 (5.155)	5.46 (5.867)	5.36 (6.416)	6.47 (7.885)
353.0	4.54 (5.664)	4.41 (5.121)	4.03 (5.741)	4.61 (5.949)	6.14 (6.700)	5.99 (7.334)	7.17 (8.872)

T/K	(b) Na^+/mol%					
	0.00	5.58	10.28	16.02	20.13	24.84
313.0	0.98 (1.017)	0.89 (0.991)	0.56 (0.925)	0.51 (0.903)	0.50 (0.811)	—
318.0	1.22 (1.333)	1.09 (1.299)	0.75 (1.219)	0.65 (1.180)	0.64 (1.082)	—
323.0	1.46 (1.675)	1.34 (1.650)	0.94 (1.555)	0.81 (1.512)	0.80 (1.399)	0.72 (1.337)
328.0	1.75 (2.078)	1.64 (2.052)	1.09 (1.944)	0.99 (1.894)	0.98 (1.766)	0.89 (1.732)
333.0	2.14 (2.545)	2.04 (2.522)	1.30 (2.407)	1.19 (2.341)	1.18 (2.187)	1.08 (2.159)
338.0	2.19 (3.080)	2.40 (3.053)	1.61 (2.923)	1.42 (2.866)	1.40 (2.679)	1.28 (2.653)
343.0	2.57 (3.659)	2.77 (3.641)	1.81 (3.487)	1.61 (3.421)	1.59 (3.222)	1.50 (3.190)
348.0	2.94 (4.286)	3.21 (4.268)	2.01 (4.096)	1.87 (4.035)	1.85 (3.783)	1.75 (3.770)
353.0	3.38 (4.998)	3.66 (4.970)	2.39 (4.772)	2.19 (4.702)	2.10 (4.436)	2.01 (4.418)

a) Fluidity data are within parentheses.

Results and Discussion

The waters of hydration in the melts were determined by the method[17] of comparison of densities.

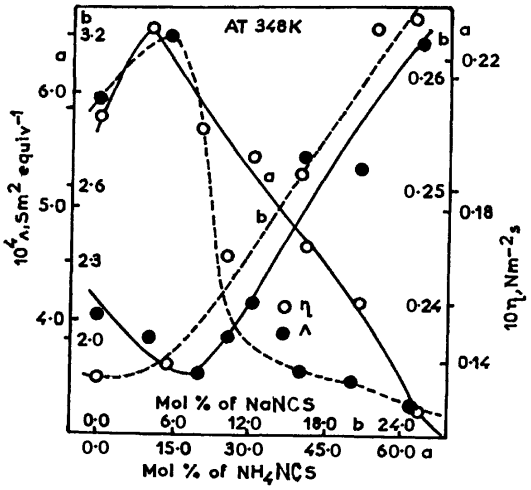

Fig. 1. Viscosity and conductance isotherms for molten (a) $Ca(NO_3)_2 \cdot 4.23H_2O$–$NH_4NCS$ and (b) $Ca(NO_3)_2 \cdot 4.1H_2O$–NaNCS systems.

The fluidities and conductances of the systems (Table 1) under investigation are found to change quite markedly with concentration (Fig. 1). The viscosity of a system is determined mainly by the bulky or less mobile entities while the ions of higher mobilities appear to be mainly responsible for the conductance behaviour. Therefore, both are expected to show an opposite trend in their behaviour with concentration as has actually been found.

In the case of the system, $Ca(NO_3)_2 \cdot 4.23H_2O$–$NH_4NCS$ fluidity and conductance both increase with increase in concentration of NH_4NCS. In this melt the hydrated solvent cation, $Ca(H_2O)_4^{2+}$ seems to be less mobile than the added solute cation, NH_4^+. Therefore, on adding NH_4NCS we are increasing the concentration of the conducting NH_4^+ ions which increase the conductance value with $[NH_4^+]$. It may, however, be pointed out that in the cases of ideal systems the resultant viscosities of the mixtures of molten salts may also depend upon the respective values of the two components. The above fact may be responsible for the increase in fluidity with $[NH_4^+]$. Both fluidity and conductance decrease with increase in the concentration of solute for the system, $Ca(NO_3)_2 \cdot 4.1H_2O$–NaNCS. Here the substitution of less mobile Na^+ for $(1/2)Ca^{2+}$ appears to be responsible for the decrease in the conductance value with increase in [NaNCS]. Decrease in the viscosity with concentration may presumably be due to an increase in the compactness or rigidity of the system.

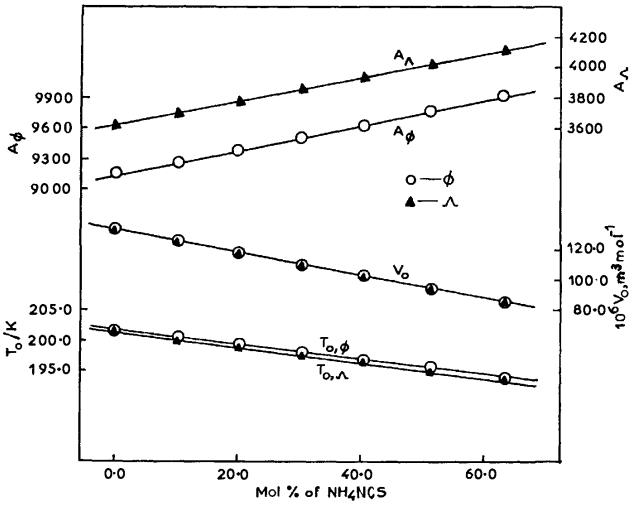

Fig. 2. Variation of A_Y, V_0, and T_0 with $[NH_4NCS]$ in molten $Ca(NO_3)_2 \cdot 4.23H_2O$–$NH_4NCS$ system.

In order to analyse the concentration dependence of fluidities and conductances the data were first least-squares fitted to the VTF and the CEM equations. The values of the parameters A_Y, A_Y', and T_0 thus obtained gave linear plots (Fig. 2) with N as expected from Eqs. 2 and 3.

Having examined the linear concentration variations of A_Y, A_Y', and T_0 the fluidities and conductances were

Table 2. Computed parameters of Eq. 5 for the equivalent conductance and the fluidity of molten salt mixtures

Melt	c	A_{0Y}	Q_{1Y}	k_Y	$T_{0(0)}$	Q_{2Y}	Std dev in ln Y
$Ca(NO_3)_2 \cdot 4.23H_2O$–$NH_4NCS$	1.7	3620.0 (9140.0)	7.720 (12.29)	567.0 (672.0)	201.3 (201.7)	0.104 (0.125)	0.019 (0.006)
$Ca(NO_3)_2 \cdot 4.1H_2O$–NaNCS	1.7	3300.0 (8357.0)	16.12 (19.48)	580.0 (670.0)	203.6 (203.9)	0.210 (0.205)	0.035 (0.004)

a) Parameters for the fluidity data are within parentheses.

Table 3. Computed parameters of Eq. 6 for the equivalent conductance and the fluidity of molten salt mixtures

Melt	c	A'_{0Y}	Q'_{1Y}	k'_Y	$T_{0(0)}$	Q_{2Y}	Std dev in ln Y
$Ca(NO_3)_2 \cdot 4.23H_2O$–$NH_4NCS$	1.7	50.10 (160.0)	0.945 (0.946)	586.2 (693.5)	201.3 (201.5)	0.122 (0.141)	0.035 (0.019)
$Ca(NO_3)_2 \cdot 4.1H_2O$–NaNCS	1.7	62.00 (180.0)	2.000 (0.530)	595.4 (694.7)	202.7 (204.0)	0.250 (0.190)	0.017 (0.017)

a) Parameters for the fluidity data are within parentheses.

Table 4. Parameters for density equation[a] and molar volumes for molten salt systems

Melt	mol%	a	$b\times10^{-3}$	10^6V_m(m³/mol) at 328 K
$Ca(NO_3)_2\cdot4.23H_2O$–NH_4NCS	NH_4^+			
	0.00	1.9635	0.7752	140.52
	10.11	1.9520	0.7841	131.93
	20.02	1.9185	0.7639	124.31
	30.35	1.8783	0.7451	116.53
	40.48	1.8424	0.7526	108.94
	51.30	1.7823	0.7054	100.60
	63.42	1.7035	0.6642	91.63
$Ca(NO_3)_2\cdot4.1H_2O$–$NaNCS$	Na^+			
	0.00	1.9813	0.7941	138.23
	5.58	1.9745	0.7884	133.53
	10.28	1.9782	0.8009	129.27
	16.02	1.9738	0.8014	124.35
	20.13	1.9704	0.7926	120.62
	24.84	1.9702	0.8002	117.03

a) The density equation is $10^{-2}\,\rho(\mathrm{kg\ m^{-3}})=a-bT(\mathrm{K})$.

least-squares fitted to Eqs. 5 and 6 at several values of constant T/T_0 $(=c)$. The corresponding temperature, T lying in the experimental range and the value of c which gave reasonably good fits were selected. The values of the relevant parameters thus obtained along with the standard deviations in $\ln\phi$ and $\ln\Lambda$ are listed in Tables 2 and 3. It should be noted that the computed values of the parameters A_{0Y}, Q_{1Y}, k_Y, Q_{2Y}, and $T_{0(0)}$ from Eq. 5 and those of A'_{0Y}, Q'_{1Y}, k'_Y, Q_{2Y}, and $T_{0(0)}$ from that of Eq. 6 are very close to those obtained from the corresponding plots (Fig. 2). Furthermore, the values of $T_{0(0)}$ obtained from Eqs. 5 and 6 are in good resemblance with those obtained by extrapolating the plots of T_0 *versus* N to zero mol% of solute in the respective melts.

It may be emphasized that the isoenergetic[18] as well as an apparently isoentropic[19] conditions used in the present systems satisfactorily represent the concentration dependence of viscosities and conductances in the glass-forming melts irrespective of the nature of the melt, whether they are ideal or non-ideal.[8] However, the isoenergetic condition appears to have a direct experimental relevance as compared to that involving an apparently constant entropy (the latter, however, is far from constant). Such an analysis emphasizes further the importance of choosing T/T_0 as a better corresponding state for the comparison of liquid properties.

Furthermore, an interesting relationship for the dependence of A_Y on T_0 obtained[11] by combining Eqs. 2 and 3,

$$A_Y=[A_{0Y}-(Q_{1Y}/Q_{2Y})T_{0(0)}]+(Q_{1Y}/Q_{2Y})T_0 \qquad (7)$$

is found (Fig. 3) to be applicable to the systems under investigation. This equation may be applied to any system in which A_Y and T_0 both vary linearly with concentration.

In view of the significance of another thermodynamic parameter, V_0 of Doolittle's equation[20] in explaining the transport behaviour, variations in the values of the parameters A''_Y and V_0 with concentration have similarly been examined. The molar volumes were obtained from the corresponding densities (Table 4). The pre-exponential term A''_Y of Doolittle's equation like those of A_Y and A'_Y terms shows a linear dependence on concentration and is, therefore, expressed as,

$$A''_Y=A''_{0Y}\pm Q_{3Y}N, \qquad (8)$$

where A''_{0Y} is the value of A''_Y for the pure solvent and Q_{3Y} is the slope of the plot of A''_Y *versus* N. It is also apparent from the plots of V_0 *versus* N (Fig. 2) that the V_0 varies linearly with concentration and may similarly be represented as,

$$V_0=V_{0(0)}\pm Q_{4Y}N, \qquad (9)$$

where $V_{0(0)}$ is the value of V_0 for the pure solvent and Q_{4Y} is the slope of the plot of V_0 *versus* N. Equations 8 and 9 may be combined to yield,

$$A''_Y=[A''_{0Y}\mp(Q_{3Y}/Q_{4Y})V_{0(0)}]\pm(Q_{3Y}/Q_{4Y})V_0 \qquad (10)$$

for the linear dependence of A''_Y on V_0.

Finally, combining Eqs. 2 and 9 a meaningful correlation between the two thermodynamic variables T_0 and V_0 may be obtained as,

$$T_0=[T_{0(0)}\mp(Q_{2Y}/Q_{4Y})V_{0(0)}]\pm(Q_{2Y}/Q_{4Y})V_0. \qquad (11)$$

The Eqs. 7, 10, and 11 represent the linear dependence of A_Y on T_0, A''_Y on V_0, and T_0 on V_0, respectively, as has actually been found in the cases of ideal (Fig. 3)

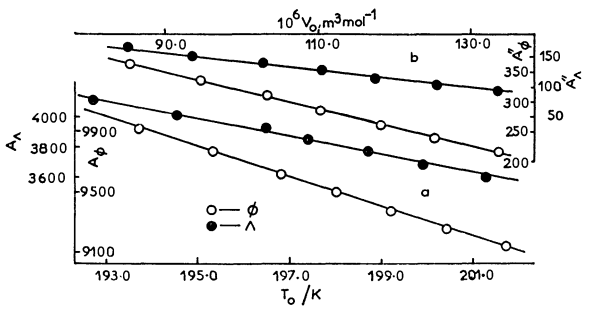

Fig. 3. Variations of (a) A_Y with $T_{0,Y}$, (b) A''_Y with $V_{0,Y}$, and (c) $T_{0,Y}$ with $V_{0,Y}$ for molten $Ca(NO_3)_2\cdot4.23H_2O$–NH_4NCS system.

as well as non-ideal systems containing either tetrahedral or octahedral complex-ions. The data for these parameters were least-squares fitted to the above derived equations and the computed values of the corresponding slopes and the intercepts are comparable with those obtained from the plots of A_Y, A''_Y, and T_0 against T_0, V_0, and V_0, respectively.

Furthermore, it is equally interesting to examine the relationship between the corrected activation energy, E_{cor} and T_0 value especially in view of their linear variations with concentration, *i.e.*, Eq. 2 and the following equation,

$$E_{cor} = E'_{cor} + Q_{5Y}N, \quad (12)$$

where E'_{cor} is the intercept while Q_{5Y} is the slope of E_{cor} *versus* N plot. Thus, combining Eqs. 12 and 2, we get,

$$E_{cor} = [E'_{cor} \mp T_{0(0)}(Q_{5Y}/Q_{2Y})] + (Q_{5Y}/Q_{2Y})T_0, \quad (13)$$

which suggests a linear increase in the corrected activation energies with T_0 as has actually been found (Fig. 4) in all the systems under investigation and also in those reported earlier.[12,13]

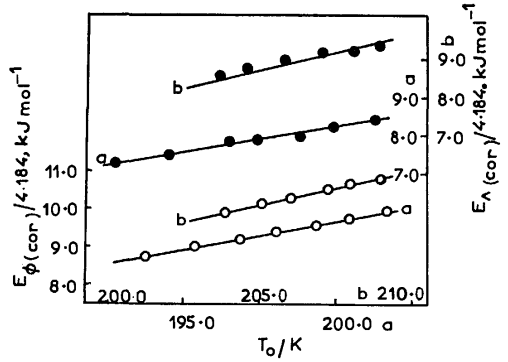

Fig. 4. Variation of E_Y with $T_{0,Y}$ for molten (a) $Ca(NO_3)_2 \cdot 4.23H_2O$–$NH_4NCS$ and (b) $Ca(NO_3)_2 \cdot 4.1H_2O$–NaCNS systems.

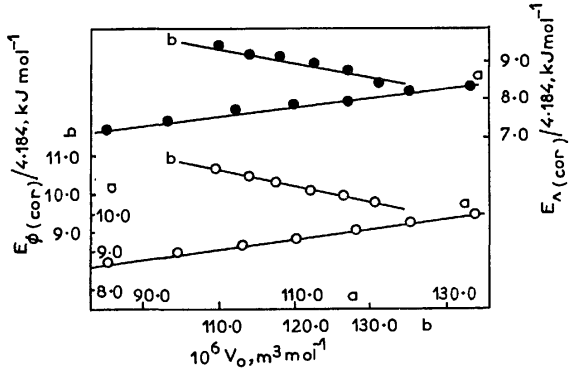

Fig. 5. Variation of E_Y with $V_{0,Y}$ for molten (a) $Ca(NO_3)_2 \cdot 4.23H_2O$–$NH_4NCS$ and (b) $Ca(NO_3)_2 \cdot 4.1H_2O$–NaNCS systems.

Similarly, in view of Eq. 11, E_{cor} may be expected to vary linearly with increase in the value of V_0 (Fig. 5) depending upon the sign in Eq. 11 for the dependence of T_0 on the V_0. Thus Eqs. 9 and 12 yield,

$$E_{cor} = [E'_{cor} \mp V_{0(0)}(Q_{5Y}/Q_{4Y})] \pm (Q_{5Y}/Q_{4Y})V_0. \quad (14)$$

It may be noted that Eq. 13 always envisages the same trend in the behaviour of E_{cor} with T_0 and is also physically understandable.

The authors wish to thank Professor W. Rahman, Head of the Chemistry Department, for providing the facilities. The financial assistance from the Council of Scientific and Industrial Research (New Delhi) to one of us (A. A.) is gratefully acknowledged.

References

1) C. A. Angell, *J. Chem. Phys.*, **46**, 4673 (1967).
2) C. A. Angell, *J. Phys. Chem.*, **70**, 3988 (1966); **69**, 2137 (1965).
3) C. A. Angell and E. J. Sare, *J. Chem. Phys.*, **52**, 1058 (1970).
4) G. Vuillard, *Ann. Chem. (Paris)*, **2**, 233 (1957).
5) The VTF equation is of the form,

$$Y = A_Y T^{-1/2} \exp[-k_Y/(T-T_0)]$$

where the terms have their usual significance.
6) C. T. Moynihan, C. R. Smalley, C. A. Angell, and E. J. Sare, *J. Phys. Chem.*, **73**, 2287 (1969).
7) N. Islam and I. Kochi, *J. Phys. Chem.*, **79**, 2180 (1975).
8) N. Islam and I. Kochi, *J. Phys. Chem.*, **80**, 1929 (1976).
9) C. A. Angell and D. B. Helphry, *J. Phys. Chem.*, **75**, 2306 (1971).
10) C. A. Angell, *J. Electrochem. Soc.*, **112**, 1224 (1965).
11) N. Islam, K. P. Singh, and S. Kumar, *J. Chem. Soc., Faraday Trans. 1*, **75**, 1312 (1979).
12) N. Islam, S. Kumar, and K. P. Singh, *Can. J. Chem.*, **56**, 1231 (1978).
13) N. Islam, M. R. Islam, B. Waris, and I. Kochi, *J. Phys. Chem.*, **80**, 291 (1976).
14) C. Tanford, "Physical Chemistry of Macromolecules," John Wiley and Sons, Inc. New York, N. Y. (1961), p. 329.
15) H. C. Cowen and H. J. Axon, *Trans. Faraday Soc.*, **52**, 242 (1956).
16) E. R. Van Artsdalen and I. S. Yaffe, *J. Phys. Chem.*, **59**, 118 (1955).
17) W. W. Ewing and R. J. Mikovsky, *J. Am. Chem. Soc.*, **72**, 1390 (1950).
18) The corrected activation energies, E_{cor}, for conductance and viscous flows were obtained as, $E_{cor}/Rk_Y = [T/(T-T_0)]^2$ from the derivative of VTF equation. R is the gas constant and k_Y is the empirical constant. Now, if we take T_0 as basis for the corresponding temperature, T in fused salts, then at constant values of T/T_0 we have, $E_{cor} = [(T/T_0)/\{(T/T_0)-1\}]^2 Rk_Y$. Therefore, E_{cor} may have a constant value at equal T/T_0 values.
19) According to the CEM, the configurational entropy of the system is given as $S_c = \Delta C_p \ln(T/T_0)$ where ΔC_p is the difference in heat capacities for the liquid and the glassy state which may be regarded as almost invariant with concentration. Therefore, at equal values of T/T_0 the configurational entropy of the system may apparently be treated as constant.
20) The Doolittle's equation is of the form.

$$Y = A''_Y \exp[-k''_Y/(V-V_0)]$$

where V is the molar volume and V_0 is the molar intrinsic volume of the melt.

Determination of Uranium and Thorium with Arsenazo III after Sequential Extraction from Acid-deficient Aluminium Nitrate Medium

T. V. RAMAKRISHNA* and R. S. SHREEDHARA MURTHY
Department of Chemistry, Indian Institute of Technology, Madras 600 036, India
(Received August 14, 1979)

Uranium has been quantitatively extracted into IBMK from ≈2.2 mol dm^{-3} aluminium nitrate solution at pH 0.8—0.9. Coextracted thorium (≈10%) is returned to the aqueous phase by addition of benzene. Subsequently, thorium is extracted into IBMK in the presence of hexadecyltrimethylammonium bromide (CTAB). This separation method has been applied to the analysis of uranium and thorium content of monazite sand.

Extensive work has been carried out on the extractive separation of uranium and thorium from each other and from accompanying elements.[1-5] A review of these methods indicates that in many instances the methods are selective either for uranium or thorium, and are therefore useful for the separation of any one of them from accompanying elements. Extraction methods have not been extensively explored for the sequential separation of uranium and thorium probably because their extraction takes place from medium of widely differing composition. This is illustrated by the studies of Cospito and Rigali[6] who extracted uranium from sulfate medium into trioctylamine in xylene and thorium with Aliquat 336, after making the aqueous phase 4 mol dm^{-3} with respect to nitric acid.

The selectivity of the extraction of uranium from 2.7 mol dm^{-3} acid-deficient aluminium nitrate into isobutyl methyl ketone (IBMK) proposed by Nietzel and De Sesa[7] was found to be far superior as compared to extraction from highly acid medium.[8] However, thorium has been coextracted to varying extents, no attempt being made to use this extraction for the separation of uranium from thorium.

The present investigation was undertaken to find suitable conditions for the selective and sequential extraction of uranium and thorium from acid-deficient aluminium nitrate solution into IBMK. The extraction behaviour of these metal ions was spectrophotometrically followed using arsenazo III.[9] The results indicate that coextracted thorium (≈10%) can be selectively returned to the aqueous phase by the addition of benzene. Further, addition of CTAB enabled the quantitative extraction of thorium into IBMK. The method was applied to the analysis of monazite sand.

Experimental

Reagents. Standard uranium and thorium solutions (10 ppm) Saturated aluminium nitrate solution Hexadecyltrimethylammonium bromide solution (0.5%) Arsenazo III solution (0.02%).

Apparatus. A Carl Zeiss PMQ II spectrophotometer with 10 mm quartz cells.

Recommended Procedure. *Separation*: Transfer a 5 cm^3 aliquot of the sample solution to a 25 cm^3 beaker. Add 10 g of aluminium nitrate and stir to dissolve. Adjust the pH to 0.8—0.9 using powdered ammonium carbonate under a pH-meter. Transfer the solution quantitatively to a 60 cm^3 separatory funnel using 1 cm^3 of saturated aluminium nitrate solution for rinsing. After extraction into 5 cm^3 of IBMK for 3 min, separate the aqueous phase (I) and treat the organic phase with 5 cm^3 each of saturated aluminium nitrate solution and benzene. Shake for 1 min. Separate the aqueous phase (II) and retain the organic phase for the recovery of uranium.

To the combined aqueous phase (I and II) in a 60 cm^3 separatory funnel, add 1 cm^3 of CTAB solution and extract into 10 cm^3 of IBMK for 5 min. Discard the aqueous phase. Retain the organic phase for the recovery of thorium.

Determination: Strip each organic phase containing uranium or thorium twice with 5 cm^3 of 0.1 mol dm^{-3} HCl and collect the resulting aqueous phases separately in a 25 cm^3 standard flask and make upto the mark with distilled water. Discard the organic phases.

Transfer an aliquot of the made-up solution containing not more than 30 μg of uranium or thorium to a 25 cm^3 conical flask. Add a few drops of concd H_2SO_4 and evaporate until fumes of sulfur trioxide evolve. For the determination of uranium, treat the residue containing uranium with 1 cm^3 of water, 5 cm^3 of concd HCl and 2 g of zinc granules. Allow the reduction to proceed for 5 min. Filter the solution through glass wool and wash thoroughly with 1: 1 HCl, collecting the filtrate and washings in a 25 cm^3 standard flask. Add 5 cm^3 of arsenazo III solution and make upto the mark with 1: 1 HCl. For the determination of thorium, dissolve the residue containing thorium in 5 cm^3 of water and transfer the solution to a 25 cm^3 standard flask using 1: 1 HCl for rinsing. Add 5 cm^3 of arsenazo III solution and dilute to the mark with 1: 1 HCl. Measure the absorbance in a 10 mm cell at 665 nm against a reagent blank. Estimate the concentration of uranium or thorium by reference to the respective calibration graphs prepared by directly subjecting 5—30 μg of uranium or thorium using 0.5—3.0 cm^3 of standard metal solution for development of coloration.

Results and Discussion

Initial studies on the extractive separation of uranium and thorium were made using 100 μg of each element. Extraction was carried out from 10 cm^3 of aqueous phase into 5 cm^3 of IBMK for 5 min, the percentage extraction of uranium or thorium being estimated.

Separation of Uranium: The effect of variation of aluminium nitrate concentration at pH 0.9 on the extraction of uranium and thorium is shown by curves A and B, respectively, in Fig. 1. It is evident that uranium extraction is quantitative provided that the aqueous phase is at least 2 mol dm^{-3} in aluminium nitrate. However, a significant amount of thorium (5—50%) was also extracted when the aluminium nitrate concen-

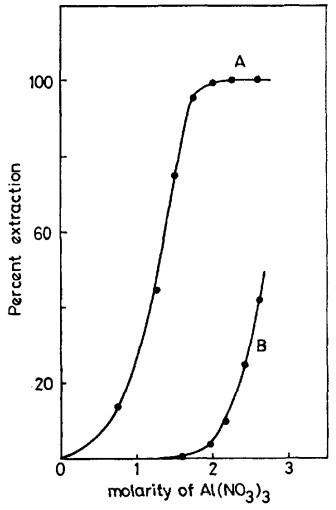

Fig. 1. Effect of aluminium nitrate concentration on the extraction of uranium (curve A) and thorium (curve B) into IBMK; pH of aqueous phase 0.9.

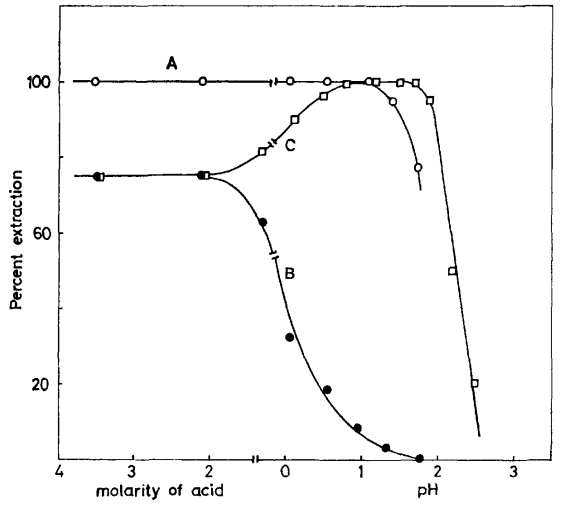

Fig. 2. Effect of acidity on the extraction of uranium (curve A), thorium (curve B), and thorium–CTAB (curve C) from 2.2 mol dm^{-3} aluminium nitrate solution into IBMK.

tration was varied from 2 to 2.6 mol dm^{-3}.

Figure 2 shows the effect of acidity on the extraction of uranium (curve A) and thorium (curve B) from aluminium nitrate solution (≈2.2 mol dm^{-3}). Variation in acidity was brought about by using concd HNO_3 or ammonia solution. It is evident that thorium extraction decreases rapidly with decreasing acidity; at pH 1.2, where uranium extraction is quantitative, only 5% of thorium is extracted. To ensure the quantitative extraction of uranium, the pH should be maintained at 0.8—0.9 where the extraction of thorium is 10—15%. Satisfactory conditions for the extraction can be conveniently brought about by dissolving 10 g of aluminium nitrate in a 5 cm^3 aliquot of the sample solution (whose volume increased to 10 cm^3) and by adjusting the pH to 0.8—0.9 using powdered ammonium carbonate with a pH-meter.

Attempts to make the organic uranium extract free from thorium revealed that retrograde extraction with a fresh aqueous phase of ≈2.2 mol dm^{-3} aluminium nitrate at pH 0.9 is ineffective, since it did not bring down thorium to the aqueous phase completely. As solvent to the organic extract in order to return the coextracted thorium selectively to the aqueous phase, benzene was chosen since it does not extract uranium or thorium. Equilibration of the phases after the addition of 5 cm^3 benzene, however, caused 10% decrease in the recovery of uranium. This was overcome by replacing the aqueous phase by 5 cm^3 of saturated aluminium nitrate solution (acidity ≈1 mol dm^{-3}) and equilibrating for 1 min with the IBMK extract after the addition of 5 cm^3 benzene. Uranium and thorium separation, however, was not quantitative when extraction was carried out from saturated aluminium nitrate solution directly into a 1 : 1 IBMK : benzene mixture, as uranium upto 20% remained in the aqueous phase along with thorium.

A shaking time of 1 min was found to be sufficient for the quantitative extraction of uranium into IBMK. Later equilibration upto 3 min with saturated aluminium nitrate and benzene did not affect the recovery of uranium.

Other solvents examined for the extraction of uranium included 1-butanol, ethyl acetate, butyl acetate, pentyl acetate, and cyclohexanone. Though extraction was quantitative with ethyl acetate and cyclohexanone, IBMK was preferred because it coextracted only 10% of thorium, while the percentage coextraction of thorium was 30% in ethyl acetate and 42% in cyclohexanone.

Separation of Thorium: Since thorium in nitrate medium would be present as the species $[Th(NO_3)_6]^{2-}$ its extraction from aluminium nitrate medium containing a cationic surfactant was considered.[10] This was examined by adding 1 cm^3 of 0.5% solution of CTAB to 10 cm^3 of ≈2.2 mol dm^{-3} of aluminium nitrate solution containing 100 μg of thorium. Extraction was carried out for 5 min using 10 cm^3 of IBMK, 1-butanol, ethyl acetate, butyl acetate, or cyclohexanone, of which only ethyl acetate and IBMK quantitatively

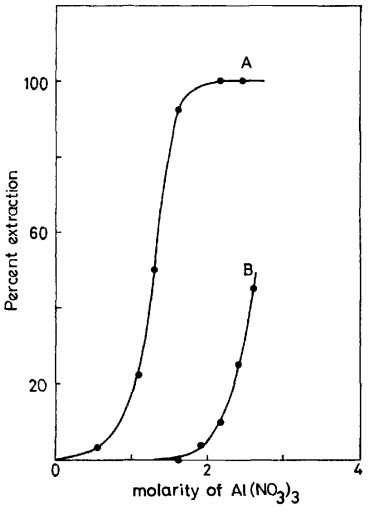

Fig. 3. Effect of aluminium nitrate concentration on the extraction of thorium–CTAB (curve A) and thorium (curve B) into IBMK; pH of aqueous phase 0.9.

extracted thorium. IBMK was preferred because of its lower solubility in the aqueous phase and rapid separation of both phases.

The effect of various parameters on the extraction of thorium indicates that the aqueous phase containing CTAB should be at least ≈2.2 mol dm^{-3} in aluminium nitrate (curve A, Fig. 3) and that the pH maintained over the pH range 0.8—1.6 for the quantitative extraction of thorium (curve C, in Fig. 2). Equilibration for 4 min and addition of at least 1 cm^3 of 0.3% solution of CTAB were sufficient for transferring thorium from the aqueous to organic phase.

TABLE 1. RECOVERY STUDIES FOR THE SEQUENTIAL EXTRACTION OF URANIUM AND THORIUM

Metal taken, μg		Metal found, μg		% Recovery	
U	Th	U	Th	U	Th
100	100	99	99	99	99
20	100	20.3	98	101.5	98
100	20	99.5	19.8	99.5	99
20	20	20	19.6	100	98
500	20	490	19.8	98	99
20	500	20.6	490	102.5	98

Sequential Extraction of Uranium and Thorium: The above results are promising for the sequential extraction of uranium and thorium. The sample solutions were subjected to extraction and determination (Experimental). The results (Table 1) indicate that the proposed method works satisfactorily.

Interference Studies: The extent of extraction of metal ions present in monazite sand which interfere with the arsenazo III procedure like zirconium, titanium and rare earths was examined. One mg of each ion (gadolinium was chosen as a representative rare earth) was subjected to extraction separately in the absence of thorium and uranium. After stripping the organic phases with 1 : 1 HCl, the concentrations of zirconium and gadolinium were estimated by the arsenazo III[9] procedure and that of titanium by the hydrogen peroxide method.[11] The interfering effect of anions such as sulfate and phosphate which are not removed by the usual means was also studied. The results (Table 2) indicate that the extraction procedure is quite selective, only phosphate inhibiting the extraction of both uranium and thorium.

Iron(III) hydroxide was used for collecting thorium and accompanying elements as hydroxide in order to overcome the interference of phosphate.[12] Aluminium hydroxide was also found to be effective for collecting thorium. The precipitate could be dissolved simply by treatment with saturated aluminium nitrate solution, so that subsequent separation and determination could be effected with no particular modification. 5 drops of saturated aluminium nitrate solution was added to samples containing uranium, thorium and phosphate. Dilute ammonia solution was then added until aluminium hydroxide precipitation was complete. The precipitate was centrifuged, washed with dilute ammonia (1 : 10) and dissolved in 8 cm^3 of saturated aluminium nitrate solution. The pH was then adjusted to 0.8—0.9 with solid ammonium carbonate and subjected to extraction. The results (Table 2) indicate that the method works satisfactorily.

TABLE 2. INTERFERENCE STUDIES

Ion added	% Extraction of		% Extraction at	
	U	Th	U stage	Th stage
Sulfate (1 mM)	99	98.5	—	—
Phosphate (1 mg)	95	94	—	—
Phosphate (2 mg)[a]	99	98.5	—	—
Titanium (1 mg)	—	—	nil	nil
Zirconium (1 mg)	—	—	nil	0.63
Gadolinium (1 mg)	—	—	0.2	1.10

a) After collection by use of aluminium hydroxide.

TABLE 3. ANALYSIS OF MONAZITE

	% ThO_2		% U_3O_8	
	Reported	Found	Reported	Found
	8.83	8.80	0.35	0.34
Sample 1[a]	—	8.84	—	0.36
	—	8.87	—	0.34
	—	8.31	—	0.33
Sample 2	—	8.34	—	0.35
	—	8.33	—	0.32

a) Supplied by Bhabha Atomic Research Center, Bombay.

Analysis of Monazite Sand: The thorium and uranium content of two monazite sand samples was determined after the removal of phosphate with aluminium hydroxide. 0.500 g of the finely ground sand was heated with 2 cm^3 of concd H_2SO_4 upto fuming of sulfur trioxide on a hot plate for 2 h. The residue was leached with ice-cold water and the leachate made up to 100 cm^3 with distilled water. A 1.0 cm^3 aliquot of the solution thus obtained was subjected to phosphate removal, then to extraction. The results (Table 3) indicate that the method works satisfactorily. In the present study, though the extraction behavior of rare earths other than gadolinium was not investigated, successful application of the extraction procedure to the analysis of monazite sand indicates that other rare earths behave in a similar way to that of gadolinium.

One of us (RSSM) is grateful to NCERT, New Delhi for financial assistance.

References

1) I. M. Kolthof and P. J. Elving, "Treatise on Analytical Chemistry," Interscience Publishers, New York (1961), Part II, Vol. 5, p. 139.

2) J. Korkisch, "Modern Methods for the separation of Rarer Metal Ions," Pergamon Press, Oxford (1969).

3) G. H. Morrison and H. Freiser, Fundamental Reviews: Extraction *Anal. Chem.*, **30**, 632 (1958); **32**, 37R (1960); **34**, 64R (1962); **36**, 93R (1964); **38**, 131R (1966); **40**, 522R (1968).

4) D. I. Ryabchikov and E. K. Gol'braikh, "The Analytical Chemistry of Thorium," Pergamon Press, Oxford (1963).
5) D. I. Ryabchikov and M. M. Senyavin, "The Analytical Chemistry of Uranium," Israel Program for Scientific Translations, Jerusalem (1963).
6) M. Cospito and L. Rigali, *Anal. Chim. Acta*, **57**, 107 (1971).
7) O. A. Nietzel and M. A. De Sesa, *Anal. Chem.*, **29**, 756 (1957).
8) W. J. Maeck, G. L. Booman, M. C. Elliot, and J. E. Rein, *Anal. Chem.*, **30**, 1902 (1958).
9) S. B. Savvin, *Talanta*, **8**, 673 (1961).
10) D. J. Carswell and J. J. Lawrence, *J. Inorg. Nucl. Chem.*, **11**, 69 (1959).
11) E. B. Sandell, "Colorimetric determination of traces of metals," Interscience Publishers, New York (1959), p. 870.
12) T. Y. Toribara and L. Koval, *Talanta*, **14**, 403 (1967).

Concentration and Spectrophotometric Determination of Molybdenum with Thiocyanate and Rhodamine 6G

T. Prasada Rao and T. V. Ramakrishna*
Department of Chemistry, Indian Institute of Technology, Madras 600 036, India
(Received August 14, 1979)

A method is described for the determination of molybdenum based on reaction with potassium thiocyanate and Rhodamine 6G in 0.55—0.8 mol dm^{-3} hydrochloric acid medium. The method is sensitive ($\varepsilon=2.63\times10^5$ l mol^{-1} cm^{-1}) and obeys Beer's law over the range 0.04—0.24 ppm of molybdenum. Selectivity can be considerably improved by collecting molybdenum on iron(III) hydroxide. In conjunction with the collection procedure, the method is useful to determine as low as 5 ppb of molybdenum present in 100 cm^3 of aqueous samples.

A number of ternary systems have been proposed for the spectrophotometric determination of molybdenum[1-5] and, amongst these, the method based on its reaction with thiocyanate and Rhodamine B in the presence of copper–thiourea complex[3] is attractive as it possesses high sensitivity ($\varepsilon=1.10\times10^5$ l mol^{-1} cm^{-1}), selectivity and, in addition, allows the determination to be completed directly in aqueous medium. Our investigation on these lines revealed that the use of Rhodamine 6G instead of Rhodamine B is advantageous, as the reaction proceeds in dilute hydrochloric acid medium without the addition of copper–thiourea complex and providing much superior sensitivity ($\varepsilon=2.63\times10^5$ l mol^{-1} cm^{-1}). Furthermore, Rhodamine 6G is less susceptible to colour changes due to slight changes in the acidity of the medium. Detailed study on this colour system showed that the few ions that interfere in the determination can be conveniently overcome by selectively collecting molybdenum(VI) on iron(III) hydroxide precipitate. In conjunction with the collection procedure, the method was found useful to determine as low as 5 ppb of molybdenum present in aqueous samples.

Experimental

Reagents. *Molybdenum(VI) Solution*: Dissolve 0.115 g of ammonium molybdate in water and dilute to 250 cm^3. Dilute appropriate volumes of this stock solution (250 ppm) with water to provide a 1.0 ppm solution.

Potassium Thiocyanate Solution (3%): Dissolve 3 g of potassium thiocyanate in water and dilute to 100 cm^3.

Rhodamine 6G Solution (0.01%): Dissolve 0.1 g of reagent (chrom a Gesellschaft, Schmid and Co., Stuttgart) in water and dilute to 1 dm^3.

Gelatin Solution (1%): Dissolve 1 g of gelatin in boiling water and dilute to 100 cm^3.

Apparatus: A Carl Zeiss PMQ-II spectrophotometer with 10 mm quartz cells and a Knick pH-meter with an Ingold combined glass-calomel electrode were used.

Recommended Procedure. *Determination*: Transfer a suitable aliquot (upto 10 cm^3) of the sample solution containing not more than 6 μg of molybdenum to a 25 cm^3 volumetric flask. Adjust the acidity to 0.55—0.8 mol dm^{-3} with hydrochloric acid and add with mixing 5 cm^3 each of potassium thiocyanate and Rhodamine 6G solution. Allow the reaction to proceed for 1 h and then add 1 cm^3 of 1% gelatin. Dilute the solution to mark with distilled water and measure the absorbance in 10 mm cells at 570 nm against a reagent blank. Prepare a calibration graph for 1—6 μg of molybdenum by the above procedure.

Concentration and Separation: To a suitable aliquot (upto 100 cm^3) of the sample add 2 mg iron(III) and adjust the pH to 4.0 under a pH-meter. Add 5 cm^3 of acetone, stir well and centrifuge the suspension. Discard the centrifugate and wash the suspension twice with 5 cm^3 of a 2% solution of ammonium chloride. Dissolve the precipitate by digesting with 5 cm^3 of 0.2 mol dm^{-3} hydrochloric acid and then treat with 2.5 cm^3 of 0.5 mol dm^{-3} sodium hydroxide to reprecipitate the iron. Centrifuge, wash the precipitate twice with 5 cm^3 of water and combine the centrifugate and washings. If the molybdenum content is large, make up the solution to a known volume and subject an aliquot to molybdenum determination. Otherwise, evaporate the solution to a small volume and complete the determination as given under "Procedure."

Results and Discussion

Preliminary Studies. Initial experiments indicated that after the addition of thiocyanate and Rhodamine 6G to molybdenum solution in 0.6 mol dm^{-3} hydrochloric acid, if the solutions were immediately diluted to 25 cm^3 with water, the colour development was quite incomplete. Omission of dilution with water caused both test and blank solution to acquire an intense pink colour but on standing, the colour of the blank slowly changed to orange red. However, later dilution with water as above to 25 cm^3 caused the pink colour of the test solution also to fade off gradually. Systematic investigation revealed that the colour system is colloidal in nature and stabilization can be achieved by the addition of small amounts of gelatin prior to dilution with water. In preliminary experiments, therefore, after the addition of reagent solutions, the reaction was allowed to proceed for 60 min to facilitate complete disappearence of the pink colour of the blank, and then treated with 1 cm^3 of 1% solution of gelatin and sufficient water to 25 cm^3.

The spectra of gelatin-stabilized solutions in 10 mm cells against distilled water is shown in Fig. 1. It is evident that the reagent blank absorbs maximally at 530 nm. In the presence of molybdenum, there is, in addition to this maximum, a new shoulder at 570 to 575 nm. The difference between the spectra of the complex and the reagent blank showed that 570 nm is the optimum wavelength for measurement.

Considerable enhancement in the absorbance of the sample at 570 nm was noticed when Rhodamine 6G concentration was increased to 5 cm^3 of 0.01%. This is

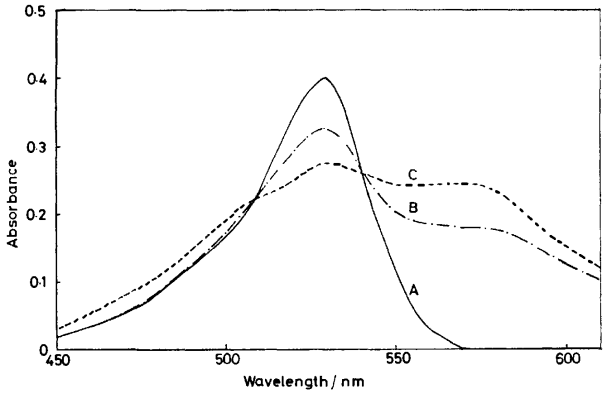

Fig. 1. Absorption spectra of molybdenum–thiocyanate–Rhodamine 6G system (0.6 mol dm^{-3} in HCl; total volume 25 cm^3; 10 mm cells).
A: 1.0 cm^3 of 2.1×10^{-4} mol dm^{-3} (0.01%) Rhodamine 6G, 1 cm^3 of 10% potassium thiocyanate and 1 cm^3 of 1% gelatin, reference: water, B,C: as in A, with 0.5 and 1 cm^3 of 1.05×10^{-4} mol dm^{-3} molybdenum, reference: water.

apparently due to increased association of the complex. Under these conditions, the blank showed an absorbance of 0.06 at 570 nm as against 0.28 and 0.61 obtained with solutions containing 0.2 and 0.5 cm^3 of 1.05×10^{-4} mol dm^{-3} of molybdenum present in 25 cm^3 respectively when measured in 10 mm cells.

Optimization of Experimental Conditions. Maximum absorbance was obtained when the acidity of the reaction medium, containing 3 μg of molybdenum, 5 cm^3 each of 3% potassium thiocyanate and 0.01%. Rhodamine 6G, was maintained from 0.55 to 0.8 mol dm^{-3} in hydrochloric acid. Similar studies at 0.6 mol dm^{-3} acidity on the variation of potassium thiocyanate and Rhodamine 6G concentration showed that the addition of 2 cm^3 of 5% potassium thiocyanate and 4 cm^3 of 0.01% solution of Rhodamine 6G was sufficient to provide maximum absorbance. Though 1 cm^3 of 0.75% solution of gelatin was found to be sufficient to stabilize the colour system, further addition did not affect the absorbance. When the recommended concentration of reagent solutions were added, maximum colour was produced after a standing time of 45 min, which after dilution remained stable for 90 min and the addition of as high as 5 cm^3 of saturated sodium chloride solution did not affect the absorbance. Under these conditions, the calibration graph was a straight line for 1—6 μg of molybdenum and passed through the origin. The molar absorptivity and Sandell sensitivity were established to be 2.63×10^5 dm^3 mol^{-1} cm^{-1} and 0.36 ng cm^{-2} respectively for the colour system at 570 nm.

Ten replicate determination of standard solutions containing 3.0 μg of molybdenum(VI) gave an average recovery of 102.5% with a relative standard deviation of 2.5%.

Effect of Diverse Ions. The effect of 40 diverse ions on the determination of 3.0 μg of molybdenum was examined. A few ions that interfered were overcome by adding thiourea, ascorbic acid or tartrate. The results obtained are summarized in Table 1. The interference due to zinc and cobalt(II) could not be masked.

Table 1. Effects of diverse ions[a)]

Ion	Amount Added (mg)	Molybdenum Found (μg)	Ion	Amount Added (mg)	Molybdenum Found (μg)
Li^+	1	3.0	W(VI)	0.1[d)]	3.0
Na^+	5	3.0	UO_2^{2+}	0.1[c)]	3.1
Be^{2+}	1	3.2	Mn^{2+}	1	3.0
Mg^{2+}	1	3.0	Fe^{3+}	0.5[c)]	3.0
Ca^{2+}	1	3.1	Co^{2+}	—	—
Sr^{2+}	1	3.0	Te^{4+}	1	3.1
Al^{3+}	1	3.3	Ni^{2+}	1[b)]	3.1
Pb^{2+}	1[b)]	3.0	Pd^{2+}	1[b)]	3.0
Bi^{3+}	1[b)]	3.1	Pt^{4+}	1[b)]	2.9
Sb(V)	1	2.9	F^-	1	3.0
Cu^{2+}	1[b)]	3.0	PO_4^{3-}	1	2.9
Zn^{2+}	—	—	SO_4^{2-}	5	3.0
Cd^{2+}	1[b)]	3.2	Br^-	5	3.0
Hg^{2+}	1[b)]	3.1	ClO_4^-	1	3.2
La^{3+}	1	3.0	NO_3^-	5	3.1
Ce^{4+}	1	3.0	Citrate	5	3.0
Th^{4+}	1	3.1	Oxalate	5	2.9
V(V)	0.1[c)]	3.2	Tartrate	5	3.1
Cr(VI)	1[b)]	3.0	Arsenate	1	3.1
Ba^{2+}	1	3.1	Arsenite	1	3.2

a) Molybdenum taken was 3.0 μg. b) 1 cm^3 of 5% thiourea. c) 1 cm^3 of 2% ascorbic acid. d) 1 cm^3 of 10% tartrate.

Composition of the Complex. The ratio of molybdenum to Rhodamine 6G was determined by both mole ratio and Job's continuous variation methods. The results obtained (Figs. 2 and 3) showed that the molar ratio of molybdenum to Rhodamine 6G is 1 : 2. The molar ratio of molybdenum to thiocyanate could not be established, as no colour developed upon treating with Rhodamine 6G, evidently due to instability of the molybdenum–thiocyanate binary complex.

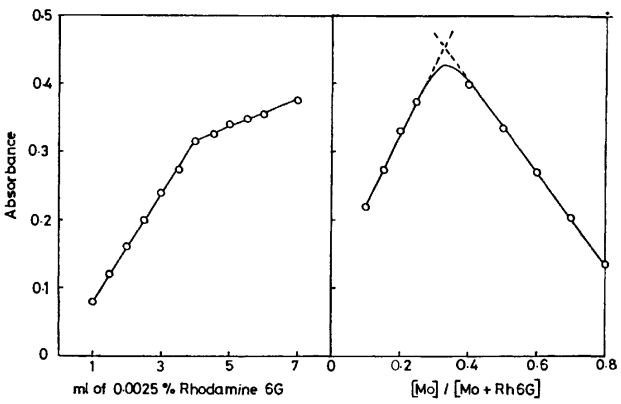

Fig. 2. Mole-ratio method (0.6 mol dm^{-3} in HCl, total volume 25 cm^3; 10 mm cells; 570 nm).
[Mo] = 1 cm^3 of 1.05×10^{-4} mol dm^{-3}, [Rh6G] = 1 to 7 cm^3 of 5.25×10^{-5} mol dm^{-3}.

Fig. 3. Continuous variation method (0.6 mol dm^{-3} in HCl; total volume 25 cm^3; 10 mm cells; 570 nm).
$[Mo+Rh6G]_{total}=2.1\times10^{-5}$ mol dm^{-3}.

With Rhodamine B colour system,[3] it has been indicated that Mo(VI) is reduced to Mo(V) by copper–thiourea complex in sulfuric acid medium to form $[MoO(SCN)_5]^{2-}$ to facilitate association with 2 molecules of Rhodamine B cation. However, with the Rhodamine 6G colour system, as the presence of copper–thiourea did not affect the sensitivity, it appeared reasonable to conclude that the reduction of molybdenum(VI) proceeds smoothly in dilute hydrochloric acid medium in the presence of thiocyanate to form $[MoO(SCN)_5]^{2-}$ which then associates with 2 molecules of Rhodamine 6G cation to produce the observed spectral shift.

Evaluation of Iron(III) Hydroxide Collection. Though solvent extraction and ion-exchange find common use to separate interferents from the desired constituent, collection of molybdenum on a sparingly soluble metal hydroxide was considered for its separation from interfering elements. Earlier studies have shown that for the collection of molybdenum from weakly acidic solutions, thorium hydroxide (99.5% collected in 30 min)[6] is much superior to iron(III) hydroxide (96.5% in 2h),[7] aluminium hydroxide (7.8% in 2 h)[6] or manganese dioxide (100% in 24 h).[8] Iron(III) hydroxide collection, however, was chosen in the present study. Detailed investigations revealed that the addition of miscible organic solvents such as acetone, methanol, ethanol, 2-propanol, 4-hydroxy-4-methyl-2-pentanone, acetonitrile, 1,4-dioxane, and *N,N*-dimethylformamide to weakly acidic solution of molybdenum promoted rapid and quantitative collection on ferric hydroxide. Addition of acetone was chosen for further investigations. Later studies revealed that the molybdenum collected on iron(III) hydroxide was quantitatively released by dissolving the precipitate in dilute hydrochloric acid and reprecipitating it with alkali.

Systematic study of collection of molybdenum was made by adding 2 mg of iron(III) to 20 cm^3 aliquots of solution and using dilute sodium hydroxide to precipitate iron(III) hydroxide. The suspensions obtained were centrifuged and the supernatant liquid was rejected. In each instance the precipitate, after washing twice with 5 cm^3 of 2% ammonium chloride, was dissolved by digesting with hydrochloric acid ($\approx$5 cm^3 of 0.2 mol dm^{-3}) and then the pH was raised to >10.0 using sodium hydroxide ($\approx$2.5 cm^3 of 0.5 mol dm^{-3}) to reprecipitate the iron. The suspension was centrifuged and washed twice with 3 cm^3 portions of water. The centrifugate and washings were combined and evaporated to about 5 cm^3. Molybdenum content was then established by the procedure described under "Experimental."

Figure 4 shows the effect of variation of pH of the medium containing 5 cm^3 of acetone on the collection of 3 μg of molybdenum by iron(III) hydroxide. It is evident that the recovery is quantitative over the pH range 4.0 to 4.5 and that iron(III) hydroxide is ineffective at pH's greater than 9.0. Subsequent studies at pH 4.0 using 2 mg of iron(III) revealed that the addition of 5 cm^3 of acetone was sufficient to recover quantitatively 0.5 μg to 1 mg of molybdenum present in 100 cm^3 of sample. Collection of molybdenum was unaffected

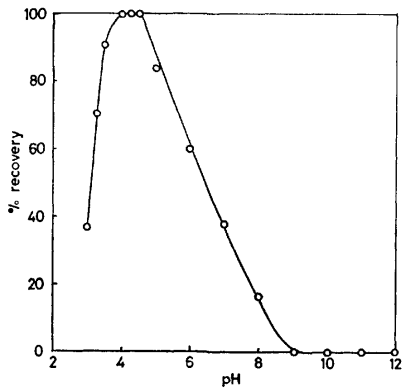

Fig. 4. Effect of pH on the collection of molybdenum on iron(III) hydroxide; 3 μg of molybdenum in 100 cm^3, 2 mg of iron(III) and 5 cm^3 of acetone.

by the presence of 5 g of sodium chloride present in 100 cm^3 of sample.

Synthetic sample solutions containing 1—6 μg of molybdenum(VI) present in 100 cm^3 were taken through the collection and determination procedure and a calibration graph was prepared. A linear relationship was obtained over the whole range and the slope was identical to that obtained from aliquots of the standard molybdenum solution analysed without the collection step. The absorbance of blanks prepared with and without the collection step were also found to be comparable.

The ions that were found to interfere in the determination of molybdenum in the absence of masking agents were re-examined in conjunction with the collection procedure. Excepting tungsten, none of the ions at 1 mg level interfered in the determination of 3 μg of molybdenum. Small quantity of tungsten was found to accompany molybdenum as was evident from the enhancement in the absorbance value (0.33 to 0.90). Addition of tartrate, as described earlier, eliminated the interference due to tungsten.

Recovery Studies. As no standard samples were available for testing the collection and determination procedure developed, it was decided to examine the recovery of molybdenum added to soil and sea water samples collected at random. 5 g of finely ground soil samples dried at 110 °C were treated with 0, 5, and 10 μg of molybdenum(VI). Each sample was heated in a platinum crucible at 400—450 °C for 3 h to decompose any organic matter present. Then 10 cm^3 of water, 2 cm^3 of concentrated sulphuric acid and 10 cm^3 of concentrated hydrofluoric acid were added and heated gently until most of the liquid was evaporated. The crucible was then heated strongly to expel the residual sulphuric acid. The residue was dissolved in 6 mol dm^{-3} hydrochloric acid, rinsed into a beaker, and heated nearly to boiling, to bring all soluble material into solution.[9] The solution was filtered through Whatman No. 42 filter paper, washed with dilute hydrochloric acid collecting the filtrate and washings in a 100 cm^3-flask. The volume was then made up with water.

Aliquots of soil solution and sea water samples were

Table 2. Recovery of molybdenum added to soil and sea water samples

Sample	Aliquot taken (cm^3)	Mo added ($\mu g/100\ cm^3$)	Mo Found (μg)	Recovery (%)
Soil extract	25	—	—	—
	25	5	1.3	104
	25	10	2.4	96
Sea water	50	—	—	—
	100	—	—	—
	50	10	5.1	102
	100	10	10.0	100
	100	1	1.05	105
	100	5	4.90	98

subjected to collection and determination procedure as described under "Experimental." The results are summarised in Table 2 which clearly indicate satisfactory recovery of molybdenum from both soil and sea water samples.

One of us (TPR) is grateful to CSIR, New Delhi for financial assistance.

References

1) B. W. Bailey, J. E. Chester, R. M. Dagnall, and T. S. West, *Talanta*, **15**, 1359 (1968).
2) A. K. Bhadra and S. Banerjee, *Talanta*, **20**, 342 (1973).
3) P. R. Haddad, P. W. Alexander, and L. E. Smythe, *Talanta*, **22**, 61 (1975).
4) M. M. L. Khosla and S. P. Rao, *Anal. Chim. Acta*, **57**, 323 (1971).
5) C. L. Leong, *Analyst*, **95**, 1018 (1970).
6) Y. S. Kim and H. Zeitlin, *Anal. Chim. Acta*, **51**, 516 (1970).
7) Y. S. Kim and H. Zeitlin, *Anal. Chim. Acta*, **46**, 1 (1969).
8) K. M. Chan and J. P. Riley, *Anal. Chim. Acta*, **36**, 220 (1960).
9) E. B. Sandell, "Colorimetric determination of traces of metals," Interscience Publishers, New York (1959), p. 660.

Polyfunctionality of α-$Zr(HPO_4)_2 \cdot H_2O$. Case of H^+/Ag^+ and H^+/Tl^+ Ion Exchange Processes†

Umberto Costantino,* Armando Isernia, and Giovanni De Meo
Dipartimento di Chimica, Università di Perugia, Via Elce di Sotto, 10-06100 Perugia, Italy
(Received August 7, 1979)

A detailed investigation of the ion exchange processes of silver and thallium(I) ions on α-$Zr(HPO_4)_2 \cdot H_2O$ has been carried out. The H^+/Ag^+ exchange occurs in $AgNO_3$ or CH_3COOAg solution with a single phase transition and leads to $Zr(AgPO_4)_2 \cdot H_2O$ (interlayer distance 8.4 Å). The H^+/Tl^+ ion exchange process has been performed by titrating the exchanger with 0.1 M ($TlNO_3$+TlOH) solution, owing to the great ionic size of Tl(I). The titration curve shows essentially a single plateau. In a similar way to that for H^+/Ag^+ exchange, the process takes place with a single phase transition, leading to $Zr(TlPO_4)_2 \cdot H_2O$ (interlayer distance 9.0 Å). Since the processes are new examples in which a univalent cation is exchanged with a single phase transition in α-$Zr(HPO_4)_2 \cdot H_2O$, the so called "polyfunctionality" of this exchanger has been discussed, considering the high polarizability of Ag^+ and Tl^+ ions. The catalytic potential applications of zirconium phosphate loaded with Ag^+ ions are outlined.

The crystal structure of α-zirconium bis(monohydrogen-orthophosphate) monohydrate, α-$Zr(HPO_4)_2 \cdot H_2O$, hereafter referred to as α-$HH \cdot H_2O$††, has been refined[1] and the position of the exchangeable hydrogen atoms and water molecule determined by means of powder neutron diffraction data[2]. From these works it was concluded that: a) the exchangeable hydrogen atoms are covalently bonded to phosphate oxygens; b) the water molecule lies in the center of the cavity formed by the arrangement of the layers and it is hydrogen-bonded to tetrahedral ≥P–OH groups belonging to the same layer; c) there are no hydrogen-bonds between the layers that are held by van der Waals forces.

Knowledge of the position of the exchangeable hydrogen atoms would help in understanding the so called "polyfunctionality" of α-$HH \cdot H_2O$. It is known that the titration curves of the exchanger with alkali metal hydroxides, in the presence of the respective chlorides, exhibit various steps at different pH values for each cation (*i.e.* 3 steps for Li^+ and Rb^+, 2 steps for Na^+ and K^+, 4 steps for Cs^+; Fig. 3, Ref. 3), as if the hydrogen atoms of α-$HH \cdot H_2O$ have different acidities for the different cations. Albertsson *et al.*[2] suggested that the exchange sites are created by the hydroxide ion, that may freely diffuse in the crystals and reacts with the ≥POH groups. The energy supplied by this reaction should allow the metal ion to be sorbed by the exchanger as hydrated ions. Troup and Clearfield[1] attributed the different acidities of the hydrogen atoms to defects of the structure that would lead to a range of hydrogen bond energies and to the shift of the phosphate groups from their normal position. Disorder would thus create exchange sites of different energies. According to Allulli *et al.*[4] the polyfunctionality of zirconium phosphate is related to the growth of various solid phases.

As a contribution to the knowledge of the exchange behaviour of α-$HH \cdot H_2O$, this paper reports two examples in which monovalent cations having a high polarizability, such as Ag^+ and Tl^+, are taken up by crystalline zirconium phosphate in one step. Furthermore the H^+/Ag^+ ion exchange process provides the first example in which a univalent cation is entirely exchanged at room temperature without addition of hydroxide ions.

Experimental

Chemicals. All reagents, except $ZrOCl_2 \cdot 8H_2O$ supplied by "Merck", were R.P.E. "C. Erba". Thallium(I) hydroxide was prepared by adding a Tl_2SO_4 solution to a hot barium hydroxide solution in a closed system filled with nitrogen.

Crystalline zirconium phosphate was prepared according to the method of slow decomposition of zirconium fluorocomplexes in the presence of phosphoric acid.[3] The microcrystals were sedimented in a countercurrent apparatus[5] and the various fractions were stored over P_4O_{10}. The fraction with a mean radius of particles of 3—5 μm was used throughout the experiments.

Ion Exchange Procedure. In order to attain different percentages of Ag^+-exchange, several samples of α-$HH \cdot H_2O$ (1 g) were equilibrated with increasing volumes of 0.100 M $AgNO_3$ or 0.050 M CH_3COOAg solutions at 25±1 °C. The thallium-uptake, as a function of pH, was obtained from the batch titration performed by contacting several samples of α-$HH \cdot H_2O$ (0.500 g) with 100 ml of 0.100 M ($TlNO_3$+TlOH) solutions. After equilibration (4 d) the solid samples were filtered off and their X-ray diffractograms recorded, the clear solutions being analyzed for their pH value and metal ion content. Kinetic experiments were performed as reported.[6]

Analytical Procedure. Silver ion was determined with a Perkin-Elmer A.A. spectrophotometer. Thallium was titrated with standard potassium bromate at 60 °C. Hydration water content was obtained by the percent-weight loss at 180 °C of the samples, previously conditioned over a NaCl saturated solution ($P/P_0 \approx 0.7$). X-Ray powder diffraction patterns were obtained with a General Electric diffractometer using Ni-filtered Cu $K\alpha$ radiation.

Results

Ag^+-uptake. The ion-exchange mechanism of Ag^+ on $HNa \cdot 5H_2O$ suggests that in acidic media Ag^+ might replace the protons of $HH \cdot H_2O$ obtained from the partial regeneration of the monosodium

† This work was supported by the National Research Council of Italy (C. N. R.).

†† The ionic forms of α-$Zr(HPO_4)_2 \cdot H_2O$ will also be indicated by their counter-ions and water content.

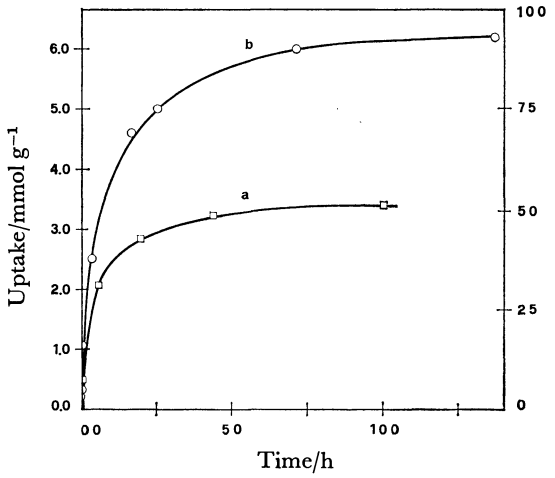

Fig. 1. Ag^+-uptake on α-$HH \cdot H_2O$ as a function of time.
Conditions: 1 g of ecxhanger equilibrated with 200 ml of 0.100 M $AgNO_3$ solution (curve a) or with 200 ml of 0.050 M CH_3COOAg solution (curve b), $t=25 \pm 1$ °C.

form.[6] For the sake of confirmation an attempt was made to convert the zirconium hydrogen phosphate into silver form by contacting the exchanger with $AgNO_3$ or CH_3COOAg solutions. Figure 1 shows the Ag^+-uptake of 1 g of $HH \cdot H_2O$, as a function of time, when the exchanger is equilibrated at 25±1 °C with 200 ml of 0.100 M $AgNO_3$ solution (curve a) or with 200 ml of 0.050 M CH_3COOAg solution (curve b). In nitrate media the uptake suddenly slows down after 20 h of equilibration, because of the accumulation in solution of the protons replaced by silver ions (after 70 h the pH was ≈1.8). Maximum Ag^+-conversion of 50% was obtained.

In acetate media, owing to the presence of the Brönsted base, CH_3COO^-, the pH of the solution remains higher than 4. The H^+/Ag^+ exchange seems to proceed in only one step, a maximum Ag^+-conversion of ≈95% being reached within 150 h.

X-Ray diffractograms of the sample withdrawn from the nitrate solution showed the presence of a not exchanged $HH \cdot H_2O$ phase and a new phase having an interlayer distance of 8.4 Å; the one withdrawn from the acetate solution showed the presence of only the 8.4 Å phase. In order to obtain further information on the ion-exchange mechanism, equilibrium experiments were carried out by contacting several samples (1 g) of $HH \cdot H_2O$ with increasing volumes of $AgNO_3$ or CH_3COOAg solution.

Figure 2 shows the millimoles of Ag^+ taken up by 1 g of exchanger against the millimoles of Ag^+ initially present in the equilibrating 0.100 M $AgNO_3$ solution (curve a) or 0.050 M CH_3COOAg solution (curve b). The following comments are given.

i) Up to 80—90% Ag^+-conversion the H^+/Ag^+ ion-exchange process seems to take place in a single step both in acetate and nitrate media; after this value of conversion the selectivity of exchanger towards Ag^+ ions strongly decreases and higher volumes of equilibrating solutions are needed to obtain the full Ag^+-phase.

ii) In the acetate medium, in the range 0—85% Ag^+-conversion the exchanger shows a high selectivity for silver ions and virtually all the added Ag^+ ions are taken up. As expected from the constancy of the H^+/Ag^+ rational selectivity coefficient, in the nitrate medium much greater amounts of silver ions (larger volumes of equilibrating solution) must be added to the exchanger in order to reach a Ag^+-conversion identical to that attained in the acetate medium.

X-Ray diffraction patterns of samples having the same Ag^+-conversion but obtained from the nitrate and acetate equilibrating solutions were found to be similar, confirming the view that the same ion exchange mechanism holds in both cases.

X-Ray powder patterns of samples at various Ag^+-loading (Fig. 3a) show that a new phase with interlayer distance 8.4 Å is present already at 10% Ag^+-conversion. This phase and the original $HH \cdot H_2O$ (7.6 Å) phase are present up to 85% Ag^+-conversion, the latter being transformed into the former as the conversion proceeds. After this value of conversion is reached, only the 8.4 Å phase is present and 100% of Ag^+-conversion is obtained without appreciable change in the X-ray diffractograms.

The water content of several samples with increasing Ag^+-loading was also determined (Fig. 4). It can be seen that the water content of the exchanger remains practically equal to one mole per mole of exchanger in all the range of composition. X-Ray powder patterns of hydrated and anhydrous silver forms are given in Table 1.

Tl^+-uptake. Preliminary experiments showed that, in constrast to silver ion, Tl^+ can not diffuse

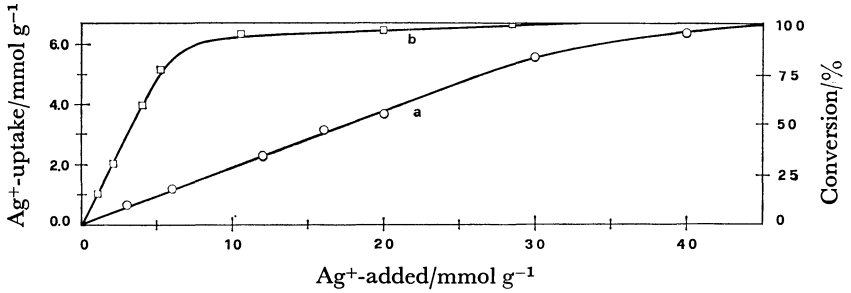

Fig. 2. Ag^+-uptake on α-$HH \cdot H_2O$ as a function of the m·moles of Ag^+ initially added.
Conditions: 1 g of exchanger equilibrated with increasing volumes of 0.100 M $AgNO_3$ solution (curve a) or 0.050 M CH_3COOAg (curve b).

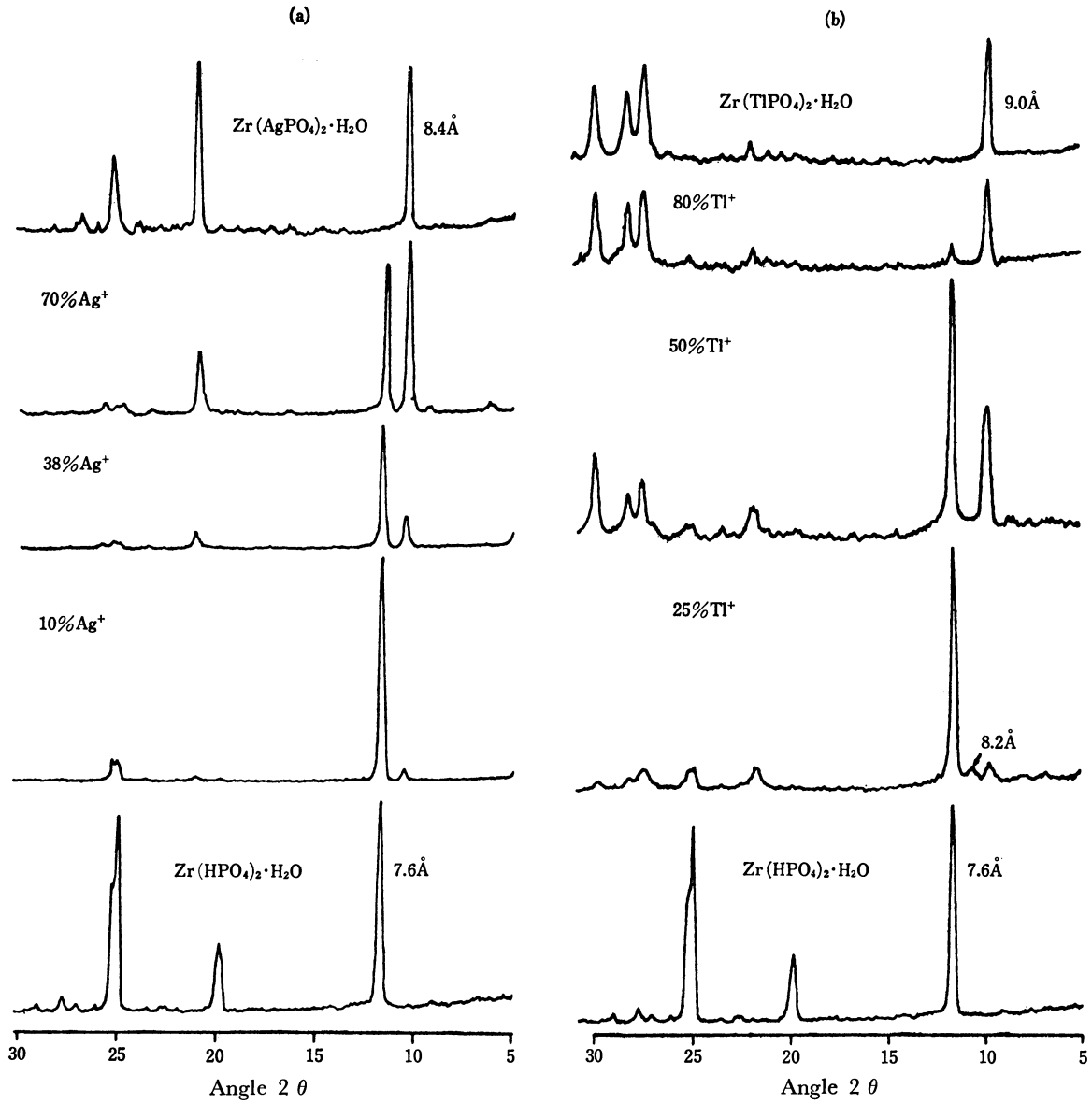

Fig. 3. Some X-ray diffractograms relative to H^+/Ag^+ (a) or H^+/Tl^+ (b) ion exchanges on α-$HH \cdot H_2O$.

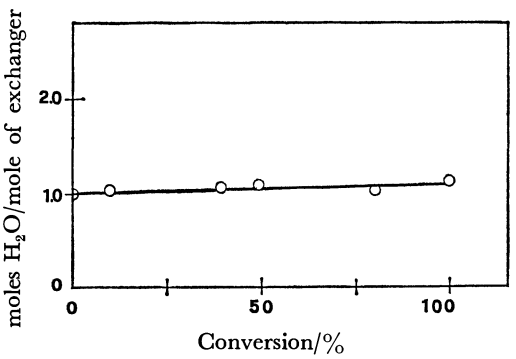

Fig. 4. Water content of α-zirconium phosphate at various stages of Ag^+-conversion.

(or diffuses very slowly owing to its greater ionic radius) within the layers of the exchanger from nitrate solutions.

When the steric hindrance prevents the free diffusion of a counter-ion in the $HH \cdot H_2O$ lattice (in this case the ionic diameter of Tl^+ ion, 3.0 Å, is much greater than the free diameter[1] of the openings connecting the cavities, 2.61 Å) it is possible to force the cations to cross these openings and to enlarge the layers of the exchanger,[3] if sufficient energy is supplied. This energy can be provided by the neutralization of the protons of the exchanger if the soluble cation hydroxide is available.

Figure 5 shows the Tl^+-uptake curve of $HH \cdot H_2O$ obtained by titrating the exchanger with 0.100 M ($TlNO_3$+TlOH) solutions at 25±1 °C. Apart from the sloping regions between 0—20% and 80—100% of Tl^+-conversion, the curve shows a single plateau at pH≈5.

X-Ray diffractograms of samples with increasing Tl^+-conversion (Fig. 3b) show that in the range 0—25% of conversion the phases, with interlayer distance of 7.6, 8.2, and 9.0 Å, are present.

In the approximate range 25—80%, two phases with interlayer distance 7.6 and 9.0 Å, respectively, are co-existent, one transforming into the other. After

Table 1. X-Ray powder diffraction patterns of hydrated and anhydrous Ag^+ and Tl^+ forms of α-zirconium phosphate

$Zr(AgPO_4)_2 \cdot H_2O$ d/Å	$Zr(AgPO_4)_2$ d/Å	$Zr(TlPO_4)_2 \cdot H_2O$ d/Å	$Zr(TlPO_4)_2$ d/Å
8.4 s	7.78 s	9.0 vs	8.9 vs
5.78 vw	5.33 w	5.86 vw	4.66 vw
5.35 w	4.51 w	5.00 vw	4.05 m
4.64 vw	4.32 vw	4.52 vw	3.58 vw
4.52 w	4.11 w	4.34 w	3.19 s
4.33 vw	3.88 s	4.20 w	2.71 vw
4.19 vs	3.79 m	4.05 m	2.61 w
3.96 vw	3.36 w	3.79 vw	
3.76 w	3.33 m	3.25 s	
3.51 w	3.24 w	3.16 m	
3.44 m	3.18 m	2.99 s	
3.36 w			
3.29 vw			
3.08 vw			

s, Strong; m, medium; w, weak; v, very.

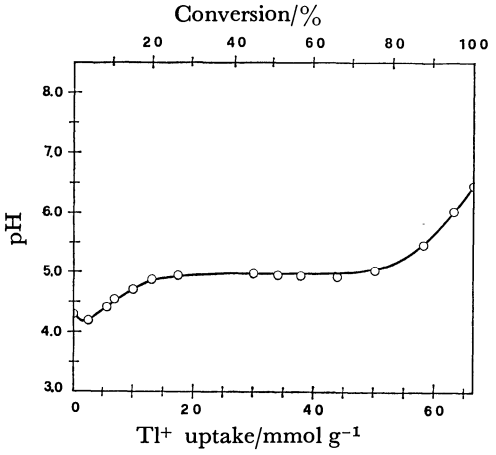

Fig. 5. Tl^+-uptake curve on α-$HH \cdot H_2O$ obtained from the batch titration curve of the exchanger with ($TlNO_3$ + TlOH) 0.100 M solutions.

80% conversion only the 9.0 Å phase is present, full conversion being reached without drastic modifications of the X-ray patterns. Determination of the water content of samples having different Tl^+-conversion, shows that as in the case of H^+/Ag^+, the H^+/Tl^+ exchange takes place without changes in water content that remains equal to one mole per mole of exchanger. The X-ray powder patterns of hydrated and anhydrous thallium forms are given in Table 1.

Discussion

The results obtained indicate that the H^+/Ag^+ and H^+/Tl^+ ion exchange processes on α-$HH \cdot H_2O$ occur in a single step with the direct transformation of the dihydrogen phase into the about fully exchanged phase. Thus, without considering the solubility of the Ag^+ ion in the $Ag_{1.7}H_{0.3} \cdot H_2O$ phase or the solubility of Tl^+ in the $Tl_{1.6}H_{0.4} \cdot H_2O$ phase, the ion exchange processes may be schematically described by the reactions:

$$\underset{7.6\,Å}{HH \cdot H_2O} + 2Ag^+ \longrightarrow \underset{8.4\,Å}{AgAg \cdot H_2O} + 2H^+ \quad (1)$$

$$\underset{7.6\,Å}{HH \cdot H_2O} + 2Tl^+ + 2OH^- \rightarrow \underset{9.0\,Å}{TlTl \cdot H_2O} + 2H_2O. \quad (2)$$

Only in the case of H^+/Tl^+ ion exchange process, the weak reflection at d=8.2 Å, present in X-ray diffractograms of samples having a Tl^+-conversion ranging from 5 to 25%, suggests that a small percentage of the HTl phase could be obtained.

In the case of the alkali metal ions, the ion exchange process on $HH \cdot H_2O$ occurs in several steps, thus the H^+/Ag^+ and H^+/Tl^+ are the first examples in which a univalent cation is taken up by α-$HH \cdot H_2O$ with a single phase transition.††† This cannot be explained in terms of ionic size, since Ag^+ and Tl^+ have effective ionic radii very similar to those of Na^+ and Rb^+, respectively, involving the difference in polarizability.

If polarizable ions constitute a ionic solid there is a further contribution to the lattice energy and discrepancies are generally found between the calculated and experimental values of lattice energy. The discrepancy is usually attributed to dispersion forces and to the possibility of some covalent bonding. The salt forms of crystalline zirconium phosphate may be considered covalent-ionic solids because the counter-ions present within the layer are ionically bonded to the macro-anions, constituting the layers themselves, that are of covalent nature.

Thus, it can be assumed that Ag^+ and Tl^+, owing to their polarizability much higher than that of alkali metal ions, give rise to higher interaction energy with the fixed groups of the matrix. Allulli *et al.*[4] found that crystalline zirconium phosphate, in molten salts, strongly prefers Tl^+ to K^+.

The strong interaction between Ag^+ and Tl^+ and

††† It should be recalled that H^+/Li^+ ion exchange on an another layered inorganic ion exchanger, α-$Ti(HPO_4)_2 \cdot H_2O$, occurs in a single step.[7,8]

the $\geq P-O^-$ groups of the exchanger, and thus their low mobility in the crystal lattice, could explain why a single step in the ion exchange processes has been obtained, in a manner similar to that recently outlined for the H^+/K^+ exchange on α-$HH\cdot H_2O$.[5,9]

Let us suppose that the energy required for exchanging the proton of the hypothetical, *i.e.* $HAg\cdot H_2O$, is lower than that furnished by the pH of equilibrating solution, in other words that the eventual second plateau of exchange lies at pH value lower than ≈ 6. In the first stages of the H^+/Ag^+ exchange, both the protons present in each cavity would be replaced by the silver ions. An appreciable amount of $AgAg\cdot H_2O$ is thus formed in the external parts of the crystals. According to the model of co-existing solid phases[3] in a single crystal of $HH\cdot H_2O$, a situation similar to that schematically shown in Fig. 6 may occur. The Ag^+ ions of the 8.4 Å phase should have a strong tendency to diffuse into the $HH\cdot H_2O$ phase, arranging themselves in a regular mode. Thus, for each cavity of the exchanger there would be one silver ion, giving rise to the HAg phase. However, if the rate of this internal diffusion is very low and the pH of the external solution remains higher than that required for the exchange of the second proton, other Ag^+ ions would be furnished by the solution, the exchange taking place, with low activation enery, in the region of separation between the $AgAg\cdot H_2O$ and $HH\cdot H_2O$ co-existing phases. In this region the cavities are very likely irregular, and the exchange of both the protons may occur with a rate greater than the diffusion of Ag^+ in the $HH\cdot H_2O$ to give the HAg phase. Thus the exchange process goes on with an advancing phase bondary (Fig. 6). This mechanism requires that, if the exchange is stopped and a crystal of zirconium phosphate, half converted into silver form, is left standing for a long time, it should be transformed into the monosilver phase according to the reaction occurring in the crystal:

$$\underset{7.6\,\text{Å}}{HH\cdot H_2O} + \underset{8.4\,\text{Å}}{AgAg\cdot H_2O} \rightarrow 2HAg\cdot H_2O. \qquad (3)$$

A sample half converted into silver form and heated at 180 °C, for 2 d, showed no co-existence of the anhydrous AgAg (7.78 Å) and HH (7.41 Å) phases. Only one phase, with inter-layer distance 7.46 Å, very likely the anhydrous HAg, was detected. This indicates that the rate of the proposed transformation (3) is very low at room temperature. Several other experiments, such as the H^+/Ag^+ exchanges performed in buffered media at different pH values for very long periods, are expected to confirm this point.

Zirconium phosphate loaded with silver ion is considered to be a promising material for catalytic processes. La Ginestra *et al.*[10] were able to reduce reversibly the silver counter-ions present between the layers of crystalline zirconium phosphate and obtain materials containing dispersed silver atoms in the structure.

The authors thank Prof. G. Alberti for helpful discussions.

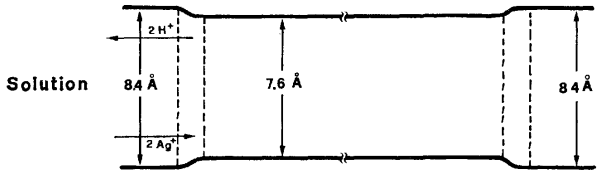

Fig. 6. Schematic representation of the co-existence of $Zr(AgPO_4)_2\cdot H_2O$ (8.4 Å) and $Zr(HPO_4)_2\cdot H_2O$ (7.6 Å) in a single crystal of the exchanger. The advancement of the phase bondary during the H^+/Ag^+ ion exchange is shown.

References

1) J. M. Troup and A. Clearfield, *Inorg. Chem.*, **16**, 3311 (1977).
2) J. Albertsson, A. Oskarsson, R. Teligren, and J. O. Thomas, *J. Phys. Chem.*, **81**, 1574 (1977).
3) G. Alberti, *Acc. Chem. Res.*, **11**, 163 (1978).
4) S. Allulli, N. Tomassini, and M. A. Massucci, *J. Chem. Soc., Dalton Trans.*, **1976**, 1816.
5) M. G. Bernasconi, M. Casciola, and U. Costantino, *J. Inorg. Nucl. Chem.*, **41**, 1047 (1979).
6) M. G. Bernasconi, M. Casciola, U. Costantino, and M. L. Luciani Giovagnotti, *Ann. Chim. (Rome)*, **69**, 9 (1979).
7) G. Alberti, P. Cardini-Galli, U. Costantino, and E. Torracca, *J. Inorg. Nucl. Chem.*, **29**, 581 (1967).
8) K. Takaguchi, and I. Tomita, *J. Chromatogr.*, **118**, 263 (1976).
9) G. Alberti, M. G. Bernasconi, M. Casciola, and U. Costantino, *J. Inorg. Nucl. Chem.*, in press.
10) A. La Ginestra, C. Ferragina, and C. Patrono, XI Congresso Nazionale di Chimica Inorganica, A. I. C. I. and S. C. I., Cosenza, Italy, 1978, Comm. 6-I.

Studies on Synthesis of 6-Bromo-2,3-disubstituted 4(3*H*)-Quinazolinones and Their Thiones

Mahmoud Zarif Amin BADR,* Hassan Ahmed Hassan EL-SHERIEF, and Abdallah Mohamed MAHMOUD

Department of Chemistry, Faculty of Science, Assiut University, Assiut, Egypt

(Received December 20, 1978)

Synthesis of some 2,3-disubstituted 6-bromo-4(3*H*)-quinazolinones is described. Treatment of some 4-quinazolinones with phosphorus pentasulfide gave the corresponding 4-quinazolinethiones. The reaction of 6-bromo-2-methyl-3,1-benzoxazin-4-one with hydroxylamine hydrochloride gave 6-bromo-3-hydroxy-2-methyl-4(3*H*)-quinazolinone which on treatment with alkyl halides, acyl chlorides and sulfonyl chlorides gave the corresponding ethers, esters, and sulfonates respectively. 2-Styryl-4(3*H*)-quinazolinone derivatives are obtained by condensation of aromatic aldehydes and corresponding 3-substituted-6-bromo-2-methyl-4(3*H*)-quinazolinones. Their antibacterial affinities are of considerable efficiency.

4(3*H*)-Quinazolinones have become of increasing importance in recent years owing to their interesting pharmacological properties,[1] and their use as analgesics,[2] potential anticonvalsant,[3] muscle relaxant,[4] and long-acting sedatives.[5]

6-Bromo-2-methyl-3,1-benzoxazin-4-ones (**1**) are known to react with amines to give the corresponding 4-quinazolinones,[6–8] which were condensed[7,9] with aromatic aldehydes to afford the corresponding 6-bromo-2-(2-arylvinyl)-4(3*H*)-quinazolinones (**2b—f**) (*cf.* Table 1).

Reaction of 6-bromo-4-quinazolinones (**2a,c—e**) with phosphorus pentasulfide in boiling pyridine gave the corresponding 4-quinazolinethiones[10–12] (**3a,c—e**) (*cf.* Table 1). The structures of **3** were established by their elemental and spectral analyses. Their IR spectra showed the stretching vibration bands of C=S (1230—1250 cm^{-1}) and C=N (1615—1630 cm^{-1}).

These compounds were reconverted to **2** by boiling with dilute hydrochloric acid. Also, condensation of **1**

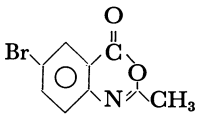

1

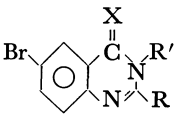

2; X=O
3; X=S

	R	R′
a	$-CH_3$	$-C_6H_4CH_3$-*p*
b	$-CH{=}CHC_6H_4OCH_3$-*p*	$-C_6H_5$
c	$-CH{=}CHC_6H_4Cl$-*m*	$-C_6H_4CH_3$-*p*
d	$-CH{=}CHC_6H_4Cl$-*p*	$-C_6H_4CH_3$-*p*
e	$-CH{=}CHC_6H_4NO_2$-*P*	$-C_6H_4CH_3$-*P*
f	$-CH{=}CHC_6H_5$	$-C_6H_4CH_3$-*p*
g	$-CH_3$	2-C_5H_4N
h	$-CH_3$	2-C_5H_4N

with heterocyclic amines,[13–15] namely, 2- and 3-aminopyridines, 2-aminothiazoles, 2-aminobenzoxazole and 2-aminobenzothiazole in dry pyridine gave the corresponding 6-bromo-4-quinazolinones (**2h, i, 4**, and **5a,b**) (*cf.* Tables 1 and 2).

TABLE 1. 6-BROMO-2-(2-ARYLVINYL)-4-QUINAZOLINONES (**2**) AND 4-THIONES (**3**)

No.	Mp °C	Molecular formula	Calcd (Found) (%) C	H	N	S	Br
2b	264—265	$C_{23}H_{17}N_2O_2Br$	63.74 (63.26)	3.92 (3.71)	6.46 (6.36)	— —	18.47 (18.21)
2c	203—204	$C_{23}H_{16}N_2OClBr$	61.13 (60.91)	3.54 (3.21)	6.20 (6.42)	— —	
2d	228—229	$C_{23}H_{16}N_2OClBr$	61.13 (61.61)	3.54 (3.45)	6.20 (6.22)	— —	
2e[a]	301—302	$C_{23}H_{16}N_3O_3Br$	59.74 (59.64)	3.46 (3.56)	9.09 (9.22)	— —	17.31 (16.76)
2f	216—217	$C_{23}H_{17}N_2OBr$	66.18 (66.23)	4.07 (4.09)	6.71 (6.81)	— —	19.18 (19.68)
2g	205	$C_{14}H_{10}N_3OBr$	53.16 (53.61)	3.16 (3.22)	13.29 (13.33)	— —	25.31 (25.61)
2h	190	$C_{14}H_{10}N_3OBr$	53.16 (53.16)	3.16 (3.36)	13.29 (13.21)	— —	25.31 (25.91)
3a	190—191	$C_{16}H_{13}N_2SBr$	52.33 (52.21)	4.04 (4.31)	8.72 (8.64)	9.96 (9.71)	24.92 (24.10)
3c	146	$C_{23}H_{16}N_2SClBr$	59.03 (58.61)	3.42 (3.31)	5.98 (5.81)	6.84 (6.61)	— —
3d	256—257	$C_{23}H_{16}N_2SClBr$	59.03 (58.61)	3.42 (3.41)	5.98 (5.81)	6.84 (6.61)	— —
3e[a]	320	$C_{23}H_{16}N_3O_2SBr$	57.74 (57.61)	3.34 (3.12)	8.78 (8.61)	6.69 (8.61)	16.73 (16.66)

a) Crystallized from pyridine.

Table 2. 3-Substituted-6-bromo-2-methyl-4-quinazolinones (**4** and **5**)

No.	Mp °C	Molecular formula	Calcd (Found) (%) C	H	N	S	Br
4a	174—176	$C_{18}H_{12}N_3OSBr$	54.27 (53.68)	3.01 (3.20)	10.55 (10.21)	8.04 (8.21)	20.10 (20.40)
4b	221	$C_{18}H_{14}N_3OSBr$	55.33 (55.61)	3.30 (3.21)	10.19 (10.14)	7.76 (7.41)	19.41 (19.31)
4c	191—192	$C_{19}H_{14}N_3O_2SBr$	53.27 (53.11)	3.27 (3.11)	9.81 (9.81)	7.47 (7.63)	18.69 (18.41)
4d	195—196	$C_{16}H_{14}N_3O_3SBr$	47.05 (47.12)	3.43 (3.33)	10.29 (10.21)	7.84 (7.61)	19.60 (19.41)
4e	241	$C_{24}H_{16}N_3SBr$	62.88 (62.41)	3.49 (3.52)	9.17 (8.81)	6.99 (6.60)	17.46 (17.14)
5a	222	$C_{16}H_{10}N_3O_2Br$	53.93 (53.42)	2.80 (2.61)	11.79 (11.61)	— —	22.47 (22.11)
5b[a]	241	$C_{16}H_{10}N_3OSBr$	51.61 (51.41)	2.68 (2.61)	11.29 (11.41)	8.60 (8.41)	21.50 (21.46)

a) Crystallized from acetic acid.

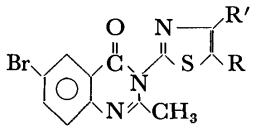

4

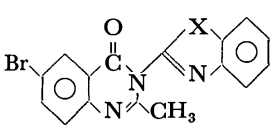

5

	R	R′
4a;	H	$-C_6H_5$
b;	H	$-C_6H_4CH_3$-*p*
c;	H	$-C_6H_4OCH_3$-*p*
d;	$-COOC_2H_5$	$-CH_3$
e;	$-C_6H_5$	$-C_6H_5$

5a; X=O

Their structures were established by elemental and spectral analyses. Their IR spectra showed the stretching vibration bands of C=O (1720—1680 cm^{-1}) and C=N (1630—1615 cm^{-1}).

On the other hand, treating 6-bromo-2-methyl-3,1-benzoxazin-4-ones (**1**) with hydroxylamine hydrochloride in presence of potassium hydroxide gave the corresponding 6-bromo-2-methyl-3-hydroxy-4(3*H*)-quinazolinones[16-17] (**6a**). Reactions of 6-bromo-4-quinazolinone (**6a**) with alkyl halides, acyl chlorides and sulfonyl chlorides gave the corresponding ethers (**6b—e**), esters (**6f—e**), and sulfonates (**6j,k**) respectively. (*cf.* Table 3).

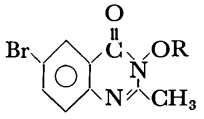

6

	R		R
a;	H	**g**;	$-COC_6H_4NO_2$-*p*
b;	*n*-C_4H_9	**h**;	$-COC_6H_4Cl$-*p*
c;	$-CH_2C_6H_5$	**i**;	$-COCH_2C_6H_5$
d;	$-CH_2C_6H_4NO_2$-*p*	**j**;	$-SO_2C_6H_5$
e;	$-CH_2C_{10}H_7$-α	**k**;	$-SO_2C_6H_4CH_3$-*p*
f;	$-COC_6H_5$		

On the other hand, when **6a** was condensed with aromatic aldehydes,[9] it gave the corresponding 6-bromo-2-(2-arylvinyl)-3-hydroxy-4-quinazolinones (**7a—d**), which reacted with alkyl halides, sulfonyl chlorides to give the corresponding ethers (**8a—e**), and sulfonates (**8f—g**) respectively (*cf.* Table 4). Moreover

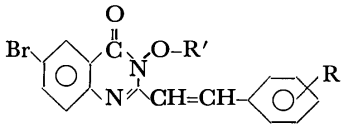

	R	R′		R	R′
7a;	H	H	**8a**;	*m*-Cl	$-CH_2C_6H_5$
b;	*p*-OCH_3	H	**b**;	*p*-OCH_3	$-CH_3$
c;	*p*-Cl	H	**c**;	*p*-OCH_3	*n*-C_4H_9
d;	*m*-Cl	H	**d**;	*p*-OCH_3	$-CH_2C_6H_5$
			e;	*p*-OCH_3	$-CH_2C_{10}H_7$-α
			f;	*p*-OCH_3	$-SO_2C_6H_4CH_3$-*p*
			g;	*p*-Cl	$-SO_2C_6H_4CH_3$-*p*

(**8a,e—g**) were also obtained by condensing (**6c,e,d**) with the corresponding aromatic aldehydes.

The IR spectra of **6a** and **7a—d** showed stretching vibration bands of OH (3360—3340 cm^{-1}), C=O (1720—1680 cm^{-1}), and C=N (1650—1620 cm^{-1}). However, the IR spectra of **6b—k** and **8a—h** did not show stretching vibration bands of OH groups.

The UV spectra of **2a,b**, **3a**, **4c**, **5a,b**, and **8d** in ethanol are similar to those of 2,3-disubstituted 4(3*H*)-quinazolinones,[9] showing two main bands in the region 280—288 and 325—350 nm, (*cf.* Table 5).

Table 5. UV spectral data of 2,3-disubstituted 4(3*H*)-quinazolinones

Compound	λ_{max} nm (ε)			
2a	285 (7000)	325 (3000)	—	—
2b	282 (9000)	350 (10000)	—	—
3a	287 (5000)	353 (4000)	370 (5000)	383 (3000)
4c	287 (7000)	340 (5000)	—	—
5a	287 (9000)	335 (4000)	—	—
5b	282 (8000)	340 (11000)	—	—
8d	287 (27000)	350 (41000)	—	—

The higher red shifts of the electronic absorption bands for the compound (**3a**) compared with that of the corresponding compound (**2a**) become understandable in view of the higher energy level of nonbonding electrons in sulfur compared to oxygen.[18] The band at 370 nm presumably arises from π-π* and n-π* transitions in the C=S group.[18]

Biological screening results: The antimicrobial activities of the prepared compounds against a variaty of microbes were determined.[19] These microorganisms include Gram-positive and Gram-negative bacteria.

The bacteria used are: *Bacillus subtilis*, *Staphylcoccus aureus*, *Escherichia coli*, *Pesudomonas aeruginosa*, *Mycobacterium pheli*, *Proteus morganii*, *Serratia* and *Bacillus megaterium*.

The results showed that most of the prepared compounds (**3a**, **4a**—**c**,**e**, **5b**, and **6c**,**g**,**h**,**k**) show from a little to a strong activity on the Gram-positive and Gram-negative bacteria. The activity expressed in percent range 40—70% inhibition was found at concentration 10^{-3} M. The more strong active compounds against *Staphylcoccus aureus* are **6c**,**g**,**h**, that against *Pesudomonas aeruginosa*, *Mycobacterium pheli* and *Escherichia coli* is **6h** and those against *Eschericha coli* are **4a**—**c** and **6k** and those against *Serratia*, *Bacillus megaterium* and *Staphylcoccus aureus* are **3a**, **4a**—**c**,**e**, and **5b**, respectively.

Table 3. 6-Bromo-2-methyl-3-hydroxy-4-quinazolinones and their ethers and esters (**6**)

No.	Mp °C	Molecular formula	Calcd (Found) (%)				
			C	H	N	S	Br
6a	249—250	$C_9H_7N_2O_2Br$	42.35 (42.41)	2.74 (2.61)	10.98 (10.18)	—	31.37 (31.21)
6b	146—147	$C_{13}H_{15}N_2O_2Br$	50.16 (50.61)	4.82 (4.61)	9.00 (9.61)	—	25.72 (25.11)
6c	174—175	$C_{16}H_{13}N_2O_2Br$	55.65 (55.41)	3.76 (3.16)	8.11 (8.12)	—	23.18 (23.22)
6d	215—216	$C_{16}H_{12}N_3O_4Br$	49.23 (49.16)	3.07 (3.41)	10.76 (10.44)	—	20.51 (20.91)
6e	190—191	$C_{20}H_{15}N_2O_2Br$	60.75 (60.11)	3.79 (3.88)	7.08 (7.11)	—	20.25 (20.46)
6f	162—163	$C_{16}H_{11}N_2O_3Br$	53.48 (53.11)	3.06 (3.21)	7.79 (7.61)	—	22.28 (22.11)
6g	227—228	$C_{16}H_{10}N_3O_5Br$	47.52 (47.41)	2.47 (2.61)	10.39 (10.61)	—	19.80 (19.66)
6h	175—176	$C_{16}H_{10}N_2O_3ClBr$	48.79 (48.11)	2.54 (2.61)	7.11 (7.14)	—	— —
6i	144—145	$C_{17}H_{13}N_2O_3Br$	57.14 (56.91)	3.64 (3.41)	7.84 (7.61)	—	22.40 (22.11)
6j	162—163	$C_{15}H_{11}N_2O_4SBr$	45.56 (45.41)	2.78 (2.61)	7.08 (7.21)	8.10 (8.61)	20.22 (20.91)
6k	165—166	$C_{16}H_{13}N_2O_4SBr$	46.94 (46.71)	3.17 (3.11)	6.84 (6.16)	7.82 (7.11)	19.55 (19.41)

Table 4. 6-Bromo-2-(2-arylvinyl)-3-hydroxy-4-quinazolinones and their ethers and esters (**7** and **8**)

No.	Mp °C	Molecular formula	Calcd (Found) (%)		
			C	H	N
7a	221—222	$C_{16}H_{11}N_2O_2Br$	55.97 (55.61)	3.20 (3.30)	8.16 (8.11)
7b	261	$C_{17}H_{13}N_2OBr$	54.66 (54.16)	3.48 (3.12)	7.50 (6.87)
7c	300	$C_{16}H_{10}N_2O_2ClBr$	50.86 (51.06)	2.64 (2.81)	6.87 (7.74)
7d	259	$C_{16}H_{10}N_2O_2ClBr$	50.86 (51.12)	2.64 (2.81)	7.41 (7.18)
8a	186—187	$C_{23}H_{16}N_2O_2ClBr$	59.03 (59.21)	3.42 (3.31)	5.98 (5.81)
8b	208—209	$C_{18}H_{15}N_2O_3Br$	55.81 (55.61)	3.87 (3.61)	7.23 (7.41)
8c	169—170	$C_{21}H_{21}N_2O_3Br$	58.74 (58.31)	4.89 (4.61)	6.52 (6.23)
8d	184	$C_{24}H_{19}N_2O_3Br$	62.20 (61.91)	4.10 (4.31)	6.00 (6.21)
8e	216—217	$C_{28}H_{21}N_2O_2Br$	67.60 (67.21)	4.22 (4.66)	5.63 (5.41)
8f	170—171	$C_{24}H_{19}N_2O_5SBr$	54.64 (54.81)	3.60 (3.41)	5.31 (5.11)
8g	243	$C_{23}H_{16}N_2O_4SBr$	55.64 (55.81)	3.22 (3.61)	5.64 (5.68)

Experimental

Melting points reported are uncorrected. Elemental analysis was carried out on a Colman C, H, and N analyser. IR spectra were recorded on a Perkin-Elmer infracord. The biological screening was carried out at the Microbiological Laboratory, Department of Botany, Assiut University.

6-Bromo-2-methyl-3,1-benzoxazin-4-one (1).[7] Pale yellow needles from carbon tetrachloride, mp 130—131 °C.

*6-Bromo-2-methyl-3-*p*-tolyl-4(3*H*)-quinazolinone (2a).*[8] Colourless needles from ethanol, mp 131—132 °C.

*3-Substituted 6-Bromo-2-(2-arylvinyl)-4(3*H*)-quinazolinones (2c—f and 7, 8):* 3-Substituted 6-bromo-2-methyl-4(3*H*)-quinazolinone (**2a**, **b**, or **6a**) was refluxed with corresponding aldehydes for 10 min. The cooled reaction mixtures gave precipitates on adding ethanol, which were filtered and crystallized from ethanol. The yield was about 80—90%. The results are listed in Table 1.

*2,3-Disubstituted 6-Bromo-4(3*H*)-quinazolinethiones (3):* A mixture of **2a**—**f** (0.01 mol) and phosphorus pentasulfide (0.01 mol) in 100 ml pyridine was refluxed for 5 h. The reaction mixture was cooled and poured into dilute acetic acid. The crude product was filtered, washed with water and recrystallized from the proper solvent. The results are listed in Table 1.

Reaction of 1 with Heterocyclic Amines (2h, i, 4, and 5): A mixture of 1 (0.01 mol) and corresponding heterocyclic amines (0.013 mol) in 100 ml dry pyridine was refluxed for 5 h. The solvent was evaporated to dryness, and the residue was washed with dilute acetic acid followed by water. The crude product was filtered, dried and recrystallized from the proper solvent. The results are listed in Tables 1 and 2.

*6-Bromo-2-methyl-3-hydroxy-4(3*H*)-quinazolinone (7a).* To a mixture of 1 (0.01 mol) and hydroxylamine hydrochloride (0.03 mol), a dilute solution of potassium hydroxide (0.05 mol) was slowly added with vigorous shaking. The reaction mixture was heated on a water bath for 30 min and then acidified with dilute acetic acid. The crude product was filtered, dried and crystallized from ethanol–benzene mixture as white needles, mp 245 °C (sublimed).

Reaction of 6a and 7 with Alkyl Halides, Acyl Chlorides, and Sulfonyl Chlorides (6b—k and 8). To a suspension of **6a** or **7a**—**d** (0.01 mol) in dry acetone (50 ml), was added 0.011 mol of anhydrous potassium carbonate and 0.011 mol of alkyl halides, acyl chloride, or sulfonyl chlorides. The mixture was heated on a steam bath for 3 h. After filtration acetone was evaporated. The crude product was recrystallized from the proper solvent, yield being about 80%. The results are listed in Tables 3 and 4.

References

1) A. P. Bhaduri, N. M. Khanna, and M. L. Dhar, *J. Sci. Ind. Res.*, **21**, 378 (1962); *Indian J. Chem.*, **2**, 159 (1964); C. Bianchi and J. David, *J. Pharmacol.*, **12**, 501 (1960); J. R. Vaughan, Jr., E. Cohen, and B. Karberg, *J. Am. Chem. Soc.*, **89**, 5508 (1959).

2) A. B. Son and O. S., Sidhu, *J. Chem. Soc.*, **25**, 407 (1948).

3) A. P. Bhaduri and M. M. Dhar, *J. Sci. Ind. Res.*, **21**, 378 (1962).

4) J. B. Taylor and D. R., Harrison, *Chem. Abstr.*, **83**, 97355 (1975), Ger. Offen. 2 450 429 (Cl.CO7D), 30 Apr 1975, Brit, Appl. 49, 338/73,23 Oct. 1973; 14 pp.

5) C. Runti, C. Nisi, and L. Sindellaria, *Ann. Chem. Rome*, **51**, 719 (1961).

6) M. T. Bogert, G. D. Beal, and C. G. Amend, *J. Am. Chem. Soc.*, **32**, 1627 (1910).

7) M. T. Bogert and W. F. Hand, *J. Am. Chem. Soc.*, **27**, 1467 (1905).

8) R. S. Salimath, S. R. Patel, and N. M. J. Shah, *Indian Chem. Soc.*, **33**, 140 (1956).

9) M. Z. A. Badr, A. A. H. El-Sherief, and M. M. Aly, *Indian J. Chem.*, **13**, 245 (1975).

10) N. J. Leonard and D. Y. Curtin, *J. Org. Chem.*, **11**, 349 (1946).

11) A. P. Bhaduri, N. M. Khanna, and M. L. Dhar, *Indian J. Chem.*, **2**, 4 169 (1964).

12) L. Legrand and N. Lozach, *Bull. Soc. Chim. Fr.*, **7**, 1400 (1961).

13) C. S. Mewad, S. R. Patel, and N. M. Shah. *J. Indian Chem. Soc.*, **32**, 199, 438 (1955).

14) M. Z. Badr, H. A. El-Sherief, C. M. El-Naggar, and A. M. Mahmoud, *Bull. Fac. Sci. Assiut University* (1978) (in press).

15) K. Noda, S. Yamasaki, A. Nakagawa, and H. Ide, *Chem. Abstr.*, **82**, 43452 (1975), Japan Kokai 7445 086 (Cl. 16E464), 27 Apr. 1974. Appl. 7290, 684, 09 Sep. 1972; 4 pp.

16) Fisons Pest Control Ltd. Fr., *Chem. Abstr.*, **62**, 9154 (1965).

17) D. Harrison and A. C. B. Smith, *J. Chem. Soc.*, **1960**, 2157.

18) R. M. Silverstein and G. C. Bassler, "Spectrometric Identification of Organic Compounds," 2nd ed, Wiley, New York (1967), p. 162.

19) J. G. Vincent and H. W. Vincent, *Prac. Expl. Biol. Med.*, **55**, 162 (1944).

The Solvent Extraction of Alkali Metal Picrates by 12-Crown-4

Yasuyuki TAKEDA

Department of Chemistry, Faculty of Science, Chiba University, Yayoi-chō, Chiba 260

(Received January 11, 1980)

Synopsis. The overall extraction equilibrium constants (K_{ex}) for 1: 1: 1 complexes of 12-crown-4 (12C4) with alkali metal picrates between benzene and water have been determined at 25 °C. The K_{ex} series for the 12C4 for the alkali metal ions are given by $Na^+ > Li^+ > K^+ > Rb^+ \geq Cs^+$.

Solvent-extraction studies of crown ether complexes with various metal ions, particularly with the alkali and alkaline earth metal ions, have been reported.[1] In some of the studies, the overall extraction equilibria have been analyzed by means of the constituent equilibria, and the extractability of the crown ether complex as well as that of the metal ion has been discussed in detail.[1b,1c,1d] Moreover, crown ethers have been used for extraction analysis.[2]

In this paper, the overall extraction equilibrium constant values for the 12-crown-4 (12C4)–alkali metal picrate system have been determined between benzene and water at 25 °C, and these extraction constant values have been compared with those of 15-crown-5 (15C5), in order to clarify the role of 12C4 in the extraction process.

Experimental

Materials. The 12C4 was obtained from Wako-Pure Chemicals, Ltd., and was used without further purification. The concentrations of the alkali metal hydroxides and picric acid solutions were determined by means of acid and basic titrations respectively. The benzene (analytical-grade) was washed twice with distilled water.

Apparatus and Procedure. The organic phase of the crown ether (1.2×10^{-2}—2.5×10^{-1} M; 1 M = 1 mol dm^{-3}) and the aqueous phase of the alkali metal hydroxide (1.1—1.7×10^{-2} M) and the picric acid (6.0×10^{-3}—1.1×10^{-2} M) in stoppered glass tubes (30 ml) were shaken in a thermostated water bath for approx. 35 min at 25±0.2 °C and then centrifuged. The initial volume of each phase was 10 ml in all cases. A portion of the aqueous phase (8 ml) was transferred into a 10-ml beaker, and the hydrogen-ion concentration determined by means of a Hitachi-Horiba F-5 pH meter. The extractions were conducted at pH 9.1—11.9. The picrate in the organic phase was back-extracted into 8 ml of a 0.01 M NaOH aqueous solution, and the picrate concentration was determined at 356 nm by means of a Shimadzu UV-200 spectrophotometer ($\varepsilon = 1.45\times10^4$ cm^{-1} M^{-1}). In blank experiments, no detectable extraction was found in the absence of 12C4.

The Distribution Coefficient of 12C4. A portion (13 ml) of a benzene solution containing 12C4 and an equal volume of distilled water were placed in a stoppered glass tube and shaken under the conditions given above. The range of concentration of the 12C4 was from 1.3×10^{-1} to 2.3×10^{-1} M. After centrifuging, a portion (12 ml) of the organic phase was transferred to a 20-ml beaker, and allowed to evaporate over several days, and the residue weighed. Since 12C4 is very hygroscopic, the water content of the residue was determined by Karl Fischer titration. The average distribution coefficient, determined in this way, was 0.15.

Results

In an equilibrium between an aqueous solution of a univalent metal ion, M^+, a picrate ion, A^-, and a benzene solution of a crown ether, L, the equilibrium constants may be defined by the following equations:

$$K_{ex} = [MLA]_o[H^+]/[M^+][L]_o[HA]_o \quad (1)$$

$$K_{D,L} = [L]_o/[L] \quad (2)$$

$$K_{ex}(HA) = [HA]_o/[H^+][A^-] \quad (3)$$

$$K_{ML} = [ML^+]/[M^+][L] \quad (4)$$

$$K_{ex'} = [MLA]_o/[ML^+][A^-] \quad (5)$$

where the subscript "o" and the lack of subscript designate the organic phase and the aqueous phase respectively; square brackets indicate the molar concentrations. Thus, K_{ex} can be written as follows:

$$K_{ex} = K_{D,L}^{-1}K_{ex}(HA)^{-1}K_{ML}K_{ex'}. \quad (6)$$

The distribution ratio of the univalent metal may be represented by:

$$D_M = [MLA]_o/([M^+]+[ML^+]) \quad (7)$$

In the case of $[M^+] \gg [ML^+]$, Eq. 7 becomes:

$$D_M = K_{ex}K_{ex}(HA)[L]_o[A^-]. \quad (8)$$

The $-\log(D_M/[A^-])$ *vs.* $-\log[L]_o$ plot in Fig. 1 shows a linear relationship with a slope of 1 in every case, indicating that 12C4 forms the 1: 1 complex with the alkali metal ion. The values of $[L]_o$ and $[A^-]$ in Eq. 8 were calculated by means of Eqs. 9 and 10 respectively:

$$[L]_o = ([L]_t-[MLA]_o)/(1+K_{D,L}^{-1}) \quad (9)$$

$$[A^-] = ([HA]_t-[MLA]_o)/\{1+(K_{HA}+K_{ex}(HA))[H^+]\} \quad (10)$$

TABLE 1. EQUILIBRIUM CONSTANTS AT 25 °C, CRYSTAL IONIC RADII OF ALKALI METALS, AND CAVITY RADII OF CROWN ETHERS

Crown ether	Cavity radius (Å)[4]	$K_{D,L}$	Cation	Crystal ionic radius (Å)[5]	log K_{ex}
12C4	0.5—0.65	0.15			
			Li^+	0.60	−1.62
			Na^+	0.95	−1.44
			K^+	1.33	−1.82
			Rb^+	1.48	−2.10
			Cs^+	1.69	−2.18
15C5	0.85—1.1	0.15[6][1d]			
			Li^+	0.60	−1.10[1d]
			Na^+	0.95	1.51[1d]
			K^+	1.33	0.19[1d]
			Rb^+	1.48	−0.25[1d]
			Cs^+	1.69	−0.49[1d]

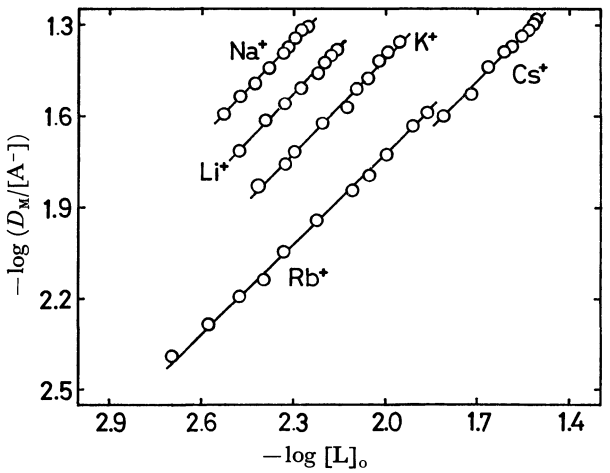

Fig. 1. Plots of $-\log (D_M/[A^-])$ *vs.* $-\log [L]_o$ for the alkali metals–12C4 system at 25 °C.

where the subscript "t" denotes the total concentration. The value of K_{ex}(HA) was spectrophotometrically determined to be 247 by using the association constant of picric acid ($K_{HA}=1.9_5$[3]). The equilibrium constants obtained from these data are summarized in Table 1, together with the literature values.

Discussion

The log K_{ex} series for the 12C4 for the alkali metal ions are given by $Na^+ > Li^+ > K^+ > Rb^+ \geq Cs^+$, indicating that the nearer the crystal radius of the alkali metal ion approaches to the cavity radius of 12C4, the more extractable the alkali metal ion is except for Li^+ (Table 1). In a previous paper,[1d] we have demonstrated that, in each case of 15C5 and 18-crown-6 (18C6), the alkali metal ion which has the optimum size for the crown ether cavity and the corresponding alkali metal ion–crown ether complex are the most extractable of all the alkali metal ions and the alkali metal ion–crown ether complexes respectively. In the case of 12C4, Na^+ is more extractable than Li^+, although Li^+ fits more closely into the 12C4 cavity than Na^+. This may be attributed to the fact that Li^+ is much more strongly hydrated than Na^+. 14-Crown-4 (14C4) and 12C4 have four donor oxygen atoms. 14C4 has a slightly larger cavity radius (0.6—0.75 Å[4]) than 12C4. However, Li^+ is the most favorable fit for the 14C4 cavity of all the alkali metal ions. It is interesting that 14C4 extracted Li^+ most effectively among the alkali metal ions.[1a] 15C5 and 18C6 show the most remarkable selectivity for Na^+ and K^+ respectively among the alkali metal ions.[1d] On the other hand, 12C4 displays no pronounced selectivity for any alkali metal ion.

Equation 6 shows that the series for K_{ex} for the same univalent metal ion for different crown ethers reflects the magnitude of $K_{D,L}$, the stability, and the extractability of the univalent metal ion–crown ether complex in the aqueous phase. It may be noted from Table 1 that the log K_{ex} value of 12C4 for the same alkali metal ion is smaller than that of 15C5. Since the $K_{D,L}$ value of 12C4 is nearly equal to that of 15C5, this may be due to the fact that the size of the 12C4 complex with the same alkali metal ion is smaller than that of the 15C5 complex and that the ability of 12C4, which has fewer donor oxygen atoms (four) than 15C5 (five), to form the complex with the same alkali metal ion in the aqueous phase is poorer than that of 15C5.

References

1) a) C. J. Pedersen, *Fed. Proc., Fed. Am. Soc. Exp. Biol.*, **27**, 1305 (1968); b) H. K. Frensdorff, *J. Am. Chem. Soc.*, **93**, 4684 (1971); c) Y. Takeda and H. Katō, *Bull. Chem. Soc. Jpn.*, **52**, 1027 (1979); d) Y. Takeda and H. Gotō, *ibid.*, **52**, 1920 (1979); e) Y. Takeda, *ibid.*, **52**, 2501 (1979).

2) a) H. Sumiyoshi, K. Nakahara, and K. Ueno, *Talanta*, **24**, 763 (1977); b) M. Takagi, H. Nakamura, and K. Ueno, *Anal. Lett.*, **10**, 1115 (1977); c)T. Kimura, K. Iwashima, T. Ishimori, and H. Hamaguchi, *Chem. Lett.*, **1977**, 563; d) Y. Takeda, S. Suzuki, and Y. Ohyagi, *ibid.*, **1978**, 1377; e) Y. Takeda, K. Oshio, and Y. Segawa, *ibid.*, **1979**, 601.

3) "Dissociation Constants of Organic Acids in Aqueous Solution," ed by G. Kortün, W. Vogel, and K. Andrussov, Butterworths, London (1961).

4) C. J. Pedersen and H. K. Frensdorff, *Angew. Chem. Int. Ed.*, **11**, 16 (1972).

5) L. Pauling, "The Nature of the Chemical Bond," 3rd ed, Cornell Univ. Press (1960).

An ESR Study of *N,N*-Bis(arylthio)aminyls. ^{33}S Hyperfine Splittings[1]

Yozo MIURA* and Masayoshi KINOSHITA

Department of Applied Chemistry, Faculty of Engineering, Osaka City University, Sumiyoshi-ku, Osaka 558

(Received October 4, 1979)

Synopsis. In the ESR spectra of *N,N*-bis(phenylthio)-, *N,N*-bis(phenyl-d_5-thio)-, and *N,N*-bis(3,5-dichlorophenylthio)aminyls, ^{33}S hyperfine splittings were detected. The spin densities in the aminyls were calculated by using the HMO calculations with and without McLachlan's correction, and the results were compared with the values derived from the ^{1}H, ^{14}N, and ^{33}S hyperfine splittings by use of the relationship $a=Q\rho$.

In a previous report on an ESR study of *N,N*-bis(arylthio)aminyls (**2**),[2,3] it was shown from the ^{1}H and ^{14}N hyperfine splitting (hfs) constants that in **2** the spin resides mainly on the central nitrogen atom and the two adjacent sulfur atoms. In continuing this study, we have tried to detect satellites due to ^{33}S (I=3/2) in ESR signals of **2**. It is well known that

$$\underset{\mathbf{1}}{\text{Ar–S–NH–S–Ar}} \xrightarrow{-H\cdot} \underset{\mathbf{2}}{\text{Ar–S–}\dot{\text{N}}\text{–S–Ar}}$$

a: Ar=C_6H_5, **b**: Ar=C_6D_5, **c**: Ar=3,5-$Cl_2C_6H_3$

the detection of satellites due to ^{33}S in natural abundance is very difficult because of the small amount present (0.74%). Fortunately, we have been successful in the detection of the satellites due to ^{33}S in the spectra of **2** without an enrichment of ^{33}S atoms. From the ^{1}H, ^{14}N, and ^{33}S hfs constants for **2**, we derived the spin densities in **2** by use of the relationship $a=Q\rho$, and compared the values with those obtained from the HMO calculations with and without McLachlan's correction.[4] In this report these results are described.

Results and Discussion

The aminyls **2** were generated by oxidation of *N*-(arylthio)arenesulfenamides (**1**) with lead dioxide and potassium carbonate.[2,5,6] Since **2** are fairly persistent, we could easily obtain high concentration solutions of **2** by this procedure. A typical ESR spectrum of **2b** is illustrated in Fig. 1a. The signal is composed of a simple 1:1:1 triplet with a small line-width (0.035 mT). On recording under high amplification, the satellite due to ^{33}S in natural abundance was detected, together with the satellite due to ^{15}N (I=1/2) in natural abundance (0.37%). The ratio of the observed splittings of $a_{^{15}N}/a_{^{14}N}$ (1.40) agrees with that of the magnetic moments of the nuclei (1.40). In the spectrum of **2a**, the satellite due to ^{33}S was also detected, but it was significantly masked by the main spectrum because of the large line-width of the spectrum (0.16 mT). However, the obtained value was in good agreement with that for **2b**. In the spectrum of **2c**,

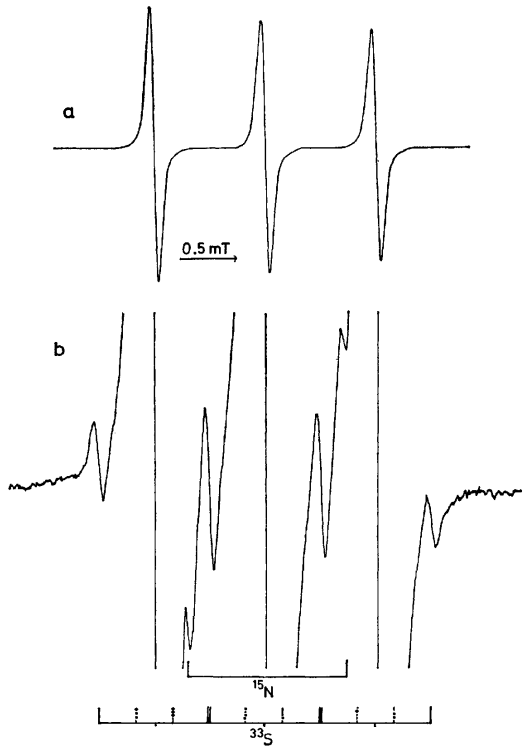

Fig. 1. ESR spectra of **2b** in benzene solution at room temperature.
(a): The main spectrum recorded under low amplification; (b): satellites due to ^{33}S and ^{15}N recorded under high amplification (100 times). The stick diagrams represent the theoretical reconstruction of satellites due to ^{33}S and ^{15}N. The experimentally observed satellites are shown by the full lines and those lost in the main spectrum are shown by the dotted lines.

TABLE 1. HYPERFINE SPLITTING CONSTANTS AND λ_{max} FOR **2**

	Solvent	$a_{^{14}N}$/mT	a_{other}/mT	*g*-value	λ_{max}/nm
2a	Benzene	1.141[a]	0.39(^{33}S)	2.0075[b]	538[a]
2b	Benzene	1.144	0.39(^{33}S), 1.60 (^{15}N)	2.0075	538
2b	Hexane	1.151		2.0074	531
2b	THF	1.143		2.0075	534
2b	Acetone	1.141		2.0075	531
2b	Acetonitrile	1.140		2.0075	527
2c	Benzene	1.140[a]	0.058 (*o*- and *p*-^{1}H),[a] 0.39(^{33}S)	2.0073[b]	531[a]

a) See Ref. 2. b) See Ref. 7.

TABLE 2. OBSERVED AND CALCULATED SPIN DISTRIBUTION IN **2a**

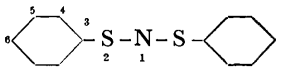

Position	Observed hfs constant / mT	Spin density	HMO	McLachlan
1	1.141(^{14}N)	0.496	0.503	0.688
2	0.39(^{33}S)	0.12	0.174	0.136
3	—		0.000	−0.014
4	0.058(^{1}H)[b]	0.021	0.025	0.018
5			0.000	−0.008
6	0.058(^{1}H)[b]	0.021	0.025	0.015

a) The spin densities (ρ) were derived from the hfs constants (a) using the relationship: $a=Q\rho$; $Q^{\pi}_{^{14}N}=2.3$ mT,[8c,d] $Q_{^{1}H}=-2.7$ mT,[10] $Q^{\pi}_{^{33}S}=3.3$ mT,[8b,11] $\lambda=0.7$. b) The value observed for **2c**.

the satellite due to ^{33}S was split into a septet, with an interval of 0.058 mT, by the interaction with the six magnetically equivalent protons. The ^{1}H, ^{14}N, ^{15}N, and ^{33}S hfs constants are listed in Table 1.

The ^{14}N hfs constant and the λ_{max} for **2b** were measured in some nonpolar and polar solvents in order to examine solvent effects on these values. As can be seen in Table 1, these values are independent of solvent. Thus, the spin distribution in **2** is little affected by the polarity of the solvent.

The HMO calculations with and without McLachlan's correction were made for **2a** using the following parameters:[8,9] $\alpha_N=\alpha+0.9\beta$, $\alpha_S=\alpha+1.3\beta$, $\beta_{NS}=0.7\beta$, $\beta_{CS}=0.75\beta$, $\lambda=0.7$; these parameters are chosen on the basis of the previously used values, but are slightly varied to give the best fit with the experimental results. In Table 2 the results are compared with the experimental values. Since, in the spectrum of **2a**, the splittings due to the ring protons were not detected, the values for **2c** are shown in Table 1. As can be seen from the comparison of the ^{14}N and ^{33}S hfs constants for **2a** with those for **2c**, the spin distributions in these aminyls are almost identical with each other. Thus, we can derive the spin densities on the phenyl rings of **2a** from the ^{1}H hfs constants for **2c**. As can be seen from Table 2, better agreement between the experimental and calculated values of the spin densities is obtained from the HMO calculation. The results indicate that in **2** *ca.* 50% of the spin resides on the central nitrogen atom and *ca.* 12% resides on each sulfur atom. The large g-values observed for **2** and other *N,N*-bis(arylthio)aminyls[2,7] (2.0073—2.0076) are well explained by this considerable delocalization of the spin onto the adjacent sulfur atoms, which have a large spin-orbit coupling parameter (382 cm^{-1}).[12,13]

Experimental

The visible spectra were obtained with a Hitachi Model ESP-3T spectrometer. The ESR spectra were obtained with a JES-ME-3X spectrometer equipped with an X-band microwave unit and 100 kHz field modulation. The hfs constants and g-values were determined in comparison with the ^{14}N hfs constant (1.309 mT) and the g-value (2.0055) of Fremy's salt. *N*-(Phenylthio)benzenesulfenamide (**1a**) and *N*-(3,5-dichlorophenylthio)-3,5-dichlorobenzenesulfenamide (**1c**) were prepared by the reported method.[2]

N-(Phenyl-d_5*-thio)benzene-*d_5*-sulfenamide (1b).* The amide was prepared in a similar manner to **1a**. Into dry ether (200 ml) was bubbled ammonia gas at −30——40 °C. To the solution was added dropwise freshly distilled benzenesulfenyl-d_5 chloride[14] (73—75 °C/3 Torr, 0.026 mol) in dry ether (30 ml). After addition, the bubbling of ammonia gas was stopped and the reaction mixture was raised to room temperature. Filtration of the reaction mixture and evaporation of solvent afforded an orange crystalline mass, which was recrystallized from hexane to give pale pink plates: mp 123—126 °C; yield 1.26 g (38%). IR (KBr): 3270 cm^{-1} (NH). Found: C, 58.85; H, 4.39; N, 5.68%. Calcd for $C_{12}HD_{10}NS_2$: C, 59.22; H, 4.56; N, 5.76%.

Generation of 2. Sulfenamide **1** (10 mg) was treated in solvent (3 ml) with lead dioxide (0.5 g) and potassium carbonate (0.5 g). After filtration, 0.5 ml of the purple solution was placed in an ESR cell and the solution was degassed by three freeze-and-thaw cycles; then the cell was sealed. ESR spectra were recorded at room temperature.

Spin density calculations were carried out on a FACOM 230-60 computer.

References

1) Part XIII of this series, "ESR Studies of Nitrogen-centered Free Radicals." For Part XII, see Y. Miura, A. Yamamoto, Y. Katsura, and M. Kinoshita, *J. Chem. Soc., Chem. Commun.*, **1980**, 37.

2) Y. Miura, N. Makita, and M. Kinoshita, *Bull. Chem. Soc. Jpn.*, **50**, 482 (1977).

3) In a previous paper,[2] the aminyls **2** were named dibenzenesulfenamidyls.

4) A. D. McLachlan, *Mol. Phys.*, **3**, 233 (1960).

5) H. Lecher, K. Köberle, and P. Stöcklin, *Chem. Ber.*, **58**, 423 (1925).

6) D. H. R. Barton, I. A. Blair, P. D. Magnus, and R. K, Norris, *J. Chem. Soc., Perkin Trans. 1*, **1973**, 1031.

7) For the corrected g-values for **2a** and **2c**, see Y. Miura, N. Makita, and M. Kinoshita, *Bull. Chem. Soc. Jpn.*, **50**, 2208 (1977).

8) a) E. T. Strom and G. A. Russell, *J. Am. Chem. Soc.*, **87**, 3326 (1965); b) P. D. Sullivan, *J. Am. Chem. Soc.*, **90**, 3618 (1968); c) C. L. Kwan, M. Carmack, and J. K. Kochi, *J. Phys. Chem.*, **80**, 1786 (1976); d) R. C. Haddon, M. L. Kaplan, and J. H. Marshall, *J. Am. Chem. Soc.*, **100**, 1235 (1978).

9) The calculations were performed without considering the sulfur d-orbital.

10) a) H. M. McConnell, *J. Chem. Phys.*, **24**, 632 (1956); b) E. T. Strom, G. R. Underwood, and D. Jurkowitz, *Mol. Phys.*, **24**, 901 (1972).

11) F. B. Bramwell, R. C. Haddon, F. Wudl, M. L. Kaplan, and J. H. Marshall, *J. Am. Chem. Soc.*, **100**, 4612 (1978).

12) The g-values for typical aromatic nitrogen-centered free radicals are in the range of 2.003—2.004. For example, the g-value for diphenylaminyl is 2.0032; F. A. Neugebauer and S. Bamberger, *Chem. Ber.*, **107**, 2362 (1974).

13) D. S. McClure, *J. Chem. Phys.*, **17**, 905 (1949).

14) Y. Miura and M. Kinoshita, *Bull. Chem. Soc. Jpn.*, **50**, 1142 (1977).

Electronic States of Crystalline Cation Radical Salts. Simple Salt of Phenothiazine$^{+\cdot}$Br$^-$ and Complex Salt of (Phenothiazine)$_2^{+\cdot}$Br$^-$

Yôichi IIDA

Department of Chemistry, Faculty of Science, Hokkaido University, Sapporo 060

(Received February 7, 1980)

Synopsis. Phenothiazine forms not only simple cation radical salt of Phenothiazine$^{+\cdot}$ Br$^-$ but also complex salt of (Phenothiazine)$_2^{+\cdot}$ Br$^-$. In this paper, less-than-half occupied Hubbard model was applied to the complex salt in order to explain its crystal electronic state.

The prominent magnetic, electrical, and optical properties of solid ion radical salts have been the subject of many theoretical and experimental investigations over the past seventeen years.[1] In such solid ion radical salts, the planar ion radical molecules are known to form, in themselves, a segregated stacking into columns so as to make a large overlap between their half-occupied molecular orbitals. In this case, any individual radical molecule interacts through charge transfer most strongly with two other neighboring radicals, and the electronic and magnetic properties of the solid salt differ distinctly from those of ion radical monomer. Moreover, in some cases, we can obtain complex ion radical salts, which include not only ion radical molecule but also its parent neutral molecule.[1-4] The optical and magnetic properties of crystalline complex ion radical salts are very interesting in comparison with those of the corresponding simple salts. In the present paper, we shall examine the electronic state of complex cation radical salt, (Phenothiazine)$_2^{+\cdot}$ Br$^-$, together with that of simple salt, Phenothiazine$^{+\cdot}$ Br$^-$.

Phenothiazine (PT) is a strong electron donating molecule and forms chemically stable cation radical salts with various diamagnetic counter anions. A simple cation radical salt of PT$^{+\cdot}$ Br$^-$ is a kind of such compounds. The electronic spectrum of solid PT$^{+\cdot}$ Br$^-$ shows a strong low-energy band at 12900 cm^{-1} and high-energy bands at 20500, 23000, and 28600 cm^{-1}.[2-5] The high-energy bands are known to come from the monomer absorptions of phenothiazine cation radical in solution, while the low-energy band at 12900 cm^{-1} is characteristic of the solid salt and was assigned to the charge-transfer transition between cation radicals.[3-5] The magnetic susceptibility of this salt was found to be almost diamagnetic, indicating that strong antiferromagnetic spin exchange interaction acts between adjacent cation radicals. According to Sato *et al.*,[6] the change in the paramagnetic susceptibility with temperature was found to fit well the curve calculated from regular one-dimensional Ising model, for which the spin-exchange coupling parameter, J, was taken to be 970 cm^{-1}. In order to understand those optical and magnetic properties, a regular one-dimensional half-occupied Hubbard model is applied to the segregated stack of phenothiazine cation radicals in simple cation radical salt of PT$^{+\cdot}$ Br$^-$. This model is a simplification of the real crystal and is described by two parameters I and T.[5] T is the transfer matrix element of an unpaired electron which describes hopping between adjacent molecular sites, while I is the on-site Coulomb repulsion between two electrons with up and down spins on the same molecule. Then, T favors electron delocalization through band formation, whereas I favors localization due to electron-electron repulsions. On the basis of this model, we can explain the reason why the intermolecular charge-transfer absorption appears in the solid-state spectrum of PT$^{+\cdot}$ Br$^-$. The peak energy of the charge-transfer absorption corresponds to $\omega=I$, and if the electron transfer matrix element, T, is not zero, the absorption has observable intensity.[5,7] As for the magnetic property of this system, Takahashi showed that, in the case of $I \gg |T|$, the half-occupied Hubbard model becomes equivalent to the following effective Hamiltonian,[8]

$$\mathcal{H}_{\text{eff}} = \frac{4T^2}{I}\sum_i \left(\boldsymbol{S}_i \cdot \boldsymbol{S}_{i+1} - \frac{1}{4}\right) + 0\left(\frac{T^3}{I^2}\right), \qquad (1)$$

where $\boldsymbol{S}_i$, $(S=1/2)$, is the spin operator of an electron at the i-th site. In other words, if the value of I is much larger than $|T|$, we can neglect such higher terms as $0(T^3/I^2)$, and the one-dimensional half-occupied Hubbard model is reduced to one-dimensional Heisenberg antiferromagnetic model with exchange interaction, $J=2T^2/I$. In this respect, our application of Hubbard model receives strong support from the fact that in PT$^{+\cdot}$ Br$^-$ there acts antiferromagnetic spin exchange interaction between adjacent PT$^{+\cdot}$ cation radicals.[6] Rigorously speaking, the J value of Heisenberg model should correspond to $2T^2/I$. However, since only the J value estimated with linear Ising model is available, we approximately use the estimated $J=970$ cm^{-1} value as $J \approx 2T^2/I$. If we use the $I=12900$ cm^{-1} value obtained spectroscopically, the T value was determined as $T \approx -2500$ cm^{-1} for the one-dimensional system of PT$^{+\cdot}$ cation radicals in simple PT$^{+\cdot}$ Br$^-$ salt.

Next, we consider the crystal electronic state of complex cation radical salt of (PT)$_2^{+\cdot}$ Br$^-$. The existence of this complex salt was earlier suggested by Matsunaga and Shono and by the present author,[2,3] and was later confirmed by Doi and Matsunaga.[4] In the electronic spectrum of the solid complex salt, the charge-transfer absorption due to the transition between cation radicals appears at 12600 cm^{-1}. In addition, a broad absorption is observed at 5200 cm^{-1}, which was assigned to the electronic transition from neutral phenothiazine to its cation radical.[4] In the complex salt, it appears that the positive charge is equally shared by the two molecules of phenothiazine and that phenothiazine molecules form, in themselves, a segregated stacking into infinite one-dimensional columns. Then, we can apply regular one-dimensional

less-than-half occupied Hubbard model to the segregated stack of phenothiazine molecules.

Shiba[9] and Klein and Seitz[10] have shown that the magnetic susceptibility of a uniform stack of lessthan-half occupied molecules (average number of unpaired electrons per site is ρ) is related to the susceptibility of a uniform stack of half-occupied molecules ($\rho=1$) in simple ion radical salt. It is assumed that the values of I and T in less-than-half occupied Hubbard model are common to those in half-occupied system, respectively. If the value of I is much larger than that of $|T|$, the less-than-half occupied one-dimensional Hubbard model becomes identical to an antiferromagnetic Heisenberg chain with exchange interaction,[11]

$$J=\frac{2T^2\rho}{I}\left(1-\frac{\sin 2\pi\rho}{2\pi\rho}\right). \quad (2)$$

In fact, if we take $\rho=1$ in Eq. 2 for half-occupied Hubbard model, we simply obtain $J=2T^2/I$, which is identical with the J value of simple ion radical salt in Eq. 1. For the complex cation radical salt of $(PT)_2^{+\cdot}$ Br^-, we can choose $\rho=1/2$, $I=12900\ cm^{-1}$ and $T\approx -2500\ cm^{-1}$ because of the assumption that the I and T values of the complex salt are almost the same as those corresponding to the simple salt of $PT^{+\cdot}$ Br^-. Then, using Eq. 2, the J value of the complex salt of $(PT)_2^{+\cdot}$ Br^- was estimated to be $485\ cm^{-1}$. Temperature dependence of the magnetic susceptibility, χ, of the complex salt can be given by Bonner and Fisher's theoretical equation with $J=485\ cm^{-1}$.[12] More practically, as an excellent fit to their equation, Torrance proposed an analytical expression of χ *versus* temperature and J.[11] If we compare the $J=970\ cm^{-1}$ value of the simple salt with the $J=485\ cm^{-1}$ value of the complex salt, we note marked decrease of the J value in the complex salt. This will give more paramagnetism to the susceptibility of the complex salt. The strong dependence of J on ρ means that the antiferromagnetic spin exchange interaction between unpaired electrons is caused mostly by the charge-transfer interaction between unpaired electrons and that less density of unpaired electron in the complex salt gives smaller J value, compared to the J value in the simple salt.

As for the optical property of the complex salt, $(PT)_2^{+\cdot}$ Br^-, the above-mentioned Hubbard model can also explain the observed charge-transfer absorption due to the transition between cation radicals. This absorption is observed at $12600\ cm^{-1}$, which is close to the $12900\ cm^{-1}$ value of the simple salt. Theoretically speaking,[7] the regular one-dimensional less-than-half occupied Hubbard model leads to the charge-transfer absorption spectrum of $\mathrm{Re}\,\sigma_{xx}(\omega)\propto \mathrm{Re}\,\sigma^+(\omega)+\mathrm{Re}\,\sigma^-(\omega)$;

$$\mathrm{Re}\,\sigma^{\pm}(\omega)=\frac{e^2}{4}\frac{I^2\rho\left(1-\frac{1}{2}\rho\right)}{\omega^2\sqrt{\omega^2-2I^2\rho\left(1-\frac{1}{2}\rho\right)}}$$
$$\times\sqrt{4T^2-\left\{-(\rho-1)I\pm\sqrt{\omega^2-2I^2\rho\left(1-\frac{1}{2}\rho\right)}\right\}^2}, \quad (3)$$

where we neglected the term of Fermi distribution function. For the simple salt of $PT^{+\cdot}$ Br^- with $\rho=1$ and $I=12900\ cm^{-1}$, the charge-transfer absorption, $\mathrm{Re}\,\sigma_{xx}(\omega)$, has a divergent peak at $\omega=I$; this spectroscopic feature was mentioned previously. For the complex salt of $(PT)_2^{+\cdot}$ Br^-, however, if we put $\rho=1/2$, $I=12900\ cm^{-1}$ and $T\approx -2500\ cm^{-1}$, the absorption peak of $\mathrm{Re}\,\sigma_{xx}(\omega)$ will take place around $\omega=\sqrt{4T^2+2IT+I^2}=11300\ cm^{-1}$. Therefore, the charge-transfer absorption of the complex salt will show red-shift in comparison with that of the simple salt. The experimental peak energy, $12600\ cm^{-1}$, of the complex salt shows a little red-shift compared to the $12900\ cm^{-1}$ value of the simple salt, but this magnitude of the red-shift is not so large as that predicted theoretically. One of the reasons for this is that the I value of the complex salt may be a little larger than that of the simple salt and that the role of counter anion of Br^- in the complex salt may be less effective to decrease on-site Coulomb repulsion than in the simple salt, because average number of Br^- anions per one site of phenothiazine in the complex salt is just half of that in the simple salt.

References

1) See, for example, Z. G. Soos and D. J. Klein, "Molecular Association," ed by R. Foster, Academic Press, London, New York, San Francisco (1975) Vol. 1, Chap. 1; "Synthesis and Properties of Low-Dimensional Materials," ed by J. S. Miller and A. J. Epstein, The New York Academy of Sciences, New York (1978).

2) Y. Matsunaga and K. Shono, *Bull. Chem. Soc. Jpn.*, **43**, 2007 (1970).

3) Y. Iida, *Bull. Chem. Soc. Jpn.*, **44**, 663 (1971).

4) S. Doi and Y. Matsunaga, *Bull. Chem. Soc. Jpn.*, **48**, 3747 (1975).

5) Y. Iida, *Bull. Chem. Soc. Jpn.*, **51**, 3637 (1978).

6) Y. Sato, M. Kinoshita, M. Sano, and H. Akamatu, *Bull. Chem. Soc. Jpn.*, **42**, 548 (1969).

7) Y. Iida, *Bull. Chem. Soc. Jpn.*, **50**, 1445 (1977); **51**, 434 (1978); **52**, 2791 (1979).

8) M. Takahashi, *Prog. Theor. Phys. (Kyoto)*, **42**, 1098 (1969); Y. Iida, *Bull. Chem. Soc. Jpn.*, **52**, 3447 (1979).

9) H. Shiba, *Phys. Rev. B*, **6**, 930 (1972).

10) D. J. Klein and W. A. Seitz, *Phys. Rev. B*, **10**, 3217 (1974).

11) J. B. Torrance, "Synthesis and Properties of Low-Dimensional Materials," p. 210. See Ref. 1.

12) J. C. Bonner and M. E. Fisher, *Phys. Rev. A*, **135**, 640 (1964).

A Further Evidence of the Vibronic Coupling through b_{3g} Vibrational Modes in the Fluorescence Spectrum of Anthracene[1)]

Tomoyuki TERADA, Motohiko KOYANAGI,* and Yoshiya KANDA

Department of Chemistry, Faculty of Science, Kyushu University, Hakozaki, Higashi-ku, Fukuoka 812

(Received February 8, 1980)

Synopsis. Angular dependence of the fluorescence polarization spectra of anthracene was investigated in polyethylene films using a sample rotation technique. An important role of a nontotally symmetric vibration, the b_{3g} ring vibration at 1655 cm^{-1}, was further confirmed by a combination of this technique and the modulation polarization technique developed previously.

Despite many studies on the fluorescence polarization spectra of anthracene, only a partially successful experiment for the assignment of b_{3g} nontotally symmetric vibrational bands has been reported by Bree and Katagiri.[2)] Very recently Ohta and Ito measured the intensity of Raman lines of crystalline anthracence in the pre-resonance excitation region and found a marked intensity enhancement of the b_{3g} Raman line at 1630 cm^{-1} for such a "resonant" excitation.[3)] The enhancement was then attributed to the vibronic coupling between two $\pi\pi^*$ excited states, *i.e.*, ^1L_a and ^1B_b, of the molecule. Previously we developed a new polarization method, *i.e.*, a modulation polarization (MP) method, and reported its application to studies of emission polarization spectra of some molecules in mixed crystals[4)] and in stretched polyethylene films.[5)] Anthracene was one of these molecules. Several bands of the long molecular axis polarization were clearly confirmed to exist in the fluorescence by the MP method. However, there remained a few ambiguous points about the molecular orientation in the stretched polyethylene films and the degrees of self-polarization of the apparatus. In the present work we examined the angular dependence of the MP spectra and confirmed the validity of the previous conclusion.

Experimental

The MP spectra were observed in a similar way to those described previously.[5)] The axis of an analyzing polarizer was fixed as inclined by 45° from the vertical axis of a Dewar for possible diminution of the systematic error of polarizations coming from the curvature of the Dewar. A sample-rotation device is homemade and it makes the 0°—180° rotation of sample films possible. An angle precision of the device is estimated to be ±3°. An angle θ is defined as that between the stretching film axis and the analyzing polarizer axis.

Results and Discussion

Anthracene is assumed to be embedded in stretched polyethylene films in such a way that its long molecular axis is oriented along the stretching film direction.[6)] Thus this system should roughly approximate a model of the oblate-spheroidal orientation of the molecule, allowing overlapping vibronic bands to be possibly separated by such polarization studies. Since $\pi\pi^*$ transitions of aromatics are of in-plane polarization,[7)] an application of such polarization techniques to oblate or prolate aromatics enables us to discriminate between the short and long molecular axis polarizations. A previous work on the MP spectrum of anthracene has partly demonstrated this possibility.[5)]

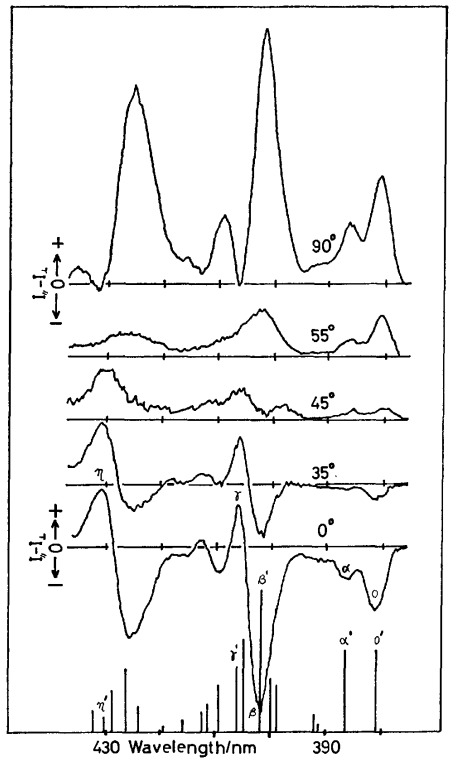

Fig. 1. Angular dependence of the fluorescence polarization spectra of anthracene in stretched polyethylene films at 77 K. For comparison, the fluorescence spectrum in heptane matrix at the same temperature is schematically shown at the bottom of this figure. The spectrum is evenly shifted so that the origin bands of both systems may coincide with one another. See text or the caption of Fig. 2 for band designations.

An angular dependence of the MP polarized fluorescence spectrum of anthracene is shown in Fig. 1. The spectrum at $\theta=0°$ resembles Fig. 3c of Ref. 5 except a better band resolution in the present work and a similar vibrational analysis is made possible by comparing the extrema of the MP spectrum with the vibrational bands of the fluorescence spectrum in heptane. Here let us devote our attention to the following extrema of the MP spectrum: the extrema at 380.6 nm (o in Fig. 1), 386.4 nm (α), 402.2 nm (β), 406.2 nm (γ), and 431.3 nm (η). These correspond nicely to five prominent bands in the anthracene/heptane system. They are the bands 0—0 (o' in Fig. 1), 0—393 cm^{-1} (α'), 0—1405 cm^{-1} (β'), 0—1637 cm^{-1} (γ'), and 0—1405—1637 cm^{-1} (η'), respectively.

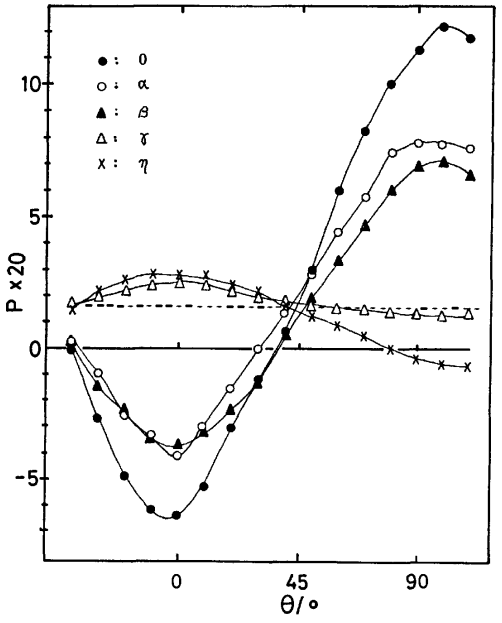

Fig. 2. Angular dependence of the polarizations of five prominent fluorescence bands. Band designations are: o, 0—0; α, 0—395 cm^{-1}; β, 0—1410 cm^{-1}; γ, 0—1655 cm^{-1}; η, 0—1655—1410 cm^{-1}.

With respect to the abscissa axis the spectrum at $\theta=0°$ is, as a whole, symmetrical to that at $\theta=90°$, as can be expected. The spectrum at $\theta=35°$, however, is seen far from such a symmetrical relation to that at $\theta=55°$. The spectrum at $\theta=45°$ shows several weak polarization peaks. These peaks were found to come mainly from the instrumental self-polarizations whose correction factor was not equal to unity, but nearly to 1.15 on an average in the present optical arrangement. This correction factor also explains the asymmetric relationship between the MP spectra at $\theta=35°$ and 55°.

Angular dependence of the polarizations of the five prominent fluorescence bands is shown in Fig. 2. Evidently there are four characteristic features to be pointed out. [1] Two types of the polarization angular dependence are found for the bands (o, α, β) and the others (γ, η). [2] All the polarization curves of the bands cross at $\theta\approx45°$. [3] The extreme value of the polarization of each band appears at $\theta\approx0°$ or $\theta\approx90°$, depending on the polarization nature of the vibrational band. [4] An even upward shift of the base-line by $P=+0.08$ seems to bring about a nice symmetric situation for the curves. The items [2] and [3] demonstrate that the molecule in the stretched polyethylene film is oriented in such a way that the long molecular axis is nearly parallel to the stretching film axis.[6] An experimental fact described in the item [4] is reasonably explained by the instrumental self-polarizations. The angular dependence of the bands γ and η (the item [1]) clearly proves these bands are certainly of b_{3g} vibrational modes.[5]

This work has been supported by the Kurata Foundation Found awarded to one of the authors (M. K.) and also by a Grant-in-Aid for Scientific Research from the Ministry of Education, Science and Culture.

References

1) A preliminary report of this work was presented at the 26th IUPAC congress, Tokyo, 1977.
2) A. V. Bree and S. Katagiri, *J. Mol. Spectrosc.*, **17**, 24 (1965).
3) N. Ohta and M. Ito, *Chem. Phys.*, **20**, 71 (1977).
4) M. Koyanagi, K. Higashi, and Y. Kanda, *Chem. Phys. Lett.*, **52**, 184 (1977).
5) T. Terada, M. Koyanagi, and Y. Kanda, *Bull. Chem. Soc. Jpn.*, **53**, 352 (1980).
6) J. J. Dekkers, G. Ph. Hoornweg, K. J. Terpstra, C. MacLean, and N. H. Velthorst, *Chem. Phys.*, **34**, 253 (1978).
7) J. R. Platt, *J. Chem. Phys.*, **17**, 484 (1949).

Infrared Studies of the Oxidation of 2-Propanol on ZnO

Hisashi MIYATA,* Kazuo HATA,† Takashi NAKAJIMA, and Yutaka KUBOKAWA
Department of Applied Chemistry, University of Osaka Prefecture, Mozuumemachi, Sakai, Osaka 591
(Received February 21, 1980)

Synopsis. The oxidation of 2-propanol and acetone on ZnO has been studied by IR spectroscopy. Surface isopropoxide was oxidized to acetate and formate ions *via* enolate complex of acetone. Formation of α-diketone-like species was proposed for oxidation with dinitrogen oxide.

By investigation of the reaction of oxygen with olefins, 2-propanol, acetone, and 2-methyloxirane on metal oxides, such as ZnO, MgO, and NiO, by IR spectroscopy,[1-3] it was found that the compounds are oxidized to carboxylates on the surface. No C–C bond scission took place in the oxidation with dinitrogen oxide.[2,3] In order to clarify the mechanism of the oxidation and the role of adsorbed oxygen species, the oxidation of 2-propanol adsorbed on zinc oxide with oxygen or dinitrogen oxide has been investigated by IR spectroscopy.

Details of the apparatus, procedures, and materials were reported.[1-3] After 0.25—0.4 cm^3/g of 2-propanol or acetone had been introduced into the IR cell, the weakly adsorbed reactants were removed by immersing the trap in liquid nitrogen. Oxygen or dinitrogen oxide of 2 kPa was then circulated over the ZnO, the temperature of which being raised in stages. Infrared spectra were recorded at ambient temperature after each treatment of the sample.

The infrared spectrum of 2-propanol adsorbed on the zinc oxide (0.35 cm^3/g) exhibited bands at 2964, 2922, 2866, 1458, 1366, 1165, and 1134 cm^{-1} (Fig. 1a), which did not change significantly on evacuation at 353 K. The bands agree with those due to the surface isopropoxide formed on metal oxides,[1,4-7] confirming the formation of the stable isopropoxide species on zinc oxide.

The temperature of the zinc oxide containing isopropoxide was raised in stages under circulation of oxygen. The bands due to isopropoxide species were slightly reduced in intensity at 353 K and disappeared at 423 K. New bands appearing at 3038, 1576, 1548, 1498, 1428, and 1308 cm^{-1} at 353 K grew with an increase in temperature of the disk to 423 K. Figure 2A shows the change in intensity of these bands with increase in temperature. The behavior is almost the same as that of the reaction of oxygen with propene and 2-methyloxirane on ZnO[2,3] and with 2-propanol on MgO.[1] Thus, the same assignment is applicable. The bands at 2976, 1548, and 1432 cm^{-1} are due to $\nu_{as}(CH_3)$, $\nu_{as}(COO)$, and $\nu_s(COO)$ of surface acetate ions, respectively, and those at 2872, 1576, and 1366 cm^{-1} to the corresponding vibrations of surface formate ions.

The spectra of acetone-d_6 adsorbed on ZnO, pretreated with D_2O, were investigated for the bands at 1498 and 1308 cm^{-1} (Fig. 1de). Bands appearing at 2666, 2502, 2245, 2216, 1464, 1352 cm^{-1} are attributed to the dissociatively adsorbed acetone, *i.e.*, the enolate complex.[7] The bands at 1466 and 1352 cm^{-1} (1498 and 1308 cm^{-1} for acetone) are assigned to the C=O and C=C coupled vibrations of $(O{=}C{=}CD_2)$-groups in the enolate complex.[7-10] CD_2= vibrations appeared at 2245 cm^{-1} (3040 cm^{-1} for acetone). The bands at 2666 and 2502 cm^{-1} are due to the surface OD groups. Similar spectra have been reported by Koga, Onishi, and Tamaru,[7] and Nagai and Miyahara.[9] Thus, the bands at 1498 and 1308 cm^{-1} can be assigned to the enolate complex. The change in intensity of the bands with increase in temperature resembles that of the isopropoxide except for the alkoxyl bands. The results together with the fact that acetone was detected during the course of temperature rise of the ZnO containing 2-propanol in the presence of oxygen leads to the following conclusion: 2-propanol is dehydrogenated to form acetone, which was oxidized to acetate and formate ions *via* the enolate complex.

Similar experiments were carried out for isopropoxide adsorbed on ZnO using dinitrogen oxide instead of oxygen. After admission of dinitrogen oxide to the ZnO containing isopropoxide, its temperature was raised in stages. The resulting spectra are shown in Fig. 3. The intensity of the bands due to the isopropoxide

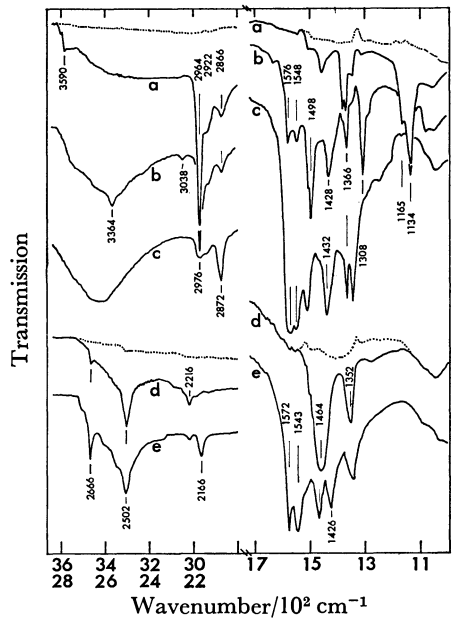

Fig. 1. Interaction of oxygen with 2-propanol or acetone adsorbed on ZnO.
(a) After 1 h adsorption of 2-propanol (0.35 cm^3/g) at 293 K followed by 1 h evacuation at 353 K; (b) followed by 1 h at 393 K in oxygen (2.1 kPa); (c) 1 h at 473 K in oxygen; (d) after 1 h adsorption of acetone-d_6 (0.3 cm^3/g) at 293 K; (e) followed by 1 h at 423 K in oxygen (2.0 kPa). In Figs. 1 and 3, the dotted lines show background spectra.

† Present address: Japan Catalytic Chemical Industry Co., Ltd., Nishitabicho, Suita, Osaka 564.

decreased with increase in temperature, disappearing completely at 523 K. The bands due to the enolate complex appeared at 353 K and passed through a maximum in intensity at 423 K (Fig. 2B). New bands appeared simultaneously at 1550 and 1436 cm^{-1} at 423 K, the ratio of intensity being constant up to 573 K. This suggests that these bands arise from the same adsorbed species. Results of similar experiments for acetone adsorbed on ZnO are also shown in Fig. 3. Essentially the same spectra are observed except for the alkoxyl bands.

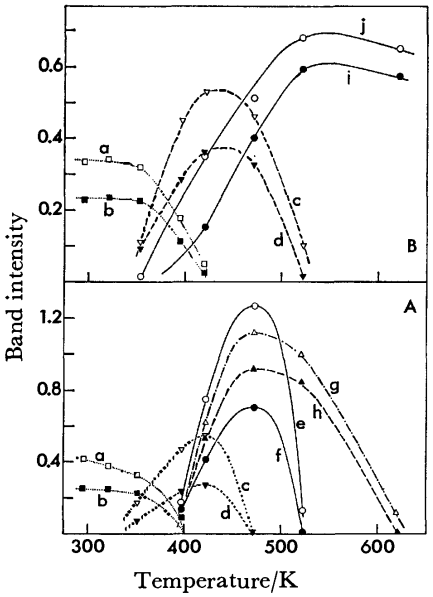

Fig. 2. Change in the band intensities with increasing temperature of ZnO.
(A) In oxygen; (B) in dinitrogen oxide; (a) 2964, (b) 1134, (c) 1498, (d) 1308, (e) 1576, (f) 1366, (g) 1548, (h) 1432, (i) 1550, (j) 1436 cm^{-1}.

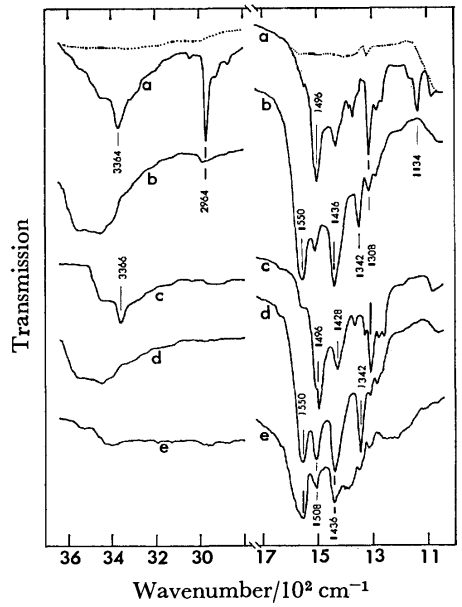

Fig. 3. Interaction of dinitrogen oxide with 2-propanol or acetone adsorbed on ZnO.
(a) After 1 h adsorption of 2-propanol (0.3 cm^3/g) at 293 K followed by 1 h at 393 K in dinitrogen oxide (2.2 kPa); (b) followed by 1 h at 523 K; (c) after 1 h adsorption of acetone (0.28 cm^3/g) at 293 K followed by 1 h at 393 K in dinitrogen oxide (2.3 kPa); (d) followed by 1 h at 523 K in dinitrogen oxide; (e) after 1 h adsorption of biacetyl (0.25 cm^3/g) followed by 1 h at 353 K in oxygen.

It was found in the reactions of dinitrogen oxide with 2-propanol or acetone that an appreciable amount of oxygen had been incorporated by the ZnO before carbon dioxide was formed. In contrast to the oxidation by oxygen, no cleavage of the C–C bond occurred, since no bands due to the formate ions appeared in the COO or CH stretching region. The results together with the change in intensity of the bands with increase in temperature (Fig. 2B) suggests that the enolate complex incorporate oxygen to form a new oxygen-containing compound having absorption at 1550 and 1436 cm^{-1}. Although the position of these bands is very similar to that for propionate ions on ZnO, the intensity of the CH stretching and the bending vibrations of the CH_3 groups is very low, in disagreement with what is expected from the propionate ions. The spectra of a number of oxygen-containing compounds such as alcohols, aldehydes, acids, and ketone were examined. Only biacetyl was found to give essentially the same spectra as those shown in Fig. 3. Thus, these bands are tentatively assigned to α-diketone-like species. Presumably, oxidation proceeds by the following scheme:

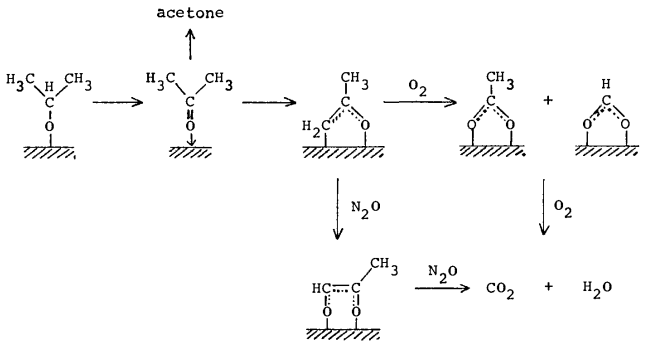

Scheme 1.

References

1) H. Miyata, M. Wakamiya, and Y. Kubokawa, *J. Catal.*, **34**, 117 (1974).
2) H. Miyata, K. Hata, and Y. Kubokawa, *J. Catal.*, **49**, 8 (1977).
3) K. Hata, S. Kawasaki, Y. Kubokawa, and H. Miyata, *Proc. Int. Congr. Catal. 6th*, 1102 (1976).
4) D. Treibmann and A. Simon, *Ber. Bunsenges. Phys. Chem.*, **70**, 562 (1966).
5) A. V. Deo, T. T. Chuang, and I. G. Dalla Lana, *J. Phys. Chem.*, **75**, 234 (1971).
6) V. N. Filimonov, *Kinet. Katal.*, **7**, 512 (1966).
7) O. Koga, T. Onishi, and K. Tamaru, *J. Chem. Soc., Faraday Trans. 1*, **76**, 19 (1980).
8) H. Miyata, Y. Toda, and Y. Kubokawa, *J. Catal.*, **32**, 153 (1974).
9) N. Nagai and K. Miyahara, *J. Res. Inst. Catal.*, **23**, 110 (1975).
10) D. M. Griffiths and C. H. Rochester, *J. Chem. Soc., Faraday Trans. 1*, **73**, 403 (1977).

Studies of the Separation Mechanism in Ion-exchange Chromatography. II. Inversion of the Elution Order of Tri- and Divalent Complex Cations with Increasing Concentration of the Eluent

Hayami YONEDA,* Chang Eon OH, and Shigeo YAMAZAKI
Department of Chemistry, Faculty of Science, Hiroshima University, Hiroshima 730
(Received January 11, 1980)

Synopsis. Two pairs of tri- and divalent complex cations $[Co(en)_3]^{3+}$, $[Ni(en)_3]^{2+}$ and $[Co(phen)_3]^{3+}$, $[Fe(phen)_3]^{2+}$ were chromatographed through the SP-Sephadex cation-exchange column using various concentrations of aqueous KBr and K_2SO_4 solutions as eluent, and the inversion of the elution order was observed for the pair of the phen complexes when eluted with KBr and for that of the en complexes when eluted with K_2SO_4.

In the first paper of this series,[1] it was reported for *cis* and *trans* isomeric pairs of some complex cations that the usual elution order in ion-exchange chromatography was reversed with the addition of dioxane to the eluent. This was interpreted as a result of the enhancement of the electrostatic interaction in the moving phase which overtook the interaction in the fixed phase. If this interpretation is valid, the inversion of the elution order is expected also for the pairs of differently charged cations under suitable conditions. This expectation was ascertained in the present study.

Experimental

All the complexes were prepared according to the literature, and identified by UV absorption spectra. Complexes used were $[Co(en)_3]Cl_3$, $[Ni(en)_3]Cl_2$, $[Co(phen)_3]Cl_3$, and $[Fe(phen)_3]Cl_2$. All the works were carried out on a laboratory-built chromatographic unit at room temperature. The column size was 10.8 cm long and 1.1 cm in diameter. SP-Sephadex C-25 (K^+-form) was used as a packing material. The detector was operated at an appropriate wavelength in the visible region for each complex. The adjusted retention volume was measured from the elution curve thus obtained. Blue dextran 2000 was used as a marker.

Results and Discussion

Figure 1 shows the adjusted retention volumes of the en and phen complex pairs as a function of KBr concentration. At low KBr concentration, both trivalent complexes, $[Co(en)_3]^{3+}$ and $[Co(phen)_3]^{3+}$ show greater retention volumes than the corresponding divalent complexes, $[Ni(en)_3]^{2+}$ and $[Fe(phen)_3]^{2+}$. This means that the trivalent complex is adsorbed more strongly on the $-SO_3^-$ group of the resin than the corresponding divalent complex. However, the retention volume of the tri- and divalent complexes decreases with increasing concentration of the eluent, and the rate of decrease in the retention volume is much larger for the trivalent complex than for the divalent complex. Thus, the inversion of the elution order can be expected for both pairs above a certain eluent concentration.[2] Here, it is worth noting that this critical concentration

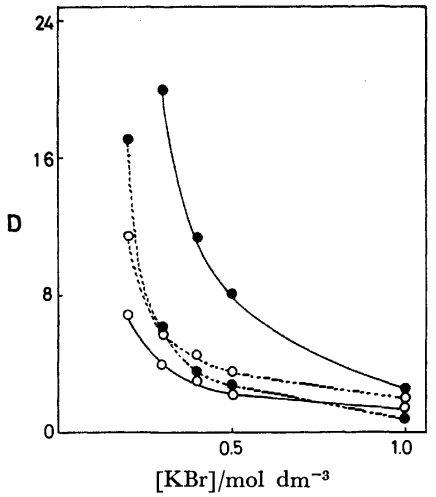

Fig. 1. Plots of *D* *vs.* concentration of KBr used as an eluent.
$[Co(en)_3]^{3+}$ (●—●), $[Ni(en)_3]^{2+}$ (○—○),
$[Co(phen)_3]^{3+}$ (●---●), $[Fe(phen)_3]^{2+}$ (○---○).

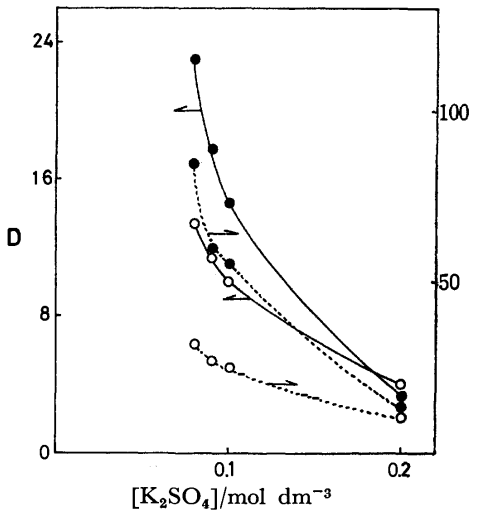

Fig. 2. Plots of *D* *vs.* concentration of K_2SO_4 used as an eluent.
$[Co(en)_3]^{3+}$ (●—●), $[Ni(en)_3]^{2+}$ (○—○),
$[Co(phen)_3]^{3+}$ (●---●), $[Fe(phen)_3]^{2+}$ (○---○).

at which the inversion takes place is different for different pairs; while the inversion takes place at 0.3 mol dm^{-3} KBr for the phen complex pair, it does not even at 1 mol dm^{-3} KBr for the en complex pair. On the contrary, as shown in Fig. 2, when K_2SO_4 solution is used as eluent, the inversion takes place at *ca.* 0.18 mol dm^{-3} for the en complex pair, but it does not even

at 0.20 mol dm^{-3} for the phen complex pair. These trends can be interpreted in the following way.

In quantitative consideration, it is convenient to use the distribution coefficient D, the ratio of the concentration of a sample ion in the resin phase to that in the moving phase, which has been demonstrated[3] to equal the adjusted retention volume per unit resin volume. Thus, we have

$$D = [M]_R/[M] = V_{adj}/V_{resin}$$

where $[M]_R$ and $[M]$ represent the concentration of a sample ion M^{m+} in the resin phase and in the moving phase, respectively, and V_{adj} and V_{resin} represent the adjusted retention volume and the volume of the ion-exchange resin packed in the column, respectively. If it is assumed that a small amount of a sample ion M^{m+} is distributed between the B^+-formed resin and the aqueous solution of an electrolyte B_nX used as an eluent, D is given by

$$D = K_B^M([B]_R)^m/[B]^m$$

where K_B^M is the selectivity coefficient of M^{m+} relative to B^+.[3] When the ion-association between M^{m+} and X^{n-} is taken into account, the distribution coefficient D of M^{m+} is expressed as[3]

$$D = K_B^M([B]_R)^m/\{[B]^m(1+\beta[X])\} \quad (1)$$

where β is the association constant. With this final equation, the elution order of the tri- and divalent complex cations can be compared.

Let D_3 and D_2, $K(3)$ and $K(2)$, and $\beta(3)$ and $\beta(2)$ represent the distribution coefficients, the selectivity coefficients, and the ion-association constants for tri- and divalent complexes, respectively. If we take the ratio of these distribution coefficients D_3 and D_2 for a particular pair, we obtain

$$D_3/D_2 = (K(3)/K(2))([B]_R/[B])(1+\beta(2)[X])/(1+\beta(3)[X]). \quad (2)$$

Here, $K(3)$ is in general larger than $K(2)$. At low concentration of B_nX, $[B]_R$ is larger than $[B]$, and $\beta[X]$ can be neglected in Eq. 2. Therefore, the value of D_3/D_2 is larger than unity, indicating that the trivalent ion is adsorbed on the resin more strongly than the corresponding divalent ion. However, as the concentration of B_nX increases, the value of $[B]_R/[B]$ becomes smaller and smaller and finally it becomes less than unity so as to make its product with $K(3)/K(2)$ very close to unity at fairly high concentration of B_nX. Thus, in principle, the value of D_3/D_2 for a particular pair can be smaller than unity at very high eluent concentration. However, when the ion-association effect is added, D_3/D_2 becomes smaller than unity at relatively low eluent concentration, since the value of $(1+\beta(2)[X])/(1+\beta(3)[X])$ in Eq. 2 is always smaller than unity for a particular pair. Using Eq. 2, our experimental results can now be explained in the following way.

Bromide anion is poorly hydrated in aqueous solution because of its large size and low electric charge, and therefore is considered to be a water-structure breaker.[4] Such a structure-breaking anion is antagonistic[4] to a water-structure-making cation like $[M(en)_3]^{m+}$ which attracts many water molecules with its many N–H bonds, and has little tendency toward association with $[M(en)_3]^{m+}$. Thus, the effect of ion-association need not be considered for the en complex pair when eluted with KBr solution and the elution order is not reversed in the ordinary concentration range of the eluent. On the other hand, SO_4^{2-} is strongly hydrated and has a great tendency to associate with a strongly hydrated complex cation like $[M(en)_3]^{m+}$ through S–O···H–N–M hydrogen bonds.[5] Thus, when the en complexes are eluted with K_2SO_4, the effect of ion-association, that is, the term $(1+\beta[X])$ becomes dominant in Eq. 2. Since the term $(1+\beta(2)[X])/(1+\beta(3)[X])$ is less than unity, the value of D_3/D_2 will become smaller than unity from a certain concentration of K_2SO_4 solution, resulting in the reversed elution order.

For the elution of the phen complex pair, we have to consider a reverse situation. Since the phen complex has no N–H bonds for hydrogen bonding and its size is large, it is poorly hydrated and is known to be a typical hydrophobic ion.[4] Such a hydrophobic cation has a big tendency toward association with a hydrophobic anion or a water-structure-breaking anion. Thus, the ion-association takes place to a considerable extent with Br^- ion, resulting in the inversion of the elution order from a certain concentration of KBr solution. On the other hand, there is little tendency toward association between a hydrophobic cation and a hydrophilic anion.[5] So, for the phen complex pair eluted with K_2SO_4 solution, the value of D_3/D_2 does not become smaller than unity, that is, the inversion of the elution order does not take place.

References

1) H. Yoneda and S. Yamazaki, *Bull. Chem. Soc. Jpn.*, **52**, 1859 (1979).

2) Actually, Searle reported the examples of the elution order variation with the change of the eluent anions for some cobalt(III) complexes of different charges. See, G. H. Searle, *Aust. J. Chem.*, **30**, 2625 (1977).

3) H. Waki, "Chelate Kagaku," Nankodo (1975), Vol. 6, Chap. 5-2.

4) K. Miyoshi, T. Taura, C. Shimada, and H. Yoneda, *Bull. Chem. Soc. Jpn.*, **48**, 1783 (1975); K. Miyoshi, C. Shimada, and H. Yoneda, *ibid.*, **48**, 3403 (1975), and references cited therein.

5) H. Yoneda, M. Muto, T. Baba, and T. Miura, *Bull. Chem. Soc. Jpn.*, **44**, 689 (1971).

Liquid Phase Peptide Synthesis by Fragment Condensation on Soluble Polymer Support. IV.[1] Relative Reactivities of *N-t*-Butoxycarbonyl-(Boc)amino Acids and Boc-Oligopeptide Acids in Their Esterification with Soluble Chloromethylated Polystyrene

Mitsuaki NARITA,* Kazuya KUSANO, Masanori HIRATA, and Makoto OKAWARA**

Department of Industrial Chemistry, Tokyo University of Agriculture and Technology, Nakamachi, Koganei, Tokyo 184
***Research Laboratory of Resources Utilization, Tokyo Institute of Technology, Nagatsuda, Midori-ku, Yokohama 227*

(Received September 14, 1979)

Synopsis. Relative reactivities of *N-t*-butoxycarbonyl-(Boc)amino acids (Gly, Val, Ile, Leu, Tyr, and Phe) and Boc-oligopeptide acids having various numbers of amino acid residues (n=2, 4, 5, 8, and 10) were determined by competitive esterification in reaction with chloromethylated polystyrene. Increase of peptide-chain lengths reduced reactivity of *C*-terminal carboxylates.

In peptide synthesis on a polymer support, the first step involves an attachment of the *C*-terminal of *N*-protected amino acid to the polymer support *via* a benzyl ester linkage.[2] Studies have been reported on the improvement of this first step in the solid phase peptide synthesis by stepwise elongation.[3-6] However, only a few studies have been made on the esterification step in peptide synthesis by fragment condensation on a polymer support.[6,7] In this paper, we report relative reactivities of Boc-amino acids in the esterification with soluble chloromethylated polystyrene and the influence of peptide-chain lengths of Boc-oligopeptide acids on the reactivity of their *C*-terminal amino acids in the esterification.

Taking advantage of polymer reaction, relative reactivities of Boc-amino acids (Gly, Val, Ile, Leu, Tyr, and Phe)[8] in their esterification with the polymer were determined by competitive esterification with use of amino acid ratios in the acid hydrolysate of the resulting resin (Table 1). We used the recovery of Gly as a standard with the intention of estimating roughly the influence of the *C*-terminal amino acid residue on the esterification. Four methods of esterification were used to obtain information on which differences in reactivity can be compensated: (1) use of potassium carbonate as a base, (2) use of potassium carbonate and 18-crown-6 as a base and catalyst, respectively,[3] (3) use of potassium fluoride as a catalyst,[4] and (4) use of potassium fluoride and 18-crown-6 as catalysts. Reactions proceeded heterogeneously in (1) and (3) and homogeneously in(2) and (4). Relative reactivities of Boc-amino acids in (1) and (3) (heterogeneous reactions) were in line with those in (2) and (4) (homogeneous reactions), respectively. In each case, Boc-amino acids having β-branched substituents (Val and Ile) and a more hydrophobic substituent (Phe) showed higher reactivity.

In order to understand the influence of the peptide-chain lengths of Boc-oligopeptide acids on the reactivity of their *C*-terminal amino acids in esterification, relative reactivities of Boc-oligopeptide acids having various numbers of amino acid residues (n=2, 4, 5, 8, and 10) and the same *C*-terminal amino acid were determined by competitive esterification using Boc-amino acid (Val or Ile) as a reference. The competitive reactions were carried out for the following.

Series A: Boc–Phe–OH (n=1), Boc–Gly–Phe–OH (n=2), Boc–Tyr–Gly_2–Phe–OH (n=4), and Boc–[Tyr(Bzl)–Gly_2–Phe]$_2$–OH (n=8)

Series B: Boc–Leu–OH (n=1), Boc–Leu_2–OH (n=2), Boc–Ala_2–Leu_3–OH[1] (n=5), and Boc–Ala_2–Leu_3–Pro_2–Leu_3–OH[1] (n=10)

Boc-oligopeptide acids of series A and B have Phe and Leu as the *C*-terminal amino acids, respectively.

Methods (1), (2), and (3) were used to estimate the effect of different reactive species on esterification. Relative reactivities of Boc-peptide acids were determined using the ratios of the carboxyl components in the resulting peptide resins taking the recovery of Val or Ile as a standard. The results are shown in Figs. 1 and 2. Total yields in the competitive esterification of the polymer with Boc-peptide acid and Boc-amino acid were 72—95%. In series A, each method showed

TABLE 1. AMINO ACID ANALYSES OF RESINS ESTERIFIED WITH BOC-AMINO ACIDS BY COMPETITIVE REACTIONS AND RELATIVE REACTIVITIES OF BOC-AMINO ACIDS

Esterification method (reaction time, h)	Amino acid content (μmol/g-resin)						Relative reactivities (Gly=1.00)				
	Gly	Val	Ile	Leu	Tyr[a]	Phe	Val	Ile	Leu	Tyr	Phe
K_2CO_3(3)	25	45	45	35	37	44	1.80	1.80	1.40	1.48	1.76
K_2CO_3(70)	72	138	136	103	100	120	1.92	1.89	1.44	1.39	1.67
K_2CO_3+18-crown-6 (1)	46	76	73	62	49	56	1.65	1.59	1.35	1.07	1.22
K_2CO_3+18-crown-6(24)	88	150	142	121	95	114	1.70	1.61	1.37	1.08	1.30
KF (7)	16	23	21	18	20	26	1.44	1.31	1.13	1.25	1.63
KF (70)	72	114	113	80	107	133	1.58	1.60	1.11	1.49	1.85
KF+18-crown-6 (70)	77	109	111	81	110	117	1.42	1.44	1.05	1.42	1.52

a) Tyr decomposes gradually by acid hydrolysis to give low recovery (90—95%) of Tyr. *Cf.* K. Watanabe and K. Inouye, *Bull. Chem. Soc. Jpn.*, **50**, 201 (1977).

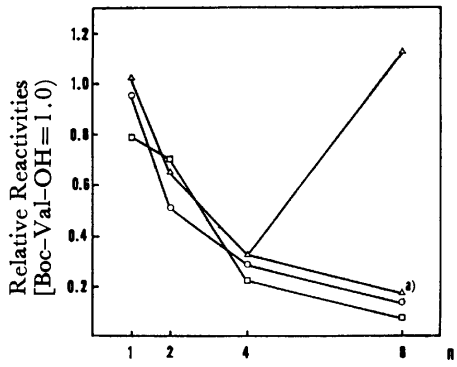

Fig. 1. The influence of the peptide-chain lengths of Boc-oligopeptide acids of series A on the estrification reaction with the chloromethylated polystyrene (Boc-Val-OH was used as a reference for the competitive reactions).
$n=1$, Boc-Phe-OH; $n=2$, Boc-Gly-Phe-OH; $n=4$, Boc-Tyr-Gly_2-Phe-OH; $n=8$, Boc-[Tyr(Bzl)-Gly_2-Phe]$_2$-OH. —○—, K_2CO_3; —□—, K_2CO_3+18-crown-6; —△—, KF; a) KF+18-crown-6.

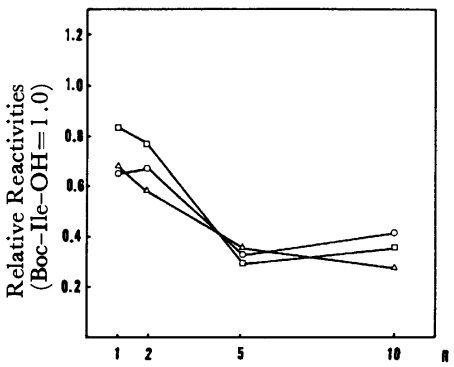

Fig. 2. The influence of the peptide-chain lengths of Boc-oligopeptide acids of series B on the esterification reaction with the chloromethylated polystrene (Boc-Ile-OH was used as a reference for the competitive reactions).
$n=1$, Boc-Leu-OH; $n=2$, Boc-Leu_2-OH; $n=5$, Boc-Ala_2-Leu_3-OH; $n=10$, Boc-Ala_2-Leu_3-Pro_2-Leu_3-OH. —○—, K_2CO_3; —□—, K_2CO_3+18-crown-6; —△—, KF.

the peptide-chain lengths of Boc-peptide acids to decrease the reactivities of their *C*-terminal carboxylates with increase in the number of amino acid residues. In series B, a similar tendency was observed except for Boc-Ala_2-Leu_3-Pro_2-Leu_3-OH, whose secondary structure was estimated to be random coil by the method of Chou and Fasman.[9] That of other Boc-peptide acids ($n=4$, 5, and 8) might be in β-sheet structure.[1] As shown in Fig. 1, an abnormal behavior was observed in the competitive reaction of Boc-Val-OH and Boc-[Tyr(Bzl)-Gly_2-Phe]$_2$-OH with the chloromethylated polystyrene using KF as a catalyst; the amount of Val incorporated was lower (total yield of Boc-Val-OH and Boc-octapeptide, 13.1%) and relative reactivity of Boc-[Tyr(Bzl)-Gly_2-Phe]$_2$-OH higher. Addition of 18-crown-6 to the reaction mixture made the reaction system homogeneous, a similar behavior being observed with methods (1) and (2) (Fig. 1).

Experimental

Relative Reactivities of Boc-amino Acids in Esterification with the Chloromethylated Polystyrene (General Method). Starting with chloromethylated polystyrene (1.00 g; chloromethyl content, 0.89 mmol/g),[10] three-fold equivalents (2.67 mmol) each of Boc-amino acids (Gly, Val, Ile, Leu, Tyr, and Phe) and an equivalent amount of potassium carbonate (8.34 mmol) with the total of the acids were added to 80 ml of DMF. The mixture was allowed to equilibrate at 40 °C in a thermostatted bath (*ca.* 30 min with magnetic stirring), followed by addition of the polymer (1.00 g) and left at 40 °C with stirring. As base and/or catalyst the following compounds were used. Method (2), an equivalent each of potassium carbonate (8.00 mmol) and 18-crown-6 (16.0 mmol). Method (3), an equivalent of anhydrous KF (16.0 mmol). Method (4), an equivalent each of anhydrous KF (16.0 mmol) and 18-crown-6 (16.0 mmol). Portions of the reaction mixture were poured into water at the reaction time given in Table 1. The precipitated resin was filtered off, washed successively with water and methanol in order to remove soluble reactants, and dried *in vacuo* at 50 °C. The resulting resin was subjected to acid hydrolysis with propionic acid–12 M HCl (2 : 1 v/v) for 72 h at 115 °C followed by amino acid analysis.

Relative Reactivities of Boc-oligopeptide Acids in Esterification with the Chloromethylated Polystyrene Using Boc-amino Acid (Val or Ile) as a Reference (General Method). The chloromethylated polystyrene (1.00 g; chloromethyl content, 0.89 mmol/g) was reacted with three equivalents (2.67 mmol) each of Boc-oligopeptide acid and Boc-amino acid in 25 ml of DMF at 40 °C. The reaction times in methods (1), (2), and (3) were 45 h, 24 h, and 45 h, respectively. The work-up was the same as that mentioned above.

References

1) Part III of this series: M. Narita, S. Itsuno, M. Hirata, and K. Kusano, *Bull. Chem. Soc. Jpn.*, **53**, 1028 (1980).
2) R. B. Merrifield, *J. Am. Chem. Soc.*, **85**, 2149 (1963).
3) R. W. Roeske and P. D. Gesellchen, *Tetrahedron Lett.*, **1976**, 3369 and references cited therein.
4) K. Horiki, K. Igano, and K. Inouye, *Chem. Lett.*, **1978**, 165.
5) S. Sakakibara, "Tanpakushithu No Kagaku IV," ed by K. Narita and T. Murachi, Tokyo Kagaku Dojin, Tokyo (1977), Vol. I, p. 420.
6) N. Izumiya, T. Kato, M. Ohno, and H. Aoyagi, "Pepuchido Gosei," Maruzen, Tokyo (1975), p. 181.
7) H. Yajima and H. Kawatani, *Chem. Pharm. Bull.*, **19**, 1905 (1971).
8) Abbreviations for amino acids and protecting groups are those recommended by the IUPAC-IUB Commission on Biochemical Nomenclature, *J. Biol. Chem.*, **247**, 977 (1972). Amino acid symbols denote the L-configuration except for Gly. Additional abbreviations: DMF, *N,N*-dimethylformamide.
9) a) P. Y. Chou and G. D. Fasman, *Biochemistry*, **13**, 211 (1974); b) P. Y. Chou and G. D. Fasman, *ibid.*, **13**, 222 (1974).
10) M. Narita, *Bull. Chem. Soc. Jpn.*, **51**, 1477 (1978).

Formation of Ketone Diperoxides from Ozonation of *O*-Methyloximes

Yoshikatsu Ito,* Hiroaki Yokoya, Yasutoshi Umehara, and Teruo Matsuura

Department of Synthetic Chemistry, Faculty of Engineering, Kyoto University, Kyoto 606

(Received February 8, 1980)

Synopsis. The ozonation of the *O*-methyloximes has been investigated. Besides the corresponding ketones, ketone diperoxides, and *N*-methoxyamides were produced. The stereochemistry of the ketone diperoxides was studied by the NMR technique.

In our previous paper,[1] it has been shown that the ozonation of valerophenone *O*-methyloxime (**1c**) in carbon tetrachloride at −20 °C gives as the major products valerophenone diperoxide (**2c**) and *N*-methoxyamides **4c** and **5c**, in addition to the corresponding ketone **3c**. Erickson *et al.*, however, reported[2] that the ozonation of acetophenone *O*-methyloxime (**1a**) in dichloromethane at −78 °C led to only the carbon–nitrogen double bond cleavage affording the corresponding ketone **3a**. This and our interest in a chemi-energized process occurring from **2c**[3] led us to study the ozonation of *O*-methyloximes in more detail.

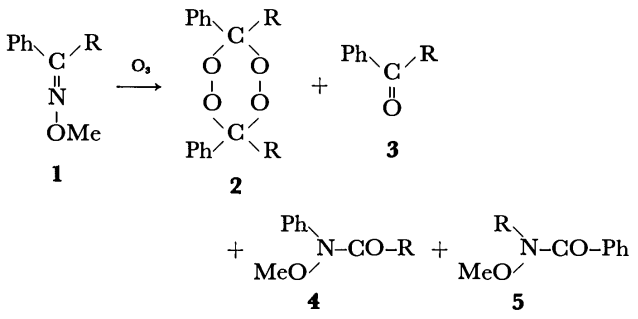

a: R=Me, **b**: R=Et, **c**: R=*n*-Bu, **d**: R=*t*-Bu

Scheme 1.

Table 1 shows the results of the ozonation of *O*-methyloximes **1a**—**d** in carbon tetrachloride or dichloromethane at low temperatures. In addition to the corresponding ketones **3a**—**d**, the ketone diperoxides **2a**—**c** and *N*-methoxyamides **4a**—**c** and **5a**—**d** were isolated, as we found previously.[1] In the case of **1d**, however, many by-products were also formed and only benzoic acid was characterizable.

The ketone diperoxides **2b** and **2c** were formed as a mixture of *cis* (**2b**-*c* and **2c**-*c*) and *trans* (**2b**-*t* and **2c**-*t*) isomers, while **2a** was obtained as a single isomer.[4] The yields of the *cis* and *trans* isomers were almost

a) *cis*-Valerophenone diperoxide (**2c**-*c*)

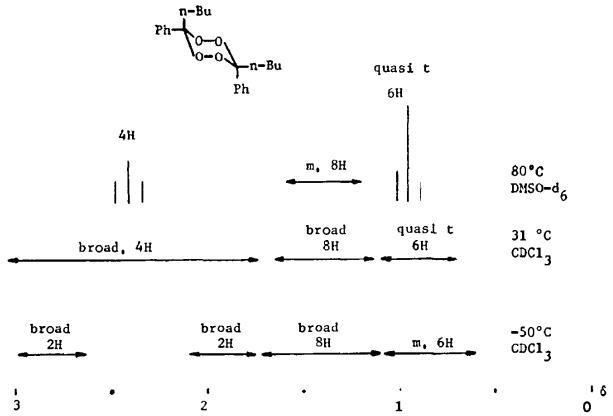

b) *cis*-Propiophenone diperoxide (**2b**-*c*)

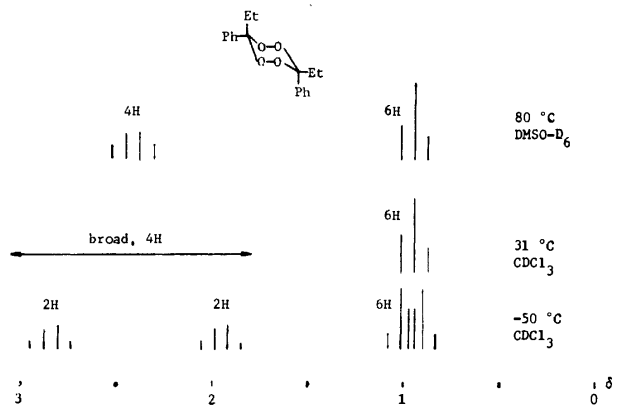

Fig. 1. NMR spectra (100 MHz) of *cis*-propiophenone diperoxide (**2b**-*c*) and *cis*-valerophenone diperoxide (**2c**-*c*) at different temperatures.

equal, *i.e.* **2b**-*t*/**2b**-*c*=1 and **2c**-*t*/**2c**-*c*=1.2. From their NMR spectra at a number of temperatures the higher melting isomers were assigned to be *trans* and the lower melting isomers to be *cis*. Similarly, the stereochemistry of acetophenone diperoxide (**2a**) was assigned to be *trans*.

The chair-to-chair conformational isomerism of acetone diperoxide was studied by Murray and coworkers by the NMR technique.[5] The NMR spectra

Table 1. The ozonation of *O*-methyl oximes **1** at low temperature

O-Methyloxime **1** (M×10²)	Solvent	O_3 passed (equiv)	Product (% yield)			
			2	**3**	**4**	**5**
1a (6.7)	CCl_4[a]	6.3	6	39	16	9
1a (8.0)	CH_2Cl_2[b]	57	10	43	11	8
1b (24.0)	CCl_4[a]	6.5	13[d]	51	11	10
1c (5.5)	CCl_4[a]	27	20[d]	34	13	16
1d (23.0)	CCl_4[c]	5.6	0	6	0	10[e]

a) At −20 °C. b) At −78 °C. c) At 0 °C. d) A combined yield of the *cis* and *trans* isomers. e) $PhCO_2H$ (15%) as a by-product.

of the *cis* isomers **2b**-*c* and **2c**-*c* (Fig. 1) indicated that they also underwent the conformational isomerization at room temperature and that the isomerization process was slowed down at low temperature (−50 °C) to the point where the chemical shifts of the axial and equatorial methylene groups can be discerned (Fig. 1. δ: **2b**-c_{eq} 2.85; **2b**-c_{ax} 1.96; **2c**-c_{eq} 2.78; **2c**-c_{ax} 1.92). According to Murray *et al.*,[5] the equatorial methylene group should be more deshielded (larger δ values). At 80 °C the peaks of the axial and equatorial methylene groups completely coalesced due to the rapid conformational isomerization (Fig. 1. δ: **2b**-*c* 2.42; **2c**-*c* 2.41). The *trans* isomers **2a**, **2b**-*t*, and **2c**-*t* showed essentially no dependency of their NMR spectra on temperatures between −50 °C and 140 °C, indicating that each of these *trans* isomers has a rigid conformation, as was found with other *trans* ketone diperoxides.[6] The alkyl substituents of the *trans* peroxides **2b**-*t* and **2c**-*t* can be regarded to be axial on the basis of the small δ values of the methylene groups adjacent to the tetroxane rings (δ: **2b**-*t* 1.62; **2c**-*t* 1.56).

The present reaction would be a convenient method for the preparation of ketone diperoxides which are not easily accessible. For example, we failed to prepare **2c** by the usual procedures for the synthesis of ketone diperoxides,[7] *i.e.*, from ozonolysis of 5,6-diphenyl-5-decene or from the reaction of valerophenone with hydrogen peroxide in the presence of sulfuric acid. As we have suggested previously,[1] a carbonyl oxide **6** seems to be a precursor of the ketone diperoxides **2**. In fact, when the ozonation of **1c** was carried out in the presence of excess acetaldehyde, the formation of **2c** was completely suppressed.[8] An oxaziridine **7** is the most probable intermediate of the *N*-methoxyamides **4** and **5**. Bailey *et al.* isolated the corresponding oxaziridine from the ozonation of *N*-benzylidene-*t*-butylamine in dichloromethane.[9]

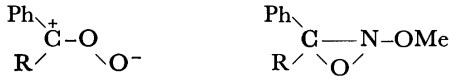

6 **7**

Experimental

O-Methyloximes **1a—d** were prepared from the corresponding ketones and *O*-methylhydroxylamine hydrochloride according to the method of Karabatsos and Hsi.[10] Pivalophenone *O*-methyloxime (**1d**) was obtained as colorless crystals from ethanol, mp 64—66 °C. NMR ($CDCl_3$) δ 1.16 (9 H, s, *t*-Bu), 3.69 (3H, s, OCH_3), 6.8—7.6 (5H, m, ArH). IR (nujol) 1480, 1070, 880 cm^{-1}. MS *m/e* 191 (M^+, relative intensity 19), 175 (9), 160 (25), 104 (100), 77 (28), 57 (69), Found: C, 75.53; H, 9.13; N, 7.05%. Calcd for $C_{12}H_{17}NO$: C, 75.35; H, 8.96; N, 7.32%.

The ozonation and isolation procedures with **1c** were described previously.[1] Similar procedures were followed with **1a** (concentration 1.5 g/150 ml of CCl_4, ozonation time 2 h), **1b** (1.6 g/40 ml of CCl_4, 2 h), and **1d** (5.0 g/120 ml of CCl_4, 2 h). The physical and spectral properties of new substances are summarized below. The NMR and IR spectra of **2a**[11] and **5a**[12] were identical with those of the authentic sample.

4a. A colorless oil, bp 44.0—45.5 °C/0.1 mmHg. NMR ($CDCl_3$) δ 2.25 (3H, s, CH_3–CO), 3.66 (3H, s, CH_3O), 7.0—7.55 (5H, m, ArH). IR (neat) 1680 cm^{-1}. MS *m/e* 165 (M^+, 12), 122 (100), 77 (64), 43 (75). Found: C, 65.20; H, 6.70; N, 8.21%. Calcd for $C_9H_{11}NO_2$: C, 65.44; H, 6.71; N, 8.48%.

2b-*t*. Colorless crystals from acetone, mp 136.5—138 °C. NMR ($CDCl_3$ at 31 °C) δ 0.55 (6H, t, J=7 Hz, CH_3) 1.62 (4H, q, J=7 Hz, CH_2), 7.24—7.72 (10 H, m, ArH). The similar NMR spectra were obtained at −50 °C ($CDCl_3$), 80 °C (DMSO-d_6), and 140 °C (DMSO-d_6).

2b-*c*. A colorless viscous oil which resisted to crystallization. NMR ($CDCl_3$ at −50 °C) δ 0.91 (3H, t, J=7 Hz, CH_3), 1.01 (3H, t, J=7 Hz, CH_3), 1.96 (2H, q, J=7 Hz, CH_2), 2.85 (2H, q, J=7 Hz, CH_2), 7.02—7.90 (10H, m, ArH). ($CDCl_3$ at 31 °C) δ 0.94 (6H, t, J=7 Hz, CH_3), 1.8—3.1 (4H, broad, CH_2), 7.27 (10H, broad s, ArH). (DMSO-d_6 at 80 °C) δ 0.94 (6H, t, J=7.5 Hz, CH_3), 2.42 (4H, q, J=7.5 Hz, CH_2), 7.40 (10H, s, ArH).

4b. A colorless oil, bp 51—52 °C/0.1 mmHg. IR (neat) 1675 cm^{-1}. NMR ($CDCl_3$) δ 1.10 (3H, t, J=7 Hz, $C\underline{H}_3CH_2$), 2.58 (2H, q, J=7 Hz, $CH_3C\underline{H}_2$), 3.70 (3H, s, CH_3O), 7.0—8.1 (5H, m, ArH). MS *m/e* 179 (M^+, 6), 57 (100). Found: C, 67.23; H, 7.52; N, 7.85%. Calcd for $C_{10}H_{13}NO_2$: C, 67.02; H, 7.31; N, 7.82%.

5b. A colorless oil, bp 49—51 °C/0.1 mmHg. IR (neat) 1640 cm^{-1}. NMR ($CDCl_3$) δ 1.28 (3H, t, J=7 Hz, $C\underline{H}_3CH_2$), 3.51 (3H, s, CH_3O), 3.72 (2H, q, J=7 Hz, $C\underline{H}_2$), 7.0—7.7 (5H, m, ArH). MS *m/e* 179 (M^+, 7), 105 (100), 77 (100). Found: C. 66.89; H, 7.52; N, 7.80%. Calcd for $C_{10}H_{13}NO_2$: C, 67.02; H, 7.31; N, 7.82%.

5d. A colorless oil, bp 83—84 °C/0.1 mmHg. IR (neat) 1645 cm^{-1}. NMR ($CDCl_3$) δ 1.55 (9H, s, *t*-Bu), 3.35 (3H, s, CH_3O), 7.2—8.2 (5H, m, ArH). MS *m/e* 207 (M^+, 4), 105 (100), 77 (32), 57 (16). Found: C, 69.31; H, 8.29; N, 6.60%. Calcd for $C_{12}H_{17}NO_2$: C, 69.54; H, 8.27; N, 6.76%.

The physical and spectral properities of **2c**-*t*, **2c**-*c*, **4c**, and **5c** were reported Previously.[1] The temperature dependences of the NMR spectra of the *cis*-diperoxide **2c—c** and the *trans*-diperoxides **2c**-*t* and **2a** were analogous to those of **2b**-*c* and **2b**-*t*, respectively.

References

1) Y. Ito, M. Konishi, and T, Matsuura, *Photochem. Photobiol.*, **30**, 53 (1979).

2) R. E. Erickson, P. J. Andrulis, Jr., J. C. Collins, M. L. Lungle, and G. D. Mercer, *J. Org. Chem.*, **34**, 2961 (1969).

3) Y. Ito, T. Matsuura, and H. Yokoya, *J. Am. Chem. Soc.*, **101**, 4010 (1979).

4) The stereoselective formation of **2a** is probably due to the less bulkiness of the methyl group.

5) R. W. Murray, P. R. Story, and M. L. Kaplan, *J. Am. Chem. Soc.*, **88**, 526 (1966).

6) M. Schulz and K. Kirschke, "Organic Peroxides," ed by D. Swern, Wiley, New York (1972), Vol. 3, p. 73.

7) M. Schulz and K. Kirschke, *Adv. Heterocycl. Chem.*, **8**, 165 (1967).

8) For the reaction and generation of a carbonyl oxide, see P. S. Bailey, "Ozonation in Organic Chemistry," Academic Press, New York (1978).

9) A. H. Riebel, R. E. Erickson, C. J. Abshire, and P. S. Bailey, *J. Am. Chem. Soc.*, **82**,1801 (1960).

10) G. J. Karabatsos and N. Hsi, *Tetrahedron*, **23**, 1079 (1967).

11) W. Dilthey, M. Inkel, and H. Stephan, *J. Prakt. Chem.*, **154**, 219 (1940).

12) P. M. Beart and A. D. Ward, *Aust. J. Chem.*, **27**, 1341 (1974).

Oxidation of Thujopsene with Lead Tetraacetate

Katsumi Yokoi* and Yoshiharu Matsubara

Department of Applied Chemistry, Faculty of Science and Technology, Kinki University, Kowakae, Higashiosaka 577

(Received September 20, 1979)

Synopsis. We inveatigated the oxidation of thujopsene with lead tetraacetate. In the hydrolysis product, two new sesquiterpenoids were found to be afforded: 6α,10,10-trimethyl-4β-acetyltricyclo[4.4.0.0^{1,3}]decane and its $C_{(4)}$-stereoisomer.

It has been reported by Nagahama *et al.*[1] that the lead tetraacetate oxidation of **1** was accompanied by ring contraction; this was a new reaction. However, the structures of the oxidation product were not well-defined. In the course of our investigation of the oxidation, therefore, we have now isolated the components of the oxidation product and defined their structures well on the basis of the MS, IR, and NMR spectra.

Results and Discussion

The reaction was carried out by adding minium trilead tetraoxide to a mixture of thujopsene, **1**, acetic acid, and acetic anhydride. The reaction product was hydrolyzed to give three components (**2**: **3**: **4**=6: 87: 7 in GLC). The hydrolysis product was fractionated by distillation under reduced pressure, and each component was isolated by GLC. Their products are shown in Fig. 1. Compound **4** was identified with authentic widdrol on the basis of the MS, IR, and NMR spectra.

Compound **2** was determined to have a molecular formula of $C_{15}H_{24}O$ on the basis of the MS spectra and the results of the elemental analysis, and it was characterized as a saturated ketone on the basis of the IR (C=O, 1700 cm^{-1}) absorption band. The ^{1}H-NMR spectra revealed the presence of the following functional groups: a *gem*-dimethyl (6H, two s), a tertiary methyl (3H, s), an acetyl (3H, s), a methine (1H, dd), and a methylene of a cyclopropane ring (2H, m). The ketone

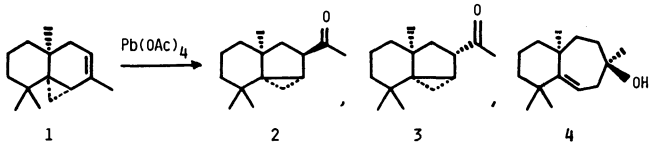

Fig. 1. Oxidation products of thujopsene **1**.

was deduced to be 6α,10,10-trimethyl-4-acethyltricyclo-[4.4.0.0^{1,3}]decane.

Compound **3** was determined to have a molecular formula of $C_{15}H_{24}O$ on the basis of the MS spectra and the results of the elemental analysis; it was characterized on the basis of the close resemblance to most of the fragment ions of the MS spectrum of **2**. Also the ^{1}H-NMR spectra revealed the presence of the same functional groups as **2**. These findness supported the idea that **3** was the $C_{(4)}$stereoisomer of **2**.

In order to define each configuration of the acetyl group and the $C_{(2)}$-methylene of **2** and **3**, the coupling constant of $C_{(4)}$-methine, the variation in the chemical shift of each proton with an increase in the concentration of the shift reagent (Eu(dpm)$_3$: Tris(dipivaloylmethanato)europium(III)), and the NOE were measured in the ^{1}H-NMR spectra (Table 1). As a result, the $C_{(4)}$-methine of **2** revealed double doublet (J=2.5 Hz, 10 Hz), while the $C_{(4)}$-methine of **3** revealed a double quartet (ddd, J=5 Hz, 8.5 Hz, 10 Hz). The chemical shift of the $C_{(10\alpha)}$-methyl of **3** was enlarged further in comparison with those of **2** with an increase in the concentration of Eu(dpm)$_3$. Besides the NOE was observed on **3**, because, when the $C_{(2)syn}$-proton of **3** at 0.33 was irradiated, the integration of the acetyl proton of **3** at δ 2.19 was increased (44% of NOE), while the $C_{(6\alpha)}$-methyl of **3** at δ 1.09 was enlarged (42% of NOE). This behavior showed their structures

Table 1. Variation in the chemical shift for different protons of (**2**) and (**3**) (1×10^{-4} mol in 0.5 ml of $CDCl_3$) with an increase in Eu(dpm)$_3$

Eu(dpm)$_3$ 10^{-4} mol	δ ppm(ΔEu(dpm)$_3$[a])							
	2				**3**			
	$COCH_3$	$C_{(6\alpha)}$–CH_3	$C_{(10\beta)}$–CH_3	$C_{(10\alpha)}$–CH_3	$COCH_3$	$C_{(6\alpha)}$–CH_3	$C_{(10\beta)}$–CH_3	$C_{(10\alpha)}$–CH_3
0	2.18	1.07	0.63	1.00	2.19	1.09	0.60	1.01
0.1	2.49 (0.31)	1.12 (0.05)	0.66 (0.03)	1.03 (0.03)	2.58 (0.39)	1.15 (0.06)	0.65 (0.05)	1.06 (0.05)
0.2	3.10 (0.92)	1.19 (0.12)	0.76 (0.13)	1.06 (0.06)	3.32 (1.13)	1.27 (0.18)	0.78 (0.18)	1.14 (0.13)
0.3	4.02 (1.84)	1.35 (0.28)	0.90 (0.27)	1.10 (0.10)	4.27 (2.08)	1.38 (0.29)	0.88 (0.28)	1.22 (0.21)
0.4	4.90 (2.72)	1.44 (0.37)	1.02 (0.39)	1.18 (0.18)	5.14 (2.95)	1.52 (0.43)	1.00 (0.40)	1.31 (0.30)
0.5	5.80 (3.62)	1.61 (0.54)	1.14 (0.51)	1.29 (0.29)	6.12 (3.93)	1.68 (0.59)	1.16 (0.56)	1.43 (0.42)

a) Δ Eu(dpm)$_3$=δ Eu(dpm)$_3$−δ $CDCl_3$.

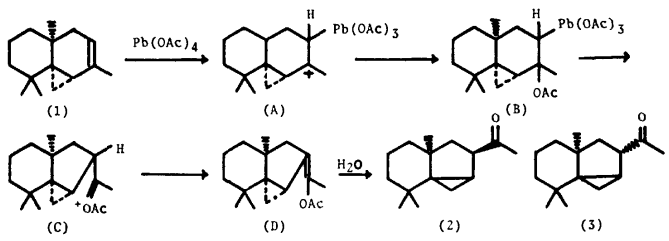

Fig. 2. Mechanism for the formation of **2** and **3**.

to be 6α,10,10-trimethyl-4-acetyltricyclo[4.4.0.0^{1,3}]-decane **2** and its $C_{(4)}$-stereoisomer, **3**.

In the reaction, the formation of the products, **2** and **3**, could be explained by the reaction sequence shown in Fig. 2: firstly, the addition of lead tetraacetate to the olefin of **1** may give an intermediate (**B**); the degration of **B** will give an enol acetate (**D**) (it was difficult to isolate **D**), accompanied by ring-contraction. The resulting stereoisomers (**2** and **3**) may be formed by the hydrolysis of **D**.

Experimental

Materials. Thujopsene, **1**, was obtained by distillation from chinese cedar wood oil (provided by the Takasago Perfumary Co., Ltd.); bp 118—120 °C/10 Torr, $d_4^{25}=0.9316$, $n_D^{25}=1.5019$, $[\alpha]_D^{29}=-77.4°$ (neat), purity in GLC 99%.

Measurements. The MS spectra were measured on a Shimadzu LKB 9000 gas chromatography mass spectrometer (acceleration voltage, 3500V; ionization potential 70 eV). The IR spectra were recorded on a Nihonbunko IRA-2 apparatus (Diffraction Grating Infrared Spectrophotometer). The ^{1}H-NMR spectra were recorded on a Hitachi Parkin-Elmer R-24 (60 MHz) spectrometer, using TMS as the internal standard, unless otherwise mentioned, in $CDCl_3$. The column chromatography depended on silica gel (Wako-gel C-300). The GLC was carried out with a separation column (3 mm×4 m) packed with 5% PEG-20M or 5% OV-17 on Chromosorb AW-DMCS (60—80 mesh).

Reaction of Thujopsene (1) with Lead Tetraacetate. To a mixture of 5 g (0.025 mol) of **1**, 48 g of acetic acid, and 17 g of acetic anhydride, we added 17.2 g of minium trilead tetra oxide in portions over a period of 1.5 h, the temperature being kept below 60 °C. Stirring was then continued for one additional hour. Water was added, and the solution was neutralized with sodium carbonate, filtered, and extracted with benzene. This benzene solution was washed with water again and dried over sodium sulfate. When the solvent was then removed, 6.4 g of a residue were obtained. $n_D^{25}=1.4941$, $d_4^{25}=0.9838$, $EV=10.6$, $[\alpha]_D^{25}=-0.07°$ (neat), The residue (3.5 g) was hydrolyzed with a 2 mol dm^{-3} sodium hydroxide–ethanol solution. After the ethanol had been removed, water and benzene were added with shaking and the organic layer was separated. This organic layer was washed and dried over sodium sulfate. The benzene was then removed; subsequent distillation gave 3.1 g of products which had three components (**2**: **3**: **4**=6: 87: 7). Bp 134—139 °C/2 Torr, $n_D^{25}=1.4975$, $d_4^{25}=0.9836$, $[\alpha]_D^{25}=-0.05°$(neat). Semicarbazone: mp 236—237 °C (dec, from 90% ethanol). A ketone regenerated from the semicarbazone had two components (**2**: **3**=2: 98) in GLC.

6α,10,10-Trimethyl-4β-acetyltricyclo[4.4.0.0^{1,3}]decane (2). Found: C, 81.59; H, 11.05%. Calcd for $C_{15}H_{24}O$: C, 81.76; H, 10.98%. MS(*m/e*) 220 (M^+, 62%), 205 ($M-CH_3$, 42), 177 ($M-COCH_3$, 100), 161 (39), 137 (83), 123 (84), 121 (87), 107 (72), 105 (56), 95 (72), 91 (56), 81 (50). IR ν(cm^{-1}) 3400, 1700 (C=O), 3050, 1020 (cyclopropane ring), 1380, 1368 (*gem*-CH_3). NMR ($CDCl_3$) δ (ppm) 0.17—0.80 (2H, m), 0.63, 1.00, 1.07 (9H, each s, *t*-CH_3), 2.18 (3H, s, $-COCH_3$), 2.63 (1H, dd, J=2.5 Hz, 10 Hz, –COCH).

6α,10,10-Trimethyl-4α-acetyltricyclo[4.4.0.0^{1,3}]decane (3). Found: C, 81.63; H, 11.01%, Calcd for $C_{15}H_{24}O$: C, 81.76; H, 10.98%. $d_4^{25}=0.9773$, $n_D^{25}=1.4918$. MS (*m/e*) 220 (M^+, 27%), 205 ($M-CH_3$, 27), 177 ($M-COCH_3$, 100), 161 (19), 137 (26), 123 (46), 121 (50), 107 (58), 105 (29), 95 (62), 93 (34), 91 (30), 81 (50), 69 (31). IR ν(cm^{-1}) 3400, 1700 (C=O), 3050, 1020 (cyclopropane ring), 1378, 1366 (*gem*-CH_3). NMR ($CDCl_3$) δ (ppm) 0.33 (1H, s, $C_{(2)syn}$–H), 0.44 (1H, br. s, $C_{(2)anti}$–H), 0.58, 1.00, 1.08 (9H, each s, *t*-CH_3), 2.17 (3H, s, $-COCH_3$), 3.05 (1H, ddd, 5 Hz, 8.5 Hz, 10 Hz, –COCH).

Widdrol (4). Mp 97.5—98 °C (colorless needle, from hexane). MS (*m/e*) 222 (M^+, 14%), 204 ($M-H_2O-CH_3$, 22), 151 (100), 121 (38), 119 (51), 93 (44). IR ν(cm^{-1}) 3350, 1100 (OH), 1382, 1368 (*gem*-CH_3). NMR ($CDCl_3$) δ (ppm) 1.08 (6H, s, $C(CH_3)_2$), 1.18 (3H, s, *t*-CH_3), 1.20 (3H, s, $C(OH)CH_3$), 1.42 (1H, s, OH), 5.48 (1H, m, =CH–).

Reference

1) S. Nagahama, H. Kobayashi, and S. Akiyoshi, *Bull. Chem. Soc. Jpn.*, **32**, 366 (1959).

Additivity Parameters for Anodic Peak Potentials in [2.2]Metacyclophanes and Tetrahydropyrene Formation[1]

Koichi TORIZUKA and Takeo SATO*

Department of Chemistry, Tokyo Metropolitan University, Setagaya-ku, Tokyo 158

(Received December 6, 1979)

Synopsis. The first anodic peak potentials $E_{pa}(O_1)$ for sixteen [2.2]metacyclophanes were surveyed in order to correlate the peak potential with the number and position of the alkyl groups. The analysis of the data gives the additivity parameters, which call for cathodic shifts of 0.14 and 0.035 V per methyl group for R_2 or R_5 (5- or 13-position) and for substitution at the rest of the positions respectively. The controlled-potential electrolysis of the representative metacyclophanes gave excellent yields of the corresponding tetrahydropyrenes.

The anodic oxidation of [2.2]metacyclophane and derivatives at the first anodic potential $E_{pa}(O_1)$ have previously been shown[2] to be a highly efficient and selective reaction to give the corresponding 4,5,9,10-tetrahydropyrenes. The current efficiency reached almost 100% as a two-electron process, and the selectivity was far better than the alternative photolytic method.[3] In this investigation, we surveyed the peak potentials, $E_{pa}(O_1)$, for a series of [2.2]metacyclophanes (**1a**—**1p**) to ascertain the effect of alkyl substitution on the one-electron transfer.

The preparation of **1** was carried out by the pyrolysis of disulfone, **3**, which had been obtained from disulfide, **2**. The cyclic voltammetry was determined in acetonitrile containing 0.1 mol dm^{-3} of Bu_4NClO_4(TBAP) at various scan rates. Of the three anodic peaks, the first peak was found to be sensitive to the impurity contained in acetonitrile. Accordingly, we carried out redeterminations for those compounds the data of which had been reported earlier.[2]

The data determined at 250 mV/s are shown in Table 1. The inspection of the data revealed the following facts:

Table 1. Observed and calculated peak potentials E_{pa} (O_1) for compound **1**

	R_1	R_2	R_3	R_4	R_5	R_6	$E_{pa}(O_1)$/V	Calcd/V	ΔE_{pa}/V
1a[2a]	H	H	H	H	H	H	1.37	—	
1b	H	Me	H	H	H	H	1.23	1.23	0
1c[2a]	H	Me	H	H	Me	H	1.09	1.09	0
1d[2b]	H	Et	H	H	Et	H	1.07	1.09	−0.02
1e[2b]	H	*t*-Bu	H	H	*t*-Bu	H	1.08	1.09	−0.01
1f	Me	H	Me	H	H	H	1.32	1.30	+0.02
1g	Me	H	H	Me	H	H	1.33	1.30	+0.03
1h	Me	Me	Me	H	H	H	1.20	1.16	+0.04
1i	Me	H	Me	H	Me	H	1.18	1.16	+0.02
1j[2b]	Me	H	Me	H	*t*-Bu	H	1.17	1.16	+0.01
1k	Me	Me	Me	H	Me	H	1.03	1.02	+0.01
1l	Me	H	Me	Me	H	Me	1.21	1.23	−0.02
1m	Et	H	Et	Et	H	Et	1.21	1.23	−0.02
1n	*i*-Pr	H	*i*-Pr	*i*-Pr	H	*i*-Pr	1.21	1.23	−0.02
1o	Me	Me	Me	Me	H	Me	1.09	1.09	0
1p	Me	Me	Me	Me	Me	Me	0.96	0.95	+0.01

Table 2. The scan-rate dependence of the peak potential shifts

Scan rate / mV/s	**1a**/V	**1c**/V	ΔE_{pa}/V	**1f**/V	ΔE_{pa}/V	**1i**/V	ΔE_{pa}/V
50	1.32	1.05	−0.27	1.26	−0.06	1.12	−0.20
100	1.34	1.07	−0.27	1.29	−0.05	1.16	−0.18
250	1.37	1.09	−0.28	1.33	−0.04	1.18	−0.19
500	1.40	1.11	−0.29	1.36	−0.04	1.20	−0.20

a) The introduction of a methyl group at the R_2 and/or R_5 positions causes a significant cathodic shift, amounting to −0.14 V per methyl group.

b) On the other hand, a methyl group at other positions (R_1, R_3, R_4, and R_6) causes less of a cathodic shift. The extent of the cathodic shift is normal for alkylated aromatics.[4] The shift is approximately one-fourth as large as that of R_2 or R_5, namely, −0.07 V for two methyl groups or −0.14 V for four methyl groups. The situation is similar for inner methyl derivatives, **4**, of which C-8, 16 methyl groups show cathodic shifts similar in magnitude to the above.

c) The cathodic shift is essentially similar for ethyl, isopropyl, and *t*-butyl derivatives, as with the corresponding methyl compound.

The predicted E_{pa} values for **1a**—**1p** are shown in Table 1. These were calculated by assuming incremental cathodic-shift changes caused by alkylation on **1a**. Such calculation at the scan of 250 mV/s is derived by means of:

$$E_{pa}(O_1) = 1.37 + m(-0.14) + n(-0.035)$$

where

m=the number of R_2 and R_5 alkyl groups

n=the number of alkyl groups other than R_2 and R_5.

For example, the effect of R_2 and R_5 methyl groups in compounds **1b**—**1e** is shown by a large cathodic shift, either by −0.14 or −0.28 V. By contrast, the cathodic shifts for **1f** and **1g** are smaller (−0.07 V). Compounds **1h** and **1i** are isomeric and contain both types of substitution, criterion a) and b), thus resulting in the potential shift of −0.21 V.

The anomalously large stabilization effect caused by

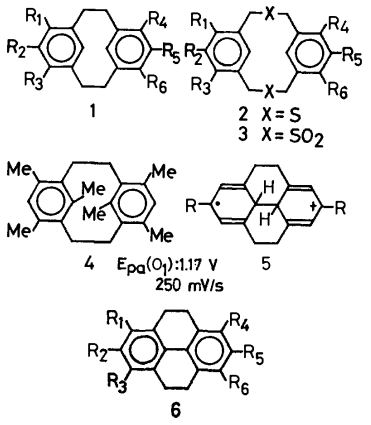

R_2 and R_5 alkyl groups is taken as an indication that the O_1 peak corresponds to the formation of the transannular cation radical, **5**, proposed earlier.[2]

The peak potentials vary with the scanning rates. Incremental changes caused by alkyl substitution were, however, found to be constant within the usual scan

TABLE 3. ANODIC OXIDATION OF 1 AND ANALYTICAL AND MELTING-POINT DATA FOR 6

Compound	Oxdn. potential V	Electricity F/mol	Product,[a] (%)	Mp °C	Formula	Calcd (%) C	Calcd (%) H	Found (%) C	Found (%) H
1g	1.34	2.0	**6g**(96)	oil	$C_{18}H_{18}$	92.26	7.74	92.27	7.76
1j	1.21	2.0	**6j** (91)	147—148	$C_{22}H_{26}$	90.98	9.02	91.35	8.97
1k	1.15	2.0	**6k**(92)	118—120	$C_{20}H_{22}$	91.55	8.45	91.88	8.40
1l	1.24	2.0	**6l**[b] (85)						
1o	1.24	2.0	**6o**(100)	173—174	$C_{21}H_{24}$	91.25	8.75	91.22	8.76
1p	1.11	2.0	**6p**[b](100)						

a) For substitution pattern see Table 1. b) See Ref. 7.

TABLE 4. MELTING POINTS AND ANALYTICAL DATA FOR COMPOUNDS 1 AND 2

Compound	Mp/°C	Yield/%	Formula	Calcd(%) C	Calcd(%) H	Found (%) C	Found (%) H
1b	64.5—66	85.0	$C_{17}H_{18}$	91.84	8.16	91.85	8.08
1h	101—101.5	72.5	$C_{19}H_{22}$	91.14	8.86	91.24	8.84
1i	62—63.5	34.5	$C_{19}H_{22}$	91.14	8.86	91.18	8.84
1k	113.5—114.5	64.0	$C_{20}H_{24}$	90.85	9.15	90.71	9.13
1o	197—198	73.0	$C_{21}H_{26}$	90.59	9.41	90.54	9.09
2b	107—108	50.2	$C_{17}H_{18}S_2$	71.28	6.33	71.38	6.37
2h	198—199.5	38.5	$C_{19}H_{22}S_2$	72.56	7.05	72.52	6.91
2i	110.5—112	53.6	$C_{19}H_{22}S_2$	72.56	7.05	72.66	7.04
2k	123—124	63.5	$C_{20}H_{24}S_2$	73.12	7.36	72.86	7.27
2o	195—196	85.5	$C_{21}H_{26}S_2$	73.63	7.65	73.90	7.62

rates. Table 2 shows the scan-rate dependence on $E_{pa}(O_1)$ and the shift differences.

When electrolyzed anodically at the potential of O_1, these [2.2]metacyclophanes gave the corresponding 4,5,9,10-tetrahydropyrenes in high yields (Table 3).

Experimental

The following compounds were prepared as previously reported: **1a**,[2a] **1c**,[2a] **1d**,[2b] **1f**,[5] **1g**,[6] **1j**,[2b] **1l**,[7] **1m**,[7] **1n**,[7] and **1p**.[7] The unsymmetrical [2.2]metacyclophanes, **1b**, **1h**, **1i**, **1k**, and **1o**, were prepared by the pyrolysis of disulfone (**3**), which had been obtained from disulfide (**2**). The physical properties and analytical data of these are summarized in Table 4. As a typical example, the preparation of 4,5,6,12,-14-pentamethyl[2.2]metacyclophane (**1o**) will be described.

5,6,7,14,16-Pentamethyl-2,11-dithia[3.3]metacyclophane (2o). A solution of 1,3-bis(chloromethyl)-4,5,6-trimethylbenzene (3.0 g, 13.8 mmol) in 200 ml of benzene and a solution of 1,3-bis(mercaptomethyl)-4,6-dimethylbenzene (2.74 g, 13.8 mmol) in 200 ml of benzene were added simultaneously and at the same rate to boiling ethanol (1 l) containing sodium hydroxide (1.1 g, 28.3 mmol) under good stirring over the course of 27 h. After a usual work-up,[2c] compound **2o** (4.0 g, 85.5%) was obtained as colorless needles; mp 195—196 °C (from benzene–hexane); ^{1}H NMR ($CDCl_3$) δ 2.10s (3H), 2.19s (6H), 2.24s (6H), 3.80s (8H), 6.62s (1H), and 6.77m (2H).

4,5,6,12,14-Pentamethyl[2.2]metacyclophane (1o) Disulfide **2o** (1.27 g) was oxidized to disulfone **3o** (mp>300 °C), using 30% hydrogen peroxide in acetic acid-benzene. The pyrolysis of **3o** used a vacuum pyrolysis furnace similar to that described by Staab *et al.*[8] at 500 °C. The purification of the sublimate gave **1o** (0.75 g, 73%) as colorless plates; mp 197—198 °C; ^{1}H NMR δ 1.77d (4H), 2.31s (15H), 3.32q (4H), 4.22s (1H), 4.28s (1H), and 7.00s (1H).

The controlled potential electrolysis of (**1**) was carried out as has been described before.[2] A typical run is as follows.

Controlled Potential Electrolysis of 1o. A solution of **1o** (55.7 mg, 0.20 mmol) in acetonitrile (60 ml) containing TBAP (0.1 mol dm^{-3}) was electrolyzed at the O_1 potential supplied from a potentiostat until 38.6 C (2.0 F mol^{-1}) had been consumed. A usual work-up and chromatography (silica gel) gave **6o** (55.0 mg, 99.5%) (mp 168.5—170 °C), which was further purified and recrystallized from hexane, thus yielding analytical samples as colorless needles; mp 173—174 °C; ^{1}H NMR δ 2.29s (15H), 2.78s (8H), and 6.90s (1H).

The physical properties and analytical data of the newly prepared tetrahydropyrenes are listed in Table 3.

References

1) Electron-organic Chemistry. VI. Part V: T. Sato, M. Kubo, and K. Nishigaki, *Bull. Chem. Soc. Jpn.* **53**, 815 (1980).

2) a) T. Sato and M. Kamada, *J. Chem. Soc., Perkin Trans. 2*, **1977**, 384; b) T. Sato and K. Torizuka, *ibid.*, **1978**, 1199; c) T. Sato, K. Torizuka, R. Komaki, and H. Atobe, *ibid.*, **1980**, 561.

3) T. Sato, K. Nishiyama, S. Shimada, and K. Hata, *Bull. Chem. Soc. Jpn.*, **44**, 2858 (1971).

4) M. R. Rifi, "Technique of Electroorganic Synthesis," ed by N. L. Weinberg, Wiley-Interscience, New York (1974), Part II, p. 690.

5) T. Umemoto, T. Otsubo, Y. Sakata, and S. Misumi, *Tetrahedron Lett.*, **1973**, 593.

6) S. Akabori, T. Sato, and K. Hata, *J. Org. Chem.* **33**, 3277 (1968).

7) T. Sato and T. Takemura, *J. Chem. Soc., Perkin Trans. 2*, **1976**, 1195.

8) H. A. Staab and M. Haenel, *Chem. Ber.*, **106**, 2190 (1973).

Naphthalene-sensitized Photolysis of Dibenzoyl Peroxide

Akihide KITAMURA, Hirochika SAKURAGI, Masayuki YOSHIDA,** and Katsumi TOKUMARU*

Department of Chemistry, The University of Tsukuba, Sakura-mura, Ibaraki 305

***Department of Chemistry, Faculty of Science, The University of Tokyo, Hongo, Bunkyo-ku, Tokyo 113*

(Received March 11, 1980)

Synopsis. Naphthyl benzoates and phenylnaphthalenes were produced, on naphthalene-sensitized photolysis of dibenzoyl peroxide, in different distribution of their isomers from its thermolysis in the presence of naphthalene, suggesting that naphthalene as sensitizer interacts with dibenzoyl peroxide in a specific orientation in the sensitization process.

Aromatic hydrocarbon-sensitized photolysis of dibenzoyl peroxide (BPO) has previously been shown to proceed by way of a singlet exciplex.[1,2] Although most photosensitized reactions are supposed to take place without any chemical change of sensitizers, the present work is concerned with the products from naphthalene-sensitized photolysis of BPO, particularly with the fate of the sensitizer.

Thus, in the sensitization process, the excited sensitizer molecule will take a favourable orientation with respect to the peroxide molecule to form efficiently an exciplex, which will subsequently undergo cleavage of the peroxide moiety into free radicals. Therefore, immediately after the cleavage, the resulting free radicals will attack the sensitizer molecule, still located in a close proximity of the radicals in a specific orientation, to give reaction products in a different distribution from random encounters of the free radicals with the sensitizer molecules. The investigation of these reaction products will give insight into the favourable orientation of the sensitizer and peroxide molecules in the exciplex, and this attempt is described below.

Results and Discussion

A solution of BPO (0.03 M) and naphthalene (0.04 M) in benzene was irradiated under nitrogen atmosphere at room temperature with a 400-W high pressure mercury lamp through a Pyrex wall. For comparison, BPO (0.03 M) was allowed to decompose thermally in the presence of naphthalene (0.04 M) in benzene at 80 °C. The products were quantitatively analyzed by GLPC. The results are summarized in Table 1.

TABLE 1. YIELD OF PRODUCTS IN PHOTOLYSIS AND THERMOLYSIS OF DIBENZOYL PEROXIDE IN THE PRESENCE OF NAPHTHALENE IN BENZENE

Product	Yield[a]	
	Photolysis	Thermolysis
Biphenyl	0.28	0.40
Phenyl benzoate	0.23	0.029
1-Phenylnaphthalene	0.036	0.006
2-Phenylnaphthalene	0.011	0.004
1-Naphthyl benzoate	0.036	0.013
2-Naphthyl benzoate	0.007	0.013
Benzoic acid	0.15[c]	
Naphthalene[b]	0.77	0.70
1,1′-Binaphthyl[b]	0.014	0.003
1,2′-Binaphthyl[b]	0.009	0.003
2,2′-Binaphthyl[b]	0.016	0.008

a) Yields in mol/mol peroxide unless otherwise noted. Average values of data obtained by duplicate runs. b) Yields in mol/mol naphthalene. c) Determined by isolation.

Production of biphenyl, phenyl benzoate, and benzoic acid is reasonably understood by a mechanism previously postulated.[3] Thus, the peroxide moiety decomposes through simultaneous two-bond cleavage into a benzoyloxyl radical and a phenyl radical, which subsequently undergo geminate recombination into phenyl benzoate or diffusion out of the solvent cage to react with benzene finally affording biphenyl and benzoic acid.

As Table 1 shows, it is remarkable that the photolysis produced larger amounts of naphthyl benzoates (1-naphthyl and 2-naphthyl benzoate) and phenylnaphthalenes (1-phenyl- and 2-phenylnaphthalene) than the thermolysis. Moreover, among the above compounds 1-naphthyl derivatives were produced in several times higher yields than their corresponding 2-naphthyl derivatives in the photolysis, in contrast with the thermolysis which gave nearly equal amounts of 1-naphthyl and 2-naphthyl derivatives. A possibility that this fact would be due to more rapid change of the resulting 2-naphthyl benzoate and 2-phenylnaphthalene than their respective 1-naphthyl derivatives under the photolytic conditions was eliminated by control experiments.

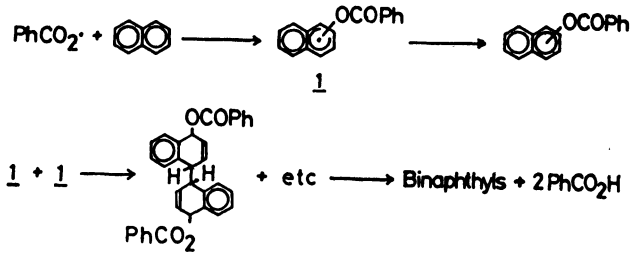

It is certain that naphthyl benzoates result from addition of benzoyloxyl radicals to naphthalene followed by loss of a hydrogen atom from the resulting cyclohexadienyl radicals (**1**).[4] Phenylnaphthalene must be similarly formed through addition of phenyl radicals to naphthalene. Production of 1,1′-, 1,2′-, and 2,2′-binaphthyl is presumably through recombination of the cyclohexadienyl radicals (**1**) followed by elimination of two moles of benzoic acid for each mole of binaphthyls formed.[4]

As mentioned above, it is reasonably supposed that when the two-bond cleavage of the peroxide moiety in the exciplex generates simultaneously benzoyloxyl and phenyl radicals in the proximity of the naphthalene

molecule, which has worked as sensitizer, these radicals will be captured by the naphthalene molecule in competing with their diffusion out of the solvent cage into the bulk of the solvent benzene. This reasoning can explain the formation of higher yields of phenylnaphthalenes and naphthyl benzoates from the photolysis than from the thermolysis, in which these compounds would result from random encounters of the radicals and naphthalene. Furthermore, the aforementioned finding that the production of higher yields of 1-phenylnaphthalene and 1-naphthyl benzoate than their respective 2-naphthyl derivatives from the photolysis might suggest that, immediately after the cleavage of the peroxide moiety, the radical centres of benzoyloxyl and phenyl radicals would be located closer to the C-1 carbon of naphthalene than to the C-2 carbon. This orientation can be taken as reflecting the conformation of the exciplex, as supposed by the construction of the molecular model, where the aromatic nucleus of the peroxide would overlap with the naphthalene molecule and the C-1 ring carbon of the peroxide would be close to the C-1 carbon of the naphthalene.

Experimental

Photolysis and Thermolysis of Dibenzoyl Peroxide with Naphthalene in Benzene. A solution of dibenzoyl peroxide (3.00 g, 0.012 mol) and naphthalene (2.00 g, 0.016 mol) in benzene (400 ml) was irradiated under nitrogen atmosphere for 2.3 h (five times half-life periods determined by iodometry) by a 400-W high pressure mercury lamp immersed in a Pyrex cooling well. Thermolysis was carried out at a half scale of photolysis at 80 °C in an oil bath for 21.7 h (five times half-life periods) under nitrogen gas bubbling. After the reaction was completed, the solution was concentrated to one-tenth of its original volume. Naphthalene, biphenyl, phenylnaphthalenes, naphthyl benzoates, and binaphthyls were determined quantitatively by GLPC. Benzoic acid was isolated by extraction with aqueous sodium hydrogencarbonate solutions and determined by gravimetry.

Irradiation of Naphthyl Benzoates in Benzene. A solution of 1-naphthyl benzoate (35.7 mg, 0.14 mmol) and 2-naphthyl benzoate (77.4 mg, 0.31 mmol) in benzene (40 ml) was similarly irradiated by a 400-W high pressure mercury lamp for 2.4 h. GLPC analysis of the irradiation mixture revealed the ratio of remaining 1-naphthyl benzoate/2-naphthyl benzoate to be 0.25.

References

1) T. Nakata and K. Tokumaru, *Bull. Chem. Soc. Jpn.*, **43**, 3315 (1970); K. Tokumaru, A. Ohshima, T. Nakata, H. Sakuragi, and T. Mishima, *Chem. Lett.*, **1974**, 571.

2) S. R. Fahrenholtz and A. M. Trozzolo, *J. Am. Chem. Soc.*, **93**, 251 (1971).

3) A. Kitamura, H. Sakuragi, M. Yoshida, and K. Tokumaru, *Bull. Chem. Soc. Jpn.*, **53**, 1393 (1980).

4) M. J. Perkins, "Free Radicals," ed by J. K. Kochi, Wiley, New York, N. Y. (1973), Vol. II, p. 231.

Synthesis of 1-Benzothiopyrylium Perchlorates and Related Compounds

Hiroyuki NAKAZUMI* and Teijiro KITAO

Department of Applied Chemistry, College of Engineering, University of Osaka Prefecture, Sakai, Osaka 591

(Received February 5, 1980)

Synopsis. The blue colored 1-benzothiopyrylium perchlorates were synthesized by the reduction of thiocoumarins with lithium aluminium hydride followed by the treatment with acid. A number of new thiocarbonyl derivatives of thiocoumarins and thiochromones were also synthesized, the spectral characterization of which has been described.

In our previous papers, we have reported the syntheses and methylation of 2*H*-1-benzothiopyran-2-ones (thiocoumarins) (**1**) and 4*H*-1-benzothiopyran-4-ones (thiochromones) (**2**), an isomer of **1**.[1,2]

In this paper, we wish to report (i) the reduction of thiocoumarins (**1**) with lithium aluminium hydride ($LiAlH_4$) and synthesis of 2*H*-1-benzothiopyran-2-thiones (**3**) and 4*H*-1-benzothiopyran-4-thiones (**4**) as reactants to prepare 1-benzothiopyrylium salts, and (ii) spectral characterization of **3** and **4** to distinguish them.

Results and Discussion

Preparation of 1-Benzothiopyrylium Perchlorates (7). In the previous paper,[2] we reported that the methylation of **2** with dimethyl sulfate gave the dimerized product **8**, while in the case of isomeric thiocoumarin **1** (X=OCH_3), none of the dimerized product but *O*-methylated product **5** was isolated by the same reaction.

We now found that a blue colored 1-benzothiopyrylium perchlorate **7** could be obtained in yields of 22—72%, by the reduction of thiocoumarin **1** with $LiAlH_4$ followed by the treatment with acid. Similar reduction of **2** with aluminium hydride or $LiAlH_4$ also gave an isomeric blue colored 1-benzothiopyrylium salt **9**.[2] Mckinnon[3] has already reported that some of thiopyrylium salts (**10**) were obtained from 2*H*(or 4*H*)-thiopyran-2(or 4)-ones under the same conditions. In the case of **1c** (X=OCH_3), both of 1-benzothiopyrylium salts **7c** and **6**, as the precursor of **7c**, were isolated in yields of 30 and 39%, respectively. Compounds **7a** and **6** also could be obtained by the cyclization of 4-(phenylthio)-2-butanones with PPA or perchloric acid.[4] A possible mechanism for the formation of **7** is given in a similar manner as described in the case of thiochromones (Scheme 1). It is shown that the condensation takes place between 4-methyl group of **1** and 2-carbon atom of the other molecule in this reaction.

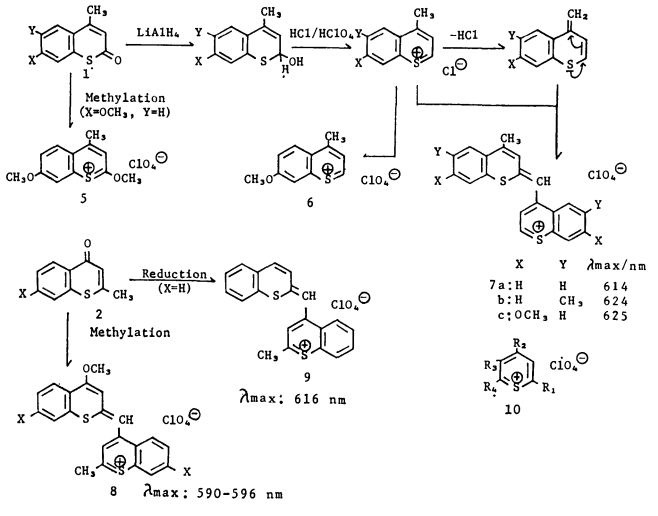

Scheme 1.

On the other hand, it is also known that the oxidation of 2*H*(or 4*H*)-thiopyran-2(or 4)-thiones give thiopyrylium salts (**10**). Then, we synthesized a number of new thiocarbonyl derivatives **3** and **4** as reagents to prepare **7** and **9**. Compounds **3** and **4** were obtained by the usual reaction of **1** and **2** with P_2S_5, respectively (Scheme 2), but an attempt to prepare **7** from **3** was failed. That is, the oxidation of **3a** with hydrogen peroxide gave an undetermined product, which showed the two λ_{max}'s of 579 and 626 nm in acetone solution and complex peaks in the NMR spectra.

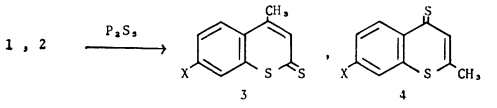

Scheme 2.

Spectral Characteristics. The spectral data of **3** and **4** are summarized in Table 1. We proposed some spectral characterization of **1** and **2** to distinguish. From **3** and **4**, the additional distinction between thiocoumarin and thiochromone nuclei became possible as follows. In the NMR spectra, the characteristic deshielding effect of benzenoid proton at the 5-position of **4** was observed similar to that of thiochromones (**2**). The proton showed the chemical shift at *ca.* 9.00 ppm. In the series of thiocoumarin **3**, however, such a proton showed the chemical shift at *ca.* 7.80 ppm. This difference may be utilized to distinguish them as well as that of **1** and **2**. The proton at the 3-position of both derivatives **3** and **4** showed the chemical shift in the aromatic region (above 7.00 ppm), compared to that of **1** and **2** in the range of 6.48—6.75 ppm, except for **3c** and **4c**.

In the mass spectra, the major fragmentation pathway for each of **3** and **4** was elimination of C=S, followed by the loss of a hydrogen atom leading to the formation of 1-benzothiopyrylium ion (Scheme 3). The series of

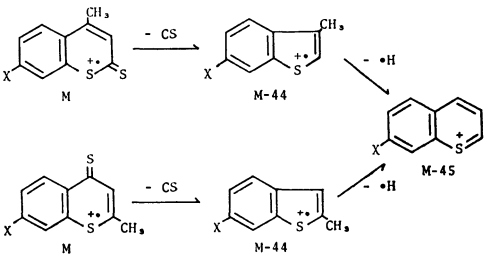

Scheme 3.

Table 1. The spectral data of 1-benzothiopyran-thione derivatives

No.	X	NMR in $CDCl_3$ δ/ppm	m/e (rel. intensity)	λ_{max}/nm[a] ($\varepsilon\times10^{-4}$)
3a	H	2.45(3H, s) 7.38—7.85(5H, m)	192 (M, 100), 191 (12) 177 (20), 148(M−44, 100) 147 (M−45, 73)	234(3.9) 302(1.7) 420(1.1)
3b	7-CH_3	2.40 (6H, s) 7.15—7.30(3H, m) 7.70 (1H, d, J=10 Hz)	206 (M, 82), 205 (10) 191 (17), 162 (M−44, 92) 161 (M−45, 50)	238(2.7) 303(1.1) 425(1.0)
3c	7-OCH_3	2.42 (3H, s) 3.88 (3H, s) 6.88 (1H, s) 7.05—7.30 (2H, m) 7.77 (1H, d, J=10 Hz)	222 (M, 82), 221 (6) 207 (8), 178 (M−44, 100) 177 (M−45, 9), 163 (45)	245(4.5) 272(1.2) 278(1.2) 309(0.82) 432(1.5)
4a	H	2.40 (3H, s) 7.43—7.70 (3H, m) 7.96 (1H, s) 9.01 (1H, m)	192 (M, 100), 191 (M−1, 58) 177 (18), 148 (M−44, 20) 147 (M−45, 57)	236(1.6) 244(2.3) 293(0.75) 412(2.1)
4b	7-CH_3	2.38 (3H, s) 2.40 (3H, s) 7.20—7.40 (2H, m) 7.85 (1H, s) 8.85 (1H, d, J=10 Hz)	206 (M, 100), 205 (M−1, 54) 191 (39), 162 (M−44, 13) 161 (M−45, 34)	238(1.3) 247(2.4) 296(0.84) 412(1.8)
4c	7-OCH_3	2.36 (3H, s) 3.90 (3H, s) 6.96 (1H, s) 7.15—7.84 (2H, m) 8.96 (1H, d, J=10 Hz)	222 (M, 100), 221 (M−1, 41) 207 (23), 178 (M−44, 13) 177 (M−45, 13), 163 (15)	253(1.9) 289(1.1) 343(0.74) 409(2.2)

a) In EtOH.

thiochromone **4** were characterized by abundant molecular ion as the base peak and the M−1 fragment ion, formula of which was not assigned. In the case of **3**, such an M−1 fragment ion was very small (below 12 (rel. intensity)). It was observed that in the case of **3** the M−44 fragment ion was much stronger than that of M−45. The M−40 fragment ion was not observed in **4**, which was found characteristically in the mass spectra of **2**.[1]

The absorption maxima of the longest wavelength of **3** were longer by *ca.* 10 nm than those of **4**.

Experimental

All the melting points are uncorrected. ^{1}H-NMR spectra were taken on a Hitachi R-24A spectrometer with tetramethylsilane as an internal standard. Absorption spectra were obtained with a Hitachi EPS-3T spectrometer. Mass spectra were taken on a Hitachi RMU-6E mass spectrometer operating at 80 eV. Elemental analyses were performed on a Yanaco CHN recorder MT-2.

The Reduction of ***1*** *with Lithium Aluminium Hydride.* Powdered $LiAlH_4$ (0.1 g) was added to a stirred solution of **1a** (1.0 g) in anhydrous diethyl ether (100 ml) at room temperature. After 1 h, ethyl acetate (2 ml) was added, and after 10 min, addition of 10% dilute HCl (10 ml) gave a blue colored mixture. After 30 min, diethyl ether was evaporated below 30 °C. The residue was dissolved in glacial acetic acid (30 ml) and 60% perchloric acid (0.5 ml) was added. After standing for 20 h at room temperature, the mixture was diluted with diethyl ether, and the resulting solid was separated and washed with a mixture of acetone and benzene (1: 2) and EtOH. The crude product was recrystallized from glacial acetic acid (80 ml) containing a small amount of perchloric acid to give **7a** (X=H, Y=H). **7a**:[4] 72%, NMR (CF_3COOH): δ=3.30 (3H, s), 5.95 (2H, s), and 7.50—9.10 (≈10H, m). Found: C, 57.01; H, 3.77%. Calcd for $C_{20}H_{15}O_4ClS_2$: C, 57.35; H, 3.58%. λ_{max} (acetone): 614 nm (ε 8.30×10^4); **7b** (X=H, Y=CH_3): 22%, NMR (CF_3-COOH): δ=2.83 (6H, s), 3.30 (3H, s), 5.88 (2H, s), and 8.0—8.8 (≈8H, m). Found: C, 58.61; H, 4.28%. Calcd for $C_{22}H_{19}O_4ClS_2$: C, 59.13; H, 4.26%. λ_{max} (acetone): 624 nm (ε 4.3×10^4). In the case of **1c** (X=OCH_3), the residue from diethyl ether was washed with glacial acetic acid (50 ml) containing perchloric acid and dissolved in glacial acetic acid (100 ml) at 70 °C. After cooling, diethyl ether was added to this solution, and then **7c** was isolated in 30% yield. The other 1-benzothiopyrylium salt **6** was isolated in 39% yield from the filtrate (washed with AcOH). **7c**: NMR (CF_3COOH): δ=3.20 (3H, s), 4.12 (3H, s), 4.22 (3H, s), 5.65 (2H, s), and 7.50—9.00 (≈8H, m). Found: C, 55.13; H, 4.03%. Calcd for $C_{22}H_{19}O_6ClS_2$: C, 55.17; H, 3.97%. λ_{max} (acetone): 625 nm (ε 6.2×10^4); **6**:[4] dec 200 °C (lit, 205 °C), NMR (CF_3COOH): δ=3.25 (3H, s), 4.20 (3H, s), 7.50—8.00 (2H, m), 8.35 (1H, d, J=10 Hz), 8.70 (1H, d, J=10 Hz), and 9.60 (1H, d, J=10 Hz). Found: C, 45.52; H, 3.85%. Calcd for $C_{11}H_{11}O_5SCl$: C, 45.44; H, 3.79%. λ_{max} (acetone): 415 nm (ε 6.4×10^3).

Oxidation of ***3a*** *with Hydrogen Peroxide.* 30% Hydrogen peroxide (0.7 ml) was added to a suspended solution of **3a** (0.5 g) in acetic acid (27 ml), and the mixture was stirred at 30 °C. After 2 h, perchloric acid (0.8 ml) was added to the solution. Dilution with diethyl ether gave a crude product, which was recrystallized from acetic acid. Found: C, 56.35; H, 3.06%. NMR (CF_3COOH): δ=2.40—3.40 (m) and 7.50—9.50 (m).

2H-1-Benzothiopyran-2-thiones (3) and 4H-1-Benzothiopyran-4-thiones (4). 4-Methyl (thiocoumarin) **1a**[5] (1.35 g, 7.7 mmol) and P_2S_5 (7.5 g, 34 mmol) were added to benzene (50 ml). The mixture was heated under reflux for 7 h and was filtered. The filtrate was evaporated, and the residue was extracted with diethyl ether. The extract was evaporated, and the resulting solid was recrystallized from EtOH to give **3a** (1.1 g, 74%). The other **3** and **4** were obtained similarly. **3a**:[6] mp 111—112 °C, Found: 62.86; H, 4.26%. Calcd for $C_{10}H_8S_2$: C, 62.50; H, 4.17%. **3b**: 67%, mp 136—137 °C, Found: C, 64.03; H, 4.94%. Calcd for $C_{11}H_{10}S_2$: C, 64.08; H, 4.85%. **3c**: 42%, mp 150—151 °C. Found: C, 59.10; H, 4.57%. Calcd for $C_{11}H_{10}OS_2$: C, 59.46; H, 4.50%. **4a**:[7] 40%, mp 107—108 °C, Found: C, 62.57; H, 4.26%. Calcd for $C_{10}H_8S_2$: C, 62.50; H, 4.17%. **4b**: 15%, mp 134—136 °C, Found: C, 63.87; H, 4.76%. Calcd for $C_{11}H_{10}S_2$: C, 64.08; H, 4.85%. **4c**: 21%, mp 138—140 °C, Found: C, 58.97; H, 4.56%. Calcd for $C_{11}H_{10}OS_2$: C, 59.46; H, 4.50%.

The authors wish to acknowledge the assistance of N. Yoshikawa and M. Hirano.

References

1) H. Nakazumi and T. Kitao, *Bull. Chem. Soc. Jpn.*, **50**, 939 (1977).
2) H. Nakazumi and T. Kitao, *Bull. Chem. Soc. Jpn.*, **52**, 160 (1979).
3) D. M. Mckinnon, *Can. J. Chem.*, **48**, 3388 (1970).
4) B. D. Tilak, H. S. Desai, C. V. Deshpande, S. K. Jain, and V. M. Vaidya, *Tetrahedron*, **22**, 7 (1966).
5) H. Nakazumi, A. Asada, and T. Kitao, *Chem. Lett.*, **1979**, 387.
6) A. Ruwet and M. Renson, *Bull. Soc. Chem. Belg.*, **79**, 89 (1970).
7) I. A. Tolmachev, V. L. Papp, V. E. Ryl'tsv, and P. Yu. Egorov, *Zh. Obshch. Khim.*, **44**, 2747 (1974).

The Stoichiometry and Promoter Role of Chlorosulfuric and Fuming Sulfuric Acids for α-Halogenation of Aliphatic Acid[1)]

Yoshiro OGATA* and Shinya WATANABE

Department of Applied Chemistry, Faculty of Engineering, Nagoya University, Chikusa-ku, Nagoya 464

(Received December 27, 1979)

Synopsis. The stoichiometry for the chlorosulfuric acid promoted α-halogenation and the role of fuming sulfuric acid instead of chlorosulfuric acid have been studied. In the α-bromination with molecular bromine, 1 mol of halogen afforded 2 mol of aliphatic α-bromo acid just as the α-iodination, but it is different from α-chlorination which affords only 1 mol of α-chloro acid. Fuming sulfuric acid instead of chlorosulfuric acid was found to be effective for α-bromination, but the yield was lower, while no α-iodination was observed with fuming sulfuric acid.

We have reported a novel method for the preparation of aliphatic α-halo acids by the reaction of molecular halogen in the presence of strong acid, *e.g.*, $ClSO_3H$,[2)] through probable intermediary formation of ketenes.[3)]

$$RR'CHCO_2H + ClSO_3H \overset{\text{fast}}{\rightleftharpoons} RR'C{=}C{=}O + HCl + H_2SO_4 \quad (1)$$

$$RR'C{=}C{=}O + X_2 \overset{\text{slow}}{\longrightarrow} \underset{\mathbf{1}}{RR'CXCOX} \quad (2)$$

The product in iodination (**1**, X=I) was found to regenerate iodine.[2g)]

$$RR'CXCOX + H_2SO_4 \longrightarrow RR'CXCO_2H + HX + SO_3 \quad (3a)$$

$$2HX + SO_3 \text{ (or } ClSO_3H) \longrightarrow X_2 + H_2O + SO_2 \ (+HCl) \quad (3b)$$

Hence 1 mol of iodine can give 2 mol of α-iodo acid (Eq. 4), but the stoichiometry is unknown for bromination and chlorination.

$$RR'CHCO_2H + 0.5I_2 + ClSO_3H \longrightarrow RR'CICO_2H + HCl + 0.5SO_2 + 0.5H_2SO_4 \quad (4)$$

Also we found that fuming H_2SO_4 could be used as an acidic promoter for the α-chlorination, but nothing is known about the yield of α-bromination and α-iodination, when fuming H_2SO_4 is used instead of $ClSO_3H$. The present note discloses these obscurities in the halogenation.

Stoichiometry of Bromination. It is known that HBr is oxidized by $ClSO_3H$ to form Br_2,[4)] so that Br_2 formed may be used again for the bromination. In fact, we confirmed that 1 mol of Br_2 can give *ca.* 2 mol of aliphatic α-bromo acid as shown in Table 1 (Runs 1, 4, and 5). Hence the stoichiometry of bromination is analogous to that of iodination (Eq. 4).

$$RR'CHCO_2H + ClSO_3H + 0.5Br_2 \longrightarrow RR'CBrCO_2H + HCl + 0.5H_2SO_4 + 0.5SO_2 \quad (5)$$

Runs 4 and 5 imply that an additional amount of aliphatic acids is consumed by the side reaction with $ClSO_3H$[5)] (*e.g.*, α-sulfonation), but since there is little difference between the yields in Runs 4 and 5, the rate of α-bromination should be faster than the side reaction.

On the other hand, unless excess aliphatic acid and $ClSO_3H$ based on Eqs. 4 and 5 are used, the yield of iodination is rather low; *e.g.*, Run 8 gives 43% and Run 9 gives 55% of iodo acid, probably because the rate of iodination is lower than that of bromination and comparable to that of the side reaction.[2h)] But when excess aliphatic acid and excess $ClSO_3H$ to iodine are used (Run 7), the yield of α-iodination based on the used iodine increases in spite of the increased side reaction.

When a mixture of halogen and aliphatic acid in a stoichiometric ratio according to Eqs. 4 and 5 was used,

Table 1. Yields of α-halogenation of aliphatic acids[a)]

Run	Substrate (mol·dm^{-3}) $CH_3(CH_2)_6CO_2H$	Halogen (mol·dm^{-3}) Br_2	Halogen (mol·dm^{-3}) I_2	Promoter (mol·dm^{-3}) $ClSO_3H$	Promoter (mol·dm^{-3}) fuming H_2SO_4	Yield (%)	Unreacted Substrate (mol·dm^{-3})
1	1.0	0.5	—	1.0	—	88.9	
2	1.0	0.5	—	0.25	—	29.2	0.76
3	1.0	0.5	—	0.1	—	9.7	0.85
4	1.0	0.25	—	1.0	—	97.8	0.11
5	1.0	0.25	—	0.5	—	93.3	0.49
6	1.0	0.25	—	0.3	—	56.5	0.66
7	1.0	—	0.25	1.0	—	100.0[b)]	
8	1.0	—	0.25	0.5	—	43.0[b)]	
9	0.5	—	0.25	0.5	—	54.5[b)]	
10	1.0	0.25	—	—	1.0	71.6	0.50
11	1.0 $CH_3(CH_2)_2CO_2H$	0.25	—	—	0.5	53.1	0.75
12	1.7	0.13	—	—	1.0	73.4[c)]	
13	1.0	0.25	—	—	1.0	27.0[c)]	
14	0.2	—	0.2	—	0.13	0.0[b)]	
15	1.7	—	0.15	—	0.6	0.0	

a) The yields were calculated on the basis of molecular halogen according to the stoichiometry of Eqs. 4 and 5.
b) Ref. 2b. c) Ref. 2f.

the yield of bromination (Run 1) was higher (88.9%) than the yield of iodination (54.5%) under analogous conditions. This is ascribed to the higher electrophilic reactivity of bromine than iodine toward C=C bond of ketene as apparent from our previous kinetic data.[2h]

Under conditions of $2[Br_2]_0 > [ClSO_3H]_0$ (Runs 2, 3 and 6), the molar yield of α-bromo acid is approximately equal to the moles of $ClSO_3H$ used, whereas the molar yield of α-chloro acid is *ca.* four fold of the moles of $ClSO_3H$ used in spite of the otherwise analogous reaction conditions.[2e] This phenomenon is tentatively explained by the following mechanism for chlorination.

$$RR'CClCOCl + RR'CHCO_2H \rightleftharpoons RR'CClCO_2H + RR'CHCOCl \quad (6a)$$

$$RR'CHCOCl \longrightarrow RR'C{=}C{=}O + HCl \quad (6b)$$

Here, α-chloroacyl chloride, which has been formed through addition of Cl_2 to ketene (Eqs. 1 and 2), can convert unreacted aliphatic acid into acyl chloride (Eq. 6a);[6] the acyl chloride thus formed is known to give again ketene (Eq. 6b),[7] which should react with Cl_2, giving again α-chloroacyl chloride.[2f] Thus only catalytic amount of $ClSO_3H$ can give a high yield of α-chloro acid because of the easier elimination of HCl from acyl chloride (Eq. 6b). On the other hand, the oxidation of α-bromoacyl bromide with chlorosulfuric acid affording Br_2 occurs at 80 °C (Eq. 3) because of the lower oxidation potential of Br^- (+1.066 V for $Br^- \rightarrow 1/2\ Br_2$; +1.358 V for $Cl^- \rightarrow 1/2\ Cl_2$); hence the bromination obeys the stoichiometry of Eq. 5, regenerating Br_2.

Bromination and Iodination with Fuming Sulfuric Acid as a Promoter. As has been observed with α-chlorination,[2a,d] the α-bromination could be carried out with fuming H_2SO_4 (Runs 10 and 11) *via* a ketene formed as shown in Eq. 7.

$$RR'CHCO_2H + SO_3 \rightleftarrows RR'C{=}C{=}O + H_2SO_4 \quad (7)$$

Since 30% fuming H_2SO_4 is expressed as H_2SO_4–$0.5SO_3$, the yield 53% of α-bromo acid in Run 11 corresponds to the moles of SO_3 contained in fuming H_2SO_4 used.

On the other hand, no iodination occurred with fuming H_2SO_4; this is ascribed to the easy decomposition of α-iodo acid with fuming H_2SO_4. In fact, when 15 mmol of fuming H_2SO_4 was introduced into the 1,2-dichloroethane solution of 4.2 mmol of α-iodobutyric acid, 0.63 mmol of iodine were easily liberated at room temperature after 5 min, but only 0.016 mmol of iodine were liberated with $ClSO_3H$. Similar decomposition giving I_2 was observed with α-iodobutyryl chloride and fuming H_2SO_4.

Also the lower yield of bromination with fuming H_2SO_4 than that with $ClSO_3H$ may be due to the slower yet noticeable decomposition of α-bromoacyl bromide by fuming H_2SO_4. Indeed, 1.8 mmol of α-bromopropionyl bromide mixed with 5 mmol of fuming H_2SO_4 gave 0.42 mmol of bromine and 0.23 mmol of α-bromopropionyl bromide at 80 C° after 30 min. But 1.4 mmol of α-bromopropionyl bromide mixed with 5 mmol of $ClSO_3H$ gave only 0.05 mmol of bromine and 0.78 mmol of α-bromopropionyl bromide at 80 °C after 30 min.

On the other hand, no molecular chlorine was detected in the reaction of chloroacetyl chloride ($CH_2ClCOCl$) with fuming H_2SO_4 or $ClSO_3H$, hence chlorine as acyl chloride produced during chlorination cannot be recycled by oxidation with $ClSO_3H$.

Experimental

Materials. Commercial first grade octanoic acid (bp 147—148 °C/35 mmHg), butyric acid (bp 73—74 °C/20 mmHg) and chlorosulfuric acid (bp 86—88 °C/33 mmHg) were distilled before use. Commerical first grade bromine, iodine, chloroacetyl chloride, and fuming H_2SO_4 were used without futher purification. α-Iodobutyric acid (mp 39—40 °C) and α-iodobutyryl chloride (bp 36—38 °C/0.38 mmHg) were prepared in thionyl chloride by the literature method.[8] α-Bromopropionyl bromide (bp 154—155 °C) was prepared by the literature method.[9] Methyl esters of those aliphatic acids had single GLC peaks. The physical properties of methyl α-bromooctanoate were: bp 136—138 °C/24 mmHg; NMR (CCl_4): δ 3.71 (s, 3H, OCH_3), 4.09 (t, J=7.8 Hz, 1H, α-H). The physical properties of other products were reported previously.[2f,h]

Products. A 1,2-dichloroethane solution (50 ml) containing aliphatic acid and halogen was thermostated at 80 °C and $ClSO_3H$ (or fuming H_2SO_4) was introduced and heated at 80 °C for 2 h. After an appropriate time, 2 ml of the solution was treated with $Na_2S_2O_3$ to remove halogen, and esterified by an ethereal solution of diazomethane.

The yield was measured by means of GLC using a Yanagimoto GCG-550 gas chromatograph equipped with a H-flame ionization detector employing a copper column 3 mm × 100 cm packed with PEG 20 M (10%) on Chromosorb WAW (60—80 mesh) with methyl caprate as an internal standard. The isolated methyl α-bromooctanoate was identified by GLC and NMR (a 60 MHz Hitachi R-24 B NMR spectrometer).

References

1) Contribution No. 270.

2) a) Y. Ogata, T. Harada, K. Matsuyama, and T. Ikejiri, *J. Org. Chem.*, **40**, 2960 (1975); b) Y. Ogata and K. Matsuyama, *Tetrahedron*, **26**, 5929 (1970); c) Y. Ogata and T. Sugimoto, *Chem. Ind. (London)*, **1977**, 538; d) Y. Ogata and T. Ikejiri, *Nippon Kagaku Kaishi*, **1975**, 1517; e) Y. Ogata, T. Sugimoto, and M. Inaishi, *Bull. Chem. Soc. Jpn.*, **52**, 255 (1979); f) Y. Ogata and T. Sugimoto, *J. Org. Chem.*, **43**, 3684 (1978); g) Y. Ogata and S. Watanabe, *ibid.*, **44**, 2768 (1979); h) Y. Ogata and S. Watanabe, *ibid.*, **45**, in press (1980).

3) Y. Ogata, T. Harada, and T. Sugimoto, *Can. J. Chem.*, **55**, 1268 (1977).

4) Gmelins Handbuch, **7**, 212 (1931).

5) a) F. Gunther and J. Hetzer, U. S. Patent 1926442 [*Chem. Abstr.*, **27**, 6001 (1933)]; b) J. K. Weil, L. P. Witnauer, and A. J. Stirton, *J. Am. Chem. Soc.*, **75**, 2526 (1953); c) E. E. Gilbert, *Chem. Rev.*, **62**, 549 (1962).

6) H. B. Watson, *Chem. Rev.*, **7**, 173 (1930).

7) a) M. S. Newman and E. A. Zuech, *J. Org. Chem.*, **27**, 1436 (1962); b) R. C. Fuson, L. J. Armstrong, D. H. Chadwich, J. W. Kneisley, S. P. Rowland, W. J. Shenk, Jr., and Q. F. Soper, *J. Am. Chem. Soc.*, **67**, 386, 1937 (1945).

8) D. N. Harpp, L. Q. Bao, C. J. Black, J. G. Gleason, and R. A. Smith, *J. Org. Chem.*, **40**, 3420 (1975).

9) C. W. Smith and D. G. Norton, *Org. Synth.*, Coll. Vol. IV, 348 (1963).

Photoinduced Decomposition of Peracetic Acid in Isopropylbenzene[1)]

Yoshiro OGATA* and Kohtaro TOMIZAWA

Department of Applied Chemistry, Faculty of Engineering, Nagoya University, Chikusa-ku, Nagoya 464

(Received February 16, 1980)

Synopsis. Irradiation of peracetic acid in isopropylbenzene with 254 nm and over 290 nm lights gave as aromatic products mainly *t*-butylbenzene, 2-phenyl-2-propanol, and 2,3-dimethyl-2,3-diphenylbutane. The yield of *t*-butylbenzene was higher in 254 nm photolysis than that with >290 nm, while the yield of hydroxylated aromatics, *i. e.*, 2-phenyl-2-propanol, was much higher with >290 nm than that with 254 nm. The distribution of products was little affected by the intensity of light. These results are discussed by a mechanism involving radicals of different reactivity derived from peracetic acid decomposition.

As reported by us previously, the photolysis of peracetic acid in aromatic hydrocarbons gives fairly stable radicals (*e.g.*, benzyl radical), which in >290 nm photolysis react with peracetic acid through an induced reaction to give hydroxylated product (*e.g.*, benzyl alcohol), but in 254 nm photolysis the contribution of this induced decomposition was less than that at >290 nm.[2-4)]

The change of decomposition rate of peracid with changing light intensity affects the rate of radical formation but affects little the distribution of products.[4)] Therefore, the marked difference in yields in 254 nm and >290 nm photolyses may depend on the wavelength.[4)]

In this paper, we selected isopropylbenzene because α-H-atom of isopropylbenzene is easily abstracted to give a stable radical, $PhMe_2C\cdot$; this solvent is suitable for examination of the possibility of exciplex formation.

Results and Discussion

The photolysis of peracetic acid (**1**) in isopropylbenzene was carried out with three sorts of light sources, *i.e.*, a 30 W low-pressure Hg lamp (254 nm light), a 300 W (>290 nm light), and a 1 kW high-pressure Hg lamp (>290 nm light). Table 1 shows the product yields which are average of six runs at $1.2—30.9\times10^{-2}$ M peracid concentration. These products were identified by GLC and GC-MS in comparison with their authentic samples.

Formed butylbenzenes (side chain methylation products) are consisted of *s*- and *t*-butylbenzene, the ratio of yields for *s*: *t* being 1: 5—7. The low ratio is due to the easier abstraction of tertiary H-atom of the side chain than that of primary H-atom. Isopropyltoluenes (cymenes), which were formed by an attack of methyl radical on the ring, gave yields of three isomers in the order; ortho>meta≈para at both 254 nm and >290 nm.

2-Phenylpropanols were formed by side chain hydroxylation. The yield of 2-propanol was much higher than 1-propanol. Isopropylphenols were obtained by hydroxylation of the ring in the order of yield: ortho≳para>meta. 2,3-Dimethyl-2,3-diphenylbutane was formed by the coupling of radical $PhMe_2C\cdot$; furthermore, an adduct of radical $PhMe_2C\cdot$ to the ring, $PhMe_2C-C_6H_4-CHMe_2$, was detected by GC-MS (see Experimental).

Table 1. Products and yields in photolysis of peracetic acid (**1**) in isopropylbenzene (**2**)[a)]

Products (%)[b)]	Light (nm)		
	254	>290(1 kW)	>290 (300 W)
Oxygen	6.4	4.2	5.7
Water	38.6	19.7	18.0
Methane	40.6	68.3	74.2
Ethane	5.9	2.8	1.6
Methanol	8.6	9.9	4.6
Butylbenzenes[c)]	21.2	7.0	5.0
Isopropyltoluenes[d)]	6.0	2.5	2.7
2-Phenylpropanols[e)]	14.1	46.6	42.5
Isopropylphenols[d)]	3.9	3.5	1.4
2,3-Dimethyl-2,3-diphenylbutane	24.6	31.1	28.1

a) The average of six runs. b) (Mol of product/mol of decomposed **1**) × 100, except with oxygen, ethane, and 2,3-dimethyl-2,3-diphenylbutane, for which this figure is doubled. c) Total amounts of *s* and *t*-isomers. d) Total amounts of ortho, meta, and para-isomers. e) Total amounts of 2-phenyl-1-propanol and -2-propanol. f) This value containes that of $PhMe_2C-C_6H_4-CHMe_2$.

In this photolysis, there were little time dependence within 80% conversion of **1** and little effect of the peroxy acid concentration on the product yields, except for 2,3-dimethyl-2,3-diphenylbutane, a dimerization product of $PhMe_2C\cdot$, yield of which increased (≈10%) with decreasing peroxy acid concentration. This decrease of peracid concentration favors the fraction of addition of $PhMe_2C\cdot$ to isopropylbenzene to form $PhMe_2C-C_6H_4-CHMe_2$ rather than coupling of $PhMe_2C\cdot$ with other radicals.

The half-times for decomposition of peracetic acid depend on the lamp in the order: 1 kW(>290 nm)<30 W(254 nm)<300 W(>290 nm); *e.g.*, *ca.* 2 h with a 1 kW lamp(>290 nm), *ca.* 4 h with a 30 W lamp(254 nm), and *ca.* 8 h with a 300 W (>290 nm) at 2.19×10^{-1} M peracid. The highest concentration of radicals is expected with a 1 kW lamp.

As apparent from Table 1, the product distribution with >290 nm(1 kW) is similar to that with >290 nm(300 W), but different from that with 254 nm; these results are inconsistent with the rate of peroxy acid decomposition, *e.g.*, the yields of butylbenzenes were higher at 254 nm than those at >290 nm, but the yields of 2-phenylpropanols were reversed. Therefore, this discrepancy between the yields and the rate of peracid decomposition suggests that, even in isopropylbenzene, the product distribution depends on the wave length rather than the light intensity.

This is explicable by the difference of excited species, *i.e.*, aromatic solvent which is in large excess is mainly excited with 254 nm light, transferring the excited energy to peroxy acid (Eqs. 1—3), but peracetic acid is excited directly by >290 nm light (Eq. 4), in view of no absorbance of >290 nm light by aromatics.

$$[PhCHMe_2] \xrightarrow{h\nu\ (254\ nm)} [PhCHMe_2]^* \qquad (1)$$

$$[PhCHMe_2]^* + CH_3CO_3H \longrightarrow PhCHMe_2 + [CH_3CO_3H]^* \quad (2)$$

$$[CH_3CO_3H]^* \longrightarrow CH_3CO_2\cdot + HO\cdot \longrightarrow CH_3\cdot + CO_2 + HO\cdot \quad (3)$$

$$CH_3CO_3H \xrightarrow{h\nu\,(>290\ nm)} CH_3CO_2\cdot + HO\cdot \longrightarrow CH_3\cdot + CO_2 + HO\cdot \quad (4)$$

Active species generated *via* Eqs. 1—3 with 254 nm light are identical with those *via* Eq. 4 with >290 nm light. Therefore, assuming that all products are formed *via* these species, the product distribution should be similar in 254 nm and >290 nm photolyses, but this is not the case (Table 1). The higher yield of methylated aromatics with 254 nm may be explained by the formation of a sort of exciplex (Eqs. 5—6).[4]

$$[PhCHMe_2]^* + CH_3CO_3H \longrightarrow [PhCHMe_2\cdot CH_3CO_3H]_{ex} \quad (5)$$

$$[PhCHMe_2\cdot CH_3CO_3H]_{ex} \longrightarrow PhCMe_3 + CO_2 + H_2O \quad (6)$$

On the other hand, a main path for *t*-butylbenzene at >290 nm may be radical coupling between $PhMe_2C\cdot$ and Me·.

The reactivity of radical HO· is higher than that of Me·; *i.e.*, both the H-abstraction by HO· and the addition of HO· to the ring are faster than those of Me·,[5] but in spite of the higher decomposition rate of peracetic acid with >290 nm(1 kW), the yields of water and isopropylphenols at >290 nm(1 kW) are lower than the yields at 254 nm. Therefore, the preferential formation of 2-phenylpropanol at >290 nm is attributable to the effective reaction of HO-group of peracetic acid; *i.e.*, to the induced decomposition of peracetic acid by $PhMe_2C\cdot$ (Eq. 7) beside radical coupling (Eq. 8) and the pathway *via* 1-methyl-1-phenylethylhydroperoxide (Eq. 9).

$$CH_3CO_2\text{–}OH + PhMe_2C\cdot \longrightarrow PhMe_2C\text{–}OH + CH_3CO_2\cdot \quad (7)$$

$$PhMe_2C\cdot + HO\cdot \longrightarrow PhMe_2C\text{–}OH \quad (8)$$

$$PhMe_2C\cdot + O_2 \longrightarrow PhMe_2C\text{–}OO\cdot \longrightarrow\longrightarrow PhMe_2C\text{–}OH \quad (9)$$

The pathway *via* Eq. 9 is possible, because the reaction of radical R· with O_2 gives ROO·, followed by the formation of hydroxylated compound.[6]

Oxygen evolved in this system may be formed *via* dark disproportionation of peroxy acid and/or decomposition of acetylperoxyl radical.[7] Therefore, the induced decomposition (Eq. 10) was confirmed by the evolution of O_2 and by the higher yields of methane and water than the total yields of aromatic products. Hence, peracetic acid is one of H-atom sources.

$$CH_3CO_3\text{–}H + R\cdot \longrightarrow CH_3CO_3\cdot + RH \quad (10)$$

These results have been observed with toluene and ethylbenzene. In conclusion, (i) the yields of methylated aromatics are higher at 254 nm than those at >290 nm. (ii) Hydroxylation of side chain occurs probably *via* Eqs. 7, 8, and 9. The higher yields of hydroxylated products at >290 nm than at 254 nm may be due to the Eq. 7, which needs CH_3CO_3H and hence favored at >290 nm than at 254 nm. Therefore, hydroxylation of side chain is a preferential pathway at >290 nm.

Experimental

Materials. The synthses of peracetic acid (**1**) and a water-free peracetic acid–isopropylbenzene solution were described in our previous paper.[2-4] Samples of commercial guaranteed reagent grade were used as authentic samples of GLC.

Apparatus. GLC analyses were performed on a Yanagimoto gas chromatograph with FID and TCD, Model G 180. A Shimadzu GC-MS 7000 gas chromatograph-mass spectrometer was used to determine and identify the photolysis products. A Halos low-pressure 30 W Hg lamp, a Halos high-pressure 300 W Hg lamp, and a Halos high-pressure 1 kW Hg lamp were used as light sources. All experiments were carried out in a cylindrical quartz vessel (2×12 cm) or a cylindrical Pyrex vessel (2×12 cm) and were repeated in triplicate.

Photolysis of Peracetic Acid in Isopropylbenzene. Peracetic acid in isopropylbenzene was photolyzed in a quartz vessel with a 30 W low-pressure Hg lamp or in a Pyrex vessel with a 300 W high-pressure Hg lamp or with a 1 kW high-pressure Hg lamp through a water jacket. After estimation of peracid remained in the solution, a given amount of Me_2SO–benzene was added to the photolysate to avoid the contamination caused by the peracid thermolysis during GLC. Gaseous products were analyzed by the method previously described[2,3] and the products in the solutions were identified and estimated by GLC with FID and TCD (Porapak QS, Bentone 34-DIDP and PEG 20M-Silicone DC 550) in comparison with authentic samples.

GC-MS Analysis of Aromatic Products. Photolysis products were characterized by means of GC-MS employing a column packed with Bentone 34-DIDP for aromatic hydrocarbons as follows: *t*-butylbenzene, *m/e* 134 (M^+), 119 (base peak), 41, and 39; *s*-butylbenzene, *m/e* 134 (M^+), 106, 105 (base peak), and 91; isopropyltoluene, *m/e* 134 (M^+), 119 (base peak), and 91, the elution order of isopropyltoluenes by GLC was para, meta, and ortho-isomer. Other aromatic products were characterized by a column packed with PEG 20M-Silicone DC 550; 2-phenyl-1-propanol, *m/e* 136 (M^+), 106, 105 (base peak), 103, 92, and 91; 2-phenyl-2-propanol, *m/e* 136 (M^+), 121, 118, 117, 115, 108, 91, and 43 (base peak); isopropylphenols, *m/e* 136 (M^+) and 121 (base peak); coupling product, 2,3-dimethyl-2,3-diphenylbutane, *m/e* 238 (M^+) and 119 (base peak); $PhMe_2\text{–}C_6H_4\text{–}CHMe_2$, *m/e* 238 ($M^+$) and 223 (base peak).

References

1) Contribution No. 256.

2) Y. Ogata and K. Tomizawa, *J. Org Chem.*, **43**, 261 (1978).

3) Y. Ogata and K. Tomizawa, *J. Org. Chem.*, **43**, 1920 (1978).

4) Y. Ogata and K. Tomizawa, *J. Org. Chem.*, **44**, 2770 (1979).

5) J. K. Kochi, "Free Radicals," John Wiley (1973), Vol. 1, pp. 70—83.

6) K. Selby and D. J. Waddington, *J. Chem. Soc., Perkin Trans. 2*, **1980**, 65.

7) a) N. A. Clinton, R. A. Kenley, and T. G. Traylor, *J. Am. Chem. Soc.*, **97**, 3746 (1975); b) N. A. Clinton, R. A. Kenley, and T. G. Traylor, *ibid.*, **97**, 3752 (1975); c) R. A. Kenley and T. G. Traylor, *ibid.*, **97**, 4700 (1975).

Photo-CIDNP Observed in *O*-Methylbenzoin-Carbon Tetrachloride System

Kazuhiro MARUYAMA, Hiroyuki FURUTA, and Tetsuo OTSUKI
Department of Chemistry, Faculty of Science, Kyoto University, Kyoto 606

(Received February 19, 1980)

Synopsis. Photo-induced decomposition of *O*-methylbenzoin in carbon tetrachloride was investigated. A reaction scheme is proposed with the aid of photo-CIDNP technique and product analysis.

Photodecomposition of benzoin and its derivatives has been investigated mainly from the standpoint as initiators of photo-polymerization.[1a-f] By means of CIDNP photo-induced α-cleavage of benzoin has already been examined in correlation with photochemical reaction of benzaldehyde, because both processes generate common radical pair, *i.e.*, pair of benzoyl radical and α-hydroxybenzyl radical.[2a-c] Though these studies were carried out in rather inert solvent, *e.g.*, benzene, methanol, or acetonitrile, here we investigated the photo-induced decomposition of *O*-methylbenzoin in good chlorine atom donor; carbon tetrachloride. From the viewpoint to investigate the escaping feature of the incage radical pair, carbon tetrachloride is a helpful solvent. In actual, chlorine atom and trichloromethyl radical incorporated with the photodecomposition processes of *O*-methylbenzoin.

When a carbon tetrachloride solution of *O*-methylbenzoin **1** was deaerated and irradiated with a high pressure Hg arc lamp for 30 min, **1** decomposed completely. Benzoyl chloride **2** (94 mol%), benzaldehyde **3** (41 mol%), 1-methoxy-1-phenyl-2,2,2-trichloroethane **4** (28 mol%), an equimolar mixture of diastereomeric *O,O'*-dimethylbenzopinacol **5** (7 mol%), hexachloroethane **6** (48 mol%), and α,α,α-trichloroacetophenone **8** (a trace) were identified in the reaction mixture (yields were calculated on the basis of **1**) (Scheme 1). This product distribution is quite different from that observed in other solvents as benzene or acetonitrile.[1b,c,d] In the latter cases, **5** is a major product (60—70%, quantum yield;≈0.35), accompanied by less amounts of benzil (<10%). This fact clearly indicates participations of chlorine atom and trichloromethyl radical in the escaping process of the incage radical pair.

The CIDNP spectrum observed during the irradiation of carbon tetrachloride solution of **1** is illustrated in Fig. 1(A). Polarized emission was observed in the methine proton of the starting material **1** (siganl 2). Besides the signal 2, three distinct polarized signals (indicated as signal 1, 3, and 5) were observed. In comparison of their chemical shifts with those of the authentic samples, the polarized signals 1 and 3 are assignable to the methine proton of 1-methoxy-1-phenyl-2,2,2-trichloroethane **4** (δ: 4.58 ppm) and that of α-chlorobenzyl methyl ether **7** (δ: 6.36 ppm), respectively. The polarized signal 5 is originated from the formyl proton of benzaldehyde **3**. Although the

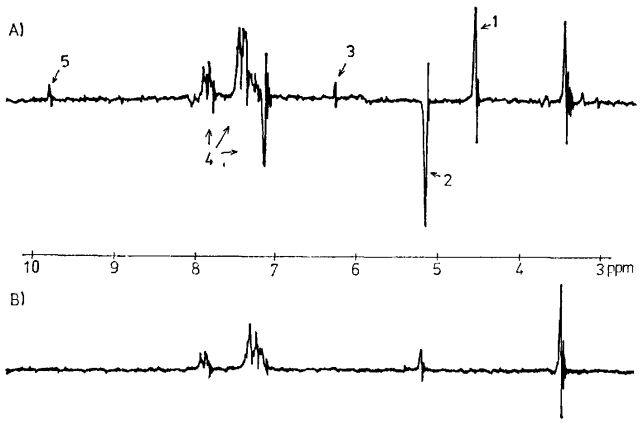

Fig. 1. Photo-CIDNP spectra of *O*-methylbenzoin in carbon tetrachloride.
A): During irradiation, B): before irradiation.

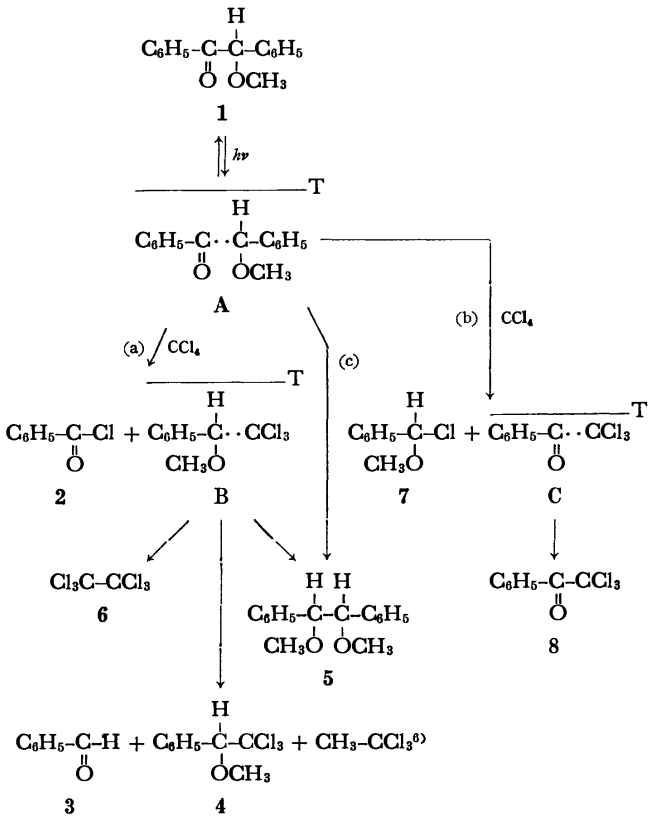

Scheme 2.

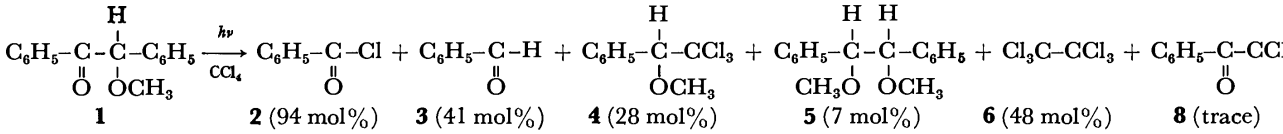

Scheme 1.

polarized signals in the region of aromatic protons cannot be assigned unambiguously, they consist of the overlapped aromatic proton signals of **1**, **2**, **3**, **4**, **7**, and **8**. The directions of the polarizations were in good agreement with the expected from the simple rule by Kaptein,[3] assuming the radical pair **A**, **B**,[4] and **C**[4] which have triplet multiplicity[5] (Scheme 2).

Observation of CIDNP signal due to **1** indicates the presence of the back process of α-cleavage, that is, regeneration of **1** from radical pair **A** once produced. Apart from the regeneration of **1**, the radical pair **A** could collapse *via* paths (a), (b), and (c) (Scheme 2). Almost quantitative yield of benzoyl chloride **2** (94 mol%) clearly shows that the major path is the path (a). α-Methoxybenzyl radical, the other moiety of the radical pair **A**, is also stabilized as benzaldehyde **3** (41 mol%), 1-methoxy-1-phenyl-2,2,2-trichloroethane **4** (28 mol%), and *O*,*O*′-dimethylbenzopinacol **5** (7 mol%). On the other hand, minor path (b) is taking place, because of detections of α-chlorobenzyl methyl ether **7** by CIDNP (signal 3) and α,α,α-trichloroacetophenone **8** by GLC.[6] Even if in part, path (b) as well as path (c) might contribute to the formation of hexachloroethane **6**. The relative intensity of polarized CIDNP signals (signal 1/signal 3) suggests again the preponderance of path (a), though the polarized intensity of CIDNP signals doesn't directly reflect the amounts of the corresponding products.

As described above photodecomposition of **1** in carbon tetrachloride takes a quite different path (path (a)) compared with those observed in other inert solvents, allowing a greater participation of carbon tetrachloride in it. This is highly suggesting that the use of carbon tetrachloride as an additive of "sensitizer," *O*-methylbenzoin, in photo-polymerization system is promising to raise the initiation rate.

Experimental

Materials. Commercially available benzaldehyde, benzoyl chloride, and hexachloroethane were used as the authentic samples without further purification. *O*-Methylbenzoin was a gift from Nippon Gosei Kagaku Co., Ltd., (Osaka, Japan) and used without further purification. 1-Methoxy-1-phenyl-2,2,2-trichloroethane,[7] *dl*- and *meso*-*O*,*O*′-dimethylbenzopinacol,[8] α-chlorobenzyl methyl ether,[9] and α,α,α-trichloroacetophenone[10] were synthesized according to the literatures. Carbon tetrachloride was dehydrated by refluxing the commercially available reagent-grade of the reagent in the presence of calcium hydride and distilled under nitrogen atmosphere.

Photochemical Reaction. A carbon tetrachloride solution (15 ml) of *O*-methylbenzoin **1** (0.13 mmol) was irradiated with a high pressure Hg arc lamp (300 W) under nitrogen atmosphere at room temperature. After the complete consumption of **1**, the reaction mixture was analyzed by GLC (Silicone DC 550-column) compared with the authentic samples. Yields of the products were estimed by means of GLC.

CIDNP Measurement. The PS-100 type of NMR spectrometer manufactured by JEOL was modified for CIDNP measurement as described previously.[11]

References

1) a) A. Ledwith, P. J. Russell, and L. H. Sutcliffe, *J. Chem. Soc., Perkin Trans. 2*, **1972**, 1925; b) H. G. Heine, *Tetrahedron Lett.*, **1972**, 4755; c) S. P. Pappas and A. Chattopadhyay, *J. Am. Chem. Soc.*, **95**, 6484 (1973); d) F. D. Lewis, R. T. Lauterbach, H. G. Heine, W. Hartman, and H. Rudolph, *ibid.*, **97**, 1519 (1975); e) F. D. Lewis, C. H. Hoyle, and J. G. Magyar, *J. Org. Chem.*, **40**, 488 (1975); f) A. Borer, R. Kirchmayr, and G. Rist, *Helv. Chim. Acta*, **61**, 305 (1978).

2) a) M. Cocivera and A. M. Trozzolo, *J. Am. Chem. Soc.*, **92**, 1772 (1970); b) G. L. Closs and D. R. Pauson, *ibid.*, **92**, 7229 (1970); c) H. D. Roth, *Mol. Photochem.*, **5**, 91 (1973).

3) R. Kaptein, *J. Chem. Soc., Chem. Commun.*, **1971**, 732.

4) The pairs **B** and **C** are generated from **A** *via* pair substitution. *Cf.* R. A. Cooper, R. A. Lawler, and H. D. Ward, *J. Am. Chem. Soc.*, **94**, 552 (1972).

5) The CIDNP signals are analyzed by assuming that *g*-values of the radicals are in the following order of magnitude: $\dot{C}Cl_3 > C_6H_5\dot{C}HOCH_3 > C_6H_5\dot{C}O$ and that the sign of the coupling constant for the α-proton of $C_6H_5\dot{C}HOCH_3$ is negative. *Cf.* H. Fischer, "Free Radicals," ed by J. K. Kochi, John-Wiley and Sons Inc., New York (1973), p. 435.

6) A trace amount of α,α,α-trichloroacetophenone could be identified by GLC from the reaction mixture. On the other hand, 1,1,1-trichloroethane colud not be identified.

7) A. Meiz and R. Tomaphgh, *Chem. Ber.*, **110**, 96 (1977).

8) D. A. Shearer and G. F. Wright, *Can. J. Chem.*, **33**, 1002 (1955).

9) E. Atraus and H. Heinze, *Justus Liebigs Ann. Chem.*, **493**, 203 (1932).

10) J. Houben and W. Fischer, *J. Prakt. Chem.*, **123**, 318 (1928).

11) K. Maruyama, T. Otsuki, A. Takuwa, and S. Arakawa, *Bull. Chem. Soc. Jpn.*, **46**, 2470 (1973).

Reaction of Phenacyltriphenylarsonium Bromides with *N*-Methylaniline and *N,N*-Dimethylaniline

Raj Kumar BANSAL* and Gope BHAGCHANDANI
Department of Chemistry, University of Rajasthan, Jaipur-302004, India
(Received February 12, 1980)

Synopsis. Reaction of phenacyltriphenylarsonium bromide with *N*-methylaniline furnished 2-phenylindole predominantly together with 1-methyl-2-phenylindole. The corresponding reaction of the arsonium salt with *N,N*-dimethylaniline did not give any indole, instead a simple nucleophilic substituted product, α-4′-(dimethylamino)deoxybenzoin was obtained. But, the latter reaction on being carried out in presence of hydrobromic acid afforded 1-methyl-2-phenylindole by the demethylation of *N,N*-dimethylaniline.

In an earlier communication,[1] we reported the reaction of phenacyltriphenylarsonium bromide with anilines leading to the formation of 2-arylindoles and it was shown that the nucleophilic addition of aniline to the carbonyl group of the arsonium salt preceded the formation of the ylide. In an attempt to extend this reaction to aromatic secondary and tertiary amines, we carried out the reactions of phenacyltriphenylarsonium bromide(s) with *N*-methylaniline and *N,N*-dimethylaniline. The results obtained were quite interesting and could be explained on the basis of the mechanism we proposed earlier.[1]

Results and Discussion

Phenacyltriphenylarsonium bromide (**1a**) reacted with *N*-methylaniline to give 2-phenylindole (**2**, 50%) and 1-methyl-2-phenylindole (**3a**, 5%). *N*-Methylaniline, like aniline, acting as a typical nucleophile interacts with the arsonium salt to form the alkylideneammonium species, **4** (Scheme 1). The formation of **2** indicates that **4** does not follow exactly the same route as observed in the case of aniline[1] because in that event 1-methyl-2-phenylindole would have been obtained exclusively. It appears that the species **4** follows two routes: (i) deprotonation of **4** gives the ylide **5** which subsequently undergoes cyclization *etc.* as observed in the case of aniline,[1] to afford **3a** (path a) and (ii) demethylation of **4** precedes the formation of the ylide **7**, the latter finally gives **2** by cyclization *etc.* (path b). The excess formation of **2** in comparison to **3a** indicates that demethylation of species **4** (path b) is preferred over its deprotonation (path a). An alternative possibility of the initial formation of **3a** followed by its demethylation to **2** is ruled out on the basis of the observations made by Chambers and Pearson[2] in connection with the dealkylation of cyclic amines.

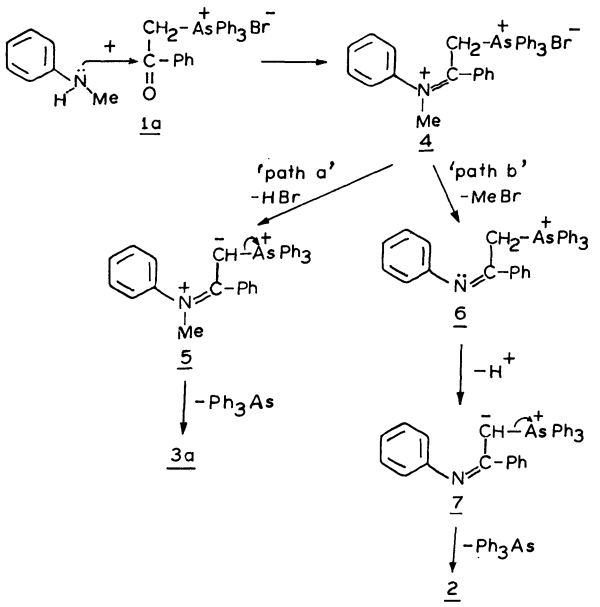

Scheme 1.

N,N-Dimethylaniline behaved in a different manner; it reacted with **1a** to afford simple nucleophilic substitution product, α-4′-(dimethylamino)deoxybenzoin (**8**) and no indole was obtained. This is in accordance with the general behaviour of $PhNMe_2$ towards nucleophilic displacement.[3] When $PhNMe_2$ was refluxed with **1a**

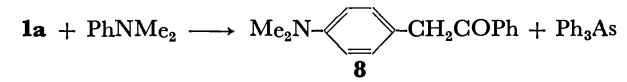

in presence of hydrobromic acid, **3a** was obtained in 36% yield. Similarly $PhNMe_2$ reacted with **1b—d** in the presence of HBr to give the corresponding 1-methyl-2-arylindoles (**3b—d**) (Table 1). The results obtained

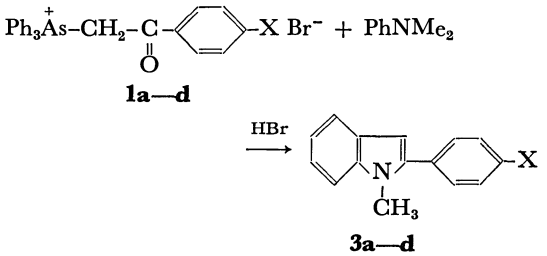

Table 1. 1-Methyl-2-arylindoles

Compound	X	Yield %	Mp/°C	Lit[4], Mp/°C
3a	H	36	100	99—100
3b	Cl	41	119	118—120
3c	Br	39	115	114—116
3d	OCH_3	35	117—118	118—119

with $PhNMe_2$ can be explained like this. The presence of two bulky methyl groups on nitrogen prevents the donation of its electron pair to the carbonyl group of the arsonium salt. But, in the presence of HBr, *N*,*N*-dimethylanilinium bromide is formed which undergoes facile demethylation to *N*-methylaniline.[2] The latter subsequently reacts with the arsonium salt as described earlier. Further, in the presence of HBr, path b is blocked due to the formation of MeBr from demethylation of $PhNMe_2$ and therefore only **3a** is formed.

$$PhNMe_2 + HBr \longrightarrow Ph\overset{+}{N}HMe_2Br^- \rightleftharpoons PhNHMe + MeBr$$

Experimental

General Procedure. Arsonium salt (10 mmol) and PhNHMe or $PhNMe_2$ (20 ml) were refluxed for 7 h. The reaction mixture was taken in chloroform, washed with 10% aqueous hydrochloric acid solution and then with water. The chloroform extract was chromatographed on silica gel. Elution with pet. ether (60—80 °C) and pet. ether–benzene (1: 1) furnished Ph_3As (mp 60 °C) and the corresponding indole(s) respectively. Reaction of the arsonium salt with $PhNMe_2$ in the presence of HBr (4 ml) was carried out in a similar manner.

We are indebted to Dr. G. Srivastava for helpful discussions. Financial support from C.S.I.R., New Delhi is gratefully acknowledged.

References

1) R. K. Bansal and S. K. Sharma, *Tetrahedron Lett.*, **1977**, 1923.
2) R. A. Chambers and D. E. Pearson, *J. Org. Chem.*, **28**, 3144 (1963).
3) Y. Pocker, *J. Chem. Soc.*, **1959**, 3944.
4) D. J. Gale, J. Lin, and J. F. K. Wilshire, *Aust. J. Chem.*, **29**, 2747 (1976).

Photocyclization of *o*-Nitrophenyl Alkyl Ethers

Shōshichi OGUCHI* and Hiroshi TORIZUKA

Department of Chemistry, Faculty of Education, The Tokyo Gakugei University, Koganei-shi, Tokyo 184

(Received January 5, 1980)

Synopsis. *o*-Nitrophenyl alkyl ethers **1a**, **1b**, and **1c** undergo photocyclization to give benzoxazoles **2a**, **2b**, and **2c**, respectively.

Nitro functions are known to undergo intermolecular and intramolecular hydrogen abstractions from the n,π^* state.[1,2] Although photochemical reaction of *o*-nitrophenyl alkyl ethers have been reported by McMahon, he didn't mention about photo-products other than dealkylation products.[3]

We here report that *o*-nitrophenyl alkyl ethers undergo photocyclization through intramolecular hydrogen abstraction by the excited nitro group. Irradiation of *o*-nitrophenyl benzyl ether **1a** in benzene under nitrogen atmosphere with a high pressure mercury lamp gave 2-phenylbenzoxazole **2a** in 62% yield together with *o*-nitrophenol **3** (trace) and benzaldehyde (4%). The latter compounds are resulted from dealkylation processes.[2] Similarly, irradiation of *o*-nitrophenyl

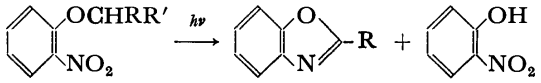

1 **2** **3**

ethers **1b** and **1c** under the same conditions gave benzoxazoles **2b** and **2c** respectively, and *o*-nitrophenol **3**. In these cases aldehydes could not be isolated. In the case of **1d**, no cyclization product was obtained.

TABLE 1. THE YIELDS OF **2** AND **3**

	1		Yield(%) of **2**	Yield (%) of **3**
	R	R′		
1a	Ph	H	62	trace
1b	CH_3	H	61	trace
1c	H	H	trace	21
1d	CH_3	CH_3	0	trace

Photocyclization of **1b** was efficiently quenched by 1,3-pentadiene (E_T=58—59 kcal, 1 cal_{th}=4.184 J),[4] and the reaction was effectively sensitized by benzophenone (E_T=69 kcal) and 4,4′-bis(dimethylamino)-benzophenone (62 kcal).[4] These results indicate that cyclization occurs from the triplet state of the nitrophenyl alkyl ethers. Nitrophenyl alkyl ethers **1b** and **1c** showed peaks of the ultraviolet absorption at 325 nm (ε 3470) and 317 nm (ε 2850), respectively, in ethanol. The peak shifted to 309 nm (ε 4200) and 304 nm (ε 2500), respectively, in cyclohexane. These results indicate that the absorptions are attributable to the π,π^* transition. Therefore, the ethers are initially excited to the π,π^* states.

Intramolecular hydrogen abstraction proceeds from the n,π^* state of aromatic nitro compounds.[1,2] The formation of benzoxazoles from the nitrophenyl alkyl ethers may be explained in terms of photocyclization through δ-hydrogen abstraction by the nitro group from the n,π^* triplet state (Scheme 1). Similar mechanism of photocyclization of *N*-substituted *o*-nitroanilines has been reported by Field *et al.*[5]

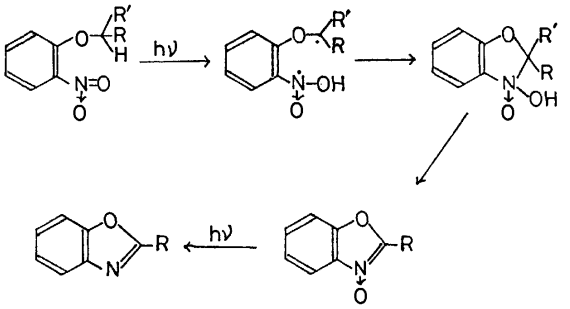

Scheme 1.

Experimental

Materials. The *o*-nitrophenyl alkyl ethers **1a**—**1d** were prepared by the usual methods from *o*-nitrohalobenzene and the corresponding sodium alkoxide. Benzoxazoles were commercially available.

General Procedure for Photolysis of o-Nitrophenyl Ether. A nitrophenyl ether (**1**) (600 mg) in hexane (400 ml) was irradiated with a high-pressure mercury vapor 450W lamp (Ushio elect. Co.) for 1.5 h. After removal of the solvent the residue was chromatgraphed on silica gel. Elution with a mixture of chloroform–benzene (volume ratio 7: 1) gave a benzoxazole (**2**) and nitrophenol (**3**). The structure of **2** was determined by comparison with an authentic sample.

References

1) R. Hurley and A. C. Testa, *J. Am. Chem. Soc.*, **88**, 4330 (1966).

2) a) "The Chemistry of the Nitro and Nitroso Groups," ed by H. Heuer, Interscience Publishers, New York and London (1969), Part 1, p. 181; b) W. A. Noyes, G. S. Hammond, and J. N. Pitts, Jr., "Advances in Photochemistry," Interscience Publishers, New York and London (1963), Vol. 1, p. 283.

3) R. E. McMahon, *Tetrahedron Lett.*, **1966**, 2307.

4) S. L. Murov, "Handbook of Photochemistry," MARCEL DEKKER, INC. New York (1973).

5) R. Fielden, O. Meth-Cohn, and Suschitzky, *J. Chem. Soc., Perkin Trans. 1*, **1973**, 696.

Hydrates of Organic Compounds. V. The Clathrate Hydration of Alcohols

Haruo NAKAYAMA* and Masayuki HASHIMOTO

Department of Chemistry, Faculty of Engineering, Yokohama National University, Tokiwadai, Hodogaya-ku, Yokohama 240

(Received November 27, 1979)

A new method for examining the ability of a given substance to form a hydrate with the same structure as that of a reference substance has been established. By using this method, for a series of alcohols ranging from methyl alcohol to pentyl alcohol, including their isomers, the ability to form a clathrate hydrate of either Structure I or Structure II has been investigated. It has been found that: (1) methyl alcohol has the ability to form both Structure I and II hydrates; (2) ethyl alcohol has the ability to form a Structure II hydrate; (3) all C_3-alcohols (propyl, isopropyl, allyl, and propargyl alcohol) can actually form Structure II hydrates with relatively high (around -10 °C) incongruent melting points, and (4) among the C_4- and C_5-alcohols, only *t*-butyl alcohol has the ability to form a Structure II hydrate. However, it is uncertain for methyl and ethyl alcohols whether they actually can form such hydrates even in the absence of a reference substance. These results strongly suggest that the size and/or shape limitation plays an important role in the formation of alcohol hydrates with a gas-hydrate structure, just as has been found for the formation of ether and ketone hydrates.

A group of polar substances, such as ethers (dimethyl ether,[1-3] tetrahydrofuran,[1,4-9] ethylene oxide,[1,8,9] 2,5-dihydrofuran,[4-6,9] propylene oxide,[4-6,9] trimethylene oxide,[4-6,9] and 1,3-dioxolane[5,6,9,10]) or ketones (cyclobutanone[5,6,11] and acetone[12-14]), are new known to form so-called "gas hydrates" with von Stackelberg's Structures I and II,[15] in which hydrogen-bonded water molecules form host lattices with specific polyhedral voids, such as tetrakaidecahedron and hexakaidecahedron.

Among a group of polar substances whose clathrate hydration has not been extensively studied is a series of alcohols. The formation of a solid different from ordinary ice in concentrated aqueous solutions of alcohols (such as ethyl alcohol, propyl alcohol, isopropyl alcohol, and allyl alcohol) was reported as early as 1896,[16] and later works have also suggested the existence of ethyl alcohol hydrate.[17] An extensive study by Potts *et al.*[18] in 1965 showed the existence of an ethyl alcohol hydrate below -73.5 °C. Its composition was near $C_2H_5OH \cdot 17H_2O$, similar to the Structure-II gas hydrates. On the other hand, from crystallographic studies Sargent *et al.*[5] concluded that the hydrate formed in the $C_2H_5OH+H_2O$ system was not Type II, and Calvert *et al.*[19] showed that there were more than one hydrate: Type I, with a structural disorder similar to that of ethylene oxide hydrate, and a modified Type II hydrate. Thus, even now there is some uncertainty concerning the structure and properties of ethyl alcohol hydrate. Of the other alcohols, though some irregular behavior has been found in the phase diagrams of alcohol+water binary systems,[20,21] no clathrate hydration has so far been reported.

In this investigation, in order to identify the clathrate hydration of alcohols phase-diagrammatically, we made use of the phenomenon of the "mixed hydrate" formation of alcohols with a reference substance like tetrahydrofuran. Since Structure II hydrates are exclusively formed by molecules with diameters in the range of 5.6—6.6 Å,[22] and since the molecular diameters of the alcohols examined in this study, except for methyl alcohol, are greater than 6 Å, we will primarily discuss the formation of a hydrate of Structure II except for the case of the clathration of methyl alcohol. In Structure II hydrates, as is also true in Structure I hydrates, the structures of the hydrogen-bonded water frameworks are all essentially the same, apart from a slight distortion caused by the nature of the individual guest molecule; they comprize an iso-structural series with similar unit-cell dimensions[5] and crystal symmetry. Thus, it can be anticipated that, when two components have molecules of a size that form Structure II hydrates, a solid solution which has an intermediate decomposition temperature will be formed by mixing them. In reality, the formation of a solid solution of this kind has already been confirmed in several systems.[23-25]

Another striking feature possessed by these hydrates is that the guest molecules nearly fully occupy large voids (16-hedra in Structure II hydrate). This means that most of these hydrates are stoichiometric[22] and that, therefore, the composition of Structure II hydrate is close to $M \cdot 17H_2O$, in which M stands for the guest molecule. From these considerations, it can reasonably be anticipated that the mixed hydrate formed from a binary-liquid mixture of M+M′, each component of which can form, for example, a Structure II hydrate ($M \cdot 17H_2O$ and $M' \cdot 17H_2O$), will have properties characteristic of a solid solution with complete miscibility and will be expressed by the $(M)_\alpha(M')_{1-\alpha} \cdot 17H_2O$ formula. Each 16-hedron will be occupied by either M or M′, and the relative content of the two will be varied continuously with the change in the conditions, such as the temperature and the composition of the mixture from which the solid solution is formed.

We have developed a new method which enables us to conclude whether one substance M′ can form a hydrate with the same structure as that of M by examining a solid-liquid-phase diagram of a ternary mixture of M+M′+water prepared under specific conditions. Palmer *et al.*[23] also selected, as a criterion for hydrocarbon-type hydrates, the condition that hydrates of mixtures exhibit behavior typical of soild solutions. However, their conclusions, derived from

thermal analyses, are not in agreement with the facts found in subsequent experiments; their method, for example, cannot lead to the fact that acetone forms a Structure II hydrate.

Experimental

Procedure. The procedure is summarized as follows: (1) A substance which has been known to form a congruently melting hydrate of a known structure is chosen as the reference component, M. It is preferable that its congruent melting point be as high as possible. (2) A solid is formed from a series of mixtures of various compositions X ($=X_M+X_{M'}$), with the restriction that the $X_M : X_{M'}$, ratio is kept constant, where X_M and $X_{M'}$, are the mole fractions of M and M′ respectively. (3) For a series of the solids, the temperature (T) at which the solid phase completely disappears is observed and is plotted against X. (4) If the value of X which gives a maximum temperature in the T-X plot for a series of mixtures is independent of the molar ratio, $X_M : X_{M'}$, and is the same as that found for the binary mixture, M+water, we may conclude that the M′ component has at least the ability to form a hydrate of the same structure as that of M, since such behavior should be observed only when a solid solution is formed between M-hydrate and M′-hydrate. In this investigation, as a reference substance (M) we chose tetrahydrofuran (which is abbreviated by THF hereafter) for a Structure II hydrate and ethylene oxide (EO) for a Structure I hydrate.

Materials and Measurements. All the organic reagents used in this report, except for ethylene oxide, were extra-pure reagent-grade and were purified by conventional methods. The ethylene oxide was kindly supplied by the Nihon Shokubai Co., Ltd., and was used without further purification. The water was doubly distilled in an all-Pyrex still. Ternary mixtures of an alcohol, either tetrahydrofuran or ethylene oxide, and water were made up by weight. No attempt was made to remove the air dissolved in the solution. Each solution (about 1—2 cm^3) was sealed in a small glass ampoule and was cooled until the solid phase appeared. Then the ampoule was gradually warmed and was kept standing for more than 10 h at a temperature several degrees lower than its approximate dissolving temperature (which had been determined by a preliminary survey) in order to obtain a well-grown solid phase in equilibrium with its solution phase. Then the ampoule was slowly warmed again (at the rate of 0.2—0.3 °C/h), with frequent shaking in a constant-temperature bath. The solid-liquid-phase diagrams were determined by measuring the temperature at which the solid phase completely disappeared. Such methods as cooling-curve measurements and temperature and calorimetric measurements by the use of a differential scanning calorimeter (Shimadzu Seisakusho, SC-20) were also employed when necessary. In order to confirm the conclusion obtained from the phase-diagrammatic behavior, the approximate content of the alcohol existing in a solid phase, as well as those of tetrahydrofuran and water, was determined by means of gas chromatography (Shimadzu Seisakusho, GC-4APT), using either a 1-m polyethylene glycol column at 60 °C or a 3-m diglycerol column at 100 °C, with a flow rate of the carrier gas (He) of 40 cm^3/min.

Results and Discussion

Confirmation of Validity of the Method. First, in order to test the validity of our method, we obtained the T-X plots for systems containing M′, which had previously been established to form a Structure II hydrate. In Fig. 1 the T-X plots are shown for the THF+1,3-dioxolane system. The 1,3-dioxolane molecule is another example whose hydrate is Structure II and which has a congruent melting point.[5,6,9,10] The top curve (marked with 1:0) and the bottom curve (marked with 0:1) indicate the solid-liquid-phase diagrams of binary mixtures of THF+water and 1,3-dioxolane+water respectively. These two curves clearly show the formation of the THF hydrate and the 1,3-dioxolane hydrate, both of which have a hydration number of 17 (X=1/18=0.056), characteristic of a Structure II hydrate. The observed congruent melting points of these hydrates (5.1 °C for the THF hydrate and −1.5 °C for the 1,3-dioxolane hydrate) are somewhat different from the reported values (4.38 °C[26] and 5.1 °C[4] for the THF hydrate; −5 °C[5] and −3 °C[10] for the 1,3-dioxolane hydrate). This discrepancy may be due to the presence of air in the hydrate, as has often been pointed out.[7] The absolute value of the melting point, however, does not have any influence on the analyses below. The other three curves in Fig. 1 are T-X plots for systems in which the molar ratios of THF:1,3-dioxolane are 1:1, 1:3, and 1:9. It is noteworthy that the dotted line which connects the points of the highest temperature in each curve is vertical around X=0.056, which corresponds to a hydration number of 17. This behavior is exactly the same as was anticipated in the above discussion.

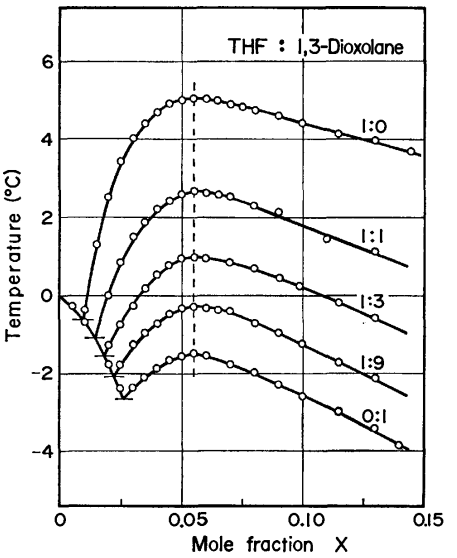

Fig. 1. The solid-liquid-phase diagrams for the THF+1,3-dioxolane+water systems.
The temperatures at which solid phase completely disappears are plotted against total mole fraction (X) of THF and of 1,3-dioxolane. The ratio attached to each curve indicates the molar ratio of THF:1,3-dioxolane in the original solution. Thus the curve marked with 1:0 is a solid-liquid equilibrium curve for THF+water binary system and one with 0:1 is that for 1,3-dioxolane+water binary system. All the following figures are made in a similar manner.

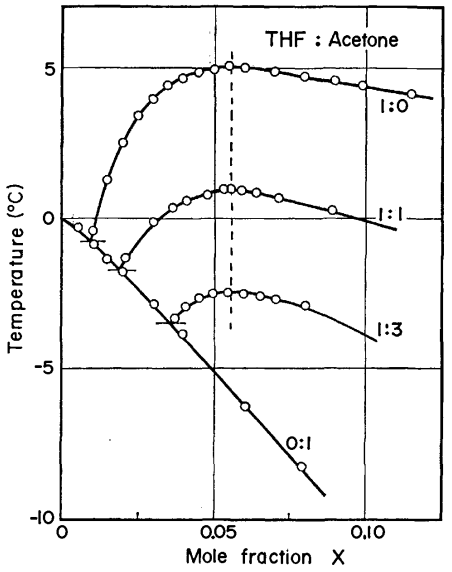

Fig. 2. The solid-liquid-phase diagrams for THF+acetone+water systems.
Explanations are given in Fig. 1.

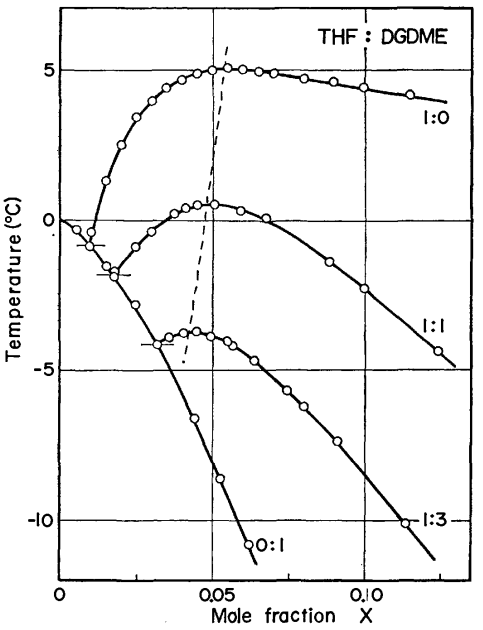

Fig. 3. The solid-liquid-phase diagrams for THF+diethylene glycol dimethyl ether+water systems.
Explanations are given in Fig. 1.

Analogous plots for the THF+acetone system are shown in Fig. 2. Since acetone forms a Structure II hydrate with an incongruent melting point (−19.8 °C[11]), we cannot, of course, observe a peak at X= 0.056 in the T-X plots for the acetone+water binary system. Only an ice-solution equilibrium curve can be obtained at a temperature higher than its incongruent melting point. However, Fig. 2 clearly shows that the T-X plots for mixtures of acetone with THF behave in the same manner as in the case shown in Fig. 1. The X which corresponds to a maximum temperature in each curve is independent of the molar ratio of THF: acetone and is around 0.056, as expected. This indicates that our principle can also be applied to a component which forms an incongruently melting hydrate. As can obviously be seen from Figs. 1 and 2, the maximum temperature in each mixture is quite high as compared with the one calculated from the proportional distribution of the melting points of both hydrates on the molar-ratio basis. This is presumably due to an enrichment of one component with a high melting point in the solid phase, as is often observed in completely miscible solid–solution systems. This effect provides a suitable condition for a temperature peak to appear beyond an ice-solution equilibrium curve, as is exemplified in Fig. 2 and in many other systems to be discussed later.

Figure 3 shows similar T-X plots for the system of THF+diethylene glycol dimethyl ether (DGDME). The latter component, which is too large to form a Structure II hydrate, was deliberately chosen in order to see the phase-diagrammatic behavior of a mixture of a hydrate former+a hydrate non-former. Figure 3 clearly shows different behavior from that found in hydrate former+hydrate former mixtures, as shown in Figs. 1 and 2; the X's which give the maximum temperatures (connected with a dotted line) depend on the THF:DGDME ratio and decrease with an increase in the DGDME content. This may be interpreted as a result of the much-depressed activities of the water molecule due to a strong interaction between water and DGDME, which is partly exemplified by the ice-solution equilibrium curve of the binary DGDME+water system. The decrease in the maximum temperature with the increase in the DGDME content may be simply interpreted as a melting-point depression of the THF hydrate upon the addition of DGDME.

From these confirmations, we may certainly conclude that the procedure employed in this report can provide information about whether or not a given substance has the ability to form a hydrate with the same structure as that of a reference substance.

Ethyl and C_3-Alcohol Hydrates. In view of the fact that the size and/or the shape of the guest species are/is the most important factor for the formation of the hydrate with a gas-hydrate structure, ethyl alcohol and a variety of C_3-alcohols are compounds which can be expected to very likely form a Structure II hydrate. The T-X plots for the systems of THF+ethyl alcohol, THF+propyl alcohol, THF+isopropyl alcohol, THF+allyl alcohol, and THF+propargyl alcohol are shown in Figs. 4—6. Despite the rather intricate discussion of the formation of ethyl alcohol hydrate with Structure II presented in an earlier section, the results shown in Fig. 4 clearly indicate that ethyl alcohol has the ability to form a Structure II hydrate with an incongruent melting point. Although it is impossible to estimate the exact value of the incongruent melting point, it is certain, by a comparison of Fig. 4 with Fig. 2, that it is considerably lower than that of acetone hydrate (−19.8 °C[11]).

As may be seen from Figs. 4—6, all the C_3-alcohols behave in a similar manner: (1) in each mixture

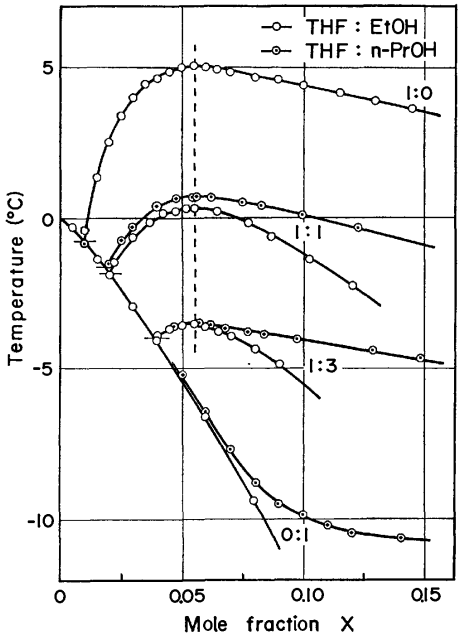

Fig. 4. The solid-liquid-phase diagrams for THF+ethyl alcohol+water systems (—○—) and THF+propyl alcohol+water systems (—⊙—). Explanations are given in Fig. 1.

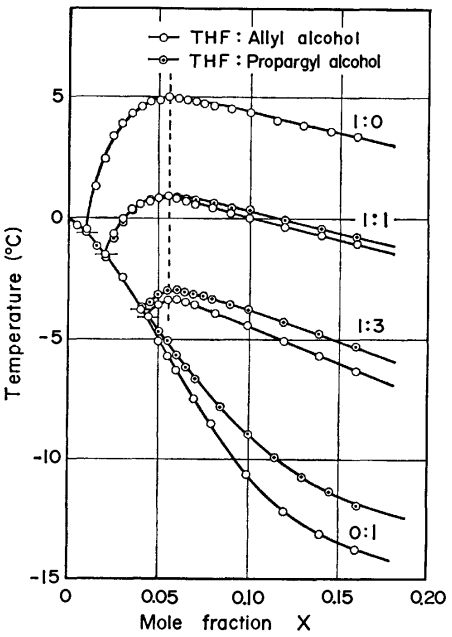

Fig. 6. The solid-liquid-phase diagrams for THF+allyl alcohol+water systems (—○—) and THF+propargyl alcohol+water systems (—⊙—). Explanations are given in Fig. 1.

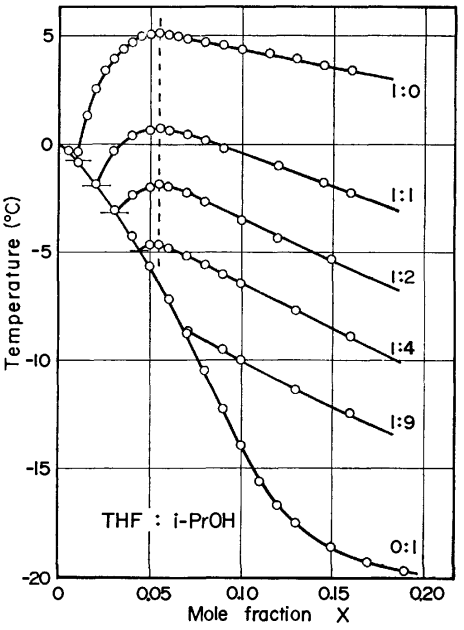

Fig. 5. The solid-liquid-phase diagrams for THF+isopropyl alcohol+water systems. Explanations are given in Fig. 1.

with THF, the X's corresponding to the maximum temperature have the same value, around 0.056, within the limits of experimental error; (2) in each binary mixture of the alcohol+water, the equilibrium curve (marked with 0:1) bends at around −10 °C for propyl, allyl, and propargyl alcohols and at about −18 °C for isopropyl alcohol. Both of these phenomena suggest that all the C_3-alcohols can form hydrates of the Structure II type. In fact, thermal analysis by means of a differential scanning calorimeter also revealed that the solid made by cooling the alcohol+water binary mixture showed a marked absorption of heat at about −11 °C for propyl alcohol, −16 °C for isopropyl alcohol, −12 °C for allyl alcohol, and −10 °C for propargyl alcohol when each solid was gradually heated. These temperatures seem to correspond to the incongruent melting point of each alcohol hydrate. In addition, more elaborate thermal analyses[30] for the propyl alcohol+water system strongly indicated that the hydration number of the propyl alcohol hydrate was 17 (Structure II). As far as we know, no formation of a C_3-alcohol hydrate with a Structure II has been reported explicitly. It is noteworthy that the incongruent melting points of these C_3-alcohol hydrates are surprisingly high as compared with that of the ethyl alcohol hydrate reported by Potts *et al.* (−73.5 °C[18]).

C_4- and C_5-Alcohols. From the standpoint of size and/or shape limitations of a guest molecule on the formation of a Structure II hydrate, it seems to be difficult for C_4-alcohols to form such hydrates. In fact, there exists no proof for its formation. The T-X plots for the THF+*t*-butyl alcohol (TBA)+water mixtures are shown in Fig. 7. The solid-liquid equilibrium curve (marked with 0:1) for the TBA+water binary system clearly shows no formation of a hydrate of Type II. The solid phase formed at high concentrations (above X=0.064) seems to be $TBA \cdot 2H_2O$, as was pointed out by Ross.[20] The T-X plots for ternary mixture of THF+TBA+water, however, behave in a manner similar to that in the systems containing ethyl alcohol and C_3-alcohols (Figs. 4—6); each T-X curve for these systems has a maximum temperature at X=0.056. Thus, from our criterion, it may be concluded that the TBA molecule has the

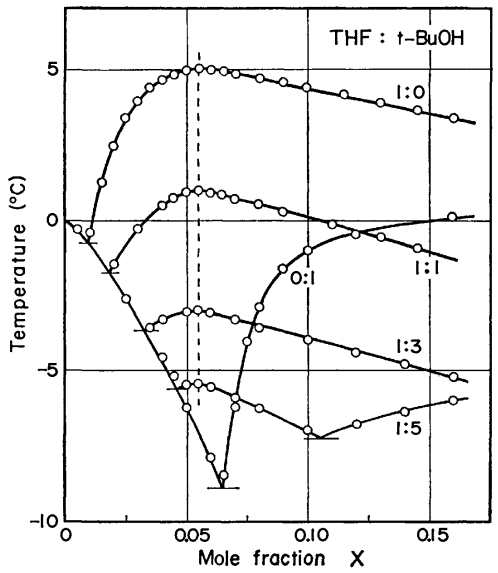

Fig. 7. The solid-liquid-phase diagrams for THF+*t*-butyl alcohol+water systems.
Explanations are given in Fig. 1.

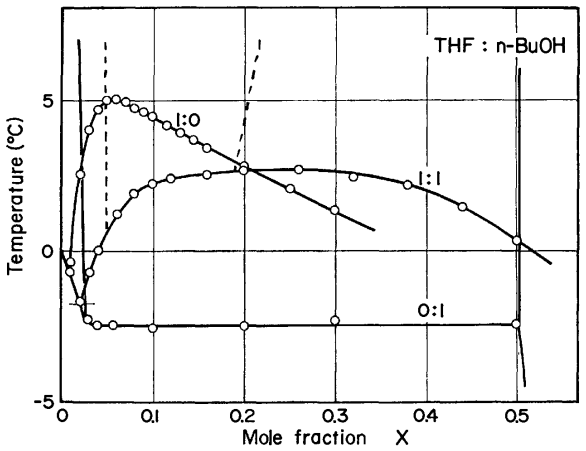

Fig. 8. The solid-liquid-phase diagrams for THF+butyl alcohol+water systems.
Explanations are given in Fig. 1.

ability to form a Structure II hydrate. Chemical analysis by means of gas chromatography also shows that the TBA molecule exists in the solid phase formed from such a ternary mixture. This can be interpreted by the following considerations. Although the TBA molecule cannot form a stable Structure II hydrate by itself because of its molecular diameter is a little larger than the limiting value of 6.6 Å, the lattice distortion caused by the TBA molecule is not so severe that the formation of a solid solution of a Structure II hydrate containing TBA is possible by incorporating the THF molecule as much as possible. The fact that TBA can form a double hydrate (Structure II) with H_2S,[31] $TBA \cdot 2H_2S \cdot 17H_2O$, gives other evidence in support of the slight distortion effect of the TBA molecule on the water structure: in this hydrate the stabilization due to the occupation of the H_2S molecule in vacant 12-hedra seems to overcome the unfavorable distortion effect of the TBA molecule.

The behavior of the *T-X* plots for the other three C_4-alcohols (butyl, isobutyl, and *s*-butyl alcohols) is quite different from that shown in Figs. 4—7. As an example, the *T-X* plots for the THF+butyl alcohol+water system are illustrated in Fig. 8. Because of the low solubility of butyl alcohol in water, the equilibrium curve (marked with 0:1) for the binary mixture with water shows the existence of a two-liquid-phase region and shows no indication of the formation of a Structure II hydrate. In Fig. 8, only the *T-X* plot for an equimolar mixture of THF+butyl alcohol is shown. Two liquid phases also exist in the region between two dotted lines. It is noteworthy that the 1:1 curve has quite a broad peak around X=0.25: this is quite different from the value corresponding to the THF+water system (0.056), indicating that the butyl alcohol does not have the ability to form a Structure II hydrate at all. The behavior of this 1:1 curve can be interpreted as follows: the solid phase formed is a simple THF hydrate (its melting point is depressed by the existence of butyl alcohol), and a high THF concentration is needed to maintain the THF hydrate in the solution since a considerable amount of THF is either distributed between the two liquid phases or extracted by liquid phase containing a large amount of butyl alcohol. The analysis by means of gas chromatography indicates, for example, for the system of X=0.14 (two liquid region) which is kept at 1.1 °C, that the molar ratio of THF:butyl alcohol:water is 1:0.04:18 for a solid sample separated from the liquid phase (the small amount of butyl alcohol may be ascribed to the incorporation of the mother liquid), 1:2.0:7.0 for an upper-liquid phase, and 1:0.75:2.2 for a lower-liquid phase (the volumes of the two phases are almost the same, and a small amount of the solid phase wafts in the upper portion of the lower-liquid phase). These results strongly support the above anticipation.

All the *T-X* plots for ternary mixtures of THF+C_5-alcohol+water also showed the same behavior, as is shown in Fig. 8.

Methyl Alcohol Hydrates. Since the molecular diameter of methyl alcohol is around 5.2—5.3 Å,[22] we first examined the possibility of the formation of a methyl alcohol hydrate of Structure I by using ethylene oxide (EO) as the reference substance. It has been known that ethylene oxide hydrate[27-29] is a Structure I with a congruent melting point of 11.1 °C.[27] The *T-X* plots for the EO+methyl alcohol+water system are shown in Fig. 9. The solid-liquid equilibrium curve (marked with 1:0) for the EO+water binary system was taken from the literature.[27] Three *T-X* curves (marked with 1:1, 1:3, and 1:5) for the ternary mixtures show the same behavior as in Figs. 4—7, indicating that methyl alcohol has the ability to form a Structure I hydrate. It is uncertain, however, whether methyl alcohol can actually form a Structure I hydrate without the assistance of EO.

On the other hand, the *T-X* plots for the ternary mixture of THF+methyl alcohol+water, shown in Fig. 10, also show that the methyl alcohol hydrate can form a solid solution with a THF hydrate of Struc-

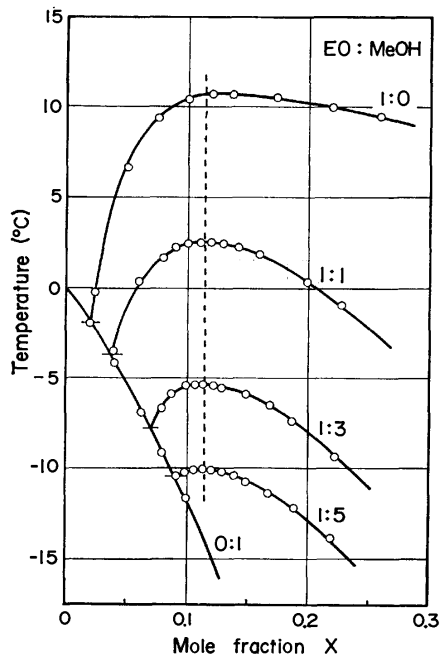

Fig. 9. The solid-liquid-phase diagrams for ethylene oxide+methyl alcohol+water systems.
Explanations are given in Fig. 1.

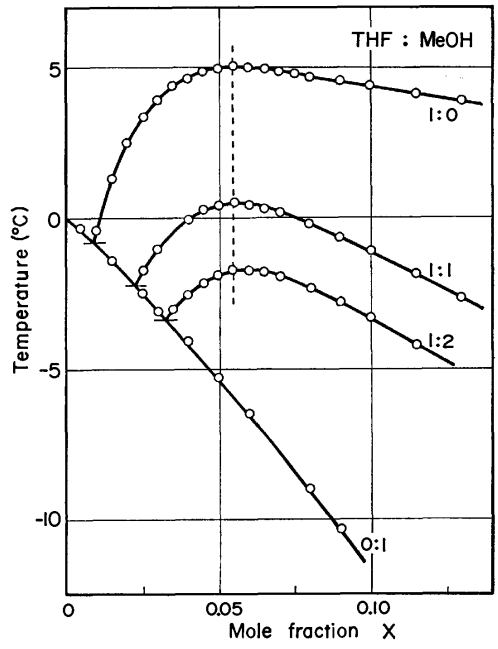

Fig. 10. The solid-liquid-phase diagrams for THF+methyl alcohol+water systems.
Explanations are given in Fig. 1.

ture II. Gas chromatographic analysis also supports this conclusion. For example, the molar ratio of THF:methyl alcohol:water is 1.0:0.85:31.0 for the solid phase formed from a solution containing X=0.07 (the molar ratio of THF:methyl alcohol is 1:3) and kept at −10.3 °C. This composition can reasonably be explained by looking upon the solid phase as a mixture of 1 mol of the THF·17H_2O hydrate and 0.85 mol of the MeOH·17H_2O, hydrate. However, this Structure II hydrate, MeOH·17H_2O, seems to be found only when a suitable other molecule such as THF coexists with methyl alcohol, since the methyl alcohol is not large enough to stabilize a Structure II hydrate by itself: stable Structure II hydrates are formed for guest molecules of 5.6—6.6 Å, as has been mentioned earlier.[22]

Summary. From these results we may classify the series of alcohols into the following four groups: (1) methyl and ethyl alcohol—these alcohols have at least the potential ability to form clathrate hydrates of either Structure I (for methyl alcohol) or Structure II (for both alcohols). It is uncertain, however, whether they can actually form such hydrates from the alcohol+water binary mixtures alone; (2) propyl, isopropyl, allyl, and propargyl alcohol—all these C_3-alcohols can form a Structure II hydrate with relatively high incongruent melting points around −10 °C; (3) *t*-butyl alcohol—though this alcohol has the potential ability to form a Structure II hydrate, it cannot form such a hydrate from the *t*-butyl alcohol+water mixture alone; and (4) other C_4- and C_5-alcohols—these alcohols do not have any potential possibilities to form the hydrates of the gas-hydrate type. These results strongly support the idea that the size and/or shape of a guest molecule also plays an important role in the formation of alcohol hydrates of Structure I and II, just as in the case of ether and ketone hydrates, and further, that the existence of a polar OH group has little influence on their formation. It is noteworthy that the experimental method employed in this study can also be applied to any other types of clathrate hydrates.

The authors wish to express their thanks to Mr. Manabu Sakai and Mr. Akira Kaneko for their preliminary experiments.

References

1) M. von Stackelberg and B. Meuthen, *Z. Elektrochem.*, **62**, 130 (1958).
2) S. L. Miller, S. R. Gough, and D. W. Davidson, *J. Phys. Chem.*, **81**, 2154 (1977).
3) S. R. Gough, S. K. Garg, J. A. Ripmeester, and D. W. Davidson, *J. Phys. Chem.*, **81**, 2158 (1977).
4) R. E. Hawkins and D. W. Davidson, *J. Phys. Chem.*, **70**, 1889 (1966).
5) D. F. Sargent and L. D. Calvert, *J. Phys. Chem.*, **70**, 2689 (1966).
6) S. R. Gough, R. E. Hawkins, B. Morris, and D. W. Davidson, *J. Phys. Chem.*, **77**, 2969 (1973).
7) S. R. Gough and D. W. Davidson, *Can. J. Chem.*, **49**, 2691 (1971).
8) D. W. Davidson, M. M. Davies, and K. Williams, *J. Chem. Phys.*, **40**, 3449 (1964).
9) L. Carbonnel and J. -C. Rosso, *J. Solid State Chem.*, **8**, 304 (1973).
10) A. Venkateswaran, J. R. Easterfield, and D. W. Davidson, *Can. J. Chem.*, **45**, 884 (1967).
11) B. Morris and D. W. Davidson, *Can. J. Chem.*, **49**, 1243 (1971).
12) A. S. Quist and H. S. Frank, *J. Phys. Chem.*, **65**, 560 (1961).

13) G. J. Wilson and D. W. Davidson, *Can. J. Chem.*, **41**, 264 (1963).
14) A. A. Ennan and V. A. Lapshin, *Zh. Fiz. Khim.*, **49**, 2295 (1975).
15) M. von Stackelberg and H. R. Müller, *Z. Elektrochem.*, **58**, 25 (1954).
16) H. P. Barendrecht, *Z. Phys. Chem.*, **20**, 234 (1896).
17) F. F. A. Wallerant, *Bull. Soc. Fr. Mineral.*, **31**, 217 (1908); A. W. Brewer and H. P. Palmer, *Proc. Phys. Soc. (London), B*, **64**, 765 (1951); G. Vuillard and N. Satragno, *C. R. Acad. Sci.*, **250**, 3841 (1960).
18) A. D. Potts and D. W. Davidson, *J. Phys. Chem.*, **69**, 996 (1965).
19) L. D. Calvert and P. Srivastava, *Acta Crystallogr., Sect. A*, **25**, S131 (1969).
20) H. K. Ross, *Ind. Eng. Chem.*, **46**, 601 (1954).
21) S. U. Pickering, *J. Chem. Soc.*, **63**, 998 (1893).
22) D. W. Davidson, "Water," ed by F. Franks, Plenum Press, New York (1973), Vol. 2, Chap. 3.
23) E. L. Lippert, Jr., H. A. Palmer, and F. F. Blankenship, *Proc. Okla. Acad. Sci.*, **31**, 115 (1950).
24) M. von Stackelberg and W. Meinhold, *Z. Elektrochem.*, **58**, 40 (1954).
25) H. Nakayama, unpublished data; solid-solution behavior was also found in $(C_4H_9)_4NF+(C_4H_9)_4NBr$ binary system. Each hydrate is known to be isostructural (R. McMullan and G. A. Jeffrey, *J. Chem. Phys.*, **31**, 1231 (1959)).
26) J. Erva, *Suom. Kemistil. B*, **29**, 183 (1956).
27) O. Maass and E. H. Boomer, *J. Am. Chem. Soc.*, **44**, 1709 (1922).
28) D. N. Glew and N. S. Rath, *J. Chem. Phys.*, **44**, 1710 (1966).
29) D. N. Glew, H. D. Mak, and N. S. Rath, *Can. J. Chem.*, **45**, 3059 (1967).
30) H. Nakayama and M. Tahara, *Bull. Chem. Soc. Jpn.*, **46**, 2965 (1973).
31) D. N. Glew, H. D. Mak, and N. S. Rath, "Hydrogen-bonded Solvent Systems," ed by A. K. Covington and P. Jones, Taylor and Francis, London (1968).

Studies of the Anodic Oxidation of the Cyanide Ion in the Presence of the Copper Ion. III. Identification of the Reaction Intermediate by Means of ESR Spectroscopy

Seiji Yoshimura, Akira Katagiri,** Yasuo Deguchi,** and Shiro Yoshizawa*

Department of Industrial Chemistry, Faculty of Engineering, Kyoto University, Yoshida, Sakyo-ku, Kyoto 606

***Department of Chemistry, College of Liberal Arts and Sciences, Kyoto University, Yoshida, Sakyo-ku, Kyoto 606*

(Received December 7, 1979)

The formation of the tetracyanocuprate(II) ion ($Cu(CN)_4^{2-}$), which was expected as a reaction intermediate in the anodic oxidation of the cyanide ion in the presence of the copper ion, has been investigated by means of ESR measurement. When a potassium cyanide solution containing a small amount of copper(I) cyanide was electrolyzed, an intermediate copper(II) species was found at the anode in the dissolved state. The ESR spectrum of the intermediate in the solidified state was obtained by freezing the solution in the resonant cavity. The intermediate was identified as $Cu(CN)_4^{2-}$ by a comparison of its spectrum to that of $Cu(CN)_4^{2-}$ already reported by other authors. When the ratio of the total copper(I) concentration to the total cyanide concentration in the solution was not too small, solid copper(II) cyanide was deposited on the anode during electrolysis.

In the investigation of the anodic oxidation of the cyanide ion, we have found a marked catalytic effect of the copper ion on this reaction.[1] We have postulated the formation of the tetracyanocuprate(II) ion ($Cu(CN)_4^{2-}$) as an intermediate in this catalytic electrochemical reaction, and have proposed the following mechanism, which is consistent with the results of several other electrochemical measurements:[2]

$$Cu^{I}(CN)_4^{3-} \longrightarrow Cu^{II}(CN)_4^{2-} + e^- \quad (1)$$

$$Cu^{II}(CN)_4^{2-} + CN^- \longrightarrow Cu^{I}(CN)_4^{3-} + \frac{1}{2}(CN)_2 \quad (2)$$

On the other hand, Longo and Buch[3] have studied the ESR and optical spectra of the unstable species produced in the chemical reaction between Cu^{II} and CN^-, and have identified the species as $Cu^{II}(CN)_4^{2-}$. The aim of the present paper is to confirm the formation of $Cu(CN)_4^{2-}$ in the anodic cyanide oxidation in the presence of the copper ion by means of ESR measurement.

Experimental

The ESR spectra were measured by the use of a JEOL JES-ME-3X spectrometer with X-band microwaves and with a field-moduration frequency of 100 kHz. A cylindrical resonant cavity of the TE_{011} mode was used. The temperature of the cavity was held constant by controlling the cold nitrogen-gas flow. In order to determine the g-values and hyperfine-coupling constants of the spectra, Mn^{2+} doped into MgO was used as the standard substance.

Two types of electrolysis cells, shown in Fig. 1, were used for the measurement of the ESR spectra during electrolysis. Both cells were made from a quartz tube (0.72 mmϕ in inner diameter) and were equipped with a platinum wire anode (0.4 mmϕ) coaxially. A platinum plate was used as the cathode. Cell (a) was set in the ESR spectrometer so that the anode was located at the center of the resonant cavity. By using this cell, the ESR spectrum of a paramagnetic substance, which was formed on the surface or in the vicinity of the anode, was measured. In the case of Cell (b) the platinum wire anode was located above the cavity, and the electrolyte was forced to flow downward. Thus, a paramagnetic substance, which was formed in the dissolved state, was detected. The temperature was kept constant at 25 °C in both cases. Electrolysis was performed at a constant current between 30 μA and 120 μA by means of a Hokuto Denko HA-104 galvanostat whose maximum output voltage was 50 V.

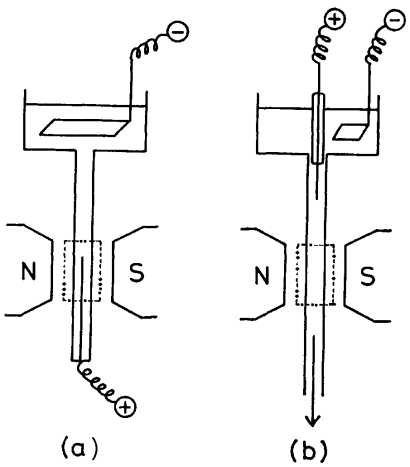

Fig. 1. Electrolysis cells for measurement of ESR absorption spectra at 25 °C.

For the purpose of measuring the ESR spectrum of a frozen solution, a polyethylene cell (2.5 mmϕ in inner diameter) was used. While a constant current was passed through at the platinum wire anode (0.4 mmϕ), the cell was brought into the cavity, whose temperature was held at −100 °C, whereby the electrolytic solution was frozen within a short time.

Electrolytic solutions were prepared from reagent-grade potassium cyanide and copper(I) cyanide. No supporting electrolyte was used, because the concentration of cyanide was sufficiently high. The compositions of the solutions were expressed in terms of the total cyanide concentration (C_{CN^-}) and the total copper(I) concentration ($C_{Cu(I)}$). C_{CN^-} and $C_{Cu(I)}$ were varied from 1.3 to 3.3 mol·dm^{-3}, and from 0.1 to 0.3 mol·dm^{-3}, respectively, while the $C_{Cu(I)}/C_{CN^-}$ ratio was varied from 1/3 to 1/33. Solid copper(II) cyanide was synthesized either by the chemical reaction of aqueous copper(II) sulfate with aqueous potassium cyanide[4] or

by the anodic oxidation of copper in an aqueous potassium cyanide solution.[5]

Results

ESR Measurement during Electrolysis. When electrolysis was started in Cell(a) at a constant anodic current of 100 μA in a solution in which $C_{Cu(I)}$ and C_{CN^-} were 0.1 and 3.0 mol·dm^{-3} respectively, ESR absorption was observed immediately. Its intensity increased with the time at first, and then a steady state was reached. Figure 2 shows the ESR spectrum in the steady state. The spectrum shows four hyperfine lines which suggest the formation of a certain copper(II) species. The same spectrum was obtained in other experiments, where the current was 30, 60, or 120 μA, and where C_{CN^-} was 1.3, 2.3, or 3.3 mol·dm^{-3}, but $C_{Cu(I)}$ was constant at 0.1 mol·dm^{-3}. The steady-state intensity of the absorption was higher for the larger current, and for the higher concentration of the total cyanide, if the total copper(I) concentration was constant. When the current was switched off, the spectrum soon disappeared.

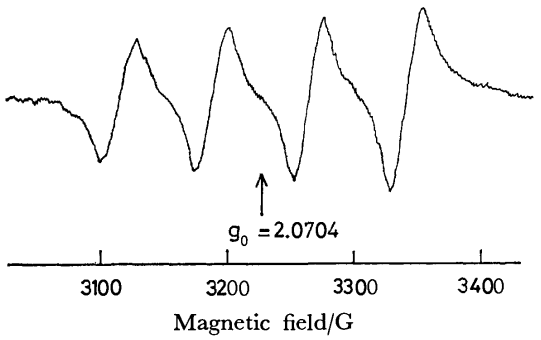

Fig. 2. ESR absorption spectrum during electrolysis at small $C_{Cu(I)}/C_{CN^-}$ ratio.
$C_{Cu(I)}$: 0.1 mol·dm^{-3}, C_{CN^-}: 3.0 mol·dm^{-3}, temp: 25 °C.

The same spectrum was observed when electrolysis was performed in a flowing solution in Cell(b), with the other conditions being the same. This indicates that the paramagnetic species was formed in the dissolved state in the solution.

Figure 3 shows the ESR spectrum measured with Cell (a) at a constant anodic current of 100 μA for the solution in which $C_{Cu(I)}$ and C_{CN^-} were 0.3 and 0.9 mol·dm^{-3} respectively. The same spectrum was obtained when the current was reduced to 50 μA and then further to 10 μA. The ESR absorption intensity increased continuously with the electrolysis time, and no steady state was reached. This spectrum agreed with that obtained independently for solid copper(II) cyanide.

ESR Measurement of the Reaction Intermediate in a Frozen Solution. Electrolysis was made in the polyethylene cell at a constant anodic current (100 μA) for a solution in which $C_{Cu(I)}$ and C_{CN^-} were 0.1 and 3.0 mol·dm^{-3} respectively. While the electrolysis was continued, the cell was inserted into the resonant cavity, held at a temperature of −100 °C, so that the anode was

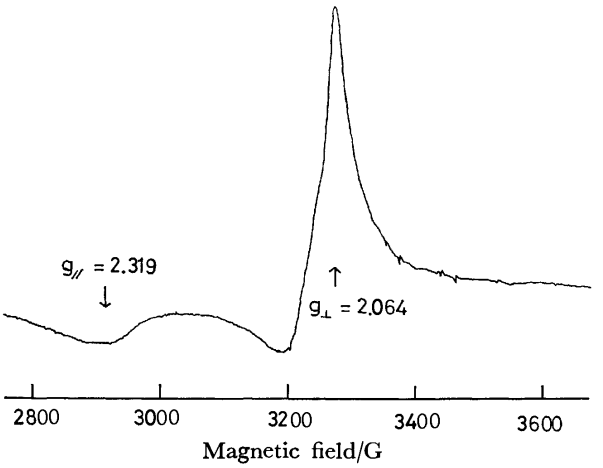

Fig. 3. ESR absorption spectrum during electrolysis at not too small $C_{Cu(I)}/C_{CN^-}$ ratio.
$C_{Cu(I)}$: 0.3 mol·dm^{-3}, C_{CN^-}: 0.9 mol·dm^{-3}, temp: 25 °C.

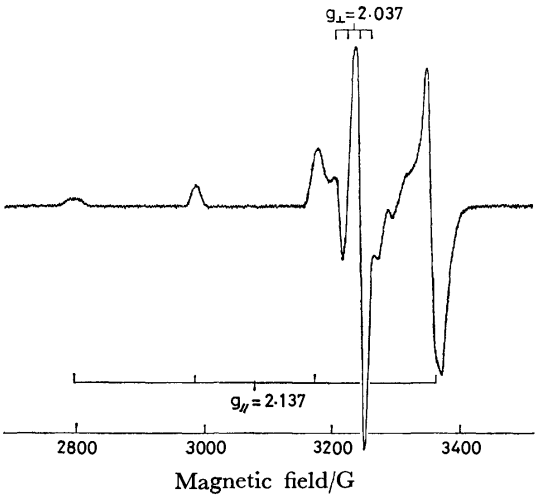

Fig. 4. ESR absorption spectrum of the frozen solution of small $C_{Cu(I)}/C_{CN^-}$ ratio.
$C_{Cu(I)}$: 0.1 mol·dm^{-3}, C_{CN^-}: 3.0 mol·dm^{-3}, temp: −100 °C.

positioned at the center of the cavity. When the solution was frozen, the current became zero. Figure 4 shows the ESR spectrum of the frozen solution thus obtained. No change was observed in the spectrum so long as the sample was held in the frozen state.

Discussion

The ESR spectrum (Fig. 2) which was observed in the case of a small $C_{Cu(I)}/C_{CN^-}$ ratio exhibits an isotropic character. This is ascribed to a certain compound of divalent copper (^{65}Cu and ^{63}Cu) with nuclear spin $I=3/2$, because the spectrum has four absorption lines equally separated. Since the anisotropic terms of spin Hamiltonian are averaged out to zero for a solution spectrum, the positions of the absorption lines are determined only by isotropic terms. The isotropic g-facter, g_0, and the isotropic hyperfine-coupling constant. A_0, are obtained from Fig. 2 with reference to the standard Mn^{2+} sample; they are shown in the left-hand column of Table 1.

Table 1. ESR parameters of the intermediate investigated in this work and of $Cu^{II}(CN)_4^{2-}$

	The intermediate investigated in this work (Figs. 2 and 4)	$Cu^{II}(CN)_4^{2-}$ (Longo and Buch)
g_0	2.0704	2.071[a]
$g_{//}$	2.137	2.146
$g_\perp$	2.037[a]	2.033
$\|A_0\|$ (10^{-4} cm^{-1})	71.4	81[a]
$\|A_{//}\|$ (10^{-4} cm^{-1})	188	190
$\|A_\perp\|$ (10^{-4} cm^{-1})	13[a]	27

a) Calculated by means of Eqs. 3 and 4.

The spectrum of the frozen solution (Fig. 4) shows the features of an axially symmetrical compound in a random orientation. The parallel and perpendicular components of the g-tensor, $g_{//}$ and $g_\perp$, and the parallel and perpendicular components of the hyperfine- coupling tensor, $A_{//}$ and $A_\perp$, are obtained from Fig. 4; they are shown in the left-hand column of Table 1. Thus, $g_{//}$ and $A_{//}$ are determined from the three low-field peaks on the spectrum. However, $g_\perp$ and $A_\perp$ are difficult to determine directly from the spectrum; therefore, they are calculated by the use of Eqs. 3 and 4,[6] together with the values of g_0 and A_0:

$$g_0 = \frac{1}{3}(g_{//}+2g_\perp) \tag{3}$$

$$A_0 = \frac{1}{3}(A_{//}+2A_\perp) \tag{4}$$

It has been known for a long time that an unstable purple compound is formed in the reaction between cyanide and the copper(II) ion (Eq. 5):

$$Cu(II) + CN^- \longrightarrow Cu(I) + \frac{1}{2}(CN)_2 \tag{5}$$

Several authors have postulated the composition of this compound from the kinetics of the reaction.[7,8] Longo and Buch[3] conducted a reaction between copper(II) sulfate and potassium cyanide in methanol, dimethylformamide, and water at a low temperature. They measured the ESR spectra of the unstable purple compound in the liquid methanol solution and in the frozen solution in each solvent, the latter being obtained by freezing the reaction mixture quickly. They thus obtained spectra with an axially symmetrical character, and concluded the purple compound to be square-planar $Cu^{II}(CN)_4^{2-}$ from a consideration based on the crystal-field theory. The ESR parameters of the compound in an aqueous solution obtained by Longo and Buch are shown in the right-hand column of Table 1. Here, the values of g_0 and A_0 are calculated from Eqs. 3 and 4, because the spectrum of a liquid solution was not measured due to the instability of the compound in an aqueous solution. Taking account of the differences in the experimental conditions, the ESR parameters obtained by Longo and Buch and those in the present work are regarded as being in substantial agreement. It is, therefore, confirmed that $Cu^{II}(CN)_4^{2-}$ is formed as a reaction intermediate in the anodic oxidation of cyanide in the presence of the copper ion.

The spectrum (Fig. 3) which was observed during electrolysis in the solution with not too small a $C_{Cu(I)}/C_{CN^-}$ ratio exhibits an anisotropic character. No hyperfine structure can be seen because of the broad linewidth. From Fig. 3, $g_{//}$ and $g_\perp$ are found to be 2.319 and 2.064 respectively. The same spectrum was obtained for solid copper(II) cyanide. Therefore, it is concluded that solid copper(II) cyanide deposits on the anode during electrolysis under these conditions. This conclusion is consistent with the fact that the intensity of the ESR absorption grows continuously with the electrolysis time. The electrode potential, which was measured under the same conditions in the H-type cell,[2] did not reach a steady value at any current, substantiating the above conclusion.

We would like to thank professor Saburo Kako for his helpful discussions, and Mr. Hideo Fujita for his assistance in measuring the ESR spectra. The present work was partly supported by a Grant-in-Aid for Scientific Research (Environmental Science) from the Ministry of Education, Science and Culture (No. 303525).

References

1) S. Yoshimura, A. Katagiri, and S. Yoshizawa, *Denki Kagaku*, **47**, 360 (1979).
2) S. Yoshimura, A. Katagiri, and S. Yoshizawa, *Denki Kagaku*, **47**, 488 (1979).
3) A. Longo and T. Buch, *Inorg. Chem.*, **6**, 556 (1967).
4) T. Chitani, "Inorganic Chemistry," Sangyō Tosho, Tokyo (1964), p. 155.
5) A. Löb, *Z. Elektrochem.*, **5**, 79 (1906).
6) R. J. Myers, "Molecular Magnetism and Magnetic Resonance Spectroscopy," Prentice Hall (1973), Chap. 8.
7) F. R. Duke and W. G. Courtney, *J. Phys. Chem.*, **56**, 19 (1952).
8) N. Tanaka, M. Kamada, and T. Murayama, *Bull. Chem. Soc. Jpn.*, **31**, 895 (1958).

 © 1980 The Chemical Society of Japan Bull. Chem. Soc. Jpn., 53, 2437—2442 (1980)

Studies of the Anodic Oxidation of the Cyanide Ion in the Presence of the Copper Ion. IV. The Kinetics and Mechanism of the Decomposition of the Intermediate Tetracyanocuprate(II) Ion

Seiji YOSHIMURA, Akira KATAGIRI,** Yasuo DEGUCHI,** and Shiro YOSHIZAWA*

Department of Industrial Chemistry, Faculty of Engineering, Kyoto University, Yoshida, Sakyo-ku, Kyoto 606

***Department of Chemistry, College of Liberal Arts and Sciences, Kyoto University, Yoshida, Sakyo-ku, Kyoto 606*

(Received February 15, 1980)

The kinetics and mechanism of the decomposition of the tetracyanocuprate(II) ion ($Cu^{II}(CN)_4^{2-}$) have been investigated by ESR measurements. Aqueous solutions of potassium cyanide with a small amount of copper(I) cyanide were electrolyzed in a cell the platinum anode of which was set in the resonant cavity of an ESR spectrometer. Since $Cu^{II}(CN)_4^{2-}$, which is formed as an intermediate, gives a definite ESR spectrum, its concentration in the anode compartment is estimated from the intensity of the first-derivative spectrum at a fixed magnetic field. From the decay curves of the ESR intensity after the steady-state electrolysis currents have been switched off, a rate equation for the decomposition of $Cu^{II}(CN)_4^{2-}$ is derived; $v=k_0[Cu^{II}(CN)_4^{2-}]^2/[CN^-]^2$, where k_0 is calculated to be 74 mol·dm^{-3}·s^{-1} at 25 °C. This rate equation is also confirmed by ESR measurements during steady-state electrolysis, where the value of $k_0=60$ mol·dm^{-3}·s^{-1} is obtained. On the basis of the kinetics, two possible mechanisms are proposed: the formation of $Cu^{II}(CN)_3^-$, followed by the rate-determining bimolecular reaction of $Cu^{II}(CN)_3^-$ to give $2Cu^{I}(CN)_2^-+(CN)_2$ (Mechanism A), and the formation of a binuclear complex, $Cu^{II}_2(CN)_6^{2-}$, followed by the rate-determining decomposition of $Cu^{II}_2(CN)_6^{2-}$ to give $2Cu^{I}(CN)_2^-+(CN)_2$ (Mechanism B). The kinetics and the mechanism are compared with those of the chemical reaction between the copper(II) ion and the cyanide ion.

In our previous investigations of the anodic oxidation of the cyanide ion in the presence of the copper ion, we have proposed the following catalytic mechanism:[2,3]

$$Cu^{I}(CN)_4^{3-} \longrightarrow Cu^{II}(CN)_4^{2-} + e^- \quad (1)$$

$$Cu^{II}(CN)_4^{2-} + CN^- \longrightarrow Cu^{I}(CN)_4^{3-} + \frac{1}{2}(CN)_2 \quad (2)$$

We have detected the intermediate tetracyanocuprate (II) ion ($Cu^{II}(CN)_4^{2-}$) by ESR measurement.[1] However, the rate of the chemical reaction, Eq. 2, was too high to be measured by chronopotentiometry or by the rotating-electrode technique under the conditions adopted.[2] In the present work, the kinetic behavior of the intermediate $Cu^{II}(CN)_4^{2-}$ have been investigated by ESR measurement, and the mechanism of the reaction, Eq. 2, discussed.

Experimental

ESR measurement was made by use of a JEOL JES-ME-3X spectrometer with X-band microwave and with a field-modulation frequency of 100 kHz. A cylindrical resonant cavity of the TE_{011} mode was used.

Figure 1 shows the electrolysis cell used. The cell was made from a quartz-glass tube (0.72 mmϕ in inner diameter) and was equipped coaxially with the platinum-wire anode (0.4 mmϕ). A platinum plate was used as the cathode. The effective surface area of the anode was controlled by means of a polyethylene sheath, as is shown in the right-hand part of Fig. 1. The cell was fixed in the spectrometer so that the working anode was positioned at the center of the resonant cavity. All experiments were made at a constant temperature of 25 °C.

The electrolytic solutions were prepared from reagent-grade potassium cyanide and copper(I) cyanide. No supporting electrolyte was used, because the concentration of cyanide was sufficiently high. The concentrations are expressed in the unit of 1 M=1 mol·dm^{-3} throughout this paper. Copper(I) must have been present almost entirely as $Cu^{I}(CN)_4^{3-}$ under the experimental conditions in this work, as can be calculated from the formation constants of the cyano copper(I) complexes.[4] Therefore, the concentration of the free cyanide ion, [CN$^-$], was simply calculated from the concentrations of the total cyanide, C_{CN^-}, and the total copper(I), $C_{Cu(I)}$, according to this equation: $[CN^-]=C_{CN^-}-4C_{Cu(I)}$.

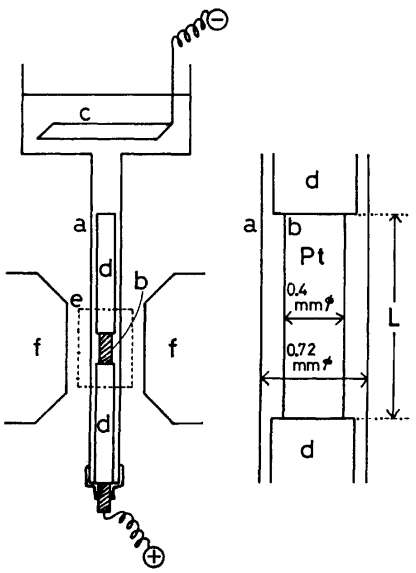

Fig. 1. Electrolysis cell for measurement of the ESR absorption intensity.
a: Quartz-glass tube, b: platinum-wire anode, c: platinum-plate cathode, d: polyethylene sheath, e. resonant cavity, f: electromagnet.

Results and Discussion

Relationship between the ESR Absorption Intensity and the Quantity of $Cu^{II}(CN)_4^{2-}$. When a potassium cyanide solution containing a small amount of copper(I) cyanide was electrolyzed in the cell shown in Fig. 1, an ESR absorption spectrum was observed, as shown in Fig. 2, which can be ascribed to the intermediate $Cu^{II}(CN)_4^{2-}$ ion.[1] Though copper(II) species other than $Cu^{II}(CN)_4^{2-}$ might possibly be formed during electrolysis, the ESR spectra did not show any evidence of such species at all under the experimental conditions in this work. In the following analysis, therefore, copper(II) is considered to be present almost totally as $Cu^{II}(CN)_4^{2-}$.

The signal intensity of the first-derivative spectrum can be regarded as proportional to the quantity of $Cu^{II}(CN)_4^{2-}$ formed,[5] because the spectrum exhibited the Lorentzian line-shape, because the peak positions did not vary with the intensity, and because the local difference in sensitivity due to the inequality of microwave field was negligible in the small anode compartment. On the basis of the above considerations, the signal intensity, I, was measured under different conditions at a fixed magnetic field, H_0, where the peak was the highest, as is shown in Fig. 2. In these experiments the conditions of the ESR spectrometer were kept strictly constant, and the unit scale (1 div) on the recorder chart was used as the unit of the signal intensity.

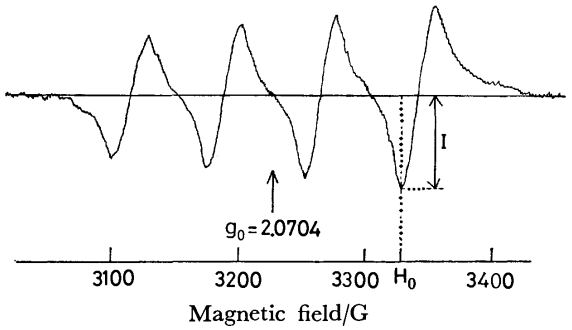

Fig. 2. ESR absorption spectrum $Cu^{II}(CN)_4^{2-}$.

Figure 3 shows a typical change in the ESR signal intensity after the switching-on and switching-off of the constant electrolysis current for a solution with a small $C_{Cu(I)}/C_{CN^-}$ ratio. The signal intensity was zero before starting electrolysis, since $Cu^{II}(CN)_4^{2-}$ was not present. When a constant anodic current was switched on, the intensity increased linearly with the time at first, and then reached a steady value. After the current was switched off, the intensity decreased, quickly at first and then slowly, to zero. Figure 4 shows the initial rate of increase in the signal intensity at the beginning of electrolysis, against the applied current. A proportionality is seen between them. It has been confirmed by other experiments that the initial rate of increase in the signal intensity is independent of the other conditions, *i.e.*, the concentrations of the free cyanide and the total copper(I), and the electrode length.

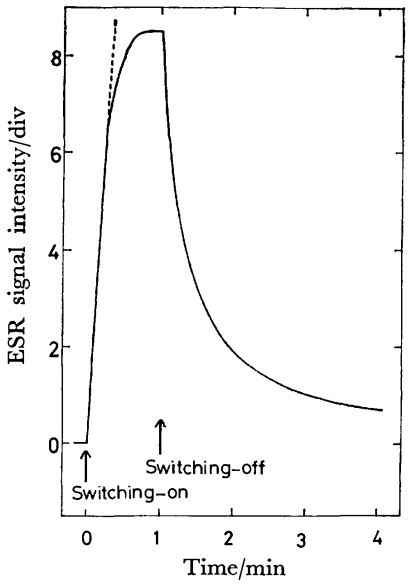

Fig. 3. Intensity of ESR absorption signal of $Cu^{II}(CN)_4^{2-}$ after switching-on and switching-off of the constant electrolysis current. (The unit intensity (1 div) corresponds to 1.55×10^{-9} mol of $Cu^{II}(CN)_4^{2-}$, *cf.* the text).
[CN^-]: 3 M, $C_{Cu(I)}$: 0.1 M, current: 60 μA, electrode length: 6 mm.

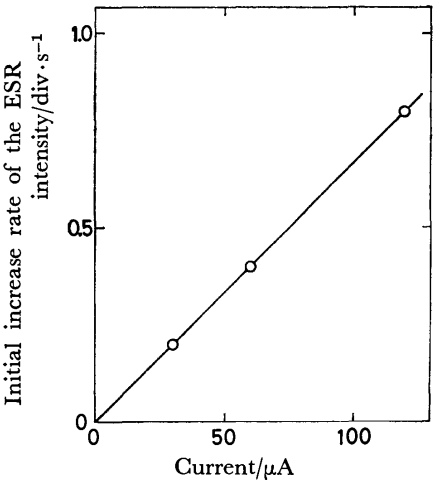

Fig. 4. Relationship between the initial increase rate of ESR signal intensity and the current.
[CN^-]: 3 M, $C_{Cu(I)}$: 0.1 M, electrode length: 6 mm.

As a method for determining the quantity of a paramagnetic species from the ESR absorption intensity, Faraday's law has been applied by some workers. Hirasawa *et al.*[6] have applied this method to the formation of the anion radical of nitrobenzene, and Dohrmann and Gallussen,[7] to the formation of the copper(II) ion. A similar method is used in this work. The results shown in Figs. 3 and 4 indicate that at the beginning of electrolysis, the rate of the decomposition of $Cu^{II}(CN)_4^{2-}$ is negligible in comparison with the rate of the formation of $Cu^{II}(CN)_4^{2-}$, and that the current efficiency of the formation (Eq. 1) of $Cu^{II}(CN)_4^{2-}$ is almost 100%. Therefore, the quantity of $Cu^{II}(CN)_4^{2-}$, m, corresponding to the unit

intensity of the ESR signal is calculated from the slope of the line in Fig. 4, on the basis of Faraday's law, as follows:

$$m = 1.55 \times 10^{-9}\ \text{mol/div.} \quad (3)$$

It may reasonably be assumed that the concentration of the intermediate $Cu^{II}(CN)_4^{2-}$ is substantially uniform in the anode compartment along the length, L (Fig. 1), because the gap between the electrode surface and the glass wall is relatively small (0.16 mm), and because the current-density distribution may be nearly uniform due to the small current and the large electrolytic conductivity of the solution. For example, the concentration of $Cu^{II}(CN)_4^{2-}$ during the steady-state electrolysis shown in Fig. 3 is calculated to be 7.8×10^{-3} M by using the value, m, of Eq. 3 and the volume, $V=1.69\times10^{-3}$ cm^3, of the anode compartment. Kinetic analyses will be made on the above assumption in the following two sections. The validity of the assumption will be discussed in more detail in a later section.

Kinetics and Mechanism of the Decomposition of $Cu^{II}(CN)_4^{2-}$. In order to investigate the kinetics of the decomposition of $Cu^{II}(CN)_4^{2-}$, the decay of the ESR signal was followed after the electrolysis current has been switched off at certain steady state. The lower the CN^- concentration, the faster the signal decayed. Figure 5 shows the reciprocal of the signal intensity against the time for three different concentrations of CN^-. A linear relationship is found, indicating that the kinetics is second-order with respect to $Cu^{II}(CN)_4^{2-}$. Thus, the rate of the reaction, which is defined as the rate of the disappearance of $Cu^{II}(CN)_4^{2-}$, may be formulated as follows:

$$v = -\frac{d[Cu^{II}(CN)_4^{2-}]}{dt} = k_2[Cu^{II}(CN)_4^{2-}]^2. \quad (4)$$

The rate constant, k_2, is calculated from the slope of each line in Fig. 5 by using the "m" and "V" values, while log k_2 is plotted against log [CN^-] in Fig. 6. Since k_2 is found to be inversely proportional to the square of [CN^-], the rate equation, Eq. 4, can be

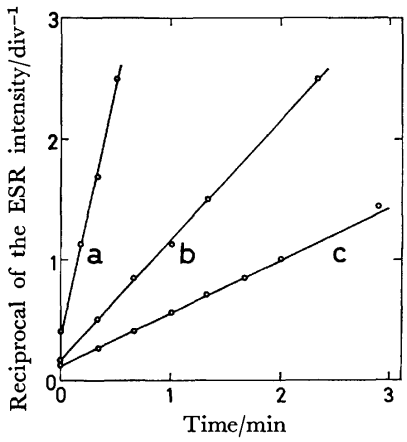

Fig. 5. Relationship between the reciprocal of ESR absorption signal intensity and time at different CN^- concentrations.
[CN^-]; a: 1 M, b: 2 M, c: 3 M, $C_{Cu(I)}$: 0.1 M, electrode length: 6 mm.

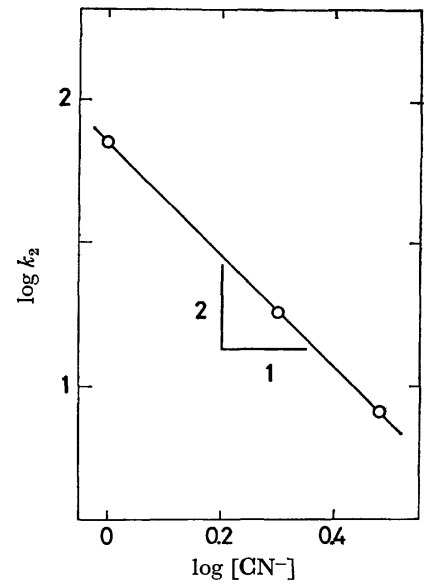

Fig. 6. Dependence of the second-order rate constant, $k_2(M^{-1}s^{-1})$ upon the CN^- concentration (M).

rewritten as Eq. 5, where k_0 is calculated to be 74 $M\cdot s^{-1}$:

$$v = k_0\frac{[Cu^{II}(CN)_4^{2-}]^2}{[CN^-]^2}. \quad (5)$$

Two types of reaction mechanisms can be considered, both of which are consistent with the rate equation, Eq. 5:

Mechanism A:

$$Cu^{II}(CN)_4^{2-} \overset{K_a}{\rightleftharpoons} Cu^{II}(CN)_3^- + CN^- \quad (6a)$$

$$2Cu^{II}(CN)_3^- \xrightarrow{k_a} 2Cu^{I}(CN)_2^- + (CN)_2 \quad (7a)$$

Mechanism B:

$$2Cu^{II}(CN)_4^{2-} \overset{K_a}{\rightleftharpoons} Cu^{II}_2(CN)_6^{2-} + 2CN^- \quad (6b)$$

$$Cu^{II}_2(CN)_6^{2-} \xrightarrow{k_b} 2Cu^{I}(CN)_2^- + (CN)_2 \quad (7b)$$

If the reaction, Eq. 6a or 6b, is in quasi-equilibrium when $[Cu^{II}(CN)_4^{2-}]\gg[Cu^{II}(CN)_3^-]$ or $[Cu^{II}(CN)_4^{2-}]\gg[Cu^{II}_2(CN)_6^{2-}]$, and if the reaction, Eq. 7a or 7b, is rate-determining, the rate equation may be described as follows:

$$v = k_aK_a^2\frac{[Cu^{II}(CN)_4^{2-}]^2}{[CN^-]^2}, \quad (8a)$$

or:

$$v = k_bK_b\frac{[Cu^{II}(CN)_4^{2-}]^2}{[CN^-]^2}. \quad (8b)$$

Here, K_a and K_b are the equilibrium constants of the reactions, Eqs. 6a and 6b, and k_a and k_b are the rate constants of the reactions, Eqs. 7a and 7b, respectively. Both Eqs. 8a and 8b agree with the experimental rate equation, Eq. 5. At present, it is not possible to decide which of the two mechanisms is correct. Another experiment has been made on this point, however, and a further discussion will be presented in a succeeding paper.

Since cyano copper(I) complexes are labile,[8] the following equilibrium may always exist:

$$Cu^{I}(CN)_2^- + 2CN^- \longrightarrow Cu^{I}(CN)_4^{3-}. \quad (9)$$

During a steady-state electrolysis, the over-all reaction may proceed through the reaction cycle of Eqs. 1, 6a, 7a, and 9, or Eqs. 1, 6b, 7b, and 9.

Kinetics during Steady-state Electrolysis. In order to confirm the rate equation, Eq. 5, the steady-state intensity of the ESR signal was measured under different conditions. Figures 7, 8, and 9 show the dependencies of the signal intensity, I, upon the anodic current, j; the electrode length, L, and the concentration of the free cyanide ion, [CN⁻]. It can be noticed from these figures that the signal intensity is proportional to $j^{1/2}$, $L^{1/2}$, and [CN⁻].

It has been assumed that the intermediate $Cu^{II}(CN)_4^{2-}$ exists uniformly in the anode compartment whose volume is $V=\pi(R^2-r^2)L$, where R is the inner radius of the quartz-glass tube and where r is the radius of the platinum-wire electrode. In a steady state when the rates of the formation and decomposition of the intermediate $Cu^{II}(CN)_4^{2-}$ are equal, the following expression should hold:

$$\frac{j}{F} = k_0 \frac{[Cu^{II}(CN)_4^{2-}]^2}{[CN^-]^2} \pi(R^2-r^2)L. \quad (10)$$

On the other hand, the steady-state intensity of the ESR signal is expressed by Eq. 11:

$$I = \frac{1}{m}[Cu^{II}(CN)_4^{2-}]\pi(R^2-r^2)L. \quad (11)$$

By combining Eqs. 10 and 11, the following equation is obtained:

$$I = \frac{1}{m}\left\{\frac{\pi(R^2-r^2)}{k_0 F}\right\}^{1/2} \cdot j^{1/2}L^{1/2}[CN^-]. \quad (12)$$

Thus, the intensity should be proportional to $j^{1/2}$, $L^{1/2}$, and [CN⁻]. These relationships are satisfied experimentally, as has been mentioned above. The rate constant, k_0, is calculated to be 60 $M \cdot s^{-1}$ from the results of Figs. 7, 8, and 9 on the basis of Eq. 12. This value is in satisfactory agreement with the value, 74 $M \cdot s^{-1}$, obtained in the previous section.

Distribution of the Concentration of $Cu^{II}(CN)_4^{2-}$ in the Anode Compartment. Kinetic analyses have been made in the preceding sections on the assumption that the concentration of $Cu^{II}(CN)_4^{2-}$ was uniform in the anode compartment. The validity of this assumption will now be discussed.

It is known that cyanogen is primarily formed in the anodic oxidation of the cyanide ion and is then hydrolyzed according to Eq. 13:[9]

$$(CN)_2 + H_2O \longrightarrow HCN + HOCN. \quad (13)$$

When the concentration of CN⁻ is sufficiently high, the hydrogen cyanide polymerizes, according to Eq. 14, to give a brown polymer, which is called "azulmin":[10]

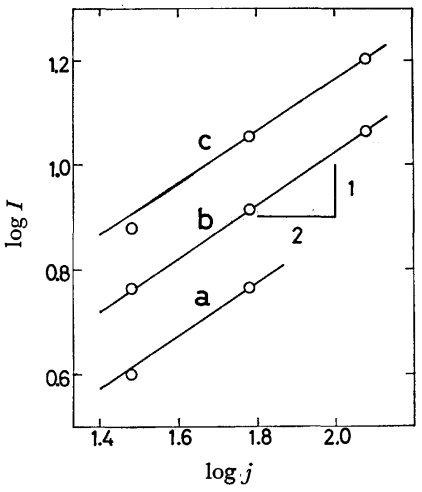

Fig. 7. Relationship between the logarithm of steady-state ESR intensity (div) and the logarithm of current (μA).
[CN⁻]: 3 M, $C_{Cu(I)}$: 0.1 M, electrode length; a: 3 mm, b: 6 mm, c: 12 mm.

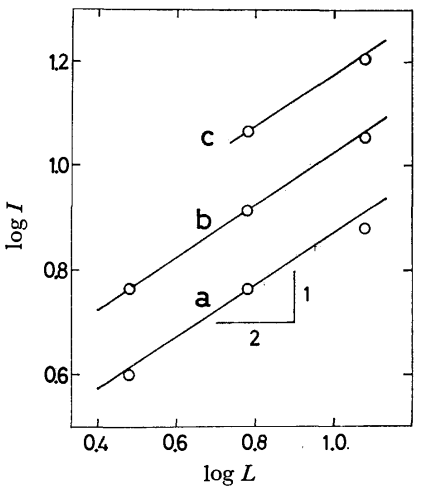

Fig. 8. Relationship between the logarithm of steady-state ESR intensity (div) and the logarithm of electrode length (mm).
[CN⁻]: 3 M, $C_{Cu(I)}$: 0.1 M, current; a: 30 μA, b: 60 μA, c: 120 μA.

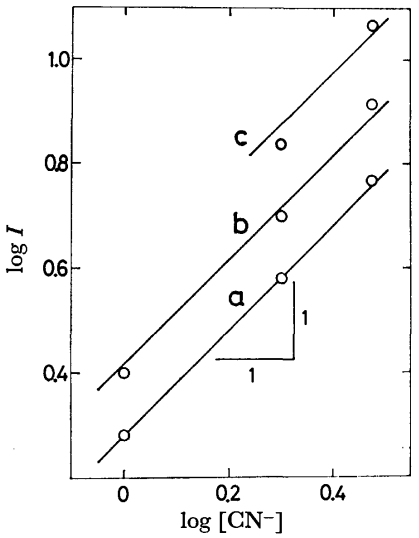

Fig. 9. Relationship between the logarithm of steady-state ESR intensity (div) and the logarithm of CN⁻ concentration (M).
$C_{Cu(I)}$: 0.1 M, electrode length: 6 mm, current; a: 30 μA, b: 60 μA, c: 120 μA.

$$x\mathrm{HCN} \longrightarrow (\mathrm{HCN})_x. \quad (14)$$

Such a brown polymer was often observed after long-time electrolysis in the present work, too. The formation of the brown polymer was almost uniform along the length of the anode, indicating that the current-density distribution was almost uniform.

The distribution of the concentration of $Cu^{II}(CN)_4^{2-}$ in the radial direction, *i.e.*, the direction normal to the electrode surface, can be calculated for steady-state electrolysis by using the rate equation, Eq. 4, and an appropriate differential equation. If the x-axis is chosen in the radical direction, with the origin at the electrode surface, and if an approximation of the linear diffusion is made, a differential equation with respect to the concentration, C, of $Cu^{II}(CN)_4^{2-}$ is established as follows:

$$\frac{\partial C}{\partial t} = D\frac{\partial^2 C}{\partial x^2} - k_2 C^2. \quad (15)$$

Here, D is the diffusion coefficient of $Cu^{II}(CN)_4^{2-}$, while k_2 is the rate constant in Eq. 4. At a steady state, when $\partial C/\partial t=0$, Eq. 15 gives Eq. 16:

$$\frac{d^2C}{dx^2} - \frac{k_2}{D}C^2 = 0. \quad (16)$$

Boundary conditions, Eqs. 17 and 18, hold:

$$\frac{dC}{dx} = -\frac{J}{DF} \quad \text{and } C=C_0 \text{ at } x=0 \quad (17)$$

$$\frac{dC}{dx} = 0 \quad \text{and } C=C_a \text{ at } x=a \quad (18)$$

where J is the current density, where a is the distance between the electrode surface and the glass wall ($a=R-r$), and where the subscripts 0 and a indicate the electrode surface and the glass wall respectively. By integrating Eq. 16 under the conditions of Eqs. 17 and 18, the following equations are derived:

$$\frac{dC}{dx} = -\sqrt{\frac{2k_2}{3D}(C^3-C_a^3)} \quad (19)$$

$$C_0^3 - C_a^3 = \frac{3}{2}\frac{J^2}{k_2DF^2}. \quad (20)$$

The integration of Eq. 19 gives Eq. 21:

$$\frac{1}{\sqrt[4]{3}}F\left\{\arccos\frac{\frac{C}{C_a}-(\sqrt{3}+1)}{\frac{C}{C_a}+(\sqrt{3}-1)}, \frac{\sqrt{3}-1}{2\sqrt{2}}\right\} = \left(\frac{2k_2C_a}{3D}\right)^{1/2}(a-x), \quad (21)$$

where $F(\varphi, k)$ indicates the elliptic integral of the first kind.[11] The concentration distribution can be calculated numerically from Eqs. 20 and 21. A typical example is shown by Curve a in Fig. 10, in which the values of $k_0=74\ \mathrm{M\cdot s^{-1}}$ and $D=10^{-5}\ \mathrm{cm^2\cdot s^{-1}}$† are used.

The horizontal line (Curve b) shows the average concentration, which was obtained from the ESR absorption intensity. The fact that Curve a lies near

† This value is estimated from the diffusion coefficients of Cu^{2+} ($D=0.72\times10^{-5}\ \mathrm{cm^2\cdot s^{-1}}$)[12] and $Cu^{II}(NH_3)_4^{2+}$ ($D=0.95\times10^{-5}\ \mathrm{cm^2\cdot s^{-1}}$),[13] both of which have the same square-planar configuration as $Cu^{II}(CN)_4^{2-}$.

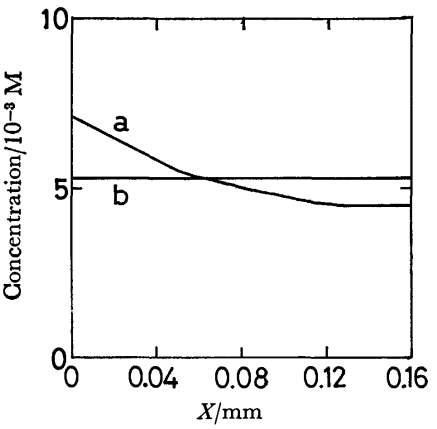

Fig. 10. Calculated concentration distribution (a) of $Cu^{II}(CN)_4^{2-}$ in the cell, compared with the experimentally observed average-value (b).
[CN⁻]: 3 M, $C_{Cu(I)}$: 0.1 M, electrode length: 6 mm, current: 30 μA.

Curve b shows the approximate validity of the assumption that the $Cu^{II}(CN)_4^{2-}$ concentration is uniform in the radial direction in the cell.

Comparison with the Kinetics and Mechanisms of the Chemical Reaction between Cu^{2+} and CN^- Ions. It is known that the copper(II) ion reacts with the cyanide ion in an aqueous solution to give copper(II) cyanide as a yellowish-brown precipitate, which then decomposes to copper(I) cyanide and cyanogen, according to Eqs. 22 and 23:[14,15]

$$Cu^{2+} + 2CN^- \longrightarrow Cu^{II}(CN)_2 \quad (22)$$

$$2Cu^{II}(CN)_2 \longrightarrow 2Cu^{I}CN + (CN)_2. \quad (23)$$

The cyanogen thus formed is evolved as a gas from an acidic solution, or it is decomposed in an alkaline solution as follows:

$$(CN)_2 + 2OH^- \longrightarrow CN^- + OCN^- + H_2O. \quad (24)$$

When the concentration of the copper(II) ion is much lower than that of the cyanide ion, not copper(II) cyanide but a purple intermediate is formed, which then gives cyanogen and a copper(I) species. Several papers have reported about this purple compound.[16–19]

The rate of the reaction between the copper(II) ion and the cyanide ion is too high under ordinary conditions to be measured by conventional methods. Duke and Courtney[20] have used the ammine copper (II) complex to diminish the reaction rate in their kinetic study, while Tanaka *et al.*[21] have used the ethylenediaminetetraacetatocopper(II) complex. Bjerrum *et al.*[22,23] have studied the kinetics in a methanol–water mixture at a low temperature. These three groups of workers have, from their kinetic considerations, expected the existence of $Cu^{II}(CN)_4^{2-}$ as an intermediate. From their measurements of ESR and optical spectra, Longo and Buch[24] have concluded the purple intermediate to be $Cu^{II}(CN)_4^{2-}$ with a square-planar configuration.

Nord and Matthes[25] have applied the stopped-flow technique to the reaction between the copper(II) ion and the cyanide ion in aqueous solutions at ambient temperatures. Thus by following the concentration of

the intermediate $Cu^{II}(CN)_4^{2-}$ by using an optical spectrometer and a oscilloscope, they obtained a rate equation, Eq. 25, from which they have proposed a reaction mechanism, Eqs. 26 and 27, the latter being rate-determining:

$$v = k_1 \frac{[Cu^{II}(CN)_4^{2-}]^2}{[CN^-]} \quad (25)$$

$$Cu^{II}(CN)_4^{2-} \rightleftharpoons Cu^{II}(CN)_3^- + CN^- \quad (26)$$

$$Cu^{II}(CN)_4^{2-} + Cu^{II}(CN)_3^- \longrightarrow \text{Product.} \quad (27)$$

There is an agreement between their work and ours in that the reaction rate is proportional to the square of $[Cu^{II}(CN)_4^{2-}]$. However, there is a disagreement in the dependency upon $[CN^-]$.

Baxendale and Westcott[26] have studied the kinetics at rather low pH values, where the concentration of the free cyanide ion is so small that the reaction rate is relatively small and can easily be measured. Thus, they followed the change in the concentration of the reaction product, $Cu^I(CN)_2^-$, by means of a UV spectrometer, and obtained the result that the reaction rate is proportional to the 6th power of $[CN^-]$ and to the square of $[Cu^{2+}]$. From this kinetic data, they have proposed the following mechanism, in which the Eq. 29 reaction is rate-determining:

$$Cu^{2+} + 3CN^- \rightleftharpoons Cu^{II}(CN)_3^- \quad (28)$$

$$2Cu^{II}(CN)_3^- \longrightarrow 2Cu^I(CN)_2^- + (CN)_2. \quad (29)$$

Their result is compatible with that of our present work. Equation 29 is the same as Eq. 7a, while their kinetic data can also be explained by the formation of $Cu^{II}_2(CN)_6^{2-}$, followed by the rate-determining reaction, Eq. 7b.

A more detailed discussion of the kinetics and the mechanisms of the chemical reaction between the copper(II) ion and the cyanide ion will be presented in a succeeding paper.

We would like to thank Professor Saburo Kako for his helpful discussions, and Mr. Hideo Fujita for his assistance in measuring the ESR spectra. The present work was partly supported by a Grant-in-Aid for Scientific Research (Environmental Science) from the Ministry of Education, Science and Culture (No. 403523).

References

1) Part III of this series: S. Yoshimura, A. Katagiri, Y. Deguchi, and S. Yoshizawa, *Bull. Chem. Soc. Jpn.*, **53**, 2434 (1980).
2) S. Yoshimura, A. Katagiri, and S. Yoshizawa, *Denki Kagaku*, **47**, 360 (1979).
3) S. Yoshimura, A. Katagiri, and S. Yoshizawa, *Denki Kagaku*, **47**, 488 (1979).
4) R. A. Penneman and L. H. Jones, *J. Chem. Phys.*, **24**, 293 (1956).
5) "Jikken Kagaku Kōza," ed by The Chemical Society of Japan, Maruzen, Tokyo (1967), Suppl. Vol. 13, p. 425.
6) R. Hirasawa, T. Mukaibo, H. Hasegawa, N. Odan, and T. Murayama, *J. Phys. Chem.*, **72**, 2541 (1968).
7) J. K. Dohrmann and F. Gallussen, *Ber. Bunsenges. Phys. Chem.*, **75**, 432 (1971).
8) A. G. MacDiarmid and N. F. Hall, *J. Am. Chem. Soc.*, **76**, 4222 (1954).
9) R. A. Nauman, *Z. Elektrochem.*, **16**, 722 (1910).
10) H. Schmidt and H. Meinert, *Z. Anorg. Allg. Chem.*, **293**, 214 (1959).
11) S. Moriguchi, K. Udagawa, and S. Hitotsumatsu, "Sugaku Koshiki I," Iwanami Shoten, Tokyo (1956), p. 148.
12) "Denki Kagaku Benran," ed by The Electrochemical Society of Japan, Maruzen, Tokyo (1964), p. 95.
13) I. M. Kolthoff and J. J. Lingane, "Polarography," Interscience (1952), p. 494.
14) "Gmelin Handbuch," Cu[B] 60, Verlag Chemie GmbH (1965), p. 1447.
15) T. Chitani, "Muki Kagaku," Sangyō Tosho, Tokyo (1964), p. 479.
16) A. G. Sharpe, "The Chemistry of Cyano Complexes of the Transition Metals," Academic Press (1976), p. 271.
17) B. N. Chadwick and A. G. Sharpe, "Advances in Inorganic Chemistry and Radiochemistry," (1966), Vol. 8 p. 83.
18) W. P. Griffith, *Quart. Rev. (London)*, **16**, 188 (1962).
19) A. Glasner and K. R. S. Asher, *J. Chem. Soc.*, **1949**, 3296.
20) F. R. Duke and W. G. Courtney, *J. Phys. Chem.*, **56**, 19 (1952).
21) N. Tanaka, M. Kamada, and T. Murayama, *Bull. Chem. Soc. Jpn.*, **31**, 895 (1959).
22) O. Mønsted and J. Bjerrum, *Acta Chem. Scand.*, **21**, 1116 (1967).
23) R. Paterson and J. Bjerrum, *Acta Chem. Scand.*, **19**, 729 (1965).
24) A. Longo and T. Buch, *Inorg. Chem.*, **6**, 556 (1967).
25) G. Nord and H. Matthes, *Acta Chem. Scand.*, **A28**, 13 (1974).
26) J. H. Baxendale and D. T. Westcott, *J. Chem. Soc.*, **1959**, 2347.

 © 1980 The Chemical Society of Japan Bull. Chem. Soc. Jpn., 53, 2443—2447 (1980)

The Reactions of NH($a^1\Delta$) with Ethane, Propane, and Isobutane in the Liquid Phase

Shigeru Tsunashima,* Jun-ichi Hamada, Mitsuhiro Hotta, and Shin Sato
Department of Applied Physics, Tokyo Institute of Technology, Ookayama, Meguro-ku, Tokyo 152
(Received December 25, 1979)

The photolysis of HN_3 was studied in liquid ethane, propane, and isobutane at the temperature of Dry Ice–methanol. In the reaction mixtures, quaternary ammonium salts were formed between the basic products and HN_3. The products were analyzed after having been passed through a trap containing NaOH, in which the salts were decomposed. The main products observed were nitrogen and amines: ethylamine from ethane, propyl- and isopropylamine from propane, and *i*-butyl, and *t*-butylamine from an isobutane solution. Ammonia and hydrogen were also formed as minor products. Possible reaction mechanisms are discussed. It is suggested that about 80% of the singlet NH is inserted into the C–H bond of paraffin to form amine and that 20% of it is deactivated to the ground triplet state by the reactions with paraffin. The relative efficiencies of the insertion into primary, secondary, and tertiary C–H bonds were estimated to be 1.0, 1.9, and 2.3 respectively.

The reactions of O and CH_2 with hydrocarbons have been extensively investigated. There are many similarities between O and CH_2 in the reactions. Triplet O(^{3}P) and $CH_2(^3B_1)$ are added to the double bond of olefin and abstract a hydrogen atom from paraffin. Singlet O(^{1}D) and $CH_2(^1A_1)$ are inserted into the C–H bond of paraffin and are added to the double bond of olefin.[1–6]

Since NH is isoelectronic with O and CH_2, the reactions of NH can be expected to be similar to those of O and CH_2.[7] Although there have been many studies of NH using the spectroscopic method,[8] the reactions of NH with hydrocarbons have not yet been established.[9–12] The main reason for this is that, except in a few studies, no NH-containing products could be detected.[13,14] This may be due to the following facts: (1) the insertion or addition products initially formed have so large an energy that only decomposition products can be observed and (2) a basic NH-containing product, if formed, may react with NH_3 or HNCO, which is often used as a source of NH, to form a quaternary ammonium salt. Because of its low vapor pressure, the salt is hard to analyze with GLC.

With these factors in mind, HN_3 was photolyzed in liquid ethane at the temperature of Dry Ice–methanol, as was briefly shown in a previous letter.[15] When less volatile products were treated with NaOH, the formation of ethylamine and ammonia could be detected. Propyl- and isopropylamine could also be detected from the propane solution. These amine formations were attributed to the insertion of the singlet NH ($a^1\Delta$) into the C–H bond of paraffin. In this paper, a kinetic study will be described and new results obtained with isobutane will be presented.

Experimental

The experimental method was the same as was briefly shown in the previous letter.[15] The details will now be given here.

HN_3 was prepared *in vacuo* by heating a mixture containing sodium azide (Koso Chemical Co.) and an excess amount of stearic acid (Tokyo Kasei Kogyo Co.) to approximately 100 °C. The HN_3 was dried with a trap containing P_2O_5, and the fraction condensable at −120 °C was stored in a Pyrex bulb covered with Al foil. The purified HN_3 was kept at a pressure of less than 50 Torr and/or was condensed at the temperature of liquid nitrogen. Pure-grade ethane, propane, and isobutane (Takachiho Shoji Co.) were used after distillation at −130, −120, and −110 °C respectively.

The mixture of HN_3 and hydrocarbon was prepared in a quartz tube 8 mm in o.d. using a mercury-free vacuum line equipped with calibrated volumes and a Wallace-Tiernan dial manometer (Nagano Keiki Co.). The quartz tube has a stopcock and a ground joint attached to it so that it was detachable from the vacuum line. The mixture was liquefied in a transparent quartz Dewar flask at the temperature of Dry Ice–methanol. The amount of the solution was about 1 ml. The solution of HN_3 thus prepared was irradiated with a medium-pressure mercury lamp (Wako Denki Co.) through a filter which cuts off the light shorter than 250 nm (Toshiba UV 27). Thus, the effective light was limited to between 320 and 250 nm.

After the irradiation, non-condensable gases at the temperature of liquid nitrogen were analyzed with a combination of a Toepler pump, a gas burette, and a CuO furnace at 300 °C. The solvents (ethane, propane, and isobutane) were evacuated at −130, −120, and −110 °C respectively, Less volatile products, including unreacted HN_3, were passed through a trap packed with NaOH-coated glass wool at 80 °C. The products thus obtained were analyzed by GLC using a column packed with amine 220 on Celite 545 (Gasukuro Kogyo Co., 5 m in length) at 40 °C. For the separation of ammonia and propane, a column packed with NaOH-coated Porapak Q (30 cm in length) was used at 80 °C. A mass spectrometer was also used for the identification of the product.

Results

When HN_3 was photolyzed in liquid ethane, propane, or isobutane at the temperature of Dry Ice–methanol, a white precipitant was observed to be formed. The non-condensable products at the temperature of liquid nitrogen were nitrogen and hydrogen. The amounts of hydrogen formed from the ethane, propane, and isobutane solutions were independent of the changes in the concentration of HN_3 and were, respectively, 5.6±1.0, 4.3±2.0, and 5.3±1.4% of that of the nitrogen formed. No methane formation was found in any case examined.

The condensable products observed were ammonia and amines: ethylamine from ethane, propyl- and isopropylamine from propane, and *i*-butyl- and *t*-

butylamine from isobutane solutions. Without having been passed through the NaOH trap, the peak of neither ammonia nor amine was observed on the gas chromatogram. Probably, a quaternary ammonium salt was formed in the reaction mixtures between the basic products and the reactant HN_3. The complete recovery of the products was checked by using authentic samples of amine and HN_3 dissolved in liquid hydrocarbon at the temperature of Dry Ice–methanol.

Because of the formation of a white precipitant in the solution and dew on the wall of the Dewar flask, the amount of the product was not reproducible; however, the product ratio was found to be reproducible. Figure 1 shows the plots of the product ratios, NH_3/N_2 and RNH_2/N_2, as functions of $[HN_3]/[RH]$. Here, R represents C_2H_5, C_3H_7, or C_4H_9. As is shown in Fig. 1, the ratio of RNH_2/N_2 decreased with an increase in the concentration ratio of $[HN_3]/[RH]$, while the ratio of NH_3/N_2 increased.

In the cases of propane and isobutane solutions, we obtained no evidence of the formation of C_6 or C_8 hydrocarbons, which are possible products of the C_3H_7 or C_4H_9 radicals, if formed. For both cases, two kinds of amines were formed, corresponding to the two types of C–H bonds present. Figure 2 shows plots of the product ratios, propylamine/isopropylamine and *i*-butylamine/*t*-butylamine, as functions of $[HN_3]/[RH]$. The product ratios were independent of the changes in the concentration ratio; they were 1.6± 0.2 and 4.0±0.4 in propane and isobutane solutions respectively.

Figure 3 shows plots of $(RNH_2+3H_2+4NH_3)/N_2$ as functions of the concentration ratio of $[HN_3]/[RH]$. The ratios were less than unity in every case examined.

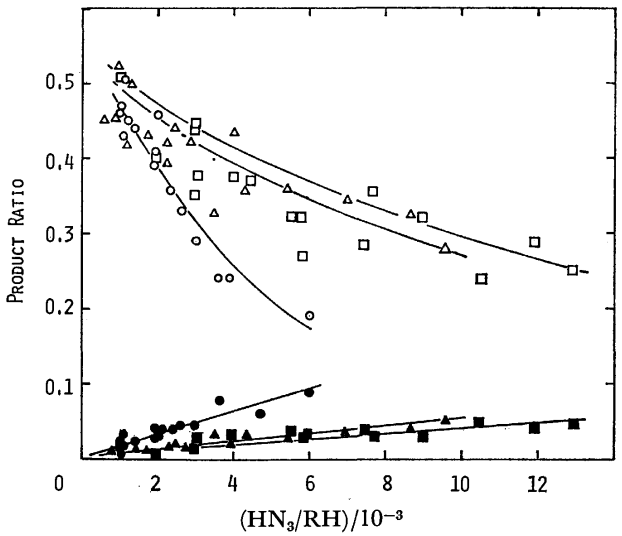

Fig. 1. Effect of concentration ratio of $[HN_3]/[RH]$ on the product ratios of RNH_2/N_2 (open symbols) and NH_3/N_2 (closed symbols).
○: R=C_2H_5, △: R=C_3H_7, □: R=C_4H_9.

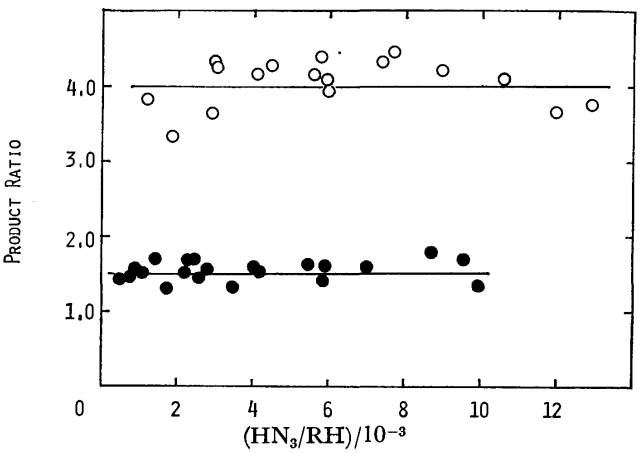

Fig. 2. Effect of concentration ratio of $[HN_3]/[RH]$ on the product ratios of propylamine/isopropylamine (●) and *i*-butylamine/*t*-butylamine (○).

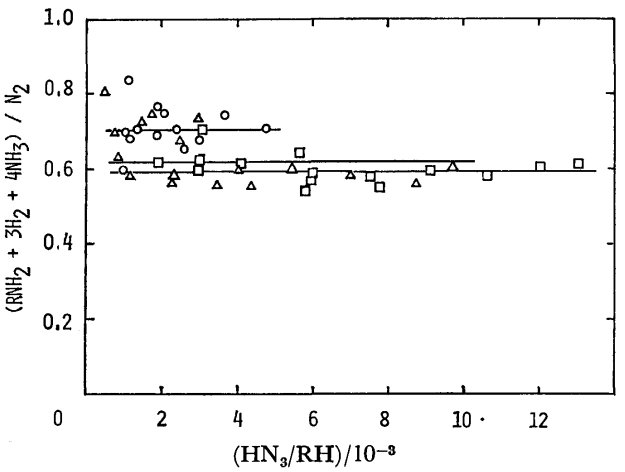

Fig. 3. Plots of $(RNH_2+3H_2+4NH_3)/N_2$ as functions of concentration ratio of $[HN_3]/[RH]$.
○: R=C_2H_5, △: R=C_3H_7, □: R=C_4H_9.

Discussion

As was discussed in the previous letter, the following reaction mechanism can explain the results obtained in the ethane and propane solutions of HN_3 at the temperature of Dry Ice–methanol:[15]

$$HN_3 + h\nu \longrightarrow {}^1NH + N_2 \qquad \alpha \qquad (1)$$

$$\longrightarrow H + N_3 \qquad (1-\alpha) \qquad (2)$$

$$^1NH + HN_3 \longrightarrow NH_2 + N_3 \qquad k_a \qquad (3)$$

$$^1NH + RH \longrightarrow RNH_2 \qquad k_h \qquad (4)$$

$$NH_2 + HN_3 \longrightarrow NH_3 + N_3 \qquad (5)$$

$$H + HN_3 \longrightarrow H_2 + N_3 \qquad (6)$$

$$2NH_2 \longrightarrow N_2H_4 \qquad (7)$$

$$2N_3 \longrightarrow 3N_2, \qquad (8)$$

where ^1NH represents an NH radical in the first excited singlet state ($a^1\Delta$).

Baronavski *et al.* showed that the 266 nm-laser photolysis of HN_3 gives rise to NH fragments exclusively in the $a^1\Delta$ state without being vibrationally excited.[14] They also showed that a similar thing could be said when HN_3 was photolyzed with the light of wavelengths

between 290 and 310 nm. Their conclusions agree well with the results obtained in the study of the flash photolysis of HN_3 using light longer than 200 nm.[16]

In the absence of added hydrocarbon, the main reaction of the singlet NH is the abstraction of a hydrogen atom from HN_3 to form an excited NH_2 which can fluoresce.[14,17] In the presence of hydrocarbon, the insertion reaction of the singlet NH into the C–H bond of paraffin is assumed for the formation of amine. The insertion reaction is similar to that observed in the case of the singlet O and CH_2.[1-6] An alternative mechanism for the amine formation is the so-called "radical-abstraction recombination" mechanism:

$$^1NH + RH \longrightarrow NH_2 + R \quad (9)$$

$$NH_2 + R \longrightarrow RNH_2. \quad (10)$$

If these reactions are predominant, more isopropylamine should be formed than propylamine and more *t*-butylamine should also be formed than *i*-butylamine, since the bond-dissociation energy of the secondary or tertiary C–H bond is smaller than that of the primary C–H bond.[18] If we found C_6 or C_8 hydrocarbons as products, Reaction 9 would be important. This was not the case in the present study, as was shown in the Results section. That is, the amine is formed mainly by Reaction 4.

Konar *et al.* proposed a reaction mechanism in which a part of the primary photodissociation of HN_3 is to N_3 and H, followed by a hydrogen-atom abstraction from HN_3. This mechanism can explain the hydrogen formation in the 213.9 nm photolysis of HN_3 at room temperature.[11] By measuring the decay of the concentration of hydrogen atoms, Bras and Combourieu have estimated the rate constant of the reaction of hydrogen atoms with HN_3 to be $1.5\times 10^{13}\exp(-2300/T)$ $cm^3\ mol^{-1}\ s^{-1}$.[19] As the exit channel of the reaction of hydrogen atoms, they proposed the formation of NH_2 and N_2, which is different from Reaction 6:

$$H + HN_3 \longrightarrow NH_2 + N_2. \quad (11)$$

When Reaction 11 is included in the mechanism instead of Reaction 6, it is necessary to consider a reaction mechanism which can explain the hydrogen formation. It was difficult to construct such a mechanism. We, therefore, conclude that the rate constant estimated by Bras and Combourieu is that for Reaction 6, but not for Reaction 11.

The abstraction of a hydrogen atom from paraffin by H or NH_2 is a possible reaction:

$$H + RH \longrightarrow H_2 + R \quad (12)$$

$$NH_2 + RH \longrightarrow NH_3 + R. \quad (13)$$

These reactions, however, can be neglected under the present experimental conditions, because of the following reasoning: (1) the bond dissociation energy of $H–N_3$ is smaller than that of R–H,[18] (2) since the activation energies of the reactions are about 20 to 40 kJ mol^{-1},[20,21] the rates of these reactions should be very slow at the temperature of Dry Ice–methanol, and (3) no possible products formed from the recombination of R could be detected in the present study, as was shown in the Results section.

In Reaction 7, a hydrazine formation was assumed, although we failed to detect the hydrazine formation. Without including Reaction 7, the following equation can be expected to hold between the amounts of the products:

$$RNH_2 + 3H_2 + 4NH_3 = N_2. \quad (14)$$

As was shown in Fig. 3, the ratios of $(RNH_2+3H_2+4NH_3)/N_2$ were less than unity for any solvent examined. That is, about 30 to 40% of the NH-containing products are missing in this study. When Reaction 7 is included in the mechanism, the following relation can be expected to hold:

$$RNH_2 + 3H_2 + 4NH_3 + 5N_2H_4 = N_2. \quad (15)$$

A steady-state treatment of the above mechanism gives the following relations:

$$\alpha = X/(X+H_2) \quad (16)$$

$$X/RNH_2 = 1 + k_a[HN_3]/k_h[RH]. \quad (17)$$

Here, X is defined as follows:

$$X = N_2 - 3(H_2+NH_3+N_2H_4). \quad (18)$$

The amount of N_2H_4 formed can be estimated using Eq. 15. The relations of Eqs. 16 and 17 are plotted in Figs. 4 and 5 respectively as functions of the concentration ratios, $[HN_3]/[RH]$.

As is shown in Fig. 4, the ratio of $X/(X+H_2)$ is independent of the changes in the $[HN_3]/[RH]$ ratio and also the changes in the solvent examined. The values of α is estimated to be 0.91 ± 0.03 from the ratio in Fig. 4. That is, about 91% of the primary photodissociation of HN_3 gives rise to the first excited singlet state, while the remaining part corresponds to the dissociation into H and N_3. This part is slightly larger than that estimated in the gas-phase photolysis of HN_3 at 213.9 nm.[11] Bradley *et al.* pointed out that the fraction of the primary photodissociation of HNCO into H and NCO decreases with the decrease in the excitation wavelength in the gas-phase photolysis of HNCO.[22] A similar effect of the wavelength might explain the difference between the results obtained by Konar *et al.* and those of the present study.

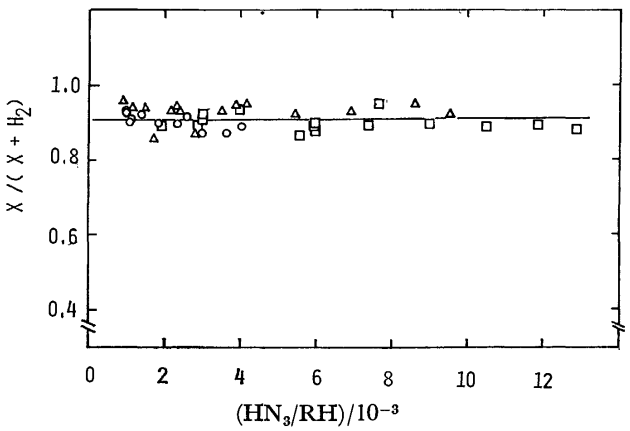

Fig. 4. Plots of $X/(X+H_2)$ as functions of concentration ratio of $[HN_3]/[RH]$.
○: $R=C_2H_5$, △: $R=C_3H_7$, □: $R=C_4H_9$.

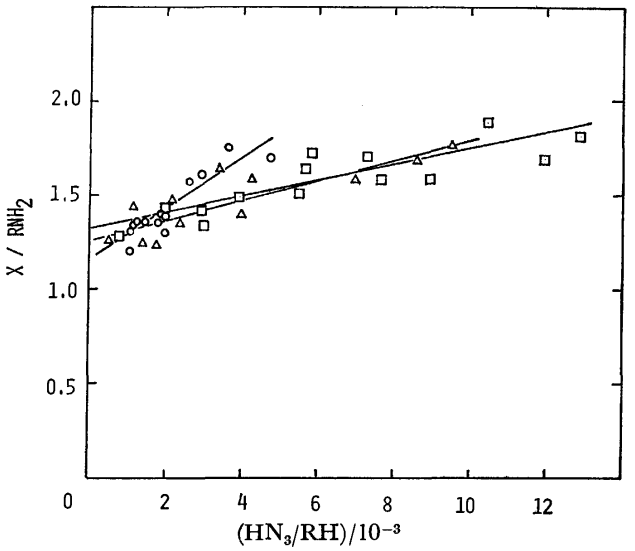

Fig. 5. Plots of X/RNH_2 as functions of concentration ratio of $[HN_3]/[RH]$.
○: R=C_2H_5, △: R=C_3H_7, □: R=C_4H_9.

As is shown in Fig. 5, the plots of X/RNH_2 give straight lines for any solvent examined, as was expected from Eq. 17. The intercepts, however, are different from unity. In order to explain the non-unity intercepts, the following reactions are considered to hold:

$$^1NH + RH \longrightarrow {}^3NH + RH \qquad k_h' \qquad (19)$$

$$^3NH + HN_3 \longrightarrow NH_2 + N_3. \qquad (20)$$

Here, ^3NH denotes NH in the ground triplet state, ($X^3\Sigma^-$). A similar deactivation process has been considered in the reactions of the singlet O and CH_2.[1-6] The triplet NH will abstract a hydrogen atom preferentially from HN_3, as was considered to hold in the case of the singlet NH. The rate constant of Reaction 20 has been estimated, in the study of the shock-wave decomposition of HN_3, to be 3.0×10^{11} exp $(-800/T)$ $cm^3\,mol^{-1}\,s^{-1}$.[23] Because of its low activation energy, Reaction 20 may be more important than Reaction 21 under the present experimental conditions:

$$^3NH + RH \longrightarrow NH_2 + R. \qquad (21)$$

By the inclusion of Reactions 19 and 20 in the mechanism, Eq. 17 changes its form as follows:

$$X/RNH_2 = (k_h+k_h')/k_h + k_a[HN_3]/k_h[RH]. \qquad (22)$$

From the slope and the intercept of the straight line in Fig. 5, the values of $k_h/(k_h+k_h')$ and k_a/k_h can be estimated. The results are summarized in Table 1. As is shown in Table 1, about 80% of the singlet NH is inserted into the C–H bond of paraffin, while the remaining part is deactivated to the ground triplet state by the reaction with paraffin. The rate constant of the reaction of the singlet NH with paraffin is about two orders of magnitude smaller than that with HN_3 at the temperature of Dry Ice–methanol.

Table 1. Summary of the rate constant ratios

Reactant	$k_h/(k_h+k_h')$	k_a/k_h	$k_h/k_{a\,rel}$	$k_{h\,rel}$
C_2H_6	0.86±0.04	125±21	1.0	1.0
C_3H_8	0.79±0.02	49± 9	2.6	1.6
i-C_4H_{10}	0.75±0.04	40± 9	3.1	1.9

The value of k_a has been estimated to be 5.6×10^{13} $cm^3\,mol^{-1}\,s^{-1}$ in the gas phase at room temperature.[14,16] Paur and Bair estimated the activation energy to be very small, if present at all.[16] In the liquid phase at the temperature of Dry Ice–methanol, the rate of Reaction 3 (k_a) may be expected to be fast and close to the diffusion-controlled rate. That is, k_a depends on the nature of the solvent, such as the viscosity. In the third column of Table 1, the relative values of k_h/k_a are listed.

Using the values of the product ratios shown in Fig. 2, it is possible to estimate the relative efficiencies of the insertion per C–H bond, k_s/k_p and k_t/k_p. Here, the subscripts p, s, and t represent the primary, secondary, and tertiary C–H bonds of paraffin respectively:

$$6k_p/2k_s = \text{propylamine/isopropylamine} = 1.6 \pm 0.2 \qquad (23)$$

$$9k_p/k_t = i\text{-butylamine}/t\text{-butylamine} = 4.0 \pm 0.4. \qquad (24)$$

Thus, $k_s/k_p=1.9\pm0.2$ and $k_t/k_p=2.3\pm0.2$. That is, the efficiencies of the insertion into the secondary and tertiary C–H bonds are about twice that into the primary C–H bond. In the case of the singlet O (^1D), a non-discriminative insertion has been observed.[24] On the other hand, the efficiency of the insertion of the singlet CH_2 ($^1A_1$) into the secondary or tertiary C–H bond is slightly larger than that into the primary C–H bond.[25] The reason for these differences is not clear at present.

The relative insertion rate of the singlet NH into ethane, propane, and isobutane can be estimated using the values of k_s/k_p, k_t/k_p and by including the numbers of the C–H bond. The results thus obtained are listed in the fourth column of Table 1. The difference between the third and fourth columns is within the factor of two and may be mainly due to the difference in k_a.

Since we included Reactions 19 and 20 in the reaction mechanism, the NH_2 radicals are formed *via* two reaction paths, Reactions 3 and 20. If Reaction 7, the formation of N_2H_4, is not included in the mechanism, the ratio of the yield, $(NH_3/RNH_2)_0$, should be equal to the k_h'/k_h ratio, where the subscript 0 denotes the value obtained by extrapolation to a zero concentration of HN_3. This is not the case, as is expected from the results shown in Fig. 1. If Reaction 7 is included, the following relations are expected to hold:

$$NH_3/(N_2H_4)^{1/2} = k_5[HN_3]/k_7^{1/2} \qquad (25)$$

$$((NH_3+2N_2H_4)/RNH_2)^{1/2} = k_h'/k_h. \qquad (26)$$

Since the yield ratios, N_2H_4/N_2, calculated were nearly independent of the change in the concentration of HN_3, the NH_3/N_2 ratio should linearly increase with an increase in the concentration of HN_3. This is the case shown in Fig. 1. Using the data of Figs. 1 and 3, the $((NH_3+2N_2H_4)/RNH_2)_0$ ratios were estimated to be 0.2, 0.3, and 0.3 respectively for the cases of ethane, propane, and isobutane. These values

are consistent with those estimated from the $k_h/(k_h+k_h')$ ratios shown in Table 1; *i.e.*, the assumption of the N_2H_4 formation well explains all of the experimental results obtained here.

References

1) R. J. Cvetanović, *Adv. Photochem.*, **1**, 115 (1963).
2) R. E. Huie and J. T. Herron, *Prog. React. Kinet.*, **8**, 1 (1975).
3) W. B. DeMore and S. W. Benson, *Adv. Photochem.*, **2**, 219 (1964).
4) H. M. Frey, *Prog. React. Kinet.*, **2**, 131 (1964).
5) "Carbene Chemistry," ed by W. Kirmse, Academic Press, New York (1971).
6) "Carbenes," ed by M. Jones, Jr., and R. A. Moss, John Wiley and Sons, New York (1973), I.
7) R. S. Berry, "Nitrenes," ed by W. Lwowski, Interscience Publishers, New York (1970), p. 13.
8) H. Okabe, "Photochemistry of Small Molecules," John Wiley and Sons, New York (1978), p. 193.
9) J. Y. Mui and R. A. Back, *Can. J. Chem.*, **41**, 826 (1963); R. A. Back, *J. Chem., Phys.*, **40**, 3493 (1964); J. L. Brash and R. A. Back, *Can. J. Chem.*, **43**, 1778 (1965); N. J. Frinswell and R. A. Back, *ibid.*, **46**, 527 (1968); W. D. Wooley and R. A. Back, *ibid.*, **46**, 295 (1968); R. A. Back and R. Ketcheson, *ibid.*, **46**, 531 (1968).
10) D. W. Cornell, R. S. Berry, and W. Lwowski, *J. Am. Chem. Soc.*, **88**, 544 (1966).
11) R. S. Konar, S. Matsumoto, and B. deB. Darwent, *Trans. Faraday Soc.*, **67**, 1698 (1971).
12) W. C. Richardson and D. W. Setser, *Can. J. Chem.*, **47**, 2725 (1969).
13) M. E. Jacox and D. E. Milligan, *J. Am. Chem. Soc.*, **85**, 278 (1963).
14) A. P. Baronavski, R. G. Miller, and J. R. McDonald, *Chem. Phys.*, **30**, 119 (1978).
15) S. Tsunashima, M. Hotta, and S. Sato, *Chem. Phys. Lett.*, **64**, 435 (1979).
16) R. J. Paur and E. J. Bair, *Int. J. Chem. Kinet.*, **8**, 139 (1976).
17) J. R. McDonald, R. G. Miller, and A. P. Baronavski, *Chem. Phys.*, **30**, 133 (1978).
18) "C. R. C. Handbook of Physics and Chemistry," 55, F213 (1974—1975).
19) G. Le Bras and J. Coumbourieu, *Int. J. Chem. Kinet.*, **5**, 559 (1973).
20) B. A. Thrush, *Prog. React. Kinet.*, **3**, 63 (1965).
21) R. Lesclaux and M. Demissy, *J. Photochem.*, **9**, 110 (1978).
22) J. N. Bradley, J. R. Gilbert, and D. Svejda, *Trans. Faraday Soc.*, **64**, 911 (1968).
23) O. Kajimoto, T. Yamamoto, and T. Fueno, *J. Phys. Chem.*, **83**, 429 (1979).
24) H. Yamazaki and R. J. Cvetanović, *J. Chem. Phys.*, **41**, 3703 (1964); G. Paraskevopoulos and R. J. Cvetanović, *ibid.*, **50**, 590 (1969).
25) B. M. Herzog and R. W. Carr, Jr., *J. Phys. Chem.*, **71**, 2688 (1967).

The Flotation of Cd^{2+} Ions in the Presence and Absence of Zn^{2+} Ions

Koichi KOBAYASHI,*,† Yoshiko SHIMIZU,†† and Tsunetaka SASAKI†††

Department of Chemistry, Faculty of Science, Tokyo Metropolitan University, Setagaya-ku, Tokyo 158

(Received December 27, 1979)

The flotation of Cd^{2+} ions was investigated in the presence and absence of Zn^{2+} ions. It was found that the flotation efficiency of Cd^{2+} ions in the Cd^{2+}–anionic surfactant system is markedly small in the presence of Zn^{2+} ions, but the flotation efficiency of Cd^{2+} ions in the Cd^{2+}–bentonite–cationic surfactant system (adsorbing particle flotation) decreased only slightly in the presence of Zn^{2+} ions. The flotation efficiency in the latter case was further increased by the addition of 3 ppm of polyacrylamide. The doubling of the flotation reagents and time did not effectively increased the flotation efficiency of Cd^{2+} ions in the presence of Zn^{2+} ions, but the two-stage flotation did. It was confirmed that the adsorbing particle flotation of Cd^{2+} ions would be an excellent method in the presence of Zn^{2+} ions.

In previous papers,[1,2] we reported that Cd^{2+} ions were effectively removed by using an anionic surfactant, a cationic surfactant with bentonite, or a cationic surfactant with bentonite and polyacrylamide.

Generally, mine water contains such heavy metal ions as Cd^{2+}, Cu^{2+}, and Zn^{2+}. In the case of removal of Cd^{2+} ions, the flotation is greatly influenced by co-existing ions.

Shimoiizaka *et al.*[3] have studied the removal of Cd^{2+} ions by precipitation flotation in the presence of co-existing ions, such as Fe^{2+} and Zn^{2+} ions, and have indicated that Cd^{2+} ions could be effectively removed by xanthate in the presence of these co-existing ions. However, no other studies have been reported on the adsorbing particle flotation of Cd^{2+} ions in the presence of co-existing ions.

In the present paper, the flotation of Cd^{2+} ions in the presence and absence of Zn^{2+} ions will be reported.

Experimental

Materials. The zinc(II) nitrate used was of an extra-pure grade $Zn(NO_3)_2 \cdot 6H_2O$; it was recrystallized twice from distilled water, and a stock solution with a concentration of 1.78×10^{-3} mol/dm^3 was prepared. For the determination of the concentration of Zn^{2+}, the chelate-titration method was carried out using Cu-PAN.[4] A stock solution of Cd^{2+} ions was prepared by dissolving Cd metal of a 99.999% purity in nitric acid. All the other reagents, such as disodium α-sulfonatododecanoate (α-SLNa), dodecyltrimethylammonium chloride (DTAC), and bentonite (Bt), were the same as have been described previously.[1] The polyacrylamide (PAA) used as a coagulating agent was a product of the Mitsubishi Kasei Co., Ltd., its average molecular weight was seven million.

Apparatus and Procedure. The apparatus and the method of flotation measurements were the same as have been reported previously.[1] The concentration of the Cd^{2+} ions was measured by using an atomic absorption spectrometer (Techtron Pty., Model-AA-100). A glass electrode pH meter (Toadenpa Co., Ltd., HM-5A) was used to measure the pH. The gas-flow rate was kept at 10 ml/min, while the gas-flow time was kept at 7 or 14 min, as the case required. The measurements of the flotation were carried out at a room temperature of about 25 °C.

The flotation efficiency of Cd^{2+} ions (F) is conventionally expressed by:

$$F = (C_i - C_f)/C_i \times 100\ (\%),$$

where C_i and C_f are the initial and final concentrations of the Cd^{2+} ions respectively.

Results and Discussion

The adsorbing particle flotation was carried out for a solution containing 1.78×10^{-5} mol/dm^3 Cd^{2+}, 1.78×10^{-5} mol/dm^3 DTAC, or 1.78×10^{-4} mol/dm^3 DTAC and 100 ppm Bt. The results are shown in Fig. 1. As can be seen in Fig. 1, the flotation efficiency of the Cd^{2+} ions increased with an increase in the pH, showed a maximum at about pH 11, and decreased with an increase in the pH above about pH 11. The maximum flotation efficiencies of the Cd^{2+} ions were 73% and 96% in the cases of 1.78×10^{-5} mol/dm^3 DTAC and 1.78×10^{-4} mol/dm^3 DTAC respectively. In the former case, the Cd^{2+} ions may be completely adsorbed on the Bt particle, considering the results presented in a previous paper,[2] but the Bt particle

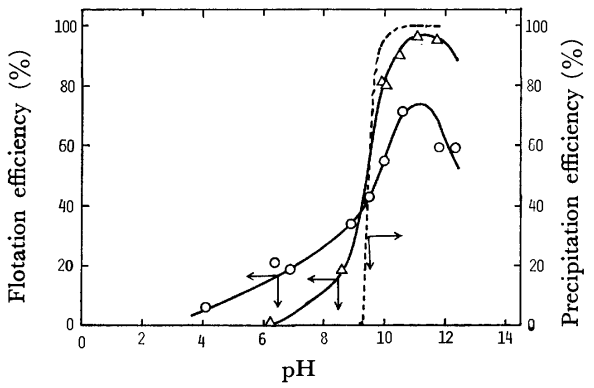

Fig. 1. Flotation efficiency *vs.* pH for Cd^{2+}–Bt–DTAC system. Cd^{2+}: 1.78×10^{-5} mol/dm^3, Bt: 100 ppm, DTAC (○: 1.78×10^{-5} mol/dm^3; △: 1.78×10^{-4} mol/dm^3), gas-flow time: 7 min, gas-flow rate: 10 ml/min. ----: Precipitation efficiency *vs.* pH curve.

† Present address: Laboratory of Chemistry, Musashi Institute of Technolgy, 1-28-1, Tamatsutsumi, Setagaya, Tokyo 158.

†† Present address: 2-7-6, Shiomidai, Isogo-ku, Yokohama, Kanagawa 247.

††† Present address: Department of Chemistry, Faculty of Science, Tokai University, Hiratsuka, Kanagawa 259-12.

could not be floated because the amount of DTAC was insufficient. When the concentration of DTAC increased to 1.78×10^{-4} mol/dm^3 DTAC, a nearly complete flotation of Bt particle could be attained. The broken curve in Fig. 1 represents the precipitation efficiency *vs.* pH curve obtained from the solubility product (7.6×10^{-15}) of $Cd(OH)_2$. It was confirmed that the flotation efficiency *vs.* pH curve of Cd^{2+} ions was in accord with the precipitation efficiency *vs.* pH curve of $Cd(OH)_2$. Judging from these facts, the polynuclear cations of Cd^{2+} may be formed and subsequently adsorbed on Bt particles. The Bt particles coagulated by DTAC are floated by bubbles.

The flotation of the Cd^{2+} ions was further carried out for the system prepared by adding 1.78×10^{-4} mol/dm^3 Zn^{2+} to a solution containing 1.78×10^{-5} mol/dm^3 Cd^{2+}, 1.78×10^{-5} mol/dm^3 DTAC, and 100 ppm Bt. The results are shown in Fig. 2(I). The flotation efficiency of the Cd^{2+} ions decreased to 62% when ten times as many Zn^{2+} ions were added as compared with 73% for the system without Zn^{2+} ions (Fig. 1). The decrease in the flotation efficiency of the Cd^{2+} ions may be due to Cd^{2+} being hindered by the adsorption of Zn^{2+} on the Bt surface. The flotation efficiency *vs.* pH curve of the system with Zn^{2+} ions shifts toward a lower pH as compared with that of the system without Zn^{2+} ions (Fig. 1). This shift in pH may be caused by the coprecipitation of Cd^{2+} with $Zn(OH)_2$, which was formed at about pH 7.7.

Figure 2(II) shows the results of the flotation of Cd^{2+} ions from a solution containing 1.78×10^{-5} mol/dm^3 Cd^{2+}, 1.78×10^{-5} mol/dm^3 α-SLNa, and 1.78×10^{-4} mol/dm^3 Zn^{2+}. The maximum flotation efficiency of 38% was obtained at pH 8.3. As may be seen, the flotation efficiency of the Cd^{2+}–α-SLNa system was lower than that of the Cd^{2+}–Bt–DTAC system in the presence of Zn^{2+} ions.

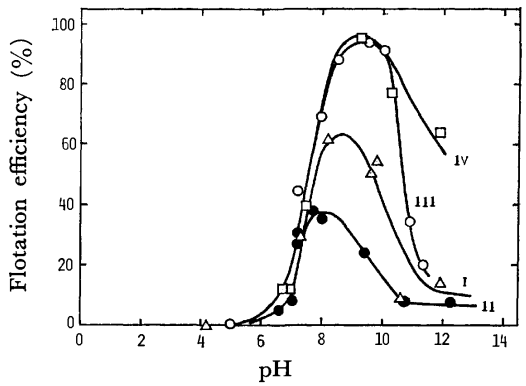

Fig. 2. Flotation efficiency *vs.* pH for Cd^{2+}–Zn^{2+}–Bt–DTAC system(I), Cd^{2+}–Zn^{2+}–α-SLNa system(II), Cd^{2+}–Zn^{2+}–Bt–DTAC–PAA system(III), and Cd^{2+}–Zn^{2+}–Bt–DTAC–PAA system(IV). Cd^{2+}: 1.78×10^{-5} mol/dm^3, Zn^{2+}: 1.78×10^{-4} mol/dm^3, gas-flow rate: 10 ml/min.
(I) DTAC: 1.78×10^{-5} mol/dm^3, Bt: 100 ppm, gas-flow time: 7 min. (II) α-SLNa: 1.78×10^{-5} mol/dm^3, gas-flow time: 7 min. (III) DTAC: 1.78×10^{-5} mol/dm^3, Bt: 100 ppm, PAA: 3 ppm, gas-flow time: 7 min. (IV) DTAC: 3.56×10^{-5} mol/dm^3, Bt: 200 ppm, PAA: 6 ppm, gas-flow time: 7 min.

In order to study the effect of PAA on the flotation efficiency, the flotation was carried out for a system prepared by adding 3 ppm PAA to a solution containing 1.78×10^{-5} mol/dm^3 Cd^{2+}, 1.78×10^{-4} mol/dm^3 Zn^{2+}, 1.78×10^{-5} mol/dm^3 DTAC, and 100 ppm Bt. As compared with Fig. 2(I) for the system without PAA, a sharp maximum of 95% flotation at about pH 9.5 is shown in Fig. 2(III). Thus, it was confirmed that the flotation efficiency of the Cd^{2+} ions increased further upon the addition of PAA.

The adsorbing particle flotation was further carried out by doubling the amount of reagents and the gas-flow time for the above system. However, the flotation efficiency of Cd^{2+} ions was not increased significantly. As can also be seen from Fig. 1 and other data,[1] the 1.78×10^{-4} mol/dm^3 DTAC is required to increase effectively the removal of 100 ppm Bt. Therefore, the further addition of DTAC is considered to increase the flotation efficiency of Cd^{2+} ions in the case of Fig. 2(IV).

As can also be seen from Fig. 1 and Fig. 2(I), the influence of the Zn^{2+} addition to the Cd^{2+}–Bt–cationic surfactant system is small in terms of the flotation efficiency. In the case of the presence of Zn^{2+}, the flotation efficiency of the Cd^{2+} ions of the Cd^{2+}–α-SLNa system was lower than that of the Cd^{2+}–Bt–DTAC system, as is shown by Fig. 2(I) and Fig. 2(II). These facts show that the adsorbing particle flotation is an effective method in the presence of Zn^{2+} ions. Further, the addition of 3 ppm PAA to the Cd^{2+}–Bt–DTAC system markedly increases the flotation efficiency of the Cd^{2+} ions, as may be seen by comparing the systems of Fig. 2(I) and Fig. 2(III). As can be seen in Fig. 2(IV), the maximum flotation efficiency of 96% was obtained when the concentration of each reagent was twice that of Fig. 2(III). Therefore, the flotation efficiency of the Cd^{2+} ions is not significantly increased by doubling the amount of the reagents and the gas-flow time.

It has also been known that the two-stage flotation is effective for the ion flotation.[5,6] Therefore, the flotation of Cd^{2+} ions from a solution containing 1.78×10^{-5} mol/dm^3 Cd^{2+}, 1.78×10^{-5} mol/dm^3 DTAC, 1.78×10^{-4} mol/dm^3 Zn^{2+}, 100 ppm Bt, and 3 ppm PAA was carried out at pH 9.55 in two stages. The flotation efficiency of Cd^{2+} ions in the first stage was 92.5%. After the underlying solution had been removed from the flotation cell, the second-stage flotation of the solution was carried out with the further addition of 1.78×10^{-5} mol/dm^3 DTAC, 100 ppm Bt, and 3 ppm PAA. It is evident from Table 1 that the flotation efficiency of the Cd^{2+} ions was 99%. From these facts, the removal of the Cd^{2+} ions can be said to have been almost complete after the two-stage flota-

Table 1. Flotation efficiency in two stages

pH	F (%)		Relative time and amount of reagents
	1st	1st+2nd	
9.55	92.5	99.0	2

tion.

In conclusion, the Cd^{2+} ions were effectively removed by using Bt and DTAC rather than the α-SLNa, and the flotation efficiency was further increased by the addition of PAA to the former system in the presence of Zn^{2+} ions. A two-stage flotation was found to be most effective.

References

1) K. Kobayashi, *Bull. Chem. Soc. Jpn.*, **48**, 1745 (1975).
2) K. Kobayashi, *Bull. Chem. Soc. Jpn.*, **48**, 1750 (1975).
3) J. Shimoiizaka, S. Hasebe, I. Matsuoka, T. Takahashi, and K. Yamamoto, *Nippon Kogyo Kaishi*, **86**, 549 (1970).
4) K. Ueno, "Chelate Titration Method," Nankodo Co., Tokyo (1972), p. 279.
5) S. Mukai and Y. Nakahiro, *Nippon Kogyo Kaishi*, **88**, 477 (1972).
6) K. Kobayashi, H. Sato, K. Kachi, M. Nakamura, and T. Sasaki, *Bull. Chem. Soc. Jpn.*, **48**, 3533 (1975).

The Effect of Sugars on the Thermal Denaturation of Lysozyme

Hatsuho UEDAIRA* and Hisashi UEDAIRA

Research Institute for Polymers and Textiles, 1-1-4, Yatabe-Higashi, Tsukuba, Ibaraki 305

(Received January 5, 1980)

Thermal denaturation of lysozyme (hen egg-white) in aqueous sugar solution was studied by DSC measurements at pH 5 and by CD measurements at pH 2.12. All of the sugars investigated show a stabilizing influence on the native conformation. The effect of sugars on the transition temperature of lysozyme almost linearly increased with the increase of the numbers of equatorial hydroxyl groups per molecule of sugars. The ellipticity of the solutions at 294 nm of lysozyme and glucose or arabinose was additive in the value of each component at pH 5. The effect of sugars in stabilizing the protein structure may be due to the intensification of the hydrophobic interactions inside the protein molecule.

There have been many investigations on the effects of alcohols and sugars on the stability of globular proteins to elucidate the nature of the interactions that stabilize the native conformation of proteins.

The effects of mono- and polyhydric alcohols on the reversible thermal denaturation of enzymes were investigated by Gelsma and Stuur,[1] Velicelebi and Sturtevant,[2] and Gekko, Morikawa and Noguchi.[3] The thermal stability of tropocollagen in these alcohols has also been measured by Harrap.[4]

A retarding effect of sucrose and glycerol on the rate of change of the optical rotation of ovalbumin in urea solution was found by Simpson and Kauzmann.[5] The effect of glucose on the denaturation of haemoglobin by urea was also tested and characterized by Simons and Naftalin.[6] The influence of polyhydric alcohols and sugars on the rate of subunit dissociation of tetrameric L-asparaginase in the presence of urea was investigated by Shifrin and Parrott.[7] In general, polyhydric alcohols have stabilizing influences on the native conformation of proteins.

No systematic investigations are available concerning the relation between the molecular conformation of sugars and their effect on the stability of globular proteins. In this work an attempt was made to explain the relation by studying the effect of various sugars on the thermal denaturation of lysozyme by differential scanning calorimetry. The interactions between some sugars and lysozyme were also studied by circular dichroism spectrometry.

Experimental

Materials. The hen egg-white lysozyme used in the present experiments was a six times recrystallized preparation obtained from Seikagaku Kogyo Co. The molecular weight of lysozyme was assumed to be 14307 and its average residue weight to be 110.9. Saccharides (G. R.) were recrystallized once or twice from water–ethanol solutions. Solutions were prepared with deionized and distilled water. The concentration of lysozyme was determined spectrophotometrically using an extinction of $E^{1\%}_{1cm}=26.9$ at 280 nm.[8] A Hitachi automatic recording spectrophotometer, model ESP-3T, or a Shimadzu double beam spectrophotometer UV 220 was used.

DSC Measurements. A Perkin-Elmer DSC Model II Calorimeter was used. 20 μl samples were packed in a stainless steel cell for high pressure use. Concentration of lysozyme was 6.188—7.986% at pH 5.0 (adjusted by adding HCl) and ionic strength was adjusted to be 0.1 by adding NaCl. It is known that aggregation of native lysozyme is favored at high pH values, above about 5.[9] On the other hand the stainless steel pan reacts with the acid solution at high temperature. Consequently, the thermal denaturation of lysozyme was measured at pH 5 with DSC.

CD Measurements. CD spectra were measured using a JASCO J-40A spectropolarimeter with a J-DPZ data processor. The recording of each spectrum was repeated four times, and the averaged spectra were obtained on the data processor. The temperature of the sample was controlled by using a Thermocircular TC-100 (Tokyo Riko Co.). The spectra were measured at protein concentrations of 0.1—0.5% in the spectral region above 250 nm and of 0.013% in the region between 200—250 nm.

Results and Discussion

Thermal Denaturation of Lysozyme without Sugars. The heating rate dependence of the denaturation temperature was observed by DSC. In Fig. 1, the foot and peak temperatures in the DSC curves for the denaturation of lysozyme at pH 5 are plotted against heating rate. The denaturation temperature increased linearly with heating rate; the extrapolated foot and peak temperatures were 64.5 and 75.4 °C, respectively. According to Velicelebi and Sturtevant,[2] T_d, the temperature at which the transition is half completed, and T_p, the temperature of maximal excess heat capacity, do not coincide, even for a two-

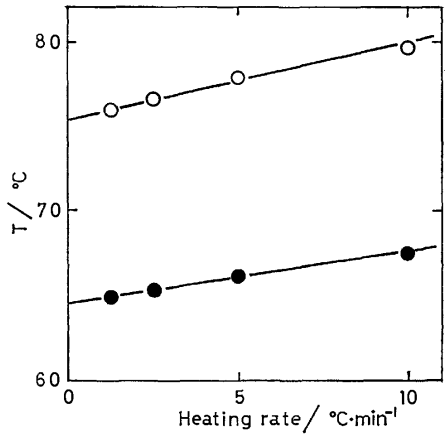

Fig. 1. Heating rate dependency of the foot (—●—) and peak (—○—) temperatures in the DSC curves for the thermal denaturation of lysozyme at pH 5 and $I=0.1$.

state process with no permanent change in heat capacity. In their work, T_d differs from T_p by 0.75—1.0 °C, but our results show the difference is within 0.1 °C. The calibration was made using the melting of In (156.7 °C) and water (0 °C). The foot and peak temperatures extrapolated to zero heating rate show 0.5 and 0.8 °C higher values for In (0.269 mg) and 1.2 and 2.3 °C higher values for water (0.7 mg), respectively. Consequently, the value of 75.4 °C of the extrapolated T_p for the denaturation of lysozyme may be a higher value still. However, due to the large difference in sample weight of lysozyme solution and of calibration substances, we use the T_p values extrapolated to zero heating rate as the denaturation temperature of lysozyme.

In Table 1, the denaturation temperature, T_d, obtained by various methods is shown. Our results are in good agreement with those in the literature.

TABLE 1. COMPARISON OF THE DENATURATION TEMPERATURES OF LYSOZYME AT pH 2.12 AND 5.0 OBTAINED BY VARIOUS METHODS

pH	2.12	5.0
T_d/°C	59.3[a]	78.5[a]
	46.8[b]	75.0[b]
	52.0[c]	
	55.8[d]	
	53.8[e]	75.4[f]

a) Calorimetry: Ref. 10. b) ORD: Ref. 11. c) UV: Ref. 1. d) Viscometry: Ref. 15. e) CD: Results of this study. f) DSC: Results of this study.

Considering the S/N ratio, we chose the heating rate of 5 degrees per minute under these conditions: The DSC sensitivity of 1 mcal/s, 20 μl of sample volume, at lysozyme concentration of 8% and ionic strength of 0.1. At this heating rate, as shown in Fig. 1, the meausured value for denaturation temperature is higher than the extrapolated value by 2.2 °C. The base line was not perfectly straight, so the evaluation of the peak area contains some uncertainty. The calorimetric enthalpy of denaturation, ΔH_{cal}, obtained from the area of DSC curve was not changed for heating rates from 1.25 to 20 degrees per minute, within experimental errors; the average value was 477±8 kJ/mol. The denaturation temperature was not changed at repeated heating about 24 h after the first run.

As most investigations are made at a more acidic condition, the denaturation was also measured by CD spectrum at pH 2.12 and ionic strength at 0.1. The value of molar ellipticity of the native lysozyme was in good agreement with the data of Shimaki *et al.*[12] and of Chen *et al.*[13]

Changes in the values of molar ellipticity, $[\theta]$, with temperature for lysozyme solution at pH 2.12 are shown in Fig. 2. The values of $[\theta]$ at 294 nm decrease with temperature and the transition temperature is 54 °C. The value of $[\theta]$ at 206 nm increases with temperature and the transition temperature is 54 °C too. The values of $[\theta]$ at 294 and 206 nm are caused by trp 62 and 108, and by the helix portion of lysozyme, respectively.[13,14] Figure 2 shows the cooperative nature of the thermal denaturation. The transition temperature T_d is taken as the temperature at which the transition is half complete. The obtained T_d values are compared with the literature values in Table 1. Table 1 shows that our results are within the values in the literature. The value of $[\theta]$ at 294 nm for the sample which was kept at 25 °C for more than 15 h after heating became the same value as that of the initial native one.

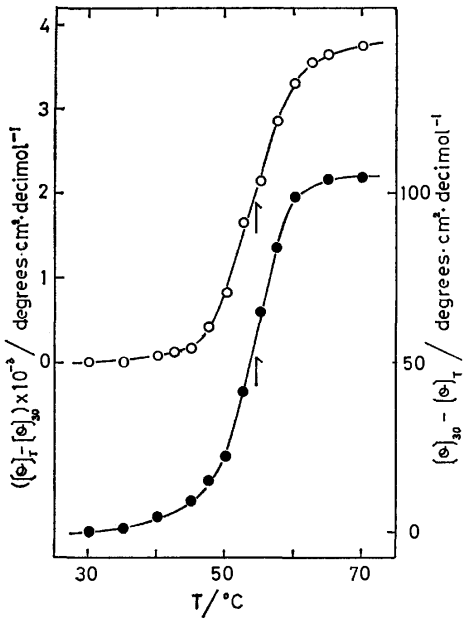

Fig. 2. Changes in the values of molar ellipticity for the lysozyme with temperature at pH 2.12 and I=0.1. —○—: At 206 nm, —●—: at 294 nm.

Plots of ln K against $1/T$, where K is the equilibrium constant for the denaturation obtained from the CD measurements, were almost linear. The values of van't Hoff enthalpy of denaturation, ΔH_{vh}, obtained from the plots were 280±8 kJ/mol from the absorption at 206 nm and 267±16 kJ/mol from the absorption at 294 nm, respectively. These values and the value of ΔH_{cal} are less than that which are obtained by Privalov[10] and by Velicelebi and Sturtevant,[2] but close to the values observed by O' Reilly and Karasz[15] and others.[16–19]

Thermal Denaturation of Lysozyme in the Presence of Sugars. DSC curves for the thermal denaturation of lysozyme (8.04%) in 1 mol kg^{-1} sugar solutions at pH 5 and I=0.1 at the heating rate of 5 degrees per minute are shown in Fig. 3. In every case studied, the thermal denaturation temperature is elevated by the addition of sugars. The values of the increasing temperature of the denaturation of lysozyme by 1 mol kg^{-1} sugar solution, ΔT_d (°C/mol), are plotted against the numbers of equatorial OH groups per molecule of sugars in Fig. 4. The numbers of equatorial OH groups are calculated from the NMR data of Angyal *et al.*[20] The values of ΔT_d are found to be closely related to the molecular conformation of sugars. From the slope in Fig. 4, T_d of lysozyme is raised about 0.8 °C per equatorial OH group. The values of ΔT_d of lysozyme by 1 mol dm^{-3} polyhydric alcohol

solutions are measured by Gelsma and Stuur,[1] and their results show that the T_d is raised by 0.8 °C per OH group, regardless of which polyhydric alcohol is added.

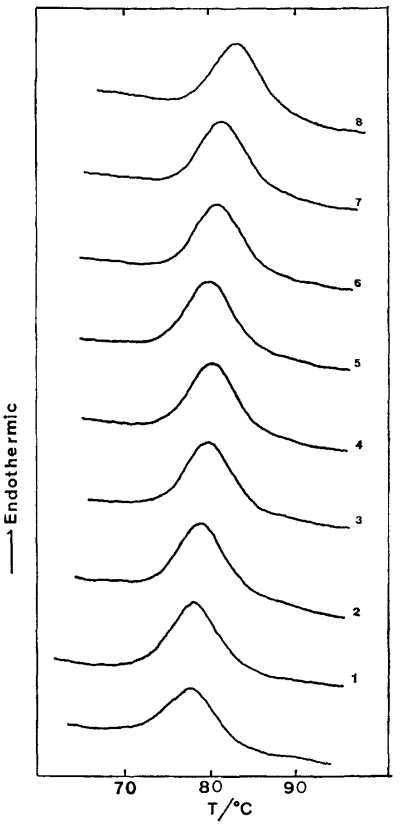

Fig. 3. DSC curves for the thermal denaturation of lysozyme in 1 mol kg^{-1} sugar solutions at pH 5 and I=0.1.
The lowest curve is for a solution without a sugar. Curves 1: with deoxyribose, 2: ribose, 3: lyxose, 4: arabinose, 5: xylose, 6: fructose, 7: glucose, and 8: sucrose.

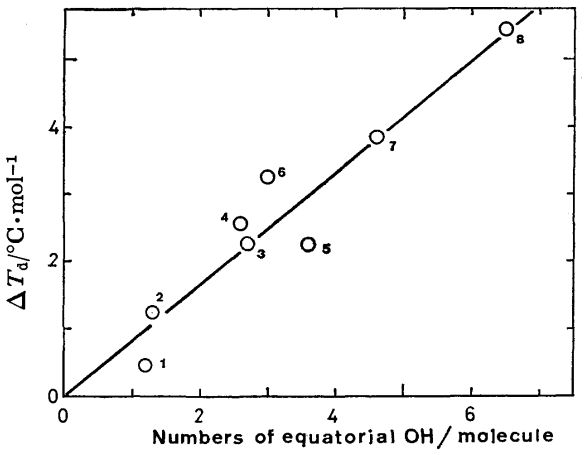

Fig. 4. The relation between the changes in the denaturation temperature of lysozyme in the presence of 1 mol kg^{-1} sugar solutions and the numbers of equatorial OH groups in a sugar molecule.
The numbers in the figure denote the same sugar as in Fig. 3.

The values of ΔH_{cal} of lysozyme in sugar solutions did not show a clear relation to the number of equatorial OH groups per added sugar molecule. In every case, sugars increased the value of ΔH_{cal} by about 10%.

Thermal denaturation for the lysozyme solution at pH 2.12 in 1 mol dm^{-1} glucose solution was also measured by the change in the values of molar ellipticity of lysozyme at 294 nm. Denaturation temperature and ΔH_{vh} were 58.5 °C and 310±16 kJ/mol, respectively. In this case, the molar ellipticity for renatured lysozyme solution was slightly lower than that for the native one. Comparing the data obtained for lysozyme with and without glucose, T_d is increased by about 5 degrees, and ΔH_{vh} increased by about 10%. The effect of the increase of T_d and ΔH_{vh} at pH 2.12 is nearly equal to the effect obtained at pH 5 by DSC measurements. The effect of polyhydric alcohols on the thermal denaturation of lysozyme is also found to be independent of pH.[1]

The Interaction between Lysozyme and Sugars. To elucidate the cause of the stabilizing effect of sugars we measured CD spectra at various concentrations of glucose and arabinose at pH 5, ionic strength 0.1, and 25 °C. CD spectra for lysozyme and arabinose solutions at various concentrations of arabinose are shown in Fig. 5. Arabinose shows a fairly negative broad band in these region, as curve h shows. Curve a is the CD spectrum for lysozyme solution and curves from b to g are the CD spectra for the mixed solutions of lysozyme and arabinose with increasing concentration of arabinose. Similarly, CD spectra for lysozyme in glucose solutions showed slightly less positive

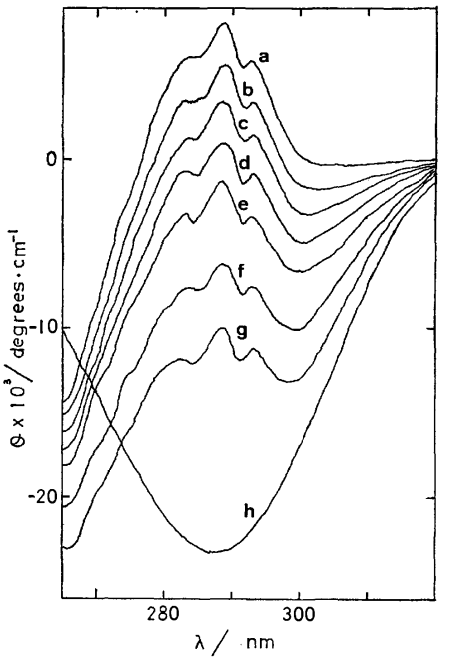

Fig. 5. The ellipticity, θ, for lysozyme and arabinose solutions at pH 5, I=0.1 and 25 °C.
Concentration of lysozyme is 8.782×10^{-3} residue mol dm^{-3}. Concentrations of arabinose are, a: 0 M (1 M=1 mol dm^{-3}), b: 0.1613 M, c: 0.3226 M, d: 0.4839 M, e: 0.6452 M, f: 0.9678 M, g: 1.290 M, and h: 1.613 M (h: without lysozyme).

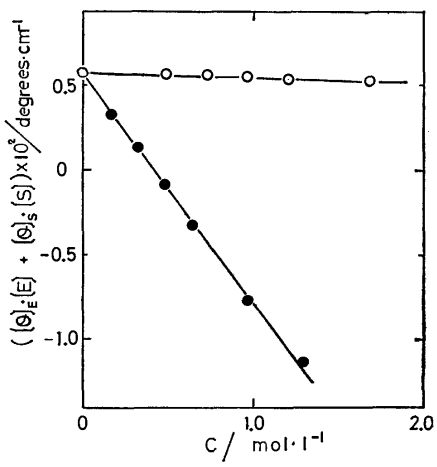

Fig. 6. The changes in the value of $[\theta]_E[E]+[\theta]_S[S]$ with sugar concentration.
Where $[\theta]_E$ and $[\theta]_S$ are molar ellipticity of lysozyme and a sugar, respectively, and [E] and [S] are molar concentrations. —O—: With glucose, —●—: with arabinose.

absorption by glucose in these wave lengths. The values of the ellipticity for the mixed solutions at 294 nm obtained by these experiments are plotted against sugar concentration in Fig. 6. Solid lines are values calculated on the assumption that the mixed solution shows the ellipticity which is simply the sum of the values of each component. The agreement between experimental and calculated values is good. These data suggest that sugars may not be bound to lysozyme at pH 5.

There have been many investigations which show the complex formation of lysozyme with sugars. Ikeda and Hamaguchi[21] found that sucrose enhanced the CD band of lyxozyme at 294 nm at pH 7.4, and that 1 mol of sucrose interacts with 1 mol of lysozyme, the association constant for the interaction was 0.4 (M^{-1}) at 25 °C. Kuramitsu *et al.*[22] showed that the binding constant for glucose and α-methyl xyloside to lysozyme was 0.5 and 1.6, respectively, from the absorption in CD spectra at 295 or 305 nm at pH 7.3 and 25 °C. Visible excited Raman spectra of lysozyme showed considerable differences in the relative intensities between that for lysozyme–glucose system and pure lysozyme, suggesting glucose–lysozyme complex formation.[23]

On the other hand, Rupley *et al.*[24] found that monosaccharide binding requires an acetamide group, and that glucose and maltose did not bind measurably. The binding constant for glucose to lysozyme is tabulated to be less than 0.1 (M^{-1}) by Chipman and Sharon.[25]

At pH 7.0, the values of ellipticity of the mixed solution of glucose and lysozyme at 304 and 294 nm are higher (less negative) that the values calculated on the assumption of additivity of $[\theta]$ of each component, in agreement with the results of Kuramitsu *et al.*[22] Also according to them, the molar ellipticity of lysozyme–α-methyl xyloside complex at 295 nm is nearly equal to that of lysozyme. The possibility remains that at pH 5, a complex is also formed but the molar ellipticity of the complex is the same as the sum of the values of each component.

As the reference values of the association constant for the complex formation of lysozyme and the saccharides studied here are very small, even if the complexes are formed, we would like to point out that there exist other interactions which stabilize the native conformation of protein in the system protein–sugar–water. The results of isopiestic measurements for the model systems[26,27] indicate that the sucrose solution environment is a more unfavorable solvent than water for amino acid with aliphatic and aromatic side chains. Consequently, it would require much more work for nonpolar groups in the interior of the protein to be exposed in the sucrose solution than in water; they would thus be caused by the sucrose solution to enter into the interior of the protein. Bull and Breese[28] suggest that the substances which stabilize proteins, such as sucrose, enhance the water structure in the immediate neighborhood of the protein and consequently contribute to protein stability. According to Tait *et al.*,[29] the distance between O–O atoms in equatorial hydroxyl groups of β-D-glucose coincides with the distance between O–O atoms in the tridimite structure of water. The structure making effect of sugars in aqueous solutions is more marked for the one which has more equatorial OH groups in the molecule.[30] Figure 4 shows that the sugars which strongly enhance the water structure raise the denaturation temperature of lysozyme more markedly. Thus in the presence of sugars the environmental effect or intensification of hydrophobic interaction inside a protein may promote a resistance against thermal denaturation of a protein.

References

1) S. Y. Gelsma and E. R. Stuur, *Int. J. Pept. Protein Res.*, **4**, 377 (1972).
2) G. Velicelebi and J. M. Sturtevant, *Biochemistry*, **18**, 1180 (1979).
3) K. Gekko, T. Morikawa, and H. Noguchi, 17th Annual Meeting of the Biophys. Soc. Japan, Nagoya, Oct. 1979, Abstr. p. 305.
4) B. S. Harrap, *Int. J. Pept. Protein Res.*, **1**, 253 (1969).
5) R. B. Simpson and W. Kauzmann, *J. Am. Chem. Soc.*, **75**, 5139 (1953).
6) N. L. Simmons and R. J. Naftalin, *Biochim. Biophys. Acta*, **419**, 493 (1976).
7) S. Shifrin and C. L. Parrott, *Arch. Biochem. Biophys.*, **166**, 426 (1975).
8) K. Imai, T. Takagi, and T. Isemura, *J. Biochem.*, **53**, 1 (1963).
9) A. J. Sophianopoulos and D. E. Van Holde, *J. Biol. Chem.*, **239**, 2516 (1964).
10) P. L. Privalov, *J. Mol. Biol.*, **86**, 665 (1974).
11) K. Hamaguchi and H. Sakai, *J. Biochem.*, **57**, 721 (1965).
12) N. Shimaki, K. Ikeda, and K. Hamaguchi, *J. Biochem.*, **71**, 265 (1972).
13) Y. H. Chen, J. T. Yang, and K. H. Chen, *Biochemstry*, **13**, 3350 (1974).
14) For example, K. Hayashi and T. Imoto, "Lysozyme," Nankodo, Tokyo (1974).

15) J. M. O'Reilly and F. E. Karasz, *Biopolymers*, **9**, 1429 (1970).
16) A. J. Sophyanopoulos and B. J. Weiss, *Biochemistry*, **3**, 1920 (1964).
17) Y. Fujita and Y. Noda, *Bull. Chem. Soc. Jpn.*, **52**, 2349 (1979).
18) C. C. McDonald, W. D. Philips, and J. D. Glickson, *J. Am. Chem. Soc.*, **93**, 235 (1971).
19) C. Tanford and K. C. Aune, *Biochemistry*, **9**, 206 (1970).
20) S. J. Angyal, *Angew. Chem. Int. Ed. Engl.*, **8**, 157 (1969); S. J. Angyal and V. A. Pickles, *Aust. J. Chem.*, **25**, 1171, 1695 (1972).
21) K. Ikeda and K. Hamaguchi, *J. Biochem.*, **68**, 785 (1970).
22) S. Kuramitsu, K. Ikeda, and K. Hamaguchi, *J. Biochem.*, **74**, 143 (1973).
23) K. G. Brown, E. B. Brown, and W. B. Person, *J. Am. Chem. Soc.*, **99**, 3128 (1977).
24) J. A. Rupley, L. Butter, M. Gerring, F. J. Hartdegen, and R. Pecoraro, *Proc. Natl. Acad. Sci. U. S. A.*, **57**, 1088 (1967).
25) D. M. Chipman and N. Sharon, *Science*, **165**, 454 (1969).
26) H. Uedaira, *Bull. Chem. Soc. Jpn.*, **50**, 1298 (1977).
27) T. S. Lakshimi and P. K. Nandi, *J. Phys. Chem.*, **80**, 249 (1975).
28) H. B. Bull and K. Breese, *Biopolymers*, **17**, 2121 (1978).
29) M. J. Tait, A. Sugget, F. Franks, S. Ablett, and P. A. Quichenden, *J. Solution Chem.*, **1**, 131 (1972).
30) H. Uedaira, Kagaku Sosetsu, No. 11, 191 (1976).

Fluctuation of Local Field and Depolarization Degree of the ν_1 Line of Carbon Tetrachloride

Shi-aki Hyodo and Tsunetake Fujiyama*,†

Department of Chemistry, Faculty of Science, Tokyo Metropolitan University, Setagaya-ku, Tokyo 158

†*Institute for Molecular Science, Okazaki 444*

(Received January 8, 1980)

The depolarization degree of a molecule having a T_d symmetry was expressed in terms of the mean square fluctuation of the local field which is felt by a molecule in the condensed phase. By the use of the mean square amplitude values observed by the X-ray diffraction method, the depolarization degree of liquid carbon tetrachloride was calculated to be 0.0021, which agrees well with the observed value of 0.0039 ± 0.0002.

The depolarization degree of Raman scattering, ρ, can be expressed in terms of a Raman scattering tensor, $\alpha'_{\rho\sigma}$, as

$$\rho = \frac{3\gamma^2}{45\bar{\alpha}^2+4\gamma^2} \tag{1}$$

where

$$\bar{\alpha} = \frac{1}{3}(\alpha'_{xx}+\alpha'_{yy}+\alpha'_{zz})$$

$$\gamma^2 = \frac{1}{2}[(\alpha'_{yy}-\alpha'_{zz})^2+(\alpha'_{zz}-\alpha'_{xx})^2+(\alpha'_{xx}-\alpha'_{yy})^2].$$

Therefore, the depolarization degree ρ should be exactly zero if the relation $\alpha'_{xx}=\alpha'_{yy}=\alpha'_{zz}$ is satisfied. The ν_1 Raman line of carbon tetrachloride is just such a case, because the vibration belongs to an a_1 symmetry of a tetrahedral molecule. The depolarization degree for the ν_1 line of liquid carbon tetrachloride, however, is not observed to be zero. With the improvement of Raman spectrometers and related attachements, the depolarization degree for this line has been observed at smaller and smaller values. But it was never observed to be zero. The most reliable value at present is $\rho=0.0039\pm0.0002$ which is reported by Murphy *et al.*[1] The finite ρ-value for the ν_1 line is believed to be real, in other words, it cannot be ascribed to any experimental errors.

There were several reports which emphasized the effect of the symmetry degradation due to the existence of the natural abundant Cl^{37}. According to the theoretical estimation of Chantry,[2] however, this effect is too small to explain the observed finite value of ρ. Douglas and Rank observed the depolarization degree of the ν_1 line of tin tetrachloride and the related isotope species and concluded that the ρ values for the three isotopic species ($SnCl_4^{35}$, $SnCl_3^{35}Cl^{37}$, $SnCl_2^{35}Cl_2^{37}$) agreed with each other within the experimental error.[3] This finite magnitude of depolarization degree has been thought to originate from some kinds of intermolecular interactions in the condensed phase, although no detailed mechanisms have been established yet. It will be shown in the present report that the fluctuation of local field is the main cause of the finite magnitude of depolarization degree observed for the ν_1 line of liquid carbon tetrachloride.

Intensity Expression for Raman Scattering. Consider a molecule irradiated by an incident light beam. In the condensed system, the electric field which is felt by the molecule is not the same as that of the incident light, because of the existence of the electric field produced on the surrounding molecuoes. Taking into account this situation, we first derive the Raman intensity expression for the liquid sample.

Imagine a space-fixed Cartesian coordinate system (x, y, z). A z-polarized incident light beam irradiates molecules along the negative x-direction (see Fig. 1). The electric vector of the incident light is expressed by $\boldsymbol{E}=\boldsymbol{E}_0\cos\omega_0 t$ ($\boldsymbol{E}_0=(0, 0, E_{0z})$). Consider now the scattering in the positive y-direction. The position vector of a molecule (i) is expressed by $\boldsymbol{r}_i$.

Generally, a polarizability $\boldsymbol{\alpha}$ is expanded as a power series of a normal coordinate Q_k as:

$$\boldsymbol{\alpha} = \boldsymbol{\alpha}^\circ + \sum_k \left(\frac{\partial\boldsymbol{\alpha}}{\partial Q_k}\right)_0 Q_k + \text{higher terms} \tag{2}$$

where Q_k is a normal coordinate corresponding to the k-th vibrational mode whose frequency is ω_ν^k, *viz.*,

$$Q_k = Q_0{}^k\cos\omega_\nu^k t.$$

If we focus our attention on a particular vibrational mode and neglect the terms higher than quadratic,

$$\boldsymbol{\alpha} = \boldsymbol{\alpha}^\circ + \boldsymbol{\alpha}'\cos\omega_\nu t \tag{2'}$$

where

$$\boldsymbol{\alpha}' = \left(\frac{\partial\boldsymbol{\alpha}}{\partial Q}\right)_0 Q_0.$$

In the case of the ν_1 vibration of carbon tetrachloride, the tensors $\boldsymbol{\alpha}^\circ$ and $\boldsymbol{\alpha}'$ have a spherical symmetry. Therefore, we can use the scalar expressions α° and α' instead of the tensors $\boldsymbol{\alpha}^\circ$ and $\boldsymbol{\alpha}'$.

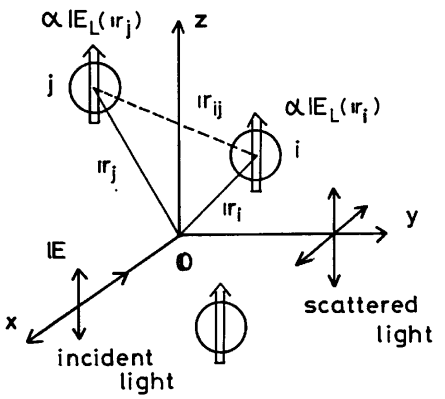

Fig. 1. Polarization of light and induced dipoles on molecules (i) and (j).

Consider a molecule (j) at $\boldsymbol{r}_j$ in the liquid phase. This molecule (j) feels the electric field $\boldsymbol{E}_L(\boldsymbol{r}_j)=\boldsymbol{E}_{L0}(\boldsymbol{r}_j)\cos\omega t$ whose frequency is the same as that of the incident light. The induced dipole, $\alpha^\circ\boldsymbol{E}_L(\boldsymbol{r}_j)$, then produces an electric field $\boldsymbol{f}(\boldsymbol{r}_i, \boldsymbol{r}_j)$ on the molecule (i) at $\boldsymbol{r}_i$. The $\boldsymbol{f}(\boldsymbol{r}_i, \boldsymbol{r}_j)$ is expressed as;

$$\boldsymbol{f}(\boldsymbol{r}_i, \boldsymbol{r}_j) = -\frac{\alpha^\circ\boldsymbol{E}_L(\boldsymbol{r}_j)}{r_{ij}^2}+\frac{3\{(\alpha^\circ\boldsymbol{E}_L(\boldsymbol{r}_j))\cdot\boldsymbol{r}_{ij}\}\boldsymbol{r}_{ij}}{r_{ij}^5} = \alpha^\circ\boldsymbol{E}_L(\boldsymbol{r}_j)\boldsymbol{l}(\boldsymbol{r}_{ij}) \quad (3)$$

where

$$\boldsymbol{r}_i \equiv \boldsymbol{r}_j-\boldsymbol{r}_i$$
$$\boldsymbol{r}_{ij} \equiv |\boldsymbol{r}_{ij}|$$
$$\boldsymbol{l}(\boldsymbol{r}_{ij}) \equiv \frac{3\boldsymbol{r}_{ij}\boldsymbol{r}_{ij}-r_{ij}^2\mathbf{I}}{r_{ij}^5}$$

and $\mathbf{I}$ is an unit tensor. As the molecule (i) is surrounded by many other molecules designated by (j), the electric field, $\boldsymbol{E}_L(\boldsymbol{r}_i)$, which is felt by the molecule (i) is

$$\boldsymbol{E}_L(\boldsymbol{r}_i) = \boldsymbol{E}+\sum_j \boldsymbol{f}(\boldsymbol{r}_i, \boldsymbol{r}_j). \quad (4)$$

As the $\boldsymbol{f}(\boldsymbol{r}_i, \boldsymbol{r}_j)$ of Eq. 4 is also the function of $\boldsymbol{E}_L(\boldsymbol{r}_j)$ which also has an expression like Eq. 4, the detailed expression of Eq. 4 becomes

$$\boldsymbol{E}_L(\boldsymbol{r}_i) = \boldsymbol{E}+\sum_j \alpha^\circ\boldsymbol{E}_L(\boldsymbol{r}_j)\boldsymbol{l}(\boldsymbol{r}_{ij}) = \boldsymbol{E}+\sum_j\{\boldsymbol{E}+\sum_k \alpha^\circ\{\boldsymbol{E}+\ldots\}\ldots\}\ldots\boldsymbol{l}(\boldsymbol{r}_{jk})\boldsymbol{l}(\boldsymbol{r}_{ij}). \quad (5)$$

If we truncate Eq. 5 at the second term,

$$\boldsymbol{E}_L(\boldsymbol{r}_i) \cong \boldsymbol{E}+\sum_j \alpha^\circ\boldsymbol{E}\boldsymbol{l}(\boldsymbol{r}_{ij}) \quad (5')$$

and

$$\boldsymbol{f}(\boldsymbol{r}_i, \boldsymbol{r}_j) = -\frac{\alpha^\circ\boldsymbol{E}}{r_{ij}^3}+\frac{3\{(\alpha^\circ\boldsymbol{E})\cdot\boldsymbol{r}_{ij}\}\boldsymbol{r}_{ij}}{r_{ij}^5}. \quad (6)$$

We consider that the dipole moment, $\alpha'\boldsymbol{E}_L(\boldsymbol{r}_i)\cos\omega_v t$, induced onto the molecule (i) scatters Raman light following the classical scattering theory. If the phases of the molecular vibrations of component molecules are independent of each other, the Raman scattering intensity from this system is proportional to the mean square amplitude of this oscillating dipole, $\alpha'\boldsymbol{E}_{L0}(\boldsymbol{r}_i)$. It sometimes happens, however, that the oscillating dipoles induced onto different molecules have the same phase; this mechanism will be shown in what follows.

The oscillating dipole induced by the electric field $\boldsymbol{E}_L(\boldsymbol{r}_i)$ onto the molecule (i), in turn, produces the electric field, $\boldsymbol{f}'(\boldsymbol{r}_j, \boldsymbol{r}_i)$, onto the molecule (j). This electric field has the same frequency as the Raman frequencies $((\omega_0+\omega_v)$ and $(\omega_0-\omega_v))$. $\boldsymbol{f}'(\boldsymbol{r}_j, \boldsymbol{r}_i)$ is expressed as

$$\boldsymbol{f}'(\boldsymbol{r}_j, \boldsymbol{r}_i) = \left[-\frac{\alpha'\boldsymbol{E}_L(\boldsymbol{r}_i)}{r_{ij}^3}+\frac{3\{(\alpha'\boldsymbol{E}_L(\boldsymbol{r}_i))\cdot\boldsymbol{r}_{ij}\}\boldsymbol{r}_{ij}}{r_{ij}^5}\right]\cos\omega_v t \cong \left[-\frac{\alpha'\boldsymbol{E}}{r_{ij}^3}+\frac{3\{(\alpha'\boldsymbol{E})\cdot\boldsymbol{r}_{ij}\}\boldsymbol{r}_{ij}}{r_{ij}^5}\right]\cos\omega_v t = \alpha'\boldsymbol{E}\boldsymbol{l}(\boldsymbol{r}_{ij})\cos\omega_v t. \quad (7)$$

The electric field, $\boldsymbol{f}'(\boldsymbol{r}_j, \boldsymbol{r}_i)$, produces an oscillating dipole $\alpha^\circ\boldsymbol{f}'(\boldsymbol{r}_j, \boldsymbol{r}_i)$ on the molecule (j). This oscillating dipole again scatters light following the classical scattering theory. It is important that the phase of this scattered light coincides with that of the molecular vibration of the molecule (i). This sort of light can be scattered from all the molecules (i). Thus, the observed Raman intensity is proportional to the mean square amplitude of the two kinds of oscillating induced dipoles, namely, $\alpha'\boldsymbol{E}_L(\boldsymbol{r}_i)\cos\omega_v t$ and $\alpha^\circ\boldsymbol{f}'(\boldsymbol{r}_j, \boldsymbol{r}_i)$. The sum of these induced dipoles is

$$\begin{aligned}&\alpha'\boldsymbol{E}_L(\boldsymbol{r}_i)\cos\omega_v t+\alpha^\circ\sum_j \alpha'\boldsymbol{E}\boldsymbol{l}(\boldsymbol{r}_{ij})\cos\omega_v t\\ &= \alpha'\boldsymbol{E}\cos\omega_v t+\sum_j \alpha'\alpha^\circ\boldsymbol{E}\boldsymbol{l}(\boldsymbol{r}_{ij})\cos\omega_v t+\sum_j \alpha^\circ\alpha'\boldsymbol{E}\boldsymbol{l}(\boldsymbol{r}_{ij})\cos\omega_v t\\ &= \alpha'\boldsymbol{E}\{1+2\sum_j \alpha^\circ\boldsymbol{l}(\boldsymbol{r}_{ij})\}\cos\omega_v t\\ &= \alpha'\boldsymbol{E}\{1+2\alpha^\circ\mathbf{L}(\boldsymbol{r}_{ij})\}\cos\omega_v t \quad (8)\end{aligned}$$

where

$$\mathbf{L}(\boldsymbol{r}_i) = \sum_j \boldsymbol{l}(\boldsymbol{r}_{ij}). \quad (9)$$

Thus, the polarized and depolarized components, I_z and I_x, of Raman scattering intensity from the liquid system can be expressed as

$$I_z \propto (\alpha')^2\{1+4\alpha^\circ\langle L_{zz}(\boldsymbol{r}_i)\rangle+4(\alpha^\circ)^2\langle(L_{zz}(\boldsymbol{r}_i))^2\rangle\}E_{0z}^2 \quad (10\text{-a})$$

$$I_x \propto 4(\alpha'\alpha^\circ)^2\langle(L_{xz}(\boldsymbol{r}_i))^2\rangle E_{0z}^2 \quad (10\text{-b})$$

where $L_{ij}(\boldsymbol{r}_i)$ represents the i,j-element of the tensor $\mathbf{L}(\boldsymbol{r}_i)$ and $\langle\ \rangle$ represents an ensemble averge. The intensity representation of Eqs. 10-a and 10-b shows that the effects of the local field on Raman intensity are completly expressed in terms of the mean and mean square values of the tensor elements, $L_{ij}(\boldsymbol{r}_i)$. In order to know $L_{ij}(\boldsymbol{r}_i)$, we have to know the relative molecular configuration of component molecules in the liquid system.

Calculation of $\langle L_{zz}(\boldsymbol{r}_i)\rangle$, $\langle(L_{zz}(\boldsymbol{r}_i))^2\rangle$, $\langle(L_{xz}(\boldsymbol{r}_i))^2\rangle$. The X-ray diffraction study of pure liquid carbon tetrachloride has clarified the existence of a local bcc lattice in the liquid at room temperature, as is shown in Fig. 2.[4] On the basis of this result,

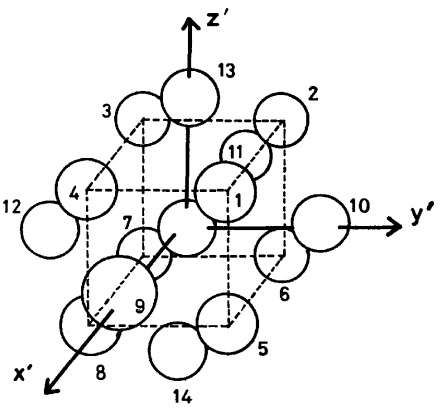

Fig. 2. Local bcc lattice structure of carbon tetrachloride obtained by X-ray diffraction study.[4] (x', y', z') refers to the lattice-fixed coordinate system. The moleucles (1—8) and (9—14) correspond, respectively, to the first and second nearest neighbours.

we calculate $\langle L_{zz}(\boldsymbol{r}_i)\rangle$, $\langle (L_{zz}(\boldsymbol{r}_i))^2\rangle$, and $\langle (L_{xz}(\boldsymbol{r}_i))^2\rangle$ values originating from displacements of component molecules from the bcc structure. Putting the molecule (i) at the center, we express the relative configuration of molecules by a vector group $\{\boldsymbol{r}_{ij}\}$, where $\boldsymbol{r}_{ij}=\boldsymbol{r}_j-\boldsymbol{r}_i$. If the lattice points of the bcc lattice is represented by a vector $\boldsymbol{r}^\circ_{ij}$, the vector $\boldsymbol{r}_{ij}$ can be written as,

$$\boldsymbol{r}_{ij} = \boldsymbol{r}^\circ_{ij} + \Delta\boldsymbol{r}_{ij} \tag{11}$$

where $\Delta\boldsymbol{r}_{ij}$ is a vector which describes the relative displacement of the surrounding molecules (j) due to thermal motion from the individual lattice points.

Now, expression of $L_{zz}(\boldsymbol{r}_i)$ or $L_{xz}(\boldsymbol{r}_i)$ with respect to $\Delta\boldsymbol{r}_{ij}$ leads to:

$$\begin{aligned} L_{zz}(\boldsymbol{r}_i) &= \sum_j l_{zz}(\boldsymbol{r}_{ij}) \\ &= \sum_j \left[l_{zz}(\boldsymbol{r}^\circ_{ij}) + \left(\frac{\partial l_{zz}}{\partial \boldsymbol{r}_{ij}}\right)_0 \Delta\boldsymbol{r}_{ij} + \text{higher terms} \right] \\ &= L^\circ_{zz}(\boldsymbol{r}_i) + \sum_j \left(\frac{\partial l_{zz}}{\partial \boldsymbol{r}_{ij}}\right)_0 \Delta\boldsymbol{r}_{ij} \end{aligned} \tag{12-a}$$

and

$$L_{xz}(\boldsymbol{r}_i) = L^\circ_{xz}(\boldsymbol{r}_i) + \sum_j \left(\frac{\partial l_{xz}}{\partial \boldsymbol{r}_{ij}}\right)_0 \Delta\boldsymbol{r}_{ij} \tag{12-b}$$

where

$$L^\circ_{zz}(\boldsymbol{r}_i) = \sum_j l_{zz}(\boldsymbol{r}^\circ_{ij}) \tag{13-a}$$

$$L^\circ_{xz}(\boldsymbol{r}_i) = \sum_j l_{xz}(\boldsymbol{r}^\circ_{ij}) \tag{13-b}$$

$$\left(\frac{\partial l_{\sigma\rho}}{\partial \boldsymbol{r}_{ij}}\right)_0 \Delta\boldsymbol{r}_{ij} \equiv \left(\frac{\partial l_{\sigma\rho}}{\partial r^x_{ij}}\right)_0 \Delta r^x_{ij} + \left(\frac{\partial l_{\sigma\rho}}{\partial r^y_{ij}}\right)_0 \Delta r^y_{ij} + \left(\frac{\partial l_{\sigma\rho}}{\partial r^z_{ij}}\right)_0 \Delta r^z_{ij}. \tag{14}$$

In the above equations, $l_{\sigma\rho}$ is a $\sigma\rho$-element of the tensor $\boldsymbol{l}(\boldsymbol{r}_{ij})$, and the shoulder index put on r_{ij} or Δr_{ij} distinguishes among the x, y, or z element of the vector. More detailed expressions of Eqs. 13-a and 13-b are

$$L^\circ_{zz}(\boldsymbol{r}_i) = \sum_j \frac{3(r^{\circ x}_{ij})^2 - (r^\circ_{ij})^2}{(r^\circ_{ij})^5} \tag{13-a'}$$

and

$$L^\circ_{xz}(\boldsymbol{r}_i) = \sum_j \frac{3(r^{\circ x}_{ij})(r^{\circ z}_{ij})}{(r^\circ_{ij})^5} \tag{13-b'}$$

where $r^{\circ x}_{ij}$ and $r^{\circ z}_{ij}$ are the x- and z-elements of a vector $\boldsymbol{r}^\circ_{ij}$.

We assume here that the molecular motions of component molecules are mutually independent and that all the displacement vectors are isotropic. This is equivalent to assuming the relations:

$$\langle \Delta\boldsymbol{r}_{ij}\rangle = 0$$

$$\langle (\Delta r^x_{ij})^2\rangle = \langle (\Delta r^y_{ij})^2\rangle = \langle (\Delta r^z_{ij})^2\rangle = \frac{1}{3}\langle (\Delta\boldsymbol{r}_{ij})^2\rangle$$

and

$$\begin{aligned} &\langle \Delta r^x_{ij}\Delta r^y_{ij}\rangle = \langle \Delta r^y_{ij}\Delta r^z_{ij}\rangle = \langle \Delta r^z_{ij}\Delta r^x_{ij}\rangle = \cdots \\ &\quad = \langle \Delta r^x_{ik}\Delta r^x_{ij}\rangle = \langle \Delta r^x_{ik}\Delta r^y_{ij}\rangle = \cdots = 0. \end{aligned} \tag{15}$$

Then, the mean values in question can be expressed as:

$$\begin{aligned} \langle L_{zz}(\boldsymbol{r}_i)\rangle &= \left\langle L^\circ_{zz}(\boldsymbol{r}_i) + \sum_j \left(\frac{\partial l_{zz}}{\partial \boldsymbol{r}_{ij}}\right)_0 \Delta\boldsymbol{r}_{ij} \right\rangle \\ &= L^\circ_{zz}(\boldsymbol{r}_i) + \sum_j \left(\frac{\partial l_{zz}}{\partial \boldsymbol{r}_{ij}}\right)_0 \langle \Delta\boldsymbol{r}_{ij}\rangle \\ &= L^\circ_{zz}(\boldsymbol{r}_i) \end{aligned} \tag{16-a}$$

$$\langle (L_{zz}(\boldsymbol{r}_i))^2\rangle = \{L^\circ_{zz}(\boldsymbol{r}_i)\}^2 + \frac{1}{3}\sum_j \left(\frac{\partial l_{zz}}{\partial \boldsymbol{r}_{ij}}\right)^2_0 \langle (\Delta\boldsymbol{r}_{ij})^2\rangle \tag{16-b}$$

and

$$\langle (L_{xz}(\boldsymbol{r}_i))^2\rangle = \{L^\circ_{xz}(\boldsymbol{r}_i)\}^2 + \frac{1}{3}\sum_j \left(\frac{\partial l_{xz}}{\partial \boldsymbol{r}_{ij}}\right)^2_0 \langle (\Delta\boldsymbol{r}_{ij})^2\rangle. \tag{16-c}$$

On the other hand, $\langle (\Delta\boldsymbol{r}_{ij})^2\rangle$ for a molecule (j) can be expressed by the use of a polar coordinate system $(\Delta r_{ij}, \theta, \phi)$ whose origin is fixed at the individual lattice point as:

$$\langle (\Delta\boldsymbol{r}_{ij})^2\rangle = \frac{\int_0^{2\pi}\int_0^{\pi}\int_0^{\infty} (\Delta r_{ij})^2 \exp\left(-\frac{\ln 2}{a_j^2}(\Delta r_{ij})^2\right)(\Delta r_{ij})^2 \sin\theta \, d(\Delta r_{ij})d\theta d\phi}{\int_0^{2\pi}\int_0^{\pi}\int_0^{\infty} \exp\left(-\frac{\ln 2}{a_j^2}(\Delta r_{ij})^2\right)(\Delta r_{ij})^2 \sin\theta \, d(\Delta r_{ij})d\theta d\phi}. \tag{17}$$

Here we assumed a Gaussian distribution for the distribution of Δr_{ij}. a_j of Eq. 17 is the half-width of the Gaussian distribution for the molecule (j). The integration of those terms related with Δr_{ij} leads to

$$\int_0^\infty (\Delta r_{ij})^2 \exp\left(-\frac{\ln 2}{a_j^2}(\Delta r_{ij})^2\right) d(\Delta r_{ij}) = \frac{1}{4}\sqrt{\pi}\left(\frac{\ln 2}{a_j^2}\right)^{-3/2}$$

and

$$\int_0^\infty (\Delta r_{ij})^4 \exp\left(-\frac{\ln 2}{a_j^2}(\Delta r_{ij})^2\right) d(\Delta r_{ij}) = \frac{3}{8}\sqrt{\pi}\left(\frac{\ln 2}{a_j^2}\right)^{-5/2}.$$

Therefore, the mean square value of the displacement vector is

$$\langle (\Delta r_{ij})^2\rangle = \frac{3a_j^2}{2\ln 2}. \tag{18}$$

In the liquid carbon tetrachloride, it is hardly possible at room temperature that the orientations of these local bcc lattices coincide with each other. It is more reasonable to assume the random orientation of the local bcc lattices. Therefore Eqs. 16-a, 16-b, and 16-c should be averaged over all the orientations of the local bcc lattices. The terms which should be averaged over all orientations are $L^\circ_{zz}(\boldsymbol{r}_i)$, $\{L^\circ_{zz}(\boldsymbol{r}_i)\}^2$, $\{L^\circ_{xz}(\boldsymbol{r}_i)\}^2$, $(\partial l_{zz}/\partial \boldsymbol{r}_{ij})^2_0$, and $(\partial l_{xz}/\partial \boldsymbol{r}_{ij})^2_0$. It is obvious from Eqs. 13-a′ and 13-b′, that $L^\circ_{zz}(\boldsymbol{r}_i)$, $\{L^\circ_{zz}(\boldsymbol{r}_i)\}^2$, and $\{L^\circ_{xz}(\boldsymbol{r}_i)\}^2$ are all zero, because $L^\circ_{zz}(\boldsymbol{r}_i)$ and $L^\circ_{xz}(\boldsymbol{r}_i)$ are zero as long as the molecular configuration has a point symmetry

with respect to $\boldsymbol{r}_1$. Thus, it is enough to consider $(\partial l_{zz}/\partial \boldsymbol{r}_{1j})_0^2$ and $(\partial l_{xz}/\partial \boldsymbol{r}_{1j})_0^2$.

The more explicit expression of $(\partial l_{zz}/\partial \boldsymbol{r}_{1j})_0^2$ or $(\partial l_{xz}/\partial \boldsymbol{r}_{1j})_0^2$ is

$$\left(\frac{\partial l_{zz}}{\partial \boldsymbol{r}_{1j}}\right)_0^2 = \frac{9}{(r_{1j}^\circ)^{12}}\{5(r_{1j}^{\circ z})^4 - 2(r_i^{\circ z})^2(r_{1j}^\circ)^2 + (r_{1j}^\circ)^4\} \tag{19-a}$$

$$\left(\frac{\partial l_{xz}}{\partial \boldsymbol{r}_{1j}}\right)_0^2 = \frac{9}{(r_{1j}^\circ)^{12}}\{(r_{1j}^{\circ x})^2(r_{1j}^\circ)^2 + (r_{1j}^{\circ z})^2(r_{1j}^\circ)^2 + (r_{1j}^{\circ z})^2(r_{1j}^\circ)^2 + 5(r_{1j}^{\circ x})^2(r_{1j}^{\circ z})^2\}. \tag{19-b}$$

Equetions 19-a and 19-b show that these quantities are proportional to r_{1j}^8, where r_{1j} is an intermolecular distance and, therefore, the effect of the molecules (j) rapidly decreases with the increase of the distance r_{1j}. Therefore, it is enough to consider the contribution from the first nearest neighbors (8 molecules) and the second nearest neighbors (6 molecules) in the bcc lattice. So far the relative configuration of molecules has been described in the lattice-fixed coordinate system. As Eqs. 19-a and 19-b are described in the space-fixed coordinate system, however, we have to transform the coordinates used for the expression of relative configuration from the lattice-fixed to the space-fixed coordinate system. Let the Cartesian coordinates of the molecule (i) be (x_1', y_1', z_1') and (x_1, y_1, z_1) in the lattice-fixed and space-fixed coordinate systems, respectively. If the orientation of the local bcc lattice is specified by the Eulerian angles (α, β, γ) of Fig. 3, the transformation of coordinates from (x', y', z') to (x, y, z) system is given by:

$$\begin{aligned} x &= x'(\cos\alpha\cos\beta\cos\gamma - \sin\beta\sin\gamma) \\ &\quad - y'(\cos\alpha\cos\beta\sin\gamma + \sin\beta\cos\gamma) + z'\sin\alpha\cos\beta \\ y &= x'(\cos\alpha\sin\beta\cos\gamma + \cos\beta\sin\gamma) \\ &\quad - y'(\cos\alpha\sin\beta\sin\gamma - \cos\beta\cos\gamma) + z'\sin\alpha\sin\beta \\ z &= -x'\sin\alpha\cos\gamma + y'\sin\alpha\sin\gamma + z'\cos\alpha. \end{aligned} \tag{20}$$

Let the distances from the center of the molecule (i) and to the centers of its first and second nearest neighbors be d_1 and d_2, respectively. Then, the coordinates of the neighboring molecues (j) in the lattice-fixed system can be calculated easily. Insertion of these coordinate values into the relations, *e.g.*, for the eight nearest neighboring molecules,

$$\sum_j (r_{1j}^{\circ x})^2 = \sum_j x_j^2 = \frac{8}{3}d_1^2$$

$$\sum_j (r_{1j}^{\circ z})^2 = \sum_j z_j^2 = \frac{8}{3}d_1^2$$

$$\sum_j (r_{1j}^{\circ z})^4 = \sum_j z_j^4 = \frac{8}{9}d_1^4\{1 + 4\sin^2\alpha\,(\sin^2\alpha\cos^2\gamma\sin^2\gamma + \cos^2\gamma)\}$$

$$\begin{aligned} \sum_j (r_{1j}^{\circ x})^2(r_{1j}^{\circ z})^2 &= \sum_j (x_j z_j)^2 \\ &= \frac{8}{9}d_1^4\{4\sin^2\alpha\cos^2\alpha\cos^2\beta(\cos^2\gamma\sin^2\gamma - 1) \\ &\quad + 1 - 4\sin^2\alpha\sin^2\alpha\cos^2\gamma\sin^2\gamma \\ &\quad + 4\sin^2\alpha\cos\alpha\sin\beta\cos\beta(\cos^3\gamma\sin\gamma \\ &\quad - \cos\gamma\sin^3\gamma)\}. \end{aligned} \tag{21}$$

If we assume that the orientation of the local bcc lattice is random, the averaging of a function $G(\alpha, \beta, \gamma)$ over all orientations is defined by

$$\overline{G}(\alpha, \beta, \gamma) = \frac{\int G(\alpha, \beta, \gamma)\,d\Omega}{\int d\Omega} \tag{22}$$

where

$$d\Omega = \sin\alpha\,d\alpha\,d\beta\,d\gamma.$$

Inserting Eq. 21 into Eqs. 19-a and 19-b, we obtain, *e.g.*, for the eight nearest neighbors

$$\begin{aligned} \overline{\sum_j \left(\frac{\partial l_{zz}}{\partial \boldsymbol{r}_{1j}}\right)_0^2} &= \frac{9}{d_1^8}\int\left[\frac{40}{9}\{1 + 4\sin^2\alpha(\sin^2\alpha\cos^2\gamma\sin^2\gamma + \cos^2\alpha)\} - \frac{16}{3} + 8\right]d\Omega \Big/ \int d\Omega \\ &= 96\frac{1}{d_1^8} \end{aligned} \tag{23-a}$$

$$\overline{\sum_j \left(\frac{\partial l_{xz}}{\partial \boldsymbol{r}_{1j}}\right)_0^2} = 72\frac{1}{d_1^8} \tag{23-b}$$

and for the six second nearest neighbors

$$\overline{\sum_j \left(\frac{\partial l_{zz}}{\partial \boldsymbol{r}_{1j}}\right)_0^2} = 72\frac{1}{d_2^8} \tag{23-c}$$

$$\overline{\sum_j \left(\frac{\partial l_{xz}}{\partial \boldsymbol{r}_{1j}}\right)_0^2} = 54\frac{1}{d_2^8}. \tag{23-d}$$

Putting $a_j = l_1$ (j=1—8) for the first nearest neighbors and $a_j = l_2$ (j=9—14) for the second nearest neighbors and inserting Eqs. 18 and 23 into Eq. 16, we obtain

$$\langle L_{zz}(\boldsymbol{r}_1)\rangle = 0 \tag{24-a}$$

$$\langle (L_{zz}(\boldsymbol{r}_1))^2\rangle = \frac{1}{2\ln 2}\left\{96\frac{l_1^2}{d_1^8} + 72\frac{l_2^2}{d_2^8}\right\} \tag{24-b}$$

$$\langle (L_{xz}(\boldsymbol{r}_1))^2\rangle = \frac{1}{2\ln 2}\left\{72\frac{l_1^2}{d_1^8} + 54\frac{l_2^2}{d_2^8}\right\}. \tag{24-c}$$

Depolarization Degree. We finally obtain the expression for depolarization degree by inserting Eqs. 24-a, 24-b, and 24-c into Eq. 10:

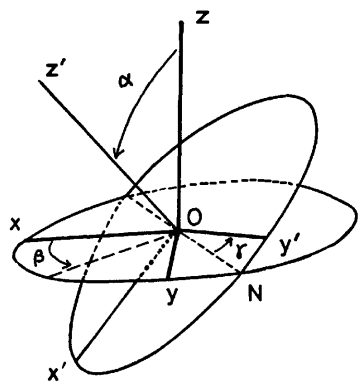

Fig. 3. Definition of Eulerian angles.
ON: Positive direction of line of nodes, the intersection of the xy and x' y' planes. α: Angle from Oz to Oz' ($0 \le \alpha \le \pi$). β: Angle in xy plane from Ox to the projection Oz on the xy plane. Also angle from Oy to ON ($0 \le \beta \le 2\pi$). γ: Angle in x' y' plane from ON to Oy'. Also angle from projection of -z on x' y' plane to Ox' ($0 \le \gamma \le 2\pi$).

$$\rho = \frac{I_x}{I_z} = \frac{\frac{2(\alpha^\circ)^2}{\ln 2}\left\{72\frac{l_1^2}{d_1^8}+54\frac{l_2^2}{d_2^8}\right\}}{1+\frac{2(\alpha^\circ)^2}{\ln 2}\left\{96\frac{l_1^2}{d_1^8}+72\frac{l_2^2}{d_2^8}\right\}}. \quad (25)$$

Eq. 25 shows that the depolarization degree ρ can be expressed in terms of the mean intermolecular distances, d_1 and d_2, the mean square amplitudes of the first and second nearest neighbors l_1 and l_2, and the polarizability, α°.

Putting the observed values of $\alpha^\circ=10.5$ Å^3,[5] $l_1=0.3$ Å, $l_2=0.35$ Å, $d_1=5.77$ Å, and $d_2=6.77$ Å,[4] into Eq. 25, ρ is calculated to be

$$\rho = 0.0021$$

for pure liquid carbon tetrachloride at room temperature. As the observed value is 0.0039 ± 0.0002, the present calculation explains the observed value very well.

Concluding Discussion. The quantities calculated in Eqs. 24-b and 24-c correspond to the magnitude of the mean square fluctuation of the local field. These fluctuations of local field are originating from the thermal displacement of carbon tetrachloride molecules from the mean local bcc structure. In other words, the main cause of the finite ρ value of the ν_1 line of liquid carbon tetrachloride is the fluctuation of local field originating from the thermal displacement of the molecular configuration.

The beautiful agreement between the observed and calculated values of depolarization degree, in turn, suggests the possibility of determining the magnitude of the thermal displacement of component molecules in the condensed system by observing the depolarization degree of liquid samples.

References

1) W. F. Murphy, M. V. Evans, and P. Bender, *J. Chem. Phys.*, **47**, 1836 (1967).
2) G. W. Chantry, *Spectrochim. Acta*, **21**, 1007 (1965).
3) A. E. Douglas and D. H. Rank, *Nature*, **162**, 453 (1948).
4) K. Nishikawa and Y. Murata, *Bull. Chem. Soc. Jpn.* **52**, 293 (1979).
5) C. P. Smyth, "Dielectric Behavior and Structure," McGraw-Hill (1955).

Some New Relationships between the Molecular Electron Densities and the Intensities of Electrons and X-Rays Scattered by Gases

Yorihiko SASAKI, Shigehiro KONAKA, and Masao KIMURA*

Department of Chemistry, Faculty of Science, Hokkaido University, Sapporo 060

(Received January 16, 1980)

Some new relations connecting the molecular electron densities and the intensities of electrons and X-rays scattered by gases have been derived by integrating analytically the scattered intensities multiplied by some functions of the momentum transfer, s, over ds.

The intensities of the electrons and X-rays scattered by gases have been known to provide information on atomic or molecular electron densities.[1] It has been proved that, in principle, the unique three-dimensional electron densities of molecules can not be derived directly from the one-dimensional scattering intensities.[2] However, the qualities of given molecular wave functions can be examined by comparing the experimental intensities with the theoretical ones calculated from the wave functions. Because of the considerably long computing time needed for such calculations, however, the theoretical scattering intensities based on molecular wave functions have been reported for only a very limited number of molecules.

A more convenient way of making such an examination is to make use of the integral relationships between the scattering intensities and the electron densities in molecules. A close connection between the integrated intensities of the total electron scattering and the total energies of molecules proved by Tavard *et al.* is an example of such a relationship.[3,4] Some relationships have also been reported by Bonham, who has mentioned the existence of other, similar relations.[5] These relations are obtained as the integral transforms of the scattering intensities by several kernels, which are functions involving momentum transfer, s. The purpose of the present paper is to present some new relations connecting the molecular electron densities with the scattered intensities by means of the integral transformation of the intensities, as well as to bring together the relations thus far reported in the form of analytical integration.

If the four σ functions are defined in terms of the elastic and total intensities of electrons (ED) and X-rays (XR) scattered by a free molecule as follows:[1,5]

$$\sigma_{\mathrm{E}}^{\mathrm{ED}}(s) = s^4 I_{\mathrm{E}}^{\mathrm{ED}}(s) - \sum_i Z_i^2, \tag{1}$$

$$\sigma_{\mathrm{T}}^{\mathrm{ED}}(s) = s^4 I_{\mathrm{T}}^{\mathrm{ED}}(s) - \sum_i Z_i^2 - N, \tag{2}$$

$$\sigma_{\mathrm{E}}^{\mathrm{XR}}(s) = I_{\mathrm{E}}^{\mathrm{XR}}(s), \tag{3}$$

$$\sigma_{\mathrm{T}}^{\mathrm{XR}}(s) = I_{\mathrm{T}}^{\mathrm{XR}}(s) - N, \tag{4}$$

to the first Born approximation, they are expressed in connection with the electron density in the molecule by:

$$\sigma_{\mathrm{E}}^{\mathrm{ED}}(s) = \sigma_{\mathrm{nn}}(s) - \sum_i Z_i^2 + \sigma_{\mathrm{ne}}(s) + \sigma_{\mathrm{E}}^{\mathrm{XR}}(s), \tag{5}$$

$$\sigma_{\mathrm{T}}^{\mathrm{ED}}(s) = \sigma_{\mathrm{nn}}(s) - \sum_i Z_i^2 + \sigma_{\mathrm{ne}}(s) + \sigma_{\mathrm{T}}^{\mathrm{XR}}(s), \tag{6}$$

where:

$$\sigma_{\mathrm{nn}}(s) - \sum_i Z_i^2 = \sum_{i\neq j}\sum Z_i Z_j \langle \mathrm{j}_0(sr_{ij})\rangle_{\mathrm{vlb}}, \tag{7}$$

$$\sigma_{\mathrm{ne}}(s) = -2\sum_i Z_i \left\langle \int \mathrm{d}\boldsymbol{r}\, \mathrm{j}_0(sr)\, \rho(\boldsymbol{r}+\boldsymbol{r}_i) \right\rangle_{\mathrm{vlb}}, \tag{8}$$

$$\sigma_{\mathrm{E}}^{\mathrm{XR}}(s) = \left\langle \int \mathrm{d}\boldsymbol{r}\, \mathrm{j}_0(sr) \int \mathrm{d}\boldsymbol{r}'\, \rho(\boldsymbol{r}')\, \rho(\boldsymbol{r}+\boldsymbol{r}') \right\rangle_{\mathrm{vlb}}, \tag{9}$$

and

$$\sigma_{\mathrm{T}}^{\mathrm{XR}}(s) = \left\langle \int \mathrm{d}\boldsymbol{r}\, \mathrm{j}_0(sr)\, \rho_{\mathrm{c}}(\boldsymbol{r}) \right\rangle_{\mathrm{vlb}}. \tag{10}$$

Here, the subscripts E and T denote elastic and total respectively; s is the momentum transfer given by $(4\pi/\lambda)\sin(\theta/2)$ (λ: wavelength, θ: scattering angle); N, the total number of electrons in the molecule; $\boldsymbol{r}_i$, the position vector of the i-th atom; Z, the atomic number; r_{ij}, an interatomic distance; $\mathrm{j}_0(x)$, the zero-order spherical Bessel function, $\sin x/x$; $\rho(\boldsymbol{r})$, the one-electron density, and $\rho_{\mathrm{c}}(\boldsymbol{r})$, the electron-pair correlation density; the brackets, $\langle\ \rangle_{\mathrm{vlb}}$, denote the averaging over thermal vibration.

To begin with, the integral of this type:

$$\Lambda(\alpha,\lambda) = \int_0^\infty \mathrm{d}s\, \sigma(s) s^\alpha \mathrm{e}^{-\lambda s}, \quad \lambda > 0 \tag{11}$$

will be considered. The factor, $\mathrm{e}^{-\lambda s}$, acts as a damping factor to reduce the error due to the termination of the integral. This type of integral has been mentioned in the literature[5] for the case where α is an integer. In general, for $\alpha \leqq -1$, the integral diverges, but for $\alpha > -1$ the integral can be expressed in terms of a hypergeometric function, ${}_2\mathrm{F}_1$.[6] By the use of the properties of ${}_2\mathrm{F}_1$, the integrals for the four kinds of σ are reduced to:[7]

$$\Lambda_{\mathrm{E}}^{\mathrm{ED}}(\alpha,\lambda) = \sum_{i\neq j}\sum Z_i Z_j \langle \mathrm{L}(\alpha,\lambda,r_{ij})\rangle_{\mathrm{vlb}} - 2\sum_i Z_i \left\langle \int \mathrm{d}\boldsymbol{r}\mathrm{L}(\alpha,\lambda,r)\, \rho(\boldsymbol{r}+\boldsymbol{r}_i) \right\rangle_{\mathrm{vlb}} + \Lambda_{\mathrm{E}}^{\mathrm{XR}}(\alpha,\lambda), \tag{12}$$

$$\Lambda_{\mathrm{T}}^{\mathrm{ED}}(\alpha,\lambda) = \sum_{i\neq j}\sum Z_i Z_j \langle \mathrm{L}(\alpha,\lambda,r_{ij})\rangle_{\mathrm{vlb}} - 2\sum_i Z_i \left\langle \int \mathrm{d}\boldsymbol{r}\mathrm{L}(\alpha,\lambda,r)\, \rho(\boldsymbol{r}+\boldsymbol{r}_i) \right\rangle_{\mathrm{vlb}} + \Lambda_{\mathrm{T}}^{\mathrm{XR}}(\alpha,\lambda), \tag{13}$$

$$\Lambda_{\mathrm{E}}^{\mathrm{XR}}(\alpha,\lambda) = \left\langle \int \mathrm{d}\boldsymbol{r}\mathrm{L}(\alpha,\lambda,r) \int \mathrm{d}\boldsymbol{r}'\, \rho(\boldsymbol{r}')\, \rho(\boldsymbol{r}+\boldsymbol{r}') \right\rangle_{\mathrm{vlb}}, \tag{14}$$

$$\Lambda_{\mathrm{T}}^{\mathrm{XR}}(\alpha,\lambda) = \left\langle \int \mathrm{d}\boldsymbol{r}\mathrm{L}(\alpha,\lambda,r)\, \rho_{\mathrm{c}}(\boldsymbol{r}) \right\rangle_{\mathrm{vlb}}, \tag{15}$$

with

$$\mathrm{L}(\alpha,\lambda,r) = \frac{1}{r}\frac{\Gamma(\alpha+1)}{(r^2+\lambda^2)^{\alpha/2}}\frac{\sin(\alpha\varphi)}{\alpha}, \quad \alpha > -1, \tag{16}$$

$$\varphi = \tan^{-1}\left(\frac{r}{\lambda}\right).$$

In the sense

$$\Sigma(\alpha) = \int_0^\infty ds\sigma(s)s^\alpha = \lim_{\lambda\to 0}\int_0^\infty ds\sigma(s)s^\alpha e^{-\lambda s}, \quad (17)$$

$\Sigma_T^{ED}(\alpha)$ *etc.* are obtained by replacing $L(\alpha,\lambda,r)$ in Eqs. 12—15 by:

$$F(\alpha,r) = \frac{\Gamma(\alpha+1)\sin(\alpha\pi/2)}{r^{\alpha+1}} \quad \alpha, \qquad 2>\alpha>-1, \quad (18)$$

and

$$F(2,r) = \frac{\pi}{r^2}\delta(r), \quad \alpha=2.$$

The result for $\Sigma_T^{ED}(0)$ is Tavard's energy relationship,[3,4] and those for $\alpha=1$ and 2 have already been given in the literature.[1,5] For $\alpha>2$, the integral over ds will diverge.

If λ in Eq. 11 is replaced by a complex number $(\lambda+ir')$, the integral over ds is expressed by a hypergeometric function, ${}_2F_1$, of $-r'^2/(\lambda+ir')^2$. By taking the imaginary part and letting λ tend to zero, in a sense similar to Eq. 17 we can obtain this integral:

$$J(\alpha,r') = \int_0^\infty ds\sigma(s)s^\alpha j_0(sr'), \quad 2\geqq\alpha>0. \quad (19)$$

This is a modification of Weber-Schafheitlin's discontinuous integral.[9] A useful relationship is obtained only for $\alpha=2$.

$$\begin{aligned} J_T^{ED}(2,r') &= \int_0^\infty ds\sigma_T^{ED}(s)s^2 j_0(sr') \\ &= \frac{\pi}{2}\sum_{i\neq j}\sum Z_iZ_j\langle r'^{-2}\delta(r'-r_{ij})\rangle_{vib} \\ &\quad - \pi\sum_i Z_i\left\langle\int d\Omega_{r'}\rho(r'+r_i)\right\rangle_{vib} \\ &\quad + \frac{\pi}{2}\left\langle\int d\Omega_{r'}\rho_e(r')\right\rangle_{vib}. \end{aligned} \quad (20)$$

Similar relations hold for the other scattering intensities, some of which have previously been reported in the literature.[10] The second and third terms of Eq. 20 are the averages over solid angles of the one-electron density around each nucleus and the electron-pair correlation density respectively. The latter is a radial inter-electron density function.[10]

In order to reduce termination errors, another integral:

$$M(\alpha,\ \mu) = \int_0^\infty ds\sigma(s)s^\alpha e^{-\mu s^2}, \quad \mu>0, \quad (21)$$

is considered, where $e^{-\mu s^2}$ is a damping factor often used in the calculations of radial distribution curves in electron-diffraction studies of gas molecules. This integral can be obtained in terms of a confluent hypergeometric function, ${}_1F_1$, of $r^2/4\mu$. For an even integer of α, $M(\alpha,\mu)$ can conveniently be expressed by replacing $L(\alpha,\lambda,r)$ in Eqs. 12—15 by the following $G(\alpha,\mu,r)$:

$$G(\alpha,\mu,r) = \frac{\partial^{(\alpha-2)/2}}{\partial\mu^{(\alpha-2)/2}}\left(\frac{1}{4}\sqrt{\frac{\pi}{\mu^3}}e^{-r^2/4\mu}\right), \quad \alpha\geqq 2. \quad (22)$$

Finally, relationships based upon finite integrals:

$$\Sigma_0(n) = \int_a^b ds\sigma(s)s^n, \quad (23)$$

and

$$\Lambda_0(n,\lambda) = \int_a^b ds\sigma(s)s^n e^{-\lambda s}, \quad (24)$$

may sometimes be used, where n is an integer. The functions, $F_0(n,r)$ and $L_0(n,\lambda,r)$, corresponding to $F(n,r)$ and $L(n,\lambda,r)$ are:

$$\begin{aligned} F_0(1,r) &= r^{-2}(\cos(ar) - \cos(br)), \\ F_0(2,r) &= r^{-1}(b^2 j_1(br) - a^2 j_1(ar)), \\ L_0(n,\lambda,r) &= (-1)^{n-1}\frac{\partial^{n-1}}{\partial\lambda^{n-1}}\{[(\lambda\sin(ar)+r\cos(ar))e^{-\lambda a} \\ &\quad -(\lambda\sin(br)+r\cos(br))e^{-\lambda b}]/r(r^2+\lambda^2)\}, \quad n\geqq 1. \end{aligned} \quad (25)$$

The various quantities closely related to the molecular electron density are obtainable from the experimental intensities. Except for small α values, the accuracy of $\Sigma(\alpha)$ is limited mainly by experimental errors at large scattering angles and the termination error at s_{max}. Such uncertainties are reducible by using $M(\alpha,\mu)$ and $\Lambda(\alpha,\lambda)$ with an appropriate choice of the parameters, μ and λ. There is no termination-error problem in $\Sigma_0(n)$ and $\Lambda_0(n,\lambda)$.

Since the calculation of the right-hand side of the above equations takes much less computing time than the calculation of the scattering intensities themselves from the molecular wave functions, these relationships must be of great use. The $J_T^{ED}(2,r')$ given by Eq. 20 is computed most easily; accordingly, it is most suitable for the first examination of a molecular wave function.

The authors wish to express their thanks to Professor Takao Iijima, Gakushuin University, for his helpful advice.

References

1) R. A. Bonham and M. Fink, "High Energy Electron Scattering," Van Nostrand Reinhold, New York (1974), Chaps. 3 and 4.
2) D. A. Kohl and L. S. Bartell, *J. Chem. Phys.*, **51**, 2891 (1969).
3) C. Tavard and M. Roux, *C. R. Acad. Sci. Paris*, **1965**, 4933.
4) C. Tavard, *Cahiers Phys.*, **20**, 397 (1966).
5) R. A. Bonham, *J. Phys. Chem.*, **71**, 856 (1967). The $\sigma_T^{ED}(s)$ defined in the present paper differs from Bonham's $\sigma_T^{ED}(s)$ by the term $\sum_{i\neq j}\sum Z_iZ_j\langle j_0(sr_{ij})\rangle_{vib}$, which is not included in his definition.
6) G. N. Watson, "Theory of Bessel Functions," 2nd ed, Cambridge Univ. Press, New York (1962), p. 381.
7) The same results are obtained for $\alpha>0$ by the use of Euler's expression of the Γ function as an infinite integral; see Ref. 8.
8) E. T. Whittaker and G. N. Watson, "A Course of Modern Analysis," 4th ed, Cambrige Univ. Press, London (1935), p. 260.
9) Ref. 6, p. 402.
10) R. F. Stewart, *Isr. J. Chem.* **16**, 111 (1977).

Direct Measurement of the Interaction Energy between Solids and Gases. VI. Calorimetric Studies on Acidic Properties of Solid Super Acids Prepared from Silica-Alumina

Hitofumi TANIGUCHI,† Tatsuo MASUDA,†† Kazuo TSUTSUMI,* and Hiroshi TAKAHASHI
Institute of Industrial Science, The University of Tokyo, 7-22-1 Roppongi, Minato-ku, Tokyo 106
(Received January 17, 1980)

Solid super acids were prepared by the reaction of gaseous antimony pentafluoride with silica–alumina and heats of adsorption of ammonia on their surfaces were measured. Solid super acids gave about 170 kJ/mol of an initial differential heat of adsorption and their adsorption energies were mainly distributed in the vicinity of 137 kJ/mol, while the initial differential heat of adsorption on original silica–alumina was about 150 kJ/mol and its adsorption energy was chiefly distributed in the vicinity of 117 kJ/mol. Therefore, it was shown that solid super acid had stronger, more homogeneous and much more acid sites than original silica–alumina.

An acid of which the strength is higher than that of 100 wt% H_2SO_4 ($H_0=-10.6$) is called "super acid," which seems to play an important role in catalyst chemistry.[1-3] The representative liquid super acids are $SbF_5 \cdot FSO_3H$ and $SbF_5 \cdot HF$, whose acid strengths were measured to be $H_0<-18$ and $H_0=-15.1$ respectively,[1-3] and others were also investigated by Gillespie *et al.*[4,5] Since liquid super acids are very difficult to deal with as catalysts in the practical reaction system, the synthesis of solid super acids has been required because of easy separation of products from a reaction system and of other advantages. Tanabe and Hattori[6,9] succeeded in the synthesis of several solid super acids such as SbF_5–TiO_2–SiO_2 and SbF_5–SiO_2–Al_2O_3 whose acid strengths are $-13.16 \geqq H_0 > -13.75$ and $-13.75 \geqq H_0 > -14.52$ respectively and which are catalytically active for the reaction of butane and isobutane at room temperature.

In this study, solid super acids (SbSA(I)—(V)) were prepared by the reaction of gaseous antimony pentafluoride with silica–alumina and heats of adsorption of ammonia on their surfaces were measured so as to clarify their surface acidic properties.

Experimental

Silica–alumina cracking catalyst (alumina 13 wt%, SA-13) supplied by Catalysts and Chemicals Ind. Co., Ltd., was evacuated at 500 °C under 10^{-3} Pa for 5 h before treatment with antimony pentafluoride. Antimony pentafluoride (SbF_5) supplied by PCR Research Chem., Inc. was used after distillation.

Solid super acids were prepared by contacting pretreated SA-13 with vapor of SbF_5 in a reaction tube made of pyrex glass for 10 minutes at room temperature, subsequently evacuating for about 20 minutes at 50 °C and repeating the above procedure twice (SbSA(I)), four times (SbSA(II)), eight times (SbSA(III)), thirteen times (SbSA(IV)) or twenty times (SbSA(V)). All of the samples were stored in the desiccator before use.

Gas adsorption calorimetries and infrared measurements were carried out as described in previous papers.[7,8] The content of antimony was determined as follows. A solid super acid was immersed into 1 mol dm^{-3} hydrochloric acid in order to extract completely surface antimony; extracted antimony was analysed by atomic absorption method.

Results

Antimony contents of each sample shown in Table 1 increased with an increase in the number of the treatment. Figure 1 shows differential heat of adsorption of ammonia on SbSA samples, which are extremely higher than that on orginal silica–alumina. Moreover, adsorbed amount of ammonia in the region of high differential heats of adsorption was much greater than that for SA-13. These results indicate the appearance of higher strong acid sites on silica–alumina surface by the treatment with SbF_5 vapor. The initial heat of readsorption of ammonia on SA-13 which was NH_3-preadsorbed and evacuated overnight at 25 °C was about 75 kJ/mol and equal to that on each of SbSA samples which were similarly pretreated. The adsorbed amount of ammonia increased linearly with an increase in antimony content as shown in Fig. 2, where A shows the adsorbed amount above

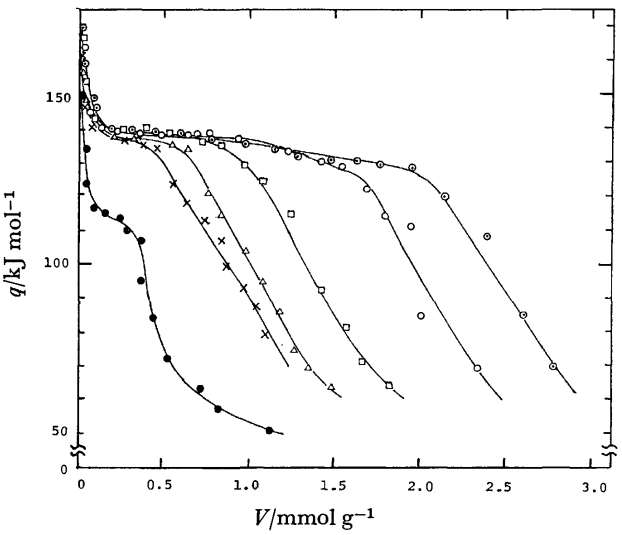

Fig. 1. Differential heats of adsorption of ammonia on solid super acids evacuated at 25 °C and SA-13 evacuated at 500 °C.
×: SbSA(I), △: SbSA(II), □: SbSA(III), ○: SbSA(IV), ⊙: SbSA(V), ●: SA-13.

† Present address: Tokuyama Soda Co., Ltd., 1-1, Mikage-cho, Tokuyama-shi, Yamaguchi 745.

†† Present address: Catalysts and Chemicals Ind. Co., Ltd., 13-2, Kitaminato-cho, Wakamatsu-ku, Kitakyushu 808.

TABLE 1. ANTIMONY CONTENT OF SOLID SUPER ACID

Sample	SbSA(I)	SbSA(II)	SbSA(III)	SbSA(IV)	SbSA(V)
Number of the treatment run	2	4	8	13	20
Sb Content / mmol g^{-1}	0.69	0.94	1.31	1.72	2.22

75 kJ/mol, B that above 130 kJ/mol and C that between 75 and 130 kJ/mol. Therefore, antimony atoms may be involved in the generation of acid sites on SbSA.

In Fig. 3, ammonia gas adsorption energy distributions on SbSA samples are shown. Fairly sharp maxima were observed for each of SbSA samples at the same heat of adsorption, 137 kJ/mol, and the number of acid sites at this region increased with antimony content. This suggests that the acid sites generated by the treatment with SbF_5 may be homogeneously distributed.

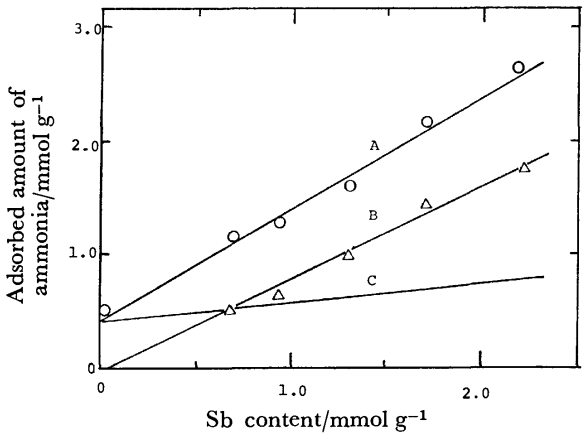

Fig. 2. Relation between Sb content and adsorbed amount of ammonia.
A: Adsorbed amount of ammonia above 75 kJ/mol, B: adsorbed amount of ammonia above 130 kJ/mol, C: adsorbed amount of ammonia between 75 and 130 kJ/mol.

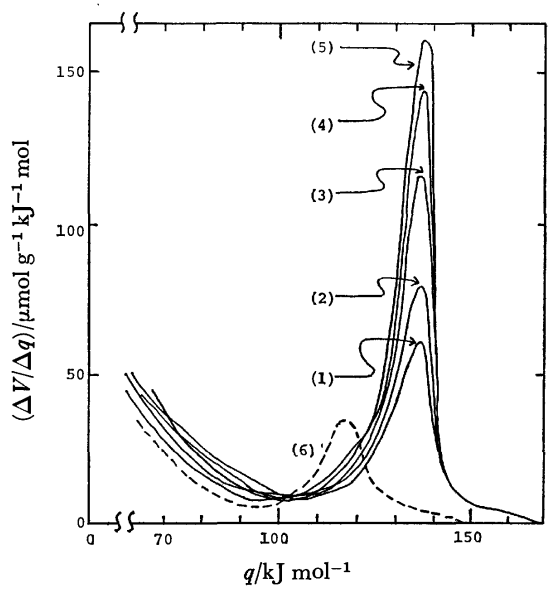

Fig. 3. Ammonia gas adsorption energy distributions for solid super acdis and SA-13.
(1): SbSA(I), (2): SbSA(II), (3): SbSA(III), (4): SbSA(IV), (5): SbSA(V), (6): SA-13.

Discussion

Tanabe *et al.*[9] proposed the following surface model of solid super acid (SbF_5–SiO_2–Al_2O_3).

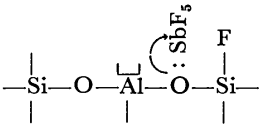

The acid strength of Lewis sites on surface aluminum ions becomes higher by an inductive effect of SbF_5 coordinated on neighboring oxygen ion. Lewis acid amount of SA-13 dehydrated at 500 °C *in vacuo* was determined to be about 180 μmol/g (from adsorbed amount of ammonia) based on the assumption described in previous paper[8] that only Lewis acid sites are present above 115 kJ/mol of differential heat of adsorption of ammonia in the case of silica–alumina (SA-13). If the surface model of SbSA is explained only by Tanabe's proposal, the adsorbed amount of ammonia above 130 kJ/mol should be about 180 μmol/g. The observed value shown in Fig. 2 implies that an another model of the acid generation would also be possible.

Infrared spectra of pyridine adsorbed on some solid super acids are shown in Fig. 4. The measurements were carried out at 25 °C after contacting SbSA samples evacuated at 50 °C with pyridine vapor for 10 min

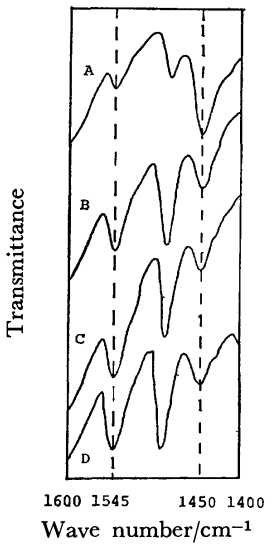

Fig. 4. Infrared spectra of adsorbed pyridine on solid super acids and SA-13.
A: SA-13, B: SbSA(II), C: SbSA(III), D: SbSA(IV).

Table 2. Ratio of the number of Brönsted acid sites to that of Lewis ones

Sample	SA-13	SbSA(II)	SbSA(III)	SbSA(IV)
B-site / L-site	4	9	11	16

and subsequent evacuation at 100 °C. All SbSA samples gave absorption peaks both at 1545 cm^{-1} and 1450 cm^{-1}, which indicates the presence of Brönsted and Lewis acid sites. The ratio of the number of Brönsted acid sites to that of Lewis ones was determined by their absorption intensity on the basis of the assumption that the ratio of the absorption coefficient of the 1450 cm^{-1} band to that of the 1545 cm^{-1} band, $\varepsilon_{1450}/\varepsilon_{1545}$, is 8.8,[10] and is shown in Table 2. The results show that the fraction of Brönsted sites on SbSA sample was greater than that on SA-13 and increased with antimony content. Hydrogen atoms are mostly present as surface hydroxyl groups on the original silica–alumina and may be involved in the generation of Brönsted acid sites by the interaction with SbF_5 molecules. The amount of residual hydroxyl groups of SA-13 after evacuation at 500 °C was gravimetrically determined to be 1.4 mmol/g by successive ignition loss *in vacuo* from 500 °C to 1200 °C by use of a Cahn electromagnetic microbalance. The transformation of surface hydroxyl groups into acid sites would be enhanced by an increase in the number of the treatment times with SbF_5 vapor, which was suggested by the finding that the site distribution at 137 kJ/mol became large with the treatment times. The maximum at 117 kJ/mol for original SA-13 disappeared by the treatment with SbF_5, accompanied by an appearance of the maximum at 137 kJ/mol. This suggests that the nature of inherent acid sites on SA-13 changed with the treatment with SbF_5.

The highest acid strength of SbF_5–SiO_2–Al_2O_3 prepared by Tanabe *et al.* was reported to be $-13.75 \geqq H_0 > -14.52$[6,9], while SbSA samples in this study gave about 170 kJ/mol of an initial differential heat of adsorption and their adsorption energies were mainly distributed in the vicinity of 137 kJ/mol. The differential heat value, $q=137$ kJ/mol, seems to correspond to the acid strength, $H_0 \fallingdotseq -14$, on the basis of the relation between q and pK_a value described in a previous paper,[11] which is similar to the value measured by Tanabe *et al.* The finding that SbF_5–SiO_2–Al_2O_3 exhibited high activity for the reaction of butane at 20 °C[6,9] might be attributed to the presence of a great number of acid sites with high differential heat of adsorption of ammonia above 130 kJ/mol.

It was concluded that solid super acid (SbSA samples) had stronger, more homogeneous and much more acid sites than original SA-13 and that most of acid sites on the former are Brönsted sites.

This work was partly supported by a Grant-in-Aid for Science Research from the Ministry of Education, Science and Culture (No. 343017).

References

1) G. A. Olah, I. R. DeMemer, and J. Sheu, *J. Am. Chem. Soc.*, **95**, 4952 (1973).
2) G. A. Olah, J. Sheu, and R. H. Schlosberg, *J. Am. Chem. Soc.*, **95**, 4957 (1973).
3) G. A. Olah, Y. Halpern, J. Sheu, and Y. K. Mo, *J. Am. Chem. Soc.*, **95**, 4960 (1973).
4) R. J. Gillespie, T. E. Peel, and E. A. Robinson, *J. Am. Chem. Soc.*, **93**, 5083 (1971).
5) R. J. Gillespie and T. E. Peel, *J. Am. Chem. Soc.*, **95**, 5173 (1973).
6) K. Tanabe and H. Hattori, *Chem. Lett.*, **1976**, 625.
7) T. Masuda, H. Taniguchi, K. Tsutsumi, and H. Takahashi, *J. Jpn. Petro. Inst.*, **22**, 67 (1979).
8) H. Taniguchi, T. Masuda, K. Tsutsumi, and H. Takahashi, *Bull. Chem. Soc. Jpn.*, **53**, 362 (1980).
9) K. Tanabe, H. Hattori, and O. Takahashi, *Hyomen*, **16**, 455 (1978).
10) M. R. Basila, T. R. Kantner, and K. H. Rhee, *J. Phys. Chem.*, **68**, 3197 (1964).
11) H. Taniguchi, T. Masuda, K. Tsutsumi, and H. Takahashi, *Bull. Chem. Soc. Jpn.*, **51**, 1970 (1978).

Study of Triplet-Triplet Energy Transfer between Like Molecules in a Rigid Glass Solution by Means of Optical Detection of Magnetic Resonance

Akinori Inoue, Nobuyuki Nishi,†,†† Minoru Kinoshita,† and Nozomu Ebara*

Department of Chemistry, College of General Education, The University of Tokyo, Komaba, Meguro-ku, Tokyo 153

†*The Institute for Solid State Physics, The University of Tokyo, Roppongi, Minato-ku, Tokyo 106*

(Received January 22, 1980)

The triplet-triplet energy transfer between like molecules was investigated for the system of quinoxaline in ethanol by using the method of optical detection of zero-field magnetic resonance at 1.4 K. The concentration dependence of the spin state population indicates that the energy transfer between quinoxaline molecules takes place at concentrations higher than about 2×10^{-2} mol/dm^3.

The triplet-triplet energy transfer between like molecules has so far been studied by the method of the concentration depolarization of phosphorescence[1,2] or by magnetophotoselection.[3] However, these methods are subject to the masking effect due to the singlet-singlet energy transfer, since molecules are initially excited into singlet states in most cases. Two of the present authors (AI and NE) have also developed a method which eliminates the effect of the S-S energy transfer by making use of isotopic mixtures.[4,5]

A more sophisticated approach would be to apply the method of optical detection of zero-field magnetic resonance (ZF ODMR), in which the use of an isotopic mixture is not necessary. As the perturbation causing the T-T energy transfer does not depend on the spin variables, the direction of the spin angular momentum is conserved during the energy transfer. Hence, the relative populations initially prepared in the spin states by optical pumping, followed by intersystem crossing, are modified as a result of the energy transfer according to the relative orientations of the solute molecules. Therefore, the modified relative populations may be used as an indication of the presence of the energy transfer, if the populations are compared with those obtained in the absence of energy transfer (*i.e.*, those in a sufficiently dilute solution).

In the present communication, we will describe an application of this method to a study of the T-T energy transfer among quinoxaline molecules dissolved in ethanol.

Experimental

Quinoxaline was distilled under reduced pressure. Ethanol was distilled after passing it through silica gel columns. The equipment for the ZF ODMR experiments has been described elsewhere.[6] Samples were excited with light from a high-pressure mercury lamp through an appropriate filter, and the phosphorescence was monitored at 474 nm.

Results and Discussion

The phosphorescent triplet state of quinoxaline has been thoroughly studied by ZF ODMR.[7] It is well established that the ordering of the spin sublevels is $T_x<T_y<T_z$ and that the phosphorescence emission occurs predominantly from T_z, where the x axis is defined as the normal to the molecular plane; the y axis, as the short axis, and the z axis, as the long axis. Most studies so far reported have been made in mixed crystals, such as quinoxaline in durene and in naphthalene-d_8.[7]

In the ethanol rigid glass solution (3×10^{-3} mol/dm^3) at 1.4 K, we observed MIDP (microwave-induced delayed phosphorescence) signals at 3.49 and 1.12 GHz; these signals indicate that the zero-field splitting parameters are not much different from those in the mixed crystals. On the other hand, the decay-rate constants were obtained as 1.2, 1.3, and 6.5 s^{-1} for the T_x, T_y, and T_z states respectively. Apparently, these values are affected by the spin-lattice relaxation. Therefore, the kinetic parameters given in Table 1 should be considered to represent just apparent properties. It is reasonable to assume that the spin-lattice relaxation does not depend on the concentration of quinoxaline. As a matter of fact, it will turn out that the spin-lattice relaxation does not significantly affect our main conclusion, since we focus our attention only on the concentration dependence of the parameters.

The steady-state population ratio, r_{ij}, of the sublevel, i, with large radiative and total decay rates, to another sublevel, j, is given by:

Table 1. The phosphorescence decay rates, k_i, relative radiative decay rates, k_i^r, and relative steady-state populations, N_i^0, of quinoxaline

	k_x/s^{-1}	k_y/s^{-1}	k_z/s^{-1}	k_x^r/k_z^r	k_y^r/k_z^r	N_x^0/N_z^0
In ethanol[a)]	1.2	1.3	6.5	0.040	0.035	0.30
In naphthalene-d_8[b)]	0.42	0.80	12.0	0.013	0.013	0.36
In durene[b)]	0.40	0.59	11.1	0.015	0.020	0.68

a) 3×10^{-3} mol/dm^3 and at 1.4 K. b) From Ref. 7.

†† Present address: Institute for Molecular Science, Myodaiji, Okazaki 444.

$$r_{ij} = N_j^0/N_i^0 \simeq h_{ij}(t_1) \exp(k_j t_1)/fI_0 + \exp(k_j - k_i)t$$

where $h_{ij}(t_1)$ is the magnitude of the MIDP signal at time t_1 ($t_1 \simeq 1$ s), where I_0 is the steady-state phosphorescence intensity tacitly approximated to be proportional to $k_i^r N_i^0$, and where f is the transfer efficiency of the population from T_j to T_i by means of a microwave pulse. In the present case, the concentration dependence of this quantity was measured for the T_x-T_z transition. The value thus obtained, r_{zx}, is also the apparent ratio of the steady-state population of T_x to that of T_z, because the above equation is valid only under the isolation conditions.

The observed r_{zx} values are plotted against the concentration in Fig. 1. The values remain almost constant ($\simeq 0.3$) in the range of 10^{-3} mol/dm^3. This indicates that the population in the T_z state is larger than that in the T_x state in the absence of any energy transfer. When the concentration is increased, the T-T energy transfer gradually becomes effective and results in *population randomization* among the spin states. As a result, the value of r_{zx} may be expected to increase, as we observed.

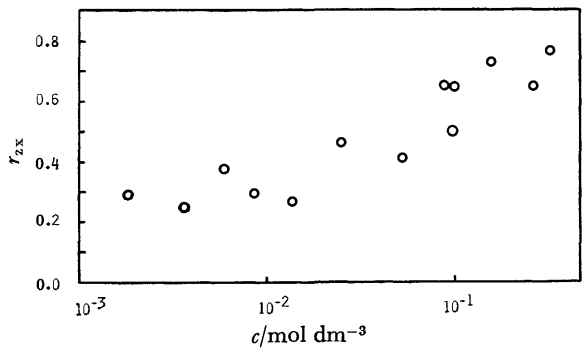

Fig. 1. Variation of the population ratio, r_{zx}, with concentration at 1.4 K.

However, before drawing any conclusion, we should discuss various possibilities which might influence the value of r_{zx} at high concentrations. As the values of f and I_0 changed from sample to sample, we used the values obtained in each measurement to estimate the value of r_{zx} from the equation. Therefore, the results in Fig. 1 cannot be due to the change in these quantities. Changes of the decay rates, k_x and/or k_z, might also affect the value of r_{zx}. However, it was found that the value of k_x does not show a significant variation in the concentration range studied. This is shown in Fig. 2. The values in Fig. 2 were obtained by plotting $\ln h_{zx}(t)$ *vs.* t in the region comparable to t_1 (*i.e.*, $\simeq 1$ s); the plots gave good straight lines. This means that, at both low and high concentrations, the effect of k_z on the magnitude of $h_{zx}(t)$ is not important and that, therefore, the second term of the equation can be neglected in this time region.

The rigid glass solutions were transparent, although cracked, at the highest concentration of 0.4 mol/dm^3, and the formation of microcrystals was not observed visually. Furthermore, the T_x-T_z transition was observed at nearly the same microwave frequency (3.48 GHz) in the 0.1 mol/dm^3 solution as in the solutions of lower concentrations. The phosphorescence spectrum of the same solution showed little difference compared with that of the samples of lower concentrations. These results suggest that the observed variation of r_{zx} is not due to a dimer or aggregate formation at high concentrations.

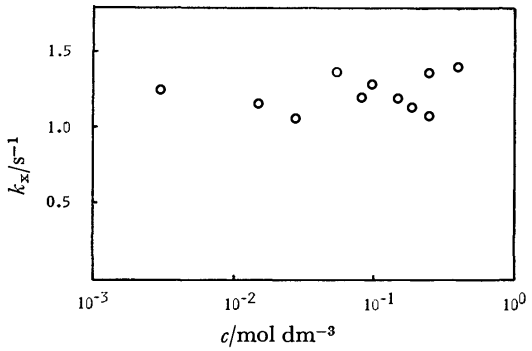

Fig. 2. Concentration dependence of the phosphorescence decay rate, k_x.

Triplet-triplet annihilation is an alternative possibility which might be responsible for the observed variation in r_{zx} with the concentration, because the population in T_z would be most effectively diminished by the annihilation. To check whether or not this possibility is operative, we measured the population ratios at different excitation light intensities and the phosphorescence decay curves at different concentrations. The intensity of the incident light was reduced to about a half by the use of an appropriate filter. The values of r_{zx} were found to be 0.55 and 0.50 for the 0.1 mol/dm^3 solution with and without the attenuation of light intensities respectively. These values are essentially in agreement with each other within the range of experimental error. The possibility of T-T annihilation is thus eliminated.

From these considerations, it may be concluded that the observed increase of r_{zx} at high concentrations is caused by the randomization of the relative populations in the spin states as a result of the triplet-triplet energy transfer among the randomly oriented quinoxaline molecules in the ethanol rigid glass. The energy transfer was found to become efficient at concentrations higher than 2×10^{-2} mol/dm^3; this finding essentially coincides with the corresponding concentration for the T-T energy transfer between dissimilar molecules.[18]

References

1) N. K. Chaudhuri and M. A. El-Sayed, *J. Chem. Phys.*, **42**, 1947 (1965).
2) Y. Gondo, M. Hirai, T. Iwao, T. Kakibaya, T. Kuroi, H. Nagatomo, and Y. Kanda, *Chem. Lett.*, **1975**, 463.
3) S. Siegel and L. Goldstein, *J. Chem. Phys.*, **44**, 2780 (1966).
4) A. Inoue and N. Ebara, *Chem. Lett.*, **1975**, 1137.
5) A. Inoue, H. Chuman, and N. Ebara, *Bull. Chem. Soc. Jpn.*, **51**, 345 (1978).
6) N. Nishi and M. Kinoshita, *Chem. Phys. Lett.*, **27**, 342 (1974).
7) J. Schmidt, D. A. Antheunis, and J. H. van der Waals, *Mol. Phys.*, **22**, 1 (1971).
8) V. L. Ermolaev and A. N. Terenin, *Trans. Faraday Soc.*, **52**, 1042 (1956).

Microwave Spectrum of Propyl Silane

Michiro HAYASHI,* Jun NAKAGAWA, and Yasunori AGUNI
Department of Chemistry, Faculty of Science, Hiroshima University, Higashi-sendamachi, Hiroshima 730

(Received January 28, 1980)

The microwave spectra of propyl silane and its four deuterated species were measured. The structure of the antiperiplanar isomer was so obtained as to reproduce the observed moments of inertia. The dipole moment and its direction were determined by Stark-effect measurements of several low J transitions.

In continuation of studies on the molecular structures of organosilicone molecules such as allyl silane[1] and ethyl fluorosilane,[2] the antiperiplanar isomer of propyl silane has been investigated by means of microwave spectroscopy.

The infrared and Raman spectra of the molecule were obtained by Murata *et al.*[3] who gave evidence of the existence of two rotational isomers, the antiperiplanar and synclinal isomers, in the gaseous phase. According to their Raman spectra, the antiperiplanar isomer is more stable than the synclinal isomer in the liquid state. We expected the structure of the synclinal isomer to be adequate for comparing it with that of allyl silane, but the observed microwave spectra of the synclinal isomer were so weak that assignments were possible for only the antiperiplanar isomer. In the present paper, the structure and the dipole moment of the antiperiplanar isomer are discussed.

Experimental

Samples of propyl silane and its deuterated species $CH_3CH_2CH_2SiD_3$ were prepared by reducing propyl trichlorosilane with lithium aluminium hydride or deuteride in dibutyl ether. Samples of $CD_3CH_2CH_2SiH_3$, $CH_3CD_2CH_2SiH_3$, and $CH_3CH_2CD_2SiH_3$ species were prepared by reacting appropriate propyl Grignard reagents with iodosilane.

The Grignard reagents were prepared in dibutyl ether from appropriate deuterated propyl bromides (98 atom % D, Merck Sharp & Dohme, Canada). Iodosilane was prepared by the method of Sternbach and MacDiarmid.[4]

The microwave spectra of the samples were measured in the region 8000—35000 MHz with a conventional Stark modulation spectrometer at the temperature of Dry Ice.

Results and Discussion

Microwave Spectra. The antiperiplanar isomer of propyl silane is a nearly prolate symmetric top molecule with the μ_a and μ_b-dipole moment components. However, the b-type transitions are actually very weak because of the smallness of the μ_b-dipole component. The observed frequencies of the transitions are given in Table 1. The rotational constants were obtained by a least-squares fit of all the observed frequencies with use of a rigid rotor formula modified by adding the first term of the centrifugal distortion $-d_J[J(J+1)]^2$. The results are given in Table 2.

Molecular Structure. The present data are not sufficient to determine the r_s structure by the substitution method. Only a part of the r_s coordinate values of the hydrogen atoms could be obtained from the solutions of the Kraitchman equations. They are given in Table 4.

In order to find a plausible structure of the molecule, five skeletal parameter values alone were adjusted so as to well reproduce the fifteen observed moments of inertia, the other parameter values being transferred from those of analogous molecules.

For the CCH_2SiH_3 part of the molecule, a set of parameter values was transferred from those of ethyl silane.[5] Since the reported parameter values of the methyl group for propane[6] gave a slightly asymmetric group, the parameter values were so corrected as to give a symmetric methyl group before the transfer of the values to the CH_3C part of our molecule.

As regards the parameter values of the CCH_2C part, r(CH) and α(HCC) values were transferred from those of the corresponding parameter values of the methyl group in ethyl silane. Since the α(CCC) value to be adjusted was related closely to the other five angle values, the change of α(CCC) was compensated by the change of α(HCH). The parameter values are given in Table 3.

When the r_s structure of a molecule is well established, the differences between the observed and calculated moments of inertia are small positive values and approximately constant for all the measured species. This was taken into consideration for the adjustment of the skeletal parameter values.

The differences between the observed and calculated moments of inertia (Table 2) are considered to be as small as those usually obtained from the r_s structure. The coordinate values of the hydrogen atoms calculated from the set of the skeletal parameter values reproduce the r_s coordinate values (Table 4).

The present set of skeletal parameter values can be regarded as the best set but their reliability cannot be shown clearly since the ambiguity arising from the transfer of the parameter values between molecules prevents estimation of the definite reliability of the values obtained.

However, even when maximum uncertainty is assumed, the r(CC) value of the CH_3C group is greater than that of propane, and the r(CC) value of the CH_2CSi group smaller than that of ethyl silane. The r(SiC) value is much greater than those of methyl silane[7] (1.8668 Å) and ethyl silane (1.866 Å).

The angle values are almost equal to those of the corresponding angle values for analogous molecules.

Dipole Moment. The dipole moments were determined by Stark-effect measurements of six low J transitions for the antiperiplanar isomers of propyl

Table 1. Observed frequencies of propyl silane (MHz)[a)]

	$CH_3CH_2CH_2SiH_3$	$CH_3CH_2CH_2SiD_3$	$CD_3CH_2CH_2SiH_3$	$CH_3CD_2CH_2SiH_3$	$CH_3CH_2CD_2SiH_3$
$2_{11}\leftarrow1_{10}$	8922.47(−8)	8291.30(−5)	8008.37(−9)	8782.71(−5)	8848.24(1)
$2_{02}\leftarrow1_{01}$	8826.73(−9)	8210.08(−4)		8680.83(−2)	8740.07(0)
$2_{12}\leftarrow1_{11}$	8731.83(−2)	8129.63(5)		8580.04(7)	8633.08(−1)
$3_{13}\leftarrow2_{12}$	13097.48(−3)	12194.14(10)	11783.68(0)	12869.62(2)	12949.23(−1)
$3_{03}\leftarrow2_{02}$	13239.20(−4)	12314.27(−4)	11897.12(−4)	13019.95(−2)	13108.59(−3)
$3_{12}\leftarrow2_{11}$	13383.52(−3)	12436.80(1)	12012.53(4)	13173.77(−2)	13271.98(2)
$4_{14}\leftarrow3_{13}$	17462.82(−2)	16258.38(−2)	15711.24(3)	17158.84(1)	17264.93(1)
$4_{04}\leftarrow3_{03}$	17650.40(−7)	16417.42(−1)	15861.55(−1)	17357.53(0)	17475.38(1)
$4_{13}\leftarrow3_{12}$	17844.20(−2)	16581.92(−2)	16016.30(1)	17564.36(−3)	17695.15(−5)
$5_{15}\leftarrow4_{14}$	21827.72(−1)	20322.29(0)	19638.43(0)	21447.52(2)	21580.06(8)
$5_{05}\leftarrow4_{04}$	22060.04(−9)	20519.16(1)	19824.77(−5)	21692.95(−4)	21839.76(3)
$5_{14}\leftarrow4_{13}$	22304.47(2)	20726.73(3)	20019.79(1)	21954.44(0)	22117.80(−1)
$6_{15}\leftarrow5_{14}$	26764.19(7)	24871.04(6)	24022.87(0)	26343.75(−2)	26539.61(1)
$6_{06}\leftarrow5_{05}$	26467.79(−2)	24619.16(4)	23786.62(−5)	26025.84(−2)	26201.15(3)
$6_{16}\leftarrow5_{15}$	26192.07(−2)	24385.67(−5)	23565.27(0)	25735.52(3)	25894.31(3)
$7_{17}\leftarrow6_{16}$	30555.90(9)	28448.58(−1)	27491.73(7)	30022.71(4)	30207.75(9)
$7_{07}\leftarrow6_{06}$	30873.21(9)	28717.04(5)	27746.81(−1)	30355.63(−3)	30558.98(4)
$7_{16}\leftarrow6_{15}$	31223.25(13)	29014.73(5)	28025.51(3)	30732.27(4)	30960.47(5)
$8_{17}\leftarrow7_{16}$		33157.76(8)	32027.57(4)	35119.73(5)	
$8_{08}\leftarrow7_{07}$		32812.50(9)	31705.04(4)	34681.80(8)	
$8_{18}\leftarrow7_{17}$		32510.86(4)	31417.58(7)	34309.01(9)	
$1_{10}\leftarrow1_{01}$	17905.89(−8)			15148.35(−3)	14845.45(−3)
$2_{11}\leftarrow2_{02}$	18001.72(2)	14468.83(1)	16023.66(−10)	15250.24(−4)	14953.58(−6)
$3_{12}\leftarrow3_{03}$	18145.96(−5)	14591.29(−1)	16139.03(−6)	15404.04(−6)	15116.97(−1)
$4_{13}\leftarrow4_{04}$	18339.73(−2)	14755.80(−9)	16293.78(−4)	15610.98(1)	15336.81(0)
$5_{14}\leftarrow5_{05}$	18584.15(8)	14963.33(−2)	16488.81(3)	15872.46(5)	15614.90(2)
$6_{15}\leftarrow6_{06}$	18880.35(−4)	15215.23(2)	16725.03(5)	16190.39(6)	15953.40(3)
$7_{16}\leftarrow7_{07}$	19230.46(7)	15512.93(3)	17003.67(3)	16567.03(7)	16354.90(5)
$8_{17}\leftarrow8_{08}$	19636.07(3)	15858.20(3)	17326.23(6)	17004.98(7)	16822.35(6)
$9_{18}\leftarrow9_{09}$	20099.58(2)	16253.02(3)	17694.20(3)	17507.10(−1)	17359.06(2)
$10_{19}\leftarrow10_{010}$	20623.36(−3)	16699.60(3)	18109.38(−4)	18076.74(−2)	17968.71(−4)
$2_{12}\leftarrow1_{01}$		22436.35(7)			
$3_{13}\leftarrow2_{02}$	30813.12(−5)	26420.25(−4)		27815.58(−12)	27580.08(−8)
$4_{14}\leftarrow3_{03}$		30364.30(−9)	31392.61(−6)	31954.45(−11)	31736.34(−12)
$5_{15}\leftarrow4_{04}$		34269.10(−14)			
$6_{06}\leftarrow5_{15}$	9314.03(12)	10869.02(−1)	8441.94(−1)	11674.33(1)	
$7_{07}\leftarrow6_{16}$	13994.91(−3)	15200.40(10)	12623.52(3)	16294.44(1)	16864.39(−5)
$8_{08}\leftarrow7_{17}$	18714.77(−3)	19564.04(−9)	16836.83(−1)	20953.44(−4)	21569.29(−12)
$9_{09}\leftarrow8_{18}$	23471.07(−5)	23958.26(−11)	21080.21(−5)	25648.28(−2)	
$10_{010}\leftarrow9_{19}$	28261.17(−5)	28380.61(−3)	25351.78(−5)	30375.26(−10)	

a) Figures in parentheses indicate the deviation of the observed frequency from the calculated one attached to the last significant figures.

Table 2. Rotational and centrifugal distortion constants of propyl silane[a)] (MHz) and moments of inertia (amu·Å^2)[b)]

	$CH_3CH_2CH_2SiH_3$	$CH_3CH_2CH_2SiD_3$	$CD_3CH_2CH_2SiH_3$	$CH_3CD_2CH_2SiH_3$	$CH_3CH_2CD_2SiH_3$
A	20065.10 (23)	16399.77 (20)	17892.13 (18)	17268.03 (20)	16976.86 (20)
B	2254.478(13)	2093.062(11)	2021.186(9)	2221.042(11)	2238.955(12)
C	2159.131(16)	2012.176(12)	1944.914(12)	2119.647(14)	2131.382(13)
$d_J\times10^3$	0.57 (14)	0.40 (12)	0.39 (9)	0.49 (11)	0.45 (19)
$I_a(\Delta I_a)$	25.1868(0.0462)	30.8160(0.0125)	28.2457(0.0143)	29.2666(0.0625)	29.7685(0.0375)
$I_b(\Delta I_b)$	224.1654(0.3359)	241.4530(0.3395)	250.0393(0.4535)	227.5400(0.3226)	225.7200(0.3022)
$I_c(\Delta I_c)$	234.0645(0.2444)	251.1589(0.1886)	259.8449(0.3628)	238.4246(0.2295)	237.1118(0.1817)

a) Figures in parentheses indicate the uncertainties calculated from 2.5 times standard deviations attached to the last significant figures. b) Figures in parentheses indicate the difference between the observed and calculated moments of inertia. $\Delta I_g=I_g(\text{obsd})-I_g(\text{calcd})$.

TABLE 3. STURCTURAL PARAMETERS OF PROPYL SILANE AND RELATED MOLECULES[a)]

	$CH_3CH_2CH_2SiH$	$CH_3CH_2CH_3$	$CH_3CH_2SiH_3$
CH_3C group			
r(CC) (Å) (adjusted)	1.534	1.526	
$r(CH_s)$ (Å)	1.094	1.089	
$r(CH_a)$ (Å)	1.094	1.094	
$\alpha(H_sCC)$	110° 8′	111°48′	
$\alpha(H_aCC)$	110° 8′	110°36′	
$\alpha(H_sCH_a)$	108°48′	108° 6′	
$\alpha(H_aCH_a)$	108°48′	107°18′	
CCH_2C group			
r(CC) (Å) (adjusted)	1.528	1.526	1.540
r(CH) (Å)	1.093	1.096	1.093
α(CCC) (adjusted)	112°10′	112°24′	
α(HCC)	109°34′	109°34′	111° 2′
α(HCH) (balanced)	106°20′	106° 6′	106°59′
CCH_2Si group			
r(SiC) (Å) (adjusted)	1.886		1.866
r(CH) (Å)	1.097		1.097
α(CCSi) (adjusted)	113°11′		113°11′
α(CCH)	110°10′		110°10′
α(HCSi)	108°46′		108°46′
α(HCH)	105°46′		105°46′
SiH_3 group			
$r(SiH_s)$ (Å)	1.483		1.483
$r(SiH_a)$ (Å)	1.480		1.480
$\alpha(H_sSiC)$	110° 3′		110° 3′
$\alpha(H_aSiC)$	110° 3′		110° 3′
$\alpha(H_aSiH_s)$	109° 9′		109° 9′
$\alpha(H_aSiH_a)$	108°20′		108°20′

a) (adjusted) indicates the parameter value which was adjusted and (balanced) indicates the parameter value used as the balance of the change of the adjusted parameter value.

TABLE 4. COORDINATE VALUES FOR HYDROGEN ATOMS (Å)

Atom		r_s[a)]	Model[b)]
$H_a(CH_3)$[c)]	x_c	±0.885	±0.890
$H(CCH_2C)$	x_a	−0.960	−0.965
	x_b	1.142	1.141
	x_c	±0.877	±0.874
$H(CCH_2Si)$	x_a	−0.071[d)]	−0.165
	x_b	−1.245	−1.249
	x_c	±0.876	±0.873
$H_a(SiH_3)$[c)]	x_c	±1.203	±1.200

a) Solved by the Kraitchman equation. b) Obtained from the structure given in Table 3. c) H_a indicates the hydrogen atom located out of the symmetry plane. d) This Kraitchman coordinate value is unreliable because of the smallness of the absolute value.

silane and its two deuterated sepcies ($CH_3CH_2CH_2SiD_3$ and $CH_3CD_2CH_2SiH_3$). The spectrometer was calibrated with OCS[8)] on the measurements. The results are given in Table 5.

The dipole moment of the $CH_3CH_2CH_2SiH_3$ species is slightly larger than that of the $CH_3CH_2CH_2SiD_3$ species though 99% reliability intervals of the dipole moments for these species slightly overlap each other. Thus the silyl group is considered to be situated at the side of the negative pole of the dipole moment.[9)]

There are two possible directions for the dipole moment (Table 5), making angles of i) 5°46′ and ii) 143°54′ with the SiC bond, respectively. The angle between the b-inertial axis and the SiC bond of the $CH_3CD_2CH_2SiH_3$ species is smaller by ca. 40′ than that of the $CH_3CH_2CH_2SiH_3$ species. The angle of $\alpha((C–Si)\times\mu)$ for the $CH_3CH_2CH_2SiH_3$ and CH_3CD_2-CH_2SiH_3 species agree with each other within experimental error for i), and disagree beyond experimental error for ii).

The dipole moment of the antiperiplanar isomer of propyl silane is thus concluded to incline by 5°46′ from the SiC bond towards the SiH bond in the symmetry plane.

The dipole moment of the antiperiplanar isomer of propyl silane (0.811 D) is close to that of ethyl silane (0.81 D),[5)] larger than that of methyl silane (0.7351 D).[9)] The angle between the dipole moment and the SiC bond is much larger than that for ethyl silane (1°18′).

Spectra due to the Excited Vibrational States. Several groups of spectra attributable to those in the excited vibrational states can be found around the ground state lines. Among them, the group of spectra

TABLE 5. DIPOLE MOMENTS AND STARK COEFFICIENTS OF PROPYL SILANE[a)]

		$CH_3CH_2CH_2SiH_3$		$CH_3CH_2CH_2SiD_3$		$CH_3CD_2CH_2SiH_3$	
Stark coefficient $(\Delta\nu/E^2)$[b)]							
	|M|	obsd	calcd	obsd	calcd	obsd	calcd
$2_{02}\leftarrow1_{01}$	0	−0.539(16)	−0.542	−0.561(8)	−0.562		
	1	0.441(4)	0.441	0.467(4)	0.454	0.437(3)	0.440
$2_{12}\leftarrow1_{11}$	0	0.450(2)	0.447	0.484(6)	0.484	0.466(5)	0.476
$2_{11}\leftarrow1_{10}$	0	0.435(4)	0.443	0.455(3)	0.446	0.437(5)	0.432
$2_{03}\leftarrow2_{02}$	0					−0.137(1)	−0.137
	1			−0.059(1)	−0.059	−0.063(1)	−0.063
	2	0.168(1)	0.166	0.162(2)	0.156	0.152(0)	0.149
$3_{13}\leftarrow2_{12}$	0	−1.498(18)	−1.496			−0.137(1)	−0.137
	1			1.379(12)	1.413	1.119(6)	1.136
$3_{12}\leftarrow2_{11}$	0					−0.024(0)	−0.025
	1	−1.248(14)	−1.306	−1.452(6)	−1.476	−1.179(8)	−1.203
Dipole moment (Debye)							
μ_a		0.783(7)		0.766(8)		0.776(6)	
μ_b		0.212(8)		0.215(22)		0.227(4)	
μ_{total}		0.811(8)		0.796(10)		0.809(6)	
$\alpha(\mu\times b)$[c)]		74°50′(45′)		74°20′(1°53′)		73°40′(25′)	
$\alpha((C\text{-}Si)\times\mu)$[d)]		5°46′ or 143°54′		5°05′ or 143°35′		5°14′ or 142°02′	
$\alpha(b\times(C\text{-}Si))$[e)]		69°01′		69°12′		68°24′	

a) Figures in parentheses indicate the uncertainties calculated from 2.5 times standard deviations attached to the last significant figures. b) In 10^{-5} MHz $(cm/V)^2$ unit. c) The angle between the dipole moment and the b-inertial axis. d) The angle between the dipole moment and the C-Si bond. e) The angle between the b-inertial axis and the C-Si bond.

predictable by the rotational constants $(A, B, C)=$ (19700, 2251, 2158) MHz for the normal species were assigned to that arising from the first excited skeletal torsional state. Actually, rough measurements of the relative intensity of the spectra gave the vibrational frequency of *ca.* 100 cm^{-1} which is close to the observed Raman frequency (102 cm^{-1}) in the liquid state for the $CH_3CH_2CH_2SiD_3$ species.[3)]

Assignments of the spectra attributed to those of the excited CH_3 and SiH_3 torsional states were attempted in order to evaluate the barrier to internal rotation of the CH_3 and SiH_3 groups. However, we have found no spectra with reasonable splittings.

The authors wish to express their thanks to Associate Professor Akinori Hasegawa for his kindness in supplying the samples.

References

1) M. Hayashi, M. Imachi, and M. Saito, *Chem. Lett.*, **1977**, 221.
2) M. Hayashi, M. Hikino, and M. Imachi, *Chem. Lett.*, **1977**, 1.
3) H. Murata, H. Matsuura, K. Ohno, and T. Sato, *J. Mol. Struct.*, **52**, 1 (1979).
4) B. Sernback and A. G. MacDiarmid, *J. Am. Chem. Soc.*, **83**, 3384 (1961).
5) H. D. Petersen, Thesis, The University of Notre Dame (1961).
6) D. R. Lide, Jr., *J. Chem. Phys.*, **33**, 1514 (1961).
7) R. W. Kilb and L. Pierce., *J. Chem. Phys.*, **27**, 108 (1957).
8) J. S. Muenter, *J. Chem. Phys.*, **48**, 4544 (1968).
9) J. S. Muenter and V. W. Laurie, *J. Chem. Phys.*, **45**, 855 (1966).

Spectroscopic and Kinetic Study of an Intramolecular Aromatic Nucleophilic Photosubstitution. Reaction Mechanism of a Photo-Smiles Rearrangement

Kenji YOKOYAMA, Ryoichi NAKAGAKI, Junko NAKAMURA, Kiyoshi MUTAI,** and Saburo NAGAKURA*

The Institute of Physical and Chemical Research, Wako, Saitama 351

***Department of Chemistry, College of General Education, The University of Tokyo, Meguro-ku, Tokyo 153*

(Received January 25, 1980)

Photo-Smiles rearrangement reaction of *N*-[ω-(*p*-nitrophenoxy)alkyl]aniline was studied by measuring the absorption spectra of transient species. Two intermediates **A** and **B** were observed and were assigned to a solvated ion pair and the Meisenheimer complex, respectively. The reaction scheme, starting material→intramolecular charge transfer on excitation→**A**→**B**→final product, was derived from the relative yields and lifetimes of **A** and **B** as well as from the effects of solvent polarity, of triethylamine and oxygen, and of the alkyl chain length on each step of reaction.

A great number of studies on aromatic nucleophilic photosubstitution have been carried out, main interest being focused on the orientation rule.[1] However, works in which the reaction mechanism has been elucidated through direct observation of intermediates are only a few. Cornelisse *et al.*[2] and also Duddel and Richards[3] studied the reactions of 3,5-dinitroanisole and *o*-, *m*-, and *p*-nitroanisoles, respectively, with the hydroxide ion by flash and laser photolysis. They concluded that the reaction proceeded *via* the triplet state except for *m*-nitroanisole.

A photo-Smiles rearrangement is known as an intramolecular nucleophilic photosubstitution reaction in which a nucleophile and a reaction center coexist within a molecule. Mutai *et al.*[4] studied the reaction in which *N*-[ω-(*p*-nitrophenoxy)alkyl]aniline (abbreviated hereafter to $(I)_n$, *n* being the number of methylene in the alkyl chain) converted into an alcohol $(II)_n$ in polar solvents by irradiation with light of about 300 nm (see Fig. 1). They reported that the reaction proceeded unimolecularly and proposed a tentative reaction scheme. In the present study, we have intended to elucidate the reaction mechanism by observing directly the intermediates with the aid of laser photolysis.

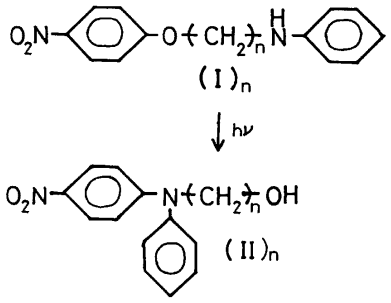

Fig. 1. Photo-Smiles rearrangement of *N*-[ω-(*p*-nitrophenoxy)alkyl]aniline, $(I)_n$.

Experimental

The starting material $(I)_n$ with $n=2$, 3, and 4 were prepared as mentioned previously[5] and purified by chromatography. Acetonitrile, benzene, cyclohexane (Wako, Spectrograde), ethanol (Nakarai, Spectrograde), and tetrahydrofuran (Wako, Special Grade) were used as solvents without further purification. Sample solution for the transient absorption measurements (about 1×10^{-3} mol·dm^{-3}) were degassed by repeating freeze-pump-thaw cycles. *N*-Methylaniline (NMA) (Wako, Special Grade) and *p*-nitroanisole (PNA) (Tokyo Kasei, Special Grade) which were regarded as two components of $(I)_n$ were used as references after distillation *in vacuo* and recrystallization, respectively.

An N_2 laser (Molectron UV-24 with peak height of 900 kw and pulse duration of 10 ns) was used as a pulse excitation source of reaction. A monitor light source was designed and constructed using a Xe flash lamp (EG & G 3CP-2). This system was able to emit rectangular shaped radiation pulses with 50 μs duration by the discharge through an LC delaying circuit.[6] By the use of this system, the transient absorption in μs region was measured with enough accuracy. A current regulated I_2-W lamp, chopped with a mechanical shutter, was used for the measurement of longer lived species (≈1 ms).

Time profile and spectra of transient species were measured by using a Jarrell-Ash JE-25 monochromator equipped with an HTV R-666S photomultiplier. A Hitachi 200-20 spectrophotometer was used for ordinary absorption measurements. All the experiments were made at room temperature.

Results and Discussion

Spectral change caused by 365 nm light irradiation of $(I)_2$ in acetonitrile is shown in Fig. 2. $(II)_2$ was produced by the irradiation of the sample in acetonitrile with the 313 or 365 nm light of Hg lamp or the defocused N_2 laser beam. Several isosbestic points were observed. This indicates that the reaction is clean and straightforward, being suited for the kinetic study of the reaction. The spectra of $(I)_2$ are safely reproduced by the superposition of those of PNA and NMA, whereas Mutai found a weak CT absorption band at 360 nm for the compounds of $n=2$ and 3.[7] This implies the existence of weak interaction in the ground state molecule. Thus it is suggested that considerable amounts of the molecules take sandwich configuration in their ground state.

Figure 3 shows the time dependence of the transient absorption of $(I)_2$ observed at 450 nm in acetonitrile.

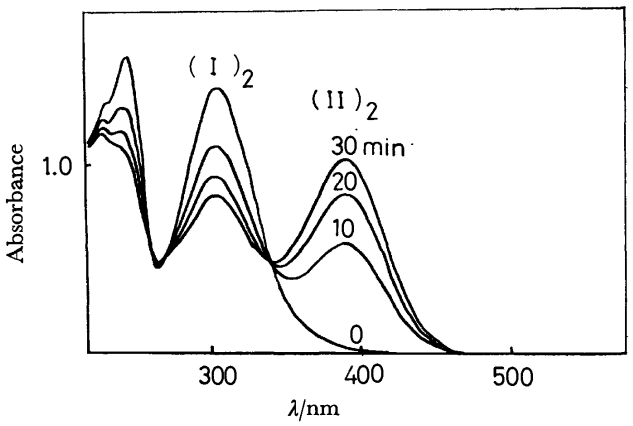

Fig. 2. Spectral change of $(I)_2$ in acetonitrile irradiated at 365 nm for 0, 10, 20, and 30 min, respectively.

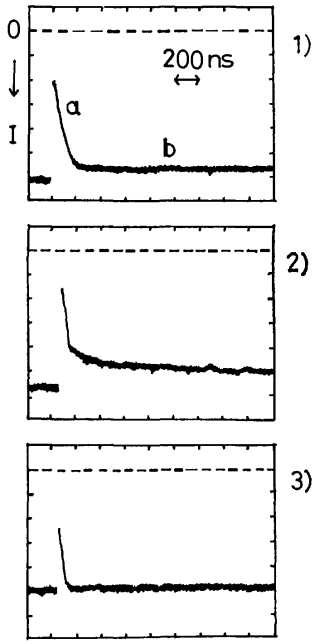

Fig. 3. Decay curve of transient absorption of $(I)_2$ in acetonitrile at 450 nm.
1) $(I)_2$ only, 2) with $N(C_2H_5)_3$ ($\approx 1\times10^{-1}$ mol·dm^{-3}), 3) with O_2.

The decay curve of the absorption can be analyzed as composed of two components, **a** and **b**. Component **a** absorbs strongly but decays very fast, whereas component **b** is weak but long lived. The observation of these two components indicates the existence of two kinds of intermediates. Hereafter the intermediates which show the **a** and **b** components are referred to as **A** and **B**, respectively.

Figure 4 shows the absorption spectrum of **A**, which has a maximum at 450 nm, a shoulder in the shorter wavelength region, and a long tail in the longer wavelength region. The spectrum was not observed when either PNA or NMA was irradiated separately by the N_2 laser under the present experimental condition. The masking of nitrogen of the NMA component by addition of 0.1 mol·dm^{-3} hydrochloric acid also resulted in the nonoccurrence of **A**. The absorption spectrum of **A** is independent of *n*, the number of the methylene group in the alkyl chain. Thus, it is concluded that decay component **a** is caused by the coexistence of PNA and NMA moieties.

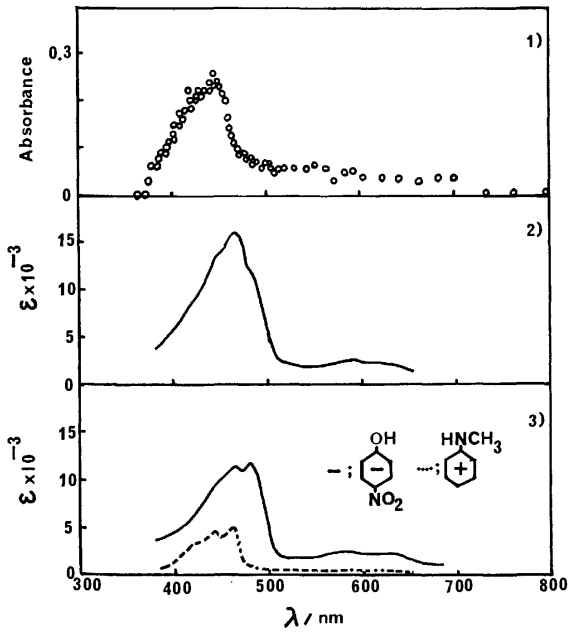

Fig. 4. Absoprtion spectra of **A** and the authentic species.
1) Absorption spectrum of **A** of $(I)_2$ in acetonitrile solution 10 ns after the excitation, 2) the 1:1 superposition of the absorption spectra of the NMA cation radical and the *p*-nitrophenol anion radical, 3) absorption spectra of the *p*-nitrophenol anion radical (Ref. 8b) and the NMA cation radical (Ref. 8a).

Transient intermediate **A** was observed clearly in polar solvents such as acetonitrile, ethanol and tetrahydrofuran, but not in nonpolar solvents such as benzene and cyclohexane. This solvent effect on the occurrence of **A** suggests the highly polar character of **A**.

Shida *et al.* reported the spectra of the *p*-nitrophenol anion radical and the NMA cation radical obtained by γ-ray irradiation at low temperature.[8] The 1:1 superposition of the spectra of both ions which are reproduced in Fig. 4, 3 is similar to the spectrum of **A** (compare Fig. 4, 1) with Fig. 4, 2)). Since the spectrum of the PNA anion radical is expected to be similar to that of the *p*-nitrophenol anion radical, the spectrum of **A** may be regarded as a superposition of those of the PNA and NMA ions. From this fact and the above-mentioned necessity of the coexistence of PNA and NMA moieties for the occurrence of **A**, we can conclude that **A** is a solvated ion pair in which both ions are bridged with the methylene chain.

Transient intermediate **A** is formed within the excitation pulse time (10 ns). Its lifetime is about 60—100 ns in the degassed acetonitrile solutions and reduces to about 20 ns after bubbling of the solution with O_2 gas for 3 min (see Table 1). In spite of the oxygen effect, **A** cannot be assigned to the lowest triplet state of $(I)_2$ in view of the fact that the spectrum of **A** is different from the T-T absorption spectra of nitro-

TABLE 1. EFFECTS OF $N(C_2H_5)_3$ AND O_2 ON THE INTERMEDIATES

	Lifetime of **A**	The relative yield of **B** to **A**
$(I)_2+N(C_2H_5)_3$	25 ns	0.15
$(I)_2$ only	65	0.07
$(I)_2+O_2$	≈20	<0.04
$(I)_3+N(C_2H_5)_3$	27	0.14
$(I)_3$ only	73	0.06
$(I)_3+O_2$	≈20	<0.03
$(I)_4+N(C_2H_5)_3$	25	0.19
$(I)_4$ only	98	0.12
$(I)_4+O_2$	≈20	<0.04

anisoles,[3] aniline and *N,N*-dimethylaniline.[9] The oxygen effect on the decay of **A** may be interpreted as the quenching of the aromatic anion by O_2.

Mutai *et al.* observed that the reaction $(I)_2 \rightarrow (II)_2$ was accelerated by addition of $N(C_2H_5)_3$.[4] We studied the effect of O_2 besides $N(C_2H_5)_3$ on the rate of the reaction by monitoring the absorbance at the peak of $(II)_2$ (at 395 nm) and the results are shown in Fig. 5. The addition of O_2 was found to decrease the rate.

Furthermore, we studied the effects of $N(C_2H_5)_3$ and O_2 on the decay of transient absorption and the results are shown in Fig. 3. The observed values of lifetime are listed in Table 1, together with the relative yield of **B** to **A** which is the ratio of absorbance of **B** observed 1 μs after the excitation to that of **A** observed 10 ns after irradiation. The addition of O_2 decreases the lifetime of **A** as well as the relative yield of **B**. The addition of $N(C_2H_5)_3$ decreases the lifetime of **A** but increases the relative yield of **B**. These results mean that O_2 quenches the ion pair and intercepts formation of **B** from **A** whereas $N(C_2H_5)_3$ accelerates the formation. The retarding effect of O_2 and the accelerating effect of $N(C_2H_5)_3$ were observed for formation of the final product, too. This is one of the evidences that intermediates **A** and **B** observed spectroscopically really participate in the reaction.

Figure 6 shows the absorption spectrum of **B** produced from $(I)_2$ in the presence of $N(C_2H_5)_3$ (1 μs after excitation). A similar spectrum of **B** was also observed in the absence of $N(C_2H_5)_3$ although S/N

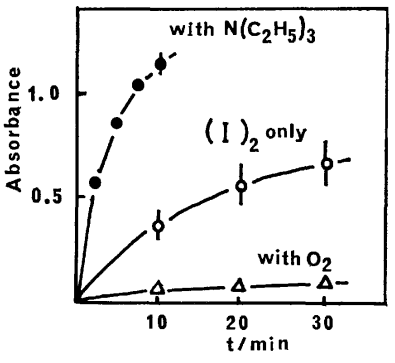

Fig. 5. Effects of O_2 and $N(C_2H_5)_3$ on the rate of reaction $(I)_2 \rightarrow (II)_2$ in acetonitrile with the irradiation of 365 nm light.

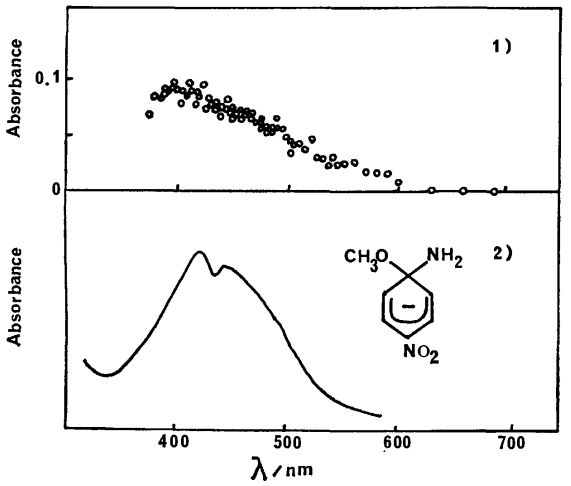

Fig. 6. Absorption spectra of **B** and the authentic species.
1) Absorption spectrum of **B**, 2) absorption spectrum of 1-methoxy-1-amino-4-nitrocyclohexadienide (Ref. 10).

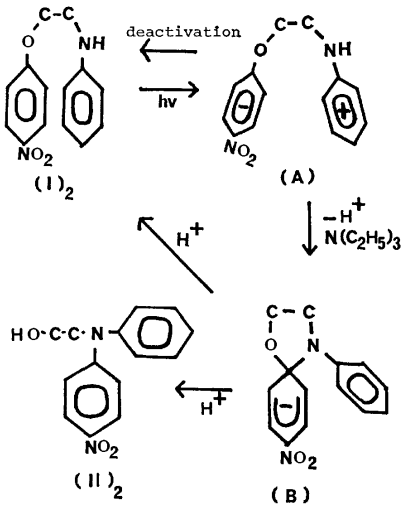

Fig. 7. A conclusive mechanism of the photo-Smiles rearrangement of $(I)_2$.

ratio became worse. As a stable intermediate of aromatic substitutions, the Meisenheimer complex (see Fig. 6) is well known. Ohsawa observed the absorption spectrum of the complex of PNA with amine with the results shown in Fig. 6.[10] We can see from the figure that the spectrum of **B** is similar to that of the complex. Therefore **B** is assigned to the Meisenheimer complex. The lifetime of **B** in the presence of $N(C_2H_5)_3$ is about 1—several ms for n=2, 3, and 4. Furthermore the spectral feature was found to be almost independent of n.

Figure 7 shows a conclusive mechanism of the reaction. A slight interaction may occur between the two ending groups in the ground state of the starting material $(I)_2$, as suggested by the appearance of a weak charge transfer band. When the sandwich type molecule is excited, a charge separation takes place efficiently through the orbital overlap and then the charge-transfer complex is solvated to form an ion pair.[11]

The process **A**→**B** corresponds to the Meisenheimer complex formation probably accompanied with abstraction of H^+ and **B** is converted into $(II)_2$ gradually by abstracting H^+ from $HN(C_2H_5)_3^+$. At the stage of **A** to **B**, the basicity of the NMA cation may be considered to be weaker than that of $N(C_2H_5)_3$. Therefore H^+ transfers from **A** to $N(C_2H_5)_3$. This may reasonably explain the enhancement of the relative yield of **B** by the addition of $N(C_2H_5)_3$. The above explanation implies that the presence of H^+ acceptor such as amine is necessary for the forward reactions. Actually, when the solvent acetonitrile was distilled repeatedly with P_2O_5, the photo-Smiles reaction rate was markedly slow. The fact that commercially available spectroscopic grade acetonitrile is positive solvent for the reaction suggests the presence of impurities which act as catalysts in thermal reaction steps, although they are not detectable by gas and liquid chromatography.

As a whole, the photosensitized Smiles rearrangement is such a reaction that a substitution takes place between the cation and anion radicals produced by irradiation of light. Nagakura and Tanaka predicted theoretically that the radicals formed by charge transfer interaction played an important role in the aromatic substitution reaction.[12] The observation of the ion pair as the reaction intermediate in the present study shows that the photo-Smiles reaction is a typical example for their prediction.

Generally speaking, the orientation rule is known to be different for thermal and photo aromatic substitutions. Mutai *et al.*, however, reported that the photo-Smiles reaction is para directing with regard to the NO_2 group as is usual for the thermal nucleophilic substitution.[4] This agrees with the theoretical prediction by Nagakura and Tanaka[12a] that the free valency of the nitrobenzene anion is largest at the para position. In other words, photo-Smiles reaction is triggered by irradiation of light and the substitution takes place through interaction between the ground state cation and anion radicals in pair.

References

1) J. Cornelisse and E. Havinga, *Chem. Rev.*, **75**, 353 (1975).
2) J. Cornelisse, G. P. de Gunst, and E. Havinga, *Adv. Phys. Org. Chem.*, **11**, 225 (1975).
3) D. A. Duddel and J. T. Richards, "Lasers in Chemistry," ed by M. A. West, Elsevier, Amsterdam (1977), pp. 349—353.
4) K. Mutai, S. Kanno, and K. Kobayashi, *Tetrahedron Lett.*, **1978**, 1273.
5) M. Ōki and K. Mutai, *Spectrochim. Acta, Part A*, **25**, 1941 (1969).
6) L. H. Luthjens, *Rev. Sci. Instrum.*, **44**, 1661 (1973); M. Sumitani, Private communication.
7) K. Mutai, *Tetrahedron Lett.*, **1971**, 1125.
8) a) T. Shida, Y. Nosaka, and T. Kato, *J. Phys. Chem.*, **82**, 695 (1978); b) T. Shida, Private communication.
9) K. D. Cadogan and A. C. Albrecht, *J. Phys. Chem.*, **73**, 1868 (1969).
10) S. Ohsawa, *Nippon Kagaku Kaishi*, **1973**, 1486.
11) Migita *et al.* reported that the stretched form molecules were also able to form ion pairs through charge separation by irradiation. (M. Migita, M. Kawai, N. Mataga, Y. Sakata, and S. Misumi, *Chem. Phys. Lett.*, **53**, 67 (1978).)
12) a) S. Nagakura and J. Tanaka, *Bull. Chem. Soc. Jpn.*, **32**, 734 (1959); b) S. Nagakura, *Tetrahedron*, **19**, Suppl. (2), 361 (1963).

Observation of Intramolecular Excimer Emission of Benzyl Radical Pair Produced by Photolysis of [2.2]Paracyclophane

Shun-ichi Ishikawa, Junko Nakamura,† and Saburo Nagakura*

The Institute for Solid State Physics, The University of Tokyo, Roppongi, Minato-ku, Tokyo 106

†*The Institute of Physical and Chemical Research, Wako, Saitama 351*

(Received February 22, 1980)

Photochemistry of [2.2]paracyclophane in glassy solvents at 77 K was studied. With irradiation, a species in which two benzyl radicals are linked together with an ethylene bridge was produced. From the ESR study, the radicals were found to form the benzyl radical pair in harder solvents. The emission spectrum and the emission lifetime of the radical species showed remarkable dependence on the solvent viscosity. In harder solvents, a new broad emission was observed on the longer wavelength side of the structured emission of the benzyl radical. From the studies of the excitation spectrum and the emission lifetime, this broad band was concluded to be the intramolecular excimer fluorescence of the radical pair. The photo-reaction of [2.2]paracyclophane was found to be biphotonic, occurring from a higher triplet state excited *via* the lowest triplet state.

[2.2]Paracyclophane (PC) is a typical molecule for studying the transannular interaction, and its electronic structure was studied by several authors both experimentally and theoretically.[1] Photochemistry of PC is also interesting in connection with its electronic structure. The biradical and the zwitter ion *etc.* were assumed by Helgeson and Cram as photochemical intermediates in the photolysis of PC in solution at room temperature.[2]

We studied the photochemistry of PC in glassy solvent at 77 K. Our main interest was laid on the confirmation of a photo-reaction intermediate, benzyl radical pair, and also on the transannular effect in the emissive state of this species.

Experimental

Materials. PC (the Aldrich Chemical Company) was purified by column chromatography and vacuum sublimation. 2-Methylpentane and 2-methyltetrahydrofuran (Tokyo Kasei) which were used as solvents, were distilled from lithium aluminium hydride. Isopentane (Tokyo Kasei) was used without further purification. The concentration of the sample was about 10^{-3} mol dm^{-3} throughout the experiment except the case of the absorption spectrum (10^{-4} mol dm^{-3}). Solutions were degassed by freeze-pump-thaw cycles. We used 2-methyltetrahydrofuran (MTHF), 2-methylpentane (2-MP), isopentane (IP), and mixed solvents of 2-MP and IP (10:0.3, 10:1, 4:1, 3:2, 1:1, and 3:7) as solvents. IP initially forms glass but gradually becomes snowy at 77 K, while other solvents form clear glass. The viscosities of these solvents at 77 K are greatly different from one another; 3.7×10^{20} cp at 77.5 K for MTHF,[3] 2.4×10^{13} cp at 77.5 K for 2-MP,[3] and $<8.9\times10^{5}$ cp at 77 K for IP.[4]

Absorption Measurements. Ultraviolet and visible absorption spectra of photolysis products of PC were measured with a Cary 14 recording spectrophotometer. For the generation of *p*-methylbenzyl radical from *p*-xylene, a light of fourth harmonics (266 nm) of a YAG laser (Quanta Ray DCR-1) was used as an exciting source, and the absorption spectrum was measured.

ESR Measurements. The ESR spectra were recorded on a JEOL JES-FE-3AX spectrometer. The magnetic field was calibrated by measuring the resonance frequency of ^{1}H NMR.

Emission and Excitation Measurements. Emission spectra of the PC photoproduct were measured by using a 100 W super high-pressure mercury lamp and a Jarrell-Ash 1/4 M monochromator as an exciting system and a Spex 1700-111 monochromator and a Hamamatsu TV R636 photomultiplier as a detecting system. As an exciting source for the excitation spectrum measurement, a 500 W xenone lamp and the Spex monochromator were used.

Emission Lifetime Measurements. A nitrogen laser (Molectron UV24) pumped dye laser (DL-14) and the second harmonic generator (KDP (KH_2PO_4) crystal) were used for the emission lifetime measurement. The excitation wavelengths are 421 nm (*p*-bis(*o*-methylstyryl)benzene), 457 nm (7-diethylamino-4-methylcoumarin), and 322 nm (Rhodamin B and Cresyl Violet Perchlorate/KDP crystal). The duration of pulse is 4—8 ns and the line-width is about 0.01 nm. The emission was observed with a Nikon G-250 monochromator and a Hamamatsu TV R666S photomultiplier.

Results and Discussion

PC in glassy solvents was irradiated at 77 K with the use of 313 nm light of a super high-pressure mercury lamp. Initially green phosphorescence of PC with long lifetime was observed. By continuing irradiation, the yellowish emission with short lifetime was observed instead of the phosphorescence of PC. After irradiation, the glassy solution was colored yellow as observed previously by Bramwell and Gendell.[5] The yellowish emission was also observed by using the longer wavelength light (365, 436 nm) for excitation. The absorption, ESR, emission, and excitation spectra of the species produced by photolysis of PC were measured and analyzed as follows.

Absorption Spectra of PC Photoproduct. By photolysis of PC in glassy solvent at 77 K, a new species was produced and existed stably in the solvent matrix. Absorption spectra of this new species produced at irradiation times of 2, 5, and 8 min in 2-MP were measured with the results shown in Fig. 1. There appear a few peaks in 260—270 nm, distinct peaks in 300—322 nm, and weak but distinct peaks near 450 nm. Kaupp *et al.* reported recently that a new species was produced by photolysis of PC in MTHF at 77 K, the absorption spectrum of which showed peaks near 320 and 450 nm.[6] Their result is consistent with ours except for the wavelength region below 300 nm which was not measured by them.

The observed spectrum consisting of the three bands at 270, 320, and 450 nm is very similar to that of the

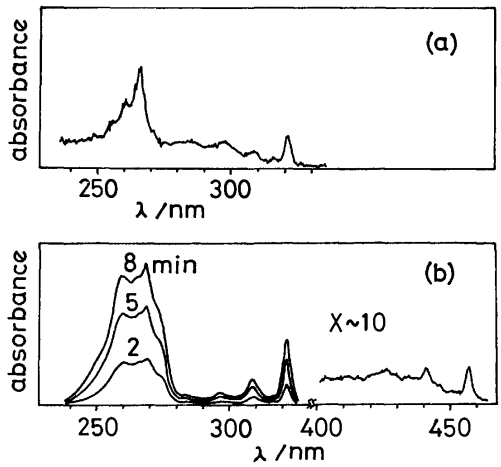

Fig. 1. Absorption spectra of (a) the *p*-methylbenzyl radical produced from *p*-xylene, (b) the PC photoproduct at respective irradiation times (2, 5, and 8 min) in 2-MP at 77 K.

benzyl radical produced from toluene or its methyl derivatives in glassy solvents at 77 K.[7] For the purpose of comparison, the observed absorption spectrum (240—340 nm) of the *p*-methylbenzyl radical produced from *p*-xylene is also shown in Fig. 1. It is evident that a species with the structure very similar to the *p*-methylbenzyl radical is produced by photolysis of PC.

It is reasonable to consider that a C–C ethylene bridge of PC is dissociated at the primary reaction step and a biradical species in which two benzyl radicals are linked together by an ethylene bridge in the *p*-position (·CH_2–C$_6$H$_4$–CH_2–CH_2–C$_6$H$_4$–CH_2·) is produced. This biradical is expected to show the absorption spectrum similar to that of the *p*-methylbenzyl radical in agreement with the above-mentioned observation. This point has been investigated further with the aid of ESR spectroscopy.

ESR Spectra of PC Photoproduct. We measured the ESR spectra of PC photoproduct in glassy solvents at 77 K in order to certify the assignment to a biradical (two benzyl radicals linked with an ethylene bridge) and to elucidate its structure.

In MTHF, 2-MP, and the harder mixed solvents of 2-MP and IP (4:1, 3:2, and 1:1), two signals are observed in the $g \approx 4$ region. One is the signal of PC in the lowest triplet state, and this signal decreases its intensity with the increasing irradiation time (PC decreases by reaction) and decays slowly with the cut-off of exciting light. Its lifetime is the same as the phosphorescence lifetime. The other signal observed in the $g \approx 4$ region increases its intensity with the increasing irradiation time and does not decay with the cut-off of exciting light. The signal can be regarded as due to the $\Delta m=2$ transition of the radical pair in triplet. There are two possibilities for the radical pair. One is that of two benzyl radicals produced from PC, and the other is that of the benzyl radical with a solvent radical which is created by reaction of the radical with solvent. By the following considerations about the reactivity of the radical with solvlent, we confirm that the $\Delta m=2$ signal is due to the radical pair, ·CH_2–C$_6$H$_4$–CH_2–CH_2–C$_6$H$_4$–CH_2·, produced by photolysis of PC, and not owing to the interaction between the benzyl radical and the solvent radical.

The absorption spectrum in each solvent does not change compared with that of the *p*-methylbenzyl radical although small shifts are observed. Consequently, the production of the radical added to the solvent is unconceivable. A possible process of reaction with solvent is the abstraction of hydrogen atom. However, it is known that the benzyl radical produced from toluene does not abstract hydrogen atom from hydrocarbon, and not even from EPA.[8] The low reactivity of benzyl radical is due to the fact that benzyl radical is π-radical and the unpaired electron density at $-CH_2$ is decreased by resonance effect. (According to Hückel MO theory, unpaired electron densities are calculated to be 4/7 on the $-CH_2$ carbon and 1/7 on each of *o*- and *p*-carbons of the benzene ring.)

From the species where unpaired electron densities exist at each *p*-position of two benzyl radicals, the remaining C–C bridge can dissociate and two molecules of quinodimethane can be produced.

CH_2=C$_6$H$_4$·–CH_2–CH_2–C$_6$H$_4$·=CH_2 ⟶

CH_2=C$_6$H$_4$=CH_2 + CH_2=C$_6$H$_4$=CH_2

Kaupp reported that quinodimethane was produced by photolysis of PC in MTHF at 85 K.[9] The reported absorption spectrum of quinodimethane has many peaks below 300 nm[9] but the production of such species could not be detected in our experiment (photolysis at 77 K).

Therefore, the photoproduct of PC is expected to remain as the biradical at 77 K without the abstraction of hydrogen atom from the solvent used here nor the degradation to smaller fragments. It is considered that the biradical with an interaction between the two benzyl radicals was observed as a radical pair in the ESR spectrum. However, there is no strong interaction between the two benzyl radicals in the ground state, because the spectral shape of the absorption spectrum is the same as that of the *p*-methylbenzyl radical produced from *p*-xylene and the spectral shift is fairly small.

In contrast with the case in the $g \approx 4$ region of the ESR spectrum, a signal increases its intensity in the $g \approx 2$ region with the increasing irradiation in all solvents used. The spectra in various solvents are broad and the detailed analysis is difficult, but the following trends can be pointed out.

1. In MTHF, an intense and broad signal in which the splitting of fine structure is about 150 G (1 G=10^{-4} T) is observed together with weak but sharply structured signals. The structured signals are considered to be due to MTHF radical. The origin of the broad signal can be assigned to the radical pair in triplet because of its spectral shape.
2. In 2-MP, only a broad signal the origin of which

can be assigned to the radical pair is observed.
3. The spectral shapes in the 4:1 and the 3:2 mixed solvents of 2-MP and IP are similar to that in 2-MP. In the softer mixed solvent (1:1), a sharp signal overlaps the broad signal. In the 3:7 mixed solvent and in IP, the sharp signal has the rather complicated structure, but it may be partly due to the benzyl radical without the interaction with the other radical linked together. These results observed in the $g \approx 2$ region also support the scheme that a biradical produced by photolysis of PC is forming a benzyl radical pair.

The Structure of the Biradical as Revealed from ESR Spectra. The homolytic cleavage of one of the C–C bridges of PC at the benzyl radical pair formation increases freedom in the motions of the benzyl radicals. Consequently, in soft matrices, the biradical is expected to take an open structure in which the two benzene rings are not parallel but separate from each other. In the hard glassy solvents, however, the molecular motion of the rings is restricted and the biradical takes a structure in which a weak interaction between the two benzyl radicals is effective. From this view, we can expect that the zero-field splitting parameter, D^*, decreases with the increasing softness and the $g \approx 4$ signal disappears in some soft solvents. This expectation is fulfilled by the present observation. The $g \approx 4$ signal is observed in MTHF, 2-MP, and in harder mixed solvents of 2-MP and IP (4:1, 3:2, and 1:1), but cannot in the soft mixed solvent (3:7) and in IP. Furthermore, the D^* value has a tendency to be larger in harder solvents, as is seen in Table 1 in which the D^* values estimated from the positions of the $g \approx 4$ signals are tabulated.

TABLE 1. D^* AND CALCULATED r VALUES OF PC PHOTOPRODUCT

Solvent	D^*/cm^{-1} a)	r/Å b)
MTHF	0.015	5.6
2-MP	0.014	5.7
4 : 1 c)	0.012	6.0
3 : 2 c)	0.013	5.8
1 : 1 c)	0.010	6.4

a) The error is estimated as ± 0.001 cm^{-1}. b) ± 0.2 Å.
c) Mixed solvent of 2-MP and IP.

In a model in which two localized radicals are separated from one another in the distance of r, D^* and r are related by the following equation:

$$D^* = 3/2(g^2\beta^2/r^3).$$

On an assumption of g=2.0023, we calculated r from observed D^* with the aid of the equation. The result is shown in Table 1. With the use of the Hückel MO theory, the center of unpaired electron distribution is calculated to locate on the C–C bond connecting $-CH_2$ and the benzene ring (see Fig. 2). r is considered to correspond approximately to the distance between the centers of unpaired electron distribution in the two benzyl radicals. As the result of cleavage of one of the C–C bridges the two benzene rings of PC gain motional freedom, facing obliquely and rotating about the remaining C–C bridge. In the non-twisted

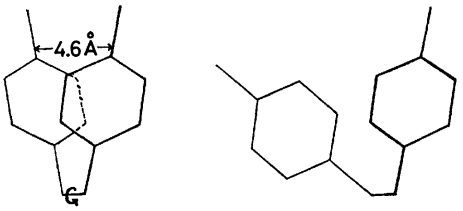

Fig. 2. Structure of the PC photoproduct in glassy solvents.
(a): Non-twisted, (b): twisted.

structure ((a) in Fig. 2), r is estimated to be about 4.6 Å. From the observed r, the two benzene rings are considered to take the twisted structure ((b) in Fig. 2). In harder solvents, the r value is smaller and this suggests that the twist angle is smaller compared with the case in softer solvents. In the 3:7 mixed solvent and in IP, the two benzyl radicals must be separated largely, so that the signal cannot be observed because of the scarce interaction.

Hope *et al.* mentioned that the better fittings of crystal structure analysis was attained for PC by assuming a small twist of two benzene rings.[10] Andrews and Westrum suggested that from an anomaly in the heat capacity (C_p) near 50 K, the twisting motion became an active vibrational mode over 50 K.[11] These facts indicate that the two benzene rings may twist after cleavage of a C–C bridge.

Emission Spectra of PC Photoproduct. The benzyl radical produced from toluene or its methyl derivatives exhibits green emission and its spectrum is sharply structured. Kaupp *et al.* mentioned that the emission of PC photoproduct was similar to that of the *p*-methylbenzyl radical, and that the excimer-like emission was not observed.[6] However, in the present experiment new excimer emission of the benzyl radical pair produced from PC was observed in some solvents.

The emission spectra of PC photoproduct in MTHF, 2-MP, IP, and in mixed solvents of 2-MP and IP are shown in Fig. 3. The emission spectrum in IP is similar in the vibrational structure to that of the benzyl radical monomer produced from toluene. The excitation spectrum of the emission is the same as the absorption spectrum of benzyl radical, and this emission is caused by the excitation of either of the two benzyl radicals produced from one PC molecule.

In solvents harder than IP, a broad emission overlaps a monomer-like emission. Especially in 2-MP and MTHF, a clear peak appears in the longer wavelength region. Because of the appearance of the new band, the emission in 2-MP and in MTHF becomes yellow rather than green. The excitation spectrum measured by monitoring the sharp band is the same as the absorption spectrum, and that measured by monitoring only the broad band component (>600 nm) also exhibits the peaks around 320 nm and 450 nm, and is the same as the absorption spectrum. Therefore, the origin of the broad band is also the benzyl radical, and not the reaction product of PC with solvent. The new broad emission is considered to be caused by the interaction in the excited state between two benzyl radicals linked with the ethylene bridge.

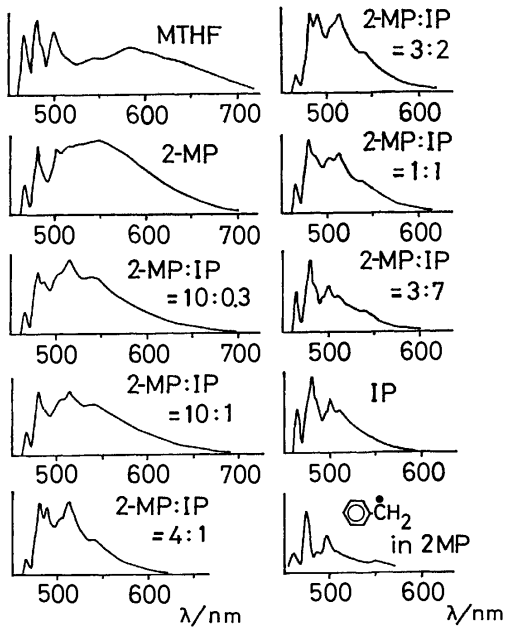

Fig. 3. Emission spectra of the benzyl radical in 2-MP and of the PC photoproduct in MTHF, 2-MP, IP, and mixed solvents of 2-MP and IP (10:0.3, 10:1, 4:1, 3:2, 1:1, and 3:7).

Both the sharp band and the broad band show single exponential decay and their decay constants are equal to each other. Furthermore they are independent of excitation wavelengths. The rise time of the broad emission is too short to be observed within the exciting pulse duration, 4 ns. These kinetic results are consistent with the case of ordinary intramolecular excimer in solution where there exists rapid equilibrium between the excited monomer state and the excimer state. Therefore, it is reasonable to consider that the broad emission observed in 2-MP and MTHF is the intramolecular excimer fluorescence of the benzyl radical pair.

The peak of the excimer band is 580 nm in MTHF and 550 nm in 2-MP. In softer solvents, the excimer band moves toward the monomer band, although the peak wavelength of excimer band cannot be determined unambiguously. This may indicate that the stabilization energy of excimer is larger in harder solvents.

The emission lifetimes of PC photoproduct in several solvents are shown in Table 2 in the decreasing order of solvent viscosity. The emission lifetime in IP is about 1.1 μs, and the emission lifetime of the benzyl radical produced from toluene is reported to be 1.28 μs in EPA.[7d] In IP, the emitting species is the benzyl radical without the interaction with the other radical, and the lifetime in IP may become similar to that of monomer. The emission lifetimes in solvents harder than IP are shorter (see Table 2). A possible reason for this is that the recombination of the two benzyl radicals is enhanced in harder solvents. In harder solvents, the two radicals are located in the closer position (from the ESR study). The probability of the recombination process from the excited states of radical (monomer or excimer) may be larger in harder solvents, and the emission lifetime of radical may be more shortened.

Table 2. Emission lifetime of PC photoproduct

Solvent	Lifetime/ns[a]
MTHF	55
2-MP	350
3 : 7[b]	560
IP	1100

a) The values cited are typical ones of several experiments. They are not always reproducible, depending on the condition of radical formation, *e.g.* irradiation time. b) Mixed solvent of 2-MP and IP.

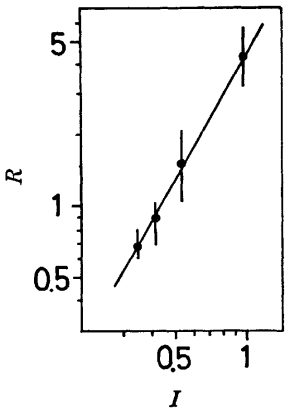

Fig. 4. Dependence of reaction rate, *R*, upon the intensity of exciting light, *I*.

Light Intensity Dependence of Reaction Rate. The absorbance at 322 nm of the PC photoproduct (biradical) increases at the initial stage linearly with irradiation time, and the initial reaction rate for the formation of the biradical can be determined. Figure 4 shows the dependence of this reaction rate, *R*, upon the exciting light intensity, *I*. The log-log plot of *R vs. I* shows a straight line, the slope of which is 1.8. This suggests the biphotonic mechanism for the formation of the biradical from PC. Therefore the photolysis of PC does not occur directly from the lowest excited state, S_1 or T_1, because of the energy deficiency. In the rigid media at low temperature, T_1 has a long lifetime (a few seconds). The higher triplet states which are populated by photon absorption of T_1 have sufficient energy for the photolysis of PC.

According to our previous paper on the $T_n \leftarrow T_1$ absorption spectrum of PC,[1b] we have a very weak band around 550 nm ($T_3 \leftarrow T_1$), an intense band around 380 nm ($T_4 \leftarrow T_1$), and a weak band around 340 nm ($T_5 \leftarrow T_1$). The 313 nm excitation corresponds to the $T_5 \leftarrow T_1$ transition the parentage of which is the local excitation corresponding to the $^3E_{2g}^- \leftarrow {}^3B_{1u}^+$ transition of the benzene ring. Therefore the locally excited T_5 state is considered to be the reactive state. Helgeson and Cram reported the wavelength-dependent photochemistry of PC in alcoholic solutions.[2] From the analysis of photoproducts at various exciting wavelengths, they proposed that the biradical composed of two benzyl radicals was produced only by the exciting light the wavelength of which is shorter than 230 nm, and that the zwitter ion (benzyl cation and

anion) is produced by the excitation with 253.7 nm light. Their suggestion that the biradical is produced from higher excited states with sufficient energy is consistent with our conclusion.

The authors should like to express their sincere thanks to Dr. Hisaharu Hayashi, the Institute of Physical and Chemical Research, for his kind advice in measuring ESR spectra.

References

1) a) S. Iwata, K. Fuke, M. Sasaki, S. Nagakura, T. Otsubo, and S. Misumi, *J. Mol. Spectrosc.*, **46**, 1 (1973); b) S. Ishikawa, J. Nakamura, S. Iwata, M. Sumitani, S. Nagakura, Y. Sakata, and S. Misumi, *Bull. Chem. Soc. Jpn.*, **52**, 1346 (1979); and the references cited therein.

2) R. C. Helgeson and D. J. Cram, *J. Am. Chem. Soc.*, **88**, 509 (1966).

3) A. C. Ling and J. E. Willard, *J. Phys. Chem.*, **72**, 1918 (1968).

4) J. R. Lombardi, J. W. Raymonda, and A. C. Albrecht, *J. Chem. Phys.*, **40**, 1148 (1964).

5) F. B. Bramwell and J. Gendell, *J. Chem. Phys.*, **58**, 420 (1973).

6) G. Kaupp, E. Teufel, and H. Hopf, *Angw. Chem. Int. Ed. Engl.*, **18**, 215 (1979).

7) a) G. Porter and E. Strachan, *Spectrochim. Acta*, **12**, 299 (1958); b) G. Porter and M. I. Savadatti, *Spectrochim. Acta*, **22**, 803 (1966); c) P. M. Johnson and A. C. Albrecht, *J. Chem. Phys.*, **48**, 851 (1968); d) T. Okamura and I. Tanaka, *J. Phys. Chem.*, **79**, 2728 (1975).

8) I. Norman and G. Porter, *Proc. R. Soc. London, Ser. A*, **230**, 399 (1955).

9) G. Kaupp, *Angw. Chem. Int. Ed. Engl.*, **15**, 442 (1976).

10) H. Hope, J. Bernstein, and K. N. Trueblood, *Acta Crystallogr., Sect. B*, **28**, 1733 (1972).

11) J. T. S. Andrews and E. F. Westrum, Jr., *J. Phys. Chem.*, **74**, 2170 (1970).

 © 1980 The Chemical Society of Japan Bull. Chem. Soc. Jpn., 53, 2481—2488 (1980)

Electronic Structure of Transition Metal Complexes II. Trans Influence in Ammine Complexes of the First Transition Metals

Eiko KAI, Tomoko MISAWA, and Kichisuke NISHIMOTO*

Department of Chemistry, Faculty of Science, Osaka City University, Sumiyoshi-ku, Osaka 558

(Received March 19, 1980)

CNDO/2 calculations of pentaammine complexes, $[M(NH_3)_5X]$ (both low and high spin states), where M= Co^{2+}, Co^{3+}, Fe^{2+}, and Fe^{3+}, and X=FH, OH_2, CO, NH_3, pyridine, OH^-, F^-, and CN^-, have been carried out in order to investigate the mutual influence between ligands. The present calculation shows that the σ-type mutual influence is remarkably affected by the oxidation number and the spin state of the metal ion and scarecely affected by the number of d electron (d electron configuration). Furthermore, the calculated results show the metal-ligand bond distance of a complex in the low spin state should be shorter than that in the high spin state.

Many experimental evidences of the trans influences in the transition metal complexes have been found in the field of inorganic chemistry from long time ago. Most of them were found at Pt complexes.[1] Recently, some experimental works have been done about the trans influence in the first transition metal complexes.[2] Shustorovich *et al.* carried out quantum chemical calculations in order to solve this problem.[3] They applied the perturbation theory based on the simple MO method to several types of complexes.

In this paper, we have investigated the trans influences in the various pentaammine complexes, $[M(NH_3)_5X]$ (both low and high spin states) where M=Co^{2+}, Co^{3+}, Fe^{2+}, and Fe^{3+}, and X=FH, OH_2, CO, NH_3, pyridine(py), OH^-, F^-, and CN^-, using CNDO/2 method. We have studied how the trans influence is affected by the oxidation number and the spin state of the metal ion and the kinds of metals and ligands.

Calculations

In the previous paper,[4] we proposed new bonding parameters associated with 4s and 4p AO's of the first transition metals in the CNDO/2 method, which give satisfactory results for the binding energies of coordination bonds of various hexaammine and hexaaqua complexes. In the present study, we have carried out CNDO/2 calculations (unrestricted SCF scheme) of pentaammine complexes (see Fig. 1) using these new parameters.

We take five neutral ligands, FH, OH_2, CO, NH_3, and py, and three ionic ones, OH^-, F^-, and CN^- into consideration. In coordination chemistry, the spin state of the transition metal complex has an important role in its physico chemical properties. Therefore, we have also calculated the electronic structure of the complexes in the low and high spin states.

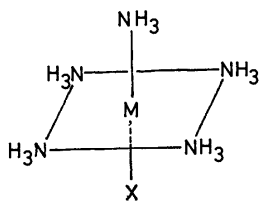

Fig. 1. Pentaammine complexes, where M=Co^{2+}, Co^{3+}, Fe^{2+}, and Fe^{3+}, X=FH, OH_2, CO, NH_3, py, OH^-, F^-, and CN^-.

We used the experimental data for Co–N distances, 2.11 Å(Co^{2+}–N)[5] and 1.97 Å(Co^{3+}–N),[6] and estimated ones for Fe–N distances, 2.15 Å(Fe^{2+}–N)[4] and 2.00 Å (Fe^{3+}–N). We have employed the experimental geometry[7] of the free molecule for that of the ligand. For the simplicity, we have put the distance of M–X bond same as that of M–N bond, that is ,we assumed a regular octahedral geometry for each complex.

Results and Discussion

The mutual influence between the trans ligands is not affected only by the characteristics of the ligand such as the ionization potential, electron affinity *etc.*, but also by the electronic structure of the central metal ion such as the oxidation number, the spin state and the number of d electrons. The mutual influence should be appeared in the charge densities of the central metal ion and the ligands and the bond orders between the metal and the ligands. The charge distribution in the complex reflects sharply the characteristics of the ligand and the central metal ion. However, it is difficult to measure experimentally the change of the charge density on the atom caused by trans influence. Many experimental evidences[2] of the mutual influence have been found by the measurement of bond distances between the metal and the ligands. However, the charge density on the atom is important for the discussion of the reactivity of the complex. Therefore, we will discuss the mutual influence from the standpoint of both the charge density and the bond order.

The most important factors affecting on the mutual

Table 1. Orbital energies of the isolated ligands

$\varepsilon^X_{HOMO}(\sigma)$/a.u.		$\varepsilon^X_{HOMO}(\pi)$/a.u.		$\varepsilon^X_{LUMO}(\pi)$/a.u.	
CN^-	−0.0365	CN^-	−0.2026	CN^-	0.7924
F^-	−0.0651	py	−0.5314	CO	0.1953
OH^-	−0.0941	CO	−0.7736	py	0.1293
py	−0.4773				
NH_3	−0.6022				
CO	−0.6346				
OH_2	−0.7127				
FH	−0.8493				

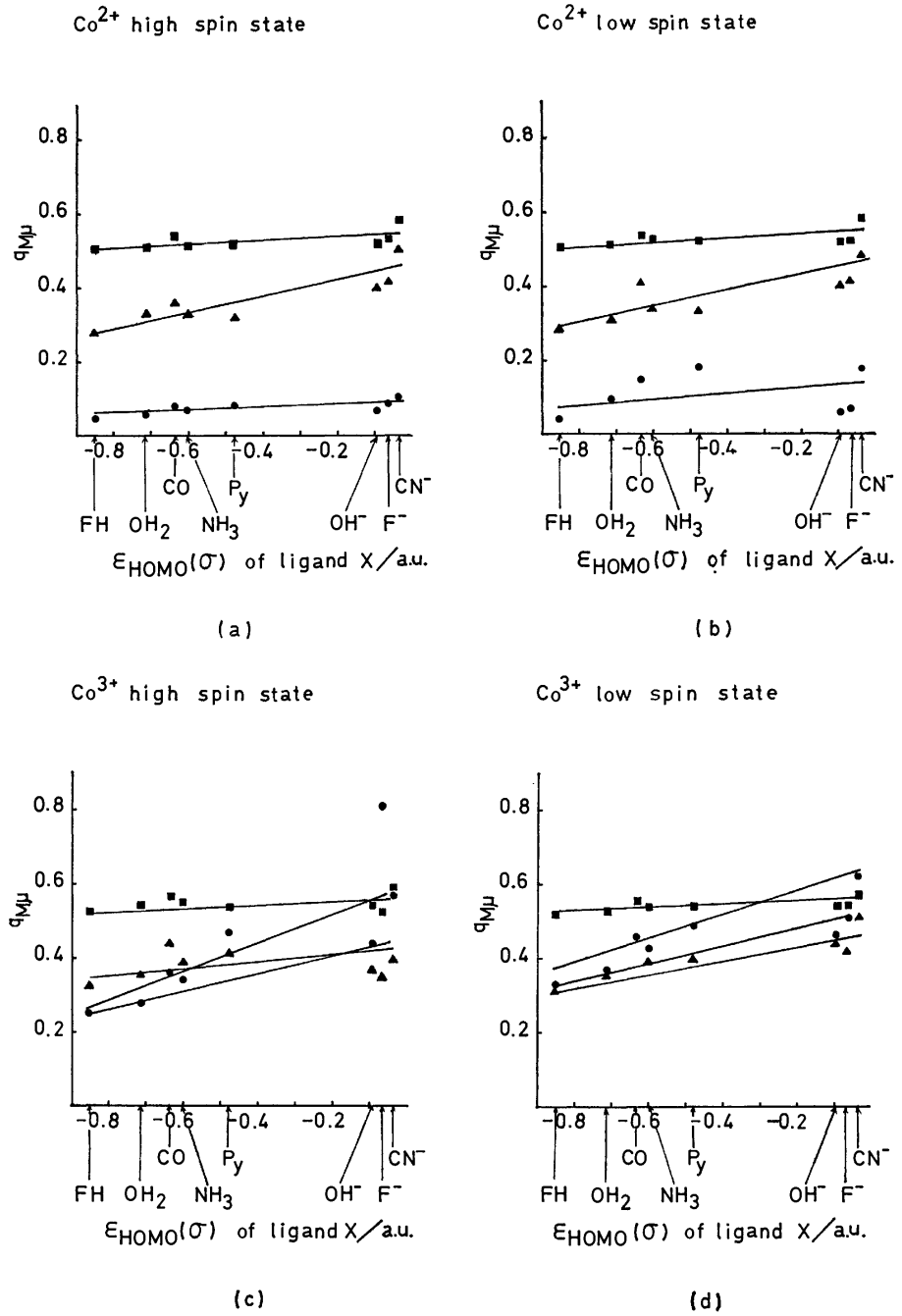

Fig. 2. The charge densities associated with 4s, $4p_z$, and $3d_{z^2}$ orbitals of cobalt.
(a): Co^{2+} (high spin), (b): Co^{2+} (low spin), (c): Co^{3+} (high spin), (d): Co^{3+} (low spin).
Marks; ●: $3d_{z^2}$, ■: 4s, ▲: $4p_z$.

influence are the ionization potential and the electron affinity of the ligand, so that, in Table 1 the highest occupied and the lowest unoccupied orbital energies of isolated ligands calculated by the CNDO/2 method are given as a reference.

Charge Density. From the chemical intuition, we expect the 4s, $4p_z$, $3d_{z^2}$, $3d_{xz}$, and $3d_{yz}$ orbitals of metal ion make the most important contribution to the trans influence. Our results show that only the variations of the charge densities associated with these orbitals are considerably large and others are negligible when ligand X is varied. Figures 2(a)—(d) show the plots of the charge densities associated with 4s, $4p_z$, and $3d_{z^2}$ orbitals of cobalt (Co^{2+} and Co^{3+}) against the highest occupied orbital energy of the ligand X, $\varepsilon^{X}_{HOMO}(\sigma)$.

From these figures, it is found that the charge density associated with $4p_z$ orbital is varied largely at the bivalent metals, while the charge density associated with $3d_{z^2}$ orbital is changed remarkably at the tervalent metals. The reason for this may be due to the following facts. In the bivalent metal, two 4s electrons are removed, so that the electrons come back to 4s and 4p orbitals by the formation of com-

plex. Because the coordination bond is largely polarized, the contribution of $4p_z$ orbital to this bond should be large. This might be the reason why the variation of population of $4p_z$ with respect to the change of the ligand is large. In the tervalent metal, the third electron is removed from 3d orbital. Therefore, by the formation of the complex, an electron comes back at first to 3d orbital. $3d_{z^2}$ orbital contributes largely to the coordination bond, X–M–N, formed by the trans ligands and the metal, but other d orbitals contribute slightly. Consequently, the variation of the population in $3d_{z^2}$ orbital is largely varied by the trans influence.

In tervalent metal complexes, when we plot the charge density associated with $3d_{z^2}$ orbital against $\varepsilon^{X}_{HOMO}(\sigma)$, we obtain two lines. One of them contains py, CO, and CN^-, and another line contains FH, OH_2, NH_3, OH^-, and F^-. The ligands belonging to the former have unoccupied π-orbitals, however, those belonging to the latter no unoccupied π-orbitals. These π-orbitals will affect $3d_{z^2}$ orbital indirectly through the interaction with $3d\pi$ orbital.

The tendency of the charge density variation of the iron (Fe^{2+} or Fe^{3+}) complex (Figs. 3(a)—(d)) is

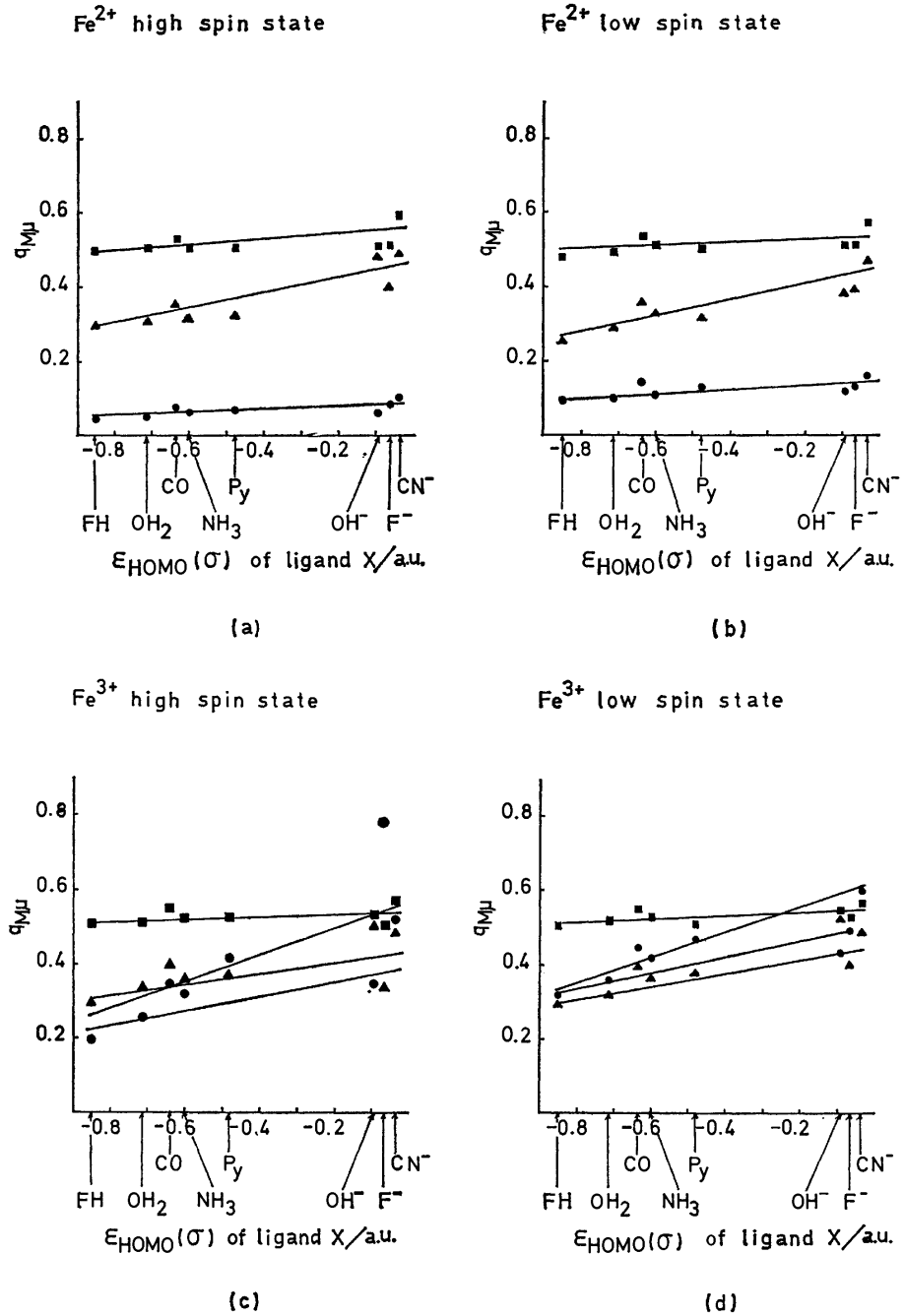

Fig. 3. The charge densities associated with 4s, $4p_z$, and $3d_{z^2}$ orbitals of iron.
(a): Fe^{2+} (high spin), (b): Fe^{2+} (low spin), (c): Fe^{3+} (high spin), (d): Fe^{3+} (low spin).
Marks: see Fig. 2.

similar to that of the corresponding cobalt complex.

Comparing the calculated charge densities of Co complex with those of the corresponding Fe complex (*cf.* Figs. 2(a)—(d) and Figs. 3(a)—(d)), we conclude that the charge population at the central metal ion is determined mainly by the oxidation and spin states of the complex.

Bond Order. The total bond order associated with the metal-ligand bond is consisted of the contributions of various orbital pairs. In Table 2, all possible orbital pairs are given. Similar to the results of charge density as mentioned above, the contributions of the particular pairs of orbitals to the trans influence are important, while those associated with other orbital pairs are negligibly small.

First of all, let us investigate about σ-type interac-

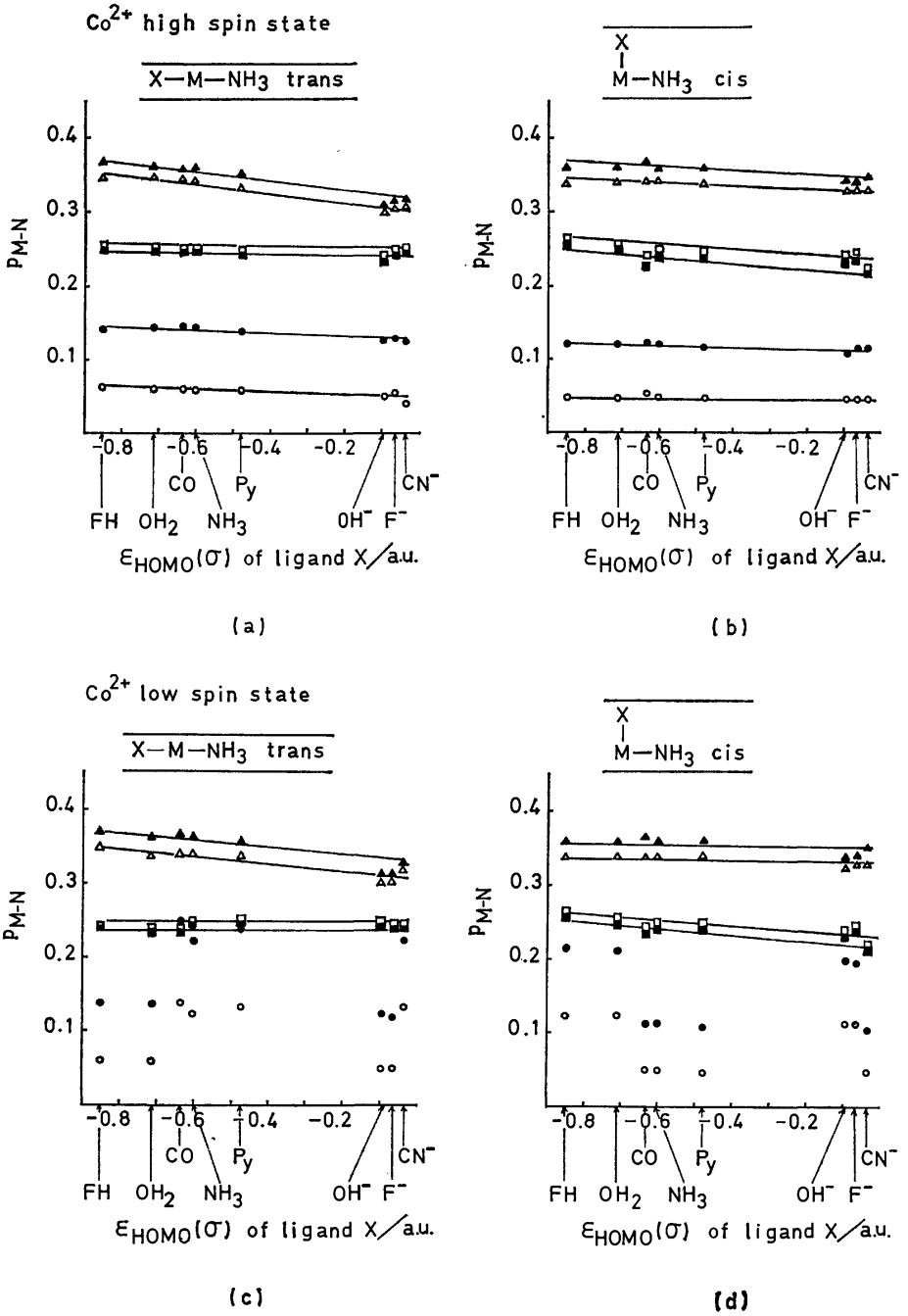

Fig. 4. The bond orders associated with various orbital pairs of M–N bond in bivalent cobalt complex.

(a): Co^{2+}–*trans*N (high spin), (b): Co^{2+}–*cis*N (high spin), (c): Co^{2+}–*trans*N (low spin), (d): Co^{2+}–*cis*N(low spin).

Marks;

M–*trans*N bond—○: $3d_{z^2}$-2s, ●: $3d_{z^2}$-$2p_z$, □: 4s-2s, ■: 4s-$2p_z$, △: $4p_z$-2s, ▲: $4p_z$-$2p_z$.

M–*cis*N bond—○: $3d_{x^2-y^2}$-2s, ●: $3d_{x^2-y^2}$-$2p_x$, □: 4s-2s, ■: 4s-$2p_x$, △: $4p_x$-2s, ▲: $4p_x$-$2p_x$.

tion between the metal and the ligand. In this case, the ligand acts as an electron donor, so that $\varepsilon^{X}_{HOMO}(\sigma)$ plays a key role. Figures 4(a)—7(d) show the plots of the bond orders associated with all possible orbital pairs against $\varepsilon^{X}_{HOMO}(\sigma)$. It is interesting to note that the gross feature of the figure of Co^{n+} at the high spin state or Co^{n+} at the low spin state is very similar to that of the corresponding Fe complex (see *cf.* Figs. 4(a) and 6(a)). Consequently, we can say that in Fe and Co complexes the nature of the coordination bond is determined mainly by the oxidation number and the spin state (low or high), but is not by the number of d electrons of the metal. It is well known that Fe, Co, and Ni form similar complexes, so that they are called a triad. Actually, our calculation shows the electronic states of Fe and Co complexes resemble each other.

In the bivalent metal complexes, the bond orders pertaining to $4p_z$ orbital are prominently varied by the trans ligand X. Figures 4(a)—(d) show that the bond orders associated with $4p_z$-$2p_z$ and $4p_z$-2s pairs are decreased with the increase of $\varepsilon^{X}_{HOMO}(\sigma)$.

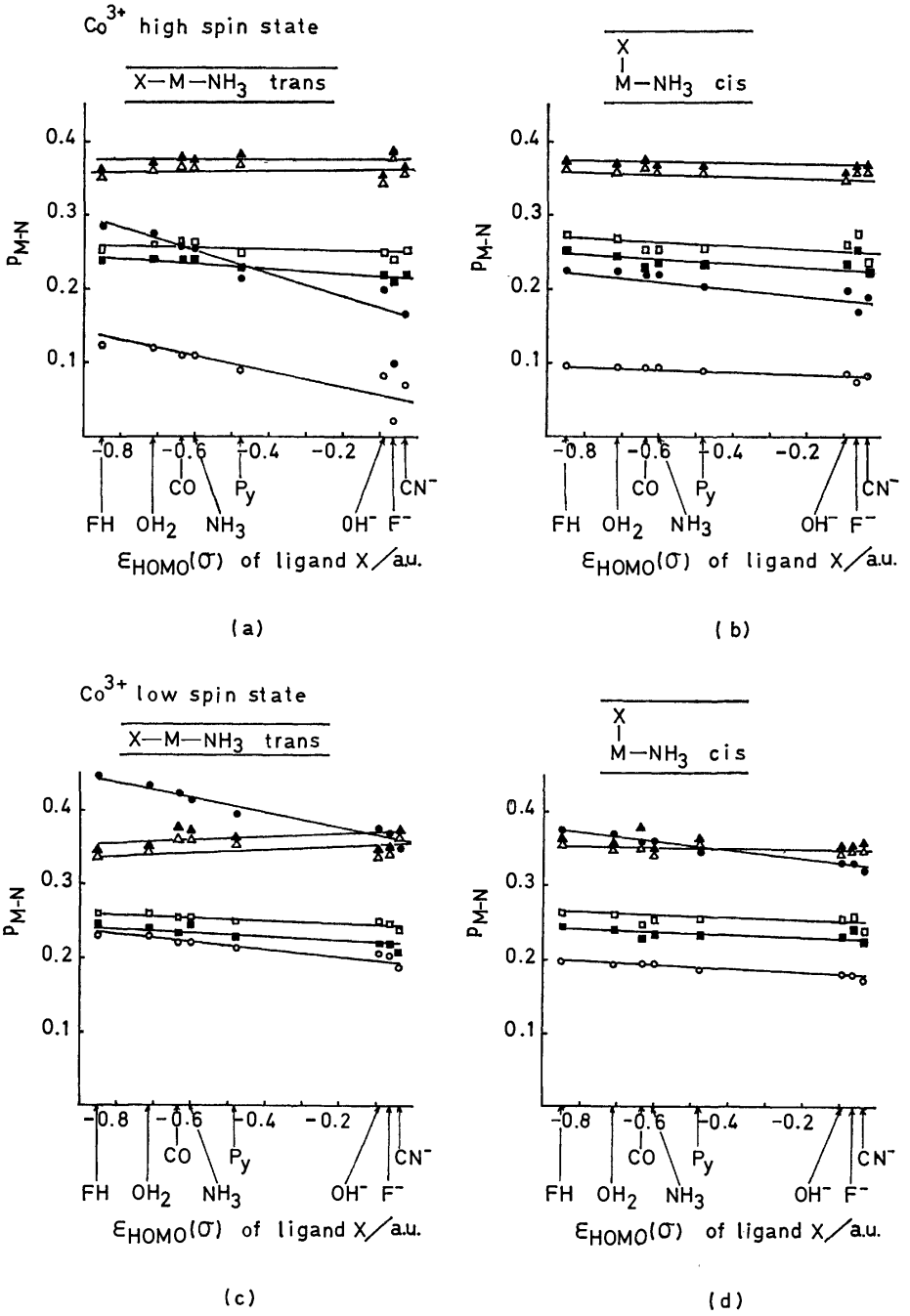

Fig. 5. The bond orders associated with various orbital pairs of M–N bond in tervalent cobalt complex.
(a): Co^{3+}–*trans*N (high spin), (b): Co^{3+}–*cis*N (high spin), (c): Co^{3+}–*trans*N (low spin), (d): Co^{3+}–*cis*N (low spin).
Marks: see Fig. 4.

This result can be understood from the standpoint of the simple MO theory. Let us consider the coordination bond X–M–N. The orbital energy, α_M, associated with metal's AO increases when $\varepsilon^X_{HOMO}(\sigma)$ is increased. Second order perturbation theory calculates this increase, $\Delta\alpha_M$, by the following equation,

$$\Delta\alpha_M = \frac{\beta_{MX}^2}{\alpha_M^0 - \varepsilon^X_{HOMO}(\sigma)}$$

where α_M^0 is the orbital energy of metal's AO in the hexaammine complex. The increase of $\Delta\alpha_M$ causes the decrease of bond order, Δp_{MN}, associated with M–N bond in the following manner,

$$\Delta p_{MN} \simeq -p_{MN}^0 \frac{\Delta\alpha_M(\alpha_M^0 - \alpha_N^0)}{4\beta_{MN}^2} = k\Delta\alpha_M,$$

where $k = -\frac{p_{MN}^0(\alpha_M^0 - \alpha_N^0)}{4\beta_{MN}^2}$ (<0) and α_N^0 is the orbital energy of the lone pair of ligand NH_3. p_{MN}^0 means the bond order of M–N bond in the hexaammine complex. On the other hand, the change of the bond order, Δp_{MX}, associated with M–X bond can be written by

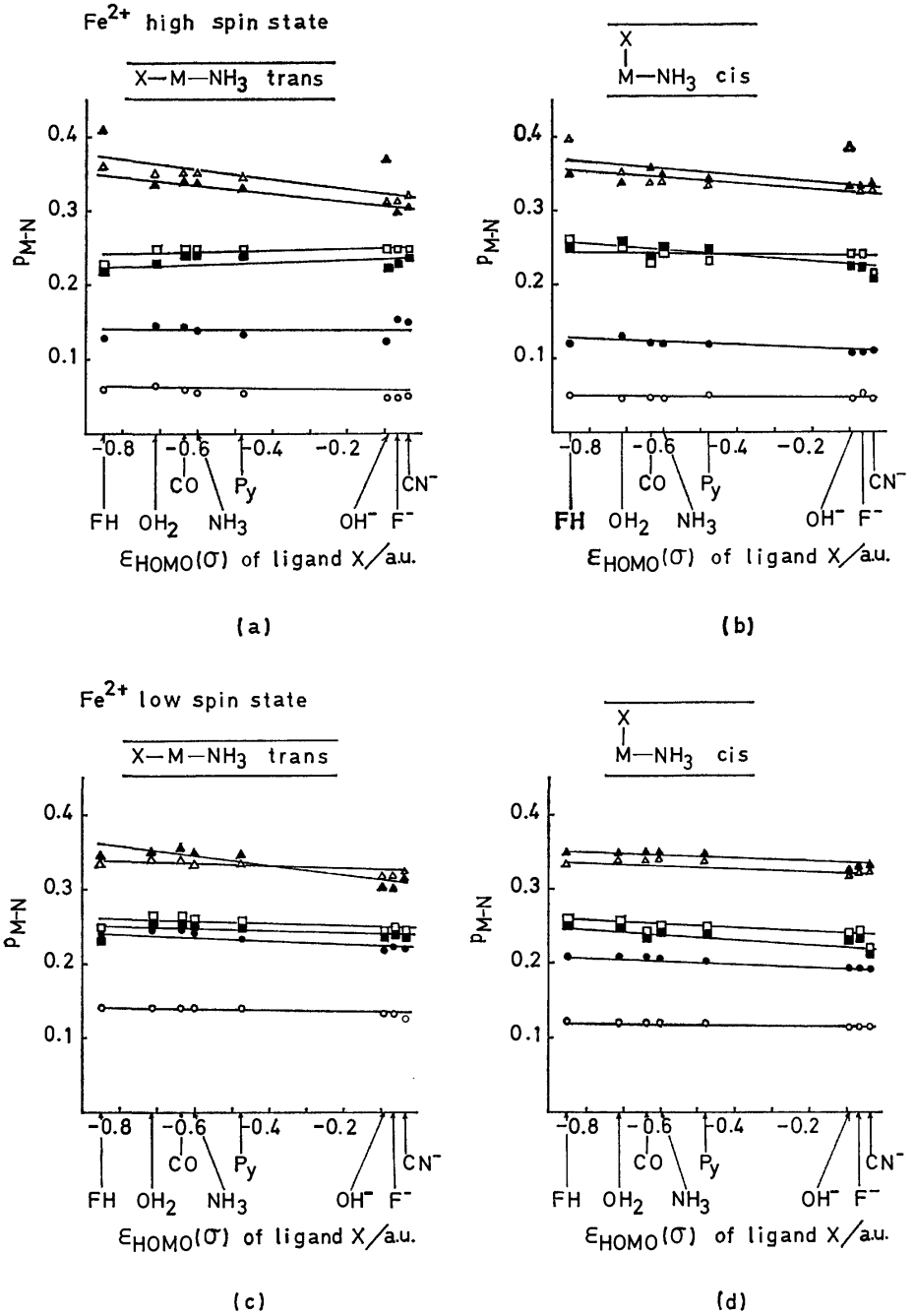

Fig. 6. The bond orders associated with various orbital pairs of M–N bond in bivalent iron complex.
(a): Fe^{2+}–*trans*N (high spin), (b): Fe^{2+}–*cis*N (high spin), (c): Fe^{2+}–*trans*N (low spin), (d): Fe^{2+}–*cis*N (low spin).
Marks: see Fig. 4.

$$\Delta p_{MX} \simeq p_{MN}{}^{0}\frac{\Delta\alpha_X(\alpha_M{}^{0}-\varepsilon^{X}_{HOMO}(\sigma))}{4\beta_{MX}{}^{2}}$$

because of $\Delta\alpha_X=\Delta\varepsilon^{X}_{HOMO}(\sigma)=\varepsilon^{X}_{HOMO}(\sigma)-\alpha_N{}^{0}=-\Delta\alpha_M$. Therefore, the bond order associated with M–N bond is decreased, when that associated with M–X bond is increased. In other words, when M–X bond is strengthened, the M–N bond is weakened.

It should be noted that the bond order associated with $3d_{z^2}$-$2p_z$ and $3d_{z^2}$-2s pairs are almost constant against the variation of $\varepsilon^{X}_{HOMO}(\sigma)$. This result is consistent with the charge variation of the bivalent metal ion. That is, in the bivalent metal complex, $4p_z$ orbital plays more important role than $3d_{z^2}$ orbital.

It is of interest to consider the effect of the spin state on the trans influence. M–*trans*N bond is greatly affected by the spin state of the metal (see Figs. 6(a) and (c)). Namely, the bond order associated with M–*trans*N bond in the low spin state is much larger than that in the high spin state. In other words, the bond distance of M–*trans*N bond in the low spin state is shorter than that in the high spin state. This

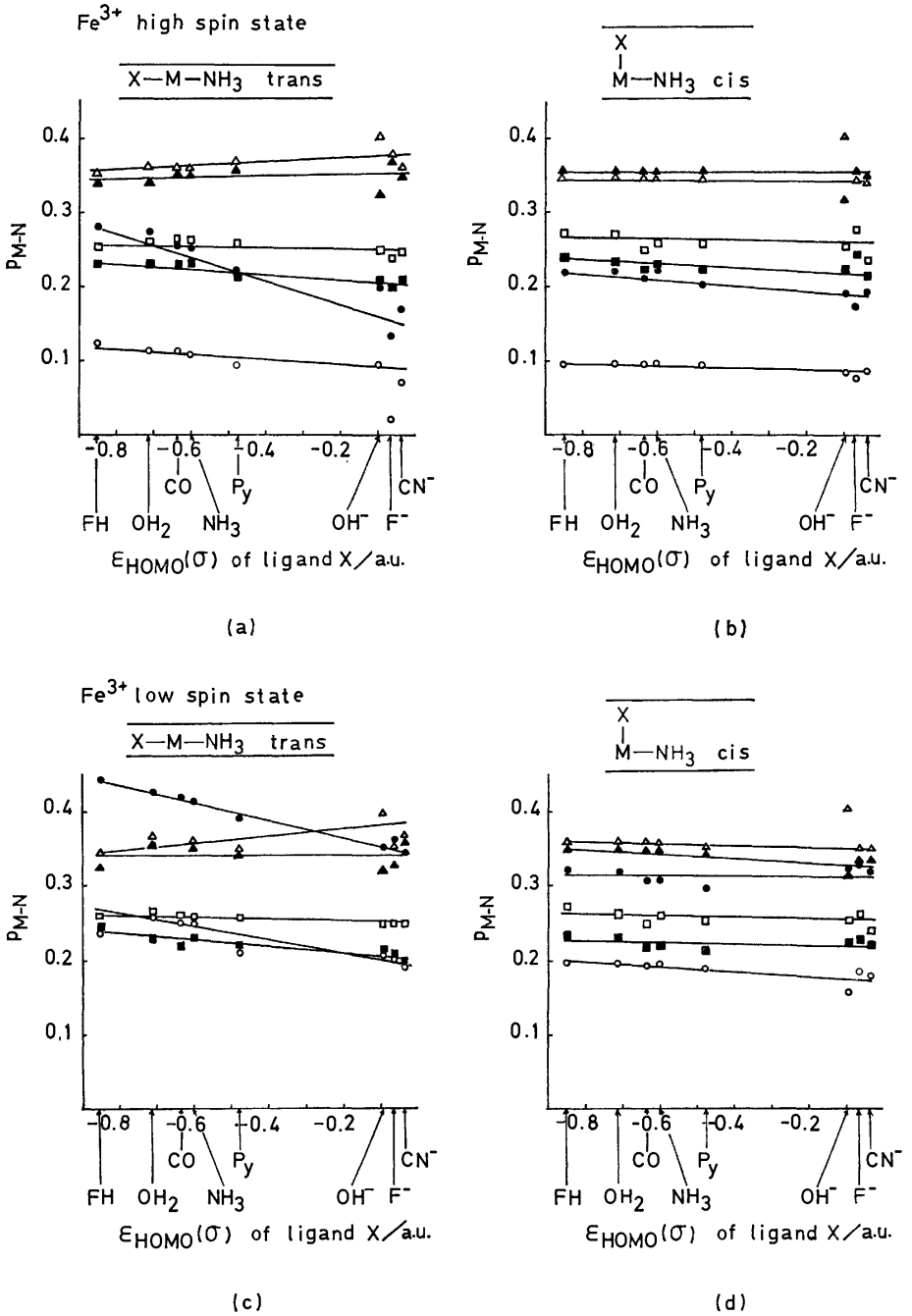

Fig. 7. The bond orders associated with various orbital pairs of M–N bond in tervalent iron complex.
(a): Fe^{3+}–*trans*N (high spin), (v): Fe^{3+}–*cis*N (high spin), (c): Fe^{3+}–*trans*N (low spin), (d): Fe^{3+}–*cis*N (low spin).
Marks: see Fig. 4.

Table 2. The various orbital pairs contributing to M-N bond

σ-Type interaction	
M-*trans*N	M-*cis*N
$4s-2s$	$4s-2s$
$4s-2p_z$	$4s-2p_x$
$4p_z-2s$	$4p_x-2s$
$4p_z-2p_z$	$4p_x-2p_x$
$3p_{z^2}-2s$	$3d_{x^2-y^2}-2s$
$3d_{z^2}-2p_z$	$3d_{x^2-y^2}-2p_x$

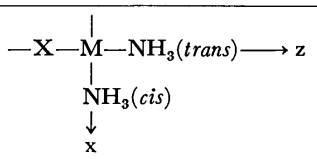

is in accord with the experiment.[8] In M–*cis*N bond, the effect of the ligand X is very small (see Figs. 4(b) and (d)).

In the M–*trans*N bond, the variation of the bond order associated with $4p_z$-2s or $4p_z$-$2p_z$ is large, but that associated with 4s-2s or 4s-$2p_z$ is rather small. Whereas, in the M–*cis*N bond, that associated with 4s-2s or 4s-$2p_x$ is considerably large (see Figs. 4(a) and (b)). From these results, we might conclude that when a p-character of M–*trans* ligand bond increases, that of M–*cis* ligand bond decreases, so that the s-character of M–*cis* ligand bond should increase and *vice versa*. In other word, when the bond distance of M–*trans* ligand bond increases, that of M–*cis* ligand bond becomes to decrease, if the contribution of $3d_{z^2}$ orbital is unchanged. This rule can be applied to the bivalent metal complexes, because the contribution of $3d_{z^2}$ orbital is very small. However, in the tervalent metal complexes, the contribution of $3d_{z^2}$ orbital is rather large, so that this rule may not be applied.

In the tervalent metal complexes, the contribution of each orbital pair to M–*trans*N bond is much complicated (see Figs. 5(a)—(d)). The bond order associated with M–*cis*N bond is also varied considerably by the change of the spin state (see Figs. 5(b) and (d)). An interesting result is that the bond order associated with $3d_{z^2}$-$2p_z$ is increased with the decrease of $\varepsilon^{x}_{\mathrm{HOMO}}(\sigma)$, while, that associated with $4p_z$-$2p_z$ is decreased. The bond order associated with M–*trans*N bond in the low spin state is larger than that in the high spin state. It is interesting to note that the contribution of $4p_z$-$2p_z$ pair to M–*trans*N bond in the low or the high spin state is almost same, but the contribution of $3d_{z^2}$-$2p_z$ or $3d_{z^2}$-2s in the low spin state is almost double of that in the high spin state. Therefore, we expect that the bond distance of M–*trans*N bond in the low spin state is shorter than that in the high spin state, and also that of M–*cis*N bond in the low spin state is shorter than that in the high spin state.

Let us consider, next, π-type influence in a complex. The ligands FH, OH_2, NH_3, OH^-, and F^- have no unoccupied π-orbitals. On the other hand, CO, py and CN^- have unoccupied π-orbitals which can accept charge from the central metal ion. Therefore, we will find some differences between the bond order p_{MX} associated with the former ligand and that associated with the latter ligand. However, the change of p_{MN} against $\varepsilon^{x}_{\mathrm{HOMO}}(\pi)$ of the ligand X is very small, because NH_3 has no available π-orbital. Thus, the ligand X having unoccupied π-orbitals has an effect on the charge density variation of the central metal ion, but no effect on the bond order of M–N bond.

The authers would like to express their gratitude to the Data Processing Center of Kyoto University for the use of the FACOM M190 computer.

References

1) a) S. S. Batsanov, *Zh. Neorg. Khim.*, **2**, 2553 (1957); b) S. S. Batsanov, *J. Inorg. Chem. (U.S.S.R.)*, **4**, 773 (1959); c) J. A. Wunderlich and D. P. Mellor, *Acta Crystallogr.*, **7**, 130 (1954); d) J. A. Wunderlich and D. P. Mellor, *ibid.*, **8**, 57 (1955); e) G. B. Bakii and G. A. Kukina, *Akad. Nauk S.S.S.R. Krist.*, **2**, 400 (1957).

2) a) S. F. A. Kettle, *Coord. Chem. Rev.*, **2**, 9 (1967); b) V. I. Nefedov and Yu. A. Buslaev, *Zh. Neorg. Khim.*, **18**, 3163 (1973).

3) a) E. M. Shustorovich, M. A. Porai-Koshits, and Yu. A. Buslaev, *Coord. Chem. Rev.*, **17**, 1 (1975); b) E. M. Shustorovich, *J. Am. Chem. Soc.*, **100**, 7513 (1978); c) E. M. Shustorovich and P. A. Dobosh, *J. Am. Chem. Soc.*, **101**, 4090 (1979).

4) E. Kai and K. Nishimoto, *Int. J. Quantum Chem.*, **16** (1980) in press.

5) N. E. Kime and J. A. Ibers, *Acta Crystallogr., Sect. B*, **25**, 168 (1969).

6) D. W. Meek and J. A. Ibers, *Inorg. Chem.*, **9**, 465 (1970).

7) "Tables of Interatomic Distances and Configuration in Molecules and Ions," ed by L. E. Sutton, The Chem. Soc., London (1965).

8) M. Mikami, M. Konno, and Y. Saito, *Acta Crystallogr., Sect. B*, **36**, 275 (1980).

Resonance Raman Spectra of Intermolecular Vibrations of Würster's Cation Dimers

Kenji YOKOYAMA,* Yoshitaka TAJIMA, Masao TAHARA, and Shiro MAEDA

Research Laboratory of Resources Utilization, Tokyo Institute of Technology, Nagatsuda, Midori-ku, Yokohama 227

(Received March 24, 1980)

The resonance Raman spectra of some Würster's cation dimers were measured in alcohol solution at 201 K and in glassy matrix at 77 K. The spectra of the dimer of *p*-phenylenediamine cation showed the resonance enhancement of the Raman line assigned to the intermolecular stretching vibration and supported the D_{2h} symmetry for the dimer. However, for the dimer of 2,3,5,6-tetramethyl-*p*-phenylenediamine cation and *N,N*-dimethyl-*p*-phenylenediamine cation, it was supposed that D_{2h} symmetry was broken down in alcohol solution and in glassy matrix, because the dimers had two Raman lines in the region of the intermolecular vibration.

Resonance Raman effect is a well known phenomenon where the Raman lines related to an electronic transition show enhancement of their intensities when wavelength of an exciting line approaches to the corresponding absorption band. Recently, the authors found the resonance enhancement of the Raman lines assigned to the intermolecular stretching vibrations for the dimers of some aromatic ion radicals, *p*-phenylenediamine cation (PD^+), 2,3,5,6-tetramethyl-*p*-phenylenediamine cation ($TMPD^+$),[1] *p*-benzosemiquinone anion[2] and tetracyanoethylene anion ($TCNE^-$),[3] by the excitation at the long wavelength absorption bands characteristic of the dimer formation. These results not only indicated the strength of the intermolecular bondings directly, but brought fine informations about the behavior of dimerization, with the detailed feature of their spectra taken into account. In the present study, the resonance Raman effect of Würster's cation dimers was further reinvestigated to study the mechanism of dimerization and the relation between the nature of the intermolecular bondings and the values of force constant for the corresponding bondings of the dimers.

Experimental

PD^+ and $TMPD^+$ were prepared with Br_2, as previously reported.[1] *N,N*-Dimethyl-*p*-phenylenediamine bromide ($DMPD^+Br^-$) was prepared by the method of Michaelis and Granick.[4] *N,N,N',N'*-Tetradeuterated PD (PD-d_4) and *N,N,N',N'*-tetradeuterated TMPD (TMPD-d_4) were prepared by repeating of dissolution and crystallization in CH_3OD. Methanol and ethanol were used as solvents for measurement at 201 K. A mixed solvent, EPA (ethanol: isopentane: diethyl ether = 10:1:1), was used for measurement at 77 K. The conditions of spectroscopic measurement were almost equal to the previous report,[1] except that the satellite lines of the exciting source were eliminated by using a prism system.

Results and Discussion

Figure 1 a) shows the resonance Raman spectrum of the dimer of PD^+Br^- in ethanol solution at 201 K by the excitation at the absorption band characteristic of the dimer at 605 nm.[1] A broad line at 161 cm^{-1} showed a striking resonance enhancement together with its progression, and a weak line appeared at 523 cm^{-1} in resonance condition. These Raman lines were all polarized, and the depolarization ratio of the line at 161 cm^{-1} was 0.31. Therefore, they were assigned to totally symmetric vibrations.

Kimura *et al.* studied the electronic structure of the dimer of PD^+ by using LCMO method, assuming a parallel structure of D_{2h} symmetry, as shown in Fig. 2[5] and showed that the absorption band at 605 nm characteristic of the dimer was assigned to a transition from ϕ_+ to ϕ_-, which had a transition dipole along the out-of-plane axis, z. A significant difference between ϕ_+ and ϕ_- is that ϕ_+ has a bonding character whereas ϕ_- has an antibonding character on the intermolecular bonding. Therefore, according to the Franck-Condon mechanism of Raman intensity, the resonance enhancement of the Raman line assigned

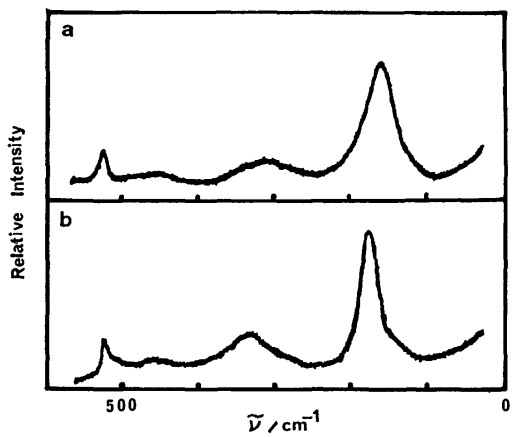

Fig. 1. Resonance Raman spectra of PD^+Br^- by the excitation with 605 nm line.
a) In ethanol solution at 201 K, b) in EPA glassy matrix at 77 K.

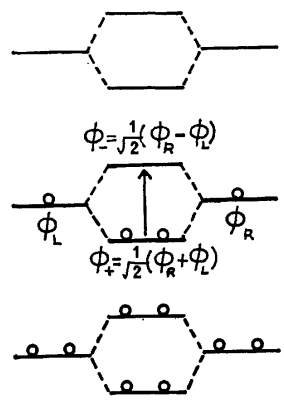

Fig. 2. MO scheme of the dimer of ion radical.

to the intermolecular stretching vibration is expected to take place by the excitation at this absorption band.

Consequently, the 161 cm^{-1} line was assigned to the intermolecular stretching vibration, as previously reported.[1] The broad line shape indicates the nature of the intermolecular vibration and the value of depolarization ratio shows the contribution of α_{zz} component to the resonance enhancement.

On the other hand, an out-of-plane NH_2 bending vibration may appear in the region about 200 cm^{-1},[6] while this mode probably increases in frequency when PD is converted to PD^+ because the conjugation between benzene ring and NH_2 is increased.[7,8] If the line is the out-of-plane NH_2 vibration, it must decrease in frequency about 6 cm^{-1} according to the deuteration. However, in the present study, the resonance Raman spectrum of the dimer of PD-d_4^+ did not show any considerable change in frequency, compared with that of the dimer of PD-h_4^+. Therefore, it was confirmed that the line observed at 161 cm^{-1} is not assigned to the out-of-plane NH_2 bending vibration.

Figure 3 a) shows the resonance Raman spectrum of the dimer of $TMPD^+Br^-$ in methanol solution at 201 K by the excitation at 605 nm. In the previous report,[1] the shoulder at 145 cm^{-1} was regarded as due to a satellite line of the exciting source. However, this shoulder did not disappear even if the satellite line was eliminated. Therefore, we have revised the assignment of this shoulder as a Raman line of the dimer of $TMPD^+$, and confirmed that the dimer of $TMPD^+$ has two lines in the region of the intermolecular vibration. Both lines at 117 and 145 cm^{-1} showed no change in spectral feature when $TMPD^+$ was converted to TMPD-d_4^+. The depolarization ratio of the band consisting of the two lines was 0.23, which is smaller than that of the dimer of PD^+, slightly.

Figure 3 b) shows the resonance Raman spectrum of the dimer of $TMPD^+Br^-$ in EPA glassy matrix at 77 K. Two lines in the region of low frequency region appeared more clearly and became to be more distiguishable from each other. Table 1 shows the observed frequencies of the Raman lines for the dimer

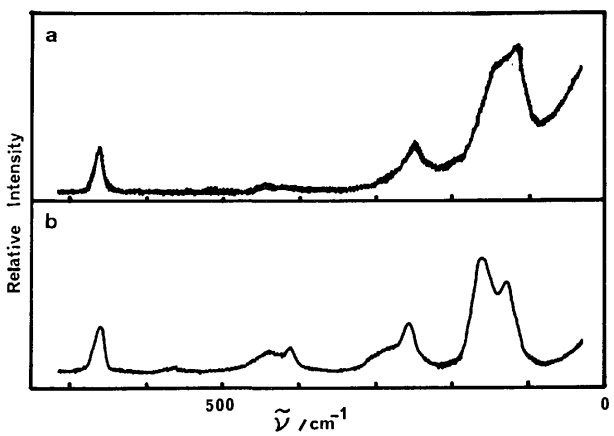

Fig. 3. Resonance Raman spectra of $TMPD^+Br^-$ by the excitation with 605 nm line.
a) In methanol solution at 201 K, b) in EPA glassy matrix at 77 K.

Table 1. The observed frequencies and their assignment for Würster's cation dimers

Species	201 K cm^{-1}	77 K cm^{-1}	Assignment
$(PD^+)_2$		≈130 sh	intermolecular vibration
	161 s p	174 s p	intermolecular str.
	322 w p	343 w	161×2 and 174×2
	523 m p	521 m	ring bend.
$(TMPD^+)_2$	117 s p	128 s p	intermolecular vibration
	145 s p	156 s p	
	250 m p	258 m p	CH_3 bend.
		≈280 w	156+128=284
		415 w	156+258=414
		445 w	156×2+128=440
	655 m p	658 m p	ring bend.
$(DMPD^+)_2$		151 s p	intermolecular vibration
		184 s p	

s; Strong, m; medium, w; weak, sh; shoulder, p; polarized.

of $TMPD^+$ at 77 K, together with those at 201 K. Both lines at 117 and 145 cm^{-1} at 201 K shifted to 128 and 156 cm^{-1} in glassy matrix, respectively. These deviations are larger than those for the lines at 250 and 655 cm^{-1}. These results mean that both lines at 117 and 145 cm^{-1} are more sensitive to the surrounding condition than the other lines, which shows that these lines relate to the intermolecular bonding closely.

As shown in the previous study,[3] the resonance Raman spectra of the dimer of $TCNE^-$ showed the resonance enhancement of two lines in the frequency region of the intermolecular stretching vibration. The two lines were assigned to the respective intermolecular stretching vibrations of two kinds of the dimers, because the relative intensities of the two lines showed remarkable alternation when the counter cation was changed from Na^+ to Cs^+. However, the two Raman lines for the dimer of $TMPD^+$ did not show any considerable change of their intensities when the counter anion was changed among Br^-, I^-, and ClO_4^-. Therefore the origin of the two lines for the dimer of $TMPD^+$ must be different from that for the dimer of $TCNE^-$.

These results are interpreted reasonably by considering that D_{2h} symmetry is broken down for the dimer of $TMPD^+$. When the D_{2h} symmetry of the dimer is degraded, vibrations belonging to other symmetry species become totally symmetric and the transition from ϕ_+ to ϕ_- becomes to contain in-plane components beside z component. Therefore the both lines at 117 and 145 cm^{-1} were assigned to mixed modes between two intermolecular vibrations. One is surely the intermolecular stretching vibration, and the other is probably the ring tilting vibration. The break down of D_{2h} symmetry for the dimer of $TMPD^+$ is probably attributed to the repulsion between the H atoms of CH_3 substituents of component radicals. The value of depolarization ratio, 0.23, is reasonably interpreted to be owing to the mixing of α_{xx} or α_{yy} to the scattering tensor, derived from the lowering

of symmetry. The alternation of intensity for these lines at 201 K and 77 K (see Fig. 3) shows that the configuration of the dimer of $TMPD^+$ is sensitive to the surrounding condition. Figure 3 b) shows that there are some weak lines at 280, 415, and 445 cm^{-1}. These lines can be assigned to combination lines, $156+128=284$, $156+258=414$, and $156\times2+128=440$ cm^{-1}, respectively. These assignments show a good correspondence with the interpretation that both lines at 128 and 156 cm^{-1} in glassy matrix should be attributed to the same species.

Figure 1 b) shows the resonance Raman spectrum of the dimer of PD^+Br^- in EPA glassy matrix at 77 K. The spectral feature at 77 K was almost the same as that at 201 K, with slight differences that 161 cm^{-1} line was observed to increase in frequency slightly and narrow its band width, and a new weak shoulder appeared at 130 cm^{-1}. These results show that the deviation of configuration from D_{2h} symmetry for the dimer of PD^+ is slight in glassy matrix.

The resonance Raman spectra of $DMPD^+Br^-$ in EPA glassy matrix at 77 K are shown in Fig. 4. The dimer of $DMPD^+$ has the absorption band characteristic of dimerization at 680 nm.[5] As the wavelength of excitation line approached to the absorption band two Raman lines appeared with resonance enhancement, same as for the dimer of $TMPD^+$. This result indicates that the dimer of $DMPD^+$ does not take D_{2h} symmetry in glassy matrix, either. Tanaka and Sakabe reported that in the crystal of $DMPD^+Br^-$, one component cation radical was displaced relatively to the other.[7] The present result is in good agreement with their conclusion.

Table 1 shows the observed values of frequency for the dimers at 77 K, together with those at 201 K.

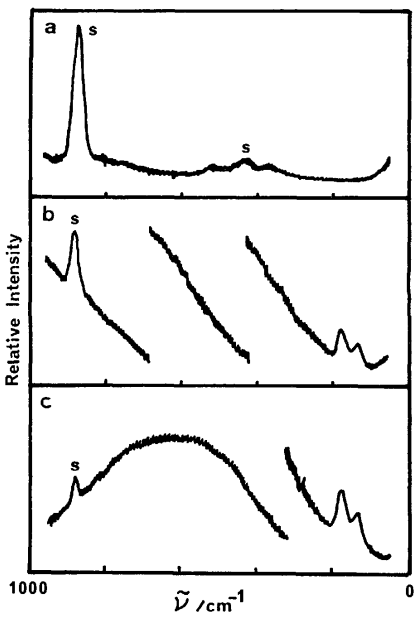

Fig. 4. Resonance Raman spectra of $DMPD^+Br^-$ in EPA glassy matrix at 77 K by the excitation with 514.5 nm a), 584 nm b), and 605 nm c) lines, respectively.
s: Solvent lines.

The Raman lines in the region of low frequency were assigned to the intermolecular vibrations, as discussed above. A 250 cm^{-1} line of the dimer of $TMPD^+$ was assigned to an out-of-plane CH_3 bending vibration because the corresponding line did not appear for the dimer of PD^+. Lines at 523 cm^{-1} for the dimer of PD^+ and 655 cm^{-1} for the dimer of $TMPD^+$ were assigned to respective ring bending vibrations because they were observed for both dimers. The corresponding line for the dimer of $DMPD^+$ was not confirmed because S/N ratio was wrong. These lines at 250, 523, and 655 cm^{-1}, assigned to intramolecular vibrations, probably borrow their intensities from the intermolecular vibrations through the mixing of vibrational modes.

Table 2 shows the force constants of the intermolecular stretching vibrations of three dimers on the basis of diatomic model. The values for the dimer of $TMPD^+$ and $DMPD^+$ were derived from the averaged frequency of the two Raman lines. Nakayama and Suzuki reported that the values of enthalpies of the dimer formation, $-\Delta H$, were nearly equal for PD^+ and $DMPD^+$, 8.0 and 8.2 kcal/mol, respectively.[9] These values show a good correspondence with the values of force constants of the dimers.

Table 2. The values of force constants for the intermolecular stretching vibrations

Species	201 K	77 K
$(PD^+)_2$	0.82 md/Å	0.96 md/Å
$(TMPD^+)_2$	0.83	0.97
$(DMPD^+)_2$		1.12

It is well known that the values of force constant of the stretching vibrations are related to the corresponding bond distances among bondings with similar nature. The values of force constant for the intermolecular bonding of these ion radical dimers are 0.8—1.1 md/Å, as shown in Table 2, and their bond distances are expected to be about 3.1 Å, according to the result of X-ray study on $DMPD^+$ crystal.[7] Yada *et al.* reported that the force constant of intermolecular stretching vibration for a CT complex, trimethylamine–iodine ($TMA-I_2$), was 0.546 md/Å, though the corresponding bond distance was 2.27 Å.[10] The inclination of force constants between these ion radical dimers and $TMA-I_2$ is not parallel to that of their bond distances. Therefore the nature of intermolecular bondings of the ion radical dimers is expected to be different from that of the CT complex. On the other hand, ferrocene is a well known sandwitch type molecule and similar with the ion radical dimers because the π orbitals of aromatic rings form a kind of covalent bond, directly. For ferrocene, the metal-ring distance is 1.66 Å and the force constant of metal-ring stretching vibration is 3.07 md/Å on the basis of linear triatomic molecule model.[11,12] At least, the inclination of their force constants are parallel to that of their bond distances. This result indicates that the intermolecular bonding of the ion radical dimer is owing to the covalency between

two π orbitals rather than CT interaction.

References

1) K. Yokoyama and S. Maeda, *Chem. Phys. Lett.*, **48**, 59 (1977).
2) S. Yamaguchi, K. Yokoyama, and S. Maeda, *Bull. Chem. Soc. Jpn.*, **51**, 3193 (1978).
3) K. Yokoyama, S. Maeda, C. Etoh, S. Matsuzaki, and K. Toyoda, *Bull. Chem. Soc. Jpn.*, **53**, 36 (1980).
4) L. Michaelis and S. Granick, *J. Am. Chem. Soc.*, **65**, 1747 (1943).
5) K. Kimura, H. Yamada, and H. Tsubomura, *J. Chem. Phys.*, **48**, 440 (1968).
6) G. Varsanyi, "Vibrational spectra of benzene derivatives," Academic Press, New York (1969).
7) J. Tanaka and N. Sakabe, *Acta Crystallogr., Sect. B*, **24**, 1345 (1968).
8) E. Mayer, R. B. Girling, and R. E. Hester, *J. Chem. Soc., Chem. Commun.*, **1973**, 192.
9) S. Nakayama and K. Suzuki, *Bull. Chem. Soc. Jpn.*, **46**, 3694 (1973).
10) H. Yada, J. Tanaka, and S. Nagakura, *J. Mol. Spectrosc.*, **9**, 461 (1962).
11) J. D. Dunitz, L. E. Orgel, and A. Rich, *Acta Crystallogr.*, **9**, 373 (1956).
12) E. R. Lippincott and R. D. Nelson, *Spectrochim. Acta*, **10**, 307 (1958).

 © 1980 The Chemical Society of Japan Bull. Chem. Soc. Jpn., 53, 2493—2498 (1980)

Precipitation and Microflotation of Egg Albumin and Hemoglobin in the Presence of Dioctadecyldimethylammonmin Chloride

Haruo NAKAYAMA,* Kazuo ITOH, Kōzō SHINODA, and Egon MATIJEVIĆ†

Department of Chemistry, Faculty of Engineering, Yokohama National University, Tokiwadai, Hodogaya-ku, Yokohama 240

† *Institute of Colloid and Surface Science and Department of Chemistry, Clarkson College of Technology, Potsdam, New York 13676, U.S.A.*

(Received March 24, 1980)

Precipitation and microflotation of egg albumin and of hemoglobin was studied as a function of pH in the presence of dioctadecyldimethylammonium chloride (DOAC). The "DOAC concentration-pH" stability domains for both protein solutions (0.05 wt%) exhibited similar boundaries. Efficient separation by precipitation (more than 80% after 24 h) occurs at pH>5.0 for albumin and at pH>6.3 for hemoglobin. The same amount of removal by microflotation required 5 min under otherwise similar conditions. The DOAC concentration for optimal separation of proteins (from 0.05 wt% solutions) is 0.02 wt% at pH 6—8 for albumin and 0.015 wt% at pH 6.5—8 for hemoglobin. It is noteworthy that both proteins can be precipitated and also foam separated even in strongly alkaline media, such as at pH 12, where the usual flocculents (*e.g.*, aluminum salts) cannot be employed. This work points out the usefulness of infinitely aggregating surfactants as microflotation agents.

Since proteins, such as hemoglobin and albumin, are major components in waste waters of food processing and related industries, their removal and/or recovery is highly desirable. It has been shown that microflotation, which is characterized by the application of small bubbles, could be successfully applied for the separation of inorganic and organic colloidal impurities from their suspensions.[1-4] In this process the materials to be removed must be in flocculated state, which can be accomplished either by the addition of a coagulant or by a change of solution pH. The precipitate is then floated with the help of a surfactant (collector).

Various types of flocculents have been applied to protein solutions, such as lignin[2] and its derivatives,[5] sodium polyacrylate,[6] cationic surfactants (*e.g.*, dodecylpyridinium bromide),[7] anionic surfactants (*e.g.*, sodium alkylbenzenesulfonate or sodium dodecyl sulfate),[7-9] nonionic surfactants,[10,11] and simple inorganic salts.[11,12] Among the listed additives the high molecular weight flocculents (such as lignin) and freshly precipitated metal hydroxides proved to be most suitable for efficient flotation.[2]

The solubility of proteins in water may be reduced by certain reagents which form a less soluble complex with the protein. In this investigation, dioctadecyldimethylammonium chloride, $(C_{18}H_{37})_2N(CH_3)_2Cl$ (DOAC), was used to precipitate and to float egg albumin and hemoglobin. Owing to two long alkyl chains in the DOAC molecules, its solution behavior is quite different from that of ordinary cationic surfactants.[13] Instead of forming micelles these long chain molecules infinitely aggregate yielding multilayer structures in aqueous media over a broad pH range. This property of DOAC makes it a useful precipitant for proteins and it also enhances their floatability by microbubbles.

Experimental

Materials. Egg albumin and hemoglobin were obtained from Tokyo Kasei Kogyo Ltd. and were used without further purification. Dioctadecyldimethylammonium chloride (DOAC), the purity of which with respect to the alkyl chain length was 98.6%, was kindly supplied by Kao Soap Co. Since the proteins used had a certain amount of impurities as shown below, DOAC was also used without further purification. To prepare the stock solutions, the precalculated amount of the protein (either albumin or hemoglobin) was dissolved in 200 cm³ of a NaOH solution (pH 11.0), stirred for 24 h, and filtered through an 1.0 μm pore membrane (Tōyō Roshi Co., TM-100P). A known amount of the filtrate was dried to constant weight *in vacuo* at 70°C from which the weight, obtained by the same procedure using only the solvent, was subtracted. The analysis showed that 1.5% of albumin and 3.2% of hemoglobin remained insoluble in the alkaline media; thus, the concentrations of the solutions of these proteins were corrected accordingly. Stock solutions of DOAC were prepared by dissolving appropriate amount of the solid surfactant in distilled water under stirring at 50 °C for 24 h.

Analyses. Since DOAC scattered light in the visible region and weakly absorbed light in the ultraviolet region, the protein concentrations in solutions containing DOAC were determined by the Lowry method[14] as described previously.[2] The absorbance at 750 nm increased linearly with the DOAC concentration; however, this increase was small and amounted to only 0.08 at 0.05 wt% DOAC, which was the maximum amount of the surfactant in most experiments. The measured absorbance of protein solutions was corrected for the presence of the surfactant.

The concentration of DOAC was determined independently in solutions containing protein by the methyl orange method developed by Wang *et al.*[15] The volume of a sample solution (usually 0.2—1.0 cm³) in a 500-cm³ separatory funnel was adjusted with distilled water to 10 cm³ and then 1.0 cm³ of a buffer solution (pH=3),[16] 0.1 cm³ of a 0.1 wt% Methyl Orange aqueous solution, and 10 cm³ of chloroform were added. After vigorous shaking for 30 sec, the mixture was allowed to stand for about 30 min to achieve complete separation of the chloroform from the water phase. The absorbance of the chloroform solution was then determined spectroscopically at 415 nm. The presence of protein in the sample did not interfere, (even at a 50 fold excess with respect to DOAC) except that it took much longer time for the phase to separate. The absorbance was linearly proportional to the DOAC concentration over the range 0—0.002 wt%; it had a value of ≈1.0 for a 0.002 wt% DOAC solution when a cell of 1.00 cm light path was used.

Stability and Microflotation Measurements. The stability of the protein was very much affected by both the pH and the DOAC concentration. Thus, a series of solutions was prepared at a constant pH and protein concentration (0.05 wt%) whereas the concentration of DOAC was varied systematically.

Desired quantities of stock solutions of the protein and of DOAC were mixed with distilled water to give a final volume of 30 cm^3. The pH was then adjusted with NaOH and HCl, as necessary, and the resulting solution was allowed to settle for 24 h after which time the visual appearance of the system, the relative volume of settled flocs, and the concentrations of both the protein and DOAC in the supernatant solutions were determined.

The microflotation apparatus and the procedure were essentially the same as described earlier[2] except that a 300 cm^3 instead of a 600 cm^3 glass Buchner funnel was employed as the flotation cell. Precalculated amounts of protein and DOAC solutions and of distilled water, which would yield a final volume of 200 cm^3, were introduced into the cell and the pH was adjusted with either NaOH or HCl. As frother/collector served 0.5 cm^3 of ethanol containing 5 mg of lauric acid.

Results

Figure 1 gives the concentration of albumin in supernatant solutions as a function of pH, 24 h after mixing the reacting components. Each curve is for a different initial DOAC concentration whereas the albumin content was kept constant (0.05 wt%) in all systems. In the absence of the surfactant, some precipitation of the protein occurs only over a relatively narrow pH range of 4.4—5.7; the maximum amount of the protein separated by gravity settling after 24 h amounted to only 26% at pH ≈ 5.0. The addition of DOAC affects the precipitation of albumin as follows: (1) no precipitation of albumin is observed at pH<4.4, regardless of the amount of DOAC present; (2) with increasing DOAC concentration, the amount of separated albumin becomes larger and the pH range over which the protein precipitates broadens; (3) although albumin dissolves at high pH, it remains precipitated even at a pH as high as 12, provided the DOAC concentration is ≥0.05 wt%; and (4) a domain of high turbidity exists over the pH region of ≈4.5—5.0 (hatched area in Fig. 1), presumably due to stable albumin–DOAC dispersions.

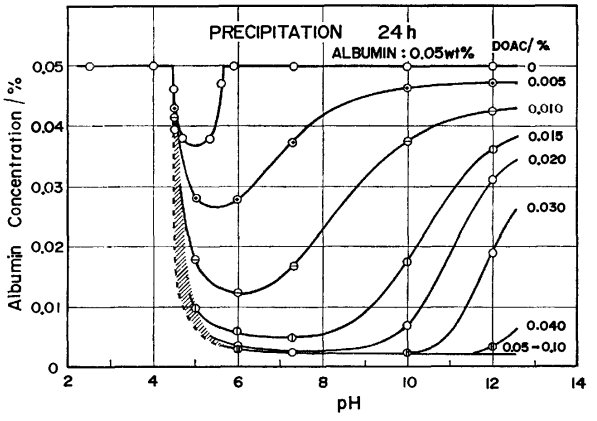

Fig. 1. The concentration of albumin left in the supernatant solutions after gravity settling as a function of pH. Each curve represents systems containing a constant concentration of albumin (0.05 wt%) but different concentrations (0—0.10 wt%) of dioctadecyldimethylammonium chloride (DOAC) 24 h after mixing of the reacting components. Hatched area indicates conditions yielding stable dispersions.

The upper part of Fig. 2 gives the concentration of albumin in the supernatant solutions, 24 h after mixing the reacting components as a function of the initial concentration of DOAC. The two curves refer to systems containing 0.05 wt% albumin at constant pH of 4.5 and 5.0, respectively. The center part of the figure shows the corresponding concentrations of DOAC in the supernatant solution. Finally, the lower part gives the percent of albumin removed after 5 min of microflotation in the same systems at pH 5.0. In Fig. 3 analogous plots refer to samples at pH 7.3 and 12.0

At pH 4.5 the addition of DOAC to protein solutions causes high turbidities. Obviously, a stable protein–DOAC precipitate is formed, which shows little tendency to settle, especially if the concentration of the surfactant exceeds 0.04 wt%. At somewhat higher pH (5.0) the removal of albumin by precipitation with DOAC and gravity settling is considerably enhanced. In these systems most of the added surfactant molecules combine with albumin leaving, for example, 0.0014 wt% and 0.0011 wt% DOAC in the supernatant solutions, at initial concentrations of 0.010 wt% and 0.015 wt%,

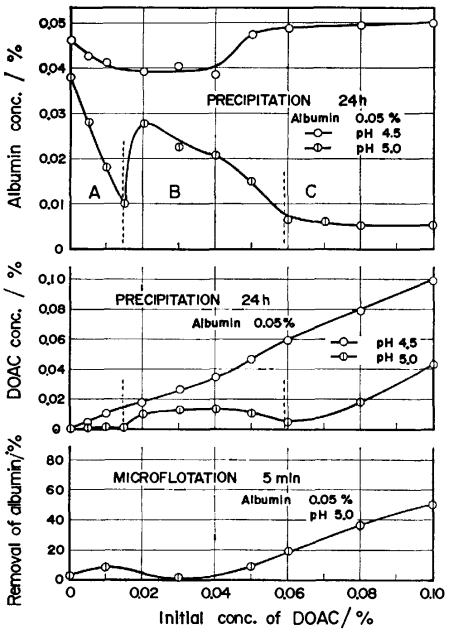

Fig. 2. The concentrations of albumin (upper part) and of dioctadecyldimethylammonium chloride (DOAC) (center part) remaining in the supernatant solutions above the precipitate separated by gravity settling 24 h after mixing of the reacting components. Lower part: the percentage removal of albumin by microflotation after 5 min. All systems contained a constant concentration of albuimn (0.05 wt%) at a constant pH (○, 4.5; ◑, 5.0), by varying amounts of added DOAC.

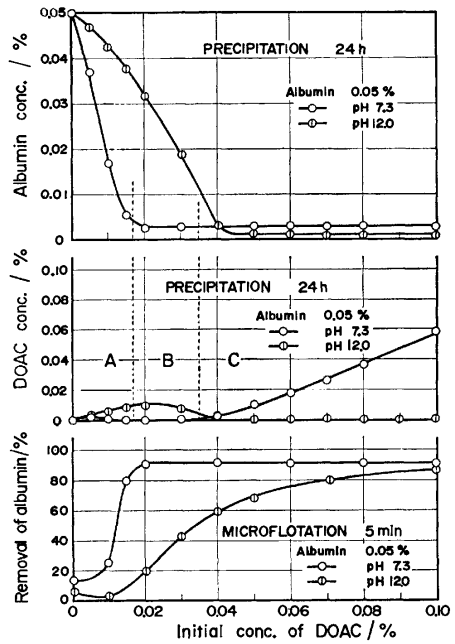

Fig. 3. Same plot as Fig. 2 for systems at pH 7.3 (○) and pH 12.0 (◐).

respectively. At intermediate amounts of DOAC a part of the precipitated albumin is peptized, giving somewhat higher concentrations of albumin and DOAC in the supernatant liquids. However, in contrast to the systems at pH 4.5, the separated albumin–DOAC phase at pH 5.0 coagulates and settles when the initial concentration of DOAC is $\geq \approx 0.06$ wt%.

The removal of albumin after 5 min of microflotation is much lower than by gravity settling after 24 h. For example, at the initial concentration of DOAC of 0.01 wt% only 8% of albumin is separated, whereas more than 60% settles out. Although the floatability of albumin improves with increasing DOAC concentration, only 50% is removed at best (in the presence of 0.10 wt% DOAC); under the same conditions $\approx$ 90% of the protein settles out.

As the pH is raised to 7.3 (upper part of Fig. 3) $\approx$ 94% of the protein is removed by settling at DOAC concentration $\geq$0.02 wt%. The surfactant content in the supernatant solutions (middle part of Fig. 3) remains low at initial concentrations <0.035 wt%, but increases nearly linearly when more DOAC is added. At this higher pH the separation of albumin by microflotation is comparable to that of settling (92% after 5 min) except that the time required is considerably shorter. The time dependence of the removal of albumin by microflotation in the absence and in the presence of different concentrations of DOAC at a constant pH of 7.3 is shown in Fig. 4.

Figure 3 also shows that at still higher pH (12.0) the precipitation and the microflotation of albumin in the presence of DOAC becomes again less efficient; thus, a minimum of 0.042 wt% of surfactant is needed for complete removal of the protein in contrast to 0.017 wt% at pH 7.3. Furthermore, at pH 12 no peptization in the presence of DOAC is detected over the concentration range studied (0—0.26 wt%).

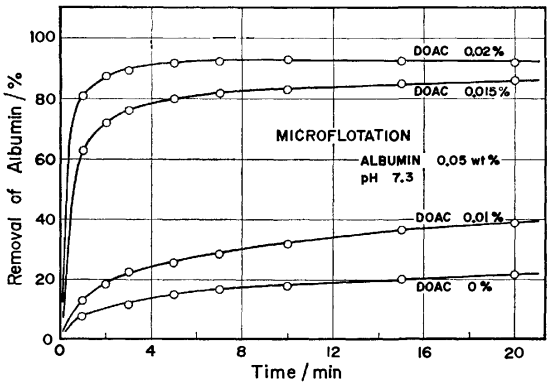

Fig. 4. Percentage removal of albumin from a 0.05 wt% protein solution at a pH of 7.3 as a function of time, in the absence and in the presence of DOAC in different concentrations.

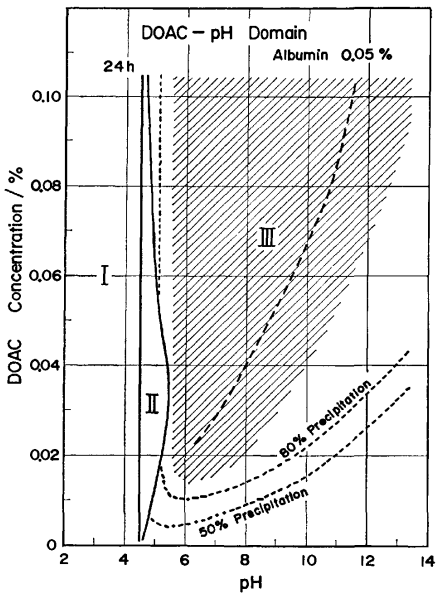

Fig. 5. DOAC-pH domain for the systems containing 0.05 wt% albumin. The solid lines delineate regions of various degree of stability, 24 h after mixing of the components. In I no precipitation takes place; in II the sols are stable; in III the albumin–DOAC floc readily settles. Dotted lines indicate the boundaries over which 50 and 80% albumin, respectively, is separated by gravity settling. Hatched area gives the conditions of 80% or greater removal of albumin after 5 min of microflotation.

In the system containing 0.20 wt% DOAC, for example, the surfactant concentration in the supernatant solution, 24 h after preparation, is only 0.0009 wt% although the settled precipitate occupies >50% of the total volume of the system. When DOAC concentration is >0.24 wt%, the entire system is solidified; *i.e.*, no supernatant solution appears 24 h after mixing the components. However, if the latter system is kept undisturbed for a longer period of time (more than 3 d), the precipitated phase gradually separates out from a transparent solution and floats as a jelly-like phase.

Figure 5 gives the entire DOAC concentration-pH

stability domain for a system containing a constant concentration of albumin (0.05 wt%), 24 h after mixing the reacting components. This plot is constructed from the data shown in Figs. 2 and 3 as well as from the analogous information for systems at pH 6.0 and 10.0. The heavy solid lines delineate conditions of different stability of albumin: in region I no precipitation is observed; in II stable albumin–DOAC aggregates are found (high turbidity); in III the complex precipitates settle by gravity. The dotted lines drawn within region III and labeled "50% precipitation" and "80% precipitation" indicate the boundary above which more than 50% (or 80%) of albumin is removed by settling 24 h after mixing. The hatched area indicates the conditions which result in 80% or better removal of albumin after 5 min of microflotation. Finally, above the dashed line an excess of DOAC is detected in the supernatant liquids (separated from the settled precipitates).

The results obtained with 0.05 wt% hemoglobin solutions are summarized in Figs. 6 and 7. A comparison with the corresponding data for albumin shows that DOAC reacts with both proteins in essentially the same manner. Minor differences noted are: (1) DOAC precipitates hemoglobin more efficiently than albumin, (2) the domain of stable dispersion (region II in Fig. 7) for hemoglobin system extends over a wider pH range than for albumin, and (3) the effective precipitation (and corresponding microflotation) region of hemoglobin is shifted by about one pH unit towards the higher pH as compared with that for albumin.

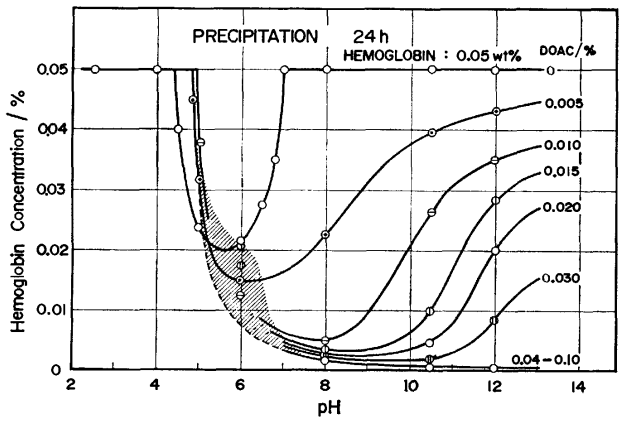

Fig. 6. Same as Fig. 1 for the hemoglobin–DOAC system.

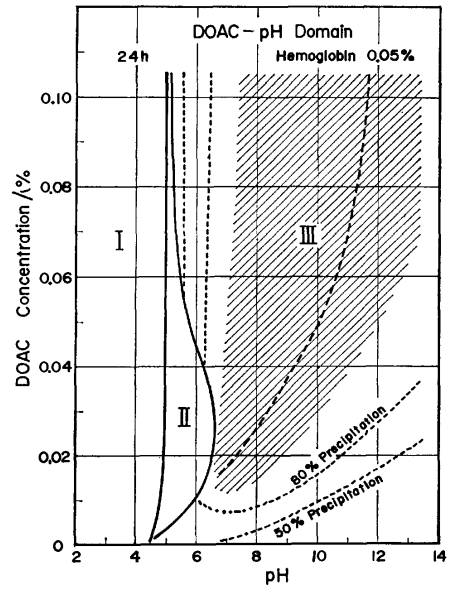

Fig. 7. Same as Fig. 5 for the hemoglobin–DOAC system.

Discussion

Dioctadecyldimethylammonium chloride (DOAC) was chosen because of its property to form very stable dispersions of liquid crystal particles that could interact with the proteins. There dispersions can be produced in aqueous solutions above or below the melting point (37 °C) of the hydrated solid DOAC. The positively charged particulate system is readily supercooled and remains unchanged for long time (over one month), even at room temperature. Thus, liquid crystals are expected to be suitable flocculents for the negatively charged proteins. The very low saturation concentration of the monomeric DOAC (2.7×10^{-4} wt% at 30 °C)[13] and the insensitivity of its liquid-crystalline phase to pH (except at a rather high concentration of base) are additional convenient properties of this surfactant for the intended purpose.

The data presented here show that the interactions between albumin (or hemoglobin) and DOAC depend strongly on the concentration of the surfactant and on the pH. Typical effects of the added DOAC on the stability of albumin are distinguished in Fig. 3 as regions *A*, *B*, and *C*. In *A* the mixing of albumin and DOAC yields rapidly settling flocs and the amount of removed albumin by gravity settling is approximately proportional to the quantity of DOAC added. The DOAC concentration in the supernatant solution is very low; the slight turbidity of the latter is most likely due to finally dispersed systems which did not settle during the 24 h of aging. In region *B* nearly the entire amount of albumin is precipitated and settled, and very little DOAC (less than 0.001 wt%) is left in the supernatant solution, even though there is an excess of the surfactant over what is necessary to react with the protein. The precipitate in this region is more voluminous than under conditions of region *A*. Finally, in *C* most of albumin is in the settled floc, but some of the DOAC can be found in the supernatant solution, the amount of which becomes larger with increasing concentration of the added surfactant.

In region *A* the negatively charged albumin reacts most likely with positively charged liquid-crystalline fragments of DOAC, as evidenced by the following observations: (1) no precipitation of albumin with DOAC takes place at pH < the isoelectric point[17] (Figs. 1 and 5); (2) the amount of DOAC which is needed to precipitate a certain amount of albumin

increases with increasing pH, *i.e.*, with increasing net negative charge on the albumin molecules (Figs. 1 and 3); and (3) at a constant pH, the amount of DOAC necessary to completely precipitate albumin is proportional to the initial protein concentration. For example, at pH=12.0, the systems containing 0.015, 0.030, and 0.05 wt% albumin, required 0.013, 0.025, and 0.042 wt% DOAC, respectively.

Although the pH dependence of the net charge on an albumin molecule (Z) is not fully established, one may assume Z to be approximately 14, 18, and 30 at pH 7.3, 10.0, and 12.0. These values are estimated by averaging the data obtained from electrophoretic mobilities[17] and from titrations.[18] Using these Z values and assuming that 60% of the positive charge on a liquid-crystalline aggregate of DOAC is electrostatically shielded by gegenions (such as Cl^- and OH^-),[19] one may calculate the DOAC content which is necessary to neutralize the negative charge on a definite amount of albumin molecules. The calculated values for a 0.05 wt% albumin solution are 0.015, 0.02, and 0.033 wt% at pH 7.3, 10.0, and 12.0, respectively. These results are in reasonable agreement with the observed DOAC concentrations (0.017, 0.022, and 0.042 wt%), which correspond to the boundary between the regions *A* and *B*.

In region *B* liquid-crystalline aggregates of DOAC may adhere to the electrically neutral albumin–DOAC floc; the onset of region *C* could, therefore, correspond to the saturated adsorption of the DOAC aggregates. The efficient multi-layer adsorption of a lammelar liquid-crystalline phase of DOAC to a surface, such as fabrics or hair, is noted elsewhere.[13] The resultant aggregate still remains in a settled state and is efficiently removed by microflotation if pH is appropriately adjusted ($\approx$6—$\approx$10). Ahmad[11] showed that the liquid-crystalline phase formed by surfactants and glycerides in association with protein was effective in the foam separation of albumin although a direct comparison with the experiments described in this work is not possible. Furthermore, some preliminary experiments indicated that the addition of $C_{18}H_{37}N(CH_3)_3Cl$, which forms micelles but does not form liquid crystalline phase in dilute aqueous solution, could also cause precipitation and settling of albumin at pH$>\approx$5. However, in excess of this surfactant, over what was needed to neutralize electric charge of the protein, peptization occurred due to the charge reversal of particles. The finely dispersed system could not be floated with microbubbles.

Stable dispersions in region *B* at pH 5 may also consist, at least in part, of small fragments of DOAC in liquid crystalline form. Since the aggregates of this surfactant contain up to 96% water, their density is very close to that of the liquid medium. Furthermore, the slight positive charge of these fragments would prevent an interaction with the finely dispersed albumin–DOAC floc of the same sign of charge. The addition of a small amount of electrolyte (*e.g.*, 1 wt% NaCl) causes a decrease in the amount of water in the swollen liquid crystals of DOAC from 96 to 70%, so that a separation of the surfactant aggregates occurs more readily. This result would indicate that the use of hard tap water rather than distilled water would be beneficial in the removal of albumin by DOAC.

Region *B* at pH 12 is considerably wider, which may be due to destabilization of liquid-crystalline aggregates of DOAC in the medium of high ionic strength. For instance, if a 0.10 wt% DOAC solution at pH 12 was aged for 24 h, a white creamy layer appeared in the upper part of the liquid; the amount of the separated phase increased with time and with increasing concentration of the surfactant.

Figure 5 shows that the conditions for an effective removal of albumin by microflotation ($\geq$80%) in the presence of DOAC coincide fairly well with those giving a floc that readily settles. The exception are either systems containing lesser amounts of the surfactant or systems at higher pH values of the media. Indeed, the higher the pH the more DOAC is needed to float the protein. The failure to separate the floc by microbubbles in this region may be due to the nature of its composition, which consists predominantly of liquid-crystalline DOAC fragments. Apparently, bubbles do not adhere to these solids sufficiently well unless the ionic strength is high enough. The addition of electrolytes (or using tap water) could improve the efficiency of microflotation under these conditions.

Since hemoglobin behaved in a very similar manner in the presence of DOAC as albumin, analogous explanation of the observed phenomena apply.

This work was supported by a joint NSF-JSPS Grant No. 01P74—24291 as a part of the United States-Japan Cooperative Science Program, by the National Science Foundation Grant CHE77 02185, and by Westvaco Foundation.

References

1) F. J. Mangravite Jr., T. D. Buzzell, E. A. Cassell, and E. Matijević, *J. Am. Water Works Assoc.*, **67**, 88 (1975).
2) H. Nakayama, E. Matijević, and K. Shinoda, *J. Colloid Interface Sci.*, **61**, 590 (1977).
3) A. J. Rubin and S. C. Lackey, *J. Am. Water Works Assoc.*, **60**, 1156 (1968).
4) E. A. Cassell, E. Matijević, F. J. Mangravite Jr., T. M. Buzzell, and S. B. Blabac, *AIChE J.* **17**, 1486 (1971).
5) For example, B. Naess, *Acta Vet. Scand.*, **12**, 572, 583 (1971); S. E. Jørgensen, *Vatten*, **1**, 58 (1971); E. I. Toenseth and H. B. Berridge, *Effluent Water Treat. J.*, **8**, 124 (1968); E. Farber, G. D. Maengwyn-Davies, and J. S. Wallerstein, *Chem. Eng. News*, **23**, 617 (1945); J. S. Wallerstein, E. Farber, G. D. Maengwyn-Davies, and A. L. Schade, *Ind. Eng. Chem.*, **36**, 772 (1944).
6) H. Nakayama *et al.*, to be published.
7) K. Aoki, *J. Am. Chem. Soc.*, **80**, 4904 (1958).
8) J. T. Yang and J. F. Foster, *J. Am. Chem. Soc.*, **75**, 5560, 5743 (1953).
9) J. F. Foster and K. Aoki, *J. Am. Chem. Soc.*, **80**, 5215 (1958).
10) F. A. Green, *J. Colloid Interface Sci.*, **35**, 481 (1971).
11) S. I. Ahmad, *Sep. Sci.*, **10**, 689 (1975).
12) E. J. Cohn, *Chem. Revs.*, **19**, 241 (1936).
13) H. Kunieda and K. Shinoda, *J. Phys. Chem.*, **82**, 1710 (1978).

14) O. H. Lowry, N. J. Rosebrough, A. L. Farr, and R. J. Randall, *J. Biol. Chem.*, **193**, 265 (1951).
15) L. K. Wang and D. F. Langley, *Ind. Eng. Chem., Prod. Res. Dev.*, **14**, 210 (1975).
16) The buffer was prepared by mixing 100 cm^3 of a 0.5 M citric acid solution with 100 cm^3 of a 0.2 M Na_2HPO_4 solution.
17) L. G. Longworth, *Ann. N. Y. Acad. Sci.*, **41**, 267 (1941).
18) C. Tanford, "Physical Chemistry of Macromolecules," John Wiley & Sons, Inc., New York (1961).
19) This estimate is based on generally accepted values for micellar solutions of ionic surfactants or for polyelectrolyte solutions.

Effect of Pressure on Mesomorphic Transitions in Cholesterol Esters of Unsaturated C_{18} Aliphatic Acids

Masaru NAKAHARA,* Katsumi MAEDA, and Jiro OSUGI

Department of Chemistry, Faculty of Science, Kyoto University, Oiwake-cho, Kitashirakawa, Sakyo-ku, Kyoto 606

(Received March 31, 1980)

The smectic to cholesteric, cholesteric to isotropic liquid, and solid to isotropic liquid transitions in the following cholesterol esters are determined by an optical method as a function of pressure up to 1 kbar; cholesteryl oleate, cholesteryl linoleate, and cholesteryl linolenate. The pressure dependence of the transition temperatures (dT/dP) is in the range of 21 to 36 K kbar^{-1}, and the volume changes (ΔV) computed by means of Clapeyron's equation are between 0.42 and 1.3 cm^3 mol^{-1} at 1 bar. The volume change for the smectic to cholesteric transition increases with the number of the double bonds in the acids, while that for the cholesteric to isotropic liquid is little affected by the double bonds.

A study of the effect of pressure on the phase behaviors of liquid-crystal forming materials was begun by Hulett[1] just 10 years after the discovery of liquid crystals.[2,3] Similar kinds of work were undertaken by Puschin and Grebenshchikov[4] and by Robberecht[5] in the former half of this century. Researches of liquid crystals at high pressure revived one decade ago, and recently developed in various ways with the aid of more advanced techniques for measurements, as briefly reviewed elsewhere.[6] A useful optical method for detecting mesomorphic transitions at high pressure was invented and applied to cholesteryl stearate in a previous paper.[6] Cholesterol esters of a homologous series of unsaturated C_{18} aliphatic acids are investigated in the present work. Hydrocarbon chains in the cholesterol esters of saturated aliphatic acids are stretched in the solid(So), smectic(Sm), and cholesteric(Ch) phases and in the isotropic liquid(IL) phase near the Ch-IL transition; all the conformations are in the *S-trans* form.[7] The conformation about a double bond is considered to be *cis* in the acids studied here.[8,9] Thus, it is interesting to see how the deviation from the linear conformation (rod-likeness) influences the phase behaviors and volume changes associated with the phase transitions.

Experimental

Cholesteryl oleate(CO), cholesteryl linoleate(CL), and cholesteryl linolenate(CLN) were obtained from Eastman Kodak. The esters were recrystallized from 1-pentanol, washed by a water-ethanol mixture (50 v/v%) and by water, and dried before use *in vacuo* for more than 10 h. As seen in Table 1, the transition temperatures at 1 bar (1 bar=10^5 Pa) of the purified materials agree well with the literature values[9] except for CLN.

The transition temperatures were determined by using an apparatus designed previously in which a He-Ne gas laser (wavelength 632.8 nm and power 3 mW) and a phototransistor were used as a source and a detector, respectively. Pressure was measured to ± 1 bar by a Heise Bourdon gage, and temperature to ± 0.1 °C by a chromel-alumel thermocouple fixed in the high-pressure optical cell. The transition temperatures were reproducible within ± 0.5 °C under any condition. The high-pressure apparatus and experimental procedure were described in detail elsewhere.[6]

Results and Discussion

A typical example of the transparency variation below and above the Sm–Ch transition is shown in Fig. 1; the transparency increases slightly with increasing temperature in the smectic phase, drops at the transition, and increases more rapidly in the cholesteric phase. The transparency minimum is reported also for the mesomorphic transition in other liquid crystals.[10–12] Causes for the appearance of the minimum would be strong light scattering and reflection at the boundaries of optically anisotropic domains being reorganized to form the cholesteric order. The positional order in the direction normal to the smectic layer is lost during the smectic to cholesteric transition. Thus, the diffusive motion of a molecule in this direction has something to do with the rate of the transparency drop. The manner how the transparency rose with time (cooling) from the minimum to its

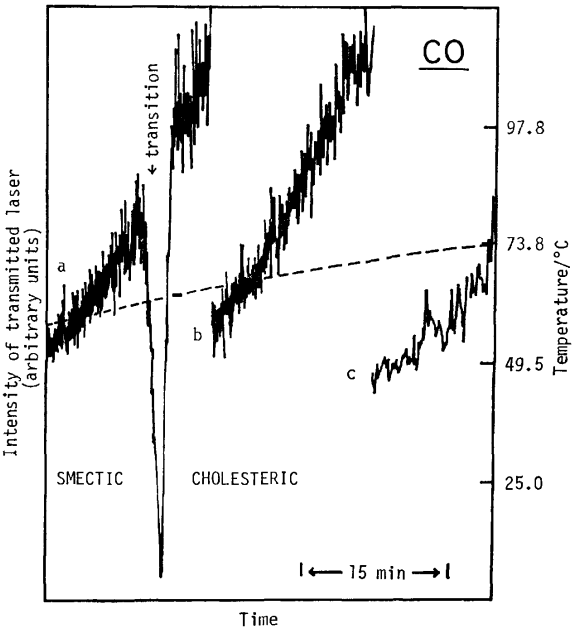

Fig. 1. Optically detected smectic-cholesteric transition in cholesteryl oleate at 920 bar.
—: Intensity of transmitted laser; --: temperature; sensitivity of detecting system, a/c=5 and b/c=2.5.

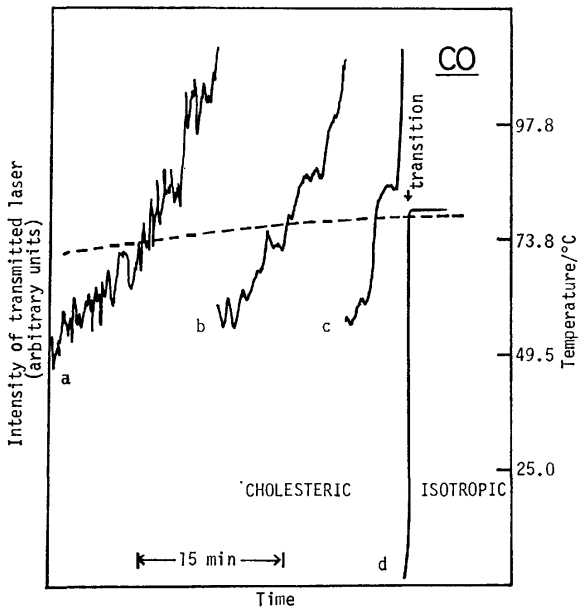

Fig. 2. Optically detected cholesteric–isotropic liquid transition in cholesteryl oleate at 1 kbar.
—: Intensity of transmitted laser; --: temperature; sensitivity of detecting system, a/d=400, b/d=200, and c/d=100.

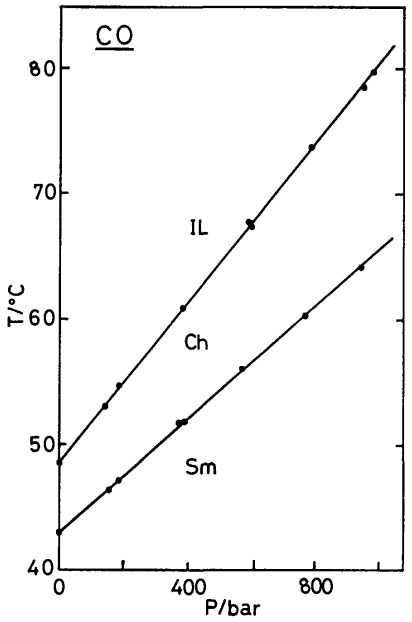

Fig. 3. Phase diagram of cholesteryl oleate.

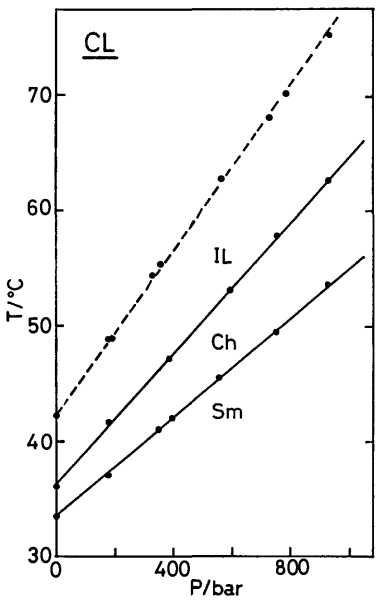

Fig. 4. Phase diagram of cholesteryl linoleate.
--: So–IL transition.

smectic value was taken as a criterion to judge a tricritical point of the Ch–Sm transition in cholesteryl oleyl carbonate.[12] No corresponding phenomena were observed in these esters at any pressure. Taschek and Williams[13] ascribed the transparency increase with temperature in liquid crystals to the decrease in the birefringent factor, the square of the difference between ordinary and extraordinary indices. Changes in the size of domains and in the pitch of the helical structure in the cholesteric phase would also contribute to the transparency increase. These factors cause the transparency jump finally at the Ch–IL transition, as seen in Fig. 2. Similar changes in transparency took place when material densities were decreased by reducing pressure at almost constant temperature. The transitions in these esters are monotropic with respect to the solid state as,

$$\text{—So}\leftarrow\text{Sm}\leftrightarrow\text{Ch}\leftrightarrow\text{IL}\leftarrow\text{ .}$$

The So←Sm transition could not be detected by the present method. The smectic phase of CO and CLN were apt to be supercooled below 0 °C, so that their So→IL transitions were not examined. The absolute value of the transparency in the smectic or cholesteric phase differed from one to another run, especially depending on the cooling rate.

The transition temperatures determined thus are plotted against pressure in Figs. 3, 4, and 5. In Fig. 4, the liquid crystalline phases look as if they were supercooled. Every boundary line in the phase diagrams is straight under the present experimental conditions. The values of the slopes (dT/dP) for the transitions are summarized together with other transition parameters at 1 bar in Table 1. In each ester, the larger the slope the higher the transition point;

$$(dT/dP)_{\text{Sm-Ch}} < (dT/dP)_{\text{Ch-IL}}[<(dT/dP)_{\text{So-IL}}].$$

In other words, the temperature range over which the liquid crystalline phases are stable is widened by the application of pressure. The trend found often experimentally is predicted by the order-disorder transition theories based on a lattice model.[14–16]

The volume changes ΔV at 1 bar accompanying the transitions are computed by putting the slopes (dT/dP) and the literature values[9] of the enthalpy changes ΔH into Clapeyron's equation,

$$\Delta V = \Delta H T^{-1}(dT/dP). \quad (1)$$

The values of ΔV computed thus are listed in the last column of Table 1. The volume change for the

Table 1. Thermodynamic data related to the phase transitions at 1 bar

Compound	Transition	Transition point[a] °C	ΔH[a] kJ mol^{-1}	dT/dP K kbar^{-1}	ΔV cm^3 mol^{-1}
Cholesteryl oleate	Ch–IL	48.5 (46.4)	0.491	32	0.49
	Sm–Ch	43.0 (41.8)	1.01	23	0.73
Cholesteryl linoleate	So–IL	42.3 (42.6)	29.9	36	34
	Ch–IL	36.3 (35.1)	0.543	28	0.50
	Sm–Ch	33.6 (34.0)	1.47	21	1.0
Cholesteryl linolenate	Ch–IL	38.0 (34.8)	0.433	30	0.42
	Sm–Ch	30.6 (33.0)	1.84	22	1.3

a) The transition points in the parentheses and enthalpy changes are from Ref. 9.

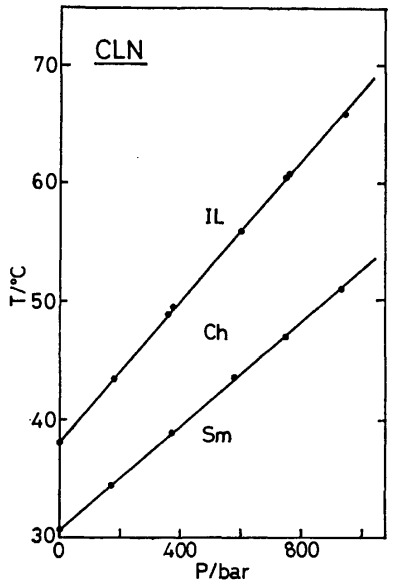

Fig. 5. Phase diagram of cholesteryl linolenate.

So–IL transition in CL is much larger than that for the Sm–Ch or Ch–IL transition, because in the former transition, the positional and rotational orders inherent in the solid state are completely lost at the same time. The ratio of the volume changes, $\Delta V_{\text{Sm-Ch}}/\Delta V_{\text{Ch-IL}}$ is larger than unity in every case, and increases as the molecular shape deviates further from rod-likeness. The former tendency indicates that one translational freedom brings about a larger volume change than two rotational freedoms. The volume change for the Sm–Ch transition increases with the number of the double bonds, while that for the Ch–IL transition is little affected. The volume changes for the Sm–Ch transition can be linearly correlated to the corresponding entropy changes in the homologous series, because the slopes (dT/dP) in Eq. 1 are all in the narrow range of 21 to 23 K kbar^{-1}.

References

1) G. A. Hulett, *Z. Phys. Chem.*, **28**, 629 (1899).
2) F. Reinitzer, *Monatsh. Chem.*, **9**, 421 (1889).
3) O. Lehmann, *Z. Phys. Chem.*, **4**, 462 (1889).
4) N. A. Pushin and J. V. Grebenshchikov, *Z. Phys. Chem.*, **124**, 270 (1926).
5) J. Robberecht, *Bull. Soc. Chim. Belg.*, **47**, 597 (1938).
6) K. Maeda, M. Nakahara, K. Hara, and J. Osugi, *Rev. Phys. Chem. Jpn.*, **49**, 85 (1979).
7) J. H. Wendorff, F. P. Price, *Mol. Cryst. Liq. Cryst.*, **22**, 85 (1973); *ibid.*, **24**, 129 (1973).
8) F. A. Vandenheuvel, *J. Am. Oil Chem. Soc.*, **40**, 455 (1963).
9) G. J. Davis, R. S. Porter, J. W. Steiner, and D. M. Small, *Mol. Cryst. Liq. Cryst.*, **10**, 331 (1970).
10) G. Chistyakov, *Soviet Physics-Chrystallography*, **8**, 57 (1963).
11) E. J. Poziomek, T. J. Novak, and R. A. Mackay, *Mol. Cryst. Liq. Cryst.*, **15**, 283 (1972).
12) P. H. Keyes, H. T. Weston, and W. B. Daniels, *Phys. Rev. Lett.*, **31**, 628 (1973).
13) R. Taschek and D. Williams, *J. Chem. Phys.*, **6**, 546 (1938).
14) J. A. Pople and F. E. Karasz, *J. Phys. Chem. Solids*, **18**, 28 (1961); F. E. Karasz and J. A. Pople, *ibid.*, **20**, 294 (1961).
15) S. Chandrasekhar, R. Shashidhar, and N. Tara, *Mol. Cryst. Liq. Cryst.*, **10**, 337 (1970); *ibid.*, **12**, 245 (1972).
16) S. Chandrasekhar, "Liquid Crystals," Cambridge University Press, London (1977), Chap. 2.

On the Origin of Differences in the Phosphorescence Band Patterns of *p*-Benzoquinone in *p*-Dihalobenzene Crystals[1)]

Yusei MIYAGI, Motohiko KOYANAGI,* and Yoshiya KANDA

Department of Chemistry, Faculty of Science, Kyushu University, Hakozaki, Higashi-ku, Fukuoka 812

(Received April 7, 1980)

The phosphorescence spectra of *p*-benzoquinone (PBQ) have been studied at 4.2 K in isostructural crystals such as *p*-dichlorobenzene (DCB), *p*-bromochlorobenzene (BCB), and *p*-dibromobenzene (DBB); and in their binary mixed crystals. The variable phosphorescence band patterns observed are interpreted in terms of anisotropic local-field effects of the host environmental molecules. A similarity of the phosphorescence intensity distribution between two systems of PBQ/BCB and PBQ/(0.5 molar fraction of DCB+0.5 molar fraction of DBB) is a manifestation of the existence of effective local-fields in the crystals.

Extensive spectroscopic studies have been carried out on the lowest excited triplet state of *p*-benzoquinone (hereafter abbreviated as PBQ) in rigid matrices[2-9)] and have served as the basis for understanding emission spectra of more complex quinoidal compounds, *e.g.*, the emission spectra of 9,10-anthraquinone[10-12)] and 1,4-naphthoquinone.[13)] No widely accepted theoretical work on the energy splitting $\Delta E(n_+ - n_-)$ has appeared so far despite a great interest in knowledge about the extent of interaction between the two zeroth order n orbitals on the two carbonyl oxygens. The energy separation between the two $n\pi^*$ states of the same spin-multiplicity, which originate mainly in the $\pi_5 \leftarrow n_+$ and $\pi_5 \leftarrow n_-$ excitations, is also controversial.[14,15)]

The phosphorescence is expected sensitive even to a feasible perturbation because PBQ has a small energy gap between $T_1(n_-\pi_5^*)$ and $T_2(n_+\pi_5^*)$ states, *e.g.*, 0.002—0.04 eV depending on environments.[3-9,14)] The perturbation may be external (*e.g.*, environmental), or internal (*e.g.*, vibrational), or a combination of both. The objectives of this paper are to examine a change in the phosphorescence spectral pattern of PBQ with a change in environmental force-fields and to demonstrate a great dependence of the PBQ spectral pattern upon environments.

Experimental

All chemicals of extra pure grade were obtained from Tokyo Kasei Co. Ltd. The guest substance PBQ was recrystallized at least twice from petroleum ether prior to several vacuum sublimations. All the host substances, *i.e.*, *p*-dibromobenzene (abbreviated as DBB), *p*-dichlorobenzene (DCB) and *p*-bromochlorobenzene (BCB), were sublimed *in vacuo* and then zone-refined more than 70 passes. The guest concentration of about 10^{-3} in mol/mol ratios was generally employed. All mixed crystals were grown using the usual Bridgman method. The apparatus and experimental conditions are similar to those described previously.[16)] No intensity correction was carried out for photomultiplier response, grating reflection property, and quantum efficiency difference because the locations of the phosphorescence origin bands in the three matrices are close to each other and only their relative intensities are referred to in this paper.

Crystal Structure of DBB, DCB, and BCB

All hosts have well been known to crystallize in the same space group of $C_{2h}^5(P2_{1/a})$ with two molecules in the unit cell and to have nearly identical unit cell dimensions.[17-19)] The representative crystal structure of these hosts is shown in Fig. 1 and the dimensional data cited are given in Table 1. If a mixed crystal is grown very slowly from the melt mixed with two types of these *p*-dihalobenzenes, each lattice point of the mixed crystal can be regarded as a statistical average of the two types of molecules.[20)] As for the BCB crystal itself, the halogen positions are filled at random by bromine or chlorine.[19,21)] Since the space group has four general positions, only a statistical symmetry is possible with a center of symmetry at the center of the average molecule. Its benzene ring is assumed as a regular hexagon of 1.41 Å in side and the C–X (halogen) bond lengths of 1.77 Å are intermediate between C–Cl (1.69 Å in DCB) and C–Br (1.88 Å in DBB).[19,22)] The permanent diplole moment of BCB has been reported to be 0.1 D.[23)] This is very close to an estimated value of 10^{-1} D from a vector combination of the dipole moments available for chlorobenzene and bromobenzene.[24)]

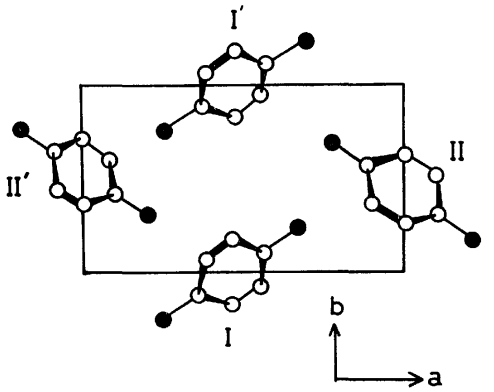

Fig. 1. Crystal structure of DCB and DBB (after Croatto *et al.*, Ref. 17).
●: Br or Cl, ○: C.

TABLE 1. THE DIMENSIONAL PARAMETERS OF THE CRYSTALS OF DCB, BCB, AND DBB

	DCB[a)]	BCB[b)]	DBB[c)]
a/Å	14.80	15.20	15.36
b/Å	5.78	5.86	5.75
c/Å	3.99	4.11	4.10
β	113°00′	113°12′	112°38′

a) Data taken from Ref. 18. b) Data taken from Ref. 19. c) Data taken from Ref. 17.

Results

Phosphorescence Spectra. The phosphorescence spectra of PBQ in BCB, DCB, and DBB at 4.2 K are shown in Fig. 2. Here two characteristic bands are designated as *a* and *q*. The band *a* lying at the shortest wavelength of the emission systems contains the origin band and the band *q* both the ν(C=O) symmetric and antisymmetric vibrational bands. At a glance the phosphorescence band pattern of PBQ/BCB resembles that of the $^3B_{1g} \rightarrow {}^1A_g$ phosphorescence of PBQ/toluquinone reported previously.[9] On the other hand, the spectra of PBQ/DCB and PBQ/DBB are of the "forbidden-type" spectral pattern whose features have been discussed somewhat minutely in the phosphorescence spectrum of PBQ/naphthalene.[9] The phosphorescence spectrum of PBQ/DCB resembles those reported previously.[2,3] However, all the spectra of this system seem to contain additional emission components with broad band feature. Such additional emissions have also been reported for other guest molecules in the same DCB host and attributed to different phases of the host crystal.[25,26] Except the band broadness, the spectral intensity distribution of PBQ/DCB is rather close to that of PBQ/DBB. The strongest band in both systems is ascribed to the ν(C=O) antisymmetric b_{1u} vibrational mode.[2,3,6-8]

Another intensity aspect is given through a study on the phosphorescence spectra of PBQ in a binary-component crystal system, *i.e.*, PBQ/(DCB–DBB). In Fig. 3 are shown the phosphorescence spectra of PBQ at various molar fractions of DCB in DBB. For convenience' sake, all the emission spectra were roughly normalized in the peak height of the band *q* around 16750 cm^{-1}. Obviously the band *a* increases in intensity, relative to the intensity of the band *q*, with an increase in DCB molar fraction x_{DCB} from 0 to 0.5. A similar concentration dependence was also observed with an increase in DBB concentration x_{DBB} from 0 to 0.5. It should be noted that the phosphorescence band pattern at $x_{DCB}=x_{DBB}=0.5$ is very similar to that of PBQ/BCB (compare the spectral curve (6) in Fig. 3 with that given in Fig. 2a).

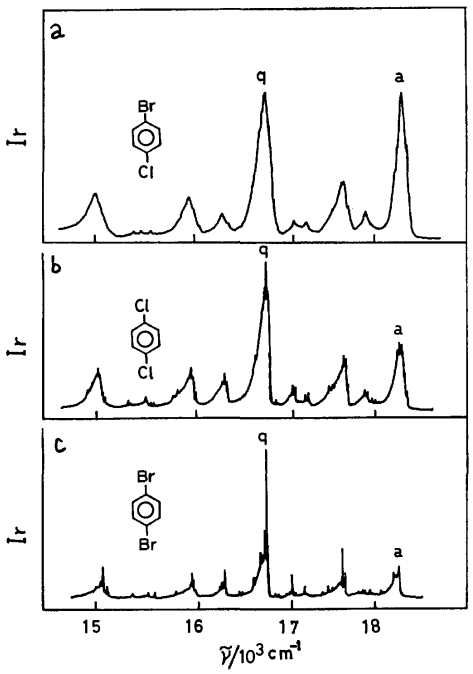

Fig. 2. Phosphorescence spectra of PBQ in (a) BCB, (b) DCB, and (c) DBB at 4.2 K. An apparent band *a* represents the origin band region containing some phonon modes and *q* the ν(C=O) band region. The ordinate I_r means a relative output signal intensity. No intensity correction is given in this Figure.

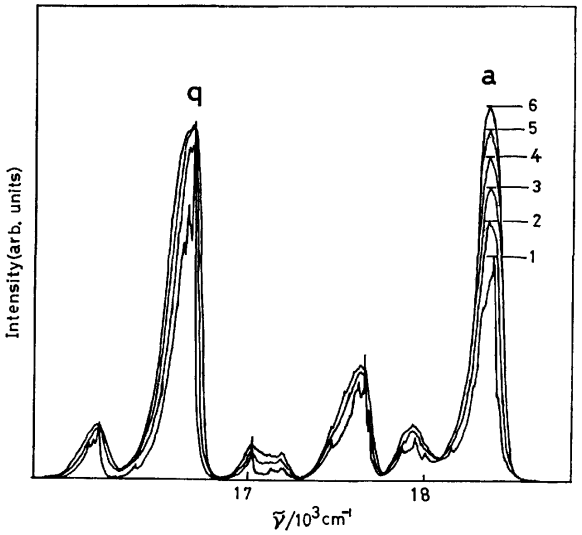

Fig. 3. Phosphorescence spectra of PBQ in binary host crystals of DCB/DBB at 4.2 K. The guest concentration is almost constant, *i.e.*, $\approx 10^{-3}$ mol/mol. The molar fractions of DCB in DBB are (1) 0.05, (2) 0.1, (3) 0.2, (4) 0.3, (5), 0.4, and (6) 0.5. To avoid the confusion of band overlappings, we employ a suitable abbreviation in this Figure.

Intensity Correlation in Binary Host Crystals. A meaningful correlation is obtained between the intensity increment of the apparent band *a* and the molar fraction of x_{DCB} (hereafter abbreviated simply as x unless noted especially) in the binary host system, *i.e.*, DCB/DBB. Since estimation of the absolute intensity of emission spectra is generally difficult, we take only a relative intensity. The intensity of the band *a* may approximately be represented as

$$\int_{\tilde{\nu}_a-\Delta}^{\tilde{\nu}_a+\Delta} f(\tilde{\nu}, x)\mathrm{d}\tilde{\nu} = F_a(x), \tag{1}$$

where $f(\tilde{\nu},x)$ is the uncorrected shape-function of the observed phosphorescence spectrum at a solvent constituent x and Δ is taken as a region much greater than any *hwhm* in all mixed crystal systems but less than 400 cm^{-1} since a next prominent band might usually appear around 400 cm^{-1} region from the band in question and we must exclude such an unnecessary component from the intensity estimation. Similarly the intensity of the band *q* is given by

$$\int_{\tilde{\nu}_q-\Delta}^{\tilde{\nu}_q+\Delta} f(\tilde{\nu}, x)\mathrm{d}\tilde{\nu} = F_q(x). \tag{2}$$

Since these bands are extremely strong in intensity and the intensities of other bands as combination

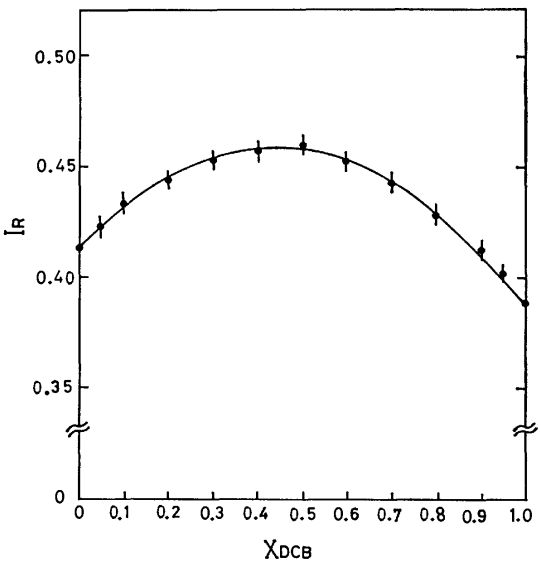

Fig. 4. A correlation between the relative intensity of the "origin" band, I_R, and the concentration of DCB in the binary host system of DCB–DBB, x. ●: Observed value, —: simulated parabola (the analytical details are given in the article).

bands are closely related to either the origin band or the false origin band, it will be reasonable to employ an approximate relative intensity of the band a as follows:

$$I_R(x) = F_a(x)/\{F_a(x)+F_q(x)\}. \quad (3)$$

The observed values of I_R against x are plotted in Fig. 4. An analytical expression for the empirical plot is given by

$$I_R(x) = -0.236x^2 + 0.212x + 0.413. \quad (4)$$

The solid curve in Fig. 4 shows this parabola.

Theoretical Consideration

General Spectral Behaviors in a Binary A–B Host System. Now let us assume that a guest molecule is surrounded by n solvent molecules. Each solvent site is occupied by either an A or a B molecule. It is, of course, statistical which molecule of them takes a certain site i. There are $N(=2^n)$ arrangements of the binary host molecules unless any symmetrical simplification is taken into account. In general the observed shape function $f(\tilde{\nu}, x)$ is represented as the arithmetic mean over all these arrangements:[27]

$$f(\tilde{\nu}, x) = \frac{1}{N}\sum_{R}^{N} f_R(\tilde{\nu}, x). \quad (5)$$

Here $f_R(\tilde{\nu}, x)$ denotes the shape function of a certain host arrangement R and is developed in terms of the binomial distribution function with two parameters n and m:

$$f_R(\tilde{\nu}, x) = \sum_m \binom{n}{m} x_A^n x_B^{n-m} f^\circ_{mR}(\tilde{\nu}), \quad (6)$$

where $f^\circ_{mR}(\tilde{\nu})$ signifies the shape function of the arrangement R with m sites of the A molecule and n-m sites of the B molecule. The actual emission shape is thus developed as a polynomial of x with degree n:

$$f(\tilde{\nu}, x) = K_n(\tilde{\nu})x^n + K_{n-1}(\tilde{\nu})x^{n-1} + \cdots + K_1(\tilde{\nu})x + K_0(\tilde{\nu}). \quad (7)$$

Here each of the expansion coefficients, K's, is constant for a fixed $\tilde{\nu}$-value:

$$K_i(\tilde{\nu}) = \sum_{m=0}^{i} \frac{n!(-1)^{i-m}}{(n-i)!(i-m)!} f^\circ_{mR}(\tilde{\nu}) \quad (8)$$

with the boundary conditions,

$$K_0(\tilde{\nu}) = f(\tilde{\nu}, 0) = f^\circ_A(\tilde{\nu}) \quad (9)$$

and

$$\sum_n K_n(\tilde{\nu}) = f(\tilde{\nu}, 1) = f^\circ_B(\tilde{\nu}). \quad (10)$$

Case of n=2. For a special case n=2 in Eq. 7, the following coefficients are obtained from Eq. 8:

$$K_2(\tilde{\nu}) = f^\circ_{0R}(\tilde{\nu}) + f^\circ_{2R}(\tilde{\nu}) - f^\circ_{1R}(\tilde{\nu}), \quad (11)$$

$$K_1(\tilde{\nu}) = 2\{f^\circ_{1R}(\tilde{\nu}) - f^\circ_{0R}(\tilde{\nu})\}, \quad (12)$$

and

$$K_0(\tilde{\nu}) = f^\circ_{0R}(\tilde{\nu}). \quad (13)$$

Discussion

If a PBQ molecule is located substitutionally at any of centrosymmetric sites in the DCB or DBB lattice of monoclinic $P2_{1/a}$, the zero-phonon origin band in the $^3B_{1g}\rightarrow{}^1A_g$ phosphorescence of the PBQ molecule is forbidden by the electric dipole selection rule. The weak origin band observed in these hosts[2,3] seems to support the assumption mentioned above for the molecular location in the hosts. When a PBQ molecule is located at any of noncentrosymmetric sites in the BCB or toluquinone lattice, however, the intensification of the origin band is remarkable (see Fig. 2a and also Ref. 9).

The intensity change observed in the binary solvent system of DCB and DBB is extremely suggestive (*cf.* Figs. 3 and 4). Supposing that one of the host molecules is substituted with a guest PBQ molecule, we can, as the zeroth approximation, consider a model in which the PBQ molecule is surrounded by eighteen neighbor host molecules: Six of them are located at "translationally equivalent" sites and the others at "translationally nonequivalent" ones. In the present case any possible guest-guest interaction is neglected since the concentration of the guest employed is dilute enough. As has been demonstrated in the previous works on the Stark experiments,[5,6,16,28] the most effective electric perturbation for the interstate coupling between $^3B_{1g}(n\pi^*)$ and $^3A_u(n\pi^*)$ states is the electric field change along the C=O axis of the guest molecule. This will be true for environmental dipolar perturbations or asymmetric host locations. As a matter of fact, a preliminary model calculation shows that the effective electric field of a permanent host molecule with 10^{-1} D over a guest molecule distant by 8 Å from it amounts to $\approx 10^6$ V/cm in external bulk scales.[29]

It is thus expected that the host arrangements concerning with four translationally equivalent molecules along the crystallographic b and c axes (*e.g.*, the molecule I′ for the assumed guest molecule I in Fig. 1) give

little contribution to the interstate mixing between $^3B_{1g}$ and ^3A_u states as well as those concerning with six translationally nonequivalent molecules (*e.g.*, the molecule II'). Furthermore, two translationally equivalent molecules along the a-axis are located too far from the guest molecule to be taken into account. There remain six translationally nonequivalent molecules on which the effective C=O axis perturbations should be assessed (*e.g.*, see the molecules II at (a/2, b/2, −c), (a/2, b/2, 0), and (a/2, b/2, c); and their inversion sites with respect to the site I). However, several investigations on the phosphorescence spectra have suggested that the $\pi_5^*\leftarrow n_\pm$ excitations are localized on the C=O groups.[6,14] Since the closest halogen-halogen intermolecular distances of DCB and DBB have been reported to be 3.85 Å and 3.76 Å, respectively, between the molecule I at (0, 0, 0) and the molecule II at (a/2, b/2, 0),[17] it seems reasonable to consider the molecule II and its inversion site molecule $\overline{\text{II}}$ at (−a/2, −b/2, 0) as the most effective components of anisotropic force-fields. There are four ways in which the molecules of DBB(B) and DCB(C) occupy these sites:

$$\text{II(B)}\text{-}\overline{\text{II}}\text{(B)},\ \text{II(C)}\text{-}\overline{\text{II}}\text{(C)},\ \text{II(B)}\text{-}\overline{\text{II}}\text{(C)},$$
$$\text{and II(C)}\text{-}\overline{\text{II}}\text{(B)}.$$

If we define the emission shape functions for these host arrangements as $f_B(\tilde{\nu})$, $f_C(\tilde{\nu})$, $f_{BC}(\tilde{\nu})$, and $f_{CB}(\tilde{\nu})$, respectively, an actual emission shape $f(\tilde{\nu}, x)$ will be represented by means of the usual statistical treatment:

$$\begin{aligned} f(\tilde{\nu}, x) &= x_{DBB}^2 f_B(\tilde{\nu}) + x_{DCB}^2 f_C(\tilde{\nu}) \\ &\quad + x_{DBB}x_{DCB}\{f_{BC}(\tilde{\nu}) + f_{CB}(\tilde{\nu})\} \\ &= x^2 f_B(\tilde{\nu}) + (1-x)^2 f_C(\tilde{\nu}) + 2x(1-x) f_{BC}(\tilde{\nu}). \end{aligned} \quad (14)$$

This just corresponds to what is given for the special case of $n=2$ in the preceding section (*cf.* Eqs. 11—13). Certainly, intensity contributions from higher orders of x than x^2 are expected small for small values of x, but this good agreement between the observed intensity change and the simulation curve of $n=2$ around $x\approx 1$ strongly supports our assumption for effective host arrangements. Since each lattice point of the mixed crystal is regarded as a statistical average of the binary components of molecules,[20] the resemblance between the phosphorescence spectra of PBQ/BCB and PBQ/(0.5 molar fraction of DCB+0.5 molar fraction of DBB) seems to be reasonable. It is suggested that the asymmetric arrangement between the molecular location II in Fig. 1 and its inversion one $\overline{\text{II}}$ is very effective for increasing the "origin band" of the PBQ phosphorescence in intensity. Similar intensification of "forbidden" bands of molecules in environments have extensively been discussed and importance of the environmental effects has been emphasized.[30-33]

The authors would like to thank Professor D. S. McClure for donating a copy of Klump's thesis (Ref. 2) and Professor H. P. Trommsdorff for sending a copy of his thesis (Ref. 4). This work has been supported by a Grant-in-Aid for Scientific Research from the Ministry of Education, Science and Culture. One of the authors (Y. M.) has been financially supported during his graduate course by the Uehara Education Foundation Fund.

References

1) Presented in part at the 40th National Meeting of the Chemical Society of Japan, Fukuoka, Oct., 1979. Taken partially from the Doctoral thesis of Y. M., Kyushu University, 1979.
2) K. N. Klump, Ph. D. thesis, University of Chicago, 1968.
3) M. Koyanagi, Y. Kogo, and Y. Kanda, *J. Mol. Spectrosc.*, **34**, 450 (1970).
4) H. P. Trommsdorff, *J. Chem. Phys.*, **56**, 5358 (1972); Ph. D. thesis, Université Scientifique et Médical de Grenoble, 1972.
5) R. M. Hochstrasser, L. W. Johnson, and H. P. Trommsdorff, *Chem. Phys. Lett.*, **21**, 251 (1973).
6) H. Veenvliet and D. A. Wiersma, *Chem. Phys. Lett.*, **22**, 87 (1973); *Chem. Phys.*, **2**, 69 (1973); *ibid.*, **8**, 432 (1975).
7) A. I. Attia, B. H. Loo, and A. H. Francis, *Chem. Phys. Lett.*, **22**, 537 (1973).
8) B. H. Loo and A. H. Francis, *J. Chem. Phys.*, **65**, 5076 (1976).
9) M. Koyanagi, Y. Miyagi, and Y. Kanda, *J. Lumin.*, **12/13**, 345 (1976).
10) O. S. Khalil and L. Goodman, *J. Phys. Chem.*, **80**, 2170 (1976).
11) E. Kanezaki, N. Nishi, and M. Kinoshita, *Bull. Chem. Soc. Jpn.*, **52**, 2836 (1979).
12) T. Murao and T. Azumi, *J. Chem. Phys.*, **70**, 4460 (1979).
13) A. Kuboyama, *Bull. Chem. Soc. Jpn.*, **51**, 2771 (1978).
14) J. Goodman and L. E. Brus, *J. Chem. Phys.*, **69**, 1604 (1978).
15) C. T. Horst and J. Kommandeur, *Chem. Phys.*, **44**, 287 (1979).
16) Y. Miyagi, M. Koyanagi, and Y. Kanda, *Chem. Phys. Lett.*, **40**, 98 (1976).
17) U. Croatto, S. Bezzi, and E. Bur, *Acta Crystallogr.*, **5**, 825 (1952); *Gazz. Chim. Ital.*, **79**, 240 (1949).
18) E. Frasson, C. Garbuglio, and S. Bezzi, *Acta Crystallogr.*, **12**, 126 (1959).
19) A. Klug, *Nature*, **160**, 570 (1947).
20) B. D. Saksena, *J. Chem. Phys.*, **18**, 1653 (1950).
21) S. B. Hendricks, *Z. Kristallogr.*, **34**, 85 (1933).
22) H. Laszlo, *Proc. R. Soc. London, Ser. A*, **146**, 690 (1934).
23) J. W. Williams, *J. Am. Chem. Soc.*, **50**, 2350 (1928).
24) J. Wilson, *Chem. Rev.*, **25**, 377 (1939).
25) B. W. Gash and S. D. Colson, *J. Chem. Phys.*, **59**, 3528 (1973).
26) T. Shigeoka, Master thesis, Kyushu University, 1968. In this thesis work, the phosphorescence spectra of pyrazine have been studied in various matrices as a function of sample-cooling-rates. In DCB three emission systems have distinctly been observed when the samples had been cooled very rapidly. These emissions have been attributed to three different phases in the host crystal. Such additional emissions have never been observed in DBB.
27) When some particular arrangements are favored by the solute/solvent system, weight-factors appropriate to them should, of course, be introduced into Eq. 5.
28) S. J. Sheng and M. A. El-Sayed, *Chem. Phys. Lett.*, **34**, 216 (1975).
29) Y. Miyagi, Doctoral thesis, Kyushu University, 1979.
30) G. W. Robinson, *J. Chem. Phys.*, **46**, 572 (1967).
31) M. Koyanagi, *J. Mol. Spectrosc.*, **25**, 273 (1968).
32) E. T. Harrigan and N. Hirota, *Mol. Phys.*, **31**, 681 (1976).
33) M. Koyanagi, K. Higashi, and Y. Kanda, *Chem. Phys. Lett.*, **52**, 184 (1977).

Studies of the Ion Flotation by Poly(ethyleneimine) Resin

Tsunetaka Sasaki,* Hisayo Kurosawa, Keiichi Miyasaka, and Minoru Mizushima

Department of Chemistry, Faculty of Science, Tokai University, 1117 Kitakaname, Hiratsuka 259-12

(Received April 1, 1980)

Flotation of Crystal violet (CV^+), neucoccin (NC^-), CrO_4^{2-}, PO_4^{3-}, Fe^{3+}, and Cu^{2+} ions was studied with use of poly(ethyleneimine) resin (PEI) as an adsorbent, Na-polyacrylate or polyacrylamide as a coagulant and sodium dodecyl sulfate or hexadecyltrimethylammonium chloride as a frother. In line with the results of adsorption studies, NC^-, PO_4^{3-}, and CrO_4^{2-} ions were effectively floated from their dilute solutions but CV^+ was not floated so much. The most effective flotation was attained for CrO_4^{2-} ions, a rapid initial decrease in concentration due to the flotation within 30 s being followed by a gradual decrease and nearly 100% flotation achieved within 10 min for a dilute solution. The rate of flotation follows a bimolecular reaction. The activation energy of flotation, 28.03 kJ mol^{-1}, is equal to that of CrO_4^{2-} ion adsorption by PEI. Flotation of Fe^{3+} and Cu^{2+} ions was effectively carried out through chelate formation of these ions with PEI.

Adsorbing particle flotation has been reported as an effective method of ion flotation,[1] bentonite being used as a cation exchange adsorbent. Further, poly(ethyleneimine) (PEI) was found to be a good anion exchange adsorbent as well as a chelating agent for metallic cations.[2] The adsorbing particle flotation of organic and inorganic anions and cations using PEI is reported in this paper.

Experimental

Materials. PEI used was supplied by Shunan Petroleum Company. The sample was prepared in a similar way to that reported.[2] Crystal Violet (CV^+) was precipitated by the addition of diethyl ether to an ethanol solution of CV^+. The precipitate was filtered and dried under reduced pressure. Neucoccin (NC^-) was recrystallized from its aqueous solution by the addition of anhydrous sodium carbonate. Crystals were filtered, washed with ethanol and dried. Potassium chromate, trisodium phosphate, Fe(III) chloride and Cu(II) sulfate of guaranteed grade were used without purification. Sodium polyacrylate (NaPA) of the degree of polymerization 2200—6600 and polyacrylamide (PAA) (Sanfloc AA-300P of Sanyo Chemical Industry Product) were used as coagulants. Pure hexadecyltrimethylammonium chloride (HTAC) (KAO Soap Co.) and sodium dodecyl sulfate (SDS) (Nikko Chemical Co.) were used.

Measurement. Flotation was carried out by adding PEI, coagulant and surfactant to the solution containing ions to be floated and shaking the solution in a stoppered test tube equipped with a stopcock at the bottom. Floatability (F) of dissolved ions was calculated from the concentrations of the solute before and after flotation by

$$F = \frac{C_i - C_f}{C_i} \times 100\%$$

where C_i and C_f denote the initial and final concentration of solute ions, respectively.

The concentrations of CV^+ and NC^- ions were measured with a Shimazu Spectronic Colorimeter 20 at wave lengths of 480 nm and 580 nm, respectively. The concentrations of CrO_4^{2-}, Fe^{3+}, and Cu^{2+} ions were measured with a Hitachi Atomic Absorption Spectrometer at wave lengths 357.9 nm, 248.3 nm, and 324.7 nm, respectively. Concentration of phosphate was determined by colorimetry at wave length 700 nm of ammonium phosphomolybdate formed by the addition of ammonium molybdate to the sample solution.

Results and Discussion

Flotation of PEI. In order to carry out the adsorbing particle flotation of ions by PEI, conditions for the flotation of PEI were studied. Flotation by hand-shaking of PEI suspension with addition of SDS alone, SDS and NaPA, and HTAC and NaPA was studied. In the flotation of PEI–SDS system, 15 cm^3 of a solution containing 0.1 g of PEI and varying amounts of SDS was shaken in a test tube for 10 s and left to stand for 5 min. The floatability was measured from the amount of PEI remaining as a suspension after flotation. In the flotation of PEI–NaPA–SDS and PEI–NaPA–HTAC systems, 15 cm^3 of the solution containing 0.1 g of PEI, 5.3 ppm of NaPA and varying amounts of SDS or HTAC was subjected to a similar treatment and the floatability was measured. All the experiments were carried out at room temperature, *ca.* 25 °C. The results are shown in Fig. 1.

The flotation percentage of PEI increases with increasing concentration of SDS or HTAC. The minimum concentration of surfactant of 100% flotation and the time required for the flotation are given in Table 1. Adsorbing particle flotation can be carried out under the conditions given. However, NaPA–SDS and NaPA–HTAC systems are preferable since flotation is quickly completed. NaPA–HTAC was used in the ion flotation studies of CV^+, NC^-, CrO_4^{2-}, and PO_4^{3-}, and PAA–SDS in the case of Fe^{3+} and Cu^{2+}

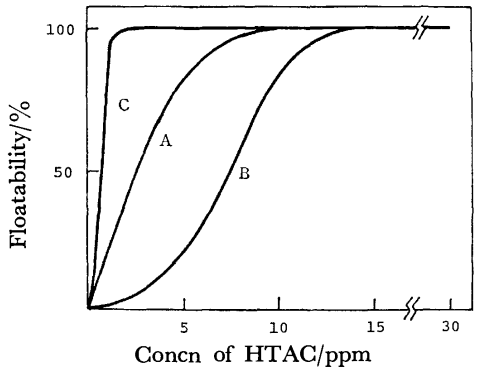

Fig. 1. Flotation of PEI.
A; SDS system, B; SDS-NaPA system,
C; HTAC-NaPA system.

Table 1. Flotation of PEI

System	Concn of SDS or HTAC	Time of flotation
SDS	8 ppm	60 s
SDS-NaPA	15	7
HTAC-NaPA	2	30

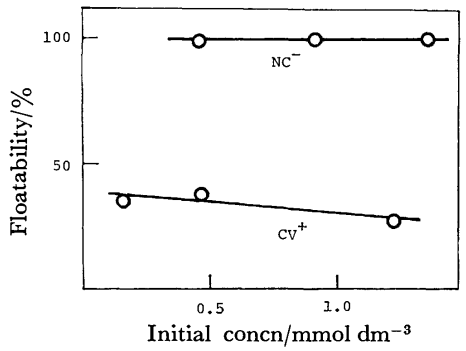

Fig. 2. Flotation of dyes.

ion flotation, neither NaPA–SDS nor NaPA–HTAC being effective in the latter case.

Flotation of Dye Ions. A 20 cm^3 solution containing 0.1 g of PEI, 14 ppm of NaPA in the case of NC^-, 40 ppm of NaPA in the case of CV^+, 20 ppm of HTAC and varying amounts of NC^- or CV^+ ions was shaken frequently for 7 min. After complete float-up of PEI, concentrations of NC^- and CV^+ ions in the underlying layers were measured, the floatability calculated being plotted against the initial concentration of respective ions (Fig. 2). Floatability of ions is nearly 100% up to the initial concentration of about 1.5 mmol dm^{-3}, while a maximum of 35% floatability was obtained for the dilute solution of CV^+ ions. Such a difference in floatability between NC^- and CV^+ ions can be expected from the anion exchange nature of PEI.[2]

Flotation of CrO_4^{2-} Ions. Since CrO_4^{2-} ions are significant as regards environmental contamination, removal of CrO_4^{2-} ions from aqueous solution by ion flotation was studied in detail.

Rate of CrO_4^{2-} Ion Flotation. A 150 cm^3 solution containing 1 g of PEI 13 ppm of NaPA, 3.3 ppm of HTAC and varying amounts of CrO_4^{2-} ions was put into an Erlenmeyer flask. Magnetic stirring for 5 min and shaking by hand was repeated. Residual concentration of Cr in the solution below PEI floated after each shaking was measured and plotted against time. Figure 3 shows the result for the solution of initial Cr concentration of 61.47 ppm.† The initial rapid fall of concentration within 30 s was followed by a gradual decrease, the concentration falling below 1/10 of the initial value within the first 10 min. Figure 4 shows the floatability of Cr after flotation for 10 min plotted against the initial concentration. The floatability increases with decreasing concentration of Cr, 98% of Cr being removed from 10.7 ppm Cr solution by flotation for 10 min.

† Concentration of Cr and the following P are expressed by ppm instead of mol dm^{-3}.

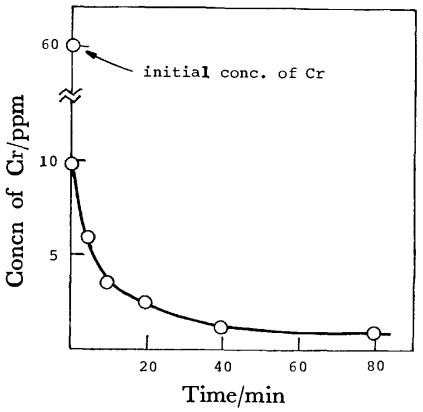

Fig. 3. Rate of CrO_4^{2-} ion flotation.

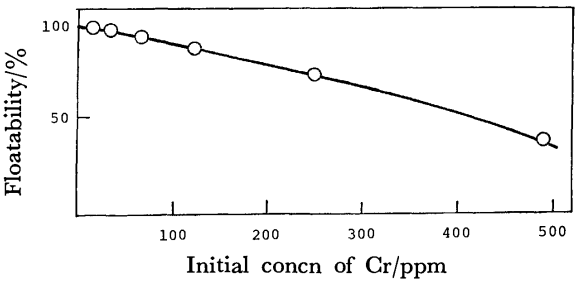

Fig. 4. Flotation of Cr.

In order to study the temperature dependence of the rate of CrO_4^{2-} ion flotation, a 500 cm^3 solution containing 54.5 ppm of Cr, 1 g of PEI, 14 ppm of NaPA and 4 ppm of HTAC was put into the Erlenmeyer flask. Stirring and shaking were carried out as mentioned above. The residual concentration determined after each flotation by shaking was measured, the result being plotted against time at a constant temperature in the range 25 °C—50 °C. Diagrams similar to that in Fig. 3 were obtained. From the results $1/(C-C_\infty)$ *vs.* t plots were made as in the case of CrO_4^{2-} ion adsorption by PEI,[2] where C and C_∞ denote the concentrations of Cr at time t and after a sufficiently long time, respectively. The results obtained at 30 °C are shown in Fig. 5. A linear relation

$$\frac{1}{C-C_\infty} = Kt + L$$

where K and L are constants, was confirmed to hold. This indicates that the reaction is bimolecular as in the case of CrO_4^{2-} ion adsorption by PEI.[2] The logarithm of K, considered as a reaction rate constant

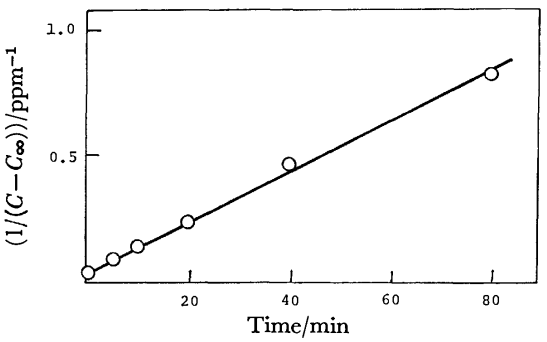

Fig. 5. $(1/C-C_\infty)$ *vs.* t plots.

of ion flotation, is plotted against the reciprocal of the absolute temperature T (Fig. 6). A straight line was obtained, the slope of which gave the activation energy of 28.03 kJ mol^{-1} in agreement with the value obtained for CrO_4^{2-} ion adsorption by PEI.[2] This suggests that the ion exchange adsorption is the rate determining step of the flotation of CrO_4^{2-}.

Effect of the Amount of PEI on CrO_4^{2-} Ion Flotation. In order to determine the amount of PEI necessary for CrO_4^{2-} ion flotation, a 500 cm^3 solution containing 5 ppm of Cr,†† 14 ppm of NaPA, 4 ppm of HTAC and varying amounts of PEI was stirred and shaken in an Erlenmeyer flask, and the residual concentration of Cr after flotation for 10 min was measured. The result is plotted against the amount of PEI in Fig. 7. It was confirmed that 0.5 g of PEI is sufficient to reduce Cr concentration from 5 ppm to below 0.5 ppm in a 500 cm^3 solution. Since neither the NaPA–HTAC–CrO_4^{2-} system nor the HTAC–CrO_4^{2-} system showed any perceptible flotation of Cr, PEI together with HTAC and NaPA is considered necessary to float Cr. A suggested model to explain the mechanism of adsorbing particle flotation of CrO_4^{2-} ions is shown in Fig. 8.

Flotation of PO_4^{3-} Ions. A 500 cm^3 solution containing 1 g of PEI, 14 ppm of NaPA, 8 ppm of HTAC and varying amount of PO_4^{3-} was treated as in the case of CrO_4^{2-} ion flotation. The residual concentration of P, determined by the measurement of PO_4^{3-} ion concentration, was plotted against the flotation time. Figure 9 shows results obtained for PO_4^{3-} solution containing 8.15 ppm of P. An abrupt decrease in the residual concentration of P within a minute is followed by a gradual decrease, the concentration becoming nearly constant after 20 min flotation. Figure 10 shows the floatability of P after 20 min flotation plotted against the initial concentration. The floatability does not reach 90% even in a dilute solution of PO_4^{3-} ions. Further experiment showed that 1 g of PEI is necessary to reduce the concentration of P from 3.26 ppm to 0.23 ppm in 500 cm^3 solution by 40 min flotation.

Rate of Fe^{3+} and Cu^{2+} Ion Flotation. While the use of NaPA and HTAC was found to be unfavorable, that of PAA and SDS was effective. Preliminary experiments showed 57 ppm of SDS and 10 ppm of

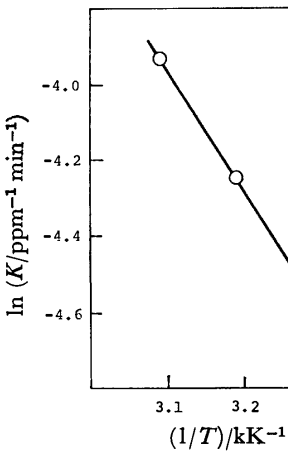

Fig. 6. Arrhenius plots.

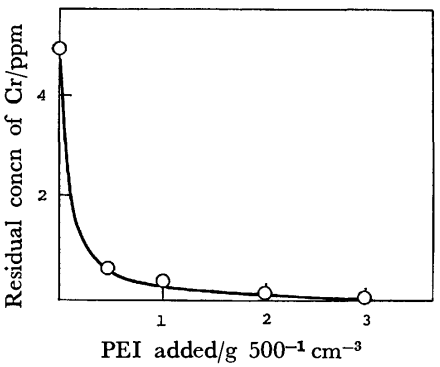

Fig. 7. Removal of Cr by flotation.

†† Ten times the maximum permissible concentration of Cr in environmental water.

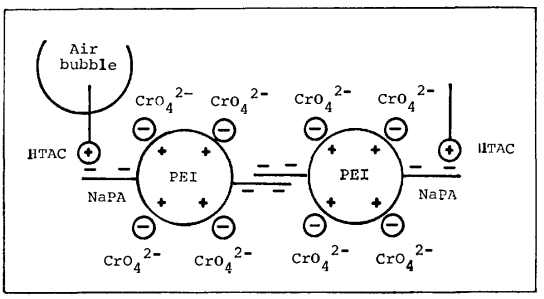

Fig. 8. Model of CrO_4^{2-} ion flotation by PEI, NaPA, and HTAC.

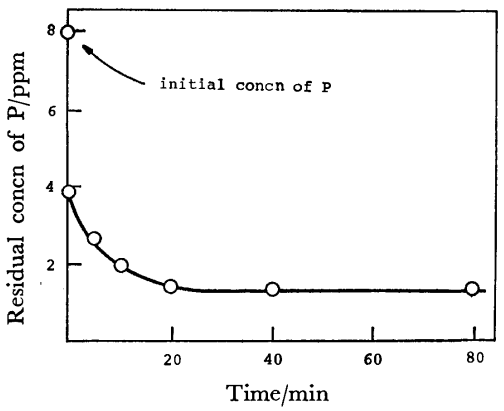

Fig. 9. Rate of flotation of P.

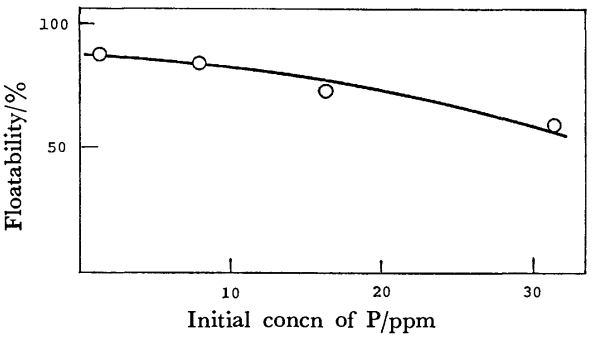

Fig. 10. Concentration *vs.* floatability of P.

PAA to be necessary.

For the measurement, a 20 cm^3 solution containing 1×10^{-4} mol dm^{-3} of Fe^{3+} ions at pH 8 or Cu^{2+} ions at pH 7, 0.06 g of PEI, 57 ppm of SDS and 10 ppm of PAA was gently shaken in a test tube for varying periods of time and then shaken vigorously for 3 s. PEI underwent flotation. The concentrations of Fe^{3+} and Cu^{2+} ions in the underlying layers after shaking were determined, floatability calculated being plotted against time. It was found that the maximum floatability reaches nearly 100% and 90% after 30 s of flotation for Fe^{3+} and Cu^{2+} ions, respectively.

Effect of pH *on* Fe^{3+} *and* Cu^{2+} *Ion Flotation.* The pH of a 20 cm^3 solution containing 1×10^{-4} mol dm^{-3} of Fe^{3+} or Cu^{2+} ions, 57 ppm of SDS, 10 ppm of PAA and 0.06 g of PEI was controlled by the addition of HCl and NaOH. The solution was gently shaken for 30 s, then vigorously for 3 s and PEI was floated. Fe^{3+} and Cu^{2+} ion concentrations were measured and the floatability calculated. The floatability is plotted against pH in Fig. 11. Flat maximum of floatability is attained in the pH range 5—9 for Fe^{3+} and 4—9 for Cu^{2+} ions. The pH dependence of floatability of Fe^{3+} and Cu^{2+} ions without the addition of PEI is also given for the sake of comparison. The floatability is far smaller than that of the system with PEI, showing the marked effect of PEI for the flotation

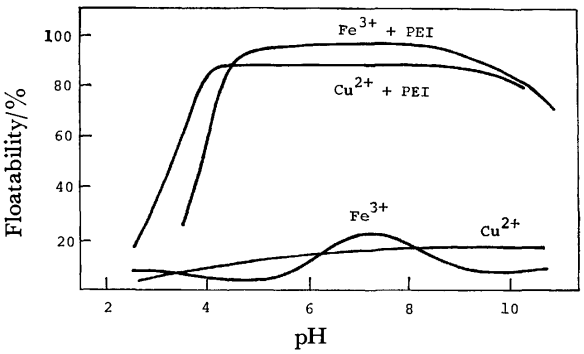

Fig. 11. pH *vs.* floatabilities of Fe^{3+} and Cu^{2+}.

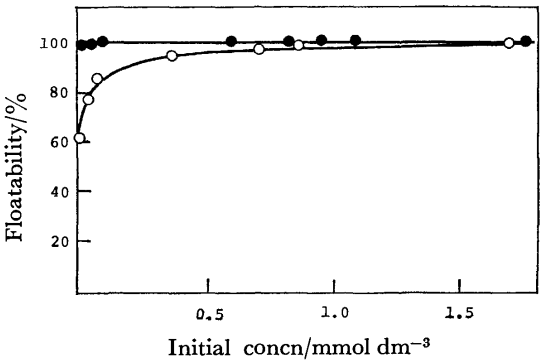

Fig. 12. Flotation of Fe^{3+} (●) and Cu^{2+} (○) ions.

of these ions.

Concentration Dependence of Fe^{3+} *and* Cu^{2+} *Ion Flotation.* A 20 cm^3 solution containing 57 ppm of SDS, 10 ppm of PAA, 0.06 g of PEI and varying amounts of Fe^{3+} ions at pH 8 or Cu^{2+} ions at pH 7 was gently shaken for 30 s, then vigorously for 3 s and PEI was floated. Fe^{3+} and Cu^{2+} ion concentrations of underlying layer were measured, the floatability calculated being plotted against the initial concentration of these ions (Fig. 12). Nearly 100% flotation was observed in wide concentration ranges of these ions, except for a lower concentration of Cu^{2+} ions where a decrease in floatability was observed. The decrease may be due to the hydrolytic formation of hydroxide which is neither adsorbed by PEI nor floated without PEI.

References

1) T. Inakazu, K. Kobayashi, and T. Sasaki, *Bull. Chem. Soc. Jpn.*, **48**, 3008 (1975); K. Kobayashi, H. Sato, K. Kachi, M. Nakamura, and T. Sasaki, *ibid.*, **48**, 3533 (1975); K. Kobayashi, N. Watabe, and T. Sasaki, *ibid.*, **49**, 2701 (1976); K. Kobayashi, K. Natori, M. Kamaya, and T. Sasaki, *ibid.*, **51**, 439 (1978).

2) T. Sasaki, O. Asakawa, H. Kurosawa, M. Mizushima, and T. Nakazono, *Bull. Chem. Soc. Jpn.*, **53**, 1867 (1980).

Studies of Thermochemical Hydrogen Production. VII. Vapor-Liquid Equilibrium for Sulfur Dioxide-Bromine-Hydrobromic Acid-Sulfuric Acid-Water System

Hiroshi Ishikawa,* Eiichi Ishii, Itsuki Uehara, and Masanori Nakane
Government Industrial Research Institute, Osaka, Midorigaoka, Ikeda, Osaka 563

(Received October 4, 1979)

In order to eliminate SO_2 from HBr gas produced by the reaction between SO_2, Br_2, and H_2O, vapor-liquid equilibrium measurements of the Br_2–H_2SO_4–H_2O system saturated with HBr have been made over a wide range of the constituent concentrations. Experiments were carried out in a semi-flow system at 25 °C under atmospheric pressure. The relative concentration of HBr saturated in the liquid phase decreased from 0.31 to 0.05 [mol]/[mol] with an increase in the relative H_2SO_4 concentration from 0.0 to 0.40 [mol]/[mol]. The solubility of Br_2, as defined by Henry's law constant, varied from 1.1 to *ca.* 150 atm/mol/mol with the above-mentioned decrease in the HBr concentration. The relation between the partial pressure of SO_2 in the gas phase and the composition of the liquid phase was found to be expressed by the following empirical formula: $P_{SO_2}=K\cdot C_{HBr}\cdot C_{H_2SO_4}/C_{Br_2}$, where the value of K is 8×10^{-4} when C is expressed as a relative molar concentration for each species in the liquid phase. The unconverted SO_2 can be effectively removed by bringing the effluent gases from the reactor into contact with a HBr-saturated aqueous solution containing an excess of Br_2.

The research and development of thermochemical hydrogen production from water by the iron-bromine family cycle has previously been carried out by the present authors.[1-3] One of the most feasible iron-bromine thermochemical cycles consists of the following four chemical reactions:

$$SO_2 + Br_2 + 2H_2O \longrightarrow H_2SO_4 + 2HBr \quad (1)$$

$$H_2SO_4 \longrightarrow H_2O + SO_2 + 1/2O_2 \quad (2)$$

$$3FeBr_2 + 4H_2O \longrightarrow Fe_3O_4 + 6HBr + H_2 \quad (3)$$

$$Fe_3O_4 + 8HBr \longrightarrow 3FeBr_2 + 4H_2O + Br_2 \quad (4)$$

Each reaction step has been investigated experimentally on a laboratory scale, and our earlier works have dealt with Reactions 2, 3, and 4.

The reaction between SO_2, Br_2, and H_2O is relatively well known as a usual method for preparing gaseous HBr in a laboratory-scale operation.[4] Recently, equilibrium determinations and reaction kinetic measurements have been carried out by Velzen *et al.*[5] during the course of the development of the electrochemical hybrid-water-splitting cycle, Mark-13, presented by Schuetz *et al.*[6] It has also been confirmed by the present authors that gaseous HBr and concentrated sulfuric acid could be prepared by using a packed column reactor.[7]

One of the problems to be solved, however, is the removal of the small quantity of unconverted SO_2 contained in the HBr gas produced in a flow reactor of SO_2 with Br_2 and H_2O. This is because the HBr gas produced by Reaction 2 is circulated for use in the bromination of Fe_3O_4, *i.e.*, Reaction 4, and the contamination of HBr by SO_2 would cause the formation of $FeSO_4$ as an undesirable side reaction. The continuous operation of the cycle would cause $FeSO_4$ to be accumulated as a by-product, and its thermal decomposition to Fe_2O_3 would be additionally required. On the other hand, the contamination of HBr by Br_2 matters little. The requirement for SO_2-free HBr gas seems to be fulfilled by bringing the effluent HBr gas from the reactor into contact with a HBr-saturated aqueous solution containing an excess of Br_2. Therefore, prior to the kinetic measurements, vapor-liquid equilibrium measurements of the HBr-saturated Br_2–H_2SO_4–H_2O system have been made over a wide range of constituent concentrations.

Some equilibrium data have already been reported by Velzen,[5] but they were confined to the liquid phase with a high concentration of H_2SO_4.

Experimental

The experiments were carried out in a semi-flow system at 25 °C under atmospheric pressure. The apparatus shown in Fig. 1 is composed of a cylindrical vessel 4 cm in diameter and 13 cm in height and equipped with a HBr-gas dispersion tube (ball filter No. 1), three PTFE tubes 1.0 mm in inner diameter for the addition of Br_2 and sulfuric acid and for the withdrawing of a liquid-phase sample, and a magnetic stirrer. The vessel was immersed in a water bath thermostatted at 25 °C.

After the liquid had been saturated with HBr, given quantities of Br_2 and 98 wt% sulfuric acid were introduced into the agitated liquid phase. Simultaneously, HBr gas was passed in at a rate of 50 ml/min. The outlet gas was led to a sampling cell of a derivative spectrophotometer (Yanagimoto Co. Ltd., Type UO-2) for the quantitative analysis of Br_2 as well as of the SO_2 evolved by the oxidation of HBr with H_2SO_4. Figure 2 shows examples of the variation in the Br_2 and SO_2 concentrations in the gas phase

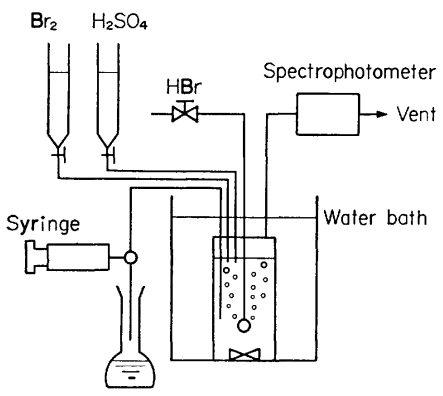

Fig. 1. Experimental appparatus for equilibrium determinations.

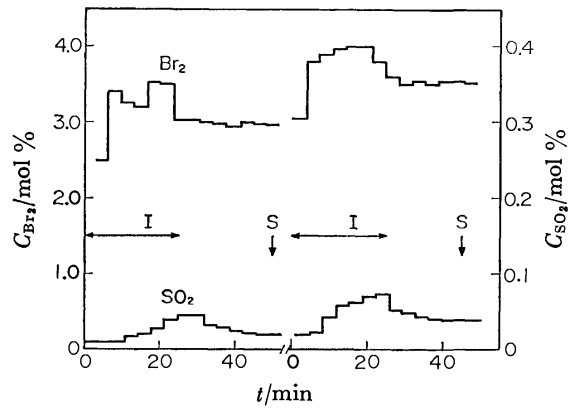

Fig. 2. Variation of Br_2 and SO_2 concentrations in gas phase.
I: Injection of sulfuric acid, S: sampling of liquid phase and determination of gas phase and liquid phase compositions.

monitored alternatively at regular intervals of 3.5 min. After about 20 min, when both the Br_2 and SO_2 concentrations had reached an equilibrium condition, the feed of the HBr gas was stopped, and the composition of the gas phase, considered to consist of only HBr, Br_2, and SO_2, was determined. At the same time, a sample of the liquid phase was taken out by using a syringe, and a weighed aliquot was diluted with a large excess of water in a volumetric flask. The composition of the liquid phase, consisting of HBr, H_2SO_4, Br_2, and H_2O, was calculated by determining the free Br_2, the total acidity, and the sulfuric-acid content. Thus, a given volume of the liquid-phase sample was taken and analyzed for Br_2 iodometrically, after which the total acid content was determined by titration with an NaOH solution. Another sample was analyzed for H_2SO_4 as follows: hydrogen bromide was oxidized by adding nitric acid. After the resulting Br_2 and the excess HNO_3 had been evaporated in a water bath, the remaining sulfuric acid was titrated. Then the HBr content was determined by subtracting the H_2SO_4 content from the total acid content.

Results and Discussion

Experiments were carried out on the liquid phase in concentrations of H_2SO_4 ranging from 0.0 to 80 wt% and in concentrations of Br_2 up to 10 wt%. The equilibrium data at 25 °C under atmospheric pressure are shown in Table 1. The content of SO_2 dissolved in the liquid phase was neglected, since the partial pressure of SO_2 evolved in the gas phase was very low. Moreover, the solubility of SO_2 in these liquid phases can be estimated to be small from the solubility data in sulfuric acid,[8] in a mixture of hydrochloric and sulfuric acids,[9] and in a mixture of hydrobromic and sulfuric acids.[5]

Solubility of HBr. The solubility data of the gaseous-phase components of the reaction mixture in the corresponding liquid phase are indispensable for the control of the mass balance of the HBr-producing system. Run No. 1 in Table 1 is an example carried out to determine the solubility of HBr in water. The numerical value obtained, 67.5 wt%, was a little higher than that of 66.0 wt% given by Haase *et al.*[10] The relation between the concentration of HBr and that of H_2SO_4 in the HBr-saturated liquid phase is shown in Fig. 3. The "relative concentration" is defined

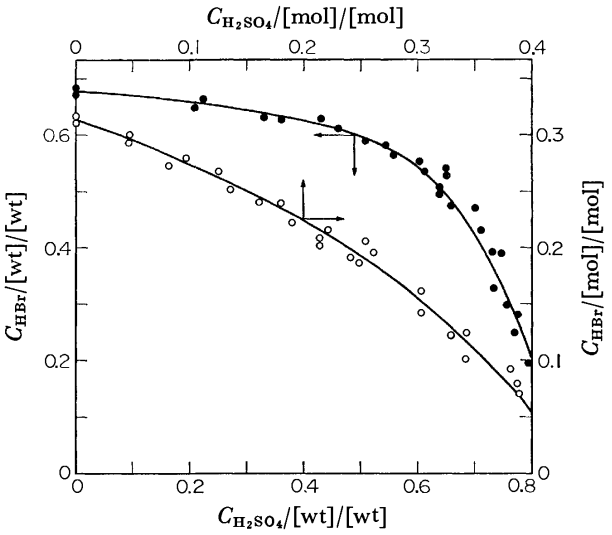

Fig. 3. Solubility of HBr in Br_2–H_2SO_4–H_2O mixture at 25 °C.
C_{Br_2} : 0—10 wt %.

Table 1. Equilibrium determinations for the SO_2-Br_2-HBr-H_2SO_4-H_2O system at 25 °C

Run No.	Liquid phase								Gas phase	
	Br_2		H_2SO_4		HBr		H_2O		Br_2	SO_2
	wt %	mol %	wt %	mol %	wt %	mol %	wt %	mol %	mol %	mol %
1	—	—	—	—	67.5	31.6	32.5	68.4	—	—
2	6.8	1.7	—	—	62.7	30.8	30.5	67.5	1.7	—
3	8.6	2.2	7.8	3.3	54.6	27.8	27.0	66.7	3.2	0.04
4	7.8	2.0	15.8	6.8	48.3	25.2	28.1	66.0	3.8	0.07
5	3.8	1.0	28.7	12.5	39.9	21.0	27.6	65.5	3.5	0.21
6	3.0	0.8	39.2	17.8	31.8	17.4	26.0	64.0	4.6	0.31
7	4.0	1.1	45.6	21.1	25.3	14.2	25.1	63.6	9.6	0.19
8	1.7	0.5	55.0	26.7	20.2	11.8	23.1	61.0	6.9	0.47
9	0.7	0.2	62.7	31.2	14.4	8.6	22.2	60.0	7.0	1.06
10[a]	1.6	0.5	67.7	34.6	9.3	5.7	21.4	59.2	28.0	0.38

a) Also present: liquid bromine insoluble in the liquid phase.

by [mol]/[mol] or [wt]/[wt], where [mol] and [wt] are the concentrations expressed in mol% and wt% respectively. The concentration of HBr saturated in the solution was reduced from 0.31 to 0.05 [mol]/[mol] with an increase in the H_2SO_4 concentration from 0.0 to 0.40 [mol]/[mol].

Henry's law constant (H) is also useful in defining the vapor-liquid equilibrium:

$$H = P_A/X_A \quad \text{(atm/wt/wt or atm/mol/mol)} \qquad (5)$$

where P_A is the partial pressure of a gas, A, in the gas phase and where X_A is the concentration of a species, A, in the liquid phase, expressed in a weight fraction or a mole fraction. Figure 4 shows the relation between Henry's law constant for HBr and the H_2SO_4 concentration in the liquid phase. The values

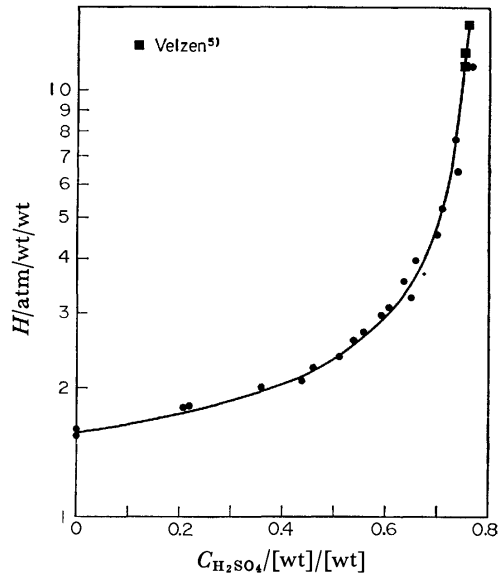

Fig. 4. Relation between Henry's law constant for HBr and concentration of H_2SO_4 in solution at 25 °C.

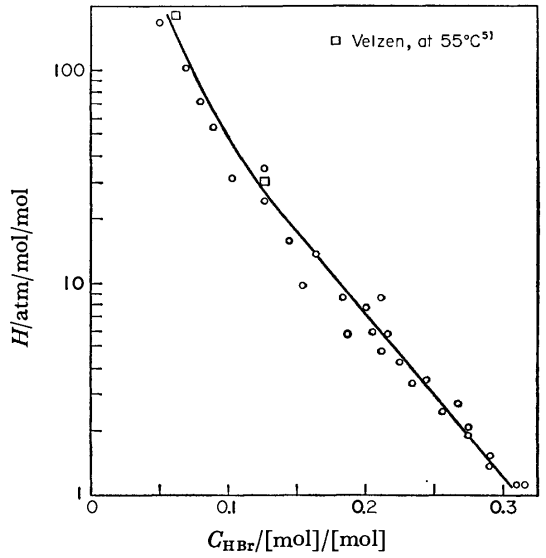

Fig. 5. Relation between Henry's law constant for Br_2 and concentration of HBr in solution at 25 °C.
$C_{H_2SO_4}$: 0.40→0.0 [mol]/[mol].

of H given by Velzen[5] in the high-H_2SO_4-concentration region were in fair agreement with our data. The presence of Br_2 up to a concentration of 10 wt% had little effect on the solubility of HBr.

Solubility of Br_2. The solubility of Br_2 in the liquid phase of the reaction mixture depends strongly on the HBr concentration. Figure 5 shows Henry's law constant for Br_2 as a function of the relative HBr concentrations, ranging from 0.05 to 0.31 [mol]/[mol]. The corresponding H_2SO_4 concentrations in the solution can be seen in Fig. 3 to range from 0.40 to 0.0 [mol]/[mol]. It has already been shown by Velzen[5] that the values of H at 23 °C and 55 °C are nearly identical; their values are also in good agreement with our data at 25 °C. It thus appears that the effect of the temperature was negligibly small.

Figure 6 gives the content of Br_2 saturated in the solution of the reaction mixture at a low HBr concentration, *i.e.*, at a high H_2SO_4 concentration. In this case, liquid Br_2 insoluble in the solution was also present, and the partial pressure of Br_2 in the gas phase was equal to that of liquid Br_2, *i.e.*, 0.28 atm at 25 °C, as shown by Run No. 10 in Table 1.

Partial Pressure of SO_2 in the Gas Phase. Since only the equilibrium partial pressure of SO_2 in the gas phase was required for the reaction kinetic measurements and the succeeding design of a reactor unit, the concentration of SO_2 in the solution of the reaction mixture was not determined. The partial pressure of SO_2 evolved in the gas phase in equilibrium with the liquid phase was strongly influenced by both the H_2SO_4 and Br_2 concentrations. It was found that the relation between the partial pressure of SO_2 in the gas phase and the composition of the liquid phase could be expressed by the following empirical formula:

$$P_{SO_2} = K \cdot \frac{C_{HBr} \cdot C_{H_2SO_4}}{C_{Br_2}} \qquad (6)$$

where the value of K was *ca.* 7×10^{-4} when C was expressed as a weight fraction or a relative weight concentration for each species in the liquid phase. The validity of this formula (6) is shown in Fig. 7. When C was defined by a mole fraction or a relative molar concentration for each species, the value of K was *ca.* 8×10^{-4}. Figure 8 shows the calculated

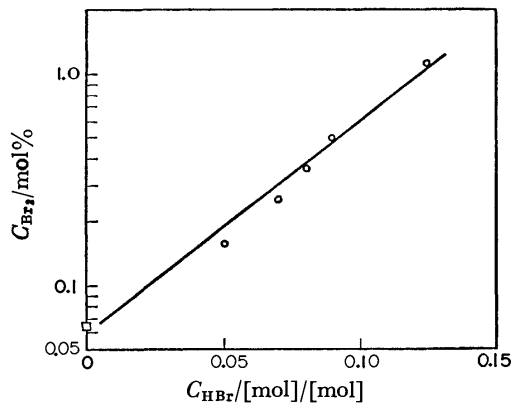

Fig. 6. Solubility of Br_2 in HBr saturated H_2SO_4-H_2O mixtures at 25 °C.
$C_{H_2SO_4}$: 0.43→0.34 [mol]/[mol].

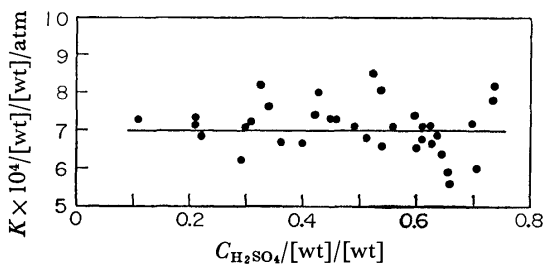

Fig. 7. Validity of empirical formula (6).

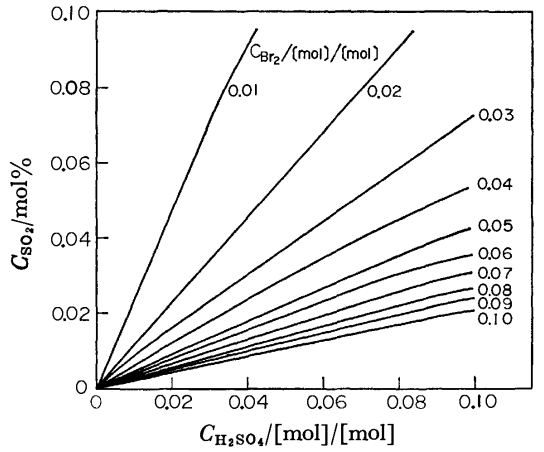

Fig. 8. Calculated equilibrium SO_2 concentration in gas phase as a function of H_2SO_4 and Br_2 concentrations in solution.

equilibrium SO_2 concentration in the gas phase as a function of the relative H_2SO_4 and Br_2 concentrations in the liquid phase.

It can be seen from Fig. 8 that, when HBr contaminated by SO_2 is placed in contact with a HBr saturated aqueous solution of H_2SO_4 and Br_2 at relative concentrations of, for example, 0.03 and 0.07 [mol]/[mol] respectively, the SO_2 content of the gas mixture in equilibrium is reduced to 0.01 mol%. The corresponding relative HBr concentration in the solution obtainable from Fig. 3 was 0.30 [mol]/[mol]; the value of H for Br_2 also obtainable from Fig. 5, was 1.2 atm/mol/mol. Therefore, the Br_2 concentration in the gas phase is expected to amount to 5.9 mol%, since the Br_2 concentration in the solution is calculated to be 4.9 mol%.

Conclusion

As a part of research and development of the thermochemical hydrogen production from water by the iron-bromine family cycle, the vapor-liquid equilibrium for the reaction of SO_2 with Br_2 and H_2O has been investigated. It could be concluded that the development of a continuously HBr-producing process was feasible by combining a packed column reactor with an absorber of unconverted SO_2. The absorbent liquid can be fed into the reactor as a reaction agent when it was condensed into concentrated H_2SO_4. Studies of the reaction kinetics are under way in order to design a practical unit.

References

1) H. Ishikawa, M. Nakane, E. Ishii, I. Uehara, and Y. Miyake, *Nippon Kagaku Kaishi*, **1977**, 1817.
2) H. Ishikawa, E. Ishii, I. Uehara, M. Nakane, and Y. Miyake, *Nippon Kagaku Kaishi*, **1978**, 530.
3) H. Ishikawa, E. Ishii, I. Uehara, and M. Nakane, *Nippon Kagaku Kaishi*, **1979**, 817.
4) E. Léger, *C. R. Acad. Sci.*, **115**, 946 (1892).
5) D. van Velzen, H. Langenkamp, and A. Ferrari, "Hydrogen Production from Water using Nuclear Heat," Progress Report, J.N.R.C. Ispra, No. 7, 51 (1978); No. 8, 97 (1979).
6) G. Schuetz and D. Fiebelmann, "Hydrogen Production from Water using Nuclear Heat," Progress Report, J.N.R.C. Ispra, No. 5, 76 (1974).
7) E. Ishii, I. Uehara, H. Ishikawa, M. Nakane, and Y. Miyake, Proceeding of 4th HESS (1977), p. 4.
8) A. Simecek, J. Michalek, B. Kadlec, and J. Vosolsobe, *Chem. -Ing. -Tech.*, **41**(19), 1077 (1970).
9) I. G. Syrkina, A. A. Krasheninnikova, and V. M. Zaliopo, *Zh. Fiz. Khim.*, **46**(3), 805 (1972).
10) R. Haase, H. Naas, and H. Tkumm, *Z. Phys. Chem. Neue Folge*, **37**, 210 (1963).

Studies on the Preparation of Cuprous Oxide. VIII. A Spectrophotometric Study of Halogenocopper(I) Complexes in Aqueous 5 M $Na(ClO_4)$ Solutions

Kazuhiko SUGASAKA* and Ayako FUJII

Government Industrial Research Institute, Shikoku, Hananomiya-cho 2-3-3, Takamatsu 761

(Received November 12, 1979)

The complex formation of copper(I) with bromide and iodide ions in aqueous 5 M (1 M = 1 mol dm^{-3}) $Na(ClO_4)$ solutions was studied spectrophotometrically over a pH range from acidic to alkaline. Over the concentration range of 0.05—5 M bromide ions in acidic solutions, the $CuBr_2^-$ and $CuBr_3^{2-}$ complexes were found. On the other hand, in the iodide system the CuI_2^-, CuI_3^{2-} complexes and a higher complex were found under the same experimental conditions, although the composition and the formation constant of the last complex could not be determined in this study. The equilibrium constants for the reactions, $CuX_2^- + X^- = CuX_3^{2-}$, were 13 and 1.6 for the bromide and iodide complexes respectively. A hydrolyzed species of copper(I), $Cu(OH)_2^-$, was found in an alkaline solution of the two systems. The formation constants, $\beta_{-22} = [Cu(OH)_2^-][X^-]^2/[CuX_2^-][OH^-]^2$, were evaluated as follows: $\beta_{-22} = (10.0 \pm 0.7) \times 10^7$ ($[Br^-] < 2$ M), $(2.6 \pm 0.7) \times 10^7$ ($[Br^-] = 3$ M), $(1.7 \pm 0.7) \times 10^7$ ($[Br^-] = 4$ M) in the bromide solutions, $(4.0 \pm 0.4) \times 10^3$ ($[I^-] < 2$ M), $(2.5 \pm 0.4) \times 10^3$ ($[I^-] = 3$ M), $(2.2 \pm 0.4) \times 10^3$ ($[I^-] = 4$ M) in the iodide solutions.

During the course of an investigation of copper(I) oxide by the hydrolysis of copper(I) halides, it was shown that the color of copper(I) oxide changed from yellow to red depending upon the concentration of halide ions in solutions.[1,2] For the precipitation of copper(I) oxide by the hydrolysis of copper(I) iodide crystals, the dissolution of the crystals is the rate-determining step in water, whereas the crystal growth of copper(I) oxide is the rate-determining step in a concentrated sodium iodide solution.[3] Based on these observations, we aimed at studying the equilibria of the formation of copper(I) halide complexes in aqueous solutions in order to obtain information on reactions between copper(I) and halide ions.

Bodländer and Storbeck[4,5] suggested the formation of the CuX_2^- and CuX_3^{2-} complexes (X denotes halide ions) on the basis of solubility measurements of copper(I) halides in sodium halide solutions. Fromherz and Menschick[6] and Doehlemann and Fromherz[7] found that a concentrated lithium bromide solution containing both copper(I) and copper(II) showed absorption maxima at 272, 338, and 512 nm. Sukhova *et al.*[8] reported that a copper(I) chloride solution has λ_{max} at 200, 235, and 273 nm and broad bands at 300—400 and 1200—2000 nm, analogous to the absorption maxima of copper(I) bromide and iodide solutions. The formation constants of copper(I) bromo-[9] and iodo-complexes[10] have been reported in the basis of solubility measurements.

In spite of the existence of many results in the literature, investigations of the complex formation of copper(I) ions with halide ions have been restricted to acidic media.

In a previous paper[11] we dealt with the complex formation of copper(I) in an aqueous 5 M Na(Cl, ClO_4) solution and found that $CuCl_2^-$ and $CuCl_3^{2-}$ complexes were formed in acidic media, together with these mixed halogeno–hydroxo complexes, $CuClOH^-$, $CuCl_2OH^{2-}$, and $CuCl(OH)_2^{2-}$, in alkaline media. In this paper we wish to describe the complex formation of copper(I) ions with bromide and iodide ions in 5 M $Na(ClO_4)$ aqueous solutions over a wide pH range, the total anionic concentration being kept constant.

Experimental

Reagents. Copper(I) bromide was recrystallized according to a procedure described ealier.[11] Copper(I) iodide was purified in the following way: reagent-grade crystals were dissolved into a saturated sodium iodide solution, and then after filtration, the solution was diluted with water. The precipitates thus formed by dilution were washed with water and then with acetic acid before being dried at 130 °C under a nitrogen atmosphere.[12] The stock solutions of copper(I) bromide and iodide were prepared by dissolving copper(I) bromide and iodide crystals into 0.5 M sodium bromide and sodium iodide solutions respectively, both types of solutions containing sufficient amounts of sodium perchlorate and perchloric acid to maintain the total anionic concentration and pH at 5 M and 1 respectively. Since the stock solutions contained pieces of pure copper wire (99.99% purity) for reducing the trace amount of copper(II) ions, the concentrations of copper(II) ions in the bromide and iodide solutions were estimated to be less than 8×10^{-8} M and 3.6×10^{-11} M respectively; these values were calculated on the basis of the equilibrium constants of copper(I) and (II) bromo- and iodo-complexes reported in the literature.[13] Sample solutions were prepared from the stock solutions; sodium bromide, sodium iodide, and sodium hydroxide solutions. The sodium bromide, sodium iodide, sodium perchlorate, and sodium hydroxide were of a reagent grade. The preparation of sample solutions and measurements were carried out under an atmosphere of nitrogen.

Spectrophotometric Measurements. These were run with a Hitachi EPS-3T spectrophotometer. The absorption spectra of the sample solutions were obtained using 1-, 2-, 10-, and 20-mm cells at 25 °C by referring to blank solutions which were the same in composition with the samples except for the copper(I) ions. Since the amount of copper(II) ions in the sample solutions prepared by the dilution of the stock solutions was estimated to be less than 2×10^{-9} M, and since the molar extinction coefficients of the copper (II) bromide complexes were estimated to be about 10^2—10^3 mol^{-1} dm^3 cm^{-1} over the wavelength region of 260—300 nm,[14–16] the influence of copper(II) ions on the measurements in the bromide solutions was neglected. Although no spectrophotometric data for copper(II) iodide complexes have been given in the literature, the absorption due to copper(II)–iodide complexes was also neglected because of the much lower concentration of copper(II) ions in the iodide

solutions than in the bromide solutions. When the sample solution came in contact with air, the solution turned yellow within 20 min. Therefore, an effort was made to avoid the contact of the sample with air by the introduction of nitrogen gas into the cells and to finish the measurements within a few minutes.

Determination of Concentrations of Ions in the Solutions. The copper(I) ions in the stock solutions were determined by atomic-absorption spectrometry. The concentration of halide ions was determined by means of argentometric titration. Since the concentration of the halide ions in the samples was in a large excess compared with that of the copper(I) ions, the concentration of the free halide ions [X^-] was assumed to be equal to the total concentration of the sodium halide in the solutions.

Results and Discussion

Spectra of Copper(I) Halide Solutions. Absorption spectra of copper(I) halide solutions containing various amounts of sodium halide and sodium hydroxide are shown in Figs. 1 and 2. In the absorption spectra of copper(I) bromide in acidic solutions, a maximum absorbance appeared at 278 nm (Fig. 1). The absorbance at 278 nm increased as the concentration of bromide ions increased. When the concentration of hydroxide ions increased, the absorbance at 278 nm decreased, while the absorbance at 240 nm increased.

The absorption maximum appeared at 274—285 nm in the copper(I) iodide solutions in acidic media, depending upon the concentration of iodide ions, as is shown in Fig. 2. The absorption at a wavelength shorter than 270 nm was not measured because the intense absorption due to the iodide ions overlapped with that of the complexes at that wavelength. The absorbance at these wavelengths decreased with the concentration of hydroxide ions.

Complex Formation in Acidic Media. The apparent molar extinction coefficient, $\bar{\varepsilon}=E/[\mathrm{Cu(I)}]_{\mathrm{TOT}}$, at 278 nm is shown in Fig. 3, where E denotes the absorbance

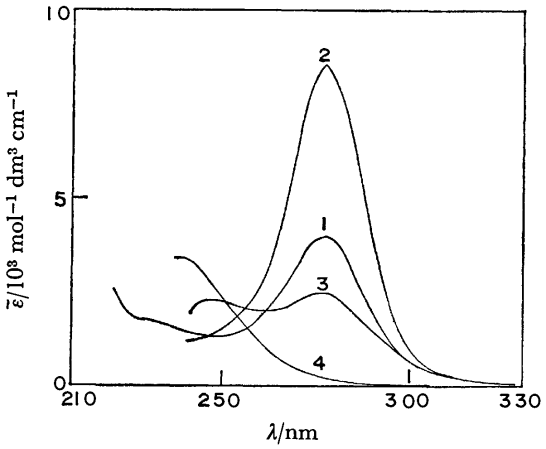

Fig. 1. UV absorption spectra of solution of copper(I) bromide and sodium bromide (at 25 °C).

No.	$[Br^-]_{TOT}$/M	$-\log[OH^-]$	$[Cu(I)]_{TOT}/10^{-4}$ M
1	0.05	11.5	2
2	5	11.5	2
3	4	2.06	0.8
4	4	0.84	0.8

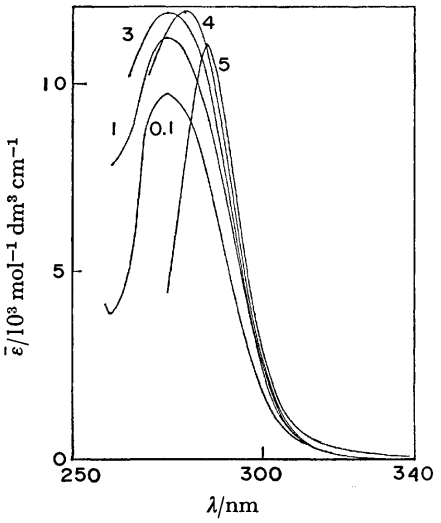

Fig. 2. UV absorption spectra of acidic solutions of copper(I) iodide and sodium iodide (at 25 °C).
$-\log[OH^-]=8$—12, $[Cu(I)]_{TOT}/10^{-4}$ M=4.8.
Numbers in the figure indicate the total concentration of iodide ions (M).

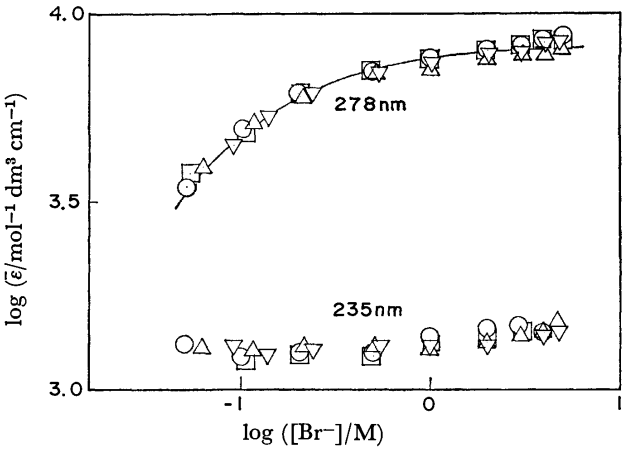

Fig. 3. Relationship between $\bar{\varepsilon}$ at 278 nm and the concentration of bromide ions (at 25 °C).
$-\log[OH^-]=8$—12, $[Cu(I)]_{TOT}/10^{-4}$ M=0.2 : ○, 0.7 : □, 2.0 : △, 6.6 : ▽.

of a solution for a unit of the optical pathlength. The plot was dependent upon the concentration of bromide ions, but independent of the total copper(I) ions. These results show that no polynuclear complex of copper(I) ions was formed in the solutions. The absorbance at 235 nm remained practically unchanged when the concentrations of both the copper(I) and bromide ions were varied. Therefore, the data were not used for analysis.

Since copper(I) halides hardly dissolve in water, but dissolve only in solutions containing an excess amount of the halide ions, the species in the solution may have the composition of $CuX_m^{(m-1)-}$ (the possibility of the formation of a polynuclear complex is excluded). Therefore, the CuX_2^- complex may be formed in the first stage of complex formation in a halide solution and then higher complexes may be formed by the further addition of halide ions to the CuX_2^- ion:

$$CuX(s) + X^- = CuX_2^- \quad (1)$$

$$CuX_2^- + nX^- = CuX_{2+n}^{(n+1)-}. \quad (2)$$

Since we used solutions without solid CuX, the equilibrium constant of the first reaction could not be determined though the constants of Reaction 2 were determined.

From the material balance of copper(I) and the absorbance, E, per unit of the path, the following equation is derived:

$$\bar{\varepsilon} = \frac{E}{[Cu(I)_{TOT}]} = \frac{\varepsilon_0 + \sum_n \varepsilon_n \beta_n [X^-]^n}{1 + \sum_n \beta_n [X^-]^n}, \quad (3)$$

as long as the ligand shows no absorbance over the entire wavelength range studied or as long as the absorbance due to the ligand has been subtracted as a blank in the measurement of ε. β_n is defined as $\beta_n = [CuX_{2+n}^{(n+1)-}]/[CuX_2^-][X^-]^n$. The molar extinction coefficient of the $CuX_{2+n}^{(n+1)-}$ complex is denoted as ε_n. The values of ε_0, ε_n, β_n, and n may be determined by comparing the plots of log ε *vs.* log $[X^-]$ with a family of the normalized curves, $y = \log\{x^n/(1+x^n)\} = f(\log x)$, because Eq. 3 may be rearranged as:

$$\log(\bar{\varepsilon} - \varepsilon_0) = \log(\varepsilon_n - \varepsilon_0) + \log \frac{\beta_n [X^-]^n}{1 + \beta_n [X^-]^n}, \quad (4)$$

by assuming that only one complex, $CuX_{2+n}^{(n+1)-}$, besides the CuX_2^- complex, is present in the solution. The plots of log $\bar{\varepsilon}$ at 278 nm against log $[Br^-]$ (Fig. 2) fit a normalized curve, $y = \log\{x/(1+x)\}$; thus, $n=1$, the molar extinction coefficient of the $CuBr_2^-$ complex, $\varepsilon_0 = 0$, $\varepsilon_1 = 8.5 \times 10^3$, and $\beta_1 = 13$ were obtained. The values were refined by means of a least-squares calculation with an electronic computer; the values are summarized in Table 1.

For the iodide system, on the other hand, the apparent molar extinction coefficient, $\bar{\varepsilon}$, at 274 nm first increased and then sharply decreased with an increase in the concentration of iodide ions (Fig. 4). This fact obviously showed that at least two complexes, one with a larger value and the other with a much smaller value of ε than ε_0, must exist in the solution. Since the ε's at both 274 and 285 nm were independent of the concentration of the copper(I) ions, the formation of any polynuclear complex of copper(I) ions was ruled out.

At first, the formation of two complexes, $CuI_{2+l}^{(l+1)-}$ and $CuI_{2+l+m}^{(l+m-1)-}$, besides the CuI_2^- complex, was assumed. The apparent molar extinction coefficient, $\bar{\varepsilon}$, of the solution may thus be given by Eq. 5:

$$\bar{\varepsilon} = \frac{\varepsilon_0 + \varepsilon_l \beta_l [I^-]^l + \varepsilon_{l+m} \beta_{l+m} [I^-]^{l+m}}{1 + \beta_l [I^-]^l + \beta_{l+m} [I^-]^{l+m}}. \quad (5)$$

Since the $\bar{\varepsilon}$ values at 274 nm steeply decreased at about $[I^-] \simeq 3$ M, we assume that the second species may be formed in a solution of $[I^-] \gtrsim 3$ M, and that, in the concentration region of $[I^-]$ lower than 3 M, the equilibrium between CuI_2^- and the first complex, $CuI_{2+l}^{(l+1)-}$ may be established, where the molar extinction coefficient of the solution may approximately be given as follows:

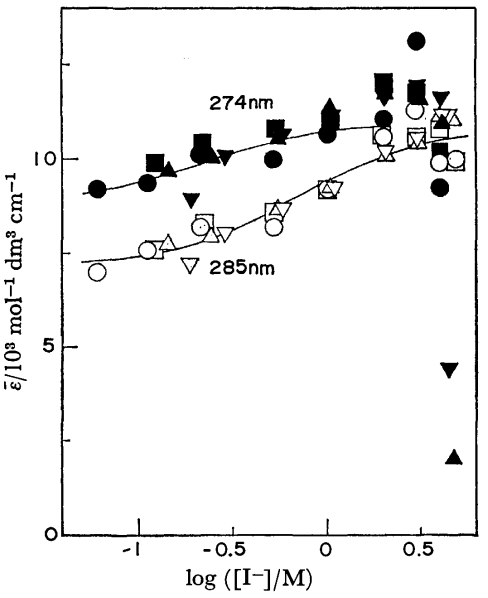

Fig. 4. The plots of $\bar{\varepsilon}$ at 274 and 285 nm *vs.* log $[I^-]$. $-\log[OH^-] = 8$—12, $[Cu(I)]_{TOT}/10^{-4}$ M = 0.6 : ○, 1.3 : □, 2.4 : △, 4.8 : ▽.

$$\bar{\varepsilon} = \frac{\varepsilon_0 + \varepsilon_l \beta_l [I^-]^l}{1 + \beta_1 [I^-]^l}. \quad (6)$$

A curve-fitting method may be applied to the plot of log $\bar{\varepsilon}$ *vs.* log $[I^-]$ in order to determine ε_0, ε_l, and β_l, as well as l, by comparing the plots with the normalized curve, $y = \log\{x^n/(1+x^n)\}$, at various n's, or by comparing $\bar{\varepsilon}$ *vs.* log $[I^-]$ with a family of normalized curves, $u = \log\{a/(1+v^n)\}$, with various sets of a and n. In both the curve-fitting procedures, the data fit the curve of $n=1$; thus, the value of l was determined to be unity. The values estimated by the curve-fitting method were as follows: at 274 nm, $\varepsilon_0 = 9.4 \times 10^3$, $\varepsilon_1 = 1.3 \times 10^4$, and log $\beta_1 = 0.22$ ($\beta_1 = 1.7$); at 285 nm, $\varepsilon_0 = 7.0 \times 10^3$, $\varepsilon_1 = 1.1 \times 10^4$, and log $\beta_1 = 0.18$ ($\beta_1 = 1.5$).

The variation in $\bar{\varepsilon}$ at 274 nm in the $[I^-] > 3$ M region was so steep that no reasonable assumption to explain the data was given; the $l+m$ value must, though, be very large ($l+m \gg 2$). However, since the data at 285 nm showed no clear indication for the formation of such a high complex, we concluded that the $l+m$ value was not so large, but that the ionic-medium principle to keep constant the activity coefficients of all reacting species did not hold in the region of $[I^-] >$ 3—5 M. Therefore, we did not use these data for the determination of the formation constant of the second complex, $CuI_{2+l+m}^{(l+m-1)-}$. The $l+m$ value was also not determined for this complex.

The formation constant, β_1, and the molar extinction coefficients, ε_0 and ε_1, at 274 and 285 nm were refined by means of a least-squares calculation with the aid of an electronic computer. The final results are summarized in Table 1 together with the results for the copper(I) chloro complexes.[11]

Halogenocopper(I) Complexes in Alkaline Solutions. The absorbance of a copper(I) bromide solution at 278 nm decreased when sodium hydroxide was added

to the solution (see Fig. 1). Typical examples of the change in $\bar{\varepsilon}$ at 278 nm of copper(I) bromide solutions with the concentration of the hydroxide ions are shown in Fig. 5. Patterns similar to those of bromide system were obtained for the iodide system at 285 nm; they are shown in Fig. 6. It is obvious from the plots that no polynuclear complex was formed,

Table 1. The molar extinction coefficients and the formation constants of the copper(I) halide complexes

Species	λ_{max} (nm)	ε (mol^{-1} dm^3 cm^{-1})	β
$CuBr_2^-$	278	0.0	—
$CuBr_3^{2-}$	278	$(8.3\pm0.1)\times10^3$	13.0 ± 0.4
CnI_2^-	274	$(9.0\pm0.4)\times10^3$	—
	285	$(7.0\pm0.1)\times10^3$	
CuI_3^{2-}	274	$(1.2\pm0.1)\times10^4$	1.6 ± 0.1
	285	$(10.0\pm0.2)\times10^3$	
$CuCl_2^-$	233	$(1.45\pm0.1)\times10^3$	—[11]
$CuCl_3^{2-}$	273	$(3.33\pm0.1)\times10^3$	1.95[11]

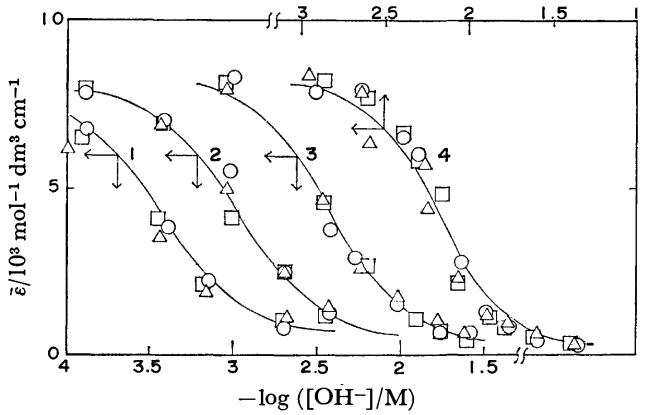

Fig. 5. Relationships between $\bar{\varepsilon}$ at 278 nm and the concentration of hydroxide ion for bromide solutions. Numbers indicated in the figure show the total concentrations of bromide ions (M).
$[Cu(I)]_{TOT}/10^{-4}$ M=0.2 : ○, 0.4 : □, 0.8 : △.

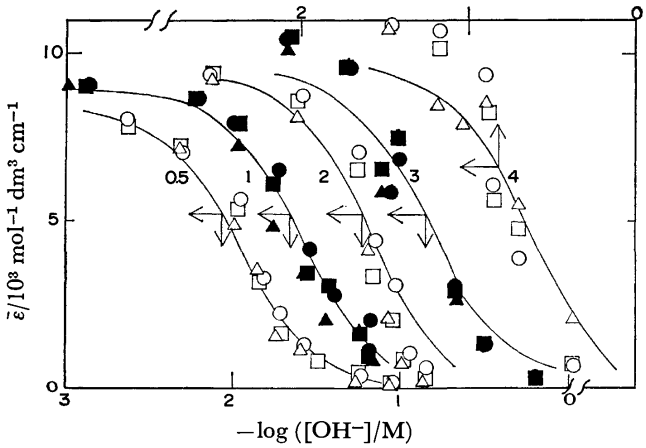

Fig. 6. Relationships between $\bar{\varepsilon}$ at 285 nm and the concentration of hydroxide ion for iodide solutions. Numbers indicated in the figure show the total concentrations of iodide ions (M).
$[Cu(I)]_{TOT}/10^{-4}$=0.3 : ○, 0.7 : □, 1.3 : △.

because $\bar{\varepsilon}$ was independent of the concentration of the copper(I) ions in both the bromide and iodide solutions. Since the curves depend on the concentration of the halide ions, we assumed the formation of complexes with the general formula of $CuX_{2+p}(OH)_q^{(p+q-1)-}$ in the alkaline solutions. The formation constant, β_{pq}, of the complex is defined as follows:

$$CuX_2^- + pX^- + qOH^- = CuX_{2+p}(OH)_q^{(p+q-1)-} \quad (7)$$

$$\beta_{pq} = [CuX_{2+p}(OH)_q^{(p+q-1)-}]/[CuX_2^-][X^-]^p[OH^-]^q. \quad (8)$$

The material balance for copper(I) ions may be represented by the following equation:

$$[Cu(I)]_{TOT} = [CuX_2^-] + \sum_n \beta_n[CuX_2^-][X^-]^n + \sum_p \sum_q \beta_{pq}[CuX_2^-][X^-]^p[OH^-]^q, \quad (9)$$

where p is either positive, zero, or negative, and where q is zero or a positive integer. The apparent molar extinction coefficient, $\bar{\varepsilon}$, is given as follows:

$$\bar{\varepsilon} = \frac{\varepsilon_0 + \sum_n \varepsilon_n\beta_n[X^-]^n + \sum_p \sum_q \varepsilon_{pq}\beta_{pq}[X^-]^p[OH^-]^q}{1 + \sum_n \beta_n[X^-]^n + \sum_p \sum_q \beta_{pq}[X^-]^p[OH^-]^q}. \quad (10)$$

$^*\beta_{pq}$ symbolizes a conditional constant, $\beta_{pq}[X^-]^p$, at a constant $[X^-]$; here $[X^-]$ is approximated to $[X^-]_{TOT}$. By inserting $^*\beta_{pq}$ into Eq. 10 and rearranging it, we obtain:

$$\frac{\bar{\varepsilon}(1 + \sum_n {}^*\beta_n) - (\varepsilon_0 + \sum_n \varepsilon_n {}^*\beta_n)}{\varepsilon_{pq} - \bar{\varepsilon}} = {}^*\beta_{pq}[OH^-]^q. \quad (11)$$

Since $\bar{\varepsilon}$ decreased with the increase in the concentration of hydroxide ions and approached zero, ε_{pq} may be assumed to be zero as a first approximation.

One function, F_1 is defined as follows:

$$F_1 = \log\left\{\frac{(\varepsilon_0 - \sum_n \varepsilon_n {}^*\beta_n) - \bar{\varepsilon}(1 + \sum_n {}^*\beta_n)}{\bar{\varepsilon}}\right\} = \log {}^*\beta_{pq} + q \log [OH^-]. \quad (12)$$

The plots of F_1 *vs.* log $[OH^-]$ are shown in Figs. 7 and 8 for the bromide and iodide systems respectively. Both plots gave straight lines with a slope of 2: thus, q=2 was estimated for both the bromide and iodide solutions. Therefore, Eq. 10 is rewritten as follows:

$$\bar{\varepsilon} = \frac{\varepsilon_0 + \sum_n \varepsilon_n {}^*\beta_n + \sum_p \varepsilon_{p2} {}^*\beta_{p2}[OH^-]^2}{1 + \sum_n {}^*\beta_n + \sum_p {}^*\beta_{p2}[OH^-]^2}. \quad (13)$$

Another function, F_2 is defined, after the rearrangement of Eq. 13, as follows:

$$F_2 = \{\bar{\varepsilon}(1 + \sum_n {}^*\beta_n) - (\varepsilon_0 + \sum_n \varepsilon_n {}^*\beta_n)\}[OH^-]^2 = \sum_p \varepsilon_{p2} {}^*\beta_{p2} - \bar{\varepsilon}_p {}^*\beta_{p2}. \quad (14)$$

Since F_2 is experimentally determinable at a given $[X^-]$, F_2 can be plotted against $\bar{\varepsilon}$. The plots are shown in Figs. 9 and 10 for the bromide and iodide systems respectively. Although the data are scattered to some extent, straight lines may be drawn through the points, as may be seen in the figures. In both plots, the lines pass a point near the original point of the coordinate: therefore, ε_{p2} may be zero or small compared with ε_0 and ε_n. The slopes of the lines,

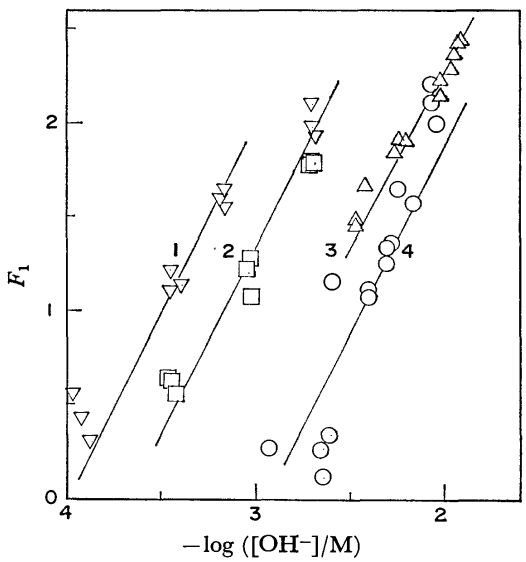

Fig. 7. Relationship between F_1 and log [OH⁻] for bromide solutions.
Numbers in the figure show the total concentrations of bromide ions (M).

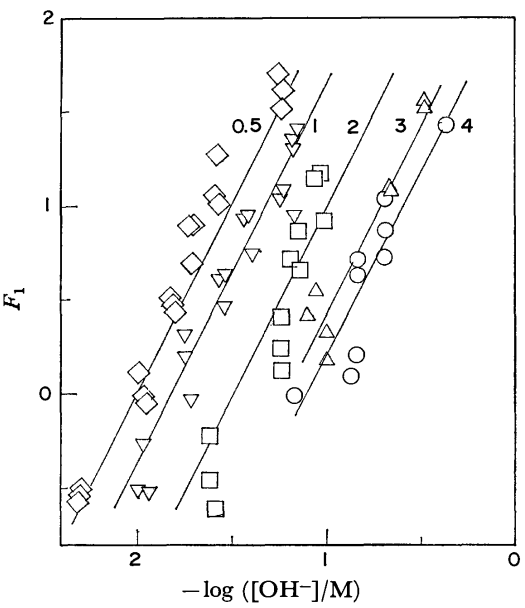

Fig. 8. Relationship between F_1 and log [OH⁻] for iodide solutions.
Numbers in the figure show the total concentrations of iodide ions (M).

$\sum_p {}^*\beta_{p2}$, thus obtained are plotted against log [X⁻] in Fig. 11. For both the bromide and iodide systems, $p=-2$ was found. Therefore, we concluded that, in the bromide and iodide solutions, $Cu(OH)_2^-$ was produced in alkaline solutions.

The formation constant of the complex proposed here was refined by means of a least-squares calculation: the final results are tabulated in Table 2, as are the values for the copper(I) chloro–hydroxo mixed complexes.[11] The solid lines in Figs. 5 and 6 show the curves calculated by using the constants finally obtained. In the solutions containing halide ions larger than 3 M, the formation constants obtained were slightly different from those found in the solutions with concentrations of the halide ions lower than 3 M;

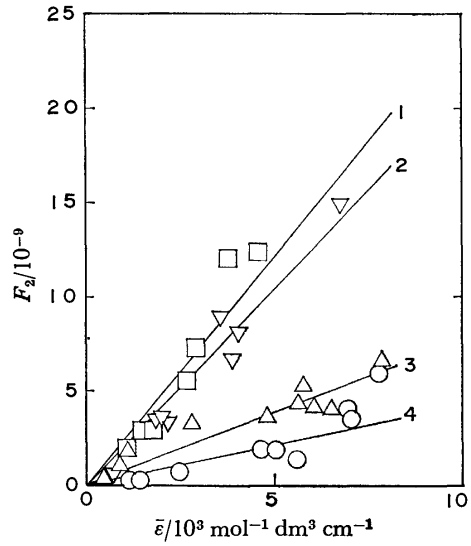

Fig. 9. Relationship between F_2 and $\bar{\varepsilon}$ at 278 nm for bromide solutions.
Numbers in the figure show the total concentrations of bromide ions (M).

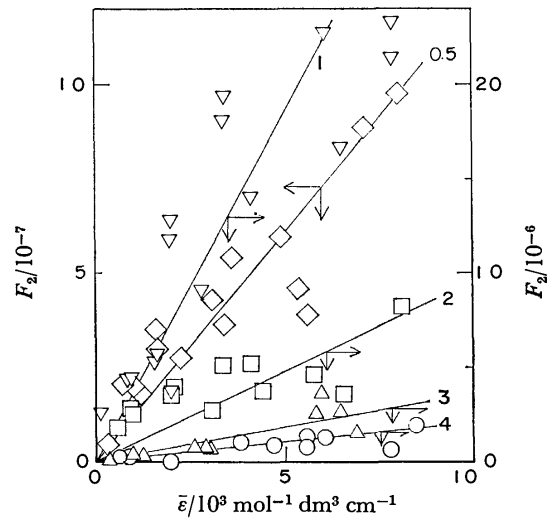

Fig. 10. Relationship between F_2 and $\bar{\varepsilon}$ at 285 nm for iodide solutions.
Numbers in the figure show the total concentrations of iodide ions (M).

TABLE 2. THE FORMATION CONSTANTS OF THE DIHYROXOCOPPER(I) COMPLEX, $Cu(OH)_2^-$

Solution	$[X^-]_{TOT}$ (M)	β_{pq}
Bromide	4	$(1.7\pm0.1)\times10^7$
	3	$(2.6\pm0.1)\times10^7$
	2–1	$(10.0\pm0.1)\times10^7$
Iodide	4	$(2.2\pm0.2)\times10^3$
	3	$(2.5\pm0.2)\times10^3$
	2–0.5	$(4.0\pm0.1)\times10^3$
Chloride[11]	$CuClOH^-$	$(1.1\pm0.1)\times10^4$
	$CuCl_2OH^{2-}$	$(4.1\pm0.3)\times10^3$
	$CuCl(OH)_2^{2-}$	$(3.8\pm0.1)\times10^6$

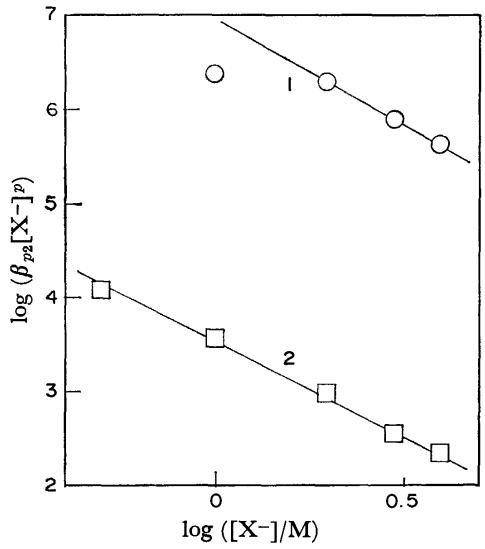

Fig. 11. Relationship between log (β_{p2}[X⁻]ᵖ) and log [X⁻].
1 : Bromide solutions, 2: iodide solutions.

this was due to the change in the property of the ionic media by the introduction of a large amount of the halide ions to the sodium perchlorate medium.

We have already reported in a previous paper[11] that the mixed halogeno–hydroxo complexes of copper(I) were found in alkaline solutions of the chloride system, whereas the dihydroxocopper(I) complex was not so found. In the bromide and iodide systems, the mixed halogeno–hydroxo complexes were not found, only the dihydroxocopper(I) complex was found in alkaline media.

The following formation constants of the $CuX_n^{(n-1)-}$ complexes have been reported in the literatures: for the chloride system, $CuCl_2^- + Cl^- = CuCl_3^{2-}$: log K_3= 0.29±0.04 by spectrophotometry;[17] for the bromide system, $CuBr_2^- + Br^- = CuBr_3^{2-}$: $K_3 = 10.2 \times 0.9\ M^{-1}$,[9] and for the iodide system, $[CuI_2^-]/[I^-] = (0.91—1.13) \times 10^{-3}$, $[CuI_3^{2-}]/[I^-]^2 = (4.32—5.9) \times 10^{-3}$. The results obtained in our experiments for the chloride and bromide systems are the same or nearly the same as the values in literature, but for the iodide system ones is smaller than the value in the literature.

The formation constant of the CuX_3^{2-} complex is smaller in the iodide system than in the bromide system. At a glance, this trend seems to be in the direction opposite to that expected from the hard-and-soft acid-and-bases concept. However, these results may be well explained on the HSAB basis as follows: a very soft acid the Cu^+ ion, may combine with a very soft base, I^-, to form the fairly stable CuI_2^- complex, which may have a linear structure; hence, the CuI_2^- complex may not be deformed by the insertion of the next iodide ion into the complex. On the other hand, the $CuBr_2^-$ complex may be less than the CuI_2^- complex, thus allowing for the addition of the third bromide ion to the complex to form the $CuBr_3^{2-}$ complex.

The much smaller formation constant of the $Cu(OH)_2^-$ complex in the iodide system than in the bromide system may be interpreted much like the fact that the stable CuI_3^{2-} complex (the overall formation constant of the CuI_3^{2-} may be large than that of the $CuBr_3^{2-}$, according to the HSAB concept) is not easily decomposed to form the $Cu(OH)_2^-$ complex with hydroxide ions by releasing the iodide ions within the complex.

It is thought that the difference in the behavior of the complex formation of copper(I) among the three halides may be related to the precipitation process of copper(I) oxide by the hydrolysis of copper(I) halide. In the precipitation of the less-soluble salt, the size of the nucleus depends on the ratio of the concentration of the supersaturation to the saturation of the solute.[18] As the halogeno complexes of copper(I) are stable in a concentrated solution of sodium halide and are much more stable in an iodide solution than in other halide solutions, the ratio of the concentration of the supersaturation to the saturation of copper(I) oxide is kept low: that is, large crystals of copper(I) oxide are easily precipitated in a concentrated solution of sodium halide, especially in an iodide solution.

The authors wish to express their gratitude to Professor Hitoshi Ohtaki of the Tokyo Institute of Technology at Nagatsuda for his guidance and helpful discussions.

References

1) K. Sugasaka, T. Kobayashi, S. Katoh, and J. Mizuguchi, *Denki Kagaku*, **36**, 250 (1968).
2) K. Sugasaka and T. Kobayashi, *Kogyo Kagaku Zasshi*, **71**, 335 (1968).
3) K. Sugasaka, A. Fujii, and N. Ninomiya, *Kogyo Kagaku Zasshi*, **74**, 339 (1971).
4) G. Bodländer and O. Storbeck, *Z. Anorg. Allg. Chem.*, **31**, 1 (1902).
5) G. Bodländer and O. Storbeck, *Z. Anorg. Allg. Chem.*, **31**, 458 (1902).
6) H. Fromherz and W. Menschick, *Z. Phys. Chem., Abt B*, **3**, 1 (1929).
7) E. Doehlemann and H. Fromherz, *Z. Phys. Chem., Abt A*, **171**, 23 (1934).
8) T. G. Sukhova, O. N. Temkin, and R. M. Flid, *Zh. Neorg. Khim.*, **1970**, 1849; *Chem. Abstr.*, **73**, 71739r (1970).
9) D. G. Peters and R. L. Caldwell, *J. Inorg. Chem.*, **6**, 1478 (1967).
10) A. M. Golub, S. M. Sazhienko, and C. I. Romanenko, *Chem. Abstr.*, **58**, 3949 (1963).
11) K. Sugasaka and A. Fujii, *Bull. Chem. Soc. Jpn.*, **49**, 82 (1976).
12) "Jikken Kagaku Koza," ed by The Chemical Society of Japan, Maruzen, Tokyo (1958), Vol. 9 pp. 384, 395.
13) "Stability Constants," The Chem. Soc., London (1974), No. 17, pp. 17, 285.
14) P. S. Farrington *J. Am. Chem. Soc.* **74**, 966 (1952).
15) R. Kruh, *J. Am. Chem. Soc.*, **76**, 4865 (1954).
16) S. Matsuo, *Nippon Kagaku Zasshi*, **82**, 1330 (1961).
17) B. Carlsson and G. Wettermark, *Z. Naturforsh., Teil A*, **31**, 297 (1976).
18) T. Kubo, E. Suito, Y. Nakagawa, and S. Hayakawa, "Fun-Tai," Maruzen, Tokyo (1962), p. 47.

The Raman Spectra of Cobalt(III) Complexes. I. Differentiation between *cis* and *trans* Isomers of Bis(ethylenediamine)cobalt(III) Complexes

Kan KANAMORI* and Kiyoyasu KAWAI

Department of Chemistry, Faculty of Science, Toyama University, Gofuku, Toyama 930

(Received November 15, 1979)

The Raman spectra of bis(ethylenediamine)cobalt(III) complexes have been studied with a view toward differentiating between the *cis* and *trans* configurations. It is shown that a correlation can be made between the configurations of the complexes and the intensity of the band due to the chelate-ring-deformation vibration, δ(cycle). Thus, *trans* isomers exhibit a strong and sharp band near 270 cm^{-1} due to this mode, while *cis* isomers exhibit no intense band at this frequency.

Several attempts have been made, with varying degrees of success, to correlate the configurations of bis(ethylenediamine)cobalt(III) complexes with the infrared spectra. Merritt and Wiberley[1] have suggested that a differentiation between *cis* and *trans* isomers of bis(ethylenediamine)cobalt(III) complexes may be made on the basis of the shift of the band in the 1500—1600 cm^{-1} region to lower frequencies from a *cis* to a *trans* configuration. Chamberlain and Bailar[2] have proposed a means for differentiating the *cis* and *trans* isomers by the number of bands in the 1120—1150 cm^{-1} region. Morris and Busch[3] and Baldwin[4] have attempted to correlate the splitting of the 1600 cm^{-1} and the 870—900 cm^{-1} bands respectively with the *cis* configuration. Hughes and McWhinnie[5] have suggested that a differentiation between the *cis* and *trans* isomers may be made on the basis of the complexity of the spectra in the 500—600 cm^{-1} region.

The present study was undertaken to correlate the configuration of the bis(ethylenediamine)cobalt(III) complex with the Raman spectrum. All the previous infrared studies, with the exception of the one by Hughes and McWhinnie,[5] have been concerned with the intra-ligand vibrations. The difference between the symmetries of the *cis* and *trans* isomers of bis(ethylenediamine)cobalt(III) complexes should, however, be reflected more sensitively in the skeletal vibrations than in the intra-ligand vibrations. It was thought worthwhile to study the metal-ligand vibrations of the *cis* and *trans* isomers, and Raman spectroscopy is suitable for this purpose. The Raman spectra were measured for the complexes whose geometrical configurations has already been determined, and on the basis of the observed Raman spectral difference between the *cis* and *trans* isomers, the Raman spectral criterion for differentiating the isomers was established. This criterion was then applied to the $[CoX(SO_3)(en)_2]$-type complexes ($X=N_3^-$, NCS^-, NH_3) obtained in the present work.

Experimental

Preparation. cis-$[Co(NCS)(SO_3)(en)_2]\cdot 0.5H_2O$: *trans*-$[CoCl(SO_3)(en)_2]$ (6 g) and NaSCN (1.7 g) were dissolved in 50 cm^3 of water, and the mixture was heated on a water bath for 3 h. The resulting mixture was cooled to room temperature. Then pale brown needles (*trans*-$[Co(NCS)(SO_3)(en)_2]$) were filtered off, and the filtrate was left standing overnight at room temperature. Orange-yellow leaflet crystals were deposited; they were then filtered off and recrystallized from hot water. Absorp. max. $10^{-3}\sigma$/cm^{-1} (log ε): 21.5 (2.44), *ca.* 29 sh (2.9), 35.0 (4.12). Found: C, 18.22; H, 5.29; N, 21.44%. Calcd for $[Co(NCS)(SO_3)(C_2H_8N_2)_2]\cdot 0.5H_2O$: C, 18.41; H, 5.25; N, 21.46%.

trans-$[Co(N_3)(SO_3)(en)_2]\cdot 0.5H_2O$: *trans*-$[Co(SO_3)(en)_2(H_2O)]ClO_4$ (6 g) was dissolved in 100 cm^3 of water, and then NaN_3 (5 g) was added. On occasional heating at 40 °C, the mixture was stirred for 1 h. On cooling and the addition of ethanol, a reddish-brown powder appeared; this was filtered off and dried. Absorp. max. $10^{-3}\sigma/cm^{-1}$ (log ε): 21.2 (2.55), *ca.* 30 sh (3.5), 36.5 (4.68). Found: C, 15.40; H, 5.54; N, 31.04%. Calcd for $[Co(N_3)(SO_3)(C_2H_8N_2)_2]\cdot 0.5H_2O$: C, 15.49; H, 5.52; N, 31.61%.

trans-$[Co(SO_3)(NH_3)(en)_2]Cl\cdot H_2O$: *trans*-$[CoCl(SO_3)(en)_2]$ (6 g) was dissolved in 50 cm^3 of liquid ammonia. The ammonia was then allowed to evaporate spontaneously, leaving behind a brown solid, which was recrystallized from hot water. Absorp. max. $10^{-3}\sigma/cm^{-1}$ (log ε): 21.6 (2.22), *ca.* 28 sh (2.3), 36.4 (4.15). Found: C, 14.58; H, 6.40; N, 21.18%. Calcd for $[Co(SO_3)(NH_3)(C_2H_8N_2)_2]\cdot H_2O$: C, 14.57; H, 6.42; N, 21.24%.

Other Complexes: *cis*-$[Co(CN)(SO_3)(en)_2]$ and *cis*-$[CoBr(CN)(en)_2]Br$ were prepared according to the method of Ohkawa, Hidaka, and Shimura.[6] *trans*-$[Co(CN)(SO_3)(en)_2]$ was prepared according to the method of Chan and Tobe.[7] *trans*-$[CoBr(CN)(en)_2]Br$ was prepared by the method of Chan.[8] *cis*-$[Co(CN)(NO_2)(en)_2]Br$ and *trans*-$[Co(CN)(NO_2)(en)_2]ClO_4$ were prepared by the method of Ohkawa, Hidaka, and Shimura.[9] *trans*-$[Co(NCS)(SO_3)(en)_2]$ and *cis*-$[Co(SO_3)(NH_3)(en)_2]Cl$ were prepared by the method of Baldwin.[10] *cis*-$[Co(N_3)(SO_3)(en)_2]$ was prepared by the method of Hughes and McWhinnie.[5] *cis*-$Li[Co(S_2O_3)_2(en)_2]$ was prepared by the method of Akamatsu, Hidaka, and Shimura.[11] All the other complexes are well known and were prepared by standard means. All the complexes were identified by means of the visible and ultra-violet spectra.

Measurements. The Raman spectra were recorded on a JASCO Laser Raman spectrometer (model R-800), using a He–Ne laser (632.8 nm) or an Ar^+ ion laser (514.5 or 457.9 nm) as the excitation source. Generally, the spectra were measured in aqueous solutions in order to avoid the appearance of lattice modes and the band splitting due to a crystal field.

Results and Discussion

The Raman spectra in the skeletal vibration region of *trans*- and *cis*-bis(ethylenediamine)cobalt(III) complexes whose geometrical configurations have previously been determined are shown in Fig. 1 and 2. The isomeric pair of complexes reveals a quite different Raman spectrum in this region. In general, the spectra of the *cis* isomers reveal more complicated

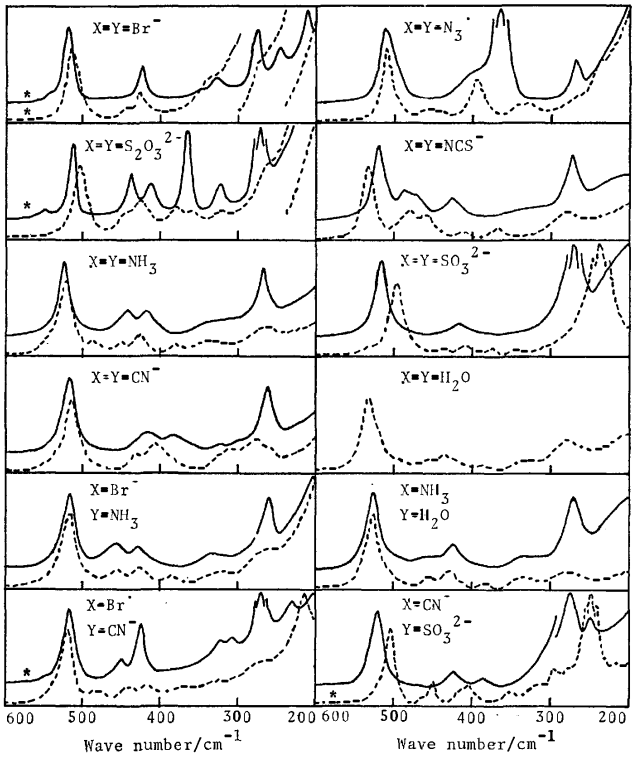

Fig. 1. Raman spectra of $[CoXY(en)_2]$-type complexes. *trans* isomer (——) and *cis* isomer (----). (* Denotes a solid-state spectrum.)

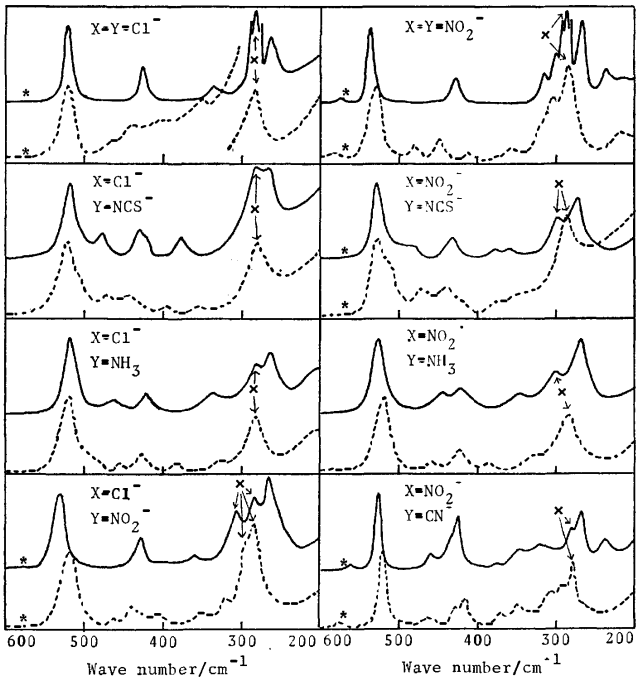

Fig. 2. Raman spectra of $[CoXY(en)_2]$-type complexes, where X or Y is a chloro or nitro group. *trans* isomer (——) and *cis* isomer (----). (* Denotes a solid-state spectrum; × denotes ν(Co–Cl) or ν(Co–NO_2).)

features than those of the *trans* isomers. The most striking difference is found near 270 cm^{-1}. That is, the Raman spectra of the *trans* isomers have a strong and sharp band near 270 cm^{-1}, while those of the *cis* isomers have no intense band at that frequency.

Two different assignments for the *ca.* 270 cm^{-1} band have been proposed. Gouteron-Vaissermann[12] has assigned the *ca.* 270 cm^{-1} band of $[Co(en)_3]^{3+}$ to the bending vibration of the N–Co–N angle, which does not include the chelate ring. On the other hand, Krishnan and Plane[13] have assigned the corresponding band to the chelate-ring-deformation vibration, δ(cycle), in their Raman study of complexes of ethylenediamine with zinc(II), cadmium(II), and mercury(II). The latter assignment is regarded as reasonable because the band at *ca.* 270 cm^{-1} in the Raman spectrum of *trans*-$[CoX_2(en)_2]$-type complexes is polarized and only the symmetric chelate-ring deformation of the nine skeletal deformation modes belongs to a totally symmetric species. Therefore, the strong band obserbed near 270 cm^{-1} in the Raman spectrum of *trans*-bis(ethylenediamine)cobalt(III) complexes may confidently be assigned to δ(cycle).

In the case of complexes containing a nitro or chloro group (see Fig. 2), careful measurements are required in estimating the intensity of δ(cycle) because ν(Co–NO_2) or ν(Co–Cl) appears as a intense band in the vicinity of δ(cycle). For example, the low-resolution Raman spectra of *cis*- and *trans*-$[Co(NO_2)_2(en)_2]^+$ are similar to each other in the *ca.* 270 cm^{-1} region; *i.e.*, the aqueous Raman spectrum of each isomer apparently shows a strong band in the region because of the band overlapping of δ(cycle) with ν(Co–NO_2). The differentiation between δ(cycle) and ν(Co–NO_2) or ν(Co–Cl) is performed by means of the Raman measurement of *N*-deuterated complexes. The band due to δ(cycle) shows a shift to a lower frequency (about 5 cm^{-1}) following a deuteration of the amino protons of the ethylenediamine group, while the band due to ν(Co–NO_2) or ν(Co–Cl) is not affected.

In conclusion, *cis-trans* isomeric pairs of $[CoX_2(en)_2]$-type and $[CoXY(en)_2]$-type complexes were successfully differentiated on the basis of the examination of the Raman intensity of the band due to δ(cycle) near 270 cm^{-1}.

It is obviously of interest to apply the present results to complexes of unknown or doubtful geometrical configurations. For the geometrical configuration of $[Co(NO_3)_2(en)_2]NO_3$, two different assignments have been proposed. Shimura and Tsuchida[14] have proposed that the complex has a *trans* configuration because the electronic absorption spectrum in the visible region shows the splitting of the first d-d absorption band. On the other hand, Krebs and Diewald[15] have regarded the complex as a *cis* isomer on the basis of the optical resolution by starch chromatography. Figure 3 shows the Raman spectrum of solid $[Co(NO_3)_2(en)_2]NO_3$. This complex is very unstable in water, and the Raman spectrum in an aqueous solution could not be obtained. The presence of the strong band at 276 cm^{-1} due to the δ(cycle) and the simple features of the spectrum reveal that the complex has a *trans* configuration. It can, therefore, be presumed that the complex which was optically resolved by Krebs and Diewald[15] might be an aquation-and-

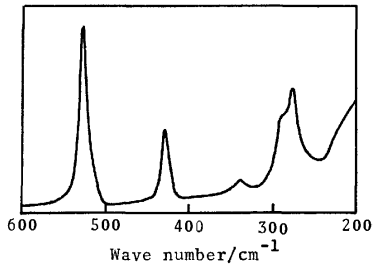

Fig. 3. Raman spectrum of solid $[Co(NO_3)_2(en)_2]NO_3$.

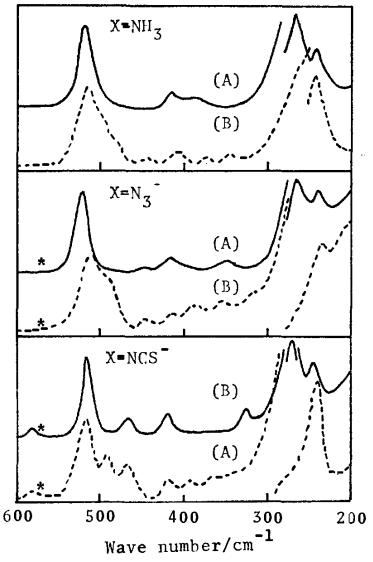

Fig. 4. Raman spectra of $[CoX(SO_3)(en)_2]$-type complexes.
trans isomer (——) and *cis* isomer (----). (* Denotes a solid-state spectrum; (A) refers to the spectra of the complexes which were prepared in the present work, and (B), to those of the complexes which were prepared by the methods in the Refs. 5 and 10.)

isomerisation product of the complex. The Raman spectrum of the aquation product of the complex does not show an intense band near 270 cm^{-1}.

Baldwin[10] has obtained a geometrical isomer of $[CoX(SO_3)(en)_2]$-type complexes ($X=H_2O$, NCS^-, NH_3) by means of substitution reactions of $[CoCl(SO_3)(en)_2]$. Hughes and McWhinnie[5] have also obtained a geometrical isomer of $[Co(N_3)(SO_3)(en)_2]$ by a similar method. These complexes have been assumed to have a *cis* configuration on the basis of the infrared spectra. However, the X-ray studies of $[Co(SO_3)(en_2)(H_2O)]ClO_4 \cdot H_2O$[16] and $[Co(NCS)(SO_3)(en)_2] \cdot 2H_2O$[17] show that these complexes have a *trans* configuration.

We have applied the Raman intensity criterion for δ(cycle) to the ammine and the azido complexes and have also prepared another isomer of the $[CoX(SO_3)(en)_2]$-type complexes ($X=NH_3$, N_3^-, NCS^-). The Raman spectra of the isomeric pairs of the complexes are shown in Fig. 4, where the (A) spectra refer to the isomers which have been prepared in the present work, and the (B) spectra, to the isomers which have been obtained by the methods in the literature. The Raman criterion indicates that the ammine and the azido complexes prepared by the present method have a *trans* configuration, while the complexes prepared by the methods in Refs. 5 and 10 have a *cis* configuration, consistent with the prediction made on the basis of the infrared spectra. It is also confirmed that the isothiocyanato complex obtained in the present work has a *cis* configuration.

The authors are indebted to Professor Yoichi Shimura of Osaka University and Dr. Isao Kanesaka of our university for their valuable discussions.

References

1) P. E. Merritt and S. E. Wiberley, *J. Phys. Chem.*, **59**, 55 (1959).
2) M. M. Chamberlain and J. C. Bailar, Jr., *J. Am. Chem. Soc.*, **81**, 6412 (1959).
3) M. L. Morris and D. H. Busch, *J. Am. Chem. Soc.*, **82**, 1521 (1960).
4) M. E. Baldwin, *J. Chem. Soc.*, **1960**, 4369.
5) M. N. Hughes and W. R. McWhinnie, *J. Inorg. Nucl. Chem.*, **28**, 1659 (1966).
6) K. Ohkawa, J. Hidaka, and Y. Shimura, *Bull. Chem. Soc. Jpn.*, **39**, 1715 (1966).
7) S. C. Chan and M. L. Tobe, *J. Chem. Soc.*, **1963**, 966.
8) S. C. Chan, *J. Chem. Soc.*, **1964**, 2716.
9) K. Ohkawa, J. Hidaka, and Y. Shimura, *Bull. Chem. Soc. Jpn.*, **40**, 2830 (1967).
10) M. E. Baldwin, *J. Chem. Soc.*, **1961**, 3123.
11) K. Akamatsu, J. Hidaka, and Y. Shimura, *Bull. Chem. Soc. Jpn.*, **50**, 533 (1977).
12) J. Gouteron-Vaissermann, *C. R. Acad. Sci., Ser. B*, **275**, 149 (1972).
13) K. Krishnan and R. A. Plane, *Inorg. Chem.*, **5**, 852 (1966).
14) Y. Shimura and R. Tsuchida, *Nippon Kagaku Zasshi*, **77**, 734 (1956).
15) H. Krebs and J. Diewald, *Z. Anorg. Allg. Chem.*, **287**, 98 (1956).
16) E. N. Maslen, C. L. Raston, A. H. White, and J. K. Yandell, *J. Chem. Soc., Dalton Trans.*, **1975**, 327.
17) S. Baggio and L. N. Becka, *Acta Crystallogr., Sect. B*, **25**, 946 (1969).

Synthesis and Circular Dichroism Spectra of [Co(a)(gly)(1,4,7-triazacyclononane)]-type Complexes

Satoru SHIMBA, Shuhei FUJINAMI, and Muraji SHIBATA*

Department of Chemistry, Faculty of Science, Kanazawa University, Kanazawa 920

(Received November 21, 1979)

Complexes of the [Co(a)(gly)(tacn)]-type, where tacn represents 1,4,7-triazacyclononane and a is CN^-, NO_2^-, NH_3, NCS^-, H_2O, OH^-, N_3^-, or Cl^-, have been prepared and resolved. The CD spectra of these complexes have been measured. On the basis of the X-ray analysis of $(-)_{589}$[Co(gly)(NH_3)(tacn)]$I_2\cdot H_2O$, the absolute configurations of the other complexes have been assigned by referring to the CD spectra. These complexes have exhibited a common CD pattern in the T_{1g}-band region, and from this fact a criterion for the assignments of the absolute configurations for the complexes of the *fac*(D)-[Co(a)(BC)(DDD)]-type has been established.

Most circular dichroism (CD) spectral studies of cobalt(III) complexes have been undertaken to investigate various sources of optical activity, such as the distribution of chelate rings, the conformation of chelate rings, the vicinal effect due to asymmetric carbon in an optically active ligand, and the vicinal effect due to an asymmetric donor atom.[1] In contrast to those investigations, little work has been reported on complexes whose optical activity arises from the arrangement of unidentate ligands. The paucity of research on such complexes seems mainly a result of the lack of preparative methods. In our laboratory some complexes of *cis-cis*-[Co(a)$_2$(b)$_2$(CC)]- and *all-cis*-[Co(a)$_2$(b)$_2$(c)$_2$]-types have been prepared through a few steps of ligand substitution, and then resolved into enantiomeric isomers.[2] Shimura *et al.*[3,4] prepared and resolved complexes of the *fac*(D)-[Co(a)(BC)(DDD)]-type, using 2-aminomethyl-2-methyl-1,3-propanediamine (1,1,1-tris(aminomethyl)ethane, TAME) or $Nb_6O_{19}^{8-}$ as the DDD ligand and glycinate as the BC ligand. However, the absolute configurations of these complexes have not been established. Very recently, we reported a complex of the *fac*(D)-[Co(a)(b)(c)(DDD)]-type, where DDD was 1,4,7-triazacyclononane (=TACN) and where a, b, and c were CN^-, Br^-, and NH_3 respectively.[5]

This paper will deal with the syntheses and optical resolution of a series of $[Co(a)(gly)(tacn)]^{n+}$ complexes (a=CN^-, NO_2^-, NH_3, NCS^-, H_2O, OH^-, N_3^-, Cl^-, or I^-). Since TACN coordinates facially in an octahedral complex, the chirality of these complexes is derived from the arrangement of the complexed gly and unidentate ligands, as is shown in Fig. 1. The absolute configurations of these complexes are assigned by referring to the CD spectra, on the basis of the results of the X-ray analysis of $(-)_{589}$[Co(gly)(NH_3)(tacn)]$I_2\cdot H_2O$.[6]

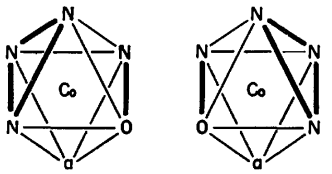

Fig. 1. Enantiomers of [Co(a)(gly)(tacn)]-type complex.

Experimental

Ligand. 1,4,7-Triazacyclononane trihydrochloride (TACN·3HCl) was prepared by the literature method.[7]

Preparation of Complexes. *1) Aquaglycinato-1,4,7-triazacyclononanecobalt(III) Perchlorate Dihydrate, [Co(gly)(tacn)$(H_2O)](ClO_4)_2\cdot 2H_2O$:* The *mer*(N)-*trans*$(NH_3)$-[Co$(CO_3)(gly)(NH_3)_2$] complex (5.0 g, 0.022 mol)[8] was dissolved in water (20 cm^3), and then the ligand, TACN·3HCl (5.0 g, 0.022 mol), was added to this solution in portions, with care taken to the evolution of carbon dioxide. After the compounds had been dissolved, the solution was adjusted to pH 2 with $HClO_4$ (60%), whereupon the diaqua complex, $[Co(gly)(NH_3)_2(H_2O)_2]^{2+}$, was formed. The solution was alkalized with 5 M (1 M=1 mol dm^{-3}) KOH until pH 9, stirred for 15 min, and then acidified with $HClO_4$ until pH 6. The resulting solution was filtered once and diluted to 2 dm^3 with water. This solution was poured into a column containing SP-Sephadex C-25 (4.5×25.0 cm, Na^+ form). The adsorbed band was eluted with 0.1 M $HClO_4$, and a red band corresponding to the bivalent cation of the desired complex was collected. The eluate was concentrated to a small volume by means of a rotary evaporator, after which a small amount of ethanol and a large amount of ether were added to the concentrate successively. This solution was kept in a refrigerator until the red material of the desired complex was deposited. The crude product was recrystallized from warm water (*ca.* 60 °C). The yield was about 2.0 g. Found: C, 18.55; H, 4.95; N, 10.62%. Calcd for $[Co(gly)(tacn)(H_2O)](ClO_4)_2\cdot 2H_2O = C_8H_{25}O_{13}N_4Cl_2Co$: C, 18.65; H, 4.90; N, 10.88%. This aqua complex was used as the starting material for the following syntheses (*2)—7)*).

2) Glycinatonitro-1,4,7-triazacyclononanecobalt(III) Chloride Monohydrate, $[Co(NO_2)(gly)(tacn)]Cl\cdot H_2O$: To a solution of the aqua complex (1.5 g in 20 cm^3 H_2O) we added $NaNO_2$ (1 g, 0.014 mol), and then the solution was adjusted to pH 4 with $HClO_4$. The solution was stirred at 50—60 °C until its color changed from red to yellow. The resulting solution was subjected to Sephadex column chromatography in a way similar to that in *1)*. The eluate obtained by elution with 0.05 M NaCl was concentrated to a small volume by means of a rotary evaporator, with the simultaneous removal of the NaCl deposited; a large amount of ethanol was then added to the concentrate. The ethanolic solution was kept in a refrigerator to obtain yellow crystals. The crystals were recrystallized from warm water (*ca.* 50 °C). The yield was *ca.* 0.8 g. Found: C, 26.25; H, 5.69; N, 19.47%. Calcd for $[Co(NO_2)(gly)(tacn)]Cl\cdot H_2O = C_8H_{21}O_5N_5ClCo$: C, 26.56; H, 5.89; N, 19.37%.

3) Ammineglycinato-1,4,7-triazacyclononanecobalt(III) Iodide Monohydrate, $[Co(gly)(NH_3)(tacn)]I_2\cdot H_2O$: The aqua complex (1.5 g) was dissolved in aqueous ammonia (28%,

100 cm³), after which the solution was allowed to stand in a flask with a stopcock at 60 °C until it turned orange (several hours). The resulting solution was poured into a column of Dowex 50W-X8 (4.5×10.0 cm, Na^+ form). The eluate obtained by subsequent elution with 0.3 M NaI was treated in a way similar to that in *2)*. When the concentrated solution was kept in a refrigerator, orange crystals were deposited; they were recrystallized from warm water (60 °C). The yield was *ca.* 1.0 g. Found: C, 17.37; H, 4.26; N, 12.52%. Calcd for $[Co(gly)(NH_3)(tacn)]I_2 \cdot H_2O = C_8H_{24}O_3N_5I_2Co$: C, 17.31; H, 4.37; N, 12.62%.

4) Glycinatoisothiocyanato-1,4,7-triazacyclononanecobalt(III) Bromide, [Co(NCS)(gly)(tacn)]Br: An aqueous solution (20 cm³) containing starting aqua complex (1.5 g) and KSCN (1.5 g, 0.015 mol) was adjusted to pH 4 with $HClO_4$ and then stirred at 50—60 °C for 2—3 h. The resulting red solution was chromatographed in the same manner as *3)*. The elution was carried out with 0.1 M NaBr. The yield of the desired complex was *ca.* 0.8 g. Found: C, 26.91; H, 4.81; N, 17.31%. Calcd for $[Co(NCS)(gly)(tacn)]Br = C_9H_{19}O_2N_5SBrCo$: C, 27.01; H, 4.79; N, 17.50%.

5) Azidoglycinato-1,4,7-triazacyclononanecobalt(III) Iodide Monohydrate, [Co(N₃)(gly)(tacn)]I·H₂O: This complex was prepared in the same manner as the isothiocyanato complex, except for the use of NaN_3 (1.0 g, 0.015 mol) in place of KSCN. The elution was carried out with 0.1 M NaI. Red-violet crystals were obtained in a yield of *ca.* 0.8 g. Found: C, 21.23; H, 4.33; N, 21.42%. Calcd for $[Co(N_3)(gly)(tacn)]I \cdot H_2O = C_8H_{21}O_3N_7ICo$: C, 21.29; H, 4.70; N, 21.73%.

6) Chloroglycinato-1,4,7-triazacyclononanecobalt(III) Chloride 1.5-hydrate, [Co(Cl)(gly)(tacn)]Cl·1.5H₂O: Starting aqua complex (1.5 g) was dissolved in 6 M HCl (20 cm³), after which the solution was stirred at 60 °C for 2—3 h. The resulting solution was poured into a column of Dowex 50W-X8 (5.5×10.0 cm, H^+ form). The eluate obtained by elution with 0.1 M NaCl was treated by the same way as *3)*. The yield of violet crystals was *ca.* 0.5 g. Found: C, 26.66; H, 5.77; N, 15.31%. Calcd for $[Co(Cl)(gly)(tacn)]Cl \cdot 1.5H_2O = C_8H_{22}O_{3.5}N_4Cl_2Co$: C, 26.68; H, 6.17; N, 15.56%.

7) Glycinatoiodo-1,4,7-triazacyclononanecobalt(III) Iodide, [Co(I)(gly)(tacn)]I: When, in the preparation of the aqua complex, elution was carried out with 0.1 M NaI and the eluate was concentrated to a small volume, the solution turned green. From the solution, powdery green crystals of the iodo complex separated out. The yield was *ca.* 1.0 g. Found: C, 18.53; H, 3.54; N, 10.92%. Calcd for $[Co(I)(gly)(tacn)]I = C_8H_{19}O_2N_4I_2Co$: C, 18.48; H, 3.69; N, 10.78%.

8) Cyanoglycinato-1,4,7-triazacyclononanecobalt(III) Chloride Dihydrate, [Co(CN)(gly)(tacn)]Cl·2H₂O: So far as this cyano complex was concerned, attempts at derivation from the aqua complex in an aqueous medium were unsuccessful. Instead, the desired complex was obtained by means of a reaction in dimethyl sulfoxide (DMSO); the chloro complex, $[Co(Cl)(gly)(tacn)]Cl \cdot 1.5H_2O$ (2.0 g, 0.0056 mol), was carefully dissolved in a minimum amount of conc. HNO_3; after the evolution of Cl_2 and NO_2 gases had ceased, ethanol (15 cm³) was added to the solution to precipitate the nitrate of the complex, $[Co(Cl)(gly)(tacn)]NO_3$. The nitrate was dissolved in DMSO (300 cm³) containing KCN (1.0 g, 0.015 mol), after which the solution was heated at 85—90 °C for 2—3 h. The resulting yellow solution was poured into a column of SP-Sephadex C-25 (4.5×25.0 cm, Na^+ form). Elution was carried out with 0.05 M NaCl to collect a portion of the desired species. When the concentrate of the fraction was kept in a refrigerator, yellow crystals separated out; yield, *ca.* 0.6 g. Found: C, 29.92; H, 6.05; N, 19.45%. Calcd for $[Co(CN)(gly)(tacn)]Cl \cdot 2H_2O = C_9H_{23}O_4N_5ClCo$: C, 30.05; H, 6.46; N, 19.47%.

Optical Resolution. Each of the cyano, nitro, and ammine complexes was resolved into two optically active forms by the column chromatography of SP-Sephadex C-25 (2.5×110.0 cm, Na^+ form), using 0.05 M $K_2[Sb_2(d\text{-tart})_2]$ as the eluent. The remaining isothiocyanato, aqua, azido, and chloro complexes were all resolved into two forms each using columns of Dowex 50W-X8 (200—400 mesh, 2.5×34.5 cm, Na^+ form) and a 0.3 M $Na_2[Sb_2(d\text{-tart})_2]$ solution as the eluent. When the adsorbed band had descended to four-fifths of the column height, the band was washed with water and eluted with 0.1 M NaCl or 0.3 M $NaClO_4$. The eluate thus concentrated was submitted to the measurement of the CD spectra, while the concentration of the complex species was evaluated from the absorption spectral data.

Derivations from Optically Active Complexes. Several optically active complexes, $(-)_{589}[Co(NO_2)(gly)(tacn)]^+$, $(-)_{589}[Co(NCS)(gly)(tacn)]^+$, $(+)_{589}[Co(N_3)(gly)(tacn)]^+$, and $(-)_{589}[Co(Cl)(gly)(tacn)]^+$, could be directly derived from the optically active aqua complex, $(-)_{589}[Co(gly)(tacn)(H_2O)](ClO_4)_2 \cdot 2H_2O$, according to the methods described in *2)*, *4)*, *5)*, and *6)* respectively. The reaction of aqueous ammonia of the $(-)_{589}[Co(gly)(tacn)(H_2O)]^{2+}$ complex resulted in the formation of the racemic $[Co(gly)(NH_3)(tacn)]^{2+}$ complex. On the other hand, the oxidation of the $(-)_{589}[Co(NCS)(gly)(tacn)]^+$ complex by aqueous H_2O_2 at *ca.* pH 3 produced the $(-)_{589}[Co(gly)(NH_3)(tacn)]^{2+}$, $(-)_{589}[Co(CN)(gly)(tacn)]^+$ and $(-)_{589}[Co(gly)(tacn)(H_2O)]^{2+}$ complexes, which were separated chromatographically.

Measurements. The absorption spectra in aqueous solutions were recorded with a Hitachi 323 recording spectrophotometer. The CD spectra were measured with a JASCO J-40C automatic recording spectropolarimeter equipped with a JASCO Model J-DPZ data processor for CD. For the measurement of the optical rotation, a JASCO Model DIP-SL automatic polarimeter was used. The absorption and CD spectra of hydroxo complex species were measured with an alkalized solution (pH 9) of the aqua complex with 5 M NaOH. The hydroxo complex species was chromatographically pure, and its absorption and CD spectra were changed into the original spectra of the parent aqua complex when the solution was again acidified with $HClO_4$. This fact suggests that the base-hydrolysis proceeds with retention of the configuration.

The CD measurement was carried out for an aqueous solution of bis(1,4,7-triazacyclononane)cobalt(III), $[Co(tacn)_2]^{3+}$,[9] in the presence of $[Sb_2(d\text{-tart})_2]^{2-}$ ($[Co(tacn)_2]Cl_3$ 4.0×10^{-3} M; $K_2[Sb_2(d\text{-tart})_2] \cdot H_2O$ 8.0×10^{-2} M).

Results and Discussion

Preparation and Resolution. A feature of the present method of preparation is that a series of complexes with various unidentates, a, $[Co(a)(gly)(tacn)]^{n+}$, could be derived from one complex, $[Co(gly)(tacn)(H_2O)]^{2+}$. An exception was the case of the cyano complex; the reaction of potassium cyanide on an aqueous solution of the aqua complex resulted in the formation of a hydroxo complex, $[Co(OH)(gly)(tacn)]^+$, which was not isolated because of its great solubility. Instead, the reaction of the chloro complex, $[Co(Cl)(gly)(tacn)]^+$, with potassium cyanide in DMSO yield-

ed the desired complex.

For the optical resolution of the complexes, column chromatography using an ion-exchanger and *d*-tartratoantimonate(III) was useful. It is worth noting that a complete resolution was attained by using a Dowex cation exchanger for the complexes containing unidentates whose ligand-field-strengths are weaker than that of ammonia. On the other hand, the chromatographic resolutions of the same complexes on Sephadex columns were partial. The attempted resolution of the iodo complex was unsuccessful becasue of the great lability of the complexed iodide ion.

Absorption and CD Spectra. The absorption spectrum of the racemic $[Co(gly)(NH_3)(tacn)]^{2+}$ complex and the CD spectra of the two resolved isomers are illustrated in Fig. 2, the CD curves being mirror images of each other. Since the same situation was encountered in the resolved pairs of the other complexes, the CD spectra for only the isomers obtained from the earlier eluates are illustrated, together with the absorption spectra, in Figs. 3—5. The numerical data are summarized in Table 1. Every complex has a rhombic ligand field in which there are three electronic transition components for each of the first absorption (T_{1g}) and second absorption (T_{2g}) bands. However, no appreciable splittings are observed even in the T_{1g} bands of the cyano and chloro complexes. The maximum positions of the first absorption bands ($\tilde{\nu}_{Imax}$) shift to a higher-frequency side in accord with the spectrochemical series[10], $I^- < Cl^- < N_3^- < OH^- < H_2O < NCS^- < NH_3 < NO_2^- < CN^-$, with respect to the unidentates used.

The observed CD spectra are classified into three groups on the basis of the patterns in the T_{1g} band region: 1) one negative broad peak, 2) a positive and a negative peak from a lower frequency, and 3) a negative, a positive, and a negative peak from a lower frequency. The $(-)_{589}[Co(CN)(gly)(tacn)]^+$ complex belongs to Group 1. The extremum is located at a lower frequency compared with the corresponding absorption maximum ($\tilde{\nu}_{Imax}$), and a shoulder is observed at a higher frequency. The

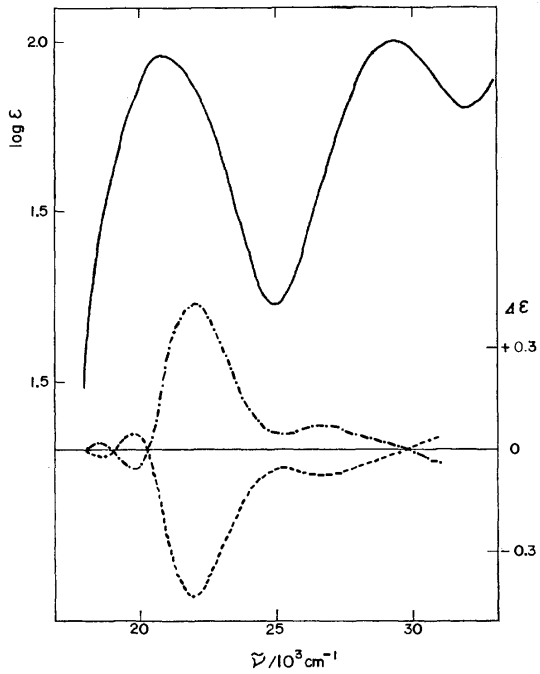

Fig. 2. Absorption spectrum of $[Co(gly)(NH_3)(tacn)]^{2+}$ (——), and CD spectra of $(-)_{589}[Co(gly)(NH_3)(tacn)]^{2+}$ (earlier eluate) (----), $(+)_{589}[Co(gly)(NH_3)(tacn)]^{2+}$ (—·—·—).

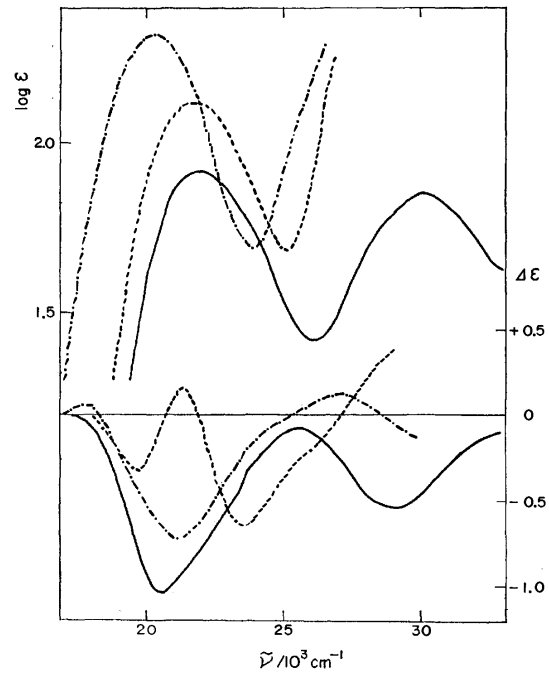

Fig. 3. Absorption and CD spectra of $(-)_{589}[Co(CN)(gly)(tacn)]^+$ (——), $(-)_{589}[Co(NO_2)(gly)(tacn)]^+$ (----), $(-)_{589}[Co(NCS)(gly)(tacn)]^+$ (—·—·—).

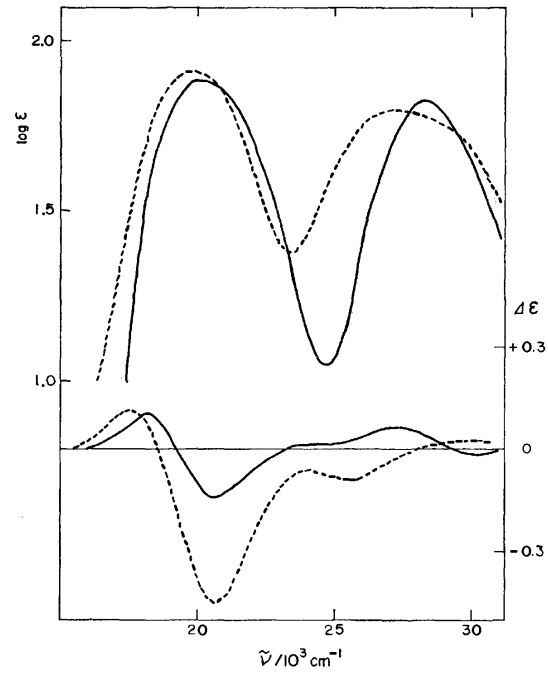

Fig. 4. Absorption and CD spectra of $(-)_{589}[Co(gly)(tacn)(H_2O)]^{2+}$ (——), $(-)_{589}[Co(OH)(gly)(tacn)]^+$ (----).

$(-)_{589}$[Co(NCS)(gly)(tacn)]$^+$, $(-)_{589}$[Co(gly)(tacn)-(H_2O)]$^{2+}$, $(-)_{589}$[Co(OH)(gly)(tacn)]$^+$, $(+)_{589}$[Co-(N_3)(gly)(tacn)]$^+$, and $(-)_{589}$[CoCl(gly)(tacn)]$^+$ complexes exhibit the pattern of Group 2. Two complexes, $(-)_{589}$[Co(NO_2)(gly)(tacn)]$^+$ and $(-)_{589}$[Co-(gly)(NH_3)(tacn)]$^{2+}$, show the pattern of Group 3. However, the negative extremum observed at the lowest frequency in the spectrum of the $(-)_{589}$[Co-(gly)(NH_3)(tacn)]$^{2+}$ complex is extremely weak. A striking characteristic in the CD spectra for the earlier-eluted enantiomers is that a major CD peak of a negative sign is observed at a higher frequency in the T_{1g}-band region, except for the case of the cyano complex, where a negative shoulder appears at a higher frequency. Another characteristic is that the intensity is very weak in comparison with that of bis- or tris-diamine complexes.

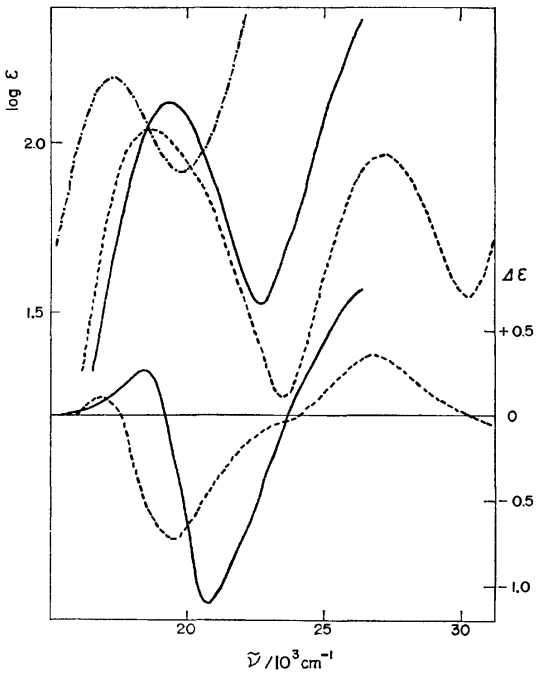

Fig. 5. Absorption and CD spectra of $(+)_{589}$[Co(N_3)-(gly)(tacn)]$^+$ (——), $(-)_{589}$[Co(Cl)(gly)(tacn)]$^+$ (----), [Co(I)(gly)(tacn)]$^+$ (—·—·—).

For the present chiral complexes, three sources of d-electron optical activity can be considered; the helical distribution of a H_2N–CH_2–COO^- chelate and the –NH–CH_2–CH_2–NH– moiety of tacn, the conformations of the three chelate rings of the tacn or glycinate ring, and the arrangement of the three donors of the glycinate and unidentate ligands. Recently, the absolute configuration of the $(-)_{589}$[Co(gly)(NH_3)-(tacn)]$I_2 \cdot H_2O$ was determined by X-ray analysis.[6] It was thereby found that the glycinate chelate ring was nearly planar (that is, it was achiral), and the five-membered chelate rings of the tacn ligand had all a δ-conformation. However, it is thought that the conformations of the tacn chelate rings are not fixed in a solution, judging from the following fact. When a solution CD spectrum of the $[Co(tacn)_2]^{3+}$ complex was measured in the presence of $[Sb_2(d\text{-tart})_2]^{2-}$, a negative peak ($\Delta\varepsilon = -0.40$) was observed

Table 1. Absorption and CD spectral data of the earlier-eluted enantiomers

Complex	Absorption		CD	
	$\tilde{\nu}/10^3$ cm^{-1}	(log ε)	$\tilde{\nu}/10^3$ cm^{-1}	($\Delta\varepsilon$)
$(-)_{589}$[Co(CN)(gly)(tacn)]$^+$	21.9	(1.9)	20.7	(−1.05)
			ca. 23.0	(*ca.* −0.5 sh)
	30.0	(1.85)	29.0	(−0.53)
$(-)_{589}$[Co(NO_2)(gly)(tacn)]$^+$	21.8	(2.12)	19.8	(−0.32)
			21.3	(+0.15)
			23.6	(−0.66)
$(-)_{589}$[Co(gly)(NH_3)(tacn)]$^{2+}$	20.8	(1.96)	18.6	(−0.02)
			19.8	(+0.06)
			22.0	(−0.42)
	29.1	(2.00)	26.4	(−0.07)
$(-)_{589}$[Co(NCS)(gly)(tacn)]$^+$	20.3	(2.31)	17.8	(+0.04)
			21.2	(−0.73)
	—	—	27.0	(+0.12)
$(-)_{589}$[Co(gly)(tacn)(H_2O)]$^{2+}$	20.0	(1.88)	18.2	(+0.10)
			20.6	(−0.14)
	28.0	(1.82)	27.1	(+0.06)
			30.3	(−0.01)
$(-)_{589}$[Co(OH)(gly)(tacn)]$^+$	19.7	(1.91)	17.6	(+0.11)
			20.6	(−0.45)
	27.1	(1.80)	25.4	(−0.09)
$(+)_{589}$[Co(N_3)(gly)(tacn)]$^+$	19.4	(2.32)	18.4	(+0.27)
			20.8	(−1.10)
$(-)_{589}$[Co(Cl)(gly)(tacn)]$^+$	18.6	(2.04)	16.9	(+0.10)
			19.6	(−0.71)
	27.0	(1.97)	26.7	(+0.36)
[Co(I)(gly)(tacn)]$^+$	17.2	(2.20)		

at 21200 cm^{-1} in the T_{1g}-band region, indicating the preferential formation of a fixed conformation (probably δ) of the chelate rings. A similar CD spectrum was observed for $[Co\{(2R\text{-Me})\text{-tacn}\}_2]^{3+}$;[11-13] it shows a very strong positive peak in the T_{1g}-band region, probably as a result of the chiral puckering of the chelate rings with the λ-conformation.[14] This experimental result indicates a small contribution from a fixed conformation to the solution CD spectrum of the present $[Co(a)(gly)(tacn)]^{n+}$ complex. There are two kinds of helical distributions in the $[Co(a)(gly)(tacn)]^{n+}$ complex, however, one is designated Δ, and the other, Λ. Therefore, the optical activity due to the helical distribution is probably very small in the complex.

On the other hand, the CD spectra of $(-)_{589}[Co(gly)(NH_3)(tacn)]^{2+}$ and $(-)_{589}[Co(gly)(NH_3)(tame)]^{2+}$, where tame is a tripod ligand, resemble each other well in both shape and peak intensity; *i.e.*, the $\Delta\varepsilon$ value for the dominant peak of $(-)_{589}[Co(gly)(NH_3)(tacn)]^{2+}$, $\Delta\varepsilon=-0.42$, corresponds well with that of $(-)_{589}[Co(gly)(NH_3)(tame)]^{2+}$, $\Delta\varepsilon=-0.44$. These facts also support the idea that the first and second sources make little contribution to optical activity. Therefore, it may be concluded that the optical activity of $[Co(a)(gly)(tacn)]^{n+}$ is due to the arrangement of the three donors of the glycinate and unidentate ligands.

Absolute Configuration. In order to investigate the relation between the Cotton signs and the absolute configuration on the $[Co(a)(gly)(tacn)]^{n+}$ complexes, we tried to obtain optically active complexes directly from the $(-)_{589}[Co(gly)(tacn)(H_2O)]^{2+}$ complex. The conversions were successful in giving the corresponding $(-)_{589}[Co(NO_2)(gly)(tacn)]^{+}$, $(-)_{589}[Co(NCS)(gly)(tacn)]^{+}$, $(+)_{589}[Co(N_3)(gly)(tacn)]^{+}$, and $(-)_{589}[Co(Cl)(gly)(tacn)]^{+}$ complexes. This fact indicates that the configurations of the gly and tacn ligands are retained in the course of the reaction. The oxidation of the $(-)_{589}[Co(NCS)(gly)(tacn)]^{+}$ complex with aqueous H_2O_2 at *ca.* pH 3 produced $(-)_{589}[Co(gly)(NH_3)(tacn)]^{2+}$, $(-)_{589}[Co(CN)(gly)(tacn)]^{+}$ and $(-)_{589}[Co(gly)(tacn)(H_2O)]^{2+}$ complexes. Similar oxidative degradation reactions have been reported by Gillard and Maskill[15]; $(-)_{589}[Co(NCS)_2(en)_2]^{+}$ was converted into $(-)_{589}[Co(NH_3)_2(en)_2]^{3+}$ and $(-)_{589}[Co(CN)_2(en)_2]^{+}$, and these three complexes have the same absolute configuration. Therefore, the four tacn complexes also have the same absolute configuration.

On the basis of the above results, it is concluded that the earlier-eluted enantiomers, whose major CD peaks have a negative sign, have the same arrangement with respect to the donors of gly and the unidentates (CN^-, NO_2^-, NH_3, NCS^-, H_2O, OH^-, N_3^-, and Cl^-), as is shown in Fig. 6. We can now assign the absolute configurations of $(-)_{589}[Co(gly)(NH_3)(tame)]^{2+}$, $(-)^{CD}_{546}[Co(Nb_6O_{19})(gly)(NH_3)]^{6-}$, and $(-)^{CD}_{546}[Co(Nb_6O_{19})(gly)(H_2O)]^{6-}$ complexes,[3,4] which belong to the *fac*(D)-[Co(a)(BC)(DDD)]-type, by comparing the sign of the CD peak in the T_{1g}-band region with that of the $(-)_{589}[Co(gly)(NH_3)(tacn)]^{2+}$ or $(-)_{589}[Co(gly)(tacn)(H_2O)]^{2+}$ complex. Thus, the three complexes, $(-)_{589}[Co(gly)(NH_3)(tame)]^{2+}$, $(-)^{CD}_{546}[Co(Nb_6O_{19})(gly)(NH_3)]^{6-}$ and $(-)^{CD}_{546}[Co(Nb_6O_{19})(gly)(H_2O)]^{6-}$, have the same arrangement with respect to the donors of the glycinate and unidentate ligands, as is shown in Fig. 6.

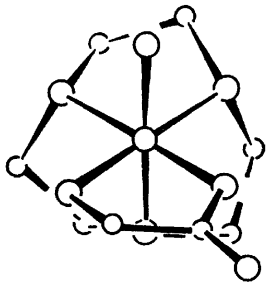

Fig. 6. Absolute configuration of the earlier eluted enantiomer of $[Co(a)(gly)(tacn)]^{n+}$ Complex.

The authors wish to express thanks to Dr. Nonoyama, Nagoya University, for his aid in the preparation of the ligand.

References

1) C. J. Howkins, "Absolute Configuration of Metal Complex," Wiley, New York, N. Y. (1971).
2) T. Ito and M. Shibata, *Inorg. Chem.*, **16**, 108 (1977).
3) K. Yamanari, J. Hidaka, and Y. Shimura, *Bull. Chem. Soc. Jpn.*, **48**, 1653 (1975).
4) Y. Hosokawa, J. Hidaka, and Y. Shimura, *Bull. Chem. Soc. Jpn.*, **48**, 3175 (1975).
5) S. Shimba, S. Fujinami, and M. Shibata, *Chem. Lett.*, **1979**, 783.
6) S. Sato, S. Ohba, S. Shimba, S. Fujinami, M. Shibata, and Y. Saito, *Acta Crystallogr., Sect. B*, **36**, 43 (1980).
7) J. E. Richman and T. J. Atkins, *J. Am. Chem. Soc.*, **96**, 2268 (1974).
8) S. Kanazawa and M. Shibata, *Bull. Chem. Soc. Jpn.*, **44**, 2424 (1971).
9) H. Koyama and T. Yoshino, *Bull. Chem. Soc. Jpn.*, **45**, 481 (1972).
10) R. Tsuchida, *Bull. Chem. Soc. Jpn.*, **13**, 388 (1938).
11) S. F. Mason and R. D. Peacock, *Inorg. Chim. Acta*, **19**, 75 (1976).
12) A. F. Drake, R. Kuroda, and S. F. Mason, *J. Chem. Soc., Dalton Trans.*, **1979**, 1095.
13) M. Nonoyama, *Inorg. Chim. Acta*, **29**, 211 (1978).
14) M. Mikami, R. Kuroda, M. Konno, and Y. Saito, *Acta Crystallogr., Sect. B*, **33**, 1485 (1977).
15) R. D. Gillard and R. J. Maskill, *J. Chem. Soc., A*, **1971**, 2813.

Voltammetric Studies of Tris(1-pyrrolidinecarbodithioato)manganese(III) and -iron(III) and Bis(1-pyrrolidinecarbodithioato)copper(II) in Nonaqueous Solvents

Akio Ichimura and Toyokichi Kitagawa*

Department of Chemistry, Faculty of Science, Osaka City University, Sumiyoshi-ku, Osaka 558

(Received December 24, 1979)

The voltammetric behavior of the title complexes has been studied. These complexes give a one-electron oxidation wave and a one-electron reduction wave in most solvents. A linear correlation between the ($E_{1/2}^{ox}$—$E_{1/2}^{red}$) values and the solubility parameters of the solvents was obtained. The ($E_{1/2}^{ox}$—$E_{1/2}^{red}$) values were interpreted in terms of the solvation energy of the complexes.

A number of electrochemical studies of transition metal complexes with *N,N*-disubstituted dithiocarbamates have been reported. Considerable work has been carried out at the platinum electrode in acetone or acetonitlile as the solvent, where the electrode reactions have been shown to be relatively simple; *e.g.*, the dithiocarbamato complexes of the first-row transition metals from chromium to copper give a one-electron oxidation wave as well as a one-electron reduction wave.[1-7] Solvent effects on the redox potential of complexes have been widely studied. Golding *et al.*[8] investigated the redox behavior of iron(III) dithiocarbamates and interpreted the variation in the redox potentials of the complexes in acetone–water solutions by considering the effect of the solvent as a perturbation of the energy-level scheme. Recently Austrian workers have described the solvent effects on the half-wave potentials of tetraethylammonium hexacyanoferate(III)[9] and hexacyanomanganate(III),[10] tris(ethylenediamine)cobalt(III) perchlorate,[11] and tris(acetylacetonato)manganese(III)[12] by means of the donor-acceptor approach. In the present paper the voltammetric behavior of manganese(III), iron(III), and copper(II) complexes with 1-pyrrolidinecarbodithioate [$Mn(pcd)_3$, $Fe(pcd)_3$, and $Cu(pcd)_2$] is examined in eleven nonaqueous solvents, and the solvent effects are discussed.

Experimental

$Mn(pcd)_3$, $Fe(pcd)_3$, and $Cu(pcd)_2$ were prepared according to previously described methods.[3,13,6] All the solvents used were purified in a conventional manner.[14,15] Tetrabutylammonium perchlorate (TBAP) was prepared by metathesis from an aqueous solution of sodium perchlorate and tetrabutylammonium bromide, which has been synthesized with tributylamine and butyl bromide, thoroughly washed with water, and recrystallized twice from ethanol. The voltammetric studies were carried out at the platinum disk electrode by the rotating electrode method, cyclic voltammetry, pulse voltammetry, and differential pulse voltammetry with a Yanagimoto P-1000-type polarograph. An aqueous SCE and a platinum wire were used as the reference electrode and the counter electrode respectively. All the sample solutions containing 0.1 M TBAP as supporting electrolyte were deoxygenated with pre-dried nitrogen and kept in the dark throughout the experiment because the complexes were relatively unstable to light.

Results and Discussion

Studies of the diffusion current are described for only $Fe(pcd)_3$ in this paper because $Cu(pcd)_2$ is slightly soluble in most solvents used and $Mn(pcd)_3$ decomposes slowly in solution except in the cases of *N,N*-dimethylformamide and dimethyl sulfoxide, in which $Mn(pcd)_3$ decomposes immediately. $Fe(pcd)_3$ underwent both a one-electron oxidation to $Fe(pcd)_3^+$ and a one-electron reduction to $Fe(pcd)_3^-$ in all the solvents studied. The limiting current at the rotating electrode was proportional to the square root of the rotation speed, and the peak current in cyclic voltammetry was proportional to the square root of the scan rate, indicating that both the electrode reactions in the respective solvents are controlled by diffusion. The differential pulse and the cyclyc voltammetric behavior shows that the electrode reaction of the oxi-

Table 1. The pulse voltammetric and the convective diffusion currents of the oxidation wave of $Fe(pcd)_3$

Solvent	$10^2\eta$ / g cm^{-1} s^{-1}	I_dC^{*-1} / A mol^{-1} cm^3	$I_1\omega^{-1/2}C^{*-1}$ / A s$^{1/2}$ mol^{-1} cm^3	$I_dC^{*-1}\eta^{1/2}$	$10^2(I_1\omega^{-1/2}C^{*-1})(\eta^{5/6}d^{-1/6})$ a)
Acetone	0.302	68.8	4.67	3.78	3.86
Acetonitrile	0.399	69.4	4.45	4.04	4.06
Dichloromethane	0.412	61.3	4.04	3.93	3.97
Isobutyl methyl ketone	0.542	50.3	2.66	3.70	3.56
Nitromethane	0.627	50.5	2.96	4.00	4.23
N,N-Dimethylformamide	0.796	43.3	2.26	3.86	4.07
Nitrobenzene	1.811	26.1	1.13	3.51	3.88
Dimethyl sulfoxide	1.996	24.3	1.01	3.43	3.81

a) d: density of the solvent in g cm^{-3}.

dation and the reduction are reversible or nearly reversible, and that the oxidation process is more reversible than the reduction process in the respective solvents. Table 1 shows that there is a marked dependence of the normalized pulse voltammetric diffusion current (I_d/C^*) and the normalized convective diffussion current ($I_l/\omega^{1/2}C^*$) of the oxidation wave for $Fe(pcd)_3$ on the viscosity of the solvents (η). $Fe(pcd)_3$ is too insoluble in the alcohols for us to obtain reliable data on the normalized diffusion currents. According to the Cottrell equation, the pulse voltammetric diffusion current is proportional to the square root of the diffusion coefficient (D). Using the Stokes-Einstein relation, $I_d\eta^{1/2}/C^*$ can be expected to be constant, provided the diffusion coefficient is due solely to a change in the viscosity. The value of $I_d\eta^{1/2}/C^*$ in Table 1 are almost constant, indicating that there is no specific interaction between $Fe(pcd)_3$ and the molecule of each solvent. As is shown in Table 1, this is also confirmed by the rotating disk electrode method with the aid of the Levich equation and the Stokes-Einstein relation.

The half-wave potential of the oxidation ($E^{ox}_{1/2}$) and the reduction ($E^{red}_{1/2}$) of the pcd complexes were found to vary appreciably with different solvents. To aviod the difficulty in evaluating the liquid-junction potential between the reference electrode used (SCE) and the solvent studied, the difference between $E^{ox}_{1/2}$ and $E^{red}_{1/2}$ was used to discuss the solvent effect. The ($E^{ox}_{1/2}-E^{red}_{1/2}$) values for $Fe(pcd)_3$, $Mn(pcd)_3$, and $Cu(pcd)_2$ are listed in Table 2, together with the solubility parameter (δ),[16,17] the relative dielectric constant (ε), the donor number (DN),[18] and the acceptor number (AN),[19] of the solvents. As may be seen from Table 2, there is a correlation only between the ($E^{ox}_{1/2}-E^{red}_{1/2}$) values and the solubility parameters. When the oxidation and the reduction processes at the rotating electrode are reversible, $E^{ox}_{1/2}$ and $E^{red}_{1/2}$ can be written as follows:

$$E^{ox}_{1/2} = E^{\circ}_{ox} + (RT/F)\ln(f_{M^+}D_M^{2/3}/f_M D_{M^+}^{2/3}) \quad (1)$$

and:

$$E^{red}_{1/2} = E^{\circ}_{red} + (RT/F)\ln(f_M D_{M^-}^{2/3}/f_{M^-}D_M^{2/3}) \quad (2)$$

where E°_{ox} and E°_{red} are the standard potentials of the M/M^+ and M^-/M couples respectively, and where f is the activity coefficient, the subscripts M, M^+, and M^- representing the neutral complex, the cation formed by oxidation, and the anion formed by reduction respectively. By applying the Born-Haber cycle, the ($E^{\circ}_{ox}-E^{\circ}_{red}$) can be written as follows:

$$F(E^{\circ}_{ox}-E^{\circ}_{red}) = I_p - E_A + \Delta G^s_{M^+} + \Delta G^s_{M^-} - 2\Delta G^s_M, \quad (3)$$

where I_P and E_A are the ionization potential and the electron affinity of the neutral complex respectively, and where ΔG^s is the solvation energy. From Eqs. 1—3, the ($E^{ox}_{1/2}-E^{red}_{1/2}$) can be expressed by:

$$F(E^{ox}_{1/2}-E^{red}_{1/2}) = I_p - E_A + \Delta G^s_{M^+} + \Delta G^s_{M^-} - 2\Delta G^s_M + 2RT\ln(f_{M^\pm}/f_M) + (2/3)RT\ln(D_M^2/D_{M^+}D_{M^-}). \quad (4)$$

Among the values of the last five terms on the right-hand side of Eq. 4, which may vary with different solvents, those of the last two terms are considered to be almost constant. The solvation energy of the ion is predominantly electrostatic in nature and is, then, expressed by the modified Born equation.[20] The variation in the ΔG_{M^+} and ΔG_{M^-} with different solvents, evaluated from the modified Born equation with the crystallographic radius of 6.42 Å for $Fe(pcd)_3$,[21] is too little to explain the difference in ($E^{ox}_{1/2}-E^{red}_{1/2}$). Consequently, the remaining term, that is, the solvation energy of the neutral complex, must be largely responsible for the difference in ($E^{ox}_{1/2}-E^{red}_{1/2}$) values. When the complex with a solubility parameter, δ_M, is transferred from the gas phase to the polar solvent of the molar volume, V_S, and solubility parameter, δ_S, ΔG_M is approximately expressed by:[22]

$$\Delta G_M = V_S\delta_S(\delta_S-\delta_M). \quad (5)$$

Since the first and second terms on the right-hand side of Eq. 4 are inherent in the complexes, and since the remaining terms except ΔG_M are considered to be almost constant in all the solvents studied, Eq. 4 can be written as:

$$F(E^{ox}_{1/2}-E^{red}_{1/2}) = -2V_S\delta_S(\delta_S-\delta_M) + k \quad (6)$$

or:

$$F(E^{ox}_{1/2}-E^{red}_{1/2}) + 2V_S\delta_S^2 = 2V_S\delta_S\delta_M + k. \quad (7)$$

Figure 1 shows the plot of the value of the left-hand side of Eq. 7 for $Fe(pcd)_3$ *vs.* $2V_S\delta_S$. It gives a straight line with a slope of 11.44 (cal $cm^{-3})^{1/2}$, corresponding to the δ_M of $Fe(pcd)_3$. The δ_M values of $Mn(pcd)_3$

Table 2. Solvent parameters and ($E^{ox}_{1/2}-E^{red}_{1/2}$) values

No.	Solvent	δ/(cal $cm^{-3})^{1/2}$	ε	DN	AN	$E^{ox}_{1/2}-E^{red}_{1/2}$/mV		
						$Cu(pcd)_2$	$Fe(pcd)_3$	$Mn(pcd)_3$
1	Isobutyl methyl ketone	8.58	13.1	—	—	1111	996	524
2	Acetone	9.62	20.7	17.0	12.5	1052	954	485
3	Dichloromethane	9.88	9.0	—	20.4	1038	930	473
4	Nitrobenzene	11.06	34.8	4.4	14.8	995	879	417
5	*N,N*-Dimethylformamide	11.79	36.7	26.6	16.0	960	860	—
6	Acetonitrile	12.11	36.0	14.1	18.9	924	841	387
7	Nitromethane	12.90	36.0	2.7	20.5	911	811	359
8	Dimethyl sulfoxide	12.97	46.6	29.8	19.3	865	766	—
9	1-Propanol	12.18	20.4	—	—	880	714	301
10	Ethanol	12.78	24.3	—	37.1	850	700	297
11	Methanol	14.50	32.6	19.0	41.3	808	645	231

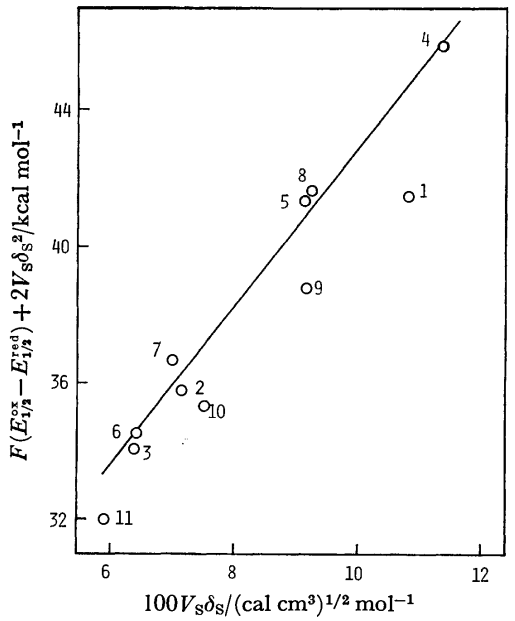

Fig. 1. Plot of Eq. 7 for $Fe(pcd)_3$.
Numbers correspond to those in Table 2.

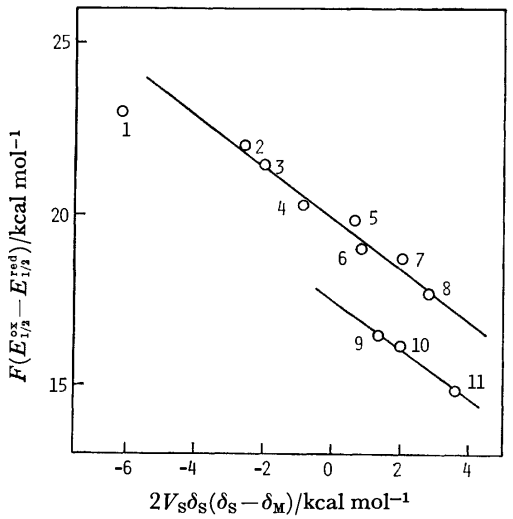

Fig. 2. Plot of Eq. 6 for $Fe(pcd)_3$.
δ_M: 11.44 (cal cm^{-3})$^{1/2}$. Numbers correspond to those in Table 2.

and $Cu(pcd)_2$, as obtained from a similar plot, are 11.40 and 11.32 (cal cm^{-3})$^{1/2}$ respectively. These δ_M values are considered reasonable compared with the value of other complexes.[23] Using the δ_M value thus evaluated, the $(E^{ox}_{1/2}-E^{red}_{1/2})$ value was plotted against $V_S\delta_S(\delta_S-\delta_M)$. The plot for $Fe(pcd)_3$ is shown in Fig. 2, which gives two straight lines, one for the aprotic solvents, and the other, for the alcohols. These linear relationship indicates that Eq. 6 is a valid expression of the solvent effect. The difference between the alcohols and the other solvents may be due to the difference in the entropy change of the solvation being neglected in Eq. 5. Similar relations were obtained for $Mn(pcd)_3$ and $Cu(pcd)_2$. It may be concluded from these results that the variation in the half-wave potential of these pcd complexes with different solvents is not dependent on the solvation energy of the ions formed by oxidation and reduction, but is dependent on the solvation energy of the neutral complexes.

The authors wish to thank Professor Sachio Murakami for his many helpful discussions.

References

1) R. Chant, A. R. Hendrickson, R. L. Martin, and N. M. Rohde, *Aust. J. Chem.*, **26**, 2533 (1973).
2) G. Cauquis and D. Lachenal, *Inorg. Nucl. Chem. Lett.*, **9**, 1095 (1973).
3) A. R. Hendrickson, R. L. Martin, and N. M. Rohde, *Inorg. Chem.*, **13**, 1933 (1974).
4) R. Chant, A. R. Hendrickson, R. L. Martin, and N. M. Rohde, *Inorg. Chem.*, **14**, 1894 (1975).
5) A. R. Hendrickson, R. L. Martin, and N. M. Rohde, *Inorg. Chem.*, **14**, 2980 (1975).
6) A. R. Hendrickson, R. L. Martin, and N. M. Rohde, *Inorg. Chem.*, **15**, 2115 (1976).
7) H. Yasuda, K. Suga, and S. Aoyagi, *J. Electroanal. Chem.*, **86**, 259 (1978).
8) R. M. Golding, L. L. Kok, K. Lehtonen, and R. K. Nigam, *Aust. J. Chem.*, **28**, 1915 (1975).
9) G. Gritzner, K. Donksagmuller, and V. Gutmann, *J. Electroanal. Chem.*, **90**, 203 (1978).
10) A. Messina and G. Gritzner, *J. Electroanal. Chem.*, **101**, 201 (1979).
11) U. Mayer, A. Kotokova, V. Gutmann, and W. Gerger, *J. Electroanal. Chem.*, **100**, 875 (1979).
12) G. Gritzner, H. Murauer, and V. Gutmann, *J. Electroanal. Chem.*, **101**, 185 (1979).
13) A. H. White, R. Roper, E. Kokot, H. Waterman, and R. L. Martin, *Aust. J. Chem.*, **17**, 294 (1964).
14) C. K. Mann, "Electroanalytical Chemistry," ed by A. J. Bard, Dekker, New York (1969), Vol. 3, p. 57.
15) J. A. Riddick and W. B. Bunger, "Organic Solvents," 3rd ed, Wiley-Interscience, New York (1970).
16) H. Ohtaki, M. Tanaka, and S. Funahashi, "Yoeki Hanno no Kagaku," University of Tokyo Press, Tokyo (1977), p. 224.
17) K. L. Hoy, *J. Paint Technol.*, **42**, 76 (1970).
18) V. Gutmann, "Coordination Chemistry in Nonaqueous Solutions," Springer, Vienna and New York (1968).
19) U. Mayer, V. Gutmann, and W. Gerger, *Monatsh. Chem.*, **106**, 1235 (1975).
20) W. H. Latimer, K. S. Pitzer, and C. M. Slansky, *J. Chem. Phys.*, **7**, 108 (1939).
21) S. Mitra, C. L. Raston, and A. H. White, *Aust. J. Chem.*, **31**, 547 (1978).
22) J. H. Hildebrand, J. M. Prausnitz, and R. L. Scott, "Regular and Related Solutions," Van Norstrand Reinhold Co., New York (1970).
23) H. M. N. H. Irving, "Ion Exchange and Solvent Extraction," ed by J. A. Marinsky and Y. Marcus, Dekker, New York (1974), Vol. 6, p. 139.

 © 1980 The Chemical Society of Japan Bull. Chem. Soc. Jpn., 53, 2531—2534 (1980)

Mixed-ligand Complexes of Cobalt(III) with 1-(2-Pyridylazo)-2-naphthol (PAN) and Diethylenetriamine (dien) or Triethylenetetramine (trien)†

Katsura Mochizuki and Masatoshi Fujimoto*

Department of Chemistry, Faculty of Science, Hokkaido University, Sapporo 060

(Received January 14, 1980)

New mixed-ligand complexes $[Co^{III}(pan)(dien)](ClO_4)_2 \cdot EtOH$ and $[Co^{III}(pan)(trien)](ClO_4) \cdot NaClO_4$ were synthesized. The ^1H NMR and the visible absorption spectra of these complexes were compared with those of the free ligand PAN and $[Co^{III}(pan)_2]Cl$. A remarkable down-field shift observed in the ^1H NMR signal for the proton H_{10} of the cobalt(III) complexes reflects the structural changes in the PAN molecule upon chelate-ring formation. The reaction between $[Co^{III}Cl_2(trien)]Cl$ and PAN gave two kinds of products, which confirmed a strong tendency for the ligand PAN to behave as a planar terdentate ligand.

In previous papers on the reaction mechanisms of the complex formation of cobalt(II) ion with PAN or its analogs, it was reported that the reaction proceeds in two steps to form a cobalt(III) complex, *i.e.*, the fast formation of a 1:2 cobalt(II) complex followed by the slower oxidation of the central cobalt(II) ion.[1] However, for the elucidation of detailed mechanisms involved in each step further information concerning the coordination fashion of the multidentate ligands like PAN in solution is required.

The complex formation of a terdentate ligand PAN with a metal ion has been assumed to involve predominantly an N,N,O-coordination by the heterocyclic nitrogen, the azo nitrogen, and the phenolic oxygen as revealed by X-ray analysis of $[Cu(pan)(OH_2)](ClO_4)$[2] supporting a terdentate structure (Fig. 1). On the other hand, another possibility remains for the terdentate ligand PAN to behave in the metal complex only as a bidentate ligand; two types of N,N-coordination and one N,O-coordination are possible.

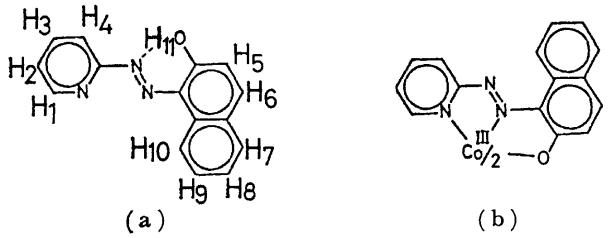

Fig. 1. Structural formulae of (a) PAN with numbering of the protons and (b) its cobalt(III) complex.

In the present study we have synthesized mixed-ligand complexes of cobalt(III) with PAN and a terdentate ligand dien or a qudridentate ligand trien and suggested the possibility for the coordination fashions of PAN as a bidentate or a terdentate ligand in these complexes based on the ^1H NMR and the spectral data.

Experimental

Materials. Reagent grade materials were used unless otherwise specified. A commercial specimen of PAN (Dojindo) was used without further purification, the purity being confirmed by elemental analysis. $[Co^{III}(pan)_2]Cl$ was prepared as reported in a previous paper.[3]

$[Co^{III}(pan)(dien)](ClO_4)_2 \cdot EtOH$ was prepared from $[Co^{III}Cl_3(dien)]$ in the same manner as in the preparation of $[Co^{III}(par)(dien)]Cl \cdot NaCl$.[4] Two grams of PAN dissolved in 200 cm^3 of ethanol was added with stirring at 50 °C to 100 cm^3 of an ethanolic suspension, containing 2.1 g of $[Co^{III}Cl_3(dien)]$ and 0.6 g of charcoal. Addition of 2.1 cm^3 of a 20% aqueous solution of $AgNO_3$ to the reaction mixture gave a deep green solution. The solution was filtered. The filtrate was evaporated to dryness. The residue was dissolved in a minimum amount of water. After the addition of 0.3 g of NaCl, the solution was filtered. Thirty cm^3 of a saturated solution of $NaClO_4$ was added to the filtrate. The precipitates were recrystallized several times from ethanol to yield crystals with green luster. Found: C, 38.38; H, 4.40; N, 13.00%. Calcd for $C_{19}H_{23}N_6O_9Cl_2Co \cdot C_2H_5OH$: C, 38.49; H, 4.46; N, 12.82%. The elemental analysis shows that the isolated mixed-ligand complex contains one mol of ethanol. The complex is soluble in water.

$[Co^{III}(pan)(trien)](ClO_4)_2 \cdot NaClO_4$ was prepared from *cis*-α-$[Co^{III}Cl_2(trien)]Cl$ as follows. The reaction mixture obtained by the same treatment as in the synthesis of $[Co^{III}(pan)(dien)](ClO_4)_2 \cdot EtOH$ was passed through a column of a cation-exchange resin SP-Sephadex C-25 in the Na-form (400×30 mm i.d.) and eluted with a 0.2 mol dm^{-3} aqueous solution of NaCl. The chromatogram consisted of two main bands, a red and a green band **A**, which were eluted in this order. The green eluate from the green **A** band evaporated to a small volume at 40—50 °C. Sodium chloride precipitated was filtered off and the filtrate was evaporated to dryness. The residue was extracted with a small amount of ethanol. The extract was filtered in order to remove residual sodium chloride. After the procedure, filtration, evaporation, and extraction, had been repeated, the final extract was dissolved in a small amount of water. To the solution was added 30 cm^3 of a saturated solution of $NaClO_4$ in order to deposit the perchlorate. The crystals were recrystallized several times from ethanol–ether (1:1 v/v). Found: C, 32.74; H, 3.98; N, 12.26%. Calcd for $C_{21}H_{28}N_7O_9Cl_2Co \cdot NaClO_4$: C, 32.56; H, 3.64; N, 12.66%.

Larger slender plates with green luster were also obtained by slow evaporation of the aqueous solution of the products containing a large amount of $NaClO_4$. Found: C, 30.05; H, 4.02; N, 11.87%. Calcd for $C_{21}H_{28}N_7O_9Cl_2Co \cdot NaClO_4 \cdot 3H_2O$: C, 30.43; H, 4.14; N, 11.83%. Elemental analysis shows that this complex contains 1 mol of $NaClO_4$ and 3 mol of water.

The red eluate from the red band was treated rapidly in the same manner as mentioned above to remove sodium chloride. The precipitate obtained was immediately subjected to measurements without further recrystallization.

The isolated perchlorates of the mixed-ligand complexes

† Presented at the 29th Annual Meeting on Coordination Chemistry, Hamamatsu, October 2, 1979, Abstract, p. 310.

with PAN and trien are soluble in water.

Measurements. 100 MHz ^{1}H NMR spectra were measured with a JEOL spectrometer model PS-100 or FX-100. Tetramethylsilane (TMS) for measurements in $CDCl_3$ or CD_3OD and sodium 2,2-dimethyl-2-silapentane-5-sulfonate (DSS) for those in D_2O solutions were used as internal standards. The perchlorates of cobalt(III) complexes were converted to the more water-soluble chlorides by passing through a column of an anion-exchange resin in the chloride-form, in order to facilitate measurements. The values of the chemical shifts hardly changed with the concentration of the complexes under the experimental conditions. Absorption spectra were measured at 25 °C with a Hitachi recording spectrophotometer Model EPS-3T.

Results and Discussion

The ^{1}H NMR spectrum of the free ligand PAN in $CDCl_3$ is shown in Fig. 2(a). First-order analysis of the spin-spin coupling constants, values of the chemical shifts, and application of a method of double irradiation allowed the assignment of signals to the protons H_1, H_5, H_6, H_{10}, and H_{11} (*cf.* Fig. 1 as regards the numbering of the protons). The spectra of the free ligand PAN and the PAN coordinated in the complexes were too complicated to attain complete assigments for the other protons of PAN. The assignment of the signals to H_1 and H_{10} was further confirmed by a comparison of the spectrum of the free PAN with that of the coordinated PAN in the cobalt(III) complexes. The values of the chemical shifts for the signals of H_1, H_5, H_6, H_{10}, and H_{11} are summarized in Table 1.

The ^{1}H NMR spectrum of $[Co^{III}(pan)(dien)]^{2+}$ in D_2O at pH *ca.* 5 is shown in Fig. 2(b). The integrated intensities of the signals show the presence of ten aromatic protons and six methylene protons (complex multiplet centered at *ca.* 3.3 ppm) corresponding to the coordinated ligands, PAN and dien, respectively.

The ^{1}H NMR spectrum of $[Co^{III}(pan)_2]^+$ in CD_3OD (Fig. 2(c)) indicates that two ligand molecules in $[Co^{III}(pan)_2]^+$ are both magnetically and chemically equivalent.

A remarkable feature found in the ^{1}H NMR spectra of the cobalt(III)–PAN complexes in comparison with those of the free PAN is a large difference in the chemical shift of the proton H_{10}. The H_{10} signal for the free ligand appeared at 8.19 ppm, while the corresponding signals for the coordinated PAN appeared at 9.37 ppm in $[Co^{III}(pan)(dien)]^{2+}$ and 9.64 ppm in $[Co^{III}(pan)_2]^+$. As shown in Fig. 1, the terdentate planar N,N,O-coordination of PAN molecule is necessarily accompanied by a rupture of the intramolecular hydrogen-bond and an internal rotation of the naphthol ring moiety around the C–N axis by 180 °. The molecular model (Fig. 3) suggests that a fairly close contact takes place between the proton H_{10} and the azo group. The proton H_{10} in such a chemical environment would be susceptible to the effect of the magnetic anisotropy due to the π-electron system of the azo group in addition to the effect of the ring current of the naphthol ring. The location of the

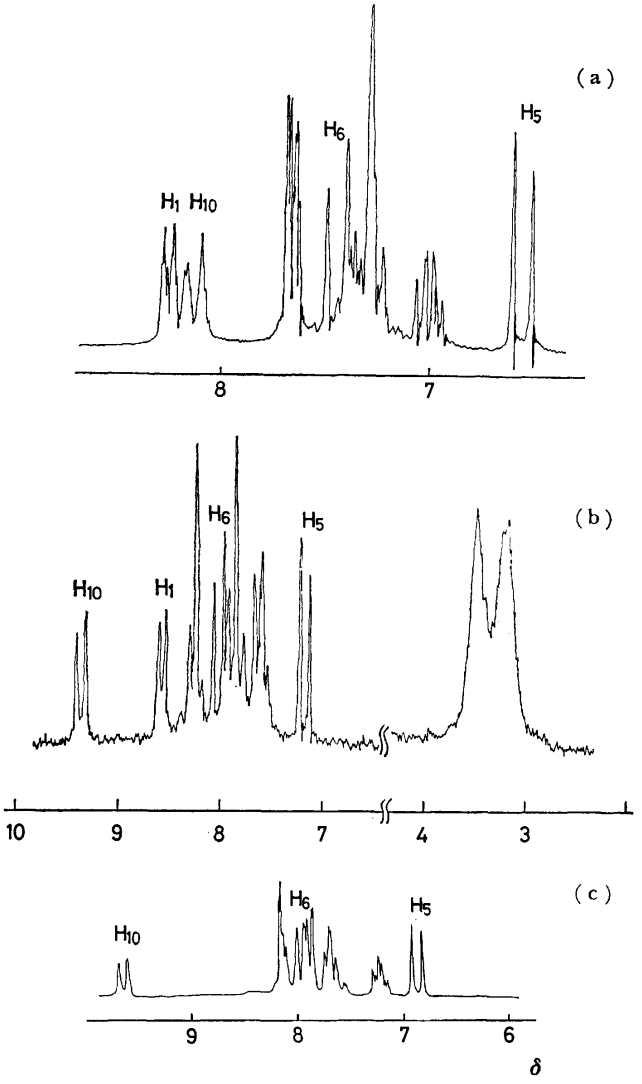

Fig. 2. ^{1}H NMR spectra of (a) PAN in $CDCl_3$, (b) $[Co^{III}(pan)(dien)]^{2+}$ in D_2O at pD *ca.* 5, and (c) $[Co^{III}(pan)_2]^+$ in CD_3OD.

Table 1. Results of chemical shifts in the ^{1}H NMR spectra (in ppm)

	5	6	1	10	11	Solvent	Standard
PAN	6.53	7.46	8.30	8.19	15.70	$CDCl_3$	TMS
$[Co^{III}(pan)(dien)]^{2+}$	7.18	8.03	8.58	9.37	—	D_2O[a]	DSS
	7.14	8.00	8.44	9.41	—	CD_3OD	TMS
$[Co^{III}(pan)_2]^+$	6.88	7.96	b)	9.64	—	CD_3OD	TMS
Red complex[c]	7.09	b)	8.58	b)	—	D_2O[a]	DSS
Green **A** complex[c]	7.18	8.06	8.58	9.46	—	D_2O[a]	DSS

a) pD *ca.* 5. b) In the complex multiplets. c) See text.

proton H_{10} in such an environment causes a down-field shift when the complexes are in the magnetic field. A similar phenomenon was observed in the case of the cobalt(III) complexes with 4-(2-pyridylazo)-resorcinol (PAR) which has a structure similar to that of PAN.[4]

The resonance signal of the H_1 in $[Co^{III}(pan)_2]^+$ shows a definite up-field shift as compared with that in the free PAN hidden among the complex multiplet appearing at the upper field. On the other hand, no such up-field shift was observed for the H_1 signal for $[Co^{III}(pan)(dien)]^{2+}$ (Fig. 1 and Table 1). We see by inspection of molecular models that the difference in the chemical shift observed for the H_1 is caused by the number of PAN molecule involved. The proton H_1 of one of the PAN molecules in $[Co^{III}(pan)_2]^+$ is disposed close to and above the azo group of the other PAN molecule, only when these two PAN molecules coordinate to the cobalt(III) ion in a planar fashion as terdentate ligands (Fig. 3). Consequently, the observed up-field shift can be explained as being caused by the magnetic anisotropy due to the π-electron system of the azo group in the neighboring ligand PAN. Similar up-field shifts have been observed for the protons in the ortho position to the pyridyl nitrogen in $[Co^{III}(par)_2]$[4] and other complexes.[5]

The observed down-field shift of H_{10} signal and the up-field shift of the H_1 signal should give a useful support for the mer configuration also in the similar complex containing ligands with a structure as in Fig. 3 (*e.g.*, the complexes of TAR, TAN, *etc.*).

The data of visible spectra for the cobalt(III) complexes are summarized in Table 2. The positions of absorption bands and the spectral features are essentially the same for these complexes. The values of absorption coefficients for the complexes containing one molecule of PAN, $[Co^{III}(pan)(dien)]^{2+}$ and $[Co^{III}(pan)(trien)]^{2+}$, were about a half of the corresponding absorption coefficients for $[Co^{III}(pan)_2]^+$. The characteristic spectra with three absorption bands at *ca.* 450, 580, and 620 nm were always obtained; in contrast with the case of $[Co^{III}(pan)_2]^+$, for the complexes containing one molecule of PAN the value of absorption coefficient of the absorption band around 580 nm was smaller than that of the absorption around 620 nm. The results indicate that the absorption for these PAN complexes is primarily due to the coordinated PAN molecule and that the PAN molecules in the complexes are in the same electronic state irrespective of the numbers of the ligand.

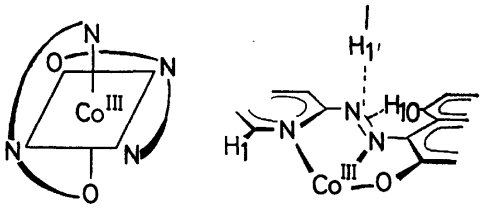

Fig. 3. The mer configuration and the disposition of two PAN molecules in $[Co^{III}(pan)_2]^+$ suggested from a molecular model.

Absence of the pH-dependence in the absorption spectra of these complexes supports the terdentate coordination of the ligand PAN to the central cobalt(III) ion.

Mixed-ligand complexes of cobalt(III) with PAN and trien were synthesized by the reaction of *cis*-α-$[Co^{III}Cl_2(trien)]Cl$ with PAN. Since the coordination sites in the cobalt(III) ion were occupied with a quadridentate triethylenetetramine, only two coordination sites are available for the coordination of the terdentate ligand PAN. If the ligand PAN coordinates to the central cobalt(III) ion as a terdentate ligand, one of the coordination sites in the trien molecule should be dissociated from the cobalt(III) ion.

The data of the ^1H NMR spectra for the red and the green **A** cobalt(III) complex are given in Table 1 (see Experimental for the red and the green **A** complex). The spectral feature and the chemical shifts of the protons H_5, H_6, H_1, and H_{10} in the green **A** complex are very similar to those of $[Co^{III}(pan)(dien)]^{2+}$, which show down-field shift of the resonance for the proton H_{10} and no up-field shift of the resonance for the proton H_1. This suggests that in the green **A** complex the ligand PAN coordinates to the cobalt(III) ion in a planar terdentate fashion and one of the sites of coordination in the ligand trien should be dissociated from the cobalt(III) ion. On the other hand, the spectral feature and the chemical shifts for H_1 and H_{10} of the red cobalt(III) complex differ from those of the green **A** complex, the free PAN, $[Co^{III}(pan)_2]^+$, and $[Co^{III}(pan)(dien)]^{2+}$; in the ^1H NMR spectrum of the red complex no corresponding down-field shift of the resonance for H_{10} was observed, suggesting the possibility of the contribution of some other coordination structure in the ligand PAN.

The visible spectrum of the green **A** complex is essentially the same as that of $[Co^{III}(pan)(dien)]^{2+}$. On the other hand, the spectrum of the red complex differs from that of (1) PAN, $[Co^{III}Cl_2(trien)]^+$, and $[Co^{III}(OH_2)_2(trien)]^{3+}$, (2) the cobalt(III) complex with nitrosonaphthol[6] which is assumed to be a decomposition product of PAN, and (3) a bivalent cobalt

Table 2. Data of absorption spectra

$[Co^{III}(pan)_2]^+$ in DMSO		$[Co^{III}(pan)(dien)]^{2+}$ in H_2O (DMSO)		$[Co^{III}(pan)(trien)]^{2+}$ in H_2O[a]	
λ_{max}/nm	$\varepsilon/10^4$ mol^{-1} dm^3 cm^{-1}	λ_{max}/nm	$\varepsilon/10^4$ mol^{-1} dm^3 cm^{-1}	λ_{max}/nm	$\varepsilon/10^4$ mol^{-1} dm^3 cm^{-1}
453	2.38	444 (448)	1.32 (1.41)	452	1.11
582	2.23	570 (574)	1.08 (1.11)	577	0.90
628	1.93	616 (624)	1.24 (1.39)	625	0.94

a) Green **A** complex (see text).

complex, $[Co^{II}(pan)_2]$.[1] The observations suggest the possibility that the ligand PAN in the red complex coordinates to the cobalt(III) ion not in a planar terdentate fashion but in some other way.

Upon standing for a long time or heating with a small amount of 0.1 mol dm^{-3} solution of NaOH, the color of the solution of the red complex turned green, showing the formation of a green complex **B**. The color of the solution of this green **B** complex was not changed reversibly to red under the experimental conditions. The visible spectrum of the solution of the green **B** complex was essentially the same as that of the green **A** complex in the eluate from the ion-exchange column. The ^1H NMR spectra of the green **B** product also showed down-field shift of the H_{10} signal, though the spectra corresponding to the trien in the green **B** complex differ a little from those in the green **A** complex in the eluate.

The results suggest that the multidentate ligand PAN in these two green complexes **A** and **B** coordinates to the cobalt(III) ion in a planar terdentate fashion and the green cobalt(III) complex is more stable than the red cobalt(III) complex. When the synthesis of the mixed-ligand PAN-trien complex of cobalt(III) was carried out in a slightly basic media containing a small amount of NaOH, only the green complexes were obtained, the formation of the red complex was no longer observed.

On the basis of these results, we conclude that the multidentate lignad PAN has a very strong tendency to function as a planar terdentate lignad in the cobalt(III) complexes.

References

1) K. Mochizuki, T. Imamura, T. Ito, and M. Fujimoto, *Chem. Lett.*, **1976**, 1207; *Bull. Chem. Soc. Jpn.*, **51**, 1743 (1978).
2) S. Ooi, D. Carter, and Q. Fernando, *Chem. Commun.*, **1967**, 1301.
3) K. Mochizuki, T. Imamura, and M. Fujimoto, *Bull. Chem. Soc. Jpn.*, **53**, 1757 (1980).
4) K. Mochizuki, T. Ito, and M. Fujimoto, *Bull. Chem. Soc. Jpn.*, **52**, 441 (1979).
5) J. D. Milter and R. H. Prince, *J. Chem. Soc.*, **1965**, 3185, 4076; H. Ito, J. Fujita, and T. Ito, *Bull. Chem. Soc. Jpn.*, **44**, 723 (1971); S. Castellano, H. Gunther, and S. Ebersole, *J. Phys. Chem.*, **69**, 4166 (1965); T. Ito and N. Tanaka, *J. Inorg. Nucl. Chem.*, **32**, 155 (1970).
6) R. Lundquist, G. E. Markle, and D. F. Boltz, *Anal. Chem.*, **27**, 1731 (1955).

 © 1980 The Chemical Society of Japan Bull. Chem. Soc. Jpn., 53, 2535—2539 (1980)

Spin-state Equilibria of the Nickel(II) Complexes of 2,12-Dimethyl-3,7,11,17-tetraazabicyclo[11.3.1]heptadeca-1(17),2,11,13,15-pentaene Analogs in Water

Katsura Mochizuki, Masatoshi Fujimoto,* Haruko Ito,† and Tasuku Ito†

Department of Chemistry, Faculty of Science, Hokkaido University, Sapporo 060

† *Institute for Molecular Science, Okazaki 444*

(Received February 21, 1980)

Spin-state equilibria between a singlet low-spin and a triplet high-spin species of the title complexes in water were investigated by means of electronic spectra. The equilibrium constants and the thermodynamic parameters, ΔH and ΔS, were evaluated from detailed analysis of the temperature-dependence of the electronic spectra. The electronic spectra of the singlet and the triplet species involved were also derived, from the same analysis. The formation of the triplet species was found to be exothermic, which reflects the predominant contribution of the exothermic change to the formation of nickel(II)–water bond over the contribution of the endothermic change in the bond length caused by the change in spin state. The absolute values of ΔS almost correspond to those expected for the effective liberation of two molecules of water in aqueous solution.

Nickel(II) complexes with the title macrocyclic quadridentate ligands, $[Ni(L+nH)]^{2+}$ (n=−2 (**1**), 0 (**2**), 2 (**3**), and 4 (**4**): Fig. 1), have been reported to be often in an equilibrium between a singlet low-spin (diamagnetic square planar) and a triplet high-spin (paramagnetic pseudo octahedral) species in coordinating solvents,[1-3] as described by

$$[Ni(L+nH)]^{2+} + 2S \rightleftharpoons [Ni(L+nH)S_2]^{2+}, \quad (1)$$

where S denotes a coordinating solvent such as water, methanol, dimethyl sulfoxide, *N*,*N*-dimethylformamide, or acetonitrile.

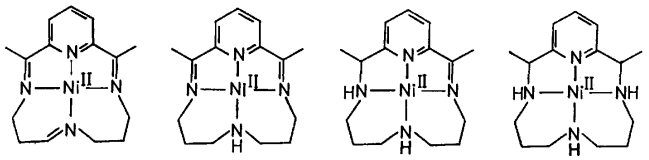

1 2 3 4

Fig. 1. Structural formulae of the complexes, $[Ni(L-2H)](ClO_4)_2$ (**1**), $[Ni(L)](ClO_4)_2$ (**2**), $[Ni(L+2H)](ClO_4)_2$ (**3**), and $[Ni(L+4H)](ClO_4)_2$ (**4**).

Though the exact electronic spectra of the component species are required for the spectrophotometric evaluation of the equilibrium constant and the thermodynamic parameters for Equilibrium 1, evaluation of such component spectra was difficult because of the equilibrium immediately attained in a coordinating solvent.

In the present study we applied detailed analysis of the temperature-dependence of the electronic spectra to the spin-state equilibria of $[Ni(L+nH)]^{2+}$ in water for the evaluation of electronic spectra of the components, which allow the evaluation of equilibrium constants and thermodynamic parameters.

Experimental

Materials. Deionized water was distilled. Sodium perchlorate for the adjustment of ionic strength was recrystallized three times after traces of heavy metal ions had been removed. The nickel(II) complexes, $[Ni(L+nH)](ClO_4)_2$ (**1**—**4**), were synthesized according to the literature.[1,2,4,5] The purity was confirmed by elemental analysis.

Measurements. The absorption spectra were measured with a Hitachi recording spectrophotometer model 340 equipped with a data printer, the absorbance being recorded within ±0.001. The temperature was measured with a copper-constantan thermocouple and a digital thermometer TAKEDA TR-2121, and maintained within ±0.1 °C. All measurements were carried out at a constant ionic strength, I=0.1 ($NaClO_4$) (see below).

Analyses of the Data

Derivation of the electronic spectra of the component species and calculations of the equilibrium constants and the thermodynamic parameters were carried out as follows, an appropriate computer program being designed for the present purpose.[6]

The equilibrium constant for Eq. 1 is defined as

$$K = [\text{triplet}]/[\text{singlet}]. \quad (2)$$

This equation is transformed into Eq. 3 by introducing the molar absorption coefficients at an arbitrary wavelength λ_n, ε_{sn} and ε_{tn}, for the singlet and the triplet species, respectively, and the apparent molar absorption coefficient, ε_{obsn}, for the solution in equilibrium,

$$K = (\varepsilon_{sn}-\varepsilon_{obsn})/(\varepsilon_{obsn}-\varepsilon_{tn}). \quad (3)$$

At the wavelength λ_0 where ε_{s0} equals 0, Eq. 3 becomes

$$K = \frac{\varepsilon_{obs0}}{\varepsilon_{t0}-\varepsilon_{obs0}}. \quad (4)$$

The temperature-dependence of the equilibrium constant, K, is given by Eq. 5, provided that the molar absorption coefficients for the singlet and the triplet species do not depend on the temperature

$$\ln K = \ln\left(\frac{\varepsilon_{obs0}}{\varepsilon_{t0}-\varepsilon_{obs0}}\right) = \frac{\Delta S_0}{R} - \frac{\Delta H_0}{RT}. \quad (5)$$

Since Eq. 3 also holds at an arbitrary wavelengh λ_n, the following relationship is immediately derived:

$$\varepsilon_{obsn} = \varepsilon_{sn} - \frac{(\varepsilon_{sn}-\varepsilon_{tn})}{\varepsilon_{t0}}\cdot\varepsilon_{obs0}, \quad (6)$$

where ε_{obsn} and ε_{obs0} denote the apparent molar absorption coefficients at T K observed at λ_n and λ_0, respectively. This equation enables the calculation of the absorption coefficients, ε_{sn} and ε_{tn}, at any arbi-

trary wavelength λ_n from the plot of ε_{obsn} against ε_{obs0} at various temperatures. The absorption spectra for the singlet and the triplet form are constructed by plotting the values of ε_{sn} and ε_{tn} against the wavelengths λ_n, respectively.

The Arrhenius equation holds also in terms of ε_{sn} and ε_{obsn}:

$$\ln K = \ln\left(\frac{\varepsilon_{sn}-\varepsilon_{obsn}}{\varepsilon_{obsn}-\varepsilon_{tn}}\right) = \frac{\Delta S_n}{R} - \frac{\Delta H_n}{RT}. \quad (7)$$

The thermodynamic parameters, ΔS_n and ΔH_n, are evaluated from Eq. 7. The values of molar absorption coefficient at λ_n could be calculated by Eq. 8 with respect to K,

$$\varepsilon_{calcn} = \varepsilon_{sn} + \frac{\varepsilon_{sn}-\varepsilon_{tn}}{1+K}. \quad (8)$$

Actual calculations were carried out according to the following directions by means of an appropriate computer program which includes the least-square fits for Eqs. 5 and 7.[6]

(1) Choose the wavelength λ_0 where $\varepsilon_{s0}=0$ (In some cases λ_0 where $\varepsilon_{t0}=0$ should be chosen).

(2) Calculate the value of K at T K by means of Eq. 4 for an appropriate value of ε_{t0} and plot the value of log K against T^{-1} by means of Eq. 5.

(3) Repeat the calculations in (2) by changing the values of ε_{t0} until a linear plot is obtained. Determine the optimum value for ε_{t0}.

(4) For the optimum value of ε_{t0} evaluated in (3), plot the values of ε_{obsn} against those of ε_{obs0} at various temperatures by means of Eq. 6. Evaluate the values of ε_{sn} and ε_{tn} at λ_n from the slope $(\varepsilon_{sn}-\varepsilon_{tn})/\varepsilon_{t0}$ and the intercept ε_{sn}.

(5) Calculate the value of K_n at T K with the values of ε_{sn} and ε_{tn} by means of Eq. 7 and plot the Arrhenius relationship. Evaluate the values of ΔH_n and ΔS_n at λ_n from the slope and the intercept. Confirm the coincidence of all values with each other for ΔH_n and ΔS_n obtained at λ_n.

(6) Calculate the values of ε_{calcn} at various λ_n with the values of K, ΔH and ΔS, and ε_{sn} and ε_{tn}. Confirm the coincidence of the calculated values of ε_{calcn} with those of ε_{obsn} measured at λ_n.

Results and Discussion

Figure 2 shows the electronic spectra of $[Ni(L)]^{2+}$ in water at various temperatures. The spectrum changes reversibly with an isosbestic point at 590 nm. With rise in temperature the absorption at 395 nm remarkably increases and the absorption at 720 nm decreases. Based on the assignment of the absorption maxima at 450 and 720 nm to the singlet and the triplet species, respectively, we deduced that the given spectral change corresponds to the temperature-dependence of the spin-state equilibrium of the given complex between the singlet square planar and the triplet pseudo octahedral species. Similar temperature-dependence in the electronic spectra was observed also for the other analogous $[Ni(L+nH)]^{2+}$–H_2O systems, indicating the temperature-dependent equilibrium between the triplet and the singlet species.

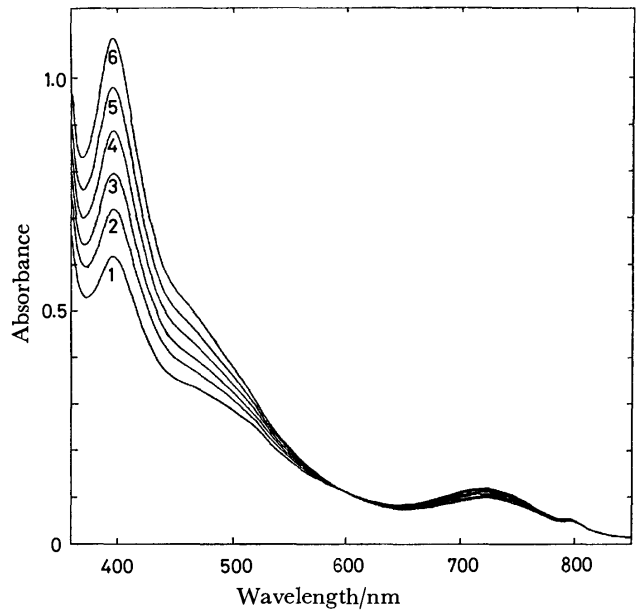

Fig. 2. Absorption spectra of $[Ni(L)](ClO_4)_2$ in H_2O (4.98×10^{-3} mol dm^{-3}) at various temperatures. At I=0.1 ($NaClO_4$). Measured at 279.2 (1), 285.6 (2), 290.0 (3), 294.8 (4), 299.3 (5), and 303.8 K (6).

The detailed analyses of the temperature-dependence of the spectra as described in the foregoing section allowed us to calculate the equilibrium constant, K, and the thermodynamic parameters, ΔH and ΔS, of Equilibrium 1 and also to derive the individual spectrum of the singlet and the triplet species. Since in the $[Ni(L)]^{2+}$–H_2O system an absorption peak at 720 nm assigned to a triplet species is well separated from the absorption peaks of the singlet species appearing at shorter wavelengths, 720 nm was adopted as an appropriate wavelength λ_0 for the $[Ni(L)]^{2+}$–H_2O system, where $\varepsilon_{s0}=0$.

Figure 3 shows a set of plots of log K for the $[Ni(L)]^{2+}$–H_2O system against T^{-1} as derived from Eq. 5 for various values of ε_{t0}. We see that only the plot for $\varepsilon_{t0}=27.6$ mol^{-1} dm^3 cm^{-1} gives a straight line; for any values of ε_{t0} larger than 27.6 mol^{-1} dm^3 cm^{-1} the plot always gives a curve with positive curvature, and for any values of ε_{t0} smaller than 27.6 mol^{-1} dm^3 cm^{-1} a curve with negative curvature. The values of ε_{sn} and ε_{tn} at an arbitrary wavelength λ_n are evaluated using this value of ε_{t0} and the values of ε_{obsn} by means of Eq. 6. The validity of the value 27.6 mol^{-1} dm^3 cm^{-1} as ε_{t0} was again confirmed for the linear dependence on T^{-1} of the values of K derived from the values of ε_{sn} and ε_{tn} using Eq. 7. The values of ΔH and ΔS were calculated as slopes and intercepts by means of Eqs. 5 and 7. The adopted wavelength λ_0 and the evaluated ε_{t0} for the series of $[Ni(L+nH)]^{2+}$–H_2O systems are summarized in Table 1.

Figure 4(a) shows the electronic spectra of the singlet and the triplet species, $[Ni(L)]^{2+}$ and $[Ni(L)(OH_2)_2]^{2+}$, reproduced by plotting against λ_n the values of ε_{sn} and ε_{tn} calculated by means of Eq. 6, respectively. The absorption maximum at 395 nm (ε=1011 mol^{-1}

$dm^3\ cm^{-1}$) and the d-d absorption band around 450 nm are clearly shown in the spectrum of the singlet species. A remarkable feature in the electronic spectrum of the triplet species is the clear discrimination of a weak absorption band around 520 nm by the analysis of electronic spectra. The band is almost included in the envelope of a very strong singlet band and is observed only as an indiscernibly weak shoulder in Fig. 2. Figure 4(b) shows the electronic spectra of the singlet and the triplet species in the *meso*-[Ni-(L+4H)]$^{2+}$-H_2O system. The weak absorption band around 500 nm of the triplet species, not recognized in the spectrum of the equilibrium mixture of the triplet and the singlet species, is also clearly discriminated by the same analysis. The results indicate that the proposed analysis is useful also for the de-

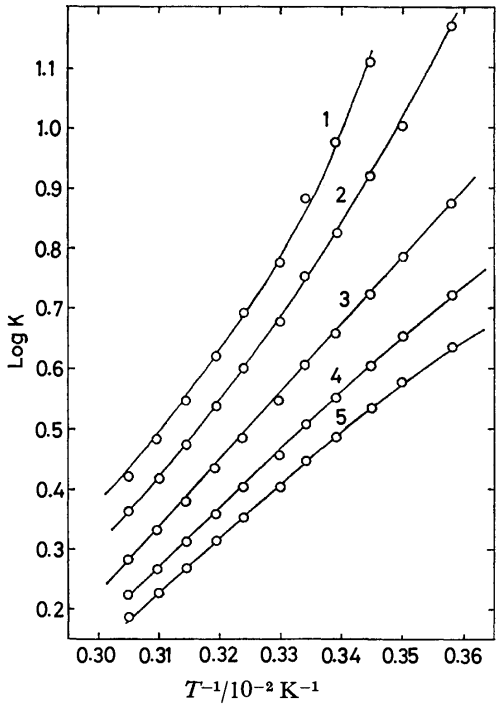

Fig. 3. Plots of $\log K$ *vs.* T^{-1} for $[Ni(L)](ClO_4)_2$ (4.98×10^{-3} mol dm^{-3}) for various values of ε_{t0} at 720 nm. The values of ε_{t0} at 720 nm: 25.0 (1), 26.0 (2), 27.6 (3), 29.0 (4), and 30.0 $mol^{-1}\ dm^3\ cm^{-1}$ (5).

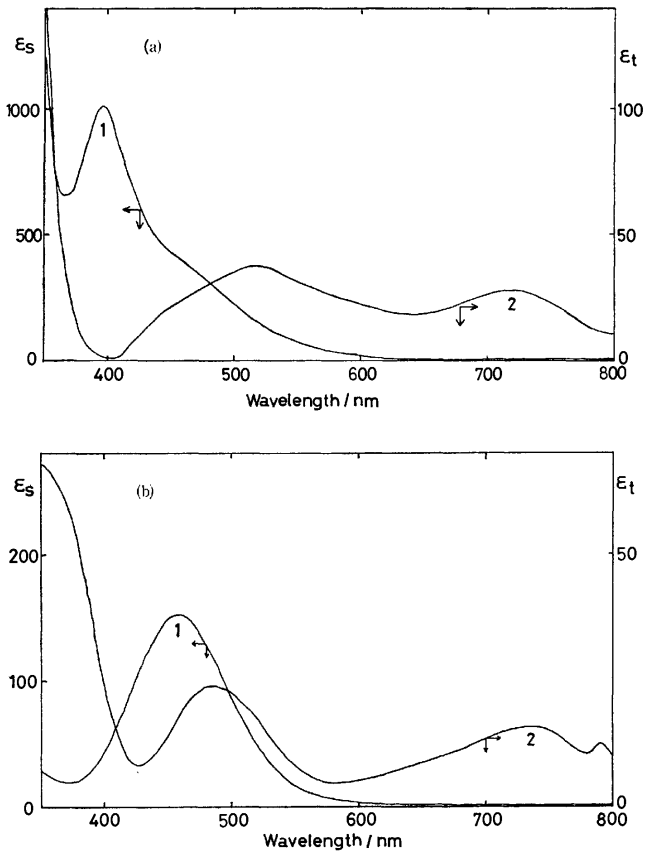

Fig. 4. Absorption spectra of the singlet (1) and the triplet (2) species obtained by the calculation (see the text). (a) $[Ni(L)](ClO_4)_2$-H_2O system. (b) *meso*-$[Ni(L+4H)](ClO_4)_2$-H_2O system.

Table 1. Evaluated ε_{t0} at λ_0 where $\varepsilon_{s0}=0$[a]

	λ_0/nm	ε_{t0}/$mol^{-1}\ dm^3\ cm^{-1}$	[Complex]/10^{-3} mol dm^{-3}
meso-$[Ni(L+4H)[(ClO_4)_2$[b]	735	11.3	8.51
rac-$[Ni(L+4H)](ClO_4)_2$[c]	730	17.6	9.11
$[Ni(L+2H)](ClO_4)_2$	725	22.4	8.07
$[Ni(L)](ClO_4)_2$	720	27.6	4.98
$[Ni(L-2H)](ClO_4)_2$	720	8.2	4.36

a) At I=0.1 ($NaClO_4$). b) α-*C-meso* isomer (see Ref. 5). c) *C-rac* isomer.

Table 2. Equilibrium constants in H_2O[a]

	K	T/K	K	T/K
meso-$[Ni(L+4H)](ClO_4)_2$[b]	0.31_2	299.4	0.28_0	303.5
rac-$[Ni(L+4H)](ClO_4)_2$[c]	0.45_9	299.4	0.41_2	303.4
$[Ni(L+2H)](ClO_4)_2$	0.55_6	299.3	0.49_4	303.5
$[Ni(L)](ClO_4)_2$	3.99_6	299.3	3.59_5	303.0
$[Ni(L-2H)](ClO_4)_2$	0.59_3	299.3	0.51_9	303.8

a) Under the same conditions as in Table 1. K=[triplet]/[singlet]. b) α-*C-meso* isomer (see Ref. 5). c) *C-rac* isomer.

tection of unknown weak absorption bands of the components hidden in the spectrum of an equilibrium mixture.

The values of equilibrium constants, K, at 299.3± 0.1 and 303.4±0.4 K are given in Table 2. The value of K at 299.3 K is larger than that at 303.4 K, indicating a decrease in the triplet form with rise in temperature. The degree of formation of the triplet species for $[Ni(L)](ClO_4)_2$ is the largest among the given $[Ni(L+nH)](ClO_4)_2$–H_2O systems. This can be interpreted as follows. The in-plane ligand-field strength is assumed to be in the order, $[Ni(L+4H)]^{2+}<[Ni(L+2H)]^{2+}<[Ni(L)]^{2+}<[Ni(L-2H)]^{2+}$.[7] On the other hand, the steric hindrance at an axial coordination site caused by the proton of secondary amine and/or methyl moiety in the ligand molecule is assumed to be in the reversed order. The ease with which an axial ligand coordinates to the central atom is expected to be the largest at $[Ni(L)]^{2+}$ having moderate effects both in the in-plane ligand-field strength and in the steric hindrance at an axial coordination site.

The thermodynamic parameters for Equilibrium 1 are given in Table 3 (see Experimental). The negative values of ΔH indicate that formation of the triplet species is exothermic for all $[Ni(L+nH)]^{2+}$–H_2O systems. For the complexes of similar quadridentate ligands the Ni–N bond length has been reported to be $(2.07—2.10)\times10^{-8}$ cm in the high-spin complexes and $(1.88—1.91)\times10^{-8}$ cm in the singlet low-spin complexes.[7,8] For the formation of a triplet species the Ni–N bonds in a complex should be elongated; this change in the bond length in the in-plane ligand should cause the endothermic effects. The negative values of ΔH obtained reflect the exothermic contribution of the formation of Ni–water bond exceeding the endothermic contribution of change in the spin-state.

Table 3. Thermodynamic parameters[a]

	$-\Delta H$ / 10^4 J mol^{-1}	$-\Delta S$ / J K^{-1} mol^{-1}
meso-$[Ni(L+4H)](ClO_4)_2$[b]	2.02	77.0
rac-$[Ni(L+4H)](ClO_4)_2$[c]	2.04	74.9
$[Ni(L+2H)](ClO_4)_2$	2.16	77.0
$[Ni(L)](ClO_4)_2$	2.12	59.4
$[Ni(L-2H)](ClO_4)_2$	2.32	82.0

a) Under the same conditions as in Table 1. b) α-*C-meso* isomer (see Ref. 5). c) *C-rac* isomer.

The absolute values of ΔS nearly correspond to those expected for the effective liberation of two water molecules from the title complexes in aqueous solution, *viz.*, $(30\sim40)\times2$ J K^{-1} mol^{-1}.[9]

Table 4 shows the effects of the addition of $NaClO_4$ on the spin-state equilibria in the $[Ni(L)]^{2+}$– and the *rac*-$[Ni(L+4H)]^{2+}$–H_2O system. In both cases addition of $NaClO_4$ enhanced the intensity of the singlet bands, which shows the increase in the singlet species in equilibrium. In a solution containing high concentrations of $NaClO_4$, *e.g.*, 6 mol dm^{-3}, no temperature-dependence of the spectrum was observed, showing the predominance of the singlet species in the equilibrium. The value of molar absorption coefficient ($\varepsilon=1167$ mol^{-1} dm^3 cm^{-1}) measured in 6 mol dm^{-3} $NaClO_4$ at 395 nm, absorption maximum for the singlet species, agreed with that evaluated from the above calculation. The decrease in K with increasing concentrations of $NaClO_4$ was almost the same in the case of the $[Ni(L)]^{2+}$– and the *rac*-$[Ni(L+4H)]^{2+}$–H_2O system. A similar effect has been reported in other spin-state equilibria such as $[Ni(trien)]^{2+}$–H_2O,[10] $[Ni(cyclam)]^{2+}$–H_2O,[11] and $[Ni(isocyclam)]^{2+}$–H_2O systems,[12] where trien, cyclam, and isocyclam denote quadridentate ligands, triethylenetetramine, 1,4,8,11-tetraazacyclotetradecane, and 1,4,7,11-tetraazacyclotetradecane, respectively. On the basis of these observations, all measurements in the preceding paragraphs were carried out at a constant ionic strength, $I=0.1$ ($NaClO_4$).

Table 4. Effect of $NaClO_4$ on the Equilibrium constants[a]

$[Ni(L)](ClO_4)_2$[b]		*rac*-$[Ni(L+4H)](ClO_4)_2$[c]	
$[NaClO_4]$ / mol dm^{-3}	K	$[NaClO_4]$ / mol dm^{-3}	K
0	6.87	0	0.623
0.040	4.83	0.040	0.479
0.080	4.21	0.080	0.422
0.161	3.41	0.200	0.323
0.282	2.66	0.400	0.229
0.402	2.17	0.800	0.144
0.805	1.21	1.200	0.082
1.207	0.75	1.552	0.051

a) $K=\dfrac{[\text{triplet}]}{[\text{singlet}]}$. b) 3.98×10^{-3} mol dm^{-3} at $T=298.8$ K. c) 2.65×10^{-3} mol dm^{-3} at $T=299.2$ K. *C-rac* isomer.

Calculations were carried out on the HITAC M-200H computer at the Computer Center, Institute for Molecular Science and on the FACOM M230-60 computer at Hokkaido University Computing Center. This work was supported by the Joint Studies Program (1978—1979) of the Institute for Molecular Science.

References

1) J. L. Karn, Ph.D. Dissertation, The Ohio State University, 1966; J. L. Karn and D. H. Busch, *Inorg. Chem.*, **8**, 1149 (1969).

2) E. K. Barefield, F. V. Lovecchio, N. E. Tokel, E. Ochiai, and D. H. Busch, *Inorg. Chem.*, **11**, 283 (1972).

3) L. Runsnak and R. B. Jordan, *Inorg. Chem.*, **10**, 2199 (1971).

4) K. Mochizuki, T. Ito, and M. Fujimoto, *Bull. Chem. Soc. Jpn.*, **53**, 543 (1980).

5) E. Ochiai and D. H. Busch, *Inorg. Chem.*, **8**, 1798 (1969).

6) The further details and improvement of this method will be reported elsewhere. T. Ito, H. Ito, J. Suzuki, and J. Fujita, unpublished study. Refer to T. Ito for the computer program for calculations.

7) For the detailed discussion, see L. Y. Martin, D. R. Seperati, and D. H. Busch, *J. Am. Chem. Soc.*, **99**, 2968 (1977).
8) P. O. Whimp, M. F. Bailey, and N. F. Curtis, *J. Chem. Soc., A*, **1970**, 1956; L. N. Swink and M. Atoji, *Acta Crystallogr.*, **13**, 639 (1960); J. M. Waters and K. R. Whittle, *J. Inorg. Nucl. Chem.*, **34**, 155 (1972); T. Ito and K. Toriumi, *Chem. Lett.*, **1978**, 1395.
9) F. P. Hinz and D. W. Margerum, *Inorg. Chem.*, **13**, 294 (1974).
10) C. K. Jørgensen, *Acta Chem. Scand.*, **11**, 399 (1957).
11) A. Anichini, L. Fabbrizzi, and P. Paoletti, *Inorg. Chim. Acta*, **24**, L21 (1977).
12) L. Sabatini and L. Fabbrizzi, *Inorg. Chem.*, **18**, 438 (1979).

Syntheses and Characterization of Some New (3-Oxo-1-cyclohexenyl)-palladium(II) Complexes

Masayoshi Onishi,* Hideharu Yamamoto, and Katsuma Hiraki*
Department of Industrial Chemistry, Faculty of Engineering, Nagasaki University, Bunkyo-machi, Nagasaki 852

(Received January 31, 1980)

trans-Chloro(3-oxo-1-cyclohexenyl)bis(triphenylphosphine)palladium(II) (**1**) reacted with 1,2-bis(diphenylphosphino)ethane (dppe), 1,10-phenanthroline (phen), sodium diethyldithiocarbamate–water (1/3), and sodium tetra(1-pyrazolyl)borate {Na[BPz_4]} (Pz=1-pyrazolyl) to give the corresponding new (3-oxo-1-cyclohexenyl)-palladium(II) complexes, [Pd(oxch)Cl(dppe)] (oxch=3-oxo-1-cyclohexenyl) (**2**), [Pd(oxch)Cl(phen)], [Pd(oxch)(S_2CNEt_2)(PPh_3)], and [Pd(oxch)(BPz_4)(PPh_3)], respectively. Complex **2** was treated with carbanions derived from methyl and ethyl cyanoacetates and malononitrile, and new diorganopalladium(II) complexes were obtained. These complexes were characterized by means of elemental analyses and IR and ^{1}H-NMR spectroscopy. The stereochemical nonrigidity of the BPz_4 complex was discussed.

In our previous study,[1] linear and cyclic (β-carbonylvinyl)chlorobis(triphenylphosphine)palladium(II) complexes were prepared by oxidative addition reactions of [$Pd(PPh_3)_4$] towards the corresponding linear and cyclic chlorovinyl ketones. Little has been known about the reactivity of the (β-carbonylvinyl)-palladium(II) complexes.

This paper deals with some new (3-oxo-1-cyclohexenyl)palladium(II) complexes, derived from the reactions of the cyclic β-carbonylvinyl palladium(II) complex, *trans*-chloro(3-oxo-1-cyclohexenyl)bis(triphenylphosphine)palladium(II) [Pd(oxch)Cl(PPh_3)$_2$] (oxch=3-oxo-1-cyclohexenyl) (**1**) towards bidentate ligands. In addition, one of the new complexes, {1,2-bis(diphenylphosphino)ethane}chloro(3-oxo-1-cyclohexenyl)palladium(II) (**2**) was treated with carbanions formed from active methylene compounds, and new stable diorganopalladium(II) complexes were obtained. Organopalladium(II) complexes have already been prepared from reactions of chloropalladium(II) complexes with the carbanions.[2-4]

Experimental

General Procedure. Melting points and IR and ^{1}H-NMR spectra were measured according to the previous paper.[1] Complex **1**, 1,2-bis(diphenylphosphino)ethane (dppe),[5] and sodium tetra(1-pyrazolyl)borate{Na[BPz_4]} (Pz=1-pyrazolyl)[6] were synthesized in the described methods. 1,10-Phenanthroline (phen), sodium diethyldithiocarbamate–water(1/3) {Na[dedc]·$3H_2O$}, and the other reagents were commercial samples, and were used without further purification.

*Reaction of **1** with dppe or phen.* A benzene solution (110 ml) containing **1** (1.68 mmol) and dppe (1.85 mmol) was stirred at room temperature for 48 h. The resulting greyish white solids were collected and washed with benzene and diethyl ether to give [Pd(oxch)Cl(dppe)] (**2**). Complex **1** reacted similarly with phen to afford [Pd(oxch)Cl(phen)] (**3**).

*Halogen Metathesis of **3**.* An acetone suspension (20 ml) involving **3** (0.08 mmol) and lithium bromide (0.80 mmol) was refluxed for 40 h. The resulting solids were separated and added to 20 ml of ethanol, followed by stirring for 20 h at room temperature. Off-white powders were collected and washed with ethanol and diethyl ether to yield [PdBr(oxch)(phen)] (**4**).

*Reaction of **1** with Na[dedc]·$3H_2O$.* A benzene suspension (35 ml) containing **1** (0.25 mmol) and Na[dedc]·$3H_2O$ (0.28 mmol) was heated at 55 °C for 8 h. After the resulting solid was filtered off, the solvent was removed under reduced pressure. The residue was recrystallized from benzene–hexane to give [Pd(oxch)(dedc)(PPh_3)] (**5**).

*Reaction of **1** with Na[BPz_4].* A benzene suspension (30 ml) involving **1** (0.23 mmol) and Na[BPz_4] (0.24 mmol) was refluxed for 3 h. After the resulting precipitate was filtered off, the solvent was evaporated to dryness. The residue was recrystallized from benzene–diethyl ether to afford [Pd(oxch)(BPz_4)(PPh_3)] (**6**).

*Reactions of **2** with Carbanions Formed from Alkyl Cyanoacetates or Malononitrile.* A methanol solution (30 ml) of sodium methoxide (0.19 mmol) was added dropwise to a THF suspension (30 ml) containing **2** (0.19 mmol) and methyl cyanoacetate (0.37 mmol). The mixture was stirred at room temperature for 20 h. After filtration, the filtrate was evaporated to dryness. The residue was extracted with dichloromethane, and the solvent was removed under reduced pressure. The resulting solids were recrystallized from THF–hexane to give [Pd{CH(CN)CO_2Me}(oxch)(dppe)] (**7**).

Complex **2** reacted similarly with ethyl cyanoacetate and malononitrile in the presence of sodium ethoxide in an equimolar amount of **2**, followed by the analogous treatments to the case of **7**, to afford [Pd{CH(CN)CO_2Et}(oxch)(dppe)] (**8**) and [Pd{$CH(CN)_2$}(oxch)(dppe)] (**9**), respectively.

Results and Discussion

General Properties. The *trans*-bis(triphenylphosphine) type complex **1** underwent substitution by the bidentate ligands, dppe, phen, [dedc]$^-$, and [BPz_4]$^-$, affording new neutral complexes **2**, **3**, **5**, and **6**, respectively. Furthermore, the dppe type complex **2** reacted with carbanions formed from methyl and ethyl cyanoacetates and malononitrile, to give novel diorganopalladium(II) complexes, **7**—**9**, respectively. The phen-type complex **3** underwent halogen metathesis to afford the bromo complex **4**. The yields, analytical data, and some properties of these new complexes are summarized in Table 1. Complexes **2** and **5**—**9** are soluble in usual organic solvents except saturated hydrocarbons, whereas **3** and **4** are highly insoluble in the solvents.

All the new complexes showed two strong IR bands near 1630 and 1540 cm^{-1}, ascribable to ν(C=O) and ν(C=C) frequencies, respectively (Table 2). In addi-

Table 1. Yields and elemental analyses of the palladium complexes

Complex		Yield %	Color	Mp[a] °C	Found (%) C	H	N	Calcd (%) C	H	N
[Pd(oxch)Cl(dppe)]	**2**	96	Off white	>205	60.57	4.95	0	60.49	4.92	0
[Pd(oxch)Cl(phen)]	**3**	13	Off white	>247	52.45	3.62	6.58	51.82	3.62	6.72
[PdBr(oxch)(phen)]	**4**	62	Pale yellow	236—240	47.20	3.35	6.19	46.83	3.28	6.07
[Pd(oxch)(dedc)(PPh_3)]	**5**	42	Pale yellow	157—160	56.70	5.34	2.35	56.91	5.27	2.29
[Pd(oxch)(BPz_4)(PPh_3)]	**6**	55	White	>180	58.39	4.64	14.74	58.20	4.61	15.08
[Pd{CH(CN)CO_2Me}(oxch)(dppe)]	**7**	56	Yellow	>109	62.07	5.14	2.01	61.95	5.05	2.01
[Pd{CH(CN)CO_2Et}(oxch)(dppe)]	**8**	28	Yellow	108—113	62.07	5.23	1.99	62.41	5.24	1.97
[Pd{$CH(CN)_2$}(oxch)(dppe)]	**9**	40	Yellow orange	>125	62.77	4.87	4.24	63.22	4.85	4.21

a) Measured in nitrogen atmosphere. All complexes except **8** decomposed without melting.

tion, each of **2** and **5**—**9** exhibited a strong band and a medium one near 1425 and 1475 cm^{-1}, respectively, characteristic of ν(P–C) frequencies.

Complexes **2**—**5**. Complexes **2**—**5** are stable in a solid state in air. However, **2** begins to decompose in deoxygenated dichloromethane at ambient temperature after 1 h, in contrast to **1** and its 5,5-dimethyl homologue. The relatively low stability of **2** is probably due to the lowering of the bond order of the palladium-carbon bond, owing to a considerably strong *trans* influence of the phosphino group located at the *trans* position to the palladium-carbon bond.

In the ^{1}H-NMR spectrum of **2** in CD_2Cl_2, the olefinic proton (2-H) of the oxch moiety resonated as a multiplet at δ 5.95{$^4J(HP_{trans})$=12.0 Hz, $^4J(HP_{cis})$=4.5 Hz, and ^4J(H-6-H)=1.3 Hz}, indicating unambiguously that two phosphino groups were coordinated at *trans* and *cis* positions to the oxch moiety. The IR spectrum of **2** exhibited a ν(Pd–Cl) band at 300 cm^{-1}, which was higher by 20 cm^{-1} than that for **1** (Table 2). This shift to the higher wave number is associated with the difference between the *trans* influence of the phosphino group in **2** and that of the oxch moiety in **1**. The ν(Pd–Cl) frequency of **3** appeared at higher wave number, corresponding to the nitrogen donor site located at a *trans* position to the palladium-chlorine bond.

The anionic bidentate ligand $[dedc]^-$ substituted both the chloro ligand and one of the two triphenylphosphine ligands in **1**, giving the neutral complex **5**, in contrast with the neutral bidentate ligand, such as dppe or phen. It is the case with the $[BPz_4]^-$ ligand, affording the neutral complex **6**, too. The ^{1}H-NMR spectrum of **5** exhibited two ethyl resonances, besides proton signals attributable to the oxch moiety (Table 3) and to the phenyl groups. This proves a double bond character of the carbon-nitrogen bond in the dedc ligand.[7]

Table 2. Characteristic IR bands of the complexes[a]

Complex	ν(C=O)	ν(C=C)	ν(C≡N)	ν(Pd-Cl)
1	1640	1540	—	280
2	1630	1540	—	300
3	1625	1540	—	325
4	1620	1538	—	—
5	1630	1535	—	—
6	1640	1545	—	—
7	1620	1535	2180	—
8	1630	1535	2180	—
9	1630	1535	2204 2150	—

a) In cm^{-1}, in KBr disk.

The [BPz_4] *Complex* **6**. Complex **6** shows a considerably high stability not only in the solid state in the air, but also in the solution of benzene, chloroform, or dichloromethane. It is worthy to note that the [BPz_4] ligand serves as a stabilizing ligand for the palladium-carbon bond, presumably owing to the electronic and steric effects of the ligand. The [BPz_4] ligand in **6** was believed to act as a bidentate chelate, since a relatively electron-rich palladium atom in **6** prevents coordination to the third pyrazolyl group in similar fassion to its related BPz_4–palladium(II) complexes.[8-10]

The ^{1}H-NMR spectra of **6** in $CDCl_3$ showed a temperature dependency in the region 50——31 °C, implying a stereochemically nonrigid motion of the BPz_4 ligand (Fig. 1). The pyrazolyl proton resonances

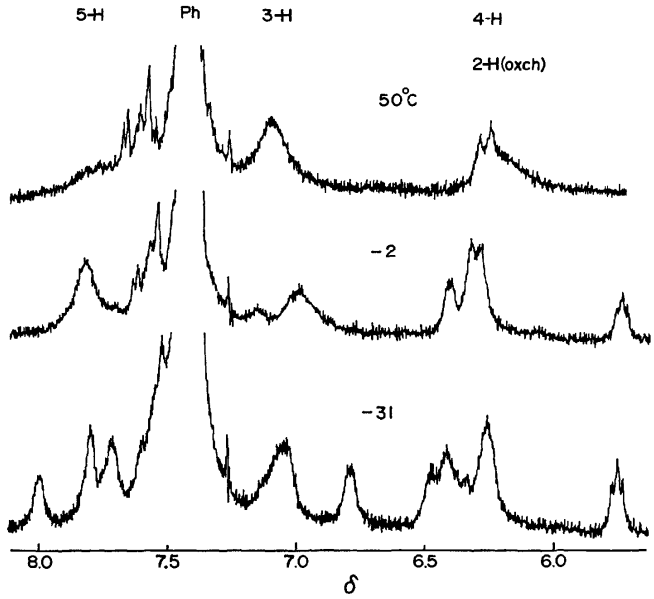

Fig. 1. Low field region of the ^{1}H-NMR spectra of **6**.

Table 3. ^{1}H-NMR data of the palladium complexes[a]

Complex	The oxch moiety							The other group[b]					
	2-H		4-H		5-H	6-H		-CH-		-CH$_2$-		-CH$_3$	
	δ/ppm	J_{PH}/Hz	δ/ppm	J/Hz	δ/ppm	δ/ppm	J/Hz	δ/ppm	J_{PH}/Hz	δ/ppm	J/Hz	δ/ppm	
2	5.95(m)[c]	12 4.5	2.4(b)[d]	—	1.5(m)	1.96(m)	6.1	—	—	—	—	—	
5[e]	6.22(d)	1.7	2.42(t)	5.5	1.5(m)	1.92(m)	6.1	—	—	3.71(q) 3.77(q)	7.3 7.3	1.21(t) 1.28(t)	
6[e,f]	6.27(d)	4.3	←——0.9—2.4(c)——→					6.21(b, 4-H) 7.10(b, 3-H) 7.75(b, 5-H)		—	—	—	
7	5.99(b, d)	11.5	←——1.5—2.5(c)——→					3.43(d)	9.8	—	—	3.34(s)	
8	5.97(b, d)	13.0	←——1.5—2.5(c)——→					3.43(d)	9.8	3.34(q)	7.0	1.15(t)	
9	6.24(b, d)	11.7	2.68(t)	8.3	1.5(m)	1.98(t)	6.7	3.71(d)	6	—	—	—	

a) δ value from TMS. In CD_2Cl_2, except for **5** and **6**. Abbreviations used; b=broad, c=complicated, d=doublet, m=multiplet, q=quartet, s=singlet, and t=triplet. b) Phenyl protons and the ethylene protons of the dppe ligand were omitted. c) Coupling constant to 6-H's was 1.3 Hz. d) Overlapping with the ethylene protons of the dppe ligand. e) In $CDCl_3$. f) At room temperature.

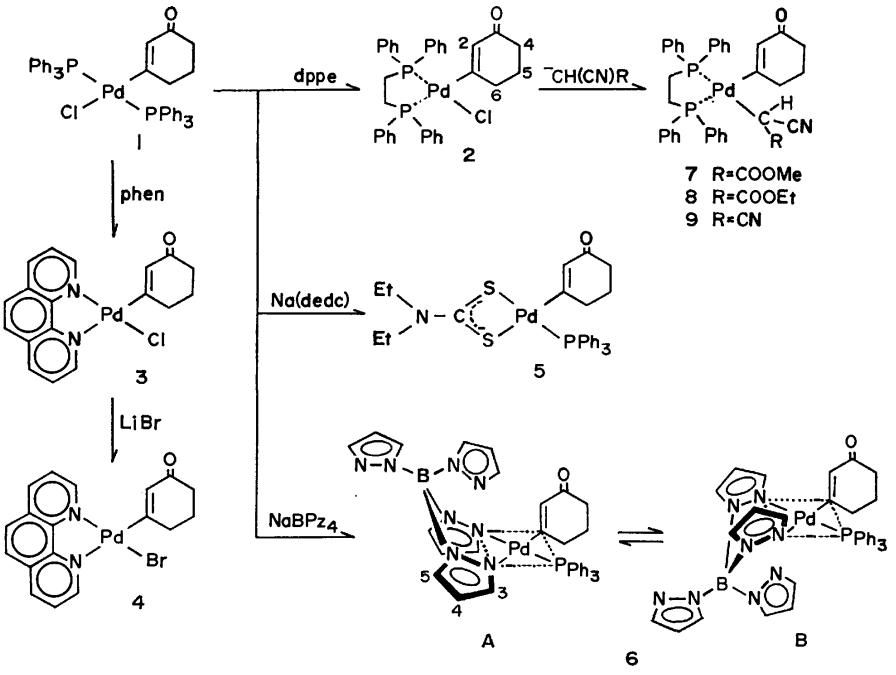

Scheme 1.

at 50 °C indicate that the four pyrazolyl groups are spectroscopically equivalent and move in a tumbling process[8] at a fairly fast rate on the NMR time scale, while the fast-exchange limiting spectrum was not obtained.

At −2 °C, the 4-H signal of the BPz_4 ligand separated into a slightly broad triplet at δ 5.76 (1H, $^3J_{HH}$=2 Hz) and two broad signals at δ 6.3 (2H, overlapping with 2-H of the oxch moiety) and 6.43 (1H). The larger broad signal at δ 6.3 was ascribed to two uncoordinated pyrazolyl groups, which exchanged rapidly with each other, accompanied both by the inversion of the Pd-(N-N)$_2$-B boat-type six-membered ring and by the fluttering of two coordinated pyrazolyl groups (**6A** and **6B** in Scheme 1). The third pyrazolyl group, corresponding to the smaller broad signal at δ 6.43, was one of the two coordinated pyrazolyl groups and exchanged slowly with the former two uncoordinated pyrazolyl ones. The fourth pyrazolyl group, associated with the triplet at δ 5.76, was virtually fixed at this temperature. Similar type of motion of the BPz_4 ligand has been reported concerning [Pd(cdamb)(BPz_4)] (cdamb=2-chloro-3-dimethylamino-3-methyl-1-butenyl-1-*C*,*N*)[10] and its related complexes.[10]

At −31 °C, the larger broad signal separated into two broad signals at δ 6.28 (1H) and 6.50 (1H), indicating that the motion of the BPz_4 ligand turned considerably sluggish. However, **6** gave no slow-exchange limit spectrum even at this temperature.[11]

The Diorganopalladium(II) Complexes 7—9. The IR and ^{1}H-NMR data of **7**—**9** indicate undoubtedly that each of **7**—**9** retains the oxch moiety unchanged and the dppe chelate, while the ^{1}H-NMR spectra of **7** and **8** exhibit complicated signals near δ 1.5—2.5 for 4-, 5-, and 6-H's of the oxch moiety. The nonionic character of these complexes was confirmed by their low molar conductivities (Λ=2.5—5.0 Ω^{-1} cm^2 mol^{-1} in 1.0 mmol/dm^3 acetone solution). The IR spectrum of **7** showed a moderate band at 2180 cm^{-1}, which was assigned to a ν(C≡N) frequency but not to a ν(C=C=N) one in a keteniminato type [Pd-N=C=CH(CO_2Me)].[2,12] In addition, the methine proton of the cyano(methoxycarbonyl)methyl moiety in **7** resonated as a doublet at δ 3.43 ($^3J_{HP}$=9.8 Hz). The chemical shift is considerably similar to those of the methine protons in [Pd{CH(CN)CO_2Me}(pip)] {pip=2-(2-picolylimino)-4-pentanonato-*N,N,O*} and its related complexes.[4] The value of the coupling constant $^3J_{HP}$ is consistent with the protons adjacent to the carbon atom located at a *trans* position to a tertiary phosphine.[13,14] This evidence comfirms unambiguously that the cyano(methoxycarbonyl)methyl moiety in **7** is bonded to the palladium atom with the methine-carbon-palladium σ-bond but not with a nitrogen-palladium bond in the keteniminato type. It is the case with **8**, the ethyl ester homologue of **7**, or with **9**, which has a dicyanomethyl moiety in place of the cyano(methoxycarbonyl)methyl one in **7**.

Complexes **7**—**9** are considerably stable both in the solid state and in the deoxygenated solution of dichloromethane. Moreover, **7**—**9** are inactive to alcohol in THF, as expected from the preparative methods, and are in contrast to [$PdMe_2(PEt_3)_2$].[15] It seems likely that the thermal stability of **7**—**9** is actually comparable with that of [$PdMe_2$(dppe)] and related dimethylpalladium complexes.[14,15] However, **7**—**9** are more sluggish to aerial oxidation than the dimethylpalladium complexes.[14] These stabilities of **7**—**9** and their insensitivity to air are possibly due to the electron-delocalization effect of the electron-withdrawing substituents in the organic moieties attached to the palladium atom.

Complex **2** reacted with the carbanion derived from dimethyl malonate in a procedure similar to the preparation of **7**, giving no isolated pure product. However, **2** did not react with the carbanion formed from methyl acetoacetate, remaining the starting complex **2** recovered. The inertness of the latter carbanion was due to its lower nucleophilicity in comparison with the former carbanion or with the carbanion conducted from methyl cyanoacetate.[16] Complex **3** did not react with the carbanion from methyl cyanoacetate, probably owing to the high insolubility.

We wish to express our gratitude to Mrs. Hisako Mazume and Miss Yumi Kojima, Nagasaki University, for their technical assistance.

References

1) M. Onishi, H. Yamamoto, and K. Hiraki, *Bull. Chem. Soc. Jpn.*, **51**, 1856 (1978).
2) W. H. Baddley and P. Choudhury, *J. Organometal. Chem.*, **60**, C74 (1973).
3) K. Suzuki and S. Nakamura, *Inorg. Chim. Acta.* **25**, L21 (1977).
4) K. Hiraki, M. Onishi, and H. Matsuo, *J. Organomet. Chem.* **185**, 111 (1980).
5) K. Sommer, *Z. Anorg. Allg. Chem.*, **376**, 37 (1970).
6) S. Trofimenko, *J. Am. Chem. Soc.*, **89**, 3170 (1967).
7) M. C. Cornock and T. A. Stephenson *J. Chem. Soc., Dalton Trans.*, **1977**, 501.
8) S. Trofimenko, *J. Am. Chem. Soc.*, **91**, 3183 (1969).
9) M. Onishi, K. Sugimura, and K. Hiraki, *Bull. Chem. Soc. Jpn.*, **51**, 3209 (1978).
10) M. Onishi, K. Hiraki, M. Shironita, Y. Yamaguchi, and S. Nakagawa, *Bull. Chem. Soc. Jpn.*, **53**, 961 (1980).
11) The quantitative analysis about the stereochemically nonrigid motion of the BPz_4 ligand in **6** was not performed owing both to the failure of the detection of the slow-exchange limit spectrum and to the overlapping with the other signal.
12) M. Lenarda and W. H. Baddley, *J. Organomet. Chem.*, **39**, 217 (1972).
13) a) K. Suzuki and H. Yamamoto, *J. Organomet. Chem.*, **54**, 385 (1973); b) R. A. Michelin, M. Napoli, and R. Ros, *ibid.*, **175**, 239 (1979).
14) T. Ito, H. Tsuchiya, and A. Yamamoto, *Bull. Chem. Soc. Jpn.*, **50**, 1319 (1977).
15) G. Calvin and G. E. Coates, *J. Chem. Soc.*, **1960**, 2008.
16) K. Hiraki, Y. Fuchita, and Y. Morita, *Bull. Chem. Soc. Jpn.*, **51**, 2012 (1978).

Deuteration Reaction of Malonate Hydrogens in Some Monomalonatocobalt(III) Compounds[1]

Ushio SAKAGUCHI, Michie NAKANO, and Hayami YONEDA*

Department of Chemistry, Faculty of Science, Hiroshima University, Hiroshima 730

(Received February 25, 1980)

The rate of deuteration at malonate hydrogens has been measured for $[Co(mal)(N)_4]^+$ and $[Co(malH)(NH_3)_5]^{2+}$ ions in aqueous solution over the pD range of 2 to 8, where mal=malonate dianion, malH=malonate monoanion, and $(N)_4=(NH_3)_4$, (ethylenediamine)$_2$, (1,3-propanediamine)$_2$, (1,10-phenanthroline)$_2$, or (2,2′-bipyridine)$_2$. For the tetraamine type complexes with a chelated malonate ligand, the deuteration process is acid-catalysed up to pD=about 4 and base-catalysed at higher pD values. This contrasts with the behavior of the unidentate malonate ligand, for which the deuteration is base-catalysed up to pD=3.5, whereupon the deprotonation of the carboxylate group takes place and the deuteration rate steps down to a constant, pH-independent value. The deuteration mechanisms are discussed.

In 1967, Yoneda and Morimoto[2] found that the methylene hydrogens of malonate chelated to a cobalt (III) ion exchange with deuterium in deuterium oxide. Since the exchange was observed simply by dissolving the cobalt(III) compounds in deuterium oxide, this facile exchange was ascribed to the electron-withdrawing power of the central metal ion. Subsequently, a similar facile deuteration was confirmed to take place for several malonatocobalt(III) complexes.[3-7] Buckingham *et al.* noted that the malonate hydrogens in $[Co(mal)_2(en)]^-$ and $[Co(mal)(en)_2]^+$ ions[4] appear to undergo acid-catalysed and probably base-catalysed exchange. Farago and coworkers[5-7] recently measured the deuteration rates for $[Co(mal)(bpy)_2]^+$, $[Co(mal)_2(en)]^-$, and $[Co(mal)(en)_2]^+$ in the pD range of about 2 to 3 at several temperatures. They confirmed that the exchange reaction is in fact acid-catalysed. We have measured the exchange rates at 36.4 °C over a wide pH region for $[Co(mal)(N)_4]^+$ type of complexes, as well as $[Co(malH)(NH_3)_5]^{2+}$, where $(N)_4$ represents $(NH_3)_4$, $(en)_2$, $(tn)_2$, $(phen)_2$, or $(bpy)_2$.

Experimental

Materials. Deuterium oxide (99.8 atom% D minimum) was obtained from E. Merck (Darmstadt). Malonic acid and other chemicals were purchased from Katayama Chemical Industries Co., Ltd. (Osaka).

Pentaamminemalonatocobalt(III) perchlorate,[8] tetraamminemalonatocobalt(III) perchlorate,[9] and bis(ethylenediamine)malonatocobalt(III) iodide hemihydrate,[10] were prepared by the literature methods and the identity was confirmed by visible absorption and NMR spectra. The en compound was optically resolved by (−)-$[Co(edta)]^-$ after Jordan *et al.*[10] The tn compound was prepared from $[Co(CO_3)(tn)_2]ClO_4$ and malonic acid. Found: N, 13.46; C, 26.46; H, 5.42%. Calcd for $[Co(mal)(tn)_2]ClO_4$: N, 13.71; C, 26.45; H, 5.43%. The bis(phen) compound was synthesized from $[CoCl_2(phen)_2]Cl\cdot 3H_2O$[11] and sodium malonate in aqueous solution. The solution was heated on a water bath until the color of the solution changed to red and then filtered while hot. Cooling the filtrate to room temperature yielded needle-like crystals. These were recrystallized from warm water and suction filtered. Found: N, 8.37; C, 48.41; H, 3.67%. Calcd for $[Co(mal)(phen)_2]Cl\cdot NaCl\cdot 3H_2O$: N, 8.37; C, 48.45; H, 3.61%. The absorption maximum in water was at 510 nm (ε=94). The bipyridine compound, $[Co(mal)(bpy)_2]Br\cdot H_2O$,[5] was prepared by a method similar to that for the phen compound. Since the chloride salt was too soluble to obtain good crystals and the iodide and perchlorate were too insoluble to allow NMR measurements, the complex was obtained in the bromide by adding excess potassium bromide to the hot, filtered reaction mixture and cooling in ice. This procedure gave the crystals of the composition consistent with $[Co(mal)(bpy)_2]Br\cdot 0.5KBr\cdot H_2O$. Recrystallization from warm water gave an analytically pure compound, for which the identity was confirmed by the visible absorption and NMR spectra, and by chemical analysis.[5]

Measurements. The solubilities of the $(N)_4$ compounds were rather small; they are about 0.10, 0.22, 0.084, 0.16, and 0.05 mol dm^{-3} for the en, tn, phen, bpy, and tetraammine complexes, respectively. Therefore these complexes were dissolved in deuterium oxide to near saturation.

Nuclear magnetic resonance spectra were taken at 36.4 °C on a Varian T-60 spectrometer operating at 60 MHz. Owing to the low solubilities of the $(N)_4$ compounds, we measured the peak height (rather than integrated intensity) of the malonate singlet at suitable time intervals after dissolution. The exchange rates were obtained from the slope of the plots of ln(intensity) *vs.* time. Chemical shifts were referred to internal sodium 2,2-dimethyl-2-silapentane-5-sulfonate (DSS). The stability of these complexes against acid- and base-hydrolysis could be checked easily by NMR spectra thanks to the fact that the chemical shifts of coordinated malonates and the uncoordinated malonic acid or malonate anion are different.

The solution pD was adjusted by appropriate amount of HCl or Na_2CO_3 and measured by a Hitachi-Horiba Model F-7 pH meter with a microelectrode accessory, immediately after kinetic measurements. The pH meter readings were converted to the pD values by the empirical formula developed by Fife and Bruice,[12] pD=pH(meter readings)+0.35(at 36.4 °C).

Absorption spectra were run on a Shimadzu UV-200 double beam spectrophotometer and circular dichroism spectra on a JASCO J-40CS spectropolarimeter.

Results and Discussion

The NMR spectrum of the pentaammine compound was reported previously for dimethyl-d_6 sulfoxide solution.[8c] In D_2O the compound gave a sharp peak at δ 3.41 due to coordinated malonate and two broad absorptions at δ 3.79 and 2.84 with an intensity ratio of 4:1. The latter two absorptions are due to coordinated *cis* and *trans* (to coordinated oxygen) ammine groups and their chemical shift differences are explained

by the magnetic anisotropy of the central cobalt(III) ion.[13] Figure 1 shows the NMR spectra of the $(N)_4$ complexes used in this work, taken in pure deuterium oxide and the chemical shift values are summarized in Table 1. The malonate hydrogens of the $(N)_4$ compounds appear as a singlet between $\delta=3.19$ and 3.33. The tetraammine compound exhibits two broad absorptions at $\delta=4.23$ and 3.29 with equal intensities and they are due to coordinated ammine groups. The high field signal at $\delta=3.29$ can be assigned to ammine groups *trans* to the oxygen atoms of coordinated malonate ion on the basis of the magnetic anisotropy effect of the cobalt(III) ion.[13] The spectrum of the en compound has been reported[2,3,7] and consists of four peaks at $\delta=5.25$ (*cis* NH_2), 4.49 (*trans* NH_2), 3.32 (malonate CH_2), and 2.62 (CH_2CH_2 of en). The tn compound showed, in addition to malonate resonance, two broad peaks at $\delta=4.70$ (*cis* NH_2) and 4.07 (*trans* NH_2) and two complex multiplets at about $\delta=2.57$ (C_1 and C_3 methylenes) and 1.87 (C_2 methylene). The latter two methylene peaks sharpen as the deuteration at NH_2 groups proceeds, as shown in the inset of Fig. 1. The assignment of the NH_2 resonances of the en and tn compounds has been made previously[13] and the high-field signals are due to *trans* NH_2 groups. In the pentaammine, tetraammine, bis(en), and bis(tn) compounds, all the ammine and amine groups undergo hydrogen-deuterium exchange in basic deuterium oxide.[14] The resonances due to phen and bpy ligands appear in fine structures between $\delta=9.15$ and 7.12, and $\delta=8.96$ and 7.32, respectively.

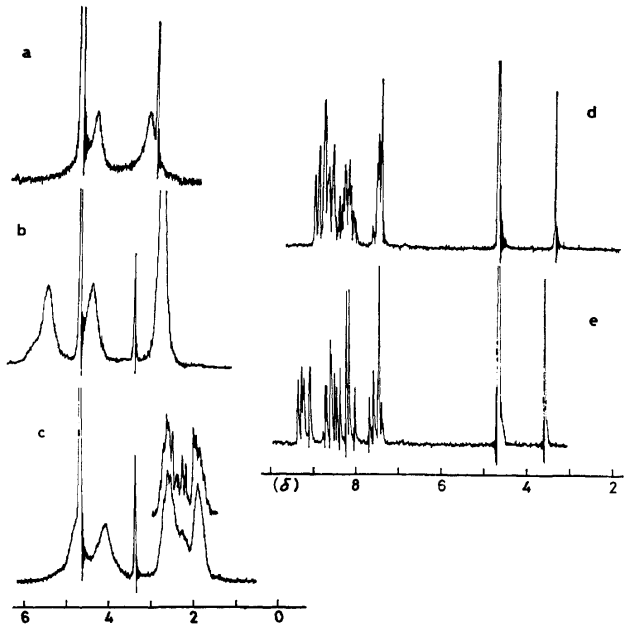

Fig. 1. The 60 MHz NMR spectra of $[Co(mal)(N)_4]^+$ complexes in deuterium oxide, where $(N)_4$ is (a) $(NH_3)_4$, (b) $(en)_2$, (c) $(tn)_2$, (d) $(bpy)_2$, and (e) $(phen)_2$. Inset of (c) illustrates the spectrum after complete deuteration of all NH_2 groups of tn. The strong peak at δ 4.62 is due to solvent HDO.

Exchange Reaction of the $(N)_4$ Compounds. The malonate singlet of all the compounds examined here decreased in intensity with time. The ln(intensity) *vs.* time plots gave a straight line, indicating that the deuteration process follows the kinetic equation

$$\frac{d}{dt}[Co\ mal_H] = -k[Co\ mal_H],$$

where $[Co\ mal_H]$ is the concentration of an undeuterated malonatocobalt(III) complex and k is the pseudo-first-order rate constant for the deuteration of malonate ligand. In Fig. 2, the $\log(k)$ values are plotted against the solution pD. The solid lines in Fig. 2 have slopes of $+1$ and -1. Though the low solubilities of the $(N)_4$ compounds made the quality of the pD-rate

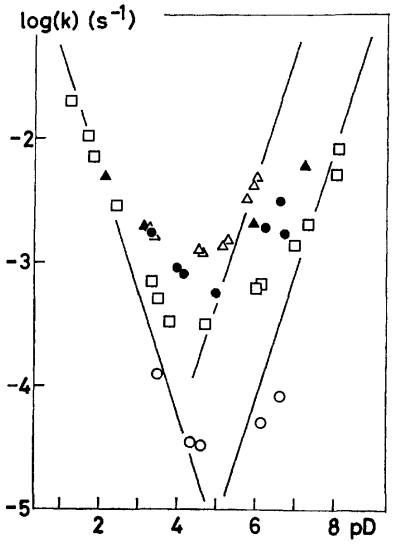

Fig. 2. The $\log(k)$ *vs.* pD plots for the deuteration of malonate hydrogens of $[Co(mal)(N)_4]^+$ complexes, where $(N)_4$ is $(NH_3)_4$ (○), $(tn)_2$ (□), $(en)_2$ (●), $(phen)_2$ (△), and $(bpy)_2$ (▲). Solid lines are with slopes of $+1$ or -1.

Table 1. Chemical shifts measured in deuterium oxide

The values are in δ (ppm) from an internal DSS.

	$(NH_3)_4$	$(en)_2$	$(tn)_2$	$(phen)_2$	$(bpy)_2$	$(NH_3)_5$
Malonate	3.19	3.32	3.33	3.28	3.32	3.41
cis Amine or ammine	4.23	5.25	4.70			3.79
trans Amine or ammine	3.29	4.49	4.07			2.84
Others		2.62[a]	2.57[b]	9.15～7.12[d]	8.96～7.32[e]	
			1.87[c]			

a) CH_2CH_2. b) C_1 and C_3 methylenes. c) C_2 methylene. d) phen. e) bpy.

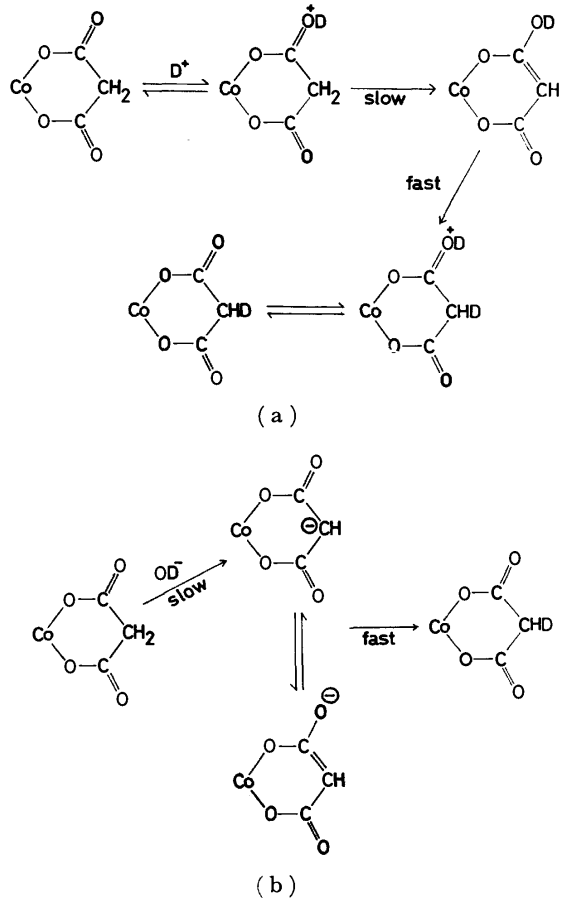

Fig. 3. A probable mechanism of hydrogen-deuetrium exchange catalysed by (a) D_3O^+ and (b) OD^- ions.

profile rather poor, Fig. 2 indicates that $\log(k)$ is proportional to $-$pD at lower pD while at higher pD it is proportional to pD. From this pD dependence it follows that k is proportional to $[D_3O^+]$ at lower pD and to $[OD^-]$ at higher pD. Therefore, the exchange reaction is acid-catalysed at pD values less than about 4 and base-catalysed at higher pD.

The mechanism of acid-catalysed deuteration will be considered in an analogous way to that proposed for the deuteration of glycine residues in $[Co(edta)]^-$ ion.[15,16] Farago and Smith[5] proposed such a mechanism as illustrated in Fig. 3(a). In this mechanism, the initial step is the rapid protonation of carbonyl oxygen, which is followed by the rate-determining step of a hydrogen abstraction to give an enol. This enol will tautomerize, upon deuteration, to regenerate the carboxyl group. The deuteration is thus effected by D_2O molecule donating D^+ to the enol intermediate.

The second mechanism proposed originally by Terrill and Reilley[15] also for $[Co(edta)]^-$ involves the carbonyl protonation and the subsequent rupture of carboxylate-cobalt bond. This mechanism seems at first sight to be adapted to the present case. Since this mechanism assumes the monodentate carbonium ligand of the form,

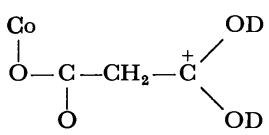

we may reasonably expect concomitant racemization at the metal center. For $[Co(edta)]^-$ ion, Terrill and Reilley in fact confirmed that deuteration is accompanied by racemization. For the optically active en compound, however, we did not observe any measurable change in the circular dichroism spectrum over the whole pD region examined here and over several half-lives of deuteration. In highly basic solution, this ion undergoes base-hydrolysis and decreases its optical activity as reproted by Farago and Keefe.[17] Though both mechanisms are consistent with the $[D_3O^+]$ dependence of the rate constant, the second mechanism does not seem to play the dominant role in our systems.

The mechanism of base-catalysed reaction will involve the carbanion intermediate, see Fig. 3(b). The first step may be a hydrogen abstraction by OD^- to give the carbanion. This carbanion can be resonance stabilized with the enol form, which favors the planar structure of the malonate moiety of this intermediate. The rate-determining step in base-catalysed reaction will be the C-H bond rupture. As for the acid-catalysed reaction, the deuteration is effected by D_2O donating D^+ to the carbanion intermediate. For the en and bpy compounds, Farago and Smith[5] made temperature dependence studies between 20 and 37 °C at around pD=2 to 3. Their results at 37 °C are in good agreement with our data shown in Fig. 2. Figure 2 indicates also that in acid-catalysed reaction the rates for all the compounds are not so different but in base-catalysed reaction the rates vary from compound to compound and the rate is in the order $(phen)_2$—$(bpy)_2$>$(en)_2$>$(tn)_2$>$(NH_3)_4$.

Deuteration Reaction of The Pentaammine Compound. Figure 4 shows the $\log(k)$ *vs.* pD plots for $[Co(malH)(NH_3)_5]^{2+}$ ion. This plots contrast with Fig. 2 in the following points; (i) the deuteration is base-catalysed even at lower pD values, (ii) at about pD=3.95, the rate constant steps down to a value of 5×10^{-5} s^{-1}, and (iii) at higher pD region the rate constant does not depend on acid or base concentration. Clearly the sudden decrease at pD=3.95 corresponds to the deprotonation of the unidentate malonate ligand, for which the pK_a value was estimated by Svatos and Taube[8a] at 3.41(μ=0.1). By applying the deuterium

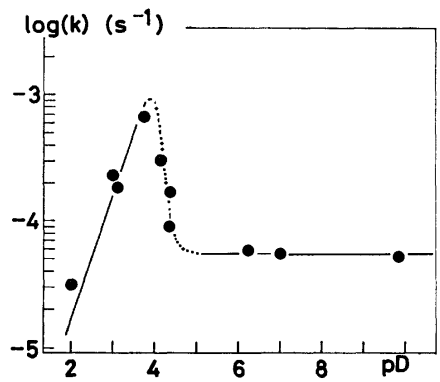

Fig. 4. The $\log(k)$ *vs.* pD plots for the deuteration of malonate in $[Co(OOCCH_2COOH)(NH_3)_5]^{2+}$. Solid lines are with slopes of +1 or zero.

isotope effect of 0.35 pH meter unit[12] to 3.41, we obtain the value 3.76. This value compares well with the pD value that corresponds to the kink in the pD-rate profile of Fig. 4. At low pD, the reaction should involve the coordinated carbanion intermediate produced by hydrogen abstraction by OD^- catalyst. The pD-independent rate at high pD region suggests that the methylene group in the $[Co(OOCCH_2COO)(NH_3)_5]^+$ ion undergoes either "water-catalysed" exchange or mixed D^+–OD^- (zwitterionic) catalysed exchange. The deuteration of methylene group of free ethyl malonate anion has been studied by Kirby and Lloyd[18] and the observed pH-independent exchange rate is reported at $3.33\times10^{-4}\ s^{-1}$ at 39.6 °C. This value is approximately an order of magnitude larger than our corresponding value for the Co(III)-$OOCCH_2COO^-$ group. In this context, the effect of the electron-withdrawing power of the cobalt(III) ion upon the exchange rate does not appear significant.

References

1) This work is Proton Magnetic Resonance Spectra of Metal Ammine Complexes. 14.

2) H. Yoneda and Y. Morimoto, *Inorg. Chim. Acta*, **1**, 413 (1967).

3) D. A. Buckingham, L. Durham, and A. M. Sargeson, *Aust. J. Chem.*, **20**, 257 (1967).

4) Abbreviations; mal=malonate dianion, malH=malonate monoanion, en=ethylenediamine, tn=1,3-propanediamine, phen=1,10-phenanthroline, bpy=2,2′-bipyridine, edta=ethylenediaminetetraacetate.

5) M. E. Farago and M. A. R. Smith, *J. Chem. Soc., Dalton Trans.*, **1972**, 2120.

6) M. E. Farago and M. A. R. Smith, *Inorg. Chim. Acta*, **14**, 21 (1975).

7) S. Amirhaeri, M. E. Farago, J. A. P. Gluck, M. A. R. Smith, and J. N. Wingfield, *Inorg. Chim. Acta.* **33**, 57 (1979).

8) a) G. Svatos and H. Taube, *J. Am. Chem. Soc.*, **83**, 4172 (1961); b) R. D. Butler and H. Taube, *ibid.*, **87**, 5597 (1965); c) C. Lavallee and E. Deutsch, *Inorg. Chem.*, **11**, 3133 (1972).

9) J. D. Edwards, Y. Sulfab, and A. G. Sykes, *Inorg. Chem.*, **14**, 1474 (1975).

10) W. T. Jordan, B. J. Brennan, L. R. Froebe, and B. E. Douglas, *Inorg. Chem.*, **12**, 1827 (1973).

11) A. V. Ablov, *Russ. J. Inorg. Chem.*, **6**, 157 (1961).

12) T. H. Fife and T. C. Bruice, *J. Phys. Chem.*, **65**, 1079 (1961). See also, W. F. K. Wynne-Jones, *Trans. Faraday Soc.*, **32**, 1397 (1936); P. K. Glasoe and F. A. Long, *J. Phys. Chem.*, **64**, 188 (1960).

13) a) U. Sakaguchi, S. Yamazaki, and H. Yoneda, *Bull. Chem. Soc. Jpn.*, **49**, 402 (1976); b) Y. Nakashima, U. Sakaguchi, and H. Yoneda, *ibid.*, **48**, 762 (1975), and references cited therein. The assignment in Ref. 5 for the two amine peaks of the en compound is opposite to the present assignment.

14) U. Sakaguchi, K. Maeda, and H. Yoneda, *Bull. Chem. Soc. Jpn.*, **49**, 397 (1976), and references therein.

15) J. B. Terrill and C. N. Reilley, *Inorg. Chem.*, **5**, 1988 (1966).

16) J. L. Sudmeier and G. Occupati, *Inorg. Chem.*, **7**, 2524 (1968).

17) M. E. Farago and M. Keefe, *Inorg. Chim. Acta*, **15**, 5 (1975).

18) A. J. Kirby and G. J. Lloyd, *J. Chem. Soc., Perkin Trans. 2*, **1976**, 1762.

Use of the Copper(II) Ion-selective Electrode for the Determination of the Stability Constant of Binuclear Copper(II) Complex with 3,6-Dioxaoctane-1,8-diamine-*N,N,N',N'*-tetraacetric Acid

Kunio Ohzeki, Masakuni Saruhashi, and Tomihito Kambara*

Department of Chemistry, Faculty of Science, Hokkaido University, Sapporo 060

(Received March 18, 1980)

The stability constant of binuclear copper(II) complex with 3,6-dioxaoctane-1,8-diamine-*N,N,N',N'*-tetraacetic acid (ethylene glycol bis[2-[bis(carboxymethyl)amino] ethyl] ether, customarily abbreviated to EGTA of Y) was determined on the basis of potentiometric titration by means of a copper(II) ion-selective electrode. In acetate buffer solution of pH 5.8 titration curves of copper(II) with EGTA show two distinct end points corresponding to Cu_2Y and CuY complexes. The formation constant of the binuclear copper(II) complex was determined from the potential response in the titration fraction between first and second end points. The logarithmic value was found to be log $K_{Cu_2Y}=6.40$ at ionic strength of 0.2 M (KNO_3–acetate buffer solution) at 25± 0.5 °C.

The response of copper(II) ion-selective electrode in the aqueous solution of complexing agent has been studied. Nakagawa *et al.*[1] found that the stability constants of copper(II) complexes with several ligands such as acetate, ammonia, ethylenediamine, *etc.* agreed very well with those given in the literature, except EDTA and NTA complexes. Similar behavior has recently been observed by Heijine and Linden.[2]

In the present paper a successful application of copper(II) ion-selective electrode to the determination of binuclear copper(II)–EGTA complex is described.

Theoretical

When copper(II) is titrated with EGTA forming only two complexes CuY and Cu_2Y, the total concentration of copper(II) and EGTA in the titration vessel can be written as:

$$C_{Cu} = [CuY] + 2[Cu_2Y] + [Cu]\alpha_{Cu} \quad (1)$$

and

$$C_Y = [CuY] + [Cu_2Y] + [Y]\alpha_Y, \quad (2)$$

where α_{Cu} denotes the side reaction coefficient of copper(II) with component of buffer system, and α_Y indicates that of titrant with hydrogen ion. The stability constants of CuY and Cu_2Y are given

$$K_{CuY} = \frac{[CuY]}{[Cu][Y]} \quad (3)$$

and

$$K_{Cu_2Y} = \frac{[Cu_2Y]}{[Cu][CuY]}. \quad (4)$$

Introducing Eqs. 3 and 4 into Eqs. 1 and 2 and eliminating [Y], one obtains

$$\frac{C_Y}{C_{Cu}} = \frac{K_{CuY}[Cu]+K_{CuY}K_{Cu_2Y}[Cu]^2+\alpha_Y}{K_{CuY}[Cu]+2K_{CuY}K_{Cu_2Y}[Cu]^2}\left(1-\frac{[Cu]\alpha_{Cu}}{C_{Cu}}\right). \quad (5)$$

Between the first and second end points, Eq. 5 can be simply written as:

$$\frac{C_Y}{C_{Cu}} = \frac{1+K_{Cu_2Y}[Cu]}{1+2K_{Cu_2Y}[Cu]}. \quad (6)$$

When a ml of copper(II) solution in the initial concentration of C_{Cu}° is diluted in the titration vessel to V ml, and then titrated with ΔV ml of titrant of the concentration of C_Y°, the titration fraction is given by

$$\frac{C_Y}{C_{Cu}} = \frac{\Delta VC_Y^\circ}{aC_{Cu}^\circ}. \quad (7)$$

Combination of Eqs. 6 and 7 yields

$$K_{Cu_2Y}[Cu] = \frac{aC_{Cu}^\circ-\Delta VC_Y^\circ}{2\Delta VC_Y^\circ-aC_{Cu}^\circ}. \quad (8)$$

When the titration is carried out in acetate or ammonia buffer solution, the formation of the mixed ligand complex such as $Cu_2Y(NH_3)$ should be considered. In this case, K_{Cu_2Y} in Eq. 8 is replaced by

$$K'_{Cu_2Y} = K_{Cu_2Y}(1+K_{Cu_2YL}[L]+K_{Cu_2YL}K_{Cu_2YL_2}[L]^2), \quad (9)$$

where K'_{Cu_2Y} is the apparent formation constant, K_{Cu_2YL} and $K_{Cu_2YL_2}$ are the formation constants of the mixed ligand complexes, and L denotes the acetate or ammonia. In the logarithmic expression of the resulting equation, one derives

$$pCu = \log K'_{Cu_2Y} - \log\frac{aC_{Cu}^\circ-\Delta VC_Y^\circ}{2\Delta VC_Y^\circ-aC_{Cu}^\circ}. \quad (10)$$

A plot of pCu against the logarithmic term in the right-hand side will show a straight line with a negative slope of unity and K'_{Cu_2Y} value is estimated from the intercept of the line.

Experimental

Reagents. A Dotite reagent EGTA (Dojindo Lab.) was used as received. Other chemicals used were all of analytical reagent grade. A 10^{-2} M (1 M=1 mol dm^{-3}) copper(II) stock solution was prepared from copper(II) sulfate pentahydrate. A 10^{-2} M EGTA solution (pH=4.8) was prepared by dissolving the acid with appropriate amount of potassium hydroxide, the ionic strength being adjusted to 0.2 M with potassium nitrate. The EGTA solution was standardized against the copper(II) solution. A solution containing 0.1 M acetate buffer solution (pH=6.0) and 0.1 M potassium nitrate was used for conditioning the copper(II) ion-selective electrode.

Apparatus. The copper(II) ion activities were measured with an Orion copper(II) ion-selective electrode, Model 94-29. A Horiba double junction SCE with the outer compartment filled with 0.2 M potassium nitrate was used as the reference electrode. The potential measurements were made by the aid of a Hiranuma recording auto titrator, Type RAT-11. A Hitachi-Horiba pH meter, F-5, was used

for pH measurements.

Procedure. All experiments were carried out in a thermostat kept at 25±0.5 °C. The electrode potential was recorded while the solution was gently stirred.

Conditioning: The surface of copper(II) ion-selective electrode was polished gently with a tooth paste and then soaked in the conditioning solution until a constant potential value was attained.

Calibration: A series of standard copper(II) solution from 10^{-3} to 10^{-7} M was prepared by diluting the stock solution immediately before the measurements, the ionic strength being adjusted to 0.2 M with potassium nitrate. The pH of final solution was in the range of 5.0—5.4. The potenital was recorded for 30 s with a Hiranuma recording auto titrator without titrant supply.

Titration: Titrations of copper(II) with EGTA were performed in acetate or ammonia buffer solution. The ionic strength of test solutions was adjusted to 0.2 M with potassium nitrate. The EGTA solution was automatically supplied to a 50-ml portion of the test solution containing copper(II) in the analytical concentration range from 2×10^{-4} to 10^{-3} M. A 30-μl portion of the titrant was delivered to a titration vessel within 0.5 s and the electrode potential was measured after 9.5 s, and the procedure was repeated. Titration curves with stepwise potential decreases were recorded automatically.

Results and Discussion

Calibration Curve. The electrode potential drifted slightly in the 10^{-7} M copper(II) solution, while above 10^{-6} M a stable potential was observed during 30 s. The Nernstian response was found to hold from 10^{-3} to 10^{-6} M of copper(II), obeying the equation:

$$E = E' + S\log a_{Cu^{2+}}$$
$$= E'' + S\log[Cu]$$
$$= 260 + 29.9\log[Cu].$$

In the equations, E' and E'' are constants, S the Nernstian coefficient, and the figures in the last equation are expressed in mV.

Titration in Acetate Buffer Solution. Titrations were made with varying acetate buffer concentrations, namely, 0.06, 0.10, 0.14, and 0.20 M. The pH values of test solutions were in the range 5.76—5.80. These values decreased slightly as titration proceeded. A typical titration curve was shown in Fig. 1. Two distinct end points were found. The ratio of amount of titrant at the second end point to that at the first end point was found to be 2.00 (number of determinations $n=6$). The first end point is due to the formation of binuclear copper(II) complex Cu_2Y. The results of log-log plot according to Eq. 10 were shown in Fig. 2. Each plot gave a straight line with a negative slope of unity as expected theoretically. The apparent formation constant is evaluated from the intercept of each line at the abscissa zero line, where the titration fraction is two-thirds. A constant K'_{Cu_2Y} value was obtained irrespective of the initial copper(II) concentration ranging from 2×10^{-4} to 10^{-3} M. However, the value increased with increasing concentration of buffer solution as shown in Fig. 2, which suggests the formation of mixed ligand binuclear copper(II) complex such as $Cu_2Y(CH_3COO)$. When the forma-

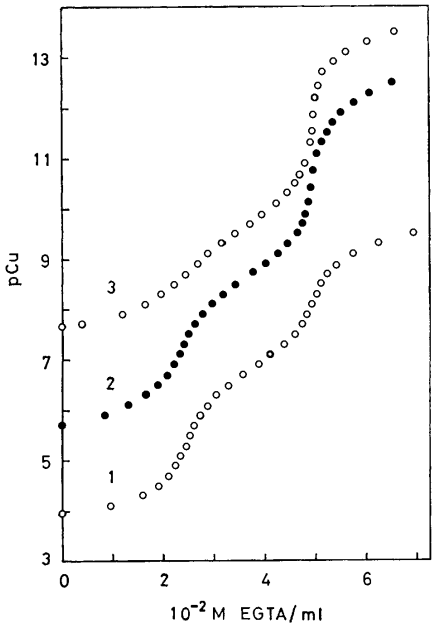

Fig. 1. Titration of a 50-ml portion of 10^{-3} M (f= 0.995) copper(II) with 10^{-2} M (f=1.000) EGTA performed in: 1; 0.10 M (CH_3COOH–CH_3COONa), pH 5.8, 2; 0.06 M (NH_3–NH_4Cl), pH 8.0, 3; 0.20 M (NH_3–NH_4Cl), pH 8.4.

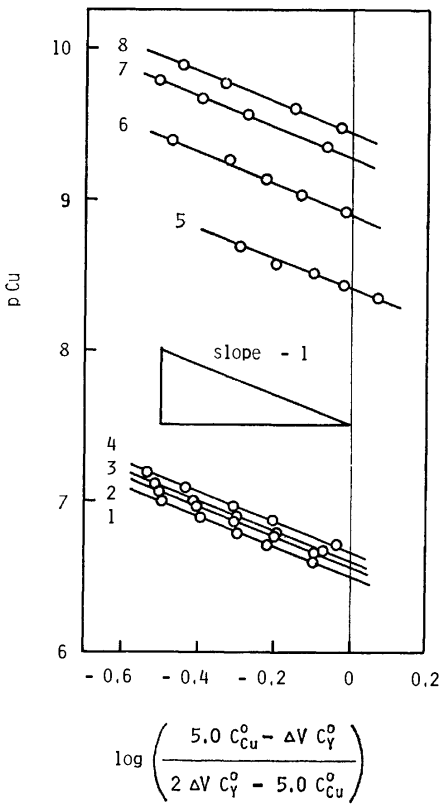

Fig. 2. Plots according to Eq. 10. Titrations were made in: 1; 0.06, 2; 0.10, 3; 0.14, 4; 0.20 M acetate buffer solution (nominal pH=5.8) and 5; 0.06, 6; 0.10, 7; 0.16, 8; 0.20 M ammonia buffer solution (nominal pH=8.5).

tion of $Cu_2Y(CH_3COO)_2$ is negligible, Eq. 9 is expressed as:

$$K'_{Cu_2Y} = K_{Cu_2Y} + K_{Cu_2Y}K_{Cu_2Y(CH_3COO)}[CH_3COO^-] \quad (12)$$

and a plot of the apparent formation constant K'_{Cu_2Y} against the concentration of acetate ion at the titration fraction of two-thirds will show a straight line. The result given in Fig. 3 supports the above assumption. The values of intercept and slope of the regression equation of Eq. 12 were determined with 95% confidence limits as $(2.50\pm0.19)\times10^6$ and $(1.29\pm0.16)\times10^7$, respectively. The logarithms of the constants were 6.40 for K_{Cu_2Y} and 0.71 for $K_{Cu_2Y(CH_3COO)}$. The value of log K_{Cu_2Y} is much greater than the value 4.31 determined by a pH-potentiometric method.[3]

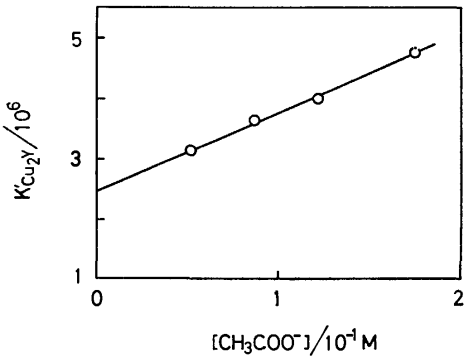

Fig. 3. Determination of K_{Cu_2Y} and $K_{Cu_2Y(CH_3COO)}$ according to Eq. 12.

Titration in Ammonia Buffer Solution. Titrations were performed with varying ammonia buffer concentrations, namely, 0.06, 0.10, 0.16, and 0.20 M. The pH values of test solutions were in the range 8.04—8.35. The values increased slightly as titration proceeded. Typical titration curves were shown in Fig. 1. Two end points were found while the potential change at the first end point decreased with increasing amount of ammonia. On the whole, the titration curves were shifted to lower potential values than those in acetate buffer solution. The formation of fairly stable mixed ligand complexes such as $Cu_2Y(NH_3)$ and $Cu_2Y(NH_3)_2$ are postulated. Equation 9 is transformed into:

$$\left(\frac{K'_{Cu_2Y}}{K_{Cu_2Y}}-1\right)[NH_3]^{-1} = K_{Cu_2Y(NH_3)}(1+K_{Cu_2Y(NH_3)_2}[NH_3]) . \quad (13)$$

From the plot of left-hand side of Eq. 13 against the concentration of ammonia, the formation constants were evaluated. The values for K'_{Cu_2Y} were obtained from the plots shown in Fig. 2. The concentration of ammonia was calculated from the solution pH and the total concentration of ammonia at the titration fraction of 2/3, where average mole ratio of copper(II) to ammonia was assumed to be unity. The result was shown in Fig. 4. The values of intercept and slope of the regression equation were determined with 95% confidence limits as $(2.99\pm0.40)\times10^4$ and $(2.55\pm0.36)\times10^6$, respectively. The logarithms of the constants were 4.48 for $K_{Cu_2Y(NH_3)}$ and 1.88 for $K_{Cu_2Y(NH_3)_2}$.

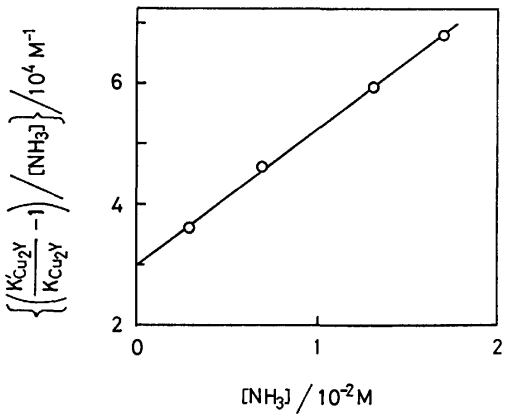

Fig. 4. Determination of $K_{Cu_2Y(NH_3)}$ and $K_{Cu_2Y(NH_3)_2}$ according to Eq. 13.

Theoretical Titration Curves. When 10^{-3} M (f= 0.995) copper(II) in a 50-ml portion of acetate or ammonia buffer solution is titrated with ΔV ml of 10^{-2} M (f=1.000) EGTA, the following equation holds:

$$\Delta V = \frac{0.995\times10^{-3}-\alpha_{Cu}[Cu]}{\frac{10^{-2}}{50}\left(\frac{K_{CuY}[Cu]+2K_{CuY}K'_{Cu_2Y}[Cu]^2}{K_{CuY}[Cu]+K_{CuY}K'_{Cu_2Y}[Cu]^2+\alpha_Y}\right)+\frac{\alpha_{Cu}[Cu]}{50}} \quad (14)$$

The values of K'_{Cu_2Y}, α_{Cu}, and α_Y were calculated from the concentration of ammonia or acetate ion and pH at the titration fraction of 2/3; namely, $K'_{Cu_2Y(CH_2COO)}=3.61\times10^6$, $\alpha_{Cu(CH_3COO)}=6.23$, and $\alpha_{Y(H)}=1.17\times10^7$ for titration in acetate buffer solution and $K'_{Cu_2Y(NH_3)}=2.64\times10^6$, $\alpha_{Cu(NH_3)}=9.23\times10^2$, and $\alpha_{Y(H)}=1.81\times10^2$ for titration in ammonia buffer solution, respectively. These values were assumed to be con-

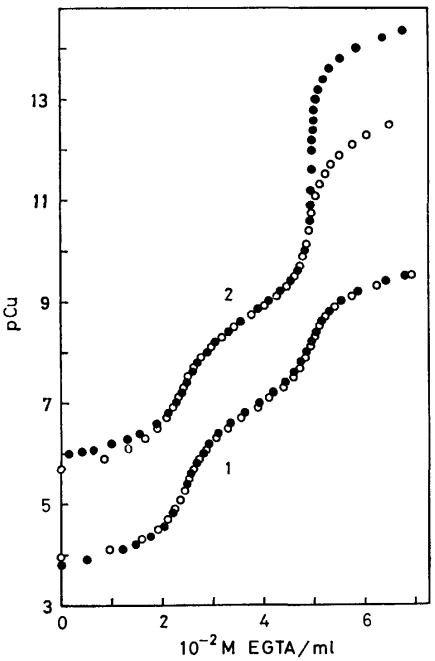

Fig. 5. Comparison of the experimental titration curves (○) with the theoretically obtained curves (●). Curves 1 (○) and 2 (○) are the same as curves 1 and 2 in Fig. 1, respectively.

stant during titration. The formation constant[4] K_{CuY} is reported to be 10^{17}. Introducing these values and copper(II) concentration into Eq. 14, one can illustrate theoretical titration curves as shown in Fig. 4. In the case of acetate buffer solution, a fairly good agreement was observed between the theoretically obtained titration curve and the experimental one. On the other hand, in ammonia buffer solution, the potential change at the second end point is much less than the theoretically expected value. Since the membrane of the Orion copper(II) electrode is made up of mixed sulfides of copper(II) and silver, the formation of silver–EGTA complex at the electrode surface may be responsible for the depression of response for copper (II).[1]

It should be noted from Eq. 14 that when titration is carried out in the acetate buffer solution of pH lower than 5, where the value of $\alpha_{Y(H)}$ is approximately equal to 10^{10}, the second end point disappears, only the first end point corresponding to the formation of Cu_2Y being obtained. On the contrary, in concentrated ammonia buffer solution where $\alpha_{Cu(NH_3)}$ is around 10^6, the first end point disappears and only the second end point is observed.

References

1) G. Nakagawa, H. Wada, and T. Hayakawa, *Bull. Chem. Soc. Jpn.*, **48**, 424 (1975).
2) G. J. M. Heijine and W. E. Linden, *Anal. Chim. Acta*, **96**, 13 (1978).
3) K. H. Schröder, *Acta Chem. Scand.*, **19**, 1347 (1965).
4) A. Ringbom, "Complexation in Analytical Chemistry," Interscience, New York and London (1963).

A New Synthesis of 1-Amino-4-butylaminoanthraquinone from 1-Aminoanthraquinone Promoted by Metal Ions

Katsuhira YOSHIDA,* Masaru MATSUOKA,*,† Yoshio YAMASHITA, and Teijiro KITAO†

Department of Chemistry, Faculty of Science, Kochi University, Akebono-cho, Kochi 780

†*Department of Applied Chemistry, College of Engineering, University of Osaka Prefecture, Sakai, Osaka 591*

(Received November 14, 1979)

In the presence of some metal ions and atmospheric oxygen, 1-aminoanthraquinone(**1**) reacts readily with butylamine to give 1-amino-4-butylaminoanthraquinone(**2a**), along with a small amount of 1,4-diaminoanthraquinone, which is produced by the dealkylation of **2a**. The activity of the metal ions decreased in the following order: Co(II)≫Ni(II)>Cu(II)>Al(III). The reaction is remarkably affected by the substitution of an alkyl group into the amino group of **1**, the addition of a chelating agent, the counter anion of metal ions, and the reaction temperature. By the use of cobalt(II) chloride, the reaction proceeds most smoothly at about 30 °C. Both anthraquinone and 2-aminoanthraquinone show no sign of the reaction under the same conditions. A possible mechanism involving the formation of a metal complex, followed by the nucleophilic attack of amine at the 4-position and the oxidative abstraction of the hydride anion by atmospheric oxygen is proposed.

Aminoanthraquinone derivatives are very important compounds as dyes or dye intermediates. A large number of papers and patents have been reported on reactions introducing amino groups into the anthraquinone nucleus. The displacement of sulfonyl, halogeno,[1] nitro, and hydroxy groups by amino groups is widely adopted.

The direct amination of anthraquinone or aminoanthraquinones with hydroxylamine in concentrated sulfuric acid catalyzed by iron(II) sulfate or vanadium pentaoxide has also been described, but it produces random substitution products.[2] Russkikh *et al.*[3] reported that the reaction of the boric esters of quinizarin with aromatic amines gave 2-arylaminoquinizarins in the presence of atmospheric oxygen. Recently, we ourselves reported a metal-promoted alkylamination of α-substituted anthraquinones, in which the amination products were obtained in good yields under mild conditions.[4] This is a useful method for preparing some 1-amino-4-alkylaminoanthraquinones from 1-aminoanthraquinone.

In this paper, we wish to report on the reaction of 1-aminoanthraquinone with butylamine in detail and to propose the possible mechanism of this direct amination.

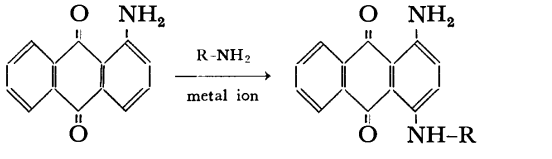

1 **2**

a: R=$CH_2CH_2CH_2CH_3$
b: R=H

Results and Discussion

The reaction of 1-aminoanthraquinone(**1**) with butylamine in the presence of metal salts gave 1-amino-4-butylaminoanthraquinone(**2a**), along with a small amount of 1,4-diaminoanthraquinone(**2b**) produced by the dealkylation of **2a**.[5] A partial dealkylation of alkylaminoanthraquinones has already been noted in previous papers.[6] The activities of metal salts in this direct amination are shown in Table 1.

Table 1. Effect of metal chlorides on the butylamination of **1**[a]

Run	Metal chloride	Recovered(%)[b] **1**	Yield(%)[b] **2a**	Yield(%)[b] **2b**
1	None	99.0	0	0
2	$CuCl_2$	70.9	5.4	3.2
3	$NiCl_2$	57.2	11.1	trace
4	$CoCl_2$	0	58.7	4.7
5	$AlCl_3$	65.9	3.1	trace
6	$FeCl_3 \cdot 6H_2O$	99.1	0	0
7	$MgCl_2 \cdot 6H_2O$	90.1	0	0
8	$ZnCl_2$	93.8	0	0

a) The reactant, **1** (9 mmol), was stirred in 1-butanol (15 ml) with butylamine (15 ml) and metal salt (9 mmol) at 80—82 °C for 24 h. b) Determined by means of a TLC-scanner.

No reaction occurred in the absence of metal salts, but in the presence of metal salts two direct amination products (**2a** and **2b**) were obtained. Metal chlorides were arranged in the order of the activity as follows: Co(II)≫Ni(II)>Cu(II)>Al(III). The activity of the cobalt(II) ion was particularly superior to those of other metal ions, while the Fe(III), Mg(II), and Zn(II) ions did not promote the reaction. As is shown in Table 2, the activity of the cobalt ion is affected by its counter anion. Cobalt(II) chloride and cobalt(II) bromide have good activity, but cobalt(II) fluoride has poor activity.

The 1-amino group plays a great role on this reaction, since both anthraquinone and 2-aminoanthraquinone show no sign of the reaction.[4a] Furthermore, the butylamination of 1-alkylaminoanthraquinones, such as 1-methylamino- or 1-butylaminoanthraquinones, gave the corresponding 1,4-bis(alkylamino)anthraquinones, though in only low yields, in the presence of copper(II) acetate, but none of them in the presence of cobalt(II) chloride. These results suggest that the formation of a metal complex in which the amino and carbonyl groups of **1** coordinate to the metal ion may play an important role during the course of this direct amination. Neither anthraquinone nor 2-aminoanthraquinone can form such a chelate complex

Table 2. Effect of the counter anion of the cobalt ion on the butylamination of **1**[a]

Run	Cobalt salt	Time (h)	Recovered(%)[b] **1**	Yield(%)[b] **2a**	Yield(%)[b] **2b**
9	$CoF_2 \cdot 3H_2O$	24	74.1	0.2[c]	0
10	$CoCl_2$	8	0	66.1	3.1
11	$CoCl_2 \cdot 6H_2O$	8	6.0	53.5	3.0
12	$CoBr_2 \cdot 6H_2O$	8	5.3	63.5	2.9
13	$Co(OCOCH_3)_2 \cdot 4H_2O$	24	19.2	32.1	1.8
14	$Co(CH_3COCHCOCH_3)_2 \cdot 2H_2O$	24	91.2	0	0

a) The reactant, **1** (4.5 mmol), was stirred in 1-butanol (5 ml) with butylamine (15 ml) and metal salt (4.5 mmol) at 30 °C. b) Determined by means of a TLC-scanner. c) Isolated yield.

with the metal ion. The substitution of an alkyl group into the amino group of **1** may prevent the formation of a chelate complex by its steric hindrance.

The addition of a small amount of ethylenediamine completely inhibited the reaction. This suggests that the metal ion is preferentially combined with ethylenediamine rather than with **1** and that, consequently, the reaction was prohibited.[4a]

The effect of the molar ratio of cobalt(II) chloride to **1** on the yield of **2a** is shown in Table 3. The yield of **2a** increases with the increase in the molar ratio of cobalt(II) chloride up to 1.0. The addition of another mole of $CoCl_2$ depresses the yield to 54% because of such undesirable side reactions as dealkylation (Run 20). The yields of **2a**, based on $CoCl_2$, are approximately kept constant at about 64% up to the molar ratio of 1.0 (Runs 15, 17, and 18). In the presence of a 0.1 molar equivalent of $CoCl_2$, a prolonged reaction time results in an increase of the yield of **2a** (Run 16) but the yield based on $CoCl_2$ does not exceed 100%. From these results, the cobalt complex (**1**: Co(II)=1:1) was proposed as an activated intermediate for this direct amination. Also, it was found that atmospheric oxygen is also necessary for this amination because, under a nitrogen atmosphere, the yield of **2a** is depressed drastically to 2.9% and 92% of **1** is recovered, even in the presence of an equimolar amount of cobalt(II) chloride (Run 19).

The reaction was also considerably affected by the reaction temperature. Figure 1 shows the effect of the reaction temperature on the butylamination of **1** in the presence of $CoCl_2$. The yield of **2a** increased up to 30 °C and then decreased gradually with the increase in the temperature. The optimum temperature for this reaction was 30 °C. The decrease in the yield of **2a** at higher temperatures seems to be caused by the fact that the chelate complex may be unstable at higher temperature.

On the basis of the experimental results described above, the following possible mechanism for this amination may be proposed (Scheme 1). The formation of the chelate complex (**3**) probably increases the electrophilicity of the substituted anthraquinone nucleus and, consequently, facilitates the nucleophilic attack of butylamine on the nucleus. Russkikh *et al.*[3,7] reported that the formation of boron-chelate rings of 1,4-dihydroxy-, 1-amino-4-hydroxy-, and 1,4-diaminoanthraquinones increases the electrophilicity of the

Table 3. Effect of the molar ratio of cobalt(II) chloride on the butylamination of **1**[a]

Run	$CoCl_2$/**1**[b]	Time (h)	Recovered (%)[c] **1**	Yield(%)[c] **2a**[d]	Yield(%)[c] **2a**[e]
15	0.1	8	86.6	6.5	64.5
16	0.1	24	78.6	9.2	91.8
17	0.5	8	32.6	32.3	64.6
18	1.0	6	0	62.6	62.6
19	1.0[f]	6	92.3	2.9	2.9
20	2.0	5	0	54.1	—

a) The reactant, **1** (4.5 mmol), was stirred with butylamine (15 ml) and $CoCl_2$ at 30 °C in the presence of air. b) Molar ratio. c) Determined by means of a TLC-scanner. d) Yield based on the **1** used. e) Yield based on the $CoCl_2$ used. f) Reaction carried out under a nitrogen atmosphere.

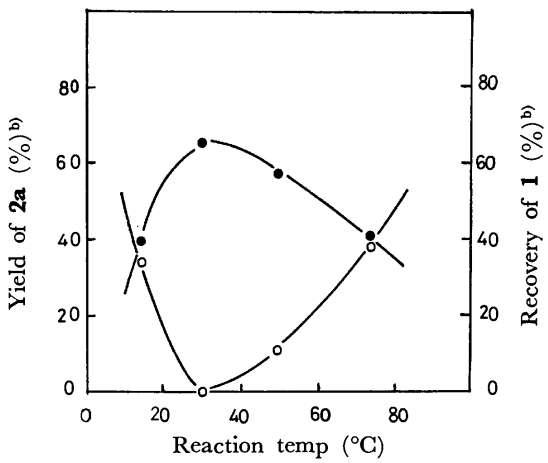

Fig. 1. Effect of reaction temperature on the butylamination of 1-aminoanthraquinone(**1**).[a]
○: 1-Aminoanthraquinone(**1**), ●: 1-Amino-4-butylaminoanthraquinone(**2a**). a) Reactant **1** (4.5 mmol) was stirred with butylamine (15 ml) and $CoCl_2$ (4.5 mol) for 6 h. b) Determined by means of a TLC-scanner.

substituted anthraquinone nucleus and facilitates the direct amination at the 2-position of these compounds.

The preferential substitution of the amino group at the 4-position, but not at the 2-position, seems to be caused by the fact that the formation of hydrogen-bonding between the *N*-hydrogen atom and the oxygen

atom of the carbonyl group stabilizes the adduct (**4**). A similar role of hydrogen-bonding has also been inferred in previous reports.[8] The oxidative abstraction of the hydride anion from the adduct (**5**) by atmospheric oxygen is proposed from the experimental results. The final step of acid hydrolysis of **6** gives rise to **2**. The details of the reaction mechanism for each step are still not clear, however, and are under investigation.

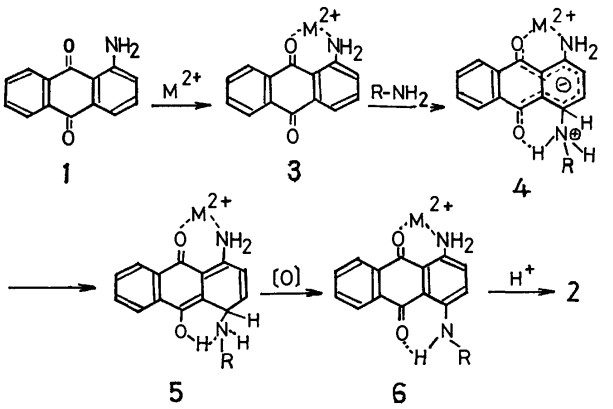

Scheme 1.

Experimental

All the melting points are uncorrected. The visible spectra were measured using a Hitachi EPS-3T spectrometer. The ^{1}H NMR spectra were taken on a JEOL Model MH-100 spectrometer, with TMS as the internal standard. The elemental analyses were recorded on a Yanaco CHN recorder MT-2. Column chromatography was carried out on activated alumina (Sumitomo KCG-30), using xylene as the eluent. Thin-layer chromatography was performed on silica gel (Merck Kieselgel 60) using the following solvent system (volume ratio); System A (benzene), and System B (cyclohexane: acetone: ethyl acetate=13:1:1). The resulting thin-layer chromatograms were measured on a chromatoscanner(Shimadzu CS-900). The yields were determined on the basis of measurements made using calibrations with standard solutions of the pure compounds.

Materials. The 1-aminoanthraquinone was supplied by the Mitsubishi Chemical Industry, Inc., and was purified by column chromatography, followed by recrystallization from xylene. 1,4-Diaminoanthraquinone (Mitsui Toatsu Chemicals), used as an authentic sample, was purified by column chromatography and subsequent recrystallization from ethanol. All the metal salts were reagent-grade and were used without further purification. The amines and solvents were purified by the ordinary methods.

Reaction of 1 with Butylamine. The general procedure was as follows. A mixture of **1**, metal salt, butylamine, and 1-butanol was stirred in a open flask (see Tables 1, 2, and 3, and Fig. 1). The mixture was then poured into a cold 3.0% hydrochloric acid solution, and the separated products were filtered, washed with water, and dried. The R_f values of the components were as follows:

1: R_f 0.43 (System A), R_f 0.26 (System B)
2a: R_f 0.26 (System A), R_f 0.20 (System B)
2b: R_f 0.10 (System A), R_f 0.05 (System B).

The yields were determined by means of a TLC-scanner or after isolation by column chromatography.

2a: λ max (Methanol) 617 (ε 17300), 573 (ε 15200); mp 140—141 °C (lit,[9] 142.6—143.1 °C(cor)); Found: C, 73.06; H, 6.14; N, 9.51%. Calcd for $C_{18}H_{18}N_2O_2$: C, 73.45; H, 6.16; N, 9.52%. PMR ($CDCl_3$): δ=0.98 (3H, t, $-CH_3$), 1.2—2.0 (4H, m, $-(CH_2)_2-$), 3.36 (2H, q, NH–CH_2-), 6.9—7.3 (4H, m, $H^{2,3}$, and NH_2), 7.72 (2H, m, $H^{6,7}$), 8.36 (2H, m, $H^{5,8}$), 10.68 (1H, broad, NH–Bu).

Compound (**2b**) was identified with the authentic sample.

Reaction of Anthraquinone (7) with Butylamine. A mixture of **7** (4.5 mmol), $CoCl_2$ (4.5 mmol), butylamine (15 ml), and 1-butanol (5 ml) was stirred under reflux for 8 h. The subsequent procedures were the same as those in the case of **1**. Reactant **7** was recovered in a 99% yield.

Reaction of 2-Aminoanthraquinone (8) with Butylamine. A mixture of **8** (4.5 mmol), $CoCl_2$ (4.5 mmol), butylamine (15 ml), and 1-butanol (5 ml) was stirred under reflux for 8 h. The reactant, **8**, was recovered quantitatively.

Reaction of 1-Methylamino-(9) or 1-Butylamino-anthraquinone (10) with Butylamine. A mixture of the reactant (4.5 mmol), metal salt (4.5 mmol), butylamine (15 ml), and 1-butanol (5 ml) was stirred under reflux for 8 h. After the solvent and the excess amine had been distilled off under reduced pressure, the mixture was poured into a cold 3.0% hydrochloric acid solution. The separated precipitate was filtered, washed with water, and dried. The crude product was extracted with xylene and separated by column chromatography. The results are shown in Table 4.

Table 4.

Reactant	Metal salt	Recovered(%) Reactant	Yield(%) 1,4-(R-NH)$_2$-AQ
9	$Cu(OCOCH_3)_2$	80	2.0[a]
10	$Cu(OCOCH_3)_2$	65	1.7[b]
9	$CoCl_2$	96	0
10	$CoCl_2$	100	0

a) 1-Butylamino-4-methylaminoanthraquinone. b) 1,4-Bis(butylamino)anthraquinone.

The authors wish to thank Miss Noriko Yamanari, Miss Yumiko Shiga, and Mr. Junichi Tagashira for their assistance in carrying out some of the experiments.

References

1) The Ullmann amination of halogenoanthraquinones using copper salts as a catalyst is a well-known industrial method of preparing intermediates and dyestuffs in the anthraquinone series.

2) A. C. Robson and S. Coffey, *J. Chem. Soc.*, **1954**, 2372.

3) V. V. Russkikh, S. A. Russkikh, and E. P. Fokin, *J. Org. Chem. USSR.*, **76**, 2502 (1971).

4) a) K. Yoshida, M. Matsuoka, T. Ueyama, Y. Yamashita, and T. Kitao, *Chem. Lett.*, **1978**, 765; b) K. Yoshida, M. Matsuoka, Y. Yamashita, and T. Kitao, *ibid.*, **1978**, 1317; c) M. Matsuoka, Y. Makino, K. Yoshida, and T. Kitao, *ibid.*, **1979**, 219; d) M. Matsuoka, Y. Makino, K. Yoshida, and T. Kitao, *ibid.*, **1979**, 1347.

5) When a mixture of **2a** (0.5 g), $CoCl_2$ (0.22 g) and 1-butanol was heated under reflux for 16 h, the dealkylation of **2a** was observed and **2b** (32 mg) was obtained, together with the **2a** (0.35 g) recovered.

6) W. Bradley and E. Leete, *J. Chem. Soc.*, **1951**, 2147; W. Bradley and R. F. Maisey, *ibid.*, **1954**, 247; W. M. Lord and A. T. Peters, *J. Chem. Soc., C*, **1968**, 783.

7) S. A. Russkikh, V. A. Loskutov, and V. V. Russkikh, *J. Gen. Chem. USSR.*, **44**, 612 (1974).

8) J. H. Gorvin and D. P. Whalley, *J. Chem. Soc., Perkin Trans. 1*, **1979**, 1364; C C. F. Bernasconi and R. H. de Rossi, *J. Org. Chem.*, **41**, 44 (1976).

9) S. Arai, T. Yamagishi, S. Ototake, and M. Hida, *Bull. Chem. Soc. Jpn.*, **50**, 547 (1977).

 © 1980 The Chemical Society of Japan Bull. Chem. Soc. Jpn., 53, 2555—2565 (1980)

Studies of Unusual Amino Acids and Their Peptides. XII. The Chemistry of *N*-(Carboxymethyl)amino Acids. I. The Preparation, Properties, and Characterization of *N*-(Carboxymethyl)amino Acids and Their Esters

Toshifumi Miyazawa

Department of Chemistry, Faculty of Science, Kōnan University, Okamoto, Higashinada-ku, Kobe 658

(Received November 16, 1979)

N-Carboxymethyl(Cm-)amino acids and their mono- and diesters were prepared by several routes, and their physical and chiroptical properties were compared with those of the parent amino acids and their esters. The isolation procedure was improved for the preparation of the free Cm-amino acids obtained from the corresponding amino acids and bromoacetic acid; the aimed-at compounds were also obtained by the catalytic hydrogenolysis of the dibenzyl esters. The isomeric pairs of monoalkyl esters of Cm-amino acids were similarly accessible via the benzyl alkyl esters. The diesters proved to be suitable for the GLC and MS analyses of Cm-amino acids. All the free Cm-L-amino acids and the dicyclohexylammonium salts of their *N*-ethylthiocarbonothioyl derivatives show positive Cotton effects at 200—225 nm and at 335—350 nm respectively in CD measurements; therefore, these correlations can be used for the configurational assignments of Cm-amino acids.

Up to the present, various kinds of unusual amino acids have been found in nature. Among them there is a group which can be represented by the general formula **1**. Some typical examples of such amino

acids are octopine ($R=CH_3$, $R'=(CH_2)_3NHC(=NH)NH_2$),[1] lysopine ($R=CH_3$, $R'=(CH_2)_4NH_2$),[2] and nopaline ($R=(CH_2)_2CO_2H$, $R'=(CH_2)_3NHC(=NH)NH_2$).[3] The importance of this group seems to have been becoming increasingly great, for the occurrence of *N*-carboxymethyl(Cm-)amino acids (**2**), simple-structured members of this group, has recently been reported.

Cm-*t*-leucine[4] has been found in a peptide antibiotic, bottromycin A_2, and Cm-alanine has been isolated from an extract of *Strombus gigas* as a fish attractant and designated as strombine.[5]

Unfortunately, though synthetic Cm-amino acids have been referred to in the literature, with regard to their physical properties and chemical behavior little has yet been investigated systematically, except for their coordination chemistry.[6] For some of the synthetic Cm-amino acids even their melting points and/or optical rotations remain undetermined. In particular, nothing is known about the chemistry of peptides containing Cm-amino acids. In connection with the synthetic work of bottromycin[7] the present author felt an interest in this kind of unusual amino acids and started a systematic investigation of them.

Preparation of Cm-amino Acids and Their Esters. The Cm-amino acids[8] listed in Table 1 were prepared by condensing the corresponding amino acids with bromoacetic acid according to the method of Snyder and Angelici.[6a] Even after 4 h, the consumption of the starting amino acid was always incomplete, as determined by following its ninhydrin reaction;[14] nevertheless, an appreciable amount of the *N,N*-biscarboxymethylated derivative was produced in some cases. For the isolation of the Cm-amino acid from the reaction mixture, ion-exchange chromatography, recommended by the above authors, was useful, but elution with aq ammonia did not always give a satisfactory separation. In general, water proved to be a better eluent; through a short column of cation-exchange resin the *N,N*-biscarboxymethylated amino acid was eluted first, and the Cm-amino acid next, while the unchanged amino acid was usually immobile. The rate of elution was quite fast for such Cm-amino acids as Cm-alanine, Cm-aspartic acid, Cm-proline, and Cm-serine. On the other hand, such Cm-amino acids with a low solubility as Cm-phenylalanine and Cm-*t*-leucine could be purified merely by recrystallizing the crude products from water.

As alternative routes[15] to the aimed-at compounds the following reactions were also attempted: the condensations of (i) an amino acid with a haloacetic ester, (ii) an amino ester with a haloacetic acid, and (iii) an amino ester with a haloacetic ester. Though the resulting esters must be hydrolyzed (or hydrogenolyzed) to obtain free Cm-amino acids, they can be used as intermediates for peptide synthesis. Especially by Method (iii) it is possible to prepare derivatives of a Cm-amino acid carrying selectively removable *C*-protecting groups.

However, Methods (i) and (ii) were of no practical use, because of the low rates of conversion, probably because of the heterogeneity of the reaction (Method (i)), or because of the difficulty in the isolation of the desired products (Methods (i) and (ii)). On the other hand, Method (iii) always gave a satisfactory result. In this method, the formation of the *N,N*-biscarboxymethylated derivative was not observed. After the crude mixture had been washed with aq citric acid to remove the unchanged amino ester, it was further purified by extracting in acid. If the product obtained here was not pure enough, it was necessary to resort to column or thin-layer chromatography. The dimethyl or diethyl esters were also accessible from the free Cm-amino acids by the usual method. The diesters (**3**) of Cm-amino acids thus obtained are listed in Table 2.

TABLE 1. *N*-(CARBOXYMETHYL)AMINO ACIDS (**2**)

Compound	Yield (%)	Mp[1] (°C)	$[\alpha]_D^{25}$ (*c* 1.0)		^{1}H-NMR, δ (-NHC$\underline{H}_2$CO-)[q]	Elemental analysis Found (Calcd)		
			H_2O	1 M HCl		C%	H%	N%
L-CmAbu	65	205.5—207 (A)	+14.5°	+9.8°	E 4.36 F 3.22	44.94 (44.71	7.04 6.88	8.81 8.69)
L-CmAla[a]	66	203.5—204(dec) (B)	+6.3°	+3.7°	E 4.34 F 3.65	40.81 (40.81	6.23 6.17	9.66 9.52)
L-CmAsp[b]	44	185—186(dec) (A)	+11.8°	+15.6°	E 4.49 F 3.38	37.60 (37.70	4.58 4.75	7.16 7.33)
L-CmIle[c]	49	189—189.5(dec) (C)	+16.0° [j]	+13.9°	E 4.31 F 3.05	50.62 (50.78	7.99 7.99	7.12 7.40)
L-CmLeu[d]	44	200.5—201.5(dec) (A)	+10.3°	+12.5° [n]	E 4.35 F 3.07	50.53 (50.78	8.17 7.99	7.55 7.40)
L-CmLys(Tos)	66	171—172.5(dec) (A)	—[k]	+14.6°	E 4.38 F 3.08	50.22 (50.27	6.23 6.19	7.82 7.82)
L-CmPhe[e]	72	223—223.5(dec) (A)	—[k]	+15.7°	E 4.24 F 3.29	58.94 (59.18	5.98 5.87	6.19 6.28)
D-CmPhg	51	227—229(dec) (A)	—[k]	−149.0° [o]	E 4.16 F 3.05	57.29 (57.41	5.03 5.30	6.52 6.70)
L-CmPro[f]	37	217.5—219.5(dec) (D)	−59.9°	−58.2°	E 4.46 F 2.91 and 3.32[r]	48.81 (48.55	6.48 6.40	8.21 8.09)
L-CmSer[g]	22	178—182(dec) (A)	+0.5°	+5.4°	E 4.55 F 3.15	36.63 (36.81	5.45 5.56	8.87 8.59)
L-CmThr	34	165.5—168.5(dec) (A)	−26.7°	−27.8°	E 4.51 F 3.12	40.38 (40.68	6.10 6.26	7.61 7.91)
L-CmTle	75	247—250(dec) (A)	−14.2° [l]	−23.3°	E 4.33[s] F 3.32 and 3.44[t]	50.83 (50.78	8.03 7.99	7.66 7.40)
DL-CmTle	71	227—229(dec) (A)				50.68 (50.78	8.11 7.99	7.36 7.40)
L-CmTyr[h]	30	243.5—245.5(dec) (A)	—[k]	+14.5° [p]	E 4.27 F 3.05	55.08 (55.23	5.36 5.48	5.58 5.86)
L-CmVal	64	212—213(dec) (C)	+6.8° [m]	+1.8°	E 4.32 F 3.51 and 3.56[r]	47.75 (47.99	7.65 7.48	7.71 8.00)

a) Lit,[9] mp 220 °C. b) Lit,[10] mp 198—199 °C, $[\alpha]_D^{27}$ +4.1° (H_2O), $[\alpha]_D^{27}$ +11° (1 M HCl). c) Lit,[11] mp 197—198 °C. d) Lit,[12] mp 201 °C (dec), $[\alpha]_D^{24}$ +8.42° (*c* 0.95, 0.2 M HCl). e) Lit,[12] mp 243 °C, $[\alpha]_D^{25}$ +15.67° (*c* 1.85, 1 M HCl); lit,[10] mp 228—233 °C (dec). f) Lit,[10] mp 220 °C (dec). g) Lit,[13] mp 167 °C, $[\alpha]_{578}$ +3° (*c* 2.2, H_2O). h) Lit,[12] mp 247 °C (dec), $[\alpha]_D^{25}$ +10.11° (*c* 0.89, 0.2 M HCl). i) Solvents for recrystallization: A, H_2O; B, aq EtOH; C, aq acetone; D, aq *i*-PrOH. j) *c* 0.77. k) Insufficiently soluble; not measured. l) *c* 0.54. m) *c* 0.80. n) $[\alpha]_D^{24}$ +11.4° (*c* 0.95, 0.2 M HCl). o) *c* 0.52. p) $[\alpha]_D^{25}$ +14.6° (*c* 0.89, 0.2 M HCl). q) E, in TFA; F, in D_2O-NaOD (pH 12). r) ABq, J=15 Hz. s) Broad. t) ABq, J=16 Hz.

To obtain a free Cm-amino acid, the diester was heated in 6 M HCl (1 M=1 mol dm^{-3}) at 110 °C for *ca.* 15 h. Even on heating with a more dilute acid or with 6 M HCl for a few hours, the diester disappeared completely, but there remained an appreciable amount of the monoester(s). Under these conditions, the formation of neither glycine nor the other amino acid was observed.[16] The rate of the acidic hydrolysis of a benzyl ester, especially of a dibenzyl ester, was quite slow compared with that of a dimethyl (or diethyl) ester.

On the other hand, its debenzylation by catalytic hydrogenolysis proceeded quite smoothly; thus, the Cm-amino acid was obtained from the corresponding dibenzyl ester in a good yield. Similarly, the monoalkyl esters (**4** and **5**) of Cm-amino acids were obtained from the corresponding benzyl alkyl esters, which are listed in Table 3. In the preparation of **5b**, the crude benzyl ethyl ester (**3f**), contaminated by benzyl valinate, was also used, because the desired compound could easily be separated from the reduction mixture. This is not the case with its isomer (**4b**).

Properties of Cm-amino Acids and Their Esters. As can be seen from Table 1, the melting (or decomposition) point of a Cm-amino acid is much lower than that of the parent amino acid. The optical rotation of a sample of Cm-phenylalanine prepared by the condensation of phenylalanine with bromoacetic acid was in good agreement with that of a different sample prepared by the hydrogenolysis of the dibenzyl ester (**3o**) or by the acidic hydrolysis of the dimethyl ester (**3l**), obtained by the condensation of a phenylalanine ester with a bromoacetic ester (see Experimental). The coincidence of the optical rotations of the Cm-amino acid prepared in these different ways apparently means that little or no racemization occurred during

Table 2. Diesters (3) of Cm-L-amino acids

Compound	Yield (%)	n_D^t (t, °C)	IR (cm^{-1})[b] ν_{NH} / $\nu_{C=O}$	^{1}H-NMR, δ[c]	Salt[d]	Mp[e] (°C)	$[\alpha]_D^{25}$ (c 1.0, MeOH)	Elemental analysis (%) Found	Calcd
OMe CmVal-OMe (**3a**)	58[a]	1.4410 (21)	3310 1743	0.96(6H, d, J=6.5 Hz), 1.97(1H, m), 2.09(1H, s), 3.04(1H, d, J=5.5 Hz), 3.35(2H, s), 3.69(6H, s)	**t**	123—125 (A)	+3.5°	C: 51.25 H: 6.78 N: 3.72	51.19 6.71 3.73
OEt CmVal-OEt (**3b**)	85	1.4330 (24)	3320 1736	0.96(6H, d, J=6.5 Hz), 1.26(6H, t, J=7 Hz), 1.98(1H, m), 2.02(1H, s), 3.02(1H, d, J=5.5 Hz), 3.33(2H, s), 4.17(4H, q)	**p**	120—121 (B)	+1.6°	C: 50.74 H: 5.83 N: 14.26	50.91 5.90 14.13
OBzl CmVal-OMe (**3c**)	75	1.4902 (24)	3310 1740	0.96(6H, d, J=6.5 Hz), 1.97(1H, m), 2.02 (1H, s), 3.05(1H, d, J=5.5 Hz), 3.40(2H, s), 3.68(3H, s), 5.12(2H, s), 7.31(5H, s)	**p**	150—151 (B)	+2.0°	C: 55.20 H: 5.58 N: 12.86	55.25 5.38 12.88
OMe CmVal-OBzl (**3d**)	62	1.4802 (24)	3330 1737	0.95(6H, d, J=6.5 Hz), 2.00(1H, m), 2.05 (1H, s), 3.07(1H, d, J=6 Hz), 3.35 (2H, s), 3.67(3H, s), 5.13(2H, s), 7.31(5H, s)	**p**	119—120 (B)	−12.3°	C: 55.13 H: 5.56 N: 12.87	55.25 5.38 12.88
OBzl CmVal-OEt (**3e**)	76	1.4849 (25)	3300 1737	0.97(6H, d, J=6.5 Hz), 1.26(3H, t, J=7 Hz), 1.98(1H, m), 2.14(1H, s), 3.05(1H, d, J=5.5 Hz), 3.42(2H, s), 4.17(2H, q, J=7 Hz), 5.13 (2H, s), 7.31(5H, s)	**t**	87.5—89 (C)	−12.4°[f]	C: 59.03 H: 6.65 N: 2.81	59.34 6.71 3.01
OEt CmVal-OBzl (**3f**)	61	1.4864 (26)	3330 1732	0.94(6H, d, J=6.5 Hz), 1.23(3H, t, J=7 Hz), 2.00(1H, m), 2.11(1H, s), 3.08(1H, d, J=6 Hz), 3.33(2H, s), 4.14(2H, q, J=7 Hz), 5.13 (2H, s), 7.31(5H, s)	**t**	117—118.5 (C)	−21.1°[f]	C: 59.09 H: 6.83 N: 2.93	59.34 6.71 3.01
OBzl CmVal-OBzl (**3g**)	72	1.5329 (19)	3320 1732	0.93(6H, d, J=6.5 Hz), 1.97(1H, m), 2.04 (1H, s), 3.07(1H, d, J=6 Hz), 3.39(2H, s), 5.10(4H, s), 7.28(10H, s)	**p**	114.5—116 (B)	−8.2°	C: 60.13 H: 5.32 N: 11.36	60.09 5.37 11.30
OBu^t CmVal-OMe (**3h**)	62	1.4410 (20)	3320 1738	0.97(6H, d, J=6.5 Hz), 1.44(9H, s), 1.97 (1H, m), 2.02(1H, s), 3.02(1H, d, J=5.5 Hz), 3.23(2H, s), 3.68(3H, s)	**p**	153—153.5 (B)	+3.8°	C: 51.75 H: 6.27 N: 13.71	51.86 6.13 13.75
OMe CmAla-OMe (**3i**)	67[a]	1.4292 (31)	3310 1735	1.33(3H, d, J=6.5 Hz), 2.11(1H, s), 3.40 (2H, s), 3.40(1H, q, J=6.5 Hz), 3.69(6H, s)	**p**	134.5 —135.5 (B)	+9.5°	C: 46.56 H: 4.83 N: 15.75	46.47 4.82 15.94

Table 2. (Continued)

Compound	Yield (%)	n_D^t (t, °C)	IR (cm^{-1})[b] ν_{NH} $\nu_{C=O}$	^{1}H-NMR, δ[c]	Salt[d]	Mp[e] (°C)	$[\alpha]_D^{25}$ (c 1.0, MeOH)	Elemental analysis (%) Found	Calcd
OBzl CmAla-OMe (**3j**)	63	1.5035 (25)	3320 1739	1.31(3H, d, J=7 Hz), 2.17(1H, s), 3.40(1H, q, J=7 Hz), 3.43(2H, s), 3.66(3H, s), 5.11 (2H, s), 7.29(5H, s)	**t**	156—157 (B)	−1.2°	C: 56.66 H: 5.91 N: 3.04	56.73 5.95 3.31
OMe CmAla-OBzl (**3k**)	64	1.5015 (25)	3290 1745	1.33(3H, d, J=7 Hz), 2.14(1H, s), 3.39(2H, s), 3.43(1H, q, J=7 Hz), 3.66(3H, s), 5.12 (2H, s), 7.30(5H, s)	**t**	159—161 (D)	−9.2°	C: 56.98 H: 6.06 N: 3.29	56.73 5.95 3.31
OMe CmPhe-OMe (**3l**)	84[a]	1.5009 (27)	3320 1741	2.06(1H, s), 2.88—3.00(2H, three peaks, J_{vic}=6 Hz and 7 Hz), 3.33(2H, s), 3.45, (1H, o), 3.60 and 3.61(6H, each s), 7.18 (5H, s)	**t**	108—108.5 (A)	+21.8°	C: 56.59 H: 6.07 N: 3.25	56.73 5.95 3.31
OBzl CmPhe-OMe (**3m**)	57	1.5426 (26)	3320 1740	2.09(1H, s), 2.91—3.02(2H, three peaks, J_{vic}=6 Hz and 7 Hz), 3.36(2H, s), 3.45 (1H, o), 3.55(3H, s), 5.05(2H, s), 7.16 (5H, s), 7.25(5H, s)	**t**	147.5—149 (A)	+18.3°	C: 62.47 H: 5.77 N: 2.65	62.51 5.85 2.80
OMe CmPhe-OBzl (**3n**)	66	1.5173 (29)	3330 1736	2.10(1H, s), 2.96(2H, d-like, $J\fallingdotseq$6.5 Hz), 3.34(2H, s), 3.50(1H, o), 3.60(3H, s), 5.04(2H, s), 7.14(5H, s), 7.22(5H, s)	**p**	149.5 —150.5 (B)	+7.1°	C: 58.88 H: 5.12 N: 11.79	58.88 4.94 11.84
OBzl CmPhe-OBzl (**3o**)	65	1.5587 (27)	3330 1737	2.24(1H, s), 2.95(2H, d-like, $J\fallingdotseq$7 Hz), 3.37 (2H, s), 3.61(1H, t-like, $J\fallingdotseq$7 Hz), 5.00 and 5.04(4H, each s), 7.12—7.24(15H, m)	**t**	123.5 —124.5 (A)	+5.2°	C: 66.74 H: 5.87 N: 2.23	66.77 5.78 2.43
OMe CmLeu-OBzl (**3p**)	56	1.4861 (28)	3310 1738	0.91(6H, bd, J=5.5 Hz), around 1.55(3H, m), 2.02(1H, s), 3.36(1H, o), 3.36(2H, s) 3.65 (3H, s), 5.12(2H, s), 7.30(5H, s)	**p**	114—116 (B)	−4.6°	C: 55.81 H: 5.79 N: 12.36	56.01 5.60 12.56
OBzl CmLeu-OBzl (**3q**)	62	1.5183 (30)	3320 1730	0.88(6H, bd, J=5.5 Hz), around 1.55(3H, m), 1.97(1H, s), 3.35(1H, o), 3.39(2H, s), 5.09 (4H, s), 7.26(10H, s)	**t**	132—133.5 (D)	−3.5°	C: 64.30 H: 6.53 N: 2.70	64.31 6.51 2.59

a) By the direct esterification of Cm-amino acids. b) Neat. c) In $CDCl_3$. The signal attributable to -NHC$\underline{H_2}$CO- is underlined. d) **t**: p-toluenesulfonate; **p**: picrolonate. e) Solvents for recrystallization: A, AcOEt; B, EtOH; C, AcOEt-petroleum ether; D, EtOH-Et_2O. f) c 1.0, AcOEt.

Table 3. Monoesters (**4** and **5**) of Cm-L-amino acids

Compound	Yield (%)	Mp[b] (°C)	$[\alpha]_D^{25}$ (c 1.0)[c]	TLC, R_f[e]	^{1}H-NMR, δ[f]	Elemental analysis (%) Found	Calcd
OH CmVal-OMe (**4a**)	42	139—140	A −0.9° B −2.7°	C 0.18 D 0.54 E 0.52	1.07(3H, d, J=6.5 Hz), 1.09(3H, d, J=6.5 Hz), 2.42(1H, m), 3.64 and 3.66 (2H, each s-like), 3.85(3H, s), 4.06(1H, d, J=4 Hz)	C: 50.62 H: 8.17 N: 7.42	50.78 7.99 7.40
OMe CmVal-OH (**5a**)	51	170—171	A −1.5° B +1.2°	C 0.15 D 0.47 E 0.53	1.06(6H, d, J=7 Hz), 2.31(1H, m), 3.58(1H, d, J=4.5 Hz), 3.81(3H, s), 4.00(2H, s)	C: 51.01 H: 8.21 N: 7.69	50.78 7.99 7.40
OH CmVal-OEt (**4b**)	81	149—150	A −7.2° B −9.2°	C 0.23 D 0.56 E 0.69	0.92(3H, d, J=7 Hz), 0.95(3H, d, J=7 Hz), 1.27 (3H, t, J=7 Hz), 1.90(1H, m), 3.08(2H, s), 3.15(1H, d, J=5 Hz), 4.20(2H, q, J=7 Hz)	C: 52.97 H: 8.66 N: 6.62	53.19 8.43 6.89
OEt CmVal-OH (**5b**)	68[a]	167—168	A +1.2° B +0.6°	C 0.27 D 0.54 E 0.71	0.91(6H, d, J=6.5 Hz), 1.23(3H, t, J=7 Hz), 1.85(1H, m), 2.81(1H, d, J=5.5 Hz), 3.33(2H, s), 4.17(2H, q, J=7 Hz)	C: 53.02 H: 8.48 N: 6.92	53.19 8.43 6.89
OH CmAla-OMe (**4c**)	82	167—169	A −2.4° B −3.6°	C 0.07 D 0.38 E 0.19	1.28(3H, d, J=7 Hz), 3.12(2H, s), 3.45(1H, q, J=7 Hz), 3.71(3H, s)	C: 44.48 H: 6.85 N: 8.65	44.71 6.88 8.69
OMe CmAla-OH (**5c**)	79	186—189	A +1.4° B +1.8°	C 0.06 D 0.36 E 0.17	1.29(3H, d, J=7 Hz), 3.31(1H, q, J=7 Hz), 3.56(2H, s), 3.74(3H, s)	C: 44.61 H: 6.97 N: 8.63	44.71 6.88 8.69
OH CmPhe-OMe (**4d**)	82	157.5—159	A +15.8° B +17.2°	C 0.28 D 0.57 E 0.72	2.91—3.03(2H, three peaks, J_{vic}=6 Hz and 7 Hz), 3.11(2H, s), 3.60(3H, s), 3.64(1H, o), 7.27(5H, s)	C: 60.82 H: 6.38 N: 6.03	60.75 6.37 5.90
OMe CmPhe-OH (**5d**)	80	207—209 (dec)	A —[d] B +15.4°	C 0.24 D 0.56 E 0.67	2.84—2.97(2H, three peaks, J_{vic}=6 Hz and 8 Hz), 3.35(2H, s), 3.37(1H, o), 3.69(3H, s), 7.29(5H, s)	C: 60.74 H: 6.39 N: 6.05	60.75 6.37 5.90

a) Based on H-L-Val-OBzl·TosOH. See Experimental. b) Solvent for recrystallization: EtOH. c) A, in H_2O; B, in 1 M HCl. d) Insufficiently soluble; not measured. e) C, on silica gel, n-BuOH-AcOH-H_2O (4:1:2); D, on silica gel, n-PrOH-H_2O (64:36); E, on cellulose, n-BuOH-AcOH-H_2O (4:1:2). f) In D_2O-K_2CO_3. The signal attributable to -NHC$\underline{H_2}$CO- is underlined.

the preparation by the former method.

The diesters of Cm-amino acids were oily substances with a low viscosity. They were far more stable than the free esters of the parent amino acids; they could be kept at room temperature for a week without any detectable change, though in a few months they had gradually changed into a solid mass.[17] The diesters formed crystalline substances with *p*-toluenesulfonic or picrolonic acid (Table 2). In general, the picrolonate crystallized more easily than the *p*-toluenesulfonate. These crystals were practically non-hygroscopic, and they could be stored for a long time.

Though the monoesters of Cm-amino acids have zwitter-ionic structures, they have low and sharp melting points and are highly soluble in hot ethanol.

Characterization of Cm-amino Acids and Their Esters. The detection of Cm-amino acids with ninhydrin was unsuccessful in most cases, while ninhydrin–formic acid[18] could generally be used for this purpose. The diesters of Cm-amino acids gave a distinct blue spot on a pink background when sprayed with cobalt(II) thiocyanate.[19] Such coloration was specific for the diesters, for neither the monoesters nor the Cm-amino acids themselves gave this coloration. In contrast to the free Cm-amino acids and the diesters, the monoesters gave a distinct coloration with ninhydrin. The initial color (on TLC) was purple for the monoesters (**4**), while it was yellow for the monoesters (**5**).

In general, a Cm-amino acid and the parent amino acid could not be satisfactorily separated by thin-layer or paper chromatography, while paper electrophoresis was useful for this purpose. The Cm-amino acid migrated a fairly long distance toward the anode in an acidic medium.

The ^{1}H-NMR spectrum of a Cm-amino acid showed a signal attributable to the methylene protons in the carboxymethyl group near δ 4.4 in trifluoroacetic acid (TFA) and near δ 3.2 in D_2O–NaOD. For Cm-proline, Cm-*t*-leucine, and Cm-valine, it appeared as an AB quartet with J=15—16 Hz in the latter solvent (Table 1).

The R_f value on TLC of the diester of a Cm-amino acid was much larger than that of the corresponding parent amino ester, so their separation was extremely easy.

It is worth noting that GLC (or even TLC) could be used to distinguish among various kinds of Cm-amino acid diesters, including the isomeric pairs (Table 4). Consequently, the diesters of Cm-amino acids seem to be an excellent derivative for the analysis of these amino acids by GLC; they were volatile and stable enough for the purpose.

The diesters of Cm-amino acids could also be well analyzed by mass spectrometry. For example, in the mass spectra of the isomeric benzyl ethyl esters (**3e** and **3f**) of Cm-valine, the benzyl fragment and the fragment resulting from the removal of the alkoxycarbonyl group of the valine moiety appeared strongly, as expected. The discrimination of the isomers was quite easy.

In the ^{1}H-NMR spectra of the isomeric pair of diesters (*e.g.*, **3e** and **3f**), there was a tendency for a signal attributable to the methylene protons in the benzyloxycarbonylmethyl group of one isomer (*e.g.*, **3e**) to appear in a slightly lower field than that in the methoxy- or ethoxycarbonylmethyl group of the other (*e.g.*, **3f**) (Table 2). On the other hand, the ^{13}C-NMR method proved to be ineffective for their discrimination.

TABLE 4. R_f AND t_R VALUES ON TLC AND GLC FOR THE DIESTERS OF Cm-L-VALINE

Compound	TLC, R_f[a]		GLC, t_R (min)[b]
	A	B	
3a	0.18	0.35	0.5
3b	0.26	0.46	0.8
3c	0.36	0.60	4.4
3d	0.34	0.61	4.2
3e	0.38	0.63	5.3
3f	0.33	0.56	4.9
3g	0.44	0.69	34.9

a) Solvent systems: A, benzene : AcOEt=9 : 1; B, $CHCl_3$: AcOEt=9 : 1. b) Column temp, 180 °C; injector temp, 250 °C; carrier gas, N_2 60 ml/min.

For the monoesters, though it was difficult to differentiate between a pair of isomers (*e.g.*, **4a** and **5a**) by TLC, they could clearly be distinguished by the difference in the chemical shifts in the ^{1}H-NMR of the methylene protons in the two types of carboxymethyl groups; a signal attributable to the methylene protons in the alkoxycarbonylmethyl group of one isomer (*e.g.*, **5a**) appeared in a lower field than that in the free carboxymethyl group of the other (*e.g.*, **4a**) (Table 3).

Configurational Assignments of Cm-amino Acids. The chiroptical behavior of α-amino acids has been widely used for their configurational assignments. Concerning the Cm-amino acids, however, no useful data are available for this purpose, except for a few reports on their metal complexes.[6c]

As can be seen from Table 1, the Clough-Lutz-Jirgensons rule[20] for α-amino acids could not be applied to the Cm-amino acids. This is also the case with the monoesters of Cm-amino acids listed in Table 3, though the absolute values of their optical rotations are generally small.

The ORD and CD techniques have been employed for the correlations of the configurations of α-amino acids,[21] and recently such methods have also been applied to *N*-methyl-[22] and *N*,*N*-dimethylamino acids.[23] Table 5 shows the ORD and CD data for Cm-L-amino acids and their monoesters, recorded in water and in a hydrochloric acid solution. Every aliphatic Cm-L-amino acid thus far examined shows one positive CD Cotton effect both in water (at 200—206 nm) and in an acidic solution (at 206—210 nm). The CD maxima appear at wavelengths approximately identical with those of the parent α-amino acids, but the intensities are somewhat enhanced. This is also the case with the wavelengths of the first extremum and the molecular rotations in ORD measurements. The relatively small changes on the carboxymethyla-

Table 5. ORD and CD data for Cm-L-amino acids and their monoesters[a]

Compound	ORD (H_2O)		CD (H_2O)		ORD (1 M HCl)		CD (1 M HCl)	
	λ(nm)	[ϕ]	λ(nm)	$\Delta\varepsilon$	λ(nm)	[ϕ]	λ(nm)	$\Delta\varepsilon$
CmAbu	221	+2350	202	+1.73	224	+2490	210	+1.61
CmAla	219	+1400	202	+1.26	226	+2000	208	+1.22
CmAsp	220	+2020	200	+1.62	224	+1870	206	+0.98
CmIle	219	+3260	200	+2.38	224	+4170	207	+2.38
CmLeu	220	+2760	202	+2.22	226	+2840	210	+1.85
CmPro	222	−240	206	+0.82	223	+220	208	+1.04
CmSer	221	+2000	200	+1.57	225	+2410	209	+1.63
CmThr	224	+1070	200	+1.37	227	+2190	210	+1.95
CmTle	223	+1810	200	+1.80	225	+2410	209	+1.84
CmVal	215	+3270	201	+2.21	225	+3680	207	+2.12
CmPhe[b]		—[d]		—[d]	226	+8530	216	+4.92
CmPhg[b,c]		—[d]		—[d]	225	+17900	216	+12.5
CmTyr[b]		—[d]		—[d]	234	+3540	226	+3.87
5a	214	+2080	199	+2.27	224	+1930	209	+1.86
5b	212	+3730	200	+2.28	224	+3210	210	+2.02
5c	213	+1670	202	+1.44	222	+1730	209	+1.24
5d[b]	224	+5140	215	+4.30	224	+9010	215	+5.41
4a	221	+3600	206	+2.21	220	+3490	208	+2.10
4b	221	+2850	207	+1.99	223	+3290	210	+2.16
4c	218	+2790	206	+1.24	221	+1600	207	+1.15
4d[b]	224	+6940	217	+4.40	224	+8380	215	+5.02

a) *c* 0.5—1, *l*=5 mm (ORD) or 1 mm (CD), unless otherwise noted. b) *c* 0.02—0.05, *l*=5 mm (ORD) or 1 mm (CD). c) The D-isomer was used for measurements. d) Insufficiently soluble; not measured.

tion of the amino group suggest the same transition, *i.e.*, the n→π^* transition of the carbonyl group, and a similar predominant conformation[24] may be responsible for the observed Cotton effect.

Similarly, the aromatic Cm-L-amino acids exhibit a positive CD band at 216 nm (Cm-phenylalanine and Cm-phenylglycine) or at 226 nm (Cm-tyrosine) in an acidic solution, the intensity being somewhat enhanced.[25]

Thus, the dominant positive Cotton effect generally observed between 200 and 225 nm can be utilized for the configurational assignments of Cm-amino acids.

Even when the carboxymethyl group is replaced by the methoxycarbonylmethyl or ethoxycarbonylmethyl group, the wavelength where the Cotton effect appears and its intensity are little affected either in water or in an acidic solution (*e.g.*, Cm-valine, **5a**, and **5b**) (Table 5). This result suggests that neither the electronic state nor the bulkiness of the carboxymethyl group has a profound influence on the predominant conformation of a Cm-amino acid.

In addition to the strong positive maximum at 210—218 nm, the CD spectra of the diesters of Cm-L-amino acids show a very weak negative band at 236—246 nm in 95% ethanol (Table 6); the occurrence of such a band has previously been reported on the free esters of some amino acids and interpreted in terms of the existence of an alternative conformation.[26] This band could not be observed in an aqueous solution of such Cm-amino acid esters as **4a** listed in Table 5.

For a preferable approach to the configurational assignments of amino acids, a number of their derivatives have been recommended which exhibit the Cotton effects at longer wavelengths. The *N*-ethylthiocarbonothioyl (ETCT) derivative of an α-amino acid has been used as one of the most suitable compounds for this purpose,[27] and this approach has recently been applied to β-amino acids also.[28] In the ETCT derivatives of these amino acids, the solvents influence the Cotton effects in a striking manner. Thus, in certain cases, the sign of the Cotton effect is inverted by changing the solvent.

The Cm-amino acids (except Cm-proline) listed in Table 1 were converted into the ETCT derivatives, and their Cotton effects examined in four different solvents (methanol, dioxane, chloroform, and benzene).

Table 6. CD data for the diesters of Cm-L-amino acids in 95% EtOH[a]

Compound				
	λ(nm)	$\Delta\varepsilon$	λ(nm)	$\Delta\varepsilon$
3a	215	+1.18	243	−0.08
3b	213	+1.27	242	−0.06
3c[b]	214	+2.46	242	−0.11
3d[b]	218	+1.44	244	−0.20
3h	212	+1.52	242	−0.14
3i	210	+0.73	236	−0.20
3l[b]	217	+3.32	246	−0.20

a) *c* 0.45—1, *l*=1 mm, unless otherwise noted. b) *c* 0.035—0.045, *l*=1 mm and 5 mm.

TABLE 7. ORD AND CD DATA FOR ETCT-Cm-L-AMINO ACIDS IN MeOH[a]

ETCT derivative of	ORD[b]		CD	
	λ(nm)	[φ]	λ(nm)	Δε
CmAbu	366	+1120	346	+0.93
CmAla	365	+2120	345	+1.41
CmAsp	364	+240	345	+0.21
CmIle	362	−2480	347	−0.47
CmLeu	367	+1900	347	+1.28
CmLys(Tos)	364	+1090	347	+0.90
CmPhe	374	−730	348	+0.29
CmPhg[c]	362	+5720	345	+2.63
CmSer	365	+3500	345	+2.29
CmThr	366	+3750	347	+1.95
CmTle	369	−3120	353	−1.38
CmTyr	376	−790[d]	350	+0.20
CmVal	366	−3320	348	−0.95

a) c 0.2—0.4, l=5 mm. b) 1st extremum. c) The D-isomer was used for measurements. d) Shoulder.

TABLE 8. EFFECTS OF SOLVENTS ON THE CD COTTON EFFECT OF ETCT-Cm-L-VALINE[a]

Solvent	λ(nm)	Δε
Methanol	348	−0.95
Ethanol	348	−0.77
Acetonitrile	346	−0.31
	378	+0.02
Acetone	348	−0.65
1,2-Dichloroethane	350	−0.60
Dichloromethane	351	−0.83
Chloroform	353	−1.42
Ethyl acetate	350	−0.72
Tetrahydrofuran	349	−0.85
Dioxane	352	−0.51
Diethyl ether	350	−0.69
Benzene	353	−1.25
Carbon tetrachloride	357	−1.81

a) c 0.25, l=5 mm.

The results obtained by measurement in methanol are summarized in Table 7. All the ETCT derivatives of Cm-L-amino acids show a CD maximum at 345—370 nm and the ORD first extremum at 360—380 nm in the above solvents, similarly to those of the parent α-amino acids. In contrast to the latter, however, the sign of the Cotton effect is independent of the solvents, though the intensity fluctuated somewhat depending on the solvents used. This is also the case with many more solvents of widely differing polarities, as is illustrated with ETCT-Cm-L-valine (Table 8). The Cotton effects of the ETCT derivatives of prolines, pipecolic acid, and *N*-methylalanine have been reported to be little influenced by solvents.[27] Consequently, the insusceptibility to solvent effects may be regarded as a feature common to the ETCT derivatives of imino acids. As can be seen from Table 8, there is a tendency for the CD maximum to be bathochromically shifted upon a decrease in the solvent polarity.

TABLE 9. EFFECTS OF ADDED AMINES ON THE CD COTTON EFFECT OF ETCT-Cm-L-VALINE IN $CHCl_3$[a]

Amine[b]		λ(nm)	Δε
N-Ethyldiisopropylamine	(10.4)	349	+1.68
N-Ethylmorpholine	(7.6)	352	+1.58
Triethylamine	(7.5)	350	+1.53
Dicyclohexylamine	(6.3)	349	+1.50
Tributylamine	(13.3)	351	+1.23
N-Ethylpiperidine	(8.6)	347	+1.01
Diisopropylamine	(13.7)	348	+0.63
Diethylamine	(14.4)	336	−0.56
None		353	−1.42
Ammonia		344	−1.99
Butylamine	(10.1)	344	−2.06
Piperidine	(9.2)	341	−2.34
Morpholine	(9.4)	343	−2.67
Isopropylamine	(10.3)	345	−2.72
Cyclohexylamine	(10.7)	344	−2.76
t-Butylamine	(7.3)	345	−3.19

a) c 0.38, l=2 mm. b) The number in the parentheses indicates the molar ratio of the amine to ETCT-L-CmVal.

TABLE 10. ORD AND CD DATA FOR ETCT-Cm-L-AMINO ACIDS IN THE PRESENCE OF DICYCLOHEXYLAMINE IN MeOH[a]

ETCT derivative of	ORD[b]		CD	
	λ(nm)	[φ]	λ(nm)	Δε
CmAbu	365	−48[c]	343	+0.15
CmAla	361	+480	340	+0.56
CmAsp	361	−170[c]	344	+0.01
CmIle	363	−680	341	+0.16
CmLeu	360	+320	339	+0.45
CmLys(Tos)	366	−73[c]	341	+0.16
CmPhe	365	−470	349	+0.22
CmSer	361	+300	341	+0.21
CmThr	363	+400	344	+0.65
CmTle	367	−850[c]	339	+0.32
CmVal	363	+71	340	+1.24

a) c 0.2—0.4, l=5 mm. b) 1st extremum. c) Shoulder.

This is also suggestive of the same transition as in the case of the ETCT derivative of the parent α-amino acid, *i.e.*, the $n \rightarrow \pi^*$ transition of the NCS_2 chromophore.[27]

Most of the ETCT derivatives of Cm-L-amino acids show a positive Cotton effect, while those of Cm-L-valine, Cm-L-isoleucine, and Cm-L-*t*-leucine show a negative one; there could be recognized no simple correlation between the sign of the Cotton effect and the configuration of the parent amino acid. In the case of the ETCT derivatives of α-amino acids[27] or β-amino acids,[28] an empirical rule correlating the sign of the Cotton effect with the configuration has been achieved through the salt formation with such a base as cyclohexylamine or dicyclohexylamine (DCHA). Table 9 shows the effects of added amines

on the Cotton effect of ETCT-Cm-L-valine. The effects are surprisingly great,[29] and some kinds of amines such as DCHA invert the sign of the Cotton effect. Therefore, the Cotton effect of all the ETCT derivatives were reexamined in the presence of three molar amounts of DCHA in the same four solvents as above. The results obtained by measurement in methanol are summarized in Table 10.

All the DCHA salts of ETCT-Cm-L-amino acids show a positive Cotton effect (with a CD maximum at 335—350 nm and the ORD first extremum at 360—370 nm) in all the solvents used, except in some cases where the insolubility of the salts made the measurements impossible. Therefore, the correlation observed here can also be used for the configurational assignments of Cm-amino acids.

Experimental

All the melting points are uncorrected. The optical rotations were measured with a JASCO DIP-4 polarimeter. The ^{1}H- and ^{13}C-NMR spectra were recorded on a Hitachi R-24B spectrometer and a JEOL JNM-PS-100 spectrometer respectively. The chemical shifts are given in δ values with respect to TMS or DSS as an internal standard. The IR spectra were recorded on a Hitachi EPI-S2 spectrophotometer, and the mass spectra (MS) on a JEOL-OIS instrument at an ionization energy of 75 eV. The ORD and CD measurements were carried out with a JASCO ORD/UV-5 spectropolarimeter with its CD attachment. The TLC and preparative TLC were performed on Merck Kieselgel 60 F_{254} and Kieselgel GF_{254} (Type 60) respectively. Merck Kieselgel 60 was used for column chromatography, and Amberlite CG-120 (Type I) in the H^+ form for ion-exchange chromatography. The GLC analyses were performed on a Hitachi 063 Gas Chromatograph equipped with a flame-ionization detector using a ϕ3 mm×1 m 10% SE-30 column. Paper electrophoresis was carried out on a Yanagimoto EC-10 instrument, using a buffer with this composition: pyridine:AcOH:H_2O=25:1:225 (pH 6.4).

Benzyl bromoacetate (bp 112.5—113 °C/3 mmHg)[30] and *t*-butyl bromoacetate (bp 73—75 °C/25—25.5 mmHg)[31] were prepared according to the literature. The optical rotations of the less common amino acids used here as starting materials are as follows: L-Abu,[32] $[\alpha]_D^{16}$ +20.8° (*c* 4.8, 6 M HCl); D-Phg,[33] $[\alpha]_D^{20}$ −111.1° (*c* 1.0, 1 M NaOH); L-Tle,[34] $[\alpha]_D^{26}$ +30.0° (*c* 1.0, AcOH).

General Procedure for the Preparation of N-*(Carboxymethyl)-amino Acids (2).* N-*Carboxymethyl-L-2-aminobutyric Acid (L-CmAbu)*: H-L-Abu-OH (2.23 g) was allowed to react with bromoacetic acid (3.01 g) at pH 11 and at *ca.* 50 °C according to the method of Snyder and Angelici.[6a] After 4 h the reaction mixture was neutralized with 6 M HCl to pH 7. Then the solution was concentrated to some extent, loaded onto a column of cation-exchange resin (ϕ 3 cm×13 cm), and eluted with water. The front of the zone containing the desired product had clearly been observed throughout the elution. The pH of the eluate first went steeply down to 1, then rose gradually near 7, became acidic again, and finally reached *ca.* 7. The second acidic eluate with pH 2—4 (1.8 l), which showed only one spot in the paper electrophoresis, was evaporated to dryness under reduced pressure; yield, 2.28 g (65%). Recrystallization from water afforded large plates; mp 205.5—207 °C, $[\alpha]_D^{25}$ +9.8° (*c* 1.0, 1 M HCl).

N-*Carboxymethyl-L-t-leucine (L-CmTle)*: H-L-Tle-OH (786 mg) was allowed to react with bromoacetic acid (840 mg) for 4 h in a manner similar to that described above. Then the reaction mixture was acidified with concd HCl to pH 2. The deposited crystals were collected, and the concentration of the filtrate afforded a second crop. They were combined and recrystallized from water to afford prisms; yield, 850 mg (75%); mp 247—250 °C (dec), $[\alpha]_D^{25}$ −23.3° (*c* 1.0, 1 M HCl). Paper-electrophoresis showed only one spot.

Cm-DL-*t*-leucine and Cm-L-phenylalanine were likewise prepared in this way.

Preparation of the Diesters (3) of N-*(Carboxymethyl)amino Acids.* To a stirred mixture of an amino ester *p*-toluenesulfonate (or hydrochloride) (10 mmol), and TEA (20 mmol) in dry THF (30 ml), we added, drop by drop, a solution of a bromoacetic ester (12 mmol) in dry THF (10 ml). Then the mixture was stirred for 4—7 d at room temperature, with an occasional filtration of the precipitates (TEA salts). After the solvent had been removed under reduced pressure, the residual syrup was distributed between AcOEt and water, and the organic layer was washed successively with water, 10% citric acid, and water. After the solvent had been removed under reduced pressure again, 4—6 M HCl was added to the residue and the resulting solution was washed with AcOEt.[35] The aqueous layer was basified with solid K_2CO_3, and the liberated oil was extracted into AcOEt. The extracts were combined, washed with water, and dried over Na_2SO_4. The subsequent removal of the solvent yielded a syrup, the purity of which was checked by TLC, GLC, or ^{1}H-NMR. If the product thus obtained was not pure enough, it was further purified by column chromatography or preparative TLC, as will be described in the examples below.

For characterization, the diester was converted into the crystalline derivatives, the *p*-toluenesulfonate and/or the picrolonate. Even when the *p*-toluenesulfonate was difficult to crystallize, the corresponding picrolonate easily became crystalline.

Some typical examples of the procedures for the isolation of the diesters will be given below.

Ethyl N-*Benzyloxycarbonylmethyl-L-valinate (3e)*: H-L-Val-OEt·TosOH (3.17 g) was allowed to react with benzyl bromoacetate for 7 d. After the work-up described above, a colorless liquid was obtained in a pure state; yield, 2.24 g (76%); n_D^{32} 1.4825, $[\alpha]_D^{25}$ −18.5° (*c* 1.0, MeOH). Found: C, 65.56; H, 7.71; N, 4.52%. Calcd for $C_{16}H_{23}NO_4$: C, 65.51; H, 7.90; N, 4.78%. *p*-Toluenesulfonate, mp 87.5—89 °C; picrolonate, mp 120—122 °C (from EtOH).

When the reaction mixture was heated under reflux for 40 h, a similar work-up yielded the diester (**3e**) in a little poorer yield (71%).

The free diester was recovered from the *p*-toluenesulfonate as follows. The salt was distributed between Et_2O (or AcOEt) and 10% K_2CO_3, and the organic layer was further washed with the alkali and water, and then dried over Na_2SO_4. The subsequent removal of the solvent, followed by the addition of $CHCl_3$ to the residue and its successive evaporation, gave the diester (**3e**); n_D^{25} 1.4849.

Methyl N-*Benzyloxycarbonylmethyl-L-phenylalaninate (3m)*: H-L-Phe-OMe·HCl (2.16 g) was allowed to react with benzyl bromoacetate for 4 d. After the work-up described above, the residual syrup (3.25 g) was chromatographed on a silica-gel column, using $CHCl_3$–AcOEt (9:1) as the eluent. The fractions which indicated coloration (on TLC) with $Co(SCN)_2$ and not with ninhydrin were collected and then evaporated under reduced pressure; yield, 1.86 g (57%). *p*-Toluenesulfonate, mp 147.5—149 °C; picrolonate, 168—169 °C (from EtOH).

Benzyl N-*Benzyloxycarbonylmethyl-*L*-phenylalaninate (**3o**)*: H–L-Phe–OBzl·TosOH (915 mg) was allowed to react with benzyl bromoacetate for 7 d. The syrup (752 mg) obtained by the work-up described above was chromatographed on preparative TLC, using benzene–AcOEt (9:1) as the developing solvent; yield, 563 mg (65%). *p*-Toluenesulfonate, mp 123.5—124.5 °C; picrolonate, mp 153—153.5 °C (from EtOH).

General Procedure for the Direct Esterification of N-*(Carboxymethyl)amino Acids. Methyl* N-*Methoxycarbonylmethyl-*L*-alaninate (**3i**)*: To a chilled solution of $SOCl_2$ (0.6 ml) in dry MeOH (5 ml), Cm-L-alanine (500 mg) was added, after which the mixture was stirred at room temperature for 2 d. After it had then been refluxed for 4 h, it was evaporated to dryness under reduced pressure. The residue was dissolved in water and basified with solid K_2CO_3 to pH 9; the mixture was extracted with AcOEt. The organic extracts were combined, washed with water, and dried over Na_2SO_4. The subsequent removal of the solvent afforded **3i** as a liquid in a pure state; yield, 397 mg (67%); $[\alpha]_D^{25}$ −24.4° (*c* 1.0, MeOH). Picrolonate, mp 134.5—135.5 °C.

Preparation of N-*(Carboxymethyl)amino Acids (**2**) via Their Diesters (**3**). N-Carboxymethyl-*L*-phenylalanine (L-CmPhe), a) by the Hydrogenolysis of the Dibenzyl Ester (**3o**)*: The dibenzyl ester (**3o**) (270 mg) was hydrogenolyzed in AcOH–H_2O (2:1) (30 ml) in the presence of 5% Pd–C (60 mg). After the absorption of hydrogen had ceased (*ca.* 2 h), the catalyst was filtered off and the filtrate was evaporated under reduced pressure, affording a white crystalline mass in a quantitative yield. It was then recrystallized from water; $[\alpha]_D^{25}$ +15.8° (*c* 1.0, 1 M HCl).

*b) By the Acidic Hydrolysis of the Dimethyl Ester (**3l**)*: The dimethyl ester (**3l**) (710 mg) was heated in 20% HCl (7 ml) at 100—110 °C. The progress of the hydrolysis was followed by TLC on cellulose or by circular paper chromatography. Within 2 h the spot due to the starting material disappeared, while those spots corresponding to the monoester(s) (**4d** and/or **5d**) and the desired compound appeared on the chromatograms. After *ca.* 10 h, the color of the former faded considerably, but it did not completely vanish even after a further 7 h. Even at this time, though, the formation of neither glycine nor phenylalanine could be detected. The reaction mixture was evaporated under reduced pressure. After the addition of water to the residue and its successive evaporation has been repeated, the residual solid mass was recrystallized from water; yield, 565 mg (90%); $[\alpha]_D^{25}$ +15.9° (*c* 1.0, 1 M HCl).

*General Procedure for the Preparation of the Monoesters (**4** and **5**) of* N-*(Carboxymethyl)amino Acids. Methyl* N-*Carboxymethyl-*L*-phenylalaninate (**4d**)*: The benzyl methyl ester (**3m**) (290 mg) was hydrogenolyzed in AcOH–H_2O (2:1) (10 ml) in the presence of 5% Pd–C (90 mg). After the absorption of hydrogen had ceased (*ca.* 3.5 h), the catalyst was filtered off and the filtrate was evaporated under reduced pressure, affording a crystalline mass (210 mg); mp 145—153 °C. It was recrystallized from EtOH; yield 139 mg (66%); mp 157.5—159 °C, $[\alpha]_D^{25}$ +17.2° (*c* 1.0, 1 M HCl).

N-*Ethoxycarbonylmethyl-*L*-valine (**5b**)*: The crude benzyl ethyl ester (**3f**) (3.96 g), obtained from 5.36 g of H–L-Val–OBzl·TosOH and contaminated by the unchanged starting ester, was hydrogenolyzed in a manner similar to that described above. The catalyst was filtered off, and the filtrate evaporated under reduced pressure. After it had been dried sufficiently, the residue was treated with hot EtOH and the insoluble materials (valine) were filtered off. From the filtrate, the desired product (**5b**) was obtained; yield, 1.94 g (68%, based on H–L-Val–OBzl·TosOH); mp 167—168 °C, $[\alpha]_D^{25}$ +0.6° (*c* 1.0, 1 M HCl).

^{13}C-NMR and MS Spectra of the Isomeric Diesters of N-*Carboxymethyl-*L*-valine, **3e** and **3f**. **3e***: ^{13}C-NMR ($CDCl_3$): δ 14.33 (q, $-OCH_2\underline{C}H_3$), 18.40 and 19.17 (each q, $-CH(\underline{C}H_3)_2$), 31.56 (d, $-\underline{C}H(CH_3)_2$), 49.80 (t, $-NH\underline{C}H_2CO-$), 60.49 (t, $-O\underline{C}H_2CH_3$), 66.45 (t, $-O\underline{C}H_2C_6H_5$), 66.70 (d, $-NH\underline{C}HCO-$), 128.30 (d, C2,6* and C4 of C_6H_5), 128.53 (d, C3,5* of C_6H_5), 135.69 (s, C1 of C_6H_5), 171.60 (s, $-\underline{C}H_2CO-$), 174.03 (s, $=CH\underline{C}O-$). An alternative assignment is probable for the peak marked with an asterisk.

MS *m/e* (rel intensity): 293 (M^+, 0.5), 250 ($M^+-(CH_3)_2CH$, 5.2), 221 ($250^+-C_2H_5$, 9.2), 220 ($M^+-COOC_2H_5$, 63.2), 202 ($M^+-C_6H_5CH_2$, 1.6), 158 (202^+-CO_2, 7.6), 130 ($221^+-C_6H_5CH_2$, 4.6), and 91 ($C_6H_5CH_2^+$, base peak).

3f: ^{13}C-NMR ($CDCl_3$): δ 14.18 (q, $-OCH_2\underline{C}H_3$), 18.36 and 19.19 (each q, $-CH(\underline{C}H_3)_2$), 31.60 (d, $-\underline{C}H(CH_3)_2$), 49.83 (t, $-NH\underline{C}H_2CO-$), 60.77 (t, $-O\underline{C}H_2CH_3$), 66.45 (t, $-O\underline{C}H_2C_6H_5$), 66.77 (d, $-NH\underline{C}HCO-$), 128.31 (d, C2, 6* of $\underline{C}_6H_5$), 128.56 (d, C3,5* and C4 of C_6H_5), 135.74 (s, C1 of C_6H_5), 171.74 (s, $-CH_2\underline{C}O-$), 174.10 (s, $=CH\underline{C}O-$).

MS *m/e* (rel intensity): 293 (M^+, 0.4), 278 (M^+-CH_3, 0.2), 250 ($M^+-(CH_3)_2CH$, 5.4), 221 ($250^+-C_2H_5$, 0.8), 220 ($M^+-COOC_2H_5$, 5.4), 202 ($M^+-C_6H_5CH_2$, 0.9), 158 (202^+-CO_2, base peak), 130 ($221^+-C_6H_5CH_2$, 2.6), and 91 ($C_6H_5CH_2^+$, 58.3).

Measurements of the ORD and CD Spectra. All the measurements were carried out at room temperature. The sample solution concentration and the length of the cell, l, are given in the footnotes of each table.

The Cm-amino acids (**2**) listed in Table 1 were converted into the corresponding ethyl dithiocarbamates according to the methods in the literature.[27] Their ORD and CD spectra were measured in several solvents, with or without the addition of three molar amounts of DCHA.

The author is grateful to Profs. (the late) Hiroshi Watanabe and Shigeru Kuwata of Kōnan University, and to Prof. Kazuhiro Maruyama of Kyoto University, for their helpful suggestions and encouragement.

References

1) a) J. P. Greenstein and M. Winitz, "Chemistry of the Amino Acids," John Wiley & Sons, New York (1961), Vol. 3, p. 2548; b) J. D. Kemp, *Biochem. Biophys. Res. Commun.*, **69**, 816 (1976).

2) K. Biemann, C. Lioret, J. Asselineau, E. Lederer, and J. Polonsky, *Bull. Soc. Chim. Biol.*, **42**, 979 (1960).

3) a) A. Goldmann, D. W. Thomas, and G. Morel, *C. R. Acad. Sci., Ser. D*, **268**, 852 (1969); b) R. E. Jensen, W. J. Zdybak, K. Yasuda, and W. S. Chilton, *Biochem. Biophys. Res. Commun.*, **75**, 1066 (1977).

4) Y. Takahashi, H. Naganawa, T. Takita, H. Umezawa, and S. Nakamura, *J. Antibiot.*, **29**, 1120 (1976). Its absolute configuration remains undetermined.

5) A. W. Sangster, S. E. Thomas, and N. L. Tingling, *Tetrahedron*, **31**, 1135 (1975).

6) See, for example, a) R. V. Snyder and R. J. Angelici, *J. Inorg. Nucl. Chem.*, **35**, 523 (1973); b) *idem.*, *Inorg. Chem.*, **13**, 14 (1974); c) K. Okamoto, J. Hidaka, and Y. Shimura, *Bull. Chem. Soc. Jpn.*, **48**, 2456 (1975), and the references cited therein.

7) T. Yamada, K. Takashima, T. Miyazawa, S. Kuwata, and H. Watanabe, *Bull. Chem. Soc. Jpn.*, **51**, 878 (1978).

8) a) The following abbreviations are used for Cm-

amino acids and their derivatives: CmAA for a Cm-amino acid derived from an amino acid (AA) and X–$\underset{\underset{\text{CH}_2\text{CO–Y}}{|}}{\overset{\overset{\text{Y}}{|}}{\text{C}}}$mAA–Z for its derivative (X–$\underset{\underset{\text{R}}{|}}{\text{NCHCO}}$–Z). b) The abbreviations given by the IUPAC-IUB Commission (*J. Biol. Chem.*, **247**, 977 (1972)) are used throughout. Additional abbreviations: Abu, 2-aminobutyric acid; Phg, phenylglycine; Tle, *t*-leucine; Tos, *p*-toluenesulfonyl; Bzl, benzyl; Bu^t, *t*-butyl; TEA, triethylamine; THF, tetrahydrofuran; TosOH, *p*-toluenesulfonic acid.

9) E. Abderhalden and E. Haase, *Hoppe-Seyler's Z. Physiol. Chem.*, **202**, 49 (1931).

10) S. Korman and H. T. Clarke, *J. Biol. Chem.*, **221**, 113 (1956).

11) W. B. Lawson, M. D. Leafer, Jr., A. Tewes, and G. J. S. Rao, *Hoppe-Seyler's Z. Physiol. Chem.*, **349**, 251 (1968).

12) S. Kanao, *Yakugaku Zasshi*, **66B**, 17 (1946).

13) E. Hardegger, F. Szabo, P. Liechti, Ch. Rostetter, and W. Zankowska-Jasinska, *Helv. Chim. Acta*, **51**, 78 (1968).

14) Ref. 12 says that, in the condensation with chloroacetic acid, the ninhydrin reaction of some amino acids became negative in 1—2 h.

15) The formation of a Cm-amino acid from the reaction of an α-amino acid with glyoxal has been reported; N. V. Chuyen, T. Kurata, and M. Fujimaki, *Agric. Biol. Chem.*, **37**, 2209 (1973).

16) The Cm-amino acid itself was also stable; for example, glycine could not be detected even after 3 days' heating of Cm-*t*-leucine.

17) This change could be avoided by storing them in a refrigerator.

18) A. G. Long, J. R. Quayle, and R. J. Stedman, *J. Chem. Soc.*, **1951**, 2197.

19) E. S. Lane, *J. Chromatogr.*, **18**, 426 (1965).

20) J. P. Greenstein and M. Winitz, "Chemistry of the Amino Acids," John Wiley & Sons, New York (1961), Vol. 1, p. 83.

21) See, for example, a) P. Crabbé, "ORD and CD in Chemistry and Biochemistry," Academic Press, New York (1972), p. 54; b) W. Klyne and P. M. Scopes, "Fundamental Aspects and Recent Developments in Optical Rotatory Dispersion and Circular Dichroism," ed by F. Ciardelli and P. Salvadori, Heyden & Son, London (1973), p. 140.

22) J. Shoji, *J. Antibiot.*, **26**, 302 (1973).

23) C. J. Hawkins and G. A. Lawrance, *Aust. J. Chem.*, **26**, 1801 (1973). See also W. Klyne, P. M. Scopes, and R. N. Thomas, *Helv. Chim. Acta*, **54**, 2420 (1971).

24) E. C. Jorgensen, *Tetrahedron Lett.*, **1971**, 863.

25) The weak band near 260 nm reported for the parent amino acid could not be observed here.

26) J. C. Craig and W. E. Pereira, Jr., *Tetrahedron Lett.*, **1970**, 1563; *Tetrahedron*, **26**, 3457 (1970).

27) K. Ishikawa, K. Achiwa, and S. Yamada, *Chem. Pharm. Bull.*, **19**, 912 (1971), and the references cited therein.

28) a) T. Yamada, S. Kuwata, and H. Watanabe, *Tetrahedron Lett.*, **1978**, 1813; b) S. Kuwata, T. Yamada, T. Shinogi, N. Yamagami, F. Kitabashi, T. Miyazawa, and H. Watanabe, *Bull. Chem. Soc. Jpn.*, **52**, 3326 (1979).

29) Profound effects of added amines on the Cotton effect of an ETCT-L-β-amino acid have been reported.[28a])

30) H. T. Clarke, *J. Chem. Soc.*, **97**, 428 (1910).

31) B. Abramovitch, J. C. Shivers, B. E. Hudson, and C. R. Hauser, *J. Am. Chem. Soc.*, **65**, 986 (1943).

32) K. Vogler, *Helv. Chim. Acta*, **30**, 1766 (1947).

33) P. A. Levene, R. E. Steiger, and L. W. Bass, *J. Biol. Chem.*, **82**, 161 (1929).

34) T. Miyazawa, K. Takashima, Y. Mitsuda, T. Yamada, S. Kuwata, and H. Watanabe, *Bull. Chem. Soc. Jpn.*, **52**, 1539 (1979); T. Miyazawa, T. Nagai, T. Yamada, S. Kuwata, and H. Watanabe, *Memoirs of Kōnan University, Science Series*, No. 23 (1979), p. 51.

35) For **3h** this procedure was omitted.

Reactions of Substituted Epoxides with Alkyl Chloroacetate

Tokuji TAKEDA,* Satoshi YASUHARA, and Shoji WATANABE
Osaka Municipal Technical Research Institute, Ogimachi, Kita-ku, Osaka 530

(Received December 14, 1979)

The reactions of substituted epoxides with alkyl chloroacetate in the presence of lithium salts, quarternary salts and zinc chloride were studied. The reaction of 1-chloro-2,3-epoxypropane (**1a**) with butyl chloroacetate (BCA) in the presence of any of these catalysts yielded exclusively butyl [2-chloro-1-(chloromethyl)ethoxy]acetate (**2a**) via the normal cleavage of **1a** followed by the reaction with the chloroacetate. On the other hand, the reaction of 1,2-epoxypropane(**1b**) with BCA yielded a mixture of isomeric products resulting from the normal and abnormal cleavages of **1b**, and the ratio of the normal and abnormal products is dependent on the type of the catalyst. Moreover, it was found that lithium salt alone catalyzed the insertion reaction in a polar aprotic solvent, whereas the reaction in aromatic solvent needed a suitable co-catalyst such as hexamethylphosphoric triamide and triphenylphosphine oxide.

Insertion of an epoxide into the carbon-halogen bond of an alkyl halide had not been investigated to any noticeable extent. In our previous papers, we reported the insertion of ethylene oxide into the carbon-halogen bond of benzyl chlorides[1] and halooctanes[2,3] using zinc halide as a catalyst. The reaction of ethylene oxide with benzyl chlorides and halooctanes in *N,N*-dimethylacetamide(DMA) gave 2-chloroethyl benzyl ethers and 1-(2-haloethoxy)octanes, respectively, while the reaction of ethylene oxide with secondary halooctanes in the absence of any solvent gave the mixture of 2-(2-haloethoxy)octane, 3-(2-haloethoxy)octane and 4-(2-haloethoxy)octane.

In this study, we obtained the novel insertion compounds from the reaction of substituted epoxides with butyl chloroacetate(BCA) and investigated the distribution of isomers of the insertion products. Moreover, we searched for more effective catalysts and reaction systems from the limitation of zinc halide hitherto used as a catalyst. It was found that the isomer distribution of the insertion product caused by the direction of ring opening was dependent on the substituent of the epoxide ring and the type of the catalyst and that lithium salt complexed with suitable co-catalyst was effective for the present insertion reaction.

Results and Discussion

*Reaction of 1-Chloro-2,3-epoxypropane(**1a**) with BCA.* The reaction of the epoxide **1a** with BCA in DMA in the presence of lithium chloride gave only product, butyl [2-chloro-1-(chloromethyl)ethoxy]acetate(**2a**), in the yield of 35.6%.

$$\underset{\textbf{1a}}{ClCH_2CHCH_2O} + ClCH_2COOC_4H_9 \xrightarrow[\text{in DMA}]{LiCl} \underset{\textbf{2a}}{(ClCH_2)_2CHOCH_2COOC_4H_9}$$

The structure of this novel compound **2a** could not be determined clearly by ^{1}H-NMR spectrum because the signals of methylene and methine proton between the chlorine and the ether oxygen of the normal and abnormal products, $(ClCH_2)_2CHO-$ and $ClCH_2CH(Cl)CH_2O-$, would appear at similar chemical shifts. However, the presence of seven signals above 80.00 in ^{13}C-NMR unambiguously supported the structure of **2a**. Chemical shifts were assigned on the basis of Lindeman-Adams' equation,[4] the substituent effect and off-resonance spectrum. The effect of catalyst on the yield of the product **2a** is shown in Table 1. Zinc chloride and triethylamine gave a small amount of **2a**. Lithium salts and tetraethylammonium bromide gave considerable amounts of **2a**. In the reaction of **1a** with BCA in DMA, a very small amount of dibutyl oxydiacetate(**3**) was detected by GLC analysis. This could be due to a trace amount of water in DMA. Thus, the reaction of **1a** with BCA was tried in benzene and toluene to avoid the formation of **3**. Lithium salt alone is insoluble in benzene and toluene, and refluxing a benzene or toluene solution of **1a** and BCA in the presence of lithium salt gave no reaction. However, by the addition of an equimolar amount of hexamethylphosphoric triamide(HMPA) to lithium salt the insertion reaction took place smoothly. These results suggest that DMA, added as a solvent in the former reaction, and HMPA, added as a co-catalyst in the latter reaction, may play the same role for the insertion reaction. DMA and HMPA act not only simply as solvents, but also specifically solvate the lithium ion to enhance the nucleophilicity of the resulting "naked" halide ion. It was reported by Rickborn[5] that a 1:1 complex of LiBr–HMPA was an efficient catalyst for the rearrangement of epoxides, but the catalytic activity of the complex was quenched by the addition of a second

Table 1. Effect of catalysts on the yield of **2a**[a]

Catalyst	Recovery of BCA (%)	Yield of **2a** (%)[b]
LiCl	43.3	33.0
LiBr	60.0	35.8
TEAB	61.0	28.6
TEA[c]	79.5	4.9
$ZnCl_2$[d]	73.3	8.2

a) Reaction temperature is 80 °C and other conditions are the same as those in the case of LiCl, described in Experimental Section. The reactions were carried out in homogeneous system. b) Based on BCA. c) Triethylamine. d) Reaction temperature is 100 °C.

Table 2. Catalysis by lithium salt-cocatalyst for the reaction of the epoxide **1a** with BCA in benzene[a)]

Catalyst	Recovery of BCA (%)	Yield of **2a** (%)[b)]
LiCl–HMPA	59.2	27.2
LiBr–HMPA	33.5	46.3
LiBr–4HMPA[c)]	16.9	48.1
LiI–HMPA	38.3	33.9
LiCl–DMF[d)]	87.8	9.9
LiCl–DMA	83.2	10.3
LiCl–NMP[e)]	87.0	10.7
LiCl–DMSO[f)]	92.4	1.7
LiBr–TMU[g)]	95.0	3.3
LiCl–TPPO	66.6	15.9
LiBr–TPPO	31.4	51.0
LiBr–TBPO[h)]	63.7	19.9
LiCl–$(EtO)_3PO$[i)]	77.3	9.0
LiCl–$(PhO)_3PO$[j)]	93.5	2.8
LiBr–12-Crown-4	95.6	4.3
LiBr–15-Crown-5	57.4	16.2
LiBr–18-Crown-6	95.0	0.4
LiBr–Dibenzo-18-crown-6	83.2	5.4

a) Reaction temperature is 90 °C and other conditions are described in Experimental section. The reaction mixtures were not clear solution because of the inadequate solubility of catalysts. b) Based on BCA. c) A mixture of 6 mmol of LiBr and 24 mmol of HMPA was used. d) *N*,*N*-Dimethylformamide. e) *N*-Methyl-2-pyrrolidone. f) Dimethyl sulfoxide. g) Tetramethylurea. h) Tributylphosphine oxide. i) Triethyl phosphate. j) Triphenyl phosphate.

equivalent of HMPA. Although such quenching was not observed in the present reaction, it was found that an equimolar amount of HMPA to lithium salt was sufficient to promote the insertion (Table 2). In DMA the yield of **2a** is not different regardless of the kind of lithium salts, as shown in Table 1, while in benzene the yield of **2a** by LiBr catalyst is higher than by LiCl catalyst. The difference in the catalysis may be ascribed to the difference in the solubility of these catalysts in DMA and benzene; both LiCl and LiBr are soluble in DMA, but LiBr is more soluble in benzene than LiCl.

The effectiveness of other polar aprotic additives, phosphates, phosphine oxides and crown ethers as promoting agents is shown in Table 2. Triphenylphosphine oxide (TPPO) was the best promoting agent except for HMPA. The best yield of **2a** was 57.6% in the reaction using LiBr–TPPO catalyst at 90 °C for 24 h. 15-Crown-5 was the most effective among the crown ethers inspected when used with lithium bromide. The effect of solvents on the yield of the insertion product **2a** is shown in Table 3. The yield of **2a** was lower in toluene at a higher temperature than in benzene at a lower temperature. This may be due to inadequate solubility of lithium bromide–HMPA in toluene. Tetrahydrofuran was effective at a lower temperature.

Quarternary salts were also effective for the insertion

Table 3. Effect of solvents on the yield of **2a**[a)]

Solvent	Recovery of BCA (%)	Yield of **2a** (%)[b)]
Toluene[c)]	41.6	29.2
Dioxane[d)]	57.8	20.5
THF[e)]	54.2	28.2

a) Lithium bromide and HMPA were used as a catalyst and a co-catalyst, respectively. The reaction mixture were not clear solutions because of the inadequte solubility of catalysts. b) Based on BCA. c) Reaction temperature is 110 °C. d) Reaction temperature is 90 °C. e) Reaction temperature is 70 °C.

Table 4. The reaction of **1a** with BCA in the presence oe quarternary salts[a)]

Catalyst	Recovery of BCA (%)	Yield of **2a** (%)[b)]
TEAB–HMPA	90.8	6.0
TBAB–HMPA	42.8	30.1
TBAB	51.6	20.7
MTPPI–HMPA	63.1	23.3

a) A mixture of 6 mmol each of quarternary salt and HMPA, 60 mmol each of BCA and **1a** in 20 ml of benzene was stirred at 90 °C for 5 h. The reaction mixtures were clear solutions, except for TEAB–HMPA and MTPPI–HMPA. b) Based on BCA.

reaction in benzene (Table 4). Tetraethylammonium bromide (TEAB) and methyltriphenylphosphonium iodide (MTPPI) are not sufficiently soluble in benzene to cause reaction, unlike tetrabutylammonium bromide (TBAB). Thus, the former two quarternary salts were not effective in benzene in the absence of HMPA, whereas TBAB alone promoted the insertion in this nonpolar solvent. However, with TBAB the yield of **2a** increased upon addition of HMPA. This result suggests that the nucleophilicity of the halide ion of TBAB was enhanced by the addition of HMPA.

*Reaction of 1,2-Epoxypropane (**1b**) with BCA.* The reaction of the epoxide **1b** with BCA in DMA in the presence of lithium chloride gave a mixture of butyl [1-(chloromethyl)ethoxy]acetate (the normal isomer, **4a**) and butyl (2-chloropropoxy)acetate (the abnormal isomer, **4b**).

These novel compounds, the normal and abnormal isomers, were separated and isolated by GLC using DEGS liquid phase. ^{1}H-NMR spectrum of the isolated **4a** showed a characteristic doublet peak at δ 1.30 due to the methyl proton adjacent to the methine carbon.

$$CH_3CH\underset{\backslash\,/}{CH_2}O + ClCH_2COOC_4H_9 \xrightarrow[\text{in DMA}]{\text{LiCl}}$$

1b

$$CH_3\underset{\displaystyle CH_2Cl}{\underset{|}{C}}HOCH_2COOC_4H_9 + CH_3\underset{\displaystyle Cl}{\underset{|}{C}}HCH_2\underset{\displaystyle COOC_4H_9}{\underset{|}{O}}CH_2$$

4a 41.2% **4b** 58.8%

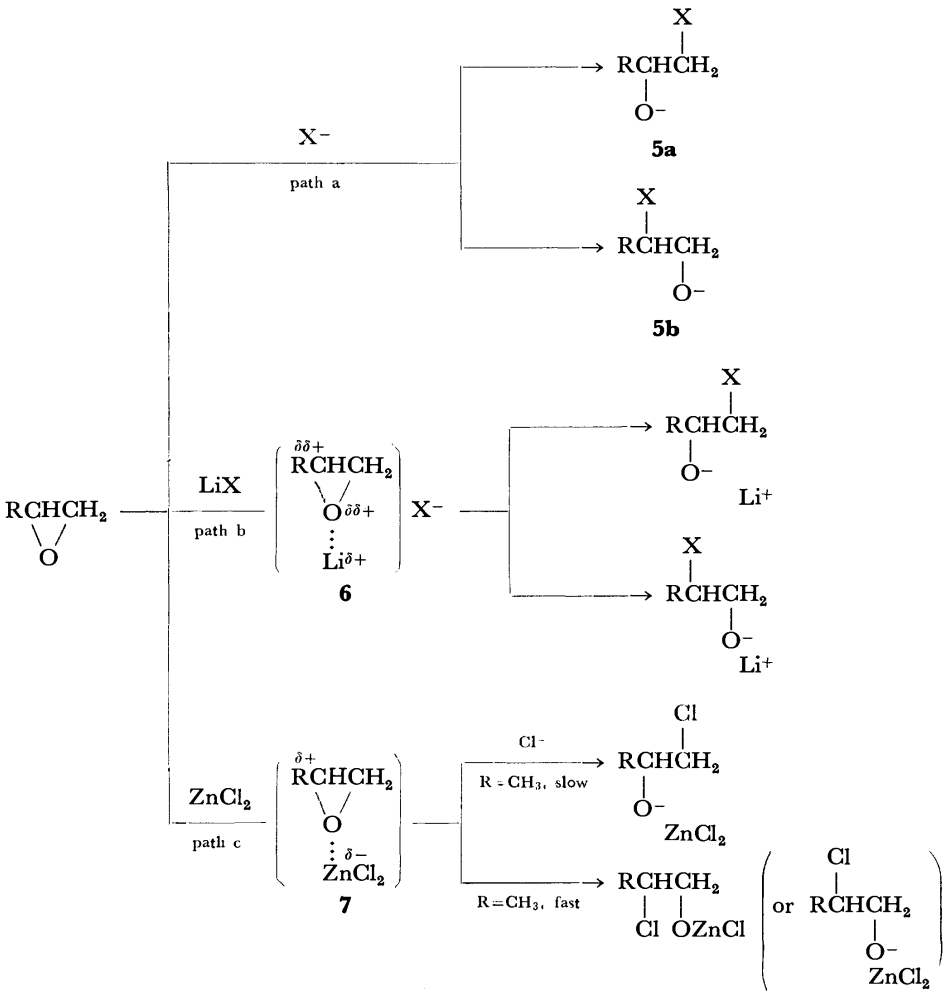

Scheme 1.

^{1}H-NMR spectrum of the isolated **4b** showed a characteristic doublet peak at 1.56 ppm due to the methyl proton adjacent to the methine carbon attached to the chlorine atom. In mass spectra, the normal isomer **4a** gave characteristic fragment peaks at *m/e* 159 and 103 based on the elimination of chloromethyl group and the abnormal isomer **4b** gave characteristic fragment peaks at *m/e* 172 and 71 based on dehydrochlorination. From these results the structures of the normal and abnormal isomers were confirmed.

Isomer Distribution and Probable Mechanism. The reaction of the epoxide **1a** with BCA exclusively gave the normal insertion product **2a**, regardless of the type of catalyst. However, the reaction of the epoxide **1b** with BCA gave the mixture of the isomeric products, **4a** and **4b**. The present reaction may proceed by the following mechanism, as shown in Scheme 1.

The exclusive formation of the normal isomer in the reaction of the epoxide **1a** may be explained by the inductive (electron-withdrawing) and large steric effects of chloromethyl group. The stability of a transition state such as **6** or **7** is disturbed by the electron-withdrawing power of chloromethyl group.

On the other hand, the formation of the normal and abnormal isomers in the reaction of the epoxide **1b** can be attributable to the inductive (electron-donating) and steric effects of methyl group. The isomer distribution of the products from the reaction of the epoxide **1b** with BCA was dependent on the type of the catalyst. The results are summarized in Table 5. Use of tetraethylammonium salts resulted in a little preferential formation of the normal isomer. In this case, the nucleophilic attack by halide ion may an important role in the ring opening of epoxide. The isomer distribution may be ascribed to the steric

Table 5. Isomer distribution of the reaction product of BCA with the epoxide **1b**[a]

Catalyst	Isomer distribution		Yield of **4a**+**4b**(%)[b]
	4a(%)	**4b**(%)	
$ZnCl_2$	20.0	80.0	34.5
LiCl	41.2	58.8	31.5
LiCl+TEAB[c]	44.8	55.2	44.2
TEAC[d]	58.5	41.5	—
TEAB	60.0	40.0	21.0

a) A mixture of 0.5 mmol of catalyst, 5 mmol each of BCA and DMA, and 20 mmol of **1b** was stirred at 100 °C for 5 h. The reactions were carried out in homogeneous system. b) Based on BCA. c) A mixture of 0.5 mmol each of lithium chloride and tetraethylammonium bromide was used. d) Tetraethylammonium chloride.

effect of methyl group which is smaller than that of chloromethyl group (path a). Use of lithium halide led to a little preferential formation of the abnormal isomer. Lithium ion, solvated by (or complexed with) DMA, HMPA, or TPPO, would coordinate to the oxygen of the epoxide ring and polarize the C–O bond of the epoxide, thus facilitating the ring opening by nucleophilic attack by halide ion. The isomer distribution may be attributable to the inductive and steric effects of methyl group of the epoxide **1b** (path b). Zinc chloride highly preferentially gave the abnormal isomer. In this case, the chloride ion seems to be less nucleophilic, which is in accord with the fact that the reaction of **1a** is very slow as shown in Table 1. Zinc chloride would coordinate stronger to the oxygen of the epoxide ring. Predominant formation of **4b** can be explained by the attack (intramolecular or not) of the chloride ion on the highly polarized transition state like **7** or the secondary carbonium ion which is preferentially formed by the inductive effect of the methyl group (path c).

Experimental

^{1}H-NMR and ^{13}C-NMR spectra were recorded with JEOL JNM-MH-100 and JNM-FT-100 Spectrometers in carbon tetrachloride and deuterochloroform solution, respectively. Mass spectra were determined with a JEOL JMS-07 Spectrometer at an ionizing voltage of 30 eV.

*Reaction of 1-Chloro-2,3-epoxypropane (**1a**) with Butyl Chloroacetate (BCA) in N,N-Dimethylacetamide (DMA).* LiCl 0.13 g (3 mmol) was dried under vacuum prior to use and was dissolved in 5.2 g (60 mmol) of DMA. Then, 9.0 g (60 mmol) of BCA and 5.5 g (60 mmol) of **1a** were added to the solution and the mixture was stirred at 100 °C for 5 h. The resulting reaction mixture was extracted (Et_2O–H_2O), and the ethereal extract was washed with H_2O and dried with $MgSO_4$. 2.5 g of BCA was recovered by distillation and 5.5 g (37.5% based on BCA) of crude butyl 2-chloro-1-(chloromethyl)ethoxy acetate (**2a**, 95% purity by GLC) was obtaned. The product purified further by distillation had the following properties: Bp 108—109 °C/2 mmHg (1 mmHg=133.322 Pa). ^{13}C-NMR (excluding COO) δ 13.68 (Off-resonance decoupling; q, CH_3), 19.14 (t, $\underline{C}H_2CH_3$), 30.65 (t, $\underline{C}H_2C_2H_5$), 43.37 (t, $ClCH_2$), 65.00 (t, $COO\underline{C}H_2$), 68.02 (t, $O\underline{C}H_2COO$), 79.58 (d, $\underline{C}HO$). ^{1}H-NMR δ 0.98 (3H, t, J=7.5 Hz, CH_3), 1.30—1.70 (4H, m, CH_2), 3.70—3.72 (5H, m, $ClCH_2CHCH_2Cl$), 4.16 (2H, t, J=7.5 Hz, $COOCH_2$), 4.26 (2H, s, OCH_2COO). Found: C, 44.26; H, 6.37; Cl, 29.1%.[6] Calcd for $C_9H_{16}O_3Cl_2$: C, 44.46; H, 6.64; Cl, 29.16%.

*Reaction of **1a** with BCA in Benzene and Other Nonpolar Solvents.* A mixture of 6 mmol of lithium salt, dried prior to use, and co-catalyst (1.0 g in the case of crown ethers), and 60 mmol of BCA and **1a** in 20 ml of a solvent was stirred at 70—110 °C for 5 h. The yield of **2a** and the recovery of BCA, as shown in Tables 2 and 3, were determined by GLC.[7]

*Reaction of 1,2-Epoxypropane (**1b**) with BCA.* A mixture of 3.15 g (15 mmol) of tetraethylammonium bromide (TEAB), 13.1 g (150 mmol) of DMA, 22.6 g (150 mmol) of BCA and 17.4 g (300 mmol) of **1b** was heated in a glass autoclave at 100 °C for 5 h. The reaction product was isolated by the same procedure as in the case of **2a** and 4.5 g (14.4%) of the pure product was obtaned. Bp 65—66 °C/20 mmHg. Found: C, 51.53; H, 8.39; Cl, 17.1%; Mol. weight, 213.3.[8] Calcd for $C_9H_{17}O_3Cl$: C, 51.80; H, 8.21; Cl, 16.99%; Mol. weight, 208.5. This product contained the normal cleavage product **4a** and the abnormal cleavage product **4b**. Each isomer was isolated by GLC using DEGS 20%, 3 m column. **4a**: ^{1}H-NMR δ 0.93 (3H, t, J=6.5 Hz, terminal CH_3), 1.30 (3H, d, J=6.0 Hz, CH_3C–O–), 1.43—1.47 (4H, m, CH_2), 3.35—3.84 (3H, m, $ClCH_2$–CHO), 4.07—4.20 (4H, m, CH_2OCOCH_2O). **4b**: 0.98 (3H, t, J=6.5 Hz, terminal CH_3), 1.56 (2H, d, J=6.0 Hz, CH_3CCl), 3.57—3.77 (3H, m, OCH_2CHCl), 4.06—4.21 (4H, m, CH_2OCOCH_2O). The reactions using various catalysts were carried out in a 20 ml sealed tube. Product distribution was determined by GLC[9] using standard mixtures, and the overall yield of the insertion products was determined by GLC.[10]

The authors would like to thank Professor Mitsuo Okahara and Assistant Professor Isao Ikeda of Osaka University for helpful discussion and to Dr. Mitsuo Komatsu of Osaka University for obtaining the C-13 NMR spectra.

References

1) I. Ikeda, T. Takeda, and S. Komori, *J. Org. Chem.*, **35**, 2353 (1970).
2) T. Takeda, I. Ikeda, S. Yasuhara, and S. Masuyama, *Nippon Kagaku Kaishi*, **1974**, 1682.
3) T. Takeda and S. Yasuhara, *Nippon Kagaku Kaishi*, **1976**, 1579.
4) L. P. Lindeman and J. Q. Adams, *Anal. Chem.*, **43**, 1245 (1971).
5) B. Rickborn and R. M. Gerkin, *J. Am. Chem. Soc.*, **93**, 1693 (1971).
6) Content of chlorine was determined by a modified semimicro butanol–Na method. W. Kimura, *Kogyo Kagaku Zasshi*, **37**, 1310 (1934).
7) Silicon DC 550 10% on Shimalite, 3 m, 190 °C. By making a calibration curve between the isolated product and the internal standard, the yield based on BCA was determined. (Internal standard; methyl tetradecanoate)
8) Molecular weight was determined by the measurement of the depression of the freezing point of benzene.
9) DEGS 20% on Shimalite, 3 m, 170 °C.
10) Silicon DC 550 10% on Shimalite, 3 m, 170 °C.

Synthesis of Muramyl Dipeptide Analogs with Enhanced Adjuvant Activity[1)]

Shigeru KOBAYASHI,* Tsunehiko FUKUDA, Hidefumi YUKIMASA, Masahiko FUJINO, Ichiro AZUMA,† and Yuichi YAMAMURA††

Chemical Research Laboratories, Central Research Division, Takeda Chemical Industries, Ltd., Yodogawa-ku, Osaka 532

† *Institute of Immunological Science, Hokkaido University, Kita-ku, Sapporo 060*

†† *The Third Department of Internal Medicine, Osaka University, Fukushima-ku, Osaka 553*

(Received December 19, 1979)

N-Acetylmuramyl-L-alanyl-D-isoglutamine (MDP) and thirteen new analogs were synthesized by the conventional organic chemical procedure using dicyclohexylcarbodiimide-*N*-hydroxy-5-norbornene-2,3-dicarboximide as a coupling agent. Their ability to induce delayed-type hypersensitivity to *N*-acetyl-3-(4-arsonophenylazo)-L-tyrosine in guinea pigs was assayed. The results indicate that the presence of an α-amino acid adjacent to the lactic acid moiety in MDP is important for the high biological activity, the valine analog having the most favorable effect. The structure-activity relationship is discussed.

Freund's complete adjuvant (FCA) is a most widely used adjuvant consisting of heat-killed mycobacterial cells in mineral oil.[2)] Ellouz *et al.*[3)] and Kotani *et al.*[4)] independently elucidated that *N*-acetylmuramyl-L-alanyl-D-isoglutamine (MDP) (**9a**) is the minimal structure responsible for the activity elicited by peptidoglycan of the bacterial cell walls. MDP can be substituted for mycobacterial cells in FCA to potentiate both B cell- and T cell-mediated immune responses.[5)] Recently, MDP has been found to have biological activities such as enhancement of the nonspecific resistance in mice infected by *Klebsiella pneumoniae*,[6)] stimulation of the thymidine uptake in mouse spleen cell cultures,[7)] and the activation of reticuloendothelial system[8)] and macrophages *in vitro*.[9)]

In view of possible clinical applications of immunomodulators, it is important to prepare MDP analogs with enhanced activities. In this report, we describe the synthesis and immunological activities of 13 new MDP analogs (Table 3). MDP has also been synthesized for the sake of comparison in our biological system.

Chemistry

MDP and its analogs were synthesized by the conventional organic chemical procedure using dicyclohexylcarbodiimide (DCC)-*N*-hydroxy-5-norbornene-2,3-dicarboximide (HONB)[10)] as a coupling agent at each step. The *t*-butoxycarbonyl (Boc) group was used for α-amino protection and the benzyl group for side chain hydroxyl and carboxyl protection. The Boc group was removed with trifluoroacetic acid prior to each coupling. The final deprotection of all the protecting groups was effected by catalytic hydrogenation.[11)] Details of the synthesis are summarized in Scheme 1.

The protected dipeptides (**4**) were synthesized by coupling D-isoglutamine benzyl (**2a**) or methyl (**2b**) ester with Boc-amino acid HONB ester (**3**). The dipeptides (**4**) thus obtained are given together with their physicochemical properties in Table 1.

The protected glycopeptides (**8**) were prepared by coupling suitably protected dipeptides (**5**) with protected muramic acid derivatives, such as benzyl 2-acetamido-4,6-*O*-benzylidene-3-*O*-[1-(*R*)-carboxyethyl]-2-deoxy-α-D-glucopyranoside (**6a**), the (*S*)-isomer (**6b**), benzyl 2-acetamido-4,6-*O*-benzylidene-3-*O*-[1-(*R*)-carboxyisopentyl]-2-deoxy-α-D-glucopyranoside (**6c**), or benzyl 4,6-*O*-benzylidene-2-benzyloxyacetamido-3-*O*-[1-(*R*)-carboxyethyl]-2-deoxy-α-D-glucopyranoside (**6d**). These protected muramic acids (**6**) were converted into the HONB active esters (**7**) for coupling.

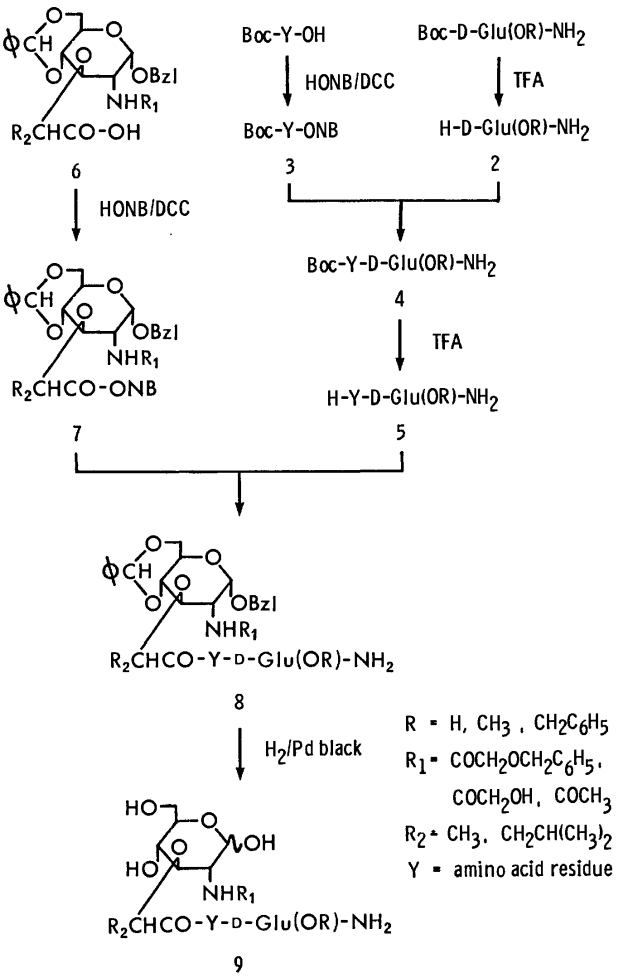

Scheme 1.

Protected *N*-acetylmuramic acid (**6a**) was prepared by the method of Flowers and Jeanloz[12)] and protected

Table 1. Yields and physicochemical properties of dipeptides, Boc-Y-D-Glu(OR)-NH_2 **4**

Compd	Y	R	Yield/%	Mp/°C	$[\alpha]_D$ (c 0.5) (temp, solvent)	Formula	Found (Calcd)[%] C	H	N
4a	L-Ala	$CH_2C_6H_5$	83.2	140—141[a]	+8.3° (20, MeOH)[a]	$C_{20}H_{29}N_3O_6$	59.41 (58.95)	7.23 7.17	10.25 10.31)
4b	β-Ala	$CH_2C_6H_5$	81.0	148—149	+11.4° (20, MeOH)	$C_{20}H_{29}N_3O_6$	58.96 (58.95)	7.18 7.17	10.24 10.31)
4c	Sar	$CH_2C_6H_5$	89.3	110—112	+4.0° (20, MeOH)	$C_{20}H_{29}N_3O_6$	50.06 (58.95)	7.39 7.17	10.10 10.31)
4d	Aib[b]	$CH_2C_6H_5$	70.2	112—113	+13.2° (27, EtOH)	$C_{21}H_{31}N_3O_6$	59.81 (59.84)	7.76 7.41	9.84 9.97)
4e	Pro	$CH_2C_6H_5$	72.3	155—156	−12.6° (27, DMF)	$C_{22}H_{31}N_3O_6$	61.04 (60.96)	7.43 7.21	9.67 9.69)
4f	L-Thr(OBzl)	$CH_2C_6H_5$	64.5	115—117	+6.0° (27. EtOH)	$C_{28}H_{37}N_3O_7$	63.92 (63.74)	7.14 7.07	7.83 7.96)
4g	L-Val	$CH_2C_6H_5$	81.2	148	+8.9° (25, DMF)	$C_{22}H_{33}N_3O_6$	60.53 (60.67)	7.74 7.64	9.54 9.65)
4h	L-Val	CH_3	84.3	117—119	+8.6° (23, DMF)	$C_{16}H_{29}N_3O_6$	53.72 (53.46)	8.10 8.13	11.44 11.69)
4i	L-Ser(OBzl)	$CH_2C_6H_5$	98.0	65—66[c]	+5.7° (23, EtOH)	$C_{27}H_{35}N_3O_7$	62.98 (63.14)	6.93 6.87	8.19 8.18)

a) Lit,[11b] mp 137.5—138.5 °C. b) Aib: α-aminoisobutyric acid. c) Lit,[11c] mp 65—66 °C; $[\alpha]_D^{25}$ +5.8°(MeOH).

N-acetylisomuramic acid (**6b**) by that of Petit and Sinäy.[13] Compound **6c** was obtained by treating benzyl 2-acetamido-4,6-*O*-benzylidene-2-deoxy-α-D-glucopyranoside[12] with sodium hydride, followed by condensation with (*S*)-2-chloro-4-methylpentanoic acid.[14] (The compound obtained after hydrogenolytic deprotection of **6c** is referred to as *N*-acetyl *C*-isobutylnormuramic acid in this text). Acylation of benzyl 2-amino-4,6-*O*-benzylidene-α-D-glucopyranoside[15] with benzyloxyacetic anhydride gave benzyl 4,6-*O*-benzylidene-2-benzyloxyacetamido-α-D-glucopyranoside (**10**), which was then treated with sodium hydride and condensed with (*S*)-2-chloropropionic acid[16] as in the synthesis of **6a** to give protected *N*-glycolylmuramic acid (**6d**). The protected glycodipeptides (**8**) obtained are given in Table 2 together with their physicochemical properties.

The *N*-acetylmuramyl dipeptides (**9a**—**9h**), *N*-acetylisomuramyl dipeptide (**9i**), *N*-glycolylmuramyl dipeptides (**9j**—**9m**) and *N*-acetyl *C*-isobutylnormuramyl dipeptide (**9n**) were obtained after elimination of all the protecting groups by catalytic hydrogenation in acetic acid. The final products (**9**) were purified by column chromatography on Sephadex LH-20 with ethanol–0.1 M acetic acid as a solvent. The physicochemical properties of the desired MDP analogs are given in Table 3.

During the hydrogenolytic deprotection of the isomuramyl derivative (**8i**) in acetic acid, TLC showed the generation of L-alanyl-D-isoglutamine (**13**), an unknown by-product (**11**) and a small amount of isomuramic acid (**12**) as well as the desired *N*-acetylisomuramyl-L-alanyl-D-isoglutamine (**9i**). Attempts to isolate the unknown by-product were unsuccessful, the only compound obtained being isomuramic acid.

Treatment of **9i** in acetic acid at 80 °C for 1 h gave nearly the same result on TLC as that obtained by the hydrogenolytic deprotection of **8i**. Quantitative analysis of the liberated L-alanyl-D-isoglutamine by means of an amino acid analyzer showed that the conversion of **9i** into **11** and **12** reaches up to 49.9%. However, hydrogenolysis of **8i** under aprotic conditions (in DMF) gave **9i** with no side reaction.

The results can be explained by assuming that the deprotected *N*-acetylisomuramyl dipeptide (**9i**) is gradually decomposed to give the intramolecular ester (**11**) and the dipeptide through *N* to *O* migration of the amide bond under acidic conditions. The resulting intramolecular ester can readily be hydrolyzed to isomuramic acid (**12**) (Scheme 2). MDP treated in a similar way gave the dipeptide in only 5% yield, suggesting that the *S*-isomer (**9i**) more easily undergoes migration than its *R*-isomer (**9a**).

Biological Results

The adjuvant activity of the synthetic MDP analogs (**9**) was assayed for the induction of delayed-type hypersensitivity to *N*-acetyl-3-(4-arsonophenylazo)-L-tyrosine (ABA–Tyr) in guinea pigs[17] (Table 4).

We see that the *N*-acetylisomuramyl derivative (**9i**) greatly reduces the adjuvant activity (compare **9a** and **9i**), indicating that the configuration of the lactic acid moiety of MDP has to be the *R*-form to elicit the activity.

Replacement of alanine by β-alanine (**9b**) led to complete loss of activity. This indicates that lengthening of the peptide chain by one methylene group (as in **9b**) is unfavorable, since glycine analog of MDP has a distinct although weak as compared with MDP,

Table 2. Yields and physicochemical properties of the protected glycodipeptides **8**

Compd	R_1	R_2	Y	R	Yield/%	Mp/°C	$[\alpha]_D$[a] (c, temp)	Formula	Found(Calcd)[%] C	H	N
8a	CH_3CO	CH_3	L-Ala	Bzl	96.1	223—230 (d)[b]	+89.2° (1.0, 20)	$C_{40}H_{48}N_4O_{11}$	62.91 (63.15	6.12 6.36	7.25 7.40)
8b	CH_3CO	CH_3	β-Ala	Bzl	78.0	276 (d)	+89.9° (0.5, 20)	$C_{40}H_{48}N_4O_{11}$	62.97 (63.15	6.39 6.36	7.27 7.40)
8c	CH_3CO	CH_3	Sar	Bzl	71.8	177—178	+90.1° (0.5, 20)	$C_{40}H_{48}N_4O_{11}$	63.10 (63.15	6.41 6.36	7.27 7.40)
8d	CH_3CO	CH_3	Aib[c]	Bzl	86.7	93 (d)	+87.7° (1.0, 21)	$C_{41}H_{50}N_4O_{11}$	63.82 (63.55	6.88 6.51	6.87 7.23)
8e	CH_3CO	CH_3	L-Pro	Bzl	65.9	82 (d)	+96.4° (0.5, 27)	$C_{42}H_{50}N_4O_{11}$	63.84 (64.11	6.44 6.41	7.07 7.12)
8f	CH_3CO	CH_3	L-Thr(OBzl)	Bzl	65.4	242 (d)	+88.0° (0.1, 27)	$C_{48}H_{56}N_4O_{12}$	65.13 (65.45	6.33 6.41	6.22 6.35)
8g	CH_3CO	CH_3	L-Val	Bzl	93.7	257 (d)	+90.5° (0.5, 20)	$C_{42}H_{52}N_4O_{11}$	63.51 (63.94	6.63 6.64	6.98 7.10)
8h	CH_3CO	CH_3	L-Val	CH_3	92.0	242 (d)	+86.1° (0.5, 22)	$C_{36}H_{48}N_4O_{11}\cdot H_2O$	59.35 (59.16	6.80 6.90	7.70 7.68)
8i[d]	CH_3CO	CH_3	L-Ala	Bzl	58.3	280—281 (d)	+58.3° (0.5, 20)	$C_{40}H_{48}N_4O_{11}\cdot \frac{1}{2}H_2O$	62.56 (62.40	6.50 6.42	7.22 7.28)
8j	$BzlOCH_2CO$	CH_3	L-Ala	Bzl	58.6	196—198	+70.4° (0.4, 27)	$C_{47}H_{54}N_4O_{12}$	64.98 (65.11	6.27 6.28	6.44 6.46)
8k	$BzlOCH_2CO$	CH_3	L-Ser(OBzl)	Bzl	68.0	216—217	+60.0° (0.4, 27)	$C_{54}H_{60}N_4O_{13}$	66.65 (66.65	6.16 6.22	5.67 5.76)
8l	$BzlOCH_2CO$	CH_3	L-Val	Bzl	75.3	199—201	+62.3° (0.4, 27)	$C_{49}H_{58}N_4O_{12}$	65.31 (65.75	6.51 6.53	6.16 6.26)
8m	$BzlOCH_2CO$	CH_3	L-Leu	Bzl	70.2	175—176	+63.2° (0.4, 27)	$C_{50}H_{60}N_4O_{12}$	65.77 (66.06	6.60 6.65	6.00 6.16)
8n	CH_3CO	CH_3>$CHCH_2$ CH_3	L-Ala	Bzl	69.3	234—235	+91.7° (0.5, 23)	$C_{53}H_{54}N_4O_{11}$	64.36 (64.32	6.76 6.78	6.99 6.99)

a) Solvent: DMF. b) Lit,[11b] mp 240 °C(d). c) Aib: α-aminoisobutyric acid. d) The chiral carbon of the lactic acid moiety of this compound has the *S*-configuration.

Table 3. Yields and physicochemical properties of MDP analogs **9**

Compd	R_1	R_2	Y	R	Yield/%	$[\alpha]_D$ (c 0.5) (temp, solvent)	Formula	Found(Calcd)[%] C	H	N
9a	CH_3CO	CH_3	L-Ala	H	85.4	+33.7°(23, H_2O)[a,b,c]	$C_{19}H_{32}N_4O_{11}\cdot\frac{1}{4}H_2O$	45.70 (45.92	6.90 6.59	11.21 11.27)
9b	CH_3CO	CH_3	β-Ala	H	95.5	+31.8°(19, H_2O)[a]	$C_{19}H_{32}N_4O_{11}\cdot H_2O$	44.64 (44.69	6.73 6.71	10.63 10.98)
9c	CH_3CO	CH_3	Sar	H	95.8	+47.7°(19, H_2O)[a]	$C_{19}H_{32}N_4O_{11}\cdot\frac{3}{2}H_2O$	43.70 (43.92	6.91 6.79	10.35 10.78)
9d	CH_3CO	CH_3	Aib[d]	H	quant	+46.3°(19, H_2O)[a,c]	$C_{20}H_{34}N_4O_{11}\cdot\frac{1}{2}H_2O$	46.58 (46.59	6.80 6.84	10.76 10.86)
9e	CH_3CO	CH_3	L-Pro	H	96.7	+60.2°(27, EtOH)	$C_{21}H_{34}N_4O_{11}\cdot\frac{1}{2}H_2O$	47.91 (47.81	7.01 6.69	10.48 10.62)
9f	CH_3CO	CH_3	L-Thr	H	66.4	+51.3°(27, EtOH)[e]	$C_{20}H_{34}N_4O_{12}\cdot H_2O$	45.49 (45.19	6.93 6.64	10.52 10.54)
9g	CH_3CO	CH_3	L-Val	H	94.2	+61.8°(23, DMF)	$C_{21}H_{36}N_4O_{11}\cdot\frac{1}{2}H_2O$	47.98 (47.63	7.41 7.04	10.32 10.58)
9h	CH_3CO	CH_3	L-Val	CH_3	86.1	+53.8°(22, DMF)	$C_{22}H_{38}N_4O_{11}\cdot\frac{1}{2}H_2O\cdot\frac{1}{2}AcOH$	48.34 (48.15	7.22 7.21	9.78 9.77)
9i[f]	CH_3CO	CH_3	L-Ala	H	89.3	−19.1°(24, H_2O)[a]	$C_{19}H_{32}N_4O_{11}\cdot 2H_2O$	43.58 (43.17	6.63 6.87	10.51 10.60)
9j	$HOCH_2CO$	CH_3	L-Ala	H	88.1	+58.1°(27, DMF)	$C_{19}H_{32}N_4O_{12}\cdot\frac{1}{2}H_2O\frac{1}{2}AcOH$	43.98 (43.87	6.88 6.45	10.25 10.23)
9k	$HOCH_2CO$	CH_3	L-Ser	H	86.7	+57.4°(27, DMF)	$C_{19}H_{32}N_4O_{13}\cdot H_2O$	42.12 (42.06	6.70 6.32	9.95 10.32)
9l	$HOCH_2CO$	CH_3	L-Val	H	90.7	+36.1°(27, DMF)	$C_{21}H_{36}N_4O_{12}\cdot H_2O\cdot\frac{1}{2}AcOH$	45.40 (45.20	7.13 6.72	9.54 9.58)
9m	$HOCH_2CO$	CH_3	L-Leu	H	97.1	+51.4°(27, DMF)	$C_{22}H_{38}N_4O_{12}\cdot\frac{1}{2}H_2O$	47.21 (47.23	7.38 7.03	9.66 10.01)
9n	$HOCH_2CO$	$CH_3\diagdown CHCH_2\diagup CH_3$	L-Ala	H	84.8	+39.7°(23, H_2O)[a]	$C_{22}H_{33}N_4O_{11}\cdot\frac{3}{2}H_2O$	47.29 (47.05	7.18 7.36	9.68 9.98)

a) Optical rotation was determined when mutarotation was completed (25 h). b) c 0.1. c) Lit,[11b] $[\alpha]_D^{15}$ +33.1° (after 25 h) (c 0.51, H_2O). d) Aib: α-amino-isobutyric acid. e) c 0.4. f) The chiral carbon of the lactic acid moiety of this compound has the *S*-configuration.

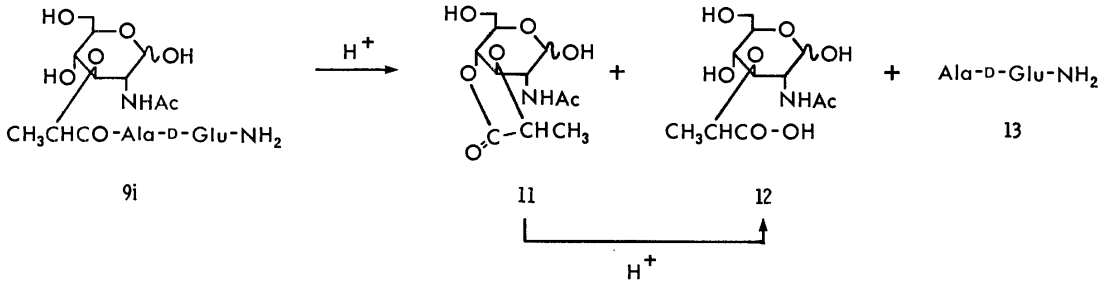

Scheme 2.

Table 4. Adjuvant activity of MDP analogs **9** in delayed-type hypersensitivity to ABA-Tyr (100 μg) in Guinea Pigs

Compd[a]	Skin reaction with BαA at 24 h (mm±SE)			
	Exp 1	Exp 2	Exp 3	Exp 4
MurNAc-L-Ala-D-Glu-NH_2 (**9a**)	18.1±1.2	22.9±1.2	18.2±0.7	17.6±0.7
MurNAc-β-Ala-D-Glu-NH_2 (**9b**)	0	—	—	—
MurNAc-Sar-D-Glu-NH_2 (**9c**)	0	—	—	—
MurNAc-Aib-D-Gul-NH_2[b] (**9d**)	21.8±1.7	—	—	—
MurNAc-L-Pro-D-Glu-NH_2 (**9e**)	—	14.1±0.5	—	—
MurNAc-L-Thr-D-Glu-NH_2 (**9f**)	—	24.0±1.1	—	—
MurNAc-L-Val-D-Glu-NH_2 (**9g**)	—	28.0±1.5	20.0±1.0	19.4±0.7
OCH_3 | MurNAc-L-Val-D-Glu-NH_2 (**9h**)	—	—	—	19.7±0.4
isoMurNAc-L-Ala-D-Glu-NH_2 (**9i**)	—	9.4±1.0	—	—
MurNGl-L-Ala-D-Glu-NH_2[c] (**9j**)	—	—	18.0±0.7	—
MurNGl-L-Ser-D-Glu-NH_2[c] (**9k**)	—	—	19.3±0.5	—
MurNGl-L-Val-D-Glu-NH_2[c] (**9l**)	—	—	19.6±0.9	—
MurNGl-L-Leu-D-Glu-NH_2[c] (**9m**)	—	—	16.4±0.5	—
C-IsobutylnorMurNAc-L-Ala-D-Glu-NH_2 (**9n**)	17.5±1.2	—	—	—
Control (ABA-Tyr+FIA)[d]	0	0	0	0

a) Dose: 100 μg. b) Aib: α-aminoisobutyric acid. c) MurNGl=*N*-glycolylmuramyl. d) FIA: Freund's incomplete adjuvant.

adjuvant activity.[18] No activity of the sarcosine analog (**9c**) and reduced activity of the proline analog (**9e**) show the necessity of the NH group adjacent to the lactic acid moiety.

The results indicate that alanine or some other α-amino acid adjacent to the lactic acid moiety is important for high biological activity. Replacement of alanine by α-aminoisobutyric acid (**9e**), threonine (**9f**) and valine (**9g**) gave rise to an increase in activity, the valine analog showing the most favorable effect on biological potency. The *N*-glycolyl leucine analog (**9m**), however, has moderate but slightly weak activity as compared with other *N*-glycolyl analogs (**9j**—**9l**), indicating that the size or lipophilicity of the amino acid adjacent to the lactic acid moiety has an effect on the activity. An increase in the size or lipophilicity of the lactic acid residue in muramic acid (**9n**) also caused a decrease in the activity.

The *N*-glycolylmuramyl analogs have activities equipotent to those of the corresponding *N*-acetylmuramyl analogs (compare **9a** with **9j**, and **9g** with **9l**), indicating that *N*-glycolyl and *N*-acetyl groups caused no marked difference in activity.[19] The methyl ester (**9h**) of the valine analog in which a carboxyl group of the D-isoglutamine residue is esterified also possesses activity equipotent to that of the carboxyl-free analog (**9g**).

Experimental

Melting points were taken in open capillaries and are uncorrected. Optical rotations were determined with a Perkin-Elmer Model 141 polarimeter. Amino acid analyses were performed on a Hitachi KLA-3B amino acid analyzer. All chemicals and solvents were of reagent grade and used without further purification with the exception of dioxane which was dried by refluxing in the presence of CaH_2. The reactions were monitored on TLC with Merck F_{254} silica gel plates, which were developed with $CHCl_3$–MeOH (19:1, v/v) for compounds **4**, $CHCl_3$–acetone–MeOH (10:3:2, v/v) for **8**, and *n*-BuOH–EtOAc–AcOH–H_2O (1:1:1:1, v/v) for **9**. Evaporation was carried out in a rotary vacuum evaporator under reduced pressure at temperatures below 45 °C.

D-*Glutamic Acid γ-Benzyl Ester.* This was synthesized according to the method of Guttman and Boissonnas:[20] mp 176—178 °C (lit for L-form 189 °C,[20] 174 °C[21]); $[\alpha]_D^{25}$ −18.6° (*c* 6.0, AcOH) [lit for L-form[20] $[\alpha]_D^{23}$ +19.6°±0.2° (*c* 6.0, AcOH)].

t-*Butoxycarbonyl*-D-*glutamic Acid γ-Benzyl Ester DCHA Salt.* A suspension of D-glutamic acid γ-benzyl ester (5.93 g, 25

mmol) in water (14 ml) was combined with a DMF solution (14 ml) of *O*-*t*-butyl *S*-(4,6-dimethyl-2-pyrimidinyl)thiocarbonate[22] (7.21 g, 30 mmol), Et_3N (3.5 ml, 25 mmol) being then added. The mixture was stirred overnight, becoming a clear solution, to which was added water (40 ml). After extraction with EtOAc (50 ml), the pH of the aqueous layer was adjusted to 2 by addition of 5 M HCl under cooling and the mixture was extracted with EtOAc (40 ml×3). The EtOAc layer was washed with 1 M HCl (25 ml×3) and satd. aq NaCl (25 ml×2), and dried over Na_2SO_4. Evaporation of the solvent gave an oil (7.00 g) of *t*-butoxycarbonyl-D-glutamic acid γ-benzyl ester, which was converted into its DCHA salt in a mixture of EtOAc (50 ml) and Et_2O (50 ml) by addition of a petroleum ether solution (10 ml) of DCHA (3.63 g, 20 mmol) under cooling. The precipitate was filtered to give crystalline *t*-butoxycarbonyl-D-glutamic acid γ-benzyl ester DCHA salt: 10.15 g (78.3%). Mp 141—143 °C (lit for L-form[23] 138—139 °C). $[\alpha]_D^{19}$ −12.5° (*c* 1.0, MeOH) [lit for L-form[23] $[\alpha]_D^{25}$ +11.9° (MeOH)]. Found: C, 67.01; H, 9.16; N, 5.56%. Calcd for $C_{29}H_{46}O_6N_2$: C, 67.15; H, 8.94; N, 5.56%.

t-*Butoxycarbonyl*-D-*glutamic Acid* α-p-*Nitrophenyl* γ-*Benzyl Diester.* A suspension of *t*-butoxycarbonyl-D-glutamic acid γ-benzyl ester DCHA salt (9.86 g, 19 mmol) in EtOAc (100 ml) was shaken with 0.2 M H_2SO_4 (100 ml). The EtOAc layer was washed with satd. aq NaCl (25 ml×2) and dried over Na_2SO_4. After filtration, *p*-nitrophenol (2.69 g, 19 mmol) and DCC (3.92 g, 19 mmol) were added under cooling, and the mixture was stirred at 0 °C for 2 h and kept in a refrigerator overnight. The resulting *N,N'*-dicyclohexylurea was filtered and the filter cake was washed with EtOAc. The combined EtOAc layer was then concentrated to 50 ml and the resulting precipitate was filtered: 7.55 g (86.8%). Mp 121—122 °C (lit for L-form[24] 120—121 °C). $[\alpha]_D^{23}$ +25.0° (*c* 0.5, EtOAc) [lit for L-form[24] $[\alpha]_D^{25}$ −32.7° (MeOH)]. Found: C, 60.19; H, 5.76; N, 6.07%. Calcd for $C_{23}H_{26}O_8N_2$: C, 60.25; H, 5.72; N, 6.11%.

t-*Butoxycarbonyl*-D-*isoglutamine Benzyl Ester.* *t*-Butoxycarbonyl-D-glutamic acid α-*p*-nitrophenyl γ-benzyl diester (4.58 g, 10 mmol) was dissolved in tetrahydrofuran (40 ml), ammonia water (25%, 6.8 ml) being added to the solution. After being stirred for 2 h at room temperature, the solution was concentrated and the residue was dissolved in EtOAc (150 ml). After the usual work-up, the residue was recrystallized from EtOAc–petroleum ether: 2.38 g (70.8%). mp 123—124 °C. $[\alpha]_D^{20}$ −28.0° (*c* 0.5, MeOH). Found: C, 60.63; H. 7.15; N, 8.07%. Calcd for $C_{17}H_{24}O_5N_2$: C, 60.70; H, 7.19; N, 8.23%.

t-*Butoxycarbonyl*-L-*valine HONB Ester.* *t*-Butoxycarbonyl-L-valine (15.2 g, 70 mmol), HONB (13.8 g, 77 mmol) and DCC (15.9 g, 77 mmol) were combined in a mixture of acetonitrile (300 ml) and DMF under cooling. The mixture was stirred at 0 °C for 1 h and at room temperature for 4 h and filtered. After evaporation of the solvent, the residue was dissolved in EtOAc. The EtOAc layer was washed with 5% $NaHCO_3$ and water, then dried over Na_2SO_4. The solvent was removed and the residue was triturated with petroleum ether giving crystalline *t*-butoxycarbonyl-L-valine HONB ester: 26.5 g (quantitative). mp 120—122 °C. $[\alpha]_D^{27}$ −33.6° (*c* 0.5, DMF). Found: C, 60.14; H, 7.21; N, 7.11%. Calcd for $C_{19}H_{26}O_2N_6$: C, 60.30; H, 6.93; N, 7.40%.

t-*Butoxycarbonyl*-D-*glutamic Acid* γ-*Methyl Ester.* This was synthesized from D-glutamic acid γ-methyl ester[25] (19.7 g, 0.1 mol) in a similar way to that described for *t*-butoxycarbonyl-D-glutamic acid γ-benzyl ester: 23.5 g (89.9%). An analytical sample was converted into its DCHA salt as described for the preparation of *t*-butoxycarbonyl-D-glutamic acid γ-benzyl ester DCHA salt: mp 155 °C (lit for L-form[26] 155—157 °C). $[\alpha]_D^{23}$ −10.2° (*c* 0.5, MeOH) [lit for L-form[26] $[\alpha]_D$ +10.5° (MeOH)]. Found: C, 62.45; H, 9.61; N, 6.17%. Calcd for $C_{23}H_{42}O_6N_2$: C, 62.47; H, 9.57; N, 6.33%.

t-*Butoxycarbonyl*-D-*glutamic Acid* α-N-*Succinimidyl* γ-*Methyl Diester.* To a solution of *t*-butoxycarbonyl-D-glutamic acid γ-methyl ester (23.0 g, 88 mmol) and *N*-hydroxysuccinimide (11.2 g, 97 mmol) in acetonitrile (200 ml) was added DCC (20.0 g, 97 mmol) under cooling, and the mixture was stirred at 0 °C for 3 h and at room temperature for 12 h. After filtration and evaporation of the solvent, the residue was dissolved in EtOAc (175 ml). The EtOAc layer was washed with 5% $NaHCO_3$ (70 ml×3), water (70 ml×3) and 10% citric acid (70 ml×3) successively, and dried over Na_2SO_4. After evaporation, the residue was triturated with petroleum ether giving the desired compound: 22.9 g (72.7%). Mp 96 °C. $[\alpha]_D^{23}$ +33.8° (*c* 0.5, DMF).

t-*Butoxycarbonyl*-D-*isoglutamine Methyl Ester.* *t*-Butoxycarbonyl-D-glutamic acid α-*N*-succinimidyl γ-methyl diester (17.9 g, 50 mmol) was dissolved in tetrahydrofuran (50 ml), ammonia water (25%, 18 ml) being added to the resulting solution. After being stirred at 0 °C for 30 min and at room temperature for 30 min, the solution was concentrated and the residue was dissolved in EtOAc (250 ml). After the usual work-up, the residue was recrystallized from EtOAc–petroleum ether: 6.4 g (49.2%). Mp 129—130 °C. $[\alpha]_D^{23}$ −4.2° (*c* 0.5, DMF). Found: C, 51.08; H, 6.25; N, 7.74%. Calcd for $C_{11}H_{20}O_2N_5$: C, 50.75; H, 6.19; N, 7.82%.

t-*Butoxycarbonyl*-L-*valyl*-D-*isoglutamine Methyl Ester (**4h**).* *t*-Butoxycarbonyl-D-isoglutamine methyl ester (5.0 g, 19.1 mmol) was dissolved in cold trifluoroacetic acid (20 ml) and the resulting solution was stirred at room temperature for 15 min. Trifluoroacetic acid was then removed and the residue was triturated with Et_2O. Oily D-isoglutamine methyl ester trifluoroacetate was dried over NaOH pellets, dissolved in acetonitrile (40 ml), and neutralized with Et_3N (2.8 ml, 20 mmol). *t*-Butoxycarbonyl-L-valine HONB ester (7.22 g, 19.1 mmol) was added to this solution and the mixture was stirred at room temperature for 15 h. The solution was then concentrated and the residue extracted with EtOAc (500 ml). The EtOAc layer was washed successively with 5% $NaHCO_3$, 10% citric acid, and water (100 ml×3), then dried over Na_2SO_4 and evaporated. The residue was triturated with petroleum ether giving crystals which were recrystallized from EtOAc–petroleum ether: 5.8 g (84.3%).

*Other protected dipeptides (**4**)* were similarly prepared from appropriate *t*-butoxycarbonylamino acid HONB esters and *t*-butoxycarbonyl-D-isoglutamine benzyl ester.

*Benzyl 4,6-O-Benzylidene-2-benzyloxyacetamido-2-deoxy-α-D-glucopyranoside (**10**).* DCC (7.48 g, 36.3 mmol) was added at 0 °C to a solution of benzyloxyacetic acid[27] (11.0 g, 66 mmol) in dichloromethane (100 ml). The mixture was stirred at 0 °C for 2 h and at room temperature for 15 h. After filtration, the solvent was removed to give oily bis(benzyloxyacetic) anhydride which was dissolved in tetrahydrofuran (300 ml) without further purification together with benzyl 2-amino-4,6-*O*-benzylidene-2-deoxy-α-D-glucopyranoside[15] (10.7 g, 30 mmol). The mixture was heated under reflux for 1 h and the solvent was evaporated. The resulting crystalline residue was collected by filtration and washed with Et_2O to give **10** in a quantitative yield: 15.2 g. Mp 161—162 °C. $[\alpha]_D^{27}$ +48.6° (*c* 0.5, $CHCl_3$). Found: C, 68.70; H, 6.31; N, 2.40%. Calcd for $C_{29}H_{31}ON_7$: C, 68.89; H, 6.18; N, 2.77%.

*Benzyl 2-Acetamido-4,6-O-benzylidene-3-O-[1-(R)-carboxyisopentyl)-2-deoxy-α-D-glucopyranoside (**6c**).* Benzyl 2-acetamido-4,6-*O*-benzylidene-2-deoxy-α-D-glucopyranoside (3.2 g, 8 mmol) was dissolved in dioxane (300 ml) at 90 °C. Sodium hydride (1.80 g, 60% in oil) was then added to the solution at 70 °C and the mixture was kept at 90 °C for 1 h. A solution of (*S*)-2-chloro-4-methylpentanoic acid[14] (6.3 g, 42 mmol) in dioxane (10 ml) was added when the temperature had cooled to 65 °C. After 1 h, additional sodium hydride (7.48 g) was added and the mixture was stirred at 65 °C for 15 h. Water was then added carefully to the reaction mixture under cooling, and the dioxane of the upper phase separated by decantation was evaporated. The residue was dissolved in water (100 ml) and the solution extracted with $CHCl_3$ (50 ml). The aqueous phase was adjusted to pH 3 with 2 M HCl under cooling, the precipitate being extracted with $CHCl_3$ (100 ml×3). The combined organic layer was washed with water and dried (Na_2SO_4). After filtration and evaporation, the residue was purified by silica-gel column (4×12 cm) chromatography using $CHCl_3$–MeOH (95:5, v/v) as solvent: 1.2 g (29.9%). Mp 156—157 °C. $[\alpha]_D^{23}$ +118.4° (*c* 0.5, DMF). Found: C, 65.56; H, 6.88; N, 2.74%. Calcd for $C_{27}H_{36}ON_8$: C, 65.48; H, 6.87; N, 2.73%.

*Benzyl 4,6-O-Benzylidene-2-benzyloxyacetamido-3-O-[1-(R)-carboxyethyl]2-deoxy-α-D-glucopyranoside (**6d**).* Sodium hydride (2.0 g, 50 mmol, *ca.* 60% in oil) was added to a dioxane (300 ml) solution of **10** (10.1 g, 20 mmol) and the mixture was stirred at 90 °C for 1 h. (*S*)-2-Chloropropionic acid (7.54 g, 70 mmol) was added when the temperature had cooled to 65 °C. After 1 h, additional sodium hydride (3.2 g, 80 mmol, 60% in oil) was added and the mixture was stirred at 65 °C for 15 h. Water (40 ml) was then added carefully under cooling, the pH of mixture being adjusted to 7 with 10% citric acid. After evaporation of dioxane, 10% citric acid (250 ml) was added. The resulting precipitate was filtered and washed with water, then with $CHCl_3$–petroleum ether. Recrystallization from MeOH gave **6d**: 6.70 g (58.1%). Mp 230 °C (dec.). $[\alpha]_D^{27}$ +67.5° (*c* 0.3, DMF). Found: C, 65.59; H, 5.89; N, 2.50%. Calcd for $C_{32}H_{35}ON_9 \cdot {}^1/_2H_2O$: C, 65.51; H, 6.19; N, 2.38%.

*Benzyl 2-Acetamido-4,6-O-benzylidene-3-O-[1-(R)-carboxyethyl]-2-deoxy-α-D-glucopyranoside HONB Ester (**7a**).* DCC (3.71 g, 18 mmol) was added to a solution of benzyl 2-acetamido-4,6-*O*-benzylidene-3-*O*-[1-(*R*)-carboxyethyl]-2-deoxy-α-D-glucopyranoside[12] (7.07 g, 15 mmol) and HONB (3.22 g, 18 mmol) in tetrahydrofuran (110 ml) under cooling, and the mixture was stirred at 4 °C for 3 h and at room temperature for 16 h. After filtration, the solvent was removed and the resulting crystalline residue was recrystallized from EtOAc–Et_2O: 7.42 g (78.4%). Mp 122—124 °C. $[\alpha]_D^{27}$ +86.0° (*c* 0.5, DMF). Found: C, 64.52; H, 5.67; N, 4.25%. Calcd for $C_{34}H_{36}O_{10}N_2$: C, 64.55; H, 5.74; N, 4.43%.

*Benzyl 4,6-O-Benzylidene-2-benzyloxyacetamido-3-O-[1-(R)-carboxyethyl)-2-deoxy-α-D-glucopyranoside HONB Ester (**7d**)* was synthesized in a similar way to that described for **7a**: 99.6%. Mp 98—99 °C. $[\alpha]_D^{27}$ +69.0° (*c* 0.5, DMF). Found: C, 66.64; H, 5.99; N, 3.77%. Calcd for $C_{41}H_{42}O_{11}N_2$: C, 66.65; H, 5.73; N, 3.79%.

*N-Acetyl-1-O-Benzyl-4,6-O-benzylidene-α-muramyl-L-valyl-D-isoglutamine Methyl Ester (**8h**).* *t*-Butoxycarbonyl-L-valyl-D-isoglutamine methyl ester (**4h**) (359 mg, 1 mmol) was treated with trifluoroacetic acid (5 ml) at room temperature for 20 min. After evaporation, the residue was triturated with Et_2O and collected. L-Valyl-D-isoglutamine methyl ester trifluoroacetate thus obtained was dissolved in acetonitrile (10 ml) and the solution was neutralized with Et_3N (0.17 ml) under cooling. A solution of **7a** (633 mg, 1 mmol) in acetonitrile (10 ml) was added and the the mixture was stirred at room temperature for 15 h. The resulting precipitate was collected and washed with hot acetonitrile to give **8h**: 656 mg (92.0%).

*Other protected muramyl dipeptides (**8**)* were similarly prepared from appropriate protected muramic acid HONB esters and protected dipeptides.

*N-Acetylmuramyl-L-valyl-D-isoglutamine Methyl Ester (**9h**).* Compound **8h** (31.2 mg, 0.05 mmol) was hydrogenolyzed in a mixture of MeOH (5 ml) and AcOH (0.5 ml) with palladium black as a catalyst at room temperature for 3 h. After filtration and evaporation, the residue was kept in a refrigerator to allow crystallization. Et_2O was then added and the crystals were filtered to give **9h**: 23 mg (86.1%).

*Other muramyl dipeptides (**9**)* were similarly prepared from appropriate protected muramyl dipeptides (**8**).

*Isolation of N-Acetylisomuramic Acid (**12**) and L-Alanyl-D-isoglutamine (**13**) from a Side Reaction.* *N*-Acetyl-1-*O*-benzyl-4,6-*O*-benzylidene-α-isomuramyl-L-alanyl-D-isoglutamine benzyl ester (**8i** 857 mg) was subjected to hydrogenolysis in AcOH (50 ml) in the presence of palladium black at room temperature for 5 d. After filtration and evaporation, the residue was applied to a column of Sephadex LH-20 (3×90 cm) and eluted with 0.1 M AcOH. The fractions from 155 to 175 ml containing the probable internal ester (**11**) and *N*-acetylisomuramic acid (**12**), identical on TLC with an authentic sample,[13] were collected and lyophilized. The residual syrup was solidified with Et_2O and filtered. The powder obtained was highly hygroscopic, showing a single spot corresponding to *N*-acetylisomuramic acid on TLC: 60 mg. Found: C, 42.25; H, 6.50; N, 4.43%. Calcd for $C_{11}H_{19}ON_8$: C, 42.44; H, 6.78; N, 4.50%.

Other 125—140 ml fractions were also collected and lyophilized. The resulting powder was applied to a column (2×40 cm) of CM-cellulose and eluted with dilute AcOH (pH 4.5). The fraction 63—98 ml was collected and lyophilized to give L-alanyl-D-isoglutamine (**13**, 95 mg), which had an R_f value on TLC identical to that of the authentic dipeptide. Amino acid analysis (hydrolysis with 6 M HCl at 110 °C for 24 h): Ala, 1.00; Glu, 1.01.

*Comparison of Degradation (Side Reaction) Rate of **9a** and **9i**.* Solutions of AcOH (0.5 ml each) containing *N*-acetylmuramyl-L-alanyl-D-isoglutamine (**9a**, 10.34 μmol) or *N*-acetylisomuramyl-L-alanyl-D-isoglutamine (**9i**, 10.10 μmol) were heated at 80 °C for 1 h. After evaporation, the residue was subjected to amino acid analysis (column length: 20 cm, buffer: pH 5.28, flow rate: 60 ml/h). The quantity of liberated dipeptide was calculated on the basis of the standard experiment using L-alanyl-D-isoglutamine[11b] (retention time: 25 min), and was 0.52 μmol (5.0%) from **9a** and 5.04 μmol (49.9%) from **9i**.

Biological Assay. Determination of the adjuvant activity on the induction of delayed-type hypersensitivity was carried out according to the method reported.[17]

We wish to thank Prof. T. Shiba, Drs. E. Ohmura, and M. Nishikawa for valuable discussions.

References

1) Previous communication in this series: S. Kobayashi, T. Fukuda, I. Imada, M. Fujino, I. Azuma, and Y. Yamamura, *Chem. Pharm. Bull.*, **27**, 3193 (1979).
2) J. Freund, *Adv. Tuber. Res.*, **7**, 130 (1956).
3) F. Ellouz, A. Adam, R. Ciorbaru, and E. Lederer, *Biochem. Biophys. Res. Commun.*, **59**, 1317 (1974).

4) S. Kotani, Y. Watanabe, F. Kinoshita, T. Shimono, I. Morisaki, T. Shiba, S. Kusumoto, Y. Tarumi, and K. Ikenaka, *Biken J.*, **18**, 105 (1975).

5) I. Azuma, K. Sugimura, T. Taniyama, M. Yamawaki, Y. Yamamura, S. Kusumoto, S. Okada, and T. Shiba, *Infect. Immun.*, **14**, 18 (1976); F. Audibert, L. Chedid, P. Lefrancier, and J. Choay, *Cellular Immunol.*, **21**, 243 (1976); A. Adam, M. Devys, Vongthip Souvnnavong, P. Lefrancier, and E. Lederer, *Biochem. Biophys. Res. Commun.*, **72**, 339 (1977); L. Chedid, F. Audibert, and A. G. Johnson, *Prog. Allergy*, **25**, 63 (1978).

6) L. Chedid, M. Parant, F. Parant, P. Lefrancier, J. Choay, and E. Lederer, *Proc. Natl. Acad. Sci. U.S.A.*, **74**, 2089 (1977).

7) C. Damais, M. Parant, and L. Chedid, *Cell Immunol.*, **34**, 49 (1976); C. Damais, M. Parant, L. Chedid, P. Lefrancier, and J. Choay, *ibid.*, **35**, 173 (1977).

8) A. Tanaka, S. Nagao, R. Saito, S. Kotani, S. Kusumoto, and T. Shiba, *Biochem. Biophys. Res. Commun.*, **77**, 621 (1977).

9) Y. Yamamoto, S. Nagao, A. Tanaka, T. Koga, and K. Onoue, *Biochem. Biophys. Res. Commun.*, **80**, 923 (1978).

10) M. Fujino, S. Kobayashi, M. Obayashi, T. Fukuda, S. Shinagawa, and O. Nishimura, *Chem. Pharm. Bull.*, **22**, 1857 (1974).

11) a) C. Merser, P. Sinäy, and A. Adam, *Biochem. Biophys. Res. Commun.*, **66**, 1316 (1975); b) S. Kusumoto, Y. Tarumi, K. Ikenaka, and T. Shiba, *Bull. Chem. Soc. Jpn.*, **49**, 533 (1976); c) P. Lefrancier, J. Choay, M. Derrien, and I. Lederman, *Int. J. Peptide Protein Res.*, **9**, 249 (1977); d) A. Hasegawa Y. Kaneda, M. Amano, M. Kiso, and I. Azuma, *Agric. Biol. Chem.*, **42**, 2187 (1978).

12) H. M. Flowers and R. W. Jeanloz, *J. Org. Chem.*, **28**, 2983 (1973).

13) J. M. Petit and P. Sinäy, *Carbohydr. Res.*, **24**, 415 (1972).

14) K. Ichimura and M. Ohta, *Bull. Chem. Soc. Jpn.*, **43**, 1443 (1970).

15) P. H. Gross and R. W. Jeanloz, *J. Org. Chem.*, **32**, 2759 (1967).

16) S. C. J. Fu, S. M. Birnbaum, and J. P. Greenstein, *J. Am. Chem. Soc.*, **76**, 6054 (1954).

17) M. Uemiya, K. Sugimura, T. Kusama, I. Saiki, M. Yamawaki, I. Azuma, and Y. Yamamura, *Infect. Immun.*, **24**, 83 (1979).

18) A. Adam, M. Devys, V. Souvannavong, P. Lefrancier, J. Choay, and E. Lederer, *Biochem. Biophys. Res. Commun.*, **72**, 339 (1976).

19) *N*-Glycolylmuramic acid is a constituent of *Nocardiae* and *Mycobacteria*, and *N*-acetylmuramic acid that of *Corynebacteria*. The cell walls of these bacteria cause induction of delayed-type hypersensitivity; for example, see Ref. 18.

20) St. Guttman and R. A. Boissonnas, *Helv. Chim. Acta*, **41**, 1852 (1958).

21) E. R. Blout and R. H. Karlson, *J. Am. Chem. Soc.*, **78**, 941 (1956).

22) T. Nagasawa, K. Kuroiwa, K. Narita, and Y. Iwasa, *Bull. Chem. Soc. Jpn.*, **46**, 1269 (1973).

23) E. Schröder and E. Klieger, *Ann.*, **673**, 196 (1964).

24) C. H. Li, B. Gorup, D. Chung, and J. Ramachandran, *J. Org. Chem.*, **28**, 178 (1963).

25) M. Goodman, E. E. Schmitt, and D. A. Yphantis, *J. Am. Chem. Soc.*, **84**, 1283 (1962).

26) J. C. Anderson, M. A. Barton, P. M. Hardy, G. W. Kenner, J. Preston, and R. C. Sheppard, *J. Chem. Soc., C*, **1967**, 108.

27) H. O. L. Fischer and B. Gohlke, *Helv. Chim. Acta*, **16**, 1130 (1933).

The Kinetics of the β-Cyclodextrin-catalyzed Decarboxylation of Trichloroacetic Acid in an Alkaline Solution

Yoshiaki MOTOZATO, Yoshiaki FURUYA,* Toshikazu MATSUMOTO, and Tsukasa NISHIHARA

Department of Synthetic Chemistry, Faculty of Engineering, Kumamoto University, Kumamoto 860

(Received December 20, 1979)

The rate of the decarboxylation of trichloroacetic acid (abbreviated as TCAH) in the presence of β-cyclodextrin(βCD) in an aqueous solution of sodium hydroxide has been followed by the determination of the remaining TCAH. The rate equation was given by

$$\text{Rate} = (k_{1T}+k_{1TC}C_{\beta CD})C_{TCAH}^{1/2} + (k_{2T}-k_{2TC}C_{\beta CD})C_{TCAH}.$$

A probable bimolecular decarboxylation mechanism which involves the unionized molecule of TCAH rather than the anion was proposed and discussed.

Since it was pointed out that TCAH was split quantitatively into chloroform and carbon dioxide when heated in organic bases,[1] the decarboxylation mechanism has been studied by many chemists. Verhoek and his co-workers have suggested that the reaction is a unimolecular reaction of the anion.[2] In opposition to this, Clark has assumed that the reaction is a bimolecular decomposition of the anion.[3]

Some facts of interest were found when we were dealing with the decarboxylation of TCAH as a part of the studies of βCD-catalyzed reactions. We should like to note that the title reaction involves a bimolecular reaction of the unionized TCAH with the solvent water molecule. We will also discuss the catalysis of βCD.

Experimental

Materials. Guaranteed reagents of TCAH (Wako Pure Chemical Industries), βCD (Tokyo Kasei Kogyo Co.), and the sodium hydroxide were used without further purification. The molarities (denoted by M, 1 M=1 mol dm^{-3}) of an aqueous solution of TCAH and of sodium hydroxide were determined by titration with aqueous solutions of sodium hydroxide or hydrochloric acid of known concentrations. The molecular weight of βCD was measured vapor pressure-osmometrically. M_n 1078; calcd 1135.

Typical Rum for the Rate Measurements. Aqueous solutions of TCAH (0.4961 M, 59.97 ml) and sodium hydroxide (0.2957 M, 100.46 ml) were kept separately in a thermostatted water bath of a specified temperature. After appropriate temperature equilibration, the two solutions were mixed together. Aliquots (9.99 ml each) were taken out at appropriate intervals of time, and to each one was added a 9.94 ml portion of a 0.4833 M aqueous solution of hydrochloric acid. Then, they were titrated by 0.4912 M aqueous sodium hydroxide, with Methyl Orange as an indicator. The initial concentration and concentration at time t are given by the following equations:

$$C^0_{TCAH} = ad_1/(d_1+d_2+w)$$

$$C^t_{TCAH} = \{bV+9.99bd_2/(d_1+d_2+w)-9.94c\}/9.99.$$

Here, C^0_{TCAH} and C^t_{TCAH} denote the concentrations of TCAH at time 0 and t, and a and b are the molarities of, and d_1 and d_2 are the quantities (in ml) of aqueous solutions of TCAH and sodium hydroxide respectively. The character, w, is the volume of water added, and c and V are the molarity of an aqueous solution of hydrochloric acid and a titer (at time t) of an aqueous solution of sodium hydroxide respectively.

Measurement of Dissociation State for TCAH in an Aqueous Solution. The degree of dissociation for TCAH in an aqueous solution containing about an equimolar amount of sodium hydroxide was measured by means of a Yanagimoto Conductivity Outfit, model MY-7, in pH 9.0 at 60 °C. The molar conductivities are plotted against the square root of the TCAH concentrations in Fig. 1. From Fig. 1, the degrees of dissociation may be found to be 0.7038—0.8694 in the range of 0.25—0.06 M TCAH at 60 °C. Therefore, it was concluded that the trichloroacetate anion may coexist with the unionized TCAH molecule.

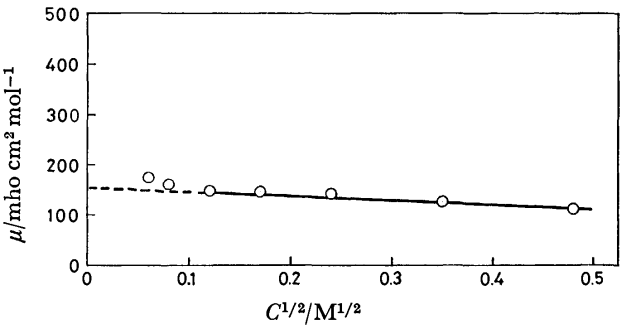

Fig. 1. The Kohlrausch plot of TCAH in aqueous solution of equimolar sodium hydroxide at 60 °C.

Results and Discussion

The pseudo first-order rate plot fit closely to a straight line, as is shown in Fig. 2. The rate data are tabulated in Table 1. The pseudo first-order rate constant, k_{1obs}, increases linearly in proportion to the reciprocal of the square root of the initial concentration of TCAH, as is shown in Fig. 3. Thus, the following equation can be derived:

$$k_{1obs} = k_1 C_{TCAH}^{-1/2} + k_2. \quad (1)$$

The values of k_{1obs} in the decarboxylation of 0.05 M TCAH (6.21×10^{-5} s^{-1} and 1.33×10^{-4} s^{-1}) at 80 °C in the absence or the presence of 0.02 M βCD agreed well with those (7.00×10^{-5} s^{-1} and 1.36×10^{-4} s^{-1}) calculated from the half-life periods given by Cramer and Kampe.[4]

The rate constant k_1 increases, while k_2 decreases, with an increase in the βCD concentration, as is shown in Figs. 4 and 5. Therefore, each constant can be divided into two terms:

Table 1. Rate data and activation parameters for the decarboxylation of trichloroacetic acid

		βCD-catalyzed				Non-catalyzed	
		$10^5 k_{1T}$ / $M^{1/2} s^{-1}$	$10^4 k_{1TC}$ / $M^{-1/2} s^{-1}$	$10^5 k_{2T}$ / s^{-1}	$10^4 k_{2TC}$ / $M^{-1} s^{-1}$	$10^5 k_1$ / $M^{1/2} s^{-1}$	$10^5 k_2$ / s^{-1}
Temp/°C	75	0.18	5.90	2.70	7.40	0.18	2.67
	80	0.40	10.67	5.80	15.73	0.41	5.60
	83	0.65	14.43	7.94	21.13	0.66	7.85
$\Delta H^{\neq}$ kcal/mol		39.4	28.5	33.8	32.5	39.4	33.8
$\Delta S^{\neq}$ e.u.		28.1	18.3	17.5	20.2	28.1	17.4
$\Delta G^{\neq}$ kcal/mol		29.5	25.6	27.6	25.3	29.5	27.6

1 cal=4.184 J.

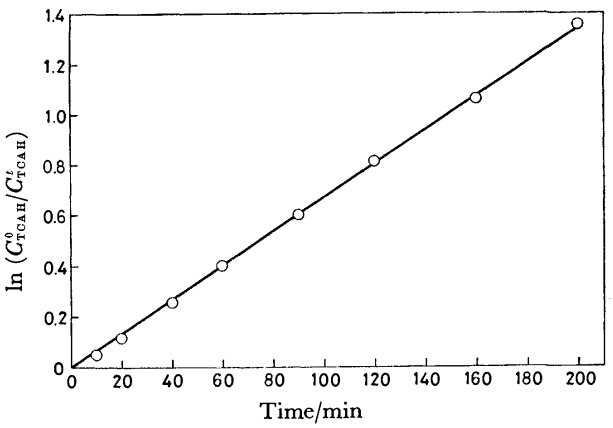

Fig. 2. The first-order rate plot for the decarboxylation of TCAH in aqueous solution of sodium hydroxide at 83 °C.
Initial concn of TCAH: 0.238 M, Concn of βCD: 0.02 M.

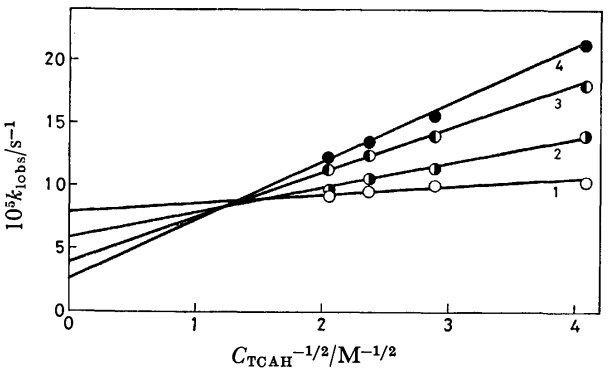

Fig. 3. The plot of k_{1obs} *vs.* $C_{TCAH}^{-1/2}$ for the decarboxylation of TCAH in aqueous solution of sodium hydroxide at 83 °C.
Concn of βCD: 1, none; 2, 0.01 M; 3, 0.02 M; 4, 0.03 M

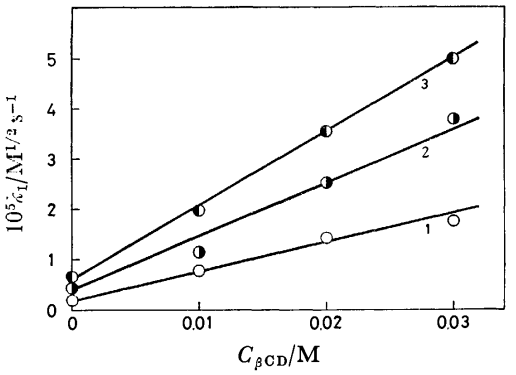

Fig. 4. The plot of k_1 *vs.* βCD concentration for the decarboxylation of TCAH in aqueous solution of sodium hydroxide. Reaction temp: 1, 75 °C; 2, 80 °C; 3, 83 °C.

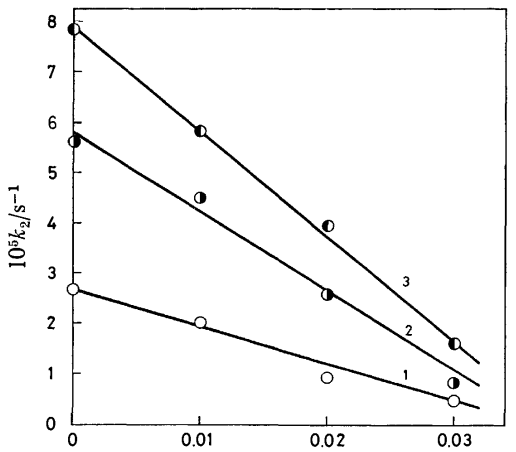

Fig. 5. The plot of k_2 *vs.* βCD concentration for the decarboxylation of TCAH in aqueous solution of sodium hydroxide.
Reaction temp: 1, 75 °C: 2, 80 °C; 3, 83 °C.

$$k_1 = k_{1T} + k_{1TC}C_{\beta CD} \quad (2)$$

$$k_2 = k_{2T} - k_{2TC}C_{\beta CD}. \quad (3)$$

From these relationships, the overall kinetics of this reaction is given by the following equation:

$$\text{Rate} = (k_{1T}+k_{1TC}C_{\beta CD})C_{TCAH}{}^{1/2}+(k_{2T}-k_{2TC}C_{\beta CD})C_{TCAH}. \quad (4)$$

The first and second terms represent the decarboxylation of the anion, for $C_{TCAH}^{1/2}$ is expressed by $K^{-1/2}C_{TCA^-}$ under our reaction conditions (Equivalent of TCAH≃ Equivalent of NaOH).[2] Here, K and C_{TCA^-} are the dissociation constant of TCAH and the anion concentration respectively. The third and fourth terms express the decomposition of the unionized molecule and concecutive reactions. In spite of its strong acidity, a measurable amount of TCAH still remains un-

Table 2. A comparison of the kinetic data for the decarboxylation of malonic acid and trichloroacetic acid in various solvents[6] at 100 °C

	Malonic acid			Trichloroacetic acid		
	$\Delta H^{\neq}$ kcal mol	$\Delta S^{\neq}$ e.u. mol	$10^4 k$ s^{-1}	$\Delta H^{\neq}$ kcal mol	$\Delta S^{\neq}$ e.u. mol	$10^4 k$ s^{-1}
1) Aniline	26.9	−4.46	1.3	24.5	−2.57	78
2) *o*-Toluidine	25.7	−7.05	2.0	23.8	−6.82	29
3) Quinoline	26.74	−2.37	5.0	23.98	−2.41	214
4) 8-Methylquinoline	24.4	−10.47	2.1	22.31	−8.43	100
5) Hexanoic acid	32.5	3.2	0.037	39.3	22.1	0.065

1 cal=4.184 J.

ionized, as has been mentioned above. Accordingly, it seems reasonable to assume that the chemical species which takes part in the decarboxylation is not only the anion, but also the unionized molecule.

The loss of a proton to form the anion increases the electron density on the oxygen of the carboxylate residue, thus decreasing the effective positive charge on the polarized carboxyl carbon atom. This leads to a weakening of the attraction between the nucleophile and the carboxylate carbon; this may account for the observed increase in the enthalpy of activation[5] of the first term as compared with that of the third term. On the other hand, a comparison of the kinetic data for the decarboxylation of malonic and trichloroacetic acids in various amines[6] showed that the steric effect hinders the approach of the nitrogen of amine to the carboxyl carbon, thus decreasing the probability of the formation of the activated complex. This leads to the decrease in the entropy of activation in the formation of the activated complex, as is shown in Table 2. Analogously to this, the smaller entropy of the activation of the third term than that of the first term, as is found in Table 1, may be ascribed to the hindrance of the approach of the oxygen of water to the carboxylic carbon of TCAH caused by the free-rotating carboxylic hydroxyl group. As a result of these findings, the pathways of the decarboxylation of TCA^- and of TCAH will be expressed by the first and the third terms respectively.

Furthermore, the kinetic behavior of TCAH bears some resemblance to that of malonic acid, as is shown in Table 2. Malonic acid apparently does not ionize not only in water and/or alcohol and dioxane containing water,[7] but also in aromatic amines and in acid solvents.[6] Therefore, an un-ionized TCAH molecule will probably take part in a decarboxylation reaction. This pathway, to be expressed as the first-order kinetics, seems to correspond to the third term, which constitutes the main part of the decarboxylation reaction (70—90%).

The values of the overlap population between two carbons in both TCAH and TCA^- were calculated by means of the CNDO/2 method in a closed system.[8] The geometries of the chemical species are cited from Sutton's Tables[9] and are fixed. When the oxygen of water, which is parallel to the Cl–C–C(=O)–O plane, approaches the carboxylic carbon of TCAH or TCA^- up to 0.2 nm on its p_z-axis, the diminution degree of the value of Mulliken's population between C–C in the free acid (0.0052) is larger than that in its anion (0.0008). Thus, the anion seems to be less liable to decarboxylate than the free acid.

The value of $\log k_{1T}$ decreases slightly and linearly with an increase in the pH, whereas $\log k_{2T}$ increases slightly and linearly with an increase in the pH value. It seems reasonable to assume that there are two kinds of water as the attacking species in a basic aqueous solution; one is the water affected by the hydroxide anion, and the other is the one unaffected by the anion. The hydroxide anion is hydrated by three molecules of water.[10] The oxygen of such water may have a larger negativity. As the ratio of the participation of such water increases with an increase in the pH,

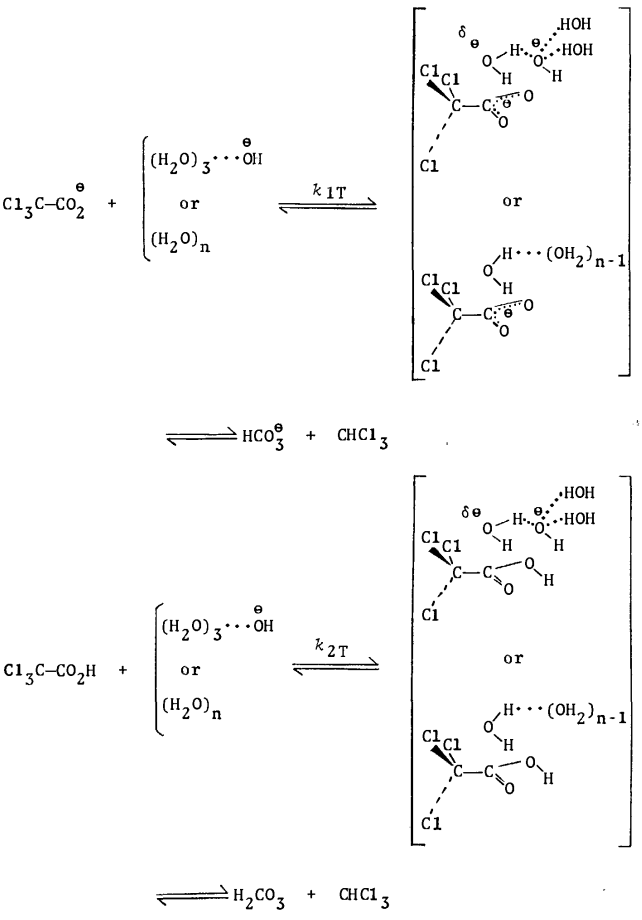

the rate constants, k_{1T} and k_{2T}, will decrease and increase respectively with an increase of the pH value.

The value of k_{1T} decreases, and that of k_{2T} increases, with a decrease in the pH value in this acidic range. The former still has some value (0.173×10^{-5} $M^{1/2}$ s^{-1}) even at pH 1.30, however, the concentration of the anion will decrease remarkably, but not to zero. The latter phenomenon is considered to be due to the formation of the protonated TCAH, which is liable to be attacked by the oxygen of water.

The second and fourth terms constitute a βCD-catalyzed mechanism. The value of log k_{1TC} is affected to a small extent by the pH. On the other hand, log k_{2TC} is independent of the basicity of the reaction medium. In the reaction catalyzed by βCD, the activated complex formed by the attack of the water molecule on the TCA^- anion included in βCD will be more stable than that in the case of free TCA^-, but the approach of the water molecule will be controlled by the severe steric factor. Therefore, both the enthalpy and the entropy of activation of the second term will have smaller values than those of the first term, as may be found in Table 1.

The fourth term of Eq. 4 may be a βCD-catalyzed hydrolysis of the trichloromethyl anion formed:[11]

$$TCAH + \beta CD \rightleftharpoons \underset{[I]}{\beta CD\cdots TCAH} \quad (5)$$

$$I + H_2O \rightleftharpoons \underset{[II]}{\beta CD\cdots Cl_3C^-} + H^+ + H_2CO_3 \quad (6)$$

$$II + H^+ \xrightarrow{\text{slow}} \beta CD + HCl + CCl_2 \quad (7)$$

$$CCl_2 + 2H_2O \longrightarrow 2HCl + HCO_2H. \quad (8)$$

In a reaction mixture, both the chloride and formate anions are detected. As the concentrations of formic and hydrochroric acids are added to the remaining TCAH concentration, the fourth term should have a minus sign.

This work has been supported financially by a grant of the Asahi Glass Foundation for Contributions to Industrial Technology.

References

1) H. Silberstein, *Chem. Ber.*, **17**, 2664 (1884).
2) F. H. Verhoek, *J. Am. Chem. Soc.*, **67**, 1062 (1945).
3) L. W. Clark, *J. Am. Chem. Soc.*, **77**, 3130 (1955); *J. Phys. Chem.*, **63**, 99, 1760 (1959); **64**, 917, 1758 (1960).
4) F. Cramer and W. Kampe, *J. Am. Chem. Soc.*, **87**, 1115 (1965).
5) K. J. Laidler, "Chemical Kinetics," 2nd ed, McGraw-Hill, New York (1965), p. 242.
6) L. W. Clark, "The Decarboxylation Reaction," in "The Chemistry of Carboxylic Acids and Esters," ed by S. Patai, John Wiley & Sons, New York (1969), pp. 589—622.
7) F. H. Westheimer and W. A. Jones, *J. Am. Chem. Soc.*, **63**, 3283 (1941).
8) J. A. Pople and D. L. Beveridge, "Approximate Molecular Orbital Theory," McGraw-Hill, New York (1970).
9) L. E. Sutton, "Tables of Interatomic Distances and Configuration in Molecules and Ions," The Chemical Society, Burlington House, London (1965).
10) G. Schwarzenbach and R. Sulzberger, *Helv. Chim. Acta*, **27**, 348 (1944).
11) J. Hine, *J. Am. Chem. Soc.*, **72**, 2438 (1950).

Thione *S*-Imide. Reaction with Heterocumulenes

Takao Saito, Isao Oikawa, and Shinichi Motoki*

Department of Chemistry, Faculty of Science, Science University of Tokyo, Kagurazaka, Shinjuku-ku, Tokyo 162

(Received December 28, 1979)

9-Fluorenethione *S*-*p*-toluenesulfonimide reacted with diphenylketene to give two regioisomeric 1,3-dipolar cycloadducts. The thione *S*-imide and symmetrical dialkylcarbodiimides produced 3-tosylimino-1,2,4-thiadiazolidines. In the reaction with ketenimines, there occurred siteselective cycloaddition reactions on C=N *vs.* C=C bonds in the imines and further rearrangement of the 1,2,4-thiadiazolidine adducts.

In the preceding papers, we reported that 9-fluorenethione *S*-*p*-toluenesulfonimides (**1**)[1] prepared by a Wittig-type reaction of phosphonium fluorenylides with *N*-sulfinyl-*p*-toluenesulfonamide underwent 1,3-dipolar and Diels-Alder type cycloaddition and ene reactions as a 4π or 2π component with the compounds containing C=C[2] or C=X[3] (X=NR, S, O) double bonds. The present report involves cycloaddition reactions of **1** with some heterocumulenes, *i.e.* diphenylketene, ketenimines, and carbodiimides.

When **1** was allowed to react with diphenylketene (**2**) in 1,2-dichloroethane at room temperature for a week, two regioisomeric (3+2)cycloadducts (**3**, **4**) were obtained. Their IR spectra showed νC=O absorptions at 1715 and 1718 cm^{-1} respectively, so four-membered structures such as **5** were excluded by a comparison with the νC=O values of the related compounds (**6**, **7**).[4] However, it was difficult to distinguish these adducts from each other strictly for the following reasons. (1) Assignment of the νC=O absorptions to Ph_2C–CO–N or Ph_2C–CO–Fl group was difficult. (2) Both adducts showed similar mass-spectral fragmentation patterns. (3) Both adducts were inert to hydrolysis and to 2,4-dinitrophenylhydrazine.

The reaction of **1** with symmetrical dialkylcarbodiimides (**8**) in 1,2-dichloroethane at room temperature afforded 1:1 cycloadducts (**9**). The IR spectra showed strong and broad absorptions at 1530—1560 cm^{-1} assigned to the νC=N–Ts but not to the νC=N–R (alkyl).[5] The mass-spectral fragmentation patterns which exhibited Fl=S$^{\cdot+}$, Ts–NCN–R$^{\cdot+}$, and Fl=NR$^{\cdot+}$ ion peaks also supported the 1,2,4-thiadiazolidine structure. Furthermore, in the NMR spectra of **9a**, the resonance for one CH_3CH_2N group appeared at a rather high field, probably due to the shielding effect exerted by the diamagnetic anisotropy of the adjacent fluorenylidene group (δ 0.56 (CH_3), δ 2.79 (CH_2)). The NMR signal of the other CH_3CH_2N group shifted to lower field (δ 1.42 (CH_3), δ 4.13 (CH_2)) than is found in the usual case. This may be attributed to the deshielding effect of the fluorenylidene ring because this ethyl group would be located near the plane of the fluorenylidene ring. The adduct **9** is considered to be the rearranged product of the hypothetical initial adduct **10**, but we cannot elucidate this at present.[6]

Reactions with diarylcarbodiimides did not proceed under the same reaction conditions, while **1** and unsymmetrical carbodiimides (**11**) afforded guanidines (**12**) and fluorenone (**13**) as unexpected products.

In the reaction of **1** with ketenimines (**14**), 1,3-thiazolidine (**15**) and 1,2,4-thiadiazolidine (**16**) deriv-

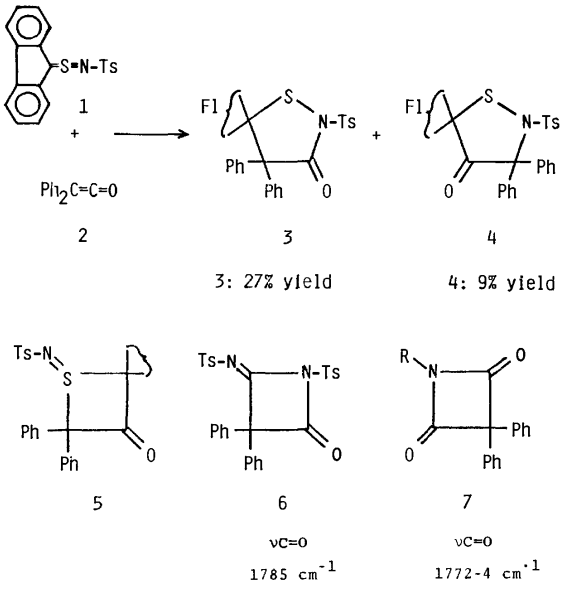

Fl: fluorenylidene group, Ts: p-toluenesulfonyl group

Scheme 1.

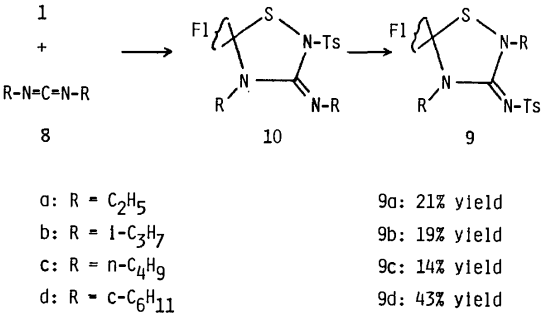

Scheme 2.

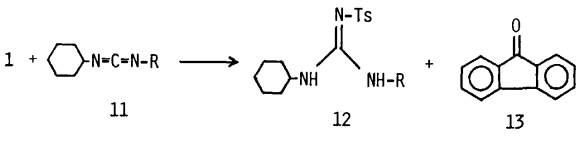

Scheme 3.

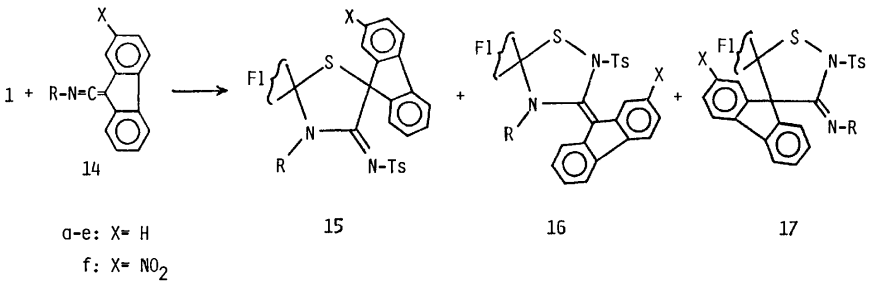

Scheme 4.

Table 1. Reaction of thione *S*-imide (**1**) with ketenimines (**14**)

	R	X	Yield (%)		
			15	**16**	**17**
a	C_6H_5	H	87	8	0
b	*p*-$CH_3C_6H_4$	H	0	55	16
c	*p*-ClC_6H_4	H	67	17	0
d	1-Naphthyl	H	93	3	0
e	*c*-C_6H_{11}	H	75	0	0
f	C_6H_5	NO_2	17	20	0

Table 2. ^{13}C NMR spectral data of **15** and **16**

	C(2)	C(3)	C(4)	C(5)	CH_3(Ts)
15a	71.8 s	—	162.9 s	69.0 s	21.3 q
15b	70.9 s	—	163.7 s	67.6 s	21.7 q
15f	72.1 s	—	163.2 s	68.4 s	21.2 q
16a	—	142.2 s	—	68.3 s	21.5 q
16b	—	150.6 s	—	67.1 s	21.8 q

s: Singlet, q: quartet in SFORD measurement.

atives were obtained (Table 1). The IR spectra of **15** and **16** displayed strong νC=N–Ts absorption at 1560—1565 cm^{-1} and νC=C at 1670—1685 cm^{-1}, respectively. The ^{13}C NMR spectra of **15a, b, f** (indicating the presence of two quarternary carbon atoms and one ring-carbon atom attached to the tosylimino group) and **16a,b** (indicating the presence of one quarternary carbon atom and one olefinic ring-carbon atom bonded with nitrogens) also supported the proposed structures (Table 2). In the reaction of **1** and **14b**, a third adduct (**17b**) which exhibits νC=N–Tol-*p* absorption at 1595 cm^{-1} was obtained. This is the 1,3-cycloadduct of **1** onto the C=C bond in **14**. The adducts **16a,b** were found to rearrange gradually into **15a,b** on standing in dichloromethane or deuteriochloroform; this conversion was confirmed by monitoring the NMR spectra and by isolating **15a,b**. The reaction is rationally explained by assuming the sulfur-nitrogen bond cleavage in **16** and a subsequent recombination of sulfur-carbon bond, as considered in the formation of **9**.[7] On the other hand, **17b**, a direct 1,3-cycloadduct, did not rearrange into **15b** (and *vice versa*) at room temperature. The sum of the yields of **15** and **16** which result from the cycloaddition of **1** onto the C=N bond in **14** is much larger than that of **17**, as shown in Table 1. Therefore the

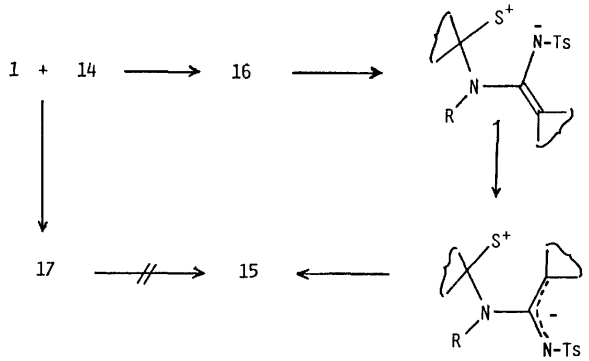

Scheme 5.

cycloaddition of **1** onto the C=N bond predominates with kinetic preference over that onto the C=C bond.

Experimental

All the melting points are uncorrected. The IR spectra were determined on a Hitachi Model 260-10 spectrometer. The ^1H NMR and ^{13}C NMR spectra were measured on JEOL JNM-PMX 60 and/or JNM-FX 100 spectrometers in δ values from Me_4Si as an internal standard in deuteriochloroform. The mass spectra were recorded on a Hitachi double-focusing mass spectrometer RMU-7M operating at an ionizing potential of 70 eV. The elemental analyses were performed using a Shimadzu universal organic micro analyzer UM-3B and a rapid-nitrogen analyzer NA-1.

Starting Materials. Diphenylketene (**2**)[8] and carbodiimides (**8, 11**)[9] were prepared by the methods in the literature. New ketenimines (**14**) were synthesized from the corresponding isocyanates and triphenylphosphonium fluorenylides by the modified method reported by Frøyen.[10]

A mixture of phenyl isocyanate (1.19 g, 0.01 mol) and triphenylphosphonium fluorenylide (4.26 g, 0.01 mol) was refluxed in 50 ml of dry benzene for 2 h until the IR absorption of νN=C=O at 2200 cm^{-1} disappeared; the ketenimine formation was recognized from the strong maximum νC=C=N absorption at 2025 cm^{-1}. After the evaporation of the benzene solvent, the residue was extracted with 60 m of hot ligroine and the yellow-orange extract was passed through a short Florisil column. From the colored fraction, the ketenimine **14a** was obtained quantitatively as yellow plates (recrystallized from hexane); mp 85.0—85.5 °C; MS (70 eV) *m/e* 267 (100, M^+), 190 (58), 164 (66). Found: C, 89.94; H, 4.73%. Calcd for $C_{20}H_{13}N$: C, 89.86; H, 4.90%. The other ketenimines **14b—f** were similarly prepared, as is shown in Table 3.

Reaction of Thione S*-Imide (1) with Diphenylketene (2).* A mixture of **1** (2.46 g, 6.7 mmol) and **2** (1.30 g, 6.7 mmol)

Table 3. Ketenimines (**14**)

Compound	Reaction time	Yield %	Mp (°C) [Bp(°C/mm)]	IR νC=C=N	Appearance
14a	2 h	98	85.0—85.5	2025	yellow plates
14b	2 h	93	—	2010	yellow oil
14c	2 h	82	84.5—85.5	2010	yellow crystals
14d	5 h	57	165—166	2030	yellow needles
14e	3 d	90	[180/0.05]	2040	yellow oil
14f	1 d	20	89—90	2010	orange needles

was stirred in dry 1,2-dichloroethane (70 ml) for a week at room temperature. After the evaporation of the solvent, the residue was chromatographed on silica gel, using benzene as the eluent, to give **3** (the latter fraction) and **4** (the former fraction) together with small amounts of fluorenone (**13**) and *N*-fluorenylidene-*p*-toluenesulfonamide.[11]

3: Colorless crystals (benzene–chloroform); mp 264—265 °C; IR (KBr) 1715 cm^{-1} (C=O), 1250 cm^{-1}; MS (70 eV) *m/e* 559 (17, M^+), 206 (100, $M^+ - Ts - Fl{=}S$), 196 (16, $Fl{=}S^+$), 194 (10, Ph_2CCO^+); NMR ($CDCl_3$) δ 2.42 (s, 3H, CH_3(Ts)), 6.8—7.7 (m, 22H, arom). Found: C, 73.01; H, 4.55; N, 2.54; S, 11.42%. Calcd for $C_{34}H_{25}NO_3S_2$: C, 72.96; H, 4.50; N, 2.50; S, 11.46%.

4: Colorless crystals (benzene–chloroform); mp 249—250 °C; IR (KBr) 1718, 1724 (shoulder) (C=O), 960 cm^{-1}; MS (70 eV) *m/e* 559 (10, M^+), 206 (46, $M^+ - Ts - Fl{=}S$), 196 (100, $Fl{=}S^+$), 194 (62, Ph_2CCO^+); NMR ($CDCl_3$) δ 2.42 (s, 3H, CH_3(Ts)), 6.7—7.8 (m, 22H, arom). Found: C, 72.99 H, 4.56; N, 2.56; S, 11.48%. Calcd for $C_{34}H_{25}NO_3S_2$: C, 72.96; H, 4.50; N, 2.50; S, 11.46%.

Reaction of Thione S-*Imide* (*1*) *with Symmetrical Carbodiimides* (*8*). *A Typical Procedure*: A mixture of **1** (1.83 g, 5 mmol) and dicyclohexylcarbodiimide (**8d**) (1.03 g, 5 mmol) was stirred in dry 1,2-dichloroethane (30 ml) for 2 h at room temperature. The solvent was evaporated *in vacuo* and the residue was chromatographed on silica gel, using benzene as the eluent, to give **9d** in a 43% yield as colorless crystals recrystallized from chloroform–ethanol. The reactions of **1** with **8a**—**c** were similarly carried out (reaction times: **a**, **b**, and **d**, 2 h; **c**, 4 h).

9a: Mp 122—124 °C; IR (KBr) 1560 (C=N), 1280, and 1145 cm^{-1} (SO_2); NMR ($CDCl_3$) δ 0.56 (t, J=7.2 Hz, 3H, CH_3), 1.42 (t, J=7.0 Hz, 3H, CH_3), 2.36 (s, 3H, CH_3 (Ts)), 2.79 (q, J=7.2 Hz, 2H, CH_2), 4.13 (q, J=7.0 Hz, 2H, CH_2), 7.1—8.1 (m, 12H, arom); MS (70 eV) *m/e* 463 (13, M^+), 308 (40, $M^+ - Ts$), 280 (2, $M^+ - Ts - Et + 1$), 224 (9, $TsNCNEt^+$), 207 (21, $Fl{=}NEt^+$), 196 (35, $Fl{=}S^+$), 155 (27, Ts^+), 122 (100, $M^+ - Ts - Fl{=}S$), 91 (64, Tol^+). Found: C, 64.81; H, 5.45; N, 8.94; S, 13.90%. Calcd for $C_{25}H_{25}N_3O_2S_2$: C, 64.77; H, 5.44; N, 9.06; S, 13.83%.

9b: Mp 208—209 °C; IR (KBr) 1540 (C=N), 1280 and 1145 cm^{-1} (SO_2); NMR ($CDCl_3$) δ 0.8 (d, J=6.8 Hz, 6H, CH_3), 1.42 (d, J=6.4 Hz, 6H, CH_3), 2.37 (s, 3H, CH_3 (Ts)), 2.90 (sep, J=6.8 Hz, 1H, CH), 5.33 (sep, J=6.4 Hz, 1H, CH), 7.1—8.0 (m, 12H, arom); MS (70 eV) *m/e* 491 (15, M^+), 449 (13), 336 (57, $M^+ - Ts$), 294 (29), 238 (35, Ts-NCNPr-*i*$^+$), 220 (46), 196 (47, $Fl{=}S^+$), 155 (48, Ts^+), 140 (79, $M^+ - Ts - Fl{=}S$), 91 (100, Tol^+). Found: C, 65.83; H, 5.90; N, 8.50; S, 13.20%. Calcd for $C_{27}H_{29}N_3O_2S_2$: C, 65.96; H, 5.95; N, 8.55; S, 13.02%.

9c: Mp 113—114 °C; IR (KBr) 1550 (C=N), 1290 and 1145 cm^{-1} (SO_2); NMR ($CDCl_3$) δ 0.2—2.1 (m, 14H, CH_2-CH_2CH_3), 2.36 (s, 3H, CH_3 (Ts)), 2.67 (t, J=7.5 Hz, 2H, CH_2), 4.06 (t, J=7.3 Hz, 2H, CH_2), 7.1—8.1 (m, 12H, arom); MS (70 eV) *m/e* 519 (4, M^+), 463 (8), 364 (65, $M^+ - Ts$), 308 (12), 235 (18, $Fl{=}NBu\text{-}n^+$), 196 (35, $Fl{=}S^+$), 168 (17, $M^+ - Ts - Fl{=}S$), 155 (54, Ts^+), 91 (100, Tol^+). Found: C, 67.21; H, 6.31; N, 8.14; S, 12.36%. Calcd for $C_{29}H_{33}N_3O_2S_2$: C, 67.03; H, 6.40; N, 8.08; S, 12.33%.

9d: Mp 195—196 °C; IR (KBr) 1530 (C=N), 1280 and 1140 cm^{-1} (SO_2); NMR ($CDCl_3$) δ 0.2—2.5 (m, 20H, $(CH_2)_5$), 2.37 (s, 3H, CH_3 (Ts)), 2.75 (broad s, 1H, CH), 4.78 (broad s, 1H, CH), 7.0—8.0 (m, 12H, arom); MS (70 eV) *m/e* 571 (4, M^+), 489 (38), 416 (47, $M^+ - Ts$), 334 (37), 260 (22), 220 (48, $M^+ - Ts - Fl{=}S$), 196 (31, $Fl{=}S^+$), 155 (52, Ts^+), 91 (100, Tol^+). Found: C, 69.74; H, 6.65; N, 7.60; S, 11.22%. Calcd for $C_{33}H_{37}N_3O_2S_2$: C, 69.32; H, 6.52; N, 7.35; S, 11.21%.

Reaction of Thione S-*Imide* (*1*) *with Unsymmetrical Carbodiimides* (*11*). The reaction was carried out in the manner used for **8** (reaction time; **a** and **b**: 30 min, **c**: 15 h). The resultant reaction mixture was subjected to chromatography on silica gel, using chloroform as the eluent, to give **12** and **13**.[11]

12a: Colorless crystals (chloroform–hexane); mp 163—165 °C; IR (KBr) 3370, 3345 (N–H), 1590 (C=N), 1260 and 1145 cm^{-1} (SO_2); NMR ($CDCl_3$) δ 0.9—2.1 (m, 10H, $(CH_2)_5$), 2.39 (s, 3H, CH_3 (Ts)), 2.80 (d, J=4.8 Hz, 3H, CH_3), 3.50 (broad s, 1H, CH), 5.3—6.6 (broad m, 2H, NH), 7.21 (d, J=7.8 Hz, 2H, arom), 7.76 (d, J=7.8 Hz, 2H, arom); MS (70 eV) *m/e* 309 (3, M^+), 162 (7), 154 (58), 98 (84), 91 (62), 28 (100). Found: C, 58.03; H, 7.45%. Calcd for $C_{15}H_{23}N_3O_2S$: C, 58.23; H, 7.49%.

12b: Colorless crystals (chloroform–hexane); mp 106—107 °C; IR (KBr) 3340 (N–H), 1580 (C=N), 1260 and 1140 cm^{-1} (SO_2); NMR ($CDCl_3$) δ 0.8—2.1 (m, 11H, $(CH_2)_5CH$), 1.10 (t, J=7.0 Hz, 3H, CH_3), 2.38 (s, 3H, CH_3 (Ts)), 2.9—3.9 (m, 3H, CH_2, NH), 6.2 (broad, 1H, NH), 7.20 (d, 2H, J=8.0 Hz, arom), 7.73 (d, 2H, J=8.0 Hz, arom); MS (70 eV) *m/e* 323 (2, M^+), 225 (3), 168 (70), 155 (18), 98 (96), 91 (47), 44 (100). Found: C, 59.55; H, 7.81%. Calcd for $C_{16}H_{25}N_3O_2S$: C, 59.42; H, 7.79%.

12c: Colorless crystals (chloroform–hexane); mp 165—166 °C; IR (KBr) 3350 (N–H), 1625 (C=N), 1250 and 1140 cm^{-1} (SO_2); NMR ($CDCl_3$) δ 0.7—2.2 (m, 10H, $(CH_2)_5$), 2.41 (s, 3H, CH_3 (Ts)), 3.8 (broad, 1H, CH), 5.0 (broad, 1H, NH), 7.0—7.5 (m, 6H, arom), 7.79 (d, 2H, J=8.2 Hz, arom), 8.66 (broad, 1H, NH); MS (70 eV) *m/e* 405 (2, M^+), 322 (2), 250 (10), 155 (13), 127 (100), 98 (24), 91 (31). Found: C, 59.22; H, 6.01%. Calcd for $C_{20}H_{24}N_3O_2SCl$: C, 59.18; H, 5.96%.

Reaction of Thione S-*Imide* (*1*) *with Ketenimines* (*14*). *A Typical Procedure*: To a partial suspension of **1** (0.92 g, 2.5 mmol) in 30 ml of 1,2-dichloroethane, a solution of **14a** (0.67 g, 2.5 mmol) in 10 ml of 1,2-dichloroethane was added dropwise at room temperature. The red suspension of **1** gradually disappeared within 2—4 h, but the mixture remained colored. The reaction mixture was stirred overnight

at room temperature to complete the reaction. The evaporation of the solvent gave the oily residue, which was subjected to column chromatography on silica gel with benzene as the eluent, followed by dichloromethane. The evaporation of the benzene elution gave **16** together with a trace amount of **14** and fluorenone (**13**). From the second dichloromethane elution, **15** (**17b**) was obtained. The crude **15**, **16**, and **17b** were recrystallized from the appropriate solvents as indicated below. In the case of **c** and **d**, the mixed elution solvent was used instead of the first benzene elution because of the low solubility of **15c**, **d** and **16c**, **d** into benzene (CH_2Cl_2/benzene; **c**: *ca.* 1, **d**: *ca.* 2).

15a: Yellow crystals (recrystallized from benzene-ether); mp 232—233.5 °C; IR (KBr) 1560 (C=N), 1320, 1150, and 1095 cm^{-1} (SO_2); NMR ($CDCl_3$) δ 2.28 (s, 3H, CH_3 (Ts)), 6.8—7.8 (m, 25H, arom); MS (70 eV) *m/e* 632 (3, M^+), 477 (6, $M^+ - Ts$), 436 (12, $M^+ - Fl{=}S$), 281 (27, $M^+ - Ts - Fl{=}S$), 139 (100). Found: C, 76.17; H, 4.40; N, 4.53%. Calcd for $C_{40}H_{28}N_2O_2S_2$: C, 75.94; H, 4.46; N, 4.43%.

15b: Yellow crystals (benzene-ether); mp 267—269 °C; IR (KBr) 1560 (C=N), 1320, 1155, and 1100 cm^{-1} (SO_2); MS (70 eV) *m/e* 646 (4, M^+), 491 (3, $M^+ - Ts$), 450 (30, $M^+ - Fl{=}S$), 295 (78, $M^+ - Ts - Fl{=}S$), 255 (100), 139 (60). Found: C, 76.21; H, 4.72; N, 4.39%. Calcd for $C_{41}H_{30}N_2O_2S_2$: C, 76.13; H, 4.68; N, 4.33%.

15c: Yellow prisms (dichloromethane-benzene); mp 240—242 °C; IR (KBr) 1565 (C=N), 1315, 1150, and 1090 cm^{-1} (SO_2); NMR ($CDCl_3$) δ 2.27 (s, 3H, CH_3 (Ts)), 6.9—8.1 (m, 24H, arom); MS (70 eV) *m/e* 666 (4, M^+), 511 (7, $M^+ - Ts$), 470 (15, $M^+ - Fl{=}S$), 315 (31, $M^+ - Ts - Fl{=}S$), 139 (100). Found: C, 72.19; H, 4.12; N, 4.08%. Calcd for $C_{40}H_{27}N_2O_2S_2Cl$: C, 72.00; H, 4.08; N, 4.08%.

15d: Yellow crystals (benzene); mp 218—220 °C; IR (KBr) 1560 (C=N), 1315, 1150, and 1090 cm^{-1} (SO_2); NMR ($CDCl_3$) δ 2.18 (s, 3H, CH_3 (Ts)), 6.7—8.3 (m, 27H, arom); MS (70 eV) *m/e* 682 (45, M^+), 527 (16, $M^+ - Ts$), 486 (29, $M^+ - Fl{=}S$), 331 (100, $M^+ - Ts - Fl{=}S$), 196 (94, $Fl{=}S^+$), 139 (19). Found: N, 3.92%. Calcd for $C_{44}H_{30}N_2O_2S_2$: N, 4.10%.

15e: Colorless crystals (benzene-hexane); mp 270—271 °C; IR (KBr) 1560 (C=N), 1300, 1155, and 1095 cm^{-1} (SO_2); NMR ($CDCl_3$) δ 2.24 (s, 3H, CH_3 (Ts)), 1.1—2.4 (m, 11H, $(CH_2)_5CH$), 6.8—7.5 (m, 20H, arom); MS (70 eV) *m/e* 638 (20, M^+), 483 (6, $M^+ - Ts$), 442 (6, $M^+ - Fl{=}S$), 196 (28, $Fl{=}S^+$), 139 (100). Found: N, 4.33%. Calcd for $C_{40}H_{34}N_2O_2S_2$: N, 4.38%.

15f: Pale yellow needles (dichloromethane-benzene); mp 221—222 °C; IR (KBr) 1560 (C=N), 1525, 1340 (NO_2), 1310, 1155, and 1095 cm^{-1} (SO_2); NMR ($CDCl_3$) δ 2.27 (s, 3H, CH_3 (Ts)), 6.7—8.3 (m, 24H, arom); MS (70 eV) *m/e* 682 (45, M^+), 527 (16, $M^+ - Ts$), 486 (29, $M^+ - Fl{=}S$), 331 (100, $M^+ - Ts - Fl{=}S$), 196 (94, $Fl{=}S^+$), 139 (19). Found: N, 6.23%. Calcd for $C_{40}H_{27}N_3O_4S_2$: N, 6.20%.

16a: Colorless plates (benzene-hexane); mp 173—175 °C; IR (KBr) 1670 (C=C), 1365, 1150, and 1085 cm^{-1} (SO_2); NMR ($CDCl_3$) δ 2.60 (s, 3H, CH_3 (Ts)), 6.5—7.9 (m, 25H, arom); MS (70 eV) *m/e* 632 (4, M^+), 477 (9, $M^+ - Ts$), 436 (13, $M^+ - Fl{=}S$), 281 (31, $M^+ - Ts - Fl{=}S$), 267 (19, $FlCNPh^+$), 196 (9, $Fl{=}S^+$), 139 (100). Found: C, 76.02; H, 4.51; N, 4.32%. Calcd for $C_{40}H_{28}N_2O_2S_2$: C, 75.94; H, 4.46; N, 4.43%.

16b: Colorless plates (benzene-hexane); mp 206—207 °C; IR (KBr) 1670 (C=C), 1370, 1150, and 1095 cm^{-1} (SO_2); NMR ($CDCl_3$) δ 1.88 (s, 3H, CH_3), 2.58 (s, 3H, CH_3 (Ts)), 5.8—8.3 (m, 24H, arom); MS (70 eV) *m/e* 646 (11, M^+), 491 (6, $M^+ - Ts$), 450 (22, $M^+ - Fl{=}S$), 295 (56, $M^+ - Ts - Fl{=}S$), 281 (25, $FlCN\text{-}Tol\text{-}p^+$), 196 (26, $Fl{=}S^+$), 139 (100). Found: C, 76.18; H, 4.70; N, 4.35%. Calcd for $C_{41}H_{30}N_2O_2S_2$: C, 76.13; H, 4.68; N, 4.33%.

16c: Colorless plates (dichloromethane-benzene); mp 193—196 °C; IR (KBr) 1670 (C=C), 1365, 1150, and 1090 cm^{-1} (SO_2); NMR ($CDCl_3$) δ 2.27 (s, 3H, CH_3 (Ts)), 6.07—8.5 (m, 24H, arom); MS (70 eV) *m/e* 666 (13, M^+), 511 (13, $M^+ - Ts$), 470 (17, $M^+ - Fl{=}S$), 315 (56, $M^+ - Ts - Fl{=}S$), 301 (25, $FlCNPh\text{-}Cl\text{-}p^+$), 196 (34, $Fl{=}S^+$), 139 (100). Found: N, 4.18%. Calcd for $C_{40}H_{27}N_2S_2Cl$: N, 4.20%.

16d: Colorless crystals (dichloromethane-hexane); mp 170—172 °C; IR (KBr) 1670 (C=C), 1365, 1165, and 1090 cm^{-1} (SO_2); NMR ($CDCl_3$) δ 2.18 (s, 3H, CH_3 (Ts)), 6.2—8.4 (m, 27H, arom); MS (70 eV) *m/e* 682 (46, M^+), 527 (20, $M^+ - Ts$), 486 (16, $M^+ - Fl{=}S$), 331 (100, $M^+ - Ts - Fl{=}S$), 317 (32, $FlCN\text{-}Naph^+$), 139 (15). Found: N, 3.95%. Calcd for $C_{40}H_{27}N_3O_4S_2$: N, 6.20%.

17b: Yellow crystals (dichloromethane-ether); mp 174—175 °C; IR (KBr) 1595 (C=N), 1290, 1165, and 1090 cm^{-1} (SO_2); NMR ($CDCl_3$) δ 2.05 (s, 3H, CH_3), 2.52 (s, 3H, CH_3 (Ts)), 6.4—8.1 (m, 24H, arom); MS (70 eV) *m/e* 646 (1, M^+), 450 (17, $M^+ - Fl{=}S$), 295 (42, $M^+ - Ts - Fl{=}S$), 256 (100), 196 (53, $Fl{=}S^+$). Found: C, 76.29; H, 4.71%. Calcd for $C_{41}H_{30}N_2O_2S_2$: C, 76.13; H, 4.68%.

References

1) T. Saito and S. Motoki, *J. Org. Chem.*, **42**, 3922 (1977).

2) a) T. Saito and S. Motoki, *Chem. Lett.*, **1978**, 591; b) T. Saito and S. Motoki, *J. Org. Chem.*, **44**, 2493 (1979).

3) T. Saito, I. Oikawa, and S. Motoki, *Bull. Chem. Soc. Jpn.*, **53**, 1023 (1980).

4) H. Grill and G. Kresze, *Tetrahedron Lett.*, **1970**, 1427, and the references cited therein.

5) Similar IR determinations were given for 1,2,4-thiadiazolidine derivatives containing *exo* C=N-R groups. a) G. L'Abbe', G. Verhelst, C-C. Yu, and S. Toppet, *J. Org. Chem.*, **40**, 1728 (1975); b) M. Komatsu, Y. Ohshiro, K. Yasuda, S. Ichijima, and T. Agawa, *J. Org. Chem.*, **39**, 957 (1974); c) T. Kinoshita, S. Sato, and C. Tamura, *Bull. Chem. Soc. Jpn.*, **49**, 2236 (1976); d) T. Kinoshita, S. Sato, and C. Tamura, *Bull. Chem. Soc. Jpn.*, **52**, 1225 (1979).

6) This type of rearrangement for 1,2,4-thiadiazolidine ring system was reported; Refs. 5b and 5d.

7) On the basis of the spectral data, we could not completely exclude the possibility of the 1,2-thiazolidine structure **i** for **15**.

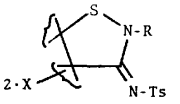

i

8) *Org. Synth.*, Coll. Vol. III, 356 (1955).

9) S. R. Sandlar and W. Karo, "Organic Functional Group Preparation," Academic Press, New York and London (1971), Vol. II, p. 205.

10) P. Frøyen, *Acta Chem. Scand.*, *B*, **28**, 586 (1974).

11) *N*-fluorenylidene-*p*-toluenesulfonamide and fluorenone (**13**) were identified by a comparison of the IR spectra with those of authentic samples.

The Dehydrochlorination of *gem*-Dichloroalkane and the Formation of Dienes from the Reactions of Butenes and Cyclohexene with Chlorine through Molten Salt

Shōichi Kikkawa, Masakatsu Nomura,* and Michimasa Shimizu

Department of Applied Chemistry, Faculty of Engineering, Osaka University, Suita, Osaka 565

(Received January 5, 1980)

The dehydrochlorination of 1,1-dichloropropane and 1,1-dichloro-3-methylbutane was carried out over molten salt catalysts (mainly $ZnCl_2$-containing melts) using a conventional flow system. The *cis*/*trans* ratio (1.8) of the resulting olefins from 1,1-dichlorobutane was found to stand between the ratio (1.4) with 1,1-dichloro-3-methylbutane and the ratio (2.2) with 1,1-dichloropropane; this can be explained by considering the stereochemistry of the adsorbed carbonium ions. The detailed results of the reactions of three butene isomers with chlorine through molten salts were presented. The selective formation of butadiene was explained in terms of the thermally assisted attack of chlorine in the allylic positions of butene, followed by the 1,2- or 1,4-elimination of HCl from chlorobutenes, a process which is strongly assisted by the $ZnCl_2$-containing melts. The reaction of 2-methyl-2-butene and cyclohexene with chlorine through molten salts was also undertaken. The addition of Zn powder to $ZnCl_2$ melts in advance was found to improve the selectivity for the formation of isoprene and cyclohexadiene. Because the HCl evolved reacts instantly with Zn powder to afford $ZnCl_2$ and hydrogen, Zn powder substantially prohibits the addition of HCl to dienes yielding chlorobutenes and chlorocyclohexenes.

In a previous paper,[1] we explained the *cis*/*trans* ratio of the 1-chloro-1-butene produced in the dehydrochlorination of 1,1-dichlorobutane in contact with zinc chloride melts by considering the surface-adsorbed carbonium ion. The former part of this paper will present additional information to support this explanation, using 1,1-dichloropropane and 1,1-dichloro-3-methylbutane as reactants.

The reaction of butenes with chlorine through zinc chloride melts containing alkali chloride has been found to yield butadiene predominantly.[2] The dependence of this reaction on the reaction conditions has been discussed. The selective formation of isoprene and cyclohexadiene from the reaction of 2-methyl-2-butene and cyclohexene with chlorine was also examined. In these cases, the addition of zinc powder to zinc chloride melts improved the yield of these dienes.

Experimental

Catalysts and Reagents. The $ZnCl_2$, $SnCl_2$, CuCl, LiCl, NaCl, KCl, $NaNO_3$, and KNO_3 were all commercially available guaranteed reagents. The nitrogen, argon, chlorine, and hydrogen chloride were dried by passing each gas from commercial cylinders through concd H_2SO_4 and anhydrous calcium chloride. The 1,1-dichloropropane was prepared by the reaction of propionaldehyde with PCl_5 (bp 83—85 °C; 98% pure).[3] The 1,1-dichloro-3-methylbutane was prepared by the reaction of isopropyl chloride and vinyl chloride in the presence of $AlCl_3$ (bp 57 °C/66 mmHg; 99% pure).[4] The addition of HCl to isoprene afforded 3-chloro-3-methyl-1-butene (bp 32 °C/40 mmHg).[5] The 1-chloro-3-methyl-2-butene was obtained by the isomerization[5] of 3-chloro-3-methyl-1-butene in the presence of HCl [bp 61—62 °C/120 mmHg; NMR ($CDCl_3$) 1.70 (6H, CH_3, m), 3.96 (2H, $ClCH_2$, d), 5.34 (H, CH=C, t)]. The 3-chloro-2-methyl-1-butene and 1-chloro-2-methyl-2-butene were separated from a mixture of them obtained by the chlorination[6] of 2-methyl-2-butene using preparative gas chromatography; they were confirmed on the basis of their respective NMR spectra [the former NMR (CCl_4): 1.60 (3H, $ClCHCH_3$, d), 1.84 (3H, $=CCH_3$, s), 4.46 (1H, CHCl, q), 4.74 (1H, HC=, s), 4.92 (1H, HC=, s); the latter NMR (CCl_4): 1.70 (6H, $=CHCH_3$, $=CCH_3$, mc), 3.96 (2H, CH_2Cl, s), 5.34 (1H, $CHCH_3$, q)]. The 3-chlorocyclohexene was prepared by the photoirradiation of a mixture of cyclohexene and *t*-butyl hypochlorite (bp 52—53 °C/25 mmHg; 95% pure).[7] The 4-chlorocyclohexene was obtained by the dehydration[8] of 4-chlorocyclohexanol, which had been synthesized according to the literature (bp 56—57 °C/39 mmHg; 97% pure).[9]

General Procedure. The reaction through molten salts was carried out using an apparatus similar to that described in the previous paper.[1] The salts tested were two ternary mixtures, 60 mol% $ZnCl_2$–20 mol% KCl–20 mol% NaCl ($ZnCl_2$ melts) and 60 mol% CuCl–20 mol% KCl–20 mol% NaCl (CuCl melts), and a binary mixture, 60 mol% $SnCl_2$–40 mol% KCl and 60 mol% CuCl–40 mol% LiCl. The melt of 50 mol% KNO_3–50 mol% $NaNO_3$ was used as a reaction medium, through which chlorination may be supposed to reflect a purely thermal reaction. For the preparation of the anhydrous $ZnCl_2$ melts,[10] a stream of HCl gas was introduced, along with a N_2 stream, at the desired temperature; then dry N_2 was bubbled in in order to eliminate the excess HCl gas. For the other salts, dry N_2 was allowed to flow through the melts until no more H_2O was seen at the exit. A total of 40—70 g of material was used, and the melt height was 8 cm from the tip of the nozzle to the melt surface.

The duration of the reaction was 30 min. After the end of the reactant-feeding, N_2-bubbling was continued for about 1 h in order to recover the reaction mixture remaining in the system. The reaction products were collected at the exit in an ice–water trap. Analysis of the gaseous products was carried out by removing aliquots from the gas stream with the aid of a syringe (every ten minutes after the start of feeding). Both the HCl evolved and the unreacted Cl_2 (in the case of chlorination) were removed prior to sampling by passing the gas stream through a $Na_2S_2O_3$ solution.

Analysis of Reaction Products. The GC column materials used for products analysis were as follows: 1. 10% Pluronic L 84 on Neopak 1 A (60/80 mesh), 2. 30% Propylene Carbonate/Uniport C (30/60 mesh), 3. 15% Silicone DC 550/Celite 545 (60/80 mesh), 4. 20% PEG 20 M/Celite 545 (30/60 mesh), 5. Silica gel (60/80 mesh).

The columns and the operating temperature used for the analysis of the liquid and gaseous products obtained from the respective reaction systems are described below

for each reaction system. 1,1-Dichloropropane (liq: 1, 40 °C, Shimadzu GC-3BT; gas: 5, 145 °C, Shimadzu GC-3AH), 1,1-dichloro-3-methylbutane (liq: 1, 70 °C, Shimadzu GC-2C; gas; 5, 145 °C, Shimadzu GC-3AH), butene (liq: 1, 60 °C, Shimadzu GC-3BT; gas: 2, room temp, Shimadzu GC-2C), 2-methyl-2-butene (liq: 1, 50 °C, Shimadzu GC-3BT; gas: 3, 50 °C, Shimadzu GC-3BT), cyclohexene (liq: 4, 110 °C, Shimadzu GC-2C; gas: 5, 145 °C, Shimadzu GC-3AH).

Identification of Products. Both *cis*- and *trans*-1-chloro-1-propene and *cis*- and *trans*-1-chloro-3-methyl-1-butene were separated by preparative gas chromatography, and their structures were confirmed by a comparison of the chemical-shift difference[11] of the olefinic proton between CCl_4 and C_6H_6. Most of the products were confirmed by having the same retention time as that of the reference and by means of the mass spectra of each fraction, obtained using GC-MS (Hitachi-RMU-6 MG type). Table 1 shows the confirmed liquid products (arranged in the order of elution in a gas chromatography) for each reaction system.

Results and Discussion

Dehydrochlorination of 1,1-Dichloropropane and 1,1-Dichloro-3-methylbutane. The results of the dehydrochlorination of 1,1-dichloropropane and 1,1-dichloro-3-methylbutane through $ZnCl_2$–KCl–NaCl, $SnCl_2$–KCl, and CuCl–LiCl are shown in Table 2 and Table 3 respectively. At 450 °C, the 1,1-dichloropropane conversion was approximately double the conversion at 400 °C through $ZnCl_2$ melts and $SnCl_2$ melts. The finding that the gaseous-product yield at 450 °C was more than twice the value at 400 °C suggests an increasing contribution of the thermal reaction at the higher temperature. Such a tendency was also observed in the dehydrochlorination of 1,1-dichloro-3-methylbutane. The dehydrochlorination with the $ZnCl_2$ melts afforded a relatively high conversion in comparison with that of the $SnCl_2$ melts.

The dehydrochlorination of alkyl halides through molten salts containing Lewis acid, such as $ZnCl_2$, $SnCl_2$, and CuCl, has been studied by Kenney,[12] Bailey,[10] and the present authors.[13] An E_1-elimination mechanism has been postulated. Since the carbonium ion formed by chloride abstraction from *gem*-dichlorides is stabilized through the conjugation with another chlorine atom, *gem*-dichloroalkanes also could proceed *via* E_1 elimination. The higher conversion of 1,1-dichloropropane and 1,1-dichloro-3-methylbutane

Table 1. The different kinds of liquid products for different reaction systems

Reaction system	Products
1,1-Dichloropropane	*cis*-1-chloro-1-propene, *trans*-1-chloro-1-propene, 3-chloro-1-propene, [1,1-dichloropropane], 1,2-dichloropropane
1,1-Dichloro-3-methylbutane	isoprene, *cis*-1-chloro-3-methyl-1-butene, *trans*-1-chloro-3-methyl-1-butene, monochloromethylbutenes (4 peaks), [1,1-dichloro-3-methylbutane]
Butene	2-chloro-1-butene, *trans*-2-chloro-2-butene, (*cis*-1-chloro-1-butene),[a] 3-chloro-1-butene, *cis*-2-chloro-2-butene(*trans*-1-chloro-1-butene),[a] 4-chloro-1-butene, 1-chloro-2-butene, *meso*-2,3-dichlorobutane, *dl*-2,3-dichlorobutane, 1,2-dichlorobutane, 3,4-dichloro-1-butene, polychloro compounds
2-Methyl-2-butene	2-methyl-1-butene, [2-methyl-2-butene], isoprene, 2-chloro-2-methylbutane and 3-chloro-3-methyl-1-butene, 3-chloro-2-methyl-1-butene, monochlorobutenes (3 peaks), 1-chloro-2-methyl-2-butene and/or 1-chloro-3-methyl-2-butene, polychloro compounds
Cyclohexene	[cyclohexene], 1,3-cyclohexadiene, 1,4-cyclohexadiene, benzene, monochloromethylcyclopentanes, chlorocyclohexane, 1-chlorocyclohexane, monochlorocyclohexadienes, 4-chlorocyclohexenene, 3-chlorocyclohexene, 1,2-dichlorocyclohexane

a) In the case of 1-butene as the starting material.

Table 2. Dehydrochlorination[a] of 1,1-dichloropropane through molten salts

Molten salts	$ZnCl_2$–KCl–NaCl		$SnCl_2$–KCl		CuCl–LiCl
Reaction temp (°C)	400	450	400	450	450
Recovery (%)	90	84	93	86	91
Conversion (%)	45.7	85.5	28.2	67.2	65.3
Distribution of products (%)					
cis-1-Chloro-1-propene	19.4	42.0	13.6	38.2	37.3
trans-1-Chloro-1-propene	8.8	20.2	5.7	17.6	15.9
3-Chloro-1-propene	3.0	6.9	1.3	2.8	3.6
1,2-Dichloropropane	12.8	11.8	6.2	5.4	6.3
Gaseous products	1.7	4.6	1.3	3.2	1.4
cis/*trans*	2.2	2.1	2.4	2.2	2.3

a) Reactant : Ar=0.036 : 0.094 mol/h, Duration of reaction: 30 min, Conv %=100−reactant in recovered liquid (%), Recovery (%)=(total C number of liquid products/total C number of reactant)×100.

over the melts containing $ZnCl_2$ can easily be understood, because $ZnCl_2$ may be supposed to abstract chloride from the substrate forming the carbonium ion due to its relatively strong Lewis acidity.

In the case of 1,1-dichloropropane, the *cis/trans* ratio of the resultant 1-chloro-1-propene was observed in the region from 2.1 to 2.4 through three kinds of melts. On the other hand, the *cis/trans* ratio of 1-chloro-3-methyl-1-butene was between 0.9 and 1.4. We have reported on the dehydrochlorination[1] of 1,1-dichlorobutane through molten salts, where the quite large ratio of *cis/trans* of 1-chloro-1-butene (1.4—1.8 with $ZnCl_2$ melts) may be explained in terms of the resultant carbonium ion adsorbed on the surface of the melts [illustrated in Fig. 1 (R representing the methyl, ethyl, and isopropyl groups)].

The release of H_b from the carbonium ion (in Fig. 1)

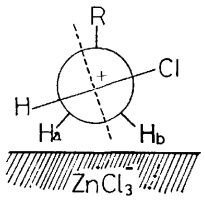

Fig. 1. Molten salts surface-adsorbed carbonium ion. Dotted line shows the vacant p orbital; R=CH_3, C_2H_5 and $(CH_3)_2CH$; Cl atom is linked to C_1, Both H_a and H_b are on C_2.

as a proton leads to the effective sharing of the free-electron pair at C_2 with the vacant p orbital at C_1. This process affords *cis*-olefin predominantly. If the alkyl group goes on from methyl to isopropyl, the location of the carbonium ion as in Fig. 1, becomes, however, somewhat unfavored because of the increasing steric repulsion between chlorine and isopropyl groups. This leads to the desorption of the carbonium ion from the melts surface, the *cis/trans* ratio of the resulting olefin nearing unity. The finding that *cis/trans* ratio with alkyl group=C_2H_5 (1.8) stands between the ratio with alkyl=CH_3 (2.2) and the ratio with alkyl=$(CH_3)_2CH$(1.4) under the same conditions is in good agreement with the explanation presented above.[14,15] The formation of isoprene from the reaction of 1,1-dichloro-3-methylbutane through $ZnCl_2$ can be explained by considering the rearrangement of the primary monochloro carbonium ion (in Fig. 1) to the more stable secondary and/or tertiary carbonium ion and the subsequent 1,4-dehydrochlorination of the 1-chloro-3-methyl-2-butene produced from the above rearranged carbonium ion.

Reaction of Butene with Chlorine. The reaction of butene with chlorine through the $ZnCl_2$ melts and the CuCl melts is shown in Tables, 4, 5, and 6. The substitution reaction by chlorine probably takes place at the allylic position of butenes (1-butene, *cis*-2-butene, *trans*-2-butene) *via* a radical mechanism whose operation was confirmed in the chlorination of cyclohexane[13]

TABLE 3. DEHYDROCHLORINATION OF 1,1-DICHLORO-3-METHYLBUTANE

Molten salts	$ZnCl_2$-KCl-NaCl[a]		$SnCl_2$-KCl[b]		CuCl-LiCl[b]
Reaction temp (°C)	400	450	400	450	450
Recovery (%)	97	97	71	70	84
Conversion (%)	44.1	80.2	21.5	64.0	75.2
Distribution of products (%)					
Isoprene	4.3	5.8	1.0	1.1	2.3
cis-1-Chloro-3-methyl-1-butene	18.0	31.6	9.3	29.2	27.6
trans-1-Chloro-3-methyl-1-butene	12.9	26.8	7.9	26.7	29.8
Monochlorobutenes	6.3	8.8	1.5	2.6	9.3
Gaseous products[c]	2.3	5.5	1.1	4.3	4.2
Others	0.3	1.7	0.7	0.1	2.0
cis/trans	1.4	1.2	1.2	1.1	0.9

a) Reactant : Ar=0.11 : 0.056 mol/h, b) Reactant : Ar=0.027 : 0.080 mol/h. c) Mainly propane, propylene.

TABLE 4. REACTION[a] OF *trans*-2-BUTENE WITH CHLORINE (450 °C)

Molten salts	$ZnCl_2$-KCl-NaCl	CuCl-KCl-NaCl	Gas-phase reaction
Recovery (%)	68	80	68
Conversion (%)	70.1	69.7	60.0
Distribution of products (%)			
1-Butene	0.8	tr	tr
cis-2-Butene	10.4	8.8	11.1
Butadiene	58.9	46.2	14.8
Monochlorobutenes	tr	2.2	27.6
meso-2,3-Dichlorobutane	tr	5.4	5.8
dl-2,3-Dichlorobutane	tr	1.0	2.0
Others	tr	0.9	tr

a) Cl_2/Reactant=0.9, Reactant : Ar=0.10 : 0.15 mol/h.

through the $ZnCl_2$ melts and the CuCl melts. The subsequent dehydrochlorination of the resulting chlorobutenes could be assisted by the melts, yielding butadiene in a high selectivity. Using the $ZnCl_2$ melts, a butadiene selectivity of more than 93% is attained if one does not take account of the degree of isomerization among butenes. With the CuCl melts, considerable amounts of unreacted chlorobutene and dichlorobutane were observed. The effects of the reaction temperature and the Cl_2/butene ratio on the extent of reaction and the degree of selectivity to butadiene were examined with the $ZnCl_2$ melts (Tables 7 and 8). The reactions at 400 °C and 450 °C gave almost the same yields of butadiene in a good material balance. With a Cl_2/feed equal to 1.15, appreciable amounts of carbonaceous material were produced; this led to a poor material balance at a high concentration of chlorine. An inspection of Table 8 reveals that the Cl_2/butene ratio between 0.59 and 0.85 is desirable in view of the material balance and butadiene yield.

There have been reported several dehydrogenation processes of butene for butadiene production. One of them is to use metal oxide catalysts[16] in the presence of oxygen and chlorine-releasing compounds (yield 27%, selectivity, 43% at 700 °C). Another procedure[17] gives a 68.0% yield of butadiene with a 89.3% selectivity (temp 638 °C, HI/butene=0.2, over 5% CeO_2/Al_2O_3). The yield and selectivity of the process presented here compares fairly well with those of the latter process under less severe conditions.

Reaction of 2-Methyl-2-butene with Chlorine. The results of experiments using both the $ZnCl_2$ melts

Table 5. Reaction[a] of *cis*-2-butene with chlorine (450 °C)

Molten salts	$ZnCl_2$-KCl-NaCl	CuCl-KCl-NaCl	Gas-phase reaction
Recovery (%)	89	79	67
Conversion (%)	73.9	74.9	70.2
Distribution of products (%)			
1-Butene	0.8	tr	tr
trans-2-Butene	14.1	12.5	15.1
Butadiene	59.0	51.2	17.2
Monochlorobutenes	tr	3.4	28.6
meso-2,3-Dichlorobutane	tr	1.4	3.5
dl-2,3-Dichlorobutane	tr	5.4	5.8
Others	tr	1.0	tr

a) Cl_2/Reactant=0.9, Reactant : Ar=0.10 : 0.15 mol/h.

Table 6. Reaction[a] of 1-butene with chlorine (450 °C)

Molten salts	$ZnCl_2$-KCl-NaCl	CuCl-KCl-NaCl	Gas-phase reaction
Recovery (%)	99	96	95
Conversion (%)	50.4	48.5	36.6
Distribution of products (%)			
trans-2-Butene	2.2	0.6	—
cis-2-Butene	1.8	0.4	—
Butadiene	46.4	38.1	16.0
Monochlorobutenes	tr	7.4	16.5
1,2-Dichlorobutane	tr	1.6	1.7
Others	tr	0.4	2.4

a) Cl_2/Reactant=0.9, Reactant : Ar=0.10 : 0.15 mol/h.

Table 7. Effects of temperatures[a] on the reactions of butenes with chlorine

Butene	1-Butene			*trans*-2-Butene		
Cl_2/C_4H_8	0.99	0.98	1.0	1.0	1.0	0.95
Temp (°C)	350	400	450	350	400	450
Recovery (%)	97	97	95	85	95	96
Conversion (%)	61.4	65.2	67.2	77.9	81.8	80.4
Distribution of products (%)						
trans-2-Butene	1.1	1.0	1.3	0.6	0.5	0.7
cis-2-Butene	0.8	0.9	1.0	9.4	8.0	8.3
Butadiene	45.2	55.3	60.7	57.8	69.3	71.4
Monochlorobutenes	11.0	6.2	3.6	5.5	2.0	tr
1,2-Dichlorobutane	1.3	0.7	0.2	3.3[b]	1.3[b]	tr[b]
Others	2.0	1.1	0.4	1.3	0.7	tr

a) Reactant : Ar=0.10 : 0.15 mol/h. $ZnCl_2$ melts. b) 2,3-Dichlorobutane

TABLE 8. EFFECT OF THE Cl_2/C_4H_8 RATIO ON THE REACTIONS[a] OF *trans*-2-BUTENE WITH CHLORINE (450 °C)

Cl_2/C_4H_8	0.30	0.59	0.95	1.15
Recovery (%)	108	112	96	81
Conversion (%)	27.0	57.8	80.4	90.5
Distribution of products (%)				
1-Butene	0.1	1.5	0.7	0.4
cis-2-Butene	8.1	9.5	8.3	4.9
Butadiene	18.8	46.8	71.4	85.2

a) Reactant : Ar=0.10 : 0.15 mol/h.

TABLE 9. REACTION[a] OF 2-METHYL-2-BUTENE WITH CHLORINE

Molten salts	$ZnCl_2$	$ZnCl_2$-Zn[b]		
Cl_2/C_5H_{10}	0.58	0.27	0.61	1.1
Recovery (%)	81	88	89	81
Conversion (%)	98.4	32.3	56.9	81.5
Selectivity to diene	11.4	86.7	82.1	64.0
Product distribution (%)				
2-Methyl-1-butene	tr	1.4	2.9	2.2
Isoprene	11.2	28.0	46.7	52.2
2-Chloro-2-methylbutane	66.7	0.2	1.4	4.9
3-Chloro-3-methyl-1-butene	1.1	0.1	0.2	1.1
3-Chloro-2-methyl-1-butene	3.5	1.5	2.9	4.0
Other chloromethylbutenes	12.3	0.1	0.1	1.7

a) Reactant : Ar=0.091 : 0.10 mol/h. b) $ZnCl_2$-KCl-NaCl-Zn=46 : 15 : 15 : 24 mol %.

and the $ZnCl_2$ melts containing a suspension of Zn powder in the reaction of 2-methyl-2-butene with chlorine are shown in Table 9.

Using the $ZnCl_2$ melts as catalysts, the reaction of 2-methyl-2-butene with chlorine gave small amounts of expected isoprene, along with great quatities of 2-chloro-2-methylbutane. The primary formation of the latter compound was supposed to be due to the addition of the HCl produced to an intermediate product, 2-methyl-2-butene, through the $ZnCl_2$ melts (at 400 °C, 76.9% yield of 2-chloro-2-methylbutane). In order to eliminate the HCl evolved during this reaction and to improve the yield of isoprene, we used $ZnCl_2$ melts containing a suspension of Zn powder instead of $ZnCl_2$ melts. As Table 9 shows, the use of those melts brough about a high yield of isoprene, as expected, and at the same time we found the formation of H_2 in an amount about the same as the quantities calculated on the basis of the following equation: $[H_2=(\text{isoprene})+(C_5H_9Cl)/2-(C_5H_{11}Cl)/2]$.

Based on these findings, this reaction may be outlined as follows:

$$2\text{C-C=C-C} + Cl_2 \longrightarrow \underset{\text{C}}{\text{C-C=C-CCl}} + \underset{\text{C}}{\text{C-C=C-CCl}} + 2HCl \quad (1)$$

$$Zn + 2HCl \longrightarrow ZnCl_2 + H_2 \quad (2)$$

$$\underset{\text{C}}{\text{ClC-C=C-C}} + \underset{\text{C}}{\text{C-C=C-CCl}} \longrightarrow 2\underset{\text{C}}{\text{C=C-C=C}} + 2HCl \quad (3)$$

TABLE 10. REACTION OF CYCLOHEXENE WITH CHLORINE[a]

Molten salts	$ZnCl_2$[b]	$ZnCl_2$-Zn[c]		
Cl_2/C_6H_{10}	0.55	0.26	0.55	1.0
Recovery (%)	90	94	90	81
Conversion (%)	39.3	21.4	46.4	67.5
Selectivity to diene	39.7	78.5	73.9	59.7
Product distribution (%)				
1,3-Cyclohexadiene	15.6	16.8	34.3	40.3
1,4-Cyclohexadiene	3.6	1.8	3.6	5.5
Benzene	5.8	1.4	5.1	14.8
1-Chlorocyclohexene	1.4	0.9	1.5	2.5
3-Chlorocyclohexene	5.5	—	0.1	1.0
4-Chlorocyclohexene	0.5	0.2	0.6	1.8
Chloromethylcyclopentanes	2.3	—	—	0.4
Chlorocyclohexane	1.5	—	—	—
1,2-Dichlorocyclohexane	tr	—	—	—
Others	3.1	0.3	1.2	1.2

a) Cyclohexene : Ar=0.095 : 0.10 mol/h. b) $ZnCl_2$-KCl-NaCl=60 : 20 : 20 mol %. c) $ZnCl_2$-KCl-NaCl-Zn=46 : 15 : 15 : 24 mol %.

Appreciable amounts of 1-chloro-2-methyl-2-butene and/or 3-chloro-2-methyl-2-butene were produced with $ZnCl_2$ melts; this was confirmed by means of GC-MS analysis.

Reaction of Cyclohexene with Chlorine. The results of the reaction through the $ZnCl_2$ melts and the Zn-powder-suspended $ZnCl_2$ melts are presented in Table 10. The presence of Zn powder increases the selectivity to cyclohexadiene in the chlorination of cyclohexene. Therefore, in a way similar to the reaction of 2-methyl-2-butene, Zn powder can react with evolved HCl, which otherwise will add to cyclohexene or/and cyclohexadiene, yielding H_2 and $ZnCl_2$. The good agreement of the hydrogen amounts with the calculated value confirms this process to be correct. Under the same conditions, the dehydrochlorination of 3-chlorocyclohexene and 4-chlorocyclohexene (at 400 °C) proceeded with an 85 and 49% selectivity to cyclohexene respectively. Therefore, it may be suggested that the chlorination of cyclohexene proceeds as in the following reaction scheme:

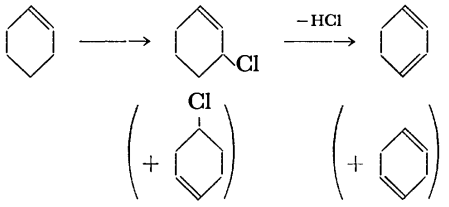

(4)

References

1) S. Kikkawa, M. Nomura, and M. Ikezaki, *Nippon Kagaku Kaishi*, **1976**, 472.
2) S. Kikkawa, M. Nomura, and M. Shimizu, *Chem. Lett.*, **1977**, 317.
3) L. Sliegler and J. M. Tinker, *J. Am. Chem. Soc.*, **61**, 938 (1939).
4) L. Schmerling, *J. Am. Chem. Soc.*, **68**, 1650 (1946).
5) R. A. Sneen and P. S. Kay, *J. Am. Chem. Soc.*, **94**, 6983 (1972).
6) M. L. Pautsma, *J. Am. Chem. Soc.*, **87**, 2161 (1965).
7) H. M. Teeter and E. W. Bell, *Org. Synth.*, Coll. Vol. IV, 125.
8) L. N. Owen and P. A. Robins, *J. Chem. Soc.*, 320 (1949).
9) S. F. Birch, R. A. Dean, and H. J. Hunter, *J. Org. Chem.*, **23** 1026 (1958).
10) R. A. Bailey and S. F. Prest, *Can. J. Chem.*, **49**, 1 (1971).
11) D. F. Ewing and K. A. W. Parry, *J. Chem. Soc.*, **B**, 970 (1970).
12) C. N. Kenny and R. Takahashi, *J. Catal.*, **22**, 16 (1971).
13) S. Kikkawa, T. Hayashi, and T. Yamada, *Kogyo Kagaku Zasshi*, **74**, 1818 (1971).
14) H. Noller, W. Low, and P. Andrew, *Angew. Chem.*, **68**, 663 (1964).
15) H. Noller, H. Hanische, and P. Andrew, *J. Catal.*, **4**, 354 (1965).
16) L. Bajars, U. S. Patent 3,211,800 (1965).
17) M. Chono, *Sekiyu Gakkaishi*, **16**, 426 (1965).

A New Synthesis of Glutathione *via* the Thiazoline Peptide

Yoichi Ozawa, Toshiaki Tsuji, and Yasuo Ariyoshi*

Central Research Laboratories, Ajinomoto Co., Inc., Suzuki-cho, Kawasaki-ku, Kawasaki 210

(Received January 18, 1980)

A convenient synthesis of glutathione (GSH) by the use of minimal protecting groups was investigated. *N*-Formyl-L-2-amino-4-cyanobutyric acid ethyl ester was condensed with ethyl L-cysteinylglycinate to give (4*R*)-2-[(3*S*)-3-ethoxycarbonyl-3-(formylamino)propyl]-4-(ethoxycarbonylmethylcarbamoyl)-2-thiazoline. This compound was saponified in aqueous acetone at −15——20 °C and subsequently treated with dilute H_2SO_4 (pH 4) to yield formylglutathione, whose formyl group was then hydrolyzed with 0.5 M (1 M=1 mol dm^{-3}) H_2SO_4 to give free GSH. For purification, this was changed to a copper thiolate, which was then decomposed with H_2S to afford pure GSH.

Glutathione (GSH) is a tripeptide with the sequence γ-L-Glu–L-Cys–Gly that occurs in many cells in a variety of species. It is currently used as a medicine for some diseases in several countries. GSH has thus been produced on a large-scale by means of both fermentation and chemical synthesis.

Although GSH is a small-sized peptide, a large-scale synthesis of it seems to be difficult because it has a free SH group that is susceptible to oxidation, and a γ-linkage in the molecule. A variety of methods[1] for synthesizing GSH have been reported so far, but only a few of them are applicable to a large-scale synthesis of GSH; in most of these reported syntheses, all the functional groups of the amino acids have been protected, and expensive benzyloxycarbonyl and benzyl groups have often been employed for protecting the amino and the mercapto groups, respectively. Moreover, in most of these methods, drastic conditions such as sodium in liquid ammonia have been used for removal of the protecting groups.

In order to find a more convenient synthetic method for GSH, we have investigated a new route which uses minimal protection. The distinctive feature of the present method is to form a tripeptide with a thiazoline ring as an intermediate peptide (**6**), which is subsequently hydrolyzed to give GSH. We concentrated our efforts on forming the thiazoline ring and opening it at the C–S bond to form a peptide linkage and a free SH group.

L-2-Amino-4-cyanobutyric acid (**1**),[2] which was prepared by dehydration of *Z*-L-Gln with *N*,*N*′-dicyclohexylcarbodiimide followed by hydrogenolysis, was employed as a starting material instead of L-Glu.

A partner peptide, L-Cys-Gly-OEt (**5**), was prepared by hydrolysis of (4*R*)-(3-formyl-2,2-dimethyl-4-ethoxycarbonylmethylcarbamoyl)thiazoline, which was prepared according to the method described in the synthesis of the corresponding methyl ester.[3]

Esterification of **1** by a conventional method was always accompanied with a considerable amount of Glu formed by hydrolysis of the nitrile group. The amino acid (**1**) was successfully esterified with EtOH–$SOCl_2$ after blocking the amino group by a formyl group to give ethyl L-2-amino-4-cyanobutyrate hydrochloride (**3**). This compound was then treated with HCOOH–Ac_2O–AcONa for formylation because the formyl group of **2** was cleaved during the esterification (Scheme 1). An attempt to convert the nitrile group into an imidic ester failed. Treatment of *N*-formyl-L-2-amino-4-cyanobutyric acid ethyl ester (**4**) with EtOH–HCl was accompanied with a considerable amount of by-products, such as Glu and Glu ester, by concomitant cleavage of the formyl group and hydrolysis of the nitrile group. Therefore, we decided to form the thiazoline ring by direct condensation of **4** with L-Cys–Gly–OEt (**5**). Compound **4** was condensed with **5** in ethanol under reflux and in an atmosphere of nitrogen to give (4*R*)-2-[(3*S*)-ethoxycarbonyl-3-(formylamino)propyl]-4-(ethoxycarbonylmethylcarbamoyl)-2-thiazoline (**6**) in 62.5% yield (Scheme 2).

Care must be taken in treating **6** with alkali, since it is known that a thiazoline ring is susceptible to racemization.[4] No appreciable racemization occurred when **6** was treated with alkali at a low temperature of −15——20 °C.

Careful saponification of the ester group of **6** at −15——20 °C in aqueous acetone and subsequent mild

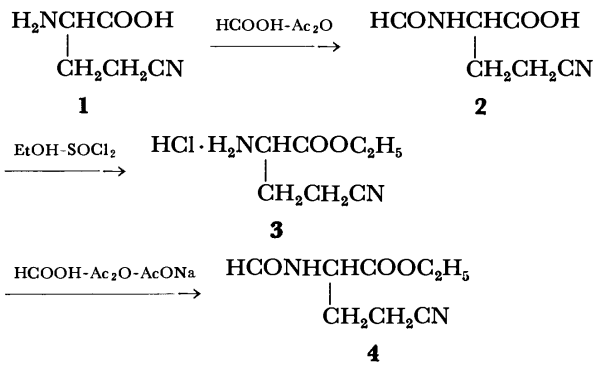

Scheme 1.

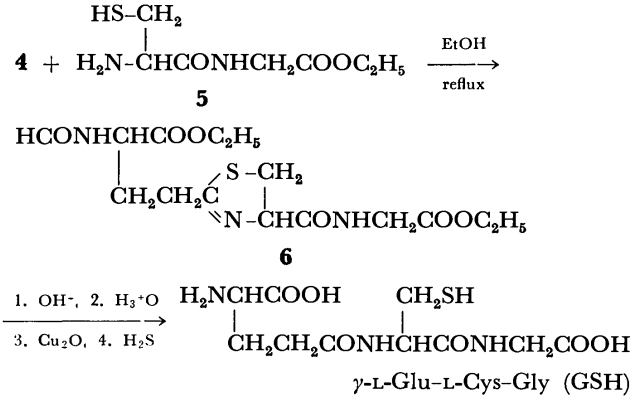

Scheme 2.

acid hydrolysis of the thiazoline ring gave *N*-formylglutathione. This was passed through a column of Diaion SK1B[5] (H^+ form) in order to remove the sodium ion which was found to cause the free SH group to change into an –S–S– bond at the final stage. Removal of the formyl group with dilute sulfuric acid gave free GSH, which was changed to a copper thiolate. Subsequent decomposition of the thiolate with hydrogen sulfide afforded pure GSH (Scheme 2).

This method shows considerable promise for large-scale syntheses of GSH.

Experimental

Melting points were measured in glass capillaries and are uncorrected. The UV-spectrum was recorded on a Shimadzu MPS-5000 spectrometer. The optical rotations were measured on a Perkin-Elmer 141 polarimeter.

N-Formyl-L-2-amino-4-cyanobutyric Acid Ethyl Ester (4). To an ice-cooled mixture of formic acid (55.2 g, 1.2 mol) and acetic anhydride (45.9 g, 0.60 mol) was added **1** (38.4 g, 0.30 mol) with stirring. After stirring for 3 h in an ice-bath, ether (500 ml) was added to the reaction mixture, and crystals (**2**) thus formed were collected by filtration; yield, 42.9 g (91.7%); mp 127—128 °C. To a suspension of **2** (42.1 g, 0.27 mol) in anhydrous ethanol (300 ml) was added dropwise thionyl chloride (21 ml) at −5——10 °C. After the addition was complete, the mixture was permitted to warm to room temperature. After the mixture was stirred at 40 °C for 40 min, the solvent was evaporated *in vacuo* at a bath temperature of 30 °C. The residue was dissolved in ethanol (140 ml) and filtered, and ether (300 ml) was added to the filtrate, which was then kept in a refrigerator overnight. Crystals (**3**) thus formed were collected by filtration and recrystallized from ethanol–ether; yield, 39.5 g (76.1%); mp 143—144 °C. To a mixture of formic acid (46.0 g, 1.0 mol) and sodium acetate (16.4 g, 0.2 mol) was added acetic anhydride (30.6 g, 0.3 mol) with cooling in an ice-bath. After stirring for 10 min, **3** (38.5 g, 0.2 mol) was added to the mixture, which was stirred with cooling in an ice-bath for 3 h. Ice water (30.6 g) was then added to the reaction mixture. After stirring at room temperature for 30 min, the reaction mixture was concentrated *in vacuo* to give an oily residue, which was dissolved in water (100 ml), adjusted to pH 6.0 with sodium carbonate, and extracted twice with 150-ml portions of chloroform. The chloroform layer was washed with water (100 ml), dried on anhydrous sodium sulfate, and evaporated *in vacuo* to give the desired compound (**4**) as an oil; yield, 30.4 g (82.6%).

L-Cys–Gly–OEt (5). (4*R*)-(3-Formyl-2,2-dimethyl-4-ethoxycarbonylmethylcarbamoyl)thiazolidine (mp 70—72 °C) prepared according to the method described for the corresponding methyl ester[3] was hydrolyzed in ethanolic hydrochloric acid to give L-Cys–Gly–OEt·HCl (83.5%; mp 135—137 °C), which was neutralized with Et_3N in ethyl acetate. The solvent was evaporated *in vacuo* to give **5** as an oil.

(4R)-2-[(3S)-3-Ethoxycarbonyl-3-(formylamino)propyl-4-(ethoxycarbonylmethylcarbamoyl)-2-thiazoline (6). A mixture of **4** (25.0 g, 0.136 mol) and **5** (33.6 g, 0.163 mol) in anhydrous ethanol (50 ml) was heated under reflux with stirring in an atmosphere of nitrogen for 16 h. After the reaction was complete, insoluble materials were filtered off, and the filtrate was concentrated *in vacuo*. The residue was taken up in chloroform (300 ml) and washed with a 20% aqueous citric acid solution (50 ml), and then twice with 100-ml portions of water. The chloroform layer was dried on anhydrous sodium sulfate and then evaporated *in vacuo* to give an oily residue, which was crystallized from ethyl acetate–petroleum ether to give **6** as crystals; yield, 31.7 g (62.5% based on **4**); mp 78—80 °C; UV (35% HCl): λ_{max} 268 nm (ε 4900); $[\alpha]_D^{18}$ +13.2° (*c* 1.0, ethanol). Found: C, 48.05; H, 6.19; N, 11.08; S, 8.69%. Calcd for $C_{15}H_{23}O_6N_3S$: C, 48.24; H, 6.21; N, 11.25; S, 8.59%.

Glutathione (GSH). To a stirred solution of **6** (70.0 g, 0.187 mol) in a mixture of acetone (617 ml) and O_2-free water (94 ml) was added dropwise 1 M (1 M=1 mol dm^{-3}) NaOH (374 ml) at −15——20 °C. After stirring at the same temperature for 1 h, the reaction mixture was acidified with 0.5 M H_2SO_4 (380 ml) to pH 4. In order to open the thiazoline ring, the mixture was stirred at room temperature for 30 min, and then the acetone was evaporated *in vacuo* from the mixture. The resulting solution, which contained formylglutathione, was passed through a column of Diaion SK1B (H^+ form) and the column was then washed with O_2-free water. The eluate and washings were combined and concentrated *in vacuo* to a small volume (336 ml), and then 5 M H_2SO_4 (37 ml) was added to the concentrate, which was stirred at 45—47 °C for 6 h in order to remove the formyl group. Copper(I) oxide (13.37 g, 0.0935 mol) was added to the reaction mixture, which was then stirred at the same temperature for 15 min. After storage in a refrigerator overnight, the copper thiolate thus formed was collected by filtration and washed thoroughly with water. The thiolate was suspended in water (500 ml) and H_2S gas was bubbled into the suspension. The copper sulfide thus formed was filtered off and the filtrate was concentrated *in vacuo* to give a syrupy residue, which was dissolved in O_2-free water (96 ml), and then ethanol (480 ml) was added to the solution at 40 °C. After standing at the same temperature for 15 min, a yellow oil was removed by decantation. Crystals of GSH (1.0 g) were added as seed to the solution, which was kept at room temperature for 2 d and then placed in a refrigerator overnight. Crude crystals along with a syrupy material were collected by filtration; yield, 20.0 g (34.7%; one gram (seed) is subtracted from the yield). The crystals (20.0 g) were dissolved in O_2-free water (60 ml) and 2-propanol (80 ml) was added at 40 °C. Crystals of GSH (1.0 g) were added as seed to the mixture, which was stirred at 40 °C for 2 h and kept at room temperature for 20 h, then kept in a refrigerator overnight. The crystals thus formed were collected by filtration; yield, 16.6 g (28.8%; one gram (seed) is subtracted from the yield). Mp 184—185 °C (dec); lit,[1] 186—190 °C (dec); $[\alpha]_D^{23}$ −21.9° (*c* 2.74, H_2O), lit,[1] $[\alpha]_D^{27}$ −21° (*c* 2.74, H_2O); Found: C, 38.88; H, 5.52; N, 13.75; S, 9.86%. Calcd for $C_{10}H_{17}O_6N_3S$: C, 39.08; H, 5.58; N, 13.67; S, 10.43%.

The authors are indebted to Mr. F. Kakizaki for his skillful technical assistance.

References

1) S. Goldschmidt, W. Lautenschlager, B. Kolb, and G. Zumach, *Chem. Ber.*, **97**, 2434 (1964). For other syntheses, see the footnotes cited here.

2) M. M. Brysk and C. Ressler, *J. Biol. Chem.*, **245**, 1156 (1970).

3) J. C. Sheehan and D. -D. H. Yang, *J. Am. Chem. Soc.*, **80**, 1158 (1958).

4) Y. Hirotsu, T. Shiba, and T. Kaneko, *Bull. Chem. Soc. Jpn.*, **40**, 2945 (1967).

5) A strong cation-exchange resin with sulfonic acid functional groups from Mitsubishi Chem. Ind. Ltd.

Electron Transfer Sensitization. II. Photo-cyclodimerization and -polymerization of *N*-Vinylcarbazole[1)]

Noboru KITAMURA and Shigeo TAZUKE*

Research Laboratory of Resources Utilization, Tokyo Institute of Technology, Nagatsuta, Midori-ku, Yokohama 227

(Received January 5, 1980)

Photoinduced ternary electron transfer reactions have been demonstrated in the system of perylene(Pe)-1,4-dicyanobenzene(DCB)-*N*-vinylcarbazole(VCZ) in acetone. Photoexcited perylene was recycled *via* two successive electron transfer reactions while VCZ-cyclodimer and/or -polymer were obtained in good yields. Quantum yields for VCZ-cyclodimer and -polymer formation were larger in the electron transfer sensitization system in comparison with the other reaction systems such as in the Pe–VCZ or the VCZ–DCB system. The photocatalytic effect of the electron transfer sensitization was clearly confirmed in the present system, by estimating the overall sensitizer efficiency as over 8000 although chain propagation steps of VCZ cation radical are involved in the present reaction processes.

The role of photosensitizer in photochemistry is unequivocally of primary importance. In the original meaning of photosensitizer(S), S is recycled by repeating photoabsorption and energy transfer to substrates.[2)] In view of utilizing low energy photons to initiate reactions *via* energy transfer processes, singlet sensitizers are by no means significant since the photoirradiation of sensitizers in a shorter wavelength region than the absorption of the substrates to be excited is required. Another category of photosensitization is the electron transfer sensitization consisting of at least two successive electron transfer processes. Although the number of examples are still limited, the most elegant example is the electron transport system in photosynthesis. It is consequently anticipated that the principle of the electron transfer sensitization will be widely applied to drive various one electron transfer redox reactions. Recently, some examples have been reported by several authors demonstrating such as dimerization of ethylenic compounds,[3)] photochemical addition of furans to electron-rich olefines,[4)] and photochemical cleavage of indene dimers,[5)] in addition to our preliminary report.[1)]

In the present article, we applied electron transfer sensitization to the Pe–DCB–VCZ system in polar media. Since VCZ cation radical is known to be the precursor of *trans*-1,2-di-9-carbazolylcyclobutane and the polymer,[6)] we expected that photo-cyclodimerization and/or -polymerization of VCZ were efficiently conducted in the electron transfer sensitization system while perylene was recycled as an electron carrier.

Experimental

Materials. Perylene (Tokyo Kasei, G. R. grade) was used without further purification. 1,4-Dicyanobenzene (Tokyo Kasei, G. R. grade) and *N*-vinylcarbazole (Koch Light Co.) were purified by several recrystallization from ethanol and hexane, respectively. Acetone was refluxed over $KMnO_4$ for several hours followed by drying over $MgSO_4$, and then distilled. Tetrahydrofuran (THF), *N*,*N*-dimethylformamide (DMF), and dimethyl sulfoxide (DMSO) were dried over appropriate drying agents and then distilled before use.

Procedure. Absorption spectra were measured by a Hitachi Spectrophotometer EPS-III. The photoreactions were carried out in a quartz cell, under the conditions of monochromatic irradiation using a JASCO Spectroirradiator CRM-FA. After photoirradiation, the reaction mixture was evaporated to dryness under reduced pressure, and then 50 ml of methanol was added. The reaction mixture in methanol was stirred vigorously and insoluble precipitates were filtered off. The precipitates were dried *in vacuo* thoroughly and then weighed. The precipitates (VCZ-cyclodimer or -polymer) were analyzed by the usual accepted procedures (IR, mp, and NMR).[7)] The light intensities for quantum yield measurements were determined by a Hatchard-Parker actinometer.[8)]

Results and Discussion

Photodecomposition of Perylene. The absorption spectra of the reaction components are shown in Fig. 1. In the Pe–DCB–acetone system, perylene was photodecomposed readily when perylene was irradiated. However, if VCZ which did not participate in photoabsorption was added to the reaction system (*i.e.* Pe–DCB–VCZ system in acetone), photodecomposition of perylene was greatly retarded (Fig. 2a). The same phenomena have been observed in the systems of pyrene–diethyl terephthalate and of pyrene–diethyl terephthalate–*N*,*N*-dimethylaniline in polar media.[9)] Since photoinduced electron transfer processes in elec-

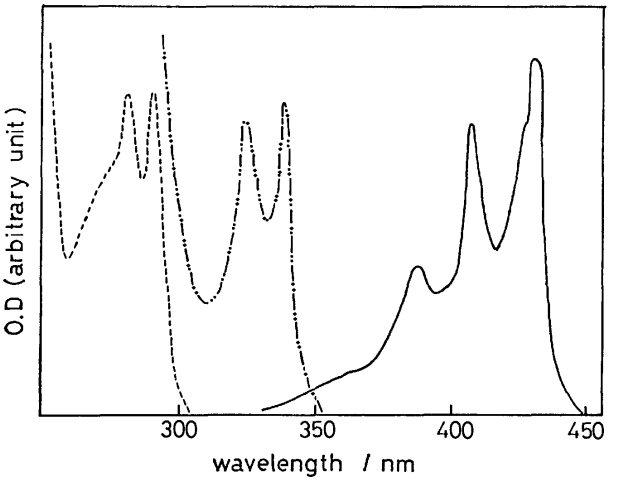

Fig. 1. Absorption spectrum in acetone.
Pe: (——), VCZ: (—··—··—), DCB: (----).

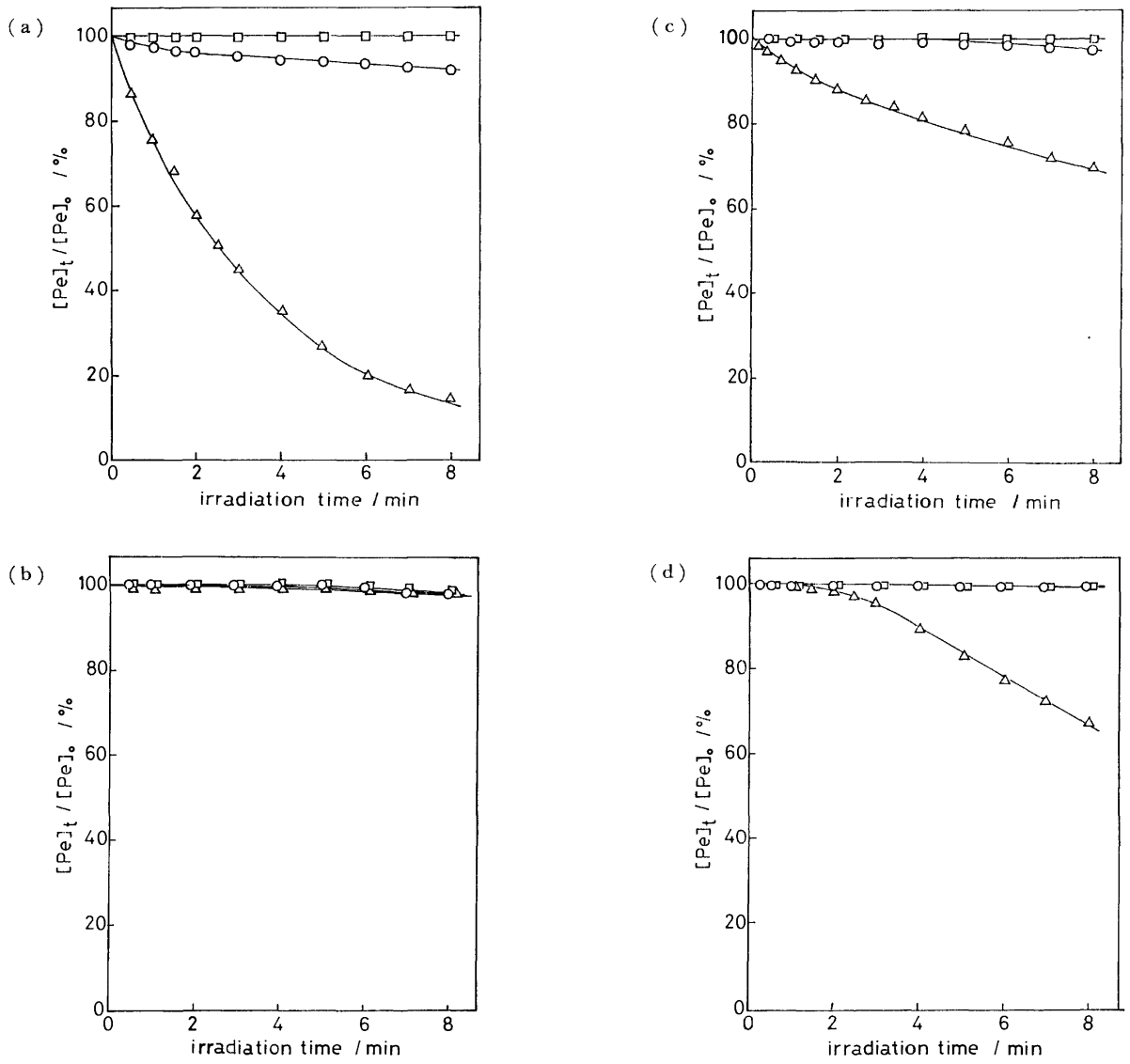

Fig. 2. Photodecomposition of perylene in various solvents. Perpendicular axis is a relative concentration of perylene(%).
Pe-VCZ-DCB: (○), Pe-VCZ: (□), Pe-DCB: (△), [Pe]$=5\times10^{-5}$ mol dm^{-3}, [VCZ]$=0.2$ mol dm^{-3}, [DCB]$=5\times10^{-4}$ mol dm^{-3}, irradiated at 435 nm in aerated conditions. a) In acetone, b) in THF, c) in DMF, d) inDMSO.

tron donor-acceptor systems in polar media are well established,[10] the results were interpreted by assuming two successive electron transfer reactions. In the present reaction system (Pe-DCB-VCZ), the reaction schemes are given as below. Namely, the successive electron transfer between perylene anion radical or cation radical and DCB or VCZ, respectively, brings about the recovery of perylene molecule, and then the photodecomposition of perylene is suppressed. In other words, perylene is recycled *via* two successive electron transfer reactions, and consequently perylene acts as an electron carrier. These mechanisms are called as "electron transfer sensitization" being contrasted to the conventional energy transfer sensitization.

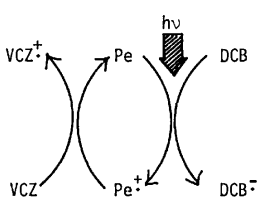

Scheme 1.

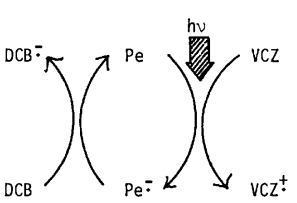

Scheme 2.

The free energy change for the electron transfer between the excited singlet state of perylene (Pe*[1]) and DCB or VCZ, calculated from Eq. 1 ($E(D^+/D)$ and $E(A/A^-)$ are oxidation potential of an electron donor and reduction potential of an electron acceptor, respectively. $e^2/\varepsilon r$ is the Coulombic term and $\Delta E_{0\text{-}0}$ is the 0.0-band energy for the photoexcited species(Pe)),[11] is -38.5 or $+5.9$ kJ/mol, respectively.

$$\Delta G = E(D^+/D) - E(A/A^-) - e^2/\varepsilon r - \Delta E_{0\text{-}0} \quad (1)$$

These values suggest that the electron transfer between Pe*[1] and DCB proceeds with a nearly diffusion

controlled rate whereas that between Pe*[1] and VCZ is a rather slow process ($\approx 10^8$ dm^3 mol^{-1} s^{-1}); as being expected from the results reported by D. Rehm and A. Weller.[12] Consequently, Scheme 1 is considered as the main reaction path with a minor contribution of Scheme 2.

In the Pe–DCB system, the rapid photodecomposition of perylene is attributed to unstable perylene cation radical which is formed by the electron transfer between Pe*[1] and DCB. On the other hand, the result that perylene is scarcely photodecomposed in the course of photoirradiation in the Pe–VCZ system requires some comments. We consider that the electron transfer between Pe*[1] and VCZ occurs to produce perylene anion radical, since perylene is a weak but definite sensitizer for photoreactions of VCZ as shown in the next section. However, under aerobic conditions, perylene anion radical will be oxidized by oxygen to reproduce perylene molecule as shown below.

$$Pe^{\cdot-} + O_2 \longrightarrow Pe + O_2^{\cdot-} \qquad (2)$$

The elctron transfer from perylene anion radical to oxygen is a highly exothermic process so that we consider that the reaction in Eq. 2 occurs efficiently.[13]

The photodecomposition of perylene was also studied in THF, DMF, and DMSO (Figs. 2b, 2c, and 2d, respectively). Similar to the case in acetone, the fast photodecomposition of perylene in the Pe–DCB system was retarded or inhibited by the addition of VCZ. However, perylene was hardly photodecomposed in THF in the Pe–DCB system. Taking into account that the photodecomposition of perylene is induced by the electron transfer between Pe*[1] and DCB or VCZ, solvent polarity is suggested to be of primary importance. The finding that the free ion yield in photo-induced electron transfer reactions in electron donor-acceptor systems is nearly zero in a low polarity solvent such as THF would explain the stability of perylene in THF even in the presence of DCB.[14] On the other hand, the fact that the free ion is produced efficiently in polar solvents such as acetone, DMF, and DMSO, is in good agreement with the present results.[14]

Photo-cyclodimerization and -polymerization of VCZ. Since VCZ cation radical is known as the precursor of VCZ-cyclodimer and -polymer,[6] it is expected that VCZ-cyclodimer and/or -polymer are produced by irradiating the present ternary system. Indeed, photoirradiation leads to the formation of VCZ-cyclodimer and/or -polymer. Quantum yields for VCZ-cyclodimerization and -polymerization under various conditions are listed in Table 1. In the Table, the quantum yields over 1.0 indicate that the cyclodimerization or -polymerization of VCZ involves chain propagation processes which have been discussed by Ledwith in detail.[6] The mechanisms are as follows. The reaction path of VCZ cation radical as function of atmosphere and solvent is identical with the previous results.[15]

In the Pe sensitized systems (Pe–DCB–VCZ, Pe–VCZ) in acetone, VCZ-cyclodimer and -polymer were formed efficiently in air and *in vacuo*, respectively. The quantum yield is larger by a factor of ≈ 6 in the Pe–DCB–VCZ system than in the Pe–VCZ system

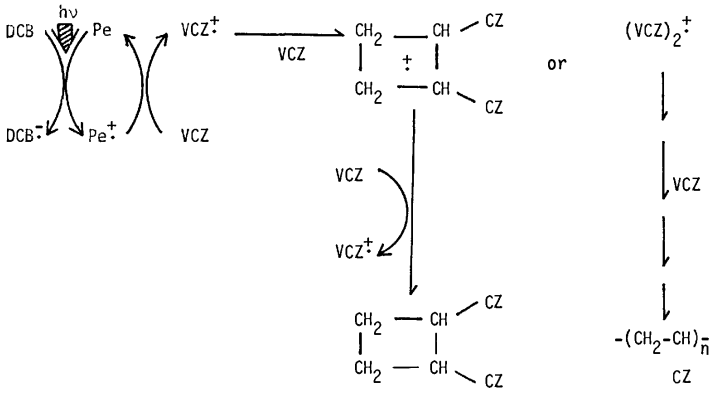

TABLE 1. QUANTUM YIELDS FOR VCZ-CYCLODIMER AND -POLYMER FORMATION

Solvent	$h\nu$ nm	Quantum yield in air (*in vacuo*)			
		Pe-VCZ-DCB	Pe-VCZ	VCZ-DCB	VCZ
Acetone	435	4.5[a] (2.3)	0.75[a] (0.38)	0 (0)	——
	365	——	——	2.57[a] (1.80)	2.57[a] (0.43)
THF	435	0 (0)	0 (0)	0 (0)	——
	365	——	——	≈0 (≈0)	≈0 (0.08)
DMF	435	0 (0)	0 (0)	0 (0)	——
	365	——	——	0.27 (0.18)	0.36 (0.09)
DMSO	435	≈0 (0.1)	≈0 (0.9)	0 (0)	——
	365	——	——	2.10 (1.00)	1.71 (0.52)

Conditions; [Pe] = 2×10^{-5} mol dm^{-3}, [VCZ] = 0.2 mol dm^{-3}, monochromatic irradiation for 16 min at room temperature. a) 1,2-*trans*-Di-9-carbazolylcyclobutane, others are poly(*N*-vinylcarbazole).

either in air or *in vacuo*. Furthermore, in comparison with the quantum yield in the VCZ–DCB system or the system containing VCZ alone, the ternary system is twice as efficient as the others. The finding that the quantum yield is the highest in the ternary system indicates the suppression of the back electron transfer between ion radicals resulting in an increase in the steady state concentration of VCZ cation radical. Namely, an electron is transffered from VCZ to DCB by perylene and consequently, charge separation is most efficient in the ternary system, which brings about high quantum yields of cyclodimerization and/or -polymerization of VCZ. These results reveal the usefulness of the electron transfer sensitization system in respect of, i) the enhancement of quantum yield, and ii) the utilization of low enrgy photons. In the electron transfer sensitization system in air, we estimated the overall sensitizer efficiency which is defined as "product per consumed perylene," to be over 8000, although the mechanisms for VCZ-cyclodimer and -polymer formation involve chain propagation processes described above. Consequently, we conclude that the sensitizer (perylene) is reproduced *via* two successive electron transfer reactions, which is the same conclusion obtained in the previous section.

In THF, since the free ion yield in electron donor-acceptor systems is nearly zero, the absence of cyclodimerization or -polymerization of VCZ is quite reasonable. However, the features of the reactions in DMF and DMSO are more complicated. In perylene sensitized systems, VCZ-polymer was scarcely produced,[16] whereas the polymer was formed in the system of VCZ–DCB and of VCZ alone by irradiating VCZ. The reasons for these results are unclear at the present time. However, since it has been reported that viscous solvents such as DMF and DMSO promote geminate recombination of the ion radical pair,[17] we consider that the back electron transfer between perylene cation radical and DCB anion radical will suppress the polymerization or cyclodimerization from VCZ cation radical.

Conclusion

Although the quantitative information on the electron transfer sensitization was not obtained, it is concluded that perylene acts as an electron carrier to induce the cation radical initiated cyclodimerization and -polymerization of VCZ. The quantum yields for VCZ-cyclodimer and -polymer formation were enhanced in the presence of electron transfer sensitizer in comparison with other systems in which VCZ was directly excited. Furthermore, the effective absorption wavelength can be extended to longer wavelength region by the use of electron transfer sensitizer. The electron transfer sensitization is a useful tool for photo-redox reactions in general. Quantitative discussions on further examples of the electron transfer sensitization systems will be reported in near future.[18]

References

1) A part of this article has been reported. S. Tazuke and N. Kitamura, *J. Chem. Soc., Chem. Commun.*, **1977**, 515.

2) A. A. Lamola, "Energy Transfer and Organic Photochemistry," ed by A. A. Lamola and N. J. Turro, Wiley-Interscience, New York (1969), Chap. 1.

3) T. Asanuma, T. Gotoh, A. Tsuchida, M. Yamamoto, and Y. Nishijima, *J. Chem. Soc., Chem. Commun.*, **1977**, 485.

4) K. Mizuno, R. Kaji, H. Okada, and Y. Otsuji, *J. Chem. Soc., Chem. Commun.*, **1978**, 594.

5) T. Majima, C. Pac, A. Nakasone, and H. Sakurai, *J. Chem. Soc., Chem. Commun.*, **1978**, 490.

6) A. Ledwith, "The Exciplex," ed by M. Gordon and W. R. Ware, Academic- Press., New York (1975), p. 209.

7) L. P. Ellinger, *Polymer*, **5**, 559 (1964); L. P. Ellinger, *Mh. Chem.*, **96**, 131 (1965).

8) C. G. Hatchard and C. A. Parker, *Proc. R. Soc. London, Ser. A*, **235**, 518 (1956).

9) S. Tazuke and K. Sato, *J. Phys. Chem.*, **80**, 1727 (1976).

10) H. Leonhardt and A. Weller, *Z. Phys. Chem. N. F.*, **29**, 277 (1961); H. Knibbe, D. Rehm, and A. Weller, *Ber. Bunsenges. Phys. Chem.*, **72**, 757 (1968); H. Knibbe, K. Röllig, F. P. Schäfer, and A. Weller, *J. Chem. Phys.*, **47**, 1184 (1969).

11) Following values were used to calculate the ΔG values. $E(Pe^+/Pe)=0.85$ V[12]; $E(Pe/Pe^-)=-1.65$ V[12]; $\Delta E(DCB/DCB^-)=-1.64$ V[12]; $E(VCZ^+/VCZ)=1.30$ V: L. P. Ellinger, *J. Appl. Polym. Sci.*, **9** 3939 (1965); $e^2/\varepsilon r=5.4$ kJ/mol; $E_{0.0}(Pe^{*1})=275.3$ kJ/mol: S. L. Murov, "Handbook of Photochemistry," Marcel Dekker, New York (1973), Sec. 1.

12) D. Rehm and A. Weller, *Ber. Bunsenges. Phys. Chem.*, **73**, 834 (1969); D. Rehm and A. Weller, *Israel J. Chem.*, **8**, 259 (1970).

13) Further details on this electron transfer process will be discussed in Part III of this series. Ref. 18.

14) N. Mataga, "The Exciplex," ed by M. Gordon and W. R. Ware, Academic-Press, New York (1975), p. 113.

15) Y. Shirota, K. Tada, M. Shimizu, S. Kusabayashi, and H. Mikawa, *J. Chem. Soc., Chem. Commun.*, **1970**, 1110.

16) In DMF or DMSO, VCZ-polymer is the only product. See also Ref. 15.

17) H. -J. Werner, Z. Schulten, and K. Schulten, *J. Chem. Phys.*, **67**, 646 (1977); Z. Schulten and K. Schulten, *ibid.*, **66**, 4616 (1977).

18) N. Kitamura and S. Tazuke, *Bull. Chem. Soc. Jpn.*, **53**, 2598 (1980).

Electron Transfer Sensitization. III. A Kinetic Study of Oxidative Dye Formation from Leuco Crystal Violet

Noboru KITAMURA and Shigeo TAZUKE*

Research Laboratory of Resources Utilization, Tokyo Institute of Technology, Nagatsuta, Midori-ku, Yokohama 227

(Received January 5, 1980)

The action of electron transfer sensitization was quantitatively discussed by measuring photooxidative dye formation of leuco Crystal Violet (LCV) in the perylene(Pe)-1,4-dicyanobenzene(DCB)-LCV combination in polar media. Under the conditions of exclusive photoexcitation of perylene (λ_{ex} at 435 nm), the kinetic study revealed that the turn over number of perylene as a sensitizer was immeasurably large in the ternary system *in vacuo*. This is an indication that perylene is indeed recycled *via* two successive electron transfer processes. The turn over number decreased to 58 in air, probably due to instability of intermediate ion radicals. The quantum yield was larger for the ternary system than for the binary system(Pe–LCV) irradiated at 435 nm. Although the absolute quantum yield of photooxidation was in the order of 10^{-3} or less in both systems, the ternary electron transfer system was apparently advantageous since the efficiency of back electron transfer would be reduced when multiple electron transfer processes are linked. Furthermore, the concept of electron transfer sensitization enables spectral sensitization and utilization of low energy photons in singlet state photoredox reactions. Such systems would be considered as a model for the primary action of photosynthesis.

In the preceding articles, we have reported the electron transfer sensitization of Pe–DCB–*N*-vinylcarbazole(VCZ) system in polar media.[1] On selective irradiation of perylene, VCZ-cyclodimer and -polymer were obtained in good yields. Since the monomer cation radical is known to be the precursor of the VCZ-cyclodimer and -polymer,[2] we assumed the scheme described below. However, the formation of

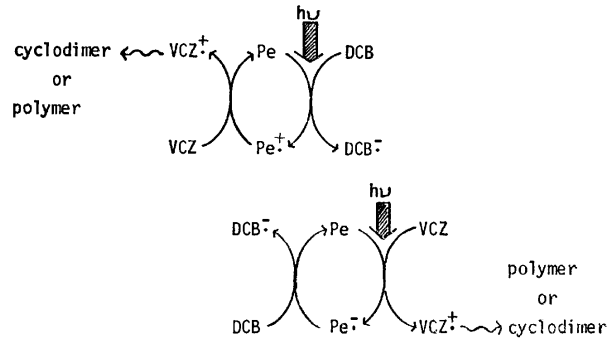

VCZ-cyclodimer and -polymer involves chain propagation processes, and consequently the mean turn over number of perylene as a sensitizer could not be determined. In the present paper, we are presenting a kinetic study of oxidative dye formation from LCV sensitized by the electron transfer sensitizer (perylene).

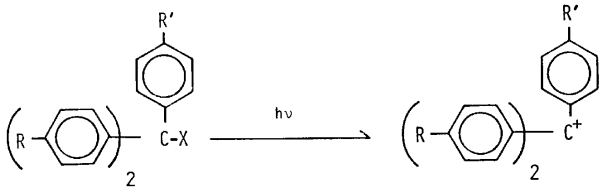

(I) CRYSTAL VIOLET R=R'=NMe$_2$

(II) MALACHITE GREEN R=NMe$_2$, R'=H

(III) BRILLIANT GREEN R=NEt$_2$, R'=H

(IV) DOEBNER'S VIOLET R=NH$_2$, R'=Ph

X=H OR CN

Since the photoreactions of leuco triphenylmethane derivatives in the presence or the absence of an electron acceptor are well established,[3] quantitative information on the action of electron transfer sensitization is expected.

Experimental

Materials. Perylene(Aldrich) was used without further purification. 1,4-Dicyanobenzene and leuco Crystal Violet (both Tokyo Kasei, guaranteed reagent) were recrystallized from ethanol several times. 9-Cyanoanthracene (CNA) was prepared according to literature,[4] and was purified by column chromatography, followed by recrystallization from ethanol and finally sublimed *in vacuo* before use. Acetonitrile was refluxed over phosphorus pentaoxide for several hours and then distilled. Benzene, tetrahydrofuran (THF), and *N*,*N*-dimethylformamide (DMF) were dried over appropriate drying reagents (CaH_2, Na and $LiAlH_4$, and CaH_2, respectively) and then distilled. Acetone was treated over $KMnO_4$ and $MgSO_4$ successively, and then distilled.

Procedure of Photoreactions. Photoreactions in air were carried out in a Teflon capped quartz cell (optical length 1 cm). Degassed samples were prepared by several freeze-pump-thaw cycles and then sealed off at the constriction of a Pyrex branch of a quartz cell. Monochromatic light source was obtained by a JASCO Spectroirradiator CRM-FA equipped with a 2-kW xenon lamp. Absorption and fluorescence spectroscopy were made by a Shimadzu UV-200S spectrophotometer and a Hitachi MPF-4 spectrofluorometer, respectively. For fluorescence quenching experiments, samples were thoroughly deaerated by argon bubbling. Light intensity for the quantum yield measurements were determined by a Hatchard-Parker actinometer (0.15 mol dm^{-3} potassium trioxalatoferrate(III) in a 0.1 mol dm^{-3} aqueous sulfuric acid solution).[5]

Results and Discussion

Oxidative Dye Formation of LCV and Photodecomposition of Perylene. Figure 1 shows the absorption spectra of the components in this electron transfer sensitization system in acetonitrile. Perylene is an electron transfer sensitizer (a photoabsorber), DCB and CNA are electron acceptors, and LCV is an electron donor. It

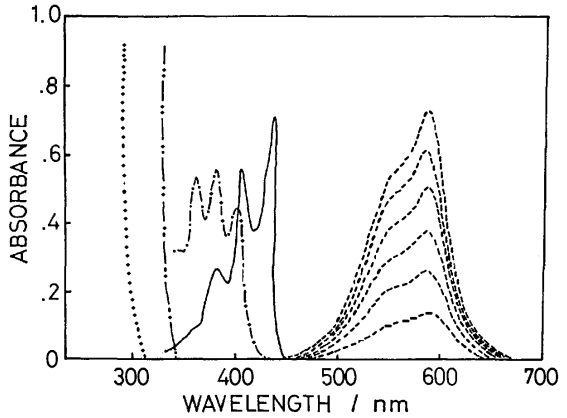

Fig. 1. Absorption spectrum of the components for the present reaction system in acetonitrile.
[Pe]$=1.7\times10^{-5}$ mol dm^{-3} (——); [CNA]$=1.0\times10^{-3}$ mol dm^{-3} (—·—·—); [DCB]$=1.0\times10^{-3}$ mol dm^{-3} (·····), [LCV]$=1.0\times10^{-3}$ mol dm^{-3} (—··—··—); CV^+ (----).

is clear from these spectra that LCV and DCB have no absorption at the absorption maximum of perylene (435 nm). CNA is also transparent at 435 nm under our experimental conditions ([CNA]$=1\times10^{-4}$ mol dm^{-3}) as manifested by the fact that the fluorescence from CNA on excitation at 435 nm is not observed at all. Hence, the selective excitation of perylene is attained in this system.

On excitation of perylene in the Pe–CNA–LCV system, the development of violet color showing an absorption maximum around 590 nm was observed. This new absorption band is identical to that observed upon direct excitation of LCV. Since LCV is easily photooxidized to give its violet colored carbonium ion, and the spectrum in Fig. 1 agrees with the reported one,[6] we identified the violet species as Crystal Violet cation (CV^+) which is one of the triphenylmethane dyes ($\lambda_{max}=590$ nm, $\varepsilon=1.1\times10^5$ dm^3 mol^{-1} cm^{-1}).[7] The dye was stable within the time scale of our experimental conditions. As the absorption intensity at 590 nm due to the dye formation increases, the absorption around 435 nm also increases and the conditions of selective excitation of perylene are no longer sustained. However, since the extinction coefficient around 435 nm is negligibly small compared with the value at 590 nm and also with the value for perylene, the inner filter effect due to the increase in the absorption at 435 nm is negligible if the dye absorbance at 590 nm is less than 0.8.

Figure 2 shows the time conversion curves of the dye formation in the Pe–CNA–LCV and the Pe–LCV systems in acetonitrile. It is obvious that the rate of the dye formation is faster in the ternary system than in the binary one, and the reactions seem to be favored in air than *in vacuo*. The photodecomposition of perylene shown in Fig. 3 indicated that the fast decomposition of perylene in the aerated system of Pe–CNA was retarded by the addition of LCV which did not concern with the light absorption. In a similar manner, the fast decomposition of perylene in the Pe–LCV system was completely inhibited in

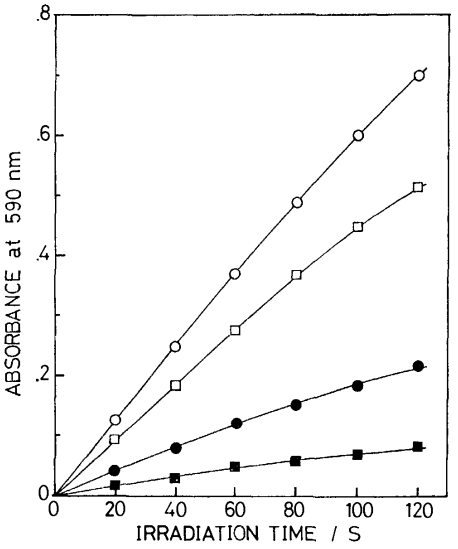

Fig. 2. Time conversion curves for the dye formation under various conditions.
Pe–CNA–LCV; (○; in air, ●: *in vacuo*), Pe–LCV; (□: in air, ■: *in vacuo*), [Pe]$=1.7\times10^{-5}$ mol dm^{-3}, [CNA]$=$[LCV]$=1.0\times10^{-3}$ mol dm^{-3} in acetonitrile.

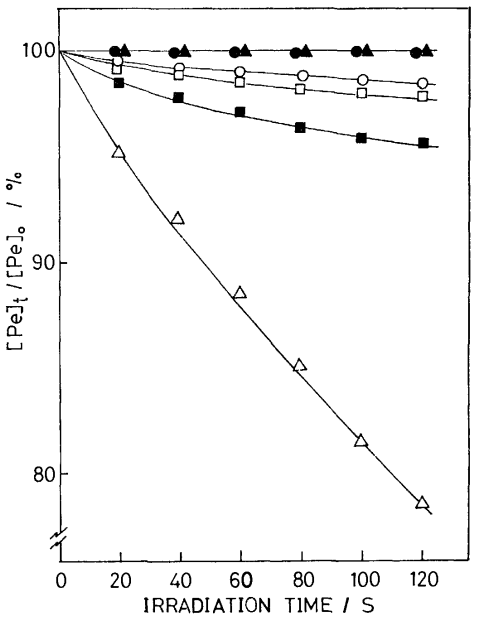

Fig. 3. Photodecomposition of perylene.
Perpendicular axis is a relative concentration of perylene(%).
Pe–CNA–LCV (○: in air, ●: *in vacuo*), Pe–LCV (□: in air, ■: *in vacuo*), Pe–CNA (△: in air, ▲: *in vacuo*).
The reaction conditions are same as Fig. 2.

the ternary system *in vacuo*. The same results were also obtained using DCB as an electron acceptor instead of CNA.

Proposed Mechanism. Either energy transfer or electron transfer should be responsible for the primary processes. However, energy transfer mechanism is excluded because the energy of the excited state of perylene is lower than the energy of LCV or the acceptors either in the excited singlet or the triplet state (see Table 1). On the other hand, the negative free

TABLE 1. EXCITED SINGLET AND TRIPLET ENERGIES, AND REDOX POTENTIALS

	$\Delta E_{0.0}$ Singlet (kJ/mol)	$\Delta E_{0.0}$ Triplet (kJ/mol)	$E(A/A^-)$[a] (V)	$E(D^+/D)$[a] (V)	ΔG[b] (kJ/mol)
Pe	275.3[c]	146.9[c]	−1.65[g]	0.85[g]	—
DCB	412.5[c]	295.0[c]	−1.64[i]	—	−40.6
CNA	297.1[d]	175.7[e]	−1.58[j]	—	−46.4
LCV	376.6[d]	309.6[f]	—	0.74[k]	−50.2

a) A half-wave potential (*versus* S.C.E. in acetonitrile). b) Calculated from Eq. 1. ΔG values for the electron transfer reactions between Pe*[1] and an electron acceptor or an electron donor. c) S. L. Murov, "Handbook of Photochemistry," Marcel Dekker, New York (1973), Sec. 1. d) Estimated from the onset of UV absorption. e) J. B. Birks, "Organic Molecular Photophysics," Wiley Interscience (1975), Vol. 2, Chap. 9. f) The value for leuco Ethyl Crystal Violet complied with MacLachlan, Ref. 6. g) See Ref. 8. h) E. S. Pysh and N. C. Yang, *J. Am. Chem. Soc.*, **85**, 2124 (1963). i) See Ref. 8. j) J. Eriksen and C. S. Foote, *J. Phys. Chem.*, **82**, 2659 (1978). k) F. D. Saeva and G. R. Olin, *J. Chem. Soc., Chem. Commun.*, **1976**, 943.

energy change (ΔG listed in Table 1) for the electron transfer between the excited singlet state of perylene (Pe*[1]) and LCV or the electron acceptors (CNA and DCB), calculated from Eq. 1,[8] indicate that electron transfer from Pe*[1] to the electron acceptor or from

$$\Delta G = E(D^+/D) - E(A/A^-) - e^2/\varepsilon r - \Delta E_{0\text{-}0} \quad (1)$$

LCV to Pe*[1] is the primary key step for the subsequent reactions. Consequently, we assumed the following ion radical mediated reaction schemes. In Scheme 1, electron transfer takes place between

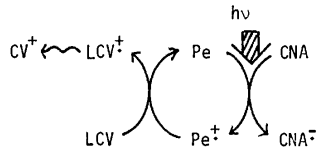

Scheme 1.

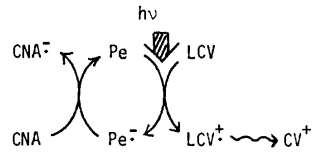

Scheme 2.

Pe*[1] and CNA in the first step, and then in the second, an electron is transferred from LCV to perylene cation radical to bring about the recovery of perylene molecule. On the other hand, Scheme 2 indicates that the first electron transfer occurs between Pe*[1] and LCV, and then the second electron transfer occurs between perylene anion radical and CNA. Since Schomburg *et al.* have also reported such electron transfer reactions in the system of pyrene–*N*,*N*-dimethylaniline–DCB in acetonitrile,[9] and the free energy change for the electron transfer between Pe*[1]–LCV or Pe*[1]–CNA (or DCB) has a negative value,[10] we considered that these schemes are plausible. Furthermore, by assuming these schemes, the retardation or the inhibition of perylene decomposition in the ternary system compared with the binary one is well interpreted.

The mechanism of Crystal Violet dye formation from LCV cation radical has been reported by MacLachlan for the system of leuco Ethyl Crystal Violet–carbon tetrachloride, based on ESR and flash photolysis study, as follows;[6]

$$LCV^{\cdot+} \overset{K}{\rightleftharpoons} CV\cdot + H^+ \quad (2)$$

$$LCV^{\cdot+} + CV\cdot \xrightarrow{k_r} LCV + CV^+ \quad (3)$$

where K denotes the equilibrium constant

$$K = [CV\cdot][H^+]/[LCV^{\cdot+}].$$

The dye is yielded by disproportionation between LCV cation radical and Crystal Violet radical (CV·) which is formed by the equilibrium Eq. 2. The participation of equilibrium is supported by the results from the temperature effects on the dye formation. The Arrehnius plots and the activation energies are shown in Fig. 4 and Table 2, respectively. The activa-

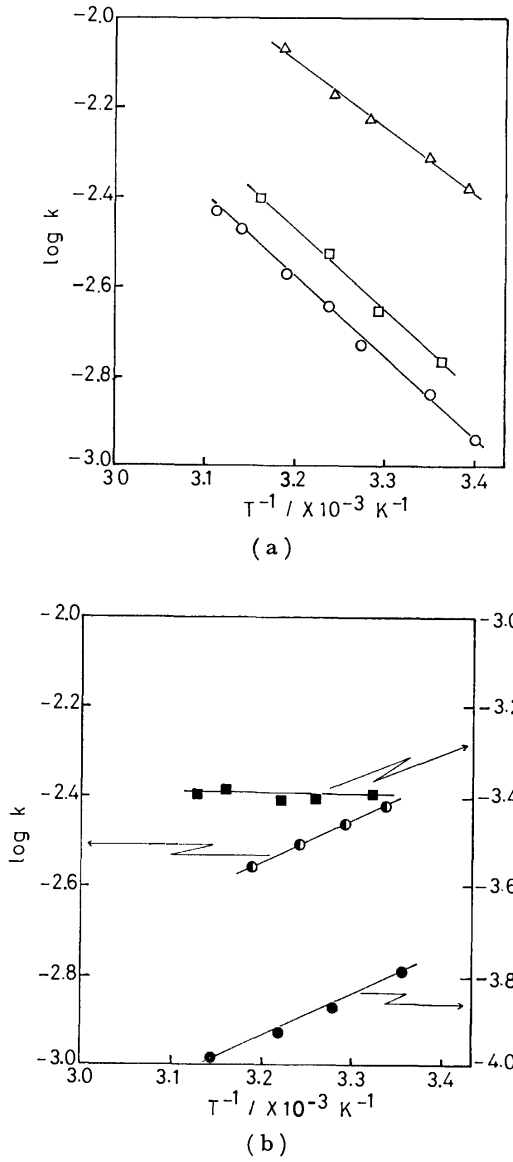

Fig. 4. Arrehnius plots for the dye formation.
a) In air, ○: Pe–LCV–DCB, □: Pe–LCV, △: LCV.
b) ●: Pe–LCV–DCB (*in vacuo*), ■: Pe–LCV (*in vacuo*), ◐: Pe–LCV–DCB (under CO_2 atmosphere). The reaction conditions are shown in Table 2.

TABLE 2. ACTIVATION ENERGIES FOR THE DYE FORMATION

Atmosphere	Activation energy (kJ/mol)		
	Pe-LCV-DCB[a]	Pe-LCV[a]	LCV[b]
Air[c]	33.9	37.2	31.4
Vacuum[d]	−18.0	1.7	
CO_2[e]	−13.8		

Irradiated at a) 435 nm, or b) 304 nm in acetonitrile. ([Pe] = 1.8×10^{-5} mol dm^{-3}, [LCV] = [DCB] = 1×10^{-3} mol dm^{-3}). c) Air saturated solution. d) Degassed by several freeze-pump-thaw cycles. e) Degassed by several freeze-pump-thaw cycles, and then CO_2 gas was introduced to atmospheric pressure.

tion energies for the dye formation were +33.5 kJ/mol under aerated conditions, while the nearly zero or slightly negative temperature dependence was observed *in vacuo*. We consider that such temperature dependence indicates the participation of equilibrium Eq. 2 in the dye formation, corresponding the positive and the negative (or zero) temperature dependence, for the forward and the backward reactions in the equilibrium, respectively.

Kinetics. The reaction Schemes 1 and 2, and the CV^+ dye formation processes from LCV cation radical lead to kinetic expressions as follows.

$$Pe \xrightarrow{I} Pe^{*1} \tag{4}$$

$$Pe^{*1} \xrightarrow{\tau^{-1}} Pe \text{ or } Pe^{*3} \tag{5}$$

Equation 5 expresses the sum of the decay processes of the excited singlet state of perylene by internal conversion to the ground state (rate constant: k_d), radiative decay (k_f), and intersystem crossing (k_{isc}) to the excited triplet state (Pe^{*3}). In the presence of an electron acceptor or LCV, we take the non-electron transfer quenching processes into account (Eqs. 6 and 7). The elementary reactions in the schemes are

$$Pe^{*1} + A \xrightarrow{k_{qa}} Pe + A \tag{6}$$

$$Pe^{*1} + LCV \xrightarrow{k_{qd}} Pe + LCV \tag{7}$$

expressed as below (Eqs. 8—11). The quantum yield

Scheme 1

$$Pe^{*1} + A \xrightarrow{k_1} Pe^{+\cdot} + A^{-\cdot} \tag{8}$$

$$Pe^{+\cdot} + LCV \xrightarrow{k_2} Pe + LCV^{+\cdot} \tag{9}$$

Scheme 2

$$Pe^{*1} + LCV \xrightarrow{k_3} Pe^{-\cdot} + LCV^{+\cdot} \tag{10}$$

$$Pe^{-\cdot} + A \xrightarrow{k_4} Pe + A^{-\cdot} \tag{11}$$

of the CV^+ dye formation (ϕ_{CV}) is expressed as Eq. 12.

$$\phi_{CV} = \frac{k_r[LCV^{+\cdot}][CV\cdot]}{I}, \tag{12}$$

where I indicates the absorbed photoenergy. Now assuming the stationary concentration for Pe^{*1}, CV radical, LCV cation radical, and perylene cation radical, we obtained the Stern-Volmer equation for the dye formation (Eq. 13).

$$\phi_{CV} = Z\left(1+\frac{k_{qa}[A]+k_{qd}[LCV]}{k_1[A]+k_3[LCV]}+\frac{1}{\tau(k_1[A]+k_3[LCV])}\right), \tag{13}$$

where

$$Z = ([H^+]+Kk_r)/K.$$

Varying the concentration of DCB or LCV (1.0×10^{-3}—1.0×10^{-4} mol dm^{-3}) while keeping the concentration of LCV or DCB constant at 1.0×10^{-4} mol dm^{-3}, respectively, the change in ϕ_{CV} was spectroscopically determined and presented in a form of Stern-Volmer plot in Fig. 5. It is shown that the slopes depend upon the concentration of DCB or LCV. Under two extreme conditions, namely [DCB] $\gg$[LCV] and [DCB]$\ll$[LCV], Eq. 13 can be simplified as Eqs. 14 and 15, respectively.

$$\phi_{CV} = Z\left(1+\frac{k_{qa}}{k_1}+\frac{1}{\tau k_1[DCB]}\right) \tag{14}$$

$$\phi_{CV} = Z\left(1+\frac{k_{qd}}{k_3}+\frac{1}{\tau k_3[LCV]}\right) \tag{15}$$

The concentration dependent terms in Eqs. 14 and 15 correspond to the initial slopes in Fig. 5 (*i.e.* the high concentration limits of DCB and LCV, respectively) and Eq. 13 to the low concentration region. Consequently, the slopes in the high concentration regions give the values $Z/\tau k_1$ and $Z/\tau k_3$ relevant to the electron transfer processes Eqs. 8 and 10, respectively. From the ratio of these slopes, we obtained $k_1/k_3=2.5$. Namely, the electron transfer between Pe^{*1} and DCB is faster than that between Pe^{*1} and LCV. These results suggest that the perylene cation radical intermediate mechanism (Scheme 1) is more plausible, although Scheme 2 participates to a lesser extent.

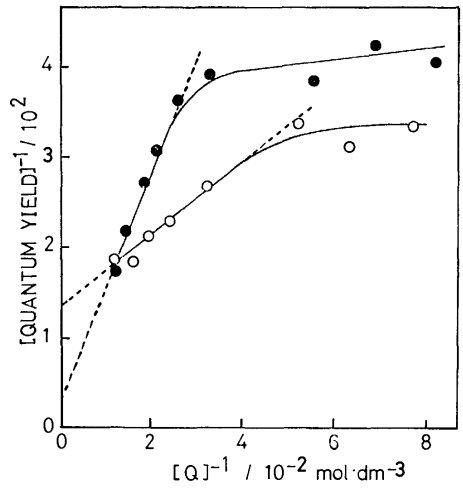

Fig. 5. Stern-Volmer plots for the dye formation. The concentration of perylene was fixed at constant (2×10^{-5} mol dm^{-3}), while the concentration of DCB (○) or LCV (●) was varied from 1×10^{-3} mol dm^{-3}—1×10^{-4} mol dm^{-3}. The reactions were carried out under air saturated conditions at 23.0 °C. Irradiation at 435 nm.

When $[Q]^{-1}$ in Fig. 5 increases, the assumptions on which the deviation of Eqs. 14 and 15 is based are no longer valid. Under the conditions of [LCV] $=1\times10^{-4}$ mol dm^{-3}, [DCB] being variable, Eq 13 indicates that ϕ_{CV}^{-1} should approach a constant value of $Z\left(1+\frac{k_{qd}}{k_3}+\frac{1}{\tau k_3[LCV]}\right)$ at the low concentration limit of DCB. Similarly, when [LCV] is variable, [DCB] being fixed, the limiting ϕ_{CV}^{-1} at [LCV]$\rightarrow$0 corresponds to $Z\left(1+\frac{k_{qa}}{k_1}+\frac{1}{\tau k_1[DCB]}\right)$. Deviation of Stern-Volmer plots in Fig. 5 with decreasing the quencher concentration is the manifestation of these.

The value of k_1/k_3 can be also estimated from the fluorescence quenching experiments of Pe*[1] as shown in Fig. 6. Since quenching of fluorescence in electron donor-acceptor systems in polar media is known to proceed *via* electron transfer process,[11] the Stern-Volmer quenching constants, K_q(DCB) and K_q(LCV), determined for DCB and LCV, respectively, will represent the relative rate of the electron transfer processes (Eqs. 8 and 10). The ratio of K_q therefore provides the value of k_1/k_3,

$$K_q(DCB)/K_q(LCV) = k_1/k_3 = 2.7.$$

Good agreement of the values obtained by reaction kinetic analysis and fluorescence quenching study strongly supports the validity of the present kinetic treatments.

It is worth noting that the electron transfer between Pe*[1] and DCB is faster than that between Pe*[1] and LCV, whereas, the values of ϕ_{CV} obtained by extraporating [LCV] to the infinite concentration, [DCB] being kept constant, is larger than the value at the infinite concentration of DCB with a fixed [LCV]. The difference between the ϕ_{CV} values is explained by the fact that two successible electron transfer processes (Eqs. 8 and 9) are necessary for the dye formation in the latter case, whereas the dye is formed directly by single electron transfer reaction (Eq. 10) in the former case. In other words, fast electron transfer between Pe*[1] and DCB does not necessarily bring about an increase in the quantum yield by Scheme 1, since another electron transfer between perylene cation radical and LCV is necessary. If the second electron transfer is slow, the overall quantum yield turns to be smaller, probably due to competing back electron transfer processes, Eqs. 16, 17, and 18. The back

$$Pe^{+\cdot} + DCB^{-\cdot} \longrightarrow Pe + DCB \quad (16)$$

$$LCV^{+\cdot} + DCB^{-\cdot} \longrightarrow LCV + DCB \quad (17)$$

$$LCV^{+\cdot} + Pe^{-\cdot} \longrightarrow LCV + Pe \quad (18)$$

electron transfer processes involving perylene cation radical (Eq. 16) would be more efficient than those involving LCV cation radical since LCV cation radical dissociates to CV radical. For the reaction to proceed by Scheme 1 at high DCB concentration, Eq. 9 has to compete with Eq. 16 at a fixed LCV concentration at 1×10^{-4} mol dm^{-3}. Apparently, the efficiency of reaction by Scheme 1 at infinite concentration of LCV is higher than that by Scheme 1 at infinite concentration of DCB in which the overall effciency is reduced by the ion recombination (Eq. 16) and also by the limited probability of Eq. 9 to occur within the lifetime of perylene cation radical at [LCV] $=1\times10^{-4}$ mol dm^{-3}. These discussions, however, could not be expressed by a kinetic treatment. Including these back electron transfer processes in the kinetic expression, the rate equation is far too complicated to be graphically presented. As a compromise, all factors reducing overall efficiency are attributed to Eqs. 6 and 7 in our present kinetic treatment. Phenomenalogically, participation of Eq. 16 is equivalent to increasing k_{qa} in Eq. 6.

Quantum Yield Measurements. The quantum yields for the dye formation (ϕ_{CV}) and perylene photodecomposition (ϕ_{Pe}) were measured in various conditions and shown in Table 3. The values of f in Table 3 confirm the turn over number of perylene by Scheme 1 or Scheme 2. In fact, the f value is about 58 in air and immeasurably large *in vacuo* in the ternary system. The finding that perylene is recycled even

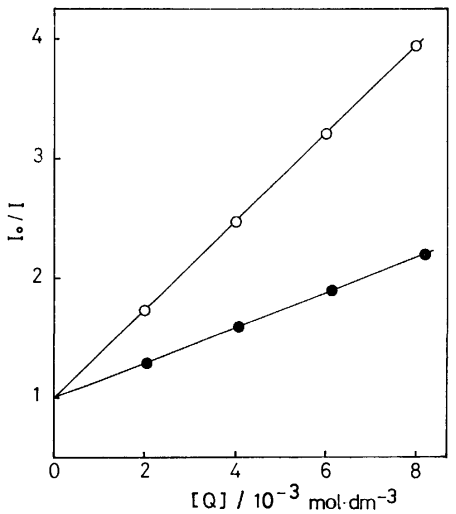

Fig. 6. Fluorescence quenching of perylene.
Quencher ○: DCB, ●: LCV, ([Pe]$=2\times10^{-5}$ mol dm^{-3} in acetonitrile).

Table 3. Quantum yields for the dye formation and perylene decomposition

	In air			*In vacuo*		
	$\frac{\phi_{CV}}{10^{-3}}$	$\frac{\phi_{Pe}}{10^{-3}}$	f[b]	$\frac{\phi_{CV}}{10^{-3}}$	$\frac{\phi_{Pe}}{10^{-3}}$	f[b]
Pe-DCB-LCV	4.4	0.15	58	3.9	~0	c)
Pe-LCV	3.0	0.42	14	0.3	1.2	0.5
Pe-DCB	—	20.8	—	—	0.3	—
LCV-DCB	0	—	—	—	—	—
LCV-DCB[a]	4.3	—	—	0.9	—	—
LCV	0	—	—	—	—	—
LCV[a]	1.2	—	—	0.1	—	—

Irradiated at absorption maximum of perylene(435 nm) at 23.0 °C ([Pe]$=2\times10^{-5}$ mol dm^{-3}, [DCB]$=$[LCV]$=2\times10^{-3}$ mol dm^{-3} in acetonitrile). a) Irradiated on LCV directly at 304 nm. b) Turn over number of perylene as an electron carrier, which is defined as $f=2\times\phi_{CV}/\phi_{Pe}$. c) Immeasurably large.

in the Pe–LCV system ($f=14$) in air requires comments. In this system, O_2 will act as an electron acceptor so that Pe anion radical formed by Eq. 10 will be oxidized to reproduce the Pe molecule by Eq. 19. Although the detection of superoxide ion (O_2^-)

$$Pe^{\cdot-} + O_2 \longrightarrow Pe + O_2^- \quad (19)$$

was not carried out, the participation of O_2 is confirmed by the facts that perylene is not recycled *in vacuo* ($f=0.5$) and Eq. 19 is a highly exothermic process ($\Delta G=-100.4$ kJ/mol).[12] Recently, the similar electron transfer reaction between O_2 and 9,10-dicyanoanthracene anion radical has been reported as an elementary process of non-singlet oxygen photooxygenation of alkenes or sulfides *via* superoxide ion.[13] We conclude that the electron transfer sensitization is also attained in this system, O_2 being an electron acceptor, as described below (Scheme 3).

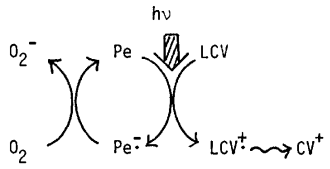

Scheme 3.

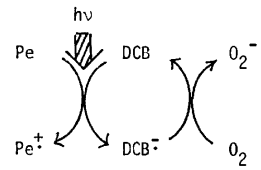

Scheme 4.

In a similar manner, a large quantum yield of perylene photodecomposition in Pe–DCB system in air is understandable by assuming Scheme 4, where DCB acts as an electron carrier instead of perylene. DCB anion radical is reproduced by the electron transfer from DCB anion radical to O_2 ($\Delta G=-100.4$ kJ/mol),[12] whereas perylene cation radical must escape from the cycle to decompose. Although the product analysis has not been carried out, perylene cation radical will be decomposed by oxygenation with superoxide ion as Eriksen *et al.* have reported.[13] The participation of oxygen (superoxide ion) in the perylene decomposition is confirmed by the difference in quantum yields of perylene photodecomposition in air and *in vacuo* (ϕ_{Pe} (in air) $=20.8\times10^{-3}$ and ϕ_{Pe} (*in vacuo*) $=0.3\times10^{-3}$, in Table 3).

The larger quantum yield of dye formation in air relative to the value *in vacuo* will be also explained by assuming the participation of superoxide ion. Superoxide ions produced by the electron transfer from acceptor anion radicals to O_2 reduce the proton concentration according to Eq. 20 and consequently

$$H^+ + O_2^{\cdot-} \longrightarrow HO_2\cdot \quad (20)$$

shift the equilibrium (Eq. 2) towards right to increase the quantum yield of dye formation. Such assumption is supported by the fact that the activation energy for the dye formation in air has a positive value whereas the rate of the dye formation *in vacuo* shows negative dependence on temperature. The negative temperature dependence of the rate is explainable only by considering equilibrium in the course of the dye formation.

In comparison with the unimolecular photodissociation of Crystal Violet leuconitrile (X=CN) to the dye which proceeds with a quantum yield close to unity,[3] the quantum yields given in Table 3 are very much smaller. ϕ_{CV} in the LCV–DCB system on direct irradiation of LCV at 304 nm is almost the same as the values in the ternary system in air. The quantum yields of these electron transfer sensitization systems are small in general, because the presence of back electron transfer between ion radicals diminishes the efficiency. The merit of electron transfer sensitization is to shift the effective absorption wavelength towards longer wavelength regions in comparison with the direct excitation of a redox pair. Singlet state sensitization by means of energy transfer is obviously impossible. The same principles of electron transfer sensitization will be applicable to redox reactions in which the excited triplet state participates.

Solvent Effects. The solvent effects on the dye formation are shown in Table 4. The free ion yields determined by the laser photolysis of electron donor-acceptor (EDA) systems are nearly zero in low polarity solvents. The threshold of the solvent polarity to promote photo-ionic dissociation of EDA systems *via* electron transfer seems to be around ≈10, which is confirmed by transient spectroscopy or photocurrent

Table 4. Solvent effect

	Solvent properties			$\phi_{CV}/10^{-3}$			
		DN	AN	Pe–LCV–DCB[a]	Pe–LCV[a]	LCV–DCB	LCV
Benzene	$\varepsilon=2.28$, $\eta=0.60$	0.1	8.2	0	0	≈0[b]	≈0[b]
THF	$\varepsilon=7.58$, $\eta=0.46$	20.0	8.0	0	0	≈0[b]	≈0[b]
Acetone	$\varepsilon=20.0$, $\eta=0.30$	17.0	12.5	1.8	3.1	1.9[c]	2.3[c]
CH_3CN	$\varepsilon=37.5$, $\eta=0.33$	14.1	19.3	4.4	3.0	4.3[b]	1.2[b]
DMF	$\varepsilon=36.7$, $\eta=0.80$	26.6	16.0	2.1	1.6	2.7[c]	1.0[c]

Irradiated under air saturated solution at 23.0 °C ([Pe] $=2\times10^{-5}$ mol dm^{-3}, [DCB] = [LCV] $=2\times10^{-3}$ mol dm^{-3}). ε and η indicate solvent polarity and solvent viscosity, respectively. Irradiation wavelength is as follows, a) 435 nm(Pe), b) 304 nm(LCV), c) 334 nm(LCV).

measurement in the pyrene–*N*,*N*-dimethylaniline system.[14] As anticipated from the preceeding discussions, the electron transfer between EDA pairs is an essential requirement for the dye formation. Consequently, the present results that ϕ_{CV} is nearly zero in benzene or THF whereas the efficient dye formation takes place in acetone, acetonitrile, and DMF are well understandable. Furthermore, the largest ϕ_{CV} in acetonitrile is in agreement with the finding that the relative free ion yield is the largest in this solvent. In addition to solvent polarity, solvent viscosity seems to influence the efficiency of the dye formation. While DMF is as polar as acetonitrile, the value of ϕ_{CV} in DMF is about half of that in acetonitrile. This difference would be attributed to the high viscosity of DMF. Recently, Schulten and Schulten have reported that ion radical recombination processes are largely affected by solvent viscosity.[16] Namely, viscous solvent like DMF, compared with acetonitrile, will promote the back electron transfer reactions between the ion radicals in geminate ion pair which will diminish the dye formation yield. Furthermore, since carbonium ions are stable and cationic reactions are favored in the solvent having a high acceptor number(AN) and a low donor number(DN) as Gutmann has suggested,[17] the high DN of DMF is also unfavorable factor for the formation of Crystal Violet cation dye.

In contrast to the case in acetonitrile or DMF, the electron transfer sensitization was not achieved in acetone, in which the ϕ_{CV} value was smaller in the ternary system than in the binary one. For electron transfer sensitization to be effective, highly polar solvent and sufficient lifetime of free ion are required. To satisfy these conditions, acetone is neither polar enough nor sufficiently electrophilic to stabilize the cations. The finding that ϕ_{CV} of Pe–LCV system in acetone is comparable to that in acetonitrile whereas the efficiency of the dye formation in the ternary system is low in acetone would indicate the participation of Scheme 1 to be inefficient. This is understandable since perylene cation radical intermediate will be unstable in acetone. From these discussions, it is a reasonable consequence that Crystal Violet dye cation formes efficiently in acetonitrile, having high polarity and low viscosity as well as having the highest AN and the lowest DN among the solvents examined.

Conclusion

On the basis of a kinetic investigation, we have shown that LCV is oxidized to Crystal Violet dye cation *via* electron transfer sensitization mechanism. Under a limited conditions, the turn over number of perylene used as the primary photoabsorber is measurably large. From the view point of singlet state sensitization, the principle of spectral sensitization of redox reactions *via* singlet state has been established. Furthermore, these systems can be considered as a kinetic model for the electron transport system in photosynthesis, which have been also reported by the present authors demonstrating the photoreduction of carbon dioxide to oxalic acid or formic acid using water as a hydrogen source,[18] or the primary action of chlorophyll using polymer bound or micellar electron transfer sensitizers to facilitate energy migration among the chromophores like in antena pigments.[19]

References

1) S. Tazuke and N. Kitamura, *J. Chem. Soc., Chem. Commun.*, **1977**, 515; N. Kitamura and S. Tazuke, *Bull. Chem. Soc. Jpn.*, **53**, 2594 (1980).
2) A. Ledwith, "The Exciplex," ed by M. Gordon and W. R. Ware, Academic Press., New York, N. Y. (1975), p. 209.
3) See for example, M. W. Geiger, N. J. Turro, and W. H. Waddel, *Photochem. Photobiol.*, **25**, 15 (1977) and the references cited therein.
4) K. E. Whitaker and H. R. Snyder, *J. Org. Chem.*, **35**, 30 (1970).
5) C. G. Hatchard and C. A. Parker, *Proc. R. Soc. London., Ser. A*, **235**, 518 (1956).
6) A. MacLachlan, *J. Phys. Chem.*, **71**, 718 (1967).
7) M. L. Herz, *J. Am. Chem. Soc.*, **97**, 6778 (1975).
8) $E(D^+/D)$ and $E(A/A^-)$ are oxidation potential of an electron donor and reduction potential of an electron acceptor, respectively. $e^2/\varepsilon r$ is the Coulombic term and we took the value as +5.4 kJ/mol. $\Delta E_{0.0}$ is the 0-0 transition band energy for the photoexcited species. D. Rehm and A. Weller, *Ber. Bunsenges. Phys. Chem.*, **73**, 834 (1969); D. Rehm and A. Weller, *Israel J. Chem.*, **8**, 259 (1970).
9) H. Shomburg, H. Staerk, and A. Weller, *Chem. Phys. Lett.*, **22**, 1 (1973).
10) The free energy change for the electron transfer between perylene cation radical and LCV, or perylene anion radical and CNA (or DCB) is estimated as −10.5 kJ/mol or −6.7 kJ/mol (0 kJ/mol), respectively.
11) H. Leonhardt, D. Rehm, and A. Weller, *Ber. Bunsenges. Phys. Chem.*, **72**, 257 (1968); H. Leonhardt and A. Weller, *Z. Phys. Chem. N. F.*, **29**, 277 (1961); H. Knibbe, K. Rölling, F. Schafer, and A. Weller, *J. Chem. Phys.*, **47**, 1184 (1967).
12) For the reduction potential of O_2, we used the value −0.57 V (*vs.* S.C.E.). See also Ref. 13.
13) J. Eriksen, C. S. Foote, and T. L. Parker, *J. Am. Chem. Soc.*, **99**, 6455 (1977).
14) Y. Taniguchi and N. Mataga, *Chem. Phys. Lett.*, **13**, 596 (1972); Y. Taniguchi, Y. Nishina, and N. Mataga, *Bull. Chem. Soc. Jpn.*, **45**, 764 (1970).
15) H. Masuhara, M. Shimada, and N. Mataga, *Bull. Chem. Soc. Jpn.*, **43**, 3316 (1970); H. Masuhara, M. Shimada, T. Tsujino, and N. Mataga, *ibid.*, **44**, 3310 (1971); M. Shimada, H. Masuhara, and N. Mataga, *Chem. Phys. Lett.*, **15**, 364 (1972); M. Shimada, H. Masuhara, and N. Mataga, *Bull. Chem. Soc. Jpn.*, **46**, 1903 (1973).
16) Z. Schulten and K. Schulten, *J. Chem. Phys.*, **66**, 4616 (1977); H. -J. Werner, Z. Schulten, and K. Schulten, *ibid.*, **67**, 646 (1977).
17) U. Gutmann, *Electrochim. Acta*, **21**, 661 (1976).
18) S. Tazuke and N. Kitamura, *Nature*, **275**, 301 (1978).
19) S. Tazuke, H. Tomono, H. Kitamura, K. Sato, and N. Hayashi, *Chem. Lett.*, **1979**, 85 and unpublished results.

 © 1980 The Chemical Society of Japan Bull. Chem. Soc. Jpn., 53, 2605—2609 (1980)

Synthesis of *erythro*- and *threo*-γ-Hydroxy-L-ornithines

Koichi MIZUSAKI, Hidefumi YAMAMOTO,† and Satoru MAKISUMI*

Department of Chemistry, Faculty of Science, Kyushu University, Higashi-ku, Fukuoka 812

(Received January 25, 1980)

γ-Hydroxy-DL-ornithine was obtained from an alkaline hydrolysate of 2,5-diamino-4-pentanolide synthesized according to the method of Talbot *et al.*[1] The amino acid preparation was found to be a racemic mixture composed of 34% *erythro* and 66% *threo* isomers by a new chromatographic assay. This assay is based on the conversion of the basic amino acid to a neutral amino acid by acetylation of the δ-amino group and the analysis of the resulting N^{δ}-acetyl derivative with an automatic amino acid analyzer by the ordinary method. Two diastereoisomers of γ-hydroxy-DL-ornithine were separated by column chromatography on Dowex 50 and isolated as their crystalline hydrochlorides. Guanidination of the separated racemic diastereoisomers gave the corresponding diastereoisomeric γ-hydroxyarginines, hydrolysis of which with arginase yielded *erythro*- and *threo*-γ-hydroxy-L-ornithines.

γ-Hydroxyornithine is a diamino monocarboxylic acid which, by virtue of its two asymmetric centers, may exist as four optically active stereoisomers or two racemic diastereoisomers (Scheme 1). Since this amino acid was first synthesized in 1916 by Hammarsten,[2] several synthetic attempts, leading to racemic mixtures in varying proportions of the two possible diastereoisomers of 2,5-diamino-4-pentanolide (**2**), have been studied by several researchers.[3–5] Although the synthesis of the two diastereoisomers of this amino acid from L-histidine and the establishment of the stereochemistry of γ-carbon, to which the secondary hydroxyl group is attached, have been achieved in 1956 by Witkop and Beiler,[5] none of the four optically active isomers has been characterized. Several years later an optically active γ-hydroxyornithine was isolated from an enzymatic hydrolysate of the natural γ-hydroxyarginine and the overall configuration of the amino acid was determined to be *erythro*-γ-hydroxy-L-ornithine by Fujita.[7,8] The occurrence of this amino acid in a plant was also reported.[9] However, none of the optically active isomers, other than the *erythro* L-isomer, has hitherto been characterized, nor has any description for the separation of the two diastereomeric racemates appeared. This paper is primarily concerned with the preparative separation of these diastereomeric racemates, and the resolution of each racemic pair to yield *erythro* and *threo* isomers of γ-hydroxy-L-ornithine.

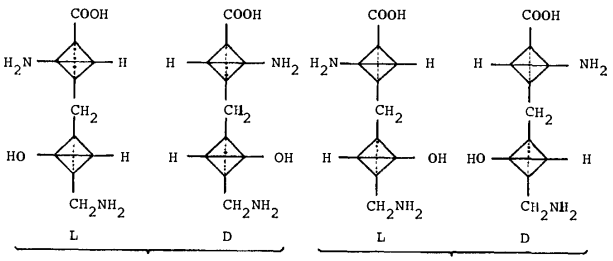

Scheme 1. Fischer projections of four stereoisomers of γ-hydroxyornithine.

Results and Discussion

*Preparation of γ-Hydroxy-DL-ornithine (**1ab**).* Compound **2** was prepared according to the directions of Talbot *et al.*[1] The preparation started from diethyl allylmalonate and involved treatment with sulfuryl

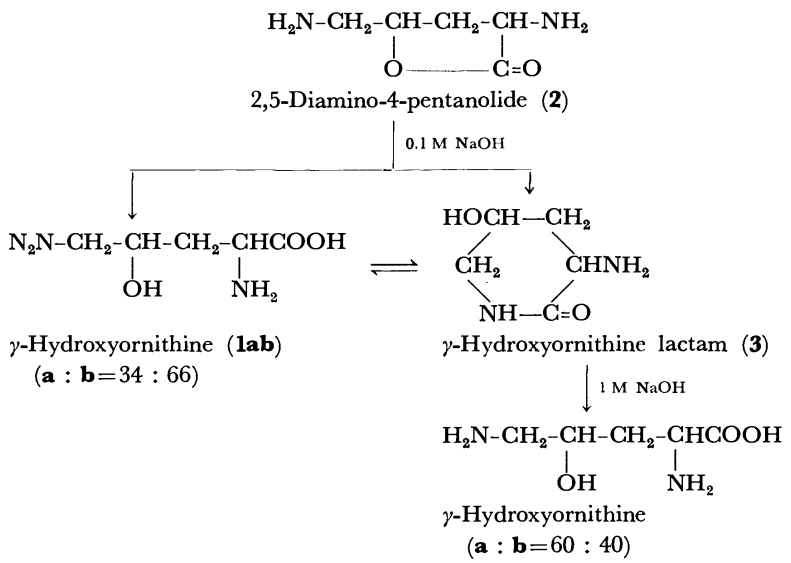

Scheme 2. Alkaline hydrolysis of 2,5-diamino-4-pentanolide.

† Present address: Sumitomo Chemical Co., Ltd., 2-40 Tsukahara, Takatsuki 569.

chloride, followed by hydrolysis and distillation to yield 2,5-dichloro-4-pentanolide. Condensation of this with potassium phthalimide gave 2,5-diphthalimido-4-pentanolide. Talbot *et al.* reported that the latter compound, on hydrolysis by a mixture of glacial acetic acid and concentrated hydrochloric acid, yielded γ-hydroxy-DL-ornithine, which was isolated as a crystalline dihydrochloride monohydrate of the corresponding **2** in a good yield (95%), mp 239 °C. But acid hydrolysis of the diphthalimido derivative in the present work gave a crude diamino lactone hydrochloride as a gummy residue. This crystallized on repeated trituration with ethanol but the crystalline product had an indistinct melting point. Additional recrystallization was impossible, and the lactone was unstable. The crude lactone hydrochloride was subjected to alkaline hydrolysis (Scheme 2). Paper chromatographic analysis of the hydrolysate in 1-butanol–acetic acid–pyridine–water system revealed many spots upon spraying with ninhydrin. Therefore, the hydrolysate neutralized with acid was freed from contaminated acidic and neutral amino acids by passage down a column of Dowex 50 (NH_4^+ form). The basic amino acid were eluted with aqueous ammonia. Further purification was performed by ion exchange chromatography on a column of Dowex 50 equilibrated with pyridinium acetate buffer of pH 4.8. The component that appeared as the first major peak was confirmed to be **lab** by the chromatographic and electrophoretic behavior on paper. From the fractions comprising the peak, a mixture of the two racemic diastereoisomers of γ-hydroxyornithine was isolated as its hydrochloride (**lab**·HCl) (see Experimental section). The isomeric composition of the sample of **lab**·HCl was estimated to be 66% *threo* and 34% *erythro* forms by the assay with an amino acid analyzer, as described below. The next major peak was found to be principally composed of a derivative of γ-hydroxyornithine. From the fractions comprising the peak, a product that gave a characteristic brown-gray color with ninhydrin on paper was isolated as the crystalline hydrochloride. The compound was identified as γ-hydroxyornithine lactam (3-amino-5-hydroxy-2-piperidone) (**3**) by elementary analysis. The characteristic amide bond (lactam) of **3** was well defined by the band at 1670 cm^{-1} in the IR spectrum. Another γ-hydroxyornithine preparation was also recovered from **3** hydrochloride by treatment with alkali. This preparation was composed of 40% *threo* and 60% *erythro* isomers. If γ-hydroxyornithine hydrochloride was treated with warm aqueous ammonia or the free base with refluxing water, a fraction of the amino acid was converted into the lactam. In the same manner, ornithine lactam (3-amino-2-piperidone) was formed from ornithine hydrochloride. Fischer and Zemplen[10] have reported that piperidone was formed from 5-aminovaleric ester and 3-amino-2-piperidone from ornithine ester as a result of spontaneous cyclization. Taking into account the isomeric compositions of the two γ-hydroxyornithine preparations, we can assert that *erythro* isomer is liable to cyclize more easily than *threo* isomer.

*Preparative Separation of Two Diastereoisomers of γ-Hydroxyornithine (**lab**).* The successful separation of the diastereoisomers of hydroxylysine on a column (3.4×115 cm) of Dowex 50 (Na^+ form) was reported by Hamilton and Anderson.[11] For the separation of the two racemic diastereoisomers of **lab**, we also tried this technique, but only partial separation was obtained. Upon passage through a long column (3.8×275 cm) of Dowex 50, a good separation of the diastereoisomers into two peaks resulted. A typical elution pattern is shown in Fig. 1. The component of the first major peak was confirmed to be **lb** and that of the second peak to be **la** by the assay with an amino acid analyzer. From the combined peak fractions, **la** and **lb** were isolated as their crystalline hydrochlorides, respectively. Their stereoisomeric purity was ascertained by the assay with an amino acid analyzer.

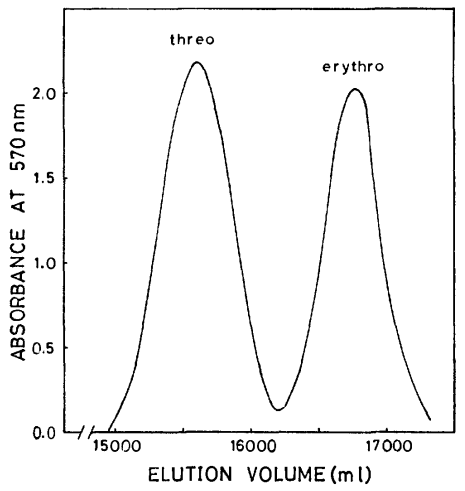

Fig. 1. Elution pattern of γ-hydroxyornithine diastereoisomers on a column (3.8×275 cm) of Dowex 50.

Assay with an Automatic Amino Acid Analyzer. The analytical separation of the diastereoisomers of γ-hydroxyornithine on a Dowex column (0.9×100 cm) by the method of Hirs *et al.*[12] as modified by Piez[13] was reported by Witkop and Beiler.[6] However, the procedure involves many time-consuming operations. A new attempt was made to assay the diastereoisomeric composition of γ-hydroxyornithine with an automatic amino acid analyzer after transformation of this basic amino acid into a neutral amino acid by acetylation of the δ-amino group. As a standard we used "natural" *erythro*-γ-hydroxy-L-ornithine, obtainable by enzymatic hydrolysis of natural γ-hydroxy-L-arginine with arginase. The elution profiles of some N^δ-acetyl derivatives of γ-hydroxyornithine are shown in Fig. 2. The separation of the two isomers was not complete, but was sufficient to allow us to estimate their compositions. The elution times were 40 min for the *threo* and 45 min for the *erythro* isomers. This is a suitable method for routine analysis of the stereochemical purity and of the composition of the diastereoisomers of γ-hydroxyornithine preparations.

Epimerization of erythro-*γ-Hydroxy-L-ornithine by Treatment with Acid and Alkali.* Hamilton and An-

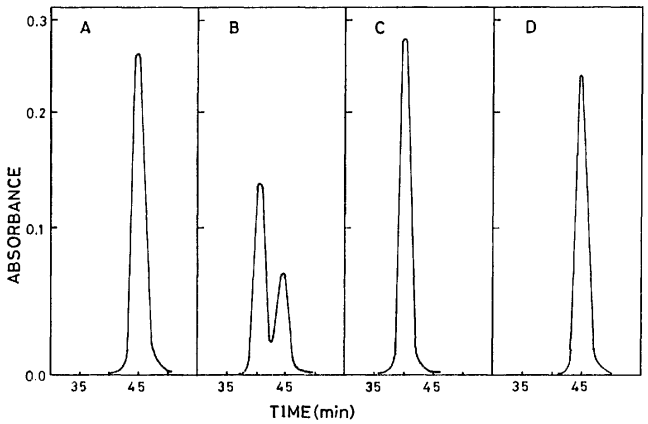

Fig. 2. Elution pattern of N^{δ}-acetyl-γ-hydroxyornithine on a long column (0.8×50 cm) of an amino acid analyzer. A: N^{δ}-Acetyl derivative of γ-hydroxyornithine derived from natural γ-hydroxyarginine, B: N^{δ}-Acetyl derivative of diastereoisomeric γ-hydroxy-DL-ornithine (**lab**), C and D: N^{δ}-Acetyl derivatives of *threo* L- and *erythro* L-isomers obtained in this study.

Table 1. Epimerization of *erythro*-γ-hydroxyornithine on refluxing in acid and alkali

Conditions time (h)	6 M HCl			0.5 M $Ba(OH)_2$	
	0	24	72	0	2
erythro Isomer, %	100	90	78	100	80
threo Isomer, %	0	10	22	0	20

derson[11] have reported that refluxing solutions of δ-hydroxy-L-lysine with 6 M (1 M=1 mol dm^{-3}) hydrochloric acid for 72 h led to epimerization at the α-carbon; a nearly equal mixture of δ-hydroxy-L-lysine and allo-δ-hydroxy-D-lysine resulted. A "natural" γ-hydroxyornithine preparation was refluxed with 6 M hydrochloric acid or 0.5 M barium hydroxide and the extent of epimerization was determined by the assay with an amino acid analyzer. The results are presented in Table 1. Epimerization of *erythro*-γ-hydroxy-L-ornithine was shown to take place more slowly in boiling 6 M hydrochloric acid than that of δ-hydroxy-L-lysine. On the other hand, after refluxing of natural γ-hydroxyarginine in 0.5 M barium hydroxide for 2 h, the content of the diastereoisomers of the resulting γ-hydroxyornithine was found to be 20% *threo* and 80% *erythro* isomers.

Preparation of γ-Hydroxy-DL-arginine. Compounds **1a** and **1b** obtained above were guanidinated with 1-amidino-3,5-dimethylpyrazole nitrate to give γ-hydroxyarginines in the usual manner.[14] After column chromatography of the reaction mixture, γ-hydroxyarginine and unchanged γ-hydroxyornithine were isolated as their hydrochlorides. Assays with an amino acid analyzer of each isomer of the unchanged γ-hydroxyornithine showed that no racemization occurred under the conditions of guanidination.

Hydrolysis of γ-Hydroxy-DL-arginine with Arginase. The optical resolution of racemic γ-hydroxyarginine into γ-hydroxy-L-ornithine and γ-hydroxy-D-arginine was performed by the L-directed hydrolytic action of beef liver arginase. Thus *threo*-γ-hydroxy-L-ornithine and *threo*-γ-hydroxy-D-arginine were obtained from the hydrolysate of *threo*-γ-hydroxy-DL-arginine, and *erythro*-γ-hydroxy-L-ornithine and *erythro*-γ-hydroxy-D-arginine from *erythro*-γ-hydroxy-DL-arginine, respectively. Two optically active isomers of γ-hydroxy-L-ornithine were isolated in crystalline state as their hydrochlorides. The *erythro* isomer obtained here was found to be optically identical with "natural" *erythro*-γ-hydroxy-L-ornithine obtained from natural γ-hydroxy-L-arginine. Rivard and Carter[15] have reported that L- and D-ornithines were obtained from L- and D-arginines, respectively, by hydrolysis with barium hydroxide and careful crystallization with ethanol. Refluxing natural γ-hydroxy-L-arginine with 0.5 M barium hydroxide for 2 h led to complete conversion to γ-hydroxyornithine, but partial epimerization in the product occurred as described above. Therefore, no attempt was made to prepare the isomers of γ-hydroxy-D-ornithine.

Experimental

All melting points are uncorrected. The amino acid analyses were carried out using a JEOL-6AS amino acid analyzer. The optical rotations were measured with a Union high sensitivity polarimeter PM-71. Paper chromatography was done by the ascending technique on Toyo Roshi No. 52 paper with 1-butanol–acetic acid–pyridine–water (4:1:1:2, v/v). Paper electrophoresis was carried out at 300 V for 2.5 h on Toyo Roshi No. 52 paper in a buffer solution of pyridine–acetic acid–water (20:10:970, v/v). The spots were made visible with ninhydrin and Sakaguchi reagents.

Preparation of 2,5-Diphthalimido-4-pentanolide. This compound was prepared from 2,5-dichloro-4-pentanolide (52 g, 30.8 mmol) and potassium phthalimide (122 g, 67.8 mmol) according to the method reported by Talbot *et al.*[1] Yield of crude product, 108 g (27.7 mmol). Recrystallization from a large volume of glacial acetic acid gave crystals, mp 261—263 °C (lit,[1] 263 °C).

Found: C, 64.14; H, 3.71; N, 7.07%. Calcd for $C_{21}H_{14}O_6N_2$: C, 64.62; H, 3.61; N, 7.18%.

*Preparation of γ-Hydroxyornithine (**1ab**) and Its Lactam (**3**).* The crude 2,5-diphthalimido-4-pentanolide (10 g, 25.6 mmol) was hydrolyzed by a mixture of glacial acetic acid (50 ml) and concentrated hydrochloric acid (100 ml) according to the literature.[1] The filtrate was evaporated to dryness *in vacuo* after the phthalic acid had been removed from the cold solution. The residue was dissolved in water and the solution was decolorized with Norit, concentrated to a small volume, and crystallized by repeated trituration with ethanol. The crystalline product was hygroscopic and had an indistinct melting point. The product (2.1 g) was dissolved in 0.1 M sodium hydroxide (30 ml); the solution was refluxed for 3 h and subsequently neutralized with dilute hydrochloric acid. The solution was washed onto a column (2×15 cm) of Dowex 50 (H^+ form); the column was washed with water and then eluted with 2 M aqueous ammonia (200 ml). The eluate was evaporated to dryness *in vacuo*. The residue taken up in a small volume of water was applied to a column (2×15 cm) of Dowex 50 (NH_4^+ form). The column was washed with water and then eluted with 2 M aqueous ammonia (200 ml), and the eluate was evaporated to dryness. The residue dissolved in a small volume of 0.3 M pyridinium acetate buffer, pH 4.8, was placed on a Dowex 50 column (3×54 cm) equilibrated with the same buffer. The column

was developed with the same buffer at a flow rate of about 10 ml/h and the effluent was collected in 5 ml fractions. The position and shape of the resulting peaks were established by ninhydrin spot test on paper of 10 μl samples taken from alternate fractions. Two major peaks appeared on the chromatogram. The component of the first major peak was proved to be **lab** and that of the second to be **3**, by means of paper chromatography and electrophoresis.

*γ-Hydroxy-*DL*-ornithine Hydrochloride (**1ab**·HCl)*: The first major peak fractions were pooled and evaporated to dryness *in vacuo*. The residue dissolved in water was passed through a column (2×10 cm) of Dowex 50 (H^+ form) and the column was washed with water. The amino acid was eluted with 2 M aqueous ammonia (100 ml) and the evaporated eluate was dissolved in water (5 ml). The solution was adjusted to pH 5.0 with 1 M hydrochloric acid, decolorized with charcoal, and concentrated to a syrup. The syrup dissolved in a small volume of 50% ethanol was subjected to crystallization in the cold with the addition of absolute ethanol; yield, 806 mg (4.4 mmol); mp 180—181 °C; *erythro*:*threo*=34:66.

Found: C, 32.77; H, 7.29; N, 15.04%. Calcd for $C_5H_{12}O_3N_2$·HCl: C, 32.53; H, 7.10; N, 15.17%.

*γ-Hydroxy-*DL*-ornithine Lactam Hydrochloride (**3**·HCl)*: The next major peak fractions were pooled and evaporated to dryness. The residue was dissolved in 2 M hydrochloric acid and the solution treated with charcoal, filtered, and evaporated to a syrup. Ethanol was added to the syrup and triturated in the cold to yield crystals. Recrystallization from water–ethanol gave 268 mg (1.6 mmol) of pure **3**·HCl; mp 217—218 °C (dec). This compound gave the characteristic brown-gray color on paper with ninhydrin reagent. IR (KBr): 3200, 1670, and 1580 cm^{-1} (lactam).

Found: C, 35.96; H, 6.66; N, 16.80%. Calcd for $C_5H_{10}O_2N_2$·HCl: C, 36.01; H, 6.60; N, 16.81%.

The combined mother liquors of the crystallization of **3**·HCl were evaporated to dryness. The residue dissolved in 1 M sodium hydroxide (30 ml) was refluxed for 3 h. After neutralization with 1 M hydrochloric acid, the solution was passed through a column (2×11 cm) of Dowex 50 (H^+ form) and the column was washed with water. The amino acid was eluted with 2 M aqueous ammonia (150 ml) and the eluate was evaporated to dryness. From the residue, racemic γ-hydroxyornithine was crystallized as its hydrochloride as described for **lab**·HCl. Yield, 486 mg (2.6 mmol); mp 168—169 °C; *erythro*:*threo*=60:40.

*Separation of Two Diastereoisomers of γ-Hydroxy-*DL*-ornithine (**1ab**).* A preparation of **lab**·HCl (600 mg) was dissolved in a small volume of water and the solution was applied to a column (3.8×275 cm) of Dowex 50 equilibrated with 0.2 M acetate buffer, pH 3.4. The column was developed at room temperature with 0.1 M phosphate buffer, pH 7.8, at a flow rate of 20 ml/h. The first 15 liters of effluent were discarded and the next 2.5 liters were collected in 20 ml fractions. The position and shape of the resulting peaks were established by the colorimetric ninhydrin analysis[16] of 0.2 ml aliquots taken from each fraction. Figure 1 shows a typical chromatogram. The component and the degree of overlap were confirmed by the assay with an amino acid analyzer of 1—2 ml aliquots of the peak fractions. Fractions comprising the fore and after peaks were found to be composed of **1b** and **1a**, respectively, and fractions that overlapped were discarded.

threo-*γ-Hydroxy-*DL*-ornithine Hydrochloride (**1b**·HCl)*: The fractions of 15100—15940 ml were collected and adjusted to pH 5.0 with 2 M hydrochloric acid. The solution was passed through a column (3.8×20 cm) of Dowex 50 (H^+ form) and the column was washed with 50% ethanol. The amino acid was eluted with 2 M aqueous ammonia (900 ml) and the eluate was treated as described for **lab**·HCl; yield of crystals, 300 mg (76%), mp 193—194 °C (dec). The stereochemical purity of the compound was ascertained by the assay with an amino acid analyzer, as shown in Fig. 2.

Found: C, 32.05; H, 7.15; N, 15.15%. Calcd for $C_5H_{12}O_3N_2$·HCl: C, 32.53; H, 7.10; N, 15.17%.

erythro-*γ-Hydroxy-*DL*-ornithine Hydrochloride (**1a**·HCl)*: The fractions of 16460—17120 ml were treated as described for **lb**·HCl; yield of crystals, 153 mg (75%), mp 175—175.5 °C (dec).

Found: C, 32.44; H, 7.04; N, 15.15%. Calcd for $C_5H_{12}O_3N_2$·HCl: C, 32.53; H, 7.10; N, 15.17%.

*Preparation of N^δ-Acetyl-γ-hydroxy-*L*-ornithine.* *erythro*-γ-Hydroxy-L-ornithine hydrochloride (92.3 mg, 0.5 mmol) obtained from natural γ-hydroxy-L-arginine hydrochloride was dissolved in a small volume of water; the solution was brought to 90 °C and copper(II) carbonate was added. Excess copper carbonate was filtered off and the filtrate chilled. With stirring in an ice–water bath, 2 M lithium hydroxide (0.5 ml, 1 mmol) and acetic anhydride (0.1 ml, 1 mmol) were added alternately in portions. After standing for 30 min at room temperature, the solution was acidified with glacial acetic acid and poured onto a column (1×3 cm) of Dowex 50 (H^+ form). After washing with water, the N^δ-acetyl derivative was eluted with 2.5 M pyridine (20 ml) and the eluate was evaporated to dryness *in vacuo*. The residue was triturated in ethanol, filtered off, and washed with ethanol and ether. The product was recrystallized from water–ethanol; yield 49.2 mg (52%); mp 211 °C (dec).

Found: C, 44.02; H, 7.38; N, 14.39%. Calcd for $C_7H_{14}O_4N_2$: C, 44.21; H, 7.37; N, 14.73%.

Amino Acid Analysis of N^δ-Acetyl-γ-Hydroxyornithines. A small amount of γ-hydroxyornithine preparation (1—2 mg) was transformed into its N^δ-acetyl derivative, as described above, on a small scale. Without crystallization, the product was dissolved in 0.2 M sodium citrate buffer (5 ml) of pH 3.25 (the first buffer). A sample of the solution was applied to a long column (0.8×50 cm) and the column was eluted with the first buffer in the usual way.

Epimerization of erythro-*γ-Hydroxy-*L*-ornithine with Strong Acid.* *erythro*-γ-Hydroxy-L-ornithine hydrochloride (9.3 mg) was refluxed in 6 M hydrochloric acid (10 ml). Two milliliter aliquots of the reaction mixture were taken out and evaporated to dryness. The product was converted to N^δ-acetyl derivative as described above and subjected to amino acid analysis. The results of the samples refluxed for 24 and 72 h are presented in Table 1.

Degradation of erythro-*γ-Hydroxy-*L*-arginine with Weak Alkali.* Natural γ-hydroxyarginine hydrochloride (12 mg) was refluxed in 0.5 M barium hydroxide (2 ml) for 2 h. The reaction mixture was no longer positive to a Sakaguchi reaction. Then it was neutralized with 0.25 M sulfuric acid and centrifuged. The concentrated supernatant was treated with copper(II) carbonate. This was followed by acetylation with acetic anhydride and alkali, as described above. N^δ-Acetyl derivative of the possible reaction product (γ-hydroxyornithine) was subjected to amino acid analysis. The result is presented in Table 1.

Preparation of γ-Hydroxyarginine from γ-Hydroxyornithine. Guanidination of γ-hydroxyornithine with 1-amidino-3,5-dimethylpyrazol nitrate and chromatographic separation of the product and unchanged amino acid on a Dowex 50 column were carried out essentially according to the literature.[14]

erythro-*γ-Hydroxy*-DL-*arginine Hydrochloride*: Compound **1a**·HCl (203 mg, 1.1 mmol) was guanidinated with 1-amidino-3,5-dimethylpyrazol nitrate (443 mg, 2.2 mmol) and the reaction mixture subjected to chromatography on a Dowex 50 column (2×16 cm). From the afterpeak fractions, the product was crystallized as its hydrochloride. The yield of hygroscopic crystals was 160 mg (64%). The homogeneity of this compound was confirmed by ninhydrin and Sakaguchi reagents by paper electrophoresis and chromatography. A small amount of **1a**·HCl was recovered from the forepeak fractions.

threo-*γ-Hydroxy*-DL-*arginine Hydrochloride*: Guanidination of **1b**·HCl (277 mg, 1.5 mmol) with the guanidinating reagent (604 mg, 3 mmol), followed by column chromatography, gave hygroscopic crystals; yield 140 mg (41%).

Optical Resolution of Racemic γ-Hydroxyarginine by Arginase. The partially purified arginase preparation was obtained as reported by Schmike.[17] Racemic γ-hydroxyarginine hydrochloride (120—140 mg) and the arginase (50 mg) were dissolved in 0.025 M Tris-Cl buffer of pH 9.6 (5 ml) containing 0.01 M manganese chloride, and incubated for 24 h at 37 °C. The progress of the hydrolysis of the susceptible L-antipode was followed by amino acid analysis as usual. To reach complete hydrolysis, arginase (25 mg) were added to the reaction mixture and it was incubated for a further 24 h. From the mixture deproteinized with 0.5 M perchloric acid, the products were recovered by chromatographic separation on a Dowex 50 column (2×16 cm) essentially according to the literature.[14]

erythro-*γ-Hydroxy*-L-*ornithine Hydrochloride.* *erythro-γ*-Hydroxy-DL-arginine hydrochloride (140 mg) was treated with arginase and the deproteinized solution was subjected to chromatographic separation. From the forepeak fractions, *erythro-γ*-hydroxy-L-ornithine was crystallized as its hydrochloride; yield 32 mg (56%); mp 175—176 °C (dec); $[\alpha]_D^{20}$ +10.5° (c 2, H_2O), lit,[8] $[\alpha]_D^{20}$ +10.6° (*c* 5, H_2O).

Found: C, 32.39; H, 7.06; N, 14.81%. Calcd for $C_5H_{12}O_3N_2 \cdot HCl$: C, 32.53; H, 7.10; N, 15.17%.

From the afterpeak fractions, *erythro-γ*-hydroxy-D-arginine was crystallized as its hydrochloride; yield of hygroscopic crystals, 42 mg (60%).

threo-*γ-Hydroxy*-L-*ornithine Hydrochloride*: *threo-γ*-Hydroxy-DL-arginine hydrochloride (120 mg) was treated as described for *erythro* racemate. The yield of *threo-γ*-hydroxy-L-ornithine hydrochloride was 48 mg (98%); mp 200—201 °C (dec); $[\alpha]_D^{20}$ −7.0° (*c* 2, H_2O).

Found: C, 32.53; H, 7.09; N, 14.99%. Calcd for $C_5H_{12}O_3N_2 \cdot HCl$: C, 32.53; H, 7.10; N, 15.17%.

The yield of hygroscopic crystals of *threo-γ*-hydroxy-D-arginine hydrochloride was 51 mg (85%).

References

1) G. Talbot, R. Gandry, and L. Berlinguet, *Can. J. Chem.*, **34**, 911 (1956).
2) E. Hammarsten, *Compt. Rend. Trav. Lab. Carlsberg*, **11**, 223 (1916).
3) W. Traube, R. Tohow, and W. Tepohl, *Ber.*, **66**, 1861 (1923).
4) W. Langenbeck and R. Hutschenreuter, *Ber.*, **162**, 305 (1929).
5) A. N. Dey, *J. Chem. Soc.*, **1937**, 1166.
6) B. Witkop and T. Beiler, *J. Am. Chem. Soc.*, **78**, 2282 (1956).
7) Y. Fujita, *Bull. Chem. Soc. Jpn.*, **32**, 439 (1959).
8) Y. Fujita, *Bull. Chem. Soc. Jpn.*, **33**, 1379 (1960).
9) E. Bell and A. S. L. Tirmanna, *Nature (London)*, **197**, 901 (1963).
10) E. Fischer and G. Zemplen, *Ber.*, **42**, 1022, 4878 (1909).
11) P. B. Hamilton and R. A. Anderson, *J. Biol. Chem.*, **213**, 249 (1955).
12) C. H. W. Hirs, S. Moore, and W. H. Stein, *J. Biol. Chem.*, **195**, 669 (1952).
13) K. A. Piez, *J. Biol. Chem.*, **207**, 77 (1954).
14) S. Ohyama, K. Mizusaki, H. Tsunematsu, and S. Makisumi, *J. Biochem. (Tokyo)*, **86**, 11 (1979).
15) D. E. Rivard and M. E. Carter, *J. Am. Chem. Soc.*, **77**, 1260 (1955).
16) E. N. Yemm and E. C. Cooking, *Analyst (London)*, **80**, 209 (1955).
17) R. T. Schimke, *J. Biol. Chem.*, **239**, 3808 (1964).

Studies of Polyphenyls and Polyphenylenes. II.[1] The Synthesis and Physical Properties of Polyphenyls Containing Para Linkage

Shigeru Ozasa,* Noriko Hatada, Yasuhiro Fujioka, and Eiichi Ibuki

Department of Organic Chemistry, Kyoto College of Pharmacy, Misasagi-nakauchi-cho, Yamashina-ku, Kyoto 607

(Received January 28, 1980)

Twelve linear polyphenyls, including quinque- to octiphenyl, were synthesized by the Ullmann cross-coupling reaction of iodobiphenyl with diiodobenzene or iodoterphenyl. Ultraviolet spectral studies of the polyphenyls indicated that the positions of the K-bands above *ca.* 260 nm, regardless of the presence of *o*- or *m*-phenylene unit(s), may be considered to be an indication of the approximate number of consecutive *p*-phenylene units. Infrared studies also showed that the locations of strong or medium bands in the 815—850 cm^{-1} region may give the same information. The HMO calculations of the longest wavelength absorption bands of twenty-four polyphenyls were carried out. A comparison between the calculated and observed wavelengths gave rather good agreement, except in the cases of two compounds. The signals of the proton magnetic resonance spectra of eighteen polyphenyls were assigned tentatively. The correlations between the arrangement of the benzene rings and the spectral patterns are discussed.

In the previous paper, a series of closely related linear sexiphenyls have been synthesized to elucidate the relation between the structures and the physical properties of polyphenyls.[1] Spectral studies have proved that the sexiphenyls having one or two *p*-phenylene rings displayed marked characteristics in both their infrared (IR) and ultraviolet (UV) absorption spectra.

In the present work, in order to investigate the spectral characteristics of a wide variety of polyphenyls, we synthesized twelve symmetrical and unsymmetrical linear polyphenyls (**1**—**12**), having one to four *p*-phenylene rings and not having them for comparison. The IR, UV, and proton magnetic resonance (^{1}H-NMR) spectra of the polyphenyls have been measured, and the relationship between the number and arrangement of the benzene rings and their physical properties, especially the characteristics due to the presence of *p*-linkage, has been discussed. In addition, we performed the HMO calculations of the longest wavelength absorption bands of the polyphenyls as well as of the closely related bi-, ter-, and quaterphenyls. The calculated results have been compared with the observed values.

For the synthesis of the polyphenyls, the Ullmann cross-coupling reaction of aryl halides has been used. Among the halides used, iodobiphenyls (2- (**13**), 3- (**14**), and 4-iodobiphenyl (**15**)) and iodoterphenyls (4-iodo-*o*- (**16**) and 4-iodo-*p*-terphenyl (**17**)) were prepared from commercial aminobiphenyls, aminonitrobenzene, and terphenyls. Diiodobenzenes (*o*- (**18**), *m*- (**19**), and *p*-diiodobenzene (**20**)) were commercially available. A mixture of iodobiphenyl and diiodobenzene in the molar ratio of 2 to 1 was subjected to the reaction at 230—275 °C with copper powder for the synthesis of symmetrical polyphenyls, while a mixture of an equimolar ratio of iodobiphenyl and iodoterphenyl was used for the synthesis of unsymmetrical ones. The polyphenyls and by-products thus obtained are given in Table 1.

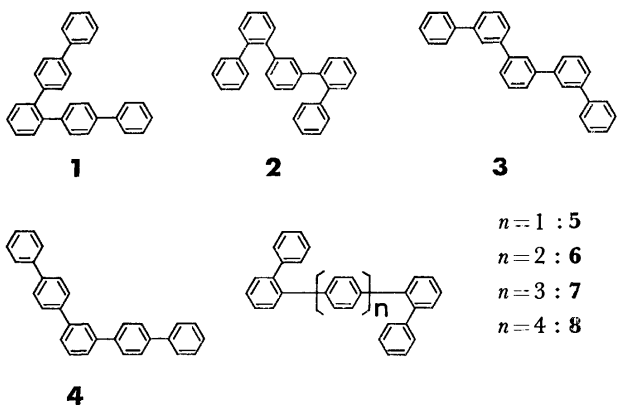

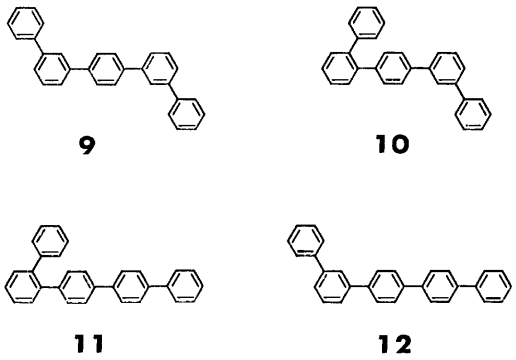

The quinque-, septi-, and octiphenyl, thus prepared, showed IR spectral data consistent with their structure and gave acceptable results from elemental analysis and molecular weight determination. An alternative synthesis of eight quinquephenyls has been reported earlier by other workers (**1**,[2] **2**,[2] **3**,[3] **4**,[3b,4] **5**,[3b] **9**,[3b,5] **10**,[2,6] **12**[6]). Although the melting point of **2**[7] does

Table 1. Ullmann synthesis of polyphenyls

Iodide	Quinquephenyl (Yield/%)	Other products
15+**18**	**1**(16.4)	**21**, **27**
13+**19**	**2**(23.8)	**22**
14+**19**	**3**(8.1)	**26**
15+**19**	**4**(13.3)	**21**, **27**
13+**20**	**5**(13.9)	**22**, **6**, **7**, **8**
13+**16**	**5**(20.0)	**21**, **24**, **22**, **6**
14+**20**	**9**(13.1)	**21**, **26**
13+**18**	——	**21**, **22**, **23**
14+**16**	**10**(18.5)	**21**, **24**, **26**, **6**
15+**16**	**11**(24.7)	**21**, **24**, **27**, **6**
14+**17**	**12**(27.0)	**21**, **25**, **26**, **28**

not coincide with that of previous authors, those of the seven remaining quinquephenyls fall within 1—2 °C of those of the other authors.

The yields of all the pure quinquephenyls except **3** (8.1%) were 13—27%, and in all of the coupling experiments an appreciable amount of quaterphenyls formed by the homo-coupling of the corresponding iodobiphenyl were isolated as by-products. Further, in the coupling reactions using **16** or **17** as one of the iodo compounds (**13**+**16**, **14**+**16**, **15**+**16**, and **14**+**17**) a significant amount of sexiphenyls were obtained. An attempted coupling of **13**+**20** gave **6** (9.8%), **7** (7.4%), and **8** (2.4%), in which two to four *p*-phenylene rings are present respectively, together with **5** (13.9%). A similar coupling of **14**+**20**, however, failed to give the analogous sexi-, septi, and octiphenyls except for quinquephenyl, **9**. In the case of **13**+**18**, no corresponding quinquephenyl was isolated, but biphenyl (**21**, 11.1%), *o*-quaterphenyl (**22**, 30.2%), and triphenylene (**23**, 23.9%) were obtained. The formation of **23** may be comparable to that of phenyltriphenylene in the Ullmann cross-coupling reaction of 2,2'-diiodobiphenyl with **14** or **15**;[1] it shows favorable cyclization by the apparent elimination of hydrogen iodide to form a triphenylene ring.

The IR spectra of the twelve polyphenyls (**1**—**12**) were measured by the KBr-disk method. Let us now discuss the most characteristic bands due to C–H out-of-plane deformation vibrations in the 675—920 cm^{-1} region.

In the spectra of **1**, **4**, **5**, **9**, and **10**, which have one or two isolated *p*-phenylene rings, the strong or medium C–H out-of-plane bending vibration bands of two adjacent hydrogen atoms of *p*-phenylene rings were observed in the range 835—850 cm^{-1}. In the cases of **11**, **12**, and **6**—**8**, in which two to four consecutive *p*-phenylene rings are present, the analogous intense bands were observed in the region 817—832 cm^{-1} (Table 2). These spectral data show that the position of strong or medium C–H bands observed in the 817—850 cm^{-1} range is shifted toward a lower wave number in accordance with the progression of *p*-phenylene rings. The shift of C–H band was considered to be quite analogous to that reported previously in the spectra of *p*-polyphenyls by Sandroni[9] and others.[10] The results also show that the position of the C–H band is nearly independent of whether the polyphenyls have *o*- or *m*-phenylene ring(s) or not.

On the basis of these results, the positions of strong or medium bands in the 815—850 cm^{-1} region of the polyphenyls, regardless of the presence of *o*- or *m*-phenylene unit(s) in them, may be considered to be an indication of the approximate number of consecutive *p*-phenylene units.

The UV spectra of the twelve polyphenyls were measured in a cyclohexane solution. The absorption curves are shown in Figs. 1—4. The longest wavelength absorption maxima above 220 nm of the polyphenyls, except the three new compounds (**7**, **8**, and **11**), coincide within 1—3 nm with those of other workers.[2,3b,5,6,8,11]

All of the polyphenyls displayed two groups of intense bands: one in the fairly narrow region of 192—207 nm with intensities approximately proportional to the number of ring units (ε 59300—129000) and another in the broad region of 230—315 nm with a high intensity. The former, whose band position was found to be independent of the structure, is considered to be the E-band, and the latter, whose band position was substantially affected by the nature and number of phenylene rings, is regarded as the K-band, as has been discussed in regard to the spectra of sexiphenyls.[1,12]

The spectrum of **3** displayed an intense K-band at substantially the same wavelength as the biphenyl

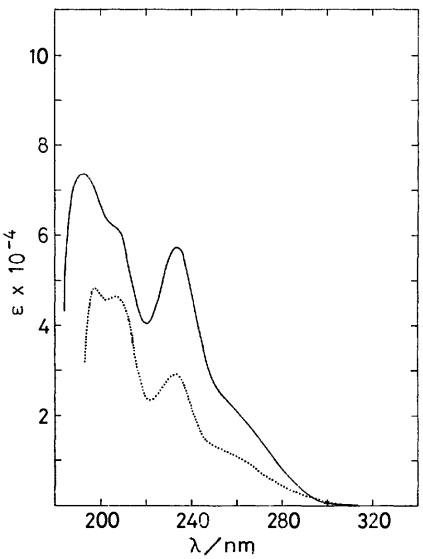

Fig. 1. UV spectra of terphenyl and quinquephenyl in cyclohexane.
——: 2,2″-Diphenyl-*m*-terphenyl (**2**), ……: *o*-terphenyl (**24**).

Table 2. IR spectra of polyphenyls containing para linkage (cm^{-1})

n	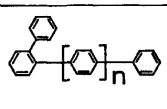	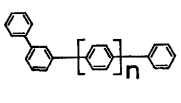	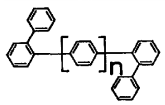	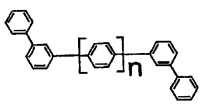	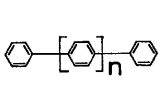	
1	841	845	841	848	842±5[a]	833—855[b]
2	826	829	832	826[d]	827±5[a]	826—833[b]
3	818[c]		823		819[a]	820[b]
4			817		814[a]	817[b]

a), b), c), and d) refer to Refs. 9, 10b, 13, and 1 respectively.

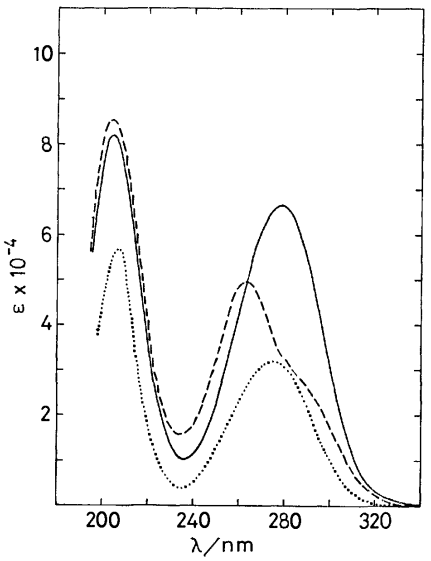

Fig. 2. UV spectra of terphenyl and quinquephenyls in cyclohexane.
——: 4,4″-Diphenyl-*m*-terphenyl (**4**), ----: 4,4″-diphenyl-*o*-terphenyl (**1**), ·····: *p*-terphenyl (**25**).

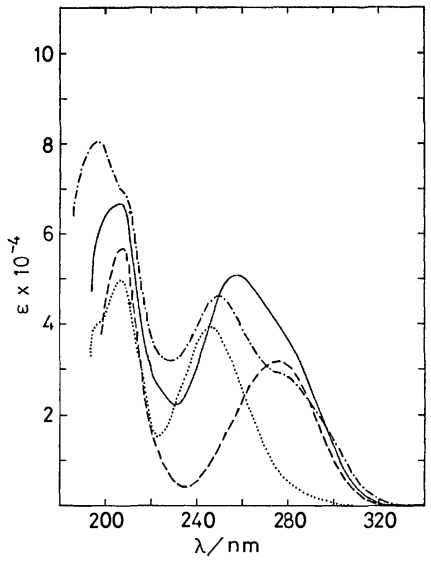

Fig. 3. UV spectra of terphenyls and quinquephenyls in cyclohexane.
——: 3,3″-Diphenyl-*p*-terphenyl (**9**), —·—·—: 2,3″-diphenyl-*p*-terphenyl (**10**), ----: *p*-terphenyl (**25**), ·····: *m*-terphenyl.

band, but with an intensity about four times greater (Table 4). Also, the K-band (234 nm, 57700; 250 nm sh, 27000) of **2**, in which two *o*-terphenyl units hold a common *m*-phenylene ring, appeared at the similar wavelength with an intensity about two times that of *o*-terphenyl (**24**) (233 nm, 29100; 251 nm sh, 13300) (Fig. 1). In the cases of **4** and **1**, in each of which two isolated *p*-phenylene rings are present, the spectrum of the former revealed a strong K-band (280 nm, 66500) at a similar wavelength with an intensity about two times that of *p*-terphenyl (**25**) (277 nm, 31600), while the spectrum of the latter

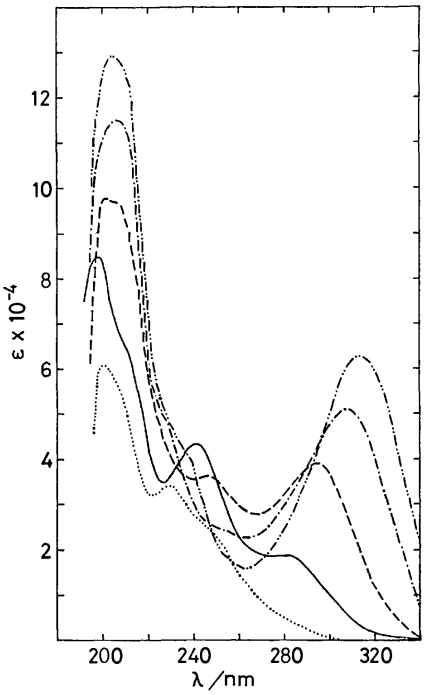

Fig. 4. UV spectra of related quater-, quinque-, sexi-, septi-, and octiphenyl in cyclohexane.
··—··: 2,2″″″-Diphenyl-*p*-sexiphenyl (**8**), —·—·—: 2,2″″-diphenyl-*p*-quinquephenyl (**7**), ----: 2,2‴-diphenyl-*p*-quaterphenyl (**6**), ——: 2,2″-diphenyl-*p*-terphenyl (**5**), ·····: *o*-quaterphenyl (**22**).

displayed a discernible shoulder near 280 nm, together with a intense K-band at about 260 nm (264 nm, 49800; 284 nm sh, 30600). The differences of the spectra might reflect the difficult extension of the two conjugated systems of *p*-terphenyl separated by *m*-phenylene ring in the former, and the reduced π-π interaction across the pivot bonds between *o*-phenylene ring and its nearest neighbors in the latter (Fig. 2). In the cases of **10** and **9**, which each have one *p*-terphenyl unit, the spectra (250 nm, 46200; 275 nm sh, 29300) (258 nm, 50800; 280 nm sh, 38200) displayed only a discernible shoulder near 280 nm together with a prominent K-band at 250 nm or at 258 nm respectively (Fig. 3).

Then, the spectra of the series of four polyphenyls **5**—**8** (series C), in which both terminals of one or two to four consecutive *p*-phenylene units are linked by *o*-phenylene rings, showed a remarkable bathochromic shift and an increase in intensity of the characteristic K-bands with an increase in the number of consecutive *p*-phenylene rings (Fig. 4). An analogous shift and increase in intensity of the K-band were also observed in the spectra of series B, A, and D, in which one or both terminals of one or more *p*-phenylene units are linked by *m*- or *o*-phenylene ring(s), as shown in Table 3. Such a characteristic shift and increase in intensity of K-band are compatible with the observation in the spectra of four *p*-polyphenyls (series E) by Gillam and Hey.[12a]

The foregoing results in the spectra of the polyphenyls show that the K-band above *ca.* 260 nm suggest the presence of *p*-phenylene unit(s), and that the positions

TABLE 3. UV SPECTRA OF POLYPHENYLS CONTAINING PARA LINKAGE IN CYCLOHEXANE (λ_{max}/nm (ε))

n	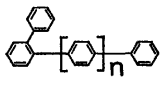 (A)	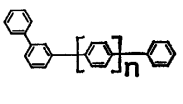 (B)	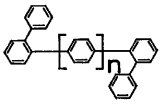 (C)	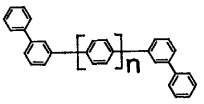 (D)	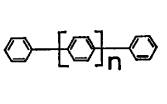 (E)
1	278 (25100)	268 (38400)	280 (18500)	280[sh] (38200)	277 (31600)
2	295 (42100)	296 (47500)	297 (38900)	296 (51900) [b]	294 (44000)
3	307 (57000) [a]		307 (51000)		310 (62000) [c,d]
4			315 (62900)		317.5 (>75600) [c,d]

a), b), and c) refer to Refs. 13, 1, and 12a respectively. d) In chloroform.

TABLE 4. CALCULATED AND OBSERVED LONGEST WAVELENGTH ABSORPTION BANDS OF THE POLYPHENYLS AND RELATED COMPOUNDS

Compound	Calcd trans. energy β [a]	Absorption band		
		Calcd	Obsd	
		λ_{max}/nm	λ_{max}/nm	ε
21	−1.4392	233	248	18500
25	−1.2254	273	277	31600
27	−1.1176	300	294	44400
ϕpppϕ [b]	−1.0550	318	310	62000 [c]
ϕmϕ	−1.3564	247	247	39100
26	−1.3222	253	248	62700
3	−1.3048	257	249	83200
24	−1.4810	226	251 sh	13300
22	−1.4192	236	245 sh	25600
ϕoooϕ	−1.3834	242	237	46200 [d]
ϕpoϕ	−1.2308	272	278	25100
ϕpmϕ	−1.2090	277	268	38400
ϕmoϕ	−1.3492	248	251 sh	32400 [d]
1	−1.1418	293	284 sh	30600
2	−1.3440	249	250 sh	27000
4	−1.1702	286	280	66500
5	−1.2354	271	280	18500
7	−1.0676	314	307	51000
8	−1.0246	327	315	62900
ϕmomϕ	−1.2922	259	249 sh	48300 [d]
9	−1.1956	280	280 sh	38200
10	−1.2150	276	275 sh	29300
11	−1.1254	298	295	41200
12	−1.1116	301	296	47500

a) For β, −3.70 eV was used as the mean value calculated from the absorption bands of the biphenyl and the first four *p*-polyphenyls. b) ϕ, p, m, and o refer to phenyl, *p*-, *m*-, and *o*-phenylene rings. c) And d) refer to Refs. 12a and 13.

of the bands may be an indication of the approximate number of continuous *p*-phenylene units.

A comparison between the calculated and observed longest wavelength bands of the polyphenyls and closely related compounds is given in Table 4. Here the HMO calculations were performed by assuming tentatively the dihedral angle of the pivot bond as follows: 50° for phenyl–*o*- and *o*-–*o*-phenylene linkages, 35° for *o*-–*p*- and *m*-–*p*-phenylene linkages, and 20° for the other linkages. The table shows rather good agreement between calculated and observed wavelengths except in the cases of **21** and **24**. The results may also be confirmed by the approximate linear relation of the wave numbers of the longest wavelength absorption bands to the calculated longest wavelength transition energies, as shown in Fig. 5.

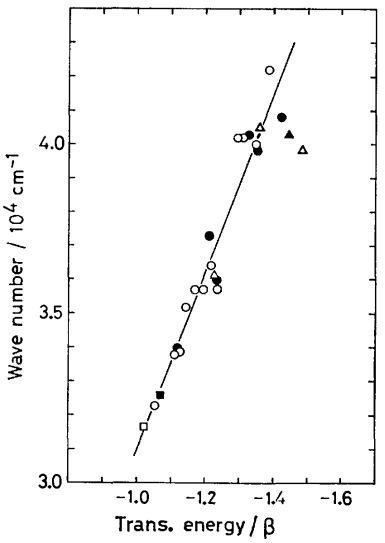

Fig. 5. Plots of wave numbers of longest wavelength absorption bands *vs.* calculated longest wavelength transition energies of the polyphenyls and related compounds.
▲: Biphenyl, △: terphenyls, ●: quaterphenyls, ○: quinquephenyls, ■: septiphenyl, □: octiphenyl.

The ^{1}H-NMR spectra of the polyphenyls and closely related compounds were measured at 80 MHz in a $CDCl_3$ solution. The chemical shifts from tetramethylsilane are summarized in Table 5.

The spectra of **1**, **5**—**8**, **10**, and **11** show one singlet peak near δ 7.44; this is assigned to the resonances of protons on one or two *o*-phenylene rings by comparison with the *o*-phenylene proton signal of **24** (δ 7.41, 4H, s, *o*-C_6H_4).

The most down field multiplet peaks (δ 7.75—7.93) found commonly in the spectra of **3**, **4**, **9**, **10**, **12**, and *m*-quaterphenyl (**26**) may be assigned to the resonances of one isolated *m*-phenylene proton by comparing with the signals of *m*-terphenyl and 1,3-di(phenyl-d_5)benzene[13] (δ 7.78—7.83, 1H, m, *m*-C_6H).

Among the spectra of the eleven polyphenyls containing *p*-linkage(s), those of **4**, **9**, **12**, and *p*-quater-

Table 5. ^{1}H-NMR spectral data of **1**—**12**, **21**, **22**, and **24**—**27** in $CDCl_3$[a)]

Compound	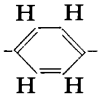	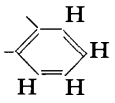	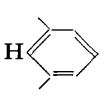	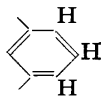	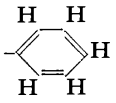
21	——	——	——	——	7.16—7.70(10H, m)
25	7.68(4H, s)	——	——	——	7.33—7.71(10H, m)
27	7.71(8H, s)	——	——	——	7.34—7.68(10H, m)
26	——	——	7.81—7.88(2H, m)		7.32—7.74(16H, m)
24	——	7.41(4H, s)	——	——	7.17(10H, s)
22	——	7.12—7.43(8H, m)	——	——	6.51—7.08(10H, m)
1	7.26 and 7.48(8H, AA′BB′-q, J=8.6 Hz, C_2, C_3-H and C_3, C_5-H)	7.47(4H, s)	——	——	7.32—7.66(10H, m)
2	——		6.78—7.48(22H, m)		
3	——	——	7.84—7.93(3H, m)		7.32—7.75(19H, m)
4	7.73(8H, s)	——	7.87—7.93(1H, m)		7.33—7.68(13H, m)
5	6.97(4H, s)	7.40(8H, s)	——	——	7.12—7.21(10H, m)
6	7.18 and 7.44(8H, AA′BB′-q, J=8.3 Hz, $C_{2'}$, $C_{6'}$-H and $C_{3'}$, $C_{5'}$-H)	7.43(8H, s)	——	——	7.20(10H, s)
7	7.21 and 7.50(8H, AA′BB′-q, J=8.8 Hz, $C_{2'}$, $C_{6'}$-H and $C_{3'}$, $C_{5'}$-H) 7.64(4H, s, middle)	7.45(8H, s)	——	——	7.21(10H, s)
8	7.23 and 7.51(8H, AA′BB′-q, J=8.7 Hz, $C_{2'}$, $C_{6'}$-H and $C_{3'}$, $C_{5'}$-H) 7.69(8H, s, inner)	7.45(8H, s)	——	——	7.22(10H, s)
9	7.75(4H, s)	——	7.84—7.89(2H, m)		7.33—7.71(16H, m)
10	7.23 and 7.51(4H, AA′BB′-q, J=8.7 Hz, $C_{2'}$, $C_{6'}$-H and $C_{3'}$, $C_{5'}$-H)	7.45(4H, s)	7.75—7.82(1H, m)		7.21(5H, s, o-$C_6\underline{H}_4\cdot C_6\underline{H}_5$) 7.33—7.71(8H, m, m-$C_6\underline{H}_3\cdot C_6\underline{H}_5$)
11	7.23 and 7.50(4H, AA′BB′-q, J=8.7 Hz, $C_{2'}$, $C_{6'}$-H and $C_{3'}$, $C_{5'}$-H) 7.66(4H, s, p-$C_6\underline{H}_4\cdot C_6H_5$)	7.45(4H, s)	——	——	7.21(5H, s, o-$C_6H_4\cdot C_6\underline{H}_5$) 7.33—7.71(5H, m, p-$C_6H_4\cdot C_3\underline{H}_5$)
12	7.72(4H, s, p-$C_6\underline{H}_4\cdot C_6H_5$) 7.75(4H, s, p-$C_6\underline{H}_4\cdot p$-$C_6H_4\cdot C_6H_5$)	——	7.84—7.90(1H, m)		7.33—7.67(13H, m)

a) δ(ppm) from internal standard TMS.

phenyl (**27**) display one or two singlet peaks near δ 7.73. These are assigned to the resonances of *p*-phenylene protons by comparison with the *p*-phenylene proton signal of **25** (δ 7.68, 4H, s, *p*-C_6H_4). On the other hand, those of **1**, **6**, and **10** reveal an apparent AA'BB'-q pattern near δ 7.22 and 7.48, which may be assigned to the resonances of the *p*-phenylene protons from analogy with the spectra of *p*-phenylene protons of 2,4'-diphenylbiphenyl and 2,4'-di(phenyl-d_5)biphenyl[13] (δ 7.21 and 7.46, 4H, AA'BB'-q, J=8.6 Hz, 2'-, 6'-H and 3'-, 5'-H). Furthermore, those of **7**, **8**, and **11** show one singlet peak near δ 7.66 in addition to an apparent AA'BB'-q pattern near δ 7.22 and 7.50, and both peak and pattern are assigned to the resonances of the protons on the different types of *p*-phenylene rings. In the case of **5**, however, the resonances of the *p*-phenylene protons are observed as a singlet peak at a rather higher field (δ 6.97) as compared with those of **25**. The marked high field shift possibly reflects the ring current effect of both terminal phenyl groups. The foregoing results suggest that the two types of *p*-phenylene proton signal, a singlet peak and an AA'BB'-q pattern, are related closely with the kinds of the two groups adjacent to the *p*-phenylene ring. The correlation may be generalized as follows: 1) In the cases of polyphenyls, in which the *p*-phenylene ring is linked by two identical groups (phenyl or phenylenes) or by two different groups (phenyl or phenylenes except *o*-phenylene), the resonances of *p*-phenylene protons are generally observed as a singlet peak. 2) The resonances of *p*-phenylene protons of polyphenyls, in which the *p*-phenylene ring is linked by two different groups (phenyl or phenylenes), of which one is an *o*-phenylene ring, are generally observed as an AA'BB'-q pattern.

The spectra of **6**—**8**, **10**, and **11** reveal one singlet peak near δ 7.21. This is assigned to the resonances of protons of phenyl group(s) adjacent to *o*-phenylene ring(s), by comparison with the phenyl proton signal of **24** (δ 7.17, 10H, s, C_6H_5). However, the phenyl proton signals of **10** and **11**, each of which has a phenyl group linked by a *m*- or *p*-phenylene group, respectively, and those of **1**, **3**, **4**, **9**, **12**, and **25**—**27** are observed as multiplet peaks in the region δ 7.32—7.75. Among them, the multiplet peaks in the δ 7.32—7.75 region of **3**, **4**, **9**, **10**, **12**, and **26**, all of which have *m*-phenylene ring(s), are assigned to the resonances not only of phenyl protons but also of three adjacent *m*-phenylene protons, from analogy with the spectra of *m*-terphenyl (δ 7.78—7.83, 1H, m, *m*-C_6H; δ 7.27—7.72, 13H, m, *m*-C_6H_3 and C_6H_5) and 1,3-di(phenyl-d_5)benzene[13] (δ 7.78—7.83, 1H, m, *m*-C_6H; δ 7.51—7.61, 3H, m, *m*-C_6H_3).

The spectrum of **22** shows multiplet peaks of 10H at a rather higher field (δ 6.51—7.08). These are assigned to the resonances of protons on two terminal phenyl rings. That of **2** displays multiplet peaks (δ 6.78—7.48, 22H, m) which are quite difficult to assign.

Experimental

Low melting points were determined with a Mettler FP-51 apparatus; for those above 300 °C, a Shimadzu DSC-30M differential scanning calorimeter was employed. The UV spectra were measured on a Shimadzu QV-50 and a Hitachi EPS-2 spectrophotometer, the IR spectra on a Leitz III-G spectrophotometer, and ^{1}H-NMR spectra on a Varian CFT-20 spectrometer at 80 MHz, using TMS as an internal standard. The molecular weights were determined with a Mechrolab 301A vapor-pressure osmometer and a Hitachi RMU-6E mass spectrometer.

2- (**13**), 3- (**14**), and 4-Iodobiphenyl (**15**) were prepared as reported previously.[1]

o- (**18**), *m*- (**19**), and *p*-Diiodobenzene (**20**) were commercially available and purified before use.

4-Iodo-o-terphenyl (16). Commercially available *o*-terphenyl was subjected to nitration[14] to give 4-nitro-*o*-terphenyl (mp 117.3 °C), which was reduced with activated iron in hot benzene[15] to prepare 4-amino-*o*-terphenyl (mp 117.4 °C). Then the amine was converted to **16** in the usual manner. Colorless plates; mp 117.6 °C (lit,[16] mp 116—116.5 °C). (Found: C, 60.51; H, 3.81%).

4-Iodo-p-terphenyl (17). 4-Iodo-*p*-terphenyl was prepared by the direct iodination[17] of *p*-terphenyl. Colorless needles; mp 246.5 °C (lit,[18] mp 246—247 °C). (Found: C, 60.67; H, 3.66%).

Preparation of 4,4"-Diphenyl-o-terphenyl (1). A mixture of **15** (8.40 g, 30.0 mmol) and **18** (4.95 g, 15.0 mmol) in a reaction tube (ϕ2.5×20 cm) was heated in an oil bath at 230—240 °C, and then copper powder (19.1 g, 300 mg-atom) was added under stirring in portions over a one hour period, after which the mixture was heated at 245 °C for an additional hour. After cooling, the reaction product was extracted with hot benzene followed by hot xylene, then the solvents were distilled off. The benzene extract (5.34 g) was treated with 60 ml of a cyclohexane–benzene (5:1 v/v) mixture (C–B(5:1)) to separate the product into soluble and insoluble parts. Recrystallization of the latter together with the xylene extract (1.09 g) from benzene provided *p*-quaterphenyl (**27**) (colorless plates; mp 319 °C (lit,[19] mp 317.7—318.7 °C); yield, 1471 mg). The former was dissolved in the C–B (5:1) and then subjected to chromatography on alumina with the same solvent as the eluent, to provide biphenyl (**21**) (colorless leaves from ethanol; mp 69.4 °C; yield, 1405 mg) and **1**. The properties of the latter are as follows.

1: Colorless needles from ethanol; mp 184.5 °C (lit,[2] mp 182—184 °C); yield, 939 mg (16.4%). IR: 675 m; 700 s (γ_{C-C}); 715 w, 727 m, 737 m, 757 s (γ_{C-H}, M, *o*); 773 s (γ_{C-H}, *o*); 837 s, 842 cm^{-1} s (γ_{C-H}, *p*).[20] UV: λ_{max} (ε) 204 (85300), 264 (49800), 284 nm (sh) (30600). Found: C, 94.34; H, 5.76%; mol wt, 382. Calcd for $C_{30}H_{22}$: C, 94.20; H, 5.80%; mol wt, 382.

Preparation of 2,2"-Diphenyl-m-terphenyl (2). A mixture of **13** (8.40 g) and **19** (4.95 g) was treated with copper powder (19.1 g) at 260—270 °C for 1 h, and the mixture was heated at 275 °C for a further 1 h. The hot benzene extract of the product (6.10 g) was chromatographed on alumina with C–B (5:1) to give *o*-quaterphenyl (**22**) (colorless cubes from ethanol; mp 118.0 °C (lit,[21] mp 118 °C); 2509 mg) and **2**.

2: Colorless prisms from ethanol; mp 164.2 °C (lit,[8] mp 155.5—156.6 °C); 1362 mg (23.8%). IR: 695 s, 704 s, 711 s (γ_{C-C}); 728 w; 745 s, 749 s, 755 sh s, 764 s (γ_{C-H}, M, *o*); 779 m, 783 m (γ_{C-H}, *o*); 803 m (γ_{C-H}, *m*); 846 w, 879 w; 908 cm^{-1} m (γ_{C-H}, *m*). UV: λ_{max} (ε) 192 (73800), 204 (sh) (63400), 234 (57700), 250 nm (sh) (27000). Found: C, 94.35; H, 5.95%; mol wt, 382. Calcd for $C_{30}H_{22}$: C, 94.20; H, 5.80%; mol wt, 382.

Preparation of m-*Quinquephenyl (3).* A mixture of **14** and **19** was heated with copper powder as has been described in the preparation of **1**. The hot benzene extract of the product (5.80 g) was subjected to distillation *in vacuo*, then the distillate was chromatographed on alumina with C–B (5:2) to afford *m*-quaterphenyl (**26**) (colorless plates from ethanol; mp 87.1 °C (lit,[22] mp 85.5—86 °C); 992 mg) and **3**.

3: Colorless needles from ethanol; mp 114.0 °C (lit,[3a] mp 114—115 °C; lit,[3b] mp 115.3—115.6 °C); 462 mg (8.1%). IR: 699 s, 707 sh m (γ_{C-C}); 729 w; 750 s (γ_{C-H}, M); 779 s, 791 w, 807 w, 810 sh w (γ_{C-H}, *m*); 884 sh m, 888 m, 899 vw, 908 cm^{-1} vw (γ_{C-H}, *m*). UV: λ_{max} (ε) 196 (59300), 205 (60400), 249 nm (83200). Found: C, 93.93; H, 6.07%; mol wt, 382. Calcd for $C_{30}H_{22}$: C, 94.20; H, 5.80%; mol wt, 382.

*Preparation of 4,4″-Diphenyl-*m-*terphenyl (4).* A mixture of **15** and **19** was treated with copper powder under conditions similar to those used in the preparation of **2**. The product was extracted with hot benzene followed by hot toluene. The benzene extract (4.41 g) was treated with 50 ml of the C–B (5:2) to separate soluble [B_1] (2.50 g) and insoluble [B_2] (1.91 g) parts. The toluene extract (1.64 g) was treated as described above to separate soluble [T_1] (0.33 g) and insoluble [T_2] (1.58 g) parts. The soluble [B_1] was chromatographed on alumina with the C–B (5:2) to give **21** (378 mg). The [B_2] and [T_1] parts were combined and chromatographed with C–B (1:1) to give **4**. Crystallization of the insoluble [T_2] from benzene afforded **27** (1523 mg).

4: Colorless prisms from benzene; mp 269.7 °C (lit,[4] mp 264—266 °C; lit,[3b] mp 273.4—273.8 °C); 764 mg (13.3 %). IR: 690 s, 698 sh s (γ_{C-C}); 725 m, 732 w; 759 s (γ_{C-H}, M); 796 s (γ_{C-H}, *m*); 826 w; 845 s, 849 s (γ_{C-H}, *p*); 893 w, 910 cm^{-1} w (γ_{C-H}, *m*). UV: λ_{max} (ε) 205 (82100), 280 nm (66500). Found: C, 94.17; H, 5.76%; mol wt, 386. Calcd for $C_{30}H_{22}$: C, 94.20; H, 5.80%; mol wt, 382.

*Preparation of 2,2″-Diphenyl-*p-*terphenyl (5). Procedure A*: A mixture of **13** (8.40 g) and **20** (5.00 g) was treated with copper powder (19.1 g) at 250—260 °C for 1 h, and then at 265 °C for another hour. The hot benzene extract (6.19 g) was digested with 60 ml of the C–B (5:2) to remove insoluble material. The soluble part (6.00 g), after removal of the solvent, was subjected to chromatography on alumina with cyclohexane to afford **22** (2526 mg). Subsequent progressive elutions with C–B(5:1), then with C–B(5:2) and C–B(5:3), and finally with C–B(1:1), provided **5**, 2,2‴-diphenyl-*p*-quaterphenyl (**6**) and 2,2⁗-diphenyl-*p*-quinquephenyl (**7**), and 2,2⁗′-diphenyl-*p*-sexiphenyl (**8**) respectively.

5: Colorless needles from ethanol; mp 185.8 °C (lit,[3b] mp 185.6—185.8 °C); 798 mg (13.9%). IR: 678 w; 700 s (γ_{C-C}); 744 s, 755 s, 763 m (γ_{C-H}, M, *o*); 778 m, 781 m (γ_{C-H}, *o*); 841 s, 848 m (γ_{C-H}, *p*); 877 cm^{-1} w. UV: λ_{max} (ε) 198 (85000), 242 (43200), 280 nm (18500). Found: C, 94.36; H, 6.06%; mol wt, 382 (M^+). Calcd for $C_{30}H_{22}$: C, 94.20; H, 5.80%; mol wt, 382.

6: Colorless leaves from benzene–ethanol; mp 236.1 °C; 670 mg (9.8%); identified by mixed-melting-point method and identical IR and UV spectra to those from the authentic sample.[1]

7: Colorless leaves from ethanol–benzene; mp 256.6 °C; 589 mg (7.4%). IR: 683 w; 706 s (γ_{C-C}); 720 m, 734 w; 747 s, 763 s (γ_{C-H}, M, *o*); 785 m (γ_{C-H}, *o*); 823 s, 830 cm^{-1} sh m (γ_{C-H}, *p*). UV: λ_{max} (ε) 206 (115800), 230 (sh) (45800), 307 nm (51000). Found: C, 94.06; H, 5.83%; mol wt, 534 (M^+). Calcd for $C_{42}H_{30}$: C, 94.34; H, 5.66%; mol wt, 534.

8: Colorless leaves from benzene; mp 309 °C; 218 mg (2.4%). IR: 684 w; 706 s (γ_{C-C}); 729 w; 743 s, 747 s, 764 s (γ_{C-H}, M, *o*); 786 m (γ_{C-H}, *o*); 817 s (γ_{C-H}, *p*); 854 cm^{-1} w. UV: λ_{max} (ε) 203 (129600), 234 (sh) (41100), 315 nm (62900). Found: C, 94.09; H, 5.55%; mol wt, 610 (M^+). Calcd for $C_{48}H_{34}$: C, 94.39; H, 5.61%; mol wt, 610.

Procedure B: A mixture of **13** (2.80 g, 10.0 mmol) and **16** (3.56 g, 10.0 mmol) was treated with copper powder (6.35 g, 100 mg·atom) at 260—265 °C for 1.5 h, and then at 270 °C for an additional hour. The hot benzene extract (3.82 g) was chromatographed as above with cyclohexane to yield **21** (40 mg) and *o*-terphenyl (**24**) (colorless needles from ethanol; mp 56.7 °C; 184 mg). Subsequent progressive elutions with C–B(9:1), then C–B(9:1) and C–B(4:1), and finally with C–B(4:1) and C–B(1:1) provided **22** (600 mg), **5** (765 mg, 20.0%), and **6** (570 mg, 12.5%) respectively.

*Preparation of 3,3″-Diphenyl-*p-*terphenyl (9).* A mixture of **14** and **20** was heated with copper powder, as has been described for the preparation of **1**. The hot benzene extract (5.50 g) was separated into soluble and insoluble parts in 150 ml of C–B(1:1). Chromatography of the former (2.90 g) with the same solvent and of the latter (2.60 g) with benzene on alumina afforded **21** (250 mg) and **26** (1600 mg), and **26** (40 mg) and **9** respectively.

9: Colorless plates from benzene; mp 235.7 °C (lit,[5] mp 235—236 °C; lit,[3b] mp 236.1—236.3 °C); 750 mg (13.1%). IR: 686 w; 699 s (γ_{C-C}); 754 s, 760 s (γ_{C-H}, M); 790 s, 798 m (γ_{C-H}, *m*); 848 m, 855 w (γ_{C-H}, *p*); 890 cm^{-1} m (γ_{C-H}, *m*). UV: λ_{max} (ε) 207 (66800), 258 (50800), 280 nm (sh) (38200). Found: C, 93.93; H, 5.94%; mol wt, 381. Calcd for $C_{30}H_{22}$: C, 94.20; H, 5.80%; mol wt, 382.

Reaction of 13 and 18. A mixture of **13** and **18** was treated under conditions similar to those used in the preparation of **2**. The hot benzene extract (6.40 g) was subjected to chromatography on alumina with cyclohexane to provide **21** (512 mg). Subsequent elution with C–B(5:1) gave **22** (1389 mg) and triphenylene (**23**).

23: Colorless needles from cyclohexane; mp 198.6 °C (lit,[23] mp 197—198 °C); 829 mg (23.9%). Found: C, 94.78; H, 5.25%; mol wt, 221. Calcd for $C_{18}H_{12}$: C, 94.70; H, 5.30%; mol wt, 228.

*Preparation of 2,3″-Diphenyl-*p-*terphenyl (10).* A mixture of **14** (2.80 g) and **16** (3.56 g) was heated as has been described in the preparation of **5** (Procedure B). The hot benzene extract (3.77 g) was chromatographed on alumina with cyclohexane to give **21** (30 mg). Subsequent elutions with C–B(9:1), then C–B(9:1) and C–B(4:1), and finally with C–B(4:1) and C–B(1:1) afforded **24** (280 mg) and **26** (270 mg), **10**, and **6** (950 mg, 20.7%) respectively.

10: Colorless plates from ethanol; mp 120.0 °C (lit,[6] mp 120.1—120.5 °C; lit,[2] mp 119.5—120.0 °C); 705 mg (18.5%). IR: 684 w, 689 w; 701 s, 704 sh s (γ_{C-C}); 736 m; 746 s, 751 sh s, 765 w (γ_{C-H}, M, *o*); 779 m (γ_{C-H}, *o*); 797 m, 812 vw (γ_{C-H}, *m*); 835 m, 841 s (γ_{C-H}, *p*); 874 w; 895 cm^{-1} m (γ_{C-H}, *m*). UV: λ_{max} (ε) 197 (81000), 250 (46200), 275 nm (sh) (29300). Found: C, 93.99; H, 5.92%; mol wt, 382 (M^+). Calcd for $C_{30}H_{22}$: C, 94.20; H, 5.80%; mol wt, 382.

*Preparation of 2-Phenyl-*p-*quaterphenyl (11).* A mixture of **15** and **16** was treated under conditions similar to those used in the preparation of **5** (Procedure B). The product was then extracted with hot benzene, followed by hot toluene. The benzene extract (3.76 g) was subjected to chromatography on alumina with C–B(9:1) to afford **21** (58 mg). Subsequent elutions with C–B(5:1), then C–B (5:1) and C–B(5:2), and finally with benzene provided

24 (273 mg), **11** and **6** (493 mg, 10.8%), and **27** (199 mg) respectively. Crystallization of the toluene extract (0.17 g) from benzene provided more **27** (110 mg).

11: Colorless needles from benzene; mp 186.9 °C; 788 mg (24.7%). IR: 692 s, 702 s (γ_{C-C}); 720 m, 728 m; 748 s, 757 s, 763 sh s, 769 m (γ_{C-H}, M, *o*); 780 m (γ_{C-H}, *o*); 826 s (γ_{C-H}, *p*); 855 w, 876 cm^{-1} w. UV: λ_{max} (ε) 205 (79900), 237 (sh) (19400), 264 (sh) (24900), 295 nm (42100). Found: C, 93.95; H, 5.98%; mol wt, 382 (M^+). Calcd for $C_{30}H_{22}$: C. 94.20; H, 5.80%; mol wt, 382.

*Preparation of 3-Phenyl-*p*-quaterphenyl (12).* A mixture of **14** and **17** was heated as has been described in the preparation of **5** (Procedure B). The hot benzene extract (5.81 g) of the product was chromatographed on alumina with cyclohexane to afford **21** (100 mg). Subsequent elutions with C–B(9:1), then C–B(9:1) and C–B(4:1), and finally with benzene provided **26** (453 mg), *p*-terphenyl (**25**) (colorless plates from ethanol; mp 212.4 °C), and **12** respectively. The benzene-insoluble part of the product, upon repeated extraction with concentrated ammonia–water, left a solid which was sublimed at 350—400 °C/0.13 Pa to afford *p*-sexiphenyl (**28**).

12: Colorless leaves from benzene; mp 258.9 °C (lit,[6] mp 259.7—259.9 °C); 1030 mg (27.0%). IR: 698 s (γ_{C-C}); 721 w, 736 w; 755 s, 759 sh s, 768 s (γ_{C-H}, M); 798 s (γ_{C-H}, *m*); 829 s (γ_{C-H}, *p*); 855 w; 890 cm^{-1} w (γ_{C-H}, *m*). UV: λ_{max} (ε)207 (75300), 253 (sh) (23200), 296 nm (47500). Found: C, 94.38; H, 5.70%; mol wt, 382 (M^+). Calcd for $C_{30}H_{22}$: C, 94.20; H, 5.80%; mol wt, 382.

28: Colorless leaves; mp 441 °C (lit,[10b] mp 439—445 °C; lit,[24] mp 465 °C); 525 mg (11.5%). Found: C, 94.31; H, 5.53%; mol wt, 458 (M^+). Calcd for $C_{36}H_{26}$: C, 94.28; H, 5.72%; mol wt, 458.

The authors would like to express their gratitude to Dr. K. Watanabe for the MO calculations, which were carried out on the FACOM 230-OS2/VS at the Inst. Chem. Res. Kyoto University. The authors are also indebted to Nippon Shinyaku Co., Ltd., for kindly performing the measurements of IR spectra. Thanks are due to Mr. Y. Fujiwara of this college for his help in ^{1}H-NMR spectral measurements.

References

1) Part I: E. Ibuki, S. Ozasa, and K. Murai, *Bull. Chem. Soc. Jpn.*, **48**, 1868 (1975).
2) G. F. Woods and F. Scotti, *J. Org. Chem.*, **26**, 312 (1961).
3) a) N. B. Sunshine and G. F. Woods, *J. Org. Chem.*, **28**, 2517 (1963); b) C. Beaudet, J. Horlait, A. Marcq, and G. Belpaire, *EUR* 31, f (1962).
4) G. F. Woods and I. W. Tucker, *J. Am. Chem. Soc.*, **70**, 3340 (1948).
5) G. F. Woods, D. D. Centola, H. E. Ruskie, and C. D. Miller, *J. Am. Chem. Soc.*, **82**, 5227 (1960).
6) C. Beaudet, J. Horlait, and A. Marcq, *EUR* 295, f (1963).
7) Woods *et al.* have noted a lower melting point range: 155.5—156.6 °C (Ref. 8).
8) G. F. Woods, A. L. Van Artsdale, and F. T. Reed, *J. Am. Chem. Soc.*, **72**, 3221 (1950).
9) S. Sandroni and F. Geiss, *Z. Anal. Chem.*, **220**, 321 (1966).
10) a) J. E. Stewart and M. Hellmann, *J. Res. Natl. Bur. Stand.*, **60**, 125 (1958); b) R. C. Doss and P. W. Solomon, *J. Org. Chem.*, **29**, 1567 (1964).
11) R. L. Alexander, Jr., *J. Org. Chem.*, **21**, 1464 (1956).
12) a) A. E. Gillam and D. H. Hey, *J. Chem. Soc.*, **1939**, 1170; b) J. Dale, *Acta Chem. Scand.*, **11**, 650 (1957); H. Suzuki, *Bull. Chem. Soc. Jpn.*, **32**, 1340 (1959); R. M. Silverstein and G. C. Bassler, "Spectrometric Identification of Organic Compounds," 2nd ed, John Wiley & Sons, Inc., New York, London, and Sydney (1967), p. 152.
13) E. Ibuki, S. Ozasa, and Y. Fujioka, unpublished work.
14) C. F. H. Allen and D. M. Burness, *J. Org. Chem.*, **14**, 175 (1949).
15) S. E. Hazlet and C. A. Dornfeld, *J. Am. Chem. Soc.*, **66**, 1781 (1944).
16) T. Sato, S. Shimada, and K. Hata, *Bull. Chem. Soc. Jpn.*, **42**, 766 (1969).
17) W. Kern, W. Gruber, and H. O. Wirth, *Makromol. Chem.*, **37**, 198 (1960).
18) H. France, I. M. Heilbron, and D. H. Hey, *J. Chem. Soc.*, **1938**, 1364.
19) J. J. E. Schmidt and J. A. Krimmel, *J. Org. Chem.*, **25**, 252 (1960).
20) γ_{C-C} and γ_{C-H} refer to vibrations which are primarily out-of-plane C–C and out-of-plane C–H bending motions. M, *o*, *m*, and *p* in parentheses refer to mono-, ortho-, meta-, and para-substituted rings.
21) J. Dale, *Acta Chem. Scand.*, **11**, 640 (1957).
22) G. F. Woods and F. T. Reed, *J. Am. Chem. Soc.*, **71**, 1348 (1949).
23) C. Hansch and C. F. Geiger, *J. Org. Chem.*, **23**, 477 (1958).
24) J. A. Cade and A. Pilbeam, *J. Chem. Soc.*, **1964**, 114.

Synthesis of 2,5-Dehydrohomoadamantane (Tetracyclo[5.3.1.$0^{2,5}$.$0^{3,9}$]undecane) from 2,4-Dehydrohomoadamantane (Tetracyclo[5.3.1.$0^{3,5}$.$0^{4,9}$]undecane)[1,2]

Takeo KATSUSHIMA, Masato YOSHIKAWA, Ryohei YAMAGUCHI, and Mituyosi KAWANISI*
Department of Industrial Chemistry, Faculty of Engineering, Kyoto University, Yoshida, Sakyo-ku, Kyoto 606
(Received January 28, 1980)

A reaction of 2,4-dehydrohomoadamantane with NBS in AcOH followed by $LiAlH_4$ reduction and subsequent CrO_3–pyridine complex oxidation gave *endo*-2-bromohomoadamantan-4-one (**9**) in good yield. A treatment of **9** with *t*-BuOK in *t*-BuOH followed by Wolff-Kishner reduction furnished 2,5-dehydrohomoadamantane.

Out of five possible "non-bridgehead" monodehydrohomoadamantanes, the strained cage compounds which incorporate a small ring in homoadamantane framework (**1**—**5**),[3-6] 2,5-dehydrohomoadamantane (**1**) is the only compound which contains a cyclobutane ring in its structure. Recently, Sasaki *et al.* reported a synthesis of **1** utilizing an intramolecular ketene cycloaddition.[3] During our search for synthesis and reactions of strained cage systems,[4b,5b,7] we have had an opportunity to investigate **1** and now wish to describe an alternative synthetic route of **1** starting from 2,4-dehydrohomoadamantane (**2**).

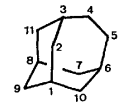

Homoadamantane
(Tricyclo[4.3.1.$1^{3,8}$]undecane)

1(2,5) **2**(2,4) **3**(2,11) **4**(2,9) **5**(2,10)

Fig. 1. "Non-bridgehead" Monodehydrohomoadamantanes.

Results and Discussion

When **2** was allowed to react with *N*-bromosuccinimide (NBS) in acetic acid, two isomeric bromo acetates, *endo*-2-bromo-*exo*-4-acetoxy- and *endo*-2-bromo-*endo*-4-acetoxyhomoadamantanes (**6a** and **6b**) were obtained in 70% combined yield in a ratio of 3:2 (GLC analysis). The structures of **6a** and **6b** were determined by the following experimental results. Reductions of **6a** and **6b** with lithium aluminum hydride gave bromo alcohols (**7a** and **8b**) in 68 and 81% yields, respectively. When a mixture of **7a** and **7b** was reduced with tributyltin hydride, only homoadamantan-4-ol (**8**)[8] was obtained in 78% yield. No other alcohol could be detected. These chemical transformations clearly indicate that the bromo acetates (**6a** and **6b**) and bromo alcohols (**7a** and **7b**) retain a homoadamantane skeleton and that the acetoxyl and hydroxyl groups are located at C_4-position in the homoadamantane system.

Each bromo alcohol (**7a** or **7b**) was further subjected to the oxidation with chromium trioxide–pyridine complex to afford the same product, *endo*-2-bromohomoadamantan-4-one (**9**) in 91 or 95% yield;

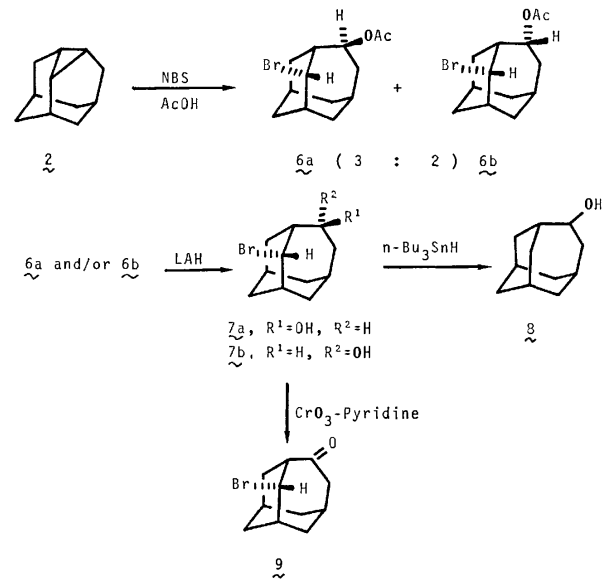

Scheme 1.

these results show that **6a** and **6b**, and **7a** and **7b** also, are isomeric in relation to C_4-position and that the bromine substituents have the same configurations. The ^{1}H-NMR (PMR) spectrum of **9** showed a singlet peak at 4.55 ppm due to the C_2 carbinyl proton. Previous studies[7a,9] showed that *exo*-C_2-proton does not couple with the adjacent protons, whereas *endo*-C_2-proton does couple, giving a triplet with a coupling constant of *ca.* 4 Hz. The configuration of the bromine substituent of **9** was thus determined to be *endo*. The configurations of substituents at C_4-positions of **6a**, **6b**, **7a**, and **7b** were deduced by comparison of their ^{13}C-NMR (CMR) and PMR spectra with each other. In a cage system such as adamantane, a γ_{syn}-carbon to a substituent has 4—7 ppm higher chemical shift than a γ_{anti}-carbon does because of a stronger interaction between the former and the substituent.[10] On the other hand, a γ_{syn}-hydrogen is reported to appear at 0.4—0.6 ppm lower field than its counterpart, a γ_{anti}-hydrogen.[11] Our results are summarized in Table 1. The chemical shifts of the carbons at the 2-positions of **6a** and **7a** are higher than those of **6b** and **7b** and the chemical shifts of the C_2-hydrogens of the former are lower than those of the latter. These facts lead to our conclusion that **6a** and **7a** are *endo*-2-bromo-*exo*-4-acetoxyhomoadamantane and *endo*-2-bromo-*exo*-homoadamantan-4-ol and that **6b** and **7b** are *endo*-2-bromo-*endo*-4-acetoxyhomoadamantane and *endo*-2-bromo-*endo*-homoadamantan-4-ol.

Table 1. Chemical shifts[a] of C_2 and C_2–H

	6a	6b	7a	7b
C-Br	56.2	59.1	56.7	60.8
CH-Br	4.75	4.40	4.87	4.38

a) ppm relative to TMS.

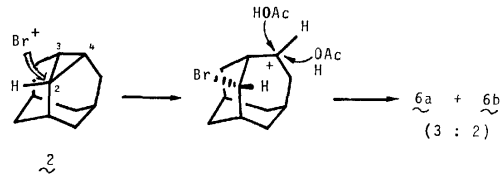

Scheme 2.

On the basis of the structures of **6a** and **6b**, we constructed the following reaction scheme with respect to the cleavage of the cyclopropane by bromonium ion (Scheme 2). An initial attack of the strained C_2–C_4 bond by bromonium ion must occur exclusively at C_2-position with inversion of configuration giving a carbocation intermediate.[12] The subsequent nucleophilic attack by the solvent from both sides will give **6a** and **6b** almost non-selectively. The remarkable regioselectivity observed in the initial bromination stage may be attributed not only to steric but also to electronic reasons, because ^{13}C–H coupling constants of C_2 and C_4 (or C_3) ($J_{C_2\text{-}H}$=163 Hz and $J_{C_{4(3)}\text{-}H}$=158 Hz) indicate that C_2-carbon with more s-character in C_2–H bond should have more p-electron density than $C_{4(3)}$-carbon.[13]

A treatment of **9** with potassium *t*-butoxide in *t*-butyl alcohol at room temperature induced an efficient cyclization to give 2,5-dehydrohomoadamantan-4-one (**10**) in 86% yield. The ketone (**10**) showed a characteristic absorption band at 1775 cm^{-1} due to cyclobutanone in its IR spectrum; the PMR spectrum was identical with that reported.[14] The final Wolff-Kishner reduction was nicely conducted to afford 2,5-dehydrohomoadamantane (**1**) in 71% yield.

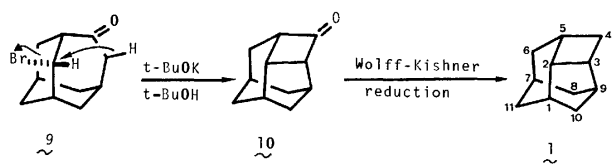

Scheme 3.

Experimental

All the temperatures were uncorrected. Melting points were measured in sealed capillaries. The IR spectra were recorded on a Shimadzu IR-27 spectrometer. The MS spectra were taken by using a Hitachi RMS-4 mass spectrometer. The PMR and CMR spectra were obtained on Varian EM-390 and CFT-20 spectrometers, tetramethylsilane being chosen as an internal standard. Micro analyses were performed in Kyoto University Elemental Analysis Center.

Reaction of Tetracyclo[5.3.1.$0^{3,5}$.$0^{4,9}$]undecane (2) with N-Bromosuccinimide (NBS). A solution of **2** (998 mg; 6.74 mmol) and NBS (1521 mg; 8.54 mmol) in AcOH (25 ml) was stirred at 60 °C under argon for 28 h. The reaction mixture was poured onto water and extracted with CH_2Cl_2. The organic solution was washed successively with brine, aqueous $NaHCO_3$, and brine, and dried (Na_2SO_4). After filtration, the solvent was evaporated and the residue (2.16 g) was chromatographed on silica gel (100 g). Elution by hexane gave the unreacted starting material (41 mg). Subsequent elution by hexane and CH_2Cl_2 (4:1) gave **6a** (480 mg), a mixture of **6a** and **6b** (324 mg), and **6b** (250 mg). The combined yield of **6a** and **6b** (1054 mg) was 55% and the ratio of **6a** and **6b** was determined to be 3:2 by GLC analysis (PEG 20 M, 220 °C) of the crude products. Similarly, the reaction of **2** (207 mg; 1.40 mmol) and NBS (282 mg; 1.58 mmol) in AcOH (5 ml) at 45—50 °C for 6 d gave a mixture of **6a** and **6b** (282 mg, 70%). *endo*-2-Bromo-*exo*-4-acetoxytricyclo[4.3.1.$1^{3,8}$]-undecane (**6a**): bp 70 °C (bath temp)/133 Pa. MS *m/e* (rel intensity): 228, 226 (M^+—AcOH, 47, 48), 165 (17), 147 (100). IR (neat): 2825, 1740, 1445, 1365, 1240, 1015, 960, 715 cm^{-1}. PMR δ (CCl_4): 4.90 (1H, d.d.d, J=10.0, 5.4, 3.6 Hz), 4.65 (1H, s), 2.02 (3H, s), 2.75—1.20 (14H, br. complex m). CMR δ ($CDCl_3$); 169.9 (C), 76.0 (CH), 56.2 (CH), 46.9 (CH), 41.3 (CH_2), 37.7 (CH_2), 36.0 (CH, CH_2), 30.4 (CH_2), 30.2 (CH_2), 28.6 (CH), 26.7 (CH), 21.3 (CH_3). Found: C, 54.25; H, 6.58%. Calcd for $C_{13}H_{19}BrO_2$: C, 54.36; H, 6.67%. *endo*-2-Bromo-*endo*-4-acetoxytricyclo[4.3.1.$1^{3,8}$]undecane (**6b**): bp 70 °C (bath temp)/133 Pa. MS *m/e* (rel intensity): 228, 226 (M^+—AcOH, 49, 48), 165 (26), 147 (100). IR (neat): 2925, 1740, 1450, 1365, 1245, 1020, 965, 720, 710 cm^{-1}. PMR δ (CCl_4): 5.02 (1H, d.d.d, J=9.0, 6.0, 3.0 Hz), 4.40 (1H, s), 1.98 (3H, s), 2.70—1.20 (14H, br. complex m). CMR δ ($CDCl_3$): 169.9 (C), 74.8 (CH), 59.1 (CH), 46.4 (CH), 40.9 (CH_2), 40.0 (CH_2), 35.5 (CH), 34.7 (CH_2), 30.2 (CH_2), 28.7 (CH), 26.5 (CH), 25.6 (CH_2), 21.3 (CH_3). Found: C, 54.53; H, 6.76%. Calcd for $C_{13}H_{19}BrO_2$: C, 54.36; H, 6.67%.

endo-*2-Bromo*-exo-*tricyclo*[*4.3.1.*$1^{3,8}$]*undecan-4-ol* (**7a**). To a suspension of $LiAlH_4$ (60 mg) in dry Et_2O (5 ml) was added dropwise a solution of **6a** (105 mg; 0.37 mmol) in dry Et_2O (5 ml). The mixture was stirred under reflux for 10 min. Aqueous Na_2SO_4 was added to the cooled reaction mixture. The organic layer was collected and dried (Na_2SO_4). After filtration, the solvent was evaporated and the residue was chromatographed on silica gel. Elution by hexane and CH_2Cl_2 (3:2) gave **7a** (61 mg, 68%): mp 147—149 °C. MS *m/e* (rel intensity): 228, 226 (M^+-H_2O, 30, 31), 147 (100). IR (KBr): 3325, 2950, 1445, 1015, 715 cm^{-1}. PMR δ ($CDCl_3$): 4.87 (1H, s) ,4.00 (1H, d.d.d, J=10.0, 5.0, 3.0 Hz), 2.70—1.20 (15H, br. complex m). CMR δ ($CDCl_3$): 74.3 (CH), 56.7 (CH), 51.0 (CH), 43.9 (CH_2), 38.1 (CH_2), 36.2 (CH, CH_2), 30.8 (CH_2), 30.6 (CH_2), 28.7 (CH), 26.9 (CH). Found: C, 54.08; H, 7.25%. Calcd for $C_{11}H_{17}BrO$: C, 53.89; H, 6.99%.

endo-*2-Bromo*-endo-*tricyclo*[*4.3.1.*$1^{3,8}$]*undecan-4-ol* (**7b**). Reduction of **6b** (111 mg; 0.39 mmol) with $LiAlH_4$ (52 mg) in a similar manner to the above gave a crude product which was chromatographed on silica gel. Elution by hexane and CH_2Cl_2 (3:2) gave **7b** (77 mg, 81%): mp 134—136 °C. MS *m/e* (rel intensity): 246, 244 (M^+, 2, 2), 228, 226 (M^+-H_2O, 8, 8), 165 (66), 147 (100). IR (KBr): 3360, 2925, 1450, 1045, 1010, 715, 680 cm^{-1}. PMR δ ($CDCl_3$); 4.38 (1H, s), 4.08 (1H, d.d.d, J=9.0, 6.0, 3.0 Hz), 2.80—1.00 (15H, br. complex m). CMR δ ($CDCl_3$): 72.9 (CH), 60.8 (CH), 50.1 (CH), 43.5 (CH_2), 40.5 (CH_2), 35.6 (CH), 34.4 (CH_2), 30.4 (CH_2), 28.6 (CH), 26.5 (CH), 24.6 (CH_2). Found: C, 54.01; H, 7.10%. Calcd for $C_{11}H_{17}BrO$: C, 53.89; H, 6.99%.

Reduction of ***7a*** *and* ***7b*** *with* n-Bu_3SnH. A solution of a mixture of **7a** and **7b** (435 mg; 1.78 mmol) and n-Bu_3SnH (2.0 g, 6.9 mmol) in benzene (50 ml) was refluxed under nitrogen for 20 h. The solvent was evaporated and the residue was chromatographed on silica gel. Elution by hexane and CH_2Cl_2 (9:1) gave tricyclo[4.3.1.$1^{3,8}$]undecan-4-ol (**8**) (229 mg, 78%).

endo-*2-Bromotricyclo[4.3.1.*$1^{3,8}$*]undecan-4-one* (***9***). To a mixture of pyridine (1.6 ml) and CH_2Cl_2 (5 ml) was added CrO_3 (160 mg; 1.6 mmol) and then a solution of **7a** (83 mg; 0.34 mmol) in CH_2Cl_2 (5 ml). The reaction mixture was stirred at room temperature for 30 min and washed with aqueous 5% NaOH, aqueous 5% HCl, and brine, and dried (Na_2SO_4). After filtration, the solution was passed through a short silica-gel column and the solvent was evaporated to give **9** (76 mg, 91%): mp 124—126 °C. MS *m/e* (rel intensity): 244, 242 (M^+, 6, 6), 163 (100). IR (KBr): 2925, 1690, 1460, 1445, 1365, 1200, 1150, 1070, 950, 930, 800 cm^{-1}. PMR δ ($CDCl_3$): 4.55 (1H, s), 3.15 (1H, d, J=6 Hz), 2.90—1.20 (13H, br. complex m). CMR δ ($CDCl_3$): 212.5 (C), 58.8 (CH), 54.4 (CH), 49.9 (CH_2), 37.3 (CH_2), 36.8 (CH_2), 36.0 (CH), 29.3 (CH_2), 27.9 (CH_2), 26.7 (CH), 25.6 (CH). Found: C, 54.63; H, 6.19%. Calcd for $C_{11}H_{15}BrO$: C, 54.33; H, 6.22%.

The oxidation of **7b** (70 mg; 0.29 mmol) in a similar manner to the above gave **9** (67 mg, 95%) also.

Tetracyclo[5.3.1.$0^{2,5}$*.*$0^{3,9}$*]undecan-4-one* (***10***). A solution of **9** (242 mg; 1.00 mmol) and potassium *t*-butoxide (179 mg; 1.59 mmol) in *t*-butyl alcohol (15 ml) was stirred at room temperature for 1.5 h. The reaction mixture was poured onto water and extracted with hexane. The organic layer was washed with brine and dried (Na_2SO_4). After filtration, the solvent was evaporated and the residue (156 mg) was chromatographed on silica gel. Elution by hexane and CH_2Cl_2 (4:1) gave **10** (139 mg, 86%): mp 223—225 °C (lit,[3] mp 224—227 °C). MS *m/e* (rel intensity): 162(M^+, 3), 134 (97), 92 (100). IR (KBr): 2930, 1775, 1445, 1190, 1165, 1120, 1100, 1050 cm^{-1}. PMR δ (CCl_4): 3.53 (1H, q, J=6.8 Hz), 3.10 (1H, m), 2.76 (1H, q, J=7.5 Hz), 2.60—1.00 (11H, br. complex m). CMR δ ($CDCl_3$): 211.3 (C), 70.9 (CH), 54.5 (CH), 46.3 (CH_2), 35.2 (CH_2), 33.8 (CH, CH_2), 33.7 (CH), 31.9 (CH), 31.0 (CH_2), 28.1 (CH). Found: C, 81.15; H, 8.56%. Calcd for $C_{11}H_{14}O$: C, 81.44; H, 8.70%.

Tetracyclo[5.3.1.$0^{2,5}$*.*$0^{3,9}$*]undecane* (***1***). A mixture of **10** (206 mg: 1.21 mmol), KOH (675 mg), and 100% hydrazine hydrate (1 ml) in diethylene glycol (8 ml) was stirred at 110 °C for 30 min and then at 180 °C for 3 h under nitrogen. The sublimed product on the condenser was dissolved in pentane and washed with brine, and dried (Na_2SO_4). After filtration, the solvent was evaporated and the residue was resublimed at 110 °C/1729 Pa to give **1** (134 mg, 71%): mp 171—172 °C (lit,[3] 177—179 °C). MS *m/e* (rel intensity): 148 (M^+, 95), 106 (100). IR (KBr): 2925, 2860, 1445 cm^{-1}. PMR δ ($CDCl_3$): 2.90—1.00 (br. complex m). CMR δ ($CDCl_3$): 44.0 (CH, CH_2), 38.4 (CH), 37.9 (CH_2), 36.8 (CH), 35.6 (CH_2), 33.5 (CH), 33.2 (CH_2), 31.6 (CH), 29.6 (CH), 28.2 (CH_2). Found: C, 88.92; H, 11.02%. Calcd for $C_{11}H_{16}$: C, 89.12; H, 10.88%.

References

1) Part of this work was presented at the 37th National Meeting of the Chemical Society of Japan, Yokohama, April 1978, Abstr. 3C14.

2) In cases where there is no ambiguity, we have used trivial nomenclatures for simplicity. The IUPAC names are described in the Experimental section.

3) For 2,5-dehydrohomoadamantane (**1**): T. Sasaki, S. Eguchi, and Y. Hirako, *J. Org. Chem.*, **42**, 2981 (1977).

4) For 2,4-dehydrohomoadamantane (**2**): a) Z. Majerski, S. H. Liggero, and P. v. R. Schleyer, *J. Chem. Soc., Chem. Commun.*, **1970**, 949; b) R. Yamaguchi, T. Katsushima, T. Imagawa, and M. Kawanisi, *Synth. Commun.*, **1974**, 83; R. Yamaguchi, T. Katsushima, and M. Kawanisi, *Bull. Chem. Soc. Jpn.*, **47**, 2830 (1974).

5) For 2,11-dehydrohomoadamantane (**3**): a) R. K. Murray, Jr., and T. M. Ford, *J. Org. Chem.*, **44**, 3504 (1979); b) T. Katsushima, M. Maki, R. Yamaguchi, and M. Kawanisi, *Bull. Chem. Soc. Jpn.*, in press.

6) For 2,9-dehydrohomoadamantane (**4**): R. K. Murray, Jr., D. L. Goff, and R. E. Ratych, *Tetrahedron Lett.*, **1974**, 763.

7) a) R. Yamaguchi, T. Katsushima, and M. Kawanisi, *Bull. Chem. Soc. Jpn.*, **48**, 2328 (1975); b) R. Yamaguchi and M. Kawanisi, *Chem. Lett.*, **1975**, 649; c) T. Katsushima, R. Yamaguchi, and M. Kawanisi, *J. Chem. Soc., Chem. Commun.*, **1975**, 692; d) T. Katsushima, R. Yamaguchi, M. Kawanisi, and E. Osawa, *ibid.*, **1976**, 39; e) T. Katsushima, R. Yamaguchi, S. Iemura, and M. Kawanisi, *ibid.*, **1980**, 133.

8) J. E. Nordlander, F. Y. Wu, S. P. Jindal, and J. B. Hamilton, *J. Am. Chem. Soc.*, **91**, 3962 (1969); P. v. R. Schleyer, E. Funke, and S. H. Liggero, *ibid.*, **91**, 3965 (1969).

9) H. Langhals and C, Rüchard, *Chem. Ber.*, **107**, 1245 (1974).

10) T. Pehk, E. Lippmaa, V. V. Sevostjanova, M. M. Krayuschkin, and A. I. Tarasova, *Org. Magn. Reson.*, **3**, 783 (1971); H. Duddeck, *ibid.*, **7**, 151 (1975).

11) F. W. van Deursen and J. Bakker, *Tetrahedron*, **27**, 4593 (1971).

12) We have already observed that a radical type cleavage of **2** also shows the same regioselectivity.[7a]

13) N. Muller and D. E. Pritchard., *J. Chem. Phys.*, **31**, 768, 1471 (1959).

14) We thank Professors T. Sasaki and S. Eguchi for sending the specimen of **10** to us.

Photo- and Thermally-induced Radical Rearrangements of Hypoiodites of 3α- and 3β-Methyl-5-cholesten-3-ols in the Presence of Mercury(II) Oxide and Iodine or Silver(II) Oxide and Iodine

Hiroshi SUGINOME*,** and Norio MAEDA

Department of Chemistry, Faculty of Science, Hokkaido University, Sapporo 060

(Received February 4, 1980)

Hypoiodites of 3α- and 3β-methyl-5-cholesten-3-ols in benzene containing mercury(II) oxide and iodine gave 3α,5-epoxy-6β-iodo-3β-methyl-*A*-homo-4-oxa-5α-cholestane in 50—66% yield on irradiation or heating in the dark. Some minor products including the 6α-epimer were also found. The corresponding reaction with silver oxide and iodine reagent gave the same epoxide in 52% yield, together with a low yield of 3,4-seco-3-methyl-3-oxo-5-cholesten-4-al. Hydrogenolysis of the 6β-iodide with Pd–C as a catalyst gave 3α,5-epoxy-3β-methyl-*A*-homo-4-oxa-5α-cholestane (52% yield), together with the 6α-epimer arising from isomerization. The former, on treatment with boron trifluoride etherate and acetic anhydride in benzene, was transformed into 2-acetyl-3-methyl-5-acetoxymethyl-4-oxa-5β-cholestan-2-one. This was converted into 2β-acetyl-3α,5-epoxy-3β-methyl-4-oxa-*A*-homo-5α-cholestane by the treatment with aqueous methanolic potassium hydroxide.

In the previous paper, the photo- and thermally-induced radical rearrangements of cholesterol, epicholesterol, and 3,4,4-trimethylcholesterol hypoiodites in the presence of mercury(II) oxide and iodine were reported.[1] Cholesterol and epicholesterol hypoiodites in the presence of mercury(II) oxide and iodine were found to give 3α,5-epoxy-6β-iodo-*A*-homo-4-oxa-5α-cholestane and its 6α-isomer on irradiation and to give 3α,5-epoxy-6β-iodo-*A*-homo-4-oxa-5α-cholestane accompanied by *A*-homo-4-oxa-5-cholesten-3α-ol and 5-cholesten-3β-yl *A*-homo-4-oxa-5-cholesten-3α-yl ether on thermal reaction. The reactions of 3α,4,4-trimethyl-5-cholesten-3α-ol hypoiodite under comparable conditions gave 2α- and 2β-acetyl-4,4-dimethyl-3-oxa-5-cholestenes together with 3α,5-epoxy-*A*-homo-4-oxa-5α-steroids. Since the effects of alkyl substituents at their C-3 and C-4 positions appear to be appreciable, we investigated the photo- and thermally-induced radical rearrangements of hypoiodites of 3α- and 3β-methyl-5-cholesten-3-ols in the presence of mercury(II) oxide and iodine or silver(II) oxide and iodine. The results are reported in this paper.

Results

3α- And 3β-methyl-5-cholesten-3-ols (**1** and **2**) were prepared by previously described procedures.[2] The mass spectra of alcohols **1** and **2** were similar and exhibited a prominent peak at *m/e* 329 (69.3 and 100%). The suggested structure and genesis are shown in Scheme 1. Irradiation of 3β-alcohol **1** in benzene containing iodine and mercury(II) oxide (each 3 mol equiv.) with a 100-W high pressure mercury arc for 5 h under an argon atmosphere afforded a mixture of products (Scheme 2). In contrast to the case of cholesterol, a recrystallization of the product from methanol–diethyl ether readily gave an epoxide (**3**), mp 116.5—118.6 °C, in *ca.* 60% yield. The structure was ascertained to be 3α,5-epoxy-6β-iodo-3β-methyl-*A*-homo-4-oxa-5α-cholestane on the basis of the following spectral and chemical evidence. The mass spectrum of epoxide **3** showed a very weak molecular ion peak of *m/e* 541 and a prominent peak of *m/e* 415 (21.5%) assignable to M^+-I. Its infrared spectrum showed three 3H singlets at τ 8.60, 9.26, and 8.64 assignable to 3β-methyl, 18-H, and 19-H and an AB quartet centred at τ 6.58 and 5.77 (J=7.9 Hz) assignable to 4a-methylene protons. Besides these signals, the spectrum showed a 1-H triplet at τ 5.69 (J=3.2 Hz) assignable to a proton attached to a carbon bearing iodine (the 6α-H). Preparative TLC of the residue from the filtrate gave a further amount of epoxide **3** and a crystalline mixture. Although separation of the mixture into its components was unsuccessful, the NMR spectrum (see Experimental) indicated that it was a 1:1 mixture of 3α,5-epoxy-6α-

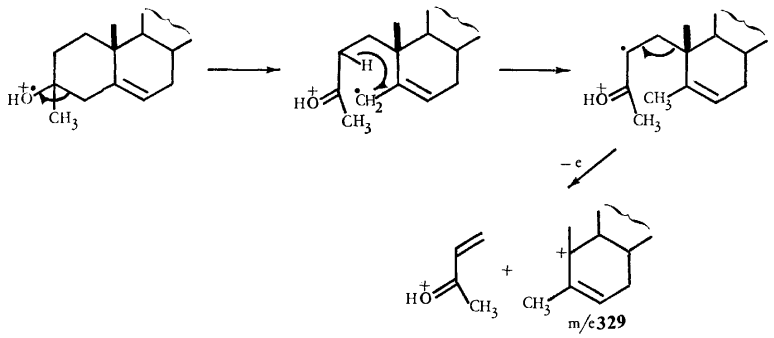

Scheme 1.

** Present address: Organic Chemistry Laboratory, Department of Chemical Process Engineering, Faculty of Engineering, Hokkaido University, Sapporo 060.

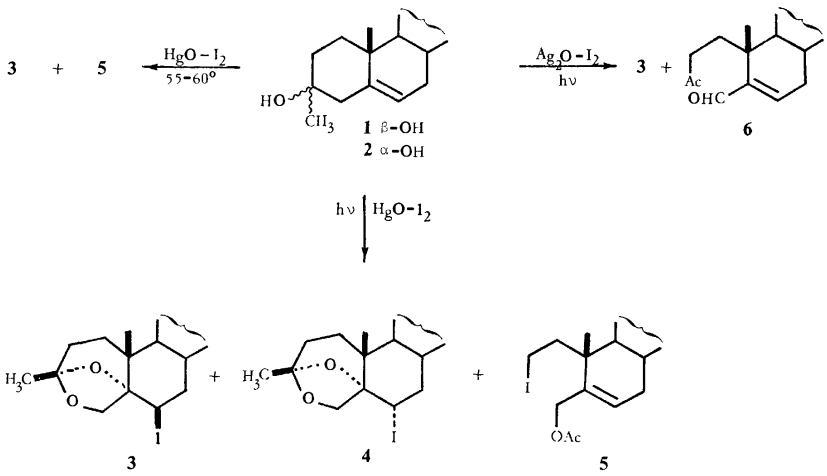

Scheme 2.

iodo-*A*-homo-4-oxa-5α-cholestane (**4**), obtained by a Pd-catalyzed isomerization of the 6β-isomer (*vide infra*), and 2-iodo-*A*-nor-2,3-seco-5-cholesten-3-ol acetate (**5**). The presence of the latter was indicated by a comparison of the signals with those of the ^{1}H NMR spectrum of 2-iodo-*A*-nor-2,3-seco-5-cholesten-3-ol formate.[1] The yields of both compounds were about 2%.

Irradiation of 3α-alcohol **2** in benzene containing iodine and mercury(II) oxide under the conditions comparable to 3β-isomer **1** gave virtually the same products (Scheme 2). The isolated yield of pure crystalline epoxide **3** was 50% and a very minor amount of seco iodide **5** was also obtained.

The photo-reaction of 3β-alcohol **1** in benzene containing iodine and silver oxide in place of mercury(II) oxide was also attempted. This reaction was found to be very slow and more silver oxide and iodine were added to the solution after 5 and 48 h in the course of the reaction; 95 h was required to complete the reaction. A recrystallization and preparative TLC of the products gave crystalline epoxide **3** (52% yield) and a new amorphous compound (**6**) (4% yield) (Scheme 2). The NMR and IR spectra indicated the new compound should be formulated as 3,4-seco-3-methyl-3-oxo-5-cholesten-4-al (**6**); the IR spectrum exhibited three bands at 1720, 1691, and 1631 cm^{-1} in the carbonyl region which can be assigned to an acetyl and an α,β-unsaturated formyl groups. The NMR spectrum showed three 3H singlets at τ 8.00, 9.40, and 8.95 (assignable to 3-methyl, 18-H, and 19-H, a 1H double doublet (J=1.8 and 6.0 Hz) at τ 3.26 assigned to 6-H, and a 1H singlet at τ 0.81 assigned to the formyl proton.

The thermal decomposition of 3α-methyl-5-cholesten-3β-ol hypoiodite in the presence of mercury(II) oxide and iodine at 55—60 °C was also studied, and a higher yield of epoxide **3** (66%) was obtained. Not even a trace of 6α-iodo isomer **4** was detected in the products (Scheme 2). The absence of 6α-isomer in the products from the thermal reaction is also found for the reaction of cholesterol and 3,4,4-trimethylcholesterol.[1]

*Some Reactions of 3α,5-Epoxy-6β-iodo-3β-methyl-*A*-homo-4-oxa-5α-cholestane (Schemes 3 and 4).* Iodo compound **3** was inert to base even under severe conditions.

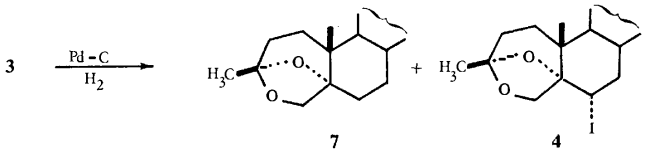

Scheme 3.

Thus, epoxide **3** in dioxan–water containing potassium hydroxide was refluxed for 25 h, but virtually no products resulting from elimination or substitution of iodine were formed and **3** was recovered unchanged.

Hydrogenolysis of iodo compound **3** with 10% Pd–C as a catalyst gave 3α,5-epoxy-3β-methyl-*A*-homo-4-oxa-5α-cholestane (**7**), mp 63.5—65.0 °C, in a 52% yield. Its NMR spectrum exhibited three 3H singlets at τ 8.57, 9.34, and 9.16 assigned to 3β-methyl, 18-H, and 19-H, and an AB quartet at τ 6.77 and 5.90 (J= 6.9 Hz). As would be expected, the signal due to the 19-H shifted upfield significantly in comparison with the corresponding signal of 6β-iodo compound **3**, proving that there is a β-oriented iodine atom in iodo compound **3**. Another amorphous product (**4**) was formed in this hydrogenolysis in a 26% yield. Iodine was still intact in product **4**; its NMR spectrum showed three 3H singlets at τ 8.52, 9.36, and 9.11 assigned to 3β-methyl, 18-H, and 19-H of 3α,5-epoxy-*A*-homo-4-oxasteroid, an AB quartet at τ 6.21 and 5.83 (J=8.3 Hz) assigned to the 4a-methylene protons, and a double doublet at τ 5.44 (J=5.3 and 12.0 Hz) assignable to a proton attached to a carbon bearing iodine. These results prove **4** to be a 6α-isomer of epoxide **3**. A homolysis of C–I bond is apparently followed by the recombination of iodine on the catalyst surface to give a more stable isomer **4**.

Treatment of iodine-free epoxide **7** with boron trifluoride etherate and acetic anhydride in benzene at room temperature for 30 min gave a crystalline product, mp 114—115 °C, in an 89% yield. All the spectral properties of the product were consistent with a dihydropyrane structure **8** (see Experimental). The mode of its formation from the epoxide has already been discussed in the previous paper.[1] Hydrolysis of product **8** with aq methanolic potassium hydroxide

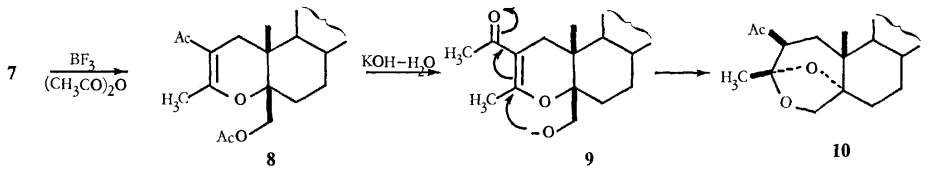

Scheme 4.

TABLE. NMR PARAMETERS (100 MHz) FOR THE 3-METHYL-5-CHOLESTENES AND THE REACTION PRODUCTS IN $CDCl_3$ SOLUTION (chemical shifts τ and splittings Hz)

Compd	3-Methyl	4 or 4a-Methylene	6-H	18-H	19-H	Others
1	8.88(s)	a)	4.74(br s)	9.32(s)	8.98(s)	
2	8.99(s)	a)	4.61(br s)	9.29(s)	8.75(s)	
3	8.60(s)	6.58(d) and 5.77(d) (7.9)	5.69(br t, 3.2) b)	9.26(s)	8.64(s)	
4	8.52(s)	6.21 5.83 (2d, 8.3)	5.44(dd, 5.3 and 1.2)	9.36(s)	9.11(s)	
6	8.00(s)	—	3.26(dd, 1.8 and 6.0)	9.40(s)	8.95(s)	0.81(s) (CHO)
7	8.57(s)	6.77 5.90 (2d, 6.9)	a)	9.34(s)	9.16(s)	
8	7.92(s)	5.98 5.78 (2d, 12.3)	a)	9.34(s)	8.91(s)	OAc 7.78(s) Ac 7.78(s)
10	8.60(s)	6.69 5.83 (2d, 7.7)	a)	9.33(s)	9.09(s)	Ac 7.83(s) 2α-H 7.23(dd, 5.44 and 12.0)

a) Unassignable. b) Superimposed with one of the 4a-methylene protons.

at room temperature for 1.5 h gave a compound (**10**), mp 131—134 °C, devoid of hydroxyl band in its IR spectrum. The mass, IR, and NMR spectra of product **10** were in full agreement with this structure: 2β-acetyl-3α,5-epoxy-3β-methyl-4-oxa-*A*-homo-5α-cholestane (**10**) formed by an intramolecular Michael addition of the first formed alcohol (**9**). Its IR spectrum showed a band at 1711 cm^{-1} due to an acetyl group and the NMR spectrum showed three 3H singlets assigned to 3β-methyl, 18-H, and 19-H, and an AB quartet assignable to 4a-methylene protons. Besides these signals, the spectrum showed a 3H singlet at τ 7.83 and a 1H double doublet at τ 7.23 (J= 5.4 and 12.0 Hz) assignable to the 2α-H. Epoxide **7** is formed in a manner entirely analogous to its 3-demethyl homologue.[1]

Discussion

The paths by which 3α,5-epoxide [*e.g.* **3** and **4**] are formed have been discussed in the previous paper.[1] Our experiments again confirmed the generality of the reaction, but the effects of a substitution by a methyl group at the C-3 of 3-hydroxy-Δ^5-steroids on the type of products and their relative yields are clear.

Thus, although thermal and photoinduced reactions of 3α- and 3β-methylcholesterol hypoiodites in the presence of mercury(II) oxide and iodine afford the products parallel to those in the corresponding reaction of cholesterol, the formation of 6β-iodo compound (*e.g.* **3**) as a single major product is noteworthy. Another feature of the present reaction is the absence of 3-oxa-5-cholesten-3β-ol under the experimental procedures comparable to the present reactions. As we suggested 4,4-dimethyl groups may be necessary in order to achieve an appropriate geometry of an intermediate to lead to 3-oxa-5-cholestenes. The absence of the 6α-isomer **4** in the products from the thermal reaction of 3α- and 3β-methylcholesterol hypoiodites[1] was again confirmed. The formation of 3α,5-epoxy-6α-iodo-*A*-homo-4-oxa-5α-steroids and 3α,5-epoxy-*A*-homo-4-oxa-5α-steroid-6-ene has been concluded to arise from an ionic reaction of intermediate carbonium ions.

No dimeric acetal, obtained from cholesterol, was formed in the thermal reaction of 3α- and 3β-methylcholesterol hypoiodites. The 3-methyl group in these hypoiodites hinders the formation of dimeric acetal in the thermal reaction and apparently facilitates the intramolecular reaction to 3α,5α-epoxy-*A*-homo-4-oxa-steroids.

Experimental

For instruments used and general procedures see Ref. 1. Mass spectra of compounds **1**, **2**, **7**, **8**, and **10** were recorded in the Faculty of Agriculture with a Hitachi JMS-D 300 spectrometer (ionizing voltage 70 eV). Mass spectra of compounds **3** and **4** were recorded in the Faculty of Pharmaceutical Sciences with a Hitachi RMU-6E spectrometer (ionizing voltage 70 eV).

*3α- And 3β-Methyl-5-cholesten-3-ols **1** and **2**.* These compounds were prepared by a described procedure.[4] 3β-Alcohol **1** mp 168.5—170.0 °C, (lit,[4] mp 167—168 °C); $[\alpha]_D^{24}$ −28.8° (*c* 1.3 in $CHCl_3$) (lit,[4] $[\alpha]_D^{25}$ −30° (*c* 1.25 $CHCl_3$); MS, *m/e* (rel intensity) 400 (M^+, 4.1%), 382 (M^+-H_2O, 100), 36.7 ($M^+-H_2O-CH_3$, 10.0), 329 (69.3), 147 (20.2), 121 (24.6), 119 (25.6), 107 (21.3) 95 (45.3), 81 (26.7), 57 (19.9), 55 (20.1), and 43 (19.9); for NMR see Table,

3α-Alcohol **2**. Mp 118.0—120.0 °C (lit,[4] mp 119—120 °C); $[\alpha]_D^{29}$ −27.2° (*c* 0.9 $CHCl_3$) (lit,[4] $[\alpha]_D^{25}$ −29° (*c* 0.94 $CHCl_3$); MS, *m/e* (rel intensity) 400 (M^+, 5.6%), 382 (M^+-H_2O, 85.9), 367 (6.8), 329 (100), 147 (19.0), 121 (25.4), 119 (34.3), 107 (22.3), 95 (39.9), 81 (25.7), 57 (20.5), 55 (23.8), and 43 (34.3); for NMR see Table.

Rearrangement of 3α-Methyl-5-cholesten-3β-ol Hypoiodite in the Presence of Mercury(II) Oxide and Iodine. By Irradiation. 3β-Alcohol **1** (1 g, 2.5 mmol), mercury(II) oxide (1.62 g, 7.5 mmol), and iodine (1.75 g, 7.5 mmol) in benzene (150 ml) were irradiated under an argon atmosphere with a 100-W high pressure mercury arc for 5 h. The solution was once filtered and the evaporation of the solvent from the filtrate at below 30 °C left a residue which was extract ed with chloroform (200 ml). The chloroform solution was washed with 5% aq sodium hydrogensulfite, water saturated with sodium chloride, and water successively, and dried (Na_2SO_4). Removal of the solvent left a residue which was recrystallized from a mixture of diethyl ether and methanol to give epoxide **3**, mp 112—114 °C, (749 mg). The specimen for analysis was obtained by recrystallizing it from methanol. Mp 116.5—118.5 °C. (Found: C, 61.82; H, 8.79; I, 23.58%. Calcd for $C_{28}H_{47}O_2I$: C, 61.98; H, 8.73; I, 23.39%); $[\alpha]_D^{34}$ −36.0° (c 1.0 $CHCl_3$); IR, 1198, 1175, 1121, 1024, and 865 cm^{-1}; MS, *m/e* (rel intensity) 541 (M^+, 0.5%), 415 (M^+-I, 21.5), 373 (100), 355 (16.7), 327 (42.9), 57 (26.2), and 43 (52.4); for NMR see Table. The filtrate from the first recrystallization was evaporated to yield a residue (570 mg). It was subjected to preparative TLC with a 2:3 mixture of hexane–benzene. The most mobile fraction (154 mg) showed two spots on TLC. This fraction was again subjected to preparative TLC to afford two fractions. The more mobile fraction was a crude acetal **3** (70 mg), which was recrystallized from methanol to yield a further amount of acetal **3** (59 mg). The less mobile fraction (47 mg) was a mixture; its NMR spectrum indicated it was almost certainly a 1:1 mixture of 3α,5-epoxy-6α-iodo-3β-methyl-*A*-homo-4-oxa-5α-cholestane and 3-acetoxy-2-iodo-*A*-nor-2,3-seco-5-cholesten-3-ol acetate. It showed three singlets at τ 9.35 (18-H), 9.09 (19-H), and 8.51 (3-methyl), an AB quartet (C-4a methylene) at τ 5.82 and 6.20 (J=8 Hz), and a double doublet at τ 5.48 (J=5 and 12 Hz) (6β-H) [a doublet at higher field was superimposed with a signal due to C-3 methylene of product **5**] of product **4**. In addition to these signals, it showed three singlets at τ 9.32, 9.01, and 7.86, a broad singlet at τ 5.48, and a diffused doublet at τ 4.11, which could be assigned to 18-H, 19-H, 3-acetoxyl, 3-H, and 6-H of seco iodide **5**. An attempted separation of these two products by means of preparative TLC was unsuccessful. More polar fractions (396 mg) were an intractable mixture.

Thermal Reaction: A reaction mixture in the same scale as that for the photo-reaction was heated at 55—60 °C under an argon atmosphere for 3 h and worked up as usual. The crude mixture (1.38 g) was recrystallized from diethyl ether–methanol to yield an acetal **3**, mp 113—115.5 °C (862 mg). Removal of the solvent left a residue (441 mg) which was subjected to preparative TLC. A fraction (52 mg) of acetal **3** was recrystallized to yield the acetal (37 mg). The less mobile fraction (22 mg) was identified to be seco ketone **6** on the basis of the NMR spectrum. In contrast to the photo-reaction results, 6α-iodo isomer **5** was absent in the product, as indicated by TLC.

Photoinduced Rearrangement of 3β-Methyl-5-cholesten-3α-ol Hypoiodite in the Presence of Mercury(II) Oxide and Iodine. 3α-Alcohol **2** (400 mg, 1 mmol), mercury(II) oxide (651 mg, 3 mmol), and iodine (762 mg, 3 mmol) in benzene (60 ml) were irradiated under an argon atmosphere for 3 h. After the usual work-up, a crude product (620 mg) was recrystallized from diethyl ether–methanol to give acetal **3** (234 mg), mp 112—115 °C. The residue from the filtrate was subjected to preparative TLC with a 2:3 mixture of hexane–benzene. The most mobile fraction (50 mg) was recrystallized to yield acetal **3** (35 mg). The next mobile fraction (10 mg) was a seco iodide, as judged by its NMR spectrum. From the less mobile fraction, the starting material (7 mg, 2%) was recovered unchanged.

*Photoinduced Rearrangement of 3β-Alcohol **1** in the Presence of Silver(II) Oxide and Iodine.* 3β-Alcohol **1** (300 mg, 0.75 mmol), silver oxide (552 mg, 2.25 mmol), and iodine (796 mg, 2.25 mmol) in benzene (40 ml) were irradiated under an atmosphere of argon for 95 h. In the course of the reaction, further amounts of silver(II) oxide and iodine were added [silver(II) oxide 340 mg and iodine 460 mg at the period of 5 h and silver(II) oxide 180 mg and iodine 400 mg at the period of 48 h]. Work-up of the reaction mixture gave a crude product (392 mg), which was recrystallized from a mixture of acetone and methanol to yield acetal **3** (203 mg), mp 116.5—118.5 °C. A residue from the filtrate was subjected to preparative TLC with a 2:3 mixture of hexane and benzene. The most mobile fraction (17 mg) was recrystallized to give acetal **3** (10 mg). The least mobile raction (50 mg) was again subjected to preparative TLC to afford an amorphous α,β-unsaturated aldehyde **6**. IR, (neat) 1720 (acetyl), 1691 and 1631 (α,β-unsaturated formyl), 1463, 1376, 1361, 1258, 1161, and 805 cm^{-1}; for NMR spectrum see Table.

*Hydrogenolysis of Epoxide **3** with 10% Palladium on Carbon Catalyst.* Epoxide **3** (543 mg) in a mixed solvent of ethanol (18 ml) and benzene (20 ml) containing potassium acetate (80 mg) and a 10% Pd–C catalyst (200 mg) was hydrogenated under an atmospheric pressure for 28 h. At the period of 24 h, a further amount of the catalyst (50 mg) was added. After removal of the catalyst and the solvent, the residue was dissolved in diethyl ether. The solution was washed with water and dried (Na_2SO_4). The residue (470 mg) was subjected to preparative TLC to give three fractions. The most mobile fraction (140 mg) was an amorphous 6α-epimer **4**. $[\alpha]_D^{20}$ −6.8° (*c* 2.0 $CHCl_3$); IR, no hydroxyl and carbonyl bands; 1276, 1234, 1134, 1039, and 734 cm^{-1}; MS *m/e* (rel intensity) 542 (M^+ +1, 0.3%), 541 (M^+, 0.1), 415 (M^+-I, 96), and 99 (100); for NMR spectrum see Table. The next mobile fraction (260 mg) was recrystallized from a mixture of diethyl ether and methanol to give 3α,5α-epoxide **7** (215 mg) in 2 crops, mp 61.5—63.0 °C. The specimen for analysis, mp 63.5—65.0 °C was obtained by further recrystallizations. (Found: C, 80.40; H, 11.70%. Calcd for $C_{28}H_{48}O_2$: C, 80.71; H, 11.61%), $[\alpha]_D^{20}$ +10.9 (*c* 1.0 $CHCl_3$); IR, 1120, 1028, and 866 cm^{-1}; MS *m/e* (rel intensity) 416 (M^+, 7.5%), 387 (55.9), 356 (28.6), 345 (100), 327 (96.7), 215 (25.1), 120 (26.2), 95 (29.2), 81 (28.1), 55 (25.3), and 43 (31.3); for NMR spectrum see Table.

*The Reaction of 3α,5α-Epoxide **7** with Boron Trifluoride Etherate and Acetic Anhydride.* 3α,5α-Epoxide (105 mg, 0.25 mmol), acetic anhydride (0.2 ml, 2 mmol), and boron trifluoride etherate, (0.05 ml, *ca.* 0.39 mmol) in benzene (10 ml) were stirred for 30 min at 22 °C. The solution was neutralized by the addition of aq sodium hydrogencarbonate and was extracted with diethyl ether. The solution was washed with aq sodium hydrogencarbonate solution and water, and dried (Na_2SO_4). Removal of the solvent gave a dihydropyrane derivative **8** (109 mg) in two crops. The specimen for analysis was obtained by further recrystalliza-

tions and melted at 114—115 °C. (Found: C, 76.53; H, 10.36%. Calcd for $C_{32}H_{52}O_4$: C, 76.75; H, 10.43%); $[\alpha]_D^{22}$ −7.7° (*c* 0.9 $CHCl_3$); UV λ_{max} (ethanol) 268 nm (ε; 11500); IR, 1754 (acetyl), 1675 and 1583 (RO-C=C-Ac), 1240, and 1043 cm^{-1}; MS *m/e* (rel intensity) 500 (M^+, 6.5%), 397 (5.2), 328 (4.9), 327 (9.6), 95 (14.2), and 43 (100); for NMR spectrum see Table.

Hydrolysis of Dihydropyrane Derivative **8**. Dihydropyrane derivative **8** (20 mg) in a mixture of diethyl ether (1 ml) and methanol (1 ml) containing water (1.1 ml) and potassium hydroxide (50 mg) was stirred for 1.5 h at room temperature. The solution was extracted with diethyl ether (20 ml). The organic layer was washed with dilute hydrochloric acid and water and dried (Na_2SO_4). The crude product (14 mg) was recrystallized from methanol to yield 3α,5α-epoxy-*A*-homo-4-oxa-steroid **10**, mp 131—134 °C. Recrystallization raised the melting point to mp 134—137 °C; IR, 1711 (acetyl), 1175 and 1026 cm^{-1}; MS *m/e* (rel intensity) 458 (10.7%), 440 (20.9), 398 (38.8), 345 (25.0), 328 (100), 327 (37.8), 247 (19.1), 215 (45.7), 121 (23.3), 120 (43.9), 119 (23.9), 95 (36.4), 81 (24.3), and 43 (55.4); for NMR spectrum see Table.

The authors are grateful to Mrs. Tomoko Okayama for the measurements of the ^1H NMR spectra.

References

1) Photoinduced Transformations. Part 52. Previous paper in this series. H. Suginome, A. Furusaki, K. Kato, N. Maeda, and F. Yonebayashi, *J. Chem. Soc., Perkin Trans. 1*, in press.

2) M. S. Patel and W. J. Peal, *Tetrahedron*, **20**, 2511 (1964).

Photo- and Thermally-induced Radical Rearrangement of 4,4-Dimethyl-5-cholesten-3β-ol Hypoiodite in the Presence of Mercury(II) Oxide and Iodine[1)]

Hiroshi SUGINOME*,** and Norio MAEDA

Department of Chemistry, Faculty of Science, Hokkaido University, Sapporo 060

(Received February 19, 1980)

Irraidation of a benzene solution of hypoiodite of 4,4-dimethyl-5-cholesten-3β-ol (**1**) in the presence of mercury(II) oxide and iodine gave a mixture of products, from which 3α,5-epoxy-6β-iodo-*A*-homo-4-oxa-5α-cholestane (2%), 4,4-dimethyl-3-oxa-5-cholestene (**3**) (10%), and 4a,4a-dimethyl-3α,5-epoxy-*A*-homo-4-oxa-5α-cholest-6-ene (**4**) (4%) were isolated. The thermally-induced reaction on **1** conducted at 55—60 °C gave **3** and **4** in lower yields. The reaction with the use of lead tetraacetate-iodine reagent also gave a complex mixture, from which only **4** was obtained in 22% yield. The formation of 4,4-dimethyl-3-oxa-5-cholestene skeleton is parallel with the case of the photo- and thermally-induced reactions of hypoiodite of 3α,4,4-trimethyl-5-cholesten-3β-ol and appears to be particular with 5-cholesten-3β-ol bearing dimethyl groups at the C-4 under similar conditions. The formation is explained in terms of radical-induced decarbonylation of initially formed 4,4-dimethyl-2-formyl-3-oxa-5-cholestene.

Previous papers[1,2)] have reported the results on the photo- and thermally-induced radical rearrangments of hypoiodite of several 5-cholesten-3-ols in the presence of mercury(II) oxide and iodine. It has been found that the reaction, regardless of whether it was induced photochemically or thermally, led generally to the formation of 3α,5-epoxy-*A*-homo-4-oxa-5α-cholestanes having α- or β-oriented iodine or 3α,5-epoxy-*A*-homo-4-oxa-5α-cholest-6-enes. Methyl substituents at their C-3 or C-4, however, affected the relative yields of the products appreciably and even resulted in the formation of new products. Thus, for example, 3α,4,4-trimethylcholest-5-en-3β-ol hypoiodite gave 2-acetyl-3-oxa-5-cholestenes together with 3α,5-epoxy-*A*-homo-4-oxa-5α-cholestanes on thermal or photoindused reaction in the presence of mercury(II) oxide and iodine. These effects of the alkyl substituents were interpreted as due mainly to steric effects on the conformation of the intermediary allyl radical generated by the β-scission of oxyl radicals.[2)]

This paper reports a study of photo- and thermally-induced reactions of the hypoiodite of 4,4-dimethyl-5-cholesten-3β-ol (**1**)[3)] in the presence of mercury(II) oxide and iodine; the study was made to assess the effect of alkyl substitution at the C-4.

Results

The reactions have been conducted under the conditions reported previously.[1,2)] Thus, irradiation of 4,4-dimethyl-5-cholesten-3β-ol (**1**) in benzene containing iodine and mercury(II) oxide (each *ca.* 3 mol equiv.) with a 100-W high pressure mercury arc for about 4 h under an atmosphere of nitrogen gave a complex mixture of products, from which three products (**2**) (2%), (**3**) (10%), and (**4**) (4%) were obtained by preparative TLC and column chromatography (Scheme 1). The structures of these products were deduced by analysis of their spectra. The crystalline product **2** contained an iodine atom in the molecule; the mass spectrum showed a weak ion of *m/e* 429 attributable to M^+-I, a base peak at *m/e* 371, and a prominent peak at *m/e* 353, indicating the structure to be a 3α,5-epoxy-*A*-homo-4-oxa-5α-cholestane. The elemental analysis was in agreement with this. The genesis and the structure of the fragments of *m/e* 371 and *m/e* 353 is depicted in Scheme 2.

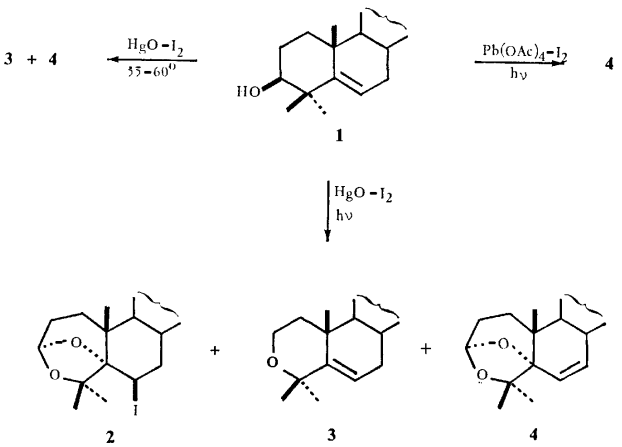

Scheme 1.

The ^{1}H NMR spectrum of **2** showed two broad singlets at τ 5.81 and 4.65. The former is ascribable to a proton attached to a carbon bearing iodine and the latter is assigned to a proton attached to a carbon bearing two oxygen atoms. Irradiation at τ 6.5 sharpened the broad singlet at τ 5.81.

A molecular formula of **3** was confirmed to be $C_{28}H_{48}O$ by high resolution mass spectrometry. The IR spectrum lacked bands arising from hydroxyl and carbonyl groups. The ^{1}H NMR spectrum of **3** indicated a 1-H double doublet centered at τ 4.65 due to an olefinic proton, a 2-H multiplet at τ 5.95—6.54 assignable to a methylene group having an ether type oxygen, and four singlets due to the four tertiary methyl groups. The fragmentation in the mass spectrum was most helpful for the assignment of the structure. The spectrum showed the base peak at *m/e* 385; no other peak whose intensity exceeded 2% was present. The fragment arises from an expulsion

** Present address: Organic Chemistry Laboratory, Department of Chemical Process Engineering, Faculty of Engineering, Hokkaido University, Sapporo 060.

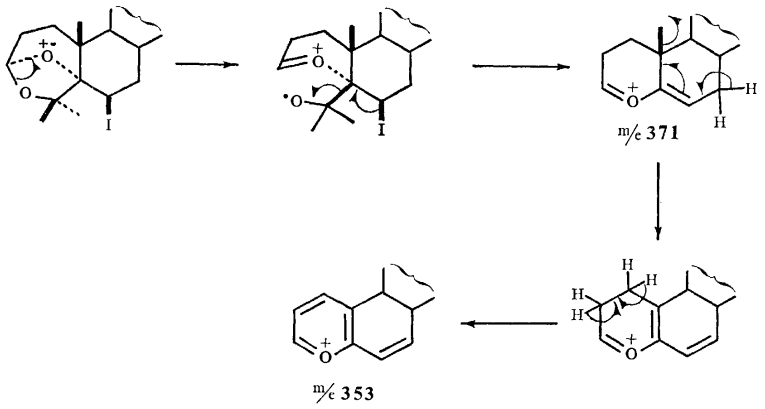

Scheme 2.

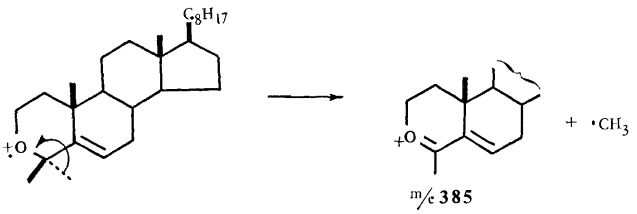

Scheme 3.

of a methyl group at the C-4, as confirmed by an accurate mass measurement which showed the ion of *m/e* 385 to be a species $C_{27}H_{45}O^+$ (*m/e* 385.3467). All these results can be accommodated in the structure 4,4-dimethyl-3-oxa-5-cholestene. The structure and a genesis of the base peak is depicted in Scheme 3.

The ^{13}C NMR spectrum of product **3** showed 28 signals, including those at δ 147.36, 117.98, 74.43, 57.99, 56,89, 55.92, and 49.83 ppm in the downfield region. By the aid of off-resonance decoupling, these signals could be assigned to the C-5, C-6, C-4, C-2, C-14, C-17, and the C-9 respectively.

The molecular formula of **4** was deduced to be $C_{29}H_{48}O_2$ by the mass spectrum (M^+, *m/e* 428) and the elemental analysis. The mass spectrum showed the base peak at *m/e* 370. The IR spectrum lacked any hydroxyl and carbonyl groups. The ^1H NMR spectrum showed a 1-H broad singlet at τ 4.70, assigned to a proton attached to a carbon having two oxygens. It also exhibited the signals assignable to two olefinic protons centered at τ 4.56 and 4.11. Their coupling constants (11.6 Hz) indicated that they are vicinal protons in a fused cyclohexene. The respective doublet showed further small splitting. These results of the ^1H NMR spectrum and the presence of a base peak at *m/e* 370 in the mass spectrum indicated that the structure of the product **4** was 4a,4a-dimethyl-3α,5-epoxy-*A*-homo-4-oxa-5α-cholest-6-ene (**4**). The ion of *m/e* 370 may arise as depicted in Scheme 4. No other well-defined products were isolated from the product mixture.

The photoinduced reaction of the hypoiodite was also attempted by the use of lead tetraacetate–iodine reagent.[4] However, the reaction again led to a complex mixture, from which only 4a,4a-dimethyl-3α,5-epoxy-*A*-homo-4-oxa-5α-cholest-6-ene (**4**) was isolated in 22% yield.

Finally, thermally-induced rearrangements were attempted. Homoallyl alcohol **1** in benzene containing mercury(II) oxide and iodine was heated at 55—60 °C for 3 h in the dark, as was previously reported for several 5-cholesten-3β-ols. Again, a mixture of products was obtained, and 4,4-dimethyl-3-oxa-5-cholestene **3** (5%) and 4a,4a-dimethyl-3α,5-epoxy-*A*-homo-4-oxa-5α-cholest-6-ene **4** (2%) were isolated from the mixture by preparative TLC.

Discussion

The paths by which 3α,5-epoxy-*A*-homo-4-oxa-5α-cholestanes and 3α,5-epoxy-*A*-homo-4-oxa-5α-cholest-6-enes are formed have been discussed in the previous papers.[1,2]

4,4-Dimethyl-3-oxa-5-cholestene (**3**) is a new type of product in this reaction, but its formation may reasonably be explained in either of the following two ways. Scheme 5 shows the first probable path. Thus, as suggested previously,[2] 3-oxa-5-cholestene skeleton (G) can be formed either *via* successive intermediates (A) to (E) or *via* (A) to (F). The second hypoiodite (B) may be formed by the reaction of iodine oxide and allyl radical intermediate (A). Radical-induced decarbonylation[5] of 4,4-dimethyl-2-formyl-3-oxa-5-cholestene (G) may take place under the experimental conditions to give the observed product **3**. The possibility of the photochemical removal of the formyl group is excluded, since **3** is also formed in the reaction under the dark.

An alternative path to 3-oxa-5-cholestene is shown in Scheme 6. In this path, 3,3-dimethyl-2-iodo-*A*-nor-2,3-seco-5-cholesten-3-ol formate (I) is formed from an intermediate (H) formed from the allyl radical (A). The transformation of the intermediate (I) into another intermediate (K) and radical or ionic cyclization of (K) may give product **3**. The formate (J) is, in fact, one of the major products in the photo-induced rearrangements of cholesterol hypoiodite in the presence of mercury(II) oxide and iodine.[2] This latter path, however, is less likely since no 3-oxa-5-cholestene is formed under the experimental conditions in the photoinduced reaction of cholesterol hypoiodite.

Thus, the present results are considered to be nearly parallel with those obtained in the reaction of 3α,4,4-

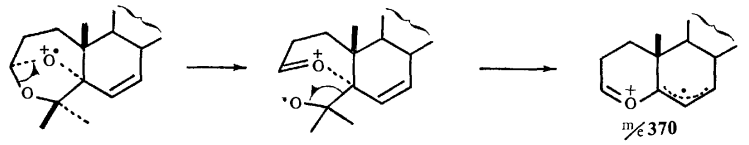

Scheme 4.

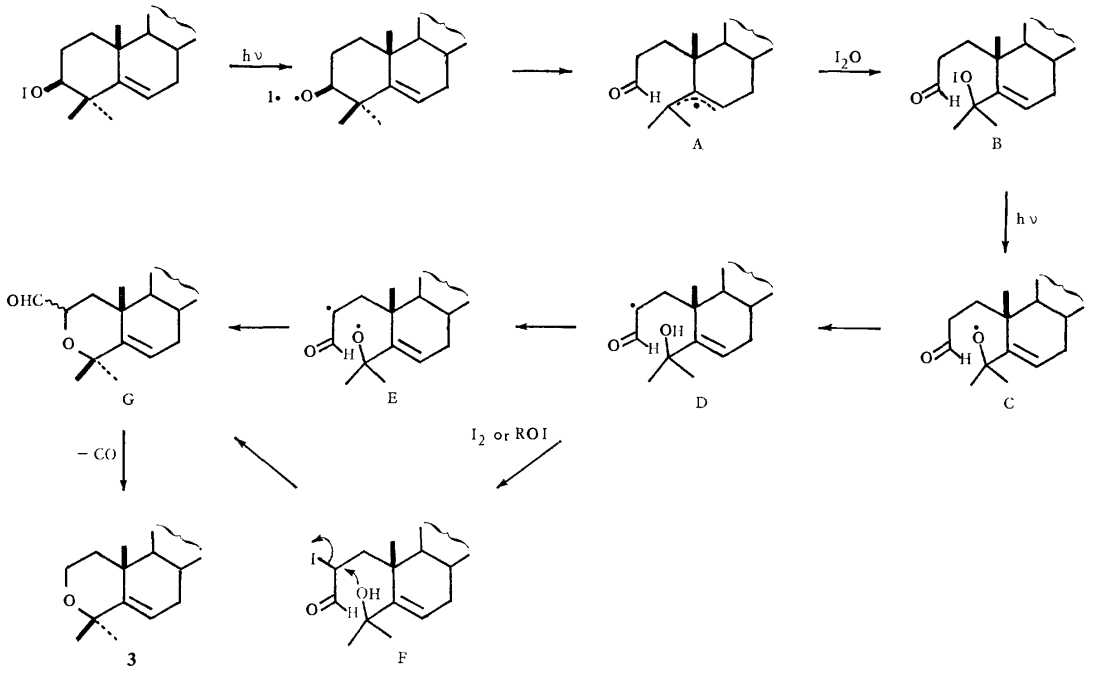

Scheme 5.

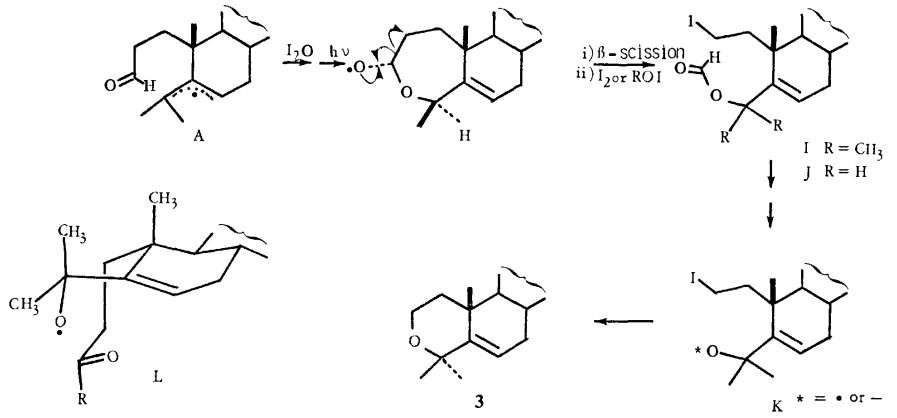

Scheme 6.

trimethyl-5-cholesten-3β-ol[2] although the yields of the products are lower than those in the reaction of the 3-methyl analogue.[2]

The formation of 3-oxa-5-cholestene (*e.g.* **3**) appears to be particular with 5-cholesten-3-ols having dimethyl groups at their C-4. The fact strengthens our previous hypothesis[2] that one of the methyl groups at their C-4 destabilizes a conformation (L), in which the oxyl radical attacks a carbonyl carbon to give an oxepane (H), by virtue of a quasi 1,3-diaxial relationship with its 10β-methyl group, and facilitates an intramolecular abstraction of the most weakly bound C-2–H by the oxyl radical.

Experimental

For instruments used and general procedure see Ref. 2. Low resolution mass spectra of compounds **2** and **3** and high resolution mass spectrum of **3** were recorded with a Hitachi JMS-D 300 spectrometer (ionizing voltage 70 eV) by Miss Yuko Chiba of the Faculty of Agriculture in this University. The mass spectrum of compound **4** was recorded with a Hitachi RMU-6E spectrometer (ion source temperature 80 °C, ionizing voltage 80 eV) by the staff of the Faculty of Pharmaceutical Sciences. The ^{13}C NMR spectrum was recorded with a Brucker SXD pulsed FT NMR spectrometer ($CDCl_3$, 22.63 MHz, ppm from TMS) in the Faculty of

Engineering of this University.

The Irradiation of 4,4-Dimethyl-5-cholesten-3β-ol Hypoiodite in the Presence of Mercury(II) Oxide and Iodine. 4,4-Dimethyl-5-cholesten-3β-ol (**1**) (1 g, 2.42 mmol), mercury(II) oxide (1.6 g, 7.38 mmol), and iodine (1.72 g, 6.78 mmol) in benzene (130 ml) were irradiated for 3 h 40 min. After the solution was filtered, the filtrate was evaporated to give a residue which was worked up in the usual way. The crude product (1.02 g) was subjected to preparative TLC with benzene. Seven fractions: A (214 mg), B (111 mg), C (75 mg), D (104 mg), E (60 mg), F (40 mg), and G (157 mg) were obtained in order of decreasing mobility. The ^{1}H NMR spectrum of fraction A indicated no proton signal due to aldehyde. Fractions B and C were combined and subjected to column chromatography. (Kiesel gel 60, 70—230 mesh). Elutions with a 5:1 mixture of hexane and benzene gave a 3α,5-epoxide **2** (19 mg, 2%), which was recrystallized from a mixture of diethyl ether and methanol to give a specimen for analysis, mp 131.5—133.5 °C. $[\alpha]_D^{22}$ −41.8° (*c* 0.5 $CHCl_3$); (Found: C, 62.60; H, 8.92; I, 23.02%. Calcd for $C_{29}H_{49}O_2I$: C, 62.57; H, 8.87; I, 22.80%); IR, 1171, 1148, 1119, 1104, 1025, 970 and 938 cm^{-1}; NMR, τ 9.27 (3H, s, 18-H), 8.69 and 8.57 (each 3H, s, C-5 dimethyl), 8.28 (3H, s, 19-H), 5.81 (1H, br s, $W_{1/2}$ 3.8 Hz, 3β-H); MS, *m/e* (rel intensity) 429 (0.2%, M^+-I), 372 (20.5), 371 (100), 353 (4.2), 57 (4.6), 55 (13.5), and 43 (51). Fraction D was an almost pure 3-oxa compound **3**. After recrystallization from diethyl ether–ethanol, it had mp 106.0—107.5 °C (61 mg). $[\alpha]_D^{21}$ −40.2° (*d* 1.0 $CHCl_3$); (Found: C, 83.87; H, 12.18%. Calcd for $C_{28}H_{48}O$: C, 83.93; H, 12.08%; *m/e* 400.3702. Calcd for $C_{28}H_{48}O$: M, 400.3704); IR, 917, 963, 1078, 1113, 1143, and 1177 cm^{-1}; NMR, τ 9.32 (3H, s, 18-H), 8.79, 8.67, and 8.64 (each 3H, s, C-4 dimethyl, and 19-H), 5.95—6.54 (2H, m, 2α- and 2β-H), and 4.65 (1H, dd, J=2 and 5 Hz, 6-H); MS, *m/e* (rel intensity), 400 (M^+, 0.2%) 399 (0.1), 386 (24.3), and 385 (M^+-CH_3 100). (Found; *m/e* 385.3467. Calcd for $C_{27}H_{45}O^+$: 385.3469). Fraction E was subjected to column chromatography (silica gel, 6 g). Elutions with a 1:1 mixture of hexane and benzene afforded an amorphous 3α,5α-epoxide **4** (43 mg, 4%); NMR, τ 9.40 (3H, s, 18-H), 9.06 (3H, s, 19-H), 8.78 and 8.60 (each 3H, s, C-4 dimethyl), 4.70 (1H, br s, $W_{1/2}$=3.7 Hz, 3β-H), 4.56 (1H, dd, J=11.6 and 3.1 Hz, 7H), and 4.11 (1H, dd, J=11.6 and 1.8 Hz, 6H); IR, (neat) 800, 969, 1025, 1105, and 1260 cm^{-1}; MS, *m/e* (rel intensity) 428 (M^+, 11.0%), 370 (100), 343 (12.8), 339 (14.6), 149 (47.7), 57 (60.6), and 43 (71.6). No single compound was obtained from other fractions.

The Thermal Decomposition of 4,4-Dimethyl-5-cholesten-3β-ol Hypoiodite in the Presence of Mercury(II) Oxide and Iodine. The 3β-ol (480 mg, 1.15 mmol), mercury(II) oxide (780 mg, 3.61 mmol), and iodine (860 mg, 3.39 mmol) in benzene (65 ml) were heated at 55—60 °C in the dark for 3 h. The reaction mixture was worked up as was described for the mixture from the photoinduced reaction. The amorphous residue (553 mg) was subjected to preparative TLC with benzene. Five fractions: A (34 mg), B (52 mg), C (37 mg), D (70 mg), and E (115 mg) were obtained in the order of decreasing mobility. Fraction B (52 mg) was subjected to preparative TLC with benzene to yield cyclic ether **3** (25 mg, 5%), identical with the specimen obtained from photolysis. The fractions C and D were combined and were again subjected to preparative TLC with a 4:1 mixture of hexane and diethyl ether to yield an amorphous 3α,5-epoxide **4** (11 mg, 2%).

The Reaction of 4,4-Dimethyl-5-cholesten-3β-ol with Lead Tetraacetate–Iodine Reagent. 4,4-Dimethyl-5-cholesten-3β-ol (**1**) (300 mg, 0.72 mmol), freshly prepared lead tetraacetate (962 mg, 2.17 mmol), and iodine (749 mg, 2.17 mmol) in benzene (40 ml) containing calcium carbonate (120 mg) were irradiated through Pyrex for 2.5 h with a 100-W Hg arc under an argon atmosphere. After the solution was filtered, the filtrate was washed three times with 5% aq sodium hydrogensulfite solution, washed with water, and dried (Na_2SO_4). The removal of the solvent left a residue (365 mg) which was subjected to preparative TLC with a 2:3 mixture of dichloromethane and benzene. Four fractions: A (48 mg), B (34 mg), C (60 mg), and D (69 mg) were obtained. The fraction D was 4a,4a-dimethyl-3α,5-epoxy-*A*-homo-4-oxa-5α-cholest-6-ene as indicated by the NMR spectrum.

We thank Mrs. T. Okayama and Miss H. Maki for the measurements of NMR spectra and spin decoupling experiments.

References

1) Photoinduced Transformations. Part 53. Previous paper in this series, H. Suginome and N. Maeda, *Bull. Chem. Soc. Jpn.*, **53**, 2621 (1980).

2) H. Suginome, A. Furusaki, K. Kato, N. Maeda and F. Yonebayashi, *J. Chem. Soc., Perkin Trans. 1*, in press.

3) R. B. Woodward, A. A. Patchett, D. H. R. Barton, D. A. J. Ives, and R. B. Kelly, *J. Chem. Soc.*, **1957**, 1139.

4) For reviews of the hypoiodite reaction see K. Heusler and J. Kalvoda, *Angew. Chem.*, **76**, 518 (1964); J. Kalvoda and K. Heusler, *Synthesis*, **1971**, 501.

5) W. v. E. Doering, M. Farber, M. Sprecher, and K. B. Wiberg, *J. Am. Chem. Soc.*, **74**, 3000 (1952).

The Reaction of 3-Hydroxyflavones with Metal Salts

Mutsumi HAMADO* and Kazu KUROSAWA

Department of Chemistry, Faculty of Science, Kumamoto University, Kurokami, Kumamoto 860

(Received February 6, 1980)

The reaction of 3-hydroxyflavones (**1a—d**) with lead(IV) acetate gave 1,2-diphenylethanediones (**2a—d**), 1,2-diphenyl-2-hydroxyethanones, 2-hydroxybenzoic acids (**7** and **9**), and benzoic acids (**8** and **10**), and the reaction with manganese(III) acetate yielded **2**, **7**, **8**, **9**, and **10**. In addition to **2**, **7**, and **10**, 6-methoxy-2-(4-methoxybenzoyloxy)-3(2*H*)-benzofuranone and 2-hydroxy-4-methoxybenzaldehyde were obtained in the reaction of **1c** with manganese(III) acetate. It has been established by the studies of ^{14}C-labelled compounds that the $C_{(3)}$ in the 3-hydroxyflavone was lost during the reaction.

In previous papers,[1,2] the decarbonylation reactions of 1,3-diphenyl-1,3-propanediones and 1,3-indandiones with lead(IV) acetate have been reported. The reaction of ^{14}C-labelled compounds showed that the $C_{(2)}$ was lost completely in the case of 2-acetoxy-1,3-diphenyl-1,3-propanedione, but that 53 percent of the $C_{(\alpha)}$ was retained in the case of β-hydroxychalcone (1,3-diphenyl-1,3-propanedione), suggesting that there may be binary reaction pathways. Similar results were obtained in the reaction of ^{14}C-labelled 1,3-indandiones and 1*H*-phenalene-1,3(2*H*)-dione with lead(IV) acetate[2] (Scheme 1). In order to obtain further information about the nature of the decarbonylation reaction, we studied the reaction of 3-hydroxyflavones with lead(IV) acetate under various reaction conditions.

When 4′,7-dimethoxy-3-hydroxyflavone (**1c**) was heated in acetic acid with lead(IV) acetate, five compounds (**2c**, **3c**, **4c**, **7**, and **10**) were obtained. The NMR spectrum of **2c** indicated the presence of a para-substituted benzoyl group [δ=7.92 (2H, m) and 6.96 (2H, m)], a 2,4-disubstituted benzyol group [δ=7.4 (1H, d, J=9 Hz) and 6.25—6.5 (2H, m)],

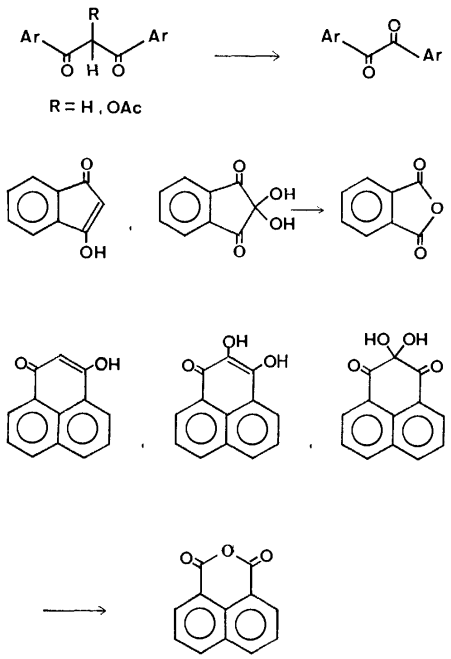

Scheme 1. Reactions of 1,3-diaryl-1,3-propanediones, 1,3-indandiones, and 1*H*-phenalene-1,3(2*H*)-dione with lead(IV) acetate.

a hydrogen-bonded hydroxyl group [δ=11.9 (1H, s)] which disappeared on deutration, and two methoxyl groups [δ=3.82 (3H, s) and 3.85 (3H, s)]. Two carbonyl functions, one of which was hydrogen-bonded, were characterized by IR absorption at 1685 and 1630 cm^{-1}. The mass spectrum of **2c** showed four prominent ions, at *m/e* 151, 135, 123, and 107, due to the α-cleavages to the carbonyls that are shown in Fig. 1. This spectroscopic evidence clearly showed that this compound was 1-(2-hydroxy-4-methyoxyphenyl)-2-(4-methoxyphenyl)ethanedione (**2c**). The structure was confirmed by an unambiguous synthesis of **2c**: the reaction of 2′-benzyloxy-4,4′-dimethoxychalocone with thallium(III) nitrate[3] gave 1-(2-benzyloxy-4-methoxyphenyl)-2-(4-methoxyphenyl)ethanedione (**2e**), which was then debenzylated to give the identical **2c**.

The NMR spectrum of **3c** showed that presence of a para-substituted phenyl group [δ=7.28 (2H, m) and 6.85 (2H, m)], three atomatic protons [δ=7.15 (1H, d, J=8 Hz) and 6.3—6.45 (2H, m)], two methoxyl groups [δ=3.76 (3H, S) and 3.75 (3H, s)], two hydroxyl groups [δ=12.1 (1H, s) and 4.25 (1H, broad s)], and a broad singlet [5.8 (1H)]. The latter singlet became sharp and the hydroxyl groups disappeared when shaken with deuterium oxide. The IR spectrum of this compound indicated the presence of hydroxyl groups (3460 and 2500—3300 cm^{-1}) and a hydrogen-bonded carbonyl group (1640 cm^{-1}). Thus, the structure of **3c** is shown as 2-hydroxyl-1-(2-hydroxy-4-methoxyphenyl)-2-(4-meth-

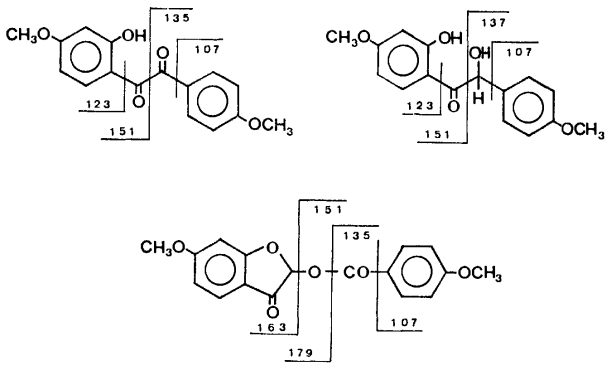

Fig. 1. The mass spectral data of 1-(2-hydroxy-4-methoxyphenyl)-2-(4-methoxyphenyl)ethanedione (**2c**), 2-hydroxy-1-(2-hydroxy-4-methoxyphenyl)-2-(4-methoxyphenyl)ethanone (**3c**), and 6-methoxy-2-(4-methoxybenzoyloxy)-3(2*H*)-benzofuranone (**5**).

oxyphenyl)ethanone. This was further confirmed by the mass spectrum of **3c**, which showed prominent ions at *m/e* 151 and 123 due to α-cleavages to the carbonyl group, and at 137 and 107 due to α-cleavages to the alcoholic hydroxyl group (Fig. 1).

The third compound was found to be 3-acetoxy-4′,7-dimethoxyflavone (**4c**), which was identified with an authentic sample by a comparison of their IR spectra. The two carboxylic acids (**7** and **10**), as a mixture, were compared with the mixture of authentic samples on NMR, and then the methyl-esterified mixture was identified by a comparison of its GC retention time with that of the authentic specimen. When the reaction was conducted in a benzene solution, the yields of these products (**2c** and **3c**) were poor so that all the reactions hereafter were carried out in acetic acid.

When **1c** was oxidized with manganese(III) acetate, five products (**2c**, **5**, **6**, **7**, and **10**) were obtained. **6** was found to be 2-hydroxy-4-methoxybenzaldehyde. The NMR spectrum of **5** indicated the presence of a para-substituted benzoyl group [δ=8.09 (2H, m) and 6.95 (2H, m)], three aromatic protons [δ=7.69 (1H, d, J=10 Hz) and 6.53—6.84 (2H, m)], and a singlet [δ=6.50 (1H)]. The mass spectrum of **5** showed prominent ions due to all the possible cleavages shown in Fig. 1. The IR spectrum of **5** showed a carbonyl absorption at 1745 cm^{-1}. These spectral data are consistent with the structure of **5** shown in Scheme 2.

Three other 3-hydroxyflavones (**1a**, **1b**, and **1d**) were also oxidized with lead(IV) acetate to give 1-(2-hydroxyphenyl)-2-phenylethanediones (**2a**, **2b**, and **2d**), 2-hydroxy-1-(2-hydroxyphenyl)-2-phenylethanones (**3a** and **3b**), 3-acetoxy-7-methoxyflavone (**4a**), 2-hydroxybenzoic acids (**7** and **9**), and benzoic acids (**8** and **10**). The oxidations of **1a**, **1b**, and **1d** with manganese(III) acetate again gave 1-(2-hydroxyphenyl)-2-phenylethanediones (**2a**, **2b**, and **2d**).

In order to establish the nature of the decarbonylation reaction, the reaction was carried out using ^{14}C-labelled 3-hydroxyflavone. When 3-hydroxy-4′,6,7-trimethoxyflavone-3-^{14}C was oxidized with lead(IV) acetate, an inactive **2d** and an active carbon dioxide were obtained (Scheme 3), indicating that the $C_{(3)}$ was lost during the oxidation. That the 2-hydroxy-1-(2-hydroxyphenyl)-2-phenylethanones (**3a**—**c**) and the aldehyde (**6**) were isolated in the reactions seems to show the complex features of the reaction. It is well known that 1,2-diphenyl-2-hydroxyethanone is oxidized to give 1,2-diphenylethanedione, benzaldehyde, and benzoic acid by lead(IV) acetate.[4] Thus, this suggests that, *via* an unknown process, 3-hydroxyflavone

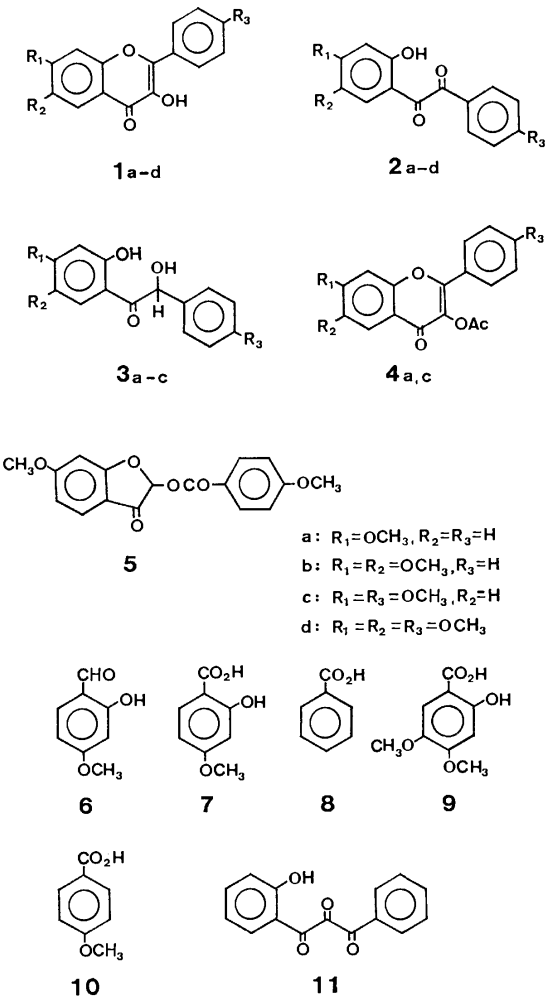

Scheme 2. 3-Hydroxyflavones and products in the oxidations of 3-hydroxyflavones with lead(IV) acetate and manganese(III) acetate.

Table 1. The reactions of 3-hydroxyflavones with lead(IV) acetate and manganese(III) acetate[a]

Substrate	Oxidant	Products (yield/%[b])								
		2	**3**	**4**	**5**	**6**	**7**	**8**	**9**	**10**
1a	$Pb(OAc)_4$	2	6	2			78	56		
1b	$Pb(OAc)_4$	13	1					17	56	
1c	$Pb(OAc)_4$	7	8	3			59			59
1d	$Pb(OAc)_4$	16							47	19
1a	$Mn(OAc)_3$	4					42	21		
1b	$Mn(OAc)_3$	1						29	14	
1c	$Mn(OAc)_3$	8			4	3	16			34
1d	$Mn(OAc)_3$	2							44	25

a) The reactions were carried out in acetic acid at the reflux temperature. b) Yields are based on the amount of 3-hydroxyflavone consumed. c) The yields of carboxylic acids (**7**, **8**, **9**, and **10**) are estimated from the NMR spectra.

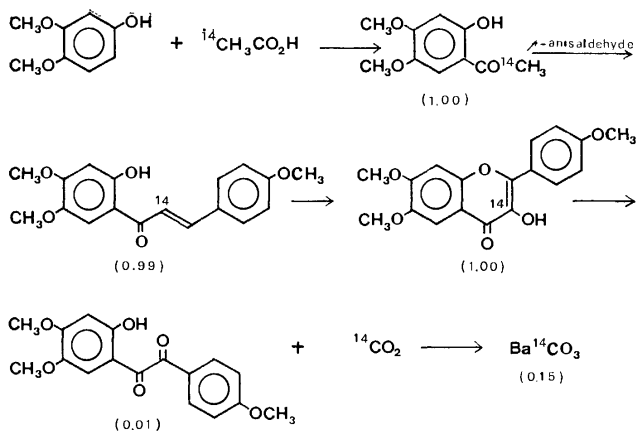

Scheme 3. Synthesis and the oxidation of 3-hydroxy-4′,6,7-trimethoxyflavone-3-^{14}C (the figures under the formulae refer to the specific radioactivities of the compounds relative to the acetophenone).

is transformed into 1,2-diphenyl-2-hydroxyethanone, with is then oxidized to 1,2-dipehnylethanedione. However, it is still possible to assume another reaction pathway in which an open-chain triketone (**11**), formed from 3-hydroxyflavone by the oxidation, could give rise to 1,2-diphenylethanedione by decarbonylation.[5]

Experimental

All the ^1H NMR spectra were recorded for the deuteriochloroform solution with a Hitachi-Perkin-Elmer R 24 NMR spectrometer, with tetramethylsilane as the internal reference. The IR spectra were recorded for the chloroform solution with a JASCO IRA-1 grating spectrometer, while the mass spectra were measured with a Hitachi RMU-6M mass spectrometer. The melting points were determined with a Yanagimoto hot-stage apparatus and were not corrected. The radioactivities were recorded, for samples crystallized to a constant specific radioactivity, with an Aloka liquid scintillation spectrometer. The scintillator consisted of 0.4% DPO and 0.01% POPOP (Dojin Laboratories, Kumamoto) dissolved in toluene. Barium carbonate samples were suspended in a gel made up with 4% w/v CAB-O-SIL (Beckmann Instruments, Inc., U.S.A.). Sample counts were repeated twice; the maximum observed error was within 0.5%.

3-Hydroxyflavones. The 3-hydroxyflavones (**1a**—**d**) were prepared by the literature methods.[6,7]

Oxidation of 3-Hydroxyflavones with Lead(IV) Acetate. A typical procedure for the oxidation of 3-hydroxyflavones was as follows. To a 3-hydroxyflavone (500 mg) dissolved in boiling acetic acid (30 ml), lead(IV) acetate (2.0 equivalents) was added. After the removal of the acetic acid *in vacuo*, the residue was treated with 2 M hydrochloric acid (60 ml) and extracted with chloroform (100 ml). The chloroform solution was washed with an aqueous sodium hydrogencarbonate solution (100 ml) three times and then evaporated. The aqueous sodium hydrogencarbonate solution was acidified, and subsequent extraction with chloroform gave acidic products. The neutral products were separated on TLC, with chloroform as the developing solvent. The acidic products were identified by a comparison of their retention times as methyl esters and their NMR spectra with those of the authentic samples.

*Oxidation Products of 3-Hydroxy-7-methoxyflavone (**1a**).* *1-(2-Hydroxy-4-methoxyphenyl)-2-phenylethanedione (**2a**)*: Mp 82—83 °C (ethanol) (Found: C, 70.18; H, 4.73%. Calcd for $C_{15}H_{12}O_4$: C, 70.30; H, 4.72%); IR 1695 and 1635 cm^{-1}; NMR δ=11.82 (1H, s, OH), 7.9—8.1 (2H, m), 7.3—7.7 (4H, m), 6.3—6.6 (2H, m), and 3.85 (3H, s, OCH_3); MS *m/e*=151, 123, 105, and 77.

*2-Hydroxy-1-(2-hydroxy-4-methoxyphenyl)-2-phenylethanone (**3a**)*: Mp 75—76 °C (ligroin) (Found: C, 69.56; H, 5.44%. Calcd for $C_{15}H_{14}O_4$: C, 69.75; H, 5.46%); IR 1640 and 3460 cm^{-1}; NMR δ=12.05 (1H, s, OH), 7.50 (1H, d, *J*=8 Hz), 7.31 (5H, s, Ph), 6.15—6.5 (2H, m), 5.85 (1H, s), 4.3 (1H, broad s), and 3.75 (3H, s, OCH_3); MS *m/e*=151, 123, 107, and 77.

*3-Acetoxy-7-methoxyflavone (**4a**)*: Mp 172—174 °C (ethanol) (lit,[5] mp 176 °C).

*2-Hydroxy-4-methoxybenzoic Acid (**7**) and Benzoic Acid (**8**). Oxidation Products of 6,7-Dimethoxy-3-hydroxyflavone (**1b**).* *1-(4,5-Dimethoxy-2-hydroxyphenyl)-2-phenylethanedione (**2b**)*: Mp 171.5—172 °C (ethanol) (Found: C, 66.97; H, 5.04%. Calcd for $C_{16}H_{14}O_5$: C, 67.12; H, 4.93%); IR 1690 and 1630 cm^{-1}; NMR δ=11.83 (1H, s, OH), 7.9—8.15 (2H, m), 7.3—7.7 (3H, m), 6.82 (1H, s), 6.56 (1H, s), 3.97 (3H, s, OCH_3), and 3.70 (3H, s, OCH_3); MS *m/e*=181, 153, 105, and 77.

*1-(4,5-Dimethoxy-2-hydroxyphenyl)-2-hydroxy-2-phenylethanone (**3b**)*: Mp 133—135 °C (ligroin); IR 1630 and 3440 cm^{-1}; NMR δ=11.94 (1H, s, OH), 7.35 (5H, s, Ph), 6.79 (1H, s), 6.4 (1H, s), 5.8 (1H, s), 4.45 (1H, broad s), 3.87 (3H, s, OCH_3), and 3.65 (3H, s, OCH_3).

*4,5-Dimethoxy-2-hydroxybenzoic Acid (**9**) and Benzoic Acid (**8**). Oxidation Products of 4′,7-Dimethoxy-3-hydroxyflavone (**1c**).* *1-(2-Hydroxy-4-methoxyphenyl)-2-(4-methoxyphenyl) ethanedione (**2c**)*: Mp 99—101 °C (ethanol) (Found: C, 66.92; H, 4.90%. Calcd for $C_{16}H_{14}O_5$: C, 67.12; H, 4.93%).

*2-Hydroxy-1-(2-hydroxy-4-methoxyphenyl)-2-(4-methoxyphenyl)-ethanone (**3c**)*: Mp 111—113 °C (ligroin) (Found: C, 66.41; H, 5.51%. Calcd for $C_{16}H_{16}O_5$: C, 66.66; H, 5.59%).

*3-Acetoxy-4′,7-dimethoxyflavone (**4c**)*: Mp 188—190 °C (lit,[7] mp 190 °C) (ethanol).

*p-Anisic Acid (**10**) and 2-Hydroxy-4-methoxybenzoic Acid (**7**). Oxidation Products of 3-Hydroxy-4′,6,7-trimethoxyflavone (**1d**).* *1-(4,5-Dimethoxy-2-hydroxyphenyl)-2-(4-methoxyphenyl)ethanedione (**2d**)*: Mp 129—131 °C (ethanol) (Found: C, 64.35; H, 5.15%. Calcd for $C_{17}H_{16}O_6$: C, 64.55; H, 5.10%); IR 1680 and 1630 cm^{-1}; NMR δ=11.85 (1H, s, OH), 7.96 (2H, m), 6.98 (2H, m), 6.86 (1H, s), 6.53 (1H, s), 3.92 (3H, s, OCH_3), 3.87 (3H, s, OCH_3), and 3.70 (3H, s, OCH_3).

*3,4-Dimethoxy-2-hydroxybenzoic Acid (**9**) and p-Anisic Acid (**10**)*: Mp 185 °C.

Oxidation of 3-Hydroxyflavones with Manganese(III) Acetate. A typical procedure for the oxidation of 3-hydroxyflavones with manganese(III) acetate was as follows. A mixture of a 3-hydroxyflavone (500 mg), manganese(III) acetate[8] (3.8 equivalents), and acetic acid (30 ml) was heated under reflux for several minutes. After the subsequent removal of the acetic acid *in vacuo*, the residue was extracted with chloroform and separated in the manner described previously. **1a** gave **2a**, **7**, and **8**. **1b** yielded **2b**, **8**, and **9**. **1c** gave **2c**, 6-methoxy-2-(4-methoxybenzoyloxy)-3(2*H*)-benzofuranone (**5**); mp 163—164.5 °C (ethanol) (Found: C, 64.91; H, 4.60%. Calcd for $C_{17}H_{14}O_6$: C, 64.96; H, 4.49%); IR 1745 cm^{-1}; NMR δ=8.09 (2H, m), 7.69 (1H, d), 6.95 (2H, m), 6.53—6.84 (2H, m), 6.50 (1H, s), 3.94 (3H, s, OCH_3), and 3.92 (3H, s, OCH_3); MS *m/e*=285, 179, 163, 151, 135, and 107, 2-hydroxy-4-methoxybenzaldehyde (**6**), mp 41 °C, **7**, and **10**. **1d** yielded **2d**, **9**, and **10**.

*1-(2-Benzyloxy-4-methoxyphenyl)-2-(4-methoxyphenyl)ethanedione (**2e**).* A mixture of 2′-benzyloxy-4,4′-dimethoxy-

chalcone[9] (1 g), thallium(III) nitrate (3.2 g), methanol (6 ml), and 35% perchloric acid (3 ml) was stirred at room temperature for 2 h. Water (150 ml) was added to the reaction mixture, and then the mixture was extracted with chloroform (30 ml). After the removal of the chloroform, the resulting substance was purified by TLC, with chloroform as the developing solvent, to give **2e**; mp 114—119 °C (ethanol) (360 mg, 36%) (Found: C, 73.14; H, 5.30%. Calcd for $C_{23}H_{20}O_5$: C, 73.39; H, 5.36%); IR 1680 cm^{-1}; NMR δ=8.02 (1H, d, J=9 Hz), 7.62 (2H, m), 6.77 (2H, m), 6.9—7.2 (5H, m), 6.4—6.73 (2H, m), 4.85 (2H, s, $-CH_2-$), and 3.80 (6H, s, $2\times OCH_3$).

Debenzylation of 2e. **2e** (50 mg) was added to a mixture of 35% perchloric acid (10 ml) and methanol (16 ml), and the mixture was heated under reflux for 2.5 h. After the removal of the methanol *in vacuo*, the residue was extracted with chloroform (60 ml) and purified on TLC to give **2c**; mp 99—101 °C (ethanol) (34 mg, 89%).

4',5'-Dimethoxy-2'-hydroxyacetophenone-2-^{14}C. A mixture of 3,4-dimethoxyphenol (10.6 g), a boron trifluoride–acetic acid complex (13 g), and sodium acetate-2-^{14}C (250 μCi, Radiochemical Center, Amersham, England) was heated at 100 °C for 25 min. The reaction mixture was then poured into 2 M hydrochloric acid (150 ml). The insoluble materials were dissolved in methanol, and the methanol solution was then added to the acid solution. After the removal of the methanol, the residue was extracted with benzene and the benzene solution was purified by means of a silica column yielding 4',5'-dimethoxy-2'-hydroxyacetophenone-2-^{14}C; mp 112—113 °C (6.85 g; 54%; specific radioactivity, 1.50 μCi/mmol).

2'-Hydroxy-4,4',5'-trimethoxychalcone-α-^{14}C. A mixture of 4',5'-dimethoxy-2'-hydroxyacetophenone-2-^{14}C (6.3 g), *p*-anisaldehyde (5.0 g), 40% aqueous potassium hydroxide (50 ml), and ethanol (50 ml) was stirred at room temperature for 2 h. The reaction mixture was then poured into cold hydrochloric acid, and the precipitates were collected. These precipitates gave 2'-hydroxy-4,4',5'-trimethoxychalcone-α-^{14}C; mp 133—135 °C (ethanol) (1.64 g; 14.3%; specific radioactivity, 1.48 μCi/mmol).

3-Hydroxy-4',6,7-trimethoxyflavone-3-^{14}C. To a mixture of 2'-hydroxy-4,4',5'-trimethoxychalcone-α-^{14}C (1.54 g), 22% aqueous potassium hydroxide (30 ml), and ethanol (90 ml), we added cold 15% hydrogen peroxide (20 ml). The reaction mixture was allowed to react for two days and then poured into 2 M hydrochloric acid. The precipitates were collected and recrystallized, giving 3-hydroxy-4',6,7-trimethoxyflavone-3-^{14}C, mp 229.5—230 °C (ethanol) (740 mg; 47%; specific radioacitivity, 1.49 μCi/mmol).

Oxidation of 3-Hydroxy-4',6,7-trimethoxyflavone-3-^{14}C *with Lead-(IV) Acetate.* To 3-hydroxy-4',6,7-trimethoxyflavone-3-^{14}C (250 mg) dissolved in boiling acetic acid (30 ml), lead(IV) acetate (676 mg) was added under a nitrogen stream, after which the reaction mixture was worked-up in a manner described previously, giving 1-(4,5-dimethoxy-2-hydroxyphenyl)-2-(4-methoxyphenyl)ethanedione (**2d**) (mp 128—130 °C (ethanol) (10 mg; 4.2%; specific radioactivity, 0.02 μCi/mmol)), carbon dioxide, which was later converted to barium carbonate (142 mg; 95%; specific radioactivity, 0.23 μCi/mmol), and *p*-anisic acid (**10**) (mp 185 °C (water) (40 mg; 28%; specific radioactivity, 0.01 μCi/mmol)).

The authors wish to thank Dr. Naotake Ogawa, Department of Pharmacology, Kumamoto University, for his kind assistance in the measurements of the radioactivities.

References

1) K. Kurosawa and A. Moriyama, *Bull. Chem. Soc. Jpn.*, **47**, 2717 (1974).
2) K. Ezoe and K. Kurosawa, *Bull. Chem. Soc. Jpn.*, **50**, 443 (1977).
3) A. McKillop, P. Swann, M. E. Ford, and E. C. Taylor, *J. Am. Chem. Soc.*, **95**, 3641 (1973).
4) K. Ichikawa and Y. Takeuchi, *Nippon Kagaku Zasshi*, **79**, 1060 (1958).
5) J. D. Roberts, D. R. Smith, and C. C. Lee, *J. Am. Chem. Soc.*, **73**, 618 (1951).
6) St. v. Kostanecki and M. L. Stoppani, *Ber.*, **37**, 1180 (1904).
7) G. Bargellini and G. B. Marini-Bettolo, *Gazz. Chim. Ital.*, **70**, 170 (1940).
8) P. J. Andrulis, Jr., M. J. S. Dewar, R. Dietz, and R. L. Hunt, *J. Am. Chem. Soc.*, **88**, 5473 (1966).
9) K. Juppen and St. v. Kostanecki, *Ber.*, **37**, 4161 (1904)

Conversion of Carbon–Sulfur Linkages into Carbon–Silicon Ones *via* Reductive Silylation. Preparation of Silyl Enol Ethers of Acyltrimethylsilanes[1)]

Isao KUWAJIMA,* Akio MORI, and Masahiro KATO
Department of Chemistry, Tokyo Institute of Technology, Ookayama, Meguro-ku, Tokyo 152
(Received February 8, 1980)

Reductive cleavage of carbon–sulfur linkages of silyl enol ethers of thiocarboxylic *S*-esters can be induced by treatment with sodium or potassium–sodium alloy in the presence of chlorotrimethylsilane, and the corresponding silyl enol ethers of acyltrimethylsilanes can be prepared in high yields.

Various organosilicon compounds have recently been employed as useful intermediates in a wide range of synthetic organic chemistry.[2)] Acyltrimethylsilanes were initially prepared from an interest of their unique spectral properties. However, it has recently been found that they have interesting properties as synthetic intermediates.[3)] Compounds of this type are usually prepared by silylation of various acyl anion equivalents,[4)] appropriate 1-trialkylsilyl-1-alkanol derivatives also being employed for their preparation.[5,6)] This paper describes a new approach to the generation of acyl anion equivalents from silyl enol ethers of thiocarboxylic *S*-esters, by which acyltrimethylsilanes can be prepared as their silylated enols.

Reductive silylation of unsaturated organic compounds[7)] with alkali metal, *e.g.* sodium or potassium–sodium alloy, has been found to be a most useful method for the synthesis of organosilicon compounds.[8)] Carbon–sulfur linkages undergo cleavage with metallic lithium in the presence of an appropriate proton source. Such a procedure has frequently been employed for removal of sulfur group from various sulfides.[9)] It was thus expected that treatment of sulfides with alkali metal and chlorotrimethylsilane would make it possible to convert the carbon–sulfur linkages into the corresponding carbon–silicon ones through silylation of the initially generated carbanionic species. Such a transformation has recently been reported by using alkyl phenyl sulfides.[10,11)]

Studies were carried out on the application of this procedure to the synthesis of silyl enol ethers of acyltrimethylsilanes **1**, used also for the preparation of parent acyltrimethylsilanes and their α-functionalized derivatives.[12)] Silyl enol ethers **3** of thiocarboxylic *S*-esters were prepared by treating the corresponding esters **2** with lithium diisopropylamide (LDA) and then with chlorosilane.[13)] Of the esters examined, succinic and glutaric esters gave no silyl enol ethers because of a facile intramolecular cyclization reaction of the ester enolate anion generated initially. Except for the above cases, various *S*-methyl and *S*-phenyl esters gave the desired silylated enols **3** in excellent yields.

A preliminary study on the effect of substituent on thiocarboxylic acid in the reductive silylation has been carried out by using the silylated enols of *S*-methyl, *S*-ethyl, and *S*-phenyl 3-phenylpropanethioates **3**. From the results, enols of *S*-methyl ester **3** ($R^1=C_6H_5CH_2$, $R^2=H$, $R=CH_3$) and of *S*-phenyl ester **3** ($R^1=C_6H_5CH_2$, $R^2=H$, $R=C_6H_5$) were found to undergo the expected reductive silylation to afford the corresponding silyl enol ether **1** ($R^1=C_6H_5CH_2$, $R^2=H$) in good yields, while that of *S*-ethyl ester **3** ($R^1=C_6H_5CH_2$, $R^2=H$, $R=C_2H_5$) was almost inert under similar reaction conditions. In the reaction with *S*-phenyl ester derivative, (phenylthio)trimethylsilane was also formed as one of the side-products, which decreased through its conversion into phenyltrimethylsilane on prolonged reaction period. On the effect of the substituent on sulfur atom in reactions of this type, the following unique features of methyl and phenyl groups have been observed. (1) In the reductive silylation of sulfides, alkyl phenyl sulfides usually undergo a facile bond cleavage between alkyl and sulfur to give alkyltrimethylsianes together with (phenylthio)trimethylsilane, but not dialkyl sulfides.[10)] (2) In the reaction with disulfides, dialkyl and diphenyl disulfides afford the corresponding thiosilanes, but dimethyl disulfide gives bis(trimethylsilyl) sulfide exclusively.[11)]

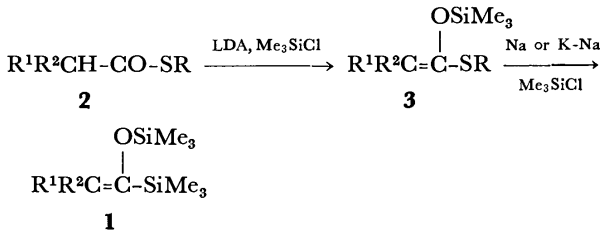

Scheme 1.

The results indicate that the phenylthio group might enhance the cleavage of another bond with sulfur of **3**, giving the corresponding carbanionic species **4** directly. On the other hand, in the reactions with the *S*-methyl ester derivative, the linkage between sulfur and methyl seems to be cleaved preferentially to the bond of sulfur with the vinyl group of **3**. 1-Trimethylsiloxy-1-trimethylsilylthio-1-alkene **5** appears to be generated as an initial intermediate and then converted into the silylated enol **1** through the bond scission between sulfur and the vinyl group. This was confirmed by the following controll experiments. Treatment of **3** ($R^1=C_6H_5CH_2$, $R^2=H$, $R=CH_3$) with 5 equiv of potassium–sodium alloy in the presence of chlorotrimethylsilane, followed by aqueous work-up of the reaction mixture gave rise to the formation of the corresponding thiocarboxylic acid **6** as a major product (66%) together with **1** ($R^1=C_6H_5CH_2$, $R^2=H$) (29%), while the reaction with 8 equiv of the same reducing agent afforded **1** ($R^1=C_6H_5CH_2$, $R^2=$

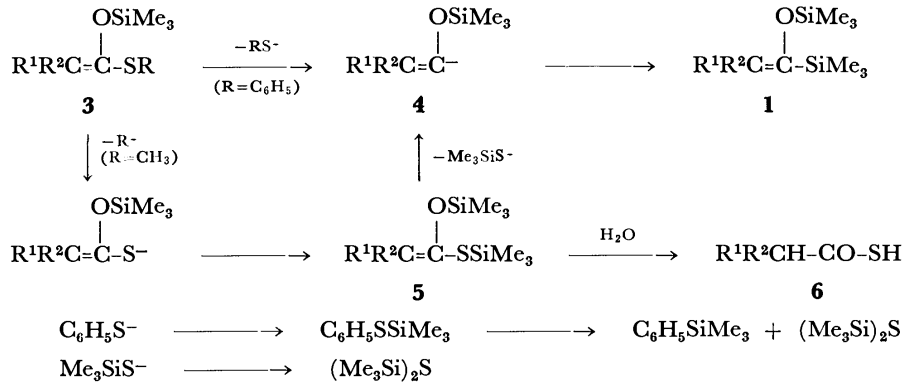

Scheme 2.

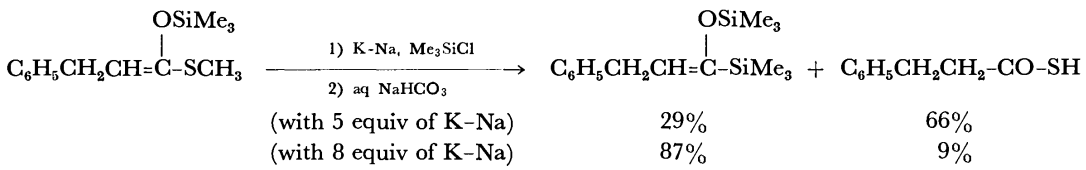

(1)

Table 1. Preparation of trimethylsilyl enol ethers of thiocarboxylic *S*-esters **3**

R^1	R^2	R	Yield (%)	Bp (°C/mmHg)[a]	Anal. (*m/e*)
CH_3	H	CH_3	83	110—112/102	Found: 176.0680. Calcd for $C_7H_{16}OSSi$: M, 176.0691.
CH_3	CH_3	CH_3	86	102—103/55	Found: 190.0822. Calcd for $C_8H_{18}OSSi$: M, 190.0848.
C_4H_9	H	CH_3	91	128—130/33	Found: 218.1143. Calcd for $C_{10}H_{22}OSSi$: M, 218.1161.
C_4H_9	H	C_6H_5	95	104—105/0.5	Found: 280.1333. Calcd for $C_{15}H_{24}OSSi$: M, 280.1317.
C_6H_{13}	H	C_6H_5	96	109—112/0.1	Found: 308.1609. Calcd for $C_{17}H_{28}OSSi$: M, 308.1630.
C_8H_{17}	H	C_6H_5	96	152—154/0.75	Found: 336.1928. Calcd for $C_{19}H_{32}OSSi$: M, 336.1943.
$C_6H_5CH_2$	H	CH_3	93	115—116/6	Found: 252.0988. Calcd for $C_{13}H_{20}OSSi$: M, 252.1004.
$C_6H_5CH_2$	H	C_6H_5	92	123—125/0.13	Found: 314.1140. Calcd for $C_{18}H_{22}OSSi$: M, 314.1161.
CH_2=CH$(CH_2)_7$-	H	C_6H_5	92	135—138/0.15	Found: 348.1931. Calcd for $C_{20}H_{32}OSSi$: M, 348.1943.
-$(CH_2)_5$-		C_6H_5	92	90—91/0.08	Found: 292.1331. Calcd for $C_{16}H_{24}OSSi$: M, 292.1317.
C_2H_5O	H	CH_3	85	110—112/35	Found: 206.0782. Calcd for $C_8H_{18}O_2SSi$: M, 206.0797.
$CH_3C(C_2H_4O_2)CH_2$	H	C_6H_5	91	123—125/10	Found: 324.1231. Calcd for $C_{16}H_{24}O_3SSi$: M, 324.1215.
CH_3S	H	CH_3	90	97—99/10	Found: 208.0430. Calcd for $C_7H_{16}OS_2Si$: M, 208.0412.
C_2H_5S	H	CH_3	92	128—130/23	Found: 222.0552. Calcd for $C_8H_{18}OS_2Si$: M, 222.0568.

a) 1 mmHg = 133.322 Pa.

H) in 87% yield accompanied by thiocarboxylic acid **6** (9%) under similar reaction conditions.

The phenylthio and trimethylsilylthio groups seem to make the cleavage of the bond between sulfur and 1-(trimethylsiloxy)vinyl group feasible, but neither ethylthio and its homologs.

Excess amount of the reducing agent should be used in order to achieve the transformation. Otherwise, the starting material is recovered in the reaction with *S*-phenyl ester derivative **3** (R=C_6H_5), or the corresponding thiocarboxylic acid is obtained in the case with *S*-methyl ester derivative **3** (R=CH_3) in a large amount, although theoretically required amounts should be 4 equiv of the reducing agent to 1 equiv of **3** even if the reaction proceeds through an initial removal of R groups of **3**. This is a great difference from acyloin condensation, which usually proceeds with almost stoichiometric amount of the reducing agent.[7a] We have used 8—9 equiv of sodium dispersion or potassium–sodium alloy to achieve an efficient conversion into **1**.

With sodium dispersion prepared by heating in tolune or xylene, the results are sometimes irreproducible probably because of the difference in the grade of dispersion of the reducing agent. Use of commercial sodium dispersion[14] could eliminate such difficulties to give the desired silylated enol **1** over 80% yields. The usual potassium–sodium alloy can advatageously be used, especially for large scale preparation, to give slightly higher yields in comparison with the commercial sodium dispersion.

As a solvent, benzene is preferable to tetrahydrofuran or ether. Some unidentified products are formed in noticeable amount when tetrahydrofuran is used.

When start from *S*-phenyl ester derivative **3**, (phenylthio)trimethylsilane and phenyltrimethylsilane were also formed as by-products, sometimes making it difficult to separate the desired silyl enol ether **1** by distillation.

In such a case, *S*-methyl ester derivative **3** (R=CH_3) would be preferable since the side-product, bis(trimethylsilyl) sulfide, can be removed by a simple hydrolytic work-up of the reaction mixture. A small amount of 1-trimethylsiloxy-1-trimethylsilylthio-1-alkene **5** sometimes still remains in the reaction mixture, but it can be removed by treatment with aq $NaHCO_3$ solution. GLPC and NMR analyses of the resulting crude mixtures show that they are pure enough for further synthetic use without purification. For example, acidic hydrolysis[5a,e] or treatment with chlorine [12a] affords the corresponding acyltrimethylsilane or its α-chlorinated derivative almost quantitatively.

Some functional groups are compatible with the present procedure (Table 2), no difficulty being encountered in the reductive silylation of the *S*-phenyl or *S*-methyl ester derivative **3** having olefinic or acetal group.

With the α-alkoxy derivative of **3**, a side reaction such as β-elimination of the intermediate **4** into the corresponding acetylenic ether might be expected. However, from a starting material such as **3** (R^1=

Table 2. Preparation of 1-trimethylsilyl-1-trimethylsiloxy-1-alkenes **1**[a]

R^1	R^2	Bp(°C/mmHg)[b]	Yield(%)	IR(neat) cm^{-1}; NMR[c] (CCl_4) δ; Elemental analyses %
CH_3	H	100—104/100	74[d]	1620, 1250, 1150, 850; 0.06(s, 9H), 0.13(s, 9H), 1.58(d, J=7 Hz, C<u>H</u>$_3$CH=C), 1.63(d, J=7 Hz, C<u>H</u>$_3$CH=C), 5.05 (q, J=7 Hz, CH_3C<u>H</u>=C), 5.43(q, J=7 Hz, CH_3C<u>H</u>=C); Found: C, 53.22; H, 10.81. Calcd for $C_9H_{22}OSi_2$: C, 53.40; H, 10.95.
CH_3	CH_3	82—83/18	81[d]	1610, 1250, 1125, 840; 0.20(s, 9H), 0.28(s, 9H), 1.65(s, 3H), 1.77(s, 3H); Found: C, 55.63; H, 11.02. Calcd for $C_{10}H_{24}OSi_2$: C, 55.47; H, 11.18.
C_4H_9	H	70—72/7	87[d] 87[e]	1605, 1250, 1115, 840; 0.10(s, 9H), 0.13(s, 9H), 0.70—1.50(m, 7H), 1.75—2.25(m, 2H), 4.85(t, J=7 Hz, CH_2C<u>H</u>=C), 5.28(t, J=7 Hz, CH_2C<u>H</u>=C); Found: C, 59.21; H, 11.77. Calcd for $C_{12}H_{28}OSi_2$: C, 58.94; H, 11.54.
C_6H_{13}	H	119—120/12	82[e]	1607, 1250, 1110, 840; 0.13(s, <u>Me</u>$_3$Si), 0.23(s, <u>Me</u>$_3$Si), 1.00 (t, J=3 Hz, 3H), 1.38(s, 8H), 1.80—2.33(m, 2H), 5.03(t, J=6 Hz, 1H); Found: C, 61.74; H, 11.79. Calcd for $C_{14}H_{32}OSi_2$: C, 61.69; H, 11.61.
C_8H_{17}	H	93—95/0.7	94[e]	1610, 1250, 1100, 850; 0.17(s, 9H), 0.26(s, 9H), 1.00(t, J=4 Hz, 3H), 1.32—1.71(m, 12H), 1.86—2.47(m, 2H), 5.02(t, J=7 Hz, 1H); Found: C, 64.09; H, 12.29. Calcd for $C_{16}H_{36}OSi_2$: C, 63.92; H, 12.07.
$C_6H_5CH_2$	H	90—92/0.25	87[d] 84[d,f] 82[e]	1590, 1245, 1115, 840; 0.15(s, 9H), 0.18(s, 9H), 3.27(d, J=8 Hz, C<u>H</u>$_2$CH=C), 3.40(d, J=6.5 Hz, C<u>H</u>$_2$CH=C), 5.10 (t, J=6.5 Hz, CH_2C<u>H</u>=C), 5.48(t, J=8 Hz, CH_2C<u>H</u>=C), 7.08(s, 5H); Found: C, 64.80; H, 9.34. Calcd for $C_{15}H_{26}OSi_2$: C, 64.68; H, 9.41.
CH_2=CH$(CH_2)_7$	H	135—138/0.15	88[e]	1639, 1609, 1250, 1110, 850; 0.20(s, 18H), 1.39(s, 10H), 1.89—2.27(m, 4H), 4.87—5.23(m, 2H), 5.55—5.97 (m, 2H); Found: C, 65.28; H, 11.63. Calcd for $C_{17}H_{36}OSi_2$: C, 65.31; H, 11.61.
-$(CH_2)_5$-		100—102/10	88[e]	1610, 1250, 1120, 850; 0.16(s, 18H), 1.17—1.86(m, 6H), 2.00—2.50(m, 4H); Found: C, 61.03; H, 11.23. Calcd for $C_{13}H_{28}OSi_2$: C, 60.87; H, 11.00.
C_2H_5O	H	80—82/28	70[d]	1626, 1245, 1150, 1110, 845; 0.18(s, 18H), 1.07(t, J=7 Hz, C<u>H</u>$_3$CH$_2$O), 1.12(t, J=7 Hz, C<u>H</u>$_3$CH$_2$O), 3.45(q, J=7 Hz, CH_3C<u>H</u>$_2$O), 3.55(q, J=7 Hz, CH_3C<u>H</u>$_2$O), 5.27(s, C<u>H</u>=C), 6.20(s, C<u>H</u>=C); Found: C, 51.80; H, 10.53. Calcd for $C_{10}H_{24}O_2Si_2$: C, 51.65; H, 10.41.
$CH_3C(C_2H_4O_2)CH_2$	H	87—89/1.5	82[d]	1600, 1245, 840; 0.05(s, 9H), 0.13(s, 9H), 1.17(s, 3H), 2.22(d, J=7 Hz, C<u>H</u>$_2$CH=C), 2.27(d, J=7 Hz, C<u>H</u>$_2$CH=C), 3.72(s, 4H), 4.98(t, J=7 Hz, CH_2C<u>H</u>=C); Found: C, 54.32; H, 9.95. Calcd for $C_{13}H_{28}O_3Si_2$: C, 54.12; H, 9.78.

a) All reactions were carried out in 10 mmol scale unless otherwise stated. b) 1 mmHg=133.322 Pa. c) Values obtained by using benzene or dichloromethane as an internal standard. d) Reactions carried out with the *S*-methyl ester derivative **3** by using potassium-sodium alloy. e) Reactions carried out with the *S*-phenyl ester derivative **3** by using commercial sodium dispersion. f) Reaction carried out in 0.1 mol scale.

OC_2H_5, R^2=H, R=CH_3), the corresponding silyl enol ether **1** (R^1=OC_2H_5, R^2=H) could be obtained satisfactorily, the yield decreasing slightly.

In contrast, with the α-alkylthio or α-phenylthio derivative **3**, β-elimination seems to take place from the intermediate **4** predominantly, no corresponding product being isolated. The solution usually turns dark purple during the course of reductive silylation, but in these cases such kind of color change has never been observed.

In contrast to the inert behavior of dialkyl sulfides to the present reducing system, various thioacetals appear to undergo a facile bond cleavage between carbon and sulfur, and the reaction with *S*-methyl ester derivative **3** having diethyl thioacetal or ethylene thioacetal group resulted in the formation of complex mixtures.

Experimental

All boiling points are uncorrected. IR spectra were recorded on a Hitachi 260-10 spectrometer, and NMR spectra on a Hitachi R-24B spectrometer using dichloromethane or benzene as an internal standard.

Materials. Tetrahydrofuran (THF) and benzene were purified shortly before use by drying and distillation over sodium-benzophenone or sodium. Chlorotrimethylsilane was purified by distillation over sodium wire. Thiocarboxylic *S*-phenyl esters were prepared by treating the corresponding acyl chlorides with benzenethiol in the presence of triethylamine in ether. *S*-Methyl esters were prepared by treating dichloromethane solution of the corresponding acyl chlorides with aqueous solution of sodium methanethiolate in the presence of tetrabutylammonium bromide.

Preparation of Trimethylsilyl Enol Ethers of Thiocarboxylic S-Esters **3**. *General Procedure*: Lithium diisopropylamide (LDA) was prepared by treating diisopropylamine (2.47 g, 24.5 mmol) and butyllithium (14.9 ml of 1.64 molar hexane solution, 24.5 mmol) in tetrahydrofuran at −78 °C under argon atmosphere. An appropriate thiocarboxylic *S*-ester (20 mmol) in tetrahydrofuran (10 ml) was added over a period of 10 min to the resulting LDA solution at −78 °C. After further addition of chlorotrimethylsilane (3.26 g, 30 mmol) for 1 min, the resulting mixture was warmed up to room temperature and stirred at that temperature for 2h. The solvent was then removed *in vacuo* and the remaining residue diluted with hexane (20 ml). The salt deposited was filtered off by means of a hyflo super cell. Removal of the solvent from the filtrate followed by fractional distillation afforded the corresponding silyl enol ether **3**. Elementary compositions of the products were determined by means of high mass spectra with use of a Hitachi RMU-7M mass spectrometer. The results are given in Table 1.

Preparation of Trimethylsilyl Enol Ethers of Acyltrimethylsilanes. **1** *(A) Reductive Silylation of* **3** *with Sodium Dispersion and Chlorotrimethylsilane*: Sodium dispersion[14] (3.68 g of 50% paraffin contained, 0.08 g atom) was washed three times with hexane (10 ml) and once with benzene (10 ml). It was then mixed with benzene (35 ml) and introduced into a flask filled with argon with a hypodermic syringe. Chlorotrimethylsilane (8.68 g, 80 mmol) was then added. To the resulting solution was added a benzene (15 ml) solution of an appropriate silyl enol ether **3** (10 mmol) during the course of 10 min. After addition was complete, the reaction mixture was heated to refluxing for 2 h. The reaction mixture was filtered through the hyflo super cell and the filtrate concentrated *in vacuo*. The residual oil was washed with 1:1 aqueous tetrahydrofuran (10 ml) solution of satd sodium hydrogencarbonate, and extracted with hexane (20 ml). After drying over anhydrous Mg_2SO_4, removal of the solvent followed by fractional distillation gave the trimethylsilyl enol ether of the corresponding acyltrimethylsilane **1**. The results are given in Table 2.

Preparation of Trimethylsilyl Enol Ethers of Acyltrimethylsilanes **1**. *(B) Reductive Silylation of* **3** *with Potassium–Sodium Alloy and Chlorotrimethylsilane*: The alloy was prepared by heating a mixture of metallic potassium (1.56 g, 0.04 g atom) and sodium (0.92 g, 0.04 g atom) in a flask filled with argon To this was added a benzene (35 ml) solution of chlorotrimethylsilane (8.68 g, 80 mmol). To the resulting solution was added an appropriate trimethylsilyl enol ether of thiocarboxylic *S*-ester **3** (10 mmol) in benzene (15 ml) at room temperature over a period of 10 min. Gentle refluxing took place immediately. After addition was complete, the reaction mixture was stirred at room temperature for 4.5 h. The reaction mixture was then treated in a similar way to that described above, the trimethylsilyl enol ether of the corresponding acyltrimethylsilane **1** being obtained (Table 2).

Controll Experiment. The reaction was carried out with the silyl enol ether of *S*-methyl 3-phenylpropanethioate **3** (R^1=$C_6H_5CH_2$, R^2=H, R=CH_3) (2.53 g, 10 mmol) by using potassium (0.975 g, 0.025 g atom) and sodium (0.575 g, 0.025 g atom) in a similar way to that described in procedure (B). The reaction mixture was filtered off and the solvent was removed *in vacuo*. The residual oil was washed with 1:1 aqueous tetrahydrofuran (10 ml) solution of satd $NaHCO_3$ and extracted with hexane. From the extracts, 1-trimethylsiloxy-1-trimethylsilyl-3-phenyl-1-propene (0.817 g, 29%) was isolated by fractional distillation. The aqueous layer was acidified with dil HCl and extracted three times with ether (10 ml). Removal of the solvent followed by bulb-to-bulb distillation afforded 3-phenylpropanethiocarboxylic acid (1.101 g, 66%). The product was identified by the following spectral data. IR (neat); 2525, 1685, and 1055 cm^{-1}. NMR (CCl_4); δ 2.78 (s, 4H, $C_6H_5C\underline{H_2}$-$C\underline{H_2}CO$–), 4.23 (s, 1H, –S<u>H</u>), and 7.02 (s, 5H, aromatic protons). MS; M^+ 166

References

1) A preliminary report dealing with certain aspects of this work: I. Kuwajima, M. Kato, and T. Sato, *J. Chem. Soc., Chem. Commun.*, **1978**, 478.

2) a) I. Flemming, *Chem. Ind. (London)*, **1976**, 449; b) P. F. Hudrlick, "New Application of Organometallic Reagents in Organic Synthesis," ed by D. Seyferth, J. Organomet. Chem. Library, Elsevier, Amsterdam (1976), Vol. 1, p. 127; c) J. K. Rasmussen, *Synthesis*, **1977**, 91; d) E. W. Colvin, *Chem. Soc. Rev.*, **7**, 15 (1978).

3) I. Kuwajima, K. Atsumi, T. Tanaka, and T. Inoue, *Chem. Lett.*, **1979**, 1239; I. Kuwajima and M. Kato, *J. Chem. Soc., Chem. Commun.*, **1979**, 708; H, J. Reich, J. J. Rusek, and R. E. Olson, *J. Am. Chem. Soc.*, **101**, 2225 (1979); I. Kuwajima and M. Kato, *Tetrahedron Lett.*, **21**, 623 (1980).

4) A. G. Brook, J. M. Duff, P. F. Jones, and N. R. Davis, *J. Am. Chem. Soc.*, **89**, 431 (1967); E. J. Corey, D. Seebach, and R. Freedman, *ibid.*, **89**, 434 (1967); E. M. Dexheimer and L. Spialter, *J. Organomet. Chem.*, **107**, 229 (1976).

5) a) I. Kuwajima, M. Arai, and T. Sato, *J. Am. Chem. Soc.*, **99**, 4181 (1977); b) I. Kuwajima, T. Abe, and N. Minami, *Chem. Lett.*, **1976**, 993; c) A. Hosomi, H. Hashimoto, and H, Sakurai, *J. Organomet. Chem.*, **175**, C1 (1979).

6) For other methods of preparation, see: G. J. D. Peddle, *J. Organomet. Chem.*, **14**, 139 (1968); J. Dunogues, M. Bolourtchian, R. Calas, N. Duffaut, and J. -P. Picard, *ibid.*, **43**, 157 (1972); P. Bourgeois, *ibid.*, **76**, C1 (1974); P. Bourgeois, J. Dunogues, and N. Duffaut, *ibid.*, **80**, C25 (1974); A. Hassner and J. A. Soderquist, *ibid.*, **131**, C1 (1977); N. Minami, T. Abe, and I. Kuwajima, *ibid.*, **145**, C1 (1978); A. Sekiguchi, Y. Kabe, and W. Ando, *Tetrahedron Lett.*, **1979**, 871, and references cited therein.

7) a) K. Ruhlmann, *Synthesis*, **1971**, 236; J. J. Bloomfield, D. C. Owsley, and J. M. Nelke, *Org. Reactions*, **23**, 259 (1976); b) I. Kuwajima, T. Sato, N. Minami, and T. Abe, *Tetrahedron Lett.*, **1976**, 1591; I. Kuwajima, N. Minami, T. Abe, and T. Sato, *Bull. Chem. Soc. Jpn.*, **51**, 2391 (1978).

8) See also: J. -P. Picard, R. Cales, J. Dunogues, N. Duffaut, J. Gerval, and P. Lapouyade, *J. Org. Chem.*, **44**, 420 (1979), and references cited therin.

9) See, for example: J. F. Bielmann and J. B. Ducep, *Tetrahedron Lett.*, **1969**, 3707.

10) I. Kuwajima, T. Abe, and K. Atsumi, *Chem. Lett.*, **1978**, 383.

11) I. Kuwajima and T. Abe, *Bull. Chem. Soc. Jpn.*, **51**, 2183 (1978).

12) a) T. Sato, T. Abe, and I. Kuwajima, *Tetrahedron Lett.*, **1978**, 259; b) N. Minami, T. Abe, and I. Kuwajima, *J. Organomet. Chem.*, **145**, C1 (1978); c) T. Sato, M. Arai, and I. Kuwajima, *J. Am. Chem. Soc.*, **99**, 5827 (1977).

13 a) H. O. House, L. J. Czuba, M. Gall, and H. D. Olmstead, *J. Org. Chem.*, **34**, 2324 (1969); b) C. Ainsworth, F. Chen, and Y. -N. Kuo, *J. Organomet. Chem.*, **46**, 59 (1972); c) M. W. Rathke and D. F. Sullivan, *Syn. Commun.*, **1973**, 67; d) R. E. Ireland, R. H. Mueller, and A. K. Willard, *J. Am. Chem. Soc.*, **98**, 2868 (1976).

14) Sodium dispersion purchased from Alfa Ventron was used.

 © 1980 The Chemical Society of Japan Bull. Chem. Soc. Jpn., 53, 2639—2641 (1980)

Branched-chain Sugars. XX. Kinetic Studies on the Epimerization of 1,2 : 5,6-Di-*O*-isopropylidene-3-*C*-nitromethyl-α-D-allofuranose[1)]

Ken-ichi SATO, Kenji KOGA,† Hironobu HASHIMOTO, and Juji YOSHIMURA*

Laboratory of Chemistry for Natural Products, Faculty of Science, Tokyo Institute of Technology, Nagatsuta, Midoriku, Yokohama 227

(Received February 15, 1980)

A study was made on the kinetics of the epimerization of 1,2: 5,6-di-*O*-isopropylidene-3-*C*-nitromethyl-α-D-allofuranose in nitromethane to its 3-epimer in the presence of a small amount of sodium methoxide. The activation energy was found to be 75±8 kJ/mol, the intermediate in epimerization being 1,2: 5,6-di-*O*-isopropylidene-α-D-*ribo*-hexofuranos-3-ulose with use of the labelled compound.

Cyanohydrin and nitromethane syntheses have been widely used in the reaction of carbohydrate field for lengthening the carbon chain of reducing sugars. The stereoselectivity in the formation of two isomers is explicable on the basis of conformational grounds, since in the zigzag conformation the β-hydroxyl groups come into unfavorable eclipsed proximity in the 2,4-*erythro* isomer but not in the 2,4-*threo* isomer.[2)] However, alteration of the reaction conditions such as pH can sometimes reverse the selectivity.[3)] Recently, these reactions were applied to branched-chain sugar synthesis.[4)] Data accumulated indicate that one epimer or a mixture of epimers is obtained depending on the rate of epimerization of the kinetically-controlled product to thermodynamically stabler isomer.

In a previous paper a report was given on the composition of isomers in the reaction of nitromethane with 1,2:5,6-di-*O*-isopropylidene-α-D-*ribo*-hexofuranos-3-ulose (**1**) in the presence of a slight excess of sodium ethoxide over the equivalent. It was found that the reaction at −78 °C for 30 min or at 20 °C for 3 min in the usual solvent gives exclusively 1,2:5,6-di-*O*-isopropylidene-3-*C*-nitromethyl-α-D-allofuranose (**2**), while the reaction at 25 °C for 30 min only the corresponding D-*gluco* isomer (**3**).[5)] The results indicate that the kinetically-controlled product **2** epimerizes rapidly into **3** at room temperature. This paper deals with the measurement of activation energy and deduction of the pathway of epimerization.

Experimental

Solutions were evaporated under reduced pressure at bath temperature not excceding 50 °C. NMR spectra were taken with a JEOL SP-100 spectrometer in deuteriochloroform containing tetramethylsilane as an internal reference. TLC was carried out on glass plates coated with Kieselgel 60F 254 (Merck) equilibrated in the atmosphere before use. The solvent system employed was ether–hexane (1:1 v/v). R_f values of compounds **1**, **2**, and **3** were 0.07, 0.26, and 0.30, respectively.

*1,2:5,6-Di-*O*-isopropylidene-3-*C*-(nitromethyl-^{14}C)-α-D-allofuranose.* To a suspension of excess silver nitrite in ether (20 ml) was added with stirring a solution of methyl iodide [0.3 ml (5.0 mmol) having total radioactivity of 500 μCi, the Radiochemical center, Amersham] in ether (10 ml). The reaction mixture was stirred for 20 h in the dark at room temperature, and then filtered. The filtrate was carefully concentrated to give crude nitromethane (44 mg).

To a solution of **1** (250 ml) in ethanol (1.5 ml) was added a solution of nitromethane-^{14}*C* (44 mg) and sodium ethoxide (15 mg sodium metal in 3 ml ethanol) at a temperature below −30 °C. The reaction mixture was kept at 0 °C for 48 h and then half of the reaction mixture was neutralized with 60% acetic acid and extracted with chloroform. The resulting solution was washed with water and evaporated after addition of an authentic sample of non-labelled **2** (600 mg) to give a solid, which was recrystallized twice from ethanol. Specific activity of **2** (370 mg) thus obtained was 8.62 nCi/mg.

From the remaining half of the reaction mixture was obtained in a similar manner **2** (272 mg) having specific activity of 10.18 nCi/mg. The recrystallized needles were checked on TLC to show one spot (R_f 0.26).

*Epimerization of ^{14}C-Labelled **2** to **3**.* To a solution of nitromethane (0.9 ml, 16.7 mmol) and sodium ethoxide (4.5 mg, 19.6 mmol sodium in 0.9 ml ethanol) was added a solution of ^{14}C-labelled **2** (8.62 nCi/mg, 355 mg, 1.11 mmol) in ethanol (9 ml) at room temperature. The reaction mixture heated at 65 °C for 30 min showed the presence of **3** and a trace amount of **1** on TLC, was then neutralized with 60% acetic acid and extracted with chloroform. The extract was washed with water and evaporated to give crystals which were recrystallized twice from ethanol–hexane to give pure **3** (48 mg, R_f 0.30) of 0.585 nCi/mg.

If the activity of ^{14}C-labelled **2** was completely reduced with non-radioactive nitromethane added to the isomerization mixture, the activity of **3** should be 0.537 nCi/mg. Thus, the conversion ratio of the activity corresponded to 99% of the theoretical value.

A similar epimerization of **2** (272 mg, 0.853 mmol. 10.18 nCi/mg) in the presence of non-labelled nitromethane (266.5 mg, 4.37 mmol) gave pure **3** (44.9 mg, 1.56 nCi/mg), its conversion ratio of activity being 101% of the theoretical value.

*Measurement of Epimerization Rate of **2** into **3** at various Temperatures.* A solution **2** (200 mg, 0.627 mmol) in nitromethane (2 ml, 38 mmol) was added into nitromethane (2 ml) containing sodium methoxide (0.109 mmol in 0.25 ml methanol) at various temperatures controlled by means of a thermostat. Each 0.4 ml of the reaction mixture was pipetted out at appropriate intervals, acidified promptly with 60% acetic acid to stop the epimerization, and then extracted with chloroform. The chloroform layer was washed with water, and then evaporated. The extent of the isomerization in the residual solid was estimated from the ratio of the intensities of H-1 (δ 5.91 for **2**, 5.82 for **3**) and OH (δ 3.55 for **2**, δ 3.30 for **3**) protons in the NMR spectrum. Measurements were carried out at 0, 45, 65, and 95 °C (±0.1 °C). The results are summarized in Table 1. No isomerization was observed at 0 °C for 10 h.

† Present address: Shinloihi Co., Ltd., Technical Department, 2-19-12 Dai Kamakura-shi, Kanagawa 247.

TABLE 1. EPIMERIZATION RATE (%)

Temp (°C)	Reaction time (min)						
	0	2	4	6	10	30	60
45	0	0	0	0	3.5	9.6	19.3
65	0	0	6.5	10.8	20.0	44.6	67.8
95	0	17.2	36.7	53.5	69.0	92.5	94.0

Discussion

Both cyanohydrin and nitromethane reactions are reversible, epimeric ratios in the asymmetric induction depending on the reaction conditions. However, except for the dependency of reaction rate on pH,[6] few kinetic studies have been carried out.

Albrecht and Moffatt[7] presumed the dehydration of the initially formed **2** to 1,2: 5,6-di-*O*-isopropylidene-3-*C*-nitromethylene-α-D-*ribo*-hexofuranose (**4**), followed by readdition of water, to be the cause of the formation of a mixture of **2** and **3** from **1** in the presence of excess butoxide. They demonstrated the conversion of **2** into **4** by treatment with dimethyl sulfoxide and acetic anhydride at 20 °C for 24 h, and that of **4** into **3** by the base-catalyzed hydration. Contrary to their presumption, our experimental results with labelled **2** showed complete reduction of the specific activity with non-labelled nitromethane, indicating that the epimerization of **2** into **3** proceeds *via* **1** (Scheme 1). Bourgeois[8] reported the epimerization of the cyanohydrin of D-*allo* configuration from **1** isomerizes into D-*gluco* isomer in aqueous potassium cyanide at room temperature. The isomerization should proceed also *via* **1**, since no equivalent intermediate to **4** can be considered in this case.

It seems likely that this type of isomerization is common in the reaction of uloses with hydrogen cyanide or nitromethane under the alkaline conditions, though the factors to control the thermodynamic stability can not be predicted correctly. The reaction of methyl 4,6-*O*-benzylidene-2-deoxy-α-D-*erythro*-hexopyranoside (**5**) and hydrogen cyanide in pyridine at room temperature gave a 21:1 mixture of methyl 4,6-*O*-benzylidene-3-*C*-cyano-2-deoxy-α-D-*ribo*-hexopyranoside (**6**) and its α-D-*arabino* isomer (**7**),[9] the predominancy of **6** being attributed to the hydrogen bonding between axial hydroxyl group at C-3 and methoxyl oxygen at C-1.[10] **7** was preponderantly obtained in the same reaction in ether and aqueous sodium hydrogencarbonate.[11]

Rosenthal and Ong[12] reported that the reaction of **5** and excess nitromethane in methanol in the presence of equimolar sodium methoxide at room temperature for 16 h gives methyl 4,6-*O*-benzylidene-2-deoxy-3-*C*-nitromethyl-α-D-*ribo*-hexopyranoside (**8**) and the D-*arabino* isomer (**9**) in 63 and 22% yields, respectively. In our experiments, however, the same reaction in chloroform in the presence of three equimolar triethylamine as a basic catalyst at room temperature for 72 h gave only **8** in 82% yield. This indicates that the isomerization rate is smaller in the presence of a weaker base. In fact, treatment of **8** in nitromethane with three equimolar sodium methoxide at room temperature for 1 h gave a 1:1 mixture of **8** and **9**.[13]

For measurement of the activation energy of the isomerization of **2** into **3**, the conditions described in Experimental were chosen. The plots of $\ln a/a-x$,

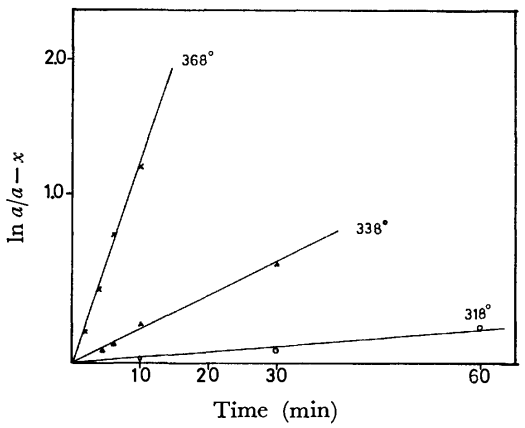

Fig. 1. Plots of a first-order rate equation for the epimerization of **2**.

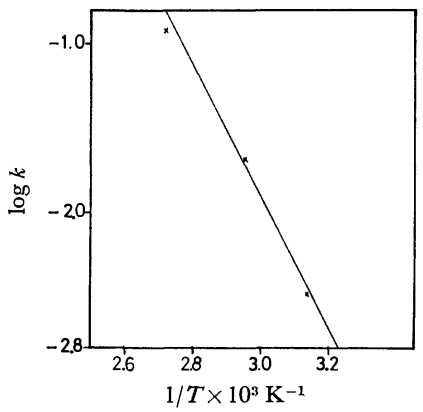

Fig. 2. Arrhenius plot.

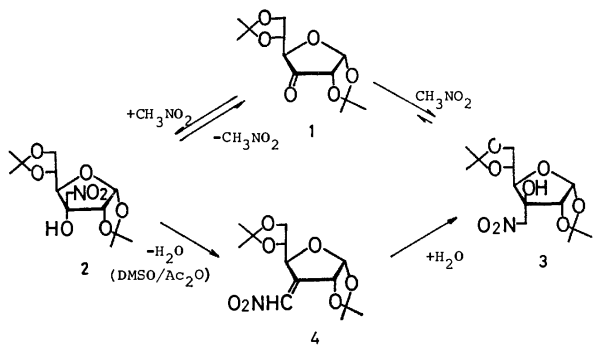

Scheme 1.

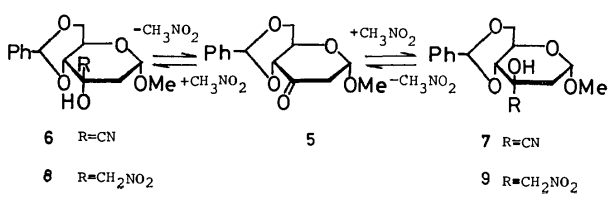

Scheme 2.

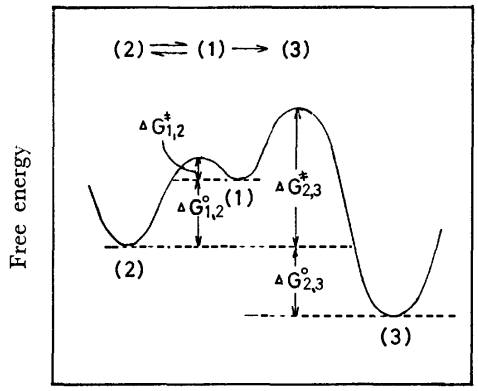

Fig. 3. Energy diagram between **1**, **2**, and **3**.

where x is the epimerization ratio, against time at three different temperatures were found to be linear at the initial stage, indicating that the reaction is of first-order (Fig. 1). The slopes of these lines give the times of half-conversion to be 5.65, 34.7, and 211 min at 95, 65, and 45 °C, respectively, and also the rate constant k. The plot of $\log k$ against the reciprocal of temperature shows a linear relationship (Fig. 2), its slope giving an activation energy of epimerization of 75±8 kJ/mol. The energy diagram of this raction system is given in Fig. 3. Since the reaction of **1** with nitromethane at −78 °C gave kinetically controlled product **2** selectively, $\Delta G^{*}_{1,2}$ value would be small as in the usual equilibration reaction. A comparison of bond energy between **1** and **2** indicates that $\Delta G^{\circ}_{1,2}$ value is *ca.* 50 kJ/mol, and the value of isomerization energy from **2** to **3**, $\Delta G^{*}_{2,3}$ we obtained is reasonable. Although $\Delta G^{\circ}_{2,3}$ value could not be measured, it would be larger than $\Delta G^{\circ}_{8,9}$ in the systems of **5**, **8** and **9**.

The present work was partially supported by a Grant-in-Aid for Encouragement of Young Scientists from the Ministry of Education, Science and Culture (No. 474244).

References

1) Part XIX. K. Sato, M. Matsuzawa, K. Ajisaka, and J. Yoshimura, *Bull. Chem. Soc. Jpn.*, **53**, 189 (1980).
2) a) J. G. Maltby, *J. Chem. Soc.*, **1929**, 2769; b) J. Kovar and H. H. Baer, *Can. J. Chem.*, **48**, 2377 (1970).
3) H. S. Isbell, *J. Res. Nat. Bur. Stand.*, **48**, 163 (1962).
4) H. Grisebach and R. Schmid, *Angew. Chem.*, **84**, 192 (1972).
5) K. Sato, J. Yoshimura, and C. Shin, *Bull. Chem. Soc., Jpn.*, **50**, 1191 (1977).
6) W. Militzer, *Arch. Biochem. Biophys.*, **21**, 143 (1949).
7) H. P. Albrecht and J. G. Moffatt, *Tetrahedron Lett.*, **1970**, 1063.
8) J. -M. Bourgeois, *Helv. Chim. Acta*, **58**, 363 (1975).
9) a) J. Yoshimura, M. Matsuzawa, K. Sato, and M. Funabashi, *Chem. Lett.*, **1977**, 1403; b) J. Yoshimura, M. Matsuzawa, and M. Funabashi, *Bull. Chem. Soc. Jpn.*, **51**, 2067 (1978).
10) J. Yoshimura, M. Matsuzawa, K. Sato, and Y. Nagasawa, *Carbohydr. Res.*, **76**, 67 (1979).
11) T. T. Tang, F. Winternitz, A. Olesker, A. Lagrange, and G. Lukacs, *J. Chem. Soc., Chem. Commun.*, **1979**, 153.
12) A. Rosenthal and K.-S. Ong, *Can. J. Chem.*, **48**, 3034 (1970).
13) K. Sato and J. Yoshimura, unpublished result.

Functionalization of *trans*-Decalin. IV. A Stereoselective Synthesis of *dl*-β-Costol, *dl*-Arctiol, and the Related Eudesmane Type Sesquiterpenes

Sigeru Torii* and Tsutomu Inokuchi

Department of Industrial Chemistry, School of Engineering, Okayama University, Tsushima, Okayama 700

(Received February 15, 1980)

The efficient synthetic procedures to *dl*-β-costol (**1a**), *dl*-arctiol (**2**), and the related eudesmane type sesquiterpenes are described. *trans*-8,8-Ethylenedioxy-4aβ-methyldecalin-2α-ol (**6a**), prepared from *trans*-1,1-ethylenedioxy-4aβ-methyl-$\Delta^{6,7}$-octalin by epoxidation and subsequent reduction of the epoxy ring, was converted into **1a** as follows: (1) deacetalization of **6a** followed with mesylation, giving 2α-methylsulfonyloxy-4aβ-methyldecalin-8-one (**7b**), (2) condensation of **7b** with methyl sodiomalonate and subsequent Wittig reaction with methylenetriphenylphosphorane affording dimethyl (*trans*-4aβ-methyl-1-methylene-7β-decalinyl)malonate (**9**), (3) reduction of sodium salt of **9** with $NaAl(OCH_2CH_2OMe)_2H_2$. Oxidation of **1a** with PCC gave *dl*-β-costal. *dl*-Arctiol (**2**), structurally related to **1a**, was prepared from *trans*-5,5-ethylenedioxy-8aβ-methyldecalin-2-one. Introduction of two equatorial substituents, such as hydroxyl and 1-hydroxy-1-methylethyl groups at the C-2 and C-3 carbons of **2**, was carried out as follows: (1) methoxycarbonylation followed by methylation of the sodium salt of keto ester with MeLi, (2) subsequent reduction with lithium in liquid NH_3, giving *trans*-5,5-ethylenedioxy-3β-(1-hydroxy-1-methylethyl)-8aβ-methyldecalin-2α-ol (**14**), and (3) deacetalization of **14** followed by the reaction with methylenetriphenylphosphorane. *dl*-Eudesma-4(14),7(11)-dien-8-one was also prepared from **2** by oxidation with PCC followed by dehydration and subsequent isomerization of double bond.

In the course of our efforts to study the stereocontrolled synthesis of *dl*-dehydrofukinone[1] and *dl*-isopetasol,[2] we have found an efficient preparative way of *trans*-8,8-ethylenedioxy-4aβ-methyldecalin-2α-ol (**6a**)[1] and *trans*-5,5-ethylenedioxy-8aβ-methyldecalin-2-one (**11**)[2] from methyl 1-oxo-$\Delta^{6,7}$-octalin-4a-carboxylate.[3] The compounds **6a** and **11** are considered to be versatile intermediates[4] for eudesmane class sesquiterpenoid syntheses.[5] Herewith, we report the stereoselective syntheses of *dl*-β-costol (**1a**), *dl*-β-costal (**1b**), a major constituent of costus root oil[6] (*Saussurea lappa* Clark), *dl*-arctiol (**2**), found in the leaves of Gobo[7] (*Arctium lappa* L.), and *trans*-3-isopropylidene-8aβ-methyl-5-methylenedecalin-2-one (*dl*-eudesma-4(14),7(11)-dien-8-one) (**3**),[8] isolated from the essential oil of *Asarum caulescens* Maxim.

A key intermediate for the preparation of *dl*-β-costol (**1a**) must be 1,1-ethylenedioxy-4aβ-methyl-$\Delta^{6,7}$-octalin (**4**), prepared from methyl 1-oxo-$\Delta^{6,7}$-octalin-4a-carboxylate (65% overall yield).[1] Epoxidation of **4** with *m*-chloroperbenzoic acid at 0—5 °C gave the corresponding 2α,3α-epoxide **5** in 91% yield. Reductive epoxy ring opening at the C-3 position of **5** with lithium metal in liquid ammonia afforded the desired alcohol **6a** in 82% yield, in accordance with the axial ring opening rule.[9] The stereochemistry for the hydroxyl group of **6a** can be assigned by comparison of ^{13}C NMR and ^1H NMR results with those of the steroisomer **6c**, prepared from **6a** by oxidation with pyridinium chlorochromate (PCC)[10] and subsequent reduction with lithium aluminium hydride. The ^{13}C chemical shift values of the C-2 and C-8a carbons of **6a** appeared at 5.3 and 5.1 ppm higher fields than those of **6c**, due to the γ-effects,[11] are consistent with the assigned stereochemistry of the axial hydroxyl group of **6a**. In addition, the significant downfield shift of ^1H NMR signal due to the C-2 equatorial proton (δ 4.15) of **6a** as compared to the C-2 axial proton of **6c** (δ 3.58) is also consistent with the structures **6a** and **6c**.

The compound **6a** is nicely functionalized for the straightforward introduction of *exo*-methylene group as well as isopropenyl function at the C-8 and C-2 carbons. In particular, in the formation of the equatorial oriented substituent at C-7 carbon of **1**, the axial hydroxyl group of **6a** is expected to be easily replaced by a nucleophile, such as sodiomalonate. Thus, hydrolysis

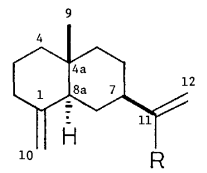

1a: R = $^{13}CH_2OH$

1b: R = CHO

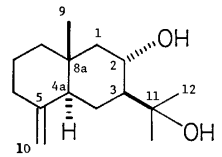

2

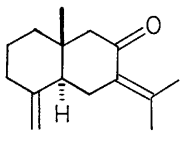

3

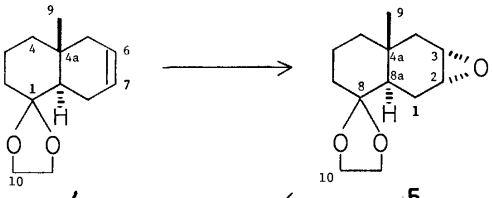

4 **5**

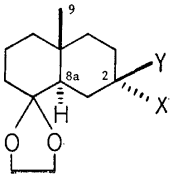

6a: X = OH, Y = H

6b: X = Y = O

6c: X = H, Y = OH

of **6a** with perchloric acid and subsequent treatment of **7a** with methanesulfonyl chloride in pyridine afforded the mesylate **7b** in 92% yield (from **6a**). The reaction of **7b** with methyl sodiomalonate in 1,2-dimethoxyethane (DME) provided the diester **8** in 82% yield. The Wittig reaction of **8** with a salt free solution of methylenetriphenylphosphorane[12] in benzene gave the *trans*-1-methylenedecalin **9** in 78% yield, accompanying with epimerization of the concomitant *cis*-fused decalin to its trans system.[13]

According to the slightly modified Marshall's procedure,[14] so called the malonic enolate reduction-elimination method, reduction of **9** with sodium bis(2-methoxyethoxy)aluminium hydride[15] and sodium hydride led to *dl*-β-costol (**1a**) in 74% yield along with the hydrogenated **10** (13%).[16] *dl*-β-Costal (**1b**) could be obtained in 84% yield by oxidation of *dl*-**1a** with PCC (Scheme 1).[6c,17]

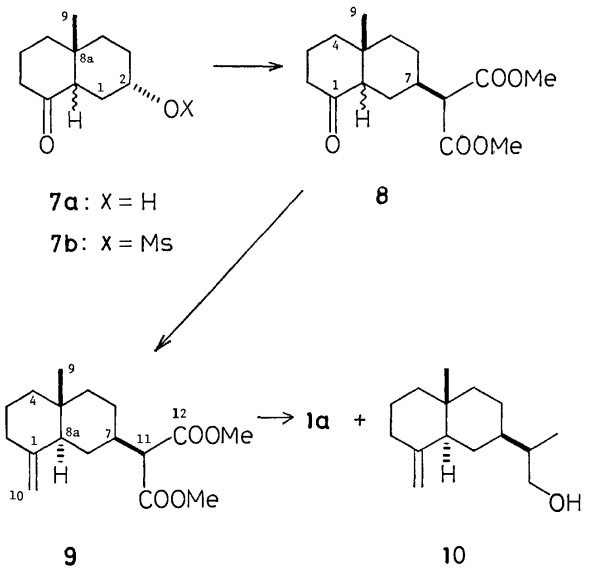

Scheme 1.

We tried to prepare another eudesmane sesquiterpenes **2** and **3**, structurally related to **1**, from the masked diketone **11**.[2] One of the structural features of *dl*-arctiol (**2**) must be the C-2 and C-3 equatorial substituents. In connection with the synthesis of *dl*-isopetasol,[2] we have experienced that the reduction of the *trans*-decalin-2-one derivative with lithium metal in liquid ammonia provides the thermodynamically more stable *trans*-decalin-2α-ol, exclusively. The analogous reaction would be expected to proceed in the case of the ketone **13**, giving the 2α-alcohol **14**, a key precursor for the target **2**.

As shown in Scheme 2, the compound **11** is considered to be a suitable precursor for the preparation of the desired **13**. Methoxycarbonylation at the C-3 position of **11** with sodium hydride in dimethyl carbonate gave the keto ester **12** (84% yield) and subsequent methylation of **12** with methyllithium afforded **13**, smoothly. The stereochemistry of the C-3 substituent of **13** is considered to be a thermodynamically stable equatorial isomer.[18] The chemical shift value of the C-4a carbon (δ 50.4) of **13** is close to the C-4a

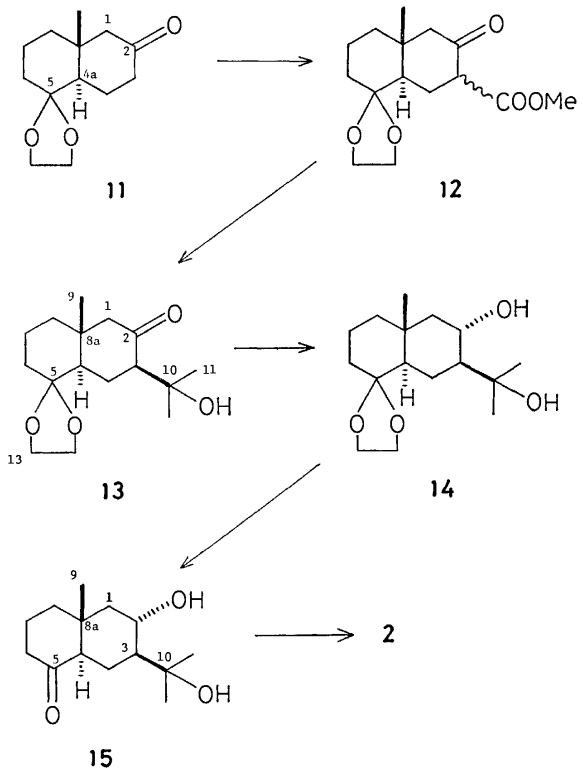

Scheme 2.

carbon (δ 50.1) of **11**, suggesting absence of the γ-effect between the C-3 substituent and the C-4a carbon of **13**.

Reduction of **13** with lithium metal in liquid ammonia provided the diol **14** in 84% yield. The tentative assignment of the equatorial hydroxyl group at C-2 of **14** is based on the comparison of ^{1}H NMR signals of the C-8a methyl group with those of **13**. In the *dl*-isopetasol synthesis,[2] we have encountered a significant 1,3-downfield shift[19] of signals due to the C-8a methyl protons of *trans*-decalin-2β-ol system in the value of 0.28 ppm compared to that of *trans*-decalin-2-one, in contrast to 0.06 ppm of the corresponding *trans*-decalin-2α-ol system. In the conversion of **13** into **14**, no remarkable shift on C-8a methyl protons was observed and the result would reveal absence of the shielding effect of C-2 axial hydroxyl group for the C-8a angular methyl protons of **14**. Hydrolysis of the ethylene acetal of **14** with perchloric acid and subsequent treatment of the ketone **15** with methylenetriphenylphosphorane afforded the desired **2** in 74% yield (from **14**), whose spectral data was identical with those of authentic specimen.[20]

dl-Eudesma-4(14),7(11)-dien-8-one (**3**), possessing a medical interest for a potential antiinflammatory activity,[21] was prepared from *dl*-arctiol (**2**) by oxi-

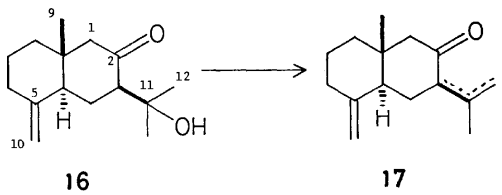

dation with PCC and subsequent dehydration of the ketol **16** on treatment with thionyl chloride in pyridine. Isomerization of the resulting *exo* and *endo* double bond isomers **17** by passing through an activated alumina column gave **3** in 41% yield (from **2**).[8a,17]

Experimental

Melting points and boiling points are uncorrected. IR spectra were determined with a JASCO IRA-I grating spectrometer. ^{1}H NMR (100 MHz) and ^{13}C NMR (25.05 MHz) spectra were measured with a JEOL Fourier transform spectrometer, Model FX-100. Samples were dissolved in $CDCl_3$ and signals are reported in parts per million (δ) downfield from the internal Me_4Si. Elemental analyses were performed in our laboratory.

trans-*2α,3α-Epoxy-8,8-ethylenedioxy-4aβ-methyldecalin (**5**).* To a solution of *m*-CPBA (199 mg, 1.15 mmol) in CH_2Cl_2 (5 ml) was added a solution of **4** (150 mg, 0.72 mmol) in CH_2Cl_2 (1 ml) at 0 °C. After being stirred at 0 °C for 1 h and 5 °C for 20 h, the mixture was quenched with water and taken up in CH_2Cl_2. The extract was washed with aqueous 10% $Na_2S_2O_3$ (3 ml), aqueous 5% NaOH, and brine, dried (Na_2SO_4), and concentrated. The residue was chromatographed (SiO_2, hexane–AcOEt 4:1) to give 147 mg (91%) of **5**: bp 75.0—77.0 °C/0.003 Torr (Kugelrohr); IR (neat) 1284, 1213, 1194, 1143, 1078, 1030, 901, 810, 797 cm^{-1}; ^{1}H NMR δ 0.86—2.24 (m, 11, CH_2, CH), 0.93 (s, 3, CH_3), 2.97—3.06 (m, 1, CH–O), 3.14—3.20 (m, 1, CH–O), 3.60—3.96 (m, 4, CH_2O); ^{13}C NMR δ 19.1 (t, C-6), 19.7 (q, C-9), 20.2 (t, C-1), 32.5 (s, C-4a), 35.4 (t, C-7), 40.5 (t, C-5), 41.9 (t, C-4), 42.9 (d, C-8a), 50.5 (t, C-2), 53.1 (d, C-3), 64.0 (t, C-10), 65.4 (t, C-11), 110.0 (s, C-8). Found: C, 69.72; H, 8.98%. Calcd for $C_{13}H_{20}O_3$: C, 69.61; H, 8.99%.

trans-*8,8-Ethylenedioxy-4aβ-methyldecalin-2α-ol (**6a**).* To a blue solution of lithium (35 mg, 5 mmol) in liquid NH_3 (35 ml) was added a solution of **5** (245 mg, 1.09 mmol) in DME (5 ml) at −78 °C. After being stirred for 1 h at −78 °C and for 1.5 h at −33 °C, the mixture was quenched with NH_4Cl (500 mg) at −78 °C, allowed to stand at room temperature until most of liquid NH_3 has removed. The residue was worked up in the usual manner. The crude product was chromatographed (SiO_2, hexane–AcOEt 2:1) to give 202 mg (82%) of **6a**: bp 104.0—106.5 °C/0.005 Torr (Kugelroher); IR (neat) 3400 (OH), 1095, 1063, 1030, 1000, 945, 914, 878 cm^{-1}; ^{1}H NMR δ 0.90—2.04 (m, 13, CH_2, CH), 0.98 (s, 3, CH_3), 1.90 (s, 1, OH), 3.64—4.01 (m, 4, CH_2O), 4.15 (m, 1, CH–O); ^{13}C NMR δ 17.0 (q, C-9), 19.5 (t, C-6), 27.3 (t), 28.1 (t), 35.2 (s, C-4a), 35.8 (t, C-7), 36.6 (t, C-4), 40.8 (t, C-5), 44.1 (d, C-8a), 64.0 (t, C-10), 65.3 (t, C-11), 66.5 (d, C-2), 110.3 (s, C-8). Found: C, 69.02; H, 9.97%. Calcd for $C_{13}H_{22}O_3$: C, 68.99; H, 9.80%.

trans-*8,8-Ethylenedioxy-4aβ-methyldecalin-2-one (**6b**).* To a suspension of $Py\cdot CrO_3\cdot HCl$ (449 mg, 1.68 mmol) and anhydrous AcONa (275 mg, 3.35 mmol) in CH_2Cl_2 (5 ml) was added a solution of **6a** (127 mg, 0.56 mmol) in CH_2Cl_2 (4 ml) at 0—5 °C. After being stirred for 30 min at 0—5 °C and for 3 h at room temperature, the mixture was diluted with ether (5 ml) and passed through a short silica gel column eluting with ether–AcOEt. The eluate was concentrated and the residue was chromatographed (SiO_2, hexane–AcOEt 3:1) to give 118 mg (94%) of **6b** as white solids: mp 65.5—66.6 °C: IR (Nujol) 1710 cm^{-1} (C=O); ^{1}H NMR δ 0.96—2.04 (m, 9, CH_2, CH), 1.16 (s, 3, CH_3), 2.12—2.32 (m, 4, $COCH_2$), 3.68—4.04 (m, 4, CH_2O); ^{13}C NMR δ 17.1 (q, C-9), 19.4 (t, C-6), 34.6 (s, C-4a), 35.0 (t), 36.8 (t), 37.9 (t), 39.8 (t, C-4), 41.4 (t, C-5), 49.8 (d, C-8a), 64.2 (t, C-10), 65.6 (t, C-11), 109.3 (s, C-8), 212.2 (s, C-2). Found: C, 69.74; H, 9.25%. Calcd for $C_{13}H_{20}O_3$: C, 69.61; H, 8.99%.

trans-*8,8-Ethylenedioxy-4aβ-methyldecalin-2β-ol (**6c**).* To a suspension of $LiAlH_4$ (15 mg, 0.40 mmol) in ether (0.5 ml) was added a solution of **6b** (17 mg, 0.076 mmol) in ether (0.5 ml) at 0—5 °C. After being stirred for 1 h at 5 °C and for 2 h at room temperature, the mixture was quenched with AcOEt and aqueous 5% $NaHCO_3$. The usual work-up gave 14 mg (82%) of **6c**: bp 106.0—107.5 °C/0.005 Torr (Kugelrohr); IR (neat) 3360 (OH), 1060, 1020, 958, 944, 887, 872, 852 cm^{-1}; ^{1}H NMR δ 0.99 (s, 3, CH_3), 1.08—2.02 (m, 13, CH_2, CH), 1.63 (br s, 1, OH), 3.58 (m, 1, CH–O), 3.72—4.01 (m, 4, CH_2O); ^{13}C NMR δ 17.8 (q, C-9), 19.5 (t, C-6), 29.3 (t), 31.1 (t), 34.6 (s, C-4a), 35.6 (t, C-7), 40.4 (t, C-4), 40.9 (t, C-5), 49.2 (d, C-8a), 64.2 (t, C-10), 65.4 (t, C-11), 71.8 (d, C-2), 109.8 (s, C-8). Found: C, 68.89; H, 9.77%. Calcd for $C_{13}H_{22}O_3$: C, 68.99; H, 9.80%.

*2α-Hydroxy-4aβ-methyldecalin-8-one (**7a**).* A solution of **6a** (175 mg, 0.77 mmol) and 70% $HClO_4$ (50 mg) in THF (5 ml) and H_2O (2.5 ml) was stirred for 12 h at 5 °C. The mixture was taken up in ether–benzene (1:1) and the extract was worked up in the usual manner to give 134 mg (95%) of **7a**: bp 114.5—115.5 °C/0.01 Torr (Kugelrohr); IR (neat) 3400 (OH), 1702 cm^{-1} (C=O); ^{1}H NMR δ 0.79, 0.98 (s, 3, CH_3), 1.08—2.48 (m, 13, CH_2, CH, OH), 2.72 (d, d, 1, J=11, 5 Hz, COCH), 4.15 (m, 1, CH–O). Found: C, 72.31; H, 10.09%. Calcd for $C_{11}H_{18}O_2$: 72.49; H, 9.95%.

*2α-Methylsulfonyloxy-4aβ-methyldecalin-8-one (**7b**).* To a solution of **7a** (154 mg, 0.85 mmol) in pyridine (3 ml) was added $MeSO_2Cl$ (200 mg, 1.74 mmol) at 0—5 °C. After being stirred for 20 h at 5 °C, the mixture was quenched with cold water and taken up in ether–benzene (1:1). The extract was worked up in the usual manner to give 214 mg (97%) of **7b** as white solids after chromatography (SiO_2, hexane–AcOEt 4:1): mp 91.5—93.5 °C; IR (Nujol) 1700 (C=O), 1354, 1170 cm^{-1}; ^{1}H NMR δ 0.80, 1.18 (s, 3, CH_3), 1.10—2.16 (m, 11, CH_2, CH), 2.32 (d, 2, J=7 Hz, $COCH_2$), 2.66 (d, d, 1, J=12, 2 Hz, COCH), 2.99 (s, 3, SO_2CH_3), 5.05 (br s, 1, CH–O); ^{13}C NMR (major peaks) δ 16.3 (q, C-9), 22.4 (t, C-6), 26.3 (t), 26.5 (t), 34.2 (t) 38.5 (q, SO_2CH_3), 39.0 (s, C-4a), 40.0 (t, C-4), 41.1 (t, C-5), 50.8 (d, C-8a), 79.0 (d, C-2), 211.3 (s, C-8). Found: C, 55.26; H, 7.88%. Calcd for $C_{12}H_{20}O_4S$: C, 55.37; H, 7.74%.

*Dimethyl (4aβ-Methyl-1-oxo-7β-decalinyl) malonate (**8**).* To a solution of dimethyl sodiomalonate prepared from dimethyl malonate (330 mg, 2.5 mmol) and NaH (55 mg, 2.3 mmol) in DME (3 ml) was added a solution of **7b** (105 mg, 0.40 mmol) in DME (1 ml). After being heated at reflux for 36 h, the mixture was quenched with 5% HCl at 0—5 °C and taken up in ether–benzene (1:1). The extract was washed with brine, dried (Na_2SO_4), and concentrated to give 97 mg (82%) of **8** as white solids after chromatography (SiO_2, hexane–AcOEt 3:1): mp 97.5—98.5 °C; IR (Nujol) 1750 (ester C=O), 1698 cm^{-1} (C=O); ^{1}H NMR δ 0.77, 1.13 (s, 3, CH_3), 1.10—2.40 (m, 14, CH_2 CH), 3.25 (d, 1, J=9 Hz, CHCOO), 3.72 (s, 6, OCH_3); ^{13}C NMR (major peaks) δ 16.8 (q, C-9), 22.5 (t, C-3), 24.7 (t), 25.0 (t), 37.5 (d, C-7), 39.2 (s, C-4a), 40.2 (t, C-2, C-4), 41.1 (t, C-5), 52.4 (q, OCH_3), 56.8 (d, C-8a), 57.7 (d, malonic ester CH), 168.7 (s, COO), 168.9 (s, COO), 211.7 (s, C-1). Found: C, 64.80; H, 8.29%. Calcd for $C_{16}H_{24}O_5$: C, 64.84; H, 8.16%.

*Dimethyl (*trans-*4aβ-Methyl-1-methylene-7β-decalinyl) malonate (**9**).* A salt free solution of methylenetriphenylphosphorane prepared from methyltriphenylphosphonium bromide (217 mg, 0.61 mmol) and $LiNH_2$ (95 mg, 2.43 mmol) in benzene (5 ml) was added dropwise to a solution of **8** (45 mg, 0.15 mmol) in benzene (1 ml). After being stirred for 20 h at room temperature, the mixture was quenched with aqueous 5% HCl and taken up in ether–benzene (1:1). The extracts were washed with brine, dried (Na_2SO_4), and concentrated. The residue was chromatographed (SiO_2, hexane–AcOEt 5:1) to give 38 mg (86%) of **9**: bp 101.0—102.5 °C/0.02 Torr (Kugelrohr); IR (neat) 3065, 1760 (ester C=O), 1738 (ester C=O), 1645 cm^{-1} (C=C); ^1H NMR δ 0.70 (s, 3, CH_3), 0.84—2.36 (m, 14, CH_2, CH), 3.25 (d, 1, J=9 Hz, CHCOO), 3.73 (s, 6, OCH_3), 4.35, 4.66 (br s, 2, H_2C=C); ^{13}C NMR δ 16.2 (q, C-9), 23.4 (t, C-3), 25.7 (t, C-6), 28.3 (t, C-8), 35.8 (s, C-4a), 36.7 (t, C-2), 38.4 (d, C-7), 40.5 (t, C-4), 41.7 (t, C-5), 49.3 (d, C-8a), 52.2 (q, OCH_3), 58.0 (d, C-11), 105.6 (t, C-10), 150.2 (s, C-1), 169.0 (s, C-12, C-13). Found: C, 69.35; H, 8.98%. Calcd for $C_{17}H_{26}O_4$: C, 69.36; H, 8.90%.

*dl-β-Costol (**1a**)* and trans-*7β-(2-Hydroxy-1-methylethyl)-4aβ-methyl-1-methylenedecalin (**10**).* A mixture of **9** (40 mg, 0.135 mmol) and NaH (25 mg, 1.04 mmol) in DME (3 ml) was heated at reflux for 24 h and to this solution was added a solution of 70% $NaAl(OCH_2CH_2OCH_3)_2H_2$ (540 mg, 1.87 mmol) in benzene. The mixture was heated at reflux for 1 h, quenched with MeOH at 0—5 °C, acidified with aqueous 5% HCl, and taken up in benzene–AcOEt (1:1). The extract was washed with brine, dried (Na_2SO_4), and concentrated. The residue was chromatographed (SiO_2, hexane–AcOEt 4:1) to give 22 mg (74%) of **1a** (R_f 0.82, hexane–ether 2:1) and 4 mg (13%) of **10** (R_f 0.69). **1a**: bp 79.5—81.0 °C/0.015 Torr (Kugelrohr) (lit,[6a] 150 °C/0.5 Torr, lit,[6d] 130 °C/0.3 Torr); IR (neat) 3300 (OH), 3060 (HC=C), 1645 (C=C), 1438, 1407, 1380, 1175, 1150, 1055, 1043, 1030, 1022, 885 cm^{-1}; ^1H NMR δ 0.74 (s, 3, CH_3), 0.84—2.41 (m, 15, CH_2, CH, OH), 4.13 (br s, 2, CH_2O), 4.41, 4.69 (br s, 2, H_2C=C), 4.93, 5.03 (br s, 2, H_2C=C); ^{13}C NMR δ 16.4 (q, C-9), 23.5 (t, C-3), 27.3 (t, C-6), 30.0 (t, C-8), 36.0 (s, C-4a), 36.8 (t, C-2), 41.2 (d, C-7), 41.7 (t, C-4), 41.9 (t, C-5), 50.0 (d, C-8a), 65.3 (t, C-13), 105.4 (t, C-10), 107.8 (t, C-12), 150.7 (s, C-1), 154.1 (s, C-11).

10: [6d] Bp 81.5—83.0 °C/0.01 Torr (Kugelrohr); IR (neat) 3300 (OH), 3060, 1644 (C=C), 1440, 1378, 1057, 1039, 884 cm^{-1}; ^1H NMR δ 0.71 (s, 3, CH_3), 0.85—2.40 (m, 19, CH_3, CH_2, CH, OH), 3.35—3.76 (m, 2, CH_2O), 4.39, 4.68 (br s, 2, H_2C=C).

*dl-β-Costal (**16**).* To a suspension of $Py\cdot CrO_3\cdot HCl$ (60 mg, 0.28 mmol) and AcONa (37 mg, 0.45 mmol) in CH_2Cl_2 (1 ml) was added a solution of **1a** (22 mg, 0.1 mmol) in CH_2Cl_2 (1 ml) at 0—5 °C. After being stirred for 0.5 h at 0—5 °C and for 3 h at room temperature, the mixture was diluted with ether. The usual work-up gave 16 mg (73%) of **1b** after chromatography (SiO_2, hexane–AcOEt 3:1): bp 53—57 °C/0.02 Torr (Kugelrohr) (lit,[6d] 110 °C/0.3 Torr); IR (neat) 3070, 2700, 1698 (C=O), 1646 (C=C), 1628 (C=C), 1440, 1380, 1208, 1150, 922, 918, 888 cm^{-1}; ^1H NMR δ 0.75 (s, 3, CH_3), 1.10—2.70 (m, 14, CH_2, CH), 4.36, 4.69 (br s, 2, H_2C=C), 5.98, 6.28 (s, 2, H_2C=C), 9.54 (s, 1, CHO); ^{13}C NMR δ 16.4 (q, C-9), 23.5 (t, C-3), 27.0 (t, C-6), 29.5 (t, C-8), 35.9 (s, C-4a), 36.5 (t, C-2), 36.9 (d, C-7), 41.0 (t, C-4), 41.9 (t, C-5), 49.8 (d, C-8a), 105.6 (t, C-10), 133.0 (t, C-12), 150.8 (s, C-1), 155.5 (s, C-11), 194.9 (s, C-13).

Methyl trans-*5,5-Ethylenedioxy-8aβ-methyl-2-oxodecalin-3-carboxylate (**12**).* A mixture of **11**[2] (210 mg, 0.94 mmol), dimethyl carbonate (270 mg, 3.0 mmol), and NaH (37 mg, 1.54 mmol) was heated at 60—65 °C for 3 h and quenched with aqueous 50% MeOH at 0—5 °C. The mixture was extracted with benzene–AcOEt (1:1) and the extract was washed with aqueous $NaHCO_3$, dried (Na_2SO_4), and concentrated. The residue was chromatographed (SiO_2, hexane–AcOEt 2:1) to give 223 mg (84%) of **12**: bp 137.0—139.0 °C/0.03 Torr (Kugelrohr); IR (neat) 1742 (ester C=O), 1710 (C=O), 1655, 1618 cm^{-1}; ^1H NMR δ 0.89—1.96 (m, 7, CH_2, CH), 0.99 (s, 3, CH_3), 2.04—2.50 (m, 4, CH_2), 3.76 (s, 3, OCH_3), 3.90—4.04 (m, CH_2O, COCH), 12.06 (s, OH). Found: C, 63.95; H, 8.03%. Calcd for $C_{15}H_{22}O_5$: C, 63.81; H, 7.85%.

trans-*5,5-Ethylenedioxy-3β-(1-hydroxy-1-methylethyl)-8aβ-methyldecalin-2-one (**13**).* To a suspension of NaH (50 mg, 2.1 mmol) in THF (5 ml) was added a solution of **12** (200 mg, 0.71 mmol) in THF (5 ml) at 0 °C. When H_2 evolution was complete, an ethereal solution of 1.4 M MeLi (3.1 ml, 4.3 mmol) was added at 5 °C. After being stirred at reflux for 12 h, the mixture was quenched with aqueous 10% NH_4Cl at 0—5 °C and taken up in AcOEt. The extract was washed with aqueous $NaHCO_3$, dried (Na_2SO_4), and concentrated. The residue was chromatographed (SiO_2, hexane–AcOEt 1:1) to give 27 mg of **11** and 146 mg (73%) of **13** as white solids: mp 87.0—88.5 °C; IR (Nujol) 3480 (OH), 1688 (C=O), 1290, 1228, 1172, 1098, 1074, 1051, 1032, 952, 855 cm^{-1}: ^1H NMR δ 0.93 (s, 3, CH_3), 1.10—2.48 (m, 12, CH_2, CH), 1.22, 1.26 (s, 6, CH_3), 3.68—4.02 (m, 4, CH_2O), 4.10 (br, 1, OH); ^{13}C NMR δ 18.6 (q, C-9), 19.5 (t, C-7), 23.7 (s, C-8a), 25.5 (q, C-11), 28.6 (q, C-12), 35.6 (t, C-4), 39.7 (s, C-8a), 40.4 (t, C-8), 50.4 (d, C-4a), 58.8 (t, C-1), 59.1 (d, C-3), 64.4 (t, C-13), 65.6 (t, C-14), 71.8 (s, C-10), 109.8 (s, C-5), 214.7 (s, C-2). Found: C, 68.19; H, 9.41%. Calcd for $C_{16}H_{26}O_4$: C, 68.06; H, 9.28%.

trans-*5,5-Ethylenedioxy-3β-(1-hydroxy-1-methylethyl)-8aβ-methyldecalin-2α-ol (**14**).* To a blue solution of lithium (19 mg, 2.71 mmol) in liquid NH_3 (20 ml) was added a solution of **13** (115 mg, 0.41 mmol) in ether (3 ml), EtOH (36 μl), and dioxane (0.5 ml) at −78 °C. After being stirred for 30 min at −78 °C and for 1 h at −33 °C, the mixture was quenched with NH_4Cl (200 mg) at −78 °C and allowed to stand at room temperature until the most of liquid NH_3 had evaporated. The residue was taken up in AcOEt–benzene and worked up in the usual manner to give 101 mg (87%) of **14** as while crystals after chromatography (SiO_2, hexane–AcOEt 1:1): mp 143.5—145.0 °C; IR (Nujol) 3330 (OH), 1380, 1174, 1088, 1037, 907 cm^{-1}; ^1H NMR δ 0.97 (s, 3, CH_3), 1.04—1.90 (m, 12, CH_2, CH), 1.26, 1.28 (s, 6, CH_3), 2.39 (br, 2, OH), 3.60—3.94 (m, 4, CH_2O), 4.02 (d, d, d, 1, J=10, 5, 5 Hz, CH–O); ^{13}C NMR δ 18.9 (q, C-9), 19.2 (t, C-7), 21.3 (t, C-4), 23.9 (q, C-10), 30.2 (q, C-12), 35.5 (t, C-6), 36.1 (s, C-8a), 40.4 (t, C-8), 50.8 (d, C-4a), 51.5 (t, C-1), 54.1 (d, C-3), 64.1 (t, C-13), 65.2 (t, C-14), 68.9 (d, C-2), 75.2 (s, C-10), 109.9 (s, C-5). Found: C, 67.55; H, 10.08%. Calcd for $C_{16}H_{28}O_4$: 67.57; H, 9.92%.

trans-*2α-Hydroxy-3β-(1-hydroxy-1-methylethyl)-8aβ-methyldecalin-5-one (**15**).* A mixture of **14** (53 mg, 0.19 mmol) and 70% $HClO_4$ (20 mg) in THF (3 ml) and H_2O (1.5 ml) was stirred for 12 h at 5—10 °C and taken up in CH_2Cl_2. The extract was worked up in the usual manner to give 38 mg (85%) of **15** as while crystals after chromatography (SiO_2, hexane–AcOEt 1:1): mp 164.5—165.5 °C (benzene); IR (Nujol) 3250 (OH), 1710 cm^{-1} (C=O); ^1H NMR δ 0.80 (s, 3, CH_3), 1.06—2.00 (m, 10, CH_2, CH), 1.28 (s, 6, CH_3), 2.22—2.40 (m, 3, CH_2CO, CHCO), 2.80 (br s, 2, OH), 3.97 (d, d, d, 1, J=10, 5, 5 Hz, CH–O); ^{13}C NMR δ 17.9 (q, C-9), 22.2 (t, C-4, C-7), 23.8 (q, C-11), 30.4 (q, C-12),

40.0 (t, C-6), 40.5 (s, C-8a), 41.1 (t, C-8), 49.5 (t, C-1), 53.2 (d, C-3), 56.9 (d, C-4a), 68.5 (d, C-2), 75.5 (s, C-10), 212.5 (s, C-5). Found: C, 70.08; H, 9.99%. Calcd for $C_{14}H_{24}O_3$: C, 69.96: H, 10.07%.

dl-*Arctiol (2)*. To a solution of **15** (46 mg, 0.19 mmol) in benzene (1 ml) was added a solution of salt-free methylenetriphenylphosphorane (555 mg, 2.01 mmol) in benzene (10 ml). After being stirred for 24 h at room temperature, the mixture was quenched with aqueous 5% HCl at 0—5 °C and taken up in AcOEt. The organic layer was washed with brine, dried (Na_2SO_4), and concentrated to give 35 mg (77%) of **2** as white crystals after chromatography (SiO_2, hexane–AcOEt 2:1): mp 135.5—136.5 °C (hexane) (lit,[7] 157.5—159.0 °C); IR (Nujol) 3250 (OH), 3060, 1642 (C=C), 1147, 1037, 1012, 913, 883 cm^{-1}; ^1H NMR δ 0.74 (s, 3, CH_3), 0.85—2.37 (m, 12, CH_2, CH), 1.28, 1.30 (s, 6, CH_3), 2.81 (br, 2, OH), 4.00 (d, d, d, 1, J=10, 5, 5 Hz, CH-O), 4.40, 4.71 (br s, 2, H_2C=C); ^{13}C NMR δ 17.3 (q, C-9), 22.9 (t, C-7), 24.0 (q, C-12), 26.0 (t, C-4), 30.3 (q, C-13), 36.6 (t, C-6), 37.7 (s, C-8a), 41.4 (t, C-8), 49.4 (d, C-4a), 50.2 (t, C-1), 54.3 (d, C-3), 69.2 (d, C-2), 75.2 (s, C-11), 105.5 (t, C-10), 150.0 (s, C-5). Found: C, 75.49; H, 11.02%. Calcd for $C_{15}H_{26}O_2$: C, 75.58; H, 10.99%.

trans-*3β-(1-Hydroxy-1-methylethyl)-8aβ-methyl-5-methylenedecalin-2-one (16)*. To a suspension of $Py \cdot CrO_3 \cdot HCl$ (73 mg, 0.34 mmol) and AcONa (37 mg, 0.45 mmol) in CH_2Cl_2 (3 ml) was added a solution of **2** (31 mg, 0.13 mmol) in CH_2Cl_2 (1 ml) at 5 °C. After being stirred for 1 h at 5 °C and for 2 h at room temperature, the mixture was worked up in the usual manner to give 27 mg (88%) of **16**: bp 55.0—57.0 °C/0.002 Torr (Kugelrohr); IR (neat) 3540 (OH), 3075, 1691 (C=O), 1642 (C=C), 1437 1378, 1210, 1145, 1052, 880 cm^{-1}; ^1H NMR δ 0.70 (s, 3, CH_3), 1.26 (s, 6, CH_3), 1.40—2.56 (m, 12, CH_2, CH), 3.40 (br, 1, OH), 4.51, 4.82 (br s, 2, H_2C=C); ^{13}C NMR δ 17.1 (q, C-9), 23.0 (t, C-7), 25.6 (q, C-12), 28.2 (t, C-4), 28.6 (q, C-13), 36.6 (t, C-6), 40.9 (s, C-8a), 41.3 (t, C-8), 48.4 (d, C-4a), 57.1 (t, C-1), 59.0 (d, C-3), 71.5 (s, C-11), 107.3 (t, C-10), 148.4 (s, C-5), 214.4 (s, C-2). Found: C, 76.13; H, 10.43%. Calcd for $C_{15}H_{24}O_2$: C, 76.23; H, 10.24%.

dl-*Eudesma-4(14),7(11)-dien-8-one (3)*. To a solution of **16** (12 mg, 0.05 mmol) in pyridine (3 ml) was added $SOCl_2$ (81 mg, 0.68 mmol) at 0 °C. After being stirred for 1.5 h at 0—5 °C, the mixture was quenched with aqueous 5% $NaHCO_3$ and taken up in ether. The extract was worked up in the usual manner to give 7 mg (65%) of **17** after chromatography (SiO_2, hexane–AcOEt 5:1): IR (neat) 3080, 1710 (C=O), 1680 (shoulder), 1645 (C=C), 890 cm^{-1}; ^1H NMR δ 4.50—4.70 (m, H_2C=C). Without further purification, **17** was passed through an activated Al_2O_3 300 (Nakarai Chemicals) column (hexane–AcOEt 5:1) to give 5 mg (71%) of **3**: bp 116—118 °C/11 Torr (lit,[8a] 92.5—95.4 °C/4.5 Torr); IR (neat) 3090, 1680, 1645, 1595, 1210, 890 cm^{-1}; ^1H NMR δ 0.78 (s, 3, CH_3), 1.00—2.80 (m, 1, CH_2, CH), 1.82, 1.98 (s, 6, CH_3), 5.60, 5.84 (br s, 2, H_2C=C).

References

1) S. Torii, T. Inokuchi, and T. Yamafuji, *Bull. Chem. Soc. Jpn.*, **52**, 2640 (1979).

2) S. Torii, T. Inokuchi, and K. Kawai, *Bull. Chem. Soc. Jpn.*, **52**, 861 (1979).

3) S. Torii, T. Kunitomi, and T. Okamoto, *Bull. Chem. Soc. Jpn.*, **47**, 2349 (1974).

4) a) J. W. Huffman and M. L. Mole, *J. Org. Chem.*, **37**, 13 (1972); b) R. G. Carlson and E. G. Zey, *ibid.*, **37**, 2468 (1972); c) R. B. Miller and R. D. Nash, *ibid.*, **38**, 4424 (1973); d) G. H. Posner and G. L. Loomis, *ibid.*, **38**, 4459 (1973); e) J. L. Cooper and K. E. Harding, *Tetrahedron Lett.*, **1977**, 3321; f) E. Huq, M. Meller, E. G. Scovell, and J. K. Sutherland, *J. Chem. Soc., Chem. Commun.*, **1978**, 526.

5) For a review of synthetic approaches to eudesmane type sesquiterpenes, see a) C. H. Heathcock, "The Total Synthesis of Natural Products," ed by J. W. ApSimon, John Wiley & Sons, Inc., New York, N. Y. (1973), Vol. 2, pp. 282—330. Recent reports on the synthesis of eudesmanes; b) G. H. Posner, G. L. Loomis, and H. S. Sawaya, *Tetrahedron Lett.*, **1975**, 1373; c) O. P. Vig, M. L. Sharma, R. Anand, and S. D. Sharma, *J. Ind. Chem. Soc.*, **53**, 81 (1976); d) W. C. Still and M. J. Schneider, *J. Am. Chem. Soc.*, **99**, 948 (1977); e) J. A. Marshall and P. G. M. Wuts, *J. Org. Chem.*, **43**, 1086 (1978); f) S. R. Wilson and D. T. Mao, *J. Am. Chem. Soc.*, **100**, 6289 (1978); g) B. D. MacKenzie, M. M. Angelo, and J. Wolinsky, *J. Org. Chem.*, **44**, 4042 (1979).

6) Isolation: a) A. S. Bawdekar and G. R. Kelkar, *Tetrahedron*, **21**, 1521 (1965); b) S. Ito, K. Endo, H. Honma, and K. Ota, *Tetrahedron Lett.*, **1965**, 3777; c) B. Maurer and A. Grieder, *Helv. Chim. Acta*, **60**, 2177 (1977); Synthesis; d) J. A. Marshall, M. T. Pika, and R. D. Carroll, *J. Org. Chem.*, **31**, 2933 (1966).

7) K. Naya, K. Tsuji, and U. Haku, *Chem. Lett.*, **1972**, 235.

8) a) J. Endo and M. Nagasawa, *Yakugaku Zasshi*, **94**, 1574 (1974); b) Y. Nishikawa, I. Yasuda, Y. Watanabe, and T. Seto, *Shoyakugaku Zasshi*, **30**, 132 (1976); c) F. Bohlmann and A. Suwita, *Phytochemistry*, **17**, 567 (1978).

9) A. S. Hallsworth and H. B. Henbest, *J. Chem. Soc.*, **1957**, 4604.

10) E. J. Corey and J. W. Suggs, *Tetrahedron Lett.*, **1975**, 2647.

11) D. K. Dalling and D. M. Grant, *J. Am. Chem. Soc.*, **94**, 5318 (1972).

12) a) H. J. Bestmann and B. Arnason, *Chem. Ber.*, **95**, 1513 (1962); b) A. Maercker, *Org. React.*, **14**, 270 (1967).

13) a) C. H. Heathcock and R. Ratcliffe, *J. Am. Chem. Soc.*, **93**, 1746 (1971); b) F. E. Ziegler and J. A. Kloek, *Tetrahedron*, **33**, 373 (1977).

14) J. A. Marshall and N. Cohen, *J. Org. Chem.*, **30**, 3475 (1965).

15) L. F. Fieser and M. Fieser, "Reagents for Organic Synthesis," John Wiley & Sons, Inc., New York, N. Y. (1972), Vol. 3, p. 260.

16) The use of $NaAl(OCH_2CH_2OMe)_2H_2$ for reduction-elimination of **9** seems to be pertinent to minimize the undesired **10** in contrast to the results obtained by the reaction of the similar functional group as a malonic ester with $LiAlH_4$[6d,14] leading to a mixture involving more than 20% of a hydrogenated product.

17) The spectra of the synthetic materials were identical with spectra of the corresponding natural products.

18) a) R. M. Coates and J. E. Shaw, *J. Am. Chem. Soc.*, **92**, 5657 (1970); b) D. J. Goldsmith and I. Sakano, *J. Org. Chem.*, **41**, 2095 (1976); c) K. Yamakawa, I. Izuta, H. Oka, R. Sakaguchi, M. Kobayashi, and T. Satoh, *Chem. Pharm. Bull.*, **27**, 331 (1979).

19) R. B. Miller and E. S. Behare, *J. Am. Chem. Soc.*, **96**, 8102 (1974).

20) We are gratefull to Proffessor K. Naya, Kwansei Gakuin University, for providing ^1H NMR and IR spectra of natural arctiol (**2**).

21) K. Endo and H. Hikino, *Bull. Chem. Soc. Jpn.*, **52**, 2439 (1979).

Production of Furan by Vapor-phase Oxidation of Crotonaldehyde Using Heteropoly Compounds as Catalysts

Mamoru Ai,* Tian-hsi Tsai, and Atsumu Ozaki

Research Laboratory of Resources Utilization, Tokyo Institute of Technology, Nagatsuta, Midori-ku, Yokohama 227

(Received February 19, 1980)

The synthesis of furan by direct vapor-phase oxidation of crotonaldehyde has been studied. It was found that heteropoly compounds such as 12-molybdophosphoric acid are more effective than the mixed oxide (MoO_3–P_2O_5, P/Mo=1/12) as catalyst for furan formation, and that the cesium salt of 12-molybdophosphoric acid with a Cs/Mo atomic ratio of 1/12 is more effective than the 12-molybdophosphoric acid catalyst. The rate of furan formation increases with increase in steam concentration in the feed, but is nearly independent of oxygen and crotonaldehyde concentrations. The yield of furan increases by decreasing the crotonaldehyde concentration, attaining 60 mol% at a concentration of 0.17 vol% in the feed. The conversion of crotonaldehyde at maximum yield is 90—95%.

Furan is a raw material for tetrahydrofuran which is in great demand as a solvent and a starting material for polymer compounds. Tetrahydrofuran has been manufactured by three methods: the furfural process, hydrolysis of 1,4-dichloro-2-butene, and hydrogenation of maleic anhydride. Attempts were also made to obtain furan by direct oxidation of butadiene.[1] Several reports have appeared on the oxidation of crotonaldehyde, but they deal exclusively with the formation of maleic anhydride.[2–5]

One of us (M.A.) reported that furan is an intermediate in the oxidation of butene, butadiene, or crotonaldehyde to form maleic anhydride,[6] and found that the MoO_3–P_2O_5 (P/Mo atomic ratio=*ca.* 1/10) catalyst is effective for furan synthesis from butadiene or crotonaldehyde.[7,8] The effects of reaction variables on the yield of furan were studied using the MoO_3–P_2O_5 catalysts, where the best result for furan yield is 30—35 mol % in the oxidation of crotonaldehyde.[8]

Recently, heteropoly compounds were found to be effective for furan formation from butadiene,[9] suggesting that the heteropoly compounds are also effective for the oxidation of crotonaldehyde to furan.

In this study, we have directed our attention to furan formation in the oxidation of crotonaldehyde and attempted to clarify the effects of catalyst and reaction variables, since no detailed information is available on the oxidation reaction.

Experimental

Catalysts. The following three catalysts were used. (A) Heteropoly acid (HPA) catalyst: 136 g of 12-molybdophosphoric acid (Kanto Chemical Co. Inc.) was dissolved in water and 0.50 l (*ca.* 190 g) of 10—20 mesh pumice from volcanic rocks was mixed with the solution, the mixture then being evaporated with vigorous stirring below 200 °C. (B) MoO_3–P_2O_5 catalyst: 80 g of $(NH_4)_6Mo_7O_{24}\cdot 2H_2O$ and 4.6 g of 85 wt% H_3PO_4 were dissolved in hot water (P/Mo atomic ratio=1/12), and 0.30 l of the pumice was added: the mixture was then evaporated. (C) Cs–HPA catalyst: 9.75 g of Cs_2CO_3 was added to the 12-molybdophosphoric acid solution (Cs/Mo atomic ratio=1/12), the subsequent procedure being the same as that for (A). All the catalysts were calcined at 380 °C for 4—5 h in a stream of oxygen. The surface areas measured by the BET method using nitrogen at −196 °C, were (A) 2.1, (B) 9.5, and (C) 3.4 m^2/g.

Reaction Procedures. Oxidation of crotonaldehyde was carried out in the conventional continuous-flow system under atmospheric pressure. The reactor, made of a steel tube lined with aluminum, length 50 cm, i.d. 1.8 cm, was mounted vertically and immersed in a molten lead bath. The oxygen–nitrogen mixed gas was fed from the top of the reactor, liquid crotonaldehyde and water being introduced into the preheater section by means of two injection syringe pumps (micro feeders). The total flow rate was kept constant at 1.0 l/min. The amount of catalyst used was 20 g and the concentration of crotonaldehyde, oxygen, steam, and nitrogen 1.66, 6.6, 7.6, and 84.1 vol%, respectively. The effluent gas from the reactor was led successively into four chilled water-scrubbers in order to recover the water soluble compounds. The contents (*ca.* 300 ml) of the water-scrubbers were collected every 1 h. Maleic anhydride was analyzed by titration with 0.10 mol dm^{-3} NaOH, and the other compounds by gas chromatography. The inlet and exit gases were intermittently analyzed. In order to measure the catalytic activity in stationary state, the data were taken more than 7 h after the start of each run.

Results

Comparison of Performance of Catalysts. Since the Cs–HPA catalyst gives a good yield of furan in the oxidation of butadiene,[9] the actions of the HPA, MoO_3–P_2O_5, and Cs–HPA catalysts in the oxidation of crotonaldehyde were examined at different temperatures. The results are summarized in Fig. 1.

The heteropoly compound, HPA catalyst, is effective for furan formation to a greater extent than the mixed oxide, the MoO_3–P_2O_5 catalyst. Addition of a small amount of Cs^+ to the heteropoly acid promotes furan formation. The results are in line with those obtained in the oxidation of butadiene to give furan.[9]

Since a good result is obtained with the Cs–HPA catalyst, the effects of reaction variable on the reaction rates and the furan yield were studied using only the Cs–HPA catalyst.

Effect of Temperature on the Reaction Products. The main products were furan, maleic anhydride, CO, CO_2, and unidentifiable polymer compounds. The amounts of other products were negligibly small. The yields of the main products are plotted as a function

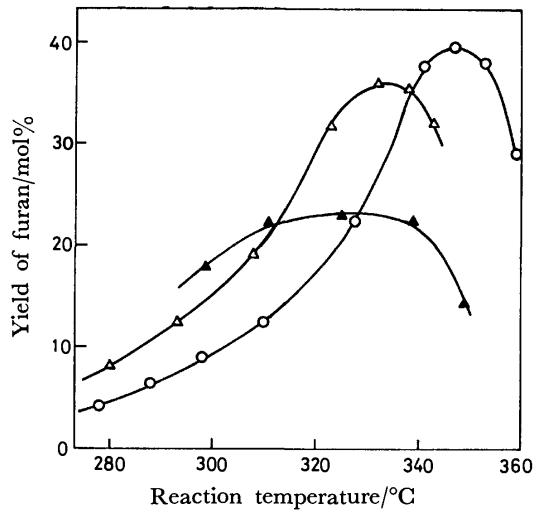

Fig. 1. Comparison of the performances of the catalysts.
Catalyst: (△)=HPA, (▲)=MoO_3–P_2O_5, (○)=Cs–HPA.

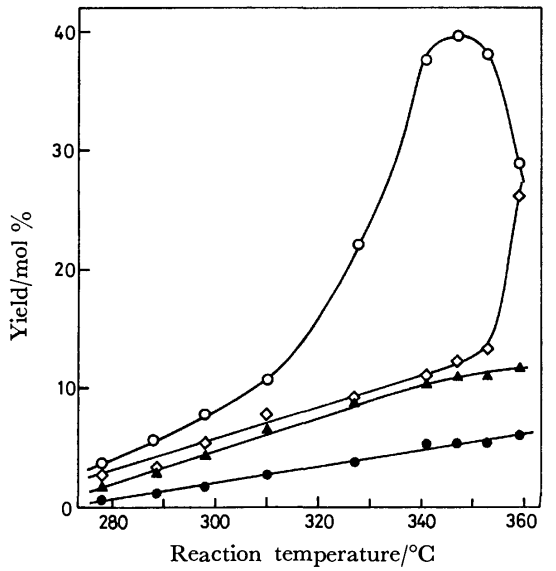

Fif. 2. Product distribution in the oxidation of crotonaldehyde over the Cs–HPA catalyst.
(○)=furan, (◇)=maleic anhydride, (●)=1/4 CO, (▲)=1/4 CO_2.

of the raction temperature in Fig. 2.

Below 310 °C, the yield of each product increases in proportion to temperature rise, indicating that the products are formed competitively but not consecutively. However, at *ca.* 347 °C, the yield of furan attains a maximum value of 40 mol % when the conversion is estimated to be *ca.* 90—95%. The yield decreases above this temperature accompanied by a sharp increase in the yield of maleic anhydride. The results suggest that maleic anhydride is formed also by the oxidation of the produced furan. The yield of maleic anhydride attains *ca.* 55 mol% at 98—100% conversion

Effect of Contact-time on the Yields of Products. The change in the yields of products with the progress of reaction was studied at 346 °C by changing the

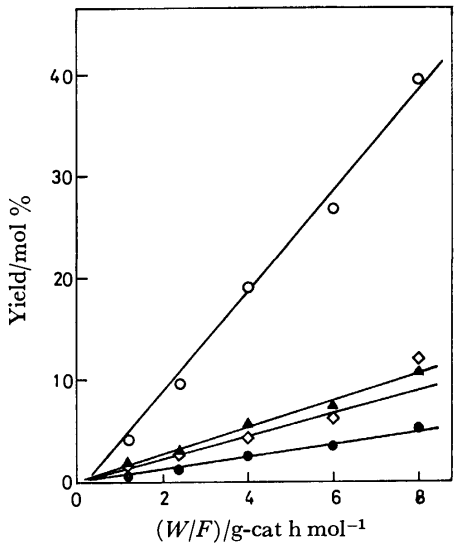

Fig. 3. Yields of products as a function of the contact time (W/F).
Temperature=346 °C, (○)=furan, (◇)=maleic anhydride, (●)=1/4 CO, (▲)=1/4 CO_2.

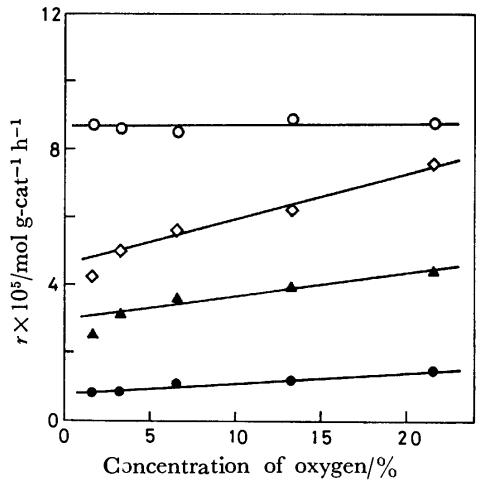

Fig. 4. Effect of oxygen concentration on the reaction rates.
Temperature=278 °C, (○)=furan, (◇)=maleic anhydride, (●)=1/4 CO, (▲)=1/4 CO_2.

amounts of catalyst from 3 to 20 g (Fig. 3). Furan, maleic anhydride, CO, and CO_2 are produced in line with the results shown in Fig. 2, suggesting zero order dependence on the crotonaldehyde concentration.

Effect of Oxygen Concentration on the Reaction Rates. The reaction was carried out by changing the oxygen concentration in the feed gas from 1.6 to 21.6 vol%. Following the principle of the differential reactor, the conversion was held at a low level. The rates of furan, maleic anhydride, CO, and CO_2 formation measured at 278 °C are plotted as a function of oxygen concentration in Fig. 4.

The rate of furan formation is independent of oxygen concentration, the rates of maleic anhydride, CO, and CO_2 formation increasing slightly with increase in the oxygen concentration.

Effect of Crotonaldehyde Concentration on the Reaction Rates. The concentration of crotonaldehyde was

varied in the range 0.34—1.66 vol%. The initial rates of formation for the main products are shown in Fig. 5. All the rates increases slightly with increase in the crotonaldehyde concentration.

Effect of Crotonaldehyde Concentration on the Furan Yield. The yield of furan was measured at five different crotonaldehyde concentrations at various temperatures. The results are shown in Fig. 6. Since the reaction order with respect to the crotonaldehyde concentration is very low (Fig. 5), it is reasonable to assume that the higher the initial crotonaldehyde concentration, the higher the temperature required to achieve sufficient conversion. The maximum yield of furan decreases with increase in the crotonaldehyde concentration. The yield of furan attains 60 mol% when the crotonaldehyde concentration is very low (0.17 vol%), becoming 40 mol% at a 1.66 vol% concentration.

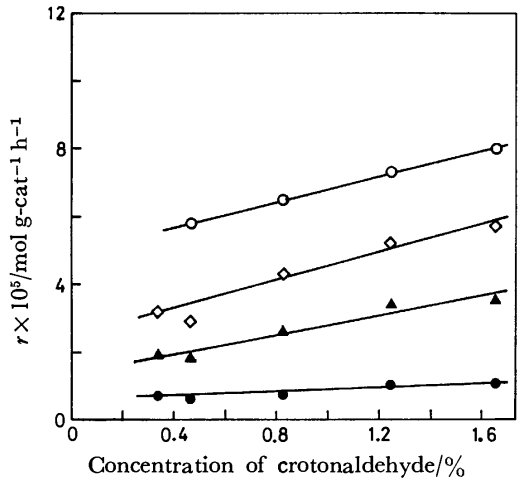

Fig. 5. Effect of crotonaldehyde concentration on the reaction rates.
Temperature=278 °C, (○)=furan, (◇)=maleic anhydride, (●)=1/4 CO, (▲)=1/4 CO_2.

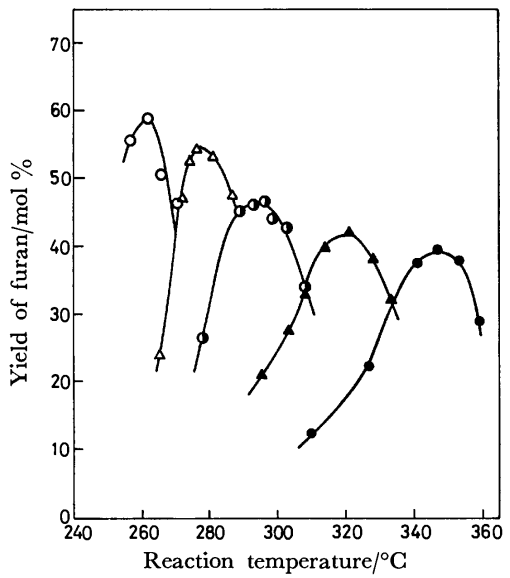

Fig. 6. Effect of crotonaldehyde concentration on the yield of furan.
Concentration of crotonaldehyde: (○)=0.17, (△)=0.25, (◑)=0.46, (▲)=0.83, (●)=1.66% in the feed.

Effect of Steam Concentration on the Reaction Rates. The effect of steam concentration on the initial rate for each product is shown in Fig. 7. The rates increase almost linearly with steam concentration, the slopes becoming more gentle at higher steam concentrations. The results are in line with those obtained in the oxidation of olefins as well as of furan over 12-molybdophosphoric acid catalyst.[10]

Effect of Steam on the Yield of Furan. The effect of steam concentration on the yield of furan was also examined. The presence of steam increases the yield of furan as well as the catalytic activity. (Fig. 8).

Discussion

The Cs–HPA catalyst as well as the HPA and MoO_3–P_2O_5 catalysts are acidic. Thus, they are active for

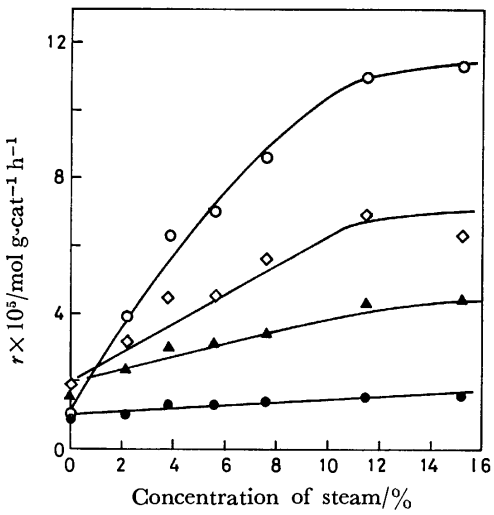

Fig. 7. Effect of steam concentration on the reaction rates.
Temperature=278 °C, (○)=furan, (◇)=maleic anhydride, (●)=1/4 CO, (▲)=1/4 CO_2.

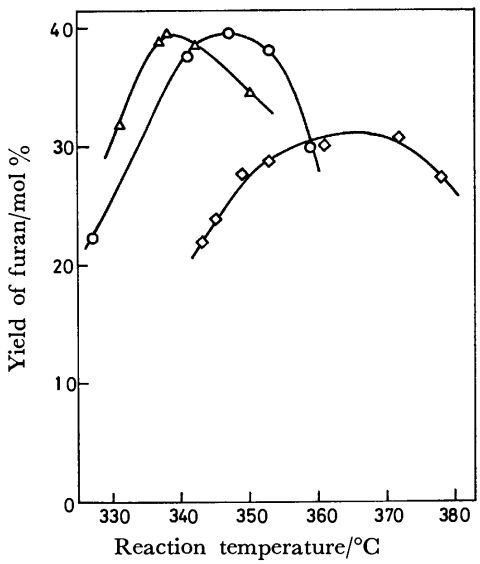

Fig. 8. Effect of steam on the yield of furan.
Concentration of steam: (◇)=3.8, (○)=7.6, (△)=15.1% in the feed.

oxidation of such basic compounds as butadiene, crotonaldehyde and furan but inactive for acidic compounds such as maleic anhydride. Their selectivity to maleic anhydride from the basic reactants at high conversion attains *ca.* 50—60 mol%.

Since furan is an intermediate product, the yield is affected by two factors:[6,11] (i) relative reactivity of furan to crotonaldehyde, and (ii) affinity of the catalyst for furan; this indicates that the stronger the furan adsorption, the larger the portion of the adsorbed furan species which goes to the next oxidation, without being desorbed to the gas phase.

The yield of furan attains a maximum at a 90—95% crotonaldehyde conversion, the catalysts being markedly more active for the oxidation of crotonaldehyde than that of furan.

On the other hand, the results indicate that the reaction rate markedly increases with increase in the steam concentration but is almost independent of the concentration of both oxygen and crotonaldehyde. This suggests that the reaction is mainly restricted by the desorption of oxidation products to gas phase, in contrast with the oxidation of butadiene which is of first order with respect to oxygen concentration.[10] The effect of steam addition on the yield of furan can be explained by assuming that the steam acts to remove the adsorbed furan.[10]

The effect of cesium addition to the heteropoly acid actalyst can also be understood on the same assumption. The addition of a basic compound such as cesium ion reduces the acidic property of catalyst and the affinity for furan, facilitating the desorption of adsorbed furan and increasing the yield of furan.

Since the character of mixed oxide has not yet been defined, it is difficult to understand the difference in catalytic behavior between the heteropoly compounds and the MoO_3–P_2O_5 mixed oxide catalyst.

Conclusion

The cesium salt of 12-molybdophosphoric acid with a Cs/Mo atomic ratio of 1/12 is an excellent catalyst for furan production by direct oxidation of crotonaldehyde as in the case of furan formation from butadiene. Reaction conditions favorable for furan formation are higher steam concentration and lower crotonaldehyde concentration. The maximum furan yield is attained at a 90—95% crotonaldehyde conversion.

References

1) T. Asano, *Yuki Gosei Kagaku Kyokai Shi*, **36**, 146 (1978).
2) W. L. Faith and A. M. Schaible, *J. Am. Chem. Soc.*, **60**, 52 (1938).
3) S. K. Bhattacharyya and N. Venkataraman, *J. Appl. Chem.*, **52**, 737 (1958).
4) S. K. Bhattacharyya and A. K. Kar, *J. Catal.*, **1**, 293 (1962).
5) J. M. Charch and P. Bitha, *Ind. Eng. Chem., Prod. Res. Develop.*, **2**, 61 (1963).
6) M. Ai, *Bull. Chem. Soc. Jpn.*, **43**, 3490 (1970).
7) M. Ai, *Kogyo Kagaku Zasshi*, **74**, 183 (1971).
8) M. Ai and M. Ichihara, *Kogyo Kagaku Zasshi*, **73**, 2152 (1970).
9) M. Ai, preprint of 13th Sanka-hanno (Oxidation reaction) Meeting, Kyoto, 1979, p. 71.
10) M. Ai, Preprint of 44th Shokubai (Catalyst) Meeting, Fukuoka, 1979, p. 84.
11) F. Hartog and P. Zwietering, *J. Catal.*, **2**, 79 (1963).

Reduction by a Model of NAD(P)H. 27. Role of Bivalent Metal Ion in the Reduction of 2-Acylpyridines and 1-Acylisoquinolines

Atsuyoshi Ohno,* Shinro Yasui, and Shinzaburo Oka
Institute for Chemical Research, Kyoto University, Uji, Kyoto 611

(Received February 22, 1980)

Reductions of 1-acetylisoquinoline (AQ), 1-benzoylisoquinoline (BQ), and isoquinoline-1-carbaldehyde have been studied kinetically and the results are compared with those of 2-acetylpyridine (AP), 2-benzoylpyridine (BP), and pyridine-2-carbaldehyde. Equilibrium constants for complexes between these substrates and zinc ion have also been studied. Kinetic deuterium isotope effects for AQ and BQ are smaller than the corresponding product isotope effects, respectively, whereas those for AP and BP are identical. The results are discussed in terms of stability and reactivity of intermediate radical-ion pair, and it is concluded that strong coordination of a metal ion onto the reaction site of a substrate facilitates the complexation but interferes the reduction.

In a previous paper of this series, it was reported that both substrate–metal ion and coenzyme model–metal ion complexes are reacting species in the zinc ion-catalyzed reductions of 2-acetylpyridine (AP) and 2-benzoylpyridine (BP) with 1-benzyl-1,4-dihydronicotinamide (BNAH).[1] Namely, computor-assisted simulation of the kinetics has revealed a key role of the metal ion-complexes on explanation of unusual behavior of metal ion in the reduction of 2-acylpyridines.[2,3]

However, relative importance between a substrate–metal ion and BNAH–metal ion complexes has not been discussed yet and the role of metal ion has still remained ambiguous. In order to obtain further insight into relative importance of complexes, we studied kinetics for the reductions of 1-acetylisoquinoline (AQ), 1-benzoylisoquinoline (BQ), and isoquinoline-1-carbaldehyde (QCA) with BNAH in acetonitrile at 50 °C in the presence of zinc perchlorate, and the results were compared with those of the corresponding pyridine derivatives; AP, BP, and pyridine-2-carbaldehyde (PCA).

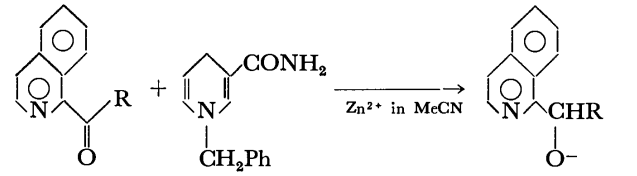

AQ; R=Me BNAH
BQ; R=Ph
QCA; R=H

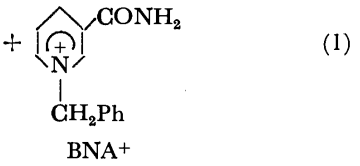

(1)

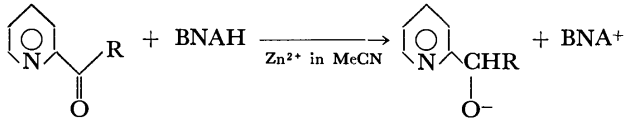

AP; R=Me
BP; R=Ph
PCA; R=H

It is expected that 1-acylisoquinolines and 2-acylpyridines form complexes with zinc ion in a different manner because isoquinoline system has bulky B-ring which would distort the interaction with zinc ion, whereas pyridine system does not. On elucidation of the mechanism of reductions, the difference mentioned above may give a crucial information.

Results and Discussion

Complex Formation. AQ, BQ, QCA, and PCA form complexes with zinc ion. The complexation constant, K_S, defined by Eq. 2

$$S + M \overset{K_S}{\rightleftharpoons} SM \qquad (2)$$

S; a substrate, M; zinc ion

was determined in acetonitrile at 50 °C spectrophotometrically[4] for each substrate and the results are summarized in Table 1 together with those of AP and BP.[1,5] It is known that the complexation constant for BNAH, K_B, defined by Eq. 3 is 500 M^{-1} under the same conditions.[1,5]

$$B + M \overset{K_B}{\rightleftharpoons} BM \qquad (3)$$

B; BNAH, M; zinc ion

It has been reported that the pyridine-ring nitrogen and carbonyl oxygen in 2-acylpyridines are oriented in *E* each other in liquid phase.[6] 1-Acylisoquinolines are also expected to have similar conformations. When the isoquinoline-ring nitrogen is oriented in *Z* to the carbonyl oxygen, a large steric repulsion arises between the isoquinoline-B-ring and the R group except for QCA. Examination with CPK molecular models indicates that AP and BP have small repulsion in their *Z* conformers and the magnitude of this repulsion is slightly larger in BP than in AP. It is important that increasing order of repulsion forces (PCA≃QCA≪AP<BP≪BQ<AQ) are just in agreement with decreasing order of the complexation constants. That is, the more stable the *Z*-conformer, the more stable

Table 1. Complexation constant, K_S

Substituent	K_S, M^{-1}	
	Pyridine	Isoquinoline
H	1900	1800
Ph	200[a]	50
Me	500[a]	30

a) See Refs. 1 and 5 for detail.

the corresponding complex with zinc ion, which may lead to the conclusion that the complexation demands the *Z*-conformation for the carbonyl compound. The conclusion is also supported by spectroscopic investigations.[7,8] Thus, the distortion angle between the planes of carbonyl group and heterocyclic ring in the complexed substrate increases in the order; PCA≃QCA< AP≲BP<BQ≲AQ. CPK molecular models predict that the angle in PCA-complex is about 0° and that in AQ-complex is nearly 90°.

Kinetics. Pseudo-first-order kinetics at 50 °C in acetonitrile was followed spectrophotometrically by observing the decrease in the intensity of absorption from BNAH at 360 nm unless otherwise indicated in Experimental Section. Each run gave a good first-order relationship (correlation coefficient; $r>0.999$) for more than at least two half-lives. Rate constant for zinc ion-catalyzed auto-decomposition of BNAH (6.94×10^{-5} s^{-1}) was small enough to be neglected.[1] Observed first-order rate constants at appropriate concentrations of reagents are summarized in Tables 2—5.

Similarly to the previous procedure,[1] we obtain a kinetic expression shown in Eqs. 4 and 5 for the present reaction (Eq. 6).

$$k_{obsd}[B]_T = k^H[B][S][M], \quad (4)$$

$$k^H = k_1K_B + k_2K_S, \quad (5)$$

$$\left.\begin{array}{l} BM + S \xrightarrow{k_1} \\ SM + B \xrightarrow{k_2} \end{array}\right\} \text{products}, \quad (6)$$

where B, S, and M denote BNAH, a substrate, and zinc ion, respectively, and the subscript T means stoichiometric concentration. Computor-assisted analysis of kinetic data[1] gave numerical value of k^H as listed in Table 6.

Although k^H's are composite constants, there is no doubt that their relative magnitudes are in the same order as those of rate-constants for rate-determining

Table 2. Reduction of 1-acetylisoquinoline (AQ)

$[AQ]_T$ $\times10^3$, M	$[Zn^{2+}]_T$ $\times10^3$, M	$[BNAH]_T$ $\times10^4$, M	k_{obsd} $\times10^4$, s^{-1}
1.98	0.401	0.990	1.73
1.98	0.603	0.990	2.01
1.98	1.00	0.990	2.63
1.98	2.01	0.990	4.39
1.98	3.11	1.00	4.74
1.98	4.02	0.990	6.10
2.02	0.601	0.970[a]	0.909
2.02	1.03	0.970[a]	1.37
2.02	2.05	0.970[a]	1.84
2.02	3.00	0.970[a]	1.92

a) BNAH-4,4-d_2 was used.

Table 3. Reduction of 1-benzoylisoquinoline (BQ)

$[BQ]_T$ $\times10^3$, M	$[Zn^{2+}]_T$ $\times10^3$, M	$[BNAH]_T$ $\times10^4$, M	k_{obsd} $\times10^4$, s^{-1}
1.99	1.01	1.02	4.64
1.99	2.01	1.02	7.12
1.99	3.02	1.02	8.15
1.99	5.04	1.02	9.19
1.98	6.22	1.02	9.09
1.98	7.76	1.02	9.51
1.99	10.1	1.02	9.15
1.99	12.1	1.02	8.71
1.99	15.1	1.02	8.48
1.99	5.01	0.970[a]	3.17
1.99	8.01	0.970[a]	3.28
1.99	10.0	0.970[a]	3.36
1.99	15.0	0.970[a]	3.11

a) BNAH-4,4-d_2 was used.

Table 4. Reduction of isoquinoline-1-carbaldehyde (QCA)

$[QCA]_T$ $\times10^3$, M	$[Zn^{2+}]_T$ $\times10^3$, M	$[BNAH]_T$ $\times10^4$, M	k_{obsd} $\times10$, s^{-1}
1.99	0.501	1.03	4.46
2.00	1.00	1.03	4.78
1.99	1.50	1.03	5.42
2.00	2.00	1.03	6.19
1.99	2.51	1.03	6.40
2.00	3.01	1.03	5.88
1.99	3.99	1.03	6.11
2.00	4.51	1.03	5.59
1.99	4.99	1.03	4.63
1.99	5.98	1.03	4.19

Table 5. Reduction of pyridine-2-carbaldehyde (PCA)

$[PCA]_T$ $\times10^2$, M	$[Zn^{2+}]_T$ $\times10^2$, M	$[BNAH]_T$ $\times10^4$, M	k_{obsd} $\times10$, s^{-1}
1.00	0.204	1.01	4.95
1.00	0.297	1.01	5.14
1.00	0.306	1.01	3.91
1.00	0.503	1.01	6.13
1.00	0.621	1.01	7.57
1.01	0.689	0.980	7.41
1.00	0.836	0.980	7.16
1.01	1.19	0.980	5.78
1.00	1.50	1.01	4.55
1.00	1.52	0.980	4.19
1.00	2.01	0.980	3.05
1.00	2.03	1.01	3.84
1.00	2.54	1.01	2.65

Table 6. Computed third-order rate constant, k^H

Substituent	k^H, M^{-2} s^{-1}		Ratio[b]
	Pyridine[a]	Isoquinoline[a]	
H	3.32×10^5	1.33×10^6	4.01
	(1.72×10^4)	(6.89×10^4)	
Ph	2.37×10^2 [c]	4.05×10^2	1.71
	(1.22×10)	(2.10×10)	
Me	1.93×10[c]	2.25×10^2	11.7
	(1.00)	(1.17×10)	

a) Numbers in parentheses are relative values. b) Ratio of k^H for a 1-acylisoquinoline to that for the corresponding 2-acylpyridine. c) Data reported in Ref. 1.

proton (or hydrogen atom) transfer from BNAH to the substrates. Namely, the reduction is associated by large kinetic deuterium isotope effect, whereas no deuterium isotope effect is observed on complexation constant, as will be descibed below in detail. Variation in complexation constants is much smaller than that in rate constants, which means that relative magnitude of k^H is determined mainly by kinetic term.

Isotope Effects. Kinetics were also followed with BNAH-4,4-d_2 to obtain rate constants, k^D. Thus calculated deuterium isotope effects, k^H/k^D, are listed in Table 7. Reproducibility of two or three experiments was satisfactory. Errors in rate constants for PCA and QCA were, however, too large to obtain precise kinetic isotope effects. In Table 7 product isotope effect, Y^H/Y^D, for AP and AQ are also listed. The product isotope effect is defined as the ratio of isotope content at the particular position of the product alcohol obtained by the reduction with BNAH-4-*d*. For the other substrates, Y^H/Y^D could not be obtained because of thermal unstability of the corresponding alcohols on VPC. Y^H/Y^D's in the reduction with an NAD(P)H-model compound have been reported to be larger than 3.0 for many substrates.[9-14] The results indicate clearly that a hydrogen nucleus is transferred from BNAH to a substrate in the rate-determining step of the reduction.

Table 7. Kinetic and product isotope effects

Substituent	Pyridine		Isoquinoline	
	k^H/k^D	Y^H/Y^D	k^H/k^D	Y^H/Y^D
H	—	—	—	—
Ph	3.28[a)]	—	2.79	—
Me	3.21[a)]	3.2	2.45	3—5

a) Data from Ref. 1.

It should be noted that k^H/k^D's are appreciably smaller than Y^H/Y^D's for AQ and BQ, whereas both isotope effects are identical for AP and BP. The discrepancy between k^H/k^D and Y^H/Y^D reveals the existence of at least one intermediate prior to the rate-determining step of the reduction.

Reactivity of the Substrates. For certain substrates it has been established that the reduction proceeds through transfer of an electron, a proton, and an electron (or an electron and a hydrogen atom) in this order.[9,15-17] Therefore, the present reduction can also be proposed to proceed similarly, on the basis of the results described above.[18] That is, the facility of a substrate toward the reduction can be substituted by the stability of substrate-originated anion-radical counterpart of the radical-ion pair intermediate, becasue the cation-radical counterpart originates from BNAH and is common to all reductions.

It has been established that zinc ion catalyzes the initial electron-transfer process.[10,17] Zinc ion would also contribute to stabilize the anion radical by neutralizing the negative charge. Such stabilization is expected to be the largest in the anion radicals formed from PCA and QCA, because these substrates can interact with zinc ion most effectively as indicated by large complexation constants. The effect of zinc ion on the stabilities of anion radicals from AP and BP are expected to be a little smaller but still significant. On the other hand, anion radicals from AQ and BQ are supposed to be much less stabilized by zinc ion, because the interaction of AQ or BQ with zinc ion forces to distort stable conformations of these substrates as discussed in the previous section.

However, contribution of an aryl group to the stability of anion radicals should also be taken into consideration. Since the plane of benzene ring in the BQ–Zn^{2+} complex can be coplanar with the plane of carbonyl group where negative charge of the anion radical appears mainly, the benzene ring can delocalize the negative charge and contribute to the stability of anion radical. It should be noted that the negative charge on anion radicals of AP, BP, PCA, and QCA can also delocalize into pyridyl or isoquinolyl moiety. Since the distorted AQ-complex has no moiety that can delocalize the negative charge, no factor is pointed out at all to stabilize the corresponding anion radical. Consequently, stability of the radical-ion pair intermediate will increase in the order: AQ<BQ<BP<AP<PCA$\simeq$QCA as a result of participation of substituent and zinc ion.

On the other hand, ratios of k^H's listed in Table 6 indicate that the value for AQ *vs.* AP is much larger than those for other substrates. The large ratio should be accounted for by unexpectedly high reactivity of AQ against other substrates, becasue the similarity of structures of 2-acylpyridine complexes cannot predict the low reactivity only for AP.

It has been predicted that an unstable radical-ion pair intermediate requires higher free energy of transition for the electron-transfer step than that for the proton (or hydrogen atom)transfer step resulting in large discrepancy between k^H/k^D and Y^H/Y^D.[10] The present result agrees with this prediction. That is, the most unstable AQ-complex is associated by the largest discrepancy.

Conclusion. From the above discussion, it may be concluded that factors which govern the facility for complexation and for reduction are independent. Rather, a corbonyl group which weakly coordinates onto metal ion has large reactivity toward the reduction within a limited framework of substrate structure. In other words, strong coordination of a metal ion onto the reaction site of a substrate facilitates the complexation but interferes the reduction. This is in contrast to the idea previously proposed; a substrate is activated by metal ion upon the coordination onto the reaction site.[2,3,19-21]

Experimental

Materials. Acetonitrile was distilled three times on phosphorus pentaoxide and once on potassium carbonate, then kept in a bottle filled by dry argon and capped by a silicone-rubber stopper. 2-Acetylpyridine (AP; bp 95 °C/34 mmHg), 2-benzoylpyridine (BP; mp 42—44 °C), pyridine-2-carbaldehyde (PCA; bp 75 °C/22 mmHg), and zinc perchlorate were commercially available (Nakarai Chem. Co. and Merck & Co., Inc.). These acylpyridines were purified

by recrystallization or distillation prior to the use. Zinc perchlorate was dried at 120 °C *in vacuo* for 15 h and kept in a desiccator over calcium chloride.

1-Benzyl-1,4-dihydronicotinamide (BNAH),[14] BNAH-4-*d*, BNAH-4,4-d_2,[10] 1-acetylisoquinoline (AQ; purified by column chromatography),[22] 1-benzoylisoquinoline (BQ; mp 74.5—75 °C),[22] and isoquinoline-1-carbaldehyde (QCA; mp 53—54 °C)[23] were prepared according to literature procedures. Deuterium contents in BNAH-4-*d* and BNAH-4,4-d_2 were 99.0±1.0% for both.

Product Analysis. Each 1 mmol of a substrate, BNAH, and zinc perchlorate was dissolved into 10 ml of acetonitrile, and the solution was kept at 50 °C for 1 d under nitrogen atmosphere in the dark. An aqueous EDTA was added to this mixture and the product was extracted with dichloromethane. The organic layer was concentrated *in vacuo*. After the purification on column chromatography, the product was identified to be the corresponding alcohol by NMR and IR spectra. The spectra were identical to those of authentic samples. Other products except for the pyridinium salt were not detected on TLC and NMR. The yields of the isolated products were 60—70%.

In the case of QCA, the product alcohol was not stable under the air and could not be isolated. The quantitative production of the corresponding alcohol, however, was confirmed on VPC.

Complexation Constant. A series of acetonitrile solutions containing zinc perchlorate, the concentrations of which varied from 20 to 200 times excess against appropriate concentration of the substrate, were prepared. Each solution was placed in a UV-cell (1 cm) equipped with a silicone-rubber stopper, and the cell was kept for at least 5 min in the cell-compartment of a Union Giken SM-401 Spectrophotometer which was kept at 50.0±0.1 °C. The reference cell was filled with acetonitrile. The substrate in acetonitrile was added to the sample cell, then the spectrum was recorded. Reproducibility was satisfactory for each run.

Kinetics. For AQ and BQ, an acetonitrile solution for kinetics was prepared and placed in a UV-cell (1 cm) equipped with a silicone-rubber stopper. Kinetics was followed spectrophotometrically with a Union Giken SM-401 Spectrophotometer, the cell-compartment of which was kept at 50.0±0.1 °C. The reference cell was filled with acetonitrile, then BNAH in acetonitrile was added to the sample cell. It was confirmed that the order of incubation of reagents did not affect the kinetics.

For PCA and QCA, the reaction was so rapid that stopped-flow method was employed on a Union Giken RA-401 Rapid Reaction Analyzer equipped by a Union Giken Kinetic Data Processer System 71. An acetonitrile solution of a substrate containing zinc perchlorate and that of BNAH were placed in two reservoirs separately. The reservoirs and UV-cell were kept at 50.0±0.1 °C under argon atmosphere. After a few minutes of incubation, both solutions were mixed and the reaction was followed spectrophotometrically.

Since the solution of substrate including a high concentration of zinc perchlorate had an absorption near 360 nm, the decrease in the intensity of the absorption from BNAH was monitored at longer wavelength (370—400 nm).

Product Isotope Effect. A product obtained by the reduction with BNAH-4-*d* was analyzed for deuterium contents by mass spectrometry on a Shimadzu LKB-9000S GC-MS Spectrometer equipped with a PACK 300DG-b Computing System and areas of appropriate peaks were measured.

Spectroscopy. NMR spectra were recorded on a Varian T-60 Spectrometer or a JASCO JNM-FX 100 FT NMR Spectrometer. IR spectra were obtained with a Hitachi EPI-S2 Spectrometer.

Correlation of Physical Units. Physical units used in this report are correlated with SI-units by the following relationship.

1 M = 1 mol dm^{-3}, t/°C = T/K − 273.15,

p mmHg = 13.5951 × 980.665 × 10^{-2} p Pa.

References

1) A. Ohno, S. Yasui, R. A. Gase, S. Oka, and U. K. Pandit, *Bioorg. Chem.*, in press.

2) R. A. Gase, G. Boxhoorn, and U. K. Pandit, *Tetrahedron Lett.*, **1976**, 2889.

3) M. Hughes and R. H. Prince, *J. Inorg. Nucl. Chem.*, **40**, 703 (1978).

4) D. J. Creighton, J. Hajdu, and D. S. Sigman, *J. Am. Chem. Soc.*, **98**, 4619 (1976).

5) These compounds form complexes of two different types, SM and S_2M. Only first complexation constants, K_{S1}, are listed in Table 1. See Ref. 1 for detail.

6) J. Barassin, G. Queguiner, and H. Lumbroso, *Bull. Soc. Chim., Fr.*, **1967**, 4707.

7) a) Y. Kidani, M. Noji, and H. Koike, *Bull. Chem. Soc. Jpn.*, **48**, 239 (1975); b) R. R. Osborn and W. R. McWhinnie, *J. Chem. Soc., A*, **1967**, 2075.

8) a) R. A. Gase and U. K. Pandit, *J. Am. Chem. Soc.*, **101**, 7059 (1979); b) R. A. Gase, Ph. D. Thesis, Uiniv. of Amsterdam, Amsterdam, The Netherlands (1979).

9) A. Ohno, H. Yamamoto, T. Okamoto, S. Oka, and Y. Ohnishi, *Chem. Lett.*, **1978**, 65.

10) A. Ohno, S. Yasui, H. Yamamoto, S. Oka, and Y. Ohnishi, *Bull. Chem. Soc. Jpn.*, **51**, 294 (1978).

11) J. Hajdu and D. S. Sigman, *J. Am. Chem. Soc.*, **98**, 6060 (1976).

12) J. J. Steffens and D. M. Chipman, *J. Am. Chem. Soc.*, **93**, 6694 (1971).

13) R. H. Abels, R. F. Hutton, and F. H. Westheimer, *J. Am. Chem. Soc.*, **79**, 712 (1957).

14) D. Mauzerall and F. H. Westheimer, *J. Am. Chem. Soc.*, **77**, 2261 (1955).

15) E. M. Kosower, A. Teuerstein, H. D. Burrows, and A. J. Swallow, *J. Am. Chem. Soc.*, **100**, 5185 (1978).

16) a) Y. Ohnishi and A. Ohno, *Chem. Lett.*, **1976**, 697; b) N. Kito, Y. Ohnishi, M. Kagami, and A. Ohno, *ibid.*, **1974**, 353; c) A. Ohno and N. Kito, *ibid.*, **1972**, 369.

17) A. Ohno, H. Yamamoto, T. Shio, and S. Oka, unpublished results which will be submitted elsewhere.

18) *Cf.* also D. J. Creighton, J. Hajdu, G. Mooser, and D. S. Sigman, *J. Am. Chem. Soc.*, **95**, 6855 (1973).

19) M. Hughes and R. H. Prince, *Chem. Ind. (London)*, **1975**, 648.

20) S. Shinkai and T. C. Bruice, *J. Am. Chem. Soc.*, **94**, 8258 (1972).

21) D. J. Creighton and D. S. Sigman, *J. Am. Chem. Soc.*, **93**, 6314 (1971).

22) A. Kaufmann, P. Dändliker, and H. Burkharodt, *Ber.*, **46**, 2934 (1913).

23) R. S. Barrows and H. G. Lindeall, *J. Am. Chem. Soc.*, **64**, 2430 (1942).

Synthetic Photochemistry. XVIII.[1] A Sensitizer Dependence in the Photooxidation of Indene and Acenaphthylene. The Occurrence of *cis*-1,2-Glycol Formation in a Rose Bengal-sensitized Reaction

Toshihide HATSUI and Hitoshi TAKESHITA*

Reaeseach Institute of Industrial Science, 86, Kyushu University, Hakozaki, Fukuoka 812

(Received February 25, 1980)

Upon Rose Bengal-sensitized photooxygenation, indene and acenaphthylene afforded substantial amounts of the expected *cis*-glycols by means of the reduction of the intermediate dioxetanes. The formerly proposed structure of one of the isomeric methoxy hydroperoxides was revised on the basis of the chemical and spectral evidence.

Recently, we have found a new photochemical oxygenation process by which to form *cis*-1,2-glycols by means of the reduction of the intermediate dioxetanes.[2-4] To demonstrate the general applicability of this new process, we have carried out the experiments with indene (**1**) and acenaphthylene (**2**); the results will be described herein. Our selection of **1** as the reactant is due to the fact that, since the 1960's, the singlet oxygen oxidation of **1** has been investigated by many workers, and it is known to be the first dioxetane-forming arylolefin.[5,6] On the other hand, **2**, with no allylic hydrogen, should form only the cycloadducts.

When a methanolic solution of **1** was irradiated by means of a tungsten lamp at 15—20 °C with a relatively large amount of Rose Bengal (RB) under an oxygen atmosphere, the occurrence of KI-starch positive species was indicated; in fact, the silica gel column chromatography of the mixture afforded a pair of methoxy hydroperoxides (**3**, 17%, and **4**, 34%), together with *cis*-1,2-indandiol (**5**, 21%),[7] homophthalaldehyde (**6**, a trace amount), and cylic acetal (**7**, 25%). Both **3** and **4** were hydroperoxy derivatives, for sodium borohydride reduction gave the 2-methoxy-1-indanols (**8** and **9**) the latter of which was characterized as *p*-nitrobenzoate. Although the NMR spectra of **8** and **9** were too ambiguous for us to assign the methine protons of oxygen functions, those of their acetates (**10** and **11**) provided clear information for use in determining the location and stereochemistry. The structure of **5** was evident on the basis of the NMR analysis as well as the chemical correlation with its diacetate. The occurrence of **6** was assured by the NMR analysis of its reduction product, 2-[2-(hydroxymethyl)phenyl]-ethanol (**12**).

The photooxidation of **1** with Methylene Blue (MB) in methanol disclosed similar product distributions, except for the absence of **5**.

Subsequently, we have carried out the oxygenation with **2**. Thus, a methanol solution of **2** was irradiated by means of a 500-W tungsten lamp in the presence of RB under an oxygen atmosphere. The four products thus formed were identified and characterized as *cis*- (**13**, 45%) and *trans*-2-methoxy-1-acenaphthenols (**14**, 2%)[8] and *cis*- (**15**, 5%) and *trans*-2-methoxy-1-acenaphthenediols (**16**, 18%). The *cis-trans* isomerism in **15** and **16** was deduced from the different magnitudes of the spin-spin coupling constants and the indication of the internal hydrogen-bond for the methoxy-alcohol function of **15**, as well as the *m*-chloroperbenzoic acid (MCPA)-oxidation of **2**, where **16** was the major product (**16**:**15**=63:37).

However, the reaction products of **2** with MB were entirely different from those with RB; except for the *cis-cisoid-cis*-dimer (**17**, 5.3%) of **2**,[9] all the oxygenation products were related to a dioxetane, *i.e.*, 1,8-naphthalenedicarbaldehyde cyclic acetal (**18**, 22%), hydroxynaphthalide (**19**, 14%),[10,11] and methoxynaphthalide (**20**, 7%),[10,12] and 1,8-naphthalenedicarboxylic anhydride (**21**, 17%).[13] **18** was independently prepared from **13** by periodic acid-oxidation in methanol. **19** and the other carboxylic derivatives are probably secondary products produced by the autooxidation of unisolable 1,8-naphthalenedicarbaldehyde. The occurrence of *cis*-glycols from **1** and **2** was again confirmed only in the RB-sensitized photooxygenation; this sensitizer dependence for the substrates constitutes another example of the RB-sensitized photoreduction process of dioxetanes.

Previously, Kearns *et al.*[5] obtained a pair of methoxyindanols in the MB-sensitized photooxygenation of **1** and assigned them the structures of *trans*-1-methoxy-2-indanol (**B**) and *trans*-2-methoxy-1-indanol (**C**) on

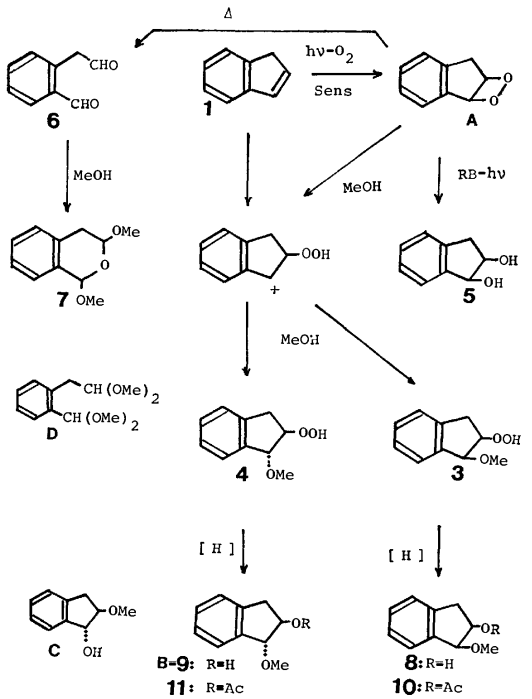

Scheme 1.

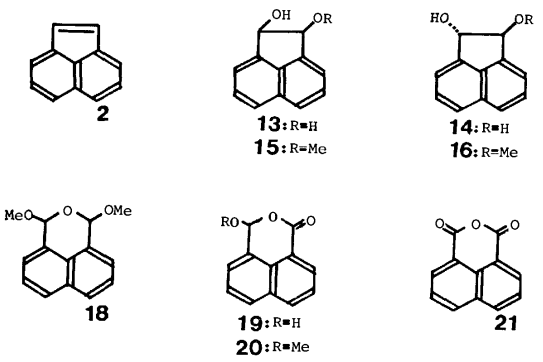

Scheme 2.

the basis of chemical correlations, following the previously known route.[14] Later, Foote *et al.*[6] suported this assignment for the structures of products derived from indene, except for that of acetal, to which Foote gave the **7** structure instead of the **D** originally given by Kearnes. The present results, however, showed some discrepancies; our **9** corresponds to **B**, but **8** does not correspond to **C**, and the structure of **7** agreed with the results of Foote. Since obtaining these indanols led Hasty and Kearns to claim a chemical trapping of the peroxirane[15] and has been cited in recent literature,[16,17] the settlement of this problem is important. The previous route of derivation involves the solvolytic substitution of 2-acetoxy-1-indanone;[18] the stable benzylic cation formed as the intermediate might therefore cause a shuffling of the substituents. Consequently, the reported formation of 2-methoxy-1-indanol based on this derivation seems to be unconvincing.

According to our reinvestigations, 2-acetoxy-1-indanone (**22**),[14,18] whose preparation from 2-bromo-1-indanone involved no rearrangement, was shown to give 2-methoxy-1-indanone (**23**, a quantitative yield) by the action of 3% hydrogen chloride in methanol under reflux for 90 min, but under less drastic conditions (40 °C for 45 min), **23** and 1-methoxy-2-indanone (**24**) were formed in a ratio of 1:1, while the additional heating of the mixture for 40 min at 40 °C caused the disappearance of **24**. In any case, we have not succeeded in finding the conditions by which to obtain

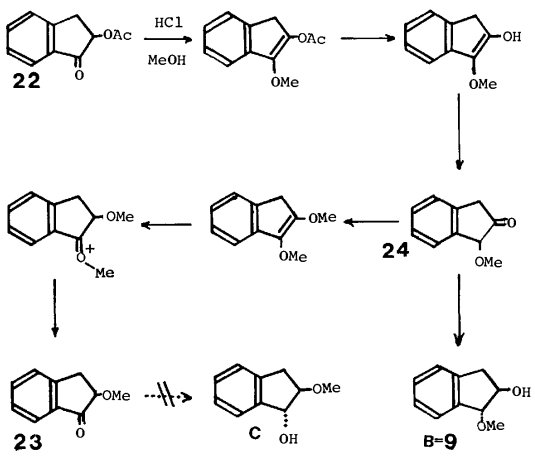

Scheme 3.

24 as a single solvolysate. Obviously, **23** is a thermodynamically stable product, while **24** is a kinetically controlled transient product, and not a simple substitution reaction, as is illustrated in Scheme 3.

The present result, the absence of an anti-Markovnikov methoxy hydroperoxide, should not only indicate the invalidity of the peroxirane hypothesis deduced on this structural basis, but should suggest also the necessity to reinvestigate the structural aspects of a related observation, *i.e.*, the formation of regioisomeric methoxy hydroperoxides from the peroxiranes of 1,3-pentadiene and 2,5-dimethyl-2,4-hexadiene.[15]

Experimental

*RB-sensitized Photooxygenation of **1** in Methanol.* A methanol solution (30 cm³) of 1 (674 mg) and RB (221 mg) was irradiated by means of a 500-W tungsten lamp at 15—20 °C for 48 h under an oxygen atmosphere. The mixture was then diluted with water and extracted with CH_2Cl_2. The extract was fractionated on a silica-gel column with hexane–ethyl acetate to give, first, a colorless oil (529 mg; 51%), which, together with a small amount of **6**, consisted mainly of **3** and **4** [δ[19]: 2.88 (1H, dd, J=17, 4 Hz), 3.32 (1H, dd, J=17, 7 Hz), 3.51 (3H, s), 4.80 (2H, m), 7.20 (4H, m), and 8.88 (1H, OH)] in a ratio of 1:2; subsequently, fractionation gave **5**, colorless crystals (mp 102.5—103 °C (lit,[7] 99—101 °C); 185 mg (21%) [δ: 2.86 (1H, dd, J=16.5, 3.5 Hz), 3.00 (1H, dd, J=16.5 6 Hz), 3.33 (2H, br. OH), 4.32 (1H, m), 4.84 (1H, d, J=5 Hz), and 7.20 (4H, m)]), together with **7**, a colorless oil (280 mg (25%) [δ: 2.92 (2H, m), 3.56 (3H, s), 3.59 (3H, s), 5.06 (1H, m), 5.64 (1H, s), and 7.2 (4H, s)]).

*Diacetate of **5**.* Prepared by acetic anhydride in pyridine as colorless needles; mp 48—48.5 °C (lit,[7] 50.8—51.6 °C) [δ: 2.06 (3H, m), 2.08 (3H, s), 3.17 (2H, m), 5.51 (1H, td, J=6.3, 5.4 Hz), 6.19 (1H, d, J=5.4 Hz), and 7.26 (4H, m)].

*Sodium Borohydride Reduction of the Mixture of RB-sensitized Photooxygenation Products of **3**.* The photooxidation mixture obtained from **1** (609 mg) with RB (164 mg) for 24 h was directly reduced with $NaBH_4$ (10 mg) at room temperature. The mixture was then evaporated *in vacuo*, and the residue was chromatographed on a silica-gel column. The products identified were **7** (123 mg; 12%), **8** (72 mg; 8.4%) [Found: M. W., 164.0820. Calcd for $C_{10}H_{12}O_2$: 164.0837. δ: 2.85 (1H, br., OH), 3.02 (2H, m), 3.52 (3H, s), 4.53 (2H, m), and 7.25 (4H, m). δ (C): 39.0, 57.0, 72.4, 84.1, 125.5, 126.5, 128.9, 139.7, and 141.0. ν: 3560. 1110, 1100, 1080 cm^{-1}]), **9** (180 mg; 21%) [Found: *m/e*, 164. δ: 2.72 (1H, dd, J=16, 5.2 Hz), 2.8 (1H, br. OH), 3.24 (1H, dd, J=16, 6.8 Hz), 3.52 (3H, s), 4.44 (1H, m), 4.58 (1H, d, J=4 Hz), and 7.20 (4H, m). ν: 3620, 3440, 1095 cm^{-1}]), and **5** (23 mg; 3%).

*Acetate (**10**) of **8**.* Prepared by the use of acetic anhydride in pyridine as a colorless oil [δ: 2.10 (3H, s), 3.12 (2H, d, J=6 Hz), 3.44 (3H, s), 4.72 (1H, d, J=5 Hz), 5.44 (1H, dt, J=6, 5 Hz), and 7.24 (4H, m). δ(C): 21.1, 35.9, 57.5, 74.3, 82.7, 125.0, 125.3, 126.9, 128.9, 139.8, and 170.9. ν: 1740, 1240 cm^{-1}].

*Acetate (**11**) of **9**.* Prepared similarly as a colorless oil [δ: 2.06 (3H, s), 2.81 (1H, dd, J=16.7, 4 Hz), 3.50 (1H, dd, J=16.7, 6.8 Hz), 3.52 (3H, s), 4.77 (1H, d, J=3.2 Hz), 5.39 (1H, ddd, J=6.8, 4, 3.2 Hz), and 7.25 (4H, m), δ(C): 21.0, 36.8, 56.9, 78.8, 87.9, 124.9, 125.3, 126.9, 129.0, 139.7, 140.3, and 170.3].

p-*Nitrobenzoate of* ***9***. Prepared by the treatment of *p*-nitrobenzoyl chloride in pyridine at room temperature as pale yellow needles; mp 84.5—85 °C [Found: C, 65.16; H, 4.68, N, 4.54%. Calcd for $C_{17}H_{15}O_5N$: C, 65.17 H, 4.82; N, 4.47%].

MB-sensitized Photooxygeanation of ***1***. A methanol solution (25 cm³) of **1** (540 mg) and MB (60 mg) was irradiated by means of 500 W tungsten lamp for 28 h under an oxygen atmosphere. The mixture was then directly reduced with $NaBH_4$ to decompose the peroxy derivatives. After the evaporation of the whole mixture, the residue was chromatographed on a silica-gel column to give **7** (59 mg; 6.5%), **12** (a colorless oil; 185 mg (27%) [δ: 2.85 (2H, t, J=6 Hz), 3.70 (2H, br. OH), 3.76 (2H, t, J=6 Hz), 4.53 (2H, s), and 7.20 (4H, m). δ(C): 35.0, 62.4, 62.8, 126.4, 128.1, 129.2, 129.9, 137.8, and 138.9]), **8** (150 mg; 20%), and **9** (153 mg; 20%).

*Bis(*p-*nitrobezoate) of* ***12***. Prepared by the usual manner as colorless prisms; mp 133.5—134 °C (lit,[20] 134—135 °C) [δ: 3.23 (2H, t, J=7 Hz), 4.51 (2H, t, J=7 Hz), 5.49 (2H, s), 7.32 (4H, m), 8.16 (4H, m), and 8.18 (4H, s)].

RB-sensitized Photooxygenation of ***2***. A mixed solution (30 cm³) of methanol and acetone (1:2) of **2** (504 mg) and RB (100 mg) was similarly irradiated by means of a tungsten lamp under an oxygen atmosphere for 90 h at 15—20 °C. The reaction mixture was then heated at 30 °C *in vacuo* to remove the solvents. The residue was chromatographed on a silica-gel column. The recovered **2** (300 mg) was obtained by elution with hexane–ethyl acetate (95:5); subsequent elution with hexane–ethyl acetate gave colorless needles of **15** (mp 91.5—92.5 °C; 14 mg (5%) [Found: C, 77.99; H, 6.11%. Calcd for $C_{13}H_{12}O_2$: C. 77.98; H, 6.04%. δ: 3.26 (1H, d, J=7 Hz, OH), 3.62 (3H, s), 5.01 (1H, d, J=6 Hz), 5.50 (1H, dd, J=7, 6 Hz), and 7.4—7.8 (6H, m). ν: 3430, 1102, 780 cm^{-1}]), a colorless oil, **16** (49 mg (18%) [Found: C, 77.77; H, 6.06%. δ: 3.15 (1H, br., OH), 3.48 (3H, s), 4.90 (1H, d, J=2 Hz), 5.31 (1H, d, J=2 Hz), and 7.2—7.7 6H, m). ν: 3620, 3430, 1110, 775 cm^{-1}]), colorless needles, **13** (mp 213—214 °C (lit,[9] 218—219 °C), 101 mg (45%) [δ: 2.76 (2H, br., OH), 5.50 2H, br. d, J=7 Hz), and 7.2—7.8 (6H, m). ν: 3330, 3200, 1110, 775 cm^{-1}]), and colorless needles, **14** (mp 158—160 °C (lit,[8] 160—163 °C), 6 mg (2%) [δ: 3.3 (2H, br., OH), 6.42 (2H, br. s), 7.4—7.6 (4H, m), and 7.7—7.9 (2H, m). ν: 3360, 985 cm^{-1}]).

Acetylation of ***13***. This yielded colorless prisms; mp 132—134 °C (lit,[8] 134.5—136.5 °C) [δ: 2.12 (6H, s), 6.60 2H, s), and 7.4—7.8 (6H, m). ν: 1775, 1240, 775 cm^{-1}]).

Acetylation of ***14***. This yielded a colorless oil (lit,[8] a colorless oil) [δ: 2.09 (6H, s), 6.54 (2H, s), and 7.4—7.9 (6H, m). ν: 1745, 1370, 1240 cm^{-1}].

MB-sensitized Photooxygenation of ***2***. A mixed solution (30 cm³) of methanol and acetone (1:2) of **2** (500 mg) and MB (60 mg) was similarly irradiated under an oxygen atmosphere for 177 h. The mixture was then heated *in vacuo* to remove the solvent, and the residue was purified through a silica-gel column; from the hexane eluent, a photodimer of **2** (**17**) as colorless needles (mp 233—235 °C (lit,[9] 232—234 °C); 13 mg) and the recovered **2** (256 mg) were thus obtained. Subsequently eluted from hexane–ethyl acetate were a dimethyl acetal of 1,8-naphthalenedicarbaldehyde, **18** (a colorless oil, 77 mg; 22%), a methoxy lactone, **20** (pale yellow prisms; mp 105—106.5 °C (lit,[10] 104 °C), 23 mg (7%) [δ: 3.66 (3H, s), 6.42 (1H, s), 7.45—7.75 (3H, m), 7.90 (1H, m), 8.08 (1H, dd, J=9, 1 Hz), and 8.40 (1H, dd, J=7, 1 Hz). ν: 1728, 1090, 1000 cm^{-1}]), a hydroxy lactone, **19** (pale yellow needles, mp 175—176 °C (lit,[12] 167 °C), 43 mg (14%) [δ: 6.86 (1H, s), 7.35—7.95 (4H, m), 8.08 (1H, dd, J=8, 1 Hz), and 8.37 (1H, dd, J=7, 1 Hz). ν: 3280, 1680, 1120, 1005, 925, 775 cm^{-1}]), and 1,8-naphthalenedicarboxylic anhydride, **21** (pale yellow needles, mp 268—270 °C (lit,[13] 271—272 °C), 55 mg; 17%).

2-Acetoxy-1-indanone (***22***) was prepared from 2-bromo-1-indanone in accordance with Ishiwara's procedure.[18] Its purity was confirmed by the NMR [δ: 2.16 (3H, s), 3.04 (1H, dd, J=17, 5 Hz), 3.60 (1H, dd, J=17, 8 Hz), 5.38 (1H, dd, J=8, 5 Hz), and 7.25—7.8 (4H, m)].

Preparation of 2-Methoxy-1-indanone (***23***). *a)*: To a methanolic 3% HCl solution (10 cm³), **22** (107 mg) was added and refluxed for 90 min. After the evaporation of the solvent, the residual mixture (95 mg) was analyzed by means of the NMR [δ: 3.00 (1H, dd, J=16, 4 Hz), 3.48 (1H, dd, J=16, 7 Hz), 3.61 (3H, s), 4.17 (1H, dd, J=7, 4 Hz), and 7.2—7.8 (4H, m)] spectrum and found to be practically pure 2-methoxy-1-indanone (**23**).

b): Similarly, **22** (80 mg) in the methanolic hydrogen chloride (8 cm³, 3%) was heated at 40 °C for 45 min. The NMR spectrometry of the mixture indicated it to be *ca.* a 1:1-mixture of **23** and 1-methoxy-2-indanone (**24**) [δ: 3.50 (2H, s), 3.57 (3H, s), 4.75 (1H, s), and 7.2—7.8 (4H, m)]. Upon prolonged heating at 40 °C with the additional introduction of a 3% methanolic HCl (5 cm³), **24** disappeared from the mixture.

MCPA-oxidation of ***2*** *in Methanol*. A methanolic solution (10 cm³) of **2** (100 mg) and MCPA (120 mg) was kept at room temperature for 24 h. Subsequently, the silica gel column chromatography of the mixture afforded **15** (31 mg; 37%), and **16** (50 mg; 60%), together with the recovered **2** (37 mg).

Cleavage of ***13*** *with Periodic Acid*. A methanol solution (5 cm³) of **13** (25 mg), containing HIO_4 (70 mg) and water (1 cm³) was kept at room temperature for 1 h. The mixture was then neutralized by $NaHCO_3$ and chromatographed on a silica-gel column to give **18** (18 mg; 49%), identical with the sample obtained by photooxygenation.

References

1) Part XVII, T. Hatsui and H. Takeshita, *Bull. Chem. Soc. Jpn.*, **53**, 2027 (1980).
2) H. Takeshita and T. Hatsui, *J. Org. Chem.*, **43**, 3080 (1978).
3) H. Takeshita, T. Hatsui, and I. Shimooda, *Tetrahedron Lett.*, **1978**, 2889.
4) H. Takeshita, T. Hatsui, and H. Mametsuka, *Heterocycles*, **11**, 323 (1978).
5) W. Fenical, D. R. Kearnes, and P. Radlick, *J. Am. Chem. Soc.*, **91**, 3396 (1969).
6) C. S. Foote, S. Mazur, P. A. Burns, and D. Lerdal, *J. Am. Chem. Soc.*, **95**, 586 (1973).
7) W. E. Rosen, L. Dorfman, and M. P. Linfield, *J. Org. Chem.*, **29**, 1723 (1964).
8) L. D. Hayward and I. G. Csizmadia, *Tetrahedron*, **19**, 2111 (1963).
9) K. Dziewonski and C. Rapalski, *Chem. Ber.*, **46**, 1990 (1913).
10) K. Bowden and A. M. Last, *J. Chem. Soc., Perkin Trans. 2*, **1973**, 358.
11) H. Bader and Y. H. Ching, *Synthesis*, **1976**, 249.
12) K. Bowden and A. M. Last, *J. Chem. Soc., Perkin Trans. 2*, **1973**, 1144.
13) N. C. Deno, *J. Am. Chem. Soc.*, **70**, 4057 (1973).
14) W. Treibs and W. Schroth, *Ann. Chem.*, **639**, 204 (1960).

15) N. Hasty and D. R. Kearnes, *J. Am. Chem. Soc.*, **95**, 3380 (1973).
16) A. P. Schaap and K. A. Zaklika, "1,2-Cycloaddition Reaction of Singlet Oxygen," in "Singlet Oxygen," ed by H. H. Wasserman and R. W. Murray, Academic Press., N. Y. (1979), p. 209.
17) A. Frimer, *Chem. Rev.*, **79**, 359 (1979).
18) F. Ishiwara, *J. Prakt. Chem.*, **108**, 194 (1924).
19) The ^{1}H- and ^{13}C-NMR spectra were obtained in $CDCl_3$ solutions, and the chemical shifts were expressed in the δ values from the internal standard, Me_4Si.
20) J. L. Warnell and R. L. Shriner, *J. Am. Chem. Soc.*, **79**, 3165 (1957).

Bondings on the TeI_4 Tetramer, as Studied by Means of NQR

Tsutomu Okuda,* Koji Yamada, and Hisao Negita
Department of Chemistry, Faculty of Science, Hiroshima University, Hiroshima 730
(Received February 29, 1980)

The ^{127}I NQR and its Zeeman effect on the TeI_4 single crystal were investigated. Ten nonequivalent iodine atoms were detected, in agreement with the X-ray analysis by Krebs and Paulat. Six of them were assigned to terminal atoms, two to bridge atoms, and the remaining two to pyramidal iodine atoms, on the basis of their quadrupole coupling constants and asymmetry parameters. One of the bridging iodine atoms takes an efg z-axis parallel to the shorter Te–I bond, but the other bridging iodine atom takes an efg z-axis perpendicular to the bridging plane. This difference can be explained by a simple model based on the Townes-Dailey treatment and is consistent with that difference to be expected from the bridging-bond length. The extremely small coupling constants for the pyramidal iodine atoms could be interpreted by covalency, assuming a hybridization of the s-orbital to the pure p-bond configuration.

According to Krebs and Paulat[1] the crystal of tellurium tetraiodide is orthorhombic (space group Pnma), with 16 TeI_4 in the unit cell. As is shown in Fig. 1, the structure is built of $(TeI_4)_4$ tetramers which are different from the $(TeCl_4)_4$ tetramer in molecular structure.[2] The $(TeI_4)_4$ tetramer has a reflection plane parallel to the ac plane. This tetramer is interesting in its structure and bonding, because it consists of three types of iodine atoms, that is, terminal, bridging, and pyramidal atoms. The last type of iodine atom was called "triply bridging iodine" by Krebs and Paulat. In the light of the NQR study, the following information has been obtained and may be discussed with the framework of the Townes-Dailey theory. (1) Angular bridging halogens are well known in dimeric compounds, M_2X_6 (M=Al, Ga, and In; X=Br and I). In these molecules, the bridging bonds are symmetrical, so that the orientations of the efg axes can be expected from the symmetry.[3,4] However, as the bridging iodine atoms in this tetramer form asymmetric bonds with two tellurium atoms, the orientations of the efg axes should depend upon the covalent character of the two Te–I bonds. In addition, it is valuable to examine the temperature dependence of the e^2Qq/h for the asymmetric bridging iodine with a definite efg axis orientation. (2) The quadrupole coupling constants for the pyramidal halogen in a normal oxidation state have been reported only for CdI_2 (X=Br and I),[5] as far as we know. The small e^2Qq/h values for the halogens in CdI_2 were interpreted in terms of covalency, assuming the hybridization of the s-orbital to the three-orthogonal-p-bonding configulation. The validity of this model was tested for the pyramidal iodine in the TeI_4 tetramer.

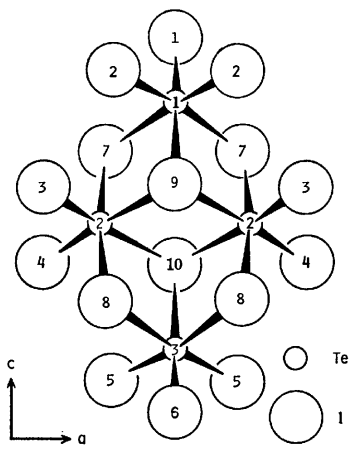

Fig. 1. Tetrameric molecular unit in the TeI_4 crystal.[1]

A part of this work has already reported elsewhere,[6] but there has been no precise discussion of the bridging iodine because of the lack of the crystal structure, which is now established.

Experimental

The TeI_4 single crystal was grown by the Bridgman-Stockbarger method in a Pyrex tube in which stoichiometric amounts of tellurium and iodine were sealed under reduced pressure. The NQR spectra and their Zeeman effect were observed according to a procedure similar to one described previously.[6,7] In the detection of the pyramidal iodine NQR signal, a Zeeman modulated Dean-type spectrometer was used. The Zeeman effect for the bridging iodine atom was observed at the temperature of liquid nitrogen in order to increase the S/N ratio of the NQR signal.

Results

The Zeeman effect on the terminal iodine was observed in order to obtaine the orientations of the crystal axes for the single crystal employed. As is to be expected from the Laue symmetry of the crystal, four zero-splitting cones were observed for the iodine in the general position. Table 1 shows the direction cosine of the efg z-axis with respect to the crystal axes, which were determined from the symmetry of the observed zero-splitting cones. As is evident from the last column of this table, the efg z-axis coincides with that of the Te–I bond within one degree.

On the other hand, in any discussion of the bridging iodine, not only the z-axis but also the x- and y-axes are necessary. In the case of an iodine atom with a pair of lines, $\nu_1(\pm 1/2 \leftrightarrow \pm 3/2)$ and $\nu_2(\pm 3/2 \leftrightarrow \pm 5/2)$, the behavior of their zero-splitting cones on η has been described elesewhere.[6] In general, efg x-, y-, and z-axes are determined only from the ν_1 cone except for $\eta \fallingdotseq 0$ and $\fallingdotseq 1$. Figure 2 shows the ν_1 patterns and the corresponding efg axes for the I(7) atom at 77 K, where the center of the pattern is pointed toward its y-axis ($\eta > 0.412$). When an η value approaches 1, such as in the case of I(8), the ν_1 and ν_2 lines both show axially symmetric cones around their y- and

Table 1. Direction cosines of the efg q_{zz}-axes and the corresponding terminal Te-I bonds (in parentheses) with respect to the crystal axes (296 K)

	e^2Qq/h / MHz	η	Direction cosine			$\angle q_{zz}$, Te-I / degree
			a	*b*	*c*	
I(1)	1522.3	0.032	−0.7035	0.001	0.7107	0.88
			(−0.6924)	(0)	(0.7215)	
I(2)	1680.9	0.029	0.5670	0.7361	0.3697	0.52
			(0.5597)	(0.7394)	(0.3741)	
I(3)	1672.0	0.014	0.6262	0.6498	0.4308	0.38
			(0.6225)	(0.6549)	(0.4285)	
I(4)	1612.8	0.056	−0.5791	0.6890	−0.4357	0.60
			(−0.5825)	(0.6921)	(−0.4262)	
I(5)	1560.1	0.056	−0.5479	0.7466	−0.3773	0.61
			(−0.5554)	(0.7404)	(−0.3786)	
I(6)	1621.8	0.012	0.6791	0.002	−0.7340	
			(0.6756)	(0)	(−0.7372)	0.32

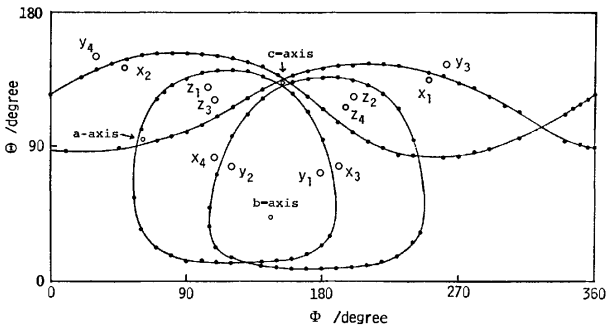

Fig. 2. Zero-splitting loci of the ν_1 line corresponding to the I(7) atom at 77 K.
○: Crystal axis, ○: efg axis.

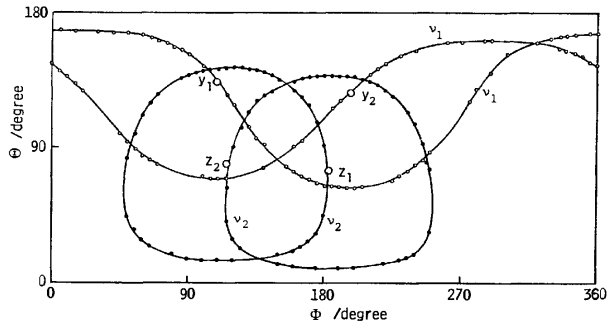

Fig. 3. Zero-splitting loci of the ν_1 and ν_2 lines corresponding to the I(8) atom.
-○-: ν_1, -●-: ν_2, ○: efg axis.

z-axes respectively. Therefore, the Zeeman effect on both ν_1 and ν_2 lines must be measured in the determination of the three orthogonal efg axes. Figure 3 shows the zero-splitting patterns corresponding to ν_1 and ν_2 for the I(8) atom. Because of the small S/N ratio, two patterns out of four were observed. The other two orientations of the patterns may be expected from the crystal symmetry. The resultant orientations of the efg axes with respect to their bridging bonds are illustrated in Fig. 4, while their angles are shown in

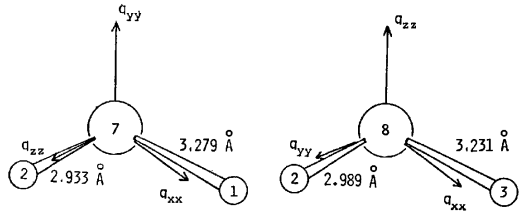

Fig. 4. Orientations of the efg axes with respect to its bridging plane.

Table 2. Bridging iodine NQR parameters (296 and 77 K) and angles between efg axes and Te-I bonds[a]

	e^2Qq/h / MHz	η	Angles: efg axis	Bridging bond	
				Te(2)-I(7)	Te(1)-I(7)
I(7)	929.6 (940.5)	0.738 (0.752)	x	90.9°	6.4°
			y	89.4°	92.9°
			z	1.2°	95.9°
				Te(2)-I(7)	Te(3)-I(8)
I(8)	775.1 (793.7)	0.949 (0.917)	x	85.5°	10.4°
			y	4.5°	98.0°
			z	90.1°	88.5°

a) NQR parameters at 77 K in parentheses.

Table 2, also with the NQR parameters. In this calculation, we assumed that there is no significant change in the crystal structure from room temperature to 77 K because of the continuous temperature dependence of the e^2Qq/h.[6]

Table 3 gives the NQR parameters of the pyramidal halogens in TeI_4 and $TeBr_4$. The crystal of tellurium tetrabromide consists of tetramers, containing terminal and pyramidal bromine atoms, and is isomorphous with tellurium tetrachloride.[8,9]

Discussion

Quadrupole Coupling Constants for the Bridging Iodine. According to the X-ray data, the bridging bond lengths

Table 3. ^{127}I and ^{81}Br NQR parameters of the pyramidal halogens at 293 and 77 K (in parentheses)[a]

Compound	$\nu_1(\pm1/2\leftrightarrow\pm3/2)$ MHz	$\nu_2(\pm3/2\leftrightarrow\pm5/2)$ MHz	e^2Qq/h MHz	η
TeI_4	8.794 (7.984)	17.008 (15.529)	57.00 (51.99)	0.163 (0.148)
	8.982 (9.278)	16.472 (17.189)	55.68 (60.22)	0.268 (0.250)
$TeBr_4$	13.539 (12.513)[b]			
	12.626			

a) Estimated error in ν: 0.01 MHz. b) Doublet.

in the Te(1)–I(7)–Te(2) are 2.933 and 3.279 Å, while those in the Te(2)–I(8)–Te(3) are 2.989 and 3.231 Å. The former bridging is more asymmetric than the latter. As is obvious from Fig. 4, the bridging atoms take their efg x-axes in the direction of their longer bonds in both cases, but the z- and y-axes change in different directions. We will explain the large asymmetry parameter and the orientations of the efg axes using a simple model. We assume that the bonding of the iodine atom is composed of pure p-orbitals, because the bridging angle is close to 90° ($\angle$Te(1)I(7)Te(2)=95.3°; $\angle$Te(2)I(8)Te(3)=95.7°). Furthermore, the p_x, p_y, and p_z orbitals of the bridging iodine atom are chosen to lie along the efg x-, y-, and z-axes of the I(7) atom. Then, Te–I–Te bonds are formed by donations from the two lone-pair electrons on the I^- ion to the orbitals of the tellurium atoms. The p_y orbital, which is normal to the bridging plane, is assumed to be occupied by a lone pair. The quadrupole coupling constants are easily obtained as follows:[10]

$$\left.\begin{aligned} e^2Qq_{xx}/e^2Qq_p &= N_x - (2+N_z)/2 \\ e^2Qq_{yy}/e^2Qq_p &= 2 - (N_x+N_z)/2 \\ e^2Qq_{zz}/e^2Qq_p &= N_z - (2+N_x)/2 \end{aligned}\right\}, \quad (1)$$

where e^2Qq_p/h is a quadrupole coupling constant for one 5p electron of iodine, and where N_x and N_z are the occupation numbers for the p_x and p_z orbitals. Then, the electrons donated to the tellurium atom from the p_x and p_z orbitals are represented by $2-N_x$ and $2-N_z$ respectively. We here introduce the parameter, k, defined by the donating-electron ratio from the I^- ion, *i.e.*:

$$k = (2-N_x)/(2-N_z), \quad (2)$$

where $0\leq k\leq 1$.

Thus Eq. 1 becomes:

$$\left.\begin{aligned} e^2Qq_{xx}/e^2Qq_p &= (2-N_z)\{(1/2)-k\} \\ e^2Qq_{yy}/e^2Qq_p &= (2-N_z)\{(1/2)+(k/2)\} \\ e^2Qq_{zz}/e^2Qq_p &= (2-N_z)\{-1+(k/2)\} \end{aligned}\right\}. \quad (3)$$

This equation holds only for the case of $0\leq k\leq 1/2$ because of the $|e^2Qq_{zz}|\geq|e^2Qq_{yy}|\geq|e^2Qq_{xx}|$ condition. In such a case, the asymmetry parameter is given by:

$$\eta = 3k/(2-k). \quad (4)$$

When $1/2\leq k\leq 1$, the absolute quadrupole coupling constant along y-axis becomes larger than that of the z-axis. Therefore, the efg z- and y-axes change their orientations in relation to each other. In this case, e^2Qq_{zz}/h is given by:

$$e^2Qq_{zz}/e^2Qq_p = (2-N_z)\{(1/2)+(k/2)\}, \quad (5)$$

with the asymmetry parameter:

$$\eta = (3-3k)/(1+k). \quad (6)$$

Using Eqs. 2—6 and the observed efg-axes orientations, we obtained k=0.395 and 0.519 for the I(7) and I(8) atoms respectively. In this calculation, the e^2Qq/h values for the I(7) and I(8) atoms were regarded as opposite in sign because of the orientation of their z-axes. These k values are consistent with the expectation from the bond length. Table 4 shows the occupation numbers of the p-orbitals.

Table 4. Bond length, p-orbital population, and net charge for the three types of iodine atoms (296 K)

Bonding type	Bond length/Å	Population	Net charge
Terminal	2.769[a]	1.30, 2.00, 2.00	−0.30
Bridge	2.933, 3.279	1.49, 1.80, 2.00	−0.29
	2.989, 3.231	1.55, 1.77, 2.00	−0.32
Pyramid[b]	3.232[a]	1.77, 1.77, 1.77	−0.30

a) Mean values. b) sp^3 hydridization assumed.

In a previous paper we reported the temperature dependence of the e^2Qq_{ii}/h values (ii=xx, yy, and zz) for the two bridging iodines, where quite different features were observed in each case. We explained it with a model in which the characteristic oscillation of the bridging atom leads to an anisotropic change in the quadrupole coupling tensor. Thus, the differnt orientations of the efg axes were predicted from the temperature dependence, although symmetrical bridging bonds were assumed at that time.

Quadrupole Coupling Constants for the Pyramidal Iodine. The mean Te–I bond length in the pyramidal iodine atoms is 3.232 Å, nearly equal to the longer bridging bond length, 3.231 Å, of Te(3)–I(8) or that of 3.279 Å of Te(1)–I(7). This fact suggests the small extent of the covalent character on the pyramidal iodine. Therefore, the extremely small e^2Qq/h value is explained by the fact that the three bonding orbitals are nearly orthogonal. We adopt an sp^3 hydridization with C_{3v} symmetry, according to Ref. 5. The quadrupole coupling constant for the pyramidal iodine is, then, given by:[11]

$$e^2Qq/e^2Qq_p = \{3\cos\theta/(\cos\theta-1)\}(N_s-N_p), \quad (7)$$

where θ is the $\angle$TeITe angle (92.08° on the average) and where N_s and N_p are the populations for the

lone pair and the Te–I bond respectively. From this equation, we get $N_p=1.766$, assuming $N_s=2.0$.

Bonding and Charge Distribution in the Tetramer. Table 4 lists the bond length, p-orbital population, and net charge on the iodine, where no s-oribtal of the terminal atom is assumed to participate in the hybridization, as was suggested by the Mössbauer parameters.[12] If we plot the p-orbital population against its bond length, a smooth line can be obtained containing all the Te–I bonds. Therefore, it seems reasonable to assume an sp^3 hybridization model on the pyramidal atom to account for its e^2Qq/h value. In addition, it is interesting that the net charges on the iodine atoms are all in the same range, in spite of their quite different bonding schemes.

References

1) V. B. Krebs and V. Paulat, *Acta Crystallogr., Sect. B*, **32**, 1470 (1976).
2) B. Buss and B. Krebs, *Inorg. Chem.*, **10**, 2795 (1971).
3) G. E. Peterson and P. M. Bridenbaugh, *J. Chem. Phys.*, **51**, 238 (1969).
4) T. Okuda, H. Terao, O. Ege, and H. Negita, *J. Chem. Phys.*, **52**, 5489 (1970).
5) R. G. Barnes, S. L. Segel, and W. H. Jones, *J. Appl. Phys.*, **33**, 296 (1962).
6) T. Okuda, K. Yamada, Y. Furukawa, and H. Negita, *Bull. Chem. Soc. Jpn.*, **48**, 3480 (1975).
7) K. Yamada, *J. Sci. Hiroshima Univ., Ser. A*, **41**, 77 (1977).
8) C. B. Shoemaker and S. C. Abrahams, *Acta Crystallogr.*, **18**, 296 (1965); A. W. Cordes, R. F. Kruh, E. K. Gordon, and M. K. Kemp, *ibid.*, **17**, 756 (1964).
9) T. Okuda, K. Yamada, Y. Furukawa, and H. Negita, *Bull. Chem. Soc. Jpn.*, **48**, 376 (1975).
10) T. P. Das and E. L. Hahn, "Nuclear Quadrupole Resonance Spectroscopy," Solid State Physics, Suppl. 1, Academic Press, New York (1957).
11) E. A. C. Lucken, "Nuclear Quadrupole Coupling Constants," Academic Press, New York (1969).
12) C. H. W. Jones and M. Mauguin, *J. Chem. Phys.*, **68**, 3067 (1978).

 © 1980 The Chemical Society of Japan Bull. Chem. Soc. Jpn., 53, 2663—2665 (1980)

The Synthesis and Decomposition of Calcium Tetraphosphate

Makoto WATANABE,* Hiroyasu SUZUMORI, Mioko MAEDA, and Tamotsu YAMADA

Department of Industrial Chemistry, Chubu Institute of Technology, Matsumoto-cho, Kasugai, Aichi 487

(Received January 24, 1980)

Calcium tetraphosphate was made by hydrolyzing cyclotetraphosphate in a 5-mol dm^{-3}-solution of sodium hydroxide, neutralizing the phosphate solution with 1 mol dm^{-3} hydrochloric acid, and then adding calcium chloride to the solution. The P/Ca molar ratio of the product was 1.4—1.5. The tetraphosphate was an amorphous substance containing 20—30% of water and was decomposed to phosphates with a shorter chain length with bound water at room temperature or at a higher temperature. Upon decomposition at 300 °C, the main product at the early stage was pyrophosphate. The hydrolysis of the tetraphosphate obeyed the first-order kinetics with respect to the concentration of the phosphate, and the activation energy of the hydrolysis was 105 kJ mol^{-1} at pH 3.5.

Studies of calcium orthophosphates have been made by many workers, but calcium polyphosphates have not been studied well, and even the synthetic methods for most of them have not yet been published. Among chain polyphosphates, the phosphates having shorter chain lengths than that of triphosphate have been investigated well because of the ease of the synthesis of these phosphates. Polyphosphates with longer chains than that of tetraphosphate are, however, very difficult to prepare. Tetraphosphate ions are made by the hydrolysis of cyclotetraphosphate in an aqueous sodium hydroxide solution, but they have not been isolated and have not yet been studied well. In this paper, we will discuss the synthesis of calcium tetraphosphate by means of the hydrolysis of cyclotetraphosphate and some properties of the phosphate.

Experimental

Materials and Procedure. All the materials used, other than the sodium cyclotetraphosphate, were of a commercial grade. The sodium cyclotetraphosphate tetrahydrate was made by the method described in the literature.[1] About 20 g of sodium cyclotetraphosphate tetrahydrate was added to 50 cm^3 of a 5-mol dm^{-3}-aqueous solution of sodium hydroxide, and the mixture was stirred at about 20 °C for 4 d. Most of the sodium cyclotetraphosphate tetrahydrate was not dissolved in the sodium hydroxide solution, while the tetraphosphate produced by the hydrolysis of the cyclophosphate was well dissolved in the alkaline solution. Therefore, the progress of the hydrolysis of the cyclophosphate to tetraphosphate was observed visually by the defecation of the solution. The solution was filtered and neutralized with 1-mol dm^{-3} hydrochloric acid at a temperature below 3 °C, and then an aqueous solution of calcium chloride, which has been made by dissolving 30 g of calcium chloride in 30 cm^3 of water, was added to the tetraphosphate solution. A white precipitate was filtered off, washed with cold water and ethanol, and then dried in an air bath at 50 °C.

Paper Chromatography. One-dimensional paper-chromatographic separation was carried out by using acidic (for the separation of chain phosphates) and basic (for the separation of ring phosphates) solvents.[2] About 0.5 g of the product was dissolved in 25 cm^3 of a 2—8% aqueous disodium dihydrogen ethylenediaminetetraacetate dihydrate (EDTA) solution. About 8 mm^3 of the solution was spotted on Toyo No. 51A filter paper (2 by 50 cm). The development was run at 5 °C for 2 d.

Colorimetric Measurement of Phosphates. Every individual spot on the chromatogram was cut at the demarcation line and placed in a 100-cm^3 beaker containing 10 cm^3 of a 0.1 mol dm^{-3}-ammonium hydroxide solution. After 1 h, the solution was transferred to a 25-cm^3 volumetric flask, together with 10 cm^3 of wash water, and a 1-cm^3 portion of Lucena-Conde and Prat's reagent[3] was added to the flask. The flask was heated in a boiling-water bath for 1 h, subsequently cooled by placing it in a bath of cold water, and diluted to the mark with water. The absorbance of the blue solution was measured by means of a Shimadzu Spectronic 88 spectrophotometer at 830 nm. The phosphate content (P%) was calculated by means of the absorbance data.

Determination of Phosphorus, Calcium, and Sodium in the Product. About 0.2 g of the product and 0.7445 g of EDTA were dissolved in water by using a 100-cm^3 volumetric flask. The amounts of phosphorus and calcium in the solution were determined by means of the molybdenum-blue method with Lucena-Conde and Prat's reagent and by means of the EDTA back-titration method with an NN indicator respectively. In the case of the back titration of a calcium ion in this system, the pH of the solution should be larger than 13, because the change in color of the solution is not clear in the pH regions smaller than 13. Atomic-absorption analysis was used for the determination of a sodium ion by using a Jarrell-Ash atomic-absorption spectrophotometer, AA80, while the analysis was performed by dissolving the product in a dilute hydrochloric acid solution.

X-Ray Diffractometry. The X-ray diffraction diagrams of the samples were taken with nickel-filtered Cu $K\alpha$ radiation by using a Toshiba X-ray diffractometer, ADG-102.

DTA and TG. The samples were heated at the heating rate of 5 °C min^{-1} in an ordinary atmosphere by using a Cho Balance $TRDA_1$-H-type apparatus.

Decomposition of the Tetraphosphate. The decomposition of the tetraphosphate at room temperature and at 300 °C in the atmosphere was measured by the paper-chromatographic and colorimetric methods described above.

Hydrolysis of the Tetraphosphate. EDTA 4.0 g was dissolved in 100 cm^3 of water, and then 3.0 g of the tetraphosphate was dissolved in the EDTA solution. The hydrolysis of the tetraphosphate was measured by using the phosphate solution at pH 3.5 and at 50, 60, or 70±0.05 °C. The separation and the determination of the tetraphosphate and its hydrolysis products were carried out by means of the method described above.

Results and Discussion

Composition of the Product. The yield of the product depended upon the pH of the phosphate solution;

it was about 27 g for pH 10—7, about 22 g for pH 8—5, and about 16 g for pH 6—3. Paper-chromatographic identification showed that the product was tetraphosphate. As will be discussed below, the tetraphosphate was decomposed to phosphates with shorter chain lengths in the atmosphere at room temperature, so it was difficult to hold pure tetraphosphate. The product thus obtained contained 20—30% of water and was X-ray-diffractometrically amorphous. An effective amount of a sodium ion was not detected in the product. The P/Ca molar ratio of the product was 1.4—1.5. The P/Ca ratio of tricalcium tetraphosphate, $Ca_3P_4O_{13}$, is 1.33, while that of the product is a little larger. The defect of calcium may be supplemented by hydrogen.

Decomposition of the Tetraphosphate at Room Temperature. As is shown in Table 1, the tetraphosphate is gradually decomposed to phosphates with shorter chain lengths in the ordinary atmosphere at room temperature. No weight change was observed in the sample. Therefore, the decomposition may be caused by the water contained in the product. Since the content (P%) of triphosphate is about three times that of orthophosphate at each decomposition time, the decomposition of triphosphate and pyrophosphate once produced to orthophosphate may not occur, and the following decomposition process can be concluded:

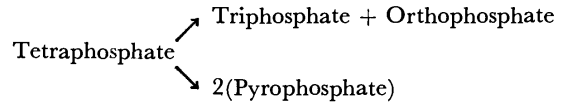

DTA and TG. DTA and TG curves of the product are given in Fig. 1. A rapid weight loss of the product and a corresponding big endothermic peak are observed below 150 °C. This reaction may be caused by removing the bound water. The succeeding gradual weight loss of the product from 150—380 °C is considered to be the condensation reaction of phosphates. An exothermic and an endothermic reaction are observed at around 560 and 740 °C respectively. The sample heated at a temperature below that of the exothermic reaction was amorphous and gave no X-ray diffraction peaks, while the sample heated at a higher temperature than that of the exothermic reaction gave some X-ray diffraction peaks. As Fig. 2 shows, these peaks are assigned to those of β-type calcium pyrophosphate (ASTM card, No. 9—346). Accordingly, the exothermic reaction is caused by the crystallization of amorphous calcium pyrophosphate to the β-form. As will be discussed below, the tetraphosphate was decomposed to phosphates with shorter chain lengths by heating it at 300 °C, and the main decomposition product was pyrophosphate in the initial stage of heating. The endothermic reaction at about 740 °C may be due to the melt of a part of the phosphate species, because the sample which was taken out and cooled after the endothermic reaction was sintered. All the X-ray diffraction peaks of the sample after the endothermic reaction were assigned to those of the β-form of calcium pyrophosphate, and an increase in the intensity of the peaks was observed in comparison with that of the peaks of the sample after the exothermic reaction described above.

Decomposition of the Product at 300 °C. As Table 2 shows, the tetraphosphate thus obtained is readily decomposed to tri-, pyro-, and orthophosphates by heating at 300 °C. Among the decomposition products, the value of the pyrophosphate content is the largest at a short heating time. Therefore, the scission of the middle P–O–P linkage of the tetraphosphate may take place in preference to that of the end P–O–P linkage. This phenomenon was not observed in the decomposition of room temperature. The decomposition products, once produced, are condensed to phos-

TABLE 1. DECOMPOSITION OF THE PRODUCT IN THE ATMOSPHERE AT ROOM TEMPERATURE

Reaction time/d	Phosphate/P%			
	Ortho	Pyro	Tri	Tetra
0	—	—	—	100
2	2.7	3.2	8.7	85.4
4	3.9	4.5	12.0	79.6
9	4.8	6.2	14.1	74.9
15	5.5	8.3	15.9	70.3
19	6.2	12.1	17.7	64.0

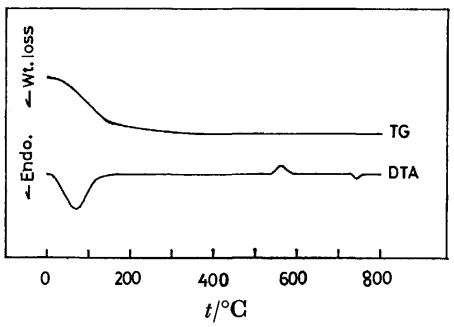

Fig. 1. DTA and TG curves of the product.

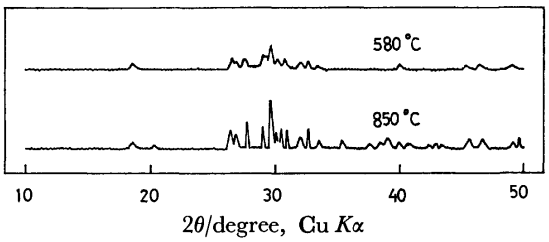

Fig. 2. X-Ray diffraction patterns of the product heated at 580 or 850 °C for 1 h.

TABLE 2. DECOMPOSITION OF THE PRODUCT IN THE ATMOSPHERE AT 300 °C

Heating time/min	Phosphate/P%				
	Ortho	Pyro	Tri	Tetra	Higher
0	1.9	4.4	8.9	84.8	—
10	29.9	48.1	15.6	6.1	0.3
20	17.5	49.5	22.1	8.2	2.7
30	12.0	45.7	24.2	11.6	6.5
40	9.3	41.2	25.4	12.5	11.6
50	5.6	33.2	25.1	14.3	21.8

Table 3. Hydrolysis of the product at pH 3.5 and 70 °C

Reaction time/min	Phosphate/P%				Rate const $\times 10^3$/min^{-1}
	Ortho	Pyro	Tri	Tetra	
0	2.7	3.2	8.2	85.9	
15	3.8	3.7	12.0	80.5	4.3
30	5.5	4.2	14.5	75.8	4.2
45	6.4	4.5	18.0	71.1	4.2
60	6.9	5.1	20.5	67.5	4.0
90	10.6	5.9	26.2	57.3	4.5
120	13.3	7.4	28.0	51.4	4.3
					mean, 4.3

phates with longer chain lengths.

Hydrolysis of the Product. According to the results listed in Table 3, the hydrolysis of tetraphosphate obeyed first-order kinetics with respect to the concentration of tetraphosphate at pH 3.5 and 70 °C. The increase in the pyrophosphate content with the reaction time is so much slower than that of tri- and orthophosphates that the scission of the end P–O–P group of tetraphosphate takes place faster than that of the middle P–O–P group in an aqueous solution. This tendency is the reverse of that of the decomposition of the product at 300 °C. The same results were obtained for the hydrolysis at 60 and 50 °C. The rate constants at 60 and 50 °C were 1.5×10^{-3} and 4.3×10^{-4} min^{-1} respectively. The activation energy was determined to be 105 kJ mol^{-1} by means of the least-squares method.

References

1) K. N. Bell, L. F. Audrieth, and O. F. Hill, *Ind. Eng. Chem.*, **44**, 568 (1952).

2) S. Ohashi, *Kagaku To Kogyo*, **21**, 878 (1968). The A_2 and B_2 solvents in Table 3 were used.

3) F. Lucena-Conde and L. Prat, *Ana'. Chim. Acta*, **16**, 473 (1957).

Studies on Diazo Type Process. VII. Electronic Spectra of 2-(Substituted phenylazo)-1-naphthol-4-sulfonic Acid

Shin SUZUKI,* Rebati C. DAS,** Kieko HARADA, and Stefan STOYANOV†,***

Department of Synthetic Chemistry, Faculty of Engineering, Chiba University, Yayoi-cho, Chiba 260

†*Department of Chemistry, Tokyo Institute of Technology, Ohokayama Meguro-ku, Tokyo 152*

(Received November 13, 1979)

The absorption of 2-(substituted phenylazo)-1-naphthol-4-sulfonic acid has been studied in neutral, acidic, and alkaline aqueous solutions as well as in solid state. Assignment of band positions to azo and hydrazone tautomers has been made by calculations using the SCF-CI-MO method. Introduction of electron-donating (or electron-withdrawing) substituent in the diazo part showed bathochromic (or hypsochromic) shift of the absorption band, which was elucidated by the charge migration and the character of the substituents taking into account azo-hydrazone tautomerism. In case of compounds containing electron-donating substituents, aggregation seems to take place in the solid state.

This paper deals with a study of the physicochemical properties of azo dyes formed in 'diazo-printing' process. Substituted benzenediazonium salt and 1-naphthol-4-sulfonic acid (NW acid) are sometimes used as the photosensitive 'diazo' and 'coupler' components, respectively.[1] Coloration of the dyes formed by the reaction between the above compounds is important.

Attempts have been made to correlate the color of azo dyes with the electronic configuration. Griffiths observed a linear relationship between the absorption maxima in the visible region and the electron-withdrawing power (σ-value) of the substituents on 4-substituted phenylazo-1-naphthols in a certain range of σ value ($\sigma > -0.16$).[2,3] His explanation is not applicable to the phenylazo-1-naphthols with strongly electron-donating substituents which are widely used for imaging processes.

The electronic spectra were measured in the visible region for 2-(substituted phenylazo)-1-naphthol-4-sulfonic acids with various electron-donating or electron-withdrawing substituents, including the dye actually used for diazo-printing process. The absorption maxima of some compounds could not be explained by Griffith's relationship. The band assignment and band shift caused by the substituents are interpreted by the SCF-CI-MO method with PPP approximation.

Experimental

Materials. Substituted benzenediazonium salts were prepared from the corresponding amines (analytical grade), precipitated as tetrafluoroborates and then coupled with NW acid. The resulting dyes were purified by repeated recrystallization from water or ethanol and stores in the dark. The other materials used were of analytical grade.

Methods. Absorption spectra in aqueous solutions were measured with Shimadzu (model UV-180) and Carl-Zeiss-Jena 'Specord UV-Vis' spectrophotometers. For solid state absorption stectra the 'Opal glass method' developed by Shibata[4] was used. A small amount of solid compound was rubbed between two sheets of transparent paper (medical wrapper, Tokyo Ikarika Kikai shoji Co.) and the resulting translucent paper was used for recording the spectrum with a Shimadzu spectrophotometer, type DPS-50L. The reflection spectra were also measured with a Shimadzu Spectrophotometer QV-50, but no distinct difference was observed.

Results and Discussion

Analysis of the Absorption Spectra. In general, azo dyes exist as an azo-hydrazone tautomer (Fig. 1). The spectra of the compounds have been determined in neutral, alkaline (0.1 mol dm^{-3} NaOH), and acidic (0.1 mol dm^{-3} $HClO_4$) aqueous solutions as well as

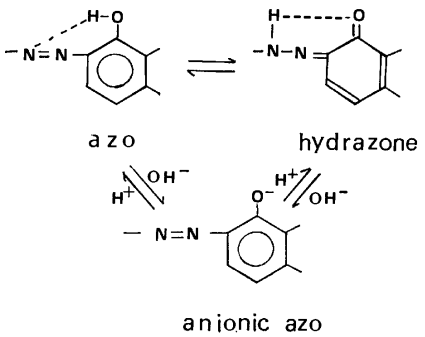

Fig. 1. Azo-hydrazone tautomerism and anionic azo form.

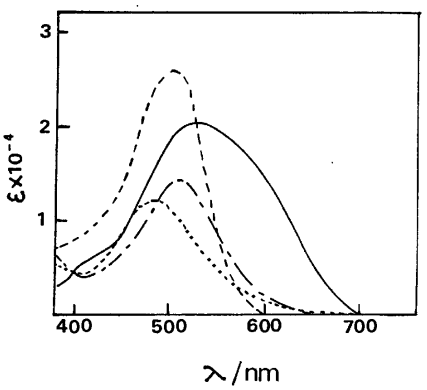

Fig. 2. Absorption spectra of 2-(*p*-dimethylaminophenylazo)-1-naphthol-4-sulfonic acid in acidic, neutral, and alkaline aqueous solutions.
·····: Below pH 4.2, —·—: at pH 4.8—5.2, ——: at pH 5.5—8.0, ----: above pH 9.0.

** Present address: Department of Chemistry, University College of Engineering, Burla 768017, Orissa, India.
*** Present address: Department of Chemistry, University of Sofia, Sofia, Bulgaria.

in the solid state. As an example, Fig. 2 shows the spectra in neutral, acidic, and alkaline solutions of (*p*-dimethylamino phenylazo)-1-naphthol-4-sulfonic acid. The positions of the main absorption maxima in the visible range are summarized in Table 1.

The main visible absorption maximum lies in the range 490—520 nm in neutral aqueous medium. This can be assigned to hydrazone tautomer of the equilibrium,[5] since hydrazone tautomer usually absorbs in a visible region greater than 460 nm, and the azo tautomer in a shorter wavelength region 400—460 nm.[6-14] In our compounds no band is seen which can be ascribed to azo tautomer, except for a very weak shoulder in a few cases. This indicates the predominance of hydrazone tautomer in neutral aqueous solutions, in line with the conclusions of Gabor *et al.*[9] and Yagi[10] on 2-phenylazo-1-naphthol in non-aqueous solvents. NMR studies also support this view.[9,15] Furthermore, the band is assigned to a π-π^* transition from the bathochromic shift caused by polar solvent.[12]

In order to confirm our assignment, quantum mechanical calculations were made by the SCF-CI-MO method with PPP approximation for both azo and hydrazone forms of the parent compound, 2-phenylazo-1-naphthol. Details of the method have been reported by one of us (S.S).[16] The values of the calculated transition energies (ΔE) and oscillator strengths (f) are given in Table 2. The calculated transition energies for the hydrazone agree with experimental data.

Table 1. Visible absorption maxima of 2-(substituted phenylazo)-1-naphthol-4-sulfonic acid

Serial No.	Substituent	σ[a]	Frequency 10^{-4}/cm^{-1} (Wavelength/nm in parentheses)			
			Neutral aqueous	Acidic aqueous	Alkaline aqueous	Solid
1	*p*-NO_2	+0.78	2.02 (495)	2.05 (489)	1.88 (531)	2.02 (495)
2	*p*-CN	+0.69	2.04 (491)	2.04 (491)	1.97 (507)	2.04 (490)
3	*p*-Br	+0.23	2.02 (496)	2.02 (496)	2.05 (487)	2.01 (497)
4	*p*-Cl	+0.22	2.02 (494)	2.02 (494)	2.06 (485)	2.04 (488)
5	*p*-F	+0.06	2.03 (492)	2.03 (492)	2.10 (476)	1.99 (502)
6	H	0	2.03 (492)	2.03 (492)	2.09 (479)	2.00 (500)
7	*p*-CH_3	−0.17	2.00 (499)	2.00 (499)	2.08 (481)	2.00 (503)
8	*p*-OCH_3	−0.27	1.98 (505)	1.98 (505)	2.08 (480)	2.00 (500)
9	*p*-$N(C_2H_5)_2$	−0.81[b] +0.78[c]	1.93 (517)	2.07 (483)	1.99 (505)	2.05 (488)
10	*p*-$N(CH_3)_2$	−0.83 +0.80[c]	1.92 (520)	2.06 (485)	2.01 (498)	2.06 (485)

a) Values taken from Ref. 20. b) For neutral and alkaline conditions: σ value of *p*-diethylamino substituent is not taken from the reference. Comparing *p*-ethyl substituent ($\sigma=-0.15$) with *p*-methyl one ($\sigma=-0.17$), the value of *p*-diethylamino substituent is estimated to be −0.18. c) For acidic condition: Hammett σ value is not taken from the reference. The value is estimated by comparing the Taft σ value[21] of protonated dimethylamino group with that of unprotonated one.

Table 2. Different parameters obtained by SCF-CI-MO calculation

Compound	Structure	ΔE(calcd)[a]/eV	f(calcd)	ΔE(expt)[a]/eV
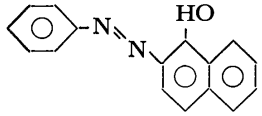	azo	2.90 (427) 3.93 (315) 4.13 (300)	0.65 0.14 0.63	
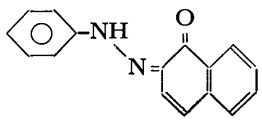	hydrazone	2.60 (477) 3.75 (331) 4.48 (277)	1.11 0.31 0.37	2.52 (492) 3.54 (350) 4.25 (291)

a) Values in the parentheses give the wavelengths(nm) of the corresponding absorption bands.

In highly alkaline solutions where the phenolic group is completely dissociated, the compounds have predominantly azo character and seem to exist in anionic azo form[3] (Fig. 1).

In highly acidic medium the visible spectrum does not change markedly from that in neutral aqueous medium except in the case of (a) *p*-dimethylamino and (b) *p*-diethylamino derivatives. Figure 2 shows this for (a). When the solution of (a) is acidified from neutral condition, the color turns from purple to pink at pH 5.2, and from pink to yellow around pH 4.2. The spectrum in highly acidic medium below pH 4.2, which shows an absorption maximum at 485 nm, differs from that around pH 5.0 (maximum at 510 nm), and from that in the neutral medium (maximum at 520 nm). The results suggest the following acid-base equilibria:

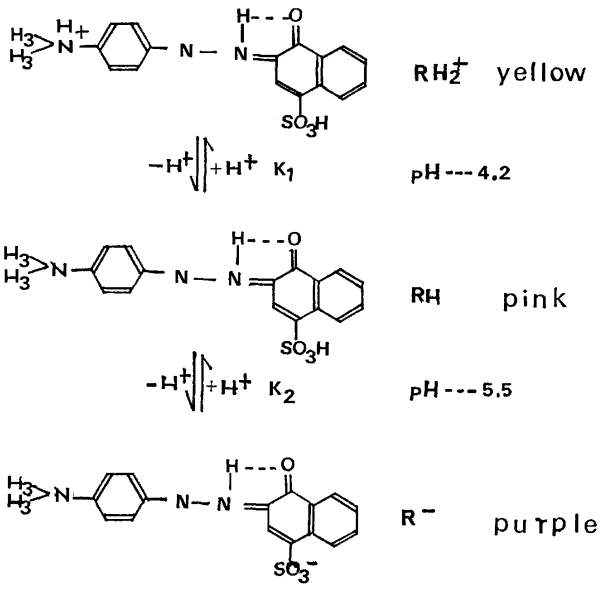

Formulae dissociation equilibria of 2-(*p*-dimethylaminophenylazo)-1-naphthol-4-sulfonic acid.

The markedly different spectrum in the acidic medium in the case of dialkylamino derivatives is ascribed to the protonation of the dialkylamino group. The protonated group behaves as an electron-withdrawing one (Table 1), the absorption peak shifting to the shorter wavelength region. A slight change is also observed in the *p*-nitro derivative [λ_{max}(neutral)= 495 nm and λ_{max} (acidic)=489 nm]. This might be due to the slight dissociation of the phenolic group even in the neutral medium since some nitro phenols are reported to be strong acids.[17]

Spectra in the solid state have been taken because of their industrial importance (Fig. 6). In the solid state spectra of these compounds, there is no clear band or shoulder which can be ascribed to the azo tautomer. Thus, in the solid state also the present compounds exist predominantly as hydrazone tautomer, in agreement with the results of NMR studies.[10,15]

Dependence of Absorption Maxima on Substituent Constants. According to the theoretical calculation[6,18] on 2-phenylazo-1-naphthol during the course of the lowest π-π^* transition ($S_0 \rightarrow S_1$), there is a charge migration from the naphthalene ring towards the azo link and, to some extent, to the benzene ring in the case of azo structure. The charge migration is in the opposite direction in the hydrazone structure, from the benzene ring and N_α atom to the N_β atom and the naphthalene ring. The approximate direction of the migration moment (movement of charge) is shown in Fig. 3.

In order to elucidate the influence of the substituents on the charge migration of 2-(*p*-substituted phenylazo)-1-naphthol, Hammett's constants were employed to estimate the character of substituents. Figure 4 shows the plots of ν_{max} in the visible region *vs.* σ values of the substituents. The plots seem scattered, but two approximate straight lines are drawn with different slopes in positive and negative ranges of σ values. This is in contrast with the linear relationship between ν_{max} and σ observed on 4-phenylazo-1-naphthol derivatives by Griffiths.[3] The present set of compounds being predominantly in hydrazone structure in neutral medium, introduction of electron-donating substituents in the diazo part facilitates charge migration, resulting in bathochromic shift of the main visible band (Fig.

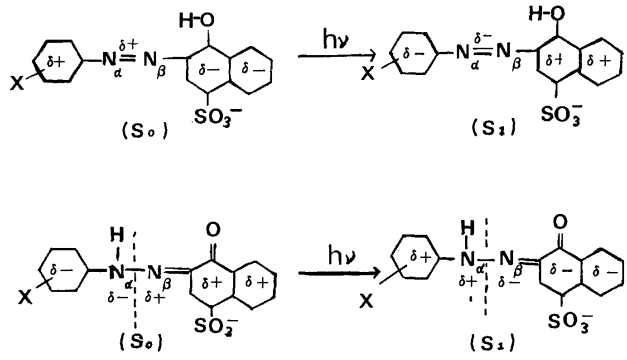

Fig. 3. Approximate scheme of charge migration during electronic transition.

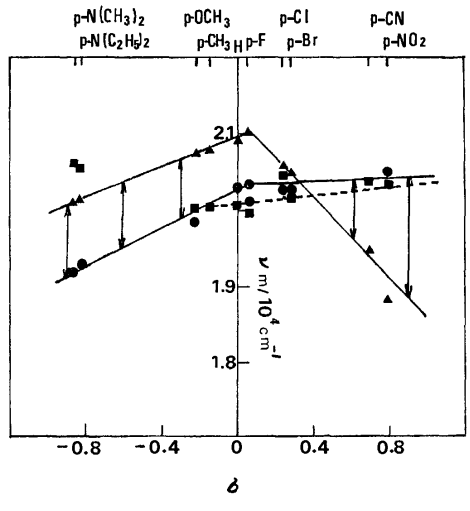

Fig. 4. Plots of ν_{max} of 2-(substituted phenylazo)-1-naphthol-4-sulfonic acid dyes agaist σ values of the substituents.
●: Neutral aqueous solution (ν_{max} of *p*-nitro derivative is in acidic solution, because the phenolic group is partly dissociated even in neutral solution), ▲: alkaline aqueous solution, ■: solid.

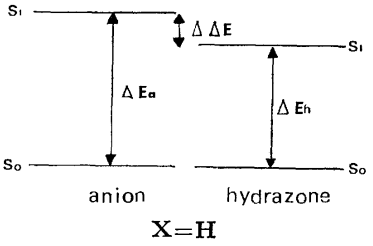

Fig. 5. Energy level diagram of the anionic azo and hydrazone forms of 2-(unsubstituted phenylazo)-1-naphthol-4-sulfonic acid.

4). The presence of electron-withdrawing substituents might cause a slight hypsochromic shift of the visible band, indicating opposition to the charge migration during the course of electronic transition. The influence of electron-withdrawing substituents in the diazo part on the visible band position is not as pronounced as that of electron-donating substituents (Fig. 4).

The dyes exist in anionic azo form in alkaline solutions (Fig. 1).[3] The unsubstituted compound (X=H) was found to show absorption at a shorter wavelength (higher ν) in alkaline solution than in neutral solution (Fig. 4 and Table 1). This is schematically explained in Fig. 5. From the foregoing discussions and Fig. 3, it is evident that electron-donating groups on hydrazone form decrease ΔE_h, while the groups on anionic azo form increase ΔE_a value. Consequently $\Delta\Delta E$ value ($\Delta E_a - \Delta E_h$) increases. Similarly ΔE_a is lowered more than ΔE_h by electron-withdrawing groups. This causes a decrease in $\Delta\Delta E$ and $\Delta\nu_{max}$ [ν_{max}(alkaline)$-\nu_{max}$(neutral)], which is proportional to $\Delta\Delta E$, with increasing σ-value (Fig. 4). The results are in line with the above discussion. Figure 4 shows that $\Delta\Delta E$ is positive for the compounds containing electron-donating and weak electron-withdrawing substituents and negative for highly electron-withdrawing substituents such as *p*-cyano and *p*-nitro groups. This is in line with the result obtained by Griffith.[2,3]

In the solid state, where the structure of the dyes is the same as in the neutral aqueous solutions as shown by the electronic spectra, the dependence of ν_{max} on σ is expected to be similar to that in neutral aqueous solution. The plot (ν_{max} *vs.* σ) in the case of compounds with electron-withdrawing substituents ($\sigma>0$) is as expected (Fig. 4). For compounds with strongly electron-donating substituents (*p*-methoxyl, *p*-dimethylamino, and *p*-diethylamino) the absorption peaks are at frequencies higher than those expected from the above consideration. The apparent anomalous behavior of these compounds is explained in the following. There is a greater scattering in the plot ν_{max} *vs.* σ in the solid state. The correlation in the solid spectra is not as good as desired. However qualitative conclusion can be drawn from it.

Aggregation in the Solid State. Distinct shoulders are present at the longer wavelength region (580—650 nm) of the main absorption bands in the solid spectra of *p*-methoxy, *p*-dimethylamino, and *p*-diethylamino derivatives. Figure 6 shows the solid absorption spectrum of *p*-dimethylamino derivative. This is not present in the other compounds. Thus the

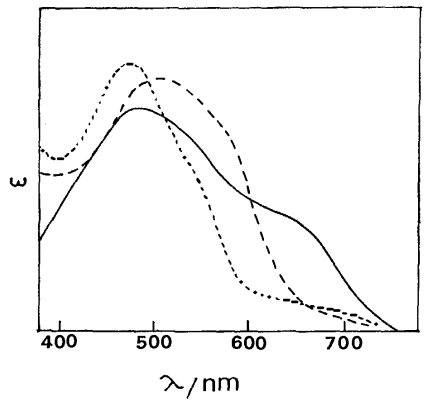

Fig. 6. Solid absorption spectra of 2-(*p*-dimethylaminophenylazo)-1-naphthol-4-sulfonic acid.
——: Untreated, ----: after treatment with alkali, ……: after treatment with acid. Molar absorptivity, arbitary.

color of the above compounds is not red as expected from the position of the main absorption bands, but purple. This shoulder does not appear in the absorption spectra in aqueous solutions.

Appearance of the additional bands might be due to the presence of aggregate species in the solid state of the compounds, as in the case of cyanine dyes used for sensitizing silver halides.[19] Only the *p*-methoxy, *p*-dimethylamino, and *p*-diethylamino derivatives of the present series of compounds form aggregate species in the solid state. The reason might be as follows. These compounds, like all other compounds, exist mainly in the hydrazone form in the solid state. There are strong donor and acceptor groups at the two ends of the molecules of these compounds. The donor groups are enhanced by the strongly electron-donating substituents. Such a situation can favor aggregation.

The aggregate band at the longer wavelength disappears in the spectrum of the *p*-dimethylamino or *p*-diethylamino derivative if a pinch of the solid compound is treated with a drop of strong acid or alkali and dried before the measurement, though no change in external appearance was observed. Figure 6 shows the solid state absorption spectra of the *p*-dimethylamino derivative before and after treatment with acid or alkali. Treatment with strong acid protonates the dialkylamino group and that with strong alkali converts the dye into anionic azo structure. In both cases, donor and acceptor groups are not simultaneously present in the molecule. The results might suport the cause of aggregation.

One of the authors (R.C. Das) is grateful to The Japan Society for Promotion of Science for the award of a Senior Co-operative Fellowship. Another author (S. Stoyanov) wishes to thank the Japanese Government for the award of UNESCO Fellowship and the Committee for Science & Technical Progress of Bulgaria for making his stay in Japan possible. Thanks are also due to Prof. H. Kobayashi, Tokyo Institute of Technology, Dr. K. Sugita and Dr. Y. Hori of Chiba University for their help and co-operation.

References

1) "Shashin Kogyo (Manual of Photographic Technology)," Shashin Kogyo Publ., Tokyo (1977), p. 157.
2) J. Griffiths, *J. Soc. Dyers Colour.*, **1971**, 801.
3) J. Griffiths, *J. Soc. Dyers Colour.*, **1972**, 106.
4) K. Shibata, "Methods of Biochemical Analysis," ed by D. Glick, Interscience Publ., New York (1959), Vol. VII, p. 77.
5) C. V. Stead, "The Chemistry of Synthetic Dyes," ed by K. Venkataraman, Academic Press, New York (1970), Vol. III p. 250.
6) D. Simov and St. Stoyanov, *J. Mol. Struct.*, **19**, 255 (1971).
7) J. N. Ospenon, *Acta Chem. Scand.*, **4**, 1351 (1950); **5**, 491 (1951).
8) A. Burawoy, A. E. Salem, and A. R. Thompson, *J. Chem. Soc.*, **1952**, 4793.
9) G. Gabor, Y. Frei, D. Gegiou, M. Kaganowitch, and E. Fischer, *Isr. J. Chem.*, **5**, 193 (1967).
10) Y. Yagi, *Bull. Chem. Soc. Jpn.*, **37**, 1875 (1964).
11) R. G. Bigelow, *J. Phys. Chem.*, **80**, 2694 (1976).
12) S. Suzuki, R. C. Das, and K. Harada, *Bull. Chem. Soc. Jpn.*, **51**, 2136 (1978).
13) A. H. Cook, P. G. Jones, and J. B. Polja, *J. Chem. Soc.*, **1949**, 1315.
14) L. Skulski, *Bull. Pol, Acad. Sci., Ser. Sci. Chim.*, **14**, 29, 37 (1966).
15) B. L. Paul, P. Madhavan Nair, A. V. RamaRao, and K. Venkataraman, *Tetrahedron Lett.*, **1966**, 3897.
16) S. Stoyanov, Thesis, XIII International UNESCO Postgraduate Course in Chemistry, Tokyo Institute of Technology, Tokyo, Japan, 1978.
17) J. Hine, "Physical Organic Chemistry," McGraw-Hill Publ., New York (1962), p. 81.
18) D. Simov and S. Stoyanov, *Izv. Bulg. Acad. Sci.* (communicated).
19) C. E. K. Mees and T. H. James, "The Theory of the Photographic Process," Macmillan., New York (1967), p. 244.
20) L. M. Stock, "Aromatic Substitution Reactions (Japanese)," trans by N. Uchino and Y. Sakakibara, Prentice Hall Publ. Tokyo (1968), p. 70.
21) John A. Dean "Lange's Handbook of Chemistry," 12 ed, McGraw-Hill Publ., New York (1979) pp. 3—135.

© 1980 The Chemical Society of Japan

NOTES

Bull. Chem. Soc. Jpn., 53, 2671—2672 (1980)

The Crystal Structure of the 1,3-Di-*p*-tolyl-5-phenylverdazyl Radical[1)]

Nagao AZUMA

Laboratory of Chemistry, Faculty of General Education, Ehime University, Bunkyo-cho, Matsuyama 790

(Received October 30, 1979)

Synopsis. The crystals of 1,3-di-*p*-tolyl-5-phenylverdazyl are monoclinic, with the space group $P2_1/c$ and with $a=10.66(1)$, $b=21.76(1)$, $c=8.171(6)$ Å, $\beta=98.8(1)°$, and $Z=4$. The crystal structure has been determined by means of X-ray diffraction. The molecular structure is similar to those of other verdazyls. The molecules are packed in a column along the c axis.

Following the conventional procedure, the paramagnetic susceptibility of 1,3-di-*p*-tolyl-5-phenylverdazyl (DTPV) has been discussed in this series.[2)] A linear chain of Ising spins has been proposed for DTPV crystals, with the suggestion of another possibility of an alternating linear chain of Heisenberg spins. The latter possibility correlates with the alternation in the molecular packing. In order to examine whether there is such an alternation in the DTPV crystal, crystal-structure analysis has been carried out by means of X-ray diffraction. No alternation appears in the revealed crystal structure.

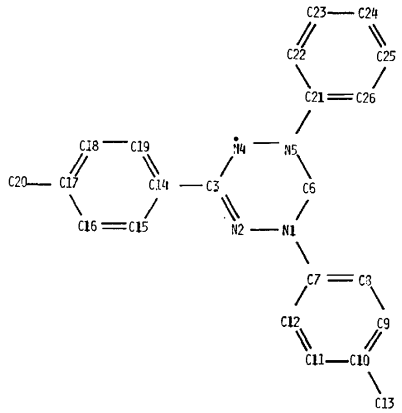

Fig. 1. The chemical structure and numbering system of 1,3-di-*p*-tolyl-5-phenylverdazyl (DTPV).

Experimental

Material and Procedure. The DTPV was prepared from *p*-tolualdehyde, *p*-toluidine, aniline, and formaldehyde, following the procedure of Kuhn and Trischmann.[3)] The crystals were purified several times through recrystallization from a methanol solution; mp=116.0—116.5 °C.

The unit-cell parameters were refined on a manually-operated four-circle diffractometer. The intensity data were collected on the same diffractometer with Zr-filtered Mo $K\alpha$-radiation up to $2\theta=45°$ through a single scan per peak for all the reflections. The background intensities around an arbitrary axis were measured as a function of the Bragg angle, and this function was assumed for all the reflections. The reflection intensities were corrected for Lorentz and polarization effects.

Crystal Data. $C_{22}H_{21}N_4$, $M=341.43$, monoclinic, space group $P2_1/c$, $a=10.66(1)$, $b=21.76(1)$, $c=8.171(6)$ Å, $\beta=98.8(1)°$, $V=1873$ Å^3, $D_m=1.2$ (by floatation), $D_x=1.210$ g/cm^3, and $Z=4$.

Structure Determination and Refinement

The structure was solved by the direct method using the *SORTE* program,[4)] with the positions of all the 26 non-hydrogen atoms located on an *E*-map. Those positions were refined by the blockdiagonal least-squares procedure. The positions of the 15 ring hydrogen atoms were deduced from a difference Fourier map. Those of the methyl hydrogen atoms were not, however, located from the difference Fourier maps and were ignored in the present refinement in view of the accuracy of the intensity data. The discrepancy index, R, for 1487 non-zero reflections was finally reduced to 0.11 by fullmatrix least-squares refinement with anisotropic thermal parameters for the non-hydrogen atoms and isotropic ones for the ring hydrogen atoms. The hydrogen isotropic thermal parameters ranged between 3.5 and 5.2 Å^2; these values were fixed in the final stage of the refinement. The atomic scattering factors were adopted from the International Tables for X-Ray Crystallography.[5)] The final positional parameters of the non-hydrogen atoms are shown in Table 1*; the numbering system refers to Fig. 1.

Discussion

Table 2 shows the bond distances and bond angles. There is no significant difference between the molecular dimensions of DTPV and those of the other verdazyls.[6)] The sums of the three bond angles around the three-coordinated nitrogen atoms, N1 and N5, are 360 and 359°. The atomic deviations of N1 and N5 from the planes defined by the N2, C6, and C7 atoms and by the N4, C6, and C21 atoms are 0.04 and 0.08 Å respectively. These two results show the sp^2 hybridization for the three-coordinated nitrogen atoms, which, accordingly, contribute two π-electrons per atom to the π-system. The conformation of the 1,2,4,5-tetrazinyl ring is an unsymmetrical boat form, with four coplanar nitrogen atoms (N-plane) and these atomic deviations from this plane: C3, −0.14; C6, −0.64; C7, 0.45; C8, 0.19; C12, 1.23; C14, −0.27; C21, 0.40; C22, 1.07; and C26, 0.14 Å. The dihedral angle between the N- and the C3-tolyl planes is 7°. Those between the N2-C6-C7 plane and the N1-tolyl plane and between the N4-C6-C21 plane and the N5-phenyl plane are 14 and 10° respectively.

* Lists of the observed and calculated structure factors (List A), of the thermal parameters (B), and of the positions of the ring hydrogen atoms (C) are kept by the office of the Chemical Society of Japan, (Document No. 8027).

Table 1. The positional parameters, with their estimated standard deviations in parentheses
The values have been multiplied by 10^4.

Atom	x	y	z
N1	5773(12)	2661(6)	4193(13)
N2	6427(9)	3182(6)	3927(12)
C3	5798(14)	3711(6)	3730(15)
N4	4523(11)	3736(5)	3441(12)
N5	3862(10)	3214(6)	3705(13)
C6	4588(16)	2788(7)	4825(18)
C7	6273(13)	2075(7)	4020(16)
C8	5775(15)	1540(7)	4637(16)
C9	6355(22)	981(7)	4394(25)
C10	7370(15)	886(7)	3546(18)
C11	7772(13)	1425(9)	2901(19)
C12	7272(14)	2021(6)	3145(18)
C13	7929(13)	249(6)	3291(16)
C14	6501(13)	4274(6)	3607(15)
C15	7796(16)	4260(6)	3657(20)
C16	8463(12)	4819(8)	3510(18)
C17	7958(14)	5404(6)	3308(16)
C18	6617(17)	5367(7)	3311(22)
C19	5910(13)	4839(8)	3435(18)
C20	8662(12)	5978(5)	3212(16)
C21	2559(12)	3204(6)	3105(16)
C22	2062(15)	3598(7)	1984(20)
C23	734(16)	3596(7)	1365(18)
C24	7(12)	3152(8)	1905(18)
C25	512(16)	2736(8)	3037(21)
C26	1798(14)	2740(6)	3651(16)

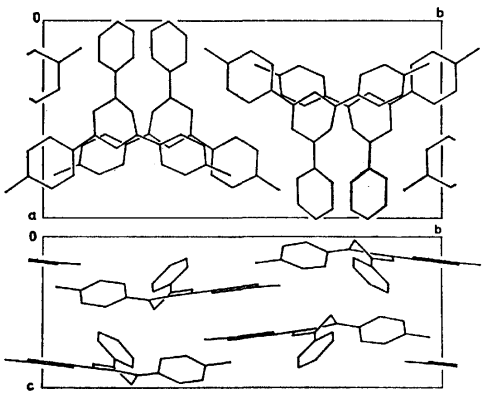

Fig. 2. The molecular packing of DTPV.

These dihedral angles can be regarded as the twist angles about the corresponding inter-ring bonds. These small twist angles and the unsymmetrical boat form of the 1,2,4,5-tetrazinyl ring have also been observed in other verdazyls.[6] Such a molecular structure of the verdazyls, containing a four-coordinated carbon atom or C6, makes the unpaired electron delocalize over the whole framework.[7]

The molecules in the crystal are packed in a column along the c axis, as is shown in Fig. 2. The shortest N...N, N...C, and C...C intermolecular atomic contacts appear in this column and are as follows: N1...N1, 4.15; N1...C12, 3.45; and C8...C3, 3.39 Å. The intermolecular contacts all seem not to be shorter than the normal van der Waals distances. There is no alternation in the molecular packing, as can be seen from Fig. 2. Therefore, the crystal structure does not support the possibility of the alternating linear chain of the spins in the DTPV crystal. For another reason, the linear chain of Ising spins is also doubtful. Based on the crvstal structure and the data from the magnetic-resonance spectroscopies, the magnetic susceptibility of the DTPV crystal will be re-

Table 2. Bond distances [l/Å] and bond angles [ϕ/°]
The estimated standard deviations are 0.02 Å and 1° respectively.

Atoms	Distance	Atoms	Distance
N1-N2	1.37	N2-C3	1.33
C3-N4	1.35	N4-N5	1.37
N5-C6	1.44	C6-N1	1.46
N1-C7	1.40	C7-C8	1.41
C8-C9	1.39	C9-C10	1.39
C10-C11	1.38	C11-C12	1.43
C12-C7	1.38	C10-C13	1.54
C3-C14	1.45	C14-C15	1.38
C15-C16	1.42	C16-C17	1.38
C17-C18	1.43	C18-C19	1.39
C19-C14	1.38	C17-C20	1.47
N5-C21	1.40	C21-C22	1.31
C22-C23	1.43	C23-C24	1.35
C24-C25	1.35	C25-C26	1.39
C26-C21	1.41		
Atoms	Angle	Atoms	Angle
N1-N2-C3	119	N2-C3-N4	122
C3-N4-N5	118	N4-N5-C6	113
N5-C6-N1	108	C6-N1-N2	113
C6-N1-C7	125	N2-N1-C7	122
N2-C3-C14	119	N4-C3-C14	118
N4-N5-C21	118	C6-N1-C21	128
N1-C7-C8	123	C7-C8-C9	118
C8-C9-C10	127	C9-C10-C11	112
C10-C11-C12	125	C11-C12-C7	119
C12-C7-C8	119	C12-C7-N1	118
C9-C10-C13	123	C11-C10-C13	124
C3-C14-C15	121	C3-C14-C19	122
C14-C15-C16	119	C15-C16-C17	127
C16-C17-C18	109	C17-C18-C19	127
C18-C19-C14	120	C19-C14-C15	118
C16-C17-C20	127	C18-C17-C20	125
N5-C21-C22	121	N5-C21-C26	119
C21-C22-C23	121	C22-C23-C24	118
C23-C24-C25	121	C24-C25-C26	121
C25-C26-C21	118	C26-C21-C22	120

examined in a separate paper.[8]

The calculations were performed at the Computer Centers of Kyoto and Ehime Universities, using the UNICS program system.[9]

The author wishes to thank Professor Yoshihiko Saito of the University of Tokyo for his help in the data collection, and Professors Yasuo Deguchi and Kazuhiko Ishizu for helpful discussions.

References

1) "Magnetic Properties of Verdazyl Free Radicals," part XII.

2) K. Mukai, N. Azuma, and K. Ishizu, *Bull. Chem. Soc. Jpn.*, **43**, 3618 (1970).

3) R. Kuhn and H. Trischmann, *Monatsh. Chem.*, **95**, 457 (1964).

4) Originally the NEAC2200/500 version by K. Nakatsu; modified by H. Shimanouchi, Lab. Chem. Natl. Prod., Tokyo Inst. of Techn.

5) "International Tables for X-Ray Crystallography," Kynoch Press, Birmingham (1962), Vol. III, p. 202.

6) D. E. Williams, *Acta Crystallogr., Sect. B*, **29**, 96 (1973); N. Azuma, Y. Deguchi, F. Marumo, and Y. Saito, *Bull. Chem. Soc. Jpn.*, **48**, 819; 825 (1975).

7) P. H. H. Fischer, *Tetrahedron*, **23**, 1939 (1967); K. Mukai, T. Yamamoto, M. Kohno, N. Azuma, and K. Ishizu, *Bull. Chem. Soc. Jpn.*, **47**, 1797 (1974).

8) N. Azuma, unpublished data.

9) "Universal Crystallographic Computation Program System (UNICS)," ed by T. Sakurai, The Crystallographic Society of Japan, Tokyo (1967).

One-electron Reduction Potentials of Several Electron Acceptor Molecules and Cation Radicals of Donors

Yôichi IIDA

Department of Chemistry, Faculty of Science, Hokkaido University, Sapporo 060

(Received January 30, 1980)

Synopsis. Reversible one-electron reduction potential values of several electron acceptor molecules and cation radicals of donors were estimated by means of the equilibrium constant of electron transfer reaction between ion radicals in acetonitrile solution, and the results were compared with the observed electrochemical data.

In previous papers reports were given on a preferred electron-transfer (*i.e.*, oxidation-reduction) reaction from an anion radical to neutral electron acceptor molecule in solution.[1] The difference in reversible one-electron reduction potentials between two acceptor molecules could be estimated by measuring the equilibrium constant of the reaction spectrophotometrically. For example, the electron-transfer reaction from 7,7,8,8-tetracyanoquinodimethane (TCNQ) anion radical to neutral cyano-substituted *p*-benzoquinone in acetonitrile solution is expressed by

$$TCNQ^{\cdot-} + p\text{-}X_2QCy_2 \rightleftharpoons TCNQ + p\text{-}X_2QCy_2^{\cdot-}, \quad (1)$$

where *p*-H_2QCy_2 (X=H) and *p*-Cl_2QCy_2 (X=Cl) stand for 2,3-dicyano-*p*-benzoquinone and 2,3-dichloro-5,6-dicyano-*p*-benzoquinone, respectively. By assuming that the activity coefficients of the solutes are unity and neglecting the effect of counter cations, the equilibrium constant of this reaction was determined spectrophotometrically to be $K=30$ at 20 ± 1 °C for X=H, while $K=(4.7\pm1.0)\times10^5$ at 15 °C for X=Cl, in acetonitrile solution.[1] By means of the Nernst equation and the estimated equilibrium constant, we obtain

$$E_0(p\text{-}H_2QCy_2, p\text{-}H_2QCy_2^{\cdot-}) = E_0(TCNQ, TCNQ^{\cdot-}) + 0.09\ V, \quad (2)$$

$$E_0(p\text{-}Cl_2QCy_2, p\text{-}Cl_2QCy_2^{\cdot-}) = E_0(TCNQ, TCNQ^{\cdot-}) + 0.32\ V, \quad (3)$$

where $E_0(A, A^{\cdot-})$ indicates reversible one-electron reduction potential of an acceptor, $A+e\rightleftharpoons A^{\cdot-}$, in acetonitrile solution.

On the other hand, studies were also made on the chemical equilibrium of electron transfer reaction from neutral electron donor molecule to another cation radical molecule in acetonitrile solution.[2,3] In a similar way to that for the chemical equilibria of electron acceptor molecules, the following relations of reversible one-electron reduction potentials were obtained for the cation radicals of donor molecules of *N,N,N',N'*-tetramethyl-*p*-phenylenediamine (TMPD), *N,N*-dimethyl-*p*-phenylenediamine (DMPD), *N,N,N',N'*-tetramethylbenzidine (TMB), and tetrathiafulvalene (TTF):

$$E_0(DMPD^{+\cdot}, DMPD) = E_0(TMPD^{+\cdot}, TMPD) + 0.078\ V, \quad (4)$$

$$E_0(TMB^{+\cdot}, TMB) = E_0(TMPD^{+\cdot}, TMPD) + 0.28\ V, \quad (5)$$

$$E_0(TTF^{+\cdot}, TTF) = E_0(TMPD^{+\cdot}, TMPD) + 0.086 \pm 0.008\ V, \quad (6)$$

where $E_0(D^{+\cdot}, D)$ stands for reversible one-electron reduction potential for cation radical of a donor, $D^{+\cdot}+e\rightleftharpoons D$, in acetonitrile solution.

So far, two series of reduction potentials have been independently obtained for the electron donor groups and the acceptor groups. In this paper, the two series are combined, for which purpose the following one-electron transfer reaction between donor TMPD and acceptor TCNQ in acetonitrile solution was considered:

$$TMPD + TCNQ \rightleftharpoons TMPD^{+\cdot} + TCNQ^{\cdot-}. \quad (7)$$

Yamagishi *et al.* examined the reaction and confirmed the occurrence of this chemical equilibrium.[4] They determined the equilibrium constant of Eq. 7 spectrophotometrically together with the enthalpy and entropy changes as

$$K = \frac{[TMPD^{+\cdot}][TCNQ^{\cdot-}]}{[TMPD][TCNQ]} = (7\pm2)\times10^{-2} \text{ at } 25\ °C, \quad (8)$$

$$\Delta H(\text{the enthalpy change}) = -17\pm4\ kJ\ mol^{-1}, \quad (9)$$

$$\Delta S(\text{the entropy change}) = -71\pm21\ J\ K^{-1}\ mol^{-1}. \quad (10)$$

Let us divide Eq. 7 into the following two reduction reactions,

$$TMPD^{+\cdot} + e \rightleftharpoons TMPD, \quad (11)$$

$$TCNQ + e \rightleftharpoons TCNQ^{\cdot-}. \quad (12)$$

The occurrence of the chemical equilibrium of Eq. 7 indicates that

$$E_0(TMPD^{+\cdot}, TMPD) - \frac{RT}{F}\ln\frac{[TMPD]}{[TMPD^{+\cdot}]} = E_0(TCNQ, TCNQ^{\cdot-}) - \frac{RT}{F}\ln\frac{[TCNQ^{\cdot-}]}{[TCNQ]}, \quad (13)$$

where R, T, and F are the gas constant, observed temperature, and Faraday constant, respectively. Using Eq. 8, we obtain

$$E_0(TCNQ, TCNQ^{\cdot-}) = E_0(TMPD^{+\cdot}, TMPD) + \frac{RT}{F}\ln K = E_0(TMPD^{+\cdot}, TMPD) - 0.07\ V. \quad (14)$$

The relation is important for connecting the reduction potentials of the donors with those of the acceptors. Another useful reaction is

$$TTF + TCNQ \rightleftharpoons TTF^{+\cdot} + TCNQ^{\cdot-}. \quad (15)$$

Yamagishi and Iida[3] examined the chemical equilibrium in acetonitrile solution spectrophotometrically, and determined the equilibrium constant to be $(2.8\pm0.1)\times10^{-3}$ at 11 °C. In a similar way to that for the TMPD/TCNQ system, we obtain

$$E_0(TCNQ, TCNQ^{\cdot-}) = E_0(TTF^{+\cdot}, TTF) - 0.14\ V. \quad (16)$$

With the aid of Eqs. 14 and 16, we can connect the reduction potential series of the acceptors (Eqs. 2 and 3) with those of the donors (Eqs. 4—6). If a standard value of reduction potential is given for E_0(TMPD$^{+\cdot}$, TMPD) or E_0(TTF$^{+\cdot}$, TTF), all the other reduction potential values can be determined from the above procedure. The reversible one-electron reduction potentials thus estimated for the donors and acceptors are given in Table 1, where E_0(TTF$^{+\cdot}$, TTF)=0.30 V is chosen as a standard. The E_0(TTF$^{+\cdot}$, TTF) value was determined by Wheland and Gillson polarographically *versus* saturated calomel electrode in acetonitrile solution using tetraethylammonium perchlorate as a supporting electrolyte.[5] Since our data of reduction potentials correspond to the free energy change in pure acetonitrile, our values should be compared with standard electrode potentials measured in the same solvent. However, since no such electrode potential data are available, we compare our data with polarographic reduction potentials measured by several authors.[5-7] These values are also given in Table 1. As for the E_0(TCNQ, TCNQ^{-}) value, the 0.16 V value estimated by our electron-transfer equilibrium method was in good agreement with the electrochemical value of Wheland and Gillson, 0.17 V.[5] The E_0(*p*-H_2QCy_2, *p*-$H_2QCy_2^{-}$)= 0.25 V value estimated by our method was somewhat smaller than the half-wave potential of 0.31 V in polarography measured by Scribner,[6] but our value of E_0(*p*-Cl_2QCy_2, *p*-$Cl_2QCy_2^{-}$)=0.48 V was found to agree almost with the 0.51 V value measured by Peover.[7] The one-electron reduction potential of phenothiazine (PT) cation radical is also given in Table 1. The value of E_0(PT$^{+\cdot}$, PT)=0.56 V was estimated by our electron-transfer equilibrium method in (1:3) ethanol-water solvent, using the relation of E_0(PT$^{+\cdot}$, PT)=E_0(TMPD$^{+\cdot}$, TMPD)+0.34 V,[2] the observed reduction potential of 0.58 V being the value in acetonitrile solution measured by Wheland and Gillson.[5] Although the solvents used differ from each other, a fairly good agreement was obtained between our value and that of Wheland and Gillson.

Table 1. One-electron reduction potential data for electron acceptor molecules and cation radicals of donors[a]

Reduction reaction	Calcd[b]	Obsd[c]
TCNQ + e $\rightleftharpoons$ TCNQ^{-}	0.16	0.17
p-H_2QCy_2 + e $\rightleftharpoons$ *p*-$H_2QCy_2^{-}$	0.25	0.31
p-Cl_2QCy_2 + e $\rightleftharpoons$ *p*-$Cl_2QCy_2^{-}$	0.48	0.51
TMPD$^{+\cdot}$ + e $\rightleftharpoons$ TMPD	0.22	—
TTF$^{+\cdot}$ + e $\rightleftharpoons$ TTF	0.30	0.30
DMPD$^{+\cdot}$ + e $\rightleftharpoons$ DMPD	0.30	—
TMB$^{+\cdot}$ + e $\rightleftharpoons$ TMB	0.50	—
PT$^{+\cdot}$ + e $\rightleftharpoons$ PT	0.56[d]	0.58

a) In unit of V *versus* saturated calomel electrode in acetonitrile solution. For abbreviations of compounds, see text. b) Values estimated by electron-transfer equilibrium method. E_0(TTF$^{+\cdot}$, TTF)=0.30 V is taken as a standard. c) Refs. 5—7. d) Value of phenothiazine cation radical (PT$^{+\cdot}$) estimated by electron-transfer equilibrium method in (1 : 3) ethanol-water solvent. The relation of E_0(PT$^{+\cdot}$, PT)=E_0(TMPD$^{+\cdot}$, TMPD)+0.34 V was used.[2]

For the reduction potentials of the other compounds, there are no experimental data for the purpose of comparison. However, the data obtained by our method are useful for predicting the degree of electron transfer when certain electron donor (D) and acceptor (A) molecules are mixed in acetonitrile solution. If E_0(A, A^{-})$-E_0$(D$^{+\cdot}$, D)$<-RT/F$, equilibrium constant of the reaction, D+A$\rightleftharpoons$D$^{+\cdot}$+A^{-}, is small, and most of the chemical species in solution will be neutral D and A molecules. If E_0(A, A^{-})$-E_0$(D$^{+\cdot}$, D)$>$ RT/F, the equilibrium constant becomes large, so that most of the chemical species in solution will be ionized D$^{+\cdot}$ and A^{-} radical molecules. In the case of E_0(A, A^{-})$-E_0$(D$^{+\cdot}$, D)$\approx$0, the equilibrium constant is *ca.* unity, and one can observe not only neutral D and A molecules but also ionized D$^{+\cdot}$ and A^{-} in solution. For example, if TTF is mixed with *p*-Cl_2-QCy_2 in acetonitrile solution, the following reaction will take place:

$$\text{TTF} + p\text{-}Cl_2QCy_2 \rightleftharpoons \text{TTF}^{+\cdot} + p\text{-}Cl_2QCy_2^{-}. \quad (17)$$

By means of the values of E_0(TTF$^{+\cdot}$, TTF)=0.30 V and E_0(*p*-Cl_2QCy_2, *p*-$Cl_2QCy_2^{-}$)=0.48 V (Table 1) and the Nernst equation, we can estimate the equilibrium constant, K, of Eq. 17 as

$$\ln K = \ln \frac{[\text{TTF}^{+\cdot}][p\text{-}Cl_2QCy_2^{-}]}{[\text{TTF}][p\text{-}Cl_2QCy_2]} = \frac{F}{RT}\{E_0(p\text{-}Cl_2QCy_2, p\text{-}Cl_2QCy_2^{-}) - E_0(\text{TTF}^{+\cdot}, \text{TTF})\}. \quad (18)$$

In acetonitrile solution at 25 °C, the magnitude of K was estimated to be as great as 1.1×10^3. Thus, in this system, one electron is transferred almost completely from TTF to *p*-Cl_2QCy_2, and most of the chemical species observed in acetonitrile will be ionized TTF$^{+\cdot}$ and *p*-$Cl_2QCy_2^{-}$.

References

1) Y. Iida and H. Akamatu, *Bull. Chem. Soc. Jpn.*, **40**, 231 (1967); Y. Iida, *ibid.*, **44**, 1430 (1971); **49**, 3691 (1976); **52**, 1875 (1979).

2) Y. Iida and A. Yamagishi, *Bull. Chem. Soc. Jpn.*, **52**, 2443 (1979).

3) A. Yamagishi and Y. Iida, *Bull. Chem. Soc. Jpn.*, **53**, 1340 (1980).

4) A. Yamagishi, F. Watanabe, and T. Masui, *J. Chem. Soc., Chem. Commun.*, **1977**, 273.

5) R. C. Wheland and J. L. Gillson, *J. Am. Chem. Soc.*, **98**, 3916 (1976).

6) R. M. Scribner, *J. Org. Chem.*, **31**, 3671 (1966).

7) M. E. Peover, *Trans. Faraday Soc.*, **58**, 1656 (1962).

MINDO/3 Prediction of the Π and Σ Electronic States of the Succinimido Radical

Osamu KIKUCHI,* Yumiko SATO, and Keizo SUZUKI
Department of Chemistry, The University of Tsukuba, Sakura-mura, Ibaraki 305
(Received March 25, 1980)

Synopsis. Restricted open-shell SCF MINDO/3 calculation gives the Σ state for the electronic ground state of the succinimido radical.

Recent works on the succinimido radical[1] has yielded a number of interesting characterizations of this radical. One of these is the recognition that two different electronic states of succinimido are being produced in the reactions of *N*-halosuccinimides, radicals with quite distinctive properties. These are considered to be the Π_N and Σ_N states.[2] Succinimido has not been detected by ESR experiment[1] and the theoretical work of this radical is worth being done.

In the simplest nitrogen radical, NH_2, the lone-pair electrons occupy the hybrid σ orbital of nitrogen and an unpaired electron occupies the nitrogen $2p_\pi$ orbital; the Π state is the ground state and the Σ state is an excited one. The *ab initio* calculation[3] gives 113 kJ mol^{-1} for the energy separation between these states; the experimental value is 130 kJ mol^{-1}.[3] The same level of the *ab initio* calculation[3] gives 46 kJ mol^{-1} for the Σ_N-Π_N energy separation of the formylaminyl (HCONH) radical. In formylaminyl, the carbonyl π^* orbital stabilizes the nitrogen $2p_\pi$ electrons, and the Σ-Π energy separation is reduced by the amount of 67 kJ mol^{-1}. In the succinimido radical, two carbonyl groups are introduced at the nitrogen atom, and its Σ-Π separation would be reduced still more; there is the possibility that the ground state of succinimido is of the Σ type.[4]

Koenig and Wielsek[5] have done the INDO calculation on the succinimido radical and concluded that the Π state is the ground state. Their results show that the energy separation between the Σ_N and Π_N states is 159 kJ mol^{-1}. This value is too large and inconsistent with the above qualitative consideration about the Σ-Π energy separation of the nitrogen radicals. We have thus examined the energy separation of succinimido using the MINDO/3 approximation.[6] The Σ and Π states of succinimido were obtained by repeated diagonalization of the correct general SCF operator which gives the optimum results for the open-shell systems.[7] The molecular structure was optimized by the use of Fletcher's variable metric method.[8] For the NH_2 radical, MINDO/3 gave the satisfactory molecular structures and the Σ-Π energy separation (Table 1). The optimized structures and the calculated heats of formation of succinimido are shown in Fig. 1. The MINDO/3 predicts the Σ ground state for the succinimido radical. This state lies 71 kJ mol^{-1} below the excited Π state.

Very recently, on the basis of the semi-empirical MNDO calculations, Clark[9] has well explained the reaction paths for the generation of the Π and Σ states of the succinimido radical from *N*-halosuccinimides. His MNDO results show that the ground state of succinimido is of Π-type, although the open-shell method employed is an approximate one. Since the present MINDO/3 calculation predicts the Σ ground state which is inconsistent with the INDO and MNDO results, another semi-empircal method, the CNDO/BW method[10] which was parametrized by Boyd and Whitehead so as to give better energetics of molecules, was also applied to succinimido. The results obtained are parallel with those of MINDO/3; the Σ state is more stable than the Π state by 41 kJ mol^{-1}.

The characterization of the ground and excited electronic states of the succinimido radical is a key factor for the analysis of the reaction mechanism in which both of the ground and excited states of succinimido are involved. The present MINDO/3 and CNDO/BW results predict the Σ state for the ground state of this radical, while the INDO[5] and MNDO[9]

TABLE 1. MINDO/3 RESULTS ON THE NH_2 RADICAL

Method	H-N-H angle/°		$E(\Sigma)-E(\Pi)$
	In Π state	In Σ state	kJ mol^{-1}
MINDO/3	102	136	100
STO-3G[a]	101	130	188
4-31G[a]	108	143	113
Experimental[a]	103	144	≈130

a) From Ref. 3.

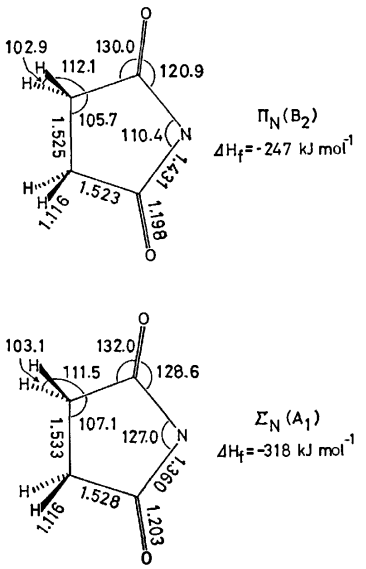

Fig. 1. The molecular structure (C_{2v}) of the Π and Σ states of the succinimido radical optimized by the restricted open-shell MINDO/3 method. These C_{2v} structures were also obtained by the geometry optimization in which the distorted (C_s) structures were used as the initial data.

calculations have predicted the Π ground state. The Σ-Π separation of succinimido is expected to be very small, and the question, whether Σ or Π is the ground state of this radical, is still open to investigation.

References

1) P. S. Skell and J. C. Day, *Acc. Chem. Res.*, **11**, 381 (1978).

2) . The stable Σ_0 structure, in which the unpaired electron locates mostly on one of the oxygen atoms, has also been predicted by INDO calculations. See Ref. 5.

3) N. C. Baird and H. B. Kathpal, *J. Am. Chem. Soc.*, **98**, 7532 (1976).

4) The possibility of the Σ ground state of succinimido has been suggested by Danen and Neugebauer: W. C. Danen and F. A. Neugebauer, *Angew. Chem. Int. Ed.*, **14**, 783 (1975).

5) T. Koenig and A. Wielesk, *Tetrahedron Lett.*, **1975**, 2007.

6) R. C. Bingham, M. J. S. Dewar, and D. H. Lo, *J. Am. Chem. Soc.*, **97**, 1285 (1975).

7) K. Hirao and H. Nakatsuji, *J. Chem. Phys.*, **59**, 1457 (1973).

8) R. Fletcher, *Computer J.*, **13**, 317 (1970).

9) T. Clark, *J. Am. Chem. Soc.*, **101**, 7746 (1979).

10) R. J. Boyd and M. A. Whitehead, *J. Chem. Soc., Dalton Trans.*, **1972**, 73.

A Photoacoustic and Fluorescent Spectroscopic Study of Uranyl Compounds

Yoshinori SUGITANI,* Hiroshi NOMURA, and Kozo NAGASHIMA
Institute of Chemistry, The University of Tsukuba, Sakura-mura, Ibaraki 305
(Received October 22, 1979)

Synopsis. The fluorescent emission spectra and fluorescent lifetimes have been measured for several available uranyl salts and natural mineral zippeite. The absolute quantum efficiency data of $UO_2SO_4 \cdot 0.5H_2O$, $H_2(UO_2)_2(PO_4)_2 \cdot 8H_2O$, and $UO_2(CH_3COO)_2 \cdot 2H_2O$ have been obtained by the simultaneous measurement of the photoacoustic and excitation spectra.

The simultaneous measurement of the intensities of the photoacoustic and fluorescent excitation signals as a function of the wavelength of the exciting light enables the determination of the absolute quantum efficiencies of fluorescence without any use of reference materials.[1] The technique was successfully applied to a series of uranyl micas: uranyl phosphate of alkali, alkaline-earth, and some other bivalent metal ions. In the present work, the simultaneous measurement of some uranyl compounds have been carried out, together with the measurement of the emission spectra and the luminescence lifetimes.

Experimental

Samples. The uranyl compounds used in the present study were all prepared according to the literature[2-5] except for a natural mineral zippeite, $3UO_2 \cdot 2SO_3 \cdot 9H_2O$.

Measurement. The fluorescent emissions were measured by means of a multi-purpose spectrometer, JASCO SS-25, using an UV light of 365 nm as the excitation source. The photoacoustic spectra and fluorescent excitation spectra were measured by means of a system, which was readily arranged by the use of the spectrometer CT-25N, a lock-in amplifier, and a sample cell designed for the simultaneous detection of photoacoustic and excitation signals.[1] The intensity of the fluorescent excitation signal was monitored at the output slit of the spectrometer adjusted at 520 ± 5 nm. A 300 w xenon lamp was used as the excitation source. The fluorescent lifetimes were measured by the multi-channel photon counting method using a microcomputer-assisted apparatus made in our laboratory, the details of the procedure will be described elsewhere.[6] All of the measurements were conducted at room temperature.

Results and Discussion

Figure 1 shows the fluorescent emission(a), fluorescent excitation(b), and photoacoustic(c) spectra of the powdered sample of uranyl acetate, $UO_2(CH_3COO)_2 \cdot 2H_2O$. The three kinds of spectra for the other uranyl compounds studied are very similar to those shown in Fig. 1, except for minor differences in peak positions and/or their relative intensities. Generally, the emission and excitation spectra of uranyl compounds have six and twelve peaks respectively, which can be explained as the transitions between $^1\Sigma_g^+$ and $^3\Pi_u$ states, the both split into sublevels by the symmetric stretching of the UO_2 species.[7] It should be noted

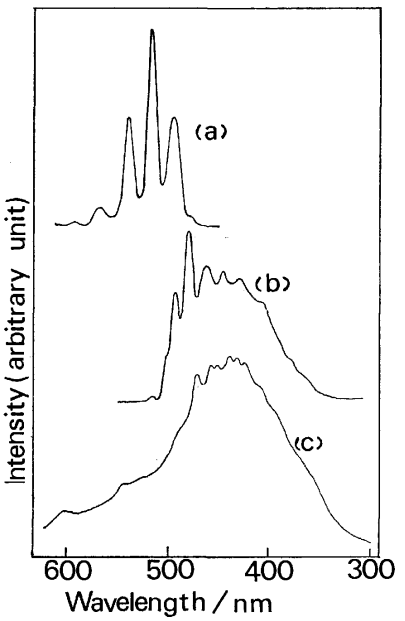

Fig. 1. Spectra of $UO_2(CH_3COO)_2 \cdot 2H_2O$.
(a) Fluorescent emission spectra, (b) fluorescent excitation spectra, (c) photoacoustic spectra (chopping frequency 80 Hz).

that the photoacoustic spectra are very similar to the excitation spectra except for a somewhat better resolution in the latter spectra, just as was the case with the uranium-mica samples. The similarity between the two spectra shows that a definite proportional amount of the energy absorbed at a certain wavelength, λ, will always be emitted as optical energy(excitation spectra), while the remaining part of the absorbed energy will be emitted as thermal energy(photoacoustic spectra). This suggests that the de-excitation processes from the twelve excited sublevels of $^3\Pi_u$ are affected by the same transition mechanism. This seems to be closely related to the fact that the six emission peaks of $Mg(UO_2)_2(PO_4)_2 \cdot nH_2O$ have the same fluorescent lifetime.[8]

The fluorescent lifetimes and quantum efficiencies of the prepared samples are given in Table 1. The lifetimes have the same order of magnitude as those of uranium-micas reported before.[8] The mineral zippeite, $3UO_2 \cdot 2SO_3 \cdot 9H_2O$, has a lifetime by an order shorter, probably because of the trace amount of impurities.

Quantum efficiency data have been obtained for the three samples through the method of the simultaneous measurement of the photoacoustic and excitation spectra, details of which have already been reported.[1] The quantum efficiency determinations for the other compounds were not successful. There is no apparent correlation between the lifetime and the

TABLE 1. FLUORESCENT LIFETIME, τ; QUANTUM EFFICIENCY, Q_f; FLUORESCENT TRANSITION PROBABILITY CONSTANT, k_f, AND EMISSION BAND POSITIONS, ν'S, OF THE URANYL COMPOUNDS

Samples	$\tau/10^{-4}$ s	Q_f/%	$k_f \times 10^3$	ν_1[a]	ν_2	ν_3	ν_4	ν_5	ν_6
$UO_2(NO_3)_2 \cdot 6H_2O$	7.0	—	—	474	490	512	534	560	587
$UO_2C_2O_4 \cdot 3H_2O$	3.0	—	—	476	492	512	535	561	589
$UO_2SO_4 \cdot 0.5H_2O$	3.1	77	2.5	475	491	512	535	560	588
$H_2(UO_2)_2(PO_4)_2 \cdot 8H_2O$	4.4	85	1.9	487	503	524	548	574	602
$UO_2(CH_3COO)_2 \cdot 2H_2O$	1.8	89	4.9	474	490	511	534	560	588
$UO_2(ClO_4)_2 \cdot 5H_2O$	2.5	—	—	472	488	510	533	558	586
$RbUO_2(NO_3)_3$	5.0	—	—	483	502	520 523	546	574	
$3UO_2 \cdot 2SO_3 \cdot 9H_2O$[b] (zippeite)	0.27	—	—			—			
UO_2CO_3[c]		—	—			—			

a) ν_1 to ν_6 correspond to the six emission bands, after Bell and Biggers.[7] b) The emission spectrum is single and broad. c) Non-fluorescent.

quantum efficiency data. However, the fluorescent transition velocity constant, k_f, which is obtained as Q_f/τ, is correlated with the lifetime value, τ, in the sense that the larger k_f value corresponds to the smaller τ value, as may be seen in Table 1.

The authors wish to thank the Ministry of Education for the financial support (No. 484032) granted to the research project which includes the present work.

References

1) Y. Sugitani and K. Kato, *Bull. Chem. Soc. Jpn.*, **52**, 3499 (1979).
2) J. M. Schreyer and C. F. Baes, Jr., *J. Am. Chem. Soc.*, **76**, 354 (1979).
3) H. R. Hoekstra, *Inorg. Chem.*, **2**, 492 (1963).
4) R. Bressat, B. Claudel, and Y. Trambouze, *Bull. Soc. Chim. Fr.*, **1963**, 464.
5) B. M. Gatehouse and A. E. Comyns, *J. Chem. Soc.*, **1958**, 3965.
6) K. Kato and Y. Sugitani, *Chem. Biomed. Environ. Instrumentation*, in press.
7) J. T. Bell and R. E. Biggers, *J. Mol. Spectrosc.*, **18**, 274 (1965); **22**, 262 (1967); **25**, 312 (1968).
8) Y. Sugitani, K. Kato, and K. Nagashima, *Bull. Chem. Soc. Jpn.*, **52**, 918 (1979).

The Crystal Structure of Bis(acetylacetonato)platinum(II)

Shigeki ONUMA, Keiji HORIOKA, Hironao INOUE, and Shuzo SHIBATA*
Department of Chemistry, Shizuoka University, Oya, Shizuoka 422
(Received January 23, 1980)

Synopsis. The crystal structure of $Pt(acac)_2$ has been determined by means of X-ray diffraction. The molecule is monomeric, the coordination geometry being square-planar. The average Pt–O distance is 1.991(8) Å. The bond lengths and angles of the chelating ligands are almost the same as those for other acetylacetone complexes.

The acac ligand in $Pt(acac)_2$ is thought to be bidentate (Hacac=acetylacetone). However, some anomalous modes of ligation have been found in platinum complexes; *e.g.*, in $K[Pt(acac)_2Cl]$,[1] one of the β-diketones is unidentate and linked to the metal through the methylene carbon; in $[Me_3Pt(acac)]_2$,[2] the β-diketone is linked to one platinum atom *via* γ-carbon atom and to the other platinum *via* oxygen atoms to yield a binuclear complex. The present study has been undertaken to elucidate the crystal structure of $Pt(acac)_2$.

Experimental

The crystals were prepared by the method of Werner.[3] Crystal Data: $Pt(C_5H_7O_2)_2$, Mol. wt. 393.3, triclinic, space group $P\bar{1}$ $a=7.13(2)$, $b=5.75(2)$, $c=7.957(4)$ Å, $\alpha=70.0(1)$, $\beta=98.9(1)$, $\gamma=113.2(2)°$, $V=282(1)$ Å^3; $D_m=2.32$, $D_c=2.31$ g cm^{-3} for $Z=1$. Found: C, 30.57; H, 3.56%. Calcd for C, 30.54; H, 3.59%. Crystal dimensions: $0.08\times0.14\times0.20$ mm^3.

Intensity data were collected on a Rigaku diffractometer with graphite monochromatized Mo $K\alpha$ radiation. Reflections were measured with the ω-scan ($2\theta\leqq30°$) and ω-2θ scan ($30°<2\theta<70°$) techniques. The scan rate was 4° min^{-1} and the scan width $(1.8+0.5\tan\theta)°$. The number of reflections with $F>3\sigma$ was 2342. The intensities were corrected for Lorentz and polarization effects, but not for absorption. The space group $P\bar{1}$ was assumed at the outset and verified by successful refinement of the crystal structure. Compliance to the centrosymmetric space group requires that the monomer possesses a crystallographic center of symmetry. The structure was solved by the heavy atom method. The positional and anisotropic thermal parameters of the eight non-hydrogen atoms were refined by the block-diagonal least-squares method. The final R value was 0.059 for 2342 reflections. The atomic scattering factors were taken from Ref. 4. Anomalous dispersion correction for platinum atom was taken into account. The resulting difference Fourier map shows no significant peaks or troughs. The final positional and thermal parameters are given in Table 1. The complete F_o-F_c data are kept at the Chemical Society of Japan (Document No. 8029).

Results and Discussion

The complex was found to be monomeric, the platinum atom having a square-planar coordination by four oxygen atoms of the acetylacetonato ligands.

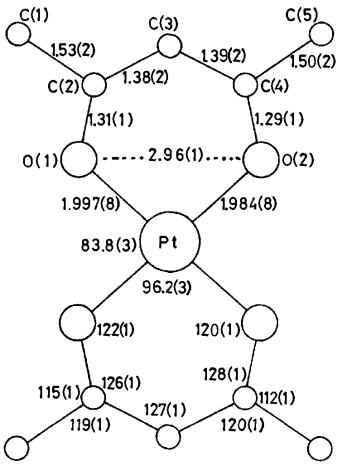

Fig. 1. Bond lengths (l/Å) and angles (ϕ/°) with their estimated standard deviations in parentheses.

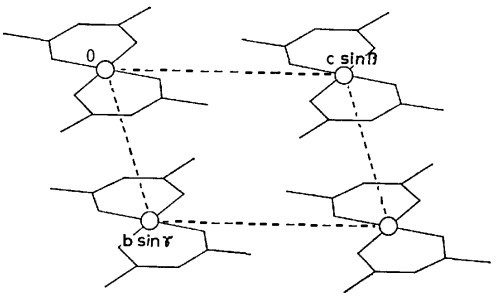

Fig. 2. Projection of the crystal structure along the a axis.

TABLE 1. THE FINAL POSITIONAL AND THERMAL PARAMETERS ($\times10^4$)
The anisotropic thermal parameters are of the form: $\exp[-(B_{11}h^2+B_{22}k^2+B_{33}l^2+B_{12}hk+B_{13}hl+B_{23}kl)]$

	x	y	z	B_{11}	B_{22}	B_{33}	B_{12}	B_{13}	B_{23}
Pt	0	0	0	181(1)	326(2)	96(1)	315(2)	−26(1)	−125(2)
O (1)	−1735(11)	1805(15)	−1709(8)	298(19)	564(35)	96(9)	587(46)	−58(21)	−160(29)
O (2)	−596(11)	572(14)	2150(8)	263(18)	488(33)	136(11)	487(42)	−64(22)	−199(31)
C (1)	−3876(18)	4257(24)	−2675(14)	326(32)	611(59)	168(18)	681(77)	−128(39)	−179(53)
C (2)	−2716(15)	2894(19)	−1147(12)	230(23)	402(40)	148(15)	405(53)	−33(30)	−132(40)
C (3)	−2791(15)	2914(20)	570(12)	238(24)	448(43)	136(15)	409(55)	−20(30)	−151(41)
C (4)	−1757(15)	1850(20)	2080(12)	251(25)	414(41)	131(14)	360(54)	22(30)	−176(40)
C (5)	−1989(19)	2142(24)	3837(14)	354(35)	579(57)	148(17)	548(76)	27(39)	−202(51)

Table 2. The average bond lengths (l/Å) and angles (ϕ/°) in $Pt(acac)_2$ and the related chelates

	Present work	$K[Pt(acac)_2Cl]$[1]	$PtCl(acac)\text{-}(H_2CCHOH)$[6]
Pt–O	1.99	2.02	2.02
C–O	1.30	1.31	1.29
C–C	1.39	1.41	1.39
$C–CH_3$	1.51	1.49	1.49
CCC	127	129	128
OCC	127	125	126
$OCCH_3$	114	116	114
OPtO	96	95	94

The molecular structure is shown in Fig. 1, atom numbering and bond lengths and angles also being given with their esd values in parentheses. The chelate ring was found to be planar, the deviations of atoms from the least-squares plane being: Pt 0.0, O(1) 0.02, O(2) 0.02, C(1) −0.03, C(2) 0.01, C(3) 0.02, C(4) 0.00, C(5) −0.02 Å. The average values of the chemically equivalent bond lengths and angles are given in Table 2, those of other β-diketonato complexes being given for the sake of comparison. They agree with each other.

The molecules are well separated. The arrangement viewed along the a axis is shown in Fig. 2. The intermolecular distances are normal, the shortest distance between methyl carbon atoms being 4.00 Å.

Most of the calculations were carried out by using the UNICS programs[5] at the Computer Center of the University of Tokyo.

References

1) R. Mason, G. B. Robertson, and P. J. Pauling, *J. Chem. Soc., A*, **1969**, 485.
2) A. G. Swallow and M. R. Truter, *Proc. R. Soc. London, Ser. A*, **254**, 205 (1960).
3) A. Werner, *Ber.*, **34**, 2584 (1901).
4) "International Tables for X-Ray Crystallography," Kynoch Press, Birmingham (1962), Vol. III.
5) "Universal Crystallographic Computing System," The Crystallographic Society of Japan, Tokyo (1967).
6) F. A. Cotton, J. N. Francis, B. A. Frenz, and M. Tsutsui, *J. Am. Chem. Soc.*, **95**, 2483 (1973).

Background Atmospheric Concentrations of Halogenated Hydrocarbons in Japan

Yoshihiro MAKIDE,* Yutaka KANAI, and Takeshi TOMINAGA
Department of Chemistry, Faculty of Science, The University of Tokyo, Hongo, Bunkyo-ku, Tokyo 113
(Received February 20, 1980)

Synopsis. The atmospheric concentrations of CCl_2F_2, CCl_3F, CCl_2FCClF_2, CH_3CCl_3, CCl_4, $CHCl{=}CCl_2$, and $CCl_2{=}CCl_2$ in remote areas in Japan and over the Japan Sea were measured in the summer of 1979. The averaged observed concentrations (in ppt: 10^{-12} v/v) for the compounds were 301 ± 12, 175 ± 7, 23 ± 2, 117 ± 11, 107 ± 6, 14 ± 10, and 19 ± 10 respectively.

Among a number of anthropogenic halogenated hydrocarbons released in large quantities into the atmosphere, greatest attention has been directed to the chlorofluoromethanes, CCl_2F_2 and CCl_3F, which have been widely used as spray propellants and refrigerants. The chlorofluoromethanes accumulated in the troposphere due to their long lifetimes rise gradually into the stratosphere, there to be decomposed by intense UV light to release atomic chlorine, which can then participate in the ClO_x-chain removal of stratospheric ozone.[1,2] While such a theoretical prediction as to stratospheric ozone depletion by chlorofluorocarbons has been essentially validated by extensive research,[3-8] precise world-wide monitoring of their background atmospheric concentrations has now become more important for the accurate estimation of possible future ozone depletion. The growing use of 1,1,1-trichloroethane (CH_3CCl_3), once classified as a 'safe' substitute for other 'labile' solvents, cannot be overlooked, since it is not decomposed completely by OH radicals in the troposphere and may similarly affect the ozone layer if the present rates of production and use continue. The development of a reliable analytical system is greatly needed in order to determine precisely its background concentration in view of the discrepancies among the reported data,[6] possibly due to contamination by the analytical systems. Measurements of unsaturated chlorocarbons, such as $CHCl{=}CCl_2$ and $CCl_2{=}CCl_2$, which are decomposed rapidly and completely in the troposphere may also be necessary for understanding their local pollution behavior, as they are extensively used as degreasing or cleaning solvents.

Since no reliable measurements of the halogenated hydrocarbons have thus far been made in Japan and Asia, we have initiated a systematic survey of the atmospheric concentrations of CCl_2F_2, CCl_3F, CCl_2FCClF_2, CH_3CCl_3, CCl_4, $CHCl{=}CCl_2$, and $CCl_2{=}CCl_2$ over Japan; we have already reported the preliminary data on more or less polluted air samples.[10] In this article we wish to describe our clean analytical system for extremely accurate measurements and our results on the averaged background atmospheric concentrations of these substances in remote areas in the summer of 1979.

Experimental

Extremely Clean Analytical System and Procedures. Stainless steel canisters were specially designed for air sampling and storage. Since Teflon stopcocks or silicone rubber plugs often cause a contamination of halogenated hydrocarbons, the sampling canister was made from a stainless steel beaker (21) by argon-arc welding and equipped with a hermetically sealed stainless steel bellows valve (Nupro SS-4H). The inside of the canister was polished electrochemically and washed ultrasonically. After the evacuation of the canister overnight to 10^{-4} Pa at 200 °C, the dead volume between the valve and a Swagelok cap was filled with ultra-high-purity nitrogen. On sampling, ambient air was introduced into the canister by simply removing the cap and opening the valve facing the wind. The composition of the atmospheric samples remain unchanged even after storage for over a year. The calibration standard was prepared by a four- or five-step static-dilution method. An extremely clean, all-stainless-steel vacuum line was built for the final stages of dilution (*e.g.*, ppb—ppt level) with ultra-high-purity nitrogen or air. Several ambient-air samples, calibrated for all components against each standard, were used as the secondary standards in routine measurements. The halogenated hydrocarbons were determined by using a constant-current-type electron capture detector (Varian 3700 EC-GC). A Silicone OV-101 column (10 wt% coated on Chromosorb W-HP, 80—100 mesh, 5 mm i.d., 3 m long) was used as the preconcentration and analytical column. The carrier-gas (nitrogen) flow rate was 80 ml/min. Methane (4 ml/min) was mixed in between the column and the detector as a make-up gas to improve the S/N ratio and to stabilize the base line without reducing the sensitivity. An aliquot of the air sample or of the standard was introduced into an evacuated sample loop until a given pressure was reached, and then it was transferred into the column cooled at −40 °C so that halogenated hydrocarbons were kept on the head of the column. The column temperature was raised linearly at a rate of 5 °C/min up to 70 °C. After the elution of the air (oxygen), ECD was connected to the analytical column by switching the four-way valve between the column and the detector, and each component was determined.

Samples. Clean-air samples were collected in the summer of 1979 at remote areas throughout Japan and over the Japan Sea. Although sampling was not always conducted under optimum meteorological conditions, we did our best to avoid local contamination within the limited sampling periods. The locations, dates, and weather conditions are listed in Table 1.

Results and Discussion

Figure 1 shows a typical EC-GC chromatogram of the atmospheric sample No. 1, collected at Nosappumisaki, together with a chromatogram of the purified nitrogen used for the dilution of the standards to ensure the absence of any halogenated hydrocarbons during the identical analytical procedure. Since impurities in the carrier gas should also have been concentrated at the head of the analytical column during preconcentration, the possible contamination from about 500 ml of purified nitrogen can not exceed the detection limit of each compound in this system: CCl_2F_2 and

Table 1. Observed concentrations of halogenated hydrocarbons in air over Japan in the summer of 1979 (in ppt = 10^{-12} v/v)

Sample[a)]	CCl_2F_2	CCl_3F	CCl_2FCClF_2	CH_3CCl_3	CCl_4	$CHCl=CCl_2$	$CCl_2=CCl_2$
No. 1	285	173	24	113	107	18	14
No. 2	304	179	23	121	103	5	23
No. 3	306	173	23	115	111	6	14
No. 4	288	166	27	103	112	7	8
No. 5	304	173	25	115	100	9	18
No. 6	311	181	21	136	96	19	36
No. 7	310	180	22	123	110	21	31
No. 8	278	162	23	100	108	6	3
No. 9	319	186	23	127	118	38	22
Average	301	175	23	117	107	14	19
S. D. (σ)	12	7	2	11	6	10	10
	(4%)	(4%)	(7%)	(9%)	(6%)	(71%)	(53%)

a) Sampling locations, dates, and weather conditions. Sample No. 1: Nosappu-misaki (Hokkaido) 43°23'N, 145°49'E, Aug. 3, 1979, clear, 15.7 °C, SSE 10 m/s. Sample No. 2: Nukabira (Hokkaido) 43°20'N, 143°10'E, Aug. 4, 1979, cloudy, 17.8 °C, SW, 3 m/s. Sample No. 3: Setana (Hokkaido) 42°29'N, 139°51'E, Aug. 6, 1979, cloudy, 19.5 °C, SSE, 8 m/s. Sample No. 4: Shiose-zaki (Akita) 39°51'N, 139°45'E, Aug. 7, 1979, cloudy, W, 5 m/s. Sample 5: Japan Sea (off Shimane) 38°25'N, 132°30'E, Jul. 4, 1979, clear, 22.8 °C, SW, 8 m/s. Sample No. 6: Tago (Shimane) 35°36'N, 133°06'E, Sep. 12, 1979, fair, 28.9 °C, ESE, 3 m/s. Sample No. 7: Iki-island (Nagasaki) 33°47'N, 129°48'E, Sep. 11, 1979, clear, 26.0 °C, E, 10 m/s. Sample No. 8: Muroto-misaki (Kouchi) 33°14'N, 134°11'E, Aug. 3, 1979, cloudy, 28.0 °C, W, 8 m/s. Sample No. 9: Noma-misaki (Kagoshima) 31°25'N, 130°07'E, Sep. 10, 1979, fair, 26.8 °C, NNW, 5 m/s.

$CHCl=CCl_2$ < 0.2 ppt, CCl_2FCClF_2, CH_3CCl_3, and $CCl_2=CCl_2$ < 0.05 ppt, and CCl_3F and CCl_4 < 0.01 ppt. The reproducibility of the measurement was within 2%. The absolute accuracy of the calibration under the present conditions may be less than 10 ppt. The observed concentrations (Table 1) were slightly affected by the sampling location and the meteorological conditions regarding the transport of the air mass. However, the small standard deviations in the CCl_2F_2 and CCl_3F concentrations (≈4%) demonstrate that the relatively low local emission in the rural areas may not appreciably raise their already high concentration levels. The averaged concentrations observed in Japan are close to the background concentrations reported in the northern hemisphere after the correction for the monthly increase in concentrations. The fluctuations in the $CHCl=CCl_2$ and $CCl_2=CCl_2$ concentrations may be ascribed to their short lifetimes and relatively high emissions even in remote areas in Japan. The averaged concentrations of these halogenated ethylenes have been observed to be hundreds-fold higher in Tokyo.[11)]

In conclusion, it is made clear that we can measure the background concentrations of the halogenated hydrocarbons even in Japan only if we carefully choose favorable locations and meteorological conditions. Further studies regarding the profile of local pollution in urban areas are also in progress in our laboratory.

We wish to thank Mr. Yukihiro Nojiri for the collection of the No. 5 sample. The present work was partially supported by the Toyota Foundation.

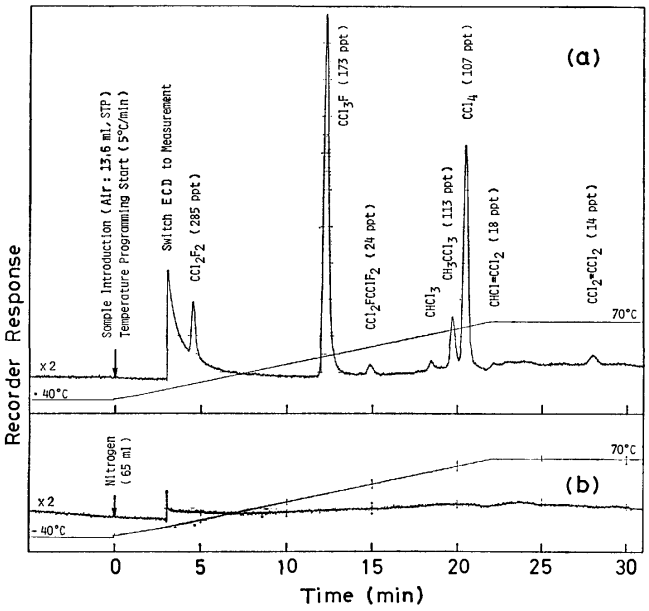

Fig. 1. Typical temperature program EC-GC chromatograms of (a) the atmospheric sample collected at Nosappu-misaki, Hokkaido (Sample No. 1 in Table 1), and (b) the instrumental background noise level in the identical analytical procedure. (Conditions are given in the text).

References

1) M. J. Molina and F. S. Rowland, *Nature*, **249**, 810 (1974).
2) F. S. Rowland and M. J. Molina, *Rev. Geophys. Space Phys.*, **13**, 1 (1975).
3) NAS Report "Halocarbons: Effects on Stratospheric Ozone," National Academy of Sciences, Washington D. C. (1976).
4) NAS Report "Halocarbons: Environmental Effects of Chlorofluoromethane Release," National Academy of Sciences, Washington D. C. (1976).
5) NASA Report "Chlorofluoromethanes and the Stratosphere," Reference Publication 1010, National Aeronautics and Space Administration, Washington D. C. (1977).
6) NAS Report "Stratospheric Ozone Depletion by Halocarbons: Chemistry and Transport," National Academy of Sciences, Washington D. C. (1979).
7) NAS Report "Protection against Depletion of Stratospheric Ozone by Chlorofluorocarbons," National Academy of Sciences, Washington D. C. (1979).
8) NASA Report "The Stratosphere: Present and Future," Reference Publication 1049, National Aeronautics and Space Administration, Washington D. C. (1979).
9) *Chem. Eng. News*, Oct. 15, 25 (1979).
10) Y. Makide, T. Tominaga, and F. S. Rowland, *Chem. Lett.*, **1979**, 355.
11) Y. Makide, Y. Kanai, and T. Tominaga, unpublished data.

Thermal Rearrangements of 1,5-Dimethyl- and 1,3,5-Trimethyl-8-vinyl-6-methylenetricyclo[3.2.1.$0^{2,7}$]oct-3-en-8-ol and Their Alkoxides

Makoto Nitta,* Nobuo Komatsu, and Ichiro Kasahara

Department of Chemistry, School of Science and Engineering, Waseda University, Shinjuku-ku, Tokyo 160

(Received December 11, 1979)

Synopsis. The reactions of 1,5-dimethyl- and 1,3,5-trimethyl-6-methylenetricyclo[3.2.1.$0^{2,7}$]oct-3-en-8-one with vinylmagnesium bromide at 0 °C afforded 1,5-dimethyl- and 1,3,5-trimethyl-8-vinyl-6-methylenetricyclo[3.2.1.$0^{2,7}$]oct-3-en-8-ol, respectively. The thermal rearrangements of IIa,b and their alkoxybromomagnesium afforded 1,5-dimethyl or 1,3,5-trimethylbenzocyclohepten-6-one. It is suggested that the pathways involve an oxy-Cope rearrangement and the subsequent hydrogen migrations.

Recently, various anionic oxy-Cope rearrangements and their related sigmatropic rearrangements have been investigated, and the rate enhancements of metal alkoxides have been precisely demonstrated from the synthetic and mechanistic points of view.[1-5] In relation to the synthesis and chemistry of polycyclic compounds containing cyclopropane ring,[6,7] we ourselves tried to prepare the skeleton of bicyclo[5.4.0]undeca-1,3,5,8,10-pentaene,[8] which has a methyl group on a bridgehead. However, benzocyclohepten-6-one derivatives were obtained by the reactions of 1,5-dimethyl- and 1,3,5-trimethyl-6-methylenetricyclo[3.2.1.$0^{2,7}$]oct-3-en-8-one (Ia and Ib) with vinylmagnesium bromide and the subsequent thermal rearrangements. Therefore, we will describe here a facile synthesis of benzocyclohepten-6-one derivatives.

The reactions of Ia and Ib with vinylmagnesium bromide in anhydrous tetrahydrofuran (THF) at 0 °C afforded 1,5-dimethyl- and 1,3,5-trimethyl-8-vinyl-6-methylenetricyclo[3.2.1.$0^{2,7}$]oct-3-en-8-ol (IIa and IIb) respectively in fairly good yields. The structures of IIa, b were assigned on the basis of their spectral properties (see Experimental). The stereochemical assignment of IIa was derived from the pseudo-contact NMR spectra obtained using Eu(fod)$_3$. The chemical shifts of the hydrogens at C-3 and C-4 were much shifted downfield compared to those of the exomethylene group and hydrogen at C-7. The attacking site of vinylmagnesium bromide on Ia is similar to the case of Ia,b with lithium aluminum hydride.[9,10] Therefore, the orientation of the hydroxyl group of IIb should be the same as in the case of IIa. On the other hand, after Ia or Ib had been reacted with vinylmagnesium bromide at 0 °C, the reaction mixtures were allowed to reflux for 5 h under a nitrogen atmosphere. The benzocyclohepten-6-one derivatives, IIIa and IIIb, were thus obtained in fairly good yields. The structures of IIIa, b were determined on the basis of the spectral properties (see Experimental). The assignment of structures was also supported by the pseudo-contact NMR spectra of IIIa obtained using Eu(fod)$_3$. The relative downfield shifts (ppm/mol) of the δ's of characteristic hydrogens are given in parentheses in the structural formula IIIa in Scheme 1. When IIa or IIb was refluxed in benzene for 5 h,

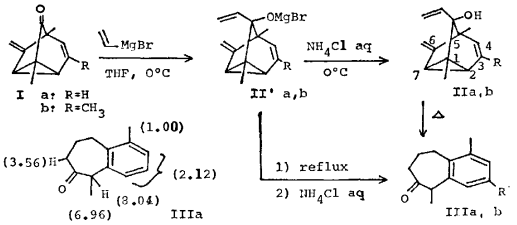

Scheme 1.

however, no thermal rearrangement into IIIa or IIIb occured, but IIa or IIb was recovered in a quantitative yield. It is known that the metal alkoxides enhance the rates of oxy-Cope rearrangements.[1-5] Therefore, IIIa, b probably originate from the anionic oxy-Cope rearrangements of the alkoxybromomagnesium derivatives, II'a and II'b.

In order to confirm this point, the thermal rearrangements of IIa and IIb were carried out at high temperatures. When IIa was heated in refluxing xylene for 30 min, a clean conversion of IIa to IIIa occured. Similarly, IIb was rearranged to IIIb in 1,2-dichlorobenzene during 15 min at the refluxing temperature.

For the facile rearrangements of IIa,b, or II'a,b, two mechanistic interpretations can be considered. In both reaction pathways, the oxy-Cope rearrangement affording IV might be the first step of the present thermal reaction, as is shown in Scheme 2. One of the possible pathways involves, perhaps, a simple stepwise aromatization of IV to III *via* V (Path a). The other possible pathway is the thermally allowed concerted [1,5]-sigmatropic rearrangement (Berson-Willcott rearrangement)[11] of IV to VI, which can give III by the cleavage of the cyclopropane ring and a concurrent hydrogen-shift.

It is known that compound IX, which has a skeleton

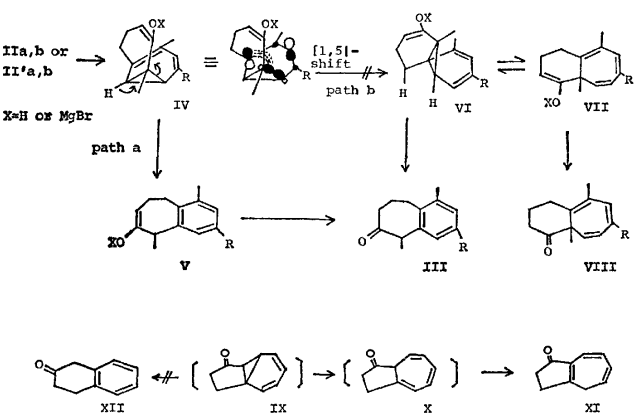

Scheme 2.

homologous with VI, affords bicyclo[5.3.0]decatrienone, XI, and does not afford XII.[12,13] Therefore, if the intermediate of norcaradiene, VI, is involved in the present thermal rearrangement, it should be possible for VI to equelibrate with cycloheptatriene, VII. However, VIII could not be obtained, hence, VI could not be involved in the present thermal rearrangement. Therefore, the present thermal rearrangement affording IIIa,b must proceed through Path a.

The much strained IV, which has a bridgehead double bond, could not undergo Berson-Willcott rearrangement. Since compounds Ia,b are synthesized very easily by the thermal reactions of 2,6-dimethylphenyl and 2,4,6-trimethylphenyl propargyl ether[14] respectively, the present reactions should be very useful for the preparation of benzocycloheptenone derivatives.

Experimental

Reactions of 1,5-Dimethyl-6-methylenetricyclo[3.2.1.0^{2,7}]oct-3-en-8-one (Ia) with Vinylmagnesium Bromide. To a stirred solution of vinylmagnesium bromide, which was prepared by a usual procedure[15] using 0.730 g (30 mg-atom) of magnesium turnings, 3.50 g (32.7 mmol) of vinyl bromide, and 50 ml of anhydrous tetrahydrofuran (THF), was added 1.60 g (10 mmol) of Ia in 10 ml of THF at 0 °C. This reaction mixture was stirred another 3 h at 0 °C and then treated with aqueous ammonium chloride, followed by ether extraction. The evaporation *in vacuo* of the dried (Na_2SO_4) organic portion gave a clean oil of IIa (1.84 g, 98%): bp 66—70 °C/7 mmHg (1 mmHg=133.32 Pa); IR (neat) 3600—3400, 1600 cm^{-1}; NMR (CCl_4) δ 1.00 (s, 3H), 1.10 (s, 3H), 1.55 (s, 1H), 1.68—1.85 (m, 2H), 4.51 (s, 1H), 4.53 (s, 1H), 4.90—5.22 (m, 4H), 6.05 (m, 1H); MS *m/e* 188 (M^+). Found: C, 82.71; H, 8.64%. Calcd for $C_{13}H_{16}O$: C, 82.93; H, 8.57%.

Reaction of Ia with Vinylmagnesium Bromide and Subsequent Thermal Rearrangement. To a stirred solution of vinylmagnesium bromide, which had been prepared using 1.75 g (16.0 mmol) of vinyl bromide, 0.356 g (15.0 mg-atom) of magnesium turnings, and 25 ml of THF, was added 800 mg (5 mmol) of Ia in 5 ml of THF at an ambient temperature. This reaction mixture was allowed to reflux for another 4 h, and then it was treated with aqueous ammonium chloride, followed by ether extraction (30 ml×3). The evaporation *in vacuo* of the dried (Na_2SO_4) organic portion gave an oil of IIIa (888 mg, 95%): bp 100 °C/4 mmHg; IR (neat) 1710 cm^{-1}; NMR (CCl_4) δ 1.36 (d, J=7.0 Hz, 3H), 1.82—2.18 (m, 2H), 2.31 (s, 3H), 2.15—2.60 (m, 2H), 2.68—2.90 (m, 2H), 3.55 (q, J=7.0 Hz, 1H), 7.00 (s, 3H); MS *m/e* 188 (M^+). Found: C, 82.87; H, 8.49%. Calcd for $C_{13}H_{16}O$: C, 82.93; H, 8.57%.

Reaction of 1,3,5-Trimethyl-6-methylenetricyclo[3.2.1.0^{2,7}]oct-3-en-8-one (Ib) with Vinylmagnesium Bromide. To a stirred solution of vinylmagnesium bromide, which had been prepared using 1.75 g (16.4 mmol) of vinyl bromide, 0.365 g (15 mg-atom) of magnesium turnings, and 25 ml of THF, was added 870 mg (5 mmol) of Ib in 10 ml of THF at 0 °C. This reaction mixture was stirred for another 4 h at 0 °C, treated with aqueous ammonium chloride, and then extracted with ether (30 ml×3). The evaporation *in vacuo* of the dried (Na_2SO_4) organic portion gave an oil of IIb (997 mg, 99%): bp 40—46 °C/4 mmHg; IR 3400, 1650 cm^{-1}; NMR (CCl_4) δ 0.95 (s, 3H), 1.22 (s, 3H), 1.95 (d, J=1.5 Hz, 3H), 1.50 (s, 1H), 1.66 (d×d, J=7.0 Hz, 3.5 Hz, 1H), 1.90 (d, J=7.0 Hz, 1H), 4.62 (s, 1H), 4.66 (s, 1H), 5.38 (m, 1H), 5.0—5.2 (m, 2H), 5.40 (m, 1H); MS *m/e* 202 (M^+). Found: C, 82.96; H, 8.67%. Calcd for $C_{14}H_{18}O$: C, 83.12, H, 8.97%.

Reaction of Ib with Vinylmagnesium Bromide and Subsequent Thermal Rearrangement. To a stirred solution of vinylmagnesium bromide, which had been prepared using 1.75 g (16.4 mmol) of vinyl bromide, 0.365 g (15.0 mg-atom) of magnesium turnings, and 25 ml of THF, was added 870 mg (5 mmol) of Ib in 10 ml of THF at an ambient temperature. After the reaction mixture had been refluxed for 4 h, it was treated with aqueous ammonium chloride and extracted with ether (30 ml×3). The evaporation *in vacuo* of the dried (Na_2SO_4) organic portion gave an oil of IIIb (950 mg, 95%); mp 60—61 °C (from hexane); IR (nujol) 1720 cm^{-1}; NMR (CCl_4) δ 1.40 (d, J=7.0 Hz, 3H), 2.30 (s, 6H), 1.75—2.10 (m, 2H), 2.10—2.60 (m, 2H), 2.80 (m, 2H), 3.55 (q, J=7.0 Hz, 1H), 6.80—7.0 (m, 2H); MS *m/e* 202 (M^+). Found: C, 83.50; H, 8.67%. Calcd for $C_{14}H_{18}O$: C, 83.12; H, 8.97%.

Thermal Reaction of Ia in Benzene. 30 mg of Ia in 1 ml of benzene was refluxed for 5 h. No rearrangement occured and Ia was recovered in a 95% yield.

Thermal Rearrangement of IIa to IIIa. 188 mg (1 mmol) of IIa in 1 ml of xylene were refluxed for 30 min in a nitrogen atmosphere. Subsequent VPC analysis (5% SE-30, column temp 120—160 °C) indicated a single component which was identified with the product derived *via* the Grignard-reagent procedure. This reaction mixture was chromatographed on alumina (2.5 g). Elution with hexane–benzene (4/1) gave 170 mg (90%) of IIIa.

Thermal Rearrangement of IIb to IIIb. 202 mg (1 mmol) of IIb in 1 ml of 1,2-dichlorobenzene were refluxed for 15 min in a nitrogen atmosphere. The subsequent evaporation *in vacuo* of the 1,2-dichlorobenzene gave an oil. This oil was chromatographed on alumina (10 g), using hexane as the eluent, to give 182 mg (90%) of IIIb.

References

1) D. A. Evans and A. M. Golb, *J. Am. Chem. Soc.*, **97**, 4765 (1975).
2) D. A. Evans and J. M. Hoffman, *J. Am. Chem. Soc.*, **98**, 1983 (1976).
3) W. C. Still, *J. Am. Chem. Soc.*, **99**, 4186 (1976).
4) D. A. Evans, D. J. Baillargeon, and J. V. Nelson, *J. Am. Chem. Soc.*, **100**, 2242 (1978).
5) T. Miyashi, A. Hazato, and T. Mukai, *J. Am. Chem. Soc.*, **100**, 1008 (1978).
6) M. Nitta, O. Inoue, and M. Tada, *Chem. Lett.*, **1977**, 59.
7) M. Nitta, O. Inoue, and M. Tada, *Chem. Lett.*, **1977**, 1065.
8) R. H. Bradbury, T. L. Gilchrist, and C. W. Rees, *J. Chem. Soc., Chem. Commun.*, **1979**, 528.
9) G. M-Müller, T. Winkler, J. Zindely, and H. Schmid, *Helv. Chim. Acta*, **59**, 1763 (1976).
10) M. Nitta, H. Sugiyama, and Y. Sekine, *Chem. Lett.*, **1977**, 55.
11) J. A. Berson and M. R. Willcott, III, *J. Am. Chem. Soc.*, **87**, 2751, 2752 (1965).
12) L. T. Scott, *J. Chem. Soc., Chem. Commun.*, **1973**, 882.
13) H. Teufel and E. F. Jenny, *Tetrahedron Lett.*, **1971**, 1769.
14) J. P-Katalinic, J. Zindely, and H. Schmid, *Helv. Chim. Acta*, **57**, 223 (1974).
15) J. W. Williams, *Org. Synth.*, Coll. Vol. IV, 258 (1963).

The Linearity of the Substituent-induced Carbon-13 Chemical Shifts of α-Carbons with Charge Densities in Aromatic Side Chains. II. 4-Substituted Phenylacetylenes

Jun NIWA

College of General Education, Nagoya University, Chikusa-ku, Nagoya 464

(Received January 25, 1980)

Synopsis. The propriety of considering the magnetic contributions to the ^{13}C chemical shift from the neighboring carbon atoms and from the 'ring-current' has been examined for the SCS of α-carbons of 4-substituted phenylacetylenes. The SCS values corrected for the above contributions are well correlated with the 2p electron densities.

In our previous papers,[1,2] we derived expressions for estimating the contribution from the magnetic term of the neighboring carbon atom, B, which is bonded to the A atom in question (σ^{AB}_{dia}) and the long-range shielding effect of the 'ring-current' ($\sigma^{A,ring}$). It was shown that the corrected SCS values of α-carbons ($\Delta\delta^{\alpha}_{corr}$) come to be linearly correlated with the electron densities on the relevant carbon atoms, A, when the observed SCS are corrected for the above two contributions in the cases of sp^2-hybridized α-carbons of 4-substituted derivatives of styrenes, α-methylstyrenes, and biphenyls.[1]

The aim of the present paper is to examine the propriety of considering the σ^{AB}_{dia} and the $\sigma^{A,ring}$ terms in interpreting the SCS of sp-hybridized α-carbons. For this purpose, we have chosen 4-substituted phenylacetylenes as a model system.

As has been shown in our previous paper,[2] the diamagnetic contribution, σ^{AB}_{dia}, from the sp-hybridized carbon atom can be expressed in the same form as the expression derived for the case of sp^2-hybridized carbon:

$$\sigma^{AB}_{dia} = (e^2/3mc^2) r_{AB}^{-1} q^B, \quad (1)$$

where r^{-1} is the inverse distance of the A atom from the point charge on the B atom and where q is the total (2s and 2p) electron density on the B atom. In the present approach, we have considered the magnetic contributions from the two neighboring carbon atoms which are directly bonded to the α-carbon of the phenylacetylene. The paramagnetic contribution, σ^{AB}_{para}, from the B atom remains almost constant so long as we assume the same average excitation-energy approximation.[3]

The carbons of the phenylacetylenes were labeled as shown below:

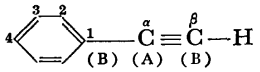

All the bond angles and the bond lengths of the phenylacetylenes are taken from the standard compilations.[4] When the bond lengths of the C_1–C_α and the C_α–C_β are taken to be 1.46 Å and 1.204 Å respectively:

$$\sum_B \Delta\sigma^{AB}_{dia} = 6.43\Delta q_1 + 7.80\Delta q_\beta. \quad (2)$$

The expression of the 'ring-current' effect on the SCS is the same as that in the previous papers:[1,2]

$$\Delta\sigma^{A,ring} = -0.4 f(\rho, z) |\sigma_\pi|. \quad (3)$$

The value of the $f(\rho, z)$ in the case of the α-carbon of phenylacetylene has been graphically estimated to be −1.08 ppm by utilizing the table of the Johnson-Bovey ring-current shift.[5] In evaluating the σ^{AB}_{dia} term, we have used the CNDO/2 formalism. The calculated values of the $\Delta\sigma^{AB}_{dia}$ and the $\Delta\sigma^{A,ring}$ terms are listed in Table 1.

It is expected that the $\Delta\delta^{\alpha}_{corr}$ values are linearly correlated with the electron densities on the α-carbon atoms, because $\Delta\delta^{\alpha}_{corr}$ reflects only the local magnetic term of the α-carbon atom. In Figs. 1 and 2, plots

Table 1. Observed and corrected chemical shifts of α-carbons in 4-substituted phenylacetylenes[a]

	Substituent	$\Delta\sigma^{AB}_{dia}$		$\Delta\sigma^{A,ring}$	$\Delta\delta^{\alpha}_{obsd}$[c]	$\Delta\delta^{\alpha}_{corr}$[b]
		$6.43\Delta q_1$	$7.80\Delta q_\beta$	$-0.4f(\rho, z)\|\sigma_\pi\|$		
1	NO_2	−0.145	−0.142	0.147	1.93	2.07
2	CN	−0.036	−0.048	0.108	1.69	1.67
3	CF_3	−0.131	−0.114	0.121	1.44	1.56
4	Cl	0.042	−0.023	0.030	1.16	1.11
5	F	0.123	0.004	0.051	1.09	0.91
6	C≡CH	0.013	−0.008	0.002	0.60	0.59
7	SCH_3	0.056	0.004	0.035	0.24	0.15
8	$CH{=}CH_2$	0.016	0.002	0.022	0.09	0.05
9	OCH_3	0.162	0.044	0.121	0.00	−0.33
10	CH_3	0.061	0.025	0.034	−0.10	−0.22
11	NH_2	0.243	0.094	0.180	−0.68	−1.20
12	$N(CH_3)_2$	0.213	0.082	0.233	−1.00	−1.53

a) All the values listed are relative to the unsubstituted compound, from the chemical shift of which the upfield shifts are represented in ppm by positive values. b) $\Delta\delta^{\alpha}_{corr} = \Delta\delta^{\alpha}_{obsd} - \sum\Delta\sigma^{AB}_{dia} - \Delta\sigma^{A,ring}$. c) Cited from Ref. 7.

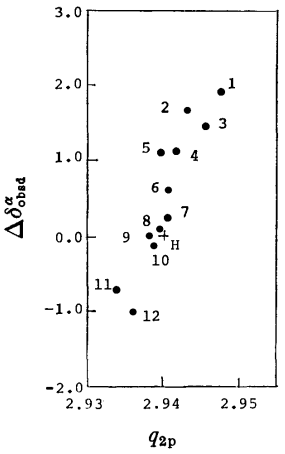

Fig. 1. Plots of $\Delta\delta^{\alpha}_{obsd}$ against the 2p electron densities on the α-carbon atoms.
Numbered points correspond to entries in Table 1.

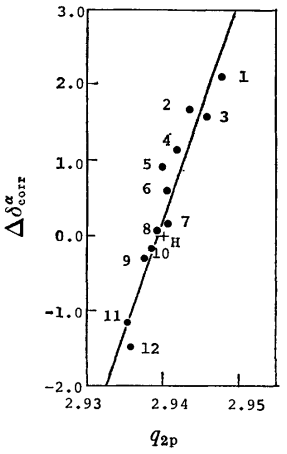

Fig. 2. Plots of $\Delta\delta^{\alpha}_{corr}$ against the 2p electron densities on the α-carbon atoms.
Numbered points correspond to entries in Table 1.

of the observed and the corrected SCS values are shown against the 2p electron densities (q_{2p})*. It may be reasonable to correlate the local magnetic terms with the 2p electron densities,[6] because the contribution of the local diamagnetic term to the SCS is very small compared with that of the local paramagnetic term. The respective correlations are expressed by least-squares fitting as:

$$\Delta\delta^{\alpha}_{obsd} = 235\Delta q_{2p} + 0.40 \quad (r=0.897,\ s=0.41) \qquad (4)$$

and:

$$\Delta\delta^{\alpha}_{corr} = 295\Delta q_{2p} + 0.23 \quad (r=0.928,\ s=0.42), \qquad (5)$$

where r is the correlation coefficient and s is the standard deviation. The values of both the intercept and the correlation coefficient in the latter case are much improved compared with those in the former case, although the values of the standard deviations are almost equal in the two cases.

This result provides further proof that it is appropriate to consider the σ^{AB}_{dia} and the $\sigma^{A,ring}$ terms in interpreting the aspect of the SCS of α-carbons in the side chains of conjugated aromatic hydrocarbons by relating the SCS to the electron densities.

The CNDO/2 calculations were carried out on a FACOM-230 75 computer at the Nagoya University Computation Center.

* The correlations between the corrected (and the observed) SCS and the total electron densities are: $\Delta\delta^{\alpha}_{corr} = 508\Delta q_{total} + 0.66$ ($r=0.868$, $s=0.5$); $\Delta\delta^{\alpha}_{obsd} = 400\Delta q_{total} + 0.72$ ($r=0.817$, $s=0.55$). In the case of the styrenes,[1] too, when the $\Delta\delta^{\alpha}_{corr}$ values are correlated with the 2p electron densities, the correlation is improved: $\Delta\delta^{\alpha}_{corr} = 135\Delta q_{total} + 0.77$ ($r=0.782$, $s=0.40$); $\Delta\delta^{\alpha}_{corr} = 122\Delta q_{2p} + 0.69$ ($r=0.844$, $s=0.34$).

References

1) Part I: J. Niwa, *Bull. Chem. Soc. Jpn.*, **51**, 2964 (1978).
2) J. Niwa, *Bull. Chem. Soc. Jpn.*, **48**, 118 (1975).
3) J. A. Pople, *J. Chem. Phys.*, **37**, 53 (1962); M. Karplus and J. A. Pople, *ibid.*, **38**, 2803 (1963).
4) "Tables of Interatomic Distance and Configuration in Molecules and Ions," Chem. Soc. London, Spec. Publ., No. 11 (1958).
5) G. E. Johnson and F. A. Bovey, *J. Chem. Phys.*, **29**, 1012 (1958); J. W. Emsley, J. Feeney, and L. H. Sutcliffe, "High Resolution Nuclear Magnetic Resonance Spectroscopy," Pergamon Press, Oxford (1965), Vol. 1, p. 525.
6) T. Yonezawa, I. Morishima, and H. Kato, *Bull. Chem. Soc. Jpn.*, **39**, 1398 (1966).
7) D. A. Davison and W. F. Reynolds, *Can J. Chem.* **53**, 373 (1975).

Relationship between Chemical Selectivity and Melting Points of Reacting Molecules

Tadashi ENDO,* Yukiko TAKEDA, Toyohiko ORII, Akio KUWAHARA, Masahiro OHTA, Miyuki SAKAI, Reiko OKADA, and Masao HASHIMOTO

Department of Chemistry, College of Science and Engineering, Aoyama Gakuin University, Chitosedai, Setagaya-ku, Tokyo 157

(Received February 21, 1980)

Synopsis. A relationship has been found to exist between the selectivity (the ratio of an unsymmetrical disulfide to symmetrical one) in the oxidation of a pair of associating thiols, 1-acyl-3-(2-sulfhydrylethyl)urea (**1**) and 1-(*p*-*N*,*N*-dimethylaminophenyl)-3-(sulfhydrylacetyl)urea, and the melting point of **1** in cases where **1** belongs to a homologous series.

As a continuing study on a correlation of reaction behavior of molecules (*i.e.*, chemical selectivity) with their physicochemical properties,[1] this paper describes a relationship between the selectivity in the oxidation of a pair of associating thiols and the melting point of one of these two thiols.

Previously we have examined the oxidation of a pair of associating thiols (**1** and **2**) with O_2 in 80% (v/v) acetonitrile–20% water. The selectivity (R) in this oxidation was represented by the ratio of an unsymmetrical disulfide (**6**) to symmetrical one (**7**) (R=**6**/**7**).[2] The result is illustrated in Fig. 1. In the case of **1a** and **2**, maximal selectivity occurred at j=2.[2] In contrast, with **1b** and **2** alternation in the selectivity was clearly observed: R was 4.5, 0.28, 0.53, 0.29, and 0.40 for k=0, 1, 2, 3, and 4, respectively.[2] Further, with **1c** and **2**, maximal selectivity (R=16) occurred at x=2.

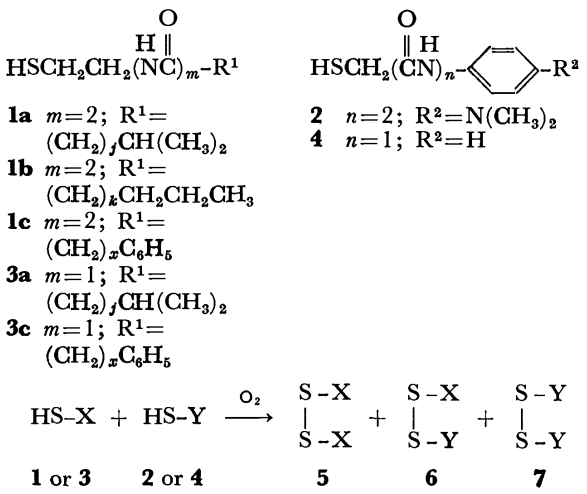

The data in Fig. 1 also indicate that the melting point of **1** depends sharply on the structure of R^1: **1a** or **1c** displayed maximal melting point at j=2 or x=2, respectively, while **1b** showed a striking alternation in melting points.[3] Therefore, Fig. 1 shows that the structure-selectivity profile for the oxidation of **1** and **2** is similar to the structure-melting point profile for **1**. It should be noted that this relationship between the selectivity and melting points does not hold for **1** having the para-substituted phenyl groups as R^1, which do not belong to a homologous series.

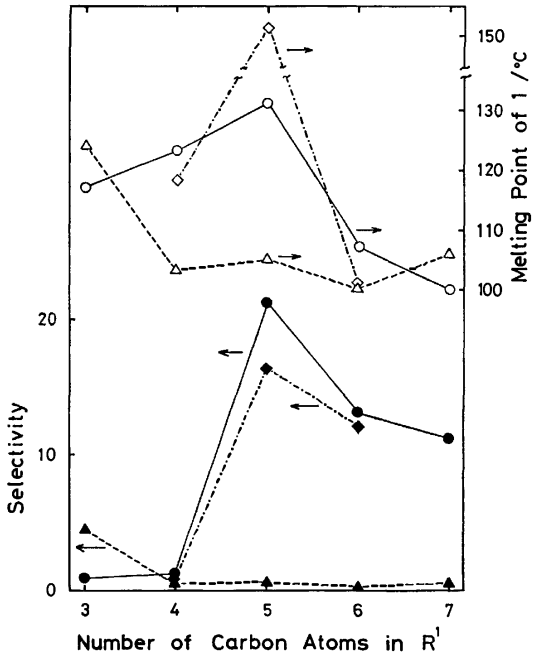

Fig. 1. Dependence of the selectivity (R=**6**/**7**), in the oxidation of a 1:1 mixture of **1** and **2** with oxygen, and of the melting point of **1** on the number of carbon atoms in R^1. With **1c** [$R^1=(CH_2)_xC_6H_5$] the number of carbon atoms in R^1 is counted as "x+3." ●, R for the oxidation of **1a** and **2**; ▲, R for the oxidation of **1b** and **2**; ◆, R for the oxidation of **1c** and **2**; ○, melting point of **1a**; △, melting point of **1b**; ◇, melting point of **1c**. Thiol **2** melted at 173 °C.

Control experiments using **1a** (or **3**) and **4** made it clear that the selectivity was insensitive to the structure of R^1 (Fig. 2): (i) in the case of **1a** and **4**, R showed a small maximum at j=1, (ii) with **3a** and **4**, R ranged only from 1.8 to 1.9, and (iii) with **3c** and **4**, R showed a small maximum at x=2. Moreover, it was found that the melting point of **3a** decreased progressively with the number of carbon atoms in R^1 and that **3c** displayed maximal melting point (66 °C) at x=2 (Fig. 2). These findings demonstrate that with **1a** (or **3**) and **4** the correlation described above does *not always* exist.[4]

^{1}H NMR results together with other experimental data revealed that **1a** (j=2) [or **1b** (k=2)] and **2** form weak complexes with each other as well as with themselves.[5] Furthermore, the degree of association (f)[6] for amide derivatives (**3** and **4**) proved to be much smaller than f for acylurea derivatives (**1** and **2**). This suggests that **1** and **2** associate strongly with themselves, while **3** and **4** associate very weakly with

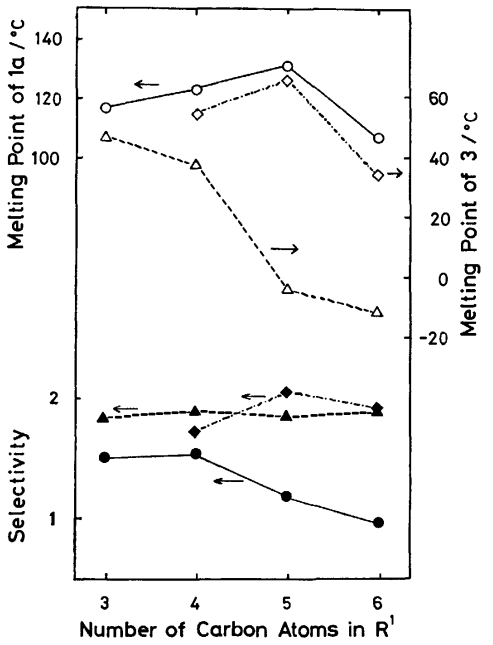

Fig. 2. Dependence of the selectivity (R=**6**/**7**), in the oxidation of a 1:1 mixture of **1a** (or **3**) and **4**, and of the melting points of **1a** and **3** on the number of carbon atoms in R^1. With **3c** [$R^1=(CH_2)_xC_6H_5$] the number of carbon atoms in R^1 is also counted as "$x+3$." ●, R for the oxidation of **1a** and **4**; ▲, R for the oxidation of **3a** and **4**; ◆, R for the oxidation of **3c** and **4**; ○, melting point of **1a**; △, melting point of **3a**; ◇, melting point of **3c**. Thiol **4** melted at 113 °C.

themselves and that **4** associates very weakly with **3**—or even with **1a** because of marked difference in f between **4** and **1a**.

All of the data presented here would suggest that chemical selectivity in the reaction of a pair of associating molecules can be correlated with the melting point of one of these two molecules in cases where one of these two molecules belongs to a homologous series.

Experimental

Materials. Thiols **1**, **2**, and **4** were prepared as described before.[5,7] Thiol **3** was synthesized according to the method previously reported.[8] Satisfactory spectroscopic data were used to support the assignment of all new compounds.

Oxidation of a Pair of Thiols. A 1:1 mixture of **1** and **2** [or of **1a** (or **3**) and **4**, 0.5 mmol each] was treated with oxygen at 35.0 °C in 12.5 ml of 80% (v/v) acetonitrile–20% water in the presence of a catalytic amount of Et_3N (0.05 mmol). When the oxidation was completed, the reaction mixture was evaporated to dryness. Yields of **6** and **7** were determined by the use of their absorption at 310 nm after separation by TLC in the oxidation of **1** and **2**,[9] and determined gravimetrically after separation by preparative TLC in the oxidation of **1a** (or **3**) and **4**.

Determination of Melting Points. Melting points of thiols (**1**—**4**) were obtained from the DTA (Differential Thermal Analysis) curves recorded with a Shimadzu DT-20B thermal analysis apparatus. The samples were finely powdered, diluted with fine-grained quartz wool in the specimen holder, and heated in a stream of nitrogen with a heating rate of 10 °C/min.

Determination of Degree of Association (f). The effective mole fraction of the solute was determined on a Hitachi Perkin-Elmer 115 molecular weight apparatus using a differential vapor pressure method at 36.0 °C and 0.01 M (1 M= 1 mol dm^{-3}) in benzene.[10]

We are grateful to Dr. Akiko Furuhashi and Miss Tomoko Nomura for helpful advice in DTA measurement and to Mr. Tomoji Murata for valuable assistance. The present work was partially supported by a Grant-in-Aid for Scientific Research from the Ministry of Education.

References

1) T. Ishigami, M. Uehara, T. Murata, and T. Endo, *J. Chem. Soc., Chem. Commun.*, **1978**, 786.

2) T. Endo, A. Kuwahara, H. Tasai, T. Murata, M. Hashimoto, and T. Ishigami, *Nature*, **268**, 74 (1977).

3) It is rather a frequent phenomenon that there is a radical difference in the structure dependence of melting points between the homologs of the branched alkyl and straight-chain alkyl groups, as is the case with *N*-phenylcarboxamides ($R^3CONHC_6H_5$): maximal melting point occurs at the isobutyl group for $R^3=i\text{-}C_3H_7$ to $i\text{-}C_6H_{13}$, whereas alternation in melting points occurs for $R^3=n\text{-}C_3H_7$ to $n\text{-}C_6H_{13}$.

4) Intermolecular association is considered to aid to correlate chemical selectivity with melting points.

5) T. Endo, Y. Takeda, T. Orii, Y. Kaneko, and M. Kondo, *Chem. Lett.*, **1979**, 1455.

6) The value of f is obtained by dividing the stoichiometric mole fraction of the solute by the effective mole fraction of the solute. The f value for **3** and **4** was less than 1.05, and the f value for **1** and **2** ranged from 1.3 to 1.5.

7) T. Endo, K. Oda, and T. Mukaiyama, *Chem. Lett.*, **1974**, 443.

8) R. Kuhn and G. Quadbeck, *Chem. Ber.*, **84**, 844 (1951).

9) T. Endo, A. Kuwahara, H. Tasai, and T. Ishigami, *J. Chromatogr.*, **140**, 263 (1977).

10) J. F. Coetzee and R. M. S. Lok, *J. Phys. Chem.*, **69**, 2690 (1965).

 © 1980 The Chemical Society of Japan Bull. Chem. Soc. Jpn., 53, 2689—2694 (1980)

Improved Resonance Energies of Nonalternant Hydrocarbons. An ω-Technique Approach

Jun-ichi AIHARA

Department of Chemistry, Faculty of Science, Hokkaido University, Sapporo 060

(Received November 22, 1979)

The ω-technique of Wheland and Mann was introduced into the graph theory of aromaticity in order to improve the resonance energies of nonalternant hydrocarbons. For these compounds, the ω-technique resonance energy was more or less smaller than the resonance energy calculated on the basis of the simplest Hückel MO model. Especially, several compounds thus far considered to be aromatic were predicted to be substantially olefinic with much reduced resonance energies. They are calicene, sesquifulvalene, azulene, dibenzo[*cd*,*gh*]-pentalene, and cyclohepta[*def*]fluorene. Many aspects of their chemistry were evidently consonant with the improved resonance energies. Possible limitation of the use of electrophilic substitution as a criterion of aromaticity was discussed. Resonance energies of alternant hydrocarbons are not modified by application of the ω-technique.

The graph theory of aromaticity[1-4] has proved very successful in rationalizing aromatic character of a wide variety of cyclic conjugated compounds. A theoretical relationship between diamagnetic susceptibility exaltation and aromatic stabilization has also been verified by means of this theory.[5] The graph theory of aromaticity in its original form is based on the simplest Hückel molecular orbital (HMO) model.[1-5] In this model the assumption is tacitly made that the Coulomb integral α is a constant characteristic of an atom and independent of a conjugated system in which it appears. A standard value of α for sp^2 carbon atoms may be denoted by α_0. This assumption is indeed reasonable for alternant hydrocarbons, each with a uniform charge distribution.

However, a simple argument[6] shows that a carbon atom in a conjugated hydrocarbon on which the charge density q is not equal to unity cannot really have $\alpha=\alpha_0$. If $q<1$, the net positive charge means that the screening seen by any one electron is reduced and the Coulombic attraction to the nucleus is increased. The Coulomb integral for such a carbon atom should have a more negative value. Conversely, a carbon atom with a net negative charge should have a less negative value of α. Wheland and Mann proposed that the value of α should be linearly related to the charge on the atom concerned, namely,[7]

$$\alpha_s = \alpha_0 + (1-q_s)\omega\beta_0, \qquad (1)$$

where ω is a dimensionless parameter whose value may be so chosen as to give the best agreement with experiment, β_0 a standard value of the resonance integral between two bonded sp^2 carbon atoms, and the subscript s used to represent the s-th carbon atom.

The value appropriately selected for the ω parameter apparently allows for an average effect of other electrons. We might say that, with one empirical parameter, this ω-technique introduces some electron repulsion within the framework of the simple HMO model.[6] The use of this technique has been shown to lead to improved calculated energy values for nonalternant hydrocarbons and conjugated cations.[6-8] In this paper I would like to revise the graph theory of aromaticity[1-5] by means of the ω-technique, and present improved resonance energies of typical nonalternant hydrocarbons in conjunction with their chemistry.

Theory

One first obtains the charge distribution of a conjugated hydrocarbon according to the simplest HMO model. This charge distribution is used to calculate new α_s's according to Eq. 1, and the new charge distribution is calculated. This process is continued until the charge distribution no longer changes, that is, the system is self-consistent.[6,7] The value of ω is taken to be 1.40 as usual.[8] On the other hand, an olefinic reference structure constructed graph-theoretically for any conjugated hydrocarbon can be regarded as a kind of alternant hydrocarbon.[1] The charge density is correspondingly equal to unity on each carbon atom of the reference structure.[9] The total π-electron energy of the reference structure was termed the reference energy.[1] It can hence be calculated without regard to the charge distribution of the reference structure. In other words, the reference energy of a conjugated hydrocarbon is independent of the ω parameter. Thus the ω-technique resonance energy of any conjugated hydrocarbon can be calculated relative to the reference energy based on the simplest HMO model.

Results and Discussion

Resonance energies thus calculated for 40 nonalternant hydrocarbons are listed in Table 1. They are compared therein with the resonance energies calculated on the basis of the simplest HMO model.[1,4] First of all, it is noteworthy that the total π-electron energy of any nonalternant hydrocarbon increases by application of the ω-technique. This might imply that the effect of electron repulsion is to diminish the resonance energy of a conjugated system because the reference energy remains unchanged. Consequently, when the absolute value of the resonance energy is small, the sign of the resonance energy is often changed by application of the ω-technique. Such compounds are **1**—**5**, **17**, **19**, and **31**.

Here a new measure of aromatic stabilization is adopted, which is defined as 100 times the resonance energy, divided by the reference energy.[10] It is termed the percent resonance energy (%*RE*). This quantity nicely gives the degree of stabilization with which a conjugated system behaves aromatically as a whole.

TABLE 1. RESONANCE ENERGIES OF 40 NONBENZENOID HYDROCARBONS

Compound	Simplest HMO		ω-Technique	
	RE[a,b]	$\%RE$[c]	RE[a]	$\%RE$[c]
1	0.063	1.29	−0.145	−2.96
2	0.020	0.27	−0.082	−1.10
3	0.009	0.09	−0.052	−0.52
4	0.005	0.04	−0.036	−0.29
5	0.009	0.12	−0.005	−0.06
6	0.000	0.00	0.000	0.00
7	−0.461	−5.81	−0.607	−7.66
8	0.433	4.13	0.038	0.36
9	−0.299	−2.28	−0.367	−2.81
10	0.272	1.73	0.023	0.15
11	−0.218	−1.20	−0.261	−1.43
12	−0.215	−2.02	−0.411	−3.85
13	0.151	1.14	0.055	0.42
14	−0.141	−0.89	−0.252	−1.60
15	0.354	2.18	0.319	1.96
16	0.339	1.80	0.317	1.69
17	0.101	0.62	−0.030	−0.18
18	0.106	0.56	0.014	0.07
19	0.055	0.34	−0.056	−0.35
20	0.106	0.55	0.065	0.33
21	0.398	1.82	0.334	1.53
22	0.134	0.55	0.110	0.45
23	0.372	1.70	0.317	1.45
24	0.376	1.72	0.312	1.43
25	0.222	1.16	0.062	0.32
26	0.247	1.13	0.063	0.29
27	0.230	0.95	0.152	0.62
28	0.217	0.99	0.131	0.60
29	0.214	0.98	0.117	0.54
30	0.122	0.56	0.034	0.16
31	0.035	0.14	−0.078	−0.32
32	0.578	2.64	0.567	2.59
33	0.418	1.92	0.326	1.49
34	0.400	1.64	0.340	1.39
35	0.416	1.71	0.382	1.54
36	0.558	2.28	0.552	2.26
37	0.310	1.42	0.275	1.26
38	0.508	1.85	0.423	1.54
39	0.506	1.84	0.434	1.58
40	0.522	1.90	0.425	1.55

a) Resonance energy. b) References 1 and 4. c) Percent resonance energy.

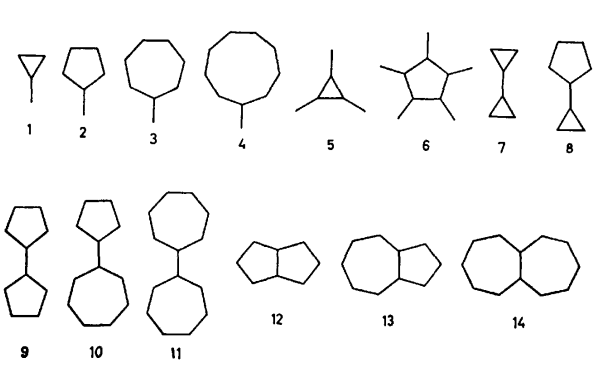

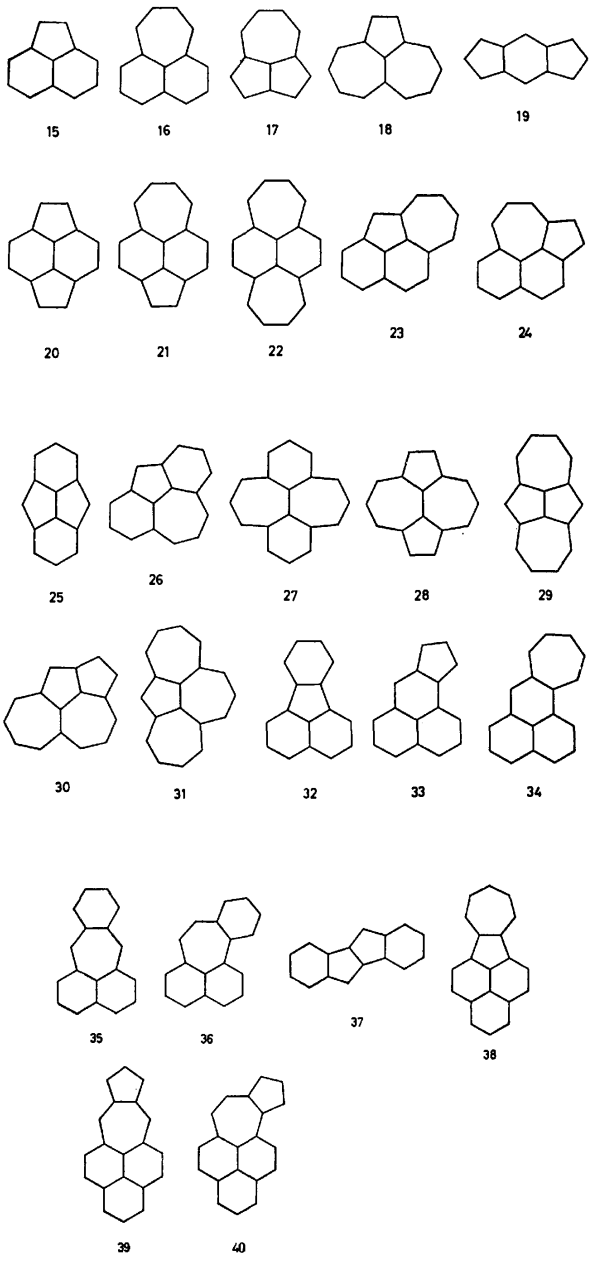

Note that the $\%RE$ neither depends upon the number of π electrons[11] nor upon the number of π bonds[12] in a conjugated system. By examining $\%RE$ values in Table 1 in detail, we can safely say that compounds with $\%RE<0.50$ might be regarded as olefinic species.

When one or more aromatic sextets[13–17] can be chosen from a nonalternant hydrocarbon, it may be called a semibenzenoid hydrocarbon.[18] Such semibenzenoid hydrocarbons are **15**, **16**, **20**—**24**, and **32**—**40**. For these compounds, a decrease in resonance energy is rather modest. Therefore, previous aromaticity considerations[1,4,11,15,17–19] are still applicable to them. They are not repeated here.

On the other hand, when a conjugated system is a combination of odd-membered π rings only, a pronounced decrease in resonance energy occurs by application of the ω-technique. Among them the following five fully nonbenzenoid hydrocarbons are

particularly noteworthy: calicene (**8**), sesquifulvalene (**10**), azulene (**13**), dibenzo[*cd,gh*]pentalene (**25**), and cyclohepta[*def*]fluorene (**26**). These compounds have been predicted to be moderately aromatic on the basis of the simplest HMO model,[1,4,11] whereas the present approach predicts them to be substantially nonaromatic with markedly reduced resonance energies. We can show below that these ω-technique resonance energies are indeed in excellent agreement with experiment.

Both calicene (**8**) and sesquifulvalene (**10**) have so far had significant $\%RE$ values.[1,11] Sesquifulvalene is known,[20] but it is not stable, polymerizing even at 30 °C. Calicene itself is not known, but a number of substituted calicene derivatives are now known.[21] Some of them, as well as sesquifulvalene, readily form adducts with tetracyanoethylene.[22] These polyene-like features of asymmetric fulvalenes are obviously consistent with the smaller $\%RE$ values. Some calicene derivatives have very large dipole moments,[23] and some have electronic spectra strongly dependent upon the solvent as might be expected for a dipolar species.[24] Such a non-uniform charge distribution in a conjugated system decreases the resonance energy when the ω-technique is applied to it.

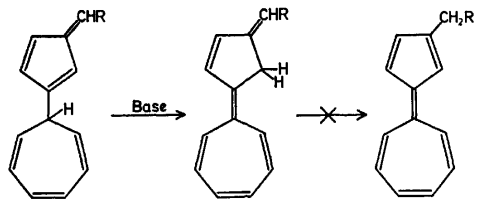

41 42 43

The prototropic rearrangement of 3-cycloheptatrienylfulvenes (**41**) gives the conjugated heptafulvenes (**42**) instead of the sesquifulvalene (**43**).[22,25] Here, R is an alkyl or an aryl group. An aromatic compound might be defined as a compound which tends to maintain its cyclic conjugated system since it has a larger binding energy than the olefinic reference structure. According to this definition, sesquifulvalenes can be classified as olefinic species. Compounds of the type **41** are obviously reluctant to attain a sesquifulvalene conjugated system. Neither triafulvalene (**7**) nor its derivatives have been prepared. The other symmetric fulvalenes **9** and **11** are extremely reactive.[22] Resonance energies of these fulvalenes were also decreased considerably. The same is true for triafulvene (**1**), which is not known yet.

Azulene has been a classical example of a non-benzenoid aromatic compound. Let the ratio of the resonance energy of azulene to that of the isomeric naphthalene be denoted by r. The r value based on the ω-technique resonance energies is about one-eighth, which is comparable to that of Dewar and de Llano calculated using the SCF resonance energies.[26] However, it is in poor accord with the r value of Hess and Schaad based on the simplest HMO model.[11] It must be noted here that they did not take the effect of electron repulsion into consideration,[11] but Dewar and de Llano did.[26] Azulene has a dipole moment of 1.0 D with the five-membered ring negative,[27] so the ω-technique resonance energy is aparently preferable as long as it is consistent with its chemistry. Thus azulene appears to have a small positive resonance energy, much less than that of naphthalene.

An experimental support for an olefinic nature of azulene is afforded by the occurrence of valence tautomerism of the simple derivatives in solution. 2-Hydroxyazulene (**44**) partly undergoes valence tautomerization to the nonaromatic heptafulvene derivative (**45**).[28] 4,8-Dimethyl-6-hydroxyazulene (**46**) coexists in solution with the tautomeric troponoid species (**47**),[29] in which an azulenoid bicyclic conjugated system is missing.

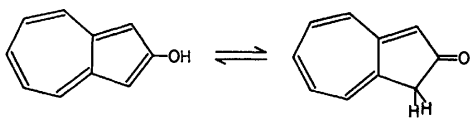

44 45

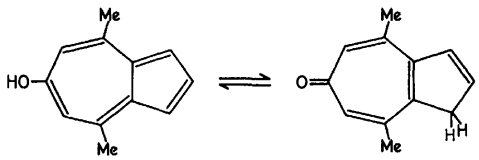

46 47

In this context, it should be remembered that 9-anthranol coexists in solution with anthrone.[30] Resonance energies of these two isomers are presumably similar to each other.[31] By analogy with this, the enol forms of hydroxyazulenes **44** and **46** must be as aromatic as the keto forms **45** and **47**, respectively. However, the latter keto forms are olefinic, so must be the former azulenoid species.

Substituted calicenes and sesquifulvalenes are protonated in acidic media to form cyclopropenium and tropylium cations, respectively.[22] Azulene itself is readily protonated, the proton adding in the 1-position of the five-membered ring to form an azulenoid cation.[32] Such a high basicity of a conjugated system is often an indication of aromaticity of the protonated species.[33] Conversely, calicene, sesquifulvalene, and azulene are not typically aromatic, in the sense that they are reluctant to maintain their original conjugated systems in acidic media.

Dibenzo[*cd,gh*]pentalene (**25**) and cyclohepta[*def*]-fluorene (**26**) have not been prepared yet. Although a dianion of **25** is known,[34] attempts to prepare the neutral hydrocarbon were unsuccessful. Such synthetic inaccessibility is not congruent with large resonance energies previously reported for them.[4] The ω-technique resonance energies are both very small in good accord with their chemistry. For these compounds, only two Kekulé structures can be written with a central double bond fixed in each Kekulé structure.

The occurrence of electrophilic substitution was a long-standing criterion of aromaticity. Azulene and some calicene derivatives undergo electrophilic substitution reactions.[35,36] This chemical feature has been

used as an irrefutable evidence of aromaticities of these compounds.[11] Electrophilic substitution usually occurs *via* a Wheland-type reaction intermediate.[37] In the case of azulene and calicenes, Wheland-type reaction intermediates are shown below:

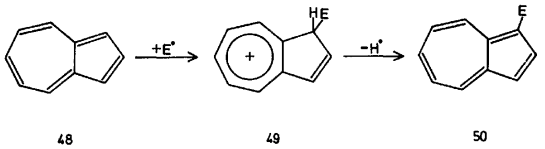

48 49 50

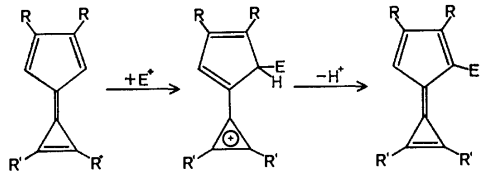

51 52 53

Here, E^+ is indicative of an electrophile.

However, it must be stressed that many olefinic compounds are now known to undergo electrophilic substitution reactions.[38] Such olefinic compounds are metal β-diketonates,[39] 2,3-dihydro-1,4-diazepinium salts,[38,40] 1,2-dihydropyrimidinium salts,[41] open-chain diazapolymethinium salts,[42] Nickel 1,19-dimethyltetradehydrocorrin salts,[43] 8-cyanoheptafulvene,[44] and ethylenic compounds such as vinyl ethers and vinyl sulfides.[45] For all these compounds, a Wheland-type intermediate is either a hetero-atom-stabilized carbonium ion or an aromatically-stabilized carbonium ion.[46] Therefore, specific stabilization of a reaction intermediate appears to be the most important condition for the occurrence of electrophilic substitution on polyenic compounds. For vinyl ethers and vinyl sulfides, a substitution reaction proceeds *via* a hetero-atom-stabilized carbonium ion.[45] 8-Cyanoheptafulvene (**54**) can be regarded as a trisubstituted ethylene. This compound undergoes several electrophilic substitution reactions at the *exo*-methylene group.[44] Each reaction intermediate is obviously an aromatically stabilized tropylium cation (**55**).

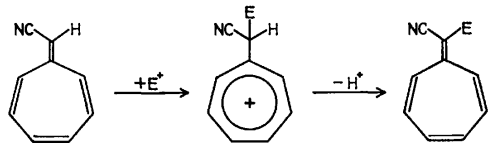

54 55 56

It is an interesting fact that a Wheland-type intermediate for azulene (**49**) is quite similar to that for 8-cyanoheptafulvene (**55**). Both are evidently stabilized by an aromatic tropylium structure. This analogy strongly suggests that aromaticity of azulene, if any, may not be necessary in order for substitution reactions to proceed on it. Calicenes undergo electrophilic substitution reactions *via* aromatically-stabilized cyclopropenium ion (**52**),[36] but this does not warrant aromaticities of the starting materials, either. Thus the occurrence of electrophilic substitution does not exclude the possibility that the starting material is olefinic as in the case of diazapolymethinium salts[40-42] and 8-cyanoheptafulvene.[44]

Further examination of various electrophilic substitution reactions disclosed the fact that, in general, less aromatic compounds are more favorable to such reactions. There have been several kinetic studies of electrophilic substitution reactions on monocyclic conjugated compounds.[47] For these compounds, the following order of reactivity has universally been established: benzene$<$thiophene$<$selenophene$<$tellurophene$<$furan$<$pyrrole.[47] If these compounds are arranged in an ascending order of aromaticity, this order is exactly reversed,[1,48] except for pyrrole which is much more aromatic than furan in all respects.[49]

When all or part of resonance energy is lost to form a Wheland-type reaction intermediate, the degree of destabilization of the intermediate necessarily depends upon the degree of aromaticity of the starting material. As stated above, it also depends upon the nature of the intermediate itself. One obvious conclusion which may be drawn here is that ready occurrence of electrophilic substitution is often inconsistent with high aromaticity. Benzene is then most aromatic and least reactive toward electrophiles. On the other hand, a Wheland-type intermediate for pyrrole is a highly stable azacarbonium ion,[50] *i.e.*, a kind of hetero-atom-stabilized carbonium ion,[46] so the reactivity is much greater than might be expected from its aromaticity. Thus there are not a few difficulties in using electrophilic substitution as a criterion of aromaticity.

Concluding Remarks

The graph theory of aromaticity based on the simplest HMO model[1-4] is free from any parametrization. In the present approach, only one parameter (*i.e.*, ω) had to be introduced in it to improve the resonance energies of nonalternant hydrocarbons. However, the revised theory can still retain all the simplicity and elegance as long as the accepted ω value of 1.40 is used.[6-8] The ω-technique resonance energies of nonbenzenoid hydrocarbons are more or less smaller than those calculated on the basis of the simplest HMO model.[1,11] In this paper, resonance energies of five nonbenzenoid hydrocarbons which are markedly sensitive to the ω-technique were analyzed in detail in conjunction with their chemistry. This analysis clearly indicated the inadequacy of the simplest HMO model, with all Coulomb integrals set equal, for dealing these nonalternant hydrocarbons. Conversely, it has firmly been established that the ω-technique resonance energies are in much better agreement with experiment.

The ω-technique approach can in principle be applied to all conjugated systems and to all cyclic conjugated ions alike. However, when a charge distribution in the reference structure is not uniform, the reference energy must be calculated self-consistently by iteratively evaluating all the Coulomb integrals[9] according to Eq. 1. The original reference energy cannot be used in

this case. It goes without saying that the resonance energy of any alternant hydrocarbon remains unchanged even if the ω-technique is applied to it.

It should be pointed up that the empirical theory of aromaticity, developed by Hess and Schaad,[11,48] can also be improved by application of the ω-technique. The ability to calculate in an additive manner the total π-electron energy of any acyclic polyene allowed them to calculate the reference energy of a cyclic conjugated system, and hence to obtain the resonance energy. Since acyclic polyenes are all alternant hydrocarbons, their additive π-bond energies[11] are not modified by application of the ω-technique. They can still be used to estimate reference energies. Accordingly, the Hess-Schaad resonance energy of a cyclic conjugated hydrocarbon is given as the difference between the total π-electron energy based on the ω-technique and the original reference energy.

When such a modified Hess-Schaad method is applied to nonalternant hydrocarbons, most results presented in this paper can be reproduced. Hess-Schaad resonance energy of azulene is changed from 0.23β to 0.14β, about one-fourth the resonance energy of naphthalene.[11] The r value becomes much closer to that estimated in this paper, and also to that estimated using the SCF resonance energies.[26]

Finally, another way of improving the graph theory of aromaticity[1-5] may be to include the overlap integrals S into HMO calculations.[51] Inclusion of overlap changes the spacing of energy levels. However, total π-electron energies and resonance energies do not seem to be affected significantly.[6]

The use of the facilities of the Hokkaido University Computing Center is gratefull acknowledged. A computer program for ω-technique calculations were taken from Dr. O. Kikuchi's book.[52]

References

1) J. Aihara, *J. Am. Chem. Soc.*, **98**, 2750, 6840 (1976); *J. Org. Chem.*, **41**, 2488 (1976); I. Gutman, M. Milun, and N. Trinajstić, *J. Am. Chem. Soc.*, **99**, 1692 (1977).
2) J. Aihara, *J. Am. Chem. Soc.*, **99**, 2048 (1977); *Bull. Chem. Soc. Jpn.*, **50**, 2010 (1977).
3) J. Aihara, *J. Am. Chem. Soc.*, **100**, 3339 (1978); *Bull. Chem. Soc. Jpn.*, **51**, 1541, 1788 (1978).
4) J. Aihara, *Bull. Chem. Soc. Jpn.*, **51**, 3540 (1978).
5) J. Aihara, *J. Am. Chem. Soc.*, **101**, 558, 5913 (1979).
6) A. Streitwieser, Jr., "Molecular Orbital Theory for Organic Chemists," Wiley, New York, N. Y. (1961), Chap. 4.
7) G. W. Wheland and D. E. Mann, *J. Chem. Phys.*, **17**, 264 (1949).
8) N. Muller, L. W. Pickett, and R. S. Mulliken, *J. Am. Chem. Soc.*, **76**, 4770 (1954); N. Muller and R. S. Mulliken, *ibid.*, **80**, 3489 (1958); A. Streitwieser, Jr., and P. M. Nair, *Tetrahedron*, **5**, 149 (1959); A. Streitwieser, Jr., *J. Am. Chem. Soc.*, **82**, 4123 (1960).
9) I. M. Gutman, *Bull. Soc. Chim. Beograd*, **43**, 191 (1978).
10) J. Aihara, *Bull. Chem. Soc. Jpn.*, **52**, 2202 (1979).
11) B. A. Hess, Jr., and L. J. Schaad, *J. Am. Chem. Soc.*, **93**, 305(1971); *J. Org. Chem.*, **36**, 3418 (1971).
12) J. Aihara, *Bull. Chem. Soc. Jpn.*, **50**. 3057 (1977).
13) E. Clar, "Polycyclic Hydrocarbons," Academic Press, London (1964), Vol. 1, Chaps. 6—9; "The Aromatic Sextet," Wiley, London (1972); J. W. Armit and R. Robinson, *J. Chem. Soc.*, **127**, 1604 (1925).
14) W. C. Herndon, *J. Am. Chem., Soc.*, **95**, 2404 (1973).
15) W. C. Herndon and M. L. Ellzey, Jr., *J. Am. Chem. Soc.*, **96**, 6631 (1974).
16) M. Randić, *Chem. Phys. Lett.*, **38**, 68 (1976).
17) M. Randić, *J. Am. Chem., Soc.*, **99**, 444 (1977): *Tetrahedron*, **33**, 1905 (1977).
18) A. DasGupta and N. K. DasGupta, *Tetrahedron*, **28**, 3587 (1972); *Theor. Chim. Acta*, **33**, 177 (1974).
19) A. DasGupta and N. K. DasGupta, *Tetrahedron*, **33**, 169 (1977).
20) M. Neuenschwander and W. K. Schenk, *Chimia*, **26**, 194 (1972).
21) H. Prinzbach, D. Seip, and U. Fischer, *Angew. Chem., Int. Ed. Engl.*, **4**, 242 (1965); W. M. Jones and R. S. Pyron, *J. Am. Chem. Soc.*, **87**, 1608 (1965) A. S. Kende and P. T. Izzo, *ibid.*, **87**, 1609 (1965); A. S. Kende, P. T. Izzo, and P. T. MacGregor, *ibid.*, **88**, 3359 (1966).
22) H. Prinzbach, *Pure Appl. Chem.*, **28**, 281 (1971).
23) E. D. Bergmann and I. Agranat, *Chem. Commun.*, **1965**, 512; *Tetrahedron*, **22**, 1275 (1966).
24) A. S. Kende and P. T. Izzo, *J. Am. Chem. Soc.*, **87**, 4162 (1965).
25) H. Prinzbach, D. Seip, and G. Englert, *Justus Liebigs Ann. Chem.*, **698**, 57 (1966).
26) M. J. S. Dewar and C. de Llano, *J. Am. Chem. Soc.*, **91**, 789 (1969).
27) H. J. Tobler, A. Bauder, and Hs. H. Günthard, *J. Mol. Spectrosc.*, **18**, 239 (1965).
28) K. Takase, T. Asao, Y. Takagi, and T. Nozoe, *J. Chem. Soc., D*, **1968**, 368.
29) W. Gerhartz, Thesis, Darmstadt, Germany (1973).
30) See, *e.g.*, Z. Majerski and N. Trinajstić, *Bull. Chem. Soc. Jpn.*, **43**, 2648 (1970).
31) W. C. Herndon, *J. Org. Chem.*, **40**, 3583 (1975).
32) See, *e.g.*, P. J. Garratt, "Aromaticity," McGraw-Hill, London (1971), Chap. 8.
33) See, *e. g.*, D. Lewis and D. Peters, "Facts and Theories of Aromaticity," Macmillan Press, London (1975), Chap. 2.
34) B. M. Trost and P. L. Kinson, *J. Am. Chem. Soc.*, **92**, 2591 (1970); **97**, 2438 (1975).
35) A. G. Anderson, Jr., and J. A. Nelson, *J. Am. Chem. Soc.*, **72**, 3824 (1950); A. G. Anderson, Jr., J. A. Nelson, and J. J. Tazuma, *ibid.*, **75**, 4980 (1953).
36) A. S. Kende, P. T. Izzo, and W. Fulmor, *Tetrahedron Lett.*, **1966**, 3697.
37) G. W. Wheland, *J. Am. Chem. Soc.*, **64**, 900 (1942).
38) See, *e. g.*, D. Lloyd and D. R. Marshall, *Ange. Chem., Int. Ed. Engl.*, **11**, 404 (1972).
39) J. P. Collman, R. A. Moss, S. D. Goldby, and W. S. Trahanovsky, *Chem. Ind. (London)*, **1960**, 1213; M. Kuhr and H. Musso, *Angew. Chem., Int. Ed. Engl.*, **8**, 147 (1969).
40) D. Lloyd, H. P. Cleghorn, and D.R. Marshall, *Adv. Heterocyclic Chem.*, **17**, 1 (1974).
41) D. Lloyd and H. McNab, *J. Chem. Soc., Perkin Trans. 1*, **1976**, 1784.
42) J. Kučera and Z. Arnold, *Collect. Czech. Chem. Commun.*, **32**, 1704 (1967).
43) A. Hamilton and A. W. Johnson, *J. Chem. Soc., C*, **1971**, 3879.
44) S. Kuroda, T. Asao, M. Funamizu, H. Kurihara, and Y. Kitahara, *Tetrahedron Lett.*, **1976**, 251; M. Oda and Y. Kitahara, *Bull. Chem. Soc. Jpn.*, **44**, 296 (1970).
45) M. Hojo, R. Masuda, and Y. Kamitori, *Tetrahedron*

Lett., **1976**, 1009; M. Hojo, R. Masuda, Y. Kokuryo, H. Shioda, and S. Matsuo, *Chem. Lett.*, **1976**, 499.
46) G. A. Olah, *Science*, **168**, 1298 (1970); *Angew. Chem., Int. Ed. Engl.*, **12**, 173 (1973).
47) G. Marino, *Adv. Heterocyclic Chem.*, **13**, 235 (1971); F. Fringuelli, G. Marino, G. Savelli, and A. Taticchi, *J. Chem. Soc., D*, **1971**, 1441.
48) B. A. Hess, Jr., L. J. Schaad, and C. W. Holyoke, Jr., *Tetrahedron*, **28**, 3657 (1972); B. A. Hess, Jr., and L. J. Schaad, *J. Am. Chem. Soc.*, **95**, 3907 (1973).
49) L. A. Paquette, "Modern Heterocyclic Chemistry," W. A. Benjamin, New York, N. Y. (1968), Chap. 4.
50) F. L. Scott and R. N. Butler, "Carbonium Ions," ed by G. A. Olah and P. v. R. Schleyer, Wiley-Interscience, New York, N. Y. (1973), Vol. 4, Chap. 30.
51) G. W. Wheland, *J. Am. Chem. Soc.*, **63**, 2025 (1941).
52) O. Kikuchi, "Bunshikidōhō," Kōdansha, Tokyo (1971), Chap. 2.

ESR Studies of a New Stable π-Conjugated 4,4′-(Biphenyl-3,3′-diyl)bis(aryloxyl) Biradical

Kazuo MUKAI* and Noriko INAGAKI

Department of Chemistry, Faculty of Science, Ehime University, Matsuyama 790

(Received December 7, 1979)

ENDOR observations were carried out for 2,6-di-*t*-butyl-4-phenylphenoxyl and some of its derivatives. Based on the proton hyperfine splittings, the structure of the aryloxyl monoradicals was investigated in terms of the McLachlan MO calculation. A new stable π-conjugated bis(aryloxyl) biradical, 4,4′-(biphenyl-3,3′-diyl)-bis(2,6-di-*t*-butylphenoxyl), was prepared, and the ***g***- and ***D***-tensor values of the biradical in toluene have been determined from its asymmetric frozen ESR spectrum. The ***D***-tensor values were calculated for the twisted "cis" and "trans" conformers of the biradical molecule, using the McLachlan spin densities of 2,6-di-*t*-butyl-4-phenylphenoxyl, which is a monoradical half of the biradical.

2,6-Di-*t*-butyl-4-phenylphenoxyl (aryloxyl radical (I)) (Fig. 1) is a fairly stable phenoxyl radical, which can be purely separated as a solid.[1] ESR[2] and NMR[3] studies of the aryloxyl radical (I) and some of its derivatives were already reported. In a recent paper, a report was given on the preparation of a new stable π-conjugated *m*-phenylenebis(aryloxyl) biradical, 4,4′-(*m*-phenylene)bis(2,6-di-*t*-butylphenoxyl), in which two aryloxyl monoradical parts strongly conjugated each other through the meta-position of central benzene ring.[4] Kothe *et al.*[5] prepared a stable benzene-1,3,5-tris(aryloxyl) triradical, 4,4′,4″-(1,3,5-benzenetriyl)tris-(2,6-di-*t*-butylphenoxyl), which is related to the *m*-phenylenebis(aryloxyl) biradical. The existence of triplet and quartet states in the bis and tris(aryloxyl) radicals, respectively, has been confirmed by ESR measurements in rigid media at 77 K.[4,6] However, no detailed study of the electronic and molecular structure of these bi- and tri-radicals seems to have been carried out so far.

First, ENDOR measurements were carried out in order to study the three aryloxyl monoradicals (I), (II), and (III) (Fig. 1), the detailed proton hyperfine splittings of the radicals being determined. The structure of the aryloxyl radicals was investigated by means of McLachlan MO calculation of the spin densities. The aryloxyl radical (I) is a monoradical half of the bis(aryloxyl) biradical (IV) (Fig. 1), and the aryloxyl radical (III) a monoradical precursor of the bis-(aryloxyl) biradical (IV).

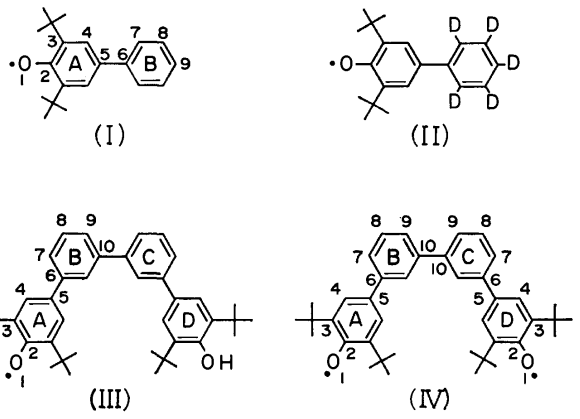

Fig. 1. Molecular structures of aryloxyl radicals (I), (II), (III), and (IV), and the atomic numbering system.

Secondly, we have prepared a new stable π-conjugated 4,4′-(biphenyl-3,3′-diyl)bis(aryloxyl) biradical (IV), and succeeded in observing the zero-field ESR spectrum in toluene rigid glass. The ESR spectrum at 77 K can be clearly analyzed as the characteristic spectrum of a non-axially symmetrical triplet, with $|D|=35.4\pm0.3$ G and $|E|=2.6\pm0.3$ G, and $g_{xx}=2.0045\pm0.0002$, $g_{yy}=2.0051\pm0.0002$ and $g_{zz}=2.0024\pm0.0002$. The D and E parameters were calculated for the assumed molecular structures, using McLachlan spin densities of the aryloxyl (I) which is a monoradical half of the biradical (IV). From the results, the conformation and electronic structure of the biradical have been discussed.

Experimental

Measurements. ESR measurements were carried out using a JES-ME-3X spectrometer equipped with a Takeda-Riken microwave frequency counter. The ENDOR spectra were recorded on a JEOL-type ES-EDX-1 spectrometer, operated with 80 Hz magnetic field modulation. About 150 W of the continuous radio wave frequency modulated at 6.5 kHz were running inside the cavity for NMR excitation. The ESR splittings were determined using $(KSO_3)_2NO$ or Mn^{+2} in MgO as a standard. The *g*-values were measuted relative to the value of Li–TCNQ powder, calibrated with $(KSO_3)_2NO$ ($g=2.0054$).[7] The aryloxyl radicals (I)—(IV) were prepared by the oxidation of the corresponding phenols with PbO_2 in toluene under a vacuum.

Preparation of Specimens. Rieker and Scheffler[2] reported the syntheses and physical properties of the phenol precursors of the aryloxyl radicals (I) and (II). Quinol (V) was synthesized by the reaction of the dimagnesium derivative of 3,3′-dibromobiphenyl with 2,6-di-*t*-butyl-*p*-benzoquinone;[8] the highly reactive magnesium investigated by Rieke and Bales[9] allows the ready preparation of many Grignard reagents which were heretofore not easily prepared or could not be prepared at all. Using their method, we have prepared the dimagnesium derivative of 3,3′-dibromobiphenyl at 20 °C.

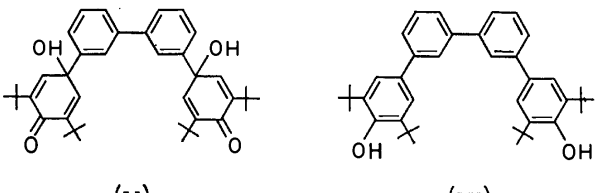

4,4′-(biphenyl-3,3′-diyl)bis(4-hydroxy-2,6-di-*t*-butyl-2,5-cyclohexadien-1-one) (quinol (V)). Freshly cut potassium (2.81 g, 0.072 mol), $MgCl_2$ (3.81 g, 0.040 mol), KI (3.32 g, 0.020 mol), and THF (tetrahydrofuran) (90 ml) were placed in an 100 ml four-necked flask equipped with reflux condensor, dropping funnel, thermometer, heating mantle, and magnetic stirrer under nitrogen atmosphere. The mixture was refluxed for 3 h with stirring, and was then left to stand at 30 °C for 0.5 h. A THF solution of 3,3′-dibromobiphenyl (3.12 g, 0.010 mol) was added dropwise below 30 °C, and the mixture was reacted for 0.5 h at 30 °C. In the same way, a THF solution of 2,6-di-*t*-butyl-*p*-benzoquinone (4.41 g, 0.020 mol) was added slowly below 30 °C, and then the reaction mixture was refluxed for 1.5 h under stirring. The grayish black solids precipitated were quickly filtered off and hydrolyzed in saturated NH_4Cl solution (200 ml). They were then taken up in diethyl ether, washed with water, and dried over anhydrous sodium sulfate. After removal of the diethyl ether, viscous oil was remained. By adding petroleum ether (bp 50—70 °C) to the viscous oil, white solids (1.5 g, 0.0025 mol) precipitated. The solids obtained were recrystallized first from ligroin (bp 90—105 °C), and then from dioxane, and finally heated at 180 °C for 11 h under vacuum (5×10^{-3} Torr; 1 Torr=133.322 Pa) in order to completely remove the dioxane solvent included in the crystal. Mp 246—248 °C. (Found: C, 80.21; H, 8.88%. Calcd for $C_{40}H_{50}O_4$: C, 80.77; H, 8.47%). UV spectrum (λ_{max}=228 nm, log ε=4.80 in THF). NMR spectrum (δ=1.27 ppm (36H, s, *t*Bu), 2.30 (2H, s, OH), 6.58 (4H, s, *m*-ring), 7.12—7.83 (8H, multiplet, biphenylene ring); δ in $CDCl_3$ with TMS as internal standard).

3,3′-Bis(3,5-di-t-butyl-4-hydroxyphenyl) biphenyl (Bisphenol (VI)). Bisphenol (VI) was synthesized by the reduction of quinol (V) (1.0 g, 0.0017 mol) with Zn powder (1.3 g, 0.020 mol) and concd HCl (15 ml) in methyl alcohol (60 ml) at 55 °C for 2 h, by a process similar to that of Rieker and Scheffler.[2] The white solid (0.75 g, 0.0013 mol) obtained was first washed with hot methyl alcohol, and then recrystallized from dioxane, and heated at 175 °C for 7 h under vacuum (5×10^{-3} Torr) in order to completely remove the dioxane solvent included in the crystal. Mp 213—215 °C. (Found: C, 85.05; H, 9.13%. Calcd for $C_{40}H_{50}O_2$: C, 85.36; H, 8.95%). UV spectrum (λ_{max}=217 nm, log ε=4.80, λ_{max}=263 nm, log ε=4.76 in THF). NMR spectrum (δ=1.48 ppm (36H, s, *t*Bu), 5.02 (2H, s, OH), 7.28 (4H, s, *m*-ring), 7.28, 7.38, 7.58 (8H, multiplet, biphenylene ring); δ in CCl_4 with TMS as an internal standard).

Results

ENDOR Spectra of Aryloxyl Monoradicals (I), (II), and (III). The ESR spectra of the aryloxyl radicals (I) and (II) have been reported by Rieker and Scheffler.[2] The spectrum of the aryloxyl radical (III) shows a sextet-doublet hyperfine pattern. Both the ring proton hyperfine splittings and the g_{iso}-values of the radicals observed in toluene at 20 °C are given in Table 1.

The ENDOR spectrum of aryloxyl radical (I) in toluene at −85 °C (Fig. 2(a)) clearly shows five different proton hyperfine splittings (1.872, 1.752, 1.620, 0.672, and 0.064 G). On the other hand, the ENDOR spectrum of deuterated aryloxyl radical (II) in toluene at −87 °C shows only two different hyperfine splittings (Fig. 2(b)). The splitting of 1.638 G in (II) is easily assigned to the two meta protons of the phenyl ring A, and that of 0.069 G to the *t*-butyl protons. Comparing

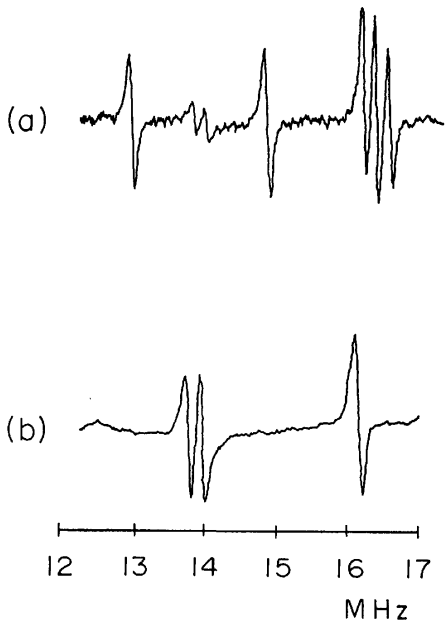

Fig. 2. ENDOR spectra of (a) aryloxyl radical (I) (at −85 °C) and (b) aryloxyl radical (II) (at −87 °C) in toluene.

Table 1. Hyperfine couplings (a_i^H) (in G), g_{iso}-values, and spin densities (ρ_i) of aryloxyl radicals (I), (II), and (III)

		a_4^H	a_7^H	a_8^H	a_9^H	a_{tBu}^H	g_{iso}
I	ESR	1.74[a]	1.74	0.74	1.74	—	2.00415[c]
	ENDOR	1.620[b]	1.752	0.672	1.872	0.064	—
	ρ(Exptl)	−0.0600	0.0649	−0.0249	0.0693	0.228	—
	ρ(Calcd)	−0.0519	0.0629	−0.0301	0.0594	0.2211	(θ_{AB}=0°)
II	ESR	1.65	—	—	—	—	2.00414
	ENDOR	1.638	—	—	—	0.069	—
III	ESR	1.76	1.76	0.69	1.76	—	2.00414
	ENDOR	1.673	1.766	0.683	1.902	0.070	—
	ρ(Exptl)	−0.0620	0.0654	−0.0253	0.0704	0.250	—
	ρ(Calcd)	−0.0511	0.0621	−0.0307	0.0592	0.2216	($\theta_{AB}=\theta_{CD}$=0°, θ_{BC}=30°)

a) Experimental errors ±0.04 G. 1 G=10^{-4} T. b) Experimental errors ±0.010 G. c) Experimental errors ±0.00003.

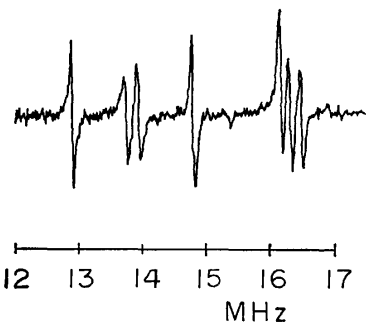

Fig. 3. ENDOR spectrum of aryloxyl radical (III) (at −65 °C) in toluene.

the ENDOR spectrum of aryloxyl radical (I) with that of aryloxyl (II), the hyperfine splittings of 1.872, 1.752, and 0.672 G of the former, which have never been observed in the latter, can clearly be identified as the proton hyperfine splittings in the substituted phenyl ring B. Of these three splittings, the smallest, 0.672 G, is also easily assigned to the two meta protons of the phenyl ring B, taking their ESR hyperfine splittings into account. In this case, we cannot distinguish the splitting due to ortho- and para-protons of the phenyl ring B. A tentative assignment was made, however, with reference to the analogous splitting of the aryloxyl radical (I) obtained by NMR measurements[3] (Table 1). The monoradical precursor (III) of the biradical (IV) shows a spectrum similar to that of aryloxyl radical (I) (Fig. 3). The value of each hyperfine splitting is very close to the corresponding value of aryloxyl radical (I). This indicates that the effects of the meta-substituion of the phenyl ring by biphenyl group are very small to induce a change in the unpaired spin distribution or molecular structure. The experimental values of the spin densities were estimated using the relation, $a_i^H = Q^H \cdot \rho_i$ and $a_{t\mathrm{Bu}}^H = Q^{t\mathrm{Bu}} \cdot \rho_i$, where Q^H and $Q^{t\mathrm{Bu}}$ were taken to be 27 and 0.28 G[10] respectively. The proton hyperfine splittings and the experimental spin densities ρ(Exp.) are summarized in Table 1.

Triplet ESR Spectrum of 4,4'-(Biphenyl-3,3'-diyl)bis-(aryloxyl) Biradical(IV). When the bisphenol precursor (VI) of bis(aryloxyl) biradical (IV) was slightly oxidized with PbO_2 in toluene under vacuum, the color of the phenol solution immediately became violet. The ESR spectrum of this solution showed a sextet-doublet hyperfine pattern (a^H=1.76±0.04 G, a^H=0.69±0.04 G, g_{iso}=2.00414±0.00003) due to the six ring protons of the monoradical precursor (III). By further oxidation, the color turned pink, a broad absorption due to the biradical being superposed on the hyperfine spectrum of the monoradical. By freezing the pink solution containing the biradical (IV) into a rigid glass (77 K), one can observe dipolar splittings as shown in Fig. 4.

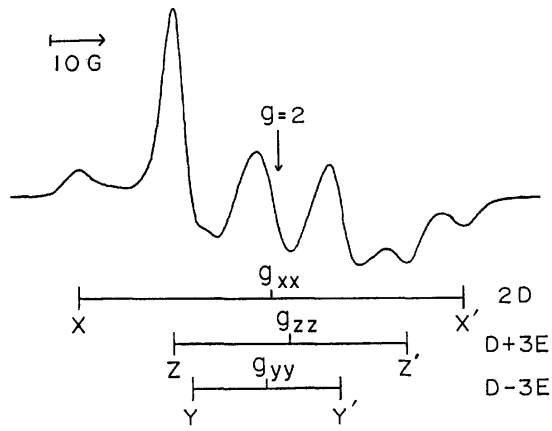

Fig. 4. ESR spectrum of 4,4'-(biphenyl-3,3'-diyl)bis-(aryloxyl) biradical (IV) in toluene at 77 K.

The biradical in a rigid glass can be treated as a two-spin system which forms a triplet and a singlet state. The usual spin Hamiltonian for the triplet state is

$$H = \beta \boldsymbol{H}\cdot\hat{\boldsymbol{g}}\cdot\boldsymbol{S} + \boldsymbol{S}\cdot\hat{\boldsymbol{D}}\cdot\boldsymbol{S} \quad (1)$$

$$= \beta \boldsymbol{H}\cdot\hat{\boldsymbol{g}}\cdot\boldsymbol{S} - XS_x^2 - YS_y^2 - ZS_z^2 \quad (S=1) \quad (2)$$

where $\boldsymbol{g}$ is the $\hat{\boldsymbol{g}}$ tensor, and $\hat{\boldsymbol{D}}$ the fine structure tensor with principal values of $-X$, $-Y$, and $-Z$, the other symbols having their usual meanings. When the radical has the property of a triplet having no axial symmetry, we usually observe three pairs of absorption lines, from whose separations the zero-field parameters (D and E) of the spin-spin dipolar interaction can be obtained.[11] In the case of biradical (IV), five out of the six lines theoretically expected for a non-axially symmetrical triplet are resolved (Fig. 4). In the spectrum, the intensity of the low-field line of the inner pair of lines is higher than the other, suggesting the overlapping of two lines. A central line at g=2 is attributable to the monoradical impurity, since the relative intensity of central line decreases when the PbO_2 oxidation proceeds from monoradical to biradical. Separation values between the three pairs of turning points (X, X'; Y, Y'; and Z, Z') in the spectrum of the biradical are 70.8±0.6, 42.6±0.6, and 27.0±0.6 G, respectively. They correspond to $2D$, $D+3E$, and $D-3E$. The D and E values were estimated to be D=35.4±0.3 G and E=2.6±0.3 G, respectively. Assuming that the principal axes of the $\boldsymbol{D}$- and $\boldsymbol{g}$-tensors are coaxial, $\boldsymbol{g}$-tensor values have been estimated from the positions of three pairs of turning points (X, X'; Y, Y'; and Z, Z').[11-13] They are g_{xx}=2.0045±0.0002 (X, X'), g_{yy}=2.0051±0.0002 (Y, Y'), and g_{zz}=2.0024±0.0002 (Z, Z'). The average g_{av} value of $1/3(g_{xx}+g_{yy}+g_{zz})$=2.0040±0.0002 agrees with the isotropic g_{iso}-value (2.00414±0.00003) measured at 20 °C, indicating that the $\boldsymbol{g}$-tensor values obtained by the above analyses are reliable.

Discussion

The Structure of Aryloxyl Monoradicals. McLachlan spin densities (ρ_i) of the aryloxyl radical (I) were calculated, varying the twist angle θ_{AB} between the phenyl rings A and B. The MO parameters were given the values $\alpha_O=\alpha+1.3\beta$, $\beta_{CO}=1.5\beta$, and λ=1.2.[14] The results are shown in Fig. 5. Comparing these spin densities and the experimental values calculated from the hyperfine splittings, the best accordance was found

for the twist angle $\theta_{AB}=0°$ (Table 1). Thus, spin densities (ρ_i) were calculated, in the case of the aryloxyl radical (III), holding one twist angle θ_{AB} at 0° and varying the other twist angles θ_{BC} and θ_{CD}; here we used the same MO parameters, $\alpha_O=\alpha+1.3\beta$, $\beta_{C-O}=1.5\beta$, for the oxygen atom (O_1), and the parameters $\alpha_{OH}=\alpha+0.9\beta$, $\beta_{C-OH}=0.4\beta$ for the oxygen atom of the OH group.[15] The results show that a very small unpaired spin density (lower than 1.5%) exists in the C and D rings, the spin density distribution not being sensitively affected by varying the twist angles θ_{BC} and θ_{CD}. The spin densities obtained for the structure $\theta_{AB}=\theta_{CD}=0°$, $\theta_{BC}=30°$ of the radical molecule (III) (Table 1) also show good agreement with those obtained from the hyperfine splittings of the radical (III).

The aryloxyl radical (I) may be considered to be a biphenyl derivative; the molecule of biphenyl is planar or nearly so in both the solid and triplet state, but twisted 30—40° around the central single bond in the vapor phase and in solution.[16] Thus, the degree of twisting of biphenyl molecule is clearly due to a delicate balance of non-bonded repulsion and conjugation. On the other hand, it is obvious that the inter-ring bond acquires some double-bond character in the aryloxyl radical (I) in view of a valence-bond. This is apparent in the quinoid valence structures (iv) and (v) for the aryloxyl radical (I):

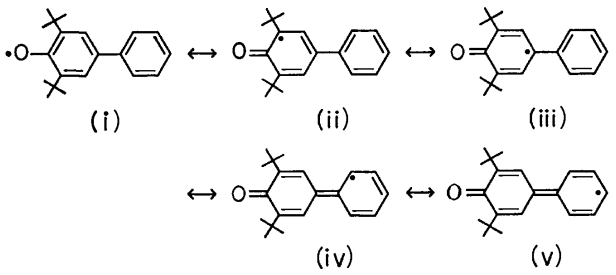

We reach a similar conclusion by calculating the bond orders due to the Hückel molecular-orbital, the result for aryloxyl radical (I) indicating that the 1—1′ and 2—3 bonds are strengthened and the 1—2 and 3—4 bonds weakened as compared to biphenyl molecule.

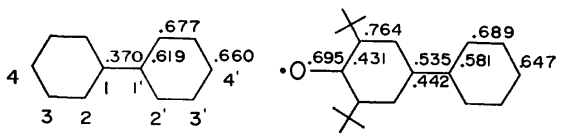

All the results indicate that the aryloxyl radical (I) has planar character.

D*-Tensor Calculation with Spin Densities.** In order to clarify the molecular structure of the 4,4′-(biphenyl-3,3′-diyl)bis(aryloxyl) biradical (IV), and determine the directions of the principal axes, X_d, Y_d, and Z_d, of the ***D-tensor in the molecule (Figs. 6 and 8), calculations of the dipolar splitting tensors were performed for the assumed molecular structures using McLachlan spin densities of the aryloxyl radical (I).

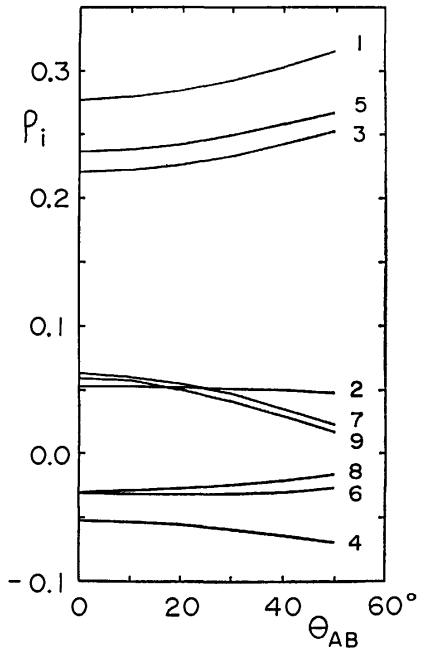

Fig. 5. Dependence of McLachlan MO spin densities (ρ_i) of carbon and oxygen atoms in aryloxyl radical (I) on twist angle θ_{AB}.

Bis(aryloxyl) (IV) is thought to be a weakly π-conjugated biradical consisting of two aryloxyl monoradical parts. The values of the hyperfine splittings of the ring protons and the isotropic g_{iso} value of the monoradical precursor (III) of the bis(aryloxyl) show an excellent agreement with the corresponding values of the aryloxyl (I), that is, a monoradical half of the biradical (Table 1). No hyperfine splitting arising from the protons in C and D rings was observed even by the ENDOR measurement with resolution higher than that of ESR measurement.[17] The results of McLachlan MO calculation of the radical (III) also supported the above anticipation, showing the existence of very small unpaired electron density (1.0—1.5%) in the C and D rings. Therefore, the dipolar magnetic system of the bis(aryloxyl) biradical may be adequately described as

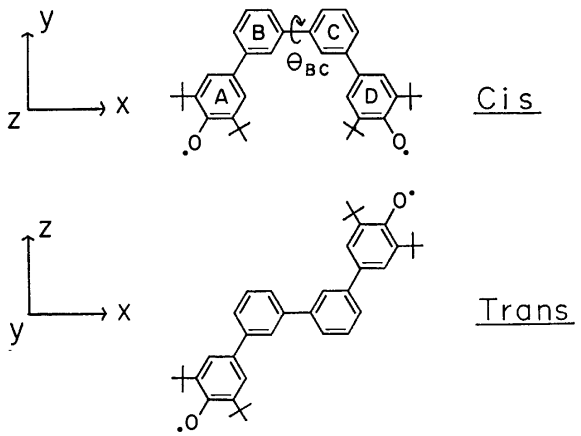

Fig. 6. Molecular structures and the coordinate systems (right-handed systems) chosen for "cis" and "trans" conformations of the 4,4′-(biphenyl-3,3′-diyl)bis(aryloxyl) biradical (IV).

an isolated two-spin system consisting of two aryloxyl groups, each containing one unpaired electron.

Aryloxyl monoradical parts of the bis(aryloxyl) (IV) seem to be planar in solution. Thus, as a most plausible case, the ***D***-tensor values have been calculated, assuming that $\theta_{AB}=\theta_{CD}=0°$ and varying θ_{BC}. Molecular structures and the coordinate systems (x, y, and z) chosen for "cis" and "trans" conformations of the bis(aryloxyl) biradical (IV) are shown in Fig. 6, where $\theta_{BC}=0°$ corresponds to a planar "cis" conformation, and $\theta_{BC}=180°$ is a planar "trans" conformer. In the planar "cis" conformation, the principal axes X_d, Y_d, and Z_d of the ***D***-tensor are parallel to the molecular axes x, y, and z, because of the symmetry of the biradical molecule[13,18] (Fig. 8). By varying the twist angle θ_{BC}, we can expect that the Y_d axis still coincides with the molecular y axis, but the X_d axis is parallel to the line inclined θ_x from the molecular x axis within xz plane.

In such a case, the ***D***-tensor components of the dipolar splitting can be calculated with the aid of the following equations.[13,19,20]

$$D_{mm} = (1/2)g^2\beta^2\sum_{i,j}\rho_i\rho_j(r_{ij}^2-3m_{ij}^2)/r_{ij}^5, \quad (m = x, y, z) \tag{3}$$

$$D_{mn} = (1/2)g^2\beta^2\sum_{i,j}\rho_i\rho_j(-3m_{ij}n_{ij})/r_{ij}^5, \quad (m, n = x, y, z; \text{ but } m \neq n) \tag{4}$$

where r_{ij} is the distance between the i and j atoms, and ρ_i and ρ_j are the McLachlan π-spin densities on the i atom in one aryloxyl group and the j atom in the other aryloxyl group, respectively, in a molecule. Here we have chosen the following parameters: the C–O bond length is 1.27 Å, and the C–C bond length is 1.40 Å on the average, as obtained by an X-ray analysis of the galvinoxyl radical.[21] The resulting tensor is then diagonalized, giving the principal values X, Y, and Z and their directions.

Several authors have carried out such calculations for the radical pairs[19,20] and the weakly π-conjugated biradicals,[13,18,22] and obtained good agreement with experiment. However, the agreement was not satisfactory[13] when the internuclear distances between two monoradical parts are small. The discrepancy between observed and calculated zero-field splitting values depends mainly on the difference between the true and the calculated zero-field splitting values for short interatomic distances. In such a case, the electron distribution within a $2p_z$ orbital has to be represented by two half-charges located above and below the plane containing the atom. This approximation has been shown to be quite good if the separation between the half-charges is 1.4 Å even when the internuclear distances are as small as 1.6 Å.[23,24]

Therefore, we calculated the ***D***-tensor values of the bis(aryloxyl) (IV), using the above approximations ((a) "point-charge" and (b) "half-charge" approximations), and compared the results obtained. How the principal values X, Y, and Z of the zero-field splitting and the value of the direction cosine ($\cos\theta_x$) of the principal axis-X_d of the zero-field splitting tensor to the molecular axis-x vary as a function of θ_{BC} is shown in Figs. 7 and 8, respectively. The results indicate that, in the above two kinds of approximations, $|X|$ is the largest

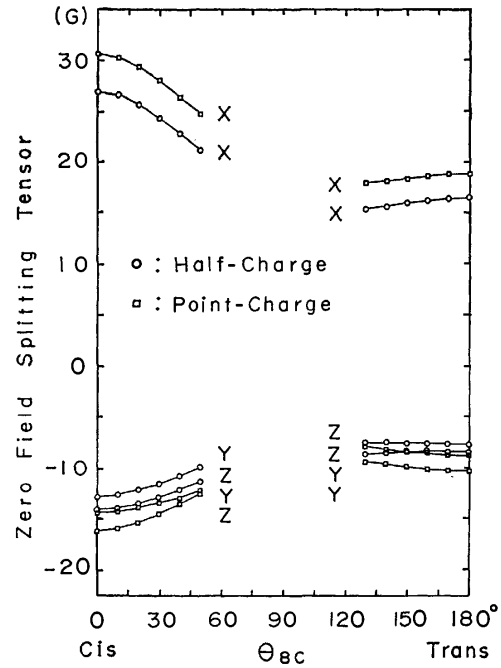

Fig. 7. The variation of the principal components of the zero-field splitting tensor as a function of the twist angle θ_{BC}.

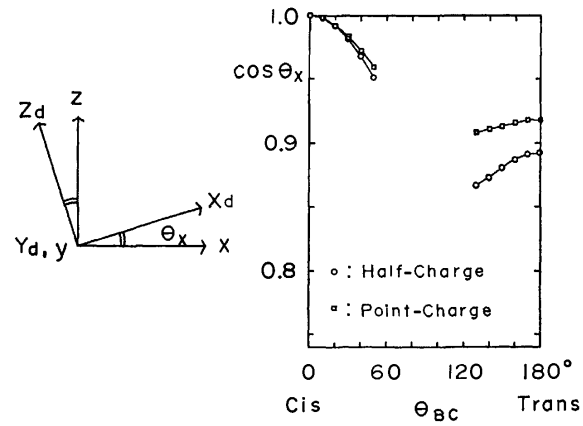

Fig. 8. The variation of the direction cosine ($\cos\theta_x$) of the pricipal axis-X_d of the zero-field splitting tensor to the molecular axis-x as a function of the twist angle θ_{BC}.

component of the zero-field splitting tensor and is consistent with our expectation. Thus, the zero-field parameters D and E are given by

$$D = -3X/2, \quad E = -(Y-Z)/2. \tag{5}$$

Figure 9 shows how the D and E parameters vary as functions of θ_{BC}. By comparing the observed D-parameter ($|D|=35.4$ G) with the calculated ones, the agreements were observed for the cases of $\theta_{BC}=35°$ in the "half-charge" approximation and $\theta_{BC}=57°$ in the "point-charge" approximation, where the θ_x values are 13° and 18°, respectively. On the other hand, in both the approximations, the absolute values of all the calculated E-parameters are smaller than the observed one ($|E|=2.6$ G). The absolute values of all the D-parameters calculated by the "point-charge" approximations are 3.6—5.4 G larger than those calculated by the "half-charge" approximation for the corresponding

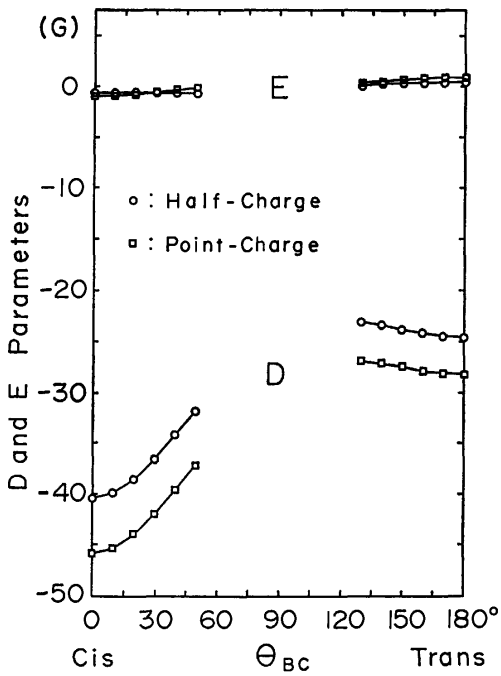

Fig. 9. The variation of the zero-field splitting parameters D and E as a function of the twist angle θ_{BC}.

twist angle θ_{BC}. For instance, in a planar "cis" conformer ($\theta_{BC}=0°$), the total D-parameters calculated are -45.8 G for the "point-charge" approximation and -40.4 G for the "half-charge" approximation, where the values of the D-parameter calculated for the nearest neighboring atoms ($C_{10B}-C_{10C}$) (Fig. 1) are -9.2 G for the former and -5.0 G for the latter. The difference (5.4 G) between the total D-parameters of the two approximations could be attributed to the difference (4.2 G) obtained for the nearest neighboring atoms ($C_{10B}-C_{10C}$). The results indicate that the "point-charge" approximation is unsatisfactory for the calculation of $\boldsymbol{D}$-tensor value of the radical molecule with short interatomic distance, such as 1.4 Å, and the "half-charge" approximation improves the calculation considerably.

Two sets of ESR spectra of the lowest excited triplet state of 2,2'-bipyridyl in poly(vinyl alcohol) (PVA) films have been observed.[25] They are interpreted to be due to its "cis" and "trans" conformations from the experimental and theoretical viewpoints, since the molecular structure in the triplet state is considered to be planar. Similar phenomena have also been observed for 3,3'-dimethylbiphenyl and 3,3'-difluorobiphenyl in rigid glass.[26,27] On the other hand, the bis(aryloxyl) biradical (IV) is considered to be a biphenyl (B and C rings) derivative. Thus, we can expect similar conformations, "cis" and "trans" forms, in the bis(aryloxyl) biradical (VI). However, the frozen-solution ESR spectrum of the bis(aryloxyl) in toluene (Fig. 4) suggests that only one conformer exists in the biradical. If two conformers exist in the aryloxyl biradical at the same time, we should, at least, observe a splitting in the X and/or X' absorption lines as the results of calculation of the D and E parameters indicate. Although the $\boldsymbol{D}$-tensor calculation presented here is of a very approximate nature for the bis(aryloxyl) biradical, the result indicates that the bis(aryloxyl) biradical has "cis" conformation rather than "trans."

We are grateful to Prof. Kazuhiko Ishizu and Dr. Fujito Nemoto for their kind advice. We also wish to thank Mr. Takayuki Yasunaga and Mr. Tsukasa Hara for their help in the preparation of aryloxyl radicals (I) and (II).

References

1) E. Müller, A. Schick, and K. Scheffler, *Chem. Ber.*, **92**, 474 (1959).
2) A. Rieker and K. Scheffler, *Liebigs Ann. Chem.*, **689**, 78 (1965).
3) S. Icli and R. W. Kreilick, *J. Phys. Chem.*, **75**, 3462 (1971).
4) K. Mukai, T. Hara, and K. Ishizu, *Bull. Chem. Soc. Jpn.*, **52**, 1853 (1979).
5) G. Kothe, C. Nowak, K. H. Denkel, E. Ohmes, and H. Zimmermann, *Angew. Chem.*, **82**, 521 (1970); *Angew. Chem. Int. Ed.*, **9**, 520 (1970).
6) C. Nowak, G. Kothe, and H. Zimmermann, *Ber. Bunsenges. Phys. Chem.*, **78**, 265 (1974).
7) J. J. Windle and A. K. Wiersma, *J. Chem. Phys.*, **39**, 1139 (1963).
8) H. Dietl and H. S. Young, *J. Org. Chem.*, **37**, 1672 (1972).
9) R. D. Rieke and S. E. Bales, *J. Am. Chem. Soc.*, **96**, 1775 (1974).
10) K. Mukai, H. Nishiguchi, K. Ishizu, Y. Deguchi, and H. Takaki, *Bull. Chem. Soc. Jpn.*, **40**, 2731 (1967).
11) E. Wasserman, L. C. Snyder, and W. A. Yager, *J. Chem. Phys.*, **41**, 1763 (1964).
12) K. Mukai, T. Mishina, and K. Ishizu, *J. Chem. Phys.*, **66**, 1680 (1977).
13) K. Mukai and J. Sakamoto, *J. Chem. Phys.*, **68**, 1432 (1978).
14) Some twenty sets of McLachlan calculations were performed before the values $\alpha_O=\alpha+1.3\beta$, $\beta_{CO}=1.5\beta$ and $\lambda=1.2$ were adopted. These values are the same as those used for the oxygen atom of the galvinoxyl radical. *Cf.* Ref. 9 and G. R. Luckhurst, *Mol. Phys.*, **11**, 205 (1966).
15) Numerous McLachlan calculations were made to obtain reasonable agreement with the experimental spin densities, and the final values of the MO parameters $\alpha_{OH}=\alpha+0.9\beta$, $\beta_{C-OH}=0.4\beta$ were adopted.
16) A. Imamura and R. Hoffmann, *J. Am. Chem. Soc.*, **90**, 5379 (1968), and references cited therein.
17) J. S. Hyde, *J. Chem. Phys.*, **43**, 1806 (1965).
18) K. Mukai and T. Tamaki, *Bull. Chem. Soc. Jpn.*, **50**, 1239 (1977).
19) D. A. Wiersma and J. Kommandeur, *Mol. Phys.*, **13**, 241 (1967).
20) N. Azuma, H. Ohya-Nishiguchi, J. Yamauchi, K. Mukai, and Y. Deguchi, *Bull. Chem. Soc. Jpn.*, **47**, 2369 (1974).
21) D. E. Williams, *Mol. Phys.*, **16**, 145 (1969).
22) W. Broser, B. Kirste, H. Kurreck, J. Reusch, and M. Plato, *Z. Naturforsch*, **13b**, 974 (1976).
23) J. Higuchi, *J. Chem. Phys.*, **38**, 1237 (1963).
24) A. Pullman and E. Kochanski, *Int. J. Quantum. Chem.*, **1**, 251 (1967), and references cited therein.
25) T. Ito and J. Higuchi, *Chem. Lett.*, **1974**, 1519.
26) B. J. Scheve and P. J. Wagner, *Chem. Phys. Lett.*, **25**, 324 (1974).
27) J. Mispelter, J.-Ph. Grivet, and J.-M. Lhoste, *Mol. Phys.*, **21**, 1015 (1971).

The r_s Structures of Fluoromethyl, Chloromethyl Ethers, and Methyl 2-Propynyl Ether

Michiro HAYASHI* and Hiroshi KATO

Department of Chemistry, Faculty of Science, Hiroshima University, Higashi-sendamachi, Hiroshima 730

(Received January 21, 1980)

^{18}O enriched samples of chloromethyl methyl ether and chloromethyl ethyl ether were prepared and their microwave spectra were measured. The r_s structures of fluoromethyl methyl ether, fluoromethyl ethyl ether, chloromethyl methyl ether, chloromethyl ethyl ether, and methyl 2-propynyl ether were re-evaluated from the observed rotational constants obtained under the common constraints and assumptions on the structures of the molecules. A comparison of the r_s structures was made between the five molecules and between the molecules and their related molecules.

In previous papers, reports were given on the r_s structures of chloromethyl methyl ether,[1] chloromethyl ethyl ether,[2] and fluoromethyl ethyl ether.[3] Studies on fluoromethyl methyl ether[4] and methyl 2-propynyl ether[5] have been completed, the r_s structures of these molecules being determined.

The most populated isomer for these five molecules is the gauche isomer around the CH_2–O bond. Since several atoms in the molecules are situated close to the principal axes, solutions of the Kraitchman equation for these atoms are not reliable for coordinates having small absolute values. Moreover, a fluorine atom has no stable isotope, and thus the coordinate values of the fluorine atom should be computed from the coordinate values of the other atoms by means of the first moment equations.

The coordinate values of the oxygen atom were also obtained from those of other atoms with certain assumptions on the structure since no ^{18}O enriched samples were available.[1,2] After our results for these molecules had been reported, we succeeded in preparing ^{18}O enriched samples. Three coordinate values for the oxygen atom could then be obtained by means of the Kraitchman equation. Since we are interested in comparison of the structures of these molecules it is important to re-evaluate their structures under a common set of constraints and assumptions on the five molecules by using new additional data. This paper deals with the structures obtained under different constraints and assumptions for each molecule. They are compared in order to find the most reliable r_s structures obtained by means of the common set of constraints and assumptions on these five molecules.

Interesting features of the structural parameters for halomethyl ethers and their related molecules are given. The dipole moment, nuclear quadrupole coupling constant tensor and internal rotation are not dealt with.

For the sake of convenience, the names of the molecules referred to are abbreviated as follows: fluoromethyl methyl ether, [F, Me]; fluoromethyl ethyl ether, [F, Et]; chloromethyl methyl ether, [Cl, Me]; chloromethyl ethyl ether, [Cl, Et]; and methyl 2-propynyl ether, [Pr, Me].

The conventional terms, trans and gauche, are used instead of the IUPAC nomenclature, antiperiplanar and synclinal, respectively, since they were used in previous papers.

Experimental

^{18}O enriched samples of [Cl, Me] and [Cl, Et] were prepared by the reaction of ^{18}O enriched methanol or ethanol and paraformaldehyde with hydrochloric acid.

^{18}O enriched methanol was prepared by the method of Sawyer.[6] Tributyl orthoformate was mixed with ^{18}O enriched water (70 atom % ^{18}O, Prochem.) in the presence of hydrochloric acid in diglyme. The resulting butyl formate-carbonyl-^{18}O was reduced by lithinum aluminum hydride. The methanol obtained contains *ca.* 60 atom % ^{18}O.

^{18}O enriched ethanol was obtained by mixing acetaldehyde with ^{18}O enriched water and the resulting aldehyde was reduced with lithium aluminum hydride. The ethanol obtained was found to contain *ca.* 30 atom % ^{18}O.

The microwave spectra were measured in the range 8500—34000 MHz with a conventional Stark modulation spectrometer at dry ice temperature. Observed frequencies and rotational constants are given in Tables 1 and 2.

Determination of r_s Structures

In spite of sufficient data for determining the r_s structures of the four halomethyl ethers by the substitution method, there are several unreliable Kraitchman atom coordinate values for each molecule. The coordinate value obtained by the Kraitchman equation is hereafter referred to as the *K*-value. The identification symbols of the atoms for the XCH_2OCH_3 and $XCH_2OCH_2CH_3$ type molecules are shown in Fig. 1 where the hydrogen atoms situated on the same side as the X atom with respect to the COC plane have

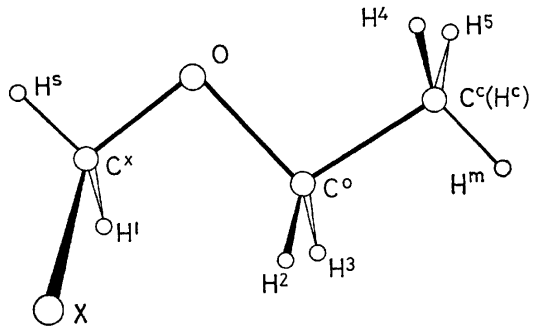

Fig. 1. Identification number of atoms in $XCH_2OCH_2CH_3$.
The symbols in parentheses indicate the atom symbols for XCH_2OCH_3.

TABLE 1. OBSERVED AND HYPOTHETICAL UNSPLIT FREQUENCIES[a] AND ROTATIONAL CONSTANTS[b] OF THE ^{18}O SPECIES OF CHLOROMETHYL METHYL ETHER (MHz)

F	$J+3/2$	$J+1/2$	$J-1/2$	$J-3/2$	ν_0	$\Delta\nu$ $(J+3/2)$	$\Delta\nu$ $(J+1/2)$	$\Delta\nu$ $(J-1/2)$	$\Delta\nu$ $(J-3/2)$
$3_{03}\leftarrow 2_{02}$	19100.02	19100.02	19098.12	19098.12	19099.60(−7)	0.42(1)	0.42(24)	−1.48(−1)	−1.48(−24)
$3_{13}\leftarrow 2_{12}$	18493.49	18491.75	18490.63	···	18492.53(−1)	0.96(2)	−0.78(6)	−1.90(−6)	—
$3_{12}\leftarrow 2_{11}$	19796.18	19794.37	19795.27	···	19795.57(10)	0.61(4)	−1.20(1)	−0.30(−4)	—
$4_{04}\leftarrow 3_{03}$	25405.69	25405.45	25404.69	···	25405.39(3)	0.30(−4)	0.06(3)	−0.70(1)	—
$4_{14}\leftarrow 3_{13}$	24642.23	24641.47	24640.73	24641.47	24641.70(−5)	0.53(−2)	−0.23(−2)	−0.97(4)	−0.23(2)
$4_{13}\leftarrow 3_{12}$	26378.16	26377.46	26377.46	26378.16	26377.82(−1)	0.34(2)	−0.36(9)	−0.36(−3)	0.34(−9)
$5_{05}\leftarrow 4_{04}$	31660.81	31660.49	31660.07	31660.49	31660.56(1)	0.25(−5)	−0.07(0)	−0.49(0)	−0.07(5)
$5_{15}\leftarrow 4_{14}$	30779.24	30778.78	30778.35	30778.78	30778.91(5)	0.33(−4)	−0.13(−7)	−0.56(6)	−0.13(6)
$5_{14}\leftarrow 4_{13}$	32945.73	32945.38	32945.38	32945.73	32945.57(−5)	0.16(−6)	−0.19(4)	−0.19(6)	0.16(−4)
$3_{22}\leftarrow 3_{12}$	31033.47	···	···	···	31033.90(−6)	−0.43(2)	—	—	—
$4_{23}\leftarrow 4_{13}$	30182.75	30182.12	···	···	30182.53(13)	0.22(−5)	−0.41(5)	—	—
$5_{24}\leftarrow 5_{14}$	29128.46	29126.74	29127.16	29128.88	29127.77(−8)	0.69(3)	−1.03(3)	−0.61(−3)	1.11(−3)
$6_{25}\leftarrow 6_{15}$	27879.27	27876.98	···	27879.83	27878.37(1)	0.90(0)	−1.39(−3)	—	1.46(3)
$7_{26}\leftarrow 7_{16}$	26446.33	26443.73	26444.26	26446.84	26445.26(25)	1.07(2)	−1.53(−2)	−1.00(−1)	1.58(1)
$8_{27}\leftarrow 8_{17}$	24844.61	24841.87	24842.34	24845.03	24843.43(70)	1.18(3)	−1.56(1)	−1.09(−1)	1.60(−3)
$9_{28}\leftarrow 9_{18}$	23093.97	23091.20	23091.57	23094.39	23092.76(158)	1.21(2)	−1.56(3)	−1.19(−5)	1.63(0)
$10_{29}\leftarrow 10_{19}$	21219.53	21216.76	21217.10	21219.88	21218.30(278)	1.23(3)	−1.54(3)	−1.20(−3)	1.58(−2)

$A=13968.12(12)$, $B=3409.25(4)$, $C=2974.86(4)$, $d_J=1.95(74)\times10^{-3}$, $d_{JK}=-1.72(43)\times10^{-2}$, $\chi_{aa}=-27.7(35)$, $\eta\chi_{aa}=-31.5(21)$

a) Since the observed components were restricted to those expected under the rule of $\Delta F=\Delta J$, the component can be designated by the F value of the lower level alone. For example, the component of the $J+1\leftarrow J$ transition labeled $F=J+3/2$ indicates the component of $F'=J+5/2\leftarrow F=J+3/2$ and so on. Dotted line indicates that the corresponding component is overlapped with the other strong line. ν_0 is the hypothetical unsplit frequency where the figures in parentheses indicate the deviations of the observed frequency from the calculated. $\Delta\nu(J+3/2)$ indicates the difference of the $F=J+3/2$ component from ν_0 where the figures in parentheses indicate the deviation of the observed frequency from the calculated one. b) Figures in parentheses indicate the uncertainties attached to the last significant figures calculated from 2.5 times the standard deviation.

TABLE 2. OBSERVED AND HYPOTHETICAL UNSPLIT FREQUENCIES AND ROTATIONAL CONSTANTS OF THE ^{18}O SPECIES OF CHLOROMETHYL ETHYL ETHER (MHz)[a]

F	$J+3/2$	$J+1/2$	$J-1/2$	$J-3/2$	ν_0	$\Delta\nu$ $(J+3/2)$	$\Delta\nu$ $(J+1/2)$	$\Delta\nu$ $(J-1/2)$	$\Delta\nu$ $(J-3/2)$
$3_{03}\leftarrow 2_{02}$	10334.40	10334.40	···	···	10334.34(−3)	0.06(−7)	0.06(−7)	—	—
$3_{13}\leftarrow 2_{12}$	10113.80	10113.80	10111.99	10111.99	10113.44(−15)	0.36(−11)	0.36(28)	−1.45(3)	−1.45(−35)
$3_{12}\leftarrow 2_{11}$	10568.18	10568.18	···	···	10568.48(18)	−0.30(−16)	−0.30(23)	—	—
$4_{04}\leftarrow 3_{03}$	13770.14	13770.14	13770.14	13770.14	13770.16(2)	−0.02(−15)	−0.02(7)	−0.02(19)	−0.02(−2)
$4_{14}\leftarrow 3_{13}$	13482.70	13482.70	13481.72	13481.72	13482.43(−8)	0.27(−3)	0.27(17)	−0.71(−2)	−0.71(−21)
$4_{13}\leftarrow 3_{12}$	14088.63	14088.63	···	···	14088.80(9)	−0.17(−8)	−0.17(11)	—	—
$5_{05}\leftarrow 4_{04}$	17198.33	17198.33	17198.33	17198.33	17198.34(12)	−0.01(−15)	−0.01(11)	−0.01(17)	−0.01(−9)
$5_{15}\leftarrow 4_{14}$	16849.60	16849.60	16849.12	16849.12	16849.46(−5)	0.14(−7)	0.14(7)	−0.34(7)	−0.34(−6)
$5_{14}\leftarrow 4_{13}$	17606.98	17606.98	17606.98	17606.98	17606.95(−11)	0.03(8)	0.03(22)	0.03(−16)	0.03(−30)
$6_{06}\leftarrow 5_{05}$	20616.91	20616.91	20616.91	20616.91	20616.92(13)	−0.01(−17)	−0.01(15)	−0.01(17)	−0.01(−14)
$6_{16}\leftarrow 5_{15}$	20214.18	20214.18	20214.18	20214.18	20214.21(2)	−0.03(−19)	−0.03(−8)	−0.03(25)	−0.03(13)
$6_{15}\leftarrow 5_{14}$	21122.66	21122.66	21122.66	21122.66	21122.64(−14)	0.02(4)	0.02(17)	0.02(−9)	0.02(−21)
$3_{22}\leftarrow 3_{12}$	26462.83	26457.41	···	···	26460.99(24)	1.84(8)	−3.58(−10)	—	—
$4_{23}\leftarrow 4_{13}$	26162.29	26156.96	···	···	26160.39(3)	1.90(−15)	−3.43(16)	—	—
$5_{24}\leftarrow 5_{14}$	25788.27	25782.77	25784.44	25789.91	25786.20(1)	2.07(−17)	−3.43(15)	−1.76(18)	3.71(−17)
$6_{25}\leftarrow 6_{15}$	25341.45	25335.44	25336.75	25342.82	25339.01(−16)	2.44(8)	−3.57(−2)	−2.26(−11)	3.81(5)
$7_{26}\leftarrow 7_{16}$	24823.03	···	24817.80	···	24820.33(−22)	2.70(25)	—	−2.53(−25)	—
$8_{27}\leftarrow 8_{17}$	24234.21	···	···	24235.37	24231.75(−14)	2.46(−12)	—	—	3.62(−2)
$9_{28}\leftarrow 9_{18}$	23577.69	23571.72	···	23578.65	23575.14(3)	2.55(−1)	−3.42(−6)	—	3.51(0)
$10_{29}\leftarrow 10_{19}$	22855.56	22849.42	22850.31	···	22852.85(22)	2.71(18)	−3.43(−7)	−2.54(−3)	—

$A=10694.92(20)$, $B=1799.47(3)$, $C=1647.90(4)$, $d_J=0.68(94)\times10^{-3}$, $d_{JK}=1.54(32)\times10^{-2}$, $\chi_{aa}=-5.7(77)$, $\eta\chi_{aa}=-50.7(54)$

a) See footnote to Table 1.

even numbers and those on the opposite side, odd numbers. For the unreliable K-values, the values should be solved by means of certain constraints and/or assumptions. However, since several different sets of constraints and/or assumptions are usually possible, a preferable set is selected by certain criterions. When

Table 3. Kraitchman values of the atom coordinates for fluoromethyl and chloromethyl ethers in Å[a]

Atom[b]	x_a	x_b	x_c	x_a	x_b	x_c
	FCH_2OCH_3(X=F)			$ClCH_2OCH_3$(X=Cl)		
X	−1.3427(33)[c]	0.4847(43)[c]	d)	−1.3485(10)	0.2480(55)	−0.0402(339)
C^x	−0.5532(44)	−0.5804(42)	0.2965(85)	e)	−0.8498(27)	0.2905(80)
H^1	−0.4705(42)	−0.4854(37)	1.3924(15)	0.1663(108)	−0.8251(20)	1.3829(14)
H^s	−1.0682(20)	1.4955(15)	±0.0636(401)[f]	−0.2582(88)	−1.8280(13)	±0.0770(352)[f]
O	0.6636(18)	−0.5536(22)	−0.3156(40)	1.1989(10)	−0.4674(26)	−0.3668(34)
C^o	1.4950(15)	0.5185(44)	0.1176(195)	1.7853(15)	0.7249(38)	0.1359(205)
H^2	1.0311(23)	1.4900(17)	−0.1705(169)	1.0783(19)	1.5877(14)	±0.0777(306)[f]
H^3	1.6230(13)	0.4735(45)	1.2104(19)	1.9915(11)	0.6106(36)	1.2156(20)
H^c	2.4503(9)	0.4041(56)	−0.3684(62)	2.7118(12)	0.8726(38)	−0.3930(88)
	$FCH_2OCH_2CH_3$(X=F)			$ClCH_2OCH_2CH_3$(X=Cl)		
X	d)	d)	d)	−1.7842(17)	0.4133(77)	−0.0443(729)
C^x	−1.1684(28)	−0.5774(56)	0.2312(145)	−0.5928(97)	−0.9500(61)	0.1922(311)
H^1	1.2076(26)	−0.5714(50)	1.3308(25)	−0.6225(104)	−1.0956(56)	1.2817(54)
H^s	−1.7098(18)	−1.4257(23)	−0.1960(186)	−1.0339(46)	−1.8002(27)	−0.3327(165)
O	0.0635(259)	−0.6061(27)	−0.2408(72)	0.6310(52)	−0.6843(48)	−0.3052(112)
C^o	0.9736(30)	0.3494(84)	0.3763(80)	1.3701(34)	0.2929(158)	0.4336(108)
H^2	0.4618(64)	1.3726(22)	0.2364(145)	0.6439(94)	1.2789(48)	0.4300(151)
H^3	0.9765(30)	0.1515(169)	1.4609(21)	1.4597(36)	e)	1.4816(36)
C^c	2.3711(12)	0.1355(224)	−0.1671(181)	2.7498(18)	0.4018(124)	−0.1798(278)
H^4	2.7135(10)	−0.8686(33)	0.1508(361)	3.2662(23)	−0.5402(146)	0.1974(402)
H^5	2.3784(12)	0.2734(93)	−1.2509(23)	2.6732(28)	0.7117(105)	−1.2241(66)
H^m	3.0622(10)	0.8474(38)	0 2824(118)	3.3404(22)	1.1456(67)	0.3447(234)

a) Figures in parentheses indicate the 99% reliability intervals attached to the last significant figures. Underlined figures indicate unreliable Kraitchman values. b) Indentification symbol is shown in Fig. 1. c) Coordinate value can be determined by means of the first moment equation. d) Coordinate value can be determined by means of the first moment equation, but will be influenced by other coordinate values to be solved with other constraints. e) Kraitchman coordinate value is imaginary. f) Kraitchman coordinate value is so small that the sign of the value is also uncertain.

the moments of inertia are calculated from atom coordinate values containing the values solved by the set of the constraints and/or assumptions, a useful criterion is the root mean square deviation of the observed and calculated moments of inertia for all the species measured (referred to as RMS).

Chloromethyl Ethyl Ether (Gauche-Trans Isomer) [*Cl, Et*]. Owing to the lack of data for the ^{18}O species, three coordinate values of the oxygen atom had to be solved from the coordinate values of the other atoms as well as three unreliable *K*-values.[2] The *K*-values of the oxygen atom are regarded as reliable ones (Table 3). The coordinate values to be solved are then those of $x_b(H^3)$, $x_c(Cl)$, and $x_c(H^4)$. $x_b(H^3)$ can be solved with the aid of the first moment equation. The $x_c(H^4)$ value is obtained in two ways: 1) by assuming $\alpha(CCH^4)=\alpha(CCH^5)$, and 2) under the $I_{ac}=0$ constraint. In both cases, $x_c(Cl)$ is solved by means of the first moment equation. Since the hydrogen atom H^m corresponds to the in-plane hydrogen if the molecule has the plane of symmetry, 1) gives a symmetric methyl group (Table 4, Structure I), while 2) gives an asymmetric methyl group (Structure II).

The structure of the CCH_3 part of the molecule is obtained by the assumption that the $x_c(H^5)$ *K*-value is reliable. The reported structure[2] (Table 4) is close to Structure II for the CCH_3 part of the molecule. As regards the other part of the molecule, Structure II is better irrespective of the choice of assumptions for the CCH_3 part of the molecule, since the reported structure was obtained under several assumptions on the structure.

It is difficult to decide which of I and II is reliable. The constraint imposed on II ($I_{ac}=0$) is not applicable to the case of [F, Et]. Thus I having a symmetric methyl group is preferable to II for [Cl, Et].

Chloromethyl Methyl Ether (Gauche Isomer) [*Cl, Me*]. There are six unreliable *K*-values for [Cl, Me].[1] The *K*-values of the oxygen atom obtained from newly additional data for the ^{18}O species seem to be reliable. For the x_c coordinates, three unreliable *K*-values are situated at the same positions as those found for [F, Me] (Table 3). The constraints used for the case of [F, Me] may also be applicable to this molecule. Then three x_c coordinates, $x_c(Cl)$, $x_c(H^s)$, and $x_c(H^2)$ are solved by the first moment equation, the $I_{bc}=0$ constraint and the $\alpha(OCH^2)=\alpha(OCH^3)$ assumption, respectively. The solutions for the x_c coordinates thus obtained are independent of the uncertainties due to three unreliable x_a *K*-values since all the x_a and x_b values related to the $\alpha(OCH^2)=\alpha(OCH^3)$ assumption are reliable.

In order to obtain the three x_a coordinate values, the first moment equation for the x_a coordinates, $\sum(x_a)_i m_i=0$ and the $I_{ab}=0$ and $I_{ac}=0$ constraints might be useful besides the assumptions on the structure. However, use of the $I_{ac}=0$ constraint may produce large uncertainties since some of the x_c coordinate

TABLE 4. STRUCTURAL PARAMETERS OF CHLOROMETHYL ETHYL ETHER[a)]

	Structure I (Proposed)	Structure II	Reported
Coordinate values (Å) obtained under the set of constraints and assumptions			
$x_b(H^3)$	−0.1417(1138)	−0.1417	0
$x_c(C^1)$	−0.0677(157)	−0.0648	−0.0740
$x_c(H^4)$	−0.0999(538)	−0.2005	−0.1974
Inertia product (amu·Å²) for the normal species			
I_{ab}	0.6841	0.6841	0.6842
I_{ac}	−0.5124	0	−0.7339
I_{bc}	0.0675	−0.0293	0.0699
Difference of the observed and calculated moment of inertia for the normal species (amu·Å²)			
ΔI_a	0.0859	0.0678	0.0377
ΔI_b	0.9416	0.9244	0.8509
ΔI_c	1.0407	1.0419	0.6453
RMS(amu·Å²)	0.8085	0.8011	0.6172
Skeleton			
r(CCl) (Å)	1.829(11)	1.829	1.830
$r(OC^x)$ (Å)	1.347(16)	1.347	1.348
$r(OC^o)$ (Å)	1.431(14)	1.431	1.421
r(CCC) (Å)	1.514(13)	1.514	1.514
α(ClCO)	113° 5′(54′)	113° 7′	113°44′
α(COC)	114°24′(1°25′)	114°24′	114°58′
α(OCC)	108° 6′(58′)	108° 6′	108°10′
τ(ClCOC)	71°49′(2°35′)	71°44′	70°18′
τ(COCC)	175°41′(3°20′)	175°41′	176°50′
Cl–CH_2–O group			
$r(CH^1)$ (Å)	1.100(31)	1.100	1.100
$r(CH^s)$ (Å)	1.092(18)	1.092	1.092
$\alpha(ClCH^1)$	102°49′(1°29′)	102°43′	103°00′
$\alpha(ClCH^s)$	104°24′(1° 2′)	104°27′	104°18′
$\alpha(OCH^1)$	114°36′(2°10′)	114°36′	113°38′
$\alpha(OCH^s)$	110° 3′(1°23′)	110° 3′	110°21′
$\alpha(H^1CH^s)$	111°14′(2°36′)	111°14′	111°14′
O–CH_2–C group			
$r(CH^2)$ (Å)	1.225(15)	1.225	1.225
$r(CH^3)$ (Å)	1.138(45)	1.138	1.092
$\alpha(OCH^2)$	104°00′(1° 8′)	104°00′	104°40′
$\alpha(OCH^3)$	104°47′(3°10′)	104°47′	109°58′
$\alpha(CCH^2)$	118°46′(1°28′)	118°46′	118°46′
$\alpha(CCH^3)$	109°11′(3°26′)	109°11′	109°28′
$\alpha(H^2CH^3)$	110°54′(7°36′)	110°54′	105°31′
CH_3 group			
$r(CH^4)$ (Å)	1.077(17)	1.074	1.074
$r(CH^5)$ (Å)	1.092(28)	1.092	1.092
$r(CH^m)$ (Å)	1.085(20)	1.085	1.085
$\alpha(CCH^4)$	110° 7′(1°41′)	112°30′	112°26′
$\alpha(CCH^5)$	110° 7′(1°41′)	110° 7′	110° 7′
$\alpha(CCH^m)$	110°27′(1°19′)	110°27′	110°27′
$\alpha(H^4CH^m)$	107°37′(2°28′)	110°24′	110°19′
$\alpha(H^5CH^m)$	107°48′(2°47′)	107°48′	107°48′
$\alpha(H^4CH^5)$	110°39′(3°54′)	105°18′	105°28′

a) Figures in parentheses indicate 99% reliability intervals. For bond lengths, the figures are attached to the last significant figures.

values are already solved by the other constraints and assumptions.

For this molecule, all the unreliable x_a values are the coordinates in the $ClCH_2O$ part of the molecule. Since all the K-values of the $ClCH_2O$ part are reliable for [Cl, Et] except the x_c(Cl) value, the structural parameters of this part of [Cl, Et] are considered to be reliable except those related to the chlorine atom.

Since the structure of the $ClCH_2O$ part of [Cl, Me] does not seem to be much affected by the substitution of OCH_3 with OCH_2CH_3, the structural parameters can be transferred between these two molecules.

Though four bond lengths and six angles belong to the $ClCH_2O$ part, seven parameters related to the Cl and H^s atoms cannot be used in order to evaluate the x_a values irrespective of the evaluation of the x_c values. The structural parameters of the skeleton are more important than the other parameters for our purpose so that the transfer of the $r(C^xO)$ value is not preferable. $r(CH^1)$ and $\alpha(OCH^1)$ are thus are the best parameters for the transfer.

Usually, the K-values for hydrogen atoms are regarded as unreliable for values less than 0.3 Å. However, they sometimes give reasonable structural parameters even when the values are less than 0.3 Å. Thus it is better to calculate structural parameters by using the unreliable K-values. If the structural parameters thus calculated are reasonable, the K-values used will be considered to be reliable.

Taking the above discussion into consideration, we tested ten possible sets of constraints and/or assumptions. 1) Use of the first moment equation and the $I_{ab}=0$ constraint requires one additional assumption on the coordinate value or structural parameter, there being four choices of assumption: i) the $x_a(H^s)$ K-value is reliable, ii) the $x_a(H^1)$ K-value is reliable, iii) the $r(CH^1)$ value is transferred, and iv) $\alpha(OCH^1)$ is transferred from that of [Cl, Et]. However, the results obtained from these four sets can be rejected since i) gives a too large $x_a(H^1)$ value and ii), iii), and iv) very small $\alpha(ClCH^s)$ values. Thus use of the $I_{ab}=0$ constraint is regarded to be inadequate. 2) Use of the first moment equation and two transferred structural parameter values, $r(CH^1)$ and $\alpha(OCH^1)$ also give a too large $x_a(H^s)$ value. 3) Use of the first moment equation and the $x_a(H^1)$ K-value assumed to be reliable requires one transferred parameter, either $r(CH^1)$ or $\alpha(OCH^1)$. These sets, however, give too small values of $\alpha(OCH^s)$ or $\alpha(ClCH^s)$ and can be rejected. 4) Use of the first moment equation, the $x_a(H^s)$ K-value assumed to be reliable requires one transferred parameter, either $r(CH^1)$ or $\alpha(OCH^1)$, (Table 5, Structures I and II). 5) The $x_a(H^1)$ values solved by the two sets of 4) are very close to the K-value. If we regard the K-values of $x_a(H^1)$ and $x_a(H^s)$ as reliable, the structural parameters obtained are close to those of Structures I and II. This set of structural parameters (Structure III) is obtained without transfer of the parameter values from the other molecules. Therefore, this is considered to be the most reliable set of parameters for [Cl, Me]. The structure reported[1)] is also given in Table 5 for the sake of comparison.

Table 5. Structural parameters of chloromethyl methyl ether[a)]

	Structure I	Structure II	Reported	Structure III (Proposed)
Coordinate values (Å) obtained under the set of constraints and assumptions				
$x_a(C^x)$	0.0665	0.0700	0.0560	0.0684(37)
$x_a(H^1)$	0.1886	0.1478	0.1780	0.1663(108)
$x_a(H^s)$	−0.2582	−0.2582	−0.2941	−0.2582(88)
$x_c(Cl)$	−0.0392	−0.0392	−0.0402	−0.0392(78)
$x_c(H^s)$	−0.0830	−0.0830	−0.0466	−0.0830(294)
$x_c(H^2)$	−0.0173	−0.0173	−0.0471	−0.0173(371)
Inertia product (amu·Å²) for the normal species				
I_{ab}	0.1501	0.1511	0.1931	0.1506
I_{ac}	0.4104	0.4554	0.4831	0.4350
I_{bc}	0	0	0.0937	0
Difference of the observed and calculated moment of inertia for the normal species (amu·Å²)				
ΔI_a	0.1349	0.1352	0.0440	0.1351
ΔI_b	0.5766	0.5849	0.1798	0.5816
ΔI_c	0.7173	0.7252	0.1855	0.7220
RMS (amu·Å²)	0.5391	0.5484	0.1508	0.5446
Skeleton				
$r(CCl)$ (Å)	1.821	1.824	1.813	1.822(5)
$r(OC^x)$ (Å)	1.364	1.361	1.379	1.362(5)
$r(OC^o)$ (Å)	1.421	1.421	1.422	1.421(8)
$\alpha(ClCO)$	112°52′	112°52′	113°22′	112°52′(21′)
$\alpha(COC)$	114° 2′	114° 2′	113°37′	114° 2′(35′)
$\tau(ClCOC)$	70°35′	70°40′	69°40′	70°37′(1°33′)
$-CH_2-$ group				
$r(CH^1)$ (Å)	1.100	1.096	1.100	1.097(8)
$r(CH^s)$ (Å)	1.096	1.097	1.092	1.097(11)
$\alpha(ClCH^1)$	104°38′	102°49′	104°41′	103°39′(44′)
$\alpha(ClCH^s)$	104°14′	104° 2′	103°45′	104° 7′(39′)
$\alpha(OCH^1)$	112°20′	114°36′	111°55′	113°34′(45′)
$\alpha(OCH^s)$	109°23′	109°31′	111°24′	109°27′(53′)
$\alpha(H^1CH^s)$	113° 2′	112°22′	111°14′	112°41′(2°24′)
CH_3 group				
$r(CH^2)$ (Å)	1.126	1.126	1.130	1.126(7)
$r(CH^3)$ (Å)	1.105	1.105	1.105	1.105(20)
$r(CH^c)$ (Å)	1.077	1.077	1.077	1.077(11)
$\alpha(OCH^2)$	109°37′	109°37′	109°30′	109°37′(46′)
$\alpha(OCH^3)$	109°37′	109°37′	109°24′	109°37′(1° 5′)
$\alpha(OCH^c)$	107°14′	107°14′	106°54′	107°14′(44′)
$\alpha(H^2CH^c)$	111°36′	111°36′	110°43′	111°36′(1° 4′)
$\alpha(H^3CH^c)$	109°28′	109°28′	109°28′	109°28′(1°32′)
$\alpha(H^2CH^3)$	109°13′	109°13′	110°43′	109°13′(2°32′)

a) See footnote to Table 4.

Fluoromethyl Methyl Ether (Gauche Isomer) [F, Me]. Of the five molecules mentioned, [F, Me] is the most favorable for the determination of its r_s structure. There are only two unreliable K-value, $x_c(H^s)$ and $x_c(H^2)$, (Table 3). For the $x_c(H^s)$ coordinate, the K-value is so small that the sign of the coordinate value is also uncertain. Three coordinate values of the fluorine atom have to be solved by means of the first moment equations.

The $x_c(H^s)$ value is found to be very sensitive to the I_{bc} inertia product but not to the I_{ac} product. On the other hand, the effect of the $x_c(H^2)$ value on the I_{bc} and I_{ac} values is reverse to that of the $x_c(H^s)$ value. In order to find the adequacy of the use of the I_{bc} and $I_{ac}=0$ constraints, the following calculations were carried out. 1) The $x_c(H^s)$ value is evaluated by $I_{bc}=0$ on the assumption that the $x_c(H^2)$ K-value is reliable (Table 6, Structure I). 2) The $x_c(H^2)$ value is evaluated by $I_{ac}=0$ with the sign of the $x_c(H^s)$ K-value taken as a) plus, (Structure II) and b) minus. Since the latter gives a very large $\alpha(H^1CH^s)$ value, a great increase of the absolute I_{bc} value and a large RMS, the structure obtained by this assumption can be rejected.

Parameter differences between Structures I and II are found mainly in the OCH_3 group. For the former, both the $\alpha(OCH^3)$ and $\alpha(OCH^2)$ values are larger than the $\alpha(OCH^c)$ value and are close to each other, while three $\alpha(HCH)$ values are close to each other. The CH^c bond is much shorter than the other two CH bonds which can be regarded to be equal if the experimental error is taken into account. Since the H^c hydrogen atom corresponds to the hydrogen atom in the molecular plane if the molecule has the plane of symmetry, the relations on the structure indicate that the symmetric methyl group tilts towards the direction of the lone pair electrons on the oxygen atom. Thus, Structure I is essentially equal to the structure obtained on the assumption $\alpha(OCH^2)=\alpha(OCH^3)$ and the $I_{bc}=0$ constraint whose parameters are listed in Table 6 as III.

On the other hand, Structure II gives an asymmetric methyl group. It is difficult to judge which structure is more reliable. The sets of constraints applied to Structures I and II cannot be used for the case of [Cl, Me]. Structure III is thus considered to be better than the other structures when a comparison of structures is made between these molecules.

Fluoromethyl Ethyl Ether (Gauche-Trans Isomer) [F, Et]. The GT isomer of [F, Et] is the most unfavorable molecule of the four halomethyl ethers for the determination of the r_s structure. There are seven unreliable K-values and three coordinate values of the fluorine atom should be solved by means of the first moment equations.

First, the reliability of the unreliable K-values was tested in order to reduce the number of coordinate values to be evaluated. For the CCH_3 part of the molecule, the unreliable K-values are $x_b(H^5)$, $x_c(H^4)$, and $x_c(H^m)$. Since the calculations indicate that the structural parameters containing $x_b(H^5)$ and $x_c(H^m)$ give quite reasonable values as compared with the corresponding parameter values of [Cl, Et], the K-values of $x_b(H^5)$ and $x_c(H^m)$ can be regarded as reliable. On the other hand, the calculated parameter values related to $x_c(H^4)$ give a very small $r(CH^4)$ and a very large $\alpha(CCH^4)$. The $x_c(H^4)$ K-value should thus be evaluated by some other means.

A similar test indicates that the $x_a(O)$ K-value is doubtful, while the $x_c(H^s)$ K-value is quite reliable though the absolute value is small.

As regards the two K-values of $x_c(H^2)$ and $x_b(H^3)$, the test gives no conclusive result and they should be evaluated by other means.

TABLE 6. STRUCTURL PARAMETERS OF FLUOROMETHYL METHYL ETHER[a)]

	Structure I	Structure II	Structure III (Proposed)
Coordinate values (Å) obtained under the set of constraints and assumptions			
$x_c(F)$	−0.1048	−0.1140	−0.1059(142)
$x_c(H^s)$	−0.0091	0.0492	−0.0026(304)
$x_c(H^2)$	−0.1705	−0.0557	−0.1578(425)
Inertia product (amu·Å²) for the normal species			
I_{ab}	−0.0768	−0.0768	−0.0768
I_{ac}	0.2908	0	0.2585
I_{bc}	0	0	0
Difference of the observed and calculated moment of inertia for the normal species (amu·Å²)			
ΔI_a	0.1840	0.1685	0.1840
ΔI_b	0.6224	0.6081	0.6226
ΔI_c	0.7849	0.7861	0.7852
RMS(amu·Å²)	0.5884	0.5843	0.5890
Skeleton			
r(CF) (Å)	1.385	1.388	1.385(7)
$r(OC^x)$ (Å)	1.362	1.362	1.362(6)
$r(OC^o)$ (Å)	1.424	1.424	1.424(7)
α(FCO)	111°19′	111° 6′	111°18′(33′)
α(COC)	113°33′	113°33′	113°33′(36′)
τ(FCOC)	69°11′	69°29′	69°13′(1°38′)
$-CH_2-$ group			
$r(CH^1)$ (Å)	1.103	1.103	1.103(9)
$r(CH^s)$ (Å)	1.094	1.079	1.092(10)
$\alpha(FCH^1)$	105°19′	105°41′	105°21′(1° 2′)
$\alpha(FCH^s)$	107° 6′	108° 9′	107°13′(43′)
$\alpha(OCH^1)$	112°11′	112°11′	112°11′(40′)
$\alpha(OCH^s)$	108° 9′	109°53′	108°20′(43′)
$\alpha(H^1CH^s)$	112°38′	109°40′	112°18′(2°19′)
CH_3 group			
$r(CH^2)$ (Å)	1.115	1.090	1.111(12)
$r(CH^3)$ (Å)	1.101	1.101	1.101(19)
$r(CH^c)$ (Å)	1.078	1.078	1.078(9)
$\alpha(OCH^2)$	109°32′	111°57′	109°48′(47′)
$\alpha(OCH^3)$	109°48′	109°48′	109°48′(1° 3′)
$\alpha(OCH^c)$	107°28′	107°28′	107°28′(39′)
$\alpha(H^2CH^c)$	110°10′	113°34′	110°33′(1° 5′)
$\alpha(H^3CH^c)$	109°52′	109°52′	109°52′(1°23′)
$\alpha(H^2CH^3)$	109°54′	104° 5°	109°16′(3°11′)

a) See footnote to Table 4.

The original set of K-values gave the RMS value of 3.4283 amu·Å² and the large inertia products (I_{ab}, I_{ac}, I_{bc})=(−0.6012, 0.4859, −0.2993) amu·Å² (Table 7).

Since the $x_c(H^4)$ K-value was also unreliable for [Cl, Et], it was obtained on the assumption $\alpha(CCH^4)=\alpha(CCH^5)$. The same assumption is also applied to $x_c(H^4)$ of the present molecule. The RMS and I_{bc} values are reduced to 3.4056 and 0.0179 amu·Å², respectively, the structural parameters of the CCH_3 part becoming reasonably closer to those of [Cl, Et]. The $x_c(H^4)$ value thus obtained is used in all the trial calculations.

In order to evaluate the most unreliable three coordinate values, $x_a(O)$, $x_b(H^3)$, and $x_c(H^2)$, the set of the $I_{ab}=0$, $I_{ac}=0$, and $I_{bc}=0$ constraints and the three first moment equations might be applied on the assumption that the other four unreliable K-values are regarded as reliable. However, simultaneous use of the zero inertia product constraints seems dangerous for the present molecule where many unreliable K-values exist in all the x_a, x_b, and x_c coordinates.

The $x_a(O)$ value is evaluated by i) $I_{ab}=0$ or ii) $I_{ac}=0$ constraint on the assumption that the K-values of $x_b(H^s)$ and $x_c(H^2)$ and the other unreliable K-values are regarded as reliable. The $x_a(O)$ value obtained from ii) is too large, that from i) being reasonable. The RMS value for the structure from i) is 1.8570 amu·Å².

Since the $I_{bc}=0$ constraint was successfully used for the $x_c(H^s)$ value of [F, Me], it is applied to one of the $x_c(H^2)$ and $x_b(H^3)$ values. The parameters related to the oxygen atom for these two cases are essentially equal to those obtained from i) but the RMS values are reduced slightly. The parameters (Structure I, Table 7) are obtained for the case where the $x_c(H^2)$ value is obtained from the $I_{bc}=0$ constraint. For Structure I, the RMS and I_{ac} values are fairly large. We see that the RMS and I_{ac} values strongly depend on the $x_a(O)$ and $x_a(F)$ values which are related with each other by means of the first moment equation.

The $x_a(O)$ value can be solved on the assumptions that the $x_b(H^3)$ and $x_c(H^2)$ values of Structure I as reliable and one of the skeletal parameter values related to the oxygen atom for analogous molecules can be transferred to that of [F, Et]. First, the α(OCC) value of [Cl, Et] is transferred. The parameter values obtained are listed under Structure II. The RMS, I_{ab} and I_{ac} values of Structure II are fairly large. Though the structure is also obtained by use of the transferred $r(C^oO)$ value of [Cl, Et], the parameter values obtained are found to be very close to those of Structure II. The $r(C^oO)$ value of [Cl, Et] is inadequate to be transferred since the influence of the substitution of the chlorine atom with the fluorine atom seems to be too serious.

The plausible structures of [Cl, Me] and [Cl, Et] indicate that the α(COC) values of these two molecules are relatively close to each other (Table 8). On the assumption that the situation is the same for [F, Me] and [F, Et], the α(COC) value of [F,Me] is transferred (Structure III, Table 7). Though the RMS value of Structure III is satisfactorily small, the I_{ab} and I_{ac} values are fairly large. Furthermore, the skeletal parameter values of Structure III do not always seem to be reasonable, when a comparison is made between the plausible structures of fluoromethyl and chloromethyl ethers. For example, the difference between $r(C^xO)$ and $r(C^oO)$ for [Cl, Et] is larger than that for [Cl, Me], while the difference for [F, Et] is smaller than that for [F, Me].

Since the (COC) value of [Cl, Et] is slightly larger (22′) than that of [Cl, Me], the α(COC) value of [F, Et] is assumed to be larger by 22′ than that of [F, Me]. By this slight change in the α(COC) value, the RMS, I_{ab} and I_{ac} values are much reduced and the difference of two CO bond lengths becomes close to that of Structure II. From the above discussion, it is

Table 7. Structural parameters of fluoromethyl ethyl ether[a)]

	Original[b)]	Structure I (Proposed)	Structure II	Structure III (Reported)
Coordinate values (Å) obtained under the set of constraints and assumptions				
x_a(O)	0.0635	0.0952	0.1057	0.1216
x_b(H^3)	0.1515	0.1515(169)	0.1515	0.1515
x_c(H^2)	0.2364	0.2588(145)	0.2588	0.2588
x_a(F)	−1.7822	−1.8088	−1.8177	−1.8311
x_b(F)	0.5804	0.5804(157)	0.5804	0.5804
x_c(F)	−0.1663	−0.1790(169)	−0.1790	−0.1790
Inertia product (amu·Å^2) for the normal species				
I_{ab}	−0.6012	0	0.1996	0.5026
I_{ac}	0.4859	−0.5175	−0.5071	−0.4913
I_{bc}	−0.2993	0	0	0
Difference of the observed and calculated moment of inertia for the normal l species (amu·Å^2)				
ΔI_a	0.1300	0.0518	0.0520	0.0532
ΔI_b	4.1963	2.2158	1.5718	0.5804
ΔI_c	4.2044	2.3105	1.6668	0.6768
RMS (amu·Å^2)	3.4283	1.8484	1.3233	0.5164
Skeleton				
r(CF) (Å)	1.369	1.385	1.389	1.396
r(C^xO) (Å)	1.319	1.349	1.359	1.374
r(C^oO) (Å)	1.456	1.437	1.431	1.421
r(CC) (Å)	1.515	1.515(8)	1.515	1.515
α(FCO)	109°27′	110°19′	110°41′	111°14′
α(COC)	114°40′	114° 4′	113°52′	113°33′ [c)]
α(OCC)	109°22′	108°25′	108° 6′ [c)]	107°36′
τ(FCOC)	70°10′	70°22′	70°16′	70° 8′
τ(COCC)	175°15′	175°41′	175°49′	176° 1′
F–CH_2– group				
r(CH^1) (Å)	1.100	1.100(15)	1.100	1.100
r(CH^s) (Å)	1.093	1.093(10)	1.093	1.093
α(FCH^1)	105°38′	105°57′	105°53′	105°47′
α(FCH^s)	108°42′	107°41′	107°26′	107° 4′
α(OCH^1)	113° 3′	112°31′	112°22′	112° 8′
α(OCH^s)	107°48′	108° 5′	108°11′	108°20′
α(H^1CH^s)	112° 8′	112° 8′(1°50′)	112° 8′	112° 8′
O–CH_2– group				
r(CH^2) (Å)	1.153	1.150(9)	1.150	1.150
r(CH^3) (Å)	1.102	1.102(9)	1.102	1.102
α(OCH^2)	104°40′	106° 0′	106°16′	106°40′
α(OCH^3)	107°30′	107°44′	107°49′	107°56′
α(CCH^2)	119°26′	119°58′(1°23′)	119°58′	119°58′
α(CCH^3)	108°58′	108°58′(1°15′)	108°58′	108°58′
α(H^2CH^3)	106°15′	105° 8′(1°27′)	105° 8′	105° 8′

CH_3 group Structural parameters are common to Structures I—III

	r(CH^4) (Å)	r(CH^5) (Å)	r(CH^m)	α(CCH^4)	α(CCH^5)
Original	1.061	1.093	1.089	115°12′	110° 8′
Others	1.086(23)	1.093(18)	1.089(17)	110° 8′(1°22′)	110° 8′(1° 5′)
	α(CCH^m)	α(H^4CH^m)	α(H^5CH^m)	α(H^4CH^5)	τ(OCCH^m)
Original	110°11′	114° 2′	108°49′	97°36′	180°17′
Others	110°11′(57′)	108°23′(1°51′)	108°49′(1°46′)	109° 7′(3°48′)	179°55′

a) See footnote to Table 4. b) The structure obtained from the original Kraitchman coordinate values and the three first moment equations. c) Assumed. See text.

found that assurance is necessary for the transferability of the skeletal parameter value in order to transfer the parameter values.

In spite of the large RMS and I_{ac} values, Structure I is considered to be plausible for the structure of [F, Et], since this structure is obtained with no assumption on the skeletal structure. It may be favorable for Structure I that the parameter values obtained are reasonable when a comparison of their values is made with those of the other three halomethyl ethers (Table 8).

TABLE 8. PLAUSIBLE STRUCTURAL PARAMETERS OF HALOMETHYL ETHERS[a)]

	FCH_2OCH_3	$FCH_2OCH_2CH_3$	$ClCH_2OCH_3$	$ClCH_2OCH_2CH_3$	$HC{\equiv}CCH_2OCH_3$
Skeleton (X=F, Cl, HC≡C)					
r(CX) (Å)	1.385(7)	1.385	1.822(5)	1.829(11)	1.459
$r(C^xO)$ (Å)	1.362(6)	1.349	1.362(5)	1.347(16)	1.410
$r(C^oO)$ (Å)	1.424(7)	1.437	1.421(8)	1.431(14)	1.410(17)
r(CC) (Å)		1.515		1.514(13)	
α(XCO)	111°18′(33′)	110°19′	112°52′(21′)	113° 5′(54′)	112°29′
α(COC)	113°33′(36′)	114° 4′	114° 2′(35′)	114°24′(1°25′)	113°30′
α(OCC)		108°25′		108° 6′(58′)	
τ(XCOC)	69°13′(1°38′)	70°22′	70′37′(1°33′)	71°49′(2°35′)	67°30′
τ(COCC)		175°41′		175°41′(3°20′)	
XCH_2 group (X=F, Cl, HC≡C)					
$r(CH^1)$ (Å)	1.103(9)	1.100(15)	1.097(8)	1.100(31)	1.101
$r(CH^s)$ (Å)	1.092(10)	1.093(10)	1.097(11)	1.092(18)	1.101
$\alpha(XCH^1)$	105°21′(1° 2′)	105°57′	103°39′(44′)	102°49′(1°29′)	108°44′
$\alpha(XCH^s)$	107°13′(43′)	107°41′	104° 7°(39′)	104°24′(1° 2′)	108°44′
$\alpha(OCH^1)$	112°11′(40′)	112°31′	113°34′(45′)	114°36′(2°10′)	109°49′
$\alpha(OCH^s)$	108°20′(43′)	108° 5′	109°27′(53′)	110° 3′(1°23′)	109°49′
$\alpha(H^1CH^s)$	112°18′(2°19′)	112° 8′(1°50′)	112°41′(2°24′)	111°14′(2°36′)	107°13′
OCH_2Y group (Y=H, C)					
$r(CH^2)$ (Å)	1.111(12)	1.150(9)	1.126(7)	1.225(15)	1.170(9)
$r(CH^3)$ (Å)	1.101(19)	1.102(9)	1.105(20)	1.138(45)	1.110(34)
$\alpha(OCH^2)$	109°48′(47′)	106° 0′	109°37′(46′)	104° 0′(1° 8′)	109°51′(1°31′)
$\alpha(OCH^3)$	109°48′(1° 3′)	107°44′	109°37′(1° 5′)	104°47′(3°10′)	109°51′(2° 2′)
$\alpha(YCH^2)$	110°33′(1° 5′)	119°58′(1°22′)	111°36′(1° 4′)	118°46′(1°28′)	113° 1′(1°48′)
$\alpha(YCH^3)$	109°52′(1°23′)	108°58′(1°15′)	109°28′(1°32′)	109°11′(3°26′)	108°52′(2°42′)
$\alpha(H^2CH^3)$	109°16′(3°11′)	105° 8′(1°27′)	109°13′(2°32′)	110°54′(7°36′)	107°50′(3°18′)
$r(CH^c)$ (Å)	1.078(9)		1.077(11)		1.078(19)
$\alpha(OCH^c)$	107°28′(39′)		107°14′(44′)		107°23′(1°28′)
$\tau(COCH^c)$	175°48′(1°47′)		174°39′(2°24′)		180.0(assumed)
CCH_3 group					
$r(CH^4)$ (Å)		1.086(23)		1.077(17)	
$r(CH^5)$ (Å)		1.093(18)		1.092(28)	
$r(CH^m)$ (Å)		1.089(17)		1.085(20)	
$\alpha(CCH^4)$		110° 8′(1°22′)		110° 7′(1°41′)	
$\alpha(CCH^5)$		110° 8′(1° 5′)		110° 7′(1°40′)	
$\alpha(CCH^m)$		110°11′(57′)		110°27′(1°19′)	
$\alpha(H^4CH^m)$		108°23′(1°51′)		107°37′(2°28′)	
$\alpha(H^5CH^m)$		108°49′(1°46′)		107°48′(2°47′)	
$\alpha(H^4CH^5)$		109° 7′(3°48′)		110°39′(3°54′)	
$\tau(OCCH^m)$		179°49′(2°55′)		180°47′(3°52′)	
RMS(amu·Å²)	0.5890	1.8484	0.5446	0.8085	0.7000

a) See footnote to Table 4.

Structure III was proposed as the plausible structure because of the smallest RMS value.[3)] However, its parameter values cannot be regarded to be adequate from a comparison of their values with those of the other three halomethyl ethers.

The large values of RMS and I_{ac} for Structure I can be understood when the experimental errors of the x_b and x_c coordinate values of the C^c carbon atom are taken into account. Experimental errors of the x_b and x_c K-values of the C^c atom are fairly large, while its absolute x_a value is large (Table 3). The experimental errors of x_b and x_c values induce large uncertainties on the x_a values of the oxygen and fluorine atoms through the inertia product constraint ($I_{ab}=0$) and the first moment equation. Actually, when $x_b(C^c)$ and $x_c(C^c)$ values are shifted by about one-fifth of the experimental errors of the K-values (+0.005 and +0.003 Å, respectively), the RMS and I_{ac} values of the structure obtained by the same procedure as Structure I are reduced to 1.2360 and −0.1160 amu·Å², while the parameters obtained are not much shifted.

The uncertainties for the "A" rotational constants of the normal and $FCH_2OCH_2{}^{13}CH_3$ species are as small as those of the other species. However, the uncertainties on the "A" rotational constants are amplified in the uncertainties on the x_b and x_c values due to the fact that the difference of the moments of inertia ΔI_a between the normal and ^{13}C species is accidentally very small (0.0444 amu·Å²). Thus, we cannot reduce the experimental errors in the x_b and x_c

K-values though it is inevitable in order to reduce the RMS and I_{ac} values of Structure I.

Methyl 2-Propynyl Ether (Gauche Isomer) [Pr, Me]. A report has been given on the microwave spectra of the gauche isomer of [Pr, Me].[5] For this molecule, the r_s structure cannot be obtained without serious assumptions on the structure since many coordinates having small absolute values exist in the $HC{\equiv}CCH_2$– part of the molecule. However, only one unreliable *K*-value exists for OCH_3 part of the molecule. This coordinate is $x_c(H^2)$. When the assumption $\alpha(OCH^2)=\alpha(OCH^3)$ is applied to this value as in the case of the halomethyl ethers, the r_s structure of the OCH_3 part can be obtained irrespective of the uncertainties of the other part of the molecule, for which the parameters are adjusted so as to reproduce the observed moments of inertia. The results are given in Table 8.

Summary of the Applied Constraints and/or Assumptions. So far we have re-evaluated the r_s structures of halomethyl ethers and the OCH_3 part of methyl 2-propynyl ether considering several sets of constraints and/or assumptions.

The sets used for the proposed structures of these molecules are given in the following, the coordinate values obtained by each constraint being shown in square brackets:

[F, Me]

The three first moment equations, $[x_a(F), x_b(F), x_c(F)]$; $\alpha(OCH^2)=\alpha(OCH^3)$, $[x_c(H^2)]$; $I_{bc}=0$, $[x_c(H^s)]$.

[Cl, Me]

The two first moment equations, $\sum mx_a=0$ and $\sum mx_c=0$, $[x_a(C^x), x_c(Cl)]$; $\alpha(OCH^2)=\alpha(OCH^3)$, $[x_c(H^2)]$; $I_{bc}=0$, $[x_c(H^s)]$; The assumption that the $x_a(H^1)$ and $x_a(H^s)$ *K*-values are reliable.

[F, Et]

The first moment equations, $[x_a(F), x_b(F), x_c(F)]$; $\alpha(CCH^4)=\alpha(CCH^5)$, $[x_c(H^4)]$; $I_{ab}=0$, $[x_a(O)]$; $I_{bc}=0$, $[x_c(H^2)]$; The assumption that the $x_b(H^3)$, $x_c(H^5)$, $x_b(H^5)$, and $x_c(H^m)$ *K*-values are reliable.

[Cl, Et]

The two first moment equations, $\sum mx_b=0$ and $\sum mx_c=0$, $[x_b(H^3), x_c(Cl)]$; $\alpha(CCH^4)=\alpha(CCH^5)$, $[x_c(H^4)]$.

[Pr, Me], OCH_3 group

$\alpha(OCH^2)=\alpha(OCH^3)$, $[x_c(H^2)]$

The above sets indicate that the plausible r_s structures of these molecules can be obtained by use of the common constraints and/or assumptions on these five molecules. As is the case of [F, Et], even when many unreliable *K*-values are contained in the atom coordinates of a molecule to which usually no reliable r_s structure can be obtained, the proposed structure seems to be fairly reliable.

Discussion on Molecular Structures

The structures of four halomethyl ethers and [Pr, Me] have different reliabilities. However, their parameters (Table 8) exhibit interesting features when comparison is made with each other or with those of the other series of molecules.

Hereafter, for the quoted parameter values, figures in parentheses indicate the experimental uncertainties, while figures with $\pm$ such as 1.391 ± 0.002 Å indicate the dispersion of the value, *viz.*, the value between 1.393 and 1.389 Å. The value referred to as that for alkyl ethers is the value taken from those for *trans*-ethyl methyl ether,[7] dimethyl ether,[8] TT-diethyl ether,[9] and TT-methyl propyl ether,[10] where TT indicates the trans-trans isomer.

Skeleton. 1) The r(CF) value of FCH_2OR(R= CH_3, CH_2CH_3) is close to that of methyl fluoride (1.384(1) Å)[11] but smaller than that of ethyl fluoride (1.398(5) Å).[12] On the other hand, the r(CCl) value of $ClCH_2OR$ is larger than those of methyl chloride (1.781(1) Å)[13] and ethyl chloride (1.788(2) Å).[14] 2) The averages of the two r(CO) values are nearly constant for all halomethyl ethers (1.391 ± 0.002 Å) and smaller than those of alkyl ethers (1.410 ± 0.002 Å). The value for [Pr, Me] is close to those of alkyl ethers. 3) r(CO) attached to the halogen atom is much smaller than the other r(CO) which is slightly larger than that of alkyl ethers. The difference between two r(CO) values (0.073 ± 0.015 Å) is much larger than that found in alkyl ethers such as *trans*-ethyl methyl ether (0.011 Å), the difference for $XCH_2OCH_2CH_3$ being larger than that for XCH_2OCH_3. For [Pr, Me], two r(CO) values may be nearly equal to each other. 4) r(CC) of $XCH_2OCH_2CH_3$ is smaller than that of propane,[15] *trans*-ethyl methyl ether and ethyl chloride, is nearly equal to that of diethyl ether, being larger than that of ethyl fluoride though the experimental uncertainty is fairly large. 5) α(COC) of halomethyl ethers is nearly equal to each other ($114°\pm28'$) and smaller than that of alkyl ethers by about 2°. α(COC) of [Pr, Me] is smaller than that of alkyl ethers. 6) α(FCO) of FCH_2OR is smaller by *ca.* 1.5° than α(ClCO) of $ClCH_2OR$. 7) α(OCC) of $XCH_2OCH_2CH_3$ is nearly equal to that of alkyl ethers. 8) Skeletal dihedral angle τ(XCOC) increases in the order [F, Me], [F, Et], [Cl, Me], and [Cl, Et], the values being much larger (about 10°) than 60° which is presumed usual for the dihedral angle value of the gauche configuration of the molecules. For [Pr, Me], this angle is smaller by *ca.* 2° than that of halomethyl ethers. 9) Skeletal dihedral angle τ(COCC) of $XCH_2OCH_2CH_3$ is not 180° which is presumed for the value of the trans configuration, being smaller by *ca.* 4° than 180°. Since the difference from 180° is beyond the experimental error, the methyl group is situated not on the C–O–C plane but on the same side of the C–O–C plane where the halogen atom is found.

XCH_2O Group. 1) $r(CH^1)$ (1.100 ± 0.003 Å) related to the out-of-plane hydrogen H^1 might be larger than the $r(CCH^s)$ on the C–O–C plane (1.094 ± 0.003 Å). 2) The average of two α(XCH) values is much smaller than the tetrahedral angle, the average for $ClCH_2OR$ ($103°45'\pm9'$) being smaller than that of FCH_2OR ($106°33'\pm16'$). α(XCH) related to the in-plane hydrogen H^s is larger than that related to the out-of-plane hydrogen H^1. On the other hand, the α(OCH) value related to the out-of plane hydrogen H^1 is much larger than the tetrahedral angle.

OCH_2Y Group. 1) r(CH), which is nearly

parallel to the CX bond, is much larger than the usual r(CH) value except for that of [F, Me] where all the CH bonds have the usual r(CH) value. On the other hand, the other r(CH) has the usual r(CH) value within experimental error. 2) $\alpha(CCH^2)$ of $XCH_2OCH_2CH_3$ ($119°22' \pm 36'$) is much larger than the tetrahedral angle, while the corresponding angle $\alpha(H^cCH^2)$ of XCH_2OCH_3 is somewhat larger than the tetrahedral angle. 3) The dihedral angle $\tau(COCH^c)$ of XCH_2OCH_3 is smaller by about 4° than 180° as in the case of the τ(COCC) value of $XCH_2OCH_2CH_3$.

Halomethyl ethers exhibit specific chemical properties. For example, the reaction velocity of these molecules on hydrolysis strongly depends on the polarity of the solvent. They are known as material having carcinogenic activity.

Since the molecular structure attained by the isotopic substitution method sometimes shows fairly large vibrational effects, we cannot conclude that irregular or unusual structural parameter values for a molecule are directly related to its chemical properties. However, as regards halomethyl ethers, specific features of the structural parameters are found for a group of molecules considered to have different vibrational effects. These specific features seem to afford some evidence of the chemical properties of halomethyl ethers.

References

1) M. Hayashi and H. Kato, *J. Mol. Spectrosc.*, **76**, 412 (1979); M. Hayashi, K. Kuwada, and H. Imaishi, *Chem. Lett.*, **1974**, 913.
2) M. Hayashi and H. Kato, *J. Mol. Struct.*, **53**, 179 (1979).
3) M. Hayashi, H. Kato, and M. Oyamada, *J. Mol. Spectrosc.*, in press.
4) J. Nakagawa, H. Kato, and M. Hayashi, *J. Mol. Spectrosc.*, in press; J. Nakagawa and M. Hayashi, *Chem. Lett.*, **1976**, 349.
5) M. Hayashi, J. Nakagawa, and H. Kato, *J. Mol. Spectrosc.* in press.
6) C. B. Sawyer, *J. Org. Chem.*, **37**, 4225 (1972).
7) M. Hayashi and K. Kuwada, *J. Mol. Struct.*, **28**, 147 (1975).
8) U. Blukis, P. H. Kasai, and R. J. Myers, *J. Chem. Phys.*, **38**, 2753 (1963).
9) M. Hayashi and K. Kuwada, *Bull. Chem. Soc. Jpn.*, **47**, 3006 (1974).
10) H. Kato, J. Nakagawa, and M. Hayashi, *J. Mol. Spectrosc.*, **80**, 272 (1980).
11) C. C. Costain, *J. Chem. Phys.*, **29**, 864 (1958).
12) L. Nygaard, *Spectrochim. Acta*, **22**, 1261 (1966).
13) R. H. Schwendeman and J. D. Kelley, *J. Chem. Phys.*, **42**, 1132 (1965).
14) R. H. Schwendeman and G. D. Jacobs, *J. Chem. Phys.*, **36**, 1245 (1962).
15) D. R. Lide, Jr., *J. Chem. Phys.*, **33**, 1514 (1961).

Selective *cis*-Isomerization of 1-Pentene Catalyzed by Ni(I)-Triphenylphosphine Complexes

Hiroyoshi KANAI,* Kenji KUSHI, Kei SAKANOUE, and Nobuji KISHIMOTO

Department of Hydrocarbon Chemistry, Faculty of Engineering, Kyoto University, Yoshida, Sakyo-ku, Kyoto 606

(Received February 16, 1980)

Selective *cis*-isomerization of 1-pentene was carried out by $NiX(PPh_3)_3$ (X=halogen and pseudohalogen). First-order plots were obtained except for the iodo-complex. The addition of tin(II) chloride increased both activities and ratios of *cis*-2-pentene to the *trans*-isomer. Protic solvents accelerated the isomerization. Isotopic exchange between C_2D_4 and C_2H_4 or 1-pentene reveals that a metal hydride addition-elimination mechanism is operative.

We have previously reported that nickel complexes prepared *in situ* from $NiX_2(PPh_3)_2$ (X=halogen), PPh_3, and zinc catalyzed isomerization of 1-butene.[1] From the point of view that the isomerization activity and the ratio of *cis*-2-butene to the *trans*-isomer were dependent upon halides, we suggested that the catalytic species were Ni(I) complexes. A remarkable characteristic of the catalytic systems in the presence of $SnCl_2$ is the highest *c*/*t* ratio reported to date for the isomerization of terminal olefins catalyzed by transition metal complexes[2] and alkali-metal alkoxides.[3]

Halogenotris(triphenylphosphine)nickel(I) isolated from the above components has been found to be an active catalyst for isomerization of 1-pentene.[4] D'Aniello and Barefield[5] have confirmed that olefin isomerization by $NiX(PPh_3)_3$ occurred by a metal hydride pathway. The characteristics of the Ni(I) complexes in the isomerization of 1-pentene will be presented here in detail.

Experimental

Reagents. Tetrahydrofuran (THF) was refluxed over sodium, distilled, and stored in a nitrogen atmosphere. Methanol and ethanol were refluxed with sodium alkoxides and distilled. Triphenylphosphine was recrystallized from methanol. 1-Pentene was obtained from Tokyo Kasei Kogyo Co. and distilled prior to use. Other chemicals were commercial materials and used without further purification.

Nickel Complexes. Dihalogenobis(triphenylphosphine)-nickel(II) was prepared according to the method given in the literature.[6,7] A typical preparation of a Ni(I) complex was as follows. A mixture of 1.5 g (2 mmol) of $NiBr_2(PPh_3)_2$ and 0.61 g (2.3 mmol) of PPh_3 in 45 ml of benzene was treated with 0.65 g (10 mmol) of zinc dust. After a few minutes of stirring, the solution changed from green to yellow; it became red-brown and then the reaction mixture was rapidly filtered into a flask containing 0.02 g of $NiBr_2(PPh_3)_2$. When the solution turned yellow, the unreacted (undissolved) $NiBr_2(PPh_3)_2$ was removed by filtration. The filtrate was concentrated to one-third of its original volume. Thirty ml of methanol was added to the suspension to precipitate a yellow solid, which was collected and washed with five 10 ml portions of cold methanol. Drying *in vacuo* gave 1.55 g (82%) of $NiBr(PPh_3)_3$. Anal. Found: C, 70.09; H, 5.14. Calcd for $C_{54}H_{45}BrP_3Ni$: C, 70.10; H, 4.90 . $NiCl(PPh_3)_3$ and $NiI(PPh_3)_3$ were prepared in a similar manner; the yields were 61 and 46%, respectively. The elementary analyses supported the presence of Ni(I) complexes.[8]

Kinetics. The general procedure for the kinetic runs was as follows. A Ni(I) complex was weighed and added to a 100 ml flask. If an additive was used in a run, it was also weighed and added at this point. THF was vacuum distilled into the flask, which had already been evacuated and chilled in liquid nitrogen. The solvent was thawed and the mixture was stirred for 5 min to give a homogeneous yellow solution. After the mixture was again frozen in liquid nitrogen, 1-pentene was vacuum distilled into the flask. We determined the start of the isomerization to be when the mixture was thawed and stirred in a thermostated water bath at 0 °C.

Analysis. The concentrations of pentenes were followed by Shimadzu Model 2B and 4A gas chromatographs equipped with TCD and FID detectors. A 5.6 m×3 mm i.d. column packed with 60/80 mesh dimethylsulfolane (30%)/C-22 was operated at ambient temperature. Mass spectrometric analysis was made on a Hokushin time-of-flight mass spectrometer using an ionizing voltage of 12 eV.

Results and Discussion

Ligand Effects. When nickel complexes $NiX_2(PPh_3)_2$ (X=Cl, Br, I) were reduced with zinc in the presence of PPh_3 in THF or benzene, the green solution turned yellow and finally red-brown. The solutions contain a mixture of Ni(0) and Ni(I) species: the former is the red-brown species[9a] and the latter is the yellow one.[9b] The Ni(I) species was presumed to be an active catalyst for the isomerization of 1-butene.[1] This presumption has been confirmed by D'Aniello and Barefield on the basis of the isomerization of 1-butene-3,3-d_2 catalyzed by $(PPh_3)_3Ni(SnCl_3)$.[5] Since $NiX(PPh_3)_3$ was prepared by a disproportionation reaction between $Ni(PPh_3)_4$ and $NiX_2(PPh_3)_2$,[9b] it is expected that only $NiX(PPh_3)_3$ might be obtained when $NiX_2(PPh_3)_2$ is added by the amount equal to that of $Ni(PPh_3)_{3-4}$ formed in the reduction of $NiX_2(PPh_3)_2$ by zinc in the presence of PPh_3.[10] Our alternative method for the preparation of Ni(I) complexes is easy to carry out, without isolation of $Ni(PPh_3)_{3-4}$.

The first-order dependence on 1-pentene was observed without any induction periods at a 1-pentene/Ni ratio of 100, except for the iodo-complex, as shown in Fig. 1. Table 1 shows activities and *c*/*t* ratios for the isomerization of 1-pentene catalyzed by $NiX(PPh_3)_3$. Complexes with anion groups other than halogens were prepared *in situ* by replacing bromine on $NiBr(PPh_3)_3$ with KSCN, $NaOCH_3$, $AgPF_6$, and $AgClO_4$, respectively. The values in Table 1 show the results at the most favorable ratios of anions to $NiBr(PPh_3)_3$. Activities and *c*/*t* ratios are dependent upon anion ligands. Although large ions

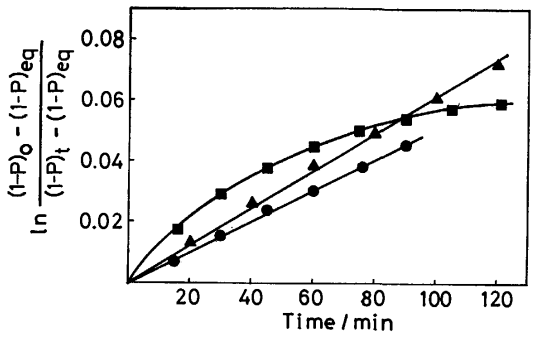

Fig. 1. Isomerization of 1-pentene catalyzed by NiX-$(PPh_3)_3$.
●: Cl, ▲: Br, ■: I.

TABLE 1. RATES AND c/t RATIOS IN THE ISOMERIZATION OF 1-PENTENE WITH $NiX(PPh_3)_3$[a]

X	k' / $10^{-3}\ s^{-1}\ M^{-1}$	c/t
Cl	1.7 (3.9)[b]	2.99
Br	2.1 (5.8)[b]	4.11
I	—[c] (4.9)[b]	5.63
SCN(5.0)[d]	1.3	1.65
OCH_3(10)[d]	1.2	3.11
PF_6(1.2)[d]	0.83	3.45
ClO_4(1.1)[d]	13.5	4.15

a) [Ni] 5×10^{-3} M, [1-pentene] 0.48—0.5 M, THF 19 ml, 0 °C. b) Conv. after 80 min. c) A first-order plot was not observed. d) Complexes were prepared *in situ* by replacing Br on $NiBr(PPh_3)_3$ with KSCN, $NaOCH_3$, $AgPF_6$, and $AgClO_4$ at given mole ratios to Ni in solution.

such as PF_6^- and ClO_4^- form counterions to $[Ni(PPh_3)_3]^+$, the high activity of the ClO_4-complex compared with that of the PF_6-complex seems to be attributed to coordinatively unsaturated nickel species, according to the abstraction of PPh_3 by $AgClO_4$.[11]

Striking increases in activities and c/t ratios were observed in the presence of $SnCl_2$ as shown in Table 2. Both activities and c/t ratios increase with the amount of $SnCl_2$ and become constant at a $SnCl_2$/Ni ratio of nearly 100 in THF. The difference of maximum c/t ratios among halogen-systems can not be regarded as significant. However, the rates increase in the following order: I<Br<Cl. Since $Ni(SnCl_3)(PPh_3)_3$ is isolated by the reaction of $NiCl(PPh_3)_3$ with $SnCl_2$ in benzene,[5] the active species responsible for high activity is $Ni(SnCl_2X)(PPh_3)_3$, shown in Eq. 1. The difference of

$$NiX(PPh_3)_3 + SnCl_2 \rightleftarrows Ni(SnCl_2X)(PPh_3)_3 \quad (1)$$

activity between halogen-systems might be attributed to that of the equilibrium constants. It is interesting to note that a first-order plot was obtained in the $NiI(PPh_3)_3$–$SnCl_2$ system, in contrast to the case of $NiI(PPh_3)_3$ alone. A small increase in rate and c/t ratio was observed at $SnBr_2/NiBr(PPh_3)_3$ ratios of 1/5—1/3, but a further addition of $SnBr_2$ retarded olefin isomerization.

TABLE 2. THE EFFECTS OF THE ADDITION OF $SnCl_2$ ON THE ISOMERIZATION OF 1-PENTENE WITH $NiBr(PPh_3)_3$[a]

X	$SnCl_2$/Ni	k' / $10^{-3}\ s^{-1}\ M^{-1}$	c/t
Cl	16	24.3	15.4
	50	44.3	22.4
	99	50.3	29.1
Br	15	11.5	16.4
	58	26.3	22.5
	97	39.9	28.4
I	15	2.69	9.6
	49	11.5	10.1
	100	14.3	24.5

a) The reaction conditions were the same as those in Table 1.

Mixtures of $NiX_2(PPh_3)_2$ (X=Cl, Br) and $SnCl_2$ are less effective catalysts than $NiX_2(PPh_3)_2$ alone in the hydrogenation and isomerization of methyl linoleate.[7] This is because $SnCl_3$ ligand, which is a soft and π-acceptor one,[12] prefers soft metal ions such as Ni(I). Catalytic properties were greatly enhanced by replacing halogen ligands with $SnCl_3$ in the hydrogenation,[13-15] isomerization,[16-19] and hydroformylation.[20-22] The $SnCl_3$ group has a labilizing effect on other ligands, especially on a ligand *trans* to it,[23] which would facilitate the formation of a hydridonickel complex and activate Ni–H or Ni–alkyl bonds.

TABLE 3. SOLVENT EFFECTS ON THE ISOMERIZATION OF 1-PENTENE WITH $NiBr(PPh_3)_3$[a]

X	Cosolvent	vol%	k' / $10^{-3}\ s^{-1}\ M^{-1}$	c/t
Cl	MeOH	21[b]	7.4	3.44
Br	MeOH	37	9.6	5.08
	CH_3CN	10[b]	11.8	2.92
	DMF	32[b]	3.1	3.66
	MEK	10	1.4	3.29
	Toluene	100	1.1	4.51
	H_2O	2.6[b]	24.6	4.48
I	MeOH	50	—(20.9)[c]	8.32

a) The reaction conditions were the same as those in Table 1. b) The vol% at which max rates were obtained. c) Conv. after 80 min.

Solvent Effects. A small difference of activity appeared between different lots. When the same lot was used in a series of experiments, the results were reproducible to ±10% on repeated runs so that they were discussed as indicating certain trends. Nickel(I) complexes are soluble in THF, aromatic hydrocarbons, DMF, and MEK, but less soluble in alcohols. Table 3 indicates solvent effects in the isomerization of 1-pentene catalyzed by $NiBr(PPh_3)_3$. None of the solvents are more suitable than THF as a one-component solvent. Maximum rates were observed at the vol% given in Table 3 for CH_3CN– and DMF–THF systems. Any amount of MEK retarded the isomerization. The c/t ratios decrease with the amount of aprotic solvents, which suggests that solvent molecules coordinate appreciably to the nickel atom. The addition of a small

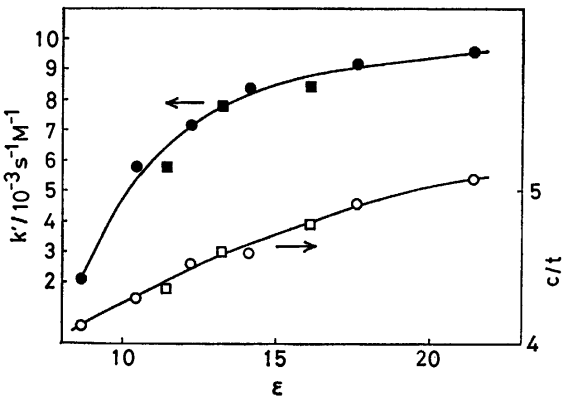

Fig. 2. Solvent effects on the rate and the *c/t* ratio in 1-pentene isomerization with $NiBr(PPh_3)_3$ in THF–alcohol system.
●, ○: MeOH, ■, □: EtOH.

amount of water led to a significant increase in activity and a slight increase in *c/t* ratio. An excess of water decreased both activity and *c/t* ratio, because the nickel(I) complex was caused to dissociate, which was followed by decomposition with butane evolution. The addition of methanol and ethanol led to the increase both in rates and *c/t* ratios, as was the case with water. Alcohols are precipitating agents for the nickel complexes, so that they are not added beyond a limited volume. Both the rate and *c/t* ratio increase with dielectric constants of THF–alcohol systems, as shown in Fig. 2. The color change was observed in protic solvent systems. The UV spectra showed λ_{max} at 343 nm ($\varepsilon=3.04\times10^3$) and 372 nm ($2.06\times10^3$) in THF, 345 nm ($4.08\times10^3$) and 370 nm ($2.79\times10^3$) in THF–MeOH, and 345 nm (4.51×10^3) and 372 nm (2.93×10^3) in THF–H_2O. Since the shifts of wavelength in λ_{max} are small, the change of the color is due to an increase of absorptivity. A similar acceleration by water or alcohols was observed in the codimerization of butadiene with ethylene catalyzed by σ-arylnickel(II) complexes–BF_3OEt_2.[24] Some complexes undergo oxidative addition of water as H and OH.[25] No results have suggested that protic solvents were used as a hydrogen source in our catalytic systems.

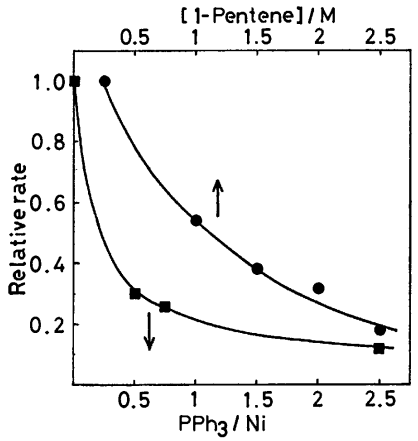

Fig. 3. Effects of excess PPh_3 and the concentration of 1-pentene on the rate of 1-pentene isomerization with $NiBr(PPh_3)_3$.

Effects of the Concentrations of Olefin and Free PPh_3. Figure 3 shows the effect of the concentlation of 1-pentene on the rate constants, where the relative rate constant is 1.0 at 0.25 M (1M=1 mol dm^{-3}) of 1-pentene. The rate constant decreases with an increase of the concentration of 1-pentene. Since no dimers of 1-pentene were observed, the retardation was due to the inhibitory impurities such as diene.[26] The presence of free PPh_3 slows activity because excess PPh_3 disturbs the coordination of olefins to the metal (Fig. 3).

Table 4. Dimerization of ethylene with $NiBr(PPh_3)_3$[a]

Solvent	Temp °C	Time h	Conv. %	Composition 1-C_4H_8 %	Composition *c/t*
THF	0	71	1.1	88	4.7
THF[b]	0	47	2.7	89	6.0
Toluene[c]	30	25	1.3	79	4.1
Toluene–MeOH (4:1)	30	25	7.7	19	3.7
THF[c]	30	25	1.4	81	4.1
THF–MeOH(4:1)[c]	30	25	11	25	3.7

a) [Ni] 2—2.5×10^{-2} M, [C_2H_4] 0.2—0.25 M, Solvent 4—5 ml. b) $NiBr(PPh_3)_2$ was prepared *in situ* from the disproportionation between $Ni(C_2H_4)(PPh_3)_2$ and $NiBr_2(PPh_3)_2$. c) A small quantity of complex was decomposed into black metal.

Dimerization of Ethylene. The dimerization of ethylene was carried out with $NiBr(PPh_3)_3$, as shown in Table 4. Though the addition of methanol accelerated dimerization and isomerization, the activity of $NiBr(PPh_3)_3$ for dimerization was on the whole low. The active species for dimerization needs one more vacant site than that for isomerization. The conversion increased at high temperatures but complexes began to decompose to give black metal. The butene composition remains over 80% unless methanol is added.

Isotopic Mixing between C_2D_4 and C_2H_4 or 1-Pentene. Two mechanisms have been proposed in the isomerization of olefins.[27] The metal hydride addition-elimination mechanism which is most common is operative in catalysis by transition metal hydrides. The second involves oxidative abstraction of C–H of olefins to form a π-allylmetal hydride, or a vinylmetal hydride intermediate.[28] Since the second mechanism involves an intramolecular 1,3-shift of hydrogen, no hydrogen scrambling occurs between olefins.

The exchange of hydrogen between C_2D_4 and C_2H_4 or 1-pentene was carried out to clarify the mechanism. Table 5 indicates: a) isotopic mixing between olefins occurs; b) the formation of metal hydride is less likely from the reaction of metal complexes and solvents; c) none of the ortho-hydrogen of PPh_3 is incorporated into olefins; d) a small amount of hydrogen from something other than olefins is incorporated into olefins. These results suggest that a metal hydride addition-elimination mechanism is operative. In this mechanism the hydride is produced from olefins *via* the reaction involving oxidative addition of an allylic

TABLE 5. ISOTOPIC MIXING BETWEEN C_2D_4 AND C_2H_4 OR 1-PENTENE CATALYZED BY Ni(I) COMPLEXES[a)]

Catalyst(mmol) Ni	Catalyst(mmol) $SnCl_2$	C_2D_4 (mmol)	C_2H_4 (mmol)	Time (h)	Isotopic distribution (%) d_0	d_1	d_2	d_3	d_4	d_5	d_6
0.1		0.15	0.15	89	6.9	25.8	37.0	24.5	5.7		
0.1[b)]	1.0		0.49	89	100						
0.1[c)]	1.5		0.48	74	100						
0.1	1.1	0.27		64			0.6	7.2	92.2		
0.1	2.0	0.45	1-C_5H_{10}	70	30.3	39.9	19.0	2.9	7.9[d)]		
			0.45		8.3	23.1	31.0	20.9	11.2	4.2	1.0[e)]

a) Deuteroethylene (C_2D_4 96.9%, C_2D_3H 3.1%) was obtained from E. Merck Co. Reactions were done in 3 ml of THF at 0 °C. b) CD_3OD (0.5 ml) was added. c) $NiBr(PPh_3)_2(P(C_6D_5)_3)$ was used. d) The isotopic distribution of ethylene. e) The isotopic distribution of pentenes (1-pentene 6.1%, *trans*-2-pentene 17.8%, *cis*-2-pentene 76.1%). d_7 0.3%, d_8 0.05%.

C–H bond of olefin to two Ni(I) centers, as D'Aniello and Barefield had confirmed.[5)] Vinylic hydrogen

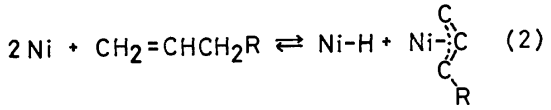

would be abstracted from ethylene which has no allylic hydrogen. The low activity in the dimerization of ethylene is also attributed to the difficulty in breaking vinylic C–H bonds. The ease of hydrogen release from olefins was related to a decrease in the induction period and an increase in the rate of ethylene dimerization with $PdCl_2(PhCN)_2$.[29)] The absence of induction period in our systems indicates that a nickel hydride forms instantly. The equilibrium of Eq. 2 is responsible for the increase of nickel hydride with the amount of olefin. The opposite result (Fig. 3) suggests the inhibition is caused by the impurities.[26)]

Stereoselectivity. Selective *cis*-isomerization of terminal olefins was observed in base catalysts,[3)] $CoH(N_2)(PPh_3)_3$,[2)] and $NiX(PPh_3)_3$–$SnCl_2$ systems. The stereoselectivity in the base-catalyzed isomerization is explained by the result that the *cis*-allylic anion is thermodynamically more stable than the *trans* form.[3,30)] With a metal hydride catalyst, an olefin inserts into an M–H bond by a concerted reaction path to give σ-alkylmetal complexes:[31)]

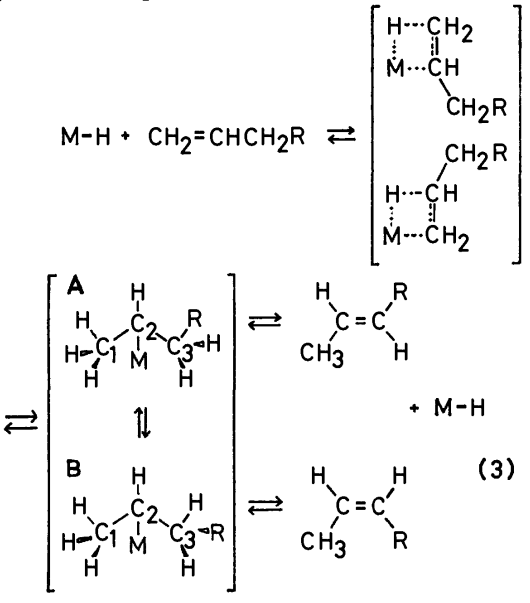

When hydrogens bonded to C_3 approach the metal in a cyclic transition state, two structures are considered to have the C_3–R bond eclipsed and *gauche* with the C_2–H bond, as shown in **A** and **B**. The conformation of **A** is thermodynamically more stable than that of **B** for the steric repulsion between C_1 methyl and R groups, so long as the steric interaction between alkyl group and ligands is neglected. The bulkiness of ligands favors the conformation of **B** to give *cis*-2-olefins in the first-period transition metal catalyst systems: the *c*/*t* ratios decrease in the order I>Br>Cl, PPh_3>PPh_2Et>$PPhEt_2$>PEt_3 in the isomerization of 1-butene by $CoX_2(PR_3)_2$– and $NiX_2(PR_3)_2$–$NaBH_4$ systems (X= halogen, $PR_3=PPh_nEt_{3-n}$).[32)] The same trend is observed in the isomerization by $NiX(PPh_3)_3$. However, the opposite trend (Cl>Br>I) which was found in the isomerization of 1-pentene by $PdX_2(PhCN)_2$ was explained in terms of Pd–olefin stability.[33)] In the isomerization of 1-olefins catalyzed by Pt–$SnCl_3$ complexes, *trans*-2-olefins are formed preferentially.[16–19)] The high yield of *trans*-2-pentene was explained in terms of the stability of the eclipsed conformation of 2-pentyl radical coordinated to pseudo-planar platinum complex.[19)] The *cis*-selectivity in the Ni–$SnCl_3$ system is due primarily to the steric bulkiness of the $SnCl_3$ group thrusting away both C_1 methyl and R groups, as shown in **B** (Eq. 3). The bulk of the $SnCl_3$ ligand tends to favor the addition which leads to the sterically less hindered terminal-carbon–Pt complex in the hydroformylation of 1-olefins.[20)]

The π-acceptor ligands require square planar configurations rather than tetrahedral ones for four-coordinated nickel complexes. Since triphenylphosphine is bulky, $NiX(PPh_3)_3$ is forced to be tetrahedral because of steric repulsion between ligands.[9b)] If the active species are PPh_3–dissociated nickel complexes, the activated intermediates with π-acceptor ligands might be different from those with σ-donor ones such as halogen. Another effect of a π-acceptor ligand, $SnCl_3$, is to labilize the alkyl–metal bonds. Facile abstraction of β-hydrogen results in the formation of isomerized olefins before the interconversion of **A**⇌**B** in Eq. 3.

The authors wish to thank Dr. Sadayuki Mori (Institute for Chemical Research, Kyoto University) for obtaining mass spectra and for helpful discussions.

References

1) H. Kanai, *J. Chem. Soc., Chem. Commun.*, **1972**, 203.
2) F. Pennella, *J. Organometal. Chem.*, **78**, C10 (1974).
3) S. Bank, A. Schriesheim, and C. A. Rowe, Jr., *J. Am. Chem. Soc.*, **87**, 3244 (1965).
4) H. Kanai, K. Kushi, and K. Sakanoue, *Shokubai*, **16**, 38 (1974).
5) M. J. D'Aniello, Jr., and E. K. Barefield, *J. Am. Chem. Soc.*, **100**, 1474 (1978).
6) L. M. Venanzi, *J. Chem. Soc.*, **1958**, 719.
7) H. Itatani and J. C. Bailar, Jr., *J. Am. Chem. Soc.*, **89**, 1600 (1967).
8) $NiCl(PPh_3)_3$: Found: C, 73.41; H, 5.43. Calcd for $C_{54}H_{45}P_3ClNi$: C, 73.62; H, 5.15. $NiI(PPh_3)_3$: Found: C, 66.79; H, 4.62%. Calcd for $C_{54}H_{44}P_3INi$: C, 66.68; H, 4.66%.
9) a) G. Wilke, E. W. Müller, and M. Kröner, *Angew. Chem.*, **73**, 33 (1961); b) P. Heimbach, *ibid.*, **76**, 586 (1964).
10) C. A. Tolman, W. C. Seidel, and D. H. Gerlach, *J. Am. Chem. Soc.*, **94**, 2669 (1972).
11) F. A. Cotton and D. M. L. Goodgame, *J. Chem. Soc.*, **1960**, 5267.
12) a) F. A. Cotton and G. Wilkinson, "Advanced Inorganic Chemistry," 2nd ed, Interscience Publishers (1966), p. 1029; b) G. W. Parshall, *J. Am. Chem. Soc.*, **88**, 704 (1966).
13) H. van Bekkum, J. van Gogh, and G. van Minnen-Pathuis, *J. Catal.*, **7**, 292 (1967).
14) L. P. van't Hof and B. G. Linsen, *J. Catal.*, **7**, 295 (1967).
15) R. D. Cramer, E. L. Jenner, R. V. Lindsey, Jr., and U. G. Stolberg, *J. Am. Chem. Soc.*, **85**, 1691 (1967).
16) R. D. Cramer and R. V. Lindsey, Jr., *J. Am. Chem. Soc.*, **88**, 3534 (1966).
17) H. C. Clark and H. Kurosawa, *Inorg. Chem.*, **12**, 1566 (1973).
18) K. Hirabayashi, S. Saito, and I. Yasumori, *Trans. Faraday Soc.*, **68**, 978 (1972).
19) G. C. Bond and M. Hellier, *J. Catal.*, **7**, 217 (1967).
20) I. Schwager and J. F. Knifton, *J. Catal.*, **45**, 256 (1976).
21) J. F. Knifton, *J. Am. Oil Chem. Soc.*, **55**, 496 (1978).
22) Y. Kawabata, T. Hayashi, and I. Ogata, *J. Chem. Soc., Chem. Commun.*, **1979**, 462.
23) F. Basolo and R. G. Pearson, "Mechanism of Inorganic Reactions," 2nd ed, John Wiley and Sons (1968), pp. 351—435.
24) N. Kawata, K. Maruya, T. Mizoroki, and A. Ozaki, *Bull. Chem. Soc. Jpn.*, **47**, 2003 (1974).
25) a) D. H. Gerlach, A. R. Kane, G. W. Parshall, J. P. Jesson, and E. L. Muetterties, *J. Am. Chem. Soc.*, **93**, 3543 (1971); b) T. Yoshida, Y. Ueda, and S. Otsuka, *ibid.*, **100**, 3941 (1978).
26) When 1-pentene from Tokyo Kasei Kogyo Co. was out of stock, we used 1-pentene available from other companies and found that no isomerization of the 1-pentene took place. D'Aniello and Barefield[5] stated that a 1 : 50 butadiene: Ni mole ratio resulted in almost complete inhibition. It was concluded that the inactivity was due to the impurities such as diene.
27) G. Henrici-Olivé and S. Olivé, "Coordination and Catalysis," Verlag Chemie, Weinheim, New York (1977), pp. 156—161.
28) a) T. H. Tulip and J. A. Ibers, *J. Am. Chem. Soc.*, **101**, 4201 (1979); b) B. Hudson, D. E. Webster, and P. B. Wells, *J. Chem. Soc., Dalton Trans.*, **1972**, 1204.
29) T. Kitamura, K. Maruya, Y. Morooka, and A. Ozaki, *Bull. Chem. Soc. Jpn.*, **45**, 1457 (1972).
30) S. Bank, *J. Am. Chem. Soc.*, **87**, 3245 (1965).
31) a) Ref. 27, pp. 122—128; b) S. Sakaki, H. Kato, H. Kanai, and K. Tarama, *Bull. Chem. Soc. Jpn.*, **48**, 813 (1975).
32) H. Kanai, S. Sakaki, and K. Tarama, *Shokubai*, **11**, 142 (1969).
33) S. Sakaki, H. Kanai, and K. Tarama, *Can. J. Chem.*, **52**, 2857 (1974).

Mechanistic Interpretations of the Dye-sensitized Formation of Hydrogen Peroxide in an Aqueous Solution

Yoshiharu Usui,* Ei-jurou Kobayashi, Akira Kazami, and Shinobu Sakuma
Department of Chemistry, Faculty of Science, Ibaraki University, Bunkyo, Mito 310
(Received February 18, 1980)

Kinetic studies of the photosensitized formation of hydrogen peroxide and hyperoxide ions in a mixed aqueous solution of eosine, oxygen, and EDTA have been attempted on the basis of a switch-over of the primary processes, *i.e.*, the so-called DD, DR, and DO mechanisms. The rate constants for reactions of $E^+\cdots E^-$ and $E^+\cdots O_2^-$ intermediates with oxygen and EDTA were obtained. The yield of hydrogen peroxide *via* the DO-initiated mechanism was enhanced as much as one order of magnitude ($\approx$0.012) by the addition of 0.15 mol dm^{-3} of sodium borate or sodium carbonate. The maximum yield, 0.08, of hydrogen peroxide was obtained in an aerated aqueous solution of 1.0×10^{-4} mol dm^{-3} of eosine, 5.0×10^{-2} mol dm^{-3} of EDTA, and 8.8×10^{-2} mol dm^{-3} of sodium borate.

The investigation of the mechanism of a photosensitized oxidation is important from the point of view of photodynamic action, and several reaction mechanisms have been proposed to account for these reactions, as have been reviewed by Grossweiner,[1] Foote,[2,3] Spikes,[4] and one of the present authors.[5] As for the dye-sensitized photooxidation, the relationship between a structure and its susceptibility to photooxidation has recently been investigated by the kinetic treatment of the eosine-sensitized photooxidation of phenylalanine and tyrosine derivatives.[6]

A reaction mechanism involving the triplet state of an organic dye should be altered with the concentrations of the dye, the reductant, and the oxidant. We have previously established that a switch-over of the primary processes can occur in the photochemical reactions of dyes, *i.e.*, the so-called DD, DR, and DO mechanisms.[5,7] The classification of the primary processes for such photoredox reactions is of significance in the interpretation of the mechanism for the dye-sensitized reactions.

On the other hand, if the hyperoxide ion, O_2^-, can be efficiently produced in the course of a photosensitized oxidation in an aerated solution, it will be synthetically useful for the purpose of the specific oxidation of an organic compound by O_2^-.

This paper is an extension of our previous papers.[8,9] Its main purpose is to show we can interpret kinetic behavior in a rather complicated system by taking a switch-over of the primary processes into account. Besides, some suggestions concerning the reaction of the transient intermediates on DD and DO mechanisms will be presented.

Experimental

Materials. Eosine (Merck) (E) was recrystallized twice from ethanol. Disodium dihydrogen ethylenediaminetetraacetate (Dotite-2Na of Wako Junyaku) (EDTA) and Tetranitro Blue Tetrazolium (Sigma Chemical Co.) (TNBT) were used without further purification.

Apparatus and Procedure. To determine the yield of H_2O_2, an irradiation apparatus was set up: ten cylindrical reaction cells (1.5 cm in radius) with an optically flat bottom were placed on a filter plate in a thermostat. The filter, made of a plastic plate, cut off any absorbance below 480 nm and was turned round at 1 rpm above the light source of a daylight fluorescent circleline (10 cm in radius) outside the thermostat set up with the transparent plastic box. The depth of the sample solutions being about 2 cm in the reaction cells, the absorption of light is practically complete in the region of the visible absorption. The quantity of light absorbed by the solutions was 1.3×10^{-9} mol cm^{-3} s^{-1}, which was estimated from the values of the photobleaching rate of eosine in a plain aqueous solution and the quantum yield. The details of the method have been described in previous papers.[8,9] For the H_2O_2-accumulation experiment, air or oxygen gas was bubbled through the solution. The determination of the concentration of H_2O_2 was performed by the spectroscopic method with titanium complexing after the separation of a precipitate of eosine by the addition of sulfuric acid. The concentration of O_2^- was determined by the measurement of the absorbance of the formazan at the wavelength of 560 nm using $\varepsilon_{560}=5.0\times10^4$ mol^{-1} cm^2, when a sample containing a small amount of TNBT was irradiated.

Results and Discussion

A considerable amount of H_2O_2 is really formed for eosine-sensitized photoredox reactions in aerated aqueous solutions containing EDTA. We have already studied the switch-over of the primary processes by means of oxygen-consumption experiments; *i.e.*, as is shown in Fig. 1, the processes of a, b, and c on triplet eosine, which correspond to the DD, DO, and DR mechanisms respectively, are known where the values of k_D^s (4.0×10^8 mol dm^{-3} s^{-1}), k_O^s (1.1×10^9 mol dm^{-3} s^{-1}), and k_E^s (5.0×10^5 mol dm^{-3} s^{-1}) are obtained respectively.[7,8] The consecutive processes can be assumed to be competitive reactions of EDTA and oxygen with the intermediate irrespective of the mechanisms of DD, DO, and DR.

Effect of EDTA and Oxygen Concentrations upon the Yield of H_2O_2 Formation via *the DD-initiated Mechanism* (Φ_h^{DD}). With the concentration of eosine fixed at 2.0×10^{-3} mol dm^{-3}, the effect of the EDTA concentration on the quantum yield of H_2O_2 formation was investigated over the wide range from 0 to 0.10 mol dm^{-3}. Figure 2 shows that Φ_h^{DD} tends to the constant value of the maximum yield ($\approx1.7\times10^{-2}$). See the scheme for DD mechanism shown in Fig. 1 in an air-saturated solution, assuming the relation of $k_D^s[E]\gg k_d$, $k_D^s[O_2]$, and $k_E^s[EDTA]$:

$$\Phi_h^{DD}=\frac{\phi_{st}k_D^r}{2k_D^s}\,\frac{k_O'^r[O_2]+\gamma(O_2)k_E'^r[EDTA]}{k_d'+k_O'^s[O_2]+k_E'^s[EDTA]}. \quad (1)$$

Denoting Φ_h^{DD} at [EDTA]=0 as Φ_0^{DD}, we can obtain

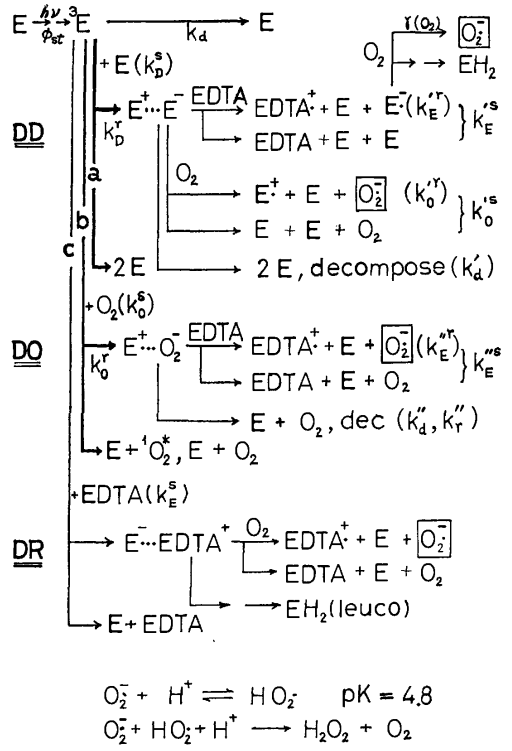

$$O_2^- + H^+ \rightleftharpoons HO_2 \quad pK = 4.8$$
$$O_2^- + HO_2 + H^+ \longrightarrow H_2O_2 + O_2$$

Fig. 1. The reaction scheme for eosine (E) photosensitized formation of hydrogen peroxide.

Eq. 2:

$$\frac{1}{\Phi_h^{DD}-\Phi_0^{DD}} = \frac{1}{\Phi_0^{DD}(\beta-\alpha)}\left(\alpha+\frac{1}{[EDTA]}\right) \qquad (2)$$

where $\alpha=k'^s_E/(k'_d+k'^s_0[O_2])$ and $\beta=k'^r_E\,\gamma(O_2)/k'^r_0[O_2]$. A linear relationship of $1/(\Phi_h^{DD}-\Phi_0^{DD})$ against $1/[EDTA]$ was obtained, as is shown in Fig. 2. This suggests that EDTA reacts with the intermediate, $E^+\cdots E^-$, competitively. From the values of Φ_0^{DD} (4.5×10^{-3}) and the slope and intercept of the line, the α and β values can be estimated. Using the value of $\phi_{st}k_D^r/k_D^s$ (0.112),[10,11] the values of k'^r_0/k'^s_E and $\gamma(O_2)k'^r_E/k'^s_E$ are estimated to be 0.665 and 0.22 respectively.

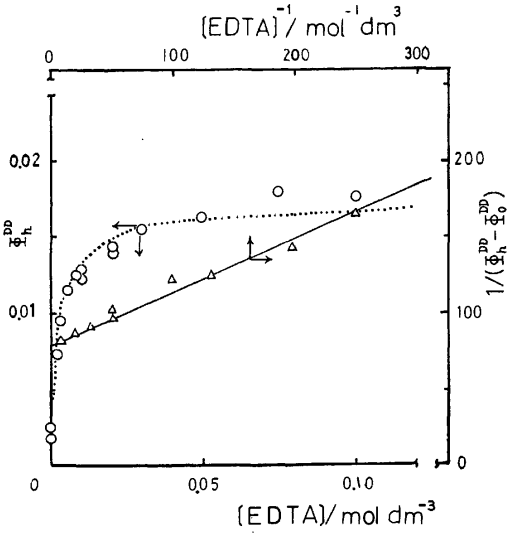

Fig. 2. Effect of EDTA concentration on Φ_h^{DD}(—○—) and the double reciprocal plots (—△—). [E]: 2×10^{-3} mol dm^{-3}, [O_2]: 2.4×10^{-4} mol dm^{-3}, pH=4.9.

At a lower concentration of EDTA (1.0×10^{-4} mol dm^{-3}) the effect of the oxygen concentration on Φ_h^{DD} was investigated under the condition of a DD-initiated mechanism. The results can be analysed by means of Eqs. 3 and 3', which are approximate to Eq. 1 as $k'^r_0[O_2]\gg k'^r_E[EDTA]\gamma(O_2)$ and $(k'_d+k'^s_0[O_2])\gg k'^s_E[EDTA]$. Equation 3 should hold without EDTA:

$$\Phi_h^{DD} \simeq \frac{\phi_{st}k_D^r}{2k_D^s}\,\frac{k'^r_0[O_2]}{k'_d+k'^s_0[O_2]} \qquad (3)$$

$$1/\Phi_h^{DD} = (2k_D^s/\phi_{st}k_D^rk'^r_0)(k'^s_0+k'_d/[O_2]) \qquad (3')$$

Judging from the data shown in Fig. 3, oxygen also reacts with the intermediate, $E^+\cdots E^-$, competitively. The slope and intercept of the linear line in Fig. 3 give the numerical values of $k'^s_0/k_d=2\times10^4$ mol dm^{-3} and $k'^r_0/k'^s_0=0.10$. Therefore, the maximum yield of Φ_h^{DD} *via* the reaction of oxygen with $E^+\cdots E^-$ should be equal to 5.5×10^{-3}, which is about one-third to that (0.017) *via* the reaction of EDTA with $E^+\cdots E^-$. Estimating the k_d value to be 1.8×10^3 s^{-1} from the data previously reported,[12,13] the rate constant for the reaction of

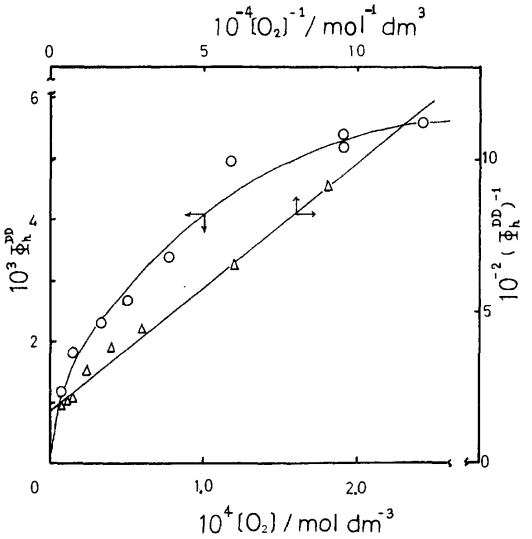

Fig. 3. Effect of oxygen concentration on Φ_h^{DD} (—○—) and the double reciprocal plots (—△—). [E]: 2×10^{-3} mol dm^{-3}, [EDTA]: 1×10^{-4} mol dm^{-3}, pH=4.9.

Table 1. Rate constants of elementary processes for the DD intermediate

Reaction	Rate constant / mol^{-1} dm^3 s^{-1}
$E^+\cdots E^-+EDTA \longrightarrow$ $E+EDTA^+\cdot+E^-$ (k'^r_E)	$\gamma(O_2)k'^r_E=$
$E^-+O_2\longrightarrow E+O_2^-$ ($\gamma(O_2)$)	8.4×10^5
$E^+\cdots E^-+EDTA \longrightarrow$ $2E+EDTA$ / $E+EDTA^+\cdot+E^-$ (k'^s_E)	2.8×10^6
$E^+\cdots E^-+O_2\longrightarrow E^++E+O_2^-$ (k'^r_0)	3.7×10^6
$E^+\cdots E^-+O_2\longrightarrow 2E+O_2$ / $E^++E+O_2^-$ (k'^s_0)	3.7×10^7

EDTA or oxygen with $E^+\cdots E^-$ listed in Table 1 are obtained.

By substituting the experimental values into Eq. 1, one can obtain the following equation:

$$\Phi_h^{DD} = (2.1\times10^5[O_2]+4.7\times10^4[EDTA])/(1.8\times10^3+3.7\times10^7[O_2]+2\ 8\times10^6[EDTA])$$

The calculated values of Φ_h^{DD} are shown with a dotted curve in Fig. 2. By comparing the k_O^s value with that of $k_E^{\prime s}$, it can be seen that oxygen can competitively attack $E^+\cdots E^-$ faster than EDTA by one order of magnitude, resulting in the production of O_2^-, as is shown in Fig. 1.

Effect of EDTA Concentration upon the Yield of H_2O_2 *Formation via DO-initiated Mechanism* (Φ_h^{DO}). When the DO-initiated mechanism is operative, Eq. 4 can be derived from the scheme in Fig. 1:

$$\Phi_h^{DO} = \phi_{st}\frac{k_O^r}{k_O^s}\frac{k_E^{\prime\prime r}[EDTA]}{k_d^{\prime\prime}+k_r^{\prime\prime}+k_E^{\prime\prime s}[EDTA]} \quad (4)$$

A linear relationship of $1/\Phi_h^{DO}$ against 1/[EDTA] was obtained by taking account of the EDTA concentration effect. The result indicates that the DO-initiated mechanism shown in Fig. 1 is operative and that the reaction of EDTA with the intermediate, $E^+\cdots O_2^-$, to produce the O_2^- ion may occur in competition with the deactivation and decomposition. Inserting the ϕ_{st} value (0.64) into the intercept of the line in Fig. 4, we obtain $k_O^r k_E^{\prime\prime r}/k_O^s k_E^{\prime\prime s}\simeq 6.2\times10^{-3}$, which leads to the inequality of $k_O^r/k_O^s \leqq 0.11$ and $0.056 \leqq k_E^{\prime\prime r}/k_E^{\prime\prime s} \leqq 1$, since the probability of singlet oxygen formation by the reaction of triplet eosine with oxygen equals 0.89.[14] The value of $(k_d^{\prime\prime}+k_r^{\prime\prime})/k_E^{\prime\prime s}$ is also obtained as 2.4 $(\pm0.3)\times10^{-3}$ mol dm^{-3} from the intercept and slope in Fig. 4. Using the numerical value of 7.0×10^5 for $k_E^{\prime\prime s}$, we obtain 1.7×10^3 s^{-1} for $(k_d^{\prime\prime}+k_r^{\prime\prime})$, which coinsides with the value of 1.2×10^3 s^{-1} for the decay constant of $E^+\cdots O_2^-$ previously reported in the experiment by means of flash photolysis.[7,9]

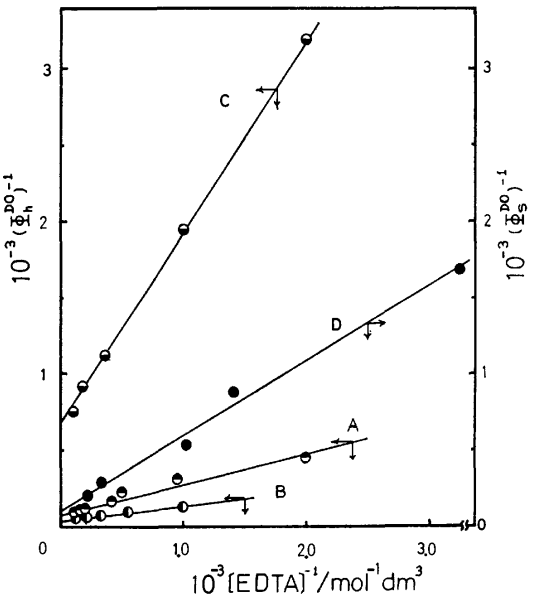

Fig. 4. Plots of $1/\Phi_h^{DO}$ (or $1/\Phi_s^{DO}$) against 1/[EDTA] for the EDTA concentration effect on Φ_h^{DO} (or Φ_s^{DO}) in 2×10^{-2} mol dm^{-3} borate buffer solution (A), 1.5×10^{-1} mol dm^{-3} borate buffer solution (B), 1×10^{-2} mol dm^{-3} acetate buffer solution (C), and 1×10^{-2} mol dm^{-3} phosphate buffer solution (D). [E]: 2×10^{-5} mol dm^{-3} and [O_2]: 2.4×10^{-4} mol dm^{-3}.

In the course of H_2O_2 production, singlet oxygen is formed simultaneously by the energy transfer between triplet eosine and oxygen. Since the yield of H_2O_2 was scarcely affected by the addition of the singlet oxygen quencher (NaN_3, 7.0×10^{-3} mol dm^{-3}), it can be said that singlet oxygen is not directly concerned in the mechanism of H_2O_2 production.

H_2O_2 Formation via the DR-initiated Mechanism. With the concentrations of eosine, oxygen, and EDTA fixed under condition when the DR mechanism is operative, the yields of H_2O_2 formation (Φ_h^{DR}) and of eosine reduction were measured. The value of Φ_h^{DR} is equal to 0.057 in the concentrations of 0.2 mol dm^{-3} of EDTA, 5.0×10^{-5} mol dm^{-3} of oxygen, and 5.0×10^{-5} mol dm^{-3} of eosine. However, the photoreduction of eosine takes place at the same time, and H_2O_2 decomposes rather rapidly after it is produced. When the deaerated solution containing 5.0×10^{-5} mol dm^{-3} of eosine, 5.0×10^{-4} mol dm^{-3} of H_2O_2, and 0.2 mol dm^{-3} of EDTA was irradiated, H_2O_2 was decomposed in the initial stage of the photoreduction of the dye. Although further investigations will be needed in order to treat Φ_h^{DR} kinetically, it may be supposed that the eosine semiquinone produced *via* the DR-initiated mechanism reacts with H_2O_2, leading to its decomposition.

Influence of Inorganic Salts on Φ_h^{DO} *via the DO-initiated Mechanism.* It was observed that the formation of H_2O_2 *via* the DO-initiated mechanism was enhanced by the addition of some inorganic salts. This effect is confirmed in the case of the DO-initiated mechanism, but not in the DD mechanism. As is shown in Table 2, the increment in the Φ_h^{DO} value was as high as one order of magnitude with 0.15 mol dm^{-3} of sodium borate or 0.16 mol dm^{-3} of sodium carbonate.

Using Eq. 4 we can analyse the effect of EDTA concentration on Φ_h^{DO} similarly and see that the DO-initiated mechanism in Fig. 1 is still operative. From the results of the kinetic analysis shown in Fig. 4, A and B, it can be seen that the value of $\phi_{st}k_O^r k_E^{\prime\prime r}/k_O^s k_E^{\prime\prime s}$ in

Table 2. Inorganic salt effect on Φ_h^{DO}

Added compound $\left(\frac{\text{concentration}}{\text{mol dm}^{-3}}\right)$	pH	Φ_h^{DO}
None	9.5	1.1×10^{-3}
$Na_2B_4O_7$ (0.15)	9.2	12×10^{-3}
Na_2CO_3 (0.16)	10.3	10×10^{-3}
Na_2SiO_3 (0.10)	11.4	5.0×10^{-3}
$Na_2P_2O_7$ (0.10)	9.9	4.5×10^{-3}
$(NH_4)_2SO_4$ (0.10)	8.5	3.4×10^{-3}
Na_2SO_4 (0.10)	8.6	2.7×10^{-3}
NaCl (0.10)	9.2	2.2×10^{-3}
CH_3COONa (0.10)	9.6	2.2×10^{-3}
Na_2HPO_4 (0.10)	7.6	2.0×10^{-3}

[E]$=5.0\times10^{-5}$ mol dm^{-3}, [EDTA]$=3.0\times10^{-3}$ mol dm^{-3}, [O_2]$=2.4\times10^{-4}$ mol dm^{-3}.

the presence of sodium borate is greater than that without the salt. For the solution to which sodium borate has been added, the yields of the triplet eosine and the semioxidized radical were checked by a flash photolysis experiment. Since no influence of the salt on these yields was observed, it may be supposed that the values of ϕ_{st} and k_0^r/k_0^s with sodium borate are equal to those without the salt. By comparing the two values of $\phi_{st}k_0^r k_E''^r/k_0^s k_E''^s$, we learn that the values of $k_E''^r/k_E''^s$ with sodium borate are seven times (at 10 °C) and twenty-five times (at 25 °C) greater than those without sodium borate. The results are shown in Table 3. The effect of the addition of sodium borate may be attributed to the enhancement of the reaction probability between $E^+\cdots O_2^-$ and EDTA.

Temperature Effect on Φ_h^{DO}. Figure 5 shows the H_2O_2 formation curves of the DO-initiated mechanism at several temperatures. The initial yield of H_2O_2 generally increases with an increase in the temperature. The Arrhenius plots for the overall rate constant, k, in the H_2O_2 formation processes, *i.e.*, $\Delta[H_2O_2]/\Delta t=kt$, give similar activation energies both in the mixed solutions of 5.0×10^{-5} mol dm^{-3} eosine, 8.0×10^{-1} mol dm^{-3} sodium borate, and 6.0×10^{-3} mol dm^{-3} EDTA ($\approx$12 kcal deg, pH=9.4), and in 5.0×10^{-5} mol dm^{-3} eosine, 1.0×10^{-2} mol dm^{-3} acetate buffer, and 6.0×10^{-3} mol dm^{-3} EDTA ($\approx$17 kcal deg, pH=5.1). With an increase in the temperature, the reaction probability, $k_0^r k_E''^r/k_0^s k_E''^s$ for $E^+\cdots O_2^-$, increases as is listed in Table 3. However, at higher temperatures ($T\gtrsim30$ °C), H_2O_2 formation curves give maximum values during irradiation and then fall, as is shown in Fig. 5. By a vacuum distillation of the irradiated solution containing the borate ion (pH=8.0), H_2O_2 was not distilled out completely; however, the residual H_2O_2 was quantitatively distilled as a result of the neutralization by the addition of hydrochloric acid. This suggests that a nonvolatile compound such as a peroxo salt of $[B_2(O_2)_2(OH)_4]^{2-}$ might be formed during the irradiation and partially dissociated.[15] It was confirmed that the peroxo compound is unstable in an aqueous solution and rapidly decomposes at temperatures higher than 20 °C. There is no maximum value in the formation curves without the borate ion even at 40 °C within the present observation time; rather, the curves rise straight. Therefore, the decomposition of H_2O_2 is negligible in this system. It may be suggested that O_2^- (or H_2O_2) makes the peroxo compound with borate ions and then decomposes at higher temperatures ($T\gtrsim20$ °C).

Supplementally, we checked the pH dependency on Φ_h. The values of Φ_h^{DO} were not practically affected by the pH in the region of pH=5—10, but those of Φ_h^{DP} became relatively small at pH$\lesssim$7.

EDTA Concentration Effect on the Yield of O_2^- *Ion Formation* (Φ_s^{DO}). Using TNBT (16 μmol dm^{-3}) as the radical trap for O_2^-, the values of Φ_s^{DO} were determined by measuring the optical absorption of the formazan at the wavelength of 560 nm.[16] Since the relationship of the $\Phi_s^{DO}/2=\Phi_h^{DO}$ is always obtained in the systems without sodium borate, it may be supposed that the disproportionation reaction between O_2^- ions occurs quantitatively in an alkaline solution. From the results of the EDTA-concentration effect on Φ_s^{DO}, a linear relationship of $1/\Phi_s^{DO}$ against 1/[EDTA] was obtained; the values of $k_0^r k_E''^r/k_0^s k_E''^s$ and $k_E''^r/(k_d''+k_r'')$ agree with those obtained from the same analytical treatment

Table 3. Rate constants of elementary processes for the DO intermediate

Conditions (pH)	T/°C	$k_0^r k_E''^r/k_0^s k_E^s$	$k_E''^s/(k_r''+k_d'')$
A) 2×10^{-2} mol dm^{-3} Borate buffer (9.2)	10	4.4×10^{-2}	3.0×10^{-2}
B) 1.5×10^{-1} mol dm^{-3} Borate buffer (9.2)	25	1.56×10^{-1}	9.0×10^{-3}
C) 1.0×10^{-2} mol dm^{-3} Acetate buffer (4.9)	25	6.2×10^{-3}	4.1×10^{-2}
D) 1.0×10^{-2} mol dm^{-3} Phosphate buffer (8.9)	25	6.0×10^{-3}	4.2×10^{-2}

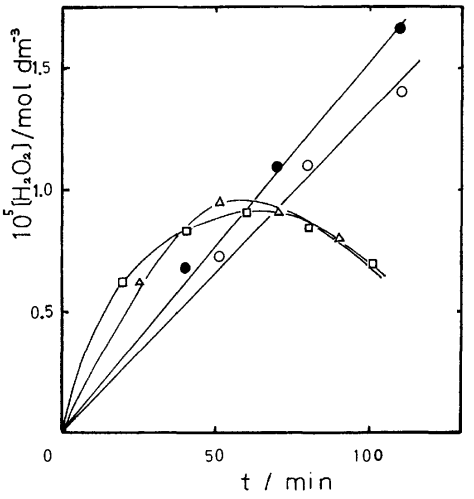

Fig. 5. H_2O_2 formation curves at several temperatures on DO started mechanism. [E]: 5×10^{-5} mol dm^{-3}, [EDTA]: 6×10^{-3} mol dm^{-3}, [O_2]: 2.4×10^{-4} mol dm^{-3}, and [$Na_2B_4O_7$]: 8×10^{-2} mol dm^{-3}. T=10 °C (—○—), 30 °C (—△—), 40 °C (—□— and —●— without $Na_2B_4O_7$).

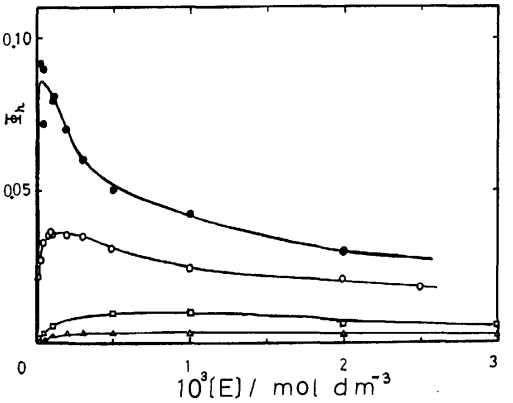

Fig. 6. Effect of eosine concentration on Φ_h in aerated aqueous solution. [EDTA]: 1×10^{-1} mol dm^{-3} (—○—), 3×10^{-3} mol dm^{-3} (—□—), and 0 mol dm^{-3} (—△—) without $Na_2B_4O_7$ (pH=4.9). [EDTA]: 5×10^{-2} mol dm^{-3} (—●—) with 8.8×10^{-2} mol dm^{-3} $Na_2B_4O_7$ (pH=7.8).

as that used for Φ_h^{po} (*cf.* Fig. 4. and Table 3, D and C). These results support the idea that the H_2O_2 formation from the O_2^- ion is exclusively due to the disproportionation between O_2^- ions in this system and that the contribution of the reaction of TNBT with the triplet eosine to make the formazan is negligible at low concentrations of 16 μmol dm^{-3}.

However, as for the addition effect of the borate ion on Φ_s^{po}, no significant increasing effect on Φ_s^{po} was observed in the system with EDTA. Under the DO mechanism in the solution without EDTA, no free O_2^- is liberated from $E^+\cdots O_2^-$; absolutely no H_2O_2 was detected.[17] In spite of such results, the formazan was still formed upon the irradiation of a sample without EDTA. It is considered that TNBT might react with $E^+\cdots O_2^-$. Furthermore, the yield of the formazan was increased by the addition of the borate ion. In the case of EDTA addition, if the borate ion could stabilize the free O_2^- liberated by the following reaction:

$$EDTA + E^+ \cdots O_2^- \longrightarrow EDTA + E + O_2^-$$

the enhancement of Φ_s^{po} by the borate ion would also be observed. Assuming that the borate ion stabilizes the O_2^- radical, which exists in an intermediate including EDTA in the above reaction, and that, in preference to the stabilization by the borate ion, TNBT reacts with O_2^- in the intermediate, no enhancement effect by the borate ion may appear. Further investigations of the reasons will be needed in the future.

Eosine Concentration Effect on Φ_h and the Accumulation Experiment of H_2O_2. In order to ascertain the conditions for the highest yield of H_2O_2 formation, Φ_h was measured at various concentrations of eosine and EDTA with or without the borate ion. As is shown in Fig. 6, the maximum yield of 0.04 (Φ_h^{max}) is obtained under the conditions of [E]: $1—2\times10^{-4}$ mol dm^{-3}, $[O_2]$: 2.4×10^{-4} mol dm^{-3}, and [EDTA]: 0.1 mol dm^{-3} without the borate ion. Further, the value of Φ_h^{max} is close to 0.08—0.10 under the conditions of [E]: 1.0×10^{-4} mol dm^{-3}, $[O_2]$: 2.4×10^{-3} mol dm^{-3}, and [EDTA]: 0.05 mol dm^{-4} with 0.088 mol dm^{-3} of the borate ion, where the maximum concentration of H_2O_2 is $\approx6\times10^{-3}$ mol dm^{-3}. Since is H_2O_2 decomposed by a catalytic reaction, the reversible fixation of gaseous oxygen was performed photochemically in the presence of EDTA, *i.e.*,

$$O_2 + 2\,EDTA + 2H^+ \xrightarrow{h\nu/\text{sensitizer}} H_2O_2 + 2\,EDTA^+$$
$$\xrightarrow{\text{catalysis}} (1/2)H_2O + (1/2)O_2.$$

This reaction leads to the consumption of EDTA.

The authors would like to express their thanks to Professor Hiroshi Kokubun of the Department of Chemistry in Tohoku University for his kind permission to use the flash photolysis apparatus. We also wish to thank to Miss Setsuko Kodera for her assistance.

References

1) L. I. Grossweiner, *Photochem. Photobiol.*, **10**, 183 (1969).
2) C. S. Foote, *Science*, **162**, 963 (1968).
3) C. S. Foote, "Free Radicals in Biology," ed by W. A. Pryor, Academic Press, New York (1976), Vol. II, p. 85.
4) J. D. Spikes and F. Rizzuto, "Progress in Photobiology," ed by G. O. Schenk, Detsuche Gesellschaft für Lichtforschung, Frankfurt (1972), No. P009.
5) M. Koizumi, S. Kato, N. Mataga, T. Matsuura, and Y. Usui, "Photosensitized Reaction," Kagaku Dohjin, Kyoto (1977).
6) F. Rizzuto and J. D. Spikes, *Photochem. Photobiol.*, **25**, 465 (1977).
7) M. Koizumi and Y. Usui, *Mol. Photochem.*, **4**, 57 (1972).
8) Y. Usui, K. Itoh, and M. Koizumi, *Bull. Chem. Soc. Jpn.*, **38**, 1015 (1965).
9) Y. Usui and M. Koizumi, *Bull. Chem. Soc. Jpn.*, **40**, 440 (1967).
10) V. Kashe and L. Lindqvist, *Photochem. Photobiol.*, **4**, 923 (1965).
11) A. G. Kepka and L. I. Grossweiner, *Photochem. Photobiol.*, **14**, 621 (1971).
12) G. I. Fisher, C. Lewis, and D. Madill, *Photochem. Photobiol.*, **24**, 223 (1976).
13) T. Ohno, S. Kato, and M. Koizumi, *Bull. Chem. Soc. Jpn.*, **39**, 232 (1967).
14) Y. Usui, *Chem. Lett.*, **1973**, 743.
15) F. A. Cotton and G. Wilkinson, "Advanced Inorganic Chemistry," John Wiley and Sons, New York (1970), Chap. 10.
16) R. W. Muller and C. T. Kerr, *J. Biol. Chem.*, **241**, 5597 (1966).
17) M. Imamura and M. Koizumi, *Bull. Chem. Soc. Jpn.*, **28**, 117 (1955).

Nuclear Quadrupole Resonance of $AlBr_3$ Molecular Complexes

Tsutomu Okuda,* Hiroshi Ohta, Hideta Ishihara, Koji Yamada, and Hisao Negita

Department of Chemistry, Faculty of Science, Hiroshima University, Higashisenda-machi, Naka-ku, Hiroshima 730

(Received February 18, 1980)

We observed the ^{81}Br NQR of several molecular complexes of $AlBr_3$ with amines such as $(CH_3)_3N$, C_5H_5N, $C_6H_5NH_2$, and $(C_6H_5)_2NH$. All the ^{81}Br resonance lines were found in the frequency range of 78—86 MHz at room temperature except for $AlBr_3 \cdot 2C_5H_5N$. From the Zeeman analysis, it was proved that $AlBr_3 \cdot 2C_5H_5N$ should be expressed with the molecular formula $2AlBr_3 \cdot 4C_5H_5N$ and contains cation species $AlBr_2(C_5H_5N)_4^+$ with two ^{81}Br resonance lines near 70 MHz and anion species $AlBr_4^-$ with four ^{81}Br resonance lines near 80 MHz. The two ^{81}Br resonance lines of $AlBr_3 \cdot (CH_3)_3N$ disappeared at about 40 °C due to hindered rotation of the whole molecule. The lower two ^{81}Br resonance lines of $AlBr_2(C_5H_5N)_4^+$ have positive temperature coefficients.

Aluminum tribromide is a Lewis acid and forms a number of molecular complexes with organic bases. The mechanism of complex formation is assumed to be mainly due to the interaction between the lone pair of the donor atom and the vacant sp^3 hybrid orbital of the Al atom.

NQR has been widely used for the study of these complexes of the $n\sigma$ type. Some NQR frequencies have been reported for molecular complexes of the type $AlBr_3 \cdot L$ (L=ethers, ketones, and pyridine).[1,2] However, no NQR result has been reported for the molecular complexes of the type $AlBr_3 \cdot 2L$.

In this investigation, we prepared several molecular complexes of $AlBr_3$ with amines and observed the ^{81}Br NQR spectra in order to examine the character of Al–Br bonds and the molecular structure.

Experimental

The complexes of $AlBr_3 \cdot (CH_3)_3N$ and $AlBr_3 \cdot 2(CH_3)_3N$ were prepared by the procedure described in the literature.[3,4] The others were obtained by melting the stoichiometric amounts of $AlBr_3$ and L (L=C_5H_5N, $C_6H_5NH_2$, and $(C_6H_5)_2$-NH) in closed glass ampoules. The single crystals of $AlBr_3 \cdot C_6H_5NH_2$ and $AlBr_3 \cdot 2C_5H_5N$ were grown by the method described previously.[5] The spectrometer used in the present experiment was a super-regenerative oscillator, and the absorption lines were observed on an oscilloscope. The Zeeman effect was examined by means of the zero-splitting cone method in a weak magnetic field of about 250 G provided by a Helmholtz coil. The temperature dependences of NQR frequencies were measured in the temperature range from liquid nitrogen temperature to the melting point. The temperature of the sample was determined using a copper-constantan thermocouple.

Results and Discussion

Table 1 shows ^{81}Br NQR frequencies and the signal-to-noise ratios in several molecular complexes of $AlBr_3$ with amines, determined at room temperature.

$AlBr_3 \cdot (CH_3)_3N$ and $AlBr_3 \cdot 2(CH_3)_3N$. $AlBr_3 \cdot (CH_3)_3N$ shows two ^{81}Br resonance lines with the intensity ratio of about 1:2. Though the crystal structure of this complex has not been determined as yet, $AlCl_3 \cdot (CH_3)_3N$ has been shown to have an ethane-like structure containing an Al–N bond, by means of X-ray diffraction.[6] The molecular structure of the bromide seems to be similar to that of the chloride in the light of the NQR results.

Table 1. ^{81}Br NQR frequencies in $AlBr_3$ molecular complexes at room temperature

Compounds		ν (MHz)	S/N
$AlBr_3 \cdot (CH_3)_3N$		79.108	4
		80.471	9
$AlBr_3 \cdot 2(CH_3)_3N$		83.168	4.5
		84.290	2.5
$AlBr_3 \cdot C_5H_5N$		79.575	7
		80.565	5
		81.424	7
$AlBr_3 \cdot 2C_5H_5N$	A	69.875	5.5
	B	69.955	5
	C	79.589	5
	D	79.667	5
	E	81.328	4.5
	F	81.331	4.5
$AlBr_3 \cdot C_6H_5NH_2$	A	79.194	3
	B	79.899	3.5
	C	84.853	4
$AlBr_3 \cdot (C_6H_5)_2NH$		78.497	4
		85.380	4.5
		85.511	4.5
Al_2Br_6[a]		79.84	(bridge)
		92.45	(terminal)
		93.61	(terminal)

a) T. Okuda *et al.*, *J. Chem. Phys.*, **52**, 5489 (1970).

The temperature dependences of ^{81}Br NQR frequencies were observed. Each resonance line began to broaden at about 30 °C and was no longer observable at about 40 °C, which is much below its melting point 156.9 °C. This disappearance is probably due to the hindered rotation of the whole molecule in the same manner as $BCl_3 \cdot (CH_3)_3N$ and $BBr_3 \cdot (CH_3)_3N$.[7,8] In the slope of the resonance frequency *versus* temperature curve we could not observe any abnormality which would be due to the reorientation of a methyl group or the rotation of a trimethylammonio group.[7]

Two ^{81}Br resonance lines were observed for $AlBr_3 \cdot 2(CH_3)_3N$. Their resonance frequencies are considerably higher than those of $AlBr_3 \cdot (CH_3)_3N$. Beattie *et al.* suggested from the study of the Raman spectra that the central Al atom in $AlBr_3 \cdot 2(CH_3)_3N$ is coordinated trigonal-bipyramidally, having two N atoms at axial sites and three Br atoms at equatorial sites.[4] This configuration about the Al atom is supported from the

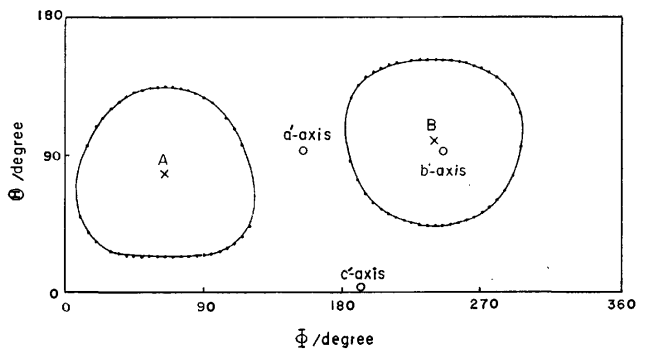

Fig. 1a. Zero-splitting patterns of ^{81}Br Zeeman lines of $AlBr_2(C_5H_5N)_4^+$ ion in $AlBr_3 \cdot 2C_5H_5N$.

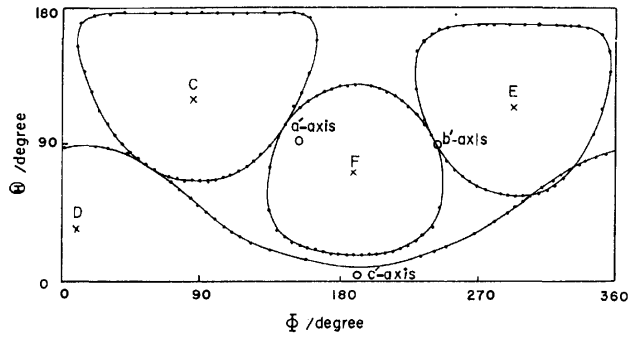

Fig. 1b. Zero-splitting patterns of ^{81}Br Zeeman lines of $AlBr_4^-$ ion in $AlBr_3 \cdot 2C_5H_5N$.

present results, because the difference in resonance frequencies is small.

$AlBr_3 \cdot C_5H_5N$ and $AlBr_3 \cdot 2C_5H_5N$. As listed in Table 1, three and six ^{81}Br resonance lines were observed in $AlBr_3 \cdot C_5H_5N$ and $AlBr_3 \cdot 2C_5H_5N$, respectively. Let us label the six resonance lines A, B, ···, F, from the lower to the higher, and label the Br atoms contributing to A, B, ···, F, Br(A), Br(B), ···, Br(F). It is found that two resonance lines, A and B, are remarkably lower than the rest. The Zeeman effect on ^{81}Br resonance lines in $AlBr_3 \cdot 2C_5H_5N$ was measured using a single crystal. Zero-splitting patterns are shown in Figs. 1a and 1b. Although four zero-splitting patterns were obtained for each resonance line, these figures show only one set of them which corresponds to a molecule in order to avoid unnecessary complexity. As all the asymmetry parameters are within ten percent, as listed in Table 2, no bridging Br atom is commonly assumed

TABLE 2. ^{81}Br NQR PARAMETERS IN $AlBr_3$ MOLECULAR COMPLEXES AT ROOM TEMPERATURE

Compounds	η (%)	e^2Qq/h(MHz)
$AlBr_3 \cdot 2C_5H_5N$	A 4.0	139.71
	B 9.8	139.69
	C 3.7	159.14
	D 7.8	159.17
	E 9.7	162.40
	F 5.9	162.57
$AlBr_3 \cdot C_6H_5NH_2$	A 10.3	158.11
	B 9.0	159.58
	C 3.2	169.68

TABLE 3. ANGLES BETWEEN THE X-AXES (X=a', b', c') AND THE Z-AXES IN $AlBr_3 \cdot 2C_5H_5N$

z-Axes	X=a'	X=b'	X=c'
Al–Br(A)	89.6°	170.7°	99.3°
Al–Br(B)	84.0	9.0	96.7
Al–Br(C)	69.0	137.4	125.0
Al–Br(D)	122.5	113.2	41.8
Al–Br(E)	129.7	52.7	118.2
Al–Br(F)	39.3	56.5	71.8

TABLE 4. BOND ANGLES IN $AlBr_3 \cdot 2C_5H_5N$

∠Br(A)–Al–Br(B)	173.5°
∠Br(C)–Al–Br(D)	109.4
∠Br(C)–Al–Br(E)	113.8
∠Br(C)–Al–Br(F)	107.9
∠Br(D)–Al–Br(E)	104.3
∠Br(D)–Al–Br(F)	113.6
∠Br(E)–Al–Br(F)	108.0

to exist in this complex, and the center of the zero-splitting pattern, *i.e.*, the direction of the z-principal axis of the electric field gradient, is regarded as the direction of Al–Br bond. Angles between Al–Br bonds were thus obtained from these patterns. The crystallographic axes were not determined from the Zeeman effect alone because of the higher class of crystal symmetry, though the axes corresponding to them were obtained from the symmetry of the zero-splitting pattern. For convenience, the axes obtained from NQR are arbitrarily termed the a'-, b'-, and c'-axis; these are perpendicular to each other. Angles between these axes and Al–Br bonds are tabulated in Table 3. The Al–Br(A) bond is perpendicular to the a'-axis and exists in the b'c' plane. Bond angles, ∠Br–Al–Br, are liested in Table 4. On the basis of the results obtained, the directions of Al–Br bonds in $AlBr_3 \cdot 2C_5H_5N$ are shown in Fig. 2. Br(A) and Br(B), whose ^{81}Br NQR

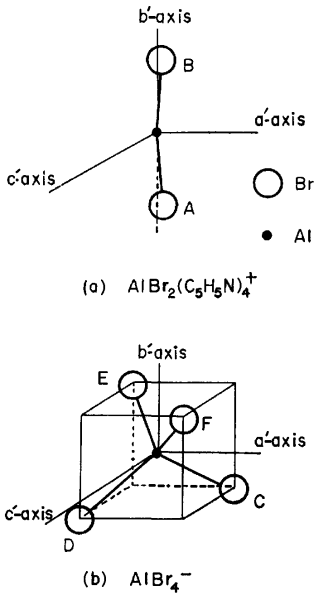

Fig. 2. Directions of Al–Br bonds with respect to the a'-, b'-, and c'-axis in $AlBr_3 \cdot 2C_5H_5N$.

frequencies are much lower than the rest, are at the axial sites and four pyridines are at the equatorial sites, near the a'c' plane, because of the well-known stableness of a six-coordinated Al atom. Br(C), Br(D), Br(E), and Br(F) are considered to belong to $AlBr_4^-$. Therefore, $AlBr_3 \cdot 2C_5H_5N$ is expressed with the molecular formula $2AlBr_3 \cdot 4C_5H_5N$ and contains cation species $AlBr_2(C_5H_5N)_4^+$ and anion species $AlBr_4^-$.

Recently, an X-ray study by Howard *et al.* revealed that the crystal of $AlCl_3 \cdot 2CH_3CN$ contains discrete $AlCl(CH_3CN)_5^{2+}$ and $AlCl_4^-$ ions together with one uncoordinated CH_3CN molecule per asymmetry unit.[9] Schmulbach reported from the phase study of $AlCl_3$–CH_3CN system that $AlCl_3 \cdot CH_3CN$ melts at 183.4 °C but $AlCl_3 \cdot 2CH_3CN$ melts incongruently at 74.2 °C.[10] The extraordinarily low melting point of the latter may be due to the solvation. On the other hand, the phase study of $AlBr_3$–C_5H_5N system showed that $AlBr_3 \cdot C_5H_5N$ and $AlBr_3 \cdot 2C_5H_5N$ melt congruently at 116.0 °C and 183.4—185.1 °C, respectively.[11] The tendency to melt in the 1 : 1 and 1 : 2 complexes is different between $AlCl_3$–CH_3CN and $AlBr_3$–C_5H_5N systems. This seems to arise from the difference in ionic structure of the 1 : 2 complex between the two systems.

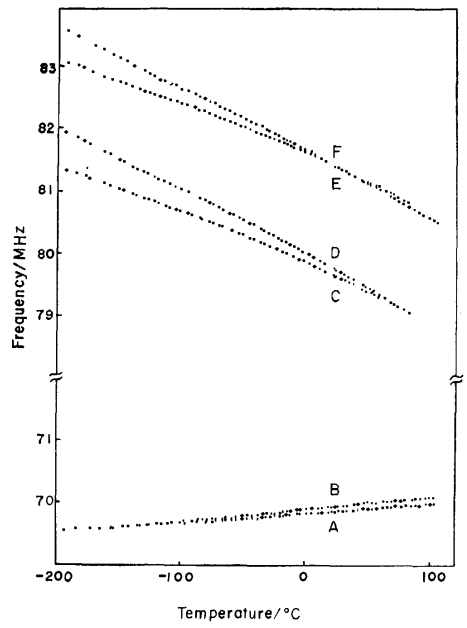

Fig. 3. Temperature dependences of ^{81}Br NQR frequencies in $AlBr_3 \cdot 2C_5H_5N$.

The temperature dependence of ^{81}Br NQR frequencies in $AlBr_3 \cdot 2C_5H_5N$ is shown in Fig. 3. In general, NQR frequencies decrease with increasing temperature as the electric field gradient of the resonant nuclei is averaged by the exciting of molecular motions. In this case, resonance frequencies corresponding to Br(A) and Br(B) increase with increasing temperature, while those of the rest decrease. Various compounds showing a positive temperature dependence have been found and the abnormality has been explained in terms of π-bonding or hydrogen bonding.[12,13] In the present case, a hydrogen bond does not occur because pyridine is not a proton donor but a proton acceptor.[14] We attributed the present positive temperature coefficient to a weak $p\pi$–$d\pi$ bond between aluminum and bromine atoms. This is probably due to π-back donation from the $4p_x$ and $4p_y$ orbitals of the bromine atom to the vacant 3d orbital of six-coordinated aluminum atom; the resonance frequency of the bromine atom thus decreases. However, this effect is cancelled with increasing temperature because the thermal vibration breakes the π-bond. Accordingly, the frequency increases with temperature will result from the stronger effect of the latter.

$AlBr_3 \cdot C_6H_5NH_2$ and $AlBr_3 \cdot (C_6H_5)_2NH$. Three resonance lines (designated as A, B, and C) were observed in $AlBr_3 \cdot C_6H_5NH_2$. There is a large difference in the frequency between the higher and the lower resonance lines. Since resonance lines were weak, we observed only a few zero-splitting patterns whose z-principal axes formed large angles to the rf coil axis. Asymmetry parameters and quadrupole coupling constants obtained are listed in Table 2. The asymmetry parameters of Br(A) and Br(B) are rather large, whereas that of Br(C) is small. This seems to be due to the difference in intermolecular interaction.

In contrast to $AlBr_3 \cdot C_6H_5NH_2$, two ^{81}Br resonance lines were observed in the high region and one line in the low region for $AlBr_3 \cdot (C_6H_5)_2NH$. This discrepancy between the two complexes may arise from a difference in intermolecular interaction or from a dimer formation like $2AlBr_3 \cdot C_6H_6$ because of a large steric effect of the ligand. The crystal structure determination is very desirable in order to discuss this problem in more detail.

References

1) Y. K. Maksytin, E. V. Bryuhova, G. K. Semin, and E. N. Gur'yanova, *Izv. Akad. Nauk SSSR, Ser. Khim.* **11**, 2658 (1968).
2) T. Deeg and A. Weiss, *Ber. Bunsenges. Phys. Chem.*, **80**, 22 (1976).
3) D. D. Eley and H. Watts, *J. Chem. Soc.*, **1952**, 1914.
4) I. R. Beattie, T. Gilson, and G. A. Ozin, *J. Chem. Soc., A*, **1968**, 1092.
5) H. Negita, T. Tanaka, T. Okuda, and H. Shimada, *Inorg. Chem.*, **5**, 2126 (1966).
6) D. F. Grant and R. C. G. Killean, *Acta Crystallogr., Sect. B*, **25**, 377 (1967).
7) D. F. R. Gilson and R. M. Hart, *Can. J. Chem.*, **48**, 1966 (1970).
8) T. Okuda, H. Ishihara, K. Yamada, and H. Negita, *Bull. Chem. Soc. Jpn.*, **52**, 307 (1979).
9) J. A. K. Howard, L. E. Smart, and C. J. Gilmore, *J. Chem. Soc., Chem. Commun.*, **1976**, 477.
10) C. D. Schmulbach, *J. Inorg. Nucl. Chem.*, **26**, 745 (1964).
11) J. Wilson and I. J. Worrall, *J. Chem. Soc., A*, **1967**, 392.
12) A. Sasane, T. Matsuo, D. Nakamura, and M. Kubo, *J. Magn. Reson.*, **4**, 257 (1971).
13) T. L. Brown and L. G. Kent, *J. Phys. Chem.*, **74**, 3572 (1970).
14) S. N. Vinogradov and R. T. Linnell, "Hydrogen Bonding," Van Nostrand Reinhold, New York (1971), p. 12.

Complexes between Nucleotide Base and Amino Acid. IV. Crystal and Molecular Structure of Cytosine : *N,N*-Phthaloyl-DL-glutamic Acid Complex Dihydrate

Akio TAKENAKA,* Minoru OHKI, and Yoshio SASADA

Laboratory of Chemistry for Natural Products, Tokyo Institute of Technology, Nagatsuta, Midori-ku, Yokohama 227

(Received February 19, 1980)

Crystals of cytosine: *N,N*-phthaloyl-DL-glutamic acid complex dihydrate were obtained from an aqueous solution of the two components. The space group is $P2_1/c$ with unit-cell dimensions of $a=5.243(1)$, $b=39.133(6)$, $c=9.192(1)$ Å, $\beta=93.66(1)°$, and $Z=4$. The structure was solved by the direct method and its parameters were refined by a block-diagonal least-squares method. The complex is formed by the two hydrogen bonds between the oxygen atoms of the ionized α-carboxyl group of glutamic acid and the nitrogen atoms, N(4) and protonated N(3), of cytosine. This binding mode is the same as that found in cytidine: *N*-benzyloxycarbonyl-L-glutamic acid complex, but quite different from that of 5-bromocytosine: *N*-acylglutamic acid complexes. The substituted bromine atom at C(5) of cytosine is thought to prescribe the binding mode in complex formation. The binding mode between cytosine and glutamic acid, which might be a possible elementary pattern of protein: nucleic acid interactions, is discussed in terms of dissociation constant.

In the studies of the elementary interaction patterns between amino acid and purine-pyrimidine base, we have found that *N*-tosyl-L-glutamic acid and *N,N*-phthaloyl-DL-glutamic acid are hydrogen-bonded to 5-bromocytosine with their γ-carboxyl group,[1,2] while Hata, Yoshikawa, Sato, and Tamura reported that in cytidine: *N*-benzyloxycarbonyl-L-glutamic acid complex dihydrate, cytosine base binds to α-carboxyl group of the amino acid.[3] It is interesting to examine what causes such different mode of cytosine: glutamic acid interactions. An X-ray analysis of the crystal structure of cytosine: *N,N*-phthaloyl-DL-glutamic acid complex has been performed, whose structure has revealed the effect of bromine atom on the complex formation.

Experimental and Structure Determination

Single crystals suitable for X-ray studies were obtained by slow evaporation of an aqueous solution containing equimolar amounts (0.2 mmol) of cytosine and *N,N*-phthaloyl-DL-glutamic acid, both of which were purchased from Tokyo Kasei Kogyo Co. The complex formation was confirmed by a preliminary X-ray experiment, an elemental analysis and IR spectrum of these crystals. Found: C, 48.0; H, 4.62; N, 13.2%. Calcd for $C_4H_5N_3O \cdot C_{13}H_{11}NO_6 \cdot 2H_2O$: C, 48.1; H, 4.75; N, 13.2%. Density was measured by the flotation method. Weissenberg photographs showed the systematic absences, $h0l$ for $l=2n+1$ and $0k0$ for $k=2n+1$, indicating the space group to be $P2_1/c$. A crystal $0.8\times0.8\times0.9$ mm was used for data collection on a Rigaku four-circle diffractometer with graphite-monochromated Mo $K\alpha$ radiation ($\lambda=0.71069$ Å). The unit-cell dimensions were calculated with 41 high-angle reflexions. The crystal data are given in Table 1.

TABLE 1. CRYSTAL DATA

Cytosine: *N,N*-Phthaloyl-DL-glutamic Acid Dihydrate	
$C_4H_5N_3O: C_{13}H_{11}NO_6: 2H_2O$	
Space group : $P2_1/c$	
$a=5.243(1)$ Å	$U=1882.2(4)$ Å^3
$b=39.133(6)$	$Z=4$
$c=9.192(1)$	$D_x=1.497$ g cm^{-3}
$\beta=93.66(1)°$	$D_m=1.49_7$

Intensities were measured in the ω scan mode with a scan width of 1° (in ω) plus α_1-α_2 divergence and a scan speed of 4° (in 2θ) min^{-1}. Five reference reflexions showed no significant intensity deterioration throughout the data collection. The intensities were corrected for Lorentz and polarization factors but not for absorption effects. Of 4306 independent reflexions in the range $2<2\theta<55°$, 1090 weak reflexions below background were considered as zero-reflexions; the observed threshold value, F_{11m}, was 2.55. The standard deviations were estimated by the equation of $\sigma^2(F_o)=\sigma_P^2(F_o)+qF_o^2$, where $\sigma_P(F_o)$ is evaluated by counting statistics and q (3.39×10^{-5}) was derived from the variations of the monitored reflexions.[4]

The structure was solved by the direct method and its parameters were refined by block-diagonal least-squares techniques. All the hydrogen atoms, found on a difference map, were included. The quantity minimized was $\sum w(|F_o|-|F_c|)^2$, with $w=1/\sigma^2(F_o)$. The zero-reflexions, for which $|F_c|>F_{11m}$, were included in the least-squares calculation by assuming $F_o=F_{11m}$ and $w=w(F_{11m})$. The final R was 0.55 for 2949 reflexions with $F_o>3\sigma(F_o)$; the maximum shift of parameters in the last cycle was 0.03σ for C, 0.45σ for H, 0.07σ for N, and 0.17σ for O atoms. Atomic scattering factors used were taken from "International Tables for X-Ray Crystallography."[5]

Atomic parameters are listed in Table 2, observed and calculated structure factors in Table 3.[6] Figure 1 shows a stereoscopic view of the cytosine: *N,N*-phthaloyl-DL-glutamic acid complex dihydrate. Bond distances and angles are shown in Fig. 2 together with the atomic numbering system. Bond angles involving hydrogen atoms are given in Table 4, least-squares planes together with deviations of atoms in Table 5, and hydrogen bond distances and angles in Table 6.

Results and Discussion

Molecular Structure. *N,N*-Phthaloyl-DL-glutamic acid is dissociated at the α-carboxyl group but not at the γ-carboxyl group, as confirmed by a difference synthesis. The bond distances and angles of the α- and γ-carboxyl groups are typical as those of the ionized and neutral carboxyl groups, respectively. The two identical C–O lengths of the α-carboxyl group suggest that the negative charges are equally localized on the two oxygen atoms.

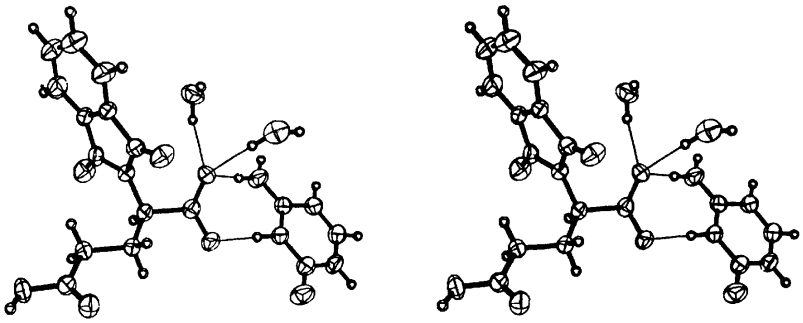

Fig. 1. Stereoview of the cytosine: *N,N*-phthaloyl-DL-glutamic acid complex dihydrate with 50% probability ellipsoids for the non-hydrogen atoms.

TABLE 2. FINAL POSITIONAL AND THERMAL PARAMETERS OF CYTOSINE: *N,N*-PHTHALOYL-DL-GLUTAMIC ACID COMPLEX DIHYDRATE

Standard deviations are given in parentheses. The anisotropic thermal factors has the form $\exp[-(\beta_{11}h^2+\beta_{22}k^2+\beta_{33}l^2+\beta_{12}hk+\beta_{13}hl+\beta_{23}kl)]$.

Atom	*x**	*y***	*z**	β_{11}*	β_{22}*	β_{33}*	β_{12}*	β_{13}*	β_{23}**
N (1)	4281 (3)	28608 (4)	3234 (2)	376 (9)	38 (1)	130 (3)	3 (2)	93 (8)	−42 (10)
C (2)	5852 (4)	26463 (5)	2533 (2)	282 (9)	49 (2)	103 (3)	2 (2)	11 (9)	0 (12)
N (3)	5507 (3)	23031 (4)	2776 (2)	304 (8)	40 (1)	96 (2)	15 (2)	97 (7)	2 (9)
C (4)	3758 (4)	21745 (5)	3660 (2)	275 (9)	48 (1)	85 (3)	10 (2)	54 (8)	23 (11)
C (5)	2196 (4)	24105 (5)	4380 (2)	303 (10)	48 (2)	103 (3)	14 (2)	120 (9)	16 (12)
C (6)	2513 (4)	27426 (5)	4145 (2)	337 (10)	53 (2)	115 (3)	17 (2)	70 (9)	−23 (12)
O (2)	7453 (3)	27482 (4)	1722 (2)	401 (8)	61 (1)	167 (3)	−6 (2)	201 (7)	115 (9)
N (4)	3567 (4)	18453 (4)	3820 (2)	444 (9)	44 (1)	147 (3)	18 (2)	246 (9)	45 (10)
C (7)	8001 (4)	15518 (5)	1519 (2)	209 (8)	41 (1)	97 (3)	5 (2)	56 (8)	−30 (10)
C (8)	8501 (4)	12757 (4)	381 (2)	231 (8)	35 (1)	73 (3)	6 (2)	16 (7)	3 (10)
C (9)	10535 (4)	13813 (5)	−653 (2)	287 (9)	36 (1)	81 (3)	0 (2)	62 (8)	−33 (10)
C (10)	10959 (4)	11072 (5)	−1774 (2)	309 (9)	44 (1)	77 (3)	−3 (2)	73 (8)	−44 (10)
C (11)	13054 (4)	11847 (5)	−2762 (2)	290 (9)	42 (1)	78 (3)	15 (2)	24 (8)	19 (11)
N (5)	9046 (3)	9433 (4)	1043 (2)	215 (6)	33 (1)	82 (2)	−2 (1)	18 (6)	7 (8)
O (3)	7526 (3)	14584 (3)	2773 (1)	356 (7)	48 (1)	86 (2)	6 (1)	129 (6)	−2 (8)
O (4)	7987 (3)	18540 (3)	1076 (2)	609 (9)	36 (1)	129 (2)	26 (2)	250 (7)	31 (8)
O (5)	13102 (3)	9550 (4)	−3823 (2)	488 (8)	58 (1)	114 (2)	−22 (2)	239 (7)	−204 (8)
O (6)	14583 (2)	14161 (3)	−2605 (2)	274 (6)	51 (1)	118 (2)	−10 (1)	75 (6)	−77 (8)
C (12)	7591 (4)	6499 (5)	726 (2)	277 (9)	44 (1)	93 (3)	−13 (2)	70 (8)	−103 (11)
C (13)	11130 (4)	8741 (5)	2032 (2)	238 (9)	44 (1)	87 (3)	2 (2)	55 (8)	9 (11)
C (14)	8846 (4)	3718 (5)	1601 (2)	320 (9)	35 (1)	93 (3)	−2 (2)	112 (8)	−36 (10)
C (15)	8182 (5)	308 (5)	1733 (3)	476 (12)	46 (2)	137 (4)	−20 (2)	90 (11)	−42 (13)
C (16)	9723 (5)	−1681 (5)	2684 (3)	756 (16)	36 (2)	160 (4)	−3 (3)	147 (13)	53 (14)
C (17)	11847 (5)	−332 (6)	3443 (3)	633 (15)	56 (2)	159 (4)	21 (3)	−8 (13)	134 (15)
C (18)	12515 (4)	3079 (5)	3303 (3)	439 (12)	53 (2)	135 (4)	15 (2)	16 (11)	106 (13)
C (19)	10955 (4)	5045 (5)	2376 (2)	280 (9)	36 (1)	89 (3)	5 (2)	81 (8)	13 (10)
O (7)	5721 (3)	6403 (4)	−111 (2)	361 (7)	62 (1)	150 (3)	−22 (2)	−112 (7)	−66 (9)
O (8)	12674 (3)	10845 (4)	2475 (2)	292 (7)	52 (1)	151 (3)	−17 (1)	−100 (7)	32 (9)
O (W1)	7221 (3)	9177 (4)	4659 (2)	440 (8)	79 (1)	96 (2)	8 (2)	107 (7)	89 (9)
O (W2)	9564 (3)	16577 (4)	5581 (2)	354 (7)	74 (1)	174 (3)	11 (2)	90 (7)	97 (10)

Atom	*x****	*y**	*z****	*B*(/Å²)*****	Atom	*x****	*y**	*z****	*B*(/Å²)*****
H (1)	448 (4)	3090 (5)	308 (2)	21 (5)	H (10B)	1142 (3)	890 (4)	−132 (2)	11 (4)
H (3)	643 (4)	2147 (5)	222 (2)	15 (5)	H (11)	1447 (5)	983 (6)	−432 (3)	64 (8)
H (5)	97 (4)	2322 (5)	503 (2)	18 (5)	H (15)	666 (4)	−54 (5)	120 (2)	18 (5)
H (6)	147 (4)	2920 (5)	462 (2)	25 (5)	H (16)	918 (4)	−407 (5)	283 (2)	31 (5)
H (4A)	462 (4)	1703 (5)	337 (2)	29 (5)	H (17)	1288 (4)	−184 (5)	414 (2)	41 (6)
H (4B)	237 (4)	1767 (6)	443 (2)	40 (6)	H (18)	1400 (4)	409 (5)	387 (2)	31 (5)
H (8)	686 (3)	1247 (4)	−21 (2)	2 (4)	H (W1A)	709 (4)	1063 (6)	395 (3)	42 (6)
H (9A)	1213 (3)	1444 (4)	−9 (2)	3 (4)	H (W1B)	857 (5)	934 (6)	505 (3)	68 (8)
H (9B)	992 (3)	1591 (4)	−116 (2)	0 (4)	H (W2A)	868 (5)	1807 (7)	612 (3)	72 (8)
H (10A)	942 (3)	1073 (4)	−241 (2)	9 (4)	H (W2B)	851 (6)	1584 (8)	466 (3)	111 (11)

*$\times 10^4$, **$\times 10^5$, ***$\times 10^3$, ****$\times 10$.

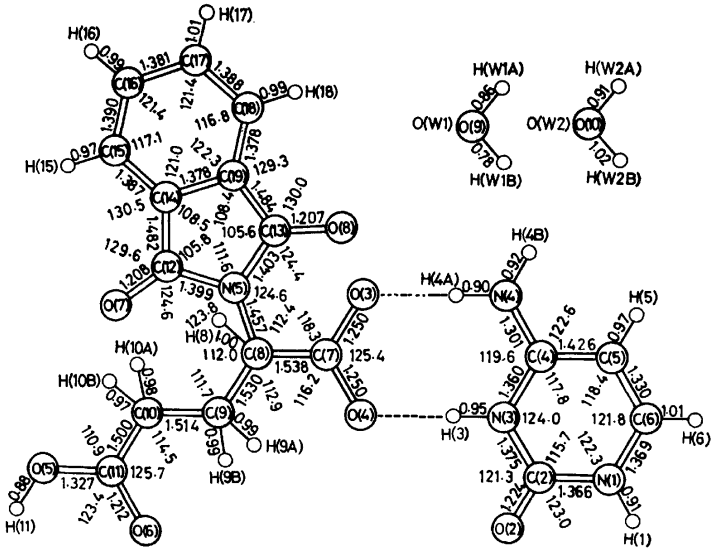

Fig. 2. Atomic numbering of the cytosine: *N,N*-phthaloyl-DL-glutamic acid complex dihydrate with bond lengths (l/Å) and angles (ϕ/°). E. s. d. 's are 0.003 Å and 0.2°, but 0.03 Å for those involving H atom. Bond angles involving H atoms are given in Table 4.

TABLE 4. BOND ANGLES INVOLVING HYDROGEN ATOMS OF CYTOSINE: *N,N*-PHTHALOYL-DL-GLUTAMIC ACID COMPLEX DIHYDRATE

	Angle (ϕ/°)		Angle (ϕ/°)
C(2)–N(1)–H(1)	117(2)	C(7)–C(8)–H(8)	106(1)
C(6)–N(1)–H(1)	121(2)	C(9)–C(8)–H(8)	108(1)
C(2)–N(3)–H(3)	118(2)	N(5)–C(8)–H(8)	106(1)
C(4)–N(3)–H(3)	118(2)	C(8)–C(9)–H(9A)	110(1)
C(4)–N(4)–H(4A)	120(2)	C(8)–C(9)–H(9B)	107(1)
C(4)–N(4)–H(4B)	117(2)	C(10)–C(9)–H(9A)	112(1)
H(4A)–N(4)–H(4B)	122(2)	C(10)–C(9)–H(9B)	109(1)
C(4)–C(5)–H(5)	119(2)	H(9A)–C(9)–H(9B)	106(2)
C(6)–C(5)–H(5)	123(2)	C(9)–C(10)–H(10A)	111(1)
C(5)–C(6)–H(6)	122(2)	C(9)–C(10)–H(10B)	112(1)
N(1)–C(6)–H(6)	116(2)	C(11)–C(10)–H(10A)	106(1)
		C(11)–C(10)–H(10B)	105(1)
H(W1A)–O(W1)–H(W1B)	109(3)	H(10A)–C(10)–H(10B)	108(2)
H(W2A)–O(W2)–H(W2B)	111(3)	C(11)–O(5)–H(11)	110(2)
		C(14)–C(15)–H(15)	119(2)
		C(16)–C(15)–H(15)	124(2)
		C(15)–C(16)–H(16)	117(2)
		C(17)–C(16)–H(16)	121(2)
		C(16)–C(17)–H(17)	119(2)
		C(18)–C(17)–H(17)	120(2)
		C(17)–C(18)–H(18)	122(2)
		C(19)–C(18)–H(18)	121(2)

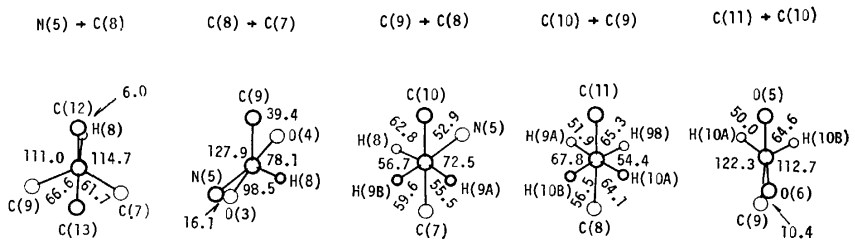

Fig. 3. Torsion angles (ϕ/°) of *N,N*-phthaloyl-DL-glutamic acid component.

TABLE 5. LEAST-SQUARES PLANES AND DEVIATIONS OF ATOMS FROM THE PLANES

X, *Y*, and *Z* are in Å along ***a****, ***b***, and ***c***, respectively. Asterisks denote atoms defining the plane. Standard deviations are given in parentheses.

Equation

Cytosine

$0.6791(6)X+0.0418(8)Y+0.7329(6)Z=4.069(8)$

Phthalimido group

$0.5646(6)X-0.2230(5)Y-0.7947(4)Z=1.339(4)$

Deviations(l/Å) of atoms from the plane

Cytosine		Phthalimido group	
N(1)*	−0.006	N(5)*	−0.012
C(2)*	0.006	C(12)*	0.007
N(3)*	0.000	C(13)*	−0.003
C(4)*	−0.004	C(14)*	0.015
C(5)*	0.003	C(15)*	0.002
C(6)*	0.004	C(16)*	−0.023
O(2)	0.007	C(17)*	−0.010
N(4)	−0.014	C(18)*	0.009
H(1)	−0.01	C(19)*	0.013
H(3)	−0.09	O(7)	0.025
H(4A)	0.01	O(8)	−0.012
H(4B)	−0.01	C(8)	0.007
H(5)	0.02	H(15)	−0.02
H(6)	0.01	H(16)	−0.09
		H(17)	−0.06
		H(18)	−0.01

The phthalimido group is almost planar, though the deviations of atoms from the mean plane indicate the slight bending of the group along its long axis (see Table 3). The N(5) and C(8) atoms also lie on this plane, suggesting an sp^2 hybridization of N(5). The bond distances and angles of the phthaloyl group are in good agreement with those in 5-bromocytosine: *N,N*-phthaloyl-DL-glutamic acid complex[2] and in the other related compounds.[7]

The torsion angles of the glutamic acid are shown in Fig. 3. The γ-carboxyl group has a synplanar C–C–C=O conformation as a common feature of carboxylic acids.[8] The extended conformation of the C–C chain is different from the folded form found in 5-bromocytosine: *N,N*-phthaloyl-DL-glutamic acid complex, where the C(9)–C(10) bond is in gauche conformation.[2] The conformation of the phthaloyl group is similar to that in 5-bromocytosine: *N,N*-phthaloyl-DL-glutamic acid.[2]

The hydrogen atom released from the α-carboxyl group is transferred to N(3) of cytosine molecule. As compared with the neutral cytosines, the protonation gives rise to a change of cytosine geometry similar to that discussed in cytosine: *N*-formylglycine complex.[9] Figure 4 compares the bond distances of cytosinium cations found in different environments. In cytosine: *N*-formylglycine complex (a), the positive and negative charges are mainly localized on the N(3) atom of

TABLE 6. HYDROGEN BOND DISTANCES AND ANGLES OF CYTOSINE: *N,N*-PHTHALOYL-DL-GLUTAMIC ACID COMPLEX DIHYDRATE

Standard deviations are given in parentheses.

Distances (l/Å)		Angles (ϕ/°)	
N(3)···O(4)	2.735(2)	O(3)···O(W2)···O(2)[f]	115.7(1)
H(3)···O(4)	1.79(2)	H(4B)[e]···O(W2)–H(W2A)	126(2)
N(4)···O(3)	2.790(2)	H(4B)[e]···O(W2)–H(W2B)	90(2)
H(4A)···O(3)	1.91(2)	O(W2)–H(W2B)···O(3)	163(3)
N(4)···O(W2)[a]	2.828(2)	O(W2)–H(W2A)···O(2)[f]	156(3)
H(4B)···O(W2)[a]	1.92(2)	O(W1)–H(W1A)···O(3)	162(3)
O(3)···O(W2)	2.838(2)	O(3)···O(W1)···O(5)[h]	111.9(1)
O(3)···H(W2B)	1.84(3)	H(W1A)–O(W1)···H(11)[h]	106(2)
O(3)···O(W1)	2.746(2)	H(W1B)–O(W1)···H(11)[h]	119(2)
O(3)···H(W1A)	1.91(2)	C(7)–O(3)···N(4)	110.9(2)
O(2)···O(W2)[d]	2.807(2)	C(7)–O(3)···O(W1)	146.2(2)
O(2)···H(W2A)[d]	1.95(3)	C(7)–O(3)···O(W2)	132.3(2)
N(1)···O(6)[c]	2.940(2)	N(4)···O(3)···O(W1)	97.2(1)
H(1)···O(6)[c]	2.04(2)	N(4)···O(3)···O(W2)	77.4(1)
O(5)···O(W1)[b]	2.649(2)	O(W1)···O(3)···O(W2)	70.8(1)
H(11)···O(W1)[b]	1.79(3)	C(7)–O(3)···H(4A)	109(1)
		C(7)–O(3)···H(W1A)	143(1)
Angles (ϕ/°)		C(7)–O(3)···H(W2B)	137(1)
N(3)–H(3)···O(4)	176(2)	H(4A)···O(3)···H(W1A)	97(1)
C(2)–N(3)···O(4)	117.5(2)	H(4A)···O(3)···H(W2B)	77(2)
C(4)–N(3)···O(4)	117.8(2)	H(W1A)···O(3)···H(W2B)	74(2)
N(3)···O(4)–C(7)	114.5(2)	O(5)–H(11)···O(W1)[b]	165(3)
H(3)···O(4)–C(7)	114(1)	C(11)–O(5)···O(W1)[b]	118.6(2)
N(4)–H(4A)···O(3)	165(2)	C(11)–O(6)···N(1)[g]	134.8(2)
N(4)–H(4B)···O(W2)[a]	172(2)	C(11)–O(6)···H(1)[g]	136(1)
C(4)–N(4)···O(3)	115.7(2)	N(1)–H(1)···O(6)[c]	170(2)
C(4)–N(4)···O(W2)[a]	112.8(2)	C(2)–N(1)···O(6)[c]	115.1(2)
O(3)···N(4)···O(W2)[a]	130.7(1)	C(6)–N(1)···O(6)[c]	122.4(2)
N(4)[e]···O(W2)···O(3)	78.5(1)	C(2)–O(2)···O(W2)[d]	143.1(2)
N(4)[e]···O(W2)···O(2)[f]	108.9(1)	C(2)–O(2)···H(W2A)[d]	136(1)

Symmetry codes (a) $-1+x, y, z$, (b) $1+x, y, -1+z$, (c) $-1+x, 1/2-y, 1/2+z$, (d) $x, 1/2-y, -1/2+z$, (e) $1+x, y, z$, (f) $x, 1/2-y, 1/2+z$, (g) $1+x, 1/2-y, -1/2+z$, (h) $-1+x, y, 1+z$.

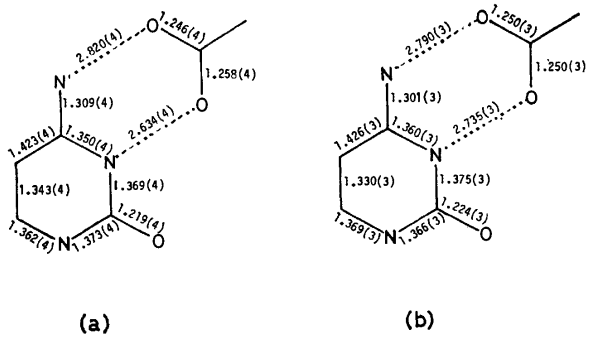

Fig. 4. A comparison of bond distances between (a) cytosine: *N*-formylglycine complex and (b) the present complex, cytosine: *N,N*-phthaloyl-DL-glutamic acid.

cytosine and its hydrogen-bonded oxygen atom of carboxyl group, respectively, and in consequence their distance becomes considerably shorter than that of N(4)···O. In the present complex (b), however, the two C–O distances of α-carboxyl group are identical and in addition these two oxygen atoms are hydrogen-bonded to N(3) and N(4) of cytosine at almost the same distances. In such a situation, the cytosinium cation is perturbed, so that the contribution from the canonical formula B increases, as compared with (a) in which the canonical formula A is predominant.

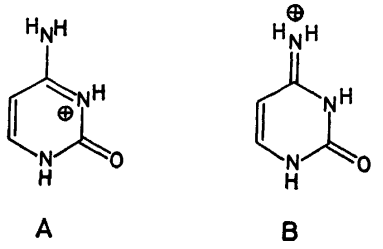

Slight differences in bond lengths seem to be consistent with this interpretation. Similar trend is also observed in cytidine: salicylic acid complex.[10]

The planarity of the present cytosine is excellent; only the N(4) atom deviates slightly from the mean plane (Table 5).

Crystal Structure. As shown in Figs. 1 and 5, the complex is formed by the two hydrogen bonds between the oxygen atoms of the dissociated α-carboxyl group of glutamic acid and the nitrogen atoms, N(4) and protonated N(3), of cytosine. This double hydrogen-bonded system is the same as that found in cytidine: *N*-benzyloxycarbonyl-L-glutamic acid complex.[3] The two N···O distances, N(3)···O(3) and N(4)···O(4), are nearly equal to each other, although the planar α-carboxyl group makes an angle of 35.3(7)° with the cytosine plane. This feature of the system is contrary to that of the above complex.[3]

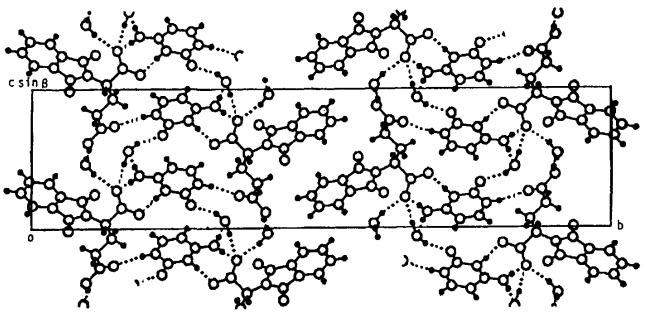

Fig. 5. Crystal structure of the cytosine: *N,N*-phthaloyl-DL-glutamic acid dihydrate, projected along the c axis.

The O(3) atom is also an acceptor of hydrogen bonds with the two water molecules. The O(W2) atom donates its hydrogen atom to O(2) of neighbouring cytosine and at the same time, accepts from N(4) of another cytosine. The γ-carboxyl group forms two hydrogen bonds; O(5) is a donor for O(W1) and O(6) is an acceptor from N(1) of adjacent cytosine. One of the two hydrogen atoms of water O(W1) is free from hydrogen bonding but directed to O(5) at $x,y,1+z$ with the O(W1)–H(W1B)···O(5) angle of 175(3)° and the distances, 3.306(2) Å for O(W1)···O(5) and 2.53(3) Å for H(W1B)···O(5).

The cytosine molecules are arranged parallel to one another on the c-glide plane. On the other hand, the phthaloyl groups come together around the inversion centres and packed parallel to form a sheet.

Complex Formation. In the present cytosine: *N,N*-phthaloyl-DL-glutamic acid complex and cytidine: *N*-benzyloxycarbonyl-L-glutamic acid complex,[3] the

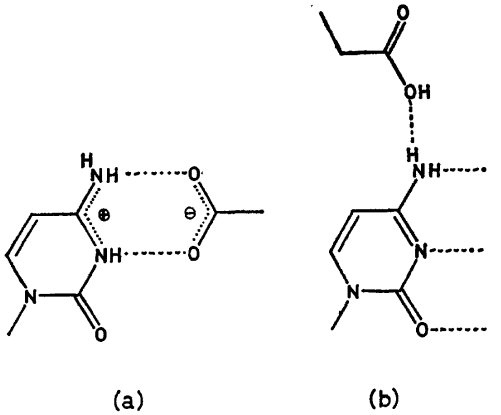

Fig. 6. Hydrogen bonding modes between cytosine and carboxyl group; (a) Type I and (b) Type II.

TABLE 7. DISSOCIATION CONSTANTS OF CYTOSINE, ITS DERIVATIVES AND *N*-ACYLAMINO ACIDS

	pK_a	Ref.
Cytosine	4.58	12
Cytidine	4.08	12
5-Bromocytosine	3.04	13
Cytidine 5′-phosphate	4.5	12
Cytidine 2′-deoxy-5′-phosphate	4.44	12
N-Acetylglycine	3.67	14
N-Benzoylglycine	3.65	14
N-Carbamoylglycine	3.88	14
N-Formylglycine	3.43	14
Glycylglycine	3.15	14
Glycylalanine	3.15	14
	pK_a^I	pK_a^{II}	Ref.
N-Benzoylglutamic acid	3.49	4.99	14

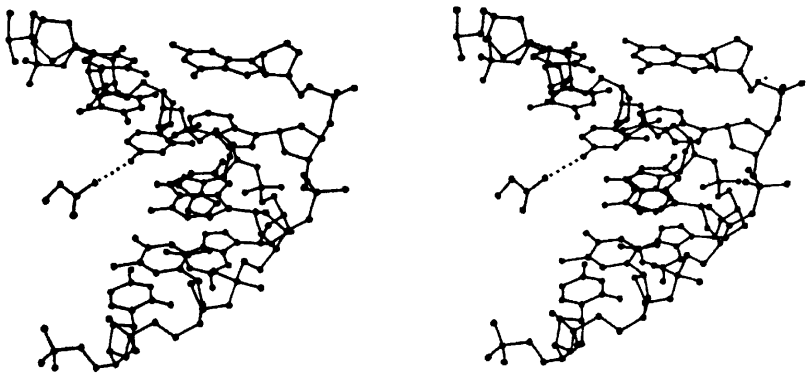

Fig. 7. A fitting feature between acidic side group of protein and cytosine moiety paired with guanine residue in the major groove of a double helical DNA (conformation B), in Type II mode.

binding modes are the same one (hereafter we designate Type I, see Fig. 6(a)) inspite of the different substitutions of glutamic acid and of cytosine, and the different crystal packings. On the other hand, the complexes with 5-bromocytosine are formed in the different mode (hereafter Type II, see Fig. 6(b)) for the two different acyl groups of the amino acids.[1,2] Consequently, it seems that the bromine atom at C(5) of cytosine determines the binding mode. The geometrical change of cytosine skeleton, which is caused by the steric and electronic effects of bromination at C(5), can be related to their dissociation constants in solution.[11] Accordingly, the complex formation modes may be interpreted in terms of pK_a values.

Table 7 lists the dissociation constants of cytosine, its derivatives and some *N*-acylamino acids. The pK_a values of *N*-acylglycines are almost invariant for different acyl groups. So, it is reasonable to assume pK_a^I and pK_a^{II} values of *N*-acylglutamic acids to be close to those of *N*-benzoylglutamic acid. Accordingly, the pK_a value of the α-carboxyl group of *N*-acylglutamic acids may be lower than that of cytosine or cytidine. In a solution containing *N*-acylglutamic acid and cytosine or cytidine, the latter molecule is easily protonated by the amino acid and both interact with each other in the Type I binding mode. On the other hand, the pK_a value of 5-bromocytosine is even less than that of the α-carboxyl group of *N*-acylglutamic acid. Therefore, 5-bromocytosine molecule could scarcely take a proton from *N*-acylglutamic acid. Consequently, the α-carboxyl groups are associated to form a dimer or tetramer[2] in the crystal, whereas 5-bromocytosine molecules are coupled with each other by the two N(4)–H···N(3) hydrogen bonds, the amino group of which are hydrogen-bonded to the γ-carboxyl group.[1,2]

Protein: Nucleic Acid Interaction. In the previous paper, we have proposed that the two binding modes, Type I and Type II, are elementary patterns of protein: nucleic acid interactions.[1,2] The pK_a values of proteins at the C terminal and at the acidic side groups respectively might be near pK_a^I of glycylglycine or glycylalanine and pK_a^{II} of *N*-acylglutamic acid. On the other hand, in nucleic acid cytosine bases would have a pK_a close to that of cytidine 5′-phosphate (CMP),

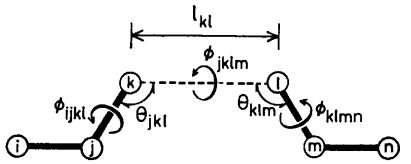

Fig. 8. Definition of the binding parameters in Table 8.

Table 8. Binding parameters between cytosine and carboxyl group in fig. 7

Binding parameter			
Interaction bond distance (/Å)			
l_{kl}			2.80
Bond angle(/°)			
θ_{jkl}			158
θ_{klm}			150
Torsion angle (/°)			
ϕ_{ijkl}			183
ϕ_{jklm}			−8
ϕ_{klmn}			−13
Atoms in cytosine		Atoms in carboxyl group	
i	N(3)	l	O
j	C(4)	m	C(1)
k	N(4)	n	C(2)

which is a value between those of carboxyl groups in proteins mentioned above. Therefore, the above discussion in terms of pK_a is also applicable and supports our previous proposal that the Type I is a binding pattern, *e.g.* between the unpaired cytosine in CCA terminus of tRNA and the C-terminal carboxyl group in enzyme, and the Type II is an elementary pattern of interaction between paired cytosine and acidic side group of amino acid residue.

To examine the above-mentioned argument, we have attempted to fit the binding geometry of Type II into a major groove of a double helical DNA (conformation B) using an interactive modelling programme[15] with computer graphics; atomic coordinates were taken from the works of Arnott and Hukins.[16] Trials show that the major groove† of B-DNA is not so wide for binding

† The major groove of B-DNA has been suggested to be a binding site from its surface accessibility[17] and from its methylation reactions.[18]

of carboxyl group to cytosine residue, due to their directional properties of hydrogen bondings. Base sequences also restrict the region. Interacting feature free from any steric hindrance, shown in Fig. 7, was constructed with small adjustment of torsional angles or bond angles. The binding data used are given in Table 8, parameters of which are defined in Fig. 8. The hydrogen bonding patterns described in the present series, together with those in adenine: indole,[19] adenine: carboxyl group,[20] and adenine: amide group[21] systems, will be useful for understanding the protein: nucleic acid interactions.

The present work was partially supported by a Grant-in-Aid for Scientific Research from the Ministry of Education and by the Kawakami Foundation, to which the authors' thanks are due.

References

1) M. Ohki, A. Takenaka, H. Shimanouchi, and Y. Sasada, *Bull. Chem. Soc. Jpn.*, **49**, 3493 (1976).
2) M. Ohki, A. Takenaka, H. Shimanouchi, and Y. Sasada, *Bull. Chem. Soc. Jpn.*, **50**, 90 (1977).
3) T. Hata, M. Yoshikawa, S. Sato, and C. Tamura, *Acta Crystallogr., Sect. B*, **31**, 312 (1975).
4) L. E. McCandlish and G. H. Staut, *Acta Crystallogr., Sect. A*, **31**, 245 (1975).
5) "International Tables for X-Ray Crystallography," Kynoch Press, Birmingham (1974), Vol. IV. p. 71.
6) Table 3 has been deposited as Document No. 8034, at the Office of the Bulletin of the Chemical Society of Japan.
7) K. Gerst and C. E. Nordman, *Acta Crystallogr., Sect. B*, **33**, 1588 (1977); M. Sikirica, I. Vicković, and D. Viterbo, *Acta Crystallogr., Sect. B*, **35**, 1735 (1979).
8) L. Leiserowitz, *Acta Crystallogr., Sect. B*, **32**, 775 (1976).
9) M. Ohki, A. Takenaka, H. Shimanouchi, and Y. Sasada, *Bull. Chem. Soc. Jpn.*, **48**, 848 (1975).
10) C. Tamura, M. Yoshikawa, S. Sato, and T. Hata, *Chem. Lett.* **1973**. 1221 (1973).
11) M. Kato, A. Takenaka, and Y. Sasada, *Bull. Chem. Soc. Jpn.*, **52**, 49 (1979).
12) A. Albert, "Synthetic Procedures in Nucleic Acid Chemistry," ed by W. W. Zorbach and R. S. Tipson, John Wiley and Sons, Inc., New York (1973), p. 1.
13) I. Wempen and J. J. Fox, *J. Am. Chem. Soc.*, **86**, 2474 (1964).
14) "Lange's Handbook of Chemistry," 11th ed, ed by J. A. Dean, McGraw-Hill Book Co., New York (1973), pp. 5—15.
15) A. Takenaka and Y. Sasada, *J. Cryst. Soc. Jpn.*, **22**, 214 (1980).
16) S. Arnott and D. W. L. Hukins, *Biochem. Biophys. Res. Commun.*, **47**, 1504 (1972).
17) C. J. Alden and S. H. Kim, *J. Mol. Biol.*, **132**, 411 (1979).
18) L. Johnsrud, *Proc. Natl. Acad. Sci. U.S.A.*, **75**, 5314 (1978).
19) M. Ohki, A. Takenaka, H. Shimanouchi, and Y. Sasada, *Bull. Chem. Soc. Jpn.*, **50**, 2573 (1977); M. Ohki, A. Takenaka, H. Shimanouchi, and Y. Sasada, *Acta Crystallogr., Sect. B*, **33**, 2954 (1977).
20) A. Takenaka and Y. Sasada, 38th National Meeting of the Chemical Society of Japan, Nagoya, October 1978, Abstr., p. 1004.
21) M. Takimoto, A. Takenaka, and Y. Sasada, Annual Meeting of the Crystallographic Society of Japan, Nagoya, November 1979, Abstr., p. 1B-13.

Thermal Decomposition of Graphite Fluoride. I. Decomposition Products of Graphite Fluoride, $(CF)_n$ in a Vacuum

Nobuatsu WATANABE,* Satoshi KOYAMA, and Hiroki IMOTO**

Department of Industrial Chemistry, Faculty of Engineering, Kyoto University, Yoshida, Sakyo-ku, Kyoto 606

(Received February 22, 1980)

The mechanism of thermal decomposition of graphite fluoride, $(CF)_n$ in a vacuum was studied by means of chemical and gas analyses, and the measurement of crystallinity. The crystallinity of $(CF)_n$ was slightly improved in the step of initial decomposition. The fluorine/carbon atomic ratio of initial gaseous product evolved by decomposition was about 2. The product is CF_2 or C_2F_4, and then it gives several compounds by secondary reaction. Every second layers of $(CF)_n$ are decomposed, and the evolved molecules or radicals abstract fluorine atoms which are bonded to the neighboring two layers.

Graphite fluoride $(CF)_n$ is obtained by the direct reaction of elemental fluorine with graphite or other carbon materials, and its atomic ratio F/C is unity.[1] Its crystal structure is shown in Fig. 1. Graphite fluoride retains the layer structure of graphite, but the layer has a zig-zag form because of the formation of C–F bond. The network of carbon atoms is therefore covered with fluorine atoms. Furthermore, the spacing between neighboring two layers is expanded from that of graphite, 3.35 Å to a larger value between 5.8 and 8.9 Å. Carbon atoms which are placed at the edge site of the layer are connected with two or three fluorine atoms.[2] However, the product actually formed is considerably strained,[3] and has a turbostratic structure.[4]

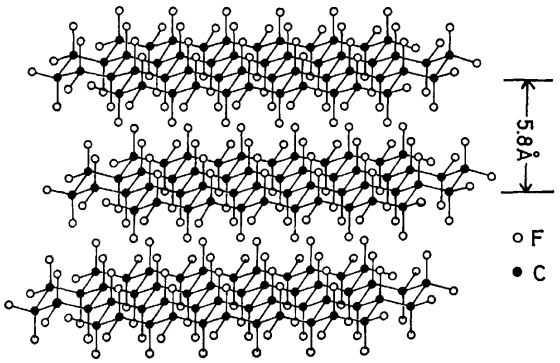

Fig. 1. Crystal structure of $(CF)_n$.
○: Fluorine atom, ●: carbon atom.

Thermal decomposition of graphite fluoride in a vacuum can be represented by:[5]

$$(CF)_n \longrightarrow \text{amorphous carbon} + C_2F_6 + CF_4 + C_3F_8 + C_2F_4 + \text{other perfluorocarbons.} \quad (1)$$

The rate of thermal decomposition is expressed by Avrami-Erofeyev's equation:

$$-\ln(1-\alpha) = (kt)^n, \quad (2)$$

where α is the fraction decomposed, k is the rate constant and n is the dimension of the nucleus growth. Kamarchik and Margrave[6] reported that n was 2 in Eq. 2. This result suggests that the decomposition proceeds two-dimensionally around an active site or a nucleus, and the reaction is auto-catalytic. However, they have not postulated a detailed mechanism for the decomposition.

In this work, the elemental and gas analyses were made in order to reveal the mechanism of the decomposition of $(CF)_n$ in a vacuum. The crystallinity of partially decomposed $(CF)_n$ was also measured.

Experimental

Powdery natural graphite whose grain size was 46—62 μm and flaky natural graphite whose grain size was 279—840 μm were fluorinated with elemental fluorine at 600 °C for 11 h for the former (sample I) and 24 h for the latter (sample II). Samles I and II thus obtained were used as the starting material for decomposition study. Interlayer spacings of samples I and II were 6.00 Å and 5.84 Å, and the F/C ratios were 0.94 and 0.93, respectively. The grain size of $(CF)_n$ is almost the same as that before fluorination.

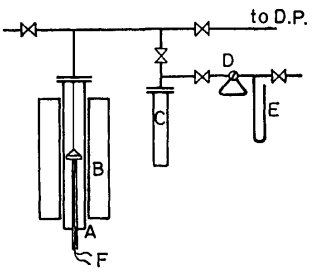

Fig. 2. Schematic diagram of apparatus for thermal decomposition.
A: Reaction tube, B: furnace, C: cold trap, D: gas sampler for gas chromatography, E: Hg manometer, F: thermocouple.

An apparatus made of Monel metal as shown in Fig. 2 was used for gas analysis. The gaseous products evolved by the decomposition were collected in a cold trap kept in liquid N_2. After the decomposition, the trapped gases were evaporated, and the total gas pressure was measured by Hg manometer. The gases were then introduced into a gas sampler, sepa rated and determined by means of gas chromatography. The identification was made by IR spectroscopy.

In another experiment, the sample was partially decomposed at 586 °C, and the residual substances were examined by X-ray diffraction and elemental analysis. The fluorine content was determined by a fluoride ion electrode after all fluorine atoms in $(CF)_n$ were allowed to form hydrogen fluoride by the oxygen flask combustion method.

** Present address: Research Laboratories of Osaka Soda Co., Ltd., Ohtakasu-cho, Amagasaki 660.

Results and Discussion

Change in Crystallinity of Graphite Fluoride and Carbon during Decomposition Process. The sample I was partially decomposed at 586 °C in a vacuum. The X-ray diffraction patterns were taken for residual substances.

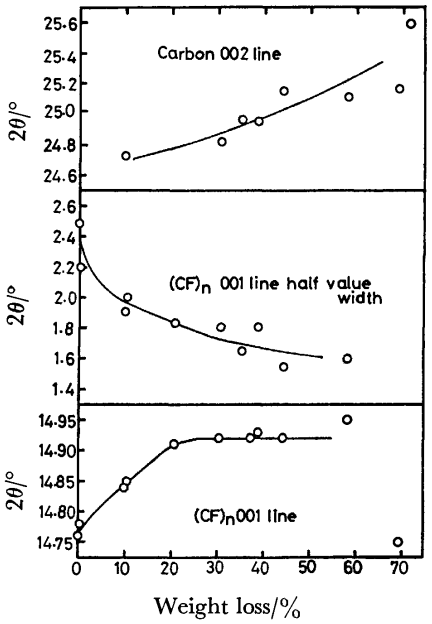

Fig. 3. Change in the crystallinity of graphite fluoride $(CF)_n$ and carbon formed during decomposition. Sample I was used.

Figure 3 shows the change in the position of the 002 line of carbon formed by decomposition, and the position and the half width of the 001 line of $(CF)_n$ during decomposition. The 002 line of carbon shifts to higher angle as the decomposition proceeds. The crystallinity of carbon is improved as the decomposition proceeds. The half width of 001 line of $(CF)_n$ becomes narrower and the position of the line profile shifts to higher angle, namely, the crystallinity of $(CF)_n$ is improved by decomposition, and the shift continues until the weight loss reaches to 20%. From the results, the decomposition is initiated at a strained region distributed in $(CF)_n$ crystal. In this region, a high stress is applied and the interlayer spacing of $(CF)_n$ tends to expand.[3] The strained region is perfectly decomposed within 20% weight loss.

The Composition Change of Graphite Fluoride. Figure 4 shows the composition change of $(CF)_n$ during decomposition at 586 °C. The plot from experiment shows a good agreement with the curve calculated under the assumption that the F/C ratio of gaseous products is 2. Therefore, the initial gaseous product is supposed to be C_2F_4 or CF_2. To confirm this, the decomposition of sample I was carried out in two different apparatus made of either pyrex glass or Monel metal shown in Fig. 2. Figure 5 shows the IR spectra of all gaseous compound by the decomposition. In the former apparatus, the absorption band of SiF_4 was more intense than that of other fluorocarbons (for example, 1250

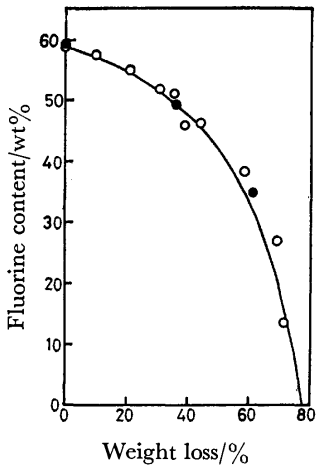

Fig. 4. Change in fluorine contents of solid products decomposed under vacuum.
—○—: Sample I, —●—: Sample II.
Solid line: Calculated under the assumption that the F/C ratio of gaseous products is 2.

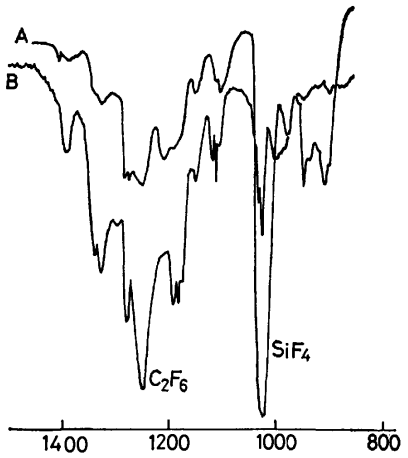

Fig. 5. Infrared spectra of total gases formed during decomposition in a vacuum.
A: Pyrex glass, B: Monel metal.

cm^{-1} for C_2F_6), and the absorption band of CO_2 was observed at 2300 cm^{-1}. They are the reaction products with glass at high temperature. However, Atkinson and Atkinson reported that C_2F_4 did not react with glass below 700 °C.[7] Therefore, the main gaseous product should be an active substance such as CF_2, beside C_2F_4.

Analysis of Gaseous Products. Reaction conditions and the amounts of each gas evolved by decomposition of 100 mg of $(CF)_n$ are shown in Table 1. C_2F_6, C_3F_8, and other saturated fluorocarbons were observed in addition to C_2F_4. They would be produced by the secondary reaction of C_2F_4 or CF_2. It is noteworthy that the amounts of unsaturated fluorocarbons, C_2F_4 and C_3F_6, formed in the experiment without trapping the gas during the reaction (run 6) are small compared with those formed in the experiment with trapping them (run 4). Moreover, the amounts of CF_4 and C_2F_6 are

TABLE 1. ANALYSIS OF GASEOUS PRODUCTS EVOLVED FROM GRAPHITE FLUORIDE DURING THERMAL DECOMPOSITION

Run	Sample	Temp/°C	t/min	Weight loss/%	Total gas/ 10^{-5} mol/100 mg	Gaseous products /10^{-5} mol/100 mg(%)			/1000 counts/100 mg	
						CF_4	C_2F_6	C_2F_4	C_3F_8	C_3F_6
1	I	663	34	73.7	37.0	9.09 (24.6)	14.64 (40.0)	3.81 (10.3)	767	264
2	I	661	10	72.5	35.8	10.14 (28.4)	13.58 (38.0)	4.16 (11.6)	729	289
3	I	611	119	72.0	28.6	6.23 (21.8)	10.10 (35.3)	3.19 (11.2)	631	291
4	I	618	82	70.1	26.9	7.58 (28.2)	10.07 (37.5)	3.10 (11.5)	625	288
5	I	618	10	13.5	4.64	1.49 (32.0)	1.70 (36.7)	0.71 (15.3)	88	22
6[a)]	I	619	82	70.1	31.8	9.11 (28.6)	11.38 (35.7)	0.01 (0.03)	729	59
7	II	616	338	74.4	34.1	7.76 (22.7)	12.49 (36.6)	2.75 (8.10)	861	180
8	I	569	920	74.4	30.7	9.20 (29.9)	8.56 (27.8)	3.10 (10.0)	387	269
9	I	569	411	53.9	24.8	9.42 (38.0)	7.68 (31.0)	3.08 (12.4)		
10	I	567	189	46.8	19.1	5.97 (33.7)	6.21 (35.0)	2.28 (12.9)	270	153

a) Without trapping the gases during the decomposition.

almost the same in both runs 4 and 6. From the result, it is clear that C_2F_4 and C_3F_6 do not form CF_4 or C_2F_6 but such compounds which have higher molecular weight. In fact, Atkinson and Atkinson[7] have reported that C_2F_4 cannot be decomposed into CF_4 at temperatures below 700 °C. Therefore, thermal decomposition of $(CF)_n$ should be expressed by the following equation,

$$2(CF)_n \longrightarrow nC^* + XCF_2 + YC_2F_4, \quad (X+2Y=n) \quad (3)$$

where C* is amorphous carbon. Kamarchik and Margrave[6] have concluded that the initial gaseous product in the decomposition of $(CF)_n$ is only C_2F_4, and that it changes to various gaseous products by secondary reactions. Their conclusion is inconsistent with the present results and those obtained by Atkinson and Atkinson.[7]

Other Products. In the decomposition of $(CF)_n$, a tarry product[8] and carbon have been found on the wall of the reaction tube in addition to the gaseous compounds. C_2F_4 or CF_2[9] formed by the initial reaction reacts with each other on the wall of apparatus or in the gas phase to form the tarry product, carbon deposit and perfluorocarbons of low molecular weight.

Process of Thermal Decomposition of Graphite Fluoride. Since the F/C ratio of gaseous compounds formed by thermal decomposition of $(CF)_n$ is 2, the remaining carbon atoms in $(CF)_n$ must be formed as perfectly amorphous carbon, and its crystallinity will never be improved even if the decomposition proceeds. However, the X-ray diffraction pattern of the residual carbon shows the improvement of the crystallinity, and moreover, the residual carbon obtained by complete decomposition has almost the same shape as that before decomposition. From these facts, every layer of $(CF)_n$ does not necessarily decompose, namely, C–C bonds in every second layer of $(CF)_n$ are ruptured by decomposition to form radicals, which abstract fluorine atoms bonded to the neighboring two layers to form CF_2 or C_2F_4 as shown in Fig. 6A.

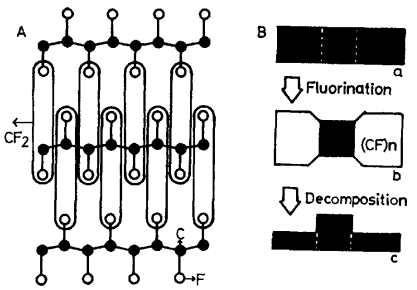

Fig. 6. Schematic illustration of thermal decomposition of graphite fluoride $(CF)_n$ (A) and thermal decomposition of partially fluorinated graphite (B).
a: Original graphite, b: partially fluorinated graphite, c: residual carbon after perfect decomposition.

Kamarchik and Margrave proposed the following mechanism as the thermal decomposition of $(CF)_n$. Fluorine atoms migrate from the interior of the particle to the edge, from which C_2F_4 is released.[6] According to their suggestion, the area of layer plane of residual carbon should become a half that of undecomposed one, and the thickness in the direction of c-axis should be the same as that of original graphite.

To confirm this, the change of the shape in the decomposition of flaky $(CF)_n$ having unreacted graphite in the sample[10] was observed by a microscope. The shape of the sample (Fig. 7) after decomposition was almost the same as that of the original one. The decomposed $(CF)_n$ region becomes thinner than the unreacted graphite. This process is shown by Fig. 6B. The mechanism of thermal decomposition of $(CF)_n$ postu-

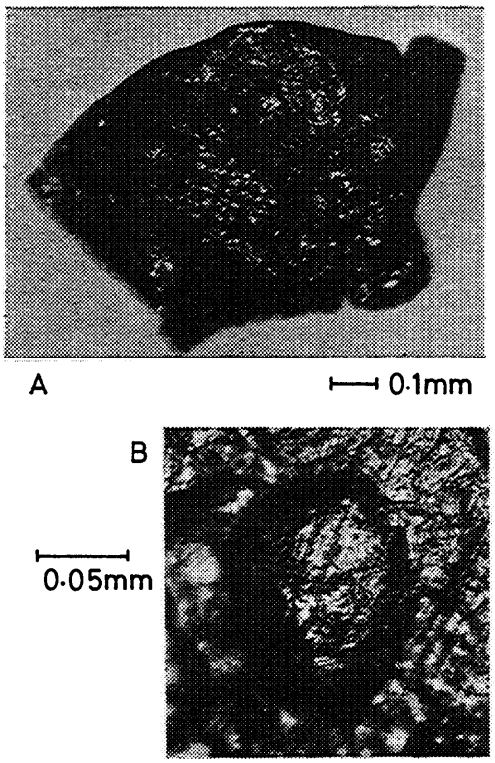

Fig. 7. Residual carbon formed from graphite fluoride having unreacted graphite.
A part of A is enlarged and shown in B.

lated by Kamarchik and Margrave cannot explain this phenomenon.

This reaction is similar to the mechanism of the decomposition of other graphite intercalation compounds.[11] In the case of thermal decomposition of $(CF)_n$, every second layers can be regarded as intercalants and the other layers as graphite layers. After releasing the intercalants, the interlayer spacing of the residual graphite decreases to that of original graphite. Owing to the decomposition of $(CF)_n$, the thickness of the particle in the direction of c-axis decreases to a half that of the original graphite. On the other hand, since the layer of unbonded carbon atoms with fluorine in $(CF)_n$ does not take part in decomposition, it maintains the original thickness.

The authors wish to express their thanks to Dr. Matae Iwasaki and Dr. Haruka Shinohara, Japan Atomic Energy Research Institute, for helpful advice.

References

1) The presence of a new type of graphite fluoride was confirmed by the authors, and its composition was found to be $(C_2F)_n$; Y. Kita, N. Watanabe, and Y. Fujii, *J. Am. Chem. Soc.*, **101**, 3832 (1979). In the present work, however, only $(CF)_n$ was dealt with.
2) N. Watanabe and H. Takenaka, 5th European Symposium on Fluorine Chemistry, Aviemore Scotland, 16—20 th September (1974).
3) N. Watanabe and H. Takenaka, *Tanso*, **92**, 2 (1978).
4) N. Watanabe, Y. Koyama, and S. Yoshizawa, *Denki Kagaku*, **31**, 756 (1963).
5) N. Watanabe and Y. Kita, *Nippon Kagaku Kaishi*, **1975**, 1896.
6) P. Kamarchik, Jr., and J. L. Margrave, *J. Therm. Anal.*, **11**, 259 (1977).
7) B. Atkinson and V. A. Atkinson, *J. Chem. Soc.*, **1957**, 2086.
8) The F/C ratio of this substance is unity, and it is similar to the compound reported by Atkinson and Atkinson.[7] Namely, it is polymeric substance having a chain of conjugated double bond.
9) The decomposition of $(CF)_n$ is an exothermic reaction. Provided that the initial product of decomposition is only CF_2, the reaction becomes endothermic. Therefore, either the formation of C_2F_4 or the reaction of the active species in the particle should be also taken into account.
10) The sample was prepared from natural graphite of 279—840 μm at 600 °C under 26.6 kPa fluorine.
11) M. Inagaki, *Carbon*, **4**, 137 (1966).

Intrinsic Quantum Efficiencies of Semiconductor Photoelectrodes Obtained by Temperature Measurement

Akira FUJISHIMA,* Yasuhisa MAEDA, and Kenichi HONDA

Department of Synthetic Chemistry, Faculty of Engineering, The University of Tokyo, Hongo, Bunkyo-ku, Tokyo 113

(Received February 20, 1980)

Quantum efficiencies of photoelectrochemical reactions on n-type and p-type semiconductor electrodes can easily be determined by the measurement of temperature changes of the surface of semiconductor electrodes by use of thermistors. The quantum efficiencies are intrinsic, since only the absorbed light quanta contribute to temperature change. The merits of the method, simplicity and applicability to the semiconductor of large surface reflectance, are discussed. The intrinsic quantum efficiencies were compared with those obtained by the usual chemical actinometric method.

Photothermal spectroscopy (PTS), a new spectroscopic method, has recently been developed.[1] A thermistor is placed on or close to a sample, and the temperature changes *i.e.*, thermistor resistance changes are measured during the course of irradiation of the sample with monochromatic light. It was found that the temperature change caused by light absorption is in line with the results of optical absorption spectroscopy. The method is applicable to cases in which samples are metal and semiconductor electrodes.[2-4]

A number of photoelectrochemical cells with use of semiconductor electrodes have been reported for the photodecomposition of water and the conversion of solar energy into electricity.[5-10] The energy conversion efficiencies and quantum efficiencies of electrochemical photocells are important for effective utilization of solar energy. Thermal measurements of semiconductor electrodes during the course of electrolysis facilitate the determination of the efficiencies.[4]

During the course of photoelectrochemical reaction only a portion of the light energy absorbed by the semiconductor can be utilized in the electrode reaction.[11] The remaining portion of energy is exhausted as heat. Thus, the efficiency of the process can be studied by monitoring temperature changes at the photoelectrodes as a function of electrode potential. In a previous paper, experimental results obtained by using CdS and TiO_2 single crystal photoanodes were presented, interpretation being given by means of a model for the energy balance within the system. The quantum efficiency and power efficiency could be determined without calibration of the irradiation source. The equation was derived by considering the energy balance within a semiconductor photoelectrode.[4] Let us consider the case in which the semiconductor electrode is illuminated with a monochromatic light pulse having an energy E (eV/photon), with an average absorbed intensity I (photon/s) for time t (s). The incoming energy (EIt) can then either be consumed by the semiconductor to promote the electrode reaction with the production of electric work (Vit) or evolved as heat in the semiconductor ($Q_{s.c.}$) *via* recombination and radiationless processes.

Thus the final equation for the overall photoelectrochemical reaction in the limiting photocurrent region is

$$E\frac{\Delta T}{\Delta T^\circ} = \frac{Q_{s.c.}+T\Delta S}{It} + e\eta_q(V-V_{fb}), \qquad (1)$$

where

ΔT: temperature change of the semiconductor surface
ΔT°: temperature change of the semiconductor surface in the open circuit
ΔS: entropy change for the semiconductor electrode reaction
$Q_{s.c.}$: heat evolved in the semiconductor *via* recombination and radiationless processes
$\eta_q\left(=\frac{i}{I}\right)$: quantum efficiency of photo-electrode reaction
V: applied potential (V *vs.* reference electrode)
V_{fb}: flatband potential (V *vs.* reference electrode).

Thus under constant illumination conditions (constant EIt) the plot $E\frac{\Delta T}{\Delta T^\circ}$ *vs.* $(V-V_{fb})$ gives the quantum efficiency, η_q, from the slope of the straight line and the loss term, $\frac{Q_{s.c.}+T\Delta S}{It}$, is obtained from the intercept of the $E\frac{\Delta T}{\Delta T^\circ}$ axis at $V=V_{fb}$ as shown in Fig. 1.

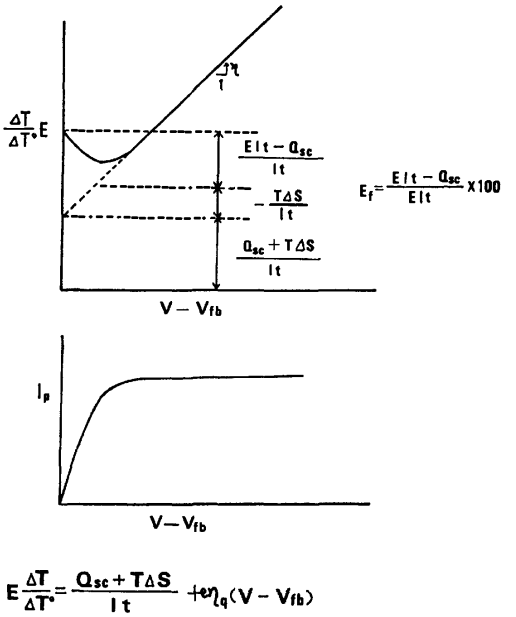

Fig. 1. Theoretical behavior of the temperature change *versus* potential.

From the loss term $\frac{Q_{s.c.}+T\Delta S}{It}$ the energy conversion efficiency

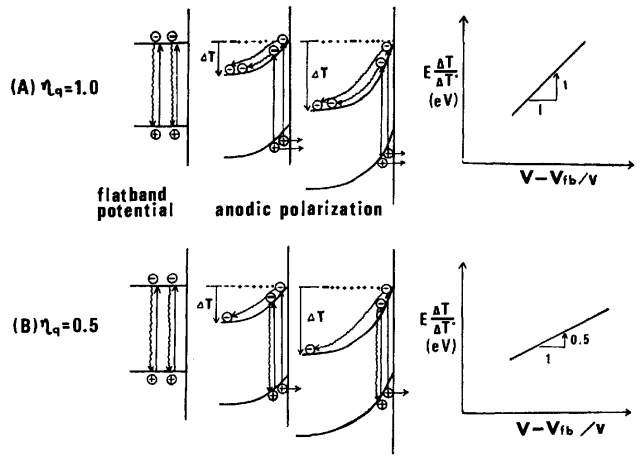

Fig. 2. Relationship between the temperature change and the applied potential in two model cases ((A), (B)). (A): Quantum efficiency is 1.0, (B): quantum efficiency is 0.5.

$$\eta_e = \frac{EIt - Q_{s.c.}}{EIt} \qquad (2)$$

can be easily obtained by making appropriate correction for the entropy change $T\Delta S$ associated with the electrode reaction.

In order to illustrate the use of Eq. 1 for obtaining quantum efficiency, two model cases are given (Fig. 2). When $\eta_q=1.0$, the slope of $E\frac{\Delta T}{\Delta T^\circ}$ against V should be 1.0, since all the electrons excited into the conduction band by light irradiation move from the surface into the bulk of the semiconductor through the space charge layer giving rise to heat generation. When $\eta_q=0.5$, the slope should be 0.5, since half of the excited electrons are recombined with the holes in the surface region.

Determination of the quantum efficiencies of various photoelectrodes [semiconductors of n-type (CdS, CdSe, GaP, GaAs, ZnO, TiO_2, and MoS_2), and p-type (GaP and GaAs)] can easily be carried out by direct measurement of temperature changes in the semiconductor electrodes.

Experimental

Procedure. The photothermal experiment on the photoelectrodes made of single crystals or polycrystals of n-CdS, n-CdSe, n-GaP, n-GaAs, n-TiO_2, n-ZnO, n-MoS_2, p-GaP, and p-GaAs (Table 1) was carried out according to the method reported.[4] Results are given for monochromatic irradiation at wavelengths shorter than that corresponding to the band gap energy (*e.g.* 340 nm for CdS). Photothermal responses were obtained for the photoelectrodes during anodic (n-type semiconductor) or cathodic (p-type) polarization, and under open circuit conditions in the electrolyte solutions. The corresponding current and temperature changes were then plotted as a function of potential *vs.* flatband potential or applied potential.

Apparatus. A block diagram of the apparatus is shown in Fig. 3. The light source employed was a 500 W high pressure mercury lamp (Ushio Electric) in an Ushio Model UI-501C lamp house. A lens to focus the light beam, interference filters (Koshin Kogaku) to select the wavelength of the exciting light, and a shutter with two timers (Ishikawa Seisakusho) to fix the irradiation period precisely were used.

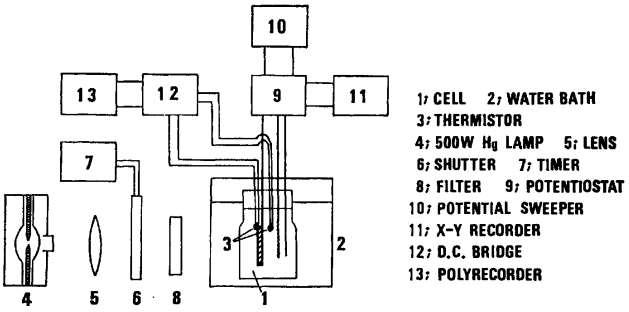

Fig 3. Measurement assembly.

The current-potential and current-time curves were measured under potentiostatic conditions with a potentiostat and a potential programmer (Nikko Keisoku, Models NPGS-301 and NPS-2). Cyclic voltammograms and current-time curves were displayed on an X-Y recorder (Yokokawa, Type 3078).

Characteristics of the semiconductor electrodes are given in Table 1. After ohmic contact, a copper wire was attached to the contact with conducting silver epoxy (Seisin Shoji, No. 4922). The back and sides of the crystal were insulated and mounted on a flat piece of glass attached to a glass rod with epoxy resin (Cemedain).

In order to measure the temperature changes, we used matched pairs of thermistors (Shibaura Electronics, Model BSB4-41A; nominal resistance 4 K Ω, sensitivity 0.052 °C/Ω). The thermistors having a time constant 0.4 s when immersed in still water were used in a differential arrangement with one held against the front surface of the semiconductor electrode and the other placed behind the electrode but not touching it. The cell was placed so that the monochromatic light beam struck only the electrode and none of the thermistors. Thus a change in temperature of the electrode caused a resistive change in the thermistor, producing a voltage imbalance in the DC bridge. The small voltage was amplified and then displayed on a strip chart recorder (Toa Electronics, Model EPR-2T).

The monochromatic light intensity was measured accurately in order to know the usual quantum efficiencies of the photoelectrodes using a chemical actinometric method (potassium ferrioxalate).[12]

All chemicals were of reagent grade and used without further purification. Where necessary, prepurified nitrogen gas was bubbled through the solution in order to remove dissolved oxygen.

Results and Discussion

CdS-Na_2SO_3 System. $E\frac{\Delta T}{\Delta T^\circ}$ was plotted against $(V-V_{fb})$ for an illuminated CdS single crystal electrode in a sodium sulfite aqueous solution in accordance with Eq. 1, where illumination conditions are constant [I: constant, E: 340 nm (3.6 eV), t: 20 s] (Fig. 4).

From the intercept of the y axis obtained by extrapolating the linear portion of the curve to the flatband potential, the energy conversion efficiency of the photoelectrode can be calculated if the heat evolved in terms of an entropy change ($T\Delta S$) attributable to the electrode reaction is obtained.[13] Though the heat

Table 1. Semiconductor electrodes employed

Semiconductor	Single or polycrystal	Manufacture	Shape dimensions /mm³	Surface oriented	Carrier density /cm⁻³	Ohmic contact	Surface treatment
n-CdS	Single	Teikoku Tsushin	$10\times10\times1$	(001)	4.8×10^{16}	In–Ga alloy	Polished with 0.3 μm[a] alumina powder; immersed for 10 s in concd HCl
n-CdS[b]	Poly		Disk $15\phi\times1.5$			In–Ga alloy	Immersed for 10 s in concd HCl
n-CdSe	Single		$10\times10\times1$			In–Ga alloy	Polished with 0.3 μm alumina powder; immersed for 10 s in concd HCl
n-GaP	Single	Sumitomo Metal Mining	Surface area 120 mm²	(111)	4.6×10^{17} (top) 1.1×10^{18} (bottom)	Au–Ge alloy evaporated; and heating in H_2 at 600 °C for 10—15 min	Polished with 0.3 μm[c] alumina powder; immersed for 30 s in aqua regia
n-GaAs	Single	Mitsubishi Metal	$10\times20\times1$	(100)	2.1×10^{17}	Au–Ge alloy evaporated; and heating at 600 °C for 10 min	Polished with 0.3 μm[d] alumina powder; immersed for 30 s in mixture of concd H_2SO_4, 30% H_2O_2, H_2O (3: 1: 1)
n-TiO_2	Single	Nakazumi Crystal	$15\times15\times1.5$	(001)		In–Ga alloy	Polished with 0.3 μm alumina powder; immersed for 10 s in concd H_2SO_4
n-ZnO[e]	Poly		Disk $15\phi\times1.5$			In–Ga alloy	Immersed for 10 s[f] in concd HCl
n-MoS_2	Single	Iwamoto Kobutsu	$10\times10\times10$	C axis	about[g] 1.3×10^{18}	In–Ga alloy	Immersed for 30 s[h] in 2 M HCl
p-GaP	Single	Sumitomo Metal Mining	Surface area 170 mm²	(100)	2.1×10^{17} (top) 3.5×10^{17} (bottom)	Au–Zn alloy evaporated; and heating in H_2 at 600 °C for 10—15 min	Polished with 0.3 μm[c] alumina powder; immersed for 30 s in aqua regia
p-GaAs	Single	Mitsubishi Metal	Surface area 150 mm²	(100)	3.34×10^{16} (front) 1.6×10^{17} (back)	Au evaporated; and heating at 500 °C for 10 min	Polished with 0.3 μm[d] alumina powder; immersed for 30 s in mixture of concd H_2SO_4, 30% H_2O_2, and H_2O (3: 1: 1)

a) Ref. 15. b) Super pure CdS powder, *ca.* 1 g (Furuuchi Chemicals) pressed at 150 kg/cm² and sintered in N_2 atmosphere at 600—700 °C for 3 h. c) Y. Nakato, S. Tonomura, and H. Tsubomura, *Ber. Bunsenges. Phys. Chem.*, **80**, 1289 (1972). d) P.A. Kohl and A.J. Bard, *J. Electrochem. Soc.*, **126**, 603 (1979). e) ZnO powder, *ca.* 1 g (Wako Pure Chemical Industries) pressed at 150 kg/cm² and sintered at 1300 °C for 3 h. f) W.P. Gomes, T. Freund, and S. R. Morrison, *J. Electrochem. Soc.*, **115**, 818 (1968). g) Calculated by Motto-Schottky plots. h) Ref. 18.

($T\Delta S$) accompanied by oxidation of sulfite ions is exothermic, the correction value for the heat ($T\Delta S$) has the opposite sign as compared with the case of oxidation of $K_4Fe(CN)_6$.[4] Energy conversion efficiencies of various kinds of semiconductor photoelectrodes obtained by the photothermal measurement were reported.[14]

A straight line with a slope equal to 1.0 can be observed in the limiting photocurrent region (Fig. 4), indicating that the quantum efficiency of the oxidation of sulfite ions on the illuminated CdS single crystal electrode is unity as shown in Fig. 2.[4]

The results were obtained under the conditions where each parameter, E, I, t, is constant. The effects of various parameters on the quantum efficiencies (slopes) were checked at first, using the CdS–Na_2SO_3 and ZnO–Na_2SO_4 system.

Effect of Exciting Wavelengths. On usual semiconductor photoelectrodes, the quantum efficiencies are almost the same in the wavelength region shorter than that corresponding to the band gap energy.

Figure 5 shows the results of the effect of exciting wavelengths on the slope using the CdS–Na_2SO_3, where t and I are constant. The wavelengths of monochromatic light irradiated were 340, 400, and 490 nm. When 340 nm was used to excite the CdS electrode, the temperature increase measured at open circuit corresponded to $E=3.6$ eV. Three parallel straight lines were observed. Use of the shortest wavelength light gave a line located in the highest position, indicating that electrons excited into the conduction band move through radiationless processes to the bottom of the conduction band, giving rise to an increase in $Q_{s.c.}$. The fact that the slope was 1.0 in all cases indicates that quantum efficiency was 1.0 at all three wavelengths. Thus we could use light of any wavelength

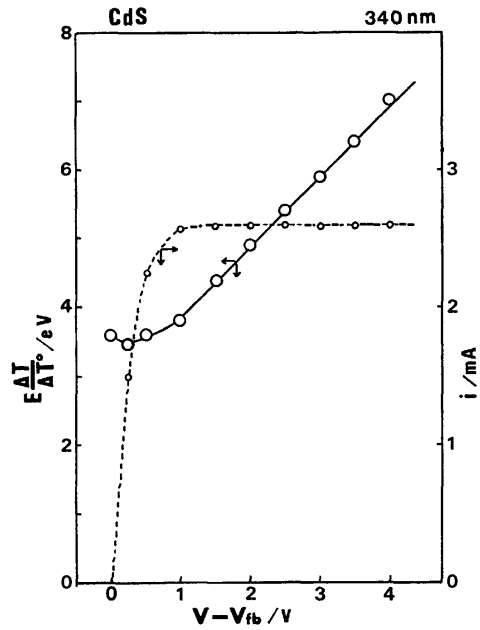

Fig. 4. Standardized temperature change *versus* potential from the flatband potential of the CdS single crystal electrode in 0.1 M Na_2SO_3 and 0.2 M Na_2SO_4.

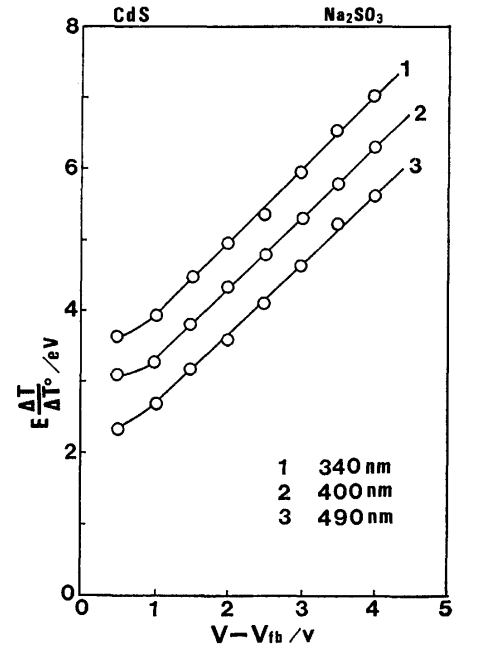

Fig. 5. The effect of exciting wavelengths on slope for the CdS single crystal electrode in 0.1 M Na_2SO_3 and 0.2 M Na_2SO_4.

shorter than that corresponding to the band gap energy to determine the quantum efficiency of a semiconductor reaction. If quantum efficiency changes with wavelengths, the slopes would also change.

Effect of Irradiation Time. The potential-ΔT relationship for the CdS–Na_2SO_3 system was measured at different irradiation times with light of constant intensity (photon numbers 5×10^{15} cm^{-2} s^{-1}), the slope being 1.0 in the irradiation time range 5—60 s (Fig. 6). A slope of 1.0 might be obtained even when irradiation

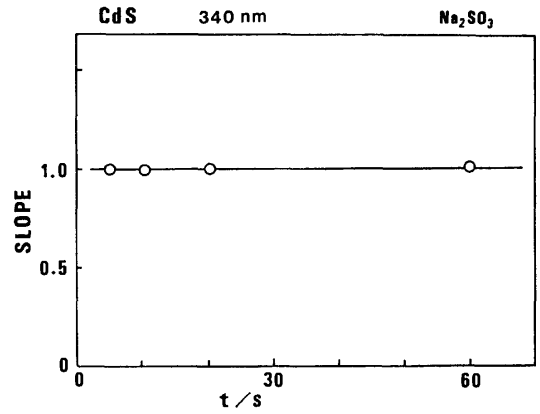

Fig. 6. The effect of irradiation time on slope for the CdS single crystal electrode in 0.1 M Na_2SO_3 and 0.2 M Na_2SO_4.

time is below 5 s. This was the case for 1.0 s irradiation time. However, in this case light of stronger intensity (1.8×10^{16} cm^{-2} s^{-1}) was introduced to the semiconductor surface to obtain a distinct rise in temperature. A slope can also be measured precisely by using a chopping system of light irradiation and a lock-in amplifier technique. When the semiconductor surface is excited for longer than 1 min (*e.g.* 2—5 min), the slope is expected to also be 1.0. However, in the irradiation time range 5—60 s, which we usually use, measurement is very easy.

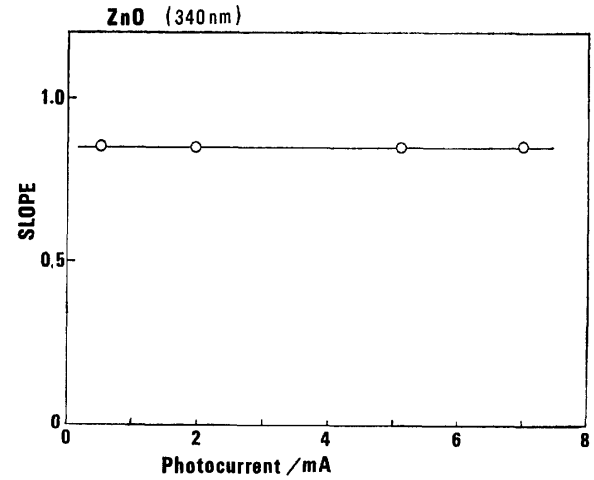

Fig. 7. The effect of light intensity on slope for the ZnO polycrystal electrode in 0.2 M Na_2SO_4.

Effect of Light Intensity. The effect of light intensity on the slope was studied using a polycrystal ZnO electrode in 0.2 M Na_2SO_4 (1 M=1 mol dm^{-3}) electrolyte solution. The results are shown in Fig. 7, where the abscissa represents the saturated photocurrent, which is proportional to the light intensity controlled by use of neutral density filters. The slope, *i.e.*, the quantum efficiency of the anodic reaction of the ZnO, was constant (0.85) at photocurrents of 500 μA cm^{-2}—7 mA cm^{-2} under the conditions of 340 nm wavelength and 20 s irradiation time (Fig. 7). The number of photons irradiated, as counted by chemical actinometry,

was between 4×10^{15}—6×10^{16} cm^{-2} s^{-1}. The magnitude of the photocurrent and the number of photons observed are of almost the same order as when measured in typical semiconductor electrode reactions.

The fact that these three parameters, *i.e.* wavelength, irradiation time, and intensity of light, can be appropriately selected depending on the characteristics of semiconductor electrodes indicates that this method is useful for obtaining quantum efficiencies.

n-Type Semiconductor Electrodes. *CdS Single Crystal*: As seen in the result for the CdS single crystal electrode, *i.e.* a slope of 1.0 (Fig. 4), oxidation of the sulfite ions occurs instead of dissolution of the CdS in a sodium sulfite solution.[15] On the other hand, quantum efficiency obtained by a comparison of the number of electrons calculated from the magnitude of photocurrent with the number of photons counted by chemical actinometry is 0.90—1.00, depending on the surface treatment.

CdS Polycrystal: The same reducing agent, SO_3^{2-}, was also used to suppress the dissolution of the polycrystal CdS electrode. The slope was 0.67, smaller than that of the single crystal CdS, probably due to the increase in surface recombination.

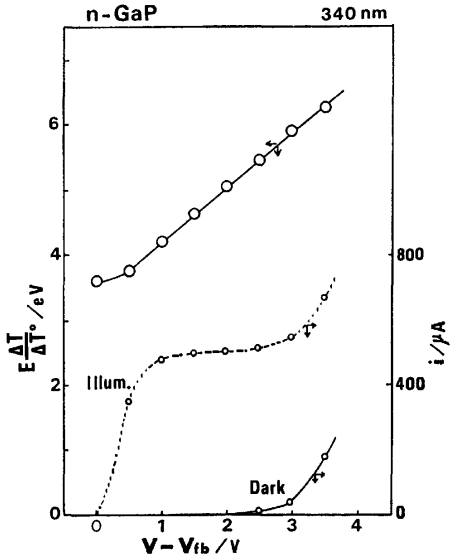

Fig. 8. Standardized temperature change *versus* potential and photocurrent *versus* potential of the n-GaP single crystal in 0.1 M Na_2S and 1 M NaOH.

n-CdSe, n-GaP, and n-GaAs Single Crystals: These semiconductor electrodes are also unstable in the usual electrolyte solution. For example, in 1 M NaOH, n-GaP dissolves under irradiation as follows:[16]

$$GaP + 11OH^- + 6p^+ \longrightarrow GaO_3^{3-} + HPO_3^{2-} + 5H_2O.$$

However, by using a strong reducing agent such as Na_2Se, the dissolution reactions can be suppressed.[17] Photothermal data and photocurrent-potential curves for the n-GaP electrode in a Na_2S aqueous electrolyte solution are shown in Fig. 8. Ellis *et al.*[17] reported that n-GaP was not stabilized perfectly in the Na_2S aqueous solution. However, we observed a constant photocurrent flow, indicating that the surface of the GaP electrode does not change during such a short irradiation period and weak intensity of light. The slope of $E\frac{\Delta T}{\Delta T^\circ}$ against potential was 0.85, which was larger than the quantum efficiency 0.62 obtained by chemical actinometry. In aqueous electrolyte solutions of the same reducing agent (Na_2S) the slope obtained for n-CdSe was 0.42 and that for n-GaAs 0.80. The value obtained for GaAs by chemical actinometry was considerably smaller (0.47). The large difference between the quantum efficiency from the slope and that from the chemical actinometry is not easy to interpret, since the surface of GaAs was not highly reflective as in the case of MoS_2.

TiO_2 Single Crystal: The slope, *i.e.* the quantum efficiency from temperature measurement, for TiO_2 changes with reduction treatment. By using TiO_2 single crystal reduced in a hydrogen atmosphere at 600 °C for 20 min, we obtained a slope of 0.7 in an aqueous solution of sulfuric acid.

ZnO Polycrystal: The results are shown in Fig. 7. The quantum efficiency from the slope is 0.85.

n-MoS_2 Single Crystal: For lustrous semiconductors, it is difficult to estimate the quantum efficiency of the photoelectrode reaction by the usual method of counting the number of photons by chemical actinometry. By the temperature method, we count only the photons absorbed in the surface of the semiconductor, with the result that value thus obtained for quantum efficiency can be taken as an intrinsic quantum efficiency. One of the most lustrous semiconductors is MoS_2, known as a layer compound semiconductor. Tributsch[18,19] reported that n-MoS_2 is a most promising photoelectrode for the electrochemical photocell because of its wide wavelength spectrum for photoactive reactions. Figure 9 shows the results with an n-type MoS_2 electrode. Under irradia-

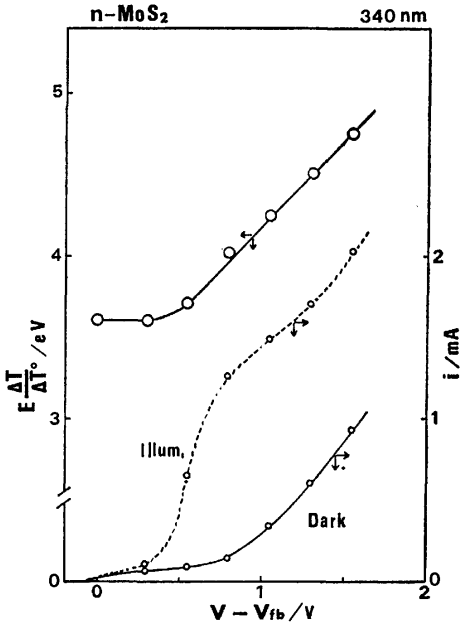

Fig. 9. Standardized temperature change *versus* potential and photocurrent *versus* potential of the n-MoS_2 single crystal in 0.2 M Na_2SO_4.

tion the limiting anodic photocurrent was obtained by substracting the anodic dark current. The slope of $E\frac{\Delta T}{\Delta T^{\circ}}$ due to a saturated photocurrent against the applied potential was 1.0. On the other hand, the quantum efficiency from the usual actinometric method was 0.54, suggesting that the temperature method is useful to determine the intrinsic quantum efficiency of a semiconductor electrode with a brilliant surface.

p-Type Semiconductor Electrodes. p-GaP and p-GaAs Single Crystal: In p-type semiconductor electrodes, the cathodic current increases by light irradiation. In the cathodic limiting photocurrent region, the relationship between temperature change and the applied potential can also give information on the intrinsic quantum efficiency. Figure 10 shows the results for a p-GaP single crystal electrode. From the linear slope, it was possible to obtain the intrinsic quantum efficiency of 0.80 for the hydrogen evolution reaction.

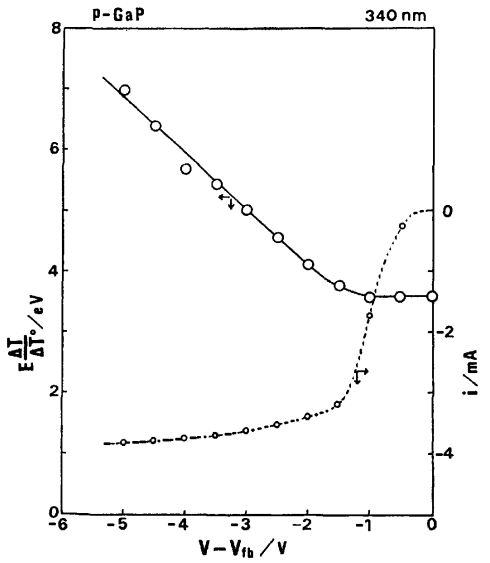

Fig. 10. Standardized temperature change *versus* potential and photocurrent *versus* potential of the p-GaP single crystal in 0.5 M H_2SO_4.

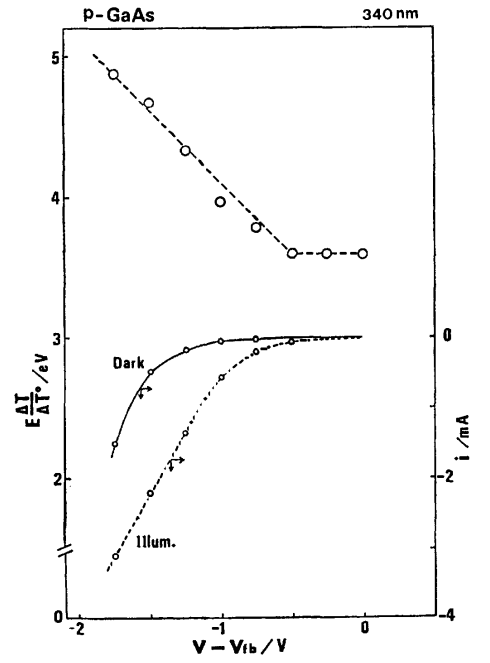

Fig. 11. Standardized temperature change *versus* potential and photocurrent *versus* potential of the p-GaAs single crystal in 0.5 M H_2SO_4.

Figure 11 shows the results for a p-GaAs single crystal electrode. Even in the limiting photocurrent region, the cathodic photocurrent increases gradually with cathodic polarization, the $E\frac{\Delta T}{\Delta T^{\circ}}$ *vs.* V curve showing no straight line. In this case, the slope of the tangent of the curve might indicate the quantum efficiency. Even in actinometric method, the quantum efficiencies showed different values depending on the applied potential, since the photocurrent is dependent on the applied potential in spite of the constant number of photons irradiated.

Summary

A comparison is made of the intrinsic quantum efficiencies obtained from the temperature measurement of the semiconductor surfaces (Table 2).

TABLE 2. COMPARISON OF QUANTUM EFFICIENCIES

340 nm

Electrode	η_t	η_a	Electrolyte
n-CdS s	1.00	1.00	Na_2SO_3
n-CdS p	0.67	0.67—0.70	Na_2SO_3
n-CdSe s	0.42	0.40—0.42	Na_2S
n-GaP s	0.85	0.62	Na_2S
n-GaAs s	0.80	0.47—0.49	Na_2S
n-TiO_2 s	0.70	0.70	H_2SO_4
n-ZnO p	0.85	0.76—0.78	Na_2SO_4
n-MoS_2 s	1.00	0.54	Na_2SO_4
p-GaP s	0.80	0.60—0.66	H_2SO_4
p-GaAs s	0.80—1.00	0.56—0.59	H_2SO_4

η_t:Quantum efficiency by temperature measurement. η_a:Quantum efficiency by actinometry. s: Single crystal. p: Polycrystal.

This temperature method has advantages over the usual actinometric method; i) simplicity, ii) no necessity of counting the number of photons irradiated and/or absorbed, iii) the possibility of obtaining intrinsic quantum efficiencies even for semiconductors which have large surface reflectance and/or scattering.

References

1) G. H. Brilmyer, A. Fujishima, K. S. V. Santhanam, and A. J. Bard, *Anal. Chem.*, **49**, 2057 (1977).
2) A. Fujishima, H. Masuda, K. Honda, and A. J. Bard, *Anal. Chem.*, **52**, 682 (1980).
3) G. H. Brilmyer and A. J. Bard, *Anal. Chem.*, **52**, 685 (1980).
4) A. Fujishima, Y. Maeda, K. Honda, G. H. Brilmyer, and A. J. Bard, *J. Electrochem. Soc.*, **127**, 840 (1980).
5) A. Fujishima and K. Honda, *Nature*, **283**, 37 (1972).

6) A. Fujishima, K. Kohayakawa, and K. Honda, *J. Electrochem. Soc.*, **122**, 1487 (1975).
7) H. Gerischer, *J. Electroanal. Chem.*, **58**, 263 (1975).
8) A. J. Bard, *J. Photochem.*, **10**, 59 (1979).
9) A. B. Ellis, S. W. Kaiser, and M. S. Wrighton, *J. Am. Chem. Soc.*, **98**, 6855 (1976).
10) B. A. Parkinson, A. Heller, and B. Miller, *J. Electrochem. Soc.*, **126**, 954 (1979).
11) A. Fujishima, G. H. Brilmyer, and A. J. Bard, "Semiconductor-Liquid Junction Solar Cells," ed by A. Heller, Electrochemical Society, Inc., Princeton, N. J. (1977), Proceeding Vol. 77-3, pp. 172—176.
12) C. G. Hatchard and C. A. Parker, *Proc. R. Soc. London, Ser. A*, **235**, 518 (1956).
13) R. Tamamushi, *J. Electroanal. Chem.*, **45**, 500 (1973); **65**, 263 (1975).
14) Y. Maeda, A. Fujishima, and K. Honda, *Rev. Polarogr.*, **24**, 87 (1978).
15) T. Inoue, T. Watanabe, A. Fujishima, K. Honda, and K. Kohayakawa, *J. Electrochem. Soc.*, **124**, 719 (1977).
16) K. Kohayakawa, A. Fujishima, and K. Honda, *Nippon Kagaku Kaishi*, **1977**, 780.
17) A. B. Ellis, J. M. Bolts, S. W. Kaiser, and M. S. Wrighton, *J. Am. Chem. Soc.*, **99**, 2848 (1977).
18) H. Tributsch and J. C. Bennett, *J. Electroanal. Chem.*, **81**, 97 (1977).
19) H. Tributsch, *Ber. Bunsenges. Phys. Chem.*, **81**, 361 (1977).

Effect of Cl^- and Br^- Ions and pH on the Flatband Potentials of Silver Halide Sheet Crystal Electrodes

Seiichi SUMI, Tadashi WATANABE, Akira FUJISHIMA,* and Kenichi HONDA

Department of Synthetic Chemistry, Faculty of Engineering, The University of Tokyo, Hongo, Bunkyo-ku, Tokyo 113

(Received February 23, 1980)

Flatband potential (E_{fb}), which coincides with the Fermi level in energy, was determined for AgCl and AgBr electrodes by electrochemical measurement of the capacitance of the space charge layer of a semiconductor in contact with a solution. The values of E_{fb} for both AgCl and AgBr electrodes in an electrolyte solution were −4.8 V *vs.* vacuum. The energy levels of the electrodes could be determined from this value. The behavior of the AgCl electrode is somewhat like an n-type semiconductor, and that of the AgBr electrode very much like an intrinsic semiconductor. The E_{fb} values for the AgCl and AgBr electrodes change cathodically in electrolyte solutions with Cl^- and Br^- ions, respectively, but not with H^+ or OH^- ions. This seems to be associated with the Ag^+ ion effect in spectral sensitization. It is concluded that the Ag^+ ion effect arises from a downward shift of the band edge of silver halides.

Studies are in progress on silver halides (AgX), major constituents of photographic emulsions, with respect to such problems as the number of silver atoms needed to form the minimum latent image,[1] and whether the ionic[2] or the electronic process[3] comes first in latent image formation. Positions of the conduction and valence bands are important for semiconductors, but, the data given by investigators for AgX differ as much as 0.1 V.[4–7]

Only a few papers have appeared on the Fermi energy level of AgX. Williams *et al.*[8] analyzed ultraviolet photoemission and reported energy differences between the Fermi energy level and the top of the valence band, 1.7 eV for AgCl, 1.2 eV for AgBr, and 1.1 eV for AgI. They determined the energy differences but not the positions of the Fermi energy levels of AgX *vs.* a reference electrode. In this study, the positions of the Fermi energy level for Ag/AgX/solution electrodes (X=Cl and Br) were determined *vs.* a saturated caromel electrode (SCE) as the flatband potential (E_{fb}) by electrochemical measurement of the capacitance of the space charge layer of a semiconductor in contact with a solution. The positions thus obtained seem to be useful for the electrochemical study of AgX.

Wagner[9] and Matejec[10] investigated the conductance of AgX (X=Cl, Br, and I) under various halogen pressures and found that there are many more electrons than holes for AgCl and somewhat more for AgBr in contact with silver at room temperature. Other investigators[11–13] reported that silver halides are n-type or p-type semiconductors. However, from the results of E_{fb} measurements, we have found the properties of AgCl and AgBr electrodes to be n-type and intrinsic semiconductors, respectively.

The spectral sensitivity of a photographic emulsion increases as the pAg (pAg=−log [Ag^+]) decreases. The Ag^+ ion effect was explained by Gilman,[5] and Collier and Gilman[14] in terms of subconduction band event, Ag^+ ions on the AgX surface acting as an electron trap. Iwasaki *et al.*[15] found that the sensitized photocurrent due to the electron injection from a photoexcited sensitizing dye increases with lowering of the pAg of the electrolyte solution. They concluded that the Ag^+ ion effect results from the anodic band edge shift of the AgCl electrode. Thus, the band edge shift due to Ag^+ ions seems to be important for clarifying the mechanism of the Ag^+ ion effect. The band edge shift of AgX could be determined by measuring E_{fb}. The Ag^+ ion effect was also investigated from the result of E_{fb} measurement.

Basic Principle

In the electrochemistry of semiconductors, the E_{fb} value is important for determining their energy levels and studying their electrode reactions. The relation between the capacitance of the space charge layer (C_s) and the surface potential ($\Delta\Phi_s$) is as follows.[16,17]

$$C_s = \frac{\varepsilon\cdot\varepsilon_0}{L}\frac{|y(e^{-V_s}-1)-y^{-1}(e^{+V_s}-1)|}{[y(e^{-V_s}-1)+y^{-1}(e^{+V_s}-1)+(y-y^{-1})V_s]^{1/2}} \quad (1)$$

where

$$y=\left(\frac{P_0}{N_0}\right)^{1/2},\ V_s=\frac{e_0\cdot\Delta\Phi_s}{k\cdot T},\ L=\left(\frac{\varepsilon\cdot\varepsilon_0\cdot k\cdot T}{2\cdot N_i\cdot e_0^2}\right)^{1/2},$$
$$\Delta\Phi_s=\Phi_s-\Phi_i,$$

and ε=dimensionless dielectric constant of semiconductor, ε_0=dielectric constant of the vacuum, P_0,N_0= equilibrium concentration of holes and electrons in bulk of semiconductor, k=Boltzmann constant, T=absolute temperature, e_0=elementary charge, $N_i=\sqrt{P_0\cdot N_0}$, Φ_s=potential of semiconductor surface, and Φ_i= potential of semiconductor bulk. When $\Delta\Phi_s$ and $1/C_s^2$ are represented by abscissa and ordinate, respectively, curves can be obtained depending on the values of y, ε, and N_i. The potential at which $\Delta\Phi_s$ becomes zero is E_{fb}. The value of $\Delta\Phi_s$ shows the potential difference between the bulk and the surface of a semiconductor, not directly showing the potential *vs.* reference electrode. This can be altered by changing the potential of a semiconductor bulk which can be changed by the electrode potentials (E) *vs.* reference electrode. The value of E_{fb} can be determined from the shape of the $1/C_s^2-E$ curve with respect to a reference electrode.

Equation 1 can be applied to n-type, intrinsic, and p-type semiconductors. However, it is so complicated that it is not generally used for n- or p-types. In the case of a highly doped n-type (or p-type) semiconductor, Eq. 1 can be simplified to the Mott-Schottky relation-

ship:

$$\frac{1}{C_s^2} = \frac{2}{\varepsilon \cdot \varepsilon_0 \cdot e_0 \cdot C_D}\left(\Delta\phi_s - \frac{k \cdot T}{e_0}\right), \quad (2)$$

where C_D=the donor concentration of an n-type semiconductor or the acceptor concentration of a p-type. It is significant that the plots of $1/C_s^2$ *vs.* $\Delta\phi_s$ or (E) derived from Eq. 2 are linear. The donor (acceptor) concentration can be calculated from the slope, giving the concentration of impurity added to the semiconductor. The potential where $1/C_s^2$ nearly approaches zero is E_{fb} in Eq. 2, the slope of the $1/C_s^2$—E curve being upward for an n-type semiconductor and downward to the right for a p-type.

Experimental

The methods of crystal preparation were the same as before,[18] except that the melting temperature was 455 °C for the AgBr crystal.

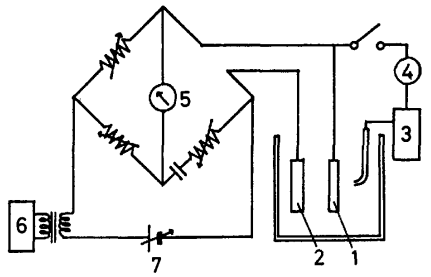

Fig. 1. Capacitance bridge circuit.
1: AgX electrode, 2: Pt counter-electrode, 3: SCE, 4: Voltmeter, 5: Null detector, 6: Oscillator (1 kHz), 7: Dry cells.

One side of the sheet crystals (diameter: 10 mm) was fastened to a lead wire with silver paste and to a glass spatula with epoxy resin, the electrodes prepared being left to stand overnight. The other surface was then etched with 1 M (1 M= 1 mol dm^{-3}) KCN for 5 min and washed thoroughly with distilled water. The AgX electrodes were immersed in electrolyte solutions of various compositions, C_S being measured by means of the capacitance bridge circuit shown in Fig. 1. The electrode potential *vs.* SCE was controlled by dry cells. During the course of measurements, contact to the voltmeter was cut to exclude extraneous capacitances. All experiments were carried out in a darkroom at room temperature. The electrolyte solutions were not deoxygenated. In addition to C_S, electrochemical cells also have counter electrode capacitance and Helmholtz layer capacitance, but they can be disregarded.

Results and Discussion

AgCl Electrode. $1/C_s^2$ is plotted against the electrode potential *vs.* SCE for the AgCl electrode in 0.1 M KCl aqueous solution (Fig. 2). The linearity of the plots shows that the Mott-Schottky relationship (Eq. 2) holds for AgCl. The E_{fb}, the potential where $1/C_s^2$ is close to zero, was 0.0 V *vs.* SCE, the value showing the position of the Fermi energy level of the AgCl electrode in 0.1 M KCl aqueous solution. The value of kT/e_0 in Eq. 2 is about 26 mV at room temperature, not being considered significant in comparison with the data of other investigators. Since the $1/C_s^2$

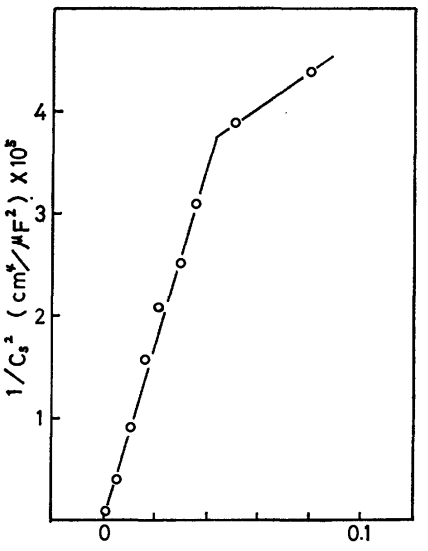

Fig. 2. Mott-Schottky plot for the AgCl electrode in 0.1 M KCl aqueous solution.

value increases with anodic polarization, the AgCl electrode can be considered as an n-type semiconductor. Assuming that ε of AgCl is 11.2[19] and the roughness factor of the electrode surface is 1, the donor concentration (C_D in Eq. 2) can be calculated from the slope to be 1.7×10^{13}, much smaller than the values for other perfectly n-type semiconductors (*e.g.*, 10^{16}—10^{17} for ZnO[20]). Though reproducibility was poor for the slope, it was good for E_{fb}. It seems that the C_D of the AgCl electrode shows either the concentration of interstitial silver ions or of divalent cation impurities.

The energy level of AgCl obtained from E_{fb} is shown in Fig. 3. The Fermi energy level *vs.* vacuum was determined in this work to be −4.8 eV. It should be noted that an energy of −4.5 eV vacuum is found to be equivalent to 0.0 eV *vs.* a standard hydrogen electrode.[21] The energy difference of 1.7 eV between the valence band and the Fermi energy level reported by Williams *et al.*[8] gives the position of the valence band. The band gap of 3.1 eV was determined from the average values of other investigators,[4-7] giving the position of the conduction band. Despite the simplicity of the method the energy levels we obtained coincide approximately with those of the other investigators.

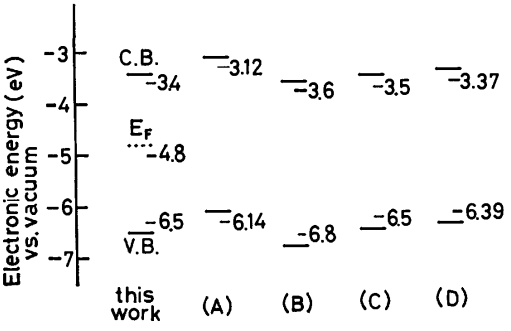

Fig. 3. Energy level of the AgCl electrode obtained from the flatband potential, C.B.: conduction band, V.B.: valence band, E_F: Fermi energy level, (A): Berry,[7] (B): Brown,[4] (C): Peterson,[6] (D): Gilman.[5]

The position of the Fermi energy level is slightly higher than the mid-point between the conduction and the valence bands (Fig. 3). In the case of a highly doped n-type semiconductor, the position of the Fermi energy level is almost identical to that of conduction band. We see that the AgCl electrode behaves like an n-type semiconductor. This coincides qualitatively with Wagner's findings that electrons are majority carriers for AgCl in contact with silver at room temperature.[9,10] Thus the conclusion that AgCl behaves like an n-type semiconductor was derived by studies of an Ag/AgCl/ solution electrode, the AgCl crystals contained in photographic emulsions not being an n-type but an intrinsic semiconductor.

The position of the conduction band obtained (Fig. 3) seems to be of great importance for studies of the spectral sensitization by electrochemical methods. The relation between sensitized photocurrents and the lowest vacant levels of sensitizing dyes was also investigated electrochemically.[18] The position of the AgCl conduction band at −3.4 eV *vs.* vacuum is also supported by the result that the sensitization of AgCl was initiated by the sensitizing dye having the lowest vacant level from −3.52 to −3.61 eV *vs.* vacuum.

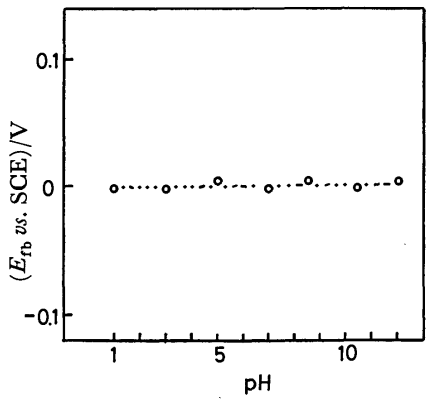

Fig. 4. pH dependence of the flatband potential (E_{fb}) of AgCl in 0.1 M KCl aqueous solution, pH control using HCl or KOH.

The E_{fb} of AgCl was measured in 0.1 M KCl aqueous solutions having different pH adjusted by the addition of HCl or KOH. As shown in Fig. 4, neither H^+ nor OH^- ions affect the E_{fb}, indicating that the band edeg of AgCl does not change with H^+ or OH^- ions, and that the photocurrent sensitized by a sensitizing dye is not dependent on the pH of electrolyte solution.[15]

E_{fb} was also measured with various concentrations of Cl^- ion (Fig. 5), and was found to shift cathodically with an increase in Cl^- ions. In order to make a comparison with the Cl^- ion effect on E_{fb}, current-potential curves were measured at various concentrations of Cl^- ion, and the relation between zero-current potential (E_z) and the concentration of Cl^- ion was plotted (Fig. 6). Measurements of photocurrent were carried out under illumination from a 500 W Xe lamp without filter. The photocurrent was measured while increase in current occurring when the AgCl electrode was exposed to the light. The photocurrent was about one-tenth of the dark current. The E_z value coincided well

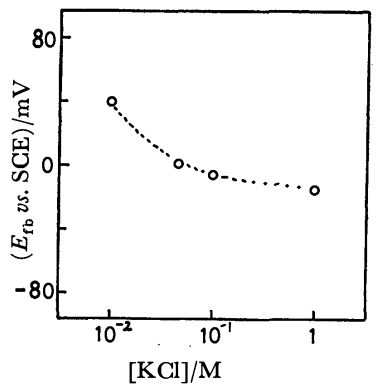

Fig. 5. Cl^- ion dependence of the flatband potential (E_{fb}) of AgCl.

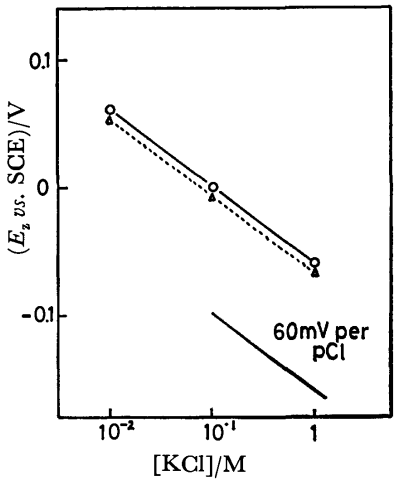

Fig. 6. Cl^- ion dependence of the zero-current potential (E_z) of AgCl, —○—: dark current, ···▲···: photocurrent.

with the E_{fb} measured in 0.1 M KCl.

Thus taking into consideration the following electrochemical reactions of Ag/AgCl/Cl^-

$$AgCl(s) \rightleftarrows Ag^+ + Cl^- \quad (3)$$

$$Ag^+ + e \rightleftarrows Ag(s) + Cl^- \quad (4)$$

$$AgCl(s) + e \rightleftarrows Ag(s) + Cl^- \quad (5)$$

and making use of the Nernst equation, we have for the shift of electrode potential ΔE,

$$\Delta E = \text{const} + \frac{RT}{F} \ln \frac{a(Ag(s))}{a(AgCl(s))} + \frac{2.3RT}{F} pCl \quad (6)$$

where AgCl(s)=solid AgCl, Ag(s)=solid Ag, e=electron, R=gas constant, F=Faraday constant, a ( )=activity, and pCl=−log [Cl^-]. Equation 6 suggests that an electrode potential shift of *ca.* 60 mV (2.3 RT/F) per unit on the pCl scale should be detected. Though the shift per pCl is *ca.* 60 mV for E_z (Fig. 6), it is about 30 mV for E_{fb} (Fig. 5). Mobile interstitial Ag^+ ions seem to be associated with the difference in the shifts in E_{fb} and E_z. The band edge of AgCl shifts cathodically with an increase in the concentration of Cl^- ion.

The Cl^- ion effect on the band edge of AgCl can be considered as a reverse effect of the Ag^+ ion effect on the

band edge of AgCl. However, the effect could not be measured directly since the Ag^+ ions in the electrolyte solution were deposited as silver on the surface of the AgCl electrode when concentrated $AgNO_3$ solution was added to the solution. Iwasaki *et al.*[15] reported that with increase in Ag^+ and Cl^- ions, the equilibrium potential of the AgCl electrode shifts anodically and cathodically, respectively. Minoura *et al.*[22] reported that with an increase in S^{2-} and Cd^{2+} ions, the E_{fb} of CdS shifts cathodically and anodically, respectively. Since the constituent ions of AgCl are Ag^+ and Cl^-, we might presume that E_{fb} of the AgCl electrode also shifts cathodically and anodically with the addition of Cl^- and Ag^+ ions, respectively. The anodic shift of the band edge gives rise to an increase in electron injection from excited sensitizing dyes,[15,18] the cathodic shift decreasing. The Ag^+ ion effect on spectral sensitization (Fig. 7) can be explained in terms of a band edge shift of the AgCl electrode.[15,18]

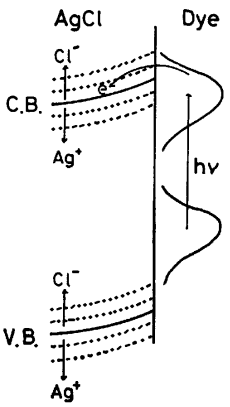

Fig. 7. Scheme of the Ag^+ and Cl^- ion effect in spectral sensitization, C.B.: conduction band, V.B.: valence band, e: electron.

Watanabe *et al.*[23] found a phenomenon similar to the Ag^+ ion effect, using TiO_2 electrode and electrochemical techniques. The sensitized photocurrent increased with decrease in the pH of the electrolyte solution. This was attributed to the shift in the E_{fb} of TiO_2 due to H^+ ions in the electrolyte solution.

AgBr Electrode. The capacitance of the space charge layer of AgBr electrodes was measured by the same procedure as for the AgCl electrode. Since the $1/C_s^2$—E plots for AgBr were not linear, Eq. 1, which can be adapted to intrinsic semiconductors, was used instead of Eq. 2. The value of y in Eq. 1 was varied from 10^{-10} to 10^{10} and the theoretical $1/C_s^2$—E curves were calculated. The capacitances were calculated on the assumption that $\varepsilon\cdot\varepsilon_0/L$ equals 1, because the N_i of the AgBr used was unknown and the value of $\varepsilon\cdot\varepsilon_0/L$ does not change the shape of $1/C_s^2$—E curve. Equation 1 can be considered to be adapted to AgBr, if the shape of the theoretical curve resembles that of the experimental one.

Figure 8 shows the theoretical $1/C_s^2$—E curves ($y=10^{-10}$—10^{10}) and the experimental values measured in 0.1 M KBr aqueous solution. Since the potential at

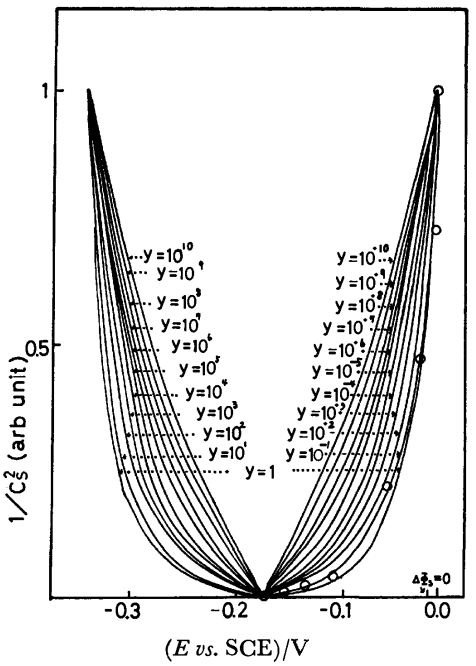

Fig. 8. $1/C_S^2$-E plot for the AgBr electrode in 0.1 M KBr aqueous solution, ——: theoretical curve, ○: measured values.

which $1/C_s^2$ is closest to zero is -0.17 V *vs.* SCE by measurement, the theoretical curve at which $1/C_s^2$ is closest to zero was based at -0.17 V. The $1/C_s^2$ of both theoretical and measured values were normalized to 1 at 0.00 V *vs.* SCE when $y<1$, and at -0.34 V when $y>1$, since the change in C_s was found only at potential more negative than 0.00 V *vs.* SCE. The experimental values coincide with the curve of $y=10^{-1}$ (Fig. 8). Not all AgBr electrodes, however, agree with the theoretical curve. More precise value than $y=10^{-1}$ could not be determined. The E_{fb} value of the $y=10^{-1}$ curve, $\Delta\phi_s=0$, was -0.01 V *vs.* SCE, and not -0.17 V. The E_{fb} of the AgBr electrode was concluded to be 0.0 V *vs.* SCE. The value for $y=10^{-1}$ coincides with that reported by Wagner[9] and others,[10] who suggested that the number of electrons is 10^1—10^2 times the number of holes when AgBr is brought into contact with silver at room temperature.

Figure 9 shows the energy level of the AgBr electrode

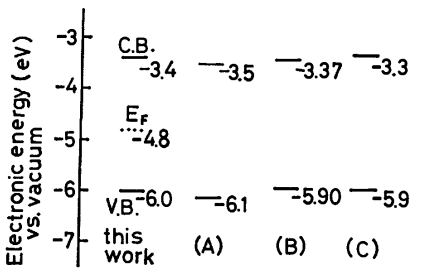

Fig. 9. Energy level of the AgBr electrode obtained from the flatband potential, C.B.: conduction band, V.B.: valence band, E_F: Fermi energy level, (A): Brown,[4] (B): Gilman,[5] (C): Berry.[7]

obtained from E_{fb}. The potential *vs.* vacuum was determined by Lohmann's value[21] as AgCl electrode. An energy difference 1.2 eV between the Fermi energy level and the valence band of AgBr was reported by Williams *et al.*,[8] giving the position of the valence band. The band gap, 2.6 eV, was determined by averaging the values of the other investigators,[4,5,7] giving the position of the conduction band. The positions of the conduction and valence bands we obtained coincide with those of other investigators.

AgBr electrode behaves almost like an intrinsic semiconductor, since the Mott-Schottky relationship could not be used for AgBr, the Fermi energy level being almost midpoint between the conduction and valence bands.

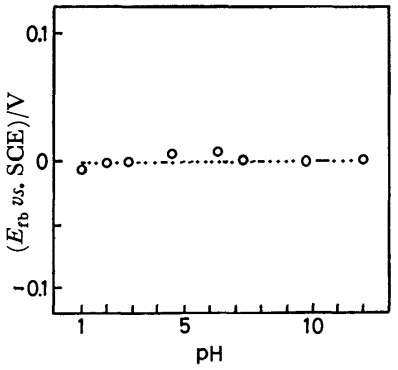

Fig. 10. pH dependence of the flatband potential (E_{fb}) of AgBr in 0.1 M KBr aqueous solution, pH control using HBr or KOH.

The E_{fb} value of the AgBr electrode, like that of the AgCl electrode, was not affected by H^+ or OH^- ions (Fig. 10). The sensitized photocurrent is expected to remain unchanged by H^+ or OH^- ions in electrolyte solution.

Figure 11 shows the Br^- ion dependence of E_{fb}. The E_{fb} shifts cathodically with an increase in Br^- ions, the slope being *ca.* 20 mV per pBr. The relation of E_z to Br^- ion concentration is shown in Fig. 12. The potentials of both photocurrents and dark currents shift cathodically with falling pAg. The photocurrents were measured as the increase in current during the course of illumination. The potential difference between dark and

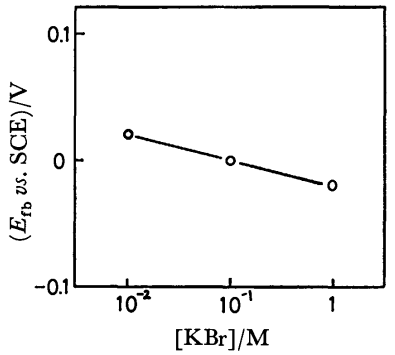

Fig. 11. Br^- ion dependence of the flatband potential (E_{fb}) of AgBr.

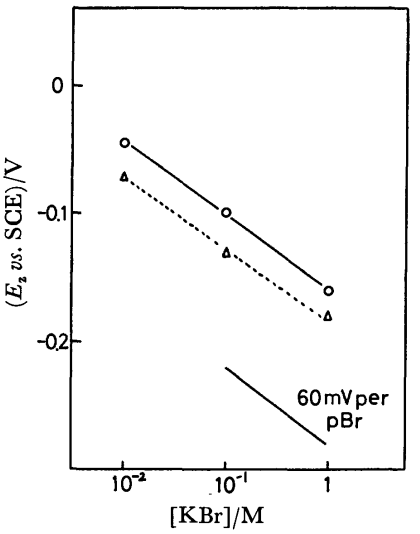

Fig. 12. Br^- ion dependence of the zero-current potential (E_z) of AgBr, —○—: dark current, ···△···: photocurrent.

photocurrents at a given concentration of Cl^- ion was based on the Dember effect, both slopes being *ca.* 60 mV per pBr. These phenomena can be explained by means of an equation similar to (6). The Br^- ion effect on the potentials suggest that sensitized photocurrent would decrease with falling pBr.

The Ag^+ ion effect in spectral sensitization is due to the anodic shift of the AgBr band edge as in the case of AgCl, since the sensitized photocurrent increases with decreasing pAg and decreases with decreasing pBr.

Conclusion

1. The flatband potentials of both AgCl (in 0.1 M KCl) and AgBr (in 0.1 M KBr) are 0.0 V *vs.* SCE, and the AgCl electrode behaves somewhat like an n-type semiconductor, while the AgBr electrode behaves almost like an intrinsic semiconductor.
2. The flatband potentials of AgCl and AgBr are affected by Cl^- and Br^- ions, respectively, in electrolyte solution. In both cases, the flatband potentials shift cathodically with an increase in halide ion concentration.
3. The effects of Cl^- ion and Br^- ion can be considered as a reverse effect of the Ag^+ ion. The Ag^+ ion effect in spectral sensitization is due to the anodic shift of the AgX band edge.

We wish to thank Dr. Kiminori Itoh for his advice and comments on the interpretation of the results, and Mr. Hiroyuki Taiko for assistance in carrying out the experiments.

References

1) T. H. James, "The Theory of the Photographic Process," 4 th ed, Macmillan, New York (1977), p. 105.
2) F. Trautweiler, *Photogr. Sci. Eng.*, **12**, 138 (1968).
3) R. W. Gurney and N. F. Mott, *Proc. R. Soc. London, Ser. A*, **164**, 151 (1938).

4) F. C. Brown, *J. Phys. Chem.*, **66**, 2368 (1962).
5) P. B. Gilman, Jr., *Photogr. Sci. Eng.*, **18**, 475 (1974).
6) C. W. Peterson, *Phys. Rev.*, **148**, 335 (1966).
7) C. R. Berry, *Photogr. Sci. Eng.*, **19**, 93 (1975).
8) D. R. Williams, J. G. Jenkin, R. C. G. Leckey, and J. Liesegang, *Phys. Lett. A*, **40**, 141 (1974).
9) C. Wagner, *Z. Electrochem.*, **63**, 1027 (1959).
10) R. Matejec, "Progress in Surface and Membrane Science," ed by J. F. Danielli *et al.*, Academic Press, New York and London (1973), Vol. 6, p. 5.
11) B. Levy and M. Lindsey, *Photogr. Sci. Eng.*, **16**, 389 (1972).
12) I. A. Akimov, V. M. Bentsa, F. I. Vilesof, and A. N. Terenin, *Phys. Status Solidi*, **20**, 771 (1967).
13) H. Meier and W. Albrecht, *Ber. Bunsenges. Phys. Chem.*, **69**, 160 (1965).
14) S. S. Collier and P. B. Gilman, Jr., *Photogr. Sci. Eng.*, **16**, 413 (1972).
15) T. Iwasaki, T. Abe, S. Sumi, A. Fujishima, and K. Honda, *Photogr. Sci. Eng.*, **24**, 67 (1980).
16) H. Gerischer, "Physical Chemistry: an Advanced Treatise," ed by H. Eyring *et al.*, Academic Press, New York and London (1970), Vol. 9A, p. 467.
17) V. A. Myamlin and Y. V. Pleskov, "Electrochemistry of Semiconductors," Plenum Press, New York (1967), p. 30.
18) S. Sumi, T. Watanabe, A. Fujishima, and K. Honda, *Bull. Chem. Soc. Jpn.*, **53**, 1892 (1980).
19) C. D. Hodgman, "Handbook of Chemistry and Physics," Chemical Rubber Publishing Co. (1956), p. 2332.
20) O. M. Tech and H. Gerischer, *J. Electrochem. Soc.*, **124**, 1612 (1977).
21) F. Lohmann, *Z. Naturforsch., Teil A*, **22**, 813 (1967).
22) H. Minoura, T. Watanabe, T. Oki, and M. Tsuiki, *Jpn. J. Appl. Phys.*, **16**, 865 (1977).
23) T. Watanabe, A. Fujishima, O. Tatsuoki, and K. Honda, *Bull. Chem. Soc. Jpn.*, **49**, 8 (1976).

An On-line Automated Adiabatic Calorimeter in the 13—300 K. Heat Capacity of Cyclohexanol†

Kōji Kishimoto, Hiroshi Suga,* and Syûzô Seki**
Department of Chemistry, Faculty of Science Osaka University, Toyonaka, Osaka 560
(Received February 22, 1980)

A computerized adiabatic calorimeter system operating in the temperature range 13—300 K is described. A digital voltmeter is used for energy measurement and the duration of energy input is determined by a program unit operated by 1 Hz pulse. Temperatures of the calorimeter are measured by a 25 Ω platinum resistance thermometer and an automated ac double bridge. The measured resistance is converted into temperature (IPTS-68) by a calibration table stored in a mini-computer. Criterion for the realization of thermal equilibration is that a temperature drift calculated from the latest six data becomes smaller than a preset value, usually 7×10^{-8} Ω s^{-1}. The system is able to measure the heat capacity of solid and liquid in an intermittent heating mode and gives the computed results during measurement. Some examples of the test runs on cyclohexanol crystal are shown and the results are compared with those obtained by manual measurements by use of dc Müller bridge. A relaxational heat capacity anomaly observed in glassy crystalline state of cyclohexanol is discussed in correlation with a secondary relaxation observed by previous dielectric measurement.

Adiabatic calorimeter with intermittent heating mode is believed to give the most accurate and precise heat capacity data at low temperatures.[1] Numerical values of the static equilibrium properties such as enthalpy, entropy and Gibbs energy function can be derived from the data. While, a series of systematic studies on glassy states of materials[2] have proved that the calorimetric technique under a good adiabatic condition provided valuable information on dynamical nature of molecular motion through the observation of relaxational behavior of enthalpy of the specimen. Thus, temperature changes due to enthalpy relaxation in cyclohexanol crystal[3] at around 150 K were followed to give calorimetric relaxation time, which was correlated with dielectric relaxation time.[4] Kinetic parameters derived from calorimetric measurement of 1,2-difluoro-1,1,2,2-tetrachloroethane crystal[5] were correlated with those obtained by NMR techniques. A relaxational process due to possible rearrangement of proton configuration in hexagonal ice[6] was persued for about a month.

The relaxation time obtained by this method ranges 5 minutes to one week (or of the order of 10^{-3} to 10^{-7} Hz in terms of frequency). Since it is almost impossible at the present stage to get such a long relaxation time by other techniques, the calorimetric method provides complementary knowledge on the dynamics of slow molecular motion in the condensed state. The prolonged observation of temperature of a system with extremely long relaxation time necessitates to build an automatic data acquisition system for calorimetry.

The development of modern electronic techniques makes possible to replace the laborious manual operations by an automatic measurement and control without loss of accuracy. There are many approaches[7-10] to the problem of automatic data acquisition in calorimetry according to the heating mode and to the method of temperature measurement. Here, a new approach of data acquisition system suitable for our purpose is reported. The system is able to give quick information of any thermal anomaly that may be encountered during measurement. The electronic system, the soft ware logic, and the method of processing the data are described. The operation of the system is illustrated by results on cyclohexanol crystal.

Automatic Heat Capacity Measurement System

An adiabatic calorimeter[11] with an immersion-type cryostat was used for the present purpose. A sample cell loaded with platinum resistance thermometer and heater is surrounded by two (inner and outer) adiabatic shields and by massive thermal station. Heat capacity of the cell is measured as a function of temperature by the standard discrete heating method. In this intermittent mode, the sequence of heat capacity measurement is composed of two successively alternating periods. One is called a drift period during which the temperature of the calorimeter cell is measured as a function of time. The other is the energy input period during which a definite amount of electrical energy is supplied to the calorimeter cell. The supplied energy is assessed on the basis of measurements of voltage and current across and through the cell heater as well as of time interval of the energy input.

Adiabatic condition of the calorimeter cell is realized by use of high vacuum and four-channels temperature controller. Each channel consists of a multi-junction thermocouple, dc amplifier and power amplifier. Controllers with proportional-integral-differential control mode are indispensable for the automatic control of the shield temperature in the discrete heating method. Small temperature difference was set between the inner and the outer shields, and the inner shield and the station, so as to produce the least temperature drift rate of the cell.

Figure 1 is a block diagram illustrating the system for automatic heat capacity measurement. This system may be divided into four major parts: (1) measuring circuits, (2) control system, (3) interface system, and (4) mini-computer.

† Contribution No. 4 from Chemical Thermodynamics Laboratory.

** Present address: Department of Chemistry, School of Science, Kwansei Gakuin University, Nishinomiya 662.

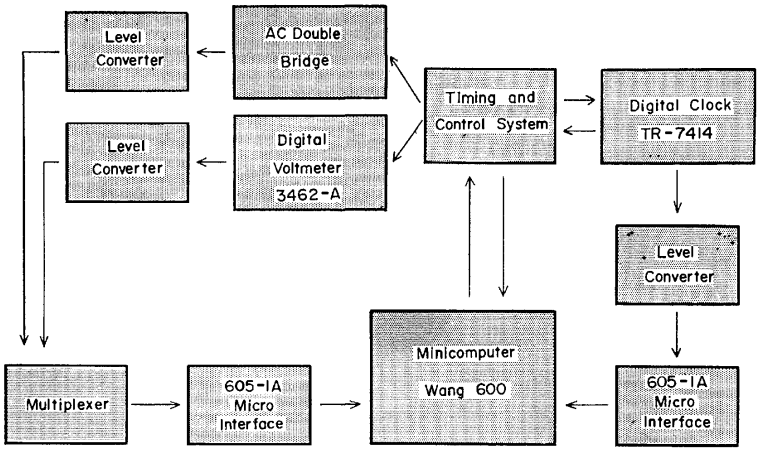

Fig. 1. Block diagram of the system for the automatic heat capacity measurement.

(1) Measuring Circuits. Resistance of the working platinum thermometer was measured by the Automatic System Laboratory A-7 precision ac double bridge. The bridge utilizes inductive voltage divider arranged as a Kelvin double bridge and is energized at 390 Hz. The bridge measures the ratio between two resistances R_t and R_s. Changes in resistance are automatically balanced and the ratio $R_t/(R_t+R_s)$ is displayed in seven digits. A capsule type platinum thermometer (Leeds and Northrup, 8164) was used in conjunction with one of four standard resistors (General Radio card-type 1440, 0.01, 0.1, 1, and 10 Ω). The four standard resistors were mounted inside a double-walled air thermostat.

The maximum temperature coefficient of the standard resistor was stated by manufacturer to be ±20 ppm/K,

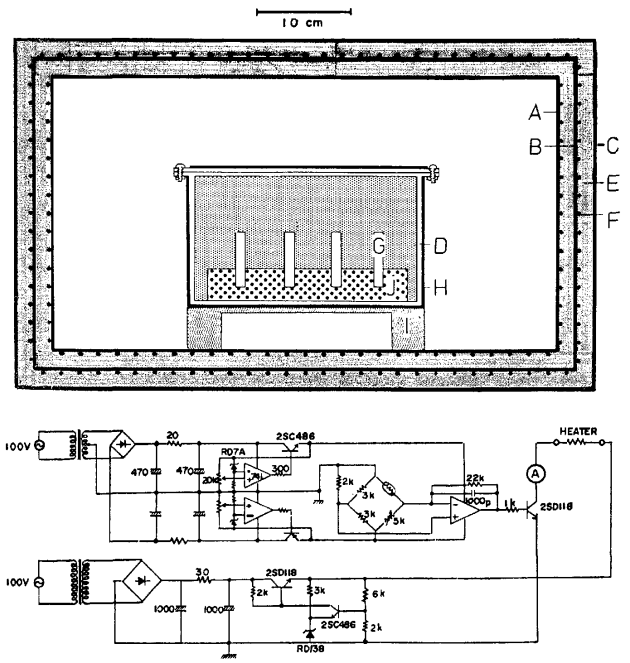

Fig. 2. Schematic drawing of an air thermostat for standard resistors and its regulator circuits.
A—C, Aluminum plates; D, copper box; E, styroform insulation; F, regulator heater; G, card-type standard resistor; H, polyurethane insulation; I, wooden pedestral; J, polyvinylchloride supporter.

while the bridge has $\pm 4\times10^{-7}$ inaccuracy. Thus, for the measurement of temperature with the accuracy better than 4×10^{-7}, the thermostat must be controlled within ±5 mK. The assembly shown in Fig. 2 consists of two parts; the boxes made of aluminum plate, A—C, and copper box, D. The spaces between A and B, and between B and C are packed with styrofoam insulation E and heater F. A and B are thermostatted independently at 36 °C and 33 °C, respectively, by use of the regulator circuit with thermistors as temperature sensors. The copper box housing the standard resistors G is wrapped by polyurethane H, and is positioned on wooden pedestral I. The thick copper wall plays a role as a buffer against fluctuation of temperature inside the aluminum box A.

The condition of the bridge balance has been given by Harris[12] in detail. Noise induced in the leads of the thermometer was liable to induce hunting in the bridge balance at the band width of 100 Hz. Since the bridge had the band widths of 100, 25, and 6.2 Hz as received from the manufacturer, it was modified so that any of setting with 30, 7.5, and 0.94 Hz could be adopted for avoiding the situation. For further improvement of the bridge balance, a normal counting logic system must be applied beside a short-cut logic system as pointed out by Martin *et al.*[8]

The electrical power supplied to the calorimeter cell was determined as follows. Values for the heater current are obtained by measuring the voltage across a 100 Ω standard resistor placed in series with the calorimeter heater. The voltages across the heater and the standard resistor are measured by means of a digital voltmeter (DVM, Hewlett-Packard 3462 A). The two DVM inputs are selected by a magnecraft mercury relay at an interval of 30 seconds during a heating period. The electrical energy dissipated in the calorimeter heater can be assessed by the equation, $E=60\sum_{i=1}^{N} V_i I_i$, where N is the total count during the heating or the heating time in unit of minute because the heating time is chosen to be multiple of one minute as will be described later.

In the drift period, the current from the power supply is circulated through a dummy resistance in

place of the calorimeter heater in order to maintain a constant drain on the power supply. The resistance used as a calorimeter heater (*ca.* 100 Ω) and the dummy resistance are switched by use of a magnecraft type MCN-IN high-speed mercury-relay, which has exceedingly low stray emf and contact resistance. All timing operations are based on a digital clock (Takeda Riken TR 7414B). As received from the manufacturer the clock had no output of one-second clock pulse which is required for the system control. One-second clock pulse fed into the Timing and Control described below are therefore taken out from the digital IC mounted in the clock.

The instrument has a claimed accuracy of 0.01% which comes from the stability of quartz crystal oscillators in it.

(2) Timing and Control System. The Timing and Control System (TCS) controls all timing operations on the basis of 1 Hz pulse generated by the digital clock. This system serves as an assistant of the mini-computer which is a data-entry-only device (or, has no interrupt system). When an energy-input command is issued from the program of the mini-computer, TCS transforms it into the electrical command signal. At the instant the energy input command signal coincides with the one-second-clock pulse, TCS makes the timer start and allows the magnecraft mercury-relay for energy input to be turned on. From this instant the energy input period starts. In the present work, the heating time interval is selected to be multiple of 1 min or 1 h. In this period, select signals are generated every 30 s from the clock and serves to select either voltage or current reading by operating a magnecraft mercury-relay.

Since the DVM can not measure voltage within a claimed accuracy (0.0004%) immediately after a sudden change in an input voltage, trigger pulses for the DVM readings are generated twice by TCS in each V and I reading period, and the second reading at the mid-time of each period is adopted. In the drift period, TCS supplies trigger pulses for DVM readings every 10 s, which are available for adjustment of the variable dummy resistance. In a normal use, an energy input is performed automatically under a program control and the heating period is fixed to the preset time interval. However, if desired, the heater on-off operation can be made manually, which is helpful in such a case as enthalpy determination of phase transition.

(3) Interface System. The interface system consists of level converter, multiplexer and micro-interface Wang 605, which interfaces the peripheral devices to a mini-computer Wang 600. The digital output levels of these measuring instruments are not directly compatible with TTL/DTL levels of Wang 600. Therefore, a level converter assembly is required between the computer and the peripheral devices. There exists no necessity of sampling of data from the ac double bridge and from the DVM in the same period. A multiplexer selects the data from the bridge in the drift period and the data from DVM in the heating period.

(4) Mini-computer and Program. The mini-computer Wang 600 takes advantages of facilities of a cassette system offering a low-cost alternative to disk and card systems. The resistance values of a working thermometer are stored on a cassette tape at an interval of 0.1 K over the temperature range from 10 to 380 K.

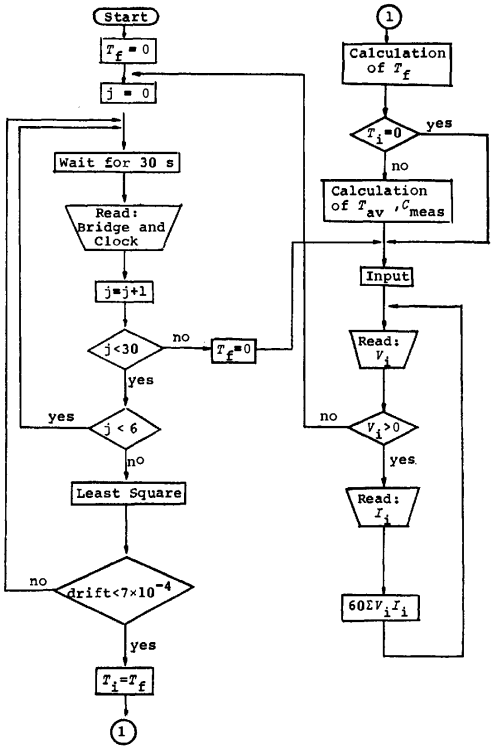

Fig. 3. Flow chart for the procedure of automatic operation of heat capacity measurement.

A flow chart for the procedure of automatic operation is drawn in Fig. 3. A typical sequence of program is as follows.

Step (1): In a drift period, the computer commands every 30 s the ac double bridge to transfer the measured resistance of a thermometer, data transfer being performed at the time when the bridge becomes at balance.

Step (2): Next the computer asks the clock to tell the time at which the measurement was made. The time is stored into a register and printed out along with the values of the measured resistance.

Step (3): The program examines whether the number of data points is smaller than six. If the answer is "yes," the program returns to step (1), after waiting for 30 s. If the answer is "no," the program proceeds to step (4).

Step (4): If the number of data points is smaller than 30, a temperature drift rate is determined from last six pairs of data by the least squares method. When a specimen accompanies with an enthalpy relaxation phenomenon, spontaneous temperature increase or decrease should be observed. In that case, 30 data points are accumulated and are used to analyse a kinetic characteristics of the relaxational process. Then, the program branches to step (7).

Step (5): A decision is made whether the drift rate is smaller than a preset value, usually 0.7 mK/ks. If

not, the program judges that the thermal equilibrium in the calorimeter cell is not established yet, and the program returns to Step (1). If so, the last six values of resistance are averaged to give an equilibrium resistance. Then, the computer converts this resistance value to temperature on the basis of T *vs.* R conversion table stored in a data bank. The corresponding value is designated as a final temperature, T_f.

Step (6): The computer calculates T_{av} which is equal to the averaged value of initial, T_i, and final, T_f, temperatures, and C_{meas} ($=60\ \Omega\ V_iI_i/(T_f-T_i)$). When the heat capacity of the empty sample cell and the weight of a sample are already known, the molar heat capacity of the sample can be calculated.

Step (7): The energy input command is issued from the program to TCS.

Step (8): Reading commands for DVM readings are generated by TCS. The computer receives these values from DVM and calculates the energy dissipated in the cell per 1 min. As Wang 600 is a data-entry-only device, a check is made whether the sign of entered data is positive or not. TCS assigns positive sign to the data from DVM and negative sign to the data from the ac double bridge. The positive sign means that the calorimeter heater is in on-state, and the input energy per 1 min must be added to give a total input energy and step (8) is repeated. In a case of negative sign the program will return to step (1) and the next cycle commences.

Calibration of the Thermometer

A platinum thermometer of 25 Ω ice-point resistance employed as working thermometer was calibrated against the laboratory standard thermometer certified at the US National Bureau of Standards according to the IPTS-68. The two thermometers were mounted in a massive copper block and the respective resistances were measured simultaneously at any fixed temperature. Since the standard thermometer is calibrated by d.c. method and since the value of resistance read with a.c. method is slightly different from that with d.c. method, the resistance of the standard thermometer was measured by Müller bridge (Leeds and Northrup, G-3), while that of the working thermometer with a.c. double bridge at fixed frequency of 390 Hz. An apparent resistance value including effects of lead impedance, self-heating and thermometer inductance *etc.* was related with IPTS-68 scale realized by the standard thermometer.

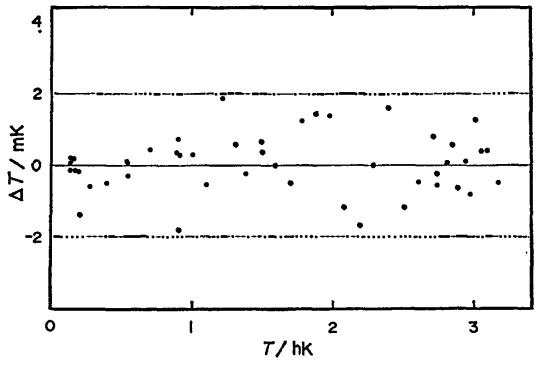

Fig. 4. Deviation plot of a working platinum resistance thermometer.

The resistance-temperature relation was established by measurements at eight fixed temperatures and by use of the interpolation formula according to the IPTS-68 in the temperature range from 13.81 to 320 K. The calibration table was given at an interval of 0.1 K and was stored in the casette tape. Figure 4 shows the deviations of the measured temperatures with use of the working thermometer from the IPTS-68 temperature scale.

Test Run for Cyclohexanol

The performance of the present automatic system was determined by measuring the heat capacity of cyclohexanol crystal. Table 1 reproduces a part of the experimental results taken with unattended operation for the low-temperature modification of cyclohexanol crystal. The bridge balance was taken at 0.94 Hz band width and the first data in an equilibration time was obtained usually about 4 min after an energy input. The notations A, B, E, C, D, G, H, and Y stand for resistance (in Ω), real time (in s), initial temperature (in K), heat capacity (in J K^{-1}), average temperature (in K), real time when an energy input was over, amount of input energy (in J) and the time duration of energy input (in s). A slight irregular variation of the bridge readings with time is not due to actual change of temperature but due to noise appearing in the thermometry circuits. This was confirmed by measuring the resistance of the thermometer with d.c. bridge. Difficulties of complete elimination of noise in the bridge circuitry lead us to take the method of averaging the latest six data points in determining an equilibrium temperature.

Figure 5 gives a graphical plot of the heat capacity data obtained for cyclohexanol crystal around liquid nitrogen temperature. In the figure, the filled circles represent the data obtained by the present automatic system with a.c. thermometry, while the open circles by the manual method with d.c. thermometry. Both of them coincide each other within 0.1% error. The accuracy of the calorimeter with d.c. thermometric technique has already been determined[11] by the use of standard benzoic acid crystal recommended by the US Calorimetry Conference.[13]

β-Relaxation Phenomenon of Cyclohexanol

A secondary (β) relaxation was observed[4] in the glassy crystalline state of cyclohexanol by dielectric measurement. The dielectric loss peak associated with the β relaxation was much smaller than that of primary (α-relaxation responsible for glass transition around 150 K. A plot of logarithm of the frequency of maximum dielectric loss against reciprocal temperature gave a linear line for the β relaxation, in contrast to the non-linear behavior for the α relaxation. Since the glass

Table 1. Reproduction of a part of the experimental heat capacity data

5.709694	A	6.149571	A
4.079	B	7.211	B
5.709691	A	6.149571	A
4.112	B	7.244	B
5.709649	A	6.149571	A
4.174	B	7.277	B
5.709674	A	6.149571	A
4.207	B	7.309	B
5.709679	A	6.149571	A
4.241	B	7.343	B
5.709679	A	6.149571	A
4.284	B	7.376	B
85.554173	E	89.522641	E
22.5004	C	23.3444	C
84.533582	D	88.539411	D
11127.0	G	20300.0	G
45.918231	H	45.886583	H
1200	Y	1200	Y
5.931621	A	6.363621	A
5.700	B	8.812	B
5.931621	A	6.363628	A
5.733	B	8.845	B
5.931621	A	6.353628	A
5.766	B	8.878	B
5.931621	A	6.363621	A
5.799	B	8.911	B
5.931621	A	6.363624	A
5.832	B	8.944	B
5.931621	A	6.363624	A
5.865	B	8.977	B
87.556242	E	91.454699	E
22.9353	C	23.7501	C
86.555207	D	90.488670	D
13748.0	G	22951.0	G
45.904483	H	45.861427	H
1200	Y	1200	Y

transition temperature of cyclohexanol observed calorimetrically corresponded to the temperature at which the dielectric relaxation time of α relaxation becomes of the order of 10^3 s, we extrapolated simply the Arrhenius plot to the same time scale. The temperature at which the mode for the β relaxation is expected to be frozen in was about 75 K.

We have pointed out[4] already that the heat capacity of the glassy crystalline cyclohexanol started to deviate from that of low-temperature modification at around 70 K and the anomalous increase may be associated with the onset of motion responsible for the β relaxation. A close examination of the previous heat capacity data of cyclohexanol in that temperature region does not disclose any anomalous behavior in temperature drift. This may be due to rather large heat leakage arizing from incomplete adiabatic condition at that time. Since the techniques in realizing adiabatic condition have been much improved, we attempted to reinvestigate the thermal behavior of glassy crystalline cyclohexanol.

The glassy crystalline cyclohexanol was prepared by cooling the high-temperature modification with an average rate of -3 K min^{-1} in the temperature interval between 270 K and 90 K and the heat capacity measurements were initiated. Table 2 lists the heat capacity data relevant to the temperatures in problem. Series I is for the specimen cooled rapidly from 90 K to 20 K with the rate of -1 K min^{-1}, while series II is for annealed specimen at 64 K for about 40 h. These data are plotted in Fig. 6 in the form of excess heat capacities over that of low-temperature modification so as to exaggerate an anomalous behavior that may be encountered. Also shown below in the figure is the rate of temperature drift. Thermal equilibrium was attained usually during 4 or 5 min after turning off the calorimeter heating. At temperature around 60 K, a marked exothermic temperature drift was observed for quenched specimen. The drift changed into an endo-

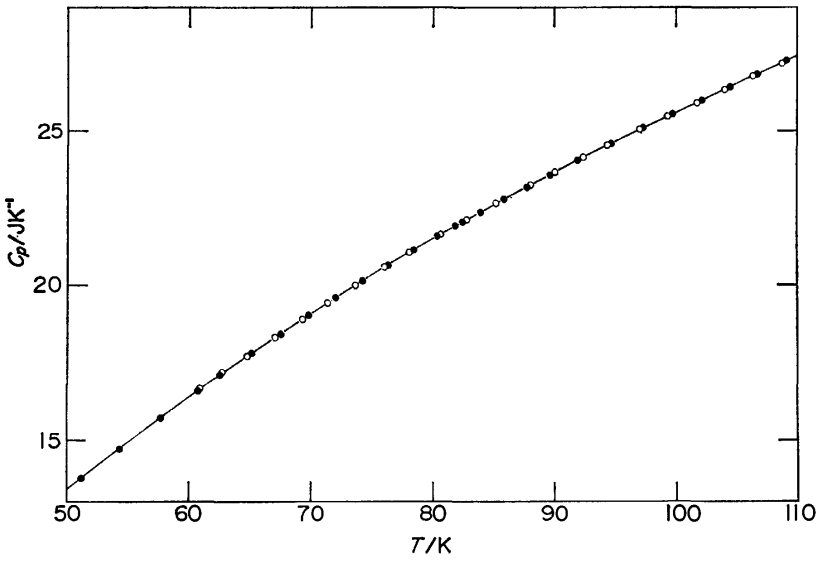

Fig. 5. Heat capacity curve of cyclohexanol crystal.
○: Measurement with d.c. thermometry, ●: measurement with a.c. thermometry.

Table 2. Heat capacities of cyclohexanol in glassy crystalline state

The samepl weight is 24.746 g. Series I is for the specimen cooled from 90 K to 20 K with the rate of -1 K min^{-1}. Series II is for the specimen annealed at 64 K for 40 h.

T / K	C_s(gl) / J K^{-1}	C_s(c) / J K^{-1}	ΔC_s / J K^{-1} mol^{-1}
	Series I quenched specimen		
57.07	16.140	15.570	2.307
60.65	17.165	16.593	2.315
63.71	18.020	17.428	2.396
66.30	18.718	18.128	2.388
68.81	19.377	18.782	2.408
71.22	19.995	19.382	2.481
73.57	20.581	19.962	2.505
75.84	21.151	20.516	2.570
78.06	21.693	21.028	2.692
80.22	22.204	21.524	2.752
82.59	22.756	22.051	2.853
85.16	23.346	22.633	2.886
87.77	23.942	23.190	3.044
90.46	24.531	23.740	3.201
	Series II annealed specimen		
58.27	16.497	15.921	2.331
60.86	17.237	16.652	2.368
63.34	17.933	17.335	2.420
65.74	18.594	17.978	2.493
68.05	19.210	18.582	2.542
71.62	20.121	19.487	2.566
75.19	20.990	20.361	2.546
77.47	21.545	20.888	2.659
79.70	22.082	21.408	2.728
81.88	22.589	21.892	2.812
84.01	23.083	22.374	2.870
86.27	23.597	22.872	2.934

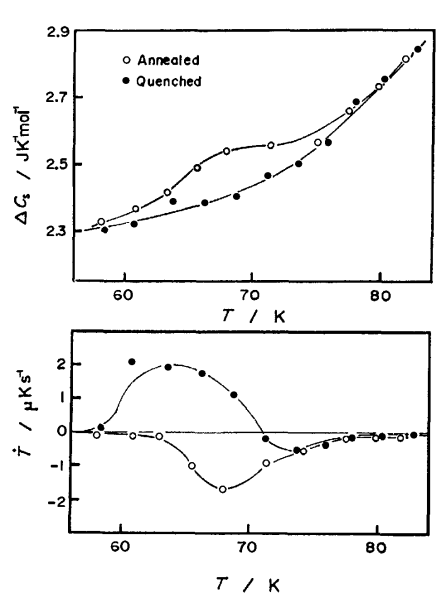

Fig. 6. Heat capacity curves of glassy crystalline cyclohexanol (above) and temperature drift rate (below). See Table 2 caption.
●: Series I (quenched specimen),
○: Series II (annealed specimen).

thermic one around 70 K on further heating and returned to normal behavior around 80 K. In this temperature interval, no energy-input command signal was issued during equilibration period and 30 data points were accumulated for each drift period. In the calculation of heat capacity, effect of the temperature drifts was treated as if they were arizen from thermal leakage.

While for the annealed specimen, a humped heat-capacity anomaly was observed and the corresponding temperature drift was endothermic in the relevant temperature interval. These thermal behavior are characteristic of a freezing phenomenon and it seems to be natural to ascribe these anomalies to the β relaxation.

Many explanations can be offered to account for the presence of secondary relaxation. We have discussed previously[4] the origin of the β relaxation of cyclohexanol crystal in terms of intramolecular motion of OH groups between two hydrogen-bonded states, in an analogous way with those traditionally invoked for polymer and molecular glasses.[14] Systematic studies[15] of a number of molecular glasses which lack either a side chain or any other internal degree of freedom have revealed a remarkable similarity in the dielectric relaxation of these glasses to those of polymers, and a surprizing uniform pattern of behavior. The conclusion drawn from the study was that the molecular mobility seen as β relaxation is intrinsic nature of the glassy state. Although a few models were proposed for the structure of amorphous solid that is consistent with the general occurrence of β relaxation phenomenon, there seems no experimental method that favors one of them. An accurate statistical mechanical approach to the description of thermodynamic and kinetic features of the frozen-in disordered system is highly desirable.

The present studies were supported in part by the Grant-in-Aid for Scientific Research from the Ministry of Education. We wish to thank Mr. N. Nakamura for helping us in a part of the experimental work.

References

1) "Experimental Thermodynamics," ed by J. P. McCullough and D. W. Scott, Butterworths, London (1968), Vol. 1.
2) H. Suga and S. Seki, *J. Non-Cryst. Solids*, **16**, 171 (1974).
3) K. Adachi, H. Suga, and S. Seki, *Bull. Chem. Soc. Jpn.*, **41**, 1073 (1968).
4) K. Adachi, H. Suga, S. Seki, S. Kubota, S. Yamaguchi, O. Yano, and Y. Wada, *Mol. Cryst. Liq. Cryst.*, **18**, 345 (1972).
5) K. Kishimoto, H. Suga, and S. Seki, *Bull. Chem. Soc. Jpn.*, **51**, 1691 (1978).
6) O. Haida, T. Matsuo, H. Suga, and S. Seki, *J. Chem. Thermodyn.* **6**, 815 (1974).
7) G. T. Furukawa, and M. L. Reilly, *J. Res. Natl. Bur. Stand.*, **74A**, 617 (1970).
8) D. L. Martin, L. L. T. Bradley, W. J. Cazemier, and R. L. Snowdon, *Rev. Sci. Instrum.*, **44**, 675 (1973).
9) J. F. Martin "Chemical Thermodynamics," ed by M. L. McGlashan, The Chemical Society, London (1973), Vol. 1, p. 133.

10) D. Moses, O. Ben-Aroya, and N. Lupu, *Rev. Sci. Instrum.*, **48**, 1098 (1977).
11) H. Suga and S. Seki, *Bull. Chem. Soc. Jpn.*, **38**, 1000 (1965).
12) F. K. Harris, "Electrical Measurements," John Wiley and Sons, New York (1952).
13) G. T. Furukawa, R. E. McCosky, and G. J. King, *J. Res. Natl. Bur. Stand.*, **47**, 256 (1951).
14) M. C. Shen and A. Eisenberg "Glass Transition in Polymers," in "Progress in Solid State Chemistry" ed by H. Reiss, Pergamon Press, Oxford (1967), Vol. 3, Chap. 9.
15) G. P. Johari and M. Goldstein, *J. Chem. Phys.*, **53**, 2372 (1970); **55**, 4245 (1971); G. P. Johari, *ibid.*, **58**, 1766 (1973); M. Goldstein, *ibid.*, **64**, 4767 (1976); M. Goldstein, *Ann. N. Y. Acad. Sci.*, **279**, 68 (1976).

Calorimetric Study on Orientationally Disordered Crystals. Cyclohexene Oxide and Cyclohexanone†

Nobuo NAKAMURA, Hiroshi SUGA,* and Syûzô SEKI**

Department of Chemistry, Faculty of Science, Osaka University, Toyonaka, Osaka 560

(Received February 22, 1980)

Low-temperature calorimetric quantities were determined for cyclohexene oxide and cyclohexanone in the temperature range between 13 and 300 K. Molar heat capacity at saturation pressure of the condensed phases, transition and melting temperatures, and enthalpies of transition and melting were measured by an on-line automated adiabatic calorimeter with intermittent heating mode. Purities of both calorimetric specimens were determined from their melting behavior. The following thermodynamic quantities, C_S°, S_S°, $[H_S^\circ(T)-H_S^\circ(0)]/T$, and $-[G_S^\circ(T)-H_S^\circ(0)]/T$ were tabulated at selected temperatures. The entropies of melting of both compounds were compared with those of cyclohexanol and cyclohexane. A factor affecting the entropy of melting was discussed from the viewpoint of non-globularity of the constituting molecules. The discussion was extended to the thermal stability of a number of orientationally disordered crystals so far studied.

Abrupt changes in the freedom of molecular motion within the crystalline solid are still among the most fascinating and least understood of physical properties. A class of crystals in which the orientational degrees of freedom of the constituent molecules are highly disordered was defined by Timmermans[1] as plastic crystals because of their high plasticity. In such a phase, the constituent molecules are located on a regular lattice with high crystallographic symmetry and reorient rapidly among several orientations. The other characteristic features of the phase are higher triple point and lower entropy of fusion in comparison with the crystal composed of less symmetric molecules. Actually it was the low entropy of fusion which led Timmermans to the recognition of plastic crystals as a unique intermediate state of matter. He set rather arbitrarily an upper limit of 5 cal K^{-1} mol^{-1} ($\simeq$21 J K^{-1} mol^{-1}) to the entropy of fusion for the criterion of plastic crystals. He recognized that such crystals are typically made up of "globular" molecules. Here, the term "globular" means either spherical or pseudo-spherical by rotation around an axis. Thus, attention of various workers in this field has been paid mainly to the crystals composed of such symmetrical tetrahedral molecules as CX_4 type, octahedral molecules as MX_6 or C_2X_6 type, cyclic molecules as cyclohexane, and caged molecules as camphor.

When we had measured the thermodynamic properties of cyclohexanol,[2] we noticed that the entropy of fusion of less symmetric and less globular cyclohexanol was smaller than that of cyclohexane. At that time, we considered that the smaller entropy of fusion originated from association effect due to intermolecular hydrogen bonding in the liquid state of cyclohexanol. This effect was found really to exist in 2-methyl-2-propanol[3] and methanol. NMR observation[4] of the cyclohexanol, however, revealed highly disordered nature of orientational and positional degrees of freedom of the molecules in the crystal. Intra- and intermolecular dipolar broadening of protons are averaged out so extensively that chemical shifts of proton—OH, CH(α), CH(β), and CH(γ)—are able to observe even in the crystalline state. There might be a possibility that less globular shape of the molecule caused to reduce the entropy of melting. In order to consider factors of the constituent molecules that diminish the entropy of melting and hence enhance their characteristics as the plastic crystals, thermal properties of cyclohexene oxide and cyclohexanone were measured with an adiabatic calorimeter in the temperature range between 13 and 300 K. Both compounds are non-globular and lack their ability of hydrogen bonding formation. Previous DTA experiments[5,6] for both compounds revealed their ability to form plastic crystalline phases. Heat capacity data of cyclohexanone are available literally[7] only for a limited temperature range.

Experimental

Materials. Cyclohexene oxide (Tokyo Kasei Co. Ltd., G. R. grade) was fractionally distilled in a double-wall glass column operated at a high reflux ratio. Temperature of the still was monitored by a thermocouple. Fractions were compared by differential thermal analysis (DTA) to monitor the purity of that part. The best fraction of the distillate was further purified by vacuum distillation and finally distilled into calorimeter cell *in vacuo*. A part of the purified specimen was transferred into a DTA tube and was used for characterization of thermal behavior. Since the material is easily polymerizable at high temperature, the sample was kept below 5 °C. The purity of the calorimetric sample was determined to be 99.97_3% from the analysis of equilibrium melting curve described later.

Cyclohexanone (Tokyo Kasei Co. Ltd., G. R. grade) was subjected to essentially the same purification process as that of cyclohexene oxide. The final purity was determined to be 99.91_9%.

Apparatus. Heat capacity measurements were made by the on-line automated calorimeter[8] built recently in our laboratory. The temperatures of the inner and the outer shields, and the tempering ring were controlled with separate temperature controllers. The electrical power supplied to the calorimeter heater was measured with a digital voltmeter operated by a program unit. Resistances of a working platinum thermometer were measured by a.c. double bridge and stored in a mini-computer. After reaching an equilibrium state, the equilibrium resistance value was converted into the

† Contribution No. 5 from Chemical Thermodynamics Laboratory.

** Present address: Department of Chemistry, School of Science, Kwansei Gakuin University, Nishinomiya 662.

IPTS-68 temperature scale and the heat capacity was calculated during the measurement. The sample cell equipped with horizontal perforated heat-distributing disks of platinum contained 29.901 g (0.30467 mol) of cyclohexene oxide and 26.081 g (0.26473 mol) of cyclohexanone, respectively.

Results

DTA. Thermal behavior of cyclohexene oxide at low temperatures was examined by use of DTA, the result being given in Fig. 1. Run 1 shows the cooling curve with a rate of -1.5 K min^{-1}. Run 2 and Run 3 are the subsequent heating curves, respectively. The heating curve Run 3 is in good agreement with that previously reported.[5] All the phase changes undercooled easily. A new intermediate phase was observed to appear always on cooling the liquid. From a comparison of respective peak areas, the intermediate phase as well as the high temperature phase are considered to be highly disordered state. Considering the manner by which the respective phase changes take place, the intermediate phase is expected to be a metastable phase.

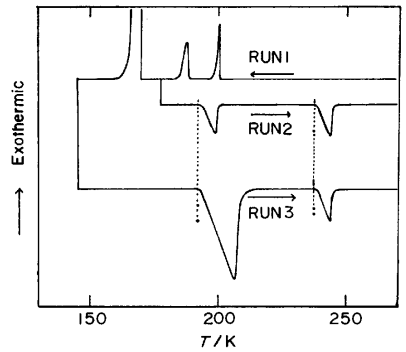

Fig. 1. DTA curves of cyclohexene oxide.

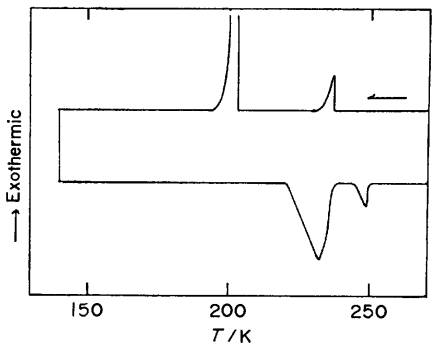

Fig. 2. DTA curves of cyclohexanone.

Figure 2 gives DTA curves of cyclohexanone for cooling and heating. Both of the solidification and solid-solid phase transition were found to undercool considerably. The peak due to the phase transition observed for heating is a little anomalous in shape and suggests a possibility that the transition proceeds in two or more steps. This possibility was examined carefully in later heat capacity measurement.

Heat Capacity. The experimental heat capacity determinations are presented in Table 1 for cyclohexene

Table 1. Molar heat capacity of cyclohexene oxide

T/K	C_s/J K^{-1} mol^{-1}	ΔT/K	T/K	C_s/J K^{-1} mol^{-1}	ΔT/K
14.37	4.063	1.148	150.37	80.525	3.095
16.99	6.128	2.088	153.44	82.058	3.047
19.00	7.943	1.936	156.47	83.643	2.999
20.80	9.706	1.665	159.44	85.320	2.951
22.60	11.560	1.937	161.85	86.751	2.219
24.64	13.694	2.145	164 06	87.930	2.195
26.81	15.932	2.199	166 24	89.147	2.171
28.88	18.040	1.928	168.51	90.598	2.381
30.97	20.061	2.257	170.88	92.262	2.347
33.10	22.142	2.022	173.21	93.756	2.318
35.04	23.836	1.858	175.51	95.344	2 286
36.94	25.595	1.953	177.78	97.120	2 254
38.83	27.164	1.822	180.02	98.784	2.224
40.60	28.019	1.715	182.23	100.88	2.189
42.53	30.148	2.150	184.40	102.70	2.159
44.62	31.556	2.029	186.54	105.16	2.121
46.69	32.948	2.108	188.66	108.06	2.080
48.75	34.412	2.001	190 63	122.33	1.904
50.70	35.679	1.913	191.75	165.58	1.460
52.80	36.870	2.286			
55.04	38.236	2.192	195.56	128.52	2.372
57.20	39.752	2.106	197.93	124.36	2.366
58.72	40.523	2.343	201.28	124.81	2.246
61.02	41.669	2.256	203.52	125.05	2.240
63.24	42.785	2.181	205.76	125.38	2.231
65.39	43.815	2.115	207.98	125.60	2.609
67.47	44.912	2.054	209.48	125.97	2.219
69.50	45.804	2.001	211.78	126.26	2.212
71.48	46.783	1.951	213.99	126.63	2.205
73.41	47.564	1.909	216.19	127.18	2.196
75.30	48.473	1.866	218.39	127.36	2.191
77.14	49.235	1.830	220.57	127.83	2.182
78.95	50.173	1.792	222.75	128.19	2.175
80.73	50.853	1.762	224.92	128.61	2.167
82.59	51.706	1.964	227.09	129.06	2.159
84.54	52.517	1.929	229.24	129.55	2.150
86.45	53.272	1.896	231.39	130.09	2.141
80.12	50.563	2.839	233.52	130.67	2.131
82.92	51.817	2.761	235.64	132.02	2.113
85.65	52.939	2.694			
88.31	54.032	2.632			
90.92	55.115	2.574	239.03	146.90	1.169
93.46	56.110	2.522	240.35	147.28	1.457
95.96	57.134	2.473	242.04	147.81	1.935
98.41	58.056	2.429	244.54	148.52	2.126
100.82	59.061	2.386	246.66	149.09	2.117
103.19	60.003	2.347	248.77	149.69	2.108
105.51	60.971	2.312	250.87	150.39	2.099
107.81	61.811	2.276	252.97	150.97	2.090
110.07	62.858	2.241	255.12	151.56	2.211
112.29	63.666	2.212	257.32	152.31	2.200
114.49	64.588	2.182	259.52	152.93	2.190
116.99	65.606	2.823	262.06	153.72	2.894
119.79	66.814	2.775	264.94	154.63	2.875
122.54	67.842	2.733	267.81	155.55	2.858
125.26	69.083	2.691	270.66	156.46	2.839
127.93	70.146	2.653	273.30	157.37	2.768
130.56	71.410	2.615	276.06	158.15	2.754
133.16	72.500	2.584	280.51	159.66	4.913
135.72	73.701	2.543	283.24	160.64	2.512
138.25	74.754	2.511	285.76	161.27	2.520
140.75	75.805	2.480	288.46	162.45	2.873
143.21	77.075	2.446	290.77	163.08	3.105
145.64	78.283	2.414	293.87	163.97	3.089
148.04	79.402	2.384	296.96	164.98	3.069

Table 2. Molar heat capacity of cyclohexanone

T/K	Cs/J K^{-1} mol^{-1}	ΔT/K	T/K	Cs/J K^{-1} mol^{-1}	ΔT/K
13.78	4.158	1.645	153.34	86.092	2.360
15.47	5.927	1.753	155.68	87.029	2.338
17.44	7.989	2.172	158.01	88.008	2.318
19.20	10.070	1.356	160.32	88.967	2.297
21.00	12.241	2.236	162.60	89.931	2.276
23.32	15.154	2.404	164.87	90.853	2.257
25.76	18.176	2.490	167.12	91.774	2.238
28.14	21.032	2.268	169.35	92.760	2.218
30.37	23.595	1.999	171.90	93.991	2.890
32.50	25.890	2.250	174.88	95.139	2.634
34.84	28.302	2.435	177.50	96.584	2.603
37.17	30.681	2.220	180.09	97.479	2.583
39.40	32.720	2.250	182.66	98.766	2.555
41.78	34.835	2.504	185.20	99.959	2.531
44.48	36.999	2.901	187.73	101.19	2.507
47.15	39.012	2.447	190.22	102.52	2.481
49.54	40.732	2.317	193.90	104.49	4.890
52.07	42.621	2.739	197.55	106.54	2.409
54.66	44.265	2.452	199.95	108.02	2.384
57.06	45.771	2.347	202.32	109.42	2.360
59.37	46.937	2.263	204.67	111.12	2.335
61.57	48.348	2.179	206.99	112.89	2.308
63.82	49.458	2.316	211.65	117.61	2.433
66.10	50.704	2.244	214.00	121.85	2.275
68.31	51.829	2.181	216.23	128.91	2.186
70.73	52.928	2.656	218.32	147.22	1.987
73.39	54.192	2.656			
76.01	56.559	2.584	222.72	147.44	2.400
78.56	56.612	2.516	225.15	142.27	2.460
81.05	57.703	2.458	227.61	141.45	2.467
83.48	58.727	2.406	230.07	142.57	2.451
85.86	59.728	2.357	232.52	143.47	2.537
88.19	60.748	2.311	234.95	144.01	2.328
90.48	61.666	2.270	237.36	146.50	2.395
92.70	62.539	2.233			
94.92	63.333	2.199			
97.10	64.225	2.164	244.75	160.18	0.684
99.25	65.120	2.132	245.67	158.49	1.259
101.37	65.881	2.104	247.46	158.92	2.208
103.46	66.739	2.075	249.66	159.95	2.197
105.55	67.145	2.114	251.96	160.52	2.401
107.86	68.394	2.453	254.36	161.59	2.405
108.05	68.473	2.446	255.39	161.69	2.318
110.48	69.395	2.420	257.70	162.51	2.308
112.88	70.426	2.381	260.02	163.14	2.391
115.25	71.266	2.353	262.40	163.99	2.380
117.59	72.225	2.323	264.95	164.77	2.710
120.28	73.264	3.066	267.65	165.95	2.693
123.16	74.321	2.698	270.34	166.70	2.682
125.84	75.428	2.661	273.01	167.51	2.669
128.49	76.383	2.628	275.67	168.55	2.654
131.10	77.445	2.595	278.32	169.55	2.640
132.88	78.081	2.579	280.95	170.24	2.629
135.44	79.209	2.546	283.58	171.35	2.614
137.97	80.169	2.519	286.18	172.17	2.602
140.48	81.095	2.492	288.78	173.35	2.586
142.95	82.182	2.465	291.31	174.27	2.577
146.61	83.368	2.429	293.87	174.96	2.541
148.58	84.267	2.405	296.40	175.96	2.527
150.97	85.313	2.381	298.92	176.72	2.517
			301.43	177.92	2.501

oxide and in Table 2 for cyclohexanone, along with the approximate temperature increments. In most cases, the temperature increments were small enough to eliminate the need of curvature correction. Correction of the vaporization was found to be negligible in both cases. The imprecision of the experimental heat capacity was usually less than 0.1%, except in the transition and melting regions. The loss of precision in these ranges was caused by slow thermal and compositional equilibration. Accuracy uncertainty in heat capacity is about 1% below 20 K and 0.2% above 50 K. The heat capacity data are reproduced graphically in Figs. 3 and 4, respectively.

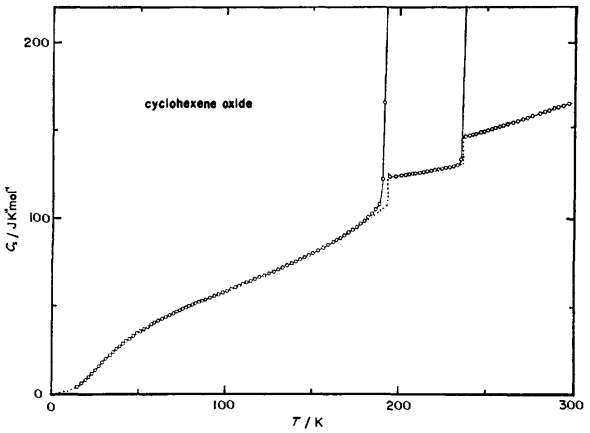

Fig. 3. Molar heat capacity of cyclohexene oxide.

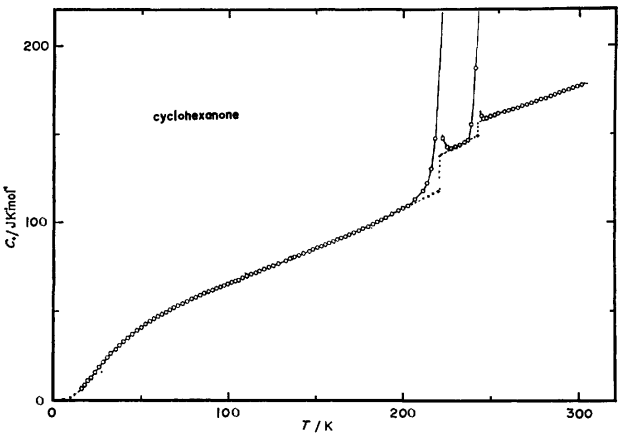

Fig. 4. Molar heat capacity of cyclohexanone.

Phase Transition. Cyclohexene oxide showed a sharp transition at 193.10 K. The thermal equilibrium was extremely difficult to attain during the transition. Hence, a temperature about 100 min after an energy input was regarded conveniently as an equilibrium temperature and was used for the calculation of apparent heat capacity. Figure 5 gives a plot of enthalpy increment against temperature during the course of phase transition of cyclohexene oxide. The transition proceeded in a single step and the temperature of transition was determined as the one at which the heat capacity reached its maximum value. The enthalpy of transition was determined from the total enthalpy

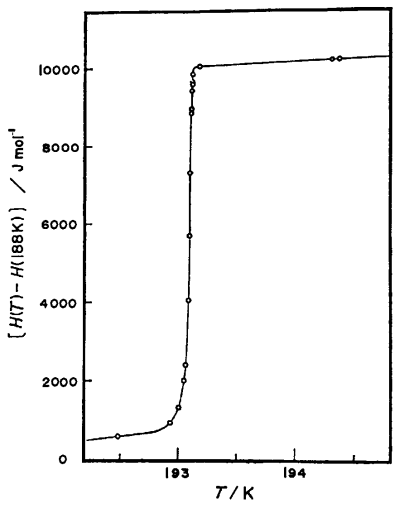

Fig. 5. Enthalpy change of cyclohexene oxide around the transition temperature.

change between equilibrium temperatures below and above the transition temperature. The isothermal increment was calculated by subtracting from the total enthalpy those part associated with the "normal" heat capacity given by dotted lines in Figs. 3 and 4, respectively. The results of replicate determinations of the enthalpies of transition for both compounds are summarized in Table 3.

TABLE 3. MOLAR ENTHALPIES OF TRANSITION

Cyclohexene oxide (T_t=193.10 K)		
T_i/K	T_f/K	ΔH_t/J mol^{-1}
180.2622	196.6566	9536.2
180.0479	197.3844	9534.0
ΔH_t=9535.1±1.1 J mol^{-1}		
ΔS_t=49.39±0.01 J K^{-1} mol^{-1}		
Cyclohexanone (Tt=220.83 K)		
T_i/K	T_f/K	ΔH_t/J mol^{-1}
211.8566	224.7534	8659.5
211.7343	224.6700	8659.7
ΔH_t=8659.6±0.1 J mol^{-1}		
ΔS_t=39.22±0.01 J K^{-1} mol^{-1}		

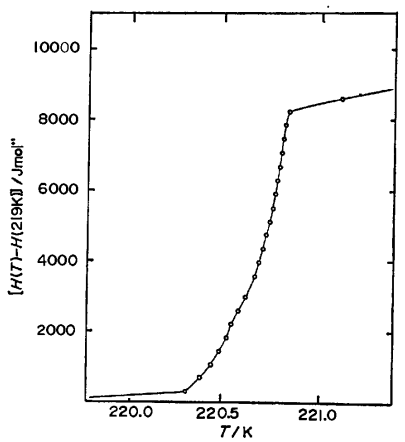

Fig. 6. Enthalpy change of cyclohexanone around the transition temperature.

Enthalpy increment during the course of the phase transition of cyclohexanone is plotted in Fig. 6 as a function of temperature. Here, the phase transition takes place over a temperature range and does not proceed uniformly. In order to make clear this situation, apparent heat capacities were calculated over the transition range and they are given in Fig. 7. Evidently, the transition proceeds in two steps. This observation accords well with suggestion by Crowe and Smyth[9] from their dielectric study and with phase diagram study of cyclohexanone–CCl_4 system by Miltenburg.[7] Würflinger and Kreutzenbeck have found a third modification of cyclohexanone by DTA under high pressures. They reported that the triple point among the three crystalline phases coincided with atmospheric pressure within the limits of experimental error. They could not reveal a superposed second solid-solid transition at atmospheric pressure by their DTA experiment, possibly because of their high heating rate.

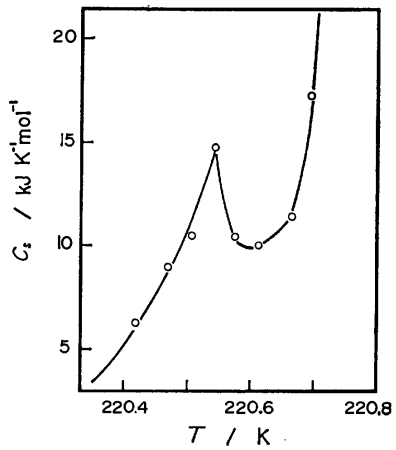

Fig. 7. Apparent heat capacity of cyclohexanone around the transition temperature.

Cataliotti and Paliani[10] reported the existence of an additional phase transition in cyclohexanone at 168 K. However, this or any other phase transition was not observed by the present calorimetric work.

Enthalpy of Melting and Sample Purity. The enthalpy of melting was determined as the isothermal

TABLE 4. SUMMARY OF MELTING EXPERIMENTS FOR CYCLOHEXENE OXIDE

f	$1/f$	$T_m(f)$/K
0.307	3.255	237.8037
0.397	2.516	237.8324
0.560	1.786	237.8620
0.722	1.384	237.8864
0.884	1.131	237.9126
$T°_m$=238.14 K		
x=0.027 mol %		
T_i/K	T_f/K	ΔH_m/J mol^{-1}
234.3244	239.0720	1064.6
234.3658	239.3133	1064.3
ΔH_m=1064.5±0.2 J mol^{-1}		
ΔS_m=4.470±0.010 J K^{-1} mol^{-1}		

Table 5. Summary of melting experiments for cyclohexanone

f	$1/f$	$T_m(f)$/K
0.2901	3.447	243.195
0.3658	2.734	243.434
0.4470	2.237	243.636
0.5342	1.872	243.802
0.6234	1.604	243.942
0.7174	1.394	244.063
0.8147	1.229	244.163
0.9124	1.096	244.253
$T°_m$=245.21 K		
x=0.081 mol %		
T_i/K	T_f/K	ΔH_m/J mol^{-1}
235.9724	247.9974	1327.91
235.8726	247.9145	1327.45
ΔH_m=1327.6±0.3 J mol^{-1}		
ΔS_m=5.414±0.010 J K^{-1} mol^{-1}		

segment of the enthalpy required to heat from an initial equilibrium temperature of the crystal to a final temperature of the liquid. Here, a normal heat capacity was assumed, being represented as the dotted lines in Figs. 3 and 4.

For the determination of the melting point and the purity of the sample, a fractional melting experiment was carried out. The equilibrium temperatures $T(f)$ were observed at several fractions f of the sample melted. The melting temperature plotted against the reciprocal fraction did not give a straight line, indicating a possibility of solid-soluble impurity scheme. Following the theoretical treatment by Mastrangelo-Dornte,[11] we have estimated the total amount of impurities x and the triple point of pure compound $T°_m$. These melting data are summarized in Tables 4 and 5.

Thermodynamic Functions. The experimental heat capacities were smoothed by a spline fit and then numerically integrated to obtain the final tabular values of the standard thermodynamic functions. They are listed in Tables 6 and 7 at selected round temperatures. Below the lowest temperature attained, the heat capacity data were extrapolated by means of the Debye law. The parameters of the Debye functions were assigned as θ=140 and 132 K for six degrees of freedom for cyclohexene oxide and cyclohexanone, respectively.

Discussion

Characterization of the plastically crystalline state is a topic of current solid-state chemical and physical interest.[12] The appearance of the plastic crystal state has been attributed to the onset of molecular reorientational motion in the solid and can be expected for globular molecules, *i.e.*, molecules of high symmetry and nearly spherical shape. The distinct difference between the phase behavior of pentane and of neopentane is cited in many textbook[13] as showing the importance of globularity of the constituent molecules in the formation of plastic crystals. A suggestion[14] that plastic crystals might better be called "crystals with globular molecules" reflects this widespread recognition.

The values of ΔS_m for cyclohexene oxide and cyclohexanone are comparable in magnitude to that of cyclohexanol,[2] 5.68 J K^{-1} mol^{-1} and less than that of cyclohexane,[15] 9.56 J K^{-1} mol.$^{-1}$ The relevant thermodynamic data are summarized in Table 8. This fact means that the calorimetric feature as the plastic crystalline behavior is enhanced by reduction of globularity of the constituent molecules. As pointed out already, the subject of plastic crystals began from the recognition by Timmermans that the crystal has considerably small entropy of melting and that the

Table 6. Molar thermodynamic functions of cyclohexene oxide

T/K	$C°_S$/J K^{-1} mol^{-1}	$S°_S$/J K^{-1} mol^{-1}	$[H°_S(T)-H°_S(0)]/T$/J K^{-1} mol^{-1}	$-[G°_S(T)-H°_S(0)]/T$/J K^{-1} mol^{-1}
20	8.921	3.450	1.656	1.794
30	19.12	8.994	5.882	3.112
40	28.10	15.82	10.32	5.498
50	35.12	22.87	14.61	8.268
60	41.11	29.82	18.54	11.28
70	46.01	36.54	22.12	14.42
80	50.53	42.98	25.39	17.59
90	54.70	49.18	28.42	20.75
100	58.71	55.15	31.25	23.90
120	66.86	66.57	36.50	30.07
140	75.56	77.51	41.45	34.06
160	85.63	88.24	46.32	41.92
180	98.83	99.04	51.38	47.66
200	124.62	159.25	104.18	55.07
220	127.67	171.26	106.17	65.09
240	147.20	187.16	112.71	74.45
260	153.08	199.17	115.58	83.59
280	159.52	210.75	118.49	92.26
300	166.12	221.98	121.44	100.53

TABLE 7. MOLAR THERMODYNAMIC FUNCTIONS OF CYCLOHEXANONE

T / K	C_S° / J K^{-1} mol^{-1}	S_S° / J K^{-1} mol^{-1}	$[H_S^\circ(T)-H_S^\circ(0)]/T$ / J K^{-1} mol^{-1}	$-[G_S^\circ(T)-H_S^\circ(0)]/T$ / J K^{-1} mol^{-1}
20	10.90	4.139	3.074	1.065
30	23.12	10.91	7.759	3.151
40	33.20	19.02	12.93	6.091
50	41.16	27.31	17.80	9.506
60	47.45	35.39	22.24	13.15
70	52.61	43.47	26.22	17.26
80	57.16	51.19	29.80	21.38
90	61.42	58.51	33.08	25.43
100	65.35	65.49	36.12	29.38
120	73.08	78.58	41.63	36.35
140	80.94	90.77	46.69	44.09
160	88.86	102.35	51.47	50.88
180	97.43	113.46	56.09	57.38
200	108.00	124.30	60.73	63.57
210	115.61	129.69	63.14	66.55
230	142.46	180.50	106.40	74.10
250	159.85	198.38	115.17	83.21
260	163.16	204.72	116.96	87.76
280	170.07	217.06	120.50	96.56
300	177.20	229.03	124.04	104.99

TABLE 8. THERMODYNAMIC DATA ASSOCIATED WITH PHASE CHANGES OF CYCLOHEXANE AND SOME OF ITS DERIVATIVES

Substance	T_t / K	ΔS_t / J K^{-1} mol^{-1}	T_m / K	ΔS_m / J K^{-1} mol^{-1}
Cyclohexane	186.09	36.20	279.84	9.56
Cyclohexanol	265.5	33.25	299.05	5.68
Cyclohexene oxide	193.10	49.39	238.14	4.47
Cyclohexanone	220.83	39.22	245.21	5.41

crystal is of high crystallographic symmetry.

The f.c.c. lattice is the one most frequently encountered for the plastic crystalline phase in which the constituent molecules have intense orientational disorder. Actually, cyclohexane, cyclohexanone and cyclohexanol are known to crystallize in f.c.c. lattice.[16] That of cyclohexene oxide has not yet been determined. However, X-ray powder diffraction experiment[5] gave a characteristic photograph of the plastic crystals; relatively intense background and a few diffuse Bragg scattering associated with large Debye-Waller factor. While the parent molecule, cyclohexane, has D_{3d} symmetry, the three oxy-derivatives can not be expected to have any symmetry element other than mirror. Microwave experiment[17] of cyclohexene oxide shows that the molecule has no symmetry.

In order to fulfil a high crystallographic site symmetry at the lattice point, molecules must reorient among several orientations. The time-averaged distribution of a molecule tends towards spherical symmetry, hence the closest packed structure is realized. A less symmetric molecule has to compensate by taking a greater number of molecular orientations than a symmetric molecule. Short-range repulsive interactions between neighboring molecules cause the reorientational motion of an asymmetric molecule to couple more closely with lattice vibrational motion, because the asymmetric molecule must reorient itself by displacing its center of mass from the lattice point. Observation of anomalously large Debye-Waller factors for these crystals reflects this coupling effect. The stronger the coupling, the smaller will be the entropy of melting, since partial positional disordering occurs concomitantly with orientational disordering at the phase transition. The stronger the coupling, the narrower will be the temperature range of plastic crystalline phase, since vibrational motion is highly excited at the phase transition. According to the simple picture by Lindemann,[18] melting might be expected when the mean amplitude of lattice vibration becomes some fraction of the lattice distance.

In order to test this intuitive idea, the relation between the entropy of melting and the temperature range of the plastic crystalline phase is examined for some plastic crystals composed of molecules with various symmetries. A list of some plastic crystals is given in Table 9, along with data for ΔS_m in units of J K^{-1} mol^{-1}. For the range of entropies of melting suggested by Timmermans for plastic crystals (<21 J K^{-1} mol^{-1}) we consider three groups: category A (ΔS_m/J K^{-1} mol^{-1} >14); category B ($14>\Delta S_m$/J K^{-1} mol^{-1} >7); category C ($7>\Delta S_m$/J K^{-1} mol^{-1}). We note that category A contains octahedral molecules or almost spherical molecules while many diatomic or tetrahedral molecules and some cyclic or caged molecules are to be found in category B. Category C contains the least globular molecules. Inert gas molecules like argon and krypton have entropies of melting between categories A and B (≈ 14 J K^{-1} mol^{-1}). They show rather high plasticity and the vapor snake phenomenon[19] near their mp. Although these crystals exhibit no phase transition, they can be legitimately considered as plastic crystals. The fact that ΔS_m values for non-globular molecules are less than those for spherical molecules (Ar, Kr) suggests strongly the importance of the orientation-position coupling effect. This coupling will also affect the temperature range in which stable plastic crystals can exist. The plastic crystals belonging to category A have a wide temperature range of existence. This is

Table 9. Entropies of fusion of some plastic crystals

A	$\frac{\Delta S_m}{J\,K^{-1}\,mol^{-1}} > 14$	C_2Cl_6(18.0)	$C_2(CH_3)_6$(18.8)
		SF_6(22.6)	MoF_6(15.3)
		$C(CH_3)Cl_3$(18.8)	$C(CH_3)_3OH$(22.4)
		bicyclo[2,2,2]octane (18.7)	
		adamantane (23.7)	*d*-borneol (17.2)
B	$14 > \frac{\Delta S_m}{J\,K^{-1}\,mol^{-1}} > 7$	N_2(9.51)	O_2(8.15)
		CH_4(10.4)	SiH_4(7.5)
		GeH_4(7.78)	CF_4(7.82)
		CCl_4(10.0)	CBr_4(10.9)
		$C(CH_3)_4$(12.7)	$C(CH_3)_3Cl$(8.11)
		$C(CH_3)_3SH$(9.04)	$C(CH_3)_2Cl_2$(9.78)
		PtF_6(13.4)	
		C_6H_{12}(9.29)	C_7H_{14}(9.09)
		d-camphor(11.7)	
		1-azabicyclo[2.2.2] octane(13.4)	
C	$7 > \frac{\Delta S_m}{J\,K^{-1}\,mol^{-1}}$	$(CH_3)_3CCOOH$(6.5)	$(CH_3)_3CC_2H_5$(3.3)
		C_5H_{10}(3.35)	$C_6H_{11}OH$(5.68)
		$C_6H_{10}O$ cyclohexanone(5.41)	
		$C_6H_{10}O$ cyclohexene oxide (4.48)	

exemplified typically by 220 K for hexamethylethane, and 335 K for adamantane. On the other hand, the compounds belonging to category C are characterized by quite narrow plastic crystal ranges: 45 K for cyclohexene oxide; 34 K for cyclohexanol; 25 K for cyclohexanone.

The present conclusion that non-globularity of the constituent molecules operates to diminish the value of ΔS_m and to narrow the plastic crystal range has some limitations. If the non-globularity of molecule exceeds some critical value, the hindering potential opposing randomization of orientation of the molecule increases too much for the orientationally disordered state to be realized before the melting point is reached. In this sense, cyclohexanone may be considered as an extreme case of a cyclohexane derivative that can exist as a plastic crystal. Pople and Karasz[20] were the first to take account of the fact in a rather qualitative way. In view of the complex nature of the intermolecular forces in this particular crystal, it is still not possible to define a critical parameter in a quantitative way.

Although the physical significance of the smallness of ΔS_m of plastic crystals has still to be clarified satisfactorily, this calorimetric feature should be correlated with the mechanical feature of the crystals. Dunning[16] suggested that the high plasticity may be analogous to the high-temperature creep of metals, which has been ascribed to the diffusional motion of vacancies through the crystalline lattice. It is this motion that also accounts for the easiness of self-diffusion observed in a number of plastic crystals and may have some correlation with the unusual freezing behavior called "vapor snake phenomenon."[19] Organic crystals in which the self-diffusion has been observed by NMR study were all characterized by their low values of ΔS_m. A kinetic parameter governing the self-diffusion in the highly disordered crystal was correlated well with the melting parameter[21] of the crystal. Valuable advances will be made by such correlation between more than one property of the plastic crystals.

References

1) J. Timmermans, *J. Phys. Chem. Solids*, **18**, 1 (1961).
2) K. Adachi, H. Suga, and S. Seki, *Bull. Chem. Soc. Jpn.*, **41**, 1073 (1968).
3) L. Q. Ameral, R. Fulfaro, and L. A. Vinhas, *J. Chem. Phys.*, **63**, 1312 (1975).
4) H. Suga and S. Seki, *Bull. Chem. Soc. Jpn.*, **35**, 1905 (1962).
5) T. Hiramoto, M. Nishii, K. Hayashi, and S. Okamura, *J. Polym. Sci.*, Part A-2, **9**, 3647 (1971).
6) A. Würflinger and J. Kreutzenbeck, *J. Phys. Chem. Solids*, **39**, 193 (1978).
7) J. C. von Miltenburg, Doctoral thesis, Rijksuniversiteit, Utrecht, 1971.
8) K. Kishimoto, H. Suga, and S. Seki, *Bull. Chem. Soc. Jpn.*, **53**, 2748 (1980).
9) R. W. Crowe and C. P. Smyth, *J. Am. Chem. Soc.*, **73**, 5406 (1951).
10) P. Cataliotti and G. Poliani, *Chem. Phys. Lett.*, **20**, 280 (1973).
11) S. V. R. Mastrangelo and R. W. Dornte, *J. Am. Chem. Soc.*, **77**, 6200 (1955).
12) M. Postel and J. G. Riess, *J. Chem. Phys.*, **81**, 2634 (1977).
13) For example; P. A. Winsor, "Liquid Crystals and Plastic Crystals," ed by G. W. Gray and P. A. Winsor, Ellis Horwood Ltd. (1974), Vol. 1, pp. 48—59 and references cited therein.
14) G. W. Smith, *Int. Sci. Technol.*, **61**, 72 (1967).
15) J. G. Aston, G. J. Szasz, and H. L. Finke, *J. Am. Chem. Soc.*, **65**, 1135 (1943); R. A. Ruehrwein and H. M. Huffman, *ibid.*, **65**, 1620 (1943).
16) W. J. Dunning, *J. Phys. Chem. Solids*, **18**, 21 (1961).
17) T. Ikeda, R. Kewley, and R. F. Curl, Jr., *J. Mol. Spectrosc.*, **44**, 459 (1972).
18) A. F. Lindemann, *Z. Phys.* **11**, 609 (1910).
19) S. Seki, *Kwagaku*, **18**, 277 (1948), *J. Chem. Phys.*, **18**, 397 (1950); M. K. Phibbs and H. I. Shiff, *ibid.*, **17**, 843 (1949); G. L. Pollack and H. P. Broida, *ibid.*, **36**, 968 (1963).
20) J. A. Pople and F. E. Karasz, *J. Phys. Chem. Solids*, **18**, 28 (1961).
21) H. Suga, M. Sugisaki, and S. Seki, *Mol. Cryst.*, **1**, 377 (1966).

Thermochemical Estimation of Destabilization Energies of 1,2-, 1,3-, and 1,4-Dicyanobenzenes Due to Interactions between Substituents. Appendix: Dipole Moments in Solution of the Dicyanobenzenes†

Tomoko SATO-TOSHIMA,** Minoru SAKIYAMA,* and Syûzô SEKI***
Department of Chemistry, Faculty of Science, Osaka University, Toyonaka, Osaka 560
(Received March 7, 1980)

Enthalpies of combustion of 1,2-, 1,3-, and 1,4-dicyanobenzenes were determined by precision oxygen-bomb calorimetry. Enthalpies of sublimation of these compounds were obtained by the measurement of temperature dependence of vapor pressure. The standard enthalpies of combustion ΔH_c°(298.15 K)/kJ mol^{-1} and the standard enthalpies of sublimation ΔH_s°(298.15 K)/kJ mol^{-1} are as follows: -4000.36 ± 0.67 and 86.9 ± 1.5 for 1,2-dicyanobenzene; -3992.29 ± 0.75 and 90.1 ± 1.5 for 1,3-dicyanobenzene; -3988.04 ± 0.59 and 88.8 ± 1.5 for 1,4-dicyanobenzene, respectively. Thermochemical destabilization energies were estimated by comparing the derived standard enthalpies of formation in gaseous state with those estimated for hypothetical non-destabilized molecules. They were discussed in terms of electrostatic interactions between highly electronegative and dipolar cyano substituents on one and the same benzene ring. Dipole moments of the dicyanobenzenes in benzene and dioxane solutions are reported in Appendix.

Determination of standard enthalpy of formation in gaseous state of a compound is the essentially sole experimental method to evaluate intramolecular energy of molecules. The method has been applied for polyhalobenzenoid compounds to study the interaction energies between substituents by Cox *et al.*,[1,2] who have shown the need to take account of electrostatic interactions between the substituents in the interpretation of standard enthalpies of formation in gaseous state.

As is well-known, a cyano group as well as halogen atoms is highly electronegative substituent. In addition, a cyano group is considered to be dipolar by itself. Thus, a cyano group has been situated at the most electronegative end of general electronegativity sequence of substituents.[3] Cyanohydrocarbons exhibit dipole moments higher than 3 Debye†† as a rule.

This study has been carried out to elucidate the interaction between cyano substituents on one and the same benzene ring. For this purpose, the standard enthalpies of combustion of 1,2-, 1,3-, and 1,4-dicyanobenzenes each in the crystalline state were measured by oxygen bomb calorimetry. Enthalpies of sublimation of the compounds were determined from the measurement of temperature dependence of vapor pressure. In this paper, results of the calorimetric and vapor pressure measurements are reported. From standard enthalpies of formation in gaseous state thus derived, destabilization energies were estimated and discussed in terms of electrostatic interactions between cyano substituents on the same benzene ring.

Experimental

Materials. Commerical 1,2-dicyanobenzene (Tokyo Kasei, G. R.) was purified by recrystallization from benzene and acetone solutions, and then by fractional sublimation *in vacuo* (0.1 Pa). Orthorhombic and monoclinic crystals are known for this compound,[4,5] though it is not clear which form is more stable. The purified sample showed neither exothermic nor endothermic anomalies between ambient and melting temperatures on DSC curves. In this respect the sample obtained is supposed to be in the stable form. 1,3-Dicyanobenzene supplied from Nihon Shokubai Kagaku Co., Ltd., and commerical 1,4-dicyanobenzene (Nakarai, G. R.) were purified by recrystallization from benzene solution, and subjected to fractional sublimation *in vacuo* (0.1 Pa), and again recrystallization from acetone solution. After brief drying *in vacuo*, a pellet drying procedure[31,32] was applied for the samples. A small endothermic peak with complicated shape was observed at *ca.* 430 K in every DSC heating curve of the latter compound, but the anomaly was not studied in further detail. Purity assessment for the three samples by DSC continuous method gave values higher than 99.9%.

Combustion Calorimetry. A rotating bomb calorimeter of isoperibol type with a platinum-lined bomb, described elsewhere,[6] was used in this study without rotating the bomb. The calorimeter was calibrated with the United States National Bureau of Standards S. R. M. 39i benzoic acid . The mean and standard deviation of mean for energy equivalents of the standard calorimetric system from six calibration experiments were (15164.84 ± 0.53) J K^{-1}.

The dicyanobenzenes are as volatile as may be purified by vacuum sublimation. However, no significant loss in mass was observed for pellets of the compounds each weighing about 1 g, when placed in air at ambient temperatures for several hours. All the combustion experiments were, therefore, carried out without enclosing the samples. An ordinary platinum crucible weighing 11.1 g was used to burn pellets of the compounds. In some of the experiments on 1,4-dicyanobenzene a deep platinum crucible with a baffle (total mass: 29.5 g) described previously[7] was employed, since the pellets showed some tendency of explosion to get out of the open crucible when partially burnt.

In order to determine a small amount of nitric acid produced as a by-product of combustion, the internal space of the bomb was washed with distilled water and the washings were adjusted to 100 cm^3. The nitric acid in the washings was titrated potentiometrically with sodium hydroxide solution, which in turn was standardized with potassium dihydrogenphosphate. Nitric acid formed in the calibration experiments was determined spectrophotometrically by using a UV absorption band

† Contribution No. 4 from Chemical Thermodynamics Laboratory.

** Present address: Sanyo Gakuen Women's Junior College, Okayama 703.

*** Present address: Department of Chemistry, School of Science, Kwansei Gakuin University, Nishinomiya 662.

†† Debye$=3.333\times10^{-30}$ cm.

Table 1. Auxiliary data for the calculation of standard energy of combustion

		ρ/g cm^{-3}	c_p/J K^{-1} g^{-1}	$(\partial E/\partial p)_T$/J MPa^{-1} g^{-1}
1,2-Dicyanobenzene	$C_8H_4N_2$	1.24	(1.19)	(−0.12)
1,3-Dicyanobenzene	$C_8H_4N_2$	1.26	(1.19)	(−0.12)
1,4-Dicyanobenzene	$C_8H_4N_2$	1.29	(1.19)	(−0.12)
Fuse	$CH_{1.860}O_{0.930}$	1.5	1.70	(−0.287)

T_h=298.15 K, V(bomb)=0.3469 dm^3, $\Delta E_C^\circ/M$(fuse)=−16507 J g^{-1}

at 202 nm.

Measurement of Temperature Dependence of Vapor Pressure. The vapor pressures of the samples were measured relatively with a DuPont Model 916 Thermal Evolution Analyzer, which was used in conjunction with a DuPont 990 Thermal Analysis System. It is based on the gas-saturation method and a flame ionization detector (F. I. D.) is used for quantitative determination of a small amount of organic species effused from the Knudsen type cell to carrier gas.[8] Increase h in the F. I. D. current caused by saturation of the carrier gas with the effused organic vapor was measured as a function of temperature. The quantity h is taken to be proportional with the saturation vapor pressure of the compound. Details of the experimental procedures were described elsewhere.[9]

Auxiliary Quantities. The experimental results were based on relative atomic weights recommended by IUPAC Commission on Atomic Weights (1970). The data of density ρ, specific heat capacity c_p, and compression energy $(\partial E/\partial p)_T$ at 298.15 K used for reduction to the standard state and for correction of weights in air to masses are shown in Table 1. The densities of the dicyanobenzenes given in Table 1 were determined by measuring the mass of a pellet of measured size as was reported by Good *et al.*[10] The procedure was examined for benzoic acid. The derived density (1.32 g cm^{-3}) agreed well with a literature value.[30] The densities thus determined were in fair agreement with the values obtained by X-ray method: 1.25 and 1.21 g cm^{-3} for orthorhomboic[4] and monoclinic[5] forms of the 1,2-isomer, respectively, and 1.283 g cm^{-3} for the 1,4-isomer.[20]

The specific heat capacities and compression energies for the dicyanobenzenes given in Table 1 are estimated values. Other auxiliary quantities used in the calculation are also collected in the table. Uncertainties given in this paper are uncertainty intervals defined by Rossini,[33] *i. e.* twice the final overall standard deviation of mean, unless otherwise stated.

Results

Standard Energies of Combustion. Six combustion experiments were carried out for 1,2- and 1,3-dicyanobenzenes, respectively. Eight combustion experiments were carried out for 1,4-dicyanobenzene, among which the deep crucible with a baffle was employed for six samples. The idealized combustion reaction at 298.15 K, to which standard energies and enthalpies of combustion refer, is expressed by the following equation:

$$C_8H_4N_2(c) + 9O_2(g) = 8CO_2(g) + 2H_2O(l) + N_2(g).$$

Results of typical combustion experiments are shown in Table 2. Symbols used in the table are similar to those used by Hubbard *et al.*[12] except for ΔE (std. state), which is the sum of items 81—85 and 87—94 as defined by Hubbard *et al.*[12] Six derived standard energies of combustion ΔE_c°/kJ mol^{-1} for 1,2-dicyanobenzene were −4000.12, −4000.36, −3999.52, −4000.08, −4001.44, and −4000.65, respectively, and mean and standard deviation of mean was −(4000.36±0.26). For 1,3-dicyanobenzene, they were −3991.43, −3991.88, −3991.60, −3992.73, −3992.66, and −3993.41, and mean and standard deviation of mean was found to be −(3992.28±0.31). For 1,4-dicyanobenzene, they were −3988.61, −3988.23, −3987.35, −3988.59, −3988.73, −3987.88, −3987.72, and −3987.23, of which the latter six were obtained by using the deep crucible with a baffle. Mean and standard deviation of mean were −(3988.42±0.19) for

Table 2. Results of typical combustion experiments

Dicyanobenzene	1,2-[a]	1,3-[a]	1,4-[a]	1,4-[b]
m^i(compd)/g	0.88438	0.87325	0.87357	0.87796
m^i(fuse)/g	0.00259	0.00257	0.00296	0.00306
m^i(H_2O, tot.)/g	1.1717	1.1527	1.1527	1.1629
p^i(gas)/MPa	3.040	3.059	3.039	3.041
θ_i/°C	23.163198	23.146460	23.156930	23.106719
θ_f/°C	25.016991	24.975439	24.983694	24.943305
$\Delta\theta_{corr}$/°C	0.026023	0.027873	0.026284	0.030085
n^f(HNO_3)/mmol	1.229	1.236	1.180	0.631
ΔE_{ign}/J	6.7	7.3	6.9	7.4
ε^i(cont.)/J K^{-1}	17.8	17.8	17.7	20.4
ε^f(cont.)/J K^{-1}	18.1	18.1	18.1	20.9
$\Delta E_{decomp.}$(HNO_3)/J	72.4	72.8	69.5	37.2
ΔE(std. state)/J	90.5	90.8	87.2	54.8
$\Delta E_{I.B.P.}$/J	−27743.8	−27338.4	−27329.1	−27425.4
ΔE_C°/kJ mol^{-1}	−4000.36	−3991.88	−3988.61	−3987.23

a) The sample was burnt in an open crucible weighing 11.1 g. b) The sample was burnt in a deep crucible with a baffle (total mass: 29.5 g).

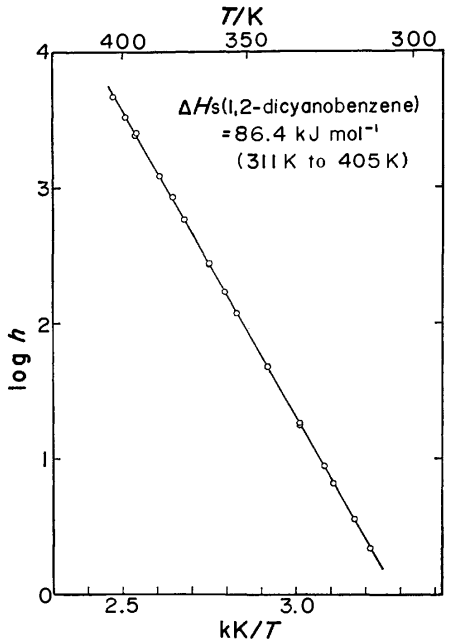

Fig. 1. Temperature dependence of vapor pressure of 1,2-dicyanobenzene. The quantity h is proportional to saturation vapor pressure of the compound and is given in arbitrary unit.

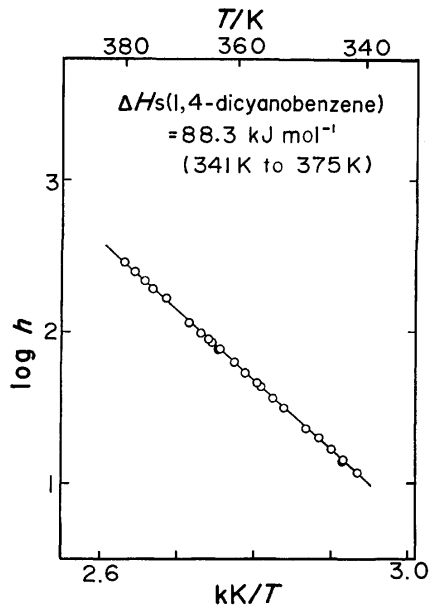

Fig. 3. Temperature dependence of vapor pressure of 1,4-dicyanobenzene. The quanitty h is proportional to saturation vapor pressure of the compound and is given in arbitrary unit.

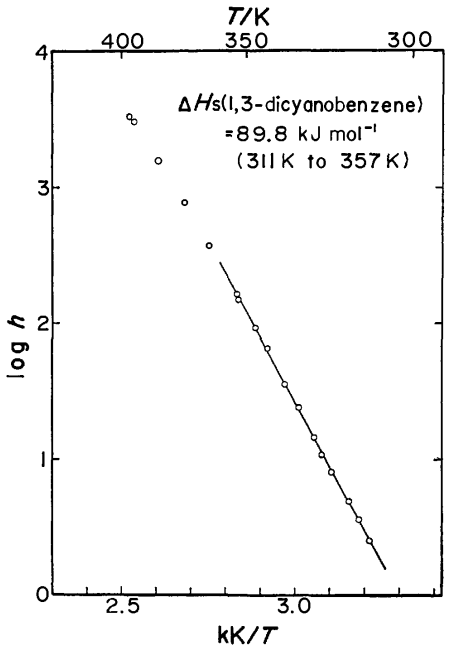

Fig. 2. Temperature dependence of vapor pressure of 1,3-dicyanobenzene. The quantity h is proportional to saturation vapor pressure of the compound and is given in arbitrary unit.

the former two and $-(3987.92\pm0.58)$ kJ mol^{-1} for the latter six experiments, respectively. In spite of difference in the mass of crucible and the amount of nitric acid formed between these kinds of experiments, the discrepancy of the derived enthalpies of combustion was not significant. Hence, the final mean and standard deviation of mean for 1,4-dicyanobenzene were calculated for all of the combustion experiments as follows: ΔE_c°/kJ mol^{-1} $=-(3988.04\pm0.21)$.

Enthalpies of Sublimation. Plots of log h against T^{-1} are given in Figs. 1, 2, and 3 for 1,2-, 1,3-, and 1,4-dicyanobenzenes, respectively. With a least squares method, the plots were fitted to straight lines and enthalpies of sublimation at mean temperatures were calculated from the slope of the straight lines on the basis of Clausius-Clapeyron equation. Vapor pressures are so low in the experimental temperature ranges that the enthalpies of sublimation were taken to be standard enthalpies of sublimation. The derived standard enthalpies of sublimation ΔH_s°/kJ mol^{-1} and mean temperatures T_m/K are as follows: 86.4 ± 1.5, 358 for 1,2-dicyanobenzene; 89.8 ± 1.5, 334 for 1,3-dicyanobenzene; 88.3 ± 1.5, 358 for 1,4-dicyanobenzene, respectively, where uncertainties are estimated values. Reduction of the standard enthalpies of sublimation at the mean temperatures to those at 298.15 K were performed by estimating molar heat capacities common to three

Table 3. Derived standard thermodynamic quantities at 298.15 K for dicyanobenzenes

Compound	$-\Delta E_c^\circ(c) = -\Delta H_c^\circ(c)$ / kJ mol^{-1}	$\Delta H_f^\circ(c)$ / kJ mol^{-1}	ΔH_s° / kJ mol^{-1}	$\Delta H_f^\circ(g)$ / kJ mol^{-1}
1,2-Dicyanobenzene	4000.36 ± 0.67	280.62 ± 1.23	86.9 ± 1.5	367.5 ± 1.9
1,3-Dicyanobenzene	3992.29 ± 0.75	272.55 ± 1.28	90.1 ± 1.5	362.7 ± 2.0
1,4-Dicyanobenzene	3988.04 ± 0.59	268.30 ± 1.19	88.8 ± 1.5	357.1 ± 1.9

dicyanobenzenes in gaseous and crystalline states. For gaseous state group contributions given by Benson *et al.*[13] were used and for crystalline state specific heat capacities were assumed to be given by the following expression: c_p/J K^{-1} g^{-1}=1.10+0.0035 (T−298.15). The corrections amounted to +0.5, +0.3 and +0.5 kJ mol^{-1} for 1,2-, 1,3-, and 1,4-dicyanobenzenes, respectively.

Derived Thermodynamic Quantities. In Table 3 are given the standard energies of combustion ΔE_c°(c) and standard enthalpies of combustion ΔH_c°(c) determined for three dicyanobenzenes together with standard enthalpies of sublimation ΔH_s° and derived standard enthalpies of formation of crystalline state ΔH_f°(c) and of gaseous state ΔH_f°(g) at 298.15 K. ICSU-CODATA key values[14] for standard enthalpies of formation of CO_2(g) and H_2O(l) were employed to calculate the standard enthalpies of formation in crystalline state.

Discussion

Comparison with Literature Values. No thermochemical determinations have been reported so far for 1,2-, 1,3-, and 1,4-dicyanobenzenes, except for the combustion calorimetric result of Salley and Gray[15] for the 1,2-isomer. The reported standard enthalpy of combustion, corrected for molar atomic masses and density, is −3995.49±1.00 kJ mol^{-1}, which is well outside the uncertainty interval of the present result, the difference being *ca.* 0.125% of the total. The calorimetric sample of Salley and Gray had been purified by recrystallization of a commercial sample from ethanol solution and had a melting point of 411.7—413.2 K. The observed nitrogen content was 99.0% of the theoretical. They stated that the accuracy of their value was almost certainly poorer than the precision (*e.g.*, 0.025% for 1,2-dicyanobenzene) of determinations, since the purity of the sample was the limiting factor.[15] In addition, 1,2-dicyanobenzene was not included in their list of compounds which was considered to be relatively pure.

Estimation of Destabilization Energies. The increment of intramolecular energy which is accompanied by the substitution of one cyano group to a benzene ring was evaluated as the difference (Δ=+135.9 kJ mol^{-1}) between the enthalpy of formation in gaseous state ΔH_f°(g) of cyanobenzene[16] and that of benzene,[17] as illustrated below:

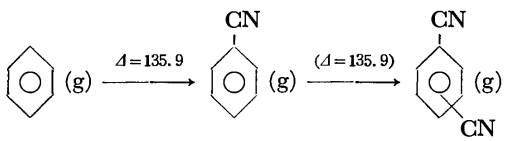

$\frac{\Delta H_f^\circ(g)}{\text{kJ mol}^{-1}}$: 82.9 218.8 (354.7)

If the increment, 135.9 kJ mol^{-1}, were assumed to be transferable to the substitution of the second cyano group, the standard enthalpy of formation in gaseous state of dicyanobenzene would be 354.7 kJ mol^{-1} as shown above. This value may be taken to be the standard enthalpy of formation in gaseous state of hypothetical "non-destabilized" dicyanobenzene. Comparison of the experimental values with this value gave destabilization energies of 12.8±1.9, 8.0±2.0, and 2.4±1.9 kJ mol^{-1} for 1,2-, 1,3- and 1,4-dicyanobenzenes, respectively.††† Among them, the 1,4-isomer is most stable and barely destabilized, the 1,3-isomer is intermediate and the 1,2-isomer is least stable. In this scheme, contributions from interactions between a benzene ring and a cyano group is eliminated automatically. Hence, the destabilization energies thus calculated are related only with interactions between the cyano-substituents.

Table 4. Destabilization energies E_{destab} of di-substituted benzenes

The energies were calculated as enthalpy changes for the following hypothetical reactions:

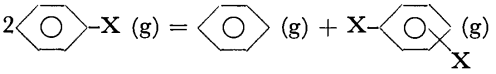

Isomer	E_{destab}/kJ mol^{-1}		
X=	F	Cl	CN
1,2-	21.2	10.4	12.8
1,3-	5.7	6.2	8.0
1,4-	8.4	2.9	2.4

Destabilization energies calculated similarly for difluoro- and dichlorobenzenes[17] were compared with those of dicyanobenzenes in Table 4. Destabilization energy of dicyanobenzene are of similar magnitude to that of the corresponding dichlorobenzene and lower than that of the corresponding difluorobenzene. It is worth noting that for difluorobenzene the 1,3-isomer is more stable than the 1,4-isomer in contrast to the trend found in dichloro- and dicyanobenzenes. Niessen[18] made *ab initio* MO calculations to obtain total energies of disubstituted benzenes including difluoro- and dicyanobenzenes. In all cases, the total energies were found to increase in the sequence of 1,3-, 1,4-, and 1,2-isomers in accordance with the trend experimentally found for difluorobenzenes. However, the differences in the total energies between 1,4- and 1,3-isomers and between 1,2- and 1,3-isomers obtained by Niessen were 0.67 and 2.72 kJ mol^{-1} for dicyanobenzenes, respectively, and 62.9 and 95.4 kJ mol^{-1} for difluorobenzenes, respectively. The latter differences are too large as compared with thermochemical values.

Interpretation of Destabilization Energies. The molecular structure of cyanobenzene was determined by Bak *et al.* from microwave spectroscopy.[19] The C–C distance of benzene is practically conserved in the structure. Changes of valence angles are definitely present, but are small (0—2.5°). The C–CN and C–N distances are 0.1455(7) and 0.1159(2) nm, respectively, where numbers in parentheses are estimated uncertainties for the final significant figures. The cyano group is coplanar with the benzene ring.

The molecular and crystal structures of 1,4-dicyano-

††† The destabilization energies are equivalent to enthalpy changes for the following hypothetical reactions:

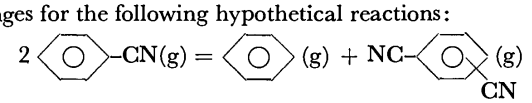

benzene were determined by van Rij and Britton[20] from X-ray diffraction method. The C–C distances in the benzene ring are all normal. The C–CN and C–N distances are 0.1438(3) and 0.1147(4) nm, respectively, where numbers in parentheses are estimated standard deviations expressed in the same way as above. The cyano groups deviated from coplanarity significantly, but slightly. 1,2-Dicyanobenzene crystallizes in two forms: orthorhombic[4] and monoclinic.[5] X-ray diffraction studies on these crystals indicated that the bond distances in the molecule are almost equal to the corresponding ones in a 1,4-dicyanobenzene molecule and the cyano groups are almost coplanar with the benzene ring.[4,5] No structural determinations have been reported for 1,3-dicyanobenzene.

These facts show that no remarkable difference in corresponding molecular parameters are observed among cyanobenzene and 1,2- and 1,4-dicyanobenzenes. It seems likely that the same would hold for 1,3-dicyanobenzene. These statements may be part of the reasonings which support the estimation of distabilization energies between substituents based on the scheme described above.

The dipole moment of a free cyanobenzene molecule is 4.14 Debye, which has been determined by Lide from microwave spectroscopy.[21] Charge distribution and dipole moment of a cyanobenzene molecule in the ground state have been studied by using molecular orbital methods of various levels. At the level of semi-empirical all valence electron MO methods, King and van Putten[22] calculated charge densities on all the atoms of the molecule (CNDO/CI method) and Klasing *et al.*[23] calculated charge densities on carbon and nitrogen atoms (CNDO/2 method). Charge densities on cyano carbon and nitrogen atoms and negative charge donated from the benzene ring to the substituent were calculated to be $+0.090e$, $-0.212e$, and $-0.122e$ by King and van Putten[22] and $+0.089e$, $-0.166e$, and $-0.077e$ by Klasing *et al.*,[23] respectively. Bloor and Breen[24] used a CNDO/2 method to calculate contributions to total dipole moment from atomic charge densities (p^σ and p^π, where σ and π denote σ and π electrons, respectively) and from the atomic dipole moment(p_{sp}) arising from the mixing of the s and p orbitals on the same atom and including lone-pair moment of the hetero-atom. The derived results were as follows: $p^\sigma=0.25$, $p^\pi=1.52$ and $p_{sp}=1.45$ Debye and total dipole moment was 3.23 Debye. At the level of *ab initio* MO method, Hehre *et al.*[25] made a calculation with the minimal STO-3G basis set to determine the total dipole moment p and total σ and π charges, q^σ and q^π, donated from the benzene ring to the substituent. Derived results were as follows: $p=3.65$ Debye, $q^\sigma=-0.104e$, and $q^\pi=-0.022e$.

As described in Appendix, the dipole moments of 1,2- and 1,3-dicyanobenzenes in benzene solution amount to *ca.* 95% of the values calculated as vector sum of the dipole moment of cyanobenzene in benzene solution and that of the 1,4-isomer is, at least, nearly equal to zero. The dipole moments in dioxane solution showed similar tendency. The charge distribution in the cyano groups of dicyanobenzene molecules is considered to be similar to that in the molecules of cyanobenzene. This is another reasoning to support the use of the scheme described above to obtain destabilization energies.

Although the destabilization of 1,2-dialkylbenzene may be ascribed to repulsive interaction between buttressed alkyl groups, that of 1,2-dicyanobenzene may hardly be due to the same cause. The molecular orbital calculations did not reproduce exactly the experimental total permanent dipole moment of 4.14 Debye, but indicated that the dipole moment of cyanobenzene comes from (1) net charge donated from the benzene ring to the substituent, (2) polarization of the C–N bond and (3) lone pair electrons on the nitrogen atom. Hence, the destabilization in the dicyanobenzenes is most likely to be due to electrostatic interactions between the substituents.

The validity of the inference may be shown by the calculation described below. For simplicity, the electrostatic interaction is assumed to be represented by dipole-dipole interaction between electric dipoles located at the positions of nitrogen atoms. Interaction energy E_{el} between two electric dipoles with moments μ_1 and μ_2, respectively, is expressed by the following equation:

$$E_{el}=\frac{\mu_1\mu_2}{r_{12}^3}(3\cos\theta_1\cos\theta_2-\cos^2\theta_{12}), \qquad (1)$$

where, r_{12} is the distance between the dipoles, θ_1 and θ_2 are the inclination angles of them to the line of centers, and θ_{12} is the angle between them.

If the dipole-dipole interaction energy and the thermochemical destabilization energy for 1,2-dicyanobenzene (12.8 kJ mol^{-1}) are equated, the dipole moment of 3.27 Debye is derived. Use of this value together with equation (1) leads in turn to dipole-dipole interaction energies of 4.3 and 2.6 kJ mol^{-1} for 1,3- and 1,4-dicyanobenzenes, respectively. In this calculation the following assumptions were made of the molecular structure of the dicyanobenzenes: (i) C–C–N moiety is linear, (ii) the molecules are planar including the substituents, (iii) C–CN and C–N distances are transferable between 1,4-dicyanobenzene and both of the 1,2- and 1,3-isomer; the reported values for the 1,4-isomer[20] were used in common, and (iv) benzene rings are regular hexagons with C–C distances of 0.1393 nm.

The derived dipole moment, 3.27 Debye, is considered to be of reasonable magnitude in view of the observed dipole moments of the dicyanobenzenes in benzene and dioxane solutions and also the result of the MO calculations on cyanobenzene. The magnitude of the calculated dipole-dipole interaction energies for 1,3- and 1,4-dicyanobenzenes are comparable with the thermochemical destabilization energies. Thus, experimental results from thermochemical and dielectric measurements have been interpreted consistently on the basis of the single model. Accordingly, it may be concluded that electrostatic interactions between the cyano substituents on one and the same benzene ring are responsible for the destabilization observed for the molecules of 1,2-, 1,3-, and 1,4-dicyanobenzenes.

The authors are indebted to Mr. Keiichi Nishiyama and Mr. Junichi Furukawa, who assisted the determinations of enthalpies of sublimation and of dipole moments, respectively. They also thank Professor Doyle Britton of University of Minnesota, Professor Kenji Osaki and Dr. Tsuneyuki Higashi of Kyoto University, and Dr. Noritake Yasuoka and Mr. Atsushi Kume of Osaka University for communicating the results of X-ray diffraction studies prior to publication and Nihon Shokubai Kagaku Co., Ltd. for their kind supply of dicyanobenzenes.

Appendix

Dipole Moments in Solution of 1,2-, 1,3-, and 1,4-Dicyanobenzenes. Dielectric constant and refractive index were measured at 298.15 K for the benzene and dioxane solutions of the dicyanobenzenes in the range up to 0.15 mol dm^{-3}. The cell used for the dielectric measurement was similar to that described by Hassion and Cole.[26] Dielectric constant was measured at 1 kHz with a General Radio Type 1615 Capacitance Bridge.

Dipole moment, p, was calculated on the basis of the Guggenheim's equation:[27]

$$\left(\frac{p}{\text{Debye}}\right)^2 = \frac{9\times10^{36}kT}{4\pi N_A}\frac{3}{(\varepsilon_1+2)(n_1^2+2)} \times\left[\frac{(\varepsilon_{12}-n_{12}^2)-(\varepsilon_1-n_1^2)}{(c/\text{mol dm}^{-3})}\right]_{c\to0},$$

where ε_1 and ε_{12} are the dielectric constants of the solvent and solution, respectively, and n_1 and n_{12} are the refractive indices of the solvent and solution, respectively; c is the concentration, k the Boltzmann constant, and N_A the Avogadro constant. In Table 5, the derived dipole moments are presented and compared with the calculated values for benzene solutions, which were obtained as the vector sums of the dipole moment of cyanobenzene in benzene solution.[28,29]

Table 5. Dipole moment p in benzene and dioxane solutions of 1,2-, 1,3-, and 1,4-dicyanobenzenes

Compound	p/Debye[a]		
	In benzene		In dioxane
	Exptl	Calcd	Exptl
Cyanobenzene	4.05[c]	4.05	
1,2-Dicyanobenzene	6.57	7.00	6.82
1,3-Dicyanobenzene	3.86	4.05	3.99
1,4-Dicyanobenzene	——[b]	0	——[b]

a) Debye/C m$=3.333\times10^{-30}$. b) The value is small and not significant. c) Refs. 28 and 29.

References

1) J. D. Cox, H. A. Gundry, and A. J. Head, *Trans. Faraday Soc.*, **60**, 653 (1964).
2) J. D. Cox, H. A. Gundry, D. Harrop, and A. J. Head, *J. Chem. Thermodyn.*, **1**, 77 (1969).
3) For example, L. N. Ferguson, "The Modern Theory of Organic Chemistry," Prentice Hall, Inc., Englewood Cliffs (1963), Chap. 2.
4) T. Higashi and K. Osaki, private communication.
5) A. Kume, private communication.
6) M. Sakiyama, T. Nakano, and S. Seki, *Bull. Chem. Soc. Jpn.*, **48**, 1705 (1975).
7) A. Kamaguchi, T. Sato, M. Sakiyama, and S. Seki, *Bull. Chem. Soc. Jpn.*, **48**, 3749 (1975).
8) F. T. Eggertsen, E. E. Seibert, and F. H. Stross, *Anal. Chem.*, **41**, 1175 (1969).
9) K. Nishiyama, M. Sakiyama, S. Seki, H. Horita, T. Otsubo, and S. Misumi, *Bull. Chem. Soc. Jpn.*, **53**, 869 (1980).
10) W. D. Good and S. H. Lee, *J. Chem. Thermodyn.*, **8**, 643 (1976).
11) "Experimental Thermochemistry," ed by F. D. Rossini, Interscience Publishers, New York (1956), Vol. 1.
12) Ref. 11, p. 75.
13) S. W. Benson, F. R. Cruickshank, D. M. Golden, G. R. Haugen, H. E. O'Neal, A. S. Rodgers, R. Shaw, and R. Walsh, *Chem. Rev.*, **69**, 279 (1969).
14) ICSU-CODATA Task Group, *J. Chem. Thermodyn.*, **4**, 331 (1972).
15) D. J. Salley and J. B. Gray, *J. Am. Chem. Soc.*, **70**, 2650 (1948).
16) F. W. Evans and H. A. Skinner, *Trans. Faraday Soc.*, **50**, 255 (1959).
17) J. D. Cox and G. Pilcher, "Thermochemistry of Organic and Organometallic Compounds," Academic Press, London (1970), Chap. 5.
18) W. von Niessen, *Theor. Chim. Acta*, **33**, 7 (1974).
19) B. Bak, D. Christensen, E. B. Dixon, L. Hansen-Nyggard, and J. Rastrup-Andersen, *J. Chem. Phys.*, **37**, 2027 (1962).
20) C. van Rij and D. Britton, *Acta Crystallogr., Sect. B*, **33**, 1301 (1977).
21) D. R. Lide, *J. Chem. Phys.*, **22**, 1577 (1952).
22) G. W. King and A. A. G. van Putten, *J. Mol. Spectrosc.*, **42**, 514 (1972).
23) L. Klasing, J. V. Knop, H. -J. Meiners, and W. Zeil, *Z. Naturforsch., A.* **27**, 1772 (1972).
24) J. E. Bloor and D. L. Breen, *J. Phys. Chem.*, **72**, 716 (1968).
25) W. J. Hehre, L. Radom, and J. A. Pople, *J. Am. Chem. Soc.*, **94**, 1496 (1972).
26) F. X. Hassion and R. H. Cole, *J. Chem. Phys.*, **23**, 1756 (1955).
27) E. A. Guggenheim, *Trans. Faraday Soc.*, **45**, 714 (1949).
28) K. B. Everard, L. Kumper, and L. E. Sutton, *J. Chem. Soc.*, **1951**, 2807.
29) C. W. N. Cumper and A. I. Vogel, *J. Chem. Soc.*, **1960**, 4723.
30) Ref. 11, p. 57.
31) M. Beckers, *Bull. Soc. Chem. Belg.*, **40**, 518, 571, 621 (1933).
32) a) C. E. Vanderzee and E. F. Westrum, Jr., *J. Chem. Thermodyn.* **2**, 681 (1970); b) C. E. Vanderzee, M. Månsson and S. Sunner, *ibid.*, **4**, 533 (1972).
33) Ref. 11, p. 297.

Liposomal Membranes. III. Permeation of Pyrene-labeled Lecithin into Matrix of Liposomal Bilayers

Junzo SUNAMOTO,* Tadashi NOMURA, and Hiroshi OKAMOTO

Department of Industrial Chemistry, Faculty of Engineering, Nagasaki University, Nagasaki 852

(Received February 27, 1980)

The permeation of a novel pyrene-labeled phosphatidylcholine, DPDL (1,2-bis[10-(1-pyrenyl)decanoyl]-*sn*-glycero-3-phosphatidylcholine), into the dipalmitoyl and egg phosphatidylcholine liposomes was studied. DPDL can adopt a sandwich conformation at the ground state, which comes in the fluorescence excimer emission. The fluorescent probe undergoes the initial rapid adsorption onto the liposome surfaces along with the instantaneous fluorescence enhancement followed by the relatively slow permeation into and diffusion in the liposomal bilayers. Through monitoring the relative quantum efficiency, I_e/I_m (see text), during the permeation, suggestive information about the bilayer structure is obtained at least around the probe. The initial binding to and the subsequent diffusion in the membrane occur mostly as the monomeric form of the probe. At lower temperature without cholesterol the bilayer structure seems to be a *lipid-separated* conformation (Fig. 1 (c)) and above the chain-melting transition the bilayer seems to exist as a *lipid-intimate* conformation (Fig. 1 (b)). These results completely coincide with those obtained in our previous study on the codispersion of the probe with phospholipids (J. Sunamoto, *et al.*, *J. Am. Chem. Soc.*, **102**, 1146 (1980)).

In a preceding paper we described syntheses of fluorescent probes, DPDL (1,2-bis[10-(1-pyrenyl)-decanoyl]-*sn*-glycero-3-phosphatidylcholine) and EP (ethyl 10-(1-pyrenyl)decanoate), and their fluorescence characteristics in the liposomal bilayers.[1] DPDL carries a pyrene moiety at the end of each fatty acyl chain of the lipid and can adopt a sandwich configuration of the pyrene moieties in the ground state, which fluorescence the excimer emission from the intramolecular ground state dimer.[1,2] When DPDL was codispersed with phosphatidylcholines, it could be intercalated in good order in the liposomal bilayers and gave meaningful informations about the structure of liposomal bilayers. (1) The relative quantum efficiency (the intensity ratio of the excimer emission at 480 nm to the monomer emission at 378 nm from DPDL, I_e/I_m) was significantly affected by the bilayer structure. (2) The addition of cholesterol into liposomes made the relative quantum efficiency larger. (3) Increasing temperature also caused an increase in the I_e/I_m ratio of DPDL in the egg phosphatidylcholine (softer) bilayers. The value always exceeded that in the dipalmitoyl phosphatidylcholine (more rigid) bilayers. (4) The observed I_e/I_m-temperature profile was thermotropically reversible. From these previous results, we proposed a conformational equilibrium of the liposomal bilayer structure as a function of temperature and as affected by cholesterol (Fig. 1). In order for the liposomal membranes to hold the observed bilayer thickness (46.5—46.8 Å)[3] with fully extended hydrocarbon chains (28.3 Å), the lipid molecule must be either the tilted conformation by about 30—35 degrees with respect to the bilayer plane (structure (a) in Fig. 1) or a shrunk one with hydrocarbon chains perpendicular to the bilayer plane ((b) or (c) in Fig. 1) at least below the chain melting transition. The codispersion studies using the probe DPDL suggested that below the chain melting transition without cholesterol the lipid bilayer structure is very probably the *lipid-separated* conformation (c), which comes in the predominant monomer emission. Above the chain melting transition or in the presence of cholesterol, on the other hand, the probability for the liposomal bilayers to be the *lipid-intimate* conformation (b) increases, which produces more excimer and results in the larger I_e/I_m ratio.

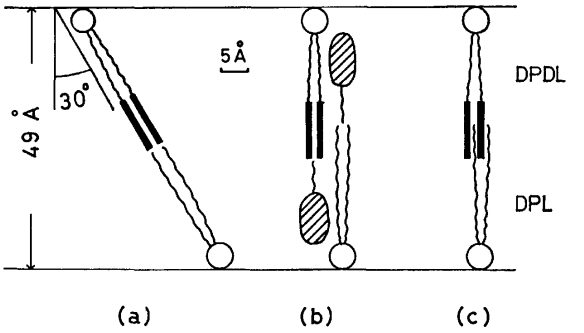

Fig. 1. Schematic representation of the structure of liposomal bilayers. The blocked group represents the pyrene moiety of DPDL. The hatched group represents the steroid nucleus of cholesterol. (a) Fully extended and tilted conformation. (b) The shrunk structure with the lipid-intimate conformation. (c) The shrunk structure with the lipid-separated conformation.

The interaction of the hydrophobic probes with liposomal membranes occurs in two successive kinetic phases; the initial rapid adsorption of probes onto the liposome surface and the second slow diffusion in the liposomal bilayer or transport across the bilayers.[4,5] In this work, we studied the permeation of DPDL or EP into the liposomal membranes and the diffusion of the probes in the bilayers in slow kinetic phase. Through the dynamic studies on the permeation and diffusion of the probes in the liposomal bilayers, the lipid conformation around the probe molecule will be discussed.

Experimental

Materials. Synthetic dipalmitoyl-DL-α-phosphatidylcholine was purchased from Sigma Chemical Company, St. Louis, Mo. and purified prior to use. Egg yolk lecithin was isolated and purified from egg yolk.[1,6,7] 1,2-Bis[10-(1-pyrenyl)decanoyl]-*sn*-glycero-3-phosphatidylcholine (DPDL) and ethyl 10-(1-pyrenyl) decanoate (EP) were the same as those used in the previous investigation.[1] Prior to use, the

purity of all the lecithins employed was inspected by TLC on silica-gel plate (Tokyo Kasei Spot Film S-160) with the solvent chloroform–methanol–water (65 : 25 : 4 by vol.).[8] All the detections by iodine staining, UV light irradiation, and Dragendorff's reagent showed only one spot of the corresponding lecithin.

Preparation of Liposomes. Multicompartment liposomes were prepared by the injection technique according to the method previously described.[1] Single compartment liposomes were formed by sonication technique and isolated by the gel-filtration using Sepharose 4B column.[7] Formations of single and multicompartment liposomes were respectively visualized by negatively staining with 2% aqueous potassium tungstophosphate on a JEOL JEM-100 V electron microscope. Phospholipid concentrations were determined as inorganic phosphate by the Allen's methods.[9]

Fluorescence Measurements. All the fluorescence measurements were made under atmospheric conditions on a Hitachi 650-10S fluorospectrometer exciting at 342 nm with the use of slits of 2 nm for excitation side and 10 nm for emission side, respectively. Under the conditions, good reproducibilities were ensured. Since the fluorescence intensity is proportional to the quantum yield when the exciting light intensity and concentration of absorbing molecule are kept constant, the fluorescence intensities for the monomer (378 nm) and the excimer (480 nm) from the pyrene moiety were determined.

For the permeation of fluorescent probes into bilayers of single-walled liposomes, an appropriate amount of ethanolic solution of the probes was injected using a microsyringe into the liposome solutions preincubated for 10 min at a given temperature. The content of ethanol in liposome solutions was depressed less than 8% (v/v). All the runs were duplicated.

Results and Discussion

Permeations of EP and DPDL. When EP was dispersed into the aqueous buffered solution, it showed the strongly quenched emission of fluorescence excimer but no monomer emission, and formation of small micelles or aggregates was electronmicrographically visualized. On the other hand, when EP was added into the liposome solutions, significant emissions of both fluorescence monomer and excimer were observed. The monomer emission as a function of time, then, gradually increased with a concomitant decrease of the excimer emission with an isolampsic (isoemissive) point at 442 nm (Fig. 2). When the fluorescent probe interacts with the liposomal bilayers, two distinct kinetic phases are observable.[4,5] They are a rapid initial adsorption of the probe onto the outer surface of liposomes and a much slower lateral diffusion in the outer half of bilayers[10] or transport across the inner layer of liposomal membranes.[4a] The instantaneous increase of fluorescence emission and the subsequent slow enhancement of the monomer emission suggest that aggregates or micelles of EP bind onto the liposome surface and subsequently the probe is intercalated in bilayers. Several typical examples of the change in individual values of I_e and I_m as a function of time are illustrated in Fig. 3. During 10 or 20 min after injection of the probe, both values usually level off and the system attains equilibrium. When EP was codispersed with phospholipids, no excimer emission was observed at

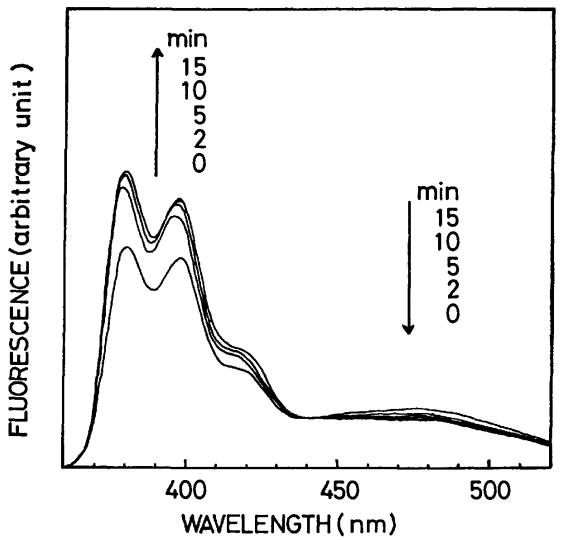

Fig. 2. Fluorescence spectra of EP as a function of time when EP was added into the multicompartment liposome solutions containing 7.84×10^{-6} M of dipalmitoyl lecithin in 0.028 M acetate buffer with 0.10 M NaCl at 25.0 °C. The final concentration of EP was 7.75×10^{-8} M in cuvette.

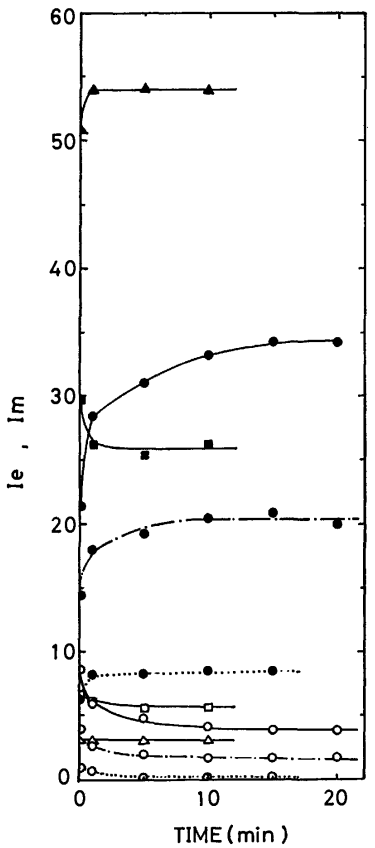

Fig. 3. Fluorescence intensities of excimer (I_e) and monomer (I_m) emissions from EP as a function of time. Conditions should be referred to Table 1. Run numbers are the same as those used in Table 1. Closed symbols are monomer emission, while open symbols are excimer emission: —●— and —○— are run 1; -·-●-·- and -·-○-·-, run 2; ···●··· and ···○···, run 3; —■— and —□—, run 4; and —▲— and —△—, run 6, respectively.

TABLE 1. RELATIVE QUANTUM EFFICIENCIES, I_e/I_m, IN EQUILIBRIUM UNDER VARIOUS CONDITIONS

Run	[Probe]/10^8M	Incubation temp °C	$\left(\frac{I_e}{I_m}\right)_{equilibrium}$	Run	[Probe]/10^8M	Incubation temp °C	$\left(\frac{I_e}{I_m}\right)_{equilibrium}$
(A): EP				(B): DPDL			
	Single-walled liposome of dipalmitoyl lecithin without cholesterol[a)]				Single-walled liposome of dipalmitoyl lecithin without cholesterol[a)]		
1	7.75	25	0.10	27	7.65	25	0.75
2	3.90	25	0.08	28	3.90	25	0.64
3	1.95	25	0.04	29	1.95	25	0.54
4	7.75	46	0.21	30	7.65	46	0.91
5	3.90	46	0.13	31	3.90	46	0.86
	Single-walled liposome of dipalmitoyl lecithin with cholesterol[b)]			32	1.95	46	0.80
6	7.75	25	0.06		Single-walled liposome of dipalmitoyl lecithin with cholesterol[b)]		
7	3.90	25	0.04	33	7.65	25	0.61
8	1.95	25	0.06	34	3.90	25	0.55
9	7.75	46	0.06	35	1.95	25	0.55
10	3.90	46	0.05	36	7.65	46	1.04
11	1.95	46	0.04	37	3.90	46	0.96
	Multilamellar liposome of dipalmitoyl lecithin without cholesterol[c)]			38	1.95	46	0.69
12	7.75	25	0.17		Multilamellar liposome of dipalmitoyl lecithin without cholesterol[c)]		
13	3.90	25	0.12	39	7.65	25	0.44
14	7.75	45	0.31	40	3.90	25	0.47
15	3.90	45	0.17	41	7.65	45	0.78
	Multilamellar liposome of dipalmitoyl lecithin with cholesterol[d)]			42	3.90	45	0.72
16	7.75	25	0.13		Multilamellar liposome of dipalmitoyl lecithin with cholesterol[d)]		
17	3.90	25	0.09	43	7.65	25	0.49
18	7.75	45	0.20	44	3.90	25	0.56
19	3.90	45	0.14	45	7.65	45	0.82
	Single-walled liposome of egg lecithin without cholesterol[e)]			46	3.90	45	0.69
20	7.75	25	0.07		Single-walled liposome of egg lecithin without cholesterol[e)]		
21	3.90	25	0.06	47	7.65	25	0.69
22	7.75	45	0.05	48	3.90	25	0.69
23	3.90	45	0.12	49	7.65	45	0.96
	Multilamellar liposome of egg lecithin without cholesterol[f)]			50	3.90	45	1.14
24	7.75	25	0.27		Multilamellar liposome of egg lecithin without cholesterol[f)]		
25	7.75	45	0.40	51	7.65	25	1.10
26	3.90	45	0.30	52	3.90	25	0.92
				53	7.65	45	1.21
				54	3.90	45	0.82

a) [dipalmitoyl lecithin]$=7.80\times10^{-6}$ M. b) [dipalmitoyl lecithin]$=7.80\times10^{-6}$ M and [cholesterol]$=3.86\times10^{-6}$ M.
c) [dipalmitoyl lecithin]$=7.84\times10^{-6}$ M. d) [dipalmitoyl lecithin]$=7.73\times10^{-6}$ M and [cholesterol]$=4.30\times10^{-6}$ M.
e) [egg lecithin]$=4.18\times10^{-6}$ M. f) [egg lecithin]$=4.02\times10^{-6}$ M.

all.[1)] In the present case, however, as reflected on the relative quantum efficiency, I_e/I_m (Fig. 4), a small extent of the excimer emission still remained even in the slow second kinetic phase. This means that a portion of EP molecules may permeate into bilayers as the small aggregates. The concentration of EP injected, temperature, existence of cholesterol, sort of employed lecithin, and state of liposomes, that is, multi or single compartment liposomes all the factors have an influence on the I_e/I_m ratio (Fig. 4 and Table 1). With an increase in the initial concentration of EP added, the I_e/I_m ratio increased. Mostly in the multilamellar liposomes than in the single-walled liposomes, in single-walled liposomes of dipalmitoyl lecithin than in that of egg lecithin, and at higher incubation temperatures than the chain melting transition temperature of the adopted lecithin, the larger I_e/I_m values are obtained (though with several exceptions).

Differently from the case of EP, when DPDL was dispersed into an aqueous buffered solution containing no liposomes, the bilayer structure was obviously visualized by electronmicrography. And the fluorescence emission from DPDL was completely quenched. On the other hand, when DPDL was injected from the exterior of liposomes, the fluorescence quantum yield of the probe significantly increased. The initial and

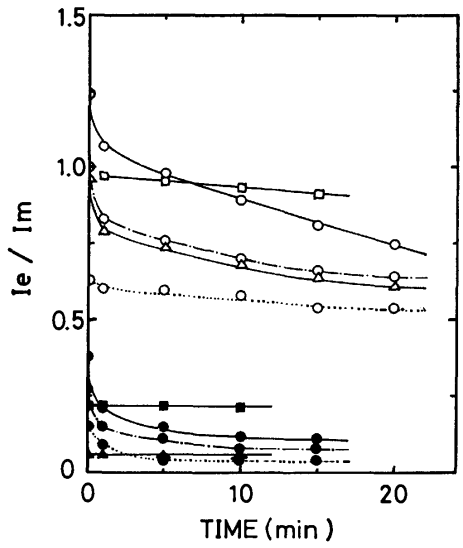

Fig. 4. The relative quantum efficiencies I_e/I_m of DPDL and EP in the single-walled liposomes of dipalmitoyl lecithin as a function of time. Open symbols are for DPDL, while closed symbols for EP: —●—, run 1; -·-●-·-, run 2; ···●···, run 3; —■—, run 4; —▲—, run 6; —○—, run 27; -·-○-·-, run 28; ···○···, run 29; —□—, run 30; and —△—, run 33, respectively. Run numbers should be referred to Table 1.

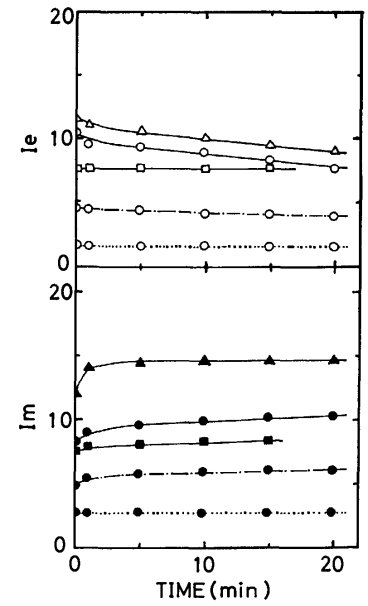

Fig. 6. Fluorescence intensities of excimer emission (I_e, open symbols) and monomer emission (I_m, closed symbols) from DPDL as a function of time in the single-walled liposome of dipalmitoyl lecithin: —●— and —○— are run 27; -·-●-·- and -·-○-·-, run 28; ···●··· and ···○···, run 29; —■— and —□—, run 30; and —▲— and —△—, run 33, respectively. Run numbers should be referred to Table 1.

instantaneous enhancement of fluorescence from DPDL is interpreted in terms of the rapid uptake of the disorganized probe by liposomes and the consequent change in polarity of the microenvironment around the probe.[4a] Similarly to the case of EP, after the instantaneous enhancement of fluorescence emission, the monomer emission gradually increased with a concomitant decrease of the excimer emission (Fig. 5). The I_e/I_m values for DPDL as a function of time are

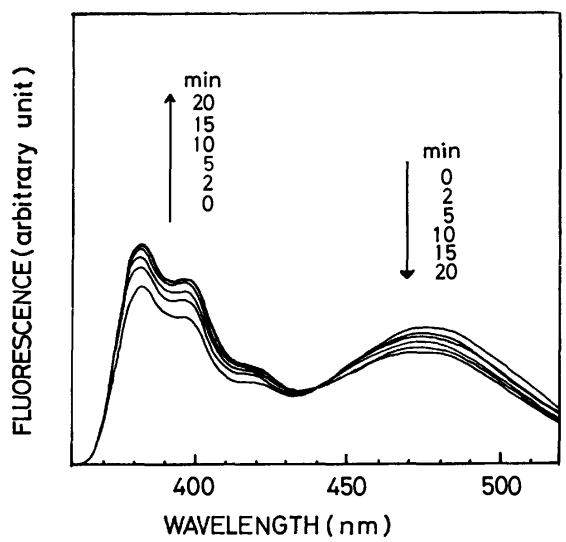

Fig. 5. Fluorescence spectra of DPDL as a function of time in the single-walled liposome of dipalmitoyl lecithin at 25 °C. DPDL (7.65×10^{-8} M) was added from exterior of the liposomes (7.80×10^{-6} M) in 0.028 M aqueous actate buffered solution containing 0.10 M NaCl.

seen in Fig. 4 along with those for EP. The I_e/I_m ratios for DPDL are always larger than those for EP (Fig. 4 and Table 1). Comparing with the case of codispersion of DPDL with lecithins, more DPDL seem to be intramolecular excimer or the ground-state dimer during the permeation. It is true also for EP. Differently from the case of codispersion experiments, in the present study even EP shows the excimer formation. The lecithin analogue probe, DPDL, seems to diffuse more slowly in liposomal bilayers comparing with the smaller and neutral probe, EP. Fluorescence intensities of excimer and monomer emissions from DPDL as a function of time are plotted, respectively, in Fig. 6. With the increase in the initial concentration of DPDL injected and with raising temperature, the I_e/I_m ratio for DPDL increased (Table 1). However, effects of state of liposomes on the I_e/I_m ratio of DPDL are rather complicated. Contrary to what would be expected, the I_e/I_m ratios for DPDL in dipalmitoyl lecithin liposomes were always higher in single compartment liposomes than in multicompartment liposomes irrespective of the incubation temperature and the presence of cholesterol. However, for egg lecithin liposomes the values were larger in multilamellar liposomes than in single-walled liposomes, which is similarly seen in the case of EP. Since the apparent surface area of single compartment liposomes is larger than that of multicompartment liposomes if the lecithin concentration in solutions were the same, the apparent concentration of the probe bound to the liposome surface should be higher in the latter liposomes than in the former ones.[11] This will lead to the higher I_e/I_m ratio. However, this is not the

case for DPDL in the dipalmitoyl lecithin liposomes.

Lenz and his coworkers previously stated that the uptake of DPH (1,6-diphenyl-1,3,5-hexatriene) by multicompartment liposomes is a more complex process than that by single-walled liposomes; the fluorescence intensity of DPH increases in stepwise fashion in multilamellar liposomes.[5] Differently from the case of DPH, permeations of DPDL and EP both were relatively simple even into multilamellar liposomes. The rate of fluorescence enhancement in the slower kinetic phase must concern with the diffusion velocity or mobility of the probes in bilayers.[4,5,10] It is, therefore, reasonable that the I_e/I_m values of the probes attain equilibrium rather rapidly in fluid liposomal bilayers containing cholesterol or being incubated at higher temperatures. From facts that trans-membrane movements of phosphatidylcholine,[12] cholesterol,[13] and lysophosphatidylcholine[14] are extremely slow, the probes (DPDL and EP) are expected to be locating mostly in the outer half of bilayers,[4] especially when they are penetrated from the exterior of liposomes at low temperature.

Conformation of DPDL in Matrix of Liposomal Bilayers. Clearly from our previous study,[1] the I_e/I_m ratio for DPDL intercalated in liposomal bilayers will give a noteworthy information about the structure of bilayers at least around the probe. The high I_e/I_m ratio suggests a conformation by which the probability to take ground-state dimer increases (structure (b) in Fig. 1). Alternately, if the low I_e/I_m ratio were obtained, it suggests that DPDL should take the lipid-separated conformation in bilayers (structure (c) in Fig. 1). The relative quantum efficiencies obtained by the present permeation technique show substantially similar tendency to those obtained by the codispersion experiment.[1] That is, in more fluid liposomes such as egg lecithin liposomes than dipalmitoyl lecithin liposomes or liposomes incubated at higher temperatures than the phase transition temperature, DPDL shows larger values of I_e/I_m in equilibrium. For DPDL, there is no large difference also in the actual value of I_e/I_m ratio between the two distinct experiments. The I_e/I_m values from DPDL lie in a range of 0.5—1.0 and never exceed the value of 1.7 obtained for DPDL in ethanol.[1] Hence, it is reasonable to consider that DPDL permeates into and laterally diffuses in liposomal bilayers mostly with a lipid-separated conformation especially at low incubation temperature in the dipalmitoyl lecithin bilayers. Increasing the mobility of lipid and probe molecules in the hydrophobic domain of bilayers enhances the probability to take more lipid-intimate conformation.

Effect of cholesterol is completely different between the codispersion[1] and permeation studies. In our previous codispersion experiments,[1] addition of cholesterol abolished the phase transition of dipalmitoyl lecithin liposomes and increased the fluidity of membranes. In the present studies, for both probes (EP and DPDL) and for both lecithin liposomes (egg lecithin and dipalmitoyl lecithin), except the permeation of DPDL into multilamellar liposomes of dipalmitoyl lecithin, the addition of cholesterol diminished the I_e/I_m value during the permeation of the probes. This means that effect of cholesterol on the diffusion of the probe is different between the two cases, the codispersion and the permeation.

References

1) J. Sunamoto, T. Nomura, H. Okamoto, and H. Kondo, *J. Am. Chem. Soc.*, **102**, 1146 (1980).
2) a) D. R. G. Brimage and R. S. Davidson, *J. Chem. Soc., Chem. Commun.*, **1971**, 1385; b) R. S. Davidson and K. R. Trethewey, *ibid.*, **1976**, 827; c) R. S. Davidson and T. D. Whelan, *ibid.*, **1977**, 361; d) M. Goldenberg, J. Emert, and H. Morawetz, *J. Am. Chem. Soc.*, **100**, 7171 (1978).
3) M. J. Janiak, D. M. Small, and G. G. Shipley, *Biochemistry*, **15**, 4575 (1976).
4) a) T. Y. Tsong, *Biochemistry*, **14**, 5409 (1975); b) **14**, 5415 (1975).
5) B. R. Lentz, Y. Barenholz, and T. E. Thompson, *Biochemistry*, **15**, 4521 (1976).
6) J. S. Chadha, *Chem. Phys. Lipids*, **4**, 104 (1970).
7) J. Sunamoto, H. Kondo, and A. Yoshimatsu, *Biochim. Biophys. Acta*, **510**, 52 (1978).
8) W. S. Singleton, M. S. Grey, M. L. Brown, and J. L. White, *J. Am. Oil Chem. Soc.*, **42**, 53 (1965).
9) R. J. L. Allen, *Biochem. J.*, **34**, 858 (1940).
10) L. A. Sklar, B. S. Hudson, and R. D. Simoni, *Biochemistry*, **16**, 819 (1977).
11) M. A. Schwartz and H. M. McConnell, *Biochemistry*, **17**, 837 (1978).
12) L. W. Johnson, M. E. Hughes, and D. B. Zilversmit, *Biochim. Biophys. Acta*, **375**, 176 (1975).
13) M. Pozansky and Y. Lange, *Nature*, **259**, 420 (1976).
14) B. de Kruyff, A. M. H. P. van den Besselaar, and L. L. M. van Deenen, *Biochim. Biophys. Acta*, **465**, 443 (1977).

Liposomal Membranes. IV. Fusion of Liposomal Membranes Induced by Several Lipophilic Agents

Junzo SUNAMOTO,* Tomiko HAMADA, and Hiroki MURASE

Department of Industrial Chemistry, Faculty of Engineering, Nagasaki University, Nagasaki 852

(Received February 27, 1980)

It was found that several lipophilic agents, such as *cis*-, *trans*-ethyl decaprenoate and their structural analogues, significantly induce the liposome-liposome fusion when incubated together a set of two different liposomes, the *A*-liposome containing a marker and the *B*-liposome involving a lipophilic agent. The rate and extent of fusion were followed spectrophotometrically by monitoring the leakage of an amphiphilic marker, Bromothymol Blue, from the fused liposomes. Fusion was also visualized directly by electronmicrographic technique. When only *A*-liposome was incubated or when a blank liposome containing no lipophilic agents was added to the *A*-liposome after the preincubation, neither the fusion nor the marker release was observed at least in periods of several hours. Also, neither fusion nor the marker release was observed when either *A*- or *B*-liposome or both were multicompartment liposome. Removing cholesterol from liposome significantly depressed the fusion. The effect of cholesterol was more prominent on the *A*-liposome side. *trans*-Ethyl decaprenoate was more effective about three-fold to induce the fusion than the *cis*-isomer. Interestingly, the effect was parallel to the antihypertensive activity of the agent.

The transformation of liposomal membranes has generated much interest because of its possible analogy to biomembrane fusion and phagocytosis of importance in both membrane biology[1] and drug delivery system.[2] Taupin and McConnell were the first to suggest that small single compartment liposomes transform to larger multicompartment liposomes involving liposome-liposome fusion process in periods of several hours when incubated at appropriate temperatures.[3] Thereafter, the Ca(II) ion,[4-6] fatty acids,[7-9] and surface-active drugs[10,11] have been found to accelerate the fusion process of liposomes. In the case of Ca(II)-induced fusion, the key event leading to membrane fusion is the isothermal phase separation induced by Ca(II) ion.[5] The fatty acid-induced fusion also required lateral separation of a fatty acid rich phase.[7] Alamethicin, which is an extracellular cyclic-polypeptide antibiotic and a kind of surface active agents, stimulated fusion of liposomes followed by the preliminary interaction with the polar choline headgroup of the lecithins.[10] These earlier investigations suggest to us that perturbation of the membrane surface by the electrostatic interaction with ionic inducers[4-6,10] or by dispersing hydrophobic components in the bulk bilayer phase and resultant phase separation[7-9] are responsible for the liposome fusion. In earlier studies, meanwhile, homogeneous fusion of liposomes has been characterized by the growth of small vesicles to larger multicompartment liposomes, which is monitored indirectly by physical changes of membrane properties using various techniques such as NMR,[7,9] DSC,[5,6,8] turbidity,[12,13] luminescence assay,[14-16] or osmotic gradient measurements[4] and also visualized directly by electronmicrographic technique.[4,6,8,10]

In certain cases the liposome fusion also is accompanied by the leakage of contents in the interior core of vesicles.[4,9] It is, therefore, possible that appropriately prepared liposomes may be used to penetrate drugs into specific cell membranes through the liposome-cell membrane fusion. However, the details of the membrane fusion process are not yet well established. If it were clarified, therefore, one may conveniently control both the release of the liposome-encapsulated drugs and the delivery of drugs to the target organ.

In a recent paper we indicated that a functional surfactant bearing an imidazole moiety at the head group plays a role as a simple lipase model to cause chemical lysis of lecithin liposomes.[17] The chemical lysis could be monitored by following a leakage of amphiphilic marker dye, Bromothymol Blue (BTB), from the bulk bilayer phase to the exterior aqueous media.[17] Not only by the lysis of liposomal membranes but also even by physico-chemically perturbing the bilayer structure, BTB being entrapped closely to the membrane surface is released from the bilayer to the exterior. In this work we would like to describe the liposome-liposome fusion induced by several lipophilic

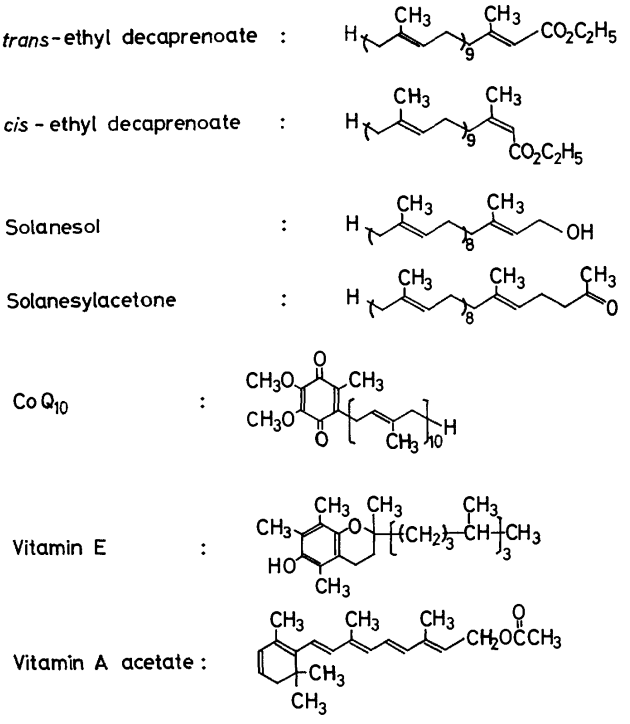

Fig. 1. Chemical structures of lipophilic agents employed in this work.

agents, where we adopted again the same marker-release technique to observe the fusion caused by the fluctuation of bilayer structure. A set of two different single compartment liposomes, the *A*-liposome encapsulating BTB and the *B*-liposome containing the neutral and lipophilic agents, respectively, was prepared. The liposome-liposome fusion can also be visualized directly by electron micrography. As the hydrophobic and neutral agents which are expected to accelerate the fusion, several kinds of polyisoprenoid pharmacological agents, *cis*- and *trans*-ethyl decaprenoate, solanesol, solanesylacetone, coenzyme Q_{10} (CoQ_{10}), vitamin E, and vitamin A acetate were employed (Fig. 1).

Experimental

Materials. All the lipophilic agents employed here were a gift from Eisai Co. Ltd., Tokyo. Egg yolk phosphatidylcholine (EL) was isolated and purified from egg yolk as described in Refs. 18 and 19. Purity of the lecithin was ascertained by TLC on silica-gel plates (Tokyo Kasei, S-160).[18,19] Bromothymol Blue was the same as that used in previous work.[17]

Preparation of Liposomes. Single and multicompartment liposomes containing BTB (*A*-liposome) or a lipophilic agent (*B*-liposome) were prepared independently according to the essentially same procedures as described in a previous paper.[17] A mixed thin film of egg phosphatidylcholine with or without cholesterol, the marker, or lipophilic agents was dispersed and swollen in 0.1 M aqueous citrate buffer solution (pH 5.0) containing 0.1 M NaCl to form multicompartment liposome, and then sonicated under nitrogen atmosphere to obtain single compartment liposomes. Single compartment liposomes were isolated by passing through a Sepharose 4B column[20] using 0.1 M NaCl as an eluant. Optically transparent liposome solutions were obtained by ultrafiltration using a Sartrius Membrane Filter SM 16315 equipped with a filter SM 11310 (0.05 μ), if necessary. By this technique, BTB was incorpotated in the bulk bilayers, not in the interior aqueous core.[17] Liposome-encapsulated BTB was determined spectrophotometrically ($\varepsilon_{617}=7.3\times10\ M^{-1}\cdot cm^{-1}$ at pH 7) after the gel-filtration, when liposomes were completely destructed by hydrolysis in strongly alkaline media at elevated temperature.[17] All the lipophilic agents employed are insoluble in water. They also were, therefore, almost quantitatively intercalated in the bulk phase of liposomal bilayers. Liposome concentrations were determined as inorganic phosphates by the modified Allen's method.[21] To obtain reliable data, for a series of experiments to compare each other, we prepared a large amount of concentrated stock solutions of liposomes as possible and diluted or devided them into several portion.

Typical Procedures to Monitor Bromothymol Blue Release upon Fusion. A 0.5 ml solution of the *A*-liposome, 1.5 ml of ethanol,[22] and 1.0 ml of aqueous buffered solution (phosphate, pH 7.0[23]) were placed in a thermoregulated cuvette cell and preincubated for 10 min at 25.0 °C unless otherwise stated. The BTB release induced by the addition of an appropriate amount of *B*-liposome solution was followed by monitoring the increase of intensity at 617 nm on a Hitachi 124 recording spectrophotometer.

During the preincubation, we could not find any spontaneous release of the marker. The percentage of BTB release was obtained by Eq. 1; where *A* is the absorbance at 617 nm, the subscripts *t* and 0 refer to the times of samples and to the instant when the *B*-liposome solution was added to the *A*-liposome solution, respectively. A_∞ stands for the absorbance of total amount of the liposome-encapsulated marker in *A*-liposome.

$$\%\ \text{BTB-release} = \frac{A_t - A_0}{A_\infty - A_0} \times 100 \qquad (1)$$

Maximum % release of BTB was the value over the plateau region after leveled off, usually after 60 min. All the runs were duplicated.

Results and Discussion

Fusion process of membranes, where the membrane of small vesicles is incorporated into larger membrane arrays, is one of the important problems to understand biological membranes.

Either when only *A*-liposome solution was incubated by itself or when a blank *B*-liposome containing no lipophilic agents was added to the preincubated *A*-liposome, no BTB release was observed at least in periods of several hours. This means that no fusion occurs. On the other hand, when an appropriate amount of liposome-encapsulated ethyl decaprenoate (a mixture of 15% *cis* and 85% *trans* isomers) was added into the *A*-liposome solution, enhanced BTB release upon the liposome-liposome fusion was observed. If we accept the mechanism of the liposomal fusion proposed by Papahadjopoulos and his co-workers,[5] it is reasonable to observe the marker release upon fusion. The liposome-liposome fusion accompanied by the BTB release was directly visualized by electron micrography,

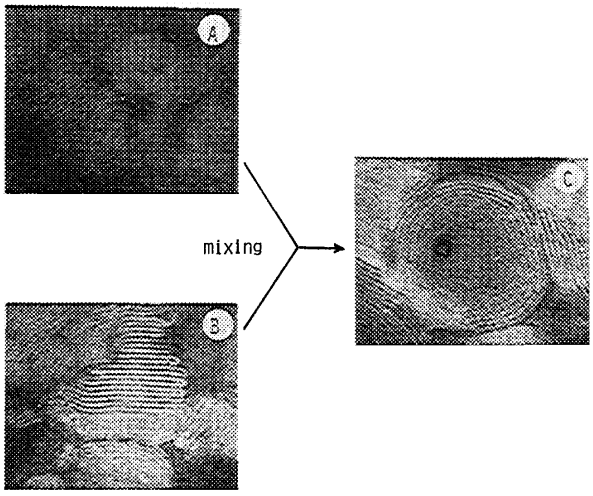

Fig. 2. Electron micrographic observation of the liposome-liposome fusion induced by a lipophilic agent, ethyl decaprenoate. Single compartment liposomes were prepared from egg phosphatidylcholine. A: The single compartment *A*-liposome containing BTB (0.82 mol %) and cholesterol (41.4 mol %). B: The single compartment *B*-liposome containing ethyl decaprenoate (28.2 mol%) and cholesterol (30.3 mol%). C: Multicompartment liposomes obtained by mixing *A*- and *B*-liposome solutions at 25 °C. All the liposome solutions were negatively stained with 2% (by wt.) aqueous sodium tungstophosphate solution. Measurements were run on a JEOL JEM 100 V electron microscope. Magnification ×250000.

which showed the evident growth of small single compartment liposomes to larger multilamellar liposomes (Fig. 2). The extent and the rate of fusion was comparable with those of the BTB release from the *A*-liposomes. The unstable state of membranes susceptible to fusion should makes the liposomal membranes highly permeable.[5] Several studies have shown that small, physiologically active, and lipophilic agents fluidize membranes.[24,25] Contrary to this, a few studies showed that lipophilic molecules may also exert a condensing effect on the liposomal bilayers.[26,27] The condensation in the bilayers may well create structural defects with resulting in fusion.[5,10] Increasing the content of the intercalated marker in the liposomal bilayer also will give rise to the instability of the membranes.[24,25] Therefore, the content of BTB in the *A*-liposomes was usually depressed less than 10 mol %. In any event, factors affecting the initial rate and the extent of the induced fusion by lipophilic agents are very complicated.

For investigating the lipophilic agent-induced fusion, all the following parameters must be perfectly controlled and kept satisfactorily constant; (i) the content of the marker in the *A*-liposome, (ii) the amount of lipophilic agents intercalated in the *B*-liposome, (iii) actual concentrations of *A*- and *B*-liposome, that is, the concentration ratio of *A*-liposome to *B*-liposome, and (iv) amount of multicompartment liposomes contaminated. Unfortunately, it was very difficult to establish

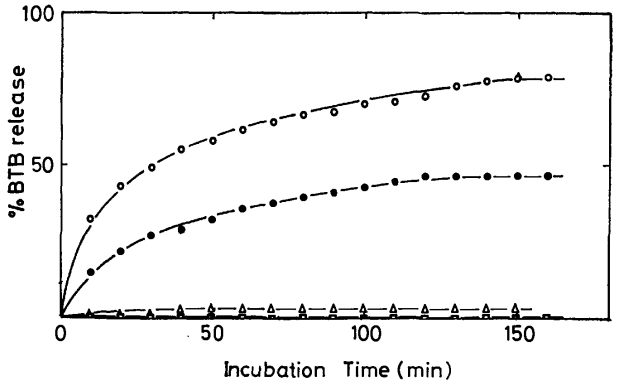

Fig. 3. Effect of cholesterol on the ethyl decaprenoate-induced fusion of egg lecithin single compartment liposomes at 25 °C and pH 7.0 (phosphate buffer). ○: *A*-Liposome consisting of 13.8 mM egg lecithin, 10.2 mM cholesterol, and 4.82 mM BTB was stimulated with *B*-liposome consisting of 1.15 mM egg lecithin, 0.83 mM cholesterol, and 0.78 mM ethyl decaprenoate. ●: *A*-Liposome consisting of 13.8 mM egg lecithin, 10.2 mM cholesterol, and 4.82 mM BTB was stimulated with *B*-liposome consisting of 1.15 mM egg lecithin and 0.78 mM ethyl decaprenoate *without* cholesterol. △: *A*-Liposome consisting of 13.8 mM egg lecithin and 4.82 mM BTB *without* cholesterol was incubated with *B*-liposome consisting of 1.15 mM egg lecithin, 0.83 mM cholesterol, and 0.78 mM ethyl decaprenoate. □: *A*-Liposome consisting of 13.8 mM egg lecithin, 10.2 mM cholesterol, and 4.82 mM BTB was incubated with a blank liposome consisting of 15.0 mM egg lecithin and 10.9 mM cholesterol without any lipophilic agent.

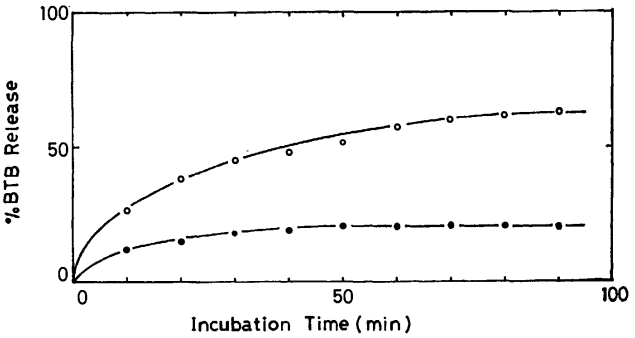

Fig. 4. Difference in efficiency of *cis*- and *trans*-ethyl decaprenoate on the liposome-liposome fusion as induced by lipophilic agents. *A*-Liposome consisting of 9.5 μM egg lecithin, 7.0 μM cholesterol, and 1.52 μM BTB was stimulated with *B*-liposomes consisting of 5.08 μM egg lecithin, 3.71 μM cholesterol, and 3.45 μM ethyl decaprenoate (*trans* (○) and *cis* (●) isomers) at 25.0 °C and pH 7.0.

the completely controlled conditions to satisfy all the above requirements. Therefore, we could discuss only the results obtained from a series of experiments employing the same liposome stock solution.

After the relatively rapid release of the marker at the initial stage, the marker release leveled off (Figs. 3 and 4). Since an excess surface free energy is the main thermodynamic driving force for fusion, the initial growth from small vesicles to diameters of negligible curvature results in the reduced surface free energy and the fusion will cease.[28,29] It is evident from the fact that we could not observe any fusion and BTB release when multicompartment liposomes were used. The rate-determining step of the fusion process is to be seen in the reaction which leads from the short-lived encounter complex of two colliding vesicles to the finally fused vesicle. According to Lawaczeck's theory[30] and if it were the liposome-liposome direct fusion in a spontaneous manner, therefore, one can establish a linear relationship between the initial rate of fusion and the square of the lecithin or liposome concentration. That is, under the assumption of a critical bilayer concentration,[30] the direct liposome fusion is considered as a reaction of second order in the lecithin or liposome concentration. If fusion is considered as one liposome is absorbed by another one,[31] however, the state of affairs may be different. In our present case, in addition, fusion is not spontaneous but induced by the lipophilic agent-encapsulated liposome and experiments were always carried out under conditions where the concentration of *A*-liposomes was higher than that of *B*-liposomes. Hence, we could not attain any linear relationship between the BTB release at a given interval and the product of concentrations of *A*- and *B*-liposomes.

At a given concentration of *A*-liposomes the maximum of % BTB release was directly affected by the concentration of *B*-liposomes (Table 1). Removing cholesterol from either side of liposomes significantly depress the fusion (Fig. 3). Its effect was more prominent on the *A*-liposome side, in which removal of cholesterol gave rise to the complete depression of the induced fusion. One role of cholesterol in membranes is to regulate the

degree of order and mobility of the acyl chains of lecithins as a modulator of the packing.[32-34] But, the orientation of the headgroup is not changed by the addition of cholesterol.[35] Above the phase transition temperature of lipids, addition of cholesterol to liposomes induces a higher molecular order in the bilayers[36] and reduces the mobility of the acyl chain.[32] In the bilayer phase, however, lipids and cholesterol are considered as totally and uniformly miscible.[37] It is certain, in any event, that the incorporation of cholesterol is considered as an important factor for fusion to initiate. Above phase transition temperature, changing the incubation temperature from 15 °C to 26 °C did not necessarily affect the extent of fusion. The concentration of *B*-liposomes rather than the incubation temperature largely affect the induced fusion.

Figure 4 indicates the difference in the efficiency on the induced fusion between *cis* and *trans* isomers of ethyl decaprenoate which were carefully isolated from the mixture by column chromatography. Very recently, Seelig and Seelig indicated that the incorporation of a *cis* double bond into a bilayer membrane leads to a general decrease in the hydrocarbon chain ordering in all parts of the bilayer and it seems to be accompanied by some increase in the rate of motion.[38] Another group found that most phospholipids derived from *cis*-parinaric acid shows the melting transition at about 1 °C lower than those from the *trans*-isomer.[39] *trans*-Parinaric acid preferentially associates with solid-phase lipid, while the *cis*-isomer shows a more equal distribution between solid and fluid lipids.[39] Judging from these previous findings,[39,40] the encapsulation of *cis*-ethyl decaprenoate is expected as more effective as to induce fusion. Contrary to what would be expected, however, *trans*-ethyl decaprenoate was more effective about three-fold than the *cis*-isomer. Though unfortunately we can not explain the reason at the present time, an interesting finding is that the antihypertensive activity of the *trans*-isomer, which was investigated *in vivo* using hypertensive rats, is higher than the *cis*-isomer.[40]

Table 1 reveals the BTB release induced by different lipophilic agent encapsulated liposomes. Spisni *et al.* recently investigated the interaction between ubiquinones and egg lecithin liposomes.[41] They found from ESR studies that the presence of ubiquinones induces the fluidity of membranes, as shown by the decrease of the $2T_{\parallel}$ parameter and the shorter correlation time of the spin-probe.[41] This means the disordering effect of the side chain of ubiquinones intercalating in the hydrocarbon region of the liposomal bilayer. As expected from the previous investigation,[41] CoQ_{10}, vitamin E, and vitamin A acetate significantly induced the liposome fusion (Table 1). Their effects were relatively large comparing with those of simple polyisoprenoids. Increasing the drug content in the *B*-liposome generally gave rise to the decrease of the apparent BTB release. When the content ratio of CoQ_{10} to egg lecithin in the *B*-liposome exceeded about 10 mol% (more than about 40 mol% for vitamines), some aggregates just like oil drops along with regular liposomes were visualized on their electron micrographies. This means that introducing a large amount of these agents causes the destruction of liposome structure itself. Relative efficiency of the BTB release upon the fusion as induced by lipophilic drugs was as follows: *cis*-ethyl decaprenoate<*trans*-ethyl decaprenoate<solanesyl-

Table 1. Maximum bromothymol blue (BTB) release upon fusion induced by lipophilic agent encapsulated liposomes under various conditions at pH 7.0

A-liposome[a]			*B*-liposome[a]			Temp °C	Maximum[b] BTB release %
[Lecithin] μM	[Cholesterol] μM	[BTB] μM	[Lecithin] μM	[Cholesterol] μM	[Additive] μM		
Ethyl decaprenoate[c]							
173 (1.0)	127 (0.73)	2.45 (0.014)	17.3 (1.0)	12.7 (0.73)	11.8 (0.68)	25.0	29
173 (1.0)	127 (0.73)	2.45 (0.014)	17.3 (1.0)	12.7 (0.73)	11.8 (0.68)	20.0	28
173 (1.0)	127 (0.73)	2.45 (0.014)	17.3 (1.0)	12.7 (0.73)	11.8 (0.68)	15.0	26
173 (1.0)	127 (0.73)	2.45 (0.014)	3.44 (1.0)	2.51 (0.73)	2.34 (0.68)	25.0	19
Solanesylacetone							
173 (1.0)	127 (0.73)	2.67 (0.015)	3.44 (1.0)	2.43 (0.71)	2.34 (0.68)	25.0	38
Solanesol							
173 (1.0)	127 (0.73)	2.45 (0.014)	3.44 (1.0)	2.57 (0.71)	2.34 (0.68)	25.0	45
22.7 (1.0)	7.57 (0.33)	17.1 (0.75)	13.6 (1.0)	4.53 (0.33)	1.49 (0.11)	25.0	33
CoQ_{10}							
22.7 (1.0)	7.57 (0.33)	17.1 (0.75)	13.6 (1.0)	4.53 (0.33)	1.49 (0.11)	25.0	45
Vitamin E							
22.7 (1.0)	7.57 (0.33)	17.1 (0.75)	13.6 (1.0)	4.53 (0.33)	1.49 (0.11)	25.0	69
Vitamin A acetate							
22.7 (1.0)	7.57 (0.33)	17.1 (0.75)	13.6 (1.0)	4.53 (0.33)	1.49 (0.11)	25.0	71

a) Numbers in parentheses are the mole ratio of the marker, lipophilic agent, or cholesterol to egg lecithins isolated as single compartment liposomes. All the concentrations are those in cuvette cell. b) The maximum BTB release was obtained at 60 min later after injection of the *B*-liposomes (see text). The marker releases were calculated by Eq. 1. Details are described under Experimental. c) Unless stated otherwise, ethyl decaprenoate was a mixture of 15% *cis* and 85% *trans* isomers.

acetone < solanesol ≪ CoQ_{10} < vitamin E ≃ vitamin A acetate. Difference of these agents in the induced liposome fusion is difficult to argue at the present time. But, one possibility is that the structure of head group of polyisoprenoids and their analogues seems to act delicately on the local property of membrane surface. Liposomal bilayers are capable of a high degree of structural discrimination, and lends support to the hypothesis that the lipid phase of cell membranes may be the site of action of these lipophilic agents.

Our thanks are due to Mr. Kazuo Egashira for the partial assistance in experiments and to Mr. Yoshio Hara for his skilled technical assistance on the electron micrographic studies. Authors also acknowledge helpful discussions of Professor Hiroshi Kaneto, Department of Pharmacology, Faculty of Pharmaceutical Sciences, Nagasaki University, and Dr. Toji Konishi, Eisai Co. Ltd., Tokyo.

References

1) G. Poste and A. C. Allison, *Biochim. Biophys. Acta*, **300**, 413 (1973).
2) G. Gregoriadis, *N. Engl. J. Med.*, **295**, 704 (1976).
3) C. Taupin and H. M. McConnell, "Mitochondria Biomembranes," North-Holland Publishing Co., Amsterdam (1972), p. 219.
4) C. Miller, P. Arvan, J. N. Telford, and E. Racker, *J. Membr. Biol.*, **30**, 271 (1976).
5) D. Papahadjopoulos, W. J. Vail, C. Newton, S. Nir, K. Jacobson, G. Poste, and R. Lago, *Biochim. Biophys. Acta*, **465**, 579 (1977).
6) D. Papahadjopoulos, *J. Colloid Interface Sci.*, **58**, 459 (1977).
7) H. L. Kantor and J. H. Prestegard, *Biochemistry*, **14**, 1790 (1975).
8) H. L. Kantor, S. Mabrey, J. H. Prestegard, and J. M. Sturtevant, *Biochim. Biophys. Acta*, **466**, 402 (1977).
9) H. L. Kantor and J. H. Prestegard, *Biochemistry*, **17**, 3592 (1978).
10) A. L. Lau and S. I. Chan, *Biochemistry*, **13**, 4942 (1974).
11) F. J. Martin and R. C. MacDonald, *Biochemistry*, **15**, 321 (1976).
12) O. Avramovic-Zikic and K. Colbow, *Biochim. Biophys. Acta*, **512**, 97 (1978).
13) N. O. Petersen and S. I. Chan, *Biochim. Biophys. Acta*, **509**, 111 (1978).
14) R. W. Holz and C. A. Stratford, *J. Membrane Biol.*, **46**, 331 (1979).
15) D. Hoekstra, A. Yaron, A. Carmel, and G. Scherphof, *FEBS Lett.*, **106**, 176 (1979).
16) T. D. Ingolia and D. E. Koshland, Jr., *J. Biol. Chem.*, **253**, 3821 (1977).
17) J. Sunamoto, H. Kondo, and A. Yoshimatsu, *Biochim. Biophys. Acta*, **510**, 52 (1978).
18) A. J. De Konig, *J. Chem. Educ.*, **51**, 48 (1974).
19) B. J. White, C. L. Tripton, and M. Dressel, *J. Chem. Educ.*, **51**, 533 (1974).
20) J. Brunner, P. Skrabal, and H. Hauser, *Biochim. Biophys. Acta*, **455**, 322 (1976).
21) R. J. L. Allen, *Biochem. J.*, **34**, 858 (1940).
22) To obtain a completely transparent solution for the optical purpose, ethanol was introduced. Under conditions adopted, that the addition of ethanol does not cause any enhanced fusion of liposomes was of course ascertained beforehand.
23) At this stage, a transmembrane pH-gradient (interior pH 5.0 and exterior pH 7.0) was retained.[17]
24) J. R. Trudell, W. L. Hubbell, and E. N. Cohen, *Biochim. Biophys. Acta*, **291**, 321 (1973).
25) D. K. Lawrence and E. N. Gill, *Mol. Pharmacol.*, **11**, 280 (1975).
26) D. K. Lawrence and E. N. Gill, *Mol. Pharmacol.*, **11**, 595 (1975).
27) M. J. Neal, K. W. Butler, C. F. Polnaszek, and I. C. P. Smith, *Mol. Pharmacol.*, **12**, 144 (1976).
28) C. Miller and E. Racker, *J. Membrane Biol.*, **26**, 319 (1976).
29) N. P. N. Gent and J. H. Prestegard, *Biochemistry*, **13**, 4027 (1974).
30) R. Lawaczeck, *J. Colloid Interface Sci.*, **66**, 247 (1978).
31) G. Poste and A. C. Allison, *Biochim. Biophys. Acta*, **300**, 421 (1973).
32) K. -Y. Y. Pang and K. W. Miller, *Biochim. Biophys. Acta*, **511**, 1 (1978).
33) S. Kawato, K. Kinoshita, Jr., and A. Ikegami, *Biochemistry*, **17**, 5026 (1978).
34) S. J. Shattil and R. A. Cooper, *Biochemistry*, **15**, 4832 (1976).
35) T. J. McIntosh, *Biochim. Biophys. Acta*, **513**, 43 (1978).
36) Y. Shimoyama, L. E. G. Eriksson, and A. Ehrenberg, *Biochim. Biophys. Acta*, **508**, 213 (1978).
37) T. Y. Tsong, *Biochemistry*, **14**, 5415 (1975).
38) A. Seelig and J. Seelig, *Biochemistry*, **16**, 45 (1977).
39) L. A. Sklar, B. S. Hudson, and R. D. Simoni, *Biochemistry*, **16**, 819 (1977).
40) Personal communication from Dr. Toji Konishi, Eisai Co. Ltd.
41) A. Spisni, L. Masotti, G. Lenaz, E. Bertoli, G. F. Pedulli, and C. Zannoni, *Arch. Biochem. Biophys.*, **190**, 454 (1978).

Liposomal Membranes. V. Interaction of Zinc(II) Ion with Egg Phosphatidylcholine Liposomes

Junzo SUNAMOTO,* Masaharu SHIRONITA, and Noriaki KAWAUCHI

Department of Industrial Chemistry, Faculty of Engineering, Nagasaki University, Nagasaki 852

(Received February 27, 1980)

The efficiency of encapsulation of several divalent metal ions, mainly Zn(II) ion, into egg lecithin liposomes has been investigated with particular attention to the stability of liposomal membranes against the transition metal(II) ions. The stronger interaction of metal ions to lecithins led to the less formation of liposomes. The addition of a suitable amount of nonionic detergent, 2-[ω-hydroxypentadeca(oxyethylene)-α-yl]-1,3-bis(dodecyloxy)propane ($2C_{12}15G$, see text), enhanced the encapsulation of Zn(II) and Cu(II) ions in liposomes. The stoichiometric measurement for the binding of Zn(II) ion to single compartment liposomes of egg lecithin suggested that a Zn(II) ion is interacting with three or four lecithin molecules on the average in both halves of liposomal bilayers. Even under the circumstances, the bilayer structure of liposomes was certainly kept stable, which was electron micrographically visualized.

Since Bangham and his coworkers reported on the bilayer structure of liposome and its resemblance to biological membranes, liposomes have attracted much attention as a suitable model of biomembranes.[1] The interaction of various metal ions with liposomal membranes has been also extensively investigated from this standpoint. The spontaneous permeability and the transmembrane movement[2-4] of metal ions, such as K^+, Na^+,[5,6] Ca^{2+}, or Mg^{2+} ion,[7] as affected by the hydrogen ion concentration,[8] the ionic strength,[9] several antibiotics providing ionophore activity,[8,10,11] and detergents[12] have been studied. Transition metals, Cr, Mn, Fe, Co, Cu, Zn, and Mo, are biologically called the "essential trace metals" since they are essentially required for enzymes or coenzymes to hold the activity.[13] The lack of these metal ions, in fact, induces specific diseases, and that the administration of the metal ions can therapeut these diseases is well known.[14,15] More recently, Gregoriadis and his coworkers have proposed that liposomes are able to be utilized as a drug carrier for therapeutic purposes.[16] Since the liposomes can encapsulate drugs,[17-19] proteins,[20] or enzymes,[21] it can be administered intravenously or orally to patients of various kinds of disease.[22] The most expedient point of liposomes as a drug-carrier is based on the following two unique features: (1) Since liposomes are constructed of amphiphilic lecithins, liposomes can also encapsulate both hydrophilic and lipophilic drugs.[19] Encapsulating water soluble drugs into the interior core of vesicles eases the permeability of these drugs across the hydrophobic cell membranes, while encapsulation of lipophilic drugs in the bulk liposomal bilayers makes the drugs easy to move in aqueous blood stream.[22] (2) If liposomes were constructed of natural phospholipids, they are biodegradable and easily metabolized. And this will promise that toxicological and immunological effects of liposomes are minimized *in vivo*.

From these aspects, we have investigated on the interaction with and the encapsulation in liposomes for several divalent metal ions which are, in a sense, thought to be a kind of hydrophilic and therapeutic drugs. This work will afford a basic knowledge on the stability of biomembranes against several divalent metal ions in one hand and on the efficiency of encapsulation of the metal ions into liposomes in other hand.

Experimental

Egg phosphatidylcholine (egg PC) was isolated and purified from fresh egg yolk according to the method in literature[23] with minor modification. Divalent metal nitrates were commercially available as analytical grade. Water used in this work was very carefully purified by deionization and redistillation using glass apparatus.

Formation of Liposomes Encapsulating Divalent Metal Ions. Liposomes were usually prepared from a mixture of egg PC and 40 mol % of chloesterol. Thirty mg of egg PC and 10 mg of cholesterol were dissolved in 1—2 ml of dry chloroform and placed in a 50 ml vol round bottom flask. Chloroform was removed off using a rotary vacuum evaporator under nitrogen atmosphere to form a thin film. The film was disperesd with 4 ml of aqueous 20 mM acetate buffer solution (pH 5.1) containing 0.1 M NaCl and 250 mM of aqueous metal ion solution by shaking on a Vortex mixer at 20 °C for 15 min. The resulting milky suspension is mostly consisted of multicompartment liposomes,[24] which was submitted to a Sephadex G-50 column (1.8×30 cm) to remove off free metal ions[10,25] and decomposed lecithins. To obtain single compartment liposomes the above milky suspension was sonified under stream of nitrogen at 2—5 °C for 15 min at 30 s intervals using a Tomy UR-200P probe-type sonifier. The sonified liposome solution (about 1.0—2.0 ml) was passed through a Sepharose 4B column (1.8×30 cm) to remove both free metal ions[10,25] and multicompartment liposomes. The amount of metal ions entrapped in liposomes was determined by atomic absorption analysis, fluorometric analysis,[26] or other spectrophotometric techniques.[27] Determination of lipid concentration was accomplished by the modified Allen's method.[28] Reproducibility of liposome formation which was ascertained by lecithin assay was rather good within about ±6% in error.

Electron Micrography of Liposomal Membranes. Liposome solution for electron micrographic measurement were negatively stained with 2% (by wt.) aqueous sodium tungstophosphate solution. A drop of the stained liposome solution was carefully put on a copper sheet-mesh using 1 μl-microsyringe, and excess sample solution was taken off with a scrap of filter paper. The sheet-mesh bearing samples was kept overnight in a vacuum desiccator and run on a JEOL JEM 100 V electron microscope.

Assay of Divalent Metal Ions; Zn(II), Cu(II), Mn(II), and Ca(II) Ions. To 0.5—1 ml of sample solution in a 3 ml-vol. Kjeldahl flask containing 0.01—250 mM metal(II) ions

was added 1 ml of 60% (v/v) perchloric acid, and heated to dryness, which was repeated thrice. After final evaporation of perchloric acid, it was diluted with 10 mM perchloric acid up to the concentration corresponding to about 10 μM of the metal(II) ions and measured on a Simadzu AA-620 atomic absorption flame spectrophotometer by regular procedures using the specific standard solution for respective metal ions.

Results and Discussion

Interaction of Liposomal Membranes with Divalent Metal Ions. The interaction of divalent metal ions and SeO_3^{2-} ion[29] with liposomal membranes of egg PC containing cholesterol was investigated focusing on the two points; (1) the amount of metal ions interacting with lecithin molecules in liposomes, $(M)_{lip}/(lecithin)_{lip}$, and (2) the % yield of lecithin molecules as recovered as liposomes after sonication and gel-filtration in the presence of metal ions. Table 1 shows the encapsulation efficiency of metal ions into liposomes. The efficiency was scarcely altered by the metal(II) ions except SeO_3^{2-} (Table 1). The stronger interaction of metal ions to liposomal membranes leads to the more destruction of liposomes, that is, the less recovery of lecithins as liposomes. Similarly, harder ultrasonication in the presence of metal ions increases the chance for metal(II) ions to interact with lecithins, but resulting in the lower lecithin recovery. The positively charged surface of egg PC liposomal membranes drastically depresses the $(Zn^{2+})_{lip}/(lecithin)_{lip}$-value comparing with the neutral surface. Contrary to what would be expected, on the other hand, the negatively charged surface hardly affect the interaction of the metal ion with membranes. The anionic phosphate moiety of phosphatidylcholines itself may present an effective binding site for metal ions. Table 1 also reveals the effect of chelating agents, EDTA and perhydrodibenzo-18-crown-6, on the encapsulation of zinc(II) ion into liposomes. EDTA was added as an aqueous solution along with zinc(II) ions during the dispersion of lipid, while dicyclohexyl-18-crown-6 was employed as a chloroform solution together with lipids during the thin lipid-film formation. The result shows that the adoption of EDTA or perhydrodibenzo-18-crown-6 rather decreases the encapsulation of zinc(II) ions. In the presence of EDTA or the crown compound, however, the lecithin recovery increased comparing with that in the absence of these chelating agents. Clearly from the fact that most of these agents adopted first are recovered during the gel-filtration, both chelating agents seem to be hardly encapsulated in liposomes. Therefore, metal ions bind predominantly to these agents in bulk aqueous solutions rather than to lecithins, which leads to saving liposomes from the destruction.

Table 1. Encapsulation of different divalent metal ions into multicompartment liposomes of egg lecithin at 25.0 °C[a]

Metal(II) ion	$\frac{(M)_{lip}}{(Lecithin)_{lip}}$[b]	Encapsulation[c] %	Lecithin[d] recovery %
None	—	—	85
Cu(II)	0.57	0.59	56
Mn(II)	0.23	0.23	81
Ca(II)	0.52	0.65	77
SeO_3^{2-}	0.03	0.03	78
Zn(II)	0.38	0.63	73
Zn(II)[e]	0.32	0.48	83
Zn(II)[f]	0.15	0.15	59
Zn(II)[g]	0.48	0.99	56
Zn(II)[g,h]	0.32	1.02	59
Zn(II)[g,i]	0.38	1.22	62
Zn(II)[g,j]	0.35	1.33	72

a) 40 μmol of egg lecithin with 26 μmol of cholesterol was dispersed in 4.0 ml of 20 mM acetate buffer containing 0.1 M NaCl and 250 mM of metal(II) nitrates at 25.0 °C. After sonication (25 W for 15 min) and gel-filtration (Sephadex G-50), concentrations of metal(II) ions and lecithin were independently determined as described under Experimental. All the values are average of duplicated or triplicated runs. b) Error which stems from assay of metal ions was as follows: ± 6.0% for Zn(II), ±0.5% for Mn(II), ±2.5% for Cu(II), and ±9.0% for Ca(II). c) Encapsulation $\% = 100 \times (M)_{lip}/(M)_{total}$. d) Lecithin recovery $\% = 100 \times (lecithin)_{lip}/(lecithin)_t$. Experimental error was within ±6.0%. e) To ensure the anionic surface charge on the liposomal membranes, 5.6 μmol of dihexadecylhydrogenphosphate was added during the lipid thin film formation. f) To ensure the cationic surface charge on the membranes, 5.6 μmol of hexadecylamine was employed during the course of thin-film formation. g) Sonicated at 60 W for 15 min. h) 10 μmol of EDTA was added. i) 25 μmol of EDTA was added. j) 10 μmol of crown ether was added.

Table 2. Effect of nonionic detergent, $2C_{12}15G$, on the encapsulation of Zn(II) ions in egg lecithin liposomes[a]

Liposomes Lecithin μmol	$2C_{12}15G$ μmol	$\frac{(Zn(II))_{lip}}{(Lecithin)_{lip}}$	Encapsulation %
40	0	0.38	0.63[b]
38	2	0.37	0.93
36	4	0.39	1.26
32	8	0.35	0.72
28	12	0.27	0.83
20	20	0.03	0.13

a) The nonionic detergent was mixed with egg lecithin in the absence of cholesterol during the course of thin film formation. Liposome solutions were sonicated at 25 W for 15 min. b) The same data as that listed in Table 1.

The effect of nonionic detergent, $2C_{12}15G$,[30] on the encapsulation of Zn(II) ion is listed in Table 2. The detergent

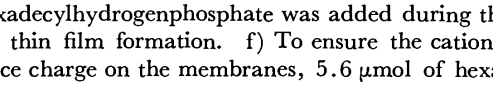

2-[ω-hydroxypentadeca(oxyethylene)-α-yl]-1,3-bis(dodecyloxy)propane ($2C_{12}15G$)

is bearing long ethylene oxide moiety as the hydrophilic part, which is expected to behave just like as an acyclic

antibiotic ionophore.[11] Intercalating up to about 10 mol% of $2C_{12}15G$ in liposomes without cholesterol enhanced the encapsulation of the metal(II) ion different from cases of the former two chelating agents. Leakage of the nonionic detergent from the liposomal bilayers to the exterior aqueous phase can be neglected under the present conditions. The totally similar effect was observed also for the encapsulation of Cu(II) ion (not shown). Addition of more detergent, however, rather decreased the efficiency of encapsulation of metal ions. Electron micrographic studies indicated that adopting the detergent up to 10 mol% against lecithins still holds reliable bilayer structure of multicompartment liposomes, but the presence of more detergent than 20 mol% gradually causes the physico-chemical damage on the bilayer structure (Fig. 1). This is very comparable to the efficiency on the metal ion encapsulation. Interestingly, in addition, as increasing the content of the detergent, the bilayer thickness determined on the electron micrograph pictures also increased: 30 Å for 100% lecithin liposomes, 34 Å for liposomes containing 10 mol% of $2C_{12}15G$, 37 Å for 20 mol%, 39 Å for 30 mol%, and 45 Å for more than 50 mol%.

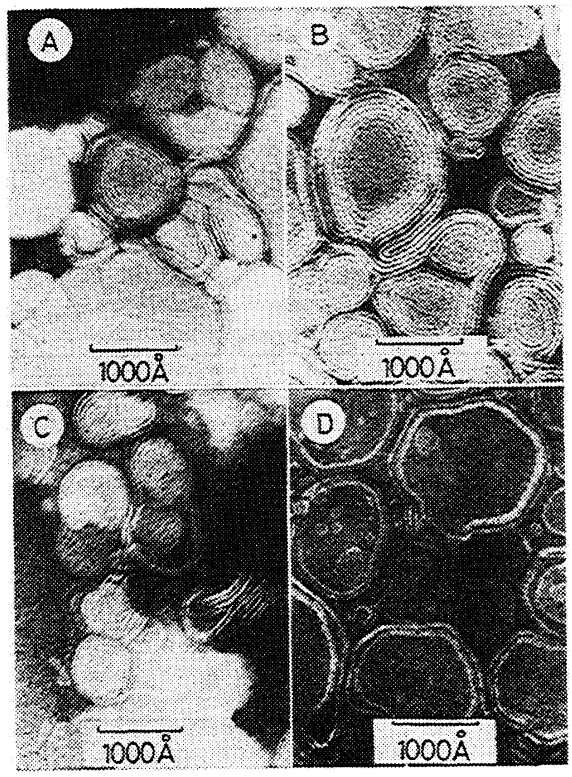

Fig. 1. Electron micrographs of egg lecithin multicompartment liposomes containing nonionic detergent, $2C_{12}15G$, at different concentrations (A, 0 mol%; B, 10 mol%; C, 30 mol%; and D, 50 mol%) in the presence of Zn (II) ion.

Adsorption of Zinc(II) Ion on the Liposomal Bilayers. Electrophoretic mobility and ^{31}P-NMR measurements were combined by McLaughlin and his coworkers[31] to test whether the combination of Henry, Boltzmann, and Grahame equations is capable of describing the adsorption of the divalent metal ions to phosphatidylcholine membrane, where they assumed a 1:1 stoichiometry for the binding of the divalent ions to phosphatidylcholine. In this work, amounts of each Zn(II) ion being in the interior of vesicles and adsorbing onto the outer surface of vesicles were independently determined by following procedures. After the gel-filtration of the single compartment liposome solutions containing Zn(II) ions, which were prepared according to the regular technique as described under Experimental, the total amount of metal ions interacting with lecithins ($(Zn(II))_{lip}$) was determined: it was 6.27 μmol. Then, the liposomes were washed by adding about 0.02 M EDTA aqueous solution[10] (about 100 times excess to total metal ions entrapped in liposomes) and contributed again to the gel-filtration in order to remove off Zn(II) ions adsorbed only on the outer surface of membranes.[10] At this stage both amounts of metal ions adsorbing on the outer surface ($(Zn(II))_{lip\cdot out}$) and locating in the interior core of vesicles ($(Zn(II))_{lip\cdot in}$) could be determined: they were 3.78 and 1.79 μmol, respectively. Hence, the yield of Zn(II) ions recovered during the above procedures was about 90%. Same experiment was repeated twice. The result also indicates that about 70% of Zn(II) ions in liposomes are binding onto the outer half of liposomal bilayers. To ascertain the result, on the other hand, the blank single compartment liposomes containing no metal ions were independently prepared. And Zn(II) ion was then added from the exterior of liposomes. After the gel-filtration to remove free metal ions off, the amount of Zn(II) ions, which corresponds to those bound only to the outer surface of liposomes ($(Zn(II))_{lip\cdot out}$), was determined: it was 4.13 μmol. This value is in good agreement with the preceding one (3.78 μmol) within experimental error (±10%). Finally, the resulting liposome solutions were washed by 0.02 M EDTA and gel-filtered again. Hence, the amount of Zn(II) ions remained in liposomes was determined: it was 0.36 μmol. This may mean that only 8.7% of Zn(II) ions permeates into the liposomes as a complex with EDTA and/or lecithins during the course of washing the outer surface of liposomes by EDTA.

Table 3. Number of Zn(II) ion binding onto respective halves of bilayers of egg lecithin single compartment liposomes

$(Zn(II))_{lip.out}$ μmol	$\frac{(Zn(II))_{lip.out}}{(lecithin)_{lip.out}}$	$(Zn(II))_{lip.in}$ μmol	$\frac{(Zn(II))_{lip.in}}{(lecithin)_{lip.in}}$
4.13(3.78)[a]	0.30—0.34	1.79	0.30—0.41

a) The parenthesized value was obtained from the codispersion experiment.

The area ratio of the outer surface to the inner surface of the single compartment liposomes is in proportion to the ratio of the number of lecithin molecules involving in respective two halves of bilayers. Assuming that the average size of single compartment liposomes is 250—300 Å[22,24] in diameter, the thickness of bilayers is 40—50 Å, and a vesicle is consisted of 3000—4000 molecules of phosphatidylcholines,[22] thus, one can estimate the

number of Zn(II) ions interacting with lecithins of both halves of bilayers (Table 3). The estimation suggests 1 to 3—4 stoichiometry for the zinc(II) ion interacting with phosphatidylcholine in both halves of liposomal bilayers. Alternatively, if assumed that all the Zn(II) ions locating in the interior water pool of liposomes are free, the estimation suggests that the initial aqueous solutions of metal ion added when forming liposomes is diluted about two-fold. But, this seems unlikely. Surprisingly, even under the circumstances, the bilayer structure of vesicles was certainly kept stable as visualized by electron micrography.

The authors are indebted to Professor Toyoki Kunitake, Kyushu University, for a gift of nonionic detergent. Thanks are also due to Analysis Center for Laboratory Waste and Noise, Nagasaki University, for measurements using atomic absorption flame spectrophotometer.

References

1) A. D. Bamghan, M. W. Hill, and N. G. A. Miller, "Methods in Membrane Biology," ed by E. D. Korn, Plenum Press (1974), Vol. 1, pp. 1—68.
2) K. Jacobson and D. Papahajopoulos, *Biochemistry*, **14**, 152 (1975).
3) S. Ohnishi and T. Ito, *Biochemistry*, **13**, 881 (1974).
4) D. Papahajopoulos, W. J. Vail, C. Neton, S. Nir, K. Jacobson, G. Poste, and R. Labo, *Biochim. Biophys. Acta*, **465**, 579 (1977).
5) A. D. Bamgham, M. M. Standish, and J. C. Watkins, *J. Mol. Biol.*, **13**, 238 (1965).
6) A. Scarpa and J. de Gier, *Biochim. Biophys. Acta*, **241**, 789 (1971).
7) A. R. de Boland, R. L. Jilka, and A. N. Martonosi, *J. Biol. Chem.*, **250**, 7501 (1975).
8) J. Wulf and W. G. Pohl, *Biochim. Biophys. Acta*, **465**, 471 (1977).
9) R. L. Jilka and A. N. Martonosi, *Biochim. Biophys. Acta*, **466**, 57 (1977).
10) T-C. Wun and R. Bittman, *Biochemistry*, **16**, 2080 (1977).
11) H. Degani, *Biochim. Biophys. Acta*, **509**, 360 (1978).
12) G. Eytan, M. J. Matheson, and E. Racker, *FEBS Lett.*, **57**, 121 (1975).
13) Y. Murakami, *Kagakuzokan*, **56**, 135 (1972).
14) R. R. C. New, M. L. Chance, S. C. Thomas, and W. Peters, *Nature*, **272**, 55 (1978).
15) R. A. Guilimette, E. A. Cerny, and Y. E. Rahman, *Life Sci.*, **22**, 313 (1978).
16) G. Gregoriadis, P. D. Leathwood, and B. E. Ryman, *FEBS Lett.*, **14**, 95 (1971).
17) K. Tsujii, J. Sunamoto, and J. H. Fendler, *Life Sci.*, **19**, 1743 (1976).
18) G. Gregoriadis, L. P. Smain, E. J. Willis, and A. S. Tvill, *Lancet* (1974), pp. 1313—1316.
19) P. Papahadjopoulos, E. Mayhew, G. Poste, S. Smith, and W. J. Vail, *Nature*, **252**, 163 (1974).
20) J. M. Boggs and M. A. Moscarello, *Biochemistry*, **17**, 5734 (1978).
21) K. Krab and M. Wikstrom, *Biochim. Biophys. Acta*, **504**, 200 (1978).
22) A. Tyrrell, T. D. Heath, C. M. Colley, and B. E. Ryman, *Biochim. Biophys. Acta*, **457**, 259 (1976).
23) W. S. Singleton, M. S. Gray, M. L. Brown, and J. L. White, *J. Am. Oil Chem. Soc.*, **42**, 53 (1965).
24) M. P. Sheetz and S. I. Chan, *Biochemistry*, **11**, 4573 (1972).
25) D. F. O'Brien, *Photochem. Photobiol.*, **29**, 679 (1979).
26) G. L. Wheeler and P. F. Lott, *Microchemical J.*, **19**, 390 (1974).
27) G. H. Ayres and A. S. Meyer, Jr., *Anal. Chem.*, **23**, 299 (1951).
28) R. J. L. Allen, *Biochem. J.*, **34**, 858 (1940).
29) The determination of Se(IV) was performed by the fluorometric analysis using 2,3-diaminonaphthalene.[25]
30) Y. Okahata, S. Tanamachi, M. Nagai, and T. Kunitake, "Polymer Preprints, Japan,"(1978), Vol. 27, p. 231.
31) A. McLaughlin, C. Greathwohl, and S. McLaughlin, *Biochim. Biophys. Acta*, **513**, 338 (1978).

The Structure of the Cyclodextrin Complex. IX. The Crystal Structure of α-Cyclodextrin-*m*-Nitroaniline (1:1) Hexahydrate Complex

Kazuaki HARATA

Research Institute for Polymers and Textiles, 1-1-4, Yatabe-Higashi, Tsukuba, Ibaraki 305

(Received March 12, 1980)

The crystal structure of α-cyclodextrin–*m*-nitroaniline hexahydrate complex was determined by X-ray analysis. The crystal is monoclinic and the space group is $P2_1$ with $Z=2$. The cell dimensions are: $a=8.054(1)$, $b=13.508(1)$, $c=25.331(2)$ Å, and $\beta=103.90(1)°$. The structure was solved by an inspection of a Patterson map and by a trial-and-error method. The refinement was done by the block-diagonal least-squares method to the final *R*-value of 0.11 for 2351 reflections ($\sin\theta/\lambda<0.49$). α-Cyclodextrin molecules are stacked along the a axis in the head-to-tail fashion to form a channel-type structure. Most of the primary hydroxyl groups of α-cyclodextrin are in a *gauche-gauche* conformation and linked by hydrogen bonds directly or through water molecules to the secondary hydroxyl groups of the next α-cyclodextrin molecule along the channel. The guest *m*-nitroaniline molecules are linearly arranged in the channel. The α-cyclodextrin ring includes the nitrophenyl group, while the amino group protrudes outside from the secondary hydroxyl side of α-cyclodextrin and is hydrogen-bonded to a primary hydroxyl group of the next α-cyclodextrin molecule. Along the channel, *m*-nitroaniline molecules are linked to each other by a weak N–H···O hydrogen bond between the amino group and the nitro group. Columns formed by the stack of α-cyclodextrin are closely packed in the crystal, and intermolecular spaces are filled with water molecules which form many hydrogen bonds with each other and with α-cyclodextrin.

Cyclodextrins form a number of inclusion complexes with a variety of guest molecules. Cyclodextrin complexes with aromatic guests have been intensively studied, mainly in relation to an enzyme model.[1] Crystal structures of α-cyclodextrin complexes with *m*- and *p*-nitrophenols[2,3] have well interpreted the stereospecific acceleration of the hydrolysis rate of nitrophenyl acetates. α-Cyclodextrin also catalyzes hydrolysis of nitroacetanilides, and it has shown to act as a true catalyst in that case.[4]

Several α-cyclodextrin complexes with para-disubstituted benzenes have been investigated by the X-ray method.[2,3,5-7] The benzene ring has been found at the same position in those complexes in spite of various substituents. On the other hand, among the α-cyclodextrin complexes with meta-isomers, only the structure of a 1:2 complex with *m*-nitrophenol has been determined.[2] In the present work, we investigated the crystal structure of the α-cyclodextrin–*m*-nitroaniline complex. Unlike the *m*-nitrophenol complex, the *m*-nitroaniline complex gives a 1:1 host-guest stoichiometry; therefore, the inclusion geometry of the complex is of particular interest, for comparison with the *m*-nitrophenol complex as well as in relation to the catalytic reaction.

Experimental

Crystals of α-cyclodextrin–*m*-nitroaniline (1:1) hexahydrate complex were prepared by slowly cooling a hot aqueous solution of α-cyclodextrin saturated with *m*-nitroaniline. They are orange prisms elongated along the a axis. The determination of the lattice parameters and the intensity measurement were carried out on a Rigaku automatic four-circle diffractometer with graphite-monochromated Mo $K\alpha$ radiation. The crystal was sealed in a quartz capillary with a drop of mother liquor since the crystal breaks up in air. 2677 independent reflections were obtained up to 40° in 2θ by using an ω-scan technique. But 324 reflections with $|F_o|<3\sigma(F)$ were treated as unobserved. No corrections were made for absorption and extinction.

Crystal Data: $C_{36}H_{60}O_{30}\cdot C_6H_7N_2O_2\cdot 6H_2O$, *F. W.* = 1220.1, monoclinic, space group $P2_1$, $Z=2$, $a=8.054(1)$, $b=13.508(1)$, $c=25.331(2)$Å, $\beta=103.90(1)°$, $V=2675.1$ Å^3, $D_x=1.515$, $D_o=1.50$ g·cm^{-3}.

Determination and Refinement of the Structure

A Patterson map showed that the α-cyclodextrin ring is located nearly perpendicular to the a axis. The position and orientation of the molecule were determined by the trial-and-error method. At this stage, the position and orientation of each glucose residue were refined by the rigid-body least-squares method. *m*-Nitroaniline and water molecules were found on Fourier and difference-Fourier maps. Two primary hydroxyl groups (O(6,G2) and O(6,G3)) of α-cyclodextrin were found to be disordered. Their occupancies were estimated from an electron-density map, but they were not refined. The refinement of atomic parameters was carried out by the block-diagonal least-squares method by using isotropic temperature factors. The quantity minimized was $\sum w(|F_o|-|F_c|)^2$, with $w=1.0$ for all the reflections used. The final *R*-value was 0.11. The atomic scattering factors were taken from "International Tables for X-Ray Crystallography."[8] The atomic parameters are listed in Table 1. A table of observed and calculated structure factors and a table of bond distances, angles, and conformation angles in α-cyclodextrin are kept at the office of The Chemical Society of Japan (Document No. 8028).

Description and Discussion of the Structure

Structure of α-Cyclodextrin. The structure and the numbering scheme of the α-cyclodextrin–*m*-nitroaniline hexahydrate complex are shown in Fig. 1. The average bond distances and angles over six glucose residues are given in Fig. 2. These values are in good agreement

Table 1. Final positional ($\times 10^4$) and thermal parameters
Estimated standard deviations are given in parentheses. OC indicates an occupancy factor for disordered atom.

	x	y	z	B	OC
C(1,G1)	1882(26)	4734(—)	1106(8)	4.9(5)	
C(2,G1)	603(24)	4298(16)	1398(8)	4.2(4)	
C(3,G1)	985(22)	4629(14)	1993(7)	3.3(4)	
C(4,G1)	2854(22)	4453(14)	2263(7)	3.4(4)	
C(5,G1)	3981(24)	4892(16)	1941(8)	4.3(4)	
C(6,G1)	5981(29)	4679(19)	2153(10)	6.4(6)	
O(2,G1)	-1110(18)	4652(12)	1130(6)	5.7(3)	
O(3,G1)	-82(17)	4146(11)	2273(5)	4.7(3)	
O(4,G1)	3174(14)	4917(9)	2787(5)	3.2(2)	
O(5,G1)	3539(17)	4432(11)	1402(5)	5.2(3)	
O(6,G1)	6283(24)	3714(15)	2177(8)	9.0(5)	
C(1,G2)	2711(30)	8268(20)	303(10)	6.7(6)	
C(2,G2)	840(28)	7886(19)	74(9)	6.0(6)	
C(3,G2)	552(28)	7076(18)	485(9)	5.6(5)	
C(4,G2)	1943(27)	6227(17)	582(9)	5.3(5)	
C(5,G2)	3738(24)	6688(16)	708(8)	4.2(4)	
C(6,G2)	5017(33)	5912(22)	640(11)	7.8(7)	
O(2,G2)	-382(23)	8636(15)	72(8)	8.3(5)	
O(3,G2)	-1008(25)	6549(17)	226(8)	9.8(5)	
O(4,G2)	1654(17)	5753(12)	1069(5)	5.4(3)	
O(5,G2)	3871(18)	7477(12)	335(6)	5.7(3)	
O(6A,G2)	5112(81)	5658(54)	225(24)	9.3(17)	0.3
O(6B,G2)	6758(35)	6265(22)	797(11)	9.0(7)	0.7
C(1,G3)	4456(29)	11206(18)	1729(9)	5.9(5)	
C(2,G3)	2628(35)	11171(22)	1329(11)	8.2(7)	
C(3,G3)	2062(30)	10129(20)	1203(10)	6.6(6)	
C(4,G3)	3338(26)	9652(17)	930(8)	5.1(5)	
C(5,G3)	5074(25)	9690(16)	1318(8)	4.4(4)	
C(6,G3)	6467(30)	9244(20)	1061(9)	6.2(5)	
O(2,G3)	1604(24)	11672(16)	1666(8)	8.9(5)	
O(3,G3)	475(24)	10204(16)	807(8)	9.3(5)	
O(4,G3)	2750(17)	8684(11)	824(6)	5.2(3)	
O(5,G3)	5567(17)	10697(12)	1466(6)	5.3(3)	
O(6A,G3)	6606(43)	9690(28)	663(14)	7.7(9)	0.5
O(6B,G3)	8046(37)	9379(25)	1422(12)	6.1(7)	0.5
C(1,G4)	6158(26)	10870(17)	3911(8)	5.2(5)	
C(2,G4)	4543(26)	11513(17)	3630(8)	5.1(5)	
C(3,G4)	3789(24)	11185(16)	3059(8)	4.3(4)	
C(4,G4)	5272(26)	11190(16)	2721(8)	4.8(5)	
C(5,G4)	6754(24)	10586(16)	3033(8)	4.5(4)	
C(6,G4)	8305(31)	10671(21)	2760(10)	7.0(6)	
O(2,G4)	3349(18)	11400(12)	3963(6)	5.9(3)	
O(3,G4)	2455(18)	11856(12)	2804(6)	5.5(3)	
O(4,G4)	4435(16)	10693(11)	2233(5)	4.5(3)	
O(5,G4)	7378(18)	10933(11)	3579(6)	5.4(3)	
O(6,G4)	8696(20)	11695(13)	2727(7)	7.1(4)	
C(1,G5)	5889(22)	7247(14)	4688(7)	3.4(4)	
C(2,G5)	4735(24)	8022(15)	4858(7)	3.9(4)	
C(3,G5)	4455(22)	8840(13)	4458(7)	3.0(4)	
C(4,G5)	6105(21)	9329(14)	4368(7)	3.0(4)	
C(5,G5)	7230(22)	8476(14)	4236(7)	3.4(4)	
C(6,G5)	9144(31)	8792(19)	4194(10)	6.7(6)	
O(2,G5)	3204(16)	7517(11)	4883(5)	4.5(3)	
O(3,G5)	3501(17)	9665(11)	4651(5)	4.8(3)	
O(4,G5)	5538(15)	9870(9)	3884(5)	3.6(3)	
O(5,G5)	7461(15)	7713(10)	4642(5)	4.0(3)	
O(6,G5)	9889(22)	9269(15)	4664(7)	7.9(4)	
C(1,G6)	3908(22)	4368(15)	3245(7)	3.6(4)	
C(2,G6)	2815(23)	4543(15)	3680(7)	3.8(4)	
C(3,G6)	3015(20)	5630(15)	3861(6)	2.6(3)	
C(4,G6)	5809(20)	5650(13)	3861(6)	2.9(3)	
C(5,G6)	5008(22)	5865(14)	4072(7)	3.5(4)	
C(6,G6)	7715(24)	5864(14)	3728(8)	4.0(4)	
O(2,G6)	1063(15)	4351(10)	3435(5)	3.7(3)	
O(3,G6)	2229(16)	5726(10)	4308(5)	4.3(3)	
O(4,G6)	5000(13)	6910(9)	4159(4)	2.8(2)	
O(5,G6)	5627(14)	4629(9)	3468(5)	3.5(3)	
O(6,G6)	8611(17)	5373(11)	4194(5)	5.1(3)	
C(1,NP)	306(26)	7559(17)	2187(8)	5.0(5)	
C(2,NP)	1943(24)	7444(16)	2085(8)	4.2(4)	
C(3,NP)	3231(22)	7824(15)	2528(7)	3.7(4)	
C(4,NP)	1303(28)	8363(19)	3055(9)	8.3(5)	
C(5,NP)	3028(35)	8301(24)	2956(11)	5.7(7)	
C(6,NP)	55(31)	7981(20)	2652(10)	6.7(6)	
N(1,NP)	-1139(18)	7185(12)	1767(6)	7.5(3)	
N(2,NP)	5013(27)	7709(17)	2453(8)	3.7(6)	
O(1,NP)	5270(18)	7316(12)	2041(6)	5.6(3)	
O(2,NP)	6199(19)	7983(13)	2831(6)	6.4(4)	
O(W1)	-18(29)	1398(18)	4696(9)	11.4(6)	
O(W2)	352(21)	2497(14)	3734(7)	7.3(4)	
O(W3)	3699(25)	3175(16)	215(8)	9.6(5)	
O(W4)	6428(20)	3295(14)	1086(7)	7.0(4)	
O(W5)	8099(23)	3295(15)	4331(7)	8.4(5)	
O(W6)	8243(38)	11863(26)	1130(12)	16.9(10)	

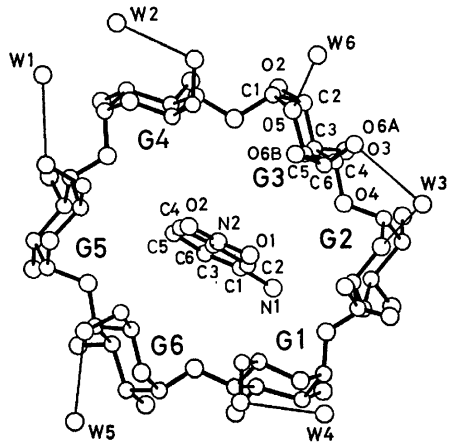

Fig. 1. Structure and numbering scheme of α-cyclodextrin–*m*-nitroaniline hexahydrate complex. O6A and O6B indicate disordered primary hydroxyl groups with *gauche-gauche* and *gauche-trans* conformations respectively. Water molecules are denoted by W1, W2, W3, W4, W5, and W6. Thin lines indicate intermolecular contacts less than 3.0 Å.

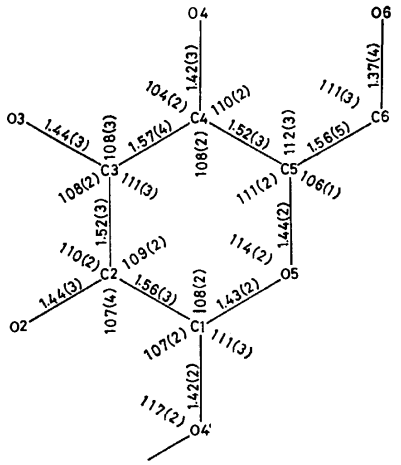

Fig. 2. Average bond distances (l/Å) and angles (ϕ/°) over six glucose residues. Standard deviations in parentheses were estimated according to the equation $\sigma=[\sum_{i=1}^{6}(x_i-\bar{x})^2/5]^{1/2}$, where x_i referes to the bond distance or angle in the i-th residue and $\bar{x}$ is the average value.

with those of other α-cyclodextrin complexes.[2,3,5-7] The primary hydroxyl groups in G2 and G3 residues are statistically disordered, and show *gauche-gauche* (O(6A)) and *gauche-trans* (O(6B)) conformations, while the others are in the *gauche-gauche* conformation. The geometrical data for the α-cyclodextrin ring are given in Tables 2 and 3. The α-cyclodextrin ring is elliptically distorted owing to the inclusion of the planar molecule, and elongated along the guest plane. The difference in the longest and shortest diagonal distances, which are measured between glycosidic oxygen atoms, is 0.99 Å. This value is nearly the same as the corresponding values found in the α-cyclodextrin complexes with para-disubstituted benzenes,[3] but is larger than the value found in the *m*-nitrophenol complex (0.40 Å).[2] The O(4)···O(4) distances between adjacent glucose residues and the torsion-angle indices indicate that the distortion of the pyranose ring is smaller than that

TABLE 2. GEOMETRICAL DATA FOR α-CYCLODEXTRIN RING

I. O(4)···O(4) distances.[a]

Distance(l/Å)		Distance(l/Å)	
O(4,G1)···O(4,G2)	4.38	O(4,G5)···O(4,G6)	4.10
O(4,G1)···O(4,G6)	4.36	O(4,G1)···O(4,G4)	8.03
O(4,G2)···O(4,G3)	4.14	O(4,G2)···O(4,G5)	8.99
O(4,G3)···O(4,G4)	4.43	O(4,G3)···O(4,G6)	8.55
O(4,G4)···O(4,G5)	4.21		

a) Estimated standard deviations are between 0.03 and 0.04 Å.

II. O(2)···O(3) distances between adjacent glucose residues.[b]

Distance(l/Å)		Distance(l/Å)	
O(2,G1)···O(3,G2)	3.45	O(2,G3)···O(3,G4)	2.81
O(3,G1)···O(2,G6)	2.74	O(2,G4)···O(3,G5)	2.91
O(2,G2)···O(3,G3)	2.80	O(2,G5)···O(3,G6)	2.84

b) Estimated standard deviations are between 0.03 and 0.04 Å.

III. Torsion-angle indices and tilt-angles for glucose residue.

Residue	Torsion-angle index (ϕ/°)	Tilt-angle (ϕ/°)
G1	132	17.6
G2	140	19.7
G3	120	10.1
G4	124	9.9
G5	126	11.2
G6	121	18.5

observed in the complexes with para-disubstituted benzenes.[3] Five O(2)···O(3) distances between adjacent glucose residues are in the range capable of hydrogen-bond formation (from 2.74 to 2.91 Å), while the O(2,G1)···O(3,G2) distance of 3.45 Å indicates no hydrogen bond. The six glycosidic oxygen atoms (O(4)) are in the same plane within the deviation of 0.16 Å. The tilt-angle of the glucose residue, which is measured between the plane through the six O(4) atoms and the plane through the O(4*), C(1), C(4), and O(4) atoms, is in the range from 9.9 to 19.7°. These values

TABLE 3. LEAST-SQUARES PLANES AND DEVIATIONS OF ATOMS FROM THE PLANE

The plane equation is of the $AX+BY+CZ=D$ form, where X, Y, and Z are the coordinates in Å units along the a, b, and c* axes, respectively.

I. The plane through the six O(4) atoms

$0.982X-0.187Y-0.038Z=-0.730$

O(4,G1)	0.07	O(4,G4)	−0.02
O(4,G2)	−0.16	O(4,G5)	−0.08
O(4,G3)	0.13	O(4,G6)	0.05

II. *m*-Nitroaniline

$0.036X+0.888Y-0.459Z=6.565$

C(1,NP)	0.00	C(6,NP)	−0.04
C(2,NP)	0.02	N(1,NP)	−0.01
C(3,NP)	0.01	N(2,NP)	0.01
C(4,NP)	0.08	O(1,NP)	0.01
C(5,NP)	−0.01	O(2,NP)	−0.07

are relatively larger than those found in the α-cyclodextrin complexes with para-disubstituted benzenes (average value of 11.3°)[9] and *m*-nitrophenol (average value of 10.7°).[2]

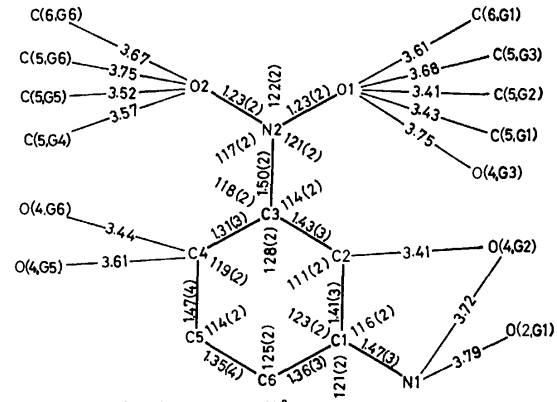

Fig. 3. Bond distances (l/Å) and angles (ϕ/°) in *m*-nitroaniline and selected intermolecular distances (l/Å) between *m*-nitroaniline and α-cyclodextrin. Estimated standard deviations in *m*-nitroaniline are given in parentheses, and those for intermolecular distances are in the range from 0.03 to 0.04 Å.

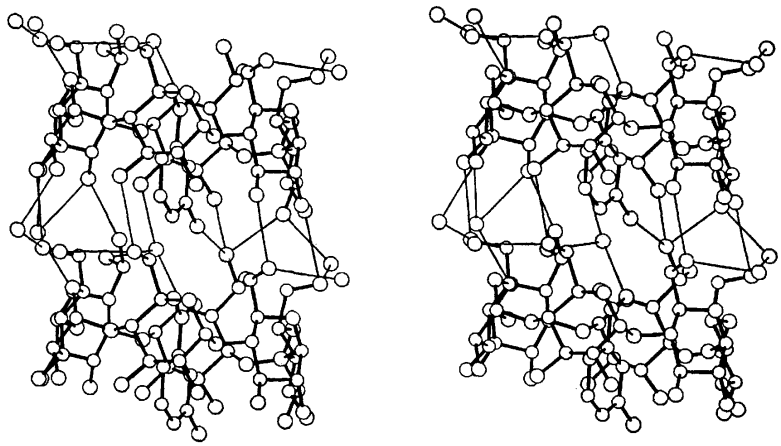

Fig. 4. A stereo-drawing of the packing feature of the complex with associated water molecules. Thin lines denote intermolecular contacts less than 3.0 Å.

Geometry of Inclusion. Figure 3 shows bond distances and angles in *m*-nitroaniline, and selected intermolecular distances between *m*-nitroaniline and α-cyclodextrin. α-Cyclodextrin molecules are stacked in head-to-tail fashion to form an endless channel, in which *m*-nitroaniline molecules are arranged as shown in Fig. 4. The nitrophenyl group is inserted into the α-cyclodextrin ring, while the amino group protrudes outside from the secondary hydroxyl side of α-cyclodextrin and forms a hydrogen bond with the primary hydroxyl group (O(6B,G2)) of the next α-cyclodextrin molecule. The nitrophenyl plane faces the G3 and G6 residues, and makes an angle of 83.5° with the plane through the six O(4) atoms. The shortest intermolecular distance is 3.41 Å, found in O(4,G2)···C(2,NP), and C(5,G2)···O(1,NP) contacts. The nitro group is surrounded by hydrogen atoms of C(5) methine groups and C(6) methylene groups. This inclusion geometry of the nitrophenyl group is quite similar to that found in the α-cyclodextrin–*p*-nitrophenol complex,[3] although the orientation of the nitrophenyl plane is slightly changed. In the *m*-nitroaniline complex, the nitrophenyl plane is parallel to the C(4)···C(4) diagonal of α-cyclodextrin, while the nitrophenyl group in the *p*-nitrophenol complex is parallel to the C(2)···C(2) diagonal. α-Cyclodextrin forms a 1:2 crystalline complex with *m*-nitrophenol[2] and also has a head-to-tail channel-type structure. Although one *m*-nitrophenol is located outside the α-cyclodextrin column, the other one is arranged in the channel. In that case, only the nitro group is inserted into the α-cyclodextrin ring, and therefore, the *m*-nitrophenol molecule is more loosely bound than the *m*-nitroaniline molecule.

In the *m*-nitroaniline complex, guest molecules are linearly arranged in the channel (Fig. 4). Some short contacts are observed between neighboring *m*-nitroaniline molecules: N(1,NP)···O(1,NP) distance of 3.14 Å and C(6,NP)···O(2,NP) distance of 3.24 Å. The O···N distance suggests a weak N–H···O hydrogen bond. The short C···O distance also shows that the *m*-nitroaniline molecules are very closely packed in the channel. Such short contacts were not observed in the *m*-nitrophenol complex.[2] The *m*-nitrophenol molecule is more tilted with respect to the channel axis, and the repetition unit along the channel (8.15 Å) is longer than that found in the *m*-nitroaniline complex (8.05 Å). As the result, the adjacent *m*-nitrophenol molecules are apart by 3.40 Å which is found between the phenolic hydroxyl group and the nitro group.

The tight packing of the guest *m*-nitroaniline molecule seems to affect its electronic state. Crystals of *m*-nitroaniline are dark yellow. When it forms the crystalline complex with α-cyclodextrin, the color changes to bright orange. This typical color change associated with the complex formation has been observed in the α-cyclodex-

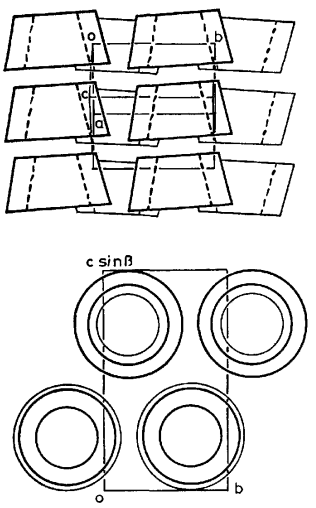

Fig. 5. Schematic drawings of the packing feature of α-cyclodextrin in the crystal.

Table 4. Intermolecular distances less than 3.0 Å

Distance(*l*/Å)	Code	Distance(*l*/Å)	Code
O(2,G1)···O(2,G7)	2.78 (c)	O(2,G4)···O(W2)	2.77 (b)
O(2,G1)···O(W4)	2.68 (c)	O(3,G4)···O(6,G4)	2.99 (c)
O(3,G1)···O(6,G1)	2.94 (c)	O(6,G4)···O(W2)	2.80 (e)
O(6,G1)···O(W1)	2.85	O(2,C5)···O(W5)	2.68 (h)
O(2,G2)···O(W3)	2.67 (f)	O(3,G5)···O(6,G5)	2.97 (c)
O(3,G2)···O(6B,G2)	2.60 (c)	O(5,G5)···O(W1)	2.92 (h)
O(5,G2)···O(W3)	2.82 (g)	O(6,G5)···O(W1)	2.88 (e)
O(6A,G2)···O(6A,G3)	2.68 (i)	O(2,G6)···O(W2)	2.72
O(6B,G2)···N(1,NP)	2.91 (a)	O(3,G6)···O(6,G6)	2.90 (c)
O(2,G3)···O(W6)	2.72 (c)	O(6,G6)···O(W5)	2.87
O(3,G3)···O(6B,G3)	2.99 (c)	O(W1)···O(W2)	2.93
O(3,G3)···O(W6)	2.93 (c)	O(W2)···O(W5)	2.84 (c)
O(5,G3)···O(W6)	2.83	O(W3)···O(W4)	2.72
O(6,G3)···O(W3)	2.99 (g)	O(W4)···O(W6)	2.61 (d)

Code	Symmetry operator			Code	Symmetry operator		
None	x,	y,	z	e	$1+x$,	$1+y$,	z
a	$1+x$,	y,	z	f	$-x$,	$1/2+y$,	$-z$
b	x,	$1+y$,	z	g	$1-x$,	$1/2+y$,	$-z$
c	$-1+x$,	y,	z	h	$1-x$,	$1/2+y$,	$1-z$
d	x,	$-1+y$,	z	i	$1-x$,	$-1/2+y$,	$-z$

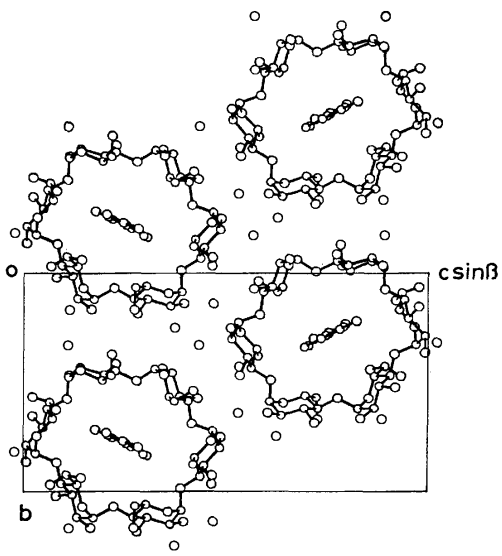

Fig. 6. Crystal structure viewed down along the a axis.

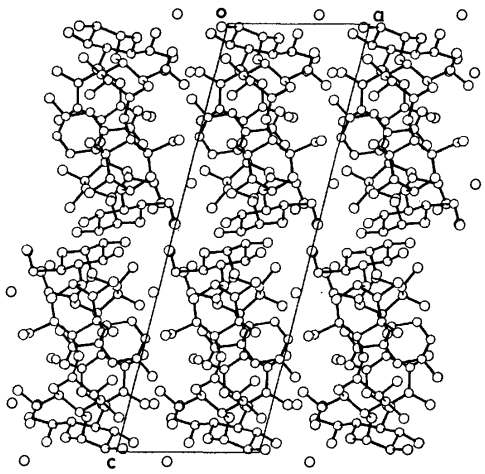

Fig. 7. Crystal structure viewed down along the b axis.

trin–polyiodide complexes,[10] where the extensive delocalization of electrons has been suggested as an explanation. In the *m*-nitroaniline complex, the charge-transfer may also occur through the hydrogen bond between the amino group and the nitro group.

Crystal Structure. Schematic drawings of the packing features of α-cyclodextrin molecules in the crystal are shown in Fig. 5. Projections of the crystal structure are given in Figs. 6 and 7. Intermolecular distances less than 3.0 Å are given in Table 4. Most of these contacts are considered to be hydrogen bonds. α-Cyclodextrin molecules are stacked along the a axis in head-to-tail fashion, thus forming an endless column. The packing of α-cyclodextrin molecules differes from other head-to-tail channel-type structures with the space group of $P2_12_12$,[2,11] in which the α-cyclodextrin molecule is located on the two-fold axis. On the other hand, the α-cyclodextrin ring in the *m*-nitroaniline complex is not perpendicular to the channel axis, but makes an angle of 79.0°. Owing to such a tilt of the α-cyclodextrin ring and the *gauche-gauche* conformation of the primary hydroxyl groups, intermolecular contacts between α-cyclodextrin molecules are quite different from those found in the $P2_12_12$ crystals. The adjacent α-cyclodextrin molecules along the channel are linked by O(2)···water···O(6) hydrogen bonds for G1, G4, and G6 residues and O(2)···water···O(5) hydrogen bonds for G2 and G3 residues, as well as by O(3)···O(6) hydrogen bonds for each glucose residue (Fig. 4). The O(2)···water···O(5) hydrogen bond is observed when the primary hydroxyl group is in the *gauche-trans* conformation. Neighboring α-cyclodextrin columns are closely packed in the crystal (Fig. 6) and are linked by hydrogen bonds directly or through water molecules. On the other hand, such close packing is not found in the $P2_12_12$ crystals, in which there is a sufficient intermolecular space to accommodate a part of the guest molecules. Water molecules fill intermolecular spaces. They are separated into two groups. W1, W2, and W5 are located in the space encircled by G4, G5, and G6 residues. They are connected to each other by a W1···W2···W5 hydrogen-bonding linkage. On the other hand, W3, W4, and W6, which are also linked by hydrogen bonds, are surrounded by G1, G2, and G3 residues.

The author wishes to thank Dr. Hisashi Uedaira for supporting this study. The computation was done on a HITAC M-160II computer in our laboratory.

References

1) M. L. Bender and M. Komiyama, "Cyclodextrin Chemistry," Springer-Verlag, New York (1978).
2) K. Harata, H. Uedaira, and J. Tanaka, *Bull. Chem. Soc. Jpn.*, **51**, 1627 (1978).
3) K. Harata, *Bull. Chem. Soc. Jpn.*, **50**, 1416 (1977).
4) M. Komiyama and M. L. Bender, *J. Am. Chem. Soc.*, **99**, 8021 (1977).
5) K. Harata, *Bull. Chem. Soc. Jpn.*, **48**, 2409 (1975).
6) W. Saenger, K. Beyer, and P. C. Manor, *Acta Crystallogr. Sect. B*, **32**, 120 (1976).
7) K. Harata, *Carbohydr. Res.*, **48**, 265 (1976).
8) "International Tables for X-Ray Crystallography," Vol. IV, Kynoch Press, Birmingham (1974), pp. 72—75.
9) K. Harata, *Bull. Chem. Soc. Jpn.*, **52**, 2451 (1979).
10) M. Noltemeyer and W. Saenger, *Nature*, **259**, 629 (1976).
11) K. Harata, *Bull. Chem. Soc. Jpn.*, **50**, 1259 (1977).

Raman Spectra of Cobalt(III) Complexes. II. Nitroammine Series of Cobalt(III) Complexes

Kan KANAMORI,* Tsutomu MORIKAWA, and Kiyoyasu KAWAI
Department of Chemistry, Faculty of Science, Toyama University, Gofuku, Toyama 930
(Received March 22, 1980)

Solid and aqueous Raman spectra of the nitroammine series of cobalt(III) complexes, $[Co(NO_2)_n(NH_3)_{6-n}]^{(3-n)+}$ (n=1—6), have been measured for the region of 1500—100 cm^{-1}. The assignments of the Raman bands due to the skeletal vibrations of the complexes have been made on an empirical basis and compared with those of the infrared bands in the literature.

Infrared investigations[1-3] of the nitroammine series and the halogenoammine series of cobalt(III) complexes, including normal coordinate treatments by Nakagawa and Shimanouchi,[2,3] have offered interesting problems in the study of coordination bonds as well as in the stereoisomerism. The facial isomer of trinitrotriamminecobalt(III) was synthesized very recently,[4] though *cis*-tetranitrodiamminecobaltate(III) has not yet obtained.

Recently, the Raman spectra of the halogenoammine series have been measured by Swaddle *et al.*[5] and Loehr *et al.*[6] and the assignments of the infrared bands have been reexamined. Therefore, a detailed Raman study of the nitroammine series seems to be required for the full assignments of the skeletal vibrations of the complexes; brief communications for *trans*-$[Co(NO_2)_4(NH_3)_2]^-$ [7] and $[Co(NO_2)_6]^{3-}$ [8,9] have already appeared.

In the present work, we have measured the solid and the aqueous Raman spectra of the nitroammine series of cobalt(III) complexes and reinvestigated the assignments of the skeletal vibrations. We have also studied the intra-ligand vibrations of the *N*-deuterated complexes in D_2O, for which the overlapping of the bands due to the ammine and the nitro groups are eliminated.

Experimental

fac-Trinitrotriamminecobalt (III) was prepared by the method of Siebert.[4] Potassium pentanitroamminecobaltate (III) was prepared by the method of Shibata *et al.*[10] All other complexes were prepared by standard means. All the complexes were identified by the visible and ultraviolet spectra and by elemental analysis. *mer*- and *fac*-trinitrotriamminecobalt (III) complexes were also identified by the ^1H-NMR spectra.

The Raman spectra were recorded for the region lower than 1500 cm^{-1} on a JASCO R-800 Raman spectrometer with a data processor, using a He–Ne (632.8 nm) laser as an excitation source. The spectra observed in the low frequency region are shown in Fig. 1. The infrared spectra were recorded on a JASCO A-3 and Hitachi FIS infrared spectrometer. The observed frequencies were calibrated by those of indene for the Raman spectra and those of polystylene film for the infrared spectra. The observed frequencies are accurate within ± 2 cm^{-1}.

Results and Discussion

Intra-ligand Vibrations. The assignment of the vibrations due to ammine or nitro groups of coordination compounds has already established by many authors.[11] Table 1 summarizes the observed frequencies for the *N*-deuterated nitroammine cobalt(III) complexes in D_2O and their approximate modes.

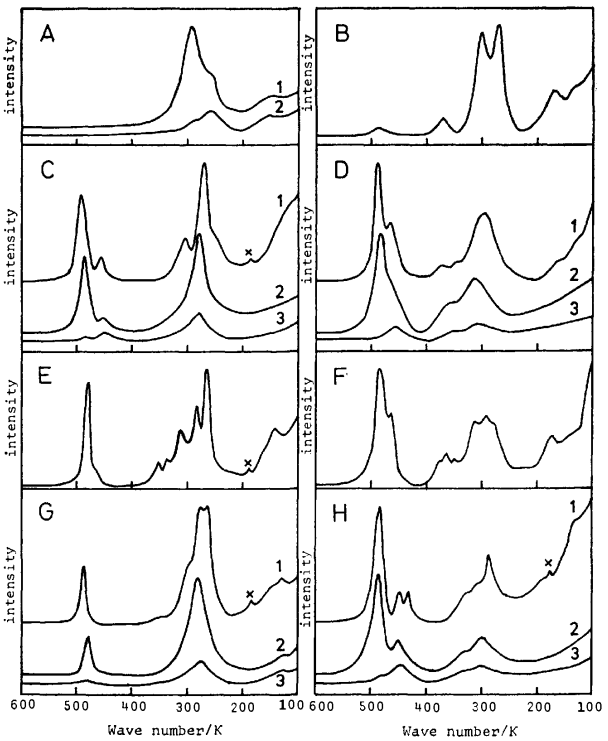

Fig. 1. Raman spectra of nitroammine cobalt (III) complexes. A: $Na_3[Co(NO_2)_6]$ in aqueous solution, //1, ⊥2. B: $K_2[Co(NO_2)_5(NH_3)]$ in solid state. C: *trans*-$[Co(NO_2)_2(NH_3)_4]NO_3$ in solid state, 1 and the fluoride in aqueous solution, //2, ⊥3. D: *cis*-$[Co(NO_2)_2(NH_3)_4]NO_3$ in solid state, 1 and the fluoride in aqueous solution, //2, ⊥3. E: *mer*-$[Co(NO_2)_3(NH_3)_3]$ in solid state. F: *fac*-$[Co(NO_2)_3(NH_3)_3]$ in solid state. G: *trans*-$NH_4[Co(NO_2)_4(NH_3)_2]$ in solid state, 1 and in aqueous solution, //2, ⊥3. H: $[Co(NO_2)(NH_3)_5]Br_2$ in solid state, 1 and the fluoride in aqueous solution, //2, ⊥3. x; no lasing line.

It is very interesting to compare the spectra of *trans* and *cis* isomers of $[Co(NO_2)_2(NH_3)_4]^+$ with a view toward differentiating between the geometric isomers. Faust and Quagliano[12] compared the solid infrared spectra of the isomeric pair. However, no essential difference was found between the spectra of the isomers, though the spectrum of the *cis* isomer is slightly more complicated than that of the *trans* isomer. The *cis* isomer of $[Co(NO_2)_2(NH_3)_4]^+$ shows two Raman bands

TABLE 1. OBSERVED FREQUENCIES (cm^{-1}) AND APPROXIMATE MODES OF THE INTRA-LIGAND VIBRATIONS OF *N*-DEUTERATED NITROAMMINE COBALT(III) COMPLEXES IN D_2O

Complex	Method	$\nu(N-O)_{as}$	$\nu(N-O)_s$	$\delta(ND_3)_s$	$\nu(NO_2)$
$[Co(NO_2)(ND_3)_5]^{2+}$	Raman	1424 vw, p	1333 m,p	1055 m,p 1015 w,dp	827 s,p
	IR	1423 s	1332 m	1025 m	827 w
trans-$[Co(NO_2)_2(ND_3)_4]^+$	Raman	1411 w,p	1340 m,p	1033 m,p 1003 w,dp	824 s,p
	IR	1422 m	1324 s	1016 m	826 m
cis-$[Co(NO_2)_2(ND_3)_4]^+$	Raman	1417 vw	1345 w,dp 1317 m,p	1037 w,p 1010 w,dp	833 s,p 827 w,dp
	IR	1425 s	1344 m 1315 s	1008 w	827 w
trans-$[Co(NO_2)_4(ND_3)_2]^-$	Raman	1408 vw,p	1357 w,dp 1308 m,p	988 vw	831 s,p 821 m,dp
	IR	1436 s	1319 s	982 vw	828 w

(one polarized and another depolarized) in both the NO_2 symmetric stretching and the NO_2 bending vibration regions; three of the four bands have counterparts in the infrared spectrum. On the other hand, the *trans* isomer shows only one band in each region of the Raman and infrared spectra; here the mutual exclusion is found.

The mutual exclusion is also found for *trans*-$[Co(NO_2)_4(NH_3)_2]^-$. If it is assumed that this complex has a D_{4h} molecular symmetry, the NO_2 symmetric stretching and the NO_2 bending vibrations transform as $(A_{1g}+B_{1g}+E_u)$. This complex shows two Raman bands but only one infrared band in the NO_2 symmetric stretching and in the NO_2 bending vibration regions. The infrared frequency in each region does not coincide with either of the two Raman frequencies; this is consistent with the molecular symmetry assumed for the complex. In conclusion, it seems to be useful for differentiation of stereoisomers of nitrocomplexes to study the aqueous Raman and infrared spectra in the NO_2 symmetric stretching and the NO_2 bending vibration regions.

No useful aqueous Raman and infrared spectra have been observed for *mer*- and *fac*-$[Co(NO_2)_3(NH_3)_3]$ because of the low solubilities of the complexes in H_2O nor for $K_2[Co(NO_2)_5(NH_3)]$ because of the instability in water. No essential difference was found between the solid Raman spectra of the isomeric pair of $[Co(NO_2)_3(NH_3)_3]$. (see Table 2)

Skeletal Vibrations. Nakagawa and Shimanouchi[2] have studied the solid infrared spectra of the nitroammine series of cobalt(III) complexes and have performed a normal coordinate analysis for $[Co(NO_2)_6]^{3-}$, $[Co(NO_2)(NH_3)_5]^{2+}$, and *trans*- and *cis*-$[Co(NO_2)_2(NH_3)_4]^+$ complexes.

In order to assign the observed Raman bands in this region, we will use two qualitative band intensity criteria. One is concerned with deformation vibrations. The skeletal bending vibrations of $[Co(NH_3)_6]^{3+}$ and $[Co(NO_2)_6]^{3-}$ appear as very weak and diffused bands in the aqueous Raman spectra.[5,13] Rocking vibrations of nitro groups of $[Co(NO_2)_6]^{3-}$ were not observed in the Raman spectrum.[9] So we can expect similar band profiles and intensities for the skeletal bending and nitro rocking vibrations of the nitroammine complexes. Therefore, the strong bands near 300 cm^{-1} in the aqueous Raman spectra of the nitroammine complexes will be confidently assigned to cobalt-nitro stretching vibrations, though skeletal bending and nitro rocking vibrations are expected to be in the same region.

Another criteria is concerned with stretching vibrations. Table 3 shows symmetry correlations related to metal-ligand stretching vibrational modes among $[Co(NH_3)_6]^{3+}$ (O_h), *trans*-$[Co(NO_2)_2(NH_3)_4]^+$ (D_{2h}), and $[Co(NO_2)(NH_3)_5]^{2+}$ (C_{2v}). For instance, the B_1 and B_2 modes due to the four equatorial Co–NH_3 bonds in C_{2v} symmetry, though formally Raman-allowed, correlate with the B_{2u} and B_{3u} modes in D_{2h} symmetry, respectively, so we expect that they will be hardly

TABLE 2. OBSERVED FREQUENCIES (cm^{-1}) AND APPROXIMATE MODES OF THE INTRA-LIGAND VIBRATIONS OF *mer*- AND *fac*-$[Co(NO_2)_3(NH_3)_3]$

Isomer	$\nu(N-O)_{as}$	$\nu(N-O)_s$ $\delta(NH_3)_s$	$\delta(NO_2)$ $\delta(NH_3)_r$
mer	1415 sh	1359 w	832 m
	1400 w	1320 sh	817 vs
		1316 s	
		1285 m	
fac	1430 sh	1355 w	834 s
	1410 w	1313 s	824 s
	1388 w	1288 s	

TABLE 3. SYMMETRY CORRELATIONS RELATED TO THE METAL-LIGAND STRETCHING VIBRATIONS OF $[Co(NH_3)]^{3+}$ (O_h), *trans*-$[Co(NO_2)_2(NH_3)_4]^+$ (D_{2h}), AND $[Co(NO_2)(NH_3)_5]^{2+}$ (C_{2v})[a]

O_h	D_{2h}	C_{2v}
A_{1g} ν(Co–N)	A_g ν(Co–N)	A_1 $\nu(Co-N)_{eq}$
	A_g ν(Co–N′)	A_1 $\nu(Co-N)_{ax}$
		A_1 ν(Co–N′)
E_g ν(Co–N)	B_{1g} ν(Co–N)	A_2 $\nu(Co-N)_{eq}$
	B_{1u} ν(Co–N′)	
F_{2u} ν(Co–N)	B_{2u} ν(Co–N)	B_1 $\nu(Co-N)_{eq}$
	B_{3u} ν(Co–N)	B_2 $\nu(Co-N)_{eq}$

a) N and N′ stand for NH_3 and NO_2 groups, respectively.

Table 4. Observed frequencies (cm^{-1}) and assignments of the skeletal vibrations of *trans*-$[Co(NO_2)_2(NH_3)_4]^+$ and *trans*-$[Co(NO_2)_4(NH_3)_2]^-$

trans-$[Co(NO_2)_2(NH_3)_4]^+$				*trans*-$[Co(NO_2)_4(NH_3)_2]^-$			
Solid[a]	Solution[b]	Assignment[c]	(D_{2h})	Solution[b]		Assignment[c]	(D_{4h})
492 s	485(453) s,p	ν(Co–N)	A_g	479(453)	s,p	ν(Co–N)	A_{1g}
461 w	453(419) w,dp	ν(Co–N)	B_{1g}				
308 m		δ(N–Co–N)	A_g				
272 vs	281(281) s,p	ν(Co–N′)	A_g	282(283)[d]	vs,p	ν(Co–N′)	A_{1g}
				276(276)[e]	w,dp	ν(Co–N′)	B_{1g}
240 sh		ν(N–Co–N′)	B_{2g} B_{3g}				
				128(129)	w,dp	δ(N′–Co–N′)	B_{2g}
121 vw		lattice vib.					

a) For nitrate. b) For *N*-deuterated compound in parenthesis. c) N and N′ stand for NH_3 and NO_2 groups, respectively. d) Peak frequency in the isotropic spectrum, e) Peak frequency in the anisotropic spectrum.

detectable in the Raman spectrum of $[Co(NO_2)(NH_3)_5]^{2+}$.

$[Co(NO_2)_6]^{3-}$: The Raman spectra of $[Co(NO_2)_6]^{3-}$ have been studied for the potassium salt by Nakagawa[9] and for the sodium salt and the aqueous solution by Krasser.[8] Krasser[8] has reported the Raman bands at 410, 300, 245, 175, and 150 cm^{-1} for the complex in aqueous solution. We have observed only three bands in this region of the aqueous spectrum (see Fig. 1A). The most intense and polarized band at 292 cm^{-1}, the somewhat intense and depolarized band at 262 cm^{-1}, and the weak and depolarized band at 158 cm^{-1} are assigned, respectively, to the $\nu(Co–NO_2)$ A_g, the $\nu(Co–NO_2)$ E_g, and the $\delta(NO_2–Co–NO_2)$ F_g modes; this assignment is consistent with the assignment of the solid spectrum by Nakagawa.[9] The weak shoulder near 230 cm^{-1} is attributed to a degradation product, since the relative intensity of the shoulder increased with time.

trans- *and* cis-*$[Co(NO_2)_2(NH_3)_4]^+$* *and* trans-*$[Co(NO_2)_4(NH_3)_2]^-$*: The observed frequencies and assignments of the skeletal vibrations for *trans*-$[Co(NO_2)_2(NH_3)_4]^+$ and *trans*-$[Co(NO_2)_4(NH_3)_2]^-$ are summarized in Table 4 and those for *cis*-$[Co(NO_2)_2(NH_3)_4]^+$ in Table 5.

The X-ray study[14] for *trans*-$[Co(NO_2)_2(NH_3)_4]NO_3 \cdot H_2O$ shows that this complex has approximately D_{2h} symmetry, with the first mirror containing the two nitro groups, the second containing the four nitrogens of the ammine groups and the last perpendicular to the other mirrors.

There appears to be no previous Raman study of this complex. If it is assumed that this complex possesses an idealized D_{2h} molecular symmetry, the metal-ligand stretching vibrations transform as shown in Table 3, with the g modes being Raman active and the u modes being infrared active. The aqueous Raman spectrum has a very simple shape (see Fig. 1C) and can be easily assigned on the basis of polarization measurements and comparison with the assignments of $[Co(NH_3)_6]^{3+}$ and $[Co(NO_2)_6]^{3-}$.

The X-ray study[15] for *cis*-$[Co(NO_2)_2(NH_3)_4]NO_3$ shows that this complex actually has a lower symmetry than C_{2v}. However, if it is assumed that this complex possesses an idealized C_{2v} symmetry, the cobalt-ligand stretching vibrations transform as $(2A_1+B_1+B_2$ for $\nu(Co–NH_3))$, and $(A_1+B_1$ for $\nu(Co–NO_2))$, all of which are Raman and infrared active. According to the normal coordinate analysis[2] based on the C_{2v} symmetry of this complex, the frequency order of the four $\nu(Co–NH_3)$ is $B_2>A_1>B_1>A_1$. The most strong and polarized band at 483 cm^{-1} is assigned to the A_1 mode

Table 5. Observed frequencies (cm^{-1}) and assignment of *cis*-$[Co(NO_2)_2(NH_3)_4]^+$

Raman				IR[d]	Assignment[e]	(C_{2v})
Solid[a]	Solid[b]	Solution[c]				
				519 m	ν(Co–N)	B_2
483 vs	485 vs	483(449)	vs,p	486 m	ν(Co–N)	A_1
464 m	464 m	459(425)[g]	sh,dp	463 s	ν(Co–N)	B_1
	445 sh			447 m	ν(Co–N)	A_1 ?
370 w				380 w	skel. def.	
350 w	358 m	357(350)	w,p	358 w	skel. def.	
310 sh	320 sh	310(317)[f]	w,dp	318 vs	ν(Co–N′)	A_1
298 s	303 s	303(310)[g]	w,dp	296 vs	ν(Co–N′)	B_1
		(268)	w,dp		skel. def.	
				153 s	lattice vib.	
128 vw	133 vw			120 m	lattice vib.	

a) For nitrate. b) For chloride. c) For *N*-deuterated compound in parenthesis. d) For chloride. e) N and N′ stand for NH_3 and NO_2 groups, respectively. f) Peak frequency in the isotropic spectrum. g) Peak frequency in the anisotropic spectrum.

of higher frequency. Nakagawa and Shimanouchi[2] have assigned the infrared band at 385 cm^{-1} to another A_1 mode. This frequency seems to be rather low for $\nu(Co-NH_3)$ and we have observed no distinct Raman band near 385 cm^{-1}. This A_1 mode may be assigned to the shoulder near 445 cm^{-1} observed in the solid Raman spectrum of *cis*-$[Co(NO_2)_2(NH_3)_4]Cl$; this would be consistent with the assignment for the Raman spectrum of *cis*-$[CoCl_2(NH_3)_4]Cl$,[5] where the band at 435 cm^{-1} has been assigned to the corresponding mode. The B_2 mode has been assigned to the infrared band at 518 cm^{-1},[2] but no distinct Raman band has been observed at the frequency. The Raman intensity of this mode is expected to be rather weak, because this mode corresponds to an antisymmetric cobalt-ammine stretching vibration of the linear NH_3–Co–NH_3 moiety.

The peak frequency of the band near 310 cm^{-1} in the isotropic spectrum of *cis*-$[Co(NO_2)_2(NH_3)_4]^+$ is 7 cm^{-1} higher than that in the anisotropic one. This discrepancy of the band maxima suggests that the band near 310 cm^{-1} consists of two components. The polarized component at 310 cm^{-1} and the depolarized component at 303 cm^{-1} are assigned to the $\nu(Co-NO_2)$ A_1 and B_1 modes, respectively.

It is interesting to compare the Raman and infrared spectra of *trans*- and *cis*-$[Co(NO_2)_2(NH_3)_4]^+$. The coincidence of the Raman frequencies with the infrared ones has not been found in the *trans* isomer, but in the *cis* isomer (see Table 5). The relative intensity of the Raman band due to $\nu(Co-NO_2)$ is stronger in the *trans* isomer than in the *cis* isomer (see Figs. 1C and D). A similar intensity difference of $\nu(Co-NO_2)$ between isomeric pairs is also found in *mer*- and *fac*-$[Co(NO_2)_3(NH_3)_3]$.

The X-ray study[16] for *trans*-$NH_4[Co(NO_2)_4(NH_3)_2]$ shows that the four nitro groups are tilted 56°, 42°, 48°, and 86° to the square plane and actually this complex has no center of symmetry. This lowering of the molecular symmetry in solid state is reflected in the complexity of the spectral features. The observed data are listed in an Appendix. On the other hand, in aqueous solution this complex can be assumed to possess a D_{4h} symmetry as stated above, and so one can expect that there will appear two bands (one polarized and another depolarized) due to the $\nu(Co-NO_2)$ and one polarized band due to the $\nu(Co-NH_3)$ in the Raman spectrum. The aqueous Raman spectrum exhibits two bands which can be attributed to the $\nu(Co-NO_2)$ and the $\nu(Co-NH_3)$, respectively. However, the discrepancy between the peak frequencies of the $\nu(Co-NO_2)$ of the isotropic and the anisotropic spectra suggests that two Raman bands are overlapped. The polarized component at 282 cm^{-1} and the depolarized component at 276 cm^{-1} are assigned to the $\nu(Co-NO_2)$ A_g and B_{1g} modes, respectively. The polarized band at 479 cm^{-1} is unambiguously assigned to the $\nu(Co-NH_3)$ A_g mode. Accordingly, the aqueous Raman spectrum of *trans*-$[Co(NO_2)_4(NH_3)_2]^-$ is explained reasonably in terms of D_{4h} symmetry in the skeletal vibration as well as in the intra-ligand vibration regions.

$[Co(NO_2)(NH_3)_5]^{2+}$ and $[Co(NO_2)_5(NH_3)]^{2-}$: The X-ray study[17] for $[Co(NO_2)(NH_3)_5]Br_2$ shows that the virtual symmetry of this complex is very close to C_{2v}, with one of the mirrors containing the NO_2 group and bisecting the NH_3–Co–NH_3 angle. On the basis of C_{2v} symmetry for this complex, the metal-ligand stretching vibrations transform as shown in Table 3, with all modes being Raman active and all but the A_2 mode being infrared active. However, we can hardly expect the Raman bands corresponding to the B_1 and B_2 modes due to the stretching vibrations of the equatorial ammine groups, according to the qualitative band intensity criteria discussed above.

The observed frequencies and the assignment of $[Co(NO_2)(NH_3)_5]^{2+}$ are summarized in Table 6 along with the infrared data. The somewhat intense band near 450 cm^{-1} is unambiguously assigned to the $\nu(Co-NH_3)_{eq}$ A_2 mode since this band is depolarized and has no counterpart in the infrared spectrum. The most intense band near 490 cm^{-1} is assigned to the $\nu(Co-NH_3)_{eq}$ A_1 mode on the basis of the correlation with the $\nu(Co-NH_3)$ A_{1g} mode of *trans*-$[Co(NO_2)_2(NH_3)_4]^+$, though the corresponding infrared band has been assigned to the $\nu(Co-NH_3)_{ax}$.[2] Our assignment is consistent with that for the $\nu(Co-NH_3)_{eq}$ of $[CoCl(NH_3)_5]^{2+}$ proposed by Swaddle *et al.*[5] and Loehr *et al.*[6] These authors have assigned the $\nu(Co-NH_3)_{ax}$ A_1 mode of $[CoCl(NH_3)_5]^{2+}$ to the medium band at 463 cm^{-1}. By the comparison

TABLE 6. OBSERVED FREQUENCIES (cm^{-1}) AND ASSIGNMENT OF $[Co(NO_2)(NH_3)_5]^{2+}$

Raman			IR[d]	Assignment[e]	(C_{2v})
Solid[a]	Solid[b]	Solution[c]			
			496 m	$\nu(Co-N)_{eq}$	B_1, B_2
482 vs	487 vs	485(453) vs,p	486 sh	$\nu(Co-N)_{eq}$	A_1
	460 sh		460 w	$\nu(Co-N)_{ax}$	A_1 ?
448 w	446 m	448(416) m,dp		$\nu(Co-N)_{eq}$	A_2
429 w					
			359 sh	skel. def.	
330 sh	340 sh	342(326) w,p	336 m	skel. def.	
310 sh				skel. def.	
287 m	299 m	303(285) m,p	294 s	$\nu(Co-N')$	A_1
132 vw	130 vw		140 s	lattice vib.	

a) For bromide. b) For nitrate. c) For *N*-deuterated compound in parenthesis. d) For nitrate. e) N and N′ stand for NH_3 and NO_2 groups, respectively.

with the assignment, the shoulder near 460 cm^{-1}, which is observed in the solid Raman spectrum of $[Co(NO_2)(NH_3)_5](NO_3)_2$, may be assigned to the $\nu(Co-NH_3)_{ax}$ A_1 mode. The band at 429 cm^{-1} of the solid Raman spectrum of nitropentaamminecobalt(III) bromide or chloride has not been observed for the aqueous solution nor for the nitrate, though the corresponding band has been observed for the infrared spectrum.[2] This band is rather low in the frequency for $\nu(Co-NH_3)$ and may not be a fundamental vibration.

No X-ray study has been done for $K_2[Co(NO_2)_5(NH_3)]$. The observed frequencies of the solid Raman spectrum are listed in the Appendix. The band at 488 cm^{-1} is confidently assigned to the $\nu(Co-NH_3)$. However, a detailed assignment of other bands is difficult, since a useful aqueous Raman spectrum could not be obtained because of the fast decomposition in water. In the aqueous Raman spectrum, the band at 488 cm^{-1} disappears and a new band appers at 467 cm^{-1}.

Table 7. Observed frequencies (cm^{-1}) and approximate mode of *mer* and *fac* isomers of $[Co(NO_2)_3(NH_3)_3]$

mer(C_{2v})		*fac*(C_{3v})		Assignment[b]
Solid	Solution[a]	Solid	Solution[a]	
482 vs	481 vs,p	489 vs	480 vs,p	ν(Co–N) A_1
470 sh	470 sh,dp	468 m	472 m,dp	ν(Co–N) B_1 for *fac.* ν(Co–N) E for *mer.*
		381 vw		skel. def. and ν(Co–N′)
352 m		363 m		
340 vw		347 w		
320 m		315 m		
285 s		291 m		
266 vs		271 m		
		179 m		lattice vib.
137 m		125 vw		

a) For DMSO solution. b) N and N′ stand for NH_3 and NO_2 groups, respectively.

mer- *and* fac-$[Co(NO_2)_3(NH_3)_3]$: The X-ray study[18] for the *mer* isomer shows that this complex has a lower symmetry than C_{2v}. No X-ray study has been reported for the *fac* isomer. We have observed the Raman spectrum of dimethylsulfoxide solution of each isomer because of the low solubility of these complexes in water. The observed frequencies and the tentative assignments are summarized in Table 7. As explained for the relative intensities of $\nu(Co-NO_2)$ of *trans*- and *cis*-$[Co(NO_2)_2(NH_3)_4]^+$, the *mer* isomer, which contains *trans* nitro groups, exhibits a very strong band due to $\nu(Co-NO_2)$, while the *fac* isomer, which contains *cis* nitro groups only, exhibit medium or weak bands (see Figs. 1E and F).

The authors are indebted to professor Yoichi Shimura of Osaka University and Dr. Isao Kanesaka of our university for their valuable discussions.

Appendix

The solid Raman data of $K_2[Co(NO_2)_5(NH_3)]$: 1400 vw, 1317 s, 836 s, 821 vs, 488 w, 383 sh, 373 w, 304 s, 273 s, 171 m, 133 w (cm^{-1}); of $NH_4[Co(NO_2)_4(NH_3)_2]$: *ca.* 1400 sh, 1360 w, 1307 s, *ca.* 1290 sh, 828 s, 817 s, 485 s, 349 w, 299 m, 277 s, 264 s, 176 w, 157 w, 128 w (cm^{-1}).

References

1) T. Shimanouchi and I. Nakagawa, *Inorg. Chem.*, **3**, 1805 (1964).
2) I. Nakagawa and T. Shimanouchi, *Spectrochim. Acta, Part A*, **23**, 2099 (1967).
3) I. Nakagawa and T. Shimanouchi, *Spectrochim. Acta*, **22**, 759 (1966).
4) H. Siebert, *Z. Anorg. Allg. Chem.*, **441**, 47 (1978).
5) T. W. Swaddle, P. J. Craig, and P. M. Boorman, *Spectrochim. Acta, Part A*, **26**, 1599 (1970).
6) T. M. Loehr, J. Zinich, and T. V. Long, *Chem. Phys. Lett.*, **7**, 183 (1970).
7) B. Belsot and P. Devrainne, *C. R. Acad. Sci., Ser. C*, **272**, 1454 (1971).
8) W. Krasser, *Z. Naturforsch., Teil A*, **24**, 1667 (1969).
9) I. Nakagawa, *Can. J. Spectrosc.*, **18**, 1 (1973).
10) M. Shibata, M. Mori, and E. Kyuno, *Inorg. Chem.*, **3**, 1573 (1964).
11) K. Nakamoto, "Infrared and Raman Spectra of Inorganic and Coordination Compounds," 3rd ed, Wiley-Interscience, New York (1978).
12) J. P. Faust and J. V. Quagliano, *J. Am. Chem. Soc.*, **76**, 5346 (1954).
13) H. Siebert and H. H. Eysel, *J. Mol. Struct.*, **4**, 29 (1969).
14) I. Oonishi, F. Muto, and Y. Komiyama, *Bull. Chem. Soc. Jpn.*, **42**, 2791 (1969).
15) I. Oonishi, H. Fujimaki, F. Muto, and Y. Komiyama, *Bull. Chem. Soc. Jpn.*, **43**, 733 (1970).
16) Y. Komiyama, *Bull. Chem. Soc. Jpn.*, **30**, 13 (1957).
17) F. A. Cotton and W. T. Edwards, *Acta Crystallogr., Sect. B*, **24**, 474 (1968).
18) Y. Tanito, Y. Saito, and H. Kuroya, *Bull. Chem. Soc. Jpn.*, **25**, 188 (1952).

Solvent Induced Structural Change of 18-Crown-6 Complexed Ion Pair with 9-Fluorenone Anion Radical as Studied by ESR Spectroscopy

Kazuo NAKAMURA

Department of Chemistry, Nagoya Institute of Technology, Gokiso-cho, Showa-ku, Nagoya 466

(Received March 24, 1980)

ESR spectra of the ion pairs of the 9-fluorenone anion radical with 18-crown-6 complexed sodium and potassium ions were examined. From the dependence of the carbonyl ^{13}C hyperfine splitting of the fluorenone anion on temperature and solvent, it was conclude that an ethereal solvent molecule can solvate the crown complexed cation on the opposite side of the anion with respect to the plane of the crown ether ring, equilibrium taking place between the solvated and unsolvated ion pairs in ethereal solution. The unsolvated species of both the potassium and the sodium ion pairs and the solvated species of the sodium ion pair are classified as contact ion pairs, the solvated species of the potassium ion pair a crown separated one. The equilibrium constant between the solvated and unsolvated ion pairs changes with temperature and solvent. From this change the enthalpy changes of solvation process were estimated for several solvents.

Recently interest has been focused on the high complexing ability of macrocyclic polyethers (crown ethers) with respect to the alkali metal ions. Since crown ethers form two dimensional complexes with cations in most cases, a counteranion and other donor molecules are capable of interacting with the cation on either or both sides of the plane of the crown ether ring, as demonstrated by X-ray crystallographic studies of a number of crown complexed inorganic salts.[1,2] This behavior of the complexes will be observed in solution.

Crown complexes alkali metal ions exist as ion pairs in ethereal solvents.[3-6] In these ion pairs it is possible that ethereal molecules can participate in coordination of the cation, since ethereal molecules are very strong cation-complexing agents[7] and one side of the two dimensional crown complex is occupied by a counteranion but the other is vacant. If this is the case, the structure of the ion pair in ethereal solvents would differ to some extent from those in solvents incapable of participating in coordination.

This paper deals with the solvation phenomena of the crown complexed ion pairs, on the basis of ESR studies of the 9-fluorenone anion radical forming an ion pair with 18-crown-6 complexed sodium and potassium ions. The carbonyl ^{13}C hyperfine splitting of the fluorenone anion is sensitive to environmental conditions, reflecting the structural changes of the ion pairs caused by cation solvation.

Experimental

Solvents. Ethereal solvents and toluene were used after being dried with sodium hydride or Na–K alloy.

Material. 15-Crown-5 and 18-crown-6 ethers (M. E. Merck) were used without further purification.

Preparation of the Anion Radical. The anion was prepared by reduction of 9-fluorenone with sodium or potassium mirror in a solution containing excess crown ether. All the operations were carried out in a high vacuum.

Measurements of ESR Spectra. A JES-PE ESR spectrometer, equipped with a magnet of a 10 in diameter pole piece and with a JES-VT-3A2 variable temperature controller was used.

Results and Discussion

Solvent Effect on the 18-Crown-6 Complexed Ion Pair. The carbonyl ^{13}C hyperfine splitting (a_C) of the fluorenone anion radical forming the ion pair with 18-crown-6 (C-6) complexed sodium ion shows an appreciable solvent dependence, ranging from 4.21 G in tetrahydrofuran (THF) to 5.00 G in toluene, diethyl ether and diisopropyl ether (Table 1). Since ethereal solvents solvate anions weakly and cations strongly, it is reasonable to assume that the solvent effect can be attributed to the difference of solvent in cation solvating power. It has been found that a_C increase with increasing cationic field acting on the carbonyl group,[8-10] the cationic field decreasing with increase in the separation between the cation and the anion. The observed decrease of a_C from toluene to THF certainly arises from the increase in the cation-anion separation caused by enhancement of cation solvation. Thus, the solvent order of decreasing a_C corresponds to that of increasing cation solvation. The solvent order of cation solvation (Table 1) differs somewhat from that observed in most cases. Polydentate solvents such as 1,2-dimethoxyethane and diglyme usually show stronger cation solvation than monodentate solvents such as THF and tetrahydropyran.[11,12] In the present system, however, the order is reversed. This suggests that the polydentate

Table 1. Solvent data on ^{13}C hfs (a_c) and ratio of solvated to unsolvated species (K) for sodium ion pair at 20 °C

Solvent	a_c(G)	K
Tetrahydrofuran	4.21	2.93
Tetrahydropyran	4.48	0.96
2-Methyltetrahydrofuran	4.51	0.86
Dioxane	4.58	0.66
1,2-Dimethoxyethane	4.58	0.66
Diglyme	4.59	0.63
1,2-Diethoxyethane	4.78	0.26
2,5-Dimethyltetrahydrofuran	4.85	0.16
Diisopropyl ether	5.00	0
Diethyl ether	5.00	0
Toluene	5.00	0

character of solvent does not work effectively, probably because most part of the coordination sphere around the cation is already occupied by the carbonyl and 18-crown-6 oxygen atoms, and the residual part can not allow more than one oxygen atom of solvent to coordinate the cation. This also indicates that only one solvent molecule can solvate the crown complexed cation forming the ion pair.

Since it is unreasonable to assume any specific interaction between an alkali metal ion and a toluene molecule, the crown complexed ion pair in toluene would exist in unsolvated state. The fact that a_C in diethyl ether and diisopropyl ether is identical with a_C in toluene indicate that these solvents can not solvate the crown complexed cation in the present system.

Hyperfine splittings due to sodium were observed, irrespective of solvent. Addition of C-6 led to the increase of the sodium hyperfine splitting (a_{Na}) in a solvent, in contrast to the decrease of a_C (for example, in the THF solution, $a_{Na}=0.49$ G in the presence of C-6, while $a_{Na}=0.41$ G in the absence of C-6 at 20 °C).[13] Since the complex formation of a crown ether with a cation causes increase in the separation of the cation and the counteranion, the increase of a_{Na} observed suggests that factors other than the cation-anion separation play an important role for deciding the magnitude of a_{Na}.[10,13]

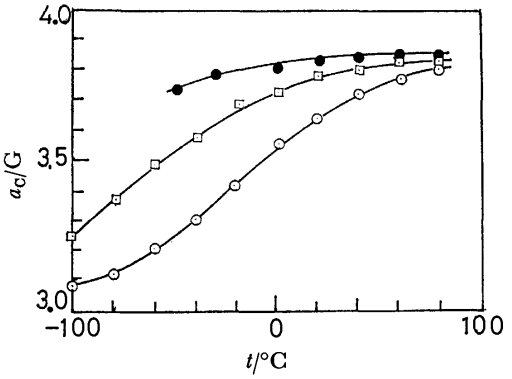

Fig. 1. Temperature dependence of the ^{13}C hfs in the fluorenone anion radical for potassium ion pair.
○: THF, □: MTHF, ●: DMTHF.

Temperature Dependence of a_C. The a_C values of both the potassium and the sodium ion pairs decrease with lowering in temperature, the magnitude of decrease varying with solvent. In a solvent with stronger cation solvation power a_C shows a larger temperature dependence. The change of a_C with temperature is significant in THF, but almost independent of temperature in diethyl ether. Figure 1 shows temperature *vs.* a_C curves of the C-6 complexed potassium ion pair in THF, 2-methyltetrahydrofuran (MTHF), and 2,5-dimethyltetrahydrofuran (DMTHF) in the temperature range −100 °C—+80 °C. At high temperature a_C of these three solutions approach each other, converging to the value nearly equal to a_C in diethyl ether ($a_C=3.90$ G); at low temperatures a_C in THF shows a value of lower limit ($a_C=3.05$ G). Similar features can be observed in the temperature *vs.* a_C curves of the C-6 complexed

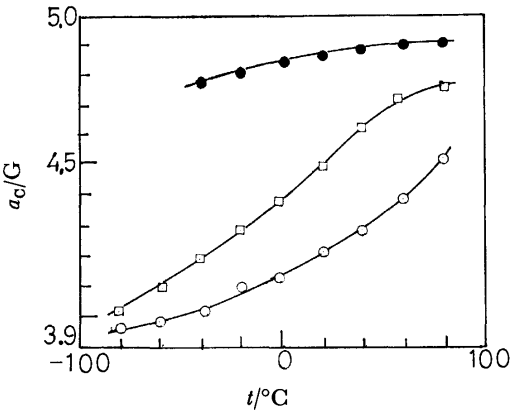

Fig. 2. Temperature dependence of the ^{13}C hfs in the fluorenone anion radical for sodium ion pair.
○: THF, □: MTHF, ●: DMTHF.

sodium ion pair (Fig. 2).

The temperature and solvent dependence of a_C could be explained in terms of the equilibrium between the solvent and unsolvated species of the C-6 complexed ion pair:

$$A^-M^+C + S \rightleftharpoons \underset{C}{A^-M^+S}, \quad (1)$$

where A^- is the fluorenone anion, M^+ an alkali metal ion, C a crown ether molecule, and S a solvent molecule. We always observe the average a_C of the solvated and unsolvated species, since the exchange rate between the both species is high in the ESR time scale. Since the solvation process is exothermic, the observed a_C approaches a_C of the unsolvated species at high temperature and a_C of the solvated species at low temperature. The equilibrium constant of Eq. 1 can be expressed by

$$K = (a_u - a_m)/(a_m - a_s), \quad (2)$$

where a_u and a_s are a_C of the unsolvated and solvated species respectively, and a_m is the observed splitting. a_u would be equal to a_C in toluene or diethyl ether, and a_s to or slightly smaller than the limiting value of a_C in THF at low temperatures. Therefore, substituting 5.00 G for a_u and 3.94 G for a_s in the sodium ion pair, and 3.90 G for a_u and 3.05 G for a_s in the potassium ion pair, we are able to calculate the equilibrium constant K of Eq. 1 by means of Eq. 2. The values of K at 20 °C for each solvent used are given in Table 1. The enthalpy change of the solvation process expressed by Eq. 1 can be estimated from the plots of ln K *vs.* $1/T$ for THF, MTHF, and DMTHF solutions of the sodium and potassium ion pairs (Table 2). The plots show that linearity holds between ln K and $1/T$ (Figs. 3 and 4).

A Possible Model. Possible models for solvation

Table 2. Enthalpy change (ΔH) of solvation process for sodium and potassium ion pairs

Solvent	ΔH (10^3 cal/mol)	
	Sodium	Potassium
Tetrahydrofuran	−3.4	−3.8
2-Methyltetrahydrofuran	−3.2	−2.6
2,5-Dimethyltetrahydrofuran	−1.4	−1.8

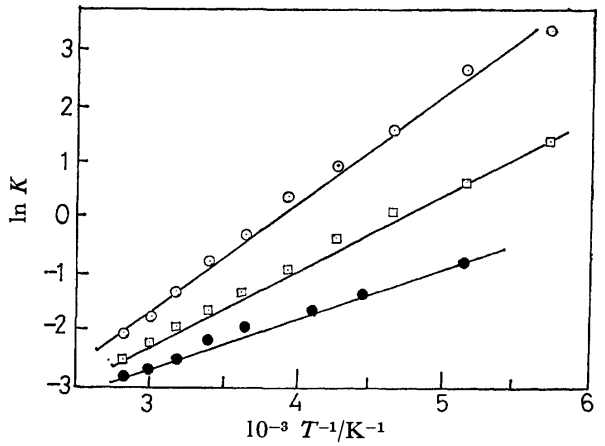

Fig. 3. Plots of ln K *vs.* $1/T$ for the potassium ion pair. The straight lines are obtained by the least squares method. ○: THF, □: MTHF, ●:DMTHF.

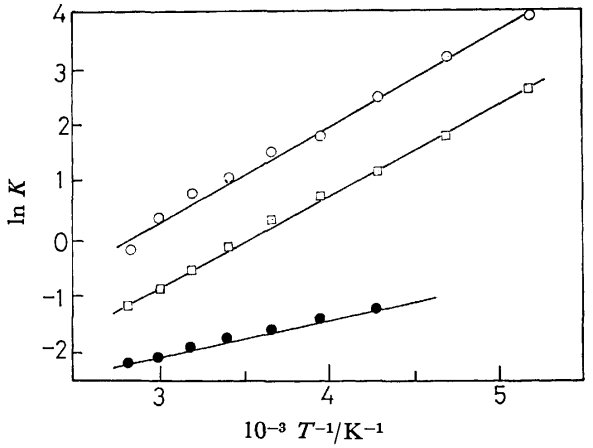

Fig. 4. Plots of ln K *vs.* $1/T$ for the sodium ion pair. The straight lines are obtained by the least squares method. ○: THF, □: MTHF, ●: DMTHF.

process of the crown complexed cation are schematically shown in Fig. 5. In the unsolvated ion pairs the cation is pulled out of the plane of the crown oxygen atoms toward the fluorenone anion (Fig. 5 (a)). When a solvent molecule solvates the cation on the opposite side of the anion with respect to the plane of the crown ether ring, the location of the cation shifts toward the center of the ring plane (Fig. 5 (b)), the cation being located on the other side of the anion with respect to the crown ether (Fig. 5 (c)). For both cases of solvation, a conformational change of the crown ether molecule would take place and the separation between the anion and the cation would increase due to steric hinderance of the crown ether. When the ion pairs are classified in terms of a contact and crown-separated ion pair, the species for Fig. 5 (a) and (b) should be referred to a contact ion pair, and the species for Fig. 5 (c) to a crown-separated one. Since the lower limit of a_C for the crown complexed sodium ion in THF (a_C=3.94 G) is close to the uncomplexed caesium ion pair in THF at 20 °C (a_C=3.90 G),[13] the solvated sodium ion pair can be classified as a contact ion pair and would have the structure of Fig. 5 (b). On the

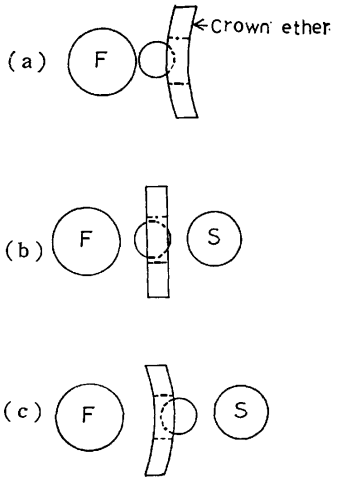

Fig. 5. Schematic representation for solvation process. Ⓕ: Fluorenone anion. Ⓢ: Solvent molecule. ○: Alkali metal cation.

other hand, the lower limit of a_C for the crown complexed potassium ion pair in THF (a_C=3.05 G) is considerably small as compared with a_C of any uncomplexed contact ion pair observed so far, and even smaller than a_C of the free anion in dimethyl sulfoxide (a_C= 3.20 G). The a_C value of the free anion is dependent on the anion solvation power of solvent. a_C of the free anion in THF is estimated to be 1.34 G, using the relation between Gutmann's acceptor number and a_C obtained previously.[14] The potassium ion pair complexed by both a crown ether and solvent molecule would have a structure such as Fig. 5 (c) classified as a crown-separated ion pair. The model, in which the anion and a solvent molecule are located on each side of the plane of the crown ether ring, is supported by the result of ESR studies on the 15-crown-5 complexed potassium ion pair, a_C of the 15-crown-5 complexed ion pair (a_C=3.92 G) being almost independent of solvent and temperature. This is probably due to the fact that, since the size of a potassium ion is too large to fit the cavity of 15-crown-5 ether, the solvent molecule can not solvate the crown complexed cation in such a manner as shown in Figs. 5 (b) and (c).[15]

The present conclusion is also supported by X-ray structures for dibenzo-18-crown-6 complexed NaNCS and $NaBr2H_2O$.[1,2] In the former the sodium ion is pulled out of the plane of the crown ether oxygen atoms toward the anion by 0.05 nm, while in the latter the sodium ion is sandwiched by a bromide ion and a water molecule and pulled out of the plane toward the bromide ion only by 0.027 nm.

The difference in a_C between the unsolvated and solvated species of the sodium ion pair is greater than that in a_C between the sodium ion pair (a_C=4.85 G) and caesium ion pair (a_C=3.90 G) in THF in the absence of C-6. This indicates that the increase of the cation-anion separation caused by the solvation of one ethereal molecule is of the same order of magnitude as the difference in ionic radius between a caesium ion and a sodium ion amounting to 0.07 nm. The reason why the interaction of one ethereal molecule with the

sodium ion can induce such a large change in the separation might be considered as follows. On the basis of measurement of the electric dipole moment of the ion pair of *p*-toluenesulfonate with a dibenzo-18-crown-6 complexed potassium ion in octanoic acid, Ting-Po I and Grunwald[16] estimated the relative stabilities of several models for the ion pairs, ignoring the solvation energy of the cation, and shown that although the contact ion pair such as shown in Fig. 5 (a) is the most stable, the energy difference between models including crown-separated ion pairs are only few kilocalories per mole. The difference in energy is comparable to the solvation energy of a cation by one ethereal molecule. If the situation is similar to the present system, the solvation of the cation by one solvent molecule would be capable of inducing the observed structural changes of the ion pairs.

References

1) D. Bright and M. R. Truter, *J. Chem. Soc., B*, **1970**, 1544.
2) M. A. Bush and M. R. Truter, *J. Chem. Soc., B*, **1971**, 1440.
3) K. H. Wong, G. Konizer, and J. Smid, *J. Am. Chem. Soc.*, **92**, 666 (1970).
4) U. Takaki, T. E. Hogen Esch, and J. Smid, *J. Am. Chem. Soc.*, **93**, 6760 (1971).
5) J. Smid, *Angew. Chem., Int. Ed,. Engl.*, **11**, 112 (1972).
6) T. E. Hogen Esch and J. Smid, *J. Phys. Chem.*, **79**, 233 (1975).
7) V. Gutmann, "Coordination Chemistry in Non-Aqueous Solution," Splinger, Wien (1968).
8) N. Hirota, *J. Chem. Phys.*, **37**, 1881 (1962).
9) N. Hirota, "Radical Ions," ed by E. T. Kaiser and L. Keven, Interscience, New York (1968), pp. 35—86.
10) W. Lubitz, M. Plato, K. Möbius, and R. Biehl, *J. Phys. Chem.*, **83**, 3402 (1979).
11) J. Smid, "Ion and Ion Pairs," ed by M. Szwarc, Wiley-Interscience, New York (1972), Vol. 1, pp. 85—151.
12) E. M. Arnett, H. C. Ko, and C. C. Chao, *J. Am. Chem. Soc.*, **94**, 4777 (1972).
13) K. Nakamura, B. F. Wong, and N. Hirota, *J. Am. Chem. Soc.*, **95**, 6919 (1973).
14) K. Nakamura, *Chem. Lett.*, **1980**, 301.
15) The ESR spectrum of the fluorenone anion radical in the solution containing 15-crown-5 ether shows the equilibrium of two species; 1: 1 and 1: 2 complexes of a potassium ion with 15-crown-5. a_C of the 1: 1 and 1: 2 complexes are 3.92 and 1.54 G, respectively.
16) Ting-Po I and E. Grunwald, *J. Am. Chem. Soc.*, **96**, 2879 (1974).

Electrical and Optical Properties of the 5,6:11,12-Bis(epidithio)-naphthacene-Bromine System (TTT-Br_n). Formation of Organic Mixed-valence Compounds (TTT)-$(TTT^+)Br^-$ and $(TTT^+)(TTT^{2+})(Br^-)_3$

Yoshio MATSUNAGA* and Kazuhiro TAKAYANAGI

Department of Chemistry, Faculty of Science, Hokkaido University, Sapporo 060

(Received April 10, 1980)

The electrical resistivity of the 5,6: 11,12-bis(epidithio)naphthacene–bromine system (TTT–Br_n) was examined over the composition range from $n=0.3$ to 2.0 using polycrystalline compactions. The room-temperature resistivity shows a minimum of about 7 Ω cm near $n=0.5$, suggesting the formation of a mixed-valence compound, (TTT)-$(TTT^+)Br^-$. The resistivity increases monotonously with n. No anomaly was found at the composition of (TTT^+)-Br^-. The formation of another mixed-valence compound, the ideal composition of which may be expressed by the formula $(TTT^+)(TTT^{2+})(Br^-)_3$, is indicated by an abrupt change of the resistivity from 100 to 4000 Ω cm around $n=1.5$. This change is accompanied by an increase of the activation energy for semiconduction by a factor of almost two and also by the change of sign in the variation of the Seebeck coefficient with the temperature from positive to negative. A further increase of the resistivity by a factor of ten was observed between $n=1.5$ and 2.0. The electronic and vibrational spectra support the coexistence of the TTT molecule and the TTT^+ ion near $n=0.5$ and that of the TTT^+ and TTT^{2+} ions near $n=1.5$.

The term "mixed-valence" has been adopted for the description of the inorganic systems containing an element in two different states of oxidation. Such systems are of great interest as their properties are frequently far from the sum of the properties of the two metal ions taken separately. The appearance of electronic conduction much higher than those in the compounds containing either valence state alone, as is exemplified by magnetite, $Fe^{II}Fe^{III}{}_2O_4$, is one of the striking features of many mixed-valence compounds. A large number of organic compounds, which contain both the molecules and the radical ions, have been prepared in the last two decades. Some of them are highly conducting. Tetrathiafulvalene–tetracyano-*p*-quinodimethane (TTF–TCNQ), complex TCNQ salts, and so-called iodine complexes are notable examples. In contrast to a great variety of valence in inorganic compounds, all the organic compounds so far studied consist of the formally neutral molecules and the monopositive or mononegative radical ions. In this work, we searched for the first example of the organic mixed-valence compounds where the mean valence would be higher than one. 5,6 : 11,12-Bis(epidithio)-naphthacene (TTT) seemed to be the best molecular species for our purpose as a number of the stable TTT^+ salts and also fairly stable TTT^{2+} salts are known from the work of Marschalk and Niederhauser.[1] The counter ions which they used to prepare both TTT^+ and TTT^{2+} salts are Cl^-, Br^-, NO_3^-, and SO_4^{2-}. We selected the bromides as the most promising component compounds.

The mixed-valence compounds of TTT with the mean valence of less than one have been studied by several workers. One of the present authors reported the preparation of the *o*-chloranil and *o*-bromanil complexes of a 3 : 1 mole ratio.[2,3] In their electronic spectra, there are strong absorption bands assignable to the TTT^+ ion. In addition, a broad electronic absorption band having a maximum around 2500 cm^{-1} is indicative of an interaction between the TTT molecule and the TTT^+ ion. The compactions exhibit resistivities of the order of one Ω cm at room temperature. The bis(1,2-ethylenedithiolato)nickel(II) complex prepared by Interrante *et al.* is another example.[4] As the complex has the empirical formula $TTT_{1.2}(NiS_4C_4H_4)$ and there is complete charge transfer from TTT to $NiS_4C_4H_4$, on the average each of the TTT molecules bears a formal charge of +5/6. The dc resistivity along the c-axis direction of the single crystal has been reported to be about 0.03 Ω cm at 25 °C. The extensively-studied iodine complex TTT–$I_{1.5}$ is also a kind of mixed-valence compound.[5-7] Because of the formation of polyiodide ions, the mean valence is less than one even if more iodine is added.[8] The single crystal resistivities measured along the needle axes in both the TTT–$I_{1.5}$ and TTT–$I_{2.7}$ phases are known to be metallic in the temperature range from 200 to 300 K. Therefore, it seemed very likely that low-resistivity mixed-valence compounds can be found with the TTT–Br_n system.

Experimental

Materials. TTT was synthesized following the method reported by Marschalk and Stumm and recrystallized three times from trichlorobenzene.[9] The dibromide was prepared by the oxidation of powdered TTT suspended in trichlorobenzene with bromine.[1] The samples with n values less than two were prepared by grinding the weighed $TTT^{2+}(Br^-)_2$ and TTT in an agate mortar in the presence of a small amount of benzene; the powders were then dried at 100 °C. The compositions were determined by microanalysis.

Measurements. The electrical resistivities and Seebeck coefficients of polycrystalline compactions were recorded as functions of the temperature from −100 to 100 °C by the procedures employed in our previous work.[8] The electronic and vibrational spectra were measured both as potassium bromide disks by means of a Beckman DK 2A spectrophotometer and a JASCO IR-G spectrophotometer respectively.

Results and Discussion

Electrical Properties. The temperature depend-

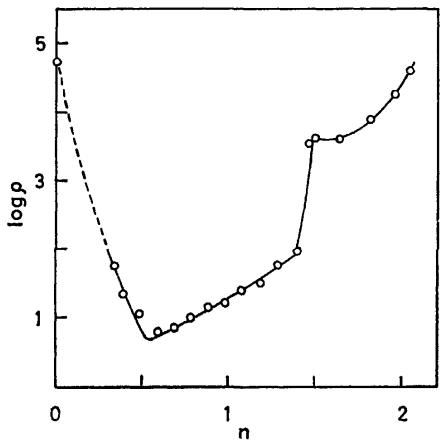

Fig. 1. Electrical resistivity at 25 °C plotted against the bromine content (n Br atoms/TTT molecule).

ence of the resistivity, ρ, of the polycrystalline compactions follows the typical semiconductor behavior: $\rho=\rho_0\exp(E_a/kT)$. In Fig. 1, the logarithm of resistivity at 25 °C is plotted against n. The drastic decrease of the resistivity compared to those at $n=0$ and 2 is clearly due to the oxidation-reduction between the TTT molecule and the TTT^{2+} ion. The solid-state and solution spectra of the mono- and dibromides are distinctly different from each other,[10] so there is no doubt about the existence of TTT^+Br^- and $TTT^{2+}(Br^-)_2$. The specimens with n values between one and two must formally consist of the TTT^+ and TTT^{2+} ions and bromide ions; those with n values less than one must consist of the TTT molecules, the TTT^+ ions, and bromide ions. As the resistivity is sensitive to the composition change, its measurement provides a simple means of detecting the possible mixed-valence compounds. An anomaly appearing in these two composition ranges can be assigned to such a compound. A minimum resistivity of about 7 Ω cm found near $n=$ 0.5 is indicative of the formation of the compound $(TTT)_2Br$. The formation of this mixed-valence compound is not unexpected. Very recently, Ritvay-Emandity *et al.* have concluded that the chloride precipitated upon mixing the methanol solutions of TTT^+ acetate and potassium chloride has the composition of $(TTT)_2Cl$.[11] In addition, a closely-related 5,6:11,12-(epidiseleno)naphthacene (TSeT) has been known to form the chloride of the same ratio, $(TSeT)_2Cl$.[12]

The electrical resistivity increases monotonously up to 100 Ω cm by $n=1.4$. No indication of a well-established compound TTT^+Br^- is found in the resistivity-composition isotherm. For this compound, Perez-Albuerne *et al.* have reported a resistivity of 50 Ω cm at 25 °C.[13] Our value at this composition is 18 Ω cm. Between $n=1.4$ and 1.5, the resistivity increases by a factor of forty. Such a behavior may arise from the formation of a nonstoichiometric compound, the lower limit of the existence region being located at $n=1.4$. The sharp edge appearing in this figure suggests that the ideal composition of this phase is $(TTT)_2Br_3$. This is the kind of compound we looked for in this system. The additional carriers introduced by the incorporation of extra TTT^+ ions into this ideal compound account for the marked decrease of the resistivity in this narrow composition range. Above $n=1.5$, the resistivity increases again and reaches about 4×10^4 Ω cm at $n=2$.

The formation of the latter mixed-valence compound is strongly supported by the variation in the activation energy for semiconduction in its existence region. The activation energy is approximately constant below $n=1$, the value being 0.115 eV. This value is in good agreement with 0.11 eV reported by Perez-Albuerne *et al.* for TTT^+Br^-. The energy increases gradually to 0.13 eV by $n=1.4$ and then abruptly to 0.21 eV by $n=1.5$. Above this composition, it remains at this value.

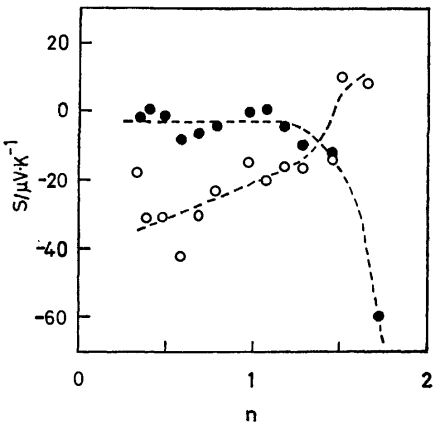

Fig. 2. Seebeck coefficients at −90 °C (○) and at 60 °C (●) plotted against the bromine content.

The whole composition range is also divided into two by the sign and temperature dependence of the Seebeck coefficient. When n is less than one, the coefficient is −20 to −30 μV K^{-1} at low temperatures and increases monotonously to about 0 μV K^{-1} at high temperatures. The direction of the temperature variation is reversed above $n=1.5$. A small positive value found below 0 °C is nearly independent of the temperature. The coefficient becomes negative above 0 °C and shows a large decrease by the further raising of the temperature. In Fig. 2, the behavior is exemplified by the values at −90 °C shown by open circles and by those at 60 °C shown by shaded circles. Thus, the existence of the mixed-valence compound, $(TTT)_2Br_3$, is manifested by the anomalous changes observed with all the electrical quantities examined.

Optical Properties. The electronic spectra of the TTT^+ and TTT^{2+} salts in both the solid and dissolved states have been examined by one of the present authors.[10] The monomeric TTT^+ ion in alcohol exhibits three weak bands at 8.0, 9.5, and 10.7×10^3 cm^{-1}, and a strong band at 17.3×10^3 cm^{-1}, followed by weaker ones at 18.7 and 21.5×10^3 cm^{-1}. The three in the near-infrared region may be ascribed to the vibrational structure of the first electronic transition.[14] The solid-state spectrum resembles the solution spectrum. By means of the transmission measurements through potassium bromide disks, we observed absorption maxima at 7.5, 9.2, 18.0, and 21.2×10^3 cm^{-1}. Except for the lowest-energy transition, these wave-

numbers are in good agreement with those obtained earlier by the diffuse reflectance method; namely, 6.3, 9.5, and 18.0×10^3 cm^{-1} and a shoulder located at 21×10^3 cm^{-1}.[10] The bands appearing in the near-infrared region are very much widened and intensified in the solid state, compared to the bands in the dissolved state. This is the region where we expect the absorption associated with the interaction between the TTT^+ ions. This expectation is consistent with the fact that the intensity ratio between the band in this region and that in the visible region depends markedly on the kind of the counter ion.[10] Furthermore, Kamaras and Grüner have recently demonstrated that an intense absorption emerges at 5.6×10^3 cm^{-1} upon cooling the methanol solution of TTT^+ acetate.[15] They attributed the new absorption to the dimer ion, $(TTT^+)_2$.

The spectrum of the brown-colored $TTT^{2+}(Br^-)_2$ is rather similar to the above-mentioned in the visible region; that is, the maxima are located at about 18 and 21×10^3 cm^{-1}. No absorption appears in the infrared region. When the salt is dissolved in dilute acid, the bands become sharper and are shifted to 20.7 and 23.6×10^3 cm^{-1} respectively. In addition, a shoulder is found at 22.7×10^3 cm^{-1}.

The mixed-valence compound, $(TTT)_2Br$, exhibits a spectrum close to that of TTT^+Br^-. However, the bands at 7.5 and 9.2×10^3 cm^{-1} are weakened compared to those in the visible region and an extra band seems to exist below 5×10^3 cm^{-1}. This new transition may be indicative of an interaction between the TTT molecule and the TTT^+ ion. The spectrum at the composition of $(TTT)_2Br_3$ looks like a superposition of those of TTT^+Br^- and $TTT^{2+}(Br^-)_2$. No sign of the interaction between the TTT^+ and TTT^{2+} ions could be seen in the electronic spectrum.

Table 1. WAVENUMBERS OF THE VIBRATIONAL BANDS IN THE SPECTRA OF TTT^+Br^-, $(TTT)_2Br_3$, AND $TTT^{2+}(Br^-)_2$ (Relative intensity: vs=very strong, s=strong, m=medium, w=weak, br=broad, sh=shoulder)

TTT^+Br^-	$(TTT)_2Br_3$	$TTT^{2+}(Br^-)_2$
1601 s	1603 s	1601 s
1550 br	1550 br	
	1473 m	1473 s
1465 s		
	1452 vs	1451 vs
1430 m		
	1390 m	1390 m
1365 s	1370 w	
	1325 s	1324 s
1312 s	1319 s	
	1305 s	1305 s
1289 vs	1290 s	
1277 vs	1280 m	
1250 s	1250 br	1249 w
1162 m	1165 m	1163 s
1129 m	1131 s	
	1110 sh	1110 br
1056 s	1060 m	
998 s	1000 s	
970 s	970 sh	
	946 w	947 w
	780 s	778 s
750 br	750 m	

Perez-Albuerne *et al.* have noted that the vibrational spectra clearly show the difference between neutral TTT and the TTT^+ salts.[13] More recently, Ritvay-Emandity *et al.* have observed that the spectrum of $(TTT)_2Cl$ consists of bands corresponding to both the TTT molecule and TTT^+ ion.[11] Our mixed-valence compound, $(TTT)_2Br$, shows a spectrum which is also a superposition of those of TTT and TTT^+Br^-. As the former spectrum is much simpler than the latter, the spectrum of $(TTT)_2Br$ is dominated by the contribution from the cation. Nevertheless, the presence of both TTT and TTT^+ ion is apparent from the relative intensities, which are markedly different from those in the spectrum of TTT^+Br^-. In Table 1, the bands found in the second mixed-valence compound, $(TTT)_2Br_3$, are listed together with those found in TTT^+Br^- and $TTT^{2+}(Br^-)_2$. Our wavenumbers for TTT^+Br^- are mostly in good agreement with those reported by Ritvay-Emandity *et al.*[11] The existence of the TTT^+ ion in this compound can be confirmed by the bands appearing at 1290, 1280, 1131, 1000, and 750 cm^{-1}. The bands assignable to the TTT^{2+} ion are also abundantly observed in this mixed-valence compound. Apparently, the bands located at 1473, 1452, 1390, 1325, and 780 cm^{-1} arise from the TTT^{2+} ion. These observations indicate that the lifetime of a definite valence state on the TTT molecule is longer than the vibrational period. An entirely different situation has been reported for some other organic mixed-valence compounds prepared by us. For example, in the spectrum of cobalticinium(3,3′,5,5′-tetrachloro-*p*-diphenoquinone)$_2$ neither the vibrational pattern due to the quinone molecule nor that due to the semiquinone anion has been found.[16] A single broad carbonyl stretching band is located at 1610 cm^{-1}; this is intermediate between that in the quinone, 1640 cm^{-1}, and that in the semiquinone salt, 1530 cm^{-1}. Similarly, the vibrational spectrum of (phenothiazine)$_2$Br is different from either that of the neutral molecule or that of its cation.[17] There is a pattern characteristic of the phenothiazine molecule bearing the charge of $+1/2$. In other words, the constituent molecules in these examples are equivalent to each other on the time scale of infrared spectroscopy. It may be added that the electrical resistivities of these two compounds are of the order of 10 or 100 Ω cm and are intermediate between the resistivity of $(TTT)_2Br$ and that of $(TTT)_2Br_3$.

The authors wish to express their thanks to Dr. Kohji Fukushi for the recording of the laser Raman spectra of some specimens in order to check for polybromide bands. This work was partly supported by a Grant-in-Aid for Scientific Research from the Ministry of Education, Science and Culture (No. 234028).

References

1) C. Marschalk and J. P. Niederhauser, *Bull. Soc. Chim. Fr.*, **1952**, 151.

2) Y. Matsunaga, *J. Chem. Phys.*, **42**, 2248 (1965).
3) Y. Okamoto, S. Shah, and Y. Matsunaga, *J. Chem. Phys.*, **43**, 1904 (1965).
4) L. V. Interrante, J. W. Bray, H. R. Hart, Jr., J. S. Kasper, P. A. Piacente, and G. D. Watkins, *J. Am. Chem. Soc.*, **99**, 3523 (1977).
5) L. I. Buravov, G. I. Zvereva, V. F. Kaminskii, L. P. Rosenberg, M. L. Khidekel, R. P. Shibaeva, I. F. Shchegolev, and E. B. Yagubskii, *J. Chem. Soc., Chem. Commun.*, **1976**, 720.
6) L. C. Isett and E. A. Perez-Albuerne, *Solid State Commun.*, **21**, 433 (1977).
7) K. Kamaras, K. Ritvay-Emandity, G. Mihaly, and G. Grüner, *Solid State Commun.*, **24**, 93 (1977).
8) T. Inabe and Y. Matsunaga, *Bull. Chem. Soc. Jpn.*, **51**, 2813 (1978).
9) C. Marschalk and C. Stumm, *Bull. Soc. Chim. Fr.*, **1948**, 418.
10) Y. Matsunaga, *Bull. Chem. Soc. Jpn.*, **45**, 770 (1972).
11) K. Ritvay-Emandity, K. Kamaras, and G. Grüner, *Chem. Phys. Lett.*, Submitted for publication (personal communication).
12) L. I. Buravov, A. I. Kotov, M. L. Khidekel, I. F. Shchegolev, and E. B. Yagubskii, *Izv. Akad. Nauk, Ser. Khim.*, **1976**, 475.
13) E. A. Perez-Albuerne, H. Johnson, Jr., and D. J. Trevoy, *J. Chem. Phys.*, **55**, 1547 (1971).
14) A. I. Kiss, M. Kertesz, P. Carsky, and H. Wedel, *Tetrahedron*, **35**, 515 (1979).
15) K. Kamaras and G. Grüner, *Solid State Commun.*, **30**, 277 (1979).
16) Y. Matsunaga and Y. Narita, *Bull. Chem. Soc. Jpn.*, **45**, 408 (1972).
17) S. Doi and Y. Matsunaga, *Bull. Chem. Soc. Jpn.*, **48**, 3747 (1975).

Direct Measurement of Interaction Energy between Solids and Gases. VII. Heats of Adsorption of Carbon Monoxide on Cu(II)-exchanged Zeolites Y

Yoji MIWA,* Kazuo TSUTSUMI, and Hiroshi TAKAHASHI
Institute of Industrial Science, The University of Tokyo, 7-22-1 Roppongi, Minato-ku, Tokyo 106
(Received April 24, 1979; revised December 22, 1979)

Differential heats of the adsorption of carbon monoxide on Cu(II)Y zeolites were calorimetrically determined. The heat of adsorption was larger on Cu(II)Y zeolites than on the NaY zeolite, and increased with the degree of Cu(II) ion-exchange. Repeated adsorption-desorption measurements revealed an increase in the heat of adsorption, which is considered to be due mainly to the migration of copper(II) ions from inaccessible sites for carbon monoxide to accessible ones in the process of adsorption-desorption.

The adsorption properties and catalytic activities of zeolites are markedly affected by the nature and the distribution of cations in the zeolites. Investigations of the interaction between simple gas molecules and the zeolite surface have often provided important information on the nature and the distribution of these cations. Carbon monoxide is an attractive choice for such investigations.[1)]

There have been a number of investigations of the adsorption of carbon monoxide on zeolites, but, as far as we know, there is only a little information about the cation migration by carbon monoxide.[1)] In this study, we have determined the heats of the adsorption of carbon monoxide on Cu(II)Y zeolites to provide calorimetric evidence for the migration of copper(II) ions under the conditions of the adsorption-desorption of carbon monoxide.

Experimental

Materials and Gas. The copper(II)-exchanged zeolites were prepared by the ion-exchange of NaY zeolite (Linde SK-40), in an excess of a 5 mM (1M= 1 mol dm^{-3}) copper-(II) nitrate solution at room temperature for 14.3 and 50.3% exchange, and at *ca.* 80 °C for 80.7%.

The Cu(II)-exchanged samples were then thoroughly washed with distilled water and dried for 6 h at 110 °C, and finally stored over a saturated ammonium chloride solution at *ca.* 25 °C for at least one week before use. The samples were sieved to 28—60 mesh for use.

The degree of exchange was determined from the chemical analysis of the sodium and the atomic absorption analysis for copper(II).

The carbon monoxide (Takachiho Chem. Co., Ltd.), which was stated to have a purity greater than 99.5% (the main impurities were air, H_2, and CO_2), was purified by passing it through a liquid nitrogen cold trap before storage.

Apparatus. The heats of adsorption were measured with a twin conduction calorimeter (Tokyo Riko Co., Ltd., MPC-10 type), which was connected to a volumetric adsorption system, with an error of *ca.* 5%. The ESR measurements were carried out at room temperature with an X-band 9.38 GHz spectrometer (Japan Electron Optics Laboratory Co., Ltd., JES-ME-3X). The phosphorescence spectra of CuY were taken with a Toshiba UV-D33S spectrophotometer at room temperature. The measurement of the electronic spectra was carried out with a spectrophotometer Shimazu MPS-5000 using the reflectance method.

Procedure. Each 0.5-g zeolite sample (including *ca.* 25% H_2O) in a sample cell was evacuated under a pressure of 10^{-1} Pa, heated up at a rate of 8 °C/min to 400 °C(or 100, 250 °C), and then held at that temperature for 5 h under a vacuum of 10^{-3} Pa. The sample cell was then cooled down *in vacuo* and set in a calorimeter thermostated at the desired temperature (25±0.01 °C) for measurements.

Results

Heats of Adsorption. The heats of the adsorption of carbon monoxide on NaY and three fresh Cu(II)Y (14.3, 50.3, and 80.7% exchanged) zeolites are plotted against the amounts adsorbed in Fig. 1. In the initial portion, the differential heats of the adsorption of carbon monoxide on Cu(II)Y were larger than on NaY, and they increased with the degree of copper(II) ion-exchange.

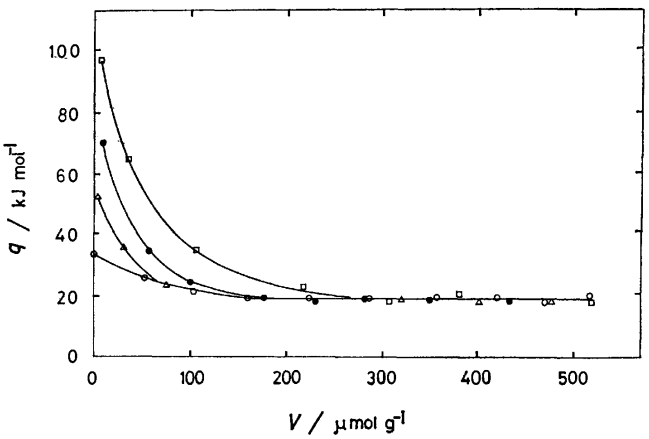

Fig. 1. Heats of adsorption of CO on Cu(II)Y and NaY.
—○—: NaY, —△—: Cu(II)Y-14.3,
—●—: Cu(II)Y-50.3, —□—: Cu(II)Y-80.7.

Figure 2 shows the adsorption isotherms of carbon monoxide on Cu(II)Y-80.7 pretreated at 400 °C under a pressure of 10^{-3} Pa for 5 h. The adsorption measurements for the second isotherm were carried out after desorbing the adsorbed CO under a vacumm of 10^{-3} Pa for *ca.* 3 d. The third was made after the desorption of the second, and so forth. The adsorption-desorption cycle increased the amount of adsorption. However, the degree of increase in the adsorbed amount became smaller with the number of cycles, and finally no such an increase was detected between the tenth and the

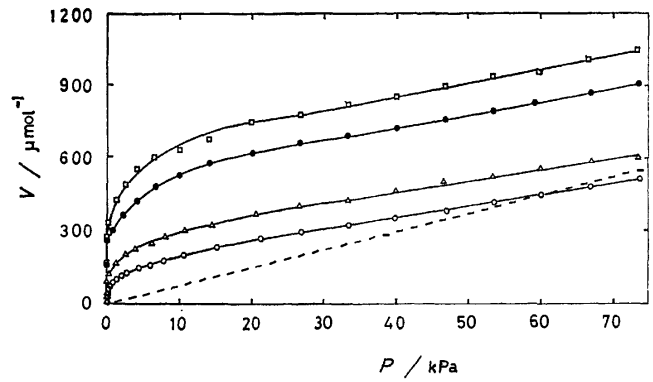

Fig. 2. Adsorption isotherms of CO on Cu(II)Y-80.7. After adsorption measurement up to *ca.* 73 kPa equilibrium pressure zeolite was evacuated at 10^{-3} Pa for *ca.* 3 d then the next run of adsorption was carried out. This procedure repeated until the isotherm practically agreed with the preceding one.
----: NaY, —○—: lst, —△—: 3rd, —●—: 7 th, —□—: 11th run.

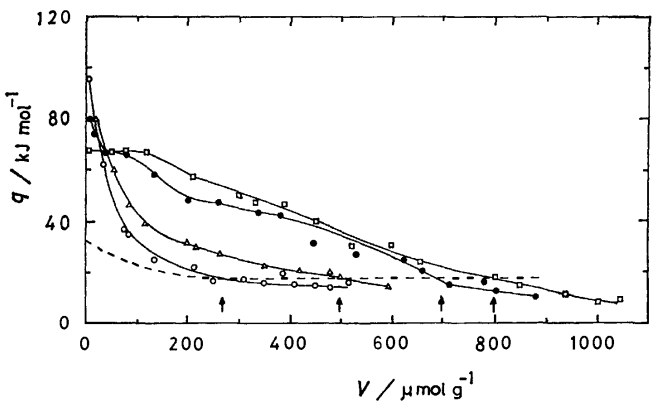

Fig. 3. Heat curves of adsorption of CO on Cu(II)Y-80.7, corresponding to Fig. 2.
----: NaY, —○—: lst, —△—: 3rd, —●—: 7th, —□—: 11th run. Arrows show the intersection of Cu(II)Y and NaY.

eleventh isotherms.

The heat curves corresponding to the above-mentioned isotherms are shown in Fig. 3. Apart from the initial portion, the heat curves were also shifted to the higher side. The initial heats of adsorption, on the contrary, gradually decreased with the number of the run. The tenth and eleventh curves agreed with each other within experimental uncertainty.

Changes in the Heats of Adsorption in the Process of Repeated Adsorption-desorption on Cu(II)Y. Thermograms of the repeated adsorption and desorption of carbon monoxide on NaY, Cu(II)Y-14.3, and Cu(II)Y-80.7 are shown in Fig. 4. After pretreatment at 400 °C, the heats of adsorption and desorption were measured by admitting measured amounts of CO: 80 μmol g^{-1} for NaY and Cu(II)Y-14.3; 20 μmol g^{-1} for Cu(II)Y-80.7. After the first thermogram had been drawn, the first heat of desorption (Q_{d1}) was measured under evacuation up to 10^{-3} Pa; then the same procedure of adsorption and desorption was repeated several times.

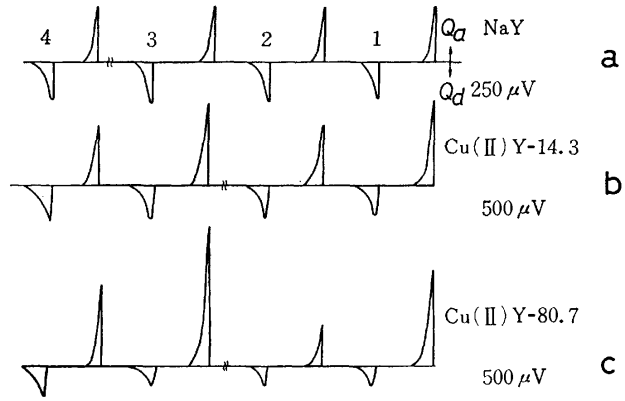

Fig. 4. Thermograms of repeated CO adsorption-desorption on NaY and Cu(II)Y, pretreated at 400 °C under a pressure of 10^{-3} Pa for 5 h. Q_a: Heat of adsorption, Q_d: heat of desorption. Admitted amount of CO: 80 μmol g^{-1} for NaY and Cu(II)Y-14.3; 20 μmol g^{-1} for Cu(II)Y-80.7. For NaY after 3 rd run and Cu(II)Y after 2 nd run the samples were evacuated overnight. 250 or 500 μV represents the full scale of the recorder response.

In the case of NaY, the heats of adsorption, Q_a, and desorption, Q_d, were practically identical at all times, not only from Q_{a1} to Q_{d3}, which were measured successively, but also at Q_{a4} and Q_{d4} which were measured after evacuation overnight under 10^{-3} Pa. In the case of Cu(II)Y-14.3, the second heat of adsorption, Q_{a2}, was smaller than the first, Q_{a1}, by 42%. This decrease occurred because of an incomplete desorption of strongly adsorbed carbon monoxide on Cu(II)Y-14.3 (Q_{d1} was smaller than Q_{a1} by 53%). However, Q_{a3}, which was measured after degassing overnight under 10^{-3} Pa, was much the same as Q_{a1}. These results showed that the carbon monoxide on Cu(II)Y-14.3 is desorbed when the sample is evacuated over a period of *ca.* 10 h (several times as long as for NaY). This was also supported by IR observation. However, when Q_{a5} (which is not shown in Fig. 4) was measured after degassing overnight under 10^{-3} Pa, an interesting phenomenon was observed: $Q_{a5}>Q_{a1}$. This phenomenon of the increase in the heat of adsorption was also, remarkably observed in the sample of higher exchanged Cu(II)Y-80.7: Q_{a2} was very much smaller than Q_{a1}, while Q_{a3}, measured after degassing overnight under 10^{-3} Pa, was *ca.* 1.5 times as large as Q_{a1}.

Figure 5 shows the changes in the thermograms with the pretreatment temperatures. The changes in the heats of adsorption markedly depended upon the pretreatment temperatures (*cf.* Fig. 4,c). In the case of the 100 °C-pretreatment in spite of the incomplete first desorption ($Q_{d1}<Q_{a1}$), the second heat of adsorption, Q_{a2}, was larger than Q_{a1}, and Q_{a3} was also larger than Q_{a2}. Furthermore, Q_{a4}, measured after evacuation overnight, was *ca.* 7.5 times as large as Q_{a1}. Intermediate behavior was observed in the case of the 250 °C-pretreatment.

The changes in the heat of adsorption, q/kJ mol^{-1}, corresponding to Figs. 4 and 5 are summarized in Table 1.

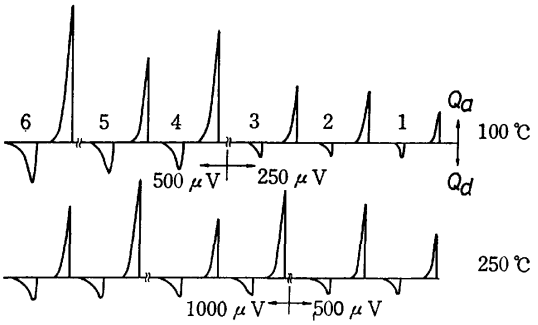

Fig. 5. Changes of thermograms of adsorption and desorption of CO on Cu(II)Y-80.7 with pretreatment temperatures 100 and 250 °C. Q_a: heat of adsorption, Q_d: heat of desorption. Admitted amount of CO: 20 μmol g^{-1}. 250, 500, or 1000 μV represents the full scale of the recorder response.

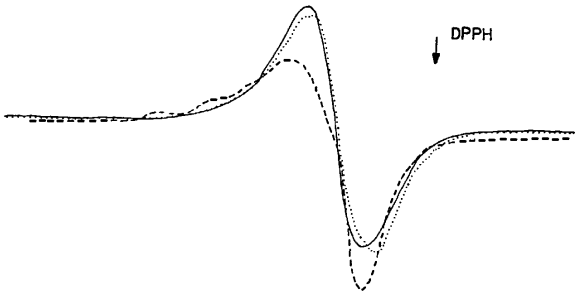

Fig. 7. ESR spectra of Cu(II)Y-80.7 recorded at room temperature.
------: (1) After evacuation at room temperature for 2 h, ——: (2) after (1) stored over saturated NH_4Cl solution at *ca.* 25 °C for 3 d, ……: (3) after evacuation at 400 °C under a pressure of 10^{-3} Pa for 5 h stored over saturated NH_4Cl solution at *ca.* 25 °C for 3 d.

Table 1. Changes in heat of adsorption (q/kJ mol^{-1}) corresponding to figs. 4 and 5

Zeolite	Cu(II) Y-14.3	Cu(II) Y-80.7	Cu(II) Y-80.7	Cu(II) Y-80.7
Pretreatment temperature/ °C	400	400	250	100
1	24.9	92.5	16.6	6.3
2	15.0	61.9	29.7	10.1
3	25.1	108.4	55.3	10.6
4	20.3	74.1	35.0	29.0
5	(26.2)		57.5	32.9
6			35.1	35.7

ESR and Phosphorescence Measurements. From the phosphorescence spectra (Fig. 6), the formation of Cu(I) was observed[2] when dehydrated Cu(II)Y-80.7 was treated with 20 kPa of CO at 400 °C for 36 h. In this case, contrary to Huang,[3] the reduction of Cu(II)Y by CO was not complete. A complete reduction was, however, achieved, as Huang[3] had reported, when NH_3 was preadsorbed in dehydrated Cu(II)Y-80.7 at a pressure of *ca.* 1.33 kPa; then the sample was treated with 20 kPa of CO at 400 °C for 1 h. However, no indication of Cu(I) formation was observed in either the sample of Cu(II)Y-80.7 evacuated at 400 °C under a pressure of 10^{-3} Pa for 5 h or, the Cu(II)Y-80.7 evacuated, followed by the adsorption of CO at room temperature. These results were in agreement with those of the ESR (Fig. 7).

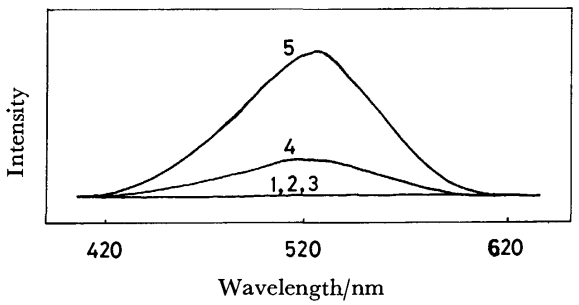

Fig. 6. Phosphorescence spectra of CuY-80.7 recorded at room temperature under the same optical conditions and nearly identical sample geometries.
(1): Cu(II)Y-80.7 untreated, (2): after evacuation of Cu(II)Y-80.7 at 400 °C under a pressure of 10^{-3} Pa for 5 h, (3): after (2) adsorption of 13.3 kPa CO at room temperature for 1 h, (4): after (2) adsorption of 20 kPa CO at 400 °C for 36 h, (5): after (2) adsorption of 1.33 kPa NH_3 at room temperature for 1 h then adsorption of 20 kPa CO at 400 °C for 1 h.

Measurement of Electronic Spectra. In the near-infrared region, the Cu(II)Y-80.7 zeolites hydrated or pretreated at 100 °C showed the absorption maxima at *ca.* 1450 and 1950 nm. However, in the case of 250 or 400 °C-pretreatment these peaks were not observed. These two bands are assigned to the overtone band ($2\nu_3$) and the combination band ($\nu_2+\nu_3$) of the adsorbed water respectively.[14]

Discussion

The synthetic Y zeolites have two sets of cavities. The larger cavities, called supercages, have a diameter of *ca.* 13 Å. The entrances to the supercages have a free diameter of approximately 9 Å. The smaller cavities, called sodalite cages, have a free diameter of 7 Å and are connected to the supercages by openings with a free diameter of 2.5 Å. The sodalite cages are joined to each other by 2.4 Å free-diameter hexagonal prisms.[4,5] The kinetic diameter of the carbon monoxide molecule is *ca.* 3.8 Å,[6] and so it must be unable to pass through these small openings. According to Smith[7] and Mortier,[8] there are five kinds of cation sites in Y zeolite; *i.e.*, SI, at the center of a hexagonal prism; SI′, displaced from a shared hexagonal face into the sodalite cage; SII′, displaced from an unshared hexagonal face into the sodalite cage; SII, slightly displaced into the supercage, and SIII′, in the supercage, formed by two O_1 and O_4 oxygens. Thus, carbon monoxide would possibly be chemisorbed, with a relatively strong interaction, on Cu(II) at the SII or SIII′ sites. The Cu(II) ions at the SI, SI′, or SII′ sites may not be accessible to carbon monoxide, as is supported by the work of Egerton and Ston.[1] They showed by experiments on a sample of synthetic sodalite that CO was not

adsorbed at temperatures below 200 °C. Also, they pointed out that a slow adsorption of CO occurring on Cu(II)Y and Ni(II)Y zeolites was to be ascribed to a gradual increase in the number of adsorption sites caused by the adsorption-induced migration of the divalent cations.

The present results and those formerly reported by other workers can well be interpreted in terms of the model to be discussed below. The difference between the adsorption properties of NaY and Cu(II)Y is primarily to be ascribed to the existence of the accessibility of Cu(II) to the visiting CO. The higher values of q in the initial portion of q *vs.* V curves are attributable to the adsorption on exchangeable cations. The curves in Fig. 1 show that Cu(II) adsorbs CO with a stronger interaction than does Na, and that the quantity of Cu(II) accessible to CO increases with the increase in the content of Cu(II). When the adsorbed amount increases, the q-value converges to 20 kJ mol^{-1} for all the samples studied. It is known that, in such a region, CO is adsorbed on the framework oxygen. Thus, the amount of the accessible Cu(II) can easily be estimated from Fig. 1; it is found to increase with the number of the adsorption-desorption cycles, as is shown in Fig. 3 and Table 2. This can be explained as follows. The Cu(II) ions at the SI, SI′, and/or SII′ sites migrate, in the course of the cycle, to the SII and/or SIII′ sites, which are accessible to the visiting CO. Though there are many possibilities, the most plausible one is that a predominant part of the Cu(II) migration occurs from the SII′ to the SII site. This change corresponds to a small displacement from one side of the 6-membered oxygen ring to the other side, and may take place with a small activation energy.

Table 2. Increase in the number of accessible Cu(II) ions with the adsorption-desorption run

Number of run	$V_{sp.ad}$ / μmol g^{-1}		Ratio of accessible Cu(II) ions compared with 1st run	
	a	b	a	b
I	270	170	1	1
III	500	280	1.9	1.6
VII	700	510	2.6	3.0
XI	800	620	3.0	3.6

a) The amount of specific adsorption was determined from the amount adsorbed where the heat curves of Cu(II)Y intersect with that of NaY. b) The amount of specific adsorption was determined by the extrapolation of the lines in the high-pressure region of the isotherms in Fig. 2 to 0 pressure.

The above discussions are based on the assumption that no reduction of Cu(II) to Cu(I) occurred; this assumption was supported by the ESR and phosphorescence studies. The ESR signal ascribed to the Cu(II) ion did not change in repeated adsorption-desorption cycles. It should have decreased if any reduction of Cu(II) had occurred. The phosphorescence spectrum in Fig. 6 shows that Cu(I) was not produced in the present treatments.

The extent of cation migration depends upon also the quantity of residual water molecules.[9-13] The present electronic spectral data show that the samples pretreated at 250 or 400 °C are considered to be dehydrated ones, and that at 100 °C, partially hydrated. This is compatible with the electronic spectral data reported by De Wilde *et al.*[15] The increase in the heat of adsorption (q) shown in Table 1 may be ascribed to another reason besides the above-mentioned migration of Cu(II): that is, the release of coordinated H_2O (or OH group). Since the samples pretreated at 250 or 400 °C are considered to be dehydrated, the phenomenon is ascribed to the Cu(II) migration, whereas in the sample pretreated at 100 °C the second reason cannot be neglected.

In conclusion, the observed results can consistently be explained by the proposed model that Cu(II) at the SII and/or SIII′ sites strongly adsorb CO, and that the number of such Cu(II) cations increases with the adsorption-desorption cycles as a result of the Cu(II) migration from the inaccessible sites to the accessible ones. In the case of partially hydrated Cu(II)Y, the replacement of coordinated H_2O (or OH group) by CO may also occur.

The authors wish to express their thanks to Professor Minoru Kinoshita and Miss Noriko Iwasaki of The Institute for Solid State Physics, The University of Tokyo, for the measurements of the phosphorescence spectra and for their helpful discussions, and to Mr. Minoru Suzuki for ESR measurements.

References

1) T. A. Egerton, and F. S. Stone, *J. Chem. Soc., Faraday Trans. 1*, **69**, 22 (1973).
2) P. A. Jacobs, W. De Wilde, R. A. Schoonheydt, J. B. Uytterhoeven, and H. Beyer, *J. Chem. Soc., Faraday Trans. 1*, **72**, 1221 (1976).
3) Y. Y. Huang, *J. Catal.*, **30**, 187 (1973).
4) L. Broussard and D. P. Shoemaker, *J. Am. Chem. Soc.*, **82**, 1041 (1960).
5) H. S. Sherry, *J. Phys. Chem.*, **70**, 1158 (1966).
6) D. W. Breck, "Zeolite Molecular Sieves, Structure, Chemistry, and Use," Wiley (1974), p. 636.
7) J. V. Smith, *Adv. Chem. Ser.*, **101**, 171 (1971).
8) W. J. Mortier and H. J. Bosmans, *J. Phys. Chem.*, **75**, 3327 (1971).
9) D. H. Olson, *J. Phys. Chem.*, **72**, 1400 (1968).
10) D. H. Olson, *J. Phys. Chem.*, **72**, 4366 (1968).
11) E. Dempsey and D. H. Olson, *J. Phys. Chem.*, **74**, 305 (1970).
12) N. G. Maksimov, V. F. Anufrienko, K. G. Ione, and N. A. Shestakova, *Zh. Strukt. Khim.*, **13**, 1020 (1972).
13) P. Gallezot, Y. Ben Taarit, and B. Imelik, *J. Phys. Chem.*, **77**, 2556 (1973).
14) Y. Sendoda, Y. Ono, and T. Keii, *J. Catal.*, **39**, 357 (1975).
15) W. De Wilde, R. A. Schoonheydt, and J. B. Uytterhoeven, "Molecular Sieves-II," ed by J. R. Katzer, ACS Symposium Series 40, ACS, Washington, D. C.(1977), p. 132.

X-Ray Diffraction Study of Liquid Water

Keiko NISHIKAWA* and Nobuko KITAGAWA

Department of Chemistry, Faculty of Science, Gakushuin University, Mejiro, Toshima-ku, Tokyo 171

(Received September 22, 1979)

The energy-dispersive X-ray diffractometer has been applied to the structural study of liquid water. The intensity data are in good agreement with those obtained by the use of an angle-dispersive method. Water has a structural correlation up to only 8 Å at 25 °C.

By using an energy-dispersive X-ray diffractometer for the determination of the liquid structure, new information was obtained about CCl_4; that is, the existence of fine structures in the diffraction pattern was obtained in the liquid for the first time.[1-3] The fine structures in the diffraction pattern reflect the long-range correlation in the liquid structure. In fact, liquid CCl_4 has a structural correlation up to 28 Å at a low temperature (−20 °C)[3] and even at room temperature.[2] The long-range correlation can be expected to exist also in liquid water, since the molecular interaction of water is a strong hydrogen bond. Therefore, it seems that it is interesting to study the diffraction pattern of water by the energy-distersive method.

At the same time, it is necessary to examine the analytical procedures of the energy-dispersive method. Some difficulties arise for the analysis of the data obtained by this method. One is the consistency of the data which were observed at different scattering angles in the overlapping region, and the other is the absorption correction. The errors caused by the difficulties mentioned above influence the intensity curve in the form of the spurious background and the discontinuity of the curve at the connected points. In this case, the radial distribution curve has ghost peaks. Therefore, it is important to compare our data obtained by the energy-dispersive method with good data obtained by the angle-dispersive method. In 1967, Narten, Danford, and Levy published their results obtained by the X-ray diffraction study of liquid water in the temperature range 4—200 °C.[4] Thereafter they published other related results.[5-7] Though the radial distribution function was also confirmed by other groups,[8-12] the work of Narten *et al.* is regarded as most precise results. It seems, therefore, that it is suitable to compare our data and the results of Narten *et al.*

Another judgement of the correctness of the data analysis can be made by a comparison of the absolute total coherent intensity at $s=0$ with the value calculated from the isothermal compressibility. Moreover, Chonacky and Beeman measured the absolute scattering intensity for water at small scattering angles.[13] This value can also be compared with our data.

Experimental

The scattering intensity of X-rays from liquid water was measured at 25 °C. An energy-dispersive diffractometer[1] with a vertical goniometer (θ—2θ scanning system) was used. A fine-focus X-ray tube with a tungsten target was used at 45 kV, 20 mA. The scattering intensity was recorded by a Si(Li) detector connected with a multi-channel pulse-height analyzer.

The scattering intensity was measured by the transmission method at the scattering angles(2θ) of 2, 4, 8, 12, 17, and 27°. The reflection method was applied at $2\theta=35$ and 70°. By using white X-rays with wavelengths ranging from 0.46 to 1 Å, these measurements cover the ranges of s ($4\pi \sin\theta/\lambda$, λ: wavelength) $=0.22$—0.48, 0.44—0.96, 0.88—1.92, 1.31—2.88, 1.85—4.07, 2.93—6.43, 3.78—8.29, and 7.20—16.00 Å^{-1} respectively. In order to avoid mistakes in the data analysis for the energy-dispersive method, the scattering angles were set so closely that the two ends of the intensity curves obtained at adjacent angles could overlap widely with each other.

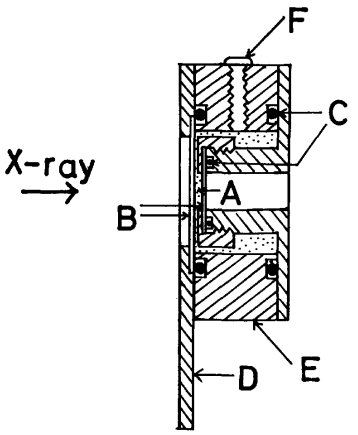

Fig. 1. A modified sample holder for the transmission method. (A): Sample, (B): Be or Myler window, (C): O-ring, (D): stainless steel plate to set the holder to the goniometer, (E): ring (The thickness of the sample can be changed by the exchange of this ring.), (F): the hole from which the sample is injected.

The sample holder used for the reflection method was the same as that used previously.[1] For the transmission method, the sample holder used in our earlier experiment was modified as shown in Fig. 1 in order to set the Be or Myler windows (B) tight and parallel to a narrow spacing. In the present study, Myler film (20 μm thick) was used; the thickness of the sample was 0.194 cm. The scattering intensity was measured for 3×10^4—10^5 s at each scattering angle, and more than 1×10^4 counts per channel were collected.

The scattering intensities from the Myler film of the sample holder and that from air, I_w, were measured, the magnitude of I_w being about 5—8% of the total scattering intensity.

Data Analysis

After smoothing, each scattering intensity curve from which the intensity, I_w, was subtracted was divided by the energy distribution curve of the incident beam (normalization).

As the linear absorption coefficient, μ, changes with the energy of the X-rays, the μ values were calculated in a way similar to that described in a previous paper,[1] in which the C parameters for oxygen and hydrogen atoms were 3.18 and 0.0127 respectively, and in which the D's were 0.0654 and 0.466×10^{-5}.[14] The values of μ, determined from the transmittance of the sample at $\theta=0°$, agree well with the calculated values in the range of wavelengths of 0.46—1 Å within the experimental error. By using the calculated values of the absorption coefficient, the normalized scattering intensity curve were corrected over the wavelength range from 0.46 to 1 Å.

The corrected intensity curve were then converted into the absolute scale (in electron units) by fitting the experimental intensity to the theoretical intensity at large s-values. In the calculation of the theoretical intensity, the internuclear distances and the mean-square amplitudes of the vibration in a water molecule obtained by gas-electron diffraction[15] were used, and the Compton scattering intensity calculated by Cromer[16] was employed. The conversion factor from the experimental to the absolute intensity, K, was easily obtained from $2\theta=2$, 4, 8, 12, and 17°; each intensity curve was successively connected with that at $2\theta=27°$ after the absorption correction. Then, K was obtained for each intensity curve. The observed total coherent intensity;

$$I_{co}(s) = \sum_n f_n(s)^2 + i_1(s) + i_2(s) \qquad (1)$$

is shown in Fig. 2, where $f_n(s)$ is the atomic scattering factor and where $i_1(s)$ and $i_2(s)$ represent the coherent intensities from atom pairs within a molecule and between different molecules respectively. The weighted structure function, $si(s)=s(i_1(s)+i_2(s))$, shown in Fig. 3, was then calculated.

The electronic radial distribution function from which the bulk density was subtracted, $4\pi r^2(\rho-\rho_0)$, was obtained by the Fourier transformation of $si(s)$:

$$4\pi r^2(\rho-\rho_0) = \frac{2r}{\pi\sum_n Z_n^2}\sum_{s=0}^{s_{max}} si(s)\cdot\sin sr\cdot\Delta s, \qquad (2)$$

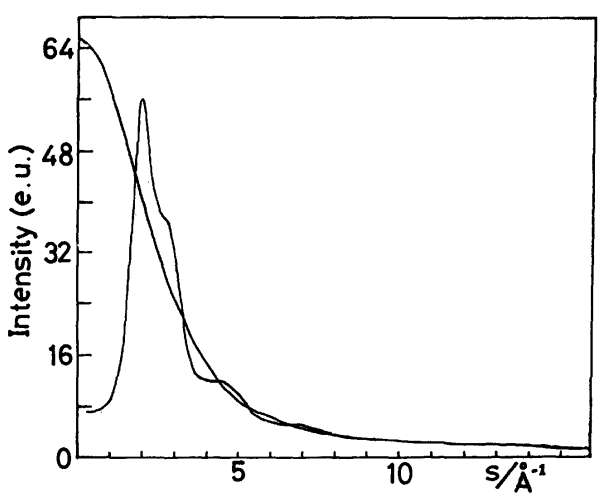

Fig. 2. Observed total coherent intensity I_{co} for liquid water at 25 °C and independent atomic scattering intensity.

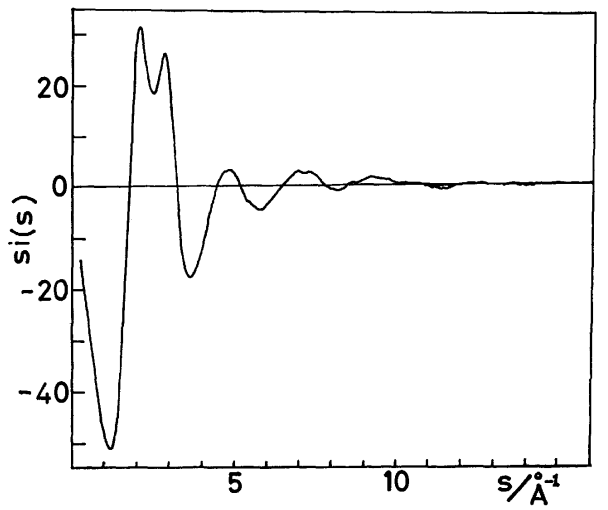

Fig. 3. Weighted structure function $si(s)$ for liquid water at 25 °C.

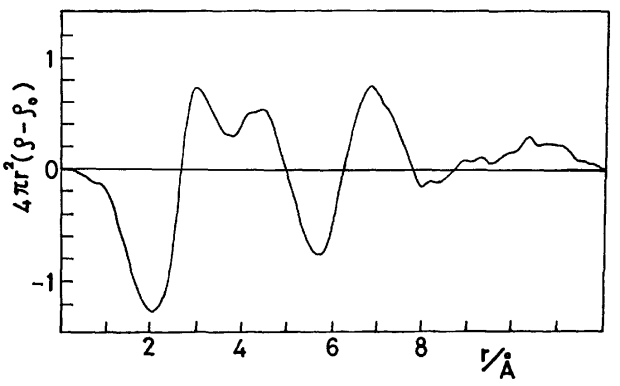

Fig. 4. Electronic radial distribution function from which the bulk density was subtracted, $4\pi r^2(\rho-\rho_0)$.

where ρ_0 is the bulk liquid density and where Z_n is the atomic number of the n-th atom. The electronic radial distribution function is shown in Fig. 4.

Results and Discussion

First, we examined to see whether or not the processing of the data obtained by the energy-dispersive method is adequate. In order to show the connection between several intensity data measured at different angles, the raw-intensity-data sets corrected for absorption are plotted in Fig. 5. The data in the $s>6$ Å^{-1} region are not shown in this figure because, in this region, the intensities are almost equal to the self-scattering ones from the corresponding atoms. In each set, the intensity at the extreme of the higher-energy region falls down slightly. In this region, the calculated values of the linear absorption coefficient, μ, are slightly smaller than the observed ones. Except for this, the intensities of the overlapped regions observed at different angles are in good agreement.

It was also confirmed that there was no spurious background which might be caused by inadequate data processing or apparatus functions. Figure 6 shows the weighted structure function, $si(s)$, which was observed

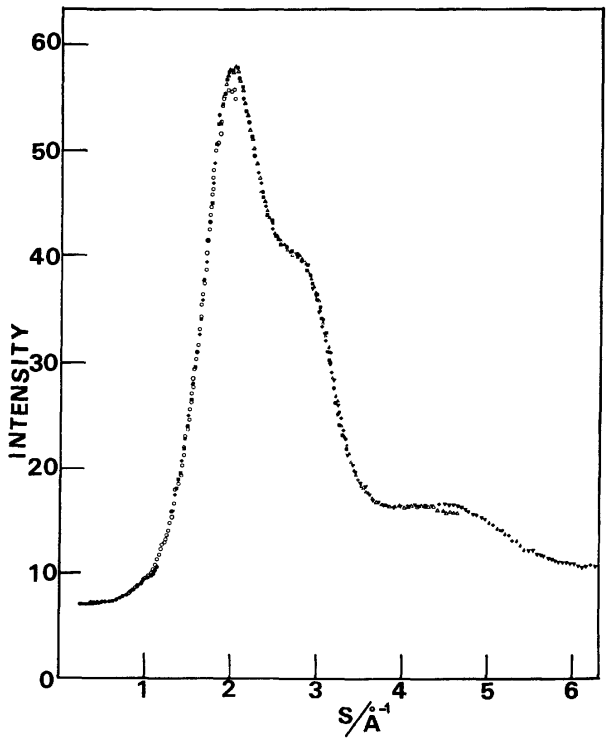

Fig. 5. The raw intensity data of liquid water after absorption correction. Each sign such as ——, ●, ○, ■, △, and ▼ shows the data obtained by angle-setting at $2\theta=2$, 4, 8, 12, 17, and 27° respectively.

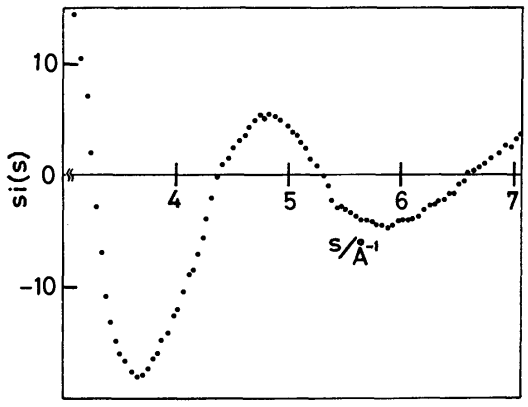

Fig. 6. The weighted structure function $si(s)$, obtained by angle setting at $2\theta=27°$. This result shows that the data do not contain apparatus functions.

at the scattering angle $2\theta=27°$. This curve was obtained as follows. In the case of water, the $i_2=0$ approximation is valid in the $s>6$ Å^{-1} region. Therefore, the data at $2\theta=27°$ could be converted into the absolute scale by adjusting the experimental intensity to the calculated intensity. If the data analysis were not correct, or if the apparatus function were contained in the data, the $si(s)$ curve would ride on a background curve and would never oscillate around the zero line as is shown in Fig. 6.

Second, the above-mentioned data obtained by the energy-dispersive method were compared with those of Narten and Levy[7] measured by the angle-dispersive method. The intensity data of the present work were, therefore, expressed in the form of $H_M(s)$. $H_M(s)$, the structure function whose Fourier transformation gives molecular-pair correlation, is difined as follows:

$$H_M(s) = [I(s)-\langle F^2\rangle]/\langle F\rangle^2. \quad (3)$$

$I(s)$ is the total coherent intensity from the liquid and $\langle F^2\rangle$ is scattered intensity from one molecule and is given by:

$$\langle F^2\rangle = \sum_i\sum_j f_i(s)f_j(s)\frac{\sin sr_{ij}}{sr_{ij}}\exp\left(-\frac{l_{ij}^2}{2}s^2\right), \quad (4)$$

where l_{ij} denotes the root mean-square amplitude of the vibration around the mean internuclear distance, r_{ij}, $\langle F\rangle$ is defined by:

$$\langle F\rangle = \sum_i f_i(s)\frac{\sin sr_i}{sr_i}\exp\left(-\frac{l_i^2}{2}s^2\right), \quad (5)$$

where r_j is the distance from the scattering center to the i-th atom. The results are listed in Table 1, with the values obtained by Narten and Levy at 25 °C. The two set of data are in good agreement with each other within 5—6% differences in the range where the intensity curve is gentle. However, a large derivation in the value of $H_M(s)$ is observed at a peak or valley in the intensity curve, for example, at the first peak at nearly $s=2.0$ Å^{-1}. It seems that this deviation is caused by an experimental error in the determination of the s-value. This determination error is within 0.02 Å^{-1} in the s-value, which corresponds to 0.05° angle-setting error for the peak at $s=2.0$ Å^{-1}. From these considerations, it may be concluded that the energy-dispersive data are in good agreement with Narten's data, within the limits of experimental error.

Finally, we have used the absolute total coherent intensity at $s=0$, $I(0)$, for judging the correctness of the data processing. $I(0)$ is related to the isothermal compressibility, κ, as follows:[17]

$$I(0)/(\sum_n Z_n)^2 = \kappa\rho_0 kT \quad (6)$$

where k is the Boltzmann constant and T the absolute temperature. The observed $I(0)$ (7.0 e.u.) does not differ significantly from the value (6.3 e.u.) calculated from Eq. 6 by the use of the reported κ-value (45.7×10^{-12} cm^2 dyn^{-1}, at 25 °C),[18] and it is also almost the same as that obtained by Chonacky and Beeman.[13]

Reproducible fine structures could not be found in the diffraction pattern of liquid water (Fig. 3). As a result of the Fourier transformation of the weighted structure function, the correlation was observed only up to 8 Å. This distance is very short compared with that in CCl_4 (28 Å).[2,3] The finding that the long-range correlation does not exist in liquid water can be interpreted as follows. A water molecule is well arranged among its neighbors according to the strong hydrogen bond, so the structure of liquid water is very bulky. This bulkiness helps to enhance the disorder of the liquid structure. This fact is supported by the density fluctuation obtained by the scattering intensity at small s-values. The observed $I_{CO}(0)$ was obtained by extrapolating the absolute total coherent intensity at small s-values and became 7.0 e.u. (electron units). This value shows that one water molecule fluctuates in a

TABLE 1. THE COMPARISON OF THE STRUCTURE FUNCTIONS FOR LIQUID WATER

s	$H_M(s)$		s	$H_M(s)$		s	$H_M(s)$		s	$H_M(s)$	
	Narten	This work		Narten	This work		Narten	This work		Narten	This work
0.00	−0.938	−0.930	0.08	−0.938	−0.930	8.16	−0.054	−0.052	8.24	−0.054	−0.053
0.16	−0.938	−0.930	0.24	−0.937	−0.930	8.32	−0.050	−0.049	8.40	−0.042	−0.040
0.32	−0.937	−0.929	0.40	−0.936	−0.929	8.48	−0.033	−0.030	8.56	−0.023	−0.024
0.48	−0.935	−0.928	0.56	−0.932	−0.928	8.64	−0.013	−0.009	8.72	−0.005	−0.004
0.64	−0.928	−0.924	0.72	−0.921	−0.920	8.80	0.003	0.002	8.88	0.010	0.009
0.80	−0.913	−0.916	0.88	−0.902	−0.906	8.96	0.017	0.018	9.04	0.023	0.025
0.96	−0.890	−0.899	1.04	−0.878	−0.888	9.12	0.028	0.027	9.20	0.031	0.033
1.12	−0.861	−0.872	1.20	−0.835	−0.846	9.28	0.032	0.030	9.36	0.031	0.029
1.28	−0.796	−0.815	1.36	−0.748	−0.770	9.44	0.029	0.029	9.52	0.027	0.024
1.44	−0.685	−0.704	1.52	−0.599	−0.622	9.60	0.025	0.023	9.68	0.021	0.019
1.60	−0.478	−0.507	1.68	−0.320	−0.371	9.76	0.015	0.017	9.84	0.007	0.010
1.76	−0.158	−0.216	1.84	−0.002	−0.039	9.92	−0.001	0.002	10.00	−0.009	−0.006
1.92	0.119	0.080	2.00	0.190	0.169	10.08	−0.014	−0.014	10.16	−0.017	−0.014
2.08	0.212	0.192	2.16	0.157	0.194	10.24	−0.018	−0.013	10.32	−0.019	−0.015
2.24	0.166	0.165	2.32	0.134	0.142	10.40	−0.020	−0.015	10.48	−0.020	−0.016
2.40	0.116	0.124	2.48	0.119	0.130	10.56	−0.020	−0.016	10.64	−0.019	−0.018
2.56	0.147	0.147	2.64	0.193	0.169	10.72	−0.016	−0.015	10.80	−0.012	−0.014
2.72	0.245	0.220	2.80	0.287	0.268	10.88	−0.009	−0.010	10.96	−0.007	−0.008
2.88	0.301	0.293	2.96	0.277	0.286	11.04	−0.005	−0.007	11.12	−0.003	−0.005
3.04	0.215	0.256	3.12	0.125	0.171	11.20	0.000	−0.003	11.28	0.003	0.002
3.20	0.022	0.073	3.28	−0.079	−0.027	11.36	0.007	0.006	11.44	0.010	0.009
3.36	−0.164	−0.119	3.44	−0.227	−0.187	11.52	0.013	0.011	11.60	0.016	0.017
3.52	−0.262	−0.232	3.60	−0.271	−0.251	11.68	0.017	0.016	11.76	0.017	0.017
3.68	−0.255	−0.356	3.76	−0.233	−0.245	11.84	0.015	0.016	11.92	0.013	0.014
3.84	−0.199	−0.230	3.92	−0.205	−0.200	12.00	0.010	0.013	12.08	0.008	0.010
4.00	−0.124	−0.171	4.08	−0.083	−0.106	12.16	0.006	0.011	12.24	0.003	0.005
4.16	−0.039	−0.060	4.24	0.005	−0.005	12.32	0.000	0.001	12.40	−0.002	0.001
4.32	0.045	0.030	4.40	0.076	0.074	12.48	−0.004	−0.002	12.56	−0.005	−0.004
4.48	0.098	0.088	4.56	0.114	0.100	12.64	−0.005	−0.006	12.72	−0.006	−0.006
4.64	0.126	0.115	4.72	0.135	0.126	12.80	−0.007	−0.005	12.88	−0.010	−0.008
4.80	0.140	0.125	4.88	0.136	0.120	12.96	−0.012	−0.009	13.04	−0.011	−0.012
4.96	0.124	0.118	5.04	0.104	0.096	13.12	−0.009	−0.010	13.20	−0.006	−0.007
5.12	0.080	0.079	5.20	0.057	0.053	13.28	−0.003	−0.005	13.36	−0.001	−0.004
5.28	0.035	0.020	5.36	0.013	−0.005	13.44	0.001	−0.001	13.52	0.002	0.000
5.44	−0.009	−0.015	5.52	−0.034	−0.039	13.60	0.005	0.003	13.68	0.007	0.005
5.60	−0.057	−0.063	5.68	−0.078	−0.078	13.76	0.008	0.007	13.84	0.008	0.009
5.76	−0.093	−0.100	5.84	−0.102	−0.108	13.92	0.007	0.008	14.00	0.005	0.007
5.92	−0.105	−0.099	6.00	−0.102	−0.093	14.08	0.004	0.007	14.16	0.004	0.005
6.08	−0.094	−0.088	6.16	−0.080	−0.078	14.24	0.004	0.006	14.32	0.004	0.005
6.24	−0.063	−0.060	6.32	−0.044	−0.045	14.40	0.002	0.004	14.48	0.000	0.002
6.40	−0.026	−0.029	6.48	−0.009	−0.011	14.56	−0.002	0.001	14.64	−0.003	−0.002
6.56	0.007	0.017	6.64	0.023	0.029	14.72	−0.004	−0.003	14.80	−0.004	−0.004
6.74	0.040	0.039	6.80	0.056	0.059	14.88	−0.004	−0.005	14.96	−0.004	−0.005
6.88	0.069	0.070	6.96	0.075	0.087	15.04	−0.004	−0.003	15.12	−0.003	−0.003
7.04	0.077	0.089	7.12	0.074	0.080	15.20	−0.003	−0.002	15.28	−0.003	−0.002
7.20	0.069	0.070	7.28	0.063	0.065	15.36	−0.003	−0.001	15.44	−0.003	−0.001
7.36	0.053	0.055	7.44	0.040	0.047	15.52	−0.002	0.000	15.60	−0.001	0.000
7.52	0.024	0.023	7.60	0.007	0.010	15.68	0.000	0.000	15.76	0.000	0.000
7.68	−0.008	−0.005	7.76	−0.020	−0.018	15.84	−0.001	0.000	15.92	−0.002	0.000
7.84	−0.030	−0.025	7.92	−0.039	−0.035	16.00	−0.003	0.000			
8.00	−0.044	−0.040	8.08	−0.050	−0.048						

volume of 467 Å^3. In other word, since 15.6 water molecules are contained in this volume, there are 15.6 ± 1 molecules in 467 Å^3 for water at room temperature. On the other hand, there are 63 ± 1 molecules in 1.00×10^4 Å^3 for liquid CCl_4.[1)]

There are many models for the structure of liquid water,[19)] and an effort to obtain the atom-atom pair correlation functions, that is $g_{OO}(r)$, $g_{OH}(r)$, and $g_{HH}(r)$ has been made experimentally.[20,21)] However, our search for a satisfactory model of liquid water must

be left for future study.

In conclusion, it was ascertained that the analysis for the energy-dispersive method was appropriate, and that data obtained by the use of energy-dispersive method were in good agreement with Narten's results within the limits of experimental error. It seems that in the present experiment the energy-dispersive method was given a sound basis for further application to more different systems.

The authors would like to express their thanks to Professor Yoshitada Murata, The Institute for Solid State Physics, The University of Tokyo and Professor Takao Iijima, Gakushuin University for their helpful discussions.

References

1) Y. Murata and K. Nishikawa, *Bull. Chem. Soc. Jpn.*, **51**, 411 (1978).
2) K. Nishikawa and Y. Murata, *Bull. Chem. Soc. Jpn.*, **52**, 293 (1979).
3) K. Nishikawa, K. Tohji, M. Shima, and Y. Murata, *Chem. Phys. Lett.*, **64**, 154 (1979).
4) A. H. Narten, M. D. Danford, and H. A. Levy, *Discuss. Faraday Soc.*, **43**, 97 (1967).
5) A. H. Narten, M. D. Danford, and H. A. Levy, ORNL Rept. ORNL-3997 (1966).
6) A. H. Narten ORNL Rept. ORNL-4578 (1970).
7) A. H. Narten and H. A. Levy, *J. Chem. Phys.*, **55**, 2263 (1971).
8) J. Morgan and B. E. Warren, *J. Chem. Phys.*, **6**, 666 (1938).
9) C. Finbak and H. Viervoll, *Tridsskr. Kjemi. Bergvessen Met.*, **3**, 36 (1943).
10) G. W. Brady and W. J. Romanov, *J. Chem. Phys.*, **32**, 306 (1960).
11) C. L. van Panthaleon van Eck, H. Mendel, and W. Boog, *Discuss. Faraday Soc.*, **24**, 200 (1957); *Proc. R. Soc. London, Ser. A*, **247**, 472 (1958).
12) J. Heemskerk, *Rec. Trav. Chim.*, **81**, 904 (1962).
13) N. J. Chonacky and W. W. Beeman, *Acta Crystallogr., Sect. A*, **25** 564 (1969).
14) "International Tables for X-Ray Crystallography," Kynoch Press, Birmingham (1962), Vol. III.
15) S. Shibata and L. S. Bartell, *J. Chem. Phys.*, **42**, 1147 (1965).
16) D. T. Cromer, *J. Chem. Phys.*, **50**, 4857 (1969).
17) J. O. Hirschfelder, C. F. Curtiss, and R. B. Bird, "Molecular Theory of Gases and Liquids," Wiley, New York (1966).
18) R. E. Gibson and O. H. Leoffer, *J. Am. Chem. Soc.*, **63**, 898 (1941).
19) A. H. Narten and H. A. Levy, *Science*, **165**, 447 (1969).
20) A. H. Narten, *J. Chem. Phys.*, **56**, 5681 (1972).
21) G. Pálinkás, E. Kálmán, and P Kovács, *Mol. Phys.*, **34**, 525 (1977).

Nuclear Magnetic Resonance in Hemihydrate Gypsum

Kenji SHIMOMURA, Toshikazu NAGASHIMA,† Akira SANJOH,††
Makoto YOSHIDA,†† and Hisao NEGITA*,††

Department of Physics, Faculty of Integrated Arts and Sciences, Hiroshima University, Higashisenda-machi, Hiroshima 730
†*Ube Research Center, Central Glass Co., Ltd., Okiube, Ube 755*
††*Department of Chemistry, Faculty of Science, Hiroshima University, Higashisenda-machi, Hiroshima 730*

(Received January 12, 1980)

The proton spin-lattice relaxation times T_1 and T_{1D} along the static and dipolar magnetic fields have been measured at 18 MHz for the water molecule in powdered hemihydrate gypsum $CaSO_4 \cdot (1/2)H_2O$. The minima of T_1 and T_{1D} were observed at $10^3/T=4.3$(233 K) and 7.0(143 K) respectively. These are ascribed to the 180° flip motion of water molecules, with an activation energy of 15.1 kJ/mol. At higher temperatures, the translational diffusion of water molecules becomes dominant; this is not observed in gypsum $CaSO_4 \cdot 2H_2O$. The activation energy of this motion is estimated to be 32.2 kJ/mol. In hemihydrate gypsum, though the diffusion is supposed to be anisotropic, the jumping distance of the water molecule is tentatively examined by Torrey's lattice diffusion theory.

In the series of crystal forms of gypsum $CaSO_4 \cdot nH_2O$, two kinds of hemihydrate gypsum, $CaSO_4 \cdot (1/2)H_2O$, are known. These are called α- and β-hemihydrate gypsum, and are obtained with different methods of preparation. The NMR method has been applied by several workers to investigate the internal motions of water molecules in gypsum. Holcomb and Pedersen[1] measured the spin-lattice relaxation time T_1 in gypsum over a wide temperature range, and showed that the relaxation is dominated by the 180° flip motion which modulates the interactions with protons on neighboring water molecules. Look and Lowe[2] examined the rotating frame spin-lattice relaxation time $T_{1\rho}$. Jeener *et al.*[3,4] evaluated the 180° flips of water molecules in gypsum and pointed out the additional relaxation due to infrequent, thermally activated jumps of water molecules at high temperatures.

It is interesting to consider the difference between the crystal structures of gypsum and hemihydrate gypsum, in which the nuclear motion affects the magnetic resonance linewidth and relaxation times. The crystal structure of gypsum consists of layers parallel to the (010) plane. The layers are bound together by bonds from water molecules, which link the Ca^{2+} ion and O atom of a SO_4^{2-} ion in one layer with an O atom of SO_4^{2-} in the adjacent layer.[5,6] A number of studies have been done on the crystal structure of hemihydrate gypsum.[7-11] The space group of the trigonal unit cell is $P3_221$ and the cell dimensions are $a=b=6.83$ Å, $c=12.70$ Å, $\gamma=120°$, and $Z=6$. These results indicate that the characteristic features of hemihydrate gypsum are due to the existence of tunnels (or systems of interconnected cavities) which serves as the passage of the water molecules through the c-axis; water molecules are held together in these tunnels, with the closest neighboring O–O distance of water molecules being 4.23 Å. Accordingly, the motion of the water molecule in hemihydrate gypsum seems to have more degrees of freedom than that in gypsum. In hemihydrate gypsum, no fundamental difference of the crystal structure has been found between α- and β-hemihydrate gypsum.[12,13] But Lasis suggests that β-hemihydrate gypsum contains more lattice defects than α-hemihydrate gypsum.[14]

Differential thermal analysis was performed in order to distinguish the α- and β-hemihydrate gypsum; this proved to be superior to the X-ray powder diffraction method. These two methods, however, gave little information on the internal motions of water molecules. Therefore, the NMR experiment was performed in order to obtain a valuable check on the motions of the water molecules. Both pulse and cw methods were employed on the powdered α- and β-hemihydrate gypsum, and the spin-lattice relaxation times T_1 along the static, T_{1D} along the dipolar magnetic fields, and the second moments were measured to examine the motion of water molecules in hemihydrate gypsum.

Experimental

The proton relaxation time T_1 was measured at 18 MHz by the solid echo method, because the free-induction decay signals were so weak in hemihydrate gypsum. T_{1D} was obtained by the 90°-45°-45° pulse method. In order to do the on-line measurement, the free decay on an oscilloscope was amplitude-to-time converted (ATC) and measured by a digital counter, while the pulse interval was measured by

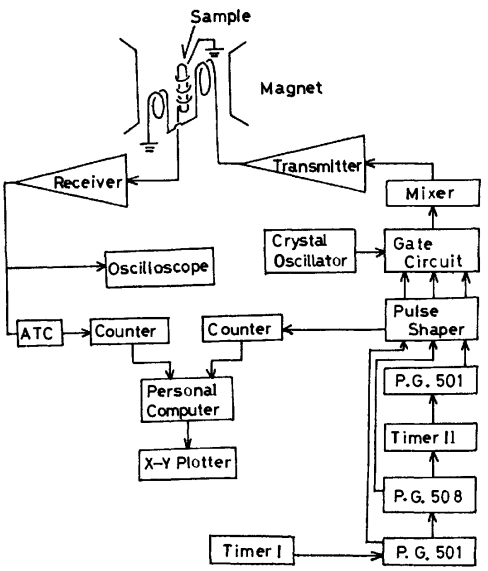

Fig. 1. Block diagram of the pulse NMR spectrometer.

another counter. These results were displayed on an X-Y plotter through a PC-7200 computer. A block diagram of the pulse NMR spectrometer is shown Fig. 1. The resonance-line-shape curve was measured at 40 MHz using a JEOL model JES-BE-1. The samples are powdered gypsum and hemihydrate gypsum from commercial sources. Three kinds of samples, K-α, P-α, and O-β, named after the makers and types of hemihydrate gypsum, were used for the experiment. A sample of hemihydrate gypsum which had been kept for about 47 h at 10^{-2}—10^{-3} Torr** was also examined. In this case, preparation was performed at about 0 °C, with care to avoid the evacuation of the water of crystallization.[15]

Results and Discussion

Second Moment. Figure 2 shows the temperature dependence of the second moments in hemihydrate gypsum. The second moments in K-α, P-α, and O-β are 24 G^2,** 25 G^2, and 23 G^2 at 123 K respectively, and the gypsum value is 30 G^2 at 173 K. This fact shows the distance between the protons in the hemihydrate gypsum is larger than that in the gypsum. But, as shown in Fig. 2, the second moments at 123 K have not reached their rigid lattice values, so we will not discuss further these values of the second moments. It is seen in Fig. 2 that the second moments of raw hemihydrate gypsum decrease suddenly above room temperature and have a minimum value (*ca.* 13 G^2) at 330 K. This remarkable anomaly is pronounced in K-α, whereas the same decrease is not observed in the evacuated hemihydrate gypsum. Recovery of the second moment occurs gradually above 330 K in the raw samples, and the curve becomes similar to that of the evacuated samples. Above 383 K the second moments decrease in the same way for both raw and evacuated hemihydrate gypsum.

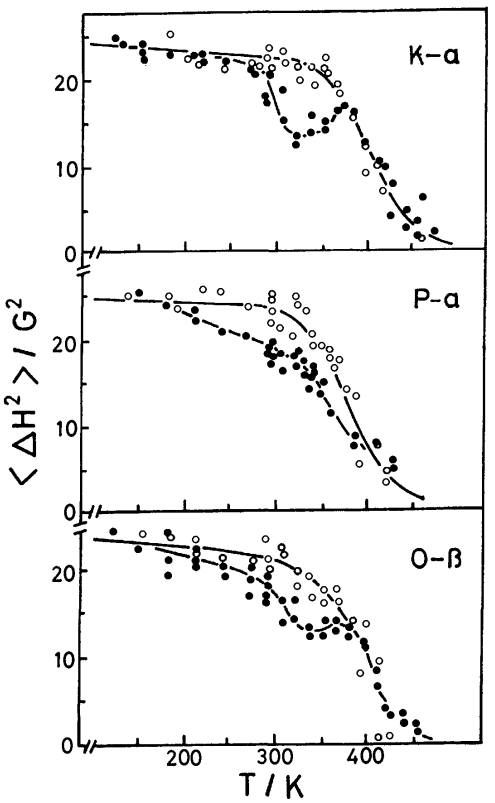

Fig. 2. Second moments of the proton resonance lines in K-α, P-α, and O-β as a function of temperature.
●: Raw samples, ○: evacuated samples.

** Throughout this paper 1 Torr = 133.322 Pa and 1 G = 10^{-4} T.

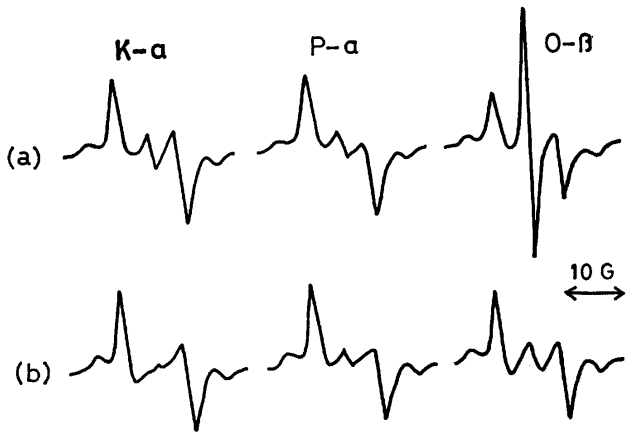

Fig. 3. Absorption derivative curves in the raw and evacuated hemihydrate gypsum at room temperature. (a) Raw samples, (b) evacuated for about 47 h at 10^{-2}—10^{-3} Torr.

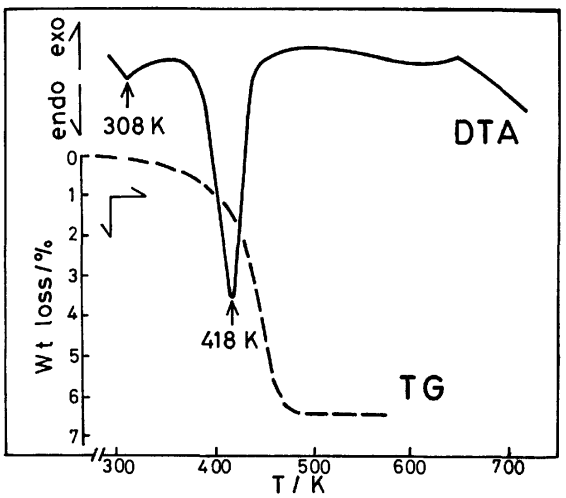

Fig. 4. DTA and TG curves in raw O-β.
Solid line indicates the DTA curve and dashed line TG curve.

Figure 3 shows the derivative curves of absorption spectra in raw and evacuated hemihydrate gypsum at room temperature; the difference in the central parts is important. It is obvious that the central part of the spectra, which is characterized by the diffusing adsorption waters, is remarkable in raw O-β, compared with both raw K-α and P-α. In an effort to explain the anomaly in the second moment at around 330 K, the thermal properties of hemihydrate gypsum were examined. Figure 4 shows the DTA and TG curves of O-β. The endothermic peaks at 308 K and 418 K correspond to dehydration of adsorption water and water of crystallization respectively. In hemihydrate

gypsum, adsorption water seems to be held on the surface as well as in the crystal lattice. When the temperature is higher than 290 K, the adsorption water molecules in the raw sample diffuse in the crystal lattice and leave from its surface, so that the motional-narrowing of the resonance line due to diffusion appears and contributes to the central part of the resonance line, resulting in the decrease of the second moment. The recovery of the second moment above 330 K in the raw sample can be ascribed to the exhaustion of the diffusing adsorption water molecules in the crystal, which restores the second moment back to that of the evacuated sample which has less mobile water molecules. The decrease of the second moment above 383 K seems to be ascribed to the diffusion of the water molecule due to the dehydration of rigidly bound water, which agrees well with the results of the DTA and TG curves.

Spin-lattice Relaxation Time. The spin-lattice relaxation times T_1 and T_{1D} *vs.* inverse temperature in gypsum are shown in Fig. 5, in which $(T_1)_{min}$($\approx$90 ms) appears at $10^3/T$=4.0(250 K) and $(T_{1D})_{min}$($\approx$1 ms) is expected to be present at $10^3/T$=7.0—8.0(143—125 K). The observed T_1 curve below 250 K gives the activation energy of 24.7 kJ/mol; we found $T_1 \approx 3T_{1D}$ on the higher temperature side of $(T_1)_{min}$. The relaxation times as a function of temperature are also shown for the three kinds of hemihydrate gypsum in Fig. 6. In hemihydrate gypsum, $(T_1)_{min}$ appears at $10^3/T$=4.3(233 K) and $(T_{1D})_{min}$ at $10^3/T$=7(143 K). These two minima are ascribed to the same mechanism. $(T_1)_{min}$ at $10^3/T$=4.3 are 0.8, 1, and 1.4 s in O-β, K-α, and P-α respectively. On the higher temperature side of $(T_1)_{min}$, T_1 decreases rapidly; this is not observed in gypsum. This tendency is seen also in T_{1D} curves. It may be concluded that $(T_1)_{min}$ may exist at $10^3/T$=2.5—2.6(*ca.* 390 K) with the value of 0.1—0.2 s, if we take the value of $(T_{1D})_{min}$ at $10^3/T$ to be 3.5(286 K). The temperature dependence

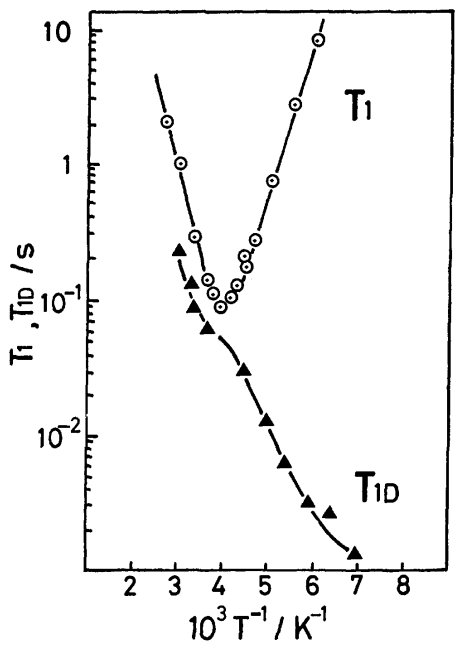

Fig. 5. Temperature dependence of the proton T_1 and T_{1D} in powdered gypsum $CaSO_4 \cdot 2H_2O$.

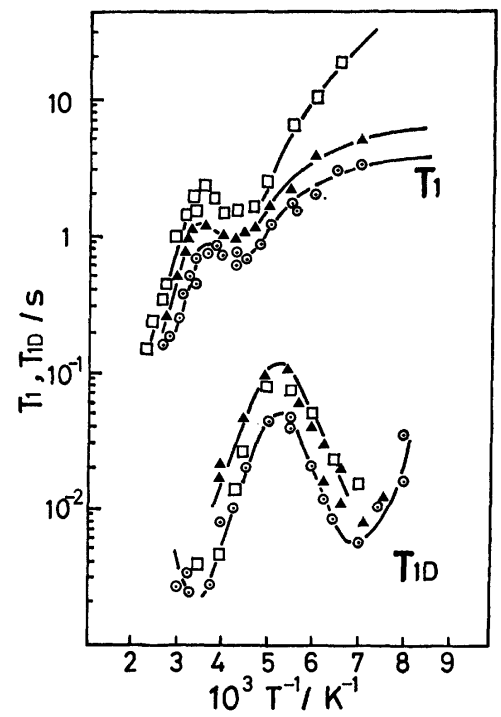

Fig. 6. Temperature dependence of the proton T_1 and T_{1D} in powdered hemihydrate gypsum $CaSO_4 \cdot (1/2)H_2O$.
⊙: O-β, ▲: K-α, □: P-α.

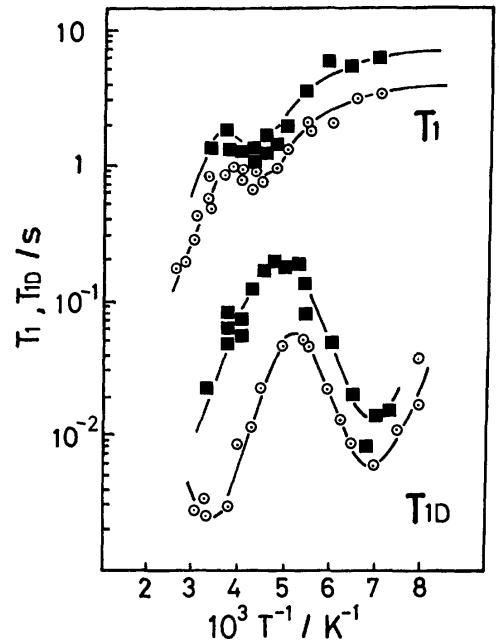

Fig. 7. Temperature dependence of the proton T_1 and T_{1D} in the evacuated O-β. Relaxation times in raw O-β are also shown.
⊙: Raw sample, ■: evacuated sample.

of T_1 and T_{1D} in evacuated O-β is shown in Fig. 7. It is obvious from Fig. 7 that T_1 and T_{1D} of the evacuated sample are longer than those of the raw sample.

At temperatures lower than 182 K, the T_1 *vs.* $1/T$ curve has a small gradient. This shows that the relaxa-

tion rate due to paramagnetic impurities predominates in this temperature region, which is important in O-β and K-α but not in P-α. Therefore, the observed relaxation time $(T_1)_{obsd}$ can be expressed as:

$$\frac{1}{(T_1)_{obsd}} = \frac{1}{(T_1)_e} + \frac{1}{(T_1)_n}, \tag{1}$$

where $1/(T_1)_e$ is the relaxation rate due to paramagnetic impurities and $(T_1)_n$ is the relaxation time due to other sources. In Fig. 8 $(T_1)_n$ were plotted after the contribution of the paramagnetic impurities was removed. In Fig. 8 we obtain $(T_1)_{min}=1$, 1.4, and 1.6 s for O-β, K-α, and P-α respectively, and 1.5 s for evacuated O-β.

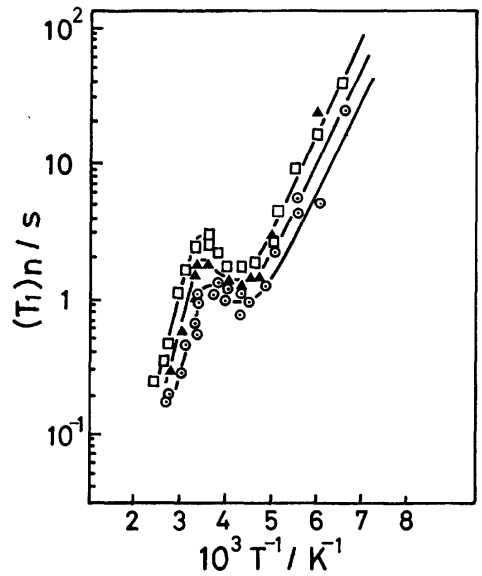

Fig. 8. Temperature dependence of the T_1 in hemihydrate gypsum. Contribution due to paramagnetic impurity is subtracted from the observed T_1 values.
⊙: O-β, ▲: K-α, □: P-α.

The proton relaxation time may be associated with two types of molecular motions: (1) the 180° flip of a water molecule about the bisector of the H-O-H angle, and (2) the translational diffusion of the water molecules. Since the intramolecular dipole-dipole interaction Hamiltonian is invariant to 180° flip motion, the intramolecular interaction makes no contribution to T_1, for which only the intermolecular interactions are responsible. The value of the second moment, which mainly comprises the intramolecular interaction, is not affected by the flip motion. Thus, as shown in Fig. 2, the observed second moment of the evacuated sample does not change appreciably up to the temperature of dehydration. Accordingly, we assign the 180° flip process to the low temperature $(T_1)_{min}$. The spin-lattice relaxation time T_1 due to this flipping is given by[2,16]

$$\frac{1}{T_1} = \gamma^4\hbar^2\frac{3I(I+1)}{16N}\sum_{i\neq j}\left[B_{ij}^{(1)}\frac{\tau_c}{1+(1/4)\omega_0^2\tau_c^2} + (2A_{ij}^{(1)}+B_{ij}^{(2)})\frac{\tau_c}{1+\omega_0^2\tau_c^2} + 2A_{ij}^{(2)}\frac{\tau_c}{1+4\omega_0^2\tau_c^2}\right], \tag{2}$$

where the notation is that of Ref. 16. Equation 2 at $\omega_0\tau_c \gg 1$ gives

$$\frac{1}{T_1} = \frac{C}{\omega_0 N\tau_c}, \tag{3}$$

where the constant C includes the proton-proton distances between water molecules. We obtained 15.1 kJ/mol for the activation energy E_a from $(T_1)_n$ data in Fig. 8 by assuming the relation $\tau_c=\tau_c^0\exp(E_a/RT)$. This value is identical to that obtained from the observed T_{1D}. The slight difference of T_1 values between α- and β-hemihydrate gypsum may be due to the amount of water molecules in the crystal lattice.

We next turn to the effect of translational diffusion on T_1 in the hemihydrate gypsum. No theoretical treatment of the diffusion has been done on a non-cubic crystal. Assuming a homogeneous distribution of nuclear dipoles, Bloom[17] obtained T_1 for the case of self-diffusion as follows:

$$\frac{1}{T_1} = \frac{8\pi}{5}\gamma^4\hbar^2 I(I+1)N \times\int_a^\infty r^{-4}\left\{\frac{\tau_c}{1+\omega_0^2\tau_c^2}+\frac{4\tau_c}{1+4\omega_0^2\tau_c^2}\right\}dr, \tag{4}$$

where N is the number of diffusing spins per unit volume and a is the distance of the closest approach of pairs of nuclei. It follows from the crystal data of hemihydrate gypsum that $N=1.17\times10^{22}/cm^3$. At the $(T_1)_{min}$ where $\omega_0\tau_c=0.62$, the following Eq. 5 is obtained from Eq. 4[18]

$$\frac{1}{(T_1)_{min}} = \frac{6\pi}{5}\gamma^4\hbar^2 N\frac{0.475}{\omega_0 a^3}. \tag{5}$$

Substituting $\tau_c=r^2/12D$[19] on the lower temperature side where $\omega_0^2\tau_c^2\gg1$, an asymptotic form is obtained from Eq. 4 as follows:

$$\frac{1}{T_1} = \frac{144\pi}{25}\gamma^4\hbar^2 ND\frac{1}{\omega_0^2 a^5}, \tag{6}$$

where D is the diffusion coefficient and can be expressed as $D_0\exp(-E_a/RT)$. On the higher temperature side where $\omega_0^2\tau_c^2\ll1$, we also obtain

$$\frac{1}{T_1} = \gamma^4\hbar^2 N\frac{\pi}{2Da}. \tag{7}$$

In order to examine the common features for both BPP (Bloembergen, Purcell, and Pound) and Torrey's theories, we consider the case where three-dimensional isotropic diffusion occurs in a space lattice. T_1 due to this motion is given for $I=1/2$ as follows:[20]

$$\frac{1}{T_1} = \frac{9}{8}\gamma^4\hbar^2\{S_1(\omega)+4S_1(2\omega)\}, \tag{8}$$

where S_1 is the spectral density of the random time function. In the limiting case $\langle r^2\rangle \gg a^2$, for which the mean flight distance is long, we obtain

$$S_1(\omega) = \frac{8\pi N}{45a^3}\left\{\frac{\tau}{1+(\omega\tau/2)^2}\right\}. \tag{9}$$

Then T_1 is given by

$$\frac{1}{T_1} = \frac{2\pi N}{5a^3}\gamma^4\hbar^2\left\{\frac{\tau/2}{1+(\omega\tau/2)^2}+\frac{2\tau}{1+(\omega\tau)^2}\right\}, \tag{10}$$

where the correlation time τ_c is equal to $\tau/2$.

At a temperature which satisfies the relation $\omega\tau=1.23$, Eq. 10 gives a $(T_1)_{min}$

$$\frac{1}{(T_1)_{min}} = \frac{2\pi N}{5a^3}\gamma^4\hbar^2\frac{1.425}{\omega} = \frac{6\pi N}{5}\gamma^4\hbar^2\frac{0.475}{\omega a^3}, \quad (11)$$

which agrees well with Eq. 5. In general, when the correlation time is short ($\omega_0^2\tau_c^2 \ll 1$), Torrey's theory agrees well with the BPP theory.[20] On the other hand, where $\omega_0^2\tau_c^2 \gg 1$, the former theory provides a much better fit than the latter. But, as shown in Eqs. 5 and 11, both theories give the same $(T_1)_{min}$ so that we can estimate the parameters a and D from this region.

In O-β, $(T_1)_{min}$ is estimated to be about 0.16 s at $10^3/T=2.25$; we obtain $a=2.56$ Å from Eq. 5 or 11. Distance a changes from 2.45 Å to 2.67 Å, if $(T_1)_{min}$ is taken from 0.14 to 0.18 s. If we put Eq. 6 equal to Eq. 7, we have an approximate condition at the $(T_1)_{min}$[18] and we obtain

$$D = \sqrt{\frac{25}{288}}\omega_0 a^2. \quad (12)$$

From this equation $a=2.56$ Å yields $D=2.1\times10^{-8}$ cm^2/s. On the other hand, we found the activation energy $E_a=32.2$ kJ/mol for diffusion from T_1 in Fig. 6 and the constant D_0 was then obtained to be 4.28×10^{-4} cm^2/s. In Fig. 9, the straight line indicates the calculated relaxation time T_1 which is followed by Eq. 6.

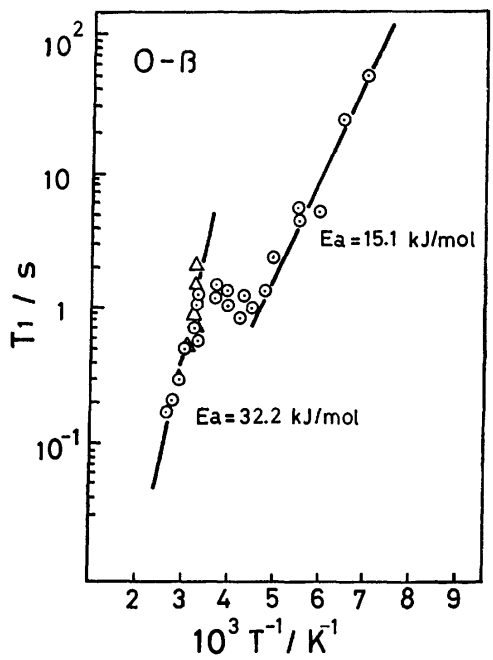

Fig. 9. Calculated T_1 values in O-β.
The straight line at the left is obtained from Eq. 6, and the right is a best fit of Eq. 3 to the data. Diffusion controlled contribution to T_1 is indicated by △.

Now we consider the case of lattice diffusion in which a spin-bearing nucleus jumps between nearest-neighbor lattice sites. We will be able to estimate the jumping distance of nucleus in the crystal lattice. The spectral density $S_1(\omega)$ is given by[21]

$$S_1(\omega) = \frac{8c}{15\omega^2\tau}\sum_i\frac{1}{r_i^6}\left\{1-\frac{1}{z}\sum_j\left(\frac{r_i}{r_j}\right)^3\left(1-\frac{3l^2}{2r_j^2}\sin^2\Theta_j\right)\right\}, \quad (13)$$

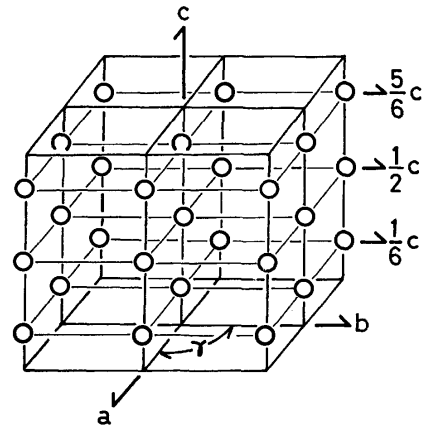

Fig. 10. The crystal structure of hemihydrate gypsum.
Positions of water molecules are shown by large circles. Cell dimensions of the trigonal unit cell are $a=b=$ 6.83 Å, $c=12.70$ Å, $\gamma=120°$, and $Z=6$.

where Θ_j is the angle between proton-proton vectors $\boldsymbol{r}_j$ and $\boldsymbol{r}_i$, z is the number of the nearest neighbors of a lattice site, and c is the ratio of the number of nuclei to the number of lattice sites. In a water molecule, we let $c=2$ as a rough estimation.[22] Figure 10 shows the positions of water molecules in hemihydrate gypsum. In order to estimate the jumping distance l, we substitute the distance r for l. Then Eq. 13 becomes

$$S_1(\omega) = \frac{124}{15\omega^2\tau}l^{-6}. \quad (14)$$

Next we evaluate the value of T_1 for two cases, that is, $l=4.23$ Å (closest O–O bond distance between the water molecules along the c-axis) and 6.83 Å (the corresponding distance on a horizontal plane). In the former case

$$S_1(\omega) = 1.437\times10^{45}\frac{1}{\omega^2\tau} \quad (15)$$

and

$$\frac{1}{T_1} = 3.234\times10^{45}\frac{\gamma^4\hbar^2}{\omega^2\tau} = 4.81\times10^8 D, \quad (16)$$

whereas for the latter case

$$S_1(\omega) = 8.144\times10^{43}\frac{1}{\omega^2\tau} \quad (17)$$

and

$$\frac{1}{T_1} = 1.832\times10^{44}\frac{\gamma^4\hbar^2}{\omega^2\tau} = 1.05\times10^7 D, \quad (18)$$

in which $\tau=l^2/6D$ is applied. For example, at $10^3/T=$ 3.0 and $D=3.82\times10^{-9}$ cm^2/s, we obtain $T_1=0.5$ s for $l=4.23$ Å and 25 s for $l=6.83$ Å. The observed value is about 0.3 s. Moreover, since $D=9.85\times10^{-10}$ cm^2/s at $10^3/T=3.35$, we obtain $T_1=2.1$ s for $l=4.23$ Å and $T_1=96$ s for $l=6.83$ Å. The observed T_1 is about 2 s. It is obvious from these results that the lattice diffusion model for $l=4.23$ Å agrees better with the experimental value.

Conclusion

The investigation of the proton magnetic resonance spectra and its relaxation times of hemihydrate gypsum

has lead to the following conclusions:

1) β-Hemihydrate gypsum contains more adsorption water in the crystal lattice than α-hemihydrate gypsum.

2) It is found that the 180° flip of the water molecule (E_a=15.1 kJ/mol) already begins at the temperature below 125 K which is the lower temperature limit of the T_{1D} measurement. In raw samples, the adsorption water which combines loosely with the crystal lattice is released at about room temperature. The translational diffusion of the water molecule (E_a=32.2 kJ/mol) begins in the crystal lattice above the temperature of 200 K, and results in the dehydration of the water of crystallization at about 380 K.

3) In O-β, we obtain $D_0 \approx 4 \times 10^{-4}$ cm^2/s and the distance of closest approach of the water molecules $a \approx 2.6$ Å. Applying 4.23 Å as the jumping distance of the water molecule between the lattice points in Torrey's theory, we can explain the observed T_1 values above 286 K successfully.

References

1) D. F. Holcomb and B. Pedersen, *J. Chem. Phys.*, **36**, 3270 (1962).
2) D. C. Look and I. J. Lowe, *J. Chem. Phys.*, **44**, 2995 (1966).
3) H. Eisendrath, W. Stone, and J. Jeener, *Phys. Rev. B*, **17**, 47 (1978).
4) H. Eisendrath and J. Jeener, *Phys. Rev. B*, **17**, 54 (1978).
5) M. Atoji and R. E. Rundle, *J. Chem. Phys.*, **29**, 1306 (1958).
6) W. F. Cole and C. J. Lancucki, *Acta Crystallogr., Sect. B*, **30**, 921 (1974).
7) P. Gallitelli, *Per. Min.*, **4**, 1 (1933).
8) O. W. Flörke, *Neues Jahrb. Mineral. Abh.*, **84**, 189 (1952).
9) P. Gay, *Min. Mag.*, **35**, 354 (1965).
10) F. G. Berschadski and O. P. Mtschedlow-Petrossian, *Zh. Prikl. Khim.*, **1966**, 1449.
11) O. P. Mtschedlow-Petrossian and F. G. Berschadski, *Silikattechnik*, **18**, 147 (1967).
12) H. Lehmann, *Tonind. Ztg.*, **91**, 6 (1967).
13) H. Miyazaki and N. Takagi, *Kogyo Kagaku Zasshi*, **73**, 1766 (1970).
14) A. Yu. Lasis, *Stroit. Mat.*, **1**, 38 (1971).
15) J. J. Gardet, B. Guilhot, and M. Soustelle, *Bull. Soc. Chim. Fr.*, **1970**, 3377.
16) K. Sagisawa, H. Kiriyama, and R. Kiriyama, *Bull. Chem. Soc. Jpn.*, **51**, 1942 (1978).
17) M. Bloom, *Physica*, **23**, 767 (1957).
18) G. W. Smith, *J. Chem. Phys.*, **36**, 3081 (1962).
19) D. F. Holcomb and R. E. Norberg, *Phys. Rev.*, **98**, 1074 (1955).
20) A. Abragam, "The Principles of Nuclear Magnetism," Oxford University Press, London (1961).
21) H. C. Torrey, *Phys. Rev.*, **92**, 962 (1953).
22) D. C. Look, I. J. Lowe, and J. A. Northby, *J. Chem. Phys.*, **44**, 3441 (1966).

 © 1980 The Chemical Society of Japan Bull. Chem. Soc. Jpn., 53, 2815—2820 (1980)

Outer-sphere Assocation of Some Achiral Cobalt(III)-Amine Complexes as Measured by Their Induced Circular Dichroism Spectra in Aqueous (*R,R*)-Tartrate Solutions

Katsuhiko MIYOSHI, Chang Eon OH, and Hayami YONEDA*

Department of Chemistry, Faculty of Science, Hiroshima University, Hiroshima 730

(Received October 11, 1979)

Outer-sphere association constants K_A of inherently achiral cobalt(III)–amine complexes, $[Co(NH_3)_6]^{3+}$, $[Co(NH_3)_4(en)]^{3+}$, and *trans*-$[Co(NH_3)_2(en)_2]^{3+}$ with (*R,R*)-tartrate anion (*d*-tart^{2-}) were determined by measuring their weak CD spectra induced when they were dissolved in aqueous *d*-tart^{2-} solutions at 25 °C. It was found that the K_A values are not so different among these three complexes, whereas their molar CD intensity $\Delta\varepsilon_{MX}$ gained by the association with *d*-tart^{2-} increases with increasing number of their chelate rings. This was tentatively interpreted to mean that the distortion of the Co(III)–N bonds brought about by outer-sphere association with chiral *d*-tart^{2-} is greater when bidentate ligands (en) are coordinated than when unidentate ones (NH_3) are, *i.e.*, when the complex has more chelate rings. Also it was found that the K_A value thus obtained for $[Co(NH_3)_6]^{3+}$ is much smaller than that determined by measuring the magnitude of its charge-transfer band which newly appears upon the addition of *d*-tart^{2-}. From the above finding and other experimental results, it was suggested that induced CD is well developed in these achiral amine complexes when the two hydroxyl oxygen atoms of *d*-tart^{2-} simultaneously form hydrogen-bonds with amine protons of the ligands.

It is well known that UV and CD spectra of metal complexes are subjected to a considerable change in shape and/or magnitude upon the addition of highly charged counterions in solution. The change is attributed to their outer-sphere association with added counterions, and has been utilized to investigate their outer-sphere interactions.[1] In particular, tris(diamine)-cobalt(III) complexes have been widely studied by many workers.[1-5] Among them, Ogino and Saito[6] were the first to find that the association constant of $[Co(en)_3]^{3+}$ with (*R,R*)-tartrate anion (*d*-tart^{2-}) is different between its two enantiomers in aqueous solution, and their pioneering work initiated extensive studies[7-11] on the discriminating interaction of chiral metal complexes with *d*-tart^{2-} in solution.

On the other hand, Mason and Norman[12] found in 1965 that weak CD is induced for inherently achiral metal complexes like $[Co(NH_3)_6]^{3+}$ when they are dissolved in aqueous (*R,R*)-tartaric acid, sodium (*R,R*)-tartrate, or diethyl (*R,R*)-tartrate solution. Since then, several attempts[13-17] have been made to elucidate the mechanisms leading to this phenomenon called induced CD (ICD) hereafter. Among several proposals made so far, outer-sphere association with the above chiral substances through hydrogen-bonding is the most plausible interpretation for the ICD of metal–amine complexes.[12-14,17,18] If this interpretation is valid, the ICD is also applied to study the outer-sphere interaction of achiral metal–amine complexes with (*R,R*)-tartrate ion (*d*-tart^{2-}) in solution.

Recently, Jonas and Norden[14a] estimated the molar ICD intensity of $[Co(NH_3)_6]^{3+}$ gained through the 1:1 association with *d*-tart^{2-} to be -1.57×10^{-2} in water at the wavelength of its maximum intensity (480 nm) by using its association constant determined by UV measurements.[10] However, the steric requisite in the association with *d*-tart^{2-} is supposed to be severer for the induction of CD than for the development of a new charge-transfer band in achiral complexes like $[Co(NH_3)_6]^{3+}$, as already pointed out by Mason and Norman.[12] In fact, it has been reported[10,19] that CD measurements are apt to give somewhat smaller association constants than UV measurements, at least for the $[Co(en)_3]^{3+}$–*d*-tart^{2-} system.[20] In the present study, the magnitude of the ICD for three achiral complexes, $[Co(NH_3)_6]^{3+}$, $[Co(NH_3)_4(en)]^{3+}$, and *trans*-$[Co(NH_3)_2(en)_2]^{3+}$ was measured in aqueous solutions as a function of *d*-tart^{2-} concentration, and their association constant K_A with *d*-tart^{2-} and accompanying molar ICD intensity $\Delta\varepsilon_{MX}$ were directly derived and compared with each other.

Experimental

Materials. All the complexes except $[Co(NH_3)_4(R\text{-pn})]Cl_3$ and $[Co(NH_3)_4(tn)]Cl_3\cdot H_2O$ were prepared in the same manner as before[21] and when necessary, they were converted to appropriate salts by ion-exchange techniques. The two tetraammine-complexes were prepared after the methods[22,23] described in the literature. They were identified by their UV and/or CD spectra. Other chemicals used were of reagent grade.

Measurements. Induced CD spectra were recorded on a JASCO J-40CS spectropolarimeter for aqueous solutions of each complex (8.0×10^{-3} mol dm^{-3}) containing varying amounts of sodium (*R,R*)-tartrate (*d*-tart^{2-}), diethyl (*R,R*)-tartrate, or (*R,R*)-tartaric acid up to 3.0 mol dm^{-3}.

To obtain the association constant from the ICD spectra, the ICD magnitudes were measured at 25 °C for aqueous solutions containing sodium (*R,R*)-tartrate or sodium (*R,R*)-tartratoantimonate(III) (Sb_2d-tart$_2^{2-}$) ranging in concentration from 0.08 to 0.15 mol dm^{-3} or from 0.05 to 0.1 mol dm^{-3}, respectively. The concentration of each complex (chloride salt) was kept constant: 8.0×10^{-3} mol dm^{-3} in *d*-tart^{2-} and 7.0×10^{-3} mol dm^{-3} in Sb_2d-tart$_2^{2-}$ solutions. The ionic strength μ was adjusted with NaCl. The pH value of sample solutions thus prepared was around 7 for *d*-tart^{2-} and 4 to 5 for Sb_2d-tart$_2^{2-}$. For the determination of the association constant by UV measurements,[6,10,19] the same experimental conditions as above were adopted except that $NaClO_4$ was added to adjust the ionic strength and perchlorate salts of respective complexes were used in place of the chloride salts.

Results and Discussion

Comparison of ICD Magnitudes. In Fig. 1 are shown the induced CD (ICD) spectra reported previously[21] in the first d-d transition region for $[Co(NH_3)_6]^{3+}$, $[Co(NH_3)_4(en)]^{3+}$, and *trans*-$[Co(NH_3)_2(en)_2]^{3+}$ (0.01 mol dm^{-3} for each) in aqueous Na_2d-tart and Na_2Sb_2d-$tart_2$ solutions (0.1 mol dm^{-3}) together with that for $[Co(NH_3)_4(tn)]^{3+}$ in d-$tart^{2-}$ solution. It is evident that the ICD magnitude increases in the following order in d-$tart^{2-}$ solutions; $[Co(NH_3)_6]^{3+} \ll [Co(NH_3)_4(en)]^{3+} < trans$-$[Co(NH_3)_2(en)_2]^{3+}$. In contrast, Taniguchi *et al.*[18] found the reversed order in acetone containing diethyl (*R,R*)-tartrate (*ca.* 5 mol dm^{-3}). However, direct comparison between their results and ours is meaningless, since the concentration of d-$tart^{2-}$ employed in our experiments is much lower. Then, the ICD magnitude was measured as a function of the concentration of the two chiral substances, Na_2d-tart and diethyl (*R,R*)-tartrate up to 3 mol dm^{-3} in aqueous solutions. For comparison, the ICD magnitude was also measured in aqueous (*R,R*)-tartaric acid solutions.

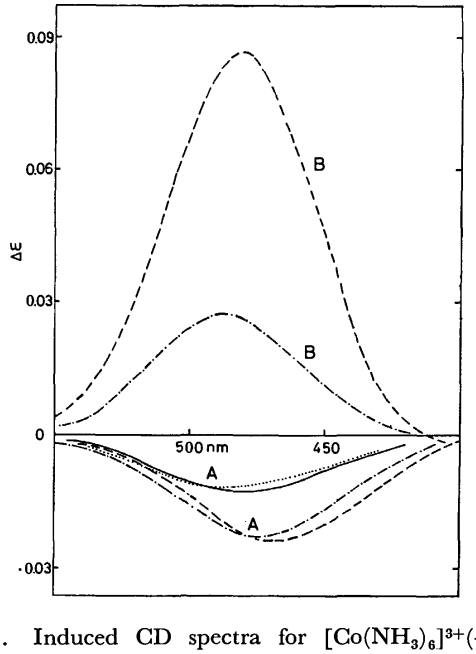

Fig. 1. Induced CD spectra for $[Co(NH_3)_6]^{3+}$(——), $[Co(NH_3)_4(en)]^{3+}$ (-•-·-), *trans*-$[Co(NH_3)_2(en)_2]^{3+}$ (——), and $[Co(NH_3)_4(tn)]^{3+}$ (·····) in aqueous d-$tart^{2-}$ (A) and Sb_2d-$tart_2^{2-}$ (B) solutions.

In Fig. 2 are plotted the ICD magnitudes obtained for $[Co(NH_3)_6]^{3+}$ (A), $[Co(NH_3)_4(en)]^{3+}$ (B), and *trans*-$[Co(NH_3)_2(en)_2]^{3+}$ (C) (8×10^{-3} mol dm^{-3} for each) at the wavelength of their maximum intensity (478, 474, and 466 nm, respectively) against the concentration of Na_2d-tart, diethyl (*R,R*)-tartrate, and (*R,R*)-tartaric acid. When their concentration is low (below *ca.* 0.3 mol dm^{-3}), the ICD magnitude is greatest in d-$tart^{2-}$ solutions for all the complexes and it increases in the following order $[Co(NH_3)_6]^{3+} < [Co(NH_3)_4(en)]^{3+} <$ *trans*-$[Co(NH_3)_2(en)_2]^{3+}$, irrespective of the kind of the

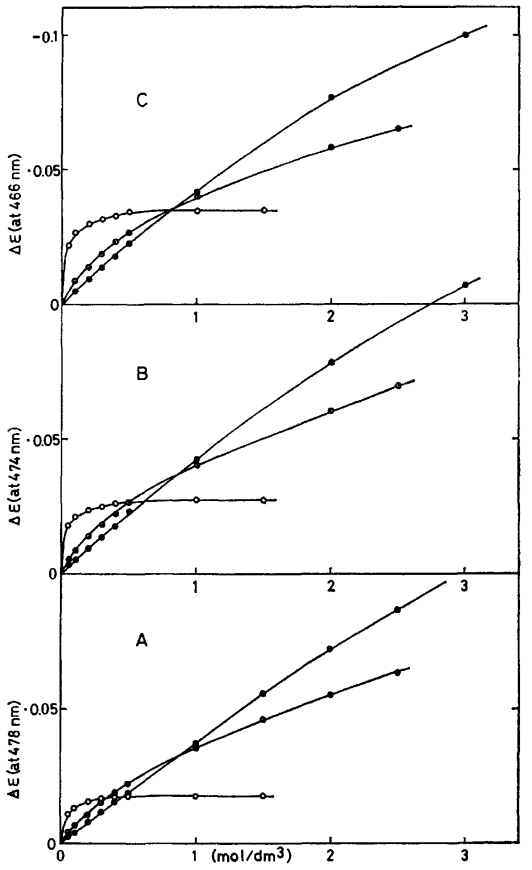

Fig. 2. Plots of the ICD magnitude for $[Co(NH_3)_6]^{3+}$ (A), $[Co(NH_3)_4(en)]^{3+}$(B), and *trans*-$[Co(NH_3)_2(en)_2]^{3+}$ (C) at the wavelength of the maximum intensity against the concentration of sodium (*R,R*)-tartrate (○), diethyl (*R,R*)-tartrate (●), and (*R,R*)-tartaric acid (⊙) in aqueous solutions.

chiral substances added. This order is in agreement with the increasing order of en chelate rings in the complexes. However, the ICD magnitude in d-$tart^{2-}$ solutions gradually ceases to increase with d-$tart^{2-}$ concentration and it finally becomes constant above *ca.* 0.5 mol dm^{-3}, the limiting ICD magnitude being -1.8×10^{-2}, -2.7×10^{-2}, and -3.5×10^{-2} for $[Co(NH_3)_6]^{3+}$, $[Co(NH_3)_4(en)]^{3+}$, and *trans*-$[Co(NH_3)_2(en)_2]^{3+}$, respectively. This indicates that no free complex (not associated with d-$tart^{2-}$) exists in such high d-$tart^{2-}$ concentration ranges. On the contrary, the ICD magnitude gained in diethyl (*R,R*)-tartrate and (*R,R*)-tartaric acid solutions keeps increasing even at 3 mol dm^{-3}. These facts imply that the interaction of these cationic complexes with d-$tart^{2-}$ anion is comparatively strong, probably due to the electrostatic attraction, while the interaction with diethyl (*R,R*)-tartrate or (*R,R*)-tartaric acid is very weak.[12] Furthermore, a close inspection of Fig. 2 reveals that the ICD magnitude gained in diethyl (*R,R*)-tartrate solution gradually becomes greater for $[Co(NH_3)_4(en)]^{3+}$ than for *trans*-$[Co(NH_3)_2(en)_2]^{3+}$ as the diethyl (*R,R*)-tartrate concentration is increased. Therefore, we suppose that the increasing order of the ICD magnitude obtained at low concentration of diethyl (*R,R*)-tartrate

will be eventually reversed and agree with the order found by Taniguchi *et al.* in more concentrated solutions.

Similar concentration dependence of the ICD magnitude could not be examined in Sb_2-*d*-$tart_2^{2-}$ solutions owing to the solubility limitation. However, it is worthy of noting that the ICD for a particular complex is certainly greater in magnitude in Sb_2-*d*-$tart_2^{2-}$ solutions than in *d*-$tart_2^{2-}$ solutions (Fig. 1). This will be discussed later.

Determination of Association Constants. If it is assumed that 1:1 association between the achiral complexes and *d*-$tart^{2-}$ is completely attained in the concentration ranges where the curves for the ICD magnitude level off in Fig. 2 (*i.e.*, above *ca.* 0.5 mol dm^{-3}), the limiting ICD magnitude in *d*-$tart^{2-}$ solutions should correspond to the molar ICD intensity of the achiral complexes gained by the association with one *d*-$tart^{2-}$ ion. In fact, the limiting ICD magnitude of $[Co(NH_3)_6]^{3+}$ (-1.8×10^{-2}) is close to its molar ICD intensity estimated by Jonas and Norden (-1.57×10^{-2}).[14a] However, this is quite an accidental coincidence, since the 1:2 association with *d*-$tart^{2-}$ is expected to take place in such high concentration ranges, as shown later. Then, we attempted to determine directly

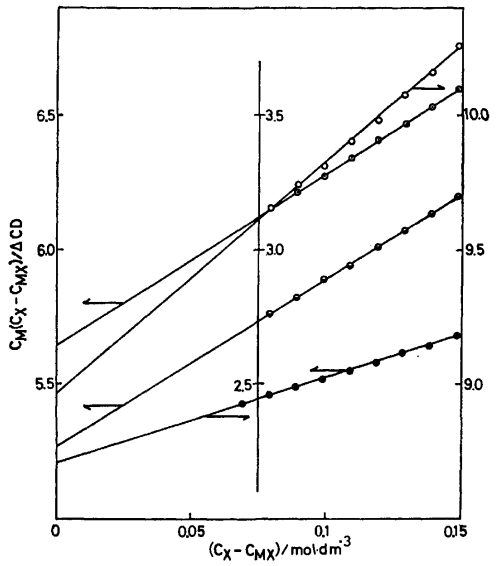

Fig. 3. Plots of Eq. 1 for $[Co(NH_3)_6]^{3+}$ (○), $[Co(NH_3)_4(en)]^{3+}$ (◎), *trans*-$[Co(NH_3)_2(en)_2]^{3+}$ (◒), and *rac*-$[Co(en)_3]^{3+}$ (●) in aqueous *d*-$tart^{2-}$ solutions.

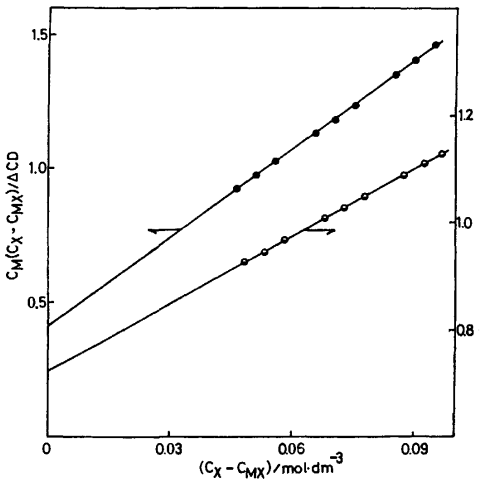

Fig. 4. Plots of Eq. 1 for *trans*-$[Co(NH_3)_2(en)_2]^{3+}$ (◒) and *rac*-$[Co(en)_3]^{3+}$ (●) in aqueous Sb_2-*d*-$tart_2^{2-}$ solutions.

the association constants K_A and accompanying ICD intensity $\Delta\varepsilon_{MX}$ by measuring the ICD spectra of the three achiral complexes in aqueous solutions containing varying amounts of *d*-$tart^{2-}$ at 25 °C. When possible, the K_A and $\Delta\varepsilon_{MX}$ values were also determined in Sb_2-*d*-$tart_2^{2-}$ solutions.

All the data obtained were analyzed by using the following general equation[11,19]

$$C_M(C_X-C_{MX})/\Delta CD = (C_X-C_{MX})/\Delta\varepsilon_{MX} + 1/K_A\Delta\varepsilon_{MX} \quad (1)$$

where C_M, C_X, and C_{MX} refer to the concentration of the complex (M), *d*-$tart^{2-}$ or Sb_2-*d*-$tart_2^{2-}$ (X), and their associated species (MX), and ΔCD and $\Delta\varepsilon_{MX}$ to the observed CD intensity and the molar ICD intensity of MX, respectively. The plots of the quantity on the left-hand side of Eq. 1 *vs.* (C_X-C_{MX}) gave fairly good straight lines (Figs. 3 and 4), indicating that only 1:1 association takes place for all the complexes under our present experimental conditions. The K_A and $\Delta\varepsilon_{MX}$ values obtained from these plots are listed in Table 1. For comparison, similar experiments were made on racemic $[Co(en)_3]^{3+}$ by using its ICD spectra arising from the differential CD change between its two enantiomers upon the addition of *d*-$tart^{2-}$ or Sb_2-*d*-$tart_2^{2-}$.[21]

Two important facts should be noted in Table 1.

Table 1. Association constant K_A and molar ICD intensity $\Delta\varepsilon_{MX}$ determined by ICD measurements

	λ/nm[a]	K_A	$\Delta\varepsilon_{MX}$	μ(NaCl)
(*R*,*R*)-$tart^{2-}$				
$[Co(NH_3)_6]^{3+}$	478	0.97±0.05	−0.116±0.005	0.49
$[Co(NH_3)_4(en)]^{3+}$	474	1.14±0.02	−0.156±0.003	0.49
trans-$[Co(NH_3)_2(en)_2]^{3+}$	466	1.19±0.02	−0.159±0.003	0.49
rac-$[Co(en)_3]^{3+}$	478	1.45±0.04	−0.314±0.009	0.49
Sb_2(*R*,*R*)-$tart_2^{2-}$				
trans-$[Co(NH_3)_2(en)_2]^{3+}$	484	5.8±1.0	0.239±0.003	0.33
rac-$[Co(en)_3]^{3+}$	461[b]	26.6±1.2	−0.091±0.002	0.32

a) Wavelength at which the ICD is measured and has its maximum intensity. b) *rac*-$[Co(en)_3]^{3+}$ has a maximum ICD intensity at 469 nm in Sb_2-*d*-$tart_2^{2-}$ solution.

The first is that the K_A values with d-tart^{2-} are not appreciably different among three achiral complexes, while the $\Delta\varepsilon_{MX}$ value of $[Co(NH_3)_6]^{3+}$ is much smaller than those of the other two complexes. Therefore, a smaller $\Delta\varepsilon_{MX}$ value of $[Co(NH_3)_6]^{3+}$ is responsible for its weaker ICD developed in d-tart^{2-} solution (Fig. 1). On the other hand, both the K_A and $\Delta\varepsilon_{MX}$ values for *trans*-$[Co(NH_3)_2(en)_2]^{3+}$ are slightly greater than the corresponding values for $[Co(NH_3)_4(en)]^{3+}$ in d-tart^{2-} solutions. Then, it is natural that the ICD similar in magnitude is developed for the two complexes as shown in Fig. 1.

Another noteworthy fact is that both the K_A and $\Delta\varepsilon_{MX}$ values for *trans*-$[Co(NH_3)_2(en)_2]^{3+}$ are much greater in Sb_2d-tart$_2^{2-}$ solution than in d-tart^{2-} solution, though the ionic strength is somewhat lower in the former solution. As a result, it is this fact that is responsible for much stronger ICD developed for *trans*-$[Co(NH_3)_2(en)_2]^{3+}$ in Sb_2d-tart$_2^{2-}$ than in d-tart^{2-} solutions. The same will probably hold for $[Co(NH_3)_4(en)]^{3+}$ whose association constant with Sb_2d-tart$_2^{2-}$ cannot be determined owing to the formation of a precipitate. Similarly, the K_A value obtained for *rac*-$[Co(en)_3]^{3+}$ is surprisingly greater with Sb_2d-tart$_2^{2-}$ than with d-tart^{2-}.[24] Therefore, we suppose that Sb_2d-tart$_2^{2-}$ interacts with these amine-complexes in quite a different fashion from d-tart^{2-}.[25] In fact, $[Co(NH_3)_4(en)]^{3+}$ and *trans*-$[Co(NH_3)_2(en)_2]^{3+}$ show a positive ICD band in Sb_2d-tart$_2^{2-}$ solution, while the two complexes and $[Co(NH_3)_6]^{3+}$ show a negative ICD band in d-tart^{2-} solution. Furthermore, the wavelength at which the ICD of these complexes has a maximum intensity is considerably different between d-tart^{2-} and Sb_2d-tart$_2^{2-}$ solutions (Fig. 1 and Table 1).

For *rac*-$[Co(en)_3]^{3+}$, however, its apparent $\Delta\varepsilon_{MX}$ value is not directly compared with those of the achiral complexes, since the mechanism leading to the ICD in racemic complexes is essentially different from that in achiral complexes.[21]

In Table 2 are given the association constants K_A of $[Co(NH_3)_6]^{3+}$ and *rac*-$[Co(en)_3]^{3+}$ with d-tart^{2-} determined in the present study by UV measurements. Also given are the K_A values reported by other workers. Here the ionic strength μ is adjusted with $NaClO_4$. Again, two noticeable facts are found in Table 2. First, the K_A value obtained for $[Co(NH_3)_6]^{3+}$ is greater than that for $[Co(en)_3]^{3+}$. Nevertheless, when the ICD measurements are applied, the resulting K_A value is greater for *rac*-$[Co(en)_3]^{3+}$ than for $[Co(NH_3)_6]^{3+}$. Another fact to be noted is that the K_A value derived from ICD measurements is much smaller than that obtained by UV measurements both for $[Co(NH_3)_6]^{3+}$ and $[Co(en)_3]^{3+}$, as seen in Tables 1 and 2. These facts strongly suggest that the steric requisite in the association with d-tart^{2-} is much severer for the induction of CD in the first d-d transition region than for the development of a new charge transfer band in the UV region for achiral complexes.[12]

Mason and Norman[12] have already found that no detectable CD is induced[26] for $[Co(NH_3)_6]^{3+}$ when mixed with (*S*)-malic acid or sodium (*S*)-malate having only one OH group on the asymmetric carbon atom. However, the addition of (*S*)-malate^{2-} as well as d-tart^{2-} gives an appreciable change in the UV spectrum of the complex, suggesting that the interaction with the two $-COO^-$ groups gives rise to the change in the UV spectrum of the complex.[6] Therefore, we suppose that the ICD is well developed only when the two OH groups on the asymmetric carbon atoms simultaneously participate in the interaction with these achiral amine complexes. The most probable interaction imagined here is the hydrogen-bonding of the hydroxyl oxygen atoms with the amine protons of the ligands.[17] In fact, ICD is well developed for $[Co(NH_3)_6]^{3+}$ and other two achiral complexes when mixed with diethyl (*R,R*)-tartrate or (*R,R*)-tartaric acid having no $-COO^-$ group.[27]

Table 2. Association constant K_A with (*R,R*)-tartrate determined by UV measurements

	λ/nm	K_A	($NaClO_4$)	Ref.
$[Co(NH_3)_6]^{3+}$	270	4.2±0.2	0.48	present study
	245	26.5±0.4	0.1	19)
	265	31 ±1	0.1	10)
rac-$[Co(en)_3]^{3+}$	277	4.2±0.1	0.48	present study
Λ-$[Co(en)_3]^{3+}$	265	22.5±0.4	0.1	19)
	265	23.4±1.0	0.1	6)[a]
	265	26 ±2	0.1	10)
Δ-$[Co(en)_3]^{3+}$	265	18.2±0.6	0.1	19)
	265	18.0±0.7	0.1	6)[a]
	265	22 ±2	0.1	10)

a) Recalcd in Ref. 6.

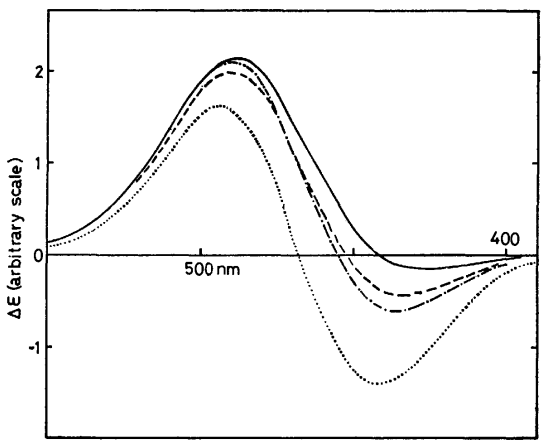

Fig. 5. CD spectra of *Λ*-$[Co(en)_3]^{3+}$ (2×10^{-3} mol dm^{-3}) in the absence (——) and presence of d-tart^{2-}; 0.0275 mol dm^{-3} (——) and 1.0 mol dm^{-3} (-·-·-), and calculated CD spectrum of *Λ*-$[Co(en)_3]^{3+}$ associated with d-tart^{2-} (……) in aqueous solutions.

Comparison of $\Delta\varepsilon_{MX}$ Values with Limiting ICD Magnitudes. Before the limiting ICD magnitudes attained in Fig. 2 are discussed and compared with the $\Delta\varepsilon_{MX}$ values listed in Table 1, the influence of added d-tart^{2-} on the natural CD spectrum of *Λ*-$[Co(en)_3]^{3+}$ is examined here. In Fig. 5 are shown the CD spectra of *Λ*-$[Co(en)_3]^{3+}$ (2×10^{-3} mol dm^{-3}) in water in the absence and presence of d-tart^{2-} (2.75×10^{-2} and 1.0 mol dm^{-3}).

The association constant of the complex with *d*-tart^{2-} has been estimated by CD measurements to be 13.0± 1.0[11] at μ=0.1 ($NaClO_4$). By using this value, the hypothetical CD spectrum of *Λ*-$[Co(en)_3]^{3+}$ associated with *d*-tart^{2-} was calculated and is shown as a dotted line in Fig. 5. It is evident that the CD spectrum in the presence of a large amount of *d*-tart^{2-} (*e.g.*, 1.0 mol dm^{-3}) is entirely different from the calculated spectrum. This unambiguously means that successive association[4a] of the complex with *d*-tart^{2-} must be taken into account at such high *d*-tart^{2-} concentrations. The same is naturally expected for the three achiral complexes in question, since all of them bear 3+ charges like $[Co(en)_3]^{3+}$. However, the association higher than 1 : 2 is improbable under our experimental conditions, as pointed out by Olsen and Bjerrum for the $[Co(en)_3]^{3+}$–$S_2O_3^{2-}$ system.[28] As a result, it follows that the 1 : 2 association with *d*-tart^{2-} is completely attained in extremely high *d*-tart^{2-} concentration ranges (Fig. 2) and that the limiting ICD magnitudes thus correspond to the molar ICD intensities of the respective achiral complexes gained by interacting with two *d*-tart^{2-} ions at a time. On the other hand, the $\Delta\varepsilon_{MX}$ values correspond to the molar ICD intensities gained by the association with only one *d*-tart^{2-} ion.

Now we are ready to compare the limiting ICD magnitudes with the $\Delta\varepsilon_{MX}$ values. First of all, it should be noted that the limiting ICD magnitude is much smaller than the $\Delta\varepsilon_{MX}$ value for all the complexes examined. If the former indeed reflects the molar ICD intensity of the achiral complex associated with two *d*-tart^{2-} ions, we are obliged to conclude that the ICD magnitude gained in the 1 : 1 association with *d*-tart^{2-} is greatly diminished (almost to one-fifth) in the 1 : 2 association, probably due to restored high symmetry[4a] of the resulting outer-sphere complex with two *d*-tart^{2-} ions. It is also highly plausible that the strain imposed on the achiral complex in the 1 : 1 association is relaxed in the 1 : 2 association owing to the electrostatic repulsion between the two *d*-tart^{2-} anions, the overall ICD magnitude being thereby diminished greatly.

Finally, the most important problem remains unanswered why the $\Delta\varepsilon_{MX}$ value for *trans*-$[Co(NH_3)_2(en)_2]^{3+}$ (−0.159) is only slightly greater than that for $[Co(NH_3)_4(en)]^{4+}$ (−0.156), while the limiting ICD magnitude is appreciably greater for the former complex (-3.5×10^{-2}) than for the latter (-2.7×10^{-2}). Though detailed mechanisms of the ICD developed in these achiral complexes are not known, some authors[13,18,29] favor the view that the ICD owes its origin to a fixed conformation (δ or λ) of the chelate rings of the complex in the presence of chiral substances. However, we are not inclined to adopt this view in the present system, since the ICD spectra obtained for *trans*-$[Co(NH_3)_2(en)_2]^{3+}$ and $[Co(NH_3)_4(en)]^{3+}$ (Fig. 1) do not resemble the natural CD spectra of *trans*-$[Co(NH_3)_2$(*R*- or *S*-pn)$_2]^{3+}$ and $[Co(NH_3)_4$(*R*- or *S*-pn)$]^{3+}$,[22] respectively, and similar CD is induced also for $[Co(NH_3)_6]^{3+}$ having no chelate. In addition, $[Co(NH_3)_4$(*R*-pn)$]^{3+}$ in which a pn chelate ring is thought to be fixed to a λ-conformation suffers a considerable change in its CD spectrum when mixed with *d*-tart^{2-} or Sb_2*d*-tart$_2^{2-}$, as shown in Fig. 6.

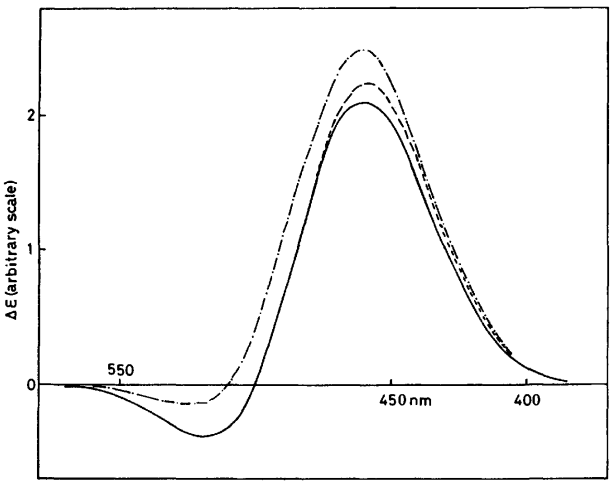

Fig. 6. CD spectra of $[Co(NH_3)_4$(*R*-pn)$]^{3+}$ in the absence (——) and presence of *d*-tart^{2-} (– – –) and of Sb_2*d*-tart$_2^{2-}$ (–·–·–) in aqueous solutions.

It is certain, however, that the ICD developed in *d*-tart^{2-} solution increases in magnitude with increasing number of en chelate rings in the complexes. This leads us to propose that the ICD magnitude depends on the degree of the distortion[13] of the Co(III)–N bonds brought about by the outer-sphere association with *d*-tart^{2-}, since a greater distortion is expected when the coordinated ligands are bidentate (en) than when they are unidentate (NH_3), *i.e.*, when the complex has more chelate rings. In accordance with this proposal, the ICD magnitude of $[Co(NH_3)_4(en)]^{3+}$ is greater than that of $[Co(NH_3)_4(tn)]^{3+}$, the strain exerted upon which is not effectively propagated to the central Co(III) ion owing to the flexibility of a tn chelate ring.

If our proposal that the strain exerted upon chelate rings is effective in inducing CD in achiral complexes is valid, a tentative answer can now be put forward to the problem mentioned above. In the 1 : 1 association with *d*-tart^{2-}, both *trans*-$[Co(NH_3)_2(en)_2]^{3+}$ and $[Co(NH_3)_4$-$(en)]^{3+}$ having at least one en chelate ring are expected to suffer a similar distortion, since *d*-tart^{2-} cannot interact with *trans*-$[Co(NH_3)_2(en)_2]^{3+}$ so as to exert a strain on the two en rings simultaneously. As a result, it is natural that CD similar in magnitude is induced for the two complexes. On the other hand, when the 1 : 2 association takes place, *trans*-$[Co(NH_3)_2(en)_2]^{3+}$ is differentiated from $[Co(NH_3)_4(en)]^{3+}$, since the former complex has another en chelate ring available for the further interaction with *d*-tart^{2-}, while the latter not. Therefore, relatively stronger CD is expected to be induced for the former complex in concentrated solution of *d*-tart^{2-}, though the overall ICD magnitude gained in the 1 : 2 association is by far smaller than that in the 1 : 1 association. In this way, an appreciably great difference in the limiting ICD magnitude between $[Co(NH_3)_4(en)]^{3+}$ and *trans*-$[Co(NH_3)_2(en)_2]^{3+}$ is reasonably interpreted.

Though the solubility limitation does not allow us to obtain the limiting ICD magnitudes in Sb_2*d*-tart$_2^{2-}$ solution, the ICD magnitude for *trans*-$[Co(NH_3)_2(en)_2]^{3+}$

is considerably greater than that for $[Co(NH_3)_4(en)]^{3+}$ even when the concentration of $Sb_2d\text{-}tart_2^{2-}$ is relatively low (Fig. 1). This tacitly means that the arguments presented above are not applied to the interpretation of the ICD developed in $Sb_2d\text{-}tart_2^{2-}$ solutions.

References

1) For reviews, J. Bjerrum, *Adv. Chem. Ser.*, **62**, 178 (1967); M. T. Beck, *Coord. Chem. Rev.*, **3**, 91 (1968).

2) S. F. Mason and B. J. Norman, *Proc. Chem. Soc.*, **1964**, 339.

3) H. L. Smith and B. E. Douglas, *Inorg. Chem.*, **5**, 784 (1966).

4) a) R. Larsson, S. F. Mason, and B. J. Norman, *J. Chem. Soc., A*, **1966**, 301; b) S. F. Mason and B. J. Norman, *ibid.*, **1966**, 307.

5) N. Tanaka, Y. Kobayashi, and M. Kamada, *Bull. Chem. Soc. Jpn.*, **40**, 2839 (1967).

6) K. Ogino and U. Saito, *Bull. Chem. Soc. Jpn.*, **40**, 826 (1967); K. Ogino, *ibid.*, **42**, 3043 (1969).

7) S. F. Mason, *Ann. Rep. Progr. Chem.*, **73**, 53 (1976).

8) Y. Yoshikawa and K. Yamasaki, *Coord. Chem. Rev.*, **28**, 205 (1979).

9) H. Yamatera and M. Fujita, *Bull. Chem. Soc. Jpn.*, **42** 3043 (1969) M. Fujita and H. Yamatera, *ibid.*, **49**, 1301, (1976); **50**, 2672 (1977).

10) B. Norden, *Acta Chem. Scand.*, **26**, 111 (1972), and references cited therein .

11) H. Yoneda and T. Taura, *Chem. Lett.*, **1977**, 63.

12) S. F. Mason and B. J. Norman, *Chem. Commun.*, **1965**, 335.

13) B. Bosnich, *J. Am. Chem. Soc.*, **89**, 6143 (1967); B. Bosnich and J. M. Harrowfield, *ibid.*, **93**, 4086 (1971).

14) a) I. Jonas and B. Norden, *Acta Chem. Scand.*, **A28**, 289 (1974), b) B. Norden, *Chem. Scr.*, **7**, 14 (1975).

15) P. E. Schipper, *Mol. Phys.*, **29**, 1705 (1975); *Inorg. Chim. Acta*, **14**, 161 (1975).

16) S. F. Mason, *Chem. Phys. Lett.*, **32**, 201 (1975), and references cited therein.

17) S. Kirschner, *J. Indian Chem. Soc.*, **51**, 28 (1974).

18) Y. Taniguchi, J. Hidaka, and Y. Shimura, *Bull. Chem. Soc. Jpn.*, **50**, 2093 (1977).

19) T. Taura, Ph. D. Thesis, Hiroshima University, 1979; *J. Sci. Hiroshima Univ.*, **A43**, 85 (1979).

20) H. Yamatera, 37 th National Meeting of the Chemical Society of Japan, Tokyo, April 1978, Abstr. No. 4V2.

21) K. Miyoshi, C. E. Oh, H. Nakazawa, and H. Yoneda, *Bull. Chem. Soc. Jpn.*, **51**, 2946 (1978).

22) C. J. Hawkins, E. Larsen, and I. Olsen, *Acta Chem. Scand.*, **19**, 1915 (1965).

23) F. Mizukami, H. Ito, J. Fujita, and K. Saito, *Bull. Chem. Soc. Jpn.*, **45**, 2129 (1972).

24) T. Taura, H. Nakazawa, and H. Yoneda, *Inorg. Nucl. Chem. Lett.*, **13**, 603 (1977).

25) H. Nakazawa and H. Yoneda, *J. Chromatogr.*, **160**, 89 (1978); H. Yoneda, *J. Liquid Chromatogr.*, **2**, 1157 (1979).

26) Weak positive CD is induced for $[Co(NH_3)_6]^{3+}$ as well as for $[Co(NH_3)_4(en)]^{3+}$ and *trans*-$[Co(NH_3)_2(en)_2]^{3+}$ in aqueous solutions containing an extremely large excess of (*S*)-malic acid, suggesting that the two simultaneous hydrogen-bonds are not necessarily essential requirements for the induction of CD in these achiral complexes. See also Ref. 14.

27) Though (*R*,*R*)-tartaric acid is partially ionized in aqueous solutions, the concentration of fully deprotonated species is very low, particularly in concentrated solutions.

28) I. Olsen and J. Bjerrum, *Acta Chem. Scand.*, **21**, 1112 (1967).

29) R. J. Geue and M. R. Show, *Inorg. Chem.*, **16**, 231 (1977).

Kinetics of the Stereoselective Deuteration of Malonate Hydrogens in Some Bis(malonato)cobalt(III) Compounds and the Reversal of Stereoselectivity Induced by the Solution pH[1]

Ushio SAKAGUCHI, Kaiji MORITO, and Hayami YONEDA*

Department of Chemistry, Faculty of Science, Hiroshima University, Hiroshima 730

(Received February 26, 1980)

The deuteration rates at malonate methylene groups have been measured for several $[Co(mal)_2(N)_2]^-$ ions over the pD range of 2 to 9 at 36.4 °C, where mal = malonate ion, $(N)_2$ = ethylenediamine, *cis*-$(NH_3)_2$, 1,3-propanediamine, *N,N'*-dimethylethylenediamine, *cis*-(pyridine)$_2$, and 1,10-phenanthroline. The malonate deuteration is acid-catalysed at pD less than about 4 and base-catalysed at higher pD in all the compounds. In the amino-containing compounds (the first four compounds), the reaction proceeds stereoselectively in both high and low pD regions. Though the degree of the stereoselectivity depends upon the compound, the fast-exchanging hydrogen is, for all the amino-containing compounds, the one which is adjacent to the coordinating nitrogen atom. The mechanisms of acid- and base-catalysed deuteration, as well as the origin of the stereoselectivity, are discussed. For the ethylenediamine and *cis*-$(NH_3)_2$ compounds, reversal of the stereoselectivity takes place at around pD = 8 and 9, respectively, and the fast-exchanging hydrogen becomes the one farthest apart from the coordinating nitrogen. Concomitant with this reversal, both malonate and amine exchange rates fall together. Thus, the rate of hydrogen-deuterium exchange at the NH_3 groups does not show the usual first-order dependence upon the OD^- concentration. These observations are explained by a mechanism in which equally reactive malonate and amine hydrogens compete for OD^- catalyst.

In the preceding paper,[2] we investigated the deuteration kinetics of malonate methylenes in monomalonatocobalt(III) compounds. The chelated and the non-chelated malonate ligands behaved quite differently and the deuteration mechanisms are discussed. The acidity of the malonate hydrogens coordinated to Co(III) has been studied by several workers. Yoneda and Morimoto[3] observed that the malonate deuteration proceeds quite easily simply by dissolving malonatocobalt(III) compounds in deuterium oxide. Buckingham *et al.*[4] noted that the malonate methylenes of $[Co(mal)_2(en)]^-$ and $[Co(mal)(en)_2]^+$ ions[5] undergo acid-catalysed and probably base-catalysed deuteration. They also found that the two types of hydrogens of coordinated malonate in $[Co(mal)_2(en)]^-$ exchange with deuterium at unequal rates. Recently, Farago and coworkers[6] made temperature dependence studies on the malonate deuteration of $[Co(mal)_2(en)]^-$, $[Co(mal)(en)_2]^+$, and $[Co(mal)(bpy)_2]^+$ in the pD region of 2 to 3. The last result confirmed that the deuteration is acid-catalysed. Here we have examined the deuteration rates of malonate ligands in $[Co(mal)_2(N)_2]^-$ type of compounds over the pD range of 2 to 9 and at 36.4 °C.

Experimental

Materials. Deuterium oxide (99.8 atom%D minimum) was obtained from E. Merck(Darmsdadt). *cis*-$K[Co(mal)_2(NH_3)_2]$[7] $2.5H_2O$, and *cis*-$K[Co(mal)_2(py)_2]3.5H_2O$[8] were prepared after Shibata *et al.* $K[Co(mal)_2(en)]H_2O$ was prepared and resolved by *levo*-$[Co(NO_2)_2(en)_2]^+$ after Dwyer and coworkers.[9] The tn complex was made after Brennan *et al.*[10] and the number of water molecules of crystallization was 2.5 instead of 2. Found: N, 6.69; C, 25.81; H, 4.38%. Calcd for $K[Co(mal)_2(tn)]\cdot 2.5H_2O$: N, 6.65; C, 25.66; H, 4.55%.

The phen compound was prepared as follows. The tris(malonato)cobalt(III) solution was prepared after Kneten and Spees[11] from 24 g(0.08M) of $Co(NO_3)_2\cdot 6H_2O$. To the filtered $[Co(mal)_3]^{3-}$ solution, 15.9 g(0.08M) of 1,10-phenanthroline monohydrate was added. After stirring at 45 °C for 1 h the solution was left standing at room temperature overnight. The precipitate, $[Co(mal)(phen)_2]$ $[Co(mal)_2(phen)]$, was filtered and redissolved in water. The double complex salt was loaded on an SP-Sephadex C-25 cation-exchange column, and eluted with water. The anionic eluent containing $[Co(mal)_2(phen)]^-$ was reloaded on a QAE-Sephadex A-25 anion-exchange column and eluted with a concentrated solution of potassium chloride. The concentrated eluent was kept in a refrigerator overnight to give needle-like crystals. Yield was about 2.0 g. Found: N, 4.84; C, 37.07; H, 2.91%. Calcd for $K[Co(mal)_2(phen)]\cdot KCl\cdot 5H_2O$: N, 4.80; C, 37.03; H, 2.59%.

Measurements. All the compounds were dissolved in deuterium oxide to about 0.20 to 0.30 mol dm^{-3}. Ionic strength was not controlled. The solution pD was adjusted by appropriate amount of HCl or K_2CO_3 and measured by a Hitachi-Horiba Model F-7 pH meter with a microelectrode accessory, immediately after kinetic measurements. The apparent pH meter readings were converted to the pD values by the empirical formula developed by Fife and Bruice,[12] pD = pH(meter readings) + 0.35(at 36.4 °C). Nuclear magnetic resonance spectra were run at 36.4 °C on a Varian T-60 spectrometer operating at 60 MHz. Chemical shifts were referred to internal sodium 2,2-dimethyl-2-silapentane-5-sulfonate(DSS).

Absorption spectra were obtained on a Shimadzu UV-200 double beam spectrophotometer and circular dichroism spectra on a JASCO J-40CS spectropolarimeter.

Deuteration Rates. The hydrogen-deuterium exchange rates at amine groups were obtained from the slope of the plots of ln(intensity) *vs.* time, as in the previous studies.[13]

For malonate exchange, we first note that $[Co(mal)_2(N)_2]^-$ contains two types of malonate hydrogens, see Fig. 1. In the figure, H_N is adjacent to the coordinated nitrogen atom and H_O is close to the malonate oxygen atom. These two types of hydrogens give rise to an AB quartet immediately after dissolution of the compounds, see Fig. 2. If only H_N is deuterated, we have the species D–C–H_O, which should yield the H_O singlet. In Fig. 2, the H_O hydrogen is assumed to resonate at a higher magnetic field, in accordance with our assignment (*vide infra*). The rate constant for this process is

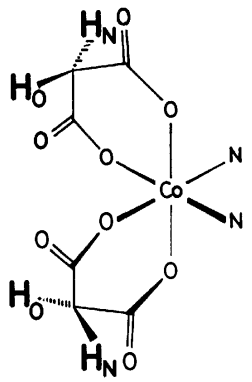

Fig. 1. A schematic presentation of the $[Co(mal)_2(N)_2]^-$ ion, showing that there are two types of malonate hydrogenes, H_N and H_O.

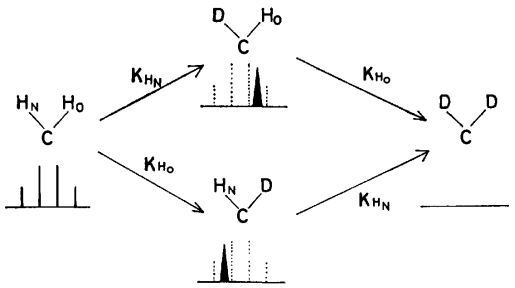

Fig. 2. The scheme for hydrogen-deuterium exchange kinetics of the H_N–C–H_O fragment. Kinetic isotope effect is not taken into account.

denoted as k_{HN}. Similarly, the species H_N–C–D produced by deuteration of only H_O would give rise to the H_N singlet. As the deuteration of H_N–C–H_O proceeds, the intensity of the initial quartet will decrease and that of the H_O and/or H_N singlet(s) will grow. This is the first stage of deuteration. Since both H_O and H_N are exchanged with deuterium in due course, these singlets diminish in intensity with time and eventually vanish. If we neglect the kinetic isotope effect[14] expected for the disappearance of H_N and H_O singlets, the rate constants for the decrease of these singlets are k_{HN} and k_{HO}, respectively. The situation is illustrated schematically in Fig. 2. We may set up simultaneous kinetic equations for the scheme of Fig. 2.

$$-\frac{d}{dt}[H_N\text{-}C\text{-}H_O] = (k_{HO}+k_{HN})[H_N\text{-}C\text{-}H_O] \quad (1)$$

$$-\frac{d}{dt}[D\text{-}C\text{-}H_O] = k_{HO}[D\text{-}C\text{-}H_O] - k_{HN}[H_N\text{-}C\text{-}H_O] \quad (2)$$

$$-\frac{d}{dt}[H_N\text{-}C\text{-}D] = k_{HN}[H_N\text{-}C\text{-}D] - k_{HO}[H_N\text{-}C\text{-}H_O], \quad (3)$$

where $[D\text{-}C\text{-}H_O]$, for example, is the concentration at time t of the species D–C–H_O and the other notations have similar meanings. Equation 1 is equivalent to

$$[H_N\text{-}C\text{-}H_O] = [H_N\text{-}C\text{-}H_O]_{t=0} \exp[-(k_{HN}+k_{HO})t]. \quad (4)$$

Namely, since H_N–C–H_O is to give either D–C–H_O or H_N–C–D or both, the rate constant for the decrease of the AB quartet, k_Q, is the sum of two rate constants k_{HN} and k_{HO},

$$k_Q = k_{HN} + k_{HO}. \quad (5)$$

Experimentally, k_Q was obtained as follows. The natural logarithms of the averaged intensity of the inner pair of the AB quartet and that of the outer pair of the quartet were plotted separately against time. These two plots gave straight lines and the slopes of these lines were the same within experimental error. The avarage of the two slopes was taken as the rate constant k_Q.

Equations 2 and 3 can be solved to give

$$[D\text{-}C\text{-}H_O] = [H_N\text{-}C\text{-}H_O]_{t=0}\{\exp(-k_{HO}t) - \exp[-(k_{HO}+k_{HN})t]\} \quad (6)$$

$$[H_N\text{-}C\text{-}D] = [H_N\text{-}C\text{-}H_O]_{t=0}\{\exp(-k_{HN}t) - \exp[-(k_{HO}+k_{HN})t]\}. \quad (7)$$

Equations 6 and 7 tell us that in the initial stage of deuteration the H_O and/or H_N singlet(s) will grow in intensity with rate constant k_{HN} and/or k_{HO}, respectively, owing to the process H_N–C–$H_O \rightarrow$D–C–H_O and/or H_N–C–D. Experimentally, it was difficult, however, to follow these initial processes over the whole pD range simply because the rates were too large in some pD region. We are forced, therefore, to estimate the separate rate constant by following the decrease in singlet intensity, which was found to be almost exponential. This corresponds to the second stage of deuteration.

Results and Discussion

Figure 3 gives the tracings of the NMR spectra in pure deuterium oxide for all the complexes investigated here. Chemical shift data are summarized in Table 1. In Fig. 3, the strong peak at δ 4.62 is due to solvent HDO. The *cis*-$(NH_3)_2$ compound, Fig. 3(a), gives the AB quartet centered at δ 3.43 and a broad resonance at δ 3.80 due to the coordinated ammonia groups. The tn compound, Fig. 3(b), shows the complex multiplets of methylene groups at δ 2.28 (C_1 and C_3 methylenes) and δ 1.95 (C_2 methylene), and a broad absorption at δ 4.62 due to the coordinated amine group (overlapped with the HDO resonance), in addition to the malonate quartet. The spectrum of the en compound, Fig. 3(c),

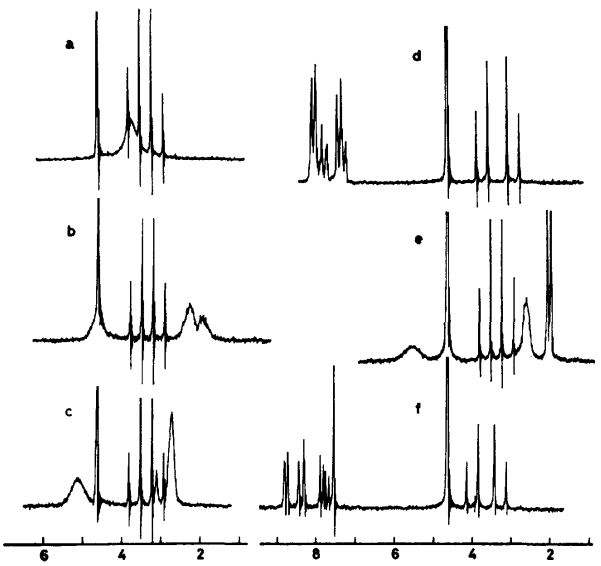

Fig. 3. The 60 MHz spectra of $[Co(mal)_2(N)_2]^-$ compounds, where $(N)_2$ stands for (a) *cis*-$(NH_3)_2$, (b) tn, (c) en, (d) *cis*-py_2, (e) dmen, and (f) phen. These spectra were taken immediately after dissolution in pure D_2O.

Table 1. Summary of the chemical shifts and the coupling constants, both values being expressed in Hz

The isotope shifts(Hz) are taken to be plus for upfield shifts in the resonance of CHD group compared with the resonance of CH_2 group, in accordance with the usual convention.

Ligand	CH_2 species		CHD species		Isotope shift		J	pD	Concn (mol dm^{-3})
	$\nu(H_N)$	$\nu(H_O)$	$\nu(H_N)$	$\nu(H_O)$	$\delta\nu(H_N)$	$\delta\nu(H_O)$			
en	218.62	187.38	—	186.98	—	+0.40	18.0	6.50	0.19
tn	216.12	184.88	215.72	184.37	+0.40	+0.51	18.3	6.83	0.12
dmen	220.44	188.31	—	187.80	—	+0.51	18.7	4.67	0.27
cis-$(NH_3)_2$	220.98	190.02	220.37	189.21	+0.61	+0.81	18.5	8.35	0.28
cis-py_2	234.04	187.96	234.65	186.38	−0.61	+1.58	18.8	6.20	0.24
phen	243.66	203.54	242.99	202.70	+0.67	+0.84	18.3	5.67	0.13

is reported[3,4,6] and consists of the malonate quartet at δ 3.38, a broad singlet at δ 2.75 due to methylene hydrogens of the coordinated ethylenediamine, and a broad peak at δ 5.12 due to the NH_2 group. The pyridine resonance of the *cis*-py_2 compound appears between δ 7.35 and 8.30, as reported previously (Fig. 3(d)).[8] The spectrum of the dmen compound consitsts of the methyl doublet (δ 2.07, $J\approx5$ Hz), a broad peak (δ 2.63) due to the methylene group, and a broad singlet (δ 5.53) due to the coordinated amine group, see Fig. 3(e). The methyl doublet collapsed into a singlet upon deuteration of the amine group. Figure 3(f) shows the spectrum of the phen compound and contains the phen multiplets between δ 7.50 and 8.90. In all the compounds, the malonate hydrogens appear as an AB quartet at around δ=3.1—4.1 and the J values assume almost constant values of about 18 Hz. The spectral parameters of these quartets (chemical shifts and J values) did not change with the solution pD. The AB quartet results from different magnetic environments seen by H_N and H_O.[3,4] The origin of this difference was discussed by Buckingham *et al.*[4] in connection with the conformation of malonate chelates. As shown in Table 1, the chemical shift differences between the H_N and H_O hydrogens are rather large, ranging from 30.96 Hz of the *cis*-$(NH_3)_2$ compound to 46.08 Hz of the *cis*-py_2 compound. Therefore, it is expected for all the compounds that the H_N hydrogen, for example, must be assigned either to the high-field pair of the quartet or the low-field counterpart. Several factors might be conceivable as the origin of the shift difference between H_N and H_O. They are the magnetic anisotropy of the central cobalt(III) ion and the anisotropic magnetic shielding of the C=O and C–O groups. The r^{-3} dependence of the former effect predicts[15] that the two hydrogens, H_N and H_O, more than 3.5 Å apart from the Co(III) ion of the *cis*-CoN_2O_4 chromophore do not exhibit the shift difference as large as 30 Hz (0.5 ppm), the value observed. The anisotropic shielding effect of the C=O and C–O groups of one malonate upon the chemical shift of the other malonate appears also unlikely, because the maximum shift difference observed for the Δ- and Λ-$[Co(ox)_2(R\text{-}pn)]^-$ pair is 0.16 ppm of the alpha hydrogen and the corresponding quantity in Δ- and Λ-$[Co(acac)_2(S\text{-}ala)]$ is 0.20 ppm.[16] The combined effect of the two COO groups within one malonate moiety would, however, amount to more than 0.6 ppm in some cases.[16d] It is rather difficult to assess quantitatively the shift difference since the shift difference of H_N and H_O depends critically on the conformation of the malonate chelate. The six-membered cobalt-malonate ring can adopt several conformation; the chair, boat, skew-boat, and intermediate stage conformations of these. The interconversion among these conformations will certainly be rapid, as discussed by Yoneda and Morimoto[3] and Buckingham *et al.*[4] In the absence of any other evidence, we can not decide the most stable conformation at present. Thus, it does not seem pertinent to discuss the chemical shift difference of H_N and H_O further.

The assignment of H_N, for example, to either the high-field or the low-field pair of the quartet will be made by comparing the chemical shift changes caused by changing nitrogen ligands. Among the en, tn, dmen, and *cis*-$(NH_3)_2$ complexes, the shift variations are relatively small and within 4.86 Hz for the low-field hydrogen and 5.14 Hz for the high-field one. For the compounds with aromatic ligands, we observed large shift variations, especially in the low-field pair. Thus, on going from the en compound to the *cis*-py_2 compound, we note that the chemical shift change of the low-field pair is 15.42 Hz while that of the high-field pair is 0.58 Hz. Likewise, the chemical shift differences between the en and phen complexes are 25.04 Hz and 16.16 Hz for the low- and the high-field pairs, respectively. The larger downfield shift of the low-field pair observed for aromatic ligands is probably due to the ring current effect[16d] of py and phen ligands and suggests that the hydrogen giving rise to the low-field pair is adjacent to the coordinating nitrogen. Therefore we propose that the hydrogen H_N undergoes a greater chemical shift change owing to its closeness to nitrogen ligands and is assigned to the low-field pair of the AB quartet.

To confirm the assignment, we have compared the chemical shift of $[Co(mal)_2(en)]^-$ and $[Co(mal)_2(meen)]^-$ ions, and of $[Co(mal)_2(gly)]^{2-}$ and $[Co(mal)_2(sar)]^{2-}$ ions.[17] In both pairs, the effect of *N*-methylation was greater for the low-field hydrogens than for the high-field ones. For example, the Meen compound exhibits two AB quartets due to malonate and the shift values of the high- and low-field hydrogens of one quartet are δ 3.11 and 3.62, respectively, and the corresponding values of the other quartet are δ 3.15 and 3.67. The latter values correspond nicely to the values

of the dmen compound (δ 3.14 and 3.67) so that this quartet is most probably due to the malonate CH_2 group adjacent to the *N*-methyl group of Meen. Thus the *N*-methylation of en caused a down-field shift of the low-field hydrogen by 0.03 ppm in both Meen and dmen compounds.

It should be pointed out that the present assignment of the AB quartet is opposite to the assignment of Farago and Smith.[6] Their assignment is based on the assumption that in the time averaged conformation of malonate-cobalt rings the H_N hydrogen is displaced, owing to the malonate-malonate repulsion, toward the NH_2 groups and is surrounded by more valence electrons than H_O. The high-field hydrogen is thus assigned to H_N. For reasons mentioned above, we do not favor their assignment.

In Table 1, the values of isotope shift[18] are also given. These values range from -0.61 to $+1.58$ Hz and they are of the magnitude usually observed.[18] In the *cis*-py_2 compound, a down-field isotope shift is found for the H_N hydrogen (-0.61 Hz). The H_O hydrogen of the same compound shows the usual upfield shift ($+1.58$ Hz). It will be interesting to note that stereochemically different hydrogens can show isotope shifts of opposite signs even if they are bonded to the same carbon atom. Generally, deuterium substitution

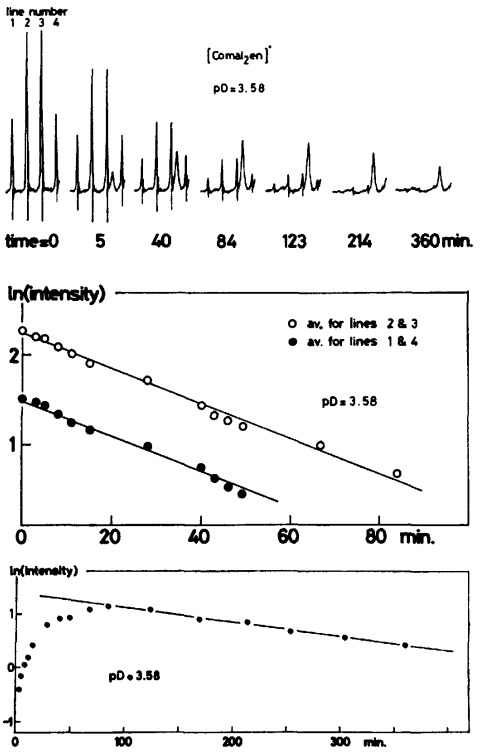

Fig. 4. An example of the kinetic analysis. The sample is $[Co(mal)_2(en)]^-$ at pD=3.58 and at 36.4 °C. (Top) The variation of the malonate portion of the spectrum with time, the H_O singlet being not numbered. (Mid-) dle) The ln (intensity) *vs.* time plots for the inner pair (lines 2 and 3, open circles) and the outer pair (lines 1 and 4, closed circles) of the quartet. (Bottom) The ln (intensity) *vs.* time plots of the H_O singlet. The solid line is the asymptote for the second stage of deuteration.

gem to a proton is reported to cause the proton resonance to be shifted upfield.[18] Only one exception is known to date; the NH_4^+ ion exhibited a downfield isotope shift.[19] This unusual isotope shift has been explained by electrostatic effects arising from hydrogen bonding with the polar deuterium oxide solvent. It appears that the isotope shifts of opposite sign exhibited by H_N and H_O of the *cis*-py_2 compound are reflecting different degrees of solvation around these hydrogens.

Stereoselectivity. The kinetic behavior expected from Eq. 4 to 7 is illustrated in Fig. 4 for the data of the en compound at pD=3.58. The top figure shows the time variation of the malonate portion of the spectrum. Immediately after dissolution we observed only the AB quartet, as expected for the presence of only H_N–C–H_O species. As time passes, the quartet decreases in intensity and at the same time a singlet appears exactly at the chemical shift of the high-field H_O hydrogen and grows in intensity with time. Then, the singlet begins to decrease in intensity and disappears eventually. The middle figure gives the time variation of the quartet intensity. In the figure, the natural logarithms of an average of the intensities of the inner and outer pair of the quartet are plotted against time by the open and closed circles, respectively. Both plots give straight lines and the slopes of both plots are the same within experimental uncertainties. Thus, the quartet intensity decreased exponentially with time over at least 2—3 half lives. As indicated by Eq. 4, these slopes correspond to k_Q or equally $k_{HN}+k_{HO}$. The bottom figure illustrates the time variation of the H_O singlet intensity. From this figure it appears rather difficult to obtain the initial rate constant, k_{HN} in this case. However, the second stage of deuteration follows the exponential law rather well, as indicated by the solid line in the figure. The slope of this asymptote corresponds to k_{HO}, as dictated by Eq. 6. The rate constant k_{HN} was obtained by $k_{HN}=k_Q-k_{HO}$, Eq. 5.

In the top figure we do not observe the H_N singlet due to the species H_N–C–H_O throughout the deuteration process. This means that the whole spectral change with time should be explained by the process

$$H_N\text{–C–}H_O \longrightarrow D\text{–C–}H_O \longrightarrow D\text{–C–}D,$$

where the species H_N–C–D was not produced during this deuteration process. Therefore, the deuteration takes place stereoselectively; the rate of deuteration of H_N is much larger than that of H_O.

The degree of the stereoselectivity can be defined by the ratio k_{HN}/k_{HO}. Qualitatively, the intensity ratio of the high- to low-field singlets can be taken as a rough measure of the degree of stereoselectivity. Figure 5 shows collectively the malonate portion of the NMR spectra of dmen, tn, *cis*-py_2, and phen compounds, taken some time after dissolution. The dmen and tn compounds exhibit marginally observable H_N singlet, in addition to the H_O singlet. This result indicates that the rate of deuteration of H_N is much faster than that of H_O in the dmen and tn compounds. The *cis*-py_2 and phen compounds show both H_N and H_O singlets in almost equal intensities, implying that the deuteration in these compounds proceeds with little or no stereoselectivity.

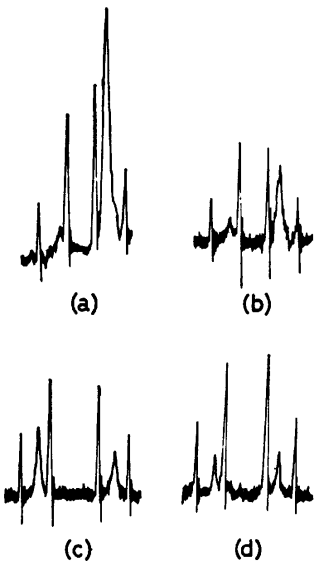

Fig. 5. The malonate portion of the NMR spectra of (a) dmen (pD=5.02), (b) tn (pD=7.18), (c) *cis*-py_2 (pD=6.55), and (d) phen (pD=6.02) complexes, taken some time after dissolution.

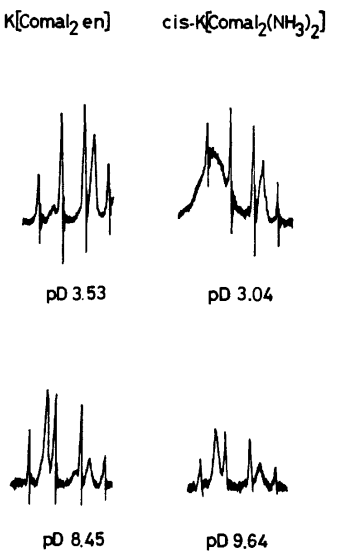

Fig. 6. The malonate portion of the NMR spectra of the en and *cis*-$(NH_3)_2$ compounds in acidified and basic deuterium oxide, taken some time after dissolution. The broad lump of the *cis*-$(NH_3)_2$ compound at pD= 3.04 is due to coordinated ammonia groups. This lump disappears in basic solution owing to the hydrogen-deuterium exchange at the ammonia groups.

Figure 6 illustrates the malonate portion of the NMR spectra of the en and *cis*-$(NH_3)_2$ compounds, taken some time after dissolution in acidified and basic deuterium oxide. At low pD, only the high-field H_O singlet can be observed for both compounds. At high pD, both the low-field H_N and the high-field H_O singlets are observed and the former is greater in intensity. These spectra are evidence that at low pD it is H_N that exchanges with deuterium first and at high pD it is H_O. Apparently the stereoselectivity in these two compounds is reversed on going from low to high pD region.

In Table 2, the second-order rate constants are given; the definition of these quantities is presented later. In terms of the second-order rate constants, the degree of the stereoselectivity is k'_{HN}/k'_{HO} or k''_{HN}/k''_{HO}. From Table 2, we see that while the degree of the stereoselectivity does not differ greatly for all the compounds in acid-catalysed reaction, it depends strongly upon the nitrogen ligand at high pD and is in the order (pD>8),

dmen > en, tn > *cis*-$(NH_3)_2$ > *cis*-py_2≈phen≈0

It is interesting to note that in *trans*-[Co(edda)(en)]$^+$ base-catalysed deuteration at glycine residues is more stereoselective than in acid-catalysed one.[20] It is reported that the degree of stereoselectivity is high and amounts to about 100 in the base-catalysis while it is about 10 in acid-catalysis.

Deuteration Mechanisms. The log(k) *vs.* pD plots for all the compounds are shown in Figs. 7 and 8, in which the deuteration rates of amine groups are also provided. The deuteration of amine groups is base-catalysed, as reported previously,[13] except for the *cis*-$(NH_3)_2$ compound at pD≈8. In other metal amine compounds, the hydrogen deuterium exchange reaction showed the first-order dependence on OD^- concentration in all instances.[13] This first-order dependence obtains even for systems where strong ion-pairing or stereoselective ion-association occurs between the amine group(s) and counter anions.[21] In the present systems,

Table 2. The second-order rate constants (s^{-1} mol^{-1} dm^3, 36.4 °C) for the deuteration of malonate hydrogens in bis(malonato)cobalt(III) complexes[a]

Ligand	Acid-catalysis			Base-catalysis			
	k'_Q	k'_{HN}	k'_{HO}	$k''_Q\times10^{-3}$	$k''_{HN}\times10^{-3}$	$k''_{HO}\times10^{-3}$	
en	1.4±0.8	(1.2)	0.2±0.1	38±20	(37)	1±0.6	pD<7
				1.3±0.7	0.25±0.14	(1.1)	pD>8
dmen	0.79±0.05	(0.7)	0.08±0.05	310±180	(300)	15±11	
tn	1.8±1.0	(1.6)	0.2±0.1	1±0.6	(0.8)	0.2±0.2	
cis-py_2	2.1±1.3	(1)[b]	(1)[b]	30±17	(15)[b]	(15)[b]	
phen	0.83±0.50	(0.4)[b]	(0.4)[b]	19±28	(10)[b]	(10)[b]	
cis-$(NH_3)_2$	3.2±3.0	(2.8)	0.4±0.3	0.55±0.32	0.32±0.14	(0.32)	pD>9

a) The values in parentheses are obtained by the relation; $k'_Q=k'_{HN}+k'_{HO}$ or $k''_Q=k''_{HN}+k''_{HO}$.b) Intensities of the H_N and H_O singlets are too small to allow rate measurements, but Fig. 5 indicates that k_{HN} is approximately equal to k_{HO}. Therefore these values are obtained on the assumption that $k_{HN}=k_{HO}$.

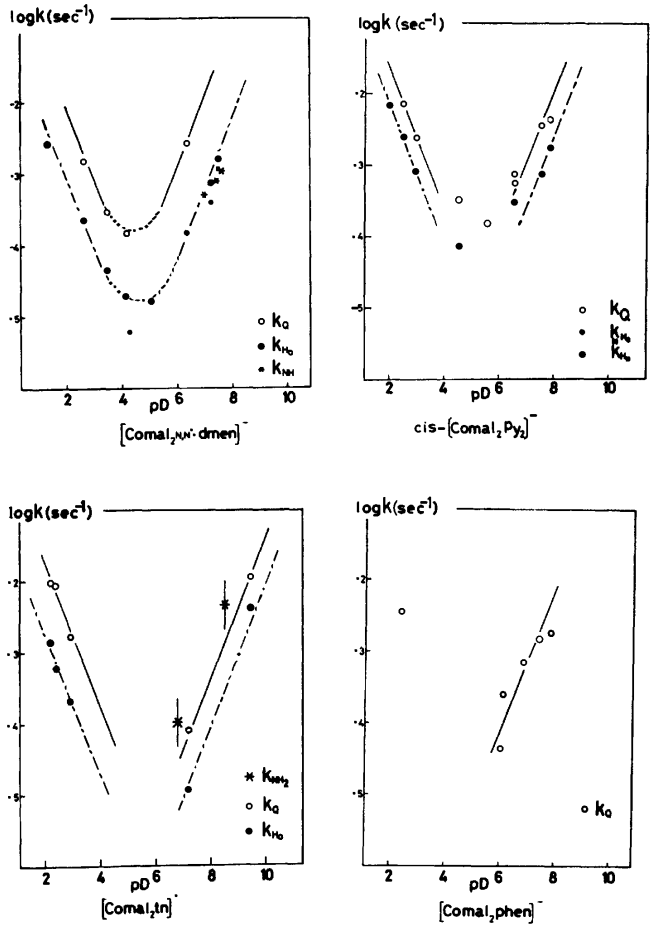

Fig. 7. The log(k) *vs.* pD plots for dmen, *cis*-py_2, tn, and phen complexes. The solid lines have a slope of $+1$ or -1.

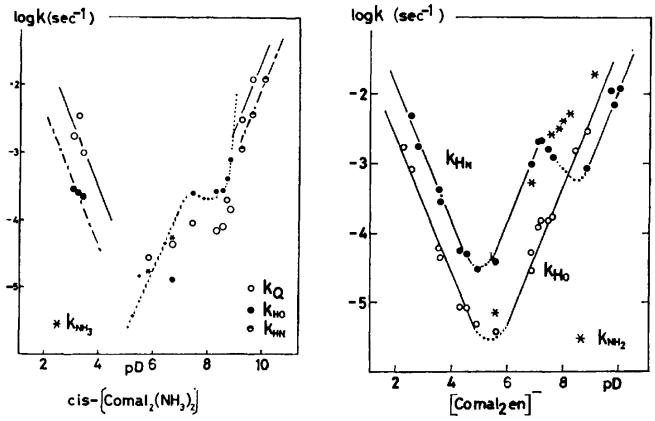

Fig. 8. The log(k) *vs.* pD plots for *cis*-$(NH_3)_2$ and en compounds. The solid lines have a slope of $+1$ or -1.

the compounds are singly-charged and it is safely assumed that the effect of ion-association upon amine exchange is minimal. The disparity found for the *cis*-$(NH_3)_2$ compound at pD$\approx$8 will be discussed later in connection with the reversal of the stereoselectivity.

It is seen that the deuteration of malonate groups is acid-catalysed at pD$<$4 and base-catalysed at pD$>$6. Thus, we have

$$k_1 = k_1'[D_3O^+] + k_1''[OD^-] \quad (i=Q,\ H_N,\ \text{or}\ H_O)$$

where k_1' and k_1'' are the second-order rate constants for the acid- and base-catalysed reactions, respectively. Apparently, this first-order dependence on catalyst concentration is not obeyed again by the en and *cis*-$(NH_3)_2$ compounds in the region of pD 7 to 8 and this point will be discussed later. The D_3O^+ and OD^- concentrations are estimated by pD and $pK_{w(D,O)}=14.37$[12c] and the second-order rate constants are obtained. In Table 2, the second-order rate constants are summarized. They do not vary greatly from compound to compound at low pD, but in base-catalysed deuteration they differ significantly. At high pD, the value of k'' decreases in the order

$$\text{dmen} > \textit{cis}\text{-py}_2,\ \text{phen} > \text{en},\ \text{tn} > \textit{cis}\text{-}(NH_3)_2$$

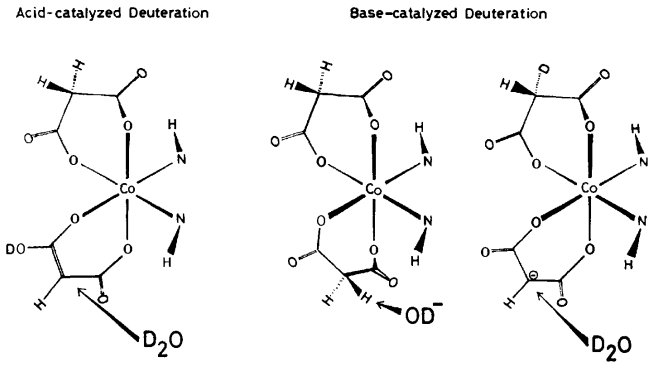

Fig. 9. A possible mechanism of acid- and base-catalysed deuteration that brings about stereoselectivity.

Mechanistically, acid-catalysed deuteration is effected by D_2O donating D^+ to the enol form, as depicted in Fig. 9. The enol results from the tautomerization of the protonated carbonyl form and is planar.[2,6] Therefore, if deuteration is to be stereoselective, it should take place preferentially either from the side adjacent to the coordinating amine group or from the side inbetween the two malonate groups. In the former case, H_N is deuterated first and we will observe the high-field H_O singlet. This is what we have found experimentally (*vide supra*).

In the acid-catalysed reaction, another mechanism will be considered. This mechanism is similar to the one proposed by Terrill and Reilley[22] for the deuteration of glycine residues in [Co(edta)]$^-$ ion. This involves the carbonyl protonation and subsequent rupture of the carboxylatocobalt bond. Since it assumes the unidentate carbonium ligand, such as

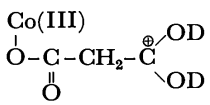

we may reasonably expect concomitant racemization at the metal center. For [Co(edta)]$^-$ ion, Terrill and Reilley in fact confirmed that deuteration is accompanied by racemization. To check the possibility of this mechanism, we resolved the en compound into optical isomers and measured the circular dichroism spectrum over the pH region of 2 to 12. Experimentally, however, we did not observe any measurable change in

the spectrum over the whole pH range and over several half lives of deuteration. This optical stability of the en compound corresponds well to the result of Dwyer *et al.*[9] It appears, therefore, that this mechanism is not appropriate at least to the en compound.

A probable mechanism of the base-catalysed deuteration is proposed previously.[2] It will suffice here to recall that the postulated mechanism involves the carbanion intermediate produced by hydrogen abstraction by OD^-. In the base-catalysed reaction, setereoselective deuteration may be effected in two ways; (a) hydrogen abstraction by OD^- is stereoselective, (b) deuteration by D_2O upon the carbanion intermediate is stereoselective. These two pathways are illustrated schematically in Fig. 9. Both processes may contribute to enhance the stereoselectivity if they occur from the N–H side(Note that the stereoselectivity is observed only for the amino-containing compounds.). It should be noted, however, that even if the hydrogen abstraction by OD^- had occurred stereoselectively, the resulting carbanion becomes most probably planar and loses its memory. The carbonion can be resonance stabilised with the adjacent carbonyl groups, which favors the planar structure. Further it is reported that retention of configuration has never been observed with simple carbanions.[23] Thus, (b) is considered the only likely process.

From the above, it is clear that the stereoselective deuteration in both acid- and base-catalysis is effected by D_2O donating D^+ to the enol and the carbanion intermediates, respectively. The present results indicate that at any pD the D_2O molecule prefers the access from the N–H side to that from the malonate side, except the high pD case of the en and *cis*-$(NH_3)_2$ compounds. The explanation of the stereoselectivity might be found in the conformation of the enol and carbanion intermediates. If the planar malonate moiety of these intermediates bends toward the coordinated nitrogen, steric repulsion is clearly expected between the amine group and the π-electron cloud of the enol or the unshared pair electron density of the carbanion. The planarity of these intermediates enforces the six-membered chelate ring to bend away from the coordinated nitrogen toward the other malonate-cobalt chelate. In this stable conformation of the intermediates, the access of D_2O molecule is likely to occur from the less-hindered side of coordinated nitrogen rather than from the more crowded malonate side.

Terrill and Reilley[22] made the variable temperature NMR studies on the stereoselective deuteration of $[Co(edta)]^-$. Sudmeier and Occupati[20] made a similar experiments on *trans*-$[Co(edda)(en)]^+$. For *trans*-$[Co(edda)(en)]^+$, $[Co(edta)]^-$, and their analogues,[24] the stereoselectivity was explained as the protection of a particular hydrogen from solvent molecules by the ethylenediamine backbone in the chelates. Farago and Smith[6] obtained the kinetic parameters for the deuteration of $[Co(mal)_2(en)]^-$ at about pD=3. This result is in good agreement with our data and indicated the stereoselectivity being entropy controlled. Further the data for the $[Co(mal)(en)_2]^+$ and $[Co(mal)(bpy)_2]^+$ ions pointed to the importance of the affinity of D_3O^+ or OD^- catalyst toward the ligands.

Origin of the Reversal of the Stereoselectivity. The reversal of the stereoselectivity as found for the en and *cis*-$(NH_3)_2$ compounds may be the most intersting aspect of the malonate exchange. In the $\log(k)$ *vs.* pD plots of Fig. 8, we note that the reversal takes place at about pD=7.5 and that the deuteration rates are retarded at around this pD. Concomitant with this anomalous pD dependence is the anomaly in the deuteration rate of coordinated amine groups. In the figure amine exchange rate is denoted by an asterisk. Above pD=8.5, a nomal first-order dependence of malonate exchange rates upon $[OD^-]$ obtains again. In the plots of the en compound, it is noteworthy that the rate of H_N is suppressed in the pD range of 7 to 8 and at pD=8, k_{HN} reverts to a $\log(k_{HN}) \propto +$pD line whereas k_{HO} appears unaffected. If we note that the reversal is accompanied by anomalous decreases in both malonate and amine exchange rates, the amine exchange may be considered to play an important role in this phenomenon. The *cis*-py_2 and phen compounds lack exchangeable N–H groups. Though the dmen and tn compounds do have these groups, their exchange rates are slower than or at most similar to those of the malonate exchange in each complex. The NH_2 resonance of the tn compound overlapped with a strong solvent HDO signal as seen in Fig. 3(b), which precluded accurate rate measurements. For *cis*-$(NH_3)_2$ compounds, it appears that the reversal of stereoselectivity takes place at such a pD value that the rate of amine exchange exceeds significantly that of malonate exchange. At this pD value, both amine and malonate hydrogens may be considered to have become equally reactive so that they might well compete for the OD^- catalyst. As a result, it is probable that both rates tend to fall together.

In the plots of the en compound, the anomaly of the amine exchange rate is less prominent than that of the malonate exchange rate. The point to be noted here is that the amine exchange rate is close to but slower than the malonate exchange even at the pD value where the k_{HN} begins to be suppressed. This observation suggests that though amine exchange does pertain in some way to the reversal, but it is not the only cause for the reversal. Some probable factors other than competition for the OD^- catalyst might be invoked. For example, one may consider the possibility that the amine and malonate hydrogens are exchanging between themselves in the pD region of 7 to 9. Under such conditions, both amine and malonate exchange rates might well be suppressed since these hydrogens are not exchanging with solvent deuterium but among themselves. By dissolving the en compound in acidified D_2O and precipitating with dry dioxane after suitable time intervals, we obtained the partially deuterated compound $K[Co(mal\text{-}d_2)_2(en)]$, for which only the malonate is deuterated completely leaving the amine group undeuterated. If the abovementioned intramolecular exchange is present, we may observe the malonate resonance to grow with time by dissolving this partially deuterated compound in D_2O at pD$\geqq$7.5. This is because the amine hydrogens that survived the partial deuteration are going to be transferred to the malonate.

We have not, however, succeeded in detecting the expected malonate resonance despite our repeated trials. We are therefore inclined to regard this intramolecular hydrogen exchange less probable. One may consider, further, that the conformation of the malonate ring changes at around pD=7 specifically in the en and *cis*-$(NH_3)_2$ compounds. It is well known[25] that conformational changes of chelate rings often show up as a change of circular dichroism spectrum. To check this possibility we have resolved the en compound into optical isomers and measured the circular dichroism spectrum over the pD range of 2 to 11. However, the circular dichroism spectrum of the optically resolved en compound exhibited no change against pD, rendering the conformational change also unlikely.

After all, our explanation at this stage is that at this pD region amine and malonate hydrogens compete for the OD^- catalyst for some reasons. In order for this process to occur, some stereochemical condition should be fulfilled. In the plots of the en compound of Fig. 8, only the rate of H_N hydrogen, which is adjacent to the amine group, is retarded while that of the H_O hydrogen, which is situated farthest apart from the amine group, remains unaffected. This will be taken to suggest that stereochemically close and, in addition, equally reactive groups are allowed to interfere with each other's exchange.

One of the authors (U.S.) acknowledges finacial support from The Ministry of Education under Grant No. 446-7054-364214 and The Matsunaga Research Grant.

References

1) This work is Proton Magnetic Resonance Spectra of Metal Ammine Complexes. 15. Part of this work has been communicated in a preliminary form; U. Sakaguchi, K. Morito, and H. Yoneda, *J. Am. Chem. Soc.*, **101**, 2767 (1979).

2) U. Sakaguchi, M. Nakano, and H. Yoneda, *Bull. Chem. Soc. Jpn.*, **53**, 2544 (1980).

3) H. Yoneda and Y. Morimoto, *Inorg. Chim. Acta*, **1**, 413 (1967).

4) D. A. Buckingham, L. Durham, and A. M. Sargeson, *Aust. J. Chem.*, **20**, 257 (1967).

5) Abbreviations; mal=malonate dianion, en=ethylenediamine, tn=1,3-propanediamine, dmen=*N*,*N*-dimethylethylenediamine, phen=1,10-phenanthroline, bpy=2,2′-bipyridine, edta=ethylenediaminetetraacetate anion, ox=oxalate anion, pn=1,2-propanediamine, acac=acetylacetonate anion, ala=alaninate anion, gly=glycinate anion, meen=*N*-methylethylenediamine, sar=*N*-methylglycine, py=pyridine.

6) a) M. E. Farago and M. A. R. Smith, *J. Chem. Soc., Dalton Trans.*, **1972**, 2120; b) M. E. Farago and M. A. R. Smith, *Inorg. Chim. Acta*, **14**, 21 (1975); c) S. Amirhaeri, M. E. Farago, J. A. P. Gluck, M. A. R. Smith, and J. N. Wingfield, *ibid.*, **33**, 57 (1979).

7) S. Kuramoto, K. Kawase, and M. Shibata, *Bull. Chem. Soc. Jpn.*, **51**, 3505 (1978).

8) Y. Ida, S. Fujinami, and M. Shibata, *Bull. Chem. Soc. Jpn.*, **50**, 2665 (1977).

9) F. P. Dwyer, I. K. Reid, and F. L. Garvan, *J. Am. Chem. Soc.*, **83**, 1285 (1961).

10) B. J. Brennan, K. Igi, and B. E. Douglas, *J. Coord. Chem.*, **4**, 19 (1974).

11) N. C. Kneten and S. T. Spees, Jr., *J. Inorg. Nucl. Chem.*, **33**, 2437 (1971).

12) a) T. H. Fife and T. C. Bruice, *J. Phys. Chem.*, **65**, 1079 (1961); b) P. K. Glasoe and F. A. Long, *ibid.*, **64**, 188 (1960); c) W. F. K. Wynne-Jones, *Trans. Faraday Soc.*, **32**, 1397 (1936).

13) U. Sakaguchi, K. Maeda, and H. Yoneda, *Bull. Chem. Soc. Jpn.*, **49**, 397 (1976), and references cited therein.

14) W. P. Jencks, "Catalysis in Chemistry and Enzymology" McGraw-Hill (1969), Chap. 4.

15) a) H. Yoneda, U. Sakaguchi, and Y. Nakashima, *Bull. Chem. Soc. Jpn.*, **48**, 209 (1975); b) U. Sakaguchi, S. Yamazaki, and H. Yoneda, *ibid.*, **49**, 402 (1976), and references cited therein.

16) a) E. A. Berends and J. G. Brushmiller, *Inorg. Nucl. Chem. Lett.*, **6**, 531 and 847 (1970); b) J. G. Stadtherr and J. G. Brushmiller, *ibid.*, **6**, 907 (1970); c) J. G. Brushmiller and L. G. Stadtherr, *ibid.*, **3**, 525 (1967); d) J. W. Emsley, J. Feeney, and L. H. Sutcliffe, "High Resolution Nuclear Magnetic Resonance Spectroscopy," Pergamon Press, N. Y. (1965), Chap. 4.

17) a) U. Sakaguchi, K. Morito, and H. Yoneda, *Chem. Lett.*, **1979**, 19; b) U. Sakaguchi *et al.*, unpublished results.

18) H. Batiz-Hernandez and R. A. Bernheim, *Prog. NMR Spectrosc.*, **3**, 63 (1967).

19) G. Fraenkel, Y. Asahi, H. Batiz-Hernandez, and R. A. Bernheim, *J. Chem. Phys.*, **44**, 4647 (1966).

20) J. L. Sudmeier and G. Occupati, *Inorg. Chem.*, **7**, 2524 (1968).

21) a) H. Yamatera and M. Fujita, *Bull. Chem. Soc. Jpn.*, **42**, 3043 (1967); b) M. Fujita and H. Yamatera, *ibid.*, **50**, 2672 (1977); c) H. Nakazawa, U. Sakaguchi, and H. Yoneda, *ibid.*, **53**, 1595 (1980).

22) J. B. Terrill and C. N. Reilley, *Inorg. Chem.*, **5**, 1988 (1966). See, also; J. L. Sudmeier and G. Occupati, *ibid.*, **7**, 2524 (1968).

23) J. March, "Advanced Organic Chemistry," McGraw-Hill, (1977), Chap. 5.

24) a) J. L. Sudmeier, A. J. Senzel, and G. L. Blackmer, *Inorg. Chem.*, **10**, 90 (1971); b) P. F. Coleman, J. I. Legg, and J. Steele, *ibid.*, **9**, 937 (1970).

25) See, for example; K. Kashiwabara, M. Kojima, and J. Fujita, *Bull. Chem. Soc. Jpn.*, **52**, 772 (1979); and references cited therein.

Studies on Characteristics of Electron Capture Responses. IV. Carrier Gas Flow-rate Dependence of Electron Capture Coefficients

Masahiro TAKEUCHI

Tokyo Metropolitan Research Laboratory of Public Health, Hyakunincho, Shinjuku-ku, Tokyo 160

(Received October 22, 1979)

The electron capture coefficients, K, defined by Wentworth *et al.* were measured on several samples in various carrier gas flow-rates at the detector temperatures of 200—320 °C. The effect of the flow-rate on the value of K was considered. The results revealed that the flow-rate dependence of K for each sample was closely related to one of the three electron capture reaction processes. In a sample undergoing the non-dissociative electron capture reaction, the values of K were generally not affected by the flow-rate; they decreased slightly with increasing the flow-rate at higher temperatures. In a sample undergoing the dissociative electron capture reaction, the values of K increased significantly with increasing the flow-rate at all temperatures. In a sample undergoing the dissociative electron capture reaction through an anion radical intermediate, the values of K were slightly or not at all affected by the flow-rate at lower temperatures, but increased gradually with increasing the flow-rate at higher temperatures.

Its high sensitivity and selectivity to halogen-containing compounds have caused the electron capture detector (ECD) to be widely used in the trace analysis of organochloro pesticides, polychlorinated biphenyls, *etc.*, remaining in various environmental samples. Though the practical applications are familiar, the theoretical details of the ECD have not received much study. The author has thus studied the responses of the ECD in order to understand the events occurring within it.

The ECD is a concentration-sensitive detector.[1-3] Its response function, studied by Wentworth *et al.*,[4-6] is given by

$$\frac{I_b - I_e}{I_e} = KC, \quad (1)$$

where I_b is the base current due to pure carrier gas, I_e is the current in the presence of a concentration C of electron capturing vapor, and K is the electron capture coefficient, which expresses the sensitivity of the detector to the vapor. In the practical gas chromatography, K is given by

$$K = \frac{1}{n}\frac{F}{S}\int \frac{I_b - I_e}{I_e} dX, \quad (2)$$

where n is the number of moles injected, F is the carrier gas flow-rate in l/min, S is the chart speed in cm/min, and X is the chart distance in cm.

Equation 2 shows that the peak areas, $\int(I_b - I_e)/I_e dX$, are inversely proportional to F under the constant conditions of S and n: If F increases to 2, 3, 4··· times as much as the initial run, the peak area will decrease to 1/2, 1/3, 1/4···, respectively. Consequently, as long as the response function of Wentworth *et al.* is correct, the value of K for a sample obtained from Eq. 2 is constant at any flow-rate. However, it was reported in the previous paper[7] that there were some samples whose values of K varied with the flow-rate. A similar result has been obtained by Devaux and Guiochon.[2] Therefore, in the present paper, the relation between the electron capture coefficient and the carrier gas flow-rate has been studied. The results have revealed that the carrier gas flow-rate dependence of K is closely related to one of the three electron capture reaction processes.

Experimental

Apparatus and Samples. A Shimadzu GC-5A gaś chromatograph equipped with an ECD was used. The ECD was of co-axial geometry and contained a 10 mCi ^{63}Ni radioactive source. Pulses were supplied by a DuMont 404 pulse generator. The pulse conditions were set up as follows in order to collect all of the electrons and to assure a steady state[4,6,8] under which Eq. 1 can be derived: the pulse period, 2000 μs; the pulse width, 2.0 μs; and the pulse amplitude, 30 V. An analog device was used for the conversion of the normal response, $I_b - I_e$, into the Wentworth response, $(I_b - I_e)/I_e$.[9] The carrier gas was pure nitrogen. Before being introduced into the system, the gas was passed through a 40 cm × 5 mm i.d. stainless steel column packed with Molecular Sieve 13 X. The flow-rate was measured at the exit end of the system with a bubble flow meter and a stopwatch. Peak areas were obtained with a Spectra-Physics Autolab System IV integrator. Two different kinds of chromatographic columns were used. One of these was a 1 m × 3 mm i.d. glass column packed with 2% Silicon OV-17 on Chromosorb W, 80—100 mesh (Column I); the other was a 1 m × 3 mm i.d. glass column packed with 2% Silicon OV-275 on Chromosorb W, 60—80 mesh (Column II). The column oven was maintained at temperatures in the range of 140—180 °C on Column I and 100—140 °C on Column II. The ECD temperature was measured with a thermometer inserted into the detector oven rather than with the thermocouple provided.

The samples used in the present study were commercially available reagents. Aldrin, γ-BHC, *p, p'*-DDE, and 2,4,6-trichlorobiphenyl were chromatographed by Column I, and nitrobenzene, azulene, iodobenzene, and 1,2,4-trichlorobenzene were chromatographed by Column II. Solutions of the samples were prepared to give suitable peak sizes, *i.e.*, $(I_b - I_e)/I_e = 1$—4.[9]

Results

Figure 1 shows the variation of I_b with the carrier gas flow-rate. Since I_b is the base current due to pure carrier gas, it ought to be kept constant. In practice, however, I_b decreased with decreasing the flow-rate, owing mainly to column bleed.[4-7] Therefore, a correction factor of I_0/I_b, where I_0 is the base current when no column bleed is observed, was utilized to adjust the value of K: the left side of Eq. 2 was multiplied by this

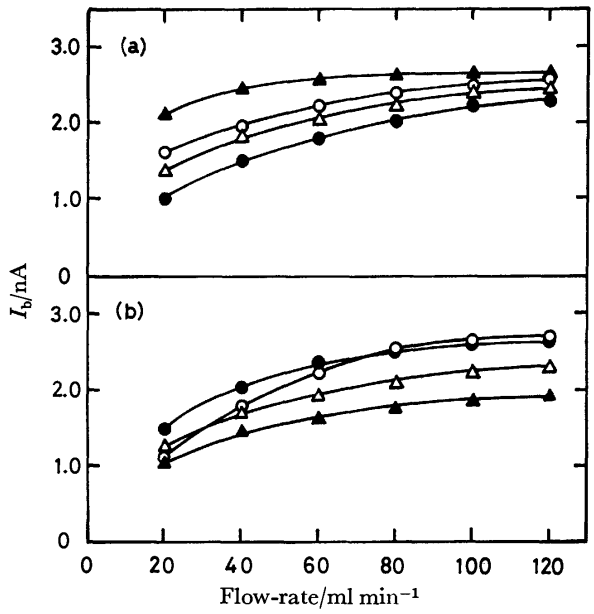

Fig. 1. Variation of base current with carrier gas flow-rate for Column I at 180 °C (a), Column II at 140 °C (b).
ECD temperatures: 200 °C (○), 240 °C (●), 280 °C (△), and 320 °C (▲).

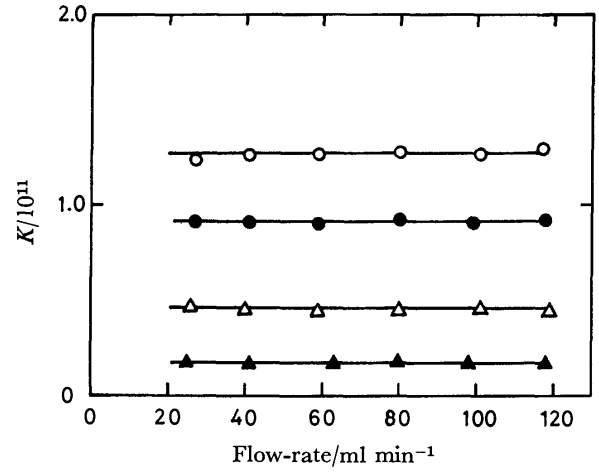

Fig. 2. Values of K for nitrobenzene *vs.* carrier gas flow-rate.
ECD temperatures: 200 °C (○), 240 °C (●), 280 °C (△), and 320 °C (▲).

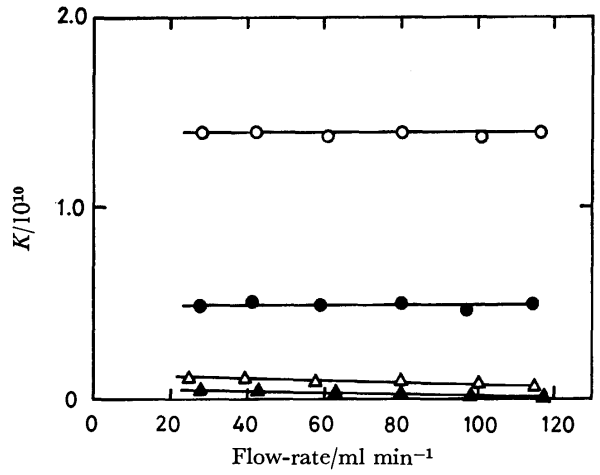

Fig. 3. Values of K for azulene *vs.* carrier gas flow-rate.
ECD temperatures: 200 °C (○), 240 °C (●), 280 °C (△), and 320 °C (▲).

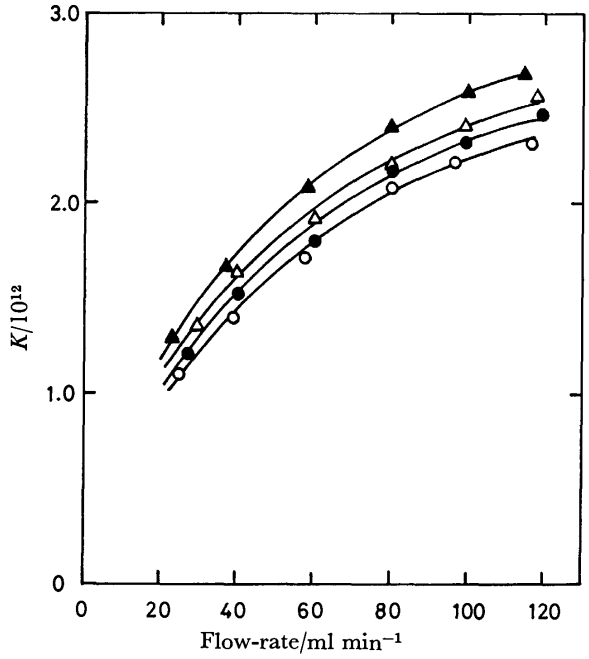

Fig. 4. Values of K for Aldrin *vs.* carrier gas flow-rate.
ECD temperatures: 200 °C (○), 240 °C (●), 280 °C (△), and 320 °C (▲).

factor.[4-6] In this paper, I_0 was regarded as I_b when the column oven was cooled to room temperature.

Figure 2 shows the values of K for nitrobenzene. No variations of K with the carrier gas flow-rate were observed at any temperature. Figure 3 shows the values of K for azulene. At lower temperatures, the values of K were not affected by the flow-rate at all. At higher temperatures, however, the values of K decreased slightly with increasing the flow-rate. Figures 4—6 show the values of K for Aldrin, γ-BHC, and p,p'-DDE, respectively. In these samples, the values of K increased significantly with increasing the flow-rate at all temperatures. Figures 7—9 show the values of K for 1,2,4-trichlorobenzene, 2,4,6-trichlorobiphenyl, and iodobenzene, respectively. In these samples, the values of K were slightly or not at all affected by the flow-rate at lower temperatures, but increased gradually with increasing the flow-rate at higher temperatures.

Discussion

The response of the ECD results from the electron capture reaction, which usually occurs through one of the three following processes:[4-6]

$$AB + e^- \rightleftarrows AB^- \quad (3)$$

$$AB + e^- \longrightarrow A\cdot + B^- \quad (4)$$

$$AB + e^- \rightleftarrows [A\cdot - B]^- \longrightarrow A\cdot + B^-. \quad (5)$$

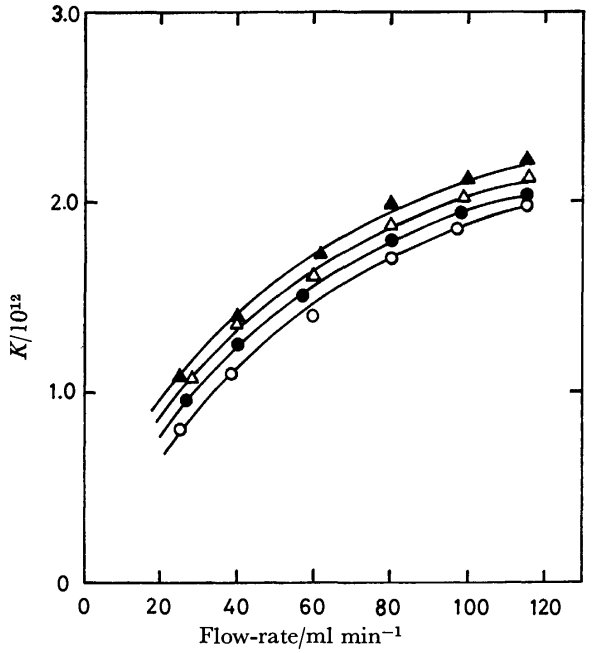

Fig. 5. Values of K for γ-BHC *vs.* carrier gas flow-rate.
ECD temperatures: 200 °C (○), 240 °C (●), 280 °C (△), and 320 °C (▲).

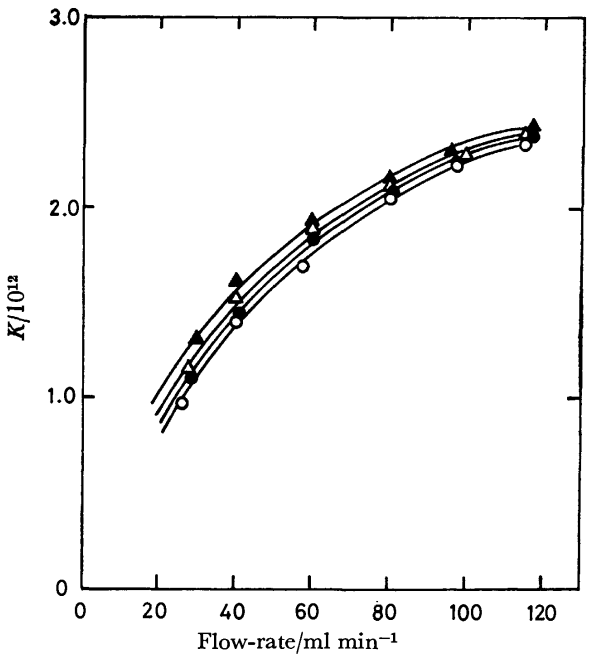

Fig. 6. Values of K for p,p'-DDE *vs.* carrier gas flow-rate.
ECD temperatures: 200 °C (○), 240 °C (●), 280 °C (△), and 320 °C (▲).

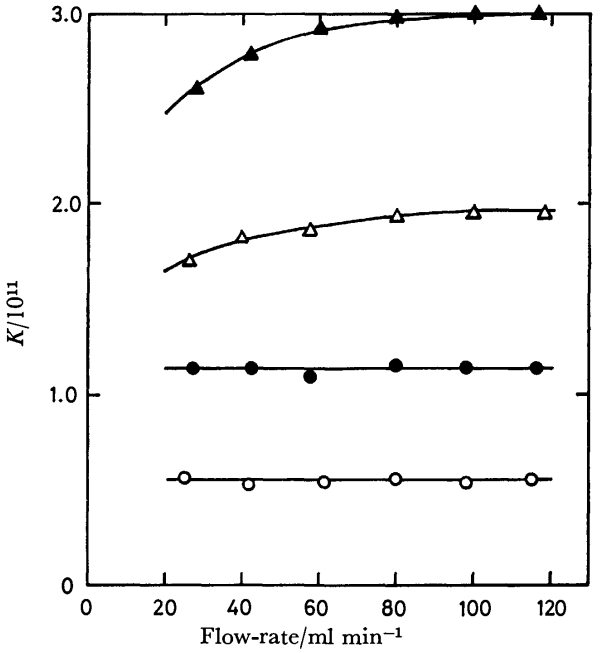

Fig. 7. Values of K for 1,2,4-trichlorobenzene *vs.* carrier gas flow-rate.
ECD temperatures: 200 °C (○), 240 °C (●), 280 °C (△), and 320 °C (▲).

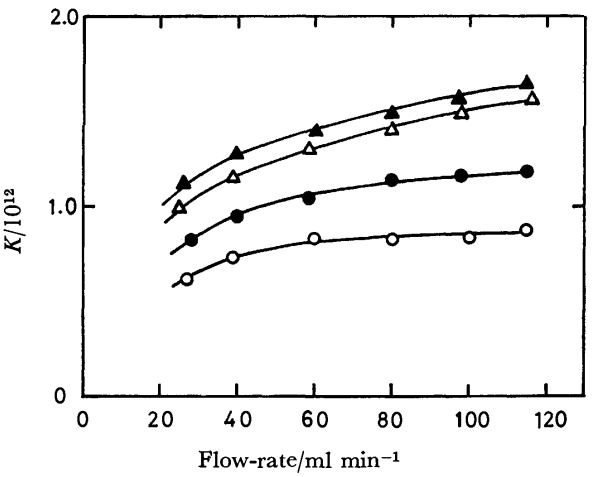

Fig. 8. Values of K for iodobenzene *vs.* carrier gas flow-rate.
ECD temperatures: 200 °C (○), 240 °C (●), 280 °C (△), and 320 °C (▲).

Equation 3, called the non-dissociative electron capture process, represents a reaction in which an electron capturing molecule, AB, reacts with an electron to form a stable molecular anion, AB^-. Equation 4, called the dissociative electron capture process, represents a reaction in which an electron capturing molecule dissociates into a radical, A·, and an anion, B^-. Equation 5, called the intermediate-dissociative electron capture process,[10] represents a reaction in which an electron capturing molecule dissociates slowly through an anion radical intermediate, [A·—B]$^-$.

These electron capture processes are closely related to the temperature dependence of K.[4-6] In the case of the non-dissociative process, the plot of ln $KT^{3/2}$ *vs.* $1/T$ has a slope of nearly zero at lower temperatures, and/or a positive slope at higher temperatures. In the case of the dissociative process, the plot has a negative slope at higher temperatures. In the case of the intermediate-dissociative process, the slope of the plot changes from zero to either negative through positive or negative directly with the rise of temperature, *i.e.*, the decrease of $1/T$. If we examine Fig. 10 from these points of

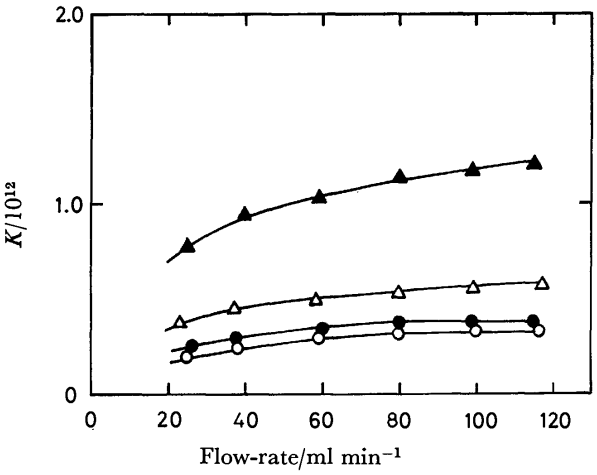

Fig. 9. Values of K for 2,4,6-trichlorobiphenyl *vs.* carrier gas flow-rate.
ECD temperatures: 200 °C (○), 240 °C (●), 280 °C (△), and 320 °C (▲).

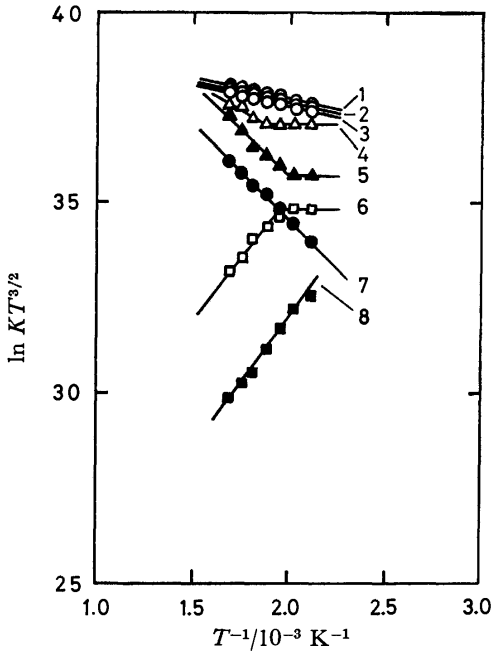

Fig. 10. Plots of ln $KT^{3/2}$ *vs.* $1/T$ for Aldrin (1), *p,p'*-DDE (2), γ-BHC (3), iodobenzene (4), 2,4,6-trichlorobiphenyl (5), nitrobenzene (6), 1,2,4-trichlorobenzene (7), and azulene (8).

view, we recognize that nitrobenzene and azulene are non-dissociative, Aldrin, γ-BHC, *p,p'*-DDE, and 1,2,4-trichlorobenzene are dissociative, and 2,4,6-trichlorobiphenyl and iodobenzene are intermediate-dissociative.

The carrier gas flow-rate dependence of K can also be related to the electron capture processes: The values of K for the samples undergoing the non-dissociative electron capture reaction are either not affected at all by the carrier gas flow-rate at any temperature, or decrease slightly with increasing the flow-rate at higher temperatures. The molecular anion formed within an ECD returns to the original molecule by recombination with a cation and/or progress of the reverse reaction before passing through the exit of the ECD. Therefore, no chemical reaction occurs, that is, the sample is unchanged by the act of detection. In such a case, the ECD acts as a concentration-sensitive detector, and consequently the values of K are either not effected by the carrier gas flow-rate, or decrease with increasing the flow-rate.[11]

The carrier gas flow-rate dependence of K for the samples undergoing the dissociative electron capture reaction are divided into two groups: One is the group whose values of K increase significantly with increasing the flow-rate (Aldrin, γ-BHC, and *p,p'*-DDE), and the other is the group whose values of K are little or not at all affected by the flow-rate at lower temperatures, but increase gradually with increasing the flow-rate at higher temperatures (1,2,4-trichlorobenzene). Each plot of ln $KT^{3/2}$ *vs.* $1/T$ for the samples belonging to the first group has a negative slope of nearly zero. Consequently the activation energy, E^*, which can be calculated from $E^* = -\text{slope} \times R$, where R is the gas constant, is very small. Therefore, it is considered that the samples in this group dissociate perfectly within the ECD. Under these circumstance, the ECD is close to coulometric in response,[12] and acts as a mass-sensitive detector rather than a concentration-sensitive detector.[13] Hence, the values of K calculated from Eq. 2, which represents the response function as the concentration-sensitive detector, increase with increasing the flow-rate. The sample belonging to the second group, *i.e.*, 1,2,4-trichlorobenzene is seemingly dissociative from Fig. 10, because it has a negative slope of the ln $KT^{3/2}$ *vs.* $1/T$ plot at higher temperatures. However, the carrier gas flow-rate dependence of K reveals that the sample is not necessarily dissociative. The values of K are not effected at all by the flow-rate at lower temperatures, although they increase gradually with increasing the flow-rate at higher temperatures. Therefore, it is considered that the reaction occurs non-dissociatively at lower temperatures and dissociatively at higher temperatures, that is, an intermediate-dissociative electron capture reaction occurs. Satouchi and Kojima[14] have pointed out from the values of E^* that the dissociative electron capture reaction for a halobenzene probably proceeds through an anion radical intermediate and that this reaction mechanism is similar to the S_N2 displacement for aromatic compounds. Furthermore, Dzidic *et al.*[15] have actually observed the anion radicals of some polychlorinated benzenes containing 1,2,4-trichlorobenzene by atmospheric pressure ionization mass spectrometry. Recently, Grimsrud and Kim[16] have suggested that the molecular anion resulting from the electron capture reaction of *p*-bromochlorobenzene survives long enough to be stabilized. These descriptions are quite in agreement with the conclusion obtained from the carrier gas flow-rate dependence of K that 1,2,4-trichlorobenzene is practically intermediate-dissociative, although it seems to be dissociative from the temperature dependence of K.

From the temperature dependence of K, iodobenzene and 2,4,6-trichlorobiphenyl should be regarded as intermediate-dissociative. Also, from the carrier gas flow-rate dependence of K, both samples seem to be intermediate-dissociative, since the values of K are not

appreciably affected by the flow-rate at lower temperatures, and increase with increasing the flow-rate at higher temperatures.

The author wishes to express his thanks to Emeritus Professor Shun Araki and Professor Shigetaka Suzuki, Tokyo Metropolitan University, for their encouragement and advice.

References

1) I. Halász, *Anal. Chem.*, **36**, 1428 (1964).
2) P. Devaux and G. Guiochon, *J. Chromatogr. Sci.*, **7**, 561 (1969).
3) L. S. Ettre, *J. Chromatogr. Sci.*, **16**, 396 (1978).
4) W. E. Wentworth, E. Chen, and J. E. Lovelock, *J. Phys. Chem.*, **70**, 445 (1966).
5) W. E. Wentworth, R. S. Becker, and R. Tung, *J. Phys. Chem.*, **71**, 1652 (1967).
6) W. E. Wentworth and E. Chen, *J. Gas Chromatogr.*, **5**, 170 (1967)
7) M. Takeuchi, *Nippon Kagaku Kaishi*, **1977**, 1484.
8) D. C. Fenimore and C. M. Davis, *J. Chromatogr. Sci.*, **8**, 519 (1970).
9) M. Takeuchi, *Nippon Kagaku Kaishi*, **1979**, 229.
10) This process is equivalent to what has been called the intermediate negative ion process in Ref. 5.
11) Whether the values of K are not affected or decrease with decreasing the flow-rate is considered to depend upon the magnitude of the rate constant for the recombination reaction, k_L, and that for the reverse reaction, k_{-1}. The details about this point will be given in the next paper.

$$AB + e^- \underset{k_{-1}}{\overset{k_1}{\rightleftharpoons}} AB^- \xrightarrow[P^+ \text{ or } R\cdot]{k_L} AB$$

where P^+ and $R\cdot$ represent positive ions and radicals, respectively.
12) J. E. Lovelock, R. J. Maggs, and E. R. Adlard, *Anal. Chem.*, **43**, 1962 (1971).
13) W. A. Aue and S. Kapila, *J. Chromatogr. Sci.*, **11**, 255 (1973).
14) M. Satouchi and T. Kojima, *Bunseki Kagaku*, **25**, 764 (1976).
15) I. Dzidic, D. I. Carroll, R. N. Stillwell, and E. C. Horning, *Anal. Chem.*, **47**, 1308 (1975).
16) E. P. Grimsrud and S. H. Kim, *Anal. Chem.*, **51**, 537 (1979).

Formation of Hydrogen Peroxide by Two-stage Acid Hydrolysis of *trans*(NO_2,O_2)-[μ-Peroxo-bis{nitrtobis(ethylenediamine)-cobalt(III)}] and Reaction Kinetics

Takashi SHIBAHARA,* Hisao KUROYA, and Masayasu MORI†

Department of Chemistry, Okayama University of Science, 1-1 Ridai-cho, Okayama 700

†*Department of Chemistry, Faculty of Science, Osaka City University, Sugimoto-cho, Sumiyoshi-ku, Osaka 558*

(Received November 10, 1979)

The aquation rate of *trans*(NO_2,O_2)-$[(NO_2)(en)_2CoO_2Co(en)_2(NO_2)]^{2+}$ has been measured in acidic aqueous solution at $[H^+]=0.003$—0.25 M and $I=0.50$ M ($LiClO_4$), the final products being *trans*-$[Co(NO_2)(OH_2)(en)_2]^{2+}$ and H_2O_2 in marked contrast to the acid decomposition of $[(NH_3)_5CoO_2Co(NH_3)_5]^{4+}$ where the final products are Co(II) and O_2. The reaction consists of two stages, each of which has preequilibrium of protonation. The observed rate constants for the first and second stages are consistent with the formula, $k_i^{obsd}=k_iK_i[H^+]/(1+K_i[H^+])$ (i=1, 2), indicating the existence of protonated reactive forms in both stages. The rate constants, activation parameters and equilibrium constants are $k_1=7.46\ s^{-1}$ (25 °C), $\Delta H_1^{\ddagger}=66.9\pm1.3$ kJ mol^{-1}, $\Delta S_1^{\ddagger}=-2.9\pm4.2$ J K^{-1} mol^{-1}, and $K_1=3.44\ M^{-1}$ (25 °C) for the first stage and $k_2=0.400\ s^{-1}$ (25 °C), $\Delta H_2^{\ddagger}=85.4\pm2.1$ kJ mol^{-1}, $\Delta S_2^{\ddagger}=33.5\pm7.1$ J K^{-1} mol^{-1}, and $K_2=2.98\ M^{-1}$ (25 °C) for the second stage. The solution of the reaction intermediate $[Co(NO_2)(O_2H)(en)_2]^+$ has been obtained by ion exchange technique and characterized by the UV and visible spectra. The factors which decide the reaction path are discussed.

While μ-hyperoxo dicobalt(III) complexes are usually resistant to acids, the μ-peroxo dicobalt(III) complexes are more or less susceptible to them. Thus $[(NH_3)_5CoO_2Co(NH_3)_5]^{4+}$ is decomposed almost instantaneously in acidic solution to give Co^{2+}, NH_4^+, and O_2, the reaction rate, however, being inverse in $[H^+]$.[1,2] On the other hand, double-bridged μ-amido-μ-peroxo dicobalt(III) complexes do not evolve oxygen but undergo isomerization.[3] A third case would be formation of hydrogen peroxide and mononuclear cobalt(III) complexes, as exemplified by μ-peroxo cyano cobalt(III) complex.[4] The kinetic study of the third case has not yet been reported.

We are now going to report a new example of this third case, *i.e.*, the reaction of *trans*(NO_2,O_2)-[μ-peroxo-bis{nitrobis(ethylenediamine)cobalt(III)}] complex with acid. The reaction gives 2 mol of mononuclear cobalt(III) complex and 1 mol of hydrogen peroxide from 1 mol of the μ-peroxo dicobalt(III) complex. This very clear-cut stoichiometry enabled us to obtain the reaction rate and the acid association equilibrium constants on a quantitative basis.

Experimental

Preparation. trans-(NO_2,O_2)-[μ-*Peroxo-bis{nitrobis(ethylenediamine)cobalt(III)}*] *Perchlorate Dihydrate*: The perchlorate salt was prepared by the addition of sodium perchlorate to an aqueous solution of the corresponding nitrate.[5] Found: C, 13.21; H, 4.86; N, 19.35%. Calcd for $[(NO_2)(en)_2CoO_2Co(en)_2(NO_2)](ClO_4)_2\cdot 2H_2O$: C, 13.40; H, 5.06; N, 19.53%.

trans-[*Aquanitrobis(ethylenediamine)cobalt(III)*] *Perchlorate Hydrate*: Sixty percent $HClO_4$ (10 ml) was added to the μ-peroxo complex (1 g, see above) and filtered. Ethanol (20 ml) was added slowly to the solution, which was then cooled for several hours. Orange crystals deposited were filtered and washed successively with ethanol and diethyl ether. Yield 0.9 g. Found: C, 10.45; H, 4.35; N, 15.42%. Calcd for $[Co(NO_2)(OH_2)(en)_2](ClO_4)_2\cdot H_2O$: C, 10.44; H, 4.38; N, 15.22%. The identification of the compound as the *trans* isomer has been made spectrophotometrically.[6] The *trans* configuration has also been confirmed by ir spectroscopy: one band (888 cm^{-1}) between 870 and 900 cm^{-1} [7] and three bands (600, 565, and 520 cm^{-1}) between 500 and 610 cm^{-1}.[8]

Analysis of the Reaction Products. *Hydrogen Peroxide*: The μ-peroxo complex $[(NO_2)(en)_2CoO_2Co(en)_2(NO_2)](ClO_4)_2\cdot 2H_2O$ was dissolved in 1 M H_2SO_4 and the hydrogen peroxide formed was titrated with permanganate, using *trans*-$[Co(NO_2)(OH_2)(en)_2]^{2+}$ solution as a reference. As expected from Eq. 1 in the following section, 0.99 ± 0.01 mol of H_2O_2 was formed for each mole of the μ-peroxo complex.

trans-[*Aquanitrobis(ethylenediamine)cobalt(III)*]$^{2+}$ *ion*: The μ-peroxo complex was dissolved in 0.1 M $HClO_4$ and the spectrum of *trans*-$[Co(NO_2)(OH_2)(en)_2]^{2+}$ formed was taken. The ε-value (at $\lambda_{max}=335$ nm 1015 cm^{-1} M^{-1}) was in good agreement with the literature value.[6]

Measurement of Reaction Kinetics. A large excess of perchloric acid over the μ-peroxo complex was used in each run ($I=0.5$ M, $LiClO_4$). The reaction was pursued by the observation of absorption changes at 305 nm at which large differences can be found between absorptivities of the complexes present. As will be described in the following section, the reaction consists of two distinct stages, each stage showing strong acid dependence. In the region of lower acid concentration ($[H^+]$[9] ≈0.003—0.01 M, and [complex] ≈0.0001 M) at 15.4 °C, both stages were followed by the conventional spectrophotometric method using a Hitachi 200-10 Spectrophotometer. In the region of higher acid concentration ($[H^+]\approx0.01$—0.25 M, and [complex] ≈0.001 M), the first stage of the reaction was followed by the stopped flow technique using Union RA 401 Instrument, while the second stage was monitored by the conventional technique.

Separation of the Intermediate. An attempt was made by use of ion exchange technique to isolate the intermediate produced at the first stage of the reaction. Thirty-six milligram (5×10^{-5} mol) of μ-peroxo complex perchlorate was dissolved in 20 ml of water, 1 ml of 0.1 M $HClO_4$ (10^{-4} mol) was added to it and the mixture was poured onto the top of a coloumn of 5 cm in length and 0.8 cm in diameter containing Dowex 50W-X2 cation exchange resin in Na-form. Elution with 0.5 M $NaClO_4$ gave a fraction of orange color, and successive elution with 1.0 M $NaClO_4$ containing 0.01 M $HClO_4$ gave another orange fraction which was spectrophotometrically identified[6] with *trans*-$[Co(NO_2)(OH_2)(en)_2]^{2+}$. The first

eluate is considered to contain the desired intermediate having charge +1 as judged from its easier elution than in the case of *trans*-$[Co(NO_2)(OH_2)(en)_2]^{2+}$.

Results

Reaction Stoichiometry and Spectra of Related Complexes. Spectrophotometry as well as permanganate titration of the final reaction products proved formation of 2 mol of *trans*-$[Co(NO_2)(OH_2)(en)_2]^{2+}$ and 1 mol of H_2O_2 from 1 mol of the dicobalt(III) complex, thus pointing to the following stoichiometry:

$$[(NO_2)(en)_2CoO_2Co(en)_2(NO_2)]^{2+} + 2H^+ + 2H_2O \longrightarrow 2\ trans\text{-}[Co(NO_2)(OH_2)(en)_2]^{2+} + H_2O_2. \quad (1)$$

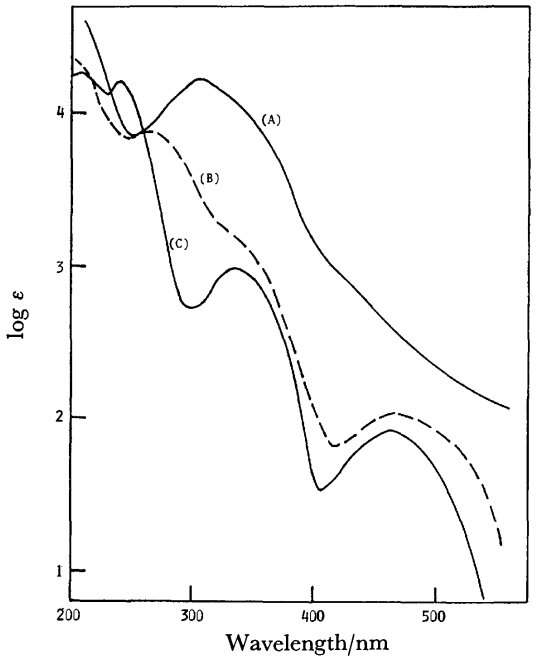

Fig. 1. UV and visible spectra.
(A): *trans*(NO_2,O_2)-$[(NO_2)(en)_2CoO_2Co(en)_2(NO_2)]^{2+}$,
(B): *trans*-$[Co(NO_2)(O_2H)(en)_2]^{+}$,
(C): *trans*-$[Co(NO_2)(OH_2)(en)_2]^{2+}$.

Spectra of the starting material and the final product are given by curves A and C in Fig. 1, respectively. Peak positions and ε-values (in parentheses) are as follows: $[(NO_2)(en)_2CoO_2Co(en)_2(NO_2)](ClO_4)_2 \cdot 2H_2O$, 307 nm (16000); *trans*-$[Co(NO_2)(OH_2)(en)_2](ClO_4)_2 \cdot H_2O$, 205 (17700), 238 (15200), 335 (975), and 463 nm (86). The ε-value (975) of the latter at 335 nm is slightly (*ca.* 4%) different from that (1015) obtained directly from the acid hydrolysis of μ-peroxo dicobalt(III) complex. This could be explained by assuming *trans* to *cis* isomerization (*ca.* 3%) during the course of the formation reaction.[10] Although the isolation of the intermediate as crystals has not yet been succesful, its absorption spectrum (Fig. 1, curve B) has been obtained.[11] The absolute ε-values of the spectrum were calculated in reference to the ε-values of *trans*-$[Co(NO_2)(OH_2)(en)_2]^{2+}$ produced therefrom by further action of perchloric acid.

Kinetic Data. As is seen in Fig. 2(A), the reaction

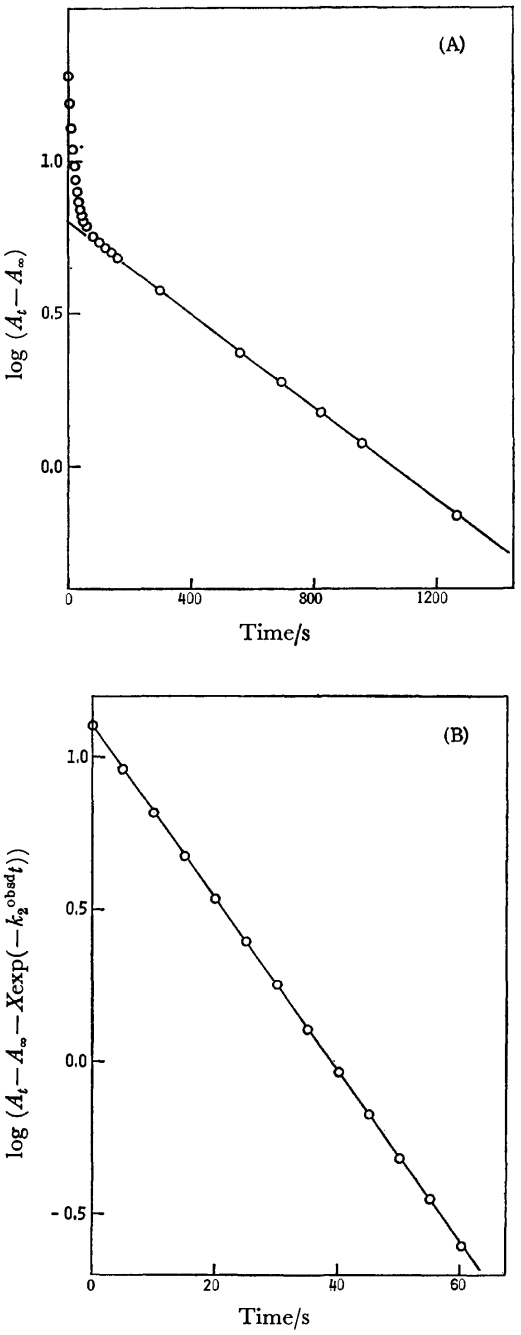

Fig. 2. Analysis of the consecutive reactions at 15.4 °C, I=0.5 M ($LiClO_4$), $[H^+]=5.69\times10^{-3}$ M, [complex]≈ 1×10^{-4} M.
(A) Plot of log (A_t-A_∞) *vs.* time for the second stage.
(B) Plot of log $(A_t-A_\infty-X\exp(-k_2^{obsd}t))$ *vs.* time for the first stage, where X=6.52 and $k_2^{bosd}=1.75\times10^{-3}$ s^{-1} obtained from (A) were used.

consists of two stages having considerably different rate, both of which are strongly acid dependent. Since the first stage dies down very quickly, the plot $\log(A_t-A_\infty)$ *vs.* t except at the initial stage forms a good straight line, from which the pseudo-first order rate constant of the second stage k_2^{obsd} can be obtained. The pseudo-first order rate constant of the first stage can then be obtained by re-plotting $\log(A_t-A_\infty-X\exp(-k_2^{obsd}t))$ *vs.* t (Fig. 2(B)), where $\log(X)$ is the intercept of the first plot

(Fig. 2(A)).[12] In the actual case, k_2^{obsd} is small enough as compared with k_1^{obsd} and the term $X\exp(-k_2^{obsd}t)$ may be regarded as nearly constant in the time scale used in the estimation of k_1^{obsd}. This approximation was used in most of the present treatment since such a treatment proved to give the same result as when the exact consecutive treatment was applied.

TABLE 1. FIRST ORDER RATE CONSTANTS, k_1^{obsd}/s^{-1} FOR THE ACID HYDROLYSIS OF *trans*(NO_2,O_2)-[μ-PEROXO-BIS{NITROBIS(ETHYLENEDIAMINE)COBALT(III)}] TO THE INTERMEDIATE, AND k_2^{obsd}/s^{-1} FOR THE ACID HYDROLYSIS OF THE INTERMEDIATE TO THE FINAL PRODUCTS; I=0.5 M ($LiClO_4$), λ=305 nm[a]

[H+]/M	Temp/°C				
	10.8	15.6	20.0	25.0	30.1
(A) k_1^{obsd}/s^{-1}					
0.030	0.201	—	—	—	1.01
0.050	0.328	0.512	0.753	1.11	1.59
0.100	0.541	0.862	1.30	1.87	2.77
0.150	0.705	1.15	1.70	2.52	3.83
0.200	0.830	1.38	2.05	3.06	4.77
0.250	0.948	1.59	2.30	3.55	5.31

[H+]/M	Temp/°C				
	5.0	10.2	15.4	20.2	25.0
(B) $k_2^{obsd}\times10^2/s^{-1}$					
0.0147	—	—	—	0.811	—
0.0294	0.267	—	—	—	2.73
0.0493	0.426	0.794	1.35	2.55	4.45
0.0985	0.769	1.40	2.41	4.48	7.85
0.148	1.01	1.87	3.27	6.09	10.3
0.198	1.18	2.23	3.87	7.27	12.4
0.247	1.32	2.49	4.45	8.49	14.5

a) Experiments at lower [H+] were made only at 15.4 °C:

$[H^+]\times10^3$/M	$k_1^{obsd}\times10^2/s^{-1}$	$k_2^{obsd}\times10^4/s^{-1}$
2.72	2.94	8.25
5.69	6.40	17.5
8.65	9.77	27.2
11.6	13.1	37.2

These data were not used in the estimation of k_1 and k_2 in Table 2.

Both rate constants k_i^{obsd} (i=1, 2) obtained in this way increased with the increase in acidity with a certain tendency of saturation (Table 1), implying the existence of preequilibrium of protonation in both stages. Linear dependence of $1/k_i^{obsd}$ (i=1, 2) against $1/[H^+]$ was observed at each temperature as consistent with (2) for both stages as can be seen in Figs. 3(A) and 3(B), and from these we could calculate the values of k_1, K_1, k_2, and K_2, *i.e.*, the rate and preequilibrium constants for the first and second stages, respectively (Table 2).

$$k_i^{obsd} = k_iK_i[H^+]/(1+K_i[H^+]). \quad (2)$$

The relevant activation and thermodynamic parameters are given in Table 3.

The Nature of the Reaction Intermediate and the Constituion of the Reaction. On addition of perchloric acid to the solution of the intermediate as described in Experimental, spectral change was observed with isosbestic points as shown in Fig. 4, and the final solution was found to contain *trans*-$[Co(NO_2)(OH_2)(en)_2]^{2+}$ and H_2O_2 as evidenced by spectrophotometry and permanganate titration. These findings and estimated charge +1 suggest that the intermediate would be *trans*-$[Co(NO_2)(O_2H)(en)_2]^+$ produced from the pro-

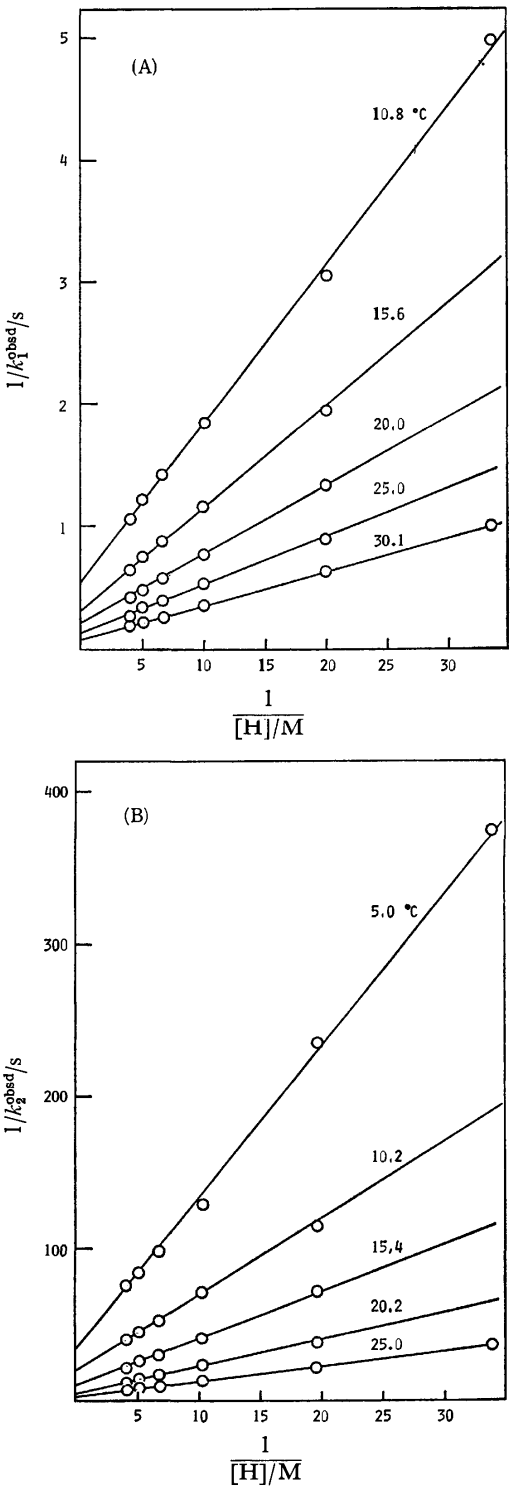

Fig. 3. Plot of $1/k_i^{obsd}$ *vs.* $1/[H^+]$ for the acid hydrolysis of the μ-peroxo complex $[(NO_2)(en)_2CoO_2Co(en)_2(NO_2)]^{2+}$, at I=0.5 M ($LiClO_4$).
(A): First stage, (B): second stage.

Table 2. Values of k_1 and k_i (i=1,2) obtained from the fit of the data in Table 1 to the Eq. 2; I=0.5 M ($LiClO_4$)

	Temp/°C	k_1/s^{-1}	K_1/M^{-1}
(A)	10.8	1.92	3.95
	15.6	3.16	3.84
	20.0	4.70	3.81
	25.0	7.46	3.44
	30.1	12.9	2.82
	Temp/°C	k_2/s^{-1}	K_2/M^{-1}
(B)	5.0	0.0307	3.22
	10.2	0.0596	3.05
	15.4	0.106	2.98
	20.2	0.208	2.77
	25.0	0.400	2.98

Table 3.

Activation parameters relevant to k_1 and k_2. I=0.5 M ($LiClO_4$).

(A) $\Delta H_1^{\ddagger}=66.9\pm1.3$ kJ mol^{-1}
$\Delta S_1^{\ddagger}=-2.9\pm4.2$ J K^{-1} mol^{-1}

(B) $\Delta H_2^{\ddagger}=85.4\pm2.1$ kJ mol^{-1}
$\Delta S_2^{\ddagger}=33.5\pm7.1$ J K^{-1} mol^{-1}

Thermodynamic parameters relevant to K_1 and K_2.

(A) $\Delta H_1=-11.7\pm2.1$ kJ mol^{-1}
$\Delta S_1=-28.9\pm22.6$ J K^{-1} mol^{-1}

(B) $\Delta H_2=-3.8\pm1.3$ kJ mol^{-1}
$\Delta S_2=-4.2\pm12.1$ J K^{-1} mol^{-1}

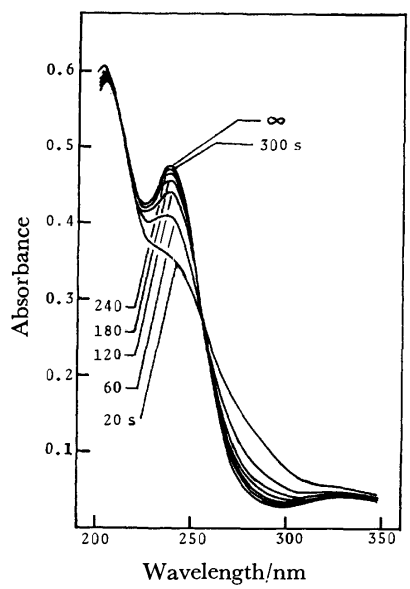

Fig. 4. Absorption changes for the acid hydrolysis of the intermediate *trans*-$[Co(NO_2)(O_2H)(en)_2]^+$ at 15 °C, I=0.5 M ($LiClO_4$), $[H^+]$=0.0294 M, and [complex]=3.0×10^{-5} M.

tonated form of the starting complex *via* protonation preequilibrium,

$$[(NO_2)(en)_2CoO_2Co(en)_2(NO_2)]^{2+} + H^+ \overset{K_1}{\rightleftharpoons} [(NO_2)(en)_2Co(O_2H)Co(en)_2(NO_2)]^{3+} \quad (3\text{-a})$$

$$[(NO_2)(en)_2Co(O_2H)Co(en)_2(NO_2)]^{3+} + H_2O \xrightarrow{k_1} trans\text{-}[Co(NO_2)(O_2H)(en)_2]^+ + trans\text{-}[Co(NO_2)(OH_2)(en)_2]^{2+} \quad (3\text{-b})$$

in conformity with the form of the rate equation. The second stage would then be the acid hydrolysis of the hydroperoxo intermediate into *trans*-$[Co(NO_2)(OH_2)(en)_2]^{2+}$ and H_2O_2, being, again, initiated by protonation:

$$trans\text{-}[Co(NO_2)(O_2H)(en)_2]^+ + H^+ \overset{K_2}{\rightleftharpoons} trans\text{-}[Co(NO_2)(O_2H_2)(en)_2]^{2+} \quad (3\text{-c})$$

$$trans\text{-}[Co(NO_2)(O_2H_2)(en)_2]^{2+} + H_2O \xrightarrow{k_2} trans\text{-}[Co(NO_2)(OH_2)(en)_2]^{2+} + H_2O_2. \quad (3\text{-d})$$

The rate of acid hydrolysis of the intermediate in the solution separated by ion exchange technique ($k^{obsd}=2.38\times10^{-2}$ s^{-1}, $[H^+]$=0.0985 M, 15.4 °C) was in good agreement with the acid hydrolysis rate of the second stage ($k_2^{obsd}=2.41\times10^{-2}$ s^{-1}, $[H^+]$=0.0985 M, 15.4 °C).

The *trans* structure of the starting μ-peroxo complex has already been established,[13] and *cis-trans* isomerization of $[Co(NO_2)(OH_2)(en)_2]^{2+}$ need not be considered here because of its slow isomerization rate.[6]

If the acid hydrolysis of the μ-peroxo compound is carried out under the exposure to sunlight, the absorbance at 335 nm of the final products decreases to *ca.* two thirds compared to the case without the sunlight exposure, indicating the appearance of an additional reaction path leading to Co(II) species. An attempt was made to find the wavelength most effective to bring about the side reaction using monochromated light from as apectrophotometer, but the intensity of the light from the spectrophotometer was found too weak to induce the side reaction.

If small amounts of acid were used for the separation of the intermediate, a different intermediate showed up, which had peaks at 337 and 462 nm and which did not give the *trans*-$[Co(NO_2)(OH_2)(en)_2]^{2+}$ even by the addition of excess amount of acids. The final products, in this case, have not yet been fully characterized.

Discussion

As stated in the introduction, the action of acid upon the μ-peroxo dicobalt(III) complexes causes in some cases the decomposition to Co(II) and O_2 (route A), and in other cases the hydrolysis to Co(III) complex and H_2O_2 (route B).

$$\left[Co^{III}\diagup O\diagdown O\diagup Co^{III}\right] + H^+ \rightleftharpoons \left[Co^{III}\diagup \overset{H}{O}\diagdown O\diagup Co^{III}\right]$$

route A: $\rightarrow Co(II)+O_2$

$+H^+$, route B: $\rightarrow Co(III)+H_2O_2$

The main factors to decide the choice among these rather different modes, *i.e.*, route A and route B, appear to be the relative stability of Co(II) and Co(III) species and the ease with which the peroxo bridge is replaced.

The first group usually contains μ-peroxo single-bridged complexes only with amine ligands. The easiness in the decomposition of these complexes, as contrasted to the stability generally seen in mononuclear Co(III) complexes towards acids, probably owes its origin to the reducing power of O_2^{2-} which itself is liable to change to O_2 by the loss of electrons, and to the more labile nature of the μ-peroxo dicobalt(III) complexes[14] as compared with other cobalt(III) complexes, because of the presence of excess electrons in the antibonding π-orbitals of O_2. The addition of acid would reduce the concentration of NH_3 in solution by the formation of NH_4^+ and promotes replacement of NH_3 by H_2O in the coordination sphere of these rather labile complexes. This makes Co(III) unstable enough to be reduced by the binding O_2^{2-} group, resulting in the formation of Co(II) and O_2. In this case, protonation to O_2 bridge itself would be rather to pull electron pair from cobalt to O_2 bridge and hinder the liberation of O_2 as proved by the experiment by Ferrer *et al.*[2] who showed that in the acid decomposition of $[(NH_3)_5CoO_2Co(NH_3)_5]^{4+}$, the protonated species is non-reactive.

In the acid hydrolysis of $[(NO_2)(en)_2CoO_2Co(en)_2(NO_2)]^{2+}$, and possibly of $[Co_2O_2(CN)_{10}]^{6-}$ and $Co_2O_2(CN)_6(en)_2]^{2-}$, on the other hand, the protonated species is reactive and the final products are Co(III) and H_2O_2 (route B). The presence of electron-withdrawing CN^- or NO_2^- group in the coordination sphere would partly cancel the above-mentioned labilizing effect of O_2^{2-} in the μ-peroxo dicobalt(III) complexes which would otherwise cause the complex to choose the route A. The stronger ligand field of these ligands at the same time is considered to stabilize Co(III) which is the product of route B.

Relatively fast acid hydrolysis of *trans*-$[Co^{III}LCl(en)_2]^{n+}$ was reported in the case of $L=NO_2^-$ or CN^- as compared to the case of $L=NH_3$, and was explained in terms of the role of π-bonding: the electron-accepting group such as nitro and cyano reduce the electron density around the group trans to the nitro or cyano group and make it easier for a solvent molecule to attach itself to cobalt and to initiate the substitution.[15]

The NO_2^- coordinated in the *trans*-position to μ-peroxo bridge in the dicobalt(III) complexes thus seems to prepare an ideal situation for the complex to be hydrolyzed to form mononuclear Co(III) complex and H_2O_2 through route B.

The acid association constants K_1 (3.44 M^{-1}, 25 °C) and K_2 (2.98 M^{-1}, 25 °C) are similar to each other and also to the acid association constants of $[(NH_3)_5CoO_2Co(NH_3)_5]^{4+}$ (11.9 M^{-1}, 25 °C, $I=0.1$ M, as calculated from acid dissociation constant),[2] and $[(en)_2Co(\mu\text{-}NH_2)(\mu\text{-}O_2)Co(en)_2]^{3+}$ (5.1 M^{-1}, 25 °C, $I=0.1$ M).[3] μ-Peroxo dicobalt complexes thus have considerably greater tendency to be protonated than hydrogen peroxide which is reported to have the acid association constant of $K\approx10^{-3}$.[16]

Ferrer *et al.*[2] reported a relatively large entropy of activation (36.4 J K^{-1} mol^{-1}) in the acid decomposition of $[(NH_3)_5CoO_2Co(NH_3)_5]^{4+}$ through route A, and attributed it to the charge neutralization within the complex. Smaller value of entropy of activation ($\Delta S_1^* = -2.9$ J K^{-1} mol^{-1}) may be due to the difference in the reaction route. Entropy of activation of the second stage ($\Delta S_2^* = 33.5$ J K^{-1} mol^{-1}), however, is not small and the situation seems to be too complicated to allow detailed discussions.

The authers are grateful to Dr. K. Takeda for the use of the stopped flow apparatus and to Prof. A. G. Sykes of the University of Newcastle upon Tyne, England, for helpful discussions.

References

1) A. B. Hoffman and H. Taube, *Inorg. Chem.*, **7**, 1971 (1968).
2) M. Ferrer, T. D. Hand, and A. G. Sykes, *J. Chem. Soc., Dalton Trans.*, **1980**, 14.
3) M. Mori and J. A. Weil, *J. Am. Chem. Soc.*, **89**, 3732 (1967).
4) A. Haim and W. K. Wilmarth, *J. Am. Chem. Soc.*, **83**, 509 (1961).
5) T. Shibahara and M. Mori, *Bull. Chem. Soc. Jpn.*, **45**, 1433 (1972).
6) S. Asperger and C. K. Ingold, *J. Chem. Soc.*, **1956**, 2862.
7) M. E. Baldwin, *J. Chem. Soc.*, **1960**, 4369.
8) M. N. Hughes and W. R. McWhinnie, *J. Inorg. Nucl. Chem.*, **28**, 1659 (1966).
9) Hydrogen ion concentrations were determined by titration with standard alkaline solution.
10) *cis*-$[Co(NO_2)(OH_2)(en)_2]^{2+}$ has peaks at 329 nm ($\varepsilon=2100$).[6]
11) Peak positions and ε-values (in parentheses) are as follows: 205 (21700), 265 (7660), 350 (1180), and 467 nm (108 M^{-1} cm^{-1}). The hydrogen peroxide anion (HO_2^-) appeares to give a slightly weaker ligand field than water does.
12) K. L. Scott, M. Green, and A. G. Sykes, *J. Chem. Soc., A*, **1971**, 3651, and the references therein.
13) T. Shibashara, S. Koda, and M. Mori, *Bull. Chem. Soc. Jpn.*, **46**, 2070 (1973).
14) Y. Sasaki, K. Suzuki, A. Matsumoto, and K. Saito, the 27 th Conference on Coordination Chemistry of the Chemical Society of Japan, Matsumoto, November (1977), Proceedings, p. 387.
15) F. Basolo and R. G. Pearson, "Mechanisms of Inorganic Reactions," 2nd ed, John Wiley and Sons, New York (1967), p. 173.
16) L. G. Sillen and A. E. Martell (compiler), "Stability Constants of Metal-ion Complexes," The Chemical Society, London (1964), Special Publication No. 17, p. 210.

Precise Determination of Dissolved Gases in Sea Water by Shipboard Gas Chromatography

Toshitaka GAMO* and Yoshio HORIBE

Ocean Research Institute, The University of Tokyo, Minamidai, Nakano-ku, Tokyo 164

(Received February 12, 1980)

A gas chromatographic system is applied to shipboard measurement of dissolved argon, oxygen, nitrogen, and total inorganic carbon dioxide in sea water. Gases are stripped from acidified sea water with helium carrier gas, separated by passing through silica-gel and molecular sieve 5A columns, and subsequently analyzed with a thermal conductivity detector and an ultrasonic detector. *Ca.* 15 min is required to analyze a 3 cm^3 sea water sample. Intercalibration by other analytical techniques for oxygen and total carbon dioxide confirmed the accuracy of this method. Vertical profiles of the gases in the Pacific Ocean demonstrate the merit of the method.

Oxygen, nitrogen, argon, and total inorganic carbon dioxide ($\sum CO_2$), which are the major dissolved gases in sea water, afford valuable information on chemical and physical processes in the ocean. O_2 and $\sum CO_2$ are involved in life processes in sea water. Near the ocean surface, photosynthesis causes enrichment of O_2 and depletion of $\sum CO_2$, while in the deep layer O_2 is consumed, changing into $\sum CO_2$ by oxidative decomposition of organic material falling from the surface. N_2 and Ar, on the other hand, are little affected by biochemical reactions because of their inertness, and can thus be used as conservative tracers. Except for O_2, however, little data on the oceanic distributions of these gases are available due to the lack of an adequate analytical method for accurate shipboard measurement.

Since Swinnerton *et al.*[1,2] developed a simple on-line gas stripping technique combined with gas chromatography, it has subsequently been adopted by a number of workers for the determination of dissolved gases in aqueous solutions.[3-7] Weiss and Craig[5] developed a set of gas chromatographs for shipboard measurement of dissolved N_2, O_2, Ar, and $\sum CO_2$. In their systems, it is necessary to inject two aliquots of a sample separately, one for the measurement of N_2, O_2, and Ar, and the other for $\sum CO_2$. It would be desirable to measure all the gases simultaneously using the same aliquot.

In this paper, a report is given on a gas chromatograph as a simpler and more convenient system for routine shipboard operations for simultaneous analysis of the four dissolved gases. Swinnerton's technique was applied to gas extraction from sea water, two detectors being employed in series: a thermal conductivity detector for the analysis of $\sum CO_2$, and an ultrasonic detector for that of Ar, O_2, and N_2. The high sensitivity of the ultrasonic detector caused significant reduction in sample volume. The dual detector system made it possible to analyze the four gases simultaneously with a single aliquot of a sample.

Experimental

Sampling and Gas Extraction. Sea water samples were taken in 60 cm^3 glass bottles with rubber stoppers from Niskin-type samplers immediately after each sampler had been brought aboard. The sample was allowed to overflow more than four times the volume of the bottle in order to avoid air contamination during the course of transfer.[8] Samples were kept in the dark before analysis for less than 10 h in order to prevent biological alteration of the dissolved gases.[9]

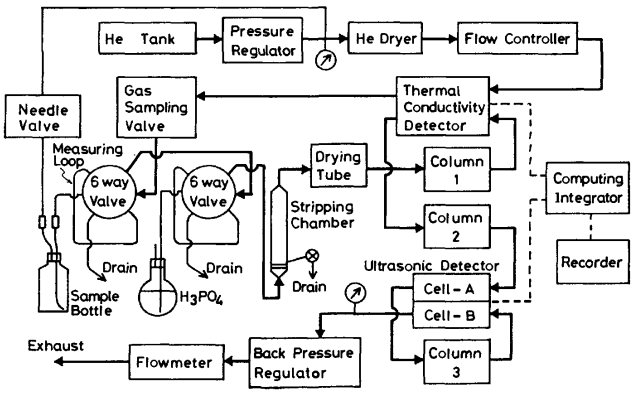

Fig. 1. Schematic diagram of the shipboard gas chromatograph. The thick arrows are the path of the carrier gas in the analysis procedure, and the broken lines are electric connections.

The gas chromatographic system is shown schematically in Fig. 1. Helium was used as a carrier gas. The head and back pressures were regulated at 3.2 and 1.5 kg cm^{-2}, respectively. A constant flow rate of 75 cm^3 min^{-1} supplied by a flow controller (Matheson, series 8287) was occasionally monitored by a soap bubble flowmeter at the end of the flow system, the average HETP of columns being the smallest at this flow rate. Helium (purity>99.995%) was dried and purified by passing through a large trap of molecular sieve 5A (10/20 mesh) at ambient temperature before it entered the flow system.

A sample bottle was connected to a six-way rotary valve. By application of helium pressure, the sample sea water was continuously made to flow out of the bottle through a measuring loop made of nylon tubing (i. d. 2 mm), its volume being calibrated accurately to 2.865 ± 0.002 cm^3. The volume was selected to maximize the Ar output of the ultrasonic detector without permitting ultrasonic phase foldover due to N_2 peak.

By turning the six-way valve, the sample was transferred to the stripping chamber, a glass cylinder (length 70 mm, i. d. 10 mm) with a coarse glass frit at the bottom. The carrier gas immediately began to strip the sample of the dissolved gases, carrying them into subsequent columns.

Carbonate and bicarbonate extractions as CO_2 were facilitated by mixing the sample with *ca.* 0.8 cm^3 of H_3PO_4 solution (1 : 10) which had been introduced into the chamber through another six-way valve (Fig. 1) and degassed similarly by carrier gas bubbling prior to the sample injection.

Separation and Detection. The gases evolved were dried by passing through a glass U-tube packed with 16/32

mesh $Mg(ClO_4)_2$. Three separation columns (stainless steel, i. d. 3 mm) were employed in series for isolating the four gas components. Column 1 (length 35 cm, packed with 40/60 mesh silica gel) separated CO_2 from the gas component (Ar, O_2, and N_2), column 2 (length 105 cm, packed with 30/60 mesh molecular sieve 5A) separated N_2 from Ar and O_2, and column 3 (length 80 cm, packed with 80/100 mesh molecular sieve 5A) separated Ar from O_2. Columns 1 and 2 were used at ambient temperature (24±1 °C), and column 3 was cooled at Dry Ice temperature.[10] It was necessary to raise the temperature of column 3 to ambient temperature for every 10 samples in order to regenerate its activity by releasing trapped N_2 out of it, while the other columns were kept activated after more than 200 analyses.

Analysis of CO_2 was carried out with a thermal conductivity cell (Gasukuro Kogyo Co., Ltd., E-121), and that of Ar, O_2, and N_2 with an ultrasonic detector (Tracor Inc., U-90) because of its high sensitivity.[11] Although the ultrasonic detector has two independent cells A and B, it is impossible to detect signals of both cells at the same time. Thus, the lengths of columns 2 and 3 were adjusted in such a way that Ar enters cell B after N_2 has finished passing through cell A.

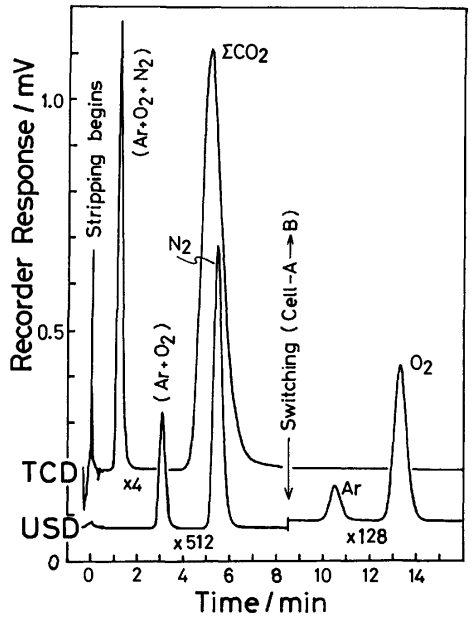

Fig. 2. Typical chromatograms of the thermal conductivity detector (TCD) and the ultrasonic detector (USD).

Typical chromatograms of both detectors are shown in Fig. 2. Retension times were 5.0, 5.4, 10.5, and 13.3 min for CO_2, N_2, Ar, and O_2, respectively. In order to calculate each peak area immediately and automatically, outputs of the detectors were connected to a computing integrator (Spectra-Physics, Autolab System IV). The relative precision of the measured values was estimated from the dispersion of shipboard analyses of a sea water sample. The standard deviations were as follows: ±0.3% for Ar and O_2, ±0.2% for N_2, and ±0.5% for CO_2.

Calibration. A calibration curve of each gas component was prepared over the proper concentration range prior to a cruise, by using a mixture of tank CO_2 and fresh air. Both gases were dried by passing through a dry ice trap before mixing. When the stripping chamber was filled with degassed sea water, a known amount of the calibration gas was injected through a gas sampling valve, and subsequently analyzed by the same procedure as used for analysis of unknown samples. Since the sensitivity of the ultrasonic detector was found not to be proportional to the amount of gas,[12] Ar, O_2, and N_2 calibrations were performed particularly in detail.

Shipboard calibration was performed every 4-5 h of operation by analyzing dried tank CO_2 or fresh air at one or two representative concentration points for each gas, in order to correct systematic shifting of the original calibration curve because of slight change in experimental conditions.

Results and Discussion

Intercalibrations with other conventional analytical methods were carried out in order to confirm the absolute accuracy of gas chromatography (GC) during routine shipboard operations. Dissolved oxygen values determined by GC were compared with those by the Carpenter-modified Winkler titration,[13] and the $\sum CO_2$ values by GC were compared with those calculated from pH and titration alkalinity.[14]

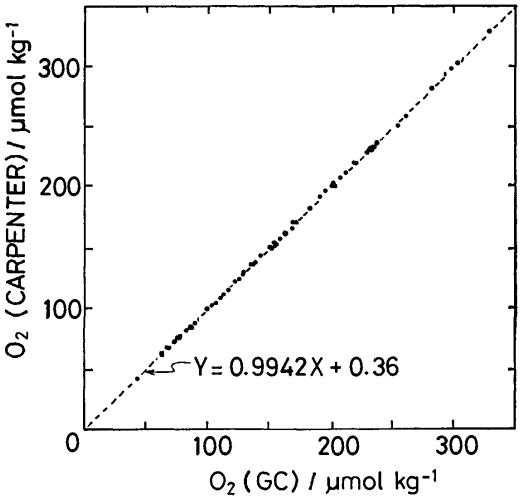

Fig. 3. Intercomparison of dissolved oxygen concentrations by the gas chromatography (GC) and the Carpenter-modified Winkler titration.
The broken line is the best fitted line by the method of least squares.

Figure 3 shows the relationship between the two sets of O_2 data obtained during the Pegasus Expedition in the Japan Sea,[15] and Vega Expedition in the Philippine Sea.[16] The estimated standard deviation of the titration method was ±1 μmol kg^{-1}. Each set of data by GC and titration was in good agreement within analytical errors of both methods. By using the method of least squares with statistical weighting,[17] a straight line of $Y=AX+B$ was fitted to the data (74 pairs), where X and Y are the GC value and the titration value, respectively. The calculated parameters with standard deviation ($\pm\sigma$) are as follows:

$$A = 0.9942 \pm 0.0017,$$
$$B = 0.36 \pm 0.28 \ (\mu\text{mol kg}^{-1}).$$

T-tests for A and B indicate that B is not significantly different from zero, while A is slightly different from unity, when α (level of significance) is 0.05. The

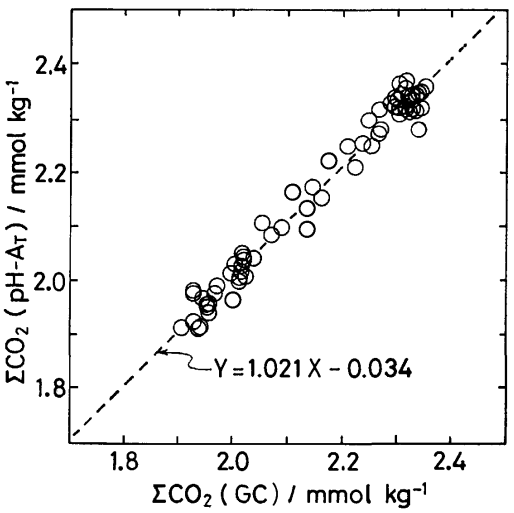

Fig. 4. Intercomparison of $\sum CO_2$ data measured by the gas chromatography (GC) and calculated from pH and titration alkalinity.
The broken line is the best fitted line by the method of least squares.

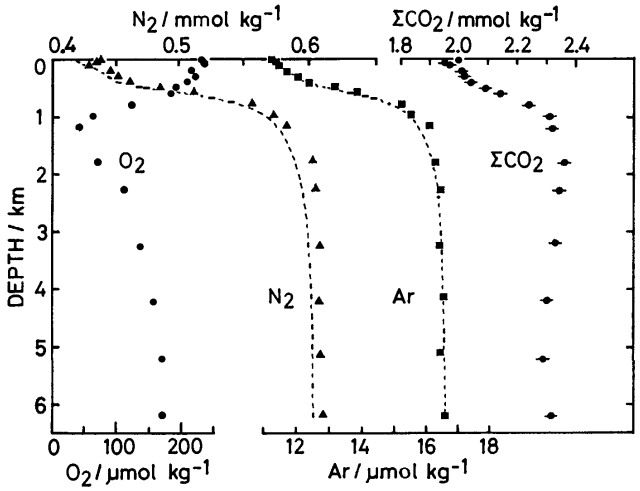

Fig. 5. Vertical profiles of O_2, N_2, Ar, and $\sum CO_2$ at Vega station 11 (29°39'N, 146°15'E).
Broken lines indicate the solubility values calculated from potential temperature and salinity at each depth.

tendency that the titration value is systematically lower than the GC value can be attributed to the loss of iodine by vaporization during the course of titration.

Figure 4 shows a comparison of $\sum CO_2$ data obtained during the Vega Expedition. The abscissa (X-axis) represents the GC value, and the ordinate (Y-axis) the value calculated by Tsubota (unpublished data) from pH and titration alkalinity measurements. The estimated standard deviation of the calculated value is $\pm 0.5\%$. The method of least squares was also applied to the sets of data (80 pairs) to give the following parameters:

$$A = 1.021 \pm 0.016,$$

$$B = -0.034 \pm 0.036 \text{ (mmol kg}^{-1}\text{)}.$$

There is a tendency that the calculated value is somewhat greater than the GC value. T-tests show, however, that A and B do not differ from unity and zero, respectively, at the level of $\alpha = 0.05$. The GC values are in good agreement with the calculated values in view of statistics.

The results of intercalibrations confirmed that the present gas chromatographic system is correctly calibrated, giving accurate and reliable O_2 and $\sum CO_2$ data on board. The accuracy of the determination of Ar and N_2 should not differ a great deal from that for O_2 and $\sum CO_2$, since all the gases were analyzed simultaneously under the same conditions.

As an example of simultaneous shipboard measurement, Fig. 5 shows vertical profiles of Ar, O_2, N_2, and $\sum CO_2$ at Vega station 11 (29°39'N, 146°15'E). The broken lines for Ar and N_2 are the saturation values calculated from the potential temperature and salinity at each depth by using the solubility equation of Weiss.[18] From surface to bottom, N_2 values are supersaturated by an average of 1.8%, Ar values being less supersaturated by an average of 0.7%. This saturation anomaly of both inert gases might reflect the effect of air injection at the ocean surface under turbulent conditions, since the N_2/Ar ratio in air bubbles is approximately twice that in sea water in equilibrium with the atmosphere.[18]

Except for the euphotic zone of the ocean surface, O_2 is only consumed by the decomposition of organic matters to produce CO_2 and nutrients. This is the reason why vertical profiles of O_2 and $\sum CO_2$ are inversely correlated with each other. By applying a vertical diffusion-advection model[19] to the deep layer (depth, 1—3 km) of station 11, the average O_2 consumption and CO_2 production rates were estimated to be 0.45 and 0.34 μmol kg^{-1} per year, respectively, when upward advection velocity of sea water was assumed to be 5 m per year. Oceanographical considerations of the results are given elsewhere in detail.[20]

The present gas chromatographic system was used for the analysis of volcanic CO_2 gas dissolved in northern Kagoshima Bay in order to calculate the CO_2 flux from bottom fumaroles.[21] With some modifications, the system will also be applicable to analysis of dissolved gases in fresh water or polluted water samples as well as sea water.

The authors wish to thank Prof. Hiroyuki Tsubota, Hiroshima University, for kindly making his unpublished $\sum CO_2$ data available. They are grateful to the officers and crew of *R. V. Hakuho Maru* for their assistances in getting sea water samples.

References

1) J. W. Swinnerton, V. J. Linnenbom, and C. H. Cheek, *Anal. Chem.*, **34**, 483 (1962).
2) J. W. Swinnerton, V. J. Linnenbom, and C. H. Cheek, *Anal. Chem.*, **34**, 1509 (1962).
3) V. J. Linnenbom, J. W. Swinnerton, and C. H. Cheek, U. S. NRL Report 6344, Washington, D. C., February 1966.
4) H. Craig, R. F. Weiss, and W. B. Clarke, *J. Geophys. Res.*, **72**, 6165 (1967).
5) R. F. Weiss and H. Craig, *Deep-Sea Res.*, **20**, 291 (1973).

6) K. Sugino, H. Kitamura, and K. Obata, *Bunseki Kagaku*, **23**, 260 (1974).
7) Y. Cohen, *Anal. Chem.*, **49**, 1238 (1977).
8) Y. Horibe, K. Kodama, and K. Shigehara, *J. Oceanogr. Soc. Jpn.*, **28**, 203 (1972).
9) T. Takahashi, R. F. Weiss, C. H. Culberson, J. M. Edmond, D. E. Hammond, C. S. Wong, Y. -H. Li, and A. E. Bainbridge, *J. Geophys. Res.*, **75**, 7648 (1970).
10) E. W. Lard and R. C. Horn, *Anal. Chem.*, **32**, 878 (1960).
11) H. W. Grice and D. J. David, *J. Chromatogr. Sci.*, **7**, 239 (1969).
12) T. Gamo and Y. Horibe, 37th National Meeting of the Chemical Society of Japan, Yokohama, April 1978, Abstr. No. 3I17.
13) J. H. Carpenter, *Limnol. Oceanogr.*, **10**, 141 (1965).
14) G. Skirrow, "The Dissolved Gases—Carbon Dioxide," in "Chemical Oceanography," 2nd ed, ed by J. P. Riley and G. Skirrow, Academic Press, London (1975), Vol. 2, Chap. 9.
15) "Preliminary Report of The Hakuhō Maru Cruise KH-77-3 (Pegasus Expedition)," ed by Y. Horibe, Ocean Research Institute, University of Tokyo, in press.
16) "Preliminary Report of The Hakuhō Maru Cruise KH-78-1 (Vega Expedition)," ed by Y. Horibe, Ocean Research Institute, University of Tokyo, in press.
17) J. W. Wolberg, "Prediction Analysis," D. Van Nostrand, Princeton, New Jersey (1967).
18) R. F. Weiss, *Deep-Sea Res.*, **17**, 721 (1970).
19) H. Craig, *J. Geophys. Res.*, **74**, 5491 (1969).
20) T. Gamo, D. thesis, University of Tokyo, Tokyo, Japan, 1978.
21) Y. Horibe, T. Gamo, and Y. Baba, "Isotope Marine Chemistry," ed by E. D. Goldberg, Y. Horibe, and K. Saruhashi, Uchida Rokakuho Pub. Co. Ltd., Tokyo (1980), Chap. 16.

The Preparation of Vanadium Tetrachloride from Vanadium Dichloride Oxide and Vanadium Trichloride and the Hydrogen Reduction Process of Vanadium Tetrachloride

Akimasa YAJIMA, Ryoko MATSUZAKI, and Yuzo SAEKI*

Research Laboratory of Resources Utilization, Tokyo Institute of Technology, 4259, Nagatsuta-cho, Midori-ku, Yokohama 227

(Received February 14, 1980)

The reactions of VCl_2O and VCl_3 with chlorine, and the reaction of VCl_3O, formed by the chlorination of VCl_2O, with chlorine in the presence of carbon were examined. The products formed by the reaction between gaseous VCl_4 and hydrogen at various temperatures, and the behavior of VCl_3 and VCl_2 on heating in a hydrogen stream were examined. The reaction between VCl_2O and chlorine occurs above *ca.* 120 °C and proceeds markedly above *ca.* 170 °C to form VCl_3O. VCl_4 can be obtained by passing the gaseous VCl_3O together with chlorine through a carbon bed held at *ca.* 700 °C. The reaction between VCl_3 and chlorine occurs above *ca.* 80 °C and proceeds markedly above *ca.* 170 °C to form VCl_4. The hydrogen reduction process of VCl_4 in the vapor phase may be represented as follows: The reaction between VCl_4 and hydrogen, $2VCl_4(g)+H_2(g)\rightarrow 2VCl_3(s)+2HCl(g)$, proceeds above *ca.* 500 °C to form VCl_3. Subsequently, the hydrogen reduction of the VCl_3, $2VCl_3(s)+H_2(g)\rightarrow 2VCl_2(s)+2HCl(g)$, and the disproportionation of the VCl_3, $2VCl_3(s)\rightarrow VCl_2(s)+VCl_4(g)$, proceed to form VCl_2. Above *ca.* 620 °C, the reaction between the VCl_2 and hydrogen, $VCl_2(s)+H_2(g)\rightarrow V(s)+2HCl(g)$, proceeds to form vanadium.

The vanadium trichloride oxide (VCl_3O) which is dissolved in the titanium tetrachloride ($TiCl_4$) prepared by the chlorination of titanium ores is commercially removed as a non-volatile vanadium-containing precipitate by bubbling hydrogen sulfide through the $TiCl_4$. The present authors[1] have previously reported that the precipitate formed by the reaction between VCl_3O and hydrogen sulfide is a mixture of vanadium dichloride oxide (VCl_2O), vanadium trichloride (VCl_3), and sulfur. The sulfur can be selectively separated by heating the mixture at *ca.* 250 °C in an argon stream.[2,3]

From the view point of resources utilization, it is important to obtain fundamental information on the preparation of vanadium tetrachloride (VCl_4) from the mixture of VCl_2O and VCl_3 and on the preparation of vanadium by the hydrogen reduction of the VCl_4.

There has been no report on the reaction between VCl_2O and chlorine. It has been reported that VCl_3 reacts with chlorine at 600 °C to form VCl_4.[4] Regarding the hydrogen reduction of VCl_4 in the vapor phase, Jantsch and Zemek[5] have reported that vanadium is obtained by the hydrogen reduction of VCl_4 at 680—700 °C. On the other hand, it has been reported that vanadium dichloride (VCl_2) is obtained by the reaction between VCl_4 and hydrogen above 650 °C,[6] or at 750—800 °C.[7]

In this paper, the reactions of VCl_2O and VCl_3 with chlorine, and the reaction of VCl_3O, formed by the chlorination of VCl_2O, with chlorine in the presence of carbon were examined. The hydrogen reduction process of VCl_4 in the vapor phase was also examined.

Experimental

Materials. The VCl_2O used was prepared from VCl_3, divanadium trioxide(V_2O_3), and VCl_3O,[8] and confirmed to be VCl_2O[9] by X-ray analysis. The chemical analysis gave V, 37.0; Cl, 51.4% (Calcd for VCl_2O: V, 36.96; Cl, 51.44%). VCl_3 was obtained by the thermal decomposition of VCl_4 at 180 °C in an argon atmosphere,[3] and confirmed to be VCl_3[10] by X-ray analysis. The chemical analysis gave V, 32.4; Cl, 67.6% (Calcd for VCl_3: V, 32.38; Cl, 67.62%). VCl_3O was prepared by the reaction between V_2O_5, which had been obtained by the thermal decomposition of guaranteed reagent ammonium metavanadate, and chlorine in the presence of carbon at 300 °C.[11] The chemical annlysis gave V, 29.4; Cl, 61.3% (Calcd for VCl_3O: V, 29.40; Cl, 61.37%). Carbon was obtained by the thermal decomposition of guaranteed reagent glucose. VCl_4 was prepared by the reaction between vanadium (V, 99.8% up) and chlorine at 500 °C.[3] The chemical analysis gave V, 26.4; Cl, 73.5% (Calcd for VCl_4: V, 26.43; Cl, 73.57%). VCl_2 was obtained by the disproportionation of VCl_3 in an argon stream at 650 °C,[3] and confirmed to be VCl_2[12] by X-ray analysis. The chemical analysis gave V, 41.8; Cl, 58.1% (Calcd for VCl_2: V, 41.81; Cl, 58.19%).

Experimental Procedures. The percentages of reacted VCl_2O or VCl_3 on heating in a chlorine stream at various temperatures for a specified period were examined as follows: The sample (1.0 g) in a quartz boat (60 mm length, 13 mm width, 7 mm depth) was placed in a straight reaction tube (17 mm i. d.) with a condenser. Chlorine was introduced into the reaction tube at a flow-rate of 50 cm^3/min. The sample part was then placed in the center of an electric furnace (300 mm in heating length) maintained at a specified temperature. The weight loss of the sample on heating in a chlorine stream for a specified period was measured. The temperature of the sample part was controlled to within ± 2 °C.

The reaction between VCl_3O and chlorine in the presence of carbon was examined as follows: Gaseous VCl_3O was formed by heating VCl_3O (27 g) at 120 °C and carried by a stream of argon (40 cm^3/min) to a carbon bed (30 mm diameter, 150 mm length) held at a specified temperature. Chlorine was simultaneously introduced at a flow-rate of 100 cm^3/min through a separate tube into the carbon bed. The mean flow-rate of gaseous VCl_3O was 10.7 cm^3/min. The reaction was allowed to proceed for 1 h.

The products obtained by the hydrogen reduction of VCl_4 in the vapor phase at various temperatures were examined as follows: Gaseous VCl_4 was formed by heating VCl_4 (28 g) at 130 °C and carried by a stream of argon (50 cm^3/min) to the reaction zone (28 mm i. d., 250 mm length) held at a specified temperature. Hydrogen was simultaneously introduced at a flow-rate of 150 cm^3/min through a separate tube into the reaction zone. The mean flow-rate of gaseous VCl_4 was 7.4

cm^3/min. A quartz or high purity alumina tube was inserted inside the reaction tube. The reaction was allowed to proceed for 2 h.

Throughout this work, the chlorides and chloride oxides of vanadium were handled in an argon atmosphere or *in vacuo* to prevent any contamination from moisture in the air.

Thermogravimetry(TG). The sensitivity of the quartz helix used for TG was approximately 67 mm/g. The sample (0.15 g) was heated at a rate of 2.5 °C/min and the flow-rate of chlorine or hydrogen was maintained at 50 cm^3/min.

Analytical. X-Ray analysis of the solid sample was performed using Ni filtered Cu radiation. The sample chamber of the diffractometer was maintained under dry nitrogen atmosphere to prevent the contamination of the sample from moisture in the air during the irradiation.

The vanadium content in the sample was determined by chelatometric titration;[13] the chlorine content was gravimetrically determined as AgCl, after dissolving the sample in dilute nitric acid.

Results and Discussion

Preparation of Vanadium Tetrachloride from Vanadium Dichloride Oxide and Vanadium Trichloride. Reaction between VCl_2O and Chlorine: On heating VCl_2O in an argon stream, the VCl_2O disproportionates above *ca.* 295 °C according to the reaction, $2VCl_2O(s) \rightarrow VClO(s) + VCl_3O(g)$, as previously reported by the present authors.[2] The TG curve of VCl_2O in a chlorine stream showed that VCl_2O began to react with chlorine before disproportionating and that the weight loss reached 100%. The percentages of reacted VCl_2O on heating VCl_2O in a chlorine stream at various temperatures for 0.25—3 h were examined. At 110 °C, no reaction product was observed. The results obtained at various temperatures above 120 °C are shown in Fig. 1.

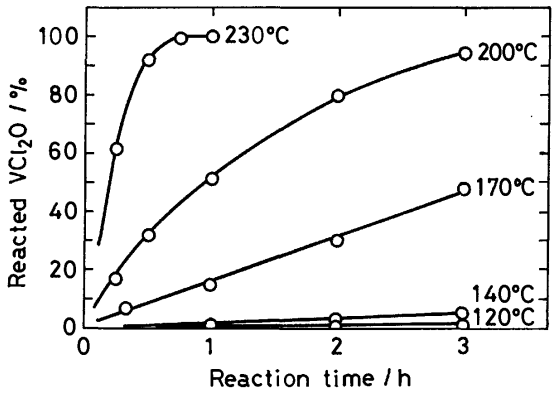

Fig. 1. Effect of temperature on the reaction between VCl_2O and chlorine.

The chemical analysis of the reaction product obtained by heating VCl_2O at 200 °C in a chlorine stream gave V, 29.4; Cl, 61.3%. From this result, the reaction product between VCl_2O and chlorine was found to be VCl_3O (Calcd: V, 29.40; Cl, 61.37%).

The above-mentioned results reveal that VCl_2O reacts with chlorine above *ca.* 120 °C according to the reaction,

$$2VCl_2O(s) + Cl_2(g) \longrightarrow 2VCl_3O(g), \quad (1)$$

and the reaction proceeds markedly above *ca.* 170 °C.

Since the vapor pressure of VCl_3O is 12.3 mmHg[8] even at room temperature (20 °C), the VCl_3O formed by heating VCl_2O (5.0 g) in a chlorine stream (100 cm^3/min) at 200 °C for 2 h was condensed in a trap held at 20 °C, 0 °C (P_{VCl_3O}=4.0 mmHg),[8] or −18 °C (P_{VCl_3O}=1.2 mmHg).[8] The percentage of the amount of VCl_3O condensed in the trap held at 20 or 0 °C to the calculated value based on the amount of reacted VCl_2O was 82 or 94%, respectively. When the temperature of the cooling trap was −18 °C, it was observed that a small amount of chlorine was dissolved in the condensed VCl_3O.[14] The amount of chlorine dissolved in the VCl_3O was determined as follows: after the chlorination was over, the VCl_3O was allowed to warm up to 0 °C in an argon atmosphere in order to liberate the chlorine from the VCl_3O. The liberated chlorine was absorbed in sodium hydroxide (NaOH) solution. A small amount of VCl_3O which vaporized during the above procedure was also absorbed in the NaOH solution. The total amount of chlorine in the NaOH solution was gravimetrically determined as AgCl, while the vanadium content in the NaOH solution was also determined by chelatometric titration. From the vanadium content, the amount of the VCl_3O absorbed in the NaOH solution was calculated. The amount of chlorine dissolved in the VCl_3O was calculated by subtracting the amount of chlorine corresponding to the VCl_3O absorbed in the NaOH solution from the total amount of chlorine in the NaOH solution. The result showed that the VCl_3O condensed in the trap held at −18 °C contained 2.0% of chlorine. The percentage of the amount of VCl_3O obtained after liberating the chlorine to the calculated value based on the amount of reacted VCl_2O was 97%.

Reaction between VCl_3 and Chlorine: On heating VCl_3 in an argon stream, the VCl_3 disproportionates above *ca.* 350 °C according to the reaction, $2VCl_3(s) \rightarrow VCl_2(s) + VCl_4(g)$, as previously reported by the present authors.[3] The TG curve of VCl_3 in a chlorine stream showed that VCl_3 began to react with chlorine before disproportionating and that the weight loss reached 100%. The percentages of reacted VCl_3 on heating VCl_3 in a chlorine stream at various temperatures for

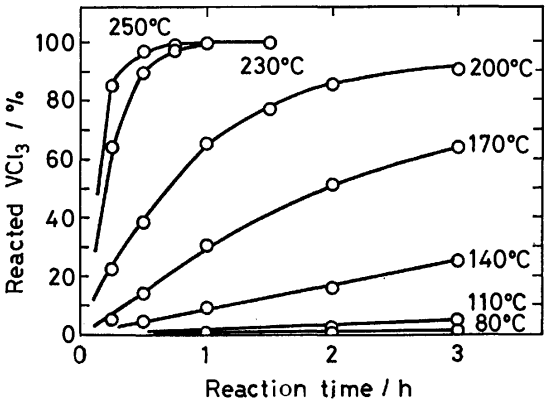

Fig. 2. Effect of temperature on the reaction between VCl_3 and chlorine.

0.25—3 h were examined. At 70 °C, no reaction product was observed. The results obtained at various temperatures above 80 °C are shown in Fig. 2.

The chemical analysis of the reaction product obtained by heating VCl_3 in a chlorine stream at 200 °C gave V, 26.4; Cl, 73.5%. From the result, the reaction product between VCl_3 and chlorine was found to be VCl_4 (Calcd: V, 26.43; Cl, 73.57%).

The above-mentioned results reveal that VCl_3 reacts with chlorine above *ca.* 80 °C according to the reaction,

$$2VCl_3(s) + Cl_2(g) \longrightarrow 2VCl_4(g), \quad (2)$$

and that the reaction proceeds markedly above *ca.* 170 °C.

Since the vapor pressure of VCl_4 is 5.4 mmHg[15] even at room temperature (20 °C), the VCl_4 formed by heating VCl_3 (5.0 g) in a chlorine stream (100 cm^3/min) at 200 °C for 2 h was condensed in a trap held at 20 °C, 0 °C ($P_{VCl_4} = 1.7$ mmHg),[15] or −18 °C ($P_{VCl_4} = 0.5$ mmHg).[15] The percentage of the amount of VCl_4 condensed in the trap held at 20 °C to the calculated value based on the amount of reacted VCl_3 was 92%. When the temperature of the cooling trap was 0 or −18 °C, it was observed that a small amount of chlorine was dissolved in the condensed VCl_4.[16] The VCl_4 formed is allowed to warm up to 20 °C in an argon atmosphere in order to liberate the chlorine. The amount of chlorine dissolved in the VCl_4 was determined in the same manner as described in the experiment on VCl_2O. From the results, the amounts of chlorine dissolved in the VCl_4 condensed at −18 and 0 °C were 0.7 and 4.0%, respectively. The percentage of the amount of VCl_4 obtained after liberating the chlorine to the calculated value based on the amount of reacted VCl_3 was 96% at 0 °C and 97% at −18 °C.

Reaction between VCl_3O and Chlorine in the Presence of Carbon: As mentioned above, VCl_3O is formed by the reaction between VCl_2O and chlorine. To obtain knowledge of formation of VCl_4 from the VCl_3O, the products obtained by passing gaseous VCl_3O together with chlorine through a carbon bed held at various temperatures were examined. The results are shown in Table 1.

Table 1. Reaction product between gaseous VCl_3O and chlorine in the presence of carbon

Temp °C	Chemical analysis/%		Product/%	
	V	Cl	VCl_4	VCl_3O
400	29.4	61.3	—	100
500	28.7	64.3	24	76
600	27.3	70.0	71	29
650	26.7	72.5	91	9
700	26.4	73.5	100	—

The chloride and chloride oxide of vanadium in the liquid state at room temperature are VCl_4 (Calcd: V, 26.43; Cl, 73.57%) and VCl_3O (Calcd: V, 29.40; Cl, 61.37%). This fact and the chemical analysis shown in Table 1 showed that VCl_4 was formed above 500 °C, and that the weight percentage of VCl_4 increased with increasing temperature. At 700 °C, VCl_4 alone was obtained. When VCl_4 formed by the chlorination of VCl_3O at 700 °C in the above manner was condensed in a trap cooled at −18 °C, VCl_4 was obtained in a 97% yield.

The above-mentioned results suggest that the following method is preferable for preparing VCl_4 from a mixture of VCl_2O and VCl_3: By heating a mixture of VCl_2O and VCl_3 at *ca.* 200 °C in a chlorine stream, VCl_4 and VCl_3O are formed. Subsequently, VCl_4 is prepared by passing the gaseous mixture of VCl_4 and VCl_3O together with chlorine through a carbon bed held at *ca.* 700 °C. The resulting VCl_4 is condensed in a trap cooled at −18 °C.

Hydrogen Reduction Process of Vanadium Tetrachloride. Reduction Products of Gaseous VCl_4 with Hydrogen: Prior to the examination of the hydrogen reduction of VCl_4 in the vapor phase, the thermal decomposition of gaseous VCl_4 was examined to know whether the thermal decomposition of gaseous VCl_4 occurs under the experimental conditions of this work. The experimental procedure was the same as that for the hydrogen reduction described in the previous paragraph, except that argon was introduced into the reaction zone instead of hydrogen at the same flow-rate as that of hydrogen.

The experimental results showed that 0.009 g of VCl_3 and 0.002 g of chlorine were formed by the thermal decomposition of gaseous VCl_4 at 200, 600, and 1000 °C, regardless of the heating temperature. The result indicated that *ca.* 0.1% of gaseous VCl_4 introduced into the reaction zone thermally decomposed. From the result, it was considered that the decomposition of gaseous VCl_4 could be neglected in the discussion about the experimental results for the hydrogen reduction of gaseous VCl_4, to be described later.

The products formed by heating gaseous VCl_4 in a hydrogen stream at various temperatures were examined by X-ray analysis and chemical analysis. At 400 °C, it was observed that the reaction between gaseous VCl_4 and hydrogen did not proceed. The results obtained above 500 °C are shown in Table 2.

Table 2. Reduction products of gaseous VCl_4 with hydrogen at various temperatures

Temp °C	Products and their yields/mol%						Unreacted VCl_4/mol%
	In the reaction zone			Outside the reaction zone			
	V	VCl_2	VCl_3	V	VCl_2	VCl_3	
500	—	<1	2	—	—	1	96
600	—	23	—	—	19	<1	56
700	2	63	—	—	34	—	—
800	4	64	—	<1	31	—	—
900	34	29	—	6	30	—	—
1000	76	—	—	23	—	—	—

The results indicate that the reaction between gaseous VCl_4 and hydrogen proceeds above *ca.* 500 °C, giving VCl_3 and VCl_2 at 500—600 °C, VCl_2 and vanadium at 700—900 °C, and vanadium alone at 1000 °C.

Behavior of VCl_3 and VCl_2 on Heating in a Hydrogen Stream: In order to reveal the hydrogen reduction process of gaseous VCl_4, the behavior of VCl_3 and VCl_2, formed during the reduction process, on heating in a hydrogen stream was examined.

The TG curve of VCl_3 in a hydrogen stream is shown in Fig. 3(a). The result showed that VCl_3 began to react with hydrogen at *ca.* 270 °C before the disproportionation described in the previous paragraph occurred. The sample heated up to 600 °C was found to be VCl_2 by X-ray analysis. The formations of hydrogen chloride and VCl_4 were observed during the weight loss. The final weight loss was 47.7%. This value was larger than the calculated value, 22.54%, based on the hydrogen reduction of VCl_3 to form VCl_2,

$$2VCl_3(s) + H_2(g) \longrightarrow 2VCl_2(s) + 2HCl(g), \quad (3)$$

and was smaller than the calculated value, 61.27%, based on the disproportionation of VCl_3 to form VCl_2,

$$2VCl_3(s) \longrightarrow VCl_2(s) + VCl_4(g). \quad (4)$$

These facts were considered to indicate that, on heating VCl_3 in a hydrogen stream, both the hydrogen reduction and the disproportionation of VCl_3 occurred. The experimental value of the weight loss showed that 35% of VCl_3 was reduced with hydrogen and 65% of VCl_3 disproportionated.

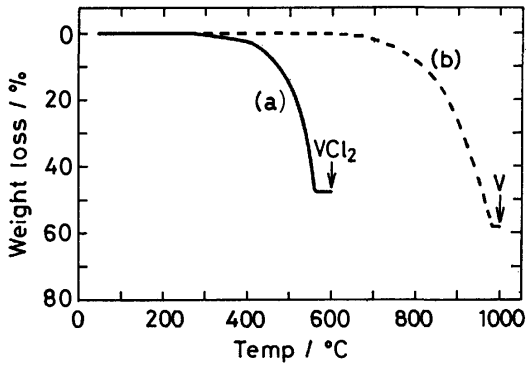

Fig. 3. TG curves of VCl_3 and VCl_2 in a hydrogen stream.
(a): VCl_3, (b): VCl_2.

From the results, on heating VCl_3 in a hydrogen stream, the hydrogen reduction of VCl_3 (Reaction 3) occurs above *ca.* 270 °C, and the disproportionation of VCl_3 (Reaction 4) occurs above *ca.* 350 °C in addition to Reaction 3. This result is contrary to the result by Pechkovskii and Vorob'ev,[17] who reported that on heating VCl_3 in a hydrogen stream above *ca.* 480 °C, VCl_2 was formed by the hydrogen reduction of VCl_3.

The TG curve of VCl_2 in a hydrogen stream is shown in Fig. 3(b). In this case, a platinum basket was used for TG, because it had been reported that vanadium reacted with quartz above *ca.* 1000 °C.[18] The sample heated up to 1000 °C was found to be vanadium[19] by X-ray analysis.

These results reveal that on heating VCl_2 in a hydrogen stream, VCl_2 reacts with hydrogen to form vanadium above *ca.* 620 °C according to the reaction,

$$VCl_2(s) + H_2(g) \longrightarrow V(s) + 2HCl(g). \quad (5)$$

Consideration on Hydrogen Reduction Process of VCl_4: From the above-mentioned results, the hydrogen reduction process of VCl_4 in the vapor phase was discussed.

As shown in Table 2, on heating VCl_4 in a hydrogen stream, VCl_3 and VCl_2 were formed at 500—600 °C. The only reaction which gave VCl_3 was thought to be

$$2VCl_4(g) + H_2(g) \longrightarrow 2VCl_3(s) + 2HCl(g), \quad (6)$$

since the thermal decomposition of gaseous VCl_4 scarcely proceeded as described before. The reactions which gave VCl_2 were considered to be the hydrogen reduction and the disproportionation of the VCl_3, since the hydrogen reduction of VCl_3 (Reaction 3) occurs above *ca.* 270 °C and the reduction is accompanied by the disproportionation (Reaction 4) above *ca.* 350 °C, as described before. As shown in Table 2, above 700 °C, vanadium was formed in addition to VCl_2, and vanadium alone was obtained at 1000 °C. Since VCl_2 is reduced with hydrogen to vanadium (Reaction 5) above *ca.* 620 °C, it was considered that the vanadium obtained was formed by the hydrogen reduction of the VCl_2 formed by Reactions 3 and 4.

These results allow us to represent the hydrogen reduction process of VCl_4 in the vapor phase as follows: the reaction between gaseous VCl_4 and hydrogen proceeds above *ca.* 500 °C to form VCl_3 (Reaction 6). Subsequently, the hydrogen reduction of the VCl_3 (Reaction 3) and the disproportionation of the VCl_3 (Reaction 4) proceed to form VCl_2. Above *ca.* 620 °C, the reaction between the VCl_2 and hydrogen proceeds to form vanadium (Reaction 5).

The present work was partially supported by the Asahi Glass Foundation for Industrial Technology.

References

1) A. Yajima, R. Matsuzaki, and Y. Saeki, *Bull. Chem. Soc. Jpn.*, **51**, 1098 (1978).
2) A. Yajima, R. Matsuzaki, and Y. Saeki, *Bull. Chem. Soc. Jpn.*, **52**, 3549 (1979).
3) A. Yajima, R. Matsuzaki, and Y. Saeki, *Bull. Chem. Soc. Jpn.*, **52**, 3292 (1979).
4) O. Ruff and H. Lickfett, *Ber.*, **44**, 506 (1911).
5) G. Jantsch and F. Zemek, *Monatsch. Chem.*, **84**, 1119 (1953).
6) R. E. McCarley and J. W. Roddy, *J. Inorg. Nucl. Chem.*, **15**, 293 (1960).
7) A. Morette, *C. R. Acad. Sci.*, **200**, 1110 (1935).
8) H. Oppermann, *Z. Anorg. Allg. Chem.*, **351**, 113 (1967).
9) R. J. Sime, *Z. Kristallogr.*, **124**, 238 (1967).
10) JCPDS, Powder Diffraction File, 15-382.
11) Y. Saeki, T. Ōno, and R. Matsuzaki, *Kogyo Kagaku Zasshi*, **74**, 828 (1971).
12) JCPDS, Powder Diffraction File, 15-215.
13) J. Krtil, *Z. Anal. Chem.*, **219**, 412 (1965).
14) F. E. Brown and J. E. Snyder, *J. Am. Chem. Soc.*, **47**, 2671 (1925).
15) A. A. Sytnik, A. A. Furman, and A. S. Kulyasova, *Russ. J. Inorg. Chem.*, **11**, 543 (1966).
16) A. Morette, *C. R. Acad. Sci.*, **202**, 1846 (1936).
17) V. V. Pechkovskii and N. I. Vorob'ev, *Russ. J. Inorg. Chem.*, **10**, 779 (1965).
18) W. Biltz and A. Köcher, *Z. Anorg. Allg. Chem.*, **241**, 324 (1939).
19) JCPDS, Powder Diffraction File, 22-1058.

Reaction between Various Copper(II) Complexes and Ascorbic Acid or 3,5-Di-*t*-butylcatechol

Naoyasu Oishi, Yuzo Nishida,* Kazuhiko Ida, and Sigeo Kida
Department of Chemistry, Faculty of Science, Kyushu University 33, Fukuoka 812
(Received February 27, 1980)

The electron transfer reactions between various copper(II) complexes and two-electron donors, such as ascorbic acid and 3,5-di-*t*-butylcatechol, were investigated. Mononuclear copper(II) complexes with a distorted tetrahedral and a trigonal bipyramidal structure, and some binuclear complexes were readily reduced to copper(I) complexes by the two-electron donors, but not mononuclear planar copper(II) complexes. The catalytic activities of these copper(II) complexes for the oxidation of 3,5-di-*t*-butylcatechol by O_2 were studied in relation to the above reactions.

Copper(II) ion in proteins are classified into three types, Type I, Type II, and Type III, Type I and Type II copper ions being isolated from other copper ions and functioning as mononuclear complexes, while a binuclear structure has been proposed for Type III because of its ESR-nondetectable nature.[1,2] The structures of two proteins containing a copper(II) ion in Type I form (plastocyanin and azurin)[3] have been determined by X-ray analysis, but the geometries around copper(II) ions are still unclarified for other copper proteins.

All the copper(II) ions have relatively high redox potentials, being readily reduced to copper(I) by ascorbic acid, hydroquinones and catechols.[1,2] We have investigated the reaction of various copper(II) complexes with two-electron donors, such as ascorbic acid and 3,5-di-*t*-butylcatechol (hereafter abbreviated as 3,5-DTBC) in order to elucidate the relationship between 1) the structure and reactivity of copper(II) complexes in the reduction to copper(I) complexes by two-electron donors, and 2) the catalytic activity for the oxidation of 3,5-DTBC by O_2 (corresponding quinone formed according to reaction (I)) and the structure of copper(II) complexes.

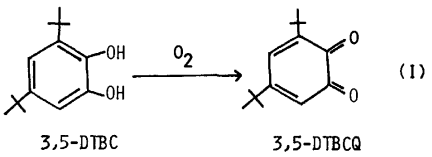

(I)

3,5-DTBC 3,5-DTBCQ

Experimental

Copper(II) Complexes. The copper(II) complexes we used are shown in Fig. 1, **5** being a new complex.

Preparation of **5**, $[Cu_2(me\text{-}ox)]X_2(X=ClO_4, PF_6)$. An ethanol solution of *N*-[2-(dimethylamino)ethyl]-1,3-propanediamine(0.01 mol) and diethyloxalate(0.005 mol) was refluxed for 1 h, and resulting solution was mixed with an aqueous solution of $Cu(H_2O)_6(ClO_4)_2$(0.01 mol). Violet prisms separated immediately were recrystallized from hot water. Found: C, 28.96; H, 5.23; N, 12.70%. Calcd for $[Cu_2(me\text{-}ox)](ClO_4)_2$: C, 28.74; H, 5.12; N, 12.56%. The magnetic moment of the perchlorate complex is 1.16 BM at 295 K. Its magnetic property can be explained in terms of the Bleaney-Bowers equation[4] (temperature range, 80—295 K, $2J=-440$ cm^{-1}, and $N\alpha=60\times10^{-6}$ cgs). By adding NH_4PF_6 to a hot water solution of the perchlorate, $[Cu_2(me\text{-}ox)](PF_6)_2$ was obtained as red needles.

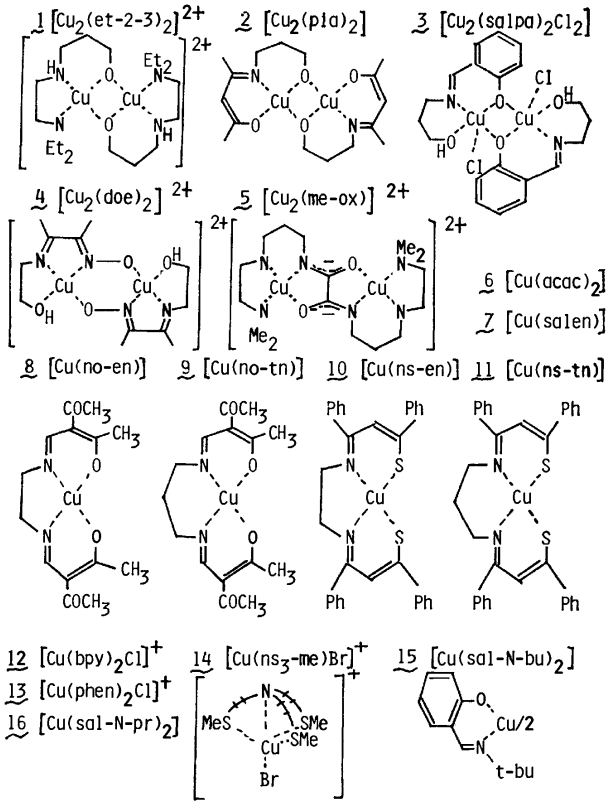

Fig. 1. Copper(II) complexes used in this study.
The abbreviations of ligands are: **6**; H(acac), acetylacetone, **7**; H_2(salen), *N*,*N*′-disalicylideneethylenediamine, **12**; bpy, 2,2′-bipyridine, **13**; phen, 1,10-phenanthroline, **16**; H(sal-N-pr), *N*-salicylideneisopropylamine.

Complexes **1**—**5** are binuclear, the structural and magnetic properties of **1**—**4** being reported (**1**,[5,6] **2**,[7] **3**,[8] and **4**[9]). In these binuclear copper(II) complexes, the strong antiferromagnetic interaction was found to be operative between two copper atoms. Complexes **6**—**11** are of four-coordinated planar structure, **6**, **7**—**9**[10], and **10**—**11**[11] having $[CuO_4]$-, $[CuN_2O_2]$- and $[CuN_2S_2]$-type coordinations, respectively. Complexes **12**—**14**[12] and **15**—**16** are of trigonal bipyramidal and distorted tetrahedral structures, respectively.

Reaction with Ascorbic Acid or Catechol. A methanol solution containing stoichiometric amount of ascorbic acid was added to a methanol solution of copper(II) complexes at 20 °C under nitrogen atmosphere and the absorption spectra of the resulting solutions were measured in the visible

region. When 3,5-DTBC was used instead of ascorbic acid, the same procedure was applied except for the addition of triethylamine[13] (3,5-DTBC: base=2: 1).

Catalytic Activity for the Oxidation of 3,5-DTBC by O_2. Oxidation was carried out according to the method of Tsuruya and Linvedt.[13] A methanol solution(20 cm^3) of 3,5-DTBC(0.1 mol/dm^3), triethylamine(0.015 mol/dm^3) and copper(II) complex (0.002 and 0.001 mol/dm^3 for mononuclear and binuclear complexes, respectively) was kept at 15 °C (in a thermostat) in a 12 mm diam. necked flask for 6—7 h. The yield of quinone(3,5-DTBCQ) formed was determined by the measurements of absorption spectra of the resulting solutions. 3,5-DTBCQ shows a characteristic absorption band at 400 nm (ε/mol^{-1} dm^3 cm^{-1}=1900 in methanol[14]).

Measurements. Absorption spectra were obtained with a Shimadzu Multipurpose spectrometer model MPS-5000.

Results and Discussion

Electron-transfer Reaction between Two-electron Donors and Various Copper(II) Complexes. Compounds **12**, $[Cu(bpy)_2Cl]Cl$ and **13**, $[Cu(phen)_2Cl]Cl$ are easily reduced to copper(I) complexes by ascorbic acid, where bpy and phen denote 2,2'-bipyridine and 1,10-phenanthroline, respectively. The green color of **14**, $[Cu(ns_3\text{-}me)Br]^+$ disappeared immediately upon addition of ascorbic acid (or 3,5-DTBC), indicating that the complex is reduced to copper(I) complex by two-electron donors.

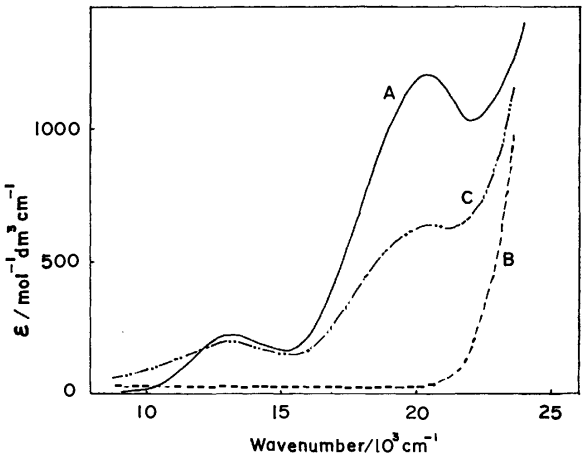

Fig. 2. Absorption spectra of **15** [Cu(sal-N-bu)$_2$] (in methanol, 15 °C).
A: [Cu(sal-N-bu)$_2$], B: [Cu(sal-N-bu)$_2$]+ascorbic acid (in N_2), C: solution (B) +O_2(in air).

Figure 2 shows that the spectral change of **15**, [Cu(sal-N-bu)$_2$], caused by the addition of ascorbic acid. The d-d band (*ca.* 13000 cm^{-1}) due to copper(II) ion disappears immediately upon the addition of ascorbic acid under nitrogen atmosphere, reappearing when the solution was exposed to the air. This indicates that the copper(II) complexes with a distorted tetrahedral structure are reduced to copper(I) by ascorbic acid (or 3,5-DTBC). On the other hand, planar mononuclear copper(II) complexes such as **6**, $[Cu(acac)_2]$ and **7**, [Cu(salen)] are not reduced by these two-electron donors at room temperature.

Patterson and Holm[15] measured the reduction potentials of various copper(II) complexes by polarography, and concluded that mononuclear copper(II) complexes with nonplanar structure (*e.g.*, distorted tetrahedron and trigonal bipyramid) are readily reduced as compared with their planar analogs. Our results seem to be in line with their conclusion. This indicates that nonplanar mononuclear copper(II) complexes can be a good model for Types I and II in biological systems.

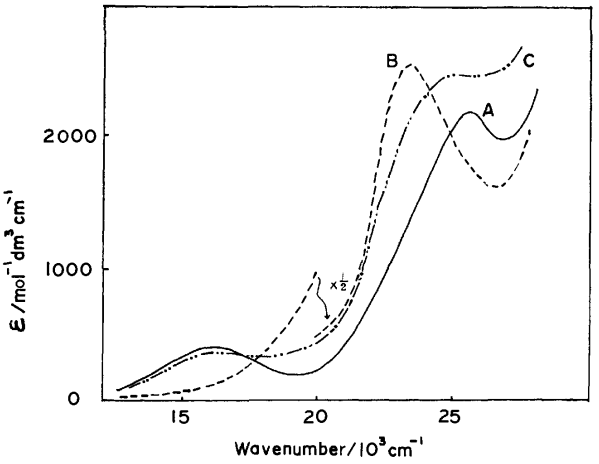

Fig. 3. Absorption spectra of **4** $[Cu_2(doe)_2](NO_3)_2$(in methanol, 15 °C).
A: $[Cu_2(doe)_2](NO_3)_2$, B: $[Cu_2(doe)_2](NO_3)_2$+ascorbic acid(in N_2), C: solution (B)+O_2(in air).

Binuclear copper(II) complexes (Fig. 1) except for **5** were also found to be readily reduced to copper(I) complexes by ascorbic acid and/or 3,5-DTBC. The spectral change of **4**, $[Cu_2(doe)_2]^{2+}$ in the reaction with ascorbic acid is shown as an example in Fig. 3. The d-d band at 16000 cm^{-1} disappears upon addition of ascorbic acid under nitrogen atmosphere, appearing again when the solution is exposed to air. It is noteworthy that planar mononuclear copper(II) complexes such as **6** and **7** are not reduced by ascorbic acid, while binuclear copper(II) complexes with planar structure such as **2**, **3**, and **4**, are readily reduced to copper(I) by ascorbic acid.

Catalytic Activity for the Oxidation of 3,5-DTBC. Since 3,5-DTBCQ shows a characteristic absorption band at 400 nm and the content of copper(II) complex is very small, the absorbance at 400 nm can be a good measure for the catalytic activity of copper(II) complexes to the oxidation of 3,5-DTBC. Examples are given in Figs. 4 and 5. Square planar mononuclear complexes (**6** and **7**) have little catalytic activity, while nonplanar copper(II) complexes (such as **12**, **14**, and **15**) and binuclear complexes (except for **5**) act as a good catalyzer for the oxidation of 3,5-DTBC. In the cases of **14** and **4**, 100% formation of 3,5-DTBCQ was observed within 6 hours. The results obtained for binuclear complexes (**1**—**4**) are in line with that of Tsuruya and Lintvedt,[13] who first pointed out the high catalytic activity of a binuclear complex, **17**, relative

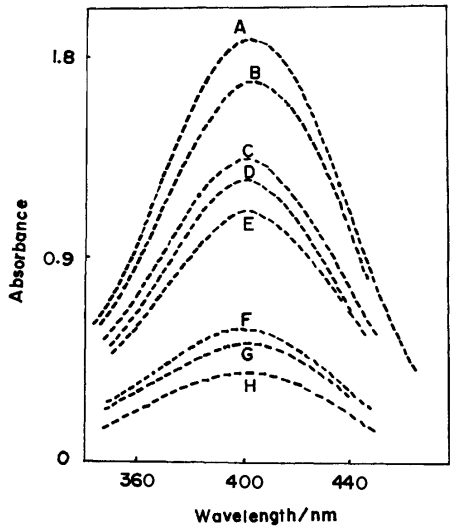

Fig. 4. Absorbance at 400 nm of the solution containing a copper (II) complex and 3,5-DTBC(in methanol, 15 °C, after 6 h).
A: **12** $[Cu(bpy)_2Cl]Cl$, B: **4** $[Cu_2(doe)_2](NO_3)_2$, C: **15** $[Cu(sal\text{-}N\text{-}bu)_2]$, D: **14** $[Cu(ns_3\text{-}me)Br]ClO_4$, E: **2** $[Cu_2(pia)_2]$, F: **6** $[Cu(acac)_2]$, G: **8** [Cu(no-en), H: no copper(II) complex.

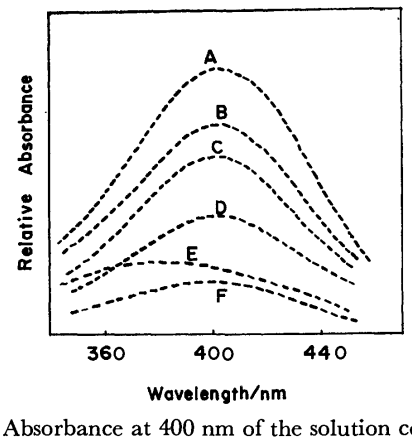

Fig. 5. Absorbance at 400 nm of the solution containing a copper (II) complex and 3,5-DTBC(in $CHCl_3$, 15 °C, after 10 h).
A: **11** [Cu(ns-tn)], B: **10** [Cu(ns-en)], C: **9** [Cu(no-tn)], D: **8** [Cu(no-en)], E: **7** [Cu(salen)], F: no copper(II) complex.

to that of a mononuclear complex, **6**, for the oxidation of 3,5-DTBC by O_2.

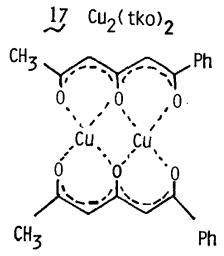

Since **10** and **11** are insoluble in methanol, the result in Fig. 5 was obtained in a $CHCl_3$ solution. Thus the catalytic activity of **11** and **10** cannot be compared directly with that of **14** and **15**. The order of catalytic activity is as follows: **12**~**13**>**14**; **15**>**16**; **11**>**10**>**9**>**8**>**7**~**6** and **4**>**1**~**2**~**3**≫**5**. Although **8** has a $[CuN_2O_2]$-type coordination similar to that of **7**, **8** is more reducible than **7** because of the presence of electron-withdrawing group in the chelate ring.[16,17] Copper(II) complexes with a $[CuN_2S_2]$-type coordination are more reducible than those with a $[CuN_2O_2]$-type coordination.[15] Complexes with 6-membered chelate ring (such as **11** and **9**) are more reducible than the corresponding complexes with 5-membered chelate ring (such as **10** and **8**).[15,16] Thus, the results indicate that more reducible mononuclear copper(II) complexes can be a better catalyzer for the oxidation of 3,5-DTBC by O_2, suggesting that the reversible change of oxidation state, *i.e.*, Cu(II)⇄Cu(I), plays an important role in the catalytic function of mononuclear copper(II) complexes. Since binuclear complexes, **1**—**4**, are reduced by 3,5-DTBC and readily oxidized by O_2 again, these binuclear copper(II) complexes act as a good catalyzer for the oxidation of 3,5-DTBC by O_2.

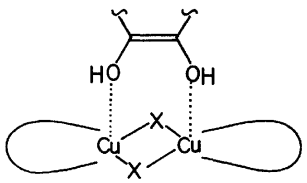

Fig. 6. "Steric match" proposed for electron transfer reaction between ascorbic acid and a binuclear copper (II) complex. This situation is impossible for ascorbic acid and a mononuclear planar copper(II) complex.

The reduction potentials of the two copper(II) complexes, **6** and **17**, are almost the same (**6**; −0.50 V, **17**; −0.48 V), **6** and **17** undergoing two-electron reduction to Cu^0 and Cu^I–Cu^I, respectively at the electrode.[18] However, the difference of reactivity between the two complexes in the electron transfer reaction with 3,5-DTBC (and/or ascorbic acid) cannot be explained by the electrochemical data. Accordingly we propose that a "steric match" between a donor and an acceptor (Fig. 6) is important in the electron transfer reaction between planar copper(II) complexes and two-electron donors, such as ascorbic acid and 3,5-DTBC. Thus on this basis the very low catalytic activity of **5** can be explained; *i.e.*, the distance between two copper atoms is estimated to be larger than 5 Å from the X-ray analysis of anologous complexes,[19] so that the "steric match" is impossible between **5** and two-electron donors.

References

1) R. Malkin and B. G. Malmstrom, *Adv. Enzymol.*, **33**, 177 (1970).
2) J. A. Fee, *Struct. Bonding*, **23**, 1 (1975).
3) P. M. Colman, H. C. Freemen, J. M. Guss, M. Murata, V. A. Morris, J. A. M. Ramshaw, and M. P. Venkatappa, *Nature(London)*, **272**, 319 (1978).
4) B. Bleaney and K. D. Bowers, *Proc. R. Soc. London, Ser. A*, **214**, 451 (1952).

5) Y. Nishida, F. Numata, and S. Kida, *Inorg. Chim. Acta*, **11**, 189 (1974).
6) A. C. Villa, L. Coghi, A. G. Manfredotti, and C. Guastini, *Cryst. Struct. Commun.*, **1974**, 543.
7) J. A. Bertrand and J. A. Kelley, *Inorg. Chim. Acta*, **4**, 203 (1974).
8) J. A. Bertrand, J. A. Kelley, and J. L. Breece, *Inorg. Chim. Acta*, **4**, 247 (1974).
9) J. A. Bertrand, J. H. Smith, and P. Garyeller, *Inorg. Chem.*, **13**, 1649 (1974).
10) L. Wolf and E-G. Jager, *Z. Anorg. Allg. Chem.*, **346**, 76 (1966).
11) E. Uhlemann, *Z. Naturforsch., Teil B*, **21**, 592 (1966).
12) M. Suzuki, H. Kanatomi, H. Koyama, and I. Murase, in press.
13) S. Tsuruya and R. L. Lintvedt, Abstracts, 176th National Meeting of the American Chemical Society, Miami Beach, FL. Sep. 1978, No. Inorg. 70.
14) W. Flaig, Th. Ploetz, and A. Kullmer, *Z. Naturforsch., Teil B*, **10**, 668 (1955).
15) G. S. Patterson and R. H. Holm, *Bioinorg. Chem.*, **4**, 257 (1975).
16) E-G. Jager, *Z. Chem.*, **18**, 229 (1978).
17) D. G. Pillsbury and D. H. Busch, *J. Am. Chem. Soc.*, **98**, 7836 (1976).
18) D. E. Fenton and R. L. Lintvedt, *J. Am. Chem. Soc.*, **100**, 6367 (1978).
19) C. Chavel, J. J. Gierd, Y. Jeannin, O. Kahn, and G. Lavigne, *Inorg. Chem.*, **18**, 3015 (1979); J. J. Gierd, O. Kahn, and M. Verdagure, *ibid.*, **19**, 274 (1979).

Electrochemical Reduction of Elemental Sulfur in Acetonitrile

Taitiro FUJINAGA, Tooru KUWAMOTO, Satoshi OKAZAKI, and Masashi HOJO*,†

Department of Chemistry, Faculty of Science, Kyoto University, Kyoto 606

(Received February 28, 1980)

Electrochemical reduction of elemental sulfur (S_8) has been carried out in acetonitrile using a platinum electrode. The products were identified by means of spectrophotometry and ESR. Sulfur is reduced voltammetrically in two steps:

$$S_8 + 2e \longrightarrow S_8^{2-}, \qquad S_8^{2-} + 2e \longrightarrow 2S_4^{2-}$$

These products turns into more stable species by the succeeding chemical reactions in a bulk solution as follows:

$$S_8^{2-} \overset{K}{\rightleftharpoons} S_6^{2-} + 1/4S_8 \qquad (K = 1.6\times10^{-2})$$

$$S_6^{2-} \overset{K_d}{\rightleftharpoons} 2S_3^{\cdot-} \qquad (K_d = 1.2\times10^{-3})$$

The S_4^{2-} species was enough active to react with S_8 into S_8^{2-}, which was regarded as the cause of a current maximum on the current-time curve in a controlled potential coulometry of S_8 at a potential of the second reduction step.

The authors have reported in the previous paper[1] that sulfur monochloride (S_2Cl_2) is reduced electrochemically into chloride ion and elemental sulfur (S_8 form) in an aprotic solvent, acetonitrile (AN), and that the produced sulfur can be further reduced at the more negative potential. Elemental sulfur has been reduced[2-5] in dimethyl sulfoxide and *N,N*-dimethylformamide to produce blue colored species, which is attributed to $S_3^{\cdot-}$ (trisulfur anion radical). However, as the system is very complicated, the different values of the equilibrium constants for the present species in a solvent are reported between two groups[3,5] of investigators.

Moreover, the authors have showed that S_8 molecule exists stably in less basic solvents, such as acetonitrile or propylene carbonate (PC), but S_8 is activated by the basicity of the solvent, not only in *N,N*-dimethylformamide but also dimethyl sulfoxide according to the conductivity data.[1] In the present work, the electrochemical reduction of S_8 in acetonitrile has been studied, and the reaction mechanism in the solution is discussed.

Experimental

Commercial acetonitrile was purified, and Et_4NClO_4 used as the supporting electrolyte was prepared by the method described previously.[1] The electrode potential was measured against a silver electrode (Ag/0.1 M $AgClO_4$–AN). A rotating platinum electrode (geometric surface area of 0.13 cm^2) and a platinum-gauze electrode were used as the working electrode. The controlled potential coulometry was carried out using a Prinston Applied Research (PAR) Model 173 Potentiostat and Model 179 Didital Coulometer. Other apparatus and equipments were the same as those in the previous report.[1]

Elemental sulfur (S_8) was dissolved in acetonitrile, heating on a hot-plate. Absorption spectra of electrolyzed sulfur solution were measured in an optical flow-cell with 1 cm path length. As the electrolytic products were affected strikingly by oxygen gas, high-purity nitrogen gas was bubbled vigorously through the solution. ESR measurements were performed with a JEOL PE-3X following the method of Umemoto.[6]

† Present address: Department of Chemistry, Faculty of Science, Kochi University, Kochi 780.

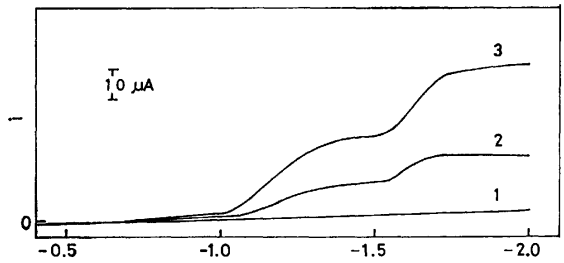

Fig. 1. Voltammograms of sulfur in 0.1 M Et_4NClO_4–AN on rotating platinum electrode.
Concn of S_8; 1: 0, 2: 0.5, 3: 1.25×10^{-4} M.

Results and Discussion

Figure 1 shows the voltammograms of S_8 in acetonitrile solution with a rotating platinum electrode. S_8 was reduced through two steps. The half-wave potential ($E_{1/2}$) of the first and second wave was -1.20—-1.16 V and -1.60 V, respectively. The first wave was irreversible (log-plot slope of 100—200 mV), whereas the second seemed to be less irreversible (the slope of *ca.* 60 mV). The wave height of both the first and second wave were proportional to the concentration of S_8. The number of electrons involved in each step was found to be both about 2 electrons by controlled potential coulometry measurements at -1.4 V and -1.8 V. Therefore, S_8 may be reduced voltammetrically through the following process;

$$\text{at the first wave,} \quad S_8 + 2e \longrightarrow S_8^{2-} \qquad (1)$$

$$\text{at the second wave,} \quad S_8^{2-} + 2e \longrightarrow 2S_4^{2-} \qquad (2)$$

Figure 2 shows the current-time curves during coulometry. The current decreases exponentially when the potential is setted at -1.4 V, which corresponds to the first wave in voltammetry. The current reached to almost zero when about 2 electrons was consumed, but it still continued to flow very slowly until about 2.7 electrons. The solution turned purple in color gradually during the electrolysis and it changed into blue after Z^{**}=*ca.* 2.0. At -1.8 V (at the second wave), a

** Z indicates the number of electrons added to for S_8.

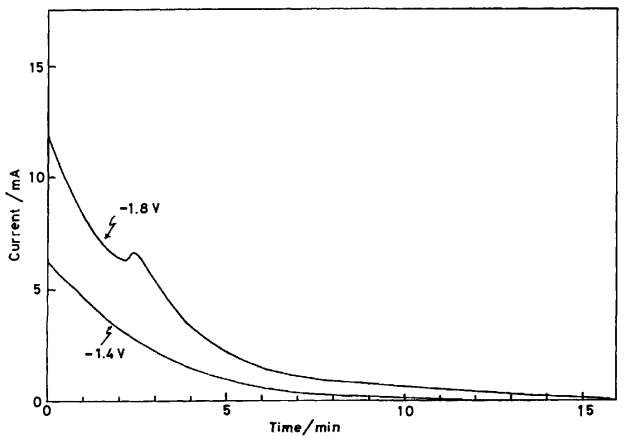

Fig. 2. Current-time relationship for the controlled potential coulometry of sulfur on Pt-gauze, $[S_8]=0.50\times10^{-4}$ M.

maximum of current was observed after a few minutes from the beginning of the electrolysis. The maximum and the minimum appeared each time at the constant number of electrons of 2.4—2.6 and 2.2—2.3, respectively, even if the position where they appear were shifted, changing the area of electrode or the concentration of the depolarizer ($[S_8]=0.1$—4.0×10^{-4} M***).

The relation between log i and t was linear for the both regions from the beginning of the electrolysis to the minimum and after the maximum. The slope of log i—t for the region after the maximum was larger than that to the minimum by the factor of 1.3—1.5. The color of the solution changed suddenly from purple to blue in the region where the current increased. These results may suggest that the electrode reaction in the region from the beginning of the electrolysis to the minimum is different from that after the maximum. The number of electrons reached 4 for S_8 after about ten minutes from the beginning of the electrolysis, but small current still continued to flow, the relation of log i—t deviating from the linearity.

The absorption spectra of the sulfur solution electrolyzed at −1.4 V are shown in Fig. 3. The spectrum had peaks of 613, 480, and 350 nm at $Z=2.0$. At about $Z=2.7$, the spectrum had peaks of 613, 450, and 270 nm and a shoulder of 340 nm. When the solution was electrolyzed at −1.8 V, it gave a spectrum similar to that of −1.4 V up to $Z=ca.$ 2.7. When the solution is completely electrolyzed at −1.8 V, however, the peak of 613 nm almost disappeared, and a peak of 330 nm and a shoulder of 400 nm appeared instead.

The change of absorbance at 613 and 480 nm during the electrolysis at −1.4 V is shown in Fig. 4. The absorbance at 613 nm increased with the increase of the number of electrons, and the increase of the absorbance was accelerated after $Z=2.0$. On the other hand, the absorbance at 480 nm reached the maximum at $Z=2$ and disappeared when the electrolysis was completed. The change of absorbance for the electrolysis at −1.8 V is also shown in Fig, 4. The same results were obtained as the case of the electrolyses at −1.4 V up to $Z=8/3$,

*** Throughout this paper 1 M = 1 mol dm^{-3}.

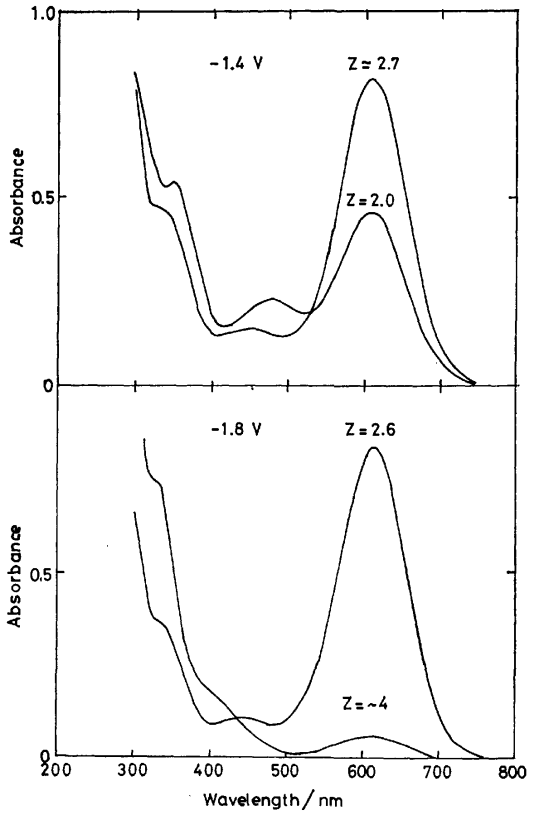

Fig. 3. Absorption spectra of sulfur solution after electrolysis at −1.4 and −1.8 V, $[S_8]=1.0\times10^{-4}$ M.

although the speed of electrolysis at −1.4 V was much slower than that at −1.8 V, especially after $Z=2.0$. The peak intensity at 613 nm began to decrease after $Z=8/3$ and almost disappeared when the electrolysis was completed. The peak at 330 nm appeared instead of the peak of 340 nm after $Z=8/3$.

These results show that the same products are obtained regardless of the potential of electrolysis so long as the same number of electrons. Considering the number of electrons, the peak at 480 nm is due to S_8^{2-}, that at 613 nm to S_6^{2-} (or a species derived from S_6^{2-}), and that at 330 nm may be to S_4^{2-}.

The color of the solution turned blue when unelectrolyzed S_8 solution was added to the solution completely electrolyzed at −1.8 V which looks yellow. Figure 5 (upper) shows the absorbance of the solution of various mixing ratio. The change of absorbance at 613, 480, and 330 nm of the mixed solution is similar to that of the solution electrolyzed at −1.8 V (see Fig. 4). This experiment shows that the following reaction occurs easily.

$$S_8 + 2S_4^{2-} \longrightarrow 2S_8^{2-} \quad (3)$$

Similary, the solution electrolyzed up to $Z=8/3$ at −1.8 V was mixed with unelectrolyzed S_8 solution (see the lower in Fig. 5). (At $Z=8/3$, all sulfur is formally S_6^{2-} state, as described in next paragraph). In this case, the resulting change of absorbance was the same as the case of the solution electrolyzed at −1.4 V. The appearence of the peak at 480 nm shows the formation of S_8^{2-} species.

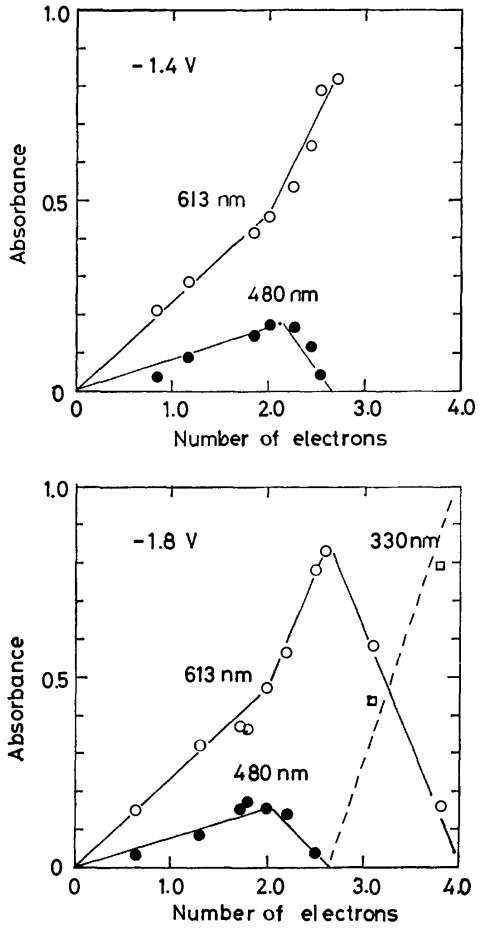

Fig. 4. Variation of absorbance during the electrolysis at -1.4 and -1.8 V.
(Absorbance at 480 and 330 nm is shown as the corrected value.)

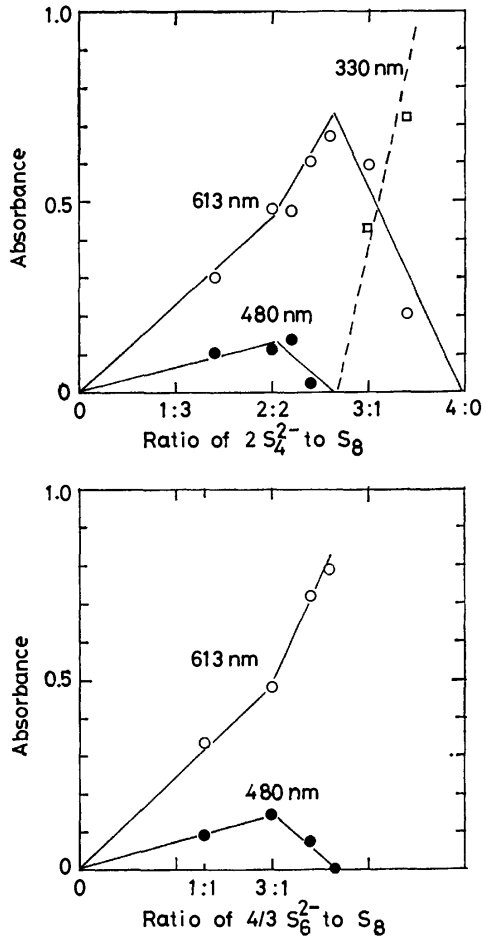

Fig. 5. Absorbance for the mixture of S_4^{2-} and S_8, and that of S_6^{2-} and S_8.
(See Fig. 4 for the absorbance at 480 and 330 nm.)

$$S_8^{2-} \overset{K}{\rightleftharpoons} S_6^{2-} + 1/4S_8 \quad (4)$$

The absorbance at $Z=8/3$ is plotted against the S_8 concentration without electrolysis in Fig. 6. At this point of the number of the electrons, all sulfur species must be formally "S_6^{2-}" state. The peak at 613 nm showed negative deviation (absorptivity falls off with increasing concentration). On the other hand, the peaks at 450 and 340 nm showed positive deviation. The spectra at $Z=8/3$ of various concentrations of S_8 showed an isosbestic point at 510 nm as shown in Fig. 7. These results suggest that S_6^{2-} dissociates into $S_3^{\cdot-}$, and the peak at 613 nm can be assigned to $S_3^{\cdot-}$ and those at 450 and 340 nm to S_6^{2-}. The presence of a radical with the g-value of *ca.* 2.03 was proved by the ESR measurement for the sulfur solution of 4×10^{-4} M at $Z=ca.$ 8/3. This g-value agrees well with that of $S_3^{\cdot-}$ species reported in the litareture.[7] Consequently, the blue species which shows the peak at 613 nm in acetonitrile is concluded to be $S_3^{\cdot-}$.

$$S_6^{2-} \overset{K_d}{\rightleftharpoons} 2S_3^{\cdot-} \quad (5)$$

The molar absorptivity of $S_3^{\cdot-}$ at 613 nm was obtained as $\varepsilon=3.9\times10^3$ and the dissociation constant for Eq. 5 as $K_d=1.2\times10^{-3}$ by the method of trial and error. The

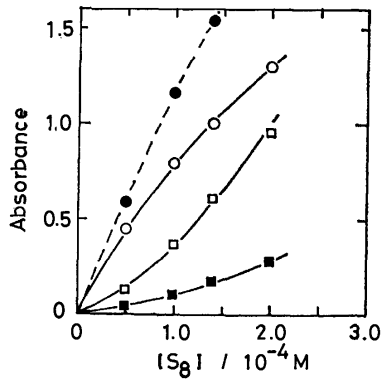

Fig. 6. Calibration curves of S_8 electrolyzed to $Z=8/3$ at -1.8 V.
●: 270, ○: 613, □: 340, ■: 450 nm.

molar absorptivity of S_6^{2-} is 3.1×10^3 at 450 nm, 1.1×10^4 at 340 nm. The peak of 270 nm may be due to $S_3^{\cdot-}$ judging from the behavior of the calibration curve.

In Fig. 8, the absorbance of electrolyzed solution at $Z=2.0$ is plotted against the initial S_8 concentration. At this point, sulfur must be electrolyzed to S_8^{2-} state.

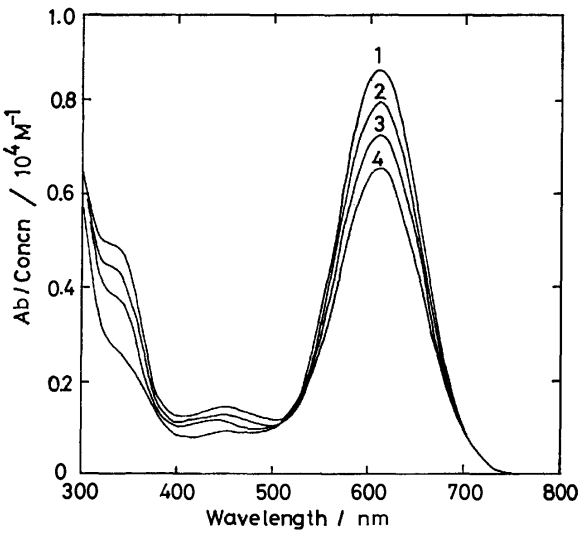

Fig. 7. Absorption spectra of S_8 electrolyzed to $Z=8/3$ at -1.8 V. Initial concn of S_8; 1: 0.5, 2: 1.0, 3: 1.4, 4: 2.0×10^{-4} M.

However, the S_8^{2-} produces more stable species, S_6^{2-} following the equilibrium of Eq. 4, so S_8^{2-}, S_6^{2-}, $S_3^{\cdot-}$, and S_8 exist together in the solution. The absorbance of $S_3^{\cdot-}$ at 613 nm deviated much more downwards from the linearity than the case of $Z=8/3$. The absorbance of 613 nm at $Z=2.0$, the molar absorptivity of $S_3^{\cdot-}$ ($\varepsilon=3.9\times10^3$) and the dissociation constant ($K_d=1.2\times10^{-3}$) enable the authors to calculate the equilibrium constant, K for Eq. 4 to be 1.6×10^{-2}. The peaks at 350 and 480 nm, due to S_8^{2-} showed positive deviation. The absorbances at 350 and 480 nm are enhanced by the additional absorption of the close peaks at 340 and 450 nm (both due to S_6^{2-}), respectively. From the corrected values of absorbance and the evaluated concentration of S_8^{2-}, the molar absorptivity of S_8^{2-} at 350 and 480 nm was obtained as 1.0×10^4 and 4.4×10^3, respectively.

As for the solution electrolyzed completely at the second wave, the absorbances at 330 and 400 nm,

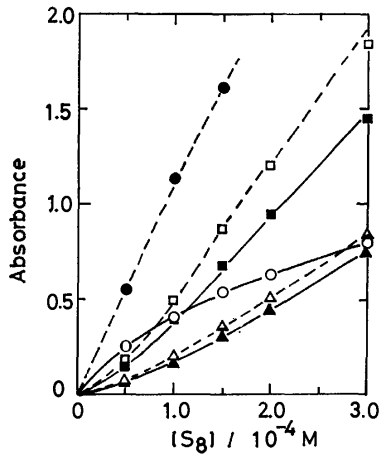

Fig. 8. Calibration curves of S_8 electrolyzed to $Z=2.0$ at -1.8 V.
●: 270, □: 350, ■: 350 corrected, ○: 613, △: 480, ▲: 480 nm corrected.

which may be due to S_4^{2-}, showed the linear dependence on the initial concentration of S_8. The molar absorptivity of S_4^{2-} at 330 and 400 is *ca.* 4.2×10^3 and 1.0×10^3, respectively. Sawyer *et al.*[3] reported the dissociation constant K_d to be 9×10^{-3}, and K in Eq. 4 to be 1.68×10^{-2} ($K^4=8\times10^{-8}$) in DMSO. However, the values obtained be Bonnaterre *at al.*[5] are much different from those by the present authors or Sawyer *et al.*[3]

The detail conditions were examined about the maximum of current in course of the coulometry at the potential of the second wave. First, the sulfur solution was electrolyzed to a certain number of electrons at -1.4 V. Then the potential was stepped to -1.8 V quickly, and the electrolysis current was recorded as shown in Fig. 9. The solution which was electrolyzed up to $Z=2.0$ at -1.4 V showed the maximum after the current decreased once. The solution electrolyzed to $Z=2.2$ showed a maximum just after the potential was stepped at -1.8 V. While, for the solution of $Z=2.5$ or more, the current decreased without the maximum.

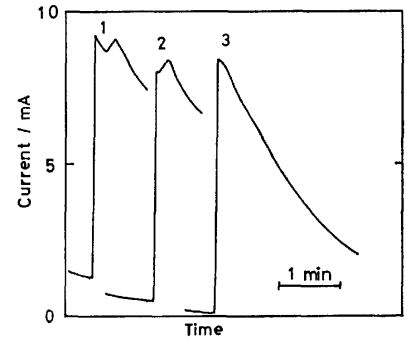

Fig. 9. Current after potential is stepped to -1.8 V from -1.4 V on various number of electrons.
$[S_8]=0.50\times10^{-4}$ M, 1: $Z=2.0$, 2: 2.2, 3: 2.5.

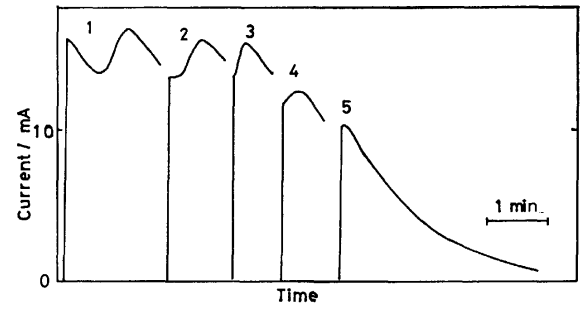

Fig. 10. Current change after addition of S_8 solutions into S_4^{2-} solutions.
Potential -1.8 V, ratio of $S_8/(2\,S_4^{2-})$; 1. 13: 7, 2. 11: 9, 3. 10: 10, 4. 8: 12, 5. 5: 15, total sulfur concn; 1.0×10^{-4} M in each case.

Similar results were obtained for the mixture of S_4^{2-} and unelectrolyzed S_8 solution as shown in Fig. 10. The solution with the mixing ratio $S_8/2S_4^{2-}$ of 10: 10, in which solution, sulfur is calculated to be $Z=2.0$ state, showed the maximum when electrolyzed at -1.8 V. The solution of the ratio of 5: 15 ($Z=3.0$ state), however, did not show the maximum any more. These

results clarify again that the appearence of the maximum in the coulometry is related to only the number of electrons up to which the sulfur is electrolyzed. As shown above, the products are same, that is, S_8, S_8^{2-}, S_6^{2-}, and $S_3^{\cdot-}$ are present each other at the same ratio of concentration when electrolyzed at -1.4 V or -1.8 V, only if the solution is in a same "electron state." The difference between the solutions electrolyzed at -1.4 and -1.8 V is whether the species of S_4^{2-} exists or not, which is observed apparently only after $Z=8/3$ at -1.8 V. It seems that the maximum current in coulometry at the second wave potential is caused by attacking of S_4^{2-} to S_8.

Lingane and Niedrach[8] observed similar i—t behavior during the electrochemical reduction of selenium (IV) in an aqueous buffer. They attributed the cause of the maximum of current to the formation of easily reduced polyselenide Se_x^{2-} by attacking of the final product Se^{2-} to elemental selenium.

The authors wish to express their thanks to Mr. Tsutomu Nagaoka for his kind assistance in the measurements of ESR spectra.

References

1) T. Fujinaga, S. Okazaki, and M. Hojo, *J. Electroanal. Chem.*, (1980), in press.
2) R. Bonnaterre and G. Cauquis, *J. Chem. Soc., Chem. Commun.*, **1972**, 293.
3) R. P. Martin, W. H. Doub, Jr., J. L. Roberts, Jr., and D. T. Sawyer, *Inorg. Chem.*, **12**, 1921 (1973).
4) M. Delemar and J. -C. Marchon, *J. Electroanal. Chem.*, **63**, 351 (1975).
5) J. Badoz-Lambling, R. Bonnaterre, G. Cauquis, M. Delamar, and G. Demange, *Electrochim. Acta*, **21**, 119 (1976).
6) K. Umemoto, *Bull. Chem. Soc. Jpn.*, **40**, 1058 (1967).
7) R. Bottcher, S. Wartewig, W. Windisch, and A. Zschunke, *Z. Naturforsch.*, **23a**, 1766 (1968).
8) J. J. Lingane and L. W. Niedrach, *J. Am. Chem. Soc.*, **71**, 196 (1949).

The Electrochemical Studies of Tetrasulfur Tetranitride in Acetonitrile

Masashi Hojo*

Department of Chemistry, Faculty of Science, Kyoto University, Kyoto 606

(Received March 1, 1980)

$S_4(NH)_4$ has been prepared in a good yield (80% or more) by the electrolytic reduction (4-electrons) of S_4N_4 in the presence of a proton donor in acetonitrile. In the proton donor, a fairly high acidity (acetic acid or a stronger acid) and a much higher concentration than would be expected from the stoichiometry was needed. With a low acidity (*e.g.*, phenol) or a low concentration of the proton donor, a side reaction occurred with the formation of H_2S and NH_3. Under these conditions, a blue species was produced in the course of the electrolysis; this species was confirmed to be S_3^-. The re-oxidation of $S_4(NH)_4$, the oxidation of S_4N_4, and the reduction of $S_4(NH)_4$ were also examined in this connection.

The present author and his co-workers have investigated the electrode reaction with disulfur dichloride (S_2Cl_2),[1] which has a bond of sulfur-chlorine, and elemental sulfur (S_8),[2] which has only a bond of sulfur-sulfur. Tetrasulfur tetranitride (S_4N_4) is the best-known nitride of sulfur, and it has formed the starting point of most previous investigations in sulfur-nitrogen chemistry.

The reduction of S_4N_4 with potassium metal in 1,2-dimethoxyethane has been reported by Chapman and Massey[3] to produce a species of color changes attributed to ions of the $S_4N_4^{n-}$ type (n=1—4). Meinzer *et al.*[4] assigned the ESR spectrum produced by the electrochemical reduction of S_4N_4 in acetonitrile to $S_4N_4^-$, which has a structure similar to S_4N_4. It was further demonstrated that this radical anion is only stable at temperatures below *ca.* −25 °C, while above 0 °C rapid decomposition occurs. Prater *et al.*[5] conclusively identified the $S_4N_4^-$ radical and showed that it decayed according to a first-order rate law. However, it was unknown what species was produced by the decomposition of the $S_4N_4^-$ radical. Very recently, Bojes *et al.*[6,7] confirmed the formation of the $S_3N_3^-$ ion as the final product of the electrochemical reduction of S_4N_4 in ethanol at room temperature.

$$S_4N_4 + 4/3e \longrightarrow 4/3\ S_3N_3^-$$

In the present paper, the mechanism of the electrochemical reaction for S_4N_4 and the related compounds in acetonitrile will be reported. The effect of proton donors on the electrode reaction will also be examined in detail.

Experimental

Reagents. S_4N_4 was prepared from S_2Cl_2 and ammonia.[8] IR absorptions (CS_2 solvent) occurred at 940 m and 700 s cm^{-1}. Found: S, 68.83, N, 30.50%. Calcd for S_4N_4: S, 69.59, N, 30.41%. $S_4(NH)_4$ was prepared by the reaction of S_4N_4 with methanolic tin(II) chloride.[9] Its IR spectrum (KBr) was coincident with in the literature.[10] Found: S, 67.88, N, 30.09, H, 2.3% . Calcd for S_4N_4: S, 68.1, N, 29.8, H, 2.1%.

The method of purifying acetonitrile and the method of preparing the Et_4NClO_4 used as a supporting electrolyte has been described elsewhere.[1] The other chemicals were of G. R. grade and were used without further purification.

* Present address: Department of Chemistry, Faculty of Science, Kochi University, Kochi 780.

Apparatus and Procedure. The apparatus and equipment used in the voltammetry, controlled potential coulometry, spectrophotometry, and ESR measurements were the same as those used before.[1,2] IR spectra were measured by a Japan Spectroscopic Co., Ltd., Diffraction Grating Infrared Spectrometer, Model IRA-1. The dropping mercury electrode had the following characteristics: m=0.70 mg/s at 60 cm in the open circuit, τ=4.3 s at −1.1 V *vs.* a Ag/0.1 M** $AgClO_4$–AN electrode in 0.1 M Et_4NClO_4–AN solution. The rotating platinum electrode had a geometric surface area of 0.10 cm^2.

The concentration of the hydrogen ion in an acetonitrile solution was determined, after a good amount of water had been added to the solution, by titration with Et_4NOH (6.75 mM aqueous solution) using a Horiba glass electrode. Ammonia and hydrogen sulfide were trapped successively in 0.005 M H_2SO_4 and 0.1 M KOH aqueous solutions respectively. The ammonia was analyzed by the Nessler method, while the hydrogen sulfide was detected by the use of sodium nitroprusside and determined by polarography.

Results and Discussion

Reduction of S_4N_4. A polarogram of S_4N_4 in acetonitrile is shown in Fig. 1; it gives main two reduction waves. The half-wave potentials of the two waves were −0.93 and −2.58 V respectively. The limiting currents for both waves were proportional to the concentration in the range from 0.5 to 5×10^{-4} M. In

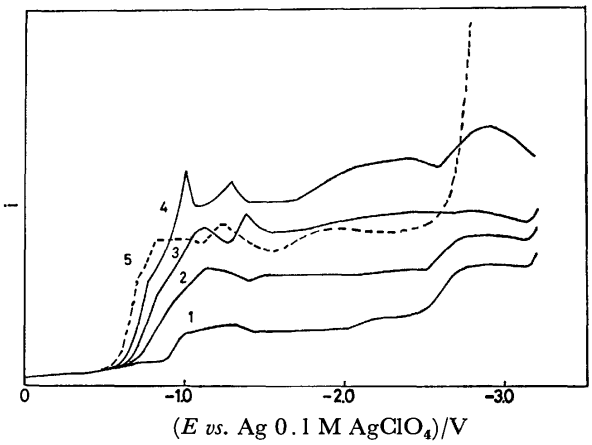

Fig. 1. Polarograms of 0.1 mM S_4N_4 with acetic acid in acetonitrile containing 0.1 M Et_4NClO_4.
(1) 0, (2) 0.2, (3) 0.5, (4) 1.0, (5) 5.0 mM of the acid.

** Throughout this paper 1 M=1 mol dm^{-3}.

order to determine the number of electrons involved in the reduction, a S_4N_4 solution was electrolyzed at the controlled potential of -1.2 V on a Hg-pool electrode; this gave a *n*-value of 1.3 for the first wave. The electrolyzed solution was pumped into an optical flow-cell, and the absorption spectrum was measured to give a peak at 360 nm. The product can be identified as $S_3N_3^-$ according to the *n*-value and the peak wavelength, with reference to the results in ethanol.[6] The absence of the $S_4N_4^{\cdot-}$ radical in the solution (the initial concn of S_4N_4 was $1—5\times10^{-4}$) at room temperature was proved by ESR measurements, as predicated by Meinzer *et al.*[4] The further reduction at the second wave caused the solution to turn colorless from yellow, with an *n*-value of 5—6 electrons.

Table 1. Voltammetric and coulometric data for S_4N_4 and $S_4(NH)_4$

Electrode	Reduction		Oxidation
	Hg	Pt	Pt
S_4N_4			
$E_{1/2}$/V	-0.93, -2.58	-0.95, (-1.48)[a]	$+1.64$
Slope[b]/mV	57.2, 120	61	170
n-Value[c]	1.3 (5—6)	1.3	*ca.* 4.0
$S_4(NH)_4$			
$E_{1/2}$/V	-2.80[d]	—[e]	$+0.95$, $+1.62$
Slope[b]/mV	127[d]		180, 140
n-Value[c]	($\approx$6)		4.0

a) A small wave appeared. b) Slope of the $-E$ *vs.* log-$[(i/(i_d-i)]$ plot. c) The number of electrons obtained by coulometry. d) Estimated value attributable to a polarographic maximum. e) With a Pt electrode, the potential can be measured to -2.0 V *vs.* Ag/0.1 M $AgClO_4$–AN at most.

The results of the voltammetry and coulometry with a platinum electrode were similar to those with mercury electrode for the first wave, as shown in Table 1, except that the absorbance at 360 nm due to $S_3N_3^-$ by the electrolysis on Hg-pool was a little smaller than that on Pt-electrode. This difference may be caused by the interaction between $S_3N_3^-$ and mercury. The molar absorptivity of $S_3N_3^-$ at 360 nm was estimated to be *ca.* 8.2×10^3 in acetonitrile, based on the experiments with Pt-gauze.

By the addition of acetic acid as a proton donor to a S_4N_4 solution, the wave height of the first wave increased and the half-wave potential shifted positively (see Fig. 1). Similar results were also obtained with benzoic acid of a degree of acidity similar to that of acetic acid.

Figure 2 shows the dependence of the wave height of the first wave on the concentration of the proton donor. With the addition of acetic acid or chloroacetic acid, the wave height increased by a factor 5—6, compared to that without a proton donor. The wave height decreased upon the further addition of the acids and then attained a constant value (*ca.* 3.5—4 times). With phenol, which is a much weaker acid, the wave

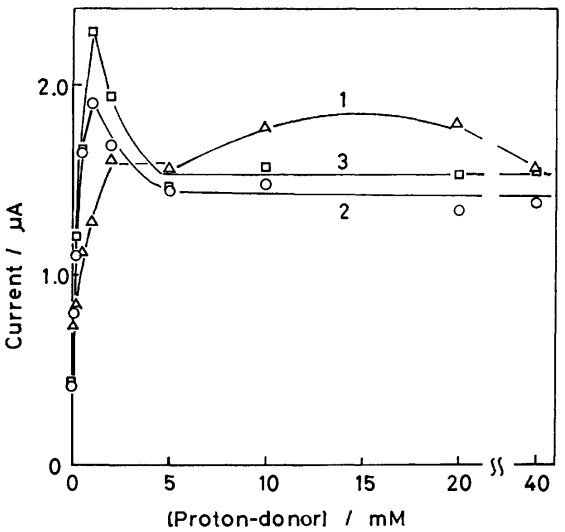

Fig. 2. Effect of proton-donor on the first wave height of S_4N_4. $[S_4N_4]=0.1$ mM, (1) phenol, (2) acetic acid, (3) monochloroacetic acid.

height increased by a factor of 4—5. The effect of water on the polarogram of S_4N_4 was very small. The presence of 5% water in acetonitrile made the first wave height increase by only a foctor of 1.6, while the second wave was not changed.

The increase in the wave height in the presence of proton donors suggested an increase in the *n*-value in the electrode precess. Figure 3 shows the *n*-values in the controlled potential coulometry with the Hg-pool electrode in the presence of proton donors. Without a proton donor, the *n*-value is 1.3, as mentioned above. However, the *n*-value increased to 8.2 with the addition of 5 mM of acetic acid to 0.1 mM of S_4N_4, and attained a constant value of 4.0 with 400 times acid, as much, when electrolyzed at -1.2 V. At -1.8 V, the *n*-value exceeded 10 with 2 mM of the acid and then decreased with more acid, but it never reached as law as 4.0.

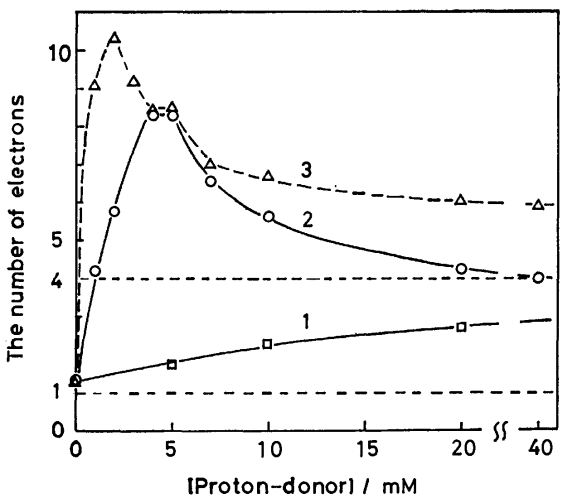

Fig. 3. The number of electrons in controlled potential coulometry. $[S_4N_4]=0.1$ mM, on Hg-pool electrode, (1) with phenol, potential at -1.2 V, (2) acetic acid, at -1.2 V, (3) acetic acid, at -1.8 V.

With phenol at −1.2 V, although the *n*-value increased from 1.3 toward a large value, a black solid was formed over the mercury electrode surface. The same black solid was also observed in the case of the presence of less than 2 mM of acetic acid.

The formation of $S_4(NH)_4$ was suggested by the *n*-value of 4 in the presence of acetic acid. The absorption spectrum of the solution electrolyzed at −1.2 V with 40 mM of acetic acid to 0.1 mM of S_4N_4 is shown in Fig. 4. $S_4(NH)_4$ gave a shoulder near 235 nm with a molar absorptivity of *ca.* 1.9×10^3 in acetonitrile, and the electrolyzed S_4N_4 solution showed the same spectrum as $S_4(NH)_4$. The yield was directly estimated to be about 90%, but the intensity of the shoulder was so small that an error may have occurred. Accordingly, the tetraimide produced was re-oxidized back to S_4N_4 at +1.2 V on the Pt electrode, and the absorbance at 250 nm was compared with that of the initial S_4N_4. The molar absorptivity of S_4N_4 at 250 nm was *ca.* 1.6×10^4. The yield in an experiment was 81%. As will be described in detail in the following section, the re-oxidation, that is, the oxidation of $S_4(NH)_4$ to S_4N_4 was established to proceed almost quantitatively. The formation of $S_4(NH)_4$ was confirmed also by voltammetry with a platinum electrode.

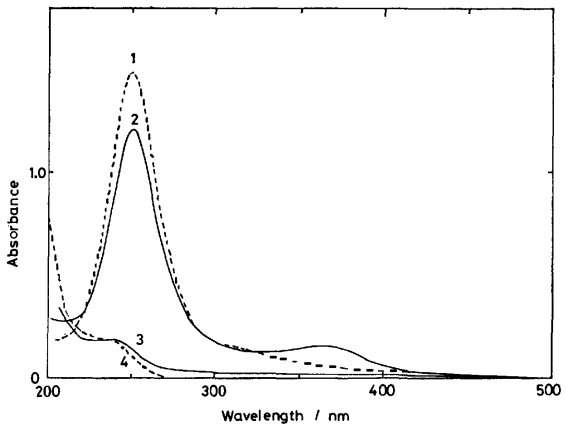

Fig. 4. Absorption spectra of the product from S_4N_4. (1) original 0.1 mM S_4N_4 solution. (2) oxidation (+1.2 V) product from (3), (3) reduction (−1.2 V) product from S_4N_4 with 40 mM acetic acid, (4) 0.1 mM $S_4(NH)_4$ solution. The absorption of the acid is corrected for (2) and (3).

For a higher concentration of S_4N_4 (*e.g.*, 0.2 or 0.5 mM), the tetraimide was obtained with about 400 times as much acid as S_4N_4. The product was isolated by being evaporated to dryness at room temperature; it was then washed with distilled water to remove the supporting electrolyte and the residues of the solvent and the acid. The IR spectrum of the product coincided with that of $S_4(NH)_4$ prepared chemically.

The above result can be summarized as follows: in the presence of a proper proton donor, S_4N_4 is reduced, and then the proton addition occurs, forming tetrasulfur tetraimide:

$$S_4N_4 + 4HA + 4e \longrightarrow S_4(NH)_4 + 4A^- \quad (1)$$

Acetic acid is such a weak acid in acetonitrile (pK_d= 22.3 by Kolthoff and Chantooni[11]) that it does not dissociate by itself to proton and acetate ions. The polarograms of the electrolyzed solution which formed $S_4(NH)_4$ showed a complicated anodic wave of mercury dissolution. This wave is thought to be caused by the acetate ion (A^-) or HA_2^-. The acetate ion is very active in an aprotic solvent. Kolthoff and Chantooni[11] have represented the constant of $K_{homo}=4.7\times10^3$ for the following homoconjugation reaction for acetic acid in acetonitrile: $A^- + HA \rightleftarrows AHA^-$

The fact that the yield of the tetraimide formation decreases, and the *n*-value far exceeds 4, with low concentrations of acetic acid suggests that the decomposition of S_4N_4 occurs as one of the side reactions. In the presence of about 40 times as much acetic acid as S_4N_4, the following reaction was confirmed to occur about 30% from the analysis of H_2S and NH_3:

$$S_4N_4 + 20HA + 20e \longrightarrow 4H_2S + 4NH_3 + 20A^- \quad (2)$$

The anodic wave in the polarogram of the solution after the electrolysis which formed H_2S and NH_3 was much higher than that in the case of Eq. 1. The acetate ion thus produced was determined by means of amperometric titration with 0.1 M $HClO_4$–AN solution. Under the conditions in which the reaction of Eq. 1 proceeds fully, the electrolyzed solution consumed 4 equivalents of the perchloric acid. On the other hand, with 40 times as much acetic acid as S_4N_4, the electrolyzed solution consumed 8 equivalents, which corresponds to the *n*-value in coulometry.

Another evidence of the decomposition reaction is the fact that the solution turned blue in the course of the electrolysis when 2—5 mM of acetic acid or 5—20 mM of phenol was added to 0.1 mM of S_4N_4. The absorption spectra gave a peak at 613 nm, as is shown in Fig. 5, with acetic acid. (The spectra with 2 mM

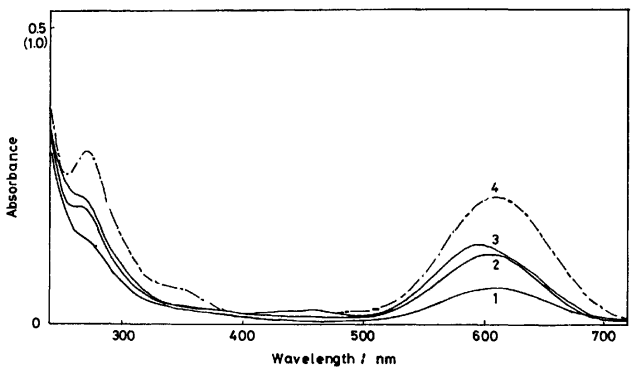

Fig. 5. Absorption spectra of S_4N_4 and S_8 solution in the course of electrolysis at −1.8 V†. (1) $[S_4N_4]$= 0.1 mM, with acetic acid 5 mM, Z=*ca.* 6.9, (2) with acetic acid 3 mM, Z=*ca.* 7.7 (3) with acetic acid 2 mM, Z=*ca.* 7.8, (4) $[S_8]$=0.05 mM, Z=2.66.†† The enlarged scale of absorbance should be used only for (4).

† As the decomposition reaction seemed to proceed more greatly at −1.8 V than −1.2 V according to Fig. 3, the results for −1.8 V are shown here. At −1.2 V, of course, the S_4N_4 solution gives same blue Species as −1.8 V.

†† S_8 is reduced to $S_3^{\cdot-}$ at Z=2.66, see Ref. 2) in detail.

of the acid gave a peak at 590 nm at $Z^{***}=7.8$, but the peak shifted to 613 nm at $Z=8.2$). Here, the blue species was confirmed to be S_3^-, for the author and co-workers have previously established[2] that the blue species is S_3^-, which gives a peak at 613 nm in the electrolytic reduction of elemental sulfur in acetonitrile. The sulfur produced by the decomposition of S_4N_4 passes through the stable species, S_3^-, before being utterly reduced to H_2S.

Proposed reduction mechanism

$$S_4N_4 \xrightarrow{e} S_4N_4^- \xrightarrow{H^+,\,e} S_4(NH)_4$$

$$\downarrow$$

$$S_3N_3^- \xrightarrow{H^+,\,e} S_3^-,\ NH_3,\ \text{and other products}$$

$$\downarrow H^+,\,e$$

$$H_2S$$

Scheme 1.

All the experiments suggest the reduction mechanism shown in Scheme 1. $S_4(NH)_4$ would be formed through the $S_4N_4^-$ radical if the radical is surrounded by a large amount of proton donors, so the protonation to $S_4N_4^-$ occurs easily. The protonated species may be reduced further at the same potential, and the protonation and the reduction will continue until $S_4(NH)_4$ is formed. Without a proton donor, $S_4N_4^-$ decomposes to $S_3N_3^-$ very rapidly at room temperature. When the $S_4N_4^-$ is not protonated enough with a small amount of the proton donor, almost all the radicals may decompose to $S_3N_3^-$. The formation of NH_3 or H_2S may occur through the species of $S_3N_3^-$. It seems reasonable to regard the species of $S_3N_3^-$ as the intermediate of the decomposition reaction, because the electrolysis of $S_3N_3^-$ in the presence of a sufficient amount of the acid did not produce the tetraimide any more, but NH_3, H_2S, and others.

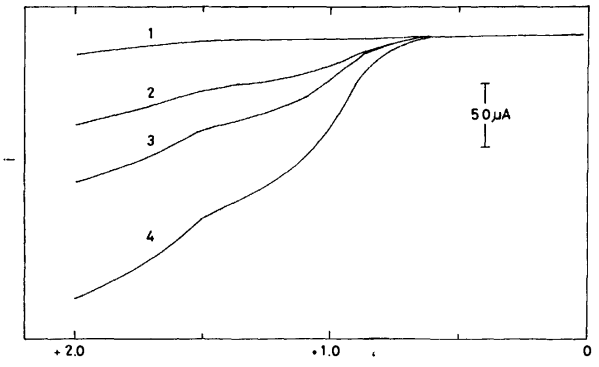

(E *vs.* Ag/0.1 M $AgClO_4$)/V

Fig. 6. Anodic waves of $S_4(NH)_4$ in acetonitile containing 0.1 M Et_4NClO_4 on the rotating platinum electrode. (1) 0, (2) 0.1, (3) 0.2, (4) 0.4 mM of $S_4(NH)_4$.

*** Z indicates the number of electrons added for S_4N_4.

The Oxidation of $S_4(NH)_4$ and S_4N_4, and the Reduction of $S_4(NH)_4$. $S_4(NH)_4$ was oxidized in two steps on the rotating platinum electrode, as is shown in Fig. 6 (see also Table 1). The limiting current of the first wave was proportional to the concentration of the depolarizer in the range of 0.1—0.7 mM. The second wave was much smaller than the first wave. The controlled potential coulometry at +1.2 V on the Pt-gauze electrode gave the n-value of 4.0 ± 0.15 for the first wave. The absorption spectrum of the solution just after the electrolysis had a peak at 250 nm, which showed the formation of S_4N_4 in a 96% yield. About 4 equivalents of the hydrogen ion were detected in the solution by acid-base titration. Therefore, the following electrode reaction is proved to occur almost quantitatively at +1.2 V:

$$S_4(NH)_4 \longrightarrow S_4N_4 + 4H^+ + 4e \qquad (3)$$

The yield for this electrode reaction was largely dependent on the potential at which the tetraimide was oxidized. For example, the yield of S_4N_4 fell to 68% at +1.3 V, and S_4N_4 was little detected by means of the UV spectrum at +1.4 V. The absorbance at 250 nm decreased with the passage of time because the proton produced behaved as a strong acid in acetonitrile and reacted with S_4N_4 to decompose. The reaction of the proton may also be related to the fact that the analyzed concentration of the proton was smaller than the calculated value by a factor of more than 10% several hours after the experiment of the electrolysis. When perchloric acid of 5 mM was present in the S_4N_4–AN solution of 0.1 mM, the absorbance at 250 nm decreased by factors of 2.7 and 4.1% after 15 min and 1 h respectively. On the other hand, hydrochloric acid of 1 mM caused the absorbance of S_4N_4 to decrease to half after 5 h. Nair and Murthy[12] reported that, when the sulfur nitride allowed to react with anhydrous hydrogen iodide in nonaqueous solvent like carbon tetrachloride, all the sulfur was reduced to hydrogen sulfide and that all the nitrogen was converted into ammonia as per the equation:

$$S_4N_4 + 20HI \longrightarrow 4H_2S + 4NH_3 + 10I_2$$

As the half-wave potential of the second wave of the imide is close to that of the anodic wave of S_4N_4, as is shown in Table 1, the S_4N_4 derived from $S_4(NH)_4$ may be thought to be further oxidized at the second wave. However, the second wave height of $S_4(NH)_4$ is much smaller than the wave height of S_4N_4, which is probably due to the proton produced at once according to Eq. 3. S_4N_4 was, furthermore, oxidized with a n-value of *ca.* 4.0 by controlled-potential coulometry at +2.0 V on the Pt-gauze electrode. The absorption spectrum of the product gave a peak at 280 nm, which might be due to the SN^+ ion, judging from the n-value of 4. The species of SN^+ has already been isolated in the $SN^+\cdot AsF_6^-$ form.[13] S_4N_4 may be oxidized as follows:

$$S_4N_4 \longrightarrow 4SN^+(?) + 4e \qquad (4)$$

$S_4(NH)_4$ gave a reduction wave accompanied by a polarographic maximum on a dropping mercury electrode before the cation of the supporting electrolyte (Et_4N^+) was reduced. The wave height was proportional

to the concentration of the depolarizer of 0.1—0.5 mM, and the number of electrons involved in the reduction step was estimated to be unity from the wave height. However, the current showed unusual behavior in coulometry at −3.0 V with a Hg-pool electrode: The current initially decreased in the usual manner, the solution turning pale red-purple. Then the current increased again with the color disappearance just after the 1-electron was consumed, and subsequently went through a maximum. Finally, an *n*-value of near 6 was obtained. This result might suggest that $S_4(NH)_4^-$ is produced by the one-electron reduction of $S_4(NH)_4$ and decomposed by the further addition of electrons. A similar current maximum in coulometry has previously reported for elemental sulfur in acetonitrile.[2)]

Conclusion

In a chemical preparation of the tetraimide, water or alcohol gives hydrogen to S_4N_4 to produce $S_4(NH)_4$. However, not even phenol can contribute to the formation of $S_4(NH)_4$; only acetic acid or a stronger acid can do so in an electrochemical reduction.

The author is indebted to Professor Taitiro Fujinaga for his invaluable advice and encouragement. Thanks are also due to Dr. Satoshi Okazaki for some valuable suggestions. The elemental analyses were made in the Laboratory for Organic Elemental Microanalysis Faculty of Pharmaceutical Science, Kyoto University. The author wishes to express his thanks to the Laboratory.

References

1) T. Fujinaga, S. Okazaki, and M. Hojo, *J. Electroanal. Chem. Interfacial Electrochem.*, in press.
2) T. Fujinaga, T. Kuwamoto, S. Okazaki, and M. Hojo, *Bull. Chem. Soc. Jpn.*, **53**, 2847 (1980).
3) D. Chapman and A. G. Massey, *Trans. Faraday Soc.*, **58**, 1291 (1962).
4) R. A. Meinzer, D. W. Pratt, and R. J. Myers, *J. Am. Chem. Soc.*, **91**, 6623 (1969).
5) J. D. Williford, R. E. VanReet, M. P. Eastman, and K. B. Prater, *J. Electrochem. Soc.*, **120**, 1498 (1973).
6) J. Bojes, T. Chivers, I. Drummond, and G. MacLean, *Inorg. Chem.*, **17**, 3668 (1978).
7) J. Bojes and T. Chivers, *Inorg. Chem.*, **17**, 318 (1978).
8) M. Villena-Blanco and W. L. Jolly, *Inorg. Synth.*, **9**, 98 (1967).
9) G. Brauer, "Handbook of Preparative Inorganic Chemistry," 2nd ed, Academic Press, New York (1963), Vol. 1, p. 411.
10) A. J. Banister and D. Younger, *J. Inorg. Nucl. Chem.*, **32**, 3763 (1970).
11) I. M. Kolthoff and M. K. Chantooni, Jr., *J. Am. Chem. Soc.*, **97**, 1376 (1975).
12) C. G. R. Nair and A. R. V. Murthy, *J. Inorg. Nucl. Chem.*, **25**, 453 (1963).
13) R. Mews, O. -L. Wagner, and O. Glemser, *Z. Anorg. Allg. Chem.*, **412**, 148 (1975).

The Determination of the Oxidation States of Neptunium in Sodium Hydroxide Solutions by Adsorption on Zirconium(IV) Hydroxide

Yoshinobu SHIOKAWA,* Akiko SATŌ, and Shin SUZUKI

The Research Institute for Iron, Steel and Other Metals, Tohoku University, Katahira, Sendai 980

(Received March 4, 1980)

An adsorption method for determining the distribution of the oxidation states of neptunium in sodium hydroxide solutions is proposed. In the range of sodium hydroxide concentrations of 1—2 M (1 M=1 mol dm^{-3}), the Np(V) was almost entirely adsorbed on zirconium(IV) hydroxide, while both Np(VI) and Np(VII) remained in the supernatant. By means of this adsorption method, it was found that Np(V) in tracer quantities, though it was most stable in acidic or neutral solutions, was not the most stable state in sodium hydroxide solutions. Also, the oxidation and reduction of Np in sodium hydroxide solutions were investigated.

Since the discovery of heptavalent neptunium in sodium hydroxide solutions,[1] the chemical behavior of neptunium in those solutions has been investigated with interest. From the polarographic study, the oxidation states found in sodium hydroxide solutions were the penta-, hexa-, and heptavalent states.[2] In order to investigate this chemical behavior it is important to find a method both for preparing the oxidation state of interest and for determining the distribution of the oxidation states in sodium hydroxide solutions. Certainly there are some oxidants suitable for the preparation of heptavalent neptunium; also, we can satisfactorily confirm its existence by means of spectrophotometry.[1]

However, no reductant or oxidant suitable for preparing penta- and hexavalent neptunium in sodium hydroxide solutions has been found, though they have been prepared by electrolysis.[3,4] Unfortunately, spectrophotometry is quite insensitive for identifying these two oxidation states because of the low solubility and low molar-extinction coefficients.[5] The absorption spectra of neither penta- and hexavalent neptunium in sodium hydroxide solutions has yet been published. Thus, in order to determine the distribution of the oxidation states of neptunium in sodium hydroxide solutions, a method different from spectrophotometry and applicable to low concentrations of neptunium is required. For this purpose it is necessary to prepare the oxidation state of interest. However, neither the determination method nor the preparation method for the oxidation states of neptunium in sodium hydroxide solutions has been established except for heptavalent neptunium of an ordinary concentration.[1]

In the first step of the present work, the oxidation states of neptunium in sodium hydroxide solutions were tentatively divided into the "reduced state" and the "oxidized state." The "reduced state" was prepared by the addition of hydrazine, and the "oxidized state," by the addition of bromine. As a result of our examination, the difference in chemical behavior necessary for discriminating these two states was found in the adsorption on zirconium(IV) hydroxide. Second, the oxidation state of the reduced and oxidized neptunium was determined by the titration of heptavalent neptunium. Third, the oxidation and reduction of neptunium in sodium hydroxide solutions were examined by utilizing the adsorption on zirconium(IV) hydroxide.

Experimental

The stock solution of sodium hydroxide was prepared by filtrating its saturated solution through a Millipore Mitex filter with a pore size of 10 μm. In order to prevent the sodium hydroxide solutions from being contaminated by carbon dioxide or neptunium from being oxidized by air, the necessary experimental procedures were carried out in an atmosphere of nitrogen or argon gas.

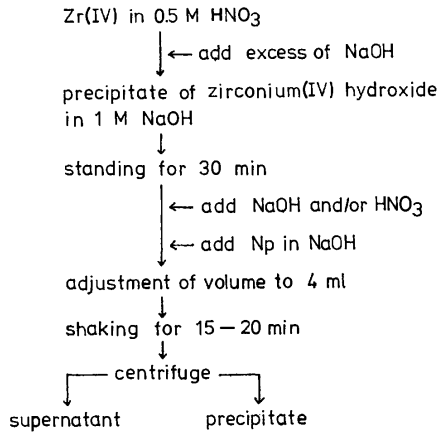

Fig. 1. Experimental procedures of the adsorption on zirconium (IV) hydroxide.

The reduced and oxidized neptunium in sodium hydroxide solutions were prepared by alkalizing a 0.5 M nitric acid solution of neptunium and by then adding hydrazine or bromine respectively. The ^{237}Np was obtained from The Radiochemical Centre, Amersham, while the ^{239}Np tracer was prepared by milking from ^{243}Am by the method of Espinosa.[6] In the preliminary experiments it was confirmed that the reduced and oxidized neptunium in sodium hydroxide solution were neither centrifuged nor adsorbed on glass.

The procedures for the adsorption on zirconium(IV) hydroxide are shown in Fig. 1. A suitable aliquot of a 0.5 M nitric acid solution of zirconium(IV) was transferred into a glass test tube equipped with a plug. In order to obtain zirconium(IV) hydroxide, a sodium hydroxide solution was added to an excess concentration of 1 M, and then, after 30 min, we added a sodium hydroxide solution and/or nitric acid solution in order to adjust the hydroxide ion-concentration. Then the sodium hydroxide solution of neptunium in the desired state was added, and the volume of the mixture was adjusted to 4 ml. The mixture was shaken for time enough to obtain an apparently constant adsorption. The recommended shaking

time was 15—20 min. By measuring the ^{239}Np activity by means of a NaI scintillation or Ge detector in both the mixture and the supernatant obtained by centrifuging, the percentage of neptunium adsorbed was determined.

The procedures for the titration of heptavalent neptunium were as follows. Heptavalent neptunium of about 5×10^{-4} M was prepared by the passage of ozone into $^{237+239}Np$ hydroxide in a 1 M sodium hydroxide solution, after which the excess ozone was swept out by argon-gas bubbling. The heptavalent solution (2—2.5 ml) was then transferred into a glass test tube equipped with a plug, and then 1×10^{-2} M hydrazine solution of 5—100 μl was added. After it was stood for 20—60 min at room temperature or 40 °C, this mixture was centrifuged, taking account of the low solubility of all the oxidation states except the heptavalent state. The supernatant was transferred into another test tube, and the adsorption on zirconium(IV) hydroxide was examined. In this experiment, the dissolved oxygen in the solution was swept out by the particularly careful passage of argon through just before use. The neptunium was determined by α- and γ-spectrometry, and the hydrazine, by iodometry.

Results and Discussion

Adsorption of the Reduced and Oxidized Neptunium on Zirconium(IV) Hydroxide. At first, the adsorption behavior on zirconium(IV) hydroxide under the various conditions was investigated for both the reduced and the oxidized neptunium in tracer quantities. Figure 2 shows the dependence of the adsorption on the amount of zirconium(IV) in a 0.96 M sodium hydroxide solution. In the range of 0.5—5 mg zirconium(IV), more than 95% of the reduced neptunium was adsorbed; on the other hand, the adsorbed fraction of the oxidized neptunium was less than 5%.

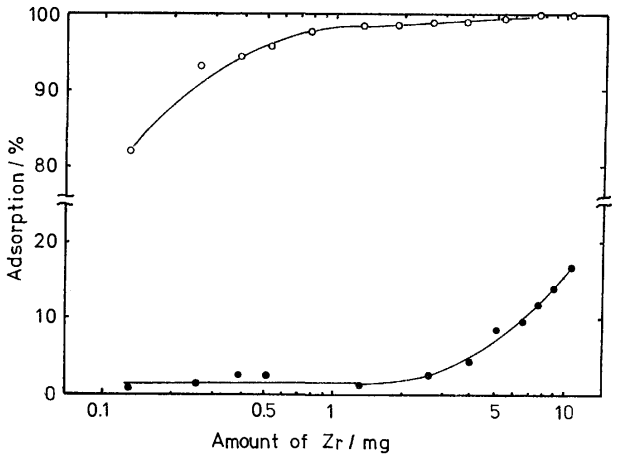

Fig. 2. Dependence of the adsorption on the amount of Zr(IV) at 0.96 M NaOH.
○: $Np+N_2H_4\cdot2HCl(1\times10^{-3}$ M),
●: $Np+Br_2(2\times10^{-2}$ M).

Figure 3 shows the dependence of the adsorption on the concentration of sodium hydroxide at a constant amount of zirconium(IV). For the reduced neptunium, the fraction adsorbed was about 99% in the range of the concentration of sodium hydroxide from 0.2 to 1 M; it decreased with the increase in the concentration,

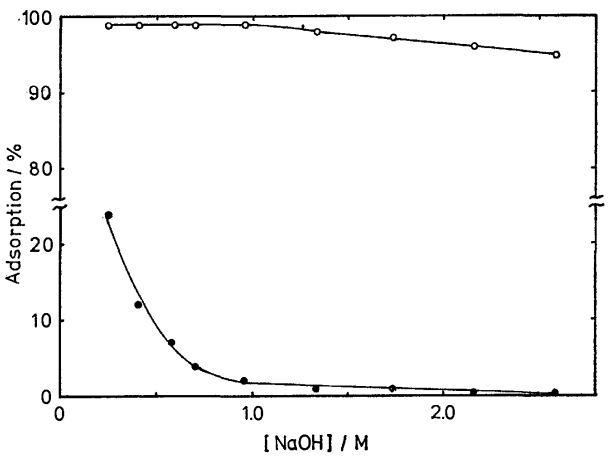

Fig. 3. Dependence of the adsorption on the concentration of NaOH using 2.9 mg Zr(IV).
○: $Np+N_2H_4\cdot2HCl(1\times10^{-3}$ M),
●: $Np+Br_2(1\times10^{-2}$ M).

reaching about 95% at 2.5 M. For the oxidized state, the fraction adsorbed was less than 2% above the concentration of 1 M, but it increased below 1 M.

Considering the dependency of the adsorption on both the amount of zirconium(IV) and the concentration of sodium hydroxide, as is shown in Figs. 2 and 3, it is possible to discriminate between the reduced and oxidized neptunium, if the adsorption is carried out with from 0.5 to 5 mg of zirconium(IV) per 4 ml of the mixture and at a sodium-hydroxide concentration from 1 to 2 M.

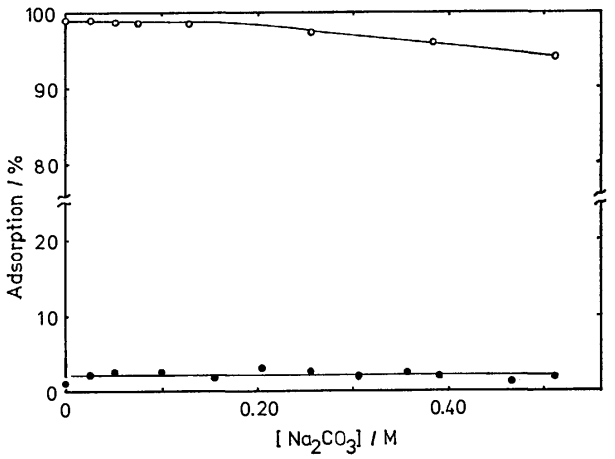

Fig. 4. Dependence of the adsorption on the concentration of Na_2CO_3 at 1.16 M NaOH using 2.6 mg Zr(IV).
○: $Np+N_2H_4\cdot2HCl(1\times10^{-3}$ M),
●: $Np+Br_2(2\times10^{-2}$ M).

The dependence of the adsorption on the concentration of the carbonate at a constant amount of zirconium(IV) and a constant concentration of sodium hydroxide is shown in Fig. 4. In the range of the carbonate concentrations examined, the fraction of the oxidized neptunium adsorbed remained constant, whereas that of the reduced neptunium was somewhat decreased

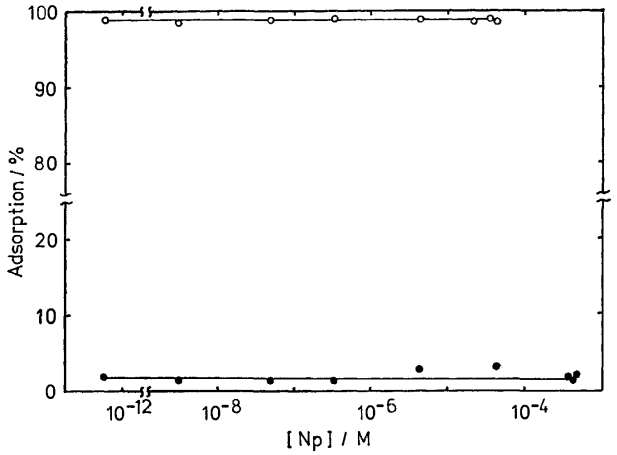

Fig. 5. Dependence of the adsorption on the concentration of Np at 1.25 M NaOH using 2.7 mg Zr(IV).
○: $Np+N_2H_4 \cdot 2HCl(1\times10^{-3}$ M),
●: $Np+Br_2(2.5\times10^{-2}$ M).

above the concentration of 0.15 M. As is shown in Fig. 4, the adsorption is little affected by the existence of the carbonate, and so this adsorption procedure may be applicable in the atmosphere of air. In the present work, however, in order to prevent the results from being disturbed, all the procedures were carried out in an atmosphere of nitrogen or argon gas.

Though the results of Figs. 2, 3, and 4 are for the reduced and oxidized neptunium in tracer quantities, the dependence of the adsorption on the concentration of neptunium is shown in Fig. 5. As is shown in Fig. 5, the fraction adsorbed was almost constant for both the reduced and oxidized neptunium over a wide range of the neptunium concentrations. Because of the low solubility of neptunium in sodium hydroxide solutions, the concentrations of neptunium examined ranged up to about 5×10^{-4} M for the oxidized neptunium and up to about 5×10^{-5} M for the reduced neptunium.

Titration of Heptavalent Neptunium by Hydrazine. As has been mentioned above, it is the only heptavalent state to be identified among some kinds of oxidation states of neptunium which occur in sodium hydroxide solutions. Therefore, if the reduced and oxidized neptunium can be prepared by adding an adequate reductant to heptavalent neptunium, it is possible to determine their oxidation states by considering the relationship between the amount of heptavalent neptunium and that of the reductant. We preferred hydrazine, which was able to reduce heptavalent neptunium quantitatively into hexavalent in sodium hydroxide solutions.[7]

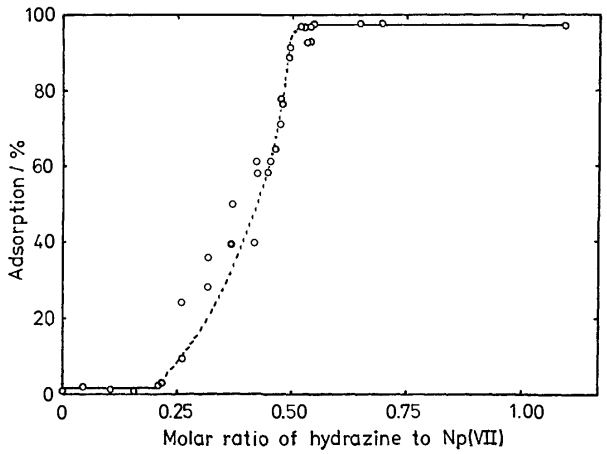

Fig. 6. Titration curve of Np(VII) by hydrazine at 1.0 M NaOH using 2.6 mg Zr(IV).

The results of the titration of heptavalent neptunium by hydrazine are shown in Fig. 6. As the equivalence point is the molar ratio of 0.25 for the reduction of heptavalent neptunium into hexavalent,[7] the adsorption at the molar ratio of 0 corresponds for heptavalent neptunium, and that at the molar ratio of 0.25, for hexavalent neptunium. Moreover, in the region of the molar ratios from 0 to 0.25, the adsorption corresponds for the mixture of hepta- and hexavalent neptunium. As is shown in Fig. 6, the fraction adsorbed in this region is very small. Consequently, both hepta- and hexavalent neptunium are hardly adsorbed at all on zirconium(IV) hydroxide.

On the other hand, the fraction adsorbed gradually increases in the region of the molar ratios between 0.25 and 0.50, and the neptunium is almost entirely adsorbed in the region of molar ratios more than 0.50. From this adsorption behavior, it is concluded that the neptunium in the oxidation state below the pentavalent state is almost entirely adsorbed on zirconium(IV) hydroxide. Moreover, if it is considered that the reduced rate of neptunium into the tetravalent state by hydrazine is negligibly small in the range of pH from weak acid to neutral solutions, and that the rate is rapid only in the strongly acid solutions,[8,9] the oxidation state of neptunium must be the pentavalent state in the region of molar ratios more than 0.5; therefore, the neptunium adsorbed on zirconium(IV) hydroxide must be in the pentavalent state.

In the region of the molar ratios between 0.25 and 0.50, the adsorption shows some scatter. This may be ascribed to the difference in the standing time and temperature on the reduction of heptavalent neptunium by hydrazine, because the solubility of hexavalent neptunium is about ten times as large as that of pentavalent neptunium in 1 M sodium hydroxide solutions, as is mentioned in the explanation of Fig. 5.

From the above discussion, it is apparent that the reduced neptunium prepared by hydrazine is in the pentavalent state, but the oxidized state cannot be assigned whether the hexavalent state, the heptavalent state, or a mixture.

Determination of the Oxidation State of Neptunium of Tracer Quantities. In the solution of neptunium without any foreign oxidants or reductants, the change of the oxidation state is as is shown in Table 1. Here, in addition to the adsorption on zirconium(IV) hydroxide, the oxidation state was determined by the adsorption on silica gel, in which hexavalent neptunium was quantitatively adsorbed, while pentavalent neptunium remained in the supernatant solution in the pH range of 6—7.[9]

At first, a solution of ^{239}Np in a 0.5 M nitric acid solution was prepared in the absence of foreign oxidants

TABLE 1. THE VARIATION IN THE OXIDATION STATE OF NEPTUNIUM IN TRACER QUANTITIES IN RELATION TO THE pH

	Adsorption[a]/%		Oxidation state
	Silica gel pH 6—7	$Zr(OH)_4$ 1 M NaOH	
Np in 0.5 M HNO_3	2		V
Np in 1 M NaOH		18	VI+(V)
Np in acetate buffer (pH 6.35)	1		V

a) The amounts of silica gel and Zr(IV) were 100 mg and 2.7 mg respectively.

or reductants; its oxidation state was acertained to be the pentavalent from the results of the adsorption on silica gel. Second, a 1 M sodium hydroxide solution of neptunium was prepared by alkalizing a 0.5 M nitric acid solution; the oxidation state was then examined by means of the adsorption on zirconium(IV) hydroxide. Because neptunium is never oxidized by oxygen into the heptavalent state,[1] the results shown in Table 1 indicate that a large portion of the neptunium in the 1 M sodium hydroxide solution exists in the hexavalent state, and a small portion, in the pentavalent state. Third, the neutral solution of neptunium was prepared by adding an acetate buffer solution to a 1 M sodium hydroxide solution; its oxidation state was found to be pentavalent.

It is well known that the most stable oxidation state of neptunium is the pentavalent state, and it has been confirmed, not only by the present work, but also by Inoue *et al.*,[9] that the oxidation state of neptunium in tracer quantities is pentavalent in the region from an acidic to a neutral solution in the absence of foreign oxidants or reductants. However, in a 1 M sodium hydroxide solution of neptunium in tracer quantities, the most stable oxidation state is not the pentavalent state, but a mixture of the pentavalent and hexavalent states, because pentavalent neptunium must be oxidized by the oxygen dissolved in the solution.

Espinosa investigated the preparation and identification of penta-, hexa-, and heptavalent neptunium in tracer quantities in alkaline solutions by means of glass fiber-electrophoresis and solvent extraction.[6] He concluded that neptunium in a sodium hydroxide solution, in the absence of foreign oxidants or reductants, was pentavalent. However, as is shown in Table 1, his method of preparation and his identification of pentavalent neptunium is questionable.

The adsorption of neptunium in tracer quantities on zirconium(IV) hydroxide in the presence of some oxidants or reductants is shown in Table 2. The pentavalent neptunium in a 1 M sodium hydroxide solution can be prepared by adding hydroxylamine and tin(II) besides hydrazine. However, it is difficult to prepare pentavalent neptunium by the use of hexacyanoferrate(II), ascorbic acid, and hydrogen peroxide, which are known as reductants capable of reducing heptavalent neptunium quantitatively into hexavalent.[1,7] The adsorption of neptunium in the presence of bromate, chlorite, and peroxosulfate is nearly equal to that in the absence of any oxidants or reductants. Therefore, these three reagents are not effective oxidants in 1 M sodium hydroxide solutions. Neptunium in tracer quantities is oxidized only to some extent by peroxosulfate at 50 °C, and in the presence of ozone, though under the same conditions neptunium of an ordinary concentration is oxidized into the heptavalent state.[1] By the use of hexacyanoferrate(III), permanganate, and bromine, neptunium is oxidized into a hexavalent or heptavalent state, as is shown in Table 2.

TABLE 2. THE REDUCTION AND OXIDATION OF NEPTUNIUM IN TRACER QUANTITIES IN 1 M NaOH

Reductant and oxidant		Adsorption[b]/% Standing time	
		15—20 min	3 h
$N_2H_4 \cdot 2HCl$	1×10^{-2} M[a]	99	99
$NH_2OH \cdot HCl$	1×10^{-2} M	99	99
$SnCl_2$	1×10^{-2} M	99	99
$K_4Fe(CN)_6$	1×10^{-2} M	95	97
L-Ascorbic acid	1×10^{-2} M	92	93
H_2O_2	1×10^{-2} M	62	57
None		18	18
$KBrO_3$	1×10^{-2} M	16	15
$NaClO_2$	1×10^{-2} M	16	13
$K_2S_2O_8$	1×10^{-2} M	15	14
$K_2S_2O_8$(50 °C)	1×10^{-2} M		9
O_3	1.5 g/h		6
$K_3Fe(CN)_6$	1×10^{-2} M	5	2
$KMnO_4$	1×10^{-2} M	3	1
Br_2	4×10^{-2} M	2	2

a) The concentrations were at the stage of reduction and oxidation, and were reduced to 1/4 of the value given at the stage of adsorption. b) The amount of Zr(IV) was 2.7 mg.

As has been mentioned above, pentavalent neptunium is found to be selectively absorbed on zirconium(IV) hydroxide, and the method proposed is effective for determining the distribution of the oxidation state of neptunium in a sodium hydroxide solution.

References

1) V. I. Spitsyn, A. D. Gelman, N. N. Krot, M. P. Mefordiyeva, F. A. Zakharova, Yu. A. Komokov, V. P. Shilov, and I. V. Smirnova, *J. Inorg. Nucl. Chem.*, **31**, 2733 (1969).

2) V. P. Peretrukhin and D. P. Alekseeva, *Radiokhimiya*, **16**, 836 (1974).

3) G. A. Simakin, I. V. Matyashchuk, and N. A. Vladimirova, *Radiokhimiya*, **15**, 98 (1973).

4) A. J. Zielen and D. Cohen, *J. Phys. Chem.*, **74**, 394 (1970).

5) D. Cohen and S. Fried, *Inorg. Nucl. Chem. Lett.*, **5**, 653 (1969).

6) E. Espinosa, Report 1973, FRNC-TH-478.

7) V. P. Shilov and N. N. Krot, *Radiokhimiya*, **11**, 399 (1969).

8) G. A. Burney and R. M. Harbour, "Radiochemistry of Neptunium," U. S. Atomic Energy Commission (1974).

9) Y. Inoue and O. Tochiyama, *J. Inorg. Nucl. Chem.*, **39**, 1443 (1977).

 © 1980 The Chemical Society of Japan Bull. Chem. Soc. Jpn., 53, 2865—2867 (1980)

A Potentiometric Study on Complex Formation of Silver(I) Ion with Glycine and β-Alanine in Aqueous Solution

Hitoshi OHTAKI,* Masayuki ZAMA, Hidemi KOYAMA, and Shin-ichi ISHIGURO

Department of Electronic Chemistry, Tokyo Institute of Technology, Nagatsuta, Midori-ku, Yokohama 227

(Received March 17, 1980)

The complex formation of silver(I) ion with glycine and β-alanine was studied at 25 °C in an aqueous solution containing 3 mol dm^{-3} $LiClO_4$ as a constant ionic medium by means of potentiometric titrations. At a relatively low pH region, the $AgHL^+$ complex (L^- represents glycinate and β-alaninate ions) was formed, in which the silver ion was coordinated with the carboxyl group of the ligands. At a medium pH range, the AgL and AgL_2^- complexes were formed. From the formation constants of the complexes, it is suggested that the silver ion within the complexes may be coordinated with the amino group of the ligands and the interaction between the metal ion and the carboxyl group within the complexes is so weak that the interaction does not appreciably stabilize the complexes. At the highest pH region, the hydrolyzed species $Ag(OH)L^-$ was formed.

In previous papers,[1,2] we have reported the complex formation reactions of silver(I) ion with some aliphatic diamines. In these cases, not only mononuclear complexes but also polynuclear, protonated, and hydrolyzed complexes were formed, and their formation constants were discussed in connection with the length of the methylene chain within the aliphatic diamines.

Although several investigations of complex formation reactions between silver(I) ion and amino acids have so far been made,[3] the pH ranges covered in most studies were rather limited, so that the formation of only AgL and AgL_2^- complexes have been reported,[4-6] and no further attention has been paid for the formation of protonated and hydrolyzed complexes.

In the present study, we examined the complex formation reactions of silver(I) ion with glycine and β-alanine in aqueous solution where the concentration of hydrogen ions was widely changed ($2 < -\log[H^+] < 11$). The $AgHL^+$ and $Ag(OH)L^-$ complexes were found together with the AgL and AgL_2^- complexes and their formation constants were obtained.

Experimental

Reagents. *Glycine and β-alanine* were recrystallized three times from an ethanol–water mixture and were dried at 80—110 °C in an electric oven. Crystals thus prepared were stored in vacuum.

Other chemicals were the same as those used previously.[1,2]

Measurements. Beckman (Nos. 40495 and 40498) glass electrodes were used in combination with an Orion Digital pH Meter Model 801. The concentration of free silver(I) ion was determined by using an Ag–AgCl electrodes in combination with Takeda Riken Digital Voltmeter (TR-6515). The Kawai-type reference half cell was used,[7] in which an Ag–AgCl electrode was set. The Ag–AgCl electrodes used were prepared according to Brown.[8]

During the potentiometric titrations the total concentration of perchlorate ion was kept constant at 3 mol dm^{-3} by using lithium perchlorate. The concentrations of silver and amino acids were changed over the range of 2.5—10 mmol dm^{-3} and 10—80 mmol dm^{-3}, respectively. The ratio of the total concentration of an amino acid to that of silver ion (C_L/C_{Ag}) ranged from 2 to 32. Measurements were performed at 25.00±0.01 °C in a paraffin oil bath set in a room thermostatted at 25.0±0.5 °C.

Details of the method of measurements were described elsewhere.[1,2]

Results

Titration curves of silver–glycine and silver–β-alanine systems are represented in Figs. 1 and 2, respectively. The value $-\log[H^+]$ was plotted against X ($=-H/C_L$; H stands for the analytical excess concentration of hydrogen ion). Titration data were first analyzed by graphical methods and the composition of the complexes

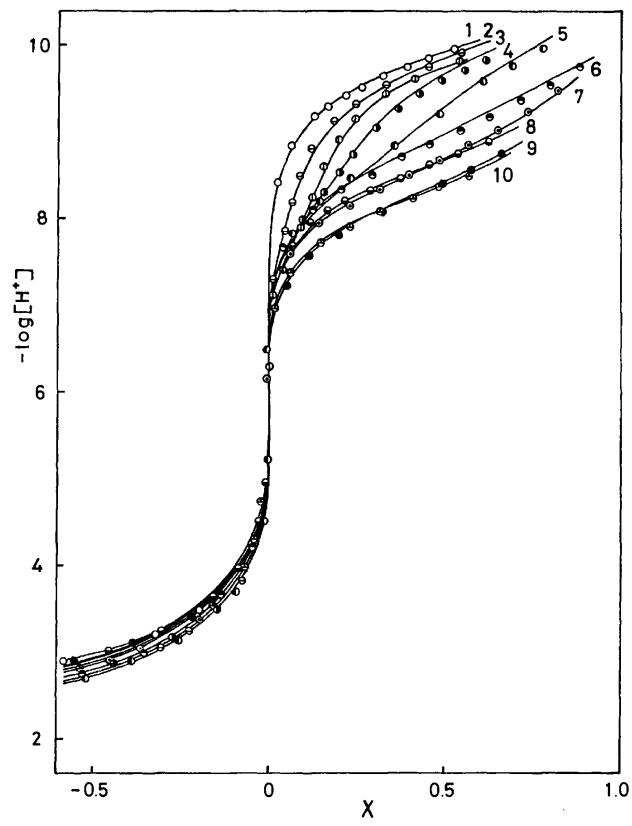

Fig. 1. Titration curves of glycine and silver–glycine solutions.
Curve 1: C_{Ag} (mmol dm^{-3}) = 0.0, C_L (mmol dm^{-3}) = 10.13; 2: 2.504, 80.00†; 3: 5.001, 80.00; 4: 2.504, 40.05; 5: 2.504, 20.04; 6: 2.507, 10.08; 7: 5.001, 20.04; 8: 5.001, 10.08; 9: 9.996; 40.05; 10: 9.996, 20.04.
† The concentration of the ligand was changed by dilution during the titration. The solid lines show calculated curves by using the constants in Table 1.

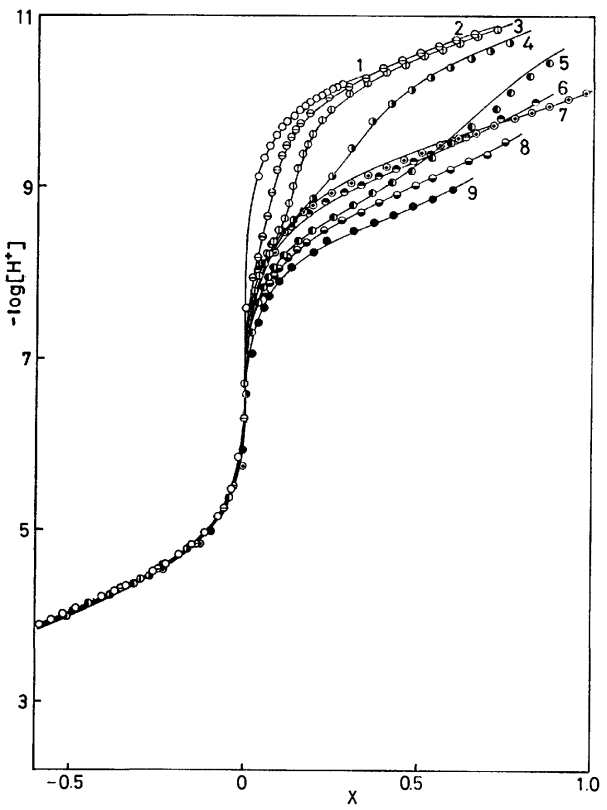

Fig. 2. Titration curves of β-alanine and silver-β-alanine solutions.
Curve 1: C_{Ag} (mmol dm^{-3})=0.0, C_L (mmol dm^{-3})= 10.26; 2: 2.546, 80.50†; 3: 5.133, 80.50; 4: 2.546, 40.14; 5: 5.133, 40.14; 6: 5.133, 10.08; 7: 2.546 5.036; 8: 10.05, 20.38; 9: 10.06, 40.14.
† See Fig. 1.

and their approximate formation constants were determined. The formation constants thus obtained were finally optimized by the least-squares method using an electronic computer (FACOM M-160). The least-squares method used was based on a modified MINIQUAD program[9] which minimizes the sum of squared residuals for all mass-balance equations.

In a lower pH range where most acids are present as HL the following equilibrium between silver ion and an amino acid may be assumed:

$$pAg^+ + rHL = Ag_pH_qL_r^{(p+q-r)+} + (r-q)H^+. \quad (1)$$

The equilibrium constant of Eq. 1 is defined as follows:

$$\kappa_{pqr} = \frac{[Ag_pH_qL_r^{(p+q-r)+}][H^+]^{r-q}}{[Ag^+]^p[HL]^r} = \beta_{pqr}/\beta^r_{011}, \quad (2)$$

where β_{pqr} denotes the overall formation constant of the $Ag_pH_qL_r^{(p+q-r)+}$ complex:

$$\beta_{pqr} = [Ag_pH_qL_r^{(p+q-r)+}]/[Ag^+]^p[H^+]^q[L^-]^r. \quad (3)$$

The material balance of the metal ion gives the following equation:

$$\frac{C_{Ag}-[Ag^+]}{[Ag^+]} = \phi - 1 = \sum_p\sum_q\sum_r p\kappa_{pqr}[Ag^+]^{p-1}[H^+]^{-(r-q)}[HL]^r. \quad (4)$$

If we assume as a first approximation that only one complex is formed in the pH range, the following equation can be readily derived:

$$\log(\phi-1) - \log[HL] = \log p\kappa_{pqr} + (p-1)\log[Ag^+] - (r-q)\log[H^+] + (r-1)\log[HL]. \quad (5)$$

Since the amount of the $Ag_pH_qL_r^{(p+q-r)+}$ complex formed was small, the concentration of the free ligand, HL, was approximated to the total concentration of the ligand, *i.e.*, $[HL]\approx C_L$. The plots of $\log(\phi-1)-\log C_L$ against $-\log[H^+]$ for the silver(I)-β-alanine system are shown in Fig. 3 as an example. The plots were practically independent of the total concentrations of both silver ion and the ligand and fell on an almost single straight line with the slope zero. Therefore, $p-1=0$, $r-1=0$ and $r-q=0$ were obtained, and thus, the complex formed was identified to be the $AgHL^+$ complex.

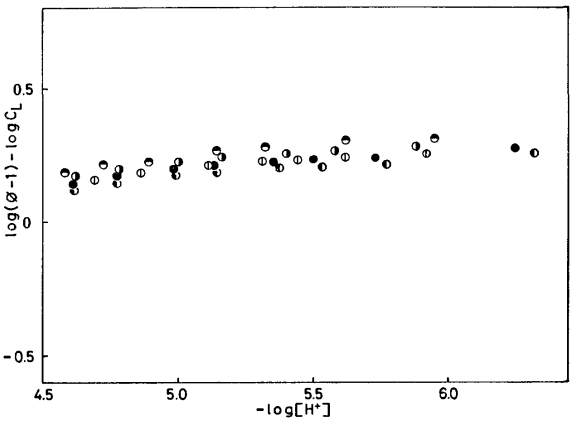

Fig. 3. Plots of $\log(\phi-1)-\log C_L$ *vs.* $-\log[H^+]$ in the silver-β-alanine system. Symbols are the same as those used in Fig. 2.

Graphical procedures were applied to the estimation of the composition and approximate formation constants of other complexes over the whole pH region. Formation of the complexes, AgL, AgL_2^- and $Ag(OH)L^-$ were estimated. The formation constants of the complexes thus evaluated by the graphical procedures were further refined by the least-squares method. The assumptions

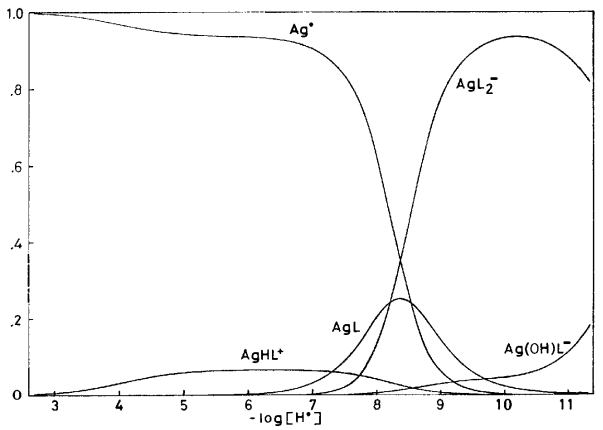

Fig. 4. Distribution of silver-β-alanine complexes.
C_{Ag}=5 mmol dm^{-3}, C_L=40 mmol dm^{-3}.

of the formation of the $AgHL_2$, $AgH_2L_2^+$, and AgOH complexes beside the complexes graphically obtained were all rejected in the course of the least-squares procedures. The final results are summerized in Table 1, together with the formation constants of ethylendiamine and 1,3-propanediamine complexes.[1,2] The solid lines in Figs. 1 and 2 were calculated by Eq. 6:

$$X_{calc}=\frac{C_L+K_1[H^+]^{-1}-[H^+]-\sum_p\sum_q\sum_r q\beta_{pqr}[Ag^+]^p[H^+]^q[L^-]^r}{C_L}, \quad (6)$$

where K_1 denotes the autoprotolysis constant of water in 3 mol dm^{-3} $LiClO_4$ aqueous solution and is $10^{-13.87\pm0.01}$ mol^{-2} dm^6,[10] and the formation constant β_{pqr} used are those in Table 1. A typical set of distribution curves of the silver–β-alanine complexes is depicted in Fig. 4.

Discussion

The equilibrium constant K(AgHL/HL) for the reaction

$$Ag^+ + HL = AgHL^+ \quad (7)$$

$$K(AgHL/HL) = [AgHL^+]/[Ag^+][HL] \quad (8)$$

can be calculated from the formation constants listed in Table 1. The values log K(AgHL/HL) for glycine and β-alanine are 0.07 and 0.23, respectively. The values are much smaller than those for diamines (*e.g.*, 2.79 for ethylenediamine), whilst they are very similar to the value for acetic acid (0.36).[11] Thus, the metal ion within the AgHL complex may be coordinated with the carboxyl group of the ligands. The value of log K(AgHL/HL) for glycine is smaller than that for β-alanine. A stronger electrostatic repulsion between silver ion and the terminal hydrogen ion at the amino group within the silver–glycine complex than that within the silver–β-alanine complex may reduce the stability of the former complex compared with the latter.

Stepwise formation constants log K(AgL/L) and log $K(AgL_2/L)$ for the reactions, $Ag^+ + L^- = AgL$ and $AgL + L^- = AgL_2^-$, respectively, are readily calculated from the data in Table 1, that is, log K(AgL/L) = 3.28 and log $K(AgL_2/L)$ = 3.68 for the silver–glycine complexes and log K(AgL/L) = 3.58 and log $K(AgL_2/L)$ = 3.88 for the silver–β-alanine complexes. The trend that the $K(AgL_2/L)$ value is larger than the K(AgL/L) value is the same as that found for silver–ammine and silver–monoamine complexes having a linear structure, and is opposite to that observed for silver–diamine complexes in the previous work[2] in which we reported that they have a distorted tetrahedral structure. These results suggest, therefore, that glycine and β-alanine essentially act as monodentate ligands to the central silver ion and the interaction between the positively charged silver ion and the negatively charged carboxyl group of the ligands may be so weak that it does not appreciably contribute to stabilization of the nitrogen-coordinated complexes.

The equilibrium constants of the hydrolytic reaction of the amino acid silver complexes, $AgL + H_2O = Ag(OH)L^- + H^+$ are given as log $^*K$(Ag(OH)L/AgL) = −9.76 and −9.70 for the glycinato and β-alaninato complexes of silver ion, respectively. These values are slightly larger than those of silver–ethylenediamine (−10.08) and 1,3-propanediamine (−10.16) complexes in the same medium.[2]

Table 1. Formation constants of the $Ag_pH_qL_r$ complexes, log β_{pqr}, in 3 mol dm^{-3} $LiClO_4$ at 25 °C[a]

$\beta_{pqr}=[Ag_pH_qL_r]/[Ag]^p[H]^q[L]^r$

Complex	gly⁻	β-ala⁻	en[2]	pn[2]
HL	9.91±0.02	10.65±0.02	10.74	10.96
H_2L	12.60±0.03	14.68±0.03	18.67	20.65
AgHL	9.99±0.20	10.88±0.15	13.53	14.32
AgL	3.28±0.02	3.58±0.03	5.26	6.59
AgL_2	6.96±0.03	7.46±0.03	9.45	9.8
Ag(OH)L	−6.48±0.15	−6.12±0.08	−4.81	−3.57

a) The charge of the complexes is omitted. Uncertainties of the formation constants were estimated as 3σ, where σ denotes the standard deviation.

References

1) H. Ohtaki and Y. Ito, *J. Cood. Chem.*, **3**, 131 (1973).
2) H. Ohtaki and K. Cho, *Bull. Chem. Soc. Jpn.*, **50**, 2674 (1977).
3) D. D. Perrin, "Stability Constants of Metal-ion Complexes: Part B, Organic Ligands," Pergamon Press (1979) and L. G. Sillén and A. E. Martell, "Stability Constants," The Chemical Society, London (1964) and (1971), Spec. Publ. No. 17 and Supplement No. 1, Spec. Publ. No. 25.
4) G. F. Thiers, L. C. Van Poucke, and M. A. Herman, *J. Inorg. Nucl. Chem.*, **30**, 1543 (1968).
5) D. J. Alner, R. C. Lansbury, and A. G. Smeeth, *J. Chem. Soc.*, A, **1968**, 417.
6) S. P. Datta and A. K. Grzybowski, *J. Chem. Soc.*, **1959**, 1094.
7) H. Tsukuda, T. Kawai, M. Maeda, and H. Ohtaki, *Bull. Chem. Soc. Jpn.*, **48**, 691 (1975).
8) A. S. Brown, *J. Am. Chem. Soc.*, **56**, 646 (1934).
9) A. Sabatini, A. Vacca, and P. Gans, *Talanta*, **21**, 53 (1974).
10) T. Kawai, S. Ishiguro, and H. Ohtaki, *Bull. Chem. Soc. Jpn.*, **53**, 2221 (1980).
11) F. Ya. Kulba, Yu. B. Yakovlev, and V. E. Mironov, *Russ. J. Inorg. Chem.*, **10**, 886 and 1624 (1965).

Indirect Spectrophotometric Determination of Phosphate Employing the Solubilization of Methylene Blue Molybdophosphate with Zephiramine

Junichi SHIDA* and Tsutomu MATSUO

Department of Applied Chemistry, Faculty of Engineering, Yamagata University, Jonan-4, Yonezawa, Yamagata 992

(Received April 4, 1980)

A highly sensitive indirect spectrophotometric method for phosphate was developed. The ion-association complex of molybdophosphate with Methylene Blue was precipitated in a nitric-acid medium. The complex was adsorbed on (1+4 v/v) cyclohexane–MIBK. The excess of Methylene Blue was removed by washing the organic phase with water. The complex was solubilized with a Zephiramine acidic aqueous solution. By measuring the absorbance of Methylene Blue in the aqueous solution at 660 nm, the phosphate was determined. The calibration curve was linear in the 0.31—3.1 μg range of phosphate, and the molar absorptivity was 2.5×10^5 l·mol^{-1}·cm^{-1}. The absorbance of the reagent blank was 0.019±0.001, and the recommended procedure was applied to the repetitive determination of 1.55 μg of phosphorus. The ten determinations produced a coefficient of variation of 1.6%. Arsenic, germanium and silicon, which form heteropolyacids like phosphorus, interfered seriously.

The studies of the solvent extraction of the ion pairs formed between complex anions and large cations are very important in analytical chemistry. Of these extractions, the one with a basic dye possessing a large molar absorptivity can be applied to the spectrophotometric determination of metals. Kirkbright *et al.*[1] have reported a method based on the formation of a complex between Rhodamine B and molybdophosphoric acid. Golkowska and Pszonicki[2] have studied the composition and properties of the ion-association complex of Rhodamine B with molybdosilicic acid, and have then used this method for the determination of silicon. Recently, Fogg *et al.*[3] have reported the spectrophotometric determination of inorganic phosphate in biological systems with Crystal Violet. The absorbance characteristics of the ion-association complex formed between molybdophosphate (MoP) and Methylene Blue (MB) are similar to those of MB itself. In a previous paper,[4] the large excess of MB co-extracted into MIBK was removed by washing it with a 2 M nitric acid solution, but the sensitivity and reproducibility were not satisfactory. This paper will report on a method for the indirect determination of phosphate by spectrophotometry. As the Methylene Blue molybdophosphate (MB·MoP) complex is only slightly soluble in the aqueous phase, it can be separated from the large excess of MB by filtration or floatation.[2] We adopted the adsorption[5] of the ion-association complex on the organic solvent; the MB·MoP complex precipitated as a thin layer on the phase boundary to separate from the large excess of MB. The MB^+ of the MB·MoP complex on the organic phase was replaced with the benzyldimethyltetradecylammonium ion (Zephiramine ion), and the free MB ion was transferred into the aqueous phase. By measuring the absorbance of the free MB ion in the aqueous phase, the amount of phosphate was determined.

Experimental

Apparatus and Reagents. A Hirama model 6B spectrophotometer with 10-mm glass cells was used. An Iwaki, model S-L type KM, shaker was used to shake the separatory funnel. All the chemicals were of analytical-reagent grades and were stored in polyethylene bottles. The nitric acid was distilled and diluted with water. The water was deionized and distilled.

Standard Phosphate Solution, 31 μg P ml^{-1}: Dissolve 0.1361 g of potassium dihydrogenphosphate in water and dilute to 1 l. This solution is then diluted as required to 0.31 μg P ml^{-1} with water.

Ammonium Molybdate Solution, 0.1 M: Dissolve 17.7 g of hexaammonium heptamolybdate tetrahydrate, $(NH_4)_6Mo_7O_{24}\cdot4H_2O$ in water and dilute to 1 l.

Methylene Blue Solution, 2×10^{-3} M: Dissolve 0.747 g of Methylene Blue (Wako Pure Chemical Industries, Ltd.; 98.5% content) in water and dilute to 1 l.

Organic Solvent: A (1+4 v/v) mixture of cyclohexane and isobutyl methyl ketone(MIBK) was used.

Zephiramine Solution, 5.0×10^{-3} M: Dissolve 1.84 g of Dotite Zephiramine (Dojindo Laboratories) in water and dilute to 1 l.

Recommended Procedure. Transfer a 20-ml portion of the sample solution(previously neutralized) containing less than 3 μg P into a 100-ml separatory funnel. Add 10 ml of 4 M nitric acid, 10 ml of a 0.1 M molybdate solution, and 5 ml of a 1 M potassium nitrate solution. Allow to stand for 10 min. Then, add 1 ml of a 2×10^{-3} M Methylene Blue solution and dilute with water to 50 ml. Mix well and add about 10 ml of the organic solvent. Shake vigorously for 10 min, allow the phases to separate, and discard the aqueous phase carefully. Then, add 25 ml of water and shake for 1 min. Allow the phases to separate and discard the aqueous phase. Repeat the washing with 25 ml of water once more. Add 5 ml of a 5.0×10^{-3} M Zephiramine solution and 5 ml of 0.5 M nitric acid, and shake vigorously for 5 min. After phase separation, transfer the aqueous phase and washings into a 25-ml volumetric flask. Dilute to the mark with water. Mix well and measure the absorbance at 660 nm against a reagent blank.

Results and Discussion

Absorption Spectra. The absorption spectra of MB in the Zephiramine acidic solution obtained by the recommended procedure are shown in Fig. 1. There are shoulders at 600—620 nm and an absorption maximum at 660 nm, where the absorbance of the reagent blank is very small; that is, the absorbance is 0.019±0.001 (ten determinations).

Effects of Reaction Variables. Concentration of Nitric Acid: The optimum acidity of the aqueous phase for

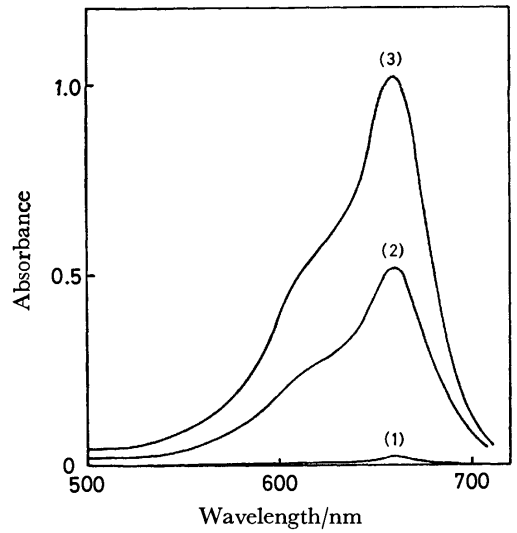

Fig. 1. Absorption spectra of Methylene Blue in Zephiramine acidic solution.
(1) Reagent blank, (2) P: 1.55 μg, (3) P: 3.10 μg. Reference: water.

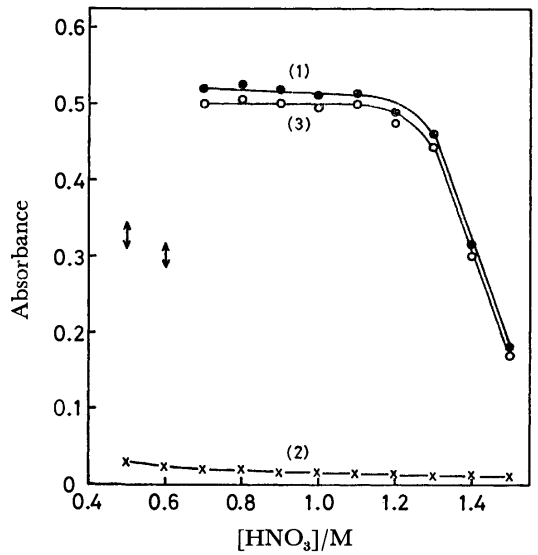

Fig. 2. Effect of nitric acid concentration on absorbance.
(1) P: 1.55 μg, (2) reagent blank, (3) net. Reference: water.

the formation of the MB·MoP complex was found to be 0.7—1.1 M nitric acid, as is shown in Fig. 2. The absorbance decreased gradually over the 1.2—1.5 M range of nitric acid. The reproducibility was poor below 0.6 M of nitric acid, because the excess of molybdate formed a precipitate with MB. A concentration of 0.8 M nitric acid in the initial solution was, therefore, chosen as the optimum.

The Amounts of Ammonium Molybdate Solution: For 1.55 μg P the absorbance increased upon the addition of 0.1 M ammonium molybdate up to 7 ml, and then remained constant for up to 20 ml of the reagent; 10 ml of the molybdate solution was used in further work.

The Amounts of Methylene Blue Solutions: As is shown in Fig. 3, a constant and maximum absorbance was

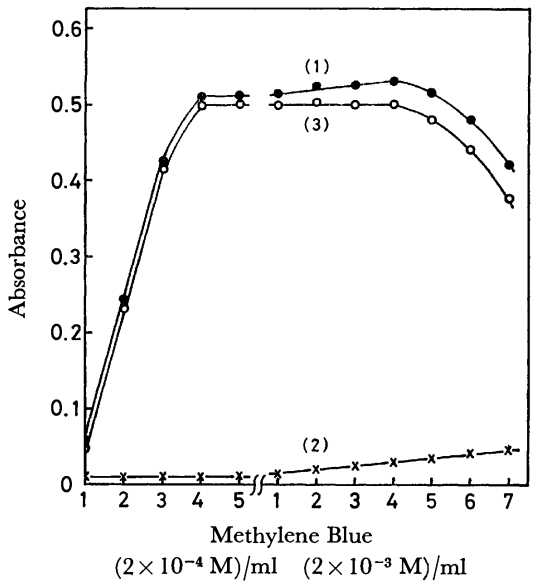

Fig. 3. Effect of the amounts of Methylene Blue solution.
(1) P: 1.55 μg, (2) reagent blank, (3) net. Reference: water.

obtained when from 4 ml of a 2×10^{-4} M solution to 3 ml of a 2×10^{-3} M MB solution were added. When a MB solution below 4 ml of 2×10^{-4} M or over 3 ml of 2×10^{-3} M was added, the absorbances decreased gradually.

Concentration of Zephiramine Solution: The effect of the Zephiramine concentration in the acidic aqueous phase on the solubilization of the MB·MoP complex was also studied. The absorbance increased up to 2.5×10^{-4} M Zephiramine, this remained constant when the reagent concentration was increased further. Therefore, 2.5×10^{-3} M Zephiramine in 0.25 M nitric acid was used. Unless the acid is added in the Zephiramine solution, it is difficult to separate the phases.

Adsorption and Separation of the MB·MoP Complex.

The Choice of Organic Solvents: The considerations for the choice of the organic solvents to adsorb the MB·MoP complex are as follows: (1) the solvent should have a smaller specific gravity of the organic solvents than that of water, such a smaller specific gravity being advantageous for washing the excess of MB, (2) there should be little extractability of the MB·MoP complex, and (3) it should be possible to separate the phases rapidly after shaking. Though there are several solvents which satisfy these conditions, the mixture of MIBK and cyclohexane was most recommended.

Effect of the Addition of Cyclohexane to MIBK: As is shown in Fig. 4, the optimum range was 20—30% (v/v) cyclohexane in MIBK, at which the absorbance of the reagent blank was very small. The emulsion forms in a yield of more than 40% upon shaking with the Zephiramine solution. Therefore, the shaking was carried out at 20%; that is, a (1+4) cyclohexane–MIBK mixture was used in further work.

Volume of (1+4)Cyclohexane-MIBK: The effect of (1+4) cyclohexane-MIBK was examined by varying the volume from 5 to 20 ml according to the recom-

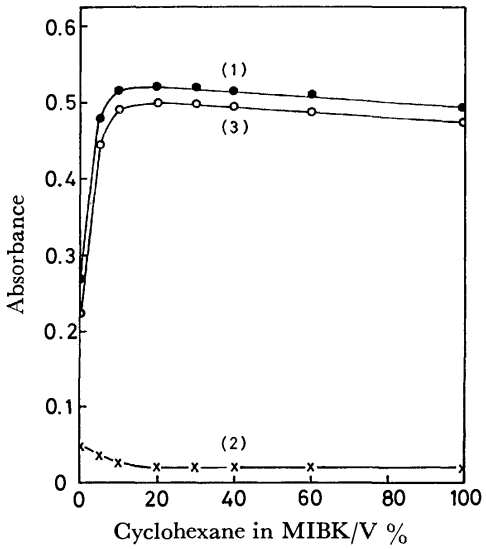

Fig. 4. Effect of the addition of cyclohexane.
(1) P: 1.55 μg, (2) reagent blank, (3) net. Reference: water.

mended procedure. However, no effect of the volume was observed. Therefore, about 10 ml of the solvent was used in further work.

Washing the Organic Phase: To remove the large excess of MB after the adsorption of the MB·MoP complex, we washed the organic phase with water. Washing twice with 25-ml portions of water was sufficient to remove the excess reagent. The shaking time for washing was 1 min.

Calibration Curve, Sensitivity, and Precision. The calibration curve obtained by the recommended procedure was linear in the range from 0.31 to 3.1 μg of phosphorus, and the molar absorptivity, as calculated from the slope of the curve, was 2.5×10^5 l·mol^{-1}·cm^{-1}. The recommended procedure was applied to the repetitive determination of 1.55 μg of phosphorus. The ten determinations produced a coefficient of variation of 1.6%.

Composition of the MB·MoP Complex. When the MB·MoP complex was dissolved with the Zephiramine solution, it was found that MB was transferred into the aqueous phase and that MoP was extracted into the organic phase. The absorbance of free MB in the aqueous phase was measured, and the concentration of MB was determined using the calibration curve of free MB. The P: MB ratio was 1: 3. After removing the organic solvent by volatilization, the analysis of MoP for molybdenum by atomic-absorption spectrophotometry, and that for phosphorus by the molybdenum blue method,[6] gave these results, P : Mo=1 : 12. The composition of the MB·MoP complex was estimated as $(MB)_3PMo_{12}O_{40}$.

Table 1. Effect of diverse ions on the recovery of phosphorus

Ion	Added as	Amount (μg)	Recovery (%)
As(V)	$Na_2HAsO_4\cdot7H_2O$	0.15	103
		1.0	119
As(III)	As_2O_3[a)]	5.0	103
		20	112
Ge(IV)	GeO_2[a)]	0.50	102
		5.0	122
Si(IV)	SiO_2[a)]	20	102
		200	122
V(V)	NH_4VO_3	2.0	104
		40	110
Cr(VI)	$K_2Cr_2O_7$	15	98
		200	87

a) Treated with NaOH. P: 1.55 μg.

Effect of Diverse Ions. The effect of diverse ions on the recovery produced from 1.55 μg of phosphorus by the recommended procedure was investigated. An ion was considered not to interfere when the error in the recovery was less than ±4% for the test solutions compared with the standards. As is shown in Table 1, arsenic, germanium and silicon, which form heteropolyacids like phosphorus, interfered seriously. These results are in agreement with those of a previous paper.[4]

Application. The method described may be used for the microanalysis of phosphate, for example, sea water and river water. Because the MB·MoP complex dissolves in alcohols (methanol, ethanol, *etc.*) or amides (*N,N*-dimethylformamide, *etc.*), phosphorus can be determined directly by measuring the absorbance of the complex in an organic solvent. Therefore, this makes possible a considerable reduction in time.

References

1) G. F. Kirkbright, R. Narayanaswamy, and T. S. West, *Anal. Chem.*, **43**, 1434 (1971).
2) A. Golkowska and L. Pszonicki, *Talanta*, **20**, 749 (1973).
3) A. G. Fogg, S. Soleymanloo, and D. Thorburn Burns, *Anal. Chim. Acta*, **88**, 197 (1977).
4) T. Matsuo, J. Shida, and W. Kurihara, *Anal. Chim. Acta*, **91**, 385 (1977).
5) T. Suzuki and T. Sotobayashi, *Bunseki Kagaku*, **12**, 376 (1963).
6) JIS K 0102 (1974).

Binuclear Metal Complexes. XXXIII.[1] Synthesis, Structure, Spectra, and Magnetism of Binuclear Copper(II) Complexes with 2-[2-(Dialkylamino)ethylthio]ethanol

Masahiro MIKURIYA, Hisashi OKAWA, and Sigeo KIDA*

Department of Chemistry, Faculty of Science, Kyushu University, Hakozaki, Higashi-ku, Fukuoka 812

(Received April 10, 1980)

Binuclear copper(II) complexes with 2-[2-(dialkylamino)ethylthio]ethanol, Cu{$R_2N(CH_2)_2S(CH_2)_2O$}X (abbreviated as Cu(R-nso)X, where R=CH_3, C_2H_5, n-C_3H_7, n-C_4H_9; X=Br, Cl, NO_3), were prepared and characterized by elemental analyses, infrared and electronic spectra and magnetic susceptibilities (80—300 K). They exhibit a band at 22—26$\times 10^3$ cm^{-1} characteristic of alkoxo-bridged structure. The magnetic data of Cu(n-C_4H_9-nso)Cl indicate that a strong antiferromagnetic interaction is operating between the copper ions. However, temperature dependence of magnetic susceptibilities of the other complexes do not obey the equation based on a binuclear structure. The crystal structure of Cu(CH_3-nso)Br was determined by the single-crystal X-ray diffraction method. The crystals are monoclinic, space group $P2_1/c$, a=10.133(2), b=7.858(2), c=14.893(3) Å, β=118.8(1)°, and Z=2. The structure was solved by the heavy atom method and refined by the block-diagonal least-squares method to an R factor of 0.042. The structure consists of alkoxo-bridged binuclear units, Cu_2-(CH_3-nso)$_2Br_2$. The coordination geometry of the copper ion is distorted square pyramid. Since the distances between the binuclear clusters are too long to give rise to an intercluster magnetic interaction, it is suggested that some structural change takes place at low temperature.

In blue copper oxidases (*e.g.*, laccase, ceruloplasmin, and ascorbate oxidase), type III copper is believed to be present as an antiferromagnetically coupled copper(II) dimer.[2] Although no exact information is available yet on the coordination geometry or the nature of the donor atoms for type III copper, models incorporating sulfur donor ligands have attracted a remarkable attention. However, few spectral and magnetic data and almost no structural data are available on binuclear copper(II) complexes with sulfur donor ligands.[3-6]

As a part of the continuing project dealing with binuclear copper(II) complexes of sulfur-containing ligands, we recently reported the synthesis and spectral and magnetic properties of the binuclear copper(II) complexes with *N*-[2-(alkylthio)ethyl]-3-amino-1-propanol, Cu{$RS(CH_2)_2NH(CH_2)_3O$}X (abbreviated as Cu(R-sno)X, where R=alkyl, X=anion).[1,7] In this study, we have prepared binuclear copper(II) complexes with 2-[2-(dialkylamino)ethylthio]ethanol, Cu{$R_2N(CH_2)_2S(CH_2)_2O$}X (abbreviated as Cu(R-nso)X, where R=CH_3, C_2H_5, n-C_3H_7, n-C_4H_9; X=Br, Cl, NO_3) and investigated their spectral and magnetic properties. In these complexes, the sulfur atom was considered to link two five-membered chelate rings upon complexation. Such a condensed-ring system should bring about a considerable strain, if all donating atoms and copper(II) ions are placed on a plane. Thus, the ligands have the potential to adopt a nonplanar arrangement about the copper ion, promoting stabilization of the copper(I) oxidation state.[8] In order to clarify the detailed molecular structure, the crystal structure of bromo{2-[2-(dimethylamino)ethylthio]ethanolato}copper(II), Cu(CH_3-nso)Br, was determined by the single-crystal X-ray diffraction method.

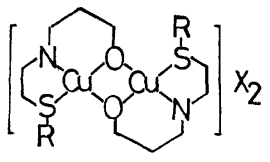

Cu(R-sno)X

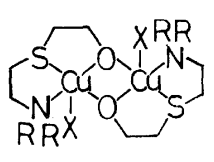

Cu(R-nso)X

Experimental

Preparation of the Ligands. *N,N*-Dialkyl-2-chloroethylamine hydrochlorides were prepared from 2-(dialkylamino)-ethanols and thionyl chloride by the method described in the literature.[9] The ligands, $R_2N(CH_2)_2S(CH_2)_2OH$ (R=CH_3, C_2H_5, n-C_3H_7, n-C_4H_9), were prepared by the reaction of *N,N*-dialkyl-2-chloroethylamine hydrochlorides and 2-mercaptoethanol by the method of Clinton *et al.*[10]

Preparation of the Complexes. The synthetic methods of the chlorides, Cu(R-nso)Cl (R=CH_3, C_2H_5, n-C_3H_7, n-C_4H_9), are nearly the same and exemplified by Cu(CH_3nso)Cl. To a solution of CH_3-nsoH (149 mg) in absolute ethanol (5 ml) was added a solution of copper(II) chloride dihydrate (85 mg) in absolute ethanol (5 ml). From the mixture, green crystals were immediately formed. They were collected by filtration and dried *in vacuo* over P_2O_5.

The nitrates and bromides, Cu(R-nso)X (X=NO_3,Br), were prepared by a method similar to that for the chlorides

TABLE 1. ANALYTICAL DATA OF Cu(R-nso)X·$n$$H_2O$

Complex R	X	n	Found (Calcd) C(%)	H(%)	N(%)
CH_3	Br	0	24.70(24.71)	4.77(4.84)	4.65(4.80)
C_2H_5	Br	0	29.61(30.05)	5.43(5.67)	4.23(4.38)
n-C_3H_7	Br	0	34.70(34.53)	6.49(6.38)	4.11(4.03)
n-C_4H_9	Br	0	38.32(38.35)	7.11(6.97)	3.81(3.73)
CH_3	Cl	0	29.07(29.15)	5.73(5.71)	5.57(5.67)
C_2H_5	Cl	0	34.84(34.90)	6.66(6.59)	5.10(5.09)
n-C_3H_7	Cl	0	39.58(39.59)	7.45(7.31)	4.60(4.62)
n-C_4H_9	Cl	0	43.43(43.49)	8.06(7.91)	4.31(4.23)
CH_3	NO_3	1/2	25.67(25.48)	5.16(5.35)	10.02(9.91)
C_2H_5	NO_3	1/2	31.03(30.91)	5.98(6.16)	9.10(9.01)
n-C_3H_7	NO_3	0	36.25(36.41)	6.75(6.72)	8.11(8.49)
n-C_4H_9	NO_3	0	39.85(40.27)	7.34(7.32)	7.50(7.83)

except for using copper(II) nitrate trihydrate and copper(II) bromide, respectively, instead of copper(II) chloride dihydrate.

Carbon, hydrogen, and nitrogen analyses were carried out at the Service Center of Elemental Analysis, Kyushu University. The results of elemental analyses for these complexes are listed in Table 1.

Measurements. Infrared spectra were measured with a Hitachi Grating Infrared Spectrophotometer Model 215 in the region 4000—650 cm^{-1} on a KBr disk. Electronic spectra were measured with a Shimadzu Multipurpose Spectrophotometer Model MSP-5000 at room temperature. Magnetic susceptibilities were measured by the Faraday method in the temperature range from liquid nitrogen temperature to room temperature. The apparatus was calibrated by the use of $[Ni(en)_3]S_2O_3$.[11] All the susceptibilities were corrected for the diamagnetism of the constituting atoms by the use of Pascal's constants.[12] Effective magnetic moments were calculated from the equation, $\mu_{eff}=2.828\sqrt{(\chi_A-N\alpha)T}$, where χ_A is the atomic magnetic susceptibility and $N\alpha$ is the temperature-independent paramagnetism. For the present complexes, $N\alpha$ was assumed to be 60×10^{-6} cgs emu.[13]

X-Ray Crystal Structure Analysis of Cu(CH$_3$-nso)Br. A photographic study using Weissenberg camera indicated monoclinic symmetry. Preliminary cell constants were obtained. The systematic absences observed, l odd for $h0l$ and k odd for $0k0$, uniquely define the space group as $P2_1/c$. The unit cell parameters and intensities were measured on a Syntex $P\bar{1}$ automated four-circle diffractometer with Mo $K\alpha$ radiation monochromated by a graphite plate ($\lambda=0.71073$ Å). The crystal was ground to a sphere (radius 0.148 mm). The unit cell parameters were determined by the least-squares refinement based on the 15 reflections in the range of $21°<2\theta<31°$. The values are $a=10.133(2)$, $b=7.858(2)$, $c=14.893(3)$ Å, $\beta=118.8(1)°$ and $V=1039.3(4)$ Å^3. The density $D_m=1.85$ g/cm^3 obtained by floatation in hexane–1,2-dibromoethane solutions agrees well with the density $D_C=1.864$ g/cm^3 calculated for two dimer units per unit cell.

Intensity data were collected by the θ-2θ scan technique with a variable scan rate of 4.0 to 24.0 °/min. Three standard reflections were monitored every 50 reflections, and their intensities showed a good stability. A total of 1943 independent reflections with $2\theta\leq50°$ were collected. The intensities were corrected for the Lorentz and the polarization effects. Absorption correction was applied with the values of the absorption-correction factors, A^*, tabulated in International Tables for X-Ray Crystallography.[14] 1595 independent reflections with $|F|>3\sigma(|F|)$ were considered as "observed" and were used for the structure analysis, where $\sigma(|F|)$ is the standard deviation of the observed structure amplitude due to counting statistics. An initial scale factor and over-all temperature factor were obtained by the Wilson statistics.

The structure was solved by the heavy atom method. The positions of the bromine and the copper atoms were obtained from a three-dimensional Patterson synthesis. The successive Fourier synthesis revealed all the nonhydrogen atoms. Refinement was carried out by the block-diagonal least-squares method. Anisotropic thermal parameters being introduced, the block-diagonal least-squares refinement yielded discrepancy factors $R_1=\sum||F_o|-|F_c||/\sum|F_o|=0.049$ and $R_2=[\sum w(|F_o|-|F_c|)^2/\sum w|F_o|^2]^{1/2}=0.082$. Hydrogen atoms were inserted in their calculated positions and included in the refinement. Further refinement with anisotropic thermal parameters for nonhydrogen atoms and isotropic temperature factors for hydrogen atoms gave final values of 0.042 and 0.072 for R_1 and R_2, respectively. In the least-squares refinement the function minimized was $\sum w(|F_o|-k|F_c|)^2$, and the weighting scheme was $w=(6.76+|F_o|+0.086|F_o|^2)^{-1}$.[15] The final shift in the atomic parameters of the nonhydrogen atoms averaged 0.024σ with the maximum of 0.127σ. The final difference Fourier synthesis showed no significant features except two peaks of 0.8 e/Å^3 in the vicinity of the bromine atom. The atomic scattering factors for Br, Cu, S, O, N, and C_{val} and the anomalous dispersion corrections, $\Delta f'$ and $\Delta f''$ for Br, Cu, and S, were taken from the International Tables for X-Ray Crystallography.[16] For the hydrogen atom, the scattering factors were adopted from the tables of Stewart *et al.*[17] All the calculations were carried out by the FACOM M-190 computer in the Computer Center of Kyushu University using the UNICS-II program system.[18] The drawings were made by the use of ORTEP program.[19] Lists of the observed and calculated structure factors are kept as Document No. 8032 at the Chemical Society of Japan. The final positional and thermal parameters with their estimated standard deviations are given in Table 2.

Results and Discussion

Description of the Structure of Cu(CH$_3$-nso)Br. A perspective drawing of the complex and the numbering system are illustrated in Fig. 1. Bond lengths and angles are listed in Table 3.

The crystal structure essentially consists of the alkoxo-bridged binuclear units, $Cu_2(CH_3\text{-nso})_2Br_2$. The $Cu_2(CH_3\text{-nso})_2Br_2$ unit is located at the crystallographic

Table 2. Fractional positional parameters and anisotropic temperature factors ($\times10^4$) of non-hydrogen atoms with their estimated standard deviations in parentheses

Temperature factors are of the form: $\exp[-(h^2B_{11}+k^2B_{22}+l^2B_{33}+2hkB_{12}+2hlB_{13}+2klB_{23})]$.

Atom	x	y	z	B_{11}	B_{22}	B_{33}	B_{12}	B_{13}	B_{23}
Br	2596(1)	2590(1)	4511(1)	175(1)	140(1)	104(1)	19(1)	87(1)	−13(1)
Cu	1268(1)	4898(1)	4751(1)	101(1)	103(1)	50.0(5)	6(1)	41(1)	8(1)
S	1556(2)	6772(2)	3657(1)	169(3)	156(3)	49(1)	−20(2)	58(1)	1(1)
O	−470(5)	6264(6)	4474(4)	120(7)	140(8)	69(3)	37(6)	58(4)	42(5)
N	3137(7)	6508(8)	6065(4)	130(9)	153(10)	51(3)	−14(8)	41(5)	−15(5)
C(1)	−760(15)	7823(14)	3987(11)	331(26)	240(20)	196(14)	158(19)	205(17)	139(14)
C(2)	28(10)	8212(13)	3442(7)	151(13)	253(19)	78(6)	21(13)	56(7)	56(9)
C(3)	3216(10)	7874(9)	4585(7)	148(12)	123(11)	95(6)	−7(10)	73(7)	19(7)
C(4)	3328(9)	8096(9)	5636(6)	148(12)	131(12)	76(5)	−5(10)	51(7)	−13(7)
C(5)	2621(12)	6894(15)	6803(6)	230(17)	328(23)	55(5)	−68(16)	73(8)	−61(9)
C(6)	4577(11)	5594(12)	6552(7)	153(13)	207(16)	71(6)	18(12)	9(7)	5(8)

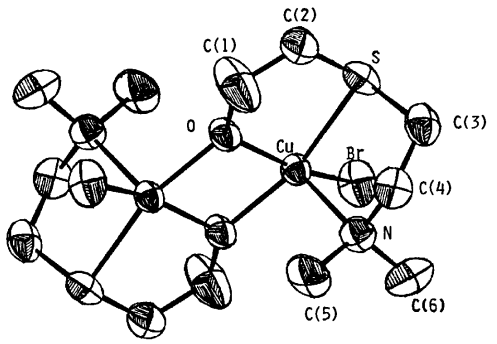

Fig. 1. Molecular structure of $Cu(CH_3\text{-nso})Br$ with thermal ellipsoids.

Table 3. Interatomic distances (l/Å) and bond angles (φ/°) with their estimated standard deviations in parentheses

Symmetry code superscript			
None	x	y	z
i	$-x$	$1-y$	$1-z$
ii	$1-x$	$1-y$	$1-z$
iii	x	$y-1$	z
iv	$-x$	$y-1/2$	$1/2-z$

(a) Copper coordination spheres

Cu···Cu^{i}	3.004(2)	Cu–O	1.930(5)
Cu–Br	2.385(1)	Cu–O^{i}	1.929(6)
Cu–S	2.316(2)	Cu–N	2.334(6)
Cu–O–Cu^{i}	102.2(2)	S–Cu–O	84.7(2)
Br–Cu–S	96.2(1)	S–Cu–N	85.4(2)
Br–Cu–O	156.0(1)	S–Cu–O^{i}	162.4(2)
Br–Cu–O^{i}	99.1(2)	O–Cu–O^{i}	77.8(2)
Br–Cu–N	104.5(2)	O–Cu–N	99.5(2)
O^{i}–Cu–N	99.2(2)		

(b) Ligand moiety

O–C(1)	1.382(13)	C(3)–C(4)	1.524(15)
C(1)–C(2)	1.418(23)	N–C(4)	1.457(11)
S–C(2)	1.818(10)	N–C(5)	1.457(15)
S–C(3)	1.803(8)	N–C(6)	1.467(11)
Cu–O–C(1)	123.1(9)	C(3)–C(4)–N	113.1(6)
Cu^{i}–O–C(1)	133.6(9)	Cu–N–C(4)	108.8(4)
O–C(1)–C(2)	117.1(12)	Cu–N–C(5)	107.7(5)
C(1)–C(2)–S	115.6(7)	Cu–N–C(6)	111.2(5)
C(2)–S–Cu	97.7(4)	C(4)–N–C(5)	108.9(7)
Cu–S–C(3)	98.8(3)	C(4)–N–C(6)	109.0(7)
C(2)–S–C(3)	103.7(4)	C(5)–N–C(6)	111.2(7)
S–C(3)–C(4)	115.0(7)		

(c) Intercluster distances

Br···Cu^{ii}	6.097(3)	Cu···Cu^{ii}	7.236(2)
Br···Cu^{iv}	6.012(7)	Cu···Cu^{iv}	7.098(4)
Cu···S^{iv}	5.097(5)		

inversion center. The Cu–S bond length (2.316(2) Å) is almost equal to the sum of the covalent-bond radii (2.32 Å) given by Pauling.[20] This distance is rather short for the copper(II)-thioether sulfur bond length.[21–27] In the present complex the thioether donor atom is placed at the inner coordination position of the tridentate ligand, so that, upon complexation, the coordination of sulfur atom is facilitated by the chelate effect. The Cu–Br bond length (2.385(1) Å) is slightly shorter than the sum of the covalent-bond radii (2.42 Å),[20] but is comparable to those found in bromo [2-(dialkylamino)ethanolato]copper(II) (2.239—2.395 Å).[28–32]

The coordination geometry around the copper ion is intermediate between a trigonal bipyramid and a square pyramid. Viewing the structure as a square pyramid, nitrogen atom occupies the apical position, and Br, S, O, and O^{i} atoms form a basal plane. On the stand point of regarding the coordination geometry as a trigonal bipyramid, Br, O, and N define the equatorial plane of the molecule. Least-squares planes with the deviations of the atoms from the planes are given in Table 4. The degree of distortion of coordination geometry from either of the limiting structures can be estimated by the bond angle Br–Cu–O. For a regular trigonal bipyramid this angle should be 120°, whereas for a square pyramid the angle should be 180°. In this complex this angle is 156.0(1)°, showing that the coordination geometry is slightly close to the latter rather than the former. In square pyramid copper(II)

Table 4. Deviations of the atoms from least-squares planes (l/Å) and dihedral angles between them (φ/°)

(I) Plane through Cu, O, Cu^{i}, O^{i}
$0.2078X+0.5701Y+0.5965Z=6.6813$[a]
[Cu 0.000, O 0.000, Cu^{i} 0.000, O^{i} 0.000, Br −0.967, S −0.072, N 2.282, C(1) 0.204, C(2) 0.061, C(3) 1.596, C(4) 2.653, C(5) 3.002, C(6) 2.608][b]

(II) Plane through Cu, S, O
$0.2247X+0.5886Y+0.5723Z=6.6032$
[Cu 0.000, S 0.000, O 0.000, Br −0.970, N 2.290, C(1) 0.239, C(2) 0.135, C(3) 1.679, C(4) 2.703, C(5) 2.980, C(6) 2.610]

(III) Plane through Cu, S, N
$0.8041X-0.5945Y-0.3934Z=-4.0380$
[Cu 0.000, S 0.000, N 0.000, Br 2.300, O −1.892, C(1) −2.571, C(2) −1.792, C(3) 0.294, C(4) −0.335, C(5) −1.032, C(6) 1.315]

(IV) Plane through Br, O, N
$0.5130X+0.5361Y-0.8346Z=-3.1672$
[Br 0.000, O 0.000, N 0.000, Cu −0.015, S 2.283, O^{i} −1.884, C(1) 1.112, C(2) 2.362, C(3) 2.456, C(4) 1.301, C(5) −1.022, C(6) −0.242]

(V) Plane through Br, S, O, O^{i}
$0.4003X+0.4117Y+0.5246Z=5.5356$
[Br −0.120, S 0.144, O −0.204, O^{i} 0.181, Cu 0.275, N 2.581, C(1) −0.199, C(2) −0.178, C(3) 1.899, C(4) 2.837, C(5) 3.073, C(6) 3.249]

Dihedral angles between the planes (φ/°)

(I) and (II)	1.8	(II) and (III)	100.1
(I) and (III)	100.2	(II) and (IV)	95.2
(I) and (IV)	96.9	(III) and (IV)	84.3

a) The equation of the plane is expressed as $LX+MY+NZ=D$, where X, Y, and Z are in Å units referred to the crystallographic axes. b) Deviations (l/Å) of atoms from the planes are listed in square brackets. Superscripts are defined as in Table 3.

complexes, the apical bonds are generally longer than basal ones.[33] The Cu–Br, Cu–S, Cu–O, and Cu–O^{i} bond legnths are in the range of those of the normal in-plane coordination, while the Cu–N bond length (2.334(6) Å) is significantly longer than values of a normal in-plane coordination. From these facts the geometry around the copper ion is best described as a distorted square pyramid.

Bond lengths of the ligand have normal values except for the O–C(1) and C(1)–C(2) distances. The O–C(1) (1.382(13) Å) and C(1)–C(2) (1.418(23) Å) bond lengths are shorter than the corresponding O–C and C–C distances observed in other alkoxo-bridged copper(II) complexes, respectively.[28–32,34–37] This is attributable to the large values of anisotropic thermal parameters for C(1). The thermal ellipsoid for C(1) (Fig. 1) gives strong indication of either disorder or large vibration approximately normal to the coordination plane. This is probably due to the strain of two adjacent five-membered chelate rings. The carbon atoms of the ethylene group, C(1) and C(2), are located above the plane through Cu, S, and O by 0.239 and 0.135 Å, respectively. Another five-membered chelate ring, Cu–S–C(3)–C(4)–N, assumes the usual gauche conformation, and C(3) and C(4) deviate from the plane through Cu, S, and N by 0.294 and −0.335 Å, respectively.

The bond angles around the nitrogen atom (Cu–N–C(4) 108.8(4), Cu–N–C(5) 107.7(5), Cu–N–C(6) 111.2(5), C(4)–N–C(5) 108.9(7), C(4)–N–C(6) 109.0(7), C(5)–N–C(6) 111.2(7)°) are close to that for a regular tetrahedron, whereas the bond angles around the sulfur atom (Cu–S–C(2) 97.7(4), Cu–S–C(3) 98.8(3), C(2)–S–C(3) 103.7(4)°) are considerably less than those around the nitrogen atom.

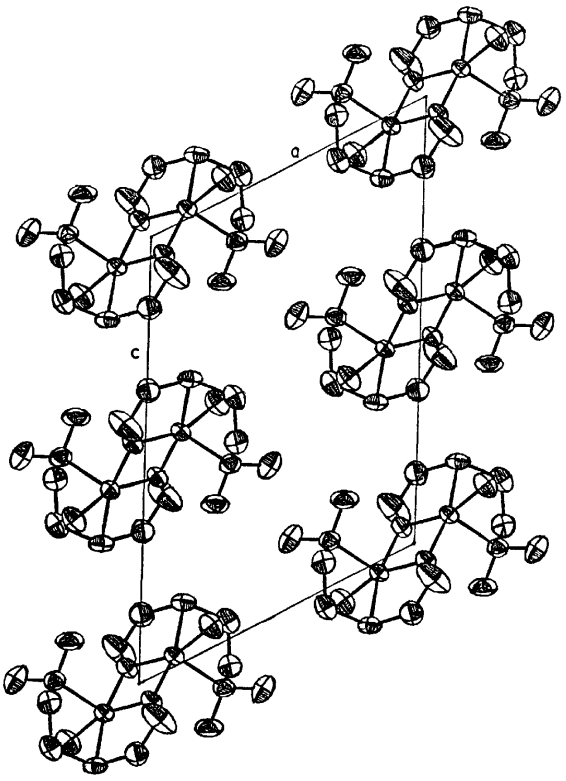

Fig. 2. A view of the packing along the b axis.

The molecular packing in the unit cell is shown in Fig. 2. As is evident from the packing diagram and the distances between the binuclear clusters (Table 3), the complex consists of discrete dimeric units.

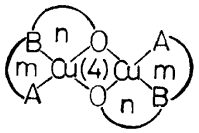

6-6-(4)-6-6

5-6-(4)-6-5 ≫ 5-5-(4)-5-5

6-5-(4)-5-6

Fig. 3. The fused chelate ring system of alkoxo-bridged copper(II) complexes.

As shown in Fig. 3, the fused chelate ring system of a binuclear copper(II) complex with amino alcohol is expressed with m–n–(4)–n–m. It is known that for the formation of the binuclear copper(II) complexes the favorable chelate ring system is 6–6–(4)–6–6 and 5–6–(4)–6–5 fused chelate ring systems.[38] The binuclear cluster consisting of 6–5–(4)–5–6 fused chelate ring system may be stable in some cases,[37,39] but it often forms a stable tetranuclear cubane structure.[34,40–44] On the other hand, it has been believed that the 5–5–(4)–5–5 fused chelate ring system is unfavorable in forming a binuclear structure, since no stable binuclear copper(II) complex containing such a fused chelate ring system has been isolated so far.[38,45–49] However, the present X-ray crystal structure analysis showed that the binuclear units containing a 5–5–(4)–5–5 fused chelate ring system exist in the crystal. This complex is the first example of such a binuclear copper(II) complex. The moderate stability of the binuclear structure can be ascribed to the "small bond angle" and the "large radius" of the sulfur atom.

Infrared Spectra. The OH stretching vibration band at ≈3350 cm^{-1} observed for the free ligands is absent in the spectra of the copper(II) complexes. This indicates that the alcoholic proton is lost upon complexation. In the case of the nitrates, Cu(R-nso)NO_3, strong bands appear at 1280—1295, 1375—1410, and 1455—1480 cm^{-1} and a sharp band at 810 cm^{-1}, which are indicative of monodentate nitrate coordination.[50]

Electronic Spectra. The band maxima of the diffuse reflectance spectra and the electronic absorption spectra in 1,2-dichloroethane solutions are given in Table 5. The band around 12.5×10^3 cm^{-1} is undoubtedly assigned to a d-d transition. Judging from the band shape and position, five-coordinate copper environment is assumed.[51] The infrared spectra of Cu(R-nso)NO_3 are consistent with this view. Moreover, the X-ray crystal structure analysis of Cu(CH_3-nso)Br confirms the five-coordinate copper(II) dimer. The position of the d-d band does not vary significantly with changing the anion X. The band at 22.3—26.2×

TABLE 5. BAND MAXIMA ($\tilde{\nu}_{max}$) OF ELECTRONIC SPECTRA OF Cu(R-nso)X·nH$_2$O

Complex R	X	n	Reflectance spectra $\tilde{\nu}_{max}/10^3$ cm^{-1}			Absorption spectra (in 1,2-dichloroethane) $\tilde{\nu}_{max}/10^3$ cm^{-1} (ε)				
CH_3	Br	0		12.1	22.4	12.2(160)	22.9(1730)	29.6sh(3090)	33.9(4480)	
C_2H_5	Br	0		12.4	22.5	12.8(153)	22.7(1850)	29.6sh(2910)	34.0(4460)	
n-C_3H_7	Br	0		12.2	22.4	13.2(159)	22.6(2090)	29.6sh(2750)	34.0(4260)	
n-C_4H_9	Br	0		12.1	22.3	13.2(142)	22.6(1940)	29.4sh(2600)	34.0(4160)	
CH_3	Cl	0		12.6	23.5	12.4(108)	24.1(1610)	31.4(3410)		37.9(3830)
C_2H_5	Cl	0		12.2	23.8	13.2(102)	23.9(1420)	31.8(2430)		37.7(2950)
n-C_3H_7	Cl	0		12.6	23.5	13.6(137)	23.9(1230)	31.7(2440)		37.7(2900)
n-C_4H_9	Cl	0		12.5	23.8	13.6(96)	23.8(1580)	31.8(3320)		37.6(4070)
CH_3	NO_3	1/2	8.9sh	12.9	26.1sh	13.4(96)	26.2(1020)		32.9(3230)	
C_2H_5	NO_3	1/2	8.7sh	13.0	26.2sh					
n-C_3H_7	NO_3	0	9.1sh	12.8	26.0sh					
n-C_4H_9	NO_3	0	8.7sh	12.8	25.6sh					

a) sh=shoulder.

10^3 cm^{-1} should correspond to the band observed at 24—25$\times10^3$ cm^{-1} for Cu(R-sno)X,[1,7] and is assigned to the p_π(O)→d(Cu) charge transfer transition. This charge transfer band of Cu(R-nso)X shifts to a lower frequency with the change of X in the order NO_3>Cl>Br. Assuming that the nonbonding p_π electron on alkoxide oxygen varies little in energy, the charge transfer band reflects the optical electronegativity of the copper ion. Since optical electronegativity of a metal increases when a donor atom is replaced with a more softer one, the optical electronegativity of the copper ion for Cu(R-nso)X should increase in the order of X=NO_3<Cl<Br. The p_π(O)→d(Cu) transition observed for Cu(R-nso)X is compatible with this expectation. The absorption around 30×10^3 cm^{-1} may be assigned to the σ(S)→d(Cu) charge transfer transition.[52-54] The ultraviolet absorptions ($\approx34\times10^3$ cm^{-1}) of Cu(R-nso)Br fall in the range for either the Br→d(Cu) or the σ(N)→d(Cu) transition. The absorption at 38×10^3 cm^{-1} of Cu(R-nso)Cl may be assigned to a superposition of the Cl→d(Cu) and the σ(N)→d(Cu) transitions.[52-56]

Magnetic Susceptibilities. The magnetic susceptibilities were measured over the temperature range 80—300 K. The magnetic moments per copper atom are subnormal at room temperature and decrease with lowering of temperature, indicating the existence of an antiferromagnetic spin-exchange interaction (Table 6). The temperature dependence of magnetic susceptibility for Cu(n-C_4H_9-nso)Cl is shown in Fig. 4. The small increase in the magnetic susceptibility at low temperature is most likely due to a small amount of mononuclear paramagnetic impurity. Accordingly, the impurity term was added to the Bleaney-Bowers equation[57] giving,

$$\chi_A = \frac{Ng^2\beta^2}{3kT}\left[1+\frac{1}{3}\exp(-2J/kT)\right]^{-1}(1-p) + \frac{0.45p}{T} + N\alpha, \quad (1)$$

where χ_A is susceptibility per copper atom, p is the

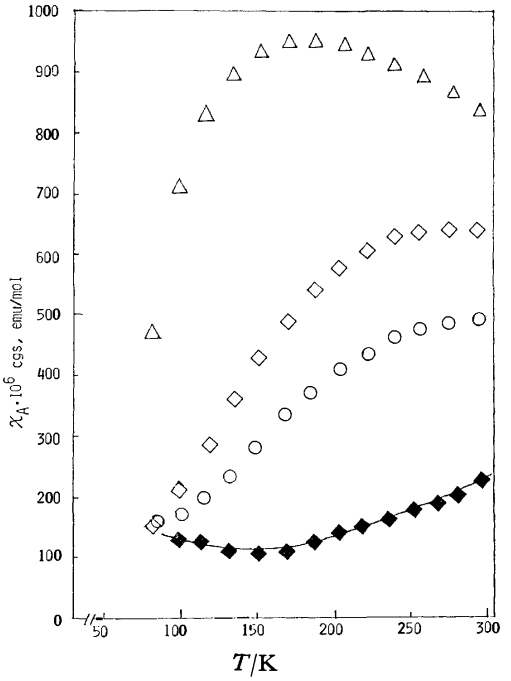

Fig. 4. Temperature dependence of magnetic susceptibilities of Cu(CH_3-nso)Br (○), Cu(CH_3-nso)Cl (◇), Cu(n-C_3H_7-nso)NO_3 (△), Cu(n-C_4H_9-nso)Cl (◆). The solid curve was calculated from Eq. 1.

TABLE 6. MAGNETIC DATA OF Cu(R-nso)X·nH$_2$O

Complex R	X	n	μ_{eff}/B.M. (T/K)	
CH_3	Br	0	1.01(294)	0.26(85)
C_2H_5	Br	0	0.84(299)	0.22(83)
n-C_3H_7	Br	0	1.25(294)	0.38(86)
n-C_4H_9	Br	0	1.17(294)	0.19(83)
CH_3	Cl	0	1.16(293)	0.25(82)
C_2H_5	Cl	0	1.07(295)	0.17(83)
n-C_3H_7	Cl	0	1.27(295)	0.66(83)
n-C_4H_9	Cl	0	0.63(297)	0.24(85)
CH_3	NO_3	1/2	1.19(296)	0.45(83)
C_2H_5	NO_3	1/2	1.00(291)	0.35(83)
n-C_3H_7	NO_3	0	1.35(294)	0.52(84)
n-C_4H_9	NO_3	0	1.50(297)	1.06(84)

ratio of mononuclear copper(II) ions to total copper(II) ions, and N, g, J, β, and $N\alpha$ have the usual meanings.[58] The $-2J$, g, $N\alpha$, and p values obtained by the best fit of the susceptibility data to Eq. 1 are 735 cm^{-1}, 2.10, 60×10^{-6} cgs emu/mol, and 0.015, respectively. The $-2J$ value, the energy separation between the spin-singlet ground state and the lowest spin-triplet state, is comparable to those of Cu(R-sno)X,[1,7] indicating that a strong antiferromagnetic interaction is operating between the copper(II) ions. However, the temperature dependence of magnetic susceptibilities of Cu(R-nso)X (R=CH_3, C_2H_5, n-C_3H_7, n-C_4H_9; X=Br, Cl, NO_3) except for Cu(n-C_4H_3-nso)Cl can not be interpreted by the equation based on a binuclear structure, in spite of the present X-ray result that Cu(CH_3-nso)Br consists of discrete binuclear clusters. Some of the examples are shown in Fig. 4. Therefore, it seems to be difficult to explain the magnetic behavior only in terms of the crystal structure obtained here. For the reasonable explanation, one should notice the crystal structure is not always independent of temperature. A remarkable variation in the coordination sphere around the copper atom may take place at low temperature, and this may cause the deviation of the χ_A-T curve from the theoretical one.

The authors wish to express sincere thanks to Prof's. Ikuhiko Ueda and Shigeaki Kawano of Kyushu University for their helpful advices and discussions. The present work was partially supported by a Grant-in-Aid for Scientific Research No. 454199 from the Ministry of Education, Science and Culture.

References

1) Part XXXII. M. Mikuriya, H. Okawa, and S. Kida, *Inorg. Chim. Acta*, **42**, 233 (1980).
2) J. A. Fee, *Struct. Bonding*, **23**, 1 (1975).
3) M. A. Ali, S. E. Livingstone, and D. J. Phillips, *Inorg. Chim. Acta*, **7**, 179 (1973).
4) M. A. Ali, S. E. Livingstone, and D. J. Phillips, *Inorg. Chim. Acta*, **7**, 531 (1973).
5) W. D. McFadyen, R. Robson, and H. Schapp, *Inorg. Chem.*, **11**, 1777 (1972).
6) W. D. McFadyen and R. Robson, *J. Coord. Chem.*, **5**, 49 (1976).
7) M. Mikuriya, H. Okawa, and S. Kida, *Inorg. Chim. Acta*, **34**, 13 (1979).
8) G. S. Patterson and R. H. Holm, *Bioinorg. Chem.*, **4**, 257 (1975).
9) D. S. Breslow, R. S. Yost, H. G. Walker, and C. R. Hauser, *J. Am. Chem. Soc.*, **66**, 1921 (1944).
10) R. O. Clinton, C. M. Suter, S. C. Laskowski, M. Jackman, and W. Huber, *J. Am. Chem. Soc.*, **67**, 594 (1945).
11) N. F. Curtis, *J. Chem. Soc.*, **1961**, 3147.
12) F. E. Mabbs and D. J. Machin, "Magnetism and Transition Metal Complexes," Chapman and Hall, London (1973).
13) B. N. Figgis and R. L. Martin, *J. Chem. Soc.*, **1959**, 1359.
14) "International Tables for X-Ray Crystallography," Kynoch Press, Birmingham (1967), Vol. II.
15) D. W. J. Cruickshank, "Computing Methods in Crystallography," ed by J. S. Rollet, Pergamon Press, Oxford (1965).
16) "International Tables for X-Ray Crystallography," Kynoch Press, Birmingham (1974), Vol. IV.
17) R. F. Stewart, E. R. Davidson, and W. T. Simpson, *J. Chem. Phys.*, **42**, 3175 (1965).
18) T. Sakurai, H. Iwasaki, Y. Watanabe, K. Kobayashi, Y. Bando, and Y. Nakamichi, *Rep. Inst. Phys. Chem. Res.*, **50**, 75 (1972).
19) C. K. Johnson, Reprt No. 3794, Oak Ridge National Laboratory, Oak Ridge, Tennessee (1965).
20) L. Pauling, "The Nature of the Chemical Bond," Cornell University Press, Ithaca, (1960).
21) J. Coetzer, *Acta Crystallogr.*, **26**, 1414 (1970).
22) A. Mangia, M. Nardelli, C. Pelizzi, and G. Pelizzi, *J. Cryst. Mol. Struct.*, **1**, 139 (1971).
23) A. C. Braithwaite, C. E. F. Rickard, and T. N. Waters, *J. Chem. Soc., Dalton Trans.*, **1975**, 1817.
24) C. C. Ou, V. M. Miskowski, R. A. Lalancette, J. A. Potenza, and H. J. Schugar, *Inorg. Chem.*, **15**, 3157 (1976).
25) E. N. Baker and G. E. Norris, *J. Chem. Soc., Dalton Trans.*, **1977**, 877.
26) D. P. Freyberg, G. M. Mockler, and E. Sinn, *Inorg. Chem.*, **16**, 1660 (1977).
27) J. F. Richardson and N. C. Payne, *Inorg. Chem.*, **17**, 2111 (1978).
28) A. Pajunen and M. Lehtonen, *Suom. Kemistil., B*, **44**, 200 (1971).
29) W. Haase, *Chem. Ber.*, **106**, 3132 (1973).
30) R. Mergehenn and W. Haase, *Z. Naturforsch., Teil B*, **30**, 155 (1975).
31) R. Mergehenn, L. Merz, and W. Haase, *Z. Naturforsch., Teil B*, **30**, 14 (1975).
32) R. Mergehenn, W. Haase, and R. Allmann, *Acta Crystallogr., Sect. B*, **31**, 1847 (1975).
33) B. J. Hathaway, *Struct. Bonding*, **14**, 49 (1973).
34) J. A. Bertrand and J. A. Kelley, *Inorg. Chim. Acta*, **4**, 203 (1970).
35) L. Merz and W. Haase, *Acta Crystallogr., Sect. B*, **34**, 2128 (1978).
36) A. C. Villa, L. Coghi, A. G. Manfredotti, and C. Guastini, *Cryst. Struct. Commun.*, **3**, 543 (1974).
37) N. Matsumoto, S. Kida, and I. Ueda, *J. Coord. Chem.*, **9**, 133 (1979).
38) Y. Ishimura, Y. Nonaka, Y. Nishida, and S. Kida, *Bull. Chem. Soc. Jpn.*, **46**, 3728 (1973).
39) Y. Nishida, F. Numata, and S. Kida, *Inorg. Chim. Acta*, **11**, 189 (1974).
40) A. Pajunen and K. Nieminen, *Finn. Chem. Lett.*, **1975**, 67.
41) K. Nieminen, *Acta Chem. Scand. A*, **31**, 693 (1977).
42) K. Nieminen and A. Pajunen, *Acta Chem. Scand. A*, **32**, 493 (1978).
43) K. Nieminen, *Acta Chem. Scand. A*, **33**, 375 (1979).
44) A. Pajunen, *Acta Crystallogr., Sect. B*, **35**, 1691 (1979).
45) M. Kato, Y. Muto, H. B. Jonassen, K. Imai, and A. Harano, *Bull. Chem. Soc. Jpn.*, **41**, 1864 (1968).
46) A. Nakahara, I. Miyachi, and T. Kohno, *Bull. Chem. Soc. Jpn.*, **42**, 573 (1969).
47) K. Yamada and H. Ojima, *Nippon Kagaku Zasshi*, **91**, 460 (1970).
48) K. Nonoyama and H. Ojima, *Nippon Kagaku Zasshi*, **92**, 612 (1971).
49) H. Ojima and K. Yamada, *Z. Anorg. Allg. Chem.*, **379**, 322 (1970).
50) N. F. Curtis and Y. M. Curtis, *Inorg. Chem.*, **4**, 804 (1965).
51) M. Ciampolini, *Struct. Bonding*, **6**, 52 (1969).
52) V. M. Miskowski, J. A. Thich, R. Solomon, and H. J.

Schugar, *J. Am. Chem. Soc.*, **98**, 8344 (1976).
53) A. R. Amundsen, J. Whelan, and B. Bosnich, *J. Am. Chem. Soc.*, **99**, 6730 (1977).
54) A. C. Braithwaite, C. E. F. Rickard, and R. N. Waters, *Inorg. Chim. Acta*, **26**, 63 (1978).
55) H. Yokoi and T. Isobe, *Bull. Chem. Soc. Jpn.*, **42**, 2187 (1969).
56) B. P. Kennedy and A. B. P. Lever, *J. Am. Chem. Soc.*, **95**, 6907 (1973).
57) B. Bleaney and K. D. Bowers, *Proc. R. Soc. London, Ser. A*, **214**, 451 (1952).
58) K. E. Hyde, G. Gordon, G. F. Kokoszka, *J. Inorg. Nucl. Chem.*, **30**, 2155 (1968).

Enrichment and Spectrophotometric Determination of a Trace Amount of Chromium(VI) as the Diphenylcarbazide Complex on a Mixed Resin Prepared from Finely Divided Anion and Cation Exchangers

Kunio Ohzeki, Toshiaki Sakuma, and Tomihito Kambara*
Department of Chemistry, Faculty of Science, Hokkaido University, Sapporo 060
(Received April 15, 1980)

A rapid and sensitive method has been developed for the determination of a trace amount of chromium(VI). It is based on the pre-concentration of chromium(VI) as the diphenylcarbazide (DPC) complex on a mixed resin prepared from finely divided anion and cation exchangers and the subsequent measurement of absorbance of the resin phase after collection on a filter paper as a uniform thin layer. The sensitivity of the method is approximately 100 times higher than the ordinary solution method using 1-cm cell. The extraction of chromium(VI) with tributyl phosphate followed by back extraction into water is effective for reducing the influence of interfering ions.

Analytical utilization of a resin mixture of finely divided anion and cation exchangers, the diameter being smaller than 30 μm, has been reported. Rapid and selective enrichment of trace amounts of copper(II)[1] and manganese(II)[2] on the mixed resin were carried out by batch method in the presence of 8-hydroxy-5-quinolinesulfonate and 4-(2-pyridylazo)resorcinol, respectively. The ions on the resin were then eluted and determined by atomic absorption spectrometry.

Yoshimura *et al.* reported ion-exchanger colorimetry[3,4] based on the pre-concentration of metal complex with negative or positive charge on respective ion exchanger ranging 200—400 mesh, and the subsequent measurement of the absorbance of the complex in the resin phase after transferring a part of the resin into a cell of 0.1 cm in thickness. The method has been successfully applied to the determination of chromium[5] and zinc[6] in water.

This article deals with a new method of ion-exchanger colorimetry[7] for chromium(VI) by means of the combined use of DPC and a mixture of finely divided anion and cation exchangers. Finely divided cation exchanger collects chromium(VI)–DPC complex rapidly by the batch method in combination with anion exchanger to form a bulky material. The coagulated resin is then separated by filtration and the resulting thin layer of the colored resin on a filter paper is directly subjected to spectrophotometric measurement.

Experimental

Reagents. A stock solution of chromium(VI) (0.5 mg/ml) was prepared by dissolving 1.415 g of analytical grade potassium dichromate in one liter of water. The solution was diluted to give 0.1 μg per ml of chromium(VI) immediately before use.

Diphenylcarbazide was used in a 0.4 (w/v)% acetone–water (1 : 1) solution, a fresh solution being made each day.

Synthetic sea water was prepared according to JIS K 2510-1971.[8]

Tributyl phosphate (TBP) saturated with 0.1 M (1 M=1 mol dm^{-3}) hydrochloric acid was used. A 150-ml portion of the ester was shaken with 50 ml of the synthetic sea water containing 0.1 M hydrochloric acid.

Ion Exchange Resin. Macroreticular type Amberlyst 15 and A-26 (both Rohm and Haas Co.) in RSO_3H and $RN(CH_3)_3Cl$ forms, respectively, were used. Suspension of the resins was prepared according to the method reported.[1] The stock suspension was stirred immediately before being pipetted off.

General Procedure. A 100-ml aliquot of the solution containing less than 1.0 μg of chromium(VI) was taken into a separatory funnel, and then 10 ml of 0.1 M sulfuric acid, 3.0 ml of anionic resin suspension (ARS), 1.0 ml of cationic resin suspension (CRS) and finally 1.0 ml of 0.4% DPC solution were added. The mixture was then shaken for 12 min and the resulting coagulated material was collected onto a filter paper (Toyo Roshi No. 5A) placed on a holder. A disk of colored resin of 17 mm diameter and about 0.3 mm in thickness was obtained. The filter strip was dipped into a dilute acetate buffer solution of pH 4.8 for 10 s in order to stabilize the coloration. Another disk of resin was prepared without addition of chromium(VI) and used as a reference. The filter strips were fixed on the glass plate and the absorbances were measured at 550 and 700 nm, the absorption maximum lying at the former wavelength and the complex having no absorption at the latter. The net absorbance was obtained by the difference.

Results and Discussion

Determination of Exchange Capacity. The ion exchange capacity of the resin in the suspension was determined by conductometric titration. A known amount of CRS and ARS was titrated with the standard solution of sodium hydroxide and silver nitrate, respectively. In both cases inverse L-shaped titration curves were obtained. The exchange capacities were 13.3×10^{-3} meq ml^{-1} for CRS and 7.22×10^{-3} meq ml^{-1} for ARS.

Coagulation. The mutual coagulation of the finely divided anion and cation exchangers was examined according to the method reported.[1] The 1.0-ml portion of CRS was most satisfactorily deposited from the solution with addition of 3.0 ml of ARS.

Exchange Capacity of the Coagulated Resin. The number of ion exchange sites consumed for the association of 3.0 ml of CRS with 9.0 ml of ARS was estimated by determining the hydrogen ion expelled from the cationic exchanger as a result of mutual coagulation. The proportions of the ion exchange sites taking part in coagulation to the total ion exchange sites in CRS and ARS were found to be 11.8% and 14.1%, respectively. The remaining sites are effective to fix cation

or anion in the solution.

Shaking Time. During the course of shaking, the cationic chromium(VI)–DPC complex is fixed on the cationic exchanger, the latter combining with anionic exchanger to form coagulated material. A constant and maximum recovery was achieved in the shaking period of 12—16 min. With prolonged shaking, the absorbance decreased slightly.

Preparation of Thin Layer. The colored coagulated material was collected onto a filter paper placed on a holder and washed with a small amount of water. The rate of filtration was about 40 ml min^{-1} with suction. At the end of washing, the suction should be stopped in order to avoid the formation of cracks in the resin phase.

Stability of the Coloration. The resin was stored wet by dipping the end of filter paper in water. The absorbance of the complex was reduced by *ca.* 4% after 30 min. When the resin was soaked for 10 s in a dilute acetate buffer solution immediately after filtration, the coloration being stable at least for 30 min. However, in the presence of a large amount of magnesium the color based on magnesium–DPC complex developed after long immersion in the acetate buffer solution. The absorbance should be measured as soon as possible.

Absorption Measurement. The thin layers of sample and reference together with filter paper were fixed with water on a glass plate fitted directly to the window of detector. The absorbance was measured with the slit width of 2.5 mm. The chromium(VI)–DPC complex in the resin phase has the absorption maximum at 550 nm. The absorbance is given by

$$A = A_{RC} + (A_{B,s} - A_{B,r}),$$

where A_{RC} denotes the absorbance of the complex in the resin phase and $A_{B,s}$ and $A_{B,r}$ denote the background absorption of the sample and reference, respectively, which are caused by the resin phase, the filter paper and the glass plate. The difference in the background absorption is estimated from the absorbance at 700 nm where the complex has no absorption. Consequently, the net absorbance of chromium(VI)–DPC complex is given by the difference in measurement at 500 nm and 700 nm.

Calibration Curve. The calibration curve deviates slightly from proportionality (Fig. 1). The relative standard deviation was 2.1% (n=6) for 1 μg of chromium(VI) and 3.3% (n=5) for 0.4 μg. The absorbance of thin layer prepared from the 100 ml of solution containing 1 μg chromium(VI) is almost the same as that for 1 ppm chromium(VI)–DPC solution in 1-cm cell. The sensitivity of the present method is approximately 100 times higher than the ordinary solution method.[9]

Sample Volume. A 1-μg portion of chromium(VI) was recovered effectively from 100—400 ml of sample solution (Fig. 2). The lower absorbance was measured with a disk prepared from 50 ml of sample solution, the reason for which is not yet clear but the result was reproducible.

Divers Ions. Effects of sodium chloride and calcium chloride examined are shown in Fig. 3. The recovery of chromium(VI)–DPC complex decreased considerably with the addition of calcium chloride, which is attributable to the competition between cations of chromium(VI)–DPC complex and calcium ion for cation exchange sites in the mixed resin. The effects of other cations are given in Table 1. Chromium-

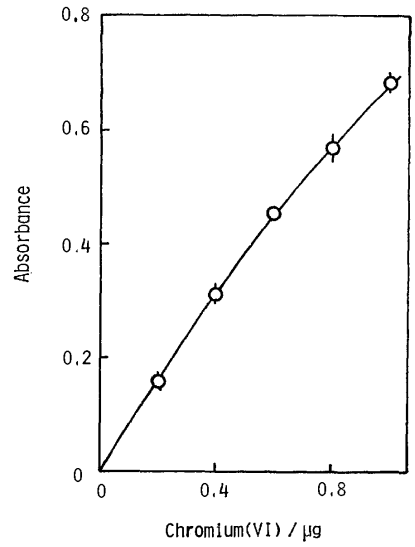

Fig. 1. Calibration curve of chromium(VI) as the complex with diphenylcarbazide. Sample volume: 100 ml. The vertical line on each plot denotes 95% confidence interval.

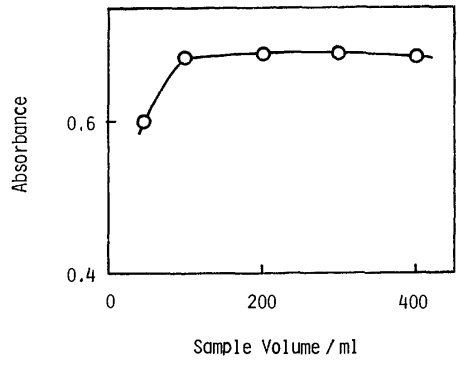

Fig. 2. The recovery of 1-μg portion of chromium(VI) from varying amounts of solution onto a coagulated resin prepared from 3.0 ml of ARS and 1.0 ml of CRS.

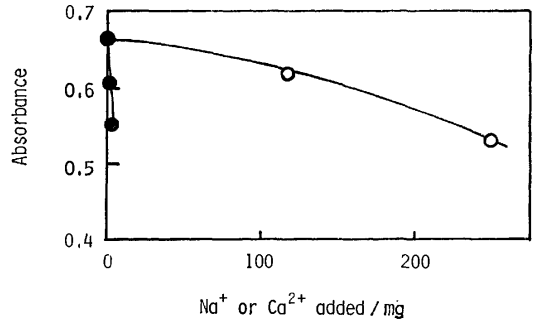

Fig. 3. Effect of sodium (○) and calcium (●) ions on the recovery of chromium(VI)–DPC complex onto a coagulated resin prepared from 3.0 ml of ARS and 1.0 ml of CRS. Amount of chromium(VI): 1.0 μg.

Table 1. Effect of foreign ions

Ions	Added as	Ratio to 0.5 μg of chromium(VI)[a]		
		40	200	400
		Relative error (%)		
Fe(III)	nitrate	−6.4	−14.5	−17.4
Cu(II)	sulfate	−8.2	−14.2	−18.6
Al(III)	nitrate	+6.8	−1.5	−11.8
Zn(II)	chloride	+7.0	+3.6	+9.4
Pb(II)	acetate	+3.1	+8.0	+9.4
Cd(II)	nitrate	+6.3	+11.6	+3.4
Cr(III)	chloride	+6.5	+14.7	+15.9

a) Sample amount: 100 ml

Table 2. Recovery of chromium(VI) from synthetic sample solution

Composition	Absorbance	r.s.d.(n) (%)	Recovery[a] (%)
A: 100 ml of saline water[b]	0.000		0.0
B: A+Cr(VI) 0.4 μg	0.298	3.1(2)	96.2
C: A+Cr(VI) 0.5 μg	0.361	3.5(4)	94.9
D: A+Cr(VI) 0.6 μg	0.428	2.0(2)	94.8
E: A+Cr(VI) 0.8 μg	0.543	1.0(3)	95.6
F: C+Cr(III) 100 μg+ Zn(II) 100 μg +Al(III) 100 μg+ Pb(II) 100 μg +Cd(II) 100 μg	0.375	4.8(8)	98.6
G: F+Fe(III) 50 μg+ Cu(II) 20 μg	0.348	3.7(5)	91.5

a) Calculated from the calibration curve in Fig. 1.
b) The sample was prepared according to JIS K 2510-1971. The components (g/l) were: NaCl 24.54, $MgCl_2 \cdot 6H_2O$ 11.10, Na_2SO_4 4.09, $CaCl_2$ 1.16, KCl 0.69, $NaHCO_3$ 0.20, KBr 0.10, H_3BO_3 0.03, $SrCl_2 \cdot 6H_2O$ 0.04, NaF 0.003.

(III), cadmium(II), lead(II), and zinc(II) have a tendency to give a positive error, iron(III), copper(II), and aluminum(III) a negative error.

Extraction of Chromium(VI) with TBP. The extraction of chromium(VI) with tributyl phosphate[10,11] was examined with synthetic sea water. General procedure is as follows: A 100-ml portion of the synthetic sea water containing less than 1 μg of chromium(VI) was mixed with 5 ml of 2 M hydrochloric acid. The solution was then shaken with 20 ml of TBP for about 3 min. Chromium(VI) in the organic phase was stripped first with 30 ml of water for 3 min and subsequently 10 ml of water for 3 min. The two aqueous phases were combined. The final sample volume was adjusted to 100 ml by addition of water, chromium(VI) being determined by the method stated above.

Chromium(VI) was most effectively extracted from 0.06—0.14 M hydrochloric acid into TBP by shaking for 2—5 min. Rapid phase separation was attained with use of 30 ml of water for the first stripping and 10 ml of water for the second stripping. Greater amount of water has no advantage.

The TBP extraction was effective to eliminate the influence of divers ions (Table 2). About 95% of chromium(VI) is recovered by the extraction-stripping procedure.

References

1) M. Abe, K. Ohzeki, and T. Kambara, *Bull. Chem. Soc. Jpn.*, **51**, 1090 (1978).
2) M. Abe, N. Takei, K. Ohzeki, and T. Kambara, *Bull. Chem. Soc. Jpn.*, **52**, 2574 (1978).
3) K. Yoshimura, H. Waki, and S. Ohashi, *Talanta*, **23**, 449 (1976).
4) K. Yoshimura, H. Waki, and S. Ohashi, *Kagaku Zokan* **78**, 95 (1978).
5) K. Yoshimura and S. Ohashi, *Talanta*, **25**, 103 (1978).
6) K. Yoshimura, H. Waki, and S. Ohashi, *Talanta*, **25**, 579 (1978).
7) K. Ohzeki, T. Sakuma, and T. Kambara, *Jpn. Analyst*, **28**, 713 (1979).
8) JIS K 2510-1971, "Testing Method for Rust-Preventing Characteristics of Turbine Oils."
9) O. G. Koch and G. A. Koch-Dedic, "Handbuch der Spurenanalyse," Springer-Verlag (1974), Teil I, p. 624.
10) A. A. Yadav and S. M. Khopher, *Indian J. Chem.*, **8**, 290 (1970).
11) K. Shimokawa, H. Mori, and H. Takada, *Jpn. Analyst*, **28**, 437 (1979).

 © 1980 The Chemical Society of Japan Bull. Chem. Soc. Jpn., 53, 2881—2884 (1980)

Preparation and Stereochemistry of Bis(1,10-phenanthroline)- and Bis-(2,2′-bipyridine)chromium(III) Complexes Containing 2,2′-Bipyridine *N,N′*-Dioxide or Its 3,3′-Dimethyl Derivative

Hideaki KANNO,† Kazuo KASHIWABARA, and Junnosuke FUJITA*

Department of Chemistry, Faculty of Science, Nagoya University, Chikusa, Nagoya 464

(Received April 16, 1980)

Bis(1,10-phenanthroline)- and bis(2,2′-bipyridine)chromium(III) complexes containing a seven-membered chelate ligand, 2,2′-bipyridine *N,N′*-dioxide(bpdo) or 3,3′-dimethyl-2,2′-bipyridine *N,N′*-dioxide(mbdo) were prepared. Each complex gave only one of two possible pairs of enantiomers resolved by SP-Sephadex column chromatography. On the basis of the circular dichroism spectra, molecular models, and recovery of the optically active free mbdo ligand from the resolved mbdo complexes, it was found that all the enantiomeric pairs consist of $\Delta(\delta)$ and $\Lambda(\lambda)$ isomers involving the skew dioxide chelate ligands in the *ob* configuration.

A seven-membered, skew chelate conformation of 2,2′-bipyridine *N,N′*-dioxide (bpdo) in metal complexes has been confirmed by X-ray analysis of $[La(bpdo)_4](ClO_4)_3$.[1] The skew conformation can exist in a pair of enantiomers, δ and λ (Fig. 1). We found that tris-type chromium(III) complexes with bpdo[2] and its derivative, 3,3′-dimethyl-2,2′-bipyridine *N,N′*-dioxide (mbdo)[3] give one and three diastereomers, respectively, of four possible ones, $lel_3(\Delta(\lambda\lambda\lambda), \Lambda(\delta\delta\delta))$, $lel_2ob(\Delta(\lambda\lambda\delta), \Lambda(\delta\delta\lambda))$, $lelob_2(\Delta(\lambda\delta\delta), \Lambda(\delta\lambda\lambda))$, and $ob_3(\Delta(\delta\delta\delta), \Lambda(\lambda\lambda\lambda))$. Δ and Λ denote the absolute configuration of a chromium(III) ion and *lel* and *ob* the diastereoisomerism of a complex with skew chelate rings analogous to that in $[M(en)_3]^{n+}$ (en=ethylenediamine).[4] The number of diastereomers formed in the dioxide complexes is related to whether a dioxide chelate ring can change the skew conformation between δ and λ.

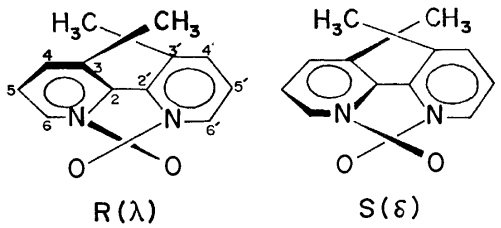

Fig. 1. A pair of enantiomers of mbdo.

This paper describes the preparation and stereochemistry of bis-phen and bis-bpy chromium(III) complexes containing bpdo or mbdo, where phen and bpy denote 1,10-phenanthroline and 2,2′-bipyridine, respectively. Since both phen and bpy ligands form planar chelate rings upon coordination to a metal ion, each of the complexes can have two diastereomers, $lel(\Delta(\lambda), \Lambda(\delta))$ and $ob(\Delta(\delta), \Lambda(\lambda))$. Bis(α-diimine) metal complexes containing a seven-membered chelate ligand do not seem to have been reported except for $[Co(bpy)_2(2,2'\text{-diaminobiphenyl})]^{3+}$ whose stereochemistry was not fully characterized because of instability.[5]

Experimental

The new complexes are photosensitive causing hydrolysis and the following procedures should be carried out in the dark.

† Present address: Department of Chemistry, Faculty of Science, Shizuoka University, Shizuoka 422.

[Cr(phen)$_2$(bpdo)]$^{3+}$ and [Cr(phen)$_2$(mbdo)]$^{3+}$. $[CrCl_2(phen)_2]Cl\cdot 2H_2O$[6] (2.0 g, 3.6 mmol) was added to an aqueous solution (50 cm^3) containing bpdo·H_2O[7] (0.75 g, 3.6 mmol) or racemic mbdo[3] (0.9 g, 4.2 mmol). The solution was adjusted to pH *ca.* 2 with hydrochloric acid in order to avoid the formation of hydroxo complexes, kept at 85 °C with stirring for 6 h, and cooled to room temperature. The resulting solution was diluted with water (0.5 dm^3) and passed through a short column (ϕ 2.7×5 cm) of SP-Sephadex C-25. The resin which adsorbed the red orange product was loaded on a column (ϕ 2.7×80 cm) of SP-Sephadex C-25 and the complexes were eluted with an aqueous 0.2 mol/dm^3 Na_2SO_4 solution adjusted to pH 2 with hydrochloric acid. The column showed two bands, red and orange, the red band being eluted faster than the orange one. The red eluate was found to involve $[Cr(H_2O)_2(phen)_2]^{3+}$ from the absorption spectrum.[8] The orange eluate was diluted with water and poured again on a small column (ϕ 2.7×3 cm) of SP-Sephadex C-25, and the complex adsorbed was eluted with an aqueous 0.5 mol/dm^3 $NaClO_4$ solution. The eluate gave an orange precipitate on standing at room temperature, which was collected and washed with a small amount of water. Recrystallization from hot water gave orange needle crystals. Yield: bpdo-complex, 0.7 g (22%); mbdo-complex, 0.6 g (17%).

[Cr(bpy)$_2$(bpdo)]$^{3+}$ and [Cr(bpy)$_2$(mbdo)]$^{3+}$. Orange needle crystals of the complexes were obtained by the same method as that for the corresponding phen complexes using $[CrCl_2(bpy)_2]Cl\cdot 2H_2O$[9] (2.7 g, 5.3 mmol) and bpdo·H_2O (1.2 g, 5.8 mmol) or racemic mbdo (1.3 g, 6.0 mmol). Yield: bpdo-complex, 1.9 g (41%); mbdo-complex, 0.9 g (18%).

Each of the phen and bpy complexes gave only one diastereomer, no indication for the formation of another isomer being detected on column chromatography.

Resolution of the Complexes. All the complexes were completely resolved by SP-Sephadex column chromatography. Each complex was loaded on a column (ϕ 2.7×130 cm) of SP-Sephadex C-25. By elution with a 0.15 mol/dm^3 sodium $(+)_{589}$-tartratoantimonate(III) solution, the column gave two separate bands of $(+)_{589}$- and $(-)_{589}$-isomers, the former being eluted faster. Each isomer was isolated as perchlorate and recrystallized from hot water by the same method as that for the racemate. Analytical data of the racemic and optically active complexes are given in Table 1.

Recovery of mbdo from the Complexes. The optically active free mbdo ligand was recovered from $(-)_{589}$-$[Cr(phen)_2(mbdo)]^{3+}$ and $(-)_{589}$-$[Cr(bpy)_2(mbdo)]^{3+}$ by the same method as that for $[Cr(mbdo)_3]^{3+}$.[3] Both mbdo recovered gave positive rotation at 589 nm.

Measurements. Absorption and circular dichroism (CD) spectra of the complexes in aqueous solutions were obtained

TABLE 1. ANALYTICAL DATA

Complexes	C/%	H/%	N/%
$[Cr(phen)_2(bpdo)](ClO_4)_3$	45.48 (45.42)	2.59 (2.70)	9.41 (9.35)
$(-)_{589}$-$[Cr(phen)_2(bpdo)](ClO_4)_3 \cdot 3H_2O$	42.91 (42.85)	2.85 (3.18)	9.19 (8.82)
$[Cr(phen)_2(mbdo)](ClO_4)_3 \cdot 2H_2O$	44.97 (44.89)	2.99 (3.36)	8.97 (8.73)
$(-)_{589}$-$[Cr(phen)_2(mbdo)](ClO_4)_3 \cdot 2H_2O$	44.84 (44.89)	2.70 (3.36)	8.97 (8.73)
$[Cr(bpy)_2(bpdo)](ClO_4)_3 \cdot H_2O$	41.63 (41.46)	2.71 (3.02)	9.50 (9.67)
$(-)_{589}$-$[Cr(bpy)_2(bpdo)](ClO_4)_3 \cdot H_2O$	41.28 (41.46)	3.05 (3.02)	9.22 (9.67)
$[Cr(bpy)_2(mbdo)](ClO_4)_3 \cdot 3H_2O$	41.22 (41.19)	3.18 (3.68)	8.73 (9.01)
$(-)_{589}$-$[Cr(bpy)_2(mbdo)](ClO_4)_3 \cdot 5H_2O$	39.28 (39.66)	3.56 (3.96)	8.74 (8.67)

( ): Calcd, bpdo=$C_{10}H_8N_2O_2$, mbdo=$C_{12}H_{12}N_2O_2$.

with a Hitachi 323 spectrophotometer and a Jasco J-40 spectropolarimeter, respectively. Optical rotations were measured with a Jasco DIP-4 polarimeter.

Results and Discussion

Each of the four new complexes, $[Cr(L)_2(bpdo)]^{3+}$ and $[Cr(L)_2(mbdo)]^{3+}$ (L=phen, bpy) gives only one pair of enantiomers stereoselectively by the reaction of the corresponding dichloro complex with the dioxide ligand in water, although there are two possible pairs of enantiomers, *lel*($\Lambda(\lambda)$, $\Lambda(\delta)$) and *ob*($\Lambda(\delta)$, $\Lambda(\lambda)$) (Fig. 1). The enantiomers are completely resolved by SP-Sephadex column chromatography using sodium $(+)_{589}$-tartratoantimonate(III) as an eluent. The complexes in aqueous solutions are stable in the dark, undergoing gradual hydrolysis in the light.

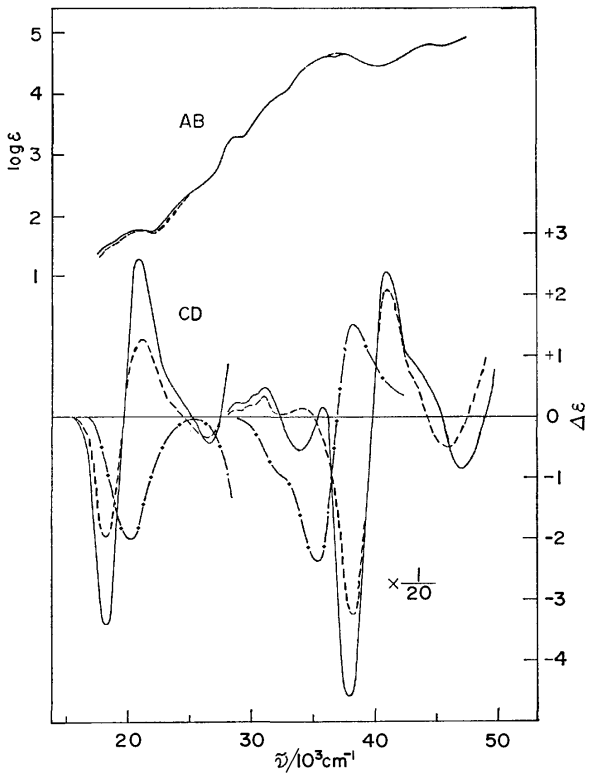

Fig. 2. Absorption and CD spectra of $(-)_{589}$-$[Cr(phen)_2(mbdo)]^{3+}$ (——) and $(-)_{589}$-$[Cr(phen)_2(bpdo)]^{3+}$ (----), and CD spectrum of Λ-$[Cr(ox)(phen)_2]^+$ (-·-·-).[12]

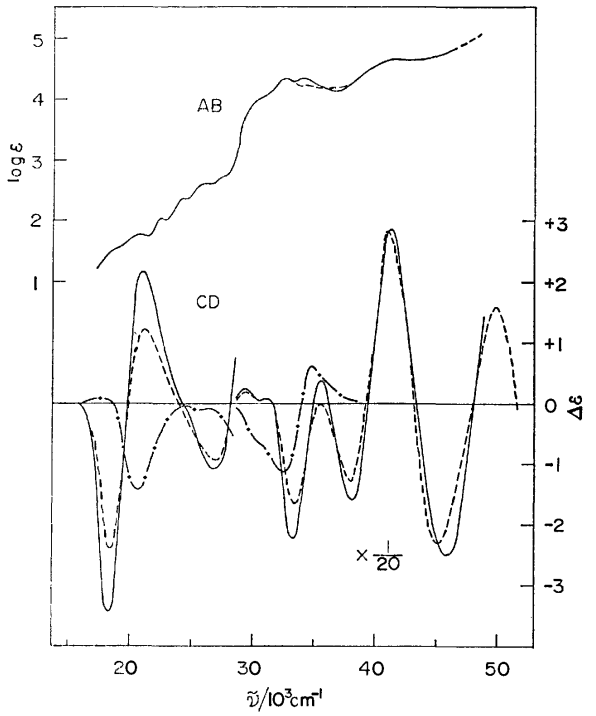

Fig. 3. Absorption and CD spectra of $(-)_{589}$-$[Cr(bpy)_2(mbdo)]^{3+}$ (——) and $(-)_{589}$-$[Cr(bpy)_2(bpdo)]^{3+}$ (----), and CD spectrum of Λ-$[Cr(ox)(bpy)_2]^+$ (-·-·-).[12]

Absorption and CD spectra of $(-)_{589}$-$[Cr(phen)_2(L)]^{3+}$ are shown in Fig. 2 and those of $(-)_{589}$-$[Cr(bpy)_2(L)]^{3+}$ in Fig. 3 (L=bpdo, mbdo). The spectral data are given in Table 2. The absorption spectra of the bpdo and mbdo complexes are nearly the same over the whole region. The bands at 20750 cm^{-1} with a shoulder (18500 cm^{-1}) and *ca.* 20850 cm^{-1} with a shoulder (18900 cm^{-1}) for the phen and bpy complexes, respectively, can be assigned to the first absorption band ($^4T_{2g} \leftarrow {}^4A_{2g}$), although the assignments are somewhat ambiguous because of adjacent strong charge-transfer bands. These first absorption bands are shifted to small wavenumbers by 450—500 cm^{-1} from those of the corresponding oxalato complexes.[10] In the ultraviolet region, all the complexes show complicated spectra due to absorptions arising from intramolecular transitions of the ligands and charge-transfer transitions from the ligands to a Cr(III) ion.

The CD spectra of all the $(-)_{589}$-isomers show a very similar pattern in the region of the first absorption band. The bpdo and mbdo complexes give similar CD spectra over the whole region. This suggests that all the $(-)_{589}$-isomers have the same absolute configuration including chirality of a skew dioxide chelate ring. The CD spectra of the dioxide complexes are compared with those of Λ-$[Cr(ox)(phen)_2]^+$ and Λ-$[Cr(ox)(bpy)_2]^+$ in Figs. 2 and 3, respectively. The absolute configurations

Table 2. Absorption and CD spectral data

	Absorption $\tilde{\nu}/10^3$ cm^{-1} (log ε)	CD $\tilde{\nu}/10^3$ cm^{-1} ($\Delta\varepsilon$)
$(-)_{589}$-[Cr(phen)$_2$-(bpdo)]$^{3+}$	13.92 (1.91)	13.77 (−0.013)
	14.62 (1.99)	14.27 (−0.013)
	18.5 (1.5) sh	18.15 (−1.94)
	20.75 (1.75)	21.16 (+1.28)
	28.41 (3.32)	26.32 (−0.34)
	32.5 (4.1) sh	28.41 (+2.82)
	36.4 (4.6) sh	29.85 (+3.96)
	37.24 (4.63)	30.86 (+6.74)
	40.8 (4.6) sh	34.36 (+2.57)
	44.54 (4.86)	38.02 (−64.6)
		40.90 (+40.2)
		42.5 (+17) sh
$(-)_{589}$-[Cr(phen)$_2$-(mbdo)]$^{3+}$	13.79 (1.91)	13.74 (−0.014)
	14.64 (1.99)	14.24 (−0.014)
	18.5 (1.6) sh	18.15 (−3.44)
	20.75 (1.77)	21.05 (+2.60)
	28.37 (3.30)	26.39 (−0.43)
	32.5 (4.1) sh	28.49 (+4.76)
	36.23 (4.62)	29.9 (+6.7) sh
	37.31 (4.63)	30.86 (+10.5)
	44.54 (4.84)	33.78 (−11.6)
		35.65 (+3.62)
		37.88 (−91.5)
		40.82 (+48.0)
		43.96 (+13.6)
		46.95 (−17.7)
$(-)_{589}$-[Cr(bpy)$_2$-(bpdo)]$^{3+}$	13.89 (1.60)	13.77 (−0.010)
	14.62 (1.71)	14.27 (−0.014)
	18.9 (1.6) sh	18.28 (−2.37)
	20.88 (1.78)	21.28 (+1.22)
	22.32 (2.03)	26.67 (−0.92)
	23.92 (2.36)	29.41 (+4.40)
	25.50 (2.56)	31.25 (+1.52)
	27.1 (2.7) sh	33.28 (−33.9)
	30.3 (4.0) sh	37.88 (−25.8)
	32.26 (4.34)	41.07 (+56.7)
	34.3 (4.3) sh	44.84 (−45.7)
	40.98 (4.63)	50.00 (+32.2)
$(-)_{589}$-[Cr(bpy)$_2$-(mbdo)]$^{3+}$	13.79 (1.54)	13.81 (−0.014)
	14.58 (1.63)	14.21 (−0.018)
	18.9 (1.6) sh	18.32 (−3.42)
	20.83 (1.76)	21.14 (+2.20)
	22.27 (2.02)	26.81 (−1.05)
	23.89 (2.36)	29.33 (+4.82)
	25.48 (2.57)	31.01 (+0.67)
	27.0 (2.7) sh	33.17 (−45.1)
	30.5 (4.0) sh	35.59 (+7.33)
	32.25 (4.33)	38.10 (−31.6)
	33.78 (4.34)	41.32 (+57.6)
	41.24 (4.63)	46.08 (−50.5)

sh: shoulder

of the oxalato complexes were assigned on the basis of the CD pattern in the regions of the first spin-allowed d-d,[11-13] the spin-forbidden d-d,[13] and the $\pi^*\leftarrow\pi$ transitions.[11,12] There seems to be little similarity in CD spectra between the dioxide and the oxalato complexes. The dioxide complexes show two CD components of similar strength with opposite signs in the region of the first absorption band; it is not clear which component is dominant. In addition the complexes do not exhibit typical exciton CD bands in the region of the $\pi^*\leftarrow\pi$ transitions of the phen (*ca.* 37000 cm^{-1}) or bpy (*ca.* 33000 cm^{-1}) ligand, although the spectra of the bpy complexes in this region somewhat resemble the spectrum of Δ-[Cr(ox)(bpy)$_2$]$^+$. Thus the absolute configuration of the dioxide complexes can not be assigned without ambiguity from the CD spectra in the region given. However, CD signs in the region of the spin-forbidden d-d transitions can be utilized for assigning the absolute configuration of chromium(III) complexes.

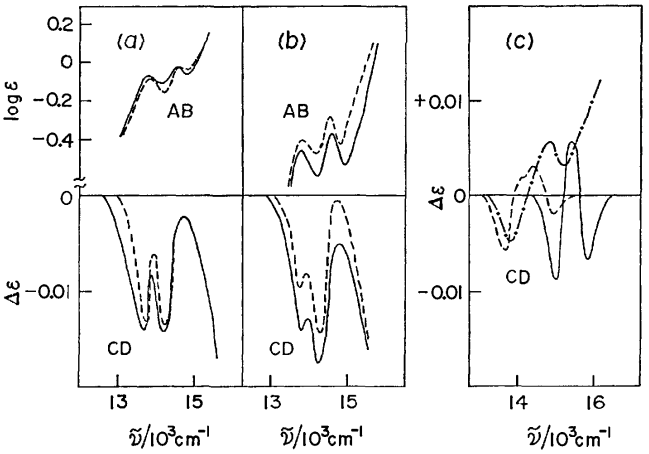

Fig. 4. Absorption and CD spectra in the region of the spin-forbidden d-d transitions. (a) $(-)_{589}$-[Cr(phen)$_2$-(mbdo)]$^{3+}$ (——) and $(-)_{589}$-[Cr(phen)$_2$(bpdo)]$^{3+}$ (----). (b) $(-)_{589}$-[Cr(bpy)$_2$(mbdo)]$^{3+}$ (——) and $(-)_{589}$-[Cr(bpy)$_2$(bpdo)]$^{3+}$ (----). (c) Δ-[Cr(en)$_3$]$^{3+}$ (——),[13] Δ-[Cr(ox)(phen)$_2$]$^+$ in 70% HClO$_4$ (-·-·-),[13] and Δ-[Cr(ox)(bpy)$_2$]$^+$ (----).[13]

Kaizaki *et al.*[14] found that in tris-chelate chromium(III) complexes except for a few complexes such as those with biguanide or acetylacetonate, the smallest wavenumber CD band in the region of the spin-forbidden d-d transitions shows the same sign as that of a dominant CD band in the region of the first spin-allowed d-d transitions. The smallest wavenumber CD bands of all the $(-)_{589}$-dioxide complexes give a negative sign in the region of the spin-forbidden bands (Fig. 4). Thus dominant CD bands of the isomers in the region of the first spin-allowed band should be negative, and the isomers can be assigned to the Δ-configuration.[15] The Δ-isomers of [Cr(ox)(L)$_2$]$^+$ (L=phen, bpy) and a typical tris-chelate complex, [Cr(en)$_3$]$^{3+}$ (en=ethylenediamine) also give negative CD bands at the smallest wavenumber in the region of the spin-forbidden d-d transitions.

The $(-)_{589}$-dioxide complexes can have two diastereomers, $\Delta(\delta)(ob)$ and $\Delta(\lambda)(lel)$. Since the free mbdo ligand is optically stable,[3] it was recovered from $(-)_{589}$-Δ-isomers of the phen and bpy complexes in order to know the absolute configuration. Both mbdo recovered show positive rotation at 589 nm. The $(+)_{589}$-mbdo

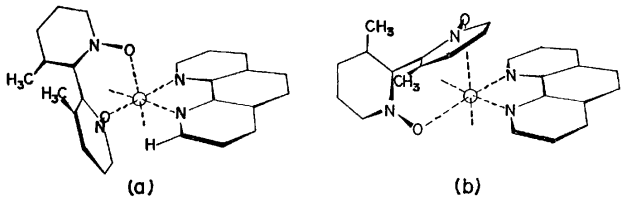

Fig. 5. Schematic drawing of the two diastereomers of Δ-[Cr(phen)$_2$(mbdo)]$^{3+}$; (a) $\Delta(\lambda)(lel)$, (b) $\Delta(\delta)(ob)$.

ligand is the same as that recovered from $(+)_{589}$-[Cr(mbdo)$_3$]$^{3+}$ which was assigned to the $\Delta(\delta\delta\delta)(lel_3)$-configuration.[3] Thus the $(-)_{589}$-Δ-isomers involve mbdo of the $\delta(S)$ chirality to form a $\Delta(\delta)(ob)$ diastereomer. Since the bpdo complexes give CD spectra similar to those of the mbdo complexes over the whole region, it is concluded that the bis-phen and bis-bpy chromium(III) complexes of these dioxides form only an *ob* isomer stereoselectively. Such stereoselectivity is in contrast with the fact that the stability of complexes with skew chelate rings decreases with an increase in the number of *ob* ligands.[4] The [Co(en)$_2$(L)]$^{3+}$ (L= 2,2′-diaminobiphenyl,[5,16] and its 6,6′-dimethyl derivative[16]) complexes, the ligands in which form skew seven-membered chelate rings similar to the dioxides, give only a *lel* isomer. The formation of only *ob* isomers for the dioxide complexes seems to be caused by steric interactions between the dioxide and the α-diimine ligands in the *lel* form. Figure 5 shows a schematic drawing of the two isomers of Δ-[Cr(phen)$_2$($(+)_{589}$-mbdo)]$^{3+}$ by Dreiding molecular models. In the $\Delta(\lambda)(lel)$ form, each 2- (or 9-) hydrogen atom of the phen ligands comes very close to the 6- and 6′-carbon (and hydrogen) atoms of mbdo. On the other hand, there is no such extreme proximity among atoms of the ligands in the $\Delta(\delta)(ob)$ form, each pyridine ring of mbdo becoming nearly parallel to each of the phen ligands to form a stable structure. Thus the bis-phen and bis-bpy complexes of bpdo and mbdo would give only one pair of *ob* enantiomers, $\Delta(\delta)$ and $\Lambda(\lambda)$, stereoselectively.

This work was partially supported by a Grant-in-Aid for Scientific Research from the Ministry of Education, Science and Culture (No. 243013).

References

1) A. R. Al-Karaghouli, R. O. Ray, and J. S. Wood, *Inorg. Chem.*, **17**, 3702 (1978).
2) H. Kanno, K. Kashiwabara, and J. Fujita, *Bull. Chem. Soc. Jpn.*, **52**, 761 (1979).
3) H. Kanno, K. Kashiwabara, and J. Fujita, *Bull. Chem. Soc. Jpn.*, **52**, 1408 (1979).
4) E. J. Corey and J. C. Bailar, Jr., *J. Am. Chem. Soc.*, **81**, 2620 (1959).
5) T. Tanimura, H. Ito, J. Fujita, K. Saito, S. Hirai, and K. Yamasaki, *J. Coord. Chem.*, **3**, 161 (1973).
6) P. Pfeiffer and B. Wedelman, *Z. Anorg. Chem.*, **262**, 31 (1950).
7) I. Murase, *Nippon Kagaku Zasshi*, **77**, 682 (1956).
8) B. Bosnich, *Acc. Chem. Res.*, **2**, 266 (1969); M. P. Hancock, J. Jusephsen, and C. E. Schaffer, *Acta Chem. Scand. Sect. A*, **30**, 79 (1976).
9) F. H. Burstall and R. S. Nyholm, *J. Chem. Soc.*, **1952**, 3570.
10) J. A. Broomhead, M. Dwyer, and N. Kane-Maguire, *Inorg. Chem.*, **7**, 1388 (1968).
11) J. Ferguson, C. J. Hawkins, N. A. P. Kane-Maguire, and H. Lip, *Inorg. Chem.*, **8**, 771 (1969).
12) S. Kaizaki, J. Hidaka, and Y. Shimura, *Inorg. Chem.*, **12**, 135 (1973).
13) S. Kaizaki, J. Hidaka, and Y. Shimura, *Bull. Chem. Soc. Jpn.*, **43**, 1100 (1970).
14) S. Kaizaki, J. Hidaka, and Y. Shimura, *Bull. Chem. Soc. Jpn.*, **42**, 988 (1969); *Inorg. Chem.*, **12**, 142 (1973).
15) C. J. Hawkins, "Absolute Configuration of Metal Complexes," Wiley-Interscience (1971), Chap. 5.
16) W. T. Jordan, C. Y. Lin, and B. E. Douglas, *J. Coord. Chem.*, **3**, 1 (1973).

Cyclization Reactions of 2,3-Bis(2-cyanophenyl)propionitriles. III.[1] Substituent Effect on the Carbanion Reactivies of the Propionitriles and Tautomerism of 5-Acetamido-11-cyanoindeno[1,2-*c*]isoquinolines

Kazuo ANDO,*,† Takashi TOKOROYAMA, and Takashi KUBOTA††
Faculty of Science, Osaka City University, Sugimoto-cho, Sumiyoshi-ku, Osaka 558
(Received June 27, 1979)

The substituent effect in the base-catalyzed cyclization reaction of 2,3-bis(2-cyanophenyl)propionitriles (**1**) to 5-amino-11-cyano-11*H*-indeno[1,2-*c*]isoquinolines has been studied and the result is discussed in terms of the dichotomic carbanion reactivities of **1**. Preparation of **1** and the tautomerism of 5-acetamido-11-cyanoindeno-[1,2-*c*]isoquinolines between 5*H* and 11*H* structures are described.

When 2,3-bis(2-cyano-3-methoxyphenyl)propionitrile (**1a**) was allowed to react with sodium ethoxide and diethyl carbonate in ethanol, a red pigment was obtained in 79.3% yield, to which we assigned the structure **2** (Scheme 1).[2]

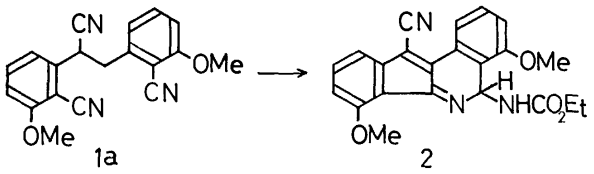

Scheme 1.

The formation of **2** from **1a** involves the preferential attack of C-3 carbanion to the cyano group on aromatic ring.

The cause for the less stable C-3 carbanion participating exclusively in the cyclization deserves further study. We have confirmed that the cyclization product derived from the more stable C-2 carbanion is also obtained and examined the relative reactivity of the dichotomic carbanions in terms of the substituent effect. We have found an interesting tautomerism between 11*H*- and 5*H*-indeno[1,2-*c*]isoquinoline systems, which is markedly influenced by the substitution patterns of the aryl rings.

Results and Discussion

Preparation of 2,3-Bis(2-cyanophenyl)propionitriles (1). The reaction of 2-cyano-3-methoxybenzyl bromide (**3a**) with sodium cyanide afforded 2,3-bis(2-cyano-3-methoxyphenyl)propionitrile (**1a**) in variable ratios to the normal product, 2-cyano-3-methoxybenzyl cyanide (**5a**), depending on the conditions.[3] Formation of the former compound is accelerated in the case of low cyanide concentration and in a polar aprotic medium such as DMSO. Since the reactivity of the benzyl cyanides (**4**) initially produced is affected to a large extent by the substituents in aryl rings, a proper modification of the reaction procedure was necessary in order to prepare propionitriles (**1**) in acceptable yields. The following methods were investigated.

A. A solution of a bromide and NaCN in ethanol–water (2: 1) was allowed to stand at −20 °C for 48 h.

B. A solution of a bromide and NaCN in ethanol–water (4: 1) was refluxed for 6 h.

C. A mixture of a bromide, NaCN, a trace of NaI, and acetone was stirred at room temperature for 48 h.

D. A mixture of a bromide, NaCN, a trace of NaI, and acetone was stirred and refluxed for 24 h.

The results obtained in the reactions of the substrates **3a**—**3f** are summarized in Table 1. Method D was generally applicable (**3a**, **3b**, **3c**, and **3f**) except when

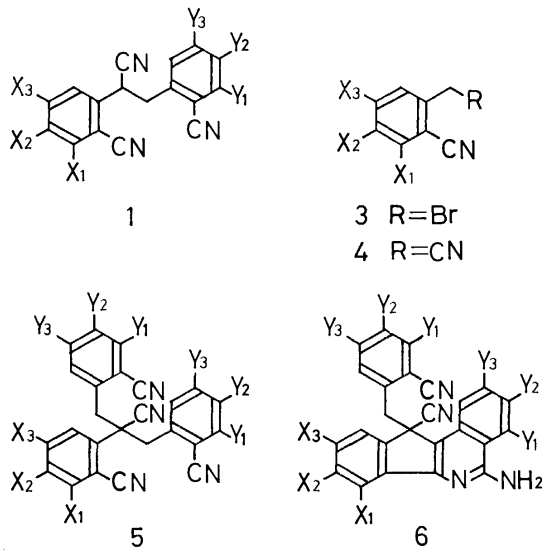

a $X_1=Y_1=OMe$, $X_2=X_3=Y_2=Y_3=H$
b $X_1=X_3=Y_1=Y_3=H$, $X_2=Y_2=OMe$
c $X_1=X_2=Y_1=Y_2=H$, $X_3=Y_3=OMe$
d $X_1=X_3=Y_1=Y_3=H$, $X_2=Y_2=Cl$
e $X_1=X_2=Y_1=Y_2=H$, $X_3=Y_3=Cl$
f $X_1=X_2=X_3=Y_1=Y_2=Y_3=H$
g $X_1=OMe$, $X_2=X_3=Y_1=Y_2=Y_3=H$
h $X_1=X_2=X_3=Y_2=Y_3=H$, $Y_1=OMe$

Fig. 1.

† Present address: Masuda Chemical Industrial Co., Ltd., 12-52, 4-chome, Asahi-machi, Takamatsu, Kagawa 760.

†† Present address: Kinki University, Medical School, Sayama-cho, Osaka 589.

Table 1. Preparation of 2,3-bis(2-cyanophenyl) propionitriles (**1**)

Entry	Substrate	Reaction conditions: Method	Reaction conditions: Ratio (NaCN/**3**)	Yield (%): **1**	Yield (%): **4**	Yield (%): **5**	Yield (%): **6**
1	**3a**	B	1.5	17.2	58.8	0	0
2	**3a**	D	2.0	78.0	0	0	0
3	**3b**	D	3.5	58.9	18.9	0	0
4	**3c**	D	5.5	42.4	0	7.4	0
5	**3d**	A	12.7	54.0	25.0	0	0
6	**3d**	C	4.7	0	0	27.0	22.8
7	**3e**	A	19.7	71.5	20.0	0	0
8	**3f**	D	3.0	77.0	0	0	0

the intermediary benzyl cyanides (**4**) were unusually reactive as in the case of compounds **3d** and **3e** with chlorosubstituents. For example, the reaction of **3d** by method C (entry 6) gave only the disubstituted compound **5d** and **6d**, which would be formed by cyclization of **5d**. Method A was introduced in such cases. Use of protic solvents and a large excess of sodium cyanide suppressed the disubstitution.

Cyclization Reactions of 2,3-Bis(2-cyanophenyl)propionitriles (1). Of the reactants used in the original red pigment formation,[2] diethyl carbonate does not seem to be essential for the cyclization reaction.

Thus, when a solution of the propionitrile (**1a**) in ethanol was refluxed in the presence of two molar equivalents of sodium ethoxide under nitrogen atmosphere for 2 h, a dark brown reaction mixture was obtained. This mixture was warmed with 1% sodium hydroxide solution for a short time in order to confirm the dissolution of the acidic product. It was then filtered. After acidification of the filtrate with dil. hydrochloric

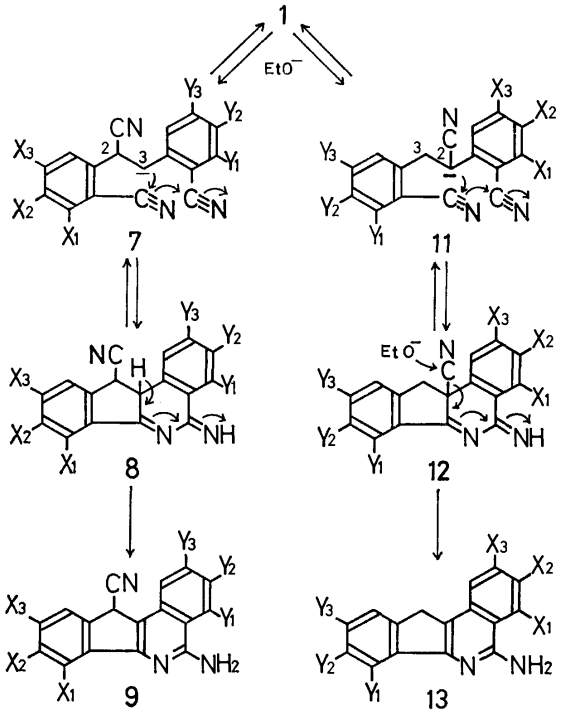

Scheme 2.

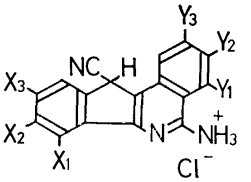

10

Fig. 2.

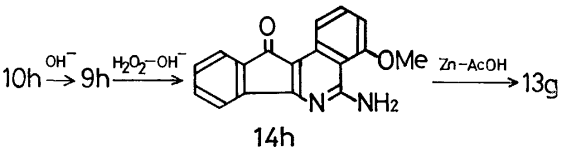

Scheme 3.

acid solution, the cyclized product **9a** was isolated as a colorless hydrochloride (**10a**) in 55% yield.[4] The undissolved material was separated by silica gel chromatography to afford a product in 3% yield, identified as **13a**. **13a** was obtained from **2** by treatment with alkaline hydrogen peroxide and the subsequent reduction with zinc-acetic acid.[2a] The formation of **13** is best interpreted by the cyclization of **1** *via* C-2 anion **11** followed by aromatization of the resulting heterocyclic ring with loss of the cyano group (Scheme 2). The possibility of the formation of **13** *via* **9** was excluded by the fact that cyclization of the propionitrile (**1g**) afforded **13g** and not **13h**. The substitution pattern was confirmed by the derivation of **13g** from **9h** through the reaction sequence used for the conversion of **2** into **13a** (Scheme 3). Thus the cyclization reaction of the 2,3-bis(2-cyanophenyl)propionitriles (**1**) with a base is dichotomic.

Cyclization experiments carried out in the same way as above for variously substituted 2,3-bis(2-cyanophenyl)propionitriles (**1**) have confirmed this to be the case.

Table 2. Cyclization reactions of 2,3-bis(2-cyanophenyl)propionitriles (**1**)

Substrate	Reaction conditions: NaOEt (mol eq.)	Reaction conditions: Time (h)	Yield (%): **9**	Yield (%): **13**	Ratio **9**/**13**
1a	2	2	55	3	18.3
1b	14	2	0	81	0
1c	2	2	66	7	9.4
1d	2	2	34	40	0.85
1e	2	2	61	6	10.2
1f	2	2	32	45	0.71
1g	4	4	23	46	0.50
1h	2	2	27	50	0.54

The results are summarized in Table 2. Formation of the dual products **9** and **13** takes place, with the exception of **1b**, which is extremely nonreactive, giving only **13b** upon reaction with use of excess base (14 molar equiv.). In the case of the propionitrile with unsubstituted aryl rings (**1f**) and the *p*-substituted analog (**1d**), the molar ratios of **9** to **13** are smaller than 1.

On the other hand, the molar ratios of *m*-substituted compounds (**1a**, **1c**, and **1e**) are larger than 1. Thus the formation ratios of **9** to **13** are considerably affected by the substitution patterns of the aryl rings, especially by the position of the substituents.

This should be interpreted in terms of the substituent effect on the relative reactivity of the intermediate anions **7** and **11**. The C-3 carbanion **7** would be formed in much smaller amount as compared to the C-2 carbanion **11**.

However, the cyclization of **7** gives the product **9**, which is in turn converted into a stabilized anion **15**.

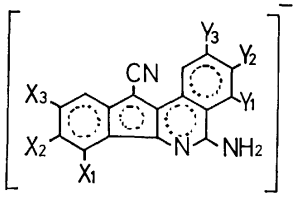

15

Fig. 3.

In contrast, the reaction of **11** leads to the formation of unstable cyclization product **12**, which could be aromatized only by the loss of the angular cyano group; **12** would be mostly reverted to **11**. The results obtained for the compounds **1g** and **1h**, in which the two aromatic rings are substituted in different ways, indicate that the formation ratios of **9** to **13** can not be explained by the substituent effect on the relative stability of the intermediate anions **7** and **11**. Unless the C-3 carbanion formation is extremely depressed by the presence of an electron-releasing group in para position as in the case of **7b**, the formation of **9** is considered to become comparable to that of **13** (**1d** and **1f**). The promoting effect of *m*-substituents, especially *m*-methoxyl group for the cyclization to **9** is remarkable (**1a**, **1c**, and **1e**) but it is difficult to give an explanation entirely in terms of inductive effect.

Tautomerism of the Acetamides 18 and 19 Derived from 9. For the purpose of identification, analogs **9** substituted in various ways were converted into acetamides by treatment with acetic anhydride and a catalytic amount of concd. sulfuric acid. The resulting solution of isoquinolinium salt (**16**) was poured into ice-water, yielding the colored acetamides (**18**). The 5*H*-indeno-[1,2-*c*]isoquinoline structures (**18**) were characterized by coloration and strong absorption near 2160 cm^{-1}. The specific formation of **18** from **16** can be accounted for by the mechanism shown in Scheme 4. The hydrolysis of **16** is initiated by the release of the proton at position 11 rather than that on ring nitrogen atom, which is trapped by strong hydrogen bonding.

When compounds **18** were dissolved in chloroform, one of them gave a colorless solution, while the others gave solutions with the same color as the original compound or a different one. Crystallization from the solutions gave either the original 5*H*-indeno[1,2-*c*]-isoquinolines (**18**), or a colorless compound. The IR spectrum of the latter compound exhibits a weak absorption band due to the nitrile group at 2250 cm^{-1},

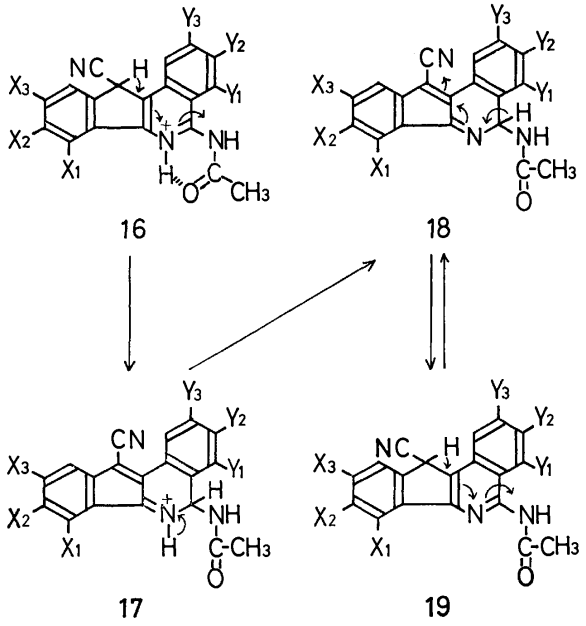

16 18 17 19

Scheme 4.

Table 3. Tautomerism of 5-acetamido-11-cyanoindeno[1,2-*c*]isoquinolines

Group	Parent amino compd.	5*H*-isomer (**18**) Color	5*H*-isomer (**18**) ν/cm^{-1} a)	Coloration of $CHCl_3$ soln.	11*H*-isomer (**19**) Color	11*H*-isomer (**19**) ν/cm^{-1} a)
(i)	**9a**	red	2165(s)	red		
(ii)	**9d**	dark green	2160(s)	pale yellow		
	9e	red	2160(s)	pale yellow		
(iii)	**9f**	purple	2180(s)	colorless	colorless	2250(w)

a) (s): strong, (w): weak.

indicating that it represents the 11*H*-indeno[1,2-*c*]-isoquinoline structure (**19**), tautomeric with **18**. The behavior of **9** by the above treatment in relation to the substitution patterns of the aryl rings can be classified into three groups (Table 3).

(i) No color change on dissolution in chloroform and recovery of the 5*H*-isomer on crystallization.

(ii) Color change to pale yellow and recovery of the 5*H*-isomer.

(iii) Change to colorless and conversion into 11*H*-isomer.

The correlation between the relative stability of 5*H*- and 11*H*-isomers, and the substitution patterns of the aryl rings is not clear from the data available.

Experimental

Melting points were uncorrected. IR spectra were measured in Nujol mull. NMR spectra were determined at 60 MHz unlesso therwise stated. Chemical shifts are given in δ-values, using TMS as an internal standard. The instruments used are the same as those reported.[2a)]

2,3-Bis(2-cyano-3-methoxyphenyl)propionitrile (1a). Method B: A solution of **3a** (8.93 g) and NaCN (2.9 g) in ethanol–

Table 4. 2,3-Bis(2-cyanophenyl)propionitriles (**1**) and 2-cyanobenzyl cyanides (**4**)

Compd No.	Mp/°C (Solv. for recryst.)[a]	Formula	Calcd (Found) (%) C	H	N	IR ν/cm⁻¹ –CN	NMR Solv.[a]	δ/ppm (J/Hz) ArH	>CH	–OCH	>CH₂
1a	161—162 (M)	$C_{19}H_{15}N_3O_2$	71.91 (71.93	4.76 4.88	13.24 13.12)	2225	$CDCl_3$	7.73— 6.81m	4.48t (7.5)	3.93s 3.90s	3.42d (7.5)
1b	133.5—134.5 (B–P)	$C_{19}H_{15}N_3O_2$	71.91 (71.91	4.76 4.84	13.24 13.26)	2230	TFA	7.67— 7.20m	4.67t (7.0)	3.93s	3.57d (7.0)
1c	152—152.5 (B)	$C_{19}H_{15}N_3O_2$	71.91 (71.79	4.76 4.78	13.24 13.16)	2220	$CDCl_3$	7.63— 6.77m	4.50t (7.5)	3.87s	3.50d (7.5)
1d[b]	147—148 (B–P)	$C_{17}H_9N_3Cl_2$	62.60 (62.47	2.78 2.85	12.88 12.76)	2230	$CDCl_3$	7.68— 7.36m	4.54t (7.5)		3.56dd, 3.36dd (7.5, 14.0)
1e[b]	197—198 (M)	$C_{17}H_9N_3Cl_2$	62.60 (62.64	2.78 2.92	12.88 12.93)	2230	TFA	7.68— 7.36m	4.73t (7.0)		3.68dd, 3.52dd (7.0, 14.0)
1f[c]	114 (M)					2250 2230	TFA	8.17— 7.23m	4.80t (7.0)		3.72d (7.0)
1g	187.5 (C–M)	$C_{18}H_{13}N_3O$	75.24 (74.94	4.56 4.65	14.63 14.71)	2240 2230					
1h	136—137 (M)	$C_{18}H_{13}N_3O$	75.24 (75.13	4.56 4.69	14.63 14.34)	2240 2230					
4a	114—116 (C–T)	$C_{10}H_8N_2O$	69.75 (69.62	4.68 4.79	16.27 16.16)	2265 2225					
4b	83.5—84.5 (B–P)	$C_{10}H_8N_2O$	69.75 (69.71	4.68 4.74	16.27 16.05)	2250 2230					
4d	67—67.5 (D–P)	$C_9H_5N_2Cl$	61.21 (61.23	2.85 2.92	15.86 15.50)	2230					
4e	119—120 (D)	$C_9H_5N_2Cl$	61.21 (61.31	2.85 2.98	15.86 15.45)	2235					

a) B: benzene, C: chloroform, D: diethyl ether, M: methanol, P: petroleum ether, T: tetrachloromethane, TFA: trifluoroacetic acid. b) The NMR spectra of **1d** and **1e** were measured at 100 MHz. c) Ref. 5, mp 114 °C.

water (4 : 1, 250 ml) was refluxed for 6 h. After extraction with chloroform and evaporation of the solvent. the residue was chromatographed on silica gel. Elution with benzene–chloroform (1 : 1) afforded **4a** (4.02 g). Further elution with the same eluent gave **1a** (1.08 g). The physical data of **1a**—**1h**, **4a**, **4b**, **4d**, and **4e** are summarized in Table 4.

Method D: A mixture of **3a** (1 g), NaCN (434 mg), NaI (45 mg), and dry acetone (12 ml) was stirred and refluxed for 24 h. After addition of water, extraction with chloroform and evaporation of the solvent, the residue on crystallization from methanol gave **1a** (547 mg).

*2,3-Bis(2-cyano-4-methoxyphenyl)propionitrile (**1b**).* *Method D*: A mixture of **3b** (7.0 g), NaCN (5.25 g), NaI (420 mg), and dry acetone (60 ml) was treated in the same way as described for **1a**. After evaporation of the solvent, the residue was chromatographed on silica gel.

Elution with benzene afforded **4b** (1.06 g). Elution of the column with benzene–chloroform (1: 1) gave **1b** (2.89 g).

*2,3-Bis(2-cyano-5-methoxyphenyl)propionitrile (**1c**).* *Method D*: **3c** (6.76 g) was cyanated as above. After evaporation of the solvent, the residue was crystallized from methanol–benzene to give 2-cyano-1,2,3-tris(2-cyano-5-methoxyphenyl)-propane (**5c**) (307 mg), mp 211—212 °C; ν_{max} 2220 cm⁻¹ (–CN); δ(CF_3CO_2H) 4.12 (4H, s, 2×$ArCH_2$–), 3.89 (3H, s, $ArOCH_3$), and 3.85 (6H, s, 2×$ArOCH_3$). Found: C, 72.80; H, 4.87; N, 12.00%. Calcd for $C_{28}H_{22}N_4O_3$: C, 72.71; H, 4.79; N, 12.12%. The filtrate was chromatographed on silica gel.

Elution with benzene–chloroform (1: 1) gave **1c** (4.0 g).

*2,3-Bis(2-cyano-4-chlorophenyl)propionitrile (**1d**).* *Method A*: A solution of **3d** (5.74 g) in ethanol (92 ml) was added to a solution of NaCN (15.5 g) in water–ethanol (1 : 1, 186 ml) and mixed. The resulting solution was allowed to stand at −20 °C for 48 h. After addition of water (300 ml), extraction with chloroform and evaporation of the solvent, the residue was chromatographed on silica gel. Elution with benzene–petroleum ether (1: 1) gave **4d** (1.1 g). Further elution with the same eluent gave **1d** (2.19 g).

Method C: A mixture of **3d** (1 g), NaCN (1 g), NaI (20 mg), and dry acetone (10 ml) was stirred at room temperature for 48 h. After addition of water, extraction with chloroform and evaporation of the solvent, the residue was chromatographed on silica gel. Elution with benzene gave 2-cyano-1,2,3-tris(2-cyano-4-chlorophenyl)propane (**5d**) (186 mg), mp 210—211 °C (from benzene–petroleum ether); ν_{max} 2230 cm⁻¹ (–CN); δ($CDCl_3$) 4.22, 3.80 (4H, ABq, J=14.0 Hz, 2×$>CH_2$). Found: C, 63.41; H, 2.90; N, 11.59%. Calcd for $C_{25}H_{13}N_4Cl_3$: C, 63.11; H, 2.75; N, 11.78%. Elution of the column with chloroform gave 5-amino-11-cyano-3,8-dichloro-11-(2-cyano-4-chlorobenzyl)-11*H*-indeno[1,2-*c*]isoquinoline (**6d**) (157 mg), mp 209—210 °C (from methanol); $\lambda_{max}^{H_2SO_4\text{-EtOH}}$ 208 (ε×10⁻³, 61.4), 225 (55.9), 233 sh (49.6), 341 (18.2) 372 (13.2), and 390 nm (10.0); ν_{max} 3490 and 3380 (–NH_2) and 2230 cm⁻¹ (–CN); δ($CDCl_3$) 8.10—6.77 (9H, m, ArH), 5.57 (2H, s, –NH_2, dissappears on D_2O exchange), 4.00 (1H, d, J=14.0 Hz, $>CH_AH_B$) and 3.45 (1H, d, J=14.0 Hz, $>CH_AH_B$). Found: C, 62.66; H, 2.76; N, 11.63%.

Calcd for $C_{25}H_{13}N_4Cl_3$: C, 63.11; H, 2.75; N, 11.78%.

*2,3-Bis(2-cyano-5-chlorophenyl)propionitrile (**1e**).* *Method A*: **3e** (1.58 g) was treated in the same way as described for **1d**. Elution of the silica gel column with benzene–petroleum ether (1 : 1) gave **4e** (245 mg). Elution of the column with benzene–chloroform (1: 1) gave **1e** (800 mg).

*2,3-Bis(2-cyanophenyl)propionitrile (**1f**).* *Method D*: **3f**

Table 5. 5-Amino-11-cyano-11*H*-indeno[1,2-*c*]isoquinoline hydrochlorides (**10**) and 5-amino-11*H*-indeno[1,2-*c*]isoquinolines (**13**)

Compd No.	Mp/°C[b]	Formula	Calcd (Found) (%) C	H	N	IR ν/cm^{-1} $-NH_3^+$ or $-NH_2$	−CN	NMR (CF_3CO_2H)[a] δ/ppm ArH	>CH or CH_2	$-OCH_3$
10a	249dec	$C_{19}H_{16}N_3O_2Cl$	64.50 (64.15	4.56 4.76	11.88 11.72)	3300 3080—2760	2245	8.27— 7.20m	5.30s	4.34s 4.13s
10c	268dec	$C_{19}H_{16}N_3O_2Cl$	64.50 (64.27	4.56 4.72	11.88 11.66)	3290, 3190 2620	2245	8.42— 7.17m	5.27s	4.13s 4.05s
10d	290dec	$C_{17}H_{10}N_3Cl_3$	56.30 (56.64	2.78 2.80	11.59 11.44)	3405, 3180 2760	2240	8.42— 7.52m	5.27s	
10e	290dec	$C_{17}H_{10}N_3Cl_3$	56.30 (56.24	2.78 2.89	11.59 11.57)	3280, 3120 2640	2240	8.48— 7.64m	5.34s	
10f	278dec	$C_{17}H_{12}N_3Cl$	69.51 (69.43	4.12 4.25	14.30 14.27)	3240, 3100 2580	2240	8.55— 7.57m	5.32s	
10g	279dec	$C_{18}H_{14}N_3OCl$	66.77 (66.61	4.36 4.48	12.98 12.68)	3180—2740	2240	8.58— 7.25m	5.40s	4.33s
10h	275dec	$C_{18}H_{14}N_3OCl$	66.77 (66.74	4.36 4.53	12.98 12.76)	3420, 3260 3160, 2440	2245	8.27— 7.28m	5.27s	4.27s
13a	229—230 dec	$C_{18}H_{16}N_2O_2$	73.95 (73.73	5.52 5.63	9.58 9.35)	3500, 3370		8.03— 6.90m	3.75s	4.13s 4.03s
13b	262dec	$C_{18}H_{16}N_2O_2$	73.95 (73.95	5.52 5.57	9.58 9.54)	3460, 3370 3290, 3130		8.08— 6.95m	3.95s	4.07s
13c	207—208 dec	$C_{18}H_{16}N_2O_2$	73.95 (73.50	5.52 5.33	9.58 9.32)	3460, 3360 3160		7.86— 6.88m	3.80s	3.92s 3.84s
13d	244—245 dec	$C_{16}H_{10}N_2Cl_2$	63.81 (63.53	3.35 3.32	9.30 9.36)	3480, 3380 3280, 3140		8.20— 7.26m	3.98s	
13e	295	$C_{16}H_{10}N_2Cl_2$	63.81 (63.70	3.35 3.42	9.30 9.29)	3480, 3280 3140		8.34— 7.48m	4.06s	
13f	207—208 dec	$C_{16}H_{12}N_2$	82.73 (82.61	5.21 5.32	12.06 12.06)	3300, 3100		8.32— 7.32m	3.85s	
13g	193.5— 195.5	$C_{17}H_{14}N_2O$	77.84 (77.79	5.38 5.49	10.68 10.49)	3480, 3280 3160		8.03— 7.00m	3.73s	4.08s
13h	209—211	$C_{17}H_{14}N_2O$	77.84 (77.51	5.38 5.49	10.68 10.41)	3360, 3200		8.27— 6.87m	3.97s	4.03s

a) The spectrum of **13c** was measured in $CDCl_3$. b) Recrystallized from methanol. dec: decomposition.

Table 6. 5-Acetamido-11-cyano-5*H*-indeno[1,2-*c*]isoquinolines (**18**) and 5-acetamido-11-cyano-11*H*-indeno[1,2-*c*]isoquinoline (**19f**)

Compd No.	Mp/°C[a]	Formula	Calcd (Found) (%) C	H	N	IR ν/cm^{-1} [b] >NH	−CN	>CO	NMR (CF_3CO_2H) δ/ppm ArH	>CH	$-OCH_3$	$-COCH_3$
18a	292—293 dec	$C_{21}H_{17}N_3O_3$	70.18 (69.84	4.77 4.86	11.69 11.77)	3300	2165s	1680 w	8.40— 7.20m	5.53s	4.37s 4.27s	2.73s
18d	263—264 dec	$C_{19}H_{11}N_3O_3Cl_2$	61.20 (60.99	3.01 2.90	11.41 10.94)	3210	2160s	1695 w	8.72— 7.74m	5.62s		2.74s
18e	280.5— 281dec	$C_{19}H_{11}N_3OCl_2$	61.20 (61.06	3.01 2.92	11.41 11.26)	3200 3120	2160s	1690 w	8.74— 7.76m	5.60s		2.74s
19f	269—270 dec	$C_{19}H_{13}N_3O$	76.24 (75.81	4.38 4.64	14.04 13.93)	3180 3100	2250 w	1690s	8.70— 7.72m	5.58s		2.74s

a) Recrystallized from chloroform. b) s: strong, w: weak.

(10.5 g) was treated in the same way as described for **1a** to give **1f** (5.54 g).

2-(2-Cyano-3-methoxyphenyl)-3-(2-cyanophenyl)propionitrile (1g) and 2-(2-Cyanophenyl)-3-(2-cyano-3-methoxyphenyl)propionitrile (1h). A mixture of **4a** (2.0 g), **3f** (2.27 g), K_2CO_3 (1.6 g), NaI (150 mg, and dry acetone (30 ml) was refluxed for 24 h. After filtration and evaporation, the residue was crystallzed to give **1g** (2.76 g, 82.6%). **1h** was similarly prepared in 72% yield from **4f**[6] and **3a**.

Cyclization Reactions of the Propionitriles (1). General Procedure: A solution of sodium ethoxide (2 mmol; 14 and 4 mmol for **1b** and **1g** respectively) in ethanol (5 ml) was added to a mixture of **1** (1 mmol) and ethanol (10 ml). The mixture was stirred and refluxed for 2 h (4 h for **1g**). When the reaction was completed,[7] 1% NaOH aqueous solution (30 ml) was added and warmed for 30 min. The solution was then cooled and allowed to stand in a refrigerator overnight. The precipitates were collected by filtration and chromatographed on silica gel. Elution with chloroform gave **13**. By acidification of the filtrate with an excess of dilute hydrochloric

Table 7. UV spectral data of **10**, **13**, **18**, and **19**

	λ_{max}[a]/nm ($\varepsilon \times 10^{-3}$)		
	10 (H_2SO_4–EtOH)[c]	**13** (H_2SO_4–EtOH)[c]	**18** or **19**[b] (EtOH)
a	220 (32.5), 263 (19.6) 332s(10.3), 344 (13.2) 380 (16.3), 398 (15.0)	220 (36.9), 259 (21.3) 328 (13.5), 342 (16.2) 386 (17.6), 405 (16.5)	217 (23.8), 250 (36.2), 279s(24.3), 286 (25.4) 325 (15.3), 384 (17.1), 520 (4.5),
b		228 (41.4), 327 (19.0) 340 (19.4), 392 (11.6) 410 (10.7)	
c	216 (25.2), 252 (21.8) 280 (38.0), 338 (18.8) 354s(16.2), 370s(14.3)	212 (25.9), 253 (22.5) 280 (38.7), 340 (20.3) 370 (15.7)	
d	223 (41.0), 233 (36.7) 325s(16.0), 337 (17.2) 372 (11.0), 390 (8.3)	223 (53.0), 234s(35.4) 324 (22.9), 338 (23.5) 380 (13.0), 400 (10.8)	220 (30.7), 234 (29.9), 265 (32.2), 282 (28.0) 303 (20.3), 320 (16.8), 330 (15.7), 366 (8.4) 428 (3.6), 460s(2.5)
e	213 (27.8), 260 (32.2) 327s(18.2), 335 (19.7) 366 (13.4), 384 (10.6)	212 (28.4), 258 (29.6) 324 (19.3), 337 (20.8) 375 (13.8), 392 (10.5)	230s(27.6), 243s(28.2), 272 (42.0), 330 (15.3) 356s (8.3), 422s(3.8), 458s(2.8), 540s(1.0)
f	213 (31.4), 239 (27.4) 316 (16.0), 330 (16.5) 364 (11.3), 382 (9.6)	213 (33.0), 244 (23.5) 316 (14.7), 330 (14.9) 374 (10.0), 388s (8.2)	212 (30.2), 261 (33.9), 293 (12.8), 301 (13.0) 314 (13.7), 357 (6.7), 420 (1.8), 460s(1.3)
g	218 (40.5), 245 (28.9) 342 (19.8), 372 (12.6) 388s(10.0)	216 (30.7), 225s(29.4) 250 (19.7), 257 (18.9) 318 (13.4), 332 (14.4) 380 (18.4), 400 (17.9)	
h	227 (29.8), 248 (16.6) 262 (16.9), 320 (10.5) 334 (11.7), 372 (16.6) 392 (15.8)	216 (35.0), 245 (25.7) 329 (16.6), 341 (18.5) 381 (10.7), 396s(8.8)	

a) s: shoulder. b) **18**: **a**, **d** and **e**; **19**: **f**. c) Containing two drops of 0.5 mol dm^{-3} H_2SO_4 per 10 ml.

acid, **10**, a hydrochloride of **9**, was obtained as a colorless precipitate. The physical data of **10** and **13** are given in Tables 5 and 7.

*Oxidative Degradation of **10h** with Alkaline Hydrogen Peroxide.* To a solution of **10h** (600 mg) in a mixture of 10% NaOH–EtOH (1: 4, 50 ml) was added 3% H_2O_2 (40 ml) and the mixture was stirred at 0 °C for 30 min. After dilution with water (400 ml) the resulting red precipitate was collected by filtration and recrystallized from chloroform to afford 5-amino-4-methoxy-11*H*-indeno[1,2-*c*]isoquinolin-11-one (**14h**) (396 mg, 77.5%), mp 247.5—248 °C; ν_{max} 3500, 3290, and 3130 ($-NH_2$) and 1685 cm^{-1} (>CO); δ(CF_3CO_2H) 8.47—7.17 (7H, m, ArH) and 4.22 (3H, s, $ArOCH_3$). Found: C, 73.74; H, 4.46; N, 10.19%. Calcd for $C_{17}H_{12}N_2O_2$: C, 73.90; H, 4.38; N, 10.14%.

*Zinc Dust Reduction of **14h**.* **14h** (440 mg), zinc dust (2.2 g), and glacial acetic acid (20 ml) were mixed and refluxed for 2 h. The insoluble material was removed by filtration. The filtrate was made basic by the addition of ammonia solution under ice-cooling. The resulting precipitate was collected by filtration and recrystallized from methanol to give pure 5-amino-4-methoxy-11*H*-indeno[1,2-*c*]isoquinoline (375 mg, 90%), mp 193.5—194.5 °C, which was identical with **13g** produced by the cyclization of **1g** in comparison of their TLCs, mps, and IR spectra.

*Acetylation of **9**. General Procedure*: To a mixture of **10** (100 mg) and Ac_2O (10 ml) was added a few drops of concd. H_2SO_4 at room temperature. After being left to stand for a certain time (1 h for **10a**, **10d**, and **10f**; a few min for **10e**), the mixture was poured into ice–water. The precipitated pigment was collected by filtration and crystallized from chloroform. The physical data of the acetamides **18** and **19** are summarized in Tables 6 and 7.

References

1) The numbering of the title compounds appearing in Parts I and II should be corrected as indicated in this paper.

2) a) Part I: K. Ando, T. Tokoroyama, and T. Kubota, *Bull. Chem. Soc. Jpn.*, **47**, 1008 (1974); b) Part II: K. Ando, T. Tokoroyama, and T. Kubota, *ibid.*, **47**, 1014 (1974).

3) T. Tokoroyama, T. Nishikawa, K. Ando, M. Nomura, and T. Kubota, *Nippon Kagaku Kaishi*, **1974**, 136.

4) The free amine (**9**) is liable to be oxidized in the air.[2]

5) D. G. Buckley, E. Ritchie, and W. C. Taylor, *Aust. J. Chem.*, **22**, 577 (1969).

6) 2-Cyanobenzyl cyanide (**4f**) was prepared by treating **3f** with KCN in aqueous ethanol; T. S. Osdene and G. M. Timmis, *J. Chem. Soc.*, **1955**, 2214.

7) Completion of the reaction was checked by TLC (silica gel, benzene, or chloroform).

Nucleophilic Reaction of Electron-deficient Pyridone Derivatives. II. Ring Transformation of 1-Substituted 3,5-Dinitro-4-pyridones with Sodio β-Keto Esters

Eizo MATSUMURA, Masahiro ARIGA,* and Yasuo TOHDA
Department of Chemistry, Osaka Kyoiku University, Tennoji-ku, Osaka 543
(Received October 16, 1979)

The reactions of 1-substituted 3,5-dinitro-4-pyridones [1-substituents: methyl (**1a**), 2-pyridyl (**1b**), 6-methyl-2-pyridyl (**1c**), and 4-pyridyl (**1d**)] with diethyl sodio-3-oxopentanedioate give 1-substituted 3,5-bis(ethoxycarbonyl)-4-pyridones and sodio-1,3-dinitro-2-propane. On the other hand, the reactions of the 4-pyridones (**1b**, **1c**, and **1d**) with ethyl sodioacetoacetate give ethyl 4-hydroxy-3,5-dinitrobenzoate together with aminopyridine homologues, and that of **1a** gives furo[3,2-*b*]pyridine derivative. On the basis of the concept of soft and hard acids and bases, a stepwise nucleophilic attack of the anion of β-keto esters at the electrophilic center of the 2 and 6-positions or 2 and 3-positions of the 4-pyridones is proposed to interpret the variations of the reaction courses.

We have previously shown that 1-substituted 3,5-dinitro-2-pyridones give nitrophenol derivatives and *N*-substituted α-nitroacetamides. A reaction course of the reaction has been elucidated by the isolation of intermediately produced meta-bridging bicyclic addition compounds.[1)]

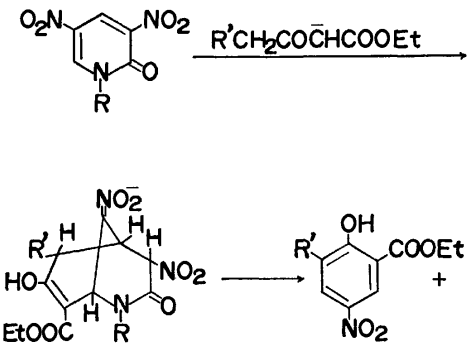

In this paper, we describe the reaction of 1-substituted 3,5-dinitro-4-pyridones with β-keto esters.

Results and Discussion

The reactions of 3,5-dinitro-1-methyl- (**1a**), 3,5-dinitro-1-(2-pyridyl)- (**1b**), 3,5-dinitro-1-(6-methyl-2-pyridyl)- (**1c**), and 3,5-dinitro-1-(4-pyridyl)-4-pyridone (**1d**) with the monosodium salts of β-keto esters were studied.

Treatment of **1a** with 1.5 equivalent amounts of diethyl sodio-3-oxopentanedioate (Na·DOPD) in pyridine gave 3,5-bis(ethoxycarbonyl)-1-methyl-4-pyridone (**2a**). The product **2a** showed strong absorption in the IR at 1735 and 1655 cm^{-1}, indicating the presence of ester carbonyl and pyridone carbonyl groups, respectively. The NMR spectrum of **2a** showed the presence of two ethyl groups. The other signals were very similar to that of the substrate **1a** except for the paramagnetic shift of the ring protons of about 1 ppm. The empirical formula of **2a**, $C_{12}H_{15}NO_5$, supports the structure indicated.

A yellow reisdue obtained after extraction of **2a** with chloroform was confirmed to be a monosodium salt of 1,3-dinitro-2-propanone (**3**), as follows. By coupling[2)] with 1 mol of benzenediazonium chloride at 0 °C, **3**

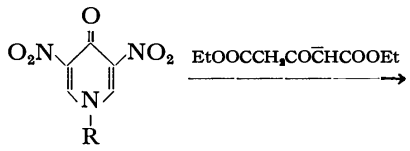

1 (a, b, c, d)

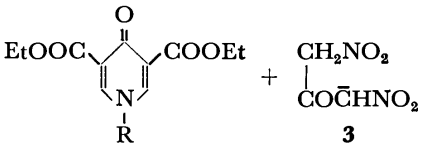

2a: Y. 84.9%
2b: Y. 66.35%
2c: Y. 58.5%
2d: Y. 61.5%

a: R=methyl
b: R=2-pyridyl
c: R=6-methyl-2-pyridyl
d: R=4-pyridyl

yielded yellow powder (**4**) of mp 167.0—168.0 °C, and with two moles of the chloride at 0 °C, another yellow powder (**5**) which decomposed at 138 °C. On the basis of their empirical formulae and their spectral properties, these products were identified as 1,3-dinitro-1-phenylhydrazono-2-propanone (**4**) and 1,3-dinitro-1,3-bis(phenylhydrazono)-2-propanone (**5**), respectively. The latter compound **5** was easily converted to 4-hydroxy-3-nitro-1-phenyl-5-(phenylazo)pyrazole (**6**) with loss of nitrous acid by heating in methanol

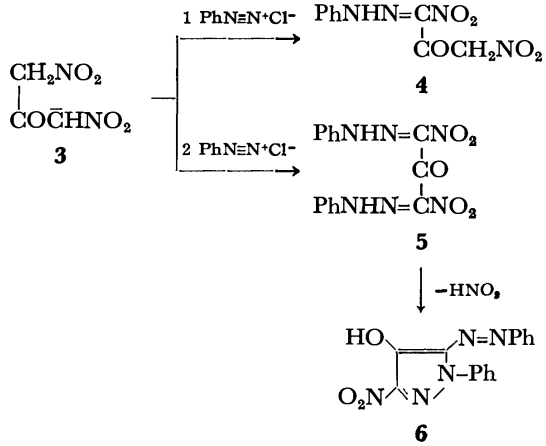

Similarly, treatment of **1b**, **1c**, and **1d** with Na·DOPD gave 3,5-bis(ethoxycarbonyl)-1-(2-pyridyl)- (**2b**), 3,5-bis(ethoxycarbonyl)-1-(6-methyl-2-pyridyl)- (**2c**), and 3,5-bis(ethoxycarbonyl)-1-(4-pyridyl)-4-pyridone (**2d**), respectively. **3** was also isolated from these reactions.

On the other hand, the reaction of **1a** with ethyl sodioacetoacetate (Na·EAA) offered different types of reaction products. First, by treatment of **1a** with Na·EAA in pyridine, colorless needles (**7a**) of mp 127.0—128.0 °C were obtained. The IR spectrum of the product showed the presence of an ester carbonyl group (1765 cm^{-1}) and a nitro group (1515, 1340 cm^{-1}). The NMR spectrum of **7a** indicated the presence of an ethoxyl group, 1.24 ppm (3H, t), 4.26 ppm (2H, q), a bridgehead proton, 6.51 ppm (1H, s), a highly deshielded proton, 8.69 ppm (1H, s), and a hydroxyl proton, 13.12 ppm (1H, s). The empirical formula of **7a** was consistent with $C_{12}H_{14}N_2O_6$. From the above data, 3-ethoxycarbonyl-7-hydroxy-2,4-dimethyl-6-nitro-3a,4-dihydrofuro[3,2-*b*]pyridine was assigned to **7a**.

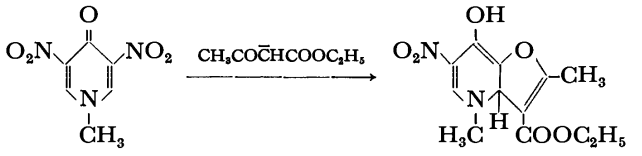

1a **7a**

The reaction of **1b** with Na·EAA was carried out at 65—70 °C in pyridine. On work-up, ethyl 4-hydroxy-3,5-dinitrobenzoate (**8**)[3] and 2-aminopyridine (**9b**) were obtained. Similar results were observed in the reaction of **1c** and **1d** with Na·EAA; the products were **8** and either 2-amino-6-methylpyridine (**9c**) or 4-aminopyridine (**9d**).

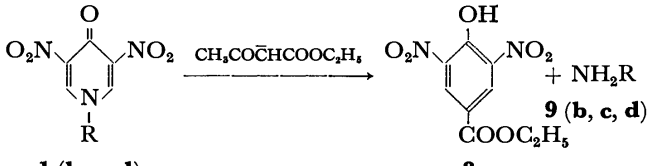

1 (b, c, d) **8** **9 (b, c, d)**

b: R=2-pyridyl
c: R=6-methyl-2-pyridyl
d: R=4-pyridyl

The formation of **2a**, **2b**, **2c**, and **2d** may proceed through a favorable nucleophilic attack of the nucleophile at the 2-position of the 4-pyridone to give the anion **10**, from which anion **11** can be derived by the prototropy. The successive steps to **2** and **3** may involve an intramolecular nucleophilic attack of an anion at the 6-position of the parent 4-pyridone. Scheme 1 may be proposed as one of the most likely reaction courses. The leaving carbanions may be considered to be soft leaving groups.

On the other hand, the formation of **7a** may proceed through the initial attack of a soft nucleophile of the enolate anion of ethyl acetoacetate ($CH_3COCHCOOEt$) at the softer 2-position of the 4-pyridone nucleus. The subsequent intramolecular nucleophilic attack of a harder *O*-anion of **12** at the 3-position of the parent

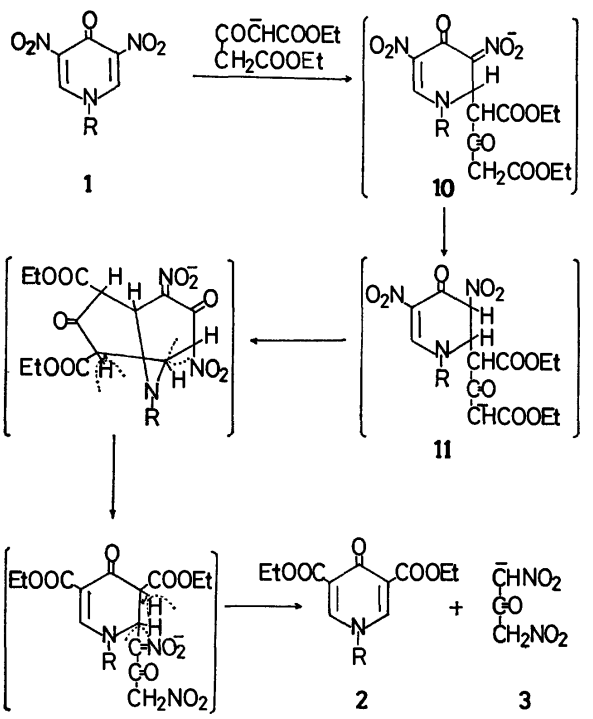

Scheme 1.

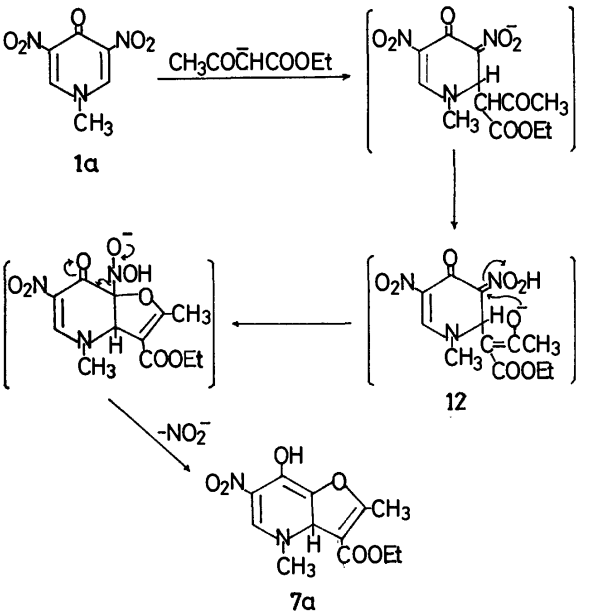

Scheme 2.

4-pyridone nucleus may lead to **7a** by loss of the harder nitrite anion (Scheme 2).

The course of the reaction of **1a** and Na·EAA is very similar to that of 3-bromo-4-nitropyridine *N*-oxide with Na·EAA.[4]

The probable course of the reaction of **1b**—**1d** with Na·EAA is shown in Scheme 3; the electron withdrawing interaction of the 5-nitro group of the parent 4-pyridone would allow the intramolecular nucleophilic attack of the carbanion **13** to lead to a cyclic intermediate **14**. Aromatization of **14** may give **8**

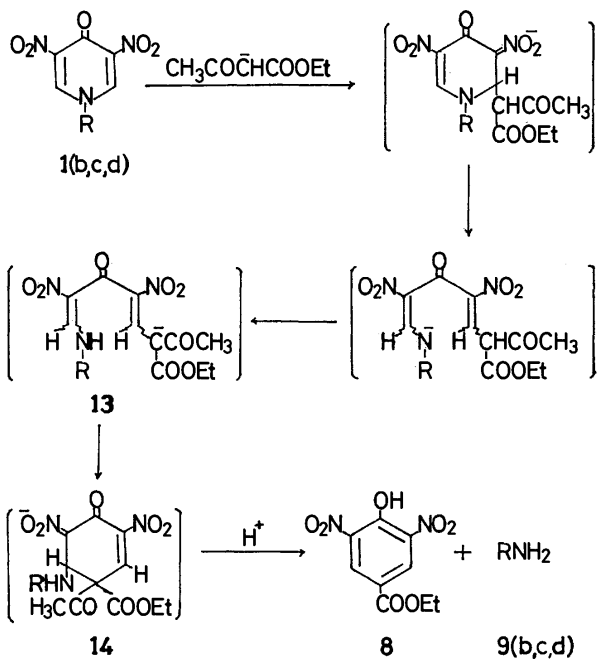

Scheme 3.

and **9**.

In the case of the reaction of **1a** with Na·EAA, the reason why the predominant attack of *O*-anion proceeds at the β-position which is substituted by the nitro group can be explained by the observation that the nature of the leaving group on the alkyl halides affects the proportion of *C* to *O* alkylation of the enolate ion. Sarthou *et al.*[5] concluded that the harder the leaving group, the lower the proportion of *C*-alkylation. A harder nitrite anion, however, classified as a border-line base, may be a favorable leaving group in the intramolecular nucleophilic substitution.

The difference between the reaction paths of **1a** with Na·EAA and those of **1b**—**1d** evidently depend upon the electronic behavior of the *N*-substituents of the 4-pyridone nucleus. The interaction of the electron donating 1-methyl group with the electron attracting β-nitro group may favor an initial attack of the soft end of the nucleophile at the 2-position of 4-pyridone nucleus without ring fission. The subsequent attack of the *O*-anion is promoted by the resonance interaction of the β-nitro group. On the other hand, the electron withdrawing 1-substituents such as 2-pyridyl and 4-pyridyl groups may reduce the resonance interaction of the 1-nitrogen atom with the β- or β′-nitro group; then the initial attack of the soft nucleophile at the somewhat harder 2-position of the 4-pyridone can not be allowed without the subsequent fission of the C_2–N bond.

In spite of the similar conditions, we find a remarkable difference of the reaction paths between the reaction of 1-substituted 3,5-dinitro-4-pyridones with Na·DOPD and those with Na·EAA. With 1-substituted 3,5-dinitro-4-pyridones and Na·DOPD, **2** were always obtained by the C_5 and C_3-anion heterolysis of the C_5–C_6 and C_2–C_3 bonds of the 4-pyridone nucleus. On the other hand, similar reactions with Na·EAA were affected not only by the nucleophile but also by the 1-substituted group.

Experimental

All the melting points are uncorrected. The IR spectra were obtained on a Hitachi EPI-S2 as Nujol muls. The NMR spectra were recorded on a Hitachi R 20-B with TMS as the internal standard.

3,5-Dinitro-1-methyl-4-pyridone (1a). Five grams of 1-methyl-4-pyridone[6] was dissolved in 50 ml of fuming sulfuric acid (30% SO_3), then 25 g of potassium nitrate was added in portions with cooling. The mixture was heated at 110 °C for 5 h and then poured onto crushed ice. Crystalline precipitates were recrystallized from water to give 4.8 g (52.1%) of **1a**, mp 214.0—215.0 °C. IR: 1680 cm^{-1} (C=O), 1550, 1360 (NO_2). NMR (DMSO-d_6): δ 3.90 (3H, s), 8.95 (2H, s). Found: C, 36.11; H, 2.63; N, 20.89%. Calcd for $C_6H_5N_3O_5$: C, 36.19; H, 2.53; N, 21.10%.

3,5-Dinitro-1-(2-pyridyl)-4-pyridone (1b). A mixture of 2-bromopyridine and sodium salt of 4-hydroxypyridine in DMSO was heated at 150 °C for 8 h to give 1-(2-pyridyl)-4-pyridone in 76.9% yield. This pyridone was treated with 10 equimolar amounts of potassium nitrate in fuming sulfuric acid (30% SO_3) at 130 °C for 10 h to give **1b** in 31.4% yield; mp 219.5—220.0 °C (water). IR: 1675 cm^{-1} (C=O), 1520, 1360 (NO_2). NMR (DMSO-d_6): δ 7.60 (1H, m), 8.12 (2H, m), 8.62 (1H, dd), 9.59 (2H, s). Found: C, 45.65; H, 2.20; N, 21.47%. Calcd for $C_{10}H_6N_4O_5$: C, 45.81; H, 2.31; N, 21.37%.

3,5-Dinitro-1-(6-methyl-2-pyridyl)-4-pyridone (1c). 1-(6-Methyl-2-pyridyl)-4-pyridone, prepared from sodium salt of 4-hydroxypyridine and 2-bromo-6-methylpyridine, was worked up according to the preceding method to give **1c** in 24.0% yield; mp 245.0—246.0 °C (aqueous acetic acid). IR: 1675 cm^{-1} (C=O), 1520, 1360 (NO_2). NMR (DMSO-d_6): δ 3.31 (3H, s), 7.4 (1H, m), 7.8 (2H, m), 9.61 (2H, s). Found: C, 47.99; H, 2.88; N, 19.90%. Calcd for $C_{11}H_8N_4O_5$: C, 47.83; H, 2.92; N, 20.24%.

3,5-Dinitro-(4-pyridyl)-4-pyridone (1d). 1-(4-Pyridyl)-4-pyridone[7] was treated as above to give **1d** in 36.2% yield; mp 242.0—243.0 °C (water). IR: 1680 cm^{-1} (C=O), 1520, 1315 (NO_2). NMR (DMSO-d_6): δ 7.81 (2H, dd), 8.82 (2H, dd), 9.31 (2H, s). Found: C, 45.49; H, 2.23; N, 21.37%. Calcd for $C_{10}H_6N_4O_5$: C, 45.81; H, 2.31; N, 21.37%.

Reaction of 3,5-Dinitro-1-methyl-4-pyridone (1a) with Na·DOPD. To a solution of 1.0 g of **1a** in 100 ml of pyridine was added a pyridine solution (20 ml) of Na·DOPD, prepared from 0.17 g of sodium and 1.7 g of diethyl 3-oxopentanedioate, with cooling. The mixture was heated at 50 °C for 5 h. The solvent was evaporated under reduced pressure, and the residue was extracted with $CHCl_3$. After the solvent was distilled off, the residual cake was rinsed with a small amount of diethyl ether, and recrystallized from benzene to give 1.08 g (84.9%) of 3,5-bis(ethoxycarbonyl)-1-methyl-4-pyridone (**2a**); colorless plates, mp 138.0—139.0 °C. IR: 1735 cm^{-1} (C=O), 1655 (C=O). NMR ($CDCl_3$): δ 1.31 (6H, t), 3.73 (3H, s), 4.28 (4H, q), 7.92 (2H, s). Found: C, 56.70; H, 5.95; N, 5.26%. Calcd for $C_{12}H_{15}NO_5$: C, 56.92; H, 5.93; N, 5.53%.

The residual powder which did not dissolve in $CHCl_3$ was washed with ethanol, and was dissolved in 50 ml of cold water. To this solution 10 g of sodium acetate was added, then aqueous benzenediazonium chloride solution formed from 0.5 g of aniline and 0.4 g of sodium nitrite was added dropwise at 0 °C. The precipitates were collected by filtration and were rinsed with methanol to give 0.40 g (31.7%) of 1,3-dinitro-1-phenylhydrazono-2-propanone (**4**); mp 167.0—

168.0 °C. IR: 3200 cm^{-1} (N–H), 1720 (C=O), 1530, 1330 (NO_2). NMR (acetone-d_6): δ 6.10 (2H, s), 7.25—7.80 (5H, m), 12.40 (1H, b, s). Found: C, 43.43; H, 3.14; N, 23.54%. Calcd for $C_9H_8N_4O_5$: C, 42.86; H, 3.20; N, 22.22%.

When three equimolar amounts of benzenediazonium chloride were used, 1,3-dinitro-1,3-bis(phenylhydrazono)-2-propanone (**5**) was obtained in 35.7% yield; dec. 138 °C. IR: 3230 cm^{-1} (N–H), 1700 (C=O), 1530, 1350 (NO_2). NMR (acetone-d_6): δ 7.1—7.7 (10H, m), 12.48 (2H, b. s). Found: C, 50.68; H, 3.10; N, 23.64%. Calcd for $C_{15}H_{12}N_6O_5$: C, 50.56; H, 3.39; N, 23.59%.

*3,5-Bis(ethoxycarbonyl)-1-(2-pyridyl)-4-pyridone (**2b**).* One gram of **1b** was treated according to the manner described above to give 0.8 g (66.3%) of **2b**; colorless prisms (benzene), mp 150.0—151.0 °C. IR: 1715 cm^{-1} (C=O), 1665 (C=O). NMR ($CDCl_3$): δ 1.32 (6H, t), 4.31 (4H, q), 7.4 (2H, m), 7.9 (1H, m), 8.53 (1H, dd), 8.93 (2H, s). Found: C, 61.03; H, 4.96; N, 8.98%. Calcd for $C_{16}H_{16}N_2O_5$: C, 60.75; H, 5.10; N, 8.86%.

*3,5-Bis(ethoxycarbonyl)-1-(6-methyl-2-pyridyl)-4-pyridone (**2c**).* From 1.0 g of **1c**, 0.75 g (58.5%) of **2c** was obtained; colorless prisms (benzene), mp 168.5—169.5 °C. IR: 1750 cm^{-1} (C=O), 1675 (C=O). NMR ($CDCl_3$): δ 1.42 (6H, t,) 2.62 (3H, s), 4.33 (4H, q), 7.2 (2H, m), 7.82 (1H, t), 8.81 (2H, s). Found: C, 62.02, H, 5.56; N, 8.54%. Calcd for $C_{17}H_{18}N_2O_5$: C, 61.81; H, 5.49; N, 8.48%.

*3,5-Bis(ethoxycarbonyl)-1-(4-pyridyl)-4-pyridone (**2d**).* From 1.0 g of **1d**, 0.75 g (61.9%) of **2d** was yielded; colorless plates (benzene), mp 201.0—202.0 °C. IR: 1755 cm^{-1} (C=O), 1650 (C=O). NMR ($CDCl_3$): δ 1.32 (6H, t), 4.33 (4H, q), 7.39 (2H, dd), 8.34 (2H, s), 8.82 (2H, dd). Found: C, 60.98; H, 5.11; N, 8.67%. Calcd for $C_{16}H_{16}N_2O_5$: C, 60.75; H, 5.10; N, 8.86%.

*4-Hydroxy-3-nitro-1-phenyl-5-(phenylazo)pyrazole (**6**).* A mixture of 0.1 g of **5** and 100 ml of methanol was refluxed for 2h, and the solvent was evaporated to half volume. 0.08 g (93.2%) of **6** was precipitated; red needles (methanol), mp 218.0—219.0 °C. IR: 3400 cm^{-1} (O–H), 1590 (C=N), 1520, 1345 (NO_2). Found: C, 58.32; H, 3.43; N, 22.63%. Calcd for $C_{15}H_{11}N_5O_3$: C, 58.25; H, 3.59; N, 22.65%.

*Reaction of **1a** with Na·EAA.* To a solution of 0.5 g of **1a** in 25 ml of pyridine was added a solution of Na·EAA, prepared from 0.17 g of sodium and 1.10 g of ethyl acetoacetate, in 25 ml of pyridine with cooling. The mixture was heated at 65—70 °C for 5 h. Pyridine was evaporated under reduced pressure, the residue was acidified to pH 3 with dil. HCl, extracted with $CHCl_3$. After the extract was dried over anhydrous sodium sulfate, the solvent was distilled off, and the residual syrup was chromatographed on a silica gel column. From the chloroform elute, 0.17 g (16.2%) of 3-ethoxycarbonyl-7-hydroxy-2,4-dimethyl-6-nitro-3a,4-dihydrofuro[3,2-*b*]pyridine (**7a**) was obtained; colorless needles (ethanol–diisopropyl ether), mp 127.0—128.0 °C. Found: C, 51.12; H, 4.90; N, 9.69%. Calcd for $C_{12}H_{14}N_2O_6$: C, 51.06; H, 5.00; N, 9.93%.

*Reaction of **1b** with Na·EAA.* A mixture of 0.5 g of **1b** and Na·EAA, prepared from 0.13 g of sodium and 0.8 g of ethyl acetoacetate, in 50 ml of pyridine was heated at 65—70 °C for 5 h. Pyridine was evaporated under reduced pressure. To the residue ethanol was added and evaporated to dryness. The residue was extracted with $CHCl_3$. Evaporation of $CHCl_3$ gave crude 2-aminopyridine (**9b**), which was purified by column chromatography on silica gel, using diethyl ether for eluent, to give 0.11 g (61.5%) of pure sample. The chloroform insoluble layer was acidified with dil. HCl to pH **3**, extracted with $CHCl_3$, and dried over anhydrous sodium sulfate. The solvent was distilled off and the residue was chromatographed on a silica gel column. From the benzene elute, 0.33 g (65.0%) of ethyl 4-hydroxy-3,5-dinitrobenzoate (**8**) was obtained; pale yellow needles (petroleum benzine), mp 88.0—89.0 °C (lit. mp 87 °C).[3] IR: 3300 cm^{-1} (O–H), 1730 (C=O), 1540, 1340 (NO_2). NMR ($CDCl_3$): δ 1.40 (3H, t), 4.41 (2H, q), 8.94 (2H, s), 11.0 (1H, b. s). Found: C, 42.37; H, 3.43; N, 10.79%. Calcd for $C_9H_8N_2O_7$: C, 42.19; H, 3.15; N, 10.94%.

When the reaction mixtrue was worked up without preceeding extraction with $CHCl_3$, 0.53 g (85.3%) of salt of 2-aminopyridine with **8** was obtained; yellow needles (ethanol), mp 217.0—218.0 °C. IR: 3400, 3250, 3200 cm^{-1} (N–H), 1720 (C=O), 1560, 1340 (NO_2). NMR (DMSO-d_6): δ 1.28 (3H, t), 4.21 (2H, q), 7.7—8.1 (2H, m), 8.7—9.2 (2H, m) 8.5—10.0 (3H, br), 9.20 (2H, s). Found: C, 48.32; H, 3.67; N, 16.29%. Calcd for $C_{14}H_{14}N_4O_7$: C, 48.00; H, 4.03; N, 16.00%.

*Reaction of **1c** with Na·EAA.* A similar treatment of 0.5 g of **1c** with Na·EAA gave 0.12 g (66.9%) of 2-amino-6-methylpyridine (**9c**) and 0.35 g (72.9%) of **8**.

*Reaction of **1d** with Na·EAA.* From 0.3 g of **1d**, 0.1 g (55.95%) of 4-aminopyridine (**9c**) and 0.26 g (51.0%) of **8** were obtained.

References

1) E. Matsumura, M. Ariga, and Y. Tohda, *Bull. Chem. Soc. Jpn.*, **52**, 2413 (1979); *Tetrahedron Lett.*, **1979**, 1393.
2) S. M. Parmeter, *Org. React.*, **10**, 1 (1959).
3) K. Ishihara, *Yakugaku Zasshi*, **49**, 902 (1929).
4) E. Matsumura and M. Ariga, *Bull. Chem. Soc. Jpn.*, **46**, 3144 (1973).
5) P. Sarthou, F. Guilbe, and G. Bram, *Chem. Comm.*, **1974**, 377.
6) T. Takahashi and F. Yoneda, *Chem. Pharm. Bull. (Tokyo)*, **6**, 365 (1958).
7) P. A. de Villers and H. J. den Hertog, *Recl. Trav. Chim. Pays-Bas*, **76**, 647 (1957).

Steric Effect in Regioselective Cyclization of 3,4-Epoxy Alcohols to Oxetanes[1)]

Tadashi MASAMUNE,* Shingo SATO, Atsushi ABIKO, Mitsunori ONO, and Akio MURAI
Department of Chemistry, Faculty of Science, Hokkaido University, Sapporo 060

(Received December 3, 1979)

A number of 3,4-epoxy alcohols, involving critical structural factors for oxetane formation by intramolecular cyclization, were prepared and treated with base under aqueous (KOH in 75% aq DMSO) and anhydrous conditions (NaH in THF). The result of the reactions of *cis*- and *trans*-4,5-epoxy-2-methyl-2-undecanols, coupled with that of 1-(2,3-epoxybutyl)- and 1-(2,3-epoxy-3-methylbutyl)-1-cyclohexanols (**1a** and **1b**), indicated that the regioselective oxetane formations of 3,4-epoxy alcohols with alkoxide anions are much insensitive to steric hindrance at the attacked oxirane rings, compared with the corresponding reactions with carbanions, while that of 1-(2,3-epoxypropyl)-1-cycloalkanols revealed that the relevant reactions depend on bulkiness of attacking alkoxide anions. Moreover, the result of the reactions of 1-(1,2-epoxycycloalkyl)-2-methyl-2-propanols under the aqueous conditions demonstrated that the oxetane formations are affected seriously by steric hindrance at the attacked oxirane rings, although the result was in striking contrast with the corresponding result with carbanions. On the other hand, the reactions of 3,4-epoxy alcohols under the anhydrous conditions proceeded in different manner, depending on the structures of the epoxides; namely, fragmentation took place as major reactions with some epoxides, while intramolecular cyclization occurred predominantly with other epoxides.

In previous papers[2a)] we reported that treatment of 1-(2,3-epoxypropyl)-1-cyclohexanol (**1**) and its methyl analogues with base in 75% aqueous dimethyl sulfoxide (DMSO) produced the corresponding four-membered ether (oxetane) (**2**) and its methyl analogues as the sole cyclized products other than hydrolysis products (**3**), while the treatment under anhydrous conditions in aprotic solvents led to formation of a dimeric five-membered ether (oxolane) (**4**) or of a simple alcoholysis product.[2b)] The regioselective formation of oxetanes was rationalized[2b)] mainly in terms of "collinearity requirement," which was proposed first by Stork and coworkers[3)] on the basis of the regioselective cyclization of 4,5-epoxy nitriles to cyclobutanes (Scheme 1, i-a), and accentuated later by Still[4)] from intramolecular cyclization of allyl 2,3-epoxyalkyl ether to a four-membered ring (oxetane) (Scheme 1, ii-a). However, Lallemand and Onanga[5)] criticized their explanation from the result of preferential cyclizations of "non-rigid" *trans*- and *cis*-3,4-epoxy nitriles to cyclopentanes and cyclobutanes, respectively, (Scheme 1, iii, *cf.*, i-b and i-c) and emphasized the importance of "steric hindrance" at the oxirane rings towards the attack of carbanions rather than the "requirement." Moreover, Stork and coworkers[3)] pointed out the effect of "bond distortion" as one of the factors which control the "requirement" on the basis of the result of the cyclizations of 4,5-epoxy nitriles. These apparently inconsistent facts on steric factors concerning the oxirane

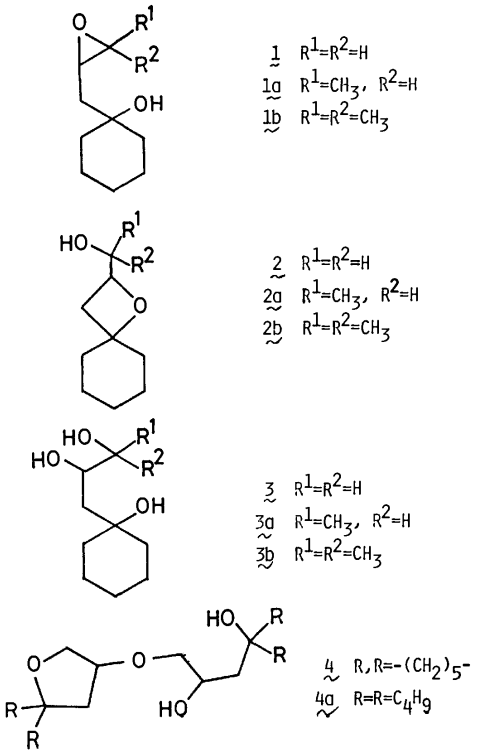

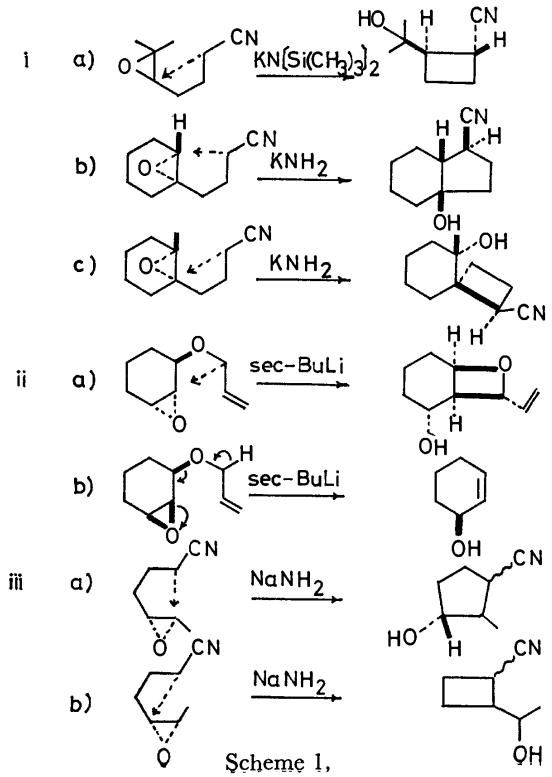

Scheme 1.

ring cleavage[6] prompted us to investigate the reactions of 3,4-epoxy alcohols, whose structures are closely related to the geometrical features of the above reactions, with base under the aqueous conditions. The results corroborating the relevant regioselectivity have recently been reported in preliminary form,[7] and the details are described in the present paper with additional results on the reactions carried out under anhydrous conditions.

Aqueous Conditions. I. Non-fused System.[8] *cis*- and *trans*-4,5-Epoxy-2-methyl-2-undecanols (**5** and **6**) were prepared by epoxidation[9] of the corresponding alkenols, *cis*- and *trans*-2-methyl-4-undecen-2-ols (**7** and **8**), as depicted in Scheme 2. These epoxy alcohols (**5** and **6**), corresponding to Lallemand's *cis*- and *trans*-4,5-epoxy nitriles (Scheme 1, iii), were submitted to base treatment under the controlled conditions [10 equiv KOH in 75% aq DMSO, 105—110 °C (bath temp), 2 h].[10] The reaction of *cis*-epoxide (**5**) proceeded as expected to give the corresponding oxetane (**9**) and hydrolysis product (triol) (**10**) in 40 and 30% yields with the recovered epoxide (**5**, 15%). In accordance with the assigned oxetane structure, compound **9** exhibited a strong absorption at 964 cm^{-1} in the IR spectrum and displayed signals due to protons at C-3 and C-2 on the oxetane (not oxolane) ring at δ 2.18 (2H, d, J=8 Hz) and 4.40 (1H, dt, J=5 and 8 Hz) in the NMR spectrum. These spectral patterns were characteristic of oxetanes, as had been demonstrated previously.[2] The same reaction of *trans*-epoxide **6** gave almost the same result; namely, the corresponding oxetane (**11**) and triol (**12**) were isolated in 50 and 19% yields, respectively, with the recovered epoxide (**6**, 8%). The structure of oxetane **11** was also clarified by the spectral data: IR, 984 and 960 cm^{-1}; NMR, δ 2.10 and 2.30 (each 1H, dAB_q, J=12 and 8 Hz, 3-H) and 4.53 (1H, dt, J=4 and 8 Hz, 2-H). The reaction result, in contrast with the Lallemand result (preferential cyclopentane formation from the *trans*-epoxy nitriles),[5] indicates that the intramolecular reactions of non-rigid 3,4-epoxy alcohols with alkoxide anions in 75% aqueous DMSO are much insensitive to steric hindrance at the attacked oxirane, compared with those with carbanions.

In connection with this, we treated 1-(2,3-epoxybutyl)-1-cyclohexanol[2] (**1a**) and its 3-methyl analogue (**1b**) with base under almost the same aqueous conditions. The latter epoxide (**1b**) could be prepared by epoxidation of the corresponding olefin[2a] with *m*-chloroperbenzoic acid (MCPBA) in an alkaline "biphasic" solvent system[11] in a 91% yield, although the compound (**1b**) was very sensitive to acid and converted readily into the corresponding oxolane, as had been described previously.[2a] Interestingly, both the epoxy alcohols (**1a** and **1b**) gave the corresponding oxetanes (**2a** and **2b**) in practically the same yields (73 and 72%) along with the simple hydrolysis products (**3a** and **3b**) (9 and 8%). This result indicates that yields of the oxetanes formed do not always increase with the number of substituents on the oxirane ring, supporting the aforementioned insensitivity to steric hindrance at the attacked oxirane rings in the oxetane formation.

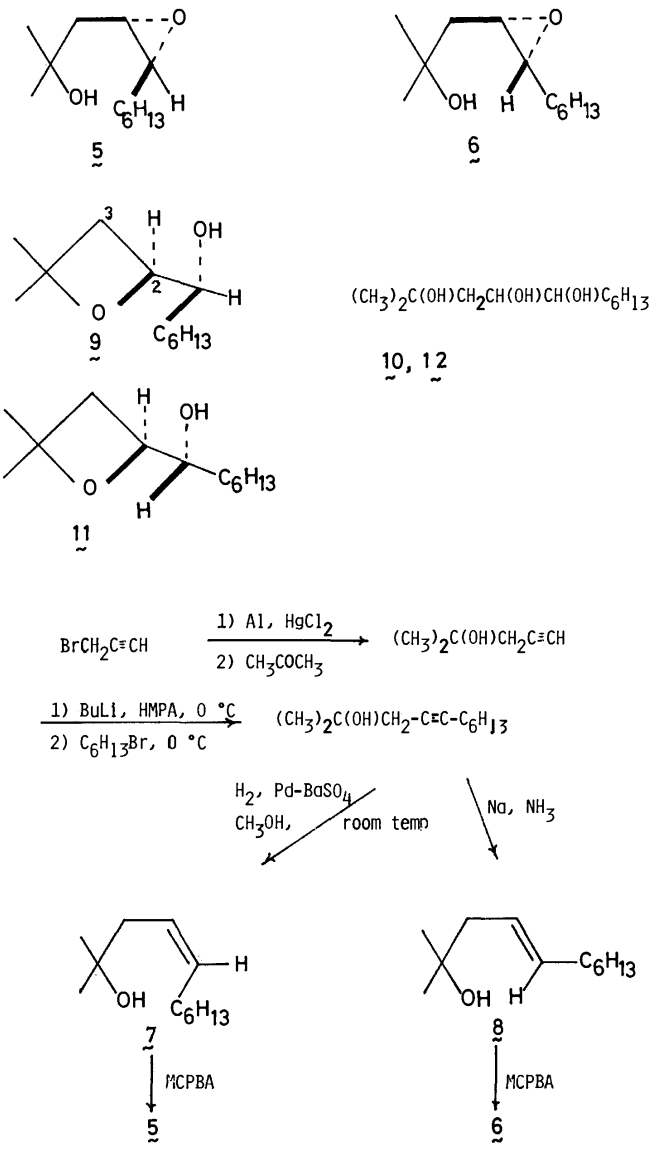

Scheme 2.

Moreover, the fact that these oxetanes (**2a** and **2b**) were formed in better yields (73%) than oxetanes **9** and **11** (40 and 50%) led us to have interest in examining the effect of the bulkiness of the attacking alkoxide anions in the relevant cyclization.

Four 1-(2,3-epoxypropyl)-1-cycloalkanols (**1**, **13**—**15**), differing only in bulkiness of the attacking anions, were used for the examination; namely, the cyclohexanol[2] (**1**), cycloheptanol (**13**), cyclooctanol (**14**), and 4-butyl-1,2-epoxy-4-octanol (**15**) were prepared from the corresponding olefins as described in Scheme 3 and treated with base under the relevant aqueous conditions. The result is summarized in Table 1. The structures of these products were deduced mainly from the spectral data, as exemplified by those of oxetane **18**, which showed a strong absorption at 965 cm^{-1} in the IR spectrum and exhibited a two-proton doublet (J=8 Hz) at δ 2.21 and one proton multiplet at δ 4.60 due to protons at C-3 and C-2 on the oxetane ring, respectively, and also two double doublets (each 1H, dAB_q, J=12, 5 and 12, 3.5 Hz) due to two hydroxymethyl

Table 1. Reactions of 1-(2,3-epoxypropyl)-1-cycloalkanols (**1**, **13**—**15**) with base under aqueous conditions[a)]

Compound	Temp/°C	Time/min	Oxetane[b)]	Triol[b)]
1	135	90	**2** (49)	**3** (32)
13	135	90	**16** (25)	**19** (55)
14	80	100	**17** (20)	**20** (60)
15	65	100	**18** (20)	**21** (60)

a) Ten equiv KOH in 75% aq DMSO. b) The figures in parentheses denote "isolated yields."

protons at δ 3.54 and 3.68, respectively. As shown in Table 1, only the corresponding oxetanes and triols were isolated in all the cases. However, the yield of oxetanes decreased in the order of increasing ring size. The result, coupled with the aforementioned one (**1a** and **2a**), implies that the increasing bulkiness of attacking alkoxide anions considerably suppresses the intramolecular reaction (oxetane formation) rather than the intermolecular (hydrolysis).

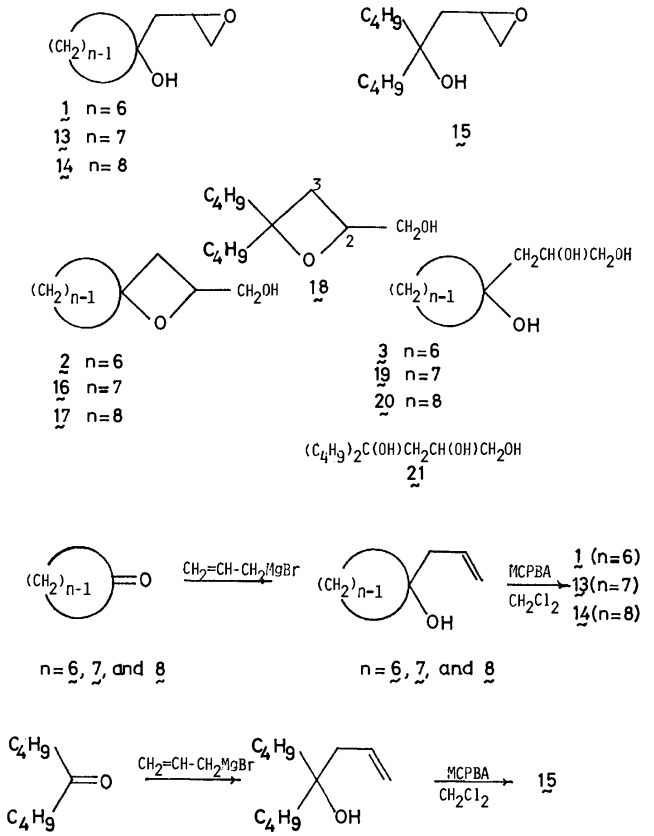

Scheme 3.

Aqueous Conditions. II. Fused System.[8)] Four 1-(1,2-epoxycycloalkyl)-2-methyl-2-propanols (**22**—**25**), were prepared from cycloalkanones *via* six-step processes as described in Scheme 4. These 3,4-epoxy alcohols, in each of which an oxirane ring is fused with a cycloalkane ring, correspond to Stork's fused 4,5-epoxy nitriles[3)] (Scheme 1, i-b). Treatment of the compounds with base under almost the same aqueous conditions produced multi-component mixtures, which were separated by preparative TLC, respectively. The structure and yield of identified products are summarized in Table 2. A typical example of the structure elucidation is illustrated by the oxolane (**29**) in the Table. The MS [*m/e* 170 (M^+), 155, and 137], IR [3600, 3420, 1150, and 1035 cm^{-1}], and NMR spectra [δ 1.35 (6H, s, $2CH_3$), 1.84 and 1.94 (each 1H, d, J=13 Hz, 3-H)] were consistent with the assigned structure. The relevant bridge-head proton on the carbon (C-7a) adjacent to the oxolane oxygen atom was observed at δ 3.79 as a triplet with J=4 Hz. The coupling constant indicates that the oxolane C-7a–O bond is oriented axial and

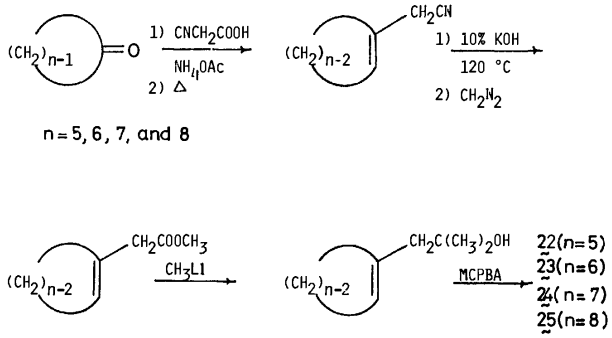

Scheme 4.

Table 2. Reactions of 1-(1,2-epoxycycloalkyl)-2-methyl-2-propanols (**22**—**25**) with base under aqueous conditions[a)]

Compound	Temp/°C	Time/min	Products[b)]			
			Oxetane	Oxolane	Triol	Diol
22	135	90	**26** (35)	—	(17)	**31** (8)
23	140	90	**27** (46)	**29** (7)	(12)	—
24	115	110	**28** (24)	**30** (22)	—	**32** (9)
25	140	150	—	—	—	—

a) Ten equiv KOH in 75% aq DMSO. b) The figures in parentheses denote "isolated yields."

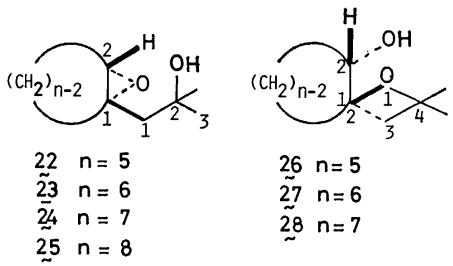

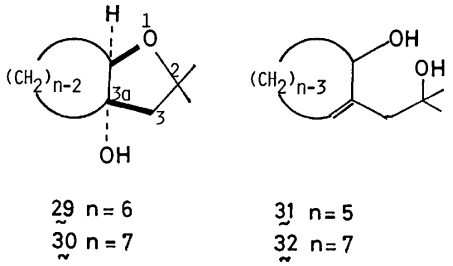

hence the oxolane C-3a–C-3 bond must be equatorial in respect to the cyclohexane ring. This assignment demonstrates that the oxolane (**29**) was formed by attack of the alkoxide anion to the oxirane ring from the back side.[6c,12] The configurations of all products in Table 2 were assigned on the basis of the spectral data and the back-side attack.

As shown in Table 2, the cyclopentene and cyclohexene oxides (**22** and **23**) afforded the corresponding oxetanes (**26** and **27**) as the sole and major cyclized products, respectively. However, the cycloheptene oxide (**24**) gave both the corresponding oxetane and oxolane (**28** and **30**) in almost the same yields, while the cyclooctene oxide (**25**) underwent no oxirane ring cleavage. In connection with this, simple (unsubstituted) cycloalkene oxides (**33**—**36**) were treated under almost the same conditions [10 equiv KOH in 75% aq DMSO, 100—110 °C (bath temp)]. While cyclohexene oxide

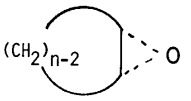

33 n = 6
34 n = 7
35 n = 8
36 n = 12

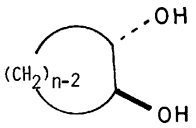

37 n = 6
38 n = 7

(**33**) was hydrolyzed rapidly to yield cyclohexane-1,2-diol (**37**) (100% within 0.5 h), cycloheptene oxide (**34**) reacted relatively slowly giving the corresponding diol (**38**) in 70 and 80% yields after 0.5 and 3 h, respectively. On the other hand, cyclooctene and cyclododecene oxides (**35** and **36**) were recovered unchanged almost quantitatively after 3 h treatment. The reactivity in the hydrolysis of these simple cycloalkene oxides clearly reflects steric hindrance against the back-side attack of hydroxide anions to the oxirane carbon atoms. Examination of the Dreiding model reveals that the hindrance also make it difficult to achieve the "collinear arrangement" for the intramolecular cyclization leading to formation of oxetane rather than that of oxolane. The result of the reactions of compounds **24** and **25** with fused medium-sized cycloalkane rings illustrates oxetane formation which is affected seriously by the "steric hindrance" under the relevant aqueous conditions. Nevertheless, the result shown in Table 2 is in striking contrast with the Stork's result. In summary, the oxetane formation from 3,4-epoxy alcohols, apart from the compounds with the afore-mentioned exceptional structural features (*e.g.*, compounds **24** and **25**), under the aqueous conditions proceeds regioselectively and would be rationalized mostly in terms of the "collinearity requirement" in the transition state, though it obviously depends on "steric effect" to some extent.

Anhydrous Conditions. Two non-fused compounds **1b** and **15** and three fused compounds **23**, **24**, and **25** were examined under anhydrous conditions. Compound **15**, when treated with sodium hydride (NaH) in tetrahydrofuran (THF) under reflux, gave the corresponding dimeric oxolane (**4a**) in a 60% yield as expected from the result of the reactions of related compounds.[2a] However, the same treatment of **1b** produced the corresponding oxetane (**2b**) in a 30% yield as a sole cyclized product, leaving a considerable amount (57%) of the starting epoxide (**1b**) unchanged. The fact offers the first example indicating importance of the steric hindrance in oxirane ring opening in anhydrous aprotic solvents. This apparently unexpected result, which is also inconsistent with "Thorpe-Ingold effect,"[13] seems to be in line with our previous rationalization proposed for the solvent dependency in ring closure;[2a] namely, "the cyclization in question in anhydrous aprotic solvents would proceed with displacement at the less-substituted carbon of the oxirane ring, leading to formation of oxygen heterocycles with less steric constraint." However, for want of other examples, we do not prefer to make further mechanistic discussion.

Treatment of the fused compounds (**23**—**25**) with base under almost the same anhydrous conditions resulted in fragmentation as the respective main reactions. The cyclohexene oxide (**23**), when treated with NaH in refluxing THF, gave a complex mixture, from which 2-methylenecyclohexanol (**39**) was isolated as a major product (38%) along with the corresponding oxetane (**27**) (27%) and 1-(2-hydroxy-2-methylpropyl)-2-cyclohexene-1-ol (**40**) (9%) by preparative TLC. The same treatment of the cycloheptene and cyclooctene oxides (**24** and **25**) afforded the corresponding 2-methylenecycloalkanols (**41** and **42**) in 55 and 18% yields, respectively, with recovery of the starting epoxides (**24** and **25**, 9 and 52%), no other compounds being detected. Formation of these 2-methylenecycloalkanols (**39**, **41**, and **42**) and cyclohexenol (**40**) might

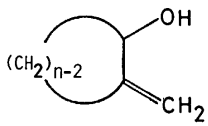

39 n = 6
41 n = 7
42 n = 8

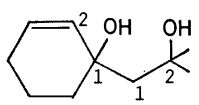

40

be understood as results of usual fragmentation reactions, route a (*cf.*, Scheme 1, ii-b) and route b, as shown in Scheme 5, indicating the special character of 75% aqueous DMSO as a solvent system. However, the

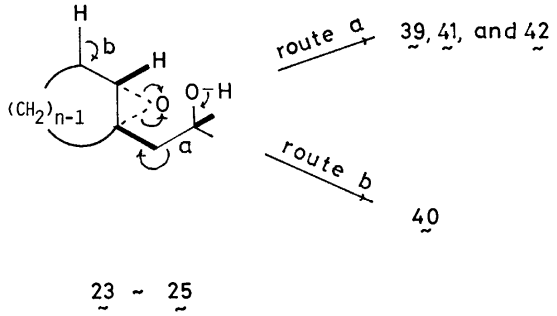

Scheme 5.

reason why the fragmentation occurred predominantly with the fused epoxy alcohols and that why the oxetane (**27**) was formed in preference to the corresponding oxolane (**29**), were explained only with difficulty. In view of the remarkable contrast of the results between the aqueous and anhydrous conditions as well as between the non-fused and fused compounds, we only emphasize that the present results provide intrinsic problems for the mechanistic studies involving steric factors, solvent effects, and others.

Experimental

All the melting and boiling points were uncorrected. The homogeneity of each compound was always checked by TLC over silica gel (Wakogel B-5F) with various solvent systems, and the spots were developed with cerium(IV) sulfate in dil sulfuric acid. The IR and NMR (100 MHz) spectra were measured in liquid state and in chloroform-*d*, respectively, unless otherwise stated. The abbreviations "s, d, t, m, and br" in the NMR spectra denote "singlet, doublet, triplet, multiplet, and broad," respectively. The preparative TLC and column chromatography were carried out over silica gel (Wakogel B-5F) and silicic acid (Merck, Kieselgel 60, 70—230 mesh), respectively. The following solvents were distilled before use after being dried; ether and THF from lithium aluminium hydride (LAH); dichloromethane from phosphorus pentaoxide; DMSO and hexamethylphosphoramide (HMPA) from calcium hydride. The latter two solvents were stored over Molecular Sieve.

*Preparation of 1-(2,3-Epoxy-3-methylbutyl)-1-cyclohexanol (**1b**).* A mixture of 1-(3-methyl-2-butenyl)-1-cyclohexanol[28a] (116 mg) in dichloromethane (5 ml) and 0.5 M aq sodium hydrogencarbonate ($NaHCO_3$, 4 ml) (pH 8.3) was stirred with MCPBA (173 mg, purity 90%) at 0 °C for 30 min.[9] The mixture was washed with 5% aq sodium thiosulfate ($Na_2S_2O_3$), 5% aq $NaHCO_3$ and water, dried and evaporated to leave **1b** (119 mg), oily; MS, *m/e* 184 (M^+) and 166; IR ($CHCl_3$), 3620, 3460, 1110, 1035, 1010, and 910 cm^{-1}; NMR, δ 1.29 and 1.35 (each 3H, s, CH_3 at C-3), and 3.04 (1H, dd, J=5 and 8 Hz, 2-H). The oil was used for the next reaction without further purification.

Preparation of cis- *and* trans-*4,5-Epoxy-2-methyl-2-undecanols (**5** and **6**). i)*: To a solution of 2-methyl-4-pentyn-2-ol[14] (3.0 g, 0.03 mol) in dry HMPA (80 ml) cooled with an ice–water bath was added 15% butyllithium in hexane (40 ml) under stirring. The mixture was stirred at 0 °C for 40 min and then warmed at *ca.* 25 °C under reduced pressure, when the hexane had been removed. To the residue was added freshly distilled hexyl bromide (8 g, 0.048 mol) dropwise at 0 °C, and the mixture was stirred at 0—15 °C for 18 h and at 40—50 °C for 1 h, and cooled.[15] The reaction mixture was mixed with water (50 ml) and extracted with ether (4×50 ml). The ether solution was washed with water and with saturated brine, dried and evaporated to leave an oily substance (4.0 g), which was purified by passing through a silica gel column to yield 2-methyl-4-undecyn-2-ol; bp 113—117 °C (bath temp) (17 Torr); MS, *m/e* 182 (M^+) and 167; IR, 3380, 1148, 1125, and 980 cm^{-1}; NMR, δ 0.90 (3H, br t, J=6 Hz, 11-H), 1.28 (6H, s, CH_3 at C-2 and 1-H), 2.04 (1H, s, OH), 2.20 (2H, m, 6-H), and 2.35 (2H, t, J=2 Hz, 3-H).

The alkynic alcohol (300 mg) was hydrogenated over Lindlar catalyst (500 mg) in methanol at room temperature for 1 h under stirring. After removal of the catalyst, the mixture was evaporated to give *cis*-2-methyl-4-undecen-2-ol (**7**, 290 mg), showing a single spot on TLC, bp 83—86 °C (bath temp) (17 Torr); MS, *m/e* 169 (M^+-CH_3) and 166 (M^+-H_2O); IR, 3380, 905, and 790 cm^{-1}; NMR, δ 1.89 (3H, br t, J=6 Hz, 11-H), 1.24 (6H, s, CH_3 at C-2 and 1-H), 2.10 (2H, m, 6-H), 2.29 (2H, d, J=6 Hz, 3-H), 5.51 and 5.63 (each 1H, dt, J=11 and 6 Hz, 5- and 4-H).

To a solution of **7** (240 mg, 1.3 mmol) in dry dichloromethane (10 ml) cooled with an ice–water bath was added MCPBA (0.51 g, 1.9 mmol), and the mixture was stirred at 0 °C for 15 min and then allowed to stand in a refrigerator for 15 h. The reaction mixture was washed with 5% aq $Na_2S_2O_3$ and then with 5% aq sodium carbonate (Na_2CO_3), and extracted with dichloromethane (3×20 ml). The dichloromethane solution was worked up as usual to leave oily residue, which was purified by chromatography over silica gel to give **5** (204 mg), bp 108—110 °C (14 Torr); MS, *m/e* 200 (M^+), 185, 167, 127, and 86 (base); IR, 3420 and 1240 cm^{-1}; NMR, δ 0.90 (3H, br t, J=6 Hz, 11-H), 1.33 and 1.36 (each 3H, s, CH_3 at C-2 and 1-H), 2.96 (1H, m, 5-H), and 3.20 (1H, dt, J=4 and 9 Hz, 4-H). Found: C, 71.55; H, 11.96%. Calcd for $C_{12}H_{14}O_2$: C, 71.95; H, 12.08%.

ii): To liquid ammonia (6 ml), distilled from sodium, containing sodium (207 mg, 9 mmol) was added the aforementioned alkynic alcohol (360 mg, 2 mmol) in dry ether, and the mixture was stirred under reflux for 2 h. After additions of ammonium chloride (2 g) and then of aq ammonia (5 ml), the reaction mixture was evaporated and extracted with ether (3×30 ml). The ether solution was washed with dil hydrochloric acid (HCl) and water, dried and evaporated to give *trans*-2-methyl-4-undence-2-ol (**8**, 230 mg), showing a single spot on TLC, bp 102—105 °C (bath temp) (17 Torr); MS, *m/e* 169 (M^+-CH_3) and 166 (M^+-H_2O); IR, 3380 and 968 cm^{-1}; NMR, δ 0.85 (3H, br t, J=6 Hz, 11-H), 1.16 (6H, s, CH_3 at C-2 and 1-H), 2.16 (4H, br m, 3- and 6-H), and 5.48 (2H, m, 4- and 5-H).

Compound **8** (150 mg) was epoxidized with MCPBA (0.40 g) in dichloromethane (10 ml) in the same manner as described above to yield **6** (110 mg), bp 126—130 °C (bath temp) (17 Torr); MS, *m/e* 200 (M^+), 185, 127, and 86 (base); IR, 3420 and 1240 cm^{-1}; NMR, δ 0.86 (3H, br t, J=6 Hz, 11-H), 1.28 and 1.31 (each 3H, s, CH_3 at C-2 and 1-H), 2.70 and 2.90 (each 1H, m, 5- and 4-H). Found: C, 71.57; H, 11.97%. Calcd for $C_{12}H_{24}O_2$: C, 71.95; H, 12.08%.

*Reaction of **5** and **6** under Aqueous Conditions. i)*: A solution of **5** (150 mg, 0.75 mmol) in DMSO (22.5 ml) and water (7.5 ml) was heated gradually from 50 °C to 115 °C (bath temp) for 2 h (at 50 °C for 0.5 h, at 80 °C for 0.5 h, at 95 °C for 0.5 h and then at 115 °C for 0.5 h), with potassium hydroxide (KOH, 520 mg, 9.3 mmol) under nitrogen with stirring, when the spot of **5** had disappeared on TLC. The reaction mixture was cooled, poured into saturated brine, and extracted with ethyl acetate (5×30 ml). The organic solution was washed with saturated brine, dried and evaporated to leave an oily residue, which was separated by chromatography over silica gel (10 g), benzene–ethyl ether mixtures being used as solvents. Fractions eluted with benzene–ether (10 : 1) gave *threo*-2-(1-hydroxyheptyl)-4,4-dimethyloxetane (**9**, 58 mg), bp 85—87 °C (bath temp) (15 Torr); MS, *m/e* 185 (M^+-CH_3) and 115; IR, 3440, 964, 940, and 910 cm^{-1}; NMR, δ 0.85 [3H, br t, J=5 Hz, $(CH_2)_5CH_3$], 1.35 and 1.47 (each 3H, s, CH_3 at C-4), 2.18 (2H, d, J=8 Hz, 3-H), 3.54 [1H, t, J=5 Hz, CH(OH)], and 4.40 (1H, dt, 5 and 8 Hz, 2-H). Found: C, 71.99; H, 12.11%. Calcd for $C_{12}H_{24}O_2$: C, 71.95; H, 12.08%. Later fractions eluted with benzene–ether (1: 1) afforded 2-methylundecane-2,4,5-triol (**10**, 64 mg), amorphous; MS, *m/e* 203 (M^+-CH_3) and 200; IR, 3380 cm^{-1}; NMR, δ 0.89 (3H, br t, J=6 Hz, 11-H), 1.28 and 1.33 (each 3H, s, CH_3 at C-2 and 1-H), 1.49 and 1.80 (each 1H, dd, J=

14, 2.5 and 14, 10 Hz, 3-H), 3.39 and 3.84 (each 1H, m, 5- and 4-H). Found: C, 65.88; H, 12.01%. Calcd for $C_{13}H_{26}O_3$: C, 66.01; H, 12.00%.

ii): Compound **6** (100 mg, 0.5 mmol) was treated with KOH (360 mg, 6 mmol) in DMSO (15 ml) and water (5 ml) in the same manner as **5**. The reaction mixture was worked up and purified as mentioned above to give *erythro*-oxetane (**11**, 50 mg), a diastereoisomer of **9**, and triol (**12**, 21 mg), which showed the following spectra. **11**, bp 106—108 °C (bath temp) (15 Torr); Ms, *m/e* 200 (M^+) and 185; IR, 3430, 984, and 960 cm^{-1}; NMR, 0.86 [3H, br t, J=6 Hz, $(CH_2)_5$-CH_3], 1.35 and 1.49 (each 3H, s, CH_3 at C-4), 2.10 and 2.30 (each 1H, dAB_q, J=12 and 8 Hz, 3-H), 3.69 [1H, m, CH(OH)] and 4.53 (1H, dt, J=4 and 8 Hz, 2-H). Found: C, 71.96; H, 12.09%. Calcd for $C_{12}H_{24}O_2$: C, 71.95; H, 12.08%. **12**, mp 50—53 °C (from ether–hexane); MS, 203 ($M^+ - CH_3$) and 200 ($M^+ - H_2O$); IR (Nujol), 3260 cm^{-1}; NMR, δ 0.88 (3H, br t, J=6 Hz, 11-H), 1.29 (6H, s, CH_3 at C-2 and 1-H), 1.76 (1H, dAB_q, J=10 and 14 Hz, one of 3-H), 3.61 (1H, m, 5-H), and 3.93 (1H, ddd, J=14, 6, and 2 Hz, 4-H). Found: C, 66.42; H, 11.82%. Calcd for $C_{12}H_{26}O_3$: C, 66.01; H, 12.00%.

Preparation of 1-(2,3-Epoxypropyl)-1-cycloheptanol (13), 1-(2,3-Epoxypropyl)-1-cyclooctanol (14), and 1,2-Epoxy-4-butyl-4-octanol (15). *i)*: A solution of freshly distilled cycloheptanone (1.12 g, 0.01 mol) in ether (10 ml) was added dropwise to a cold suspension of allylmagnesium bromide, prepared from allyl bromide (2.44 g) and magnesium (0.5 g), activated by heating, in ether (16 ml), and the whole mixture was stirred at room temperature for 13.5 h.[16] After dropwise addition of dil aq ammonia (7 ml), the reaction mixture was extracted with ether (4×10 ml). The ether solution was worked up as usal to leave an oily residue, which was distilled fractionally under reduced pressure to give 1-allyl-1-cycloheptanol (1.12 g), bp 85—88 °C (11 Torr); MS, *m/e* 154 (M^+) and 136; IR, 3380, 3060, 1640, and 905 cm^{-1}; NMR, δ 2.22 (2H, d, J= 8 Hz, CH_2=CHCH_2), 5.04 and 5.12 (each 1H, dd, J=4, 17 and 4, 10 Hz, CH_2=CHCH_2), and 5.80 (1H, ddt, J=17, 10, and 8 Hz, CH_2=CHCH_2). Found: C, 77.66; H, 11.75%. Calcd for $C_{10}H_{18}O$: C, 77.86; H, 11.76%.

The allyl cycloheptanol (1.01 g, 6.60 mmol) in dichloromethane (35 ml) was epoxidized with MCPBA (2.26 g) at room temperature under stirring in a usual manner. The reaction mixture was worked up as usual and purified by chromatography over silica gel (35 g) to give **13** (985 mg), bp 83—85 °C (15 Torr); MS, *m/e* 170 (M^+) and 152; IR, 3440 and 1250 cm^{-1}; NMR, δ 1.89 [2H, d, J=7 Hz, CH_2CH-(–O–)CH_2], 2.05 and 2.77 [each 1H, dd, J=5, 2 and 5, 5 Hz, CH_2CH(–O–)CH_2], and 3.13 [1H, m, CH_2CH(–O–)CH_2]. Found: C, 70.32; H, 10.54%. Calcd for $C_{10}H_{18}O_2$: C, 70.54; H, 10.66%.

ii): 1-Allyl-1-cyclooctanol (2.35 g) was prepared by treatment (room temp, 17 h) of cyclooctanone (2.27 g, 0.018 mol) with allylmagnesium bromide, prepared from allyl bromide (4.36 g, 0.036 mol) and magnesium turnings (0.9 g, 0.036 mol) in ether (50 ml), followed by fractional distillation, and had the following properties: bp, 99—101 °C (12 Torr); MS, *m/e* 168 (M^+) and 150; IR, 3400, 3070, 1640, and 910 cm^{-1}; NMR, δ 2.20 (2H, d, J=8 Hz, CH_2CH=CH_2), 5.07 and 5.11 (each 1H, dd, J=17, 1 and 10, 1 Hz, CH_2CH=CH_2), and 5.88 (1H, m, CH_2CH=CH_2). Found: C, 78.56; H, 11.91%. Calcd for $C_{11}H_{20}O$: C, 78.51; H, 11.98%.

The olefin (612 mg, 3.3 mmol) was oxidized with MCPBA (1.13 g, 5.0 mmol) in dichloromethane (20 ml) at room temperature for 17 h. The reaction mixture was worked up as usual and purified by chromatography to yield **14** (656 mg), bp 117—119 °C (14 Torr); MS, *m/e* 184 (M^+) and 166; IR, 3440, 1255, and 1015 cm^{-1}; NMR, δ 1.91 [2H, d, J=8 Hz, CH_2CH(–O–)CH_2], 2.49 and 2.81 [each 1H, dd, J=5, 2 and 5, 2 Hz, CH_2CH(–O–)CH_2], and 3.19 [1H, m, CH_2-CH(–O–)CH_2]. Found: C, 71.77; H, 10.89%. Calcd for $C_{11}H_{20}O_2$: C, 71.69; H, 10.94%.

iii): 5-Nonanone (1.1 g) was reacted with allylmagnesium bromide, prepared from allyl bromide (2 g) and magnesuim (0.4 g) in ether, in the same manner as mentioned above to give 4-butyl-1-octen-4-ol (1.2 g), which was used for the next epoxidation without further purification. The alkenyl alcohol (1.2 g) was treated with MCPBA (2.4 g) in dichloromethane (60 ml) at room temperature for 15 h. The reaction mixture was worked up as usual and purified by chromatography to give **15** (637 mg), bp 128—131 °C (bath temp) (18 Torr); MS, *m/e* 182 ($M^+ - H_2O$); IR, 3445 and 1250 cm^{-1}; NMR, δ 0.88 [6H, br t, J=7 Hz, $(CH_2)_3CH_3$ and 8-H], 2.45 and 2.77 [each 1H, dd, J=6, 3 and 6, 6 Hz, CH_2CH(–O–)CH_2], 3.09 [1H, m, CH_2CH(–O–)CH_2]. Found: C, 71.80, 12.06%. Calcd for $C_{12}H_{24}O_2$: C, 71.95; H, 12.08%.

Reactions of 1b, 13, 14, and 15 under Aqueous Conditions.

i): A solution of **1b** (104 mg, 0.56 mmol) in DMSO (17.25 ml) and water (5.75 ml) was stirred with KOH (370 mg, 5.6 mmol) at room temperature for 10 min and then at 108 °C (bath temp) for 1.4 h under nitrogen, when the spot of **1b** had disappeared on TLC. The mixture was cooled, poured into ice–water, and extracted with ethyl acetate. The acetate solution was washed with water, dried and evaporated to leave an oily residue (114 mg), showing two spots on TLC, which was separated into two fractions by preparative TLC over silica gel (20×20 cm^2, 5 plates), a 1:1 mixture of benzene and ether being used as a solvent. A more mobile fraction gave 2-(1-hydroxy-1-methylethyl)-4,4-pentamethyleneoxetane (**2b**, 74 mg), bp 98—102 °C (10 Torr); MS, *m/e* 184 (M^+), 166, 99, and 98; IR ($CHCl_3$), 3580, 3460, 1020, and 990 cm^{-1}; NMR, δ 1.02 and 1.16 (each 3H, s, CH_3), 2.06 and 2.32 (each 1H, dd, J=10.5 and 8 Hz, 3-H). Found: C, 71.44; H, 10.82%. Calcd for $C_{11}H_{20}O_2$: C, 71.74; H, 10.87%. A less mobile fraction afforded 1-(1-hydroxycyclohexyl)-3-methyl-2,3-butanediol (**3b**, 10 mg), amorphous; MS, *m/e* 202 (M^+) and 184; IR ($CHCl_3$), 3440 cm^{-1}; NMR, δ 1.14 and 1.18 (each 3H, s, CH_3 at C-3 and 4-H), and 3.73 (1H, dd, J=10 and 4 Hz, 2-H),

ii): A solution of **13** (172 mg, 1 mmol) in DMSO (30 ml) and water (10 ml) was heated up to 140 °C for 75 min with KOH (690 mg, 10 mmol) under nitrogen with stirring. The reaction mixture was worked up as described before and purified by chromatography over silica gel (7 g) with benzene–ether. More mobile fractions eluted with benzene–ether (5:1) gave 2-hydroxymethyl-4,4-hexamethyleneoxetane (**16**, 43 mg), bp 131—135 °C (bath temp) (17 Torr); MS, *m/e* 170 (M^+) and 152; IR, 3400, 1044, 965, and 876 cm^{-1}; NMR, δ 2.19 and 2.36 (each 1H, d, J=12 Hz, 3-H), 3.52 and 3.72 (each 1H, dd, J=12 and 4 Hz, CH_2OH), and 4.60 (1H, m, 2-H:). Found: C, 70.39; H, 10.71%. Calcd for $C_{10}H_{18}O_2$: C, 70.54; H, 10.66%. Less mobile fractions eluted with benzene–ether (1 : 1) afforded 4,4-hexamethylene-1,2,4-butanetriol (**19**, 103 mg), mp 69—72 °C (from hexane); MS, *m/e* 188 (M^+), 170, and 157; IR (Nujol), 3280 cm^{-1}; NMR δ 3.40 and 3.58 (each 1H, dd, J=11, 6 and 11, 4 Hz, 1-H), 3.52 and 4.49 (2H and 1H, each br s, OH), and 4.04 (1H, m, 2-H). Found: C, 63.56; H, 10.76%. Calcd for $C_{10}H_{20}O_3$: C, 63.79; H, 10.71%.

iii): Compound **14** (190 mg) in DMSO (30 ml) and water (10 ml) was heated up to 85 °C (bath temp) (at 50 °C for 0.5 h, at 80 °C for 0.5 h, and 85 °C for 0.5 h) with KOH (690 mg) in the same manner as mentioned above. The reaction mixture was worked up and purified as usual to give

2-hydroxymethyl-4,4-heptamethyleneoxetane (**17**, 38 mg), bp 142—144 °C (bath temp) (17 Torr), and 4,4-heptamethylene-1,2,4-butanetriol (**20**, 122 mg), mp 86—88 °C (from hexane). **17**, MS, *m/e* 184 (M^+) and 166; IR, 3390, 957, and 910 cm^{-1}; NMR, δ 2.22 (2H, d, J=8 Hz, 3-H), 3.64 (2H, dd, J=7 and 3 Hz, CH_2OH), and 4.66 (1H, m, 2-H). Found: C, 71.30; H, 11.04%. Calcd for $C_{11}H_{30}O_2$: C, 71.69; H, 10.94%. **20**, MS, *m/e* 202 (M^+) and 171; IR (Nujol), 3260 cm^{-1}; NMR, δ 3.44 and 3.57 (each 1H, dd, J=11, 6 and 11, 4 Hz, 1-H), and 4.06 (1H, m, 2-H). Found: C, 65.33; H, 11.00%. Calcd for $C_{11}H_{22}O_3$: C, 65.31; H, 10.96%.

iv): Compound **15** (202 mg) in DMSO (30 ml) and water (10 ml) was heated with KOH (690 mg) almost in the same manner (at 40 °C for 0.5 h, at 60 °C for 0.5 h, and at 80 °C for 0.25 h) as mentioned above, and the reaction mixture was worked up and purified as described before to give 4,4-dibutyl-2-hydroxymethyloxetane (**18**, 43 mg), bp 113—116 °C (bath temp) (17 Torr), and 4-butyl-1,2,4-octanetriol (**21**, 154 mg), amorphous. **18**, MS, *m/e* 200 (M^+), 182, and 143; IR, 3410, 965, and 928 cm^{-1}; NMR, δ 2.21 (2H, d, J=8 Hz, 3-H), 3.54 and 3.68 (each 1H, dd, J=12, 5 and 12, 3.5 Hz, CH_2OH), and 4.60 (1H, m, 2-H). Found: C, 71.58; H, 12.10%. Calcd for $C_{12}H_{24}O_2$: C, 71.95; H, 12.08%. **21** MS, *m/e* 218 (M^+) and 187; IR, 3360 cm^{-1}; NMR, δ 0.87 (6H, br t, J=7 Hz, CH_3), 2.95 and 4.25 (2H and 1H, each br s, OH), 3.40 and 3.56 (each 1H, dd, J=11.5, 7 and 11.5, 3.5 Hz, 1-H), and 4.03 (1H, m, 2-H). Found: C, 65.88; H, 12.30%. Calcd for $C_{12}H_{26}O_3$: C, 66.01; H, 12.00%.

Preparation of 1-(1,2-Epoxycyclopentyl)-, 1-(1,2-Epoxycyclohexyl)-, 1-(1,2-Epoxycycloheptyl)-, and 1-(1,2-Epoxycyclooctyl)-2-methyl-2-propanols (22—25). *i)*: A suspended mixture of cyclopentanone (8.4 g, 0.1 mol), cyanoacetic acid (8.5 g, 0.1 mol), and ammonium acetate (1.5 g, purity 95%) was refluxed in dry benzene (12 ml) on an oil-bath (145—155 °C) for 2 h under stirring, water being removed by a Dean-Stark apparatus.[7] The reaction mixture was evaporated to remove benzene, leaving yellow solid residue, which was submitted to distillation with concomitant decarboxylation at 155—165 °C (bath temp) under reduced pressure (40—55 Torr). Fractions distilled at 60—80 °C (40—55 Torr) were collected and dissolved in ether (25 ml), washed with 10% aq Na_2CO_3 and water, dried, evaporated and again distilled to give 2-(1-cyclopentenyl)acetonitrile (5.85 g), bp 68—71 °C (12 Torr); MS, *m/e* 107 (M^+); IR, 2240 and 1638 cm^{-1}; NMR, δ 3.14 (2H, s, 2-H) and 5.76 (1H, m, C=CH).

The nitrile (5.5 g) was stirred with 10% aq KOH (160 ml) on an oil bath (120—130 °C) for 4.5 h under nitrogen. The reaction mixture was cooled, washed with ether (50 ml), made acidic to pH ≈2 with 2M aq HCl, and extracted with chloroform (5×30 ml). The chloroform solution was dried and evaporated to give crude 2-(1-cyclopentenyl)acetic acid (5.79 g); IR (Nujol), 3040, 2640, and 1710 cm^{-1}; NMR, δ 3.18 (2H, s) and 5.60 (1H, br s). The crude acid was converted into the methyl ester as follows. To a solution of water (5 ml), ether (5 ml), and ethanol (35 ml) containing KOH (purity 85%) heated at 60—65 °C was added dropwise *p*-tolylsulfonylmethylnitrosamide (10.8 g) in ether (82 ml) under stirring, and the distilled diazomethane was dissolved in cold ether.[18] To the diazomethane solution cooled with an ice–salt bath was added dropwise the crude acid (2.0 g) in ether (14 ml), and the ether solution was evaporated to give crude methyl 2-(1-cyclopentenyl)acetate (2.3 g), which was used for the next reaction without further purification; IR, 1745 and 1655 cm^{-1}; NMR, δ 3.17 (2H, s), 3.72 (3H, s), and 5.62 (1H, m).

To lithium (6.6 g) in dry ether (252 ml) was added dropwise methyl iodide (29 ml, 64.9 g) in ether (50 ml) under gentle reflux with stirring, and the mixture was then refluxed for 2 h. The methyllithium solution (170 ml) was added to a cold solution of the crude acetate (2.0 g) in ether (80 ml), and the whole solution was stirred at 0 °C for 1 h. After addition of water (50 ml), the reaction mixture was separated into two layers, and the aqueous layer was extracted with ether (3× 50 ml). All the ether solutions were combined, washed with water, dried and evaporated to leave an oily residue, which was purified by chromatography over silica gel (70 g) to give 1-(1-cyclopentenyl)-2-methyl-2-propanol (1.22 g), bp 74—76 °C (bath temp) (12 Torr); MS, *m/e* 140 (M^+), 125, and 122; IR, 3380, 1645, and 1370 cm^{-1}; NMR, δ 1.22 (6H, s, CH_3 at C-2 and 3-H), 1.70 (1H, s, OH), 2.36 [6H, br, m, $(CH_2)_3$], and 5.50 (1H, t, J=5 Hz, CH=C). Found: C, 77.12; H, 11.61%. Calcd for $C_9H_{16}O$: C, 77.09; H, 11.50%.

The unsaturated alcohol (570 mg) was epoxidized with MCPBA (1.7 g) in dichloromethane (30 ml) at 0 °C for 3 h in the same manner as described before. The reaction mixture was worked up and purified as usual to give **22** (578 mg), bp 90—92 °C (12 Torr) (bath temp); IR, 3440, 1210, and 1115 cm^{-1}; NMR, δ 1.28 and 1.35 (each 3H, s, CH_3 at C-2 and 3-H), 1.97 (2H, s, 1-H), and 3.31 (1H, s, CH(–O–)C). Found: C, 69.27; H, 10.33%. Calcd for $C_9H_{16}O_2$: C, 69.19; H, 10.32%.

ii): 2-(1-Cyclohexenyl)acetonitrile, bp 96—98 °C (bath temp) (15 Torr), was prepared according to the reported procedure.[18] The nitrile (8.6 g) was refluxed (bath temp, 120—130 °C) with 10% aq KOH for 4.5 h under nitrogen with stirring. The reaction mixture was cooled and washed with ether (50 ml). The aqueous solution was acidified with 2 M aq HCl to pH ≈2, and extracted with chloroform (4×50 ml). The chloroform extracts were worked up as usual to give crude 2-(1-cyclohexenyl)acetic acid (10.3 g); IR, 3000 and 1713 cm^{-1}; NMR δ 1.65 and 2.07 (each 4H, m), 3.02 (2H, s), 5.64 (1H, m), and 10.70 (1H, br, W_H=30 Hz). The crude acid (2.0 g) was then converted with diazomethane in ether[18] into the corresponding crude methyl ester (2.3 g), which was used for the next reaction without further purification; IR, 1745 and 1645 cm^{-1}; NMR, δ 1.61 and 2.02 (each 4H, m), 2.97 (2H, s), 3.67 (3H, s), and 5.56 (1H, m).

To a solution of the crude ester (2.3 g) in dry ether (100 ml) cooled with an ice-bath was added a methyllithium solution in ether (100 ml) (1.5 M CH_3Li in ether) under stirring, and the mixture was stirred at room temperature for 1 h. After dropwise addition of water (50 ml), the mixture was separated into two layers, and the aqueous solution was extracted with ether (3×50 ml). All the ether solutions were combined, washed with water (2×50 ml), dried and evaporated to leave an amorphous residue, which was purified by chromatography to give 1-(1-cyclohexenyl)-2-methyl-2-propanol (1.16 g), bp 46—48 °C (bath temp) (0.15 Torr); MS, *m/e* 154 (M^+), 139, and 136; IR, 3400, 1660, and 1150 cm^{-1}; NMR, δ 1.01 (6H, s, CH_3 at C-2 and C-1), 1.62 [4H, CH_2-$(CH_2)_2CH_2$], 2.08 [4H, m, $CH_2(CH_2)_2CH_2$], 2.13 (2H, s, 3-H), and 5.52 (1H, br s, W_H=8 Hz, C=CH). Found: C, 77.49; H, 11.72%. Calcd for $C_{10}H_{18}O$: C, 77.86; H, 11.76%.

The unsaturated alcohol (505 mg) was oxidized with MCPBA (1.4 g) in chloroform (30 ml) at 0 °C for 5 h under stirring. The reaction mixture was worked up and purified as described above to give **23** (506 mg), bp 95—97 °C (bath temp) (15 Torr); MS, *m/e* 170 (M^+), 155, and 152; IR, 3440, 1380, 1370, and 1250 cm^{-1}; NMR, δ 1.27 and 1.37 (each 3H, s, CH_3 at C-2 and 3-H), 1.72 and 1.86 (each 1H, d, J=15 Hz, 1-H), and 3.06 [1H, t, J=2 Hz, $CH_2CH(–O–)$]. Found: C, 70.43; H, 10.58%. Calcd for $C_{10}H_{18}O_2$: C, 70.54; H, 10.66%.

iii): Cycloheptenylacetonitrile (4.3 g), bp 98—100 °C (12

Torr), was prepared by treatment of cycloheptanone (5.6 g) with cyanoacetic acid (4.3 g) and ammonium acetate (1.0 g) in benzene (10 ml) at 165—175 °C (bath temp) for 2 h in almost the same manner as cyclopentylacetonitrile; IR, 2440 and 1615 cm^{-1}; NMR, δ 3.05 (2H, s) and 5.92 (1H, t, J=6 Hz). The acetonitrile (4.2 g) was then hydrolyzed by heating (120—130 °C) (bath temp) in 15% aq KOH (80 ml) for 16 h to yield the corresponding crude acid (3.54 g); IR, 3000, 2660, 1715, and 1630 cm^{-1}; NMR, δ 3.05 (2H, s) and 5.74 (1H, t, J=6 Hz). The crude acid (0.6 g) was converted into the methyl ester (0.64 g); IR, 1745 cm^{-1}; NMR, δ 3.02 (2H, s), 3.68 (3H, s), and 5.69 (1H, t, J=7 Hz). The crude methyl ester (0.62 g) was transformed by treatment with methyllithium, prepared from methyl iodide (15 g) and lithium (1.63 g) in ether (80 ml), at room temperature for 15 h into 1-(1-cycloheptenyl)-2-methyl-2-propanol (0.49 g), bp 88—91 °C (bath temp) (12 Torr); MS, *m/e* 168 (M^+), 153, and 150; IR, 3380 and 1370 cm^{-1}; NMR, δ 1.22 (6H, s), 2.20 (2H, s), and 5.68 (1H, t, J=8 Hz). Found: C, 78.33; H, 12.01%. Calcd for $C_{11}H_{20}O$: C, 78.51; H, 11.98%. The unsaturated alcohol (0.44 g) was oxidized with MCPBA (1.3 g) in chloroform (15 ml) at 0 °C for 4 h under stirring. The reaction mixture was worked up and purified as usual to give **24** (0.38 g), bp 105—107 °C (bath temp) (12 Torr); MS, *m/e* 169 ($M^+ - CH_3$) and 166 ($M^+ - H_2O$); IR, 3440, 1240, and 1150 cm^{-1}; NMR, δ 1.21 and 1.38 (each 3H, s), 1.79 (2H, s), and 2.99 (1H, dd, J=4 and 6 Hz). Found: C, 71.39; H, 10.87%. Calcd for $C_{11}H_{20}O_2$: C, 71.69; H, 10.94%.

iv): Cyclooctanone (2.5 g) was refluxed with cyanoacetic acid (1.7 g) and ammonium acetate (0.3 g) in benzene (10 ml) at 170—180 °C (bath temp) for 2 h and then at 100 °C (bath temp) for 1 h under stirring. After removal of benzene, the mixture was gently heated to *ca.* 190 °C (bath temp) under reduced pressure (20—40 Torr) until evolution of carbon dioxide gas ceased, and was then distilled. Fractions boiling at 90—105 °C (15 Torr) were collected and dissolved in ethyl acetate (50 ml). The acetate solution was washed with 10% aq Na_2CO_3 (2×10 ml) and with water (10 ml), dried and evaporated to leave an oily residue, which was distilled fractionally to give 1-cyclooctenylacetonitrile (1.89 g), bp 103—105 °C (13 Torr); IR, 2240 cm^{-1}; NMR, δ 1.51 (8H, br s), 3.06 (2H, s), and 5.74 (1H, t, J=8 Hz).

The nitrile (2.1 g) was heated with 15% aq KOH (70 ml) at 120—130 °C (bath temp) for 11 h under nitrogen with stirring. After being shaken with ether (100 ml), the mixture was made acidic (pH ≈2) with 2 M aq HCl and extracted with dichloromethane (100 ml). The dichloromethane solution, after usual work-up, left crude cyclooctenylacetic acid (1.81 g); IR, 3000 and 1713 cm^{-1}; NMR, δ 1.50 (8H, s), 3.05 (2H, s), and 5.58 (1H, t, J=8 Hz). The crude acid (1.9 g) in ether (10 ml) was converted into the methyl ester (1.97 g), oily, by treatment with diazomethane, prepared from *p*-tolylsulfonylmethylnitrosamide (11 g), ethanol (15 ml), KOH (4 g), water (6 ml), and ether (6 ml);[18] IR, 1745 cm^{-1}; NMR, δ 1.49 (8H, s), 3.04 (2H, s), 3.70 (3H, s), and 5.56 (1H, t, J=8 Hz). To the crude methyl ester (1.0 g) in ether (20 ml) was added dropwise a methyllithium solution in ether (1.5 M, 110 ml) at ice–water bath temperature under stirring during 0.5 h. The mixture was stirred at the temperature and mixed with ice–water (30 ml). The whole reaction mixture was poured into saturated brine and extracted with ether (3×50 ml). The ether solution was worked up and purified by chromatography over silica gel (30 g) as mentioned above to give 1-(1-cyclooctenyl)-2-methyl-2-propanol (0.78 g), bp 113—115 °C (bath temp) (12 Torr); MS, *m/e* 182 (M^+), 167, and 164; IR, 3420 cm^{-1}; NMR, δ 1.13 (6H, s), 1.45 (8H, s) and 5.40 (1H, t, J=8 Hz). Found: C, 79.14; H, 12.08%. Calcd for $C_{12}H_{22}O$: C, 79.06; H, 12.16%.

The unsaturated alcohol (620 mg) in dichloromethane (22 ml) was oxidized with MCPBA (1.73 g) at 0 °C under stirring for 2.5 h. The reaction was ceased by addition of 5% aq $Na_2S_2O_3$ (5 ml) and the mixture was worked up as usual and purified by chromatography over silica gel (20 g). Fractions eluted with benzene and benzene–ether (10 : 1) gave **25** (411 mg), bp 125—127 °C (bath temp) (12 Torr), showing a single spot on TLC; MS, *m/e* 198 (M^+), 183, and 180; IR, 3460 and 1260 cm^{-1}; NMR, δ 1.24 and 1.39 (each 3H, s) and 2.80 (1H, dd, J=4 and 8 Hz). Found: C, 72.40; H, 11.05%. Calcd for $C_{12}H_{22}O_2$: C, 72.68; H, 11.18%.

*Reactions of **22**, **23**, **24**, and **25** under Aqueous Conditions.*

i): A solution of **22** (156 mg) in DMSO (30 ml) was heated with KOH (680 mg, 85% purity) in water (10 ml) at 130 °C (bath temp) for 0.5 h and then at 135 °C (bath temp) for 1 h under nitrogen with stirring. The reaction mixture was cooled, poured into brine, and extracted with ethyl acetate (6×50 ml). The acetate solution was washed with saturated brine (2×50 ml), dried and evaporated to leave an oily residue (320 mg), which was separated by chromatography over silica gel (8 g) with benzene–ether (5: 1). Most mobile fractions gave 2,2-(2-hydroxytetramethylene)-4,4-dimethyloxetane (**26**, 55 mg), bp 85—87 °C (bath temp) (12 Torr); MS, *m/e* 156 (M^+), 141, and 138; IR, 3420, 970, 950, and 930 cm^{-1}; NMR, δ 1.42 and 1.46 (each 3H, s, C<u>H</u>$_3$ at C-4), 2.13 and 2.67 (each 1H, ABq, J=11 Hz, 3-<u>H</u>), and 4.02 [1H, t, J=4 Hz, C<u>H</u>(OH)]. Found: C, 68.92; H, 10.35%. Calcd for $C_9H_{16}O_2$: C, 69.19; H, 10.32%. Compound **26** (16 mg) was converted by treatment with acetic anhydride (0.3 ml) and pyridine (0.6 ml) at 20 °C for 16 h into the monoacetate (**26a**), oily; MS, *m/e* 198 (M^+), 183, and 138; IR, 1745 and 850 cm^{-1}; NMR, δ 1.42 (6H, s), 2.07 (3H, s), 2.20 and 2.54 (each 1H, ABq, J=12 Hz), and 5.16 (1H, m).

Middle fractions afforded 2-(2-hydroxy-2-methylpropyl)-2-cyclopenten-1-ol (**31**, 13 mg), bp 81—83 °C (bath temp) (15 Torr); MS, *m/e* 141 ($M^+ - CH_3$) and 138 ($M^+ - H_2O$); IR, 3280, 1115, and 840 cm^{-1}; NMR, δ 1.22 and 1.30 (each 3H, s, C<u>H</u>$_3$ at C-2 and 3-<u>H</u>), 3.73 (2H, br, W_H=16 Hz, O<u>H</u>), 4.68 (1H, m, 1-<u>H</u>), and 5.83 (1H, br s, 3-<u>H</u>). Found: C, 68.83; H, 10.46%. Calcd for $C_9H_{16}O_2$: C, 69.19; H, 10.32%. The glycol (**31**, 10 mg) was converted into the monoacetate (**31a**, 10 mg), oily; MS, *m/e* 183 ($M^+ - CH_3$), 180, and 138; IR, 3440, 1735, 1120, and 855 cm^{-1}; NMR, δ 1.20 and 1.24 (each 3H, s), 2.05 (3H, s), 5.74 (1H, m), and 5.84 (1H, br s).

Least mobile fractions gave 1-(2-hydroxy-2-methylpropyl)-cyclopentane-1,2-diol (30 mg), mp 71—73 °C (from hexane); MS, *m/e* 174 (M^+), 159, and 156; IR ($CHCl_3$), 3620 and 3400 cm^{-1}; NMR, δ 1.35 and 1.43 (each 3H, s, C<u>H</u>$_3$ at C-2 and 3-<u>H</u>), 2.91 (3H, br, W_H=8 Hz, O<u>H</u>), and 4.03 (1H, m, 2-<u>H</u>). Found: C, 62.41; H, 10.44%. Calcd for $C_9H_{16}O_3$: C, 62.04; H, 10.41%. The triol (16 mg) gave the monoacetate (18 mg), amorphous; MS, *m/e* 190 (M^+), 175, 172, and 130; IR (Nujol), 3280 and 1735 cm^{-1}; NMR, δ 1.24 and 1.36 (each 3H, s), 1.86 (2H, s), 2.06 (3H, s), and 5.00 (1H, dd, J=5 and 1 Hz).

ii): Compound **23** (170 mg) in DMSO (30 ml) was heated with KOH (685 mg, purity 85%) in water (10 ml) at *ca.* 140 °C for 1.5 h under nitrogen with stirring. The reaction mixture was worked up as described above and separated into three fractions by chromatography over silica gel (7 g), a 5 : 1 mixture of benzene and ether being used as solvent. The most mobile fraction gave 2,2-(2-hydroxypentamethylene)-4,4-dimethyloxetane (**27**, 78 mg), bp 83—85 °C (bath temp) (12 Torr); MS, *m/e* 170 (M^+), 155, and 152; IR, 3420, 967, and 880 cm^{-1}; NMR, δ 1.40 and 1.47 (each 3H, s, C<u>H</u>$_3$

at C-4), 1.88 and 2.40 (each 1H, d, J=11 Hz, 3-H), and 3.36 [1H, dd, J=11 and 4 Hz, CH(OH)]. Found: C, 70.63; H, 10.71%. Calcd for $C_{10}H_{18}O_2$: C, 70.54; H, 10.66%. Compound **27** (15.5 mg) was converted into the monoacetate (**27a**, 15 mg), oily; MS, 212 (M^+); IR, 1745, 970, and 880 cm^{-1}; NMR, δ 1.40 and 1.44 (each 3H, s), 2.13 (3H, s), 1.99 and 2.30 (each 1H, d, J=10 Hz), and 4.72 (1H, dd, J=10 and 4 Hz).

The middle fraction afforded 2,2-dimethyl-1-oxaperhydroinden-3a-ol (**29**, 12 mg), mp 69—71 °C (from hexane); MS, *m/e* 170 (M^+), 155, and 137; IR ($CHCl_3$), 3600, 3420, 1150, and 1105 cm^{-1}; NMR, δ 1.35 (6H, s, CH_3 at C-2), 1.84 and 1.94 (each 1H, ABq, J=13 Hz, 3-H), and 3.79 (1H, t, J=4 Hz, 7a-H). Found: C, 70.22; H, 10.69%. Calcd for $C_{10}H_{18}O_2$: C, 70.54; H, 10.66%. The least mobile fraction gave 1-(2-hydroxy-2-methylpropyl)cyclohexane-1,2-diol (22 mg), amorphous; MS, *m/e* 188 (M^+), 173, and 170; IR (Nujol), 3360 cm^{-1}; NMR, δ 1.28 and 1.38 (each 3H, s, CH_3 at C-2 and 3-H), 3.20 (3H, br, OH), and 3.46 (1H, dd, J=8 and 4 Hz, 2-H). Found: C, 63.51; H, 10.75%. Calcd for $C_{10}H_{20}O_3$: C, 63.79; H, 10.71%. The triol (15 mg) afforded the monoacetate (16 mg), amorphous; MS, *m/e* 215 ($M^+ - CH_3$) and 212 ($M^+ - H_2O$); IR, 3410 and 1737 cm^{-1}; NMR, δ 1.28 and 1.34 (each 3H, s), 2.07 (3H, s), and 4.75 (1H, dd, J=8 and 4 Hz).

iii): Compound **24** (186 mg) was heated at *ca.* 115 °C (bath temp) for 2 h with KOH (685 mg, purity 85%) in DMSO (30 ml) and water (10 ml) under nitrogen with stirring. The reaction mixture was worked up as usual and separated by chromatography over silica gel (6 g) with benzene–ether (10: 1) to yield the unchanged starting material (**24**, 25 mg) and the following three products: 4,4-(2-hydroxyhexamethylene)-2,2-dimethyloxetane (**28**, 39 mg), 2,2-dimethyl-1-oxaperhydroazulen-3a-ol (**30**, 36 mg), and 2-(2-hydroxy-2-methylpropyl)-2-cyclohepten-1-ol (**32**, 15 mg), **28**, bp 109—112 °C (bath temp) (12 Torr); MS, 184 (M^+), 169, and 151; IR ($CHCl_3$), 3600, 3440, 988, and 955 cm^{-1}; NMR, δ 1.36 and 1.47 (each 3H, s, CH_3 at C-2), 1.96 and 2.52 (each 1H, d, J=12 Hz, 3-H), and 3.41 [1H, J=10 and 4 Hz, CH(OH)]. Found: C, 71.37; H, 11.00%. Calcd for $C_{11}H_{20}O_2$: C, 71.69; H, 10.94%. Monoacetate (**28a**) of **28**, oily, MS, *m/e* 226 (M^+), 211, 208, and 166; IR, 1740, 1040, and 850 cm^{-1}; NMR, δ 1.24 and 1.42 (each 3H, s), 2.10 (3H, s), 2.29 (1H, d, J=12 Hz), and 4.19 (1H, dd, J=10 and 4 Hz). **30**, mp 60—62 °C (from hexane); MS, *m/e* 184 (M^+), 169, and 166; IR ($CHCl_3$), 3600, 3440, 1105, and 1070 cm^{-1}; NMR, δ 1.28 and 1.39 (each 3H, s, CH_3 at C-2), 1.82 and 1.91 (each 1H, d, J=12 Hz, 3-H), and 3.96 (1H, dd, J=9 and 3 Hz). Found: C, 71.46; H, 10.98%. Calcd for $C_{11}H_{20}O_2$: C, 71.69; H, 10.94%. **32**, mp 76—78 °C (from hexane); MS, 169 ($M^+ - CH_3$) and 166 ($M^+ - H_2O$); IR ($CHCl_3$), 3620 and 3400 cm^{-1}; NMR, δ 1.20 and 1.22 (each 3H, s, CH_3 at C-2 and 3-H), 2.24 and 2.36 (each 1H, ABq, J=14 Hz, 1-H), 4.40 [1H, dd, J=6 and 2 Hz, CH(OH)], and 5.56 (1H, t, J=7 Hz, 3-H). Found: C, 71.32; H, 10.69%. Calcd for $C_{11}H_{20}O_2$: C, 71.69; H, 10.94%.

iv): Compound **25** (198 mg) was heated at *ca.* 140 °C (bath temp) for 2.5 h with KOH (685 mg, purity 85%) in DMSO (30 ml) and water (10 ml) under nitrogen with stirring. The reaction mixture was worked up as mentioned above and purified by chromatography as usual to give the starting material (**25**, 170 mg) unchanged.

Hydrolysis of Cycloalkene Oxides (33—36). Each (112—182 mg) of compounds **33**,[19] **34**,[20] **35**,[21] and **36**[22] in DMSO (15 ml) was added rapidly to an aqueous KOH (10 mol equiv) solution (5 ml) heated at 100—110 °C (bath temp), and the whole solution was stirred at the temperature for 0.5 h or for 3 h. After being cooled, the mixture was worked up as usual to give the hydrolysis product (**37**[23] or **38**[24]) and/or the starting epoxides. The result is summarized in the text.

*Reactions of **1b** and **15** under Anhydrous Conditions. i)*: A suspension of **1b** (186 mg, 1 mmol) and sodium hydride (NaH, 120 mg, purity 50%, 2.5 mmol) in dry THF (30 ml) was heated gently under reflux for 11 h. The reaction mixture was cooled, poured into ice–water, and extracted with ethyl acetate. The acetate solution was worked up as usual to leave an oily residue (170 mg), showing two spots, which was separated into two fractions by preparative TLC (5 plates) over silica gel. The less mobile fraction gave **2b** (53 mg) and and the more mobile the starting epoxide (**1b**, 102 mg).

ii): A suspended mixture of **15** (100 mg, 0.5 mmol) and NaH (60 mg, purity 50%, 1.25 mmol) in THF (10 ml) was refluxed for 13 h under nitrogen. The reaction mixture was worked up as mentioned above and purified by chromatography over silica gel (6 g) with benzene–ether (2: 1) to yield the starting epoxide (**15**, 17 mg) and 4,4-dibutyl-2-(4-butyl-2,4-dihydroxyoctyloxy)oxolane (**4a**, 64 mg), amorphous; MS, *m/e* 400 (M^+), 382, and 364; IR (Nujol), 3460, 1135, and 1070 cm^{-1}; NMR, δ 0.90 (12H, br t, J=7 Hz, CH_3), 3.48 [4H, m, CH_2(–O–)], 3.64 [1H, m, CH(OH)], and 4.21 [1H, m, CH(–O–)]. Found: C, 71.63; H, 12.10%. Calcd for $C_{24}H_{48}O_4$: C, 71.95; H, 12.10%.

*Reactions of **23**, **24**, and **25** under Anhydrous Conditions. i)*: A solution of **23** (120 mg) in THF (10 ml) was added to a stirred suspension of mineral-oil free NaH (85 mg) in THF (10 ml). The mixture was refluxed gently for 15 h, cooled and mixed with water (2 ml). After removal of THF by evaporation, the mixture was poured into brine and extracted with ethyl acetate, dried and evaporated to leave oily residue (125 mg), which was separated by column chromatography over silica gel (4 g) with benzene–ether (2: 1) and subsequent preparative TLC to yield three products, 2-methylenecyclohexanol (**39**, 38 mg), oxetane **27** (33 mg), and 2-(2-hydroxy-2-methylpropyl)-2-cyclohexen-1-ol (**40**, 12 mg). **29**, bp 65—67 °C (bath temp) (12 Torr); MS, *m/e* 112 (M^+) and 94; IR, 3340, 3080, 1640, and 897 cm^{-1}; NMR, δ 4.07 (1H, m, 1-H), 4.73 and 4.86 (each 1H, s, $=CH_2$). Found: C, 74.61; H, 10.83%. Calcd for $C_7H_{12}O$: C, 74.95; H, 10.78%. **40**, bp 97—98 °C (bath temp) (12 Torr); MS, *m/e* 170 (M^+), 155, and 152; IR, 3300 cm^{-1}; NMR, δ 1.21 and 1.28 (each 3H, CH_3 at C-2 and 3-H), 3.72 (2H, br, OH), 4.10 and 5.56 (each 1H, t, J=4 Hz, 1- and 3-H). Found: C, 70.18; H, 10.71%. $C_{10}H_{18}O_2$: C, 70.54; H, 10.66%.

ii): A suspension of **24** (170 mg) in dry THF (20 ml) containing NaH (110 mg) was heated under reflux for 15 h. The mixture was worked up as mentioned above and separated by column chromatography over silica gel (6 g) with benzene–ether (10: 1) to yield the unchanged epoxide (**24**, 17 mg) and 2-methylenecycloheptanol (**41**, 69 mg), bp 73—76 °C (bath temp) (12 Torr); MS, *m/e* 126 (M^+) and 108; IR, 3360, 3060, 1645, and 895 cm^{-1}; NMR, δ 4.28 (1H, t, J=6 Hz, 1-H), 4.88 (1H, s, $C=CH_2$), and 5.00 (1H, t, J=1.5 Hz, $C=CH_2$). Found: C, 75.83; H, 11.30%. Calcd for $C_8H_{14}O$: C, 76.14; H, 11.18%.

iii): Compound **25** (199 mg) was treated with NaH (130 mg) in THF (20 ml) in the same manner as **24**. The reaction mixture was worked up as mentioned above and separated by chromatography over silica gel (5.5 g) with benzene–ether (10 : 1), giving the starting epoxide (**25**, 103 mg) and 2-methylenecyclooctanol (**42**, 26 mg): **42**, bp 92—95 °C (12 Torr); MS, *m/e* 140 (M^+) and 122; IR, 3400, 3060, 1630, and 895 cm^{-1}; NMR, δ 4.19 (1H, dd, J=8 and 6 Hz, 1-H), 4.96 and 5.12 (each 1H, s, $C=CH_2$). Found: C, 76.87; H, 11.56%. Calcd for $C_9H_{16}O$: C, 77.09; H, 11.50%.

References

1) Part IV of "Intramolecular Cyclization of Epoxy Alcohols," Part III, Ref. 7.

2) a) A. Murai, M. Ono, and T. Masamune, *J. Chem. Soc., Chem. Commun.*, **1976**, 864; A. Murai, M. Ono, and T. Masamune, *Bull. Chem. Soc. Jpn.*, **50**, 1226 (1977). b) Treatment of compound **1** with sodium methoxide (10 equiv) in dry methanol under reflux for 1 h led to only methanolysis to give 4-methoxy-1,1-pentamethylene-1,3-butanediol in an 85% yield.

3) G. Stork, L. D. Cama, and D. R. Coulson, *J. Am. Chem. Soc.*, **96**, 5268 (1974); G. Stork, and J. F. Cohen, *ibid.*, **96**, 5270 (1974).

4) W. C. Still, *Tetrahedron Lett.*, **1976**, 2115.

5) J. Y. Lallemand and M. Onanga, *Tetrahedron Lett.*, **1975** 585.

6) a) For oxirane ring cleavage followed by (or with concurrent) oxetane formation, see: *e. g.*, H. H. Henbest and B. Nicholis, *J. Chem. Soc.*, **1959**, 221; J. G. Buchanan and E. M. Oakes, *Tetrahedron Lett.*, **1964**, 2013; P. W. Austin, J. G. Buchanan, and E. M. Oakes, *J. Chem. Soc., Chem. Commun.*, **1965**, 374; J. G. Buchanan and H. Z. Sable, "Selective Organic Transformation," ed by B. S. Thyagarajan, John Wiley and Sons, Inc., New York (1972), Vol. 2, p. 53; J. -P. Bate, J. Moulines, and J. -C. Pommier, *Tetrahedron Lett.*, **1976**, 2249; A. K. Saksena, P. Mangiaracina, and R. Brambilla, *ibid.*, **1978**, 1729. b) For intramolecular cyclization accompanied by oxirane ring cleavage, see: *e. g.*, G. B. Payne, *J. Org. Chem.*, **27**, 3819 (1962); T. Masamune, M. Takasugi, A. Murai, and K. Kobayashi, *J. Am. Chem. Soc.*, **89**, 4521 (1967); G. Büchi, D. Minster, and J. C. F. Young, *ibid.*, **93**, 4319 (1971); G. L. Hodgson, D. F. MacSweeney, and T. Money, *Tetrahedron Lett.*, **1972**, 3683; M. C. Sacquet, B. Craffe, and P. Maitle, *ibid.*, **1972**, 4453; M. F. Grundon and H. M. Okely, *J. Chem. Soc., Perkin Trans. 1*, **1975**, 150; R. Achini and W. Oppolzer, *Tetrahedron Lett.*, **1975**, 369; J. H. Babler and A. J. Tortorello, *J. Org. Chem.*, **41**, 885 (1976); B. Capon and J. W. Thomson, *J. Chem. Soc., Perkin Trans. 2*, **1977**, 917; J. Carnduff and D. G. Leppard, *J. Chem. Soc., Perkin Trans. 1*, **1977**, 1325; P. Bravo, C. Ticozzi, and D. Maggi, *J. Chem. Soc., Chem. Commun.*, **1976** 789. c) For mechanistic studies on oxirane ring cleavage, see: *e. g.*, G. L. Browne and R. E. Lutz, *J. Org. Chem.*, **17**, 1187 (1952); P. L. Nichols, Jr. and J. D. Ingham, *J. Am. Chem. Soc.*, **77**, 6547 (1955); G. Gee, W. C. E. Higginson, P. Levesly, and K. J. Taylor, *J. Chem. Soc.*, **1959**, 1338; P. A. Cruickshank and M. Fishman, *J. Org. Chem.*, **34**, 4060 (1969); D. L. Whalen and A. M. Ross, *J. Am. Chem. Soc.*, **98**, 7859 (1976); V. Markowski and R. Huisgen, *J. Chem. Soc., Chem. Commun.*, **1977**, 439; C. Battistini, P. Crotti, M. Ferretti, and F. Macchia, *J. Org. Chem.*, **42**, 4067 (1977); C. Anselmi, G. Berti, G. Catelani, L. Lecce, and L. Monti, *Tetrahedron*, **33**, 2271 (1977); U. Sankawa and T. Sato, *Tetrahedron Lett.*, **1978**, 981; J. M. Janusz, A. R. Becker, and T. C. Bruice, *J. Am. Chem. Soc.*, **100**, 8269 (1978); M. Weissenberg, P. Krinsky, and E. Glotter, *J. Chem. Soc., Perkin Trans. 1*, **1978**, 565; G. Bellucci, G. Berti, M. Feretti, G. Ingrosso, and E. Mastroilli, *J. Org. Chem.*, **43**, 422 (1978); M. Apparu and M. Barrelle, *Tetrahedron*, **34**, 1691 (1978).

7) T. Masamune, M. Ono, S. Sato, and A. Murai, *Tetrahedron Lett.*, **1978**, 371.

8) In this paper "fused and non-fused" systems are defined as groups of compounds, in each of which an oxirane ring is fused and not fused with a cycloalkane ring, respectively.

9) a) *Cf.*, R. G. Carlson and N. B. Behn, *J. Org. Chem.*, **32**, 1363 (1967); H. B. Henbest and J. J. McCullough, *Proc. Chem.Soc.*, **1962**, 74.

10) The solvent system (75% aq DMSO) was selected for carrying out the reactions in homogeneous state and found to be the most suitable for oxetane formation. *Cf.*, T. J. M. Pouw and P. Zuman, *J. Org. Chem.*, **41**, 1614 (1976).

11) W. K. Anderson and T. Veysoglu, *J. Org. Chem.*, **38**, 2267 (1973).

12) *Cf.*, G. Berti, B. Macchia, and F. Maccia, *Tetrahedron Lett.*, **1965**, 3421; *Tetrahedron*, **24**, 1755 (1968).

13) *Cf.*, H. Nilson and L. Smith, *Z. Phys. Chem.*, **166a**, 136 (1936); B. Capon, *Quart. Rev.*, **18**, 45 (1964).

14) D. F. Schneider and B. C. L. Weedon, *J. Chem. Soc., C*, **1967**, 1986.

15) *Cf.*, D. N. Brattesani and C. H. Heathcock, *Synth. Commun.*, **3**, 245 (1973).

16) *Cf.*, E. A. Braude and O. H. Wheeler, *J. Chem. Soc.*, **1955**, 320.

17) *Cf.*, A. C. Cope, A. A. D'Addieco, D. E. Whyte, and S. A. Glickman, *Org. Synth.*, Coll. Vol. IV, 234 (1963).

18) Th. J. De Boer, and H. J. Backer, *Org. Synth.*, Coll. Vol. IV, 250 (1963).

19) A. E. Osterberg, *Org. Synth.*, Coll. Vol. I, 185 (1941).

20) P. B. Talukdar and P. E. Fanta, *J. Org. Chem.*, **24**, 555 (1959).

21) A. C. Cope, S. W. Fenton, and C. F. Spencer, *J. Am. Chem. Soc.*, **74**, 5884 (1952).

22) H. Nozaki and R. Noyori, *J. Org. Chem.*, **30**, 1052 (1965).

23) S. J. Angyal and N. K. Matheson, *J. Am. Chem. Soc.*, **77**, 4341 (1955).

24) A. C. Cope, T. A. Liss, and G. W. Wood, *J. Am. Chem. Soc.*, **89**, 6287 (1957).

Dehydrooligopeptides. I. The Facile Coupling of α-Amino Acids with α-Dehydroamino Acids to Dehydrodipeptides

Yasuchika YONEZAWA, Chung-gi SHIN,* Yuji ONO, and Juji YOSHIMURA†

Laboratory of Organic Chemistry, Faculty of Technology, Kanagawa University, Rokkakubashi, Kanagawa-ku, Yokohama 221

†*Laboratory of Chemistry for Natural Products, Faculty of Science, Tokyo Institute of Technology, Nagatsuta, Midori-ku, Yokohama 227*

(Received December 14, 1979)

N-Cbz- or *N*-Tos-α-dehydroamino acid (DHA) and its ester were prepared by the condensation of 2-oxo carboxylic acid or ester with benzyl carbamate or *p*-toluenesulfonamide. Subsequently, the N-protected DHA and its N-free ester thus obtained were coupled with several L-α-amino acid esters and N-protected (Boc or Cbz)-L-α-amino acid respectively by the usual peptide synthetic methods to give a number of different types of dehydrodipeptide. The configurations of all the new DHA and dehydrodipeptides obtained were shown to have (*Z*)-geometry.

Recently, much interest has been directed to the synthesis and bioactivity of dehydropeptide (DHP), containing α-dehydroamino acid (DHA) residues, which are very important constituents in an increasing number of antibiotic and phytotoxic peptides.[1-3] The previous methods of synthesizing the simple DHP has been almost exclusively indirect, *i.e.*, methods using the reaction of unsaturated azlactone with α-amino acid[4,5] and the β-elimination of peptide, which has a leaving group.[6-8] Concerning the direct condensation, no report has been published on the coupling of DHA with α-amino acid, except for two examples[9,10] involving earlier work by one of the present authors (C. S.).

In a previous paper, we briefly reported the direct coupling of (*Z*)-2-(benzyloxycarbonylamino)-2-alkenoic acid (**4**) as a carbonyl component with the L-leucine ethyl ester by the usual synthetic method.[11]

In the present paper, we wish to report in detail on the general preparation of the DHA N-protected with the benzyloxycarbonyl (Cbz) group (**2** and **4**) or the *p*-tolylsulfonyl (Tos) group (**3** and **5**), and on the facile synthesis of the two kinds of N-protected DHP from the N-protected DHA (ΔAA)[12] and several L-α-amino acid (AA) esters, and from N-protected AA and ethyl (*Z*)-2-amino-2-alkenoate (**1**)[13,14] by the mixed anhydride, DCC, or azide method.

Results and Discussion

N-Protected (Z)-α-Dehydroamino Acids. In order to prepare the DHA with a useful protecting group as a carboxyl component, according to the method reported previously by us,[15] the condensation reaction of α-oxoalkanoic acids with amides under various acidic conditions have been extensively reinvestigated. As a result, the optimum experimental conditions for the preparation of 2-Cbz- or 2-Tos-amino-2-alkenoic acids (**4** and **5**) and ethyl 2-Cbz- or 2-Tos-amino-2-alkenoates (**2** and **3**) were established as follows. The condensation reaction of equimolar 2-oxoalkanoic acid with benzyl carbamate or *p*-toluenesulfonamide in benzene in the presence of *p*-toluenesulfonic acid (PTS) as the catalyst under reflux for *ca.* 4 h gives **4** and **5** in yields *ca.* 75 and *ca.* 51% respectively. On the other hand, in the case of the reaction of ethyl 2-oxoalkanoate with benzyl carbamate or *p*-toluenesulfonamide, it was found that a similar condensation readily occurred in the presence of phosphoryl chloride rather than PTS to give **2** and **3** in *ca.* 69 and 72% yields respectively. However, the attempt to effect a similar direct condensation of 2-oxoalkanoic acid or its ester with *t*-butyl carbamate failed because of the unstability of the *t*-butoxycarbonyl (Boc) group under acidic conditions.

The α-dehydroamino acid structure of **2**—**5** was supported by the characteristic signals of olefinic (δ 5.63—6.94), vinyl (δ 5.68—6.22), and γ-protons (δ 1.68—3.19) in the NMR spectra and the characteristic absorption bands of NH (3220—3310 cm^{-1}), ester (1720—1740 cm^{-1}), carbonyl (1705—1710 cm^{-1}), and carbon-carbon double bond (1640—1665 cm^{-1}) functions in the IR spectra. Although the configuration of **2**—**5** could not be determined from the above spectroscopic data, the geometric structures of the esters were unambiguously determined to have (*Z*)-geometry by comparison with **2** and **3** prepared independently by the acylation of (*Z*)-**1**[14] with benzyloxycarbonyl chloride (Cbz-Cl) or tosyl chloride (Tos-Cl) respectively in the usual way. Moreover, the configurational structures of the free acid prepared by the hydrolysis

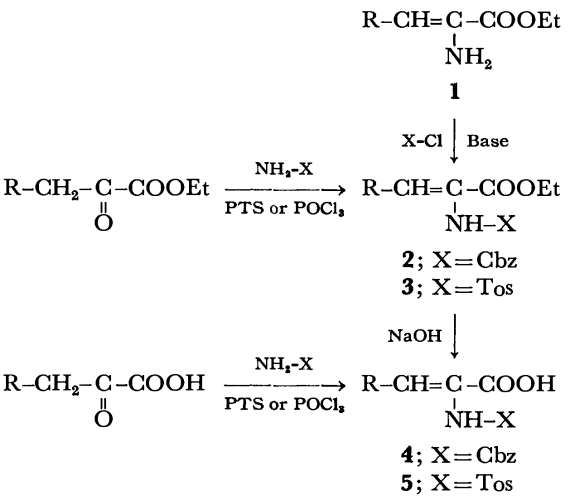

a; R=H, **b**; R=CH_3, **c**; R=C_2H_5, **d**; R=*n*-C_3H_7, **e**; R=*i*-C_3H_7, f; R=C_6H_5

Scheme 1.

TABLE 1. ETHYL (*Z*)-2-(Cbz-AMINO)- AND (*Z*)-2-(Tos-AMINO)-2-ALKENOATES (**2** and **3**)

Compd No.	Yield(%) A[a]	Yield(%) B[b]	Mp/°C	Formula	Found (Calcd), % C	H	N	NMR spectrum, δ in $CDCl_3$ Olefinic proton (J_{Hz})	γ-Proton (J_{Hz})	NH
2a	61		34—35[c]	$C_{13}H_{15}NO_4$	62.51 (62.64	6.16 6.07	5.48 5.62)	6.22s, 5.80d		
2b	69	96	syrup	$C_{14}H_{17}NO_4$	63.76 (63.86	6.55 6.51	5.12 5.23)	6.67q (7.2),	1.78d (7.2),	6.32s
2c	69	85	syrup	$C_{15}H_{19}NO_4$	65.02 (64.96	6.77 6.91	4.98 5.05)	6.58t (7.5),	2.10p (7.5),	6.64s
2d	72	88	syrup	$C_{16}H_{21}NO_4$	66.01 (65.95	7.23 7.27	4.99 4.81)	6.64t (7.8),	2.26q (7.5),	6.28s
2e	70	81	syrup	$C_{16}H_{21}NO_4$	66.07 (65.95	7.34 7.27	4.69 4.81)	6.45d (9.8),	2.70m,[e]	6.28s
2f	71	22	60—62[c]	$C_{19}H_{19}NO_4$	70.22 (70.14	5.65 5.89	4.27 4.31)	7.14—7.60m,		6.44s
3a	51		76—77[d]	$C_{12}H_{15}NO_4S$	54.00 (53.53	5.51 5.62	5.31 5.20)	5.69s,		7.40bs
3b	76	66	93—95[d]	$C_{13}H_{17}NO_4S$	55.31 (55.12	6.12 6.05	4.90 4.95)	6.94q (7.5),	2.09d (7.5),	6.21s
3c	77	63	45—46[d]	$C_{14}H_{19}NO_4S$	56.50 (56.56	6.41 6.44	4.68 4.71)	6.82t (7.5),	2.55p (7.8),	6.11s
3d	75	62	59—60[d]	$C_{15}H_{21}NO_4S$	57.80 (57.86	6.88 6.80	4.42 4.50)	6.82t (8.0),	2.49q (7.8),	6.22s
3e	71	64	79—80[d]	$C_{15}H_{21}NO_4S$	57.81 (57.86	6.71 6.80	4.45 4.50)	6.58d (11.0),	3.19m,	6.14s
3f	80	80	89—91[d]	$C_{18}H_{19}NO_4S$	62.71 (62.60	5.08 5.55	4.12 4.06)	7.12—7.90m,[e]		6.37s

a) Yield from ethyl 2-oxoalkanoate and benzyl carbamate or *p*-toluenesulfonamide. b) Yield from ethyl 2-amino-2-alkenoate and Cbz-Cl or Tos-Cl. c) Colorless needles from hexane–ethyl acetate (5: 2 v/v). d) Colorless needles from diisopropyl ether. e) Overlapped with phenyl protons.

TABLE 2. (*Z*)-2-(Cbz-AMINO)- AND (*Z*)-2-(Tos-AMINO)-2-ALKENOIC ACIDS (**4** and **5**)

Compd No.	Yield(%) A[a]	Yield(%) B[b]	Mp/°C	Formula	Found (Calcd), % C	H	N	NMR spectrum, δ in $CDCl_3$ (**4**) or DMSO-d_6 (**5**) Olefinic proton (J_{Hz})	γ-Proton (J_{Hz})	NH
4a	42		100—101[c]	$C_{11}H_{11}NO_4$	59.65 (59.72	5.19 5.01	6.25 6.33)	5.92s, 5.68s,		8.62bs
4b	73	84	152—153[d]	$C_{12}H_{13}NO_4$	61.29 (61.27	5.63 5.57	5.68 5.96)	6.50q (7.0),	1.68d (7.0),	8.54s
4c	80	92	100—101[d]	$C_{13}H_{17}NO_4$	62.44 (62.64	5.60 6.07	6.02 5.62)	6.40t (7.0),	2.19p (7.0),	8.55s
4d	82	91	126—127[d]	$C_{14}H_{17}NO_4$	63.81 (63.86	6.67 6.51	5.08 5.32)	6.41t (7.0),	2.10q (7.0),	8.54s
4e	79	93	105—106[d]	$C_{14}H_{17}NO_4$	63.62 (63.86	6.46 6.51	5.30 5.32)	6.27d (10.0),	2.62m,	8.50s
4f	92	92	170—171[d]	$C_{17}H_{15}NO_4$	68.60 (68.67	5.21 5.08	4.68 4.71)	7.35—7.70m,[h]		8.94s
5b	41	18	138—140[e]	$C_{11}H_{13}NO_4S$	51.71 (51.76	5.22 5.13	5.44 5.49)	6.93q (7.2),	1.68d (7.2),	9.11s
5c	45	17	128—129[f]	$C_{12}H_{15}NO_4S$	53.48 (53.53	5.70 5.62	5.26 5.20)	6.77t (7.8),	2.14p (7.8),	9.13s
5d	50	16	149—150[f]	$C_{13}H_{17}NO_4S$	55.25 (55.12	6.10 6.05	4.90 4.95)	6.63t (7.8),	2.05q (7.8),	8.90s
5e	47	21	140—141[f]	$C_{13}H_{17}NO_4S$	55.29 (55.12	6.13 6.05	4.88 4.95)	6.53d (10.8),	2.64m,	7.42s
5f	71	80	208—209[g]	$C_{16}H_{15}NO_4S$	60.41 (60.56	4.75 4.77	4.48 4.41)	7.02—7.78m,[h]		9.23s

a) Yield from 2-oxoalkanoic acid and benzyl carbamate or *p*-toluenesulfonamide. b) Yield from the hydrolysis of **2** or **3**. c) Colorless needles from chlorobenzene. d) Colorless needles from cyclohexane–benzene. e) Colorless prisms from chloroform. f) Colorless prisms from benzene. g) Colorless prisms from 50% ethanol. h) Overlapped with phenyl protons.

of (*Z*)-**2** and **3** were identical with those of **4** and **5** respectively.

The yields, physical constants, and NMR spectral data of **2**—**4** and **5** are listed in Tables 1 and 2.

Coupling of (Z)-DHA with L-α-*Amino Acid.* As has been reported in the preceding communication,[11] Compound **4** as a carboxyl component was subjected to a reaction with the appropriate L-α-amino acid (Gly, Ala, Ser, Leu, Met, Cys(benzyl), Phe, Trp, and Tyr) esters (methyl and ethyl). As expected, the equimolar coupling of N-protected DHA with the amino acid ester by either the mixed anhydride (MA) method (in the presence of triethylamine and ethyl chloroformate in THF–chloroform at 0 °C for 1 h), the DCC method (in the presence of dicyclohexylcarbodiimide and triethylamine in chloroform at 0 °C for 3 h), or the usual azide method occurred to give Cbz-(*Z*)-dehydroaminoacylamino acid esters (**6**) as colorless syrup or crystals in *ca.* 70% yields.

On the other hand, N-protected L-α-amino acid (Leu, Cys(benzyl), and Phe) was first coupled with (*Z*)-**1** as an amine component by the similar DCC method to

Table 3. Cbz–(*Z*)-ΔAA–L-AA–OR (**6**)

ΔAA–L-AA–OR	Yield (%)	Mp/°C	Formula	Found (Calcd), %			NMR spectrum, δ in $CDCl_3$			$[\alpha]_D^{24}$ f)
				C	H	N	Olefinic proton (J_{Hz})	α-Proton (J_{Hz})	NH	
ΔAla–Ser–OMe	43	syrup	$C_{15}H_{18}N_2O_6$	55.97 (55.89	5.62 5.63	8.88 8.69)	6.08d (2.0), 5.34d	4.57dd (9.0, 2.6),	7.62	−15.0
ΔBut–Gly–OEt	82	106—107 b)	$C_{16}H_{20}N_2O_5$	60.11 (59.99	6.21 6.29	8.71 8.75)	6.69q (7.0),	4.07d (5.2),	6.99s 7.11d	
ΔBut–Ala–OEt	65	syrup	$C_{17}H_{22}N_2O_5$	60.97 (61.06	6.51 6.63	8.19 8.38)	6.55q (7.0),	4.62m,	6.78s 6.91d	
ΔBut–Phe–OEt	61	95—96 c)	$C_{23}H_{26}N_2O_5$	67.25 (67.30	6.46 6.39	6.88 6.83)	6.54q (7.0),	4.95m,	6.65s 6.81d	−0.2
ΔBut–Tyr–OMe	71	syrup	$C_{22}H_{24}N_2O_6$	63.99 (64.06	5.68 5.83	7.01 6.79)	6.46q (7.2),	4.81m,	6.63s 6.78d	
ΔBut–Trp–OMe	72	147—148 e)	$C_{24}H_{25}N_3O_5$	65.91 (66.19	5.90 5.79	10.11 9.65)	6.40q (7.2),	4.86m,	6.63s 6.78d	+6.3
ΔLeu–Leu–OEt	67	74—75 c)	$C_{22}H_{32}N_2O_5$	65.38 (65.32	8.22 7.97	7.14 6.93)	6.25d (10.2),	4.58dt (6.0, 8.0),	6.67s 6.72d	−29.1
ΔLeu–Cys–OEt | Bzl	83	syrup	$C_{26}H_{32}N_2O_5S$	64.59 (64.45	6.99 6.66	5.81 5.78)	6.32d (10.0),	4.81m,	6.55s 7.19d	−41.3
ΔPhe–Gly–OEt	85	118—119 b)	$C_{21}H_{22}N_2O_5$	66.00 (65.95	5.84 5.80	7.27 7.33)	7.31s,	4.09d (5.2),	6.95s 7.21t	
ΔPhe–Ala–OEt	85	116—117 b)	$C_{22}H_{24}N_2O_5$	66.57 (66.65	6.15 6.10	7.01 7.01)	7.27s,	4.68m,	6.87s 7.17d	+21.8
ΔPhe–Met–OMe	61	81—82 d)	$C_{23}H_{26}N_2O_5S$	62.51 (62.43	5.81 5.92	6.25 6.33)	7.35s,	4.89m,	6.95s	−30.9

a) Yield by the DCC method. b) Colorless needles from CCl_4. c) Colorless prisms from diisopropyl ether. d) Colorless prisms from diethyl ether. e) Colorless needles from ethyl acetate. f) Measured in ethanol (*c* 1.0).

Table 4. Boc- and Cbz–L-AA–(*Z*)-ΔAA–OR (**7**)

L-AA–ΔAA–OR	Yield h) (%)	Mp/°C	Formula	Found (Calcd), %			NMR spectrum, δ in $CDCl_3$			$[\alpha]_D^{27}$ g)
				C	H	N	Olefinic proton (J_{Hz})	α-Proton (J_{Hz})	NH	
Phe–ΔBut–OEt a)	67	61—62 c)	$C_{20}H_{28}N_2O_5$	62.99 (63.81	7.44 7.50	7.31 7.44)	6.86q (7.6),	4.60dt (7.5, 7.0),	5.36d 7.81s	−18.9
Phe–ΔVal–OEt	72	150—151 d)	$C_{21}H_{30}N_2O_5$	64.27 (64.59	8.00 7.74	7.45 7.17)	—	4.50dt (7.5, 7.0),	5.24d 7.58s	−20.2
Phe–ΔnorVal–OEt a)	46	96—97 e)	$C_{21}H_{30}N_2O_5$	64.70 (64.59	7.80 7.74	7.02 7.17)	6.76t (7.5),	4.58dt (7.5, 7.0),	5.30d 7.72s	−19.4
Phe–ΔnorLeu–OEt a)	55	82—83 e)	$C_{22}H_{32}N_2O_5$	65.12 (65.32	7.72 7.97	6.73 6.93)	6.83t (7.5),	4.58dt (7.5, 7.0),	5.33d 7.76s	−19.5
Phe–ΔLeu–OEt a)	57	94—95 e)	$C_{22}H_{32}N_2O_5$	65.50 (65.32	7.81 7.97	6.71 6.93)	6.58d (10.0),	4.56dt (7.5, 7.0),	5.33d 7.61s	−20.6
Cys–ΔnorLeu–OEt a) | Bzl	56	79—80 f)	$C_{23}H_{34}N_2O_5S$	61.40 (61.31	7.51 7.61	6.10 6.22)	6.86t (7.0),	4.46dt (7.5, 7.0),	5.54d 7.90s	−28.1
Leu–ΔLeu–OEt b)	39	98—99 e)	$C_{22}H_{32}N_2O_5$	65.20 (65.32	8.09 7.97	7.21 6.93)	6.48d (10.0),	4.36m,	5.80d 7.86s	−7.4

a) Protected with the Boc group. b) Protected with the Cbz group. c) Colorless needles from hexane. d) Colorless needles from carbon tetrachloride. e) Colorless needles from cyclohexane. f) Colorless prisms from diisopropyl ether. g) Measured in methanol (*c* 1.0). h) Yield by the DCC method.

give N-protected L-leucyl-, benzylcysteinyl-, or phenylalanyl-(*Z*)-dehydroamino acid esters (**7**) as colorless crystals in *ca.* 56% yields. However, the coupling of the α-dehydrophenylalanine ester with N-protected amino acid scarcely proceeded at all because of the weak basicity of the amino group in the amine component.

In the IR spectral data, the characteristic differences between **6** and **7** could not be recognized. The presence of secondary amide absorption bands in the 1620—1670 and 1520—1560 cm^{-1} regions indicated the formation of the peptide bond. Moreover, the absorption bands of NH (3200—3400 cm^{-1}), ester carbonyl (1735—1750 cm^{-1}), and carbon-carbon double bond (1640—1685 cm^{-1}) functions are constituent with the assignment of the dehydrodipeptide structure.

The chemical shifts and the coupling constants of **6** and **7** were assigned as is shown in Tables 3 and 4. In the NMR spectrum of **6**, the signals in the δ 4.07—4.95 region as multiplets and in the δ 6.72—7.21 region as doublets are attributable to methine and NH protons of the α-AA residue, while the signals at δ 5.34 and in the 6.08—7.35 and 6.55—6.99 regions are attributable as singlets to vinyl, olefinic, and NH protons of the ⊿AA residue respectively. On the other hand, in the case of **7**, the corresponding signals of the α-AA residue appeared in the δ 4.36—4.60 as double triplets and in the δ 5.24—5.80 region as doublets, while those of the ⊿AA residue appeared in the δ 6.48—6.86 and 7.58—7.90 regions as singlets.

The configurations of **6** and **7** were readily determined to have (*Z*)-geometry, since the chemical shifts and the spectral patterns of the DHA residue in **6** and **7** were quite similar to the those of the corresponding (*Z*)-configurational **2**—**5**. Accordingly, it was found that the (*Z*)-configuration of DHA residue has been maintained during the peptide formation reaction.

The yields, physical constants, and NMR spectral data of **6** and **7** are listed in Tables 3 and 4.

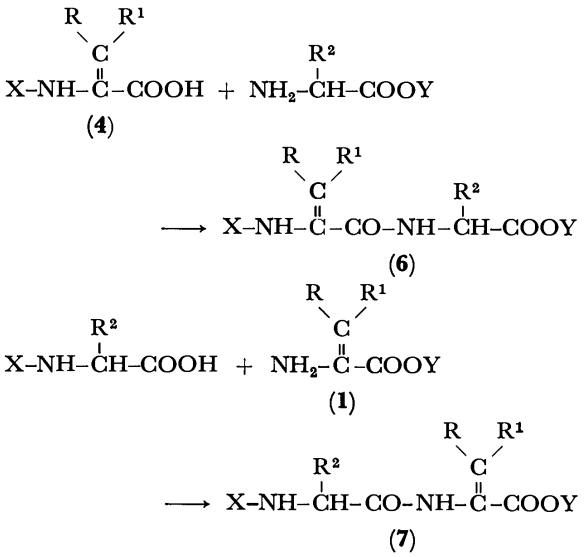

α-Amino acid residues=Gly, Ala, Ser, Leu, Met, Cys-(benzyl), Phe, Tyr, and Trp. α-Dehydroamino acid residues=⊿Ala, ⊿But, ⊿Val, ⊿norVal, ⊿norLeu, ⊿Leu, and ⊿Phe. X=Cbz and Boc groups. Y=Me and Et.

Scheme 2.

Experimental

All the melting points are uncorrected. The IR spectra were recored with a Hitachi EPI-G3 Spectrometer. The NMR spectra were measured with a JNM-PS-100 Spectrometer (Japan Electron Laboratory Co. Ltd.), using tetramethylsilane as the internal standard. The specific rotations were measured in a 0.5 dm using a JASCO DIP-4 Polarimeter (Japan Spectroscopic Co., Ltd.).

Preparation of **2**. *Procedure A*: A solution of ethyl 2-oxoalkanoate (50 mmol), benzyl carbamate (60 mmol), and $POCl_3$ (3 ml) in dry benzene (70 ml) was refluxed for 4 h. To the reaction solution we then added benzene at room temperature, after which the resultant solution was washed with saturated aqueous $NaHCO_3$ and three times with water. The benzene layer was dried over anhydrous Na_2SO_4 and concentrated under reduced pressure to give a syrupy residue, which was purified on a silica gel column, using benzene as the eluent, to give **2** as a colorless viscous oil or colorless crystals.

Procedure B: Into a solution of (*Z*)-**1** (20 mmol) and pyridine (30 mmol) in dry diethyl ether (14 ml), we stirred Cbz-Cl (20 mmol), drop by drop, under cooling. After stirring at room temperature for 6 h, more diethyl ether (40 ml) was added to the reaction solution. The pyridinium salt thus deposited was filtered off, and the filtrate was successively washed with chilled 3 M HCl, saturated aqueous $NaHCO_3$, and water, and finally dried over anhydrous Na_2SO_4. The syrupy residue thus obtained was similarly worked up to give **2**.

Preparation of **3**. *Procedure A*: In a manner analogous Procedure A described for **2**, the solution of ethyl 2-oxoalkanoate (50 ml), *p*-toluenesulfonamide (60 mmol), and $POCl_3$ (3 ml) in dry benzene (60 ml) was worked up for 9 h to give **3** as colorless crystals.

Procedure B: Into a solution of (*Z*)-**1** (20 mmol) in dry pyridine (14 ml) we stirred Tos-Cl (20 mmol) under cooling. After stirring at room temperature for 12 h, the excess pyridine was evaporated under reduced pressure. The syrupy residue thus obtained was dissolved in ethyl acetate (40 ml), and then the resultant solution was similarly worked up to give **3**.

Preparation of **4**. *Procedure A*: A solution of 2-oxoalkanoic acid (50 mmol), benzyl carbamate (50 mmol), and PTS (2 g) in dry benzene (70 ml) was refluxed for *ca.* 4 h, by which time the theoretical amount of water has separated out. After the solution had then been allowed to stand at room temperature, the crystals deposited were filtered. The filtrate was further extracted twice with saturated aqueous $NaHCO_3$ and the aqueous layer was washed once with ethyl acetate. The resultant aqueous layer was acidified to pH 2 with 6 M HCl and extracted well with ethyl acetate. The organic layer was washed with 20% aqueous NaCl and then dried over anhydrous Na_2SO_4. After the removal of the ethyl acetate, more crystals were obtained. The recrystallization of the combined crystals from chlorobenzene or cyclohexane–benzene gave **4** as colorless needles.

In an analogous manner, pyruvic acid (250 mmol) was treated with benzyl carbamate (100 mmol) in the absence of PTS to give **4a**.

Procedure B: A solution of **2** (10 mmol) in dioxane (20 ml) was treated with 1 M NaOH (30 ml) with stirring at *ca.* 35 °C for 2 h. After cooling with ice water, the reaction solution was acidified to pH 2 with 3 M HCl, and the resultant solution was extracted three times with ethyl acetate (30 ml). The extracts were washed with saturated aqueous NaCl, dried over anhydrous Na_2SO_4, and then concentrated under reduced

pressure to give **4**.

Preparation of **5**. *Procedure A*: A solution of 2-oxoalkanoic acid (50 mmol), *p*-toluenesulfonamide (50 mmol), and PTS (2.4 g) was worked up exactly according to Procedure A above to give **5** as colorless prisms.

Procedure B: The hydrolysis of **3** (10 mmol) with 1 M NaOH (30 ml) in dioxane (20 ml) was done exactly according to Procedure B above to give **5**.

Preparation of **6**. *Procedure A*: Into a solution of **4** (20 mmol) and triethylamine (20 mmol) in dry THF (60 ml) we vigorously stirred ethyl chloroformate (20 mmol), below −15 °C. After stirring had been continued for 15 min, a solution of an appropriate α-amino acid ester (20 mmol) in dry $CHCl_3$ (60 ml) was stirred into the resultant solution at 0 °C. After stirring at 0 °C for 1.5 h and then at room temperature for a further 12 h, the reaction solution was concentrated under reduced pressure to give a residual syrup, which was subsequently dissolved in a mixture of ethyl acetate (300 ml) and water (150 ml). The resulting organic layer was successively washed with 4% aqueous $NaHCO_3$, water, 10% aqueous citric acid, and water, and finally dried over anhydrous Na_2SO_4. The evaporation of the ethyl acetate under reduced pressure gave crude crystals or a syrup, subsequently purified on a silica gel column, using benzene as the eluent, to give **6**. Cbz–⊿Leu–Leu–OEt; yield, 52%. Cbz–⊿phe–Gly–OEt; yield, 56%. Cbz–⊿But–Ala–OEt; yield, 50%.

Procedure B: Into a solution of **4** (10 mmol) and an appropriate α-amino acid ester (10 mmol) in DMF (10 ml) we stirred DCC (11 mmol), portion by portion, under cooling. After the mixture had been stirred at room temperature for 12 h, the urea deposited was filtered off and washed well with ethyl acetate. The filtrate was poured into water (70 ml), and the aqueous solution was extracted twice with ethyl acetate (60 ml). The combined extracts were successively washed with 2% aqueous HCl, water, saturated aqueous $NaHCO_3$ and water, and finally dried over anhydrous Na_2CO_3. The evaporation of the ethyl acetate under reduced pressure gave crystals or a syrup, subsequently purified on a silica gel column, using benzene–ethyl acetate (4 : 1 v/v), to give **6**. See Table 3.

Procedure C: Into a solution of ethyl α-(Cbz-amino)cinnamate (**2f**; 5 mmol) in ethanol (20 ml) we stirred hydrazine hydrate (5.5 mmol) at room temperature. After the mixture had been stirred for 5 h, the ethanol was evaporated to give a residual syrup. To a solution of the syrup obtained in 1 M HCl (15 ml) and ethyl acetate (20 ml) we added a solution of $NaNO_2$ (5.5 mmol) in water (12 ml) by stirring below 0 °C. After stirring had been continued for 30 min, chilled ethyl acetate (15 ml) was added to the reaction solution and the resulting organic layer was dried over anhydrous Na_2SO_4 at 0 °C. Finally, to the resultant chilled solution we added a solution of Gly–OEt (6 mmol) in dry diethyl ether (16 ml), and then the solution was stirred at 0 °C for 12 h and then at room temperature for 12 more h. The reaction solution was washed successively with 2 M HCl, 3% aqueous $NaHCO_3$, and water, and then dried over anhydrous Na_2SO_4. The subsequent evaporation of the solvent gave Cbz–⊿Phe–Gly–OEt in a 61% yield.

Preparation of **7**. *Procedure A*: Into a solution of Boc–L-AA (20 mmol) in dry THF (60 ml) and triethylamine (20 mmol) we vigorously stirred ethyl chloroformate (20 mmol) at −15 °C. After stirring had been continued for 5 min, a solution of (*Z*)-**1** (20 mmol) in dry $CHCl_3$ (50 ml) was stirred into the resultant solution. The reaction solution was then worked-up exactly according to Procedure A above to give **7**. Boc–Phe–⊿But–OEt; yield, 33%. Boc–Phe–⊿Leu–OEt; yield, 34%.

Procedure B: Into a solution of (*Z*)-**1** (10 mmol) and an appropriate N-protected L-AA (10 mol) in CH_2Cl_2 (10 ml) we vigorously stirred DCC (11 mmol), portion by portion, below 0 °C. After stirring had been continued at room temperature for 20 h, the reaction solution was worked-up exactly according to Procedure B above to give **7**. See Table 4.

References

1) T. Kitagawa, T. Tamura, and H. Taniyama, *J. Biochem.*, **81**, 1757 (1977).

2) "Bioactive Peptides Produced by Microorganisms," ed by H. Umezawa, T. Takita, and T. Shiba, Kodansha, Tokyo (1978).

3) Y. Shimohigashi and N. Izumiya, *Yuki Gosei Kyokaishi*, **36**, 1023 (1978).

4) D. G. Doherty, J. E. Tietzmann, and M. Bergmann, *J. Biol. Chem.*, **147**, 617 (1943).

5) M. L. English and C. H. Stammer, *Biochem. Biophys. Res. Commun.*, **83**, 1464 (1978).

6) A. Srinivasan, R. W. Stephenson, and R. K. Olsen, *J. Org. Chem.*, **42**, 2253 (1977).

7) D. H. Rich and J. P. Tam, *Tetrahedron Lett.*, **1975**, 211.

8) S. Nomoto, A. Sano, and T. Shiba, *Tetrahedron Lett.*, **1979**, 521.

9) C. Shin, M. Masaki, and M. Ohta, *J. Org. Chem.*, **32**, 1860 (1967).

10) H. Poisel, *Chem. Ber.*, **110**, 942 (1977).

11) C. Shin, Y. Yonezawa, K. Unoki, and J. Yoshimura, *Tetrahedron Lett.*, **1979**, 1049.

12) In this paper, the symbol ⊿ indicates a double bond of the α-position in the DHA or DHA residue.

13) C. Shin, Y. Yonezawa, and J. Yoshimura, *Chem. Lett.*, **1976**, 1095.

14) C. Shin, Y. Yonezawa, K. Unoki, and J. Yoshimura, *Bull. Chem. Soc. Jpn.*, **52**, 1657 (1979).

15) C. Shin, M. Fujii, and J. Yoshimura, *Tetrahedron Lett.*, **1971**, 2499.

New Methods for Stereoselective Synthesis of α-Alkylidene-γ-butyrolactones Using Monoanion of *O*-Ethyl *S*-(Tetrahydro-2-oxo-3-furanyl) Thiocarbonate and Dianion of α-Mercapto-γ-butyrolactone

Kazuhiko TANAKA,* Hideki UNEME, Nobuyuki YAMAGISHI, Rikuhei TANIKAGA, and Aritsune KAJI

Department of Chemistry, Faculty of Science, Kyoto University, Sakyo-ku, Kyoto 606

(Received January 12, 1980)

The lithium enolates of *O*-ethyl *S*-(tetrahydro-2-oxo-3-furanyl) dithiocarbonate and thiocarbonate were found to be efficient reagents for the stereoselective synthesis of α-alkylidene-γ-butyrolactones from carbonyl compounds. The dianion of α-mercapto-γ-butyrolactone was successfully generated by treatment of α-mercapto-γ-butyrolactone with 2.2 equivalents of lithium diisopropylamide in the presence of *N,N,N',N'*-tetramethylethylenediamine at −78°C in THF. The dianion thus formed has been utilized for the efficient and stereoselective synthesis of α-alkylidene-γ-butyrolactones from carbonyl compounds.

Much attention has been focused on the synthesis of α-methylene-γ-butyrolactone (dihydro-3-methylene-2(3*H*)-furanone) and α-alkylidene-γ-butyrolactones (3-alkylidenedihydro-2(3*H*)-furanone) since these compounds serve as useful intermediates in organic synthesis[1] and constitute the biologically active natural products.[2] Since carbonyl compounds such as aldehydes and ketones are readily available in organic synthesis, the direct procedure for the preparation of these unsaturated lactones from carbonyl compounds is very attractive. Several methods have been reported for the direct introduction of an alkylidene group α to a γ-butyrolactone. These have included (1) the base-catalyzed condensation of γ-butyrolactone with aldehydes[3] and (2) the reaction of aldehydes with the anion of α-triphenylphosphoranylidene-γ-butyrolactone,[4] the anion of diethyl (tetrahydro-2-oxo-3-furanyl)phosphonate,[5] or the anion of α-trimethylsilyl-γ-butyrolactone.[6] However, there has been no general method for the stereoselective introduction of an alkylidene moiety onto the α-position of γ-butyrolactone.

We have reported in the preliminary communications[7,8] that lithium enolates of *O*-ethyl *S*-(tetrahydro-2-oxo-3-furanyl) dithiocarbonate and the corresponding thiocarbonate as well as the dianion of α-mercapto-γ-butyrolactone are useful and convenient reagents for the direct synthesis of α-alkylidene-γ-butyrolactones with high stereoselectivity. This report will provide, in greater detail, the scope and limitations of these useful and stereoselective α-ylidenation of γ-butyrolactone.

Results and Discussion

Lithium Enolates of O-*Ethyl* S-*(Tetrahydro-2-oxo-3-furanyl) Dithiocarbonate and Thiocarbonate.* Treatment of *O*-ethyl *S*-(tetrahydro-2-oxo-3-furanyl) dithiocarbonate (**1**)[9] with lithium diisopropylamide (LDA) at −78 °C in THF produced the yellow solution of lithium enolate **4**, which reacted with benzaldehyde to afford exclusively (*E*)-α-benzylidene-γ-butyrolactone (**5a**)[5] in 60% isolated yield. The starting material **1** can easily be prepared by the addition of α-bromo-γ-butyrolactone to potassium *O*-ethyl dithiocarbonate in ethanol. Attempts to purify the dithiocarbonate **1** by distillation, however, failed due to decomposition. This material can be purified by column chromatography on silica gel using benzene as eluent, but the procedure is unsuitable for the large scale preparation of **1**. Attempts to transform the dithiocarbonate **1** into the volatile liquid or the readily crystallizable material by preparing *O*-methyl *S*-(tetrahydro-2-oxo-3-furanyl) dithiocarbonate (**2**) or *O*-isopropyl analogue **3** were also fruitless. We have found that a monothiocarbonate (**7**), readily prepared from α-mercapto-γ-butyrolactone (**6**)[10] and ethyl chloroformate in high yield, can be easily purified

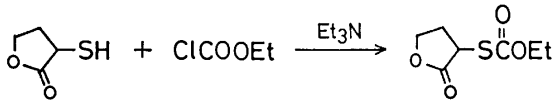

6 7 (91%)

by distillation. Reaction of **7** with lithium amide afforded the enolate **8** which smoothly reacted with benzaldehyde to give exclusively (*E*)-**5a**. Among the various lithium amides examined, lithium diethylamide is the most efficient base for converting thiocarbonate **7** into the enolate **8** as shown in Table 1. To show the generality of this method, a series of carbonyl compounds was utilized for α-ylidenation of γ-butyrolactone. In all cases examined, (*E*)-isomers were obtained predominantly. The *E*/*Z* ratio of a product **5** was determined by NMR and GLC analysis. For example, the ^{1}H-NMR spectrum of **5b** shows the vinyl proton β to the carbonyl

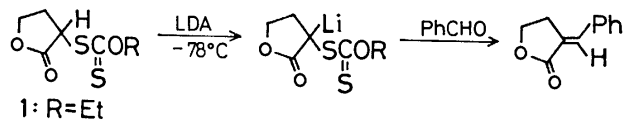

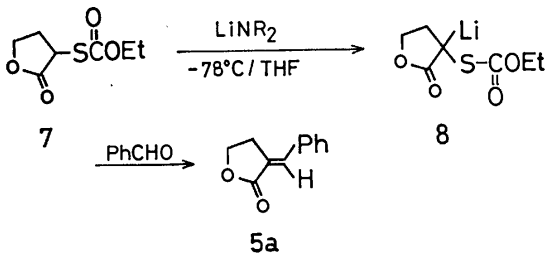

Table 1. Effect of lithium amide in the reaction of **7** with benzaldehyde

Lithium amide	% Yield of **5a**
$(i\text{-Pr})_2NLi$	53
$(i\text{-Pr})_2NLi$–TMEDA	54
$(Me_3Si)_2NLi$	39
Et_2NLi	84

at δ 6.48 for *E*-isomer and at δ 6.00 for *Z*-isomer, respectively. Integration of the vinyl proton gave a 93: 7 mixture of *E*-**5b** and *Z*-**5b**, being identical with the ratio obtained by GLC analysis (*E*/*Z*=94/6). The reaction appears to follow the pathway outlined in Scheme 1. The lithium reagent **8** attacks at the carbonyl carbon leading to **10** with transfer of the ethoxycarbonyl group from sulfur to oxygen. The intramolecular displacement affords a thiirane **11** which loses sulfur to give α-alkylidene-γ-butyrolactone (**5**). The extrusion of sulfur from thiiranes having electron-attracting substituents such as alkoxycarbonyl or cyano groups is a well-recognized process.[11,12]

Table 2. Synthesis of α-alkylidene-γ-butyrolactones from *O*-ethyl *S*-(tetrahydro-2-oxo-3-furanyl) thiocarbonate (**7**) and carbonyl compounds

Carbonyl compound	(mmol)	Product (5)		Yield %	E/Z ratio
Benzaldehyde	25	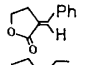	(5a)	84	100/0
Propanal	26	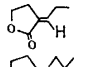	(5b)	78	94/6
Butanal	25	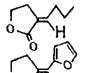	(5c)	76	95/5
2-Furancarbaldehyde	25	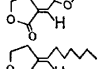	(5d)	75	100/0
Heptanal	25	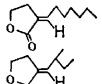	(5e)	83	94/6
2-Methylbutanal	26	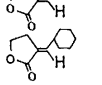	(5f)	93	85/15
Cyclohexanecabaldehyde	25	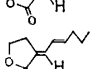	(5g)	82	92/8
(E)-2-Hexenal	25	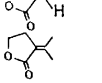	(5h)	76	91/9
Acetone	26	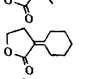	(5i)	75	
Cyclohexanone	25	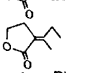	(5j)	65	
2-Butanone	25	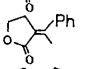	(5k)	59	48/52
Acetophenone	25	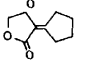	(5l)	22	100/0
Cyclopentanone	25		(5m)	16	

Stability of Lithium Enolate 8. In the case of cyclopentanone, we obtained 39% of α-ethoxycarbonyl-γ-butyrolactone (**12**)[13] in addition to 16% of α-cyclopentylidene-γ-butyrolactone (**5m**). This result suggests that the self-rearrangement of lithium enolate **8** takes place competitively. In order to examine the stability of lithium reagent **8**, the thiocarbonate **7** was treated with 1.1 equiv of lithium diethylamide in THF at

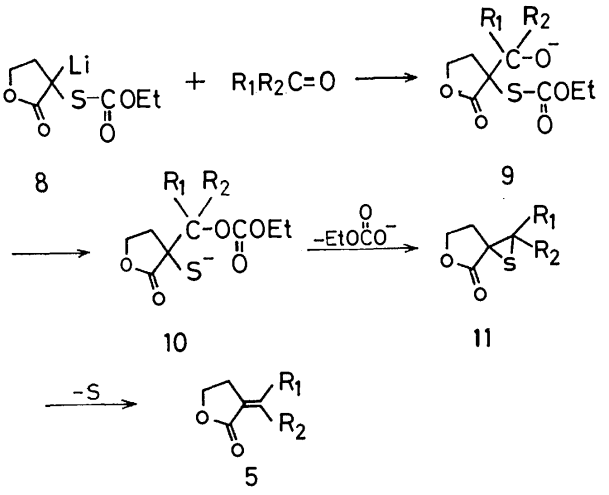

Scheme 1.

−78 °C, allowed to reach room temperature, and then quenched with saturated aqueous ammonium chloride solution. Upon workup, the lactone **12** was isolated in 45% yield. This transformation appears to involve the formation of a thiirane by intramolecular cyclization, followed by expulsion of sulfur.

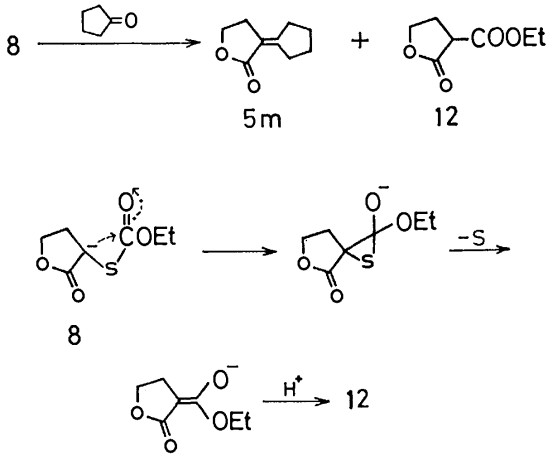

Dianion of α-Mercapto-γ-butyrolactone. The dianion of α-mercapto-γ-butyrolactone (**6**) is readily produced under mild conditions. Thus, treatment of **6** with 2.2 equiv of LDA in the presence of 2.2 equiv of *N*,*N*,*N*′,*N*′-tetramethylethylenediamine (TMEDA) in THF at −78 °C generated the dianion **13**, which afforded the dialkylated products (**14**) in high yields upon quenching

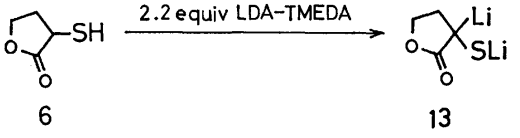

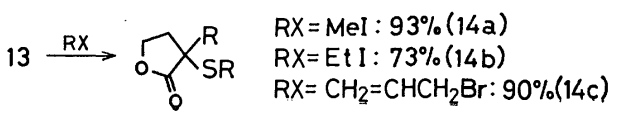

with excess of alkyl halides. The yield of the dialkylated compound (**14b**), however, decreased to 73% when ethyl iodide was used, providing a significant amount of the mono-alkylated derivatives, α-ethylthio-γ-butyrolactone (**15**) (22%). The dimethylated product **14a**

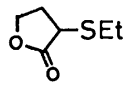

15

can be converted into α-methylene-γ-butyrolactone (Tulipalin A, **17**) by the reported procedure.[14] Thus, oxidation of **15a** and dehydrosulfenylation of **16** afforded Tulipalin A (**17**) and **18** in a ratio of 15:85. The dianion **13** is highly reactive toward carbonyl compounds. Thus, treatment of **13** with carbonyl compounds

TABLE 3. SYNTHESIS OF α-ALKYLIDENE-γ-BUTYROLACTONES FROM DIANION (**13**) AND CARBONYL COMPOUNDS

Carbonyl compound	(mmol)	Product (5)		Yield %	E/Z ratio
Benzaldehyde	40		(5a)	54	100/0
Propanal	22		(5b)	36	92/8
Butanal	25		(5c)	61	97/3
2-Furancarbaldehyde	40		(5d)	57	100/0
Heptanal	30		(5e)	67	92/8
2-Methylbutanal	40		(5f)	51	93/7
2-Methylbutanal	25		(5f)	43	96/4[a]
(E)-2-Hexenal	40		(5h)	45	78/22
Acetone	50		(5i)	50	
2-Butanone	50		(5k)	49	50/50
Acetophenone	50		(5l)	40	100/0
Cyclopentanone	25		(5m)	43	
Formaldehyde	30		(5n)	7	
Acetaldehyde	25		(5o)	30	92/8
2-Methylpropanal	25		(5p)	61	95/5
Pentanal	40		(5q)	69	95/5
3-Methylbutanal	30		(5r)	64	95/5
Hexanal	25		(5s)	64	97/3
Nonanal	25		(5t)	69	94/6
(E)-2-Butenal	40		(5u)	40	88/12
(E)-3-Phenyl-3-propenal	40		(5v)	38	b

a) Lithium diethylamide was used as a base. b) Not determined.

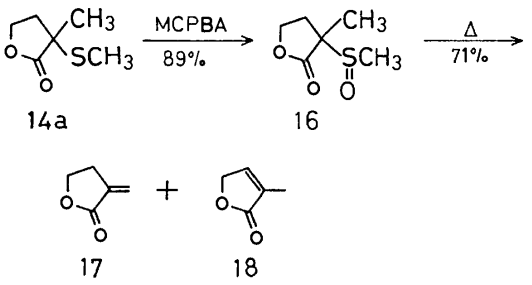

14a 16

17 18

at −78 °C and subsequent treatment of the reaction mixture with ethyl chloroformate gave predominantly (*E*)-α-alkylidene-γ-butyrolactones (**5**) in good yields. The scope of this experimentally simple synthesis of **5** is illustrated in Table 3. This reaction can be applied to a variety of aliphatic, aromatic, and heteroaromatic aldehydes, as well as α,β-unsaturated aldehydes, and afforded the desired products in moderate to good yields. However, the reaction of the dianion **13** with gaseous formaldehyde gave a disappointing yield of 7% for α-methylene-γ-butyrolactone (**5n**), probably due to polymerization of formaldehyde.

As can be seen from the data listed in Tables 2 and 3, the predominant geometry of the α-alkylidene unsaturation in **5** is *E* configuration. Such a result can be rationalized by considering the conformations of two possible stereoisomeric precursors (**19a** and **19b**) leading to **5** as shown in Scheme 2. In both cases, if the conformation, in which the OCO_2Et and S^- groups are anti-periplanar, is favorable one for the subsequent intramolecular attack of S^- group and elimination of the $^-OCO_2Et$ species, the orientation of R group is represented as **19a** and **19b**, respectively. The equilibrium between the stereoisomers **19a** and **19b**, if present with or without the participation of the *S*-ethoxycarbonylated derivative such as **9**, would surely favor **19b**, since the steric interaction between a bulky R group and a lactone carbonyl is minimized in **19b**. On the other hand, the stereoisomer **19a**, in which the alkyl and carbonyl group are *gauche*, would exhibit severe

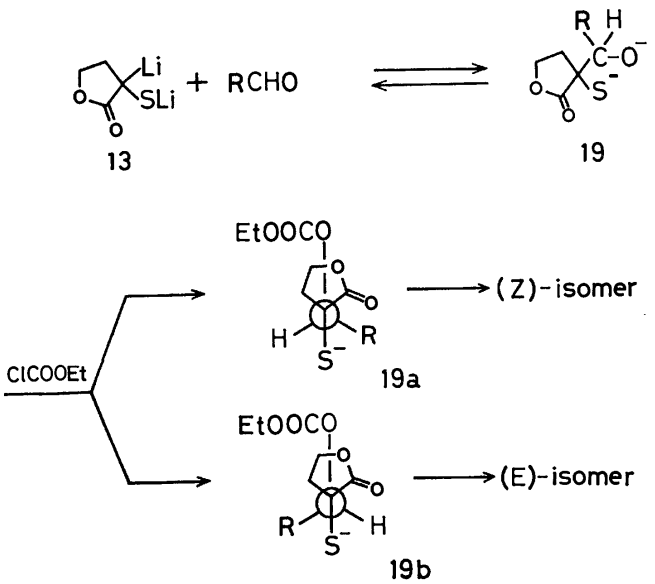

13 19 19a 19b

Scheme 2.

interactions. Thus, the *E*-isomer of α-alkylidene-γ-butyrolactone predominates.

In the case of the reaction of the carbanion **8** with carbonyl compounds, the predominant formation of the *E*-isomer is also explained by the same argument.

Evidence for the adduct **19** rests on quenching the reaction mixture of **13** and pentanal at −78 °C with methyl iodide and isolating the lactone **20q** in 84% yield. The ^{1}H-NMR spectrum of **20q** shows a doublet at δ 2.10 which indicates a mixture of diastereoisomers. An attempt to determine the ratio of this mixture by gas chromatography, however, failed due to decomposition.

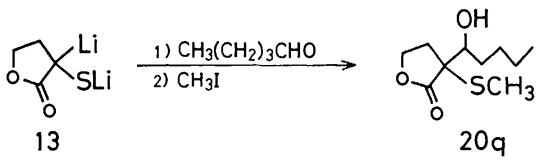

13 20q

When the reaction mixture of **13** and an aldehyde was quenched with saturated aqueous ammonium chloride solution at −78 °C, the adduct **21** was obtained in good yield as shown below. Reaction of adduct **21a**

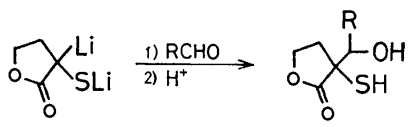

13

21a : R = C_6H_5 (76%)
21c : R = $CH_3CH_2CH_2$ (87%)

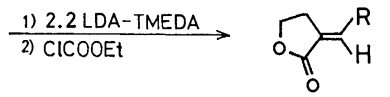

5a: R = C_6H_5 (35%; E/Z=100/0)
5c: R = $CH_3CH_2CH_2$ (42%; E/Z=96/4)

and **21c** with 2.2 equiv of LDA in the presence of TMEDA at −78 °C followed by the addition of ethyl chloroformate afforded the corresponding α-alkylidene-γ-butyrolactone **5a** and **5c**.

Experimental

General. Melting points were determined with a Yanagimoto melting point apparatus and are uncorrected. Boiling points were determined during distillation and are uncorrected. Nuclear magnetic resonance spectra were determined on a JEOL Model PS-100 spectrometer. Chemical shifts are given in δ units, part per million relative to tetramethylsilane as internal standard. Infrared spectra were determined on a Hitachi Model 215 spectrophotometer. Gas chromatograms were obtained using a Varian Aerograph Model 920 instrument with a 0.15 cm × 120 cm glass column (20% Silicone DC-550 on Celite 545). Mass spectra were determined on a Hitachi Model M-52 mass spectrometer. Tetrahydrofuran (THF) was dried by distillation from calcium hydride and by subsequent distillation from lithium aluminum hydride under a nitrogen atmosphere. Diisopropylamine, diethylamine, and *N,N,N',N'*-tetramethylethylenediamine were distilled from calcium hydride and stored over molecular sieves. All reactions were performed under a nitrogen atmosphere. The glassware was dried by flaming in a nitrogen stream.

Preparation of O-*Ethyl* S-*(Tetrahydro-2-oxo-3-furanyl) Dithiocarbonate (1).* To an ethanol solution of freshly prepared potassium *O*-ethyl dithiocarbonate (0.167 mol) was added a solution of 25 g (0.152 mol) of α-bromo-γ-butyrolactone in 100 ml of ethanol at 0 °C. After the reaction mixture was stirred for 7 h at room temperature, the ethanol was removed under reduced pressure, the residue was extracted with ether three times, washed, and dried (anhydrous Na_2SO_4), and evapoarated to give **1** as a viscous yellow oil which was unstable toward distillation. The crude product was chromatographed twice on silica gel using benzene as eluent to give an analytical sample of dithiocarbonate **1**: ^{1}H-NMR(CCl_4) δ 4.60 (q, J=7 Hz, 2H, CH_2O), 4.30 (m, 3H, CH_2 and CH), 2.00—3.00 (m, 2H, CH_2), 1.40 (t, J=7 Hz, 3H, CH_3). IR (neat); 2990, 1775, 1220, 1040 cm^{-1}. Found: C, 40.63; H, 5.03%. Calcd for $C_7H_{10}O_3S_2$: C, 40.76; H, 4.89%.

Synthesis of α-Benzylidene-γ-butyrolactone Using Lithium Enolate 4. To a solution of diisopropylamine (3.4 ml, 20 mmol) in 40 ml of THF at −78 °C was added butyllithium (20 mmol, 14 ml, 1.43 mol dm^{-3} in hexane) over 5 min. After the resulting pale yellow solution was stirred at −78 °C for 20 min, a solution of 4.13 g (20 mmol) of *O*-ethyl *S*-(tetrahydro-2-oxo-3-furanyl) dithiocarbonate (**1**) in 5 ml of THF was added over 6 min. After 30 min, a solution of 2.33 g (20 mmol) of benzaldehyde in 3 ml of THF was added over 2 min. The reaction mixture was stirred at −78 °C for 2 h and at room temperature for 1 h before quenching with saturated aqueous ammonium chloride solution (10 ml) and 0.6 mol dm^{-3} hydrochloric acid (100 ml). The resulting mixture was extracted four times with 50 ml portions of ether. The combined organic extracts were washed three times with saturated aqueous sodium chloride solution, dried (Na_2SO_4), and concentrated. Silica gel chromatography (benzene) gave 2.10 g (60%) of α-benzylidene-γ-butyrolactone, mp 117.5—118.5 °C. The product was identified by comparison of ^{1}H-NMR spectrum with the corresponding data from independently synthesized material.[8]

Preparation of O-*Ethyl* S-*(Tetrahydro-2-oxo-3-furanyl) Thiocarbonate (7).* To a mixture of 13 g (0.11 mol) of α-mercapto-γ-butyrolactone[10] (**6**) and 11.9 g (0.11 mol) of ethyl chloroformate in 80 ml of dry benzene at 0 °C was added a solution of 11.1 g (0.11 mol) of dry triethylamine in 20 ml of dry benzene. When addition was complete, the ice-bath was removed, and reaction mixture was stirred at room temperature for 2 h. Product isolation gave an oil that was distilled twice (bp 122 °C/0.6 Torr) (1 Torr=133.322 Pa), afforded 19 g (91%) of **7**: ^{1}H-NMR(CCl_4) δ 4.30 (q, J=7 Hz, 2H, CH_2), 4.20 (m, 2H, CH_2O), 4.00 (t, J=9 Hz, 1H, CH), 2.80 (m, 1H), 2.42 (m, 1H), 1.36 (t, J=7 Hz, 3H, CH_3). IR (neat); 2990, 1790, 1727, 1160, 1010 cm^{-1}. Found: C, 44.07; H, 5.45%. Calcd for $C_7H_{10}O_4S$: C, 44.20; H, 5.30%.

Reaction of Lithium Enolate of 7 with Carbonyl Compounds. *General Procedure*: Lithium diethylamide (22 mmol) was prepared as usual in 40 ml of THF at −78 °C. After 20 min, a solution of 3.80 g (20 mmol) of *O*-ethyl *S*-(tetrahydro-2-oxo-3-furanyl) thiocarbonate (**7**) in 5 ml of THF was added over a period of 3 min. After stirring at −78 °C for 1 h, a solution of a carbonyl compound (25 mmol) in 3 ml of THF was added. The reaction mixture was stirred at −78 °C for 2 h and then at room temperature for 1 h. The reaction mixture was poured into a separatory funnel containing 100 ml of 0.6 mol dm^{-3} hydrochloric acid and extracted four times with 50 ml portions of ether. The extracts were washed

with saturated sodium chloride solution, dried (Na_2SO_4), and evaporated. The crude product was purified by distillation and/or column chromatography over silica gel.

Decomposition of Lithium Enolate 8. The lithium enolate **8** was generated as usual from 3.80 g (20 mmol) of **7** and 22 mmol of lithium diethylamide in 40 ml of THF. After stirring at −78 °C for 1 h, the cooling bath was removed, and the reaction mixture was stirred at room temperature for 1 h. The reaction was quenched by adding 10 ml of saturated aqueous ammonium chloride solution. Product isolation gave 1.42 g (45%) of α-ethoxycarbonyl-γ-butyrolactone (**12**): bp 105—110 °C/1.5 Torr (lit,[13] bp 175 °C/25 Torr); ^{1}H-NMR(CCl_4) δ 4.0—4.5 (m, 4H, CH_2 and CH_2O), 3.47 (t, J=9 Hz, 1H, CH), 2.4—2.7 (m, 2H, CH_2), 1.32 (t, J=7 Hz, 3H, CH_3); IR(neat); 1770(COO), 1730(COO) cm^{-1}; MS(20 eV) *m/e* (relative intensity) 158 (M^+, 2), 86 (100). Found: C, 52.97; H, 6.54%. Calcd for $C_7H_{10}O_4$: C, 53.16; H, 6.37%.

Generation of Dianion of α-Mercapto-γ-butyrolactone (6) and Dialkylation. In a nitrogen atmosphere, 44 mmol of butyllithium was added to a solution of 4.5 g (44 mmol) of diisopropylamine and 5.1 g (44 mmol) of TMEDA in 40 ml of THF at −78°C. After stirring at −78 °C for 20 min, a solution of 2.4 g (20 mmol) of α-mercapto-γ-butyrolactone (**6**) in 7 ml of THF was added slowly with a syringe. After stirring for 1 h at −78 °C, 11.4 g (80 mmol) of methyl iodide was added. The reaction mixture was stirred for 30 min and then at room temperature for 1 h. To this was added 10 ml of saturated aqueous ammonium chloride solution, and the mixture was poured into 0.6 mol dm^{-3} hydrochloric acid (100 ml) and extracted four times with ether. The ether extracts were washed twice with saturated aqueous sodium chloride solution, dried (Na_2SO_4), and concentrated. The residue was distilled to give 2.7 g (93%) of α-methyl-α-methylthio-γ-butyrolactone (**14a**)[14]: bp 80—81 °C/2.5 Torr; ^{1}H-NMR (CCl_4) δ 4.24 (m, 2H, CH_2O), 2.0—2.5 (m, 2H, CH_2), 2.13 (s, 3H, SCH_3), 1.51 (s, 3H, CH_3). IR (neat); 1760 (COO) cm^{-1}. Similar procedures to the above were used for diethylation and diallylation.

α-Ethyl-α-ethylthio-γ-butyrolactone (14b): Bp 77—80 °C/0.75 Torr; ^{1}H-NMR(CCl_4) δ 4.2—4.5 (m, 2H, CH_2O), 1.5—2.8 (m, 6H, $3CH_2$), 1.23 (t, J=7 Hz, 3H, CH_3), 1.02 (t, J=7 Hz, 3H, CH_3); MS(20 eV) *m/e* (relative intensity) 174 (M^+, 6), 114 (100). IR (neat); 1760 (COO) cm^{-1}. Found: C, 55.43; H, 8.45%. Calcd for $C_8H_{14}O_2S$: C, 55.14; H, 8.10%.

α-Ethylthio-γ-butyrolactone (15): ^{1}H-NMR (CCl_4) δ 4.2—4.5 (m, 2H, CH_2O), 3.3—3.5 (m, 1H, CH), 1.9—3.0 (m, 4H, $2CH_2$), 1.30 (t, J=7 Hz, 3H, CH_3). IR (neat); 1765 (COO) cm^{-1}. MS (20 eV) *m/e* (relative intensity) 146 (M^+, 26), 86 (100).

α-(2-Propenyl)-α-(2-propenylthio)-γ-butyrolactone (14c): Bp 93—95 °C/0.75 Torr; ^{1}H-NMR (CCl_4) δ 5.5—6.0 (m, 2H, 2CH=C), 4.9—5.4 (m, 4H, $2CH_2$=C), 4.0—4.5 (m, 2H, CH_2O), 3.1—3.5 (m, 2H, SCH_2), 2.55 (d, J=7 Hz, 2H, CH_2), 1.9—2.5 (m, 2H, β-CH_2). MS (20 eV) *m/e* (relative intensity) 198 (M^+, 2), 126 (100). IR (neat); 1760 (COO), 1640 (C=C) cm^{-1}. Found: C, 60.46; H, 7.32%. Calcd for $C_{10}H_{14}O_2S$: C, 60.58; H, 7.12%.

Preparation of α-Alkylidene-γ-butyrolactones from Dianion 13 and Carbonyl Compounds. The example of benzaldehyde is given here as a typical experiment. To a magnetically stirred solution of the dianion **13** prepared from 44 mmol of LDA and 44 mmol of TMEDA in 40 ml of THF at −78 °C was added a solution of benzaldehyde (40 mmol) in 3 ml of THF. Stirring was continued at −78 °C for 2 h and then a solution of ethyl chloroformate (2.2 g, 20 mmol) in dry THF (5 ml) was added dropwise at −78 °C. The reaction mixture was stirred at −78°C for 30 min and the cooling bath was removed. After 1 h the reaction mixture was quenched with saturated aqueous ammonium chloride solution (10 ml) and extracted with ether (4×50 ml). The combined ether extracts were washed with brine, saturated $NaHCO_3$ solution, and brine. The dried (Na_2SO_4) solvent were removed and the residue was purified by column chromatography (silica gel, chloroform) to afford pure **5a** (1.89 g, 54%) as colorless crystals.

Physical Properties of α-Alkylidene-γ-butyrolactones. The analytical samples were obtained by silica gel chromatography and/or distillation.

(E)-α-Benzylidene-γ-butyrolactone (5a): Recrystallization from ethanol–acetone afforded an analytical sample of **5a**. Mp 117.5—118.5 °C (lit,[5] mp 118.5°C). ^{1}H-NMR ($CDCl_3$) δ 7.2—7.6 (m, 6H, aromatic and CH=C), 4.46 (t, J=6.8 Hz, 2H, CH_2O), 3.25 (dt, J=6.8, 3 Hz, 2H, CH_2); ^{1}H-NMR (C_6D_6) δ 7.59 (t, J=3 Hz, 1H, CH=C), 7.12 (s, 5H, aromatic), 3.65 (t, J=6.5 Hz, 2H, CH_2O), 2.28 (dt, J=6.5, 3 Hz, 2H, CH_2). IR (KBr pellet); 1740 (COO), 1650 (C=C) cm^{-1}. MS (20 eV) *m/e* 174 (M^+). Found: C, 75.55; H, 5.78%. Calcd for $C_{11}H_{10}O_2$: C, 75.84; H, 5.79%.

α-Propylidene-γ-butyrolactone (5b): Bp 70—75 °C/0.6 Torr. (lit,[5] bp 60 °C/0.5 Torr). The *E*- and *Z*-isomers of **5b** were separated by gas chromatography. *E*-Isomer: ^{1}H-NMR (CCl_4) δ 6.48 (m, 1H, CH=C), 4.22 (t, J=7 Hz, 2H, CH_2O), 2.80 (m, 2H, CH_2), 2.20 (m, 2H, CH_2), 1.10 (t, J=7 Hz, 3H, CH_3). MS (20 eV) *m/e* 126 (M^+). IR (neat); 1750 (COO), 1680 (C=C) cm^{-1}. *Z*-Isomer: ^{1}H-NMR (CCl_4) δ 6.0 (m, 1H, CH=C), 4.2 (t, J=7 Hz, 2H, CH_2O), 2.8 (m, 4H, $2CH_2$), 1.0 (t, J=7 Hz, 3H, CH_3). MS (20 eV) *m/e* 126 (M^+). IR (neat); 1750 (COO), 1670 (C=C) cm^{-1}.

α-Butylidene-γ-butyrolactone (5c):[15] Bp 88—94 °C/0.8 Torr. ^{1}H-NMR (CCl_4) δ 6.12 (m, 0.05H, CH=C for *Z*-isomer), 6.53 (m, 0.95H, CH=C for *E*-isomer), 4.27 (t, J=7 Hz, 2H, CH_2O), 2.84 (m, 2H, CH_2), 2.18 (m, 2H, CH_2), 1.2—1.7 (m, 2H, CH_2), 0.98 (t, J=7 Hz, 3H, CH_3). MS (20 eV) *m/e* 140 (M^+). IR (neat); 1755 (COO), 1680 (C=C) cm^{-1}. Found: C, 68.18; H, 8.57%. Calcd for $C_8H_{12}O_2$: C, 68.53; H, 8.63%.

α-(2-Furylmethylene)-γ-butyrolactone (5d): Mp 94—95 °C (lit,[4a] mp 91—92 °C). ^{1}H-NMR ($CDCl_3$) δ 7.54 (m, 1H, furan), 7.30 (m, 1H, CH=C), 6.6 (m, 2H, furan), 4.42 (t, J=7 Hz, 2H, CH_2O), 3.26 (m, 2H, CH_2). MS (20 eV) *m/e* 164 (M^+). IR (KBr pellet); 1730 (COO), 1645 (C=C) cm^{-1}. Found: C, 66.07; H, 5.10%. Calcd for $C_9H_8O_3$: C, 65.85; H, 4.91%.

α-Heptylidene-γ-butyrolactone (5e): Bp 108—112 °C/0.4 Torr. ^{1}H-NMR (CCl_4) δ 6.52 (m, 1H, CH=C), 4.26 (t, J=7 Hz, 2H, CH_2O), 2.83 (m, 2H, CH_2), 2.18 (m, 2H, CH_2), 1.2—1.6 (m, 8H, $4CH_2$), 0.09 (m, 3H, CH_3). MS (20 eV) *m/e* 182 (M^+). IR (neat); 1760 (COO), 1680 (C=C) cm^{-1}. Found: C, 72.31; H, 9.65%. Calcd for $C_{11}H_{18}O_2$: C, 72.49; H, 9.95%.

α-(2-Methylbutylidene)-γ-butyrolactone (5f): Bp 80—85 °C/0.6 Torr. ^{1}H-NMR (CCl_4) δ 6.25 (m, 1H, CH=C for *E*-isomer), 5.8 (m, CH=C for *Z*-isomer), 4.2 (t, J=7 Hz, 2H, CH_2O), 2.80 (m, 2H, CH_2), 2.2 (m, 1H, CH), 1.1—1.6 (m, 2H, CH_2), 0.7—1.1 (m, 6H, $2CH_3$). IR (neat); 1760 (COO), 1680 (C=C) cm^{-1}. Found: C, 70.18; H, 9.25%. Calcd for $C_9H_{14}O_2$: C, 70.10; H, 9.15%.

α-(Cyclohexylmethylene)-γ-butyrolactone (5g): Bp 110—111 °C/0.5 Torr. ^{1}H-NMR (CCl_4) δ 6.33 (dt, J=9.5, 2.7 Hz, 1H, CH=C), 4.25 (t, J=7 Hz, 2H, CH_2), 2.86 (dt, J=7, 2.7 Hz, 2H, CH_2), 2.20 (m, 1H), 0.7—1.9 (m, 10H). MS (20 eV) *m/e* 180 (M^+). IR (neat); 1760 (COO), 1680 (C=C) cm^{-1}.

α-[(E)-2-Hexenylidene]-γ-butyrolactone (5h): Bp 113—115 °C/0.8 Torr. The *E*- and *Z*-isomers of **5h** were separated by

silica gel chromatography using benzene as eluent. *E*-Isomer: ^{1}H-NMR (CCl_4) δ 6.9 (m, 1H, CH=C), 5.9—6.3 (m, 2H, CH=C), 4.03 (t, J=7 Hz, 2H, CH_2O), 2.93 (m, 2H, CH_2), 2.20 (m, 2H, CH_2), 1.48 (m, 2H, CH_2), 0.96 (t, J=7 Hz, 3H, CH_3). MS (20 eV) *m/e* 166 (M^+). IR (neat); 1750 (COO), 1650 (C=C) cm^{-1}. *Z*-Isomer: ^{1}H-NMR (CCl_4) δ 7.2—7.6 (m, 1H, CH=C), 6.45 (m, 1H, CH=C), 5.78 (m, 1H, CH=C), 4.24 (t, J=7 Hz, 2H, CH_2O), 2.92 (m, 2H, CH_2), 2.19 (m, 2H, CH_2), 1.48 (m, 2H, CH_2), 0.94 (t, J=7 Hz, 3H, CH_3). MS (20 eV) *m/e* 166 (M^+). IR (neat); 1740 (COO), 1650 (C=C) cm^{-1}.

α-(1-Methylethylidene)-γ-butyrolactone (**5i**): Bp 70—73 °C/0.7 Torr. ^{1}H-NMR (CCl_4) δ 4.06 (t, J=7 Hz, 2H, CH_2), 2.78 (m, 2H, CH_2), 2.06 (t, J=2 Hz, 3H, CH_3), 1.80 (t, J=1.5 Hz, 3H, CH_3). MS (20 eV) *m/e* 126 (M^+). IR (neat); 1740 (COO), 1660 (C=C) cm^{-1}. Found: C, 66.57; H, 8.21%. Calcd for $C_7H_{10}O_2$: C, 66.65; H, 7.99%.

α-Cyclohexylidene-γ-butyrolactone (**5j**): Bp 115—120 °C/2.5 Torr (lit,[5] bp 106 °C/0.5 Torr). ^{1}H-NMR (CCl_4) δ 4.18 (t, J=7 Hz, 2H, CH_2O), 2.86 (m, 4H, $2CH_2$), 2.22 (m, 2H, CH_2), 1.64 (m, 6H, $3CH_2$). MS (20 eV) *m/e* 166 (M^+). IR (neat); 1745 (COO), 1660 (C=O) cm^{-1}.

α-(1-Methylpropylidene)-γ-butyrolactone (**5k**): Bp 70—75 °C/0.7 Torr. ^{1}H-NMR (CCl_4) δ 4.08 (t, J=7 Hz, 2H, CH_2), 2.0—3.0 (m, 4H, $2CH_2$), 1.8—2.2 (m, 3H, CH_3), 0.9—1.4 (m, 3H, CH_3). MS (20 eV) *m/e* 140 (M^+). IR (neat); 1740 (COO), 1660 (C=C) cm^{-1}. Found: C, 68.31; H, 8.82% Calcd for $C_8H_{12}O_2$: C, 68.55; H, 8.63%.

α-(1-Phenylethylidene)-γ-butyrolactone (**5l**): Bp 120 °C/0.2 Torr; mp 75—78 °C. ^{1}H-NMR ($CDCl_3$) δ 7.1—7.5 (m, 5H, aromatic), 4.22 (t, J=7 Hz, 2H, CH_2O), 2.88 (m, 2H, CH_2), 2.57 (t, J=2.4 Hz, 3H, CH_3). MS (20 eV) *m/e* 188 (M^+). IR (KBr pellet); 1735 (COO), 1665 (C=C) cm^{-1}. Found: C, 76.56; H, 6.47%. Calcd for $C_{12}H_{12}O_2$: C, 76.57; H, 6.43%.

α-Cyclopentylidene-γ-butyrolactone (**5m**): Bp 110—135 °C/1.1—1.3 Torr. ^{1}H-NMR (CCl_4) δ 4.15 (t, J=7.6 Hz, 2H, CH_2O), 2.70 (m, 4H, $2CH_2$), 2.26 (m, 2H, CH_2), 1.70 (m, 4H, $2CH_2$). IR (neat); 1730 (COO), 1680 (C=C) cm^{-1}.

α-Methylene-γ-butyrolactone (**5n**): Bp 60 °C/4 Torr (lit,[4c] bp 50—53 °C/0.45 Torr). ^{1}H-NMR (CCl_4) δ 6.14 (t, J=3 Hz, 1H, CH=C), 5.62 (t, J=3 Hz, 1H, CH=C), 4.32 (t, J=7 Hz, 2H, CH_2O), 2.92 (m, 2H, CH_2). IR (neat); 1760 (COO), 1665 (C=C) cm^{-1}.

α-Ethylidene-γ-butyrolactone (**5o**)[15]: Bp 85—86 °C/2.5 Torr. ^{1}H-NMR (CCl_4) δ 6.64 (m, 0.92H, CH=C), 6.27 (m, 0.08H, CH=C), 4.30 (t, J=7 Hz, 2H, CH_2O), 2.86 (m, 2H, CH_2), 1.85 (dt, J=2, 7 Hz, 3H, CH_3). MS (20 eV) *m/e* 112 (M^+). IR (neat); 1750 (COO), 1680 (C=C) cm^{-1}. Found: C, 63.96; H, 7.47%. Calcd for $C_6H_8O_2$: C, 64.27; H, 7.19%.

α-(2-Methylpropylidene)-γ-butyrolactone (**5p**): Bp 83—84 °C/1.0—1.1 Torr. ^{1}H-NMR (CCl_4) δ 6.34 (dt, J=2, 10 Hz, 0.95 H, CH=C for *E*-isomer), 5.94 (m, 0.05H, CH=C for *Z*-isomer), 4.27 (t, J=7 Hz, 2H, CH_2O), 2.87 (dt, J=2, 7 Hz, 2H, CH_2), 2.3—2.7 (m, 1H, CH), 0.8—1.2 (d, J=7 Hz, 6H, $2CH_3$). MS (20 eV) *m/e* 140 (M^+). IR (neat); 1750 (COO), 1680 (C=C) cm^{-1}.

α-Pentylidene-γ-butyrolactone (**5q**): Bp 83—85 °C/0.35 Torr. ^{1}H-NMR (CCl_4) δ 6.47 (m, 0.95H, CH=C for *E*-isomer), 6.08 (m, 0.05H, CH=C for *Z*-isomer), 4.24 (t, J=7 Hz, 2H, CH_2O), 2.82 (m, 2H, CH_2), 1.9—2.3 (m, 2H, CH_2), 1.1—1.6 (m, 4H, $2CH_2$), 0.95 (m, 3H, CH_3). MS (20 eV) *m/e* 154 (M^+). IR (neat); 1750 (COO), 1680 (C=C) cm^{-1}. Found: C, 69.80; H, 9.03%. Calcd for $C_9H_{14}O_2$: C, 70.10; H, 9.15%.

α-(3-Methylbutylidene)-γ-butyrolactone (**5r**): Bp 93—94 °C/0.8 Torr. ^{1}H-NMR (CCl_4) δ 6.64 (m, 0.95H, CH=C for *E*-isomer), 6.10 (m, 0.05H, CH=C for *Z*-isomer), 4.30 (t, J=7 Hz, 2H, CH_2O), 2.83 (m, 2H, CH_2), 2.07 (m, 2H, CH_2), 1.6—2.0 (m, 1H, CH), 0.93 (d, J=6.5 Hz, 6H, $3CH_2$). MS (20 eV) *m/e* 154 (M^+). IR (neat); 1760 (COO), 1680 (C=C) cm^{-1}. Found: C, 70.43; H, 9.19%. Calcd for $C_9H_{14}O_2$: C, 70.10; H, 9.15%.

α-Hexylidene-γ-butyrolactone (**5s**): Bp 115—117 °C/1.1 Torr. ^{1}H-NMR (CCl_4) δ 6.46 (m, 0.96H, CH=C for *E*-isomer), 6.10 (m, 0.04H, CH=C for *Z*-isomer), 4.23 (t, J=7 Hz, 2H, CH_2O), 2.83 (m, 2H, CH_2), 1.9—2.3 (m, 2H, CH_2), 1.1—1.7 (m, 6H, $3CH_2$), 0.90 (m, 3H, CH_3). MS (20 eV) *m/e* 168 (M^+). IR (neat); 1750 (COO), 1680 (C=C) cm^{-1}. Found: C, 71.44; H, 9.55%. Calcd for $C_{10}H_{16}O_2$: C, 71.39; H, 9.59%.

α-Nonylidene-γ-butyrolactone (**5t**): Bp 140—149 °C/1.5 Torr. ^{1}H-NMR (CCl_4) δ 6.46 (m, 0.95H, CH=C for *E*-isomer,) 6.08 (m, 0.05H, CH=C for *Z*-isomer), 4.22 (t, J=7 Hz, 2H, CH_2O), 2.91 (m, 2H, CH_2), 1.9—2.3 (m, 2H, CH_2), 1.1—1.7 (m, 12H, $6CH_2$), 0.87 (m, 3H, CH_3). MS (20 eV) *m/e* 210 (M^+). IR (neat); 1760 (COO), 1685 (C=C) cm^{-1}. Found: C, 74.06; H, 10.65%. Calcd for $C_{13}H_{22}O_2$: C, 74.24; H, 10.54%.

α-[(E)-2-Butenylidene]-γ-butyrolactone (**5u**): Bp 100—106 °C/1.2—1.3 Torr. ^{1}H-NMR (CCl_4) δ 6.7—7.3 (m, 1H, CH=C), 5.7—6.2 (m, 2H, CH=C), 4.27 (m, 2H, CH_2O), 2.91 (m, 2H, CH_2), 1.90 (m, 3H, CH_3). MS (20 eV) *m/e* 138 (M^+). IR (neat); 1740 (COO), 1650 (C=C) cm^{-1}.

α-(3-Phenyl-2-propenylidene)-γ-butyrolactone (**5v**): Mp 135—136 °C (lit,[5] mp 135—136 °C). ^{1}H-NMR ($CDCl_3$) δ 7.1—7.7 (m, 6H, aromatic and CH=C), 6.6—7.0 (m, 2H, CH=C), 4.43 (t, J=7 Hz, 2H, CH_2O), 3.08 (dt, J=7, 2 Hz, 2H, CH_2). MS (20 eV) *m/e* 200 (M^+). IR (neat); 1740 (COO), 1640 (C=C) cm^{-1}. Found: C, 77.81; H, 5.97%. Calcd for $C_{13}H_{12}O_2$: C, 77.98; H, 6.04%.

Preparation of α-(1-Hydroxypentyl)-α-methylthio-γ-butyrolactone (**20q**): Into a solution of 22 mmol of the dianion **13** of α-mercapto-γ-butyrolactone (generated from 44 mmol of LDA and 44 mmol of TMEDA) in 40 ml of THF, was added at −78 °C 2.1 g (25 mmol) of pentanal. After 1 h at −78 °C, a solution of 3.1 g (22 mmol) of methyl iodide in 3 ml of THF was added with a syringe over a 3-min period. The resulting solution was stirred at −78 °C for 30 min and at room temperature for 1 h. The usual workup and distillation gave 3.65 g (84%) of **20q**: bp 125—132 °C/1.0—1.1 Torr. ^{1}H-NMR (CCl_4) δ 4.22 (m, 2H, CH_2O), 3.78 (m, 1H, CH), 3.45 (brs, 1H, OH), 2.2—2.9 (m, 2H, CH_2), 2.06 and 2.14 (s, 3H, SCH_3), 1.0—2.0 (m, 6H, $3CH_2$), 0.9 (m, 3H, CH_3). IR (neat); 3520 (OH), 1750 (COO) cm^{-1}.

α-(α-Hydroxybenzyl)-α-mercapto-γ-butyrolactone (**21a**): The dianion of 4.2 g (44 mmol) of **6** was generated with 88 mmol of LDA and 88 mmol of TMEDA in 80 ml of THF at −78 °C. A solution of benzaldehyde (4.2 g, 40 mmol)in dry THF (40 ml) was added dropwise and the reaction mixture was stirred at −78 °C for 2 h. The cooling bath was removed and the reaction mixture was quenched with 20 min of saturated aqueous ammonium chloride solution, diluted with chloroform (40 ml). The product was extracted with chloroform (4×50 ml), and the combined chloroform solution was washed with brine and dried (Na_2SO_4). The residue obtained after evaporation was chromagraphed on a silica gel column using benzene as eluent to afford pure **21a** (3.14 g, 76%): mp 125—125.5 °C. ^{1}H-NMR ($CDCl_3$) δ 7.34 (m, 5H, aromatic), 4.97 (s, 1H, CH), 3.98—4.5 (m, 3H, CH_2 and OH), 1.6—2.8 (m, 3H, CH_2 and SH). IR (KBr pellet) 3535 (OH), 2550 (SH), 1740 (C=O) cm^{-1}. Found: C, 58.93; H, 5.32%. Calcd for $C_{11}H_{12}O_3S$: C, 58.91; H, 5.40%.

α-(1-Hydroxybutyl)-α-mercapto-γ-butyrolactone (**21c**): A similar reaction utilizing 44 mmol of the dianion **13** and 3.60 g (50 mmol) of butanal gave 6.63 g (87%) of **21c**: bp 128—131 °C/

2.0 Torr. ^{1}H-NMR (CCl_4) δ 4.1—4.6 (m, 2H, CH_2O), 3.4—4.0 (m, 1H, OH), 1.1—3.0 (m, 8H), 0.97 (m, 3H, CH_3). IR (neat) 3520 (OH), 2555 (SH), 1755 (COO) cm^{-1}.

Preparation of (E)-α-Benzylidene-γ-butyrolactone (5a) from α-(α-Hydroxybenzyl)-α-mercapto-γ-butyrolactone (21a): Into a solution of 20.5 mmol of LDA in 19 ml of THF and 2.8 ml (20.5 mmol) of TMEDA, 2.09 g (9.30 mmol) of **21a** in 6 ml of THF was added at −78 °C. After stirring at −78 °C for 30 min, ethyl chloroformate (9.3 mmol) in 3 ml of THF was added. After stirring at −78 °C for 30 min and then at room temperature for 1 h, the usual workup and chromatographic isolation yielded 0.57 g (35%) of **5a**, which was identical by spectroscopic comparison with an authentic sample.

α-Butylidene-γ-butyrolactone (5c): A similar reaction utilizing 21.1 mmol of LDA, 2.9 ml of TMEDA, 1.82 g (9.57 mmol) of **21c**, and 9.6 ml of ethyl chloroformate gave 0.56 g (42%) of **5c**.

This work was supported in part by a research grant from the Ministry of Education.

References

1) a) O. E. Edwards and P.-T. Ho, *Can. J. Chem.*, **55**, 371 (1977); b) Y. S. Rao, *Chem. Rev.*, **76**, 625 (1976); c) T. G. Back, O. E. Edwards, and G. A. MacAlpine, *Tetrahedron Lett.*, **1977**, 2651; d) T. R. Hoye and A. J. Caruso, *Tetrahedron Lett.*, **1978**, 4611.

2) a) P. A. Grieco, *Synthesis*, **1975**, 67; b) R. B. Grammil, C. A. Wilson, and T. A. Bryson, *Synth. Commun.*, **5**, 245 (1975); c) S. S. Newaz, *Aldrichica Acta*, **10**, 64 (1977); d) R. A. Amos and J. A. Katzenellenbogen, *J. Org. Chem.*, **43**, 560 (1978); e) J. L. Herrmann, M. H. Berger, and R. H. Schlessinger, *J. Am. Chem. Soc.*, **101**, 1544 (1979); f) P. A. Grieco, M. Nishizawa, T. Oguri, S. D. Burke, and N. Marinovic, *J. Am. Chem. Soc.*, **99**, 5773 (1977); g) S. Danishefsky, T. Kitahara, P. F. Schuda, and S. J. Etheredge, *J. Am. Chem. Soc.*, **98**, 3028 (1976); h) S. Danishefsky, P. F. Schuda, T. Kitahara, and S. J. Etheredge, *J. Am. Chem. Soc.*, **99**, 6066 (1977); i) G. R. Kieczykowsky and R. H. Schlessinger, *J. Am. Chem. Soc.*, **100**, 1938 (1978); j) Y. Ohfune, P. A. Grieco, C.-L. J. Wang, and G. Majetich, *J. Am. Chem. Soc.*, **100**, 5946 (1978).

3) H. Zimmer and J. Rothe, *J. Org. Chem.*, **24**, 28 (1959),

4) a) D. C. Lankin, M. R. Scalise, J. C. Schmidt, and H. Zimmer, *J. Heterocycl. Chem.*, **11**, 631 (1974); b) H. Zimmer and T. Pampalone, *J. Heterocycl. Chem.*, **2**, 95 (1965); c) P. A. Grieco and C. S. Pogonowski, *J. Org. Chem.*, **39**, 1958 (1974).

5) T. Minami, I. Niki, and T. Agawa, *J. Org. Chem.*, **39**, 3236 (1974).

6) P. A. Grieco, C.-L. J. Wang, and S. D. Burke, *J. Chem. Soc., Chem. Commun.*, **1975**, 537.

7) K. Tanaka, N. Yamagishi, H. Uneme, R. Tanikaga, and A. Kaji, *Chem. Lett.*, **1978**, 197.

8) K. Tanaka, H. Uneme, N. Yamagishi, N. Ono, and A. Kaji, *Chem. Lett.*, **1978**, 653.

9) E. M. Enger, V. V. Patel, J. R. Andersen, R. R. Schumaker, and A. A. Fukushima, *J. Am. Chem. Soc.*, **100**, 3769 (1978).

10) G. Fuchs, *Ark. Kemi*, **26**, 111 (1966); *Chem. Abstr.*, **66**, 28363g (1967).

11) K. Tanaka, R. Tanikaga, and A. Kaji, *Chem. Lett.*, **1976**, 917.

12) K. Tanaka, N. Yamagishi, R. Tanikaga, and A. Kaji, *Bull. Chem. Soc. Jpn.*, **52**, 3619 (1979).

13) W. Traube and E. Lehmann, *Chem. Ber.*, **34**, 1971 (1901).

14) B. M. Trost, T. N. Salzmann, and K. Hiroi, *J. Am. Chem. Soc.*, **98**, 4887 (1976).

15) G. M. Ksander, J. E. McMurry, and M. Johnson, *J. Org. Chem.*, **42**, 1180 (1977).

Synthesis of Lipophilic Muramyl Dipeptide Derivatives *via* *O*-Aminoacyl Intermediates[1)]

Shigeru KOBAYASHI,* Tsunehiko FUKUDA, Hidefumi YUKIMASA, Isuke IMADA, Masahiko FUJINO, Ichiro AZUMA,† and Yuichi YAMAMURA††

Central Research Division, Takeda Chemical Industries, Ltd., Yodogawa-ku, Osaka 532
†*Institute of Immunological Science, Hokkaido University, Kita-ku, Sapporo 060*
††*The Third Department of Internal Medicine, Osaka University, Fukushima-ku, Osaka 553*

(Received January 21, 1980)

Incorporation of an amino acid into the 6 position of the muramic acid moiety of muramyl dipeptide has been achieved, providing an effective means for the synthesis of various new derivatives. Six new muramyl dipeptide derivatives with an *N*-acylated amino acid were synthesized using these intermediates and their immunological activity was examined. All the derivatives exhibited adjuvant activity on the induction of delayed-type hypersensitivity to *N*-acetyl-3-(4-arsonophenylazo)-L-tyrosine.

N-Acetylmuramyl-L-alanyl-D-isoglutamine (muramyl dipeptide or MDP) was found to be of the adjuvant-active minimal structure of bacterial cell wall peptidoglycans.[2)] Efforts to develop a new antitumor agent by modifying the MDP molecule led to the discovery of mycoloyl derivatives[3)] and synthetic mycoloyl-mimic long-chain fatty acid derivatives.[4)] Recently it was found that quinonyl derivatives of MDP display potent antitumor activity on the suppression of tumor growth (Meth-A fibrosarcoma) in syngeneic BALB/c female mice.[5)]

In these compounds, the 6 position of the muramyl moiety of MDP was acylated to render a lipophilic nature to the molecule. Acylation with mycolic acids, however, involves several steps and the use of 18-crown-6,[3)] the type of acid that can be introduced being restricted by the final deprotection by catalytic hydrogenolysis. The synthesis of quinonyl MDP derivatives also requires catalytic hydrogenolysis in the final stage.[5)] Thus, we tried to incorporate benzyloxycarbonylamino acids into the 6 position of the muramic acid moiety as a linking unit to introduce a lipophilic acyl group (Scheme 1). After the hydrogenolytic deprotection of all protecting groups, *O*-aminoacyl derivatives of MDP (**4**) can be coupled with various carboxylic acids as well as sulfonic and phosphoric acids, providing a valuable means for the synthesis of new derivatives of MDP. The insertion of various amino acids would affect the immunological activity.

In this paper, we describe the synthesis of six new MDP derivatives *via* *O*-aminoacyl intermediates (**4**) and their immunological activities.

The starting protected MDP derivatives (**1**) were synthesized according to the method described in a previous paper.[6)] Heating of **1** in aqueous acetic acid removed the benzylidene moiety to give partially protected MDP derivatives[7)] (**2**), which were then coupled with benzyloxycarbonylamino acid *p*-nitrophenyl ester in the presence of 1-hydroxybenzotriazole (HOBt) and *N*-ethylmorpholine (NEM) in *N*,*N*-

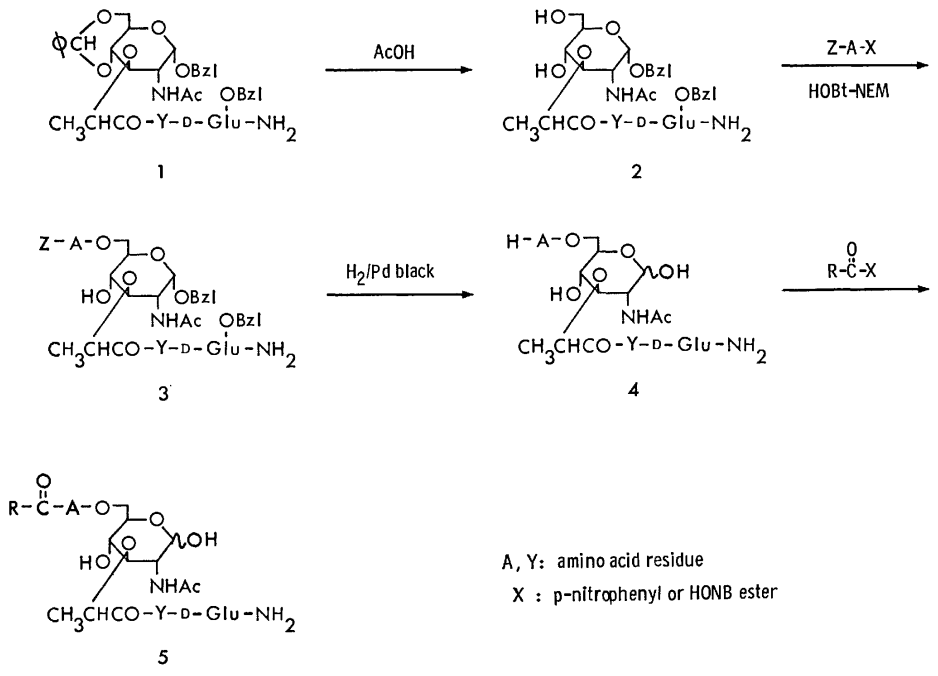

Scheme 1.

TABLE 1. YIELDS AND PHYSICOCHEMICAL PROPERTIES OF THE INTERMEDIATES **2**, **3**, AND **4**[a]

Compd	A	Y	Yield (%)	Mp/°C	$[\alpha]_D$[b] (temp)	Formula	Found (Calcd) (%) C	H	N
2a	—	Aib[c]	98	113(d)	+92.2°(20)	$C_{34}H_{46}N_4O_{11}$	59.09 (59.46	6.93 6.75	7.92 8.16)
2b	—	Ser	67	188—191	+89.8°(23)	$C_{40}H_{50}N_4O_{12}\cdot 1/2H_2O$	61.07 (60.98	6.38 6.53	7.00 7.11)
2c	—	Ala	93	222—223(d)[d]	+103.6°(23)[d]	$C_{33}H_{44}N_4O_{11}\cdot 1/2H_2O$	58.17 (58.14	6.48 6.65	8.11 8.22)
3a	Gly	Aib[c]	68	67(d)	+75.8°(23)	$C_{44}H_{55}N_5O_{14}$	60.25 (60.19	6.25 6.31	7.95 7.98)
3b	Leu	Aib[c]	57	98—100	+61.3°(20)	$C_{48}H_{63}N_5O_{14}$	61.63 (61.72	6.80 6.80	7.63 7.50)
3c	Leu	Ser	62	177—178	+58.7°(23)	$C_{54}H_{67}N_5O_{15}$	63.01 (63.20	6.49 6.58	6.71 6.83)
3d	Aud[e]	Ala	60	144—145	+67.3°(21)	$C_{52}H_{71}N_5O_{14}$	63.18 (63.07	7.31 7.23	6.97 7.07)
3e	β-Ala	Ala	71	152—154	+75.5°(23)	$C_{44}H_{55}N_5O_{14}$	59.79 (60.19	6.31 6.31	7.82 7.98)
4a	Gly	Aib[c]	69	128(d)	+61.0°(23)	$C_{22}H_{37}N_5O_{12}\cdot 1/2H_2O$	46.26 (46.15	6.93 6.69	12.29 12.23)
4b	Leu	Aib[c]	99	150—153(d)	+56.9°(20)	$C_{26}H_{45}N_5O_{12}\cdot 3H_2O$	46.14 (46.35	7.45 7.63	10.20 10.40)
4c	Leu	Ser	99	154(d)	+28.8°(23)[f]	$C_{25}H_{43}N_5O_{13}\cdot H_2O$	47.00 (46.93	7.19 7.09	10.52 10.94)
4d	Aud[e]	Ala	88	120(d)	+20.7°(21)	$C_{30}H_{53}N_5O_{12}\cdot H_2O$	51.85 (51.93	8.00 7.99	9.82 10.10)
4e	β-Ala	Ala	99	87—91(d)	+33.2°(23)	$C_{22}H_{37}N_5O_{12}\cdot 1/2H_2O$	46.46 (46.15	6.99 6.69	11.95 12.23)

a) Amino acid symbols denote the L-configuration unless otherwise stated. b) Solvent; DMF, *c* 0.5. c) Aib: α-aminoisobutyric acid. d) Lit,[7] mp 221.5—223 °C (d); $[\alpha]_D^{22}$ +93.6° (*c* 0.5, DMF). e) Aud: 11-aminoundecanoic acid. f) Solvent: H_2O, *c* 0.5 (after 25 h).

dimethylformamide (DMF) in 50—70% yields. α, β, or ω-Amino acid was coupled as a linking unit (Table 1). This procedure was originally adopted by Klausner and Chorev for the preparation of depsipeptides.[8] Efficient acylation of MDP components was accomplished with a twofold excess of protected amino acid active esters in a minimum amount of DMF. HOBt and NEM were added in a fourfold excess over the amount of MDP components. The resulting protected *O*-aminoacyl derivatives (**3**) were subjected to catalytic hydrogenolysis in acetic acid or methanol with palladium black as a catalyst in order to remove all the protecting groups. The physicochemical properties of the *O*-aminoacyl derivatives (**4**) thus obtained are given in Table 1 together with those of partially protected MDP derivatives (**2**) and protected *O*-aminoacyl derivatives (**3**).

The *O*-aminoacyl derivatives have been coupled with various carboxylic acids such as 10-(2,3-dimethoxy-5-methyl-1,4-benzoquinon-6-yl)decanoic acid[9] (**5a** and **5c**), 9-(2-methyl-1,4-naphthoquinon-3-yl)nonanoic acid[9] (**5b**), 3-(2,3-dimethoxy-5-methyl-1,4-benzoquinon-6-yl)propionic acid[9] (**5d**), all-*trans*-5,9,13,17-tetramethyl-4,8,12,16-octadecatetraenoic acid[10] (geranylgeranylacetic acid, **5e**), and retionic acid[11] (**5f**), by means of the active ester method in an attempt to obtain a variety of immunologically active compounds, especially with autitumor activity. Structures of carboxylic residues of **5a**—**f** are given in Table 2. Purification of the final products was carried out by column chromatography over silica gel and Sephadex LH-20. The structures of the compounds are given in Table 2 together with their physicochemical properties.

Their adjuvant activity on the induction of delayed-type hypersensitivity to *N*-acetyl-3-(4-arsonophenylazo)-L-tyrosine (ABA–Tyr) in guinea pigs was assayed according to a method described earlier.[6] All the compounds tested were found to be immunoadjuvant active, compounds **5a**, **5b**, and **5d** being more active than MDP (Table 3). Attachment of the lipophilic quinonyl moiety to the MDP molecule with 11-aminoundecanoic acid as a linking unit (**5d**) was found to be most favorable. Replacement of L-alanine of MDP by α-aminoisobutyric acid combined with the incorporation of quinonyl acids (**5a** and **5b**) also had a favorable effect on the biological potency.

The results show that the approach should provide a practical means for obtaining various MDP derivatives with immunological activities.

Experimental

Melting points were taken in open capillaries and are uncorrected. Optical rotations were determined with a Perkin-Elmer Model 141 polarimeter. All chemicals and solvents were of reagent grade and used without further purification. The reactions were monitored on TLC with Merck F_{254} silica gel plates, which were developed with

Table 2. Yields and physicochemical properties of MDP derivatives 5[a]

Compd	RCO-	A	Y	Yield (%)	$[\alpha]_D$[b] (temp, solvent)	Formula	Found(Calcd) (%) C	H	N
5a	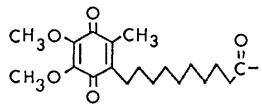	Gly	Aib[c]	55	+30.2° (23, EtOH)	$C_{41}H_{63}N_5O_{13}\cdot 3H_2O$	52.14 (52.21	7.20 7.37	7.25 7.34)
5b	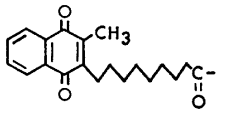	Leu	Aib[c]	47	+23.4° (20, EtOH)	$C_{45}H_{71}N_5O_{17}\cdot H_2O$	55.60 (55.59	7.49 7.57	7.14 7.21)
5c	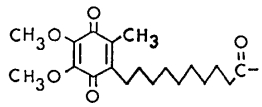	Leu	Ser	56	+16.7° (23, H_2O)[d]	$C_{44}H_{69}N_5O_{13}\cdot 2H_2O$	53.40 (53.27	7.09 7.42	7.05 7.06)
5d	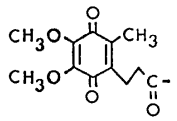	Aud[e]	Ala	51	+25.4° (23, 70%EtOH)	$C_{42}H_{65}N_5O_{17}\cdot H_2O$	54.42 (54.24	7.38 7.26	7.50 7.53)
5e	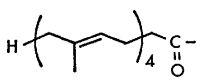	β-Ala	Ala	34	+25.8° (27, 70%EtOH)	$C_{44}H_{71}N_5O_{13}\cdot 2H_2O$	57.59 (57.81	7.95 8.27	7.62 7.66)
5f[f]	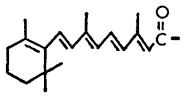	β-Ala	Ala	27	+23.9° (27, H_2O)[d]	$C_{42}H_{63}N_5O_{13}\cdot 5H_2O$	53.47 (53.85	7.19 7.86	7.43 7.48)

a) Amino acid symbols denote the L-configuration unless otherwise stated. b) *c* 0.5. c) Aib: α-aminoisobutyric acid. d) Optical rotation determined when mutarotation was completed (25 h). e) Aud: 11-aminoundecanoic acid. f) Preparation carried out in a dark place.

Table 3. Adjuvant activity of MDP derivatives for the induction of delayed-type hypersensitivity to ABA–Tyr in guinea pigs

Compound[a]	Skin reaction (mm±SE) 24 h	48 h
5a	20.5±0.8	19.5±1.4
5b	19.6±0.4	18.8±0.6
5c	18.0±1.0	18.2±1.7
5d	20.5±0.5	22.3±1.2
5e	18.8±0.7	18.6±1.1
5f	18.9±0.5	16.3±0.4
MDP	20.0±0.4	17.3±0.4
Control 1 (ABA–Tyr+FIA)[b]	9.0±1.6	1.8±1.2
Control 2 (ABA–Tyr only)	0	0

a) Dose: MDP, 100 μg; **5**, equimolar to MDP. b) FIA: Freund's incomplete adjuvant.

$CHCl_3$–acetone–MeOH (10 : 3 : 2, v/v) for compounds **2**, $CHCl_3$–MeOH–AcOH (18: 2: 1, v/v) for **3**, *n*-BuOH–AcOH–EtOAc–H_2O (1:1:1:1, v/v) for **4** and **5**, and EtOAc–pyridine–H_2O–AcOH (30 : 10 : 5 : 3, v/v) for **5**. Evaporation was carried out in a rotary vacuum evaporator under reduced pressure below 45 °C.

N-Acetyl-1-O-benzyl-α-muramyl-α-aminoisobutyryl-D-isoglutamine Benzyl Ester (2a). *N*-Acetyl-1-*O*-benzyl-4,6-*O*-benzylidene-α-muramyl-α-aminoisobutyryl-D-isoglutamine benzyl ester[5] (8.60 g, 11.1 mmol) was suspended in 75% AcOH (200 ml). The suspension was heated on a boiling water bath for 30 min, during which it gradually became clear. After evaporation of the solvent, the residue was flushed with H_2O and dissolved in a mixture of EtOAc (150 ml) and *n*-BuOH (50 ml). The solution was then washed successively with satd NaCl, 5% $NaHCO_3$–satd NaCl (1 : 1, v/v) and satd NaCl, and then dried over anhyd Na_2SO_4. Concentration followed by addition of Et_2O gave a white precipitate of **2a**: 6.90 g, 90.5% (Table 1).

Other partially protected MDP derivatives (2b and 2c) were prepared from appropriate protected MDP derivatives in a similar manner.

N-Acetyl-1-O-benzyl-6-O-benzyloxycarbonylglycyl-α-muramyl-α-aminoisobutyryl-D-isoglutamine Benzyl Ester (3a). A mixture of **2a** (412 mg, 0.6 mmol), benzyloxycarbonylglycine *p*-nitrophenyl ester (396 mg, 1.2 mmol), HOBt (324 mg, 2.4 mmol) and NEM (0.31 ml, 2.4 mmol) in DMF (3 ml) was stirred at room temperature for 40 h. After evaporation of the solvent, the residue was dissolved in EtOAc (15 ml) and the solution was washed with 5% $NaHCO_3$ (1×10 ml) then satd NaCl (1×10 ml), and dried over anhyd Na_2SO_4. The residue was purified by column chromatography of silica gel (30 g) with $CHCl_3$–acetone–MeOH (10 : 3 : 2, v/v) as an eluent, giving **3a**, 356 mg, 67.6% (Table 1).

Other protected MDP derivatives (3b—3e) were prepared from appropriate *N*-protected amino acid *p*-nitrophenyl ester and the partially protected MDP derivatives in a similar manner.

N-Acetyl-6-O-glycylmuramyl-α-aminoisobutyryl-D-isoglutamine (4a). Compound **3a** (307 mg, 0.55 mmol) was hydrogenated in acetic acid (10 ml) with palladium black as a

catalyst at room temperature for 3 h. After filtration and evaporation, the residue was purified by column chromatography of Sephadex LH-20 (1.8 cm×45 cm) with EtOH–0.1 M AcOH (3 : 2, v/v) as an eluent, giving **4a**, 184 mg, 69.3% (Table 1).

*Other MDP derivatives with an amino acid (**4b**—**4e**)* were prepared from appropriate protected MDP derivatives with an *N*-protected amino acid in a similar manner.

N-*Acetyl-6*-O-[*10-(2,3-dimethoxy-5-methyl-1,4-benzoquinon-6-yl) decanoylglycyl*]*muramyl-α-aminoisobutyryl-*D-*isoglutamine (**5a**).* 10-(2,3-Dimethoxy-5-methyl-1,4-benzoquinon-6-yl)decanoic acid *p*-nitrophenyl ester (47.4 mg, 0.1 mmol) was added to a solution of **4a** (56.4 mg, 0.1 mmol) and NEM (12.8 μl, 0.1 mmol) in DMF (1 ml). The mixture was stirred at room temperature for 16 h and evaporated. The residue was applied onto silica-gel column, the column being developed with EtOAc–pyridine–H_2O–AcOH (30 : 20 : 5 : 3, v/v) as an eluent. The fractions containing the product were collected and evaporated. The residue was rechromatographed over Sephadex LH-20 with EtOH–0.1 M AcOH (3: 2, v/v) as an eluent, giving **5a**, 50.5 mg, 55.4% (Table 2).

Other MDP derivatives with an N-*acylated amino acid (**5b**—**5f**)* were prepared from appropriate carboxylic acid active esters and MDP derivatives with an amino acid in a similar manner.

Biological Assays. Determination of the adjuvant activity on the induction of delayed-type hepersentivity was carried out according to the reported method.[6]

The authors thank Prof. Tetsuo Shiba, Osaka University, and Drs. Einosuke Ohmura, Katsura Morita, and Masao Nishikawa for descussions.

References

1) Part of this work was presented at the lst International Kyoto Conference on New Aspects of Organic Chemistry, Kyoto, December 1979, Abstr, No. C-209.

2) F. Ellouz, A. Adam, R. Ciorbaru, and E. Lederer, *Biochem. Biophys. Res. Commun.*, **59**, 1317 (1974); S. Kotani, Y. Watanabe, F. Kinoshita, T. Shimono, I. Morisaki, T. Shiba, S. Kusumoto, Y. Tarumi, and K. Ikenaka, *Biken J.*, **18**, 105 (1975).

3) Y. Yamamura, I. Azuma, K. Sugimura, M. Yamawaki, M. Uemiya, S. Kusumoto, S. Okada, and T. Shiba, *Proc. Jpn. Acad.*, **53**, 63 (1977); T. Shiba, S. Okada, S. Kusumoto, I. Azuma, and Y. Yamamura, *Bull. Chem. Soc. Jpn.*, **51**, 3307 (1978).

4) S. Kusumoto, M. Inage, T. Shiba, I. Azuma, and Y. Yamamura, *Tetrahedron Lett.*, **1978**, 4899.

5) S. Kobayashi, T. Fukuda, I. Imada, M. Fujino, I. Azuma, and Y. Yamamura, *Chem. Pharm. Bull.*, **27**, 3193 (1979).

6) S. Kobayashi, T. Fukuda, H. Yukimasa, M. Fujino, I. Azuma, and Y. Yamamura, *Bull. Chem. Soc. Jpn.*, in press.

7) S. Kusumoto, S. Okada, K. Yamamoto, and T. Shiba, *Bull. Chem. Soc., Jpn.*, **51**, 2122 (1978).

8) Y. S. Klausner and M. Chorev, *J. Chem. Soc., Chem. Commun.*, **1975**, 973.

9) I. Azuma, K. Sugimura, Y. Yamamura, R. Bando, M. Watanabe, I. Imada, and H. Morimoto, *Internat. J. Vit. Nutr. Res.*, **48**, 255 (1978).

10) Geranylgeranylacetic acid was synthesized from geranylgeranyl bromide and diethyl malonate in the presence of NaH by the conventional method.

11) Purchased from SIGMA Chemical Company, St. Louis, Mo. 63178, U. S. A.

Aromatic Nucleophilic Substitution. XIII.[1] Confirmation of the Anionic σ Complexes in the Reactions of 2,4-Dinitro- and 2,4,5-Trinitro-1-(1-piperidyl)naphthalenes with Piperidine in Dimethyl Sulfoxide

Shizen SEKIGUCHI,* Reiko HIKAGE, Kenmi OBANA, Kohji MATSUI, Yumiko ANDO, and Noboru TOMOTO**

Department of Synthetic Chemistry, Gunma University, Tenjin-cho Kiryu, Gunma 376
***Faculty of Engineering, Miyazaki University, 1-1-1 Kirishima, Miyazaki 880*

(Received January 25, 1980)

In the reactions of 2,4-dinitro- and 2,4,5-trinitro-1-(1-piperidyl)naphthalenes with piperidine in dimethyl sulfoxide, the 1,1-disubstituted anionic σ complex was confirmed to exist with visible absorption and NMR spectra. Especially in the latter case the 1,3-disubstituted anionic σ complex was formed, the cause of formation of which was ascribed to the deactivating effect of 1-piperidyl group on C_1-position of a napthtalene ring and the steric effect of 1-piperidyl group on the nucleophilic attack of piperidine on C_1-position. These factors make the 1,1-disubstituted anionic σ complex unstable.

Many Jackson-Meisenheimer complexes have been prepared by nucleophilic attack on aromatic polynitro compounds.[2] In 1970 Orvik and Bunnett[3] carried out the detailed kinetics of the reactions of 1-ethoxy-2,4-dinitronaphthalene (**1**) with primary amines in dimethyl sulfoxide (DMSO), and confirmed the presence of relatively stable Meisenheimer complex (**3**, hereafter referred to as anionic σ complex) during the course of reaction (Eq. 1).

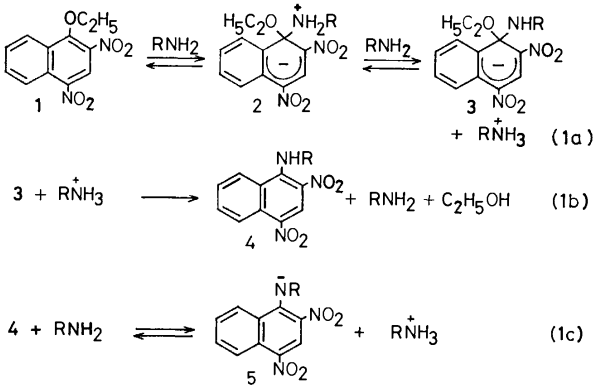

Before and since then much attention of many chemists has been concentrated on the properties and reactions of anionic σ complexes. As for anionic σ complexes found before 1970, Strauss' excellent review already appeared.[4] The later development in the chemistry of anionic σ complexes have been recently summarized by Sekiguchi.[5]

However, almost all the familar aromatic nucleophilic reactions studied so far have been limited to those of activated alkoxyarenes with primary and secondary amines or metal alkoxides[6] or to those of activated dialkylaminoarenes with metal alkoxides.[7-10] Therefore, anionic σ complexes obtained are such as **3** and **6** (hereafter referred to as 1,1-disubstituted anionic σ complex).

Although it was confirmed spectrophotometrically that in the reaction (Eq. 1) the final species is **5**,[3] what would become the final species, when a secondary amine is used in place of a primary one? In such a case, an

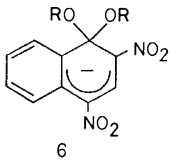

amine could not abstract a proton from **4** (Eq. 1c). Furthermore, how would 1-secondary amino group affect the rate of nucleophilic attack of corresponding amine compared with 1-alkoxyl group?

Prior to carrying out the kinetics of the reactions of 2,4-dinitro- (**7**) and 2,4,5-trinitro-1-(1-piperidyl)naphthalenes (**8**) with piperidine in DMSO, respectively, we have examined their reaction courses using NMR and visible absorption spectra.

This paper reports the presence of stable 1,1-disubstituted anionic σ complexes (**9** and **10**) in both reactions, and the presence of 1,3-disubstituted anionic σ complex (**11**) in the reaction of **8** with piperidine in addition to **10**.

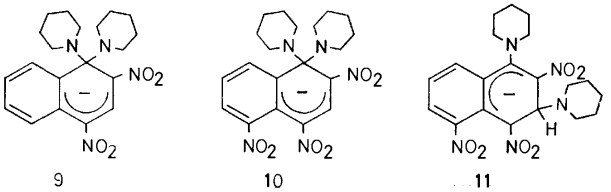

Results and Discussion

Visible Absorption Spectra Relevant to the Reactions of 2,4-Dinitro- (7) and 2,4,5-Trinitro-1-(1-piperidyl)naphthalenes (8) with Piperidine in DMSO. Figure 1 shows the time-dependent spectral change of the reaction of **7** (6.63×10^{-5} M; hereafter M means mol dm^{-3}) with piperidine (1.01 M) in DMSO at room temperature. In our previous work,[11] the electronic structure of 1,1-disubstituted 2,4-dinitronaphthalene anionic σ complexes such as **3** and **6** was determined and the electronic transitions in them were assigned. From this MO calculation and the NMR spectral evidence as will be shown later, the spectrum (d)

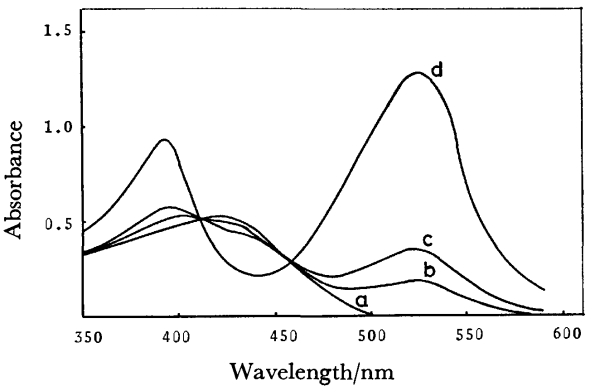

Fig. 1. Absorption spectra of 2,4-dinitro-1-(1-piperidyl)-naphthalene (**7**) with piperidine in DMSO.
a **7**; b, c, and d 10, 24, and 480 h after addition of piperidine.

obtained in 480 h after mixing of **7**, piperidine and piperidinium chloride can be clearly attributed to **9**. As a result, the reaction is considered to proceed as follows: piperidine slowly attacks C_1-position of **7** (rate-determining), followed by the fast abstraction of ammonium hydrogen by piperidine.[3]

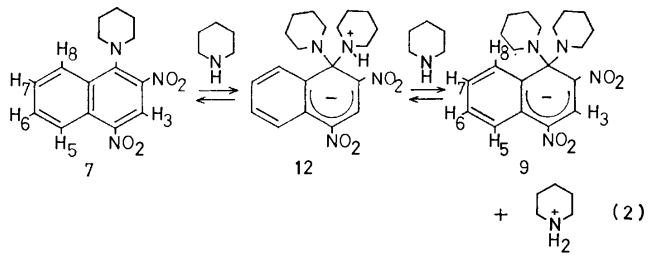

For comparison, we tried to carry out the reaction of 1-ethoxy-2,4-dinitronaphthalene [**1**, 2.87×10^{-5} M, λ_{max} 358 nm (ε 8.9×10^{-3})] with piperidine (1.01 M) in the presence of piperidinium chloride (8.08×10^{-2} M), in which immediately after mixing, the similar spectrum was obtained [λ_{max} 524 (ε 2.50×10^{4}), 365 (ε 1.55×10^{4}), and 357 nm (sh)]. Accordingly it is found that 1-piperidyl group deactivates C_1-position of a naphthalene ring considerably, compared with 1-ethoxyl one.

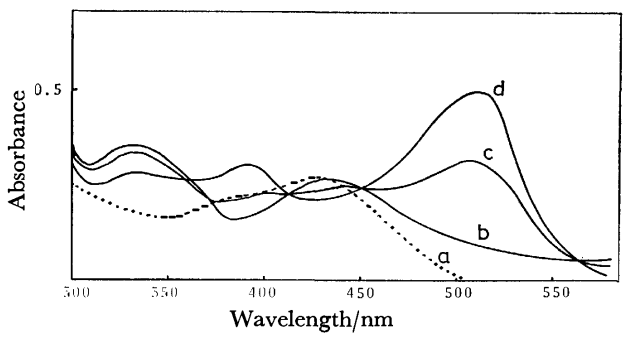

Fig. 2. Absorption spectra of 2,4,5-trinitro-1-(1-piperidyl)naphthalene (**8**) with piperidine in DMSO.
a **8**; b, c, and d immediately, 46, and 260 h after addition of piperidine.

Figure 2 shows the time-dependent spectral change of the reaction of **8** (3.11×10^{-5} M) with piperidine (0.37 M) in the presence of piperidinium chloride (0.01 M) in DMSO at room temperature. Immediately after piperidine and piperidinium chloride has been added to the DMSO solution of **8**, it turned out red at once and the spectrum with double maxima [λ_{max} 434 (ε 1.00×10^{4}) and 330 nm (ε 1.29×10^{4})] was obtained. As will be shown later by NMR spectral evidence, the spectrum (b) can be attributed to **11** (Eq. 3a). There is no isosbestic point among curves a, b, c and d. That is to say, after excess piperidine is added to the DMSO solution of **8**, the equilibrium (**8**⇄**11**) is rapidly established. Just after then, **11** slowly changes into **10** *via* **8** (**11**⇄**8**⇄**14**⇄**10**). Therefore, the isosbestic points are seen among curves b, c, and d.

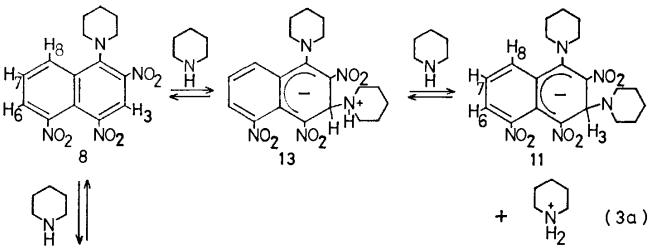

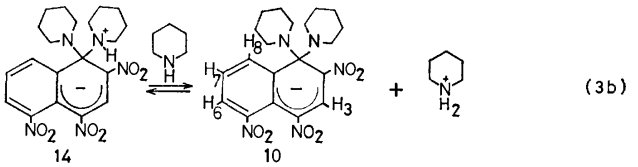

This is the first case in which a 1,3-disubstituted naphthalene anionic σ complex is found on the nucleophilic attack of an amine.

The spectrum (d) obtained in 260 h after mixing is attributed to **10** by considering the NMR spectral evidence in the next paragraph. In order to get the detailed information, we tried to carry out the following reaction in DMSO[12,13] (Eq. 4). In the case of the reaction of **15** with $NaOC_2H_5$ such an anionic σ complex

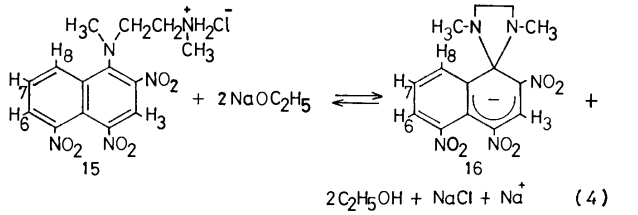

as **11** could not be formed but such one as **10** should be always formed. In 20 min after 20 equivalents of ethanolic $NaOC_2H_5$ had been added to the DMSO solution of **15** (2.57×10^{-5} M) at room temperature, the solution turned out red at once, indicating the absorption with double maxima [λ_{max} 511 (ε 2.34×10^{4}) and 352 nm (ε 9.6×10^{3})]. This result strongly supports that the spectrum (d) in Fig. 2 is due to **10** and the spectrum (b) due to **11**.

Furthermore, in the reaction of 1-ethoxy-2,4,5-trinitronaphthalene (**17**, 3.12×10^{-5} M) with piperidine

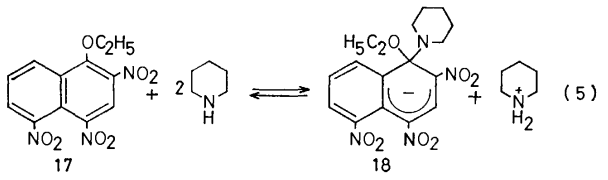

(0.377 M) and piperidinium chloride (0.020 M) in DMSO at room temperature the solution instantly turned out red after mixing, indicating the absorption with double maxima [λ_{max} 506 (ε 2.35×10^4) and 354 nm (ε 1.00×10^4)], which is attributed to **18** by the NMR spectral evidence in the next paragraph. As with **1**, 1-ethoxyl group activates C_1-position of a naphthalene ring of **17** considerably, compared with 1-piperidyl group (Eq. 3). Together with the less steric hindrance exerted by 1-ethoxyl group compared with 1-piperidyl one, this effect makes the formation of 1,1-disubstituted anionic σ complex much easier than that of 1,3-disubstituted one.

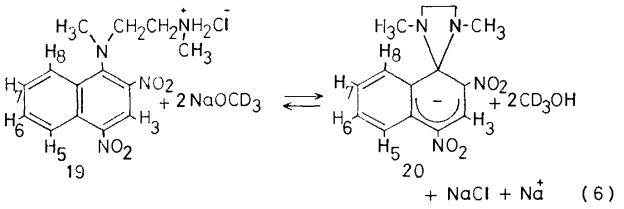

NMR Spectra Relevant to the Reaction of 7 and 8 with Piperidine in DMSO. For comparison, the time-dependent NMR spectra of the reactions of **19** and **15** with $NaOCD_3$ in DMSO-d_6 are shown in Figs. 3A—B and 3C—D, respectively. In these cases, on addition of methanolic $NaOCD_3$ (2 equivalents) to the DMSO-d_6 solution of **19** or **15** the solution turned out red at once, indicating the formation of σ complex. In the reaction course (Eq. 6) each singlet of the two CH_3 groups of **19** [not shown in Fig. 3A, δ 3.17 (N–CH_3) and 3.42 ($\overset{+}{N}$–CH_3, overlapped with the signal of $-CH_2-CH_2-$ group)] coalesced to one sharp singlet [δ 1.98 (6H)], indicating the change in hybrid orbital of C_1 ($sp^2\rightarrow sp^3$). The broad singlet of ammonium hydrogen (δ 9.30) of **19** disappeared in the spectrum of **20** (Fig. 3B). In the transformation of **19** to **20**, the H_3 singlet and H_8 doublet [δ *ca.* 8.81, $J_{8,7}$=8 Hz, the signal is finely splitted by the long-range coupling between the H_8 and H_6 protons] shifted downfield (δ 8.74→9.23 and 8.81→8.83), and the H_5 doublet (δ 8.56, $J_{5,6}$=8 Hz, $J_{5,7}$=2 Hz) and $H_{6,7}$ multiplet shifted upfield (δ 8.56→7.68 and 7.96→7.17) (Fig. 3B), respectively. With **15**, too, the similar change was found [δ 3.23 (N–CH_3) and 3.45 ($\overset{+}{N}$–CH_3, overlapped with the signal of $-CH_2-CH_2-$ group)→2.02 (6H, sharp singlet for N–CH_3 in **16**)]. The broad singlet of ammonium hydrogen of **15** [δ 9.30, overlapped with the H_6 doublet ($J_{6,7}$=8 Hz)] disappeared in the spectrum of **16** (Figs. 3C and D)]. In the transformation of **15** to **16**, the H_3 singlet shifted downfield (δ 8.83→9.03), and the H_6 ($J_{6,7}$=8 Hz) and H_8 ($J_{7,8}$=8 Hz) doublets and H_7 triplet ($J_{6,7}=J_{7,8}$=8 Hz) shifted upfield (δ 9.30→7.92, 8.65→7.68, and 8.01→7.21), respectively.

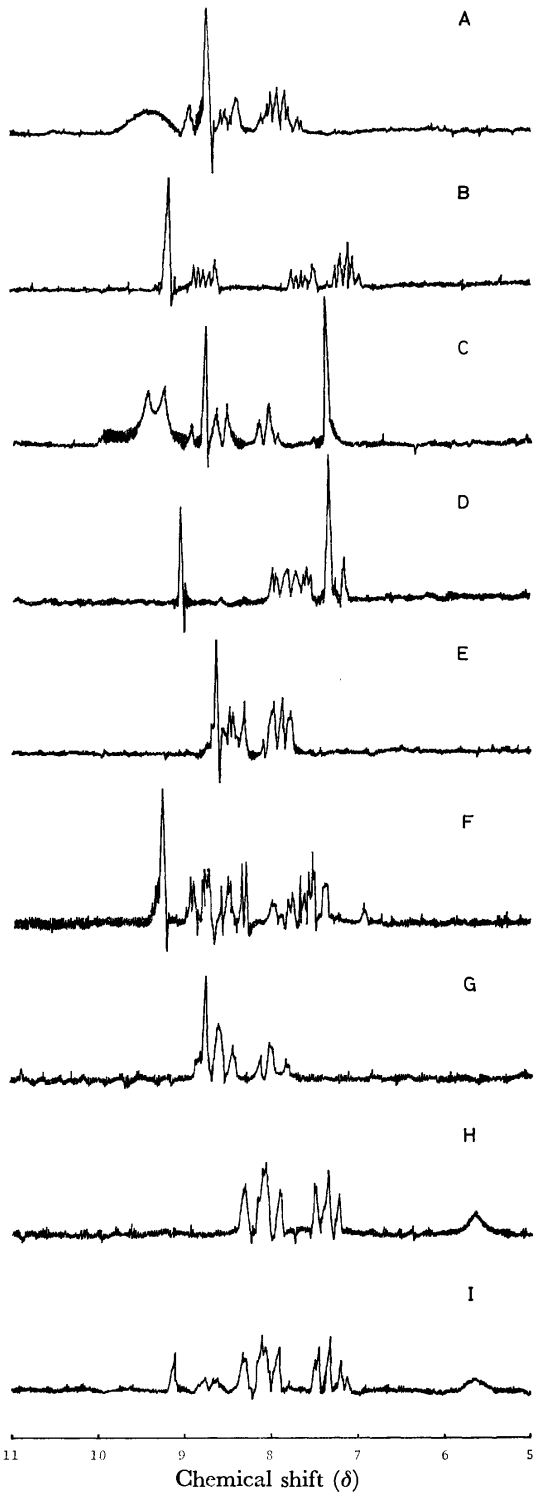

Fig. 3. NMR spectra of the reactions of *N*-methyl-2-[*N*-methyl-*N*-(2,4-dinitro-1-naphthyl)amino]ethyl-(**19**) and *N*-methyl-2-[*N*-methyl-*N*-methyl-*N*-(2,4,5-trinitro-1-naphthyl)amino]ethylammonium chlorides (**15**), and of the reactions of 2,4-dinitro- (**7**) and 2,4,5-trinitro-1-(1-piperidyl)naphthalenes (**8**) with piperidine in DMSO-d_6. A **19**; B immediately after addition of $NaOCD_3$ to the DMSO solution of **19**; C **15**; D immediately after addition of $NaOCD_3$ to the DMSO solution of **15**; E **7**; F 64 d after addition of piperdine to the DMSO solution of **7**; G **8**; H and I 8 and 14 d after addition of piperidine.

The difference between the chemical shifts of the H_8 doublets in **15** and **16** is much larger, compared with that in **19** and **20**. In **15**, 4- and 5-nitro groups deviate from coplanarity with a naphthalene ring by steric hindrance. However, when one negative charge is donated by an amino group (**15**⇄**16**), it is delocalized over three nitro groups, especially over 4-nitro one.[4] As a result, the coplanarity of 4-nitro group with a naphthalene ring increases. Accordingly 5-nitro group in **16** deviates from coplanarity to a larger extent and then comes to exert a less electron-attracting effect to H_8, which may bring about the larger upfield shift. The sharp singlet (δ 7.39) in Figs. 3C and D is due to the protons of benzene, which remained in the preparation of **15** (see Experimental).

The change in chemical shifts in both transformation is characteristic of the formation of 1,1-disubstituted anionic σ complexes.[4,5,14]

With **7**, the H_3 singlet and $H_{6,7}$ multiplet appeared at δ 8.60 and 7.90, respectively, and the $H_{5,8}$ multiplet at δ 8.47 (Fig. 3E). Sixty four days after 20 equivalents of piperidine had been added to the DMSO-d_6 solution of **7**, the H_3 singlet and H_8 doublet shifted downfield, respectively [δ 8.60→9.26 and 8.47→8.82 (d-d, $J_{7,8}$= 8 Hz, $J_{6,8}$=2 Hz)], the H_5 doublet (d-d, $J_{5,6}$=8 Hz, $J_{5,7}$=2 Hz) appeared at δ 8.49, and the $H_{6,7}$ multiplet shifted upfield (δ 7.90→7.56) (Fig. 3F). Even after a long time (64 d) the $H_{6,7}$ signals of **7** still remained (δ *ca.* 7.96), indicating the very slow nucleophilic attack of piperidine (Fig. 3F).

On the other hand, with **8** the conspicuously different signal pattern was obtained. Figures 3G, H, and I show the time-dependent NMR spectra of the reaction of **8** (6.6×10^{-5} M) with piperidine (18 equivalents) in DMSO-d_6 at room temperature. Five days after piperidine had been added to the DMSO solution of **8**, the H_3 singlet (δ 8.77), H_6 (δ 8.71) and H_8 (δ 8.58) doublets (d-d, $J_{6,7}=J_{7,8}$=8 Hz, $J_{6,8}$=2 Hz), and H_7 triplet (δ 8.05, $J_{7,8}=J_{6,7}$=8 Hz) shifted upfield (δ 5.70 singlet for H_3, δ 8.00, multiplet for $H_{6,8}$, and δ 7.43, triplet for H_7 (Figs. 3G—H)).

The extraordinary upfield shift of the H_3 singlet indicates the formation of **11**.[4,5,8,9,16-19] The intensity of the H_3 singlet corresponds to one proton. As was already mentioned, **11** slowly rearranges to **10** just after the equilibrium (**8**⇄**11**) is established. Therefore, the sharpness of the H_3 signal of **11** may depends upon the life time of **11** and the NMR resolving power. Formation of 1,3-disubstituted anionic σ complexes such as **11** is usually kinetically controlled,[15] and such complexes, therefore, are so unstable as to rearrange to 1,1-disubstituted ones, which are equilibrium-controlled.[5,8] However, even after 8 days had passed after mixing, a considerable amount of the 1,3-disubstituted anionic σ complex (**11**) still remained (Fig. 3H). Figure 3I shows that 14 d after mixing a small part of **11** rearranged to **10**, the H_3 singlet of which appeared at δ 9.13. Here, the summation of the intensities of the H_3 signals at δ 5.79 and 9.13 nearly corresponds to one proton. Fifty days after mixing, the same pattern as that in Fig. 3D was obtained. It is, therefore, considered that 1-piperidyl group considerably deactivates C_1-position of a naphthalene ring and furthermore **10** becomes more unstable owing to steric crowding of two piperidyl groups, compared with **18**. As a result, such factors would make the rearrangement of 1,3- to 1,1-disubstituted anionic σ complex slower.

In conclusion, the 1,1-disubstituted anionic σ complex is confirmed to exist in the reaction course of **7** or **8** with piperidine in DMSO and, in the latter case, the 1,3-disubstituted one confirmed additionally to be formed.

Experimental

NMR spectra were recorded on a Varian A-60D spectrometer. Visible absorption spectra were measured on a Hitachi Model 200-10 spectrophotometer. Capillary Mps were uncorrected. Elemental analyses were conducted at the Microanalytical Center of Gunma University.

*Materials. 2,4-Dinitro- (**7**) and 2,4,5-Trinitro-1-(1-piperidyl)naphthalenes (**8**)*: To a stirred 50 ml DMSO solution of 2.52 g (0.01 mol) of 1-chloro-2,4-dinitronaphthalene (CDNN, Eastman Kodak) was dropwise added 2 equivalents of piperidine (*ca.* 2 ml) at room temperature. Furthermore, the mixture was poured into *ca.* 500 ml of ice water to form the yellow precipitate. It was filtered, dried, and recrystallized from ethanol to give 2.4 g of **7** (80%); MP 136—136.5 °C, λ_{max} 422 nm (ε 7.88×10^3, DMSO). Found: C, 60.05; H, 5.35; N, 14.13%. Calcd for $C_{15}H_{15}N_3O_4$: C, 59.80; H, 5.02; N, 13.95%.

Compound **8** was prepared by the similar method to the above-described one; yield 75%, mp 194—195 °C, λ_{max} 430 nm (ε 8.4×10^3, DMSO). Found: C, 52.21; H, 4.25; N, 16.33%. Calcd for $C_{15}H_{14}N_4O_6$: C, 52.02; H, 4.08; N, 16.18%.

*1-Ethoxyl-2,4-dinitronaphthalene (**1**)*: Compound **1** was prepared by the action of C_2H_5ONa on an ethanolic solution of CDNN;[20] yield 76%, mp 91—92 °C (92 °C[20]).

*N-Methyl-2-[N-methyl-N-(2,4-dinitro-1-naphthyl)amino]-ethylammonium Chloride (**19**)*: To a stirred 400 ml ethanol solution of 2.5 g (0.0147 mol) of CDNN was dropwise added 1.3 g (0.0099 mol) of commercial *N,N'*-dimethylethylenediamine (DMED) at room temperature. The mixture was further stirred for 3 h at room temperature to form the precipitate. The filtrate was acidified with HCl and the alcohol was evaporated to *ca.* 30 ml. Then, the solution was allowed to stand 1 d. Of two kinds of crystals formed (orange and yellow) the orange ones were seperated with tweezers. If the yellow crystals were precipitated at frist, they were filtered off and the filtrate was concentrated and allowed to stand. The orange cubic crystals were obtained and recrystallized from HCl-acidified ethanol, yielding an analytical sample (1.3 g, 39%); mp 199.5—201 °C. Found: C, 49.51; H, 5.25; N, 16.60%. Calcd for $C_{14}H_{17}ClN_4O_4$: C, 49.34; H, 5.03; N, 16.44%.

*N-Methyl-2-[N-methyl-N-(2,4,5-trinitro-1-naphthyl)amino]-ethylammonium Chloride (**15**)*: 1-Chloro-2,4,5-trinitronaphthalene (CTNN) was prepared by Rindl's method;[21] yield 60%, mp 143.5—144.5 °C (143—144 °C[20]). The compound (**15**) was prepared from CTNN and *N,N'*-dimethylethylenediamine according to the method for **19** except for the following procedure: at the later stage the concentrated filtrate was allowed to stand overnight. The orange crystals were formed and filtered, and the residue was dissolved in the solution of benzene (30 ml), ethanol (10 ml) and a small amount of aqueous HCl. Then, the mixture was refluxed for 1.5 h. After the evaporation of the solvent the oily product (**15**) was

obtained, the crystallization of which was unsuccessful. Then, the product was dried over P_2O_5 in an evacuated desiccator for 7 d. The NMR spectrum shows that **15** has a certain amount of benzene. Found: C, 45.06; H, 4.64; N, 17.75%. Calcd for $C_{14}H_{16}ClN_5O_6 \cdot 1/6C_6H_6$: C, 44.61; H, 4.72; N, 17.34%.

Piperidinium Chloride. To a stirred 20 ml solution of piperidine (0.201 mol) was added dropwise 17 ml (0.205 mol) of concd HCl at room temperature and then the mixture was cooled in an ice-water bath. After 10 min's stirring the precipitate formed was filtered and washed with cooled ethanol. Recrystallization from ethanol gave 5.43 g (22%) of an analytical sample: Mp 246—247 °C. Found: C, 49.59; H, 10.10; N, 11.77%. Calcd for $C_5H_{12}ClN$: C, 49.38; H, 9.95; N, 11.52%.

NMR Measurement. A certain amount of a sample (*ca.* 35 mg) was dissolved in a small amount of DMSO-d_6 (*ca.* 0.25 ml) in a NMR tube. After excess amine (*ca.* 200 μl) had been added into the solution through a microsyringe and shaken vigorously, the mixture was measured.

Absorption Spectra Measurement. With **7**, just after *ca.* 28 μl of piperidine had been added to *ca.* 3 ml of the DMSO solution of **7** (nearly equal to 6.63×10^{-5} M) throughout a microsyringe and the mixture stirred rapidly, the spectra were taken. With **8**, the DMSO solution of **8** (6.22×10^{-5} M) and the other solution of piperidine (0.74 M) and piperidinium chloride (0.02 M) were prepared. Just after 1.5 ml of the latter solution had been added to 1.5 ml of the former one and the mixture stirred rapidly, the spectra were taken. With **1**, the spectra were measured by the similar procedure to that with **8**.

This research was supported in part by Grant-in-Aid for Scientific Research (No. 455330) from the Ministry of Education, Japan, to which the author (S.S.) is so grateful.

References

1) Part XII, S. Sekiguchi, T. Hirose, K. Tsutsumi, T. Aizawa, and H. Shizuka, *J. Org. Chem.*, **44**, 3921 (1979).

2) For general reviews on nucleophilic aromatic substitution: a) F. Pietra, *Q. Rev., Chem. Soc.*, **23**, 504 (1969); b) T. J. deBoer and I. P. Dirkx, "The Chemistry of the Nitro and Nitroso Groups," ed by H. Feuer, Interscience, New York (1968) Part I, c) J. Miller, "Aromatic Nucleophilic Substitution," American Elsevier, New York (1968); d) E. Buncel, A. R. Norris, and K. E. Russell, *Q. Rev., Chem. Soc.*, **22**, 123 (1968); e) S. D. Ross, *Prog. Phys. Org. Chem.*, **1**, 31 (1963); f) J. F. Bunnett, *Q. Rev., Chem. Soc.*, **49**, 273 (1951); g) J. F. Bunnett and R. E. Zahler, *Chem. Rev.*, **49**, 273 (1951); h) C. F. Bernasconi, *Acc. Chem. Res.*, **11**, 147 (1978).

3) J. A. Orvik and J. F. Bunnett, *J. Am. Chem. Soc.*, **92**, 2417 (1970).

4) M. J. Strauss, *Chem. Rev.*, **70**, 667 (1970).

5) S. Sekiguchi, *J. Soc. Org. Syn. Chem. Tokyo*, **36**, 633 (1978).

6) C. F. Bernasconi, *MTP Int. Rev. Sci.: Org. Chem., Ser. One*, **3**, 33 (1973).

7) S. Sekiguchi, K. Shinozaki, T. Hirose, K. Matsui, and K. Sekine, *Bull. Chem. Soc. Jpn.*, **47**, 2264 (1974).

8) S. Sekiguchi, K. Shinozaki, T. Hirose, K. Matsui, and T. Itagaki, *Tetrahedron Lett.*, **1974**, 1745.

9) S. Sekiguchi, S. Fujisawa, and Y. Ando, *Bull. Chem. Soc. Jpn.*, **49**, 1451 (1976).

10) S. Sekiguchi, T. Takei, T. Aizawa, and K. Okada, *Tetrahedron Lett.*, **1977**, 1209.

11) S. Sekiguchi, K. Tsutsumi, H. Shizuka, K. Matsui, and T. Itagaki, *Bull. Chem. Soc. Jpn.*, **49**, 1521 (1975).

12) C. F. Bernasconi and C. L. Gehringer, *J. Am. Chem. Soc.*, **96**, 1092 (1974).

13) C. F. Bernasconi and H. -C. Wang, *J. Am. Chem. Soc.*, **98**, 6265 (1976).

14) S. Sekiguchi, T. Itagaki, T. Hirose, K. Matsui, and K. Sekine, *Tetrahedron*, **29**, 3527 (1973).

15) D. J. Cram and G. S. Hammond, "Organic Chemistry," McGraw-Hill, New York (1964), p. 235.

16) F. Terrier, J. -C. Halle, and M. -P. Simonnin, *Org. Magn. Reson.*, **3**, 361 (1971).

17) F. Terrier, F. Millot, and W. P. Norris, *J. Am. Chem. Soc.*, **98**, 5883 (1976).

18) M. -P. Simonnin, M. J. Lecourt, F. Terrier, and C. A. Dearing, *Can. J. Chem.*, **50**, 3558 (1972).

19) M. -P. Simonnin, F. Terrier, and C. Paulmier, *Tetradron Lett.*, **1973**, 2083.

20) F. Ullmann and W. Bruck, *Ber.*, **41**, 3923 (1908).

21) M. Rindl, *J. Chem. Soc.*, **103**, 1913 (1913).

Synthetic Identification of Bitter Heptapeptide in Tryptic Hydrolysate of Casein

Akio HASHIMOTO,† Haruhiko AOYAGI,* and Nobuo IZUMIYA

Laboratory of Biochemistry, Faculty of Science, Kyushu University, Higashi-ku, Fukuoka 812

(Received January 26, 1980)

A heptapeptide, H-Gly-Pro-Phe-Pro-Ile-Ile-Val-OH (**1**), was synthesized and found to be indistinguishable from the natural peptide (**2**), isolated from a tryptic hydrolysate of Hammersten casein by means of chromatography, amino acid analyses, and mass spectrometric measurements. Both peptides (**1** and **2**) have a strong bitter taste.

Bitter peptides have been found widely in proteolytic hydrolysates of proteins. Two bitter peptides were isolated from the proteolytic hydrolysates of casein and their structures determined to be H-Gly-Pro-Phe-Pro-Val-Ile-OH (**3**)[1] and H-Arg-Gly-Pro-Pro-Phe-Ile-Val-OH (**4**).[2] Ribadeau Dumas *et al.* determined the whole primary structure of bovine β-casein[3] which contains the partial sequence of Arg(202)-Gly(203)-Pro-Phe-Pro-Ile(207)-Ile-Val(209)-OH in the *C*-terminal portion. No amino acid sequence of **3** or **4** can be found in the structure of the casein, but **3** and **4** are very similar to the *C*-terminal portion of the casein. Reports have been given on the synthesis of a natural hexapeptide (H-Arg-Gly-Pro-Phe-Pro-Ile-OH) as a sex factor in yeast, its sequence being identical with the 202—207 portion of casein.[4,5] Natural hexapeptide also has a strong bitter taste. Thus, we assumed that a heptapeptide, H-Gly-Pro-Phe-Pro-Ile-Ile-Val-OH (**1**), corresponding to the *C*-terminal portion (203—209) of casein and isolated from tryptic hydrolysate of casein, might show bitterness.

This paper deals with the synthesis of **1** by the conventional method and a comparison of the synthetic peptide with the natural peptide (**2**), isolated from tryptic hydrolysate of casein, by means of chromatography, amino acid analyses, mass spectrometric (MS) measurements and biological assays.

The synthetic route of **1** is shown in Fig. 1.[6] MA and EDC methods were used for the coupling reaction, Boc groups of the intermediates being removed by the action of HCl in EtOAc. Hydrogenation of **11** afforded **1** as dihydrate. The homogeneity of **1**·$2H_2O$ was confirmed by thin-layer chromatography (TLC) and paper chromatography (PPC). For tryptic digestion of casein and the subsequent isolation of the natural bitter peptide (**2**), the methods reported by Ribadeau Dumas *et al.*[3] and Matoba *et al.*[1] were used with slight modifications.

A comparison of **2** with **1** was carried out by TLC, PPC, and amino acid analysis. Compounds **1** and **2** are essentially the same, although **2** contains minor constituents as observed in TLC and amino acid analysis, and both have a strong bitter taste in almost the same threshold value. Field desorption mass spectra (FDMS) of **1** and **2** were measured at two different anode heating currents at 20 and 23 mA, respectively. Patterns of FDMS at 20 mA are shown in Fig. 2. Some peaks assigned to **1** and **2** at 20 mA are as follows: *m/e* 742 ([(M+H)$^+$] of the heptapeptide), 724 (loss of H_2O from [(M+H)$^+$]), and 697 (loss of CO_2 from [M$^+$]). A peak

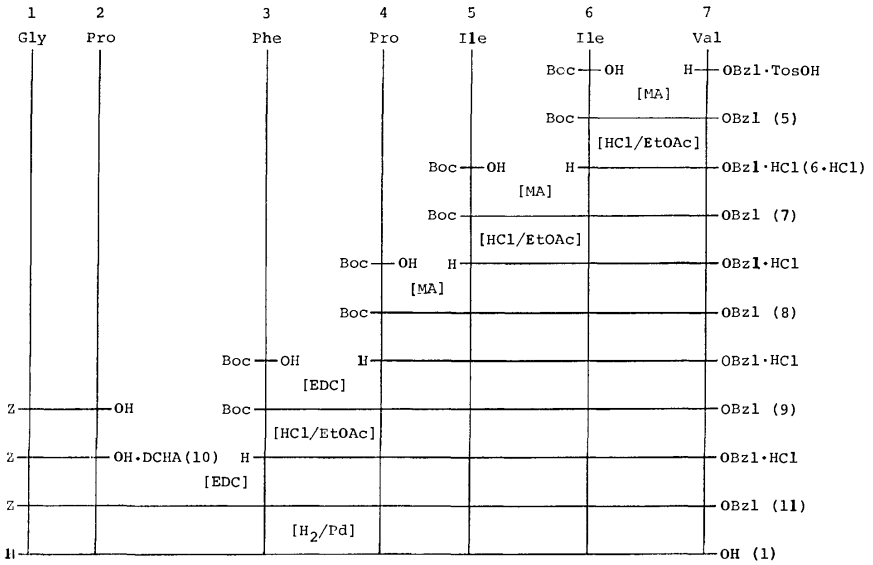

Fig. 1. Synthesis of a heptapetide, **1**.

† Present address: The Kitakyushu Municipal Institute of Environmental Health Sciences, Shin-ike, Tobata-ku, Kitakyushu 804.

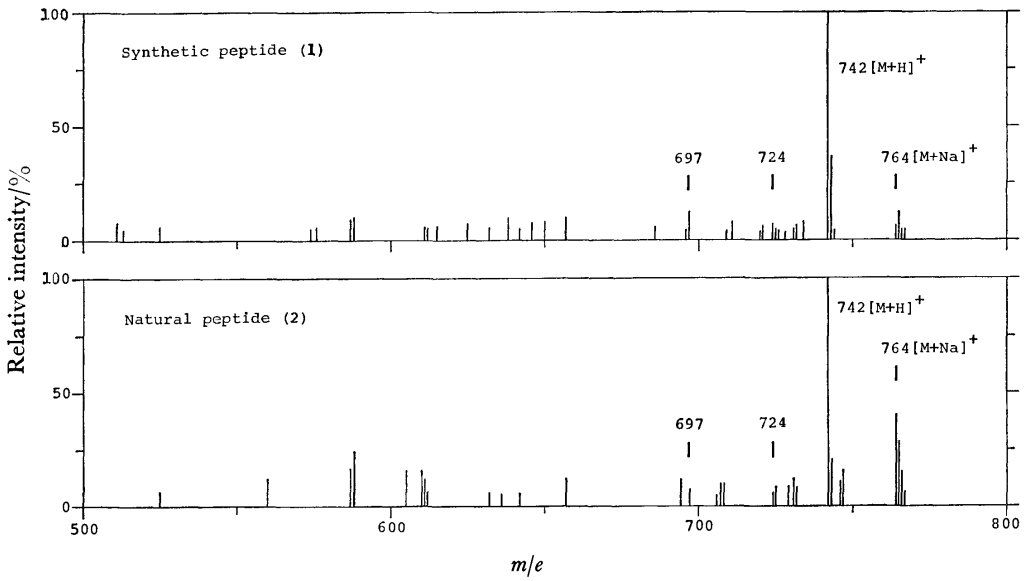

Fig. 2. FDMS of synthetic peptide (**1**) and natural peptide (**2**) measured at anode heating current of 20 mA.

at 23 mA is as follows: *m/e* 640 (loss of CO_2 from H–Pro–Phe–Pro–Ile–Ile–Val–OH which revealed *N*-terminal amino acid as Gly).

The results indicate that **2** is a new bitter peptide having the structure of H–Gly–Pro–Phe–Pro–Ile–Ile–Val–OH, the presence of several hydrophobic amino acids being important for showing bitterness as pointed out by Clegg *et al.*[7,8]

Experimental

TLC was carried out on Merck silica gel G with the systems, R_f^1, $CHCl_3$–MeOH (5 : 1); R_f^2, $CHCl_3$–MeOH (9 : 1); R_f^3, *n*-BuOH–AcOH–pyridine–H_2O (15 : 3 : 10 : 12), and on micro crystalline cellulose (AVICEL) (Funakoshi Yakuhin Co. Ltd., Tokyo) with the system R_f^4, *t*-pentyl alcohol–pyridine–H_2O (10: 4: 5). PPC was performed on Toyo Roshi No. 52 paper with the system R_f^5, the same solvent as used for R_f^4. Optical rotations were measured on a Union high sensitivity polarimeter, PM-71. Amino acid analyses were performed with a Hitachi amino acid analyzer, KLA-5. Crystalline trypsin (Sigma Chemical Co., U. S. A.) and Hammersten casein (E. Merck AG, Darmstadt, Germany) were used.

Boc–Ile–Val–OBzl (5). **5** was prepared from Boc–Ile–OH and H–Val–OBzl·TosOH by the usual MA method;[9] yield, 75%; R_f^1 0.95. Physical constants and elemental analyses of crystalline compounds are given in Table 1.

Boc–Ile–Ile–Val–OBzl (7). Compound **5** (5.0 mmol) was dissolved in 2 M HCl in EtOAc (25 ml). The solution was left to stand at room temperature for 1 h, and evaporated; yield of a solid H–Ile–Val–OBzl·HCl (**6**·HCl), 98%. **7** was then prepared from Boc–Ile–OH and **6**·HCl by the MA method; yield, 75%; R_f^1 0.75.

Boc–Pro–Ile–Ile–Val–OBzl (8). **8** was prepared from Boc–Pro–OH and H–Ile–Ile–Val–OBzl·HCl derived from **7** by the MA method; yield, 84%; R_f^2 0.75.

Boc–Phe–Pro–Ile–Ile–Val–OBzl (9). **9** was prepared from Boc–Phe–OH and H–Pro–Ile–Ile–Val–OBzl·HCl derived from **8** by the usual EDC method;[10] yield, 93%; R_f^2 0.67.

Z–Gly–Pro–OH·DCHA (10). **10** was prepared from Z–Gly–Pro–OH[11] and DCHA by the usual procedure;[12] yield, 66%.

Z–Gly–Pro–Phe–Pro–Ile–Ile–Val–OBzl (11). **11** was prepared from **10** and H–Phe–Pro–Ile–Ile–Val–OBzl·HCl derived from **9** by the EDC method; yield, 88%; R_f^2 0.52.

H–Gly–Pro–Phe–Pro–Ile–Ile–Val–OH (1). Compound **11** (0.31 g, 0.31 mmol) dissolved in a mixture of MeOH (8 ml), AcOH (4 ml), and H_2O (1 ml) was hydrogenated in the presence of Pd black. The filtrate from the catalyst was evaporated to leave a solid. Recrystallization from EtOH–EtOAc gave 0.22 g (91%); R_f^3 0.75, R_f^4 0.81, R_f^5 0.71; mass spectrum, *m/e* 741 (calcd, 741.4). Amino acid ratios in an acid hydrolysate: Pro (2.08), Gly (1.00), Val (1.03), Ile (2.09), Phe (0.99).

Isolation of Bitter Peptide from Tryptic Hydrolysate of Casein. A mixture of casein (10 g) and trypsin (150 mg) in H_2O (1000 ml) was incubated at pH 8.5 and 37 °C for 2 d. After the

Table 1. Analytical data of synthetic peptides

Compound	Mp/°C	$[\alpha]_D^{20}$ in EtOH	Formula	Found (%)			Calcd (%)		
				C	H	N	C	H	N
5	89—91	−48° (*c* 1.9)	$C_{23}H_{36}O_5N_2$	65.55	8.58	6.54	65.69	8.63	6.66
7	173—174	−77° (*c* 2.2)	$C_{29}H_{47}O_6N_3$	64.83	8.84	7.75	65.26	8.88	7.87
8	191—193	−82° (*c* 1.1)	$C_{34}H_{54}O_7N_4$	64.58	8.59	8.78	64.73	8.63	8.88
9	165—166	−81° (*c* 2.0)	$C_{43}H_{63}O_8N_5 \cdot 1/2H_2O$	65.94	8.11	8.79	65.62	8.20	8.90
10	125—126	−37° (*c* 2.6)	$C_{27}H_{41}O_5N_3$	66.15	8.45	8.45	66.50	8.48	8.62
11	133—134	−106° (*c* 1.0)	$C_{53}H_{71}O_{10}N_7 \cdot H_2O$	64.75	7.42	9.86	64.68	7.48	9.96
1	160—163	−116° (*c* 0.5)	$C_{38}H_{59}O_8N_7 \cdot 2H_2O$	58.58	7.99	12.30	58.67	8.16	12.60

solution had been adjusted to pH 7.0, it was extracted with 1-butanol (1000 ml × 3). The butanol phase was concentrated *in vacuo* and lyophilized. A solution of the residue in H_2O (100 ml) was adjusted to pH 10, and then acidified slowly to pH 5.4. The precipitates were removed by filtration, and the filtrate was concentrated and lyophilized. The residue obtained was purified by a series of column chromatography as follows: Sephadex G-25 (2 × 35 cm) with 0.01 M phosphate buffer (pH 7.5), Dowex 50X8 (1 × 45 cm) with 1 M pyridine–AcOH (pH 4.1), Dowex 50X8 (1 × 45 cm) with 0.4 M pyridine–AcOH (pH 3.5), Sephadex G-10 (1.6 × 12 cm) with H_2O, AVICEL (1.6 × 17 cm) with *t*-pentyl alcohol–pyridine–H_2O (10 : 4 : 5), Dowex 1X2 (1.6 × 17 cm) with 0.1 M AcOH and finally Sephadex G-10 (2.0 × 10 cm) with H_2O. In each case, the eluate fractions showing the same R_f values as that of **1** by TLC were collected, concentrated and lyophilized. The residue was dissolved in a small amount of EtOH. EtOAc was added to the solution until precipitates appeared. The precipitates were collected by filtration; yield, 8 mg; R_f[3] 0.73, R_f[4] 0.81, R_f[5] 0.71; mass spectrum, *m/e* 741 (calcd, 741.4). Amino acid ratios in an acid hydrolysate: Pro (2.27), Gly (1.00), Val (1.35), Ile (2.15), Phe (1.27). Minor amounts of Asp, Thr, Ser, Glu, and Ala were also found in the hydrolysate.

FDMS Measurements. Measurements were carried out on a Nihondenshi mass spectrometer Model JMS-01SG-2 equipped with a combined EI/FI/FD source. The mass spectra of **1**·2H_2O and **2** in MeOH (5 mg/ml) were measured at anode heating currents at 20 and 23 mA, respectively.

Bitterness Evaluation. The degree of bitterness was determined according to the method reported by Matoba *et al.*[1] Compounds **1**·2H_2O and **2** have the same degree of bitterness at 0.17—0.34 mM (0.13—0.25 mg/ml).

We wish to thank Mr. M. Koga, The Kitakyushu Municipal Environmental Health Sciences, for the FDMS measurements.

References

1) T. Matoba, R. Hayashi, and T. Hata, *Agric. Biol. Chem.*, **34**, 1235 (1970).
2) N. Ninamiura, Y. Matsuura, J. Fukumoto, and T. Yamamoto, *Agric. Biol. Chem.*, **36**, 588 (1972).
3) B. Ribadeau Dumas, G. Brignon, F. Grosclade, and J. C. Mercier, *Eur. J. Biochem.*, **25**, 505 (1972).
4) H. Aoyagi and N. Izumiya, *Bull. Chem. Soc. Jpn.*, **50**, 2387 (1977).
5) H. Aoyagi, N. Izumiya, A. Sakurai, K. Sakata, and S. Tamura, *Experientia*, **33**, 870 (1977).
6) Abbreviations given by the IUPAC-IUB Commissoin (*J. Biol. Chem.*, **247**, 977 (1972)) are used. Additional abbreviations: EDC, 1-ethyl-(3-dimethylaminopropyl)carbodiimide; DCHA, dicyclohexylamine; MA, mixed anhydride method. Amino acid symbols except Gly denote the L-configuration.
7) K. M. Clegg, C. L. Lim, and W. Manson, *J. Dairy Res.*, **41**, 238 (1974).
8) We assumed the structure of the natural peptide isolated by Matoba *et al.*[1] to be H–Gly–Pro–Phe–Pro–Ile–Ile–Val–OH (**1**) and not H–Gly–Pro–Phe–Pro–Val–Ile–OH (**3**), but the assumption cannot be verified at present since a sample of their natural peptide is not available and a comparison with the heptapeptide (**1**) we obtained is impossible.
9) J. R. Vaughan, Jr., and R. L. Osato, *J. Am. Chem. Soc.*, **74**, 676 (1952).
10) J. C. Sheehan, J. Preston, and P. A. Cruickshank, *J. Am. Chem. Soc.*, **87**, 2492 (1965).
11) T. Wieland, L. Lapastanis, J. Faesel, and W. Konz, *Justus Liebigs Ann. Chem.*, **747**, 194 (1971).
12) E. Klieger, E. Schröder, and H. Gibian, *Justus Liebigs Ann. Chem.*, **640**, 157 (1961).

Highly Strained Ring Systems. Hydrolysis of *endo*-Tetracyclo-[5.2.0.0^{2,4}.0^{3,5}]non-8-en-6-yl *p*-Nitrobenzoate. Importance of Anchimeric Assistance by Bicyclobutane Ring. II[1]

Masayoshi Isobe and Kazuyuki Yano*

Department of Chemistry, Saitama Medical School, 981 Kawakado, Moroyama, Iruma-gun, Saitama 350-04

(Received January 26, 1980)

Solvolytic reactivity of *endo*-tetracyclo[5.2.0.0^{2,4}.0^{3,5}]non-8-en-6-yl *p*-nitrobenzoate(**1**-OPNB), *endo*-bicyclo-[4.1.0]hept-2-yl *p*-nitrobenzoate(**2**-OPNB), and *endo*-bicyclo[4.2.0]oct-7-en-2-yl *p*-nitrobenzoate(**4**-OPNB) was investigated in 50% aqueous acetone. **1**-OPNB was less reactive than **2**-OPNB that has no cyclobutene ring and more reactive than **4**-OPNB that has no bicyclobutane ring. Product study in solvolysis of **1**-OPNB was undertaken leading to the rearranged tricyclic alcohol as a major product. The importance of conformational factor for anchimeric assistance by bicyclobutane ring is discussed.

In spite of many studies of solvolytic reactions of cyclopropyl systems,[2] only a few investigations with bicyclo[1.1.0]butane derivatives, which involve the highest strain energy in bicyclic ring systems, have been reported.[3]

Masamune *et al.*[3a] reported that in ethanolysis of 5,6-diphenyltricyclo[2.1.1.0^{5,6}]hexan-2-yl *p*-toluenesulfonate a portion of the driving force for the reaction could arise from relief of angle strain on ring opening of the bicyclobutane ring. In contrast, Breslow *et al.*[3b] reported that none of the overall strain relief was found at the transition state for solvolyses of bicyclo[1.1.0]but-2-ylcarbinyl derivatives in spite of the fact that all products were derived from ring expanded cations. These studies have been made with the bicyclobutane derivatives substituted with phenyl groups or alkyl groups on the bridge heads of the bicyclobutane ring. Thus, there may be some influence on the reactivity due to π-electron systems or alkyl groups, and the effect of the bicyclobutane itself to the reaction center has some ambiguous factors.

On the other hand, we previously demonstrated importance of anchimeric assistance by bicyclobutane ring in solvolysis of a tricyclic system.[1] Taking these results into consideration, we have synthesized *endo*-tetracyclo[5.2.0.0^{2,4}.0^{3,5}]non-8-en-6-yl *p*-nitrobenzoate (**1**-OPNB),[4] *endo*-bicyclo[4.1.0]hept-2-yl *p*-nitrobenzoate(**2**-OPNB),[5] and *endo*-bicyclo[4.2.0]oct-7-en-2-yl *p*-nitrobenzoate(**4**-OPNB),[6] which have a partial structure of **1**-OPNB, and investigated their solvolytic reactivity to assess the effect of bicyclobutane and cyclobutene[7] in a polycyclic ring system.

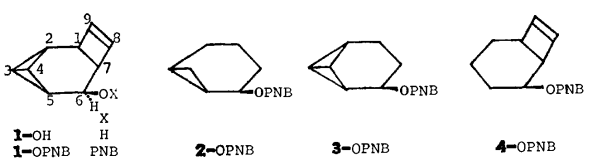

1-OH H
1-OPNB PNB **2**-OPNB **3**-OPNB **4**-OPNB

Results and Discussion

The synthesis of tetracyclo[5.2.0.0^{2,4}.0^{3,5}]non-8-en-6-one (**5**) has been previously described.[4] Sodium borohydride reduction of **5** afforded exclusively the *endo* alcohol (**1**-OH). The stereochemical assignment of the *endo* isomer (geometry of the hydroxyl group relative to the cyclobutenyl group of **1**-OH) was based upon lanthanoid-induced chemical shift studies of ^{1}H NMR (Table 1). From the values of increment in chemical shift, it was predicted that the distances of the hydrogens (H_7, H_8) from the oxygen are shorter than that of H_4($\overline{OH}_7$, $\overline{OH}_8$<$\overline{OH}_4$).[8] This prediction was supported by an examination of the oxygen-hydrogen distances from the molecular model of the *endo* alcohol (**1**-OH) using Frame work Molecular Models. The stereospecific reduction of **5** from the less hindered side of the carbonyl group by sodium borohydride also suggested the *endo* isomer.[9] Additional information about the *endo* structure was gained from the coupling constants ($J_{6,5}$ and $J_{6,7}$) of the C_6 proton signal on the NMR spectrum of **1**-OPNB. From the corresponding dihedral angles (θ) obtained from the molecular model (FMM) of **1**-OPNB, the vicinal coupling constants were calculated as $J_{6.5}^{endo}$=2.50 Hz (θ=55°) and $J_{6.7}^{endo}$=7.21 Hz (θ=20°), and $J_{6.5}^{exo}$=1.83 Hz (θ=60°) and $J_{6.7}^{exo}$=0 Hz (θ=100°) using the Karplus equation.[10] The NMR data of **1**-OPNB showed $J_{6,5}$=2.0 Hz and $J_{6,7}$=9.4 Hz supporting the *endo* structure. Contrary to our all effort, attempts to prepare the *exo* epimer of **1**-OPNB encountered with failure.

The hydrolysis of **1**-OPNB, **2**-OPNB, and **4**-OPNB were measured in 50% aqueous acetone by titrating released *p*-nitrobenzoic acid using Bromothymol Blue as an indicator. All runs showed nice first-order plots. The kinetic data were summarized in Table 2 with literature values for a related compound. From Table 2, **1**-OPNB is 38 times more reactive than **4**-OPNB suggesting that this bicyclobutane ring stabilizes the transition state of the solvolysis of **1**-OPNB by *ca.* 2.7 kcal/mol (100 °C). On the other hand, the rate of **1**-OPNB decreases to one sixth comparing with that of **3**-OPNB in spite of the fact that **4**-OPNB is more reactive than cyclohexyl *p*-nitrobenzoate.[11] The difference in the reactivity of **1**-OPNB and **3**-OPNB is rationalized by considering the following two factors. First, when compared to **3**-OPNB, **1**-OPNB has a more rigid six-membered ring caused by the cyclobutene ring, and, as a result, it has a less favorable geometry for the "bisected" ion type interaction (**10**) that is the most stable structure of its transition state.[12] Second, the reactivity of **1**-OPNB probably decreases due to an inductive effect by the double bond (*ca.* by a factor

Table 1. Lanthanoid-induced chemical shifts in 1-OH[a)]

Weight of $Eu(dpm)_3$ (mg)	Chemical shifts of hydrogen								
	H_1	H_2	H_3	H_4	H_5	H_6	H_7	H_8	H_9
0	2.84	2.48	1.67	1.67	2.76	3.70	3.04	6.18	6.18
19.6	5.50	5.25	3.90	5.00	8.54	16.25	10.15	12.52	8.75
Increment in chemical shifts	2.66	2.77	2.23	3.33	5.78	12.55	7.11	6.34	2.57

a) 1-OH (9.2 mg) in CCl_4 (0.136 ml).

Table 2. Kinetic data for hydrolysis of *p*-nitrobenzoates in 50% aqueous acetone (v/v)

Substrate	Temp/°C[a)]	k_1/s^{-1}	$\Delta H^{\neq}$, kcal/mol	$\Delta S^{\neq}$, eu	k_{rel}
1-OPNB	100	$(5.18\pm0.12)\times10^{-5}$ [b)]	25.0	−11.5	38
	125	$(5.10\pm0.06)\times10^{-4}$ [b)]			
2-OPNB	80	6.59×10^{-4}			
	100	$(3.31\pm0.09)\times10^{-3}$ [b)]	20.4	−15.7	2400
3-OPNB	80	4.93×10^{-5} [c)]			
	100	2.96×10^{-4} [c)]	22.7	−14.2	218
4-OPNB	100	1.36×10^{-6} [d)]	31.4	−1.6	1
	125	$(2.08\pm0.02)\times10^{-5}$ [b)]			

a) ±0.2 °C. b) The errors are deviation from the average of two runs. c) Reference 1. d) Extrapolated value using the data at higher temperature ($k_1=2.30\times10^{-4}$ s^{-1} at 150 °C).

2—3).[7d,7e,13)] The rate acceleration of **4**-OPNB compared to the cyclohexyl *p*-nitrobenzoate by a factor of 7×10^4 might be mainly related to a relief of back side strain[14)] and rate retarding effect by the double bond (by a factor 2—3) would be small enough compared with the back side strain. In the case of **1**-OPNB, however, the ground-state strain resulting from nonbonded interaction between the cyclobutene ring and the leaving group would bend the leaving group to the conformationally undesirable direction for the interaction between the bicyclobutane ring and p orbital at C_6 in the transition state. In consequence, the anchimeric assistance by the bicyclobutane ring in **1**-OPNB was so important that the cyclobutene ring would influence the ionization rate of **1**-OPNB negatively. Similar relation exists in the rigid molecules such as *endo*-bicyclo[3.1.0]hex-2-yl *p*-nitrobenzoate and *endo*-tricyclo[4.2.0.$0^{2,4}$]octan-5-yl *p*-nitrobenzoate.[2f)] In them the ionization rate of the latter involving the cyclobutane ring appears comparable with the former under allowance for solvent differences.

The cyclopropylcarbinyl derivative (**2**-OPNB) which is a partial structure of **1**-OPNB underwent solvolysis at a rate *ca.* 60 times as fast as **1**-OPNB (100 °C), and its reactivity was even greater than that of **3**-OPNB by a factor of 10. In the other words, **1**-OPNB and **3**-OPNB which involve the bicyclobutane ring that has greater strain energy than the cyclopropane ring were less reactive than **2**-OPNB involving the cyclopropane ring. This result indicates that the most important factor ruling the solvolytic reactivity of **1**-OPNB is the conformational factor for stabilization of its transition state by the anchimeric assistance of the cyclopropyl ring in the bicyclobutane rather than the relief of its ring strain.[1,3b)]

Hydrolysis of **1**-OPNB produced predominantly *endo, syn*-tricyclo[4.2.1.$0^{2,5}$]nona-3,7-dien-9-ol (**9**) (91%, GLC analysis) and two unidentified minor products (<5%). Although **1**-OH was found to be unstable under the solvolysis conditions, it did not produce **9** (from GLC and TLC) suggesting that **9** is a solvolysis product of the C–O bond cleavage rather than that of alkaline hydrolysis of the ester. The structural assignment of **9** was based upon its NMR spectrum and physical property. The *endo* fusion of the cyclobutene ring to the norbornene moiety in **9** was supported by its NMR data of vinyl protons (δ 5.76, s, 4H) shifting toward up-field from that of *exo*-fused alcohol (δ 6.66 or 6.24)[7a)] due to the long range shielding effects by the other double bond.[15)] The disposition of the hydroxyl group *syn* to the cyclobutene ring was determined by its physical property (mp 87.5—88.5 °C) since the *anti* epimeric alcohol has a different melting point (41.5—42.5 °C).[16)] This assignment was also in agreement with the following mechanism: the backside participation of a–b bond of **1**-OPNB affords the "bicyclobutonium" ion **6**,[1,12)] which rearranges to **7**, and further the ion **7** gives predominantly **9** through stable bishomocyclopropenyl ion **8**.[17)] In this process, the fused cyclobutene ring is thought to act only as a stereochemical marker. The deuterated **1**-OPNB (C_6-*d*) was hydrolyzed to the C-1 (C-6) labeled alcohol **9** (C_1-*d*).

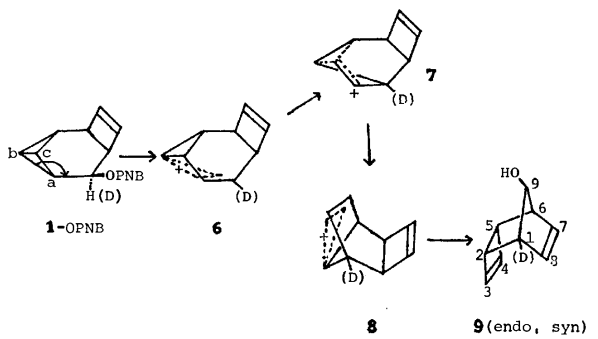

In summary, the difference in the solvolytic reactivity of **1**-OPNB, **2**-OPNB, and **3**-OPNB may depend on their effective conformations, which are related to the deviation from the most stable "bisected" structure (**10**) toward the less stable "bicyclobutonium" structure (**11**) in the transition state, for anchimeric assistance. The hydrolysis product study of **1**-OPNB also suggests the importance of anchimeric assistance by the bicyclobutane ring.

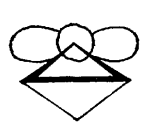

10

"bisected" ion

11

"bicyclobutonium" ion

Experimental

Melting points were taken on a Yamato MP-21 melting point apparatus and are uncorrected. Infrared spectra were recorded on a Shimadzu IR-400 spectrophotometer and nuclear magnetic resonance spectra were recorded using a Hitachi R-24 instrument with chemical shift (δ) given in parts per million downfield from Me_4Si. Gas-liquid chromatography was performed on a Shimadzu GC-4B instrument. Microanalyses were determined in the microanalytical laboratory of the Institute of Physical and Chemical Research, Wako-shi, Saitama.

endo-*Tetracyclo*[*5.2.0.0*^{2,4}*.0*^{3,5}]*non-8-en-6-yl* p-*Nitrobenzoate (1-OPNB).* To a solution of *endo*-tetracyclo[5.2.0.0^{2,4}.0^{3,5}]-non-8-en-6-one[4] (639 mg, 4.84 mmol) in 15 ml of methanol was added sodium borohydride (114 mg, 3.02 mmol) at 0 °C. The resulting solution was allowed to stir at room temperature for 15 h. After addition of 15 ml of saturated sodium chloride solution, the resulting solution was extracted with ether three times. The ethereal solution was washed with saturated sodium chloride solution, dried ($MgSO_4$), and concentrated under vaccum to give 554 mg (85%) of the crude alcohol (**1**-OH) as a colorless liquid. Owing to unstability of **1**-OH, the NMR spectrum of **1**-OH was examined without purification. **1**-OH: IR (neat) 3370 (OH), 2990, 2920, 1275, 1140, and 1040 cm^{-1}; NMR (CCl_4) δ 6.19 and 6.07 (2d, 2H, vinyl, J=3.0, 7.0 Hz), 3.95—3.35 (m, 1H), 3.30—2.25 (m, 5H), and 1.63 (t, 2H, J=2.8 Hz).

To a solution of **1**-OH (554 mg, 4.13 mmol) in 15 ml of dry pyridine was added *p*-nitrobenzoyl chloride (1060 mg, 5.71 mmol) in small portions at 0 °C. The resulting solution was allowed to stand in a refrigerator for 3 d, and then poured onto 60 g of ice with 2 ml of concentrated hydrochloric acid. The product was extracted with chloroform (60 ml×3), washed with 5% HCl solution (twice), water, 5% $NaHCO_3$ solution (twice), water (twice), dried ($MgSO_4$), and concentrated give 831 mg (71%) of **1**-OPNB: mp 90.0—91.0 °C; IR (KBr) 1710 (C=O), 1515, 1340, 1285, 1260, 1100, and 715 cm^{-1}; NMR ($CDCl_3$) δ 8.28 (s, 4H, aromatic), 6.18 and 6.05 (2d, 2H, vinyl, J=3.0, 7.4 Hz), 5.22 and 5.07 (2d,1H, J=2.0, 9.4 Hz), 3.31 and 3.16 (2d, 1H, J=4.0, 9.4 Hz), 3.04—2.54 (m, 3H), 1.94—1.74 (m, 2H). Found: C, 67.58; H, 4.74%. Calcd for $C_{16}H_{13}O_4N$: C, 67.84; H, 4.63%.

endo-*Bicyclo*[*4.2.0*]*oct-7-en-2-yl* p-*Nitrobenzoate(4-OPNB).* To a solution of *endo*-bicyclo[4.2.0]oct-7-en-2-one[6] (1.23 g, 10 mmol) in 15 ml of methanol was added sodium borohydride (266 mg, 7 mmol) at 0 °C. The resulting solution was stirred at room temperature for 15 h. After the addition of the saturated sodium chloride solution, ether extraction gave 1.17 g (94%) of the crude alcohol as a colorless liquid. This alcohol was purified by chromatography on a silica gel column to yield the *endo*-alcohol (61%): IR (neat) 3350 (OH), 3040, 2920, 2870, 1445, 1325, 1040, 785, and 725 cm^{-1}; NMR (CCl_4) δ 6.22 (s, 2H, vinyl), 3.97 (m, 1H), 2.87—3.25 (m, 2H), 2.56 (s, OH), 1.62 (bs, 6H). The *endo* alcohol (410 mg, 3.3 mmol) was converted to its corresponding *p*-nitrobenzoate (**4**-OPNB) as described above for **1**-OPNB to yield 512 mg (57%): mp 52.0—54.0 °C; IR (KBr) 1725 (C=O), 1525, 1355, 1280, 1120, 1110, and 730 cm^{-1}; NMR (CCl_4) δ 8.29 (s, 4H, aromatic), 6.43—6.17 (m, 2H, vinyl), 5.45 (br d, 1H, J=4.6 Hz), 3.56—3.07 (m, 2H), 2.17—1.57 (m, 6H). Found: C, 65.63; H, 5.52%. Calcd for $C_{15}H_{15}O_4N$: C, 65.92; H, 5.53%.

Kinetic Measurements. The *p*-nitrobenzoates were hydrolyzed in aqueous acetone, and the rates were measured as previously described.[7b] The kinetic data are shown in Table 2.

Solvolysis Product Study. *p*-Nitrobenzoate (**1**-OPNB) (300 mg, 1.06 mmol) in 150 ml of 50% aqueous acetone containing 267 mg of sodium hydrogencarbonate was divided and sealed into nine test tubes under nitrogen and the tubes were heated for 30 h at 100 °C. After cooling, the contents were evaporated for removal of acetone and added saturated sodium chloride solution. The resulting slurry was extracted with three portions of chloroform (40 ml). The combined extracts were washed with saturated sodium chloride solution, dried ($MgSO_4$), and evaporated. The product was purified by chromatography on a silica gel column eluting with 30% ether in hexane to give 58 mg (41%) of **9** as white crystals (mp 87.5—88.5 °C). The low isolated yield were attributed to sublimation during drying and an unidentified hydrocarbon which had a very short retention time in GLC. **9**: IR (KBr) 3280 (OH, br), 2975, 2950, 1286, 1225, 1065, 1055, 782, and 740 cm^{-1}; NMR (CCl_4) δ 5.76 (s, 4H, vinyl), 3.98 (br s, 1H), 3.21 (d, 2H, J=4.0 Hz), 2.55—2.30 (m, 2H), 1.99 (br s, 1H, OH).

The NMR spectrum of **9** from hydrolysis of the deuterium labeled **1**-OPNB (C_6-*d*) showed that the proton intensity at δ 2.55—2.30 (2H) was reduced to 1H indicating the deuterium staying on C_1 (or C_6).

Stability of 1-OH under the Solvolysis Conditions. Alcohol (**1**-OH) (44 mg) in 16 ml of 50% aqueous acetone containing 82.7 mg of sodium hydrogencarbonate was sealed in a test tube under nitrogen and the tube was heated at 100 °C for 30 h. After work up, the crude product was examined by GLC and TLC analyses to indicate no existance of **9** and **1**-OH.

References

1) Previous paper in this series: K. Yano and K. Yoshida, *J. Org. Chem.*, **42**, 363 (1977).

2) a) K. B. Wiberg, B. A. Hess, Jr., and A. J. Ashe, III, "Carbonium Ions," ed by G. A. Olah and P. V. R. Schleyer, Wiley-Interscience, New York, N. Y. (1972), Vol. III, pp. 1295—1345; b) H. G. Richey, Jr., *ibid.*, pp. 1201—1294; c) E. C. Friedrich and M. A. Saleh, *J. Am. Chem. Soc.*, **95**, 2617 (1973); d) R. D. Bach, J. H. Siefert, M. T. Tribble, R. A. Greengard, and N. A. LeBel, *ibid.*, **95**, 8182 (1973); e) D. F. Eaton and T. G. Traylor, *ibid.*, **96**, 1226 (1974); f) L. A. Paquette, O. Cox, M. Oku, and R. P. Henzel, *ibid.*, **96**, 4892 (1974); g) H. C. Brown, *Tetrahedron*, **32**, 179 (1976); h) K. Ohkata, *Bull. Chem. Soc. Jpn.*, **49**, 235 (1976); i) H. Yamaoka, K. Ohkata, and T. Hanafusa, *ibid.*, **49**, 245 (1976); j) H. C. Brown, E. N. Peters, and M. Ravindranathan, *J. Am. Chem. Soc.*, **99**, 505 (1977).

3) a) S. Masamune, K. Fukumoto, Y. Yasunari, and D.

Darwish, *Tetrahedron Lett.*, **1966**, 193; b) R. Breslow, H. Bozimo, and P. Wolf, *ibid.*, **1970**, 2395; c) Y. Sugihara, N. Morokoshi, and I. Murata, *ibid.*, **1977**, 3887; d) M. C. Böhm and R. Gleiter, *ibid.*, **1978**, 1179; e) H. Volz, J. Shin, H. Prinzbach, H. Babsch, and M. Christl, *ibid.*, **1978**, 1247; f) A. Greenberg, *ibid.*, **1978**, 3509; g) H. Irngartinger and K. L. Lukas, *Angew. Chem. Int. Ed. Engl.*, **18**, 694 (1979).

4) Following IUPAC nomenclature, the name of tetracyclo-[5.2.0.$0^{2,4}$.$0^{3,5}$]non-8-en-6-yl *p*-nitrobenzoate seemed to be more suitable than the previous one, tetracyclo[6.1.0.$0^{2,9}$.$0^{4,7}$]-non-5-en-3-yl(K. Yano, *Tetrahedron Lett.*, **1974**, 1861). Thus, we used this new name.

5) L. Birladeanu, T. Hanafusa, B. Johnson, and S. Winstein, *J. Am. Chem. Soc.*, **88**, 2316 (1966).

6) B. A. Hess, Jr., *J. Am. Chem. Soc.*, **93**, 1000 (1971).

7) a) R. M. Coates and K. Yano, *J. Am. Chem. Soc.*, **95**, 2203 (1973); b) K. Yano, *J. Org. Chem.*, **40**, 414 (1975); c) B. J. A. Cooke and P. R. Story, *ibid.*, **40**, 2656 (1975); d) K. Yano, *ibid.*, **42**, 1728 (1977); e) K. Yano, M. Isobe, and K. Yoshida, *J. Am. Chem. Soc.*, **100**, 6166 (1978).

8) J. K. M. Sanders and D. H. Willams, *Chem. Commun.*, **1970**, 422.

9) H. C. Brown and J. Muzzio, *J. Am. Chem. Soc.*, **88**, 2811 (1966).

10) M. Karplus, *J. Chem. Phys.*, **30**, 11 (1959).

11) Using a factor of 1/500 for converting a rate of the cyclohexyl tosylate in acetic acid at 25 °C ($k=4.88\times10^{-8}$ s^{-1})[18] to that of 3,5-dinitrobenzoate in 60% aqueous acetone at 100 °C (J. E. Baldwin and W. D. Foglesong, *J. Am. Chem. Soc.*, **89**, 6372 (1967); **90**, 4303, 4311 (1968)), a rate of the 3,5-dinitrobenzoate was converted to that of the *p*-nitrobenzoate by a factor of 0.09 under the allowance of the next assumption, $(k_{OPNB}/k_{ODNB})_{60\%} = (k_{OPNB}/k_{ODNB})_{80\%} = 0.09$,[2f] and k_{OPNB}(60% aqueous acetone) was converted to a rate in 50% aqueous acetone by a factor of 2.2 for the solvent change.[1] Thus, a value for the rate of cyclohexyl *p*-nitrobenzoate in 50% aqueous acetone at 100 °C was roughly estimated to be 1.93×10^{-11} s^{-1}.

12) P. v. R. Schleyer and G. W. Van Dine, *J. Am. Chem. Soc.*, **88**, 2321 (1966).

13) H. J. Reich and J. M. Renga, *Tetrahedron Lett.*, **1974**, 2747.

14) P. v. R. Schleyer, *J. Am. Chem. Soc.*, **86**, 1854 (1964).

15) M. Avram, I. G. Dinulescu, E. Marica, G. Mateescu, E. Sliam, and C. D. Nenitzescu, *Chem. Ber.*, **97**, 382 (1964).

16) M. Sakai, A. Diaz, and S. Winstein, *J. Am. Chem. Soc.*, **92**, 4452 (1970).

17) W. G. Woods, R. A. Carboni, and J. D. Roberts, *J. Am. Chem. Soc.*, **78**, 5653 (1956).

18) S. Winstein, B. K. Morse, E. Grunwald, H. W. Jones, J. Corse, D. Trifan, and H. Marshall, *J. Am. Chem. Soc.*, **74**, 1127 (1952).

Low-temperature Photolysis of *ortho*-Substituted Azidobiphenyls. Formation of Phenazines from 2,2′-Diazidobiphenyls[1]

Akira YABE

National Chemical Laboratory for Industry, 1-1 Yatabe-Higashi, Tsukuba, Ibaraki 305

(Received January 30, 1980)

It was found that the unexpected phenazines were formed as minor products by the low-temperature photolysis of 2,2′-diazidobiphenyls in a rigid matrix. The phenazine formation results from the 1,1′-C–C bond fission of the biphenyl nucleus and suggests the aziridine intermediates. The low-temperature photolysis of 2-azido-2′-methylbiphenyl and 2-azido-2′,4′,6′-trimethylbiphenyl leads to the triplet-derived phenanthridine derivatives as major products.

It has been reported that 2-azido-2′,4′,6′-trimethylbiphenyl (**1**) gives the phenanthridine **2** (48%), as well as the carbazole **3** (5%) and the hydrogen abstraction product **4** (29%), on thermolysis.[2] When, on the other

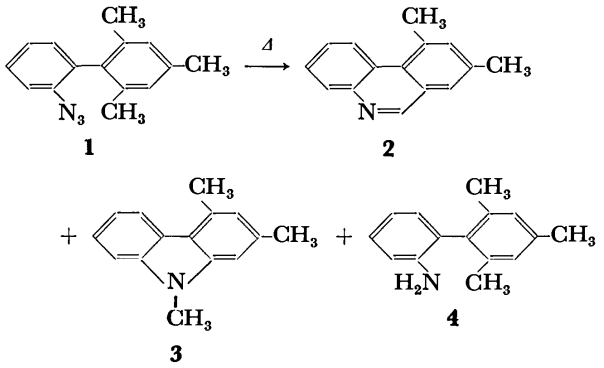

hand, the related 2,2′-diazido-6,6′-dimethylbiphenyl (**5**) was heated alone or in a number of solvents, tar rather than expected 4,9-diazapyrene (**6**) or *N*,*N*′-dimethylpyrrolo[2,3,4,5-*def*]carbazole (**7**) was obtained.[3] However, it was found, in the course of work on the low-temperature photochemistry of 2,2′-diazidobiphenyl,[4] that the photolysis of **5** in EPA at 77 K gave 1,10-dimethylbenzo[*c*]cinnoline (**8**) in a 60% yield. The

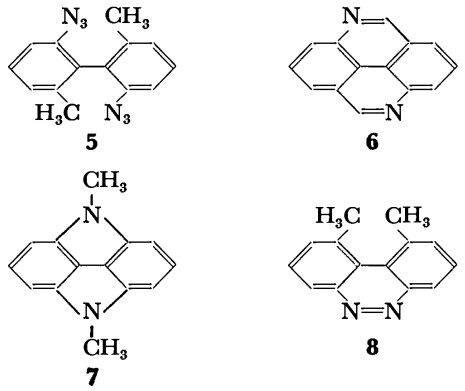

present author has now reinvestigated the possibility of forming the compound **6** or **7** as a minor product. The present paper reports that the unexpected 1,6-dimethylphenazine instead of the expected **6** and **7** was formed, together with the major product, **8**, by the low-temperature photolysis of **5** in glassy matrices. The phenazine formation involving the unusual 1,1′-C–C bond fission of the biphenyl nucleus will be discussed in terms of the interesting intermediate aziridine in nitrene chemistry. Moreover, the low-temperature photolysis of 2-azido-2′,4′,6′-trimethylbiphenyl will briefly be reported.

Results and Discussion

The previous paper reported that 2,2′-diazidobiphenyl afforded benzo[*c*]cinnoline (98%) almost quantitatively upon irradiation in glassy matrices at 77 K, and that, in the case of **5**, the yield of **8** was decreased to 60% by the steric effects.[4] The 3.18×10^{-4} mol dm^{-3} EPA (5: 5: 2) solution of **5** was irradiated at 77 K with a low-pressure mercury lamp. The residue remaining after the removal of solvents from the irradiated solution was examined by thin-layer chromatography. Initial TLC (silica gel) results using ether–hexane eluants indicated the unchanged starting material, **5**, as the first elute, and **8** as the second elute, plus a chromatographically nonmobile material, as described in the previous paper. However, the TLC results using the eluent benzene indicated a new fraction as the second elute, and bright yellow crystals were isolated in an 8% yield. It was identified as 1,6-dimethylphenazine (**9**) on the basis of the microanalysis and spectral properties. The chromatographically nonmobile material is, from the intermediate, presumed to be a polymeric product, because the existence of another remaining azido group was ascertained from the IR absorption spectrum (2120 cm^{-1}).

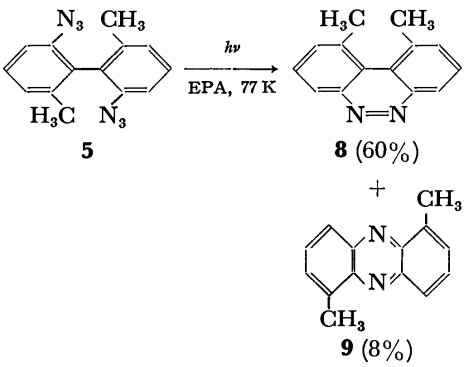

Similarly, the irradiation of 2,2′-diazidobiphenyl (**10**) in EPA at 77 K and the separation by TLC were reexamined in order to confirm that the phenazine formation was a general reaction of 2,2′-diazidobiphenyls. The parent phenazine (**12**) was detected in the second fraction, along with the major product, benzo-

[*c*]cinnoline (**11**), in the third fraction. The yield, which was determined by absorption spectroscopy, consisted of trace amounts (less than 1%).

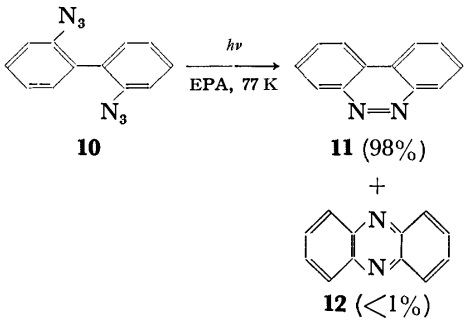

10 **11** (98%) + **12** (<1%)

The photochemical reaction with the increase in the irradiation time was followed by absorption spectroscopy. From the spectra shown in Fig. 1, it becomes apparent that 1,6-dimethylphenazine (**9**) is formed not by the thermal reaction of some photoproducts from **5**, but by the irradiation of **5** in a rigid matrix. The absorption maximum at 308 nm that is observed in the early stages is a transient absorption which disappears on warming to room temperature. It is tentatively identified as the nitrene, **13**, based on its similarity to other nitrenobiphenyls.[5] With the increase in the irradiation time the absorption maximum of the transient is obscured by the appearance of the absorption in the 320—330 nm range; this shows the formation of the major photoproduct, **8**. In addition, a small absorption at 362 nm is also observed on the tail of the large absorption of **8**. That is, the absorption (λ_{max} 362 nm) which is attributed to phenazine appears, together with that of **8**, as a secondary product from the nitrene, **13**.

The irradiations of **5** in different solvents, at different temperatures, and more different light intensities were carried out in order to find the factors governing the phenazine formation. The results in Table 1 seem to show that the nature of the solvent plays no substantial role. The difference in the room-temperature *vs.* low-temperature photolysis is represented by the rigidity of the reaction medium together with the reaction

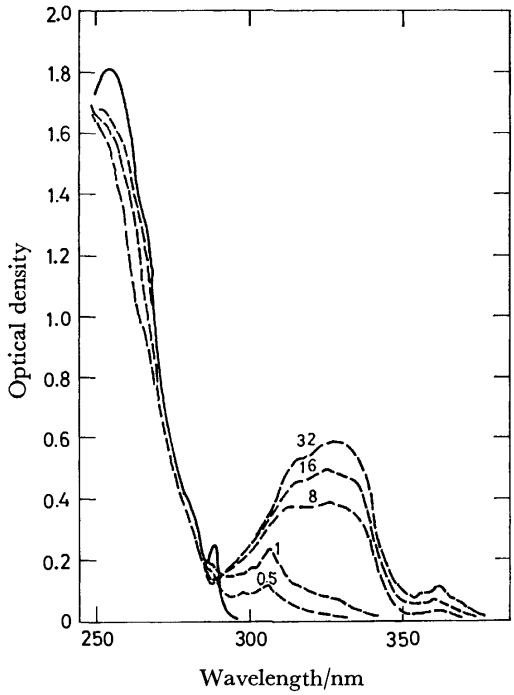

Fig. 1. Absorption spectra of 2,2′-diazido-6,6′-dimethylbiphenyl prior to (——) and after (——) photolysis in EPA at 77 K. Numbers refer to irradiation time in minute.

temperature. In a series of photolyses in IP-3MP matrices whose viscosities are varied in the range of five orders, the ratios of the yields of **8** and **9** are very similar, within the range of experimental error. However, the formations of both **8** and **9** are subject to suppression in more viscous media. The rise in the temperature, although the reaction medium is still highly rigid, changed the photolytic reaction, which could not be characterized. The formation of **8** and **9** was no longer detectable. In conclusion, the reaction is found to be highly sensitive to the reaction temperature rather than the rigidity. Table 2 shows the dependency of the product yields on the light intensity in the photolysis at 77 K in EPA. It is of interest that the yield of

TABLE 1. IRRADIATIONS OF 2,2′-DIAZIDO-6,6′-DIMETHYLBIPHENYL (**5**) AT LOW TEMPERATURES IN RIGID MATRICES

Run	Solvent[a] (Composition in parts by volume)	T/K	Viscosity[b] / Pa s	Yield/% Cinnoline **8**	Yield/% Phenazine **9**
1	EPA (5:5:2)	77	(8×10^7)	60	8
2	MCH, IP (1:3)	77	(1×10^7)	60	8
3	IP, 3MP (97:3)	77	8.9×10^4	60	7.5
4	IP, 3MP (3:2)	77	1.8×10^7	56	7.5
5	IP, 3MP (3:7)	77	1.4×10^9	55	7
6	IP, 3MP (1:9)	77	2.4×10^{10}	50	6.5
7	EtOH, MeOH (1:1)	77	($>1\times10^{13}$)	55	7
8	3MP	93.5	7.7×10^4	—	—[c]
9	EtOH, MeOH (1:1)	115	2×10^{11}	—	—[c]
10	Glycerol, MeOH (10:1)	201	1×10^{12}	—	—[c]

a) EPA (diethyl ether, isopentane, ethanol), MCH (methylcyclohexane), IP (isopentane), 3MP (3-methylpentane). b) Cited from Ref. 6. The values in parentheses are estimated from the figures cited in the literature. c) Not detectable, or negligible even if formed.

Table 2. Dependence of product distributions on the light intensity
(Irradiations of **5** at 77 K in EPA)

Run	Light[a)]	Yield/% Cinnoline **8** : Phenazine **9**
1	L-P(100%)	60 : 8
2	L-P(50%)	62 : 3
3	L-P(12.5%)	58 : *ca.* 1
4	L-P(100%) H-P	55 : 14

a) L-P (a 15 W low-pressure mercury lamp); H-P (a 500-W high-pressure mercury lamp through a UV-31 filter). The light intensity of the low-pressure mercury lamp was regulated with slits (transmittances of 50 and 12.5%).

phenazine **9** rises to 14% when the sample is simultaneously irradiated with strong long-wavelength light (λ>310 nm) in addition to the usual source of 254 nm light.

The phenazine formation by the decomposition of 2,2′-diazidobiphenyls is quite unexpected and unusual, involving the 1,1′-C–C bond fission of the biphenyl structure. A plausible mechanism to account for the phenazine formation is depicted in Scheme 1.

As the intermediate, **13**, is stable indefinitely at 77 K in rigid medium, the **13**→**14** conversion is a photochemical process. It is well-known that the ground states of arylnitrenes are triplet.[7)] Although **13** is once

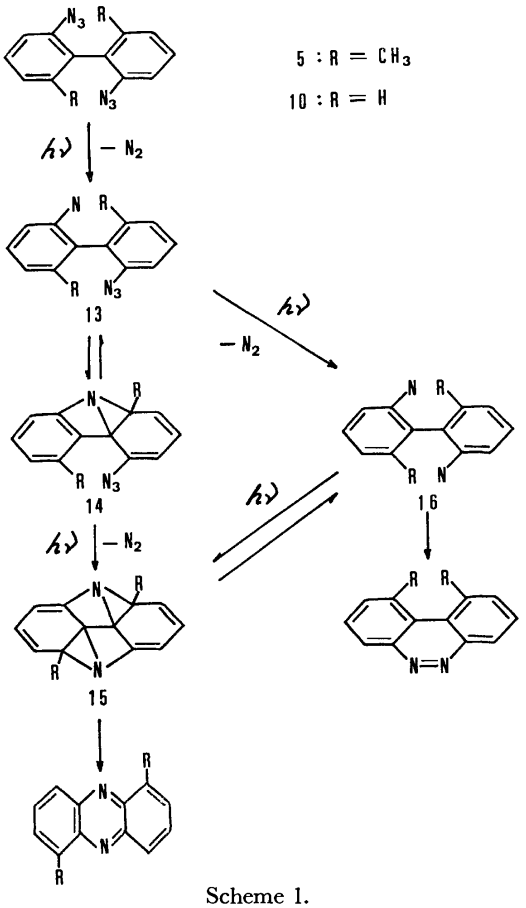

Scheme 1.

populated from the ground state to the excited triplet state (T*) by light absorption, the excited singlet state may also be efficiently populated *via* T*. Therefore, the multiplicity of the nitrene leading to the aziridine intermediate can not be concluded easily without the direct observation of the excited state. In rigid matrices at 77 K the **13**→**14** process must be less effective, much like the carbazole formation from 2-nitrenobiphenyl,[5)] than the process to benzo[*c*]cinnoline *via* **16**. The dependence on the light intensity obtained from Table 2 is revealed in the two competitive processes: the **13**→**14** conversion and the decomposition of the second azido group. The strong long-wavelength light appreciably facilitates the less effective process, **13**→**14**. Moreover, the light-intensity dependency may mean that the **16**→**15** conversion occurs by light absorption, while the reverse conversions, **14**→**13** and **15**→**16**, occur spontaneously as nonphotonic processes. In the competitive processes from **13**, the steric effects by the 6,6′-dimethyl substitution, which suppresses the coupling of nitrenes to lead to the cinnoline, contribute to the difference in the yields between **8** and **12**. As the **14** structure is highly strained, the 1,1′-C–C bond must be bent. Therefore, the **14**→**15** process may be relatively facile compared with the **13**→**14** process, although the **15** structure must be much more strained than **14**. Once the intermediate, **15**, is formed, the phenazine formation will follow to stabilize it by aromatization. The finding that **8** and **9** are formed only at a restricted low temperature is ascribable to facile side reactions from the reactive intermediates, **13**—**16**, although the details of the mechanism remain unknown.

The mechanism of the phenazine formation contains two aziridine intermediates, **14** and **15**. The structure of **14** is similar to that (**17**) proposed in the carbazole formation from 2-azidobiphenyl.[8b)] However, Sundberg and his co-workers[8)] proposed another aziridine, **18**, rather than **17**, as a result of their estimation that **17**

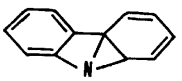

17

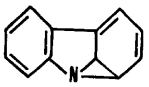

18

is about 10 kcal/mol less stable than **18**. The aziridine intermediate **17** has not been well-confirmed in the carbazole formation from azidobiphenyls. The phenazine formation, however, results from the attack of the nitrene on 1′-C and the 1,1′-C–C bond fission of the biphenyl nucleus; consequently, the **14** and **15** structures may be suggested as appropriate intermediates. These intermediates are of great interest in nitrene chemistry, although the direct evidence for them and further mechanistic aspects remain to be elucidated.

In the low-temperature photolysis of *ortho*-substituted azidobiphenyls, there has been considerable interest in the possibility of intramolecular arylnitrene insertion into a suitably located methyl group. The intramolecular reaction between the arylnitrene and the methyl group could not occur in the case of **5**, so that neither 4,9-diazapyrene nor phenanthridine derivatives were

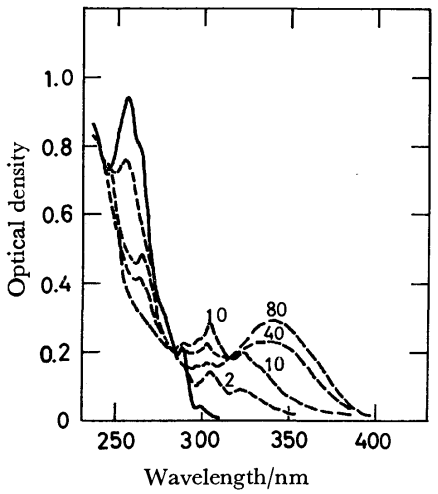

Fig. 2. Absorption spectra of 2-azido-2′-methylbiphenyl prior to (——) and after (----) photolysis in EPA at 77 K. Numbers refer to irradiation time in minute.

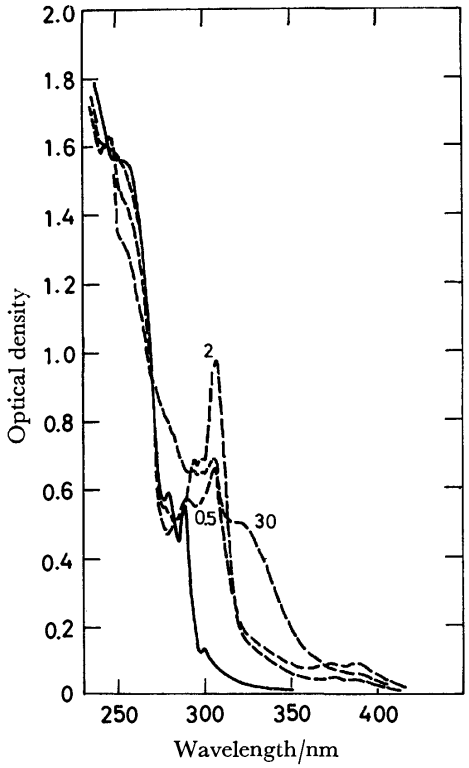

Fig. 3. Absorption spectra of 2-azdio-2′,4′,6′-trimethylbiphenyl prior to (——) and after (----) photolysis in EPA at 77 K. Numbers refer to irradiation time in minute.

detected. In this connection, the low-temperature photolysis of 2-azido-2′-methylbiphenyl (**19**) and 2-azido-2′,4′,6′-trimethylbiphenyl (**20**) was briefly studied. Figures 2 and 3 show the spectral changes in **19** and **20** respectively in EPA at 77 K with the increase in the irradiation time. In both cases, the formation of intermediate nitrenes with transient absorptions is observed in the early stages; they become photoproducts with absorption at the longer wavelengths after long irradiation times. By separate experiments with a preparative scale, the photoproducts were isolated as follows.

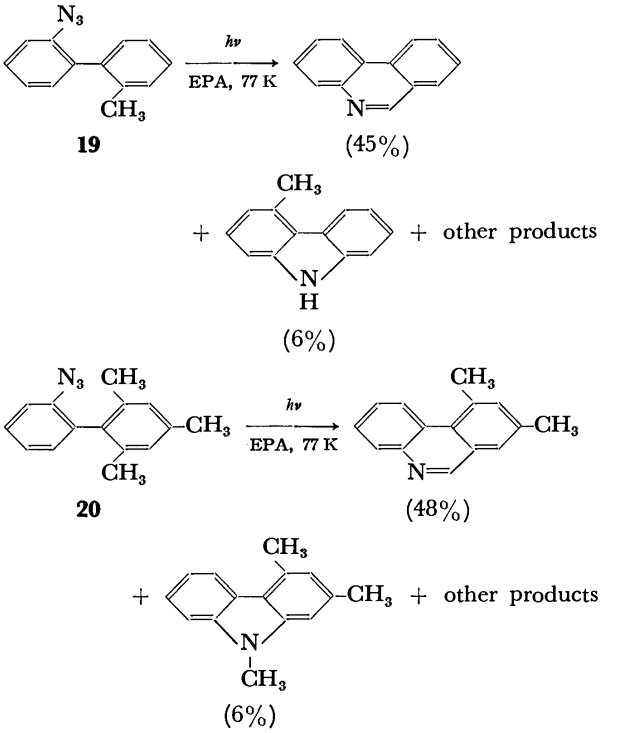

It should be noted that these products contain thermally reacted products in addition to the photoproducts formed in a rigid matrix, because an appreciable amount of the intermediate nirenes remains when the irradiation is stopped. Although the details of these photolyses can not be discussed in this report, it has become apparent that the phenanthridine formation occurs with a higher selectivity than the thermolysis[2,3] or triplet-sensitized photolyses at room or high temperatures.[9] Consequently, the intramolecular arylnitrene insertion into a methyl group occurs effectively in these compounds in a rigid matrix at a low temperature. It is of interest, therefore, that, in the case of **5**, the phenazine formation occurs instead of the insertion into methyl groups.

Experimental

Measurements. The IR and UV spectra were recorded on Hitachi Model 260—30 and Shimadzu Model UV-300 spectrophotometers respectively. The ^{1}H-NMR and ^{13}C-NMR spectra were recorded on Varian Model XL-100-12 (100 MHz) and JEOL Model FX-100 (25 MHZ) spectrometers, respectively, using TMS as the internal standard. The mass spectrum was recorded on a Hitachi Model RMU-6M spectrometer. The microanalysis was performed at the Institute of Physical and Chemical Research.

Materials. 2,2′-Diazido-6,6′-dimethylbiphenyl (**5**),[3] 2-azido-2′-methylbiphenyl (**19**),[3] and 2-azido-2′,4′,6′-trimethylbiphenyl (**20**)[2] were prepared according to the literature. The crude materials were purified by column chromatography on silica gel.

Irradiation of Azides. Low-temperature irradiations on a preparative scale were carried out in a doughnut-shaped quartz vessel (volume: about 160 ml; thickness: 7 mm) which was immersed in liquid nitrogen with a 30-W low-pressure

mercury lamp (Riko UVL-30LA) protected with a transparent quartz Dewar vessel. Irradiations at 77 K for spectroscopy were carried out with a cell (path length: 10 mm) which had been immersed in liquid nitrogen in a quartz Dewar vessel equipped with optical windows on opposite sides. An Oxford Instruments DN-704 liquid nitrogen cryostat was used for the spectroscopic measurements by the irradiation at low-temperatures over 77 K.

Products Analysis. The separation and the yield determination of the photoproducts were carried out with a preparative thin-layer chromatograph (Merck Silicagel 60 F_{254}), and were followed by UV analysis. The identification of the known compounds were confirmed by comparison with authentic samples. *1,6-Dimethylphenazine (9)* was determined on the basis of the following microanalysis and spectral properties.[10] Found: C, 79.23; H, 5.85; N, 12.74%. Calcd for $C_{14}H_{12}N_2$: C, 80.74; H, 5.81; N, 13.45%. MS, *m/e* 208 (M^+). IR (KBr) 2955, 2880, 1730, 1624, 1538, 1480, 1450, 1375, 1348 cm^{-1}. UV (MeOH) 362 (ε 11700), 254 nm (108000). ^{1}H-NMR ($CDCl_3$) δ 2.93 (s, 6H), 7.6—7.8 (m, 4H), 8.0—8.2 (m, 2H) ppm. ^{13}C-NMR ($CDCl_3$) δ 17.6 (q), 128.0 (d), 129.2 (d), 129.7 (d), 137.7 (s), 142.8 (s), 142.9 (s) ppm.

The author wishes to thank Dr. Ikuo Sakai (Toray Research Center) for his measurements and assignment of the NMR spectra.

References

1) Photolysis of Organic Azides. V. Part IV: A. Yabe, *Bull. Chem. Soc. Jpn.*, **52**, 789 (1979).
2) G. Smolinsky, *J. Am. Chem. Soc.*, **82**, 4717 (1960).
3) B. Coffin and R. F. Robbins, *J. Chem. Soc.*, **1965**, 1252.
4) a) A. Yabe and K. Honda, *Tetrahedron Lett.*, **1975**, 1079; b) A. Yabe and K. Honda, *Bull. Chem. Soc. Jpn.*, **49**, 2495 (1976).
5) a) A. Reiser, H. Wagner, and G. Bowes, *Tetrahedron Lett.*, **1966**, 2635; b) A. Reiser, G. Bowes, and R. J. Horne, *Trans. Faraday Soc.*, **62**, 3162 (1966).
6) a) J. R. Lombardi, J. Raymonda, and A. C. Albrecht. *J. Chem. Phys.*, **40**, 1148 (1964); b) H. Greenspan and E. Fischer, *J. Phys. Chem.*, **69**, 2466 (1965); c) W. G. Herkstroeter, "Creation and Detection of the Excited State," ed by A. A. Lamola, Marcel Dekker, New York, N. Y. (1971), p. 43.
7) G. Smolinsky, E. Wasserman, and W. A. Yager, *J. Am. Chem. Soc.*, **84**, 3220 (1962).
8) a) R. J. Sundberg, D. W. Gillespie, and B. A. DeGraff, *J. Am. Chem. Soc.*, **97**, 6193 (1975); b) D. Gillespie, Ph. D. Thesis, University of Virginia, U. S. A. (1974).
9) J. M. Lindley, I. M. McRobbie, O. Meth-Cohn, and H. Suschitzky, *Tetrahedron Lett.*, **1976**, 4513.
10) a) Y. Kindani and H. Otomasu, *Hoshi Yakka Daigaku Kiyo*, **6**, 39 (1957); *Chem. Abstr.*, **52**, 1181d (1958); b) E. Breitmaier and U. Hollstein, *J. Org. Chem.*, **41**, 2104 (1976).

Photoreactions of Flavanones

Ryoka MATSUSHIMA,* Tsuneo KISHIMOTO, Morio SUZUKI, Motonobu MORIOKA, and Hideo MIZUNO

Department of Industrial Chemistry, Faculty of Engineering, Shizuoka University, Hamamatsu 432

(Received February 27, 1980)

Parent and substituted flavanones undergo photochemical opening of the pyrone ring to give corresponding 2'-hydroxychalcones in benzene, pyridine, acetonitrile *etc.*, the yields varying from 0 to 70% with substituents. The reaction is depressed by the addition of 1,3-pentadiene, nitrosobenzene, or acrylonitrile. On the other hand, flavanone and 4-chromanone undergo photoreduction in 2-propanol to give reductive coupling products and solvent adducts as isomeric mixtures. 7,8-Benzoflavanone does not undergo photoreduction in 2-propanol but the ring opening reaction instead. Mechanisms have been discussed in terms of the relative contribution of n,π^* and π,π^* character in the lowest triplet states.

Flavanones have been shown to undergo photochemical ring opening reaction to give 2'-hydroxychalcones in inert solvents such as benzene[1-4] and photoreduction to give reductive coupling products in hydrogen-donating solvents.[2,3] Both biradical[1,2] and concerted[3] mechanisms have been suggested for the photochemical ring opening reaction, though not proved.

On the other hand, photoisomerization of substituted 3-chromanones have extensively been studied and the mechanism has been shown to involve prior photochemical enolization.[5] In this view, interesting mechanisms involving enolization followed by 6π-electrocyclic reactions have been postulated for the photochemical ring opening reaction of flavanones[3] and for the photochemical cyclization of 2'-hydroxychalcones to flavanones.[6]

The present work reports on the photochemistry of parent and substituted flavanones, with discussion on the mechanisms in terms of n,π^* and π,π^* character in the lowest triplet states.

Results

Photochemical Ring Opening Reaction. Dilute solutions of parent or substituted flavanones in benzene

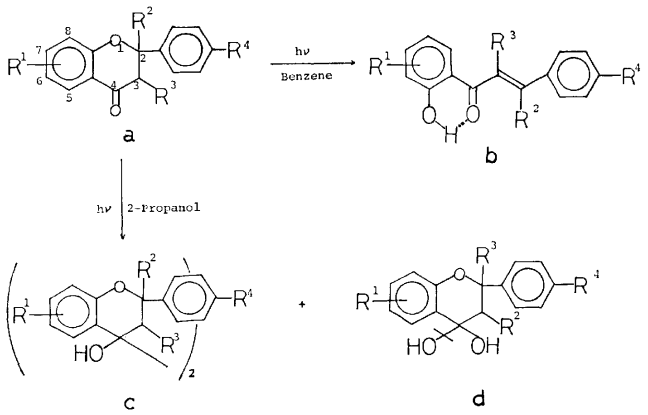

Scheme 1.

underwent photochemical ring opening reaction to give corresponding 2'-hydroxychalcones, on irradiation under a nitrogen atmosphere at room temperature with a high pressure mercury lamp (Scheme 1). The products proved identical with independently prepared authentic samples of 2'-hydroxychalcones. Irradiation of **5a**, **7a**, **8a**, **11a**, **12a**, and 4-chromanone **14a** resulted in the recovery of the starting materials: their NMR spectra remained unchanged. The yields for the reaction depended on the substituents (Table 1). Thus, electron-

Table 1. Substituent effects on the photochemical ring opening of flavanones in benzene[a]

Flavanone	Substituent				2'-Hydroxychalcone	Yield[b] %
	R^1	R^2	R^3	R^4		
1a	H	H	H	H	**1b**	14
2a	H	H	H	OMe	**2b**	40
3a	H	H	H	OCOMe	**3b**	70
4a	6-OMe	H	H	H	**4b**	15
5a	6-OCOMe	H	H	H	**5b**	0
6a	7-OMe	H	H	H	**6b**	11
7a	5-OH, 7-OMe	H	H	H	**7b**	0
8a	5,6-Benzo	H	H	H	**8b**	0
9a	7,8-Benzo	H	H	H	**9b**	5
10a	7-OMe	Me	H	H	**10b**	13
11a	7-OMe	H	*cis*-Me	H	**11b**	0
12a	7-OMe	H	*trans*-Me	H	**12b**	0
13a	7-Cl	H	H	H	**13b**	2

a) Each flavanone solution (8.8×10^{-3} mol/dm^3) was irradiated under a nitrogen atmosphere for 16.5 h at room temperature with a 100-W high pressure mercury lamp. b) Estimated from the NMR signal intensities of the phenolic protons at δ 12—15 ppm.

withdrawing groups in R^1 seem to depress the reaction (**5a**, **13a**), while electron donating groups do not (**4a**, **6a**, **10a**).

Substitution of methyl group at the C_3-position retards the reaction (**11a**, **12a**), whereas methyl substitution at the C_2-position permits the reaction (**10a**). The photochemical intertness of **11a**, **12a**, and **7a** is ascribable to a reversible intramolecular hydrogen transfer *via* a five-membered (**11a**, **12a**) or six-membered (**7a**) cyclic configuration. The low or nil reactivity of **8a** and **9a** may, at least partly, be relevant to their low-lying or less reactive π,π^* triplet states.

Table 2. Photochemical ring opening of **2a** in different solvents[a)]

Solvent	Yield of **2b**/%
Carbon tetrachloride	31
Benzene	69
Benzene (air)[b)]	49
Pyridine	66
Acetonitrile	48

a) Irradiated in ampule with a 400 W high pressure mercury lamp for 3 h at 15 °C; [**2a**] = 10^{-3} mol/dm^3. b) Without deoxygenation.

Table 2 lists the solvent effects on the photochemical ring opening reaction of **2a**. No simple correlation with solvent polarity or basicity is found. Dissolved oxygen seems to depress the reaction to some extent.

Addition of 1,3-pentadiene (1.5×10^{-3} mol/dm^3) to a benzene solution of **2a** (10^{-3} mol/dm^3) resulted in significant depression of the photoreaction (Table 3). Both acrylonitrile and nitrosobenzene, which are known to inhibit a free radical reaction, significantly depress the photoreaction.

Table 3. Effects of additives on the photochemical ring opening of **2a**

Additive	Concn of additive / 10^{-3} mol dm^{-3}	Yield of **2b** / %
1,3-Pentadiene	0.0	64[a)]
	1.5	35[a)]
Acrylonitrile	0.0	40[b)]
	4.5	5[b)]
Nitrosobenzene	0.0	46[c)]
	6.4	5[c)]

a) Benzene solution of **2a** (10^{-3} mol/dm^3) was irradiated in ampule with a 400-W high pressure mercury lamp for 70 min. b) A 50 ml benzene solution of **2a** (3×10^{-4} mol/dm^3) was irradiated with a 100-W high pressure mercury lamp for 16 h. c) A 6 ml benzene solution of **2a** (10^{-3} mol/dm^3) was irradiated in ampule with a 400-W high pressure mercury lamp for 40 min.

Photolysis of Flavanones and 4-Chromanone in 2-Propanol. A deoxygenated solution of flavanone **1a** (4.5×10^{-3} mol/dm^3) in 2-propanol gave reductive coupling product **1c** (as isomeric mixture) and solvent adduct **1d** (as 1 : 1 isomeric mixture) besides unidentified products, on irradiation with a 100 W high pressure mercury lamp at room temperature (Scheme 1 and Table 4).

Table 4. Photolyses of flavanones and 4-chromanone in 2-propanol

Starting material	Concentration / 10^{-3} mol/dm^3	Irrad. time / h	Products	ϕ_{dis}[a)]
1a	4.5	5	**1c**(39%)[b)] **1d**(8%)[c)] Unknown (20%)	0.43
7a	7.4	5	None[d)]	0.00
8a	10	12	None[d)]	0.00
9a	9.4	16	**9b** (33%)	0.02
14a	4.8	5.5	**14c** (89%)[e)]	0.24

a) Quantum yield for the disappearance of each starting material during 10 min irradiation. b) Sum of the meso and the racemic mixtures of 4,4′-biflavanol isomers. c) Sum of 1 : 1 *cis*- and *trans*-4-hydroxy-4-(1-methyl-1-hydroxyethyl)flavanes. d) The NMR spectra remained unchanged and no TLC spot was detected other than that of the starting material. e) The sum of the meso (53%) and the racemic (36%) forms of 4,4′-bichromanol isomers.

Similar photolysis of 4-chromanone **14a** gave corresponding coupling product **14c** in a high yield. Photolysis of **6a**, **13a**, and 5,7-dimethylflavanone **15a** gave too complex mixtures to permit their analyses, while **7a** and **8a** did not react. The results are summarized in Table 4, together with the quantum yield for the disappearance of each starting material at an initial stage of the reaction. Interestingly, 7,8-benzoflavanone **9a** underwent ring opening reaction to give **9b** in 2-propanol, instead of the photoreductive coupling reaction. In addition, the yield for the ring opening reaction of **9a** is higher in 2-propanol than in benzene by a factor of 6.

Discussion

Owing to the rapid and efficient intersystem crossing, the singlet lifetimes of aromatic carbonyl compounds are usually too short ($\leqq10^{-8}$ s)[7] to permit bimolecular singlet quenching in low concentrations of donor and quencher. The significant quenching effect of 1,3-pentadiene (1.5 mmol/dm^3) supports for a triplet mechanism.[2] The depression effects of acrylonitrile and nitrosobenzene favors for radical processes,[1] in accord with the triplet mechanism.

The variation in the relative reactivities in Table 1 may simply be interpreted as due to the inductive and electromeric effects of substituents in some cases (**4a**—**6a**, **10a**, **13a**); such simple interpretation, however, does not hold for some others (**1a**—**3a**).

It seems more reasonable to interpret as due to the relative contribution (importance) of n,π^* and π,π^* character: the ring opening reaction takes place from π,π^* triplet states while reductive coupling reaction from n,π^* triplet states. Benzoflavanones **8a** and **9a**, for example, are expected to have a dominant π,π^* character in the lowest triplet states in any solvents, because of the extended π-conjugation in the molecules. Thus, the lack of the photoreduction of **8a** and **9a** in 2-propanol is ascribable to nil or insufficient contribution of n,π^* character in the lowest triplet states.

Instead, **9a** undergoes photochemical ring opening reaction in 2-propanol, reflecting a dominant contribution of π,π^* character.

The higher efficiency for the ring opening reaction of **9a** in 2-propanol than in benzene may be attributable at least partly, to the more stabilization and contribution of the π,π^* state.

All other flavanones in Table 1 are also assumed to have considerable π,π^* character in their lowest triplet states, since the lowest triplet states of methoxy-substituted acetophenones are mostly of π,π^* in nature.[8] Relative importance of n,π^* and π,π^* character depends on solvent and substituents. Thus, reductive coupling reaction, as a reflection of n,π^* character, dominates in a hydrogen-donating solvent such as 2-propanol. In benzene, the n,π^* character in the lowest triplet states would increase (the π,π^* would decrease) in favor of hydrogen atom abstraction. However, the C–H bond of benzene is much stronger (*e.g.*, by 22 kcal/mol or more in the gas phase) than the C_2–H bond of 2-propanol, and hydrogen atom abstraction from benzene is unfavorable even though the n,π^* character is somewhat increased. Thus, the alternative pathway which does not involve hydrogen atom abstraction, *i.e.*, the ring opening reaction, would become dominant in benzene even though the π,π^* character is somewhat decreased.

The lack of the photochemical ring opening reaction of **14a** is ascribable to the less stability of the intermediate species, *e.g.*, biradical **16** as compared with **17** having benzyl radical stability.

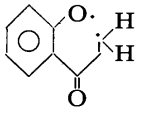

16

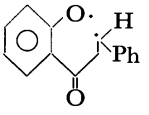

17

On the other hand, the high efficiency for the reductive coupling reaction of **14a** in 2-propanol is due partly to a small steric hindrance of the chromanone ketyl radicals compared to that of the flavanone ketyl radicals in bimolecular coupling processes, and partly to the essential n,π^* character in its lowest triplet state.

As an alternative to the unimolecular mechanism above discussed it might be thought that the photochemical ring opening reaction proceeds *via* bimolecular hydrogen atom abstraction. Hydrogen atoms at the C_3-position of ground state flavanones could be abstracted by n,π^* triplets of another flavanone molecules, followed by β-cleavage or hydrogen atom transfer of radical intermediates giving eventually 2′-hydroxychalcones. However, such mechanism seems less likely.

The recovery of each starting isomer **11a** or **12a** without *cis-trans* isomerization, or the lack of inversion at the C_3-center, suggests that hydrogen atom abstraction from the C_3-position is less important.

Bimolecular hydrogen atom abstraction from the C_2-position (the weakest C–H bond) might be thought to occur and affect the ring opening reaction. However, substitution of the hydrogen atom at the C_2-position by methyl group did not affect the efficiency (compare **10a** with **6a**), thus bimolecular C_2–H abstraction seems irrelevant to the ring opening reaction.

Experimental

Chemicals. Flavanones and 4-chromanone were prepared according to the reported methods as summarized in Table 5 together with the UV absorption maxima. Typical methods for the preparation of 2′-hydroxychalcones are shown in Table 6 together with their melting points and spectral data. Solvents and other chemicals were of guaranteed grade without further purification, except that acrylonitrile was purified just before use to eliminate polymerization inhibitors.[28]

TABLE 5. UV ABSORPTION MAXIMA OF FLAVANONES AND 4-CHROMANONE

Compound	Method of preparation[a]	Solvent[b]	λ_{max} nm	$\left(\frac{\varepsilon_{max}\times 0.01}{mol^{-1}dm^2}\right)$
1a	10, 11	E	320(3.53),	252(8.98)
2a	10, 12	E	320(33.2)	
3a	10, 13	E	310(1.09)	
4a	10, 14	E	352(3.53),	254(6.16)
5a	15	E	319(6.91),	233(83.2)
6a	10, 16	P	310(5.69),	272(11.8)
7a	10, 17	P	320(3.01),	285(17.0)
8a	18	P	340(4.20),	312(7.57)
9a	19	P	360(4.74),	280(7.08)
10a	10, 20	E	314(6.94),	277(13.2)
14a	10, 21	E	320(3.67),	250(8.81)

a) Indicated are the Reference numbers. b) Solvent used for the measurements of UV spectra; E: ethanol, P: 2-propanol.

TABLE 6. PHOTOCHEMICAL RING OPENING PRODUCTS OF FLAVANONES

Product	Mp °C	Vinyl-H δ	Ar–OH[a] δ	IR(C=O) cm^{-1}	Method of preparation[b]
1b	90—91	5.40	12.8	1630	10, 22
2b	71	5.45	13.8	1700	10, 23
3b	143—146	5.45	12.7	1720	10, 13
4b		5.50	12.0		10, 24
6b	102—105	5.45	13.6		10, 25
9b	115—125	5.45	14.8		26
10b	92—98	6.40	13.2	1680	10, 19

a) The NMR signals of the phenolic protons disappeared on addition of D_2O. b) Indicated are the Reference numbers.

Apparatus and Procedures. The IR, UV, and NMR spectra were measured by means of a JASCO IRA-I spectrometer, a Hitachi 124 spectrometer, and a Hitachi R-24 NMR spectrometer, respectivery. The light source was a 100 W high pressure mercury lamp (Riko) immersed in the reaction vessel, for preparative photoreactions; or a 400 W high pressure mercury lamp with a merry-go-round irradiation apparatus thermostated at 20 °C, for small scale experiments. Quantum yields were measured by the usual method[29] using aqueous tris(oxalato)ferrate(III) solution and with the light beams of 313 and 334 nm paralleled and through a glass filter (Toshiba UV-D2).

Photochemical Ring Opening Reaction. Typical procedures are as follows. A 100 ml benzene solution of **1a** (197 mg, 0.88 mmol) was irradiated with a 100 W high pressure mercury

Table 7. Photoreductive coupling products of flavanone and 4-chromanone in 2-propanol

Product	Mp[a] °C	Found (Calcd) %	IR (KBr) ν/cm^{-1}	NMR ($CDCl_3$)[b] δ
1c (*meso*-I)[c]	270—272	C: 80.41 (79.98) H: 5.92 (5.82)	3550	1.41—2.41 (m, H_3H_3', 4H), 3.03 (s, OH, 1H),[d] 3.67 (s, OH, 1H),[d] 4.86—5.41 (m, H_2H_2', 2H), 6.86—7.50 (m, Ar, 16H), 7.70—8.30 (m, Ar, 2H)
1c (*meso*-II)	78—80		3380	1.55—2.40 (m, H_3H_3', 4H), 3.32 (s, OH, 1H),[d] 3.86 (s, OH, 1H)[d], 4.88—5.35 (m, H_2H_2', 2H), 6.94—7.45 (m, Ar, 16H), 7.65—810 (m, Ar, 2H)
1c (racemic)[c]	237—238	C: 79.40 (79.98) H: 5.80 (5.82)	3590, 3445	2.39—3.90 (m, H_3H_3', 4H), 5.24 (s, OH, 2H)[d], 5.80—6.22 (m, H_2H_2', 2H), 6.50—7.50 (m, Ar, 16H)
1d (*cis*)	125—128		3520, 3450	1.35 (s, CH_3, 3H), 1.43 (s, CH_3, 3H), 2.1—2.2 (m, OH, 2H)[d], 2.20, 2.80 (each dd, $J_{2,3}$=3.7 and 12.3 Hz, H_3, 2H), 5.60 (dd, $J_{2,3}$=3.7 and 12.7 Hz, H_2, 1H), 6.76—7.75 (m, Ar, 9H)
1d (*trans*)	125—130		3400	1.00 (s, CH_3, 3H), 1.30 (s, CH_3, 3H), 1.90—2.24 (m, H_3, 2H), 2.45—3.20 (m broad, OH, 2H),[d] 4.78—5.20 (m, H_2, 1H), 6.68—7.58 (m, Ar, 9H)
14c (*meso*)[c]	201—204	C: 72.21 (72.46) H: 6.12 (6.08)	3550	1.50—2.35 (m, H_3H_3', 4H), 2.68 (s, OH, 1H),[d] 3.28 (s, OH, 1H),[d] 3.88—4.20 (m, H_2H_2', 4H), 6.5—7.4 (m, Ar, 7H), 8.00—8.12 (m, Ar, 1H)
14c (racemic)[c]	184—186	C: 72.51 (72.46) H: 6.17 (6.08)	3500, 3450	1.82—2.32 (m, H_3H_3', 4H), 3.87—4.27 (m, H_2H_2', 4H) 5.24 (s, OH, 1H),[d] 6.32—7.32 (m, Ar, 8H)

a) Uncorrected. b) DMSO-d_6 was used for **1c** ((racemic) and **14c** (racemic). c) Treatment with lead tetraacetate in acetic acid gave starting material at room temperature. d) Disappeared on addition of D_2O.

lamp for 16.5 h. Oxygen-free nitrogen current was passed through the solution before and during the photolysis.

The products were separated on silica gel–benzene. Similarly the photochemical ring opening products of other flavanones were isolated. They were identified by comparing their mp, IR, and NMR spectra (Table 6) with those of authentic samples independently prepared. The amounts of the products were determined by measurement of either the UV absorption at near 360 nm after separation on silica gel or the NMR signal intensities of the phenolic protons at near 13 ppm as mixture solutions.

*Photoreduction of **1a** and **14a** in 2-Propanol.* A 100 ml solution of **14a** (1 g, 4.8 mmol) in 2-propanol was irradiated with a 100 W high-pressure mercury lamp for 5.5 h. Separation of the products on silica gel–benzene and crystalization from methanol yielded colorless crystals A (53%) and B (36%).

The spectral and CH analysis data in Table 7 show that A and B are 4,4′-bichromanol isomers. Relative rates of oxidative decomposition with lead tetraacetate can serve as a method of identification of a series of isomeric 1,2-diols: the rate is rapid for gauche structure (with respect to the two hydroxyl groups) and slow for anti one.[27] Both A and B gave **14a** on treatment with lead tetraacetate with relative rates A : B = 1 : 4 in acetic acid at room temperature. Thus, A and B are ascribable to anti (meso) and gauche (racemic) forms, respectively.

Molecular models implied that the racemic form favors for intramolecular hydrogen bonding while the meso form is sterically unfavorable. Thus, the O–H streching absorption appearing in two bands (3500 and 3450 cm^{-1}) and the low-field shift of the hydroxyl protons (5.24 ppm as compared to 2.3—3.3 ppm for A) of B are ascribable to intramolecular hydrogen bonding of the racemic isomer.[30,31]

Similar photolysis of **1a** (1 g, 4.5 mmol) in 2-propanol for 5 h gave a mixture of 4,4′-biflavanols **1c** and 4-hydroxy-4-(1-hydroxy-1-methylethyl)flavanones **1d**. By separation on silica gel and crystallization, **1c** gave colorless crystals E (from benzene), F (from acetone), and G (from ligroin), while **1d** gave K and L (both from petroleum benzine).

The product E is assumed to have racemic form since the low-field shift of the hydroxyl protons (5.24 ppm) and the O–H streching appearing in two bands (3590 and 3445 cm^{-1}) are comparable with those of the racemic isomer of **14c**. On the other hand, F and G are assumed to have meso forms since their IR and NMR spectra are comparable to those of the meso isomer of **14c**.

According to Bolger *et al.*,[32] the coupling constants of the C_3-methylene protons of 4-flavanols are generally large for isomers with equatrial 4-hydroxyl group but small for isomers with axial 4-hydroxyl group: J_{eq}=15—17, J_{ax}=5—6 Hz.

Thus, relatively large coupling constant of K (12.3 Hz) is ascribable to the *cis* isomer (in which 4-hydroxyl group is equatrial) of **1d**. Molecular models of the isomers of **1d** implied that the *cis* form is favorable but the *trans* form is sterically unfavorable for intramolecular hydrogen bonding between two hydroxyl groups. Thus, the O–H stretching absorption (3520 and 3450 cm^{-1}) is ascribable to the *cis* isomer.

References

1) P. O. Mack and J. T. Pinhey, *J. Chem. Soc., Chem. Commun.*, **1972**, 451.

2) R. Matsushima, T. Kishimoto, and M. Suzuki, *Chem. Lett.*, **1976**, 579.

3) R. Nakashima, K. Okamoto, and T. Matsuura, *Bul Chem. Soc. Jpn.*, **49**, 3355 (1976).

4) A. C. Jain, H. T. Saini, and R. C. Gupta, *J. Scient. Ind. Res.*, **37**, 264 (1978).

5) A. Padwa and A. Au. *J. Am. Chem. Soc.*, **96**, 1633, 1634 (1974); A. Padwa, A. Au. G. A. Lee, and W. Owens, *ibid.*, **98**, 3555 (1976); A. Padwa and W. Owens, *J. Org. Chem.*, **42**, 3076 (1977).

6) R. Matsushima and I. Hirao, *Bull. Chem. Soc. Jpn.*, **53**, 518 (1980).

7) M. Koizumi, S. Kato, N. Mataga, T. Matsuura, and Y. Usui, "Photosensitized Reactions," Kagaku Dojin, Kyoto (1978), pp. 59—68.

8) D. O. Cowan and R. L. Drisko, "Elements of Organic Photochemistry," Plenum Press, New York, N. Y. (1976), pp. 92—100; Ref. 7, pp. 88—97.
9) J. B. Gallivan and J. S. Brinen, *Chem. Phys. Lett.*, **10**, 455 (1971); *Can. J. Chem.*, **50**, 3601 (1972).
10) S. Fujise, "Zikken Kagaku Koza," ed by M. Kotake, Maruzen, Tokyo (1963), Vol. 21, Part III, pp. 132—152.
11) A. Löweinbein, *Ber.*, **57**, 1515 (1924).
12) T. A. Geissman and R. O. Clinton, *J. Am. Chem. Soc.*, **68**, 697 (1946).
13) S. Tsujimoto, Graduation thesis, Shizuoka University, Hamamatsu, 1974.
14) M. K. Seikel, M. J. Lonnsbung, and S. Wang, *J. Org. Chem.*, **27**, 2952 (1962).
15) E. Owada, H. Nakashima, Y. Kiriyama, T. Suzuki, and S. Kokubu, *Yuki Gosei Kagaku Kyokai Shi*, **30**, 959 (1972).
16) J. Shinoda, *Yakugaku Zasshi*, **48**, 35 (1928).
17) J. Shinoda, *Yakugaku Zasshi*, **48**, 791 (1928).
18) J. Tambor, G. Plattner, and C. Zäch, *Helv. Chim. Acta*, **9**, 463 (1926).
19) G. Woker, *Ber.*, **39**, 1649 (1906).
20) S. Hishida, *Nippon Kagaku Kaishi*, **76**, 206 (1955).
21) J. D. Loudon and R. K. Razdan, *J. Chem. Soc.*, **1954**, 4299.
22) W. Feuerstein and S. V. Kostanecki, *Ber.*, **31**, 715 (1898).
23) W. Feuerstein and S. V. Kostanecki, *Ber.*, **32**, 315 (1899).
24) H. Simonis and S. Danischewski, *Ber.*, **59**, 2914 (1926).
25) T. Emilewicz and S. V. Kostanecki, *Ber.*, **32**, 309 (1899).
26) S. V. Kostanecki, *Ber.*, **31**, 705 (1898); S. Fujise, "Zikken Kagaku Koza," ed by M. Kotake, Maruzen, Tokyo (1963), Vol. 21, Part III, pp. 112—113.
27) R. Griegee, E. Büchner, and W. Walther, *Ber.*, **73**, 571 (1940).
28) W. R. Sorenson, T. W. Cambell, "Preparative Methods of Polymer Chemistry," John Wiley and Sons, Inc., New York, N. Y. (1961), p. 149.
29) J. G. Calvert and J. N. Pitts, Jr., "Photochemistry," John Wiley and Sons, Inc., New York, N. Y. (1966), pp. 783—786; M. Koizumi, S. Shida, S. Kato, N. Mataga, and M. Imamura, "Zikken Kagaku Koza," Maruzen, Tokyo (1956), Vol. 6, pp. 282—286.
30) H. Agahigian, J. F. Moraveck, and H. Gauthier, *Can. J. Chem.*, **41**, 194 (1963); W. A. Mosher and N. D. Heindel, *J. Org. Chem.*, **28**, 2154 (1963).
31) H. Göth, P. Cerutti, and H. Schmidt, *Helv. Chim. Acta*, **48**, 1395 (1965).
32) B. J. Bolger, A. Hirwe, K. G. Marathe, E. M. Philbin, M. A. Vickars, and C. P. Lillya, *Tetrahedron*, **22**, 621 (1966).

 © 1980 The Chemical Society of Japan Bull. Chem. Soc. Jpn., 53, 2943—2952 (1980)

Layered Compounds. LXIV.[1] Syntheses and Charge Transfer Spectra of Multilayered Paracyclophanequinones[2]

Hideki MACHIDA, Hitoshi TATEMITSU, Tetsuo OTSUBO,†
Yoshiteru SAKATA, and Soichi MISUMI*
The Institute of Scientific and Industrial Research, Osaka University, Suita, Osaka 565
(Received March 4, 1980)

Three isomeric triple-layered and two isomeric quadruple-layered charge transfer cyclophanes containing benzoquinone and dimethoxybenzene moieties have been synthesized together with two triple-layered and two quadruple-layered paracyclophanequinones. The structures of the isomers were determined by ^{1}H- and ^{13}C-NMR spectra and/or alternative syntheses. By comparing the CT bands of a series of dimethoxycyclophanequinones with those of the corresponding cyclophanequinones, it is concluded that the CT stabilization of multilayered dimethoxyquinones should be attributed mainly to the π-basicity of the durene ring which faces the acceptor quinone ring and partly to the decreasing π-basicity of dimethoxybenzene ring as the layer number increases. No orientational dependence of quinone and dimethoxybenzene moieties on CT transition was observed in the multilayered series.

A wide variety of charge transfer (CT) cyclophanes with both donor and acceptor moieties have been synthesized for studying the relationship between the structure and the CT interaction on intermolecular CT complexes.[3] A marked difference, dependent upon the donor-acceptor orientation, was observed in the electronic spectra of double-layered CT cyclophanes, *e.g.*, **1** and **2**.[4] In the previous paper of this series, we reported that a series of multilayered [2.2]paracyclophanes showed the increase of the transannular interaction with an increase of layer number.[5] This change in their electronic spectra was interpreted as due to the configurational interactions of charge transfer and neutral excitation states.[6] The CT cyclophanes, in which the two outer benzene rings of the multilayered paracyclophanes are replaced by a donor and an acceptor moiety, are particularly interesting in connection with both the CT and the transannular interactions. We now report the syntheses and properties of three isomeric triple-layered (**3**—**5**) and two isomeric quadruple-layered CT cyclophanes (**6** and **7**) having parabenzoquinone moiety as an acceptor as well as two isomers of triple-layered (**8** and **9**) and two isomers of quadruple-layered quinones (**10** and **11**) as spectral references.

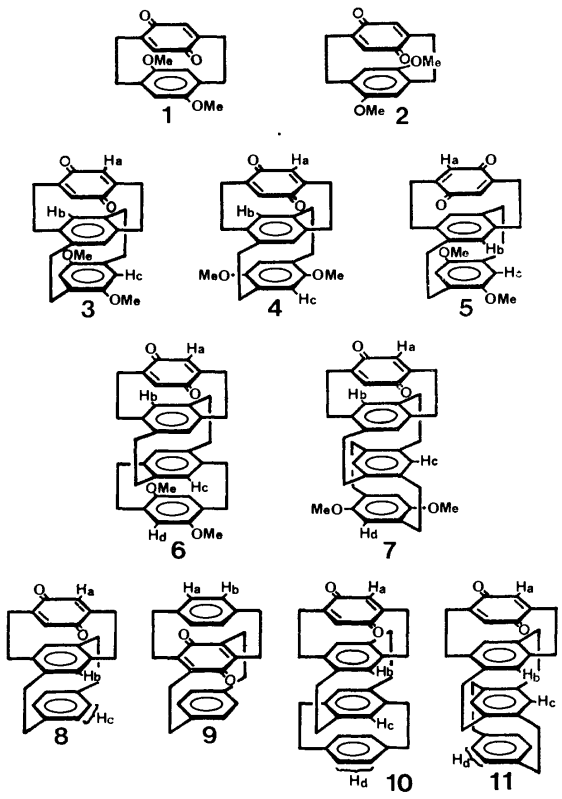

For the same purpose, we previously reported other examples of triple-layered CT cyclophanes which have tetracyanoquinodimethane moiety as an acceptor.[7] During the course of the present study, Staab and his coworkers independently reported the syntheses of **3**,[8] **4**,[8] **6**,[9] and **7**.[9]

Results and Discussion

Syntheses. The synthetic routes of dimethoxyquinones (**3**—**7**) and quinones (**8**—**11**) are shown in Schemes 1—3. A key intermediate of the routes, dimethoxy double-layered cyclophane **15b**, was prepared by two general methods, *i.e.*, the Hofmann elimination and the photodesulfurization.[10] Thus, the pyrolytic cross-breeding reaction of two quarternary ammonium hydroxides, **16** and **17**,[11] gave **15b** in 11.7% yield, whereas sulfur photo-extrusion from a mixture of isomeric disulfides, **14a** and **14b**, prepared by coupling of dithiol **12**[12] and dichloride **13**, gave the identical compound **15b** in 63% yield. The product by the latter method consisted of only the staggered isomer **15b**, indicating the intramolecular overcrowding of methyl and methoxyl groups in the eclipsed isomer **15a**.

Pyrolysis of **16** with ammonium hydroxide **20**, derived from **15b**, afforded a mixture of tetramethoxy triple-layered paracyclophane, **21** of D_2 symmetry and **22** of C_2 symmetry, in 6.1% yield, together with 7.7% of tetramethoxy double-layered and 2.5% of tetramethoxy quadruple-layered paracyclophanes. The separation of **21** and **22** was accomplished by repeated

† Present address: Department of Applied Chemistry, Faculty of Engineering, Hiroshima University, Sendamachi, Hiroshima 730.

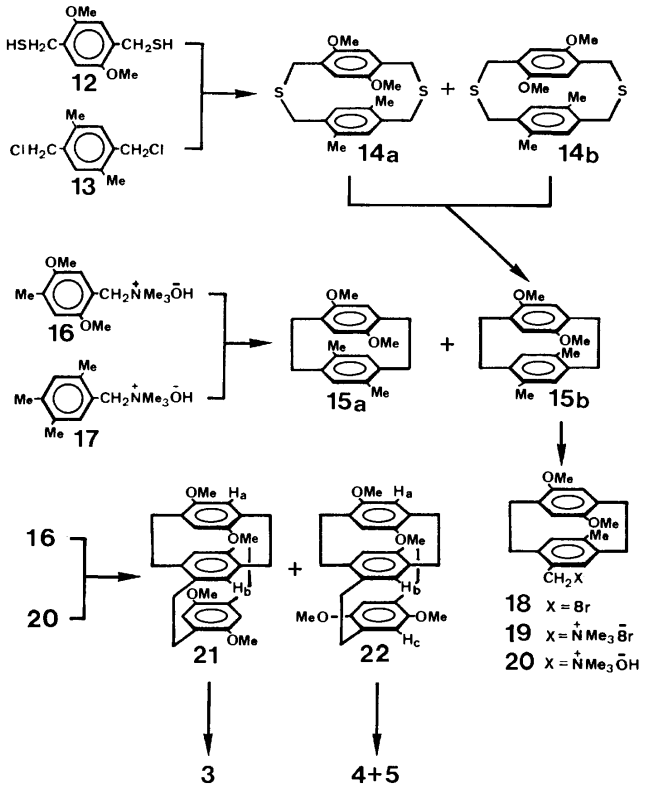

Scheme 1.

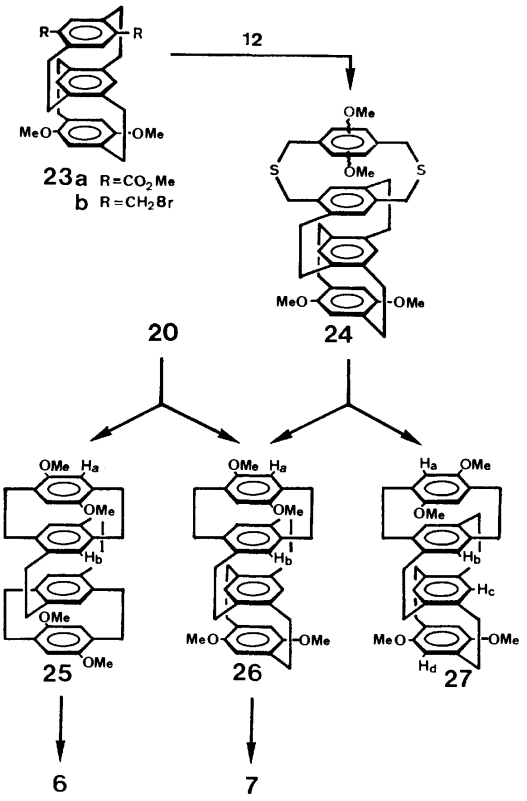

Scheme 2.

recrystallization from ethanol. Their structures were easily assigned by ^{1}H-NMR spectra, as described later. Treatment of **21** with boron tribromide followed by oxidation with silver oxide gave triple-layered dimethoxyquinone **3** in 33% yield. According to the same procedure, on the other hand, **22** gave two isomeric triple-layered dimethoxyquinones, **4** and **5**, in 41.7% total yield. The preparation of dimethoxyquinones **3** and **4** was also reported by Staab *et al.*[8] but with no isolation of the third isomer **5**. The formations of a single dimethoxyquinone from **21** and of two isomeric dimethoxyquinones from **22** provide chemical evidence to support the NMR assignment of **21** and **22**.

Pyrolysis of quarternary ammonium hydroxide **20** in boiling xylene gave a mixture of two isomeric tetramethoxy quadruple-layered paracyclophanes, **25** of C_{2h} symmetry and **26** of D_2 symmetry, in 21.8% total yield. The separation of these isomers was barely accomplished by fractional recrystallization from toluene, after many unfruitful attempts using column and liquid chromatographies. The structures of the isomers could not be unequivocally determined by ^{1}H- and ^{13}C-NMR spectra, although they were tentatively assigned by the chemical shifts of methylene carbons as described later. To confirm this ^{13}C-NMR assignment, an alternative synthesis of **26** was carried out. Here a photodesulfurization of a mixture of two isomeric disulfides **24**, prepared by coupling of dithiol **12** and triple-layered dibromide **23b**, which has a well-determined structure,[7] gave a mixture of two isomeric tetramethoxy quadruple-layered paracyclophanes (1 : 1 ratio) in 47% yield. The less soluble isomer, separated by repeated recrystallization of the mixture from hexane, was identical with **26** on the basis of various spectral data; thus **26** undoubtedly has the D_2 symmetric structure. The other two isomers, **25** and **27**, are, consequently, assigned to C_{2h} and C_2 symmetric structures, respectively. Demethylation and oxidation of **25** and **26** in a similar manner as done for the triple-layered analogues gave dimethoxy quadruple-layered paracyclophanequinones, **6** and **7**, in 10 and 9% yields, respectively. Staab and Zapf[9] also reported the preparation of **6** and **7** from **25** and **26** in the same way, after an X-ray crystallographic determination that the precursor **25** had a centrosymmetric structure.

Triple-layered paracyclophane derivatives, **30** and **8**, were prepared for spectral reference, as shown in Scheme 3. A mixture of two isomeric disulfides **29**, prepared by coupling of dibromide **28**[13] with dithiol **12**, was irradiated with a high pressure mercury lamp to give one of two possible isomers of dimethoxy compound, **30**, in 75% yield. Treatment of **30** with methylmagnesium iodide afforded, without oxidation with silver oxide, reddish orange quinone **8** in 72% yield. Dichloride **31** obtained by chloromethylation of 2,5-dimethoxy-*p*-xylene[14] was coupled with dithiol **32** to afford disulfide **33** in 65% yield. Sulfur photo-extrusion of **33** gave 60% yield of dimethoxydimethyl[2.2]-paracyclophane **34**. Disulfide **36** was obtained by bromination (86%) of **34** with NBS, followed by coupling (49%) with **32**. Photodesulfurization of **36** was performed in a similar manner to give dimethoxy triple-layered paracyclophane **37** in 69% yield. Demethylation of **37** with methylmagnesium iodide at 160 °C, followed by treatment with silver oxide, afforded yellow

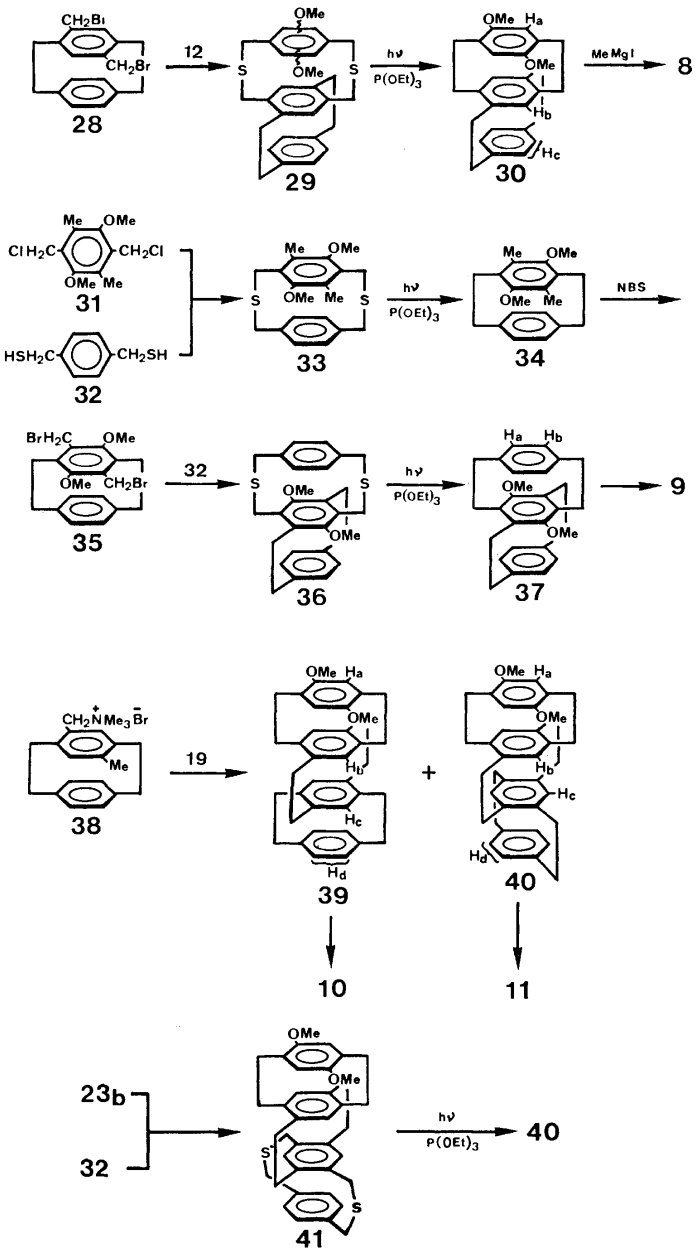

Scheme 3.

inner-quinone **9** in 12.3% yield.

Dimethoxy quadruple-layered cyclophanes, **39** and **40**, were prepared by cross-breeding pyrolysis of a mixture of two quarternary ammonium hydroxides prepared from ammonium bromides, **19** and **38**.[5] After removal of non-substituted and tetramethoxy quadruple-layered cyclophanes from the reaction mixture by column chromatography, a mixture of the desired dimethoxy compounds, **39** and **40**, was separated by fractional crystallization from hexane. The structures of both isomers were assigned by ^{13}C-NMR spectra. In order to confirm this assignment, isomer **40** was prepared by an alternative route, as shown in Scheme 3. Photodesulfurization of disulfide **41**, prepared by coupling of dibromide **23b** and dithiol **32**, gave dimethoxy quadruple-layered paracyclophane in 25% yield. This product was identical, in all respects, with a more soluble isomer **40** obtained by the cross-breeding pyrolytic method. Quadruple-layered paracyclophanequinones **10** and **11** were obtained as red needles in 28 and 29% yields, respectively, by successive demethylation and oxidation from **39** and **40** in a similar manner as done for dimethoxy triple-layered one **6**.

NMR Spectra. *^{1}H-NMR*: The chemical shifts of multilayered quinones **3**—**11** and related compounds are summarized in Table 1. We previously reported that there is an additivity among the chemical shifts of aromatic protons in a series of multilayered [2.2]-paracyclophanes and that the additivity is based on the anisotropic effect of facing benzene rings as well as the steric compression and magnetic anisotropic effects of pseudo-gem and pseudo-ortho substituents.[8] Reich and Cram also described such effects of various substituents on the chemical shifts of aromatic protons in a

Table 1. ^{1}H-NMR data of multilayered paracyclophanequinones and related compounds in deuteriochloroform (δ value)

Compd		Obsd Shift	Calcd Shift	Compd		Obsd Shift	Calcd Shift
3	Ha	5.56		**21**	Ha	5.51	
	Hb	6.12	6.19		Hb	5.98	6.02
	Hc	5.62			OCH_3	3.57	
	OCH_3	3.59		**22**	Ha	5.50	
4	Ha	5.57			Hb	5.65	5.74
	Hb	5.86	5.81		Hc	5.50	
	Hc	5.65			OCH_3	3.56	
	OCH_3	3.59		**25**	Ha	5.39	
5	Ha	5.63			Hb	5.48	
	Hb	6.04	6.04		OCH_3	3.50	
	Hc	5.63		**26**	Ha	5.39	
	OCH_3	3.59			Hb	5.47	
6	Ha	5.43			OCH_3	3.49	
	Hb	5.65		**27**	Ha	5.39	
	Hc	5.60			Hb	5.15	
	Hd	5.43			Hc	5.46	
	OCH_3	3.52			Hd	5.39	
7	Ha	5.43			OCH_3	3.49	
	Hb	5.65		**30**	Ha	5.47	
	Hc	5.61			Hb	5.71	
	Hd	5.43			Hc	6.24	
	OCH_3	3.51			OCH_3	3.54	
8	Ha	5.53		**37**	Ha	6.61	
	Hb	5.88			Hb	6.19	
	Hc	6.37			OCH_3	3.99	
9	Ha	6.56		**39**	Ha	5.38	
	Hb	6.33			Hb	5.41	
10	Ha	5.43			Hc	5.17	
	Hb	5.60			Hd	6.12	
	Hc	5.32			OCH_3	3.48	
	Hd	6.17		**40**	Ha	5.37	
11	Ha	5.42			Hb	5.41	
	Hb	5.61			Hc	5.19	
	Hc	5.34			Hd	6.12	
	Hd	6.17			OCH_3	3.47	

series of substituted [2.2]paracyclophanes.[9]

As seen in Table 1, the inner aromatic protons of three triple-layered dimethoxyquinones, **3**—**5**, and their precursors, two tetramethoxy compounds, **21** and **22**, show relatively large differences in chemical shift compared to the outer ring protons. In order to determine their structures, the magnetic effects ($\Delta\delta$) of dimethoxy and quinone groups on pseudo-ortho protons of facing benzene rings were evaluated from the observed chemical shifts of reference compounds, as shown in Fig. 1. Using these values, we calculated the chemical shifts of the inner aromatic protons of the above-mentioned triple-layered paracyclophane derivatives. For example, the calculated value of Hb in **4** is given from the chemical shift (δ 5.40) of the inner proton of **42** as follows;

$$\delta(\text{Hb of } \mathbf{4}) = \delta(\text{Hb of } \mathbf{42}) + \Delta\delta_{\text{H}\rightarrow\text{OMe}}(\text{pseudo-ortho effect}) + \Delta\delta_{\text{H}\rightarrow=\text{O}}(\text{pseudo-gem effect}) = 5.40+0.30+0.48 = 5.91 \text{ ppm}$$

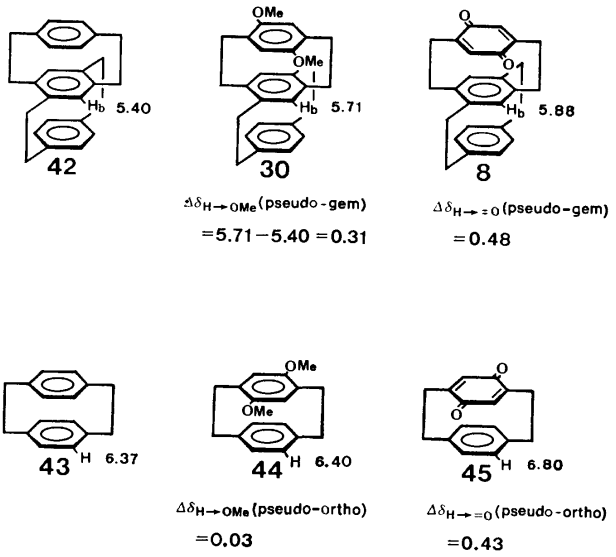

Fig. 1. ^{1}H-NMR chemical shifts of aromatic protons of five reference compounds in deuteriochloroform.

The calculated values in Table 1 are in good agreement with the observed values. The assignment of isomeric structures is consequently achieved.

On the other hand, the structures of four pairs of isomeric quadruple-layered cyclophanes, **6** and **7**, **10** and **11**, **25** and **26**, and **39** and **40**, could not be assigned only by ^{1}H-NMR spectra, because the chemical shifts of all corresponding protons are almost equal to each other in each pair. But the inner and outer aromatic protons of tetramethoxy compounds, **25**—**27**, were easily assigned on the basis of the solvent effect as described for non-substituted multilayered paracyclophanes.[8] As shown in Table 2, aromatic protons displaying larger chemical shift differences in two solvents, carbon tetrachloride and deuteriochloroform, were assigned to the outer benzene protons, while those displaying smaller differences (*ca.* 0.06 ppm) were assigned to inner benzene protons.

Table 2. Solvent effect of aromatic protons of tetramethoxy quadruple-layered paracyclophanes (δ value)

Compd		Solvent		$\Delta\delta$
		$CDCl_3$	CCl_4	($\delta_{CDCl_3} - \delta_{CCl_4}$)
25	outerH	5.39	5.23	0.16
	innerH	5.48	5.43	0.05
26	outerH	5.39	5.24	0.15
	innerH	5.47	5.41	0.06
27	innerH	5.15	5.08	0.07
	outerH	5.39	5.23	0.16
	innerH	5.46	5.40	0.06

^{13}C-NMR: To determine the structures of isomeric quadruple-layered cyclophanes, **25** and **26**, and **39** and **40**, ^{13}C-NMR spectra were examined. The data are shown in Fig. 2 together with those of reference compounds. The assignment was performed by an off-resonance technique and by comparing with the

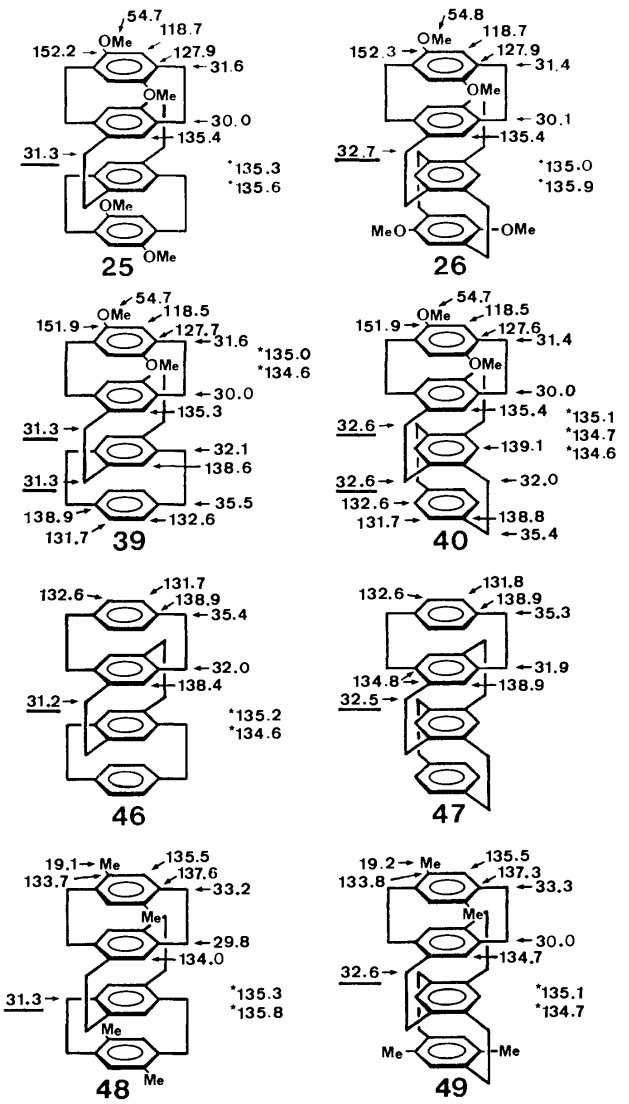

Fig. 2. ^{13}C-NMR data of quadruple-layered cyclophanes in deuteriochloroform. Values marked with star are difficult to assign.

chemical shifts which were calculated by adding the substituent effect to the chemical shifts of the parent hydrocarbons, **46** and **47**.[15] Each isomeric pair showed chemical shifts very close to each other, except for the underlined signals of the methylenes bridging two inner benzene rings.

The difference in carbon chemical shifts of the inner bridging methylenes, though slight, can be used to assign isomeric structures of reference compound pairs, **46** *vs.* **47** and **48** *vs.* **49**; these structures were clearly determined by X-ray analysis[16] or by an alternative stepwise synthesis.[5] Thus, the chemical shifts of the inner methylenes under consideration are 31.2 ppm for C_{2h} symmetric cyclophanes (**46** and **48**) and about 32.5 ppm for D_2 symmetric ones (**47** and **49**), though the relationship between structure and chemical shift is not clear. On the basis of this result, we assigned the cyclophanes displaying an inner methylene signal at 31.3 ppm to C_{2h} symmetric parent structure (**25** and **39**) and those having a signal around 32.6 ppm to D_2 symmetric parent structure (**26** and **40**). These assignments were satisfactorily supported by the alternative syntheses of **26** and **40** described before.

Electronic Spectra. The electronic spectra of **3**—**11** are shown in Figs. 3—5. All the broad and structureless bands in the longer wavelength region are associated with intramolecular charge transfer interactions, because neither the component chromophore nor the parent multilayered paracyclophane shows such an intensive band in the longer wavelength region.

It was reported that CT transitions of various double-layered CT cyclophanes such as **1** and **2** are markedly affected by the orientation of the donor and the acceptor moieties. However, the isomeric pairs (**3** *vs.* **5** and **6** *vs.* **7**) of the present triple- and quadruple-layered CT cyclophanes do not follow such a case. Thus, these isomeric pairs show nearly superimposable absorption curves, indicating no orientational dependence of the presumed main donor (dimethoxybenzene) and acceptor

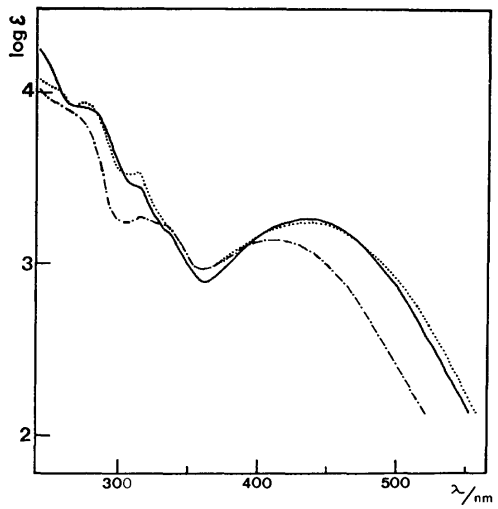

Fig. 3. Electronic spectra of three isomers of dimethoxy triple-layered [2.2]paracyclophanequinone in dichloromethane (**3**, ·····; **4**, -·-·-, **5**, ——).

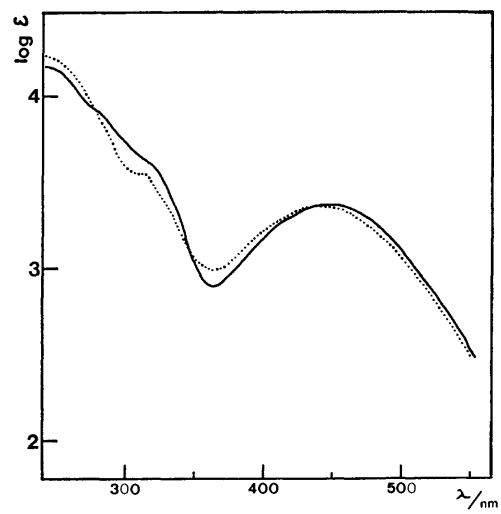

Fig. 4. Electronic spectra of two isomers of dimethoxy quadruple-layered [2.2]paracyclophanequinone in dichloromethane (**6**, ·····, **7**, ——).

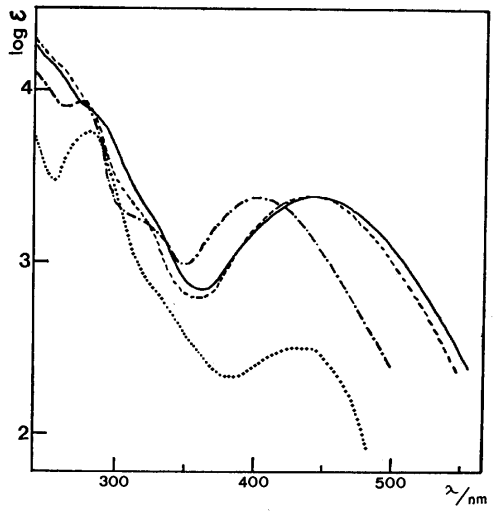

Fig. 5. Electronic spectra of two triple-layered (**8**, -·-·-; **9**, ·····) and two quadruple-layered [2.2]paracyclophanequinones (**10**, ——; **11**, ——) in dichloromethane.

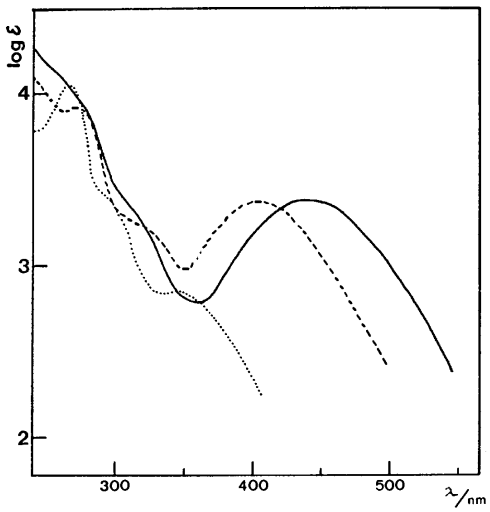

Fig. 6. Electronic spectra of double- to quadruple-layered [2.2]paracyclophanequinones in dichloromethane (**45**, ·····; **8**, ——; **10**, ——).

(benzoquinone). The only exception is the blue shifted CT band of dimethoxyquinone **4**, where the two methoxyl groups are substituted at the positions pseudogem to the bridged methylenes. The reason of the blue shift is probably the decrease of the π-basicity of dimethoxybenzene ring which results from the overcrowding interaction between the methoxyl and the methylene groups. A similar blue shift was also observed in the spectrum of TCNQ cyclophane **50**, which has the same steric relationship between dimethoxyl and bridged methylene groups.[7]

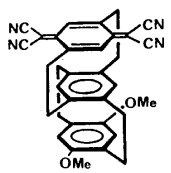

50

The electronic spectra of CT cyclophane analogues with different numbers of layers are shown in Figs. 6 and 7. In a series of paracyclophanequinones (Fig. 6), the CT bands shifted to longer wavelengths as the number of layers increased. This indicates that the π-basicity of the benzene ring facing the acceptor quinone ring becomes larger with the increase of layer number. A similar result was observed in the spectra of intermolecular CT complexes between a series of multilayered [2.2]paracyclophanes and π-acceptors.[5]

For a series of dimethoxyquinones (Fig. 7), on the other hand, the order of CT band maxima does not correspond to that of layer number, that is, **1**>**6**>**3**. In compound **1**, the dimethoxydimethylbenzene moiety having a relatively lower ionization potential is so closely fixed to the acceptor quinone that the CT band of **1** shifts to a longer wavelength compared to those of the others, **3** and **6**. In contrast to **1**, multilayered dimethoxyquinones (**3** and **6**) have two types of donors: durene moiety (the inner benzene ring faced to quinone

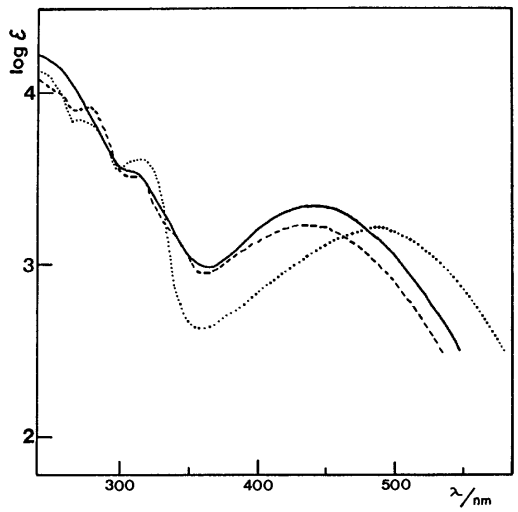

Fig. 7. Electronic spectra of double- to quadruple-layered dimethoxy[2.2]paracyclophanequinones in dichloromethane (**1**, ·····; **3**, ——; **6**, ——).

ring) and dimethoxydimethylbenzene moiety. In the case of the quadruple-layered compound **6**, the durene moiety is concluded to be the main donor, from the fact that the absorption curves of two quadruple-layered quinones, **6** and **10**, are roughly superimposable over each other. In other words, the two methoxyl groups show no contribution to the CT transition. The same conclusion for triple-layered compound **3** is obtained by comparing the spectra of **3** and **8**, but in this series, the dimethoxydimethylbenzene ring increases the π-basicity of the durene moiety by the transannular electron release. In conclusion, the blue shifts of CT bands of **3** and **6** are attributed to the durene moiety acting as the main donor in place of the dimethoxydimethylbenzene ring which has a lower ionization potential but is more remote from the acceptor. Undoubtedly, this is why there is no orientational dependence of the quinone and the dimethoxybenzene moieties on the CT transitions of **3**—**7** mentioned before.

Experimental

All melting points are uncorrected. The IR, NMR, mass and electronic spectra were recorded with a Hitachi EPI-G2, a JEOL JNM-FX-100 (100 MHz for ^1H; 25 MHz for ^{13}C) and a Hitachi R-20, a Hitachi RMU-7 or JEOL JMS-01SG-2 and a Hitachi EPS-3T spectrometer, respectively. Liquid chromatography was performed with a Nihonbunsekikogyo LC-08 of GPC type and a Waters Prep 500.

Staggered and Eclipsed 5,8-Dimethoxy-14,17-dimethyl-2,11-dithia-[3.3]paracyclophanes (14a and 14b). All the solvents were bubbled with nitrogen before use. A solution of 2,5-bis-(chloromethyl)-*p*-xylene **13** (8.13 g, 40 mmol) and 2,5-bis-(mercaptomethyl)-1,4-dimethoxybenzene **12** (9.22 g, 40 mmol) in benzene (800 ml) was added to a stirred solution of sodium hydroxide (3.92 g, 44 mmol) in water (50 ml) and ethanol (2 l) with reflux under nitrogen for 28 h. Reflux was continued for an additional 18 h. After removal of the solvents, the residue was taken up with benzene and chromatographed on silica gel with benzene–hexane (1 : 1). The crude product was recrystallized from benzene–hexane to give 9.82 g (68.1%) of **14a** and **14b**. The mixture was separated into the two isomers by repeated chromatography on silica gel.

14a: Colorless prisms, mp 188.0—189.0 °C. NMR ($CDCl_3$, δ): 6.71 (s, 4H, ArH), 3.79 (s, 6H, OCH_3), 2.33 (s, 6H, CH_3). Found: C, 66.38; H, 6.71; S, 17.50%. Calcd for $C_{20}H_{24}S_2O_2$: C, 66.63; H, 6.71; S, 17.79%.

14b: Colorless prisms, mp 202.0—202.5 °C. NMR ($CDCl_3$, δ): 6.86 (s, 2H, dimethylArH), 6.59 (s, 2H, dimethoxyArH), 3.71 (s, 6H, OCH_3), 2.20 (s, 6H, CH_3). Found: C, 66.48; H, 6.72; S, 17.79%. Calcd for $C_{20}H_{24}S_2O_2$: C, 66.63; H, 6.71; S, 17.79%.

4,7-Dimethoxy-12,15-dimethyl[2.2]paracyclophane (15a and 15b). *By Photodesulfurization*: A mixture of **14a** and **14b** (2.21 g, 5.8 mmol) in benzene–triethyl phosphite (300 ml, 1 : 1 vol ratio) was irradiated with a high pressure mercury lamp for 2 h while nitrogen was bubbled through the solution. After removal of the solvents, the residue oil was chromatographed on silica gel with benzene and recrystallized from methanol to give 1.15 g (63.3%) of **15b**.

15b: Colorless needles, mp 123.5—124.0 °C. NMR ($CDCl_3$, δ): 6.32 (s, 2H, dimethylArH), 6.08 (s, 2H, dimethoxyArH), 3.68 (s, 6H, OCH_3), 2.08 (s, 6H, CH_3). Found: C, 80.78; H, 8.03%. Calcd for $C_{20}H_{24}O_2$: C, 81.04; H, 8.16%.

By Hofmann Elimination: An aq solution of (2,4,5-trimethylbenzyl)trimethylammonium chloride[11] (364 g, 1.6 mol) and (2,5-dimethoxy-4-methylbenzyl)trimethylammonium bromide (242 g, 0.8 mol) was passed through a column of anion exchange resin (Dowex 1-X8) to give an aq solution of quarternary ammonium hydroxides **16** and **17**. This solution was dropwise added to a boiling solution of phenothiazine (5 g) in xylene, (2.8 l) which was placed in a three-necked flask equipped with a condenser, a mechanical stirrer, and a water separater. During the reaction, the bath temperature was kept at 140 °C. After water removal was over, heating was continued for 3 h. To the mixture was added benzene (1 l) and the solution was filtered off to remove insoluble solid. The filtrate was concentrated to dryness and the residue was treated with boiling hexane (2 l) and filtered. After removal of the solvent, the residue was passed through a short column of silica gel with benzene. Evaporation of the solvent gave an oil, to which hexane (50 ml) was added, the mixture was left overnight. The resulting precipitate was recrystallized from benzene to give 5 g (2.3%) of the less soluble isomer **15a**.

15a: Colorless prisms from benzene, mp 205.0—206.0 °C. NMR ($CDCl_3$, δ): 6.15 (s, 2H, dimethylArH), 5.87 (s, 2H, dimethoxyArH), 3.64 (s, 6H, OCH_3), 2.23 (s, 6H, CH_3). Found: C, 80.80; H, 8.04%. Calcd for $C_{20}H_{24}O_2$: C, 81.04; H, 8.16%.

The more soluble isomer **15b** was obtained by addition of hexane to the filtrate of **15a** and by liquid chromatography of the second mother liquor: yield, 27 g (11.7%).

Quarternary Ammonium Bromide 19. A mixture of **15b** (3 g, 10 mmol) and NBS (1.44 g, 8.1 mmol) in carbon tetrachloride (40 ml) was refluxed for 2.5 h under irradiation with a tungsten lamp. The resulting imide was filtered off and the filtrate was cooled on ice. A cold ethereal solution (14 ml) of trimethylamine (4 ml, 45.5 mmol) was added to the above solution. After the mixture was allowed to stand overnight, the precipitate was collected and dried in vacuum to yield 3.2 g (73.7%) of **19**.

Tetramethoxy Triple-layered [2.2]Paracyclophanes (21 and 22). To a refluxing solution of phenothiazine (350 mg) in xylene (240 ml) was added dropwise an aq solution of two quarternary ammonium hydroxides, **16** and **20**, which was produced by passing an aq solution of ammonium bromides, **19** (28.5 g, 65.6 mmol) and (2,5-dimethoxy-4-methylbenzyl)trimethylammonium bromide (40.2 g, 132.1 mmol) through a column of anion exchange resin (Dowex 1-X8). After water was removed by azeotropic distillation, heating was continued for an additional 2 h. Benzene (500 ml) was added to the cooled reaction mixture and the polymer was filtered off. The solvent was evaporated and the residue was chromatographed on silica gel with benzene–hexane. The crude product was separated into two tetramethoxy double-layered (1.67 g, 7.7%), triple-layered (1.84 g, 6.1%), and quadruple-layered paracyclophanes (0.49 g, 2.5%) by liquid chromatography. Separation of two isomeric triple-layered cyclophanes was carried out by fractional crystallization from ethanol to give the sparingly soluble isomer **22** and the more soluble isomer **21**.

21: Colorless needles, mp 204.0—204.5 °C. Found: C, 78.80; H, 7.70%. Calcd for $C_{30}H_{34}O_4$: C, 78.57; H, 7.47%.

22: Colorless needles, mp 226.5—226.7 °C. Found: C, 78.36; H, 7.43%. Calcd for $C_{30}H_{34}O_4$: C, 78.57; H, 7.47%

Dimethoxy Triple-layered [2.2]Paracyclophanequinone (3). A solution of **21** (49.3 mg, 0.11 mmol) in dry dichloromethane (4 ml) was added dropwise for 10 min to a stirred solution of boron tribromide (120 mg, 0.48 mmol) in dry dichloromethane (0.5 ml) under ice-salt cooling. After the addition was over, the stirring was continued for 1.5 h; then the mixture was treated with water and extracted with diethyl ether. The extract was washed with water and dried on $MgSO_4$. After removal of the solvents, acetone (5 ml) and silver oxide (126 mg) were added to the residue and the mixture was stirred for 30 min at room temperature and then for 30 min at 50 °C. Insoluble material was filtered off and the filtrate was concentrated to dryness. The crude product was chromatographed on silica gel with benzene to give 15.2 mg (33.0%) of **3**.

3: Red needles from ethanol, dec>220 °C. Found: M^+, 428.19880. Calcd for $C_{28}H_{28}O_4$: 428.19874.

Dimethoxy Triple-layered [2.2]Paracyclophanequinones (4 and 5). A solution of **22** (48.7 mg, 0.106 mmol) in dry dichloromethane was added to a stirred solution of boron tribromide (100 mg, 0.4 mmol) in dry dichloromethane (0.5 ml) at −20 °C for 5 min. The stirring was continued at that temperature for 2.5 h and then at 0 °C for 50 min. The reaction mixture was worked up as described for **3**. Silica gel chromatography of the oxidation product with benzene gave **4** from the initial eluate and **5** from the following eluate in a total yield of 19.0

mg (41.7%).

4: Red needles from ethanol, dec>225 °C. Found: M+, 428.19933. Calcd for $C_{28}H_{28}O_4$: 428.19874.

5: Red needles from ethanol, dec>210 °C. Found: C, 78.24; H, 6.35%; M+, 428.19971. Calcd for $C_{28}H_{28}O_4$: C, 78.48; H, 6.59%; M+, 428.19874.

Tetramethoxy Quadruple-layered [2.2]Paracyclophanes (25 and 26). Pyrolysis of quarternary ammonium hydroxide **20** was carried out as described for **15**. The crude product was chromatographed on silica gel with benzene–hexane to give a mixture of **25** and **26** in a total yield of 5.3 g (21.8%). Recrystallization of the mixture from toluene gave colorless plates of **25** and colorless needles of **26**, which were separated with a pincette and purified by recrystallization from ethyl acetate.

25: Colorless prisms, dec>260 °C. Found: C, 81.76; H, 7.58%. Calcd for $C_{40}H_{44}O_4$: C, 81.60; H, 7.53%.

26: Colorless needles, dec>260 °C. Found: C, 81.56; H, 7.36%. Calcd for $C_{40}H_{44}O_4$: C, 81.60; H, 7.53%.

4,7-Bis(bromomethyl)-20,23-dimethoxy Triple-layered[2.2]-Paracyclophane (23b). A solution of dimethoxy bis(methyl ester) **23a**[7] (316.1 mg, 0.6 mmol) in dry THF (20 ml) was dropwise added to a suspension of $LiAlH_4$ (1 g) in dry THF (10 ml) under reflux and stirring. After cooling, the mixture was worked up in the usual manner and extracted with ether. The extract was washed with water, dried ($MgSO_4$), and concentrated to dryness. To the solution of the residue in benzene (30 ml) was dropwise added a solution of PBr_3 (700 mg) in benzene (10 ml). The mixture was stirred at 45 °C overnight and worked up in the usual manner to give dibromide **23b** (298.4 mg, 83.2%).

23b: Colorless fine crystals from benzene–hexane, dec >280 °C. NMR ($CDCl_3$, δ): 6.14 (s, 2H, ArH), 5.86 (s, 2H, ArH), 5.48 (s, 2H, ArH), 4.35, 4.07 (AB, $J=10$ Hz, 4H, CH_2Br), 3.54 (s, 6H, OCH_3).

Tetramethoxy Quadruple-layered [2.2]Paracyclophanes (26 and 27). A solution of dibromide **23b** (407.6 mg, 0.7 mmol) and dithiol **12** (160.6 mg, 0.7 mmol) in benzene (40 ml) was added to a stirred solution of potassium hydroxide (142.6 mg) in methanol (100 ml) for 5 h under reflux and nitrogen atmosphere. After an additional reflux for 2 h, the mixture was worked up in the usual manner. The crude product was chromatographed on silica gel with benzene to give colorless disulfide **24** (86.1 mg, 18.8%) as a mixture of two isomers.

A solution of **24** (86.1 mg, 0.13 mmol) in benzene (12 ml) and triethyl phosphite (40 ml) was irradiated with a high pressure mercury lamp under bubbling of nitrogen for 75 min. After removal of the solvents, the residue was chromatographed on silica gel to give a mixture of **26** and **27** (1: 1 ratio) in 47.0% yield (36.5 mg). The mixture was separated into the two isomers by fractional crystallization from hexane.

The less soluble isomer was in all respects identical with **26** obtained by pyrolysis of **20**. The more soluble isomer **27** was recrystallized from ethyl acetate.

27: Colorless columns, dec>260 °C. Found: M+ 588.32559. Calcd for $C_{40}H_{44}O_4$: 588.32394.

Dimethoxy Quadruple-layered [2.2]Paracyclophanequinone (6). A solution of boron tribromide (180 mg, 0.72 mmol) in dry dichloromethane (12 ml) was dropwise added to a stirred solution of **25** (104.5 mg, 0.18 mmol) in dry dichloromethane (3 ml) at 0 °C for 5 min and the stirring was continued at that temperature for 20 min. The reaction mixture was treated with water and extracted with diethyl ether. After drying ($MgSO_4$) and removal of the solvent, acetone (30 ml) and silver oxide (500 mg) were added to the residue, then the mixture was stirred at room temperature for 30 min and at 50 °C for 30 min. Insoluble material was filtered off and the filtrate was concentrated to dryness. The crude product was purified by column chromatography on silica gel with benzene–hexane to give 10.3 mg (10.4%) of **6**.

6: Red needles from ethanol, dec>220 °C. Found: M+, 558.2770. Calcd for $C_{38}H_{38}O_4$: 558.2771.

Dimethoxy Quadruple-layered [2.2]Paracyclophanequinone (7). Demethylation and oxidation of **26** were carried out as described for **6**. The crude product was chromatographed on silica gel with benzene to give **7** in 8.7% yield.

7: Red needles from ethanol, dec>230 °C. Found: M+, 558.2770. Calcd for $C_{38}H_{38}O_4$: 558.2771.

Triple-layered Dimethoxy Disulfide 29. A solution of 4,7-bis(bromomethyl)[2.2]paracyclophane **28**[13] (1.60 g, 4.06 mmol) in benzene (50 ml) and a solution of dithiol **12** (0.85 g 3.70 mmol) and potassium hydroxide (0.46 g) in aq ethanol (50 ml) were dropwise and simultaneously added to ethanol (150 ml) for 2.5 h under reflux and nitrogen atmosphere. After further reflux for 10 h, the solvents were evaporated and the residue was chromatographed on silica gel with benzene–hexane (1 : 1) to give a mixture of isomeric disulfide **29**.

29: Colorless prisms from benzene–hexane (1 : 1), mp 216—221 °C (dec). NMR ($CDCl_3$, δ): 6.6—6.1 (A_2B_2, 4H, ArH), 6.29 (s, 2H, ArH), 5.93 (d, 2H, ArH), 4.3—2.2 (m, 16H, CH_2), 3.64 (s, 6H, OCH_3); MS *m/e* 462 (M+), 263. Found: C, 72.98; H, 6.54; S, 14.00%. Calcd for $C_{28}H_{30}O_2S_2$: C, 72.69; H, 6.54; S, 13.86%.

4,7-Dimethoxy Triple-layered [2.2]Paracyclophane (30). A solution of disulfide **29** (56 mg, 0.12 mmol) in triethyl phosphite (15 ml) was irradiated with a high pressure mercury lamp for 2 h under nitrogen bubbling. After removal of the solvent, the residue was chromatographed on silica gel with benzene–hexane (1: 2) to give **30**, 36 mg (75%).

30: Colorless prisms from benzene–hexane (1: 1), mp 250 °C (dec). NMR ($CDCl_3$, δ): 6.24 (s, 4H, ArH), 5.71 (s, 2H, ArH), 5.47 (s, 2H, ArH), 3.54 (s, 6H, OCH_3), 3.4—2.1 (m, 16H, CH_2); MS *m/e* 398 (M+), 294, 234. Found: C, 84.13; H, 7.36%. Calcd for $C_{28}H_{30}O_2$: C, 84.38; H, 7.59%.

Outer Triple-layered [2.2]Paracyclophanequinone (8). A solution of dimethoxy compound **30** (21 mg, 0.06 mmol) and methylmagnesium iodide (from methyl iodide 410 mg and magnesium 100 mg) in dry diethyl ether (10 ml) was refluxed for 30 min. After removal of the solvent, the residue was heated at 160 °C for 1.5 h. To the cooled product were added diethyl ether (10 ml), water (10 ml), and dil HCl, successively. The ether layer was separated and the aqueous layer was extracted with ether several times. The combined ether solution was washed with water and dried over anhyd Na_2SO_4. After solvent removal the residue was chromatographed on silica gel to give **8**, 14 mg (72%).

8: Reddish orange crystals from benzene, mp *ca.* 225 °C (dec), MS *m/e* 368 (M+). NMR ($CDCl_3$, δ): 6.37 (s, 4H, ArH), 5.88 (s, 2H, ArH), 5.53 (s, 2H, quinone), 3.4—2.3 (m, 16H, CH_2). Found: C, 84.75; H, 6.51%. Calcd for $C_{26}H_{24}O_2$: C, 84.75; H, 6.57%.

2,5-Bis(chloromethyl)-3,6-dimethoxy-p-xylene (31). Into a solution of 2,5-dimethoxy-*p*-xylene[14] (119.4 mg, 0.72 mmol) and paraformaldehyde (222.1 mg, 3.6 mmol) in dioxane (12 ml) and concd HCl (6 ml) was bubbled hydrogen chloride gas at room temperature and then at 70 °C under stirring for 5 h. In the course of this process, an additional amount (222 mg, 3.6 mmol) of paraformaldehyde was added to the mixture. After adding ice, the mixture was extracted with diethyl ether and the extract was washed with sodium hydrogencarbonate and sat NaCl aq solution and dried (Na_2SO_4). After removal of the solvent, the residue was chromatographed on silica gel to give a colorless solid of **31**

(151.1 mg, 80.0%).

31: Colorless needles from benzene–hexane (1 : 2), mp 168.0—168.5 °C, MS *m/e* 262 (M^+), 264. NMR ($CDCl_3$, δ): 4.71 (s, 4H, CH_2), 3.83 (s, 6H, OCH_3), 2.36 (s, 6H, CH_3). Found: C, 54.48; H, 5.91%. Calcd for $C_{12}H_{16}O_2Cl_2$: C, 54.76; H, 6.13%.

5,8-Dimethoxy-6,9-dimethyl-2,11-dithia[3.3]paracyclophane ***33***. A solution of dichloride **31** (1.048 g, 3.98 mmol) in benzene (100 ml) and a solution of dithiol **32** (681 mg, 4.00 mmol) and sodium hydroxide (399 mg, 9.97 mmol) in aq ethanol (104 ml) were simultaneously and dropwise added to a boiling ethanol (100 ml) for 1 h under nitrogen; the mixture was refluxed under stirring for 6 h. After removal of the solvent, the residue was chromatographed on silica gel (40 g) with benzene. Disulfide **33** was obtained as a colorless oil (941 mg, 65.5%) which crystallized on standing or by adding a small amount of hexane.

33: Colorless prisms from methanol, mp 137—138 °C, MS *m/e* 360 (M^+); UV (THF, λ_{max} nm): 303 (ε 1010), 279 sh (1390), 260.5 (4000), 223.5 (16900). NMR ($CDCl_3$, δ): 7.04 (A_2B_2, 4H, ArH), 4.13 (d, J=13.8 Hz, 2H, CH_2), 3.79 (s, 4H, CH_2), 3.56 (s, 6H, OCH_3), 3.51 (d, J=13.8 Hz, 2H, CH_2), 2.19 (s, 6H, CH_3). Found: C, 66.43; H, 6.55; S, 17.75%. Calcd for $C_{20}H_{24}O_2S_2$: C, 66.63; H, 6.71; S, 17.79%.

4,7-Dimethoxy-5,8-dimethyl[2.2]paracyclophane ***(34)***. Disulfide **33** (102 mg, 0.29 mmol) in triethyl phosphite (10 ml) was irradiated with a high pressure mercury lamp under nitrogen bubbling for 2.5 h. The residue obtained by solvent removal was chromatographed on silica gel (15 g) with benzene–hexane (1 : 1) and then benzene. The benzene eluate was condensed and recrystallized from methanol to give **34** (50.1 mg, 59.8%).

34: Colorless prisms, mp 126—127 °C, MS *m/e* 296 (M^+); UV (THF, λ_{max} nm): 313 (ε 660), 291 (420), 254 sh (4260), 229 (17600). NMR ($CDCl_3$, δ): 6.64 (s, 4H, ArH), 3.52 (s, 6H, OCH_3), 2.93 (m, 8H, CH_2), 1.92 (s, 6H, CH_3). Found: C, 80.83; H, 8.04%. Calcd for $C_{20}H_{24}O_2$: C, 81.04; H, 8.16%.

4,7-Dimethoxy-5,8-bis(bromomethyl)[2.2]paracyclophane ***(35)***. A mixture of **34** (309.8 mg, 1.05 mmol), NBS (413.3 mg, 2.32 mmol), and a catalytic amount of benzoyl peroxide in carbon tetrachloride (60 ml) was refluxed for 3 h. The mixture was worked up in the usual manner. The solid thus obtained was recrystallized from hexane to give dibromide **35** (407.2 mg, 85.8%).

35: Colorless cubic crystals from hexane, mp 176—177 °C, MS *m/e* 452 (M^+), 454, 456. NMR ($CDCl_3$, δ): 6.68, 6.36 (A_2B_2, J=8, 2 Hz, 4H, ArH), 4.59, 4.02 (AB, J=9.6 Hz, 4H, CH_2Br), 3.71 (s, 6H, OCH_3), 2.6—3.4 (m, 8H, CH_2). Found: C, 52.69; H, 4.69; Br, 35.29%. Calcd for $C_{20}H_{22}O_2Br_2$: C, 52.88; H, 4.88; Br, 35.19%.

Triple-layered Dimethoxy Disulfide ***(36)***. A solution of dibromide **35** (212.2 mg, 0.47 mmol) in benzene (25 ml) and a solution of dithiol **32** (81.4 mg, 0.48 mmol) and NaOH (56.8 mg, 1.42 mmol) in aq ethanol (24 ml) were added simultaneously and dropwise to a boiling ethanol (20 ml) for 67 min under nitrogen. The mixture was refluxed for 6.5 h and worked up as described for **33** to give disulfide **36**, 106.5 mg (49.3%).

36: Colorless fine crystals from benzene–methanol (1 : 3), mp 211—213 °C, MS *m/e* 462 (M^+); UV (THF, λ_{max} nm): 351 (ε 1140), 311 sh (950), 290 sh (2020), 225 (20300). NMR ($CDCl_3$, δ): 6.83 (s, 4H, ArH), 6.54, 6.26 (A_2B_2, J=8, 2 Hz, 4H, ArH), 3.96 (s, 6H, OCH_3), 3.72, 3.30 (AB, J=14 Hz, 4H, CH_2), 3.70 (s, 4H, CH_2), 2.82 (m, 8H, CH_2). Found: C, 72.43; H, 6.29; S, 13.87%. Calcd for $C_{28}H_{30}O_2S_2$: C, 72.69; H, 6.54; S, 13.86%.

12,15-Dimethoxy Triple-layered [2.2]Paracyclophane ***(37)***. Dimethoxy disulfide **36** (31.7 mg, 6.5 mmol) in triethyl phosphite (10 ml) was irradiated with a high pressure mercury lamp for 2 h. The mixture was worked up as described for **34**.

37: Colorless fine crystals from hexane, mp 230 °C (dec), MS *m/e* 398 (M^+); UV (THF, λ_{max} nm): 385 sh (ε 800), 375 (970), 315 sh (1280), 294 (1680), 226 (17500). NMR ($CDCl_3$, δ): 6.61 6.19 (A_2B_2, J=8, 2 Hz, 8H, ArH), 3.99 (s, 6H, OCH_3), 2.3—3.1 (m, 16H, CH_2). Found: C, 84.12; H, 7.57%. Calcd for $C_{28}H_{30}O_2$: C, 84.38; H, 7.59%.

Inner Triple-layered [2.2]Paracyclophanequinone ***(9)***. A solution of dimethoxy compound **37** (52.6 mg, 0.13 mmol) in diethyl ether (30 ml) was worked up as described for **8**. The resulting brown oil in acetone (10 ml) was refluxed with silver oxide (0.5 g) and magnesium sulfate (1 g) for 1 h. After removal of insoluble material by filtration and washing with benzene, the combined solution was chromatographed on silica gel (5 g) with benzene to give yellow quinone **9**, 6.0 mg (12.3%) from benzene–hexane (1: 2).

9: Yellow prisms, dec>250 °C with sublimation, MS *m/e* 368 (M^+). NMR ($CDCl_3$, δ): 6.56, 6.33 (A_2B_2, J=8.0, 1.4 Hz, 8H, ArH), 3.3—2.2 (m, 16H, CH_2). Found: C, 84.54; H, 6.53%. Calcd for $C_{26}H_{24}O_2$: C, 84.75; H, 6.57%.

Dimethoxy Quadruple-layered [2.2]Paracyclophanequinones ***(39 and 40)***. Cross-breeding reactions of quarternary ammonium bromides, **19** and **38**,[5] were done as described for **15**. After the reaction was over, benzene was added to the reaction mixture and the insoluble polymer was filtered off. The filtrate was condensed and passed through a short column of silica gel to remove the polymer. The crude product was chromatographed on silica gel with benzene–hexane to separate non-substituted and tetramethoxy quadruple-layered paracyclophanes from the desired dimethoxy compound. The dimethoxy compound was separated by recrystallization from hexane into two isomers, the less soluble isomer **39** and the more soluble one **40**.

39: Colorless prisms, mp 205.5—206.5 °C with decomp. Found: C, 86.14; H, 7.54%. Calcd for $C_{38}H_{40}O_2$: C, 86.32; H, 7.63%.

40: Colorless columns, mp 205.0—205.5 °C. Found: C, 86.10; H, 7.44%. Calcd for $C_{38}H_{40}O_2$: C, 86.32; H, 7.63%.

Alternative Synthesis of ***40***. Coupling of dibromide **23b** and dithiol **32** was carried out as described for **14**. The crude product was chromatographed on silica gel with benzene to give quadruple-layered disulfide **41** in 33.1% yield. Without further purification, **41** was used for the following reaction. A solution of **41** (117.1 mg) in benzene (30 ml) and triethyl phosphite (70 ml) was irradiated with a high pressure mercury lamp under bubbling of nitrogen for 1.3 h. The solvent was removed under vacuum and the crude product was purified by column chromatography on silica gel to give a 25.2% yield of **40** which was in all respects identical with the more soluble isomer described above.

Quadruple-layered [2.2]Paracyclophanequinone ***(10)***. To a methylmagnesium iodide solution (from 101.3 mg, 4.2 mmol of magnesium and excess of methyl iodide in dry diethyl ether, 50 ml) was added crystals of **39** (109.1 mg, 0.21 mmol) in a portion. After stirring for 40 min and removal of the solvent, the residue was heated at 160—170 °C for 50 min. The mixture was worked up as described for **6**. The crude product was chromatographed on silica gel with benzene to give 29.1 mg (28.3%) of **10**.

10: Red needles from ethanl, odec>235 °C. Found: M^+, 498.2570. Calcd for $C_{36}H_{34}O_2$: 498.2558.

Quadruple-layered [2.2]Paracyclophanequinone ***(11)***. Demethylation and oxidation of **40** were carried out as described

for **6**. The crude product was chromatographed on silica gel with benzene to give **11** in 29.0% yield.

11: Red needles from ethanol, dec>230 °C. Found: M^+, 498.2558. Calcd for $C_{36}H_{34}O_2$: 498.2558.

The present work was partially supported by Grants-in-Aid for Developmental Scientific Research No. 274153 and 374164 from the Ministry of Education, Science and Culture, for which the authors are grateful.

References

1) Part LXIII: T. Otsubo, H. Horita, Y. Koizumi, and S. Misumi, *Bull. Chem. Soc. Jpn.*, **53**, 1677 (1980).

2) A part of this work was preliminarily reported: H. Tatemitsu, T. Otsubo, Y. Sakata, and S. Misumi, *Tetrahedron Lett.*, **1975**, 3059; H. Machida, H. Tatemitsu, Y. Sakata, and S. Misumi, *ibid.*, **1978**, 915.

3) For review, see S. Misumi, *Kagaku No Ryoiki*, **32**, 651 (1978).

4) H. A. Staab and W. Rebafka, *Chem. Ber.*, **110**, 3333 (1977); H. A. Staab, C. P. Herz, and H.-E. Henke, *ibid.*, **110**, 3351 (1977) and references cited therein.

5) T. Otsubo, S. Mizogami, I. Otsubo, Z. Tozuka, A. Sakagami, Y. Sakata, and S. Misumi, *Bull. Chem. Soc. Jpn.*, **46**, 3519 (1973).

6) S. Iwata, K. Fuke, M. Sasaki, S. Nagakura, T. Otsubo, and S. Misumi, *J. Mol. Spectrosc.*, **46**, 1 (1973).

7) H. Tatemitsu, B. Natsume, M. Yoshida, Y. Sakata, and S. Misumi, *Tetrahedron Lett.*, **1978**, 3459.

8) H. A. Staab, U. Zapf, and A. Gurke, *Angew. Chem.*, **89**, 841 (1977).

9) H. A. Staab and U. Zapf, *Angew. Chem.*, **90**, 807 (1978).

10) For review, see a) V. Boekelheide, "Topics in Nonbenzenoid Aromatic Chemistry," Hirokawa Publ. Co., Tokyo (1973), Vol. 1, p. 47; b) F. Vögtle and P. Neumann, *Synthesis*, **1973**, 85; c) S. Misumi, *Kagaku No Ryoiki*, **28**, 927 (1974); *Mem. Inst. Sci. Ind. Res., Osaka Univ.*, **33**, 53 (1976); d) S. Misumi and T. Otsubo, *Acc. Chem. Res.*, **11**, 251 (1978).

11) D. T. Longone and H. S. Chow, *J. Am. Chem. Soc.*, **86**, 3898 (1964); *ibid.*, **92**, 994 (1970).

12) Henkel and Cie, G. m. b. H., Brit. 807720, Jan. 21, 1959; *Chem. Abstr.*, **54**, 412 h (1960).

13) N. Kannen, T. Umemoto, T. Otsubo, and S. Misumi, *Tetrahedron Lett.*, **1973**, 4397; N. Kannen, T. Otsubo, Y. Sakata, and S. Misumi, *Bull. Chem. Soc. Jpn.*, **49**, 3307 (1976).

14) W. Rebafka and H. A. Staab, *Angew. Chem. Int. Ed. Engl.*, **13**, 203 (1974).

15) T. Kaneda, T. Otsubo, H. Horita, and S. Misumi, *Bull. Chem. Soc. Jpn.*, **53**, 1015 (1980).

16) H. Mizuno, K. Nishiguchi, T. Toyoda, T. Otsubo, S. Misumi, and N. Morimoto, *Acta Crystallogr., Sect. B*, **33**, 329 (1977); H. Mizuno, K. Nishiguchi, T. Otsubo. S. Misumi and N. Morimoto, *Tetrahedron Lett.*, **1972**, 4981.

17) T. Otsubo, S. Mizogami, Y. Sakata, and S. Misumi *Bull. Chem. Soc. Jpn.*, **46**, 3831 (1973).

 © 1980 The Chemical Society of Japan Bull. Chem. Soc. Jpn., 53, 2953—2957 (1980)

Oxidative Cleavage of Tin-Tin Bonds in Hexaalkyldistannane with Several 1,4-Benzoquinones. Detection of the Semiquinone Radicals and 4-(Trialkylstannoxy)phenoxyl Radicals by ESR spectroscopy.

Sinpei KOZIMA,* Hideo FUJITA, Torazô HITOMI, Kazuhiko KOBAYASHI,† Kazuko KOBAYASHI (née KUNÔ),† and Mituyoshi KAWANISI†

Department of Chemistry, School of Liberal Arts and Sciences, Kyoto University, Sakyo-ku, Kyoto 606
†Department of Industrial Chemistry, Faculty of Engineering, Kyoto University, Sakyo-ku, Kyoto 606

(Received March 8, 1980)

The mechanism of the oxidative cleavage of tin-tin bonds in hexamethyldistannane ($Me_3SnSnMe_3$) and hexabutyldistannane ($Bu_3SnSnBu_3$) with several 1,4-benzoquinones was investigated. Chlorine-substituted 1,4-benzoquinones exerted higher reactivity, implying that the electron-acceptability of quinone is a factor governing the reaction. Stoichiometric treatments of chloranil with the distannanes ruled out the alleged isolation of the free radical, 4-(trimethylstannoxy)phenoxyl radical, reported by Cornwell *et al.* The final products were not the free radical entity but normal compounds, 1,4-bis(trimethylstannoxy)benzenes. Measurements of ESR spectra revealed the formation of the semiquinone radical anions and the subsequent formation of 4-(tributylstannoxy)phenoxyl radicals as reactive intermediates in the reaction pathway.

Oxidative cleavage of the Sn–Sn bonds in hexaorganodistannanes ($R_3Sn–SnR_3$) with halogens, oxygen, and other oxidative materials has been widely investigated.[1–7] Recently, the ability of the σ(Sn–Sn) bond as an electron donor has been obviously demonstrated by the reaction of $R_3Sn–SnR_3$ with powerful π-electron acceptors such as tetracyanoethylene (TCNE),[8] and tetracyanoquinodimethane (TCNQ).[9] In these papers, formations of charge transfer complexes, $(R_3Sn–SnR_3)^+(TCNE)^-$[8] and $(Ph_3Sn–SnPh_3)^+(TCNQ)^-$,[9] were reported, referring also to the formations of free radicals, $R_3Sn–TCNE\cdot$[8] and $R_3Sn–TCNQ\cdot$.[9]

Concerning the reaction with less powerful π-electron acceptors, *viz.* 1,4-benzoquinones and its chlorinated compounds, quite limited information has ever been available. The anion radical of 1,4-benzoquinone was detected by an ESR spectroscopy in the photolytic reaction of $Bu_3Sn–SnBu_3$ in the presence of di-*t*-butyl peroxide and 1,4-benzoquinone.[10,11] A stable free radical, Me_3Sn–chloranil·, was reported to be isolated by simple mixing of $Me_3Sn–SnMe_3$ with chloranil in molar ratio of 1 : 2, however, no structural information except elemental analysis was presented.[9] Recent report on the ESR spectrum of Me_3Sn–9,10-phenanthrenequinone radical[12] prompted us to disclose our results of the oxidative cleavage of σ(Sn–Sn) bond of R_3SnSnR_3 with several 1,4-benzoquinones. We would like to show that the free radicals, R_3Sn–1,4-benzoquinone·, could be successfully detected by ESR spectroscopy in tetrahydrofuran at low temperature, but was too unstable to be isolated at room temperature. The reaction scheme is discussed on the basis of ESR and ^{1}H-NMR spectra.

Results and Discussion

An equimolar solution of $Me_3SnSnMe_3$ and 2,3,5,6-tetrachloro-1,4-benzoquinone (chloranil, **1a**) in benzene was stirred at room temperature under ambient daylight in a nitrogen atmosphere. Gradual color change from the pale greenish yellow of **1a** into brown was observed.

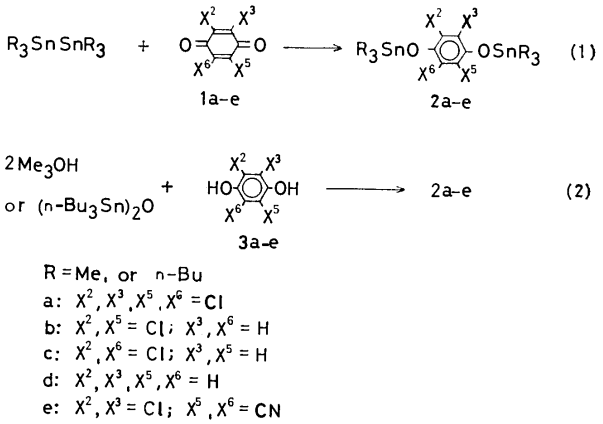

Scheme 1.

Grayish white solid began to appear in about 2 h, and precipitation almost completed within 30 h. The precipitates were identified as 1,4-bis(trimethylstannoxy)-2,3,5,6-tetrachlorobenzene (**2a**) by elemental analysis and by comparing the IR and ^{1}H-NMR spectra with those of the sample prepared by the dehydration method (Eq. 2 in Scheme 1).[13]

Cornwell, Harrison, and Richards reported the isolation of pale creamy solid which they referred to a free radical, Me_3Sn–chloranil·, by the reaction of 1 mol of $Me_3SnSnMe_3$ with 2 mol of **1a** in benzene. Repetition of this reaction allowed us to obtain similar colorless crystals. This crystalline product, however, has now been identified as the normal compound **2a**. One mol of excess **1a** was recovered unchanged from the supernatant solution of the reaction mixture. The analogous reaction of 1 mol of $Me_3SnSnMe_3$ with each 2 mol of 2,5-dichloro-1,4-benzoquinone (**1b**), 2,6-dichloro-1,4-benzoquinone (**1c**), 1,4-benzoquinone (**1d**), and 2,3-dichloro-5,6-dicyano-1,4-benzoquinone (**1e**) were carried out to give the regular products **2b**—**e**, and 1 mol of each **1b**—**e** was recovered unchanged.

^{1}H-NMR studies on the reaction of 1 mol of Me_3Sn-$SnMe_3$ with 2 mol of these 1,4-benzoquinones (**1b**—**d**)

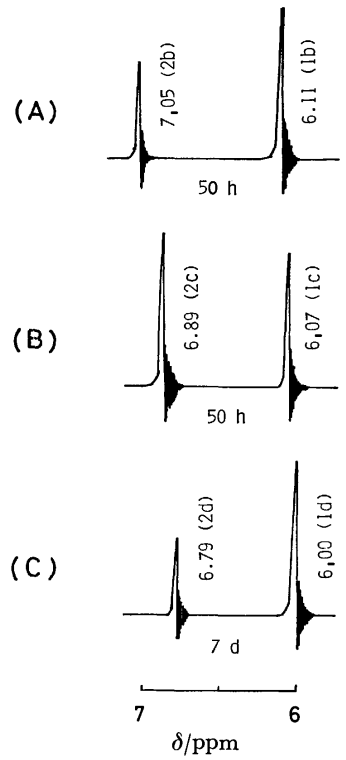

Fig. 1. ^{1}H-NMR spectra of the reaction mixtures of $Me_3SnSnMe_3$ (1 mol) with 1,4-benzoquinones (**1b—d**) (2 mol) in C_6D_6. (A): 2,5-Dichloro-1,4-benzoquinone, (B): 2,6-dichloro-1,4-benzoquinone, (C): 1,4-benzoquinone.

in C_6D_6 solution clearly showed that final products were not the free phenoxyl radicals but **2b—d**, and hence that 1 mol of the excess free 1,4-benzoquinones (**1b—d**) was always present in the solution (Fig. 1).

The electron affinity of the 1,4-benzoquinones is nicely correlated to the reaction times necessary for completing quantitative conversion in the reaction with **2e** (20 h), **2a** (1 d), **2b** (3 d), **2c** (3 d), and **2d** (a week). Particularly in the case of **2d**, the reaction was not induced in the dark even after 5 d at room temperature. These reactions were accelerated by heating and, more effectively, by UV irradiation. When the benzene solution was irradiated with a high pressure mercury lamp, the reaction was completed in less than 60 min.

Similar treatment of an equimolar solution of $Bu_3SnSnBu_3$ with 1,4-benzoquinones in benzene gave brownish (**2a—d**) and reddish oily products (**2e**).

The following scheme (Scheme 2) delineates a possible pathway. This is analogous to the proposed

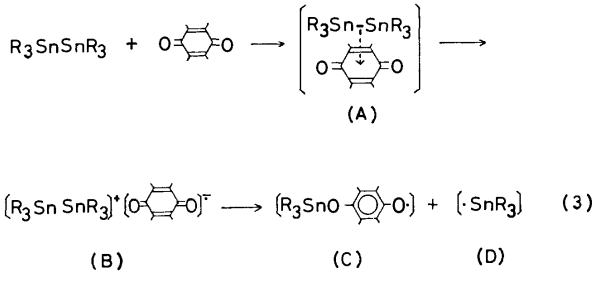

Scheme 2.

mechanism for the similar reaction of $Me_3SnSnMe_3$ with 9,10-phenanthrenequinone:[10] The electron-donating σ(Sn–Sn) bond of R_3SnSnR_3 might interact with the electron defficient 1,4-benzoquinones (acceptor) to form (σ-π) charge transfer complexes (**A**) at the initial step. The transient appearance of the dark brown color in the reaction mixture could be attributed to the formation of **A**. Then, one electron transfer from the Sn–Sn bond into the 1,4-benzoquinone to produce the semiquinone radical anion along with the radical cation of the distannane (**B**). The succeeding cleavage of the Sn–Sn bond of the cation radical in **B** affords both 4-(trialkylstannoxy)phenoxyl radical (**C**) and trialkylstannyl radical (**D**).

ESR measurements have supported the above reaction scheme. The intermediary formation of the semiquinone radical anions (**B**) and the subsequent phenoxyl radicals (**C**) has been clearly demonstrated.

The ESR spectrum of a solution of $Me_3SnSnMe_3$ and **1b** in benzene measured at room temperature displayed a triplet signal (1 : 2 : 1, a_H=1.98 G) assignable to the radical anion of **1b**.[14] The intensity of the signals gradually increased to reach a maximum in 24 h, and then began to decrease, and became finally undetectable after 3 d. Analogous semiquinone radical anion of **1c** has been observed (Table 1). In the case of **1d**, feeble signal of the semiquinone radical was detected with difficulty.

TABLE 1. ESR DATA OF THE SEMIQUINONE RADICALS OBSERVED IN THE REACTION OF $Me_3SnSnMe_3$ OR $Bu_3SnSnBu_3$ WITH 1,4-BENZOQUINONES

Radicals	$(Me_3Sn)_2$	$(Bu_3Sn)_2$
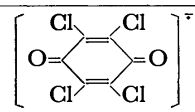		g=2.0061 singlet
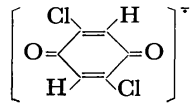	g=2.0055 triplet (1 : 2 : 1) a_H=1.98 G	g=2.0055 weak and complicated
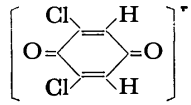	g=2.0053 triplet (1 : 2 : 1) a_H=2.38 G	g=2.0053 weak and complicated
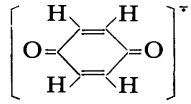	very weak	g=2.0050 quintet (1 : 4 : 6 : 4 : 1) a_H=2.32 G
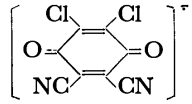		g=2.0052 quintet (1 : 2 : 3 : 2 : 1) a_N=0.61 G

By contrast, in the ESR spectra of $Bu_3SnSnBu_3$–1,4-benzoquinones systems, stronger and more clearly detectable quintet signal of the semiquinone radical of **1d** (Table 1) was observed, when a benzene solution of **1d** and $Bu_3SnSnBu_3$ was warmed up from a liquid nitrogen temperature and was kept at room temperature for 1 h. The ESR spectra of the benzene solution of $Bu_3SnSnBu_3$ with **1b** or **1c** displayed broad and weak signals. The concentration of **B** from **1b** or **1c** was too

low to be detected by ESR spectra, since **B**, if formed, could be comparatively labile and readily converted into the corresponding **C**. These different results of $Bu_3SnSnBu_3$ from those of $Me_3SnSnMe_3$ could be interpreted by taking account of the more electron donating ability of $Bu_3SnSnBu_3$ than that of $Me_3SnSnMe_3$.[7]

When the ESR spectroscopy was carried out in toluene at lower temperature, mixtures of **1b** or **1c** with $Bu_3SnSnBu_3$ afforded complicated spectra consisting of the mixed signals of **B** and **C**. The ESR spectra of the $Bu_3SnSnBu_3$–**1d** and –**1e** systems in toluene displayed strong quintet signals of the corresponding semiquinone radical anions.

In order to obtain the more detectable ESR spectra of less stable phenoxyl radical (**C**) at low temperature, tetrahydrofuran (THF) was used as a solvent. It could be expected that THF could accelerate both the electron transfer from the Sn–Sn bond and the heterolytic cleavage of Sn–Sn bond to readily convert **B** into **C**, then the concentration of **C** increased in the sample. The ESR signals of the unstable phenoxyl radicals (**C**) have now been observed at low temperature, as described below.

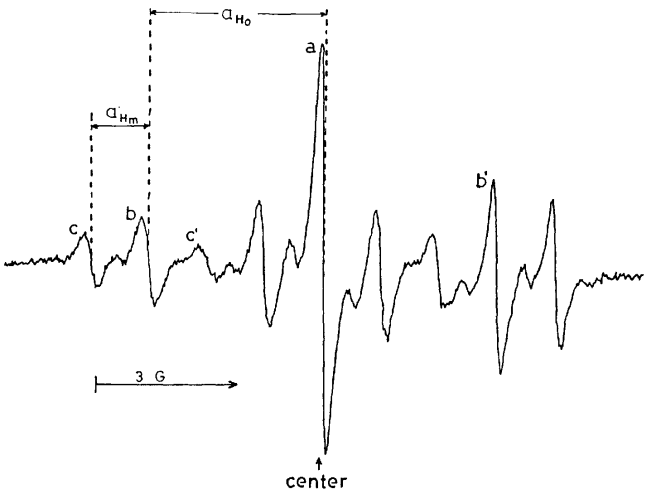

Fig. 2. The ESR spectrum of a THF solution of $Bu_3SnSnBu_3$ and 1,4-benzoquinone at −80 °C.

When a freshly prepared THF solution of $Bu_3SnSnBu_3$ and **1d** was warmed from liquid nitrogen temperature up to about 50 °C for 1 min, and was subjected to the ESR measurement at −80 °C, there were obtained ESR signals (Fig. 2). The triplet (1:2:1) of triplet (1:2:1) pattern of the signal is clearly different from that of **B** which displays the quintet, but is consistent with that of the 4-(tributylstannoxy)phenoxyl radical (**C**) (Table 2), as compared with those of the other phenoxyl radicals.[15] As the temperature of the cavity was raised from −80 °C, the ESR signals collapsed to become broad, and completely disappeared at about −20 °C. This could be due to the unstability of **C** above −20 °C. When the cavity was cooled back to −80 °C, the same spectral pattern reappeared. A short time irradiation by UV light of the solution kept in the cavity at −80 °C resulted in the increase of these ESR signals. When the reaction had been completed by 20 min irradiation with UV light in the cavity, ESR signal was no longer observed.

Table 2. Hyperfine splitting constants in 4-(tributylstannoxy)phenoxyl radicals

Radicals	g	a_{H_o}/G	a_{H_m}/G	a^{119}_{Sn}/G, a^{117}_{Sn}/G	Pattern
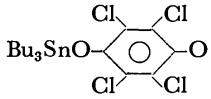	2.0050	—	—	2.21 2.11	singlet
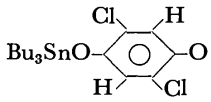	2.0054	3.12	1.04	1.94 1.85	doublet of doublet
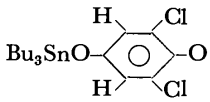	2.0053	—	1.28	1.35 1.29	triplet
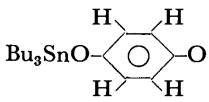	2.0047	3.67	1.22	1.36 1.30	triplet of triplet
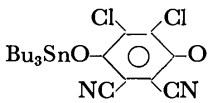	not detected				

When the reaction of $Bu_3SnSnBu_3$ with **1e** was carried out in THF, the ESR spectrum exhibited a clearly detectable quintet of **B** at −30 °C——80 °C, but no signal of **C** even at −80 °C. Warming up the solution at 50 °C for 2 min resulted in collapse of the quintet signals. This result might be attributed to the rapid conversion of the phenoxyl radical into the final product (**2e**).

The transient free phenoxyl radical (**C**), assigned by ESR spectroscopy in THF, could be converted into the product (**2**) either by the coupling with the radical (**D**), or by the reaction of **C** with R_3SnSnR_3 (Eqs. 4 and 5 in Scheme 3).

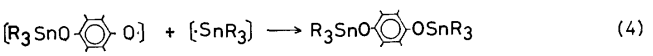

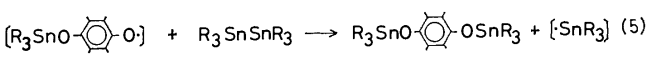

Scheme 3.

In all cases of $Me_3SnSnMe_3$ with **1b**—**e**, no definite ESR spectrum for the free phenoxyl radical was obtained even in THF solution at low temperature. This could be attributed to the more rapid consumption of **C** (R=Me) with $Me_3Sn\cdot$ or $Me_3SnSnMe_3$ than that of **C** (R=Bu) with $Bu_3Sn\cdot$ or $Bu_3SnSnBu_3$, probably because $Me_3Sn\cdot$ group or $Me_3SnSnMe_3$ has much less steric hindrance than $Bu_3Sn\cdot$ or $Bu_3SnSnBu_3$.

Experimental

All reactions were carried out in a nitrogen atmosphere. 1,4-Benzoquinones (**1a**—**e**) were purified either by vacuum sublimation or recrystallization immediately before use. The ^{1}H-NMR spectra were measured with JEOL-C60HL spectrometer operating at a resonance frequency of 60 MHz. The ^{13}C-NMR spectra were recorded in the pulse Fourier transform mode using a JEOL-FX60 spectrometer operating at a resonance frequency of 15.03 MHz. Chemical shifts were referred to tetramethylsilane.

The ESR measurements were made using a JEOL X-band spectrometer (Model ME-3) equipped with 100 kHz field modulation. The magnetic field was calibrated by the hyperfine splittings of Mn^{2+} doped in MgO and of ^{14}N of the peroxylaminedisulfonate ion.

The samples for the ESR measurements were prepared as follows. To a mixture of R_3SnSnR_3 and 1,4-benzoquinones in a quartz tube attached to a high vacuum line, anhydrous benzene, toluene, or THF was transferred. The solution was degassed at least four times. The sealed benzene solution was kept at room temperature under ambient diffused light. The ESR spectra of the benzene solution were measured at room temperature. The sealed THF solution was kept in a liquid nitrogen bath. Just before the measurement, the solution was taken out from the cold bath and warmed up at 50°C. After the solution was kept at 50 °C for several minutes in a water bath, it was cooled to −80 °C in a cavity.

*Reaction of **1a** with $Me_3SnSnMe_3$.* An equimolar mixture of $Me_3SnSnMe_3$ (0.800 g, 0.24 mmol) and **1a** (0.053 g, 0.22 mmol) in benzene (10 ml) was kept at room temperature under ambient daylight. The color of the solution gradually darkened and became dark brown in 2 h. Colorless crystals began to appear in 3 h, and were completely precipitated in 1 d. After 2 d, the crystals were collected and washed twice with benzene, and dried *in vacuo* to give colorless hexagonal plates (0.111 g), which was identified as 1,4-bis(trimethylstannoxy)-2,3,5,6-tetrachlorobenzene (**2a**). This compound (**2a**) was also prepared by the dehydration method[13] from trimethyltin hydroxide and 2,3,5,6-tetrachloro-1,4-benzenediol (**3a**) (Eq. 2 in Scheme 1). Both samples displayed the same IR and ^{1}H-NMR spectra (Table 3). Benzene of the supernatant solution was evaporated off to give brown solid (0.034 g), which was rinsed with benzene to afford **2a** (0.021 g). Total yield of **2a** was 0.132 g (94%).

A solution of $Me_3SnSnMe_3$ (0.073 g, 0.22 mmol) and **1a** (0.096 g, 0.39 mmol) in benzene (30 ml) was kept at room temperature. The reaction proceeded in the same process as the equimolar reaction. After 2 d, the crystals (**2a**, 0.109 g) were collected by decantation. Benzene of the yellowish brown supernatant solution was evaporated off *in vacuo* to give yellow crystals (0.078 g), which was dissolved in benzene (5 ml). The insoluble **2a** (0.004 g) was separated [total yield of **2a** was 0.113 g (85%)]. The benzene solution was subjected to column chromatography (silica gel, benzene) to recover the excess amount of analytically pure **1a** (0.048 g).

*Reaction of **1b** with $Me_3SnSnMe_3$.* An equimolar mixture of $Me_3SnSnMe_3$ (0.072 g, 0.22 mmol) and **1b** (0.035 g, 0.20 mmol) in benzene (10 ml) was kept at room temperature. The color of the solution darkened gradually from yellow to brown, and finally reddish brown. After 4 d, the solvent was evaporated off *in vacuo* to give pale brown solid (0.110 g) of **2b** identified by IR and ^{1}H-NMR spectra (Table 3).

A solution of $Me_3SnSnMe_3$ (0.061 g, 0.19 mmol) and **1b** (0.058 g, 0.31 mmol) in benzene (10 ml) was kept at room temperature. After 4 d, the solvent was evaporated off *in vacuo* to give pale brown solid (0.122 g). This solid was rinsed with a mixed solvent of cyclohexane (4 ml) and benzene (2 ml), and was recrystallized from benzene to give pale brown crystals (**2b**, 0.063 g). The solvent of the supernatant solution was evaporated off and the residue was redissolved in the mixed solvent to give the insoluble solid (**2b**, 0.010 g). The solvent of the rinsed solution was evaporated off to give brown solid (0.040 g), whose ^{1}H-NMR spectrum ($CDCl_3$) had two singlets; the one (+6.00 ppm) was assigned to **1b**, the other (+0.63 ppm) was assigned to Me_3SnOH.

*Reaction of **1c** with $Me_3SnSnMe_3$.* An equimolar solution of $Me_3SnSnMe_3$ (0.154 g, 0.47 mmol) and **1c** (0.083 g, 0.47 mmol) in benzene (15 ml) was kept at room temperature. The color of the solution darkened gradually from yellow to brown, and finally dark brown. After 4 d, the solvent was evaporated off *in vacuo* to give dark violet solid (0.230 g) identified as **2c** by IR and ^{1}H-NMR (Table 3 . ^{13}C-NMR ($CDCl_3$): δ −2.3 (methyl carbons), +119.5 (3,5-carbons), +126.3 (2,6-carbons).

A solution of $Me_3SnSnMe_3$ (0.097 g, 0.30 mmol) and **1c** (0.092 g, 0.52 mmol) in benzene (10 ml) was kept at room temperature. After 4 d, the solvent was evaporated off *in vacuo* to give brown solid (0.187 g). Mixed solvent of cyclohexane (2.5 ml) and benzene (1.5 ml) was added to the brown solid and insoluble solid was collected, rinsed with benzene to give pale brown solid (**2c**, 0.077 g). The solvent of the supernatant solution was evaporated off to give brown solid, which was rinsed with the mixed solvent, and further with benzene to afford **2c** (0.013 g) [total yield of **2c** was 0.090 g (63%)]. The solvent was evaporated off from the rinsed solution to give brown solid (0.091 g), whose ^{1}H-NMR ($CDCl_3$) showed two singlets; the one (+6.05 ppm) was assigned to **1c**, the other (+0.58 ppm) was assigned to Me_3SnOH.

*Reaction of **1d** with $Me_3SnSnMe_3$.* An equimolar solution of $Me_3SnSnMe_3$ (0.165 g, 0.50 mmol) and **1d** (0.055 g, 0.51

Table 3. Melting points, analytical and ^{1}H-NMR (THF) data of **2a**—**e** (R=Me)

Compound	Mp/°C	Found (%)			Calcd (%)			Sn-CH_3		CH
		C	H	N	C	H	N	δ/ppm	J_{Sn-CH_3}/Hz	δ/ppm
2a	173—174	25.03	3.37		25.12	3.14		0.56	66.0	—
2b	172—173	28.86	3.94		28.57	4.00		0.41	64.5	6.55
2c	193—194	29.93	3.79[a]		28.57	4.00		0.48	63.9	6.63
2d[b]	190—191[c]							0.42[18]	62.0	6.42[18]
2e	190—200[d]	30.46	3.40	5.08	30.30	3.27	5.05	0.62	68.0	—

a) Elemental analyses did not give satisfactory results in spite of efforts of repeated preparations and analysis. The deviation found in the elemental analyses might be due to the partial hydrolysis of the sample during recrystallization procedures.[16] b) **2d** was partially hydrolyzed during repeated recrystallizations to give analytically pure 4-(trimethylstannoxy)phenol, dp 200 °C—215 °C.[18] c) Lit, 187 °C.[17] d) Dp.

mmol) in benzene (10 ml) was kept at room temperature. The solution darkened slightly in a week. After 2 weeks the solvent was evaporated off to give pale brown solid (0.210 g). This was rinsed with cyclohexane to give pale brown solid (0.168 g, 77%) identified as **2d** by ^{1}H-NMR (Table 3) and IR spectra.[17]

Reaction of ***1e*** *with* $Me_3SnSnMe_3$. An equimolar solution of $Me_3SnSnMe_3$ (0.070 g, 0.21 mmol) and **1e** (0.046 g, 0.20 mmol) in benzene (10 ml) was kept at room temperature. The solution gradually turned brown in 15 min and reddish yellow crystals began to precipitate. The solution turned yellow in 3 h. When the mixture was kept for 20 h, the reaction was completed. The crystals were separated and recrystallized with benzene to give orange yellow needles (0.109 g, 98%) identified as **2e** (Table 3).

A solution of $Me_3SnSnMe_3$ (0.067 g, 0.20 mmol) and **1e** (0.092 g, 0.40 mmol) in benzene (10 ml) was kept at room temperature. After 2 d, crystalline **2e** (0.100 g, 90%) was collected. Benzene of the reddish brown supernatant solution was evaporated off *in vacuo* to recover the excess amount of **1e** (0.052 g).

Reaction of ***1a—d*** *with* $Me_3SnSnMe_3$ *under Irradiation.* An equimolar solution of **1a** (0.049 g, 0.20 mmol) and $Me_3SnSnMe_3$ (0.075 g, 0.23 mmol) in benzene (10 ml) in a sealed Pyrex glass tube was irradiated externally with a high pressure mercury lamp (450 W) at 20 °C. After 10 min irradiation, colorless solid precipitated and the solution turned almost colorless. After 20 min, the precipitates were collected by decantation, rinsed with benzene and dried *in vacuo* to give pure **2a** (0.083 g, 73%). The solvent of the supernatant solution was evaporated off and washed with benzene to give **2a** (0.030 g, 26%).

The reactions of **1b—d** with $Me_3SnSnMe_3$ were carried out analogously as described above: The reactions were completed within 1 h to obtain **2b**, **2c**, and **2d** in the yields of 86%, 82%, 74%, respectively.

Reaction of $Bu_3SnSnBu_3$ *with* ***1a—e***. A solution of $Bu_3SnSnBu_3$ (0.18 mmol) and **1a** (0.17 mmol) in benzene (10 ml) was stirred at room temperature being exposed to ambient diffused light. Almost quantitative yield of a brown viscous liquid, **2a** also was obtained in 25 h.

The reactions of $Bu_3SnSnBu_3$ with **1b—e** were carried out in the same manners as mentioned above. The reactions were completed in 66, 63, 140, and 24 h, respectively. Brown oily products were identified as **2b—e**, by comparing the IR and ^{13}C-NMR spectra with those of the samples prepared by Eq. 2 in Scheme 1.[13]

Reaction of $Bu_3SnSnBu_3$ *with* ***1a*** *under Irradiation.* A solution of $Bu_3SnSnBu_3$ (0.37 mmol) and **1a** (0.37 mmol) in benzene (15 ml) was irradiated. After 10 min irradiation, the color of the solution changed from pale greenish yellow to brown, and $\nu_{C=O}$ absorption of **1a** (1690 cm^{-1}) in the IR spectrum disappeard completely. Removal of the solvent *in vacuo* gave almost quantitative yield of **2a**.

Thermal Reaction of $Bu_3SnSnBu_3$ *with* ***1a***. An equimolar mixture of $Bu_3SnSnBu_3$ (0.31 mmol) and **1a** (0.27 mmol) in benzene was heated under reflux for 1.5 h. The $\nu_{C=O}$ absorption in the IR spectrum was absent, and the solvent was evaporated off to give **2a** quantitatively.

References

1) G. Tagliavini, S. Faleschini, G. Pilloni, and G. Plazzogna, *J. Organomet. Chem.*, **5**, 136 (1966).

2) H. H. Anderson, *Inorg. Chem.*, **3**, 108 (1964).

3) P. Bamberg, B. Ekström, and B. Sjöberg, *Acta Chem. Scand.*, **22**, 367 (1968).

4) G. Tagliavini and L. Doretti, *Chem. Commun.*, **1966**, 562.

5) L. Doretti and G. Tagliavini, *J. Organomet. Chem.*, **12**, 203 (1968).

6) N. A. D. Carey and H. C. Clark, *Can. J. Chem.*, **46**, 643 (1968).

7) A. Peloso, *J. Organomet. Chem.*, **67**, 423 (1974); **74**, 59 (1974).

8) P. J. Krusic, H. Stoklosa, L. E. Manzer, and P. Meakin, *J. Am. Chem. Soc.*, **97**, 667 (1975); V. F. Traven and R. West, *ibid.*, **95**, 6824 (1973); *Zh. Obshch. Khim.*, **44**, 1837 (1974); O. A. Reutov, V. I. Rozenberg, G. V. Gavrilova, and V. A. Nikanorov, *J. Organomet. Chem.*, **177**, 101 (1979).

9) A. B. Cornwell, P. G. Harrison, and J. A. Richards, *J. Organomet. Chem.*, **140**, 273 (1977).

10) J. Cooper, A. Hudson, and R. A. Jackson, *J. Chem. Soc., Perkin Trons. 2*, **1973**, 1933.

11) K. S. Chen, T. Foster and J. K. S. Wan, *J. Chem. Soc., Perkin Trans, 2*, **1979**, 1288.

12) K. Mochida, J. K. Kochi, K. S. Chen, and J. K. S. Wan, *J. Am. Chem. Soc.*, **100**, 2927 (1978).

13) G. Weissenberger, U. S. Patent 3129236 (Cl. 260—429.7), Apr. 14, (1964); Swiss Appl. Dec. 31, (1960), 6 pp; *Chem. Abstr.*, **61**, 686 e, (1964).

14) W. E. Geiger, Jr., and W. M. Gulik, Jr., *J. Am. Chem. Soc.*, **91**, 4657 (1969).

15) T. J. Stone and W. A. Waters, *J. Chem. Soc.*, **1964**, 213; H. B. Stegmann and K. Scheffler, *Tetrahedron Lett.*, **1964**, 3387.

16) The elemental analyses always showed the intermediate values between the calulated ones of **2c** and those of 4-trimethylstannoxy-3,5-dichlorophenol (Calcd for $C_9H_{12}O_2Cl_2Sn$: C, 31.67; H, 3.52%).

17) N. Wiberg and M. Veith, *Chem. Ber.*, **104**, 3191 (1971).

18) ^{1}H-NMR (THF): δ 0.43 (s, 9H, J_{Sn-CH_3}=60.0 Hz), 6.40 (d, 2H, 2,6-protons, J=9 Hz), 6.50 (d, 2H, 3,5-protons). Found: C, 39.84; H, 5.33%. Calcd for $C_9H_{14}O_2Sn$: C, 39.61; H, 5.17%.

A Facile Synthesis of 1,2-Divinylcycloalkanols and Their Behavior in the Oxy-Cope Rearrangement[1]

Tetsuya KATO,* Hisao KONDO, Masaki NISHINO, Minoru TANAKA, Go HATA, and Akihisa MIYAKE

Basic Research Laboratories, Toray Industries, Inc., Tebiro, Kamakura 248

(Received March 12, 1980)

The reaction of 2-chlorocycloalkanones with vinylmagnesium chloride gives 1,2-divinylcycloalkanols. Divinylation proceeds *via* a rearrangement of initially formed 2-chloro-1-vinylcycloalkanols to 2-vinylcycloalkanones followed by further vinylation of 2-vinylcycloalkanones. Thermal sigmatropic rearrangement of 1,2-divinylcycloalkanols gives 5-cycloalken-1-ones in good yields. The influence of the size of rings on the reaction pathways is discussed.

The oxy-Cope rearrangements are powerful reactions for the preparation of α,ε-unsaturated carbonyl compounds and α,δ-dicarbonyl derivatives.[2] Marvell and Whally extended this utility to the formation of ten-menbered rings from *trans*- and *cis*-1,2-divinylcyclohexanols.[3] Although good yields can be obtained in these reactions, the preparation of 1,2-divinylcyclohexanols requires multistep reactions, *i.e.*, vinylation of cyclohexene oxide with vinyllithium and oxidation of the resulting 2-vinylcyclohexanol with chromium trioxide followed by vinylation of 2-vinylcyclohexanone with vinylmagnesium bromide. We wish to report on the one-step synthesis of 1,2-divinylcycloalkanols and their behavior in the oxy-Cope rearrangement. The influence of the size of rings on the reaction pathways is also discussed.

Results and Discussion

Divinylation of 2-Chlorocycloalkanones. The reaction of 2-chlorocycloalkanones **1** with vinylmagnesium chloride in tetrahydrofuran (THF)[4] gives 1,2-divinylcycloalkanols **5**. Divinylation was carried out in the presence of more than 2 molar equiv of vinylmagnesium chloride at temperatures above 50 °C. The results are summarized in Table 1.

The results suggest that the yields of 1,2-divinylcycloalkanols **5** are markedly influenced by the size of rings, decreasing in the order: n=4>5>10>3>9>2. The reaction of 2-chlorocyclobutanone **1a** showed an exceptional trend, affording no detectable amount of 1,2-divinylcyclobutanol **5a**.

Divinylation of 2-chlorocycloalkanones **1**, except for the case of 2-chlorocyclobutanone **1a**, was found to proceed *via* the vinyl group rearrangement of the initially formed chlorohydrin derivatives **2**, followed by further vinylation of the resulting 2-vinylcycloalkanones **4**. The reaction pathways can be reasonably accounted for by the following observations. Treatment of 2-chlorocycloalkanones **1** with vinylmagnesium chloride in THF below room temperature predominantly affords chlorohydrins **3**.[5,6] The direct attack of vinylmagnesium chloride on chlorine atom is a minor reaction pathway.[7] For example, when 2-chlorocyclododecanone **1f** was treated with 1.15 molar equiv of vinylmagnesium chloride in THF at 0 °C, 2-vinylcyclododecanone **4f** was obtained in less than 1.6% yield, whereas 2-chloro-1-vinylcyclododecanol **3f** was obtained in 87—94% yield.

1,2-Migration of the vinyl group in chlorohydrins **3** takes place smoothly to afford 2-vinylcycloalkanones **4** when the magnesium salts of the chlorohydrins **3** (n= 3, 4, 5, 9, 10) are heated[5-9] in a solution above 50 °C. On the other hand, the reaction of 2-chlorocyclobutanone **1a** with vinylmagnesium chloride predominantly affords 1-cyclopropyl-4-penten-1-one **7**. Formation of **7** can be rationalized by assuming that the reaction proceeds *via* the ring contraction of the chlorohydrin derivative **2** (n=2) in place of the vinyl group rearrangement, followed by the conjugate addition of vinylmagnesium chloride to the resulting 1-cyclopropyl-2-propen-1-one **6**.[10] In the reaction of 2-chlorocycloalkanones **1** (n=3, 4, 5, 9,10) the ring contraction is a minor pathway. For example, 2-chlorocyclododecanone **1f** upon treatment with vinylmagnesium chloride at 55 °C gave 1-cycloundecyl-4-penten-1-one **8** only in 2% yield.

2-Vinylcycloalkanones **4** were easily converted into 1,2-divinylcycloalkanols **5** with vinylmagnesium chloride

Table 1. Divinylation of 2-chlorocycloalkanones with vinylmagnesium chloride

	n	Molar ratio CH_2=CHMgCl/**1**	Temp/°C	Yield **5** (%)
1a	2	2.60	55	0
1b	3	2.32	55	31
1c	4	2.50	55	90
1d	5	2.52	55	75
1e	9	2.20	55	7
1f	10	2.20	55	53

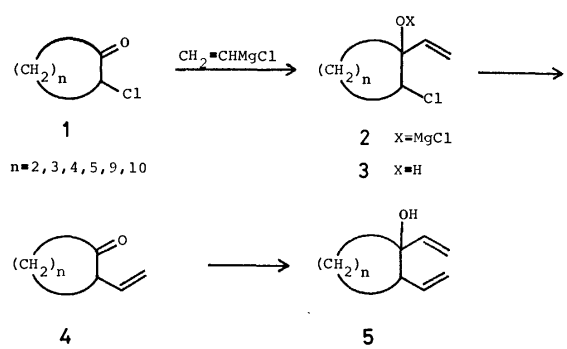

Scheme 1.

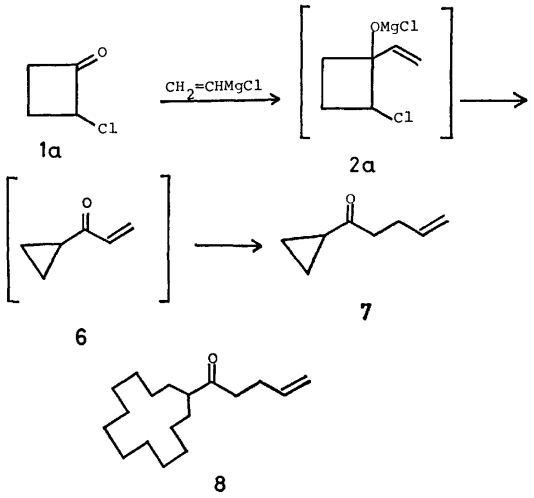

Scheme 2.

in THF at 0 °C. The major side reaction in the vinylation of **4** is the formation of enolates **9**[11] which upon hydrolysis lead to the recovery of **4** as well as the formation of 2-ethylidenecycloalkanones **10.**

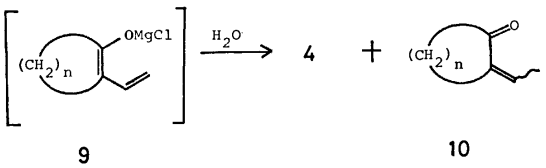

Scheme 3.

The Oxy-Cope Rearrangement of 1,2-Divinylcycloalkanols. Thermal [3,3] sigmatropic rearrangement of 1,2-divinylcycloalkanols **5** at 165—220 °C gave 5-cycloalken-1-ones **11.** The rearrangement was carried out by using a mixture of *trans-* and *cis*-1,2-divinylcycloalkanols prepared by the direct divinylation of 2-chlorocycloalkanones **1.** The results are summarized in Table 2. When 1,2-divinylcyclohexanol **5c** was used, the highest yield (82%) was obtained. The yields of **11** decreased

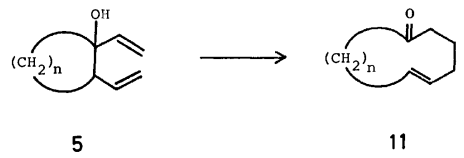

Scheme 4.

Table 2. Thermal [3,3] sigmatropic rearrangement of 1,2-divinylcycloalkanols

	n	Temp/°C	Time/h	Yield **11** (%)
5b	3	200	4	60
5c	4	220	2	82
5d	5	220	2	80
5e	9	180	2	74
5f	10	165	6	77

in the order: n=4>5>10>9>3.

Marvell and Whally examined the thermal rearrangement of *trans-* and *cis*-1,2-divinylcyclohexanols to 5-cyclodecen-1-one **11c** in detail.[3] We have examined the thermal rearrangement of *trans*-**12** and *cis*-1,2-divinylcyclododecanols **13**, and *trans*-**20** and *cis*-1,2-divinylcyclopentanols **21** in order to clarify the influence of the size of rings on the oxy-Cope rearrangement. Divinylation of 2-chlorocyclododecanone **1f** afforded a 40 : 60 ratio of *trans*-**12** and *cis*-1,2-divinylcyclododecanols **13.** When the minor isomer was heated at 180 °C for 3 h, the single product, (*E*)-5-cyclohexadecen-1-one **18** was obtained in 92% yield. The major isomer, under the same conditions, provided a mixture containing (*E*)-**18** and (*Z*)-5-cyclohexadecen-1-ones **19** in 24: 76 ratio in 67% yield. Infrared spectroscopy was used to distinguish (*E*)- (970 cm^{-1}) **18** from (*Z*)-5-cyclohexadecen-1-ones (720 cm^{-1}) **19.** Assuming that the rearrangement involves a concerted stereospecific Cope reaction *via* a chair-like transition state (**15, 16,** and **17**),[12] which minimizes 1,3-pseudo-diaxial interactions, the major isomer can be assigned to *cis*-1,2-

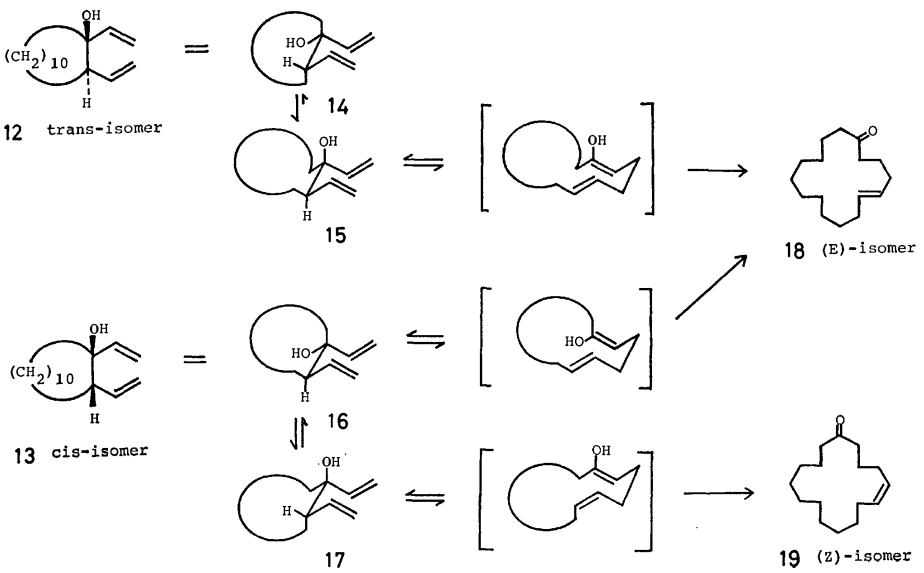

Scheme 5.

divinylcyclododecanol **13**. The stereochemical results are similar to those of 1,2-divinylcyclohexanols.[3]

Divinylation of 2-chlorocyclopentanone **1b** afforded an 81: 19 ratio of *trans*- **20** and *cis*-1,2-divinylcyclopentanols **21**. The major isomer was assigned to *trans*-1,2-divinylcyclopentanol **20** on the basis of the predominance of *trans* products in the addition of the Grignard reagents to 2-alkylcyclopentanones.[13] The thermal rearrangement of both *trans*- **20** and *cis*-1,2-divinylcyclopentanols **21** provided the single product (*E*)-5-cyclononen-1-one **22**,[14] in 46 and 72% yields, respectively, no detectable amount of (*Z*)-5-cyclononen-1-one being obtained. The stereochemistry of the product can be rationalized by assuming that chair-like transition geometries (**20** and **21**) are involved in the rearrangement of *trans*- and *cis*-1,2-divinylcyclopentanols.[15]

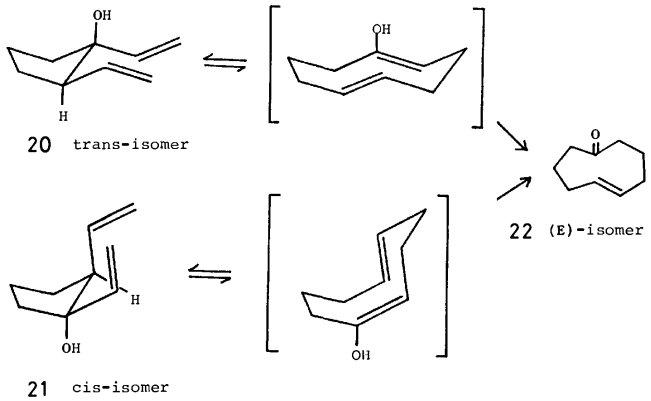

Scheme 6.

Experimental

Melting and boiling points are uncorrected. Gas-liquid chromatography (GLPC) analyses were performed on a Shimadzu 3BT instrument using 10% Silicone OV-17 or 5% PEG-20M coated on Chromosorb WHP (80—100 mesh) packed in glass columns (1.2 m). The following spectrometers were used: IR, Hitachi 215; NMR, Varian XL-100 or JEOL FX-100 (TMS as an internal standard); mass spectra, Hitachi RMU-7M or RMS-4. Silica gel (Merck, 70—230 mesh) was used for column chromatography. Unless otherwise stated, 2-chloro-1-vinylcycloalkanols **3**, 1,2-divinylcycloalkanols **5**, and 5-cycloalken-1-ones **11** consist of *trans*- and *cis*-isomers, or (*E*)- and (*Z*)-isomers.

2-Chlorocycloalkanones (1). 2-Chlorocycloalkanones **1** were prepared by the chlorination of cycloalkanones.[16-18]

Chlorohydrins (3). Typical Procedure: A solution of 2-chlorocycloundecanone **1e** (16.0 g, 79.0 mmol) in THF (20 ml) and a solution of vinylmagnesium chloride in THF (1.73 mol/l, 54.8 ml, 94.8 mmol) were added dropwise to THF (183 ml) at 0 °C during a period of 1 h. The mixture was stirred at 0 °C for 1.5 h, poured into an aqueous ammonium chloride solution and extracted with hexane. The hexane extracts were washed with water, dried over anhydrous sodium sulfate and concentrated to give 16.95 g of oil. GLPC analysis showed two major peaks due to 2-chloro-1-vinylcycloundecanol **3e** (69.3%). The oil was chromatographed on silica gel (benzene) to give a mixture of *trans*- and *cis*-2-chloro-1-vinylcycloundecanols (7.18 g, 39%). **3e**: bp 112—113 °C/0.6 Torr, mp 37—40 °C; IR (neat) 3570, 3080, 1643, 1140, 988, 922 cm^{-1}; NMR (CCl_4) δ 1.1—2.4 (m, 18H), 2.02 (s, 1H), 4.18 (dd, J=3 and 8 Hz, 1H), 5.10 (dd, J=2 and 11 Hz, 1H), 5.30 (dd, J=2 and 17 Hz, 1H), 5.96 (dd, J=11 and 17 Hz, 1H); MS *m/e* 232, 230 (M^+). Found: C, 67.92; H, 10.06; Cl, 15.34%. Calcd for $C_{13}H_{23}OCl$: C, 67.66; H, 10.05; Cl, 15.36%.

2-Chloro-1-vinylcyclobutanol (3a): Bp 65—75 °C/21 Torr; IR (neat) 3445, 1638, 985, 925, 855 cm^{-1}; NMR (CCl_4) δ 1.7—2.7 (m, 5H), 4.16—4.38 (m, 1H), 4.98—5.46 (m, 2H), 5.85 (dd, J=10 and 16 Hz, 1H). MS *m/e* 134, 132 (M^+). Found: C, 54.49; H, 6.91; Cl, 26.64%. Calcd for C_6H_9OCl: C, 54.34; H, 6.79; Cl, 26.79%.

2-Chloro-1-vinylcyclododecanol (3f, trans-*Isomer)*: Mp 55—55.5 °C; IR (KBr) 3550, 1640, 1118, 988, 919, 758 cm^{-1}; NMR (CCl_4) δ 1.1—2.3 (m, 21H), 4.03 (d, J=8 Hz, 1H), 5.10 (dd, J=2 and 11 Hz, 1H), 5.29 (dd, J=2 and 17 Hz, 1H), 5.92 (dd, J=11 and 17 Hz, 1H); MS *m/e* 246, 244 (M^+). Found: C, 68.47; H, 10.07; Cl, 14.63%. Calcd for $C_{14}H_{25}OCl$: C, 68.69; H, 10.29; Cl, 14.48%. (*3e*, cis-*isomer*): mp 63—65 °C; IR (KBr) 3550, 1638, 994, 908, 768 cm^{-1}; NMR (CCl_4) δ 1.0—2.3 (m, 21H), 4.03 (d, J=8 Hz, 1H), 5.05 (dd, J=2 and 11 Hz, 1H), 5.27 (dd, J=2 and 17 Hz, 1H), 5.90 (dd, J=11 and 17 Hz, 1H); MS *m/e* 246, 244 (M^+). Found: C, 68.51; H, 10.08; Cl, 14.52%. Calcd for $C_{14}H_{25}OCl$: C, 68.69; H, 10.29; Cl, 14.48%.

2-Vinylcycloalkanones (4). Typical Procedure: A solution of 2-chloro-1-vinylcycloundecanol **3e** (6.99 g, 30.3 mmol) in benzene (98 ml) was added to a stirred solution of ethylmagnesium bromide in ether (1.87 mol/l, 15.1 ml, 28.3 mmol) at 0 °C during a period of 1 h. After being stirred at 0 °C for 10 min, the reaction mixture was heated at 70 °C for 30 min, cooled, poured into an aqueous ammonium chloride solution and extracted with benzene. The benxene extracts were washed with water and dried over anhydrous sodium sulfate. After removal of the solvent, the residue was distilled (bp 91—93 °C/0.5—0.6 Torr) to give 5.16 g of oil. GLPC analysis showed one major peak due to 2-vinylcycloundecanone **4e** (82.7%). The yield of **4e** was 74%. The oil was chromatographed on silica gel (benzene) to give pure **4e** (2.60 g). **4e**: bp 88—89 °C/0.5 Torr; mp 35—37 °C; IR (neat) 3080, 1720, 1635, 995, 915 cm^{-1}; NMR (CCl_4) δ 1.1—2.3 (m, 16H), 2.3—2.7 (m, 2H), 3.29 (t, J=9 Hz, 1H), 4.91—5.18 (m, 2H), 5.50—5.90 (m, 1H); MS *m/e* 194 (M^+). Found: C, 80.51; H, 11.56%. Calcd for $C_{13}H_{22}O$: C, 80.36; H, 11.41%.

2-Vinylcyclododecanone (4f): Bp 80—84 °C/0.2 Torr; n_D^{20}= 1.4943; IR (neat) 3080, 1712, 1638, 995, 915 cm^{-1}; NMR (CCl_4) δ 1.0—2.1 (m, 18H), 2.25—2.60 (m, 2H), 3.10—3.40 (m, 1H), 4.90—5.20 (m, 2H), 5.53—5.94 (m, 1H); MS *m/e* 208 (M^+). Found: C, 67.84; H, 10.20; N, 15.88%. Calcd for $C_{15}H_{27}ON_3$ (semicarbazone, mp 182—184 °C): C, 67.84; H, 10.27; N, 15.84%.

1,2-Divinylcycloalkanols (5). Typical Procedure: A solution of 2-vinylcycloundecanone **4e** (2.40 g, 12.4 mmol) in THF (10 ml) was added dropwise to a stirred solution of vinylmagnesium chloride in THF (1.00 mol/l, 23.2 ml, 23.2 mmol) at 0 °C during a period of 1 h. After being stirred at 0 °C for 1.5 h, the reaction mixture was poured into an aqueous ammonium chloride solution and extracted with hexane. The hexane extracts were washed with water and dried over anhydrous sodium sulfate. After removal of the solvent, the residue was distilled (oil bath 140 °C/0.5 Torr) to give 1.71 g of oil. GLPC analysis showed a peak due to 1,2-divinylcycloundecanol **5e** (23.5%). The yield of **5e** from **4e** was 14.6%. The oil was chromatographed on silica gel (benzene) to give pure **5e**. **5e**: IR (neat) 3470, 3070, 1638, 1175, 1125, 995, 915 cm^{-1}; NMR (CCl_4) δ 1.0—2.0 (m, 19H), 2.0—2.3 (t, J=4 Hz, 1H), 4.65—5.10 (m, 4H),

5.30—5.85 (m, 2H); Found: C, 80.99; H, 11.65%. Calcd for $C_{15}H_{26}O$: C, 81.02; H, 11.78%.

*1,2-Divinylcyclopentanol (**5b**, trans-Isomer)*: $n_D^{23}=1.4810$; IR (neat) 3500, 3080, 1648, 1000, 920 cm^{-1}; NMR (CCl_4) δ 1.5—2.0 (m, 7H), 2.10—2.45 (m, 1H), 4.80—5.24 (m, 4H), 5.42—5.90 (m, 2H). Found: C, 78.42; H, 10.19%. Calcd for $C_9H_{14}O$: C, 78.21; H, 10.21%.

*(**5b**, cis-Isomer)*: $n_D^{23}=1.4859$; IR (neat) 3430, 3080, 1645, 995, 918 cm^{-1}; NMR (CCl_4) δ 1.3—2.6 (m, 8H), 4.70—5.18 (m, 4H), 5.30—5.90 (m, 2H). Found: C, 77.71; H, 10.23%. Calcd for $C_9H_{14}O$: C, 78.21; H, 10.20%.

*1,2-Divinylcyclohexanols (**5c**, trans- and cis-Isomers)*: The IR and NMR spectra of **5c** were identical with those of authentic samples.[3]

*1,2-Divinylcyclododecanol (**5f**, trans-Isomer)*: Mp 51—52 °C; IR (KBr) 3400, 3060, 1638, 997, 980, 918, 906 cm^{-1}; NMR (CCl_4) δ 1.0—2.0 (m, 21H), 2.15 (t, $J=10$ Hz, 1H), 4.70—6.02 (m, 6H). Found: C, 81.59; H, 11.99%. Calcd for $C_{16}H_{28}O$: C, 81.29; H, 11.94%.

*(**5f**, cis-Isomer)*: Bp 122—123 °C/0.7 Torr; mp 15—16 °C; $n_D^{20}=1.5023$; IR (neat) 3540, 3060, 1638, 998, 920 cm^{-1}; NMR (CCl_4) δ 0.95—1.9 (m, 21H), 2.30 (t, $J=10$ Hz, 1H), 4.88—6.02 (m, 6H). Found: C, 81.51; H, 11.91%. Calcd for $C_{16}H_{28}O$: C, 81.29; H, 11.94%.

*Direct Divinylation of 2-Chlorocycloalkanones (**1**) with Vinylmagnesium chloride. Typical Procedure*: A solution of 2-chlorocycloundecanone **1e** (10.1 g, 50.0 mmol) in THF (12 ml) and a solution of vinylmagnesium chloride in THF (1.73 mol/l, 34.7 ml, 60.0 mmol) were added dropwise to THF (60 ml) at 0 °C during a period of 1 h. Stirring was continued at 0 °C for 1.5 h. After a solution of vinylmagnesium chloride in THF (1.73 mol/l, 28.9 ml, 50.0 mmol) had been added during a period of 10 min, the reaction mixture was heated at 55 °C for 15 h, poured into an aqueous ammonium chloride solution and extracted with benzene. The benzene extracts were washed with water and dried over anhydrous sodium sulfate. After removal of the solvent, the residue was distilled (bp 100—106 °C/0.5 Torr) to give 6.28 g of oil. GLPC analysis showed a peak due to 1,2-divinylcycloundecanol **5e** (12.9%). The yield of **5e** from **1e** was 7.3%.

*Thermal Rearrangement of 1,2-Divinylcycloalkanols (**5**).*

Typical Procedure: *trans*-1,2-Divinylcyclopentanol **20** (3.00 g, 16.7 mmol) was heated at 200 °C for 3 h. The reaction mixture was distilled (bp 61 °C/3 Torr) to give 1.47 g of oil. GLPC analysis showed one major peak (94.5%) due to (*E*)-5-cyclononen-1-one **22**. The yield was 46%. *cis*-1,2-Divinylcyclopentanol **21** (1.00 g, 5.55 mmol), under the same conditions, gave an oil (0.68 g) containing (*E*)-5-cyclononen-1-one **22** (94.6%) as a major product, the yield being 72%. The IR and NMR spectra of (*E*)-5-cyclononen-1-one **22** were identical with those of an authentic sample.[14]

*5-Cyclodecen-1-one [**11c**, (E)- and (Z)-Isomers]*: The IR and NMR spectra of **11c** were identical with those of authentic samples.[3]

*5-Cycloundecen-1-one (**11d**)*: Bp 74 °C/1 Torr; $n_D^{25}=1.4904$; IR (neat) 3025, 1718, 1625, 980, 762 cm^{-1}; NMR (CCl_4) δ 1.1—2.6 (m, 16H), 4.88—5.48 (m, 2H); MS *m/e* 166 (M^+). Found: C, 79.93; H, 10.93%. Calcd for $C_{11}H_{18}O$: C, 79.46; H, 10.92%.

*5-Cyclopentadecen-1-one (**11e**)*: Mp 28—29 °C; IR (Nujol) 3025, 1720, 970, 739 cm^{-1}; NMR (CCl_4) δ 1.1—2.5 (m, 24H), 5.18—5.34 (m, 2H); MS *m/e* 194 (M^+). Found: C, 81.35; H, 11.76%. Calcd for $C_{15}H_{26}O$: C, 81.01; H, 11.78%.

*5-Cyclohexadecen-1-one [**11f**, (E)-Isomer]*: BP 114 °C/0.1 Torr; mp 11—12.5 °C; $n_D^{20}=1.4883$; IR (neat) 3040, 2940, 2880, 1710, 970 cm^{-1}; NMR (CCl_4) δ 1.1—1.8 (m, 18H), 1.8—2.1 (m, 4H), 2.1—2.4 (m, 4H), 5.18—5.34 (m, 2H). Found: C, 81.27; H, 11.64%. Calcd for $C_{16}H_{28}O$: C, 81.29; H, 11.94%.

*5-Cyclohexadecen-1-one [**11f**, (Z)-Isomer]*: Bp 137 °C/0.5 Torr; mp 36—37 °C, IR (neat) 3040, 2940, 1710, 1460, 720 cm^{-1}; NMR (CCl_4) δ 1.1—1.8 (m, 18H), 1.8—2.1 (m, 4H), 2.2—2.4 (m, 4H), 5.18—5.36 (m, 2H). Found: C, 81.35; H, 11.75%. Calcd for $C_{16}H_{28}O$: C, 81.29; H, 11.94%.

*1-Cyclopropyl-4-penten-1-one (**7**)*. A solution of vinylmagnesium chloride in THF (1.73 mol/l, 120 ml, 208 mmol) was added to a stirred solution of 2-chlorocyclobutanone **1a** (8.34 g, 79.9 mmol) in THF (70 ml) at 0 °C during a period of 2 h. The mixture was heated at 55 °C for 20 h, poured into an aqueous ammonium chloride solution and extracted with ether. The ether extracts were washed with water and dried over anhydrous sodium sulfate. After removal of the solvent, the residue was distilled (bp 60—90 °C/20 Torr) to give 5.60 g of oil. The oil was chromatographed on silica gel to give pure **7**. **7**: IR (neat) 3075, 1705, 1642, 1085, 1000, 915 cm^{-1}; NMR (CCl_4) δ 0.5—1.1 (m, 4H), 1.7—2.0 (m, 1H), 2.14—2.44 (m, 2H), 2.44—2.70 (m, 2H), 4.82—5.16 (m, 1H); MS *m/e* 124 (M^+). Found: C, 77.02; H, 9.61%. Calcd for $C_8H_{11}O$: C, 77.37; H, 9.74%.

*1-Cycloundecyl-4-penten-1-one (**8**)*: Bp 116—118 °C/0.3 Torr; $n_D^{25}=1.4873$; IR (neat) 3070, 1710, 1640, 995, 910 cm^{-1}; NMR (CCl_4) δ 1.1—1.8 (m, 20H), 2.2—2.5 (m, 5H), 4.82—5.12 (m, 2H), 5.55—5.96 (m, 1H); MS *m/e* 236 (M^+). Found: C, 81.29; H, 11.93%. Calcd for $C_{16}H_{28}O$: C, 81.27; H, 11.82%.

References

1) A part of this work was reported in a preliminary communication: M. Nishino, H. Kondo, and A. Miyake, *Chem. Lett.*, **1973**, 667.

2) S. T. Roads and N. R. Paulines, *Org. React.*, **22**, 61 (1975).

3) E. N. Marvell and W. Whalley, *Tetrahedron Lett.*, **1970**, 509.

4) A. Marcou and H. Normant, *Bull. Soc. Chim. Fr.*, **1965**, 3491.

5) M. Tiffeneau, B. Tchoubar, and S. LeTellier, *C. R. Acad. Sci.*, **216**, 856 (1943).

6) R. L. Huang, *J. Org. Chem.*, **19**, 1363 (1954).

7) A. S. Hussey and R. R. Herr, *J. Org. Chem.*, **24**, 843, (1959).

8) T. A. Geissman and R. I. Akawie, *J. Am. Chem. Soc.*, **73**, 1993 (1951).

9) A. J. Sisti, *Tetrahedron Lett.*, **1967**, 5237; A. J. Sisti, *J. Org. Chem.*, **33**, 453, 3953 (1968); A. J. Sisti, *ibid.*, **35**, 2670 (1970).

10) K. Suga, S. Watanabe, Y. Yamaguchi, and M. Tohyama, *Synthesis*, **1970**, 189.

11) M. S. Karasch and O. Reinmuth, "Grignard Reactions of Nonmetallic Substances," Constable and Company, Orange Street, London (1954), pp. 166—176.

12) W. von E. Doering and W. R. Roth, *Tetrahedron*, **18**, 67 (1962).

13) T. Shono and M. Mitani, *J. Am. Chem. Soc.*, **93**, 5284 (1971); T. Shono, I. Nishiguchi, H. Ohmizu, and M. Mitani, *ibid.*, **100**, 545 (1978).

14) G. L. Lange and T. W. Hall, *J. Org. Chem.*, **39**, 3819 (1974).

15) E. Vogel, W. Grimme, and E. Dinné, *Angew. Chem. Int. Ed. Engl.*, **2**, 1739 (1963).

16) H. W. Wanzlick, G. Gollmer, and H. Milz, *Chem. Ber.*, **88**, 72 (1955).

17) P. D. Bartlett and R. H. Rosenwald, *J. Am. Chem. Soc.*, **56**, 1992 (1934).

18) G. Hesse and D. Krehbiel, *Ann.*, **593**, 42 (1955).

The Chemical Conversion of the Photo-dimer of 2-Acetyl-5-methyl-1,4-benzoquinone. The Determination of the Regiochemistry of the Dimer

Yo Miyagi,* Kazuhiro Maruyama,† and Sachiko Yoshimoto
Faculty of Education, Kanazawa University, Kanazawa 920
†*Department of Chemistry, Faculty of Science, Kyoto University, Kyoto 606*

(Received March 21, 1980)

From the photo-dimer (**2a**) of 2-acetyl-5-methyl-1,4-benzoquinone, mono- and diacetyl derivatives and 2,6-dimethyl-1,4,5,8,9-pentaacetoxyphenanthrene (**3**) were prepared. **3** was oxidized to 2,6-dimethyl-1,4,5,8-tetraacetoxy-9,10-phenanthrenequinone (**4**). The acetoxyl groups of **4** were partly deuterated to assign their ^{1}H NMR signals. A series of chemical conversions of **2a** to **4** *via* **3** unambiguously clarified the regiochemistry of **2a**.

Previously we reported[1] that 2-acyl-1,4-benzoquinones (**1**) underwent a regioselective and stereoselective photo-dimerization to give 4aα-acyl-10β-alkyl-5,8-dihydroxy-4aα,10aα-dihydro-1,4,9(10*H*)-phenanthrenetriones (**2**). Although the structure of **2** was finally established by X-ray structure analysis, its regiochemistry had been determined by a certain sequence of reactions, which converted the dimer of **1a**, (**2a**), to a 9,10-phenanthrenequinone (**4**) through a phenanthrene (**3**).[2] This conversion excluded another possible alternative (**2'**), because **2'a** should give **4'** through **3'**. The series of reactions used in this chemical conversion are unusual and worth to describe. In this paper, the details of these unique and interesting reactions will be given.

On treatment with acetic anhydride containing a crop of *p*-toluenesulfonic acid at room temperature for 24 h, **2a** gave a monoacetyl derivative (**5**).[3] When the solution was further left to stand for 24 h after the addition of a small amount of pyridine, a diacetyl derivative (**6**) was obtained. Their structures were straightforward, judging from their ^{1}H NMR spectra: they were similar to that of **2a** except for the presence of a chelated hydroxyl signal of **5** as well as the lack of hydroxyl signals of **6**.

When a solution of **2a** in Ac_2O–pyridine was left standing over 10 d, 2,6-dimethyl-1,4,5,8,9-pentaacetoxyphenanthrene (**3**) was obtained.[4] Some plausible paths of the reactions are shown in Scheme 1. The structure

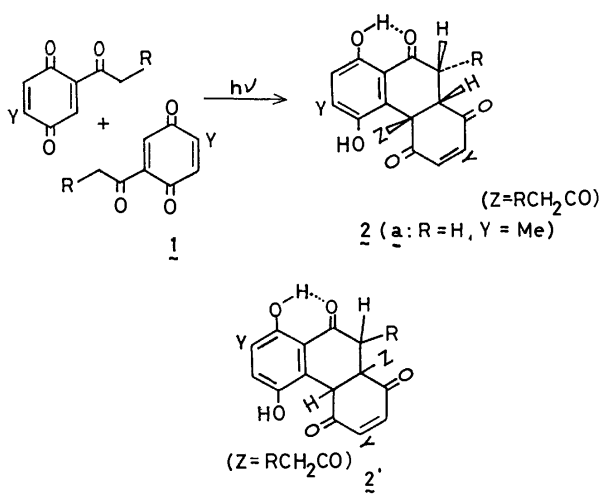

1 2 (a: R=H, Y=Me) 2'

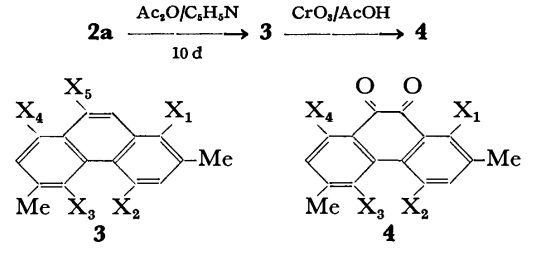

3, **4**: $X_1=X_2=X_3=X_4=X_5=AcO$

3-d_3-**1**, **4**-d_3-**1**: $X_1=X_2=X_4=X_5=AcO$, $X_3=AcO$-d_3
3-d_3-**2**, **4**-d_3-**2**: $X_1=X_3=X_4=X_5=AcO$, $X_2=AcO$-d_3
3-d_6-**1**, **4**-d_6-**1**: $X_1=X_2=X_5=AcO$, $X_3=X_4=AcO$-d_3
3-d_6-**2**, **4**-d_6-**2**: $X_1=X_3=X_5=AcO$, $X_2=X_4=AcO$-d_3
3-d_{15}, **4**-d_{12}: $X_1=X_2=X_3=X_4=X_5=AcO$-d_3

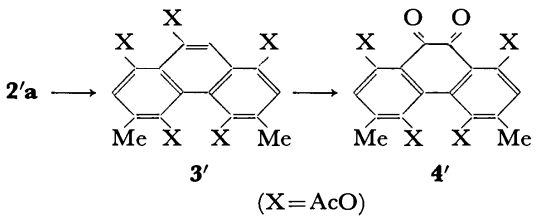

(X=AcO)

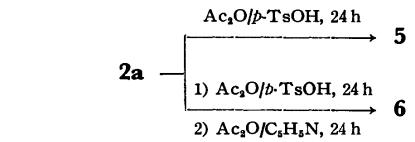

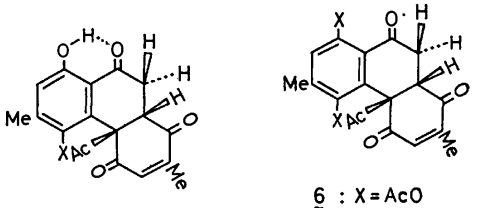

5 : X=AcO
5-d_3: X=AcO-d_3

6 : X=AcO
6-d_6: X=AcO-d_3

of **3** was clarified by its elemental analysis and spectroscopic data. The mass spectrum indicated the presence of five acetoxyl groups. The ^{13}C NMR spectrum was compatible with **3**, showing three doublets and eleven singlets of aromatic carbons (Table 1). The ^{1}H NMR spectrum showed complex signals due to methyl and acetoxyl groups between 2.1 and 2.5, though three singlets due to aromatic protons were observed at 7.12,

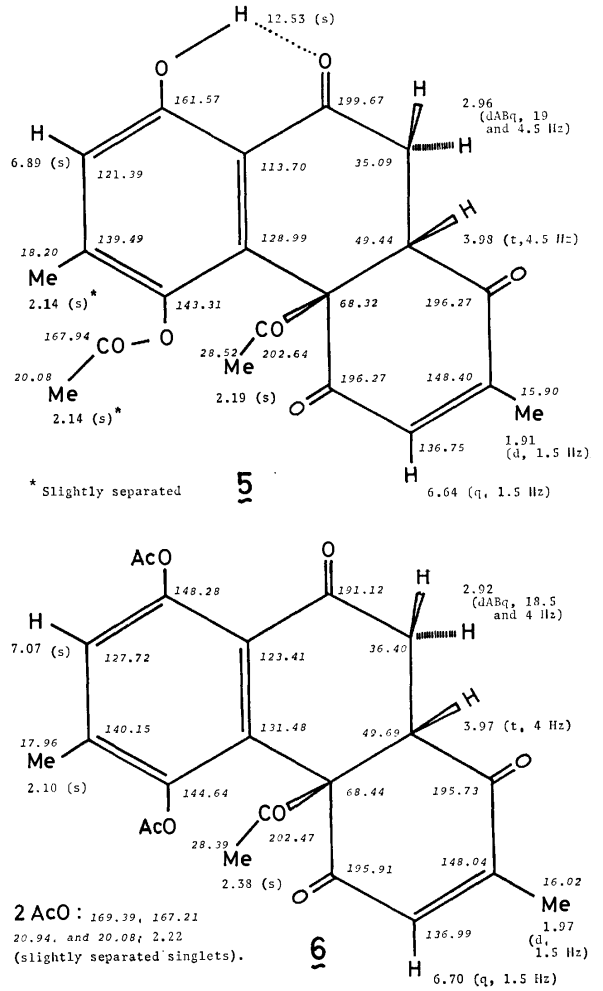

Fig. 1. The ^1H and ^{13}C NMR signals of **5** and **6** in $CDCl_3$ (δ); the ^1H NMR signals of **2a** were shown in Ref. 1; **2a** is not soluble in $CDCl_3$ enough for a ^{13}C NMR measurement and decomposes slowly in acetone.

7.28, and 7.31 in chloroform-*d*. A partially deuterated homologue of **3**, (**3**-d_{15}), was similarly prepared from **2a** with the aid of Ac_2O-d_6. The methyl groups of **3**-d_{15} showed two singlets, at 2.24 and 2.27, in pyridine-d_5; by chance, these singlets arose at the same position (2.30) in chloroform-*d*.

When **3** was oxidized by chromium trioxide, 2,6-dimethyl-1,4,5,8-tetraacetoxy-9,10-phenanthrenequinon (**4**) was obtained. Its ^{13}C NMR spectrum showed two

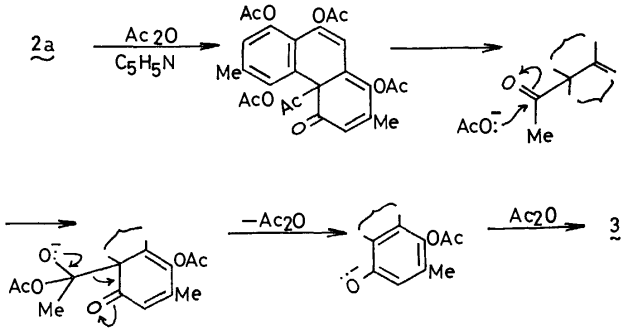

Scheme 1.

Table 1. Carbon chemical shifts in $CDCl_3$ δ

	3	**4**
$\underline{C}H_3$	16.55	16.11
	16.88	17.74
$\underline{C}H_3CO_2$	20.45	20.34
	21.10	20.67
		21.32
C-3, C-7, and C-10	112.97	120.60
	118.83	122.39
	120.28	125.32
	123.04	126.79
	124.34	128.58
C-1, C-2, C-4, C-5, C-6, C-8, and C-9	124.99	129.39
	126.77	132.97
	128.23	135.25
	129.86	
	130.51	
C-4a, C-4b, C-8a, and C-10a	141.22	142.25
	142.36	144.69
	143.98	146.80
	144.95	148.43
$CH_3\underline{C}O_2$	167.85	168.13
	168.33	169.27
	168.98	170.08
		180.33
		181.31

C-1, C-2, C-4, C-5, C-6, and C-8

C-3 and C-7

C-9 and C-10

doublets and ten singlets of aromatic carbons and two singlets of quinonoid carbonyl carbons (Table 1).

The ^1H NMR spectrum of **4** in chloroform-*d* showed two singlets[5] due to the aromatic protons at 7.08 and 7.48. In addition, it showed three singlets due to four acetoxyl groups at 2.16, 2.30, and 2.42, and two slightly split singlets due to two methyl groups at 2.27, with the relative-intensity ratio of 1 : 1 : 2 : 2. This assignment was made by a comparison of the spectrum with that of a partially deuterated homologue of **4**, (**4**-d_{12}), which was similarly prepared from **3**-d_{15}; the methyl signals of **4**-d_{12} arose clearly separated at 2.15 and 2.22 in pyridine-d_5. To assign the three singlets at 2.16, 2.30, and 2.42 to the individual acetoxyl groups, partial deuterium labellings of the acetoxyl groups of **4** were undertaken (Scheme 2).

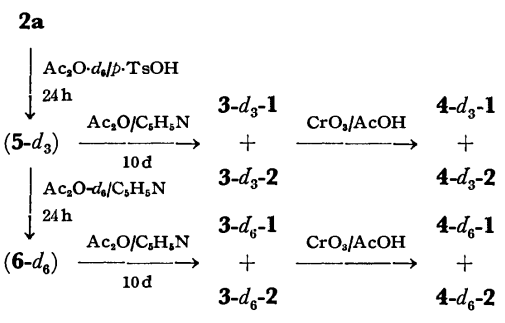

Scheme 2.

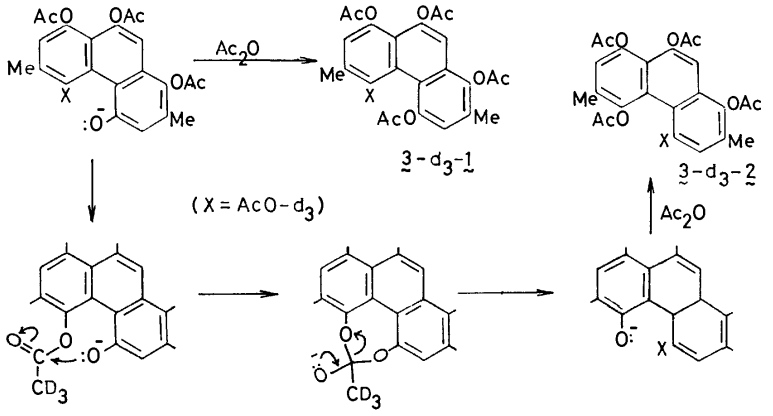

Scheme 3.

At first, after letting a solution of **2a** in Ac_2O-d_6–*p*-TsOH stand for 24 h, the concentrated residue[6] (the main component, **5**-d_3) was further treated with Ac_2O–pyridine for 10 d. At this stage, the scrambling of the CD_3CO group between the C-4 and C-5 positions was expected to give a mixture of **3**-d_3-**1** and **3**-d_3-**2**, as is shown in Scheme 3. The mixture thus obtained was oxidized by chromium trioxide to give a mixture of **4**-d_3-**1** and **4**-d_3-**2**, which showed a ^{1}H NMR spectrum in chloroform-*d* identical with that of **4**, with the exception of the decreased intensities of the signals at 2.16 and 2.30. Consequently, these two signals were ascribed to the acetoxyl groups at the C-4 and C-5 positions of **4**.

Secondly, after letting a solution of **2a** in Ac_2O-d_6–*p*-TsOH stand for 48 h, while meanwhile adding a small amount of pyridine, the concentrated residue[6] of the solution (the main component, **6**-d_6) was treated again with Ac_2O–pyridine for 10 d. A scrambling of the CD_3CO group similar to that described above was expected to give a mixture[7] of **3**-d_6-**1** and **3**-d_6-**2**, which was also oxidized to a mixture of **4**-d_6-**1** and **4**-d_6-**2**. The ^{1}H NMR spectrum of the mixture in chloroform-*d* showed the signals at 2.16, 2.30, and 2.42 with decreased intensities. Accordingly, the signal at 2.42 was assignable to two acetoxyl groups at the C-1 and C-8 positions of **4**.

The above spectroscopic studies excluded the reaction sequence of **2'a**→**3'**→**4'**, for the ^{13}C and ^{1}H NMR spectra obtained for **4** were inconsistent with **4'**; **4'** should show a doublet and five singlets of the aromatic carbons and a singlet of the quinonoid carbonyl carbons because of its molecular symmetry, while the ^{1}H NMR spectrum should give a singlet due to the methyl groups, two due to the acetoxyl groups, and one due to the aromatic protons.

Experimental

The Monoacetyl Derivative of ***2a****, 5-Acetoxy-4aα-acetyl-2,6-dimethyl-8-hydroxy-4aα,10aα-dihydro-1,4,9(10H)-phenanthrenetrione (5).* A homogeneous solution was made by occasionally swirling a suspension of **2a** (0.5 g) in acetic anhydride (30 ml) containing a crop of *p*-toluenesulfonic acid. After the solution had stood for 24 h, the solvent was evaporated by bulb-to-bulb distillation through a vacuum-line. The syrupy residue became a semi-solid on standing overnight. After rinsing with benzene, the solid was dissolved in a minimum amount of chloroform. After the addition of petroleum ether, the solution was stored in a refrigerator. Colorless crystals obtained in 10—30% yields gradually melted at 110—130 °C in a vacuum-sealed capillary. Found: C, 64.57; H, 4.66%. Calcd for $C_{20}H_{18}O_7$: C, 64.86; H, 4.90%. MS: *m/e* 370 (M^+), 328, 286.

The Diacetyl Derivative of ***2a****, 4aα-Acetyl-5,8-diacetoxy-2,6-dimethyl-4aα,10aα-dihydro-1,4,9(10H)-phenanthrenetrione (6).* After the above solution of **2a** in Ac_2O–*p*-TsOH had stood for 24 h, the solution was left further to stand for 24 h with the addition of pyridine (0.5 ml). Colorless crystals were thereafter obtained in 10—30% yields by the same procedure as above. They melted at 110—130 °C in a vacuum-sealed capillary. Found: C, 63.84; H, 4.76%. Calcd for $C_{22}H_{20}O_8$: C, 64.07; H, 4.89%. MS: *m/e* 412 (M^+), 370, 328, 286.

2,6-Dimethyl-1,4,5,8,9-pentaacetoxyphenanthrene (3). The above solution of **2a** in Ac_2O–pyridine was left standing for 10 d. The solvent was then evaporated by bulb-to-bulb distillation through a vacuum-line. The black semi-solid residue was rinsed with benzene and purified by column chromatography on silica gel (10ϕ × 100 mm; petroleum ether–diethyl ether (1 : 1)). Colorless crystals obtained in 20—40% yields were rectystallized from acetone. Mp 233—234 °C. Found: C, 62.78; H, 4.86%. Calcd for $C_{26}H_{24}O_{10}$: C, 62.90; H, 4.87%. MS: *m/e* 496 (M^+), 454, 412, 370, 328, 286. ^{1}H NMR: δ ($CDCl_3$) 2.18 (3H, s, AcO), 2.32 (6H, two slightly split s, 2 Me), 2.37 (9H, m, 3 AcO), 2.44 (3H, s, AcO), 7.12 (1H, s, ArH), 7.18 (1H, s, ArH), 7.32 (1H, s, ArH).

2,6-Dimethyl-1,4,5,8-tetraacetoxy-9,10-phenanthrenequinone (4). **3** (0.3 g) was dissolved in acetic acid (10 ml) by slight warming. CrO_3 (0.5 g) was dissolved in a minimum amount of water and diluted with acetic acid (5 ml). The CrO_3 solution was added dropwise to the solution of **3** over 1 h at 15 °C. After stirring for an additional hour, the solution was poured into water. The product was immediately extracted with choroform, washed, dried, and concentrated. The solid residue was dissolved in benzene (30 ml), while an amorphous solid remained undissolved. The yellow supernatant was concentrated to a solid, which was dissolved again in benzene. The yellow crystals obtained by repeating this procedure were rinsed with dry acetone and then washed with hot ligroine. Yield, 20—30%; mp 259—264 °C (in a vacuum-sealed capillary; softening, 240 °C). Recrystallization from hot solvents was unsuccessful because of decomposition. Found: C, 61.29; H, 4.15%. Calcd for $C_{24}H_{20}O_{10}$: C, 61.54; H, 4.30%. MS: *m/e* 468 (M^+), 426, 384, 342, 300. ^{1}H NMR:

δ ($CDCl_3$) 2.16 (3H, s, AcO), 2.27 (6H, slightly separated s, 2 Me), 2.30 (3H, s, AcO), 2.42 (6H, s, 2 AcO), 7.08 (1H, s,[5] ArH), 7.48 (1H, s,[5] ArH); δ (pyridine-d_5) 2.15 (6H, s, AcO and Me), 2.22 (3H, d, J=0.7 Hz, Me), 2.32 (3H, s, AcO), 2.38 (6H, s, 2 AcO), 7.68 (1H, s,[5] ArH[8]).

2,6-Dimethyl-1,4,5,8,9-penta(acetoxy-d_3)phenantherene (3-d_{15}). It was prepared from **2a** using Ac_2O-d_6 by the same method as that used for **3**, and it gave satisfactory results in mass analysis; ^{1}H NMR: δ ($CDCl_3$) 2.30 (6H, s, 2 Me), 7.09 (1H, s, ArH), 7.15 (1H, s, ArH), 7.30 (1H, s, ArH); δ (pyridine-d_5) 2.24 (3H, s, Me), 2.27 (3H, s, Me), 7.36 (1H, s, ArH), 7.52 (1H, s, ArH[8]).

2,6-Dimethyl-1,4,5,8-tetra(acetoxy-d_3)-9,10-phenanthrenequinone (4-d_{12}). It was prepared from **3**-d_{15} by the same method as that used for **4**, and it gave satisfactory results in mass analysis; ^{1}H NMR: δ ($CDCl_3$) 2.27 (6H, s, 2 Me), 7.04 (1H, s,[5] ArH), 7.48 (1H, s,[5] ArH); δ (pyridine-d_5) 2.15 (3H, s, Me), 2.22 (1H, s, Me), 7.70 (1H, s, ArH[8]).

The Partially Deuterated Homologues of 3 and 4, (3-d_3-1+3-d_3-2), (3-d_6-1+3-d_6-2), (4-d_3-1+4-d_3-2), and (4-d_6-1+4-d_6-2). These were prepared by the method described in the preceding section.

NMR measurements were made with a JEOL JNM-PS 100 spectrometer. We wish to thank Dr. Y. Itatani, Faculty of Pharmaceutical Sciences, Kanazawa University, for the NMR measurements and for his valuable discussions.

References

1) Y. Miyagi, K. Maruyama, H. Ishii, S. Mizuno, M. Kakudo, N. Tanaka, Y. Matsuura, and S. Harada, *Bull. Chem. Soc. Jpn.*, **52**, 3019 (1979).

2) Y. Miyagi, K. Kitamura, K. Maruyama, and Y. L. Chow, *Chem. Lett.*, **1978**, 33.

3) By the same procedure, **2** (R=Me, Y=Cl) gave the monoacetyl derivative corresponding to **5**.[1]

4) Similarly, 1,4,5,8,9-pentaacetoxyphenanthrene (mp 192—194.5 °C) and 10-methyl-1,4,5,8,9-pentaacetoxyphenanthrene (mp 190—193 °C) were obtained from **2** (R=Y=H) and **2** (R=Me, Y=H) respectively. The mass spectroscopic analysis of the latter phenenthrene indicated the contamination with methyl(propanoyloxy)tetraacetoxyphenanthrene, which supports the reaction mechanism of Scheme 1: acetic propionic anhydride and a phenanthrolate are formed by the Retro-Cleisen condensation, and the reaction between them gives the third phenanthrene and an acetate anion.

5) They seemed to be quartets in expanded measurements.

6) Because the isolation of the partially deuterated products (**3**-d_3 and **4**-d_6) in each step did not produce yields good enough to obtain the final products, the concentrated residue was submitted to further reactions. The evaporation of the solvent was effected by bulb-to-bulb distillation through a vacuum-line.

7) The complex signals of **3** at 2.37 did not become enough simpler to assign them to the individual acetoxyl groups by deuteration.

8) The signal of another aromatic proton might be behind the signals of the residual protons of pyridine.

Total Synthesis of Furanoeremophilane and 14-Norfuranoeudesmane Derivatives by a Route Involving Alkylation of 2,4-Dimethyl-3-furoic Acid[1]

Masahiro TADA,* Yayoi SUGIMOTO,† and Takeyoshi TAKAHASHI*,†

Tokyo University of Agriculture and Technology, Laboratory of Bioorganic Chemistry, Fuchu, Tokyo 183

†*Department of Chemistry, Faculty of Science, The University of Tokyo, Bunkyo-ku, Tokyo 113*

(Received March 26, 1980)

(±)-14-Norfuranoeudesmane-4,6-dione, (±)-furanoeremophilane-3,6-dione, and (±)-furanoeremophilan-14, 6α-olide were synthesized by a route involving alkylation of a dianion obtained from 2,4-dimethyl-3-furoic acid.

Various types of sesquiterpenes possessing a furan or γ-lactone moiety have been isolated from many species of higher and lower plants.[2] Although the true mechanism of biogenetical formation of a γ-lactone ring of sesquiterpenes is not clarified, furan ring is considered to be a possible precursor of the γ-lactone ring.[3] In fact oxidation of the furan ring with peracid[4] or oxygen[5] gives a γ-lactone ring. A number of syntheses of sesquiterpene lactones have been reported, but only a few of furanosesquiterpenes have been described.[6] We have undertaken the construction of furanoeremophilane- and furanoeudesmane-frameworks by combination of two moieties, **A** and **B**, to give **C**, successive transform ation of the substituent (X) into methyl group leading to furanoeremophilane- (**D-1**) and furanoeudesmane-skeletons (**D-2**), and the corresponding γ-lactones being derived from these furans. This paper deals with the synthesis of (±)-14-norfuranoeudesmane-4,6-dione (**1**), (±)-furanoeremophilane-3,6-dione (**2**),[7a] and (±)-furanoeremophilan-14,6α-olide (**3**).[8]

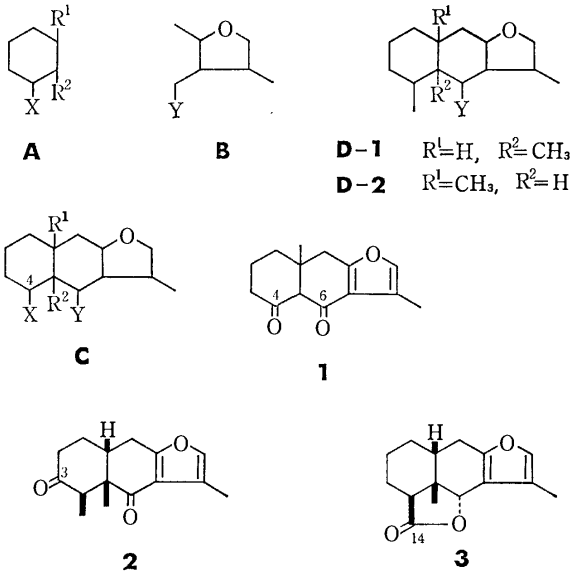

A dianion (**B'**) generated from 2,4-dimethyl-3-furoic acid (**4**) was used as a synthon corresponding to **B**. Treatment of 2,4-dimethyl-3-furoic acid (**4**)[9] with two equivalent mole of lithium diisopropylamide in a mixture of tetrahydrofuran and hexane (9: 2) at −78 °C gave an orange homogeneous solution. Alkylation of the dianion (**B'**) was then studied. The orange solution was quenched with one equivalent mole of methyl iodide at 0 °C and acidified with hydrochloric acid to give 2-ethyl-4-methyl-3-furoic acid (**5**) in 96% yield, suggesting a dianion nature for **B'**. Similar alkylation of **B'** with cyclohexanone gave a hydroxy acid (**6**) in 80% yield. Treatment of **B'** with 2-methyl-2-cyclohexen-1-one gave a 1,2-addition product in 70% yield, identified as its methyl ester (**7**). Although 1.1 or 2.5 equivalent moles of copper(I) iodide was added to **B'** before alkylation, the same 1,2-addition product was obtained as the main product.

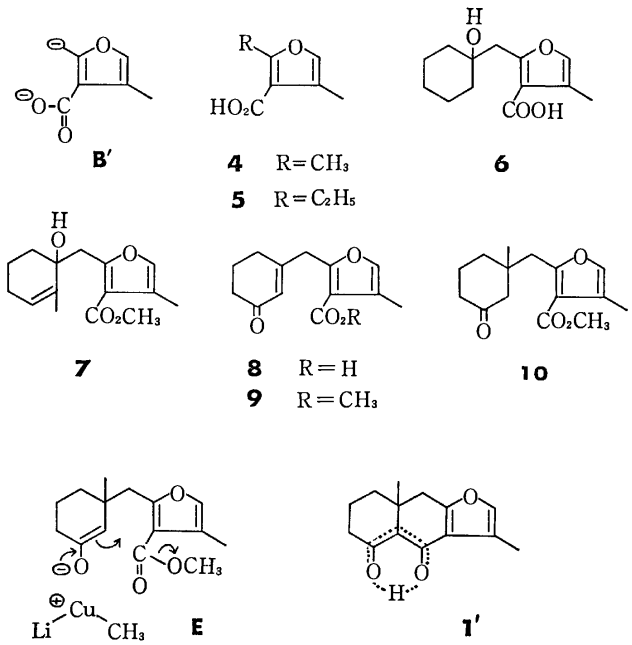

(±)-14-Norfuranoeudesmane-4,6-dione. The dianion **B'** was treated with 3-methoxy-2-cyclohexen-1-one and then acidified with hydrochloric acid to give an acid (**8**) in 78% yield. The acid (**8**) should be formed by concomitant dehydration of the addition product. Treatment of an ester (**9**) derived from **8** with lithium dimethylcuprate(I) at 0 °C for 45 h gave (±)-14-norfuranoeudesmane-4,6-dione (**1**) in 73% yield, *via* an intermediate anion (**E**) which underwent cyclization. When the reaction was carried out for 3 h, a keto ester (**10**) and **1** were obtained in 71 and 26% yields, respectively. The ^{1}H-NMR spectrum of the diketone (**1**) shows that **1** in deuteriochloroform exists in equilibrium between **1** and an enol ketone (**1'**) in the ratio 3: 7.

(±)-Furanoeremophilane-3,6-dione. (±)-Furanoeremophilane-3,6,9-trione and (±)-furanoeremophilane-3,6-dione[7a] (**2**) have been synthesized from resorcinol by Yamakawa and Satoh,[6a] *via* a diene adduct of 3,5-dimethylbenzofuran-4,7-dione and 3-ethoxy-1,3-pentadiene in overall yields of *ca.* 5 and *ca.* 4%, respectively. Synthesis of **2** starting from **4** was carried out as follows.

Alkylation of the dianion (**B'**) with 3-methoxy-2-methyl-2-cyclohexen-1-one gave an acid (**11**) in 74% yield, which was hydrogenated over 5% palladium–charcoal in ethanol to afford its dihydro derivative (**12**) quantitatively. The acid (**12**) was cyclized by treatment with *p*-toluenesulfonic acid in diphenyl ether under reflux to give 14-norfuranoeremophilane-4,6-dione (**13**) in 44% yield as the sole product. A *cis* A/B ring juncture was observed for **13** by its conversion into **2**. Preferential attack of the intermediate cation produced from **12** should be accomplished from the side opposite to the hydrogen atom at C-10 to give **13** as depicted in **F**.

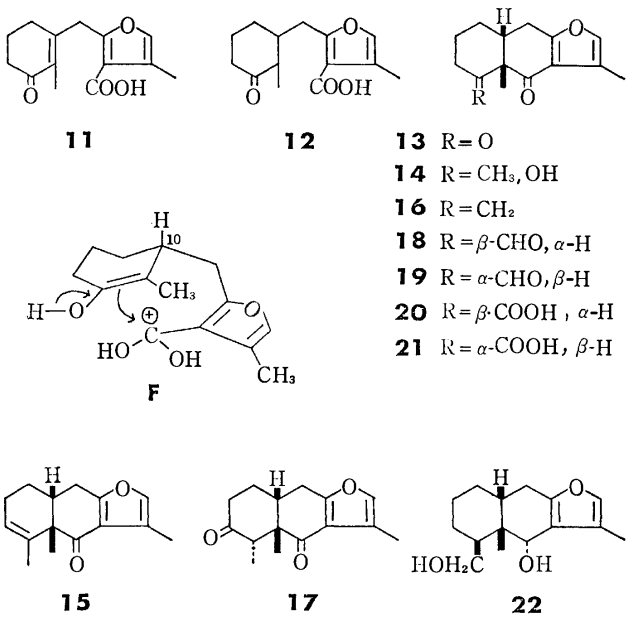

The diketone (**13**) was methylated regioselectively with 1.2 equivalent moles of methyllithium in ether at −78 °C for 1 h, giving 4-hydroxy 4-methyl ketone (**14**) in 99% yield. Dehydration of **14** with phosphoryl chloride in pyridine under reflux gave a mixture of olefins, which was separated by preparative thin-layer chromatography to afford an *endo*-olefin (**15**) in 69% yield and an *exo*-olefin (**16**) in 12% yield. The *endo*-olefin (**15**) was subjected to hydroboration with diborane in tetrahydrofuran at 0 °C and then alkaline hydrogen peroxide oxidation to give a mixture of alcohols. This mixture was oxidized, without further purification, with pyridinium chlorochromate[10] in dichloromethane to give (±)-furanoeremophilane-3,6-dione (**2**)[6a,7a] in 4% yield and (±)-4β*H*-furanoeremophilane-3,6-dione (**17**)[6a] in 78% yield. Isomerization of **17** into **2** was effected in refluxing benzene containing a catalytic amount of *p*-toluenesulfonic acid in 94% yield.[6a] (±)-Furanoeremophilane-3,6-dione (**2**) was synthesized from **4** in 7 steps in an overall yield of 17%.

Since the dione (**2**) has been converted into (±)-ligularone[11] (furanoeremophilan-6-one), (±)-ligularol[11] (petasablin; furanoeremophilan-6β-ol), and (±)-furanofukinol[7] (furanoeremophilane-3β,6β-diol) by Yamakawa and Satoh,[6] the synthesis of **2** indicates the formal total synthesis of these furanoeremophilane derivatives.

(±)-Furanoeremophilan-14,6α-olide. Furanoeremophilan-14,6α-olide (**3**) has been isolated from *Ligularia Hodgsoni* Hook, f.[8] Synthesis of the furanoeremophilane with an extra γ-lactone ring was studied.

The Wittig reaction of (±)-14-norfuranoeremophilane-4,6-dione (**13**) with methylenetriphenylphosphorane in tetrahydrofuran at room temperature proceeded regioselectively to give the *exo*-olefin (**16**) in 45% yield besides unchanged **13**. The olefin (**16**) was subjected to hydroboration with diborane in tetrahydrofuran and then alkaline hydrogen peroxide oxidation. The product, without further purification, was oxidized with pyridinium dichromate (PDC)[12] in *N,N*-dimethylformamide at room temperature to give a mixture of aldehydes and carboxylic acids, which was separated by preparative thin-layer chromatography, giving 6-oxofuranoeremophilan-14-al (**18**) in 3% yield, 6-oxo-4β*H*-furanoeremophilan-14-al (**19**) in 46% yield, 6-oxofuranoeremophilan-14-oic acid (**20**) in 10% yield, and 6-oxo-4β*H*-furanoeremophilan-14-oic acid (**21**) in 7% yield.

The stereochemistry at C-4 of **18** and **20** was determined to be 4α*H* based on the formation of **18** and **20** on oxidation of known furanoeremophilane-14,6α-diol (**22**)[8] with PDC in *N,N*-dimethylformamide. This led to 4β*H*-configuration for **19** and **21**. A preferential attack of borane to the olefin (**16**) occurred from the less hindered β-side to give **19** and **21**. Both **19** and **21** were found to be stable on acid (*p*-TsOH–PhH, under reflux) and alkaline (KOH–MeOH, under reflux) treatment. On treatment with potassium hydroxide in methanol at room temperature, **18** isomerized into **19**. Thus the conversion of **19** (or **21**) into **18** (or **20**) with desired 4α*H*-configuration was unsuccessful. Finally, reduction of **20** with lithium borohydride in tetrahydrofuran followed by acidification with acetic acid afforded (±)-furanoeremophilan-14,6α-olide (**3**)[8] in 71% yield. The overall yield of **3** from **13** was 3%. This constitutes the first total synthesis of **3**.

In conclusion, two key intermediates, 14-norfuranoeudesmane-4,6-dione (**1**) and 14-norfuranoeremophilane-4,6-dione (**13**), were obtained from **4** in 56 and 32.5% yields, respectively; **2**, **15**, and **16** were derived from **13** in reasonable yields. This presents a useful route for the synthesis of sesquiterpene lactones and furans of an eudesmane- and an eremophilane-type with oxygenated functional groups on C-3, C-4, C-6, C-14, *etc.*

Experimental

Melting points were measured on a Mel-temp capillary melting point apparatus (Laboratory Devices) and are uncor-

rected. IR spectra were measured with a Hitachi EPI-G2 or a Hitachi 260-30 spectrometer, ^{1}H-NMR spectra with a Hitachi R-20B (60 MHz) or a Varian EM-390 (90 MHz) spectrometer in deuteriochloroform solution containing tetramethylsilane as an internal standard, low resolution mass spectra with a Hitachi RMU-6-Tokugata mass spectrometer at 70 eV with a direct inlet system and high resolution mass spectra with a JEOL JMS-D300 mass spectrometer; the relative peak intensities in the mass spectra are given in parentheses. Thin-layer chromatography was carried out on Kieselgel GF_{254} (E. Merck, Darmstadt) in 0.25 mm thickness for analytical use and 0.5 mm thickness for preparative use. Wakogel C-200 and Florisil "mesh 100—200" (Wako Pure Chemical Industries) were used for column chromatography. All experiments were carried out under nitrogen atmosphere.

Alkylation of 2,4-Dimethyl-3-furoic Acid (4) with Methyl Iodide, Cyclohexanone, and 2-Methyl-2-cyclohexen-1-one. Butyllthium (4.2 mmol) in hexane (2.8 ml) was added to a solution of diisopropylamine (0.6 ml; 4.2 mmol) in dry tetrahydrofuran (15 ml) with cooling in an ice-bath. After being stirred at room temperature for 20 min, the solution was cooled to −78 °C and then treated with 2,4-dimethyl-3-furoic acid (**4**; 280 mg, 2 mmol) in tetrahydrofuran for 30 min, the color of the solution turning to orange due to formation of the dianion (**B′**).

Methyl iodide (0.14 ml; 2.2 mmol) was added to the dianion solution, and the solution was stirred at 0 °C for 1 h. The orange color of the dianion solution disappeared almost immediately. After addition of water, the mixture was acidified with hydrochloric acid and extracted with ether. The ethereal solution was washed with brine, dried ($MgSO_4$) and evaporated. The residue was purified by sublimation (100 °C, 3 mmHg) to give **5** (296 mg) in 96% yield. 2-Ethyl-4-methyl-3-furoic acid (**5**): mp 69.5—70.5 °C; IR (Nujol) *ca.* 3000 (broad) and 1680 cm^{-1}; ^{1}H-NMR ($CDCl_3$) δ 1.25 (3H, t, J=7 Hz), 2.15 (3H, d, J=1.5 Hz), 3.00 (2H, q, J=7 Hz), and 7.03 (1H, m). Found: *m/e* 154.0640. Calcd for $C_8H_{10}O_3$: M, 154.0630.

Cyclohexanone (0.23 ml) was added to a solution of dianion **B′** (2 mmol) (*vide supra*) at 0 °C. After being stirred for 30 min at 0 °C, a 10% sodium hydrogencarbonate solution was added to the reaction mixture and the mixture was extracted with ether. The ethereal solution was further treated with a 10% sodium hydrogencarbonate solution. The combined aqueous solution was acidified with hydrochloric acid and extracted with ether. The ethereal solution was treated in the usual way to give a residue which was chromatographed on a column of silica gel (20 g). Elution with hexane–ether gave **6** (380 mg) in 80% yield. 4-Methyl-2-(1-hydroxycyclohexylmethyl)-3-furoic acid (**6**): an oil; IR (neat) *ca.* 3500 (broad), *ca.* 3000 (broad), and 1680 cm^{-1}; ^{1}H-NMR ($CDCl_3$) δ 2.12 (3H, d, J=1.2 Hz), 3.16 (2H, s), 7.14 (1H, m), and *ca.* 7.5 (2H, broad signal). Found: *m/e* 238.1224. Calcd for $C_{13}H_{18}O_4$: M, 238.1206.

The solution of dianion **B′** (2 mmol) (*vide supra*) was treated with 2-methyl-2-cyclohexen-1-one (2.1 mmol) at 0 °C for 20 min. The reaction mixture was treated as in the preparation of **6**, giving a carboxylic acid, which was methylated with diazomethane. The product was purified by column chromatography (silica gel) to give **7** (365 mg) in 70% yield. Methyl 4-methyl-2-(1-hydroxy-2-methyl-2-cyclohexenylmethyl)furan-3-carboxylate (**7**): an oil; IR (neat) *ca.* 3450 (broad) and 1710 cm^{-1}; ^{1}H-NMR ($CDCl_3$) δ 1.83 (3H, broad signal), 2.13 (3H, d, J=1.2 Hz), 3.03 (1H, d, J=14.5 Hz), 3.53 (1H, d, J=14.5 Hz), 3.84 (3H, s), 5.50 (1H, m), and 7.11 (1H, m). Found: *m/e* 264.1350. Calcd for $C_{15}H_{20}O_4$: M, 264.1360.

When 1.1 equivalent mole (420 mg) or 2.5 equivalent mole (1 g) of copper(I) iodide was added to the solution of **B′** before the treatment with 2-methyl-2-cyclohexen-1-one, the same 1,2-addition product was obtained as the main product identified as its methyl ester (**7**).

Methyl 4-Methyl-2-(3-oxo-1-cyclohexenylmethyl)furan-3-carboxylate (9). 3-Methoxy-2-cyclohexen-1-one (1.8 g; 14 mmol) in tetrahydrofuran (5 ml) was added at 0 °C to a solution of dianion **B′**, prepared by treatment of **4** (1.96 g, 14 mmol) in tetrahydrofuran (15 ml) with lithium diisopropylamide (33 mmol) in tetrahydrofuran (90 ml)–hexane (22 ml) (*vide supra*). After being stirred at 0 °C for 1 h, water was added to the reaction mixture and the mixture was acidified with hydrochloric acid and extracted with ether. The ethereal solution was washed with brine, dried, and evaporated. The residue was chromatographed on a column of silica gel (100 g, elution with hexane–ether) to give **8** as yellow crystals (2.55 g) in 78% yield. Crystallization from hexane–ether gave pure **8**. 4-Methyl-2-(3-oxo-1-cyclohexenylmethyl)-3-furoic acid (**8**): mp 89—91 °C; IR ($CDCl_3$) *ca.* 3100 (broad), 1710, 1670, and 1615 cm^{-1}; ^{1}H-NMR ($CDCl_3$) δ 2.18 (3H, d, J=1.2 Hz), 3.94 (2H, broad singlet), 5.85 (1H, m), 7.15 (1H, m), and *ca.* 10.2 (1H, broad signal). Found: *m/e* 234.0888. Calcd for $C_{13}H_{14}O_4$: M, 234.0891.

The carboxylic acid (**8**) was treated with diazomethane in ether to give a methyl ester (**9**). Methyl 4-methyl-2-(3-oxo-1-cyclohexenylmethyl)furan-3-carboxylate (**9**): an oil: IR (neat) 1725, 1670, 1625, and 1610 cm^{-1}; ^{1}H-NMR ($CDCl_3$) δ 2.15 (3H, d, J=1.5 Hz), 3.82 (3H, s), 3.88 (2H, s), 5.78 (1H, m), and 7.12 (1H, m). Found: *m/e* 248.1057. Calcd for $C_{14}H_{16}O_4$: M, 248.1049.

14-Norfuranoeudesmane-4,6-dione (1). The ester (**9**) (310 mg; 1.25 mmol) in ether was added to a solution of lithium dimethycuprate (I) (3.8 mmol) in ether at 0 °C to form a yellow suspension. This was stirred at 0 °C for 45 h. The mixture was acidified with 2 M hydrochloric acid, stirred at room temperature for 1 h, and then extracted 6 times with ether. The combined ethereal solution was washed with a 5% sodium sulfite solution and brine, dried, and evaporated. The residue was purified by chromatography on a column of silica gel (20 g, elution with hexane–ether) to give **1** (213 mg) in 73% yield. Crystallization from hexane–ether gave pure **1**. (±)-14-Norfuranoeudesmane-4,6-dione (**1**): mp 91.5—93 °C; IR (KBr) *ca.* 2960 and 1612 cm^{-1}; ^{1}H-NMR ($CDCl_3$) δ 1.18 (3H, s), 2.23 (3H, d, J=1.8 Hz), 2.69 (2H, s), 3.82 (0.3H, s), 7.07 (1H, m), and 15.26 (0.7H, s). Found *m/e* 232.1108. Calcd for $C_{14}H_{16}O_3$: M, 232.1100.

When the reaction was carried out for 3 h and interrupted by addition of hydrochloric acid, the reaction product from **9** (290 mg) gave, after separation by column chromatography, a keto ester (**10**, 220 mg) and **1** (70 mg) in 71 and 26% yields, respectively. Methyl 4-methyl-2-(1-methyl-3-oxocyclohexylmethyl)furan-3-carboxylate (**10**): an oil; IR (neat) 1720 (broad) cm^{-1}; ^{1}H-NMR ($CDCl_3$) δ 0.97 (3H, s), 2.15 (3H, d, J=1.2 Hz), 3.51 (2H, broad singlet), 3.83 (3H, s), and 7.16 (1H, m). Found: *m/e* 264.1348. Calcd for $C_{15}H_{20}O_4$: M, 264.1360.

4-Methyl-2-(2-methyl-3-oxo-1-cyclohexenylmethyl)-3-furoic Acid (11). 3-Methoxy-2-methyl-2-cyclohexen-1-one (1.80 g, 12.3 mmol) was added to the solution of dianion **B′** (14 mmol) (*vide supra*) at 0 °C and the mixture was stirred for 1 h. The reaction mixture was poured into water, acidified with hydrochloric acid and extracted with ether. The ethereal solution was treated in the usual way to give a residue, which was chromatographed on a column of silica gel (150 g). Elution with hexane–ether (1 : 1) afforded a carboxylic acid (**11**; 2.55 g) in 74% yield. 4-Methyl-2-(2-methyl-3-oxo-1-cyclohexenyl-

methyl)-3-furoic acid (**11**): mp 115—116 °C (crystallized from hexane–ether); IR (Nujol) 1670, 1602, and 1557 cm^{-1}; IR ($CHCl_3$) 1680 and 1660 cm^{-1}; ^{1}H-NMR ($CDCl_3$) δ 1.90 (3H, s), 2.00 (3H, d, J=2 Hz), 4.03 (2H, s), 6.85 (1H, broad signal), and 7.10 (1H, m); MS *m/e* 248 (M^+; 100), 175 (43), 149 (34), 109 (85), and 53 (60). Found: C, 67.47; H, 6.64%. Calcd for $C_{14}H_{16}O_4$: C, 67.73; H, 6.50%.

Hydrogenation of the Carboxylic Acid (11). The carboxylic acid (**11**; 1 g) in ethanol (50 ml) was hydrogenated in the presence of 5% palladium–charcoal (*ca.* 150 mg) at room temperature for 4 h. After filtration of the catalyst, the solvent was removed to give a dihydro derivative (**12**; 1 g) in quantitative yield. 4-Methyl-2-(2-methyl-3-oxocyclohexylmethyl)-3-furoic acid (**12**): mp 123—127 °C (crystallized from hexane–ether); IR (Nujol) 1700, 1678, 1598, and 1550 cm^{-1}; IR ($CHCl_3$) 1710 and 1680 cm^{-1}; ^{1}H-NMR ($CDCl_3$) δ 1.16 (3H, d, J=6 Hz), 2.17 (3H, d, J=2 Hz), 2.94 (1H, dd, J=18 and J=8 Hz), 3.31 (1H, dd, J=18 and J=5 Hz), 7.07 (1H, m), and 7.36 (1H, broad signal; disappeared on addition of D_2O); MS *m/e* 250 (M^+; 26), 178 (57), 122 (74), and 111 (100). Found: C, 67.11; H, 7.51%. Calcd for $C_{14}H_{18}O_4$: C, 67.18; H, 7.25%.

Cyclization of the Dihydro Carboxylic Acid (12). The dihydro carboxylic acid (**12**; 270 mg) was dissolved in diphenyl ether (20 ml) containing *p*-toluenesulfonic acid (*ca.* 50 mg), and the mixture was refluxed under a Dean-Stark water separator for 3.5 h. The reaction mixture was extracted with ether. The etheral solution was washed with a 5% aqueous sodium hydroxide solution and brine, dried, and evaporated to give an oil, which was chromatographed on a column of silica gel (20 g). Fractions eluted with hexane–ether (1 : 1) were combined and subjected to purification by chromatography under the same conditions as mentioned above to give **13** (111 mg) in 44% yield. (±)-14-Norfuranoeremophilane-4,6-dione (**13**): mp 105.5—106 °C (crystallized from ether); IR (Nujol) 1715, 1665, 1608, and 1565 cm^{-1}; ^{1}H-NMR ($CDCl_3$) δ 1.37 (3H, s), 2.19 (3H, d, J=2 Hz), 2.70 (1H, dd, J=18 and J=2 Hz), 3.22 (1H, dd, J=18 and J=6 Hz), and 7.18 (1H, m); MS *m/e* 232 (M^+; 16), 122 (100), and 94 (30). Found: C, 72.22; H, 7.04%. Calcd for $C_{14}H_{16}O_3$: C, 72.39; H, 6.94%.

Methylation of 14-Norfuranoeremophilane-4,6-dione (13). 14-Norfuranoeremophilane-4,6-dione (**13**; 127 mg) in ether (20 ml) was treated with methyllithium (0.6 mmol) in ether (1.2 ml) at −78 °C for 1 h. The reaction mixture was poured into water and extracted with ether. The ethereal solution was treated in the usual way to give a hydroxy ketone (**14**; 134 mg) in 99% yield. The product showed one spot on thin-layer chromatogram and ^{1}H-NMR methyl signals corresponding to one configurational isomer. However, the configuration at C-4 remained undetermined. 4ξ-Hydroxyfuranoeremophilan-6-one (**14**): mp 115—116.5 °C (crystallized from hexane); IR (Nujol) 3450, 1648, 1608, and 1565 cm^{-1}; ^{1}H-NMR ($CDCl_3$) δ 1.21 and 1.37 (each 3H, s), 2.18 (3H, d, J=2 Hz), 2.53 (1H, dd, J=18 and J=2 Hz), 3.16 (1H, dd, J=18 and J=6 Hz), 5.74 (1H, s-like; disappered on addition of D_2O), and 7.13 (1H, m); MS *m/e* 248 (M^+; 27), 205 (16), 163 (100), and 135 (30). Found: C, 72.35; H, 8.35%. Calcd for $C_{15}H_{20}O_3$: C, 72.55; H, 8.12%.

Dehydration of the Hydroxy Ketone (14). Phosphoryl chloride (0.3 ml) was added dropwise to a solution of the hydroxy ketone (**14**; 113 mg) in pyridine (5 ml) and the mixture was heated under reflux for 2 h. The reaction mixture was poured into ice water, and the product was extracted with ether. The ethereal solution was treated in the usual way to give a residue, which was subjected to separation by preparative thin-layer chromatography [developed with hexane–ether (4 : 1)] to give an *endo*-olefin (**15**; 73 mg; R_f 0.53) in 69% yield and an *exo*-olefin (**16**; 13 mg; R_f 0.47) in 12% yield. Furanoeremophil-3-en-6-one (**15**): mp 69—69.5 °C (crystallized from hexane); IR (Nujol) 1675, 1610, and 1565 cm^{-1}; ^{1}H-NMR ($CDCl_3$) δ 1.39 (3H, s), 1.73 (3H, d, J=2 Hz), 2.17 (3H, d, J=2 Hz), 2.74 and 2.98 (each 1H, dd, J=18 and J=6 Hz), 5.49 (1H, m), and 7.10 (1H, m); MS *m/e* 230 (M^+; 23), 122 (100), and 94 (31). Found: C, 78.14; H, 7.93%. Calcd for $C_{15}H_{18}O_2$: C, 78.23; H, 7.88%. Furanoeremophil-4(14)-en-6-one (**16**): an oil; IR (neat) 1675, 1615, 1568, and 902 cm^{-1}; ^{1}H-NMR ($CDCl_3$) δ 1.39 (3H, s), 2.20 (3H, d, J=2 Hz), 2.61 (1H, dd, J=18 and J=3 Hz), 3.14 (1H, dd, J=18 and J=6 Hz), 4.79 and 5.00 (each 1H, s), and 7.13 (1H, m); MS *m/e* 230 (M^+; 25), 122 (100), and 94 (41). Found: C, 78.50; H, 8.14%. Calcd for $C_{15}H_{18}O_2$: C, 78.23; H, 7.88%.

(±)-Furanoeremophilane-3,6-dione (2). A solution of diborane (0.8 mmol) in tetrahydrofuran (0.4 ml) was added to a solution of the *endo*-olefin (**15**; 67 mg) in tetrahydrofuran (10 ml) at 0 °C. The mixture was stirred at 0 °C for 1.5 h and then at room temperature for 30 min to complete the reaction. Excess of the reagent was destroyed by careful addition of water (0.5 ml). After addition of a 3 M aqueous sodium hydroxide solution (0.2 ml), hydrogen peroxide (30%, 0.2 ml) was added dropwise to the mixture with stirring at a rate such that the temperature of the reaction mixture did not exceed *ca.* 40 °C. The reaction mixture was then heated at 40—50 °C and maintained in this temperature range for 30 min to complete the oxidation reaction. The reaction mixture was treated in the usual way to give an oil, which, without further purification, was oxidized with pyridinuim chlorochromate (PCC,[10] 356 mg) in dichloromethane (1.5 ml) at room temperature for 5 h. After addition of 2-propanol (1 ml) in order to destroy excess of the oxidant, the reaction mixture was passed through a column of Florisil, the solvent being removed by evaporation. The residue was subjected to separation by preparative thin-layer chromatography [developed with hexane–ether (1: 9)] to give **2** (3.1 mg; R_f 0.54) in 4% yield and **17** (56.2 mg; R_f 0.45) in 78% yield. (±)-Furanoeremophilane-3,6-dione (**2**):[6a] mp 176—177 °C (crystallized from hexane–ether): IR (Nujol) 1710, 1660, 1605, and 1565 cm^{-1}; ^{1}H-NMR ($CDCl_3$) δ 0.92 (3H, d, J=7 Hz), 1.12 (3H, s), 2.18 (3H, d, J=2 Hz), 2.91 (1H, dd, J=18 and J=6 Hz), 3.27 (1H, dd, J=18 and J=10 Hz), and 7.11 (1H, m); MS *m/e* 246 (M^+; 31), 122 (100), and 94 (17). Found: C, 73.02; H, 7.52%. Calcd for $C_{15}H_{18}O_3$: C, 73.14; H, 7.37%. The compound was found to be identical with (±)-furanoeremophilane-3,6-dione (**2**) prepared by Yamakawa and Satoh.[6a] (±)-4βH-Furanoeremophilane-3,6-dione (**17**):[6a] mp 119.5—120 °C (crystallized from hexane–ether); IR (Nujol) 1705, 1665, 1604, and 1560 cm^{-1}; ^{1}H-NMR ($CDCl_3$) δ 1.37 (3H, d, J=7 Hz), 1.14 (3H, s), 2.12 (3H, d, J=2 Hz), 2.71 (1H, dd, J=18 and J=6 Hz), 3.30 (1H, dd, J=18 and J=5 Hz), and 7.07 (1H, m); *m/e* 246 (M^+; 22), 122 (100), and 94 (25). Found: C, 72.87; H, 7.55%. Calcd for $C_{15}H_{18}O_3$: C, 73.14; H, 7.37%.

Isomerization of 4βH-Furanoeremophilane-3,6-dione (17). According to the procedure of Yamakawa and Satoh,[6a] the diketone (**17**; 43.3 mg) dissolved in benzene (6 ml) containing *p*-toluenesulfonic acid (8 mg) was treated under reflux for 1 h. The crude product mixture was subjected to separation by preparative thin-layer chromatography [developed with hexane–ether (1 : 9)] to give **2** (40.5 mg) in 94% yield and unchanged **17** (2.2 mg).

Wittig Reaction of 14-Norfuranoeremophilane-4,6-dione (1). Butyllithium (7.3 mmol) in hexane (4.7 ml) was added to a solution of methyltriphenylphosphonium iodide (3.02 g; 7.5

mmol) in dry tetrahydrofuran (120 ml) at room temperature, and the mixture was stirred for 6.5 h. The diketone (**1**; 324 mg) in tetrahydrofuran (10 ml) was then added to this solution, the mixture being stirred for 11 h. The reaction mixture was treated in the usual way to give a residue, which was chromatographed on a column of silica gel (60 g). Elution with hexane–ether (4 : 1) gave furanoeremophil-4(14)-en-6-one (**16**; 146 mg) in 45% yield and the unchanged diketone (**1**; 56 mg).

Hydroboration and Successive Oxidation of Furanoeremophil-4(14)-en-6-one (16). The *exo*-olefin (**16**; 85 mg) in tetrahydrofuran (10 ml) was subjected to hydroboration with diborane (3.6 mmol) in tetrahydrofuran (3.6 ml) at room temperature for 1 h. Excess of the reagent was destroyed by addition of water (1 ml). After addition of a 3 M aqueous sodium hydroxide solution (0.4 ml) and hydrogen peroxide (30%, 0.4 ml), the mixture was heated at 40—50 °C for 30 min. The reactions mixture was treated in the usual way to give a residue, which was oxidized with pyridinium dichromate (PDC,[12] 1.0 g) in *N,N*-dimethylformamide at room temperature for 2 d. The reaction mixture was poured into water and extracted with ether. The ethereal solution was treated in the usual way to give a residue, which was subjected to separation by preparative thin-layer chromatography (developed with ether) to afford **18** (2.7 mg, R_f 0.89) in 3% yield, **19** (41.6 mg; R_f 0.79) in 46% yield, **20** (9.3 mg, R_f 0.71) in 10% yield, and **21** (7 mg; R_f 0.57) in 7% yield. 6-Oxofuranoeremophilan-14-al (**18**): an oil; IR (neat) 1720, 1670, and 1563 cm^{-1}; ^{1}H-NMR ($CDCl_3$) δ 1.38 (3H, s), 2.18 (3H, d, J=2 Hz), 2.57 (1H, dd, J=18 and J=3 Hz), 3.15 (1H, dd, J=18 and J=6 Hz), 3.23 (1H, t, J=4 Hz), 7.08 (1H, m), and 9.84 (1H, d, J=2 Hz); MS *m/e* 246 (M^+; 0.1), 122 (100), and 94 (42). Found: *m/e* 246.1257. Calcd for $C_{15}H_{18}O_3$: M, 246.1254. 6-Oxo-4βH-furanoeremophilan-14-al (**19**): an oil; IR (neat) 1715, 1662, 1608, and 1562 cm^{-1}; ^{1}H-NMR ($CDCl_3$) δ 1.50 (3H, s), 2.15 (3H, d, J=2 Hz), 2.54 (1H, dd, J=18 and J=1.5 Hz), 3.32 (1H, dd, J=18 and J=6 Hz), 3.44 (1H, t, J=7 Hz), 7.03 (1H, m), and 10.04 (1H, s); MS *m/e* 246 (M^+; 1), 232 (35), 218 (13), 122 (100), and 94 (16). Found: *m/e* 246.1249. Calcd for $C_{15}H_{18}O_3$: M, 246.1254. 6-Oxofuranoeremophilan-14-oic acid (**20**): an oil; IR (neat) 1705, 1670, 1610, and 1568 cm^{-1}; ^{1}H-NMR ($CDCl_3$) δ 1.30 (3H, s), 2.18 (3H, d, J=2 Hz), 2.52 (1H, dd, J=18 and J=2 Hz), 3.16 (1H, dd, J=18 and J=5 Hz), 3.46 (1H, t, J=4 Hz), 7.04 (1H, m), and 7.23 (1H, broad signal); MS *m/e* 262 (M^+; 22), 244 (11), 122 (100), and 94 (35). Found: *m/e* 262.1211. Calcd for $C_{15}H_{18}O_4$: M, 262.1205. 6-Oxo-4βH-furanoeremophilan-14-oic acid (**21**): an oil; IR (neat) 1712, 1663, 1615, and 1565 cm^{-1}; ^{1}H-NMR ($CDCl_3$) δ 1.43 (3H, s), 2.17 (3H, d, J=2 Hz), 2.54 (1H, dd, J=18 and J=1.5 Hz), 3.30 (1H, dd, J=18 and J=5 Hz), 3.38 (1H, t, J=4 Hz), 7.07 (1H, m), and 7.40 (1H, broad signal); MS *m/e* 262 (M^+; 0.3), 218 (37), 203 (27), and 122 (100). Found: *m/e* 262.1211. Calcd for $C_{15}H_{18}O_4$: M, 262.1205.

Oxidation of Furanoeremophilane-14,6α-diol (22). Furanoeremophilane-14,6α-diol[8] (**22**; 19.5 mg) was oxidized with PDC[12] (1 g) in *N,N*-dimethylformamide (1 ml) at room temperature for 8 h. After treatment in the usual way, the product mixture was separated by preparative tihn-layer chromatography [developed with hexane–ether (2: 3)] to afford 6-oxofuranoeremophilan-14-al (**18**; 8.3 mg) as a main product in 44% yield and 6-oxofuranoeremophilan-14-oic acid (**20**; 2.2 mg) in 11% yield.

(±)-Furanoeremophilan-14,6α-olide (3). Lithium borohydride (*ca.* 10 mg) was added to a solution of 6-oxofuranoeremophilan-14-oic acid (**20**; 6.4 mg) in tetrahydrofuran (10 ml) at room temperature, and the mixture was stirred for 45 min. After addition of acetic acid (8 ml), the mixture was stirred for 12 h at room temperature, and extracted with ether. The ethereal solution was treated in the usual way to give an oil, which was subjected to separation by preparative thin-layer chromatography [developed with hexane–ether (1: 1)] to give **3** (4.3 mg; R_f 0.47) in 71% yield and unchanged **20** (0.8 mg). (±)-Furanoeremophilan-14,6α-olide (**3**): mp 125—127 °C (crystallized from hexane–ether); IR (CCl_4) 1768, 1638, and 1562 cm^{-1}; ^{1}H-NMR ($CDCl_3$) δ 1.27 (3H, s), 2.02 (3H, d, J=2 Hz), 2.66 (2H, dd, J=18 and J=2 Hz), 5.07 (1H, m), and 7.06 (1H, m); MS *m/e* 246 (M^+; 100) 202 (28), and 95 (31). Found: *m/e* 246.1262. Calcd for $C_{15}H_{18}O_3$: M, 246.1257. The spectral data of (±)-**3** were found to be identical with those of natural (−)-**3**.[8]

The authors wish to thank Prof. Koji Yamakawa and Dr. Tsuyoshi Satoh, Science University of Tokyo, for the supply of spectral data of **2** and **17** together with an authentic specimen of **2**. The authors are also indebted to Dr. Hiroshi Hirota, the University of Tokyo, for measurements of high-resolution mass spectra.

References

1) A preliminary account of this paper: M. Tada and T. Takahashi, *Chem. Lett.*, **1978**, 275; M. Tada, Y. Sugimoto, and T. Takahashi, *ibid.*, **1979**, 1441.

2) *E.g.* T. K. Devon and A. I. Scott, "Handbook of Naturally Occurring Compounds," Academic Press, New York (1972), Vol. II; E. Rodoriguez, G. H. N. Towers, and J. C. Mitchell, *Phytochemistry*, **15**, 1573 (1976).

3) V. Herout in "Pharmacognosy and Phytochemistry" ed by H. Wagner and L. Hörhammer, Spriger-Verlag, Berlin (1971), p. 93.

4) K. Takeda, H. Minato, M. Ishikawa, and M. Miyawaki, *Tetrahedron*, **20**, 2655 (1964).

5) H. Hikino, Y. Hikino, and I. Yosioka, *Chem. Pharm. Bull.*, **10**, 641 (1962).

6) a) K. Yamakawa and T. Satoh, *Chem. Pharm. Bull.*, **25**, 2535 (1977), and references cited therein; b) K. Yamakawa and T. Satoh, *ibid.*, **27**, 1747 (1979).

7) a) K. Naya, M. Nakagawa, M. Hayashi, K. Tsuji, and M. Naito, *Tetrahedron Lett.*, **1971**, 2961. b) K. Naya, Y. Makiyama, T. Matsuura, N. Ii, H. Nagano, and T. Takahashi, *Chem. Lett.*, **1978**, 301.

8) Y. Ishizaki, Y. Tanahashi, T. Takahashi, and K. Tori, *J. Chem. Soc., Chem. Commun.*, **1969**, 551; Y. Ishizaki, Y. Tanahashi, T. Tsuyuki, T. Takahashi, and K. Tori, *Bull. Chem. Soc. Jpn.*, **52**, 1182 (1979).

9) F. G. González, F. J. L. Aparicio, and F. Sánchez-laulhe, *Anales Real Soc. Españ. Fis. y Quím. (Madrid), Ser. B*, **50**, 407 (1954); *Chem. Abstr.*, **49**, 13206g (1955). *Cf.* T. Sato, M. Tada, T. Tsuyuki, and T. Takashi, *Nippon Kagaku Kaishi*, **1979**, 1618.

10) E. J. Corey and J. W. Suggs, *Tetrahedron Lett.*, **1975**, 2647.

11) H. Ishii, T. Tozyo, and H. Minato, *Tetrahedron*, **21**, 2605 (1965).

12) E. J. Corey and G. Schmidt, *Tetrahedron Lett.*, **1979**, 399.

Transformation of *D* : *A*-Friedo-18β-lup-19-en-3-one into *D* : *B*-Friedo-18β,19α*H*-lup-5-en-3β-ol and a Comment on the Structure of Guimarenol[1)]

Yasushi YOKOYAMA, Yoshihiko MORIYAMA,†† Takahiko TSUYUKI, Takeyoshi TAKAHASHI,* Akiko ITAI,† and Yoichi IITAKA†

Department of Chemistry, Faculty of Science, The University of Tokyo, Hongo, Bunkyo-ku, Tokyo 113
†Faculty of Pharmaceutical Sciences, The University of Tokyo, Hongo, Bunkyo-ku, Tokyo 113
††Institute of Chemistry, Kyoto Prefectural University of Medicine, Taishogun, Kita-ku, Kyoto 603

(Received March 28, 1980)

D:*A*-Friedo-18β-lup-19-en-3-one was transformed into *D*:*B*-friedo-18β,19α*H*-lup-5-en-3β-ol by two routes, 1) bromination-dehydrobromination of an enol benzoate of *D*:*A*-friedo-18β,19α*H*-lupan-3-one and 2) $BF_3 \cdot Et_2O$-catalyzed backbone rearrangement of 3β,4β-epoxy-*D*:*A*-friedo-18β,19α*H*-lupane. The 18β*H*,19α*H*-configuration in these *D*:*A*- and *D*:*B*-friedo-type lupane derivatives was determined by means of X-ray diffraction for a 3α,4α-epoxide derived from *D*:*A*-friedo-18β,19α*H*-lupan-3β-ol. The synthetic *D*:*B*-friedo-18β,19α*H*-lup-5-en-3β-ol was found to be not identical with guimarenol isolated from *Ceropegia dichotoma*.

From the viewpoint of acid-catalyzed backbone rearrangement of triterpenes, we are interested in the structure of guimarenol (**1**), a triterpene alcohol obtained from *Ceropegia dichotoma* by González *et al.*[2)] They proposed a novel *D*: *B*-friedolupane framework with a double bond between $C_{(5)}$ and $C_{(6)}$ and a 3β-hydroxyl group for guimarenol (**1**), though the stereochemistry at $C_{(13)}$, $C_{(14)}$, $C_{(17)}$, $C_{(18)}$, and $C_{(19)}$ remained undetermined.

Only a few reports have been given on investigations on the migrated lupane derivatives, such as isolation of guimarenol (**1**) and lup-18-en-3β-ol (**2**)[2)] and preparation of 3β-acetoxy-19α*H*-lup-13(18)-ene (**3**) from lupenyl acetate (**4**).[3)] The synthesis of *D*: *A*-friedo-18β-lup-19-ene (**5**) and its 3-oxo derivative (**6**) from friedelin (**7**) and also the conversion of **5** into a migrated baccharane derivative, methyl trinorshionanoate (**8**) were recently reported.[4)]

Biosynthesis of lupeol (**9**) is presumed to proceed *via* a pentacyclic intermediate (**A**) carrying a positive charge on $C_{(20)}$ or its equivalent species.[5)] Deprotonation of a proton on $C_{(29)}$ would afford lupeol (**9**), while a sequential shift of methyl groups and hydrides followed by removal of a proton on $C_{(6)}$ would give *D*: *B*-friedo-18β,19α*H*-lup-5-en-3β-ol (**10**) as shown in Fig. 1. Thus, the 18β*H*- and 19α*H*-configuration could be biogenetically assumed for migrated lupane derivatives including guimarenol (**1**). This paper describes the synthesis of *D* : *B*-friedo-18β,19α*H*-lup-5-en-3β-ol (**10**) from *D* : *A*-friedo-18β-lup-19-en-3-one (**6**)[4b)] and determination of the configuration at $C_{(18)}$ and $C_{(19)}$ of 3α,4α-epoxy-*D* : *A*-friedo-18β,19α*H*-lupane (**11**) derived from a synthetic intermediate by means of X-ray crystallography. Discrepancy of physical constants and spectral data between the synthetic triterpene (**10**) and guimarenol (**1**) is also described.

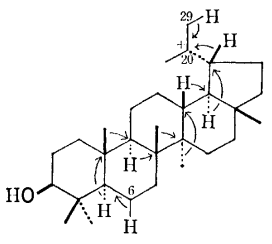

A

Fig. 1

The synthesis starts from the conversion of *D* : *A*-friedo-18β-lup-19-en-3-one (**6**) into an acetate (**13**) *via* an alcohol (**12**). The next step, hydrogenation of the acetate (**13**) seems crucial, since the hydrogenation is likely to occur from both α- and β-sides. However, it was inferred by use of a Dreiding model that hydrogenation from the α-side to generate a 19β-isopropyl group would take place more easily than that from the β-side. The acetate (**13**) in acetic acid was hydrogenated under atmospheric pressure over platinum catalyst at 40 °C. Although the product (**14**), $C_{32}H_{54}O_2$ (determined by elemental analysis and mass spectrometry), was found

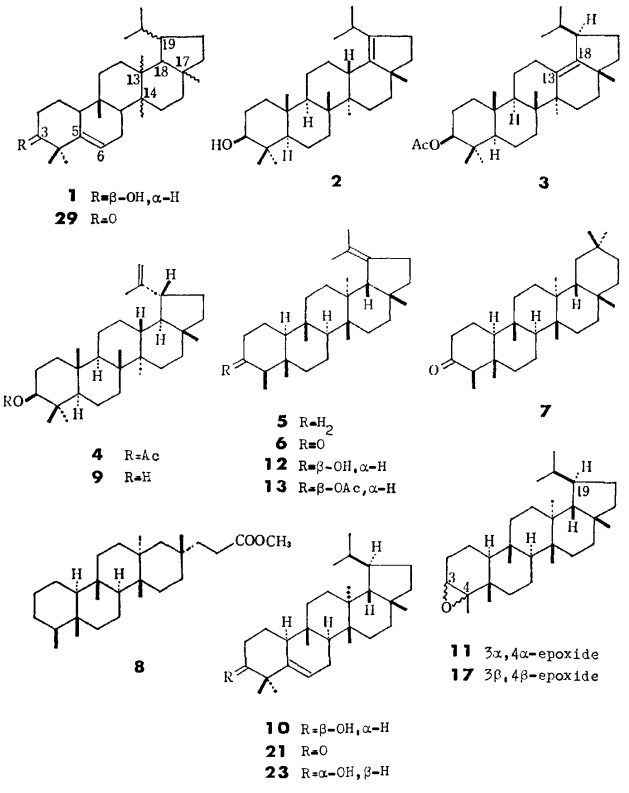

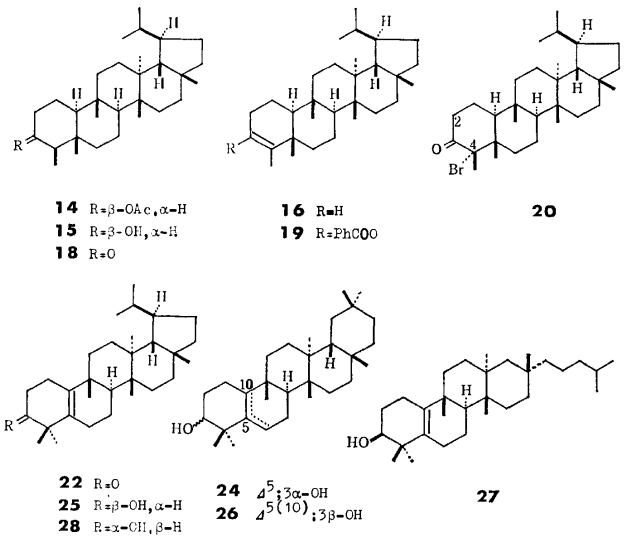

to be single by GLC and ^{1}H NMR measurement, the configuration of the 19β-isopropyl group could not be fully established until X-ray analysis clarified that 3α,4α-epoxy-*D* : *A*-friedo-18β,19α*H*-lupane (**11**) derived from the hydrogenation product possesses the desired 19α*H*-configuration (*vide infra*).

Saturated acetate (**14**) was treated with lithium aluminium hydride to give *D* : *A*-friedo-18β,19α*H*-lupan-3β-ol (**15**), which on treatment with phosphoryl chloride in pyridine under reflux, gave *D* : *A*-friedo-18β,19α*H*-lup-3-ene (**16**), $C_{30}H_{50}$, showing ^{1}H NMR signals at δ 5.18 (1H, m, $W_{1/2}$=9 Hz). The dehydration product (**16**) was treated with *m*-chloroperbenzoic acid in chloroform to afford a mixture of two epoxides in a 9: 5 ratio, their configurations being easily assigned by ^{1}H NMR measurement.[6] The major epoxide with a signal at δ 2.85 (t, J=2.5 Hz) was 3α,4α-epoxide (**11**) and the minor one with a signal at δ 2.90 (t, J=1 Hz) 3β,4β-epoxide (**17**).

The stereochemistry of the isopropyl group of **14** was unambiguously determined by X-ray diffraction analysis of 3α,4α-epoxy-*D* : *A*-friedo-18β,19α*H*-lupane (**11**). A single crystal of **11** belongs to the monoclinic space group $P2_1$ with cell parameters a=13.996(6), b=11.461(5), c=8.199(4) Å, β=106.34(6)° the two molecules being contained in the cell. The intensity data were collected on a Phlips PW1100 automatic diffractometer using graphite-monochromated Cu $K\alpha$ radiation. A total of 2494, non-zero, independent reflections with $2\theta \leq 156°$ were measured by means of θ-2θ scanning.

Table 1. Atomic positional parameters($\times 10^4$) and anisotropic temperature factors[a] ($\times 10^4$) with estimated standard deviations in parentheses

Atom	x	y	z	B_{11}	B_{22}	B_{33}	B_{12}	B_{13}	B_{23}
C(1)	3418(6)	5633(0)	9079(9)	67(5)	94(7)	147(13)	16(5)	30(7)	29(9)
C(2)	4167(6)	4633(9)	9790(11)	53(5)	113(9)	245(18)	5(6)	31(8)	57(11)
C(3)	4917(6)	4420(8)	8815(11)	58(5)	81(7)	217(17)	5(5)	17(7)	4(9)
C(4)	4946(5)	5074(7)	7301(10)	50(4)	70(6)	194(14)	4(4)	24(6)	−11(8)
C(5)	4204(5)	6078(7)	6693(9)	51(4)	70(6)	161(12)	0(4)	28(6)	−9(8)
C(6)	3997(5)	6202(8)	4732(9)	49(4)	113(8)	171(13)	1(5)	42(6)	18(9)
C(7)	3126(5)	7077(8)	3985(10)	57(4)	96(8)	189(14)	−5(5)	49(7)	32(9)
C(8)	2176(5)	6565(6)	4345(8)	45(4)	58(5)	119(10)	1(4)	39(5)	10(6)
C(9)	2304(5)	6566(6)	6298(8)	48(4)	46(5)	136(11)	−2(4)	35(5)	−5(6)
C(10)	3218(5)	5777(6)	7113(8)	50(4)	56(5)	139(11)	−4(4)	35(5)	1(7)
C(11)	1355(5)	5980(6)	6591(8)	46(4)	68(6)	111(10)	3(4)	33(5)	22(6)
C(12)	367(5)	6491(7)	5442(7)	48(4)	77(6)	93(10)	7(4)	30(5)	10(7)
C(13)	276(5)	6395(6)	3533(7)	50(4)	45(5)	105(10)	4(3)	37(5)	5(6)
C(14)	1179(5)	7093(6)	3180(8)	52(4)	51(5)	117(10)	4(4)	42(5)	11(6)
C(15)	1129(5)	6880(7)	1277(8)	61(4)	100(8)	97(10)	10(5)	42(6)	13(8)
C(16)	162(6)	7385(8)	69(10)	69(5)	115(9)	116(11)	14(6)	52(6)	38(8)
C(17)	−827(5)	7143(6)	514(8)	63(4)	64(6)	116(11)	6(5)	39(6)	10(7)
C(18)	−726(5)	6963(6)	2481(7)	50(4)	51(5)	95(10)	4(4)	33(5)	7(6)
C(19)	−1669(5)	6249(6)	2514(8)	51(4)	65(6)	126(11)	−2(4)	32(5)	10(7)
C(20)	−2494(5)	6945(7)	3021(10)	55(4)	77(7)	179(13)	3(5)	36(6)	13(8)
C(21)	−2080(6)	5688(8)	709(9)	77(5)	92(7)	137(12)	−21(6)	29(7)	−17(8)
C(22)	−1328(6)	6016(8)	−321(9)	89(6)	82(7)	122(12)	−10(6)	39(7)	−17(8)
C(23)	5924(6)	5112(9)	6755(12)	58(5)	124(10)	259(19)	20(6)	58(8)	−9(12)
C(24)	4739(6)	7208(8)	7601(12)	71(5)	69(7)	277(19)	−15(5)	34(8)	−20(10)
C(25)	2381(6)	7803(7)	7141(10)	68(5)	61(6)	191(14)	8(5)	35(7)	−32(8)
C(26)	1095(6)	8408(6)	3431(10)	75(5)	42(5)	183(14)	0(4)	47(7)	9(7)
C(27)	303(5)	5082(6)	3088(9)	63(4)	42(5)	181(13)	9(4)	45(6)	3(7)
C(28)	−1517(6)	8190(7)	−138(10)	77(5)	83(7)	153(13)	26(5)	43(7)	48(8)
C(29)	−2130(6)	7383(8)	4868(10)	71(5)	116(9)	167(14)	18(6)	57(7)	−14(10)
C(30)	−3423(6)	6185(10)	2848(13)	65(5)	137(11)	322(22)	−22(7)	72(9)	−20(14)
O	4518(4)	3926(5)	7117(7)	64(3)	61(4)	258(12)	7(3)	17(5)	−18(6)

a) The form of the anisotropic temperature factor is: $T=\exp(-B_{11}h^2-B_{22}k^2-B_{33}l^2-2B_{12}hk-2B_{13}hl-2B_{23}kl)$.

The intensities were corrected for Lorentz and polarization factors, but not for absorptions. The structure was solved by the direct method using program MULTAN.[7] An *E*-map calculated from 323 reflections with $|E| \leq 1.5$ revealed the locations of 25 nonhydrogen atoms out of 31, and all the other nonhydrogen atoms emerged in successive Fourier maps. The structural parameters were refined by the block-diagonal least-squares calculations assuming anisotropic thermal vibrations. The final *R*-factor was 9.9% excluding hydrogen atoms.[8] The weighting scheme $\sqrt{w}=20.0/|F_0|$ when $|F_0| \geq 20.0$, $\sqrt{w}=1.0$ when $20.0>|F_0| \geq 3.0$, and $\sqrt{w}=0.8$ when $|F_0|<3.0$ was applied. The atomic scattering factors were taken from International Tables for X-ray Crystallography.[9] The atomic positional and thermal parameters are given in Table 1. There are no abnormal bond lengths and angles as compared with those found in this type of compound except for the bond lengths $C_{(17)}$–$C_{(18)}$ and $C_{(13)}$–$C_{(14)}$ of 1.592 and 1.589 Å, respectively (Figs. 2a and 2b). The lengthening of the C–C bond at the fully substituted ring juncture is commonly observed in triterpenes, and for the above mentioned two bonds; the effect of repulsions between the 1,3-diaxial substituted groups may be responsible for the lengthening. Figure 3 shows a computer-generated perspective drawing of the molecule of the epoxide (**11**), with the 19α*H*-configuration as well as the 18β*H*-configuration.

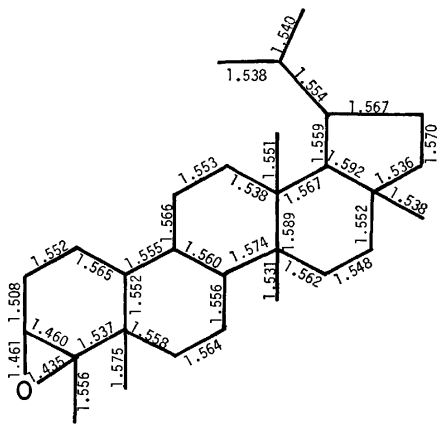

Fig. 2a. Bond lengths (*l*/Å) of **11**.

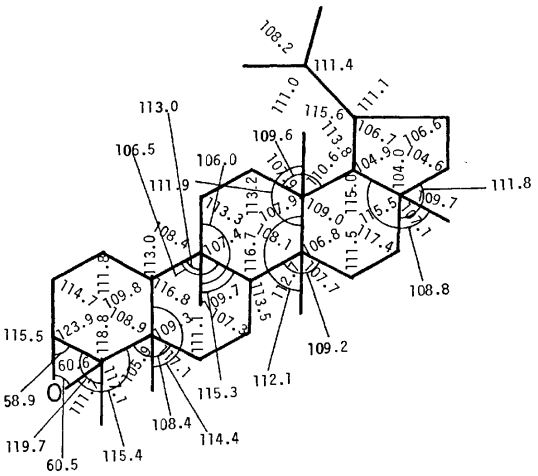

Fig. 2b. Bond angles (Φ/°) of **11**.

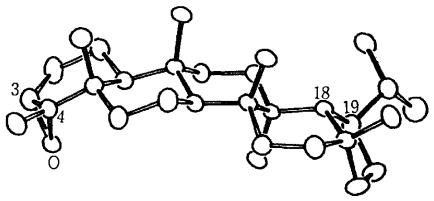

Fig. 3. Perspective view of **11**.

The saturated alcohol (**15**) was subjected to oxidation with the Jones reagent to give a ketone (**18**). The ketone is formulated *D* : as *A*-friedo-18β,19α*H*-lupan-3-one, corresponding biogenetically to the ultimate rearranged product in the migrated lupane series.

The conversion of a *D*: *A*-friedo type 3-keto triterpene into a *D* : *B*-friedo type ketone was carried out by the bromination-dehydrobromination reaction.[10,11] On treatment with benzoyl chloride under reflux, *D* : *A*-friedo-18β,19α*H*-lupan-3-one (**18**) gave 3-benzoyloxy-*D* : *A*-friedo-18β,19α*H*-lup-3-ene (**19**) selectively in a good yield. The absence of Δ^2-isomer was indicated by ^{1}H NMR measurement. The reaction product, after recrystallization from methanol, was brominated with bromine in pyridine at room temperature[10] to afford a monobromide (**20**), $C_{30}H_{49}OBr$ (M^+ 506.2946 and 504.2992), ^{1}H NMR δ 1.71 (3H, s) and δ 3.38 (1H, ddd; J=20, 13, and 8 Hz). The 4α-orientation of the bromine atom was deduced by the ^{1}H NMR spectrum: the signals at δ 3.38 were assignable to a $C_{(2\alpha)}$–H and the down-field shift was ascribed to a 1,3-diaxial relationship between the $C_{(4\alpha)}$–Br and the $C_{(2\alpha)}$–H.

The 4α-bromo derivative (**20**) was subjected to reaction with silver acetate in a mixture of diethyl ether and acetic acid.[11] The reaction product was purified by preparative TLC to afford a mixture of *D* : *B*-friedo-18β,19α*H*-lup-5-en-3-one (**21**) and -5(10)-en-3-one (**22**). The relative amount of two isomeric ketones (**21** and **22**) was estimated to be about 1 : 2 by GLC examination and ^{1}H NMR measurement. Since the mixture gave only one spot on TLC and only one peak on HPLC examination, separation of the mixture was abandoned.

The mixture was therefore reduced with sodium borohydride to afford a mixture of two pairs of epimeric alcohols. Although the alcohol mixture could not be separated into four components by a single procedure, it could be separated into two fractions by TLC, each fraction being further separated into two components by HPLC. Thus, the mixture was subjected to separation by preparative TLC into two fractions, a major fraction (R_f 0.3) and a minor one (R_f 0.4). The major fraction with a smaller R_f value on TLC was further separated by preparative HPLC into two alcohols, **23** and **25**. **23** seems to be *D*: *B*-friedo-18β,19α*H*-lup-5-en-3α-ol from the ^{1}H NMR spectrum: an olefinic proton at $C_{(6)}$ (δ 5.61, 1H, m, $W_{1/2}$=9 Hz) and $C_{(3\beta)}$-proton (δ 3.20, 1H, dd, J=10 and 4 Hz) attached to a hydroxyl-bearing carbon atom resembled those of *D*: *B*-friedo-olean-5-en-3α-ol (**24**)[12] (δ 5.63, 1H, m, $W_{1/2}$=9 Hz; δ 3.21, 1H, dd; J=10 and 5 Hz). **25** seems to be *D* : *B*-friedo-18β,19α*H*-lup-5(10)-en-3β-ol from a comparison of the ^{1}H NMR spectral data (δ 3.48, 1H, dd, J=10 and

4 Hz) with those of *D* : *B*-friedoolean-5(10)-en-3β-ol (**26**)[6b] (δ 3.45, 1H, dd; J=9.5 and 4.5 Hz) and *D* : *B*-friedobacchar-5(10)-en-3β-ol (**27**)[6a] (δ 3.48, 1H, dd; J=10 and 4 Hz).

The other fraction with a larger R_f value on TLC separation was found to be a 2:1 mixture of two alcohols by HPLC examination and was separated by preparative HPLC into two alcohols **28** (R_t=22.8 min) and **10** (R_t=20.3 min). The major alcohol (**28**) was found to be *D* : *B*-friedo-18β,19α*H*-lup-5(10)-en-3α-ol from the ^{1}H NMR spectrum and chemical conversion. The two alcohols **25** and **28** gave the same original ketone (**22**) on oxidation with chromium trioxide–pyridine complex. The fourth alcohol (**10**) should be the desired *D* : *B*-friedo-18β,19α*H*-lup-5-en-3β-ol. However, yield was less than 3% from the bromide (**20**). No satisfactory characterization could be achieved.

Treatment of 3β,4β-epoxides of *D* : *A*-friedo-type triterpenes with boron trifluoride etherate gives a mixture of backbone-rearranged products, from which *D* : *B*-friedo-Δ^5- and -$\Delta^{5(10)}$-triterpene 3β-alcohols are obtained. For example, *D* : *B*-friedobacchar-5-en-3β-ol was obtained from 3β,4β-epoxyshionane[13] and *D*: *B*-friedoolean-5-en-3β-ol from 3β,4β-epoxyfriedelane[6b] together with their 5(10)-ene isomers, respectively. 3β,4β-Epoxy-*D* : *A*-friedo-18β,19α*H*-lupane (**17**) was treated with boron trifluoride etherate in benzene to give a complex mixture, from which an alcohol was obtained. The ^{1}H NMR spectrum of the alcohol showed the presence of an olefinic proton [at δ 5.65 (1H, m, $W_{1/2}$=7 Hz)] and a proton attached to a hydroxyl-bearing carbon atom [at δ 3.45 (1H, m, $W_{1/2}$= 7 Hz)].[6b] The structure, *D*: *B*-friedo-18β,19α*H*-lup-5-en-3β-ol was established for this alcohol (**10**) by the following evidence. **10** was oxidized with chromium trioxide–pyridine complex to give a ketone, *D*: *B*-friedo-18β,19α*H*-lup-5-en-3-one (**21**), identical with that obtained by the oxidation of *D*: *B*-friedo-18β,19α*H*-lup-5-en-3α-ol (**23**). Retention times on GLC and HPLC examinations and R_f value on TLC of **10** were identical with those of the fourth alcohol obtained by the bromination-dehydrobromination reaction of the ketone (**18**) (*vide supra*).

The ^{1}H NMR, mass spectral data, and melting points of the four alcohols (**10**, **23**, **25**, and **28**) and the ketones (**21** and **22**) together with those of guimarenol (**1**) and guimarenone (**29**) are given in Table 2. The physical and spectral data of guimarenol (**1**) and the corresponding ketone, guimarenone (**29**), differ distinctly from those of the synthetic *D*: *B*-friedo-18β,19α*H*-lup-5-en-3β-ol (**10**) and the corresponding 3-one (**21**), respectively. The structure of guimarenol (**1**)[2] should be reinvestigated.

Experimental

General Procedure. Melting points were measured on a Mel-temp capillary melting point apparatus (Laboratory Devices) and are uncorrected. IR spectra were measured in Nujol mull with a Hitachi-EPI-G2 spectrometer or a Hitachi 260-30 spectrometer, mass spectra on a Hitachi RMU-6-Tokugata mass spectrometer at 70 eV with a direct inlet system, and high resolution mass spectra on a JMS-D300 (JEOL) mass spectrometer. Relative intensities are given in parentheses. ^{1}H NMR spectra were measured with a Hitachi R-20B (60 MHz) spectrometer, a Varian EM-390 (90 MHz) spectrometer or a JNM-FX60 FT-NMR (60 MHz) spectrometer (JEOL). Chemical shifts are given in δ downfield from TMS as an internal standard and coupling constants in Hz. GLC analyses were carried out with a Shimadzu Gas Chromatograph GC-6A equipped with a hydrogen flame ionization detector (column: Dexsil 300GC, temperature 270—290 °C). HPLC analysis and preparation were carried out on a Waters Liquid Chromatograph ALC/GPS 202/401 at room temperature with an RI detector (column: μ-Porasil 1/4 (inch)×1 (foot); solvent system: 1.5% diethyl ether–hexane (unless otherwise described); flow rate: 3 ml/min (unless otherwise described); pressure: *ca.* 700 psi). TLC was carried out on Kieselgel 60 GF_{254} (E. Merck) coated in 0.25 mm thickness (for analytical) and in 0.5 mm thickness (for preparative). Wakogel C-200 (Wako) was used for column chromatography.

D: A-*Friedo-18β-lup-19-en-3β-yl Acetate (13).* Excess of sodium borohydride (*ca.* 10 mg) was added to a solution of *D*: *A*-friedo-18β-lup-19-en-3-one (**6**; 7.5 mg) in methanol (30 ml) at room temperature, the mixture being stirred

Table 2.

Compound	Mp (°C)	^{1}H NMR	MS
Guimarenol (**1**)	276—278	δ 5.60 (1H, m) δ 3.55 (1H,t, $W_{1/2}$=6 Hz)	426 (M^+; 8%) 274 (100%)
5-en-3β-ol (**10**)	166—167	δ 5.65 (1H, m) δ 3.45 (1H, m, $W_{1/2}$=7 Hz)	426 (M^+; 7%) 274 (100%)
5-en-3α-ol (**23**)	181—182	δ 5.61 (1H, m, $W_{1/2}$=9 Hz) δ 3.20 (1H, dd, J=10, J=4 Hz)	426 (M^+; 10%) 274 (100%)
5(10)-en-3β-ol (**26**)	191—193	δ 3.48 (1H, dd, J=10, J=4 Hz)	426 (M^+; 13%) 408 (100%) 205 (72%)
5(10)-en-3α-ol (**28**)	195.5—196	δ 3.48 (1H, dd, J=10, J=4 Hz)	426 (M^+; 10%) 205 (100%)
Guimarenone (**29**)	196—200	δ 5.75 (1H, m)	424 (M^+; 26%) 274 (100%)
5-en-3-one (**21**)	149—153	δ 5.63 (1H, m)	424 (M^+; 11%) 274 (100%)
5(10)-en-3-one (**22**)	180—182		424 (M^+; 68%) 205 (100%)

overnight. The usual work-up and purification by preparative TLC (benzene: diethyl ether=9 : 1) gave *D* : *A*-friedo-18β-lup-19-en-3β-ol (**12**; 7.2 mg) in 95% yield: mp 173—175 °C (crystallized from acetone); IR 3460 cm^{-1}; ^1H NMR ($CDCl_3$) δ 0.8—1.0 (18H, 6×CH_3), 1.65 (6H, br s; >C=C(CH_3)$_2$), and 3.75 (1H, m, $W_{1/2}$=6 Hz); MS *m/e* 426 (M^+; 17) and 275 (100).

19-En-3β-ol (**12**; 7.2 mg) dissolved in pyridine (1 ml) was treated with acetic anhydride (1 ml) at room temperature and the mixture was left overnight. The usual work-up and purification by preparative TLC (benzene) gave *D* : *A*-friedo-18β-lup-19-en-3β-yl acetate (**13**; 6.8 mg) in 86% yield; mp 240—242.5 °C (crystallized from acetone); IR 1738 cm^{-1}; ^1H NMR ($CDCl_3$) δ 0.75—0.95 (18H, 6×CH_3), 1.63, 1.67 (each 3H, br s; >C=C(CH_3)$_2$), 2.04 (3H, s), and 4.92 (1H, m, $W_{1/2}$=7 Hz); MS *m/e* 468 (M^+; 60) and 317 (100); Found: C, 81.74; H, 11.09%. Calcd for $C_{32}H_{52}O_2$: C, 81.99; H, 11.18%.

D : A-*Friedo-18β,19α*H-*lupan-3β-yl Acetate* (**14**). The acetate (**13**; 632.2 mg) in acetic acid (350 ml) was hydrogenated in the presence of catalyst [prepared from platinum dioxide (851 mg)] under atmospheric pressure at 40 °C for 3.5 d. The catalyst was filtered off, and the solvent distilled off. The residue was purified by silica gel (35 g) column chromatography to give quantitatively a dihydro derivative, *D* : *A*-friedo-18β,19α*H*-lupan-3β-yl acetate (**14**; 637 mg); mp 251—253 °C (crystallized from acetone); IR 1735 cm^{-1}; ^1H NMR ($CDCl_3$) δ 0.8—1.0 (18H, 6×CH_3), 2.03 (6H, s), and 4.94 (1H, m, $W_{1/2}$=6 Hz); MS *m/e* 470(M^+; 58) and 410 (100); Found: C, 81.70; H, 11.81%. Calcd for $C_{32}H_{54}O_2$: C, 81.64; H, 11.56%.

D : *A-Friedo-18β,19α*H-*lupan-3β-ol* (**15**). The saturated acetate (**14**; 370 mg) dissolved in tetrahydrofuran (200 ml), was treated with lithium aluminium hydride (616 mg) under reflux for 1 h. The usual work-up gave *D* : *A*-friedo-18β,19α*H*-lupan-3β-ol (**15**; 327 mg) in 97% yield; mp 225—227 °C (crystallized from acetone); IR 3440 cm^{-1}; ^1H NMR ($CDCl_3$) δ 0.8—1.1 (24H, 8×CH_3) and 3.75 (1H, m, $W_{1/2}$= 7 Hz); MS *m/e* 428 (M^+; 100).

D : A-*Friedo-18β,19α*H-*lup-3-ene* (**16**). Freshly distilled phosphoryl chloride (1.8 ml) was added to a solution of 3β-ol (**15**; 317.3 mg) in dry pyridine (60 ml), the mixture being refluxed for 40 min. The residue obtained by the usual work-up was chromatographed on silica gel (60 g) impregnated with 25% silver nitrate to give *D* : *A*-friedo-18β,19α*H*-lup-3-ene (**16**; 254 mg) in 84% yield; mp 169—170 °C (crystallized from acetone); IR 795 cm^{-1}; ^1H NMR ($CDCl_3$) δ 0.95—1.15 (21H, 7×CH_3), 1.56 (3H, d; *J*=1.5 Hz), and 5.18 (1H, m, $W_{1/2}$=9 Hz); MS *m/e* 410 (M^+; 65) and 318 (100); Found: C, 87.78; H, 12.34%. Calcd for $C_{30}H_{50}$: C, 87.73; H. 12.27%.

Epoxidation of D : A-*Friedo-18β,19α*H-*lup-3-ene* (**16**). *m*-Chloroperbenzoic acid (578 mg) was added to a solution of the 3-ene (**16**; 254 mg) in chloroform (150 ml) at 0 °C, the solution being stirred at the same temperature for 1.5 h. A saturated aqueous sodium thiosulfate (50 ml) and a saturated aqueous sodium hydrogencarbonate (30 ml) were added to the solution, the mixture being stirred for 30 min at room temperature. Extraction with chloroform and the usual work-up gave a residue which was purified by preparative TLC [Kieselgel G (E. Merck); hexane: chloroform=3 : 2] to give 3α,4α-epoxy-*D* : *A*-friedo-18β,19α*H*-lupane (**11**; 157.5 mg) and 3β,4β-epoxy-*D* : *A*-friedo-18β,19α*H*-lupane (**17**; 87.5 mg) in 60 and 33% yields, respectively. 3α,4α-Epoxy-*D* : *A*-friedo-18β,19α*H*-lupane (**11**): mp 200—202 °C (crystallized from acetone); ^1H NMR ($CDCl_3$) δ 0.85 (15H, 5×CH_3), 0.96, 1.07, 1.19 (each 3H, s) and 2.85 (1H, t; *J*=2.5 Hz); MS *m/e* 426 (M^+; 77) and 411 (100); Found: C, 84.72; H, 11.95%. Calcd for $C_{30}H_{50}O$: C, 84.44; H, 11.81%. 3β,4β-Epoxy-*D* : *A*-friedo-18β,19α*H*-lupane (**17**): mp 215—216 °C crystallized from acetone); ^1H NMR ($CDCl_3$) δ 0.88 (15H, 5×CH_3), 0.96, 1.05, 1.17 (each 3H, s) and 2.90 (1H, t; *J*=1 Hz); MS *m/e* 426 (M^+; 100); Found: C, 84.67; H, 11.94%. Calcd for $C_{30}H_{50}O$: C, 84.44; H, 11.81%.

D : A-*Friedo-18β,19α*H-*lupan-3-one* (**18**). The 3β-ol (**15**; 246 mg) dissolved in acetone (150 ml) was treated with the Jones reagent at 0 °C for 1 h. The usual work-up gave *D*:*A*-friedo-18β,19α*H*-lupan-3-one (**18**; 236 mg) in 96% yield; mp 260—262 °C (crystallized from acetone); IR 1715 cm^{-1}; ^1H NMR ($CDCl_3$) δ 0.72 (3H, s) and 0.8—1.0 (21H, 7×CH_3); ^1H NMR ($CDCl_3$) using Eu(fod)$_3$-d_{27}/**18**=0.2 (M/M) δ 1.72 (3H, d; *J*=7 Hz; 4β-CH_3); MS *m/e* 426 (M^+; 100); Found: C, 84.66; H, 11.79%. Calcd for $C_{30}H_{50}O$: C, 84.44; H, 11.81%.

3-Benzoyloxy-D : A-*friedo-18β,19α*H-*lup-3-ene* (**19**). *D*:*A*-friedo-18β,19α*H*-lupan-3-one (**18**; 144 mg) was treated with benzoyl chloride (2 ml) under reflux for 2 h. The solution was cooled to 0 °C, methanol (*ca.* 5 ml) being added in order to destroy excess benzoyl chloride. When the mixture was allowed to stand for 30 min, crystals began to precipitate. The precipitate was collected on a filter paper and washed with methanol. 3-Benzoyloxy-*D*:*A*-friedo-18β,19α*H*-lup-3-ene (**19**; 168 mg) was obtained in 94% yield; mp 255—256 °C (crystallized from acetone); IR 1732 cm^{-1}: ^1H NMR ($CDCl_3$) δ 0.9—1.0 (18H, 6×CH_3), 1.09, 1.49 (each 3H, s), 7.4—7.7 (3H, m), and 8.0—8.3 (2H, m); MS *m/e* 530 (M^+; 5) and 105 (100); Found: C, 83.75; H, 10.13%. Calcd for $C_{37}H_{54}O_2$: C, 83.72; H, 10.25%.

4α-Bromo-D : A-*friedo-18β,19α*H-*lupan-3-one* (**20**). A mixture of bromine (0.1 ml) and pyridine (0.5 ml) was added to a chloroform solution (5 ml) of the enol benzoate (**19**; 50.3 mg) at room temperature. After being stirred for 3 h, a small amount of aqueous sodium thiosulfate was added and the mixture was stirred for several hours. The usual work-up and purification by preparative TLC (hexane: benzene=1:1) gave 4α-bromo-*D* : *A*-friedo-18β,19α*H*-lupan-3-one (**20**; 31.6 mg) in 66% yield; mp 192.5—194.5 °C (crystallized from methanol); IR 1715 cm^{-1}; ^1H NMR ($CDCl_3$) δ 0.8—1.0 (21H, 7×CH_3), 1.71 (3H, s), and 3.38 (1H, ddd; *J*=20, 13, and 8 Hz); MS *m/e* 506 (M^+; 12), 504 (M^+; 12), and 123 (100); Found: *m/e* 506.2946. Calcd for $C_{30}H_{49}O^{81}Br$: M, 506.2903. Found: *m/e* 504.2992. Calcd for $C_{30}H_{49}O^{79}Br$: M, 504.2967.

Dehydrobromination of 4α-Bromo-D : A-*friedo-18β,19α*H-*lupan-3-one* (**20**). A mixture of silver acetate (34 mg), water (0.3 ml), and acetic acid (16 ml) was added to an ethereal solution (12 ml) of the 4α-bromo ketone (**20**; 31.6 mg). The solvent was distilled off until the vapor temperature reached *ca.* 100 °C, the solution then being refluxed for 1 h. The usual work-up gave a residue (24.6 mg) which was purified by preparative TLC (benzene) to give a *ca.* 1: 2 mixture (19.6 mg) of *D*:*B*-friedo-18β,19α*H*-lup-5-en-3-one (**21**) and *D*:*B*-friedo-18β,19α*H*-lup-5(10)-en-3-one (**22**) in 74% yield. The relative ratio of the product was estimated from the peak area of GLC and the integrated area of olefinic proton signal in the ^1H NMR spectrum. These two olefinic isomers, however, could not be separated from each other by TLC or HPLC.

Readuction of the Mixture of Keto Olefins (**21** *and* **22**). A mixture (19.6 mg) of two olefinic isomers (**21** and **22**) was dissolved in methanol (5 ml) and kept at 0 °C. Excess sodium borhydride (*ca.* 30 mg) was added and the solution was stirred for 1 h. The usual work-up and purification by preparative TLC (benzene) gave a pair of mixtures. GLC examination showed that a mixture (16.6 mg) with a smaller R_f value on TLC consists of *D*: *B*-friedo-18β,19α*H*-lup-5-en-3α-ol (**23**) and *D*: *B*-friedo-18β,19α*H*-lup-5(10)-en-3β-ol (**25**), and the other

mixture (2.1 mg) with a larger R_f value consists of *D*:*B*-friedo-18β,19α*H*-lup-5-en-3β-ol (**10**) and *D*:*B*-friedo-18β,19α*H*-lup-5(10)-en-3α-ol (**28**). The former mixture was separated by preparative HPLC into *D*:*B*-friedo-18β,19α*H*-lup-5-en-3α-ol (**23**; 5.2 mg) and *D*:*B*-friedo-18β,19α*H*-lup-5(10)-en-3β-ol (**25**; 9.8 mg). *D*:*B*-Friedo-18β,19α*H*-lup-5-en-3α-ol (**23**): mp 181—182 °C (crystallized from acetone); IR 3320 and 825 cm^{-1}; ^1H NMR ($CDCl_3$) δ 0.8—1.0 (24H, 8$\times CH_3$), 3.20 (1H, dd; J=10 and 4 Hz), and 5.61 (1H, m, $W_{1/2}$=9 Hz); MS *m/e* 426 (M^+; 10) and 274 (100); HPLC (solvent system: 10% diethyl ether–hexane; flow rate: 2 ml/min) R_t=38.9 min; Found: *m/e* 426.3808. Calcd for $C_{30}H_{50}O$: M, 426.3860. *D*:*B*-Friedo-18β,19α*H*-lup-5(10)-en-3β-ol (**25**); mp 191—193 °C (crystallized from acetone); IR 3350 cm^{-1}; ^1H NMR ($CDCl_3$) δ 0.8—1.05 (24H, 8$\times CH_3$) and 3.48 (1H, dd, J=10 and 4 Hz); MS *m/e* 426 (M^+; 13), 408 (100), and 205 (72); HPLC (solvent system: 10% diethyl ether–hexane; flow rate: 2 ml/min) R_t=41.3 min; Found: *m/e* 426.3846. Calcd for $C_{30}H_{50}O$: M, 426.3860.

The latter mixture of **10** and **28** was separated by preparative HPLC into *D*:*B*-friedo-18β,19α*H*-lup-5-en-3β-ol (**10**; less than 0.5 mg) and -5(10)-en-3α-ol (**28**; 1.1 mg). *D*:*B*-Friedo-18β,19α*H*-lup-5(10)-en-3α-ol (**28**): mp 195.5—196 °C (crystallized from acetone); IR 3620 cm^{-1}; ^1H NMR ($CDCl_3$) δ 0.90 (6H, d; J=7 Hz, ($C\underline{H}_3$)$_2$CH–), 0.97, 1.03 (each 3H, s), 0.89, 1.00 (each 6H, s, 2$\times CH_3$), and 3.48 (1H, dd; J=10 and 4 Hz); MS *m/e* 426 (M^+; 10) and 205 (100); HPLC (solvent system: 10% diethyl ether–hexane; flow rate: 2 ml/min) R_t= 22.8 min; Found *m/e* 426.3880. Calcd for $C_{30}H_{50}O$: M, 426.3860.

Boron Trifluoride Etherate-catalyzed Backbone Rearrangement of 3β,4β-Epoxy-D:A-*friedo-18β,19α*H*-lupane (**17**) in Benzene.* A solution of 3β,4β-epoxy-*D*:*A*-friedo-18β,19α*H*-lupane (**17**; 47 mg) in benzene (25 ml) was treated with boron trifluoride etherate (0.3 ml) at room temperature for 1 h. The usual work-up gave a mixture, which was separated by preparative TLC (benzene) into *D*:*A*-friedo-18β,19α*H*-lupan-3-one (**18** 0.5 mg), *D*:*B*-friedo-18β,19α*H*-lup-5-en-3β-ol (**10**; 4.4 mg), and a complex mixture of alcohols (37.2 mg). *D*:*B*-Friedo-18β,19α*H*-lup-5-en-3β-ol (**10**): mp 166—167 °C (crystallized from acetone); IR 3400 (br), 1195, 1045, 973, and 825 cm^{-1}; ^1H NMR ($CDCl_3$) δ 0.88, 1.03, 1.13, 1.24 (each 3H, s; *t*-CH_3), 0.90 (6H, d; J=6 Hz; ($C\underline{H}_3$)$_2$CH–), 0.97 (6H, s, 2$\times$*t*-CH_3), 3.45 (1H, m, $W_{1/2}$=7 Hz), and 5.65 (1H, m, $W_{1/2}$=7 Hz); MS *m/e* 426 (M^+; 7) and 274 (100); HPLC (solvent system: 10% diethyl ether–hexane; flow rate: 2 ml/min) R_t=20.3 min; Found: *m/e* 426.3852. Calcd for $C_{30}H_{50}O$: M, 426.3860.

D: B-*Friedo-18β,19α*H*-lup-5-en-3-one* (**21**). *a)*: A large excess of chromium trioxide–pyridine complex in pyridine (0.5 ml) was added to a solution of *D*:*B*-friedo-18β,19α*H*-lup-5-en-3α-ol (**23**; 4.3 mg) in dichloromethane (3 ml), the solution being stirred at room temperature for 6 h. The usual work-up and preparative TLC (benzene) gave *D*:*B*-friedo-18β,19α*H*-lup-5-en-3-one (**21**; 1.6 mg).

b): The same oxidation of *D*:*B*-friedo-18β,19α*H*-lup-5-en-3β-ol (**10**; 4.4 mg) in dichloromethane (3 ml) with a large excess of chromium trioxide–pyridine complex in pyridine (0.5 ml) gave **21** (1.6 mg); mp 149—153 °C (crystallized from acetone); IR 1718 cm^{-1}; ^1H NMR ($CDCl_3$) δ 0.82. 0.90 (each 3H, s), 0.83 (6H, d; J=7 Hz; ($C\underline{H}_3$)$_2$CH–), 1.21 (12H, s, 4$\times CH_3$), and 5.63 (1H, m, $W_{1/2}$=11 Hz); MS *m/e* 424 (M^+; 11), 274 (100), and 123 (93); Found: *m/e* 424.3731. Calcd for $C_{30}H_{48}O$: M, 424.3705.

D: B-*Friedo-18β,19α*H*-lup-5(10)-en-3-one* (**22**). *a)*: Pyridinium chlorochormate[14] (16 mg) was added to a solution of *D*:*B*-friedo-18β,19α*H*-lup-5(10)-en-3α-ol (**28**; 12.5 mg) in dichloromethane (3 ml), the solution being stirred at room temperature for 5 h. The usual work-up and silica gel chromatography gave *D*:*B*-friedo-18β,19α*H*-lup-5(10)-en-3-one (**22**; 10.1 mg).

b): A solution of *D*:*B*-friedo-18β,19α*H*-lup-5(10)-en-3β-ol (**25**; 5.2 mg) in dichloromethane (3 ml) was oxidized with pyridinium chlorochromate (41 mg) in the same way as above to give **22** (5 mg); mp 180—182 °C (crystallized from acetone); IR 1715 cm^{-1}; ^1H NMR ($CDCl_3$) δ 0.8—0.95 (12H, 4$\times CH_3$), 0.97, 1.03, 1.13, and 1.16 (each 3H, s); MS *m/e* 424 (M^+; 68) and 205 (100); Found: *m/e* 424.3705. Calcd for $C_{30}H_{48}O$: M, 424.3705.

This work was partially supported by a Grant-in-Aid for Scientific Research No. 343008 from the Ministry of Education.

References

1) This work was reported in a preliminary form: Y. Yokoyama, Y. Moriyama, T. Tsuyuki, T. Takahashi, A. Itai, and Y. Iitaka, *Chem. Lett.*, **1979**, 1463.

2) A. G. González, F. G. Jerez, and M. L. Escalona, *An. Quim.*, **69**, 921 (1973); *Chem. Abstr.*, **80**, 24792n (1974).

3) E. Suokas and T. Hase, *Acta Chem. Scand.*, **B31**, 633 (1977).

4) a) Y. Yokoyama, T. Hirao, T. Tsuyuki, Y. Moriyama, T. Murae, and T. Takahashi, *Tetrahedron Lett.*, **1977**, 273; b) Y. Yokoyama, T. Tsuyuki, Y. Moriyama, T. Murae, H. Toyoshima, and T. Takahashi, *Bull. Chem. Soc. Jpn.*, **52**, 1720 (1979).

5) L. Ruzicka, A. Eschenmoser, and H. Heusser, *Experientia*, **9**, 362 (1953); A. Eschenmoser, L. Ruzicka, O. Jeger, and D. Arigoni, *Helv. Chim. Acta*, **38**, 1890 (1955); L. Ruzicka, *Proc. Chem. Soc.*, **1959**, 341.

6) Signals due to $C_{(3)}$–H: a) S. Yamada, S. Yamada, K. Tachibana, Y. Moriyama, Y. Tanahashi, T. Tsuyuki, and T. Takahashi, *Bull. Chem. Soc. Jpn.*, **49**, 1134 (1976); 3α,4α-epoxyshionane, δ 2.83, t, J=3 Hz; 3β,4β-epoxyshionane, δ 2.89, t, J=*ca.* 1 Hz; b) M. Tori, T. Torii, K. Tachibana, S. Yamada, T. Tsuyuki, and T. Takahashi, *Bull. Chem. Soc. Jpn.*, **50**, 469 (1977); 3α,4α-epoxyfriedelane, δ 2.86, t, J=2.5 Hz; 3β,4β-epoxyfriedelane, δ 2.90, m, $W_{1/2}$=3 Hz.

7) P. Main, M. M. Woolfson, L. Lessinger, G. Germain, and J. P. Declercq (1974). MULTAN 74. A System of Computer Programs for the Automatic Solution of Crystal Structures from X-ray Diffraction Data. Univs. of York, England, and Louvain-la-Neuve, Belgium.

8) The oberved and calculated structure factors are available at the office of this Bulletin as Document No. 8030.

9) "International Tables for X-Ray Crystallography," Vol. III. Birmingham, Kynoch Press (1962).

10) E. J. Corey and J. J. Ursprung, *J. Am. Chem. Soc.*, **78**, 5041 (1956); C. W. Shoppee and G. A. R. Johnston, *J. Chem. Soc.*, **1962**, 1252.

11) J. M. Beaton, F. S. Spring, R. Stevenson, and J. L. Stewart, *Tetrahedron*, **2**, 246 (1958).

12) On oxidation with chromium trioxide–pyridine complex, *D*:*B*-friedoolean-5-en-3β-ol[6b] gave the corresponding ketone, which was reduced with lithium aluminium hydride to afford a mixture of the 3β-ol and a 3α-ol in a 1: 15 ratio. The mixture was separated by column chromatography on silica gel impregnated with 20% silver nitrate to give *D*:*B*-friedoolean-5-en-3α-ol (**24**), mp 193—195 °C; IR 3430 cm^{-1}; MS *m/e* 426 (M^+), 274, and 205.

13) K. Tachibana, M. Tori, Y. Moriyama, T. Tsuyuki, and T. Takahashi, *Bull. Chem. Soc. Jpn.*, **50**, 1552 (1977).

14) E. J. Corey and J. W. Suggs, *Tetrahedron Lett.*, **1975**, 2647.

Restricted Rotation Involving the Tetrahedral Carbon. XXXIII.[1] Restricted Rotation about a C_{sp^3}–C_{sp^2} Bond in 10,10-Disubstituted 9-(2,6-Xylyl)-9,10-dihydroanthracene Derivatives[2]

Mikio NAKAMURA and Michinori ŌKI*,†

Department of Chemistry, School of Medicine, Toho University, Omorinishi, Ota-ku, Tokyo 143
†*Department of Chemistry, Faculty of Science, The University of Tokyo, Hongo, Bunkyo-ku, Tokyo 113*

(Received April 12, 1980)

A series of 10,10-disubstituted 9-(2,6-xylyl)-9,10-dihydroanthracene derivatives have been prepared and their conformations and barriers to internal rotation about the C_{xylyl}–C_9 bond have been examined. These compounds exist predominantly as a pseudo-equatorial form in the ground state for rotation. A large effect is inserted by the substituents in 10 position on barriers to rotation and is interpreted in terms of a rotation-inversion mechanism rather than a simple rotation mechanism for the methyl-exchange process which is observed by ^1H NMR spectra. The highest barrier to rotation has been found in the compound having two peri-chloro groups and a hydroxyl group in 9-position. The high barrier is ascribed to destabilization of the transition state, where 9-aryl group takes axial conformation, due to the three electronegative groups which are forced to be arranged parallelly in quite a near region. The change of 9-OH to 9-H thus decreases the barrier to rotation when peri-chlorines are present, while the increase in barrier is observed as in the case of 9-arylfluorenes and 9-arylxanthenes when they are absent.

It is well known that the barrier to rotation of 9-alkyltriptycenes (**1**) are extraordinarily high and in some cases rotational isomers have been isolated as stable entities at room temperature.[3] Barriers to rotation of aryl groups in 9-aryltriptycenes are, on the other hand, lower than those expected.[4] Although the molecular model of 9-(*o*-tolyl)triptycenes (**2**) indicated the existence of extremely high repulsion between the methyl and a peri hydrogen in the transition state for rotation, the barriers were in the range of 54—63 kJ mol^{-1} depending on the substituents in the peri position. These facts were interpreted in terms of destabilization of the ground state due to repulsive interaction between

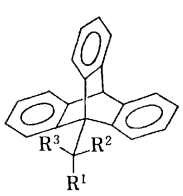

1

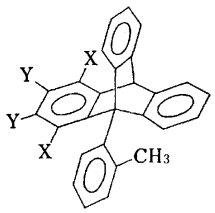

2

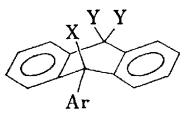

3

6′ and peri hydrogens. This means that the removal of a benzo group from 9-aryltriptycene, which leads to 9-aryl-9,10-dihydroanthracene skeleton (**3**), eliminates the repulsion mainly in the ground state and should lead to an increase in barriers to rotation. But a previous paper which dealt with restricted rotation of the aryl group in 9-(2,6-xylyl)xanthenes (**4**), 10-oxa analogs of **3**, showed relatively low barriers to rotation.[5] McKinley *et al.* explained the low barriers in this system, comparing with those of the structurally similar 9-mesitylfluorene derivatives (**5**),[6] on the basis of the difference in the direction of the substituents: the aryl group in the xanthene system takes an axial conformation both in the ground state and in the transition state for rotation. If the aryl group is axial in the boat form of the 9,10-dihydroanthracene type molecules,[7] the steric repulsion between 1,8-substituents of the xanthene ring and 2′,6′-substituents of the aryl ring will not

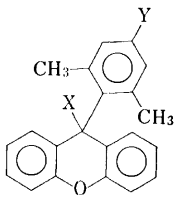

a X=OH
Y=H
b X=H
Y=CH$_3$

4

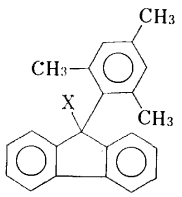

a X=OH
b X=H

5

increase in the transition state for rotation in contrast to the case of the 9-arylfluorene system.

The consideration described above leads to the idea that the barrier to rotation of the 9-aryl group in a 9,10-dihydroanthracene type molecule may be increased if the 9-aryl group is forced to take an equatorial conformation. It seems possible to realize such a situation by the introduction of two substituents in the 10 position. If a bulky group in the 9-position takes an axial conformation, it opposes a substituent in the 10 position which is also axial. Therefore, introduction of two bulky substituents in the 10 position, which assures that one of the two groups is always axial irrespective of the ring inversion, a bulky substituent in the 9 position will inevitably take the equatorial conformation. Under such expectation, we synthesized several 10,10-disubstituted 9-aryl-9,10-dihydroanthracenes (**6**—**11**) and measured the barriers to rotation about the C_9–C_{ar} bond by dynamic NMR method. This paper reports the results of the investigation and discusses the mechanism for rotation.

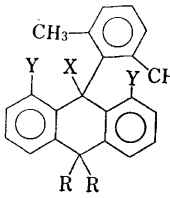

6 X=OH, Y=H, R=CH$_3$
7 X=H, Y=H, R=CH$_3$
8 X=OH, Y=Cl, R=CH$_3$
9 X=H, X=Cl, R=CH$_3$
10 X=OH, Y=H, R=PhCH$_2$
11 X=OH, Y=Cl, R=PhCH$_2$

Experimental

General. Melting points are uncorrected. ^{1}H NMR spectra were recorded either on a Hitachi R-20B spectrometer operating at 60 MHz or on a Varian EM 390 spectrometer at 90 MHz. IR spectra were measured on a Hitachi EPI-G3 grating infrared spectrophotometer. High and low temperature ^{1}H NMR spectra were measured in hexachlorobutadiene and chloroform-*d* solutions, respectively. The probe temperature was measured by the peak separation of methanol or ethylene glycol or by a thermocouple.

Syntheses. 9-(2,6-Xylyl)-10,10-dimethyl-9,10-dihydroanthracen-9-ol (6): To a vigorously stirred tetrahydrofuran solution of 2,6-xylylmagnesium bromide, prepared from 1.0 g (0.0054 mol) of 2-bromo-*m*-xylene and 0.144 g (0.0060 mol) of magnesium, was added 0.299 g (0.00135 mol) of 10,10-dimethylanthrone[8] at 0 °C. The reaction mixture was stirred for 3 h at room temperature, heated with stirring at 80 °C for 1 h, cooled, and treated with aqueous ammonium chloride. The organic layer was separated and the water layer was extracted with ether. The combined ether solution, after dried over sodium sulfate, was evaporated and the resulting oil was separated by chromatography on silica gel. Elution with hexane and benzene (10 : 1) gave white crystals which were recrystallized from hexane. The yield was 78% based on anthrone. The melting point was 153—154 °C. Found: C, 87.76; H, 7.48%. Calcd for $C_{24}H_{24}O$: C, 87.76; H, 7.37%. NMR($CDCl_3$, δ at 0 °C): 1.35 (3H, s), 1.70 (3H, s), 1.83 (3H, s), 1.9 (1H, s), 2.92 (3H, s), 7.0—7.8 (11H, m).

9-(2,6-Xylyl)-10,10-dimethyl-9,10-dihydroanthracene (7). To a solution of 102 mg (0.31 mmol) of **6** in 10 ml of acetic acid was added 2.0 ml of 57% hydriodic acid. The solution was stirred for 5 h at room temperature. The reaction mixture was poured into water and extracted with ether. The ether layer was washed with aqueous sodium hydrogencarbonate and then with aqueous sodium hydrogensulfite, and dried over sodium sulfate. After evaporation of the solvent, the products were separated by chromatography on silica gel. Elution with hexane followed by recrystallization from ethanol afforded 79 mg (81%) of white fluorescent crystals, mp 133—134 °C. Found: C, 92.18; H, 7.78%. Calcd for $C_{24}H_{24}$: C, 92.26; H, 7.74%. NMR ($CDCl_3$, δ): 1.40 (3H, s), 1.54 (3H, s), 1.90 (3H, s), 2.57 (3H, s), 5.80 (1H, s), 6.6—7.8 (11H,m).

1,8-Dichloro-9-(2,6-xylyl)-10,10-dimethyl-9,10-dihydroanthracen-9-ol (8), mp 199—200 °C, was prepared by treating 2,6-xylyllithium, prepared from 1.0 g (0.0054 mol) of 2-bromo-*m*-xylene and 0.081 g (0.012 mol) of lithium, with 0.103 g (0.00035 mol) of 1,8-dichloro-10,10-dimethylanthrone[9,10] in 30 ml of ether. The reaction mixture was separated by chromatography on silica gel. The white crystals thus obtained were recrystallized from ethanol. The yield was 63% based on anthrone. Found: C, 72.85; H, 5.44; Cl, 17.38%. Calcd for $C_{24}H_{22}Cl_2O$: C, 72.55; H, 5.58; Cl, 17.85%. This compound could not be obtained from the Grignard reaction as in the case of compound **6**. NMR ($CDCl_3$, δ): 1.40 (3H, s), 1.62 (3H, s), 1.93 (3H, s), 2.9 (1H, s), 3.10 (3H, s), 6.5—7.6 (9H, m).

1,8-Dichloro-9-(2,6-xylyl)-10,10-dimethyl-9,10-dihydroanthracene (9), mp 206—207 °C, was similarly prepared by the reaction of **8** with 57% hydriodic acid in acetic acid followed by similar treatment as **7**. Recrystallization from hexane gave white crystals in 78% yield. Found: C, 75.77; H, 5.86; Cl, 18.63%. Calcd for $C_{24}H_{22}Cl_2$: C, 75.59; H, 5.82; Cl 18.60%. NMR-($CDCl_3$, δ): 1.51 (3H, s), 1.63 (3H, s), 2.00 (3H, s), 2.87 (3H, s), 5.90 (1H, s), 6.6—7.6 (9H, m).

9-(2,6-Xylyl)-10,10-dibenzyl-9,10-dihydroanthracen-9-ol (10), mp 216—217 °C, was prepared by treating 2,6-xylylmagnesium bromide, prepared from 3.2 g (0.0173 mol) of 2-bromo-*m*-xylene and 0.411 g (0.0173 mol) of magnesium, with 2.0 g (0.0057 mol) of 10,10-dibenzylanthrone[8] in 50 ml of THF. The reaction mixture was separated by chromatography on silica gel. Elution with hexane and benzene (10 : 1) gave white crystals which were recrystallized from ethanol. The yield was 55% based on anthrone. Found: C, 89.76; H, 6.46%. Calcd for $C_{36}H_{32}O$: C, 89.96; H, 6.71%. NMR ($CDCl_3$, δ): −0.2 (1H, s), 0.26 (3H, s), 2.55 (3H, s), 3.45 (2H, s), 3.86 (2H, s), 6.1—7.6 (19H, m), 8.1 (2H, dd).

1,8-Dichloro-9-(2,6-xylyl)-10,10-dibenzyl-9,10-dihydroanthracen-9-ol (11), mp 283—285 °C, was synthesized by treating 2,6-xylyllithium, prepared from 2.20 g (0.012 mol) of 2-bromo-*m*-xylene and 173 mg (0.025 mol) of lithium, with 1.22 g (0.0028 mol) of 1,8-dichloro-10,10-dibenzylanthrone in 30 ml of ether. The product was recrystallized from benzene–hexane. The yield was 60% based on anthrone. Found: C, 78.92; H, 5.26; Cl, 12.76%. Calcd for $C_{36}H_{30}Cl_2O$: C, 78.68; H, 5.50; Cl, 12.90%. NMR ($CDCl_3$, δ): −0.2 (1H, s), 0.35 (3H, s), 2.78 (3H, s), 3.30 (2H, s), 5.00 (2H, s), 6.1 (2H, m), 6.3 (1H, dd), 6.7—7.6 (14H, m), 8.1 (2H, dd).

Results and Discussion

Ground State Conformation. Before discussing the barriers to rotation of these compounds, it is necessary to consider the ground state conformation. These compounds could exist as two conformers, pseudo-equatorial (**12**) and pseudo-axial (**13**), with respect to 9-aryl orientation. The molecular model indicates that, while extremely large repulsion exists in **13**, such large repulsive interaction can not be expected in **12** and suggests that the 9-aryl group takes the conformation which bisects the 9,10-dihydroanthracene ring. That the preferred conformation of these compounds is pseudo-equatorial is clearly demonstrated by the ^{1}H NMR spectra, especially in the case of **10** and **11**. In

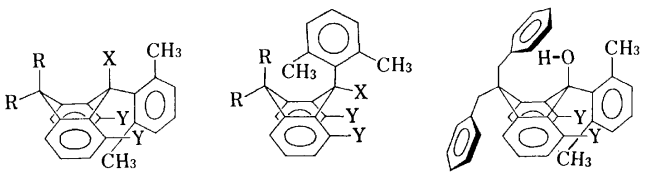

12 13 14

both compounds one of the methyl signals appeared at an abnormally high magnetic field. In addition, the hydroxyl signals of these compounds also appeared at quite a high field ($\delta = -0.2$). The high chemical shifts of these protons can be explained by the 9-aryl equatorial form with the conformation of benzyl groups which is discussed below. Two benzyl groups are arranged in such a manner that the two bulky benzene rings take the conformation anti to each other to avoid severe steric interaction. As a result one benzene ring of the benzyl group faces the methyl in the 2′ position and another the OH group, making these protons shift to quite a high field. In fact there are no such signals in 10,10-dimethyl derivatives **6** and **8**. Thus the most plausible conformation of **10** and **11** are considered to be **14**. Another piece of evidence for the conformation can be supplemented by the IR spectra. As are shown

Table 1. ν_{OH} Absorption[a)]

Compound	6	8	10	11
ν_{OH}/cm^{-1}	3596	3586	3547	3542

a) Carbon tetrachloride solutions of which concentrations were *ca.* 10 mmol l^{-1}

in Table 1, those compounds which carry benzyl groups exhibit ν_{OH} absorptions at around 3545 cm^{-1}, whereas those carrying methyl groups in the 10 position at around 3590 cm^{-1}. The latter absorption is characteristic of tertiary benzylic alcohols[11] but the former is too low to assign to the normal tertiary benzylic alcohols. Instead, the existence of the OH···π interaction[12] is suggested. Then the benzylic phenyl and the hydroxyl groups must be located in proximity. The existence of two aromatic protons which appeared at a field lower than δ 8.0 as a double doublet can also be explained by this conformation. These signals are assigned to the protons in 4 and 5 positions, because in **14** they reside in the deshielding zone of the benzene ring of the benzyl group.

In the case of the 10,10-dimethyl derivatives (**6**—**9**), it is very difficult to decide whether or not the 9-aryl groups of these compounds take the equatorial conformation on the basis of their ^1H NMR spectra, because there are no so characteristic signals as to suggest a conformation. But comparison of barriers to rotation of **6** and **7** with those of the corresponding xanthene derivatives **4a** and **4b** clearly indicates that the 9-aryl groups also take the equatorial conformation, the reason of which will be mentioned in the later part of this paper.

Barriers to Rotation. In every compound examined, two methyl signals in 2′ and 6′ positions broadened when the temperature was raised. However, no change in chemical shifts and spectral widths was observed in the signals in 10 position. This clearly shows that the coalescent phenomenon of this system is not due to the slow inversion of 9,10-dihydroanthracene ring but due to the restricted rotation of the 9-aryl ring.

In Table 2, activation free energies of these compounds including structurally similar **4** and **5** are listed together with the coalescence temperatures and the chemical shift differences between two methyl signals in 2′ and 6′ positions. Inspection of Table 2 reveals that the replacement of two methyl groups in 10 positions by benzyl groups causes the increase in energy barrier by 17.6 kJ mol^{-1} (**6**→**10**) and by more than 4.6 kJ mol^{-1} (**8**→**11**). Since the substituents in 10 positions are located far away from the two methyls in the pseudo-equatorial 9-aryl group, the increase in energy observed here seems to be too large as the substituent effect on barriers to rotation.

Table 2. Chemical shifts and barriers to rotation

Compd	2′-CH_3	6′-CH_3	10-R	T_c/°C	$\Delta G^{\ddagger}_c$/ kJ mol^{-1}
4a	1.35	2.93		−20	45.6[a)]
4b	1.63	2.58		95	73.6[a)]
5a	1.15	2.90		145	84.5[b)]
5b	1.13	2.69		>190	>104.6[b)]
6	1.35	2.92	1.70, 1.83	48	64.4
7	1.40	2.57	1.54, 1.90	126	82.0
8	1.40	3.10	1.62, 1.93	172	90.4
9	1.63	2.87	1.51, 2.00	36	62.8
10	0.26	2.55	3.45, 3.86	138	82.0
11	0.35	2.78	3.30, 4.00	>200	>95.0

a) Data from McKinley *et al.*[5)] b) Data from Rieker and Kessler.[6c)]

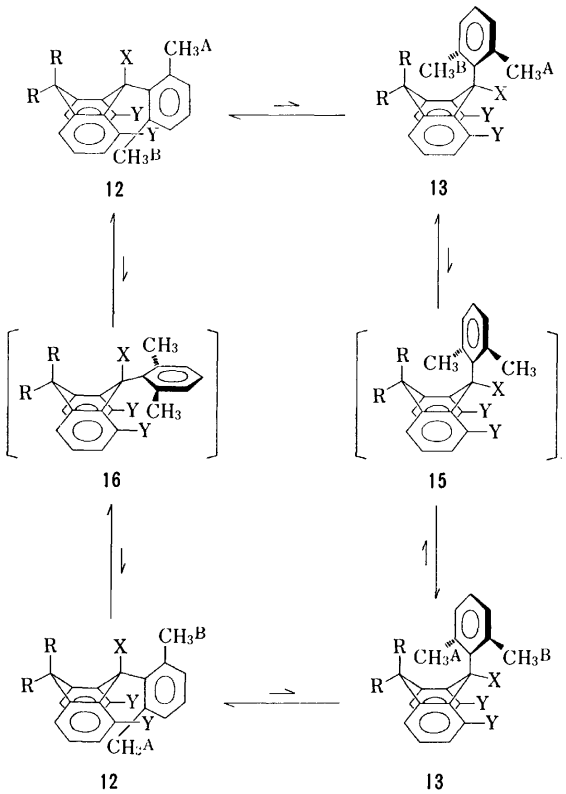

Fig. 1. Mechanism for the exchange of two methyls in the 2,6-xylyl group.

Two paths may be possible as the methyl-exchange mechanism as shown in Fig. 1. One is a simple rotation process during which the 9-aryl group is fixed in the equatorial form. The conformation of the transition state of this process is shown as **16**. The other is an inversion-rotation process which indicates that the methyl-exchange occurs through inversion of the 9,10-dihydroanthracene ring followed by rotation in the pseudo-axial conformation and then inversion to the methyl-exchanged ground state. The conformation of the transition state in this process is **15**. If the former is the case, the substituent effect in 10 position is, as mentioned, too large. In fact extremely large repulsion is expected between the xylyl group and 1,8-substituents in the conformation **16**. The barrier would have been very high in this case. If, on the other hand, the latter is occuring, the large substituent effect can be explained on the basis of the bulkiness of the benzyl groups in 10 position. In the transition state for the

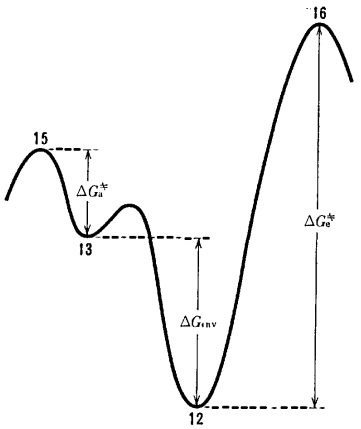

Fig. 2. Free energy profile for the rotation in 10,10-disubstituted 9-(2,6-xylyl)-9,10-dihydroanthracenes.

exchange, the two methyl groups in the pseudo-axial 9-aryl ring interact with the atoms in 1,8-positions as shown in **15**. In such a conformation two benzyl groups in **10** and **11** can not be arranged as in the ground state **14**; inside benzyl group takes the conformation in which the bulky benzene ring rotates away from the 9-aryl ring to avoid steric interaction and the rotation causes, in turn, repulsion between the two benzyl groups to result in an increase in energy of this state. In compounds **6** and **8**, on the other hand, such an additional increase in energy caused by the interaction between the two methyl groups in 10 position does not occur in the transition state for rotation. This may be the reason why **10** and **11** have higher barriers to rotation than those of the corresponding **6** and **8**. The energy profile in this system thus becomes the one described in Fig. 2, where ΔG_{inv}, ΔG_a^*, and ΔG_e^* stand for the difference in free energy between **12** and **13**, the barrier to rotation in the pseudo-axial state, and that in the pseudo-equatorial state, respectively.

The reason why we take ΔG_a^* smaller than ΔG_{inv} is as follows. If we assume that two methyls exchange only through the inversion of dihydroanthracene ring as described above, the free energy of activation (ΔG^*) in Table 2 are given by

$$\Delta G^* = \Delta G_{inv} + \Delta G_a^*.$$

Since the barrier to rotation of the xylyl group in structurally similar **4a**, where the 9-aryl group is axial both in the ground and in the transition state for rotation, was reported to be 45.6 kJ mol^{-1}, ΔG_a^* in this system is expected to be far lower than this value because of the existence of two substituents in 10 position which destabilize the aryl-axial form **13**. Therefore, the main portion of ΔG^* is occupied by ΔG_{inv}. A similar discussion has been made recently by Miller for the restricted rotation in 3-mesityl-1*H*,3*H*-naphtho-[1,8-*de*]pyrans.[13] The above discussion clearly indicates that the ground state conformation of 10,10-dimethyl derivatives (**6**—**9**) is also equatorial. If the 9-aryl groups of these compounds were axial, the ΔG^* should have been equal to ΔG_a^* which must be lower than that of **4a**. Actually, however, the reverse is true in this system.

Introduction of two chloro groups in 1 and 8 positions causes a strange effect on barriers to rotation: the increase in energy by more than 13.0 kJ mol^{-1} (**10**→**11**) and by 26.0 kJ mol^{-1} (**6**→**8**) was observed in the 9-OH derivatives, while the decrease in energy by as much as 19.2 kJ mol^{-1} was found in the 9-H derivatives (**7**→**9**). These results may be explained as follows. Introduction of two chloro groups raises the energy state of both the ground state **12** and the transition state **15** for rotation. But the degree of the increase is much greater in the latter than in the former when X is OH, because in **15** three bond dipoles are forced to be arranged parallelly in quite a narrow region. Since such a repulsion in **15** is not expected in the 9-H compound (**9**), the increase in energy of the ground state is large relative to the transition state, resulting in a low barrier to rotation.

The change in barriers, observed on the change in the 9-substituent from OH to H, is also interesting. In the case of a pair of **6** and **7**, the increase in energy of *ca.* 17.6 kJ mol^{-1} is ascribed mainly to the stabilization of the ground state. Such a stabilization of the ground state due to loss of repulsion between 9-OH and 2'-methyl is well known in **4** and **5**. On the contrary, relatively large decrease in rotational barrier (27.6 kJ mol^{-1}) was found when **8** was changed to **9**. Probably, the role of parallel arrangement of the three dipoles in the transition state of **8** exceeds that of the increase in the steric interaction in the ground state of **8** in contribution to the barrier to rotation.

References

1) Preceding paper: G. Yamamoto, M. Suzuki, and M. Ōki, *Angew. Chem. Int. Ed. Engl.*, submitted.
2) Presented in part as a preliminary form: M. Nakamura and M. Ōki, *Tetrahedron Lett.*, **1979**, 527.
3) M. Ōki, *Angew. Chem. Int. Ed. Engl.*, **15**, 87 (1976).
4) M. Nakamura and M. Ōki, *Bull. Chem. Soc. Jpn.*, **48**, 2106 (1975).
5) S. V. McKinley, P. A. Grieco, A. E. Young, and H. H. Freedman, *J. Am. Chem. Soc.*, **92**, 5900 (1970).
6) a) E. A. Chandross and C. F. Sheley, Jr., *J. Am. Chem. Soc.*, **90**, 4345 (1968); b) T. H. Siddall, III, and W. E. Stewart, *J. Org. Chem.*, **34**, 233 (1969); c) A. Rieker and H. Kessler, *Tetrahedron Lett.*, **1969**, 1227.
7) P. W. Rabideau, *Acc. Chem. Res.*, **11**, 141 (1978) and references cited therin.
8) D. Y. Curtin, R. C. Tuites, and D. H. Dybvig, *J. Org. Chem.*, **25**, 155 (1960).
9) E. De B. Barnett and M. A. Matthews, *J. Chem. Soc.*, **123**, 2549 (1923).
10) D. Y. Curtin and Z. M. Holubec, *J. Org. Chem.*, **34**, 3093 (1969).
11) M. Ōki and H. Iwamura, *Bull. Chem. Soc. Jpn.*, **35**, 1552 (1962).
12) M. Ōki and H. Iwamura, *Bull. Chem. Soc. Jpn.*, **33**, 681 (1960).
13) A. Miller, *J. Org. Chem.*, **44**, 1934 (1979).

Nuclear Magnetic Resonance Studies of Hydrosilanes. III.[1] A Correlation of Hammett σ Constants with ^{29}Si–H Coupling Constants for Substituted Phenoxy- and (Phenylthio)dimethylsilanes

Hamao WATANABE,* Ryoichi AKABA, Takao IEZUMI, and Yoichiro NAGAI*
Department of Applied Chemistry, Faculty of Engineering, Gunma University, Kiryu 376
(Received April 19, 1980)

The ^{29}Si–H coupling constants and Si–H chemical shifts have been determined for a series of substituted phenoxy- and (phenylthio)dimethylsilanes. The $J(^{29}Si–H)$ values are shown to be correlated well with the Hammett σ constants for the substituent on benzene ring in compounds Ar–Y–$SiMe_2H$, where Y=O and S. In comparison with the data for the analogs of the other types of organodimethylsilanes, such as aryldimethylsilanes, substituted benzyldimethylsilanes, and aryltetramethyldisilanes, the present results are discussed on the basis of the substituent effects through the intervening oxygen and sulfur. The transmission efficiency of Y was in the order, $S > CH_2 \approx SiMe_2 > O$. For the series of (phenylthio)dimethylsilanes, the $J(^{29}Si–H)$ values observed were larger than those for the predicted ones. This deviation was interpreted in terms of the sulfur d-orbital participation *via* the electron-acceptor, "σ-π" conjugation.

There have been many reports on Hammett treatment NMR data, proton chemical shifts and ^{13}C–H coupling constants, for a variety of substituted aromatics, such as toluenes, *t*-butylbenzene, *N,N*-dimethylanilines, anisoles, methylthiobenzenes, phenyltrimethylsilanes, *etc.*[2–10] We have recently determined the ^{29}Si–H and ^{13}C–H coupling constants and SiH chemical shifts for a series of substituted phenylsilanes, phenylmethylsilanes and phenyldimethylsilanes and found that there exist excellent correlations between the coupling constants and the Hammett σ constants of the ring substituents for these series.[11,12] Cartledge and Riedel have also shown that the ^{29}Si–H and ^{13}C–H coupling constants for a series of substituted benzyldimethylsilanes and phenyltetramethyldisilanes are directly proportional to the Hammett σ constant for the *meta* and *para* substituents and that the ρ values for the relationships can be interpreted in terms of transmission of electronic substituent effects through C–Si and Si–Si bonds.[13]

The transmission of substituent effects is quite an interesting subject in silicon chemistry and one of the problems in this fields concerns the role of d-orbitals in transmitting the electronic effects of substituents. In view of our continuing interest in the chemistry of organosilicon hydrides[11,14] we have prepared two series of compounds, phenoxy- (**1**) and (phenylthio)dimethylsilanes (**2**) and have determined the ^{29}Si–H coupling constants and Si–H chemical shifts. In the present paper, we will describe the Hammett dependence of the ^{29}Si–H coupling constants for the two series of compounds. The transmission efficiency of substituent effects of oxygen and sulfur was compared with those for the structurally related compounds in which $Y=CH_2$ and $SiMe_2$, and the electronic structure of Y which affects the magnitude of the $J(^{29}Si–H)$ values is also discussed.

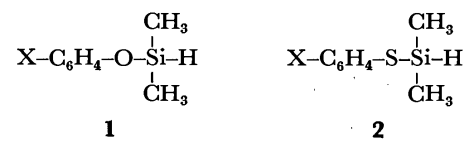

1 **2**

Results and Discussion

Transmission Efficiency of Y. Table 1 summarized all the NMR parameters determined for the two series, phenoxy- and (phenylthio)dimethylsilanes, and lists the Hammett σ constants for the substituent on benzene ring of these compounds. The Si–H coupling constants (J) for the two series of compounds are plotted against the Hammett σ constants in Fig. 1, giving the respective straight-line relationships. The slope (ρ), intercept (C) and correlation coefficient (γ) were determined by the method of least-squares and are given in Table 2, in

Table 1. NMR data for substituted phenoxy- and (phenylthio)dimethylsilanes ($XC_6H_4–Y–SiMe_2H$)

X	Y=O		Y=S		σ
	$J(^{29}Si–H)$ (Hz)	δ(Si–H) (ppm)	$J(^{29}Si–H)$ (Hz)	δ(Si–H) (ppm)	
p-MeO	−207.6	294.6	−207.8	277.8	−0.268
m-Me_2N	−207.8	296.4			−0.211
p-Me	−207.8	294.0	−208.3	280.2	−0.170
m-Me			−209.0	280.2	−0.069
H	−208.0	298.8	−209.7	283.2	−0.000
p-Cl	−209.4	295.8	−210.1	280.2	+0.227
m-Cl	−209.6	298.2			+0.373

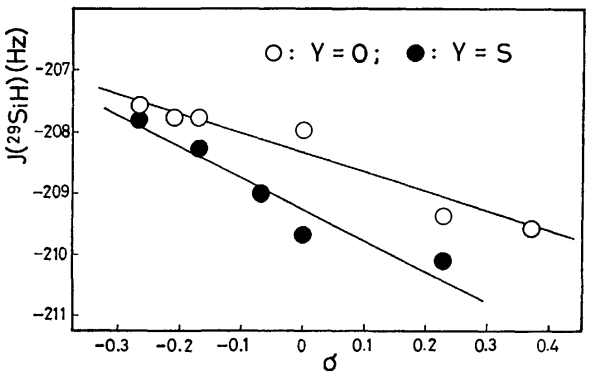

Fig. 1. Hammett plot of the $J(^{29}Si–H)$ in Ar–Y–$SiMe_2H$ *vs.* σ constant for the substituent on the benzene ring.

which the data for aryldimethylsilanes obtained by our previous work[11] and those for substituted benzyldimethylsilanes and aryltetramethyldisilanes by Cartledge and co-worker[13] were listed together.

The Si–H coupling constants presented in the Table 1 exhibited the expected trend in the two series. The presence of an electron-donating substituent (X) leads to a decrease in absolute magnitude of the coupling constant, whereas the presence of an electron-attracting substituent increases it. For example, the ^{29}Si–H coupling constants for *p*-methoxyphenoxy-, phenoxy-, and *m*-chlorophenoxysilane are −207.6, −208.0, and −209.6 Hz, respectively.

TABLE 2. THE ρ VALUES AND INTERCEPTS FOR Ar–Y–$SiMe_2H$ OBSERVED FOR $J(^{29}Si–H)$

Y	$-\rho$ (Hz/σ)	$-C$ (Hz)	γ[a]	Ref.
S	4.9	209.3	0.956	this work
O	3.3	208.4	0.989	this work
CH_2	4.4	186.7	0.978	13
$SiMe_2$	4.0	174.8	0.967	13
none	6.7	188.5	0.990	11

a) Correlation coefficient.

As seen from Fig. 1, the $J(^{29}Si–H)$ values of phenoxy- and phenylthiosilanes correlate well with Hammett σ constant. The ρ values obtained from phenoxy- and phenylthiosilanes were −3.3 and −4.9 Hz/σ with γ= 0.989 and 0.956, respectively, and can be compared with those of the other related silanes listed in Table 2. It is seen from the ρ values that the transmitting efficiency of the intervening Y (atom or group) in Ar–Y–$SiMe_2H$ decreases in the order:

$$S > CH_2 \approx SiMe_2 > O.$$

With respect to the transmission of substituent effect through Y in the type of compounds, XC_6H_4–Y–H, Marcus *et al.* have paid particular attention to oxygen and sulfur when they form part of Y.[2] Thus, by comparing the ρ values for anisoles (Y=OCH_2) with that for methylthiobenzene (Y=SCH_2) in the Hammett dependence of the methyl proton chemical shifts, they found that the efficiency of oxygen in transmitting the substituent effects is greater than that of sulfur. This observation was explained in terms of the balance of various factors, such as nonconjugative and conjugative effects of Y, medium effect, *etc.* They also discussed the transmission efficiency of these atoms by citing several experimental results other than chemical shifts and commented that the sulfur atom must show greater efficiency when it acts as an electron acceptor in conjugated systems ("conjugative-acceptor case").

Fueno *et al.* have also determined the proton chemical shifts for a series of aryl vinyl ethers and aryl vinyl sulfides and found a good carrelation between the chemical shifts for β-proton and Hammett σ constants.[9] It has been shown that the ρ-value of the sulfide series is greater than that of the ethers, and that the result supports the above Marcus' conjecture regarding an enhanced transmission efficiency of sulfur relative to oxygen. In the sulfur compounds, various electronic contributions, such as electron-donating, electron-accepting Pπ-dπ, and through-conjugative interaction[15,16] were taken into consideration to explain the transmission efficiency. They have concluded that the transmission through sulfur is enhanced by the contribution of the canonical structure involving "through-conjugative" interaction which was defined as Pπ-dπ-Pπ conjugation:

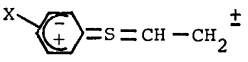

Subsequently, by comparing the Hammett dependence of the ^{13}C chemical shifts in the two series of compounds, they have obtained a similar results which supports the "through-conjugative" participation of sulfur d-orbitals in π-conjugation.[17]

In our system, the transmission efficiency of subsituent effect of sulfur was shown to be greater than that of oxygen. This fact would be attributed to the presence of sulfur atom attached to the silicon. Considering that sulfur has electron-accepting d-orbitals and lone-pair electrons available for electron donation and that silicon also electron-accepting d-orbitals,[18] the contribution of a canonical structure containing the electron-accepting conjugation is possible. This is the structure A. In addition, this conjugation could be reached to the silicon, forming a new type of "through-conjugative" interaction, or Pπ-dπ-dπ conjugation (B), as the resonance structure of A, which is similar to that of aryl vinyl sulfides as shown by Fueno and coworkers.[9,17] However, it is not clear at the present time whether the contribution of such conjugation (B) is necessary or not to explain the enhanced transmission of substituent effect.

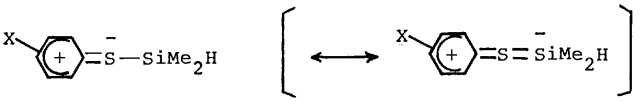

Pπ-dπ conjugation (A)

Pπ-dπ-dπ conjugation (B) (or "through-conjugative" interaction)

Similarly, oxygen in the phenoxide series serves as an electron donor to form Pπ-Pπ (C) and Pπ-dπ (D) conjugations. However, there can be no contribution by such a "through-conjugative" interaction as above mentioned.

Pπ-Pπ conjugation (C)

Pπ-dπ conjugation (D)

The ρ values of −4.4 and −4.0 Hz/σ for the two series of Y=CH_2 and $SiMe_2$, respectively, suggest roughly equal transmitting abilities for carbon and silicon.[13] This result is consistent with that obtained from the ^{13}C chemical shifts for the type of compounds, XC_6H_4–Y–$(CH_3)_3$ where Y=C and Si.[19] It is interesting, however, that the transmission efficiency of the two systems falls between those for the systems of Y=S and O.

It is worthwhile to note that the ρ value (-6.7 Hz/σ) for phenyldimethylsilanes is to be the greatest one (Table 2). The transmitting ability of the system is easily rationalized by the structure and the SiH group is one atom closer to the benzene ring than it is in the other series.

In contrast, the plots of the Si–H chemical shifts, listed in Table 1, *vs.* Hammett σ constants in the two series of oxygen and sulfur exhibited essentially no good correlation. In these cases, the correlations of the δ(SiH) with Hammett σ constants were too poor.

Electronic Behavior of Y. Although factors governing the magnitude of Si–H coupling constants cannot be said to be fully understood, the effective electronegativity of the substituent attached to silicon affects it,[11,14,20,21] as has been shown by Jensen's equation.[22] In the present system, Ar–Y–$SiMe_2H$, the magnitude of the Si–H coupling constants can be definitely related to the effective electronegativity of Y because of only change of Y. Thus, the greater this electronegativity, the greater the coupling constant. This is readily seen from an examination of the Si–H coupling constants in Table 3. The J values for (phenylthio)dimethylsilane, phenoxydimethylsilane, phenyldimethylsilane, benzyldimethylsilane, and phenyltetramethyldisilane are -209.7, -208.0, -188.3, -186.9, and -175.0 (Hz), respectively.

The decreasing trend in the absolute magnitude follows the order of decreasing electrogegativity of Y, except the case of Y=S. The ^{29}Si–H coupling constant of phenylthiosilane is greater than what would be predicted on the basis of the electronegativity of Y. Table 3 shows the correlation of the J values for the five hydrosilanes with the electronegativity of respective Y's on the Pauling scale. The plots of $J(^{29}\text{Si–H})$ for the compounds of Y=$SiMe_2$, none, CH_2, and O *vs.* the electronegativity (En) of the respective key atoms in Y show approximately a linear relationship, while the plot for the sulfur compound anormally deviates from the relationship. This deviation is attributable to sulfur attached to silicon. Within the framework of the "through-conjugation," it is possible to assume that the contribution of the structure *via* the interaction between d-orbital of sulfur and Si–H bond electrons, "σ-π" interaction, appears to play an important role affecting the silicon hybrid orbitals bonded to the hydrogen. The direction of the electron shifts *via* the conjugation is opposite to those of the conjugation A and B, and the following canonical structures can be illustrated as E and F. Thus, the charge-separated contributors would tend to increase the s character of the Si–H bond due to the structure change around the silicon ($sp^3 \rightarrow sp^2$), producing the enhancement of the absolute magnitude of the Si–H coupling constant.

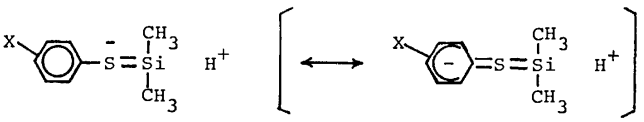

"σ-π" conjugation (E) "through-conjugative" interaction (F)

Table 3. Comparisons of the $J(^{29}\text{Si–H})$ for the related compounds

Compound	$J(^{29}\text{Si–H})$ (Hz)	En[a]	Ref.
Ph–S–$SiMe_2H$	-209.7	2.5	this work
Ph–O–$SiMe_2H$	-208.0	3.5	this work
Ph–CH_2–$SiMe_2H$	-186.9	2.5	13
Ph–$SiMe_2$–$SiMe_2H$	-175.0	1.8	13
Ph–$SiMe_2H$	-188.3	2.5	11

a) Electronegativity (Pauling scale) of the key atom in the intervening Y atom or group.

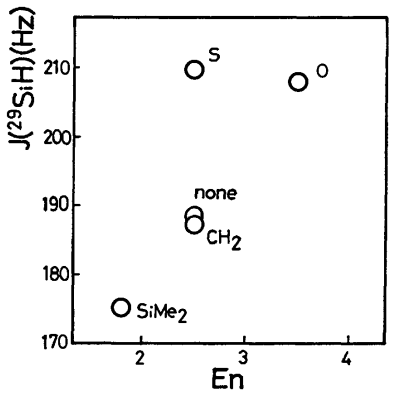

Fig. 2. Plot of the $J(^{29}\text{Si–H})$ *vs.* the electronegativity (En) of the key atom in Y.

Recently, Ojima, Nihonyanagi, and Nagai have determined the $J(^{29}\text{Si–H})$ for two series of sulfur compounds, RR'(PhS)SiH and RR'(EtS)SiH, and showed that these compounds have considerably large J values compared to that for triethylsilane.[23,24] They have stated that the large absolute values may reflect the large fraction of s character employed by silicon in the Si–H bond. This explanation is consistent with the idea of the "σ-π" interaction and provides supporting evidence for our present results.

On the other hand, the electron-accepting "σ-π" conjugation cannot occur in the series of phenoxysilanes, but oxygen serves as an electron donor, forming the Pπ-Pπ (C) and Pπ-dπ (D) conjugations. Although the two conjugations actually seem possible as has been shown by many workers in a variety of oxygen-bonded silicon compounds, the Pπ-dπ conjugation (D) in the present system should contribute to decrease the magnitude of the Si–H coupling constant. However, as the plot of the $J(^{29}\text{Si–H})$ for phenoxydimethylsilane *vs.* the electronegativity of oxygen appears to be in line of the correlation as shown in Fig. 2, the contribution of the conjugative interaction (D) might not be so important.

Experimental

All boilling points are uncorrected. IR spectra were recorded using neat liquid films with a Hitachi EPI-G3 spectrometer. Mass spectra were obtained with a Hitachi RMU-6L spectrometer. GLC analyses were conducted using Ohkura Model 807 and 1700 gas chromatographs.

TABLE 4. SUBSTITUTED PHENOXYDIMETHYLSILANES, XC_6H_4–O–$SiMe_2H$, AND THEIR ANALYTICAL RESULTS

Substituent X	Bp (°C/mmHg)	Formula	Found (Calcd) % C	Found (Calcd) % H	Mol wt[a] Found (Calcd)	n_D^{20}
P-MeO	87/13	$C_9H_{14}O_2Si$	59.34 (59.30)	7.64 (7.74)	182 (182.3)	1.5042
m-Me_2N	93/5	$C_{10}H_{17}NOSi$	61.53 (61.49)	8.65 (8.77)	195 (195.3)	1.5253
p-Me	—[b]	$C_9H_{14}OSi$	65.12 (64.99)	8.45 (8.50)	—[c]	1.4847
H	72—74/32	$C_8H_{12}OSi$	62.87 (63.10)	7.72 (7.94)	—[c]	1.4859
m-Cl	80/14	$C_8H_{11}OSiCl$	51.47 (51.46)	5.76 (5.94)	186 (186.7)	—
p-Cl	—[b]	$C_8H_{11}OSiCl$	51.58 (51.46)	6.00 (5.94)	—[c]	1.5018

a) By mass spectrum. b) Isolated by preparative GLC. c) No molecular peak was observed, but the peak corresponding to M^+-15.

TABLE 5. SUBSTITUTED PHENOXYDIMETHYLSILANES, XC_6H_4–O–$SiMe_2H$, AND THEIR SPECTRAL DATA

Substituent X	NMR (CCl_4, TMS) (δ ppm) $SiCH_3$[a]	SiH[b]	$X-C_6H_4-$	IR (neat) (cm^{-1}) Others	νSiH
p-MeO	0.30	4.91	6.71(s, 4H)	3.72 (s, 3H)	2118
m-Me_2N	0.33	4.94	6.95—7.15 (m, 4H)	2.91 (s, 6H)	2115
p-Me	0.29	4.90	6.63; 6.74 (quart, 4H)	2.24 (s, 4H)	2118
H	0.33	4.98	6.50—7.40 (m, 5H)		2120
p-Cl	0.32	4.93	6.74; 7.16 (quart, 4H)		2115
m-Cl	0.35	4.97	6.45—7.30 (m, 4H)		2120

a) (d, 6H). b) (m, 1H).

TABLE 6. SUBSTITUTED (PHENYLTHIO)DIMETHYLSILANES, XC_6H_5–S–$SiMe_2H$, AND THEIR SPECTRAL DATA

Subst. X	NMR (CCl_4, TMS) (δ, ppm)	IR (neat, sandwich) (cm^{-1})	MS (100 °C, 70 eV) *m/e* (intensity)
p-MeO[a]	0.28,[b] 3.75 (s, 3H, MeO), 4.63,[c] 7.00 (q, 4H, PhH)	3060, 2956, 2131,[d] 1599, 1497, 1464, 1289, 1250,[e] 1176, 1036, 896, 866, 826, 768.	59(83), 67(32), 73(22), 97(31), 108(78), 119(49), 125(72), 133(45), 139(29), 140 (M^+-SiMe_2)(100), 167(24), 168(46), 183(22), 198[f](85).
p-Me	0.30,[b] 2.30 (s, 3H, *p*-Me), 4.67,[c] 7.13 (q, 4H, PhH)	3020, 2960, 2135,[d] 1493, 1253,[e] 1092, 898, 868, 808, 767, 663.	45(24), 59(14), 61(27), 73(16), 75(21), 91(100), 119(48), 123(23), 124(87) (M^+-SiMe_2), 133(38), 182[f](weak).
m-Me[g]	0.32,[b] 2.30 (s, 3H, *m*-Me), 4.67,[c] 7.04 (m, 4H, PhH)	3055, 2960, 2135,[d] 1595, 1478, 1255,[e] 1080, 900, 870, 840, 780, 690.	45(28), 59(13), 61(44), 71(35), 91(100), 119(38), 124(M^+-SiMe_2)(93), 133 (32),182[f](weak).
H	0.32[b], 4.72[c], 7.30 (m, 5H, PhH).	3063, 2956, 2131,[d] 1582, 1472, 1439, 1251,[e] 1022, 897, 863, 836, 767, 757, 731, 680, 660.	45(16), 59 (15), 61(18), 75(15), 77(14), 84(16), 109(26), 110(M^+-SiMe_2) (100), 119(52), 133(41), 168[f](weak).
p-Cl[h]	0.32,[b] 4.67,[c] 7.25 (q, 4H, PhH).	3022, 2952, 2127,[d] 1472, 1384, 1249,[e] 1091, 1008, 890, 860, 832, 817, 760.	45(23), 59(19), 61(19), 73(26), 75(35), 108(33), 109(56), 119(65), 133(52), 144 (M^+-SiMe_2) (100), 146(37), 202[f] (weak).

a) Found: C, 54.55; H, 6.88%. Calcd for $C_9H_{14}OSSi$: C, 54.49; H, 7.11%. b) (d, 6H, SiMe). c) (m, 1H, SiH). d) (νSiH). e) (SiMe). f) Molecular peak. g) Bp 85—86 °C/13 mmHg. h) Found: C, 48.00; H, 5.52%. Calcd for $C_8H_{11}ClSSi$: C, 47.39; H, 5.47%.

Materials. *sym*-Tetramethyldisilane was prepared *via* $LiAlH_4$-reduction of the corresponding dichlorosilane obtained by chlorination of hexamethyldisilane.[25] Hexamethyldisilane was obtained by MeMgBr-methylation of chlorodisilane fraction (bp 148—160 °C) in the "Direct Synthesis."[26] *p*-Methoxybenzenethiol (bp 85—88 °C/3 mmHg; lit,[27] bp 89 °C/5 mmHg) was prepared by the literature method from anisole *via* chlorosulfonation with chlorosulfuric acid and then Zn–H_2SO_4 reduction of the resulting *p*-methoxybenzenesulfonyl chloride.[28] *m*-Methylbenzenethiol (bp 80—84 °C/24 mmHg; n_D^{25} 1.5715; lit,[29] bp 90—93 °C/25 mmHg; n_D^{25} 1.568—1.571) was also prepared from toluidine *via* diazotization

followed by treatment with potassium *O*-ethyl dithiocarbonate. All the other materials were commerically available.

Preparation of Substituted Phenoxydimethylsilanes. The method used for the reaction to give phenoxydimethyldisilane is representative.[30] Under argon, a mixture of phenol (10 mmol) and *sym*-tetramethyldisilane (10 mmol) was added with chlorotris(triphenylphosphine)rhodium, RhCl $(PPh_3)_3$, 0.5 mol% relative to the substrate used) and magnetically stirred at room temperature for 30 min at the stage of which gas evolution of dimethylsilane (Me_2SiH_2) ceased. GLC analysis for the resulting mixture thus obtained showed that almost of it was the reaction product, phenoxydimethylsilane, in a quantitative yield. The pure sample was obtained by distillation. Pertinent physical, spectral, and analytical data for all the compounds thus prepared are give in Tables 4 and 5.

Preparation of Substituted (Phenylthio)dimethylsilanes. Similarly, (phenylthio)dimethylsilanes were prepared by reacting substituted benzenethiols (4—15 mmol) with tetramethyldisilane (10—20 mmol) in the presence of RhCl-$(PPh_3)_3$ catalyst (0.2—0.5 mol% relative) to the benzenethiols (r. t.; 10—60 min).[23,30] The yield of the products by GLC analyses were fairly high (40—70%), but the products, except *m*-methyl derivative which could be isolated by distillation (bp 85—86 °C/13 mmHg), were only isolable by preparative GLC in 90—98% purity and further purification could not be achieved because of their instabilities under the GLC conditions. Therefore, the pure samples for elemental analyses could not be obtained, but they are enough in purity for spectral determinations. Table 6 lists the physical and spectral data which were carefully determined.

NMR Measurements. NMR constants were determined from spectra obtained on a Varian A-60D spectrometer. Measurements of the coupling constants $J(^{29}Si-H)$ and Si–H chemical shifts were made in CCl_4 solution by the method described previously.[11]

References

1) References. 11 and 12 in the present paper are designated as "Nuclear Magnetic Resonance Studies of Hydrosilanes. I and II," respectively.

2) C. H. Yoder, R. H. Tuck, and R. E. Hess, *J. Am. Chem. Soc.*, **91**, 539 (1969).

3) S. H. Marcus, W. F. Reynols, and S. I. Miller, *J. Org. Chem.*, **31**, 1972 (1966).

4) K. L. Williamson, N. C. Jacobus, and K. T. Soucy, *J. Am. Chem. Soc.*, **86**, 4121 (1964).

5) C. Heathcook, *Can. J. Chem.*, **40**, 1865 (1962).

6) I. D. Rae and L. K. Dyall, *Aust. J. Chem.*, **19**, 835 (1966).

7) H. Sakurai and M. Ohtsuru, *J. Organomet. Chem.*, **13**, 81 (1968).

8) M. E. Freeburger and L. Spialter, *J. Am. Chem. Soc.*, **93**, 1894 (1971).

9) T. Fueno, O. Kajimoto, K. Izawa, and M. Masago, *Bull. Chem. Soc. Jpn.*, **46**, 1418 (1973).

10) H. Sakurai, S. Deguchi, M. Yamagata, S. Morimoto, M. Kira, and M. Kumada, *J. Organomet. Chem.*, **18**, 285 (1969).

11) Y. Nagai, M. Ohtsuki, T. Nakao, and H. Watanabe, *J. Organomet. Chem.*, **35**, 81 (1972).

12) Y. Nagai, H. Matsumoto, T. Nakano, and H. Watanabe, *Bull. Chem. Soc. Jpn.*, **45**, 2560 (1972).

13) F. K. Cartledge and K. H. Riedel, *J. Organomet. Chem.*, **34**, 11 (1972).

14) Y. Nagai, H. Matsumoto, M. Hayashi, E. Tajima, and H. Watanabe, *Bull. Chem. Soc. Jpn.*, **44**, 3113 (1971).

15) C. C. Price and S. Oae, "Sulfur Bonding," Ronald Press, N. Y., (1962).

16) S. Oae and Y. Yano, *Tetrahedron*, **24**, 5721 (1968).

17) O. Kajimoto, M. Kobayashi, and T. Fueno, *Bull. Chem. Soc. Jpn.*, **46**, 1425 (1973).

18) C. H. Yoder and R. J. Schenck, *J. Inorg. Nucl. Chem.*, **33**, 2697 (1971).

19) C. D. Schaeffer, Jr., and J. J. Zuckermann, *J. Organomet. Chem.*, **80**, 29 (1974).

20) B. K. Hunter and L. W. Reeves, *Can. J. Chem.*, **46**, 1399 (1968).

21) E. A. Ebsworth and S. G. Frankiss, *Trans. Farady Soc.*, **63**, 1574 (1967).

22) M. A. Jensen, *J. Organomet. Chem.*, **11**, 423 (1968).

23) I. Ojima, M. Nihonyanagi, and Y. Nagai, *J. Organomet. Chem.*, **50**, C26 (1973).

24) H. Kono, M. Nihonyanagi, I. Ojima, and Y. Nagai, 28 th National Meeting of Chemical Society of Japan, Tokyo, April 1973, Abstracts III, 3I48, p. 1475.

25) H. Sakurai, T. Watanabe, and K. Kumada, *J. Organomet. Chem.*, **7**, 15 (1967).

26) M. Kumada and M. Yamaguchi, *Kogyo Kagaku Zassi* **87**, 175 (1963).

27) C. M. Suter and H. L, Hansen, *J. Am. Chem. Soc.*, **54**, 4100 (1932).

28) M. S. Morgan and L. H. Cretcher, *J. Am. Chem. Soc.*, **70**, 315 (1948).

29) E. C. Horning, *Org. Synth.*, Coll. Vol. 3, 809 (1955).

30) I. Ojima, S. Inaba, T. Kogure, M. Matsumoto, H. Matsumoto, H. Watanabe, and Y. Nagai, *J. Organomet. Chem.*, **55**, C4 (1973).

Removal and Recovery of Organic Pollutants from Aquatic Environment. V. Crosslinked Poly(hydroxystyrene) as a Polymeric Adsorbent for Removal and Recovery of ε-Caprolactam from Aqueous Solution

Nariyoshi KAWABATA* and Yukihiko TAKETANI

Laboratory of Environmental Chemistry, Department of Chemistry, Faculty of Polytechnic Science, Kyoto Institute of Technology, Matsugasaki, Sakyo-ku, Kyoto 606

(Received April 10, 1980)

Crosslinked poly(hydroxystyrene) (PHS resin) was found to be useful as a polymeric adsorbent for removal and recovery of ε-caprolactam from aqueous solution. The breakthrough capacity of PHS resins with <1-mg/l leakage in the effluent was 50—90 mg/dry g, which was scarcely affected by the presence of hydrochloric acid, sodium hydroxide, and inorganic salts such as sodium chloride, potassium chloride, calcium chloride, and magnesium chloride. Elution of the adsorbed ε-caprolactam from PHS resin was easily accomplished by a simple treatment with methanol, and PHS resin was efficiently regenerated. ε-Caprolactam was concentrated into 10—30 g/l solution.

In this series of investigations, attempts have been made to find new polymeric adsorbents which are useful for removal and recovery of organic pollutants from aquatic environment. This methodology is important not only in the protection of the environment from pollution, but also in the effective use of raw materials, because the organic pollutants can be recovered without chemical change. This paper deals with the removal and recovery of ε-caprolactam from aqueous solution by polymeric adsorbents.

ε-Caprolactam is the most important lactam in use by chemical industry. The wastewater from the manufacturing process contains some amount of the lactam, which is usually treated with activated sludge. However, the biological treatment needs a long time and a wide space. The adsorption process using a suitable polymeric adsorbent may be more convenient because the process saves time and space of the treatment, and makes it possible to reuse the recovered ε-caprolactam. We have tried to use various polymeric adsorbents for this purpose, and found that the crosslinked poly(hydroxystyrene) (PHS resin) was most useful.

Experimental

Materials. *p*-Acetoxystyrene provided by Maruzen Oil Co., Tokyo, was purified by distillation before use. Commercial products of divinylbenzene and toluene were purified by distillation before polymerization. Methanol, petroleum ether, ε-caprolactam, 2,2′-azobisisobutyronitrile, sodium hydroxide, hydrochloric acid, calcium hydride, and other chemicals were used without further purification.

Crosslinked Poly(hydroxystyrene) (PHS Resin). PHS resin was prepared by hydrolysis of the copolymer of *p*-acetoxystyrene with divinylbenzene according to the procedure of Packham[1] with minor modification. Dried copolymer of *p*-acetoxystyrene with divinylbenzene was ground using an ishiusu (a Japanese classical hand mill made of stone) and sifted out to 60—80 mesh. The sifted copolymer was hydrolyzed to give PHS resin. One sample of PHS resin (PHS-9) was prepared by a direct radical copolymerization of *p*-vinylphenol with divinylbenzene in benzene, which was ground and sifted out to 20—30 mesh. These PHS resins were rinsed with 10 Bed Volume (BV) of methanol by a batch method followed by washing with 30—40 BV of water by the continuous flow column method. Mole fraction of *p*-acetoxystyrene in the copolymer of *p*-acetoxystyrene with divinylbenzene before hydrolysis, and that of *p*-vinylphenol in PHS-9 were determined by elemental analysis. Content of water in the swollen state and the mean particle diameter of these PHS resins were determined, and results are given in Table 1.

Commercial Polymeric Adsorbents. For comparison with PHS resin, four commercial resins provided by Rohm and Haas Co., Philadelphia, Pa. were used. Amberlite IR-120B was used as a strong acid cation exchange resin which had a styrene–divinylbenzene matrix with sulfonate group. This

Table 1. Characteristics of crosslinked poly(hydroxystyrene) (PHS resin)

Crosslinked polyhydroxystrene	PHS-1	PHS-2	PHS-3	PHS-4	PHS-5	PHS-6	PHS-7	PHS-8	PHS-9[a)]
Mole fraction of *p*-acetoxystyrene before hydrolysis	0.93	0.82	0.73	0.56	0.43	0.35	0.25	0.14	0.79[b)]
Content of water in the swollen state (wt %)	44	32	25	33	41	29	47	52	62
Mean particle diameter in the dry state (mm)	0.28	0.30	0.23	0.33	0.25	0.30	0.33	0.30	0.65
Mean particle diameter in the wet state (mm)	0.38	0.40	0.33	0.40	0.38	0.38	0.35	0.38	1.03
Breakthrough capacity for sodium hydroxide adsorption (meq/dry g)	1.23	0.77	0.51	0.34	0.31	0.17	0.16	0.12	2.46
Total capacity for sodium hydroxide adsorption (meq/dry g)	1.45	0.87	0.70	0.49	0.38	0.31	0.25	0.16	2.60

a) Prepared by a direct copolymerization of *p*-vinylphenol with divinylbenzene. b) Mole fraction of *p*-vinylphenol.

resin was used in the hydrogen ion form. Amberlite IRC-50 was used as a weak acid cation exchange resin which had a styrene–divinylbenzene matrix with carboxyl group. This resin was also used in the hydrogen ion form. Amberlite XAD-2 and XAD-4 were used as porous styrene–divinylbenzene resins with no ion exchange functional group. The surface area of XAD-2 and XAD-4 were claimed by the supplier to be 300 and 784 m^2/g, respectively.

Amberlite IR-120B was preconditioned and transferred to the hydrogen ion form as follows: (1) placing it in a column of 2.5-cm diameter with a fritted glass filter; (2) washing with 10 BV of methanol; (3) washing with 10 BV of deionized water; (4) slowly contacting with 10 BV of 2 mol/l hydrochloric acid; (5) washing with 10 BV of deionized water; (6) slowly contacting it with 10 BV of 2 mol/l sodium hydroxide; (7) washing with 10 BV of deionized water; (8) repeating steps 4 through 7 several times; (9) slowly contacting it with 20—30 BV of 2 mol/l hydrochloric acid; (10) extensive washing with deionized water until the effluent pH was close to the influent pH. The ion exchange capacity of the resin was 4.4 meq/dry g, which was determined by back titration with 0.1 mol/l hydrochloric acid using phenolphthalein as indicator in 1 mol/l sodium hydroxide after the addition of standard sodium hydroxide solution. Percentage moisture of the resin was determined after drying *in vacuo* to constant weight. Amberlite XAD-2 and XAD-4, and Amberilte IRC-50 in the hydrogen ion form were preconditioned by washing with 10 BV of methanol followed by washing with 30 BV of deionized water.

For comparison with the non-ionic XAD resins, we also used pulverized copolymer of styrene with divinylbenzene containing 57 mol% styrene, which was prepared as was described in a previous paper of this series.[2)]

Adsorption Tests. Column studies were conducted using a 1.0-cm diameter glass column with a fritted glass filter connected with a 200-ml dropping funnel in a down-flow fashion at room temperature. The preconditioned polymeric adsorbent was placed in the column. The bed was carefully backwashed to eliminate entrained air and then tapped to ensure packing of the bed. The dropping funnel was used to contain influent solution. Samples were taken manually and were checked for the concentration of ε-caprolactam. The flow rate was 3 BV/h throughout this work. The influent concentration of ε-caprolactam was controlled to be about 2000 mg/l.

The capacity of polymeric adsorbents for the adsorption of ε-caprolactam was determined by continuous flow column method in two ways: (i) the breakthrough capacity, which was based upon the total amount of adsorbed ε-caprolactam before the effluent concentration reached 1 mg/l; (ii) the total capacity, which was determined based upon the total amount of adsorbed ε-caprolactam until the effluent concentration became close to the influent concentration.

The breakthrough capacity and the total capacity of the PHS resin for sodium hydroxide adsorption were determined using aqueous 0.02 mol/l sodium hydroxide solution by the continuous flow column method. Results are given in Table 1.

Equilibrium adsorption tests were conducted by placing weighed quantities of polymeric adsorbent and samples of aqueous solution of ε-caprolactam in a 300-ml Erlenmeyer flask sealed by rubber stopper in a water bath maintained at 30 ± 1 °C with magnetic stirring. After the mixture reached equilibrium, the concentration of ε-caprolactam was determined.

Recovery of Adsorbed ε-Caprolactam from Polymeric Adsorbents. Polymeric adsorbents were saturated with ε-caprolactam by the continuous flow column method carried out until the effluent concentration became 1 mg/l using about 2000 mg/l of aqueous ε-caprolactam solution. Elution of the adsorbed ε-caprolactam from the polymeric adsorbents was conducted by the continuous flow column method using methanol as the eluant with flow rate of 3 BV/h in a down-flow fashion.

Analyses. Elemental analyses were performed at the Elementary Analyses Center of Kyoto University. Quantitative analysis of ε-caprolactam in aqueous and/or methanolic solution was performed with Shimadzu Model UV-200S spectrophotometer based upon the absorptivities at 203 nm. The pH value of solutions was determined with a Horiba Model F-7AD pH meter.

Results and Discussion

Adsorption of ε-Caprolactam on Various Polymeric Adsorbents Studied by the Continuous Flow Column Method. The breakthrough curves are illustrated in Fig. 1. PHS resin and XAD-4 showed the ability to adsorb ε-caprolactam in aqueous solution, but the cation exchange resins IR-120B and IRC-50 did not adsorb ε-caprolactam under our experimental conditions. We calculated the breakthrough capacity and the total capacity for the adsorption of ε-caprolactam. Results are summarized in Table 2. The adsorption capacity of the PHS resin was not very sensitive to the content of *p*-acetoxystyrene before hydrolysis, but showed a maximum at the content of about 40 mol%.

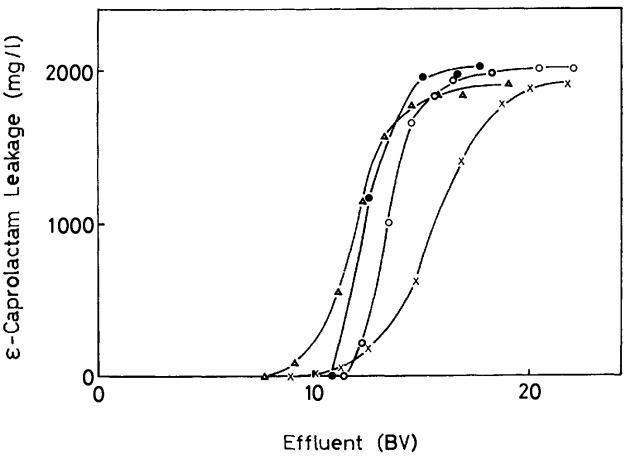

Fig. 1. Examples of the removal of ε-caprolactam from aqueous solution by polymeric adsorbents.
Conditions: influent concentration of ε-caprolactam, 2000 mg/*l*; flow rate, 3 BV/h; (▲) PHS-1; (○) PHS-4; (●) PHS-5; (×) XAD-4.

Among the styrene–divinylbenzene resins with no ion exchange functional group, XAD-4 (claimed by the supplier to have the surface area of 784 m^2/g) showed a breakthrough capacity of 55 mg/dry g, but XAD-2 (claimed by the supplier to have a surface area of 300 m^2/g) showed a much lower capacity to adsorb ε-caprolactam. This result indicates the importance of the surface area of the polymeric adsorbents. In this work, we used the PHS resins in the pulverized form, but they showed breakthrough capacities of 50—90 mg/dry g as can be seen in Table 2. If we supposed a

TABLE 2. CAPACITIES OF POLYMERIC ADSORBENTS FOR ε-CAPROLACTAM ADSORPTION[a]

Polymeric adsorbent	Breakthrough capacity (mg/dry g)	Total adsorption capacity (mg/dry g)
PHS-1	53	81
PHS-2	52	91
PHS-3	55	93
PHS-4	70	90
PHS-5	87	96
PHS-6	65	75
PHS-7	73	84
PHS-8	73	81
PHS-9	38	65
XAD-2[b]	12	—
XAD-4[c]	55	91

a) Determined by the continuous flow column method using about 2000 mg/l of aqueous ε-caprolactam solution. The flow rate was 3 BV/h. b) Claimed to have the surface area of 300 m^2/g. c) Claimed to have the surface area of 784 m^2/g.

spherical form for PHS resins, the surface area of PHS-1—PHS-8 were assumed to be about 30 cm^2/g. Thus the actual surface area of the PHS resins would be less than 0.1 m^2/g. If porous PHS resins with large surface area were used, the adsorption capacity could be further improved. PHS-9 showed a lower capacity than the other PHS resins for the adsorption of ε-caprolactam. The result can be ascribable, at least partly, to the smaller surface area, because the particle size of PHS-9 was much larger than those of the other PHS resins as can be seen in Table 1.

Effect of Some Inorganic Salts in Aqueous Solution on the Breakthrough Capacity of Polymeric Adsorbents for ε-Caprolactam Adsorption. In the practical use of polymeric adsorbents for removal and recovery of ε-caprolactam from wastewater, it is difficult to avoid the presence of some inorganic salts. Inorganic cations in wastewater might reduce the capacity of PHS resin for the adsorption of ε-caprolactam if it adsorbed through an ion exchange mechanism. In order to obtain some information on this subject, we have investigated the effect of the presence of some inorganic salts in aqueous solution on the breakthrough capacity of PHS resin for ε-caprolactam adsorption.

TABLE 3. CAPACITIES OF POLYMERIC ADSORBENTS FOR ε-CAPROLACTAM ADSORPTION IN THE PRESENCE OF INORGANIC SALTS[a]

Polymeric adsorbent	Inorganic salt	Breakthrough capacity (mg/dry g)	Total adsorption capacity (mg/dry g)
PHS-5	none	87	96
PHS-5	NaCl	85	101
PHS-5	KCl	87	103
PHS-5	$MgCl_2$	89	103
PHS-5	$CaCl_2$	89	103
XAD-4	none	55	91
XAD-4	NaCl	57	96

a) Determined by the continuous flow column method using about 2000 mg/l of aqueous ε-caprolactam solution containing 0.1 mol/l of inorganic salts. The flow rate was 3 BV/h.

Since major inorganic cations commonly appearing in natural water are sodium, potassium, calcium, and magnesium cations, we first determined the breakthrough capacities of PHS resins, and XAD-4 for comparison, for the adsorption of ε-caprolactam in the presence of sodium chloride, potassium chloride, calcium chloride, and magnesium chloride. Results are given in Table 3. The capacity did not decrease in the presence of these inorganic salts.

Effect of Acid and Alkaline Materials in Aqueous Solution on the Breakthrough Capacity of Polymeric Adsorbents for the Adsorption of ε-Caprolactam. In the practical use of polymeric adsorbents for wastewater treatment, it is also difficult to avoid the presence of acid and alkaline materials. In order to obtain some information on this subject, we have investigated the effect of hydrochloric acid and sodium hydroxide in aqueous solution on the capacity of PHS resin, and XAD-4 for comparison, for the adsorption of ε-caprolactam. Results are summarized in Table 4. The breakthrough capacity was scarcely affected by the presence of these acid and alkaline materials.

TABLE 4. EFFECT OF ACID AND ALKALINE METERIALS IN AQUEOUS ε-CAPROLACTAM SOLUTION ON THE CAPACITY OF POLYMERIC ADSORBENTS FOR ε-CAPROLACTAM ADSORPTION[a]

Polymeric adsorbent	HCl (mmol/l)	NaOH (mmol/l)	pH of the solution		Breakthrough capacity (mg/dry g)	Total adsorption capacity (mg/dry g)
			influent	effluent[b]		
PHS-5	20.1		2.77	2.78	82	103
PHS-5	1.58		4.05	4.05	91	101
PHS-5			5.48	5.69—5.87	87	96
PHS-5		0.009	6.40	5.79—6.29	89	102
PHS-5		0.18	10.40	6.84—6.87	81	99
XAD-4	15.3		3.00	2.78—2.89	42	96
XAD-4	0.57		4.22	5.74—5.78	40	94
XAD-4			5.62	5.50—5.62	55	91
XAD-4		0.07	7.43	6.00—6.03	32	93
XAD-4		1.07	10.77	10.08—10.35	41	94

a) Determined by the continuous flow column method using about 2000 mg/l of ε-caprolactam solution containing acid or alkaline materials. The flow rate was 3 BV/h. b) Before the breakthrough point.

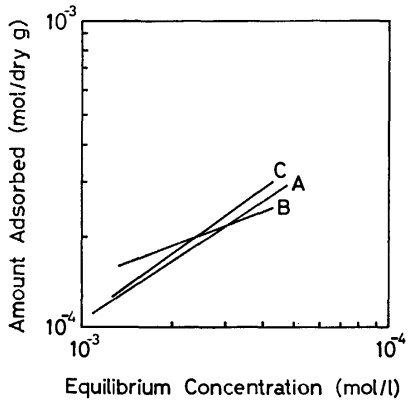

Fig. 2. ε-Caprolactam adsorption isotherms on polymeric adsorbents at 30±1°C.
(A) PHS-4; (B) PHS-5; (C) XAD-4.

Adsorption Equilibrium for ε-Caprolactam and Polymeric Adsorbents. The experimental isotherms of ε-caprolactam adsorption on PHS resin are shown in Fig. 2. Similar results were obtained with PHS resins and XAD-4.

Recovery of ε-Caprolactam from Polymeric Adsorbents. In addition to the removal of ε-caprolactam from aqueous solution, the major objective of this work is to recover as much ε-caprolactam as possible from the polymeric adsorbents. This is necessary not only in the effective regeneration of the polymeric adsorbents, but also in the reuse of the recovered ε-caprolactam. We examined the elution of ε-caprolactam from PHS resin and XAD-4 by the continuous flow column method using methanol as the eluant. Results are shown in Fig. 3. The adsorbed ε-caprolactam was quantitatively recovered using 2—3 BV of methanol as the eluant, and PHS resin and XAD-4 were efficiently regenerated. ε-Caprolactam was concentrated into 10—30 g/l solution.

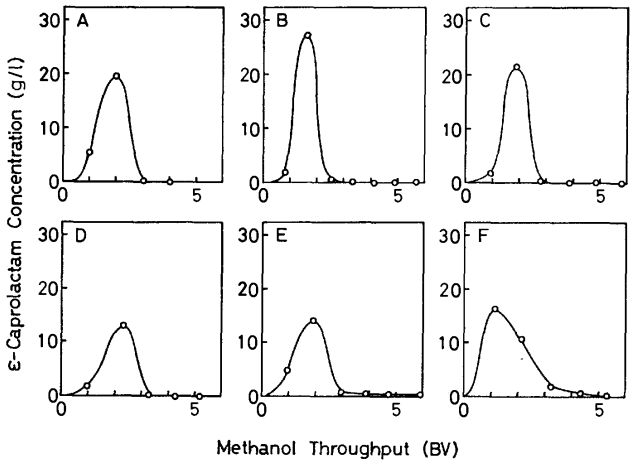

Fig. 3. Elution of adsorbed ε-caprolactam from polymeric adsorbents using methanol as the eluant by the continuous flow column method.
Flow rate was 3 BV/h; (A) PHS-5; (B) PHS-6; (C) PHS-7; (D) PHS-8; (E) PHS-9; (F) XAD-4.

Mechanism of the Adsorption of ε-Caprolactam on PHS Resin. Although mechanism of the adsorption of ε-caprolactam on PHS resin has not been elucidated as yet, experimental results gave some suggestions on this problem. It is reasonable to speculate that the adsorption of ε-caprolactam by PHS resin was derived from an intermolecular interaction between ε-caprolactam and phenolic hydroxyl group of PHS resin, because PHS resin showed a comparable or a rather higher capacity than the porous styrene–divinylbenzene resin with no ion exchange functional group, in spite of the fact that we used PHS resin in a pulverized form.

Although we used PHS resin in a pulverized form, it showed a high hydrophilicity and considerably swelled in water as can be seen in Table 1. Thus the effective surface area in water might be unexpectedly large. However, this high hydrophilicity would not wholly explain the adsorption capacity of PHS resin for ε-caprolactam, because a vinylpyridine–divinylbenzene copolymer in a pulverized form[2] did not adsorb ε-caprolactam under similar conditions, in spite of the fact that the copolymer also showed a high hydrophilicity. Therefore, the high hydrophilicity of PHS resin can not wholly explain its capacity for ε-caprolactam adsorption. The intermolecular interaction between ε-caprolactam and phenolic hydroxyl group of PHS resin appears to be an important factor for the adsorption.

Since phenol is a weak acid, and ε-caprolactam is a very weak base, the following interaction was hypothesized between PHS resin and ε-caprolactam:

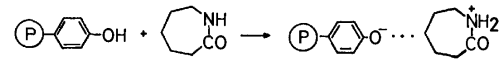

Here, ε-caprolactam uptakes a proton from phenolic hydroxyl group of PHS resin and forms a complex with phenoxide anion as the associated counterion.

On the other hand, since weak acid and strong acid cation exchange resins did not adsorb ε-caprolactam under our experimental conditions, the following ion exchange mechanism would not be suitable for the adsorption of ε-caprolactam by PHS resin.

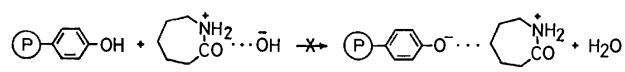

Further research is required to determine the mechanism of the interaction between ε-caprolactam and PHS resin.

References

1) D. I. Packham, *J. Chem. Soc.*, **1964**, 2617.
2) N. Kawabata and K. Ohira, *Environ. Sci. Technol.*, **13**, 1396 (1979).

Assignment of Fundamental Vibrations of *N,N'*-Dimethylthiourea

Kolar Ramakrishnaiaa Gayathri Devi and Dixit Narayanarao Sathyanarayana*
Department of Inorganic and Physical Chemistry, Indian Institute of Science, Bangalore 560012, India
(Received December 10, 1979)

The infrared spectra of symmetric *N,N'*-dimethylthiourea (s-DMTU) and its *N*-deuterated (s-DMTU-d_2) species have been measured. The fundamental frequencies have been assigned by comparison with the assignments in structurally related molecules and the infrared band shifts on *N*-deuteration, *S*-methylation, available Raman data and with the aid of theoretical band assignments from normal coordinate treatments for s-DMTU-d_0 and -d_2. A force field is derived for s-DMTU by transferring the force constants chiefly from *N*-methylthiourea and the subsequent refinement of the force constants by a least squares procedure.

There is continued interest in the vibrational spectra of thiourea derivatives. The infrared and Raman spectra and normal coordinates of thiourea (TU)[1-3] and its *N*-methyl compounds namely, *N*-methylthiourea (NMTU),[4] unsymmetric *N,N*-dimethylthiourea (u-DMTU),[5] and *N,N,N',N'*-tetramethylthiourea (TMTU)[6,7] have been published. In this context, it was felt desirable to obtain a more complete assignment for symmetric *N,N'*-dimethylthiourea (s-DMTU), and compare the results with its oxygen analogue, symmetric *N,N'*-dimethylurea (DMU),[8] and with thiocarbohydrazide (TCH, $H_2NNHCSNHNH_2$),[9] with which it is isoelectronic.

The infrared spectrum of s-DMTU was previously reported by Rao *et al.*[7] These authors have also carried out a normal coordinate treatment for only the in-plane vibrations employing a point mass approximation for the methyl group on a molecular model with a point group symmetry C_{2v}. Afterwards, Ritchie *et al.*[10] reinvestigated the vibrational spectra of s-DMTU-d_0 and -d_2 and performed a vibrational analysis for mainly the in-plane vibrations also assuming a molecular symmetry C_{2v}. However, they point out that the available Raman depolarization data suggests that the molecule is likely to have a lower molecular symmetry (C_s). There are some significant differences between the assignments of Rao *et al.* and Ritchie *et al.* And further, a complete interpretation of the vibrational spectra of this interesting molecule is lacking.

The results of the force field calculations for all the fundamentals of s-DMTU-d_0 and -d_2 are presented for the more stable *cis-trans* conformation in this paper. The present assignments for s-DMTU are compared with the earlier ones and are discussed in relation to the assignments available for other thioureas and related compounds. In order to obtain some support for the C=S and C–N stretching bands from the band shifts, the infrared spectrum of the *S*-methyl derivative of s-DMTU is also studied.

Experimental

s-DMTU was synthesized starting from methyl isothiocyanate and methylamine.[11] It was recrystallized from dry ethanol mp 62°.

s-DMTU was *N*-deuterated by dissolving it in D_2O and evaporating the solution *in vacuo*. The process was repeated several times till the infrared spectrum showed practically no bands due to NH vibrations. The *S*-methyl derivative of s-DMTU was prepared according to the method of Brand and Brand.[12] It was dried under vacuo over phosphorus pentaoxide.

Spectra: The infrared spectra were measured on a Carl-Zeiss UR 10 spectrophotometer in the range 4000 to 400 cm^{-1} by Nujol mull and KBr pellet techniques. The bands in the far infrared region and also the Raman frequencies were taken from the recently published spectra.[13] The solution infrared spectra in $CHCl_3$ were recorded for different concentrations between 4000—500 cm^{-1} using NaCl windows of path length 0.4 mm.

Normal Coordinate Analysis

Wilson's GF matrix method was employed.[14] A stable *cis-trans* conformation may be expected for s-DMTU.[10,15-19] The molecular geometry for s-DMTU was constructed on the basis of the results of the X-ray diffraction structural information on the metal complexes[18,19] of s-DMTU and free TMTU.[20] The molcular parameters employed are, C=S 0.171, C–N 0.133, N–CH_3 0.147, C–H 0.109, N–H 0.101 nm, HCH, HCN 109°28′, and all interbond angles of 120° for the planar skeleton.

The 36 normal modes of s-DMTU are classified in the point group C_s into 23 of species a′ (in-plane) and 13 of species a″ (out-of-plane) vibrations. All the normal modes are infrared and Raman allowed. The internal displacement coordinates are shown in Fig. 1, and the symmetry coordinates employed are not listed here for the sake of brevity. A simple Urey-Bradley force field (UBFF) was employed. For the out of plane vibrations of the planar skeleton, valence force constants were used. Pilot calculations were made for the in-plane vibrations of s-DMTU by transferring the force constants from NMTU[4] (set 1) and *N*-(methyl)thioacetamide[21,22] (NMTA) (set 2). It was pleasing to note that the agreement between the observed and calculated frequencies for the zero order sets was good indicating the transferability property of the force constants.

The initial values of the valence force constants for a″ modes were obtained from NMTU.[4] The transferred values of the force constants (set 1) were refined for the in-plane vibrations by a least squares procedure[23,24] by keeping some of the force constants such as stretching (CS, CN, NH, and CH), bending (HCH) and repulsion (SCN, NCN) force constants fixed. For the out-of-plane vibrations the force constants were refined by progressive adjustments to obtain a desired agreement between the observed and calculated frequencies. For simplicity, the same force constants

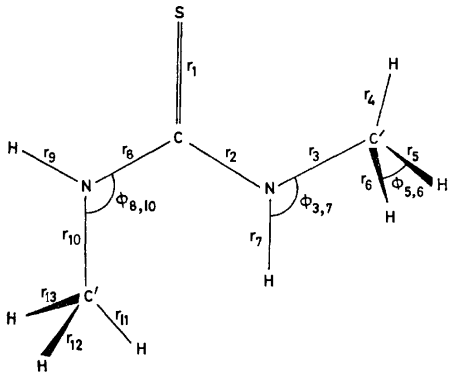

Fig. 1. Molecular structure and internal coordinates of s-DMTU.

were employed for both the *cis* and the *trans*-NH and -CH_3 moieties. For this reason the deviation between the observed and calculated frequencies is larger, particulary for the 1188, 1020, and 237 cm^{-1} bands. During the refinement process, it was noted that the potential energy distributions largely remain unaffected.

The computations were performed on an IBM 360/44 digital computer using Fortran programs similar to those of Shimanouchi.[25]

Results and Discussion

Force Field. The previous applications of the normal coordinate procedures for *N*-alkylated thioureas and thioamides have successfully employed the Urey-Bradley force.[1,3-5,7,21,22,26,27] The same has been utilized in the present study. The final values of the force constants are listed in Table 1. The values of the force constants seem reasonable.

The characteristic C=S and C–N stretching constants may now be compared. The C=S stretching constant of s-DMTU (2.65 mdyn/Å) is somewhat lower compared to that of thioacetamide (TA)[26,27] and TCH[9] (3.45 mdyn/Å). The C–N stretching constant of s-DMTU (5.45 mdyn/Å) is closer to that of TCH[9] and NMTU[4] (5.35 mdyn/Å) and *N*-(alkyl)thioamides[21,27] (5.50—5.75 mdyn/Å). The lower C=S and C–N stretching constants of s-DMTU compared to those of TA seem reasonable in relation to their π bond orders. The π bond orders of the C=S group in TA and s-DMTU are 0.637 and 0.514, respectively, while that of C–N bond is 0.585 and 0.550, respectively, as obtained by the CNDO/2 method.[28]

Vibrational Assignments. In Table 3, the results of the present investigation given in Table 2 are compared with the earlier assignments for s-DMTU and also for s-DMU. A satisfactory interpretation of all the frequencies is made by referring to the band shifts on *N*-deuteration and *S*-methylation and the characteristic group frequencies of related thioamides and thioureas.

In-plane Thioureide Group Vibrations. NH and CN Vibrations: The infrared spectrum of s-DMTU in the solid phase exhibits a broad band centred at 3005 cm^{-1}, which could easily be assigned to in- and out-of-phase vibrations of the NH group. The spectrum in $CHCl_3$ at different concentrations gives a strong sharp peak at 3450 cm^{-1} and a broad medium band centered at 3335 cm^{-1}. The intensity of the sharp peak increases and that of the broad band decreases with dilution, indicating the existence of strong hydrogen bonding in the solid state. On *N*-deuteration this broad band is replaced by the new absorptions at 2440 and 2420 cm^{-1}.

According to the normal coordinate calculations, the band at 1560 cm^{-1} is attributable to thioamide III band (B band of Jensen and Nielsen)[29] of the secondary thioamide group. It is slightly coupled with NH bending mode. The analogous band in NMTU[4] (1567 cm^{-1}) and TCH[9] (1547 cm^{-1}) is found in the same region. The potential energy distribution reveals that the 1506 cm^{-1} band could be attributed to a mixed mode of NH bending and C–N stretching. The assignment for the C–N stretching bands may be substantiated by the spectrum of the *S*-methyl derivative. On *S*-methylation, the 1560 cm^{-1} band of s-DMTU shows a larger shift and is found at 1610 cm^{-1} while 1506 cm^{-1} band is found around 1520 cm^{-1}.

The assignment of NH bending vibrations differs from the previous ones.[7,10] Alternate assignments for the NH bending mode were probed through the force field calculations. The assignments described below seemed acceptable.

The potential energy distributions (PEDs) reveal that the *trans*-NH bending mode contributes predominantly (51%) to the 1355 cm^{-1} band which disappears on *N*-deuteration. A new strong band is noted at 936 cm^{-1} in the spectrum of s-DMTU-d_2 as is to be expected consequent to the mass change on replacement of H by D. This assignment of NH bending is in good agreement with that of s-DMU[8] (1328 cm^{-1}), TCH[9] (1333 cm^{-1}) and somewhat higher than in NMTU[4] (1302 cm^{-1}). The other NH bending vibration *cis* to the thiocarbonyl group is coupled mainly with C–N stretching and contributes nearly equally ($\approx$36%) to the bands at 1506 cm^{-1} and a doublet at 1287 and 1260 cm^{-1}.

C=S Stretching: Of particular interest in the spectrum of s-DMTU is the assignment of the C=S stretching (Thioamide I band). Jensen and Nielsen[29] have qualitatively assigned for s-DMTU by comparison with its selenium analogue (s-DMSU), a band at 637 cm^{-1} to C=S stretching. However, the difference in frequency between s-DMTU and s-DMSU (605 cm^{-1}) is rather small (32 cm^{-1}).

According to the potential energy distribution the C=S stretching coordinate contributes substantially ($\approx$40%) to the 725 cm^{-1} absorption. The C=S stretching also contributes significantly ($\approx$20%) to the low frequency bands at 550 and 445 cm^{-1} and to a lesser extent to the high frequency bands at 1020 and 1274 cm^{-1}. Hence the 725 cm^{-1} band may qualitatively be assigned to the C=S stretching vibration. This assignment is in agreement with Ritchie *et al.*[10] and is concordant with the Raman data.[10,13] Further evidence for the assignment of C=S mode comes from the infrared spectrum of the *S*-methyl derivative. The 725 cm^{-1} band shifts to 708 cm^{-1} with the decreasing C=S bond

Table 1. Force constants for s-DMTU

Urey-Bradley constants (mdyn/Å)								
K	Initial	Final	H	Initial	Final	F	Initial	Final
CS	3.40	2.650	NCS	0.24	0.238	NCS	1.02	1.050
CN	5.50	5.450	NCN	0.50	0.693	NCN	0.60	0.550
C'N	3.45	4.124	CNH	0.20	0.265	CNH	0.45	0.432
NH	5.20	5.600	HNC'	0.12	0.203	HNC'	0.60	0.366
CH	4.40	4.250	CNC	0.25	0.264	CNC	0.25	0.207
			NCH	0.28	0.268	NCH	0.55	0.595
			HCH	0.41	0.410	HCH	0.05	0.057
k (Intramolecular tension) (mdyn Å)								
CH_3	−0.040	−0.042						
Valence constants (mdyn Å)								
$f(\pi^cNH)$	0.062	$f(\pi^tNH)$	0.057	$f(\tau^cCN)$	0.105	$f(\tau^tCN)$	0.098	
$f(\pi CS)$	0.0935	$f(\pi^tCH_3)$	0.0065	$f(\tau^cCH_3)$	0.0070			

Abbreviations: π, τ, C', c, and t as in Table 2.

Table 2. Observed and calculated frequencies (cm^{-1}) and assignments of s-DMTU-d_0 and -d_2

s-DMTU-d_2		s-DMTU-d_0		Assignment (PED, %)
Obsd	Calcd	Obsd	Calcd	
A' Species				
2420	2424	3305	3311	$\nu^tNH(63)$, $\nu^cNH(36)$
2420	2419	3305	3309	$\nu^cNH(63)$, $\nu^tNH(36)$
2938	2923	2940	2923	$\nu_a{}^cCH_3(76)$, $\nu_a{}^tCH_3(24)$
2938	2923	2940	2923	$\nu_a{}^tCH_3(76)$, $\nu_a{}^cCH_3(24)$
2860	2857	2850	2857	$\nu_s{}^cCH_3(73)$, $\nu_s{}^tCH_3(27)$
2860	2857	2850	2857	$\nu_s{}^tCH_3(73)$, $\nu_s{}^cCH_3(27)$
1540	1535	1560	1561	$\nu CN(53)$, $\delta^tNH(18)$
1475	1463	1506	1505	$\delta^cNH(34)$, $\nu CN(28)$
1460	1444	1455	1450	$\delta_a{}^tCH_3(76)$, $r^tCH_3(17)$
1445	1425	1445	1445	$\delta_a{}^cCH_3(74)$, $r^cCH_3(13)$
1412	1412	1418	1412	$\delta_s{}^cCH_3(48)$, $\delta_s{}^tCH_3(41)$
1412	1407	1418	1412	$\delta_s{}^tCH_3(48)$, $\delta_s{}^cCH_3(41)$
936	926	1355	1367	$\delta^tNH(47)$, $\nu CN(27)$
936	922	1287,1260	1259	$\delta^cNH(40)$, $\nu CN(21)$, $\delta NCN(11)$
1221	1248	1188	1170	$\nu^cNC'(58)$, $\delta^tNH(13)$
1152	1142	1148	1143	$\nu^tNC'(44)$, $r^tCH_3(16)$, $r^cCH_3(12)$
1068	1082	1035	1046	$r^tCH_3(53)$, $\nu^tNC'(12)$, $\delta_a{}^cCH_3(12)$
1030	1071	1020	1039	$r^cCH_3(53)$, $\delta_a{}^cCH_3(13)$, $\nu C{=}S(11)$
712	709	725	736	$\nu C{=}S(37)$, $\nu CN(25)$, $\delta NCN(11)$
550	527	550	537	$\nu C{=}S(23)$, $\delta NCS(22)$, $\delta CNC(19)$, $\delta^tNCN(15)$
442	441	445	449	$\delta NCS(36)$, $\nu C{=}S(18)$, $\delta^cCNC(13)$
211	236	211	238	$\delta^cCNC(38)$, $\delta^tCNC(27)$, $\delta NCS(26)$
193	182	193	184	$\delta^tCNC(37)$, $\delta NCN(28)$, $\delta^cCNC(27)$
A'' Species				
2938	2940	2940	2940	$\nu_a{}^cCH_3(99)$
2938	2940	2940	2940	$\nu_a{}^tCH_3(99)$
1445	1453	1455	1453	$\delta_a{}^tCH_3(42)$, $\delta_a{}^cCH_3(40)$
1445	1453	1455	1453	$\delta_a{}^cCH_3(42)$, $\delta_a{}^tCH_3(40)$
1068	1078	1035	1078	$r^tCH_3(53)$, $r^cCH_3(25)$
1068	1076	1035	1076	$r^cCH_3(53)$, $r^tCH_3(25)$
550	537	662	662	$\nu CN(45)$, $\pi^cNH(31)$
485	480	642	645	$\tau CN(47)$, $\pi^tNH(34)$
418	403	445	448	$\pi C{=}S(80)$
193	185	193	189	$\pi^cNH(42)$, $\tau CN(24)$, $\pi^tNH(15)$
150	149	150	150	$\tau^cCH_3(42)$, $\tau^tCH_3(22)$, $\tau CN(17)$
140	141	142	140	$\tau^cCH_3(49)$, $\tau^tCH_3(21)$
130	129	130	130	$\tau^tCH_3(40)$, $\pi^tNH(21)$, $\pi^cNH(17)$

Abbreviation: ν-stretching, δ-bending, r-rocking, π-out-of-plane bending, τ-torsion, s-symmetric, a-asymmetric; c-*cis* and t-*trans*, C' denotes methyl carbon, *cf.* Table 3.

Table 3. Comparison of the vibrational assignments for s-DMTU

Mode	s-DMU Mido *et al.* [a]	Rao *et al.* [b]	s-DMTU Ritchie *et al.* [c]	Present work	Main assignment
In-plane (A')	3360	3282	—	3305	νNH
	2980	—	—	2940	$\nu_a CH_3$
	2930	—	—	2850	$\nu_s CH_3$
	1596	1568	1554	1560	νCN+δNH
	1455	1446	—	1455 1445	$\delta_a CH_3$
	1410	1358	—	1418	$\delta_s CH_3$
	1328	1506	1504	1506	δNH+νCN
	1266	1420	1287	1355	
				1287 1260	δNH+νCN
	1170	1082	1186 1151	1188 1148	νNC'+rCH_3
	1132 1037	1038 851	—	1035 1020	rCH_3+νNC'
	1625	754	722	725	νC=O/νC=S
	672	551	550 220	445 550	δNCO/δNCS
	504 202	446	443 248	550 193	δNCN
	282 202	667	550	211 193	δCNC
Out-of-plane (A'')	—	—	—	2940	$\nu_a CH_3$
	—	—	—	1455	$\delta_a CH_3$
	—	—	—	1035	rCH_3
	—	726	—	662 642	πNH+τCN
	—	416	493	445	πC=S
	—	—	—	193 150	τCN
	—	—	—	140 130	τCH_3

a) Ref. [8]. b) Ref. [7]. c) Ref. [10].

order upon *S*-methylation. The C=S stretching frequency of s-DMTU is thus in the same region as in TA[26] (719 cm^{-1}), TU[1] (736 cm^{-1}), and NMTA[21] (699 cm^{-1}).

Skeletal Bending: The skeletal bending modes occur as highly coupled vibrations. Calculations indicate that NCN bending is highly delocalized and contributes to the frequencies at 193, 445, 550, 725, and 1274 cm^{-1}. In contrast, in s-DMU, NCN bending contributes mainly (46%) to 504 cm^{-1} band and to some extent (22%) to the 202 cm^{-1} frequency.[8] The characteristic NCS bending is also a highly mixed mode and contributes to the bands at 550, 445, and 211 cm^{-1}. The 445 cm^{-1} band could qualitatively be assigned to NCS bending in comparison with the 460 cm^{-1} of TA.[26] The contribution of NCS bending vibration to 550 and 445 cm^{-1} bands is evidenced by the shifting of these bands to slightly higher wave numbers (567 and 452 cm^{-1}) in the infrared spectrum of the *S*-methyl derivative.

According to the coordinate treatment, the 211 and 193 cm^{-1} bands correspond to CNC bending vibrations. This assignment compares reasonably with that of s-DMU[8] assigned at 282 and 202 cm^{-1}.

Out-of-plane Vibrations. There are five a'' modes for the planar skeleton. The present study indicates that the 662 and 642 cm^{-1} bands have their origin in the N–H vibrations as inferred by deuteration studies and normal coordinate analysis. On deuteration these bands disappear and the intensity of the 445 cm^{-1} band of s-DMTU increase in the spectrum of s-DMTU-d_2 indicating overlapping of ND out-of-plane bending with the 445 cm^{-1} fundamental. The present assignment for NH bending is at a lower frequency than the analogous band of TCH (768, 579 cm^{-1}).

The out-of-plane C=S bending is assigned to the 445 cm^{-1} band in the infrared (at 450 cm^{-1} in the Raman) in comparison with that in NMTU (400 cm^{-1}). The two CN torsional vibrations are strongly coupled with out-of-plane NH bending modes and contribute to low frequencies at 193, 150, and 142 cm^{-1}. These assignments are comparable with those in TMTU[6] at 144 and 127 cm^{-1} and in TCH[9] at 194 and 140 cm^{-1}.

Methyl Group Vibrations. The stretching and bending vibrations of the CH_3 group are easily assigned as shown in Table 2. The CH_3 rocking vibrations occur as coupled vibrations. They contribute principally to the bands at 1035 and 1020 cm^{-1} coupled with C'N stretching vibrations. The frequencies of the rocking vibrations are in the same region as observed for

NMTU[4] at 980 cm^{-1}, NMTA[21] at 1023 cm^{-1} and TMTU[6] at 1061 and 1035 cm^{-1}. The band at 1035 cm^{-1} may be attributed to both the out-of-plane CH_3 rocking (wagging) vibrations overlapping with an in-plane fundamental. The analogous rocking vibrations are observed for u-DMTU at 1068 and 1035 cm^{-1}, and in NMTU and TMTU near 1040 cm^{-1}.

The calculations suggest that the CH_3 torsional vibrations could be assigned to the bands near 140 and 130 cm^{-1}. The 144 and 127 cm^{-1} bands of TMTU are the corresponding ones. The CH_3 torsion is found near 130 cm^{-1} in NMTU[4] and *N,N*-dimethylselenoformamide.[30]

References

1) A. Yamaguchi, R. B. Penland, S. Mizushima, T. J. Lane, C. Curran, and J. V. Quagliano, *J. Am. Chem. Soc.*, **80**, 527 (1958).

2) G. B. Aitken, J. L. Duncan, and G. P. McQuillan, *J. Chem. Soc., A*, **1971**, 2695.

3) D. Hadzi, J. Kidric, Z. V. Knezvic, and B. Barlic, *Spectrochim. Acta, Part A*, **32**, 693 (1976).

4) K. Dwarakanath and D. N. Sathyanarayana, *Bull. Chem. Soc. Jpn.*, **52**, 2084 (1979).

5) K. Dwarakanath and D. N. Sathyanarayana, *Indian J. Pure Appl. Phys.*, **17**, 171 (1979).

6) U. Anthoni, P. H. Nielsen, G. Borch, J. Gustavsen, and P. Klaboe, *Spectrochim. Acta, Part A*, **33**, 403 (1977).

7) R. K. Gosavi, U. Agarwala, and C. N. R. Rao, *J. Am. Chem. Soc.*, **89**, 235 (1967).

8) Y. Mido and H. Murata, *Bull. Chem. Soc. Jpn.*, **42**, 3372 (1969).

9) K. Dwarakanath, D. N. Sathyanarayana, and K. Volka, *Bull. Soc. Chim. Belg.*, **87**, 667 (1978).

10) R. K. Ritchie, H. Spedding, and D. Steele, *Spectrochim. Acta, Part A*, **27**, 1597 (1971).

11) M. L. Moore and F. S. Crossley, *Org. Synth.*, Coll. Vol. **3**, 617 (1955).

12) E. Brand and F. C. Brand, *Org. Synth*, Coll. Vol. **3**, 440 (1955).

13) "Raman/IR-Atlas," ed by B. Schrader and W. Heiler Verlag Chemie, GmbH, Weinhein/Bergstr., (1974).

14) E. B. Wilson, Jr., *J. Chem. Phys.*, **7**, 1047 (1939); **9**, 76 (1941).

15) W. Walter and K. P. Ruess, *Justus Liebigs Ann. Chem.*, **746**, 54 (1971).

16) M. V. Andreocci, M. Bossa, G. Ramunni, M. Scazzocchio, D. Gattegno, and A. M. Giuliani, *J. Chem. Soc., Dalton Trans.*, **1974**, 41.

17) M. Bonamico, G. Dessy, V. Fares, and L. Scaramuzza, *J. Chem. Soc., A*, **1971**, 3195.

18) R. L. Girling and E. L. Amma, *Inorg. Chem.*, **10**, 335 (1971).

19) M. Bonamico, G. Dessy, V. Fares, and L. Scaramuzza, *J. Chem. Soc., Dalton Trans.*, **1973**, 876.

20) Z. V. Zvonkova, L. I. Astakhova, and V. P. Glushkova, *Kristallografiya*, **5**, 547 (1960).

21) I. Suzuki, *Bull. Chem. Soc. Jpn.*, **35**, 1456 (1962).

22) C. N. R. Rao and G. C. Chaturvedi, *Spectrochim. Acta, Part A*, **27**, 520 (1971).

23) T. Shimanouchi and I. Suzuki, *J. Chem. Phys.*, **42**, 296 (1965).

24) D. E. Mann, T. Shimanouchi, J. H. Meal, and L. Fano, *J. Chem. Phys.*, **27**, 43 (1957).

25) T. Shimanouchi, "Normal Coordinate Treatment," University of Tokyo, July (1968).

26) I. Suzuki, *Bull. Chem. Soc. Jpn.*, **35**, 1449 (1962).

27) W. Walter and P. Staglich, *Spectrochim. Acta, Part A*, **30**, 1739 (1974); and references therein.

28) V. C. Jyothi Bhasu, Ph. D. Thesis, Indian Institute of Science, Bangalore, India (1978).

29) K. A. Jensen and P. H. Nielsen, *Acta Chem. Scand.*, **20**, 597 (1966).

30) U. Anthoni, L. Henriksen, P. H. Nielsen, G. Borch, and P. Klaboe, *Spectrochem. Acta, Part A*, **30**, 1351 (1974).

Differential Refractometric Studies on Some Strong and Weak Molecular Complexes

Ram Sahai,* Vinod Singh, and Rekha Verma
Department of Chemistry, V.S.S.D. College, Kanpur University, Kanpur-208002, India
(Received January 18, 1980)

A more adequate model has been developed to determine the equilibrium constant (K_1) and stoichiometry of molecular complexes. This model involves the assumption:

$$\Delta\phi_a/C_D^\circ = \{K_1C_A^\circ/\alpha(1+K_1C_A^\circ)\} - \{K_1\Delta\phi_a/(1+K_1C_A^\circ)^2\}$$
$$\Delta\phi_d/C_D^\circ = \{K_1C_A^\circ/\alpha(1+K_1C_A^\circ)\} - \{K_1\Delta\phi_d/(1+K_1C_A^\circ)^2\}$$

where $\Delta\phi_a$ is the difference in the refraction per cm^3 of solution and acceptor; $\Delta\phi_d$ is the difference in the refraction per cm^3 of solution and donor; α is the extent of electronic polarization. C_A° and C_D° are the initial concentrations of acceptor and donor respectively. This model has been verified on some strong and weak complexes and was found better than that of earlier methods. $\Delta\phi_a$, $\Delta\phi_d$, and $\Delta\Omega C_{DA}$ (refraction per cm^3 due to charge-transfer complex) have also been used to Yoshida and Ōsawa's method. The K_1 obtained from the plot of $\Delta\phi_a$ or $\Delta\phi_d$ *versus* molar ratio of solutes were found more reliable for weak complexes than K_1 calculated from Yoshida and Ōsawa's plot. From these plots the percentage of contribution of donor or acceptor in total 30% solute aggregation as proposed by Yoshida and Ōsawa has been calculated. It is also noted that Yoshida and Ōsawa's method may give the reliable value for strong complexes but for weak complexes only differential refractometric method can provide the best values.

In our previous investigations,[1-4] refractometric[1,4] and differential refractometric[2-4] methods have been used to determine the stoichiometry and formation constant of molecular complexes. In our first paper on refractometric technique,[1] the refraction per cm^3 due to donor (D), acceptor (A) and donor–acceptor (DA) complex, $\delta\phi$, has been collectively considered, but in second paper,[3] a differential refractometric method has been developed to get the refraction per cm^3 due to donor–acceptor complex, $\Delta\Omega C_{DA}$. In these papers the refractions per cm^3 due to D and DA ($\Delta\phi_d$) and A and DA ($\Delta\phi_a$) have not been considered. The purpose of this paper is to consider these refractions, to determine equilibrium and the results are compared with those of previous techniques.

Recently we have applied $\Delta\Omega C_{DA}$ to Yoshida and Ōsawa's method to calculate the K_1 of weak molecular complexes (phenol–naphthalene) and better results were noted.[2] The purpose of the present paper is also to use $\Delta\Omega C_{DA}$, $\Delta\phi_a$, and $\Delta\phi_d$ to Yoshida and Ōsawa's method[5] and to observe the effect on the equilibrium constant. An attempt has also been made to calculate the contribution of donor and acceptor separately in the total 30% solute (donor+acceptor) aggregation as proposed by Yoshida and Ōsawa[5] for weak complexes.

Theoretical

Consider the condition of equilibrium for 1:1 complex DA, for the interaction of a donor (D) and an acceptor (A), $D+A \overset{K}{\rightleftharpoons} DA$; K is given by Eq. 1:

$$K = K_1K_\gamma; K_\gamma = \frac{\gamma_{DA}}{\gamma_D\gamma_A}. \quad (1)$$

In Eq. 1 γ is the Raoult's activity coefficient of species, i. In general, K_1 and $K\gamma$ are not constant but are functions of concentrations of reactants and products. Until recently complexes had been studied almost entirely in solution. It generally has been assumed that $K\gamma$ is unity; so that the calculations of equilibrium constants were based on the Eq. 2.

$$K_1 = C_{DA}/[(C_A^\circ - C_{DA})(C_D^\circ - C_{DA})] \quad (2)$$

where C_A° and C_D° represent the initial concentrations of acceptor and donor respectively and C_{DA} is the equilibrium concentrations of the complex.

In refractometric investigation, the refraction per cm^3 due to solution (donor+acceptor), ϕ; donor, ϕ_D; acceptor, ϕ_A, have been calculated as reported earlier.[1-4] The difference in the refraction per cm^3 of solution and acceptor, $\Delta\phi_a$, may be calculated using the method of Colter and Grunwald.[6]

$$10^3(\phi-\phi_A) = 6000(n-n_A)n_A/(n_A^2+2)^2 = \Delta\phi_a \quad (3)$$

Similarly $\Delta\phi_d$, the difference in the refraction per cm^3 of solution and donor may be calculated as:

$$10^3(\phi-\phi_D) = 6000(n-n_D)n_D/(n_D^2+2)^2 = \Delta\phi_d. \quad (4)$$

Now it can be assumed that the extent of charge-transfer from donor will measure the concentration of the complex and hence it will be proportional to the difference in the refraction per cm^3 of solution and acceptor, $\Delta\phi_a$, or donor, $\Delta\phi_d$. Now taking the case of $\Delta\phi_a$ we have,

$$C_{DA} = \alpha\Delta\phi_a, \quad (5)$$

where α is a constant determined by the extent of electronic polarization due to incidence of light. Hence Eq. 2 becomes,

$$K_1 = \alpha\Delta\phi_a/(C_A^\circ - \alpha\Delta\phi_a)(C_D^\circ - \alpha\Delta\phi_a). \quad (6)$$

On solving Eq. 6 as it was done in NMR,[7] spectrophotometric,[8] refractometric[1] and differential refractometric[3] techniques, Eq. 7 is obtained:

$$\Delta\phi_a/C_D^\circ = \{K_1C_A^\circ/\alpha(1+K_1C_A^\circ)\} - \{K_1\Delta\phi_a/(1+K_1C_A^\circ)^2\}. \quad (7)$$

Similarly, Eq. 8 can be obtained when $\Delta\phi_d$ was considered:

$$\Delta\phi_d/C_D^\circ = \{K_1C_A^\circ/\alpha(1+K_1C_A^\circ)\} - \{K_1\Delta\phi_d/(1+K_1C_A^\circ)^2\}. \quad (8)$$

Equations 9 and 10 as derived earlier[1,3] have also

been used to calculate K_1 for strong and weak molecular complexes.

$$\delta\phi/C_D^\circ = \{K_1C_A^\circ/\alpha(1+K_1C_A^\circ)\} - \{K_1\delta\phi/(1+K_1C_A^\circ)^2\} \quad (9)$$

$$\Delta\Omega C_{DA}/C_D^\circ = \{K_1C_A^\circ/\alpha(1+K_1C_A^\circ)\} - \{K_1\Delta\Omega C_{DA}/(1+K_1C_A^\circ)^2\} \quad (10)$$

As expected a plot of $\Delta\phi_a$ *versus* $\Delta\phi_a/C_D^\circ$, $\Delta\phi_d$ *versus* $\Delta\phi_d/C_D^\circ$, $\delta\phi$ *versus* $\delta\phi/C_D^\circ$ and $\Delta\Omega C_{DA}$ *versus* $\Delta\Omega C_{DA}/C_D^\circ$ gave a straight line with a slope $-\{K_1/(1+K_1C_A^\circ)^2\}$ and intercept, $K_1C_A^\circ/\alpha(1+K_1C_A^\circ)$ (Fig. 1).

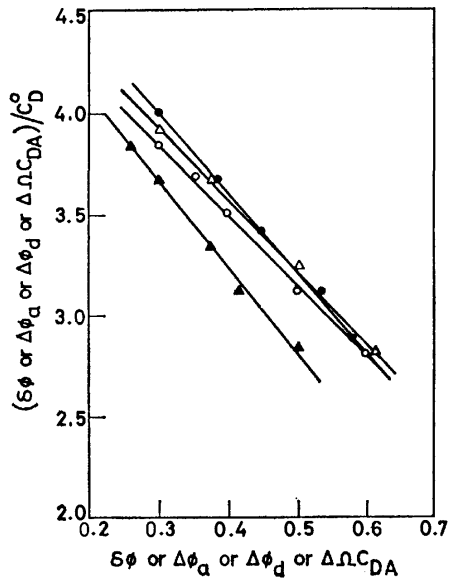

Fig. 1. Plots of $\delta\phi$ *versus* $\delta\phi/C_D^\circ$ (▲-▲-▲), $\Delta\phi_a$ *versus* $\Delta\phi_a/C_D^\circ$ (△-△-△), $\Delta\phi_d$ *versus* $\Delta\phi_d/C_D^\circ$ (●-●-●), and $\Delta\Omega C_{DA}$ *versus* $\Delta\Omega C_{DA}/C_D^\circ$ (O-O-O) for phenol-naphthalene complex in cyclohexane at 35 °C.

The equilibrium constant have also been calculated by Yoshida and Ōsawa's[5] method using Eq. 11.

$$K_1 = 2\sqrt{k}\{\sqrt{k}(C+C') - (C+kC')\}/(C-kC')^2 \quad (11)$$

where C and C' are the maximum concentrations of both the systems and k is the maximum deviation from additive or base line when molar ratio of solutes is plotted against n^2 or $\Delta\phi_a$ or $\Delta\phi_d$ or $\Delta\Omega C_{DA}$. Equation 11 has also been used to calculate K_1 after getting more reliable value of k through the plots of $\Delta\phi_a$ or $\Delta\phi_d$ *versus* molar ratio of solutes. Differential refractometric[2] method has also been used to calculate K_1. In this method, the refraction per cm³ due to charge-transfer, $\Delta\Omega C_{DA}$ has been plotted against molar ratio of solutes.

Experimental

The method of experimentation was essentially the same as it was reported earlier.[1-4]

Results and Discussion

Strong Interaction. The equilibrium constant (K_1) calculated for some strong complexes from Eqs. 7, 8, 9, and 10 are listed in Table 1. From this table it is clear that K_1 calculated from these equations are almost the same. Their percentage deviation from the spectrophotometric value comes under the experimental error (10—15%). For strong complexes, the concentration of solutes was kept low (10^{-3} mol dm^{-3}). Therefore the possibility of solute aggregation becomes quite low. The difference noted in K_1's values, obtained from these equations may be due to the bet-

Table 1. Equilibrium constant (K_1) and solute aggregation data for 1:1 molecular complexes in different solvents at 35 °C

Complex	Solvent	K_1/dm³ mol⁻¹						SA_d	SA_a
		Refractometric methods				Spectrophotometric method			
		Eq. 9	Eq. 7	Eq. 8	Eq. 10		T/°C		
Phenol-naphthalene	Cyclohexane	5.8	6.2	5.2	4.6			11.25	18.75
Ethanol-naphthalene	Cyclohexane	5.2	4.8	3.8	3.2			9.00	21.00
Indole-chloranil	CCl_4	3.8	3.2	3.0	2.3	2.86(15)	25	14.0	16.0
Ph_3As-I_2	CCl_4	1100	840	830	770	790(12)	30		
Ph_3As-I_2	$CHCl_3$	8540	7530	7510	7142(3)	8330(12)	26		
Ph_3Sb-I_2	$CHCl_3$	1140	1020	1000	909(3)	1700(12)	26		
Et_3N-I_2	Cyclohexane	3250	2850	2820	2500(3)				
Et_3N-I_2	Heptane	2800	2350	2310	2000(3)	1740(13)			
Tryptophan-chloranil	50% (aq) Ethanol	221(4)	208	200	156(4)	176(14)	25		
Tyrosine-chloranil	50% (aq) Ethanol	172(4)	168	166	142(4)				
Phenylalanine-chloranil	50% (aq) Ethanol	166(4)	164	151	131(4)				

Number in parenthesis indicates the reference number.

terment of respective equations. The K_1 calculated from Eq. 9, in which refraction per cm^3 due to solvent was considered, show maximum percentage of error. But for the same complex if Eq. 7, in which the refraction per cm^3 of solution and acceptor was considered, the percentage error is less. The value of K_1 calculated from Eq. 8 were noted to be the same as calculated from Eq. 7. This indicates that the contribution of donor or acceptor in the solute aggregation is almost negligible. The best values have been obtained when Eq. 10 has been used in which differential refractometric method has been applied to evaluate $\Delta\Omega C_{DA}$.

The equilibrium constant calculated from Yoshida and Ōsawa's plot[5] and from the plot of $\Delta\phi_a$ or $\Delta\phi_d$ or $\Delta\Omega C_{DA}$ *versus* molar ratio of solutes are listed in Table 2. The K_1 calculated from the plot of n^2 *versus* molar ratio of solutes and from the plot of $\Delta\Omega C_{DA}$ *versus* molar ratio of solutes, show slight difference. This difference may again be interpreted due to the betterment of the differential refractometric method. Consequently for strong complexes Yoshida and Ōsawa's method can give the reliable value of K_1, but to get accurate results, the differential refractometric method should be used. We could not get different values for the maximum deviation from the base line (k), when plotted $\Delta\phi_a$ or $\Delta\phi_d$ *versus* molar ratio of solutes. Thus, it was not possible to calculate the different K_1 values through these plots. This was due to the limited accuracy of the instrument.

In strong complexes, a positive deviation was observed at 1:1 molar ratio of solutes indicating 1:1 stoichiometry of these complexes (Fig. 2). But in case of Et_3N–I_2 system a negative deviation was observed (Fig. 3). A similar observation was also made by Singh and Bhat.[9] After applying the differential refractometric method, negative $\Delta\Omega C_{DA}$ values were calculated and have been plotted against molar ratio of solutes (Fig. 4). From this figure it is clear that the deviation is large which indicates strong interaction between Et_3N and I_2. The molar refraction is a measure of deformability of the electronic seath. The

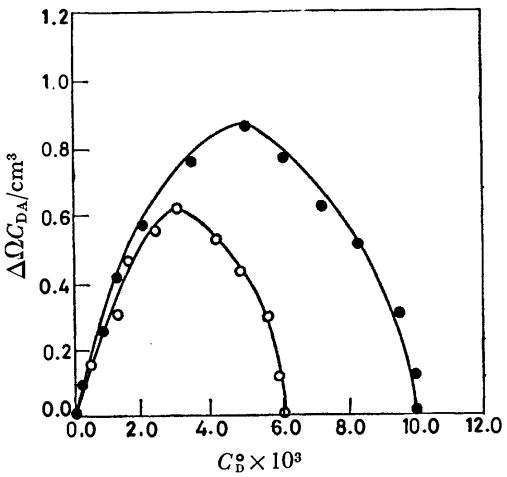

Fig. 2. Plot of $\Delta\Omega C_{DA}$ *versus* molar ratio of solutes indicating 1:1 stoichiometry of Ph_3Sb–I_2 complex in $CHCl_3$ at 35 °C.

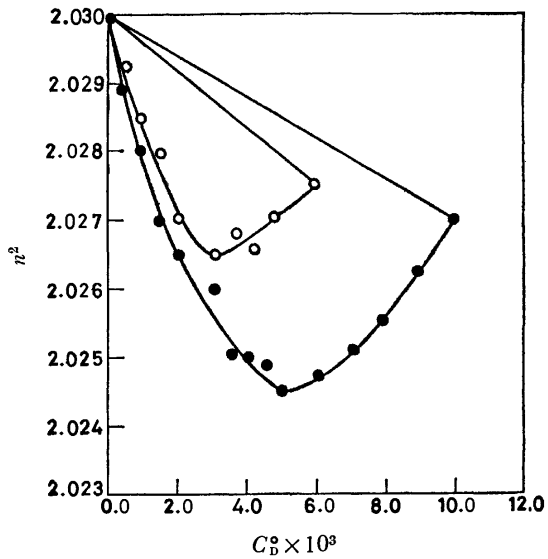

Fig. 3. Plot of n^2 *versus* molar ratio of solutes indicating 1:1 stoichiometry through negative deviation of Et_3N–I_2 in cyclohexane at 35 °C.

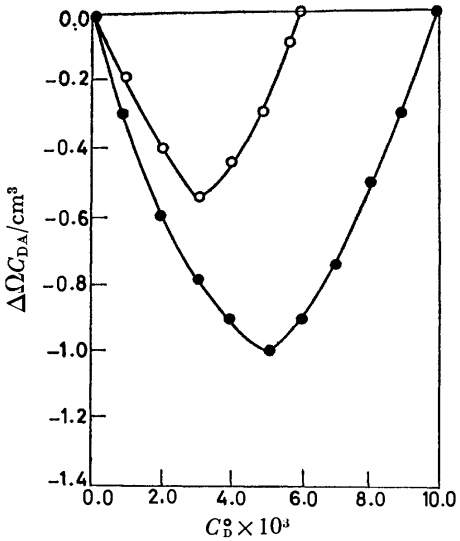

Fig. 4. Plot of $\Delta\Omega C_{DA}$ *versus* molar ratio of solutes indicating 1:1 stoichiometry through negative deviation of Et_3N–I_2 complex in cyclohexane at 35 °C.

decrease in refractive index of Et_3N–I_2 complex shows the increase of molar refractivity. Thus the complex is more polar. Similar results was obtained earlier through dipole moment studies on this system.[10]

Weak Interaction. From Table 1 it is evident that K_1 calculated for weak complexes from Eqs. 7, 8, 9, and 10 show greater difference. In order to get appropriate variation in scale due to limited accuracy of the instrument and low K_1 values, the solute concentration was raised (10^{-1} mol dm^{-3}).[2,5,11] As pointed out by Yoshida and Ōsawa[5] that at such a higher concentration, the solute aggregation occurs (about 30%) which prevents to give the reliable value of K_1. Therefore K_1 calculated from Eq. 9 shows maximum percentage of error. This error becomes less when Eq. 7 or 8 has been used but the best values were noted when Eq. 10 was used.

Table 2. Equilibrium constant (K_1) and solute aggregation data for 1:1 molecular complexes obtained on the basis of Yoshida and Ōsawa's equation in different solvents at 35 °C

Complex	Solvent	K_1/dm³ mol⁻¹ Refractometric methods 1[a]	2[b]	3[c]	4[d]	SA_d	SA_a
Phenol-naphthalene	Cyclohexane	6.2	5.6	5.2	4.9(2)	6.93	23.07
Ethanol-naphthalene	Cyclohexane	5.2	4.6	4.1	3.2	13.50	16.50
Indole-chloranil	CCl_4	3.6	3.1	2.8	2.3	11.53	18.47
Ph_3As-I_2	CCl_4	842	—	—	746.00		
Ph_3As-I_2	$CHCl_3$	8730	—	—	8710.00		
Ph_3Sb-I_2	$CHCl_3$	2127	—	—	1830.00		
Et_3N-I_2	Heptane	2550	—	—	2000.00		
Et_3N-I_2	Cyclohexane	2917	—	—	2552.00		
Tryptophan-chloranil	50% (aq) Ethanol	208(4)	—	—	157.54(4)		
Tyrosine chloranil	50% (aq) Ethanol	191.30(4)	—	—	140.72(4)		
Phenylalanine-chloranil	50% (aq) Ethanol	157.54(4)	—	—	127.16(4)		

Number in parenthesis indicates the reference number. a) Calculated from the plot of n^2 *versus* molar ratio of solutes. b) Calculated from the plot of $\Delta\phi_a$ *versus* molar ratio of solutes. c) Calculated from the plot of $\Delta\phi_d$ *versus* molar ratio of solutes. d) Calculated from the plot of $\Delta\Omega C_{DA}$ *versus* molar ratio of solutes.

The K_1 calculated for weak complexes from the plots of n^2 or $\Delta\phi_a$ or $\Delta\phi_d$ or $\Delta\Omega C_{DA}$ *versus* molar ratio of solutes are listed in Table 2. For weak complexes we could get different K values for the same system when plotted $\Delta\phi_a$ or $\Delta\phi_d$ *versus* molar ratio of solutes. Thus for the same system, different K_1 values calculated from these plots are noted in Table 2. It was not observed for strong complexes. For weak complexes, the best K_1 values have been observed when differential refractometric method was used in which the refraction per cm³ due to charge-transfer complex ($\Delta\Omega C_{DA}$) is plotted against molar ratio of solutes. The present study indicates that the contribution of refraction per cm³ of donor, acceptor and solvent is more important for moderate and weak complexes than that for strong complexes. Now, we can conclude that Yoshida and Ōsawa's method[5] can give satisfactory results for strong complexes only and not for weak complexes. But more accurate values for strong complexes can be obtained by using differential refractometric method.[2] For weak complexes only the differential refractometric method[2] can provide the best values.

Assuming that K_1 calculated from the plot of $\Delta\Omega C_{DA}$ *versus* molar ratio of solutes are absolute, and that the K_1 calculated from the plot of n^2 *versus* molar ratio of solutes incorporates 30% solute aggregation, then the contribution of donor or acceptor in the total 30% solute aggregation may be calculated as:

$K_n2=K_1$ calculated from the plot of n^2 *versus* molar ratio of solutes or from Eq. 8.

$K_{\Delta\phi_a}=K_1$ calculated from the plot of $\Delta\phi_a$ *versus* molar ratio of solutes or from Eq. 7.

$K_{\Delta\phi_d}=K_1$ calculated from the plot of $\Delta\phi_d$ *versus* molar ratio of solutes or from Eq. 9.

$K_{\Delta\Omega C_{DA}}=K_1$ calculated from the plot of $\Delta\Omega C_{DA}$ *versus* molar ratio of solutes or from Eq. 10.

Thus,

$\Delta K_{da}=K_n2-K_{\Delta\Omega C_{DA}}$=Total 30% solute aggregation.

$\Delta K_a=K_n2-K_{\Delta\phi_d}$=Solute aggregation due to acceptor.

$\Delta K_d=(\Delta K_{da}-\Delta K_a)$=Solute aggregation due to donor.

Thus the contribution of acceptor (SA_a) and donor (SA_d) in total 30% solute aggregation may be expressed by Eqs. 12 and 13 respectively.

$$SA_a = 30\times\Delta K_d/\Delta K_{da} \quad (12)$$

$$SA_d = 30\times\Delta K_a/\Delta K_{da} \quad (13)$$

The values of SA_d and SA_a calculated from Eqs. 12 and 13 are listed in Tables 1 and 2. From these tables it is evident that in case of weak complexes the contribution of donor in total 30% solute aggregation is less than that of acceptor.

The authors are grateful to Kanpur University, Kanpur for the award of UGC-JRF to VS and CSIR-JRF to RV. They also wish to thank Prof. P. C. Nigam (I.I.T., Kanpur) for providing some experimental facilities.

References

1) R. Sahai, P. C. Pande, and V. Singh, *Indian J. Chem.*, **18A**, 217 (1979).
2) R. Sahai and V. Singh, *Bull. Chem. Soc. Jpn.*, **53**, 1785 (1980).
3) R. Sahai and V. Singh, *Indian. J Chem.*, in Press.
4) R. Sahai and V. Singh, *Indian J. Pure Appl. Phys.*, **18**, 504 (1980).
5) Z. Yoshida and E. Ōsawa, *Bull. Chem. Soc. Jpn.*, **38**, 140 (1965).

6) A. K. Colter and E. Grunwald, *J. Phys. Chem.*, **74**, 3637 (1970).
7) R. Sahai, G. L. Loper, S. H. Lin, and H. Eyring, *Proc. Natl. Acad. Sci. U.S.A.*, **71**, 1499 (1974).
8) R. Sahai and V. N. Badoni, *Indian J. Chem.*, **15A**, 731 (1977).
9) R. A. Singh and S. N. Bhat, *Indian J. Chem.*, **15A**, 1106 (1977).
10) A. Funtsu and K. Toyoda, *Bull. Chem. Soc. Jpn.*, **43**, 279 (1970).
11) R. A. Singh and S. N. Bhat, *J. Phys. Chem.*, **82**, 2322 (1978).
12) K. R. Bhaskar, S. N. Bhat, S. Singh, and C. N. R. Rao, *J. Inorg. Nucl. Chem.*, **28**, 1915 (1966).
13) S. Nagakura, *J. Am. Chem. Soc.*, **80**, 520 (1958).
14) J. B. Birks and M. A. Slifkin, *Nature*, **197**, 42 (1963).
15) R. Foster and P. Henson, *Trans. Faraday Soc.*, **60**, 2189 (1964).

Synthesis and Studies of Some Novel Analogues of Phthalein Dyes

R. P. Chamoli,*,† S. J. Rai, and P. C. Gupta
Department of Chemistry, University of Allahabad, Allahabad, India

(Received October 11, 1979)

Some novel analogues of phthalein dyes have been synthesized by condensing a γ-keto acid, 2-(2-thenoyl) benzoic acid with various phenols. The dyes so obtained are unsymmetrically substituted phthalides where the central carbon atom is attached with two different rings and these dyes have been named as phthal-as-eins; -'as' representing unsymmetry, and-'ein' class of the compound (phthal-ein). The structures of these products have been established on the basis of their elemental analysis and chemical reactions. Absorption maxima of these new dyes have been determined and compared with those of true phthaleins.

The γ-keto acids have been found to exist in open **1** and cyclic **2** form due to keto-lactol tautomerism.[1] Generally it has been observed that γ-keto acids exist chiefly as lactol or equilibrium mixture of keto and ctol forms.a[2,3] These lactols give crystalline acetyl derivatives **3**[4,5] retaining their cyclic structure. Hence it has been concluded that the lactol form of the γ-keto acids is more stable than their open form.[5] The cyclic derivatives, pseudo chlorides (**4**)[6] and pseudo esters (**5**)[7-9] are obtained through the lactol form.

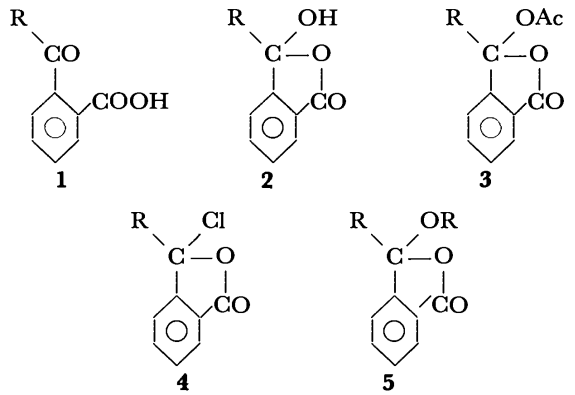

1 **2** **3** **4** **5**

Many chemical reactions[10,11] of γ-keto acids have been explained on the basis of their cyclization to lactol. IR,[8,12] Raman,[9] and NMR[13] spectra have further confirmed the formation of cyclic isomers.

It has been observed that ring tautomerism of γ-keto acids is further exalted by changing R to larger alkyl or aryl groups.[14] It increases further when hydrogen atoms on carbon atoms α to carboxyl group (in γ-keto acids of the type, R–CO–CH_2–CH_2–COOH), are also changed to larger alkyl groups or α,β-ethylenic bond.[15] In continuation of previous work[16-23] on synthesis of mixed phthaleins and succineins, we report in this paper synthesis of a new series of phthal-as-eins from a γ-keto acid, 2-(2-thenoyl)benzoic acid.

Results and Discussion

2-(2-Thenoyl)benzoic acid has also been found spectroscopically to exist as a mixture of keto **6** and lactol form **7**. IR spectrum of the acid shows notable absorption band at 1695, 1680, and 1740 (weak) cm^{-1} indicating the presence of carboxyl >C=O, diaryl ketonic >C=O, and lactonic >C=O respectively. Absorption peaks due to -OH of carboxyl group and -OH

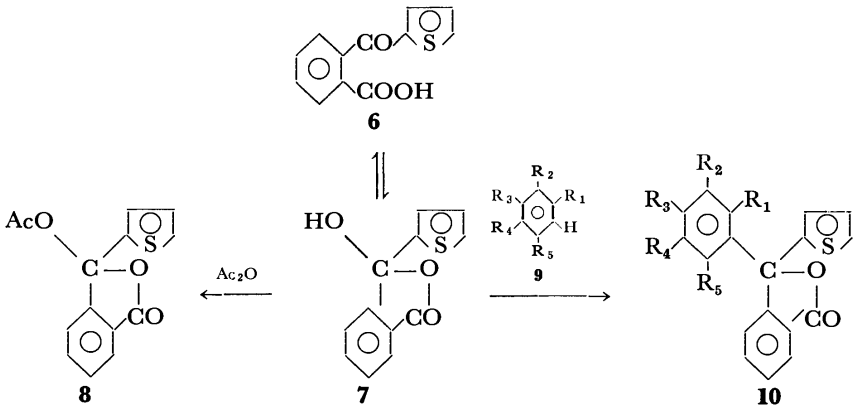

6 **8** **7** **9** **10**

11 $R_1=R_2=R_4=R_5=H$; $R_3=OH$
12 $R_2=R_4=R_5=H$; $R_1=R_3=OH$
13 $R_3=R_4=R_5=H$; $R_1=R_2=OH$
14 $R_2=R_3=R_5=H$; $R_1=R_4=OH$
15 $R_2=R_4=H$; $R_1=R_3=R_5=OH$
16 $R_4=R_5=H$; $R_1=R_2=R_3=OH$
17 $R_2=R_4=R_5=H$; $R_1=R_3=OCOCH_3$
18 $R_5=H$; $R_2=R_4=Br$; $R_1=R_3=OH$

Scheme 1.

† Department of Chemistry, Government Postgraduate College, Gopeshwar (Chamoli), U.P., India.

of lactol appear at 2640 (weak) and 3090 (broad) cm^{-1} respectively. In the NMR spectrum of the acid besides other peaks, there is a broad singlet of low intensity at τ 5.5 (1H) which may be assigned to hydroxyl proton of lactol form present in the acid.

IR spectrum of the acetyl derivative of the acid shows a very sharp peak at 1760 cm^{-1} which has been assigned to lactonic >C=O. Peaks at 1750, 1235, 1205, and 1010 cm^{-1} are due to presence of acetate group. Peaks present in the IR spectrum of the acid at 3090, 2640, 1695, and 1680 cm^{-1} are found to be absent in the IR spectrum of the acetyl derivative of the acid. In the NMR spectrum of the acetyl derivative there is no signal at τ 5.5 (present in the NMR spectrum of the acid) but there is new signal as a singlet at τ 7.5 (3H) due to acetate group.

On the basis of above spectral studies it has been concluded that acetyl derivative of the acid possesses a cyclic structure and its formation takes place through the lactol form **7** of the acid **6** (Scheme 1).

The phthal-as-eins have been prepared by condensing the acid with phenols (**9**). The condensation follows through the equilibrium process of lactol form **7** of acid (**6**) and with excess of phenols, the entire acid taken reacts as lactol. The purity of the dyes has been confirmed by TLC and paper chromatography. Their structures have been confirmed on the basis of elemental analysis, bromination, acetylation and KOH degradation studies. Formation of diacetyl derivative (**17**) and dibromo derivative (**18**) support the presence of only one resorcinol molecule in the dye molecule (**12**). KOH fusion of dye (**12**) gave acid (**6**) and resorcinol (**19**).

The absorption maxima (λ_{max}) of the phthal-as-eins are given in Table 2. Table 3 shows λ_{max} of true phthaleins prepared in similar manner. Absorption maxima of phthal-as-eins **11**, **12**, and **18** have been compared with those of phenolphthalein, fluorescein, and eosin respectively and a closeness has been observed.

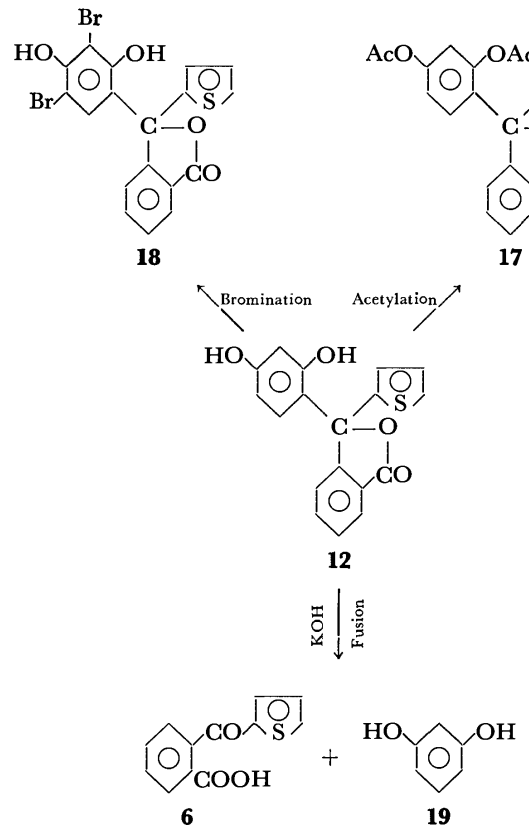

Scheme 2.

Experimental

All melting points are uncorrected. The absorption maxima (visible) have been measured with the help of model DU Beckman spectrophotometer in absolute ethanol (neutral and alkaline media). IR spectra were recorded in KBr on a Perkin Elmer infracord. NMR spectra were run in DMSO-d_6 on Varian A-60 spectrophotometer using TMS as internal standard. For TLC, plates coated with Alumina G-Silica gel G (1:1) layers were run in ethyl acetate–meth-

Table 1. Preparation and properties of 3-(substituted phenyl)-3-(2-thienyl)phthalides (**10**)

	Substituents on phenyl group	Condensation Temp °C	Condensation Duration h	Appearance (Micro-crystalline)	Mp °C	Yield %	Formula	Found (%) / Calcd (%) C	H	S
11[a]	*p*-Hydroxy	160—170	6	Greyish white	210—211	57	$C_{18}H_{12}O_3S$	70.36 70.13	3.56 3.89	10.12 10.37
13	2,3-Dihydroxy	220—230	2	Brown	215—216	40	$C_{18}H_{12}O_4S$	66.31 66.66	3.98 3.70	9.62 9.87
14	2,5-Dihydroxy	230—240	3	Light brown	195—196	35	$C_{18}H_{12}O_4S$	66.89 66.66	3.46 3.70	9.97 9.87
15	2,4,6-Trihydroxy	190—200	2	Brown	>300 dec.	50	$C_{18}H_{12}O_5S$	63.64 63.82	3.26 3.52	9.23 9.41
16	2,3,4-Trihydroxy	180—190	1½	Blackish-brown	>300 dec.	50	$C_{18}H_{12}O_5S$	64.10 63.82	3.21 3.52	9.55 9.41
17	2,4-Diacetoxy	130—140	4	Light-yellow	175—176	50	$C_{22}H_{16}O_6S$	64.92 64.70	3.65 3.92	7.60 7.84
18	3,5-Dibromo-2,4-dihydroxy	130—140	1	Brick-red	235—236	67	$C_{18}H_{10}O_4SBr_2$		Br, Br,	33.32 33.15

All the compounds crystallized from rectified ethanol. a) Excess phenol after condensation was removed by steam distillation.

Table 2. Absorption maxima of 3-(substituted phenyl)-3-(2-thienyl)phthalide
(G. F.=Green Fluorescence)

Dyes	Color in ethanol		Color with 2% NaOH	λ_{max}/nm	
	Neutral	Alkaline		Neutral	Alkaline (pH)
11	Yellow-orange	Reddish-pink	Reddish-pink	510	540 (10.0)
12	Yellowish-brown (G. F.)	Red-brown ((G. F.)	Red-brown (G. F.)	480	490 (9.5)
13	Yellow	Green	Green	400	700 (10.5)
14	Yellow	Purple	Purple	a)	— —
15	Yellow	Red-brown	Red-brown	a)	— —
16	Yellow	Purple	Purple	a)	— —
17	Yellow	Yellow	Colorless	a)	— —
18	Red (G. F.)	Red (G. F.)	Dark red	520	520 (9.5)

a) Correct λ_{max} could not be measured due to decomposition of these dyes in solution.

Table 3. Absorption maxima of known phthaleins

Name of dye	Color in ethanol		Color with 2% NaOH	λ_{max}/nm	
	Neutral	Alkaline		Neutral	Alkaline (pH)
Phenolphthalein	Colourless	Pink	Pink	—	550 (10.5)
Fluorescein	Yellow red (G. F.)	Red (G. F.)	Reddish pink (G. F.)	480	500 (10.0)
Eosin	Light pink (G. F.)	Orange pink (G. F.)	Pink	530	530 (9.5)

anol–5 mol dm^{-3} aqueous ammonia solution (60:30:10) and spots were developed with 5% aqueous NaOH.

2-(2-Thenoyl)benzoic acid was prepared according to reported procedure.[24] Its acetyl derivative prepared by refluxing it with acetic anhydride in presence of fused sodium acetate. The phenols (phenol, resorcinol, catechol, hydroquinone, phloroglucinol, and pyrogallol) have been taken in slight excess of molecular proportion than the acid (**6**) and concentrated sulfuric acid (4—5 drops) has been used as condensing agent throughout. Analogous to phthaleins, the condensation is supposed to have taken place as shown in Scheme 1.

*Synthesis of 3-(2,4-Dihydroxyphenyl)-3-(2-thienyl) phthalide (**12**).* An intimate mixture of 2-(2-thenoyl)benzoic acid (4.6 g) and resorcinol (3.0 g) was taken in a hard glass boiling tube and heated to 240 °C. Concentrated sulfuric acid (4—5 drops) was added and heating was continued between 240—250 °C for about 2 h till the contents became hard and brittle on cooling. The condensed mass was crushed, and washed thoroughly with water to remove excess of resorcinol. Then it was extracted with 2% aqueous sodium hydroxide and filtered. The dye was precipitated from red-brown (green fluorescent) filtrate by acidification with dilute hydrochloric acid. It was filtered, washed with water and purified by repeated crystallization from rectified ethanol, dried in an oven at 120 °C and then in a vacuum desiccator (3.6 g, 56% of the theoretical yield).

The yellow-brown dye, mp >300 °C is microcrystalline. The ethanolic solution is yellowish brown with light green fluorescence which on addition of alkali gives red-brown color with intensified green fluorescence. Found: C, 66.92; H, 3.50; S, 9.52%; mol wt, 315.00 (Rast). Calcd for $C_{18}H_{12}O_4S$: C, 66.66; H, 3.70; S, 9.87%; mol wt, 324.

The preparation of rest of the dyes, given in Table 1 has been done in the identical manner as already described.

*Paper Chromatography of Dye (**11**).* On test paper Whatman No. 1, 1-butanol–ammonia was allowed to run for 13 h (descending) to give two corresponding red-pink spots of the dye (**11**) and reference dye phenolphthallein, R_f: (**11**), 0.89, phenolphthalein, 0.91 (lit,[26] R_f, 0.92).

*Acetylation of Dye (**12**).* The dye (XII) (1.0 g) was refluxed with acetic anhydride (15 ml) and fused sodium acetate (3.0 g) at 130—140 °C for 4 h to give yellowish white microcrystalline diacetyl compound (0.6 g), mp, 175—176 °C (from rectified ethanol). It is soluble in ethanol, acetone, and acetic acid. Found: C, 64.92; H, 3.65; S, 7.60; acetyl, 20.70%. Calcd for $C_{22}H_{16}O_6S$ or $C_{18}H_{10}O_4S$ $(COCH_3)_2$: C, 64.70; H, 3.92; S, 7.84; Acetyl, 20.58%.

*Bromination of Dye (**12**).* The dye (XII) (1.0 g) and 10% solution of bromine in acetic acid (10 ml) were refluxed at 130—140° for 1 h. The reaction mixture on cooling and dilution with water gave brick red dibromo compound (1.0 g), mp 235 °C (from rectified ethanol). The ethanolic solution of the dibromo compound is red with light green fluorescence which is intensified on addition of alkali. Found: Br, 33.32%. Calcd for $C_{18}H_{10}O_4SBr_2$: Br, 33.15%.

*Caustic potash treatment of Dye (**12**).* The dye (XII) (1.5 g) was taken in a platinum cruciblle and mixed with a paste of caustic potash pellets (10.0 g). The contents were heated at aobut 250 °C for 3 h until the red color of the dye disappeared completely. The residue was cooled and dissolved in water (50 ml) and filtered. The excess of alkali was just neutralized by dilute hydrochloric acid when a yellowish brown residue (A) settled down which was filtered and washed with water. The filtrate was further acidified by adding an excess of hydrochloric acid giving a white residue (B); it was also filtered and washed with water. The filtrate was shaken with ether and on evaporation of excess of solvent a brownish red residue (C) was obtained. Residues A, B, and C were identified as unreacted residual dye (**12**), acid (**6**), and resorcinol (**19**) respectively by direct comparison (m. m. p, co-TLC, co-IR) with their authentic samples.

References

1) P. R. Jones, *Chem. Rev.*, **63**, 465 (1963).
2) K. Von Auwers and Heinge, *Ber.*, **52**, 584 (1919).
3) I. Heilbron and H. M. Bunbury, "Dictionary of Organic Compounds," Oxford Univ. Press, New York (1953), Vol. 3, p. 178.
4) S. Gabriel, *Ber.*, **14**, 919 (1881).
5) P. R. Jones and S. L. Congdon, *J. Am. Chem. Soc.*, **81**, 4291 (1959).
6) R. C. Martin, *J. Am. Chem. Soc.*, **38**, 1142 (1916).
7) M. S. Newman and C. D. McCleary, *J. Am. Chem. Soc.*, **63**, 1537 (1941).
8) M. S. Newman and C. W. Muth, *J. Am. Chem. Soc.*, **73**, 4627 (1951).
9) P. M. Maginnity and T. G. Gair, *J. Am. Chem. Soc.*, **74**, 4958 (1952).
10) H. Burton and D. A. Munday, *Chem. Ind.*, **1956**, 316; *J. Chem. Soc.*, **1957**, 1727; G. Cauquil, H. Barrera, and R. Barrera, *Bull. Soc. Chim. Fr.*, **1951**, 173.
11) F. Ullman, *Ann.*, **17**, 291 (1896).
12) Y. K. Syrkin, *Russ. J. Phys. Chem.*, **17**, 347 (1943); *Chem. Abstr.*, **38**, 5701 (1944).
13) R. Kuhn and H. Schretzmann, *Chem. Ber.*, **90**, 557 (1957).
14) S. Dutt and J. F. Thorpe, *J. Chem. Soc. (London)*, **125**, 2524 (1924).
15) E. Ott, *Ann.*, **392**, 245 (1912).
16) E. Singh and P. C. Gupta, *Ann. Chim.*, **6**, 427 (1971).
17) E. Singh and P. C. Gupta, *Ann. Chim.*, **7**, 359 (1972).
18) E. Singh and P. C. Gupta, *Z. Naturforsch*, **27**, 405 (1972).
19) P. C. Gupta, R. Gopal, and S. P. Garg, *J. Indian Chem. Soc.*, **50**, 410 (1973).
20) R. Gopal, P. C. Gupta, and S. P. Garg, *Z. Naturforsch*, **28**, 468 (1973).
21) R. Gopal, P. C. Gupta, and S. P. Garg, *Bull. Chem. Soc., Jpn.*, **47**, 1789 (1974).
22) R. Gupal, P. C. Gupta, and S. P. Garg, *Bull. Chem. Soc. Jpn.*, **48**, 2227 (1975).
23) R. Gopal, P. C. Gupta, and S. P. Garg, *Bull. Chem. Soc. Jpn.*, **49**, 2077 (1976).
24) Steinkopf, *Ann.*, **94**, 407 (1915).
25) M. M. Brubacker and R. Adams, *J. Am. Chem. Soc.*, **49**, 2279 (1927).
26) M. M. Hubacher, *J. Am. Chem. Soc.*, **65**, 1655 (1943).

Ortho Effects in Organic Molecules on Electron Impact. VIII. Intramolecular Aromatic Substitution in (Arylmethylene)barbituric Acids

Devalla Venkata RAMANA* and Somayajula KASI VISWANADHAM
Department of Chemistry, Indian Institute of Technology, Madras-600 036, India

(Received January 14, 1980)

Mass spectral decomposition process involving intramolecular aromatic substitution with the ejection of either the hydrogen or the substituent in the ortho position from the $M^{+\cdot}$ ion is noticed in the eleven 5-(arylmethylene)barbituric acids studied. It has been generally noticed that for such a cyclization to occur, the presence of an α,β-unsaturated carbonyl function, in conjugation with the ring, is essential in aromatic systems.

The mass spectral behaviour[1-5] of cinnamic acid, methyl cinnamate, benzylideneacetophenone, and benzylideneacetone is characterized by the formation of intense $M-H^{\urcorner+}$ ion. An intramolecular cyclization mechanism has been proposed for the above mentioned decomposition process leading to a benzopyrylium ion. Similar observation has also been made in the case of *o*-methoxycinnamic acid[6] and alkyl *o*-chlorostyryl ketones.[7] In order to understand this process more clearly and to establish the generality of this process, the mass spectral study of 5-(arylmethylene)barbituric acids has been chosen in the present work, where the carbonyl function is a part of the ring system.

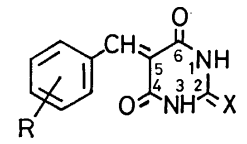

	R	X
I	H	O
II	H	S
III	o-Cl	O
IV	p-Cl	O
V	o-NO_2	O
VI	m-NO_2	O
VII	o-OCH_3	O
VIII	p-OCH_3	O
IX	m-OH	O
X	p-OH	O

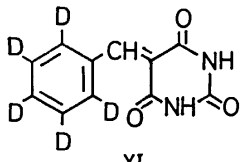

XI

Scheme 1.

Results and Discussion

The mass spectra of all the substituted (arylmethylene)barbituric acids (I—XI) (Scheme 1) present intense molecular ions except in the case of the ortho-isomers. The expected intense $M-H^{\urcorner+}$ or $M-R^{\urcorner+}$ (in the case of the ortho substituent) ions are noticed in all the spectra. In fact, in the case of *o*-chloro(III) and *o*-nitro(V) compounds, the molecular ion is non-existent and the $M-R^{\urcorner+}$ ions happen to be the base peaks. A cyclization mechanism involving an intramolecular aromatic substitution is being proposed for the formation of the above mentioned ions. It is envisaged that the oxygen of the heterocyclic ring attacks the ortho-carbon atom of the phenyl ring giving rise to a cyclized molecular ion, which then expels either the ortho hydrogen or the substituent affording the intense ion 'a' (Scheme 2). That the hydrogen, which is expelled for the formation of 'a' comes from the phenyl ring is substantiated by the fact that the compound(XI) gives exclusively $M-D^{\urcorner+}$ on electron impact and the $M-H^{\urcorner+}$ ion in this compound is totally absent. Furthermore, that the cyclization takes place with the ortho-carbon is supported by the observation that only the ortho substituents are lost during this mode of fragmentation, while in the case of meta- and para- isomers $M-H^{\urcorner+}$ ion only is noticed. These observations provide indirect proof for the mechanism suggested for the formation of the ion 'a'. The driving force for the cyclization appears to be the formation of the stable ion 'a', which is fully conjugated.

The other general mass spectral fragmentation processes noticed in these compounds are the formation of the ion 'b', by the ejection of a NHCO moiety from 'a', and the fragments 'c' and 'd' from the molecular ion (Scheme 3). Although no metastable evidence is seen for the formation of 'c' and 'd' directly from the $M^{+\cdot}$ ion, these ions are shifted to *m/z* 134 and *m/z* 107 (Table 1) respectively in the d_5-compound(XI), while the ion 'b' is shifted only the *m/z* 176. That the NHCO, that is expelled from 'a' for the formation

TABLE 1. PARTIAL MASS

Ions		I	II	III	IV	V	VI	VII	VIII	IX
				Cl^{35}	Cl^{35}					
$M^{+\cdot}$	Rel Int	70	100	0.33	86	—	70	20	100	100
	(*m/z*)	(216)	(232)	(250)	(250)	(261)	(261)	(246)	(246)	(232)
a	Rel Int	100	55	100	100	100	45	100	56	75
	(*m/z*)	(215)	(231)	(215)	(249)	(215)	(260)	(215)	(245)	(231)
b	Rel Int	64	16	70	55	78	22	60	43	52
	(*m/z*)	(172)	(172)	(172)	(206)	(172)	(217)	(172)	(202)	(188)
c	Rel Int	14	10	3	28	—	7	2	11	20
	(*m/z*)	(129)	(129)	(163)	(163)	—	(174)	(159)	(159)	(145)
d	Rel Int	25	45	6	38	—	—	5	11	19
	(*m/z*)	(102)	(102)	(136)	(136)	—	—	(132)	(132)	(118)

of the fragment 'b', is from the 1 and 2 positions of the hetero ring is adduced from the fact that compound II loses exclusively NHCS from 'a' but not the NHCO moiety.

In order to examine the general nature of the electron impact cyclization process, the mass spectra of compounds XII—XIX (Scheme 4) were studied. The mass spectra of cinnamyl alcohol[8,9] and cinnamyl phenyl ether(XII) do not show any prominent M–H^{+} ion indicating that the alcohol and ether oxygens do not readily take part in the cyclization reaction. The base peak in the mass spectrum of 2-benzylidene-1,3-indandione(XVIII) is the M–H^{+} ion, suggesting that the cyclization process is very facile in this compound. Furthermore, 5,5,5′,5′-tetramethyl-2,2′-benzylidenedi(1,3-cyclohexanedione) eliminates a molecule of dimedone during the electron impact[10] giving rise to an intense fragment at m/z 228 (72%) which corresponds to the molecular ion of 2-benzylidene-5,5-dimethyl-1,3-cyclohexanedione. This ion loses a hydrogen radical to give the base peak for which a cyclized structure has been proposed. Cinnamamide(XIII), whose mass spectrum was not studied hitherto, showed M–H^{+} ion as the base peak. This observa-

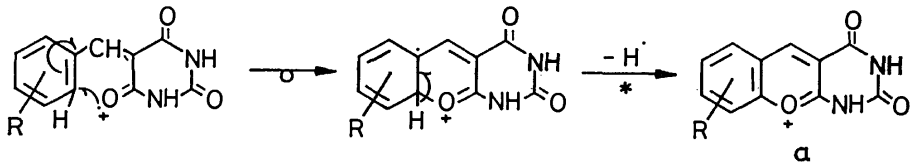

Scheme 2.

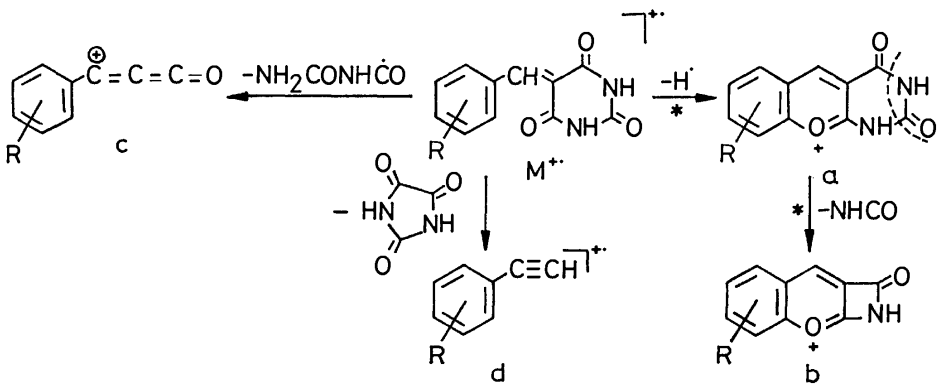

Scheme 3.

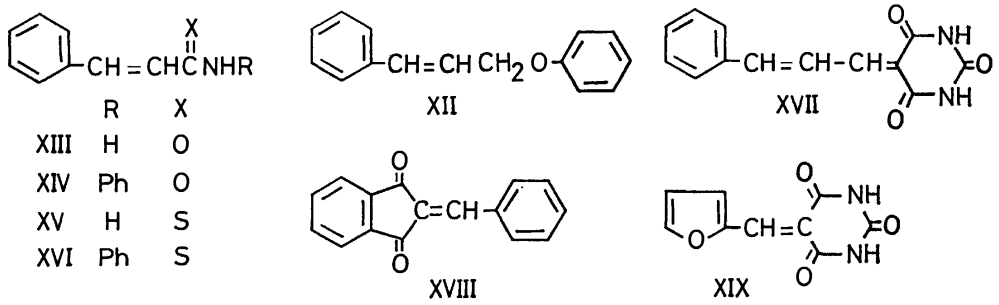

Scheme 4.

SPECTRA OF COMPOUNDS I—XIX

X	XI	XII	XIII	XIV	XV	XVI	XVII	XVIII	XIX
100 (232)	100 (221)	2 (210)	78 (147)	31 (223)	64 (163)	59 (239)	100 (242)	64 (234)	100 (206)
75 (231)	97 (219)	—	100 (146)	1 (222)	100 (162)	53 (238)	—	100 (233)	—
59 (188)	63 (176)	—	—	—	—	—	—	—	—
19 (145)	28 (134)	—	—	—	—	—	—	—	—
19 (118)	42 (107)	—	—	—	—	—	—	—	—

tion, together with the earlier ones reveal that any carbonyl oxygen (aldehyde, ketone, acid, ester, and amide) takes part readily in the cyclization in the absence of any other facile fragmentation process. However, the loss of $H\cdot$ from the $M^{+\cdot}$ of cinnamanilide-(XIV) is not a facile process, perhaps, due to a more favourable α-cleavage with respect to the carbonyl function, which leads to stable species. On the contrary the thioanalogues XV and XVI of XIII and XIV respectively exhibit more intense $M-H^{\urcorner+}$ ions in their mass spectra (Table 1). In fact the ratio of the intensity of the $M-H^{\urcorner+}$ ion with that of the $M^{+\cdot}$ ion $[(M-H^{\urcorner+})/(M^{+\cdot})]$ is 1.28 for XV and 1.563 for XVI. This may, most probably, be due to the greater size and the lower electronegativity of the sulfur atom.

The formation of six-membered ring during the cyclization reaction is energetically more favourable than the formation of an eight-membered ring and hence the mass spectrum of XVII does not contain any $M-H^{\urcorner+}$ ion. It is also noticed that 5-furfurylidenebarbituric acid(XIX) does not eject a hydrogen radical from the molecular ion implying that an aromatic hydrogen is required for the cyclization process. 3-Phenylpropionic acids and their corresponding methyl esters, where the double bond in the side chain is reduced, do not lose[11] any hydrogen radical from the $M^{+\cdot}$ on electron impact suggesting that the α,β-unsaturation is necessary for the cyclization process to occur.

From these observations, it can be generalized that the cyclization of the type discussed above becomes facile in the presence of an α,β-unsaturated carbonyl function in conjugation with the aromatic ring and in the absence of other favourable competing fragmentation processes.

Experimental

All the compounds discussed in this work are known in literature and were prepared by the methods already reported.[12,13] The purity of all the compounds was confirmed by TLC. The mass spectra were taken on a VARIAN MAT CH-7 mass spectrometer. The spectra were run at 70 eV with the emission current of 100 μA. The temperature of the ion source was 125 °C. The samples were introduced into the mass spectrometer through direct probe insertion at temparatures between 100 °C—170 °C.

One of us (S. K. V.) thanks the C. S. I. R., New Delhi (India), for a fellowship.

References

1) J. Ronayne, D. H. Williams, and J. H. Bowie, *J. Am. Chem. Soc.*, **88**, 4980 (1966).
2) Helmut Schwarz, "Topics in current chemistry," Springer-Verlag, Berlin, Heidelberg and New York (1978), Vol. 73, p. 231.
3) H. Budzikiewicz, C. Djerassi, and D. H. Williams, "Mass Spectrometry of Organic Compounds," Holden-Day Inc., Sanfrancisco (1967), p. 202.
4) E. M. Emery, *Anal. Chem.* **32**, 1495 (1960).
5) Bernd Schaldach, Ph. D., Dissertation, University of Bielefeld, W. Germany, 1976.
6) D. V. Ramana and M. Vairamani, *Indian J. Chem.*, **14B**, 448 (1976).
7) P. J. Smith, J. R. Dimmock, and W. G. Taylor, *Can. J. Chem.*, **50**, 871 (1972).
8) E. F. H. Brittain, J. P. Kelly, and W. L. Mead, *Org. Mass. Spectrom.*, **2**, 325 (1969).
9) Helmut Schwarz, Claus Koppel, and Ferdinand Bohlmann, *Org. Mass. Spectrom.*, **7**, 881 (1973).
10) D. J. Blythin and E. S. Waight, *J. Chem. Soc., C*, **8**, 993 (1968).
11) J. A. Ballantine and R. F. Curtis, *Org. Mass. Spectrom.*, **3**, 1215 (1970).
12) V. M. Vvedenskii, *Khim Geterotsikl Soedin*, **6**, 1092 (1969); *Chem. Abstr.*, **72**, 111406t.
13) N. Pravdic and V. Hann, *Croat. Chem. Acta.*, **34**, 85 (1962); *Chem. Abstr.*, **57**, 12378a.

Synthesis of Some Disperse Anthraquinone Dyes

Saoud A. M. METWALLY,* Mohamed S. K. YOUSSEF, and Mansour I. YOUNES
Chemistry Department, Assiut University, Assiut, Egypt

(Received October 22, 1979)

1-Hydroxy- and/or 1-aminoanthraquinones was allowed to react with formaldehyde in an alkaline medium to give 1-hydroxy- or 1-amino-2-hydroxymethyl-9,10-anthracenediols, which gave by air oxidation, (hydroxymethyl) anthraquinone derivatives. Interaction of 1-amino-2-(hydroxymethyl)anthraquinone or its 4-bromo derivative with carbonyl compounds in the presence of an acid catalyst gave 1,3-oxazine derivatives (**2**). The methylene group in position-2 of the 1,3-oxazine ring was found to be highly reactive and reacted with carbonyl compounds to form the corresponding 2-arylmethylene derivatives. Selective oxidation of dimethyloxazine derivatives with SeO_2 gave the corresponding dialdehyde, which interacted with aromatic amines to give the corresponding Schiff's bases. The bromine atom in the 6-position of **2** was easily replaced by aromatic amines to give blue disperse dyes.

Originally introduced as dyes for acetate fibers, disperse anthraquinone dyes are now used for a wide range of fiber types, such as polyamide, polyester, triacetate, and acrylics. The lightfastness of this class of disperse dyes is dependent on the substrate. Dyeings on acetate exhibit marginally higher lightfastness than those on nylon 66, while those on polyester are highest. Giles and Rahman[1] suggest that one parameter controlling the lightfastness of a disperse-dyed fiber is the regain of the substrate. Hence the rate of photofading on polyester may be retarded because access of water vapour to the dye particle is restricted.

Most anthraquinone disperse dyes contain either one or two amino groups (free or substituted), usually in the 1- and 4-positions. The substitution pattern can have a marked effect on the lightfastness of such dyes as shown by nature and position of both *N*- and nuclear substituents.[2] The aim of this work is to prepare some new disperse anthraquinone dyes provided by annellation of heterocyclic moiety namely the oxazine ring to the anthraquinone nucleus. The selection of oxazine ring is based on the fact that little is known in the literature concerning the structural factors that influence their application as disperse dyes for synthetic fibers. This paper is devoted for the chemistry of these dyes, while application and factors affecting fastness properties on synthetic fibers will be delt later. An extension of this area of investigation will be a comparison of the electron impact-induced fragmentation patterns of these dyes with their lightfastness on polyester.

1-Hydroxy- and 1-aminoanthraquinones react in an alkaline medium with formaldehyde or formaldehyde/aliphatic amines to give 2-(hydroxymethyl)- or 2-(aminomethyl)-substituted 9,10-anthracenediols which undergo an intramolecular redox reaction to yield the corresponding methyl-substituted anthraquinones.[3] If the reaction is interrupted by oxidation, (hydroxymethyl)- or (aminomethyl)anthraquinones can be isolated[4] (*cf.* Table 1). Interaction of carbonyl compounds with 1-amino-2-(hydroxymethyl)anthraquinone or its 4-bromo derivative in the presence of dilute hydrochloric acid as a catalyst gave 1,3-oxazine derivatives (**2**).[5] The reaction mechanism probably involves an amino aldehyde addition reaction to give intermediate (a) which under acidic conditions loses water to form the carbonium ion (b). Deprotonation of this ion leads to the 1,3-oxazine derivatives (**2**). The reaction course can be represented as follows:

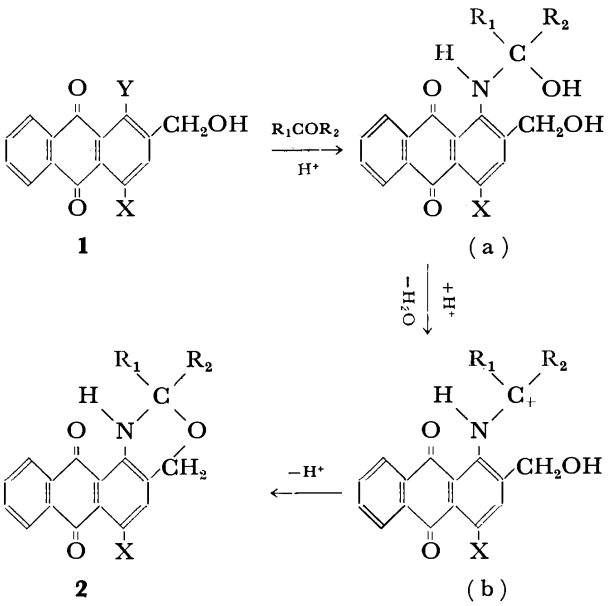

In favour of the formation of the postulated carbonium ion intermediate in the proposed mechanism is the fact that such reactions occured faster and with higher yields in case of ketones which gave the more stable tertiary carbonium ion. With formaldehyde, the reaction was found to be the lowest among the other aldehydes.

The 1,3-oxazine ring is responsible for a considerable bathochromic shift in the absorption spectra of such derivatives as compared with the starting 1-amino-2-(hydroxymethyl)anthraquinones. The IR spectra indicated the presence of NH absorption bands beside the methylene hydrogen (*cf.* Table 2).

The methylene group in the oxazine nucleus proved to be active and react with carbonyl compounds in the presence of anhydrous zinc chloride as a catalyst to give the corresponding 2-arylmethylene derivatives (**3**). The reaction can be represented as follows:

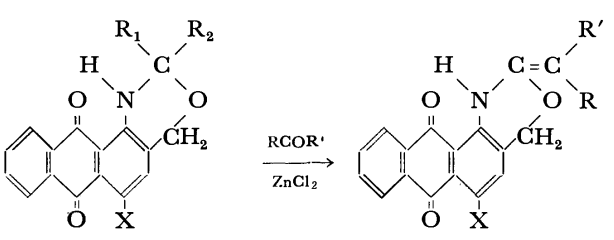

TABLE 1. (HYDROXYMETHYL)ANTHRAQUINONE DERIVATIVES (**1**)

X	Y	Z	Mp °C	Solvent of crystallization[a]	Yield %	Mol formula	N/%[b] Calcd	N/%[b] Found	λ_{max}^{EtOH}/nm (log ε)
H	NH_2	H	200—201	A	95	$C_{15}H_{11}O_3N$	5.53	5.50	472 (3.86)
NH_2	NH_2	H	224—227	B	49	$C_{15}H_{12}O_3N_2$	10.44	10.22	548 (4.16)
H	NH_2	NH_2	210	C	14	$C_{15}H_{12}O_3N_2$	9.39	9.60	—
Cl	NH_2	NH_2	242	C	22	$C_{15}H_{11}O_3NCl$	4.87	4.82	475 (3.86)
Br	NH_2	H	242	D	94	$C_{15}H_{10}O_3NBr$	4.22	4.17	472 (3.86)
H	OH	H	210—212	B	60	$C_{15}H_{10}O_4$	—	—	408 (3.83)
OH	OH	H	203—205	C	38	$C_{15}H_{10}O_5$	—	—	480 (3.98)

a) A, Ethanol; B, acetone; C, benzene; D, toluene. b) Satisfactory analyses for C, H, and Br were obtained.

TABLE 2. 1,3-OXAZINE DERIVATIVES (**2**)

R_1	R_2	Mp °C	Solvent of crystallization[a]	Yield %	Mol formula	N/%[b] Calcd	N/%[b] Found	λ_{max}^{EtOH}/nm (log ε)	ν (IR) cm^{-1}
H	H	250	A	85	$C_{16}H_{10}O_3NBr$	4.07	4.33	489 (3.69)	N-H 3320 C-O 1080
C_6H_5	C_6H_5	215	B	76	$C_{28}H_{18}O_3NBr$	2.82	3.20	488 (3.74)	N-H 3240 C-O 1090
H	C_4H_3O	183	C	82	$C_{20}H_{13}O_4NBr$	3.41	2.99	486 (3.69)	N-H 3260 C-O 1100
H	$C_{14}H_8NO_2$	168	D	72	$C_{30}H_{17}O_5N_2Br$	3.01	3.06	488 (4.14)	N-H 3300 C-O 1090
H	*p*-$(CH_3)_2N$-C_6H_4	120	B	82	$C_{24}H_{19}O_3N_3Br$	6.05	6.50	480 (3.56)	N-H 3340 C-O 1090
H	*o*-Cl-C_6H_4	95	E	86	$C_{22}H_{14}O_3NClBr$	3.07	2.91	486 (3.81)	N-H 3300 C-O 1080
H	*p*-NO_2-C_6H_4	220	D	92	$C_{22}H_{13}O_5N_2Br$	6.02	6.17	486 (4.77)	N-H 3300 C-O 1100
CH_3	CH_3	160—162	E	92	$C_{18}H_{14}O_3NBr$[1]	3.77	3.65	490 (3.88)	N-H 3290 C-O 1100
H	*o*-HO-C_6H_4	210	D	82	$C_{22}H_{14}O_4NBr$	3.21	3.11	482 (3.91)	N-H 3280 C-O 1090
H	*p*-Cl-C_6H_4	180—182	E	80	$C_{22}H_{14}O_3NClBr$	3.07	3.62	478 (3.95)	N-H 3280 C-O 1100
H	*p*-HO-C_6H_4	223—225	F	82	$C_{22}H_{14}O_4NBr$	3.21	3.45	478 (3.95)	N-H 3280 C-O 1060
H	*p*-CH_3-C_6H_4	260	G	78	$C_{23}H_{16}O_3NBr$	3.22	3.44	478 (3.89)	N-H 3320 C-O 1100
H	*m*-NO_2-C_6H_4	235	D	78	$C_{22}H_{13}O_5N_2Br$	6.02	6.64	482 (3.91)	N-H 3280 C-O 1060
H	*o*-NO_2-C_6H_4	230—232	D	80	$C_{22}H_{13}O_5N_2Br$	6.02	6.54	478 (3.96)	N-H 3280 C-O 1100
H	C_6H_5	220	D	83	$C_{22}H_{14}O_3NBr$	3.33	2.99	488 (3.86)	N-H 3300 C-O 1080
H	C_2H_5	186	D	88	$C_{18}H_{14}O_3NBr$	3.78	3.88	488 (4.64)	N-H 3300 C-O 1100
H	*p*-CH_3O-C_6H_4	220	G	90	$C_{23}H_{16}O_4NBr$	3.11	3.45	488 (3.93)	N-H 3300 C-O 1090
H	*m*-HO-C_6H_4	230	G	88	$C_{22}H_{14}O_4NBr$	3.21	3.41	488 (3.93)	N-H 3300 C-O 1080
CH_3	C_6H_5	208	G	80	$C_{23}H_{16}O_3NBr$	3.22	3.15	477 (3.89)	N-H 3290 C-O 1080
C_6H_5	CH-C_6H_5 OH	135	D	78	$C_{29}H_{20}O_4NBr$	2.66	3.03	488 (3.64)	N-H 3300 C-O 1080
H	H	162		82	$C_{16}H_{11}O_3N$[2]	5.28	4.94	495 (3.95)	
CH_3	CH_3	155		91	$C_{18}H_{15}O_3N$[1]	4.77	4.71	494 (3.92)	
H	CH_3	172		91	$C_7H_{13}O_3N$	5.02	5.12	494 (3.84)	
H	C_2H_5	183		85	$C_{18}H_{15}O_3N$	4.78	4.83	477 (4.02)	
H	C_6H_5	210		92	$C_{22}H_{15}O_3N$	4.10	4.23	498 (4.12)	

a) A, Toluene; B, benzene; C, dil methanol; D, dil acetic acid; E, acetone; F, dil ethanol; G, ethanol. b) Satisfactory analyses for C, H, and Br were obtained.

The resulting products are highly coloured and have high melting points. Their structures were established by elemental analyses as well as (IR) spectral data (*cf.* Table 3).

Oxidation of 2,2-dimethyl-1,2-dihydro-4*H*-anthra-[1,2-*d*][1,3]oxazine-7,12-dione or its 6-bromo analogue with selenium dioxide gave the corresponding dialdehyde derivatives (**4c, d**).

The dialdehyde derivative (**4d**) was found to be highly reactive and condense readily with *o*-phenylenediamine, *p*-aminophenol, and *p*-anisidine to give the corresponding Schiff's bases (**5e—g**), respectively.

1,3-Oxazine derivatives prepared in this work and

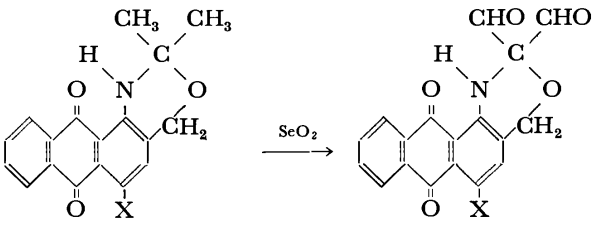

4

containing bromine atom in the 6-position were subjected to reaction with amines, whereby the bromine atom was substituted by amino group. The introduc-

TABLE 3. 2-ARYLMETHYLENE-1,3-OXAZINES (**3**)

R	R′	Mp °C	Solvent of crystallization[a)]	Mol formula	N%/[b)] Calcd	N%/[b)] Found	ν (IR) cm^{-1}
H	*p*-CH_3O-C_6H_4	260	A	$C_{24}H_{16}O_4NBr$	3.09	3.87	N-H 3400 C-O 1100 C=C 1660
H	*p*-CH_3-C_6H_4	270	B	$C_{24}H_{16}O_3NBr$	3.21	2.70	N-H 3400 C-O 1060 C=C 1660
H	*p*-HO-C_6H_4	280	C	$C_{23}H_{14}O_4NBr$	3.21	3.34	N-H 3400 C-O 1060 C=C 1670
H	*o*-Cl-C_6H_4	285—288	C	$C_{23}H_{13}O_3NBrCl$	3.00	2.54	N-H 3400 C-O 1100 C=O 1670
H	C_6H_5	295	C	$C_{23}H_{14}O_3NBr$	3.24	2.94	N-H 3400 C-O 1100 C=C 1670
H	*o*-HO-C_6H_4	235	A	$C_{23}H_{14}O_4NBr$	3.12	2.67	N-H 3400 C-O 1100 C=C 1660
C_6H_5	C_6H_5	300	C	$C_{29}H_{18}O_3NBr$	2.75	2·87	N-H 3400 C-O 1110 C=C 1660
H	C_5H_5O (2-furyl)	>300	D	$C_{21}H_{12}O_4NBr$	3.31	3.38	N-H 3400 C-O 1100 C=C 1670
CH_3	C_6H_5	305	E	$C_{24}H_{16}O_3NBr$	3.13	3.06	N-H 3400 C-O 1110 C=C 1665
H	$C_{14}H_8O_2N$ (1-amino-9,10-dioxo-2-anthryl)	270	A	$C_{31}H_{17}O_4N_2Br$	4.99	4.83	N-H 3390 C-O 1100 C=C 1670
H	*p*-NO_2-C_6H_4	283	C	$C_{23}H_{13}O_5N_2Br$	5.87	5.71	N-H 3390 C-O 1100 C=C 1660
H	*m*-HO-C_6H_4	290	A	$C_{23}H_{14}O_4NBr$	3.14	2.96	N-H 3400 C-O 1060 C=C 1670
H	*o*-NO_2-C_6H_4	265	C	$C_{23}H_{13}O_5N_2Br$	5.87	5.43	N-H 3400 C-O 1100 C=C 1680
H	*m*-NO_2-C_6H_4	280	F	$C_{23}H_{13}O_5N_2Br$	5.87	5.27	N-H 3420 C-O 1100 C-C 1670
H	*p*-Cl-C_6H_4	285	C	$C_{23}H_{13}O_3NBrCl$	3.00	3.27	N-H 3410 C-O 1100 C=C 1670

a) A, Dil acetic acid; B, toluene-pet. ether; C, DMF; D, pyridine; E, benzene-pet. ether; F, 1-butanol. b) Satisfactory analyses for C, H, and Br were obtained.

TABLE 4. BLUE ANTHRA[1,2-*d*][1,3]OXAZINE-7,12-DIONE DISPERSE DYES (**6**)

R_1	R_2	R	Mp °C	Yield %	Mol formula	N/%[a] Calcd	N/%[a] Found	λ_{max}^{EtOH}/nm (log ε)	ν (IR) cm^{-1}
CH_3	CH_3	C_6H_5	180	85	$C_{24}H_{20}O_3N_2$	7.29	7.36	620(4.02)	N-H 3290 C-O 1110
CH_3	C_6H_5	C_6H_5	170	82	$C_{29}H_{22}O_3N_2$	6.27	5.65	609(3.85)	N-H 3400 C-O 1090
C_6H_5	C_6H_5	C_6H_5	125	78	$C_{34}H_{24}O_3N_2$	5.51	5.80	608(3.79)	N-H 3400 C-O 1090
CH_3	CH_3	*o*-ClC_6H_4	120	68	$C_{24}H_{19}O_3N_2Cl$	6.69	6.46	578(3.96)	N-H 3410 C-O 1100
CH_3	C_6H_5	*o*-ClC_6H_4	130	60	$C_{24}H_{19}O_3N_2Cl$	5.85	5.36	608(3.84)	N-H 3400 C-O 1100

a) Satisfactory analyses for C, H, and Cl were obtained.

tion of the amino group in the 6-position changes the colour of the molecule to the intense blue shade. The reaction is carried out by heating the bromo derivative of 1,3-oxazines (**2**) with the amine derivative in an alkaline solution and in the presence of a copper salt as catalyst to give anthraquinone disperse dyes (**4**) (*cf.* Table 4). Such amination can be carried on the brominated 1-amino-2-(hydroxymethyl)anthraquinone derivative and the oxazine ring can be further constructed by the action of carbonyl compounds.

As the previously prepared anthraquinone derivatives are water insoluble they were tested as disperse dyes for dyeing synthetic fibers in shades ranging from yellowish brown to intense blue. Samples of polyamide, polyester and acrylic fibers were dyed satisfactory using these derivatives. A comprehensive application program involving such disperse dyes is now in progress with the aim of investigating the relation between structure, fastness properties, and dyeing behaviour. This forthcoming study will include a comparison of the electron impact induced fragmentation patterns of these dyes with their lightfastness on polyester fibers.

Experimental

The infrared absorption spectra were determined with a Unicam SP 1200 spectrophotometer using the KBr wafer technique. Absorption spectra in visible region were determined with a Unicam SP 8000 ultraviolet recording spectrophotometer. All melting points are uncorrected.

(Hydroxymethyl)anthraquinone Derivatives (1). Dissolve (0.1 mol) of 1-amino(or 1-hydroxy)anthraquinone derivatives in about 160 ml (0.1 mol dm^{-3} KOH) and 150 ml ethanol, warm the solution and pass nitrogen gas through it for about 15 min. Add formaldehyde solution (40%, 0.1 mol), followed by addition of sodium dithionite solution (0.1 mol in about 40 ml 0.2 mol dm^{-3} KOH) and pass nitrogen gas for further 12 min. The reaction mixture was oxidized by air for about 30 min. The product was filtered, dried and crystallized from the proper solvent. The results are given in Table 1.

1,3-Oxazine Derivatives (2). A mixture of 1-amino-2-(hydroxymethyl)-4-bromo (or non-brominated) anthraquinone (0.1 mol) and the carbonyl compounds (0.1 mol) was dissolved in dioxane (80 ml) in presence of 10 ml HCl (1 mol dm^{-3}). The mixture was concentrated, cooled and then added to excess of cold water. The product was filtered, washed with water and dried, then crystallised from suitable solvent. The results are listed in Table 2.

2-Arylmethylene-1,3-oxazines (3). A mixture of 6-bromo-1,2-dihydroanthra[1,2-*d*][1,3]oxazine-7,12-dione (250 mg, 0.1 mol) and the carbonyl compound (0.1 mol) was fused for about 5 min in the presence of anhydrous zinc chloride (0.5 g). The melt was triturated with ethanol to dissolve the excess aldehyde, then filtered, washed with hot water and dried. The product was crystallized from the proper solvent. The results are given in Table 3. 2,2-Diformyl-1,2-dihydro-4*H*-anthra[1,2-*d*][1,3]oxazine-7,12-dione and its 6-bromo-analogue (**4c, d**) and the corresponding Schiff's bases (**5e—g**).

0.01 Mol of the dimethyl derivative (II, $R_1=R_2=CH_3$; X=H or Br) was dissolved in ethanol and the solution was added to a solution of SeO_2 (0.02 mol) in ethanol. The reaction mixture was boiled under reflux for 1.5 h. The solution was cooled and the precipitated selenium was eliminated by filteration. The filtrate was concentrated and cooled, then the product was collected and crystallized from ethanol.

4c; mp 95 °C; ν NH 3300, ν C–O 1110, and ν –COH 1730 cm^{-1}. Found: N, 3.99%. Calcd for $C_{18}H_{11}NO_5$: N, 4.36%.

4d; mp 112 °C; ν N–H 3280, ν C–O 1110, and ν –C–H 1730 cm^{-1}. Found: N, 2.99%. Calcd for $C_{18}H_{10}NO_5Br$: N, 3.50%.

0.1 Mol of the dialdehyde (**4d**) was condensed with 0.2 mol of *o*-phenylenediamine, *p*-aminophenol and *p*-anisidine by the usual way to give the corresponding Schiff's bases (**5e—g**) respectively.

5e; mp 105 °C; ν NH 3400, ν C–O 1100, and ν C=N 1550 cm^{-1}. Found: N, 7.92%. Calcd for $C_{24}H_{14}O_3N_3Br$: N, 8.26%.

5f; mp 120 °C; ν NH 3290, ν C–O 1080, and ν C=N 1550 cm^{-1}. Found: N, 8.12%. Calcd for $C_{30}H_{20}O_5N_3Br$: N, 8.35%.

5g; mp 118 °C; ν NH 3300, ν C–O 1150, and ν C=N 1550 cm^{-1}. Found: N, 7.41%. Calcd for $C_{32}H_{23}O_5N_3Br$: N, 7.92%.

Blue Anthra[1,2-d][1,3]*oxazine-7,12-dione Disperse Dyes.* A mixture of 6-bromo-1,3-oxazine derivative (0.02 mol) and the amine derivative (0.02 mol) was dissolved in ethanol (50 ml). The solution was turned alkaline by the addition of sodium carbonate. Copper carbonate (1 g) was added and the reaction mixture was refluxed for 4 h, whereby the brown colour was changed to deep blue. The mixture was filtered while hot and the filtrate was concentrated and diluted with cold water to give a blue precipitate. It was

filtered, washed with water and dried. The product was crystallized from dilute ethanol. The results are given in Table 4.

Application of the Prepared Anthraquinone Derivatives as Disperse Dyes. These derivatives could be used for colouring synthetic fibers, *e.g.* polyamide. This is done by immersing the textile material in a dyebath containing an aqueous dispersion of these dyes and an ionic surface-active reagent. The dyeing process was performed by boiling for 45 min. The fibers are soaped and rinsed with cold water then dried and tested for light and wash fastness.

References

1) C. H. Giles and S. M. K. Rahman, *Text. Res. J.*, **31**, 1012 (1961).
2) K. Naiki, *Sen'i Gakkai Shi*, **15**, 203 (1959); *Chem. Abstr.*, **53**, 9675 (1959).
3) C. Marschalk, *Bull. Soc. Chim. Fr.*, **6**, 655 (1939).
4) K. Bredereck, S. A. Metwally, E. Koch, and R. Weckmann, *Ann. Chem.*, **1975**, 972.
5) S. A. Metwally and K. Bredereck, *Bull. Chem. Soc. Jpn.*, **48**, 2939 (1975).

Bulk Copolymerization of Acrylonitrile with α-Chloroacrylonitrile

Masao OKAMOTO* and Osamu ISHIZUKA

Department of Fiber and Polymer Engineering, Faculty of Engineering, Yamagata University, Jonan, Yonezawa 992

(Received April 18, 1980)

Synopsis. Copolymerization of acrylonitrile (M_1) with α-chloroacrylonitrile (M_2) was carried out at 60 °C using 4.3×10^{-2} mol% of α,α'-azobisisobutyronitrile. The four copolymers obtained were analyzed, their mole fractions of α-chloroacrylonitrile units being 0.196, 0.377, 0.532, and 0.722, and the monomer reactivity ratios r_1 and r_2 were found to be 0.31 and 3.25, respectively.

Copolymerization of acrylonitrile (M_1) with α-chloroacrylonitrile (CAN (M_2)) was carried out in order to obtain model compounds of chlorinated polyacrylonitrile. The monomer reactivity ratios r_1 and r_2 were evaluated by the Mayo-Lewis method.[1] So far the values have been reported only once.[2]

Experimental

Preparation of Copolymers. Commercial acrylonitrile and CAN were distilled in nitrogen atmosphere and then kept in a refrigerator. Both monomers were charged in the amounts given in Table 1 in the reaction vessel which was alternately evacuated with an oil pump and flushed with nitrogen. The bulk copolymerization was carried out at 60 °C in the presence of 4.3×10^{-2} mol% of α,α'-azobisisobutyronitrile (AIBN). The reaction vessel was sealed in order to prevent the loss of both monomers during the course of copolymerization, the reaction system being stirred magnetically. After the lapse of the required reaction time, hydroquinone was added in an amount equivalent to AIBN in order to terminate copolymerization. Copolymer was filtered, washed thoroughly with methanol, and finally dried in a vacuum at 30 °C to constant weight.

Chlorine Analysis. The method was reported in a previous work.[3]

Results and Discussion

The analytical data of products are summarized in Table 1. The mole fraction of CAN units in each copolymer was calculated by means of chlorine content. Figure 1 shows the relationship between the mole fraction obtained and that of CAN in monomer mixture at the start of reaction. Since the monomer concentrations, $[M_1]$ and $[M_2]$, at the time when polymerization ceased can be determined by means of the yield and the composition of copolymer, the lines on r_1-r_2 plots are obtained by means of Mayo-Lewis's integrated equation.[1] The lines have a common intersection near $r_1=0.31$, $r_2=3.25$, except for Experiments 6 and 7 in which light brown and brown products, respectively, were obtained. Coloration of the products in Experiments 2—5 was very faint. A side reaction would proceed simultaneously with copolymerization, being enhanced when the initial mole fraction of CAN is over 0.5.

Table 1. Copolymerization of acrylonitrile with CAN by AIBN at 60 °C

Expt No.	Reaction conditions: Acrylonitrile (M_1) / g	Reaction conditions: CAN (M_2) / g	Reaction conditions: Time / h	Analytical data of product: Yield / wt%	Analytical data of product: Chlorine content / wt%
1	20.15	0	0.25	4.7	0
2	18.13	2.75	10	22.0	11.60
3	16.12	5.39	24	9.7	20.25
4	14.10	8.25	48	4.8	26.40
5	10.07	13.76	19	2.9	32.85
6	8.06	16.51	24	4.3	33.45
7	4.03	22.02	24	4.6	33.37

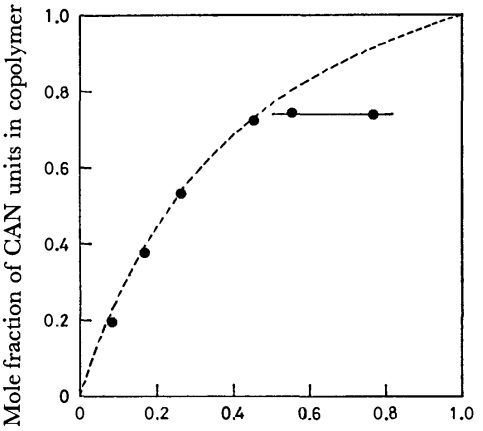

Fig. 1. Composition of copolymers.
A broken line is the initial copolymer composition curve for $r_1=0.31$, $r_2=3.25$.

In copolymers obtained in Experiments 2, 3, 4, and 5, the mole fractions of CAN units were 0.196, 0.377, 0.532, and 0.722, respectively. It seems that CAN units are distributed at random in the copolymer chain, since the reactivity ratio product (r_1r_2) is approximately equal to unity.

References

1) F. R. Mayo and F. M. Lewis, *J. Am. Chem. Soc.*, **66**, 1594 (1944).

2) "Vinyl and Diene Monomers, Part 1," ed by E. C. Leonard, John Wiley & Sons, Inc., New York (1970), p. 65.

3) M. Okamoto, C. Aoki, and O. Ishizuka, *Nippon Kagaku Kaishi*, **1977**, 103.

Interaction between Aromatics and Zinc Chloride. II. The Formation of σ-Complexes and Cation Radicals on Supported Zinc Chloride

Mikio MORITA,* Kunio HIROSAWA, Toshio SATO, and Koji OUCHI†

Government Industrial Development Laboratory, Hokkaido, 2-17 Tsukisamuhigashi, Toyohira-ku, Sapporo 061-01

†*Department of Applied Chemistry, Faculty of Engineering, Hokkaido University, Sapporo 060*

(Received June 11, 1979)

Synopsis. Anhydrous zinc chloride supported in the solid state was found to produce colored intermediates by reactions with aromatics (anthracene, naphthacene, pentacene, pyrene, pelyrene, and chrysene) at 60 °C. The measurements of their electronic absorption spectra and ESR spectra confirmed that these were the same aromatics–zinc chloride σ-complexes and aromatics cation radicals as those formed in molten zinc chloride.

It has been known that Lewis acids, such as boron trifluoride[1] and aluminum chloride,[2] react with aromatic hydrocarbons to form σ-complexes (electron donor–acceptor (EDA) complexes) and aromatics cation radicals. Our previous work revealed that molten zinc chloride also produced similar intermediates by means of reactions with aromatic hydrocarbons at higher temperatures.[3]

In order to advance further studies of the catalytic behavior of zinc chloride, we wish to confirm the reactivity of the aromatics–zinc chloride system with anhydrous zinc chloride supported on a porous Vycor glass at lower temperatures. Its high surface area and good transmission of light enabled us to measure better the electronic and ESR spectra.

The electronic absorption spectra of aromatics–zinc chloride colored complexes produced on the zinc chloride supported in the solid state were essentially similar to those of molten zinc chloride[3] and of aluminum chloride in the solid state.[2] Furthermore, the ESR signals were detected for the colored complexes. Based on these results, it was concluded that the zinc chloride supported in the solid state reacted directly with aromatic hydrocarbons to form the σ-complexes (EDA-complexes) and the cation radicals.

Experimental

Materials. The anthracene, naphthacene, pentacene, pyrene, perylene, chrysene, zinc metal, and silver chloride were all purchased and were all of a G. R. grade; they were used without further purification.

The rod of porous Vycor glass (Corning No. 7930) used as a support was ground to 100 mesh. The powdered Vycor glass was treated with a concd HNO_3 solution at room temperature overnight and washed with distilled water to remove foreign metal ions as impurities. Having been dried at 140 °C, it was heated in air at 600 °C for 6 h to burn off the organic contaminants. Its surface area was 154 m^2/g.

Preparation of Supported Zinc Chloride. Anhydrous zinc chloride was prepared by the reaction of zinc metal with siliver chloride at about 500 °C in a vacuum at 10^{-3} Torr and vaporized so as to be supported on the purified Vycor glass preliminarily heated at 500 °C for 4 h in a vacuum. The anhydrous zinc chloride content was 5—10 wt% in the present support.

Reaction. About 500 mg of the supported zinc chloride was transferred into a 1-mm-thick quartz cell in a vacuum and thoroughly mixed with 5 mg of an aromatic compound in the cell. After the cell had then been evacuated below 10^{-3} Torr, its neck was fused so as to seal it off. Then the cell was heated at a constant temperature above 60 °C. The formation of a colored product could be observed on the supported zinc chloride.

Electronic Spectra and ESR Signals. The electronic spectra of the colored products were measured at room temperature with a Hitachi 624 spectrometer equipped with an integrating sphere. The ESR signals were detected also at room temperature with a JES-ME-3X spectrometer for samples prepared in ESR tubes by a way similar to that described above.

Results and Discussion

The rate of the formation of aromatics–zinc chloride complexes was found to be depend on the aromatic hydrocarbon source. Under the present conditions, aromatic compounds with higher ionization potentials, such as benzene, naphthalene, and phenanthrene, could not be observed to form colored products. At higher temperatures and longer contact times, the transmittance of the samples gradually decreased and the characteristic absorption spectra of the complexes became obscure because of the formation of other compounds, such as condensed products of aromatics.

Figure 1 shows the absorption spectra of the colored products on the supported zinc chloride for anthracene, naphthacene, pentacene, pyrene, perylene, and chrysene; the positions of these absorption bands are summarized in Table 1 for comparison. These absorp-

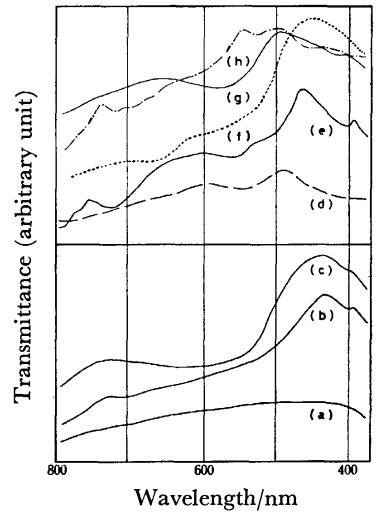

Fig. 1. Electronic absorption spectra of aromatics–$ZnCl_2$ complexes.
(a): Original, (b) and (c): anthracene at 60 °C for 10 min and for 120 min, (d): naphthacene, (e): pentacene, (f): chrysene, (g): pyrene, (h): perylene, each at 100 °C for 30 min.

Table 1. Comparison of the absorption bands of σ-complexes and radicals in supported zinc chloride with those in the molten zinc chloride, aluminum chloride, and Na–THF systems

Specie	Systems[a)]	Anthracene	Naphthacene	Pentacene	Pyrene	Perylene	Chrysene
σ-Complex	A	430	470	493	495	505	455
	B	425	460				
	C	420	468	440	481	637	
Radicals,	A	730	395, 755, 775			545, 635, 735	690
or ions	B	725	710				
	C	735	395, 670, 769				
	D	366, 705	398, 793	431, 847	492, 719	581, 675, 724	
				(unit; nm)			

a) A: zinc chloride supported on a porous Vycor glass, B: molten zinc chloride,[3)] C: aluminum chloride in the solid state,[2)] D: Na–THF.[5,6)]

tion bands disappeared when the colored products were placed in contact with water vapor.

The supported zinc chloride itself did not give any absorption band within the entire wavelength region measured in this work. When anthracene came in contact with the supported zinc chloride at 60 °C, a broad absorption band at 430 nm appeared at first, and then another absorption band developed at 730 nm after prolonged contact time. Similarly, in the reaction with the supported zinc chloride at 100 °C for 30 min, naphthacene gave three weak and sharp absorption bands at 395, 755, and 775 nm, in addition to a strong, broad absorption band at 470 nm and a broad absorption band at 650 nm. Pentacene gave two broad absorption bands at 493 and 590 nm; pyrene gave two broad absorption bands at 495 nm and 650 nm; perylene gave a strong absorption band at 505 nm, a strong sharp absorption band at 545 nm and two weak absorption bands at 635 and 735 nm, and chrysene gave two absorption bands at 455 and 690 nm.

σ- or EDA-Complex Formation. As may be seen in Table 1, the absorption bands observed at 430 nm for anthracene, at 470 nm for naphthacene, at 493 nm for pentacene, and at 495 nm for pyrene on the supported zinc chloride were found to be almost the same as those at 420 nm, at 468 nm, at 440 nm, and at 481 nm respectively of the corresponding aromatics–aluminum chloride complexes in the solid state.[2)] Furthermore, the absorption bands seen at 430 nm for anthracene and at 470 nm for naphthacene were consistent with those at 425 nm and at 460 nm of the corresponding aromatics–molten zinc chloride complexes.[3)] The colored complexes on solid aluminum chloride or in molten zinc chloride are assigned to the σ-complexes (π, v-, or EDA-complexes), and the characteristic absorption bands, to the charge-transfer ones.[2,3)]

Figure 2 shows the linear correlation between the characteristic absorption energy of the present complexes, $h\nu_{CT}$, and the ionization potential, I_D, of the corresponding aromatics; although the absorption energy of the pyrene– and chrysene–zinc chloride complexes and the slope of the line deviate somewhat from the law of the charge-transfer complexes,[4)] these aromatics–zinc chloride complexes seem to be EDA-complexes, *i.e.*, σ-complexes (*cf.* Ref. 3).

Ion or Radical Formation. When the colored complexes on the supported zinc chloride were treated at higher temperatures, the spectra changed to those characteristic to cation radicals. Except for perylene,

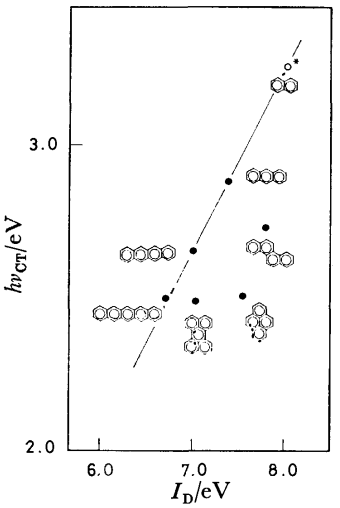

* Cited from Ref. 3.

Fig. 2. Relation between the position of CT bands and ionization potentials of donors.

all the present samples also gave a broad singlet paramagnetic signal whose *g*-value was about 2.0036 for anthracene, 2.0037 for naphthacene, 2.0031 for pentacene, 2.0031 for pyrene, and 2.0032 for chrysene. The perylene on the supported zinc chloride gave the same ESR spectrum, split into seven signals with equal hyperfine splitting (0.3 mT), as was detected on silica–alumina.[7)] The *g*-value was about 2.0038.

These findings support the idea that aromatics–cation radicals can be formed in the aromatics–supported zinc chloride system, where the radical cations are supposedly produced by the ionization of the σ- or EDA-complexes.

The assignment of the electronic spectra for cation radicals of the aromatics is well established.[3,5,6)] The positions of the bands are also summarized in Table 1.

Anthracene in molten zinc chloride gave another electronic absorption band at 620 nm;[3)] this band is attributed to the dipositive ion[5,7)] or to a secondary σ- or π-complex produced by anthracene and the anthracene–zinc chloride σ-complex.[8)] This band did not appear in the anthracene–supported zinc chloride system; therefore, such intermediates cannot be considered for the supported zinc chloride under the present conditions.

References

1) W. I. Aalbersberg, G. J. Hoijtink, E. L. Mackor, and W. P. Weijland, *J. Chem. Soc.*, **1959**, 3055.
2) H. H. Perkampus and T. Kranz, *Z. Phys. Chem., N. F.*, **34**, 213 (1962); **38**, 295 (1963).
3) M. Morita, K. Hirosawa, and T. Sato, *Bull. Chem. Soc. Jpn.*, **50**, 1256 (1977).
4) R. S. Mulliken, *J. Am. Chem. Soc.*, **74**, 811 (1952).
5) P. Balk, G. J. Hoijtink, and J. W. H. Scherurs, *Rec. Trav. Chim.*, **76**, 813 (1957).
6) K. H. Buschow, J. Dieleman, and G. H. Hoijtink, *J. Chem. Phys.*, **42**, 1993 (1965).
7) W. K. Hall, *J. Catal.*, **1**, 53 (1962).
8) H. Sato and Y. Aoyama, *Bull. Chem. Soc. Jpn.*, **46**, 631 (1973).

Relative Electron-capture Efficiency of Disubstituted Benzene in γ-Irradiated MTHF Glass at 77 K

Toshinari SHIMOKAWA

Tokyo Metropolitan Isotope Research Center, 2-11-1 Fukazawa, Setagaya-ku, Tokyo 158

(Received December 28, 1979)

Synopsis. The relative electron-capture efficiencies of disubstituted benzenes were measured by a competitive method. It was found that the efficiencies of the disubstituted benzenes are correlated with the reactivity towards nucleophilic species as expressed by Hammett's substituent constant. The logarithmic values of the efficiency are roughly proportional to the polarographic half-wave reduction potentials and to the electron affinities.

A number of investigations aimed at determining the rate constant of the electrons ejected by the irradiation of ionizing radiation with various compounds in aqueous and organic solutions have been performed by the competitive-reaction or pulse-radiolysis technique. In a previous paper,[1] a study was made of electron-capture reactions by polychlorinated benzenes and halogenated benzenes in MTHF glass at 77 K by a competitive method, and the relationship between the reactivity and the electron affinity of these molecules was discussed.

In this paper, the electron-capture efficiencies of many disubstituted benzenes relative to that of biphenyl will be determined in the MTHF glass, and the effects of the substituents on the efficiency will be described.

Experimental

The disubstituted benzenes, except for *p*-chlorobenzonitrile (an Eastman reagent chemical), were of a guaranteed grade and were obtained from the Tokyo Kasei Kogyo Co., Ltd. These chemicals were used without further purification. The measurement of the relative electron-capture efficiency was carried out by the competitive method, biphenyl being used as the reference material (0.04 M).[1,2] The sample preparation, γ-irradiation, and other experimental conditions were described in a previous paper.[1] (1 M = 1 mol/dm³)

Results and Discussion

The relative electron-capture efficiency, K_s/K_{ϕ_2}, and the ratio to the parent compound, K/K_0, are summarized in Table 1.

In a chlorobenzene series, the substituents, NO_2, $COCH_3$, and CN, markedly increased the efficiency for electrons. This result is consistent with the inductive effect of these substituents. The substitution of halogen atoms also increased the efficiency. The order of efficiency for halogen substituents was Br>Cl≫F.

On the other hand, all the electron-donating groups such as OH decreased the efficiency for electron-capture except for *p*-chlorotoluene. The decrease in the efficiency is generally in the order of $OH>OCH_3>CH_3$. This result is probably due to the resonance effect of the substituent on the ring.

In the other series, the effect of the substituent on the electron-capture efficiency is compatible with that obtained from the chlorobenzene series except for the nitrobenzene series. In the case of the nitrobenzene series, the secondary substituent scarcely changed the efficiency of the parent molecule at all.

Table 1. Relative electron-capture efficiency as determined by the competitive method

Compound	K_s/K_{ϕ_2} [a]	K/K_0 [b]	$-E_{1/2}$ [c]/V
Chlorobenzene	0.490	1	2.13
p-Nitro	12.2	24.9	1.08
p-Cyano	4.81	9.82	1.36
p-Acetyl	6.30	12.9	
p-Bromo	1.10	2.25	1.61
p-Chloro	1.03	2.10	1.81
m-Chloro	1.09	2.22	
p-Fluoro	0.569	1.16	
m-Fluoro	0.800	1.63	
p-Methyl	0.482	1.19	2.16
p-Methoxy	0.390	0.796	2.15
p-Hydroxy	0.270	0.551	
Bromobenzene	0.844	1	1.81
p-Iodo	2.73	3.24	1.08
p-Bromo	1.30	1.54	1.54
p-Chloro	1.10	1.30	1.61
p-Fluoro	0.840	0.995	
p-Methyl	0.735	0.871	1.84
p-Methoxy	0.667	0.790	1.84
p-Hydroxy	0.640	0.758	
Fluorobenzene	0.054	1	
p-Bromo	0.840	15.5	
p-Chloro	0.569	10.5	
p-Methyl	0.029	0.537	
Nitrobenzene	12.6	1	1.15
p-Chloro	12.2	0.968	1.08
p-Acetyl	12.8	1.02	
p-Methyl	11.8	0.936	
p-Methoxy	13.6	1.07	
Acetophenone	5.90	1	
p-Nitro	12.8	2.17	
p-Acetyl	10.9	1.85	
p-Bromo	7.20	1.22	
p-Chloro	6.30	1.07	
p-Methyl	5.82	0.986	
p-Methoxy	4.60	0.789	
p-Hydroxy	3.65	0.619	
Benzonitrile	2.40	1	2.17
p-Chloro	4.81	2.00	
p-Methyl	2.14	0.892	2.28
m-Methyl	3.10	1.29	2.22
p-Methoxy	1.30	0.542	

a) K_s/K_{ϕ_2}: Relative electron-capture efficiency (0.04 M biphenyl as reference). b) K/K_0: Ratio of the electron-capture coefficient for the parent molecule. c) Chlorobenzenes and bromobenzenes, Ref. 4; nitrobenzenes, Ref. 5; benzonitriles, Ref. 6.

In order to examine the substitution effects in detail, we attempted to determine whether or not the Hammett linear relation was applicable to the electron-capture reaction in MTHF glass. In Fig. 1, the log K/K_0 for a

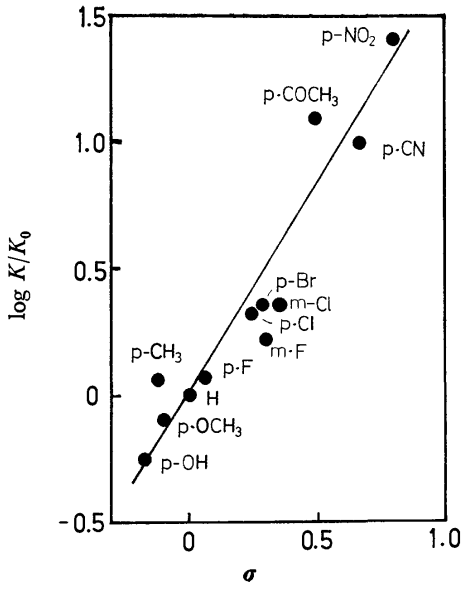

Fig. 1. Plot of log K/K_0 *vs.* Hammett substituent constant for a series of chlorobenzene.

series of chlorobenzene is plotted as a function of the Hammett substituent constant (σ).[3] A linear correlation between the log K/K_0 and σ was observed, and the reaction constant, ρ, was obtained as 1.58 from the slope. The Hammett linear relation also conforms to the electron-capture reactions of the other series except for the nitrobenzene and benzonitrile series. For the acetophenone, bromobenzene, and fluorobenzene series, the ρ values obtained in the same way are 0.49, 0.52, and 3.12 respectively. One can find that the ρ value decreases with an increase in the electron-capture efficiency of the parent molecule in the order of acetophenone, bromobenzene, chlorobenzene, and fluorobenzene.

In a previous paper,[1] it was found that the log $K_s/K_{\phi 2}$ of polychlorinated benzene correlated well with the polarographic half-wave reduction potential ($E_{1/2}$). In the forth column in Table 1, the $E_{1/2}$ values are also listed.[4-6] A good correlation between the log $K_s/K_{\phi 2}$ and the $E_{1/2}$ is observed in the case of disubstituted benzenes.

Streitwieser confirmed that the $E_{1/2}$ was well correlated to the electron affinity, A, for many aromatic hydrocarbons.[7] Therefore, it is possible to replace $E_{1/2}$ by A, and the plot of log $K_s/K_{\phi 2}$ against A was found to be roughly linear (Fig. 2). This linear correlation suggests that the initial process of the electron-capture is related to the lowest unoccupied orbitals of the molecule (LUMO), since the A value corresponds to the energy of LUMO.[8]

The correlation in Fig. 2 can be expressed by the following empirical equation:

$$\log K_s/K_{\phi_2} = 1.10A + 0.04 \quad (1)$$

However, the slope of the line in Fig. 2 greatly deviates from a predictable slope for a diffusional process in the gas phase.[1] In the case of the glassy state at low temperatures, a treatment similar to that in the gas phase may be inapplicable, for Kira and Imamura indicated that the electron-tunneling process is important in

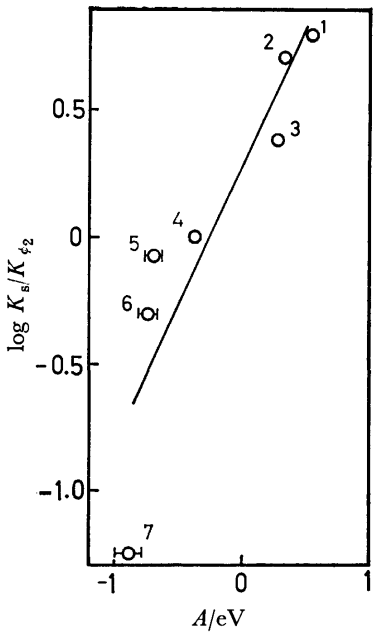

Fig. 2. Plot of log $K_s/K_{\phi 2}$ *vs.* the electron affinity for disubstituted benzenes.
1: *p*-$ClC_6H_4COCH_3$,[a] 2: $C_6H_5COCH_3$,[a] 3: C_6H_5CN,[a] 4: $C_{12}H_{10}$,[b] 5: C_6H_5Br,[c] 6: C_6H_5Cl,[c] 7: C_6H_5F.[c]
a) Thermal electron capture (Ref. 10). b) Theoretical (Ref. 11). c) Electron transmission spectroscopy (Ref. 12).

MTHF glass at 77 K.[9]

Although the relative electron-capture efficiency does not directly correspond to the absolute rate constant, the relative magnitude of these values in Table 1 is a measure of the effects of the substituent on the parent molecule. The present results, however, do not provide sufficient data for discussing the nature of the electron-capture process in organic glasses.

The author is grateful to Dr. Takeshi Sawai for his valuable discussion.

References

1) T. Shimokawa and T. Sawai, *Bull. Chem. Soc. Jpn.*, **50**, 3073 (1977).
2) W. H. Hamill, "Radical Ions," ed by E. T. Kaiser and L. Kevan, Wiley, New York (1968), Chap. 9.
3) D. H. McDaniel and H. C. Brown, *J. Org. Chem.*, **23**, 420 (1958).
4) J. W. Sease, F. G. Burton, and S. L. Nickol, *J. Am. Chem. Soc.*, **90**, 2595 (1968).
5) M. E. Peover, *Trans. Faraday Soc.*, **60**, 479 (1964).
6) H. Kojima and A. J. Bard, *J. Am. Chem. Soc.*, **97**, 6317 (1975).
7) A. Streitwieser, Jr., "Molecular Orbital Theory for Organic Chemists," Wiley, New York (1961), p. 173.
8) R. E. Buher, "The Chemistry of the Carbon-Halogen Bond," ed by Saul Patai, Wiley Interscience (1973), Part 2, Chap. 12.
9) A. Kira and M. Imamura, *J. Phys. Chem.*, **82**, 1966 (1978).
10) W. E. Wentworth, L. W. Kao, and R. S. Becker, *J. Phys. Chem.*, **79**, 1161 (1975).
11) S. Ehrenson, *J. Phys. Chem.*, **66**, 705 (1962).
12) K. D. Jordan, J. A. Michejda, and P. D. Burrow, *J. Am. Chem. Soc.*, **98**, 7189 (1976).

The Hydrolytic Rate of Barbituric Acid and the Extrathermodynamic Relationship

Shozo ASADA, Midori YAMAMOTO, and Jujiro NISHIJO*
Kobe Women's College of Pharmacy, Higashinada-ku, Kobe 658

(Received September 6, 1979)

Synopsis. The enthalpy-entropy relationship of activation was subjected to discussion in connection with the alkaline hydrolysis of 10 barbituric acids. The extrathermodynamic linear equation was derived by using several parameters; the dissociation constant (pK), the ^{13}C shift value [$\delta_c(5)$] at the 5-position of the ring, and/ or the molecular connectivity index (χ).

The alkaline hydrolysis of 5-substituted 5-ethylbarbituric acids (I) were investigated. It is known that Taft-type parameters can not be used to evaluate the substituent effects in this series of compounds.[1] Therefore, as physicochemical parameters which might reflect the electronic or steric effect of the substituent, the acid-dissociation constant (pK),[2] the value of the ^{13}C chemical shift [$\delta_C(5)$] at the 5-position,[3] and the molecular connectivity index (χ) given in the literature[4] were used to discuss them.

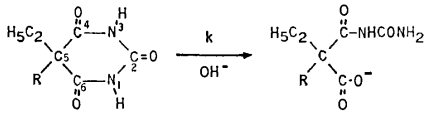

(I)

Experimental

Materials. Ten barbituric acids (I) described previously[5] were used; they are listed in Table 1. All the other chemicals were of an analytical grade.

Hydrolysis Procedures. An appropriate quantity of (I) was weighed in a volumetric flask, dissolved, and diluted with 0.4 mol dm^{-3} NaOH to produce 1×10^{-3} mol dm^{-3}. This flask was placed in a thermostatic water bath at 30, 40, or 50 $\pm$ 0.1 °C. Samples were withdrawn periodically and diluted with 0.4 mol dm^{-3} NaOH to produce a final barbiturate concentration of about 8×10^{-5} mol dm^{-3}. Spectrophotometric readings (A) at the absorption maximum (255 nm) were taken with a Hitachi Model UV-200 spectrophotometer. Plots of $\log(A-A_\infty/A_0-A_\infty)$ *vs.* the time were reasonably linear for each compound, where A_0 or A_∞ is the initial or the final asymptotic absorbance respectively. The apparent first-order rate constant (k) was obtained from the slope.

Calculation of the Molecular Connectivity Index (χ). The χ values were calculated using the previously reported method.[4] In the case of a double-bond structure, twice the value calculated as a double bond was taken into account. These values are listed in Table 2.

Results and Discussion

Relationship between Enthalpy and Entropy of Activation. According to the absolute rate theory, the enthalpy (ΔH^*) and entropy (ΔS^*) of activation[6] may be expressed by Eq. 1:

$$\log(k/T) = -(\Delta H^*/2.303RT) + (\Delta S^*/2.303R) + \log(k_B/h), \quad (1)$$

Table 1. Rate constants, k in h^{-1}, at three different temperatures in 0.4 mol dm^{-3} NaOH, and activation parameters for the hydrolyses of barbituric acids (I)

Compd No.	Substituent R	$10^3(k\pm SE)$[a] 30 °C	40 °C	50 °C	ΔH^* (kJ mol^{-1})	ΔS^*_{323} (J K^{-1} mol^{-1})
1	Ethyl	11.3 ±0.16	34.6 ±0.53	89.9 ±2.1	81.96	−79.75
2	Allyl	37.0 ±0.25	104.9 ±1.8	236.8 ±2.6	73.09	−99.16
3	Propyl	10.3 ±0.34	30.3 ±0.6	72.8 ±0.9	77.11	−96.52
4	3-Methyl-butyl	8.72 ±0.28	26.5 ±0.22	70.0 ±0.5	82.34	−80.75
5	1-Methyl-butyl	0.237 ±0.015	0.797 ±0.042	2.37 ±0.20	91.34	−81.09
6	1-Cyclo-hexenyl	1.30 ±0.09	3.09 ±0.29	10.1 ±0.6	80.75	−102.5
7	Cyclohexyl	0.267 ±0.018	0.877 ±0.036	2.65 ±0.17	90.92	−81.42
8	Phenyl	26.5 ±0.51	72.5 ±0.91	157.8 ±2.2	70.17	−111.5
9	Benzyl	7.80 ±0.18	23.9 ±0.41	62.8 ±0.8	82.42	−81.34
10	α-Methyl-benzyl	0.304 ±0.022	1.45 ±0.17	4.93 ±0.42	93.22	−69.50

a) The rate constants were determined at least in duplicate. The values are averaged. Standard errors were calculated from a linear regression analysis of the data.

Table 2. Acid dissociation constant (pK), ^{13}C chemical shift [$\delta_C(5)$] at the 5-position, molecular connectivity index (χ), and log k at 50 °C of barbituric acids (I)

Compd No.	pK[a]	$\delta_c(5)$[b]	χ[c]	log k
1	12.03	56.6	2.121	−1.046
2	11.98	55.8	2.639	−0.626
3	12.06	55.9	2.621	−1.138
4	12.13	55.8	3.477	−1.155
5	12.38	59.3	3.542	−2.625
6	11.89	61.5	4.150	−1.996
7	12.32	59.5	4.166	−2.577
8	11.60	60.0	4.177	−0.802
9	12.21	57.8	4.634	−1.202
10	12.52	60.1	5.081	−2.307

a) The apparent second acid-dissociation constants were determined by spectrophotometry at 20 °C for the ionic strength of 0.75. b) These values were reported previously.[5] c) The values are computed from the partial structure:

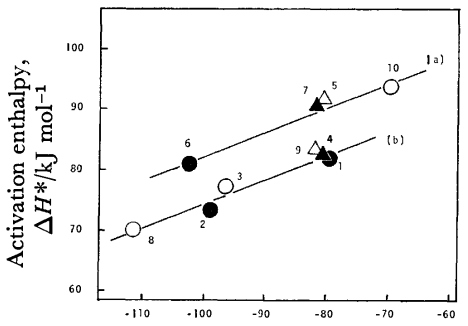

Fig. 1. Plots of the compensation effect of activation parameters.
Numbers adjacent to the marks indicate the compound numbers listed in Table 1.
Line (**a**): $\Delta H^* \times 10^3 = 122.3(\pm 5.9) \times 10^3 + 398(\pm 69)\Delta S^*$, $n=4$, $\gamma=0.971$; Line (**b**): $\Delta H^* \times 10^3 = 114.5(\pm 3.8) \times 10^3 + 401(\pm 39)\Delta S^*$, $n=6$, $\gamma=0.981$.

where k_B is the Boltzmann constant and where h is the Planck constant. Plots of log (k/T) *vs.* T^{-1} are drawn; ΔH^* was calculated from the slope, and ΔS^* was calculated by means of Eq. 1 at 50 °C, the results being given in Table 1. The ΔH^*-ΔS^* relation is shown in Fig. 1. The linear relationship between ΔH^* and ΔS^* is well known as the isokinetic relationship or the compensation effects.[7] It is possible to draw two isokinetic lines for the plots in Fig. 1. The **a** line is applied for 4 compounds (**5**, **6**, **7**, and **10**) which have a branched substituent group at the α-position, the isokinetic temperature being 398 K. The **b** line is for the other 6 compounds (**1**, **2**, **3**, **4**, **8**, and **9**), the isokinetic temperature being 401 K.

General Structure-Hydrolytic Reactivity Correlation. The extrathermodynamic linear Eq. 2 was proposed to express the relation between the hydrolytic rate constant (k) and the parameters, pK, $\delta_C(5)$, and χ. Regression analysis was then applied to this equation.

$$\log (k/k_0) = b_1[\mathrm{p}K - \mathrm{p}K_0] + b_2[\delta_c(5) - \delta_c(5)_0] + b_3[\chi - \chi_0] \quad (2)$$

or

$$\log k = b_0 + b_1\mathrm{p}K + b_2\delta_c(5) + b_3\chi = b_0 + b_1x_1 + b_2x_2 + b_3x_3, \quad (3)$$

where the subscript zero refers to the values of the standard compound, where b_i (i=0, 1, 2, and 3) are constants, and where x_1, x_2, and x_3 are predictor variables equivalent to pK, $\delta_C(5)$, and χ respectively. The correlation matrix is shown in Table 3. The smallest correlation exists between x_1 and x_2; therefore, both the variables make nearly independent contributions to log k. The regression between log k and each of the predictor variables is given by Eqs. 4—6 (Table 4). The regression including all the variables is also given by Eq. 7; its F-value is significant at the 1% level. When the variable x_3, which has the smallest t-value for the regression coefficient, is eliminated from Eq. 7, Eq. 8 is obtained and the contribution ratio of 86% is obtained. The F-value for Eq. 8 is 21.2, which is not greatly different from that obtained for Eq. 7. Therefore, no further elimination of variables was carried out. Thus, it is found that, among the parameters which may reflect the substituent effect, the combination of pK and $\delta_C(5)$ shows a good correlation with log k in the case of the compounds examined here.

Table 3. Correlation matrix for each combination of variables

	pK	$\delta_c(5)$	χ	log k
pK	1.000			
$\delta_c(5)$	0.034	1.000		
χ	0.301	0.720*	1.000	
log k	−0.691*	−0.639*	−0.490	1.000

The asterisk indicates the significance at the 5% level.

The use of the facilities of the Osaka University Computing Center is acknowledged.

References

1) C. D. Ritchie and W. F. Sager, "An Examination of Structure-Reactivity Relationships," in "Progress in Physical Organic Chemistry," ed by S. G. Cohen, A. Streitwieser, Jr., and R. W. Taft, Interscience Publishers, New York (1964), Vol. 2.
2) J. T. Carstensen, E. G. Serenson, and J. J. Vance, *J. Pharm. Sci.*, **53**, 1547 (1964).
3) J. Okada and T. Esaki, *Chem. Pharm. Bull. (Tokyo)*, **22**, 1580 (1974).
4) W. J. Murray, *J. Pharm. Sci.*, **66**, 1372 (1977).
5) S. Asada and J. Nishijo, *Bull. Chem. Soc. Jpn.*, **51**, 3379 (1978).
6) R. C. Petersen, *J. Org. Chem.*, **29**, 3133 (1964).
7) J. E. Leffler, *J. Org. Chem.*, **20**, 1202 (1955).

Table 4. Multiple regression analyses of Eq. 3[a)]

b_0 +	b_1x_1 (t value) +	b_2x_2 (t value) +	b_3x_3 (t value)	γ^2 Contribution ratio	V_e Variance	$F_{p,n-p-1}$[b)] Variance ratio	Eq.
22.3	−1.97 pK (2.70*)			0.478	0.333	7.31*	4
11.7		−0.228 $\delta_c(5)$ (2.35*)		0.408	0.377	5.52*	5
−0.139			−0.385 χ (1.59)	0.240	0.484	2.53	6
42.6	−2.21 pK (6.04**)	−0.317 $\delta_c(5)$ (5.03**)	0.302 χ (2.07)	0.917	0.071	21.9**	7
34.3	−1.92 pK (4.72**)	−0.218 $\delta_c(5)$ (4.33**)		0.860	0.103	21.2**	8

a) The number of observations is n=10, and log k at 50 °C is applied. b) p is the number of predictor variables included in the equation. One asterisk indicates the significance at the 5% level; two asterisks, that at the 1% level.

The Solvent Effects of Water-Dimethyl Sulfoxide Mixtures on the Keto-Enol Tautomerization Rate of Di-*n*-alkyl β-Diketones

Hitoshi WATARAI

Department of Chemistry, Faculty of Science, Tohoku University, Sendai 980

(Received November 21, 1979)

Synopsis. The kinetic solvent effects of water–dimethyl sulfoxide (DMSO) mixtures on the ketonization and the enolization rate constants of eight di-*n*-alkyl β-diketones were analyzed in terms of the group-transfer free energy from water to the mixed solvents. The transfer free energy of the transition state, as calculated from the rate constant and the partition coefficient of the keto or enol form, is found to be divided into three contributions: the two group-transfer free energies of the "transition state skeleton" and the methylene group, and the transfer free energy change due to the inductive effect of the *n*-alkyl group.

In the course of our study aimed at elucidating the kinetic behavior of β-diketones in a liquid-liquid partition system, it was found that the partition rate is controlled by the keto-enol tautomerization in the aqueous phase[1] and the important kinetic influence of aqueous solvent on the reaction was demonstrated.[2] Although it is well recognized that a kinetic solvent effect results from the difference in solvent effects on the reactant state and on the transition state, there have been only a few studies aimed at assessing the solvent effect on the two states individually. Previously, we ourselves demonstrated that a kinetic solvent effect can be experimentally assessed in terms of the free energies of transfer for a reactant and a transition state from a standard solvent to others, as calculated from the liquid-liquid partition coefficient and the rate constant.[2,3]

The purpose of this study is to elucidate the solvent effect and the substituent effect in the keto-enol tautomerization of di-*n*-alkyl β-diketones in a water–DMSO mixed solvent in terms of the transfer free energy.

Experimental

Chemicals. The acetylacetone and eight β-diketones were obtained from the same sources described elsewhere.[1] The solvents used were purified by the ordinary method. The mixed solvents were prepared by weight at the desired mole fraction of DMSO within ±0.0005.

Measurement of the Tautomerization Rate. The tautomerization rate constants were obtained from the absorption decreases of the enol form in 3 ml of a solution contained in quartz cell thermostated at 25±0.1 °C. The tautomerization reaction was initiated by the vapor injection method[2] for 2,3-hexanedione as well as for acetylacetone. For the other β-diketones, a minute quantity of pure liquid of β-diketone was quickly dissolved into a mixed solvent by means of a Teflon spatula designed to mix the solution effectively. Since the enol fraction in the pure liquid state of β-diketone is about 0.8, an enol-rich solution which shows an intense absorbance at 273 nm is produced by the dissolution procedure. First-order analysis of the absorbance change gave the tautomerization rate constant, $k_{obsd}(s^{-1})$. Measurements were repeated from two to five times.

TABLE 1. TAUTOMERIZATION RATE CONSTANTS OF DI-*n*-ALKYL β-DIKETONES IN WATER–DMSO MIXED SOLVENTS AT 25 °C

No.	β-Diketone	$k_{obsd}\times10^3/s^{-1}$					
		x_s=0.000	0.100	0.200	0.300	0.400	0.500
1	2,4-Pentanedione	9.93	7.42	5.45	3.17	1.92	1.08
2	2,4-Hexanedione	7.72	5.00	3.45	1.93	1.03	0.467
3	3,5-Heptanedione	5.72	3.23	1.98	1.04	0.532	0.233
4	2,4-Heptanedione	7.35	4.73	3.08	1.83	0.888	0.415
5	3,5-Octanedione	5.02	2.85	1.82	0.945	0.475	0.202
6	2,4-Octanedione	6.87	4.82	3.12	1.70	0.972	0.412
7	4,6-Nonanedione	4.92	2.80	1.67	0.867	0.443	0.188
8	2,4-Nonanedione	7.17	4.42	3.08	1.75	0.892	0.415

Results

The observed rate constants are listed in Table 1. The ketonization and enolization rate constants, k_k and k_e, were calculated from the following equations:

$$k_k = (1-f)k_{obsd}, \quad k_e = fk_{obsd}, \tag{1}$$

where f is the enol fraction in the mixed solvent determined previously.[4]

The transfer free energies (kcal mol^{-1}) of the keto form, the enol form, and the transition state from water to mixed solvents were calculated by means of following equations,[3]

$$\delta\Delta G_K = 0.592 \ln\left(\frac{P}{P_o}\frac{1-f_o}{1-f}\right),$$

$$\delta\Delta G_E = 0.592 \ln\left(\frac{P}{P_o}\frac{f_o}{f}\right), \tag{2}$$

$$\delta\Delta G_x = 0.592 \ln\left(\frac{P}{P_o}\frac{1-f_o}{1-f}\frac{f_o}{f}\frac{k_{obsd,o}}{k_{obsd}}\right),$$

where P is the apparent partition coefficient of β-diketone in the heptane/water–DMSO system and where the subscript O refers to water as the standard solvent. The data of the partition coefficient were reported previously.[4] The calculated results are listed in Table 2, where the partition coefficient for 2,4-nonanedione was assumed to be equal to that of 4,6-nonanedione. The error in the calculation is less than 0.05 kcal mol^{-1}.

Discussion

Solvent Composition Dependence of Transfer Free Energies. In Table 2, $\delta\Delta G_E$ is a negative value in all systems, while $\delta\Delta G_x$ is positive for the smaller β-diketone and slightly negative for the larger β-diketone. $\delta\Delta G_K$ takes medium values between $\delta\Delta G_E$ and $\delta\Delta G_x$. When we recall that the activation energy changes are represented by $\delta\Delta G_x-\delta\Delta G_K$ or $\delta\Delta G_x-\delta\Delta G_E$, the variation in the tautomerization rate with the solvent composition is found to be primarily governed by those in $\delta\Delta G_K$ and $\delta\Delta G_E$, because the variation in $\delta\Delta G_x$ is smaller than the two others.

Recently, we proposed a new solvent parameter for a mixed solvent, $-(P_i/\alpha T)\ (v^E/v)$, where P_i, α, v^E, and v correspond to the internal pressure, the coefficient of

Table 2. Transfer free energies (kcal mol^{-1}) from water to water–DMSO mixed solvents at 25 °C

No.[a]	State	X_s 0.100	0.200	0.300	0.400	0.500
1	$\delta\Delta G_K$	0.11	0.19	0.15	0.03	−0.13
	$\delta\Delta G_E$	−0.11	−0.25	−0.50	−0.77	−1.04
	$\delta\Delta G_X$	0.11	0.21	0.36	0.44	0.56
2	$\delta\Delta G_K$	0.03	0.08	−0.07	−0.16	−0.34
	$\delta\Delta G_E$	−0.25	−0.41	−0.75	−1.02	−1.30
	$\delta\Delta G_X$	0.05	0.14	0.21	0.37	0.44
3	$\delta\Delta G_K$	−0.05	−0.10	−0.25	−0.51	−0.75
	$\delta\Delta G_E$	−0.32	−0.58	−0.93	−1.31	−1.69
	$\delta\Delta G_X$	0.04	0.11	0.22	0.24	0.32
4	$\delta\Delta G_K$	−0.06	−0.09	−0.25	−0.53	−0.81
	$\delta\Delta G_E$	−0.30	−0.56	−0.91	−1.32	−1.71
	$\delta\Delta G_X$	0.01	0.07	0.10	0.16	0 29
5	$\delta\Delta G_K$	−0.16	−0.26	−0.51	−0.89	−1.15
	$\delta\Delta G_E$	−0.42	−0.76	−1.22	−1.68	−2.11
	$\delta\Delta G_X$	−0.05	−0.06	−0.07	−0.08	0.04
6	$\delta\Delta G_K$	−0.14	−0.25	−0.49	−0.79	−1.17
	$\delta\Delta G_E$	−0.39	−0.74	−1.16	−1.63	−2 09
	$\delta\Delta G_X$	−0.13	−0.15	−0.15	−0.22	−0.13
7	$\delta\Delta G_K$	−0.20	−0.37	−0.71	−1.10	−1.50
	$\delta\Delta G_E$	−0.53	−0.96	−1.48	−2.03	−2.52
	$\delta\Delta G_X$	−0.13	−0.18	−0.24	−0.32	−0.26
8	$\delta\Delta G_K$	−0.19	−0.37	−0.71	−1.10	−1.51
	$\delta\Delta G_E$	−0.44	−0.83	−1.37	−1.91	−2.40
	$\delta\Delta G_X$	−0.10	−0 22	−0 35	−0.43	−0.43

a) The numbers correspond to those in Table 1.

the thermal expansion, the excess molar volume, and the mean molar volume of the mixed solvent respectively.[5] For the transfer free energy, we can derive the following relation:

$$\delta\Delta G - \phi_s\delta\Delta G_1 = -q(r)\frac{P_1}{\alpha T}\left(\frac{v^E}{v}\right), \quad (3)$$

where $\delta\Delta G_1$ is the transfer free energy from water to DMSO and where $q(r)$ is a correction factor depending on the molar volumes of the solute and the solvent.[4] The plot of $\delta\Delta G-\phi_s\delta\Delta G_1$ against the pressure factor gave a linear relationship for $\delta\Delta G_K$ and $\delta\Delta G_E$ (the figure is not shown). This suggests that the variation in the solvent-solvent interaction energy in a water–DMSO mixture is an important factor govering the solvent-composition dependence of the tautomerization rate.

Substituent Effect. The relationship between $\delta\Delta G$ and the total number of carbon atoms, n, in β-diketones is summarized as follows:

(i) $\delta\Delta G_K$ and $\delta\Delta G_E$ decrease in proportion to n, *i.e.*,

$$\delta\Delta G_K = \delta\Delta G(\text{-COCH}_2\text{CO-}) + n\delta\Delta G(\text{-CH}_2\text{-}), \quad (4)$$
$$\delta\Delta G_E = \delta\Delta G(\text{-COCHCOH-}) + n\delta\Delta G(\text{-CH}_2\text{-}),$$

where $\delta\Delta G$(-COCH$_2$CO-), $\delta\Delta G$(-COCHCOH-), and $\delta\Delta G$(-CH$_2$-) are the transfer free energies of the diketone skeleton, the enol skeleton, and the methylene group.

(ii) $\delta\Delta G_X$ does not show a simple linear relationship with n, but it can be represented by the next equation:

$$\delta\Delta G_X = \delta\Delta G(\bar{X}) + \delta\Delta G(x) + n\delta\Delta G(\text{-CH}_2\text{-}), \quad (5)$$

where $\delta\Delta G(\bar{X})$ is the transfer free energy of the transition-state skeleton, calculated by subtracting $2\delta\Delta G$(-CH$_2$-) from the $\delta\Delta G_X$ of acetylacetone, and where $\delta\Delta G(x)$ is an increment in $\delta\Delta G(\bar{X})$ induced by an alkyl group other than the methyl group. For methyl group, $\delta\Delta G(x)$ is equal to zero, from the definition. Since the charge distribution in the transition state is expected to be highly delocalized, $\delta\Delta G(x)$ may be sensitive to the electronic property of the alkyl substituent. Therefore, we tested the correlation between $\delta\Delta G(x)$ and the

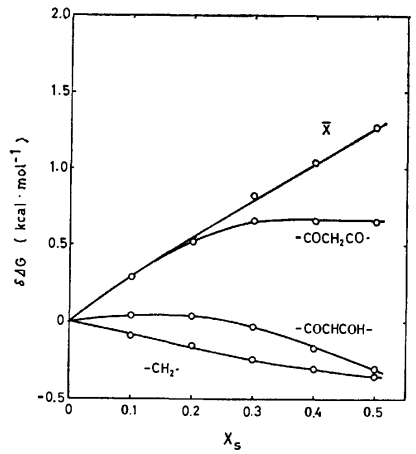

Fig. 1. Variation of the group transfer free energies with mole fraction of DMSO.

inductive parameter of the substituent proposed by Taft.[6] The plot of $\delta\Delta G(x)$ calculated from Eq. 5 against the sum of Taft σ^* (*vide infra*) for two alkyl groups of

n-Alkyl group	CH_3	C_2H_5	C_3H_7	C_4H_9
Taft's σ^*	0 000	−0 100	−0 115	−0.130

R_1 and R_2, $(\sigma_1^*+\sigma_2^*)$, in R_1-COCH$_2$COR$_2$ showed a linear relationship. Therefore, Eq. 5 can be rewritten as:

$$\delta\Delta G_x = \delta\Delta G(\bar{X}) + \rho(x_s)(\sigma_1^*+\sigma_2^*) + n\delta\Delta G(\text{-CH}_2\text{-}), \quad (6)$$

where $\rho(x_s)$ is a characteristic coefficient depending on the solvent composition. Because of the repulsive property of the interaction energy between DMSO and the anion,[7] $\delta\Delta G(\bar{X})$ is expected to be large and positive when Taft's σ^* value of the substituent is large and negative. Hence, the apparent proportionality between the tautomerization rate constant and the number of the methyl group can be ascribed to the large difference between the Taft σ^* values of the methyl group and those of the other substituents.

The group transfer free energies obtained on the basis of Eqs. 4 and 5 are shown in Fig. 1 as a function of the mole fraction of DMSO. The decreasing order of $\delta\Delta G(\bar{X})>\delta\Delta G$(-COCH$_2$CO-)$>\delta\Delta G$(-COCHCOH-)$>\delta\Delta G$(-CH$_2$-) may correspond to the decreasing order of the extent of charge delocalization. It is noticeable that the inductive effect has been clearly shown to be effective only in the transition state.

The author thanks Professor Nobuo Suzuki of Tohoku University for his helpful advice.

References

1) H. Watarai and N. Suzuki, *J. Inorg. Nucl. Chem.*, **38**, 301 (1976).
2) H. Watarai and N. Suzuki, *J. Inorg. Nucl. Chem.*, **38**, 1683 (1976).
3) H. Watarai and N. Suzuki, *Bull. Chem. Soc. Jpn.*, **50**, 757 (1977).
4) H. Watarai and N. Suzuki, *Bull. Chem. Soc. Jpn.*, **53**, 1848 (1980).
5) H. Watarai and N. Suzuki, *Chem. Lett.*, **1977**, 321.
6) R. W. Taft, Jr., *J. Am. Chem. Soc.*, **75**, 4231 (1953).
7) A. J. Parker, *Chem. Rev.*, **69**, 1 (1969).

Mössbauer Effect in Fluorotrimethyltin(IV)

Hisao NEGITA,* Ryukei BOKU, Masahiro SUGIYA, and Sumio ICHIBA
Department of Chemistry, Faculty of Science, Hiroshima University, Hiroshima 730
(Received January 10, 1980)

Synopsis. The angular dependent Mössbauer spectra of ^{119}Sn in needle crystals of fluorotrimethyltin(IV) were studied at 110 K. The principal axis of the electric-field gradient was observed at about 20° from the a axis. ^{19}F NMR spectra of the solid were also studied. From the temperature dependence of the linewidth, the activation energy for the motion of the F atom was estimated to be 6.7±1.3 kJ mol^{-1}.

The X-ray diffraction[1] of fluorotrimethyltin(IV), Me_3SnF, showed that the molecule consists of Me_3Sn groups and F atoms arranged alternately in a chain-like manner along the a axis. Yasuda *et al.*[2] proposed a structure for Me_3SnF on the basis of the X-ray diffraction study. Mössbauer studies[3,4] confirmed a trigonal bipyramidal configuration of the tin atom, and related the intensity asymmetry of the doublet resonance spectrum to the intermolecular bonding, F–Sn···F. ^{1}H NMR study[5] supported the proposed structure from the viewpoint of motions of the Me_3Sn group. The purpose of the present study is to examine the validity of the proposed structure in more detail by means of the angular dependent Mössbauer spectra and ^{19}F NMR of the solid.

Experimental

The angular dependent Mössbauer spectra were obtained from 4—6 mm long needle crystals which were attached in the same direction with nail enamel on an absorber holder and kept at 110 K in a cryostat.

The measurement of the ^{19}F NMR was made at 13.00 MHz by a broad line NMR spectrometer (Japan Electron Optics Lab. Co., Ltd.). The linewidth was measured between maximum and minimum deflection points of the derivative tracing, using an amplitude which was narrow compared to the linewidth. The scanning rate was set to 0.8—2.0 G per second to avoid the saturation broadening.

Results and Discussion

Me_3SnF is an orthorombic crystal, space group Pmcn, with four molecules in a unit cell.[1] If the space group is reasonable, the unit cell comprises two equivalent sites and a 180° rotation about the a axis transforms one into the other. If the areas of the $\sigma(\pm1/2\rightarrow\pm1/2)$ and $\pi(\pm1/2\rightarrow\pm3/2)$ transitions are expressed by A_σ and A_π, and the recoilless fraction is assumed to be isotropic in the first approximation,[6] then, for a single-crystal absorber, the area ratio after Zory[7] is given by Eq. 1 as a function of the polar and azimuthal angles, Θ and Φ, of the incident γ-ray with respect to the crystal axes system O_{bca} (see Fig. 2).

$$\frac{A_\sigma}{A_\pi}=\frac{4\left(1+\frac{1}{3}\eta^2\right)^{1/2}-(3K-1+\eta K')}{4\left(1+\frac{1}{3}\eta^2\right)^{1/2}+(3K-1+\eta K')}, \quad (1)$$

where

$$K=(Z_b^2\cos^2\Phi+Z_c^2\sin^2\Phi)\sin^2\Theta+Z_a^2\cos^2\Theta+Z_bZ_c\sin^2\Theta\sin2\Phi,$$

$$K'=[(X_b^2-Y_b^2)\cos^2\Phi+(X_c^2-Y_c^2)\sin^2\Phi]\sin^2\Theta+(X_a^2-Y_a^2)\cos^2\Theta+(X_bX_c-Y_bY_c)\sin^2\Theta\sin2\Phi.$$

The symbol X_a, for instance, stands for the direction cosine of the angle between the axis of the electric-field gradient (EFG) and the corresponding crystal axis. In the case of needle crystals grown along the a axis, the area ratio is given by integrating Eq. 1 from 0 to 2π on Φ. Expressing each of the direction cosines as a function of the Euler angles (α, β, γ), the resulting area ratio is:

$$\frac{A_\sigma}{A_\pi}=\frac{8\left(1+\frac{1}{3}\eta^2\right)^{1/2}-(3I-2+\eta I')}{8\left(1+\frac{1}{3}\eta^2\right)^{1/2}+(3I-2+\eta I')}, \quad (2)$$

where

$$I=2\cos^2\beta\cos^2\Theta+\sin^2\beta\sin^2\Theta,$$

$$I'=\sin^2\beta\cos2\gamma(2\cos^2\Theta-\sin^2\Theta).$$

In the case of $\eta=0$, this equation becomes equal to that[8] obtained by integrating the transition probabilities.

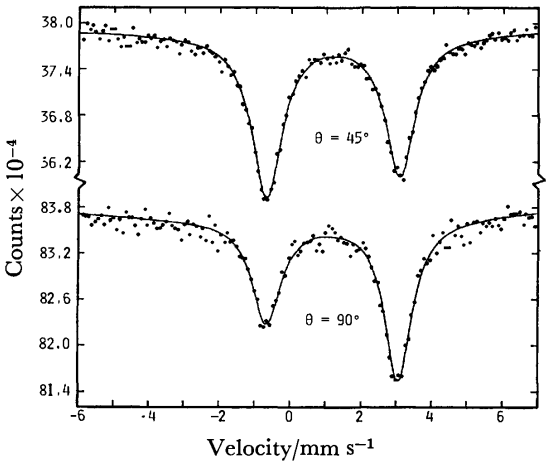

Fig. 1. The Mössbauer absorption spectra of Me_3SnF needle crystals at 110 K.

Figure 1 shows two typical spectra obtained for the γ-ray propagation direction at angles of 45° and 90° from the needle axis. In Fig. 2, the experimental values of the ratio of the high-energy absorption area to the low, A_H/A_L, are plotted against the angle Θ along with the theoretical curves calculated from Eq. 2, assuming that the molecule has C_{3v} symmetry, *i.e.*, $\eta=0$. The experimental points fit closely to the curve of $\beta=20°$.

Figure 3 shows the crystal structure proposed by Yasuda *et al.*[2] The Me_3Sn group forms a planar equilateral triangular structure and is inclined by 21° to the plane perpendicular to the a axis, and the Me_3Sn

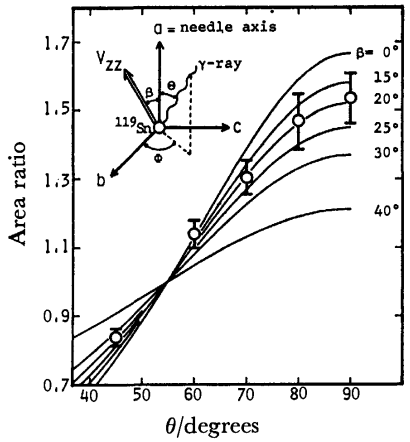

Fig. 2. The angular dependence of the area ratio for Me_3SnF needle crystals at 110 K.

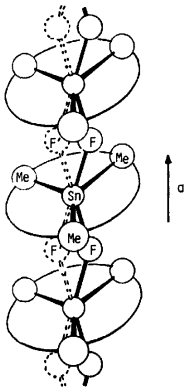

Fig. 3. Arrangement of Me_3SnF molecules.[2] F and F′ indicate the two possible possitions of the fluorine atom.

groups and F atoms are arranged alternately along the a axis. According to this structure, the molecular symmetry about the tin atom is not C_{3v}. However, it is expected that the departure from C_{3v} is not very great, and hence V_{zz} is approximately perpendicular to the plane of the Me_3Sn group, *i.e.*, the angle β is estimated to be about 21°. The value agrees well with our result, and the fact that A_H/A_L is equal to A_σ/A_π means that the σ transition lies at a higher energy than the π transition, *i.e.*, the sign of the principal component of the EFG tensor is positive, $V_{zz}>0$.

In order to explain the anomaly[1] in the electron-density distribution of the F atom, Yasuda *et al.*[2] predicted that the F atom would occupy two positions of minimum potential energy at room temperature, as

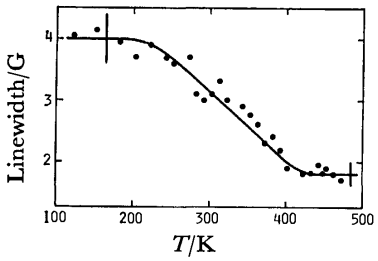

Fig. 4. The ^{19}F NMR linewidth as a function of temperature for Me_3SnF.

seen in Fig. 3. To examine the question of the motion of the F atom, ^{19}F NMR spectra were investigated in the temperature range 123—473 K. The linewidth is plotted as a function of temperature in Fig. 4. Limits of experimental error are shown at low and high temperatures by error bars in the figure. At low temperature the linewidth is constant at 4.0 G, presumably due to the rigid-lattice value. At temperatures around 450 K, the linewidth decreases to 1.8 G. The reduction of the linewidth seems likely to be caused by the switching motion of the F atoms. Accordingly, the molecular symmetry at the tin atom is expected to approach to C_{3v} by such motion. This is reflected also at the IR spectra[4] of the compound: the Sn–C asymmetric streching vibration occurs as a nearly singlet peak in the room-temperature spectrum, whereas in the liquid-nitrogen spectrum it is resolved into a doublet. The activation energy for the motion of the F atom was estimated to be 6.7 ± 1.3 kJ mol^{-1} on the basis of the theory[9] relating linewidth and correlation frequency.

References

1) H. C. Clark, R. J. O'Brien, and J. Trotter, *Proc. Chem. Soc.*, **1964**, 85; *J. Chem. Soc.*, **1964**, 2332.
2) K. Yasuda, Y. Kawasaki, N. Kasai, and T. Tanaka, *Bull. Chem. Soc. Jpn.*, **38**, 1216 (1965).
3) H. A. Stöckler and H. Sano, *Phys. Rev.*, **165**, 406 (1968).
4) R. H. Herber and S. Chandra, *J. Chem. Phys.*, **54**, 1847 (1971).
5) S. E. Ulrich and B. A. Dunell, *J. Chem. Soc., Faraday Trans. 2*, **1972**, 680.
6) The anisotropy of the recoilless fraction was pointed out in Refs. 3 and 4, but it was neglected in the theoretical derivation of the Eq. 1 for simplicity.
7) P. Zory, *Phys. Rev.*, **140**, A1401 (1965).
8) H. Sano and R. Kuroda, *Chem. Phys. Lett.*, **11**, 512 (1971).
9) For example, G. W. Smith, *J. Chem. Phys.*, **36**, 3081 (1962).

Kinetic Studies of the Electron Transfer Reaction in Iron(II) and Iron(III) Systems. X. The Electron Transfer Reaction between Iron(II) and Iron(III) in the Presence of Pyridine in Aqueous Solution

Goro WADA* and Aiko KAWAUCHI
Department of Chemistry, Nara Women's University, Nara 630
(Received February 9, 1980)

Synopsis. When pyridine is added to the reaction system of the electron transfer between Fe(II) and Fe(III) in aqueous solution at constant $[HClO_4]_o$, the apparent rate constant k grows rapidly with $[Py]_o$ at $[Py]_o<[HClO_4]_o$, while k suddenly diminishes to a small and constant value at $[Py]_o>[HClO_4]_o$. The predominant paths of the reaction will be discussed.

We have been investigating the reaction mechanisms of the electron transfer between iron(II) and iron(III) complexes Fe(II)+*Fe(III)→Fe(III)+*Fe(II) in various solutions.[1] In this note, we will report on an interesting phenomenon observed in the case that pyridine(Py) is added to the reaction system. Namely, when the total concentration of pyridine $[Py]_o$ is increased in aqueous solutions of iron(II) and iron(III) at a constant concentration of perchloric acid $[HClO_4]_o$, the apparent rate constant of the electron transfer reaction k grows rapidly at first, and becomes almost infinitely large until $[Py]_o$ reaches to values closely equal to $[HClO_4]_o$. After that, nevertheless, it suddenly diminishes to a constant value as small as $k=4.5\pm1.6$ $M^{-1}s^{-1}$ (1 M=1 mol dm^{-3}) indifferent to both $[Py]_o$ and $[HClO_4]_o$. A few cases of the phenomenon are shown in Fig. 1, in which k is plotted against $[Py]_o$ when $[HClO_4]_o$ is kept at 0.05, 0.10, and 0.20 M respectively, at $\mu=0.2$ M and 25 °C.

The apparent rate constant k was determined by the method using radioactive tracer Fe-59, as described elsewhere.[2,3]

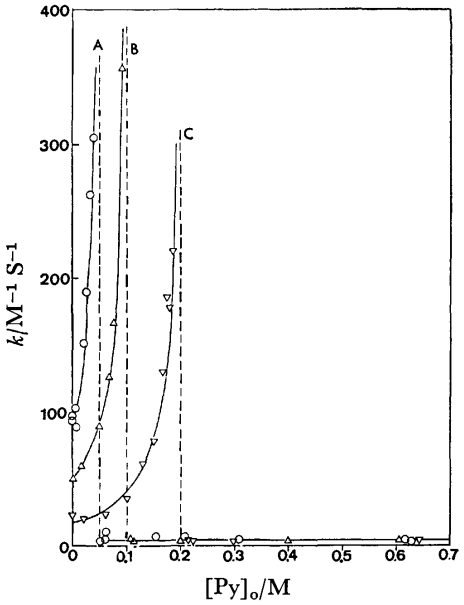

Fig. 1. The variation of k with $[Py]_o$ at $[HClO_4]_o=0.05$ M (a), 0.10 M (b), and 0.20 M (c).

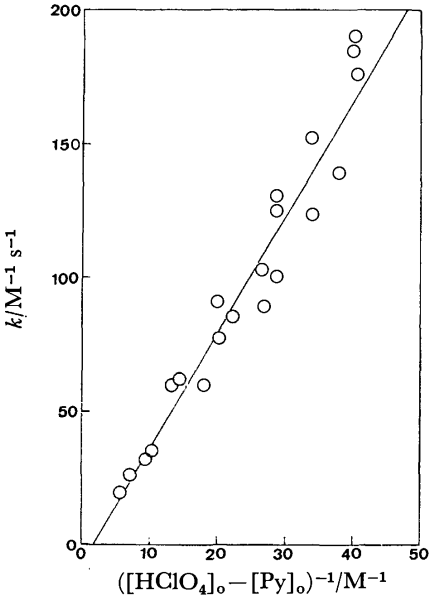

Fig. 2. The linear relationship of k with $([HClO_4]_o-[Py]_o)^{-1}$ at $[Py]_o<[HClO_4]_o$.

The observed fact that k varies peculiarly with the increase in $[Py]_o$ at a constant $[HClO_4]_o$ should be reasonably understood by the following consideration. At the concentration range of $[Py]_o<[HClO_4]_o$, the concentration of hydrogen ion $[H^+]$ becomes smaller by as much as $[Py]_o$ than $[HClO_4]_o$, because pyridine is a considerably strong base with a basicity constant $K_b=2.8\times10^5$ M^{-1} at $\mu=0.5$ M and 25 °C where $K_b=[PyH^+]/[Py][H^+]$.[4,5] Therefore, the actual value of the hydrogen ion concentration in the reaction system is approximately equal to $[HClO_4]_o-[Py]_o$. Consequently, when k is plotted against $([HClO_4]_o-[Py]_o)^{-1}$ instead of plotting against $[HClO_4]_o^{-1}$, a single straight line is obtained as is shown in Fig. 2. This indicates that k can be expressed by the following equation:

$$k = k_o + \frac{k_H K_H}{[HClO_4]_o - [Py]_o}$$

where k_o and k_H denote the reaction rate constants of the electron transfer Fe^{2+}/Fe^{3+} and $Fe^{2+}/FeOH^{2+}$ respectively, and K_H the hydrolysis constant of Fe^{3+}, $K_H=[FeOH^{2+}][H^+]/[Fe^{3+}]$.

The slope of the straight line is found to be 4.4 s^{-1} which is fairly close to the value $k_HK_H=6.0$ s^{-1} observed in aqueous solutions, using the value $K_H=2.2\times10^{-3}$ M.[6] Therefore, the equation suggests that the reaction path between Fe^{2+} and $FeOH^{2+}$ (Path B) takes an important part in parallel with the reaction path between Fe^{2+} and Fe^{3+} (Path A) in the electron transfer

reaction in the present system, the asterisked iron *Fe expressing the species labelled by radiotracer.

$$Fe^{2+} + *Fe^{3+} \longrightarrow Fe^{3+} + *Fe^{2+} \quad (A)$$

$$Fe^{2+} + *FeOH^{2+} \longrightarrow FeOH^{2+} + *Fe^{2+} \quad (B)$$

When $[Py]_o$ becomes larger than $[HClO_4]_o$, the apparent rate constant k suddenly diminishes and keeps almost constant value, as shown in Fig. 1. In this concentration range of $[Py]_o > [HClO_4]_o$, a part of pyridine is protonated with H^+ to be pyridinium ion and the rest of pyridine coordinates to Fe^{2+} to be $Fe(Py)_n^{2+}$.[7] Since $[H^+]$ decreases to a considerable extent due to the protonation of pyridine, Fe^{3+} is forced to be hydrolyzed to give $FeOH^{2+}$. Consequently, each of the equilibria of the following three reactions declines towards the right-hand side.

$$Py + H^+ \rightleftharpoons PyH^+$$

$$Fe^{2+} + nPy \rightleftharpoons Fe(Py)_n^{2+}$$

$$Fe^{3+} \rightleftharpoons FeOH^{2+} + H^+$$

Thus, the main path of the electron transfer reaction should be the reaction between $Fe(Py)_n^{2+}$ and $FeOH^{2+}$ (Path C),

$$Fe(Py)_n^{2+} + *FeOH^{2+} \longrightarrow \text{Products}, \quad (C)$$

the rate constant of which may be approximately equal to the apparent rate constant observed after $[Py]_o$ surpasses $[HClO_4]_o$. Although pyridine may be supposed to coordinate to $FeOH^{2+}$, the occurrence of the coordinated species has not been ascertained yet as far as the spectrophotometric observation was performed.

References

1) The previous paper of this series: G. Wada, Y. Ohta, S. Hayashida, H. Sugino, T. Mizui, and Y. Aihara, *Bull. Chem. Soc. Jpn.*, **53**, 1278 (1980).

2) J. Menashi, W. L. Reynolds, and G. Van Auken, *Inorg. Chem.*, **4**, 299 (1965).

3) G. Wada, N. Yoshizawa, and Y. Sakamoto, *Bull. Chem. Soc. Jpn.*, **44**, 1018 (1971).

4) R. J. Bruehlman, and F. H. Verhoek, *J. Am. Chem. Soc.*, **70**, 1401 (1948).

5) M. S. Sun, and D. G. Brewer, *Can. J. Chem.*, **45**, 2729 (1967).

6) G. Wada, and A. Endo, *Bull. Chem. Soc. Jpn.*, **45**, 1073 (1972).

7) J. Bjerrum, *Chem. Rev.*, **46**, 381 (1950); *Acta Chem. Scand.*, **27**, 970 (1973).

A.c. Polarographic Determination of Cyanide Ion after Conversion to Mercury(II) Cyanide by Use of Hg-form Resin

Goro HANAGATA,** Kunio OHZEKI, and Tomihito KAMBARA*
Department of Chemistry, Faculty of Science, Hokkaido University, Sapporo 060
***Division of Environmental Conservation, Graduate School of Environmental Science, Hokkaido University, Sapporo 060*

(Received April 11, 1980)

Synopsis. Cyanide ion was converted to mercury(II) cyanide by shaking with Hg(II)-form resin and determined by a.c. polarography at pH 9.0. The recovery was 80.5%. A linear calibration curve was obtained in the cyanide concentrations ranging from 10^{-4} to 10^{-3} M (1 M=1 mol dm^{-3}).

As to the polarographic determination of cyanide ion, several methods have been reported,[1-4] which were mainly based on the anodic oxidation of mercury in the presence of cyanide. As early as 1937 the reduction of mercury(II) cyanide was studied in detail by Tomes.[5]

Experimental

Reagents. All chemicals used were of analytical reagent grade. A 10^{-2} M nickel(II) solution was prepared from sulfate and standardized against EDTA. A 10^{-2} M potassium cyanide solution was standardized against the nickel(II) solution. The solution of other metal ions was prepared from sulfate or nitrate and standardized against EDTA. A stock solution of mercury(II) cyanide was prepared by mixing the mercury(II) nitrate and potassium cyanide in the stoichiometric ratio. Buffer solutions used were 0.2 M boric acid —0.2 M sodium hydroxide (pH=8.0—11.0).

A cation exchanger Dowex 50 W-X8 (100—200 mesh) was washed as usual, converted into H-form and then air-dried. Five grams of the resin (2.79 meq/g) were treated with mercury (II) nitrate. The Hg-form resin was then washed with water and finally dispersed in water to give a suspension of 500-ml volume. The mixture was stirred each time before pipetting out.

Apparatus. The polarograph used was a Yanagimoto product, type P-8. Characteristics of the dropping mercury electrode were: m=1.88 mg s^{-1} and t=3.97 s in 0.5 M potassium nitrate solution containing the borate buffer in 0.02 M (pH=9.0) at an open circuit with a mercury column height of 72.5 cm. Polarograms were recoded at 25±0.1 °C. A Hitachi-Horiba glass electrode pH-meter, F-5 was used.

General Procedure. A 20-ml portion of smaple solution containing cyanide ion in the concentrations ranging from 10^{-4} to 10^{-3} M was taken into a separatory funnel and 5 ml of the Hg-form resin suspension was added. The mixture was shaken for 5 min at a room temperature. The resin was then separated by filtration through glass wool, and washed with about 10 ml of water. The filtrate and washings were transferred into a 50-ml volumetric flask containing 10 ml of 2.5 M potassium nitrate and 5 ml of the borate buffer (pH=9.0). The volume was adjusted to mark with water. A part of the solution was taken into a cell and oxygen was purged by passing nitrogen gas for 5 min. The dissolved oxygen interfered slightly when the concentration of mercury(II) cyanide is low. The a.c. polarograms were recorded succssively three times and the average peak current was measured.

Results and Discussion

Polarographic Behavior of Mercury(II) Cyanide. The direct current polarographic reduction of mercury(II) cyanide has been studied by Tomes[5] and Newman *et al.*[6] In the pH range 6.0—9.5 was found a reversible wave corresponding to the over-all electrode reaction

$$Hg(CN)_2 + 2H^+ + 2e \longrightarrow Hg + 2HCN. \quad (1)$$

In alkaline solution $Hg(CN)_3^-$ and $Hg(CN)_4^{2-}$ are also reducible at the dropping mercury electrode.[6]

A well-defined a.c. polarogram with a stable and constant peak height was obtained in the pH range of 8.8 to 9.3, while the peak potential was shifted from —354 to —339 mV *vs.* Hg-pool. When mercury(II) ion is added in excess, however, precipitation of mercury(II) hydroxide takes place which causes the erroneous results. From the practical viewpoint, it is necessary to convert cyanide ion completely into mercury(II) cyanide without addition of excess mercury(II) ion.

Use of Hg-form Resin. The mercury(II) cyanide being strongly stable,[7] it is expected that when cyanide ion is mixed with Hg-form resin mercury(II) ion is expelled form the resin into the solution forming mercury(II) cyanide as follows:

$$(RSO_3)_2Hg + 2KCN \longrightarrow 2RSO_3K + Hg(CN)_2, \quad (2)$$

where R denotes the resin matrix.

A 20-ml portion of sample solution containing 237 μg of cyanide was converted to mercury(II) cyanide and determined according to the above-stated general procedure. The procedure was repeated five times. The average peak current was 140 μS and relative

Table 1. Recovery of cyanide ion

Metal-cyano complex[a]	Temperature (°C)	Shaking time (min)	Conversion to $Hg(CN)_2$ (%)
KCN	room temp[b]	5	80.5
$K[Ag(CN)_2]$	room temp	5	81.1
$K_2[Ni(CN)_4]$	room temp	5	31.6
	room temp	60	81.0
	50	5	80.3
$K_2[Cd(CN)_4]$	room temp	5	80.3
$K[Cu(CN)_2]$	room temp	5	63.7
	50	5	67.9
$K_3[Co(CN)_6]$	room temp	5	4.5
	50	5	3.1
$K_4[Fe(CN)_6]$	room temp	5	28.3
	room temp	60	52.0
	50	5	37.5
$K_3[Fe(CN)_6]$	room temp	5	8.6
	room temp	60	81.1

a) Total cyanide ion concentration in the electrolysis solution was 4×10^{-4} M. Cyano complex was prepared by mixing the metal ion in small excess to the stoichiometric ratio. b) 17±2 °C.

standard deviation was 4.0%. On the other hand, the corresponding sample solution prepared from the stoichiometric mixture of cyanide and mercury(II) gave peak current of 174 μS ($n=3$). The conversion ratio was calculated to be 80.5%. The prolonged shaking time and the increased amount of resin have no effect on the improvement of recovery. The loss is not clearly explained, while the incomplete recovery is partly attributable to the formation of $Hg(CN)^+$.

A linear calibration curve of good proportionality was obtained in the cyanide ion concentrations ranging from 10^{-4} to 10^{-3} M. This means that the conversion ratio is constant in the above concentration range.

Silver(I) and cadmium(II) do not interfere with the formation of mercury(II) cyanide as shown in Table 1. In the presence of niekel(II) and iron(III) a prolonged shaking time or an elevated temperature is effective. Cobalt(III) combining with cyanide ion stronger than mercury(II) reduces the recovery seriously. Copper(II) and iron(II) also interfere.

When the concentration of chloride or thiocyanate exceeds twice that of cyanide, the recovery begins to decrease. An equimolar amount of sulfide interferes seriously.

References

1) I. M. Kolthoff and J. J. Lingen, "Polarography," Interscience (1952).
2) W. H. Jura, *Anal. Chem.*, **26**, 1121 (1954).
3) J. H. Karchmer and M. T. Walker, *Anal. Chem.*, **27**, 37 (1955).
4) T. Kambara and S. Tanaka, *Rev. Polarog.*, **16**, 116 (1970).
5) T. Tomes, *Collect. Czech. Chem. Commun.*, **9**, 81 (1937).
6) L. Newman, J. U. Cabral, and D. H. Hume, *J. Am. Chem. Soc.*, **80**, 1814 (1958).
7) L. G. Sillén and A. E. Martell, "Stability Constants of Metal–Ion Complexes," 2nd ed, The Chemical Society, London (1964).

Halogenation of Alkyl *p*-Tolyl Sulfones with Carbon Tetrahalides. Application to the Synthesis of Aromatic Ketones

Hiroshi KOTAKE, Katsuhiko INOMATA,* Hideki KINOSHITA,
Yasuko SAKAMOTO, and Yoko KANETO
Department of Chemistry, Faculty of Science, Kanazawa University, Kanazawa 920

(Received April 11, 1980)

Synopsis. Carbanions of alkyl *p*-tolyl sulfones reacted with carbon tetrahalides to give the corresponding polyhalogenated products in good yields. Some chlorinated sulfones were converted to unsymmetrical ketones by treatment with silver perchlorate in trifluoroacetic acid.

Arnold and Kulenovic have reported that carbanions of esters reacted with carbon tetrahalides to give the corresponding α-monohalo esters.[1)]

TABLE 1. CHLORINATION OF ALKYL *p*-TOLYL SULFONES WITH CCl_4[a)]

RTs (**1a—f**) —i) BuLi (−78 °C, 15 min), ii) CCl_4 (−78 °C—r.t.)→ Chlorinated product (**2a—f**)

RTs	Product	Mp(°C)	Yield[b)] (%)
1a, CH_3Ts	**2a**, CCl_3Ts	143—144	62
1b, CH_3CH_2Ts	**2b**, CH_3CCl_2Ts	106.5—108	91
1c, $PhCH_2Ts$	**2c**, $PhCCl_2Ts$	142—143	57
1d, $PhCH_2CH_2Ts$	**2d**, $PhCH_2CCl_2Ts$	184—185	81
1e, 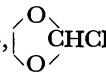	**2e**, 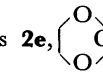	109—110.5	85
1f, $(CH_3)_2CHTs$	**2f**, $(CH_3)_2CClTs$	105—106.5	93

a) Tenfold molar quantity of CCl_4 was used. b) Isolated yields by preparative TLC.

In connection with our continuing interest to extend the synthetic utility of sulfones,[2)] we have tried a similar halogenation reaction to sulfones. When an alkyl *p*-tolyl sulfone (**1**) was lithiated with an equimolar amount of butyllithium in THF at −78 °C followed by addition of tenfold molar quantity of carbon tetrachloride, the corresponding polychlorinated sulfone (**2**) was obtained (Table 1), being in contrast with the report mentioned above.[1)]

TABLE 2. HALOGENATION OF **1b** UNDER THE VARIOUS CONDITIONS

CH_3CH_2Ts (**1b**) —i) BuLi, ii) CX_4→ CH_3CX_2Ts (X=Cl, **2b**; X=Br, **3**)

Molar ratio			Yield(%)	
1b	BuLi	CX_4	Product	Recovered **1b**
1	1	10 (X=Cl)	**2b**, 91	—
1	*ca.* 0.1	10 (X=Cl)	**2b**, 12	82
1	1	1 (X=Cl)	**2b**, 51	38
1	1	10 (X=Br)	**3**, 54	41

The result of halogenation of ethyl *p*-tolyl sulfone (**1b**) under the various conditions (Table 2) suggested that the polyhalogenation proceeds through the following scheme[3)] and that the order of acidities are $CH_3CHClTs$ (**5**)>$HCCl_3$ (**7**)>CH_2CH_2Ts (**1b**).

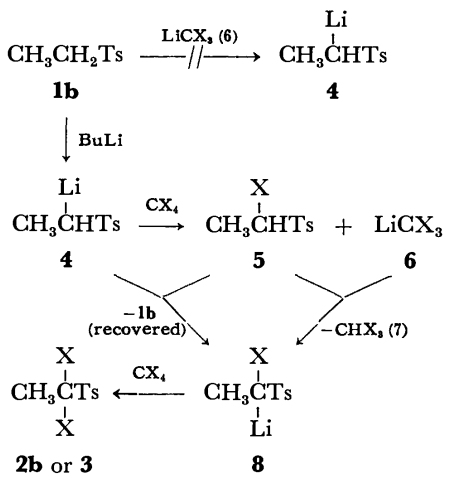

The halogenation of alkyl *p*-tolyl sulfone with carbon tetrahalide was successfully applied to the synthesis of unsymmetrical aromatic ketones as illustrated in the following scheme: the alkylated intermediate (**9**),

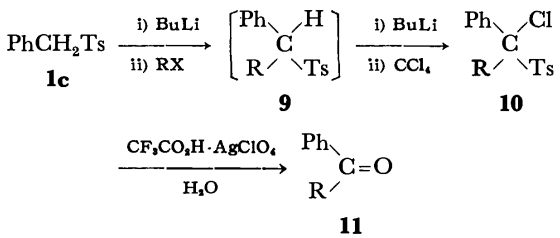

without isolation, was lithiated again with butyllithium followed by the addition of carbon tetrachloride to give the chlorinated sulfone (**10**) in good yield (Table 3). The chloro sulfone (**10**) was treated with silver perchlorate in refluxing trifluoroacetic acid containing a small amount of water to afford the corresponding aromatic ketone (**11**) in good yield (Table 3).[5)]

TABLE 3. SYNTHESIS OF AROMATIC KETONES

RX	Isolated yield/(%)	
	10	**11**
$PhCH_2Br$	87	85
$PhCH_2CH_2Br$	98	79
$CH_3(CH_2)_4I$	quant.	88

Experimental

All the melting points are uncorrected. The NMR and IR spectra were recorded on JEOL JNM/MH-60 and JASCO IRA-1 spectrometers, respectively.

Materials. Freshly distilled THF with lithium aluminum hydride under nitrogen was used. Thin-layer chromatography (TLC) was performed on Merck's Silicagel 60 PF_{254} (Type 7749).

Alkyl p-*Tolyl Sulfones (1a—f).* All of them were readily prepared from equimolar amounts of alkyl halides and sodium *p*-toluenesulfinate tetrahydrate by refluxing in methanol for 8—19 h except **1e** previously described.[4] 2-Phenylethyl *p*-tolyl sulfone (**1d**) is an only new compound. Mp 73.0—73.5 °C. Found: C, 69.23; H, 6.14%. Calcd for $C_{15}H_{16}O_2S$: C, 69.23; H, 6.15%.

1,1-Dichloroethyl p-*Tolyl Sulfone (2b).* Ethyl *p*-tolyl sulfone (**1b**, 184 mg, 1 mmol) was lithiated by stirring with an equimolar amount of butyllithium in THF (10 ml) at −78 °C for 15 min under nitrogen. After addition of carbon tetrachloride (1.538 g, 10 mmol), the reaction mixture was allowed to warm to room temperature and then stirred for 15 min at room temperature. After evaporation of the solvent, the resulting residue was treated with pH 7 buffer solution followed by extraction with ethyl acetate. The crude residue obtained by concentration of the extract was subjected to preparative TLC (hexane–ether 5 : 4 v/v) to give **2b** (229 mg, 91%, mp 100—105 °C). NMR ($CDCl_3$) δ 2.39 (s, 3H), 2.45 (s, 3H), 7.29 (d, 2H, J=9 Hz), 7.82 (d, 2H, J=9 Hz). Recrystallization from heptane gave the pure substance (187 mg, 74%, mp 106—108.0 °C) for elemental analysis. Found: C, 42.81; H, 3.92%. Calcd for $C_9H_{10}Cl_2O_2S$: C, 42.69; H, 3.95%.

In a silmilar manner, **2a,c—f** and **3** were prepared from the corresponding alkyl *p*-tolyl sulfones (Tables 1 and 2).

CCl_3Ts (2a): Found: C, 35.40; H, 2.54%. Calcd for $C_8H_7Cl_3O_2S$: C, 35.10; H, 2.56%.

$PhCCl_2Ts$ (2c): Found: C, 53.39; H, 3.73%. Calcd for $C_{14}H_{12}Cl_2O_2S$: C, 53.33; H, 3.81%.

$PhCH_2CCl_2Ts$ (2d): NMR ($CDCl_3$) δ 2.44 (s, 3H), 3.71 (s, 2H), 7.25 (s, 5H), 7.30 (d, 2H, J=9 Hz), 7.83 (d, 2H, J=9 Hz). Found: C, 54.90; H, 4.24%. Calcd for $C_{15}H_{14}Cl_2O_2S$: C, 54.71; H, 4.26%.

$CHCH_2CCl_2Ts$ (2e): NMR ($CDCl_3$) δ 2.45 (s, 3H), 2.82 (d, 2H, J=4 Hz), 3.91 (broad, 4H), 5.32 (t, 1H, J=4 Hz), 7.34 (d, 2H, J=9 Hz), 7.87 (d, 2H, J=9 Hz). Found: C, 44.41; H, 4.39%. Calcd for $C_{12}H_{14}Cl_2O_4S$: C, 44.31; H, 4.31%.

$(CH_3)_2CClTs$ (2f): Found: C, 51.76; H, 5.53%. Calcd for $C_{10}H_{13}ClO_2S$: C, 51.61; H, 5.59%.

CH_3CBr_2Ts (3): Mp 121—122 °C (recrystallized from heptane). NMR ($CDCl_3$) δ 2.45 (s, 3H), 2.65 (s, 3H), 7.31 (d, 2H, J=9 Hz), 7.87 (d, 2H, J=9 Hz). Found: C, 31.78; H, 2.88%. Calcd for $C_9H_{10}Br_2O_2S$: C, 31.58; H, 2.92%.

1-Chloro-1,2-diphenylethyl p-*Tolyl Sulfone (10, R=CH_2Ph).* Benzyl *p*-tolyl sulfone (**1c**, 246 mg, 1 mmol) was lithiated by stirring with an equimolar amount of butyllithium in THF (20 ml) at −78 °C for 20 min and then at room temperature for 20 min under nitrogen. After cooling to −78 °C, a THF (2 ml) solution of benzyl bromide (171 mg, 1 mmol) was added. The reaction mixture was allowed to warm to room temperature to complete the alkylation and then cooled again to −78 °C followed by the addition of carbon tetrachloride (1.538 g, 10 mmol). After stirring for 20 min, the mixture was treated with 1 mol dm^{-3} HCl–MeOH at −78 °C and partitioned between ether and water. The organic layer was dried over Na_2SO_4 followed by evaporation of the solvent under reduced pressure. The resulting residue was subjected to preparative TLC (hexane–ethyl acetate 5 : 1 v/v) to give **10** (322 mg, 87%, mp 133 °C). NMR ($CDCl_3$) δ 2.35 (s, 3H), 3.82 (d, 1H, J=15 Hz), 4.30 (d, 1H, J=15 Hz), 6.85—7.65 (m, 14H). Recrystallization from heptane gave the pure substance (mp 136—137 °C) for elemental analysis. Found: C, 67.89; H, 5.00%. Calcd for $C_{21}H_{19}ClO_2S$: C, 68.01; H, 5.16%.

In a similar manner, other chlorinated sulfones (**10**, R=CH_2CH_2Ph, $(CH_2)_4CH_3$ and **12**) were prepared.

$PhCH_2CH_2CPhClTs$: Mp 114—115 °C (recrystallized from cyclohexane). NMR ($CDCl_3$) δ 2.32 (s, 3H), 2.4—3.2 (m, 4H), 6.8—7.6 (m, 14H). Found: C, 68.51; H, 5.44%. Calcd for $C_{22}H_{21}ClO_2S$: C, 68.66; H, 5.46%.

$CH_3(CH_2)_4CPhClTs$: Mp 66—67 °C (recrystallized from hexane). NMR ($CDCl_3$) δ 0.6—1.6 (m, 9H), 2.36 (s, 3H), 2.15—3.20 (m, 2H), 7.07 (d, 2H, J=9 Hz), 7.1—7.5 (m, 5H), 7.35 (d, 2H, J=9 Hz). Found: C, 65.09; H, 6.57%. Calcd for $C_{19}H_{23}ClO_2S$: C, 65.05; H, 6.56%.

$CH_3(CH_2)_4(CH_2Ph)ClTs$: Oil. NMR ($CDCl_3$) δ 0.82 (t, 3H, J=5 Hz), 0.95—2.25 (m, 8H), 2.39 (s, 3H), 3.17 (d, 1H, J=14 Hz), 3.53 (d, 1H, J=14 Hz), 7.14 (s, 5H), 7.23 (d, 2H, J=8 Hz), 7.77 (d, 2H, J=8 Hz).

1,2-Diphenylethanone (11, R=CH_2Ph). To a solution of **10** (100 mg, 0.27 mmol) in trifluoroacetic acid (2 ml) were added silver perchlorate (112 mg, 0.54 mmol) and water (0.5 ml). After refluxing for 1 h, the reaction mixture was diluted with ether, neutralized with a saturated $NaHCO_3$ solution, washed with water, and dried over Na_2SO_4. The crude residue obtained by evaporation of ether was subjected to preparative TLC (hexane–ethyl acetate 5 : 1 v/v) to give **11** (45 mg, 85%, mp 50—54 °C (lit, 55—56 °C)). IR and NMR spectra were in accordance with those of authentic sample.

In a similar way, other aromatic ketones (**11**, R=CH_2CH_2-Ph, $(CH_2)_4CH_3$) were obtained as shown in Table 3.

References

1) R. T. Arnold and S. T. Kulenovic, *J. Org. Chem.*, **43**, 3687 (1978).

2) a) H. Kotake, K. Inomata, Y. Murata, H. Kinoshita, and M. Katsuragawa, *Chem. Lett.*, **1976**, 1073; b) K. Inomata, Y. Nakayama, M. Tsutsumi, and H. Kotake *Heterocycles*, **12**, 1467 (1979) and references cited therein; c) H. Kotake, K. Inomata, and M. Sumita, *Chem. Lett.*, **1978**, 717; d) K. Inomata, H. Kinoshita, H. Takemoto, Y. Murata, and H. Kotake, *Bull. Chem. Soc. Jpn.*, **51**, 3341 (1978).

3) Meyers and his co-workers proposed the radical/anion-radical/pair (RARP)mechanism for halogenation of carbanions with carbon tetrahalide: a) C. Y. Meyers, A. M. Malte, and W. S. Mathews, *J. Am. Chem. Soc.*, **91**, 7510 (1969); b) C. Y. Meyers and L. L. Ho, *Tetrahedron Lett.*, **1972**, 4319; c) C. Y. Meyers and V. M. Kolb, *J. Org. Chem.*, **43**, 1985 (1978).

4) K. Inomata, S. Aoyama, and H. Kotake, *Bull. Chem. Soc. Jpn.*, **51**, 930 (1978).

5) The chloro sulfone (**10**) was not hydrolyzed by the method described for chloro sulfide hydrolysis; P. Bakuzis, M. L. F. Bukuzis, C. C. Fortes, and R. Santos, *J. Org. Chem.*, **41**, 2769 (1976).

Evidence for Electron-transfer Process in Abnormal Grignard Reactions. Enolization and α-Diketone Formation

Masao Ōkubo,* Yoshiaki Morigami, and Reiko Suenaga

Department of Chemistry, Faculty of Science and Engineering, Saga University, Honjō-machi, Saga 840

(Received January 30, 1980)

Synopsis. The effect of 2,6-dimethyl groups on enolization *vs.* addition in the reaction of PhMgBr with $PhCH_2COPh$, and also the formation of α-diketone from $2,4,6\text{-}Me_3C_6H_2COCl$ by the treatment with MeMgX and *i*-PrMgX in the presence of $CoCl_2$, were studied. The results were discussed on the basis of electron-transfer mechanism.

In Grignard reaction of carbonyl compounds, steric hindrance affects greatly the concentration as well as the spin distribution of initially formed ketyl radicals and consequently the course of reaction.[1,2] Correlation between the spin density and the product distribution was discussed in the studies on aromatic substitution,[1] replacement of anionoid substituents,[2] and conjugate addition.[2] Among representative abnormal Grignard reactions, enolization of ketones[3] and α-diketone formation from hindered aroyl chloride[4] remanined to be studied on the same basis. Some results obtained in these reactions will be reported and discussed in this paper.

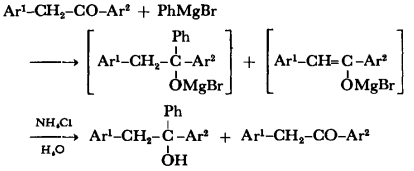

Scheme 1.

Enolizable ketones studied are benzyl phenyl ketone and its *o*-methyl derivatives (Table 1, **1**, **2**, **3**, and **4**), the reaction with PhMgBr being shown in Scheme 1. The reaction was carried out in tetrahydrofuran (THF) under nitrogen atmosphere, the reaction mixture being heated at 50 °C for 30 min. The cooled reaction mixture was quenched with saturated aqueous NH_4Cl. A mixture of products obtained after removal of solvent was heated with 50% H_2SO_4 to convert the alcohols (normal adducts) into the corresponding triarylethylenes (Scheme 2). The product mixtures were finally submitted to GLC analysis. The product distributions thus determined are summarized in Table 1.

Table 1. Product distribution in the reaction of hindered benzyl phenyl ketones

No.	$Ar^1\text{-}CH_2\text{-}CO\text{-}Ar^2$ structure	[PhMgBr]/[Ketone]	Product distribution (%) Recovered ketone	Product distribution (%) $Ar^1\text{-}CH\text{=}C(Ar^2)Ph$
1	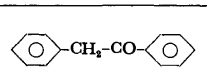	1	36	64
		1.5	27	73
		2	3	97
		3	2	98
2	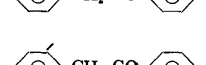	1	78	22
		5	66	34
		10	54	46
3	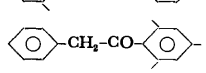	10	100	0
4	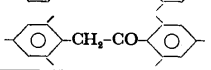	10	100	0

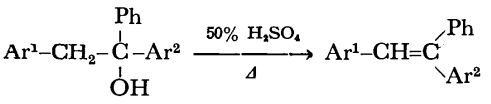

Scheme 2.

The results show that the presence of 2,6-dimethyl groups affect remarkably the product distribution: the groups on the benzoyl moiety do much more greatly than those on the benzyl moiety, thus inhibiting normal addition completely. In order to estimate the extent of enolization, the reaction mixtures of **3** and **4** were quenched with $D_2O\text{–}D_2SO_4$. Analyses of the NMR spectra show that the recovered **3** has been enolized quantitatively while **4** to *ca.* 60%.

ESR signals were detected in the reactions of **3** and **4** at room temperature. Failure to detect ESR signals in the cases of **1** and **2** is quite reasonable, since it is known that ketones having α-hydrogen atom cannot give stable metal ketyls due to rapid decomposition.[5,6] Existence of the initial electron-transfer step from Grignard reagent to substrates is generally accepted on the basis of recent mechanistic studies.[7,8] The failure to detect ESR signals in the cases of **1** and **2** is thus ascribable to the rapid subsequent processes: enolization and addition.

ESR signal observed in the case of **3** ($a_{\alpha\text{-H}}=2.6$) disappeared completely after heating the reaction mixture at 50 °C for 30 min, whereas that in the case of **4** ($a_{\alpha\text{-H}}=7.5$[9]) did not. In spite of the expected high spin density on the carbonyl carbon atom due to the sterically suppressed spin delocalization on the hindered phenyl group, the fair stability of these ketyls at room temperature could be ascribed to their conformation (Fig. 1): the direction of the $C_\alpha\text{–}H_\alpha$ bond is not in trans to that of the free spin orbital and the free spin may be stabilized by the spatial assistance of the π-electrons of the aryl group on the benzyl moiety (**3a** and **4a**). Predominance of these eclipsed conformations is rationalized since at least two THF molecules affect greatly the bulkiness of the –OMgBr group. By heating the reaction mixture of **3**, however, the conformational rotation to the staggered form (**3b**) occurs, allowing the direction of the $C_\alpha\text{–}H_\alpha$ bond to be in full trans to

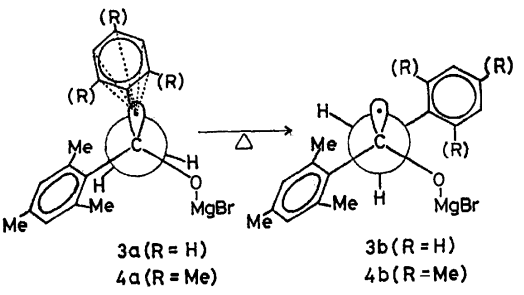

Fig. 1. Conformation of the ketyl radicals of **3** and **4**.

that of the free spin orbital. This conformation is responsible for the β-scission of the α-hydrogen atom, the original ketone **3** being thus enolized. The great stability of the ketyl of **4** is thus ascribed to the sterically retarded conformational change from **4a** to **4b** (Fig. 1) caused by the hindered aryl group of the benzyl moiety. It should be noted that the electron-transfer process was confirmed for the first time in the reaction of enolizable ketones.

The formation of α-diketone(2,2′,4,4′,6,6′-hexamethylbenzil) from hindered 2,4,6-trimethylbenzoyl chloride by the treatment with Grignard reagents (Scheme 3; R=Me, X=Br and I) in the presence of a catalytic amount of $CoCl_2$ was reported.[4] If isopropylmagnesium halide (Scheme 3; R=*i*-Pr, X=Cl, Br, and I) is used, the bulkier isopropyl group is expected to raise the yield of α-diketone.

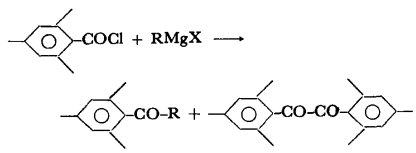

Scheme 3.

The reaction was carried out in diethyl ether to compare our result with the previous one.[4] A very high yield of the α-diketone was realized by the treatment with *i*-PrMgI (Table 2). This result, however, is explicable in terms of the electron-transfer ability of the reagent instead of ambiguous effect of bulkiness. The thermographic[10] and electrolytic[11] studies of Grignard reagents show that the isopropyl reagent is much more electron-donating than the methyl reagent. Iodide ion has an oxidation potential much lower than that of bromide ion,[12] and is favorable to the α-diketone formation as shown in Table 2. It is thus reasonable to consider that the combination of isopropyl group and iodide ion can transfer single electron to the aroyl chloride most effectively among the five reagents examined.

Table 2. Yields of the α-diketone

Grignard Reagent	Yield of 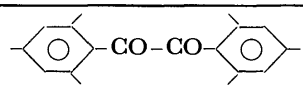 (%)
Me_2CHMgI	87
$Me_2CHMgBr$	38
$Me_2CHMgCl$	22
MeMgI	63[a]
MeMgBr	31[a]

a) The previous results[4] were reproducible.

Though volatile products[4] could result from *i*-Pr· as well as the equivocal role of $CoCl_2$ remains still to be examined, initial electron-transfer from Grignard reagent to the benzoyl chloride followed by releasing of chloride anion should be emphasized, consequently producing the hindered aroyl radical (Scheme 4) to dimerize to give the α-diketone.

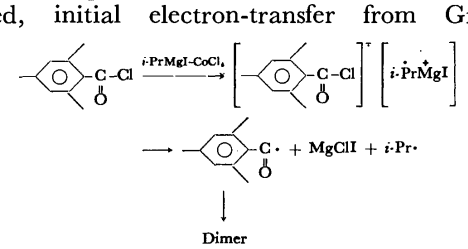

Scheme 4.

Experimental

Materials. Melting points are uncorrected. Friedel-Crafts' method using phenylacetyl chloride was applied to prepare **1** and **3**; **1**: mp 57—59 °C, **3**: mp 101—103 °C. 2,4,6-Trimethylphenylacetyl chloride was used to prepare **2** and **4**; **2**: mp 164.5—165 °C, **4**: mp 181—182 °C. Anthydrous $CoCl_2$ was prepared from commercial hydrated salt.[4] Authentic sample of the α-diketone was prepared according to the reported method[4] using isopropylmagnesium iodide: mp 120.5—122 °C (lit,[4] mp 119—120 °C).

Procedures. PhMgBr (0.0276 mol) in 20 ml THF was prepared in the usual manner. The Grignard solution was cooled to 0 °C and the ketone **1** dissolved in 20 ml THF was added rapidly; the resulting mixture was heated at 50 °C for 30 min. The subsequent procedures were described in the text. The other ketones were treated similarly. The ketones **3** and **4** were recovered quantitatively even by the treatment with 10 molar equivalents of PhMgBr. The apparatus used for ESR measurements was reported previously.[13]

i-PrMgX (0.021 mol) was prepared in diethyl ether (25 ml). $CoCl_2$ (0.0002 mol) was added under N_2, and the resulting black solution was transferred under N_2 into a dropping funnel, the reaction with the aroyl chloride (0.007 mol) in diethyl ether (25 ml) being carried out in the manner of reverse addition.[4] The product mixtures obtained in the reactions of the respective Grignard reagents were submitted to high pressure liquid chromatography on silica gel by use of methyl alcohol–water (65 : 35) as eluent under the pressure of 30 kg/cm^2. The yield of the α-diketone was estimated by comparison with a straight calibration line obtained by injection of the authentic sample solutions in benzene.

References

1) M. Ōkubo, *Bull. Chem. Soc. Jpn.*, **48**, 1057, 1327, 2057 (1975).
2) M. Ōkubo, *Bull. Chem. Soc. Jpn.*, **50**, 2379 (1977).
3) E. P. Kohler and R. B. Thompson, *J. Am. Chem. Soc.*, **59**, 887 (1939); F. C. Whitmore and L. P. Block, *ibid.*, **64**, 1619 (1942).
4) M. S. Kharasch, R. Morrison, and W. H. Urry, *J. Am. Chem. Soc.*, **66**, 368 (1944).
5) J. E. Bennett, B. Mile, and A. Thomas, *J. Chem. Soc., A*, **1968**, 298.
6) G. A. Russell and G. R. Stevenson, *J. Am. Chem. Soc.*, **93**, 2432 (1971).
7) T. Holm and I. Crossland, *Acta Chem. Scand.*, **25**, 59 (1971).
8) E. C. Ashby, Lecture given at the Conference of Organometallic Chemistry, Dijon, France, Aug. 1979.
9) The $a_{\alpha\text{-H}}$ values were found from poorly resolved ESR spectra. The value of $a_{\alpha\text{-H}}$ of **4** appreciably greater than that of **3** may be due to the twisting of 2,4,6-$Me_3C_6H_2$-group on the benzyl moiety, delocalization of the free spin being thus suppressed.
10) T. Holm, *Acta Chem. Scand.*, **23**, 579 (1969).
11) T. Holm, *Acta Chem. Scand., B*, **28**, 809 (1974).
12) F. A. Cotton and G. Wilkinson, "Advanced Inorganic Chemistry," 2nd ed, John Wiley and Sons, New York (1966), Chap. 22.
13) K. Maruyama, *Bull. Chem. Soc. Jpn.*, **37**, 897 (1964).

A Convenient One-step Preparation of Oxacyclanes by Dehydration of Diols over Alumina

Yoshihisa INOUE,* Shokichiro DEGUCHI, and Tadao HAKUSHI

Department of Applied Chemistry, Himeji Institute of Technology, Shosha 2167, Himeji, Hyogo 671-22

(Received April 14, 1980)

Synopsis. Dehydration of 1,4-, 1,5-, or 1,6-alkanediols over alumina at 220—250 °C in a distillation apparatus gave the corresponding 5- to 7-membered oxacyclanes in good yield of 51—71%. Diethylene glycol also gave 1,4-dioxane in 49% yield, whereas attempted one-step synthesis of crown ethers from polyethylene glycols in a similar manner resulted in the predominant formation of 1,4-dioxane without any trace of crown ether.

Most aliphatic ethers are prepared by the removal of water from alcohol under acidic conditions.[1] However, this method has not been used extensively and is actually unsuccessful as a general method for the preparation of oxacyclanes from α,ω-alkanediols.[2,3] Oxacyclanes have been synthesized so far from diols *via* many steps.[4-6] Recently, the synthesis of oxacyclanes has been accomplished by the use of dimethyl sulfoxide,[7] sulforane,[8] or carbodiimide,[9] but these syntheses require the use of relatively inaccessible reagents and do not give satisfactory yield for the synthesis of larger-sized oxacyclanes. The use of alumina as a dehydrating agent appears to be well established for the preparation of tetrahydrofuran derivatives from 1,4-diols.[10,11] An attempted extension of the method to prepare smaller-sized oxacyclanes has been unsuccessful[11] and further attempts have not been made so far.

We wish now to present a convenient one-step method for preparing 5- to 7-membered oxacyclanes from diols and also an attempted one-step synthesis of crown ethers from polyethylene glycols. The use of alumina in liquid phase makes the method easy to use and gives good yields.

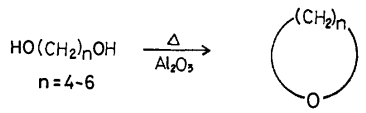

In a typical experiment, a diol was mixed with an equal weight of activated alumina and the mixture was heated up to 220—250 °C in a distillation apparatus fitted with a heating mantle until distillation ceased (*ca.* 5—30 h) to give a corresponding oxacyclane and water as an azeotropic distillate. Dehydration by alumina of 1,4-, 1,5-, or 1,6-alkanediol, *i.e.* **3**, **5**, **7**, or **9**, afforded the oxacyclane, *i.e.* **4**, **6**, **8**, or **10**, in 51—71% isolated yield, although 1,3-butanediol failed to give 2-methyloxetane in a satisfactory yield, probably due to the strain of the four-membered ring. The introduction of other functional group, *i.e.* an additional hydroxyl group or a double bond, resulted in diminished yield of 18—25%.

We also carried out the dehydration of polyethylene glycol by alumina, since this method seemed quite attractive as a simple method for preparing crown ethers. Although the reaction of diethylene glycol over alumina gave 1,4-dioxane in good yield, similar treatment with tri- or tetraethylene glycol resulted in the predominant formation of 1,4-dioxane without any trace of crown ether.

TABLE 1. DEHYDRATION OF DIOLS OVER ALUMINA AT 220—250 °C

Diol		Reaction time/h	Product		(% yield)	Bp/°C
1,4-Butanediol	**3**	20		**4**	(71)	65—66
2,5-Hexanediol	**5**	6	a)	**6**	(58)	92—94
1,5-Pentanediol	**7**	5		**8**	(52)	87—88
1,6-Hexanediol	**9**	18		**10**	(53)	112
1,2,6-Hexanetriol	**11**	30	OH	**12**	(18)	187
3-Hexene-2,5-diol	**13**	12	a)	**14**	(25)	73—75
1,3-Butanediol	**1**	20		**2**	(0.8)[b]	—
Diethylene glycol	**15**	21		**16**	(49)	98—100

a) From ^{13}C NMR spectrum, this ether is shown to be a 1:1 mixture of *cis*- and *trans*-isomers. b) Yield determined by GLC.

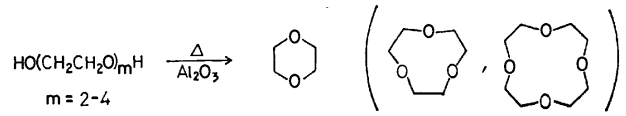

We may conclude this method offers a simple and convenient procedure especially for the preparation of 5- to 7-membered oxacyclanes and its alkyl derivatives.

Experimental

All the diols were commercially available and fractionally distilled prior to use. Commercial alumina for chromatography of 200 mesh (Nakarai Chimicals Co.) was used as a dehydration catalyst after dried for 10 h in an oven at 200 °C.

Dehydration of Diols ***1***, ***3***, ***5***, ***7***, ***9***, ***11***, *and* ***13***. Preparation of oxacyclanes, **2**, **4**, **6**, **8**, **10**, **12**, or **14**, was accomplished in a distillation apparatus by heating a diol with an equal weight of activated alumina at 220—250 °C. The product ether and water was distilled as an azeotropic mixture. The distillate was saturated with salt, and the organic layer was dried, filtered and then fractionally distilled to give the product oxacyclane. The isolated yield and boiling point of the

product are presented in Table. The product ethers (95—99% pure by GLC on polyethylene glycol-20M column) were identified by IR, ^{13}C NMR and, if needed, mass spectra and GLC comparison with the authentic samples.

1,4-Dioxane (16). Dehydration of diethylene glycol (20 g) over alumina (12 g) and the subsequent work-up gave 8.1 g (49%) of 1,4-dioxane. The IR and NMR spectra and GLC retention time were identical with those of the authentic dioxane.

Attempted Synthesis of Crown Ether. The facile preparation of 1,4-dioxane from diethylene glycol prompted us to the one-step synthesis of crown ethers from polythylene glycols. Dehydrations of tri- and tetraethylene glycols over alumina were performed merely to give 1,4-dioxane as a major dehydration product in both cases. Repeated attempts at a reduced pressure also gave dioxane; no cyclic polyethers, *e.g.* 9-crown-3 or 12-crown-4, were produced in any cases.

References

1) Schorigin and Makaroff-Semljanski, *Ber.*, **65**, 1293 (1932); J. F. Norris and G. W. Rigby, *J. Am. Chem. Soc.*, **54**, 2088 (1932); F. S. Birch, R. A. Dean, and E. V. Whitehead, *J. Org. Chem.*, **19**, 1449 (1954).

2) J. Colonge and R. Marey, *Org. Synth.*, Coll. Vol. 4, 350 (1963).

3) A. Frank and A. Kroupa, *Monatsh. Chem.*, **69**, 1741 (1936); *Chem. Abstr.*, **31**, 1360 (1937).

4) C. S. Marvel and H. O. Calvery, *Org. Synth.*, Coll. Vol. 1, 533 (1932); C. F. Allen and F. W. Spangler, *ibid.*, Coll. Vol. 3, 203 (1955); C. R. Noller, *ibid.*, Coll. Vol. 3, 835 (1955).

5) N. L. Drake, H. D. Anspon, J. D. Draper, S. T. Haywood, J. V. Hook, S. Melamed, R. M. Peck, J. Sterling, Jr., E. W. Walton, and A. Whiton, *J. Am. Chem. Soc.*, **68**, 1536 (1946); A. Kirrmann and N. Hamaide, *Bull. Soc. Chim. Fr.*, 789 (1957).

6) M. Fétizon, M. Golfier, and J. M. Louis, *Tetrahedron*, **31**, 171 (1975), R. Nakao, R. Fukumoto, and J. Tsurugi, *J. Org. Chem.*, **37**, 76 (1972).

7) B. T. Gillis and T. E. Beck, *J. Org. Chem.*, **28**, 1388 (1963); V. J. Traynelis, W. L. Herhenrother, J. R. Livingston, and J. A. Valicenti, *J. Org. Chem.*, **27**, 2377 (1962).

8) J. C. Martin, J. A. Franz, and R. J. Arhart, *J. Am. Chem. Soc.*, **96**, 4604 (1974).

9) R. C. Schnur and E. E. van Tamelen, *J. Am. Chem. Soc.*, **97**, 464 (1975).

10) R. H. Clarke, W. E. Graham, and A. G. Winter, *J. Am. Chem. Soc.*, **47**, 2748 (1925); V. N. Ipatieff and R. L. Burwell, Jr., *ibid.*, **63**, 969 (1941); R. C. Olberg, H. Pines, and V. N. Ipatieff, *ibid.*, **65**, 2260 (1943); E. A. Fehnel, S. Goodyear, and J. Berkowitz, *ibid.*, **73**, 4978 (1951).

11) E. L. Wittbecker, H. K. Hall, Jr., and T. W. Campbell, *J. Am. Chem. Soc.*, **82**, 1218 (1960).

A New Synthesis of Allethrolone

Noboru ONO,* Yo TANABE, Rikuhei TANIKAGA, Aritsune KAJI, and Takashi MATSUO**

Department of Chemistry, Faculty of Science, Kyoto University, Kyoto 606
***Institute of Biological Science, Sumitomo Chemical Ind., Takarazuka, Hyogo 665*

(Received May 6, 1980)

Synopsis. A new synthesis of 2-allyl-4-hydroxy-3-methyl-2-cyclopenten-1-one, so called allethrolone is described, in which the Michael addition of 3-phenylthio-5-hexen-2-one to 1-nitro-1-propene followed by conversion of the nitromethyl group in the adduct to an aldehyde function is involved as the key step.

Allethrolone (**4**) is the alcohol component of the allethrine which is a commercially important synthetic homologue of natural occurring pyrethrines. Allethrolone is now prepared in industry by the method of Schechter, which starts from allyl chloride, methyl acetoacetate, and methylglyoxal.[1] Owing to low overall yield of this method, a new efficient method to prepare **4** is desired. Recently, some elegant methods have been devised by Büchi[2] or Schlessinger.[3] Though the yield has been greatly improved by these methods, they require rather expensive starting materials or reagents. This paper presents a new synthesis of **4** starting from readily available materials and by a simple procedure. This new method is outlined in Scheme 1.

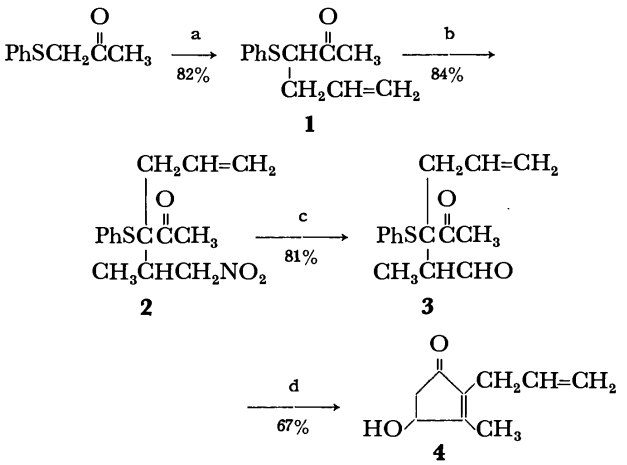

a: CH_2=$CHCH_2Br$, 30% NaOH, b: NaH, CH_3CH=$CHNO_2$ in DMF, c: CH_3ONa-CH_3OH/H_2SO_4-CH_3OH, 1 mol dm^{-3} HCl, d: C_2H_5ONa-C_2H_5OH

Scheme 1. A new synthesis of allethrolone (**4**).

3-Phenylthio-5-hexen-2-one (**1**) was obtained in 82% yield by alkylation of α-(phenylthio)acetone with allyl bromide under phase transfer conditions. The Michael addition of **1** to 1-nitro-1-propene took place at 0 °C in DMF using sodium hydride as a base to give the adduct **2** in 84% yield. The key step of the new method is conversion of the nitromethyl group in **2** to an aldehyde function. In general, a Nef type reaction of 1-nitro-4-alkanones involves some difficulties due to formation of a stable cyclic intermediates.[4] After several unsuccessful trials,[5] **2** could be converted to γ-keto aldehydes (**3**) by treating the *aci*-nitro anion of **2** with sulfuric acid in methanol followed by hydrolysis of the crude product with 1 mol dm^{-3} hydrochloric acid. The conventional method to convert 1-nitro-4-alkanones to γ-keto aldehydes requires protection of the ketone function as an acetal before a Nef type reaction.[4] However, protection of the ketone function of **2** is not required in the present procedure, for the reaction proceeds *via* an intermediate **5** in which the ketone function is already protected.[6]

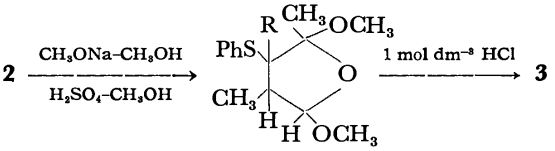

5 R= CH_2CH=CH_2

Finally, **4** was obtained in 67% yield on treatment of **3** with sodium ethoxide in ethanol.

The reactions devised here to prepare **4** can be applied to the synthesis of other related compounds: especially high reactivity of nitroolefins as Michael acceptors for ketone enolates and the simple method to prepare γ-keto aldehydes from 1-nitro-4-alkanones are of special use in organic synthesis.[7]

Experimental

NMR spectra were recorded on a JEOL PS-100 spectrometer. Chemical shift (δ) are given in ppm relative to an internal standard of TMS. IR spectra were recorded on a Hitachi 215 spectrometer, and MS on a Hitachi M-52 spectrometer with 20 eV.

3-Phenyltio-5-hexen-2-one (1). A mixture of α-(phenylthio)acetone[8] (10 g, 0.066 mol), allyl bromide (8.6 g, 0.072 mol), triethylbenzylammonium chloride (0.2 g) in 30% NaOH (100 ml) and benzene (100 ml) was stirred vigorously at 5—10 °C for 10 h. The reaction mixture was poured into water and worked up as usual. Distillation of the crude product afforded **1** (10.1 g, 82%), bp 120—121 °C/2 mmHg (1 mmHg=133.322 Pa); IR (neat) 1710 cm^{-1} (C=O); NMR (CCl_4) 2.20 (s, 3H), 2.4 (m, 2H), 3.60 (t, J=7.2 Hz, 1H), 4.9—5.2 (m, 2H), 5.5—6.0 (m, 1H), 7.5 (m, 5H). Found: C, 69.52; H, 6.82%. Calcd for $C_{12}H_{14}SO$: C, 69.86; H, 6.84%.

3-Allyl-4-methyl-5-nitro-3-phenylthio-2-pentanone (2). A solution of **1** (10 g, 0.048 mol) in 50 ml of DMF was added dropwise to a stirred suspension of NaH (0.05 mol, 50% dispersion in mineral oil) in 200 ml of DMF at room temperature, and the resulting mixture was kept stirring to cease evolution of hydrogen. A solution of 1-nitro-1-propene[9] (4.0 g, 0.048 mol) in 20 ml of DMF was added dropwise to the above DMF solution of the sodium salt of **1** under colling with an ice–salt bath (about −5 °C) and the resulting solution was stirred for 1 h at −5 °C, and then quenched with acetic acid (6 ml). After the usual work up, the crude product was subjected to column chromatography (sliica gel using benzene as an eluent) to give **2** (11.76 g, 84%): IR (neat)

1705 cm^{-1} (C=O), 1555, 1380 cm^{-1} (NO_2); NMR (CCl_4) 1.04, 1.14 (d, d, J=7.0 Hz, 3H), 2.30, 2.35 (s, s, 3H), 2.55 (m, 2H), 2.85 (m, 1H), 4.2—4.5 (m, 2H), 4.9—5.2 (m, 2H), 5.5—6.0 (m, 1H), 7.5 (m, 5H). The product was about 1: 1 mixture of two diasteroisomers and it was used for the next step without further purification.

3-Acetyl-2-methyl-3-phenylthio-5-hexenal (3). A solution of **2** (4.0 g, 0.014 mol) in 15 ml of methanol was added to a stirred solution of sodium methoxide (1 mol dm^{-3}, 16 ml) at −5 °C. The above solution of *aci*-nitro anion was added dropwise at a rate of one drop per second to a stirred solution of 30 ml of sulfuric acid in 120 ml of methanol at −5 °C. When the addition was complete the mixture was poured into 300 ml of dichloromethane and washed with ice water and dilute aqueous sodium hydroxide. The organic layer was dried over anhydrous magnesium sulfate and concentrated *in vacuo* to yield 3.9 g of the product **5**. The crude product was hydrolyzed with 1 mol dm^{-3} HCl (40 ml) at 50 °C for 1 h. After the usual work up, the crude product was subjected to column chromatography (silica gel using benzene as an eluent) to give **3** (2.9 g, 81%): IR (neat) 1720, 1700 cm^{-1} (C=O), NMR (CCl_4) 1.20, 1.38 (d, d, J=7.0 Hz, 3H), 2.40 (s, 3H), 2.55 (m, 2H), 2.8 (m, 1H), 4.9—5.1 (m, 2H), 5.8—6.0 (m, 1H), 7.3 (m, 5H), 9.55, 9.85 (s, s, 1H). The product was aboult 1: 1 mixture of two diastereoisomers.

Allethrolone (4). Compound **3** (2.62 g, 0.01 mol) was dissolved in 30 ml of ethanol which contained 0.01 mol sodium ethoxide. The resulting solution was stirred at room temperature for 1 h and quenched with 1 mol dm^{-3} HCl. After the usual work up, the crude product was subjected to column chromatography (silica gel using benzene–ether as an eluent) to give **4** (1.02 g, 67%); IR (neat) 3400 cm^{-1} (OH), 1720 cm^{-1} (C=O), 1650 cm^{-1} (C=C); NMR (CCl_4) 2.05 (s, 3H), 2.38 (m, 1H), 2.62 (m, 1H), 2.85 (m, 2H), 3.4 (s, 1H), 4.60 (m, 1H), 4.9—5.1 (m, 2H), 5.6—6.0 (m, 1H). MS m/e= 152 (M^+, 30), 137 (23), 124 (27), 123 (12), 111 (12), 109 (100). The spectral data of the product were identical in all respects with authetic allethrolone.

References

1) M. S. Schechter, N. Green, and F. B. Laforge, *J. Am. Chem. Soc.*, **71**, 3165 (1949).

2) G. Büchi, D. Minster, and J. C. F. Young, *J. Am. Chem. Soc.*, **93**, 4319 (1971).

3) R. F. Romanet and R. H. Schlessinger, *J. Am. Chem. Soc.*, **96**, 3701 (1974), other methods, see R. A. Ellison, *Synthesis*, **1973**, 397.

4) E. Keinan and Y. Mazur, *J. Am. Chem. Soc.*, **99**, 3861 (1977).

5) Unsuccessful trials: Reductive method using $TiCl_3$, the classical procedure of a Nef reaction carried out in water, and oxidative methods. Recent development of this field is reviewed, D. Seebach, E. W. Colvin, F. Lehr, and T. Weller, *Chimica*, **36**, 1 (1979), N. Ono and A. Kaji, *Yuki Gosei Kyokai Shi*, **38**, 115 (1980).

6) R. M. Jacobsen, *Tetrahedron Lett.*, **1974**, 3215, where primary nitro compounds were converted to the acetals by a Nef reaction in methanol.

7) Synthetic utility of nitroolefins has been noted in recent years, see Ref. 5. 1-Nitro-1-propene is the best enolonium ion synthon ($CH_3\overset{+}{C}HCHO$) among those known to date. Other known synthons, for example, $CH_3CH{=}C(SCH_3)\overset{\overset{O}{\|}}{S}CH_3$ and $CH_3\underset{\underset{Br}{|}}{C}HCH(OCH_3)_2$ were inert to the sodium salt of **1**.

8) R. C. Fuson and J. H. Koehncke, *J. Org. Chem.*, **14**, 706 (1949).

9) G. D. Buckley and C. W. Scaife, *J. Chem. Soc.*, **1947**, 1471.

Monoterpenoid Synthesis by Transition Metal Catalyzed Coupling of Enediylmagnesium with C_5-Organic Halides

Yasushi KAJIHARA, Katsuhiro ISHIKAWA, Hajime YASUDA, and Akira NAKAMURA*

Department of Macromolecular Science, Faculty of Science, Osaka University, Toyonaka, Osaka 560

(Received May 6, 1980)

Synopsis. A series of isoprene coupling dimers bonded at 1-2, 1-3, 1-4, 2-4, 3-4, or 4-4 position was prepared by regiocontrolled catalysis of trasition metals or without catalysts in the reaction of 2-methyl-2-butene-1,4-diylmagnesium or 3-methyl-2-butenylmagnesium chloride with C_5-alkenyl halides.

Organolithium-[1] or organomagnesium-[2] assisted terpenoid synthesis by insertion of isoprene to metal-carbon bond have recently been extensively studied and transition metal catalysts have been found to be effective for selective 1,4-addition of isoprene to these organometals. We have investigated the monoterpene synthesis using unique bifunctional 2-methyl-2-butene-1,4-diylmagnesium **1**, which is now readily obtainable by direct reaction of magnesium with isoprene.[3] The compound **1** is more reactive than the usual alkyl- or allylmagnesium compounds due to the higher ionicity of metal-carbon bond[3] and has four reactive sites, C_1, C_2, C_3, and C_4, arisen from the following rapid equilibrium, though the most part of it assumes the structure **1b** in tetrahydrofuran. This paper describes the selective synthesis of 1-4 (head to tail), 3-4, and 2-4 bonded isoprene dimers consisting of the same carbon skeleton as naturally occurring monoterpenoids by regiocontrolled catalysis in the reaction of **1** or 3-methyl-2-butenylmagnesium chloride.

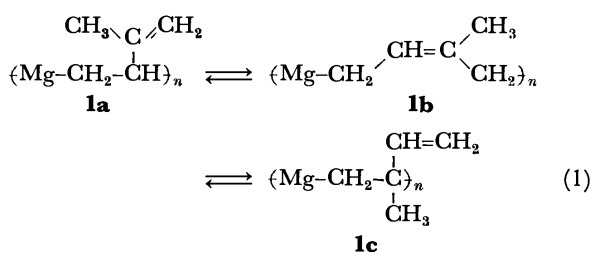

(1)

The 1:1 reaction of **1** with 1-chloro-3-methyl-2-butene in THF at 30 °C for 1 h followed by hydrolysis gave a 4-3 bonded isoprene dimer, 2,3,6-trimethyl-1,5-heptadiene **2** (78%), and a 4-4 bonded dimer, 2,7-dimethyl-1,6-octadiene **3** (22%) in 99% combined yield. Thus, C_3-carbon atom of **1** reacts predominantly. To realize the regioselective control of the various reaction sites in equilibrium, catalysis of Ni(II), Pd(II), and Ti(IV) complexes was examined since these are known as effective catalysts for regio- or stereoselective coupling of allyl halides with organomagnesium compounds.[2,4] The reaction required lower temperatures (0—5 °C) for the effective catalysis because **1** is reactive at 30 °C towards alkenyl halides without catalysts. As shown in Table 1, the addition of Ni(II) or Pd(II) complexes was effective for selective 4-4 coupling of the isoprene units and hydrolysis of the product with dilute aqueous (2 mol dm^{-3}) HCl gave **3** exclusively. This result may be explained by considering **4** as the intermediate. $TiCl_2(\eta^5\text{-}C_5H_5)_2$ and $ZrCl_2(\eta^5\text{-}C_5H_5)_2$ were not so effective for this system presumably due to the formation of catalytically inactive Cp_2M(isoprene) complexes.[5]

Table 1. Regioselection in reaction of **1** with 1-chloro-3-methyl-2-butene in THF[a]

Catalyst	% Ratio of regioisomer		Yield/%
	2	**3**	
None[b]	78	22	99
$NiCl_2(PPh_3)_2$	12	88	72
$NiCl_2$	29	71	65
$PdCl_2(PPh_3)_2$	6	94	75
$PdI_2(PPh_3)_2$	17	83	83

a) Reaction was carried out at 0 °C for 10 h in the presence of catalst (2 mol%) and the reaction mixture was hydrolyzed. b) Reacted at 30 °C for 5 h.

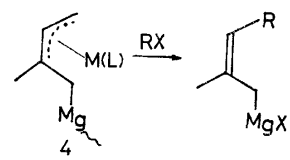

The successful control of the regioselectivity prompted us to prepare myrcene by reaction of **1** with 2-chloromethyl-1,3-butadiene using the Ni(II) catalysts. The reaction proceeds in good yield (75—78%) and myrcene **6** was obtained in 93—95% selectivity by hydrolysis (Table 2). The ratio of α-(**6a**) to β-myrcene **6b** was 8:2 but the ratio changed to 3:7 by protonation with piperidine or pyrrolidine depending on the basicity of protonolysis agents. Similar interconversion have been observed in the protonolysis of enediylmagnesium.[3] In the absence of catalyst, C_3-atom of **1** predom-

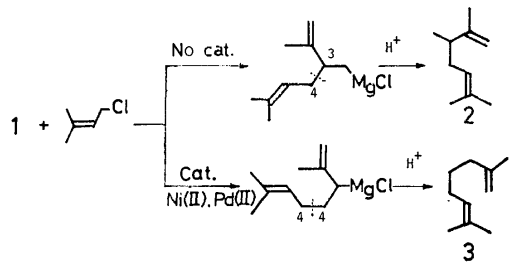

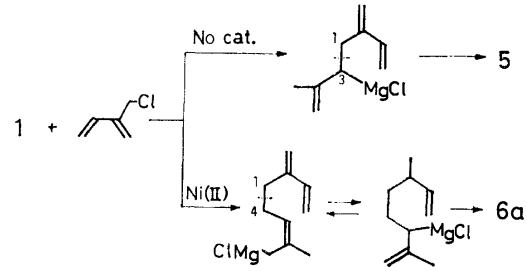

Table 2. Products of transition-metal catalyzed reaction of **1** with 2-chloromethyl-1,3-butadiene in THF[a)]

Catalyst	% Products ratio 5	6	Yield/%
None[b)]	92	8	99
$NiCl_2(dppe)$[c)]	5	95	75
$NiCl_2(PPh_3)_2$	7	93	78
$PdCl_2(PPh_3)_2$	41	59	89
$(\eta^5\text{-}C_5H_5)_2TiCl_2$	73	27	62

a) The reaction mixture was hydrolyzed, after carrying out the reaction at 0 °C for 10 h in the presence of catalyst (2 mol%). b) Reaction was done at 30 °C for 1 h. c) 1,2-Bis(diphenylphosphino)ethane complex.

inantly was alkylated with 2-chloromethyl-1,3-butadiene to give a 1-3 bonded dimer, 2,3-dimethyl-5-vinyl-1,5-hexadiene **5**, consistent with the reaction shown in Eq. 1. The reaction of 3-methyl-2-butenylmagnesium chloride with 2-chloromethyl-1,3-butadiene also produced pure β-myrcene in 92% yield without catalyst. The addition of 2.0 mol% of $PdCl_2(PPh_3)_2$ catalyst caused the production of 2-1 bonded isoprene dimer **7**

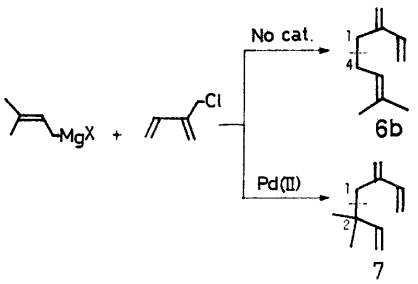

in 80% regioselectivity (68% yield). If this Pd(II) catalyzed reaction is applicable also to the reaction of 3-methyl-2-butenylmagnesium chloride with 1-chloro-3-methyl-2-butene, the 2-4 bonded isoprene dimer whose carbon skeleton is identical with yomogi alcohol or artemisia alcohol should be formed. Actually the 2-4 bonded dimer formed but the selectivity was poor (25%) presumably due to the rapid reaction in the absence of catalyst to give a 4-4 bonded dimer even at 0 °C. The dimer **3** was obtained in 75% selectivity (70% yield) in this case.

One of the most important characteristics of the reaction shown in Eqs. 1 and 2 is that the products still retain the reactivity towards a further attack of dienes or electrophiles for preparation of various derivatives of sesqui- or diterpenes. The regioselectivity observed in the present Ni(II) or Pd(II)-catalyzed reaction is considered to be due to the combined steric and electronic effects of the $-CH_2MgCl$ substituent on the η^3-allyl moiety.

Experimental

2-Methyl-2-buten-1,4-diylmagnesium **1** was prepared as previously noted.[3)] 1-Chloro-3-methyl-2-butene prepared according to the method of Tanaka[6)] and 2-chloromethyl-1,3-butadiene by Alieva's method[7)] were purified by distillation after drying over calcium hydride. All the reaction products were characterized by ^1H NMR, IR, and MS in essentially the same way as described previously.[3)]

*Reaction of **1** with 1-Chloro-3-methyl-2-butene.* To the THF (40 ml) solution of **1** (1.0 g, 11 mmol) was added 1-chloro-3-methyl-2-butene (1.1 ml, 10 mmol) at −70 °C and then transition metal catalysts (2.0 mol% of **1**). The mixture was allowed to react at 0 °C for 10 h under magnetic stirring and was hydrolyzed with 2 mol dm^{-3} HCl after the addition of pentane (50 ml). The pentane fraction was distilled and the products were finally separated by gas chromatography. Resulting 2,3,6-trimethyl-1,5-heptadiene **2** and 2,7-dimethyl-1,6-octadiene **3** were identified with authentic samples obtained from **1** and isoprene.[3)]

*Reaction of **1** with 2-Chloromethyl-1,3-butadiene.* The reaction of **1** (1.0 g, 11 mmol) with 2-chloromethyl-1,3-butadiene (1.0 ml, 10 mmol) was carried out under the same reaction conditions as above mentioned reaction. Piperidine (2.0 ml, 20 mmol) or pyrrolidine (1.7 ml, 20 mmol) was added and the mixture was heated to 50 °C for 30 min for the complete protonation. Resulting α- and β-myrcene were identified with authentic samples purchased from Takasago Perfumary Co. with NMR and IR. Characterization of the 1-3 bonded isoprene dimer was made from the following data.

2,3-Dimethyl-5-vinyl-1,5-hexadiene: IR (neat) 1644, 1595, 992, 891 cm^{-1}; NMR($CDCl_3$) δ=6.38 (d of d, 1, J=10.3 and 16.9, CH), 5.23 and 5.00 (two d, 4, CH_2), 4.69 (d, 2, J_{gem}= 1.9, CH_2), 2.26 (d, 2, J=7.8, CH_2), 2.02 (m, 1, CH), 1.69 (s, 3, CH_3), 0.99 (d, 3, CH_3); M^+ 136. Calcd for $C_{10}H_{16}$; M, 136.

Reaction of 3-Methyl-2-butenylmagnesiumchloride with Alkenyl Halides. To the 3-methyl-2-butenylmagnesiumchloride (1.4 g, 11 mmol) in THF (40 ml) was added THF solution (5 ml) of 2-chloromethyl-1,3-butadiene (1.0 ml, 10 mmol) or 1-chloro-3-methyl-2-butene (1.1 ml, 10 mmol) at −70 °C. Reaction was carried out at 0 °C for 10 h. The reaction products were distilled, isolated with preparative GC and identified with authentic samples[3)] except the followings.

*3,3-Dimethyl-5-vinyl-1,5-heptadiene **7**.* IR (neat) 1640, 1593, 1415, 1382, 1366, 990, 895 cm^{-1}; NMR ($CDCl_3$) δ= 6.36 (d of d, 1, CH), 5.87 (d of d, 1, CH), 5.25 and 5.00 (two d, 2, CH_2), 5.03 and 4.85 (two d, 2, CH_2), 4.96 (bs, 2, CH_2), 2.21 (s, 2, CH_2), 1.01 (s, 6, CH_3); M^+, 136. Calcd for $C_{10}H_{16}$; M, 136.

3,3,6-Trimethyl-1,5-heptadiene(2-4 Bonded Dimer). IR (neat) 1674, 1643, 995, 908, 884, 830 cm^{-1}; NMR ($CDCl_3$) δ=5.80 (d of d, 1, CH), 5.51 (t, 1, CH), 4.68 and 4.91 (two d, 2, CH_2), 2.25 (d, 2, CH_2), 1.98 (bs, 12, CH_3); M^+, 138. Calcd for $C_{10}H_{18}$; M, 138.

References

1) K. Takabe, T. Katagiri, and J. Tanaka, *Chem. Lett.*, **1975**, 1031, 3005.

2) S. Akutagawa and S. Otsuka, *J. Am. Chem. Soc.*, **97**, 6870 (1975).

3) H. Yasuda, Y. Nakano, K. Natsukawa, and H. Tani, *Macromolecules*, **11**, 586 (1978).

4) K. Tamao, K. Sumitani, and M. Kumada, *J. Am. Chem. Soc.*, **94**, 4374 (1972); M. Yamamura, I. Moritani, and S. Murahashi, *J. Organomet. Chem.*, **91**, C39 (1975).

5) H. Yasuda, Y. Kajihara, and A. Nakamura, Abstract C47, IXth International Conference on Organometallic Chemistry, Dijon, France, 1979.

6) J. Tanaka, T. Katagiri, and M. Yamada, *Nippon Kagaku Zassi*, **87**, 877 (1966).

7) S. I. Sadykh-Zade, N. T. Sultanov, and M. Alieva, *Azerb. Khim. Zr.*, **4**, 42 (1966).

ESR Studies of Abnormal Methyl Radicals on Various Solid Surfaces

Duro A. ODUWOLE* and Barrie WISEALL†

Department of Chemistry, Queen Mary College, Mile End Road, London, E1 4NS, U. K.

†*Department of Chemistry, City of London Polytechnic, Jewry Street, London, EC1N 2EY, U. K.*

(Received November 5, 1979)

Synopsis. Direct spectroscopic evidence is presented that strongly caged methyl iodide (or methane) molecules in *porous* surfaces are the precursors of abnormal methyl radicals. The implication of this result as concerns the nature of radical surface interaction is discussed in terms of a matrix effect.

The ESR spectra of methyl radicals trapped on solid surfaces are of interest because of their potential usefulness in surface studies. Previous independent studies using different surface types reported a number of inconsistent observations[1-3] and no collective study of these surfaces has appeared in literature. The most stable radical, the normal methyl radical (Me_n, a $\approx$2.3 mT) has been observed over a wide range of temperatures on different surfaces.[1,2,4] Interactions between the Me_n radical and surface silanol groups characterized by observable satellite lines, led to acceptable models of stabilization of this species. The formation of abnormal methyl radicals (Me_{ab}, a $\approx$1.9—2.1 mT) which are not commonly observed even at liquid nitrogen temperatures, is far less understood. Studies of this species on porous Vycor glass[1] and silica gel[2] surfaces suggested inconsistent mechanisms of stabilization. The present study of the formation of Me_{ab} radicals on various surfaces (Table 1) demonstrates a surface porosity dependence and shows for the first time, the stabilization of this species on a low temperature pretreated surface. A very low surface coverage of methyl iodide ($\approx$0.2%) is found necessary for their stabilization while larger coverages lead to complex radical kinetics which depend markedly on surface type, photolysis time and intensity since this radical is quickly swamped by the growth of Me_n radicals.

After the initial thermal pretreatment of the various silica surfaces under vacuum at specified temperatures (T_d) as generally described,[1-4] the surfaces were given an approximately 0.2% surface coating of methyl iodide which was left in contact for 1 h. The samples were then pumped under vacuum for 3 h at 373 K to remove physisorbed species. Studies showed that prolonged pumping at higher temperatures up to 500 K reduced only the yield of Me_n radicals but *not* the yield of Me_{ab} radicals on photolysis. Radicals were produced by UV photolysis with the full focussed radiation from a Hanovia medium pressure lamp.

A study of the yield as a function of pretreatment temperature shows enhanced yields on high T_d surfaces (Fig. 1), consistent with an expected decrease in the number of surface –OH groups. The relative yield

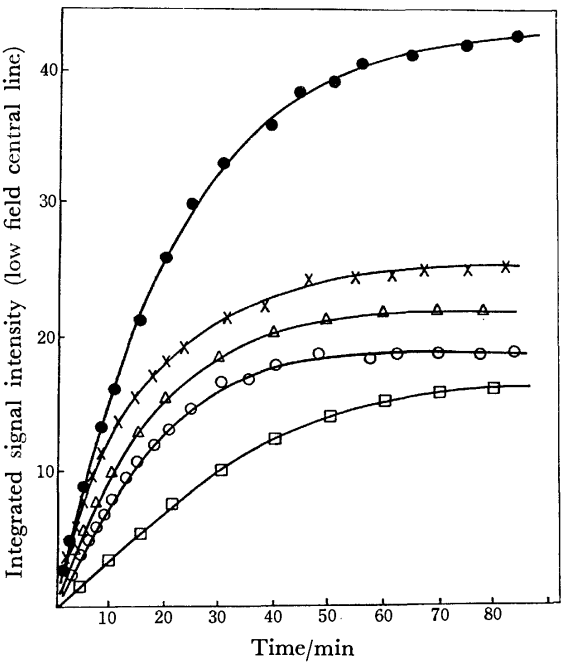

Fig. 1. The yield of abnormal methyl radicals at 77 K on macroporous silica gel surfaces pretreated at various temperatures (T_d).
T_d; ●: 1073 K, ×: 873 K, △: 773 K, ○: 673 K, □: 473 K.

TABLE 1. A LIST OF THE VARIOUS SILICA SURFACES AND THE CONSTANT RATIO OF Me_{ab} AND Me_n RADICALS STABILIZED ON THEM AFTER PROLONGED PHOTOLYSIS AT 77 K

Surface type	Manufacturer	Mean pore diameter[a] (nm)	Purity (%)		Me_{ab}/Me_n ratios at various T_d			
			SiO_2	B_2O_3	473 K	673 K	873 K	1073 K
Macroporous silica gel	Davidson/Grace Ltd.	11.5	99.8	—	7.3	15.5	23.0	35.5
Normal porosity silica gel	Hopkin & Williams Davidson/Grace Ltd.	2.2	99.8	—	0.8	2.5	4.4	6.8
Porous Vycor glass (Code 7930)	Corning Glass Works Ltd.	4.0	96.3	3	2.0	5.1	8.3	12.0
Cabosils	Cabot Carbon Ltd.	(non-porous)	99.8	—	b)	b)	b)	b)
B_2O_3 enriched glass	Glass Tubes and Components Ltd.	(non-porous)	77.5 66.8	16.5 21.8	b)	b)	b)	b)

a) Quoted by manufacturers. b) Me_n radical only observed for these cases.

TABLE 2. THE HYPERFINE CONSTANTS AND LINE WIDTH PARAMETERS (ΔH_{pp}) OBSERVED FOR ABNORMAL METHYL RADICALS STABILIZED ON POROUS VYCOR GLASS AND SILICA GEL SURFACES AT 77 K

Surface type	Pretreatment temperature / K	$a_H \pm 0.005$ mT	$\Delta H_{pp} \pm 0.005$ mT (for lines to increasing field)			
Porous Vycor glass	673	1.925	0.170	0.106	0.183	0.306
	1073	1.930	0.171	0.127	0.172	0.333
Silica gels (normal porosity and macroporous)	673	2.050	0.195	0.110	0.112	0.207
	1073[a]	2.025[b]	0.155	0.060	0.042	0.115
		2.080[c]	0.140	0.060	0.054	0.082

a) Two types of the radical (Me_{ab_1} and Me_{ab_2}) are identified on the surfaces pretreated above 870 K. b) Me_{ab_1} radical. c) Me_{ab_2} radical.

of radicals $\frac{Me_{ab}}{Me_n}$ obtained after prolonged photolysis of identically prepared samples of the various surface types (Table 1) increases with the surface porosity. No evidence of Me_{ab} radical formation on non-porous surfaces was found under any condition of sample preparation; the absence of this species on B_2O_3 enriched glass throws some doubt on the impurity-stabilization mechanism previously suggested.[1] The results strongly suggest that caged methyl iodide molecules which were not removed by prolonged pumping under vacuum at temperatures up to 500 K are precursors of Me_{ab} radicals.

It has been shown previously[5] that Me_n radicals trapped on various silica surfaces exhibit identical spectral parameters (ignoring small distortions caused by second order effects). The parameters observed for Me_{ab} radicals (Table 2) however, depend markedly on surface type; these suggest that Me_{ab}, rather than Me_n radicals,[4] are more effective labels for surface studies. These spectral differences may be explained by a matrix effect[6] in which interactions between the radical and the matrix particles can restrict radical rotations (causing line broadening) and reduce the hyperfine constants as compared to the Me_n radical. Since porous Vycor glass also contains boron (^{11}B has $I=3/2$), coupling with the quadrupole moments could produce the additional line broadening observed for Me_{ab} radical on this surface. This interpretation is in accord with the work of Fujita *et al.*[7] who showed that the reduced hyperfine constants observed for Me_{ab} radicals on porous Vycor glass and other matrices represent charge transfer to their environments. It can thus be deduced from our data that the charge transfer effect is greater for porous Vycor glass than for silica gel surfaces.

Two species of the abnormal radical, namely Me_{ab_1} and Me_{ab_2} are identified on silica gel pretreated above 870 K (Table 2). It is suggested that Me_{ab_2} radical observed only on these surfaces interacts with siloxane bridges known to occur under these conditions. A variable temperature study shows that Me_{ab_2} is relatively unstable and is not observed even under continuous photolysis at 98 K. Previous authors[2] have suggested the presence of the Me_{ab_2} radical but their results have been open to various interpretations such as a further splitting of Me_{ab_1} spectrum by a nuclear spin $I=1/2$ which produces line separations increasing to high field due to second order effects. This is the first study to identify this radical unambiguously. Matrix effects probably preclude resolution of Me_{ab_2} radical on porous Vycor glass.

Fujieda *et al.*[3] previously reported that the ESR spectra of methyl radicals produced from one monolayer of methane adsorbed on alumina surfaces show a partially resolved sextet structure and deduced that the three methyl protons in this system are not equivalent, one or two interacting more strongly with the surface than the other. However, the present study shows that by pumping off weakly adsorbed CH_4 a well resolved quartet (a ≈ 2.0 mT) is observed. Thus the non-equivalence of the 3 methyl protons suggested by Fujieda arises from their experiment conditions and could be due to dipolar interactions and other secondary causes.

References

1) a) M. Fujimoto, H. D. Gesser, G. B. Garbutt, and A. Cohen, *Science*, **154**, 381, (1966); b) G. B. Garbutt and H. D. Gesser, *Can. J. Chem.*, **48**, 2685 (1970).

2) S. Kubota, M. Iwaizumi, and T. Isobe, *Bull. Chem. Soc. Jpn.*, **44**, 2684 (1971).

3) S. Fujieda, M. Setaka, and T. Kwan, *Chem. Lett.*, **1972**, 43.

4) G. R. Joppien and J. E. Willard, *J. Phys. Chem.*, **78**, 1391 (1974).

5) D. Oduwole, J. D. Barnes, and B. Wiseall, *J. Chem. Soc., Chem. Commun.*, **1978**, 164.

6) F. J. Adrian, *J. Colloid Interface Science*, **26**, 317 (1968).

7) Y. Fujita, T. Katsu, and M. Sato, *J. Chem. Phys.*, **61**, 4307 (1974).

The Hydrothermal Activation of Silica–Alumina for Butene Isomerization. A Device to Prepare a Standard Sample

Shozo Furuyama,* Osamu Murashita,** Yuko Yukumoto, and Tetsuo Morimoto
Department of Chemistry, Faculty of Science, Okayama University, Tsushima, Okayama 700
(Received October 11, 1979)

Three kinds of silica–alumina catalysts were prepared by hydrothermal treatment (heating a sample in hot water) over the range of 25—250 °C for various periods. It was found that the hydrothermal treatment significantly increased its catalytic activity for butene isomerization. The dependencies of various surface properties (the production ratio of 2-butene isomers, the surface acidity, the surface area, the pore-size distribution, and the shape and size of the catalyst particle) on the hydrothermal conditions and the kind of starting catalyst sample were systematically investigated, too. It was concluded that the increase in the catalytic activity might be due to the progress of the Si/Al isomorphic substitution in the tetrahedral surface silica network. Hot water might serve as a solvent for the cations and facilitate their movements. Since the hydrothermal treatment can erase the effects of the blending method on the catalytic activity and other surface properties almost completely, this treatment can be used to prepare a standard sample.

Structural change in minerals is accelerated by the action of hot water.[1] Numerous minerals, including optically active quartz and various kind of zeolites, are synthesized using this action in the laboratory.[2,3] We have attempted similarly to use the action of hot water for the preparation and/or activation of various metal oxide catalysts.

Silica–alumina is a strong solid acid and is widely used as a catalyst for various reactions.[4] From the similarities to zeolite in composition, acidic nature, and other aspects, it has been accepted by many workers that the acid center of silica–alumina originates from the isomorphic substitution of a silicon atom by an aluminum atom in the tetrahedral silicate network.[4,5] To obtain an active catalyst, one must devise a method to promote the isomorphic substitution effectively. The action of hot water may be appropriately used for this purpose.

In the present paper, we will demonstrate that hydrothermal treatment (heating a sample in hot water) significantly increases the catalytic activity for butene isomerization. The reasons for this increase were studied by measuring systematically the variations in the surface acidity, the production ratio of 2-butne isomers, the surface area, *etc.* with the hydrothermal time and temperature. A systematic elucidation of the relationship between the structure of an acid site and its catalytic function for butene isomerization has been made elsewhere, using a catalyst prepared by means of the hydrothermal activation technique.[6]

Experimental

Materials. Three kinds of hydrothermally activated silica–alumina (SA) materials were prepared as follows. Silica hydrogel was prepared by the hydrolysis of one part of doubly distilled tetraethyl silicate by five parts of water at 100 °C under vigorous agitation.[7] Alumina hydrogel was prepared by the hydrolysis of vacuum-distilled aluminum isopropoxide by dropping water into it under vigorous agitation. To prepare the SA-25MHT sample, these two hydrogels were mixed thoroughly (alumina content: 25 wt%) and dried at 110 °C for 1 d. Then, the sample was calcined at 400 °C for 20 h and at 550 °C for 5 h in air, and finally exposed to wet air in a rotary kiln at 110 °C for 5 h. The silica–alumina dry gel (SA-25M) thus prepared was heated in hot water over the range of 25—250 °C in a Pyrex ampoule for various periods. To prepare the SA-*n*KHT sample, silica and alumina hydrogels were dried separately at 110 °C and then blended using an agate mortar and pestle for 30 min. (*n* denotes the alumina content, ranging from 0.1 to 50 wt%). The blended dry gel (SA-*n*K) was heated in hot water at 110 °C for various periods. To prepare the SA-*n*JHT sample, the silica and alumina hydrogels were mixed thoroughly (the alumina content, *n*, ranged from 0.1 to 50 wt%) and then heated in hot water in a Pyrex ampoule at 110 °C for 3 d. All these three kinds of samples were dried at 110 °C for 1 d before storage. Tokyo Kasei reagent-grade 1-butene was kept in a 3-L Pyrex bulb after having been passed through dry molecular sieves 3A. Nakarai reagent-grade butylamine was dried with sodium hydroxide and distilled before use. Nakarai reagent-grade color indicators (methyl red, dicinnamylideneacetone, and anthraquinone) were used without further purification.[8]

Procedure. A conventional vacuum apparatus equipped with a circulation reactor (240 ml) was used to measure the catalytic activity for the 1-butene isomerization. A catalyst (0.15 g) was degassed at 300 °C for 2 h and kept at 0 °C during the reaction. At appropriate intervals after the introduction of about 16×10^3 Pa of 1-butene, small portions of the reacting gas were withdrawn in sequence into gas samplers kept at 77 K. The composition of the reacting gas was analyzed by means of a gas chromatograph equipped with a 5-m dioctyl phthalate column kept at 0 °C. To measure the acidity, the catalyst (0.2 g) was degassed at 300 °C for 2 h. After having been cooled to room temperature, the catalyst was covered with 10 ml of dry benzene. The acidity was, then, determined by the conventional butylamine titration method.[9,10] The pore-size distribution of the catalyst was determined by applying the Cranston-Inkley method.[11] An electron microscopic photograph was taken by a Hitachi HU-11A with 11,000-times magnification. The X-ray powder pattern was measured by means of a Rigaku Geigerflex.

Results and Discussion

SA-25MHT Series. The variation in the catalytic activity for 1-butene isomerization was measured at 0 °C as functions of the hydrothermal time and the hydrothermal temperature. Since the isomeriza-

** Present address: Scientific Investigation Research Laboratory, Hyogo Prefectural Police, Ikuta-ku, Kobe 650.

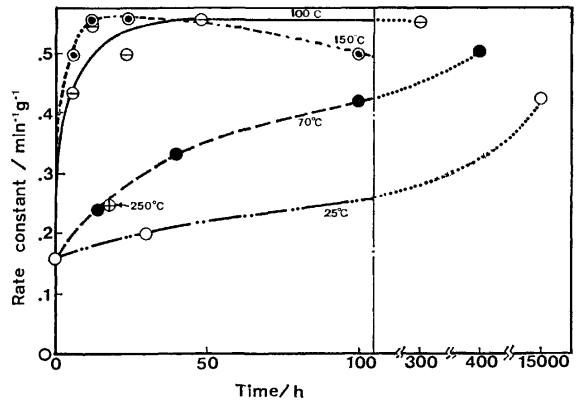

Fig. 1. Variation of apparent rate constant for 1-butene isomerization at 0 °C with hydrothermal time and temperature on SA-25 MHT.

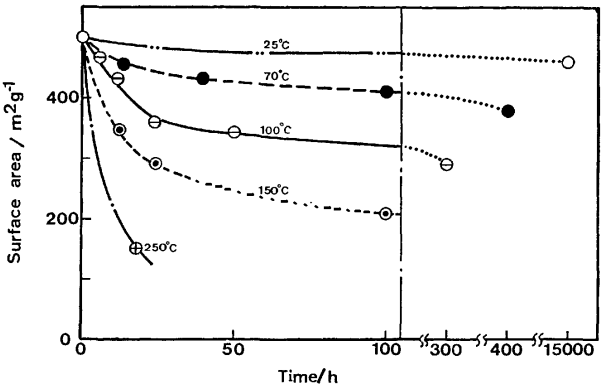

Fig. 2. Variation of surface area with hydrothermal time and temperature on SA-25 MHT.

tion of 1-butene to 2-butenes could be approximated to a simple first-order reaction at the initial stage, the apparent rate constant, k_1, was obtained from Eq. 1:

$$k_1 = (1/t) \ln (P_0/P_t). \quad (1)$$

Here, P_0 and P_t are the partial pressures of 1-butene at times zero and t respectively. The results are shown in Fig. 1. The figure shows that the catalytic activity of SA-25MHT increased with the increase in the hydrothermal time at first, reached a maximum, and then gradually decreased. This variation became prominent with the increase in the hydrothermal temperature. For instance, it took 50 h at 100 °C to attain the maximum activity, while it took only 12 h at 150 °C.

To elucidate the reason for the increase in the catalytic activity, the changes in the "macroscopic" surface structure (surface area, pore-size distribution, and particle shape), the production ratio of *cis*-2-butene *vs.* *trans*-2-butene (c/t), and the surface acidity with the hydrothermal treatment were measured.

The BET surface area decreased with the increase in the hydrothermal time, as is shown in Fig. 2. Its rate of decrease became prominent with the increase in the hydrothermal temperature. For instance, the surface area decreased to one-third after 18 h at 250 °C, while it remained almost constant even after 15000 h (one year and eight months) at 25 °C. It

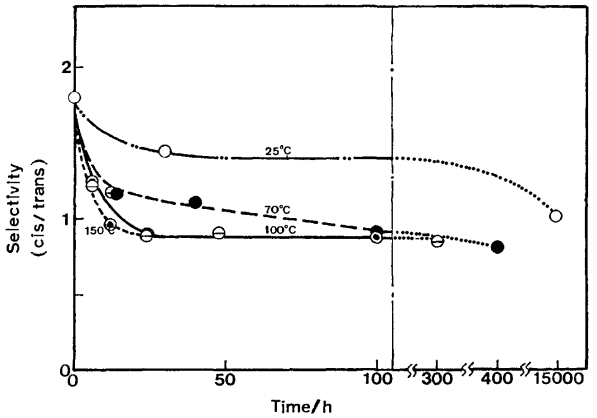

Fig. 3. Variation of selectivity to produce *cis*-2-butene against *trans*-2-butene at 0 °C with hydrothermal time and temperature on SA-25 MHT.

has been observed by several workers that the surface area of silica–alumina decreases significantly when exposed to hot water-vapor, too.[12] However, to attain the same effect as hot liquid-water, vapor needs a much higher temperature (480—950 °C).[12] The measurement of the pore-size distribution showed that the most probable size changed from 4 to 7 nm in diameter over a period of 14 d at 100 °C. Electron microscopic measurement showed that the shape of the elementary particle of the catalyst powder was quite thin and slender before the hydrothermal treatment, but became fat and thick after 14 d at 100 °C. These results clearly showed that the "macroscopic" surface structure changed significantly with the hydrothermal treatment.

The dependency of the c/t ratio upon the hydrothermal treatment is shown in Fig. 3. The value decreased from 1.8 to 0.9 with an increase in the hydrothermal time. It has been observed by many workers that the c/t ratio depends strongly upon the structure of the active site. For instance, the ratio was larger than 3.5 on dry active alumina, while it was around 1 on a typical silica–alumina catalyst.[13] It can be concluded that the hydrothermal treatment changed the structure of the active site ("microscopic" surface structure) from the active-alumina type to the typical silica–alumina type.

The acid amounts, as determined by the butylamine titration method using methyl red ($pK_a=4.8$), dicinnamylideneacetone ($pK_a=-3.0$), and anthraquinone ($pK_a=-8.2$), were 0.95, 0.55 and 0.35 meq g^{-1} respectively before the hydrothermal treatment, but became 0.60, 0.35, and 0.35 meq g^{-1} respectively after the hydrothermal treatment at 100 °C for 14 d. This means that the less active SA-25M had more numerous active sites than the more active SA-25MHT. It was, therefore, concluded that the increase in the catalytic activity with the hydrothermal treatment did not arise from the change in quantity, but resulted from the change in quality, of the active sites in the case of the SA-25MHT series.

The dependencies upon the degassing temperature of the catalytic activity and the c/t ratio for the butene isomerization, the numbers of the surface hydroxyl

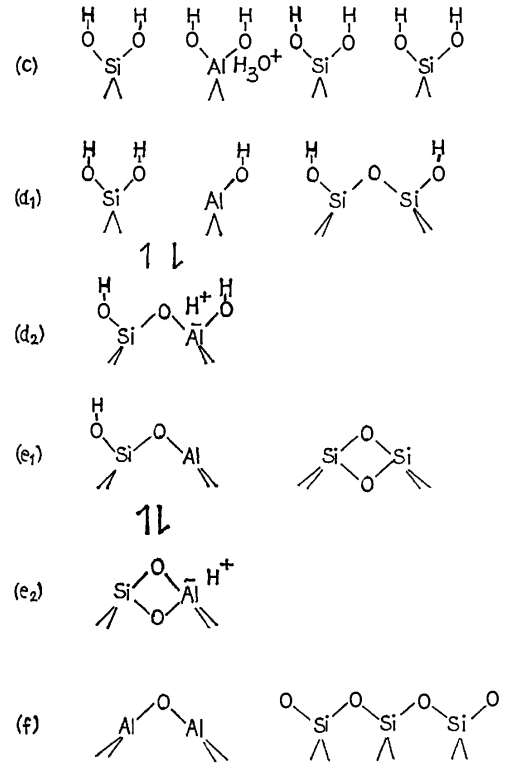

Fig. 4. A schematic representation of the structures of active site existed on SA-25 MHT before and after the hydrothermal treatment.

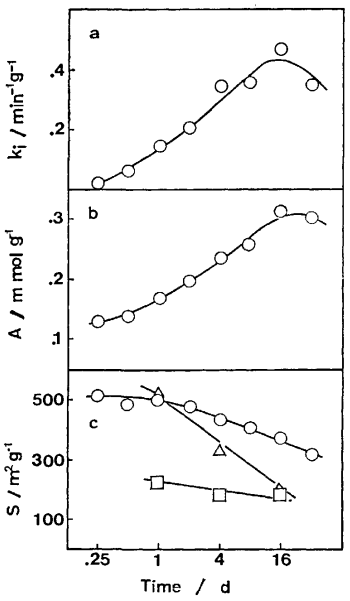

Fig. 5. Variations of (a): apparent rate constant for 1-butene isomerization (k_1) at 0 °C, (b): amount of acid site ($A(H_0 \leq -3.0)$), (c): surface area (S), with hydrothermal time at 110 °C.
○: SA-10KHT, △: silica gel, □: alumina gel.

group and acid sites, and the catalytic activity for the butene polymerization have been studied elsewhere.[6] It has been concluded that the structure of the acid site (*i.e.*, the active site for the butene isomerization) changed thus: (c)→(d)→(e)→(f) with an increase in the degassing temperature from 25 to 700 °C (Fig. 4).[6] The most active site is the (d) site, which has the most suitable structure for the occurrence of proton-donation-acception to promote the isomerization.[6] The (f) site lacks a proton, resulting in quite a low catalytic activity with a high c/t ratio for the isomerization.[6] However, the acid strength of both (d) and (f) sites are equivalent to, or higher than, 48 wt% of sulfuric acid.[6,8] The present results, when combined with those of a study made elsewhere (Ref. 6), can lead to the conclusion that the active site had a structure like (f) (the pseudo-active alumina type) before the hydrothermal treatment, but changed to the (d) site upon the action of hot water. That is, all results could be explained consistently by the assumption that the Si/Al isomorphic substitution was promoted by the hydrothermal treatment.

SA-10KHT Series. The effect of hot water in increasing the catalytic activity was more clearly demonstrated in the experiment using the SA-10KHT sample. Variations in the catalytic activity, the acid amount, and the surface area with the hydrothermal time at 100 °C are shown in Fig. 5. Figure 5a shows that the catalytic activity was negligibly low before the treatment, but increased gradually with the increase in time. It reached a maximum after 16 d and then started to decline. Although the rate of increase was very low (about one-eighth as low as that for the SA-25MHT series), the values of maximum activity did not differ much from each other. The c/t ratio was around 0.9, irrespective of the hydrothermal time.

Figure 5b shows that the acid amount, $A(H_0 \leq -3.0)$, as determined using dicinnamylideneacetone, also increased with the increase in the hydrothermal time.[14] The trend was quite similar to the trend of the catalytic activity.[15] Moreover, the maximum value was comparable with that of SA-25MHT, as in the case of the catalytic activity. As was noted in the experimental section, the SA-10K was prepared by a simple mechanical blending of dry silica and alumina gels only. It was unlikely that the active site originating from the Si/Al isomorphic substitution existed before the hydrothermal treatment. The appearances of the catalytic activity with a low c/t ratio and of the acid site ($H_0 \leq -3.0$) on SA-10KHT, therefore, may be proofs of the progress of the isomorphic substitution with the hydrothermal treatment.

The same conclusion was obtained from the trends of the variations in the surface area and the crystallinity of the silica, alumina, and SA-10K samples with the hydrothermal treatment. Figure 5c shows that the surface area of SA-10KHT decreased from 500 to 350 $m^2 g^{-1}$ upon the hydrothermal treatment at 110 °C for 16 d. The surface area of silica decreased very rapidly from 530 to 200 $m^2 g^{-1}$ while that of alumina remained almost constant (200 $m^2 g^{-1}$) during the same period. The combined surface areas of 90 wt% of silica and 10 wt% of alumina before and after the treatment were, therefore, 500 and 200 $m^2 g^{-1}$ respectively. This decrease (300 $m^2 g^{-1}$) was almost twice as large as the decrease for SA-10KHT (150 $m^2 g^{-1}$). The X-ray powder pattern showed that

silica and SA-10KHT kept their amorphous structures, while alumina was altered to boehmite during the hydrothermal treatment. These two facts may show that no pure silica and alumina surfaces were exposed on SA-10KHT.[16] During the hydrothermal treatment, either the Si and Al cations moved from the original particles to different particles and formed a new surface with an aluminosilicate network both on the parent silica and alumina particles.[16] This surface might be quite resistant to the action of hot water. Therefore, the surface area of SA-10KHT did not decrease so rapidly as that of silica,[17] and the boehmite phase was not formed in this sample.

Finally, we should discuss the mechanism of the effect of the hydrothermal process on the present silica–alumina samples. The kinetic behavior of the Si and Al cations in the solid and liquid phases was not paticularily explored in the present study. However, it may not be unrealistic to infer that Si and Al cations can be dissolved in hot water and move from surface to surface *via* the liquid phase (the liquid-phase mechanism). In other words, the role of hot water may be as a medium to take out the cations from the catalyst surface and transfer them to another surface. The idea that hot water is a solvent for metal cations is very common in studies of the hydrothermal syntheses of quartz and zeolite.[2,3] It is possible to imagine other mechanisms, for instance, that the metal cations move *via* surface and/or the bulk of a solid (the solid-phase mechanism). However, it is quite doubtful that those solid-phase mechanisms can account for the following facts more consistently than the liquid-phase mechanism can: (1) the Si/Al isomorphic substitution did occur, even in the SA-10KHT sample, in which Si and Al cations were originally separated in different particles, and (2) the "macroscopic" surface structure changed significantly and simultaneously with the isomorphic substitution. To attain the same effect with hot water-vapor (with which the solid-phase mechanisms actually work), a much higher temperature has been needed.[12] Therefore, the most reasonable conclusion may be that the isomorphic substitution mainly progressed through the liquid-phase mechanism, as far as the present study is concerned.

SA-nKHT and SA-nJHT Series. A series of SA-*n*KHT samples was prepared by hydrothermal treatment at 100 °C for 16 d, and their catalytic activity, surface acidity, and surface area were compared with those of the corresponding SA-*n*JHT samples. Figures 6a and b show that the dependencies of the catalytic activity and surface acidity upon the alumina content in the two series are quite similar to each other. Before the hydrothermal treatment, the catalytic activity and acid amount were about one-third as low as the maximum value in the SA-*n*JHT series, while they were quite low in the SA-*n*KHT series. The hydrothermal treatment could erase, easily and almost completely, the differences in the catalytic activity and surface acidity originating from the difference in the blending method. Thus, it may be concluded that the hydrothermal treatment can be a useful device for preparing a standard sample of the silica–alumina catalyst. The small but parallel difference between their surface areas shown in Fig. 6c may arise from the different hydrothermal times, 16 d for the SA-*n*KHT series and 3 d for the SA-*n*JHT series.

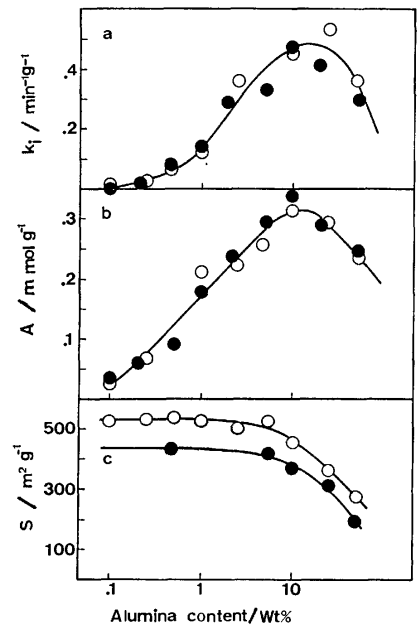

Fig. 6. Variations of, (a): apparent rate constant for 1-butene isomerization (k_1) at 0 °C, (b): amount of acid site ($A(H_0 \leq -3.0)$), (c): surface area (S), with alumina content.
●: SA-0KHT received hydrothermal activation at 110 °C for 16 d, ○: SA-*n*JHT received hydrothermal activation at 100 °C for 3 d.

The authors wish to thank Dr. Koichi Funakoshi (The University of Tokyo) for his measurement of an electron-microscopic photograph.

References

1) H. J. Greenwood, "The Evolution of the Crystalline Rocks," ed by D. K. Baily and Macdonald, Academic Press, New York (1976).

2) a) A. C. Walker and E. Buehler, *Ind. Eng. Chem.*, **42**, 1369 (1950); b) A. C. Walker, *J. Am. Ceram. Soc.*, **36**, 250 (1953).

3) a) R. M. Barrer, *J. Chem. Soc.*, **1948**, 2158; b) D. W. Breck, W. G. Eversole, and R. Milton, *J. Am. Chem. Soc.*, **78**, 2338 (1956).

4) K. Tanabe, "Solid Acids and Bases," Kodansha, Tokyo, and Academic Press, New York (1971).

5) a) C. L. Thomas, *Ind. Eng. Chem.*, **41**, 2564 (1949); b) M. W. Tamele, *Discuss. Faraday Soc.*, **8**, 270 (1960); c) J. J. Fripiat, A. Leonard, and J. B. Uyterhoven, *J. Phys. Chem.*, **69**, 3274 (1965).

6) S. Furuyama, O. Murashita, K. Ichisaka, and T. Morimoto, unpublished.

7) T. Morimoto, M. Nagao, and J. Imai, *Bull. Chem. Soc. Jpn.*, **44**, 1282 (1971).

8) The acid strengths of the acid site, as determined by these indicators, are equivalent to, or higher than, those of 10^{-6}, 48, and 90 wt% of sulfuric acid; H. A. Benesi, *J. Am. Chem. Soc.*, **78**, 5490 (1956).

9) S. Furuyama, T. Tange, O. Murashita, and Y.

Yukumoto, Rept. Res. Lab. Surface Sci., Okayama Univ., **5**, 21 (1980).

10) O. Johnson, *J. Phys. Chem.*, **59**, 827 (1955).

11) R. W. Cranston and F. A. Inkley, *Adv. Catal.*, **9**, 143 (1957).

12) a) W. G. Schlaffer, C. Z. Morgan, and J. N. Wilson, *J. Phys. Chem.*, **61** 714 (1957); b) C. R. Adams and H. H. Voge, *ibid.*, **61**, 723 (1957); c) A Elo and P. Clements, *ibid.*, **71**, 1078 (1967).

13) H. R. Gerberich and W. K. Hall, *J. Catal.*, **5**, 99 (1966).

14) The acid amount, $A(H_0 \leq 4.8)$, determined with methyl red was independent of the hydrothermal time, while that, $A(H_0 \leq -8.2)$, determined with anthraquinone increased, similarly to the acid amount, $A(H_0 \leq -3.0)$, with the increase in the hydrothermal time.

15) Figure 5b shows that there apparently existed about 0.1 meq g^{-1} of acid sites ($H_0 \leq -3.0$) before the hydrothermal treatment. Perhaps, some kind of acid site other than (d) and (f), with a weak catalytic activity, was formed on the interface between silica–alumina particles during the mechanical blending.

16) Hall *et al.* obtained a similar conclusion that silica–alumina is not an intimate mixture of microcrystals of silica and alumina, but a more nearly homogeneous substance; W. K. Hall, H. P. Leftin, F. J. Cheseleske, and D. E. O'Reilly, *J. Catal.*, **2**, 506 (1963).

17) Iler observed the related phenomenon that the solubility of silica in hot water decreased when the Al cation was also present; R. K. Iler, *J. Coll. Interf. Sci.*, **43**, 399 (1973).

 © 1980 The Chemical Society of Japan Bull. Chem. Soc. Jpn., 53, 3044—3049 (1980) [Vol. 53, No. 11

Catalysis by Mixed Oxide Perovskites. I. Hydrogenolysis of Ethylene and Ethane on $LaCoO_3$

Kenji Ichimura,* Yasunobu Inoue, and Iwao Yasumori
Department of Chemistry, Tokyo Institute of Technology, Ookayama, Meguro-ku, Tokyo 152
(Received November 8, 1979)

Catalysis by a mixed oxide with a perovskite structure, $LaCoO_3$, was studied for the hydrogenolysis of ethylene and ethane at temperatures 300—600 K using the hydrogen-excess mixtures. The high and stable activity was obtained by evacuating $LaCoO_3$ at 600 K. Ethylene hydrogenolysis above 420 K proceeded consecutively *via* the intermediate, ethane, to produce methane, whereas only the hydrogenation to form ethane occurred below 420 K. Different temperature dependence of the rate was observed, *i.e.*, the activation energy of -19.3 kJ·mol^{-1} in the range 420—600 K and 33.6 kJ·mol^{-1} in the range 300—420 K. The mechanistic analysis and tracer study using D_2 showed that the slow step of the hydrogenation shifts, with increasing temperature, from the adsorption of hydrogen to the surface reaction between hydrogen atom and ethyl radical. The hydrogenolysis of ethane produced only methane and no ethylene was observed in gas phase; the reaction orders with respect to hydrogen and ethane pressures were, respectively, -0.5 and 1.0. In the reaction with D_2, methane [D_4] was the main product and an equilibrium among the formed H_2, HD, and D_2 was quickly established. The adsorption of ethane to undergo the rupture of the carbon-carbon bond and to form monocarbon species was proposed to be a slow step. The catalytic activities of the component oxides, La_2O_3 and Co_2O_3, were also examined for a comparison. The structure and electronic states of $LaCoO_3$ were investigated by means of X-ray diffraction and X-ray photoelectron spectroscopy in connection with the catalytic activity. It was proposed that the hydrogenation proceeded mainly on a pair of La^{3+} and O^{2-} ions, whereas the hydrogenolysis was accelerated by the Co^{3+} ion; the (110) plane is suggested to be the most favorable for the catalysis.

Recently, the mixed oxides which have a perovskite structure have been recognized as promising catalysts for the reactions involving hydrogen such as the equilibration between H_2 and D_2, the hydrogenation and isomerization of olefins and the hydrogenolysis of hydrocarbons and also as suitable ones for the fundamental research of catalytic activity because of their well-defined structures.[1-7] It has been theoretically shown that the valence band structures of some perovskites are similar to those of transition metals.[8-11] Among these perovskites, those containing the lanthanoid elements R, $RCoO_3$, were reported to be more active for the hydrogenolysis of *cis*-2-butene than several kinds of transition metals.[1] We have found that $LaCoO_3$ catalyzed the hydrogenolysis of ethylene and ethane to produce methane. The hydrogenolysis of the hydrocarbons on this perovskite, however, has not been studied in detail, and thus the function of the catalyst has not been revealed yet.

In the present work, being the first one in our series, the detailed kinetic study for the hydrogenolysis of ethylene and ethane was performed, and was supplemented by the analysis of deuterium distributions in the reaction with deuterium. The crystal and electronic structures of the oxide were examined by X-ray diffraction and X-ray photoelectron spectroscopy (XPS). On the basis of the obtained results, the structures of the active site for the hydrogenation and hydrogenolysis were discussed.

Experimental

Material. $LaCoO_3$ was prepared by calcining the mixed hydroxides of La and Co at 1170 K for 3 h and then 1370 K for more than 12 h. The hydroxides were coprecipitated from the mixture of equimolar solutions of $La(NO_3)_3 \cdot 6H_2O$ and $Co(NO_3)_2 \cdot 6H_2O$ by adding an aqueous solution of ammonia and the precipitate was washed with distilled water and dried at 330 K. The X-ray diffraction pattern of the calcined product coincided with that of $LaCoO_3$ reported by Askham *et al.*[12] and any other compounds were not detected. The surface area of the catalyst was estimated at 0.33 m^2·g^{-1} by BET method using Kr adsorption at 77 K.

X-Ray photoelectron spectra of the catalyst were recorded on a Hewlett-Packard 5950A ESCA spectrometer with monochromatized Al $K\alpha$ radiation (1486.6 eV) in an ultra high vacuum of 10^{-9} Torr (1 Torr = 133.3 Pa). An electron flood gun was used to compensate the charging-up shifts of the spectra due to photoelectron emission. The values of observed binding energies were corrected using that of C 1s, 284.7 eV, as a standard.

The property of synthesized $LaCoO_3$ was examined simultaneously by DTA and TGA using a Rigaku-Denki thermal analyser in air for the sample of 50 mg which was inserted in a platinum vessel together with the reference alumina. When the catalyst was heated from 300 to 1300 K and then cooled to 300 K at a rate of 10 K·min^{-1}, two weak endothermic peaks appeared around 610 and 910 K, accompanied by the respective decreases of 0.03 and 0.06% in weight. Further, a strong endothermic peak appearing around 1190 K with increasing temperature caused a decrease of 0.21% in weight. The endothermic change at 1190 K was reversible and attributed to the first order transformation of the crystal resulting in the elimination of oxygen. Before and after the DTA and TGA measurements, no change of X-ray diffraction pattern was observed. From the $LaCoO_3$ sample which was prepared in air by calcining at 1370 K, H_2O, CO, and CO_2 were desorbed on heating; H_2O appeared around 540 and 600 K, while CO and CO_2 desorbed around 410 and 590 K. Samples after cooling to 300 K *in vacuo* evolved scarcely any gas on the second heating up to 800 K.

Hydrogen (99.99% pure), deuterium (99.6%), methane (99.95%), ethylene (99.8%), ethane (99.7%), and *cis*-2-butene (99%) were purchased from Takachiho Chem. Ind., Ltd. and used without further purification.

Procedure. Kinetic studies were carried out in the reaction temperatures from 300 to 600 K using a closed circulation system connected to a high vacuum line. The catalyst sample, 100 to 300 mg in weight, was evacuated in a reaction tube at various temperatures between 300

Table 1. The reaction of ethylene with deuterium

I[a]	Ethylene	Ethane	Methane	Hydrogen	II[b]	Ethylene	Ethane	Hydrogen
D_0	31.9%	3.3%	1.4%	0.2%	D_0	19.5%	11%	1%
D_1	28.5%	10.6%	29.1%	8.4%	D_1	42.8%	25%	4%
D_2	38.5%	14.3%	3.5%	91.4%	D_2	28.8%	32%	95%
D_3	0 %	19.5%	24.1%		D_3	8.1%	22%	
D_4	1.1%	24.9%	42.0%		D_4	0.8%	9%	
D_5		16.4%			D_5		2%	
D_6		11.1%			D_6		0%	

a) Reaction I. Reaction temperature=573 K, conversion=24%, $P_{C_2H_4}=10.0$ Torr, $P_{D_2}=103.5$ Torr.
b) Reaction II. Reaction temperature=353 K, conversion=42%, $P_{C_2H_4}=10.0$ Torr, $P_{D_2}=113.1$ Torr.

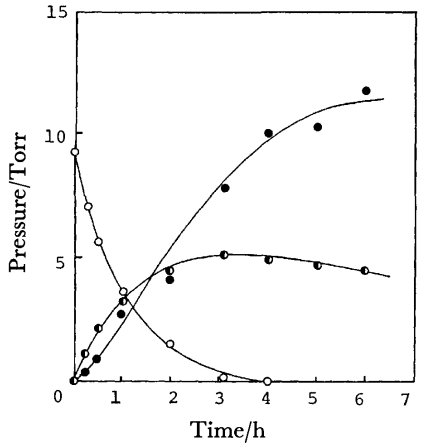

Fig. 1. Reaction of ethylene with H_2 at 573 K.
○: C_2H_4, ◐: C_2H_6, ●: CH_4.

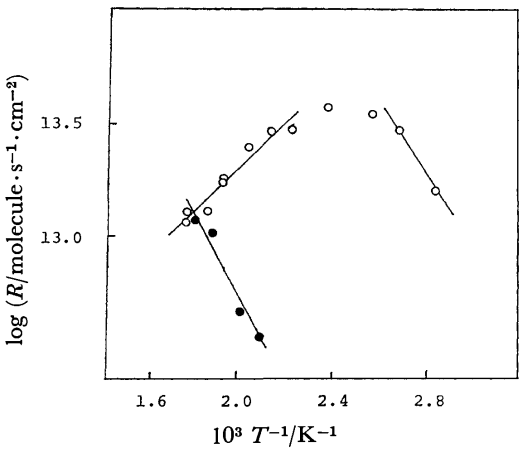

Fig. 2. Arrhenius plots for the hydrogenation of ethylene and the hydrogenolysis of ethane.
$P_{C_2H_4}=P_{C_2H_6}=10$ Torr, $P_{H_2}=100$ Torr.
○: Hydrogenation, ●: hydrogenolysis.

and 800 K for 1 to 6 h. When the catalyst was evacuated at 600 K for 1 h before each run, the activity was satisfactorily reproduced in successive ten kinetic runs and remained constant on heating the catalyst up to 800 K under vacuum.

The partial pressures of hydrocarbons were changed from 5 to 15 Torr and those of hydrogen and deuterium from 50 to 150 Torr. The composition of the reaction products was determined gas-chromatographically for the sample taken out periodically from the reaction system during the course of reaction. In addition to the hydrogenolysis of ethylene and ethane, the same reactions with D_2, the exchange reaction between methane and D_2, the equilibration of H_2 and D_2 were also examined. These reaction mixtures were analyzed by means of a mass spectrometer, Hitachi RMU-7M, and a gas chromatograph was used to analyze the isotopic molecules of hydrogen, H_2, HD, and D_2.

A preliminary study on the reaction of *cis*-2-butene (10 Torr) with hydrogen (100 Torr) over $LaCoO_3$ at 573 K confirmed that the hydrogenolysis and isomerization of butene took place simultaneously to form the main product, methane and butene isomers, as previously reported by Pedersen and Libby.[1]

Results

Hydrogenolysis of Ethylene and Ethane. Figure 1 shows the change in the gas-phase composition with time in the reaction of ethylene with hydrogen at 573 K. Ethane and methane were produced during the course of hydrogenolysis. The solid lines in the figure are the simulated curves by assuming the consecutive reaction pathway from ethylene to methane *via* an intermediate, ethane, as is described later in detail. The reaction at temperatures lower than 420 K gave only ethane as the product. Figure 2 shows the change in the initial rate of ethylene consumption with reaction temperature. The maximum in the rate appeared at about 420 K. The apparent activation energy was estimated at 33.6 kJ·mol^{-1} below 420 K and −19.3 kJ·mol^{-1} above 420 K. The kinetics of the reaction was studied at 353 and 573 K to clarify the nature of the reaction in the respective temperature ranges above and below 420 K. The rates of ethylene consumption at 573 K and 353 K are respectively expressed as

$$R_{573} = kP_{C_2H_4}P_{H_2} \quad (1)$$

and

$$R_{353} = k'P^0_{C_2H_4}P_{H_2}, \quad (2)$$

where k and k' denote the rate constants and P_i represents the partial pressure of molecule i (i=C_2H_4 or H_2).

The kinetic study of the ethane hydrogenolysis was carried out at temperatures between 473 K and 573 K. Methane was the sole product of the hydrogenolysis, and ethylene was not detected during the course of reaction. The rate of ethane consumption was given by

$$R = k^*P_{C_2H_6}P_{H_2}^{-0.5}, \quad (3)$$

with the activation energy of 34.9 kJ·mol^{-1} as shown in Fig. 2.

Isotopic Exchange Reactions of Ethylene, Ethane, or Methane with Deuterium and Equilibration between Hydrogen and Deuterium. Reaction of ethylene with D_2 was investigated at 353 K and 573 K. The observed deuterium distributions are summarized in Table 1. In the reaction at 573 K, no significant kinetic isotope effect was observed. The deuterium atoms were quite widely distributed in ethylene, ethane, and methane, whereas the produced HD and H_2 were in equilibrium with D_2 during the course of reaction. On the other hand, in the reaction at 353 K, the normal isotope effect was observed; the rate of ethylene hydrogenation with H_2 was about twice as large as that with D_2. The composition among H_2, HD, and D_2 in the gas phase was far from an equilibrium value.

The reaction of ethane with D_2 at 573 K produced methane[D_4] as main product but a negligibly small amount of deuterium-exchanged ethane. A separate experiment showed that the exchange reaction between methane and D_2 was also negligible at this temperature.

The equilibration between H_2 and D_2 was also separately examined at temperatures between 170 K and 573 K, and was found to take place rapidly on $LaCoO_3$ with activation energy of 16.0 kJ·mol^{-1}. The rate of equilibration was about 100 times as large as that of ethylene hydrogenation at 573 K.

Catalytic behavior of Component Oxides, La_2O_3 and Co_2O_3. The catalytic activities of La_2O_3 and Co_2O_3 were also examined in order to compare with that of $LaCoO_3$. La_2O_3 showed neither hydrogenation nor hydrogenolysis activity after outgassing at temperatures below 773 K, but it became catalytically active only for the hydrogenation when heated *in vacuo* at temperature as high as 973 K. Ethylene hydrogenation on thus activated La_2O_3 exhibited a maximum in the reaction rate, 2.3×10^{14} molecule·s^{-1}·cm^{-2}, at around 548 K (P_{H_2}=98.4 Torr and $P_{C_2H_4}$=13.6 Torr), giving the activation energy of −33.1 kJ·mol^{-1} above 548 K and 16.2 kJ·mol^{-1} below this temperature. It should be noted that these reaction behavior quite resembled those for the hydrogenation on $LaCoO_3$. When Co_2O_3 was evacuated at 600 K for 1 h, the hydrogenolysis of ethylene took place at 573 K to produce ethane and methane. The catalytic activity of this oxide, however, was unstable, and this was due to the reduction of Co_2O_3 to metallic cobalt during the course of reaction, since H_2O was formed, and X-ray diffraction of the oxide employed for the reaction showed characteristic peaks associated with developed cobalt metal particles. For the initial stage of reaction, rough estimation gave a rate of ethane formation, 4×10^{11} molecules·s^{-1}·cm^{-2} at 573 K, and about 30% of reacted ethylene was consumed by the direct formation of methane *via* the adsorbed ethylene.

Structural and Chemical Changes of the Catalyst. In order to see the relationship between the structure and the activity of $LaCoO_3$, the fresh catalyst, (A), the 50% deactivated catalyst by repeated run of the reaction, (B), and the completely deactivated one (C) were examined by X-ray diffraction. Each X-ray diffraction peak of samples B and C splitted into two or three peaks which appeared at lower diffraction angles. These results suggest that the activity decreases as the lattice expands to some extent.

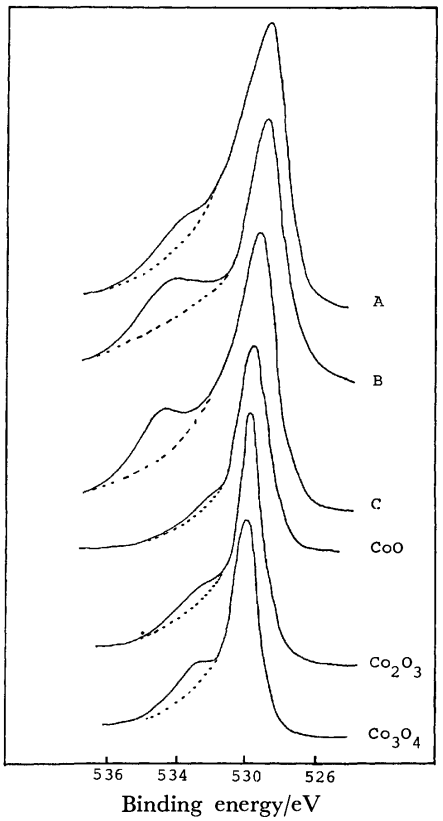

Fig. 3. X-Ray photoelectron spectra in O 1s region. Spectra A, B, and C denote the fresh $LaCoO_3$, the 50%-deactivated catalyst and the completely deactivated one, respectively.

The electronic states of samples A, B, and C were also inspected by means of XPS in comparison with those of CoO, Co_3O_4, and Co_2O_3. The O 1s spectra are illustrated in Fig. 3. The spectra of these $LaCoO_3$ samples evacuated at 300 K indicate the presence of two kinds of oxygen species; the O 1s peak of lower binding energy shifted to higher energy side with decreasing activity and the spectrum of sample became similar to those of cobalt oxides. The O 1s peak of higher binding energy diminished in intensity to the level shown by the dotted lines upon evacuation at 770 K. From the comparison with the spectra of Cu_2O, CuO, and NiO obtained by Robert *et al.*,[13] this peak was assigned to the adsorbed oxygen and the peak of lower binding energy to the lattice oxygen.

Figure 4 shows the spectral peaks from Co 2p levels. The values of spin-orbit splitting and FWHM for the fresh $LaCoO_3$ (A) are 15.3 eV and 3.2 eV, respectively, and the value of the splitting is simialr to that for Co_2O_3, 15.2 eV. However, the corresponding spectrum of catalyst C, in which the respective values are 15.9 eV and 4.7 eV, is almost the same as that of CoO with those values of 16.0 eV and 4.7 eV and is accompanied by the characteristic shake-up satellites. These differences can be used to distinguish the oxidation states of Co atoms, as reported

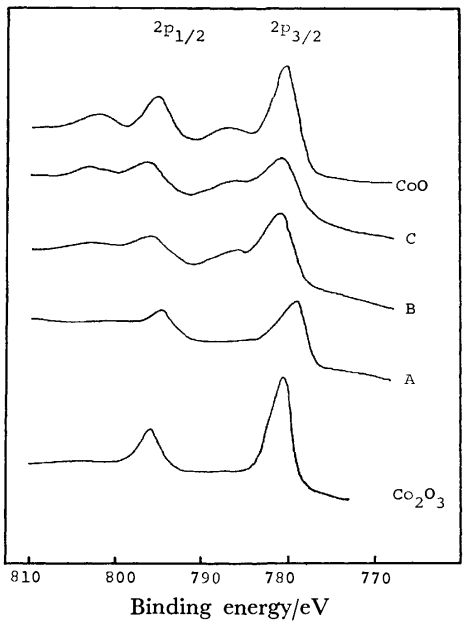

Fig. 4. X-Ray photoelectron spectra in Co 2p region. Spectra A, B, and C: see caption in Fig. 3.

by several workes,[14-16] and lead to the conclusion that the reduction from a trivalent ion, Co^{3+}, to a bivalent ion, Co^{2+}, occurred, resulting in the structural change and the degradation of catalytic activity.

No significant change of La 3d spectra was observed for all the catalysts in comparison with that for La_2O_3.

The property of $LaCoO_3$ surface was inspected from the adsorption of H_2, C_2H_4 and CO at room temperature. All the adsorbed species were removed on heating at 600 K and, from the amounts for saturation, the number of adsorption sites was estimated at 4×10^{14} cm^{-2} which corresponds to about 40% of the total surface ions.

Discussion

Mechanism of Ethylene Hydrogenolysis. The hydrogenolysis of ethylene proceeds in the following sequence;

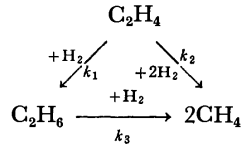

Since the observed hydrocarbon orders were unity for both the hydrogenation of ethylene and the hydrogenolysis of ethane in the high temperature range and the reacting system contained a large excess of hydrogen, the rates of ethylene and ethane consumption are expressed in the form of the pseudo-first order reaction,

$$\frac{d[C_2H_4]}{dt} = -(k_1+k_2)[C_2H_4], \quad (4)$$

$$\frac{d[C_2H_6]}{dt} = +k_1[C_2H_4] - k_3[C_2H_6], \quad (5)$$

$$\frac{d[CH_4]}{dt} = +2k_2[C_2H_4] + 2k_3[C_2H_6]. \quad (6)$$

The apparent rate constants, k_1, k_2, and k_3 as parameters, were determined by applying the nonlinear least square method to the experimental data. Estimated value of k_2, 0.014 h^{-1}, was smaller than k_1, 0.15 h^{-1}, which clearly indicates that the direct conversion of C_2H_4 to CH_4 gives a minor contribution to the entire reaction. The value of k_3, 0.12 h^{-1}, was found to coincide with the rate constant evaluated from the hydrogenolysis of ethane under the same conditions. By using these parameters, the changes in the partial pressures of reactants and products with time were calculated as shown in Fig. 1. A good agreement between the observed and calculated curves confirmed that the hydrogenolysis of ethylene proceeds consecutively, as shown in the sequence,

$$C_2H_4 \xrightarrow{+H_2} C_2H_6 \xrightarrow{+H_2} 2CH_4. \quad (7)$$

The reaction of ethylene with deuterium in the high temperature region showed wide deuterium distributions in ethylene and ethane as well as the nearly established equilibrium among gaseous H_2, HD, and D_2. Thus, these results lead to the associative mechanism which involves the following reaction steps:

$$H_2 \rightleftharpoons 2H(a) \quad (8)$$

$$C_2H_4 \rightleftharpoons C_2H_4(a) \quad (9)$$

$$C_2H_4(a) + H(a) \rightleftharpoons C_2H_5(a) \quad (10)$$

$$C_2H_5(a) + H(a) \longrightarrow C_2H_6 \quad (11)$$

where (a) denotes the adsorbed state. The above-mentioned deuterium distributions also indicate that Step 11 is a rate-determining process, and the reaction rate is given by

$$R_h = k_{11}\theta_{C_2H_5}\theta_H = \frac{k_{11}K_{10}K_eK_hP_{C_2H_4}P_{H_2}}{(1+K_eP_{C_2H_4}+\sqrt{K_hP_{H_2}}+K_{10}K_eP_{C_2H_4}\sqrt{K_hP_{H_2}})^2} \quad (12)$$

where θ_i represents the fraction of surface coverage of the i species on the hydrogenation site. Under the condition of

$$1 \gg K_eP_{C_2H_4} + \sqrt{K_hP_{H_2}} + K_{10}K_eP_{C_2H_4}\sqrt{K_hP_{H_2}}, \quad (13)$$

Eq. 12 is simplified to

$$R_h = k_{11}K_{10}K_eK_hP_{C_2H_4}P_{H_2} = k_hP_{C_2H_4}P_{H_2}. \quad (14)$$

In the low temperature region, the fraction of gaseous H_2 and HD was small in contrast to the wide deuterium distributions in the ethylene and ethane, which leads to the assumption that the adsorption of hydrogen in Step 8 is a slow step. Thus, the rate equation is expressed as

$$R_l = k_8P_{H_2}(1-\theta_{C_2H_4})^2 = \frac{k_8P_{H_2}}{(1+K_eP_{C_2H_4})^2}. \quad (15)$$

Under the condition of

$$1 \gg K_eP_{C_2H_4}, \quad (16)$$

Eq. 15 becomes

$$R_l = k_8P_{H_2}. \quad (17)$$

Equations 14 and 17 are in agreement with the observed pressure dependences in respective temperature regions.

It is of nessesity to assess this mechanism in con-

nection with that of ethylene and ethane hydrogenolysis. The striking features of catalysis by $LaCoO_3$ were the restriction imposed on the direct path from adsorbed ethylene to methane and were also the feasibility of ethane hydrogenolysis without producing ethylene in the gas phase. With this in mind, Step 10 in the associative mechanism would appear to contradict the behavior of the hydrogenolysis, if the available sites are the same for both reactions, since the intermediate described in Step 10 would rapidly undergo the rupture of carbon-carbon bond, which turned out to give a direct pathway for methane formation. Thus, it is suggested that the active sites for hydrogenation are different from those for the hydrogenolysis. A comparison of ethylene hydrogenation on La_2O_3 and $LaCoO_3$ indicated that the kinetic behavior was quite similar each other and that the catalytic acitivity was compatible when it was evaluated as the reaction rate per La^{3+} ion exposed at surface. On the contrary, Co_2O_3 exhibited a considerable selectivity to the hydrogenolysis of the adsorbed ethylene to methane but much lower activity for the hydrogenation. Therefore, these findings enable us to conclude that a pair of La and oxygen ions is mainly responsible for the hydrogenation activity of $LaCoO_3$. In this regard, it should be noted that the conditions, (13) and (16), are established for these sites of $LaCoO_3$ oxide.

Mechanism of Hydrogenolysis of Ethane. In the hydrogenolysis of ethane over transition metals, Sinfelt *et al.* proposed the mechanism involving the dissociative adsorption of ethane to produce ethyl radical which changed to hydrogen-deficient species and further to monocarbon surface fragments.[17] In the hydrogenolysis on $LaCoO_3$, however, emphasis should be put on the results that no ethylene is formed during the reaction. The facts that the hydrogenolysis of ethane is catalyzed by Co_2O_3 but not La_2O_3, and that the H_2-D_2 equilibration takes place on these oxides and $LaCoO_3$ suggest the co-functional role of component ions in the hydrogenolysis; Co^{3+} ion is mainly responsible for the C–C bond scission, while the other La^{3+} and O^{2-} ions contribute as the sites to supply the dissociatively adsorbed hydrogen. Thus, by taking the above-mentioned pathway of ethylene hydrogenation and these findings into consideration, we propose the following reaction mechanism.

$$H_2 \rightleftharpoons 2H(a) \tag{18}$$

$$C_2H_6 + H(a) \longrightarrow CH_3(a^*) + CH_3(a^*)\cdots H(a) \tag{19}$$

$$CH_3(a^*) \rightleftharpoons CH_2(a^*) + H(a) \tag{20}$$

$$CH_3(a^*) + H(a) \longrightarrow CH_4 \tag{21}$$

where (a*) represents the adsorbed state on Co^{3+} site and (a) denotes that on La^{3+} or O^{2-} site. Since methane[D_4] is the main species in the reaction of C_2H_6 with D_2, the hydrogenolysis comprise necessarily a rapid hydrogen exchange, as expressed in Eq. 20, between surface monocarbon species, *i.e.*, adsorbed carbene and methyl radicals. The absence of deuterium-exchanged ethane strongly suggests that the Step (19) is rate-determining, and the rate equation of hydrogenolysis is given by

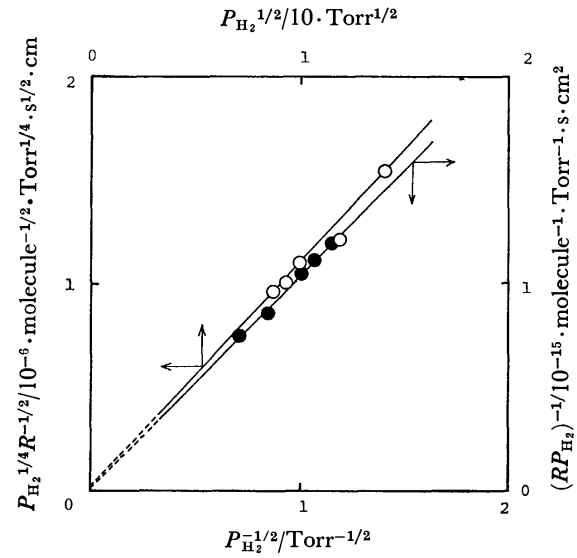

Fig. 5. Plots of $P_{H_2}^{1/4}R^{-1/2}$ *vs.* $P_{H_2}^{1/2}$ and $(RP_{H_2})^{-1}$ *vs.* $P_{H_2}^{-1/2}$. R and P_{H_2} represent the initial rate and the partial pressure, respectively.

$$R = k_{19}P_{C_2H_6}\theta_v^{*2}\theta_H \tag{22}$$

where θ_v^* denotes a fraction of vacant Co^{3+} sites and θ_H represents that of the other sites occupied by hydrogen atoms. These fractions are respectively described as

$$\theta_v^* = 1/(1+\sqrt{K_h^*P_{H_2}}) \text{ and } \theta_H = \sqrt{K_hP_{H_2}}/(1+\sqrt{K_hP_{H_2}}), \tag{23}$$

provided the fraction of sites covered with hydrocarbon species to be negligible. Under the condition of strong hydrogen adsorption on Co^{3+} sites, $1 \ll \sqrt{K_h^*P_{H_2}}$, the rate equation is rewritten into the form as,

$$\frac{1}{RP_{H_2}} = (K_h^*/k_{19}\sqrt{K_hP_{C_2H_6}})(\sqrt{K_h}+1/\sqrt{P_{H_2}}). \tag{24}$$

Under the condition of $1 \gg \sqrt{K_hP_{H_2}}$ as an approximation of weak adsorption on the other sites, on the other hand, the rate equation is recasted into the form

$$P_{H_2}^{1/4}/\sqrt{R} = (K_h^*/k_{19}\sqrt{K_hP_{C_2H_6}})^{1/2}(1/\sqrt{K_h^*}+\sqrt{P_{H_2}}). \tag{25}$$

Figure 5 shows good linear relationships for the plots of $(RP_{H_2})^{-1}$ *vs.* $P_{H_2}^{-1/2}$ on Eq. 24 and $P_{H_2}^{1/4}/\sqrt{R}$ *vs.* $\sqrt{P_{H_2}}$ on Eq. 25. Since the evaluated values of K_h and K_h^* at 573 K are 4×10^{-6} and 10, respectively, and P_{H_2} is 100 Torr, the relation

$$\sqrt{K_h^*P_{H_2}} \gg 1 \gg \sqrt{K_hP_{H_2}}$$

is held, which justifies the approximations used. By introducing these approximations, the rate equation (22) is finally simplified as

$$R = k_{19}\frac{\sqrt{K_h}}{K_h^*}P_{C_2H_6}P_{H_2}^{-0.5} \tag{26}$$

which accords with the observed partial pressure dependence.

It is interesting to compare the activity of $LaCoO_3$ for the hydrogenolysis of ethane with those of platinum and palladium; the specific rate for the hydrogenolysis over $LaCoO_3$ at 573 K is evaluated at 1×10^{13} molecule$\cdot s^{-1}\cdot cm^{-2}$ by using a reactant mixture of C_2H_6 (10 Torr) and H_2 (100 Torr). The values for Pt and

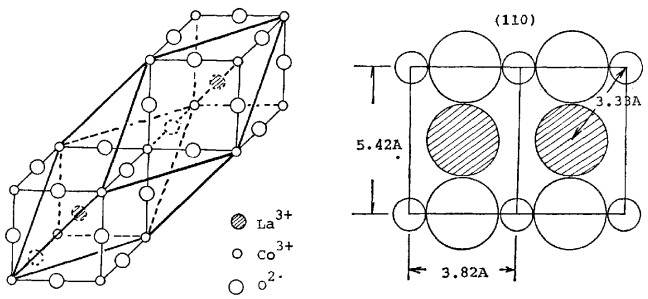

Fig. 6. Structure and geometry of $LaCoO_3$. $LaCoO_3$ have a perovskite structure, D^5_{3d}-$R\bar{3}m$, but the (110) plane is drawn as cubic structure for simplicity.

Pd catalysts are respectively 2×10^{11} and 4×10^{11} molecule$\cdot s^{-1}\cdot cm^{-2}$ which were obtained by correcting the Sinfelt's data[17] to the present reaction conditions. As the reaction temperature rises, the difference among these rates will be smaller because of large activation energy for Pt and Pd, *i.e.*, 227 and 244 kJ$\cdot$mol^{-1}, respectively.

Structure of Active Sites. At present, knowledge on $LaCoO_3$ catalyst has not been accumulated sufficiently to mention the nature of active sites for the hydrogenolysis in detail. We give here only a speculative description to their structure and behavior. The number of adsorption sites for hydrogen or ethylene on $LaCoO_3$ corresponds to about 40% of the total surface ions. These results predict that most of the exposed surface are available for the reaction and, especially, the (110) lattice plane as illustrated in Fig. 6 is likely the most favorable for the catalysis. Among the ion pairs of Co^{3+}–O^{2-} (1.91 Å), La^{3+}–O^{2-} (2.71 Å), and La^{3+}–Co^{3+} (3.16 Å), the former two pairs seem to be suited for the dissociative adsorption of hydrogen as seen in the case of transition metal oxides. As mentioned earlier, the hydrogenation mainly proceeds on the sites consisting of La and oxygen ions. It is likely that the Co^{3+} ion in $LaCoO_3$ somewhat affects the surface states of both ions in a way to provide the hydrogenation activity in accordance with a trend that a heat treatment at high temperature changed La_2O_3 to be catalytically active. For the hydrogenolysis, the geometric arrangement of the (110) plane substantiates the co-functional role in which the Co^{3+} ion ruptures the carbon-carbon bond, and the nearby La and oxygen ions supply hydrogen atoms to the resulting monocarbon species. These synergetic effect by the three component ions in $LaCoO_3$ was found to be pronounced in the hydrogenolysis of C_3 to C_5-alkanes with longer carbon chains.[18]

The thermal desorption and IR studies of adsorbed species on $LaCoO_3$ are in progress, and the obtained information will be useful in revealing the contributions of these species to the reaction and the function of active sites.

References

1) L. A. Pedersen and W. F. Libby, *Science*, **175**, 1355 (1972).
2) R. J. H. Voorhoeve, J. P. Remeika, P. E. Freeland, and B. T. Mattias, *Science*, **177**, 353 (1972).
3) R. J. H. Voorhoeve, J. P. Remeika, L. E. Frimble, A. S. Cooper, F. J. Dialvo, and P. K. Gallagher, *J. Solid State Chem.*, **14**, 395 (1975).
4) T. Shimizu, T. Nishida, and Y. Moriwaka, *Nippon Kagaku-Kaishi*, **1974**, 1836.
5) Y. Y. Yao, *J. Catal.*, **36**, 266 (1975).
6) S. Ishiyama, Tokyo Institute of Technology M. Thesis (1975).
7) R. J. H. Voorhoeve, C. K. N. Patel, L. E. Trimble, R. J. Kerl, and P. K. Gallagher, *J. Catal.*, **45**, 297 (1972).
8) J. B. Goodenough and P. M. Raccah, *J. Appl. Phys.*, **36**, 1031 (1965).
9) L. F. Mattheiss, *Phys. Rev.*, **6**, 4718 (1972).
10) V. G. Bhide and D. S. Rajaria, *Phys. Rev. B*, **6**, 1021 (1972).
11) E. A. Kraut, T. Wolfram, and W. Hall, *Phys. Rev. B*, **6**, 1499 (1972).
12) F. Askham, I. Fankuchen, and R. Ward, *J. Am. Chem. Soc.*, **72**, 3799 (1950).
13) T. Robert, M. Bartel, and G. Offergelt, *Surface Sci.*, **33**, 123 (1972).
14) D. C. Frost, A. Ishitani, and C. A. McDowell, *Mol. Phys.*, **24**, 861 (1972).
15) D. Briggs and V. A. Gibson, *Chem. Phys. Lett.*, **25**, 493 (1974).
16) Y. Okamoto, N. Nakano, T. Imanaka, and S. Teranishi, *Bull. Chem. Soc. Jpn.*, **48**, 1163 (1975).
17) J. H. Sinfelt, *Adv. Catal.* **23**, 91 (1973).
18) K. Ichimura, Y. Inoue, and I. Yasumori, unpublished.

 © 1980 The Chemical Society of Japan Bull. Chem. Soc. Jpn., 53, 3050—3053 (1980)

The Collection of Uranium from Sea Water with Hydrous Metal Oxide. IV. Physical Properties and Uranium Adsorption of Hydrous Titanium(IV) Oxide

Hisao YAMASHITA,* Yoshihiro OZAWA,** Fumito NAKAJIMA, and Toshifumi MURATA**

Hitachi Research Laboratory, Hitachi, Ltd., Kujimachi, Hitachi 319-12

*** Energy Research Laboratory, Hitachi, Ltd., Moriyama-cho, Hitachi 316*

(Received November 16, 1979)

The adsorption of uranium from sea water with hydrous titanium(IV) oxide(HTO) was studied. HTO was prepared by mixing titanium(IV) chloride and aqueous ammonia at different pHs and temperatures. The fundamental property of HTO was investigated for apparent crystal size, specific surface area, and pore size. The uranium uptake of HTO was found to depend more strongly on the temperature than on the pH in the preparation. HTO prepared at higher temperatures exhibited larger pores and a higher uranium uptake. A kinetic study of the uranium adsorption revealed that the rate of adsorption was controlled by the particle diffusion. The diffusion coefficients were calculated.

There are a large number of elements dissolved in sea water. Though the concentration of uranium in sea water is very low (3 ppb), the total amount of uranium is estimated to be about 4×10^9 t. The recovery of uranium from sea water has been studied, and several techniques for the extraction have been proposed.[1-4] Among these techniques, the adsorption method has been considered most feasible.

Hydrous titanium(IV) oxide (HTO) may be the most suitable uranium adsorbent because of its higher selectivity and adsorption capacity. Ogata[5] has shown that the uranium uptake depends strongly on the method of the preparation of HTO. However, no systematic study has been reported of the relation between the physical properties and uranium adsorption of HTO.

In the present work, the relationship between the uranium adsorption and the physical properties of HTO, such as the apparent crystal size, the specific surface area, and the pore size, is investigated.

Experimental

Preparation of HTO. HTO was prepared by the addition of 7% aqueous ammonia to a solution of 0.6 mol dm^{-3} titanium(IV) chloride at different temperatures. The pH values at the end of precipitation was controlled between 3 and 9. The precipitate was filtered off, washed with distilled water, and finally dried at room temperature for about 10 d. The dried samples were crushed and sieved, a fraction of 150—200 mesh size being used in the following experiments.

Sample Solution. The sea water used in the present work was obtained at the seashore of Hitachi city. The uranium concentration was found to be 3.1 ppb, and the pH value, 8.1. In the adsorption experiments, the initial concentration of uranium was set as 10—30 ppb by the addition of uranyl(VI) chloride solution to the sea water.

Adsorption Experiment. The HTO samples of 0.04 g were introduced into 1000 ml of sea water at 25 °C. The solution was stirred by means of a vertical stirrer. The adsorption equilibrium was attained within 8 h under the present experimental conditions. The solution was filtered to separate the adsorbents, and the uranium in the solution was determined spectrophotometrically, with Arsenazo III as an indicator.[6]

Measurement of X-Ray Diffraction. The X-ray diffraction pattern of HTO was measured with a Rigaku Denki Geiger Flex X-Ray Diffractometer, filtered Cu $K\alpha$ being used. The apparent crystal size was calculated by the Sheller equation from a peak corresponding to the (101) plane of anatase.

Measurement of Specific Surface Area and Mean Pore Radius. The specific surface area and pore volume of HTO were measured by means of the N_2 adsorption at −195 °C. The mean pore radius, r, was calculated from the $r=2V/S$ equation, where V is the pore volume and S the specific surface area.

Results and Discussion

Uranium Uptakes of HTO Prepared at Different pHs, and Temperatures. The effects of the final preparation pH of HTO on the specific surface area and the uranium uptake are shown in Fig. 1. The specific surface area (about 400 $m^2\,g^{-1}$) of HTO is independent of the pH values of the preparation. It can be seen that uranium uptakes also do not depend on the pH values of the preparation.

The effect of the preparation of HTO on the uranium uptake was investigated as well. The uranium uptake

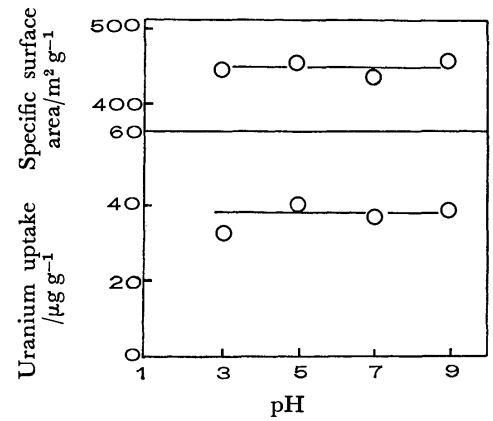

Fig. 1. Effect of preparation pH on uranium uptake and specific surface area.
Uranium adsorption;
concentration of uranium: 10 ppb, temperature: 25 °C, stirring time: 8 h.
Preparation of hydrous titanium(IV) oxide;
temperature: 25 °C, particle size: 150—200 mesh.

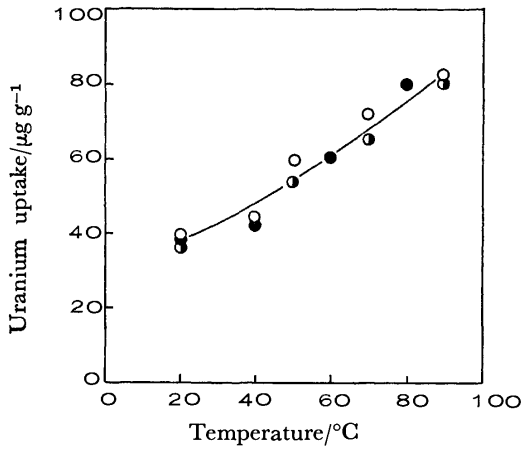

Fig. 2. Effect of preparation temperature on uranium uptake.
Uranium adsorpttion; same as Fig. 1.
Preparation of hydrous titanium(IV) oxide; pH: ○: 5, ●: 7, ◑: 9, particle size: 150—200 mesh.

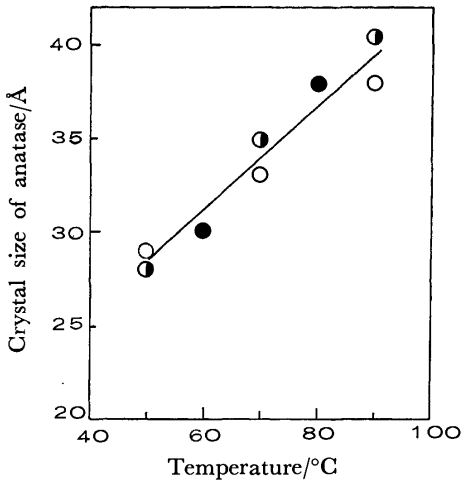

Fig. 3. Effect of preparation temperature on apparent crystal size of hydrous titanium(IV) oxide.
Preparation pH, ○, ●, ◑: same as Fig. 2.

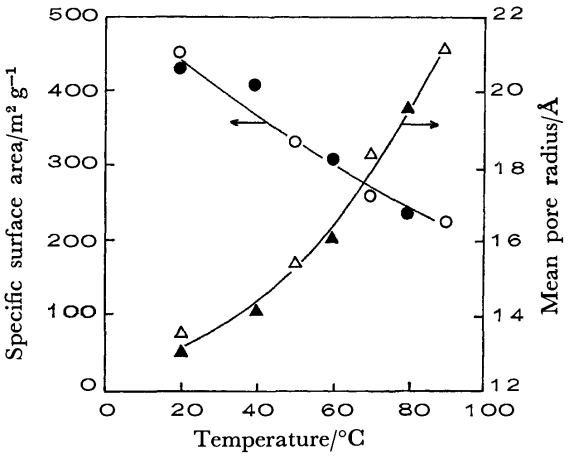

Fig. 4. Effect of preparation temperature on specific surface area and mean pore radius of hydrous titanium(IV) oxide.
Preparation pH, ○, △: 5, ●, ▲: 9.

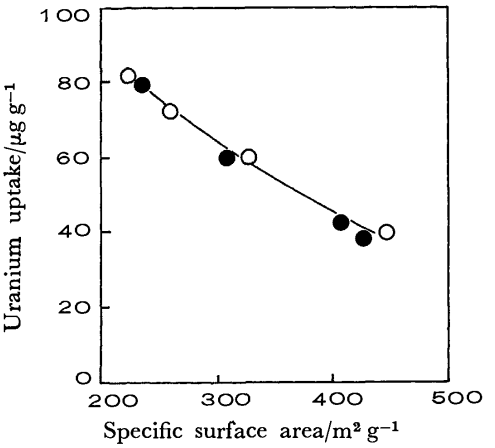

Fig. 5. Relation between uranium uptake and specific surface area of hydrous titanium(IV) oxide.
Preparation pH, ○: 5, ●: 9.

by HTO increased with an increase in the temperature of the preparation (Fig. 2). That is, HTO prepared at 20 °C and pH 5 had the uranium uptake of 40 μg g^{-1}; at 50 °C, 60 μg g^{-1}; at 70 °C, 73 μg g^{-1}, and at 90 °C, 82 μg g^{-1}. It is thus found that the uranium uptake depends strongly on the preparation temperature.

Physical Properties and Uranium Adsorption. In order to investigate the effect of the preparation temperature on the uranium uptake, the apparent crystal size, the specific surface area, and the mean pore radius of HTO were measured.

HTO prepared at 20 °C was found to be an amorphous structure, while that prepared above 50 °C showed some weak diffraction lines, indicating a crystal growth of an anatase type. The apparent crystal size of the anatase type is plotted against the temperature in Fig. 3. The crystal size of anatase increased with the temperature from about 28 Å at 50 °C to about 40 Å at 90 °C. The uranium uptake increased with the crystal growth of HTO under the present experimental conditions.

The specific surface area of HTO shows an inverse relationship with the pore radius and the crystal size (Fig. 3 and Fig. 4). The specific surface area decreased with the increase in the temperature from about 450 m^2 g^{-1} at 20 °C to about 220 m^2 g^{-1} at 90 °C. At the same time, the mean pore radius increased with the preparation temperature, *i.e.*, the values of the mean pore radius of the samples prepared at pH 5 were found to be 13.5 Å at 20 °C, 15.3 Å at 50 °C, 18.2 Å at 70 °C, and 21 Å at 90 °C. The preparation temperature thus had a large effect on the specific surface area and the mean pore radius of HTO.

The relation between the specific surface area and the uranium uptake of HTO is shown in Fig. 5. The uranium uptake decreased with the increase in the specific surface area, while it increased with the mean pore radius, as is shown in Fig. 6. The results show that the uranium uptake is low when the mean pore radius is small, despite the high specific surface area.

In consequence of the relatively high carbonate

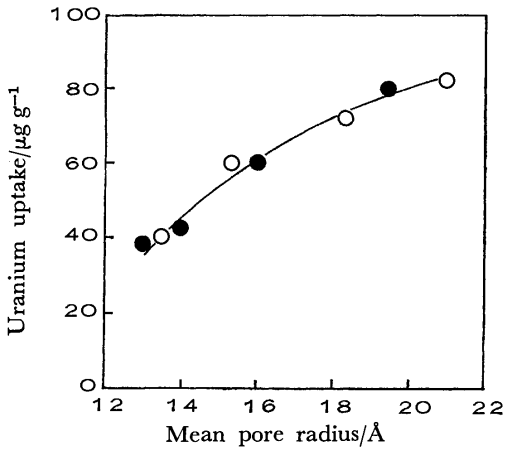

Fig. 6. Relation between uranium uptake and mean pore radius of hydrous titanium(IV) oxide.
○, ●: Same as Fig. 5.

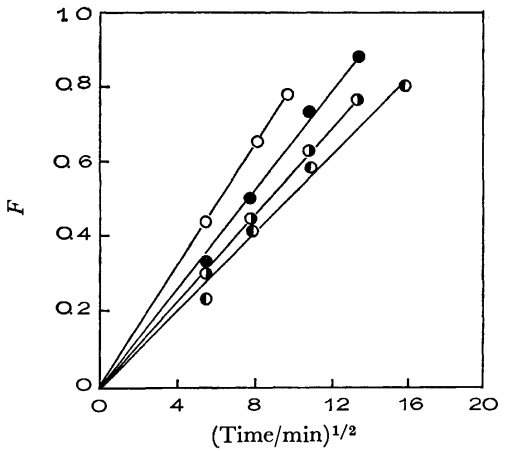

Fig. 7. Plot of F *vs.* $t^{1/2}$.
Uranium adsorption; concentration of uranium: 30 ppb, temperature: 25 °C.
Preparation of hydrous titanium(IV) oxide; particle size: 150—200 mesh, temperature: ○ 90 °C, ● 70 °C, ◑ 50 °C, ◐ 20 °C.

concentration in sea water (2.3×10^{-3} mol dm^{-3}), uranium exists in the form of tris(carbonato)dioxouranate(VI) $[UO_2(CO_3)_3]^{4-}$.[7] The ionic radius of the ion is estimated to be more than 4.7 Å.[8] It is supposed that $[UO_2(CO_3)_3]^{4-}$ can easily enter the pores with a larger diameter of HTO. However, in the case of HTO prepared at a lower temperature, the entrance of $[UO_2(CO_3)_3]^{4-}$ into the small pores is difficult. Therefore, it is considered that HTO prepared at a higher temperature exhibits a higher uranium uptake.

Kinetic Studies. Kinetic measurements were made of the uranium adsorption by HTO. When the adsorption is controlled by the particle diffusion, the following equation holds:[9]

$$F=\frac{Q_t}{Q_\infty}=\frac{6}{R}\sqrt{\frac{D_1 t}{\pi}},$$

where F is the extent of adsorption, Q_t the uranium uptake in time t and Q_∞ the uranium uptake at equilibrium. R is the radius of the adsorbent, and D_1 the diffusion coefficient. A plot of F *versus* $t^{1/2}$ will be a straight line if the adsorption is controlled by the particle diffusion, and the diffusion coefficient can be obtained from the slope of the line.

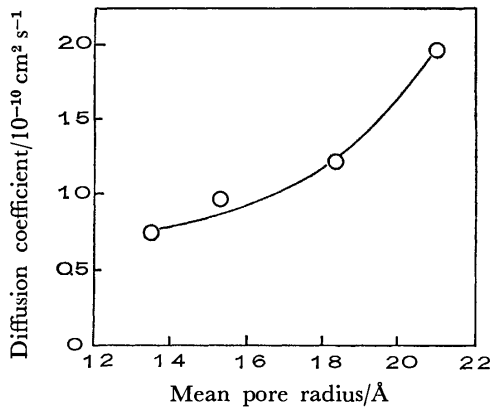

Fig. 8. Relation between diffusion coefficient and mean pore radius.

The rate of the uranium adsorption with HTO prepared at pH 5 and at 20—90 °C is shown in Fig. 7, which gives a linear relationship of F with $t^{1/2}$. The calculated diffusion coefficients are found to be 0.73×10^{-10} cm^2 s^{-1} for HTO prepared at 20 °C, 0.95×10^{-10} cm^2 s^{-1} at 50 °C, 1.24×10^{-10} cm^2 s^{-1} at 70 °C, and 1.98×10^{-10} cm^2 s^{-1} at 90 °C.

Figure 8 shows the relation between the diffusion coefficient and the mean pore radius of HTO prepared at 20—90 °C. It can be seen that the diffusion coefficients increase with the mean pore radius, *i.e.*, HTO prepared at a high temperature has larger pores and exhibits a higher uranium adsorption rate than that prepared at a low temperature. The diffusion coefficients in the present work are of the same magnitude as for the adsorption of methylene blue (with an ionic radius of about 4.5 Å) on the activated carbon (pore radius 10—30 Å, $D_1=1.1\times10^{-10}$ cm^2 s^{-1}).[10]

The rate of the uranium adsorption increased with the temperature of the solution. The diffusion coefficient for HTO prepared at 90 °C was found to be 2.53×10^{-10} cm^2 s^{-1} at 40 °C of the solution in the adsorption experiment shown in Fig. 7. The activation energy was calculated to be 12.6 kJ mol^{-1}. The relatively small activation energy indicates that the adsorption rate is controlled by the particle diffusion.

The authors wish to thank Professor Shosuke Imoto of Osaka University and Dr. Simpei Matsuda and Dr. Kazunori Fujita of the Hitachi Research Laboratory, Hitachi, Ltd., for their many helpful discussions and suggestions.

References

1) N. Ogata and H. Kakihana, *J. At. Energy. Soc. Jpn.*, **11**, 82 (1969).
2) N. J. Keen, *J. Brit. Nucl. Energy. Soc.*, **7**, 178 (1968).
3) M. Ishibashi, T. Fujinaga, T. Kuwamoto, and Y. Ogino, *Nippon Kagaku Kaishi*, **88**, 73 (1967).
4) Y. S. Kim and H. Zeitlin, *Anal. Chem.*, **43**, 1390 (1971).

5) N. Ogata, *J. At. Energy. Soc. Jpn.*, **13**, 121 (1971).
6) Y. Miyake, Y. Sugimura, and T. Uchida, *Record. Oceanog. Works. Jpn.*, **11**, 53 (1972).
7) N. Ogata, N. Inoue, and H. Kakihana, *J. At. Energy. Soc. Jpn.*, **13**, 560 (1971).
8) R. Ganzini, G. Bombieri, and E. Forsellini, *J. Chem. Soc., Dalton Trans.*, **1972**, 2059.
9) G. E. Boyd, L. L. Myers, and A. N. Adamson, *J. Am. Chem. Soc.*, **69**, 2836 (1947).
10) K. Urano and R. Kiyoura, *Kogyo Kagaku Zasshi*, **73**, 1921 (1970).

The Raman Spectra of Aligned Thin Films of Nematic Liquid Crystals

Haruka YAMADA,* Keiji FUKUMURA, and Bun-ichi TAMAMUSHI†

Department of Chemistry, Kwansei Gakuin University, Nishinomiya, Hyogo 662

† *Nezu Chemical Institute, Musashi University, Tokyo 176*

(Received November 27, 1979)

The Raman spectra of thin films of nematic liquid crystals, MBBA and NP-5A, have been measured for samples sandwiched between two glass (or quartz) plates, which had been pretreated in several ways. The intensities of the fundamental bands of the molecules and the polarization components of each band depend on the molecular orientation structures, such as the homogeneous and homeotropic alignments. The intensity ratio provides a semi-quantitative measure for the molecular orientation, and the Raman results are compared with those from polarizing microscopic observations and infrared spectra. The molecular orientation of the liquid crystals varies with the concentrations of surface-active agents as well as the materials used for the pretreatment of the plates. The molecular interactions, which give rise to the orientation structures, are briefly discussed.

The molecular orientation structures in nematic liquid crystals depend on the nature of the substrate surfaces resulting from previous treatment, and they can usually be distinguished by observation with a polarizing microscope.[1,2] They have, however, not always been clarified in molecular dimensions, because X-ray studies are not so effective for the thin films. Recently, the Raman spectra of liquid crystals have been actively studied,[3–7] but most of the work has been performed with bulk samples. For the vibrational spectra of liquid crystal films, we have reported a preliminary Raman result,[8] while some works on the far-infrared spectra have been reported[9–11] and the infrared ATR spectra on the In_2O_3 surface have been studied.[12] However, with the samples between glass or quartz plates, infrared measurement is not so useful. In order to obtain more precise information regarding the molecular orientation structures, the Raman spectra of thin films of nematic liquid crystals on glass or quartz surfaces have been studied in our present work.

Experimental

MBBA(*N*-(*p*-methoxybenzylidene)-*p*-butylaniline; Kodak and Tokyo Chem. Co.) and NP-5A (a mixture of 4-methoxy-4′-butylazoxybenzene with 4-methoxy-4′-ethylazoxybenzene; Merck) were used. Optically flat glass (or quartz) plates ($25 \times 75 \times 1$ mm) were cleaned by using a chromium trioxide solution and then treated by one of the following ways: (i) Silk treatment (rubbed with a silk cloth in the direction parallel to the long edges of the plate surface); (ii) HTAB treatment (dipped in an aqueous solution (0.007—1.4 mM; 1 M=1 mol dm^{-3}) of HTAB (hexadecyltrimethylammonium bromide; Wako Chem.) and then carefully dried); (iii) Lecithin treatment (dipped in an ethanol solution (0.001—1.0 mM) of lecithin (Wako 1st grade, extracted from eggs) and dried), or (iv) Silane treatment (dipped in a solution of 2 mM diphenyldichlorosilane (Wako Chem. special grade) in toluene and dried). A drop of MBBA or NP-5A was sandwiched by two pretreated plates, slightly pressed, and then fastened with a plastic tape along the edges. The thicknesses of the films were measured roughly by observing the interference fringes in the visible and infrared regions, 1—100 μm.

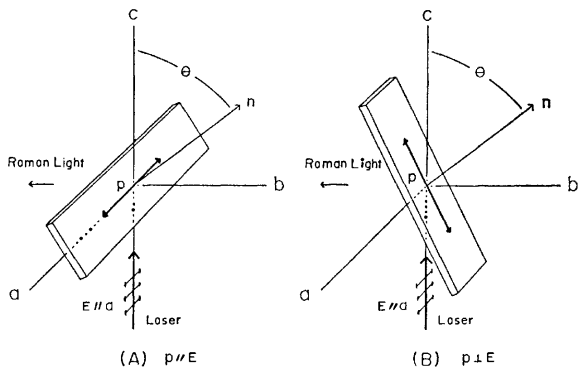

Fig. 1. Setting and irradiation of samples: (A) $\boldsymbol{p}//\boldsymbol{E}$, (B) $\boldsymbol{p} \perp \boldsymbol{E}$.

For polarizing microscopic observation, the samples were examined between crossed nicols under a Carl Zeiss photomicroscope (64 fold).

The Raman spectra were measured by means of a JASCO R-300 spectrophotometer with a JEOL-04 Ar ion laser. All the observations of the films were made in oblique settings, where the plane normal of the film, n, made an angle, θ, with the incident beam (θ=30°—80°). The laser beam irradiated the sample along the c axis (a, b, and c are the space fixed Cartesian coordinates, and n lies on the bc plane), and the scattered light was gathered in the b direction, as is shown in Fig. 1.

For the measurements of the polarization components of the Raman bands, a usual polarizer was inserted in front of the sample and an analyzer was placed near the entrance slit of the monochromator. The electric vector of the laser beam, $\boldsymbol{E}$, was taken as the a direction and could be rotated in the b direction by means of a $\lambda/2$ plate made of white mica.

The infrared spectra were measured with a JASCO DS-402G infrared spectrophotometer for the samples on quartz plates. The polarized spectra were measured with an AgCl polarizer which was located in front of the thermocouple detector.

Results and Discussion

Examination in a polarizing microscope showed different patterns for the samples, as is shown in Table 1. For example, the sample of MBBA on the glass treated with silk showed a characteristic thready texture parallel to the long edges, $\boldsymbol{p}$, and is called as a homogeneous sample, while the sample of MBBA on the glass treated with the 0.7 mM HTAB solution showed only dark stars and is designated as a homeotropic sample. In Table 1 the samples which showed colorful patterns (including texture) are classified as //, and the samples with dark stars, as ⊥. There can be seen

Table 1. Results of observations by means of a polarizing microscope

Surface treatment		MBBA	NP-5A
HTAB (aq soln)	0.0070 mM	△	⊥
	0.070	⊥	⊥
	0.70	⊥	∥
	1.4	⊥	∥
Lecithin (C_2H_5OH soln)	0.0010 mM	∥	⊥
	0.010	∥	⊥
	0.10	⊥	⊥
	1.0	⊥	∥
Silane		∥	∥
Silk		∥ (texture)	∥ (texture)

⊥: Dark stars, ∥: colorful pattern, △: dark colorful pattern.

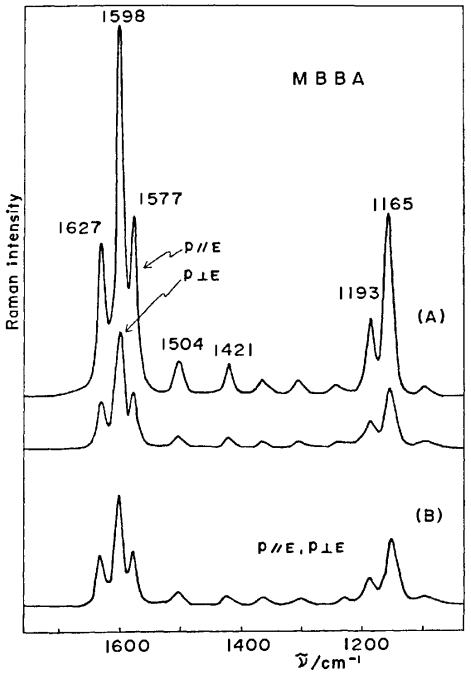

Fig. 2. Raman spectra of aligned thin (*ca.* 1 μm) films of MBBA.
(A): Homogeneous, (B) homeotropic samples.

only a very small difference in the observation between glass and quartz substrates. △ is used for the sample showing a dark colorful pattern.

The Raman spectra reported so far are for the films more than 25 μm thick. The oblique setting used here made it possible to measure the spectra of the thinner films. The Raman spectra for the MBBA thin (*ca.* 1 μm) film with a polarized incident light are shown in Fig. 2 ($\theta=60°$) for the 1700—1000 cm^{-1} region. (A) and (B) show the spectra for homogeneous (silk treatment) and homeotropic (0.7 mM HTAB treatment) samples respectively. For the homogeneous sample, the band intensities at 1598 cm^{-1} and 1577 cm^{-1} for $\boldsymbol{p}//\boldsymbol{E}$ are about three times larger than those for $\boldsymbol{p}\perp\boldsymbol{E}$, while for the homeotropic sample they are almost the same for $\boldsymbol{p}//\boldsymbol{E}$ and $\boldsymbol{p}\perp\boldsymbol{E}$, taking the electric vector of the incident light as $\boldsymbol{E}//\boldsymbol{a}$ and the long axis of the plate as $\boldsymbol{p}$. These spectra were independent of θ. The 1598 cm^{-1} and 1577 cm^{-1} bands are assigned to the benzene ring-vibrations,[3,4,12] the Raman-scattering tensors of which have the largest element $|\alpha'_{zz}|$ ($|\alpha'_{zz}| \gg |$other element$|$), taking z as the molecular long axis.

The Raman-scattering tensor (polarizability tensor derivative) is expressed by;

$$\alpha'_{mol} = \begin{pmatrix} \alpha'_{xx} & \alpha'_{xy} & \alpha'_{xz} \\ \alpha'_{yx} & \alpha'_{yy} & \alpha'_{yz} \\ \alpha'_{zx} & \alpha'_{zy} & \alpha'_{zz} \end{pmatrix}, \quad (1)$$

where x, y, and z are the principal molecular axes. Assuming an axial symmetry about the z axis resulting from the free rotation around the z axis, we obtain $\alpha'_{zz}=A$, $\alpha'_{zx}=\alpha'_{yz}=\alpha'_{zy}=\alpha'_{xz}=B$, $\alpha'_{xx}=\alpha'_{yy}=C$, and $\alpha'_{xy}=\alpha'_{yx}=D$; then,

$$\alpha'_{mol} = \begin{pmatrix} C & D & B \\ D & C & B \\ B & B & A \end{pmatrix}. \quad (2)$$

The Raman-scattering tensor in the laboratory coordinates (space fixed, a, b, c);

$$\alpha'_{lab} = \begin{pmatrix} \alpha'_{aa} & \alpha'_{ba} & \alpha'_{ac} \\ \alpha'_{ba} & \alpha'_{bb} & \alpha'_{bc} \\ \alpha'_{ac} & \alpha'_{bc} & \alpha'_{cc} \end{pmatrix} \quad (3)$$

is transformed from (1) or (2) using Euler's angles (α, β, γ).[19]

$$\begin{aligned}
\alpha'_{aa} &= (1/3)(2C+A) + (1/3)(A-C)(3\sin^2\beta\cos^2\alpha - 1) \\
&\quad - D[\sin 2\gamma(\cos^2\beta\cos^2\alpha - \sin^2\alpha) + \cos 2\gamma\cos\beta\sin 2\alpha] \\
&\quad + B\sin\beta(2\cos\gamma\cos\beta\cos^2\alpha - \sin\gamma\sin 2\alpha) \\
&\quad - B\sin\beta(2\sin\gamma\cos\beta\cos^2\alpha + \cos\gamma\sin 2\alpha). \\
\alpha'_{ac} &= (A-C)\sin\beta\cos\beta\cos\alpha \\
&\quad + D\sin\beta(\sin 2\gamma\cos\beta\cos\alpha + \cos 2\gamma\sin\alpha) \\
&\quad + B(\cos\gamma\cos 2\beta\cos\alpha - \sin\gamma\cos\beta\sin\alpha) \\
&\quad - B(\sin\gamma\cos 2\beta\cos\alpha + \cos\gamma\cos\beta\sin\alpha). \\
\alpha'_{bc} &= (A-C)\sin\beta\cos\beta\sin\alpha \\
&\quad + D\sin\beta(\sin 2\gamma\cos\beta\sin\alpha - \cos 2\gamma\cos\alpha) \\
&\quad + B(\cos\gamma\cos 2\beta\sin\alpha + \sin\gamma\cos\beta\cos\alpha) \\
&\quad - B(\sin\gamma\cos 2\beta\sin\alpha - \cos\gamma\cos\beta\cos\alpha). \\
\alpha'_{ba} &= (1/2)(A-C)\sin^2\beta\sin 2\alpha \\
&\quad - (D/2)[\sin 2\gamma(1+\cos^2\beta)\sin 2\alpha - 2\cos 2\gamma\cos\beta\cos 2\alpha] \\
&\quad + B\sin\beta(\cos\gamma\cos\beta\sin 2\alpha + \sin\gamma\cos 2\alpha) \\
&\quad - B\sin\beta(\sin\gamma\cos\beta\sin 2\alpha - \cos\gamma\cos 2\alpha).
\end{aligned}$$

α'_{bb} and α'_{cc} are omitted.

In our Raman measurements, shown in Fig. 1, we observe $(\alpha'_{aa})^2+(\alpha'_{ac})^2$ as the intensities. Assuming the molecular long axis, z, to be parallel to $\boldsymbol{p}$ for the homogeneous samples and perpendicular to $\boldsymbol{p}$ for the homeotropic samples, Euler's angles for the sample settings are given as follows:

$\alpha = 0°$, $\beta=90°$ for homogeneous $\boldsymbol{p}//\boldsymbol{E}$,

$\alpha = 270°$, $\beta = 30°$ for homogeneous $\boldsymbol{p}\perp\boldsymbol{E}$,

$\alpha = 90°$, $\beta = 60°$ for homeotropic $\boldsymbol{p}//\boldsymbol{E}$ and $\boldsymbol{p}\perp\boldsymbol{E}$.

The $(\alpha'_{aa})^2+(\alpha'_{ac})^2$ are calculated by averaging over $\gamma(0\rightarrow 2\pi)$

$$(\alpha'_{aa})^2 + (\alpha'_{ac})^2 = A^2 + B^2, \text{ for homogeneous } \boldsymbol{p}//\boldsymbol{E}$$
$$= (3/4)B^2 + C^2 + (5/8)D^2, \text{ for homogeneous } \boldsymbol{p}\perp\boldsymbol{E}$$
$$= (1/4)B^2 + C^2 + (7/8)D^2, \text{ for homeotropic } \boldsymbol{p}//\boldsymbol{E} \text{ and } \boldsymbol{p}\perp\boldsymbol{E}.$$

Since we have $|A_1| \gg |B_1|$ and negligibly small $|C_1|$ and $|D_1|$ values for the 1598 cm^{-1} band (using the suffix 1), the larger intensity observed for the homogeneous $\boldsymbol{p}//\boldsymbol{E}$ than that for the homogeneous $\boldsymbol{p}\perp\boldsymbol{E}$ can well be interpreted. The intensity ratio between 1598 cm^{-1} and 1577 cm^{-1} bands should be constant for all the sample settings, which is in harmony with the observation. The observed Raman spectra, therefore, certainly confirm the molecular alignments suggested by the observation by a polarizing microscope; the molecular long axis is parallel to $\boldsymbol{p}$ for the homogeneous sample and perpendicular to $\boldsymbol{p}$ for the homeotropic sample.

The observed peak intensity ratios between the 1627 cm^{-1} and 1598 cm^{-1} bands are given in Table 2 for

Table 2. Intensity ratios between 1627 cm^{-1} and 1598 cm^{-1} bands, $I(1627)/I(1598)$, of MBBA films

	Bulk Isotropic	Film	
		Homogeneous	Homeotropic
$\boldsymbol{p}//\boldsymbol{E}$	0.417	0.402	0.445
$\boldsymbol{p}\perp\boldsymbol{E}$		0.414	0.445

the MBBA thin films at $\theta=60°$, together with the value for the isotropic bulk (50 °C). If the 1627 cm^{-1} band is assigned to the C=N stretching vibration (using the suffix 2), $|B_2|$ and $|C_2|$ are quite large, though $|A_2|$ is the largest among $|A_2|$, $|B_2|$, $|C_2|$, $|D_2|$, because the C=N bond lies on the phenyl plane and makes an angle of 30° with the z axis.[12] The intensity ratio between the 1627 cm^{-1} and 1598 cm^{-1} bands, $I(1627)/I(1598)$, therefore, should vary with the molecular orientation, having the largest value for the homeotropic sample ($\boldsymbol{p}//\boldsymbol{E}$ and $\boldsymbol{p}\perp\boldsymbol{E}$). Based on the expressions for $(\alpha'_{aa})^2+(\alpha'_{ac})^2$ and the observed relation $|A_1|>|A_2|$, the following relation for the intensity ratio, $I(1627)/I(1598)$, can be derived:

(homogeneous $\boldsymbol{p}//\boldsymbol{E}$) < (homogeneous $\boldsymbol{p}\perp\boldsymbol{E}$) < (homeotropic $\boldsymbol{p}//\boldsymbol{E}$ and $\boldsymbol{p}\perp\boldsymbol{E}$).

The relation derived above is in good agreement with the observed values in Table 2. This fact also confirms that the 1627 cm^{-1} band is to be assigned to the C=N stretching vibration, though there may be some vibrational coupling with the benzene-ring vibration. The treatment described above is rather rough, and we have neglected the molecular precessional motion[5,12] around the optic axis.

The molecular orientation of the liquid crystals depends on the concentrations of HTAB or lecithin solutions as well as on the materials used for the pretreatment of the plates, as has been reported by Proust and Ter-Minassian-Saraga.[13] The Raman intensity ratios, $I(1627)/I(1598)$, observed for the samples treated with various concentrations of HTAB and lecithin are shown in Table 3. For the sample treated with

Table 3. Relation between Raman intensity ratios of MBBA films and concentrations of HTAB and lecithin

Treatment	Concentration	$\frac{I(1627)}{I(1598)}$	Microscopic observation
HTAB (aq soln)	0.0070 mM	0.43_6	△
	0.070	0.44_1	⊥
	0.70	0.445	⊥
	1.4	0.44_5	⊥
Lecithin (C_2H_5OH soln)	0.0010 mM	0.39_7	∥
	0.010	0.40_1	∥
	0.10	0.43_2	⊥
	1.0	0.43_8	⊥

Table 4. Polarization components of 1598 cm^{-1} band of MBBA films (relative values)

	Homogeneous $\boldsymbol{p}//\boldsymbol{E}$	Homeotropic $\boldsymbol{p}//\boldsymbol{E}$, $\boldsymbol{p}\perp\boldsymbol{E}$
(aa)	1.0	1.0
(ac)	0.37	0.90
(bc)	0.29	1.6
(ba)	0.59	1.3

0.7 mM HTAB, the measurements were made for a number of samples, while for the other cases several samples were measured for each concentration. With the HTAB treatments the MBBA molecules were almost perpendicular to the plate surface, but with the lecithin treatments they were perpendicular only if a concentration of lecithin larger than 0.1 mM was used. Moreover, with 0.01 or 0.001 mM lecithin treatment the MBBA molecules were parallel to the plate surface. With low concentrations, the amount of the adsorbed HTAB or lecithin must be small, giving rise to an incomplete surface treatment.

Thus, the intensity ratio provides a semi-quantitative measure of the molecular orientation. It was, however, found that the Raman results did not always coincide with those suggested by the polarizing microscopic observations. For example, the MBBA sample treated with 0.007 mM HTAB showed the Raman intensity ratio of 0.436, corresponding to the almost perpendicular orientation structure, though the examination by the polarizing microscope did not enable us to distinguish the molecular orientation.

The Raman intensity ratio varies with the change in the thickness of the samples. For the MBBA samples treated with 0.7 mM HTAB, the intensity ratio $I(1627)/I(1598)$ was 0.445 for the *ca.* 1 μm film and 0.427 for the 25—100 μm films ($\boldsymbol{p}//\boldsymbol{E}$, $\theta=60°$), showing that the molecular orientations were incomplete with the thicker films, because the ratio becomes largest when the molecules are perpendicular to the plate surface. On the other hand, the samples treated with silk did not show any appreciable change in the intensity ratio for 1—100 μm films.

The polarization components were measured for (aa), (ac), (bc), and (ba), where (ac) means the spectrum observed with a incident and c scattered components. The relative intensities of the 1598 cm^{-1} band observed among the polarization components

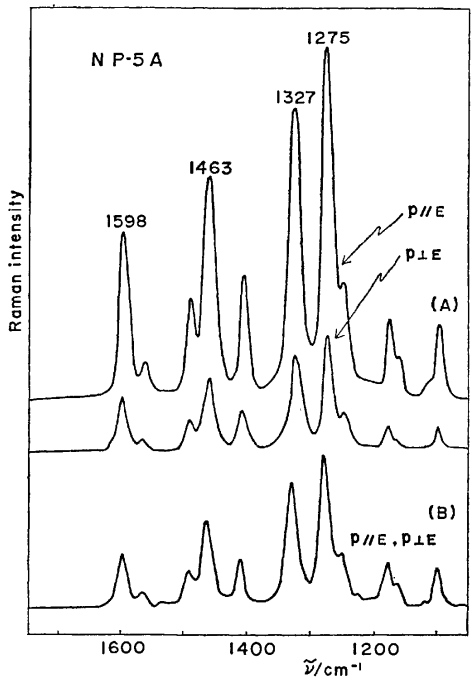

Fig. 3. Raman spectra of aligned thin (*ca.* 1 μm) films of NP-5A.
(A): Homogeneous, (B) homeotropic samples.

for $\theta=60°$ are shown in Table 4. The polarization components are calculated from the elements of α'_{ab} derived above. For homogeneous $\boldsymbol{p}//\boldsymbol{E}$, $(\alpha'_{bc})^2=D_1^2/2$ and $(\alpha'_{ba})^2=B_1^2$ while for homeotropic $\boldsymbol{p}//\boldsymbol{E}$ and $\boldsymbol{p}\perp\boldsymbol{E}$,

$$(\alpha'_{bc})^2 = (3/16)A_1^2 + (1/4)B_1^2 + (3/16)C_1^2 + (3/32)D_1^2$$

$$(\alpha'_{ba})^2 = (3/4)B_1^2 + (1/8)D_1^2.$$

Then, for the 1598 cm^{-1} band, the following relations can be derived theoretically:

$(\alpha'_{bc})^2 < (\alpha'_{ba})^2$ for homogeneous $\boldsymbol{p}//\boldsymbol{E}$, and

$(\alpha'_{bc})^2 > (\alpha'_{ba})^2$ for homeotropic $\boldsymbol{p}//\boldsymbol{E}$ and $\boldsymbol{p}\perp\boldsymbol{E}$.

These relations are in harmony with the observed relations:

$I(\mathrm{bc}) < I(\mathrm{ba})$ for homogeneous $\boldsymbol{p}//\boldsymbol{E}$, and

$I(\mathrm{bc}) > I(\mathrm{ba})$ for homeotropic $\boldsymbol{p}//\boldsymbol{E}$ and $\boldsymbol{p}\perp\boldsymbol{E}$.

In this case, the values depend on θ. These results also confirm the molecular arrangements described above.

The results obtained for the NP-5A film samples are shown in Fig. 3 and Tables 5 and 6. For the NP-5A film, the Raman bands have not yet been assigned to the normal vibrations of the molecules. However, as is shown in Fig. 3 for the homogeneous sample treated with silk, the Raman intensities of the 1598, 1463, 1327, and 1275 cm^{-1} bands were much stronger for $\boldsymbol{p}//\boldsymbol{E}$ than those for $\boldsymbol{p}\perp\boldsymbol{E}$, while no appreciable intensity changes in these Raman bands could be observed for the homeotropic sample treated with 0.1 mM lecithin. The strong bands observed for the $\boldsymbol{p}//\boldsymbol{E}$ of the homogeneous sample can be assigned to the vibrations, of which the Raman-scattering tensors have the largest $|\alpha'_{zz}|$ values. This homogeneous sample showed a colorful texture in the polarizing microscopic examination and had its molecular

Table 5. Intensity ratios for NP-5A films

	Silk		0.7 mM HTAB	0.1 mM Lecithin
	$\boldsymbol{p}//\boldsymbol{E}$	$\boldsymbol{p}\perp\boldsymbol{E}$	$\boldsymbol{p}//\boldsymbol{E}$, $\boldsymbol{p}\perp\boldsymbol{E}$	$\boldsymbol{p}//\boldsymbol{E}$, $\boldsymbol{p}\perp\boldsymbol{E}$
$\frac{I(1278)}{I(1598)}$	2.4_4	2.1_6	2.1_8	2.3_5
$\frac{I(1327)}{I(1598)}$	1.9_0	1.8_3	1.8_6	2.0_5
$\frac{I(1463)}{I(1598)}$	1.3_9	1.3_9	1.4_5	1.4_9

Table 6. Polarization components of 1275 cm^{-1} band of NP-5A films (relative values)

	Homogeneous (silk) $\boldsymbol{p}//\boldsymbol{E}$	Homeotropic (lecithin) $\boldsymbol{p}//\boldsymbol{E}$, $\boldsymbol{p}\perp\boldsymbol{E}$
(aa)	1.0	1.0
(ac)	0.6	0.8
(bc)	0.4	1.0
(ba)	0.6	0.7

axes parallel to $\boldsymbol{p}$. The sample treated with 0.7 mM HTAB also showed a colorful pattern, but not a colorful texture, and it was a kind of homogeneous sample where the molecular long axes must be randomly oriented on the plane parallel to the plate surface. In the homogeneous (texture) sample, the Raman intensity ratios are different for $\boldsymbol{p}//\boldsymbol{E}$ and $\boldsymbol{p}\perp\boldsymbol{E}$, while they are the same in the other cases, as is shown in Table 5.

The polarization components of the 1275 cm^{-1} band are shown in Table 6. $I(\mathrm{ba})>I(\mathrm{bc})$ was observed for the homogeneous sample and $I(\mathrm{bc})>I(\mathrm{ba})$ for the homeotropic sample, similar to those for the 1598 cm^{-1} band of MBBA films, confirming the molecular orientations suggested by the polarizing microscopic observations.

The infrared transmission spectra were observed at normal incidence for the MBBA films between quartz windows, but only in the C–H stretching region. They are shown in Fig. 4. The bands at 3022 and 3000 cm^{-1} can be assigned to the C–H stretching vibrations in =C–H or aromatic C–H groups. These bands have their transition moments on the molecular plane, because the C–H bands must be on the plane which approximately coincides with the benzene-ring planes. These bands are stronger for the homogeneous sample than for the homeotropic sample, as is shown in Fig. 4(A). The dichroic spectra for the homogeneous sample are observed to be as in Fig. 4(B), where these bands are stronger for $\boldsymbol{p}\perp\boldsymbol{E}$ than for $\boldsymbol{p}//\boldsymbol{E}$, taking the electric vector as $\boldsymbol{E}$. Bulkin and Lok, after measuring the far-infrared spectra of aligned films of MBBA, reported that the spectra of the homogeneous and homeotropic samples did not show any measurable difference in the intensity of the intermolecular mode.[9] However, the present infrared results for the intramolecular modes can confirm the molecular orientations described above.

It may thus be considered that the Raman spectra certainly give information on molecular orientation

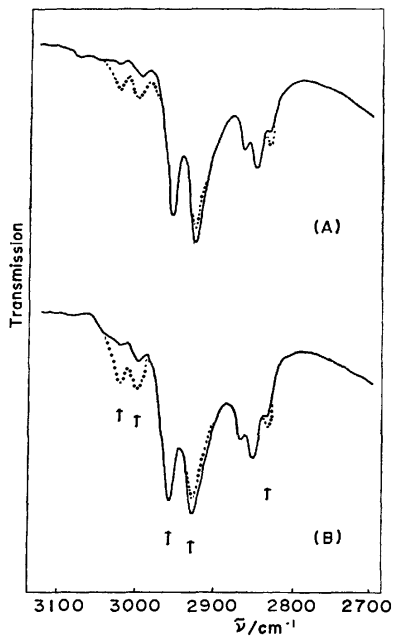

Fig. 4. Infrared spectra of aligned thin (*ca.* 1 μm) films of MBBA.
(A): Homeotropic —— and homogeneous ---- samples, (B): dichroism of homogeneous sample; $p//E$ ——, $p \perp E$ ----.

structures semiquantitatively. For the completely oriented structures, perpendicular or parallel, the Raman results agree well with the suggestions of the polarizing microscopic observations. Although the examination by a polarizing microscope is a simple and convenient method for distinguishing the orientations, it can not always be used, especially for the intermediate orientations. On the other hand, the Raman intensities measured can serve as a degree of alignment for the structural study of liquid crystal films. Furthermore, measurements of the thinner layers, more specific for the surface species, can be performed by observing the resonance Raman spectra, since the resonance Raman effect has been effectively used in the studies of small amounts of surface species.[14-17] Moreover, some theoretical work which assumes the molecular model parameters, such as the order parameter, developed by Pershan *et al.*[5] and Hatta,[12] will be able to quicken progress in studying the structures in their molecular dimensions.

Lastly, let us add some consideration of the mechanism of the formation of the two types of molecular orientation structures, homogeneous and homeotropic. The homogeneous structures appeared in thin films between two silk-treated clean plates, while the homeotropic structures appeared in thin films between plates previously treated with HTAB or lecithin solutions of certain concentration ranges. In the former case, it is supposed that the long molecules of liquid crystals with dipoles whose moment vectors being considered are in the direction of their long axes will be attracted to the plate surface mainly by the electrostatic forces between their dipoles and induced dipoles at the surface, and that they will also be oriented parallel to the surface in the inner part of the films by means of the dipole-dipole interactions, so that they will realize the homogeneous structures. On the other hand, in the latter case, where the plates are pretreated with HTAB or lecithin, whose molecules are amphiphilic in nature, the plate surfaces will be covered by these molecules anchored by their polar groups and will, accordingly, become hydrophobic because of the hydrocarbon chains oriented outside. Then, the liquid-crystal molecules with also hydrophobic groups (hydrocarbon chains at the end of their long molecules) will be attracted to the hydrophobic surfaces by the London-van der Waals attraction forces,[18] so that they will be oriented perpendicular to the surface to form homeotropic structures. However, if the concentration of the HTAB or lecithin solution used for pretreatment is too low, the surface density of the adsorbed molecules will be too small to realize the favorable orientation of the homeotropic alignment of the liquid-crystal molecules. Moreover, the difference observed between HTAB and lecithin in the concentration ranges (0.01 mM<for HTAB, 0.1 mM< for lecithin) required for the homeotropic alignment may be considered to be due to the difference in their molecular structures regarding the possibility of taking favorable orientations at the solid surface.

We wish to acknowledge the financial support from the Mitsubishi Foundation.

References

1) L. Verbit, *J. Chem. Educ.*, **49**, 36 (1972).
2) T. Uchida, H. Watanabe, and M. Wada, *Jpn. J. Appl. Phys.*, **11**, 1559 (1972).
3) G. Vergoten and G. Fleury, *Mol. Cryst. Liq. Cryst.*, **30**, 213 (1975); **36**, 327 (1976).
4) G. Vergoten and G. Fleury, *J. Mol. Struct.*, **30**, 347 (1976).
5) S. Jen, N. A. Clark, P. S. Pershan, and E. B. Priestley, *J. Chem. Phys.*, **66**, 4635 (1977); *Phys. Rev. Lett.*, **31**, 1552 (1973).
6) J. Le Brumant, N. A. Tuan, and M. Jaffrain, *C. R. Acad. Sci., Ser. B*, **280**, 719 (1975).
7) F. Cavatorta, M. P. Fontana, and N. Kirov, *Mol. Cryst. Liq. Cryst.*, **34**, 241 (1977).
8) H. Yamada, Y. Yamamoto, K. Fukumura, and B. Tamamushi, *Chem. Lett.*, **1978**, 345.
9) B. J. Bulkin and W. B. Lok, *J. Phys. Chem.*, **77**, 320 (1973).
10) M. Evans, M. Davies, and L. Larkin, *J. Chem. Soc., Faraday Trans. 2*, **69**, 1011 (1973).
11) E. Sciesinska, J. Sciesinski, J. Twardowski, and J. A. Janik, *Mol. Cryst. Liq. Cryst.*, **27**, 125 (1974).
12) A. Hatta, *Bull. Chem. Soc. Jpn.*, **50**, 2522 (1977); A. Hatta, H. Nohara, and W. Suětaka, *ibid.*, **51**, 967 (1978).
13) J. E. Proust and L. Ter-Minassian-Saraga, *J. Phys. (Paris)*, **36**, Cl-77 (1975).
14) T. Nagasao and H. Yamada, *J. Raman Spectrosc.*, **3**, 153 (1975).
15) Y. Yamamoto and H. Yamada, *J. Chem. Soc., Faraday Trans. 1*, **74**, 1562 (1978); H. Yamada and Y. Yamamoto, *ibid.*, **75**, 1215 (1979).
16) H. Yamada, T. Amamiya, and H. Tsubomura, *Chem. Phys. Lett.*, **56**, 591 (1978).
17) H. Yamada, *Indian J. Pure Appl. Phys.*, **16**, 159 (1978).
18) F. London, *Z. Phys.*, **63**, 245 (1930).
19) M. E. Rose, "Elementary Theory of Angular Momentum," Wiley, New York (1957), p. 50.
20) K. Fukumura, Master's thesis, Kwansei Gakuin University (1980).

 © 1980 The Chemical Society of Japan Bull. Chem. Soc. Jpn., 53, 3059—3063 (1980)

A New Assisted Reaction in the Photodecomposition Reaction of Dibenzoyl Peroxide

Yoshio SAKAGUCHI, Hisaharu HAYASHI,† and Saburo NAGAKURA*

The Institute for Solid State Physics, The University of Tokyo, Roppongi, Minato, Tokyo 106

† *The Institute of Physical and Chemical Research, Wako, Saitama 351*

(Received February 2, 1980)

2,2′-, 2,3′-, and 3,3′-Dimethylbiphenyls were found in the photodecomposition reaction of dibenzoyl peroxide using toluene as solvent. We carried out the experiments to study the external magnetic field, oxygen scavenging, and excitation light intensity effects on their yields. It is concluded that they are produced through the dimerization of (benzoyloxy)methylcyclohexadienyl radicals. This is a new case of the assisted reaction by benzoyloxyl radical. The yields of dimethylbiphenyls were found to be affected remarkably by the small variation of the concentration of benzoyloxyl radical through the three experiments.

The external magnetic field effect upon chemical reactions is one of the most challenging subjects of modern chemistry. We have studied the magnetic field effects upon the photolysis of dibenzoyl peroxide, and have found that the yields of some products in the reaction are dependent upon external magnetic field,[1,2] particularly the yields of newly found products of the reaction, dimethylbiphenyls, show very large magnetic field dependence.[3] In the present paper, the identification and formation mechanism of the newly found products will be discussed in detail, special attention being paid to the scavenger and the excitation light intensity effects on the product yields of this reaction.

During the study of the magnetic field effects upon the photolysis of dibenzoyl peroxide, we found that the yields of some products were sensitive to excitation light intensity. Therefore we have constructed a stabilized light source necessary for excitation and have measured the yields under constant light intensity.

Experimental

The toluene solution (0.5 ml) of dibenzoyl peroxide (**1**) (0.04 mol dm^{-3}) containing chrysene (**2**) (0.002 mol dm^{-3}) as a singlet sensitizer[4] in a Pyrex cell was degassed with the freeze-thaw technique, and was sealed under a nitrogen atmosphere. The irradiation system used in this study is shown in Fig. 1. The cell was set in a water bath with a quartz window. The temperature of the bath was kept 16.5±0.3 °C. The solution was irradiated with an ORC CHM-506-15 1 kW super high pressure mercury lamp through a water filter with Pyrex windows. In order to stabilize the excitation light intensity, we made a feed-back power supply. The light intensity was monitored by a Toshiba TPS 601 phototransister and its signal was returned to the power supply of the lamp. The response time of the feed-back system was about 1 s. The fluctuation of the light intensity was less than ±1.5% and its drift was less than ±2.5% per hour. The excitation light intensity was reduced by placing a copper mesh in front of the sample.

The decrease of **1** was monitored by iodometric titration. In order to decompose **1** almost completely, the irradiation time was set fivefold of the half life time of its disappearance.

The photodecomposition products with molecular weights less than 214 were identified with a Shimadzu 4CMPF gaschromatograph and a Hitachi RMU-6MG gaschromatograph-mass spectrometer. For the former, a 3 mm diameter×1 m PEG 20 M and Silicone OV-1 columns and 3 mm diameter×2 m Apiezone L, Polyphenylether 6-ring,

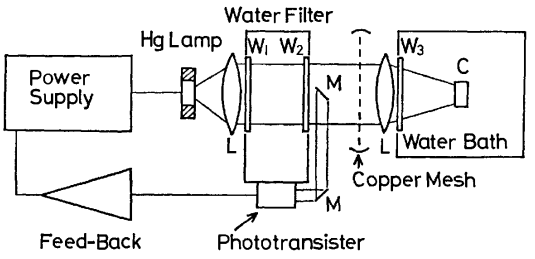

Fig. 1. Reaction apparatus of photodecomposition reaction.
C: Sample cell, L: quartz lens, M: mirror, W_1, W_2: Pyrex windows, W_3: quartz window.

Silicone OV-17, and Bentone 34 columns were used. For the latter, 3 mm diameter×1 m Silicone OV-1 column was used.

In addition to the established authentic samples[5,6] (biphenyl, 1,2-diphenylethane, diphenylmethane, *o*-, *m*-, and *p*-methylbiphenyls, phenyl benzoate, and *o*-, *m*-, and *p*-tolyl benzoates), 2,2′-, 2,3′-, 2,4′-, 3,3′-, 3,4′-, and 4,4′-dimethylbiphenyls, 2-, 3-, and 4-methyldiphenylmethanes, and benzyl benzoate were prepared for the authentic samples in the present study. Dimethylbiphenyls except for 4,4′-one (Tokyo Kasei) were synthesized after the method described in the literature.[7] 3- and 4-Methyldiphenylmethane were made by Wolff-Kishner reduction of the corresponding ketones.[8] 2-Methyldiphenylmethane was given by Dr. Sakuragi, The University of Tsukuba.[9] Benzyl benzoate was prepared from benzyl alcohol and benzoyl chloride.

The yields were measured by the gaschromatograph with a 3 mm diameter×1 m PEG 20 M column, terephthalonitrile being used as an external standard. The respective peaks were integrated by a Shimadzu chromatopac EIA integrator and these data were treated statistically using a YHP 9825A desktop computer.

Results and Discussion

In this study, we identified 14 products with molecular weights less than 212.[3] They are listed in Table 1 together with their yields under the high and low excitation light intensities. At first, our consideration will be confined to the case of high intensity excitation. Among the products given in Table 1, dimethylbiphenyls (**3**'s) and benzyl benzoate (**10**) were found for the first time in the present study, while the others have already been identified.[5,6]

The photolysis of **1** proceeds as follows:[5]

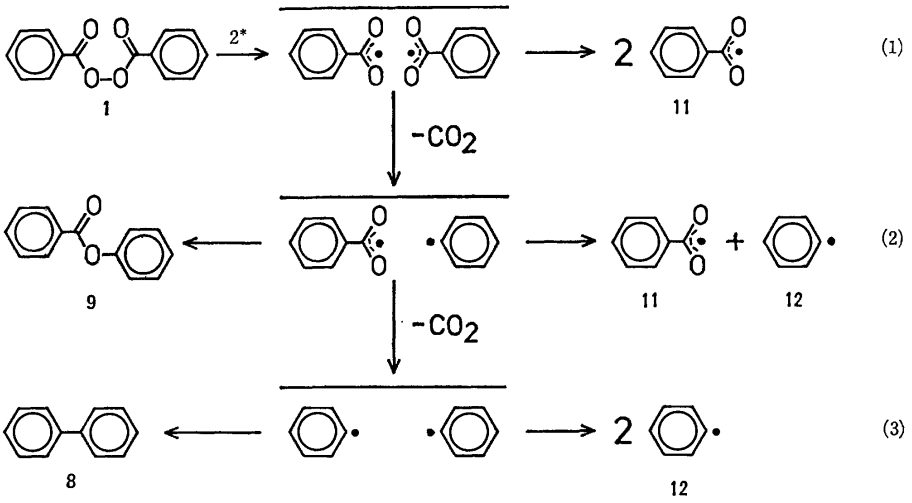

As is seen in Eq. 1, the O–O bond of **1** is dissociated to produce a benzoyloxy-benzoyloxy radical pair ($\overline{PhCO_2\cdot\ PhCO_2\cdot}$). It releases carbon dioxide and produces benzoyloxy-phenyl and phenyl-phenyl radical pairs.(See Eqs. 2 and 3.) By the recombination within the cages, **8** and **9** are formed as cage products. The pair which retains from recombination, dissociates to escaping radicals. The escaping benzoyloxy (**11**) and phenyl (**12**) radicals react with solvent (toluene) and form new radicals as shown in the following equations.

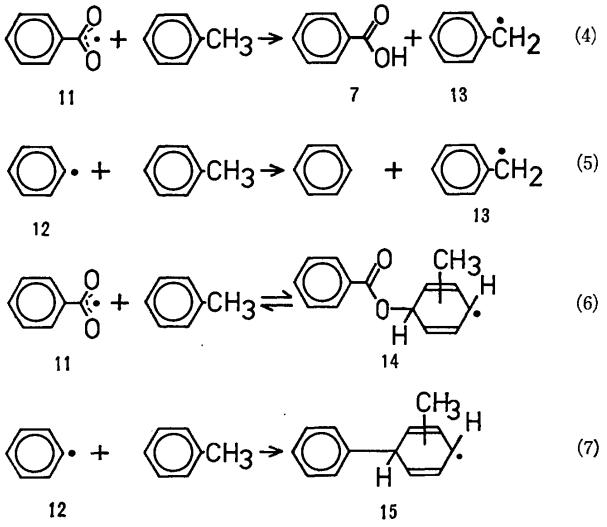

The existence of benzyl radical (**13**) was proved by the formation of 1,2-diphenylethane (**5**).[10] Beside the formation of **13**, the cyclohexadienyl radicals (**14** and **15**) are formed as is shown in Eqs. 6 and 7. Their existences were proved by the formation of tolyl benzoates (**6**'s) and methylbiphenyls (**4**'s).[5,11-13] It is worth while to point out that diphenylmethane was not found under the present experimental conditions.[6] This suggests that the reactions of Eqs. 5 and 7 are very fast and the back reaction of Eq. 7 can be disregarded.[13] On the other hand, **11** can be supplied not only by the escaping from the cage but also by the back reaction of Eq. 6.[13]

TABLE 1. PRODUCT YIELDS AND THEIR DEPENDENCES ON THE EXCITATION LIGHT INTENSITY[a]

Products		I_0	$1/3.5\,I_0$	
2,2'-Dimethylbiphenyl	(2,2'-**3**)	0.2 %	0.1 %	
2,3'-Dimethylbiphenyl	(2,3'-**3**)	2.36	1.44	(61)
3,3'-Dimethylbiphenyl	(3,3'-**3**)	3.56	2.23	(63)
2-Methylbiphenyl	(2-**4**)	6.21	6.86	(110)
Mixture[b]		23.22	24.30	(105)
o-Tolyl benzoate	(*o*-**6**)	4.09	3.26	(80)
Benzoic acid	(**7**)	102.10[c]	97.00[c]	(95)
Biphenyl	(**8**)	1.19	1.22	(103)
Phenyl benzoate	(**9**)	16.13	15.73	(98)
m-Tolyl benzoate	(*m*-**6**)	—[d]		
p-Tolyl benzoate	(*p*-**6**)	—[d]		
Benzyl benzoate	(**10**)	—[d]		

a) The yields are presented in mole percent taking benzoyl peroxide as reference. Values in the parentheses are the percentages of the yields under $1/3.5\,I_0$ divided by those under I_0. The experimental errors are less than 5% of respective values for dimethylbiphenyls and biphenyl and less than 3% of those for the others. b) Given value is the sum of the yields of 3- and 4-methylbiphenyls (3- and 4-**4**'s) and 1,2-diphenylethane (1,2-**5**) because of incomplete separation under our VPC conditions. c) The absolute yield of benzoic acid is not so precise as others owing to the VPC conditions, but the relative value in the parentheses are as precise as others. d) These products were identified but their yields were not measured because of their low yields and the incomplete separation between them under our VPC conditions.

Concerning **3**'s six isomers (2,2'-, 2,3'-, 2,4'-, 3,3'-, 3,4'-, and 4,4'-**3**'s) may be expected to exist. But actually, the only three isomers (2,2'-, 2,3'-, and 3,3'-**3**'s) were detected in the present experiment and no para-substituted compounds (2,4'-, 3,4'-, and 4,4'-**3**'s) could be found. The observed ratio of the detected isomers is; 2,2'-**3**:2,3'-**3**:3,3'-**3**=6.8:60.2:100, showing that the yields of the meta-isomers are larger than those of the ortho-isomers.

The most intuitive path for formation of **3**'s is the addition of the methylphenyl (tolyl) radical (**16**) to toluene as follows:[14]

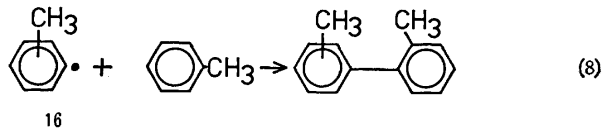

(8)

The consideration on the partial rate factors of tolylation, however, rejects the application of this mechanism to formation of **3**'s. The partial rate factors of the reaction shown by Eq. 8 can safely be considered to be similar to those of phenylation of toluene (f_t), the ratio of which was measured to be $f_o:f_m:f_p=3.3:1.1:1.3$.[15] Thus this mechanism predicts that the yield of 2,x'-**3** should be larger than that of 3,x'-**3**. This prediction contradicts the observed ratio. Therefore, the direct tolylation mechanism is disregarded.

Another possible mechanism for formation of **3**'s is an assisted reaction mechanism which have been applied to formation of tetraarylmethanes[16] and *N*-aryldiphenylmethanimines[17] by **11**. For example, 3,3'-**3** can be formed through the 4-benzoyloxy-3-methyl-2,5-cyclohexadienyl radical (*o*-**14**) as follows:

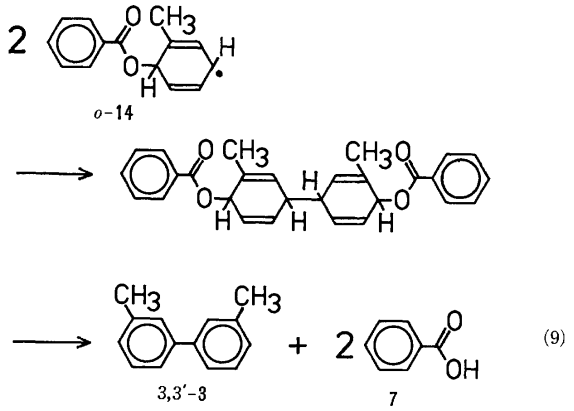

(9)

The benzoyloxylation of toluene preferably occurs on the *o*-position through the hyperconjugation of the methyl group. The steric hindrance of the methyl group may block benzoyloxylation on the methylsubstituted ring carbon atom leading to 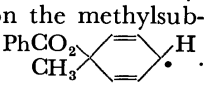 . Furthermore, the steric hindrance of benzoyloxy residue in **14** is considered to disturb the dimerization reaction at its ortho-position

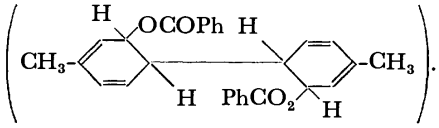

The above consideration on steric hindrance can explain the fact that formation of the **3**'s with a methyl group on the 4-position (2,4'-, 3,4'-, and 4,4'-**3**'s) is prohibited. Thus the assisted reaction scheme explains the observed yields of **3**'s. According to this mechanism, **3**'s are escape products.

In order to prove this assisted reaction scheme, we have studied the following effects on the reaction yields.

1) The effect of external magnetic field.
2) The effect of oxygen scavenging.
3) The effect of excitation light intensity.

The yields of **3**'s were decreased and increased by the application of the low (9.75 and 78 mT) and high (4.3 T) magnetic field, respectively.[3] Since this reaction occurs through a singlet precursor in which two radicals in the benzoyloxy-benzoyloxy, benzoyloxy-phenyl, or phenyl-phenyl radical pair have the anti-parallel unpaired electron spins, the observed magnetic field dependence corresponds to that of the escape product belonging to the (a-3) type of the theoretical classification.[2,3] Therefore, from the magnetic field effect, **3**'s are proved to be escape products in accordance with the above mentioned assisted reaction mechanism.

Table 2. Oxygen scavenging effect on the yields of the products[a]

Products		Degassed	Aerated	
2,3'-Dimethylbiphenyl	(2,3'-**3**)	2.26%	1.45%	(64)
3,3'-Dimethylbiphenyl	(3,3'-**3**)	3.47	2.37	(68)
2-Methylbiphenyl	(2-**4**)	5.68	9.34	(165)
Mixture[b]		20.06	13.92	(68)
o-Tolyl benzoate	(*o*-**6**)	3.24	9.57	(296)
Benzoic acid	(**7**)	81.27[c]	84.80[c]	(104)
Biphenyl	(**8**)	1.23	1.12	(91)
Phenyl benzoate	(**9**)	16.28	15.50	(95)

a) The yields and the values in the parentheses have similar meanings as those in Table 1. The experimental errors are the same as those in Table 1. b) Given value is the sum of the yields of 3- and 4-methylbiphenyls (3- and 4-**4**'s) and 1,2-diphenylethane (1,2-**5**) because of incomplete separation under our VPC conditions. c) Same as the note c) in Table 1.

Next, we tried to scavenge escaping radicals. Because this reaction yields various kinds of products, organic scavenger may disturb analysis of the products. So the dissolved oxygen in the solution was used as a radical scavenger. The product yields from the samples with and without degassing are listed in Table 2.[18] The excitation light intensity was kept constant during the two series of the experiments. The reaction time was 30 min for these experiments. We can see from Table 2 that the yields of 2,3'- and 3,3'-**3**'s were decreased by the dissolved oxygen. This decrease and the increase of the yield of *o*-**6** seem to indicate that **14**'s react with oxygen forming **6**'s and the dimerization reaction of **14**'s to form **3**'s are inhibited by the oxidation. **15**'s are also oxidized forming **4**'s. The increase of 2-**4** is remarkable as is shown in Table 2. But the sum of the yields for 3- and 4-**4** and 1,2-**5** is decreased by oxygen, because **13** is oxidized forming benzyl alcohol and benzaldehyde as final products[19] and like the case of **14**'s, the dimerization of **13** is also inhibited. On the other hand, the yields of **8** and **9** were not so much changed by oxygen. Therefore, the yields of cage products can be considered to be nearly insensitive to dissolved oxygen. This is also one of the proofs of the fact that **3**'s are escape products.

In order to determine whether **3**'s are formed through the dimerization of **14**'s, we studied the excitation light intensity dependence of their yields. On the assumption that **1** decomposes exponentially and the concentration of radical **n**, [**n**], is proportional to the decomposition rate of **1**, then the yield of the products coming from **n** has the following excitation light intensity dependence.[20] When the formation rate of the product has a first order dependence on [**n**], the product yield does not depend on the excitation light intensity. When the rate has a second order dependence on [**n**], the product yield depends linearly on the excitation light intensity. The above-mentioned excitation light intensity dependence is calculated through an oversimplified model. Thus the actual dependence may be more complex than the above prediction. But it can be used for a qualitative argument.

On the second column of Table 1 are listed the yields in the low excitation light intensity experiment in which the light intensity was reduced to 1/3.5 of that in the high intensity experiment and the reaction time was increased to 70 min from 20 min in the high intensity experiment. We can see from Table 1 that the yields of **3**'s are reduced by lowering the excitation light intensity. The yield of *o*-**6** is also somewhat decreased. These findings may be explained by the following consideration. Owing to the elongation of reaction time, the concentrations of the initially prepared benzoyloxy and phenyl radicals decrease. Thus bimolecular termination reactions between escaping radicals are retarded and the probability of the decomposition of **11** to **12**, which is an unimolecular reaction, increases relatively. This means that the yields of **3**'s and *o*-**6** coming from **11** decrease. Table 1 shows that the decrement is much larger for **3**'s than *o*-**6** which is considered to be produced depending linearly on the concentration of **14**. Therefore it is most probable that the formation rates of **3**'s are nearly proportional to the square of the concentration of **14**. This supports the mechanism that **3**'s are formed by the dimerization of **14**.

The decrease in the yields of the products which come from **11** reflected on the increase in the yields of the products coming from **12**. As is shown in Table 1, by lowering the excitation light intensity the yield of 2-**4** increased a little and the sum of the yields of 3- and 4-**4** and 1,2-**5** increased slightly. The yields of **8** and **9** are not affected so much by the change of the excitation light intensity. This can be interpreted by the fact that they are cage products.

The above-mentioned three experiments show that dimethylbiphenyls are escape products which are formed through the dimerization of (benzoyloxy)methylcyclohexadienyl radicals. This shows the rationality of the assumed assisted dimerization scheme.

This is a new assisted reaction by the benzoyloxy radical. The other cases which have hitherto been studied are formation of tetraarylmethane through the reaction with the triphenylmethyl radical[16] and formation of *N*-aryldiphenylmethanimine through the reaction with the diphenylmethaniminyl radical.[17] Compared with these two cases, the present process is more essential, because **3**'s are produced from two **14**'s and their formation does not need the other radicals.

The excitation light dependence of the radical reaction induced by photodecomposition can be anticipated as the possibility to elucidate the mechanism, although the experiments concerning the change in the excitation light intensity have not been preferred because it can provoke complexities in the reaction by the change in the radical concentrations. The present study shows that the experiment of light intensity dependence is useful for the classification of reaction mechanisms.

The authors wish to express their sincere thanks to Professor Katsumi Tokumaru and Dr. Hirochika Sakuragi, The University of Tsukuba, and Professor Masayuki Yoshida, The University of Tokyo, for helpful discussion and for supplying some of the authentic samples.

References

1) Y. Tanimoto, H. Hayashi, S. Nagakura, H. Sakuragi, and K. Tokumaru, *Chem. Phys. Lett.*, **41**, 267 (1976).
2) H. Hayashi and S. Nagakura, *Bull. Chem. Soc. Jpn.*, **51**, 2862 (1978).
3) Y. Sakaguchi, H. Hayashi, and S. Nagakura, *Bull. Chem. Soc. Jpn.*, **53**, 39 (1980).
4) T. Nakata and K. Tokumaru, *Bull. Chem. Soc. Jpn.*, **43**, 3315 (1970); K. Tokumaru, A. Ohshima, T. Nakata, H. Sakuragi, and T. Mishima, *Chem. Lett.*, **1974**, 571.
5) T. Nakata, K. Tokumaru, and O. Simamura, *Tetrahedron Lett.*, **1967**, 3303.
6) D. H. Hey, B. W. Pengilly, and G. H. Williams, *J. Chem. Soc.*, **1955**, 6; **1956**, 1463.
7) J. L. Laseter, U. Mende, and G. W. Griffin, *Org. Mass Spectrom.*, **4**, 599 (1970).
8) Huang-Minlon, *J. Am. Chem. Soc.*, **68**, 2487 (1946).
9) The authors express their heartily thanks to Dr. H. Sakuragi for his kindness in synthesizing 2-methyldiphenylmethane.
10) H. Langhals and H. Fidcher, *Chem. Ber.*, **111**, 543 (1978).
11) D. H. Hey, M. J. Perkins, and G. H. Williams, *J. Chem. Soc.*, **1964**, 3412.
12) J. Saltiel and H. C. Curtis, *J. Am. Chem. Soc.*, **93**, 2056 (1971); M. E. Kurz, E. M. Steele, and R. L. Vecchio, *J. Org. Chem.*, **39**, 3331 (1974).
13) K. Tokumaru, *Nippon Kagaku Zasshi*, **92**, 73 (1971).
14) The dimerization of **16**'s can also be considered. But the yields of **3**'s are low, so the concentration of **16** must be low during the reaction. Then the addition would favor than dimerization.
15) R. Ito, T. Migita, N. Morikawa, and O. Simamura, *Tetrahedron*, **21**, 955 (1965).
16) T. Suehiro, S. Igeta, O. Kuwabara, and M. Hirai, *Tetrahedron*, **26**, 963 (1970).
17) S. Ishikawa, H. Sakuragi, M. Yoshida, N. Inamoto, and K. Tokumaru, *Chem. Lett.*, **1975**, 819.
18) The values in the left columns in Tables 1 and 2 except for **7** are somewhat different from each other. This is due to the difference in the excitation light intensity. The fairly large discrepancy of the yield of **7** comes from the VPC conditions. However the values presented in left and right columns within each table do not have such discrepancies between them, because they were obtained under

the same experimental conditions.

19) We identified them under the existence of oxygen but we did not measure their yields.

20) The concentration of **1**, [**1**], decays as follows:

$$[\mathbf{1}](t)=[\mathbf{1}](0)\exp(-\alpha It),$$

here [**1**](0) is its initial concentration. I is the excitation light intensity, and α is the decomposition rate constant. When **n** is formed in proportion to [**1**], [**n**] can be given as follows:

$$[\mathbf{n}](t)=C_{\mathbf{n}}\left(-\frac{\mathrm{d}[\mathbf{1}](t)}{\mathrm{d}t}\right)=C_{\mathbf{n}}\alpha I\exp(-\alpha It),$$

here $C_{\mathbf{n}}$ is the fractional coefficient. If a product is produced in proportion to [**n**] or to the square of [**n**], the yield, ${}^{1\text{ or }2}Y$ is given respectively as follows:

$${}^{1}Y=\lambda_1\int_0^\infty[\mathbf{n}](t)\mathrm{d}t=\lambda_1C_{\mathbf{n}}$$

$${}^{2}Y=\lambda_2\int_0^\infty([\mathbf{n}](t))^2\mathrm{d}t=\lambda_2C_{\mathbf{n}}^2\frac{I}{2},$$

here λ_t is the reaction probability.

Thus ${}^{1}Y$ is independent of I, and ${}^{2}Y$ is linearly dependent on I.

CNDO and INDO Calculations of the Magnetic Circular Dichroism of Several Purine Derivatives

Akira KAITO and Masahiro HATANO*

Chemical Research Institute of Non-aqueous Solutions, Tohoku University, Sendai 980

(Received February 4, 1980)

Calculations of the magnetic circular dichroism(MCD) of methylpurines and methyladenines were carried out not only by the CNDO/S-CI procedure, but also by the INDO/S-CI procedure. The CNDO/S-CI procedure correctly predicted the signs and magnitudes of the MCD spectra of 1-, 3-, and 7-methylpurines and of 9-methyladenine which cannot be improved by the parameter adjustment. On the other hand, the signs of the MCD spectra and transition energies of all these purine derivatives were clearly explained by the INDO/S-CI procedure.

The magnetic circular dichroism (MCD) spectra of purine derivatives have been extensively studied by many investigators because the MCD spectra give valuable information on the electronic structure of these compounds.[1-3] By MCD the electronic absorption bands which overlap with each other have been resolved, and the presence of several electronic transitions in the ultraviolet region has been clarified.

On the other hand, there have been many attempts to calculate the Faraday parameters of the organic aromatic compounds by means of quantum mechanical SCF-MO calculations. The Pariser-Parr-Pople(PPP) procedure[4] has been successfully applied to explaining the signs of the MCD spectra of the derivatives and hetero atom analogues of alternant and nonalternant aromatic hydrocarbons.[5] The complete neglect of the differential overlap (CNDO) method,[6,7] an SCF-MO procedure for all valence electrons, has also predicted the correct signs of the MCD spectra of indole,[8] azines,[9] substituted benzenes,[10,11] some alternant hydrocarbons,[12] and azanaphthalenes.[13]

However, the original CNDO/S-CI procedure[7] proposed by Jaffé and his co-workers has failed to reproduce the MCD spectra of methyladenines and some 8-azapurines.[3] In order to overcome the difficulty, Djerassi and his co-workers have set the scaling constant, κ, for the π-type overlap integrals back to unity, as in the CNDO/2 method, and scaled the state energies and all the quantities derived from energies by means of an adjustable parameter, κ', after the CI calculation had been performed.[3] Although the new method, labeled the CNDO/S' method, has correctly predicted the signs of the MCD spectra of methyladenines and 8-azapurines, it cannot give wavefunctions which take account of the transition energies as well as the sign of the MCD spectra.

In this work, we calculate the transition energies and the Faraday B terms of purine, methylpurines, and methyl adenines not only by means of the CNDO procedure, but also by means of the intermediate neglect of the differential overlap(INDO) approximation,[14,15] and compare the results with the experimental data which have appeared in the literature.

Theoretical

The Faraday B terms were calculated using wavefunctions obtained from the INDO/S-CI approximation. The one-center core integrals and one-center electron repulsion integrals were evaluated from the valuence-state energy data[16] and the experimental Slater-Condon parameters.[17] The two-center electron repulsion integrals were calculated by means of the Nishimoto-Mataga equation.[18] The resonance integrals, $\beta_{\mu\nu}$, between atomic orbitals, μ and ν, were evaluated by means of the following equation:

$$\beta_{\mu\nu} = \frac{1}{2}(\beta_A + \beta_B)\bar{S}_{\mu\nu}, \quad (1)$$

where β_A is a bonding parameter of the atom, A, to which the atomic orbital, μ, belongs and where $\bar{S}_{\mu\nu}$ is an overlap integral obtained as follows:

$$\bar{S}^{ss}_{\mu\nu} = S^{ss}_{\mu\nu}, \quad (2)$$

$$\bar{S}^{sp}_{\mu\nu} = S^{sp}_{\mu\nu} \quad (3)$$

$$\bar{S}^{pp}_{\mu\nu} = S^{\sigma\sigma}_{\mu\nu} g^{\sigma\sigma}_{\mu\nu} \kappa_{\sigma\sigma} + S^{\pi\pi}_{\mu\nu} g^{\pi\pi}_{\mu\nu} \kappa_{\pi\pi}, \quad (4)$$

where $g^{\sigma\sigma}_{\mu\nu}$ and $g^{\pi\pi}_{\mu\nu}$ are the geometric factors and where $\kappa_{\sigma\sigma}$ and $\kappa_{\pi\pi}$ are the semiempirical scaling factors. The bonding parameters, β, and the scaling factors are determined so that the ionization potentials and transition energies of benzene and pyridine are well reproduced ($\beta_H = -6.6$ eV, $\beta_C = -15.4$ eV, $\beta_N = -23$ eV, $\kappa_{\sigma\sigma} = 1.23$, $\kappa_{\pi\pi} = 0.67$). The configuration interaction(CI) among singly excited configurations below 10 eV was taken into account.

We also calculated the Faraday B terms of the purine derivatives within the framework of the CNDO/S-CI approximation. The one-center repulsion integrals and one-center core parameters were taken from the values determined by Sichel and Whitehead.[19] The two-center electron integrals were evaluated by the Nishimoto-Mataga equation.[18] The bonding parameter, β, and the scaling factor for the π-type overlap integrals, κ, were empirically chosen in the same way as the INDO/S calculation ($\beta_H = -6.6$ eV, $\beta_C = -17.8$ eV, $\beta_N = -28$ eV, $\kappa_{\sigma\sigma} = 1.0$, $\kappa_{\pi\pi} = 0.59$).

The molecular structures of 7*H*-purine[20] and 9-methyladenine[21] have been clarified by X-ray crystal analysis. However, no experimental data for the structures of the remaining compounds have been reported. The bond lengths and the bond angles of the 7*H*-purine ring of 7-methylpurine and 7-methyladenine were taken from those of 7*H*-purine. The molecular structure of the 9*H*-purine ring of 9-methylpurine was set equal to those of 9-methyladenine. The geometries of 1- and 3-methylpurines were assumed to be the combinations of the geometry of the tautomeric forms of isocytosine[22] for the pyrimi-

Table 1. Experimental and theoretical results for purine and methylpurines

Compd	Exptl[a]		Calcd (INDO/S)		Calcd (CNDO/S)		
	$\bar{\nu}\times10^{-3}$ / cm^{-1}	$B\times10^{4}$ / βD^2 cm	$\bar{\nu}\times10^{-3}$ / cm^{-1}	$B\times10^{4}$ / βD^2 cm	$\bar{\nu}\times10^{-3}$ / cm^{-1}	$B\times10^{4}$ / βD^2 cm	
Purine			30.7	−2.4	33.0	−1.4	A″
			35.2	−0.4	37.5	0.2	A″
	37.9	−8.7	36.7	−10.6	37.2	−7.6	A′
			40.0	0.2	41.2	−0.7	A″
	41.2	16.8	42.0	25.0	43.0	15.0	A′
			43.3	−0.7	44.2	−0.3	A″
1-Methylpurine			27.9	−0.3	30.3	0.2	A″
			29.8	−0.6	31.5	0.0	A″
	33.9	−	30.8	−9.0	32.5	−13.9	A′
			32.3	0.7	36.5	3.6	A″
	35—37	+	35.4	11.8	35.9	16.6	A′
			38.5	−23.2	42.0	1.4	A″
	41—43	−	39.2	17.2	41.0	−12.1	A′
			43.7	−2.9	45.0	−0.5	A′
3-Methylpurine			29.0	−0.4	31.6	0.1	A″
	33.6	−	30.7	−18.8	32.9	−48.5	A′
	36—39	+	34.2	59.9	34.2	67.8	A′
			34.4	−20.0	36.8	−0.1	A″
			36.3	−8.1	37.5	−5.7	A″
			40.9	−0.4	42.2	−0.4	A″
	42—	−	42.2	−39.9	42.5	−26.8	A′
7-Methylpurine			30.7	−2.4	33.1	−1.5	A″
			35.2	−0.3	37.5	−0.2	A″
	37.3	−	36.4	−14.5	39.1	−9.8	A′
			39.7	−2.9	41.4	−1.4	A″
	40—43	+	40.7	32.6	42.2	22.8	A′
			43.4	−0.4	44.2	−0.1	A″
			45.4	−0.9			A″
	47—	−	46.5	−58.9	47.1	−25.9	A′
			47.4	56.3	49.4	55.9	A′
9-Methylpurine			30.9	−2.3	33.5	−1.2	A″
			34.9	−0.1	36.7	0.2	A″
	37.1	−	37.0	−2.6	37.7	8.4	A′
	40—42	+	40.7	6.8	41.5	−12.3	A′
			41.0	−2.4	42.0	−5.8	A″
			43.0	0.6	44.7	0.0	A″
	47—	−	46.1	−11.3	47.2	6.1	A′

a) The experimental data of the methylpurines are taken from Ref. 2.

dine ring with that of 7*H*-purine for the imidazole ring. The bond lengths and bond angles of the methyl and amino groups were assumed to be the same as those of 9-methyladenine.

The Faraday B term of a transition from the ground state, a, to the excited state, j, is given by:[23]

$$B_{j\leftarrow a} = \sum_{k\neq a,j} B_{j,k} + \sum_{k\neq a,j} B_{k,a} + B_{j,a} \quad (5)$$

$$B_{j,k} = \mathrm{Im}\langle j|\boldsymbol{\mu}|k\rangle\cdot\langle a|\boldsymbol{m}|j\rangle \times \langle k|\boldsymbol{m}|a\rangle/(E_k-E_j) \quad (6)$$

$$B_{k,a} = \mathrm{Im}\langle k|\boldsymbol{\mu}|a\rangle\cdot\langle a|\boldsymbol{m}|j\rangle \times \langle j|\boldsymbol{m}|k\rangle/(E_k-E_a) \quad (7)$$

$$B_{j,a} = \mathrm{Im}\langle j|\boldsymbol{\mu}|a\rangle\cdot\langle a|\boldsymbol{m}|j\rangle \times (\langle j|\boldsymbol{m}|j\rangle-\langle a|\boldsymbol{m}|a\rangle)/(E_j-E_a) \quad (8)$$

In Eqs. 6—8, $\boldsymbol{m}$ and $\boldsymbol{\mu}$ are the electric and magnetic moment operators respectively, and E_a, E_j, and E_k are energies of the a, j, and k states respectively. $B_{j,k}$ stands for the magnetic mixing of the k state with the excited state, j, and $B_{k,a}$ represents the coupling of the k state to the ground state, a. $B_{j,a}$ arises from the magnetic mixing between the ground state, a, and the excited state, j.

The electric transition moments were evaluated by the dipole length method. The LCAO-MO coefficients regarding the orthogonalized INDO atomic orbital basis were deorthogonalized by the inverse Löwdin transformation[24], and the atomic integrals

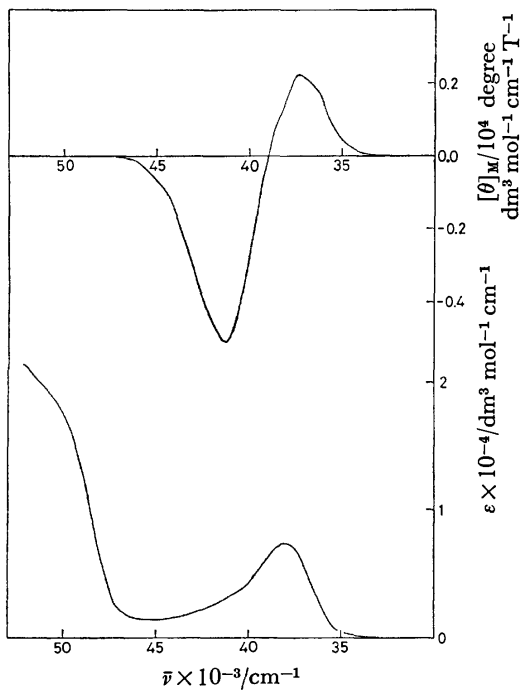

Fig. 1. MCD (upper) and absorption (lower) spectra of purine in aqueous solution (pH 7) at room temperature.

were calculated using Slater atomic orbitals,[25] in accordance with the description of Refs. 26 and 27.

The Faraday B terms calculated for non-centric molecules using a limited basis set are origin-dependent.[28,29] In this work, the origin was placed at the center of the electron cloud in the molecule, according to the theoretical argument of Caldwell and Eyring.[29]

Computations were carried out using an ACOS 700 computer in the computer center of Tohoku University.

Results and Discussion

The MCD and absorption spectra of purine are presented in Fig. 1. The molar ellipticity $[\theta]_M$ per unit of magnetic field is shown in degree dm^3 mol^{-1} cm^{-1} T^{-1}. The intense absorption band observed at 38100 cm^{-1} is resolved into two in the MCD spectrum. The positive MCD band is assigned to the lowest $\pi^*\leftarrow\pi$ transition, and the negative one, to the second $\pi^*\leftarrow\pi$ transition.

The results calculated for purine and methylpurines are given in Table 1, along with the experimental data. The experimental values of the Faraday B terms of purine were obtained by a gaussian curve-fitting procedure. The experimental data for methylpurines were taken from the spectra reported by Townsend *et al.*[2] The sign pattern of the MCD of methylpurines is the same as that of purin itself. The transition energies of 7-methylpurine and 9-methylpurine are close to those of purine, whereas the MCD bands of 1-methylpurine and 3-methylpurine are shifted to a lower wavenumber region relative to purine. For purine, 1-methylpurine, 3-methylpurine, and 7-methylpurine, both INDO/S-CI and CNDO/S-CI procedures correctly predict the sign of the MCD spectra and the band positions of these compounds. On the other hand, a remarkable difference between the INDO/S-CI result and the CNDO/S-CI result is found for 9-methylpurine. Although the INDO/S-CI procedure explains the sign of the MCD of 9-methylpurine well, the sign of the MCD of 9-methylpurine calculated by the CNDO/S-CI procedure is the opposite of that of the experiments.

In the lowest wavenumber region, two $\pi^*\leftarrow$n transitions with A″ symmetry are predicted. In the MCD and absorption spectra, $\pi^*\leftarrow$n transitions are hidden behind the stronger $\pi^*\leftarrow\pi$ transitions, and none of them is observed separately. However, 7-ribosyl purine exhibits a negative CD band, at 35200 cm^{-1}, which arises from the $\pi^*\leftarrow$n transition.[30] A weak out-of-plane polarized band was observed at 34000 cm^{-1} in the polarized absorption spectrum of the crystal of 7-methylpurine and assigned to the $\pi^*\leftarrow$n transition.[31] The calculated transition energy of the lowest $\pi^*\leftarrow$n transition agrees fairly well with these experimental findings.

The magnitudes of the calculated Faraday B terms of the $\pi^*\leftarrow$n transitions are smaller than those of the $\pi^*\leftarrow\pi$ transitions, except for the fourth $\pi^*\leftarrow$n transition of 1-methylpurine and the second $\pi^*\leftarrow$n transition of 3-methylpurine. The relatively large B terms of the $\pi^*\leftarrow$n transitions of 1- and 3-methylpurines are interpreted as mainly arising from the magnetic coupling of the neighbouring $\pi^*\leftarrow\pi$ state with the $\pi^*\leftarrow$n state.

The experimental and theoretical results for methyladenines are shown in Table 2. The experimental transition energies and Faraday B terms are taken from Ref. 3. The substitution of the amino group on the purine ring reverses the sign of the MCD spectra and causes a slight red shift. The INDO/S-CI procedure takes good account of the sign of the MCD spectra of these methyladenines, except for the lowest $\pi^*\leftarrow\pi$ transition of 7-methyladenine. The CNDO/S-CI method cannot reproduce the sign of three lowest MCD bands of 7-methyladenine.

The effects of the bonding parameter of the nitrogen atom, β_N, on the B terms calculated by the INDO/S-CI procedure are given in Table 3. In the INDO/S-CI calculation, the signs of the Faraday B term of 7-methyladenine are sensitive to the bonding parameter of the nitrogen atom, β_N. The unsatisfactory results for the sign of the lowest MCD band of 7-methyladenine are improved by increasing the value of $|\beta_N|$. We have also calculated the B terms of 7-methyladenine and 9-methylpurine by the CNDO/S-CI method with $\beta_N=-20$ eV and -35 eV. However, the calculated signs of the B terms of these compounds were not improved.

Recently Michl has shown that the sign of the Faraday B term of $\pi^*\leftarrow\pi$ transitions in cyclic π-systems with $(4N+2)\pi$ electrons can be predicted by a simple rule.[5] The sign of the B term of the lowest $\pi^*\leftarrow\pi$ transition is the same sign as the difference in the energy gap of the two lowest unoccupied molecular orbitals (ΔLUMO) from that of the two highest occupied molecular orbitals (ΔHOMO), (ΔHOMO—

TABLE 2. EXPERIMENTAL AND THEORETICAL RESULTS FOR METHYLADENINES

Compd	Exptl[a]		Calcd (INDO/S)		Calcd (CNDO/S)		
	$\bar{\nu}\times10^{-3}$ / cm^{-1}	$B\times10^{4}$ / βD^2 cm	$\bar{\nu}\times10^{-3}$ / cm^{-1}	$B\times10^{4}$ / βD^2 cm	$\bar{\nu}\times10^{-3}$ / cm^{-1}	$B\times10^{4}$ / βD^2 cm	
7-Methyladenine			33.4	−1.3	35.8	−0.2	A″
	36.2	2.6	35.1	−1.2	36.1	−4.8	A′
			35.4	0.0	38.3	−0.6	A″
	38.6	−4.0	39.9	−9.4	41.6	0.3	A′
			40.4	4.9	41.9	7.8	A″
			41.1	0.2	45.2	0.0	A″
	41.8	4.5	43.9	11.1	45.8	−30.5	A′
			44.3	1.3			A″
	45.5	14.7	45.8	42.7	46.6	61.8	A′
			46.8	−0.6			A″
	49.0	−6.2	47.1	−60.0	49.6	−38.6	A′
9-Methyladenine			34.0	−0.2	36.8	0.0	A″
			35.5	−1.1	37.4	−12.2	A″
	36.6	8.6	36.2	33.0	37.4	57.4	A′
	39.2	−7.4	38.2	−45.8	39.2	−59.0	A′
			41.8	−1.1	42.1	−1.3	A″
			43.8	0.1	45.7	−0.1	A″
			44.3	0.7			A″
	42.9	0.8	44.9	11.1	45.7	8.5	A′
			45.5	7.6			A″
	46.2	17.8	47.1	37.1	49.5	53.3	A′
			47.5	−9.5	50.2	−6.2	A″
	49.5	−15.0	48.7	−47.3	51.5	−43.3	A′

a) Ref. 3.

TABLE 3. DEPENDENCE OF THE FARADAY B TERMS CALCULATED BY THE INDO/S PROCEDURE ON THE BONDING PARAMETER OF THE NITROGEN ATOM, β_N

Compd		Calcd ($\beta_N=-23$ eV)		Calcd ($\beta_N=-25$ eV)		Calcd ($\beta_N=-27$ eV)		Exptl[a]
		$\bar{\nu}\times10^{-3}$ / cm^{-1}	$B\times10^{4}$ / βD^2 cm	$\bar{\nu}\times10^{-3}$ / cm^{-1}	$B\times10^{4}$ / βD^2 cm	$\bar{\nu}\times10^{-3}$ / cm^{-1}	$B\times10^{4}$ / βD^2 cm	$B\times10^{4}$ / βD^2 cm
7-Methyladenine	A″	33.4	−1.3	33.7	−1.1	34.1	−0.9	
	A′	35.1	−1.2	36.1	3.7	36.9	7.7	2.6
	A″	35.4	0.0	35.9	−1.4	36.3	−0.9	
	A′	39.9	−9.4	40.7	−13.9	41.2	−19.0	−4.0
	A″	40.4	4.9	41.3	0.7	41.9	−2.6	
	A″	41.1	0.2	43.5	0.1	45.0	1.1	
	A′	43.9	11.1	45.1	14.7	46.3	20.1	4.5
	A″	44.3	1.3	44.7	2.1	45.3	1.0	
	A′	45.8	42.7	47.4	54.2	48.5	67.8	14.7
	A″	46.8	−0.6	48.3	10.5	48.1	−11.6	
	A′	47.1	−60.0	48.5	−88.0	49.8	−70.2	−6.2

a) Ref. 3.

ΔLUMO). Although the purine derivatives may deviate somewhat from the weakly perturbed 10 electron annulenes, it is a fact that the energy of the frontier molecular orbitals is an important factor in determining the sign of the MCD spectra. The values of (ΔHOMO−ΔLUMO) calculated by the INDO/S-CI method are negative or almost zero for methylpurines and positive for methyladenines. However, the CNDO/S-CI method predicts a large positive value for the difference, (ΔHOMO−ΔLUMO), of 9-methylpurine, leading to the positive B value for the lowest $\pi^*\leftarrow\pi$ transition.

The two LUMO's and the two HOMO's of 9-methylpurine obtained from the INDO/S calculation are shown in Fig. 2. The LCAO-MO coefficients obtained by the CNDO/S method are analogous to

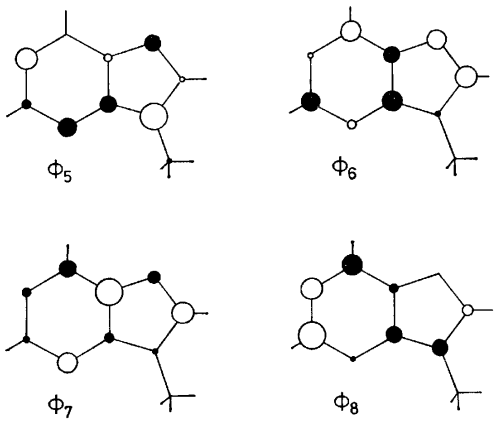

Fig. 2. LCAO-MO coefficients of the highest occupied π molecular orbitals, ϕ_5 and ϕ_6, and the lowest unoccupied π molecular orbitals, ϕ_7 and ϕ_8 of 9-methylpurine. White and black circles represent positive and negative signs, respectively.

those obtained by the INDO/S method and so are not shown here. The orbital energies of the HOMO, ϕ_6, and the LUMO's, ϕ_7 and ϕ_8, calculated by the CNDO/S method are almost the same as those calculated by the INDO/S method, whereas the CNDO/S method predicts the energy of the molecular orbital, ϕ_5, to be lower by 0.53 eV than that calculated by the INDO/S method. This is because the CNDO/S method does not discriminate the energy of one π-electron in the pyrrole-type nitrogen atom having two π-electrons from that in the pyridine-type nitrogen atom with one π-electron, and gives poor results for the energy of the molecular orbital, ϕ_5, in which the LCAO-MO coefficients of the nitrogen atoms are larger than in other molecular orbitals; although the semi-empirical valence-state ionization potentials, $I_p\{N(SP^2PP)\rightarrow N(SPPP)\}$ and $I_p\{N(SP^2PP)\rightarrow N(SP^2P)\}$, are 12.48 eV and 14.42 eV respectively,[16] the CNDO/S method does not distinguish between them.

The INDO/S-CI procedure is superior to the CNDO/S-CI procedure in that the former can discriminate the ionization potential of the pyrrole-type nitrogen atom from that of the pyridine-type nitrogen atom, and predicts correct signs of the Faraday B terms of 9-methylpurine and 7-methyladenine.

This work was supported in part by a grant from the Japan Society for the Promotion of Science.

References

1) W. Voelter, R. Records, E. Bunnenberg, and C. Djerassi, *J. Am. Chem. Soc.*, **90**, 6163 (1968); W. Voelter, G. Barth, R. Records, E. Bunnenberg, and C. Djerassi, *ibid.*, **91**, 6165 (1969); D. L. Elder, E. Bunnenberg, C. Djerassi, M. Ikehara, and W. Voelter, *Tetrahedron Lett.*, **10**, 727 (1970).

2) L. B. Townsend, D. W. Miles, S. J. Manning, and H. Eyring, *J. Heterocyclic Chem.*, **10**, 419 (1973).

3) R. E. Linder, H. Weiler-Feilchenfeld, G. Barth, E. Bunnenberg, and C. Djerassi, *Theoret. Chim. Acta*, **36**, 135 (1974); H. Weiler-Feilchenfeld, R. E. Linder, G. Barth, E. Bunnenberg, and C. Djerassi, *ibid.*, **46**, 79 (1977).

4) R. Pariser and R. G. Parr, *J. Chem. Phys.*, **21**, 466, 767 (1953); J. A. Pople, *Trans. Faraday Soc.*, **49**, 1375 (1953).

5) J. Michl, *Chem. Phys. Lett.*, **39**, 386 (1976); **43**, 457 (1976); J. Michl, *J. Am. Chem. Soc.*, **100**, 6801 (1978) and the references cited therein.

6) J. A. Pople, D. P. Santry, and G. A. Segal, *J. Chem. Phys.*, **43**, S129 (1965); J. A. Pople and G. A. Segal, *ibid.*, **43**, S136 (1965); **44**, 3289 (1966).

7) J. Del Bene and H. H. Jaffé, *J. Chem. Phys.*, **48**, 1807 (1968).

8) F. M. Sprinkel, D. D. Shillady, and R. W. Strickland, *J. Am. Chem. Soc.*, **97**, 6653 (1975).

9) A. Kaito, M. Hatano, and A. Tajiri, *J. Am. Chem. Soc.*, **99**, 5241 (1977).

10) J. H. Obbink and A. M. F. Hezemans, *Theor. Chim. Acta*, **43**, 75 (1976).

11) A. Kaito and M. Hatano, *J. Am. Chem. Soc.*, **100**, 2034 (1978).

12) J. H. Obbink and A. M. F. Hezemans, *Chem. Phys. Lett.*, **50**, 133 (1977).

13) A. Kaito and M. Hatano, *J. Am. Chem. Soc.*, **100**, 4037 (1978).

14) J. A. Pople, *J. Chem. Phys.*, **47**, 2026 (1969).

15) J. Ridley and M. Zerner, *Theor. Chim. Acta*, **32**, 111 (1973).

16) J. Hinze and H. H. Jaffé, *J. Am. Chem. Soc.*, **84**, 540 (1962); J. Hinze and H. H. Jaffé, *J. Phys. Chem.*, **67**, 1501 (1963).

17) J. Hinze and H. H. Jaffé, *J. Chem. Phys.*, **38**, 1834 (1963).

18) N. Mataga and K. Nishimoto, *Z. Phys. Chem. (Frankfurt am Main)*, **12**, 335 (1957).

19) J. M. Sichel and M. A. Whitehead, *Theor. Chim. Acta*, **7**, 32 (1967).

20) D. G. Watson, R. M. Sweet, and R. E. Marsh, *Acta Crystallogr.*, **19**, 573 (1965).

21) R. F. Stewart and L. H. Jensen, *J. Chem. Phys.*, **40**, 2071 (1964).

22) B. D. Sharma and J. F. McConnell, *Acta Crystallogr.*, **19**, 797 (1965).

23) A. D. Buckingham and P. J. Stephens, *Annu. Rev. Phys. Chem.*, **17**, 399 (1966).

24) P. O. Löwdin, *J. Chem. Phys.*, **18**, 365 (1950).

25) J. C. Slater, *Phys. Rev.*, **36**, 57 (1930).

26) A. Imamura, T. Hirano, C. Nagata, and T. Tsuruta, *Bull. Chem. Soc. Jpn.*, **45**, 396 (1972).

27) M. Suzuki, Y. Nihei, and H. Kamada, *Bull. Chem. Soc. Jpn.*, **42**, 323 (1969).

28) L. Seamans and A. Moscowitz, *J. Chem. Phys.*, **56**, 1099 (1972).

29) D. J. Caldwell and H. Eyring, *J. Chem. Phys.*, **58**, 1149 (1973).

30) D. W. Milles, W. H. Inskeep, L. B. Townsend, and H. Eyring, *Biopolymers*, **11**, 1181 (1972).

31) H. H. Chen and L. B. Clark, *J. Chem. Phys.*, **51**, 1862 (1969).

Studies of the Magnetic Circular Dichroism and Tautomerism of Pyridinols (Pyridinones) and Pyrimidinols (Pyrimidinones)

Akira KAITO and Masahiro HATANO*

Chemical Research Institute of Non-aqueous Solutions, Tohoku University, Sendai 980

(Received February 4, 1980)

The magnetic circular dichroism(MCD) spectra of pyridinols (pyridinones) and pyrimidinols (pyrimidinones) were measured in the wavenumber region of 27000—50000 cm^{-1}. The transition energies, the oscillator strengths, and the Faraday B terms were calculated within the framework of the INDO/S-CI approximation. The calculated results for the $\pi^* \leftarrow \pi$ transitions were in good agreement with the experimental results. The lactim-lactam tautomerism of 3-pyridinol(3(1H)-pyridinone) and 2-pyrimidinol (2-pyrimidinone) was discussed.

The electronic structures of the derivatives of pyridine and pyrimidine have been extensively studied by many investigators.[1-11] In particular, some of these compounds, such as uracil, cytosine, thymine, and vitamin B_6, have attracted special interest because of their biological importance. The ultraviolet spectra of the pyridine and pyrimidine derivatives have been interpreted[2-5, 7-10] by means of SCF-MO calculations of the Pariser-Parr-Pople(PPP) procedure[12] and the complete neglect of the differential overlap (CNDO) method.[13,14]

Considerable attention has also been paid to the problem of tautomerism between lactam and lactim forms, which can be expected in these heterocyclic compounds because of the presence of labile hydrogen atoms. Mason and his co-workers have investigated pyridinol-pyridinone and pyrimidinol-pyrimidinone tautomerism in aqueous solutions by the measurements of the UV-absorption spectra.[1] The measurements of the UV and IR spectra have suggested that some of the hydroxy derivatives of pyrimidine favor the lactam-pyrimidinone forms.[15] The tautomerism of 4-pyrimidinol(4-pyrimidinone) and 4,6-pyrimidinediol(6-hydroxy-4-pyrimidinone, *etc.*) has been investigated by NMR spectroscopy.[16,17] The tautomeric stability of substituted pyridines and pyrimidines has been discussed on the basis of the SCF-MO calculation in the CNDO/2 approximation.[11]

On the other hand, magnetic circular dichroism (MCD) spectroscopy has made remarkable progress in providing valuable information on the electronic structures of ions and molecules.[18,19] The MCD spectra of derivatives of pyrimidine and purine and other heterocyclic compounds have been reported, and the electronic and molecular structures of these compounds studied.[20-26] In addition, the signs and magnitudes of the MCD spectra of azines,[22] azanaphthalenes,[23] aza-replaced alternant hydrocarbons,[24] indole,[25] and purine derivatives[26,27] have been calculated by the quantum mechanical SCF-MO procedures.

More recently, Jonas and Michl have reported the MCD spectra of pyridinones and pyrimidinones and interpreted them in terms of the π-electron theory.[28] Although the present work partially overlaps with their work, they have investigated mainly the keto forms of these compounds in acetonitrile solutions.

In this work we measured the MCD spectra of 2- and 4-pyridinols(2- and 4-pyridones), 3-pyridinol(3-(1H)-pyridinone), 2- and 4-pyrimidinols(2- and 4-pyrimidinones), and uracil, both in aqueous and in relatively nonpolar solvents. We also calculated the signs and the magnitudes of the MCD of the tautomers of these pyridine and pyrimidine derivatives within the framework of the intermediate neglect of the differential overlap (INDO) procedure.[29,30] The lactam-lactim tautomerism of these heterocyclic compounds is also discussed.

Experimental

The 2-pyridinol(2-pyridone), 3-pyridinol(3(1H)-pyridinone), and 4-pyrimidinol(4-pyrimidinone) were purified by recrystallization from benzene. The 4-pyridinol(4-pyridone) and uracil were also recrystallized from water. The 2-pyrimidinol(2-pyridone) was liberated with sodium hydroxide from its hydrochloride and was purified by vacuum sublimation and recrystallization from ethanol. Spectro-grade dioxane, heptane–dioxane (7:3 in volume), ethanol, and a phosphate buffer solution (pH 6—7) were used as solvents.

The MCD spectra were recorded with a JASCO J-20A recording circular dichrometer equipped with a 1.25 T electromagnet. The absorption spectra were measured on a Hitachi EPS-3T recording spectrophotometer.

The experimental values of the Faraday B terms were obtained from the MCD spectra by the use of the method of moments,[18] after the overlapping bands had been resolved by the Gaussian curve-fitting procedure.

Theoretical

The wavefunctions obtained from the INDO/S-CI approximation were used for calculating the Faraday B terms. The bonding parameter for the oxygen atom was determined so that the transition energies of some ketones are well reproduced ($\beta_0 = -31$ eV). The other parameters of the INDO/S calculation are the same as those of the previous work.[27] The configuration interaction among singly excited configurations below 12 eV was taken into consideration.

The molecular structures of uracil and 2-pyrimidinone were taken from the experimental data[31,32] obtained by the X-ray crystal analysis. However, no experimental data have been reported for the remaining compounds. The bond lengths and bond angles of pyridinones and 4-pyrimidinone were taken from those of 2-pyrimidinone.[32] The molecular structures of 3-pyridinol and 2-pyrimidinol were estimated from those of pyridine, pyrimidine, and phenol.

The Faraday B terms were calculated according to the expression derived by Buckingham and Stephens.[18]

TABLE 1. OBSERVED AND CALCULATED TRANSITION ENERGIES, OSCILLATOR STRENGTHS, AND FARADAY B TERMS

Compd	$\bar{\nu}_{obsd} \times 10^{-3}$ / cm^{-1}	$\bar{\nu}_{calcd} \times 10^{-2}$ / cm^{-1}	f_{obsd}	f_{calcd}	$B_{obsd} \times 10^4$ / βD^2 cm	$B_{calcd} \times 10^4$ / βD^2 cm	Symmetry
2-Pyridone		26.0		0.001		−0.4	A″
	34.5[a]	32.7	0.123	0.204	8.6	12.7	A′
		40.0		0.000		−0.1	A″
		41.2		0.004		2.8	A″
	45.2[a]	43.0	0.137	0.319	−5.2	−15.4	A′
3(1*H*)-Pyridinone		22.0		0.002		−4.0	A″
	32.0[a] 27.4[e]	23.6	0.083	0.152	6.7	16.7	A′
		26.3		0.001		0.8	A″
		33.0		0.002		2.0	A″
	41.1[a]	34.8	0.080	0.241	−9.8	−13.6	A′
4-Pyridone		21.0		0.000		0.0	A″
	38.6[a]	35.9	0.133	0.032	14.3	14.0	A′
		36.3		0.003		7.0	A″
	40.6[a]	38.6	0.148	0.438	−13.5	−24.2	A′
		41.7		0.000		0.1	A″
2-Pyrimidinone		27.3		0.000		0.0	A″
		31.4		0.004		−5.0	A″
	34.3[a]	32.6	0.100	0.146	7.5	13.2	A′
		41.5		0.003		0.3	A″
		43.9		0.000		0.6	A″
	47.4[a]	45.8	0.223	0.378	−2.2	−8.9	A′
4(3*H*)-Pyrimidinone		26.1		0.001		−0.2	A″
		34.0		0.007	6.8	9.4	A″
	36.4[d]	34.4	0.082	0.166		0.5	A′
		39.5		0.000		−0.2	A″
	45.3[d]	42.4	0.122	0.009	−2.1	−6.6	A″
		43.7		0.301		−1.4	A′
		44.1		0.011		−2.4	A″
Uracil		25.4		0.001		−0.1	A″
		31.4		0.000		0.0	A″
	39.0[a]	39.8	0.165	0.298	7.4	7.6	A′
		45.0		0.000		0.1	A″
		46.1		0.094		6.3	A′
	49.1[a]	47.6	0.255	0.162	−2.2	−16.4	A′
3-Pyridinol		34.4		0.008		−1.7	A″
	36.4[b]	37.5	0.065	0.083	4.8	6.8	A′
		41.9		0.000		0.0	A″
		45.6		0.000		0.7	A″
	45.8[b]	46.3	0.129	0.262	−4.5	−19.5	A′
2-Pyrimidinol		32.8		0.013		−3.2	A″
		37.6		0.000		0.0	A″
	37.4[c]	39.2	0.081	0.085	6.8	6.8	A′
		44.2		0.000		0.0	A″
		48.9		0.001		−20.0	A″
		49.0		0.342		4.3	A′

a) In an aqueous solution. b) In an ethanol solution. c) In a heptane–dioxane (7:3 in volume) solution. d) In a dioxane solution. e) The absorption maximum in a cyclohexane-saturated solution. Taken from Ref. 8.

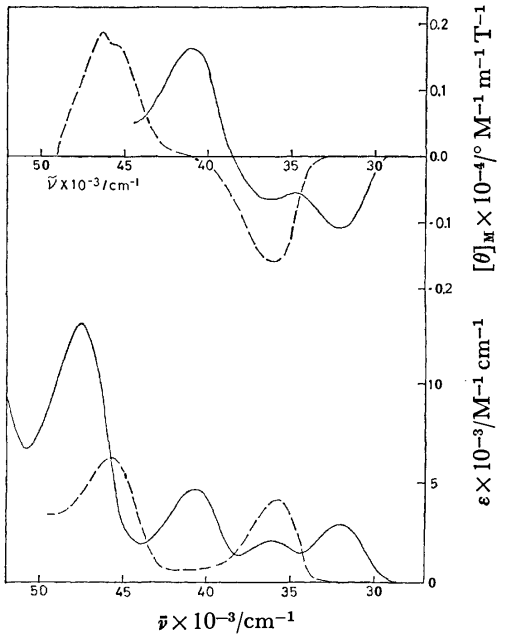

Fig. 1. MCD (upper) and absorption (lower) spectra of 3-pyridinol (3(1*H*)-pyridinone) in aqueous (——) and ethanol (----) solutions.

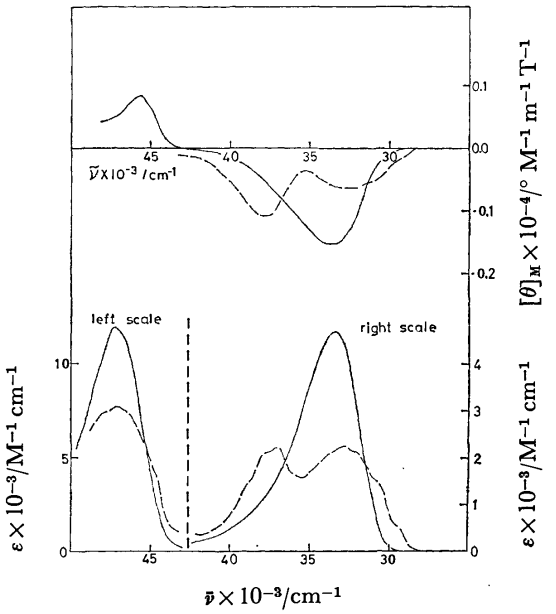

Fig. 2. MCD (upper) and absorption (lower) spectra of 2-pyrimidinol (2-pyrimidinone) in aqueous (——) and heptane-dioxane (7:3 in volume) (----) solutions.

The details of the calculation of the *B*-terms were reported in a previous paper.[27]

Results and Discussion

The experimental MCD and absorption spectra of 3-pyridinol(3(1*H*)-pyridinone) are presented in Fig. 1. The molar ellipticity $[\theta]_M$ per unit of magnetic field is shown in ° M^{-1} m^{-1} T^{-1}, and the molar extinction coefficient, ε, in M^{-1} cm^{-1} (1 M=1 mol dm^{-3}).

Four electronic transitions are identified in the MCD and absorption spectra of 3-pyridinol (3(1*H*)-pyridinone) in an aqueous solution, while only two bands are observed in an ethanol solution. The lactim 3-pyridinol and lactam 3(1*H*)-pyridinone forms have been shown to exist in equilibrium in an aqueous solution.[1] The two MCD bands observed at 36400 cm^{-1} and 45800 cm^{-1} in an ethanol solution are assigned to the $\pi^*\leftarrow\pi$ transitions of the lactim 3-pyridinol form. On the other hand, the two MCD bands at 32000 cm^{-1} and 41100 cm^{-1} which appear in an aqueous solution are attributable to the $\pi^*\leftarrow\pi$ transitions of the lactam 3(1*H*)-pyridinone form.

The MCD and absorption spectra of 2-pyrimidinol (2-pyrimidinone) are presented in Fig. 2. 2-Pyrimidinol (2-pyrimidinone) exhibits positive and negative MCD bands at 34300 cm^{-1} and 47400 cm^{-1} respectively in an aqueous solution. It has been shown by a UV spectrographic comparison with 1-methyl-2-pyrimidinone that 2-pyrimidinol (2-pyrimidinone) predominantly exists in the lactam 2-pyrimidinone form in an aqueous solution.[1] On the other hand, in a heptane-dioxane (7:3 in volume) solution the lowest MCD bands decrease in intensity, and a new negative MCD band appears at 37400 cm^{-1} (Fig. 2), This band can reasonably be assigned to the lowest $\pi^*\leftarrow\pi$ transitions of the lactim 2-pyrimidinol form, which is in equilibrium with the lactam 2-pyrimidinone form in heptane–dioxane (7:3 in volume).

The MCD spectra of the remaining compounds were in agreement with those reported by Jonas and Michl.[28]

The experimental and calculated results are summarized in Table 1. The calculated transition energies of 3(1*H*)-pyridinone are much smaller than the experimental ones. A similar difficulty has been met with in the CNDO/S-CI calculation reported by Cignitti and Paoloni.[8] They have also reported that the lowest absorption band of 3(1*H*)-pyridinone, observed at 32000 cm^{-1} in an aqueous solution, shows a large hypsochromic shift in a saturated cyclohexane solution.[8] The solvent shift can be explained by the fact that ground state has a larger dipole moment than the low-lying excited states and is stabilized by the dipole-dipole interaction with the polar solvent. However, the calculated results for the $\pi^*\leftarrow\pi$ transitions of the remaining compounds are in satisfactory agreement with the experimental data. In particular, the calculated signs of the Faraday *B* terms agree perfectly with the experimental results. The signs of the Faraday *B* terms of the first and second $\pi^*\leftarrow\pi$ transitions are positive and negative respectively, both for the lactam form and for the lactim form.

On the other hand, several $\pi^*\leftarrow$n transitions are predicted in the ultraviolet region. The lowest $\pi^*\leftarrow$n transition of pyridinones and pyrimidinones is characterized by the transition from the nonbonding 2p orbital of oxygen to the unoccupied π orbitals. The second $\pi^*\leftarrow$n transition of pyrimidinones and the low-lying $\pi^*\leftarrow$n transitions of 3-pyridinol and 2-pyrimidinol correspond to the transition from the nonbonding orbital of the aza nitrogen atom to unoccupied π orbitals.

Although the first $\pi^*\leftarrow$n transition of pyridinone and pyrimidinone is predicted in the wavenumber

region of 21000—27000 cm^{-1}, no distinct MCD or absorption band is found in this spectral region. The first $\pi^*\leftarrow$n transition is probably hidden behind the tail of the lowest absorption band; otherwise, it has too small an intensity to be observed. It should be noted that the calculated transition energy of the lowest $\pi^*\leftarrow$n transition of these compounds is not very reliable, because it has been shown to be sensitive to the choice of the two-center electron repulsion integrals.[8)]

We have calculated the magnetic mixing among excited electronic states caused by the external magnetic field. The Faraday B terms of the two lowest $\pi^*\leftarrow\pi$ transitions proved to be mainly induced by the magnetic mixing between the two lowest $\pi^*\leftarrow\pi$ states, leading to the opposite sign of the B terms of these transitions. The magnetic mixing between the $\pi^*\leftarrow\pi$ state and the $\pi^*\leftarrow$n state is small except when the energy separation of the two states is very small, and it does not make a large contribution to the MCD spectrum.

This work was supported in part by a grant of the Japan Society for the Promotion of Science.

References

1) D. J. Brown, E. Hoerger, and S. F. Mason, *J. Chem. Soc.*, **1955**, 211; S. F. Mason, *ibid.*, **1957**, 5010; **1959**, 1253.
2) C. Nagata, A. Imamura, Y. Tagashira, and M. Kodama, *Bull. Chem. Soc. Jpn.*, **38**, 1638 (1965).
3) J. Ladik and K. Appel, *Theor. Chim. Acta*, **4**, 132 (1966).
4) H. Berthod, C. Giessner-Prettre, and A. Pullman, *Theor. Chim. Acta*, **5**, 53 (1966).
5) E. M. Eveleth, *Theor. Chim. Acta*, **11**, 145 (1968).
6) L. Paoloni, M. L. Tosato, and M. Cignitti, *Theor. Chim. Acta*, **14**, 221 (1969).
7) J. S. Kwiatowski, *Theor. Chim. Acta*, **16**, 243 (1970).
8) M. Cignitti and L. Paoloni, *Theor. Chim. Acta*, **25**, 277 (1972).
9) M. Kamiya, *Bull. Chem. Soc. Jpn.*, **46**, 2235 (1973).
10) W. Hug and I. Tinoco, Jr., *J. Am. Chem. Soc.*, **95**, 2803 (1973); **96**, 665 (1974).
11) M. Berndt, J. S. Kwiatkowski, J. Budzinski, and B. Szczodrowska, *Chem. Phys. Lett.*, **19**, 246 (1973).
12) R. Pariser and R. G. Parr, *J. Chem. Phys.*, **21**, 466, 767 (1953); J. A. Pople, *Trans. Faraday Soc.*, **49**, 1375 (1953).
13) J. A. Pople, D. P. Santry, and G. A. Segal, *J. Chem. Phys.*, **43**, S129 (1965); J. A. Pople and G. A. Segal, *ibid.*, **43**, S136 (1965); **44**, 3289 (1966).
14) J. Del Bene and H. H. Jaffé, *J. Chem. Phys.*, **48**, 1807 (1968).
15) J. R. Marshall and J. Walker, *J. Chem. Soc.*, **1951**, 1004; L. N. Short and H. W. Thompson, *ibid.*, **1952**, 168 and the references cited therein.
16) Y. Inoue, N. Furutachi, and K. Nakanishi, *J. Phys. Chem.*, **31**, 175 (1966).
17) G. M. Kheifets, N. V. Khromov-Borisov, A. I. Koltsov, and M. V. Volkenstein, *Tetrahedron*, **23**, 1197 (1967).
18) A. D. Buckingham and P. J. Stephens, *Annu. Rev. Phys. Chem.*, **17**, 399 (1966).
19) P. N. Schatz and A. J. McCaffery, *Q. Rev., Chem. Soc.*, **23**, 552 (1966).
20) W. Voelter, R. Records, E. Bunnenberg, and C. Djerassi, *J. Am. Chem. Soc.*, **90**, 6163 (1968); W. Voelter, G. Barth, R. Records, E. Bunnenberg, and C. Djerassi, *ibid.*, **91**, 6165 (1969); D. L. Elder, E. Bunnenberg, C. Djerassi, M. Ikehara, and W. Voelter, *Tetrahedron Lett.*, **10**, 727 (1970).
21) L. B. Townsend, D. W. Miles, S. J. Manning, and H. Eyring, *J. Heterocyclic Chem.*, **10**, 419 (1973); D. W. Miles, W. H. Inskeep, L. B. Townsend, and H. Eyring, *Biopolymers*, **11**, 1181 (1972).
22) A. Kaito, M. Hatano, and A. Tajiri, *J. Am. Chem. Soc.*, **99**, 5241 (1977).
23) A. Kaito and M. Hatano, *J. Am. Chem. Soc.*, **100**, 4037 (1978).
24) J. Michl, *Chem. Phys. Lett.*, **39**, 386 (1976); E. W. Thulstrup, J. W. Downing, and J. Michl, *Chem. Phys.*, **23**, 307 (1977).
25) F. M. Sprinkel, D. D. Shillady, and R. W. Strickland, *J. Am. Chem. Soc.*, **97**, 6653 (1975).
26) R. E. Linder, H. Weiler-Feilchenfeld, G. Barth, E. Bunnenberg, and C. Djerassi, *Theor. Chim. Acta*, **36**, 135 (1974); H. Weiler-Feilchenfeld, R. E. Linder, G. Barth, E. Bunnenberg, and C. Djerassi, *ibid.*, **46**, 79 (1977).
27) A. Kaito and M. Hatano, *Bull. Chem. Soc. Jpn.*, **53**, 3064 (1980).
28) I. Jonas and J. Michl, *J. Am. Chem. Soc.*, **100**, 6834 (1978).
29) J. A. Pople, *J. Chem. Phys.*, **47**, 2026 (1969).
30) J. Ridley and M. Zerner, *Theor. Chim. Acta*, **32**, 111 (1973).
31) R. F. Stewart and L. H. Jensen, *Acta Crystallogr.*, **23**, 1102 (1967).
32) S. Furberg and J. Solbakk, *Acta Chem. Scand.*, **24**, 3230 (1970).

 © 1980 The Chemical Society of Japan Bull. Chem. Soc. Jpn., 53, 3073—3078 (1980)

The Application of Magnetic Circular Dichroism to the Study of the Tautomerism of Cytosine and Isocytosine

Akita KAITO, Masahiro HATANO,* Toru UEDA,** and Susumu SHIBUYA**

Chemical Research Institute of Non-aqueous Solutions, Tohoku University, Sendai 980

*** Faculty of Pharmaceutical Science, Hokkaido University, Sapporo 060*

(Received March 5, 1980)

The MCD and absorption spectra of cytosine and isocytosine and their *N*-substituted derivatives were measured in the wave-number region of 30000—50000 cm^{-1}. On the basis of the experimental results, the tautomerism of cytosine and isocytosine was discussed. The transition energies, the oscillator strengths, and the Faraday *B* terms of the tautomeric forms of cytosine and isocytosine were calculated within the framework of the intermediate neglect of the differential overlap(INDO) approximation. The calculated results are in good agreement with the experimental data.

The magnetic circular dichroism (MCD) spectra of purine and pyrimidine derivatives, which are the constituents of nucleic acids, have been extensively studied by many investigators.[1-4] Some overlapping absorption bands have been resolved in the MCD spectra, and valuable information about the electronic structure of these compounds has been obtained. Recently, also quantum mechanical calculations of the MCD of some purine derivatives[4,5] and pyrimidine derivatives[6] have been reported.

On the other hand, the minor tautomers of nucleic acid bases are biological interest because they have been considered to be a source of the imperfect base pairing which leads to genetic mutations.[7] The tautomerism of cytosine in solution has been studied by the aid of the electronic absorption spectra.[8-10] Morita and Nagakura[10] have shown that, in an aqueous solution, cytosine takes the [1*H*]-2-keto 4-amino form(I) at room temperature, but with a rise in the temperature the 2-keto 4-imino form(II) coexists with Form I, while cytosine takes Form I and Form II in trimethyl phosphate and in acetonitrile respectively. It has been proposed from the unusual line broadening of the NMR spectra of the H5 proton of cytosine that Form II coexists with Form I to the extent of 15±3% at room temperature in a neutral aqueous solution of cytosine.[11] However, Wong[12] has shown that the line broadening is caused by the paramagnetic impurities, and this has raised questions about the existence of 15% of the minor tautomer of cytosine, Form II, at room temperature in a neutral aqueous solution.

The tautomerism of isocytosine has also been extensively studied by measurements of the electronic absorption spectra.[9,10,13] It has been shown that isocytosine takes the [3*H*]-2-amino 4-keto form(IV) in ethanol and in a diethyl ether solution, but in an aqueous solution, the [1*H*]-2-amino 4-keto form(V) coexists with Form IV.[9,10,13]

The tautomeric forms of cytosine and isocytosine in the crystalline state are of interest. X-Ray crystal analysis studies have shown that cytosine takes Form I in crystals,[14] while Forms IV and V coexist at a ratio of 1:1 in the isocytosine crystal.[15]

In this work, we measure the MCD spectra of cytosine, isocytosine, and their derivatives and discuss the tautomerism of cytosine and isocytosine on the basis of the MCD spectra. We also calculate the Faraday *B* terms of three tautomers of cytosine and two tautomers of isocytosine, which are shown in Fig. 1, using wavefunctions obtained by the intermediate neglect of the differential overlap (INDO) procedure.[16,17]

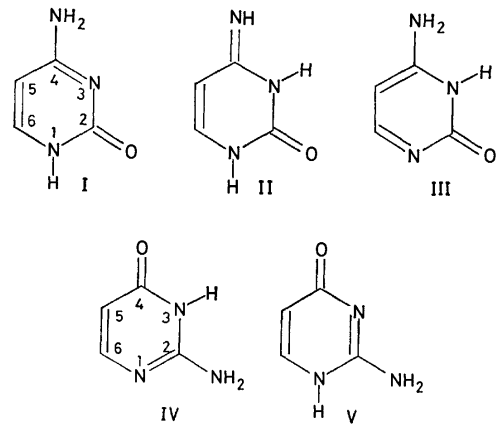

Fig. 1. Tautomeric forms of cytosine and isocytosine.

Experimental

Cytosine and isocytosine were purified by recrystallization from water. 3-Methylcytosine and 3-methylcytidine methosulfate were also recrystallized from a methanol-ethyl acetate solution. 3-Methylisocytosine was prepared according to the procedure by Angier and Curran.[18] Isocytosine was synthesized by the ammonolysis of 2,5′-cyclouridine.[19]

Acetonitrile, ethanol, a Na_2HPO_4–KH_2PO_4 buffer solution(pH 7), and a NaOH–Na_2HPO_4 buffer solution(pH 11) were used as solvents. The pH values of the buffer solutions were controlled so that the neutral form was dominant.

The MCD spectra were recorded with a JASCO J-20A recording circular dichrometer equipped with a 12.5 kG electromagnet. The absorption spectra were measured on a Hitachi EPS-3T recording spectrophotometer.

The experimental values of the Faraday *B* terms were obtained by the gaussian curve-fitting procedure or the method of moments.

Theoretical

The Faraday *B* terms were calculated using wavefunctions obtained by the INDO/S-CI approximation.[16,17] The bonding parameter of the oxygen atom, β_0, was determined so that the transition energies of the $\pi^* \leftarrow \pi$ transitions of some ketones were well reproduced ($\beta_0 = -31$ eV). The other parameters in

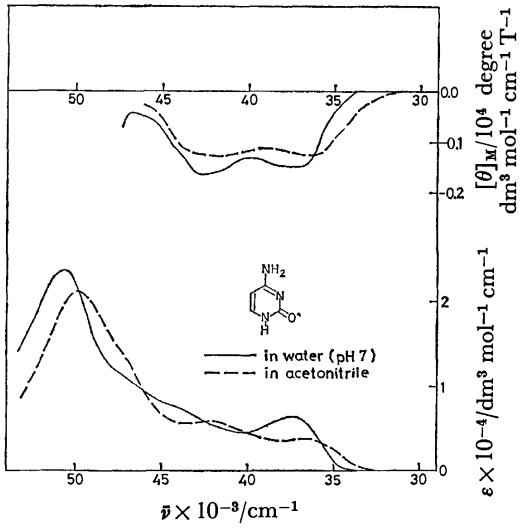

Fig. 2. MCD (upper) and absorption (lower) spectra of cytosine in aqueous solution (pH 7) (——) and in acetonitrile (– – –) at room temperature.

the calculation were described in a previous paper.[5]

The molecular structures of Form I of cytosine and Forms IV and V of isocytosine were taken from the experimental data obtained by X-ray crystal analysis.[14,15] The bond lengths and bond angles of Forms II and III of cytosine were estimated from the experimental values of Forms I, IV, and V.[14,15]

The configuration interaction among singly excited configurations below 12 eV was taken into account.

The Faraday B terms were calculated according to the expression derived by Buckingham and Stephens.[20] The procedures of the calculation of the Faraday B terms have been reported in the previous paper.[5]

Results and Discussion

The MCD and absorption spectra of cytosine are shown in Fig. 2. The molar ellipticity per unit of the magnetic field, $[\theta]_M$, is expressed by 10^4 degree dm^3 mol^{-1} cm^{-1} T^{-1} unit, and the extinction coefficient, ε, by dm^3 mol^{-1} cm^{-1} unit. The spectra in the aqueous solution are in agreement with those measured by Voelter *et al.*[1] In the wavenumber region of 32000—46000 cm^{-1}, two negative MCD bands are observed. In the absorption spectrum, we can observe an intense peak and a shoulder at 50700 cm^{-1} and at about 47000 cm^{-1} respectively, while no distinct MCD band is detected in the wavenumber region of 47000—50000 cm^{-1}. The MCD and absorption spectra in an acetonitrile solution are red-shifted and decrease in intensity relative to the spectra in an aqueous solution.

The MCD, CD, and absorption spectra of 3-methylcytidine methosulfate in an aqueous solution (pH 11) are presented in Fig. 3. 3-Methylcytidine shows a negative MCD band and a positive MCD band at 37400 cm^{-1} and at 43400 cm^{-1} respectively.

On the other hand, Morita and Nagakura[10] have concluded that the most stable form of cytosine in acetonitrile is Form II. The MCD and absorption

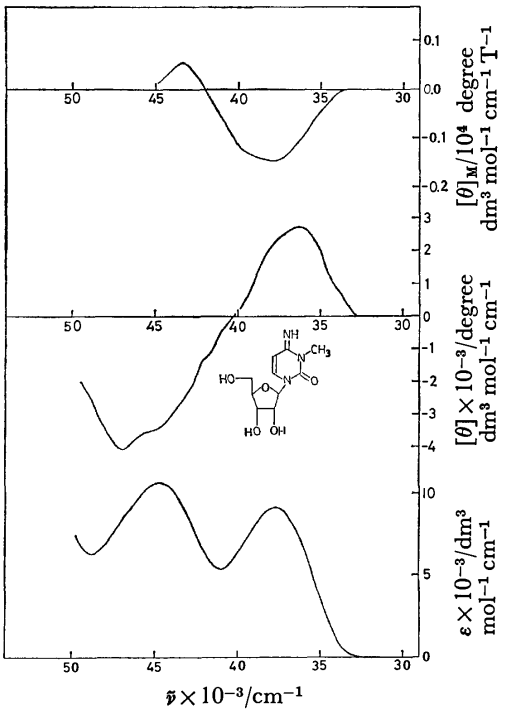

Fig. 3. MCD (top), CD (middle), and absorption (bottom) spectra of 3-methylcytidine in aqueous solution (pH 11) at room temperature.

spectra of Form II should resemble those of 3-methylcytidine, because the tautomeric form of 3-methylcytidine is fixed to Form II. However, the sign of the second MCD band of cytosine in acetonitrile is the opposite of that of 3-methylcytidine. In addition, the absorption spectrum of cytosine in acetonitrile is not very similar to that of 3-methylcytidine with respect to the absorption intensity and the position of the absorption peak observed in the wavenumber region higher than 40000 cm^{-1}. The MCD spectrum of cytosine in acetonitrile resembles that of cytosine in an aqueous solution rather than the MCD spectrum of 3-methylcytidine.

These results suggest that the most stable tautomer of cytosine is Form I, not only in a neutral aqueous solution, but also in acetonitrile. We can consider several reasons for the solvent dependence of the MCD and absorption spectra of cytosine: a change in the polarity of the solvent, the specific interaction of the cytosine molecule with the solvent molecules, such as the formation of hydrogen bonding, the association of cytosine molecules, or the contamination of small amount of minor tautomers.

The MCD and absorption spectra of 3-methylcytosine, whose tautomeric form is fixed to Form III,[21] are shown in Fig. 4. Morita and Nagakura[10] have reported that Form III coexists with Forms I and II, to a much smaller extent, in an acetonitrile solution of cytosine at a higher temperature. The sign pattern of the MCD spectrum of 3-methylcytosine is the same as that of 3-methylcytidine (Form II), while the lowest MCD and absorption bands lie at lower wavenumbers than those of cytosine (Form I) and 3-methylcytidine (Form II). The presence of

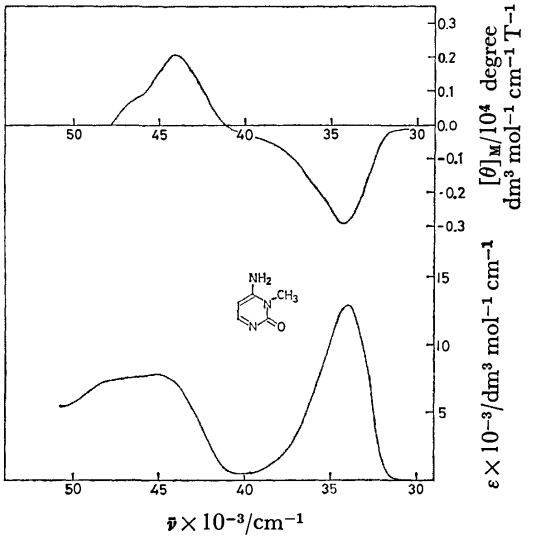

Fig. 4. MCD (upper) and absorption (lower) spectra of 3-methylcytosine in aqueous solution (pH 11) at room temperature.

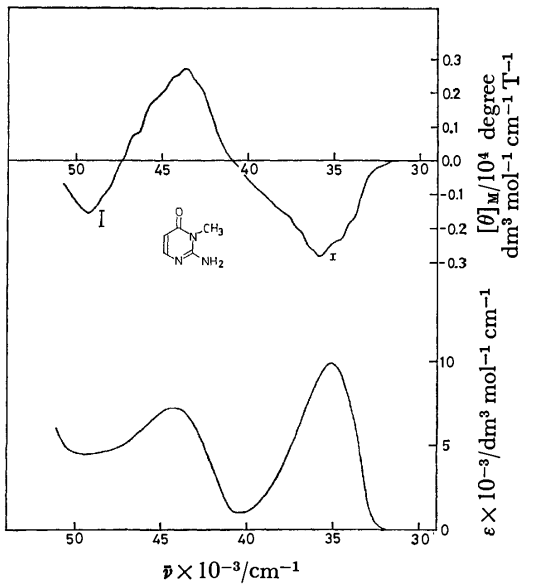

Fig. 5. MCD (upper) and absorption (lower) spectra of 3-methylisocytosine in aqueous solution (pH 7) at room temperature.

Form III in cytosine is not confirmed by the results of this work.

The MCD and absorption spectra of 3-methylisocytosine, whose tautomeric form is fixed to Form IV, are exhibited in Fig. 5. The MCD and absorption spectra of 3-methylisocytosine are very similar to those of 3-methylcytosine, because these two compounds have the same valence-bond structure.

The MCD, CD, and absorption spectra of isocytidine, whose tautomeric form is fixed to Form V, are shown in Fig. 6. Although the lowest negative MCD band almost corresponds to the lowest absorption band at 39100 cm^{-1}, the second negative MCD band lies intermediate between the absorption peak at 48500 cm^{-1} and a shoulder at 43600 cm^{-1}.

The MCD and absorption spectra of isocytosine in

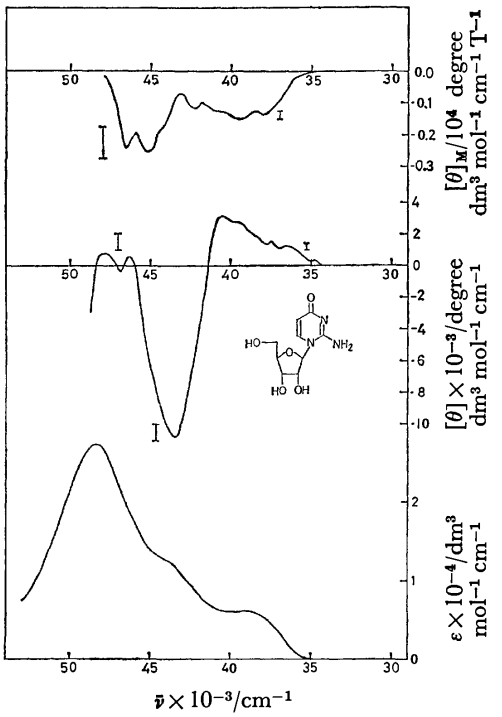

Fig. 6. MCD (top), CD (middle), and absorption (bottom) spectra of isocytidine in aqueous solution (pH 7) at room temperature.

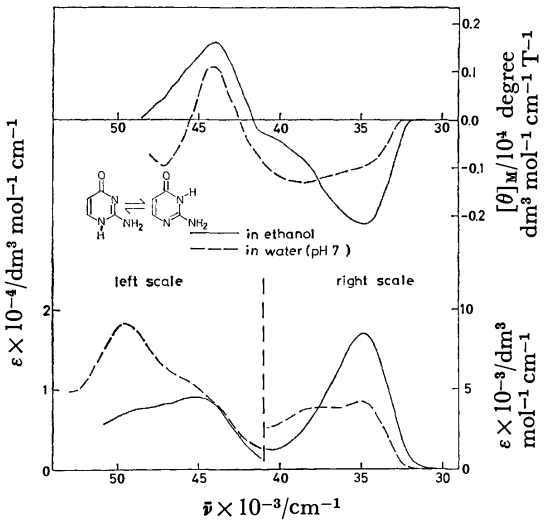

Fig. 7. MCD (upper) and absorption (lower) spectra of isocytosine in aqueous solution (pH 7) (– – –) and in ethanol (——) at room temperature.

an ethanol and in an aqueous solution (pH 7) are shown in Fig. 7. In the ethanol solution, negative and positive MCD bands are observed at 35400 cm^{-1} and at 44500 cm^{-1} respectively. The MCD and absorption spectra of isocytosine in ethanol resemble those of 3-methylisocytosine, suggesting that the prevailing tautomeric form of isocytosine in ethanol is Form IV. In the aqueous solution, the two MCD bands at 35400 cm^{-1} and at 44500 cm^{-1} decrease in intensity, and two negative MCD bands appear at about 38700 cm^{-1} and at 47200 cm^{-1}. These MCD bands appearing in the aqueous solution are analogous to the MCD bands of isocytidine, and they can rea-

TABLE 1. THE CALCULATED AND OBSERVED VALUES OF THE TRANSITION ENERGIES, OSCILLATOR STRENGTH, AND THE FARADAY B TERMS OF FORMS I—V

$\bar{\nu}_{obsd} \times 10^{-3}$ / cm^{-1}	f_{obsd}	$B_{obsd} \times 10^4$ / βD^2 cm	$\bar{\nu}_{calcd} \times 10^{-3}$ / cm^{-1}	f_{calcd}	$B_{calcd} \times 10^4$ / βD^2 cm	
Cytosine in H_2O			Form I			
			29.2	0.000	0.0	A″
			33.1	0.002	−3.2	A″
37.4	0.096	4.1	34.0	0.094	9.2	A′
			42.6	0.003	0.6	A″
42.0	0.100	6.5	43.4	0.090	−1.1	A′
			44.5	0.000	0.7	A″
47.0	0.211		46.9	0.931	0.2	A′
			48.7	0.004	−0.7	A″
52.1	0.639		50.4	0.052	−10.5	A′
3-Methylcytidine			Form II			
			30.6	0.000	0.0	A″
			31.2	0.002	−2.1	A″
37.4	0.17	5.6	37.5	0.305	8.3	A′
			42.6	0.000	5.3	A″
			42.6	0.254	−1.9	A′
45.1	0.39	−1.0	44.6	0.114	−8.4	A′
			47.6	0.018	6.3	A″
			48.6	0.009	−0.1	A″
3-Methylcytosine			Form III			
			27.8	0.000	0.0	A″
34.6	0.198	10.3	31.8	0.254	−23.6	A′
			32.0	0.004	31.8	A″
			43.4	0.002	0.0	A″
			43.7	0.000	0.0	A″
44.1		−4.6	44.8	0.357	−6.5	A′
	0.275		49.3	0.013	13.6	A″
48.5[a]			49.4	0.201	−31.9	A′
			49.6	0.005	6.4	A″
Isocytosine in ethanol			Form IV			
			27.3	0.001	−0.3	A″
35.4	0.169	9.3	33.4	0.264	12.1	A′
			39.2	0.004	−2.1	A″
44.5		−3.9	42.6	0.306	−14.3	A′
			42.8	0.002	−0.3	A″
	0.303		43.4	0.004	−2.5	A″
			44.3	0.019	7.5	A″
			47.7	0.000	−0.2	A″
49.0[a]			49.8	0.188	−8.6	A′
Isocytidine			Form V			
			23.4	0.000	0.0	A″
			33.8	0.002	−0.3	A″
39.1	0.126	5.7	37.3	0.021	4.6	A′
43.6[a]	0.159		41.4	0.387	−29.0	A′
			41.5	0.004	17.4	A″
			44.1	0.003	1.7	A″
45.7[b]		5.2	45.1	0.244	19.0	A′
			46.7	0.012	0.7	A″
			48.4	0.007	0.2	A″
48.5			49.5	0.348	−16.9	A′

a) Wavenumber at the shoulder of the absorption spectrum. b) Wavenumber at the peak of the MCD spectrum.

TABLE 2. THE CALCULATED AND OBSERVED VALUES OF THE TRANSITION ENERGIES, OSCILLATOR STRENGTH, AND THE FARADAY B TERMS OF 3-METHYLCYTIDINE AND 3-METHYLISOCYTOSINE

$\bar{\nu}_{obsd} \times 10^{-3}$ / cm^{-1}	f_{obsd}	$B_{obsd} \times 10^4$ / βD^2 cm	$\bar{\nu}_{calcd} \times 10^{-3}$ / cm^{-1}	f_{calcd}	$B_{calcd} \times 10^4$ / βD^2 cm	
3-Methylcytidine			3-Methyl-4-imino-2-pyrimidinone			
			30.5	0.000	−0.2	A″
			30.7	0.002	−1.6	A″
37.4	0.17	5.6	37.2	0.241	6.9	A′
			42.1	0.000	3.4	A″
			42.3	0.188	36.9	A′
45.1	0.39	−1.0	42.6	0.246	−41.1	A′
			45.5	0.007	2.8	A″
			47.8	0.003	−4.8	A″
3-Methylisocytosine			3-Methylisocytosine			
			27.4	0.001	−0.3	A″
35.2	0.174	10.6	33.3	0.238	10.7	A″
			39.3	0.002	−1.5	A″
			41.9	0.005	4.0	A″
44.3	0.254	−6.7	42.3	0.278	−19.0	A′
			42.9	0.000	0.0	A″
			44.1	0.015	5.6	A″
			47.8	0.000	2.2	A″
			48.0	0.199	−10.1	A′

sonably be assigned to the MCD bands of Form V. Thus, the MCD spectrum of isocytosine in an aqueous solution can be well interpreted by assuming that Form V is in equilibrium with Form IV in an aqueous solution of isocytosine.

The calculated transition energies, oscillator strengths, and Faraday B terms of Forms I—V are listed in Table 1, along with the experimental values. It should be noted that the positive B terms give negative MCD bands. In the ultraviolet region, the present calculation predicts three or four $\pi^* \leftarrow \pi$ transitions for Forms I—V; these transitions can reasonably be assigned to the peaks and the shoulder observed in the absorption and MCD spectra. On the other hand, several transitions with A″ symmetry are predicted below 50000 cm^{-1}. Most of them are characterized by a transition from the nonbonding orbitals of carbonyl oxygen and azanitrogen to the unoccupied π orbitals. Although the lowest $\pi^* \leftarrow$n transition of Form V is predicted at a much lower wavenumber than the lowest $\pi^* \leftarrow \pi$, no MCD or absorption band assignable to the lowest $\pi^* \leftarrow$n transition is identified.

A large B value is predicted for the second $\pi^* \leftarrow$n transition of Form III, whose oscillator strength is much smaller than that of the $\pi^* \leftarrow \pi$ transitions. The large B term of the second $\pi^* \leftarrow$n transition is mainly induced by the magnetic mixing of the second $\pi^* \leftarrow$n state with the first $\pi^* \leftarrow \pi$ state, which lies close to the second $\pi^* \leftarrow$n state, and this large B term is partially cancelled out by the negative B term of the first $\pi^* \leftarrow \pi$ transition in the MCD spectrum; the net contribution to the MCD spectrum from these two electronic transitions is about $+12.2 \times 10^{-4}$ βD^2 cm.

The calculated values of the transition energies and the oscillator strengths of the $\pi^* \leftarrow \pi$ transitions of Forms I—V are in good agreement with the experimental values. The magnitudes of the experimental B terms of the second MCD band of cytosine are larger than the theoretical B values of the electronic transitions predicted in the spectral region of 42000—45000 cm^{-1}. The second $\pi^* \leftarrow \pi$ transition of Form V, whose B term is predicted to be negative and large, is not identified in the MCD spectrum of isocytidine. However, the agreement between the calculation and the experiment is satisfactory as a whole.

In order to study the effect of the methylation at the nitrogen atom on the calculated results, we have carried out a similar calculation for 3-methyl-4-imino-2-pyrimidinone (the N-methylated derivative of Form II) and for 3-methylisocytosine (the N-methylated derivative of Form IV); the results are shown in Table 2. The calculated transition energies of the N-methylated compounds tend to be slightly smaller than those of Form II and Form IV themselves. The calculated energy difference between the second and the third $\pi^* \leftarrow \pi$ transitions of Form II becomes smaller upon N-methylation, which increases the magnetic mixing between the second and the third $\pi^* \leftarrow \pi$ states. However, the calculation shows that the spectral features of Form II and Form IV are not much affected by the N-methylation.

References

1) W. Voelter, R. Records, E. Bunnenberg, and C. Djerassi, *J. Am. Chem. Soc.*, **90**, 6163 (1968); W. Voelter, G. Barth, R. Records, E. Bunnenberg, and C. Djerassi, *ibid.*, **91**, 6165 (1969); D. L. Elder, E. Bunnenberg, C. Djerassi, M. Ikehara, and W. Voelter, *Tetrahedron Lett.*, **10**, 727 (1970).

2) L. B. Townsend, D. W. Miles, S. J. Manning, and H. Eyring, *J. Heterocyclic Chem.*, **10**, 419 (1970).

3) D. W. Miles, W. H. Inskeep, L. B. Townsend, and

H. Eyring, *Biopolymers*, **11**, 1181 (1972).
4) R. E. Linder, H. Weiler-Feilchenfeld, G. Barth, E. Bunnenberg, and C. Djerassi, *Theoret. Chim. Acta*, **36**, 135 (1974); H. Weiler-Feilchenfeld, R. E. Linder, G. Barth, E. Bunnenberg, and C. Djerassi, *ibid.*, **46**, 79 (1977).
5) A. Kaito and M. Hatano, *Bull. Chem. Soc. Jpn.*, **53**, 3069 (1980).
6) S. L. Wallace, A. Castellan, D. Müller, and J. Michl, *J. Am. Chem. Soc.*, **100**, 6828 (1978); I. Jonas and J. Michl, *ibid.*, **100**, 6834 (1978).
7) J. D. Watson and F. H. Crick, *Cold Spring Harbor Symp. Quant. Biol.*, **18**, 123 (1953).
8) C. Hélène, A. Haug, M. Delbrück, and P. Douzou, *C. R. Acad. Sci. Paris*, **259**, 3385 (1964).
9) C. Hélène and P. Douzou, *C. R. Acad. Sci. Paris*, **259**, 4853 (1964).
10) H. Morita and S. Nagakura, *Theor. Chim. Acta*, **11**, 279 (1968).
11) G. C. Y. Lee, J. H. Prestegrad, and S. I. Chan, *J. Am. Chem. Soc.*, **94**, 951 (1972).
12) Y. P. Wong, *J. Am. Chem. Soc.*, **95**, 3511 (1973).
13) C. Hélène and P. Douzou, *C. R. Acad. Sci. Paris*, **259**, 4387 (1964).
14) D. L. Barker and R. E. Marsh, *Acta Crystallogr.*, **17**, 1581 (1964).
15) B. D. Sharma and J. F. McConnell, *Acta Crystallogr.*, **19**, 797 (1965).
16) J. A. Pople, *J. Chem. Phys.*, **47**, 2026 (1969).
17) J. Ridley and M. Zerner, *Theor. Chim. Acta*, **32**, 111 (1973).
18) R. B. Angier and W. V. Curran, *J. Org. Chem.*, **26**, 1891 (1961).
19) T. Ueda and S. Shibuya, unpublished experimental data.
20) A. D. Buckingham and P. J. Stephens, *Annu. Rev. Phys. Chem.*, **17**, 399 (1966).
21) T. Ueda and J. J. Fox, *J. Am. Chem. Soc.*, **85**, 4024 (1963).

 © 1980 The Chemical Society of Japan Bull. Chem. Soc. Jpn., 53, 3079—3084 (1980)

Liquid Crystal Formation in Binary Systems. II. Induction of Nematic and Smectic Phases by Electron Donor-Acceptor Interaction between the *p*-Dimethylamino and *p*-Nitro Derivatives of *N*-Benzylideneaniline

Kotaro Araya and Yoshio Matsunaga*

Department of Chemistry, Faculty of Science, Hokkaido University, Sapporo 060

(Received February 28, 1980)

The formation of solid molecular complexes and the induction of nematic and smectic phases have been demonstrated with a number of binary mixtures of potentially-mesomorphic electron donors and acceptors of the type *N*-(*p*-X-benzylidene)-*p*-Y-aniline. One of the components contains a dimethylamino group as X or Y, and the other a nitro group as X or Y. The remaining substituents are methoxyl, ethoxyl, or propoxyl groups. The maximum temperature of the nematic phase induced in these electron donor-acceptor systems is higher by 23 to 45 °C than the straight line joining the latent transition temperatures of the two components. The tendency to form a solid complex and that to induce a nematic phase are both shown to a large extent by the propoxy derivatives, to a lesser extent by the methoxy derivatives, and least by the ethoxy derivatives. All the solid molecular complexes are reddish brown and exhibit an additional electronic absorption band located at about 500 nm. The mesophases are similarly colored. The enhanced thermal stability of the nematic and smectic phases in these binary mixtures is ascribed to the complex formation by an electron donor-acceptor interaction.

The liquid crystalline state is a state of matter intermediate between crystalline solids and isotropic liquids. Intermolecular attractions are supposed to be essential for producing the parallel molecular arrangement characteristic of such a state. If the interactions are not strong enough to produce the orientation, the compound may be monotropically mesomorphic. Upon heating such a compound, the crystalline solid melts to an isotropic liquid but the latter may undergo the transition to a liquid crystal if it is sufficiently supercooled. Even when the expected metastable liquid crystalline state is not achieved, the compound may be considered to be potentially mesomorphic. This paper deals mostly with the compounds of the last category. It seemed likely to us that the parallel molecular arrangement required by liquid crystal formation should become observable in the binary systems consisting of potentially mesomorphic compounds if the orientational cohesive forces were supplemented by an electron donor-acceptor interaction. This sort of intermolecular force may particularly suit the alignment of the planar component molecules. The enhancement of nematic-phase stability found by Park *et al.* with the binary system of *N*-(*p*-methoxybenzylidene)-*p*-butylaniline and 4-cyano-4′-pentylbiphenyl and several other, closely related systems is apparently in support of our postulate.[2,3] They have attributed the increased thermal stability to molecular complexing by a weak electron donor-acceptor interaction. A similar observation has been made by us with the azoxydianisole-*N*-(*p*-nitrobenzylidene)-*p*-anisidine mixtures.[1] It must be noted that both or one of the component compounds in these systems are enantiotropically mesomorphic, in contrast to those to be described in this paper.

Because of the simplicity of molecular structure and the ease of preparations, *N*-(*p*-X-benzylidene)-*p*-Y-aniline

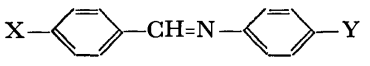

lines were chosen for the present study. In order to maximize the proposed intermolecular attraction, a dimethylamino group was introduced to one of the components, which is regarded as the electron donor, and a nitro group to the other, which is regarded as the electron acceptor. The remaining terminal groups were selected from short alkoxyl groups: namely, methoxyl, ethoxyl, and propoxyl groups, to avoid making the component compounds themselves mesomorphic.

Experimental

Materials. The *N*-benzylideneanilines listed in Table 1 were prepared by a condensation reaction between a *p*-X derivative of benzaldehyde and a *p*-Y derivative of aniline, and were purified by repeated recrystallization from a suitable solvent and by sublimation in a vacuum if necessary. Hereafter, the compounds are represented by their terminal groups (X,Y). Binary mixtures in known proportions were melted in small test tubes, shaken well to insure homogeneity, and then rapidly cooled.

Measurements. The calorimetric curves were recorded on a Rigaku Thermoflex differential scanning calorimeter during the processes of heating and cooling. The heating rate in this work was 2.5 °C min^{-1}. The temperature was calibrated as described in a previous paper.[1] The induced mesophases were identified by examining the texture with the aid of a polarizing microscope and/or by studying the continuous miscibility with a reference mesophase. The diffuse reflectance of the solid component compounds and molecular complexes was measured by means of a Beckman DK 2A spectroreflectometer. The spectrum was then plotted using the Kubelka-Munk function.

Results and Discussion

Methoxy Derivatives. The phase diagrams of all the possible electron donor-acceptor combinations of the methoxy derivatives are presented in Fig. 1. The open and shaded circles indicate the transitions found during the processes of heating and cooling respectively. Therefore, the phase appearing below the transition, indicated solely by shaded circles, is metastable. The shaded circles are omitted when they coincide exactly with the open circles. The systems of (dimethylamino, methoxy) with (nitro, methoxy) and also of (methoxy,

Table 1. Melting points and isotropic liquid-nematic liquid crystal transition temperatures of *N*-(*p*-X-benzylidene)-*p*-Y-anilines

Substituents X	Substituents Y	Mp/°C	Tp/°C[a]
$(CH_3)_2N$	CH_3O	141[b]	(55)
NO_2	CH_3O	133[c]	(80)
CH_3O	$(CH_3)_2N$	143.5	(60)
CH_3O	NO_2	124[d]	(82)
$(CH_3)_2N$	C_2H_5O	147[e]	(97.5)
NO_2	C_2H_5O	122[f]	(85)
C_2H_5O	$(CH_3)_2N$	138	(102)
C_2H_5O	NO_2	114[g]	(90)
$(CH_3)_2N$	C_3H_7O	122	(75)
NO_2	C_3H_7O	103[h]	(50)
C_3H_7O	$(CH_3)_2N$	115	(75)
C_3H_7O	NO_2	110[i]	57.5[j]

a) The values in parentheses were estimated by studies on the binary systems with azoxydianisole. b) 140.2 °C Dave and Lohar (Refs. 4 and 8). c) 135.7 °C by Dave and Dewar (Ref. 5); 134.4—136 °C by Schroeder and Schroeder (Ref. 6); 135 °C by Malthete *et al.* (Ref. 7). d) 124.5—125 °C by Schroeder and Schroeder (Ref. 6); 124 °C by Malthete *et al.* (Ref. 7). e) 147.4 °C by Dave and Lohar (Ref. 4). f) 123.5 °C by Dave and Lohar (Refs. 4 and 8). g) 121 °C by Malthete *et al.* (Ref. 7). h) 105 °C by Malthete *et al.* (Ref. 7). i) 97 °C by Malthete *et al.* (Ref. 7). j) 62 °C by Malthete *et al.* (Ref. 7).

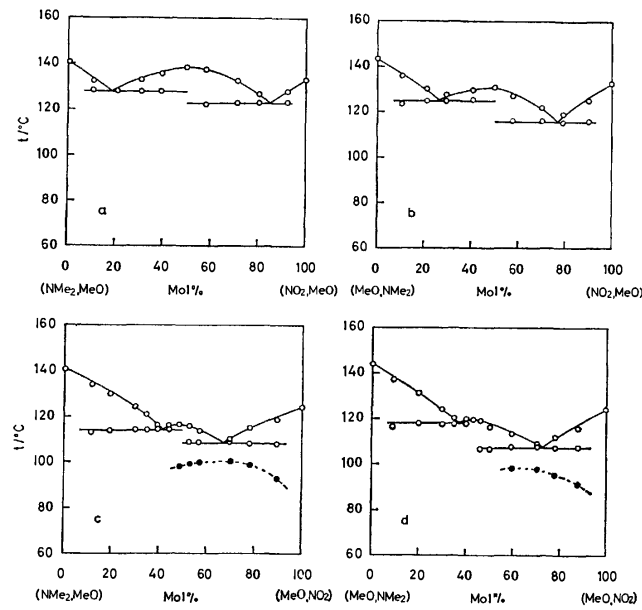

Fig. 1. Phase diagrams of (a) the *N*-[*p*-(dimethylamino) benzylidene]-*p*-anisidine–*N*-(*p*-nitrobenzylidene)-*p*-anisidine, (b) *N*-(*p*-methoxybenzylidene)-*p*-(dimethylamino)aniline–*N*-(*p*-nitrobenzylidene)-*p*-anisidine, (c) *N*-[*p*-(dimethylamino)benzylidene]-*p*-anisidine–*N*-(*p*-methoxybenzylidene)-*p*-nitroaniline, and (d) *N*-(*p*-methoxybenzylidene)-*p*-(dimethylamino)aniline–*N*-(*p*-methoxybenzylidene)-*p*-nitroaniline systems. The open and shaded circles are transitions observed in the processes of heating and cooling respectively.

dimethylamino) with (nitro, methoxy) yield only solid 1:1 molecular complexes (see Figs. 1a and 1b). The eutectic points in the former system are located at 128 °C and 18.5 mol% and at 123 °C and 84.5 mol% of the acceptor component. The melting point of the complex is 138.5 °C; this is a few degrees higher than the mean value of those of the components. In the latter system, the eutectic points are found at 125 °C and 26 mol% and at 115.5 °C and 77 mol%. The complex melts congruently at 131 °C. This temperature is several degrees below the straight line joining the melting points of the components. Disregarding small variations in the melting point of the component compounds, one may say that the higher the melting point and the wider the region of the existence of the solid complex (the composition difference between the two eutectics), the more stable is the complex.[9] Therefore, the solid complexes formed in the (dimethylamino, methoxy)–(methoxy, nitro) and (methoxy, dimethylamino)–(methoxy, nitro) systems shown in Figs. 1c and 1d are of considerably lower stability. Note that the composition of the complex in the last system is not 1:1 but 3:2. When the melts of these two systems are supercooled, the isotropic liquid-nematic liquid crystal (I-N) transition curves are partially observable. Since the latent I-N transition temperatures of (dimethylamino, methoxy) and (methoxy, nitro) were estimated as 55 °C and 82 °C respectively by the method to be mentioned in the last paragraph of this paper, the maximum deviation from linearity in the transition temperature is as much as 30 °C at 50 mol%. The corresponding value in the (methoxy, dimethylamino)–(methoxy, nitro) system is not available, but the deviation at 60 mol% is 25 °C. The flat maximum is indicative of a high degree of dissociation of molecular complex in the isotropic liquid phase. The I-N transition curve is observable only in the high mol% range of the acceptor compound. The large temperature difference between the freezing point curve and the metastable I-N transition curve may account for the solidification of supercooled melts without reaching the latter in the left half of the diagram.

Ethoxy Derivatives. As is shown in Fig. 2, all the combinations of the ethoxy derivatives can produce nematic phases. The I-N transition is monotropic in the system of (dimethylamino, ethoxy) with (nitro, ethoxy) but enantiotropic in the other three. The nematic liquid crystals are stable in the hatched areas in Figs. 2b, 2c, and 2d. The I-N transition curves are very much alike. The maximum is located near a 1:1 mole ratio, and is a little above 120 °C in the two systems with (nitro, ethoxy), but a little below 120 °C in the two systems with (ethoxy, nitro). One factor that should not be ignored is the fact that the latent I-N transition in the donor compound occurs at an appreciably higher temperature than that of the corresponding methoxy compounds. The thermal stability enhancement by mixing of the donor and acceptor compounds is therefore not large; it ranges from 23 to 32 °C.

It must be added that the system (dimethylamino,

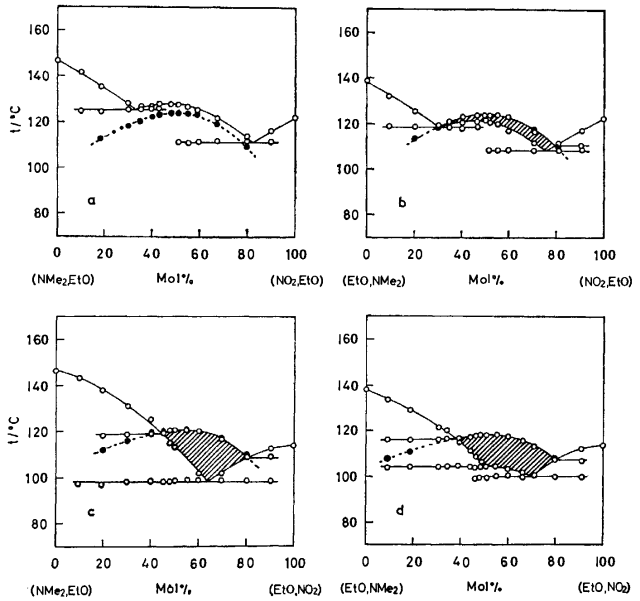

Fig. 2. Phase diagrams of (a) the *N*-[*p*-(dimethylamino)benzylidene]-*p*-phenetidine–*N*-(*p*-nitrobenzylidene)-*p*-phenetidine, (b) *N*-(*p*-ethoxybenzylidene)-*p*-(dimethylamino)aniline – *N*-(*p*-nitrobenzylidene)-*p*-phenetidine, (c) *N*-[*p*-(dimethylamino)benzylidene]-*p*-phenetidine–*N*-(*p*-ethoxybenzylidene)-*p*-nitroaniline, and (d) *N*-(*p*-ethoxybenzylidene)-*p*-(dimethylamino)-aniline–*N*-(*p*-ethoxybenzylidene)-*p*-nitroaniline systems. In the hatched area, the nematic phase is stable. As to the open and shaded circles, see the caption of Fig. 1.

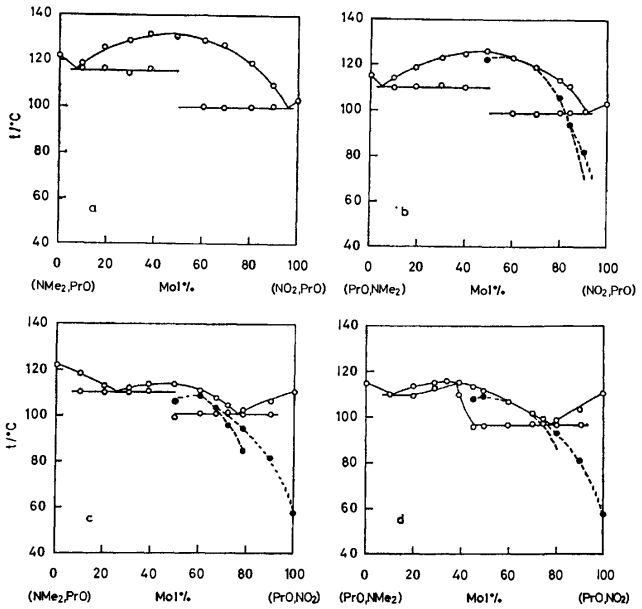

Fig. 3. Phase diagrams of (a) the *N*-[*p*-(dimethylamino)benzylidene]-*p*-propoxyaniline – *N*-(*p*-nitrobenzylidene)-*p*-propoxyaniline, (b) *N*-(*p*-propoxybenzylidene)-*p*-(dimethylamino)aniline – *N*-(*p*-nitrobenzylidene)-*p*-propoxyaniline, (c) *N*-[*p*-(dimethylamino)-benzylidene]-*p*-propoxyaniline – *N*-(*p*-propoxybenzylidene)-*p*-nitroaniline, and (d) *N*-(*p*-propoxybenzylidene)-*p*-(dimethylamino)aniline–*N*-(*p*-propoxybenzylidene)-*p*-nitroaniline systems. As to the open and shaded circles, see the caption of Fig. 1.

ethoxy)–(nitro, ethoxy) shown in Fig. 2a has been studied by Lohar.[8] The agreement in the melting points of the component compounds is good and that in the freezing point curve above 60 mol% of the acceptor compound is fair. He has located a eutectic at 114.5 °C and 83 mol%. These values compare well with ours: namely, 111.5 °C and 82.5 mol%. However, Lohar's freezing point curve below 60 mol% is at significantly higher temperatures. The eutectic we found at 125.5 °C and 33 mol% is missing in his result. In addition, the metastable nematic phase has not been detected at all.

The tendency to form a solid complex is markedly diminished compared with that of the methoxy derivatives. While the region of the existence of the solid complex in the system of (dimethylamino, ethoxy) with (nitro, ethoxy) is 49.5 mol%, that in the system of the corresponding methoxy compounds extends over 66 mol% (compare Figs. 1a and 2a). The fact that the melting point of the complex, 127 °C, is several degrees below the mean value of those of the components reflects also a decreased stability of the solid complex. This tendency is shown most when (dimethylamino, ethoxy) is mixed with (ethoxy, nitro), as is illustrated in Fig. 2c. The resulting phase diagram is of the eutectic type, no solid complex being formed. The complex in the (ethoxy, dimethylamino)–(ethoxy, nitro) system shown in Fig. 2d is also not of high stability. It melts incongruently at 104 °C. Here again, the composition does not appear to be a 1:1 mole ratio.

Propoxy Derivatives. Among the examined alkoxyl groups, the propoxyl group is the substituent which best stabilizes a solid complex. The diagrams illustrated in Fig. 3 indicate the formation of a congruently melting molecular complex in all the systems. The one formed in the (dimethylamino, propoxy)–(nitro, propoxy) system is the most stable, melting at 132 °C (see Fig. 3a). While this value is lower than the melting point of the complex formed in the (dimethylamino, methoxy)–(nitro, methoxy) system shown in Fig. 1a, it is higher by 17 °C than the mean value of those of the components. The eutectic points are at 115.5 °C and 7 mol% and at 100 °C and 96 mol%. As the result, the freezing point curve of the complex occupies a large part of the diagram. No liquid crystalline phase is observed in this system, while the other three systems yield not only nematic but also smectic phases. The difference between the latent I-N transition temperature and the melting point in the acceptor compound is larger than that in the donor compound; nevertheless, the mesophases were found solely on the nitro derivative-rich side. (Propoxy, nitro) is the only compound in this work whose liquid phase could be cooled to the I-N transition temperature without solidification occurring. The melt, which is relatively rich in the donor component, is directly transformed into the smectic phase. In other words, only the isotropic liquid-smectic liquid crystal (I-S) transition curve is observable in such a composition range. The maximum temperatures of nematic and smectic phases in the system containing

(propoxy, nitro) as the acceptor component do not differ much from each other (see Figs. 3c and 3d). These nematic phases are stabilized as much as 40 °C near the maximum with respect to the ideal linear relationship. The latent nematic liquid crystal-smectic liquid crystal (N-S) transition temperatures of the component compounds are not known, but they are certainly located below the I-N transition temperatures. The extrapolation of the N-S transition curve in Fig. 3c to 100 mol% of (propoxy, nitro) suggests that the latent transition temperature of this acceptor compound is not higher than 20 °C.

The thermal stability enhancement of a smectic phase has been reported by several workers in binary mixtures in which both or one of the components give stable nematic liquid crystals.[6,10-12] For example, a paper by Schroeder and Schroeder has referred to the appearance of a smectic phase by mixing of mesomorphic 4,4'-bis(hexyloxy)azoxybenzene and non-mesomorphic (methoxy, nitro).[6] Engelen *et al.* have proposed that such phases be called induced smectic phases.[11] They have concluded that mixtures of terminal polar with terminal nonpolar nematic liquid crystals usually induce smectic phases. While nitro and cyano derivatives are considered to be polar, the derivatives carrying only alkyl and alkoxyl groups are nonpolar. Contrary to these authors' conclusion, Domon and Billard have shown recently that the existence of a strong terminal dipole for only one of the components is not always correlated with the induction of smectic phases.[12] Among the twenty-eight systems listed by them, over ten have been shown to yield an induced smectic phase without a terminal polar compound. Our systems are entirely different from theirs; that is, all our component molecules bear a dimethylamino or nitro group and are strongly polar. Secondly, the nematic phases of the components are metastable with respect to the crystalline phases at any temperature.

General Remarks. As the whole, the tendency of a solid complex formation decreases in the following order:

(dimethylamino, alkoxy)-(nitro, alkoxy) > (alkoxy, dimethylamino)-(nitro, alkoxy) > (alkoxy, dimethylamino)-(alkoxy, nitro) > (dimethylamino, alkoxy)-(alkoxy, nitro).

Among the compounds examined, this tendency is shown to a large extent by the propoxy derivatives, to a lesser extent by the methoxy derivatives, and least by the ethoxy derivatives.

The latent I-N transition temperatures of the ethoxy derivatives are higher than those of the methoxy and propoxy derivatives, thus making the observation of the induced mesophases easiest. The effects of dimethylamino and nitro groups on the transition temperature are also appreciable. Consequently, the order is ethoxy > propoxy > methoxy for the donor compounds, while ethoxy > methoxy > propoxy for the acceptor compounds.

The observations made with the ethoxy derivatives suggest that the thermal stability enhancement of nematic phases is larger in the first two combinations of the donor and acceptor compounds: namely, (dimethylamino, alkoxy)-(nitro, alkoxy) and (alkoxy, dimethylamino)-(nitro, alkoxy). Concerning the effects of alkoxyl groups, the comparison is possible with the other two combinations, as listed in Table 2. The order of the alkoxy derivatives in the thermal stability enhancement of nematic phases agrees exactly with that of the tendency of a solid complex formation: that is,

propoxy > methoxy > ethoxy.

Qualitatively speaking, therefore, the effects of substituents on the formation of a solid complex and the induction of mesophases are dependent on each other. The special feature of smectic phase is its stratification. This structure makes the phase to be much closer to the crystalline state than is the nematic phase. The appearance of smectic phase in the mixtures of the propoxy derivatives seems to be correlated with the fact that the tendencies to form a solid complex and to induce a mesophase are both high.

Table 2. Thermal stability enhancement of nematic phases: the deviation at 50 mol% from a linear relationship between the transition temperatures of the component compounds

(The values in parentheses were estimated by the extrapolation of the I-N transition curves.)

Combination	Methoxy deriv.	Ethoxy deriv.	Propoxy deriv.
(Dimethylamino, alkoxy) + (nitro, alkoxy)	(33 °C)	32 °C	(45 °C)
(Alkoxy, dimethylamino) + (nitro, alkoxy)	(32 °C)	31 °C	(40—45 °C)
(Dimethylamino, alkoxy) + (alkoxy, nitro)	30 °C	27 °C	(40 °C)
(Alkoxy, dimethylamino) + (alkoxy, nitro)	(27 °C)	23 °C	(40 °C)

The solid molecular complexes are reddish brown, while the component compounds are yellow. A study of the diffuse reflection spectra has revealed the appearance of an additional electronic absorption band due to complexing. As is exemplified by the combination of (dimethylamino, ethoxy) and (nitro, ethoxy) in Fig. 4, the maximum is located around 20×10^3 cm^{-1} (500 nm). This band is assigned to the charge-transfer transition associated with the electron donor-acceptor pairs. The persistence of color in mesophases is considered as the evidence that the molecular complexing in them is also of the electron donor-acceptor type. Naturally, the loss of color is seen when the separation of donor and acceptor molecules into two phases occurs by the solidification.

Estimation of Latent Transition Temperatures. The failure to observe mesophases in the systems (dimethylamino, methoxy)-(nitro, methoxy), (methoxy, dimethylamino)-(nitro, methoxy), and (dimethylamino, propoxy)-(nitro, propoxy), shown in Figs. 1a, 1b, and 3a respectively, must be attributed to the strong tendency to form a crystalline solid, which overshadows the transformation of the melt to a metastable mesophase. The existence of such a induced mesophase has been confirmed by a study of the phase diagram of

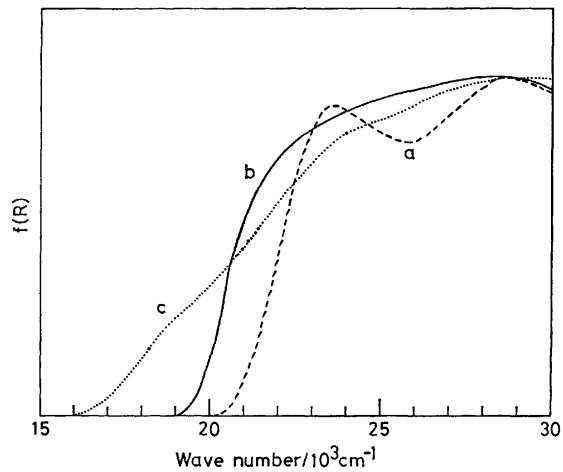

Fig. 4. Diffuse reflection spectra of (a) *N*-[*p*-(dimethylamino)benzylidene]-*p*-phenetidine, (b) *N*-(*p*-nitrobenzylidene)-*p*-phenetidine, and (c) their 1:1 complex.

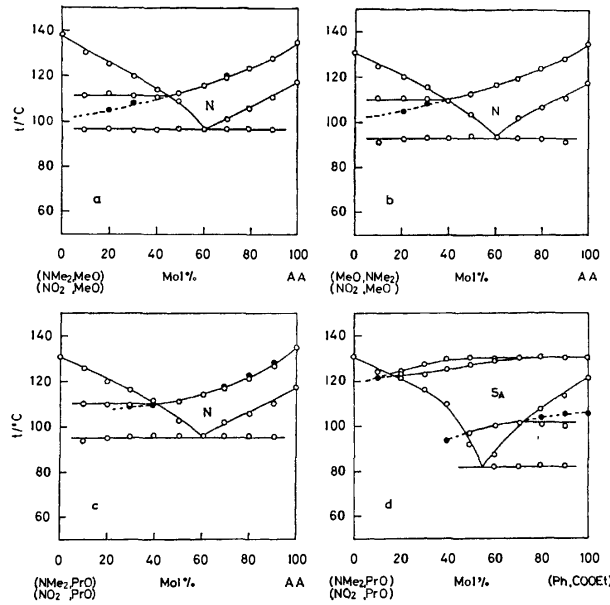

Fig. 5. Phase diagrams of (a) the system consisting of the *N*-[*p*-(dimethylamino)benzylidene]-*p*-anisidine–*N*-(*p*-nitrobenzylidene)-*p*-anisidine (1:1) complex and azoxydianisole, (b) the system consisting of the *N*-(*p*-methoxybenzylidene)-*p*-(dimethylamino)aniline–*N*-(*p*-nitrobenzylidene)-*p*-anisidine (1:1) complex and azoxydianisole, (c) the system consisting of the *N*-[*p*-(dimethylamino)benzylidene]-*p*-propoxyaniline – *N*-(*p*-nitrobenzylidene)-*p*-propoxyaniline (1:1) complex and azoxydianisole, and (d) the system consisting of the *N*-[*p*-(dimethylamino)benzylidene]-*p*-propoxyaniline–*N*-(*p*-nitrobenzylidene)-*p*-propoxyaniline (1:1) complex and *N*-(*p*-phenylbenzylidene)-*p*-ethoxycarbonylaniline. As to the open and shaded circles, see the caption of Fig. 1.

the pseudo-binary system consisting of the 1:1 complex and a mesomorphic compound. We employed for this purpose azoxydianisole (AA), which exhibits a nematic phase stable between 117.5 and 135 °C, and *N*-(*p*-phenylbenzylidene)-*p*-ethoxycarbonylaniline (phenyl, ethoxycarbonyl), which exhibits a smectic phase stable between 121.6 and 131.0 °C.[13] The diagrams displayed in Fig. 5 are of the eutectic type and clearly prove the latent induction of mesophases in all the three systems. The I-N transition temperature in the (dimethylamino, methoxy)–(nitro, methoxy) complex is estimated by the extrapolation of the transition curve to 0 mol% of AA to be 101 °C (see Fig. 5a). This temperature is higher by 33 °C than the straight line joining the latent transition temperatures of the two components of the complex. As the matter of fact, the molten complex solidifies at 112.5 °C, thus making the I-N transition not detectable. In the case of the (methoxy, dimethylamino)–(nitro, methoxy) complex shown in Fig. 5b, the I-N transition temperature obtained by the extrapolation is 102 °C, which is 32 °C above the mean value of those of the two components. It must be emphasized that the thermal stability enhancement in these two complexes is larger than that in the other two systems of the methoxy derivatives, in agreement with the order of tendency of a solid-complex formation.

The (dimethylamino, propoxy)–(nitro, propoxy) complex is expected to have latent I-N and I-S transition temperatures. The former temperature is located at about 107 °C by the diagram with AA and the latter at 119 °C by the diagram with (phenyl, ethoxycarbonyl), as are shown in Figs. 5c and 5d. The stability enhancement of the nematic phase is about 45 °C, the largest among all the examined combinations. The diagram shows that the induced mesophase is of the type smectic A. When the smectic A phase of (phenyl, ethoxycarbonyl) is supercooled, another smectic phase appears at 106 °C (see Fig. 5d). The eutectic point of this pseudo-binary system is considerably lower than this transition curve; therefore, the new smectic phase becomes enantiotropic in the range of 50 to 70 mol% of (phenyl, ethoxycarbonyl).

With the exception of (propoxy, nitro), the I-N transition of the component compounds could not be observed by supercooling of the melt. Consequently, the transition temperatures listed in Table 1 have been deduced by the extrapolation of the transition curves observed in the binary systems with mesomorphic AA. Such systems have been extensively studied by Dave and Lohar and the diagrams with the following five compounds can be reproduced from their data:[4,5] (dimethylamino, methoxy), (nitro, methoxy), (methoxy, dimethylamino), (dimethylamino, ethoxy), and (nitro, ethoxy). Especially for the last two, the transition temperatures have been estimated by Lohar to be 97.5 °C and 85 °C respectively.[8] We have worked on all the other systems. The diagrams are of the eutectic type. When the Schiff base is a dimethylamino derivative, the I-N transition curve deviates negatively from the ideal linear relationship. In other words, the curve is slightly concave upwards. On the other hand, the transition curve is markedly convex upwards with the nitro derivative, indicating the attractive interaction between the Schiff base and AA molecules. The I-N and solid-liquid transition temperatures read from the phase diagrams are summarized in Table 3

Table 3. Isotropic liquid-nematic liquid crystal transition temperatures in the binary systems with azoxydianisole

(Monotropic transitions are given in parentheses.)

Substituents		Mol% of azoxydianisole								
X	Y	10	20	30	40	50	60	70	80	90
CH_3O	NO_2	(93.0)	(100.5)	(107.0)	112.0	116.0	119.8	123.6	127.4	131.2
C_2H_5O	$(CH_3)_2N$			(105.5)	(108.0)	110.5	114.0	118.7	124.0	129.2
C_2H_5O	NO_2		(107.5)	112.8	117.0	121.5	124.7	127.3	129.5	132.3
$(CH_3)_2N$	C_3H_7O			(86.5)	(91.5)	97.5	104.5	112.3	120.2	128.0
NO_2	C_3H_7O	(76.5)	(93.5)	102.5	111.0	117.7	122.5	126.3	129.7	132.5
C_3H_7O	$(CH_3)_2N$			(85.0)	(90.2)	96.3	103.5	110.7	118.0	126.5

Table 4. Solid-liquid transition temperatures in the binary systems with azoxydianisole

Substituents		Mol% of azoxydianisole									Eutectic	
X	Y	10	20	30	40	50	60	70	80	90	Mol%	Temp/°C
CH_3O	NO_2	118.5	113.8	108.5	103.0	91.5	97.5	103.0	106.7	112.3	51.0	90.0
C_2H_5O	$(CH_3)_2N$	135.0	130.2	124.7	118.5	110.5	102.0	102.0	107.8	113.0	64.0	98.0
C_2H_5O	NO_2	112.0	109.5	106.0	99.5	88.5	95.3	101.5	107.0	112.0	51.0	87.0
$(CH_3)_2N$	C_3H_7O	118.7	115.0	110.5	104.0	95.5	101.5	106.5	111.0	114.5	50.0	95.5
NO_2	C_3H_7O	101.0	96.5	92.5	86.0	89.5	96.5	102.0	107.5	112.5	43.5	82.5
C_3H_7O	$(CH_3)_2N$	110.5	105.7	100.5	93.5	94.0	98.5	102.7	107.5	112.5	43.0	89.5

and 4 respectively. The latent I-N transition temperatures of the Schiff bases presented in Table 1 were obtained by the extrapolation of the transition curves to 0 mol% of AA. They are in good agreement with those located from the phase diagrams of the binary mixtures of the Schiff bases given in Figs. 1, 2, and 3.

References

1) Part I: K. Araya and Y. Matsunaga, *Bull. Chem. Soc. Jpn.*, **53**, 989 (1980).

2) J. W. Park, C. S. Bak, and M. M. Labes, *J. Am. Chem. Soc.*, **97**, 4398 (1975).

3) J. H. MacMillan and M. M. Labes, *Mol. Cryst. Liq. Cryst.*, **56**, 7 (1979).

4) J. S. Dave and J. M. Lohar, *J. Chem. Soc., A*, **1967**, 1473.

5) J. S. Dave and M. J. S. Dewar, *J. Chem. Soc.*, **1955**, 4305.

6) J. P. Schroeder and D. C. Schroeder, *J. Org. Chem.*, **33**, 591 (1968).

7) J. Malthete, J. Billard, J. Canceill, J. Gabard, and J. Jacques, *J. Phys. (Paris), Colloq.*, **37**, C3-1 (1976).

8) J. M. Lohar, *J. Phys. (Paris), Colloq.*, **36**, C1-393 (1975).

9) C. Shinomiya, *Bull. Chem. Soc. Jpn.*, **15**, 92 (1940).

10) F. Hardouin, G. Sigaud, M. F. Achard, and H. Gasparoux, *Ann. Phys. (Paris)*, **3**, 381 (1978).

11) B. Engelen, G. Heppke, R. Hopf, and F. Schneider, *Ann. Phys. (Paris)*, **3**, 403 (1978).

12) M. Domon and J. Billard, *J. Phys. (Paris), Colloq.*, **40**, C3-413 (1979).

13) D. Demus and H. Sackmann, *Z. Phys. Chem. (Leipzig)*, **222**, 127 (1963).

 © 1980 The Chemical Society of Japan Bull. Chem. Soc. Jpn., 53, 3085—3088 (1980)

Charge Transfer and Proton Transfer in the Formation of Molecular Complexes. XII.[1] *o*-Aminobenzoic Acid–Picric Acid and Related Complexes

Yoshio MATSUNAGA* and Reiko USUI

Department of Chemistry, Faculty of Science, Hokkaido University, Sapporo 060

(Received April 9, 1980)

The combination of *o*-aminobenzoic acid and picric acid was found to yield four kinds of adducts. These were a stable yellow (1:1) salt, formed by the proton transfer from the picric acid to the *o*-aminobenzoic acid molecule, two red (1:1) molecular complexes of markedly different stability, and a red (2:1) complex consisting of the *o*-aminobenzoic acid molecule, its protonated ion, and the picrate ion. The enthalpy change and the activation energy for the isomerization from the salt to the charge-transfer complex by a solid-solid transformation were shown to decrease during storage. The 1,3,5-trinitrobenzene complexes with *o*-(methylamino)benzoic acid, *o*-, *m*-, and *p*-(dimethylamino)benzoic acids, and their sodium and potassium salts were prepared. Their electronic spectra were measured, along with those of the complexes with *o*- and *p*-aminobenzoic acids and their salts presented in the work of Sudborough and Beard. The displacement of the charge-transfer absorption maxima to the lower wavenumber side by the salt formation is 2×10^3 cm^{-1} on the average and seems to be consistent with our proposition that the picrate ion acts as an electron acceptor in aromatic amine-picric acid (2:1) complexes.

One of the most striking properties of *o*-aminobenzoic acid is the formation of both a yellow salt and a red molecular complex with picric acid;[2] and another is the formation of the 1,3,5-trinitrobenzene complexes of the potassium salt as well as of the acid itself.[3] They have received no further attention, however. When picric acid is combined with an aromatic amine, the acid-base interaction generally predominates in the solid state. With this acid, only three other anilines and three naphthylamines are known to exhibit the phenomenon of complex isomerism: that is, the formation of both a salt and a charge-transfer complex.[4,5] In some cases, the two forms are enantiotropically related to each other, while in the others, the molecular complex is metastable with respect to the salt at every temperature. One of the aims of the present work was to clarify the relation between the two forms of the *o*-aminobenzoic acid–picric acid reported by Issa and El-Essawey.[2]

1-Naphthylamine was shown by Kofler to form the yellow 1:1 and red 2:1 adducts with picric acid.[6] The former is a simple salt, while the latter consists of naphthylamine molecule, naphthylammonium cation, and picrate anion.[7] The red color presumably arises from the charge-transfer interaction between the amine molecule and the picrate ion. We assumed that the electron acceptor in this 2:1 adduct is the picrate ion. Our proposition that the acceptor strength of picric acid is not much affected by the salt formation seems to be consistent with numerous examples subsequently accumulated by us; however, this is in serious conflict with Tanaka's recent theoretical view.[8] On the basis of his molecular orbital calculations, he suggested that the picrate anion is a donor and the indole moiety an acceptor in the tryptophan picrate. If so, the change in the electronic structure of picric acid by salt formation must be substantial, because indole is known to act as a donor in the complex formation with picric acid.[9] The second aim of the present work was to find out experimentally how large the change in the donor strength of aminobenzoic acid by salt formation is. The spectral measurements of the trinitrobenzene complexes of *o*- and *p*-aminobenzoic acids and their potassium salts originally prepared by Sudborough and Beard will provide the means of giving a certain answer to this question. Both the acids and the salts undoubtedly function as electron donors in forming the complexes. If the energy differences in the charge-transfer absorption maxima observed with them are significantly smaller than the magnitude predicted by Tanaka for picric acid, our proposition becomes more likely than his.

Experimental

Materials. The *o*- and *p*-aminobenzoic acids, *m*- and *p*-(dimethylamino)benzoic acids, and picric acid were obtained from commercial sources. The methylation of *o*-aminobenzoic acid with a calculated amount of dimethyl sulfate yields the *N*-methyl derivative, while that with an excess of methyl iodide yields the *N,N*-dimethyl derivative.[10] The latter was isolated as the polyiodide. After removing iodine by steam distillation, the acid was freed from hydrogen iodide by the treatment with silver oxide. The *o*-(dimethylamino)benzoic acid thus separated was purified by the precipitation from a methanol solution by the addition of diethyl ether. The synthesis of 1,3,5-trinitrobenzene was carried out starting from 2,4,6-trinitrotoluene, Eastman yellow label, through 2,4,6-trinitrobenzoic acid.[11] The alkali-metal salts of the aminobenzoic acids were obtained by dissolving equimolar amounts of the acid and the hydroxide in water and then evaporating to dryness. The use of an excess of the latter reagent must be carefully avoided; otherwise, a small amount of Meisenheimer complex is formed in the step of the trinitrobenzene-complex preparation and interferes with the measurements of the electronic spectra. The complexes were isolated by concentration or by evaporation of a solution containing equimolar amounts of the components in an appropriate solvent.

Measurements. The spectroscopic, calorimetric, and X-ray measurements were made using the procedures reported in a previous paper of this series.[12] As the red form of *o*-aminobenzoic acid–picric acid is too unstable to be ground, the thin layers of the complex were prepared by evaporating the warm solution on sodium chloride or quartz plates for the spectroscopic measurements.

Results and Discussion

When a hot methanol solution of equimolar amounts of *o*-aminobenzoic acid and picric acid is concentrated, red crystals appear. They are not stable at room temperature and are gradually transformed into yellow crystals. Found: C, 43.13; H, 2.78; N, 15.00%. Calcd for $C_7H_7NO_2$–$C_6H_3N_3O_7$: C, 42.63; H, 2.75; N, 15.30%. In agreement with the observation made by Issa and El-Essawey, the former form exhibits an asymmetric N–H stretching band and a symmetric one at 3485 and 3375 cm^{-1} respectively, while the latter shows broad bands covering the region from 2925 to 2625 cm^{-1}, to be assigned to the NH_3^+ group. The red form deposited on a quartz plate shows an electronic absorption band which is not present in either of the components. The maximum is hidden under a strong higher-energy band, but is possibly at about 22×10^3 cm^{-1}. This wavenumber is not far from that of the charge-transfer absorption band in the orange-yellow *o*-aminobenzoic acid–trinitrobenzene complex, about 24×10^3 cm^{-1}. As the acceptor strength of picric acid is known to be comparable with that of 1,3,5-trinitrobenzene, the band may be ascribed to the charge-transfer transition from the *o*-aminobenzoic acid molecule to the picric acid molecule.

Upon heating the yellow crystals at a scanning rate of 2.5 °C min^{-1}, an endothermic peak extending from 156 to 171 °C is observed on the calorimetric curve. Above this temperature range, the red form produced by the phase transition starts to decompose exothermally. The enthalpy change of the transition from the yellow salt to the red molecular complex decreases during storage. The fresh samples give a value of 10.2 kJ mol^{-1}. On the other hand, the value obtained after one-month storage at room temperature is 6.6 kJ mol^{-1}. These enthalpy changes are rather small compared to those so far examined. The values recorded earlier range from 9.2 kJ mol^{-1} of *o*-chloroaniline-2,4,6-trinitrobenzoic acid to 34 kJ mol^{-1} of 1-bromo-2-naphthylamine-picric acid.[1,12] It is apparent that these isomeric forms are enantiotropically related to each other. Previously we showed that the picrates of all the anilines with pK_a values of less than 3 isomerize into charge-transfer complexes upon melting, if they do not isomerize by an enantiotropic solid-solid transition.[13] The pK_a value reported by Schwarzenbach *et al.* for *o*-aminobenzoic acid is 2.09,[14] and nicely fits into the range where complex isomerization is expected to occur.

The endothermic peak due to the transformation covers a temperature range as wide as 15 °C and is asymmetric, in contrast to those of Hertel's picric acid complexes described earlier.[1] The slope changes very gently on the lower-temperature side and sharply on the other side. Up to near the maximum, the curve is characteristic of a transition whose extent increases linearly with time under isothermal conditions. In other words, the rate constant, k, is given by

$$k=B(dH/dt),$$

where B is a constant and where (dH/dt) is the rate of change of enthalpy with time and is proportional to the departure of the peak from the baseline at the associated temperature.[15] The activation energy of such a transition can be estimated by a plot of log (dH/dt) *versus* $1/T$. The energy given by the fresh samples is relatively large and is scattered in a wide range. At the heating rate of 2.5 °C min^{-1}, six independently-prepared samples gave 449, 600, 640, 719, 879, and 931 kJ mol^{-1} (see Plots a and b in Fig. 1). This energy decreases during storage at room temperature and becomes more reproducible. After one month, the six runs performed at the scanning rates of 2.5, 5, 10, and 20 °C min^{-1} yielded the mean value of 306 ± 15 kJ mol^{-1} (see Plots c and d in Fig. 1). The over-all activation energy of a solid-solid transformation depends mostly upon the kinetics of the nucleation, which takes place heterogeneously and preferentially at grain boundaries.[16] When the red charge-transfer complex is transformed into the yellow salt below the transition temperature, the initially-formed crystals are supposed to be highly strained because of the change of molecular arrangement. Upon storage, such a stress may be largely reduced by the spontaneous growth of the grain boundaries. The relatively large and markedly scattered activation energies observed with the fresh samples suggest that the growth of the grain boundaries proceeds rather slowly and irregularly. This postulate seems to be in accordance with the observations made earlier with some Hertel's picric acid complexes that the endothermic peak due to the transformation from the salt to the charge-transfer complex is appreciably broadened and weakened by the grinding of the crystals.[1]

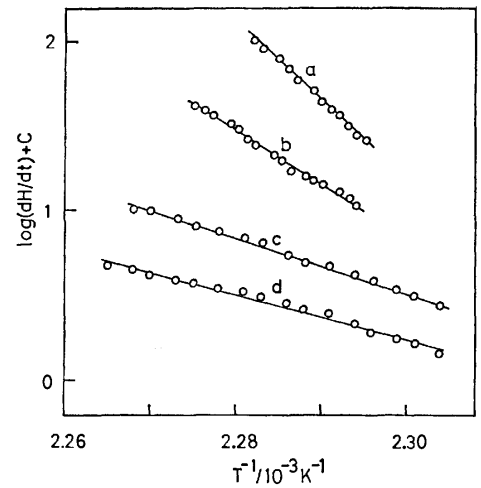

Fig. 1. Arrhenius plots constructed from the endothermic peak due to the isomerization from the yellow salt to the red molecular complex of the *o*-aminobenzoic acid–picric acid (1:1). a) and b), fresh samples at a heating rate of 2.5 °C min^{-1}. The estimated activation energies are 931 and 600 kJ mol^{-1} respectively. c) and d), samples stored for one month at room temperature. The heating rates are 10 and 5 °C min^{-1}, and the activation energies are 275 and 271 kJ mol^{-1} respectively.

The vermillion crystals deposited from a chloroform solution are also of the 1:1 mole ratio. Found: C,

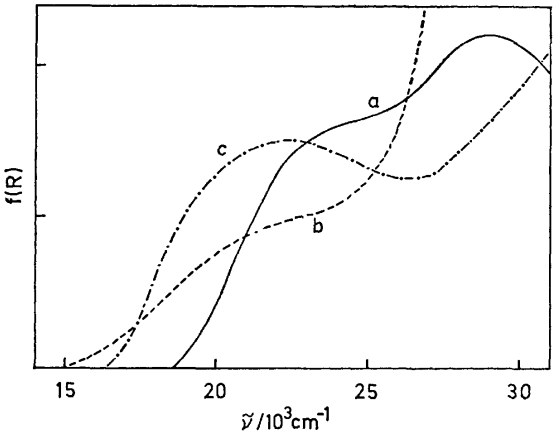

Fig. 2. Kubelka-Munk plots of diffuse reflectance of the 1,3,5-trinitrobenzene complexes with a) *o*-aminobenzoic acid, b) the sodium salt, and c) the potassium salt.

42.62, 42.49; H, 2.71, 2.70; N, 15.25, 15.32%. Contrary to the red-colored form from a methanol solution, the crystals could be kept at room temperature over several months without the transformation to the yellow salt. However, they are easily transformed into yellow powder by crushing. A comparison of the X-ray diffraction patterns revealed that the molecular complex is polymorphic. The N–H stretching bands are found at 3500 and 3380 cm^{-1}. The maximum of the charge-transfer absorption band in the second form of the molecular complex is not separable from a strong higher-energy band, but is possibly located around 21×10^3 cm^{-1}.

Stable scarlet crystals can also be obtained from a methanol solution if *o*-aminobenzoic acid is dissolved in excess. The compound is of the 2:1 mole ratio. Found: C, 47.61; H, 3.41; N, 13.99%. Calcd for $(C_7H_7NO_2)_2$–$C_6H_3N_3O_7$: C, 47.72; H, 3.40; N, 13.91%. The vibrational bands due to the NH_2 group, 3475 and 3375 cm^{-1}, and also the pattern characteristic of the NH_3^+ group in the range from 2875 to 2625 cm^{-1} are found in the infrared spectrum. Without doubt, the proton-transfer and charge-transfer interactions operate simultaneously in this solid. The electronic absorption band appearing as a shoulder at about 20×10^3 cm^{-1} is assigned to the charge-transfer transition between the *o*-aminobenzoic acid molecule and the picrate ion. Following our earlier view,[7] we tentatively suppose that the latter species acts as an electron acceptor in this complex. This point will be discussed in detail later.

Sudborough and Beard noted that the trinitrobenzene complex of *o*-aminobenzoic acid is orange yellow and that of its potassium salt is deep red.[3] Their electronic spectra are presented in Fig. 2, which includes the spectrum of the complex formed with the sodium salt. The charge-transfer absorption maximum of the potassium-salt complex is seen at 22.3×10^3 cm^{-1}. In the other two, the absorption maximum is not explicit because of overlapping with a stronger absorption band; nevertheless, it is very likely that the sodium-salt complex gives a maximum at the same wavenumber as that of the potassium-salt complex. The maximum in the *o*-aminobenzoic acid complex is probably at about 24×10^3 cm^{-1}. Thus, the difference which should reflect the relative ionization potentials of the acid and its salts is only about 2×10^3 cm^{-1} or 0.2 eV. Some additional spectral measurements were made in which the *N*-methyl and *N,N*-dimethyl derivatives were employed as donors. Here again, no large shift due to salt formation can be found. The observed wavenumbers are listed in Table 1.

Table 1. The wavenumbers of the charge-transfer absorption maxima in the solid trinitrobenzene complexes

Donor	Wavenumber /10^3 cm^{-1}	Color
o-Aminobenzoic acid	24	yellowish orange
Sodium *o*-aminobenzoate	22	dull red brown
Potassium *o*-aminobenzoate	22.3	scarlet
o-(Methylamino)benzoic acid	23	orange
Sodium *o*-(methylamino)-benzoate	21.2	brown carmine
Potassium *o*-(methylamino)-benzoate	21.2	brown carmine
o-(Dimethylamino)benzoic acid	23.5	orange brown
Potassium *o*-(dimethylamino)-benzoate	23	violet black
m-(Dimethylamino)benzoic acid	21.5	violet black
Sodium *m*-(dimethylamino)-benzoate	19.5	blackish violet
Potassium *m*-(dimethylamino)-benzoate	20.5	violet black
p-Aminobenzoic acid	25	orange
Sodium *p*-aminobenzoate	22.0	violet brown
Potassium *p*-aminobenzoate	24	brown orange
p-(Dimethylamino)benzoic acid	21.5	deep carmine
Sodium *p*-(dimethylamino)-benzoate	21.3	dark violet red
Potassium *p*-(dimethylamino)-benzoate	21.0	violet black

Although *m*-aminobenzoic acid does not form a molecular complex with trinitrobenzene, the potassium salt is known to give a dark reddish brown complex.[3] With the *N,N*-dimethyl derivative, however, both the acid and the salts yield the complexes. Sudborough and Beard have isolated the trinitrobenzene complexes of *p*-aminobenzoic acid and its potassium salt. The former is red and the latter dark red. The *N,N*-dimethyl derivative and its salts form more deeply colored complexes. Their spectral data are also given in Table 1. In all cases, the charge-transfer absorption maxima of the salt complexes are consistently displaced to the lower wavenumber side, but only by 2×10^3 cm^{-1} on the average, compared to those of the corresponding acid complexes. The results may be understood from the fact that the ionization potentials of the salts are lower than those of the acids by the same magnitude.

Tanaka has presented the location of the highest occupied molecular orbital (HOMO) of picrate anion and that of the lowest unoccupied molecular orbital (LUMO) of the indole moiety of tryptophan as the

criteria of electron donor and acceptor strength.[8] His conjecture of the donor character of the picrate anion comes from the calculations that its HOMO is located 3.78 eV above the HOMO of the indole moiety and its LUMO is 2.30 eV above the LUMO of the latter. However, the charge-transfer absorption in the tryptophan picrate appears in the same region as that of the indole–picric acid.[9] Furthermore, indole is well-known to behave as an electron donor in forming molecular complexes with a number of compounds including picric acid.[9,17] If it is assumed that picric acid is an acceptor but its anion is a donor with respect to essentially the same species, then the relative locations between the HOMO of indole and the LUMO of picric acid must resemble those between the HOMO of picrate ion and the LUMO of indole moiety calculated by Tanaka. As a consequence, the LUMO of picrate ion should be located at an energy higher by about 6 eV than the LUMO of the acid. If so, the HOMO of picrate ion should be also higher to a similar extent than the HOMO of picric acid. Analogously, one may expect a considerable difference, presumably of the order of 1 eV, in the location of the HOMO between an aminobenzoic acid and its anion. The experimental results summarized in Table 1 are definitely not in accord with the assumption made above. Thus, an alternative explanation that the picrate anion is not an electron donor but an electron acceptor in the tryptophan picrate and also in the *o*-aminobenzoic acid–picric acid (2:1) complex appears to be more likely. In this regard, it should be noted that the picrate anion in the solid complex is under the strong influence of the counter ion.[18] The charge on the anion in such solids may be largely localized by the polarizing power of the cation. The resultant situation would be more or less similar to the electronic structure of a picric acid molecule. Therefore, we feel that Tanaka's theoretical work on either an isolated picrate anion or a composite molecule does not reflect the situation in the solid salt complexes.

The authors wish to express their thanks to Dr. Jun-ichi Aihara for his helpful discussion.

References

1) Part XI: Y. Matsunaga, E. Osawa, and R. Osawa, *Bull. Chem. Soc. Jpn.*, **48**, 37 (1975).
2) R. M. Issa and M. M. El-Essawey, *Z. Phys. Chem. (Leipzig)*, **253**, 96 (1973).
3) J. J. Sudborough and S. H. Beard, *J. Chem. Soc.*, **97**, 773 (1910).
4) E. Hertel, *Ann.*, **451**, 179 (1926).
5) Y. Matsunaga, G. Saito, and N. Sakai, *Bull. Chem. Soc. Jpn.*, **47**, 2873 (1974).
6) A. Kofler, *Z. Elektrochem.*, **50**, 200 (1944).
7) Y. Matsunaga and G. Saito, *Bull. Chem. Soc. Jpn.*, **45**, 963 (1972).
8) M. Tanaka, *Bull. Chem. Soc. Jpn.*, **50**, 3194 (1977).
9) Y. Matsunaga, *Bull. Chem. Soc. Jpn.*, **46**, 998 (1973).
10) R. Willstätter and W. Kahn, *Ber.*, **37**, 401 (1904).
11) H. T. Clarke and W. W. Hartman, *Org. Synth.*, Coll. Vol., 1, 541 (1941).
12) Y. Matsunaga and R. Osawa, *Bull. Chem. Soc. Jpn.*, **47**, 1589 (1974).
13) G. Saito and Y. Matsunaga, *Bull. Chem. Soc. Jpn.*, **44**, 3328 (1971).
14) G. Schwarzenbach, A. Willi, and R. O. Bach, *Helv. Chim. Acta*, **30**, 1303 (1947).
15) J. M. Thomas and T. A. Clarke, *J. Chem. Soc., A*, **1968**, 457.
16) C. N. R. Rao and K. J. Rao, *Prog. Solid State Chem.*, **4**, 131 (1967).
17) M. A. Slifkin, "Charge Transfer Interactions of Biomolecules," Academic Press, London and New York (1971), pp. 97—102.
18) G. Saito and Y. Matsunaga, *Bull. Chem. Soc. Jpn.*, **45**, 2214 (1972).

A Study of the Ligand Exchange of Bromo(*o*-tolyl)bis(triphenylphosphine)nickel(II) with Amine by Means of ^{31}P- and ^{13}C-NMR Spectroscopy

Yoshiyuki NAKAMURA,* Ken-ichi MARUYA, and Tsutomu MIZOROKI

Research Laboratory of Resources Utilization, Tokyo Institute of Technology, Nagatsuta-cho, Midori-ku, Yokohama 227

(Received March 21, 1980)

The amine substitution of bromo(*o*-tolyl)bis(triphenylphosphine)nickel(II) was investigated by the use of ^{31}P- and ^{13}C-NMR. The triphenylphosphine ligands are readily replaced by sterically less crowded amines, such as primary amines, secondary amines, pyridine, and *γ*-picoline, at room temperature in chlorobenzene, while no replacement at all takes place with tertiary amines. The equilibrium constants with *γ*-picoline, pyridine, or dibutylamine, as defined by Eq. 2, show that the entropy change contributes predominantly to the constant. The substitution with pyrrolidine, as monitored by means of ^{13}C-NMR, indicates that the amine coordinates to the nickel(II) atom.

It is well known that organo transition-metal complexes are stabilized by the coordination of the tertiary phosphine ligand to the metal atoms. For example, halogeno(aryl)bis(triphenylphosphine)nickel(II), first prepared by Chatt[1] twenty years ago, is quite stable in organic solvents. This compound acts as a precursor to an active catalyst for the selective dimerization and codimerization of olefin[2-4] and gives a cationic nickel(II) complex with an amine ligand on treatment with $AgClO_4$.[5] Little attention has, however, been paid to organo transition-metal complexes with amine ligands, presumably because they are too unstable to be easily isolated and characterized. Little information is, accordingly, available with respect to the coordination states of amines, although amine is expected to behave much like phosphine.

Triphenylphosphine ligands on bromo(*o*-tolyl)bis(triphenylphosphine)nickel(II) are readily replaced by other tertiary phosphines, with the driving force for the replacement being steric in nature.[6] The same procedure may be extended to the substitution of amine for phosphine. Thus, the substitution reactions of various amines, as represented by:

$$[NiBr(o\text{-tolyl})(PPh_3)_2] \underset{PPh_3}{\overset{amine}{\rightleftharpoons}} [NiBr(o\text{-tolyl})(amine)(PPh_3)] \underset{PPh_3}{\overset{amine}{\rightleftharpoons}} [NiBr(o\text{-tolyl})(amine)_2] \quad (1)$$

have been investigated in order to elucidate the nature of the amine coordination.

Experimental

Materials. Bromo(*o*-toly)bis(triphenylphosphine)nickel(II) was prepared by the oxidative addition of *o*-bromotoluene to tetrakis(triphenylphosphine)nickel(0) according to the literature.[7]

All the experiments were conducted under a nitrogen atmosphere. Chlorobenzene which has been dried by P_2O_5 before distillation was used as the solvent. No reaction of chlorobenzene with amines was observed under the present experimental conditions. The pyridine, *γ*-picoline, pyrrolidine, piperidine, butylamine, and dibutylamine were dried by CaH_2 before distillation. The other amines, such as quinoline, 4-methoxyaniline, 3,4-dimethylaniline, 4-methylaniline, aniline, 4-chloroaniline, *N*-methylpyrrolidine, *N*-methylpiperidine, tributylamine, t-butylamine, propylamine, dipropylamine, and *N,N,N',N'*,-tetramethylethylenediamine, obtained from commerical sources, were used without further purification.

Procedures. All the samples were prepared under a nitrogen atmosphere. To bromo(*o*-tolyl)bis(triphenylphosphine)nickel(II) (50 mg) placed in a two-necked flask (20 ml) are added chlorobenzene (5.00 ml) containing a known amount of an amine, the solution was then stirred at room temperature for about 1 h before ampouling the solution with C_6D_6 (D-lock) and TMS into a NMR tube (10 mm. O.D.).

The ^{31}P- and ^{13}C-NMR spectra were obtained on a Japan Electron Optics Laboratory FX-100 spectrometer operating the pulsed Fourier transform mode at 40.26 and 25.00 MHz, the repetitions being 6 s (^{31}P-; 400—1000 pulses) and 2 s (^{13}C-; 10000—35000 pulses). The ^{31}P-NMR spectra were taken without proton-decoupling, if necessary. The ^{31}P- and ^{13}C-NMR chemical shifts were reported in ppm, downfield from internal triphenylphosphine (−5.86 ppm from H_3PO_4) and TMS respectively.

Results and Discussion

General Features of the Substitution. Figure 1 shows the ^{31}P-{^{1}H}NMR spectra of the chlorobenzene solutions of *trans*-[NiBr(*o*-tolyl)$(PPh_3)_2$] (to be denoted by the M-complex here after) and pyridine (pK_b= 8.8) at −20 °C. The increase in the molar ratio of pyridine to the nickel complex results in a decrease in the intensity of resonance, S_0, at 29.4 ppm due to the M-complex, accompanied by an increase in that of the resonance, L_p, at 0 ppm due to free triphenylphosphine. The resonance, S_1, at 36.9 ppm can be attributed to the monosubstituted M-complex with pyridine, [NiBr(*o*-tolyl)(pyridine)(PPh_3)].

The degree of amine coordination to nickel is represented by the relative intensities, h_p and h_1, of L_p and S_1 the resonances:

$$h_p = \frac{h(L)_p}{h(L_p)+h(S_0)+h(S_1)}, \quad h_1 = \frac{h(S_1)}{h(L_p)+h(S_0)+h(S_1)},$$

where $h(L_p)$, $h(S_0)$, and $h(S_1)$ are the peak heights of the resonances for free triphenylphosphine, the M-complex, and the monosubstituted M-complex respectively.

With respect to the amines with a pyridine ring, the following coordination sequence may be deduced from

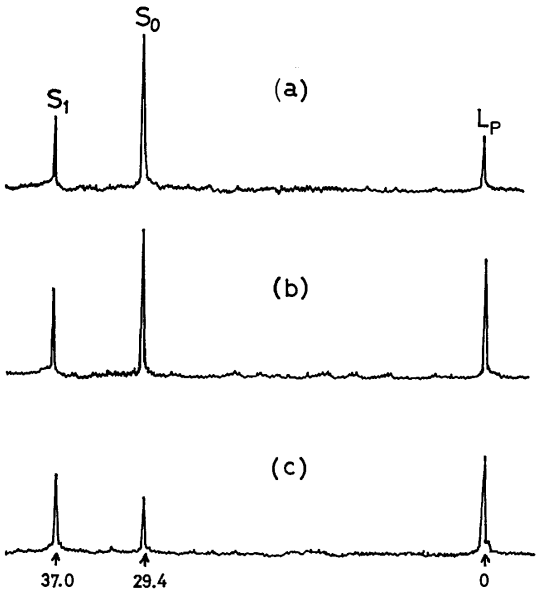

Fig. 1. ^{31}P-{^1H} NMR spectra in the substitution of M-complex with pyridine at −20 °C at the molar ratio of $[pyridine]_0/[M]_0=5$(a), 10(b), or 20(c).

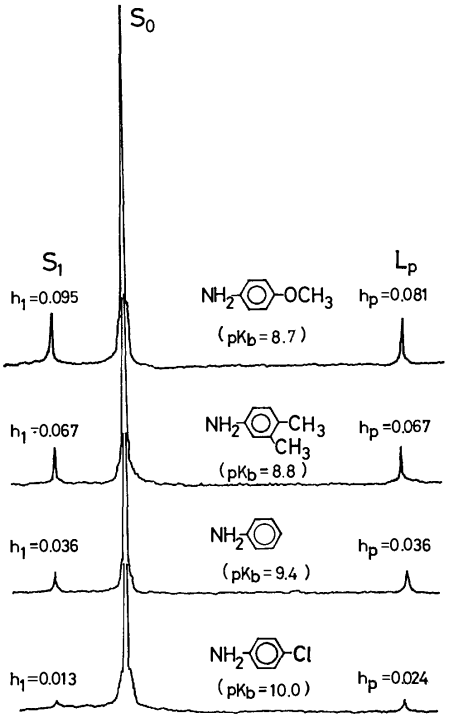

Fig. 2. ^{31}P-{^1H} NMR spectra in the substitution of M-complex with substituted aniline at the molar ratio of $[aniline]_0/[M]_0=20$ at −20 °C.

the relative intensities at −20 °C;

$$\gamma\text{-picoline} > \text{pyridine} \gg \text{quinoline}$$
$$(pK_b=7.9) \quad (pK_b=8.8) \quad (pK_b=9.2)$$

where the molar ratio of the amine to the M-complex is 10. This sequence appears to imply that the more basic the amine, the stronger the coordination. In order to confirm this tendency, *p*-substituted anilines with equal steric crowding were chosen as the substitutes.

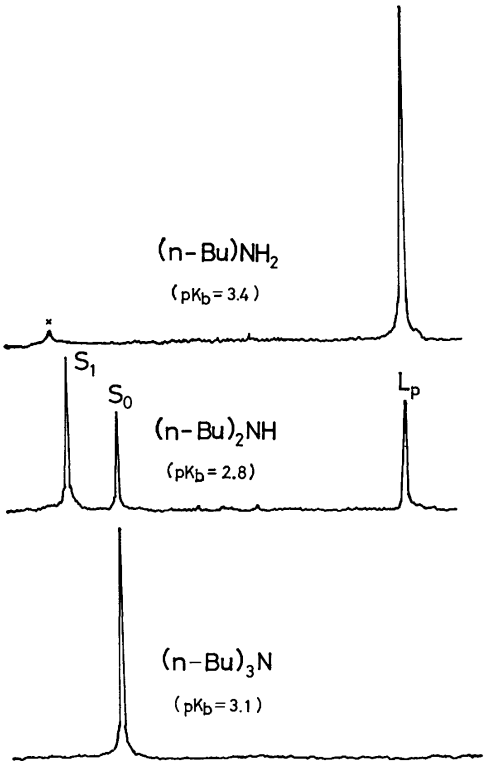

Fig. 3. ^{31}P-{^1H} NMR spectra in the substitution with $NH_{3-n}(n\text{-Butyl})_n$($n$=1, 2, and 3) at molar ratio of $[amine]_0/[M]_0=6$ at −20 °C.

The ^{31}P-{^1H} NMR spectra of the M-complex p-substituted aniline system are shown in Fig. 2. The stronger electron donor results in the higher relative intensities, h_p and h_1, of the free triphenylphosphine and the monosubstituted M-complex.

On the other hand, most of the triphenylphosphine on M-complex is replaced by butylamine ($pK_b=3.4$) at the molar ratio of [butylamine]/[M]=6, while no replacement by tributylamine ($pK_b=3.1$) takes place at all, as is shown in Fig. 3. Essentially the same sequence was observed with mono-, di-, and tri-propylamines. Other sterically crowded amines, such as *N*,*N*-dimethylaniline, *N*-methylpyrrolidine, and *N*-methylpiperidine, gave neither the resonance due to free triphenylphosphine nor that due to the mono-substituted M-complex. From comparisons of the ^{31}P-NMR spectra (Fig. 1) with pyridine ($pK_b=8.8$) and (Fig. 3) with butylamine ($pK_b=3.4$), it seems that the triphenylphosphine on the M-complex is replaced more readily by a strong amine base. Figure 3 clearly shows that the steric factor is predominant in the substitution with amine, as well as with other tertiary phosphine ligands.[6]

When *N*,*N*,*N*′,*N*′,-tetramethylethylenediamine was used, both L_p and S_0 resonances were observed, while no S_1 resonance corresponding to the monosubstituted M-complex was detected, suggesting some chelation of the diamine, although no further study was done.

The ^{31}P- chemical shifts (S_1) of the monosubstituted M-complex with various amines, [NiBr(*o*-tolyl)(amine)(PPh_3)], were almost the same (independent of the strength of the amine base): 34.7 ppm ($NH(n\text{-Pr})_2$),

TAELB 1. EQUILIBRIUM CONSTANTS WITH AMINE; $K_1=\frac{[S_1][L_p]}{[S_0][L_N]}$

Amine	$[N]_0/[M]_0$	K_1 24 °C	10 °C	0 °C	−10 °C	−20 °C
NH(*n*-Bu)$_2$	1.53	0.71	—	0.48	—	0.48
	3.07	0.80	0.60	0.55	0.59	0.55
	mean	0.75	0.60	0.51	0.59	0.51
Pyridine	5.0	0.21	0.23	0.24	0.27	—
	10.0	0.24	0.22	0.19	—	—
	mean	0.23	0.23	0.22	0.27	—
γ-Picoline	3.0	0.85	0.78	0.69	0.51	—
	6.0	0·79	0.72	0.61	0.61	—
	mean	0.82	0.75	0.65	0.57	—

34.4 ppm (NH(*n*-Bu)$_2$), 36.5 ppm (pyrrolidine), 36.7 ppm (piperidine), 37.2 ppm (γ-picoline), and 36.9 ppm (pyridine).

Evaluation of Equilibrium Constant. Since substituted M-complexes with amines were too unstable to be isolated, we attempted to evaluate the equilibrium constants of Eq. 2 using pyridine, γ-picoline, or dibutylamine in order to confirm Eq. 2.

The concentrations of free triphenylphosphine, the M-complex, and the monosubstituted M-complex at equilibrium can be calculated from the relative peak areas of ^{31}P-NMR (without ^{1}H-decoupling) and from the initial concentrations of the M-complex and the amine, because they are proportional to the concentrations (mol/l), $[L_p]$, $[S_0]$, and $[S_1]$. The relative peak areas are as follows:

$$\underset{[S_0]}{[NiBr(o\text{-tolyl})(PPh_3)_2]} + \underset{[L_N]}{Amine} \underset{\text{in } C_6H_5Cl}{\overset{K_1}{\rightleftarrows}} \underset{(cis \text{ and } trans)}{\underset{[S_1]}{[NiBr(o\text{-tolyl})(amine)(PPh_3)]}} + \underset{[L_p]}{PPh_3} \quad (2)$$

$HL_p=H(L_p)/(H(S_0)+H(S_1)+H(L_p))$, $HS_0=H(S_0)/(H(S_0)+H(S_1)+H(L_p))$, and $HS_1=H(S_1)/(H(S_0)+H(S_1)+H(L_p))$, where $H(L_p)$, $H(S_0)$, and $H(S_1)$ are the peak areas of the resonances of L_p, S_0, and S_1 recorded on ^{31}P-NMR charts. Each concentration is a function of HL_p, HS_1, or HS_0, as represented by Eqs. 3—7.

$$[L_p] = 2[M]_0 \times HL_p \quad (3)$$

$$[S_0] = [M]_0 \times HS_0 \quad (4)$$

$$[S_1] = 2[M]_0 \times HS_1 \quad (5)$$

$$[S_2] = [M]_0 - [S_0] - [S_1] \quad (6)$$

$$[L_N] = [N]_0 - 2[S_2] - [S_1] \quad (7)$$

$[M]_0$ is the total concentration of nickel(II) complex and is given by the amount of M-complex initially charged, and $[N]_0$ is the concentration of amine initially charged. $[S_2]$ and $[L_N]$ are the concentrations of the disubstituted M-complex and the free amine at equilibrium respectively.

The equilibrium constants $K_1=\left(\frac{[S_1][L_p]}{[S_0][L_N]}\right)$ thus obtained at different values of $[N]_0/[M]_0$ are summarized in Table 1. Despite the two-fold change in $[N]_0/[M]_0$ the values of K_1 are almost constant at any temperature, as was expected.

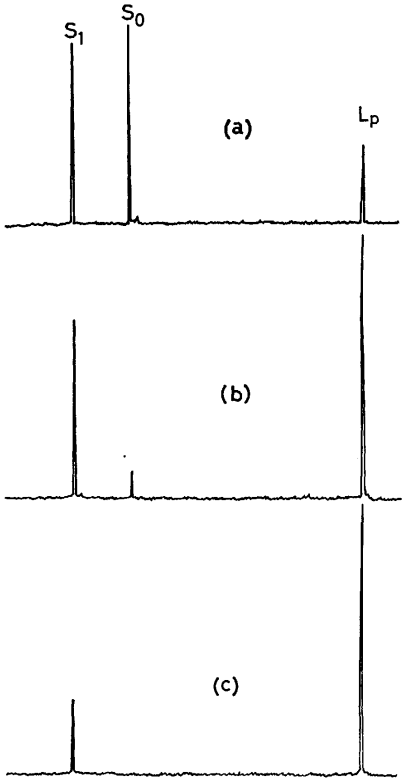

Fig. 4. ^{31}P-{^{1}H} NMR spectra in the substitution of M-complex with pyrrolidine at the molar ratio of 1(a), 2(b), or 4(c) at −24 °C.

It is notable that the effect of the temperature on K_1 is very small, indicating that the entropy change is the predominant factor in the equilibrium constant. This feature is in accord with the fact that bulky amines do not result in the substitution. On the other hand, the equilibrium constants for sterically less crowded amines, such as propylamine, butylamine, pyrrolidine, and piperidine, appear to be too large, rendering the evaluation difficult because of the difficulty in evaluating the value of $[L_N]$, even in a system with added PPh_3. They are, however, presumably one order of magnitude larger than that for γ-picoline. It may be imagined that more than two molecules of a sterically less crowded amine coordinate to the nickel(II) atom, whereas no new resonance in ^{31}P-{^{1}H} NMR was observed in addition to the S_0, S_1, and L_p resonances,

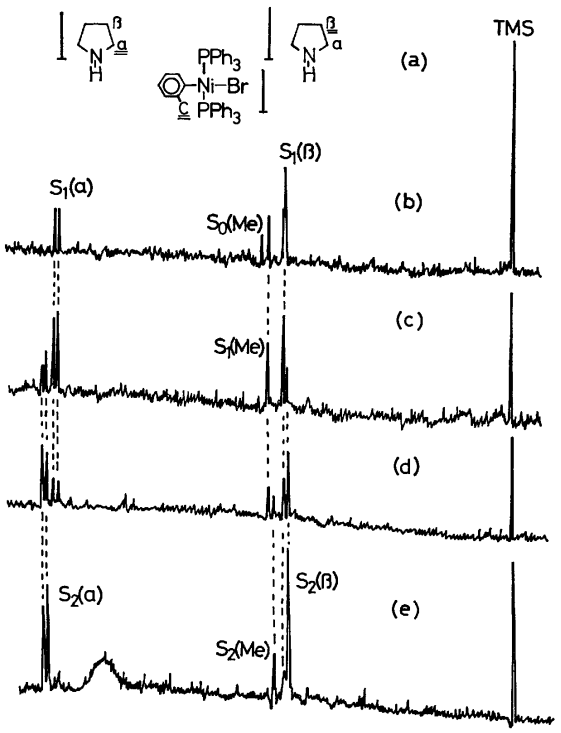

Fig. 5. ^{13}C-{^1H} NMR spectra in the substitution of M-complex with pyrrolidine at the molar ratio of 1(b), 2(c), 4(d), and 8(e), and free pyrrolidine(a) at −20 °C.

as is shown in Figs. 1—4, giving no indication of such coordination.

Evidence of Amine Coordination Obtained by Means of ^{13}C-{^1H} NMR. More direct evidence for the coordination of amine to the nickel(II) atom will be provided by ^{13}C-{^1H} NMR. Pyrrolidine was selected as the candidate amine, because it has only two kinds of carbon atoms exhibiting a strong coordination ability to the nickel(II) atom, thus making the ^{13}C-{^1H} NMR analysis simpler. The results are shown in Fig. 5. The methyl carbon (26.27 ppm, S_0(Me)) of the M-complex and the α-carbon (47.12 ppm, $L_N(\alpha)$) and the β-carbon (25.78 ppm, $L_N(\beta)$) of free pyrrolidine are observed in the range of 0—50 ppm, as is shown Fig. 5(a).

In Fig. 5(b) for $[N]_0/[M]_0=1$, the α-carbon of the pyrrolidine ligand of the monosubstituted M-complex is split into two resonances (47.56 ppm and 48.00 ppm, $S_1(\alpha)$), while the β-carbon is shifted to 23.98 ppm (broad)($S_1(\beta)$), and the methyl carbon, to 25.58 ppm (S_1(Me)). In Fig. 5(c) for $[N]_0/[M]_0=2$, three new resonances are observed. The two resonances at 49.17 ppm and at 48.82 ppm ($S_2(\alpha)$) are due to the α-carbon of pyrrolidine of the disubstituted M-complex, while the other at 23.54 ppm (broad)($S_2(\beta)$), is that of the β-carbon.

It should be noticed that the resonance at 26.27 ppm (S_0(Me)) observed in Fig. 5(b) mostly disappears in Fig. 5(c). In Fig. 5(d) for $[N]_0/[M]_0=4$, one new resonance (25.00 ppm, S_2(Me)) is detected; it can be assigned to the methyl carbon of the disubstituted M-complex. The relative intensities of the $S_2(\alpha)$ and $S_2(\beta)$ resonances are larger than those in Fig. 5(d).

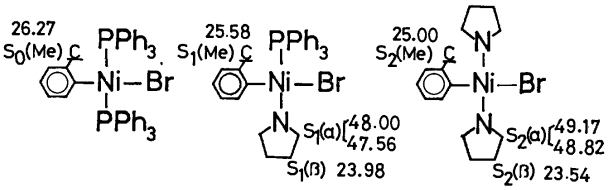

Fig. 6. Assignment of ^{13}C-{^1H} NMR.

This change in the ^{13}C-NMR spectra with the amine concentration is in accord with the results for ^{31}P-{^1H} NMR shown in Fig. 4.

The assignment of these ^{13}C-{^1H} NMR resonances is summarized in Fig. 6. The assignment is based on the following facts; 1) three resonances (S_0(Me), S_1(Me), and S_2(Me)) are observed, with their relative intensities depending reasonably on the molar ratio of pyrrolidine, and 2) the intensities of $S_2(\alpha)$ and $S_2(\beta)$ relative to $S_1(\alpha)$ and $S_1(\beta)$ increase with the increase in the molar ratio of pyrrolidine. Since the ^{13}C-resonances ($S_1(\alpha)$ and $S_2(\alpha)$) of the α-carbons of pyrrolidine are observed to split into two peaks upon coordination to nickel(II), it may be suggested that this is a mixture of *cis-* and *trans-* forms of mono- and disubstituted M-complexes, although only one resonance of the ^{31}P-{^1H} NMR spectra is observed with the monosubstituted M-complex (Fig. 4). It is also possible that no rotation is allowed about the N–Ni bonds of the substituted M-complexes, thus resulting in the split. No clear explanation of the split can, however, be made at present.

At a high molar ratio of pyrrolidine (Figs. 5(d) and 5(e)), no resonance due to free pyrrolidine (25.78 ppm (α) and 47.12 ppm (β)) is detected, while a broad resonance is observed in the range from 39 to 45 ppm (Fig. 5(e)). This resonance remains unclarified. Free pyrrolidine is possibly polymerized during the ^{13}C-{^1H} NMR measurements (about 10 hours at room temperature for each measurement) because of its reactivity is higher than that of the coordinated pyrrolidine.

It may be concluded at least that the driving force for the substitution is predominantly the steric factor of amine rather than the electronic factor, as is the case with the substitution of triphenylphosphine ligands with other tertiary phosphines.

References

1) J. Chatt and B. L. Shaw, *J. Chem. Soc.*, **2**, 1718 (1960).
2) K. Maruya, T. Mizoroki, and A. Ozaki, *Bull. Chem. Soc. Jpn.*, **43**, 11, 3630 (1970).
3) N. Kawata, K. Maruya, T. Mizoroki, and A. Ozaki, *Bull. Chem. Soc. Jpn.*, **47**, 413 (1974).
4) N. Kawata, K. Maruya, T. Mizoroki, and A. Ozaki, *Bull. Chem. Soc. Jpn.*, **47**, 2003 (1974).
5) a) M. Wada, *Inorg. Chem.*, **14**, 1415 (1975); (b) M. Wada, K. Oguro, and Y. Kawasaki, *J. Organomet. Chem.*, **178**, 261 (1979).
6) a) Y. Nakamura, K. Maruya, and T. Mizoroki, *J. Organomet. Chem.*, **104**, C-5(1975); b) *Nippon Kagaku Zasshi*, **11**, 1486 (1978).
7) M. Hidai, T. Kashiwagi, T. Ikeuchi, and Y. Uchida, *J. Organomet. Chem.*, **30**, 279 (1971).

 © 1980 The Chemical Society of Japan Bull. Chem. Soc. Jpn., 53, 3093—3099 (1980)

Thermal Decomposition of Graphite Fluoride. II. Kinetics of Thermal Decomposition of $(CF)_n$ in a Vacuum

Nobuatsu WATANABE* and Satoshi KOYAMA

Department of Industrial Chemistry, Faculty of Engineering, Kyoto University, Yoshida, Sakyo-ku, Kyoto 606

(Received April 3, 1980)

The rate of thermal decomposition of $(CF)_n$ prepared under several reaction conditions was measured in a vacuum. The rate was expressed by Avrami-Erofeyev's equation of second-order for highly oriented sample and of first-order for disordered one. The apparent activation energies of the decomposition reaction were about 50 kcal/mol (1 cal=4.184 J) for the former, and about 14 kcal/mol in higher temperature region and about 100 kcal/mol in lower temperature region for the latter. Thermal decomposition of $(CF)_n$ proceeds two-dimensionally around a nucleus of carbon which is formed at the initial stage of decomposition. The rate of thermal decomposition of various samples is dependent on the number of the nucleus forming sites. The nucleation of carbon takes place on a grain boundary between two small crystallites of $(CF)_n$. The rate of the growth of the nucleus is fast along the grain boundary but slow in other directions. The activation energy was estimated to be about 100 kcal/mol for the former and almost 0 kcal/mol for the latter.

It is well-established that the physicochemical properties of graphite fluoride depend both on those of original carbon materials and fluorination conditions.[1,2] DTA studies revealed that decomposition temperature of $(CF)_n$ samples varied widely between 320 and 610 °C. Detailed analyses of the decomposition products of $(CF)_n$ in a vacuum have also been made, and it was found that thermal decomposition can be expressed by the following equation,[3]

$$2(CF)_n \longrightarrow nC^* + XCF_2 + YC_2F_4, \quad (1)$$

where $X+2Y=n$ and C* is amorphous carbon. Then, these gaseous products give various compounds such as CF_4, C_2F_6, C_3F_8, *etc.*

Recently this reaction was also studied by Kamarchik and Margrave.[4] They have used Avrami-Erofeyev's equation to analyze their kinetic data.

$$-\ln(1-\alpha) = (kt)^n, \quad (2)$$

where α is the fraction decomposed, k is the rate constant, and n is the dimension of the nucleus growth. The value of n was found to be 2. This result suggests that the decomposition proceeds two-dimensionally around an active site or a nucleus, and the reaction is of an auto-catalytic type. However, they could not make clear the reason why the rate of thermal decomposition of $(CF)_n$ samples varied with their formation conditions.

In this work, thermal decomposition of $(CF)_n$ prepared from various carbon materials was investigated in more detail. Based on the kinetic studies, we will discuss how the reaction (Eq. 1) proceeds in a particle or crystal of $(CF)_n$, and why the thermal behavior of samples differs from each other. In addition, microscopic observation has been made with $(CF)_n$ before and after the decomposition, and we also discuss where the decomposition begins, and how the nucleus grows.

Experimental

Preparation and Some Properties of $(CF)_n$ Samples. The samples used for the measurement of decomposition rate were prepared from (I) flaky natural graphite whose grain size was 279—840 μm, (II) powdery natural graphite whose grain size was 46—62 μm, and (III) petroleum coke (<37 μm).

The samples I and II were prepared by using a rotary reactor for fluorination.[5] Table 1 shows some properties and formation conditions of these samples. Crystallinity was measured by means of X-ray diffractometry. The crystallinity of the samples increases in the order of I>II>III. While the fluorine/carbon atomic ratio (F/C) of sample III is the highest. This is due to the presence of CF_2 or CF_3 groups on the particle surface of this $(CF)_n$ sample.[6]

In addition to the samples described in Table 1, another $(CF)_n$ sample has been prepared for microscopic observation in the following manner. A grain of flaky natural graphite of 2 mm in diameter was directly fluorinated in a thermo-balance type apparatus at 610 °C, for 48 h. Fluorine pressure was 26.6 kPa. The sample of $(CF)_n$ thus prepared was of flaky type. The size was about 2 mm in diameter (a and b axes) and about 0.5 mm in thickness (c axis), respectively.

Measurement of the Decomposition Rate and Microscopic Observation. A thermo-balance was used to measure the weight loss *vs.* time curve. The apparatus has been described in detail previously.[7] About 30 mg of $(CF)_n$ sample on a nickel boat was placed in the reaction tube of the apparatus. A pressure of 0.13 Pa was kept throughout the decomposition.

TABLE 1. PREPARATION CONDITION AND SOME PROPERTIES OF GRAPHITE FLUORIDE SAMPLE

Sample	Starting materials	Preparation condition		Crystallinity		F/C ratio	Color
		Temp/°C	t/h	d_{001}/Å	β_{001}/°		
I	Natural graphite (279—840 μm)	600	24	5.84	1.4	0.93	White
II	Natural graphite (46—62 μm)	600	11	6.00	2.5	0.94	Gray
III	Petroleum coke	420	Several	6.64	3.1	1.14	White

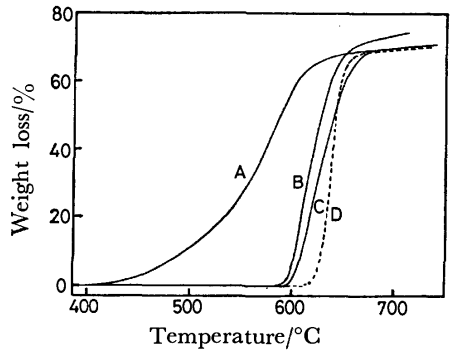

Fig. 1. TG curves for thermal decomposition of graphite fluoride in a vacuum.
A: Sample III, B: sample II, C: sample from natural graphite of 62—74 μm, D: sample I. Heating rate: 5 °C/min.

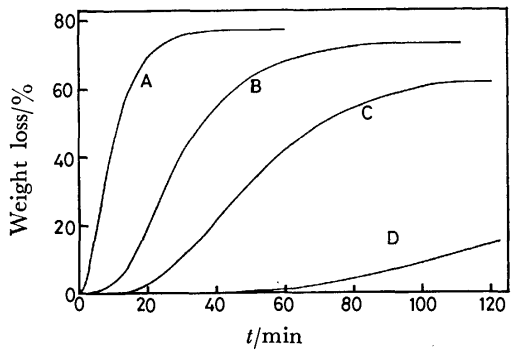

Fig. 2. Thermal decomposition of graphite fluoride (sample I) in a vacuum.
A: 668 °C, B: 654 °C, C: 616 °C, D: 599 °C.

The sample for microscopic observation was cleaved vertically along c axis. To do this, two fine rods of steel were sticked on both basal planes of a particle, then they were pulled off. These procedures were continued until the sample became sufficiently transparent. The sample thus formed was about 0.05 mm in thickness. The microscopic observation was carried out through this thin flake by means of either transmitted or reflected light, and in some cases, polarized light was used. The distribution of fluorine and carbon atoms in $(CF)_n$ sample was determined by X-ray microanalyzer.

Results and Discussion

Figure 1 shows TG curves for the decomposition of $(CF)_n$ sample given in Table 1 and of a sample from natural graphite of 62—74 μm. The heating rate was 5 °C/min. The decomposition of sample III which has a low crystallinity begins at lower temperature. However, the decomposition ended at the same temperature for all the samples, and their final weight loss was also constant value of about 70%. In the following discussion, the fraction decomposed, α is defined by $\alpha=w/w_f$, where w is the weight loss and w_f is the final weight loss. Since the final weight loss was 70%, α was given by $\alpha=w/0.7$.

Decomposition Rate of Samples I and II. Figure 2 shows the weight loss *vs.* time curves for the decomposition of sample I. Each curve has induction period, followed by acceleratory period and deceleratory period, that is, the curves are of sigmoid type. These curves are characteristic of the thermal decomposition of solids such as magnesite,[8] barium azide,[9] and other ionic crystals. The presence of induction and acceleratory periods shows that the reaction proceeds heterogeneously,[10] namely, a nucleus of the decomposition product is formed at a specific point in the crystal and spreads around the point.[11] In heterogeneous reactions, it is known that the rate equation for the decomposition of various kinds of compound is expressed by

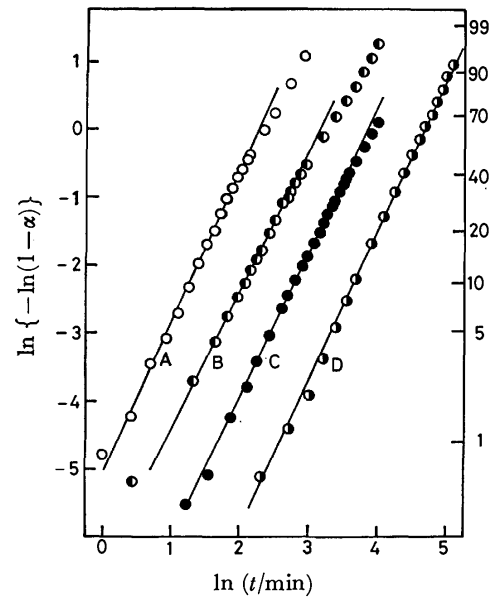

Fig. 3. $\ln\{-\ln(1-\alpha)\}$ *vs.* $\ln t$ plots for thermal decomposition of graphite fluoride (sample I).
A: 668 °C (n=2.24), B: 654 °C (n=2.05), C: 616 °C (n=2.12), D: 599 °C (n=2.18).

$$\alpha = \frac{\sigma N_0}{V_0}(k_1 t)^n, \tag{3}$$

or

$$-\ln(1-\alpha) = \frac{\sigma N_0}{V_0}(k_1 t)^n, \tag{4}$$

where α is the fraction decomposed, σ is the shape factor of a nucleus, N_0 is the number of nucleus forming sites, V_0 is the final volume of the reaction products, k_1 is the linear rate constant of the growth of the nucleus and n is the dimension of the growth of nucleus. The curves shown in Fig. 2 could be expressed by Eq. 3 only for the region that the weight loss is less than 20%. However, the n value was varied from 1.5 to 2.1. This is because the overlapping of nuclei is not taken into account, and it becomes difficult to neglect the effect of overlapping as the nucleus grows. Equation 4 was derived by Avrami considering this effect.[12]

Then Eq. 4 was applied to the decomposition of $(CF)_n$, and $\ln\{-\ln(1-\alpha)\}$ was plotted against $\ln t$ in Fig. 3, in order to obtaine the n value. The plot gives a straight line for the region that α is less than 40% for samples I and II. For sample I, values in the range from 2.05 to 2.24 were obtained from the

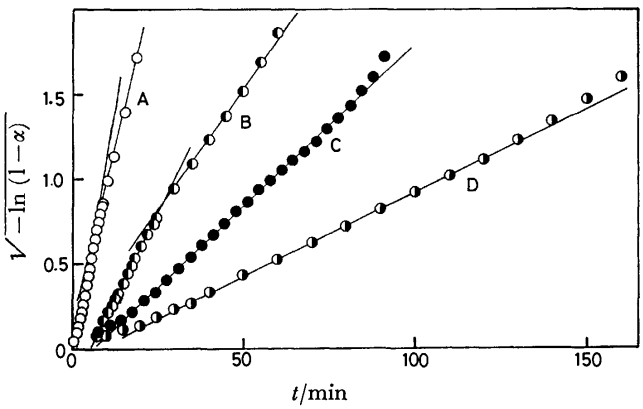

Fig. 4. $\sqrt{-\ln(1-\alpha)}$ *vs.* time plots for thermal decomposition of graphite fluoride (sample I) in a vacuum.
A: 668 °C, B: 654 °C, C: 616 °C, D: 599 °C.

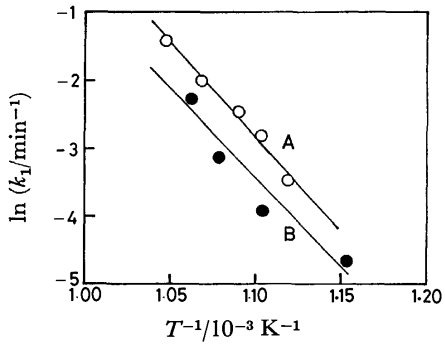

Fig. 5. The Arrhenius plots for decomposition of graphite fluoride.
A: Sample II, B: sample I. According to Eq. 3 (n=2).

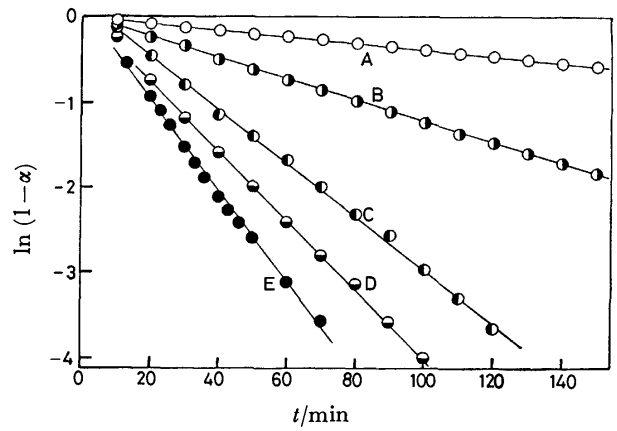

Fig. 6. $\ln(1-\alpha)$ *vs.* time plots for thermal decomposition of graphite fluoride (sample III) in a vacuum.
A: 438 °C, B: 458 °C, C: 504 °C, D: 522 °C, E: 543 °C.

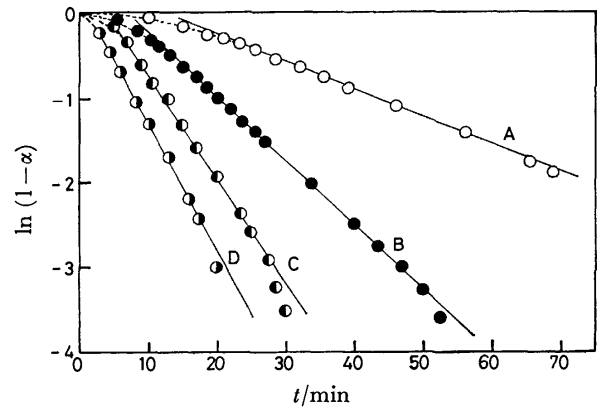

Fig. 7. $\ln(1-\alpha)$ *vs.* time plots for thermal decomposition of graphite fluoride (sample II) in a vacuum.
A: 621 °C, B: 633 °C, C: 644 °C, D: 663 °C.

slopes of these plots as the dimension of the nucleus growth. This result suggests that the rate of the nucleation is sufficiently fast and that the dimension of the growth of nucleus is 2. Then $\sqrt{-\ln(1-\alpha)}$ was plotted against time in order to obtain the apparent rate constant in Fig. 4. This plot gives a straight line in the range of α=0—40% for sample I. The same plot for sample II also gives a straight line in the same range and the rate constant can be obtained from the slope. Figure 5 shows the Arrhenius plots for these two samples. The activation energy was 52.8 kcal/mol for sample II and 49.7 kcal/mol for sample I. The intercept to the ordinate $1/T$=0 was 26.8 and 24.0 for sample II and I, respectively. These values are given by $\ln A\sqrt{\sigma N_0/V_0}$, where A is the frequency factor of k_1. Since A, σ, and V_0 can be regarded as constant for these samples, the difference in the intercepts and the apparent reaction rate between the samples are due to the difference in N_0. It was found from the value of 26.8 and 24.0 that the number of nucleus forming site in sample II was about 300 times that in sample I.

It was found that the dimension of the nucleus growth is two and that the number of nucleus forming sites is different in each sample. These results suggest that the decomposition is initiated at CF_2 and CF_3 groups on the surface of $(CF)_n$ crystal or at a point on the region which is highly strained as reported on the decomposition by γ-ray[13] and by heat.[14] They also suggest that the nuclei formed spread two-dimensionally in parallel with the layer plane.

Decomposition Rate of Samples II and III. In contrast to the samples I and II, smaple III is a fine powdery sample prepared from petroleum coke. The weight loss *vs.* time curve for this sample has almost no acceleratory period and exhibits deceleratory curve from the beginning since the overlapping will take place as soon as the decomposition starts. The reaction rate is then expressed by the first-order equation:

$$-\ln(1-\alpha) = kt, \qquad (5)$$

where k is the apparent rate constant. Figure 6 shows $\ln(1-\alpha)$ *vs.* time plots for this sample. The same plots for sample II also gave straight lines in the region where the weight loss is more than 20% (see Fig. 7). The Arrhenius plots for sample III at 480 °C or above can be approximated by a straight line (see Fig. 8), and the activation energy was calculated to be about 14 kcal/mol. On the other hand, it was about 100 kcal/mol below this temperature. This fact suggests that the rate-determining step at higher temperatures differs from that at lower tem-

Table 2. Rate equation for thermal decomposition of graphite fluoride in a vacuum

Sample	% decomposed					
	0—30%		30—40%		40—100%	
	Equation	E_a/kcal/mol	Equation	E_a/kcal/mol	Equation	E_a/kcal/mol
I	$\alpha=(kt)^2$					
	$\ln(1-\alpha)=-(kt)^2$	49.7	$\ln(1-\alpha)=-(kt)^2$	49.7		
II	$\alpha=(kt)^2$		$\ln(1-\alpha)=-kt$	100	$\ln(1-\alpha)=-kt$	100
	$\ln(1-\alpha)=-(kt)^2$	52.8	$\ln(1-\alpha)=-(kt)^2$	52.8		
III	$\alpha=(kt)^2$					
	$\ln(1-\alpha)=-kt$	14.4[a]	$\ln(1-\alpha)=-kt$	14.4[a]	$\ln(1-\alpha)=-kt$	14.4[a]
		100[b]		100[b]		100[b]

a) Above 480 °C. b) Below 480 °C.

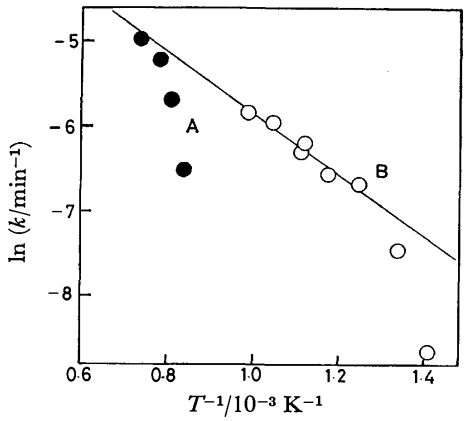

Fig. 8. The Arrhenius plots for decomposition of graphite fluoride.
A: Sample II, B: sample III. According to Eq. 5.

peratures. For sample II the activation energy was calculated to be about 100 kcal/mol. The same plot for sample I did not give a straight line. The results obtained above are summarized in Table 2.

Microscopic Observation of the Formation and Growth of Nucleus. Graphite fluoride belongs to optically uniaxial crystals and its optic character is negative. The principal refractive index, ω is 1.543—1.544.[15] In the following observation, since sample was exposed with the light in parallel with the optic axis (or crystallographical c axis) of $(CF)_n$, it apparently looks optically isotropic. Therefore, it looks always dark in the observation between crossed nicols. Figure 9 shows the photomicrographs of the sample before decomposition. The bright lines in Fig. 9B showed double refraction and were extinguished in the rotation of the sample by 90°. A bright line showing double refraction corresponds to the black line in Fig. 9A, and is regarded as grain boundary in $(CF)_n$ crystal.

The sample was heated up to 400 °C in a vacuum with a heating rate of 10 °C/min, and it was then quenched to room temperature. Photomicrographs of the sample after these treatments are shown in Fig. 10. In the case of observation with transmitted light, the black lines in Fig. 10A were widened, and light lines in Fig. 10B were darkened in the observation between crossed nicols. These results suggest that the decomposition nucleus of carbon is formed on the grain boundary.

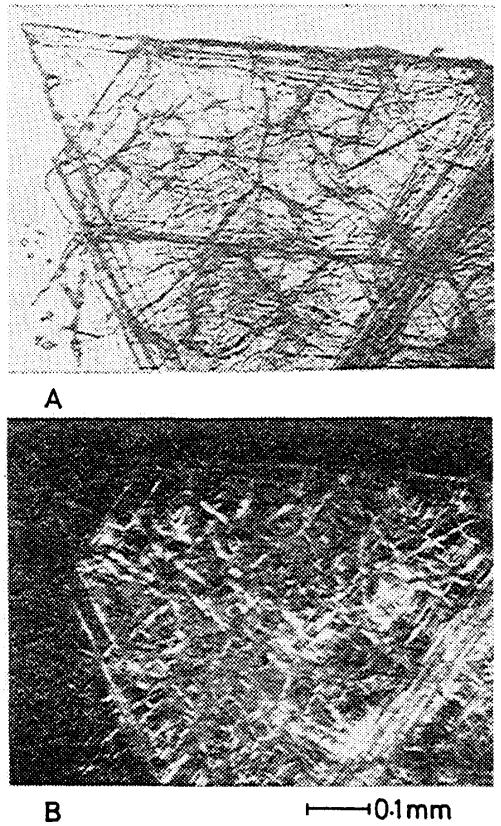

Fig. 9. Photomicrographs of graphite fluoride thin flake.
A: Transmission, B: reflection between crossed nicols.

Figure 11 shows the shape of the nucleus. The main part of the photomicrograph is sketched; the solid line shows the outline of a nucleus, and the broken line shows a grain boudary. Nuclei spread long along the grain boundary, and is anisotropic in shape. Therefore, a nucleus should be formed at a point on a grain boundary and then grow along the grain boundary. The growth of the nucleus is not isotropic, that is, fast along the grain boundary and slow in other directions. Figure 12 shows a scanning electron micrograph and changes in composition of carbon

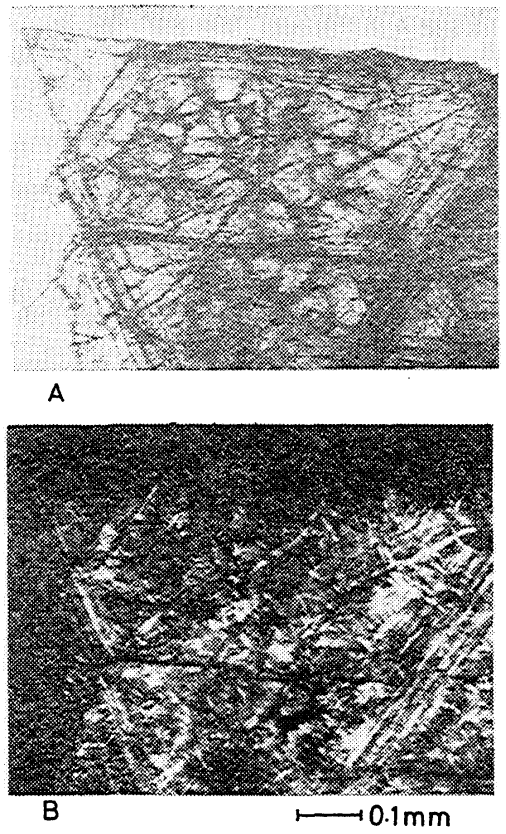

Fig. 10. Photomicrographs of partially decomposed graphite fluoride flake.
A: Transmission, B: reflection between crossed nicols.

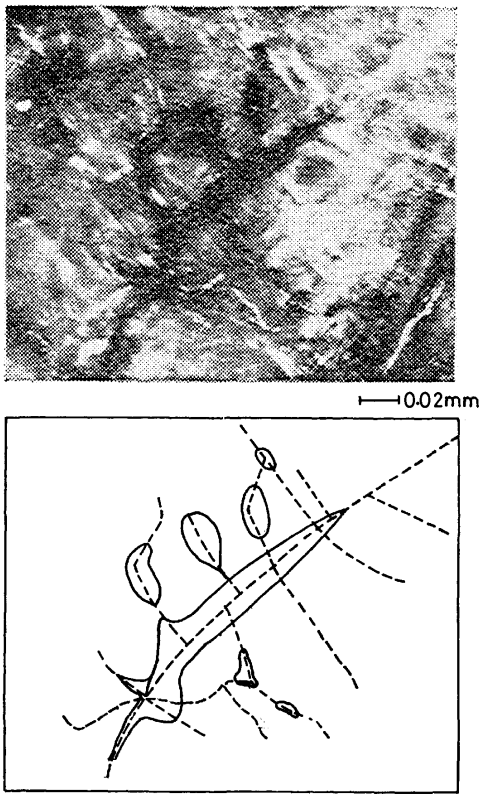

Fig. 11. Photomicrograph of graphite fluoride showing the shape of nuclei (reflection between crossed nicols). Broken line: grain boundary, solid line: nucleus of carbon.

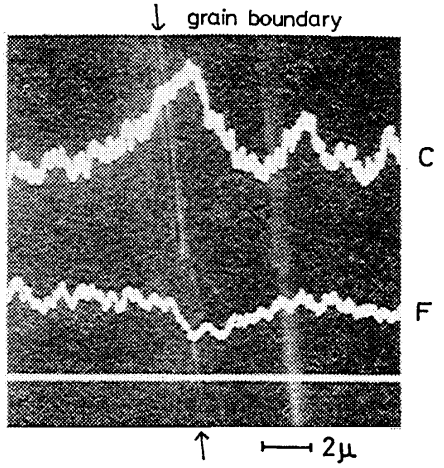

Fig. 12. Scanning electron micrograph of the grain boundary and elemental analysis by X-ray micro-analyzer.

and fluorine atoms determined by means of the X-ray microanalysis. The straight line shows the place where the analysis is done. Two curves above the straight line show the distribution of carbon and fluorine atoms. Fluorine concentration near the grain boundary is low and carbon concentration is high as compared with other parts. No such a change was observed for the original graphite fluoride.

It should be due to the strain energy[15] that the decomposition begins at a point on the grain boundary. This region is energetically activated. The nucleation takes place at the point to which extremely high stress is applied. When the layer plane of $(CF)_n$ is decomposed to that of graphite, the C–C bond length decreases from 1.54 to 1.42 Å, and the plane shrinks.[2] Therefore, the stress applied to the point where the decomposition occurs is relaxed. Next the stress remains in the vicinity along the grain boundary, and then the vicinity will decompose in turn. Thus the nucleus grows along the grain boundary. Because of the relaxation of the stress which expands the layer spacing, the crystallinity of $(CF)_n$ is improved as described in the preceding paper.[3]

Kinetics of Thermal Decomposition of $(CF)_n$. The rate of thermal decomposition of highly oriented $(CF)_n$ is expressed by Eq. 4 with $n=2$. In this equation, it is assumed that the volume $V(t)$ of the nucleus at time t is given by:

$$V(t) = \sigma(k_1 t)^2 \qquad (6)$$

This equation also involves the assumption that the growth of the nucleus is isotropic. When the nucleus grows anisotropically, the volume should not be given by this equation. Figure 13 shows a model of the nucleus shape in $(CF)_n$. A nucleus formed at A at time 0 grows at a rate of k_a along the grain boundary and at a rate of k_b in other directions, where $k_a > k_b$. At time y ($y<t$), the growth of the nucleus reaches to B. At time t, the front of the nucleus spreads by $k_b(t-y)$ from B and by $k_b \cdot t$ from A in other directions than grain boundary. Therefore, the shape of the nucleus

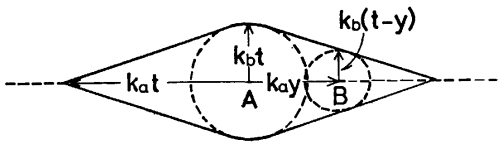

Fig. 13. Schematic model of a nucleus at time t, which was formed at $t=0$.
Broken line: grain boundary.

at time t is rhomb-like as given by the solid line in Fig. 13. The volume of the nucleus having this shape is given by:

$$V(t) = 2\sigma k_a k_b t^2, \qquad (k_a \gg k_b). \tag{7}$$

Then Eq. 4 can be rewritten as[10]

$$-\ln(1-\alpha) = \frac{2\sigma N_0 k_a k_b}{V_0} \cdot t^2. \tag{8}$$

The apparent rate constant, k_1 in Eq. 4 is given by:

$$k_1 = \sqrt{k_a k_b} = A\{\exp(E_{aa}+E_{ab})/2RT\}, \tag{9}$$

where E_{aa} and E_{ab} are the value of activation energy involved in k_a and k_b, respectively. The apparent activation energy according to Eq. 4 is about 50 kcal/mol, that is,

$$E_{aa}/2 + E_{aa}/2 \simeq 50 \text{ (kcal/mol)}. \tag{10}$$

The degree of the nuclei overlapping on the grain boundary becomes larger as the decomposition proceeds because the nucleus forming sites are distributed on the grain boundary. In Avrami-Erofeyev's equation, the overlapping of nuclei has been taken into account.[10] However, Eq. 7 is not applicable if nuclei overlap only on the grain boundary. The number of nucleus forming sites, N_0 of the sample II is greater than that of sample I. The shape of a nucleus of the sample with a large number of nucleus forming sites is shown in Fig. 14. The nuclei overlapping on the grain boundary is negligible in an earlier part of the decomposition as shown in Fig. 14A. On the other hand, it becomes nonnegligible in the later part of the decomposition as shown in Fig. 14B. If the length L of the grain boundary is sufficiently large, the nucleus shown in Fig. 14B is given by:

$$V(t) = 2L\sigma k_b t. \tag{11}$$

Then the rate equation can be written as:

$$-\ln(1-\alpha) = \frac{2L\sigma N_0 k_b}{V_0} \cdot t. \tag{12}$$

This equation has the same form as Eq. 5 and has been applied to the decomposition of sample II (decomposed above 30%) and sample III (decomposed above several percent). The activation energy according to this equation has been obtained to be about 100 kcal/mol, which means $E_{ab} \simeq 100$ kcal/mol. Substituting this value into Eq. 10, a value of almost 0 kcal/mol is obtained as the activation energy for the growth of the nucleus along the grain boundary, that is, $E_{aa} \simeq 0$ kcal/mol.

Characteristics of thermal decomposition of $(CF)_n$. Graphite fluoride, $(CF)_n$ can be regarded as a two-dimensional sheet-like ploymer, and carbon atoms are bonded to fluorine atoms covalently. Chain polymers are generally depolymerized by heat treatment, and

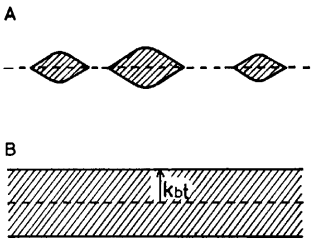

Fig. 14. Schematic illustration of nucleus when the sample has a large number of nucleus forming sites, N_0.
A: Overlapping of nuclei along grain boundary can be neglected, B: grain boundary has perfectly nucleated.

release their corresponding monomer. It seems strange that the decomposition reaction of $(CF)_n$ is heterogeneous as known about magnesite, barium azide, and other ionic crystals.

"Cage effect" is one of the most important phenomena which take place during γ-ray irradiation on some polymers.[16] This effect is essentially the trapping of radicals or molecules formed by the rupture of the polymer chain in polymer molecules. Then these are to recombine with the polymer radicals resulting from the rupture. This is also the case for thermal decomposition of $(CF)_n$. Carbon atoms in the layer is hardly released because they are bonded to neighboring three carbon atoms. Even if one C–C bond is ruptured, the remaining two bonds hold the carbon atom. The probability of recombination should increase, and the decomposition takes place preferentially at the interface between the nucleus and reactant. In fact, decomposition is also initiated on the surface of the crystal and proceeds to the inner part when γ-ray is irradiated on $(CF)_n$.[13] In the case of $(CF)_n$, this effect should be called as "chain effect" rather than "cage effect."

It is due to the strong stress to the grain boundary that thermal decomposition of $(CF)_n$ is initiated at grain boundary. The strain in grain boundary also leads to the decomposition at such a low temperature as 400 °C and zero activation energy E_{aa}. The strain energy remains in the vicinity, and the nucleus grows along the grain boundary.

The actual decomposition mechanism might be more complicated because the grain boundary does not have regular form, and therefore, the shape of the nucleus must change with that of the grain boundary. Consequently, it is not enough to consider only the simple model shown in Fig. 13 for the explanation of the whole reaction. Both Eqs. 8 and 12 could not be applied in the region $\alpha=40$—100% for sample I.

Conclusion

Thermal decomposition of $(CF)_n$ is initiated at a point on a grain boundary or at CF_2 or CF_3 group on the surface of a particle. The nucleus of carbon formed spreads two-dimensionally but anisotropically; the rate of the nucleus growth is larger along the grain boundary than in other directions. As a result,

the shape of nucleus varies with the degree of nucleus overlapping along grain boundary, and the reaction is expressed by either of two different equations. The apparent rate of thermal decomposition is determined by the number of nucleus forming sites in $(CF)_n$ sample.

References

1) N. Watanabe and A. Shibuya, *Kogyo Kagaku Zasshi*, **71**, 963 (1968).
2) M. Takashima and N. Watanabe, *Nippon Kagaku Kaishi*, **1975**, 432.
3) N. Watanabe, S. Koyama, and H. Imoto, *Bull. Chem. Soc. Jpn.*, **53**, 2731 (1980).
4) P. Kamarchik Jr., and J. L. Margrave, *J. Therm. Anal.*, **11**, 259 (1977).
5) Y. Kita, N. Watanabe, and Y. Fujii, *J. Am. Chem. Soc.*, **101**, 3832 (1979).
6) N. Watanabe and H. Takenaka, 5th European Symposium on Fluorine Chemistry, Aviemore Scotland, 16—20th Sept. (1974).
7) M. Takashima and N. Watanabe, *Nippon Kagaku Kaishi*, **1976**, 1222.
8) H. Hashimoto, *Kogyo Kagaku Zasshi*, **63**, 471 (1960).
9) F. E. Harvey, *Trans. Faraday Soc.*, **29**, 653 (1933).
10) Heterogeneous reactions which are seen in decomposition of solids begin at definite localized spot where the activation energy is least. These spots are called nuleus forming sites. A nucleus forming site becomes a small nucleus of reaction product by initial reaction. Once the nucleation takes place, the nucleus spreads 1-, 2-, or 3-dimensionally since the reactant becomes active at the interface with the product. The detailed description about the mechanism of the nucleation and the growth of the nucleus is given in: P. W. M. Jacobs and F. C. Tompkins, "Classification and Theory of Solid Reactions," in "Chemistry of Solid State," ed by W. E. Garner, Butterworth (1955), pp. 184—212.
11) In the case of $(CF)_n$, a small particle of carbon formed by initial decomposition can be regarded as a nucleus.
12) M. Avrami, *J. Chem. Phys.*, **8**, 212 (1940).
13) N. Watanabe, S. Koyama, Y. Kita, and M. Iwasaki, *Nippon Kagaku Kaishi*, **1978**, 1618.
14) N. Watanabe and Y. Kita, *Nippon Kagaku Kaishi*, **1975**, 1896.
15) N. Watanabe and H. Takenaka, *Tanso*, **92**, 2 (1978).
16) K. Shinohara and H. Kashiwabara, "Hoshasen to Kobunshi," Maki Shoten (1968), p. 68.

Thermal Decomposition of Graphite Fluoride. III. Thermal Decomposition of $(CF)_n$ in Oxygen Atmosphere

Nobuatsu WATANABE,* Toshihiko KAWAMURA, and Satoshi KOYAMA
Department of Industrial Chemistry, Faculty of Engineering, Kyoto University, Yoshida, Sakyo-ku, Kyoto 606
(Received April 3, 1980)

Thermal decomposition of $(CF)_n$ was carried out under an oxygen atmosphere. The decomposition temperature was found to be a decisive factor to control the decomposition mechanism and the structure of residual substances. The decomposition reaction proceeded faster in oxygen than in a vacuum at temperatures higher than 588 °C. However, it was reversed below 588 °C. The decomposition mechanism in high temperature region was similar to that in a vacuum. The ESCA spectra of residual substances prepared above 588 °C indicated the presence of carbon atoms which were not bonded with fluorine, namely the nuclei comprised of carbon still remained even in oxygen. The rate of the weight decrease was larger in oxygen than in a vacuum because of the reaction of carbon nuclei, which was formed by thermal decomposition, with oxygen. On the other hand, it considerably decreased below 588 °C, where no nuclei was found for any sample.

A high temperature reaction of graphite fluoride with elemental fluorine gives the $(CF)_n$ type graphite fluoride having a layered structure of hexagonal network. The low surface energy is the most characteristic nature of the product.[1] Therefore, while it is useful as a solid lubricant on one hand, it is on the other hand a troublesome substance which brings about the anode effect in the electrolysis of molten fluorides. Currently, there is a necessity of studying the decomposition of $(CF)_n$ in order to produce in good yield and to elucidate the phenomenon of anode effect. Graphite fluoride, $(CF)_n$, decomposes in a vacuum at high temperature to form several kinds of volatile fluorocarbons and amorphous carbon.[2] Previous studies revealed that the Avrami-Erofeyev equation could be applied to the isothermal TG curves for the decomposition of $(CF)_n$ in a vacuum, and that fluorine and carbon atoms were eliminated from $(CF)_n$ in the ratio of 2 to 1 during the decomposition.[3-5] In this study, thermal decomposition of $(CF)_n$ was performed under oxygen atmosphere and comparison was made with the decomposition behavior in a vacuum.

Experimental

The starting material was natural graphite from Madagascar, whose particle size was 46—62 μm, and the purity was 99.5% from ash treatment. Graphite fluoride, $(CF)_n$, was prepared by the fluorination of natural graphite at 600 °C for 10 h (sample I) or for 15 h (sample II) under the stream of mixed gas of fluorine (5.1×10^4 Pa) and argon (5.1×10^4 Pa). Some properties of these samples were summarized in Table 1. Sample I was used for the measurement of TG and DTA, and sample II was used for X-ray diffractometry, elementary analysis, photoelectron and infrared spectroscopy.

Isothermal TG curves for thermal decomposition of $(CF)_n$ were measured with a thermobalance under oxygen flow. The flow rate was between 15 and 20 ml/min. The residual substances were obtained from the partially decomposed $(CF)_n$. They were analyzed with the methods mentioned above. DTA was carried out under reduced pressure of 6.7×10^2 Pa, using α-Al_2O_3 as a reference material. Infrared spectra were taken with the KBr disc method. The fluorine content of residual substance was determined with the oxygen flask method.

TABLE 1. SAMPLES USED FOR THE EXPERIMENT

Sample	Fluorine content/%	Crystallinity		Color
		d_{001}/Å	β_{001}/°	
I	56.3	6.02	2.40	Gray
II	59.7	5.97	1.67	Gray

Results

Isothermal TG Curves for Thermal Decomposition of $(CF)_n$ in Oxygen. Figure 1 shows isothermal TG curves both in oxygen and in a vacuum at several temperatures. The final weight loss was about 75% in a vacuum, whereas it was almost 100% in oxygen at temperatures above 588 °C. The Arrhenius plot for the TG curves in oxygen is given in Fig. 2. The rate constant was defined to be the slope at the inflexion point of the TG curve. As shown in the figure, it has a distinct break point at 588 °C. This means that the mechanism of thermal decomposition is different from each other in the two regions divided at this tempera-

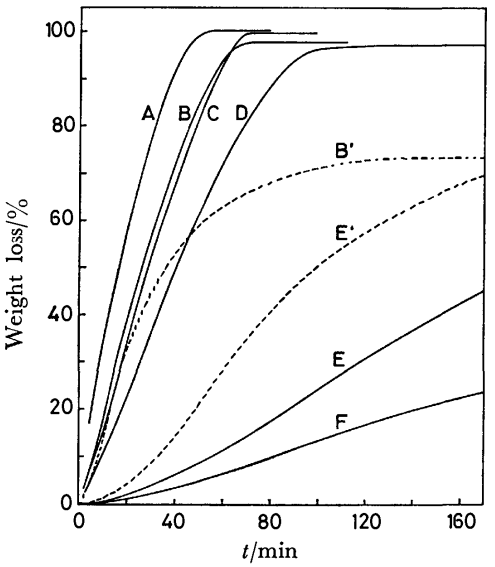

Fig. 1. Isothermal TG curves for thermal decomposition of $(CF)_n$ in oxygen and in a vacuum.
——: Oxygen, ----: vacuum.
A: 623 °C, B,B': 610 °C, C: 602 °C, D: 588 °C, E,E': 575 °C, F: 562 °C.

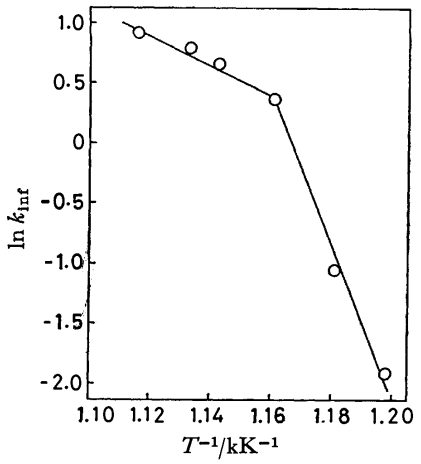

Fig. 2. Arrhenius plot for thermal decomposition of $(CF)_n$ in oxygen.

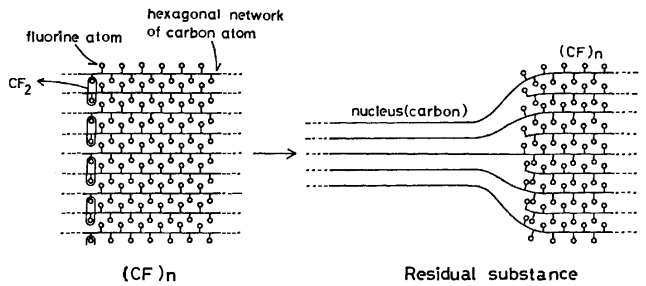

Fig. 3. Schematic illustration of thermal decomposition of $(CF)_n$ in a vacuum.

ture. As seen in Fig. 1, the decomposition proceeds faster in oxygen than in a vacuum at temperatures higher than 588 °C, though the reverse is ture below 588 °C.

The thermal decomposition of $(CF)_n$ has been studied under vacuum previously,[3-5] and the Avrami-Erofeyev equation[6]

$$-\ln(1-\alpha) = (kt)^n$$

is applied to the isothermal TG curves. Here α is the fraction decomposed, k is the rate constant and n is the dimension of nucleus growth. The mechanism shown in Fig. 3 is suggested for the structural changes during the decomposition from the facts that n is equal to 2 and $(CF)_n$ has a layered structure.[7] The above equation can also be applied to the isothermal TG curves in oxygen. The result is shown in Fig. 4, where straight lines are obtained at temperatures above 588 °C. This means that the decomposition at higher temperatures is also due to the formation and growth of nuclei. No such plots can be obtained at temperatures below 588 °C, because the decomposition rates are too small to measure the final weight loss.

Structural Analysis of Residual Substance. In order to elucidate the difference in the mechanism of the thermal decomposition due to a temperature, the residual substance was analyzed by several methods. The sample were those prepared by the thermal decomposition of $(CF)_n$ in oxygen at 560 and 610 °C.

Table 2 shows the fluorine contents and color of the residual substance. The fluorine contents are

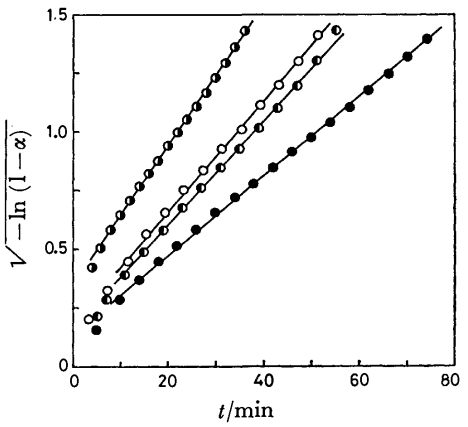

Fig. 4. $\sqrt{-\ln(1-\alpha)}$ *vs.* t for thermal decomposition of $(CF)_n$ in oxygen.
◑: 623 °C, ○: 610 °C, ◐: 602 °C, ●: 588 °C.

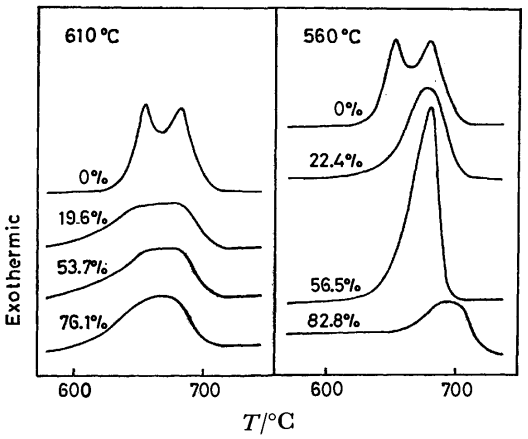

Fig. 5. DTA curves for residual substance formed in oxygen. Numerical value for each curve indicates the weight loss of residual substance.

Table 2. Fluorine content and color of residual substance

T / °C	Weight loss / %	Fluorine content / %	Color
560	15.4	57.6	Gray
	31.1	59.5	White
	59.3	59.9	White
	62.6	57.9	White
610	12.2	58.6	Black
	28.7	59.3	Black
	42.2	57.8	Black
	59.4	57.9	Black
Before decomposition		59.7	Gray

almost constant and independent of decomposition temperature or weight loss. This fact indicates that fluorine and carbon atoms are eliminated in the ratio of 1 to 1 during the decomposition in oxygen. In addition, it was observed that $(CF)_n$ turned black as soon as the decomposition started at 610 °C and this color did not change during the decomposition as observed in a vacuum.[4] On the other hand, $(CF)_n$ gradually turned white at 560 °C as the decomposition

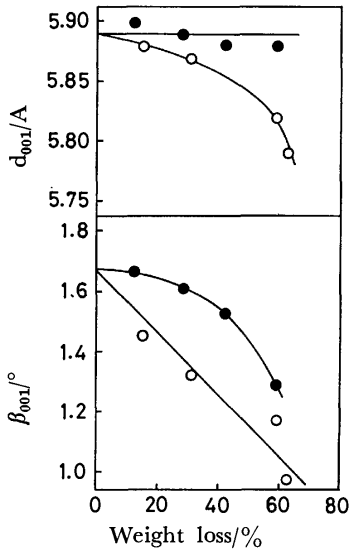

Fig. 6. Change in crystallinity of residual substance formed in oxygen.
●: 610 °C, ○: 560 °C.

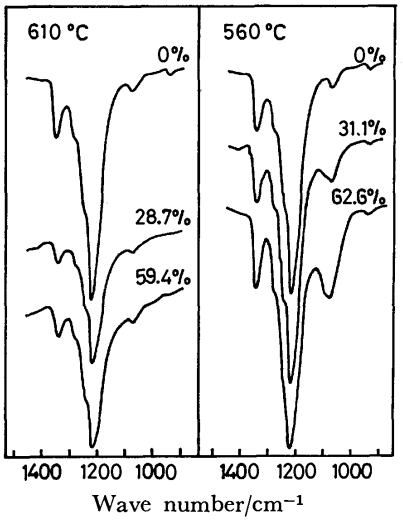

Fig. 7. IR spectra of residual substance formed in oxygen. Numerical value for each spectrum indicates the weight loss of residual substance.

proceeded.

The DTA curves are shown in Fig. 5, where the residual substance formed at 610 °C is thermally less stable than that formed at 560 °C.

Figure 6 shows the results obtained from X-ray diffractometry. Only the lines correspond to $(CF)_n$ can be observed and those of carbon are not observed at both temperatures. The interlayer spacing and half width were calculated from the diffraction profile of the 001 line of $(CF)_n$. The decrease in the half width means that the strain of $(CF)_n$ is removed. The rate at 560 °C is larger than that at 610 °C.

Figure 7 shows the IR spectra of residual substances. The pattern of the peak at 1075 cm^{-1} for the sample prepared at 560 °C varies with the decrease in weight, whereas the pattern is hardly changed by heating at 610 °C. However, there is no peak for carbonyl group as observed in graphitic oxide.[8]

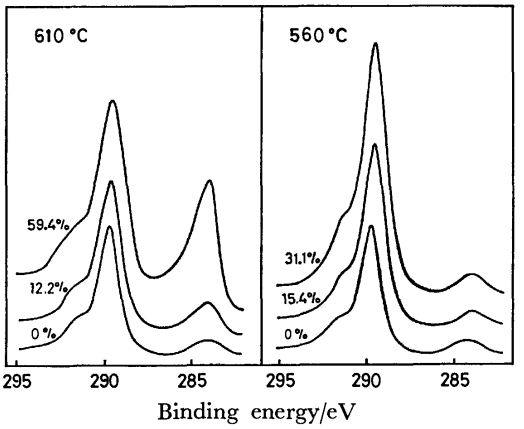

Fig. 8. C_{1s} ESCA spectra of residual substance formed in oxygen. Numerical value for each spectrum indicates the weight loss of residual substance.

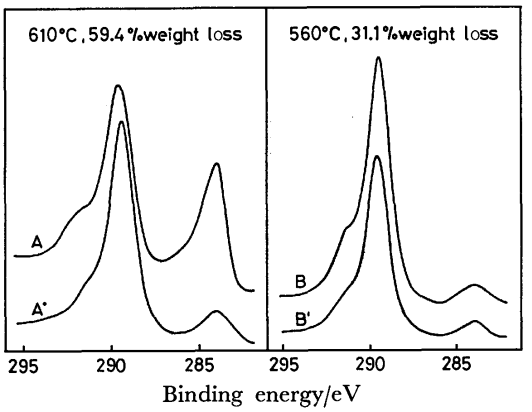

Fig. 9. C_{1s} ESCA spectra of residual substance formed in oxygen.
A,B: Before grinding, A',B': after grinding.

The ESCA spectra of the residual substances are shown in Fig. 8, where two peaks are observed at 284 and 289.5 eV. The former is due to C_{1s} electrons of graphite or hydrocarbons, and the latter is due to those of tertiary C–F group.[9,10] No changes are observed in the spectra of the residual substances formed at low temperature, whereas in the case of the sample prepared at high temperature, the intensity of the peak at 284 eV increases as the decomposition proceeds. Figure 9 shows the change in the C_{1s} ESCA spectra for samples ground with an agate mortar. For the sample prepared at 610 °C, there is a decrease in the intensity of the peak at 284 eV. In general, the information obtained from ESCA is limited to the surface layer of the sample. Therefore, the ESCA spectra show that carbon atoms having no bond with fluorine atoms are present only on the surface of the residual substance formed at 610 °C. However, since the amount of such carbon atoms is regarded to be negligible compared with that of carbon bonded with fluorine, the fluorine contents are not dependent on the weight loss, as shown in Table 2. For the sample formed at 560 °C, no such carbon atoms are found. This is consistent with the result of the elementary analysis.

All the evidences shown above indicate that the

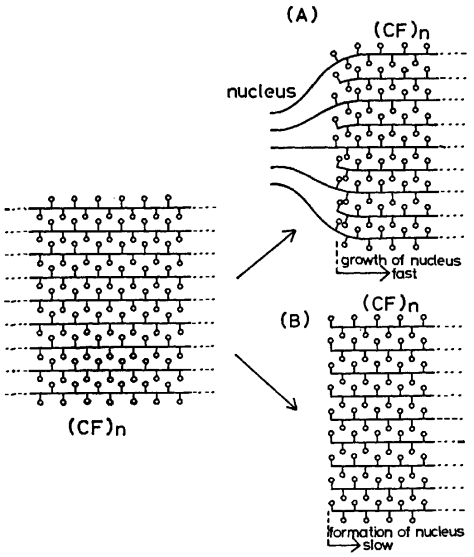

Fig. 10. Schematic illustration of thermal decomposition of $(CF)_n$ in oxygen.
(A): Residual substance formed in high temperature region, (B): residual substance formed in low temperature region.

mechanism of the thermal decomposition of $(CF)_n$ in oxygen at temperatures higher than 588 °C is different from that below this temperature as suggested from the Arrhenius plot.

Discussion

Mechanism of Thermal Decomposition of $(CF)_n$ in Oxygen. From the results described above, the mechanism shown in Fig. 10 is suggested for the thermal decomposition in oxygen. The decomposition is initiated by the nucleus formation at the edge plane or strained regions of $(CF)_n$ as is discussed in the study under vacuum.[4] The result of X-ray diffractometry supports the above view. The nucleus consists of carbon atoms. Since fluorine and carbon atoms are eliminated in the ratio of 2 to 1 during the decomposition in a vacuum, the ratio of carbon atoms in the residual substance increases as the decomposition proceeds. In the presence of oxygen, it is expected that the decomposition rate in oxygen is larger than that in a vacuum because of the reaction of carbon with oxygen. This inference seems to be reasonable because no peak due to carbonyl group is observed in the IR spectra and fluorine and carbon atoms are eliminated in the ratio of 1 to 1. However, since the decomposition in a vacuum proceeds faster than that in oxygen at 575 °C as shown in Fig. 1, the inference is not valid for the decomposition at low temperatures.

In the case of the thermal decomposition in oxygen at high temperatures, the mechanism is considered to be similar to that in a vacuum from the following results; (i) the decomposition proceeds faster in oxygen than in a vacuum, (ii) the isothermal TG curves are fit to the Avrami-Erofeyev equation, (iii) the change in the color of residual substances in oxygen is similar to that in a vacuum and (iv) carbonaceous parts are present on the surface of residual substances. If the nuclei grow at a rate larger than that of the reaction of carbon with oxygen, they will still remain even in the presence of oxygen. Therefore, the weight loss in oxygen is almost equal to a sum of that in a vacuum and that by the elimination of carbon dioxide. and the rate of the weight loss in oxygen is larger than that in a vacuum.

On the other hand, in the low temperature region, the nuclei grow at a rate smaller than that of the reaction of carbon with oxygen. That is, since the nuclei are consumed as soon as they are formed, the rate of weight loss is smaller than that in a vacuum. From this reason, the ESCA spectra of residual substances formed at 560 °C show no peak corresponding to the carbon atoms which are not bonded with fluorine atoms.

Structural Aspect of Residual Substance. The differences in the properties of the residual substances formed at 560 °C and 610 °C are discussed in relation to the nucleus described above. The residual substances formed at 610 °C have carbonaceous parts which can change to nuclei, whereas those formed at 560 °C have no such parts. The strain energy produced by the difference in the crystal structure between reactant and product is one of the sources for the activation of nucleus in the thermal decomposition of solids.[11] Since the residual substances formed at 610 °C have such strain energy in the particle, their crystallinity is inferior to that of the residual substances formed at 560 °C, and the former is thermally less stable than the latter.

References

1) N. Watanabe, H. Takenaka, and S. Kimura, *Nippon Kagaku Kaishi*, **1975**, 1655.
2) N. Watanabe, and Y. Kita, *Nippon Kagaku Kaishi*, **1975**, 1896.
3) P. Kamarchik Jr., and J. L. Margrave, *J. Therm. Anal.*, **11**, 259 (1977).
4) N. Watanabe, S. Koyama, and H. Imoto, *Bull. Chem. Soc. Jpn.*, **53**, 2731 (1980).
5) N. Watanabe and S. Koyama, *Bull. Chem. Soc. Jpn.*, **53**, 3093 (1980).
6) The Avrami-Erofeyev equation is derived on the assumption that the reaction in question is initiated by the formation of nucleus which grows either n-dimensionally or $(n-1)$-dimensionally. The nucleus is the fragment of the product.
7) Nuclei are formed at the edge of layers or at the strained parts of $(CF)_n$ when the rupture of C–C bond occurs, and at the same time, fluorocarbon radical (*i.e.* CF_2) or fluorocarbon molecule (*i.e.* C_2F_4) are formed. The nuclei mainly consist of carbon atoms. Since the interface between $(CF)_n$ and nuclei is more reactive than the bulk of $(CF)_n$, it is more likely that the decomposition proceeds by two dimensional growth of the nuclei in the layers. From another experiment, it was found that the rupture of C–C bond takes place at every second layer of $(CF)_n$.
8) D. Hadzi and A. Novak, *Trans. Faraday Soc.*, **51**, 1614 (1955).
9) D. T. Clark and J. Peeling, *J. Polym. Sci., Polym. Chem. Ed.*, **14**, 2941 (1976).
10) P. Cadman, J. D. Scott, and J. M. Thomas, *Carbon*, **15**, 75 (1977).
11) P. W. M. Jacobs and F. C. Tompkins, "Chemistry of Solid State," ed by W. E. Garner, Butterworths (1955), Chap. 7; D. A. Young, "Decomposition of Solids," Pergamon, Press (1966), Chap. 1.

Structural Studies on Fortimicins. III. The Crystal and Molecular Structure of Fortamine Dihydrochloride

Noriaki HIRAYAMA,* Kunikatsu SHIRAHATA, Yuji OHASHI,† and Yoshio SASADA†

Tokyo Research Laboratory, Kyowa Hakko Kogyo Co., Ltd., 3-6-6 Asahimachi, Machida, Tokyo 194

† *Laboratory of Chemistry for Natural Products, Tokyo Institute of Technology, Nagatsuta, Midori-ku, Yokohama 227*

(Received April 11, 1980)

Fortamine dihydrochloride, $C_8H_{18}N_2O_4 \cdot 2HCl$, is obtained by the hydrolysis of fortimicin B with hydrochloric acid. The space group is *C2* with $a=16.109(2)$, $b=10.047(1)$, $c=8.603(1)$ Å, $\beta=108.69(1)°$, and $Z=4$. The structure was solved by the heavy atom method, and least-squares refinement using 1564 reflexions led to the final R value of 0.030. The ring conformation of fortamine dihydrochloride is an inversed chair form of fortamine. The chair form is significantly compressed to relax the non-bonded interactions between axial substituents.

In the studies on the structures of fortimicins, potent aminocyclitol antibiotics, Egan *et al.* have reported that the ring conformation of 1,4-diaminocyclitol in fortimicin B must be inversed when its amino groups are protonated in its sulfate.[1] Similar unusual conformational inversion occurs in fortimicin A (4-*N*-glycylfortimicin B).[1] We have achieved X-ray analyses of fortimicin B[2] and fortamine,[3] and found that 1,4-diaminocyclitol rings take a normal conformation as shown in Fig. 1. We will denote this conformation as 'B' type and inversed one as 'A' type. Because of the inherent 1,3-diaxial interactions, 'A' type conformation seems to be unstable and it is necessary to examine the validity of the assignment by Egan *et al.*[1] Unfortunately, attempts to crystallize fortimicin B sulfate and fortimicin A were unsuccessful, but crystals of fortamine dihydrochloride were obtained. Its structure determination would throw light on the effect of protonation on the ring conformation.

Experimental and Structure Determination

Fortamine dihydrochloride was obtained by the hydrolysis of fortimicin B with hydrochloric acid. The prismatic crystals were grown from a methanol solution. A crystal of $0.5 \times 0.4 \times 0.3$ mm^3 sealed in a glass capillary was used for data collection on a Rigaku four-circle automated diffractometer with graphite monochromated Mo $K\alpha$ radiation ($\lambda=0.71069$ Å). Preliminary unit-cell dimensions and space group were obtained from photographs. The space group was determined from the systematic absences (*hkl* for $h+k=2n+1$). Accurate cell dimensions were determined by least-squares calculation with the 2θ values of 15 high angle reflexions measured on the diffractometer. Crystal data are summarized in Table 1. All reflexions within the range of $2\theta \leqq 55°$ were collected by the use of the ω-2θ scan mode with a scanning rate of $4°(2\theta)$ min^{-1}. Stationary background counts were accumulated for 10 s before and after each scan. Periodic checks of the intensity values of three standard reflexions did not reveal any significant X-ray damage or crystal decay. Any corrections for absorption or extinction were not applied. A total of 1610 independent reflexions were obtained, of which 1564 ($|F_o| \geqq 3.0\sigma(|F_o|)$) were considered as observed.

The structure was solved by the heavy atom methods and refined by the block-diagonal least-squares methods with the modified HBLS program. All the hydrogen atoms were found by the difference Fourier synthesis. Refinement was brought to completion using anisotropic and isotropic thermal parameters for the non-hydrogen and hydrogen atoms, respectively. In the later stage of the refinement, the following weighting system was adopted;
$w=0.3$ for $|F_o|<3.72$ and $|F_o|>37.16$, and

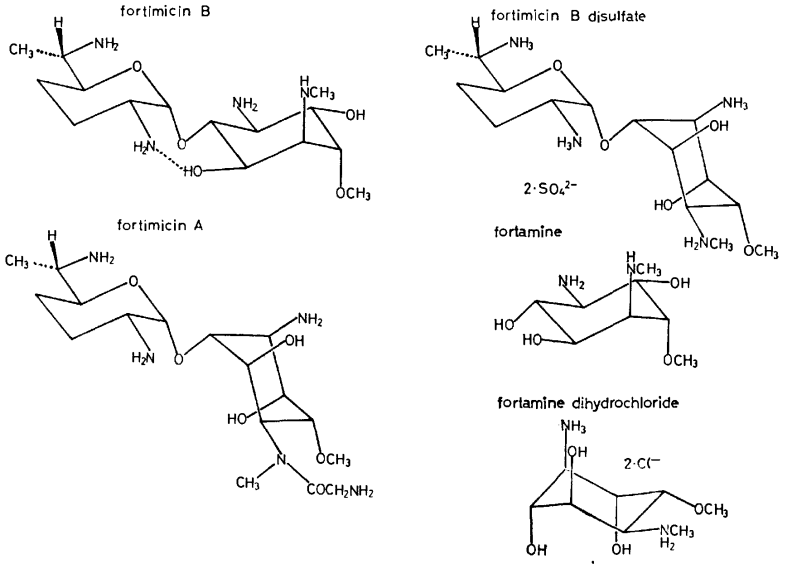

Fig. 1. Structures of fortimicins and fortamines.

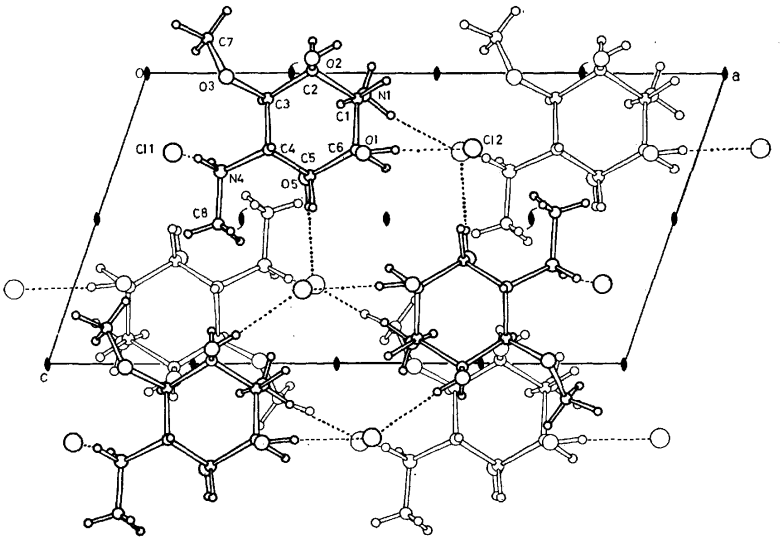

Fig. 2. The crystal structure projected along the b axis.

Table 1. Crystal data

$C_8H_{20}N_2O_4Cl_2$	$b=10.047(1)$
M.W.=277.15	$c=8.603(1)$ Å
C2	$\beta=108.69(1)°$
$Z=4$	$D_x=1.396$ g cm^{-3}
$a=16.109(2)$	μ(Mo $K\alpha$)=4.961 cm^{-1}

$w=(0.00833(F_o)^2-0.34114|F_o|+4.48559)^{-1}$ for $3.72\leqq|F_o|\leqq37.16$. The final R value was 0.030. Atomic scattering factors were taken from "International Tables for X-Ray Crystallography."[4] Differences in the intensities of six Friedel pairs of reflexions measured on a diffractometer using Cu $K\alpha$ radiation confirmed the absolute configuration previously determined by CD measurements.[1] The final positional and thermal parameters are given in Table 2. A list of the observed and calculated structure factors is kept as Document No. 8035 at the Chemical Society of Japan.

Results

Hydrogen Bond and Crystal Structure. The crystal structure viewed along the b axis is shown in Fig. 2. Hydrogen bond lengths and angles are listed in Table 3. All functional groups are involved in intermolecular hydrogen bonds with the chloride anions, but there is no hydrogen bond between functional groups. The N(4) atom makes bifurcated hydrogen bonds with Cl(1) and Cl(2). Two short contacts are found between O(5) and N(1), and between O(3) and N(4); O(5)···N(1) and O(3)···N(4) distances being 2.802 and 2.703 Å, and O(5)···H–N(1) and O(3)···H–N(4) angles 109.2 and 97.8°, respectively. Judging from these geometries, it is not plausible to assign hydrogen bonding to these interactions.

Bond Lengths and Angles. The bond lengths and angles are shown in Table 4, in which corresponding values of fortamine are also given. The average endocyclic C–C bond length of 1.527 Å in the dihydrochloride is essentially equal to that of 1.524 Å in fortamine. This indicates that protonation at the amino groups hardly affects the endocyclic C–C bond lengths. Although the C(1)–C(2) length of fortamine is significantly short (1.505 Å), that of the dihydrochloride (1.542 Å) is notably long. The C(1)–N(1), C(4)–N(4) and N(4)–C(8) bond lengths of the dihydrochloride becomes longer than those of fortamine under the influence of protonation. All C–O (hydroxyl) bond lengths except C(5)–O(5) are significantly shorter than those of fortamine. The C(2)–O(2) bond length (1.411 Å) is particularly short.

The average endocyclic C–C–C bond angles is 112.1°. This value is larger than 111.4° of fortamine. The effect of protonation is seen in the endocyclic bond angles, too. In epi-inositol, the C–C–C angle between 1,3-diaxial hydroxyl group is 114.7°.[5] Similar 1,3-diaxial interaction between O(1) and O(2) (O(1)···O(2) distance being 3.01 Å) in the present molecule widen the C(6)–C(1)–C(2) angle to 114.3°. On the contrary, the C(1)–C(6)–C(5) angle of 112.4(2)° is not so large and does not seem to suffer from the N(1)···O(5) non-bonded interaction, although the N(1)···O(5) distance is shorter (2.820 Å).

All of the exocyclic bond angles except O(3)–C(3)–C(4) and C(7)–O(3)–C(3) in the dihydrochloride are significantly different from those in the free base, fortamine. The bond angles around N(4)–C(4) and O(3)–C(3) are remarkably asymmetrical. This seems to indicate that there is some attractive force between N(4) and O(3).

Conformation of the Molecule. The ring conformation of fortamine dihydrochloride, as shown in Fig. 3, is inverse of the free base conformation. The signs of torsional angles listed in Table 5 also represent the ring inversion. Figure 4 shows the important torsional angles between substituents and the *d* values, defined by deviations of the two atoms from the least-squares plane through other four atoms consisting of the seat of a chair. The average C–C–C–C torsional angles in the ring is 52.7° and average *d* is 0.627 Å. Both of these values are smaller than those of the free base, 54.9° and 0.655 Å, respectively. The ring of the dihydrochloride is flattened to some extent

TABLE 2a. FINAL ATOMIC COORDINATES WITH THEIR ESTIMATED STANDARD DEVIATIONS, MULTIPLIED BY 10^5 FOR Cl ATOMS, 10^4 FOR C, N, AND O ATOMS, AND 10^3 FOR H ATOMS

Atom	x	y	z	B_{eq}[a] or B	Atom	x	y	z	B_{eq}[a] or B
C(1)	1250(2)	1949(2)	9154(3)	2.18	HC(3)	289(2)	108(3)	911(3)	2.1
C(2)	2198(2)	2355(3)	1012(3)	2.08	HC(4)	246(2)	355(3)	742(3)	2.1
C(3)	2821(1)	2066(2)	9154(3)	1.87	HC(5)	135(2)	235(4)	538(3)	3.2
C(4)	2487(1)	2596(2)	7406(3)	1.82	HC(6)	34(2)	197(3)	672(3)	2.3
C(5)	1592(2)	2033(3)	6470(3)	2.09	HAC(7)	430(3)	109(5)	1086(6)	8.3
C(6)	940(2)	2397(3)	7349(3)	2.26	HBC(7)	403(2)	181(4)	1215(5)	5.7
C(7)	4215(2)	1886(4)	11223(4)	3.86	HCC(7)	483(2)	231(5)	1166(4)	5.4
C(8)	2911(2)	2395(4)	4807(3)	3.33	HAC(8)	243(2)	169(3)	423(4)	3.3
N(1)	1165(1)	461(2)	9256(3)	2.24	HBC(8)	340(2)	240(4)	450(4)	3.9
N(4)	3169(1)	2242(3)	6619(2)	2.09	HCC(8)	266(2)	326(3)	453(4)	3.5
O(1)	840(1)	3798(2)	7259(3)	3.36	HAN(1)	59(2)	18(4)	860(4)	4.2
O(2)	2263(1)	3721(2)	10525(3)	3.07	HBN(1)	117(2)	26(3)	1026(3)	2.2
O(3)	3662(1)	2638(2)	9897(2)	2.27	HCN(1)	157(2)	2(4)	900(4)	3.7
O(5)	1667(1)	618(2)	6409(2)	2.43	HAN(4)	365(2)	276(3)	708(3)	1.9
Cl(1)	41486(4)	50057(8)	72985(7)	2.73	HBN(4)	340(2)	131(4)	692(4)	4.5
Cl(2)	−10356(4)	43746(9)	74524(9)	3.11	HO(1)	29(2)	399(4)	732(5)	4.6
HC(1)	87(2)	229(3)	974(3)	2.4	HO(2)	193(2)	386(4)	1102(4)	3.8
HC(2)	238(2)	190(3)	1114(3)	2.6	HO(5)	141(2)	35(4)	541(4)	4.1

a) $B_{eq}=\frac{1}{3}(2\pi^2)^{-1}\sum_i\sum_j \beta_{ij}\boldsymbol{a}_i\cdot\boldsymbol{a}_j$, here $\boldsymbol{a}_i$ and $\boldsymbol{a}_j$ are the base vectors in real space, and β_{ij}'s are anisotropic thermal parameters.[8]

TABLE 2b. FINAL THERMAL PARAMETERS WITH THEIR ESTIMATED STANDARD DEVIATIONS. ANISOTROPIC THERMAL PARAMETERS ARE MULTIPLIED BY 10^4 AND ISOTROPIC ONES MULTIPLIED BY 10^3

Atom	U or U_{11}	U_{22}	U_{33}	U_{12}	U_{13}	U_{23}
C(1)	274(11)	230(13)	373(12)	−15(9)	181(10)	−30(9)
C(2)	333(11)	215(12)	278(10)	−48(10)	148(9)	−33(10)
C(3)	227(10)	189(11)	279(10)	−18(8)	64(8)	−14(9)
C(4)	243(10)	199(10)	279(10)	14(8)	132(9)	2(8)
C(5)	257(10)	255(13)	268(10)	0(9)	65(9)	15(9)
C(6)	224(10)	238(13)	408(13)	21(9)	116(10)	40(10)
C(7)	362(15)	515(20)	481(16)	−10(13)	−34(13)	116(14)
C(8)	427(14)	582(20)	298(12)	−31(14)	176(11)	8(14)
N(1)	293(10)	261(10)	327(10)	−62(8)	143(9)	7(9)
N(4)	250(9)	282(9)	288(9)	−21(9)	127(8)	−17(9)
O(1)	377(10)	261(9)	707(14)	109(8)	281(11)	117(10)
O(2)	476(11)	260(9)	539(11)	−105(8)	325(10)	−174(9)
O(3)	238(7)	261(9)	329(8)	−44(7)	40(7)	6(7)
O(5)	362(9)	243(8)	299(9)	−28(8)	80(8)	−51(7)
Cl(1)	346(3)	367(3)	292(2)	−111(3)	62(2)	40(3)
Cl(2)	349(3)	337(3)	564(4)	47(3)	248(3)	6(3)
HC(1)	28(7)					
HC(2)	31(7)					
HC(3)	24(7)					
HC(4)	25(7)					
HC(5)	38(8)					
HC(6)	29(7)					
HAC(7)	122(19)					
HBC(7)	72(13)					
HCC(7)	73(11)					
HAC(8)	43(9)					
HBC(8)	51(9)					
HCC(8)	44(9)					
HAN(1)	53(9)					
HBN(1)	28(7)					
HCN(1)	47(9)					
HAN(4)	23(7)					
HBN(4)	55(10)					
HO(1)	67(11)					
HO(2)	45(9)					
HO(5)	52(10)					

from the free base. As seen from the d values, C(4) and C(5) are puckered and C(1) and C(2) flattened. Small C(5)–C(4)–N(4)–C(8) torsional angle of 44.8° is probably due to the bifurcated hydrogen bond of N(4). Some exocyclic torsional angles between axial substituents in the dihydrochloride are fairly larger than those in the free base. This indicates the exocyclic torsional angles also suffer from 1,3-diaxial interaction to a large extent. Therefore, the smallest exocyclic O(2)–C(2)–C(3)–O(3) torsional angle of 46.5° is due to the O(1)···O(2) repulsion.

Table 3. Distances and angles of hydrogen bond A-H···B

	l(A···B)/Å	ϕ(A–H···B)/°
N(4)···Cl(1)^{I}	3.155(3)	141.9
O(1)···Cl(2)^{I}	3.132(3)	175.5
N(4)···Cl(2)^{II}	3.141(3)	175.6
N(1)···Cl(1)^{III}	3.176(2)	165.7
O(5)···Cl(1)^{IV}	3.096(2)	169.8
O(2)···Cl(2)^{V}	3.094(2)	174.3

Symmetry code

I:	(x	y	z)
II:	($1/2+x$	$-1/2+y$	z)
III:	($-1/2+x$	$-1/2+y$	z)
IV:	($1/2-x$	$-1/2+y$	$1-z$)
V:	($-x$	y	$2-z$)

Discussion

Fortamine dihydrochloride takes the 'A' type conformation in the crystal structure. This result shows that the protonation at the two nitrogen atoms makes

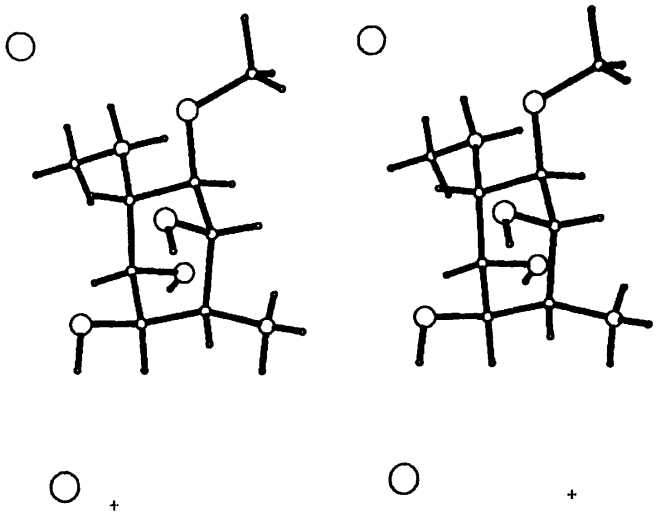

Fig. 3. A stereoscopic drawing of the molecule. This was drawn by TSD: XTAL, which is a computer-graphics interactive modeling program for NOVA 3 computer.[7]

Table 4. Bond lengths (l/Å) and angles (ϕ/°) with their estimated standard deviations in parentheses. Bond angles including the hydrogen atoms are omitted for clarity

	Fortamine dihydrochloride	Fortamine		Fortamine dihydrochloride	Fortamine
C(1)-C(2)	1.542(4)	1.505(4)	O(5)-HO(5)	0.89(4)	0.92(3)
C(2)-C(3)	1.523(4)	1.513(4)	C(7)-HAC(7)	0.92(5)	0.96(4)
C(3)-C(4)	1.521(3)	1.532(4)	C(7)-HBC(7)	0.93(5)	1.11(4)
C(4)-C(5)	1.518(4)	1.528(4)	C(7)-HCC(7)	1.04(5)	0.92(5)
C(5)-C(6)	1.522(4)	1.521(4)	C(8)-HAC(8)	1.06(4)	0.98(3)
C(6)-C(1)	1.538(4)	1.545(4)	C(8)-HBC(8)	0.90(4)	1.05(4)
C(1)-N(1)	1.506(4)	1.470(4)	C(8)-HCC(8)	0.94(4)	1.00(3)
C(2)-O(2)	1.411(3)	1.432(3)	C(1)-C(2)-C(3)	111.5(2)	112.6(2)
C(3)-O(3)	1.421(3)	1.434(4)	C(2)-C(3)-C(4)	112.8(2)	111.1(2)
O(3)-C(7)	1.420(4)	1.414(4)	C(3)-C(4)-C(5)	111.7(2)	109.9(2)
C(4)-N(4)	1.506(4)	1.485(4)	C(4)-C(5)-C(6)	109.7(2)	112.0(2)
N(4)-C(8)	1.487(5)	1.469(4)	C(5)-C(6)-C(1)	112.4(2)	111.2(2)
C(5)-O(5)	1.430(3)	1.429(3)	C(6)-C(1)-C(2)	114.3(2)	111.4(2)
C(6)-O(1)	1.417(4)	1.434(3)	N(1)-C(1)-C(2)	108.9(2)	110.4(2)
C(1)-HC(1)	0.97(4)	0.92(3)	N(1)-C(1)-C(6)	110.0(2)	108.7(2)
C(2)-HC(2)	0.94(3)	0.99(3)	O(1)-C(6)-C(1)	109.9(2)	109.1(2)
C(3)-HC(3)	1.01(3)	1.05(3)	O(1)-C(6)-C(5)	107.2(2)	109.1(2)
C(4)-HC(4)	0.96(3)	1.05(3)	O(5)-C(5)-C(6)	109.7(2)	112.5(2)
C(5)-HC(5)	0.95(4)	1.08(3)	O(5)-C(5)-C(4)	108.2(2)	112.0(2)
C(6)-HC(6)	1.03(3)	1.04(3)	N(4)-C(4)-C(5)	112.3(2)	110.3(2)
N(1)-HAN(1)	0.97(4)	1.03(3)	N(4)-C(4)-C(3)	106.5(2)	111.8(2)
N(1)-HBN(1)	0.87(3)	0.89(3)	C(8)-N(4)-C(4)	116.6(2)	112.2(2)
N(1)-HCN(1)	0.89(4)		O(3)-C(3)-C(4)	106.7(2)	107.2(2)
N(4)-HAN(4)	0.92(3)	0.94(3)	O(3)-C(3)-C(2)	112.1(2)	109.6(2)
N(4)-HBN(4)	1.02(4)		C(7)-O(3)-C(3)	114.2(2)	114.5(2)
O(1)-HO(1)	0.93(4)	0.82(3)	O(2)-C(2)-C(3)	108.1(2)	110.7(2)
O(2)-HO(2)	0.81(4)	0.83(3)	O(2)-C(2)-C(1)	111.9(2)	108.7(2)

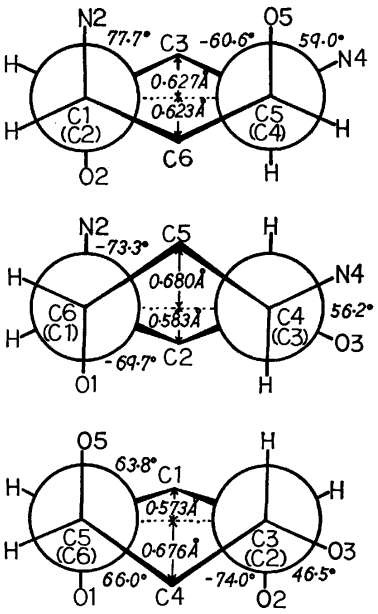

Fig. 4. Schematic drawings of chair forms of fortamine and fortamine dihydrochloride.

the 'B' type conformation unstable and inverse the fortamine ring into the 'A' type conformation. It seems that the electrostatic repulsion between the charge at the amino groups is responsible for the ring inversion. We calculated the electrostatic repulsion energies of the fortamine dihydrochloride in the 'A' type and in the 'B' type conformations. To simplify the treatment 1 e.s.u. charge due to protonation is assumed to be localized at each nitrogen atom. The geometry of the 'B' type dihydrochloride is taken as that of fortamine except the C–N distances which are replaced by the values observed in fortamine dihydrochloride. The calculation indicates that the electrostatic repulsion energy in the 'B' type conformation is 0.50 kcal/mol higher than that in the 'A' type conformation.

In the 'A' type conformation, however, the non-bonded interactions between the axial substituents seem to be more crucial than those in the 'B' type conformation. We estimated them by calculating the non-bonded interaction energy between the axial substituents. Giglio's potentials[6] were used and the effect of axial hydrogen atoms were also included. The value obtained was 1.19 kcal/mol. This is not so high; in other words, the non-bonded interactions between the axial substituents in the 'A' type conformation are fully relaxed by deforming the endocyclic angles and torsional angles as described in the previous section. Although further studies on the energy of molecular deformation would be required, it is most probable that the electrostatic force is ineviatble to stabilize fortamine dihydrochloride molecule in the 'A' type conformation. The inversed chair form significantly compressed to relax the 1,3-diaxial interactions would serve the basis to construct the structure of fortimicin A.

Table 5. Torsional angles (ϕ/°)

	Fortamine dihydrochloride	Fortamine
C(1)-C(2)-C(3)-C(4)	49.4	−56.1
C(2)-C(3)-C(4)-C(5)	−57.4	56.3
C(3)-C(4)-C(5)-C(6)	59.0	−56.4
C(4)-C(5)-C(6)-C(1)	−54.9	54.6
C(5)-C(6)-C(1)-C(2)	49.6	−52.6
C(6)-C(1)-C(2)-C(3)	−45.8	53.9
N(1)-C(1)-C(2)-O(2)	−161.1	−62.2
O(2)-C(2)-C(3)-O(3)	46.5	−59.8
C(2)-C(3)-O(3)-C(7)	80.6	129.2
C(4)-C(3)-O(3)-C(7)	−155.4	−110.1
O(3)-C(3)-C(4)-N(4)	56.2	173.9
C(3)-C(4)-N(4)-C(8)	167.3	−70.9
C(5)-C(4)-N(4)-C(8)	44.8	166.5
N(4)-C(4)-C(5)-O(5)	59.0	−60.1
O(5)-C(5)-C(6)-O(1)	−175.3	−57.9
O(1)-C(6)-C(1)-N(1)	167.4	65.2

We thank Dr. H. Sano, Tokyo Research Laboratory of Kyowa Hakko Kogyo Co., Ltd., for providing the crystals.

References

1) R. S. Egan, R. S. Stanaszek, M. Cirovic, S. L. Mueller, J. Tadanier, J. R. Martin, P. Collum, A. W. Goldstein, R. L. De Vault, A. C. Sinclair, E. E. Fager, and L. A. Mitscher, *J. Antibiot.*, **30**, 552 (1977).

2) N. Hirayama, K. Shirahata, Y. Ohashi, Y. Sasada, and J. R. Martin, *Acta Crytallogr., Sect. B*, **34**, 2648 (1978).

3) N. Hirayama, K. Shirahata, Y. Ohashi, and Y. Sasada, *Bull. Chem. Soc. Jpn.*, **53**, 1514 (1980).

4) "International Tables for X-Ray Crystallography," The Kynoch Press, Birmingham (1974), Vol. IV, pp. 72—102.

5) G. A. Jeffrey and H. S. Kim, *Carbohydr. Res.*, **15**, 310 (1970).

6) E. Giglio, *Nature*, **222**, 339 (1969).

7) A. Takenaka and Y. Sasada, Annual Meeting of the Crystallographic Society of Japan, Hiroshima, November 1978, Abstr., p. 32.

8) B. T. M. Willis and A. W. Pryor, "Thermal Vibrations in Crystallography," Cambridge University Press, Cambridge (1975), p. 102.

Electronic Spectra of Single Crystals of 1,1′-Diethyl-2,2′-Cyanine Iodide, Bromide, and Chloride

Jiro TANAKA,* Masashi TANAKA, and Masuo HAYAKAWA

Department of Chemistry, Faculty of Science, Nagoya University, Chikusa-ku, Nagoya 464

(Received April 18, 1980)

Reflection spectra of single crystals of 1,1′-diethyl-2,2′-cyanine iodide, bromide and chloride were measured in order to find the origin of the J band. The spectra were obtained by the Kramers-Kronig transformation of reflectivity. The positions of absorption peaks and the shapes of vibronic envelope for each crystalline faces are explained by a calculation of surface exciton splitting with a weak coupling model. The intensity of each bands is interpreted by the oriented gas model, however, a peculiar anomalous band shape characteristic of J band is explained by the charge resonance (CR) and the molecular exciton interaction. The J band is found along particular crystalline direction, in which the dye molecules are stacked face to face, showing importance of interplanar π electron interaction. The molecular exciton band shape is changed significantly to give a J band because the higher vibronic bands are blurred off by the enhanced relaxation mechanism of the CR interaction.

Jelly[1] and Scheibe[2] found a sharp electronic absorption band of cyanine dye on a concentrated solution of 1,1′-diethyl-2,2′-cyanine, and it has been called J band. The J band shows several peculiar spectral characteristics; the band appears only in an aggregate system and it is unusually sharp as an electronic transition of organic molecule modified by association. The emission spectra of the aggregate is also sharp without Stokes shift. The spectra and physico-chemical properties of cyanine dye aggregate system have been investigated by many people, particularly by Scheibe and his coworkers[3] in view of finding the relation between the structure and the spectra and the mechanism of spectral sensitization for silver halide crystals. Cooper[4] investigated the aggregate state in solution at low temperature and found a doublet structure in the J band and a sharp emission band. Daltrozzo *et al.*[5] studied the condition of J-aggregation in solution and proposed a model of the aggregate.

Theoretical investigation on the band shift of the aggregate was first presented by McRae and Kasha[6] based on a molecular exciton theory, and further development was proceeded by Norland, Bird and their group[7] and Kuhn and his group.[8] These authors suggested that a lateral displacement of adjacent dye molecules shifts a monomer absorption band (M band) to red and produces the J band, while a pairwise stacking of the dye causes a hypsochromic H band. A theory of the band shape of the J band was developed by Briggs and Herzenberg[9] with coherent exciton scattering (CES) method and it has been suggested that the band will be sharp when the exciton interaction is much stronger than the coupling with the molecular vibration. Sumi[10] extended a model calculation with coherent potential approximation (CPA) including several coupling parameters and obtained a band shape which looks like the J band. A similar calculation was carried out by Ito *et al.*[11]

In order to study the nature of the electronic transitions of the J aggregate, spectral measurement of the single crystals of these dyes will be particularly useful, because the directional properties of the electronic transition may be clearly demonstrated and a peculiar characteristics of the J band may be found. Several years ago Dr. Jörg Preuss in Münich suggested to one of the authors (J. T.) that a sharp J type absorption band could be found in the crystal of 1,1′-diethyl-2,2′-cyanine chloride along the stacking axis of the molecules. Recently Marchetti *et al.*[12] reported the crystalline spectra of the same dye iodide and chloride and correlated the J band in solution to the crystalline exciton state.

In this paper the spectra of the above dye iodide, bromide and chloride are presented with a theoretical consideration of the band splitting and the band shape, together with assignments of each band. A particular emphasis will be given on the importance of the charge resonance (CR) interaction between the dye molecules in the crystals.

Experimental

Materials. 1,1′-Diethyl-2,2′-cyanine iodide (dye iodide) was a product of Japanese Research Institute for Photosensitizing Dyes Co. (Okayama). The crystals of the dye iodide were obtained by recrystallization from methanol solution. The crystals of the dye bromide and the chloride were obtained by metathesis with potassium bromide or chloride after precipitation of the iodide by silver nitrate as silver iodide. The crystalline forms and faces were confirmed by taking X-ray photographs on Weissenberg camera and compared with the published X-ray data.[13–15] The shape of the crystalline forms are sketched as shown in Fig. 1.

Measurements. The reflection spectra were measured with a microscopic spectrophotometer constructed in this laboratory. It consists of an Olympus microscope, a Carl Zeiss Ultrafluar lens (×10), a Nikon crystal mount, a HTV 928 photomultiplier tube as detecting device and an Intel 8080 microcomputer for data processing. The reflectivities were converted to molar absorption coefficients by using Kramers-Kronig transformation on a FACOM 230-60 and 230-75 computers of Nagoya University Computation Center.

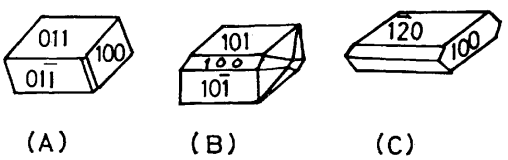

Fig. 1. Crystalline habit and developed faces of (A) dye iodide, (B) dye bromide, and (C) dye chloride.

Table 1. Crystalline data of 1,1'-diethyl-2,2'-cyanine halide

	a(Å)	b(Å)	c(Å)	α(°)	β(°)	γ(°)	Space group	Ref.
Dye iodide	10.787	11.626	16.484	90.0	107.48	90.0	$P2_1/c$	15
Dye bromide	13.530	10.500	14.070	90.0	90.6	90.0	$P2_1/n$	14
Dye chloride	13.586	19.167	10.517	90.0	90.0	134.35	$P2_1/b$	13

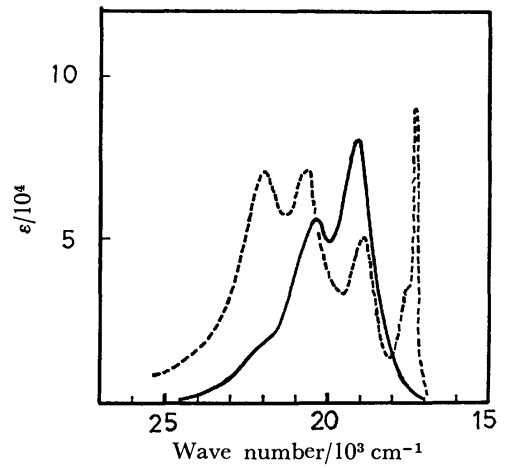

Fig. 2. Solution spectra of the dye iodide in EGW solution at 298 K (2×10^{-5} M, ——) and at 77 K (2×10^{-3} M, ----).

The spectra in a ethyleneglycol–water (EGW) solution at room temperature and 77 K were measured with a Cary 16 spectrophotometer equipped with a Cryo-tip refrigerator (Fig. 2).

Theoretical Considerations on Crystalline Excited States

Molecular Orbital and the Excited State of the Dye Molecule. The molecular orbitals of π electron system of the dye were calculated by Pariser-Parr-Pople[16] method with Nishimoto-Mataga[17] potential. The atomic coordinates determined by the X-ray crystal structure analyses were used for the calculation, and the results were nearly the same for the molecules in the iodide, bromide and chloride crystals. Two quinoline rings are twisted, hence the directions of π electron envelopes were settled along the direction perpendicular to one of the quinoline ring plane, another quinoline ring plane and the plane composed of the central carbon and the adjacent carbons of the quinoline rings. By this choice a pseudo-two-fold symmetry of the MO was conserved.

The highest occupied orbital (orbital 11, HOMO) and the lowest unoccupied orbital (orbital 12, LUMO) have a pseudo-symmetry of S_y and A_y, respectively, where the y axis is the short molecular axis, and the charge density spreads over the whole molecule. The second and the third HOMO are nearly degenerate, and the charge densities are localized on either one of quinoline rings.

The energy of the lowest allowed transition, which is composed of mainly one electron transition from the HOMO to LUMO, was calculated at 18600 cm^{-1} (2.30 eV) and the polarization is along the long axis of the molecule. The calculated value is nearly in agreement with the value found in solution spectra (*cf.* Fig. 2, peak at 19000 cm^{-1}). We consider only this transition in this paper because other bands are weak and locate at higher energy region.

Molecular Exciton States and Intermolecular Exciton Interaction. The crystals treated in this paper are all monoclinic with space groups and lattice constants as shown in Table 1 and they contain four molecules per unit cell. The molecular exciton (MX) state in the crystal, one of them is allowed along the monoclinic axis (A_u state) and another is allowed perpendicular to it (B_u state), are written as

$$\left.\begin{aligned} A_u:\ \Psi_b &= \frac{1}{\sqrt{N}}(\Psi_{1i}-\Psi_{2i}+\Psi_{3i}-\Psi_{4i})e^{ik\cdot R_i} \\ B_u:\ \Psi_{ac} &= \frac{1}{\sqrt{N}}(\Psi_{1i}-\Psi_{2i}-\Psi_{3i}+\Psi_{4i})e^{ik\cdot R_i} \end{aligned}\right\}, \quad (1)$$

where N is the number of molecules in the crystal under consideration, i is the numbering of unit cell and 1, 2, 3, and 4 designate the molecular site. Ψ_{1i} means the original site of the i-th cell is excited and others are in the ground state. Ψ_{2i}, Ψ_{3i}, and Ψ_{4i} are the wavefunction in which the excitation occurs at sites related by the crystal symmetries of inversion, screw-axis rotation and glide-reflection, respectively. The exponential factor shows the translational symmetry of the crystal, and if we consider N molecules with a spacing of a, then $k=2\pi n/Na$ where $n=0,1,2,\cdots N$.

The most significant term of the interaction Hamiltonian is the dipole-dipole type between the transition moment on different molecules. If we denote the HOMO by ϕ_m and LUMO by ϕ_n, the excitation transfer matrix element between the i-th and the j-th molecules will be written as

$$\begin{aligned} b_{ij} &= \int \phi^*_{jn}(r_j)\phi^*_{im}(r_i)\frac{e^2}{r_{ij}}\phi_{jm}(r_j)\phi_{in}(r_i)\,dv_i dv_j \\ &= \frac{1}{R^3_{ij}}\left(\boldsymbol{p}_i\cdot\boldsymbol{p}_j-\frac{3(\boldsymbol{p}_i\cdot\boldsymbol{R}_{ij})(\boldsymbol{p}_j\cdot\boldsymbol{R}_{ij})}{R^2_{ij}}\right) \end{aligned} \quad (2)$$

Here $\boldsymbol{R}_{ij}$ is the vector connecting between the i-th and the j-th molecules, $\boldsymbol{p}_i$ and $\boldsymbol{p}_j$ are the transition moments of these transitions, respectively.

For the strong molecular transition of the dye in the crystal, the dipole interaction is most significant, and the calculation of surface exciton states by a slab sum method is appropriate for the present analysis.[18] Marchetti *et al.*[12] calculated the surface exciton state of the dye iodide to explain the spectral shifts. We have calculated the surface exciton energies for the measured crystalline faces of the dye iodide and bromide and the results of calculation are shown in Table 2. Because the measured crystalline spectra showed a weak coupling type, the estimation of exciton band

Table 2. Calculated and observed band splittings

	Crystalline face	Calculated shift B_n axis	Vib. level n	(cm^{-1})	Observed shift (cm^{-1})	Shift used for simulation
Dye iodide[a]	(100)	b	0-0	−1425	−1650	−1500
			0-1	−1000	−1300	
		c	0-0	1319	1350	1500
			0-1	910	1050	
	(011)	b	0-0	−1034	−1600	
		a, c	0-0	750	1000	
			0-1	520	500	
					1000	
	(011)	b	0-0	−1633	−1600	
		a, c	0-0	123	1000	
Dye bromide[b]	(100)	b	0-0	−1590	−1000	−1000
			0-1	−1113	−900	
			0-2	−398	−200	
		c	0-0	−974	−1040	−1000
			0-1	−682	−700	
			0-2	−244	−400	
	(10$\bar{1}$)	b	0-0	−1590	−1000	
		c	0-0	−260	−200?	
	(101)	b	0-0	−1575	−1000	
		a, c	0-0	1880	2300?	3000
			0-1	1316		
			0-2	470		
Dye chloride[c]	(100)	c	0-0	−1766	−1400	
			0-1	−1236	−1250	
		b	0-0	2184	2500	
	(1$\bar{2}$0)	c	0-0	−2092	−1400	
		a, b	0-0	−520	−500?	

a) D=20 Å, R=100 Å, and E_0=19000 cm^{-1}. b) D=20 Å, R=200 Å, and E_0=18500 cm^{-1}. c) D=20 Å, R=200 Å, and E_0=19000 cm^{-1}.
D=Depth of Slab. R=Radius of summation of molecules. E_0=The center of crystalline transition to compare with the observed spectra.

energies were presented for each vibronic band. The listed values B_n for each vibronic levels were obtained by using $\boldsymbol{p}$ values estimated from the oscillator strength for each vibronic band.

The summation of molecules was taken for the limited radius of sphere (100—200 Å) or the finite depth (10—20 Å) of the slab which gave a convergent result. The energy band structure for each exciton levels is illustrated in Fig. 3. The state density for the single exciton level will be given by $N/2B_n$, but when the higher vibronic exciton band overlaps with the lower ones, the density will be increased in the superposed region.

Charge Resonance State. When molecules in the crystals strongly overlap with neighboring ones, the charge transfer (CT) state becomes important. The crystals now considering are composed of same species, and the CT should occur between each other, hence the CT state should be called as the charge resonance (CR) state. The CR effect in molecular crystal will be two or three-fold; one is for the ground state to stabilize the stacked structure and others are an appearance of the CR exciton band and the modification of the molecular exciton bands.

The CR transition in a neat molecular crystal is not so frequently found; the out of plane transition

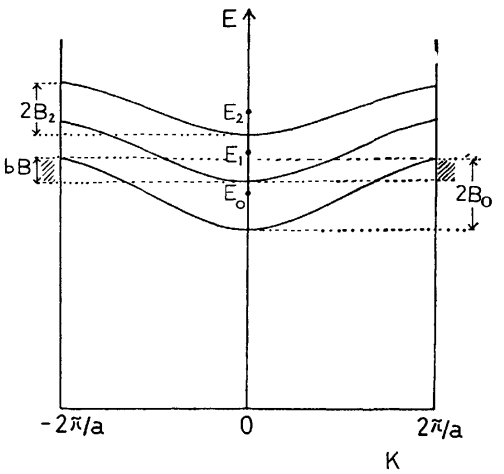

Fig. 3. Molecular exciton (MX) band structure with vibronic exciton splittings.

of the α form crystal of 9,10-dichloroanthracene[19–21] is known to be the case. In anthracenophane molecules where the interplanar distances are very close, the CR absorptions are found but they are rather weak and broad.[22] Apparently the CR transitions are found in cases where a peculiar polarization is

TABLE 3. ENERGY LEVELS OF CHARGE RESONANCE STATE

Dye halide crystals	Axis relating stacked molecules	Energy levels of CR states without polarization correction
Dye iodide	b-axis	3.33 eV
	c-axis	3.36
Dye bromide	a-axis	3.32
	b-axis	3.43
Dye chloride	a-axis	3.20
	c-axis	3.44

expected or a borrowing of intensity from nearby strong allowed transition is accessible. In the present crystals the intermolecular overlap is appreciably large along one-dimensional chain and the CR effect may be found on particular crystalline directions.

The energy level of the CR state is estimated by using the calculated MO and Nishimoto-Mataga[17] potential as shown in Table 3. The potential may underestimate the Coulomb term between molecules, hence the estimated levels may be too high. Moreover the CR state will be stabilized by a polarization force in a highly polarizable crystal as much as 1—2 eV.[23] Therefore the CR level may be at about 2.3 eV and they will be close to or coincident with the molecular exciton levels.

The mixing of the CR state wavefunction Φ to the ground state wavefunction Ψ_0 can be described by the wavefunction of the stabilized ground state as

$$\Psi_G = \Psi_0 + \frac{\langle \Psi_0 | H' | \Phi \rangle}{E_{CR} - E_0} \Phi. \tag{3}$$

The CR matrix element between the stacked molecules will be related to the transfer integral t and it is actually estimated by the overlap integrals between the π electrons of stacked molecules. Namely, the charge transfer matrix will be written, for example, between the HOMO of the i-th molecule and the LUMO of the j-th molecule as $t_{im,jn}$ or simply as t_{mn}. The calculated results of overlap integrals between the neighboring molecules are shown in Table 4, where a single exponent AO and four term expanded AO[24] were used for the calculation and compared in the Table. The empirical values of energy of t integrals are given by

$$t = kS, \tag{4}$$

where the proportional constant k is about $k = -10$ eV for S evaluated by the four term expanded AO and $k = -15$ eV for S obtained by single exponent AO. Referring to Table 2 the largest value is about -0.10—0.15 eV between the HOMO (t_{mm}) and about -0.10 eV between the HOMO and LUMO (t_{mn}). These values are fairly large as the intermolecular interaction in molecular crystal between the same species. The matrix element in Eq. 3 is relevant for t_{mn} and the coefficient of the CR configuration in the ground state is estimated as about 0.1.

The wavefunctions for the optically allowed CR exciton states are written as

$$\left.\begin{aligned} A_u:\ \Phi_b &= \frac{1}{\sqrt{N}} \sum_i (\Phi_{1i} - \Phi_{2i} + \Phi_{3i} - \Phi_{4i}) e^{ik \cdot R_i} \\ B_u:\ \Phi_{ac} &= \frac{1}{\sqrt{N}} \sum_i (\Phi_{1i} - \Phi_{2i} - \Phi_{3i} + \Phi_{4i}) e^{ik \cdot R_i} \end{aligned}\right\}. \tag{5}$$

Here Φ_{1i} implies that an electron in the 1st site of the i-th cell is transferred to the adjacent molecules. The CR exciton band width is estimated with these wavefunctions and only the nearest neighbor interactions are taken into account to give

$$C = b_{CR} + S_{mm} t_{nn} + S_{nn} t_{mm}. \tag{6}$$

Here b_{CR} is the dipole-dipole interaction between the CR transitions on different sites and it is much less as compared to the values of strong molecular HOMO to LUMO transition. The terms $S_{mm}t_{nn}$ are second order to the electron overlap, therefore the CR exciton band width C will be one or two order of magnitudes smaller than B. On this ground the CR exciton band will be much narrow than the MX band. When they are mixed the CR band will be wider than before the interaction.

Mixing of the CR State with Molecular Exciton States. When the CR level is located nearby the MX level, the interaction between the two states will be significant and it may modify the shape of MX band. The wavefunction for the mixed exciton states will be given for A_u state as

$$\left.\begin{aligned} &\Psi_b + \frac{\langle \Psi_b | H' | \Phi_b \rangle}{E_{CR} - E_{MX}} \Phi_b \\ \text{and} \\ &\Phi_b + \frac{\langle \Phi_b | H' | \Psi_b \rangle}{E_{MX} - E_{CR}} \Psi_b \end{aligned}\right\}. \tag{7}$$

The off-diagonal matrix elements between the CR and the MX states include both the dipole interaction and the transfer terms and they will be written as

$$b_{MC} + \sum_{ij} (t_{in,jn} - t_{im,jm}), \tag{8}$$

where b_{MC} is the dipole interaction between the molecular and CR exciton transitions of A_u symmetry and the transfer integrals may be taken over i and j molecules related by translation, inversion, screw-axis and glide reflection, respectively, but actually the transfer interaction between the nearest neighbors is much larger than for other type. This is one of the reason why the mixing occurs anisotropically; the electron overlap between the stacked molecules is significant along particular direction. The dipole-dipole interaction between the two type of transitions may be another probable source of the anisotropy of mixing. The b-axis of the dye iodide and bromide and the c-axis of the dye chloride are the direction along which the CR effect seems important because t_{nm} is large between the molecules stacked along these directions, hence the ground state will have an anisotropic CR character by this mechanism. The intrinsic CR band will be stronger along this direction than others, therefore the mixing through b_{MC} term will be larger along this particular crystalline directions than others.

One of the consequence of the CR and the MX mixing will appear in the exciton band structure. The CR exciton band is narrow and flat, and the

Table 4. Overlap integrals between the MO of stacked dye molecules

Molecules related by inversion symmetry Stacking directions		Overlap integrals between MO			
Dye crystals	MO	Single term AO 11	12	Four term AO 11	12
Chloride					
c-axis	11	0.0059	0.0049	0.0093	0.0079
	12		0.0030		0.0052
a-axis	11	0.0023	0.0002	0.0026	0.0006
	12		−0.0005		−0.0006
Bromide					
b-axis	11	0.0047	−0.0038	0.0077	−0.0066
	12		0.0024		0.0046
a-axis	11	0.0022	−0.0004	0.0027	−0.0008
	12		−0.0007		−0.0010
Iodide					
b-axis	11	0.0069	0.0043	0.0115	0.0061
	12		0.0027		0.0032
c-axis	11	0.0049	−0.0020	0.0057	−0.0016
	12		0.0006		−0.0002

state density may be greatly modified around the interacting region. For instance the energy levels in Fig. 4 show that the CR exciton level exists on the top region of the MX 0-0 band, and after the interaction, by non-crossing rule, the energy curves become plateu and the state density increases greatly in this range. If the 0-1 exciton level is located close to it, the radiationless exciton scattering may be enhanced and the higher vibronic band shape will be broadened significantly by the radiationless transitions.

One of another consequence of the CR and MX mixing may be an appearance of Fano's effect[25] in the begining of the absorption band. An interference which produces a dip or sharpening of the absorption band may be an indication of such interaction.

Band Splitting and Band Shape Analysis of Exciton States. Electronic transitions of large oscillator strength exhibit directional dispersion in anisotropic crystals. Weiser *et al.*[26] analysed the spectra of pentamethine cyanine dye crystal showing that the band shift is changed with the direction of the propagation of light to the crystalline face, however, this method is applicable only for uniaxial crystal.

For the present crystals the surface exciton state is calculated by a slab sum method.[18] The vibrational pattern of the monomer absorption band of the dye is simulated by a Lorentzian type shape function as

$$\left.\begin{aligned} \langle g\rangle &= \sum_{n=0}^{2}\langle g\rangle_n \\ \langle g\rangle_n &= Im\frac{|\boldsymbol{p}_n|^2}{E-E_0-n\lambda-i\gamma_n} \end{aligned}\right\}, \qquad (9)$$

where E_0 is the transition energy of the monomer dye, λ is the vibrational quanta of the coupled normal vibration and γ_n is the half-width of each band. The band width γ_n manifests the coupling of each vibronic level with other low frequency intramolecular and solvent modes. The present monomer spectrum was simulated by using $E_0=19000\ \mathrm{cm^{-1}}$, $\lambda=1300\ \mathrm{cm^{-1}}$ and $\gamma_n=500\ \mathrm{cm^{-1}}$. We took the square of the transition moment $|\boldsymbol{p}_n|^2$ as proportional to the observed vibronic band intensities. Actually each absorption band has a Gaussian shape, but it was approximated by a Lorentzian shape. In the molecular exciton states, following a weak coupling model, each band peak is expected to shift as proportional to the vibronic band intensity and the shift is given by B_n, where the CR effect is not taken into account. Then the absorption shape of the molecular surface exciton states is written as follows.

$$\langle G\rangle = \sum_{n=0}^{2} Im\frac{|\boldsymbol{p}_n|^2}{E-E_0-n\lambda-B_n-i\Gamma_n} \qquad (10)$$

Here Γ_n is the half-width for the n-th vibronic level. The band shapes are simulated for several crystalline faces of the dye bromide and iodide and the results are shown in Fig. 5, where the crystalline Γ_n is taken equal to γ_n of solution spectra.

Results of this simulation may be summarized as follows. (1) When B_n is negative and large, the red shift of the split band is accompanied with increasing separation of the vibrational progressions. The band intensities are distributed among each vibronic levels as in solution spectra. (2) When B_n is positive and large, the blue-shifted vibronic levels are overlapped and converged into a single peak. Some of the measured spectra shown in the following section are consistent with this theoretical band shape analysis, but the J type band is different from this calculation. As regard to the sharpness of the J band, Briggs and Herzenberg[9] and also Sumi[10] attributed it solely to the increased exciton band shift, B, and B/λ was taken as a measure of the interaction, however, actually the same B/λ value does not give the same band shape. The J type absorption shape is found when the higher vibronic transitions lose intensity

and the 0-0 vibronic transition becomes sharp. In fact the J type absorption band appears when the CR level is coincident or close to the MX 0-0 band and the interaction is significant.

The CR band shape is not explained in the above treatment. Apparently extra absorption bands are found in the present crystals in addition to the MX bands, because the electron overlap is appreciably large. They are regarded as the CR bands. Normally the CR transition is rather broad in many molecular crystals, but it is found to be sharp when the CR exciton band width is increased by the mixing with the MX band. Toyozawa[27] pointed out that the half-band width of the exciton absorption band is given by an exciton scattering mechanism and is proportional to the state density of the exciton band. For the localized CR exciton state the band width will be given by

$$\gamma_{CR} = \frac{2\pi}{\hbar} \sum d_{CR}^2 / \Delta_{CR}, \tag{11}$$

where d_{CR} is the matrix element with phonon and Δ_{CR} is the energy of the coupled phonon modes. When the CR level is below the MX 0-0 level and they interact each other, the mixed CR+MX states are formed, and the exciton band-width of CR state may be increased as aB_0, and γ_{CR} will be reduced significantly. The localized CR state is changed into the mobile molecular coupled exciton state. The band-width Γ_{CR} will be narrowed because $aB_0 > \Delta_{CR}$ and $d_{kk'} < d_{CR}$ where $d_{kk'}$ is the exciton scattering matrix. The band-width will be given by

$$\Gamma_{CR} = \frac{2\pi}{\hbar} \sum d_{kk'}^2 / aB_0. \tag{12}$$

The intensity of the mixed transitions is mostly due to the MX 0-0 band, and the absorption appears as a single band or separate bands depending on the coupling of the CR and MX transition dipoles.

The band-width of the MX 0-0 level may be reduced from its original molecular band-width γ_0 by several mechanisms. One is discussed by Toyozawa[27] that when B_0 is large the state density is reduced and Γ_0 will be decreased as

$$\Gamma_0 = \frac{2\pi}{\hbar} \sum d_{kk'}^2 / B_0. \tag{13}$$

For the higher vibronic MX levels, when $B_0 > \lambda$, the 0-0 exciton band will overlap with the 0-1 level, and additional scattering route may be provided through the inter-band scattering and the absorption band-width may be increased as

$$\Gamma_1 = \frac{2\pi}{\hbar} \{ \sum d_{kk'}^2 / B_1 + \sum d_{kk_0}^2 / bB_0 \} \tag{14}$$

The increase of Γ_1 is contrast to the decrease of Γ_0, thus the narrowing of the MX 0-0 band may be interpreted by the exciton band scattering mechanism and the peak intensities of higher vibronic bands will be suppressed by the increase of Γ_1.

However, as is described previously, the CR interaction with the MX band may change the exciton band structure. If the exciton band becomes flat by the CR mixing, the inter-band scattering will be enhanced because the state density is increased around

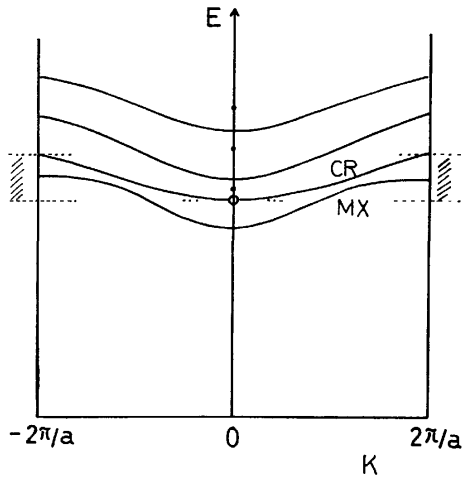

Fig. 4. Mixing of the CR and MX levels and band structures.

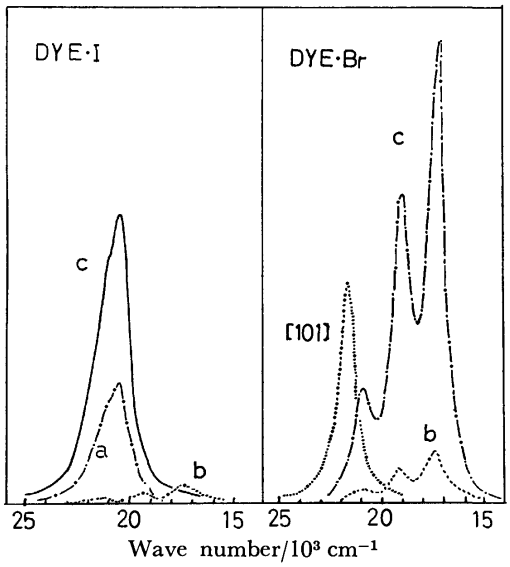

Fig. 5. Simulated absorption spectra of the dye iodide and the dye bromide. The ordinate is absorption coefficient in arbitrary unit.

the interacting region and higher vibronic band has additional decay terms represented by

$$\Gamma_n = \frac{2\pi}{\hbar} \sum t_{CR,MX}^2 / \delta_n,$$

where $t_{CR,MX}$ is the inter-band scattering matrix between the CR and MX states and δ_n is a small energy difference of two levels of nearly iso-energetic condition. The increased Γ_n will make the higher vibronic exciton band very broad and the absorption intensity will be lost except the mixed MX 0-0 band. Moreover the band-width of the MX 0-0 band may be sharpened by the following CR interaction mechanism. When the CR level is above and close to the MX 0-0 band, another mechanism is conceivable as follows. Suppose some phonon coupled 0-0 band may have energy of $E_0 + \Delta_n$, and it is equal to that of the CR level. The mixing with the CR level will take place, and the band-width will be broadened by the inter-band scattering mechanism as is discussed above. Then the MX 0-0 band will be sharper

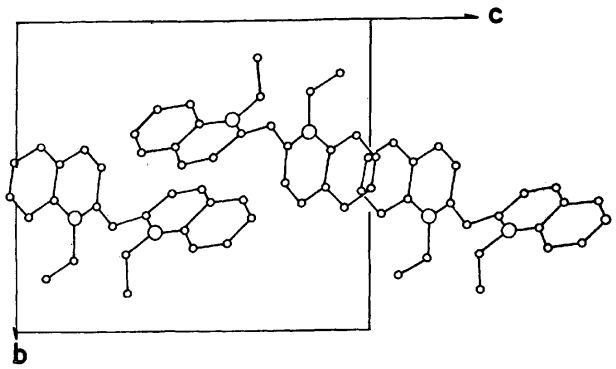

Fig. 6. Projection of molecules in the dye iodide crystal onto the (100) plane.

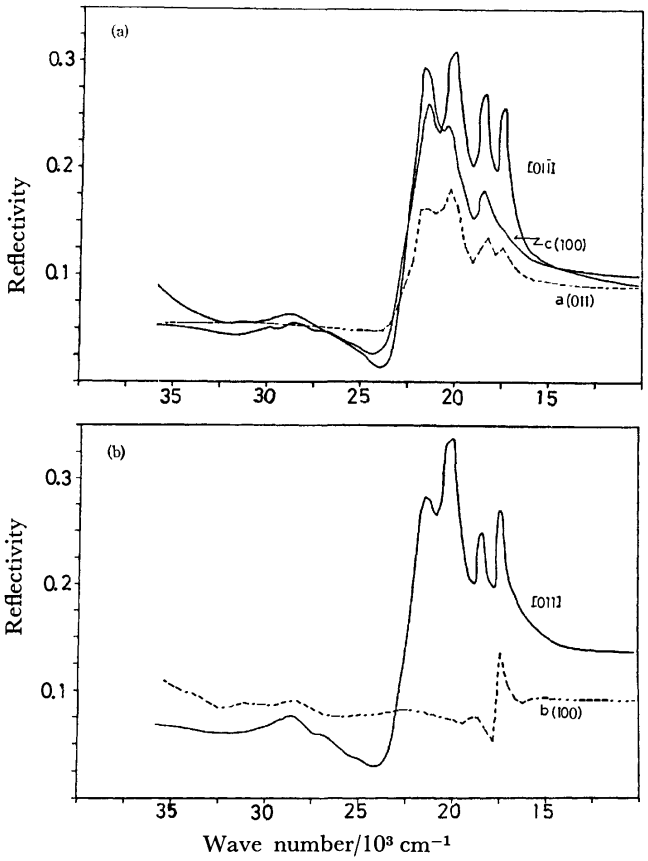

Fig. 7. Reflection spectra of the dye iodide taken with (a) (011), (a,b) (100), and (b) (01$\bar{1}$) faces.

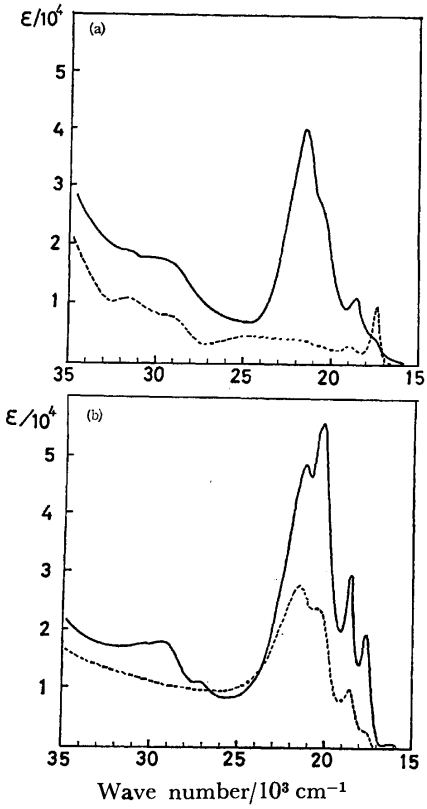

Fig. 8. Absorption spectra of the dye iodide obtained with the (100) and (011) faces.
(a) (100) face, ---- b-axis, —— c-axis.
(b) (011) face, ---- a-axis, —— [01$\bar{1}$] direction.

because some phonon coupled modes lose the peak intensity. These arguments may throw some light on the peculiar band shape of the J band.

Results and Discussion

Crystalline Spectra of the Dye Iodide. The crystals obtained from methanol solution were used for the reflectivity measurement with crystalline faces, (100), (011), and (01$\bar{1}$) as shown in Fig. 1. The projection of molecules onto the (100) plane is shown in Fig. 6 according to the X-ray crystal analysis of Nakatsu *et al.*[15] Two quinoline rings of the dye molecule are twisted each other, and each ring stacks with another quinoline ring of the adjacent molecules. The double array of molecules extend along [101].

The reflection spectra with (100), (011), and (0$\bar{1}\bar{1}$) faces are shown in Fig. 7. The Kramers-Kronig transformation of the reflectivity gives the absorption spectra as shown in Fig. 8. The spectra along the [011] axis is similar to that of along the [01$\bar{1}$]. The absolute values of reflectivity and hence the molar absorption coefficients are dependent on the quality of surface of crystal, therefore the comparison of intensities with different crystalline faces may be less accurate than to obtain the dichroic ratio with the same face.

The spectra with the (100) face (Fig. 8(a)) showed a strong dichroism; the intensity is much stronger along the c-axis than along the b-axis. Actually the intensity along the b-axis is much intensified than the value expected from the oriented gas model; and it may be due to the influence of the CR state which may exist around the 17000—19000 cm^{-1} region. The exciton splitting for the (100) face is calculated as shown in Table 2; the red shift for the b-axis is well explained and the blue shift of the c-axis will be right if we take the 20350 cm^{-1} band along the c-axis as the 0-0 band because it should be fairly strong as compared to other bands. Then the band at 17400 and 18600 cm^{-1} along the c-axis is regarded as the CR band. The broad absorption bands in the 18000—26000 cm^{-1} region appeared along the b-axis are regarded as the mixed band of the CR and MX states, because an enhancement of the intensity and the

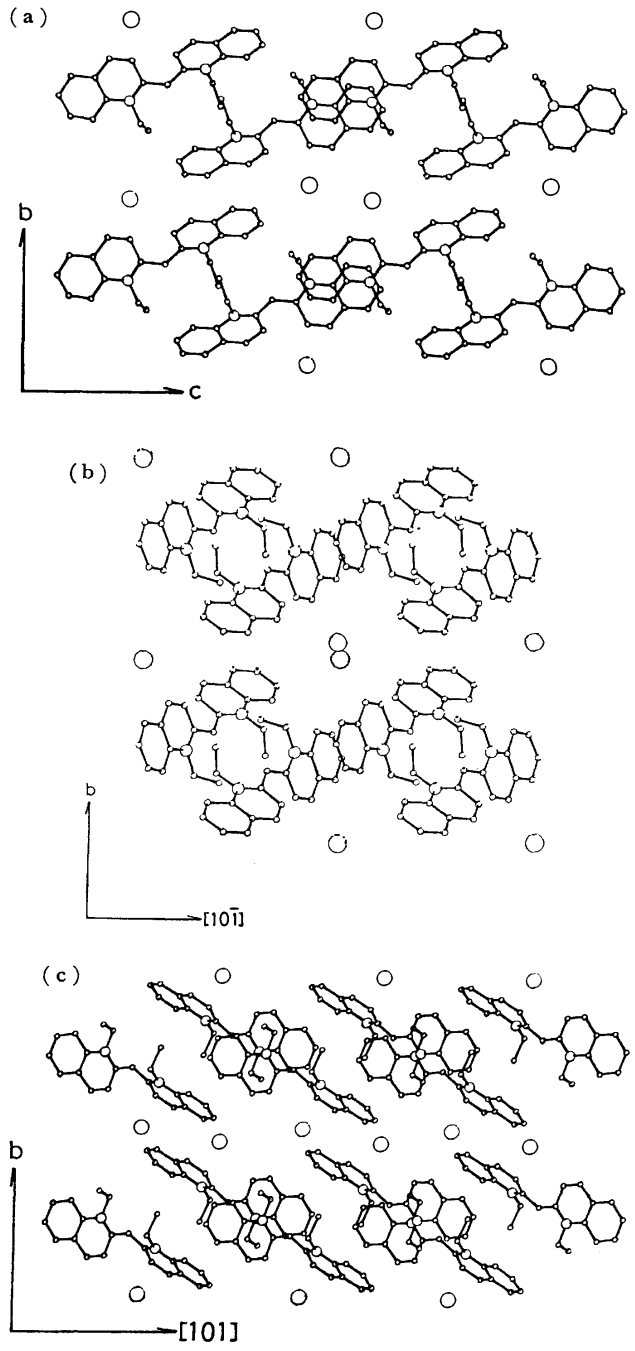

Fig. 9. Projection of molecules onto the developed crystalline faces of the dye bromide.
(a) (100) face, (b) (101) face, and (c) (10$\bar{1}$) face.

sharpening of the 0-0 band may be explained by the interaction between the CR and MX states as is discussed previously.

The spectra with the (011) face is shown in Fig. 8(b). The absorption band along the a-axis is similar to the c-axis band, and the weak humps at 17500 and 18600 cm^{-1} are regarded as the CR band. Along the [01$\bar{1}$] direction both the A_u and the B_u transitions are allowed, the peak at 17400 cm^{-1} is ascribed to the A_u type, while peaks at 18700, 20100, and 21100 cm^{-1} are ascribed to the B_u type transitions. The calculated splittings for the MX bands are approxi-

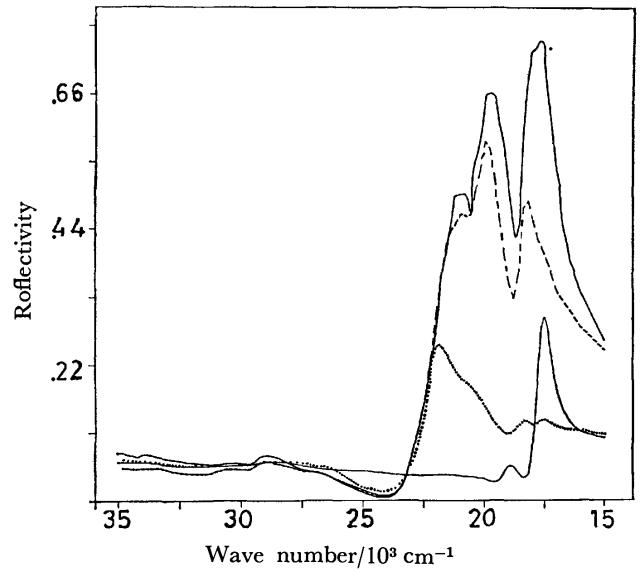

Fig. 10. Reflection spectra of the dye bromide measured with (100) face —— c-axis, —— b-axis, and (10$\bar{1}$) face---- [101] direction (101) face····· [10$\bar{1}$] direction.

mately in agreement with the observed spectral tendency.

The simulated absorption curve by Eq. 10 for the MX vibronic band is shown in Fig. 5, where the intensity is taken as proportional to the oriented gas value. We took the values of B_0 as -1500 cm^{-1} for the b-axis and 1500 cm^{-1} for the c-axis. The calculated curve is in agreement with the observed spectra except that the CR effect is seen along the b-axis and the CR bands are seen along other axes as extra bands. The original CR band starts at about 17000 cm^{-1} and appears in the range of 17500—27000 cm^{-1} as a broad band. Along the b-axis the CR state interacts strongly with the MX state in the 17000—19000 cm^{-1} region and a sharp mixed band is observed, because the electron overlap is largest along this direction. Examination of these spectra shows that the J-type sharp absorption can be found only along the b-axis. It means an importance of CR effect through the electron overlap, since the calculated overlap integrals given in Table 4 show that the b-axis value is larger than for the c-axis and the obtained value is large enough to give effective interaction between molecules.

Crystalline Spectra of the Dye Bromide. The projection of molecules onto the measured crystalline faces are shown in Fig. 9 according to the X-ray structural result of Nakatsu *et al.*[14] The crystalline reflection spectra were measured with (100), (101) and (10$\bar{1}$) faces as shown in Fig. 10 and the absorption spectra calculated by the Kramers-Kronig transformation are shown in Fig. 11. The simulated absorption curve (Fig. 5) is obtained with the reduced surface exciton shift of -1000 cm^{-1} and the 0-0 band origin assumed at 18500 cm^{-1}.

The transition to the A_u excited state, which is allowed along the b-axis, appears at the same position for all measured faces and the calculated value is

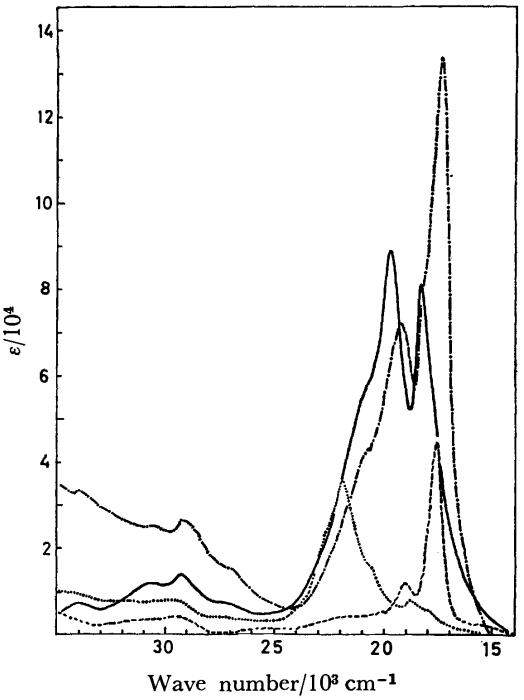

Fig. 11. Absorption spectra of the dye bromide obtained with (100) face —·—·— c-axis, ---- b-axis, (10$\bar{1}$) face —— [101] direction, and (101) face ····· [10$\bar{1}$] direction.

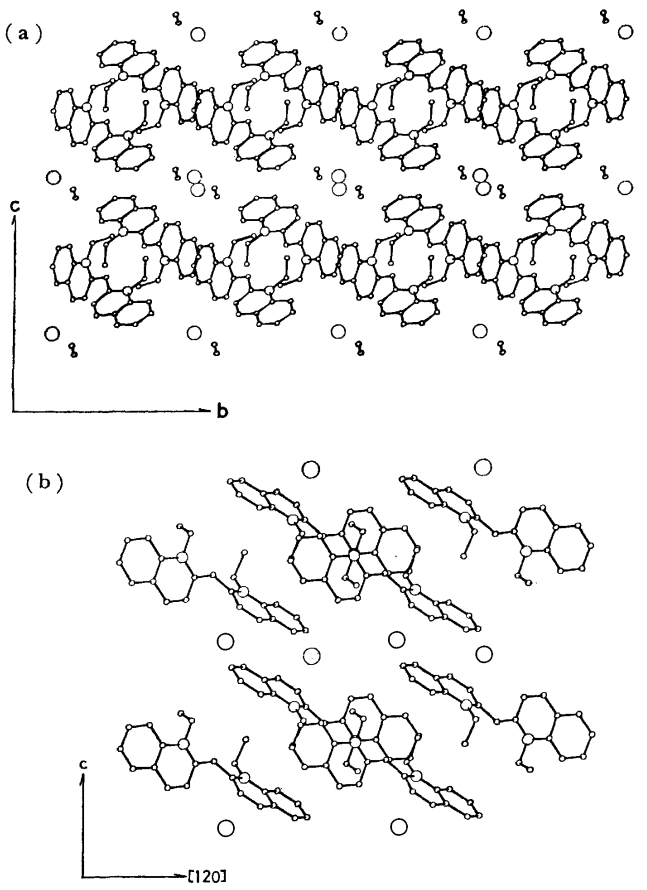

Fig. 12. Projection of molecules onto the developed crystalline faces of the dye chloride (a) (100) plane, (b) (1$\bar{2}$0) plane.

$-1590\ cm^{-1}$, while the observed shift is about $-1000\ cm^{-1}$. Comparison of the intensity of simulated spectra with the observed spectra showed that the 0-0 band is intensified and sharpened. The CR state may exist in this region and the enhancement and the sharpening of the b-axis transition may be due to the interaction of the CR and MX states. The band shape along the b-axis is a typical of J band that the intensity is concentrated around the 0-0 transition and higher vibronic bands are broad and weak.

The transition to the B_u state on the (100) face is allowed along the c-axis, and it shows vibronic structures starting 0-0 at $17460\ cm^{-1}$. Although the exciton shift B_0 is almost same for b and c-axes, the band shape is different. The simulated spectra with a shift of $-1000\ cm^{-1}$ shown in Fig. 5 is in good agreement with the observed spectra, except that the 0-0 band is actually much sharp and intense than the simulated spectra. For the c-axis the mixing of the CR and MX states seems smaller than for the b-axis, presumably because the electron overlap is smaller along this direction.

The B_u type transition on the (10$\bar{1}$) face showed peaks at 18300 and $19700\ cm^{-1}$ and a shoulder at $21000\ cm^{-1}$. We may assign the $18300\ cm^{-1}$ band as the 0-0 band and the $19700\ cm^{-1}$ band as the 0-1 band, because the calculated shift for the 0-0 band is $-260\ cm^{-1}$, but the band progression is not normal as compared to other directions. An alternative plausible interpretation may be that the 18300 cm^{-1} band is the CR mixed band and the MX 0-0 band is shifted to $19700\ cm^{-1}$. The vibronic pattern is normal by this choice, and the CR band is fairly strong because of borrowing intensity from the MX 0-0 band.

With the (101) face along the [10$\bar{1}$] direction a peak is found at $21800\ cm^{-1}$, a shoulder at $20800\ cm^{-1}$ and weak humps around $18800\ cm^{-1}$. The simulated absorption spectra (Fig. 5) is in agreement if we take a shift of $+3000\ cm^{-1}$, but actually the calculated shift is $+1880\ cm^{-1}$ for the 0-0 band. A shoulder at $20800\ cm^{-1}$ may be the shifted 0-0 band. Thus a calculated tendency of overlap of peaks for the blue-shifted bands is actually exemplified. The weak humps around $18500\ cm^{-1}$ region may be the CR band, and it will be weak because the strong MX band shifts to blue and does not mix with it.

In this spectra again the value of B/λ does not show a good correlation with the observed spectral bandwidth. Moreover the directional property of the J band will show the detailed mechanism of the CR and MX mixing that the electron overlap and the dipole interaction anisotropy are important.

Crystalline Spectra of the Dye Chloride. The crystalline structure of the dye chloride was analysed by Dammeier and Hoppe[13] although the crystalline axes were chosen differently from other crystals. The crystal structure is isomorphous with the dye bromide, and the c-axis of the chloride corresponds to the b-axis of the bromide. The [120] and b-axes of the chloride are correlated to the [101] and [10$\bar{1}$] axes of the bromide. The projection of molecules onto the measured

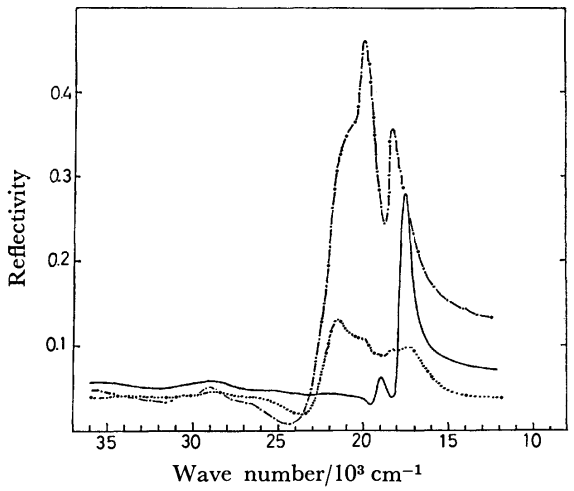

Fig. 13. Reflection spectra of the dye chloride measured with (100) face ····· b-axis, —— c-axis and (1$\bar{2}$0) face —·—·— [120] direction.

faces are shown in Fig. 12. The reflection spectra were measured with the (1$\bar{2}$0) and (100) faces as shown in Fig. 13.

The absorption spectra obtained by the Kramers-Kronig transformation look like the bromide spectra (Fig. 14). The surface exciton splitting on (100) and (1$\bar{2}$0) faces were calculated as shown in Table 2. If we take the molecular 0-0 transition at 19000 cm^{-1} the agreement between the calculated and the experimental values of the shift is quite satisfactory.

The transition along the c-axis is red shifted and the sharp J band appears by the interaction of the CR and the MX states, because the electron overlap is significantly large along the c-axis (Table 4). The band along the [120] axis showed several peaks and a plausible explanation for this pattern may be that the 18400 cm^{-1} band is the mixed CR state and the 19800 cm^{-1} band is the MX 0-0 vibronic transition. The spectra along the b-axis is blue-shifted at 21400 cm^{-1}, and the calculated shift is in reasonable agreement with the observed value. A single peak is appeared because the large blue-shifted vibronic transitions are overlapped as is discussed previously. Another weak shoulder around 18400 cm^{-1} may be due to the CR band. Thus the observed spectra showed a similarity with the bromide spectra reflecting isomorphous crystalline structure.

Spectra of the Dye Iodide in Solution. The J band in solution may be compared with the crystalline spectra in order to find the structure of the J aggregate in solution. The spectra of the dye iodide in a 1:1 ethyleneglycol water (EGW) solution shown in Fig. 2 are nearly in agreement with the earlier results of Zimmerman and Scheibe[3] and Cooper;[4] the J band appears at 77 K. However, the detail of the spectra is slightly different between independent studies and it may be due to the difference in experimental conditions such as the kind of solvent and the concentration of counter ions. For instance the intensity of the J band is varied case by case; it is strongest in water with chloride ion[3] and is weak in ethanol with

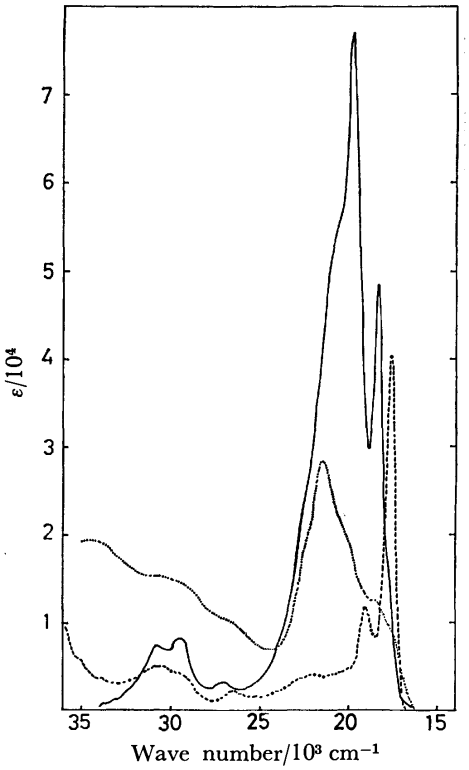

Fig. 14. Absorption spectra of the dye chloride with (100) face ····· b-axis, ---- c-axis and (1$\bar{2}$0) face —— [120] direction.

iodide ion[12] and is intermediate in EGW solution. Cooper[4] observed a doublet structure of the J band on the dye bromide in EGW at 77 K, but we found a weak doublet in dye iodide in the same solution at 77 K. It appears that the change of spectra reflects a variation of the fine structure of the aggregate. Marchetti *et al.*[12] did not report the doublet presumably because their solution contained 0.1 M KI and they proposed that the spectra resemble to the crystalline spectra of the dye iodide, hence the J aggregate will have a similar structure of the iodide crystals. Our results showed that the positions of the aggregate band are very close to the bands found in the iodide crystal rather than that of the bromide, but the intensity of the J band at 17400 cm^{-1} in solution is much stronger than in the crystal. We agree with their opinion that the aggregate in solution may have a similar structure of the iodide crystal.

We have estimated how many molecules might be involved in the aggregate by calculating the band splitting using the same arrangement of molecules in the crystal of the dye iodide. The splitting for the A_u and B_u transitions were calculated for the spherical assemblies of molecules of radius 10—18 Å, which includes 4 to 50 molecules inside. The results of the calculation showed that the sphere of the radius 16 Å containing 36 molecules gives a maximum splitting, the red shift of −1220 cm^{-1} and the blue shift of 1640 cm^{-1}. In solution the splitting of the J band and the blue-shifted 0-0 vibronic band is 3400 cm^{-1}, hence the calculated valuc is smaller than the observed value, but the agreement is not so bad. If we use the crys-

talline data of the dye bromide or chloride, the result is much smaller than for iodide. Although the agreement is not in perfect, but the similarity of the band shape supports the iodide structure and it may be inferred that the J-aggregate of 2,2'-cyanine in solution is conformed of at least 30 molecules assembled like the dye iodide crystal. Scheibe and his coworkers[3,5] discussed the minimum size of the J-aggregate and suggested that it might include at least 7 molecules. Further studies will be required to clarify these points.

Summary of the J Band of 2,2'-Cyanine Dye Crystals. The results of spectral investigation on 2,2'-cyanine dye iodide, bromide, and chloride crystals are summarized as follows. (1) Molecular electronic transition of the dye is split on crystalline surfaces by the exciton interaction. The splittings on the developed crystalline faces are reasonably explained by the dipole-dipole interaction with a slab sum method. The vibronic band shapes are well simulated by a weak coupling model; each vibronic level interacts individually. A red shifted band shows expanded vibronic intervals while a blue shifted one converges into a single peak. In addition, extra bands, which are not found in solution spectra, appear because of the electron overlap effect, that is the CR band.

(2) The J type band is found with particular crystalline directions of specific surfaces. A characteristic of the crystalline J band may be a sharpened 0-0 band and diminished higher vibronic bands. It appears when the CR state is mixed with the split MX state. An extensive electron overlap between the neighbor molecules is an important necessary condition for the appearance of the J band. A coincidence of the MX and CR state is another requisite for the sharp J band. It may be said that the sharp J band will be found only when these several dominating conditions are satisfied, but a widely used nomenclature for the J band may infere the red shifted strong transition with exciton sharpening without the CR mixing. We believe our view is more extensive.

Anyhow, several conditions, a lateral displacement of molecules, which is necessary for a large red shift, an extensive stacking of molecules to give a strong electron overlap, and a coincidence of the MX and CR levels, are satisfied only for rare cases. Therefore the appearance of the J band may be an unusual spectral phenomena associated with specific aggregation of cyanine dyes.

The authors thank to Profs. K. Nakatsu, Y. Toyozawa, and Dr. H. Sumi for helpful information and kind discussions. This research was supported from the Grant-in-Aid of the Ministry of Education, Science and Culture (No. 254144, 1977).

References

1) E. E. Jelly, *Nature*, **138**, 1009 (1936).
2) G. Scheibe, *Angew. Chem.*, **49**, 563 (1936).
3) G. Scheibe, *Z. Elektrochem.*, **47**, 73 (1941), **73**, 52 (1948); H. Zimmerman and G. Scheibe, *Z. Elektrochem.*, **60**, 566 (1956).
4) W. Cooper, *Chem. Phys. Lett.*, **7**, 73 (1970).
5) E. Daltrozzo, G. Scheibe, K. Gschwind, and F. Haimerl, *Photogr. Sci. Eng.*, **18**, 441 (1974).
6) E. D. McRae and M. Kasha, *J. Chem. Phys.*, **28**, 721 (1958).
7) K. Norland, A. Ames, and T. Taylor, *Photogr. Sci. Eng.*, **14**, 295 (1970).
8) G. R. Bird, K. S. Norland, A. E. Rosenoff, and H. B. Michaud, *Photogr. Sci. Eng.*, **12**, 196 (1968).
9) J. S. Briggs and A. Herzenberg, *Mol. Phys.*, **21**, 865 (1971).
10) H. Sumi, *J. Phys. Soc. Jpn.*, **38**, 825 (1975).
11) H. Ito, T. Eri, and Y. J. I'Haya, *Chem. Phys.*, **8**, 68 (1975).
12) A. P. Marchetti, C. D. Salzberg, and E. I. P. Walker, *J. Chem. Phys.*, **64**, 4693 (1976); *Photogr. Sci. Eng.*, **20**, 107 (1976).
13) B. Dammeier and W. Hoppe, *Acta Crystallogr., Sect. B*, **27**, 2364 (1971).
14) H. Yoshioka and K. Nakatsu, *Chem. Phys. Lett.*, **11**, 255 (1971).
15) K. Nakatsu, H. Yoshioka and H. Morishita, *Acta Crystallogr., Sect. B*, **33**, 2181 (1977).
16) R. Pariser and R. G. Parr, *J. Chem. Phys.*, **21**, 466 (1953); *ibid.*, **21**, 767 (1953); J. A. Pople, *Trans. Faraday Soc.*, **49**, 1375 (1953).
17) N. Mataga and K. Nishimoto, *Z. Phys. Chem., N. F.*, **13**, 140 (1957).
18) M. R. Philpott, *J. Chem. Phys.*, **58**, 588 (1973).
19) J. Tanaka and M. Shibata, *Bull. Chem. Soc. Jpn.*, **41**, 34 (1968).
20) S. C. Abbi and D. M. Hanson, *J. Chem. Phys.*, **60**, 319 (1974).
21) K. Syassen and M. R. Philpott, *Chem. Phys., Lett.*, **50**, 14 (1977).
22) M. Morita, T. Kishi, M. Tanaka, J. Tanaka, J. Ferguson, Y. Sakata, S. Misumi, T. Hayashi, and N. Mataga, *Bull. Chem. Soc. Jpn.*, **51**, 3449 (1978).
23) F. Gutmann and L. E. Lyons, "Organic Semiconductors," John Wiley, New York (1967), p. 345.
24) E. Clementi, *IBM Journal of Res. Dev.*, **9**, Suppl, 2 (1965).
25) U. Fano, *Phys. Rev.*, **124**, 1866 (1961).
26) H. J. Hesse, W. Fuhs, G. Weiser, and L. von Szentpaly, *Phys. Status Solidi B*, **76**, 817 (1976).
27) Y. Toyozawa, "Proc. IVth International Conf. on Vacuum Ultraviolet Radiation Physics," ed by E. E. Koch, R. Haensel, and C. Kunz, Pergamon (1974), p. 317.

The J-aggregate 5,5′,6,6′-Tetrachloro-1,1′-diethyl-3,3′-bis(4-sulfobutyl)-benzimidazolocarbocyanine Sodium Salt in Aqueous Solution

Shigetoshi Makio, Nobuaki Kanamaru, and Jiro Tanaka*

Department of Chemistry, Faculty of Science, Nagoya University, Chikusa-ku, Nagoya 464

(Received April 18, 1980)

The aggregation of the title dye in a dilute alkaline aqueous solution is investigated at 283—303 K by measuring the electronic absorption spectra. The association number is estimated to be 8, the heat of formation and the entropy change for the association are found as $\Delta H = -91.5$ kcal mol^{-1} (1 cal=4.184 J) and $\Delta S = -139.3$ cal K^{-1} mol^{-1}, respectively. The structure of the octamer is discussed from a view of spectral shift, intermolecular force and the crystalline structural data. The lifetimes, quantum yields and polarization of fluorescence are investigated on the monomeric and the J-aggregate state of the dye. The energy transfer between several J-aggregate units is indicated in the excited state.

The appearance of the J band is an extraordinary spectral phenomenon caused by molecular association. Since Jelly[1] and Scheibe[2] found the J band, its origin has been discussed by many people. Herz[3] has reviewed the aggregation of organic dyes in solution, but only a few dyes are known to form the J-aggregate in solution. The aggregation number of the J-aggregate is not firmly fixed; different numbers, $n=3$—7, have been proposed for 2,2′-cyanine chloride[4,5] and $n=4$ for the dye discussed in this paper.[3] 5,5′,6,6′-Tetrachloro-1,1′-diethyl-3,3′-bis(4-sulfobutyl)benzimidazolocarbocyanine sodium salt is a good sensitizer for silver halide crystals and easily forms the J-aggregate in aqueous solution,[3] in a monomolecular film and on silver halide crystals.[6] We have investigated the equilibrium of the dye in a dilute alkaline aqueous solution and obtained the aggregation number, the equilibrium constant and the heat of formation. A model of the aggregate is suggested based on the crystal structural data and a theoretical calculation of the molecular interaction.

Experimental

The dyes used were gifted from Fuji Film Co. and were used without further purification. The water used for the solvent was twice distilled with potassium permanganate to remove oxidant and carbon dioxide. The dilute NaOH aqueous solution was prepared by carefully adjusting the pH of solution at 11.0. The dyes were dissolved immediately before experiment into the prepared solvent to attain the concentration to be measured. The temperature of the dye solution was kept constant with an accuracy of ±0.04 °C by circulating thermostated water around the cell compartment. The temperature was measured with a copper-constantan thermocouple by a Hewlett-Packard type 3465 B digital multimeter. The visible absorption spectra were recorded with a Cary 16 spectrophotometer. The fluorescence, the fluorescence excitation, and polarization spectra were measured with a Shimadzu spectrofluorometer RF-501. The band-width of the fluorescence was measured with a Spex double spectrometer under a narrow band excitation of the dye laser, Spectra Physics model 375 at the Institute of Molecular Science. The lifetime of fluorescence was measured by a HTV streak camera excited with a p s pulse of the second harmonics of YAG laser at the Institute of Molecular Science. The condition for the aggregation is dependent on several unexpected factors: *e.g.* a careful removal of the oxidant from the water is essential and the stability of the dye solution must be checked before each measurement.

Results and Discussion

A typical spectral change by the dye aggregation is shown in Fig. 1 for the concentration range of 10^{-7}—10^{-3} mol/dm^3 at 293 K. The monomer absorption peak was found at 19490 cm^{-1}, and a shoulder was observed at 20900 cm^{-1}. The peak of the J absorption band was observed at 17040 cm^{-1} with a half-band width of 240 cm^{-1}. An isosbestic point was found at 18590 cm^{-1}, and the tail of the absorption of the J-aggregate extended to 21000 cm^{-1} region (curve 9 of Fig. 1).

The equilibrium between the monomer and the J-aggregate is described as

$$nM \rightleftharpoons J, \tag{1}$$

where the equilibrium constant, K, is given by

$$K = \frac{C_J}{(C_M)^n}. \tag{2}$$

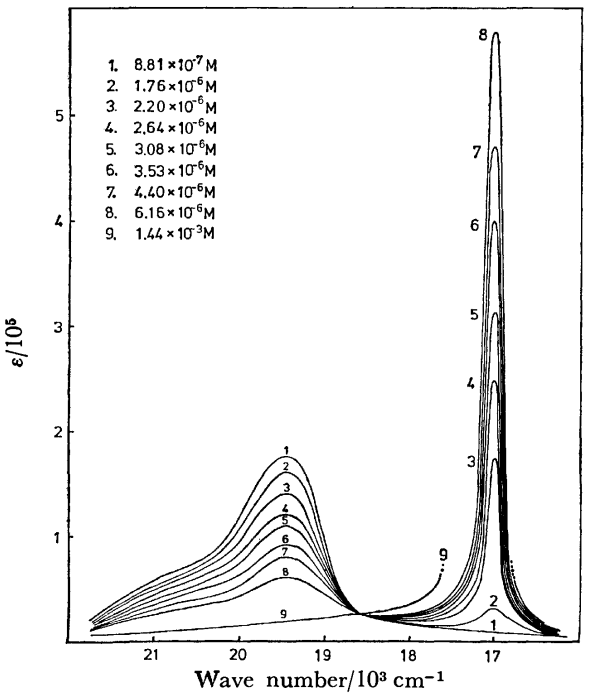

Fig. 1. Change of electronic absorption spectra with the concentration of the dye in a dilute alkaline aqueous solution (pH=11.0). (The concentrations are given in unit of monomer.)

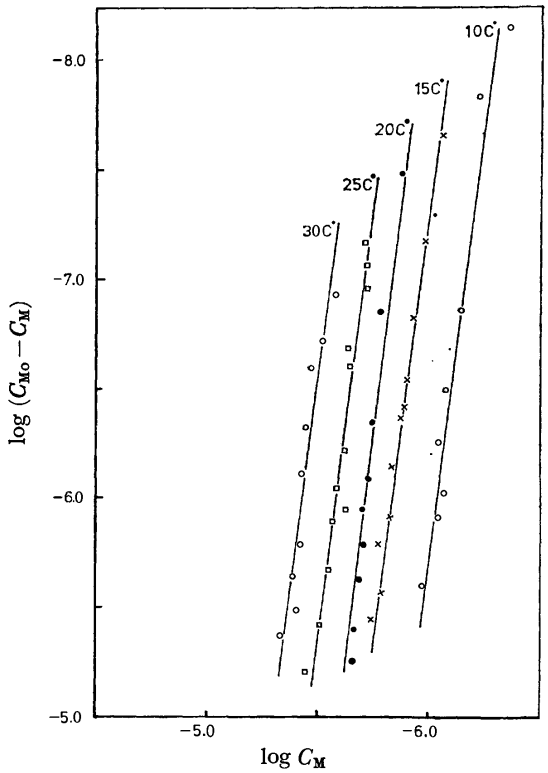

Fig. 2. Plots of $\log(C_{Mo}-C_M)$ against $\log C_M$.

Here C_J and C_M are the concentrations of the J-aggregate and the monomer, respectively. If the nominal concentration of the dye is shown by C_{Mo}, then

$$C_{Mo} = C_M + nC_J = C_M + nK(C_M)^n. \quad (3)$$

By taking the logarithms we obtain

$$\log(C_{Mo}-C_M) = n\log C_M + \log(nK). \quad (4)$$

We have carefully measured C_M by using the monomer's molar absorption coefficient, $\varepsilon_M=175000$, at 19490 cm^{-1} and used them to obtain constants in Eq. 4. A plot of $\log(C_{Mo}-C_M)$ *versus* $\log C_M$ is shown in Fig. 2, where the contribution of the tail of the J-band to the absorption at 19490 cm^{-1} is estimated by the absorption spectrum of a high concentration solution, which indicated a slight absorption of the J-band as shown in curve (9) of Fig. 1. Although Herz[3] plotted $\log(nC_J)$ *versus* $\log C_M$ in his analysis, we used $(C_{Mo}-C_M)$ instead of nC_J, because the concentration of the J-aggregate at the initial stage of the aggregation is liable to experimental artifact. When we use the intensity of the J band for equilibrium measurements, the results were not quantitatively reproducible for small absorbance. It appears that the concentration of the residual monomer which does not aggregate in solution is more precisely determined than that of the aggregate in the early stage of aggregation.

The gradient of the straight lines drawn for these plots gives the association number $n=8$, which is different from the value $n=4$ reported by Herz.[3] Since the present experiment covers wider temperature and concentration ranges, we believe that 8 is more reliable. Actually the gradient of the plot is easily influenced by uncertain experimental conditions, and it has tendency to give rather larger value more than 8.

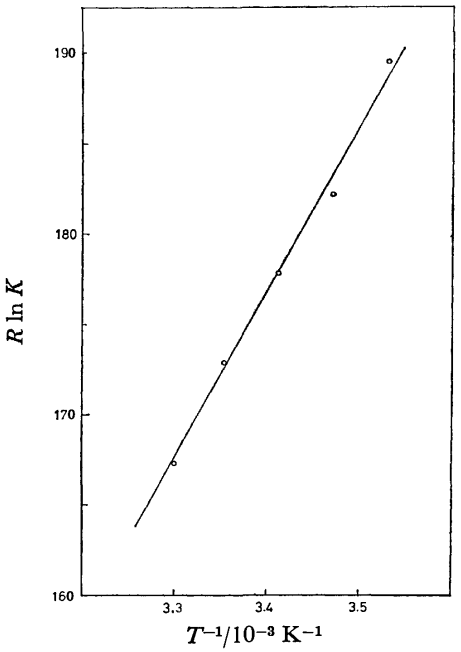

Fig. 3. A plot of $R\ln K$ against T^{-1}.

Table 1. Equilibrium constants and free energies of association

Temp K	Association number	$10^{-4}\varepsilon_J/8$	$\log K$	$-\Delta G$ (kcal mol^{-1})
283	8	85.3	41.4	53.7
288	8	85.3	39.8	52.5
293	8	85.2	38.8	52.0
298	8	78.7	37.8	51.5
303	8	75.9	36.6	50.7

By using this number, the equilibrium constants K were determined at several temperatures (Table 1). In the Table the molar absorption coefficients of the octamer are shown confirming that the values are reasonably constant. The plot of $R\ln K$ against $1/T$ gives the heat of formation and entropy change for the aggregation. The values are $\Delta H=-91.5$ kcal mol^{-1} and $\Delta S=-139.3$ cal K^{-1} mol^{-1} for the octamer. These values are much larger than those of dimerization ($\Delta H=-3$——-8 kcal mol^{-1}, $\Delta S=-10$ cal K^{-1} mol^{-1})[7-11] and of trimerization ($\Delta H=-11$ kcal mol^{-1})[11] for other dyes. This result indicates that the octamer is formed concertedly without an intermediate stage as is consistent with the appearance of the isosbestic point in Fig. 1.

The J type absorption band was found in the crystal of5,5′,6,6′-tetrachloro-1,1′,3,3′-tetraethylbenzimidazolocarbocyanine iodide solvated with two molecules of methanol,[12] and it was realized that the intermolecular arrangement and contact is very important for the appearance of the J band. It seems certain that the J-aggregate in solution takes a similar conformation as was seen in the crystal structure determined by Smith and Luss.[13]

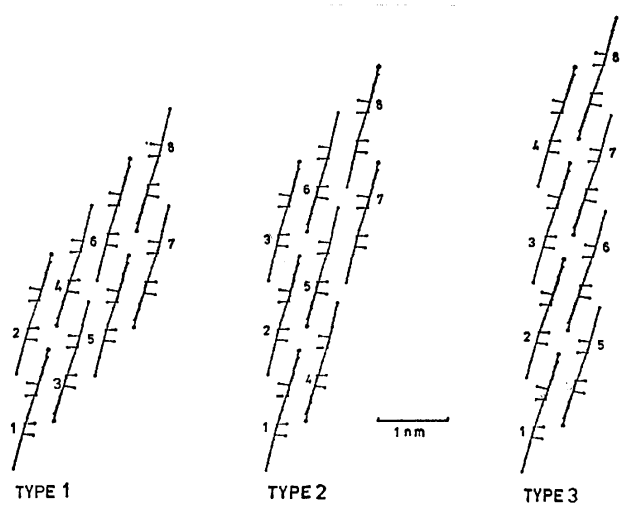

Fig. 4. Three types of model of J-aggregate

We have tried to correlate the observed J band shift with the calculated band shift in the models of the octamer. The calculation is not merely to evaluate the spectral shift by a theoretical calculation, but to estimate the magnitude of the intermolecular attraction by a dispersive and charge transfer forces.

Now we assume three models of the J-aggregate as shown in Fig. 4, where the dyes are placed face to face on a sheet as in the crystal of the dye solvated with two methanol molecules.[13] Eight dye molecules are arranged as in the crystalline bc plane; the choices of lateral displacement are different for three kinds of models. The exciton states are presumed for the octamer; the wavefunction of the ground and the excited states are written as

$$\Phi_G = \prod_{i=1}^{8} \phi_i^\circ$$
$$\Phi_E = \sum_{j=1}^{8} \left(\prod_{i \neq j}^{8} \phi_i^\circ \right) \phi_j^e \qquad (5)$$

where ϕ_i° and ϕ_j^e mean the ground and the excited states of the i-th and the j-th molecules. The calculation of the energy shift is carried out for the allowed in phase state given by Eq. 5 by a dipole-dipole approximation and by a somewhat rigorous transition density method.[14] In the dipole-dipole approximation the length of the transition dipole was estimated as 2.42 Å from the solution spectral oscillator strength of the monomer absorption band. Here we take the strong coupling model for the aggregate, in which all transition intensities are concentrated in the 0-0 band. In the transition density model we take it as $\pm 0.32\,e$ charges separated by 7.54 Å in the molecular plane based on the MO calculation. The results of calculation is shown in Table 2, and it is found that the type 1 model gives the largest stabilization of the excited state and the two methods give identical results. Experimentally the observed shift is $-2460\ \mathrm{cm}^{-1}$, hence the magnitude of the shift is well explained by these models. So far no rigorous proof for the in-phase Φ_E to be real eigenstate of the system is given. However, the 8-th order eigenvalue problem was solved for the type 1 model, and the result gave practically the same energy ($-2950\ \mathrm{cm}^{-1}$) and the intensity of 84% as given by in-phase Φ_E. The lowest energy state has the largest transition dipole, and the wavefunction shows that the excitation distributes more in the middle of the aggregate.

Table 2. Shift of absorption spectra calculated by exciton type interactions

Model	Dipole-dipole approximation	Transition density method
1	$-3000\ (\mathrm{cm}^{-1})$	$-2800\ (\mathrm{cm}^{-1})$
2	-2700	-2650
3	-2500	-2400

Table 3. Overlap integrals between dye molecules

Overlap types	A	B	C
Overlap integrals S	-0.0003	-0.0036	0.0074

Table 4. Comparison of overlap index

Model	Overlap index
1	24.6×10^{-5}
2	19.1×10^{-5}
3	22.0×10^{-5}

The stabilization energy of the aggregate by the dispersion force in the ground state may be estimated by the perturbation theory as follows. The van der Waals force (dispersion force) for the pair-wise molecules i and j will be given by

$$E_{v.d.w} = \sum_e \frac{|\langle \phi_i^e \phi_j^e | V | \phi_i^\circ \phi_j^\circ \rangle|^2}{E_{ei} + E_{ej} - E_{oi} - E_{oj}} \qquad (6)$$

where the values of matrix element are the same for the calculated ones given in Table 2. Therefore the larger the shift the greater will be the dispersion force, and the type 1 model seems to be most stable from this point of view.

The charge transfer force between the dye pair may be estimated by the following formula

$$E_{CR} = \frac{4\beta_{ij}^2}{E_{CT} - E_o} = \frac{4(kS_{ij})^2}{E_{CT} - E_o} \qquad (7)$$

where the dye molecules are presumed to play roles of both the electron donor and acceptor. Here β_{ij} is Mulliken's charge transfer integral approximated by the overlap integral between the HOMO and LUMO of the paired dye molecules, i and j. There are three types of overlap of dye molecules, A, B, and C in the order of increasing overlap integrals in the crystal of the dye with two methanol molecules.[13,15] The numerical calculation of the overlap integrals will be published in a separate paper and only the values are shown in Table 3. For three types of models we evaluate the overlap index given by $\sum_{ij} S_{ij}^2$ as shown in Table 4. The result of the calculation shows that type 1 is most stable from a view of the charge resonance interaction.

One more important force for the molecular association in aqueous solution is hydrophobic force which is produced by the surface tension of water.[16]

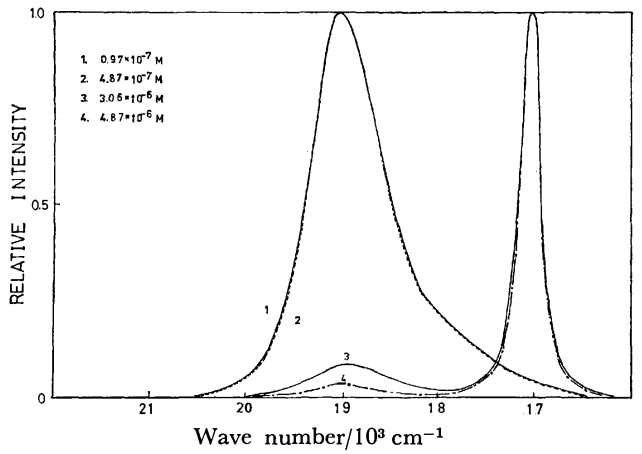

Fig. 5. Change of fluorescence spectra with the concentration of the dye.

The force will be greatest if the surface area of the aggregate is smallest and the type 1 model is most favorable from this point. On these grounds we may guess that the shape of the J-aggregate in aqueous solution correspond to type 1 model.

Fluorescence Spectra. The fluorescence spectra at various concentration of the dye measured by the excitation at 21740 cm^{-1} is shown in Fig. 5. The monomer fluorescence band shows a Stokes shift of 620 cm^{-1}, while the sharp J-band emission shows no Stokes shift. The band shape of the J-emission band was measured by a sharp dye laser excitation at 17340 cm^{-1} and 17182 cm^{-1} for the solution of 2.14×10^{-6} mol/dm^3, but it did not show any shift or broadening by changing the excitation energy. The band-width of the emission was only 150 cm^{-1}, which is smaller than the absorption band-width. Anomalous sharpening and zero-Stokes shift by aggregation are quite unusual as a complex organic molecule. An importance of charge resonance effect on the excitation transfer is discussed on various crystals as is discussed in separate papers.[12]

The excitation spectra for this sharp fluorescence band was in perfect agreement with the absorption spectra of the J-aggregate, and a long tail of absorption extended into the 22000 cm^{-1} region. The excitation profile of the J-emission was completely different from that of the monomer emission, therefore a possibility of energy transfer from the monomer to the J-aggregate may be rejected.

The quantum yields of fluorescence were measured relative to that of rhodamine B (0.97) in ethanol:

Monomer $\Phi^M = 0.03 \pm 0.006$

Aggregate $\Phi^J = 0.25 \pm 0.05$.

The lifetimes were measured at ambient temperature by a p s YAG laser as follows;

Monomer $\tau^M = 0.12 \pm 0.03$ ns

Aggregate $\tau^J = 0.062 \pm 0.01$ ns.

The lifetime of emission is correlated to the absorption oscillator strength f and fluorescence quantum yield. The natural lifetime is approximately given as

$$\tau_0 = 1.500/\bar{\nu}^2 f$$

and the fluorescence lifetimes are

$$\tau^M = \Phi^M \cdot \tau_0(M)$$
$$\tau^J = \Phi^J \cdot \tau_0(J).$$

The oscillator strength of the aggregate absorption is conserved as compared to the monomer absorption, *i.e.* $f(M)=1.02$ and $f(J)=8.16$, from these and observed quantum yields we obtain $\tau^M=0.12$ ns and $\tau^J=0.16$ ns as calculated values. The agreement is excellent for the monomer and is not good for the J-aggregate.

The radiative (k_r) and non-radiative (k_{nr}) decay rates of the excited state are related to the quantum yield of fluorescence Φ and fluorescence life time τ as follows.

$$\Phi = \frac{k_r}{k_r+k_{nr}}$$
$$\tau = \frac{1}{k_r+k_{nr}}.$$

By using the observed values, these rates are evaluated for the monomer and the J-aggregate as

	$k_r[s^{-1}]$	$k_{nr}[s^{-1}]$
Monomer	2.5×10^8	8.1×10^9
Aggregate	4.0×10^9	1.2×10^{10}.

It is apparent that the J-aggregate has 16 times larger radiative rate as compared to the monomer. A most plausible explanation for this enhancement is that the fast excitation transfer takes place between more than two J-aggregate units within the life time of the excited state, and the coherent excited state has a larger radiative transition probability than the value expected for the octamer ($f(J)=8.16$). The extent of the excitation transfer might be more than two units, because two is an ideal number expected for the parallel arrangement which will be never realized in solution. Therefore the delocalization of the excited energy between several J-aggregate is the most acceptable reason for the discrepancy between τ^J (calcd) and τ^J (obsd).

Further support for the fast excitation transfer between the J-aggregate is given by the polarization measurement. The polarization of the emission bands were measured at different temperatures; the p-values were

p(monomer) $= 0.40\pm0.04$ for 275—303 K

p(aggregate) $= 0.20\pm0.02$ at 303 K

p(aggregate) $= 0.23\pm0.02$ at 275 K

in dilute alkaline solution. The relation given by Perrin[17,18] on the rotational relaxation of the chromophore and the p-value is

$$p = p_0\left[1+\left(1-\frac{p_0}{3}\right)\left(\frac{\tau_{fl}}{\tau_{rot}}\right)\right]^{-1}$$

where p_0 is an ideal polarization value for rigid chromophore, τ_{fl} and τ_{rot} are the fluorescence and rotational relaxation lifetimes. From this equation and putting $p_0=0.45$ we may estimate the rotational relaxation times for the monomer to be 1.18 ns, while that of the J-aggregate is 0.04 ns. If we assume the excitation of the J-aggregate is confined within octamer, this result is quite unreasonable since the large aggregate

has a much shorter rotational time constant than a small monomer. If the energy transfer between several J-aggregate is very efficient, the low p-value is reasonably accepted as a polarization quenching by a fast energy transfer.

The authors thank to Profs. E. Hirota and K. Yoshihara of the Institute for Molecular Science for the use of the dye and YAG lasers. This research was supported in part from the Grant-in-Aid of the Ministry of Education, Science and Culture (No. 254144, 1977).

References

1) E. E. Jelly, *Nature*, **138**, 1009 (1936).
2) G. Scheibe, *Angew. Chem.*, **49**, 563 (1936).
3) A. Herz, *Photogr. Sci. Eng.*, **18**, 323 (1974).
4) H. Zimmerman and G. Scheibe, *Z. Elektrochem.*, **60**, 566 (1956).
5) E. Daltrozzo, G. Scheibe, K. Gschwind, and F. Waimerl, *Photogr. Sci. Eng.*, **18**, 441 (1974).
6) D. F. O'Brien, *Photogr. Sci. Eng.*, **18**, 16 (1974).
7) K. Rohatgi and G. Singhal, *J. Phys. Chem.*, **70**, 1695 (1966).
8) K. Rohatgi and K. Mukhopadhyay, *Chem. Phys. Lett.*, **12**, 259 (1971).
9) E. Rabinowitch and L. Epstein, *J. Am. Chem. Soc.*, **63**, 69 (1941).
10) B. Robinson, A. Loffler, and G. Schwarz, *J. Chem. Soc., Faraday Trans. 1*, **69**, 56 (1973).
11) J. Paddy, *J. Phys, Chem.*, **72**, 1259 (1968).
12) J. Tanaka, M. Tanaka, and M. Hayakawa, *Bull. Chem. Soc. Jpn.*, **53**, 3109 (1980). J. Tanaka, M. Tanaka, and N. Kanamaru, "Relaxation of Elementary Excitations," ed by R. Kubo and E. Hanamura, Springer, Berlin (1980), pp. 181—194.
13) D. L. Smith and H. R. Luss, *Acta Crystallogr. Sect. B*, **28**, 2793 (1972).
14) V. Czikklely, H. D. Forsterling, and H. Kuhn, *Chem. Phys. Lett.*, **6**, 207 (1970).
15) T. Kaneda, S. Yoon, and J. Tanaka, *Acta Crystallogr., Sect B*, **33**, 2065 (1977).
16) O. Sinanoglu, "Molecular Association in Biology," Academic Press, New York (1968), p. 427.
17) F. Perrin, *J. Phys. Radium*, **5**, 497 (1934).
18) G. Porter, P. J. Sadkowski, and C. J. Tredwell, *Chem. Phys. Lett.*, **49**, 416 (1977).

Behavior of Sulfate Ions during Formation of Anodic Oxide Film on Aluminium

Yoshio FUKUDA* and Toshiro FUKUSHIMA

Corrosion Division, National Research Institute for Metals, 2-3-12, Nakameguro, Meguro-ku, Tokyo 153

(Received April 21, 1980)

The incorporation of sulfate into anodic film formed on aluminium in an H_2SO_4–$MgSO_4$ solution was investigated by infrared spectroanalysis using the compensation method. The sulfate content of the film was very small at the initial stage of anodizing, but increased with time to a nearly constant value. This result is explained in terms of the variation of strength of electric field and the mobility of each anion in the barrier layer. The distribution of sulfate across the cell wall also was examined. The sulfate content was relatively small near the wall/solution interface, but increased with the distance across the wall from the surface, reached a maximum value on the intermediate layer between the wall/solution interface and the cell boundary, and decreased gradually. Such distribution is considered to be similar to that across the barrier layer. The SO_4 distribution and the transfer of anions from the barrier layer to the porous layer are explained.

When aluminium is anodized in an aqueous solution of an acid such as sulfuric or oxalic acid, porous-type films are formed. These films consist of hexagonal columnar cells, each of which contains a cylindrical pore. At the bottom of the pore there is a thin layer, called the "barrier layer."[1] Probably only the barrier layer forms immediately after the start of electrolysis, but in a short time pores are developed by the solvent action of the electrolyte on the layer, and then close-packed cells are established. While the formation and dissolution of the barrier layer occur simultaneously, the porous layer grows toward the metal. Accordingly, the initially formed film is located near the outer surface. Such porous-type films contain more electrolyte anions than barrier-type films which are formed in neutral salt solutions.[2] This fact suggests that the anions involved in the film affect the dissolution behavior of the film and determine the type of the film. Therefore, a study of the anodic behavior of electrolyte anions during the pore development is important to understand the pore-formation process and the properties of the films. From this point of view, the time dependence and distribution of the oxalate content of the film formed in oxalic acid were elucidated in a previous paper.[3] The distribution of anions in the film formed with phosphoric acid also has been described.[4,5]

Although the incorporation of sulfate into the initially formed film has been studied by Brace and Baker[6] using ^{35}S as a radioactive tracer, the time dependence and distribution of sulfur content of the film are not obvious. Whether or not the behavior of anions at a constant current density is different from that of anions at a constant voltage also is not obvious.

The time dependence of sulfate content of the film during anodization in an H_2SO_4–$MgSO_4$ solution at a constant current density or a constant voltage was examined by infrared spectroanalysis using the compensation method. The anion distribution across the cell wall was examined by gravimetric analysis and the manner of transfer of anions from the barrier layer to the porous layer was speculated about.

Experimental

Foil specimens of 99.99% aluminium (annealed, 150 mm × 70 mm × 0.1 mm or 150 mm × 35 mm × 0.1 mm) were treated with a hot solution of mixture of phosphoric acid and chromic acid to remove natural oxide film, and then were anodized. For Auger electron spectroscopy and electron microscopic observation, electropolished aluminium sheets (25 mm × 10 mm × 0.5 mm) of the same purity were used. A 3 dm^3 beaker was used as an electrolytic cell, the cathodes being made of two plates of carbon (200 mm × 45 mm × 10 mm).

Anodizing was carried out in a mixed solution of 0.6 mol dm^{-3} H_2SO_4 and 0.4 mol dm^{-3} $MgSO_4$ at 30 °C for 3 s—30 min by applying a constant current density of 1 A dm^{-2} or a constant bath voltage of 18 V while the solution was stirred at a nearly constant rate. In every process, after the steady state was reached, the current density was 1 A dm^{-2} and the bath voltage was 18 V. Magnesium sulfate was added to sulfuric acid in order to retard the arrival at the critical point ('c' in Figs. 6 and 7) by suppression of the dissolution of the film.[7] Since the Mg content of the film was extremely small and the sulfate content of the film was nearly the same as that of sulfuric acid film,[7] the film-forming characteristics of this mixture are considered to be essentially the same as those of sulfuric acid alone.

After the anodized specimens were rinsed in running water for 10 min,[6] the films were isolated by the mercury (II) chloride method. The films were rinsed, dried, and fully crushed. Thereafter, the SO_4 content of the films was determined by gravimetric analysis ($BaSO_4$) and by infrared spectroanalysis (KBr disk; sample = 3.5 mg, KBr = 800 mg). The chemical composition of the film near the surface and the film/metal interface were analyzed by a PHI Auger spectrometer during or after Ar^+ ion sputtering (E_p = 3 kV). The thin films isolated were observed directly with a transmission electron microscope at an accelerated voltage of 50 or 100 kV.

Results

Electron Microscopic Observation. At the constant current density, numerous pores of small radii were observed in the 3 s-film (Fig. 1). The radii of some pores increased with time and the number (surface density) of pores decreased (Fig. 2). The total area of pores decreased with time to a nearly constant value after 20 s.

At the constant bath voltage, the average radius of the pores and its variation with time were nearly the same as those obtained by the constant current process. Altough the number of pores in the 3 s and 10 s films was smaller than that obtained by the constant current process, the number decreased with time,

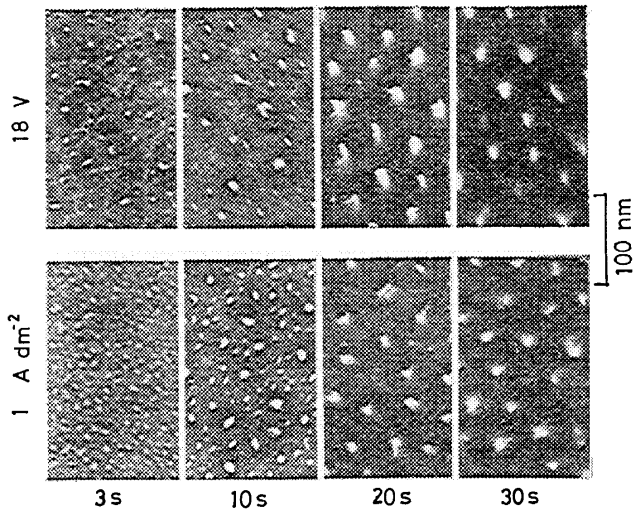

Fig. 1. Transmission electronmicro-photos showing the growth of pores at the initial stage of anodizing in 0.6 mol dm^{-3} H_2SO_4–0.4 mol dm^{-3} $MgSO_4$ at 30 °C (accelerated voltage=50 kV).

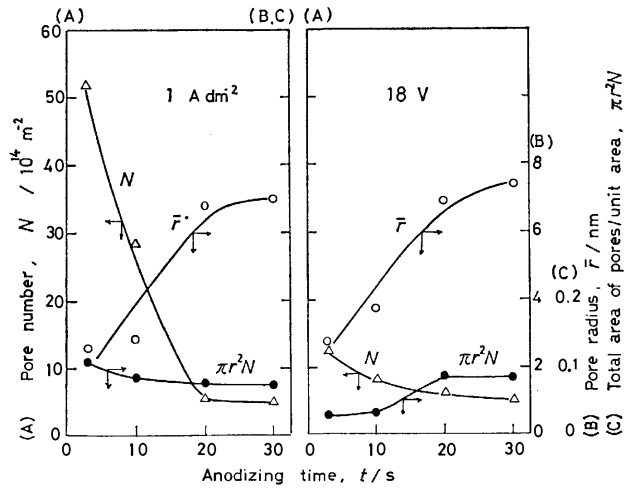

Fig. 2. Time dependence of the number, radius, and total area of pores (0.6 mol dm^{-3} H_2SO_4–0.4 mol dm^{-3} $MgSO_4$, 30 °C).

reaching nearly the same value as that obtained by the constant current process. From these results, it was found that near the outer surface of the film there were smaller pores than in the inner part of the film.

Further, the number of pores in 30 s-films was smaller than that reported[1,8] previously. This is probably due to the low ability of transmission of the electron beam at 50 kV. Therefore, the values of the dissolution rate shown in Fig. 10 were calculated by using the data ($r=7$ nm, $N=9.2\times10^{14}$ m^{-2}) obtained with 100 kV-observation on the films formed for 80 s.

Infrared Spectra of the Films. Curve 1 in Fig. 3 shows a spectrum of a film formed in sulfuric acid, obtained by using KBr as reference. The absorption band 1150 cm^{-1} is considered to be due to sulfate, because it also exists in the spectrum of $Al_2(SO_4)_3$ (broken line). Dorsey[9] also assigned such bands to sulfate. However, the determination of the SO_4 content of the film using this band was difficult, because

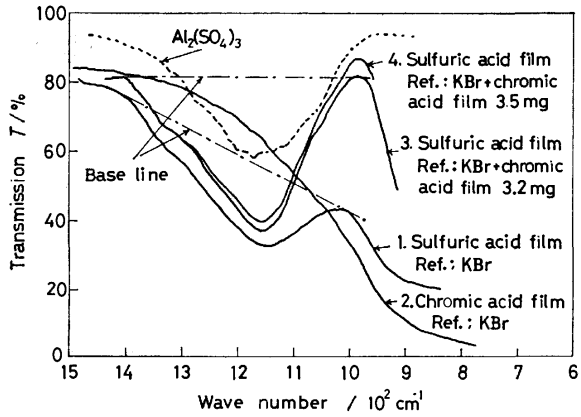

Fig. 3. Infrared spectra obtained by the compensation method.

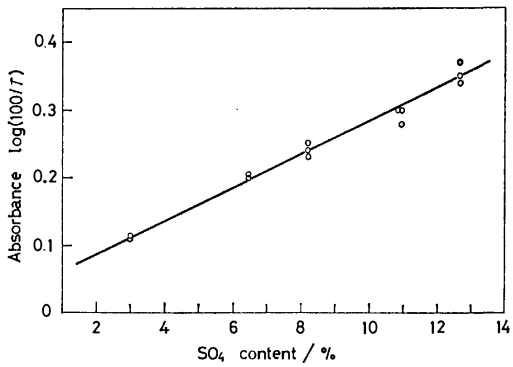

Fig. 4. Calibration of absorbance at 1150 cm^{-1} in IR spectra against the SO_4 content determined by gravimetric analysis ($BaSO_4$).

not only was its band weak, but also a strong and wide absorption band due to Al-OAl (stretching) was present below 900 cm^{-1}.[10] Therefore, the appropriate amount (1—3.5 mg) of the film formed in chromic acid, which did not absorb infrared rays over the 1400—1000 cm^{-1} region (curve 2), was added to the KBr reference so as to make the base line of the spectrum nearly horizontal, as shown by the curve 3, compensating the absorption by Al-OAl. When the amount of the film formed in chromic acid was in excess, such spectra as the curve 4 were obtained. However, the slight deviation of the base line from the horizontal did not appreciably change the absorbance at 1150 cm^{-1}. By such a compensation method, the IR spectra of the films whose SO_4 content had been already determined by gravimetric analysis were obtained. The absorbance at 1150 cm^{-1} was then calibrated against the SO_4 content of the film (Fig. 4). By using this relation, the SO_4 content of the film could be determined with errors below 10%.

Time Dependence of the SO_4 Content. Figure 5 shows the IR spectra of the films formed at 1 A dm^{-2} for 5 s—30 min. Nearly the same spectra were obtained in the case of 18 V-anodizing. The time dependence of the SO_4 content obtained from these spectra is shown in Figs. 6 and 7. At the initial stage of every anodizing process, the SO_4 content was very small, but it increased with time to a nearly

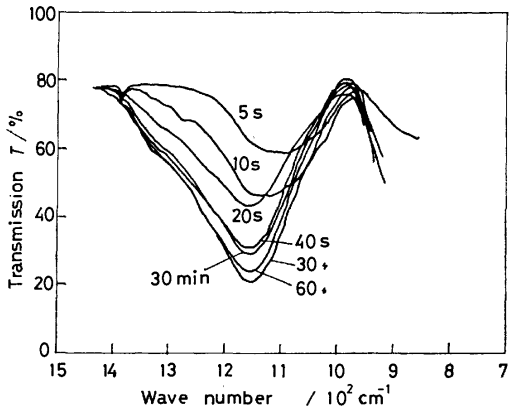

Fig. 5. Infrared spectra of films formed in 0.6 mol dm^{-3} H_2SO_4–0.4 mol dm^{-3} $MgSO_4$ at 30 °C and 1 A dm^{-2} for various times (Ref.; KBr+chromic acid film).

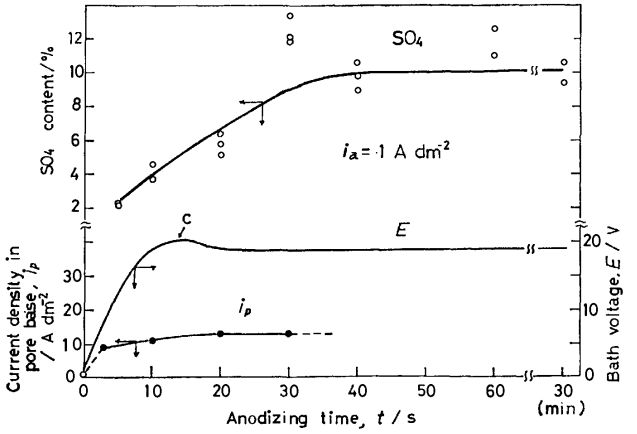

Fig. 6. Time dependence of the SO_4 content, current density in pore base, and bath voltage during constant current anodizing (0.6 mol dm^{-3} H_2SO_4–0.4 mol dm^{-3} $MgSO_4$, 30 °C).

constant value after 30 s at 1 A dm^{-2} and after 10 s at 18 V, respectively. These results were similar to those obtained with oxalic acid. However, in the case of 5 s and 10 s-films, the band due to sulfate shifted to a lower wave number. Perhaps the binding state of sulfate to the film is different. Therefore, strictly speaking, the relation between the absorbance at such a lower wave number and the SO_4 content may be different to some extent from that shown in Fig. 4. However, the results shown in Figs. 6 and 7 were consistent with the fact (Fig. 8) that the Auger peak to peak height of sulfur in the film near the outer surface, which was formed initially, was smaller than that of sulfur in the inner part of the film, which was formed later.

Anion Distribution across the Cell Wall. The distribution of electrolyte anions across the cell wall was examined in the same way as in the previous paper. Namely, after the specimen was anodized for 30 min, it was immersed in 1 mol dm^{-3} H_2SO_4, keeping the temperature at 30 °C. Then the time dependences of both the amount of the dissolved film and the SO_4 content of the remaining film were determined by

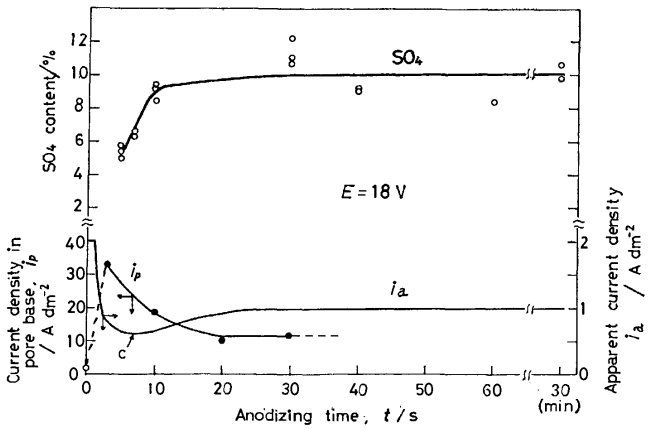

Fig. 7. Time dependence of the SO_4 content, current density in pore base, and apparent current density during constant voltage anodizing (0.6 mol dm^{-3} H_2SO_4–0.4 mol dm^{-3} $MgSO_4$, 30 °C).

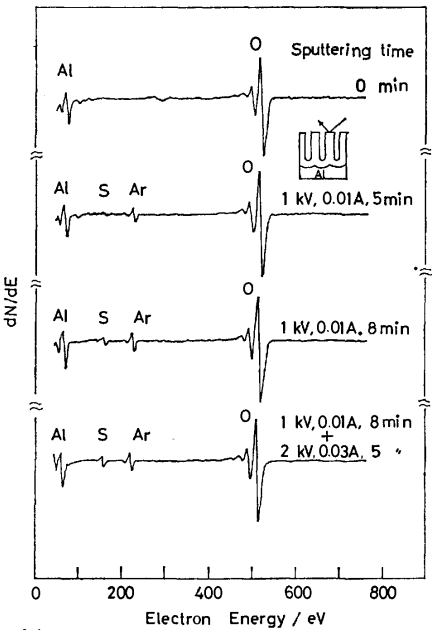

Fig. 8. Auger spectra obtained during Ar^+ ion sputtering from the surface of the film (0.6 mol dm^{-3} H_2SO_4–0.4 mol dm^{-3} $MgSO_4$, 30 °C, 1 A dm^{-2}, 30 s).

weight measurement and gravimetric analysis, respectively (Fig. 9). From these results, the SO_4 content of the film dissolved for a certain period was calculated. Further, the rate of chemical dissolution of the film was calculated every 10 min with reference to the method by Nagayama and Tamura[11] and the thickness of the wall consumed was thereby determined. The SO_4 content and chemical dissolution rate of the film for a certain period were plotted against the mean distance from the surface of the wall (Fig. 10).

The SO_4 content was relatively small near the wall/solution interface, but increased with the distance across the wall from the surface, reached a maximum value on the intermediate layer between the wall/solution interface and the cell boundary, and decreased gradually. This result is similar to that obtained with phosphoric acid[4] or oxalic acid.[3]

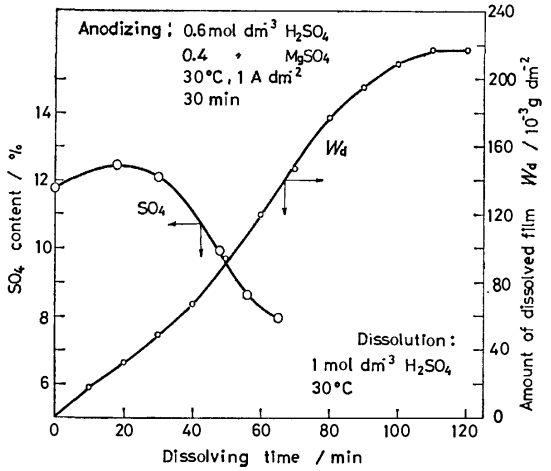

Fig. 9. Variation of the amount of the dissolved film and the SO_4 content of the remaining film with dissolving time.

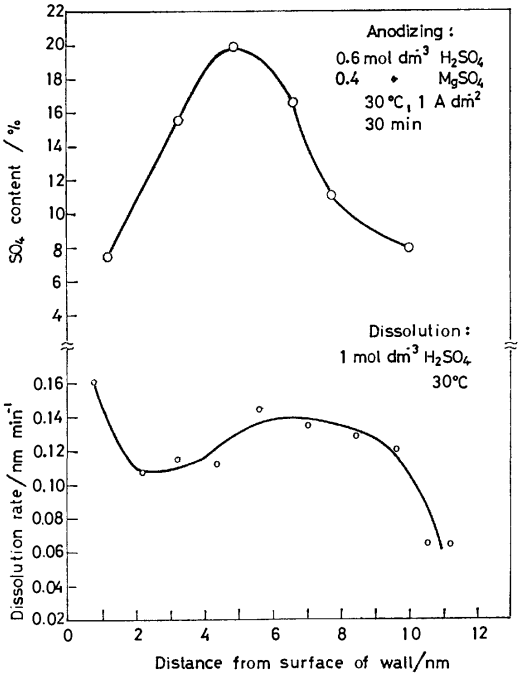

Fig. 10. Distribution of anions across the cell wall (upper) and the variation of dissolution rate of the film with the distance from the surface of the wall (lower).

As shown in Fig. 10 (lower), the chemical dissolution rate of the wall was highest near the surface, decreased with the distance from the surface, increased slightly, and decreased again near the boundary of the cells.

Little sulfur was detected near the barrier layer/metal interface (Fig. 11). The rate of sputtering of the film near the barrier layer/metal interface was lower than that of the bulk of the film.

Discussion

Mobility of Electrolyte Anions. It is impossible that the sulfate ions enter from the surface of the cell wall to which no electric field is applied. It is considered that the anions are pulled under the electric field from the surface of the barrier layer into the bulk of the layer, migrate through the layer, and remain in the porous layer by being released from the electric field.

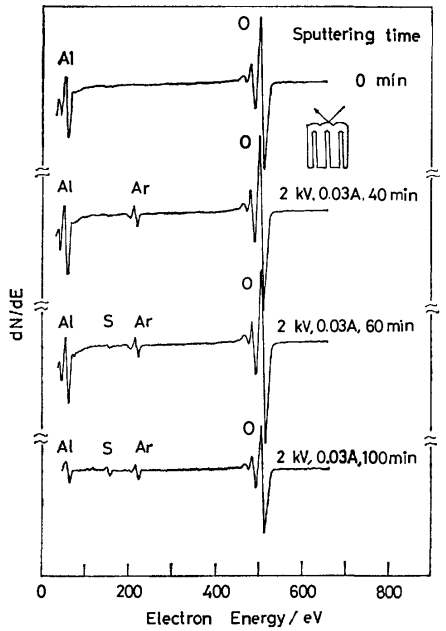

Fig. 11. Auger spectra obtained after Ar^+ ion sputtering from the barrier layer/metal interface (0.6 mol dm^{-3} H_2SO_4–0.4 mol dm^{-3} $MgSO_4$, 30 °C, 18 V, 30 min).

Although the mechanism of movement of electrolyte anions is not known well, if the anions are mobile, the anion content of the film would increase with the strength of the electric field. This seems to be reasonable on the basis of the following two facts. (1) According to Hoar and Yahalom,[12] the electrical properties of the barrier layer formed in sulfuric acid and sulfate solutions are similar to those of the barrier layer formed in neutral borate solution, and the relation, $\log i$ (A m^{-2}) $\propto E/y$ (V m^{-1}), is not changed remarkably for different incorporated anions. In other words, as the current density becomes higher, the strength of the electric field increases. (2) According to Mason,[13] the SO_3 content of the film increases with the current density. Therefore, it can be said that the stronger electric field at the higher current density causes the increased SO_3 content of the film.

Time Dependence of the SO_4 Content. In this experiment, even if the apparent current density (i_a) is constant, the real current density varied with the pore development at the initial stage (Fig. 6). Namely, when the anodizing is started, pores should not be present, so the current density is 1 A dm^{-2}. However, as pores were developed with time (3—20 s), the current density in the pore base (i_p) increased to a nearly constant value after 20 s (Fig. 6). Therefore, the strength of electric field would be small immediately after the start of anodizing, so that the SO_4 content is very small. Probably, this is due to small mobilities of HSO_4^- and SO_4^{2-} compared with

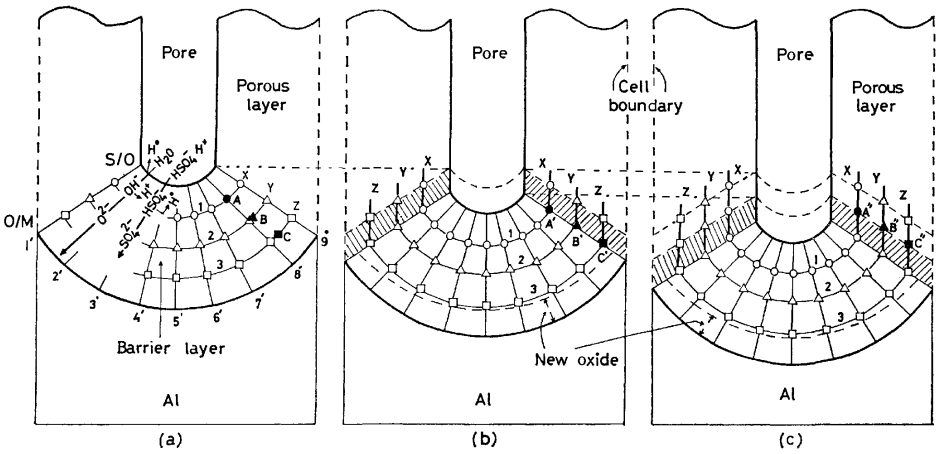

Fig. 12. Schematic representation of the transfer of anions from the barrier layer to the porous layer.

those of OH^- and O^{2-}. However, as pores are developed (3—20 s), the i_p increases and the strength of the electric field would increase, causing the increase of the SO_4 content. After 20 s, the i_p value is nearly constant. Therefore, it is considered that the film containing about 10% SO_4 (sulfate content of the 30 min-film) grows beneath the 20 s-film at a constant rate. The proportion of the initially formed film (outer layer) to the total film decreases with time so that the value of SO_4 content of the film, which was about 6% at 20 s, would approach with time to 10% as follows: $(6\%\times20+10\%\times10)/30=7.3\%$ at 30 s, $(6\%\times20+10\%\times40)/60=8.7\%$ at 60 s, and $(6\%\times20+10\%\times100)/120=9.3\%$ at 2 min. This is in fairly good agreement with the experimental result (Fig. 6).

In the case of constant voltage (Fig. 7), the i_a stayed at about 2 A dm^{-2} for the first 2 s, then abruptly decreased to a minimum value, and afterwards increased slightly to a constant value. For the first 2 s, the current density is low and the strength of electric field would be small, so that the SO_4 content of the film is small at the initial stage of anodizing. However, the i_p increases and the strength of the electric field would increase, so that the SO_4 content increases with time. In this case, the time to saturation of the SO_4 content was shorter than in the constant current process. This is due to the higher current density in the pore base at the initial stage of anodizing.

Anion Distribution across the Cell Wall. In steady state, the barrier layer, of constant thickness, moves toward the metal while it is renewed continuously. According to Siejka and Ortega,[14] the new oxide is formed at the oxide/metal (O/M) interface by the migration of oxygenated anions (O^{2-}, SO_4^{2-}), while at the solution/oxide (S/O, pore base), only the dissolution of the film occurs and there the oxide is not formed by the migration of cations.

Figure 12a shows the cross section of the barrier layer and its neighborhood in steady state. The curves 1, 2, and 3 show isopotential planes,[15] the lines of 1′—9′ show the current flow (the direction of the electric field). The anion content is the same everywhere on a certain isopotential plane. Since the current density in the barrier layer decreases with the distance from the surface of the layer, the strength of the electric field is considered to decrease with the distance from the surface.

In the steady state, OH^- (by decomposition of H_2O) and HSO_4^- ions are supplied from the solution into the barrier layer. The former is dissociated into O^{2-} and the latter is dissociated into SO_4^{2-} by releasing H^+, and then they migrate into the barrier layer. However, SO_4^{2-}, which is larger than O^{2-}, becomes gradually immobile since the strength of electric field decreases with the distance from the surface. On the intermediate layer between the interfaces of O/M and S/O, the strength of electric field is probably so small that SO_4^{2-} ions are delayed and accumulated there. On the contrary, O^{2-} ions migrate farther inward, so that the film with a very small SO_4 content is formed near the O/M interface (Fig. 11).

When the electrolysis is continued, the interfaces of S/O and O/M move gradually, while the distance between these interfaces is kept constant and the shaded portions become porous, as shown in Figs. 12b and 12c. During this period, the direction and strength of electric field applied to the anions at the position of A turn to the cell boundary and increase, so that the anions migrate toward the cell boundary and the metal, resulting in the movement on the isopotential plane 1 to A′ in Fig. 12b. Al^{3+} ions which take part in the formation of the film are replaced continuously by new cations transported from the metal. Most anions located at A may be transferred to A′; however, some anions may migrate inward further than the isopotential plane 1 and some anions may be supplied from the solution. The SO_4 content on the plane 1 is always kept constant. Thereafter, the anions at A′ remain in the porous layer by being released from the electric field, as shown by A″ in Fig. 12c. In the same manner, most anions located at the positions B and C in Fig. 12a are transferred to B′ and C′ in Fig. 12b, and remain in the porous layer as B″ and C″ in Fig. 12c, respectively. Accordingly, the anions located nearer to the surface of the barrier layer and farther from the center (5′

in Fig. 12a) of the layer are more rapidly transferred to the porous layer. The SO_4 contents on the planes X, Y, and Z in the porous layer are the same as those on the planes 1, 2, and 3 in the barrier layer, respectively. The composition of the wall surface is the same as that of the barrier layer surface.

The surface of the wall is soluble, since HSO_4^- ions would be incorporated into the oxide. The chemical dissolution rate of the wall decreases with the distance from the surface of the wall as the number of HSO_4^- ions became fewer, increases owing to the increase in the SO_4 content of the film, and decreases again near the cell boundary owing to the decrease in the SO_4 content.

Thus, the distribution of anions across the cell wall is considered to be similar to that established in the barrier layer.

Conclusions

The time dependence and distribution of SO_4 content of the anodic oxide film formed on aluminium in an H_2SO_4–$MgSO_4$ solution were the same as those of the film formed in oxalic acid and in phosphoric acid. From these results, it is speculated that the behavior of sulfate ions during anodizing was as follows.

(1) Immediately after the start of anodizing, a film containing a number of micropores and a small quantity of SO_4 was formed, and then the number of pores decreased. During this period, the current density in the pore base increased and the strength of electric field increased so that the SO_4 content of the film increased. When the current and voltage were in steady state, the SO_4 content of the film became constant.

(2) Under the electric field, HSO_4^- ions were pulled from the surface of the barrier layer into the layer, were dissociated into SO_4^{2-} by releasing H^+, and then migrated into the layer. However, since the strength of electric field was smaller with the distance from the surface of the barrier layer, SO_4^{2-} ions gradually became immobile and accumulated. Therefore, the SO_4 content of the film reached a maximum value on the intermediate layer between the pore base and the barrier layer/metal interface. When the barrier layer became porous by being released from the electric field, the distribution of anions across the barrier layer remained in the porous layer across the cell wall.

(3) The surface of the wall was soluble since HSO_4^- ions would be incorporated into the oxide. The chemical dissolution rate of the wall decreased with the distance from the surface of the wall as the number of HSO_4^- ions became fewer, increased owing to the increase in the SO_4 content of the film, and decreased again near the cell boundary owing to the decrease in the SO_4 content.

The authors are indebted to Dr. Kazuhiro Yoshihara and Dr. Masayasu Kurahashi of this institute for the performance of the Auger electron spectroscopy.

References

1) F. Keller, M. S. Hunter, and D. L. Robinson, *J. Electrochem. Soc.*, **100**, 411 (1953).
2) S. Tajima, "Advance in Corrosion Science and Technology," ed by M. G. Fontana and R. W. Staehle, Plenum Press, New York (1971), Vol. 1, p. 281.
3) Y. Fukuda, *Nippon Kagaku Kaishi*, **1974**, 1868; *Trans. Nat. Res. Ins. Metals*, **17**, 239 (1975).
4) H. Takahashi and M. Nagayama, *Nippon Kagaku Kaishi*, **1974**, 453.
5) G. E. Thompson, R. C. Furneaux and G. C. Wood, *J. Electrochem. Soc.*, **125**, 1480 (1978).
6) A. W. Brace and H. Baker, *Trans. Inst. Met. Fin.*, **40**, 31 (1963).
7) Y. Fukuda and T. Fukushima, Preprint for 52th Lecture Meeting of Metal Fin. Soc. Jpn., p. 80 (1975).
8) G. C. Wood and J. P. O'Sullivan, *Electrochimica Acta*, **15**, 1865 (1970).
9) G. A. Dorsey Jr., *Plating*, **57**, 1117 (1970).
10) A. J. Maeland, R. C. Rittenhous, and K. Bird, *Plating and Surface Fin.*, **63**, May, 56 (1976).
11) M. Nagayama and K. Tamura, *Electrochimica Acta*, **12**, 1097 (1967).
12) T. P. Hoar and J. Yahalom, *J. Electrochem. Soc.*, **110**, 614 (1963).
13) R. B. Mason, *J. Electrochem. Soc.*, **102**, 671 (1955).
14) J. Siejka and C. Ortega, *J. Electrochem. Soc.*, **124**, 883 (1977).
15) Although the exact shapes of S/O and O/M interfaces are not obvious, they are drawn as concentric.

 © 1980 The Chemical Society of Japan Bull. Chem. Soc. Jpn., 53, 3131—3137 (1980)

Raman Scattering Study on Coordination Structures of Cu(II)–L-Histidine(1 : 2) in Aqueous Solutions

Masao ITABASHI* and Koichi ITOH

Department of Chemistry, School of Science and Engineering, Waseda University, Shinjuku-ku, Tokyo 160

(Received April 30, 1980)

The pH and pD dependences of the Raman spectra of Cu(II)–L-histidine (1:2) and Cu(II)–L-histidine-d_{3-5} (1:2) were analyzed based on the pH titration data. Several ring vibrations of the imidazolyl group with cationic, neutral and anionic forms, the out-of-plane bending vibration of the bound carboxylate, and the Cu(II)–N stretching vibrations of the bound amino groups are used to study the chelation structures of the species taken by the solutions. From the results it was concluded that MHA^{2+}, the major species below pH 3, assumes a glycine-like chelation structure with an unbound imidazolium cation. The results also indicate that the species MHA_2^+, which is prominent in the pH region 4.0—4.5, takes a mixed-type structure, in which one histidine molecule coordinates to Cu(II) as a terdentate ligand and another binds as a substituted glycine. MA_2, the major species around pH 7, is determined to have the chelation structure in which two nitrogen atoms of the amino groups and two nitrogen atoms of the imidazole rings are bound to the Cu(II) ion in the square-planar trans position and at least one carboxyl group in the axial position.

The imidazolyl group, as a histidine moiety, functions as a ligand toward transition metal ions in a variety of metalloproteins including carbonic anhydrase,[1] carboxypeptidase,[2] and thermolysine.[3] Yoshida *et al.*[4] and Salama and Spiro[5] measured the Raman spectra of cobalt(II)–imidazole and cobalt(II)–L-histidine complexes as model compounds of metalloproteins and studied the relationship between the spectra and the coordination geometries of the complexes. Recently we also analyzed the Raman spectra of hexakis(4-methylimidazole)cobalt(II) complex, $Co(4MeImH)_6^{2+}$, and bis(L-histidinato) metal complexes, M(L-His)$_2$ (M=Ni(II), Zn(II)), in solid state.[6] From this study we concluded that some vibrational modes of the bound imidazolyl group clearly reflect the coordination site of this group to central metal ions. We also mentioned the possibility of elucidating the coordination geometries of the above-mentioned metalloproteins by means of Raman spectroscopy.

In this paper we measured Raman spectra and studied the coordination structures of Cu(II)–L-histidine(1:2) in aqueous solutions. Physiological studies suggest that a fraction of Cu(II) ions in human plasma is bound to human serum albumin and at the same time bound to amino acids consisting mostly of L-histidine.[7,8] Therefore, many physicochemical methods have been applied to Cu(II)–L-histidine(1:2) in aqueous solutions. Several pH-titration studies indicate that the solution contains MHA^{2+}, MA^+, MHA_2^+ and MA_2 as major species near and below the physiological pH[9,10] (Cu(II) abbreviated to M^{2+} and anionic histidine to A^-). The precise structures of these species, however, are still uncertain because the physical parameters obtained for the system (*e.g.*, formation constants, absorption maxima, and circular dichroism extrema) give only indirect informations about the coordination geometries. The use of ^{1}H-NMR spectroscopy is restricted only to the Cu(II)–L-histidine system with the ligand to metal ion ratio greater than 10^3 because the long electron spin relaxation time of Cu(II) ion causes too large line broadening of ligand resonances to permit their observation at stoichiometric concentration ratios.[11,12] The analysis of the Raman spectra provide us with some new and direct informations about the coordination structures of several species. The results clearly show that Raman spectroscopy is one of the powerful method for the structural study of coordination compounds containing L-histidine molecules and L-histidine residues as ligands.

Experimental

Materials. L-Histidine monohydrochloride monohydrate and $CuCl_2 \cdot H_2O$ were of reagent grade and obtained from Kanto Chemical Co., Inc. D_2O (99.75%), and concentrated D_2O solutions of NaOD (40%), and DCl (37%) were from E. Merck AG, Darmstadt. The measurement of the Raman spectra was made on the aqueous solutions of L-histidine and those containing L-histidine (0.4 M†) and $CuCl_2$ (0.2 M). The measurement was also performed on the D_2O solutions of L-histidine-d_{3-5} and those containing L-histidine-d_{3-5} (0.4 M) and $CuCl_2$ (0.2 M). L-Histidine-d_{3-5} and $CuCl_2 \cdot D_2O$ were prepared by Iyophilizing two times the D_2O solutions of L-histidine and $CuCl_2 \cdot H_2O$. The pH and pD values of the sample solutions were adjusted with 2—5 M NaOH and HCl and 2—5 M NaOD and DCl, respectively.

Measurement of Raman Spectra. All the spectra were taken by using a JEOL 400D Raman spectrophotometer equipped with a Spectra Physics model 164 argon ion laser. The 488.0 nm emission line was used as an excitation source. A spinning cell or a flow technique was used for the measurement.

Results and Discussion

Species Distribution of Cu(II)–L-Histidine (1:2) in Aqueous Solutions. A histidine molecule is considered to have three potential coordination sites in aqueous solutions. As pH rises, the carboxyl oxygen (pK_a=1.9), the imidazole nitrogen (pK_a=6.1) and the amino nitrogen (pK_a=9.1) become available for coordination to a metal ion.[10,13] The neutral imidazolyl group exists in the tautomeric equilibrium between the N(1) protonated form and the N(3) protonated one (Scheme 1).[14] Either one of these nitrogens

† 1 M=1 mol dm^{-3}.

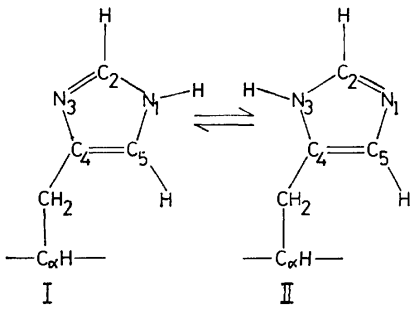

Scheme 1.

forms the chelation site.

In order to analyze the Raman spectra of Cu(II)–L-histidine complexes in aqueous solutions, it is first necessary to know the type of species which appears in various pH values of the solutions. As mentioned in the previous section, the solutions possess the predominant species, MHA^{2+}, MA^{+}, MHA_2^{+}, and MA_2. Below pH 3 the only major species is MHA^{2+} with a frequency approaching 50%. Just above pH 3, the solution contains the species MA^{+} in its maximum amount where about 25% of the Cu(II) ion is so bound. The species MHA_2^{+} appears to the extent of 90% from pH 4 to 4.5, and its deprotonation leads to MA_2 with $pK_a=5.5$. From pH 7 to 8 the species MA_2 is the most stable and its existence ratio approaches to 100%. In a pH region higher than 9, the formation of species $MH_{-1}A_2^{-}$, $MH_{-1}A$, and $M_2H_{-2}A_2$ are possible due either to hydroxylation or pyrrole hydrogen ionization ($pK_a=11.7$).[15,16]

It is known that a Cu(II) ion prefers a square-planar or a grossly distorted octahedral geometry to bind a maximum of two amino acid ligands. For a steric reason the three donor atoms of a terdentate histidine anion (A^{-}) cannot all occupy a planar site simultaneously, and these atoms have the equal possibility of being bound to the Cu(II) ion in the axial position. It has been strongly favored that the species MA^{+} involves the amino and imidazolyl groups in the square plane (histamine-like) with the carboxyl group in an apical position.[17] In contrasts, the site of protonation in MHA^{2+} is more controversial. The most popular view has been that the Cu(II) ion is bonded through an imidazole nitrogen and a carboxyl oxygen, while the amino nitrogen is protonated (Scheme 2 Ia).[9,18–20] The imidazole-carboxylate chelation, however, forms an unstable 7-membered ring and the binding at the glycine locus with an unbound protonated imidazolium cation has also been suggested to MHA^{2+} (Scheme 2 Ib).[17] Scheme 2 II shows one of the structures proposed to the species MHA_2^{+}, in which one histidine molecule coordinates to the Cu(II) ion as a terdentate ligand while another binds as a substituted glycine with an unbound imidazolium cation (mixed type).[15] The structure of the species MA_2 has so far received the most attention as a model for the transport form of Cu(II) ions in human blood. Great controversy, however, has been centered around its structure and several different proposals have been made to it.[17,21–23] The structure shown in Scheme 2 III is one of the proposals.[15]

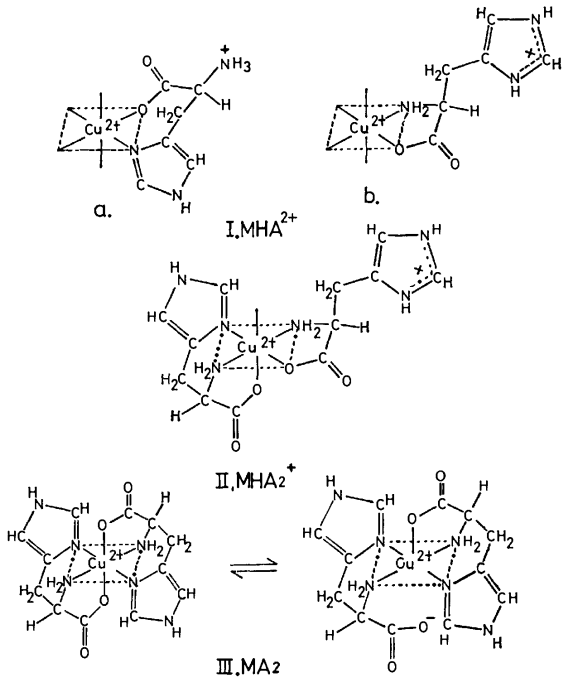

Scheme 2.

Raman Spectra of L-*Histidine and Cu(II)–*L-*Histidine (1:2) in H_2O.* Figure 1 shows the Raman spectra of L-histidine in H_2O at the pH values of 3.90(A), 8.15(B), and 11.98(C). Ashikawa and Itoh analyzed the pH dependence of Raman spectra of L-histidine.[24] On the basis of the normal coordinate treatment they assigned the bands observed at 1627, 1264, and 994 cm^{-1} in Fig. 1(A) to the C=C stretching, the ring breathing, and the C–H in-plane bending vibrations of the protonated imidazolium cation, respectively. They also stated that the doublet bands around 1580, 1270, and 990 cm^{-1} observed in Fig. 1(C) reflect the tautomerism of the neutral imidazolyl group of L-histidine, the 1570-, 1285-, and 988-cm^{-1} components corresponding to the tautomer I and the 1585-, 1262-, and 1004-cm^{-1} to the tautomer II (Scheme 1). At pH 8.15, where the tautomer I is predominant, the spectrum shown in Fig. 1(B) gives rise to the strong and sharp bands at 1570, 1282, and 988 cm^{-1}. These results are useful for monitoring the coordination mode of each species assumed by the Cu(II)–L-histidine (1:2) system.

Figure 2 shows the Raman spectra of the Cu(II)–L-histidine(1:2) aqueous solutions with various pH values. The spectrum observed at pH 2.48 (Fig. 2(F)), where the species MHA^{2+} is predominant, shows the prominent bands at 1628, 1483, 1268, 1189, 990, and 629 cm^{-1}. The spectrum is quite similar to that of the ligand containing a protonated imidazolium cation (Fig. 1(A)) with the exception that a well-defined band at 561 cm^{-1} is observed in Fig. 2(F). The 561-cm^{-1} band is observed throughout the pH range 2.48—7.23 (Figs. 2(C)—(F)), where the carboxyl group of the ligand is bound to the Cu(II) ion. This band can be assigned to the out-of-plane bending mode of the bound carboxylate by comparing with the same vibrational mode observed at 570 cm^{-1} for bis-

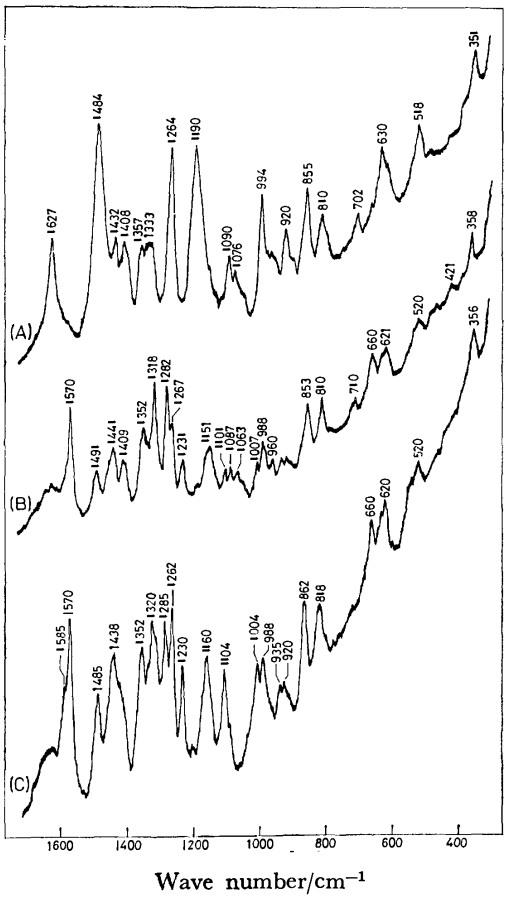

Fig. 1. Raman spectra of L-histidine in aqueous solutions (*ca.* 10 wt%) at a room-temperature: (A) pH= 3.90, (B) 8.15, (C) 11.98.

(glycino) complex of Cu(II).[25] From these results it is clear that in the species MHA^{2+} the Cu(II) ion is bound through an amino nitrogen and a carboxyl oxygen (glycine-like chelation), while the protonated imidazolium cation is not involved in the coordination. Therefore, the structure of this species is concluded to be the one shown in Scheme 2 Ib.

On raising the pH values (Figs. 2(D) and (E)) the band at 1628 cm^{-1} decreases its intensity and another band begins to appear at about 1585 cm^{-1} (the C=C stretching vibration of the neutral imidazole ring). The latter band is attributable to the bound imidazolyl group because the group with the pK_a value of 6.1 cannot exist as a free and neutral form at pH 4.55 and 3.72. One of the pH titration studies[10] reports that at pH 3.72 there exist appreciable amounts of three species, MA^+, MHA^{2+}, and MHA_2^+ in the Cu(II)-L-histidine(1:2) system. Therefore, it is difficult to assign each Raman scattering band in Fig. 2(E) to either one of the species. At pH 4.55, MHA_2^+ is the only major species. As Fig. 2(D) shows, the intensities of the two C=C stretching bands at 1628 and 1583 cm^{-1} are almost identical with each other, which is consistent with the mixed-type chelation structure shown in Scheme 2 II.

The Raman spectrum measured at pH 7.23 (Fig. 2(C)), where the species MA_2 exists almost exclusively, exhibits the vibrational modes of the neutral imidazole

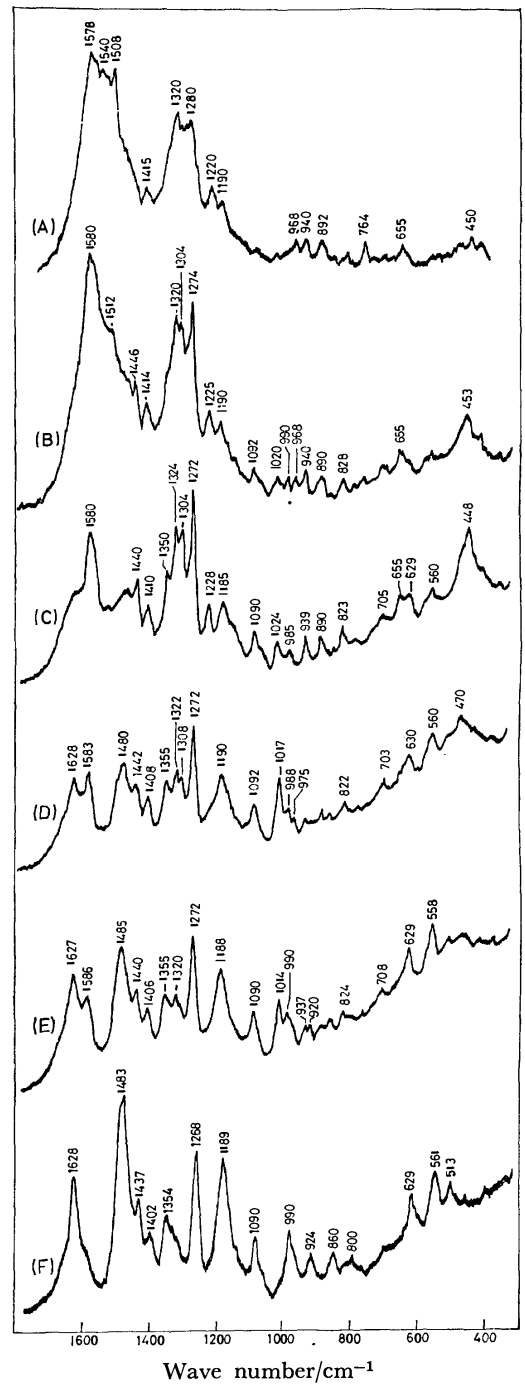

Fig. 2. Raman spectra of Cu(II)-L-histidine(1:2) in aqueous solutions (0.2 M) at a room-temperature: (A) pH=11.12, (B) 9.52, (C) 7.23, (D), 4.55, (E) 3.72, (F) 2.48.

ring (1580 and 1272 cm^{-1}, *etc.*). As already mentioned, the free imidazolyl group of L-histidine in a basic aqueous solution (Fig. 1(C)) gives rise to the doublets near 1580, 1270, and 990 cm^{-1}. The singlet bands observed at 1580 and 1272 cm^{-1} in Fig. 2(C) indicates that the imidazolyl group of the species MA_2 takes either one of the two tautomeric forms shown is Scheme 1. The strong band at 448 cm^{-1} in Fig. 2(C) can be ascribed to one of Cu(II)-ligand stretching vibrations because the free L-histidine with

the neutral imidazolyl group does not show any band in this region (Figs. 1(B) and (C)). This band shifts down to 432 cm^{-1} in D_2O (see the next section and Fig. 4(B)), suggesting that the 448 cm^{-1} band can be assigned to the Cu(II)–N stretching vibration of the bound amino groups. Generally two amino groups coordinated to the central Cu(II) ion with cis position show two Cu–N stretching bands (symmetric and asymmetric) while the amino groups occupying the trans position give only one Cu–N symmetric stretching vibration. This is supported by the observations that *trans*-Cu(II)(glycine)$_2 \cdot 2H_2O$ gives rise to only one Cu(II)–N stretching mode at 462 cm^{-1} while *cis*-Cu(II)(glycine)$_2 \cdot H_2O$ shows two Cu(II)–N stretching bands at 477 cm^{-1} (asymmetric) and 455 cm^{-1} (symmetric).[25] In Fig. 2(C) the only one Cu(II)–N stretching band appears at 448 cm^{-1} indicating that the trans position to the central Cu(II) ion is taken by the bound amino groups. The band at 560 cm^{-1} in Fig. 2(C), the intensity of which is a little weaker than that of the corresponding band in Fig. 2(D), can be assigned to the out-of-plane bending vibration of the bound carboxylato group. From the above-mentioned results it can be concluded that the coordination structure of the species MA_2 is similar to that proposed by Kruck and Sarkar,[15] in which two nitrogen atoms of the amino groups and two nitrogen atoms of the imidazole rings are bound to the Cu(II) ion in square-planar trans position and at least one, if not both, carboxyl group is bound in the axial position (Scheme 2 III).

Salama and Spiro have measured the Raman spectrum of octahedral Co(L-histidinato)$_2$ complex in H_2O with a UV excitation (363.8 nm).[5] They observed a band at 1574 cm^{-1}, which corresponds to the one observed at 1580 cm^{-1} in Fig. 2(C), and assigned it to the bound carboxylate mode. Cu(II)–histamine (1:2) in the aqueous solution with the pH values where the imidazolyl group of the ligand has the neutral form[26] and Co(4MeImH)$_6^{2+}$ complex[6] also show a well-defined peak in the region from 1590 to 1570 cm^{-1}. These results exclude the assignment made by Salama and Spiro and confirm that the 1580-cm^{-1} band in Fig. 2(C) are due to the C=C stretching vibration of the bound imidazolyl group.

At pH 9.52 (Fig. 2(B)) the 1580-cm^{-1} band is remarkably enhanced with a shoulder at 1512 cm^{-1} and, as the pH value is increased further (pH 11.12, Fig. 2(A)), a broad band centered around 1540 cm^{-1} begins to appear. The Raman spectrum of histidine with the imidazolide anion gives rise to the C=C stretching vibration of the group at 1527 cm^{-1}, which corresponds to the 1540-cm^{-1} band in Fig. 2(A). The shift to the higher frequency ($\Delta\nu = 13$ cm^{-1}) can be ascribed to the chelation of the anionic group in the Cu(II)–L-histidine(1:2) system. Salama and Spiro[5] also measured the Raman spectrum of tetrahedral Co(L-histidinato)$_2^{2-}$ complex and observed the scattering peak at 1545 cm^{-1}, to which they assigned the anti-symmetric mode of the free carboxylate anion. The frequency of 1545 cm^{-1} is too low to be assigned to the free carboxylate mode because the infrared spectra of L-histidine and Cu(II)–L-histidine(1:2) in

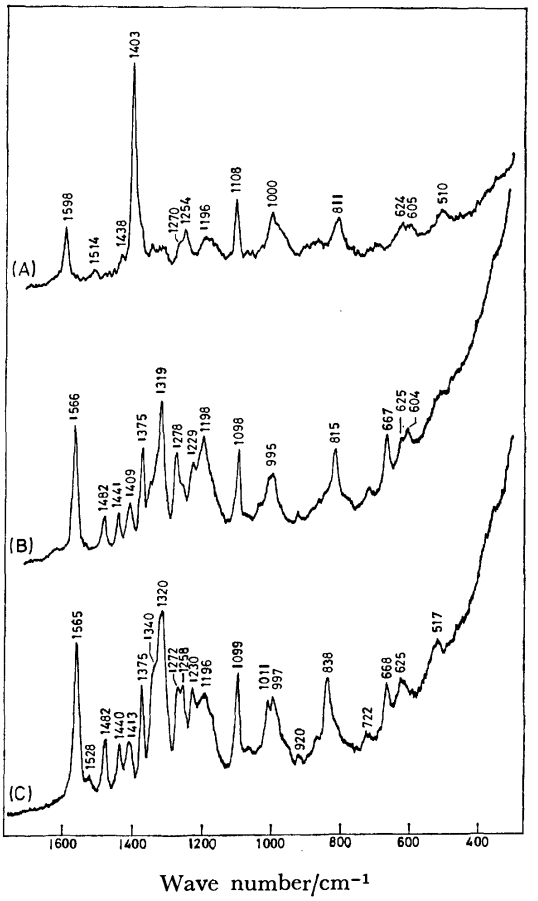

Fig. 3. Raman spectra of L-histidine-d_{3-5} in D_2O (*ca.* 10 wt%) at a room-temperature: (A) pD=2.80, (B) 8.34, (C) 13.20.

D_2O solutions show the free and the bound carboxylate mode at 1578 and 1590 cm^{-1}, respectively.[15] The appearance of the 1540-cm^{-1} band in Fig. 2(A) is accompanied by the shift and disappearance of several bands in Fig. 2(C). The bands observed at 1272 and 985 cm^{-1} in Fig. 2(C) shift to 1280 and 968 cm^{-1}, respectively. The 1090- and 1024-cm^{-1} bands in Fig. 2(C) almost disappear in Fig. 2(A). These results can be ascribed to the change in the chelation structure caused by the deprotonation of the imidazolyl group. Above pH 8, however, the Cu(II)–L-histidine(1:2) system becomes unstable (sometimes we observed a slight precipitation just above pH 9 presumably due to the copper(II) hydroxide formation) and we could not make a detailed analysis of the Raman spectra of Cu(II)–L-histidine (1:2) in which all the imidazolyl groups have the anionic form.

Raman Spectra of L-*Histidine*-d_{3-5} *and Cu(II)–*L-*Histidine*-d_{3-5} *(1:2) in* D_2O. Figure 3 shows the Raman spectra of L-histidine-d_{3-5} in D_2O at the pD values of 2.80(A), 8.34(B), and 13.20(C). The spectrum observed at pD 2.80 shows the bands at 1598, 1403, 1254, and 1000 cm^{-1}. They correspond to the 1627-, 1484-, 1264-, and 994-cm^{-1} bands in Fig. 1(A) and are assigned to the C=C stretching, the N–D in-plane bending, the ring breathing, and the C–H in-plane bending vibrations of the imidazolyl group,

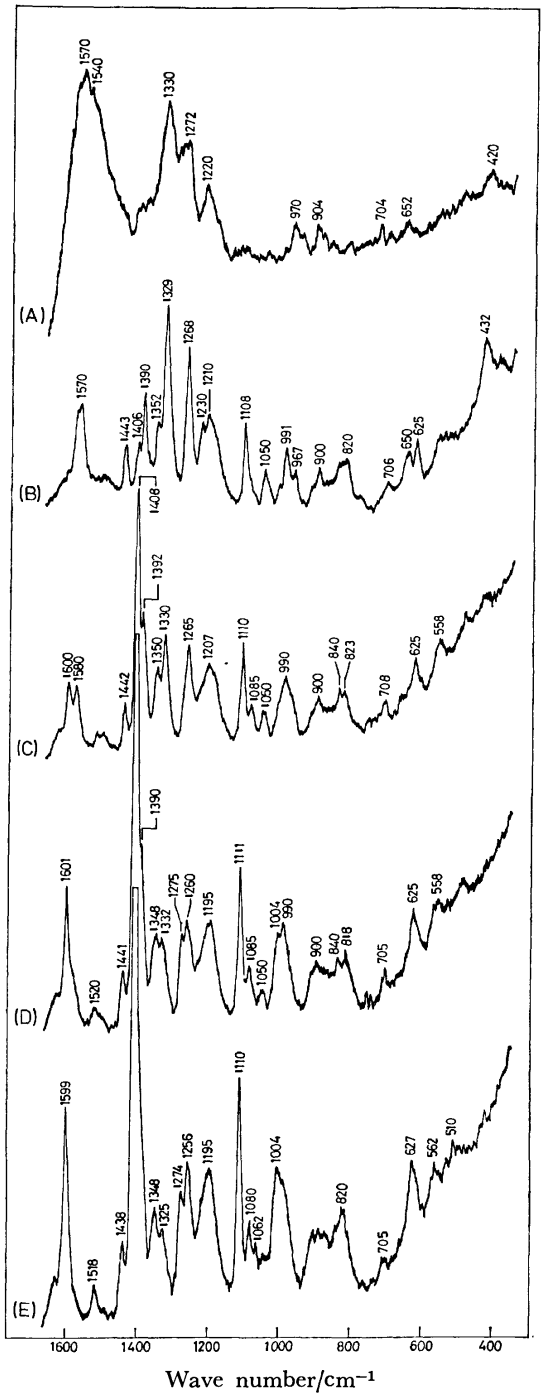

Fig. 4. Raman spectra of Cu(II)–L-histidine-d_{3-5} (1:2) in D_2O at a room-temperature: (A) pD=10.6, (B) 7.7, (C) 4.4, (D) 3.3, (E) 2.5.

respectively. At pD 8.34, where the neutral imidazolyl group favors the tautomeric form I, the spectrum (Fig. 3(B)) gives rise to the bands at 1566, 1278, and 995 cm^{-1} which are due to the C=C stretching, the breathing and the C–H in-plane bending modes of the neutral imidazolyl group with the tautomeric form I. On raising the pD value to 13.2, where both the tautomers I and II coexist, the Raman spectrum (Fig. 3(C)) shows the 1258- and 1011-cm^{-1} bands ascribable to the tautomer II in addition to the 1272- and 997-cm^{-1} bands due to the tautomer I. In the D_2O solution the tautomer I has the C=C stretching vibration with the frequency virtually identical with that of the tautomer II, giving rise to a sharp and strong band at 1565 cm^{-1} in Fig. 3(C).

Figures 4(A)—(E) show the Raman spectra of Cu(II)–L-histidine-d_{3-5}(1:2) in D_2O measured at pD values from 2.5 to 10.6. The bands at 1599, 1408, 1256, 1110, and 1004 cm^{-1} in Fig. 4(E) correspond to those at 1598, 1403, 1254, 1108, and 1000 cm^{-1} in Fig. 3(A), all of which are assigned to a protonated imidazolium cation. The out-of-plane bending vibration of the bound carboxylato group is observed at about 560 cm^{-1} in Fig. 4(E). Therefore, the Raman spectrum shown in Fig. 4(E) also confirms that the glycine-like binding occurs in MHA^{2+} which is the major species at pD 2.5.

In Fig. 4(D) the 1601- and 1408 cm^{-1} bands decrease their intensities, and there appear a shoulder band near 1580 cm^{-1} and a band at 990 cm^{-1}. The latter two bands can be ascribed to the bound neutral imidazolyl group. This is consistent with the result of the pH titration study[10] which brought the conclusion that in the pH region just above 3 there exist appreciable amounts of multiple species consisting of MHA^{2+} (Scheme 2 Ib), MHA_2^+ (Scheme 2 II) and MA^+ in which an L-histidine molecule is bound to Cu(II) as a terdentate anion.

At pD 4.4 (Fig. 4(C)), the intensity of the C=C stretching vibration observed at 1600 cm^{-1} (ascribed to the protonated imidazolium cation) is almost the same as that of the 1580-cm^{-1} band (assignable to the bound neutral imidazolyl group). This is consistent with the mixed-type structure (Scheme 2 II) proposed to MHA_2^+ which is the major species at pD 4.4.

The spectrum observed at pD 7.7 (Fig. 4(B)) also confirms the structure (Scheme 2 III) which was proposed to MA_2, the major species at pD 7.7. First, well-defined bands at 1570, 1268, and 991 cm^{-1} indicate that the species contains the neutral imidazolyl group with the tautomeric form I and the N(3) atom is bound to the Cu(II) ion. Second, the band near 560 cm^{-1} shows that in the species MA_2 at least one carboxylato group is bound to the central ion. Third, the sharp band at 432 cm^{-1} can be ascribed to the symmetric Cu(II)–N stretching vibration of the bound amino groups occupying the trans position to the Cu(II) ion. In Fig. 4(B) we cannot find the band which corresponds to the sharp band at 1482 cm^{-1} in Fig. 3(C). L-Histidine in a basic aqueous solution (Fig. 1(C)) also gives rise to a sharp band at 1485 cm^{-1} which reduces its intensity appreciably or almost disappears in Fig. 2(C). The 1482-cm^{-1} band in Fig. 3(C) (and the 1485 cm^{-1} in Fig. 1(C)) is presumably ascribed to one of the imidazole ring vibrations,[27] to which the N(3)=C(2) stretching mode contributes. On coordination of the imidazolyl group *via.* the N(3) atom, this band either shifts or decreases its intensity. The 1375-cm^{-1} band observed for the free ligand in D_2O (Fig. 3(C)) shifts to 1390 cm^{-1} in Fig. 4(B). The frequency shift can also be used to monitor the chelation of the imidazolyl group in D_2O.

In a higher pD region (Fig. 4(A)), there appears

Table 1. Obsd Raman frequencies of L-His and Cu(II)-L-His(1:2) system (1600—300 cm^{-1})

L-Histidine monomer						Cu(II)-L-Histidine(1:2) system						Assignments
H_2A^+		HA		A^-		MHA^{2+}		MHA_2^+		MA_2		
H_2O	D_2O	H_2O	D_2O	H_2O	D_2O	H_2O	D_2O	H_2O	D_2O	H_2O	D_2O	
1627	1598			1585[b]		1628	1599	1628	1600			R(ν(C=C))
		1570	1566	1570[a]	1565			1583	1580	1580	1570	
1484	1403	1491	1482	1485	1482	1483	1408	1480	1408			δ(N-H or N-D)+R
1432	1438	1441	1441	1438	1440	1437	1438	1442	1442	1440	1443	$\delta(CH_2)$
1408		1409	1409		1413	1402		1408		1410	1406	$\nu(CO_2)$
			1375		1375				1392		1390	R+δ(N-D)
1357		1352		1352		1354	1348	1355	1350	1350	1352	
1333		1318	1319	1320	1320		1325	1322	1330	1324	1329	R+$\delta(C_\alpha$-H)
	1270						1270	1308		1304		
1264	1254	1282[a]	1278	1285[a]	1272[a]	1268	1256	1272	1265	1272	1268	R(ring breathing)
		1267[b]		1262[b]	1258[b]							
		1231	1229	1230	1230					1228	1230	
	1196		1198		1196		1195		1207		1210	R, δ(N-H)
1190	1108	1151	1098	1160	1099	1189	1110	1190	1110	1185	1108	ν(NCN)+δ(N-H)
1090		1101				1090	1080	1092	1085	1090		ν(C-H)
		1087										
1076		1063					1062	1017	1050	1024	1050	$\nu(C_\alpha$-N)
994	1000	1007[b]		1004[b]	1011[b]	990	1004	988	990	985	991	$\delta(C_{2,5}$-H)
		988[a]	995	988[a]	997[a]							
		960						975			967	$r(CH_2)$
				935						939		
920				920	920	924			900	890	900	π(N-H), ν(C-C)
855		853		862	838	860			840			
810	811	810	815	818		800	820	822	823	823	820	
702		710			722		705	703	708	705	706	$\delta(CO_2)$
		660	667	660	668					655	650	ring deform.
630	624	621		620		629	627	630	625	629	625	+ν(C-C)
						561	562	560	558	560		$\pi(CO_2)$
518	510	520		520	517	513	510					$r(CO_2)$
										448	432	ν(Cu-N)
351		358		356								

Abbreviations: R, ring stretching; ν, stretching; δ, bending; π, out-of-plane bending; r, rocking. a) Assigned to Tautomer I. b) Assigned to Tautomer II.

a strong and broad band around 1540 cm^{-1}, giving a large background in the frequency range from 1600 to 1500 cm^{-1}. This band corresponds to the one at 1540 cm^{-1} in Fig. 2(A) and it can be assigned to the C=C stretching vibration of the bound imidazolide anion. As is the case with the Raman spectrum observed for the H_2O solution at a high pH value (Fig. 2(A)), the spectral features of Fig. 4(A) are different from those of Fig. 4(B) in several respects. The bands at 1268, 991, and 432 cm^{-1} in Fig. 4(B) shift to 1272, 970, and 420 cm^{-1} in Fig. 4(A), respectively. The bands observed at 1108 and 1050 cm^{-1} in Fig. 4(B) almost disappear in Fig. 4(A). Although these results clearly reflect the change in the coordination mode of the sample, the clear-cut explanation to these changes based on the assumed species (*i.e.*, $MH_{-1}A_2^-$, $MH_{-1}A$, and $M_2H_{-2}A_2$) could not be made because of the same reason given to the H_2O solution with a high pH value.[15] Sometimes the sample forms a dark-colored precipitation above pD 8.

Conclusions

The frequencies and tentative assignments of the Raman bands observed for L-histidine and Cu(II)–L-histidine(1:2) in H_2O and L-histidine-d_{3-5} and Cu(II)–L-histidine-d_{3-5}(1:2) in D_2O are listed in Table 1. As mentioned above, the C=C stretching and the breathing vibrations of the free and bound imidazolyl groups, the out-of-plane bending vibration of the bound carboxylato group, and the Cu(II)–N stretching vibrations of the bound amino groups can be used to determine the chelation structures of the species taken by the Cu(II)–L-histidine(1:2) system. The following are the conclusions. (1) The species MHA^{2+}, the major one below pH 3, assumes the structure shown in Scheme 2 Ib. The results obtained from the Raman spectra are incompatible with the structure shown in Scheme 2 Ia, which has been one of the most popular structures proposed to MHA^{2+}. (2) The Raman spectra measured at pH 4.55 and pD 4.4 (Figs. 2(D) and 4(C)) correspond quite well to the mixed-type chelation structure shown in Scheme 2 II, which is proposed to MHA_2^+, the major species in the pH region from 4 to 4.5. (3) From the Raman spectra measured at pH 7.23 and pD 7.7, where the species MA_2 is present almost to the extent of 100%,

it is concluded that the species assumes the chelation structure shown in Scheme 2 III. The intensity of out-of-plane bending vibration of the bound carboxylato group observed at 560 cm^{-1} in Fig. 2(C) is smaller than that of the corresponding band in Fig. 2(D), which suggests that one of the carboxylato groups exists in the equilibrium between the bound and free states.

We wish to express our sincere thanks to Professor M. Tasumi, Faculty of Science, The University of Tokyo, and Mr. S. Muraishi, JEOL Co. Ltd., for allowing us to use their Raman spectrophotometers.

References

1) A. Liljas, K. K. Kannan, P. C. Bergstein, I. Waara, K. Fridborg, B. Strandberg, V. Carlbom, L. Jarup, S. Lovgren, and M. Petet, *Nature (London), New Biol.*, **235**, 131 (1972).
2) W. N. Lipscomb, J. A. Hartsuck, F. A. Quiocho, and G. N. Reeke, Jr., *Proc. Natl. Acad. Sci. U.S.A.*, **64**, 28 (1969).
3) B. W. Matthews, J. N. Jansonius, P. M. Colman, B. P. Schoenbom, and D. Duporque, *Nature (London), New Biol.*, **238**, 41 (1972).
4) C. M. Yoshida, T. B. Freedman, and T. M. Loehr, *J. Am. Chem. Soc.*, **97**, 1028 (1975).
5) S. Salama and T. G. Spiro, *J. Am. Chem. Soc.*, **100**, 1105 (1978).
6) M. Itabashi and K. Itoh, *Chem. Lett.*, **1979**, 1331.
7) A. G. Bearn and H. G. Kunkel, *Proc. Soc. Exp. Biol. Med.*, **88**, 44 (1954).
8) P. Z. Neumann and A. Sass-Kortasak, *J. Clin. Invest.*, **46**, 646 (1967).
9) D. D. Perrin and V. S. Sharma, *J. Chem. Soc., A*, **1967**, 724.
10) H. C. Freeman and R. -P. Martin, *J. Biol. Chem.*, **244**, 4823 (1969).
11) H. Sigel and D. B. McCormick, *J. Am. Chem. Soc.*, **93**, 2041 (1971).
12) H. Aiba, Y. Kuroda, and H. Tanaka, *Bull. Chem. Soc. Jpn.*, **49**, 1313 (1976).
13) P. J. Morris and R. B. Martin, *J. Inorg. Nucl. Chem.*, **32**, 2891 (1970).
14) Throughout this paper the imidazole ring of histidine is labeled according to IUPAC nomenclature (see Scheme 1).
15) T. P. A. Kruck and B. Sarkar, *Can. J. Chem.*, **51**, 3563 (1973).
16) P. J. Morris and R. B. Martin, *J. Am. Chem. Soc.*, **92**, 1543 (1970).
17) E. W. Wilson, Jr., M. H. Kasperian, and R. B. Martin, *J. Am. Chem. Soc.*, **92**, 5365 (1970).
18) R. Leberman and B. R. Rabin, *Trans. Faraday Soc.*, **55**, 1660 (1959).
19) D. R. Willams, *J. Chem. Soc., Dalton Trans.*, **1972**, 790.
20) H. Siegel, R. Griesser, and D. B. McCormick, *Arch. Biochem. Biophys.*, **134**, 217 (1969).
21) K. M. Wellman and B. -K. Wong, *Proc. Nat. Acad. Sci. U.S.A.*, **64**, 824 (1969).
22) H. Siegel, R. E. Mackenzie, and D. B. McCormick, *Biochem. Biophys. Acta*, **200**, 411 (1970).
23) B. Sarkar and Y. Wigfield, *J. Biol. Chem.*, **242**, 5572 (1967).
24) I. Ashikawa and K. Itoh, *Biopolymers*, **18**, 1859 (1979).
25) J. R. Kincaid and K. Nakamoto, *Spectrochim. Acta, Part A*, **32**, 227 (1976).
26) Unpublished data.
27) A. -M. Bellocq, Ph. D. Thesis, University of Bordeaux, Bordeaux, France, 1969.

Possible Role of Denatured Albumin in Formation of "Heat-resistant" Serum Albumin

Hiroshi TERADA,* Kazuhiko WATANABE, and Fujio KAMETANI
Faculty of Pharmaceutical Sciences, University of Tokushima, Shomachi-1, Tokushima 770

(Received May 8, 1980)

Studies with the probe dye 2-(4-hydroxyphenylazo)benzoic acid, which can detect small conformational differences in serum albumin, showed that the conformation of "heat-resistant" serum albumin (form N') was not constant, but depended on the heating temperature, becoming similar to that of the denatured monomer as the heating temperature was increased from 55 °C to 70 °C in buffer of pH 7.0. Denatured albumin was suggested to protect native serum albumin from full denaturation. In the presence of denatured albumin, native albumin was found to undergo only a slight conformational change to give the N' form. This protective effect may explain why a constant amount of serum albumin remains as "heat-resistant" serum albumin even after prolonged heating.

From studies on changes in the solubility and sedimentation velocity of serum albumin on denaturation, Levy and Warner[1,2] concluded that a certain amount of serum albumin remains undenatured even after prolonged heating at 65 °C in solutions of various pH values, and that denatured albumin consists of monomer, dimer and higher aggregates. These findings have been confirmed by electrophoresis of albumin heat denatured between 65 °C and 75 °C.[3-5] The presence of an undenatured, heat-stable fraction in heat-treated albumin has been interpreted as due to the existence of "heat-resistant" serum albumin, and it has sometimes been taken as support for the concept of the heterogeneity of serum albumin.[6,7]

In studies using probe dyes, such as 2-(4-hydroxyphenylazo)benzoic acid (HABA), Bromcresol Green and 8-anilinonaphthalene-1-sulfonate,[8-10] we found that there are at least two forms, N and N', in the native fraction of heat-treated serum albumin, and that during heating N' is formed from N by slight conformational modification. The N' form is "heat-resistant" albumin itself. Although "heat-resistant" albumin (N' form) is very similar to N in properties, such as its helical content, electrophoretical mobility and absorption spectrum in the ultraviolet region,[5] it can be distinguished from N with these probe dyes. Among the probe dyes examined, HABA is the most useful, since it shows a new spectral band at about 480 nm with N or N', but not with denatured albumin.[8,11] The affinity of HABA for N', determined from the absorbance of the dye at about 480 nm, was found to be about 60% of that of N in heat-treated albumin at 65 °C in buffer of pH 7.0 or pH 9.0.[8]

Since heat denaturation of serum albumin is characterized by the presence of "heat-resistant" serum albumin and the formation of aggregated albumin, it is very important for understanding the mechanism of heat denaturation of albumin to determine various properties of these molecular species, and especially of "heat-resistant" albumin. This paper deals with the effect of the heating temperature of the properties of "heat-resistant" serum albumin, and the effect of denatured albumin on formation of "heat-resistant" albumin, examined by electrophoresis and with the probe dye HABA. The importance of denatured albumin in formation of "heat-resistant" albumin is suggested.

Experimental

Materials. Bovine serum albumin (Armour, crystalline, Lot no. H72803 and H72009) was used without further purification. Its molecular weight was assumed to be 6.6×10^4. The concentration of albumin in solution in 0.1 mol/dm^3 potassium phosphate buffer, prepared just before use, was determined spectrophotometrically as described previously.[8] The concentration of denatured albumin was expressed in terms of monomer. HABA was obtained from Wako Chemical Co., Osaka (Japan). The other reagents used were standard commercial products.

Method. Heat denaturation was carried out at pH 7.0 as described previously.[8] Acrylamide gel electrophoresis (gel concentration: 7.5%) was conducted at pH 8.3, and quantitative analysis of protein bands of heat-treated albumin, stained with Amidoblack 10B, was carried out in a Shimadzu dual-wavelength TLC scanner, model CS-900, using a wavelength pair of 590 and 700 nm.[10] The absorption spectrum of HABA was recorded at pH 7.0 and 25 °C in a Union spectrophotometer, model SM 4012.

Results

Effect of Temperature on Properties of N'. Figure 1 shows the time-course of heat-denaturation of 1.5×10^{-4} mol/dm^3 bovine serum albumin at various temperatures at pH 7.0, determined by acrylamide gel electrophoresis. At all temperatures, denaturation was first rapid and then slowed down, finally reaching a steady level. The existence of an undenatured fraction of serum albumin after prolonged heating is regarded as due to the formation of modified native albumin N' ("heat-resistant" albumin) from native albumin.[8] The results in Fig. 1 indicate that the amount of N' decreases as the heating temperature increases; at 55 °C, 92% of native albumin (N) changes to N', whereas at 70 °C, only 20% changes to N' and 80% is denatured. At 80 °C all the native albumin is denatured (Table 1). This temperature-dependent denaturation is essentially the same as that at pH 8.9.[4] However, denaturation proceeded more rapidly at pH 8.9, probably because the exchange of disulfide bonds associated with denaturation of serum albumin was greater due to the higher concentration of OH^- (Refs. 5 and 12).

As reported previously, the spectrum of the probe dye HABA shows a new spectral band at about 480

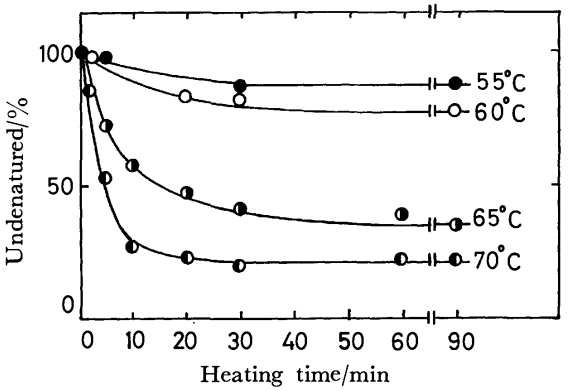

Fig. 1. Time course of heat denaturation of serum albumin at various temperatures determined by acrylamide gel electrophoresis.

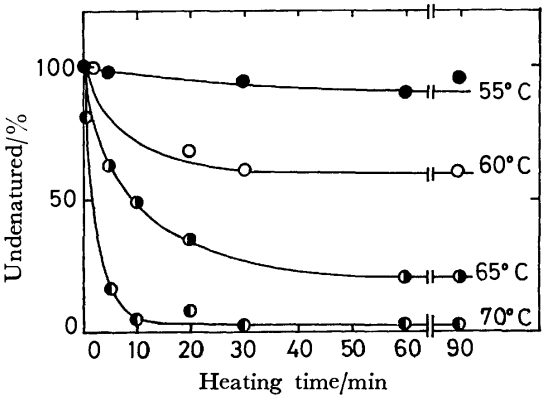

Fig. 2. Time course of heat denaturation of serum albumin at various temperatures determined from the absorbance of HABA.

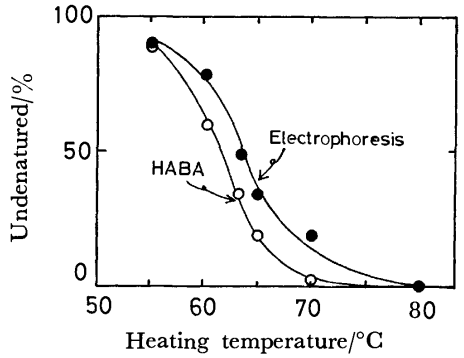

Fig. 3. Temperature-dependence of change in amount of undenatured albumin after heating for 90 min, determined by electrophoresis and from the absorbance of HABA.

nm on binding with undenatured albumin (N and N').[8] Using the same heat-treated albumin as for the experiments in Fig. 1, the absorbance of 10^{-3} mol/dm^3 HABA at 480 nm was measured. The relative absorbance of HABA induced by 10^{-5} mol/dm^3 heat-treated albumin to that induced by the same concentration of unheated albumin was taken as the relative amount of undenatured albumin remaining during heat-treatment, and is plotted as a function of the heating period at various temperatures in Fig. 2. The results in Fig. 2 are very similar to those in Fig. 1 determined by acrylamide gel electrophoresis, but the changes are more rapid.

Table 1. Relative amount of N' formed after prolonged heating

Heating temp/°C	Relative amount of N'/%		Ratio (A/B)
	From absorbance of HABA (A)	By electrophoresis (B)	
55	89	92	0.97
60	60	79	0.76
63	35	50	0.70
65	20	35	0.57
70	3	20	0.15
80	0	0	—

Figure 3 shows the temperature dependences of the relative amount of N' after heating for 90 min, determined by electrophoresis and from the absorbance of HABA. These values and the ratio of the relative amount of N' determined with HABA to that determined by electrophoresis are listed in Table 1. Values for the relative amount of N' determined by the two methods decreased similarly with the heating temperature, but the value determined with HABA was always smaller than that determined by electrophoresis, because the molar extinction coefficient of HABA induced by N' is smaller than that induced by N.[8] If the conformation of N' around the binding sites for HABA is the same in N' formed at all temperatures, the ratio of N' determined with HABA to that determined by electrophoresis should be the same between 55 °C and 70 °C, even though the relative amount of N' determined by the two methods changes with the heating temperature. However, the results in Table 1 show that this ratio becomes smaller with increase in the heating temperature, indicating that the structure of N' is not the same at different heating temperatures, and that the affinity of N' to HABA becomes smaller as the denaturating temperature increases.

Effect of Denatured Albumin on Denaturation. Figure 4 shows the time course of denaturation of serum albumin at 65 °C monitored by measuring the absorbance of HABA at 480 nm; the relative absorbance of HABA induced by heat-treated albumin to that induced by unheated albumin is plotted against the heating time. In this experiment, solutions containing various amounts of denatured albumin (final concentration, D_0) and native albumin (final concentration, N_0) at a constant total protein concentration of 5.0×10^{-5} mol/dm^3 were heated. The denatured albumin used was obtained by heating serum albumin at 80 °C for 15 min in buffer of pH 7.0 to denature it completely. It is apparent from the figure that the extent of denaturation decreases with increase in the amount of denatured albumin; with solutions containing 75% and 50% $D_0(N_0/(N_0+D_0)=$ 0.25 and 0.50, respectively) before heating, the absorbance of HABA due to the undenatured fraction ($N+N'$) after heating for 25 min is decreased to 43%

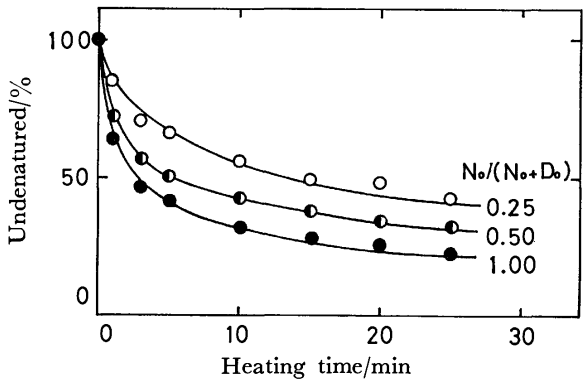

Fig. 4. Time course of heat denaturation of serum albumin at 65 °C and pH 7.0 in the presence of various amounts of heat denatured albumin. Denaturation was monitored by the absorbance of 10^{-4} mol/dm^3 HABA.
N_0: Initial concentration of native albumin, D_0: initial concentration of heat-denatured albumin.

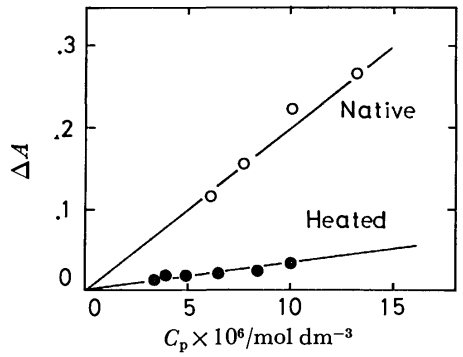

Fig. 5. Concentration dependence of heat denaturation of serum albumin at 65 °C and pH 7.0. The denaturation was monitored as the absorbance of 5.0×10^{-4} mol/dm^3 HABA induced by 10-fold diluted samples of heat-treated albumin. The concentrations of heat-denatured albumin(C_p) shown in the figure are those at the time of measuring the absorbance of HABA, and the C_p values during heat-denaturation were 10 times greater. The absorbance of HABA induced by native albumin is also shown.

and 32%, respectively, while in the absence of denatured albumin ($N_0/(N_0+D_0)=1$) it is decreased to 23%. The addition of denatured albumin before heating seems to inhibit denaturation. However, in this experiment the decrease in denaturation could be due to an effect of concentration on denaturation of serum albumin, since the experiments were carried out keeping N_0+D_0 constant and thus N_0 decreased with increase in D_0.

For examination of this possibility, we measured the heat denaturation at 65 °C of solutions of serum albumin at concentrations of 3.0×10^{-5} mol/dm^3 to 10^{-4} mol/dm^3. The solutions were heated for 100 min, and then mixed with a solution of HABA and the absorbance of HABA was measured at 480 nm. The absorbance induced by various concentrations of native albumin was also measured. As shown in Fig. 5, the absorbance of HABA increased linearly with increase in concentration of the heat-treated albumin,

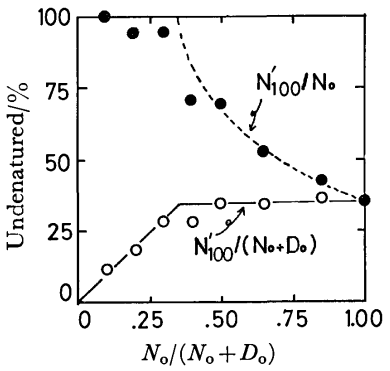

Fig. 6. Effect of heat-denatured albumin on denaturation of serum albumin at 65 °C and pH 7.0.
D_0: Initial concentration of heat-denatured albumin, N_0: initial concentration of native albumin, N'_{100}: concentration of N' after heating for 100 min.

indicating that denaturation does not depend on the concentration of albumin under these experimental conditions. The ratio of the slope of the straight line obtained with denatured albuimn to that with native albumin was 0.18, coinciding well with the value of 0.20 obtained on denaturation of 1.5×10^{-4} mol/dm^3 serum albumin for 90 min at 65 °C (*cf.* Table 1). Thus the decreased denaturation of native albumin in the presence of denatured albumin shown in Fig. 4 could be due to an inhibitory effect of denatured albumin, not to dilution of the native albumin. Thus the effect of denatured albumin on denaturation was next studied in more detail.

Various amounts of native albumin(N) were mixed with denatured albumin(D), obtained by heat-treatment at 80 °C for 10 min, keeping the total albumin concentration at 1.5×10^{-4} mol/dm^3. The mixtures were heated at 60 °C or 65 °C for 100 min, where the albumin remaining undenatured was N' form. Then they were subjected to polyacrylamide gel electrophoresis and the amount of undenatured albumin (N'_{100}) was determined from the absorbance of the stained Amidoblack 10B. The ratio N'_{100}/N_0 (the amount of undenatured albumin as a percentage of that before heating), and the ratio $N'_{100}/(N_0+D_0)$ (the amount of undenatured albumin as a percentage of the total concentration of albumin) are plotted as functions of $N_0/(N_0+D_0)$ (=the relative amount of native albumin before heat-treatment) in Figs. 6 and 7.

On heating at 65 °C (Fig. 6), the value of N'_{100}/N_0 became greater as the value $N_0/(N_0+D_0)$ decreased; in the absence of denatured albumin before heat-treatment ($N_0/(N_0+D_0)=1.00$) N'_{100}/N_0 was 35%, whereas when the albumin solution contained more than 65% denatured albumin ($N_0/(N_0+D_0)\leq0.35$) N'_{100}/N_0 was almost 100%. However, when the percentage of undenatured albumin was expressed in terms of the total albumin content, $N'_{100}/(N_0+D_0)$, 35% of the albumin consistently remained undenatured in the region where the content of the original native albumin was greater than 35% ($N_0/(N_0+D_0)\geq0.35$). Moreover, in the region where $N_0/(N_0+D_0)$ was less than 0.35, the plot of change in the percentage of undenatured albumin after heating for 100 min

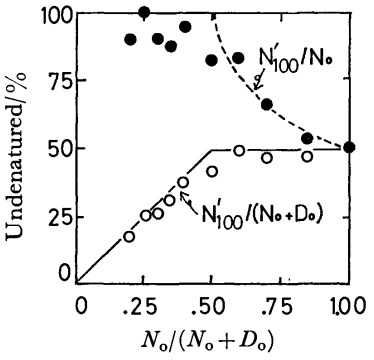

Fig. 7. Effect of heat-denatured albumin on the denaturation of serum albumin at 63 °C and pH 7.0. Experimental conditions were similar to those in Fig. 6, except heating temperature.

against $N_0/(N_0+D_0)$ was linear with a slope of one; that is, the percentage of undenatured albumin was the same as before heat-treatment, since no denaturation took place. In the figure, the solid and dotted lines were drawn assuming that at less than 0.35 $N_0/(N_0+D_0)$, the serum albumin was not denatured.

On denaturation at 63 °C, results were similar to those on denaturation at 65 °C, as shown in Fig. 7, and about 50% of the albumin was denatured when no denatured albumin was added before heat-treatment (the solid and dotted lines in the figure were drawn assuming that at less than 0.50 $N_0/(N_0+D_0)$, the serum albumin was not denatured.). The scatter of experimental results on denaturation at both temperatures in the region of small values of $N_0/(N_0+D_0)$ is due to the difficulty in determining the exact amount of undenatured albumin, since before heating the sample contained only a small amount of native albumin.

Discussion

The results of Figs. 1 and 2, and Table 1 show that form N' ("heat-resistant" serum albumin) remaining in heat-treated albumin after prolonged heating changes in conformation and loses affinity for HABA with increase in the heating temperature. Under the experimental conditions for Fig. 2, where the concentration of the probe dye HABA was much greater than that of the protein, the change in affinity of the protein for the dye reflects change in the number of binding sites for the dye.[8,10] Thus decrease in the affinity of N' for HABA with increase in heating temperature from 55 °C to 70 °C indicates that the number of binding sites on N' became smaller as the heating temperature increased. Since the denatured monomer did not have any binding sites for HABA that induced the characteristic absorption band of the dye, it can be concluded that the conformation of N' became similar to that of the denatured monomer, at least with regard to the microenvironment around the binding site for HABA, with increase in the heating temperature. As reported previously,[9] heat-treatment of native albumin(N) first causes formation of N' and denatured monomer. There must be some regulatory effect determining the amounts of denatured monomer and N' formed from N. Thus the mechanism of formation of N' from N is important for understanding the mechanism of heat-denaturation of serum albumin.

The results of this study, especially those in Figs. 6 and 7, indicate that denatured albumin has a protective effect on heat-denaturation of serum albumin, and that the denaturation proceeds until the ratio of the amount of native albumin to denatured albumin attains a certain value depending on the heating temperature; at 65 °C, 35% was native and 65% denatured, whereas at 63 °C, 50% was native and 50% denatured. Kratochvil *et al.*[13] reported that albumin that had been heated at 65 °C retarded the aggregation of serum albumin induced by heating at 75 °C. This report and our results suggest that denatured albumin stabilizes native albumin, preventing the latter from complete denaturation.

Some biopolymers are known to be stable in solution containing protein or starch.[14] Recently, Martinek *et al.*[15] reported that α-chymotrypsin and trypsin became stable against thermo-inactivation, when they interacted non-covalently with polyacrylamide gel. Similarly, our preliminary experiments showed that the presence of polyvinylpyrrolidone reduced the rate of heat-denaturation of serum albumin. In view of these findings, it is suggested that denatured albumin (D) which mainly consists of aggregated albumin protects native albumin(N) from heat-denaturation probably by a certain non-covalent interaction between D and N, but this "interaction" is not strong enough to prevent the denaturation completely and thus N changes slightly in conformation to form N'. With increase in the heating temperature, the "interaction" between D and N will become weaker, and thus the conformational change of N' will increase, the conformation of N' finally becoming similar to that of the denatured monomer, as indicated by the results in Table 1.

Though it is not clear at present how denatured albumin protects native albumin from denaturation, the stabilizing effect of denatured albumin could be one of the decisive reasons why serum albumin is not completely denatured and "heat-resistant" serum albumin (form N') exists between 55 °C and 70 °C. Since our recent results[10] have suggested that fatty acids also influence the process of heat-denaturation of serum albumin, further studies are necessary on the mechanism of formation of N' during heat-denaturation of serum albumin.

The authors thank Miss Yukari Maeda for technical assistance. The present work was partially supported by a Grant-in-Aid for Scientific Research No. 167273 from the Ministry of Education, Science and Culture.

References

1) M. Levy and R. C. Warner, *J. Phys. Chem.*, **58**, 106 (1954).
2) R. C. Warner and M. Levy, *J. Am. Chem. Soc.*, **80**, 5735 (1958).
3) B. Sedlacek, *Collect. Czech. Chem. Commun.*, **25**, 1008

(1960).
4) K. Aoki, K. Hiramatsu, K. Kimura, S. Kaneshina, Y. Nakamura, and K. Sato, *Bull. Inst. Chem. Res., Kyoto Univ.*, **47**, 274 (1969).
5) K. Aoki, K. Sato, S. Nagaoka, M. Kamada, and K. Hiramatsu, *Biochim. Biophys. Acta*, **328**, 323 (1973).
6) S. Stokrova and J. Sponar, *Collect. Czech. Chem. Commun.*, **28**, 659 (1963).
7) S. Stokrova and J. Sponar, *Collect. Czech. Chem. Commun.*, **32**, 2386 (1967).
8) H. Terada, K. Aoki, and M. Kamada, *Biochim. Biophys. Acta*, **342**, 41 (1974).
9) H. Terada, E. Iwakaji, K. Hiramatsu, and K. Aoki, *Biochim. Biophys. Acta*, **453**, 26 (1976).
10) H. Terada, K. Hiramatsu, and K. Aoki, *Biochim. Biophys. Acta*, **622**, 161 (1980).
11) H. Terada, *Life Sci.*, **11**, 417 (1972).
12) L. O. Andersson, *Biochim. Biophys. Acta*, **200**, 363 (1970).
13) P. Kratochvil, P. Munk, S. Stokrova, J. Sponar, and B. Sedlacek, *Collect. Czech. Chem. Commun.*, **28**, 972 (1963).
14) P. A. Albertsson, "Partition of Cell Particles and Macromolecules," (Japanese Edition), Tokyo University Press, Tokyo (1971), p. 127.
15) K. Martinek, A. M. Klibanov, V. S. Goldmacher, A. V. Tchernysheva, V. V. Mozhaev, I. V. Berezin, and B. O. Glotov, *Biochim. Biophys. Acta*, **485**, 13 (1977).

The Kinetics of Oxygen-exchange Reaction between Chromate Ions and Water

Akiko Okumura,* Mie Kitani, Yuiko Toyomi, and Nobukazu Okazaki

Department of Chemistry, Nara Women's University, Nara 630

(Received January 5, 1980)

The oxygen-exchange reaction between chromate ions and water has been studied under the following conditions: 25 °C, pH=7—12, [Cr(VI)]=0.075 mol dm^{-3}, I=0.2 and 1 mol dm^{-3}. The rate law of the exchange reaction has been found to be:

$$R = k_1[CrO_4^{2-}] + k_2[HCrO_4^-] + k_3[H^+][HCrO_4^-] + k_4[HCrO_4^-][CrO_4^{2-}] + k_5[HCrO_4^-]^2.$$

The exchange rate has been analyzed in terms of this rate law to obtain the values of k_1—k_5. The presence of the third-order rate term in [Cr(VI)] has been suggested. The activation energy of the overall exchange reaction (I=1 mol dm^{-3}) is (25.5±0.7) kJ/mol at pH 7.4 and (98.9±1.0) kJ/mol at pH 11.0. The salt effect is negative at pH<10.5 and absent at pH>10.5.

In a series of papers on the oxoanion catalysis of the oxygen-exchange reaction of arsenate ions,[1,2] it has been suggested that a study of the oxygen-exchange reaction of an oxoanion in the presence of a catalytic amount of another oxoanion may provide a means of elucidating the interactions of these two oxoanions. As a preliminary to a study of the interaction of chromate ions with another oxoanion by the oxygen-exchange reaction,[3] we have examined the oxygen exchange of chromate ions with water.

This reaction has been studied by several authors.[4–6] Holyer and Baldwin[5] have interpreted the exchange reaction (pH 6.7—12, [Cr(VI)]=0.64—2.7 M,** 25 °C) in terms of these reactions:

$$HCrO_4^- + CrO_4^{2-} \rightleftharpoons Cr_2O_7^{2-} + OH^-,$$

$$HCrO_4^- + HCrO_4^- \rightleftharpoons Cr_2O_7^{2-} + H_2O,$$

and $$CrO_4^{2-} + H_2{}^{18}O \rightleftharpoons CrO_3{}^{18}O^{2-} + H_2O.$$

Mak[6] has extended the study up to pH 4.5 ([Cr(VI)]= 0.1 and 0.2 M, 25 °C), and proposed these exchange paths:

$$Cr_2O_7^{2-} + HCrO_4^- \rightleftharpoons Cr_3O_{10}^{2-} + OH^-,$$

and $$HCr_2O_7^- + HCrO_4^- \rightleftharpoons Cr_3O_{10}^{2-} + H_2O,$$

the former being important at pH 6.7—7.6, and the latter, at pH<6.0. The chloride-ion catalysis of the oxygen-exchange reaction of chromate ions has been noted by this author at pH>6.8. The absence of the salt effect on the exchange reaction has been claimed in these papers.

In the present paper, the uncatalyzed and acid-catalyzed oxygen exchanges of hydrogenchromate ions with water have been proposed as additional exchange paths, the presence of the third-order rate term in [Cr(VI)] has been suggested, and the salt effect on the exchange reaction has been established.

Experimental

Materials. The sodium chromate tetrahydrate (guaranteed reagent, Merck), sodium chloride (guaranteed reagent JIS), and other chemicals (guaranteed reagent JIS) were used without further purification. Sodium chromate enriched in oxygen-18 was prepared by the exchange reaction of sodium chromate with $H_2{}^{18}O$ at 100 °C for 2 h.

** 1 M=1 mol dm^{-3}.

Procedure. The procedures were almost the same as those previously reported.[7] The exchange reaction was initiated by dissolving a weighed amount of the enriched sodium chromate in normal water. The normal water was boiled before use to expel the dissolved carbon dioxide. The pH of the solution was fixed by adding a small amount of a hydrochloric acid or sodium hydroxide solution. The pH of the solution was measured with a Hitachi-Horiba pH-meter (Model F-7) or with a Radiometer PHM-26 pH-meter equipped with a glass electrode (Type 202 C) and a reference electrode (Type K 401). The ionic strength was adjusted to 1 M by the addition of sodium chloride. The ionic strength of 0.2 was maintained by means of the chromate. The reactions were carried out at 25 °C. At appropriate intervals, aliquots were drawn and the chromate ion was precipitated as barium chromate by adding a solution of barium chloride. The above series of operations were carried out under an atmosphere of nitrogen.

To avoid the precipitation-induced oxygen exchange of the chromate ion, which becomes appreciable at pH values smaller than 8, the pH of the solution was, when necessary, brought to ≈9 before the addition of the precipitant by adding an appropriate amount of a sodium hydroxide solution.

The precipitate was separated by means of a centrifuge, washed three times with absolute ethanol, dried in an oven at 110 °C, and converted into carbon dioxide by the guadinium-chloride method.[8] The isotopic analysis of the carbon dioxide was done on a Hitachi RMS-I-type mass spectrometer.

The rate of the oxygen exchange was calculated by means of this formula:

$$R = -\frac{1}{t}\cdot\frac{[Cr(VI)][H_2O]}{4[Cr(VI)]+[H_2O]}\cdot\ln\left(1-\frac{O_0-O_t}{O_0-O_\infty}\right),$$

where O_0, O_t, and O_∞ are the oxygen-18 contents of the chromate at the times 0, t, and infinity respectively, and where [Cr(VI)] and [H_2O] are the molar concentrations of the chromate and water respectively.

Dissociation and Condensation Constants of Hydrogenchromate Ions. The values of the equilibrium constants, K_1 and K_d, defined by:

$$K_1 = [HCrO_4^-]/a_{H^+}[CrO_4^{2-}],$$

and $$K_d = [Cr_2O_7^{2-}]/[HCrO_4^-]^2,$$

were obtained as follows. The values at I=0.2 M and 25 °C were interpolated from the literature values[9] by means of the Debye-Hückel equation. The literature values at 20 °C were corrected to 25 °C and used in the interpolation. The results are $\log(K_1/M)=6.03$ and $\log(K_d/M)=1.75$.

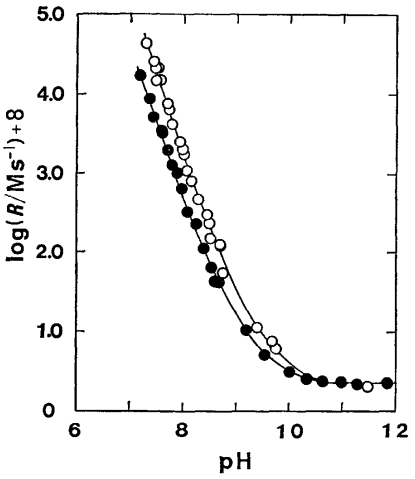

Fig. 1. The rate of oxygen exchange reaction of chromate ions with water *versus* pH.
([Cr(VI)]=0.075 M, 25 °C)
○: I=0.2 M, ●: I(NaCl)=1.0 M.

The values at I(NaCl)=1.0 M and 25 °C were determined by means of potentiometric titrations with a glass electrode. Solutions of sodium chromate of known concentrations and a unit ionic strength were titrated with standardized hydrochloric acid. Seven series of titrations were carried out with chromate solutions of varied concentrations, ranging from 1.157×10^{-3} M to 6.198×10^{-2} M. The titration curves were treated by the method of Sillén[10] and Sasaki[11] to obtain the values of K_1 and K_d. The value of the activity coefficient of the hydrogen ion in the medium of I(NaCl)=1.0 M necessary for the treatment was obtained by the potentiometric titration of a 1 M NaCl solution with standardized hydrochloric acid. The results are $\log(K_1/M)=5.73$ and $\log(K_d/M)=2.14$.

Results and Discussion

pH *Dependence of the Exchange Rate.* The dependence of the exchange rate on the pH was studied at I=1.0 and 0.2 M, the concentration of Cr(VI) being kept at ≈0.075 M. The rate-pH profiles are shown in Fig. 1. In the pH region smaller than 8.7, $\log(R/M\ s^{-1})$ decreases linearly with the increase in pH. The slopes of the lines obtained by the method of the least-squares are -1.89 ± 0.04 (I=0.2 M) and -1.82 ± 0.03 (I=1.0 M). From pH=8.7 upwards, the rate decreases increasingly less rapidly, and above pH=10.5, where CrO_4^{2-} is the predominating ionic species, it becomes independent of the pH. The exchange rate in this region is so slow (half-life=*ca.* 25 d) that it was difficult to follow the reaction for more than a half-period without the interference of the atmospheric carbon dioxide. In these runs, the final values were borrowed from the runs under more acidic conditions.

[*Cr(VI)*] *Dependence of the Exchange Rate.* This was studied at four different pH's: 7.2, 7.4, 7.7, and 8.0 (25 °C, I=1.0 M). The concentration of Cr(VI) was varied from 0.036 to 0.14 M at pH=7.2, 7.7, and 8.0, and from 0.010 to 0.14 M at pH=7.4. Plots of $\log(R/M\ s^{-1})$ against log([Cr(VI)]/M) are shown in Fig. 2. The slopes of the four straight lines through

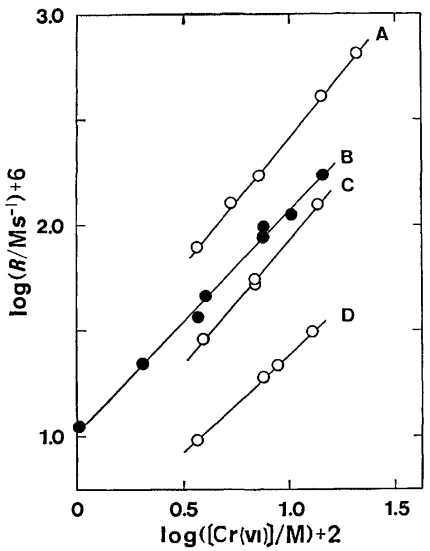

Fig. 2. Dependence of the exchange rate on [Cr(VI)].
(25 °C, I(NaCl)=1 M)
○ A: pH=7.2, C: pH=7.7, D: pH=8.0 ([Cr(VI)]=0.036—0.14 M).
● B: pH=7.4 ([Cr(VI)]=0.010—0.14 M).

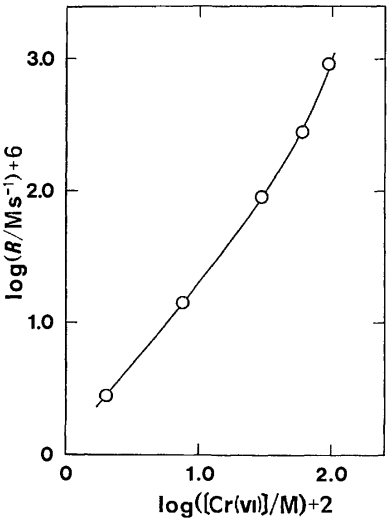

Fig. 3. Dependence of the exchange rate on [Cr(VI)].
[Cr(VI)]=0.02—0.96 M, I(NaCl)=4 M, pH=7.5, 25 °C.

each set of plotted points are 1.23 ± 0.02 (pH: 7.2), 1.05 ± 0.03 (pH: 7.4), 1.17 ± 0.02 (pH: 7.7), and 0.93 ± 0.01 (pH: 8.0). It may be inferred that the order of the exchange reaction with respect to [Cr(VI)] tends to the value of unity with the increase in the pH.

Holyer and Baldwin[5] have reported a value of 1.98 ± 0.07 for the corresponding slope at pH=7.5 with Cr(VI) concentrations ranging from 0.15 to 2.7 M. In order to explain the apparent discrepancy between this and the present results, we have studied the [Cr(VI)] dependence over a wider range of Cr(VI) concentrations (0.02—0.96 M, I(NaCl)=4.0 M). The logarithmic plot of R against [Cr(VI)] gives a curve concave upwards (Fig. 3), the slope of the curve in-

Table 1. Effect of the supporting electrolytes on the rate of the oxygen exchange of chromate ions

[Cr(VI)] / M	pH[a]	Supporting electrolyte (I=1.0 M)	$R/10^{-5}$ M s^{-1}
0.0721	7.60	$NaClO_4$	0.828±0.006
0.0739	7.60	NaCl	0.792±0.006
0.0720	7.51	$NaClO_4$	1.83±0.06
0.0741	7.51	NaCl	1.75±0.05

a) In measuring the pH, the inner solution of the reference electrode was replaced by 4 M NaCl.

creasing from unity to 2.6 with the increase in the concentration of Cr(VI). It appears that the observed [Cr(VI)] dependence of the exchange reaction is dependent on the value of [Cr(VI)]. The kinetics of the oxygen exchange of chromate ions involves both the first-order and the higher-order rate terms in [Cr(VI)]. At lower concentrations of Cr(VI), the first-order term predominates, while at higher concentrations the second- and third-order terms come into play.

Effect of Chloride Ions on the Exchange Rate. Since hydrogenchromate ions react with chloride ions to form trioxochlorochromate(VI) ions in acidic aqueous solutions,[12,13] it may be suspected that the $HCrO_4^- + Cl^- + H^+ \rightleftharpoons CrO_3Cl^- + H_2O$ reaction might contribute to the oxygen exchange of chromate ions. Perlmutter-Hayman and Wolff[14] have noted the absence of chloride-ion catalysis of the hydrolysis of dichromate ions.

In order to examine the possibility of nucleophilic catalysis by chloride ions, the exchange rate was studied in the perchlorate media and compared with the rate in NaCl media (Table 1). The results indicate that the catalysis of the oxygen exchange of chromate ions by chloride ions is absent, at least under the present experimental conditions.

Mechanism of the Oxygen-exchange Reaction. The above results may be summarized as follows:

pH: 7.2—8.7 $R \propto [H^+]^{1.8}[Cr(VI)]^{1.2-1.0}$,

pH: 8.7—10.5 $R \propto [H^+]^{1.8-0}[Cr(VI)]$,

pH: >10.5 $R \propto [H^+]^0[Cr(VI)]$.

In the pH region greater than 10.5, the exchange reaction may be interpreted in terms of the process:

$$CrO_4^{2-} + H_2{}^{18}O \rightleftharpoons CrO_3{}^{18}O^{2-} + H_2O. \quad (1)$$

Since the more acidic species of an oxoanion is usually more reactive in the oxygen-exchange reaction, it is natural to assume the exchange mechanism:

$$HCrO_4^- + H_2{}^{18}O \rightleftharpoons HCrO_3{}^{18}O^- + H_2O, \quad (2)$$

along with Reaction 1.

The nearly first-order dependence on [Cr(VI)] (see Fig. 2, [Cr(VI)]<0.14 M) and the nearly second-order dependence on [H$^+$] observed at pH<8.7 suggest that the acid-catalyzed oxygen exchange of hydrogenchromate ions with water:

$$CrO_4^{2-} + H^+ \rightleftharpoons HCrO_4^-,$$

$$HCrO_4^- + H_2{}^{18}O + H^+ \rightleftharpoons HCrO_3{}^{18}O^- + H_2O + H^+, \quad (3)$$

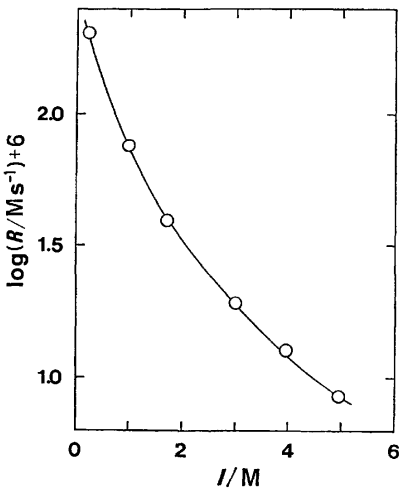

Fig. 4. The effect of ionic strength on the exchange rate.
I=0.2—5 M, [Cr(VI)]=0.075 M, pH=7.5, 25 °C.

plays a dominant role in this pH region.

The order of the exchange reaction with respect to [Cr(VI)] is definitely greater than unity at pH<7.7. This fact suggests that there is some contribution of the two dimerization mechanisms, 4 and 5, to the exchange reaction:

$$HCrO_4^- + CrO_4^{2-} \rightleftharpoons Cr_2O_7^{2-} + OH^-, \quad (4)$$

$$HCrO_4^- + HCrO_4^- \rightleftharpoons Cr_2O_7^{2-} + H_2O. \quad (5)$$

The rate law of the oxygen exchange of chromate ions with water may now be written as:

$$R = R_1 + R_2 + R_3 + R_4 + R_5$$
$$= k_1[CrO_4^{2-}] + k_2[HCrO_4^-] + k_3[H^+][HCrO_4^-] + k_4[HCrO_4^-][CrO_4^{2-}] + k_5[HCrO_4^-]^2. \quad (6)$$

Salt Effect. The effect of the ionic strength on the exchange rate can be seen from Fig. 1. The salt effect is negative at pH<10.5 and is absent above pH=10.5. The salt effect at pH=7.50 has been studied over a wider range of ionic strength (I(NaCl)= 0.2—5.0 M) (Fig. 4), [Cr(VI)] being kept at 0.075 M. The exchange rate decreases with the increase in the ionic strength.

At pH 7.50, the exchange reaction proceeds for the most part through the k_3 and k_5 paths (*ca.* 65% and 30% respectively). The kinetic salt effect on the k_3 path may be expected to be negative, and that on the k_5 path, to be positive. The equilibrium salt effect on K_1 and K_d reduces the concentration of $HCrO_4^-$, which is the more active species in the oxygen exchange of chromate ions. The observed salt effect is a result of these effects.

Temperature Dependence of the Exchange Rate. This has been studied at pH 7.38 (0 °C, 15 °C, and 25 °C) and at pH 11.0 (25 °C, 35 °C, and 45 °C). The concentration of chromium(VI) was kept at 0.075 M, the ionic strength being fixed at 1.0 M. The Arrhenius plots are shown in Fig. 5. The activation energies are (25.5±0.7) kJ/mol at pH 7.38 and (98.9±1.0) kJ/mol at pH 11.0.

Since the oxygen exchange proceeds exclusively through the k_1 path at pH=11.0, the value obtained

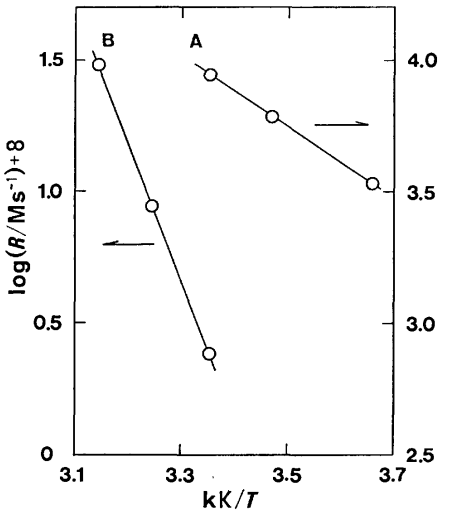

Fig. 5. Temperature dependence of the exchange rate at pH=7.4(A) and pH=11.0(B). ([Cr(VI)]=0.075 M, I(NaCl)=1 M).

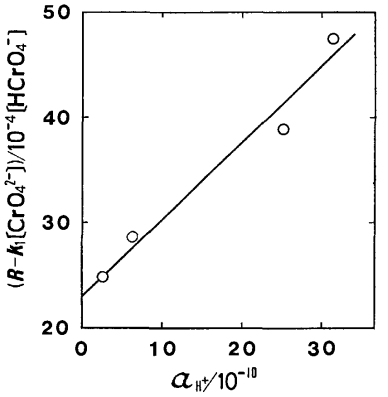

Fig. 6. A plot of $(R-k_1[CrO_4^{2-}])/[HCrO_4^-]$ against a_{H^+}. 25 °C, [Cr(VI)]=0.075 M, I(NaCl)=1 M, pH=8.5—9.6.

above (98.9 kJ/mol) may be interpreted as the energy of activation of this path. The entropy of activation of this path, ΔS^*_1 (298 K), is calculated to be (-45.1 ± 3.3) J/K mol, assuming the first-order dependence on $[H_2O]$.

Analysis of the Exchange Rate. The exchange rates plotted in Fig. 1 were analyzed as follows. The concentrations of the ionic species of Cr(VI) were calculated by the relations:

$$[Cr(VI)] = [HCrO_4^-] + [CrO_4^{2-}] + 2[Cr_2O_7^{2-}],$$

$$K_1 = [HCrO_4^-]/a_{H^+}\cdot[CrO_4^{2-}],$$

$$K_d = [Cr_2O_7^{2-}]/[HCrO_4^-]^2.$$

In the pH region greater than 10.5, the exchange reaction proceeds exclusively through the k_1 path. The appropriate rate law is:

$$R = k_1[CrO_4^{2-}].$$

The average of five values of k_1, calculated from the data in Fig. 1, pH>10.5, is:

$$k_1 = (3.2\pm 0.2)\times 10^{-7}\ s^{-1}.$$

Since the order of the exchange reaction with respect to [Cr(VI)] is 0.93 at pH=8.0, the contribution of the condensation mechanism (k_4 and k_5 paths) may be ignored in the pH region greater than 8.0. The rate law (6) then reduces to:

$$R = k_1[CrO_4^{2-}] + k_2[HCrO_4^-] + k_3[H^+][HCrO_4^-],$$

or $$(R-k_1[CrO_4^{2-}])/[HCrO_4^-] = k_2 + k_3[H^+].$$

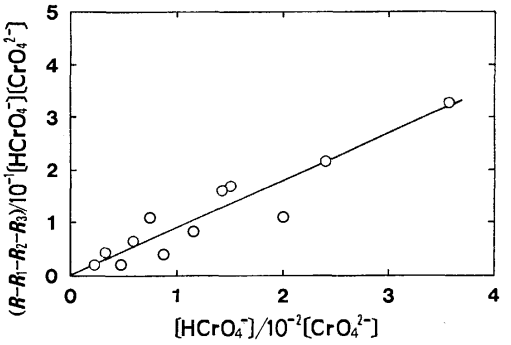

Fig. 7. $(R-R_1-R_2-R_3)/[HCrO_4^-][CrO_4^{2-}]$ as a function of $[HCrO_4^-]/[CrO_4^{2-}]$.
25 °C, [Cr(VI)]=0.075 M, I(NaCl)=1 M, pH=7.2—8.5.

In Fig. 6, the left-hand side of the equation is plotted against a_{H^+} for the runs at pH 8.5—9.57 and I=1.0 M. The least-squares treatment of the plot yields the values:

$$k_2 = (2.30\pm 0.19)\times 10^{-3}\ s^{-1},$$

and $$k_3 = (0.37\pm 0.09)\times 10^{6}\ M^{-1}\ s^{-1}.$$

The rate law (6) may then be written as:

$$\frac{R-k_1[CrO_4^{2-}]-k_2[HCrO_4^-]-k_3[H^+][HCrO_4^-]}{[HCrO_4^-][CrO_4^{2-}]} = k_4 + k_5[HCrO_4^-]/[CrO_4^{2-}]. \quad (7)$$

The left-hand side of the equation was calculated by using the values of k_1, k_2, and k_3 obtained above; in Fig. 7 it is plotted against $[HCrO_4^-]/[CrO_4^{2-}]$ for the runs at pH 7.2—8.5 and I=1.0 M. From the intercept and the slope of the straight line, the values of k_4 and k_5 are found to be $(0.8\pm 17)\times 10^{-3}\ M^{-1}\ s^{-1}$ and $(9.0\pm 1.1)\ M^{-1}\ s^{-1}$ respectively.

The runs at I=0.2 M were treated similarly. The values of the rate constants thus obtained are summarized in Table 2. The sign of the salt effect for each of these rate constants is as would be expected for the charge type of each reaction. In Fig. 1 the curves show the exchange rates calculated by using the rate constants obtained above. The agreement with the experimental values is satisfactory.

Our values of k_1 and k_4 agree satisfactorily with those of the earlier works.[5,15,16] Table 3 shows the value of k_5 obtained by various methods. The values of k_5 obtained in this study are larger by one order of magnitude than those determined by the methods other than oxygen-exchange. We have obtained a k_5 value of a similar magnitude (k_5=8.4 $M^{-1}\ s^{-1}$, at I=1.0 M and 25 °C) in the KCl medium. The discrepancy must be due to the occurrence of the third-order rate terms, $k_a[HCrO_4^-]^3$ and/or $k_b[HCrO_4^-]^2[CrO_4^{2-}]$, which increase in importance as the total concentration increases. It has been noted above that

Table 2. Rate constants of the oxygen-exchange reaction of chromate ions with water at 25 °C

I(NaCl)/M	k_1/s^{-1}	k_2/s^{-1}	k_3/$M^{-1}s^{-1}$	k_4/$M^{-1}s^{-1}$	k_5/$M^{-1}s^{-1}$
0.2	$(3.2\pm0.2)\times10^{-7}$	$(2.4\pm0.9)\times10^{-3}$	$(1.9\pm0.2)\times10^{6}$	$\approx10^{-3}$	5.0 ± 1.1
1.0		$(2.3\pm0.2)\times10^{-3}$	$(0.73\pm0.09)\times10^{6}$	$\approx10^{-3}$	9.0 ± 1.1

Table 3. Rate constants of the dimerization of hydrogenchromate ions at 25 °C

k_5/$M^{-1}s^{-1}$ a)	[Cr(VI)]/M	I/M	Reference
9.0	0.075	1.0(NaCl)	This work b)
5.0	0.075	0.2	This work b)
1.3	1—2.7	Not controlled 2.5—6.0	5 b)
5.5	0.1, 0.2	0.15, 0.45	6 b)
0.45 c)	0.02	0.1(KNO_3)	17
0.25	$(3—4)\times10^{-4}$	0.2($NaNO_3$)	18
0.38	0.002	0.1(KNO_3)	15

a) While the value of k_5 obtained by the oxygen-exchange method usually refers to the transfer of four oxygen atoms between chromate ions and water, the rate constant of the $2HCrO_4^- \rightleftharpoons Cr_2O_7^{2-} + H_2O$ reaction corresponds to the transfer of one atom of oxygen. In this column, the rate constants obtained by other methods are divided by 4 for comparison. b) Oxygen-exchange method. c) 23 °C.

the order of the exchange reaction in [Cr(VI)] increases above 2 with the increase in [Cr(VI)].

Perlmutter-Hayman *et al.*[14,19] have noted the general acid and base catalyses of the hydrolysis of dichromate ions. From the catalytic constants of other acids, Pladziewicz and Espenson[20] estimated the value of the rate constant of the hydrogenchromate-catalyzed hydrolysis of dichromate ions to be 0.1 $M^{-1}s^{-1}$. This value is, however, too small to account for the discrepancy noted above.

Mak[6] has determined the rate constant of the reaction:

$$HCrO_4^- + Cr_2O_7^{2-} \rightleftharpoons Cr_3O_{10}^{2-} + OH^-,$$

to be 13.6 $M^{-1}s^{-1}$ at 25 °C. This reaction might explain a part of the discrepancy.

The remaining possibility is the chromate-ion catalysis of the dimerization of hydrogenchromate ions:

$$2HCrO_4^- + CrO_4^{2-} \rightleftharpoons Cr_2O_7^{2-} + H_2O + CrO_4^{2-}.$$

On the assumption that the discrepancy is due entirely to the general-base catalysis, Eq. 7 may be written as:

$$\frac{R-(R_1+R_2+R_3)}{[HCrO_4^-][CrO_4^{2-}]} = k_4 + (k_5+k_b[CrO_4^{2-}])\frac{[HCrO_4^-]}{[CrO_4^{2-}]}.$$

Under the present experimental conditions, the dominating ionic species of Cr(VI) is CrO_4^{2-} (>95%), and $[CrO_4^{2-}]$ may be regarded as nearly constant. The plot of $(R-(R_1+R_2+R_3))/[HCrO_4^-][CrO_4^{2-}]$ against $[HCrO_4^-]/[CrO_4^{2-}]$ (Fig. 7) remains linear. Using 0.36 (the average of the last three values in Table 3) as the value of k_5, the upper limit of the value of k_b may be calculated as 65 $M^{-2}s^{-1}$, or 2.6×10^2 $M^{-2}s^{-1}$ (referred to the transfer of 1 atom of oxygen)

Table 4. Effect of protonation on the reactivity of oxoanions towards water

Reaction	Rate constants/s^{-1}	Temp/°C	I/M	Reference
$HCrO_4^- + H_2O \rightarrow$	2.4×10^{-3}	25	1.0, 0.2	This work
$CrO_4^{2-} + H_2O \rightarrow$	3.2×10^{-7}	25	1.0, 0.2	This work
$H_2AsO_4^- + H_2O \rightarrow$	1×10^{-4}	30	0.55	7
$HAsO_4^{2-} + H_2O \rightarrow$	1.2×10^{-5}	30	0.55	7
$AsO_4^{3-} + H_2O \rightarrow$	1.5×10^{-6}	30	0.55	7
$HSeO_3^- + H_2O \rightarrow$	2×10^{-4}	0	0.16	21
$SeO_3^{2-} + H_2O \rightarrow$	1.5×10^{-4}	0	0.16	21

(I=0.2 M).

On the contrary, if it is assumed that the rate term, $k_a[HCrO_4^-]^3$, accounts for all of the discrepancy, Eq. 7 becomes:

$$\frac{R-(R_1+R_2+R_3)}{[HCrO_4^-][CrO_4^{2-}]} = k_4 + (k_5+k_a[HCrO_4^-])\frac{[HCrO_4^-]}{[CrO_4^{2-}]}.$$

As $[HCrO_4^-]$ changes 20-fold between pH=7.2 and 8.5, the plot of $(R-(R_1+R_2+R_3))/[HCrO_4^-][CrO_4^{2-}]$ against $[HCrO_4^-]/[CrO_4^{2-}]$ should be a concave curve upwards. Figure 7 does not show such a trend.

The rate-determining step of the nucleophilic catalysis of the dimerization of hydrogenchromate ions[15] is the attack of a nucleophile on the hydrogenchromate ion. In the case of chromate ions as the nucleophile this is nothing but the dimerization of chromate ions and does not result in the acceleration of the rate of oxygen exchange between chromate ions and water. The analysis of the third-order rate terms is beyond the scope of this work.

The hydrogen-ion-catalyzed oxygen exchange of hydrogenchromate ions with water which has been found in this work may be formulated as:

$$H^+ + HCrO_4^- \rightleftharpoons H_2CrO_4,$$

$$H_2CrO_4 + H_2{}^{18}O \rightleftharpoons H_2CrO_3{}^{18}O + H_2O.$$

The dissociative mechanism seems unlikely because of the small activation energy (25.5 kJ/mol) at pH=7.38.

$$H_2CrO_4 \rightleftharpoons H_2O + CrO_3.$$

Table 4 shows the effect of protonation on the reactivity of oxoanions towards water. The enhanced reactivity of hydrogenchromate ions as compared with that of chromate ions is noteworthy. Since the role of a proton in facilitating the oxygen exchange of oxoanions probably consists in the polarization of the bond between the oxygen and the central atom, this bond seems to be more polarizable in chromate ions than in arsenate and selenite ions.

References

1) A. Okumura, N. Yamamoto, and N. Okazaki, *Bull. Chem. Soc. Jpn.*, **46**, 3633 (1973).
2) A. Okumura, S. Watanabe, M. Sakaue, and N. Okazaki, *Bull. Chem. Soc. Jpn.*, **52**, 2783 (1979).
3) Some preliminary results have been reported in Ref. 2.
4) M. R. Baloga and J. E. Earley, *J. Phys. Chem.*, **67**, 964 (1963).
5) R. H. Holyer and H. W. Baldwin, *Can. J. Chem.*, **45**, 413 (1967).
6) S. Y. C. Mak, Ph. D. thesis, The University of Western Ontario, 1967. The authors wish to thank Prof. J. O. Edwards, Brown University, for the information about this thesis.
7) A. Okumura and N. Okazaki, *Bull. Chem. Soc. Jpn.*, **46**, 2937 (1973).
8) P. D. Boyer, D. J. Graves, C. H. Suelter, and M. E. Dempsey, *Anal. Chem.*, **33**, 1906 (1961).
9) L. G. Sillén and A. E. Martell, "Stability Constants," *Chem. Soc.*, Spec. Publ. No. 17 (1964).
10) L. G. Sillén, *Acta Chem. Scand.*, **10**, 803 (1956).
11) Y. Sasaki, *Acta Chem. Scand.*, **16**, 719 (1962).
12) G. P. Haight, D. C. Richardson, and N. H. Coburn, *Inorg. Chem.*, **3**, 1777 (1964).
13) J. Y. Tong and R. L. Johnson, *Inorg. Chem.*, **5**, 1902 (1966).
14) B. Perlmutter-Hayman and M. A. Wolff, *J. Phys. Chem.*, **71**, 1416 (1967).
15) P. Moore, S. F. A. Kettle, and R. G. Wilkins, *Inorg. Chem.*, **5**, 220 (1966).
16) A. Lifshitz and B. Perlmutter-Hayman, *J. Phys. Chem.*, **65**, 2098 (1961).
17) J. H. Swinehart and W. Castellan, *Inorg. Chem.*, **3**, 278 (1964).
18) B. Perlmutter-Hayman, *J. Phys. Chem.*, **69**, 1736 (1965).
19) R. Baharad, B. Perlmutter-Hayman, and M. A. Wolff, *J. Phys. Chem.*, **73**, 4391 (1969).
20) J. R. Pladziewicz and J. H. Espenson, *Inorg. Chem.*, **10**, 634 (1971).
21) A. Okumura and N. Okazaki, *Bull. Chem. Soc. Jpn.*, **46**, 1084 (1973).

 © 1980 The Chemical Society of Japan Bull. Chem. Soc. Jpn., 53, 3149—3153 (1980)

Restricted SCF and MC-SCF Study of the Σ and Π States of the Formyloxyl and Formylaminyl Radicals

Osamu KIKUCHI

Department of Chemistry, The University of Tsukuba, Sakura-mura, Ibaraki 305

(Received February 22, 1980)

Open-shell restricted SCF and MC-SCF methods with the semi-empirical MINDO/3 approximation have been applied to the Σ and Π states of the formyloxyl and formylaminyl radicals. In the MC-SCF formalism, the $\pi\rightarrow\pi^*$ singly- and doubly-excited configurations are included. The optimized molecular structures and spin distributions predicted by the SCF and MC-SCF methods are compared. For the Π state of formyloxyl, the restricted SCF method gives a distorted C_s structure as the most stable Π structure, while the MC-SCF gives a symmetric C_{2v} structure. The use of the MC wavefunctions is recommended for the evaluation of the molecular and electronic structures of these radicals, in which a doublet instability of the restricted SCF solution is expected to occur.

Aminyl radicals[1] are unique in that the central nitrogen atom possesses both an unpaired electron and a lone pair of electrons in its pure $2p_z$ AO and hybrid σ AO; they are, therefore, capable of existing in either a Π or Σ ground electronic state. Since the σ hybrid AO is lower in energy than the pure $2p_z$ AO, the Π state is the ground state of alkylaminyl radicals.[1]

Π Σ

When one of the alkyl groups is replaced by a carbonyl group, an electron-withdrawing group, the $2p_z$ AO is stabilized by the carbonyl π^* orbital. Thus, the Π and Σ states of the acylaminyl radicals[2] may be expected to lie very close to each other, and their ground state can not easily be predicted. The same Σ-Π problem occurs in the acyloxyl radicals,[3,4] which are important intermediates in the thermal and photochemical decompositions of acyl peroxides.

Several semi-empirical and *ab initio* calculations have been reported for solving the Σ-Π problem for the acylaminyl[5,6] and acyloxyl[7-9] radicals. One theoretical problem involved in these radicals is the doublet instability expected in the RHF wavefunction for the three-electron π system. It has been pointed out[10-12] for the allyl radical that the doublet instability occurs in its π system for some region of its geometrical space, and this instability does not depend upon the approximation employed in the semi-empirical or *ab initio* RHF methods.[12] In this study, a multi-configuration(MC)-SCF formalism for the doublet states is applied to the formylaminyl and formyloxyl radicals in the hope of obtaining molecular and electronic structures which are not disturbed by the doublet instability of three-electron π system. The Π and Σ states of these radicals are calculated by a three-configuration MC-SCF equation with the semi-empirical MINDO/3 approximation.[13] Since the energy difference between the Π and Σ states of these radicals is expected to be very small,[5-9] it is difficult to derive any ultimate conclusion about the Σ-Π problem of these radicals by the present semi-empirical approximation. Attention is paid especially to the molecular and electronic structures of these radicals, obtained by both the open-shell restricted SCF and the MC-SCF methods.

Procedure

The distortion of the nuclear framework of the allyl radical leads to a further lowering of the RHF energy,[11,14] which is inconsistent with the ESR experimental evidence.[15] This instability of the RHF solution seems to be general in three-electron π systems.[12] The instability problem which appears in the three-electron system has been examined in detail for the H_3 system by Yamaguchi and Fukutome.[16] They showed that the RHF solution is stable in only a small region of the geometrical space of the H_3 system. The CCC angle of the allyl radical, and also the corresponding angles of formylaminyl and formyloxyl, are expected to be $\approx 120°$. The UHF solution of the H_3 system[16] indicates that the correct wavefunction of this region has the ASDW configuration, which is expressed in terms of the RHF orbitals by a mixture of three electron configurations. In the present formylaminyl and formyloxyl systems, these three configurations correspond to the ground configuration and the $\pi\rightarrow\pi^*$ singly- and doubly-excited configurations. Thus, the following four configuration functions are taken into account in the present MC-SCF formalism:

$$^2\Psi_g = |\cdots i\bar{i}\cdots m|$$

$$^2\Psi_i^k(1) = \frac{1}{\sqrt{2}}\{|\cdots i\bar{k}\cdots m| + |\cdots k\bar{i}\cdots m|\}$$

$$^2\Psi_i^k(2) = \frac{1}{\sqrt{6}}\{|\cdots i\bar{k}\cdots m| - |\cdots k\bar{i}\cdots m| - 2|\cdots ik\cdots \bar{m}|\}$$

$$^2\Psi_{\bar{i}}^{k} = |\cdots k\bar{k}\cdots m|,$$

and the wavefunction is expressed by:

$$^2\Phi = C_0\Psi_g + C_1\Psi_i^k(1) + C_2\Psi_i^k(2) + C_3\Psi_{\bar{i}}^{k}. \quad (1)$$

The electronic energy of Eq. 1 is written as:

$$E_{\mathrm{elec}} = E_g + \sum_{p,q} A_{pq}L_{pq} + \sum_{p,q,r,s} B_{pqrs}\langle pq|rs\rangle, \quad (2)$$

where p, q, r, and s run over the i, m, and k orbitals, and where A_{pq} and B_{pqrs} are expressed by the configuration expansion coefficients (they are given in the Appendix). Also,

$$E_g = \sum_{p=1}^{m-1} 2H_{pp} + \sum_{p,q}^{m-1}(2J_{pq} - K_{pq}) + H_{mm} + \sum_{p}^{m-1}(2J_{pm} - K_{pm})$$

$$L_{pq} = H_{pq} + \sum_{r}^{m-1}\{2\langle rr|pq\rangle - \langle rq|pr\rangle\} + \frac{1}{2}\{2\langle mm|pq\rangle - \langle mq|pm\rangle\},$$

$$I_{pq} = \int \phi_p^*(1) H_{\mathrm{core}}(1)\phi_q(1)d\tau$$

$$\langle rs|tu\rangle = \int \phi_r^*(1)\phi_s(1)\frac{1}{r_{12}}\phi_t^*(2)\phi_u^*(2)d\tau_1 d\tau_2.$$

A troublesome aspect of implementing the MC-SCF formalism involves the handling of the off-diagonal Lagrangian multipliers, which insure orthonormality between open- and closed-shell orbitals of the same symmetry.[17] Segal[18] has put forward the "partitioning basis-set" technique, which simplifies the calculation of the wavefunctions of the excited states of molecules. His method corresponds to a partial variation method, in which the variations of open-shell orbitals are expanded by virtual orbitals. Thus, the MO's obtained by this method are not optimum ones. However, its simplicity makes it possible to obtain many types of MC-SCF wavefunctions easily. This technique, which has been applied to the calculation of MC-SCF wavefunctions by Basch[19] and also by the present author,[20] was used in the present study. After treatment the same as that described previously,[20] Fock-type eigenvalue equations are obtained:

$$\left.\begin{aligned} &F_\lambda|\phi_\lambda\rangle = \varepsilon_\lambda|\phi_\lambda\rangle \quad (\lambda=1,2,\cdots,m-1;\ \neq i)\\ &F_i|\phi_i\rangle = \varepsilon_i|\phi_i\rangle\\ &F_m|\phi_m\rangle = \varepsilon_m|\phi_m\rangle\\ &F_k|\phi_k\rangle = \varepsilon_k|\phi_k\rangle. \end{aligned}\right\} \quad (3)$$

The operators, F_λ F_i, F_m, and F_k, are given by:

$$F_\lambda = F_c + \sum_{r,s}^{i,k}\frac{1}{2}A_{rs}(2f_{rs}-g_{rs})$$

$$F_c = H_{\mathrm{core}} + \sum_{p=1}^{m-1}(2J_p - K_p) + \frac{1}{2}(2J_m - K_m)$$

$$F_m = \frac{1}{2}F_\lambda - \frac{1}{4}(2J_m - K_m) + B_{miim}g_{ii} + B_{mkkm}g_{kk} + \frac{1}{2}B_{mikm}(g_{ik}+g_{ki})$$

$$F_i = F_{ii} + F_{ik}|\phi_k\rangle\langle\phi_i| + |\phi_i\rangle\langle\phi_k|F_{ki}$$

$$F_k = F_{kk} + F_{ki}|\phi_i\rangle\langle\phi_k| + |\phi_k\rangle\langle\phi_i|F_{ik}$$

$$F_{ii} = F_\lambda + \frac{1}{2}A_{ii}F_c + B_{iiii}f_{ii} + \frac{1}{2}B_{iikk}f_{kk} + \frac{1}{2}B_{iiki}(f_{ik}+f_{ki}) + \frac{1}{2}B_{ikki}g_{kk} + B_{miim}g_{mm}$$

$$F_{kk} = \frac{1}{2}A_{kk}F_c + B_{kkkk}f_{kk} + \frac{1}{2}B_{iikk}f_{ii} + \frac{1}{2}B_{ikkk}(f_{ik}+f_{ki}) + \frac{1}{2}B_{ikki}g_{ii} + B_{mkkm}g_{mm}$$

$$F_{ik} = \frac{1}{2}A_{ik}F_c + \frac{1}{2}B_{mikm}g_{mm} + \frac{1}{2}B_{iiki}f_{ii} + \frac{1}{2}B_{ikkk}f_{kk} + B_{ikik}f_{ik}$$

$$F_{ki} = \frac{1}{2}A_{ki}F_c + \frac{1}{2}B_{mikm}g_{mm} + \frac{1}{2}B_{kiii}f_{ii} + \frac{1}{2}B_{kiki}f_{kk} + B_{kiki}f_{ki},$$

where r and s run over two orbitals, i and k, and where p runs over orbitals which are doubly occupied in the Ψ_g configuration. The J_p, K_p, and H_{core} operators have their usual meanings, and the f_{rs} and g_{rs} operators are defined by:

$$f_{rs}(1)\phi_t(1) = \left(\int\frac{1}{r_{12}}\phi_r(2)\phi_s(2)d\tau_2\right)\phi_t(1)$$

$$g_{rs}(1)\phi_t(1) = \left(\int\frac{1}{r_{12}}\phi_r(2)\phi_t(2)d\tau_2\right)\phi_s(1).$$

If the variation method is applied so as to minimize the E_{elec} with respect to the LCAO coefficients, $\mathbf{c}$, of:

$$\phi_r = \chi c_r,$$

equations equivalent to Eq. 3 are obtained:

$$\left.\begin{aligned} &\boldsymbol{F}_\lambda\boldsymbol{c}_\lambda = \boldsymbol{c}_\lambda\boldsymbol{\varepsilon}_\lambda\\ &\boldsymbol{F}_i\boldsymbol{c}_i = \boldsymbol{c}_i\boldsymbol{\varepsilon}_i\\ &\boldsymbol{F}_m\boldsymbol{c}_m = \boldsymbol{c}_m\boldsymbol{\varepsilon}_m\\ &\boldsymbol{F}_k\boldsymbol{c}_k = \boldsymbol{c}_k\boldsymbol{\varepsilon}_k, \end{aligned}\right\} \quad (4)$$

where the matrices, $\boldsymbol{F}_\lambda$, $\boldsymbol{F}_i$, $\boldsymbol{F}_m$, and $\boldsymbol{F}_k$, are evaluated with the corresponding operator and the set of AO's. The configuration expansion coefficients and the orbital expansion coefficients are determined by an iterative procedure described elsewhere.[20] The spin density at the rth AO is obtained by means of:[21]

$$\rho_r = \left(1-\frac{4}{3}C_2^2\right)c_{rm}^2 + \left(\frac{2}{3}C_2^2 + \frac{2}{\sqrt{3}}C_1C_2\right)c_{ri}^2 + \left(\frac{2}{3}C_2^2 - \frac{2}{\sqrt{3}}C_1C_2\right)c_{rk}^2 + \frac{4}{\sqrt{6}}(C_2C_3 - C_0C_2)c_{ri}c_{rk}.$$

The open-shell restricted SCF solutions, which are being compared with the MC-SCF results, are obtained by the repeated diagonalization of the correct general SCF operator for the doublet state given by Hirao and Nakatsuji.[22] This gives correct converged solutions even when the usual Roothaan open-shell treatment diverges.

The semi-empirical MINDO/3 approximation[13] is used to evaluate the matrix elements. The calculation of the simplest nitrogen-center radical, NH_2, by this approximation gives satisfactory results for both the molecular structures of the Π_N and Σ_N states and the energy separation between these two states.[24]

Results and Discussion

Formyloxyl Radical. Formyloxyl has the possibility of existing in the symmetric C_{2v} structure and is a good example for use in examining the difference between the results obtained by the SCF and MC-SCF methods. In the Ψ_g configuration for the Π state of formyloxyl, the lowest π MO(π), the second π MO(π^0), and the highest π MO(π^*) are doubly-occupied, singly-occupied, and unoccupied MO's respectively. In the MC-SCF formalism, the π, π^0, and π^* MO's are assigned to the i, m, and k MO's of Eq. 1 respectively. In the calculation of the $\Sigma(B_2)$ state, the π^0, $\sigma(b_2)$, and π^* MO's are assigned to the i, m,

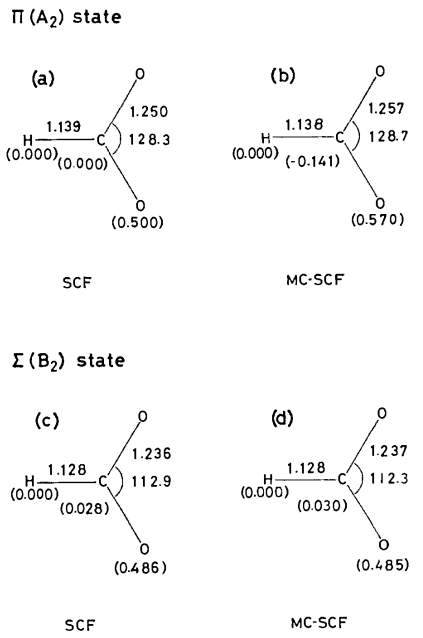

Fig. 1. The structures and spin distributions of the Π and $\sum$ states of the C_{2v} formyloxyl radical. Atomic spin densities are in parentheses. Bond lengths are in Å, and bond angles in degrees.

and k MO's respectively.[25] The optimized[26] molecular structures and spin distributions for the C_{2v} Π and $\sum$ states are shown in Fig. 1. The SCF and MC-SCF methods predict a very similar molecular structure for the $\Pi(A_2)$ state and also for the $\Sigma(B_2)$ state. The spin distribution of the $\Sigma(B_2)$ state by SCF and MC-SCF also resemble each other. The negative spin density appears at the central carbon atom in the MC-SCF Π state. Although the molecular structure and spin distribution of the C_{2v} formyloxyl are not greatly afected by the inclusion of the excited configurations, the relative energy between the $\Sigma(B_2)$ and $\Pi(A_2)$ states is greatly reduced by the MC-SCF formalism (Table 1).

The SCF calculation gives a stable Π(A″) structure for the distorted C_s formyloxyl.[27] This is shown in Fig. 2. This distorted C_s structure is 19.6 kJ mol^{-1} more stable than the SCF C_{2v} $\Pi(A_2)$ state, and the unpaired electron is located mostly (90%) at one of the oxygen atoms in this structure. These results indicate that the SCF calculation predicts the distorted C_s structure instead of the symmetric C_{2v} one, as the most stable Π state. The C_{2v} structure of the allyl π radical has been determined from the experimental ESR coupling constants of allyl.[15] When the open-shell restricted SCF procedure is applied to the allyl radical, the distorted C_s structure is obtained, while the MC-SCF MINDO/3 procedure presented here gives the C_{2v} structure,[14] which is consistent with the experimental evidence for the allyl radical. Thus, the C_s(Π) structure of the acyloxyl radical predicted by the present SCF calculation may not be correct for the Π state of acyloxyl.

When the MC-SCF optimization of the nuclear framework, using the C_s structure in Fig. 2 as the initial structure, was carried out for the Π state, the

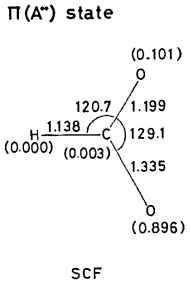

Fig. 2. The optimized structure and spin distribution (in parentheses) of the Π(A″) state of the distorted C_s formyloxyl radical. The MC-SCF formalism does not give the stable structure for the distorted form.

Table 1. Relative energies (kJ mol^{-1}) of the $\sum$ and Π states of the formyloxyl radical

	SCF	MC-SCF
$\Sigma(B_2)$	0.0	0.0
$\Pi(A_2)$	59.8	9.2
Π(A″)	40.2	—

symmetric Π structure shown in Fig. 1-(b) was obtained as the optimized one. It may be concluded that the stable C_s Π structure of formyloxyl predicted by the SCF calculation results from the doublet instability expected in the RHF solution for the C_{2v} structure of the three-electron π system, and that this instability is removed by the MC-SCF treatment. The wavefunction of the C_{2v} $\Pi(A_2)$ state, Fig. 1-(b), is:

$$0.974\Psi_g + 0.039\Psi_i^k(1) + 0.210\Psi_i^k(2) - 0.081\Psi_{ii}^{kk}$$

The contribution of the doubly-excited configuration, Ψ_{ii}^{kk}, to this state is small. It was found that the exclusion of the doubly-excited configuration from the present MC-SCF formalism also gives the $C_{2v}(A_2)$ structure, instead of the C_s(A″) one, as the most stable Π state. Thus, the inclusion of the singly-excited configuration in the MC-SCF formalism appears to be sufficient to remove the doublet instability expected in the RHF solution of C_{2v} three-electron radicals. It should be noted that, if the symmetry of formyloxyl is restricted to C_{2v}, a reliable structure for the Π state is obtained by the restricted SCF calculation, since the SCF and MC-SCF structures of the Π states (Fig. 1) closely resemble each other. The reliable spin distribution can be obtained by the SCF calculation, followed by the CI calculation.

Formylaminyl Radical. The optimized structures and spin distribution for the Π and $\sum$ states of formylaminyl are shown in Fig. 3. The difference in the molecular structures between the SCF and MC-SCF Π states is not very large, but it is important; the lengthening of the CO bond and the shortening of the CN bond are more obvious in the MC-SCF structure than in the SCF structure. This indicates

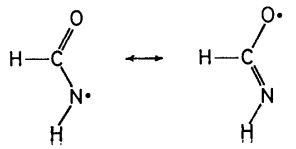

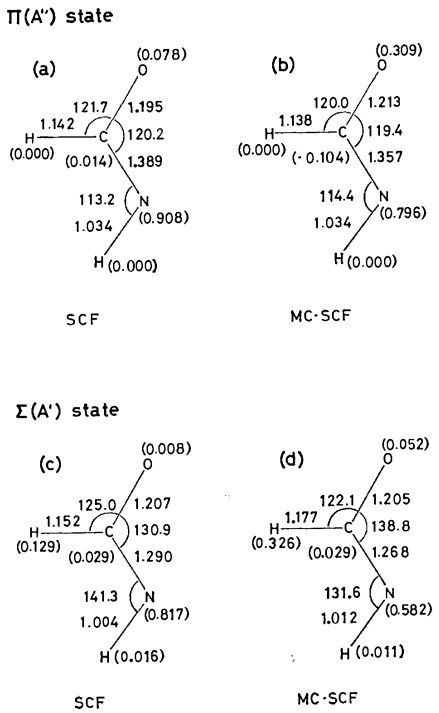

Fig. 3. The structures and spin distribution of the Π and Σ states of the formylaminyl radicals. Atomic spin densities are in parentheses. Bond lengths are in Å, and bond angles in degrees.

that the single-determinant SCF calculation overestimates the contribution of one of the canonical structures to the Π electronic state of this radical. This trend also appears in the calculated spin distribution; the larger spin density on the oxygen atom is obtained in the MC-SCF structure. As is to be expected from the analysis of the formyloxyl radical, the difference between the SCF and MC-SCF structures for the Π state of the acylaminyl radical may result mainly from the unstable nature of the restricted SCF method for this radical. A large difference is observed in the SCF and MC-SCF spin distributions in the Σ(A') state (Figs. 3c and 3d). This may come from the difference between the SCF and MC-SCF structures. The decrease in the HCN and CNH angles causes a larger interaction between the 1s AO of the H–C hydrogen atom and the hybrid odd-electron AO of the nitrogen atom, and the spin delocalization occurs from the nitrogen to the hydrogen atom. A similar trend has been observed in the spin distributions in the SCF Σ(A') state, which are calculated as functions of the CNH angle.

The ESR spectra of several acylaminyl radicals have been obtained.[1,5] The nitrogen splittings are ≈15 G (1 G=10^{-4} T), and the N–CH_3 proton splittings are ≈29 G. These values are very similar to those of the dialkylamino radicals,[1,5] whose ground state is of the π-type, and also indicate that the odd-electron AO at the nitrogen atom is not the sp hybrid AO, but almost pure 2p AO. These ESR results support the Π_N ground state for the acylaminyl radical, although it is not possible absolutely to exclude a Σ_N structure with the CNC angle of ≈180°. The MC-SCF results

Table 2. Relative energies (kJ mol^{-1}) of the Σ and Π states of the formylaminyl radical

	SCF	MC-SCF
Σ(A')	0.0	7.1
Π(A'')	26.4	0.0

in Table 2 indicate that the ground state of formylaminyl is of the Π(A'') type, which is consistent with the results of the ESR experiments. However, the energy difference between Σ and Π is very small.

The *ab initio* STO-3 G and 4-31G calculations by Baird and Kathpal[6] show that the Σ_N state is much (>40 kJ mol^{-1}) higher than the Π state, while the present results predict they will lie very close to one another. In their calculations of the formylaminyl radical, all the bond angles around the carbon atom were assumed to be 120°. As may be seen from Fig. 3, the bond angles around the carbon atom deviate greatly from 120°; the optimization of these angles is important in estimating the relative energy between the Π and Σ states.

Significant differences have been observed between the SCF and MC-SCF molecular electronic structures for the formyloxyl and formylaminyl radicals. They come mainly from the doublet instability of the restricted SCF solutions for the 3π-electron radicals. The allyl 3π-electron system is described correctly by the present MC-SCF procedure;[14] the use of the multi-configuration wavefunction is recommended for the evaluation of the molecular and electronic structures for the lower-lying Π and Σ states of acyloxyl and acylaminyl radicals.

Appendix

A_{pq} and B_{pqrs} in Eq. 2 are expressed by the following configuration expansion coefficients; all the other values are zero.

$$A_{ii} = -C_1^2 - C_2^2 - 2C_3^2$$
$$A_{kk} = C_1^2 + C_2^2 + 2C_3^2$$
$$A_{ik} = A_{ki} = \sqrt{2}\,(C_0C_1 + C_1C_3)$$
$$B_{iiii} = B_{kkkk} = C_3^2$$
$$B_{iikk} = -C_1^2 - C_2^2 - 4C_3^2$$
$$B_{miim} = B_{immi} = \frac{1}{2}(C_2^2 - \sqrt{3}\,C_1C_2)$$
$$B_{mkkm} = B_{kmmk} = \frac{1}{2}(C_2^2 + \sqrt{3}\,C_1C_2)$$
$$B_{mikm} = B_{immk} = \frac{\sqrt{6}}{2}(C_0C_2 - C_2C_3)$$
$$B_{ikii} = B_{kiii} = -\sqrt{2}\,C_1C_3$$
$$B_{ikkk} = B_{kikk} = \sqrt{2}\,C_1C_3$$
$$B_{ikik} = B_{kiki} = C_0C_3$$
$$B_{ikki} = 2(C_1^2 + C_3^2).$$

References

1) For a review for the aminyl radical, see W. C. Danen and F. A. Neugebauer, *Angew. Chem., Int, Ed, Engl.*, **14**, 783 (1975).

2) For a review for the acylaminyl radical, see P. Mackiewicz and R. Furstoss, *Tetrahedron*, **34**, 3241 (1978).
3) J. M. McBride and R. A. Merrill, *J. Am. Chem. Soc.*, **102**, 1723 (1980), and the references cited therein.
4) O. Kikuchi, *J. Synth. Org. Chem.*, **37**, 678 (1979).
5) T. Koenig, J. A. Hoobler, C. E. Klopfenstein, G. Hedden, F. Sunderman, and B. R. Russell, *J. Am. Chem. Soc.*, **96**, 4573 (1974).
6) N. C. Baird and B. Kathpal, *J. Am. Chem. Soc.*, **98**, 7532 (1976).
7) T. Koenig, R. A. Wielesek, and J. G. Huntington, *Tetrahedron Lett.*, **1974**, 2283.
8) O. Kikuchi, *Tetrahedron Lett.*, **1977**, 2421.
9) O. Kikuchi, K. Utsumi, and K. Suzuki, *Bull. Chem. Soc. Jpn.*, **50**, 1339 (1977).
10) J. Paldus and J. Cizek, *J. Chem. Phys.*, **52**, 2919 (1970).
11) J. McKelvey and W. J. Hehre, *Mol. Phys.*, **25**, 983 (1973); J. M. McKelvey and G. Berthier, *Chem. Phys. Lett.*, **41**, 476 (1976).
12) J. Paldus and A. Veillard, *Chem. Phys. Lett.*, **50**, 6 (1977).
13) R. C. Bingham, M. J. S. Dewar, and D. H. Lo, *J. Am. Chem. Soc.*, **97**, 1285 (1975).
14) O. Kikuchi, *Chem. Phys. Lett.*, **72**, 487 (1980).
15) R. W. Fessenden and R. H. Schuler, *J. Chem. Phys.*, **39**, 2147 (1963).
16) K. Yamaguchi and H. Fukutome, *Prog. Theor. Phys.*, **54**, 1599 (1975).
17) G. Das and A. C. Wahl, *J. Chem. Phys.*, **56**, 1769 (1972).
18) G. A. Segal, *J. Chem. Phys.*, **53**, 360 (1970).
19) H. Basch, *J. Chem. Phys.*, 55, 1700 (1971).
20) O. Kikuchi and K. Aoki, *Bull. Chem. Soc. Jpn.*, **47**, 2915 (1974).
21) O. Kikuchi, Thesis, Tokyo Kyoiku University (1969).
22) K. Hirao and H. Nakatsuji, *J. Chem. Phys.*, **59**, 1457 (1973).
23) C. C. J. Roothaan, *Rev. Mod. Phys.*, **32**, 179 (1960).
24) The HNH angle of the NH_2 radical estimated by MINDO/3 is 102° for the Π state and 136° for the $\sum$ state, and the energy difference between these states is estimated to be 24 kcal/mol. The corresponding experimental values[6] are 103°, 144°, and 31 kcal/mol respectively.
25) In the $\sum$ state of formyloxyl and formylaminyl, four electrons occupy the π orbitals, and the doublet instability may not occur. When the OCO or OCN angle becomes small, the energy difference between the π^0 and π^* levels decreases and the doubly-excited configuration from π^0 to π^* becomes important to the $\sum$ state. Moreover, the preliminary CI calculations showed that the singly-excited $\pi \rightarrow \pi^*$ configuration is important for the acylaminyl radical. For the above reasons, the π^0 and π^* MO's are assigned to the i and k orbitals in Eq. 1 for the $\sum$ state of the acyloxyl and acylaminyl radicals.
26) The variable metric method proposed by Fletcher was employed; R. Fletcher, *Computer J.*, **13**, 317 (1970).
27) The SCF MINDO/3 energies of $\sum(A_1)$ and the distorted $\sum(A')$ states are lower than those of the $\sum(B_2)$ and $\Pi(A_2)$ states. In these states, the CH distance is >1.2 Å and the OCO angle is $>150°$. These are, thus, transient states dissociative to $H+CO_2$.

Hydrogenation Activity and Selectivity of Cobalt Boride and Cobalt Nickel Binary Boride Catalysts

Yuriko NITTA, Toshinobu IMANAKA, and Shiichiro TERANISHI*

Department of Chemical Engineering, Faculty of Engineering Science, Osaka University, Toyonaka, Osaka 560

(Received March 10, 1980)

Co–B catalyst has higher selectivity than Ni–B catalyst for the formation of α,β-unsaturated alcohols from α,β-unsaturated aldehydes and lower selectivity for the formation of olefins from acetylenes. The differences between the two catalysts can be ascribed to the differences in the adsorption strength of reactants on Co and Ni metals. The hydrogenation activities of the Co–Ni–B catalysts vary through a maximum, but the selectivities vary monotonously with nickel content. These features are explained in terms of the surface composition measured by XPS and of the surface area of the catalysts. The enrichment of nickel on the surface and the increase of the surface area are observed for the Co–Ni–B catalysts. Co–B catalysts modified by a small amount of metal salts (Fe, Cr, Cu, *etc.*) are more effective for the selective hydrogenation of α,β-unsaturated aldehydes than co-precipitated binary boride catalysts.

Paul *et al.* reported in 1951[1] that cobalt boride (Co–B) prepared by the liquid-phase reduction of cobalt salt with sodium tetrahydroborate has catalytic activity for the hydrogenation of safrole. Since then, the Co–B catalyst has been used in several reactions, such as in selective hydrogenation of nitriles to primary amines,[2] in the reduction of nitro compounds[3] and carbon monoxide,[4] and in hydrogenolysis of hydrogen peroxide.[5] With regards to the hydrogenation of olefins, aldehydes and ketones on Co–B catalyst, however, there have been only a few reports, probably because the activity of the Co–B catalysts is much lower than that of the Ni–B catalyst.

On the other hand, there have been some reports showing the difference between nickel and cobalt catalysts in the activity and selectivity for hydrogenations of various compounds.[6] We have reported the surface state of Ni–B catalyst and its catalytic activity and selectivity for hydrogenation reactions in comparison to other nickel catalysts.[7] In this work, we studied the selective hydrogenation of α,β-unsaturated aldehydes to unsaturated alcohols and that of acetylenes to olefins on the Co–B catalyst, which might exhibit higher selectivity than the Ni–B catalyst.

Furthermore, although a small amount of a metal such as Mo, W, Cr, or Rh, added to the Co–B or Ni–B catalyst is known to promote the catalytic activity,[1,5,8] there has been no detailed report on the catalytic activity and selectivity of binary boride catalysts with various compositions. In the present work, a series of co-precipitated cobalt nickel boride (Co–Ni–B) catalysts was examined in order to elucidate the relation between the catalytic activity or selectivity and the surface state of the binary boride catalysts. The effects of metal salt additives to the Co–B and Ni–B catalysts on their selectivities were also studied in order to reveal the influence of preparation methods of binary boride catalysts and to find a more effective catalyst for the selective hydrogenation of α,β-unsaturated aldehydes to unsaturated alcohols.

Experimental

Catalysts. Co–B catalyst was prepared by reducing cobalt(II) acetate with sodium tetrahydroborate in water at 30 °C according to the method described previoursly.[7e] Co–Ni–B catalysts were prepared in a similar way from mixtures of measured amounts of cobalt acetate and nickel acetate. The total weight of reduced metal was held constant. A freshly prepared catalyst was used for each experiment, immediately after washing with water and ethanol. The modification of Co–B or Ni–B catalyst by metal salts was carried out by stirring the washed catalyst with a measured amount of metal acetate or chloride in 20 cm^3 of ethanol for 20 min under a hydrogen atmosphere prior to the hydrogenation reaction.

BET surface areas of the catalysts were measured by N_2 adsorption at 77 K after they were washed with acetone and after evacuation by a diffusion pump for 4 h at ambient temperature. The surface areas of several catalysts were also measured after heating at 300 °C for 2 h *in vacuo*.

Apparatus, Procedure, and Materials. The hydrogenation reactions of acetone (2 cm^3), crotonaldehyde, cinnamaldehyde, and acetylenes (0.5 cm^3 for each) were carried out at 30 °C in 20 cm^3 of 99% ethanol under atmospheric pressure of hydrogen by using an apparatus similar to that described previously.[9] A sufficient amount of hydrogen was adsorbed on each catalyst prior to the hydrogenation reactions. The amount of catalyst used was 0.2 g of metal for the hydrogenation of crotonaldehyde and acetylenes, and 0.5 g for that of acetone and cinnamaldehyde. The reaction rates were found not to be controlled by diffusion under these reaction conditions.

The initial hydrogenation rates were measured manometrically by the uptake of hydrogen in the initial stage of the reaction. The decomposition rate of hydrogen peroxide was also measured for comparison from the volume of oxygen evolved on 0.2 g of catalyst at 0 °C in 20 cm^3 of ethanol.

The selectivity of a catalyst for the hydrogenation of α,β-unsaturated aldehydes (S_1) was determined as the ratio of the yield of unsaturated alcohols to the total yield of the products based on GLC analysis at about 50% conversion. With the hydrogenation of acetylenes, the olefin selectivity (S_2) of a catalyst was defined as the molar ratio of olefin in olefin plus paraffin.

All reactants and solvent used for the hydrogenation reactions were dried and distilled before use. Metal salts and $NaBH_4$ were commercially obtained guaranteed or extra pure grade reagents (Nakarai Chemicals) and were used without further purification.

Analysis. Analysis of the reaction products was carried out by GLC using a Shimadzu 4APT gas chromatograph with a 2 m column of 20% PEG 20 M on Celite 545,

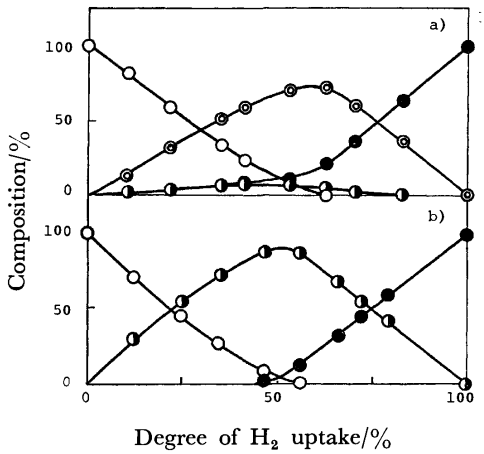

Fig. 1. Hydrogenation of cinnamaldehyde on (a) Co–B and (b) Ni–B catalysts.
○: Cinnamaldehyde, ◑: 3-phenylpropionaldehyde,
◎: cinnamyl alcohol, ●: 3-phenyl-1-propanol.

X-Ray photoelectron spectra(XPS) of some of the Co–Ni–B catalysts were measured to estimate the surface composition of the catalysts by using a Hitachi 507 photoelectron spectrometer. The detailed procedures were reported elsewhere.[7e] The surface concentration of nickel in a Co–Ni–B catalyst was estimated from the relative peak area intensities of Ni $2p_{3/2}$ and Co $2p_{3/2}$ and from the relative atomic sensitivities obtained by measuring the X-ray induced spectra of $NiSO_4$ and $CoSO_4$.

Results

Co–B Catalyst. The Co–B catalyst prepared from cobalt(II) acetate is a fine, nonpyrophoric, and nonferromagnetic precipitate, and appears amorphous from the X-ray diffraction pattern. These properties of Co–B catalyst are similar to those of the Ni–B catalyst reported previously.[1,7] The Co–B catalyst prepared from cobalt(II) chloride is, however, ferromagnetic and has a little lower activity for hydrogenation reactions than the one prepared from cobalt(II) acetate. Although the BET surface area of the Co–B catalyst is 38 m^2/g, twice as large as that of the Ni–B catalyst, the catalytic activity of the Co–B catalyst for hydrogenation reactions is considerably lower than that of the Ni–B catalyst. For example, the relative specific hydrogenation rates over the Co–B catalyst to that over the Ni–B catalyst are 1/3 for acetone, 1/15 for cinnamaldehyde, and 1/35 for crotonaldehyde. The low hydrogenation activity and the low resistivity to fatigue of cobalt catalyst may be partly attributed to the strong affinity of cobalt metal for oxygen,[10] as is expected from the following result of the decomposition reaction of hydrogen peroxide.

The hydrogenation profiles of cinnamaldehyde on the Co–B and Ni–B catalysts are shown in Fig. 1. A considerable amount of unsaturated alcohol, *i.e.*, cinnamyl alcohol, was produced together with much smaller amounts of saturated aldehyde and saturated alcohol from the initial to the middle of the reaction stage on the Co–B catalyst, whereas no unsaturated alcohol was detected at all for the reaction on the Ni–B catalyst. In the case of crotonaldehyde, we also

Table 1. Hydrogenation of acetylenes on cobalt and nickel catalysts

Reactant	Catalyst	Hydrogenation rate r/H_2-ccSTP $min^{-1}\cdot g^{-1}$	Olefin selectivity $S_2/\%$
Phenylacetylene	Co-B	46.1	79.0
	R-Co	0.4	76.6
	Ni-B	117.0	90.0
1-Heptyne	Co-B	35.5	68.5
	R-Co	8.9	61.0
	Ni-B	57.0	72.5
2-Heptyne	Co-B	17.7	97.3
	R-Co	0.7	93.4
	Ni-B	63.7	95.3

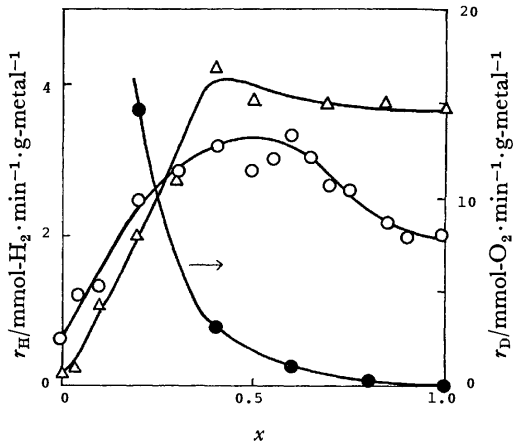

Fig. 2. Initial reaction rates as a function of nickel content x.
Substrate: ○, acetone(×10); △, crotonaldehyde; ●, hydrogen peroxide.

obtained crotyl alcohol with 21% of selectivity on the Co–B catalyst as well as on the platinum boride catalyst modified by copper(II) salt or iron(II) salt, as reported in our previous paper.[11]

On the other hand, the selectivities to olefins(S_2) in the hydrogenation of acetylenes on the Co–B catalyst were somewhat lower than those on the Ni–B catalyst, while somewhat higher than those on Raney cobalt(R-Co) catalyst (Table 1). With regards to the hydrogenation rate of acetylenes, the Co–B catalyst showed considerably high activity, while the R-Co catalyst showed very low activity.

Co–Ni–B Catalysts. Figure 2 shows the initial hydrogenation rates (r_H) of acetone and crotonaldehyde and the initial decomposition rate(r_D) of hydrogen peroxide on the Co–Ni–B catalysts against nickel content (x=Ni/Co+Ni) in the catalyst. A maximum activity for hydrogenation reactions was obtained with a catalyst containing nickel in a concentration around x=0.5; however the shape of maximum was not sharp. X-Ray diffraction analysis showed that no crystalline phase existed in any of the Co–Ni–B catalysts used.

With respect to the decomposition reaction of hydrogen peroxide, however, the Co–B catalyst has the maximum activity, while a catalyst containing more nickel shows much lower activity. This feature cannot

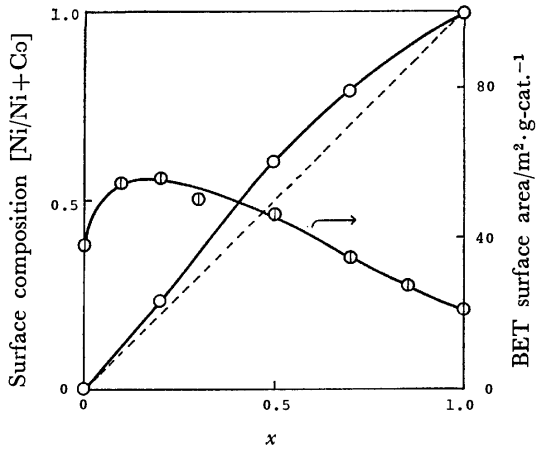

Fig. 3. Surface composition and BET surface area of Co–Ni–B catalyst as a function of nickel content x.

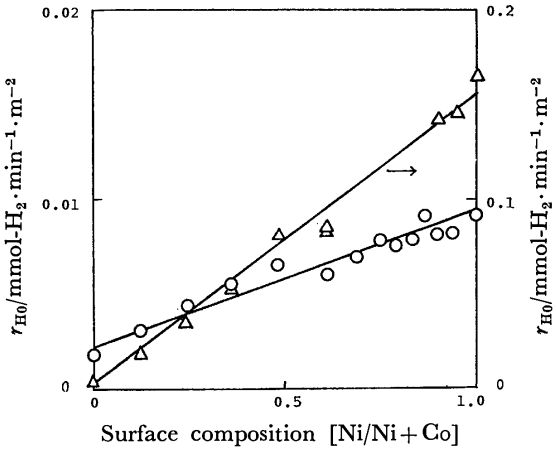

Fig. 4. Intrinsic hydrogenation activity r_{H0} of Co–Ni–B catalyst for acetone(○) and crotonaldehyde(△) as a function of surface composition.

be explained only by the increase of surface area of Co–Ni–B catalysts. It can be seen from Fig. 2 that the degree of variation in activity with nickel content is larger for the catalysts containing less nickel.

In Fig. 3, surface compositions of some Co–Ni–B catalysts obtained by XPS measurement are plotted, together with the BET surface areas of the catalysts, against nickel content in the bulk. The nickel content on the catalyst surface was found to be larger than that in the bulk.

Since the catalytic activities should be compared with the surface states of the catalysts, the intrinsic hydrogenation activities(r_{H0}) of Co–Ni–B catalysts per unit surface area were calculated based on the data in Fig. 2 and Fig. 3, and are plotted against the nickel content on the surface of the catalyst (Fig. 4).

The catalytic selectivities of the Co–Ni–B catalysts for the hydrogenations of α,β-unsaturated aldehydes(S_1) and phenylacetylene(S_2) are also plotted against nickel content(x) in Fig. 5. Both selectivities (S_1 and S_2) vary monotonously with nickel content in the catalysts. Each selectivity, S_1 or S_2, of the Co–Ni–B catalysts is lower than that of the Co–B or the Ni–B catalyst. The degree of variation in these selectivities with nickel content is also larger for the catalysts containing less

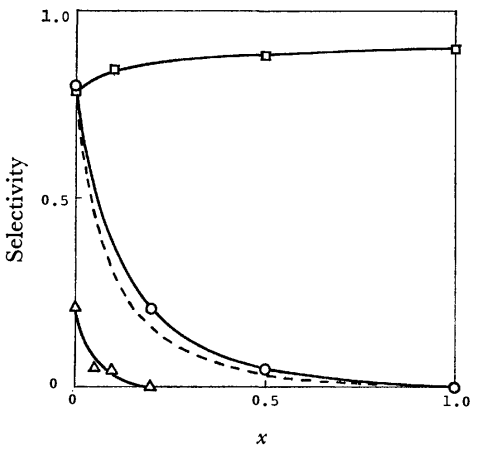

Fig. 5. Selectivity of Co–Ni–B catalyst as a function of nickel content x.
○: Selectivity to cinnamyl alcohol from cinnamaldehyde(S_1), △: selectivity to crotyl alcohol from crotonaldehyde(S_1), □: selectivity to styrene from phenylacetylene(S_2).

nickel.

In addition, the resistivity against sintering of the Co–Ni–B catalysts was studied by measuring the BET surface areas of the catalysts heated at 300 °C for 2 h *in vacuo*. The resistivity to the fatigue due to oxidation of the catalyst surface was also evaluated by measuring the decomposition rate of hydrogen peroxide repeatedly on once-used catalyst. Both resistivities increased rapidly with the increase of nickel content.

Co–B Catalyst Modified with Metal Salt. Table 2 lists the products distribution for the hydrogenation of crotonaldehyde and cinnamaldehyde on Co–B catalysts modified by various metal salts (0.17 mmol/g-Co). The addition of certain metal salts was found to increase the yield of unsaturated alcohols(UA) on the Co–B catalyst, as reported on R-Co catalyst,[12] while it was not effective at all in the case of the Ni–B catalyst. The effectiveness of metal salts added to the Co–B catalyst decreased in the order: Fe≃Cr>Cu>Cd>Zn>Ru>Co.

When the amount of the metal salts added was more than 0.17 mmol/g-Co (1 mol% of the amount of the Co–B catalyst), it was less effective. In the case that metal salts were added to the aqueous solution of cobalt acetate prior to the reduction with $NaBH_4$, the resulting coprecipitated binary boride catalysts, even Co–Ni–B or Co–Cr–B catalyst, were not so selective as the modified cobalt boride catalyst.

Discussion

From the fact that the plots in Fig. 4 give a straight line, the variation of the specific activity of the Co–Ni–B catalysts with nickel content shown in Fig. 2 is evidently explained in terms of the surface area and the surface composition of the catalysts. In other words, the maximum hydrogenation activity of the Co–Ni–B catalyst containing nickel in concentrations around x=0.5 is due not only to the increase of the

Table 2. The modifying effect of metal salt added to Co-B catalyst on the selectivity for the hydrogenation of α,β-unsaturated aldehydes

Run[a]	Modifier	Reaction time/min	Conversion/%	Product yield/%		
				SD	UA	SA[c]
1)	None	73	50	60	21	19
2)	$CuCl_2 \cdot 2H_2O$	220	48	50	37	13
3)	$FeCl_2 \cdot nH_2O$	254	26	36	47	17
4)	$CrCl_3 \cdot 6H_2O$	220	52	42	44	14
5)	$Cd(CH_3COO)_2 \cdot 2H_2O$[b]	120	20	60	28	12
6)	$Zn(CH_3COO)_2 \cdot 2H_2O$	150	40	60	26	14
7)	$RuCl_3 \cdot H_2O$	45	55	71	22	7
8)	$Co(CH_3COO)_2 \cdot 4H_2O$	155	55	61	22	17
9)	None	120	39	15	78	7
10)	$FeCl_2 \cdot nH_2O$	360	19	6	87	6
11)	$CrCl_3 \cdot 6H_2O$	147	65	6	90	4

a) Reactants are crotonaldehyde(6 mmol) for run 1 to run 8 and cinnamaldehyde(4 mmol) for run 9 to run 11. b) The amount of cadmium salt added is 0.085 mmol/g-Co instead of 0.17 mmol/g-Co. c) SD: saturated aldehyde, UA: unsaturated alcohol, SA: saturated alcohol.

surface area but also to the enrichment of nickel on the surface of the catalyst.

The features of the dependence of the selectivities (S_1 and S_2) on nickel content mentioned before (Fig. 5) are also explicable by the enrichment of nickel on the catalyst surface and by the higher hydrogenation activity of Ni metal than that of Co metal in the catalyst. The dashed line in Fig. 5 represents the variation of the calculated selectivity with nickel content for the hydrogenation of cinnamaldehyde, based on the surface composition of the catalysts and the values of selectivities and activities of Co–B and Ni–B catalysts.

The rapid increase in the resistivities against sintering or the fatigue with the increase of nickel content in Co–Ni–B catalysts can also be understood as a result of the enrichment of nickel on the surface of the catalysts, because the Ni–B catalyst is well known to have high resistivities against sintering or fatigue.

An advantage of the coprecipitated binary boride catalyst, Co–Ni–B, is the increase of hydrogenation activity. As for the catalytic selectivity, these binary boride catalysts were found to be ineffective. On the other hand, another type of binary boride catalysts, prepared by the modification of the Co–B catalyst with a small amount of metal salt, has an increased selectivity for the hydrogenation of α,β-unsaturated aldehydes. In this case, since the added metal cations interact with cobalt metal only on the surface of the catalyst, the addition of only small amounts of metal salt was more effective, compared to the case of the coprecipitated binary boride catalyst. It can be concluded, therefore, that the coprecipitated binary boride catalysts are effective for the increase of hydrogenation activity but that the modified binary boride catalysts are effective for the increase of the catalytic selectivity.

As can be seen from Fig. 5, the variations of the catalytic selectivities, S_1 and S_2, with nickel content of the catalysts are quite different; S_1 is the largest for the Co–B catalyst, whereas S_2 is the largest for the Ni–B catalyst. In the competitive hydrogenation of acetophenones over Ni and Co catalysts, Kajitani *et al.* reported that the characteristic difference in the susceptibility to the effects of substituent groups and solvents between R-Ni and R-Co catalysts can be mainly attributed to the differences between nickel and cobalt metals.[6c] In the previous work, we reported that the hydrogenation activities and selectivities over various nickel catalysts, as well as the high resistivity of the Ni–B catalyst to poisoning,[7f] are explained in terms of the surface *d*-electron density of the catalyst.[7g] The characteristic differences in the hydrogenation activities and selectivities between the Co–B and Ni–B catalysts may, therefore, be due to the difference in the surface *d*-electron density of the two metals; the surface *d*-electron density of Co is smaller than that of Ni. That is to say, the reactants are adsorbed more strongly on the Co–B catalyst than on the Ni–B catalyst, resulting in lower hydrogenation rates on the Co–B catalyst than on the Ni–B catalyst. This is consistent with the results reported previously.[7g] Blyholder and Shihabi pointed out in their study of IR spectra that a metal-oxygen bond rather than a metal-carbon bond is responsible for the bonding between acetone and the metal surface of silica-supported nickel and cobalt.[13] Moreover, cobalt has stronger affinity for oxygen than nickel, as mentioned earlier. Therefore, the carbonyl group of α,β-unsaturated aldehydes will be adsorbed as strongly as the carbon-carbon double bond on the Co–B catalyst. This will relatively favor the hydrogenation of the carbonyl group on the Co–B catalyst, since the stronger adsorbate has an advantage in competitive hydrogenations. Especially for the hydrogenation of cinnamaldehyde, which has a large steric hindrance around the carbon-carbon double bond, the carbonyl group will be hydrogenated much more easily than the carbon-carbon double bond. On the Ni–B catalyst, however, the carbonyl group is adsorbed too weakly to be hydrogenated prior to the hydrogenation of the carbon-carbon double bond.

With regard to the hydrogenation of acetylenes, since a carbon-carbon triple bond is adsorbed on

metal much more strongly than the double bond, the hydrogenation of an acetylenic bond will be much more difficult than that of an olefinic bond on the Co–B catalyst, as compared with those on the Ni–B catalyst. Moreover, the olefinic bond is also adsorbed too strongly on the Co–B catalyst to desorb before being hydrogenated to the single bond. This will favor the hydrogenation of an olefinic bond formed by the hydrogenation of an acetylenic bond, resulting in the lower olefin selectivity(S_2) on the Co–B catalyst than on the Ni–B catalyst. This idea is supported by the fact that the olefin selectivities(S_2) for the hydrogenation of 1-heptyne, which is comfirmed to be adsorbed on catalysts more strongly than 2-heptyne by the result of competitive hydrogenation of 1-heptyne and 2-heptyne, are lower than those for the hydrogenation of 2-heptyne, as shown in Table 1.

We wish to thank Dr. Yasuaki Okamoto for his advice concerning the XPS measurement and for his valuable discussion. We also thank Miss Akiko Ohara for her technical assistance.

References

1) R. Paul, P. Buisson, and M. N. Joseph, *C. R. Acad. Sci.*, **232**, 627 (1951).

2) B. D. Polkovnikov, L. Kh. Freidlin, and A. A. Balandin, *Izv. Akad. Nauk SSSR, Otdel. Khim. Nauk*, **1959**, 1488; C. Barnett, *Ind. Eng. Chem., Prod. Res. Dev.*, **8**, 145 (1969).

3) T. Satoh, S. Suzuki, Y. Suzuki, Y. Miyagi, and Z. Imai, *Tetrahedron Lett.*, **1969**, 4555; T. Satoh, S. Suzuki, T. Kikuchi, and T. Okada, *Chem. Ind.*, **1970**, 1626.

4) H. Kurita and Y. Tsutsumi, *Nippon Kagaku Zasshi*, **82**, 1461 (1961).

5) J. M. Pratt and G. Swinden, *J. Chem. Soc., Chem. Commun.*, **1969**, 1321.

6) a) K. Hotta and T. Kubomatsu, *Bull. Chem. Soc. Jpn.*, **44**, 1348 (1971); b) S. Imaizumi and H. Murayama, *Shokubai*, **20**, 231 (1978); c) M. Kajitani, N. Suzuki, T. Abe, Y. Kaneko, K. Kasuya, K. Takahashi, and A. Sugimori, *Bull. Chem. Soc. Jpn.*, **52**, 2343 (1979); d) M. Kajitani, Y. Watanabe, Y. Iimura, and A. Sugimori, *ibid.*, **48**, 2848 (1975).

7) a) Y. Murakami, S. Kishida, T. Imanaka, and S. Teranishi, *Nippon Kagaku Zasshi*, **89**, 263 (1968); b) Y. Nitta, T. Imanaka, and S. Teranishi, *Kogyo Kagaku Zasshi*, **74**, 777 (1971); c) Y. Nitta, T. Imanaka, and S. Teranishi, *Nippon Kagaku Zasshi*, **1976**, 1362; d) Y. Nitta, Y. Okamoto, T. Imanaka, and S. Teranishi, *Nippon Kagaku Kaishi*, **1978**, 634; e) Y. Okamoto, Y. Nitta, T. Imanaka, and S. Teranishi, *J. Chem. Soc., Faraday Trans. 1*, **75**, 2027 (1979); f) T. Imanaka, Y. Nitta, and S. Teranishi, *Bull. Chem. Soc. Jpn.*, **46**, 1134 (1973). g) Y. Okamoto, Y. Nitta, T. Imanaka, and S. Teranishi, *J. Catal.*, **64**, 397 (1980).

8) R. W. Mitchell, L. J. Pandolfi, and P. C. Maybury, *J. Chem. Soc., Chem. Commun.*, **1976**, 172.

9) S. Kishida and S. Teranishi, *J. Catal.*, **12**, 90 (1968).

10) E. I. Klabunovskii, V. I. Neupokoev, and Y. I. Petrov, *Izv. Akad. Nauk SSSR, Ser. Khim*, **1971**, 2067.

11) Y. Nitta, T. Imanaka, and S. Teranishi, *Kogyo Kagaku Zasshi*, **72**, 2363 (1969); S_1=21—25% for *ca.* 10% conversion at 30 °C under atmospheric H_2 pressure.

12) K. Hotta and K. Kubomatsu, *Bull. Chem. Soc. Jpn.*, **45**, 3118 (1972); **42**, 1447 (1969).

13) G. Blyholder and D. Shihabi, *J. Catal.*, **46**, 91 (1977).

The Rate Constants of the Reactions of the Metastable Nitrogen Atoms, ^2D and ^2P, and the Reactions of $N(^4S)+NO\rightarrow N_2+O(^3P)$ and $O(^3P)+NO+M\rightarrow NO_2+M$

Ko-ichi SUGAWARA, Yo-ichi ISHIKAWA, and Shin SATO*

Department of Applied Physics, Tokyo Institute of Technology, Ookayama, Meguro-ku, Tokyo 152

(Received March 29, 1980)

The pulse-radiolysis technique was used for the measurement of the quenching rates of the metastable nitrogen atoms, ^2D and ^2P, both in nitrogen and in helium. The rate constants obtained for $N(^2D)$ were $(1.3\pm0.2)\times10^{-14}$ cm^3 molecule^{-1} s^{-1} (1 cm^3 molecule^{-1} s^{-1} = 6.022×10^{17} m^3 mol^{-1} s^{-1}) in nitrogen and $(4.6\pm0.4)\times10^{-17}$ in helium; these values were larger than those for the higher energy metastable nitrogen atoms, $N(^2P)$, $(3.3\pm0.3)\times10^{-17}$ in nitrogen and $(4.2\pm1.3)\times10^{-18}$ in helium. The room temperature rate constants of the reactions of these atoms with nitrogen monoxide and with ethylene were also measured. All of these rate constants were found to be of the order of 3×10^{-11} cm^3 molecule^{-1} s^{-1}. The rate constants of the reactions, $N(^4S)+NO\rightarrow N_2+O(^3P)$ and $O(^3P)+NO+M\rightarrow NO_2+M$, were also measured and compared with literature values.

Recently we used a pulse-radiolysis technique combined with the resonance absorption method for the measurement of the rate constants of the reactions of the ground state-nitrogen atoms with several olefins.[1] In that experiment, we recognized that the metastable nitrogen atoms, ^2D and ^2P, generated together with the ground state-nitrogen atoms, ^4S, decayed very rapidly in a high pressure nitrogen gas. Since then, our technique was improved, so that the measurement of the reactions of these metastable atoms could be attempted.

The quenching of the metastable nitrogen atoms by simple molecules and atoms is attracting the attention of many researchers. This is not only because of their occurrence in discharge systems, but also because of the significant roles which these atoms play in the chemistry of the upper atmosphere.[2-7]

A number of investigations have been reported on the reaction of the NO-titration for $N(^4S)$ atoms.[8-22] Since our apparatus can easily be applied for the measurement of this reaction, we have measured the rate constants of the reactions of $N(^4S)+NO\rightarrow N_2+O(^3P)$ and $O(^3P)+NO+M\rightarrow NO_2+M$, where M stands for N_2 or He.

Experimental

The apparatus, the set-up of which is shown schematically in Fig. 1, has been described previously.[23] To measure the time dependence of the concentration of $N(^2D)$ and $N(^2P)$ atoms, the emission lines at around 149.3 and 174.3 nm, respectively, were used; these were excited in flowing He containing a trace of N_2. Although both lines consisted of fine structures (149.262, 149.267, and 149.467 for the $^2P_J\rightarrow{}^2D$ transition and 174.272, 174.273, 174.526, and 174.527 for the $^2P_J\rightarrow{}^2P$ transition), they were not resolved for the measurement of the concentration of the atoms. For $N(^4S)$ and $O(^3P)$ atoms, the resonace lines were used.[1,23]

Figures 2, 3, and 4 show the optical densities for $N(^2D)$, $N(^2P)$, and $N(^4S)$ atoms generated immediately after the irradiation of the high-energy electrons, the peak energy

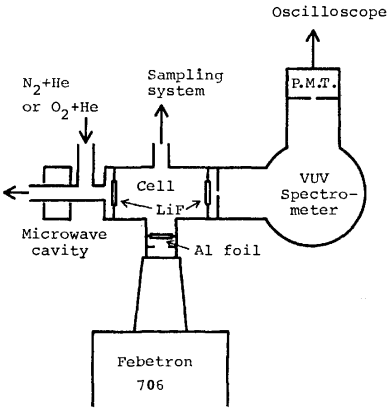

Fig. 1. Schematic diagram of the experimental apparatus. P.M.T., Photomultiplier.

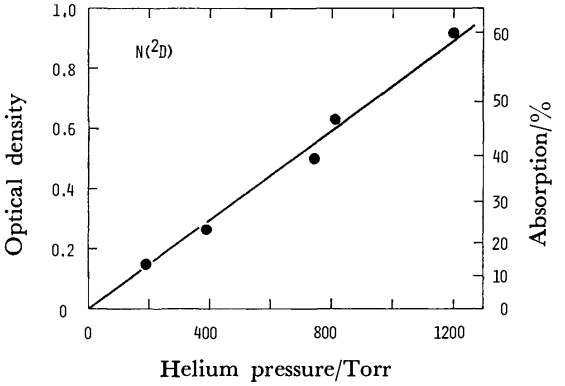

Fig. 2. The optical densities of $N(^2D)$ atoms generated immediately after the electron irradiation in the mixture of 2.0 Torr N_2 and He as a function of the He pressure.

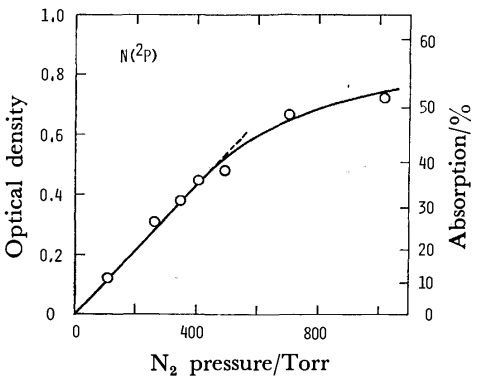

Fig. 3. The optical densities of $N(^2P)$ atoms generated immediately after the electron irradiation in N_2 as a function of the N_2 pressure.

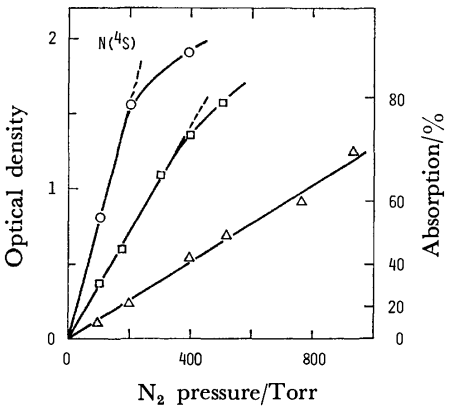

Fig. 4. The optical densities of N(⁴S) atoms generated immediately after the electron irradiation in N_2 as a function of the N_2 pressure. The d.c. charging voltages of Febetron 706 were set at 20 (△), 25 (□), and 28 (○) kV.

being 600 keV, from Febetron 706 as functions of the pressure of nitrogen or helium in the reaction cell. Since the penetration length of 600 keV-electrons is longer than 1 m in the atmosphere, probably most of the electrons ejected from Febetron 706 discharge at the wall of the reaction cell after having penetrated the reactant gas. Consequently, the energy transfer from the electrons to the gas should be proportional to the pressure of the gas in the cell.

The spectral lines used for the measurement of the optical densities of N(²P) and N(⁴S) atoms are not completely isolated from other spectral lines; therefore, some contamination could not be avoided. This is probably the reason for the apparent saturation of the optical densities for N(²P) and N(⁴S) atoms shown in Figs. 3 and 4. In the present experiments, optical densities less than 0.5 were always used for the measurement of the relative concentrations of atoms. Even if the light intensity of the contaminated spectral lines is 40%, the errors introduced in the estimation of the decay rate do not exceed 10%, since the first-order decay plots are always made in the optical density of 0.5—0.05.

The high-purity dried He (Nihon Helium Co.) and N_2 (Nihon Sanso Co.) were passed through traps filled with molecular sieve 4A at 77 K before use. The research grade NO and C_2H_4 (Takachiho Shoji Co.) were used without further purification.

Results

Figure 5 shows a typical example of the oscillograms obtained for the decay of N(²D) atoms in the mixture of He and N_2. The decay rate may be expressed as follows:

$$k = k_{He}[He] + k_{N_2}[N_2] + k_{dif}.$$

Here, k is the apparent decay rate, k_{He} and k_{N_2} are the rate constants of the quenching by He and N_2, and k_{dif} is the decay rate due to the diffusion of N(²D) atoms from the optical path. The last term may be ignored in the present experiment, since the k_{dif} value of the ground-state N(⁴S) atoms in N_2 at one atmosphere is only 0.3 s^{-1},[1] and k_{dif} is known to be roughly proportional to the reciprocal of the pressure of the solvent gas. In Fig. 6, the apparent decay rates are plotted as a function of the nitrogen pressure. The slope

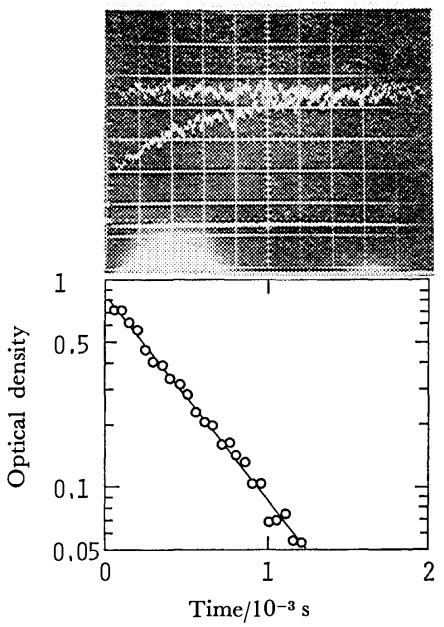

Fig. 5. The oscillogram and the first-order plot for the decay of N(²D) atoms in the mixture of 2.00 Torr N_2 and 1200 Torr He.

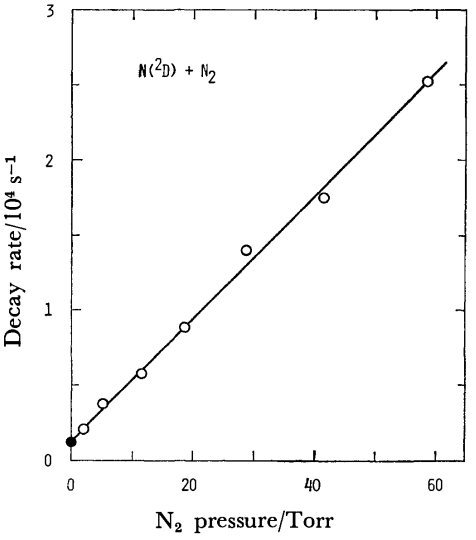

Fig. 6. The decay rates of N(²D) atoms in the mixture of 800 Torr He and N_2 as a function of the N_2 pressure. The filled circle corresponds to the quenching rate by He at 800 Torr, which has been calculated from the data shown in Fig. 7. This plot is not included for the estimation of the quenching rate constant by N_2.

of this linear relation corresponds to the quenching rate constant of N(²D) atoms by N_2, while the intercept corresponds to the quenching rate by He at 800 Torr (1 Torr=133.3 Pa). Figure 7 shows the helium pressure-dependence of the quenching rate. The slope of this linear relation gives the quenching rate constant of N(²D) atoms by He.

Similar measurements were carried out for the decay rates of N(²P) atoms. Table 1 summarizes the quenching rate constants thus obtained, where the error limits are the standard deviation. It is noticeable

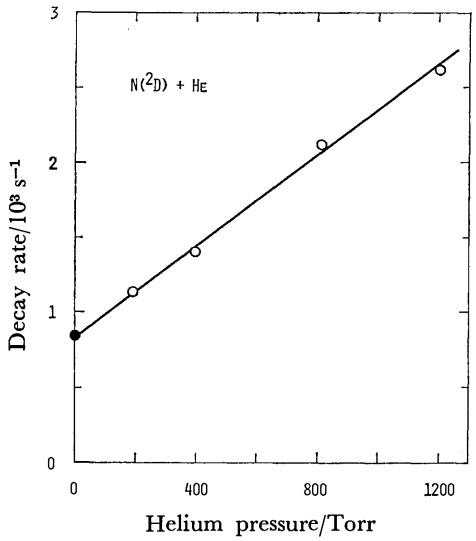

Fig. 7. The decay rates of $N(^2D)$ atoms in the mixture of 2.0 Torr N_2 and He as a function of the He pressure. The filled circle corresponds to the quenching rate by N_2 at 2.0 Torr, which has been calculated from the data shown in Fig. 6. This plot is not included for the estimation of the quenching rate constant by He.

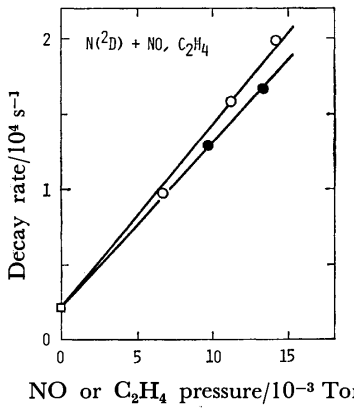

Fig. 8. The decay rates of $N(^2D)$ atoms as functions of the NO (●) or C_2H_4 (○) pressure. The N_2 pressure is 2.0 Torr and the He pressure, 800 Torr.

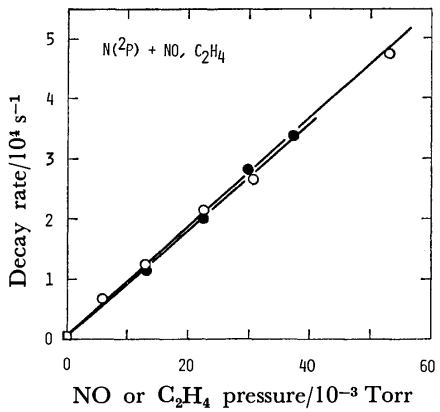

Fig. 9. The decay rates of $N(^2P)$ atoms as functions of the NO (●) or C_2H_4 (○) pressure. The N_2 pressure is 700 Torr.

Table 1. Quenching rate constants of $N(^2D)$ and $N(^2P)$ in N_2 and in He at room temperature

	k/cm³ molecule⁻¹ s⁻¹		Ref.
	$N(^2D)$	$N(^2P)$	
N_2	$\leq 6\times10^{-15}$		2
	$(1.6\pm0.7)\times10^{-14}$		3
	$(2.3\pm1.1)\times10^{-14}$	$\leq 3\times10^{-16}$	4
	$(1.5\pm0.1)\times10^{-14}$	10^{-16}	5
	$(1.6\pm0.25)\times10^{-14}$		7
	$(1.3\pm0.2)\times10^{-14}$	$(3.3\pm0.3)\times10^{-17}$	This work[a]
He	$\leq 2\times10^{-16}$		2
	$\leq 1.6\times10^{-16}$		3
	$(4.6\pm0.4)\times10^{-17}$	$(4.2\pm1.3)\times10^{-18}$	This work[a]

a) 298 ± 2 K.

Table 2. Rate constants of the reactions of $N(^2D)$ and $N(^2P)$ with NO and C_2H_4 at room temperature

	$k/10^{-11}$ cm³ molecule⁻¹ s⁻¹		Ref.
	$N(^2D)$	$N(^2P)$	
NO	18 ± 5		2
	7 ± 2.5		3
	6.1 ± 3.7	3.4 ± 1.1	4
	5.9 ± 0.4	3.2 ± 0.1	5
		2.8 ± 0.6	6
	3.5 ± 0.3	2.7 ± 0.2	This work[a]
C_2H_4	12 ± 3		2
	3.7 ± 0.3	2.8 ± 0.2	This work[a]

a) 298 ± 2 K.

that the ^2P state, which is higher than the ^2D state by 1.20 eV, is quenched more slowly than the ^2D state. Since the energy level of the ^2P state is higher than that of the ^2D state, the quenching of the ^2P state might produce the ^2D state; therefore, we carefully observed the decay of the ^2D state in the long time-range. But no indication of the production of the ^2D state by the quenching of the ^2P state could be observed in any case.

When a small amount of NO or C_2H_4 was added in the systems studied above, the rapid decays of both metastable states could be observed. The experimental results are shown in Figs. 8 and 9, and the quenching rate constants calculated from these figures are summarized in Table 2. The four rate constants are all of the order of 3×10^{-11} cm³ molecule⁻¹ s⁻¹. About a quarter of all collisions are efficient for the quenching.

Among the reactions of the ground state-nitrogen atoms with molecules, the reaction with nitrogen monoxide has been well established. In order to ascertain whether our apparatus works properly, we have measured the rate constant of this reaction. Figure 10 shows one of the combined oscillograms; one of the traces is for the decay of $N(^4S)$ atoms and the other for the formation and decay of $O(^3P)$ atoms. The measurement of the concentration of the $O(^3P)$

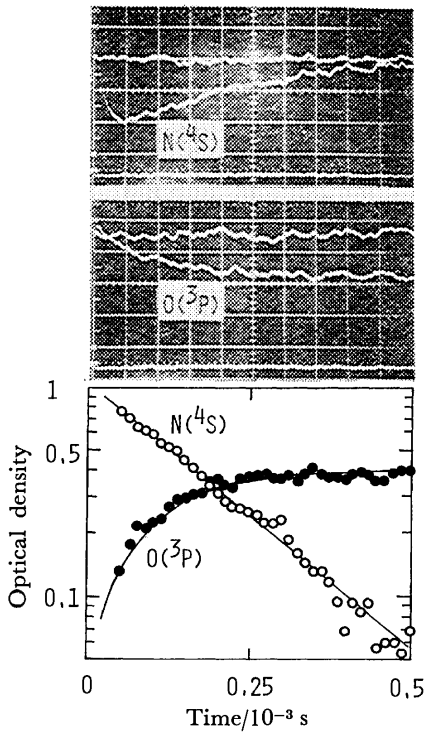

Fig. 10. The oscillograms and the plots of the logarithm of the optical densities for the decay of $N(^4S)$ atoms and for the formation and decay of $O(^3P)$ atoms. The NO pressure is 10.5 mTorr and the N_2 pressure, 198 Torr.

atoms has been discussed previously.[23] These traces correspond to the following reactions:

$$N(^4S) + NO \longrightarrow N_2 + O(^3P), \quad (1)$$

$$O(^3P) + NO + N_2 \longrightarrow NO_2 + N_2. \quad (2)$$

The solid curve for the time dependence of the concentration of $O(^3P)$ atoms was calculated by using the rate constants obtained below.

According to Reactions 1 and 2, the time dependence of the concentration of $O(^3P)$ atoms should be expressed as follows:

$$I_t = I_0[\exp(-k_2[NO][N_2]t) - \exp(-k_1[NO]t)].$$

Here, I_t is the time dependent variable proportional to the concentration of $O(^3P)$ atoms, I_0 is a constant, k_1 and k_2 are the rate constants of Reactions 1 and 2, and [NO] and $[N_2]$ are the concentrations of NO and N_2. When the solid curve for the $O(^3P)$ atoms shown in Fig. 10 was drawn by substituting the rate constants into the above equation, the constant I_0 was adjusted so as to fit the plot obtained at 0.50 ms.

Figure 11 shows the decay rates of $N(^4S)$ atoms as a function of the NO pressure. Here, three different nitrogen pressures and two different charging voltages of Febetron 706 were used; however, as shown in Fig. 11, all the decay rates obtained gave a consistent value. From this linear plot, the rate constant of Reaction 1 was estimated. In this estimation, the reaction of $N(^4S)$ atoms with NO_2, which is the product of Reaction 2, was ignored, since the reaction of N+NO_2 is known to be slower than that of N+NO ($k(N+NO_2) = (1.4\pm0.2)\times10^{-12}$ cm^3 molecule^{-1} s^{-1}),[13] and the concentration of NO_2 produced does not exceed 5% of that of NO. Table 3 compares the present result with those previously reported.

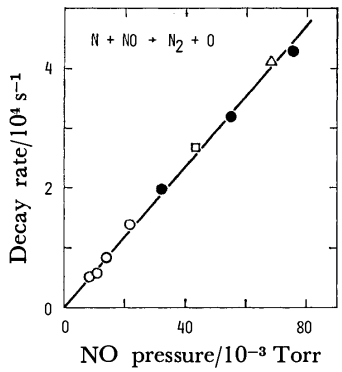

Fig. 11. The decay rates of $N(^4S)$ atoms as a function of the NO pressure. The N_2 pressures are 200 (□), 600 (○,●), and 1000 (△) Torr. The filled symbols denote 20 kV for the d.c. charging voltage of Febetron 706, while the open symbols, 25 kV.

TABLE 3. RATE CONSTANT OF THE REACTION OF N+NO→N_2+O AT ROOM TEMPERATURE

Author[a]	Method[b]	Pressure/Torr	$k/10^{-11}$ cm^3 s^{-1}
CT	DF/CL	1.5—6.5	3.6[c]
H	DF/MS	0.33—0.87	1.7±0.8
PS	DF/MS	0.026—0.31	2.2±0.6
LPK	DF/RA	1.1—2.7	3±1
CM	DF/MS	≲5	2.2±0.2
LMPS	DF/RF	1.12—2.61	2.7±0.4
LMPS	FP/RF	20—70	4.0±0.2
This work[d]	PR/RA	200—1000	1.9±0.2

a) CT: Clyne and Thrush, Refs. 8 and 9; H: Herron, Ref. 10; PS: Phillips and Schiff, Ref. 11; LPK: Lin, Parkes, and Kaufman, Ref. 12; CM: Clyne and McDermid, Ref. 13; LMPS: Lee, Michael, Payne, and Stief, Ref. 14. b) DF: Discharge flow; CL: chemiluminescence; MS: mass spectrometry; RA: resonance absorption; RF: resonance fluorescence; FP: flash photolysis; PR: pulse radiolysis. c) Calculated from the Arrhenius expression. d) 298±2 K.

Since Reactions 2 and 3 were much slower than Reaction 1 under the conditions of the present experiments,

$$O(^3P) + NO + He \longrightarrow NO_2 + He, \quad (3)$$

the concentration of NO was increased in the measurement of the rate constants of Reactions 2 and 3. In the time-range used for the measurement of the data shown in Figs. 12 and 13, Reaction 1 is already finished.

Figure 12 shows the decay rates of $O(^3P)$ atoms as functions of the pressures of NO and N_2. From these two linear relations, the rate constant of Reaction 2 can be derived. It is known that the rate constant of the reaction between $O(^3P)$ and NO_2 is comparable to that of Reaction 1 ($k(O+NO_2) = (9.5\pm1.1)\times10^{-12}$ cm^3 molecule^{-1} s^{-1}).[24] Consequently, the NO_2 produced in Reaction 2 might disturb the estimation of the rate constant of Reaction 2. However, as will be shown later, the concentration of NO_2 produced cannot exceed 2×10^{13} molecules cm^{-3}; therefore, the

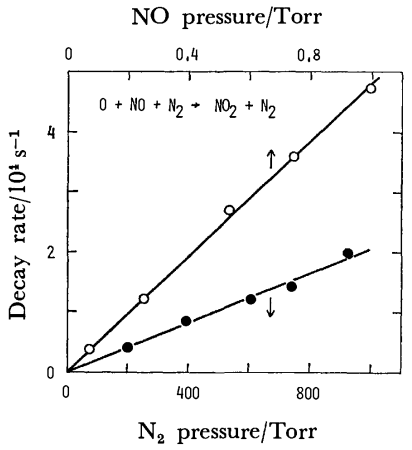

Fig. 12. The decay rates of $O(^3P)$ atoms as functions of the NO (○) or N_2 (●) pressure. When the NO pressure was varied, the N_2 pressure was fixed at 600 Torr, while when the N_2 pressure was varied, the NO pressure was fixed at 0.25 Torr.

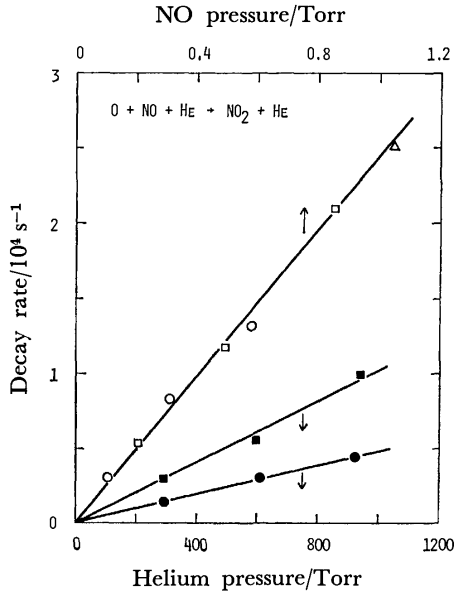

Fig. 13. The decay rates of $O(^3P)$ atoms as functions of the NO or He pressure. The symbols, ○ and ● stand for the mixture of 2.0 Torr O_2, He, and NO; □ and ■ for the mixture of 10 Torr N_2, He, and NO; △ for the mixture of NO and He. The open symbols denote that the He pressure is 600 Torr, while the filled ones denote that the NO pressures are fixed at 0.10 (●) and 0.20 (■) Torr.

disappearance of $O(^3P)$ atoms due to the reaction with NO_2 is less than 10% of that due to Reaction 2, even if the reactant gas consists of 0.25 Torr NO and 200 Torr N_2.

Figure 13 shows the experimental results which can be used for the estimation of the rate constant of Reaction 3. In order to establish the rate constant, various experimental conditions were used, as stated in the figure caption. In six measurements, oxygen was used as the source of oxygen atoms. Since NO is reactive with O_2, the experiments were performed immediately after the mixture of O_2 and He was introduced in the reaction cell containing a known amount of NO.

Table 4. Rate constants of the reactions of $O+NO+M\rightarrow NO_2+M$ (M=N_2, He) at room tfmperature

Author[a]	Method[b]	Pressure/Torr	$k/10^{-32}$ cm^6 s^{-1}
	$O+NO+N_2\rightarrow NO_2+N_2$		
KV	DF/MS	~2	13
FE	P/PA		5.0
K	DF/CL	~0.5	6.9
CT	DF/CL	2	8.6±1.2
KH	DF/MS	2—3	10.3±0.4
This work[c]	PR/RA	200—1000	7.7±0.5
	$O+NO+He\rightarrow NO_2+He$		
OS	DF/IC	1.21—3.21	5.10±0.28
CT	DF/CL	2	5.0±0.9
SN	FP/CL	~10	6.7±1.4
SN	FP/CL	0.3—31	6.65±0.67
This work[c]	PR/RA	300—1000	4.2±0.5

a) KV: Kistiakowsky and Volpi, Ref. 15; FE: Ford and Endow, Ref. 16; K: Kaufman, Ref. 17; CT: Clyne and Thrush, Ref. 18; KH: Klein and Herron, Ref. 19; OS: Ogryzlo and Schiff, Ref. 20; SN: Stuhl and Niki, Refs. 21 and 22. b) P: photolysis; PA: product analysis; IC: isothermal calorimetry. c) 298±2 K.

The apparent decay rate of $O(^3P)$ atoms in this case may be expressed as follows:

$$k = k_{NO}[NO][M] + k_{O_2}[O_2][M].$$

Here, k_{NO} and k_{O_2} are the rate constants of the third-order reactions for the disappearance of $O(^3P)$ atoms, and $[M]=[He]+[NO]+[O_2]$. Since the He pressure is much higher than those of NO and O_2, the following equations may hold: $[M]=[He]$, $k_{NO}=k_3$, and $k_{O_2}=k_4$.

$$O(^3P) + O_2 + He \longrightarrow O_3 + He. \quad (4)$$

Using the rate constant of Reaction 4, which was determined in the previous paper,[23] the decay rate due to Reaction 3 can be estimated. These calculated results are plotted in Fig. 13. All the data obtained under different experimental conditions were found to be consistent with each other. The rate constants calculated from the slopes of the linear relations shown in Figs. 12 and 13 are compared with previous measurements in Table 4.

Discussion

In the previous paper,[23] we estimated the initial concentration of oxygen atoms generated in the mixture of 3 Torr oxygen and 900 Torr He to be about 3×10^{13} molecules cm^{-3}, when the d.c. charging voltage of Febetron 706 was set at 25 kV. In that calculation, the G-value of oxygen atoms was assumed to be 12.8. According to a theoretical calculation,[25] the G-value of nitrogen atoms under similar conditions is about 9; therefore, the initial concentration of nitrogen atoms at 25 kV of the d.c. charging voltage may be in the order of 2×10^{13} molecules cm^{-3}. The concentration of nitrogen atoms is not so high that the quenching of the metastable $N(^2D)$ and $N(^2P)$ atoms by $N(^4S)$

atoms may be ignored. If the quenching by $N(^4S)$ atoms is an important process, the decay rates shown in Figs. 6 and 7 should not be linearly dependent upon the pressure of the solvent gas.

As Table 1 shows, the $N(^2D)$ atoms are quenched by N_2 or He more easily than the higher state $N(^2P)$ atoms, while it is known that the radiative lifetime of $N(^2D)$ is longer than that of $N(^2P)$.[26] Such a reverse order can also be found between $O(^1D)$ and $O(^1S)$ atoms.[27] The quenching rate constants for the metastable oxygen atoms, however, are generally much larger than those for the metastable nitrogen atoms.

The rate constants of the reactions of $N(^2D)$ and $N(^2P)$ with NO and C_2H_4 obtained in the present experiments are a little smaller than those reported previously. One possible reason is that some other reactions contaminate the process; they might participate in the formation of $N(^2D)$ and $N(^2P)$ atoms in the present system. The neutralization reactions such as $N^+ + e^- + M \rightarrow N(^2D \text{ or } ^2P) + M$, however, may be ignored, since the time-range used for the measurement of $N(^2D)$ and $N(^2P)$ atoms is 20 μs–10 ms, while it is believed that the neutralization is completed within 10 μs.[28] If the metastable states higher than ^2P state are produced and if they are quenched to the ^2D and ^2P states in the time-range of ms, the discrepancy stated above may be explained, but it is difficult to imagine that the irradiation of high energy electrons is considerably different from the microwave discharge, which was used by previous investigations in producing the metastable atoms.

The rate constant obtained for the reaction $N(^4S) + NO \rightarrow N_2 + O(^3P)$ is in good agreement with the literature value. Since the rate constant of this reaction is comparable to those of the quenching reactions of $N(^2D)$ and $N(^2P)$ atoms by NO, the following reactions might affect the estimation of k_1:

$$N(^2D \text{ or } ^2P) + NO \longrightarrow N_2 + O \quad (5)$$

$$\longrightarrow N(^4S) + NO. \quad (6)$$

In the present experiments, we can measure only the time dependence of the relative concentrations of N or O atoms, but not the absolute concentrations; therefore, we cannot eliminate the possibility of the participation of Reaction 6 in the formation of $N(^4S)$ atoms. If Reaction 6 is a predominant process compared to Reaction 5, the data shown in Table 3, probably including the results reported from other investigations, need serious corrections. Further studies are obviously necessary.

As Fig. 11 shows, the initial concentration of $N(^4S)$ atoms, which is controlled by the charging voltage of Febetron 706, does not affect the observed rate constant; this fact seems to suggest that the active species such as $N_2(^3\Sigma_u^+)$ state produced by the pulse-irradiation have no effect on the reaction between $N(^4S)$ and NO.

The reaction between $O(^3P)$ atoms and NO is important in the chemistry of the atmosphere. So far, the rate constant of this famous third-order reaction has been measured mainly at low pressures. It may be worthwhile to mention that the present result, which was obtained at higher pressures, is in good agreement with the values obtained at low pressures. In other words, the reaction between $O(^3P)$ atoms and NO does not reach its high pressure limit even at 1000 Torr.

References

1) S. Sato, K. Sugawara, and Y. Ishikawa, *Chem. Phys. Lett.*, **68**, 557 (1979).
2) G. Black, T. G. Slanger, G. A. St. John, and R. A. Young, *J. Chem. Phys.*, **51**, 116 (1969).
3) C. -L. Lin and F. Kaufman, *J. Chem. Phys.*, **55**, 3760 (1971).
4) D. Husain, L. J. Kirsch, and J. R. Wiesenfeld, *Faraday Discuss. Chem. Soc.*, **53**, 201 (1972).
5) D. Husain, S. K. Mitra, and A. N. Young, *J. Chem. Soc., Faraday Trans. 2*, **70**, 1721 (1974).
6) R. A. Young and O. J. Dunn, *J. Chem. Phys.*, **63**, 1150 (1975).
7) T. G. Slanger and G. Black, *J. Chem. Phys.*, **64**, 4442 (1976).
8) M. A. A. Clyne and B. A. Thrush, *Nature*, **189**, 56 (1961).
9) M. A. A. Clyne and B. A. Thrush, *Proc. R. Soc. London, Ser. A*, **261**, 259 (1961).
10) J. T. Herron, *J. Chem. Phys.*, **35**, 1138 (1961).
11) L. F. Phillips and H. I. Schiff, *J. Chem. Phys.*, **36**, 1509 (1962).
12) C. -L. Lin, D. A. Parkes, and F. Kaufman, *J. Chem. Phys.*, **53**, 3896 (1970).
13) M. A. A. Clyne and I. S. McDermid, *J. Chem. Soc., Faraday Trans. 1*, **71**, 2189 (1975).
14) J. H. Lee, J. V. Michael, W. A. Payne, and L. J. Stief, *J. Chem. Phys.*, **69**, 3069 (1978).
15) G. B. Kistiakowsky and G. G. Volpi, *J. Chem. Phys.*, **27**, 1141 (1957).
16) H. W. Ford and N. Endow, *J. Chem. Phys.*, **27**, 1156 (1957).
17) F. Kaufman, *Proc. R. Soc. London. Ser. A*, **247**, 123 (1958).
18) M. A. A. Clyne and B. A. Thrush, *Proc. R. Soc. London, Ser. A*, **269**, 404 (1962).
19) F. S. Klein and J. T. Herron, *J. Chem. Phys.*, **41**, 1285 (1964).
20) E. A. Ogryzlo and H. I. Schiff, *Can. J. Chem.*, **37**, 1690 (1959).
21) F. Stuhl and H. Niki, *Chem. Phys. Lett.*, **7**, 197 (1970).
22) F. Stuhl and H. Niki, *J. Chem. Phys.*, **55**, 3943 (1971).
23) K. Sugawara, Y. Ishikawa, and S. Sato, *Bull. Chem. Soc. Jpn.*, **53**, 1344 (1980).
24) P. P. Bemand, M. A. A. Clyne, and R. T. Watson, *J. Chem. Soc., Faraday Trans. 2*, **70**, 564 (1974).
25) K. Okazaki and S. Sato, *Bull. Chem. Soc. Jpn.*, **48**, 3523 (1975).
26) R. H. Garstang, "The airglow and the aurorae," Pergamon Press, London (1956), p. 324.
27) K. Schofield, *J. Photochem.*, **9**, 55 (1978).
28) Y. Ishikawa, M. Yamabe, A. Noda, and S. Sato, *Bull. Chem. Soc. Jpn.*, **51**, 2488 (1978).

 © 1980 The Chemical Society of Japan Bull. Chem. Soc. Jpn., 53, 3165—3170 (1980)

Interaction of 9-Aminoacridinium and 10-Methylacridinium Cations with Polyelectrolytes, with Emphasis on the Bound-dye Spectra[1)]

Kiwamu YAMAOKA,* Mineo TAKATSUKI, and Kinya NAKATA

Faculty of Science, Hiroshima University, Higashisenda-machi, Hiroshima 730

(Received April 7, 1980)

Visible and UV absorption spectra of two dyes, 9-aminoacridinium (AA) and 10-methylacridinium (MeA) cations, were measured at 25 °C in the presence of three different polyelectrolytes—sodium salts of poly(*p*-styrenesulfonate) (NaPSS), polyphosphate (NaPP), and polyacrylate (NaPA)—for polymer residue-to-dye ratios from zero to near unity. The optical titration curves of AA–polyanion systems showed a slightly sigmoidal curvature. The method of extended principal component analysis was applied to the experimental spectra of the AA–NaPSS, –NaPP, –NaPA and MeA–NaPSS systems. Only two absorbing component dyes, *i.e.*, bound and unbound, were verified to exist in each system. The equilibrium constant of the binding between dye and polyanion, the pure spectrum of bound dye, and the adjustable parameter α, by which the sigmoidal titration curve is characterized, were determined. In each of the above systems, the bound-dye spectrum behaves in opposition to the common notion of "metachromasy," showing a bathochromic shift without any new band. The spectra of MeA changed only moderately by the addition of NaPSS. The ultrafiltration of the MeA–NaPP and –NaPA solutions confirmed that most of the MeA cations remain unbound.

Although the physicochemical basis of metachromasy still remains to be clarified becasue of its extraordinary complexity, it has become apparent that the metachromatic behavior of a cationic dye depends on the combination between its chemical structure and the charged functional group and conformation of the associated polyelectrolyte.[2–4)] The metachromasy of acridine dyes is known to be most marked in the presence of charged polyanions of various types when the dyes possess the exonuclear amino or disubstituted amino groups at the 3- and 6-positions.[5)] Indeed, the symmetric 3,6-substituted aminoacridines and their derivatives such as Proflavine (PF),[6)] Trypaflavine (TF),[2–4,7)] and Acridine Orange (AO)[6,8)] have been most extensively documented. Their interactions with both natural and synthetic polyanions have been studied theoretically and experimentally from two points of view: metachromatic changes of absorption spectra[8)] and binding reactions.[10)]

By means of the extended principal component analysis (the EPCA procedure), the interactions between TF, one of the most typical 3,6-diaminoacridines, and various polyanions were recently studied to extract the bound-dye spectrum out of a family of experimental spectra.[2)] The result is surprising in that each unmasked spectrum of bound TF always shows two broad but distinct bands whose maxima are located on both the longer- and shorter-wavelength sides of the original peak of TF without polymer. This finding requires some modifications to be made in the concept of metachromasy, which has been defined as the hypsochromic and hypochromic changes in color.[11)] The complexity of spectral changes of the dye–polymer systems is mainly associated with the elusive behavior of the visible absorption spectra of the above dyes, which belong to the C_{2v} point symmetry group and should, therefore, have two orthogonally polarized transition moments. A recent work on the film dichroism of those dyes ascertained beyond doubt that both the short-axis polarized band (the ^1L_a band) and the long-axis polarized band (the ^1L_b band) are involved in the seemingly simple absorption band.[12,13)]

It is now clear that use of some acridine dyes optically simpler than TF will help to understand the physical basis of metachromasy and, possibly, the binding mechanism. Both 9-aminoacridinium (AA) and 10-methylacridinium (MeA) cations are suited to this purpose. Each absorption spectrum shows two unequivocally assigned bands (the ^1L_a and ^1L_b bands) which are widely separated, so that the observed spectral changes may be related to each transition.[12–14)] Furthermore, both AA and MeA have been shown to bind to DNA and other polyelectrolytes.[15–21)] In this work, the observed absorption spectra of these dyes in the presence of three different polyanions were treated by the EPCA procedure to extract the spectra of AA and MeA bound to the polymers; the polymer residue-to-dye mixing ratios from zero to near unity were investigated. The optical titration data were analyzed to evaluate the apparent equilibrium constant and the molar fraction of the bound dye species.

Experimental

Materials. The three polymer and two dye samples used in this work are sodium poly(*p*-styrenesulfonate) (NaPSS, the degree of polymerization DP=1360),[2)] sodium polyphosphate (NaPP, DP=154),[2)] sodium polyacrylate (NaPA, DP=7700),[2)] 9-aminoacridinium chloride (denoted simply as AA),[4,20)] and 10-methylacridinium chloride (denoted as MeA).[12,20,21)]

Preparations of Sample Solutions. The dye concentration was determined by the use of the molar absorption coefficients, ε in $M^{-1}cm^{-1}$ (1 M=1 mol dm^{-3}), 10500 at 401 nm for AA and 21000 at 357 nm for MeA. The absorption of the dye–polymer solution was expressed with the apparent ε of the dye present in the solution, unless otherwise stated. The dye–polymer solution contained neither extra neutral salts nor buffer salts to avoid any side effects.[7)] A concentrated polymer solution (*ca.* 2 mM) was delivered dropwise to a dye solution (7 or 14 ml) in an optical cell (either 2 cm or 5 cm in path length) through a microburet (20 μl in each portion). The mixture was stirred for a few minutes before measuring each absorption spectrum. The molar mixing ratio of polymer residues to dye (P/D) was thus varied from zero to slightly over unity without appreciable volume increase. The volume correction for the observed absorbance was always made according to the procedure given in Ref. 2.

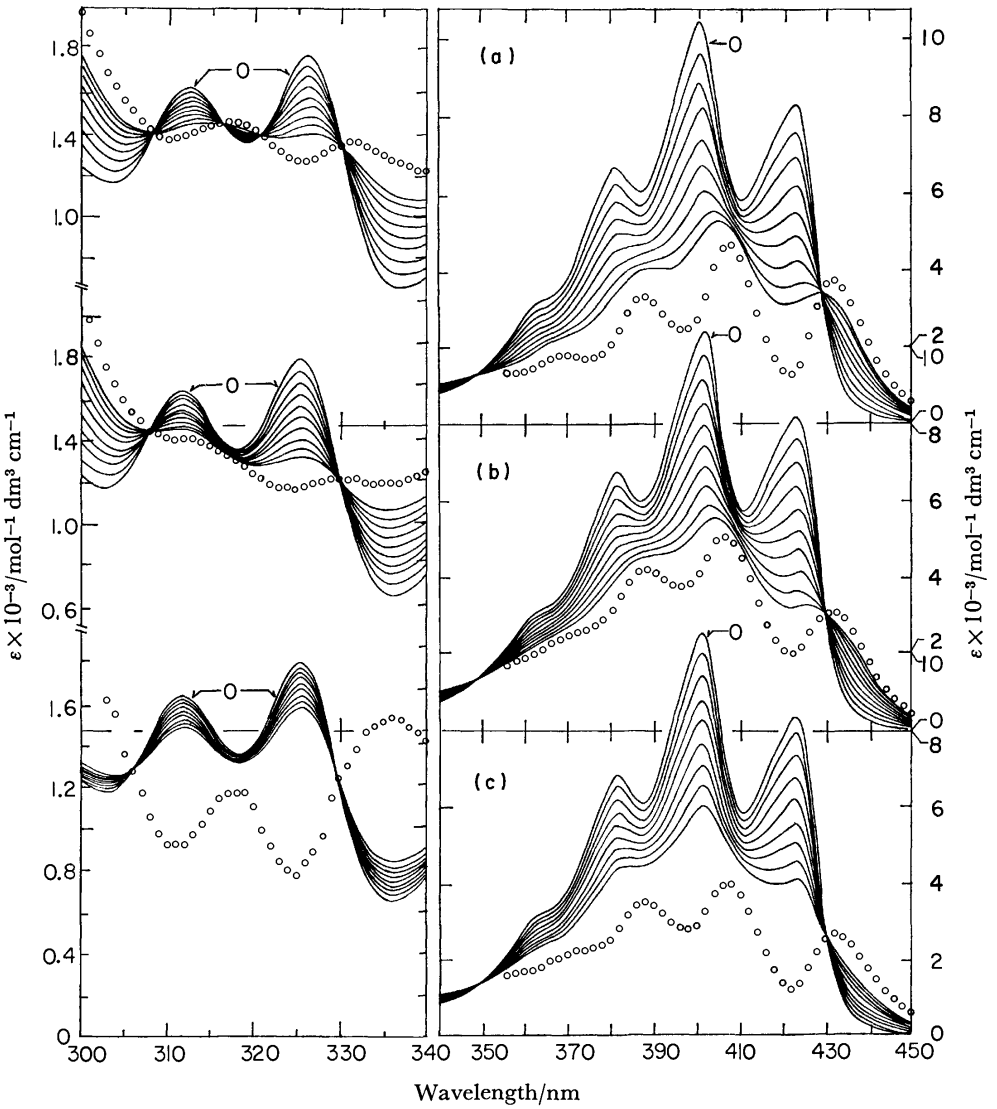

Fig. 1. The observed visible and UV absorption spectra of AA in the presence of (a) NaPSS, (b) NaPP, and (c) NaPA in the *P/D* range between 0 and nearly unity as specified below, together with the corresponding bound-dye spectra (circles).
The dye concentrations in mol/dm³ are: (a) 3.83×10^{-5}, (b) 4.43×10^{-5}, and (c) 3.78×10^{-5}. The pH values of the dye-polyanion systems are in the range of 6—7. In each family of spectra, the *P/D* values are in the following order which corresponds to the decrease in absorptions at 401 and 326 nm: (a) 0, 0.122, 0.243, 0.365, 0.486, 0.608, 0.730, 0.851, 0.973; (b) 0, 0.113, 0.226, 0.339, 0.451, 0.564, 0.677, 0.789, 0.902, 1.015; (c) 0, 0.160, 0.320, 0.481, 0.641, 0.801, 0.961, 1.120, 1.280. The isosbestic points in nm are: (a) 429, 349, 330, 320.6, 316, 308.3; (b) 429, 351, 330, 308; (c) 430, 351, 330, 306.

Ultrafiltration. Filtration experiments were performed, whenever needed, to detect the presence of unbound dye in the dye–polymer solutions in a manner similar to a previous case.[7]

Measurements. The absorption spectra were measured at 25 °C in the same manner as before.[2-4] The 5 cm and 2 cm cells were used for the visible and UV regions, respectively.

Data Analysis by the EPCA Procedure. The EPCA method utilized in this work has been described in detail elsewhere.[2-4,22] Since the number of the absorbing components involved in the present dye–polymer system was determined to be two (*vide post*), a generalized empirical expression (Eq. 1) was employed to describe the binding equilibrium between a dye D and a dye–polymer complex PD*:

$$K = \frac{[DP^*]}{[D][P]^{\alpha}}, \qquad (1)$$

where the notations have the same meaning as before.[2] The α is an empirical, adjustable parameter.

Results and Discussion

Visible and UV Absorption Spectra of the AA–Polymer Systems. The observed visible and UV spectra of AA in the presence of NaPSS, NaPP, and NaPA are shown over a *P/D* range of 0—1 in Figs. 1(a)—(c). The longest-wavelength band of AA in the 450—350 nm region is the short-axis polarized transition (the

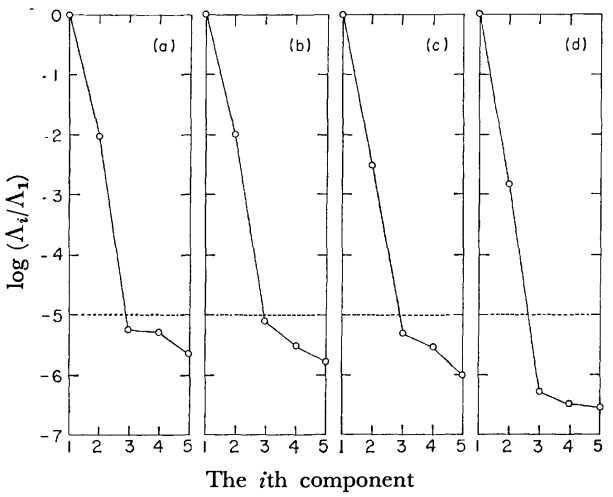

Fig. 2. Variations in the eigenvalue Λ_i (i=1, 5) with the ith absorbing component for three AA–polyanion systems [(a) NaPSS, (b) NaPP, and (c) NaPA] and for the MeA–NaPSS systems (d).

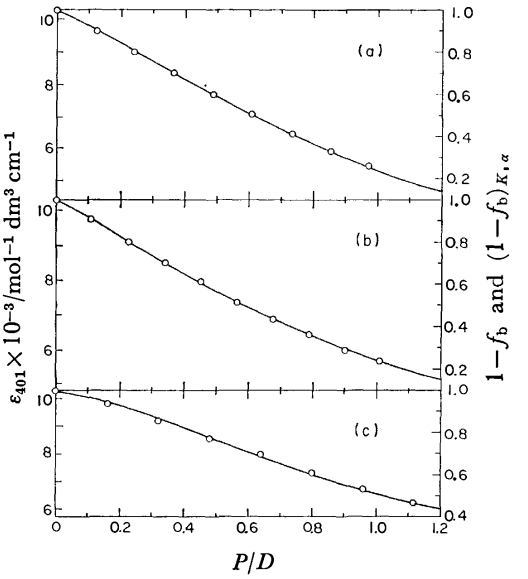

Fig. 3. Optical titration data of three AA–polyanion systems [(a) NaPSS, (b) NaPP, and (c) NaPA] and the fraction of bound AA.
The titration data (open circles) are plotted in terms of ε_{401} (left ordinate) against P/D. The fractions of unbound dye are also plotted against P/D (right ordinate). They were calculated by two different methods; $(1-f_b)_{K,\alpha}$ from the values of K and α according to Eq. 2 of Ref. 3 (it is drawn with the solid curve) and $(1-f_b)$ directly from the EPCA procedure with the aid of Eq. 4 of Ref. 3 (it is actually undistinguishable with the circle).

^1L_a band), *i.e.*, the axis is in the direction bisecting the 10-nitrogen and 9-carbon atoms of the acridine nucleus, while the short-wavelength band in the 340–300 nm region is the long-axis polarized band (the ^1L_b band), *i.e.*, the axis is perpendicular to the short axis in the molecular plane.[14] The ^1L_a band of AA with a vibrational structure and the ^1L_b band both decreased batho- and hypochromically by the dropwise addition of any of the three different polyanions. The peaks and shoulders of these bands were shifted toward the long wavelengths, but all fine structure was clearly retained. These spectral changes are contrary to the previous results for the 3,6-disubstituted acridine dye-polymer systems for which the hypso- and hypochromic effects were noted in a P/D range below unity.[2,3,6,8–10,23]

In each family of the spectra in Fig. 1, the isosbestic points (*cf.* the caption of Fig. 1) exist for both the ^1L_a and ^1L_b bands. The existence of these isosbestic points strongly indicates that two dye species, *i.e.*, unbound and bound, are present in each dye–polymer system.[2,3] Comparison of these points between three AA–polymer systems also indicates that the spectral profiles of AA bound to three polyanions are similar to one another, in spite of the marked differences in their ionized monomer units and molecular weights. In order to ascertain the number of absorbing species in each system, the PCA procedure was applied to the data spectra given in Fig. 1.

The Number of Absorbing Species in the AA–Polyanion Systems. In each system, the data matrix $\boldsymbol{D}$ was constructed with a set of absorbances at 48 selected wavelengths, at 2 nm intervals, between 356 nm and 450 nm and with a set of ten or nine experimentally obtained absorption spectra. The variation of the ith eigenvalue, Λ_i, with the ith component is shown in Fig. 2, where the ratios of Λ_i to Λ_1 are plotted on a logarithmic scale against components. It is clear from Figs. 2(a)—(c) that a large gap in eigenvalues exists between the second and third components (i=2 and 3) for each AA–polyanion system. In addition, the ratio of the eigenvalue of the third component Λ_3 to that of the first component is at most 1×10^{-5} (the dotted lines), which does not fulfill the criterion previously set for a genuine component.[2,22] These results can be taken as evidence that there are indeed two light-absorbing species in each system, *i.e.*, bound and unbound AA.

Optical Titration Curves and the Fraction of Bound AA. The optical titration curves of the AA–polyanion systems are shown in Fig. 3, where the apparent ε values at 401 nm, the peak position of free AA, were plotted against P/D. The ε values decrease with a slightly sigmoidal curvature with the increase in P/D, as was already noted for other dye–polymer systems.[2,3] To reproduce these titration data, the EPCA procedure was applied to the visible absorption spectra of each system shown in Fig. 1 with the aid of Eq. 1. The values of the parameter α and the equilibrium constant K were evaluated and are given in Table 1. The α values are larger than unity, as is expected from the sigmoidal curvature of the titration data.[2,3] The K' value at P/D=1 is a measure which can be compared with the commonly used equilibrium constant for a binding reaction, *viz.*, $K'=[DP^*]([D]\cdot[P])^{-1}=K[P]^{\alpha-1}$. The K' values are of the same order of magnitude as those obtained for other acridine dye–polyanion systems, indicative of a high binding ability of AA.[2]

The molar fraction of bound dye, f_b, is defined as the ratio of the concentration of bound dye to the

TABLE 1. EMPIRICAL PARAMETER, α, AND EQUILIBRIUM CONSTANTS, K AND K', AT 25 °C FOR THE DYE–POLYANION SYSTEMS

Polymers	Dyes: AA α	AA K [a]	AA K' [b]	MeA α	MeA K [a]	MeA K' [b]
NaPSS	1.5	1.1×10^{8}	3.4×10^{5}	1.5	8.2×10^{6}	0.31×10^{5}
NaPP	1.2	3.0×10^{6}	3.0×10^{5}	—	—	—
NaPA	1.7	9.2×10^{7}	0.50×10^{5}	—	—	—

a) The dimension is $[dm^3\ mol^{-1}]^{\alpha}$. b) $K'=[DP^*]/([D]\cdot[P])=K[P]^{\alpha-1}$ at $P/D=1$.

TABLE 2. BAND PEAKS AND SEPARATIONS BETWEEN SUCCESSIVE PEAKS IN THE SPECTRA OF FREE AND BOUND DYES

Free and Bound Dyes	Bands: ^1L_a Subbands 1	2	3	4	^1L_b [d] Subbands 1	2
AA[a]	422.5[b]	400.5	381	362	326	312.5
	1.30[c]	1.28	1.37		1.33	
AA-NaPSS	432[b]	408	388	369	331	317.5
	1.36[c]	1.26	1.33		1.29	
AA-NaPP	431.5[b]	406	387.5	370	331	313.5
	1.45[c]	1.18	1.22		1.69	
AA-NaPA	432[b]	407	388	372.5	335	318
	1.42[c]	1.20	1.08		1.60	
MeA[a]	440[b]	415	397	—	357	342
	1.37[c]	1.09	—		1.23	
MeA-NaPSS	451[b]	425	405	—	362.5	346
	1.36[c]	1.16			1.31	

a) Free dye as the reference. b) The values in this row are the peak wavelength expressed in nm. c) The values in this row are the separation of the successive subbands expressed in (wave number) $\times 10^{-3}$ (cm^{-1}). d) The positions of this band are only apparent, because of the overlap by an intense band in the shorter wavelength region.

sum total of the concentrations of bound and free dyes in solution. The values of $(1-f_b)$ were calculated by two different methods, which are described in detail in Ref. 3 (*cf.* Eqs. 2 and 4 given therein). The calculated $(1-f_b)$ curves are shown for three AA–polyanion systems in Fig. 3. It is clear from Fig. 3 that AA binds to these polyanions by 50% or more at a P/D of unity in spite that AA is rather simple and small in molecular size as compared with TF.[2)]

Visible and UV Spectra of Bound AA. A major advantage of the EPCA method is the simultaneous determination of the bound-dye spectrum and the equilibrium constant for a given dye–polymer system.[2–4,22)] The pure spectra of bound AA in three AA–polyanion systems, extracted from the observed absorption spectra in the visible region, are shown by open circles in Figs. 1(a)—(c). Since the changes in the observed UV spectra of the same systems are not large enough for the EPCA method to be applied with high accuracy, the bound-AA spectra in the UV region were calculated by the use of the value of f_b, which was obtained from the binding curve $(1-f_b)$, and the observed ε_λ at a given wavelength λ. The molar absorption coefficient of the bound dye, ε^b_λ, at the same wavelength can be expressed as

$$\varepsilon^b_\lambda = \varepsilon^f_\lambda + \frac{\varepsilon_\lambda - \varepsilon^f_\lambda}{f_b}, \qquad (2)$$

where ε^f_λ is the molar absorption coefficient of the unbound dye at λ.

The unmasked bound-AA spectra reveal a number of interesting points. First, they all show a large bathochromic, but not hypsochromic, shift. As the spectral data in Table 2 indicate, the ^1L_a bands are shifted by 10 nm toward the red. Secondly, both ^1L_a and ^1L_b bands of the bound spectra retain the spectral profile of the original AA as regards the vibrational structure and the separation of successive subbands. In particular, no new band appears in the bound-AA spectra. Thirdly, the ^1L_a and ^1L_b bands of the bound spectra are both hypochromic, *i.e.*, the intensity of AA is decreased tremendously by its binding to a polymer site. The first and second features are in contrast with the definition of metachromasy[11)] and also with the observed metachromatic behavior of the 3,6-diaminoacridine and its derivatives which

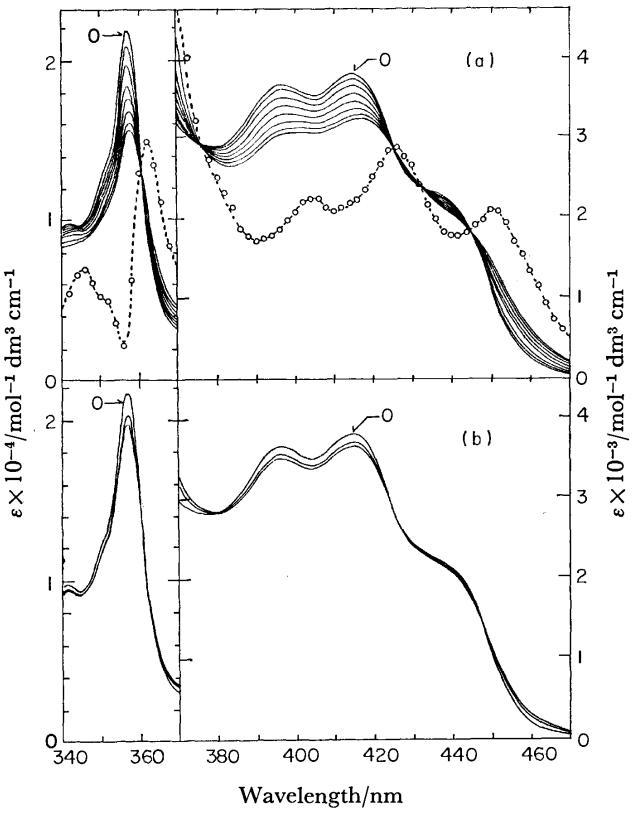

Fig. 4. The observed visible and UV absorption spectra of MeA in the presence of (a) NaPSS and (b) NaPP in the *P/D* range between 0 and nearly unity as specified below, together with the corresponding bound-dye spectrum (circles).
The dye concentrations are 2.20×10^{-5} mol dm^{-3} for both (a) and (b). The isosbestic points in nm are 445, 430.5, 426, 376.5, 360.5 in (a). The *P/D* values are in the following order which corresponds to the decrease in absorptions at 357 and 415 nm: (a) 0, 0.171, 0.342, 0.513, 0.685, 0.856, 1.027, 1.20.

are bound to synthetic polyelectrolytes in the low *P/D* range.[2,3,24]

Visible and UV Absorption Spectra of the MeA–Polyanion Systems. The observed visible and UV absorption spectra of MeA in the presence of NaPSS and NaPP are shown in Figs. 4(a) and (b), respectively. The absorption band of MeA in the 470—370 nm region is the short-axis polarized transition (^1L_a), while the band in the 370—340 nm region is the ^1L_b band.[12,13] In contrast with the cases of AA, the spectra of MeA changed only moderately by the dropwise addition of NaPSS and only silghtly with NaPP. It should be noted that the spectra of the MeA–NaPA system changed less than 10% in the *P/D* range between 0 and near 2. This trend is peculiar in the sense that all three polymers can be bound to AA in very favorable proportions and that the chemical structure of MeA does not seem to differ from that of AA. Thus, it appears that the observed discrepancy should be accounted for by some other reasons.

The ultrafiltration of both the MeA–NaPP and –NaPA solutions at a *P/D* value near 3 was performed. The filtrated solutions all showed the absorption spectrum characteristic of MeA free from either NaPP or

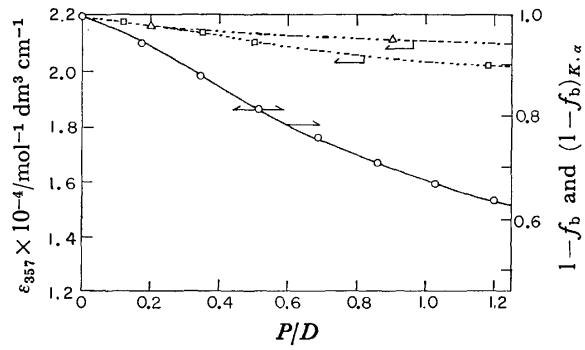

Fig. 5. Optical titration and the fraction of bound MeA.
The titration data (open symbols) are plotted with ε_{357} (left ordinate) against *P/D*.
(○) NaPSS, (□) NaPP, (△) NaPA. The fraction of unbound MeA was calculated only for the MeA–NaPSS system in the same manner as noted in Fig. 3.

NaPA. This result thus leads to the conclusion that most of the MeA cations in the NaPP or NaPA solution remain unbound and are filterable through a semipermeable membrane. Under considerations of the degree of polymerization of these polymers (see Experimental), this conclusion can not be explained by the size (or chain length) effect. Hence, it is most reasonable to attribute the difference in binding abilities to the geometry and the chemical properties of the ionized binding site of the polymer (sulfonate *versus* phosphate and carboxylate residues).

The experimental spectra of MeA–NaPSS system are, however, sufficient to reveal the spectral behavior of the bound MeA. As the *P/D* values increase, the intensity of both the ^1L_a and ^1L_b bands of MeA decreases with a concomitant shift toward the red, similarly to the case of the AA–NaPSS system. The result of the PCA treatment is shown in Fig. 2(d), where a large gap exists between the second and third components. Hence, the MeA–NaPSS system is indeed verified to contain two absorbing species, bound and unbound MeA.

Optical Titration, Fraction, and Spectrum of MeA Bound to NaPSS. The optical titration data of the MeA–polyanion systems are shown in Fig. 5, where the apparent ε values at 357 nm, a peak wavelength of free MeA, were plotted against *P/D*. The ε values of MeA in the presence of NaPSS decrease sigmoidally, which is in accord with an α value larger than unity. The fractions of MeA bound to NaPSS, $(1-f_b)_{K,\alpha}$, were calculated with the values of α and K given in Table 1. It is clear from Fig. 5 that more than 30% of MeA are bound to NaPSS at $P/D=1$ and that the calculated curve agrees well with the observed ε values. This latter result assures us that the EPCA procedure was applied properly. As are shown in Fig. 5, the changes in ε values with *P/D* are very small for the MeA–NaPP and –NaPA systems; for these, therefore, the α and K values could not be evaluated by the EPCA method.

The visible spectrum of MeA bound to NaPSS was extracted from the observed spectra, while the UV spectrum of the bound MeA was calculated with Eq.

2 from the f_b values in Fig. 5. The bound spectrum of MeA (circles in Fig. 4) is again, as in the case of bound AA, bathochromic and hypochromic relative to the unbound MeA. The optical data are given in Table 2, which shows that the separations of the successive peaks of the visible band (^1L_a) remain nearly constant for each of the unbound and bound MeA species. Thus, it can be concluded that the bound MeA retains the spectral features of unbound MeA itself showing neither a new "metachromasy band" nor metachromatic behavior, *viz.*, the blue shift of the absorption bands, in the presence of NaPSS.

Closing Remarks on Bound-dye Spectra and Binding Ability of AA and MeA. The bound-AA and -MeA spectra should result from the dyes which are bound to polymer sites to a maximal extent, since they are extracted in the P/D range between 0 and near unity. Yet, the AA and MeA spectra bound to various synthetic polyanions show the bathochromic and hypochromic changes, *i.e.*, both the short-axis and long-axis polarized bands shift toward the red rather than the blue. This trend is evidently opposite to the previous results obtained for 3,6-diaminoacridines, TF[2] and AO,[23] and contradicts the widely prevailing notion of metachromasy, *i.e.*, the shift of the visible absorption maximum toward the blue with a concomitant decrease in its intensity.[11] The spectrum of MeA bound to NaPSS (Fig. 4) is surprisingly close to that of MeA bound to DNA, in spite of a vast difference in their primary and secondary structures.[21] Hence, the bound-AA and -MeA spectra are rather insensitive to the structure of the ionizable groups of polymers and their overall conformations. The apparent equilibrium constants are in the order of NaPSS>NaPP>NaPA for AA, and NaPSS>NaPP≈NaPA for MeA. As regards the dye species, the fraction of bound AA is about equal to that of previously reported TF[2] at a P/D value of unity, but much higher than that of MeA, which is the simplest of all acridine dyes. The binding reactions between both AA and MeA and three polyanions seem to resemble the previous cases in which TF and Crystal Violet were employed,[2,3] although spectral changes of the former differ from those of the latter. Hence, it may be inferred that the binding mechanism formally expressed by Eq. 1 prevails in many dye–polymer combinations.

References

1) Part VII of *Metachromasy*. For the preceding paper of this series, K. Yamaoka and T. Matsuda, *Biophys. Chem.*, in press (1980).
2) K. Yamaoka and M. Takatsuki, *Bull. Chem. Soc. Jpn.*, **51**, 3182 (1978).
3) M. Takatsuki and K. Yamaoka, *Bull. Chem. Soc. Jpn.*, **52**, 1003 (1979).
4) M. Takatsuki, *Bull. Chem. Soc. Jpn.*, **53**, 1922 (1980).
5) Reports on this subject are too numerous to be listed here. For detailed references, see those cited in Refs. 2—8.
6) G. Weill and M. Calvin, *Biopolymers*, **1**, 401 (1963).
7) K. Yamaoka, M. Takatsuki, and M. Miura, *Bull. Chem. Soc. Jpn.*, **48**, 2739 (1975).
8) D. F. Bradley and M. K. Wolf, *Proc. Natl. Acad. Sci. U.S.A.*, **45**, 944 (1959).
9) B. C. Myhr and J. G. Foss, *Biopolymers*, **10**, 425 (1971).
10) G. Schwarz and S. Klose, *Eur. J. Biochem.*, **29**, 249 (1972).
11) J. A. Bergeron and M. Singer, *J. Biophys. Biochem. Cytol.*, **4**, 433 (1958).
12) Y. Matsuoka and K. Yamaoka, *Bull. Chem. Soc. Jpn.*, **52**, 3163 (1979).
13) Y. Matsuoka and K. Yamaoka, *Bull. Chem. Soc. Jpn.*, **53**, 2146 (1980).
14) H. Kokubun, *Z. Elektrochem.*, **62**, 599 (1958).
15) A. R. Peacocke and J. N. H. Skerrett, *Trans. Faraday Soc.*, **52**, 261 (1956).
16) S. C. Riva, *Biochem. Biophys. Res. Commun.*, **23**, 606 (1966).
17) K. Yamaoka and R. A. Resnik, *Biopolymers*, **8**, 289 (1969).
18) D. G. Dalgleish, H. Fujita, and A. R. Peacocke, *Biopolyners*, **8**, 633 (1969).
19) K. Jackson and S. F. Mason, *Trans. Faraday Soc.*, **67**, 966 (1971).
20) K. Yamaoka, *Biopolymers*, **11**, 2537 (1972).
21) K. Yamaoka and M. Masujima, *Biopolymers*, **17**, 2485 (1978).
22) M. Takatsuki and K. Yamaoka, *J. Sci. Hiroshima Univ. Ser. A*, **40**, 387 (1976).
23) V. Vitagliano, L. Costantino, and A. Zagari, *J. Phys. Chem.*, **77**, 204 (1973).

Singlet Energy Transfer in *p*-Terphenyl Crystal Doped with Tetracene

Hiroyuki SHINOHARA and Masahiro KOTANI*

Faculty of Science, Gakushuin University, Mejiro, Toshima-ku, Tokyo 171

(Received April 21, 1980)

The transfer of singlet energy in *p*-terphenyl crystal was measured as a function of the dopant (tetracene) concentration and the temperature. The simple hopping model yields a value of 3×10^{-14} s. This value is believed to be correct within a factor of 5. In the low temperature phase of the crystal, the energy transfer is temperature dependent with an activation energy of 66 cm^{-1} in undeuterated *p*-terphenyl and 90 cm^{-1} in perdeuterated *p*-terphenyl. It seems probable that in the low temperature phase the freedom of the conformational change of the molecule plays an important role in the energy migration.

p-Terphenyl is known as one of the fastest scintillators. Its short fluorescence lifetime (5 ns in the crystalline state) and the consequent excellent pulse pair separation makes the measurement of very high count-rates possible. The energy migration in *p*-terphenyl crystal is interesting because the molecule has some freedom of conformational change. There is some evidence that the three benzene rings of the free molecule are not coplanar in the electronic ground state, whereas the molecule tends to be planar in its electronic excited states.[1] Thus it is possible that the migration of the electronic excitation energy is accompanied by some molecular deformation. The energy migration in *p*-terphenyl crystal, however, has not been well investigated, seemingly just because the short lifetime makes the detailed investigation difficult.

Long range migration of excitation energy in organic crystals has been commonly studied with either of the two experimental approaches. One is based on the observation of sensitized luminescence from doped crystals, wherein guest molecules act as emission centers. The intensity[2] or the lifetime[3-5] of the host and the guest emission is measured as a function of the guest concentration. A bimolecular reaction between a singlet exciton which migrates over the host lattice and a guest molecule is thought to give rise to the guest emission. The other involves the analysis of the bimolecular annihilation of two singlet excitons.[6-9] This approach is superior to the former in the sense that doping is not necessary and the possible complications therefrom need not be considered. However, the precise knowledge of the initial concentration and the temporal behavior of the excitons which is needed limits the application of this method to materials with relatively long lifetimes.

In the present work the singlet energy migration in *p*-terphenyl crystal doped with tetracene was investigated with the steady state excitation. This system is ideal in that the solubility of tetracene in *p*-terphenyl crystal is very high. This makes the segregation of microcrystals of the dopant improbable, which is the major difficulty when data for a wide range of dopant concentration is needed. It also means that the distortion of the host lattice caused by the doping will be minimal. Another advantage of the system is the small overlap of the absorption and the emission spectra of *p*-terphenyl crystal. This feature makes the reabsorption of the fluorescence unimportant. It is to be noted also that the host and the guest fluorescence are well separated. The correction for the overlap of the respective fluorescence and for the absorption are accordingly unimportant and hence the quantitative determination of the relative intensity is possible.

Experimental

p-Terphenyl (GR grade, Tokyo Kasei Co.) was purified by column chromatography with activated alumina and by zone melting. The trace amount of tetracene in the starting material was removed by refluxing with maleic anhydried. Perdeuterated *p*-terphenyl (Merck Sharp and Dohme) was purified by chromatography and by zone melting. After extensive zone melting the crystal gave the same fluorescence spectrum as that of the undeuterated compound. The tetracence (Eastman) used as dopant was sublimed *in vacuo*. "Pure" *p*-terphenyl showed no detectable sensitized fluorescence and had a triplet lifetime of $\approx$100 ms. A weighed amount of tetracence was added to the "pure" *p*-terphenyl to give a sample with a dopant concentration of 10^{-2} mol/mol. Doped crystals of various concentrations were made by successively diluting this highly doped sample with the "pure" *p*-terphenyl. This procedure may be justified because the solubility of tetracene in *p*-terphenyl is practically unlimited, as described below. Crystals with tetracene concentration of 10^{-7} mol/mol prepared with this procedure exhibit faint sensitized fluorescence, whereas the "pure" sample showed no detectable guest fluorescence. This observation eventually showed that the concentration of tetracence in the "pure" sample was less than 10^{-7} mol/mol.

Melting point of doped crystals were measured in a stirred silicone oil bath and were observed visually.

Emission spectra were measured with a fluorescence spectrophotometer (Hitachi, MPF 2A). Temperature was controlled either by flowing cold nitrogen gas in a quartz cryostat or by thermal conduction using liquid nitrogen. The fluorescence lifetime was measured with the single photon counting technique with an air gap spark (pulse width 6 ns) as the excitation light source.

Results

Melting points for the samples with tetracene concentration up to 30 mol% were measured (Fig. 1). The fluorescence spectra of *p*-terphenyl crystal and of tetracene doped in *p*-terphenyl crystal are shown in Fig. 2. Also shown in the figure are the absorption spectrum of *p*-terphenyl and the excitation spectrum of the fluorescence of tetracene doped in *p*-terphenyl monitored at 530 nm. Figure 3 shows the concentration dependence of the ratio I_G/I_H, the intensity of the guest fluorescence observed at 570 nm

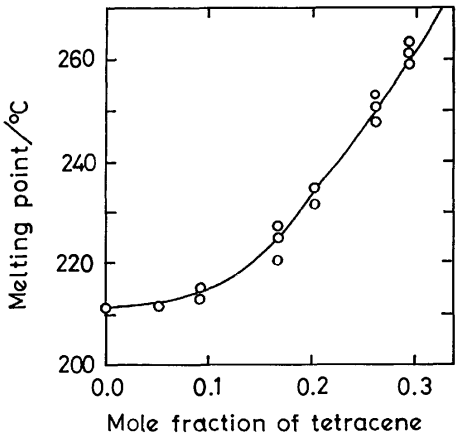

Fig. 1. Melting point of *p*-terphenyl doped with tetracene. The melting point goes up with the concentration of tetracene, indicating that *p*-terphenyl forms a solid solution in this concentration range.

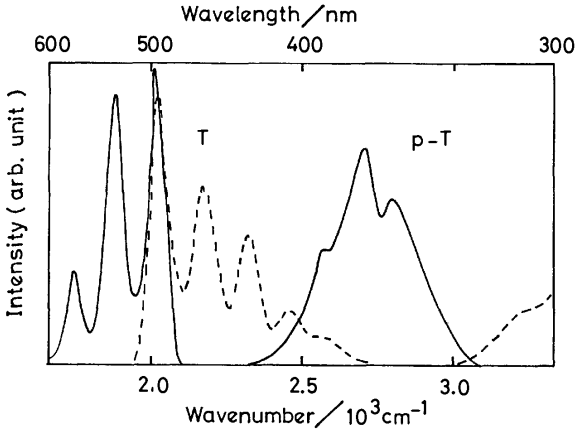

Fig. 2. Full lines (——) show the fluorescence spectra of *p*-terphenyl crystal (*p*-T) and of tetracene (T) doped in *p*-terphenyl. Dashed lines (----) show the absorption spectrum of *p*-terphenyl crystal and the excitation spectrum of the fluorescence of tetracene (as doped in *p*-terphenyl) monitored at 530 nm. The radiative transfer is not important in the system *p*-terphenyl doped with tetracene. The reabsorption of the fluorescence of *p*-terphenyl by *p*-terphenyl itself is also small.

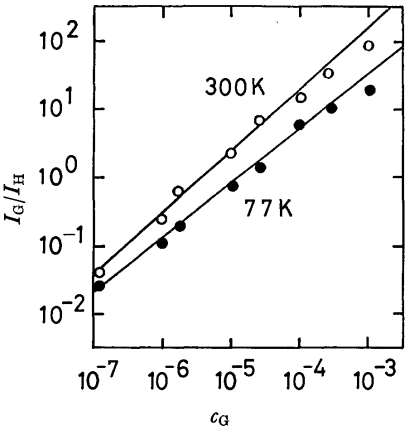

Fig. 3. The relative intensity of the guest fluorescence (I_G) over the host fluorescence (I_H) as a function of the mole fraction of tetracene (c_G).
The intensities are coreected for the detector sensitivity. ○; 300 K, ●; 77 K.

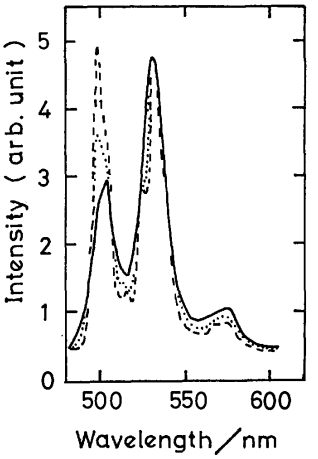

Fig. 4. Fluorescence spectra of tetracene doped in *p*-terphenyl (not corrected) showing the effect of reabsorption at different temperatures. The fluorescence was excited with 460 nm light (direct excitation of the guest).
---- 77 K, ····· 135 K, —— 300 K. $c_G = 1 \times 10^{-3}$ mol/mol. The intensity of the guest fluorescence (I_G) throughout this work was monitored at 530 nm.

over that of the host fluorescence observed at 370 nm, each corrected for the spectrometer sensitivity and expressed in a unit proportional to photons/s. The result is best fitted by

$$I_G/I_H = Ac_G^n, \quad (1)$$

with

$$A = 5.6 \times 10^5,\ n = 0.91 \pm 0.1,$$

for 300 K and

$$A = 9.4 \times 10^3,\ n = 0.81 \pm 0.1,$$

for 77 K; c_G is the mole fraction of the guest. The above wavelengths were chosen in order to minimize the effect of reabsorption. Figure 4 shows an effect of the reabsorption. It shows the emission spectra of the guest at different temperatures, excited at 460 nm (direct excitation of tetracene). The intensity of 570 nm peak relative to that at 530 nm is constant, whereas the relative intensity at 500 nm decreases with rising temperature. This is caused by the reabsorption of emitted fluorescence by tetracene itself. Reabsorption is significant at higher temperatures. Figure 5(a) shows the temperature dependence of I_H for an "pure" sample. Figure 5(b) shows the variation of I_H and I_G with temperature for a sample with the guest concentration of 10^{-5} mol/mol. The temperature dependence of I_G/I_H is shown in Fig. 6. Activation energies of 66 cm^{-1} for undeuterated *p*-terphenyl (*p*-T-h_{14}) and 90 cm^{-1} for perdeuterated *p*-terphenyl (*p*-T-d_{14}) were obtained from the slope of the straight parts of the figures corresponding to temperatures lower than 200 K.

Discussion

Solubility. *p*-Terphenyl exhibits a higher melt-

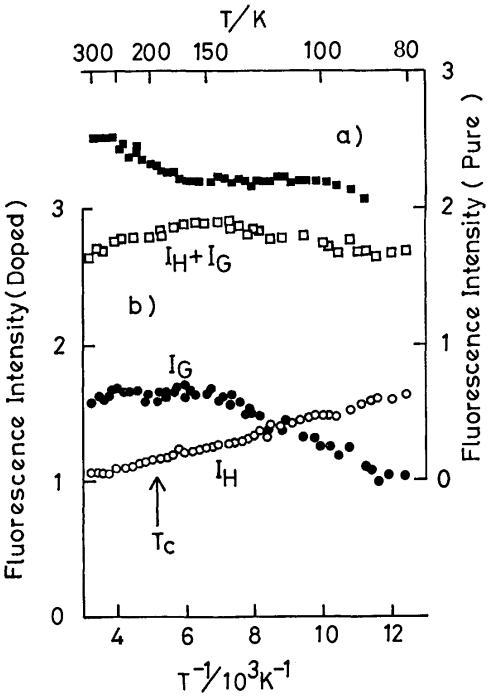

Fig. 5. (a) Temperature dependence of the fluorescence intensity (right ordinate) of an undoped *p*-terphenyl crystal. It is seen that the fluorescence quantum yield is constant within 15%. (b) Temperature dependence of the host (I_H) and the guest (I_G) fluorescence intensity of a doped crystal (left ordinate). Note that the sum (I_H+I_G) is nearly independent of temperature, showing that the radiationless decay is not important. T_c denotes the phase transition temperature.

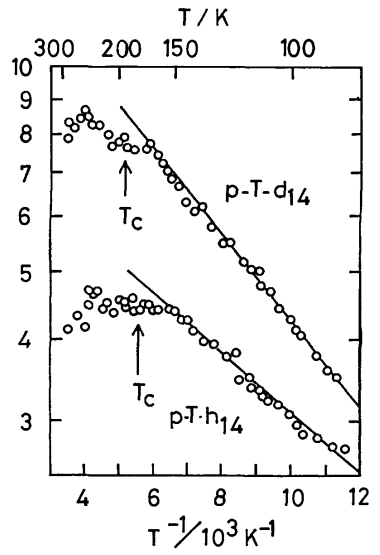

Fig. 6. Temperature dependence of the relative fluorescence intensity (I_G/I_H). Activation energies are 66 cm^{-1} for *p*-T-h_{14} and 90 cm^{-1} for *p*-T-d_{14}. T_c denotes the phase transition temperature.

ing point when it is doped with tetracene (Fig. 1). During zone refining it was noticed that the distribution coefficient k (concentration in the solid phase/concentration in the liquid phase) is larger than unity; tetracene accumulated at the top of the zone refining tube. These facts indicate that the solubility of tetracene in *p*-terphenyl crystal is very high. In this respect this system is basically different from the classical system of tetracene in anthracene, in which the solubility of tetracene is reported to be $\approx 10^{-5}$ mol/mol.[10] *p*-Terphenyl crystallizes in monoclinic form and tetracene has a triclinic lattice, so they are not isomorphic. Accordingly, they can not form a solid solution for the entire concentration range. However, the similar size and shape of the molecules of the two compounds seem to make possible the formation of the solid solution in a rather wide concentration range.

Kinetics. If a *p*-terphenyl crystal (host, hereafter with subscript H) doped with tetracene (guest, hereafter with subscript G) is illuminated with light of intensity I, the rate equations for the concentrations of the host and the guest singlet excited states are[2]

$$dS_H/dt = \alpha I - k_H S_H - k_{HG} S_H, \quad (2)$$

and

$$dS_G/dt = k_{HG} S_H - k_G S_G, \quad (3)$$

where α is the absorption coefficient, k_H and k_G are the monomolecular decay constants, and k_{HG} is the rate constant of the energy transfer. In the steady state condition

$$dS_H/dt = dS_G/dt = 0,$$

and the ratio of the fluorescence intensity I_G/I_H is given by

$$I_G/I_H = k_G^* S_G/k_H^* S_H = k_G k_{HG}/k_H^* k_G = \eta_G k_{HG}/\eta_H k_H, \quad (4)$$

where k^*'s are the radiative rate constants and η's are the fluorescence quantum yields.

The observed concentration dependence of I_G/I_H (Fig. 3) comes from the concentration dependence of k_{HG}, if η_G is constant. This is likely for the low concentration range of concern (10^{-7} to 10^{-3} mol/mol), where the trap-trap interaction must be negligible. If it is assumed that k_{HG} is proportional to the guest concentration, *i.e.*, $k_{HG}=c_G/t_h$, where t_h is the hopping time of the exciton,

$$I_G/I_H = \eta_G c_G/t_h \eta_H k_H. \quad (5)$$

From the fact that I_G/I_H is unity at the concentration of 5×10^{-6} mol/mol and the observed fluorescence decay time of 5.3 ns ($=1/k_H$) the hopping time, t_h, of an exciton on a lattice site is obtained to be 3×10^{-14} s (300 K) or 6×10^{-14} s (77 K), with an assumption $\eta_G/\eta_H=1$. It is possible that, with this assumption, we underestimate t_h by a factor of 3—5. The hopping time is shorter than that in anthracene, which is in accord with the result by Belitz, who measured the effect of doping on the fluorescence lifetime by using the phase method.[10] The spectral overlap of the host fluorescence and the guest absorption, which is the key factor in determining the host-guest energy transfer efficiency, is larger in anthracene–tetracene mixed crystal than in *p*-terphenyl–tetracene system. In the above analysis we have assumed that the last step of the energy migration, namely the transfer of the excitation energy to the guest molecule, is diffusion-limited. If it is not diffusion-limited, the result in Fig. 3 implies that t_h is even smaller than that given above.

The hyperlinear concentration dependence, *i.e.*, $n<1$ in Eq. 1, has been observed in several materials.[11-14] The deviation is small, but definitely present. It introduces an uncertainty of a factor of 2 in determining the value of k_{HG}. The attempt to explain it by a simple diffusion theory or by random walk consideration has not been successful so far.[15] In this work we analyze the result in terms of the simple hopping model, although the fact $n<1$ is not compatible with the assumption $k_{HG}=c_G/t_h$, at least in principle. The understanding of this feature awaits further investigation. It is interesting that Auweter *et al.* have found that the time dependent part of k_{HG} in naphthalene crystal is important for low dopant (anthracene) concentrations and that it is not simply proportional to the guest concentration.[9] It is to be noted that the hyperlinear dependence has been observed only for singlet energy transfer, but not for triplet.

Temperature Dependence of the Energy Transfer. The temperature dependence is quite different from that for anthracene and for naphthalene. In anthracene crystal the rate constant for the bimolecular annihilation, γ_{ss}, has been found to be proportional to $T^{-1/2}$; this has been explained in terms of the scattering of excitons by phonons.[16] In naphthalene, γ_{ss} is almost temperature independent.[9] Figure 4 shows that the fluorescence quantum yield of tetracene in *p*-terphenyl lattice, when corrected for the reabsorption, is independent of temperature. It is shown in Fig. 5(b) that I_G and I_H change with temperature, whereas the sum, I_H+I_G, shows only a slight variation in the temperature range 85—300 K. This shows that the quantum yield of the total fluorescence from the mixed crystal does not change within this temperature range and indicates that the effect of the traps for singlet excitons that may act as quenchers is not significant. Thus it seems reasonable to assume that the observed temperature dependence of I_G/I_H (Fig. 6) corresponds to that of k_{HG}. We may thus conclude that the energy transfer in *p*-terphenyl crystal is almost temperature independent in the temperature range 300—160 K (*p*-T-h_{14}) or 300—170 K (*p*-T-d_{14}) and that at lower temperatures the temperature dependence changes to that with an activation energy.

p-Terphenyl undergoes a phase transition around 190 K.[17-20] In the high temperature phase the molecules are planar. However, the amplitude of the rotational vibration of the central benzene ring about the molecular long axis is large and is better analyzed with the model in which the rotational vibration has a double well potential.[21] The sign of the resulting tilt of the central ring is random and no long range order is present. Below the transition temperature, however, the tilt of the central ring occurs in an ordered fashion, similar to the spins in antiferromagnetic materials. It has been observed that the order parameter grows as the temperature goes down. Hence the transition is thought to be of the order-disorder type.[22,23] It is proposed that a *p*-terphenyl molecule in its electronic ground state is non-planar, whereas in the excited state it is planar. This is based on the observation that the absorption spectrum of the compound in the solution lacks any vibrational structure, whereas its fluorescence spectrum is clearly structured.[1] It is also known that the absorption spectrum becomes more structured when the molecule in a viscous solution is excited to higher excited states.[24] In view of this conformational change accompanying the electronic excitation, the following mechanism of the energy transfer seems to be probable. A *p*-terphenyl molecule in a crystal takes the planar conformation when it is excited. Energy transfer to a neighboring molecule takes place equienergetically only when the latter takes the planar conformation. In this simplified model the energy barrier for the rotation of the central ring is expected to manifest itself in the temperature dependence of the energy transfer. When the four hydrogen atoms attached to the central benzene ring are replaced by four deuterium atoms, the moment of inertia about the molecular long axis increases by some 20% and the zero point energy becomes correspondingly lower. Accordingly, the activation energy ΔE is expected to be larger in *p*-T-d_{14} compared to *p*-T-h_{14} (Fig. 7), which is consistent with our observation. One could argue that the temperature dependence is caused by the presence of traps for excitons and the observed activation energies correspond to the trap depth. This possibility is denied by estimating the number of traps. Let us assume that the fraction x of the molecular sites is occupied by traps (impurities or displaced molecules), the depth of which is ΔE. The fraction 1-x is thus occupied by normal host molecules. An exciton migrates with occasional trapping. Detrapping is possible because ΔE (66 cm^{-1} or 90 cm^{-1}) is comparable to, or smaller than, kT for the temperature range investigated. The average hopping time of an exciton will be

$$t_h = (1-x)t_h^0 + xt_h^0\exp(-\Delta E/kT), \quad (6)$$

where t_h^0 is the hopping time between two normal

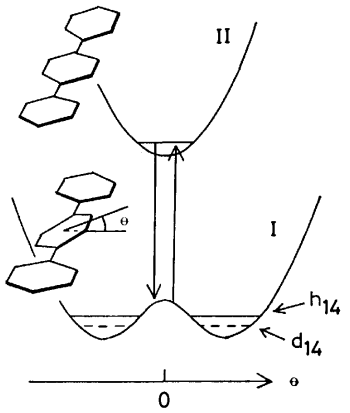

Fig. 7. A model for the intermolecular energy transfer in *p*-terphenyl crystal. In the electronic ground state (I) the molecule has a double well potential as regards the rotation of the central ring around the molecular long axis (θ). A molecule in the excited state (II) transfers its energy to a neighboring molecule equienergetically when the latter takes the planar conformation. The difference in the librational zero point energy of *p*-T-h_{14} and of *p*-T-d_{14} may account for the difference in the activation energies.

molecules. The observed temperature dependence of I_G/I_H could not be fitted with this model with x smaller than 0.8. This obviously contradicts the idea that a very low concentration of unidentified impurity is affecting the results. The fact that the temperature below which the plot log (I_G/I_H) *vs.* $1/T$ is linear corresponds roughly, although not exactly, to the transition temperature also seems to support our view that the temperature dependence, as well as the effect of deuterium substitution, is not determined by impurities, but is intrinsic.

References

1) I. Berlman, *J. Phys. Chem.*, **74**, 3035 (1970).
2) H. C. Wolf, *Adv. Atomic Mol. Phys.*, **3**, 119 (1967).
3) R. C. Powell and R. G. Kepler, *Mol. Cryst. Liq. Cryst.*, **11**, 349 (1970).
4) R. C. Powell and Z. G. Soos, *Phys. Rev. B*, **5**, 1547 (1971).
5) Z. G. Soos and R. G. Powell, *Phys. Rev. B*, **6**, 4035 (1972).
6) A. Bergmann, M. Levine, and J. Jortner, *Phys. Rev. Lett.*, **18**, 593 (1967).
7) S. D. Babenko, V. A. Benderskii, V. I. Gordanskii, A. G. Lavrushko, and V. P. Tyshinskii, *Phys. Status Solidi B*, **45**, 91 (1971).
8) A. Inoue, K. Yoshihara, and S. Nagakura, *Bull. Chem. Soc. Jpn.*, **45**, 1973 (1972).
9) H. Auweter, A. Braun, U. Mayer, and D. Schmid, *Z. Naturforsch., Teil A*, **34**, 761 (1979).
10) K. W. Benz and H. C. Wolf, *Z. Naturforsch., Teil A*, **19**, 177 (1964).
11) F. Belitz, *Z. Naturforsch., Teil A*, **25**, 955 (1970).
12) K. W. Benz and H. C. Wolf, *Z. Naturforsch., Teil A*, **19**, 181 (1964).
13) W. Klöpffer, *J. Chem. Phys.*, **50**, 1689 (1969).
14) H. Port, H. Schneckenburger, and H. C. Wolf, *Chem. Phys. Lett.*, **61**, 503 (1979).
15) H. Port, M. Bader, G. Weber, and H. C. Wolf, *Z. Naturforsch., Teil A*, **30**, 277 (1975).
16) A. Inoue, S. Nagakura, and K. Yoshihara, *Mol. Cryst. Liq. Cryst.*, **25**, 199 (1974).
17) J. L. Baudour, Y. Delugeard, and H. Cailleau, *Acta Crystallogr., Sect. B*, **32**, 150 (1976).
18) J. O. Williams, *Chem. Phys. Lett.*, **42**, 171 (1976).
19) S. Ramdas and J. M. Thomas, *J. Chem. Soc., Faraday Trans. 2*, **72**, 1251 (1976).
20) H. Cailleau and A. Dworkin, *Mol. Cryst. Liq. Cryst.*, **50**, 217 (1979).
21) J. L. Baudour, H. Cailleau, and W. B. Yelon, *Acta Crystallogr., Sect. B*, **33**, 1773 (1977).
22) H. Cailleau, J. L. Baudour, A. Girard, and W. B. Yelon, *Solid State Commun.*, **20**, 577 (1976).
23) A. Girard, H. Cailleau, Y. Marqueton, and C. Ecolivet, *Chem. Phys. Lett.*, **54**, 479 (1978).
24) K. Razi-Naqvi, J. Donatsch, and U. P. Wild, *Chem. Phys. Lett.*, **34**, 285 (1975).

Ylide-Metal Complexes. IV. The Preparation and Properties of IIb-group Metel (Zn, Cd, Hg) Complexes of Alkylidenetriphenylphosphoranes

Yoshihisa YAMAMOTO* and Hideo SUGIMOTO†

Faculty of Pharmaceutical Sciences, Higashi Nippon Gakuen University, Ishikari, Tobetsu, Hokkaido 061-02

(Received December 3, 1979)

Ylide-IIb-group metal (Zn, Cd, Hg) complexes, bis(triphenylphosphonium alkylide)metal dichloride, $[(C_6H_5)_3\overset{+}{P}-\underset{R}{\underset{|}{CH}}-M-\underset{R}{\underset{|}{CH}}-\overset{+}{P}(C_6H_5)_3](Cl^-)_2$ (M: Zn, Cd, Hg), and chloro(triphenylphosphonium isobutylide)metal dichloride, $[(C_6H_5)_3\overset{+}{P}-\underset{CH(CH_3)_2}{\underset{|}{CH}}-M-Cl]Cl^-$ (M: Zn, Cd), have been obtained from alkylidenetriphenylphosphoranes, $(C_6H_5)_3P=CH-R$ (R: H, CH_3, $CH(CH_3)_2$), and $ZnCl_2$, $CdCl_2$, or $HgCl_2$. In these organometallic complexes, the alkylidenetriphenylphosphoranes are attached to the IIb-group metals atom through the carbanionic donor atom. They are thermally stable.

The complexes of alkylidenetriphenylphosphorane and IIb-group metals have been investigated by Schmidbaur[1-4] and some other researchers.[5-7] The complexes of alkylidenetriphenylphosphorane $(C_6H_5)_3P=CH-R$ (R: H, CH_3, $CH(CH_3)_2$), and $ZnCl_2$, $CdCl_2$, or $HgCl_2$ have, however, been the subject of little research.

Previous papers have been concerned with the preparation and physical properties of stable 2/1- and 1/1-gold(I), silver(I) and copper(I) complexes of alkylidenetriphenylphosphoranes[8] and arsoranes.[9] The present paper will deal with the preparation and ^1H- and ^{13}C-NMR measurements of bis(triphenylphosphoniumalkylide)metal dichloride, $[(C_6H_5)_3\overset{+}{P}-\underset{R}{\underset{|}{CH}}-M-\underset{R}{\underset{|}{CH}}-\overset{+}{P}(C_6H_5)_3](Cl^-)_2$ (M: Zn, Cd, Hg) and chloro(triphenylphosphonium isobutylide)metal chloride, $[(C_6H_5)_3\overset{+}{P}-\underset{CH(CH_3)_2}{\underset{|}{CH}}-M-Cl]Cl^-$ (M: Zn, Cd).

Results and Discussion

Synthesis and Properties. 2/1 complexes of bis(triphenylphosphonium alkylide)metal dichloride (**1a**—**1b**, **2a**—**2b**, and **3a**—**3c**) and 1/1 complexes of chloro(triphenylphosphonium isobutylide)metal dichloride (**1d** and **2d**) have been isolated from a reaction mixture of alkylidene triphenylphosphorane ($(C_6H_5)_3P=CH-R$, **La**; R=H, **Lb**; R=CH_3 and **Lc**; R=$CH(CH_3)_2$) and $ZnCl_2$, $CdCl_2$, or $HgCl_2$. Attempts to obtain the bis(triphenylphosphonium isobutylide)metal dichloride

$$2(C_6H_5)_3P=CH-R \xrightarrow{MCl_2} [(C_6H_5)_3\overset{+}{P}-\underset{R}{\underset{|}{CH}}-M-\underset{R}{\underset{|}{CH}}-\overset{+}{P}(C_6H_5)_3](Cl^-)_2$$

M	R = H	R = CH_3	R = $CH(CH_3)_2$
Zn	**1a**	**1b**	—
Cd	**2a**	**2b**	—
Hg	**3a**	**3b**	**3c**

† Present address: Yoshitomi Pharmaceutical Industries Ltd., 3-35, Hirano-cho, Higashi-ku, Osaka 541.

$$2(C_6H_5)_3P=\underset{CH(CH_3)_2}{\underset{|}{CH}} \xrightarrow{MCl_2} [(C_6H_6)_3\overset{+}{P}-\underset{CH(CH_3)_2}{\underset{|}{CH}}-M-Cl]Cl^-$$

M	
Zn	**1d**
Cd	**2d**

from **Lc** and $ZnCl_2$ or $CdCl_2$ invariably resulted in the isolation of a 1/1 complex of **1d** or **2d** respectively.

All the complexes except **1a** and **2a** are insoluble in most organic solvents and change to the corresponding phosphonium salts, *i.e.*, $[(C_6H_5)_3PCH_2R]Cl$, in chloroform and dichloromethane at room temperature or at a low temperature. **1a** and **2a** change slowly to the corresponding phosphonium salt in dichloromethane, but they are stable at −40 °C. All the complexes are thermally stable in the solid state. The stability of these complexes and bis(triphenylphosphonium methylide)metal chloride, $[(C_6H_5)_3\overset{+}{P}-CH_2-\bar{M}-CH_2-\overset{+}{P}(C_6H_5)_3]Cl^-$ (M: Cu; **4**,[10] Ag; **5**[11] and Au; **6**[8]), in dichloromethane is **6**≫**1a**≈**2a**>**4**≈**5**≫**3a**. **5** is sensitive to light, but **2a** is stable.

Also, **3a'** was prepared from **La** and $HgBr_2$ by Seyferth and Grim.[12] Although they reported that the **3a'** was somewhat soluble in hot methanol, **3a** can be decomposed in that solvent (*cf.* the ^1H-NMR section).

NMR Spectra. The ^1H-NMR spectrum of **1a** showed a doublet signal for the CH_2P at 0.76 ppm and a multiplet signal for the phenyl groups at 7.5 ppm in a ratio of 2:15 at room temperature. The ^1H-NMR spectrum of **2a** showed satellites caused by the spin-spin coupling of the $^{111/113}Cd$ nuclei with CH_2 protons in the complex, in addition to a doublet signal for the CH_2P at 0.70 ppm and a multiplet signal for the phenyl groups at 7.5 ppm. The ^1H-NMR spectrum of **3a** could not be measured at −45 °C because it was not soluble in dichloromethane-d_2. The ^1H-NMR spectrum of **3a** showed a doublet signal (J_{HCP}: 13.5 Hz) at 3.3 ppm in dichloromethane-d_2 at room temperature or at 3.0 ppm in hot methanol-d_4 for the methyl group and a multiplet signal for the phenyl groups at 7.5 ppm in dichloromethane-d_2 or at 7.7 ppm in methanol-d_4 in a ratio of 3:15. The chemical shift (δ) and the coupling constant (J_{HCP}) of methyltriphenylphosphonium bromide in methanol-

TABLE 1. ^{1}H- AND ^{13}C-NMR DATA OF COMPLEXES AND YLIDE

^{1}H	CH_2P			C_6H_5
	δ/ppm	$^2J_{HCP}$/Hz	$^2J_{HCM}$/Hz	δ/ppm
1a	0.76 d (2H)	16	—	7.3—8.0 m (15H)
2a	0.70 d (2H)	14	54.2	7.2—7.9 m (15H)
6	1.70 d	13.0		7.5—7.9 m
La	0.13 d	7.5		

^{13}C	CH_2P		C_6H_5 δ/ppm (J_{PC}/Hz)				Temp
	δ/ppm	J_{PC}/Hz	c-1	*o*	*m*	*p*	
1a	−1.17 d	48.8	124.3	132.5	128.5	134.8	−60 °C
			(85.0)	(8.8)	(12.7)	(—)	
2a	−2.01 d	44.9	118.6	132.3	128.7	134.6	−60 °C
			(87.9)	(9.8)	(12.7)	(—)	
6	9.5 d	39.1					
La	−4.3 d	98.6					

Standard: ^{1}H-NMR; int-TMS (δ=0), ^{13}C-NMR; CD_2Cl_2 (δ=53.6 ppm). Solvent: CD_2Cl_2. M: $^{111/113}$Cd.

d_4 are 3.0 ppm and 13.5 Hz for the methyl group and a multiplet signal for the phenyl groups at 7.7 ppm.

The coupling constants (J_{HCP}) of **1a** and **2a** were larger than that (7.5 Hz) of **La**, and their proton signals shifted to a lower field than that (0.13 ppm) of **La**. These spectra are similar to those[8,10,11] of **4**—**6**. It seems that the alkylidenetriphenylphosphoranes are attached to the metal atom through the carbanionic donor atom.[8,11,12] The cadmium atom in **2a** is considered to have the *SP* configuration from the following facts: the coupling constant (J_{HCM}) of **2a** is larger than those (35.4,[13] 34.9 Hz[14]) of the ylide-complexes with a tetrahedral-configurational cadmium atom, and it is close to those (49.4 Hz for $J_{HC^{111}Cd}$, 51.2 Hz for $J_{HC^{113}Cd}$) of diethylcadmium,[15] while the equivalent conductance of **2a** is 15 S cm^2 in dichloromethane at −50 °C. The chemical shifts (CH_2P) of **1a** and **2a** are at a higher field than those[8,10,11] of **4**—**6**. The change in the chemical shifts of these complexes is similar to that of the chemical shifts of other ylide-Ib-group and -IIb-group metal complexes.[13,14]

The ^{13}C-NMR spectra of **1a** and **2a** were measured in dichloromethane-d_2 at −60 °C. The coupling constants (J_{PC}) of these complexes were much smaller than that[8] of **La**. This finding is also similar to those[8,10,11] in the cases of **4**—**6**. The chemical shifts (CH_2P) of these complexes are at a higher field than those of **4**—**6**. The ^{1}H- and ^{13}C-NMR data of **1a** and **2a** are summarized in Table 1.

Experimental

Measurements. The NMR spectra were measured with an FX-60 spectrometer (JEOL) for ^{13}C-NMR, and with a JNMOMX-60 (JEOL) spectrometer and an R-40 (Hitachi) spectrometer for ^{1}H-NMR. The equivalent conductance was measured with a CM-30 (Schimadzu) conductometer.

Starting Materials. The methylene-,[16] ethylidene-,[10,17] isobutylidenetriphenylphosphoranes[10] were prepared from the corresponding phosphonium bromides by the sodium-amide method.[8,9]

The reaction mole ratio, the yield, the decomposition temperature, and the analytical data of complexes are collected in Table 2.

*Preparation of 1/2 Complexes. Bis(triphenylphosphonium methylide)zinc Dichloride (**1a**), Bis(triphenylphosphonium methylide)cadmium Dichloride (**2a**), and Bis(triphenylphosphonium methylide)mercury Dichloride (**3a**)*: $ZnCl_2$, $CdCl_2$, or $HgCl_2$ was added to a dry THF (20 cm^3) solution of methylenetriphenylphosphorane at room temperature under nitrogen. The color of the methylenetriphenylphosphorane changed from yellow to colorless. The white complex thus precipitated was filtered under nitrogen, washed with THF, and pentane, and dried under a vacuum.

*Bis(triphenylphosphonium ethylide)zinc Dichloride (**1b**), Bis(triphenylphosphonium ethylide)cadmium Dichloride (**2b**), Bis(triphenylphosphonium ethylide)mercury Dichloride (**3b**), and Bis(triphenylphosphonium isobutylide)mercury Dichloride (**3c**)*: These complexes were prepared according to the procedure for complexes **1a**, **2a**, and **3a**.

*Chloro(triphenylphosphonium isobutylide)zinc Chloride (**1d**)*: A dry ether (30 cm^3) solution of isobutylidenetriphenylphosphorane was added to $ZnCl_2$ at room temperature under nitrogen. The white complex precipitated after 8 d was filtered under nitrogen, washed with ether, and then pentane, and dried under a vaccum.

*Chloro(triphenylphosphonium isobutylide)cadmium Chloride (**2d**)*: A dry THF (20 cm^3) solution of isobutylidenetriphenylphosphoranes was added to $CdCl_2$ at room temperature under nitrogen. After 4 d, the precipitated white complex was filtered under nitrogen, washed with THF and then pentane and dried under a vacuum.

The present work was partially supported by a Grant-in-Aid for Scientific Research from the Ministry of Education, Science and Culture.

References

1) H. Schmidbaur and K. H. Räthlein, *Chem. Ber.*, **107**, 102 (1974).

2) H. Schmidbaur and J. Eberlein, *Z. Anorg. Allg. Chem.*, **434**, 145 (1977).

TABLE 2. REACTION MOLE RATIO, SOLVENT, REACTION TIME, YIELDS, DECOMPOSING TEMPERATURES, AND ANALYTICAL DATA OF COMPLEXES

No.	M	MCl_2 g (mmol dm^{-3})	R	$(C_6H_5)_3PCHR$ g (mmol dm^{-3})	Solvent	Reaction time d	Yield g (%)	Dt/°C	Formula (Molecular weight)	Found (%) C	Found (%) H	Calcd (%) C	Calcd (%) H
1a	Zn	0.068 (0.499)	H	0.276 (1.00)	THF	1	0.32 (93.1)	190	$C_{38}H_{34}P_2ZnCl_2$ (688.92)	66.56	5.27	66.25	4.97
1b	Zn	0.080 (0.59)	CH_3	0.39 (1.34)	THF	1	0.34 (80.4)	163	$C_{40}H_{38}P_2ZnCl_2$ (716.97)	66.63	5.09	67.01	5.34
1d	Zn	0.14 (1.03)	i-C_3H_7	0.70 (2.2)	Ether	8	0.44 (94.0)	180	$C_{22}H_{23}PZnCl_2$ (454.68)	57.69	5.51	58.11	5.10
2a	Cd	0.09 (0.491)	H	0.316 (1.14)	THF	3	0.34 (94.1)	114	$C_{38}H_{34}P_2CdCl_2$ (735.94)	61.84	5.06	62.02	4.66
2b	Cd	0.09 (0.491)	CH_3	0.410 (1.41)	THF	8	0.32 (85.3)	114	$C_{40}H_{38}P_2CdCl_2$ (763.99)	62.64	5.24	62.88	5.01
2d	Cd	0.09 (0.491)	i-C_3H_7	0.37 (1.16)	THF	4	0.20 (81.2)	115	$C_{22}H_{23}PCdCl_2$ (501.70)	53.00	4.87	52.67	4.62
3a	Hg	0.135 (0.497)	H	0.276 (1.00)	THF	1	0.36 (87.9)	182	$C_{38}H_{34}P_2HgCl_2$ (824.13)	54.99	4.47	55.38	4.14
3b	Hg	0.136 (0.501)	CH_3	0.290 (1.00)	THF	3	0.36 (84.3)	185	$C_{40}H_{38}P_2HgCl_2$ (852.18)	56.68	4.69	56.38	4.49
3c	Hg	0.136 (0.501)	i-C_3H_7	0.40 (1.26)	THF	a)	0.40 (87.9)	199	$C_{44}H_{46}P_2HgCl_2$ (908.29)	58.22	5.26	58.18	5.10

a) 7 h.

3) H. Schmidbaur and W. Wolf, *Chem. Ber.*, **108**, 2851 (1975).
4) H. Schmidbaur and W. Richter, *Z. Anorg. Allg. Chem.*, **429**, 222 (1977).
5) E. T. Weleski, J. L. Silver, M. D. Jansson, and J. L. Burmeister, *J. Organomet. Chem.*, **102**, 365 (1975).
6) N. A. Nesmeyanov, V. M. Novikov, and O. A. Reutov, *Izv. Akad. Nauk SSSR, Ser. Khim.*, **1964**, 772 [*Chem. Abstr.*, **61**, 3143 (1964)].
7) H. Daniel and J. Paetsch, *Chem. Ber.*, **98**, 1915 (1965).
8) Y. Yamamoto and Z. Kanda, *Bull. Chem. Soc. Jpn.*, **52**, 2560 (1979).
9) a) Y. Yamamoto and H. Schmidbaur, *J. Chem. Soc., Chem. Commun.*, **1975**, 669; b) W. Richter, Y. Yamamoto, and H. Schmidbaur, *Chem. Ber.*, **110**, 1312 (1977).
10) Y. Yamamoto and H. Schmidbaur, *J. Organomet. Chem.*, **96**, 133 (1975).
11) Y. Yamamoto and H. Schmidbaur, *J. Organomet. Chem.*, **97**, 479 (1975).
12) D. Seyferth and S. O. Grim, *J. Am. Chem. Soc.*, **83**, 1610 (1961).
13) H. Schmidbaur, O. Gasser, C. Kruger, and J. C. Sekutowski, *Chem. Ber.*, **110**, 3517 (1977).
14) H. Schmidbaur, H. J. Fuller, V. Bejenke, A. Franck, and G. Huttner, *Chem. Ber.*, **110**, 3536 (1977).
15) "Advances in Organometallic Chemistry," ed by F. G. A. Stone and R. West, Academic Press, New York and London (1965), Vol. 3, p. 19.
16) a) H. Schmidbaur, H. Stuhler, and W. Vornberger, *Chem. Ber.*, **105**, 1084 (1972); b) R. Koster, D. Simic, and M. A. Grassberger, *Justus Liebigs Ann. Chem.*, **739**, 211 (1970).
17) H. Bock and H. Tom Dieck, *Z. Naturforsch., Teil B.*, **21**, 739 (1966).

The Temperature Dependence of the Mixed and Intervalence State in Mono-oxidized *trans*-μ-(*as*-Indacene)bis(cyclopentadienyliron)

Sei'ichiro IIJIMA,† Izumi MOTOYAMA, and Hirotoshi SANO*

Department of Chemistry, Faculty of Science, Tokyo Metropolitan University, Fukasawa, Setagaya-ku, Tokyo 158

(Received January 18, 1980)

The temperature dependence first observed in the Mössbauer spectrum for mono-oxidized *trans*-μ-(*as*-indacene)bis(cyclopentadienyliron) was interpreted in terms of the increase in the rate of intervalence-electron transfer between two irons with an increase in the temperature. The cyclic voltammetric study of *trans*-μ-(*as*-indacene)bis(cyclopentadienyliron) indicates that the metal-metal interaction in the monocation of the compound is greater than that in the monocation of biferrocene at room temperature.

The so-called "mixed-valence" compounds have been extensively investigated in connection with the increased interest in superconductive materials and biological "mixed-valence" systems.[1–6] The monocation salts of binuclear ferrocenes, in which two kinds of iron atoms, formally Fe(II) and Fe(III), are simultaneously present, have attracted much attention in the field of "mixed-valence" chemistry and have been investigated by using several physico-chemical measurements.[7–19]

As is known by means of Mössbauer spectroscopy, some of the monocation salts of binuclear ferrocenes give two different valence states of irons, corresponding to bi- and trivalent irons, while the others give iron atoms in an intervalent state averaged between these two valence states. In the latter compounds, the "intervalence state" has been interpreted by assuming a thermal-electron transfer between the two iron atoms on a time scale shorter than the life-time of the excited Mössbauer nuclear level, *ca.* 10^{-7} s. There has, however, been no direct experimental proof for this speculative interpretation of the mechanism, because there has been no binuclear ferrocene derivatives' monocation which shows a typical temperature-dependent Mössbauer spectrum from an isolated mixed-valence state to a single averaged valence state.

It is known by means of Mössbauer spectroscopy that the mono-oxidized biferrocenylene(bis(μ-bicyclopentadienyl)-diiron(II)) gives iron atoms in an intervalent state[16,18] and the averaging has been speculated to proceed either through the cyclopentadienyl rings or directly through the overlapped *d*-orbitals of each iron atom. It was recently demonstrated, based on Mössbauer spectroscopic studies of the mono-oxidized salts of acetylene-bridged binuclear ferrocenes, that the π-conjugated system(s) between two ferrocenyl moieties plays an important role in the appearance of the intervalent state.[20,21]

During the process of verifying the role of the π-conjugated system bridged between two ferrocene moieties in the molecule which has a *trans*-conformation with respect to iron atoms, in contrast with biferrocenylene's and [2.2]ferrocenophane-1.13-diyne's monocation, a model compound of biferrocene derivatives with the conformation fixed in the *trans* form, *trans*-μ-(*as*-indacene)bis(cyclopentadienyliron), $(C_{12}H_8)Fe_2(C_5H_5)_2$ (**1**) and its monocation salt, $(C_{12}H_8)Fe_2(C_5H_5)_2{}^+I_3{}^-0.5I_2$ (**2**) were first synthesized.[22] The latter monocation salt (**2**) shows a trapped mixed-valence-type spectrum at 4.2 K and an intervalence-type spectrum at room temperature. The present paper will describe the temperature dependence of the valence state of the salt (**2**) as determined by means of Mössbauer spectroscopy. Cyclic voltammograms of the compound (**1**) will also be reported in order to elucidate the degree of the metal-metal interaction in the monocationic species.

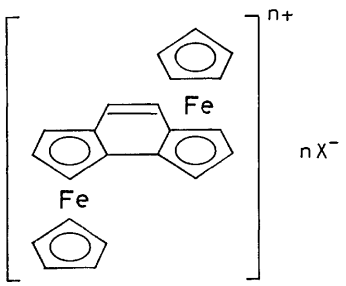

(1) n = 0

(2) n = 1, $X^- = I_3{}^-0.5I_2$

Fig. 1. The structure of **1** and **2**.

Experimental

Materials. *trans*-μ-(*as*-Indacene)bis(cyclopentadienyliron) (**1**) was prepared by the reaction of iron(II) chloride with a mixture of lithium cyclopentadienide and dilithium *as*-indacenide prepared by the reaction of dihydro-*as*-indacene with *n*-butyllithium. To a solution of tetrahydrofuran containing 0.62 g (4 mmol) of dihydro-*as*-indacene and cooled to −70 °C, 2.64 g (40 mmol) of cyclopentadiene was added. 32 ml of solution of 1.5 M *n*-butyllithium in hexane was added in drops over a period of 15 min. The mixture was allowed to stand for about 15 min until the temperature rose to room temperature. After the mixture had then been left for another 10 min, it was poured, at room temperature, into a suspension of iron(II) chloride prepared immediately before use. After the mixture had been allowed to stand for 30 min under stirring, the solvent was evaporated off and the residues were extracted with hexane. The extract was rapidly separated from ferrocene by column chromatography on alumina. **1** was thus obtained in the form of reddish needles in a yield of 3%. Mp 210—211 °C. Found: C, 66.79; H. 4.73%. Calcd for $C_{22}H_{18}Fe_2$: C, 67.05; H, 4.60%.

† Present address: Research Institute for Polymer and Textiles, Yatabe-Higashi, Tsukuba, Ibaraki 305.

Table 1. Half-wave potentials for *trans*-μ-(*as*-indacene)-bis(cyclopentadienyliron) (**1**) and related compounds in a CH_3CN solution containing 0.1 M *n*-Bu_4NClO_4

Compound	$E_{1/2}(1)$[a]	$E_{1/2}(2)$[a]	$\Delta E_{1/2}$[b]
trans-μ-(*as*-Indacene)-bis(cyclopentadienyliron)	0.29	0.70	0.41
Biferrocene	0.36	0.68	0.32
1′,1‴-Diacetylbiferrocene	0.62	0.92	0.30
1′,1‴-Diethylbiferrocene	0.28	0.63	0.35
2,2″-Dimethylbiferrocene[c]	0.37	0.63	0.26

a) Volts *vs.* Ag/AgCl electrode at 250 mm/s. b) $\Delta E_{1/2} = E_{1/2}(2) - E_{1/2}(1)$. c) Cited from Ref. 15, where CV was determined in CH_3CN containing Et_4NClO_4 (0.1 M) in volts *vs.* SCE at 100 mm/s.

The monocation salt, $(C_{12}H_8)Fe_2(C_5H_5)_2{+}I_3^- \cdot 0.5I_2$ (**2**), was prepared through the oxidation of **1** in benzene with iodine. Found: C, 29.23; H, 2.23%. Calcd for $C_{22}H_{18}Fe_2I_4$: C, 29.31; H, 2.06%.

Biferrocene derivatives,[23-26] polyethylferrocenes,[27] and aminoferrocene[38] were prepared according to the methods previously reported in the literature.

Measurements. The ^{57}Fe Mössbauer measurements were carried out by using a ^{57}Co(Pt) source moving in a constant acceleration mode. The isomer shifts are determined relative to metallic iron foil. The experimental errors of the isomer shifts and quadrupole splittings are ±0.05 mm/s for Compound **2** and ±0.02 mm/s for the other compounds.

Cyclic voltammograms of biferrocene, 1′,1‴-diacetyl- and 1′,1‴-diethylbiferrocene, and Compound **1** were obtained using a Hokuto Denki HB-107A function generator and a Hokuto Denki HA-201 potentiostat combined with a standard three-electrode configuration. The working electrode, a platinum button (Beckman), and the reference, an Ag/AgCl electrode, were connected *via* a salt bridge containing *n*-Bu_4NClO_4 (0.1 M) in CH_3CN. The half-wave potentials given in Table 1 were calculated from the peak potentials.

Results and Discussion

The half-wave potentials obtained by means of cyclic voltammetry for Compound **1** and related compounds are summarized in Table 1. The number of positions of substituents in biferrocenes shown in Table 1 are illustrated in Fig. 2. In the cyclic voltammograms of the compounds in CH_3CN solutions containing 0.1 M *n*-Bu_4NClO_4, two steps of the one-electron oxidation were observed. It is known that the difference in the half-wave potentials ($\Delta E_{1/2}$) can be used as the measure of the metal-metal interaction in a mono-oxidized binuclear ferrocene.[14] The larger value of $\Delta E_{1/2}$ in **1** (0.41 V) compared to that in biferrocene (0.32 V) suggests that the metal-metal interaction in the monocation of **1** is greater than that in the monocation of biferrocene. The $\Delta E_{1/2}$ of **1** is also somewhat greater than those of the substituted biferrocenes listed in Table 1, indicating that the large $\Delta E_{1/2}$ of **1** should be ascribed to the *trans*-conformation of the ferrocenyl moieties of **1** rather than to a simple substituent's effect of the fused ring in **1**. The values of $\Delta E_{1/2}$ reported for other substituted biferrocenes by LeVanda *et al.* are also lower than

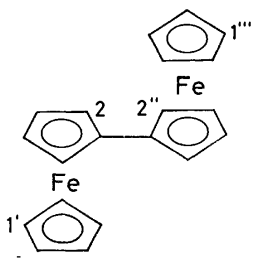

Fig. 2. The number of positions of substituents in the biferrocenes.

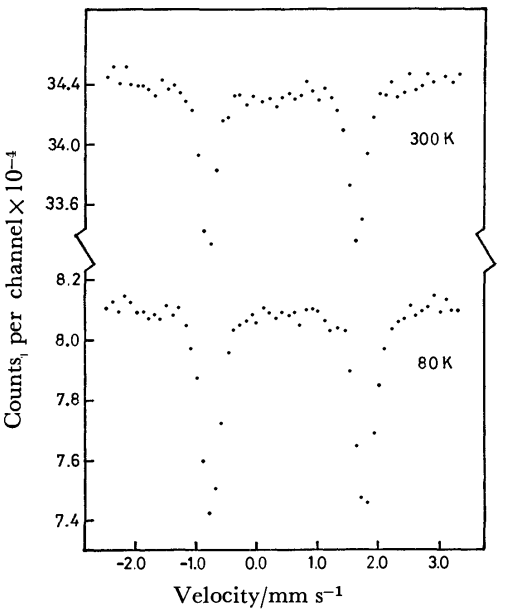

Fig. 3. Mössbauer spectra of $(C_{12}H_8)Fe_2(C_5H_5)_2$ (**1**) at 80 and 300 K.

that of **1**,[15] although their experimental conditions were a little different from those of the present studies. The small $\Delta E_{1/2}$ (0.26 V) found on 2,2″-dimethylbiferrocene[15] may be ascribed to the incomplete *trans*-conformation caused by the steric hindrance attributable to substituted rings. The results obtained for the compounds listed in Table 1 suggest that the two ferrocenyl moieties are twisted from a coplanar conformation with respect to the two combined cyclopentadienyl rings, except for **1**.

The Mössbauer parameters of Compound **1** and **2** are summarized in Table 2, with the data of biferrocene shown also for comparison. The neutral species (**1**) gives biferrocene-like spectral parameters, as may be seen in Fig. 3, although the quadrupole splitting (qs) is rather greater than that of biferrocene. This is similar to the relation between the qs of cyclopentadienyl(indenyl)iron(II) or bis(indenyl)iron(II) and that of biferrocene.[28,29] As may be seen in Table 3, it is found in the present studies that some ferrocene derivatives with electron-donating substituents give larger values of qs than that of ferrocene; that is, such a substituent increases the qs of ferrocene. On the other hand, it has been reported that the electron-attracting substituents decrease the qs of ferrocene.[30] Thus, the large qs of **1** is ascribable to the electron-donating effect of the fused ring in **1** to the ferrocenyl

Table 2. Mössbauer data for *trans*-μ-(*as*-indacene)-bis(cyclopentadienyliron) $(C_{12}H_8)Fe_2(C_5H_5)_2$ (**1**), its monocation salt, $(C_{12}H_8)Fe_2(C_5H_5)_2^+I_3^- 0.5I_2$ (**2**), and biferrocene

Compound	Temperature K	δ[a] mm s^{-1}	ΔE_Q mm s^{-1}
$(C_{12}H_8)Fe_2(C_5H_5)_2$ (**1**)	300	0.46	2.37
	80	0.55	2.42
$(C_{12}H_8)Fe_2(C_5H_5)_2^+$ I_3^--0.5I_2 (**2**)	300	0.35	0.86
	200	0.48[b]	0.76[b]
		ca. 0.5[c]	*ca.* 2.1[c]
	100	0.44[b]	0.56[b]
		0.49[c]	2.25[c]
	4.2	0.58	0.29
		0.65	2.30
Biferrocene	298	0.45	2.30
		0.45[d]	2.30[d]
	78	0.55	2.34
		0.52[d]	2.36[d]

a) The isomer-shift data are reported with respect to metallic iron foil. b) Apparent inner doublet. c) Apparent outer doublet. d) See G. K. Wertheim and R. H. Herber, *J. Chem. Phys.*, **38**, 2106 (1963).

Table 3. Mössbauer data for ferrocene and its derivatives at 78 K

Compound	δ[a] mm s^{-1}	ΔE_Q mm s^{-1}
Ferrocene[b]	0.52	2.39
Aminoferrocene	0.55	2.43
Diethylferrocene	0.52	2.42
Tetraethylferrocene	0.53	2.44
Hexaethylferrocene	0.53	2.47
Octaethylferrocene	0.54	2.48
Decaethylferrocene	0.52	2.48
Decamethylferrocene	0.53	2.50

a) The isomer-shift data are reported with respect to metallic iron foil. b) This value agrees well with the value reported in Ref. 30.

moieties.

The Mössbauer spectra of the monocation salt (**2**) were determined at 4.2, 100, 200, and 300 K. As is shown in Fig. 4, the shape of the spectrum of **2** greatly depends upon the temperature. The spectrum at 4.2 K consists of inner and outer doublets in nearly a 1:1 ratio; these doublets are ascribed to the ferrocenium-type and ferrocene-type irons (Fe(III) and Fe(II)) in **2** respectively. This is a typical trapped-valence type spectrum. On the other hand, only a single quadrupole doublet with a large half-line width (hlw) is observed in the spectrum at 300 K. The spectra at 100 and 200 K apparently consist of an intense "inner doublet" and a weak "outer doublet."

It is obvious that the results obtained for **2** cannot be interpreted essentially in terms of trapped-valence states with different spectral areas which are simply temperature-dependent. First of all, we cannot explain why the qs of the "inner doublet" increases considerably as the temperature increases (0.57 mm/s in qs from 4.2 to 300 K), despite the fact that qs slightly decreases as the temperature increases in most cases. Secondly, the anomalously large hlw of the "inner doublet" at higher temperatures cannot be explained either, because the hlw of ^{57}Fe absorption in most mono-oxidized binuclear ferrocenes has been reported to be in the range from *ca.* 0.3 to 0.4 mm/s, while the hlw of the "inner doublet" at 300 K is as large as 0.65 mm/s. Thirdly, such an extreme difference between the spectral areas in each component can only be explained by assuming a greatly different dependence in recoil-free fractions between the outer ferrocene-like and inner ferrocenium-like components, although a nearly equal recoil-free fraction for the two irons is to be expected from the point of view of the importance of the intermolecular interaction on the recoil-free fraction.[31]

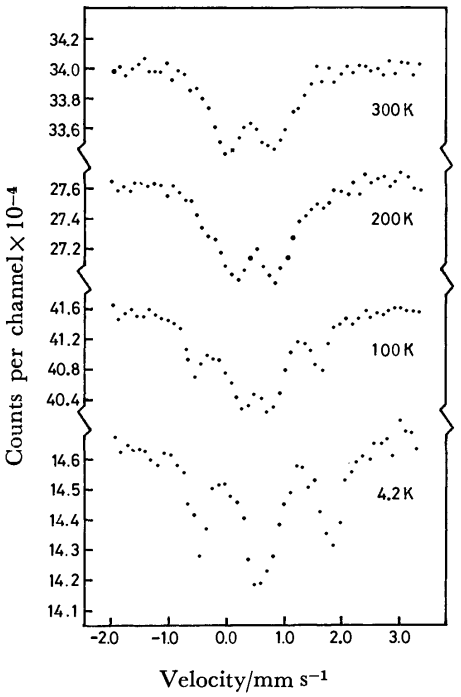

Fig. 4. Mössbauer spectra of $(C_{12}H_8)Fe_2(C_5H_5)_2^+$-$I_3^-$ 0.5I_2 (**2**) at 4.2, 100, 200, and 300 K.

On the other hand, the Mössbauer spectroscopic behaviour of some "mixed-valence" compounds (*e.g.*, Fe_3O_4,[32] $Fe_3(CH_3COO)_6 \cdot O \cdot 5H_2O$,[33] and Eu_3S_4[34]) has already been interpreted successfully in terms of an electron-hopping model. The temperature dependence of the Mössbauer spectra of the salt (**2**) was examined by applying this model to clarify the rate of thermal electron-transfer between two irons.

The shapes of the spectra of 100 and 200 K can well be described as the consequences of an increased electron-transfer rate with the increased temperature, which makes the qs values of the ferrocene-like and ferrocenium-like components closer to each other, causing the line to broaden on each component, while the rate of the electron-transfer is much smaller than *ca.* 10^7 s^{-1} at 4.2 K. The line components of the two

types of iron atoms virtually merge into a single resonance line at 300 K at a transfer rate larger than *ca.* 10^7 s^{-1}. The broadened line shape of the spectrum at 300 K can be explained in terms of the remaining relaxation effects caused by electron-hopping. The qs value at this temperature is slightly smaller than the average of the qs values of the two doublets at 4.2 K. This inconsistency can probably be ascribed to the simplicity of the model, since essentially no temperature-dependence is assumed for the basic electronic configurations of the pure ferrocene-like and ferrocenium-like components.

The general formula given by Wickman for the relaxation Mössbauer spectrum[35] has been applied to the explanation of the electron-hopping mechanism in Eu_3S_4 by Berkooz *et al.*[34] Both the relations derived from Wickman's formula of the transfer-rate with the peak positions and the half-line width of the spectral line component,[36] were used in the present study for the estimation of the electron-transfer rate in **2**, based on the assumption that the transfer rate at 4.2 K is much less than *ca.* 10^7 s^{-1}. In the calculation of the transfer rate, it is also assumed that the magnetic quantum number (m_I) of the excited Mössbauer nucleus does not change during the relaxation processes, *i.e.*, the relaxation between ferrocene-like and ferrocenium-like iron atoms occurs independently in each transition, $m_I=\pm1/2\rightarrow\pm1/2$ and $m_I=\pm1/2\rightarrow\pm3/2$, in Compound **2**.

The sign of the electric-field gradient (efg) of the ferrocenium-like component, like that of the ferrocene-like component in **2**, is assumed to be positive, because the ferrocenium-like component in biferrocene monocation salt is known to have a positive sign of efg.[19]

The electron-transfer rates, κ, were estimated to be 1.4×10^7 s^{-1} and 2.0×10^8 s^{-1} at 100 K and 300 K respectively. The values of the transfer rate derived from each transition coincide with each other within the range of experimental error.

The activation energy, E_p, of the electron-hopping in **2** was evaluated to be roughly 1 kcal mol^{-1} (0.04 eV) by using the following equation, as in the case of Eu_3S_4;[34]

$$\kappa = \kappa_0\exp(-E_p/kT).$$

The rate of the intermolecular electron transfer was determined at various temperatures in the NMR studies between ferrocene and ferrocenium ions in solutions of acetonitrile and of methanol.[37] The E_p value for the intermolecular electron-transfer was estimated to be 5 kcal mol^{-1} in acetonitrile and 3 kcal mol^{-1}. The lower value of E_p estimated in the present work may be ascribed to the smaller intramolecular Fe–Fe distance of the salt (*ca.* 5.0 Å) than that of the ferrocene-ferrocenium association complex (*ca.* 7.8 Å) and also the intramolecular π-conjugated system in **2**.

References

1) M. B. Robin and P. Day, *Adv. Inorg. Chem. Radiochem.*, **10**, 247 (1967).
2) G. C. Allen and N. S. Hush, *Prog. Inorg. Chem.*, **8**, 357 (1967).
3) N. S. Hush, *Prog. Inorg. Chem.*, **8**. 391 (1967).
4) I. F. Shchegolev, *Phys. Status Solidi A*, **12**, 9 (1972).
5) R. H. Holm and J. A. Ibers, "Iron-Sulfer Proteins," ed by W. Lovenberg, Academic Press, New York (1977), Vol. 3, Chap. 7.
6) J. Cambray, R. W. Lane, A. G. Wedd, R. W. Johnson, and R. H. Holm, *Inorg. Chem.*, **16**, 2565 (1977).
7) D. O. Cowan, R. L. Collins, and F. Kaufman, *J. Phys. Chem.*, **75**, 2025 (1971).
8) D. O. Cowan, G. A. Candela, and F. Kaufman, *J. Am. Chem. Soc.*, **93**, 3889 (1971).
9) D. O. Cowan, J. Park, M. Barber, and P. Swift, *Chem. Commun.*, **1971**, 1444.
10) D. O. Cowan and C. LeVanda, *J. Am. Chem. Soc.*, **94**, 9271 (1972).
11) D. O. Cowan, C. LeVanda, J. Park, and F. Kaufman, *Acc. Chem. Res.*, **6**, 1 (1973).
12) D. O. Cowan, C. LeVanda, R. L. Collins, G. A. Candela, U. T. Mueller-Westerhoff, and P. Eilbracht, *J. Chem. Soc., Chem. Commun.*, **1973**, 329.
13) C. LeVanda, D. O. Cowan, C. Leitch, and K. Bechgaard, *J. Am. Chem. Soc.*, **96**, 6788 (1974).
14) C. LeVanda, K. Bechgaard, and D. O. Cowan, *J. Org. Chem.*, **41**, 2700 (1976).
15) C. LeVanda, K. Bechgaard, D. O. Cowan, and M. D. Raush, *J. Am. Chem. Soc.*, **99**, 2964 (1977).
16) W. H. Morrison, Jr., and D. N. Hendrickson, *J. Chem. Phys.*, **59**, 380 (1973).
17) W. H. Morrison, Jr., and D. N. Hendrickson, *Chem. Phys. Lett.*, **22**, 119 (1973).
18) W. H. Morrison, Jr., and D. N. Hendrickson, *Inorg. Chem.*, **14**, 2331 (1973).
19) A. W. Rudie, A. Davison, and R. B. Frankel, *J. Am. Chem. Soc.*, **101**, 1630 (1979).
20) I. Motoyama, M. Watanabe, and H. Sano, *Chem. Lett.*, **1978**, 513.
21) M. Watanabe, S. Iijima, I. Motoyama, and H. Sano, *J. Phys. (Paris), Colloq.*, **C2**, 392 (1979).
22) S. Iijima, I. Motoyama, and H. Sano, *Chem. Lett.*, **1979**, 1349.
23) M. D. Rausch, *J. Org. Chem.*, **26**, 1802 (1961).
24) A. N. Nesmeyanov, V. N. Drozd, V. A. Sazonova, V. I. Romanenko, A. K. Prokof'ef, and L. A. Nikonova, *Izv. Akad. Nauk SSSR, Otd. Khim. Nauk*, **1962**, 45.
25) S. I. Goldberg and R. L. Matteson, *J. Org. Chem.*, **29**, 324 (1964).
26) A. N. Nesmeyanov, V. A. Sazonova, and U. N. Drozd, *Chem. Ber.*, **93**, 2717 (1960).
27) K. Schlögl and M. Peterlik, *Monatsh. Chem.*, **93**, 1328 (1962).
28) R. B. King, L. M. Epstein, and E. W. Gowling, *J. Inorg. Nucl. Chem.*, **32**, 441 (1970).
29) R. H. Herber, R. B. King, and G. K. Wertherim, *Inorg. Chem.*, **3**, 101 (1964).
30) A. V. Lesikar, *J. Chem. Phys.*, **40**, 2746 (1964).
31) H. Sano and H. Yamamoto, *Chem. Lett.*, **1977**, 67.
32) G. A. Sawatzky, J. M. D. Coey, and A. H. Morrish, *J. Appl. Phys.*, **40**, 1402 (1969).
33) D. Lupu, D. Barb, G. Filoti, M. Morariu, and D. Tarina, *J. Inorg. Nucl. Chem.*, **34**, 2803 (1972).
34) O. Berkooz, M. Malamud, and S. Shtrikman, *Solid State Commun.*, **6**, 185 (1968).
35) H. H. Wickman, "Mössbauer Effect Methodology," ed by I. J. Gruverman, Plenum Press, New York (1966), p. 39.
36) J. A. Pople, W. G. Schneider, and H. J. Berstein, "High-Resolution Nuclear Magnetic Resonance," McGraw-Hill Book Company, New York (1959).
37) E. S. Yang, M-S. Chan, and A. C. Wahl, *J. Phys. Chem.*, **79**, 2049 (1975).
38) E. M. Acton and R. M. Silverstein, *J. Org. Chem.*, **24**, 1487 (1959); A. N. Nesmeyanov, E. G. Perevalova, R. V. Golovnya, and L. S. Shilovtseva, *Dokl. Akad. Nauk SSSR*, **102**, 535 (1955).

Nitrogen Determination by Pyrolysis Using Steam. I.

Akira NOMURA,* Yazaemon MORITA, and Yukitoshi KOGURE
Department of Analytical Chemistry, National Chemical Laboratory for Industry, Yatabe, Ibaraki 305

(Received January 31, 1980)

Pyrolysis of nitrogen compounds with use of steam and $FeCl_3$–Al_2O_3 catalyst was investigated in detail in order to develop a new method for nitrogen determination. The catalyst was prepared by mixing an aqueous $FeCl_3$ solution and porous active Al_2O_3 for column chromatography and drying the mixture. A sample solution containing nitrogen was added to the catalyst in a boat and was then covered with an additional catalyst after removal of the solvent, leaving the sample adsorbed on the catalyst. The boat was then inserted into a pyrolysis tube, the sample being pyrolyzed in the presence of steam also used as carrier gas. The nitrogen in the sample converted into ammonia by the pyrolysis reaction was determined by titration after steam distillation under alkaline conditions. The nitrogen compounds except for N–O and N–N bonded compounds were converted quantitatively into ammonia by the pyrolysis under optimum conditions. The reaction was applied to the determination of nitrogen in various compounds.

Nitrogen determination of organic compounds was carried out mainly by the classical Kjeldahl, Dumas and ter Meulen method. Modification of their method has been investigated. Hozumi and Kirsten[1] reported the sealed tube method. Microcoulometry combined with hydrogenation of nitrogen compounds[2] and chemiluminescence measurement of nitrogen monoxide with ozone[3] were applied to nitrogen determination. Nitrogen in coke was determined by the semimicro gasification method[4] using steam as a carrier gas.

A new method for nitrogen determination of organic compounds is described in this paper. Its principle is based on the fact that nitrogen compounds are converted into ammonia by pyrolysis using $FeCl_3$–Al_2O_3 catalyst in the presence of steam.

Experimental

Materials. Porous active aluminium oxides (Al_2O_3) for column chromatography (Merck) were used. Methyl Red–Methylene Blue mixed indicator was used for acidimetric titration. Other reagents were of reagent grade.

Apparatus. The apparatus for pyrolysis is shown in Fig. 1. The nitrogen contents in the reagents were determined with a microcoulometric titrating system (Model TN-01, Mitsubishi Chemical Industrial Co. Ltd.) or a Kjeldahl digestion and distillation apparatus.

Ammonia converted from the nitrogen compounds by pyrolysis was identified by gas chromatography (Shimadzu GC-4CMPF) with a nitrogen-selective detector (Envirotech Corp., Dohmann Microcoulometric Titration System-10) based on the investigation by Martin.[2] A glass column, length 1 m, i.d. 3 mm, packed with 10% by weight PEG-20M (Gas Chro. Industrial Co. Ltd.) on Chromosorb-W precoated with 5% of KOH was used, argon being used as carrier gas at 40 ml/min. A glass precolumn (3 mm i.d. × 90 mm) installed in the sample inlet zone of the gas chromatograph was packed with soda lime and heated at 200 °C to release the basic compounds in the samples.

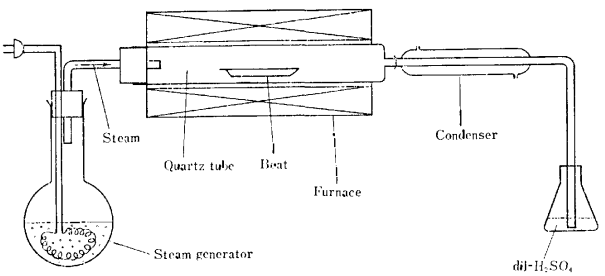

Fig. 1. Schematic diagram of apparatus for pyrolysis.

Preparation of Catalysts. Aqueous $FeCl_3$ solutions (50 ml) of various concentrations were added to Al_2O_3 (100 g), thoroughly mixed with a pestle and dried at 60 °C for 5 h. It is desirable to prepare the catalysts as required. Otherwise they should be stored in a desiccator containing silica gel.

Procedure. The catalyst (1.5 g) was uniformly distributed in an alumina boat (Japan Chemical Ceramic Co. Ltd., SSA-H5B). A sample solution of 0.5 ml containing approximately 1 mg of nitrogen dissolved with a suitable solvent was added to the catalyst with a micro pipette (Toa Medical Electronic Co. Ltd., Type 1058-F500) and dried at 60 °C in order to remove the solvent. The catalyst supporting the sample was covered uniformly with an additional catalyst (2.0 g). The boat was pushed with a stainless steel wire attached to the tail of the boat into a quartz pyrolysis tube (28.5ϕ × 475 mm), heated at 700—1000 °C in a furnace. Steam of 2.5 g/min, regulated with a Slidac, was immediately supplied from a steam generator for 10 min by connecting a hose to the open end of the pyrolysis tube. The pyrolyzed products were carried by the steam through a condenser to a flask containing dilute H_2SO_4 for absorption of ammonia in the reaction products. Ammonia was determined by the conventional titration method after steam distillation under alkaline conditions, since acidic materials such as HCl are produced during the course of pyrolysis by the decomposition of $FeCl_3$ and the sample. In order to obtain a blank value, the same procedure was carried out for the catalyst without sample.

Results and Discussion

Nitrogen compounds are classified into three types[5]—Type I: N–H and N–C bonded; Type II: N–O bonded; and Type III: N–N bonded. Ammonium sulfate, urea, pyridine, aniline, *p*-dinitrobenzene, and azobenzene were selected as typical compounds.

Identification of Ammonia by Gas Chromatography with Nitrogen-selective Detector. Since the method is based on the fact that nitrogen compounds are converted into ammonia by the pyrolysis reaction utilizing the $FeCl_3$–Al_2O_3 catalyst, the detection and identification of ammonia by gas chromatography with a nitrogen-selective detector would help confirm the validity of the method.

Samples for chromatographic analysis were prepared

Table 1. Effect of aluminium oxide properties on pyrolysis

No.	Properties of Al_2O_3			Concentration of $FeCl_3(Fe/Al_2O_3)$/wt%	Recovery of N/%			
	Activity[a]	Pore diameter/Å	Acidity		Pyridine	*p*-Dinitrobenzene	Azobenzene	Urea
1	I	90	Neutral	1	76.1	57.6	82.3	100.4
				2	93.2	73.8	91.6	98.7
				4	99.3	76.3	84.9	81.6
				6	95.7	87.0	72.3	83.4
2	I	90	Aacidic	1	86.3	79.4	88.0	95.5
				2	97.2	89.8	92.3	86.7
				4	97.7	91.9	81.0	81.2
				6	96.5	85.5	61.2	78.3
3	I	90	Basic	1	— [b]	80.2	74.7	98.0
				2	92.6	85.2	90.1	96.2
				4	94.9	88.1	85.5	92.9
				6	95.3	85.4	75.3	90.1
4	I	60	Basic	1	70.5	63.4	76.7	97.6
				2	89.1	73.3	78.0	99.0
				4	97.7	88.8	83.8	94.8
				6	95.9	87.9	63.0	79.2
5	I	150	Basic	1	— [b]	87.0	82.6	99.5
				2	83.7	85.9	88.6	97.0
				4	81.7	87.2	84.2	98.3
				6	81.4	90.0	56.2	97.9
6	II—III	90	Basic	1	— [b]	74.7	71.0	98.6
				2	93.4	85.6	84.7	98.7
				4	96.0	90.0	81.3	91.2
				6	96.7	84.7	73.7	91.3

a) Determined according to the method of Brockmann and Schodder.[6] b) End point not clear due to the presence of unreacted pyridine.

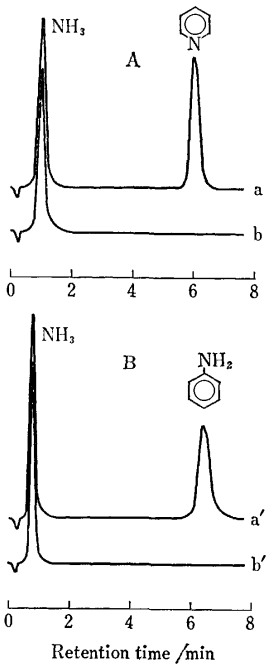

Fig. 2. Identification of ammonia by gas chromatography with nitrogen-selective detector.
A; Column temperature: 100 °C, a: standard sample (ammonium sulfate 100 ng N, pyridine 100 ng N), b: reaction products of pyridine at 800 °C, B; column temperature: 170 °C, a′: standard sample (ammonium sulfate 100 ng N, aniline 100 ng N), b′: reaction products of aniline at 800 °C.

as follows. The pyrolyzed products of 1 mg N of pyridine or aniline, absorbed in dilute H_2SO_4, were distilled. The distillate was neutralized with slight excess of acid (H_2SO_4) in an adaptor, then codensed to 10 ml. If the nitrogen in the pyridine or aniline is quantitatively recovered as ammonia, 100 ng/μl of nitrogen should be contained in the condensed solution.

The sample of 1 μl (100 ng N) was injected through the inlet of the gas chromatograph and the chromatogram obtained was compared with that of a standard sample (Fig. 2). Peaks of both pyridine and aniline (chromatograms A and B) disappeared, only that of ammonia appearing after the pyrolysis. The peak height of ammonia converted from pyridine or aniline was nearly the same as that of ammonia (100 ng N) in a standard sample.

The results indicate that both pyridine and aniline are converted into ammonia giving no other basic nitrogen compounds detectable with a nitrogen-selective detector. The conventional acidimetric titration is simpler and more precise for determination of ammonia as compared with chromatographic determination when only ammonia exists as a basic compounds.

Effect of Aluminium Oxide Properties. Aluminium oxides used were porous sorbents for column chromatography (particle size: 0.04—0.15 mm). The properties of aluminium oxides (Merck) are summarized in Table 1, together with catalytic efficiencies. The concentration of $FeCl_3$ supported on Al_2O_3 was in the range 1—6% of Fe/Al_2O_3. The temperature for the pyrolysis was 800 °C, the steam flow rate being 2.5 g/min.

TABLE 2. EFFECTS OF THE AMOUNT OF CATALYST AND THE HEATING TEMPERATURE ON PYROLYSIS

Compound	Amount of catalyst/g	Recovery of N/%				
		600 °C	700 °C	800 °C	900 °C	1000 °C
Pyridine	0	— a)	— a)	— a)	— a)	— a)
	1	— a)	81.3	90.2	90.4	82.0
	2	54.7	94.7	99.3	101.3	88.6
	3	48.7	90.3	99.3	100.6	82.8
p-Dinitrobenzene	0	64.2	61.0	55.1	48.0	57.1
	1	45.6	68.3	63.0	62.8	80.9
	2	33.8	69.9	76.3	59.4	68.5
	3	33.6	71.2	77.6	56.0	51.0
Azobenzene	0	38.5	56.6	68.0	59.1	51.0
	1	51.0	75.3	82.4	74.1	50.6
	2	38.2	62.3	84.9	74.7	56.9
	3	31.6	71.9	82.3	68.4	56.4
Urea	0	32.3	93.0	97.6	96.9	94.8
	1	72.6	88.8	93.6	82.3	62.0
	2	43.4	89.4	81.6	69.1	46.3
	3	41.0	91.9	81.5	56.3	35.9
Ammonium sulfate	0	73.8	101.1	96.8	89.3	77.2
	1	68.4	98.3	90.4	77.7	59.2
	2	61.4	79.9	80.9	53.8	38.1
	3	70.5	70.5	69.5	38.2	27.7

a) End point not clear due to the presence of unreacted pyridine.

The nitrogen in pyridine was recovered quantitatively by 4%-Fe/Al_2O_3 except for No. 5 whose pore size is the largest among the Al_2O_3 we used. The reason for the low recovery of pyridine by No. 5 has not been clarified. We assume the removal of some pyridine from the catalyst during the drying process due to larger pore size (low adsorptivity for pyridine), since 8-quinolinole (oxine), having lower vapor pressure than pyridine, was recovered quantitatively.

The activity and acidity of Al_2O_3 did not remarkably affect the recovery of the nitrogen compounds. On the other hand, both *p*-dinitrobenzene and azobenzene could not be recovered quantitatively under the conditions in Table 1.

In urea (Type I), which is the same as pyridine except for the fact that it contains only one carbon atom in a molecule, the recovery increased as $FeCl_3$ concentration decreased except for No. 5. Iron(III) chloride supported on Al_2O_3 is assumed to undergo oxidation to Fe_xO_y during the course of pyrolysis, urea or its intermediates being considered to be partly oxidized due to the excessive presence of Fe_xO_y causing the low recovery of ammonia. Low concentration of $FeCl_3$ is recommended. The results obtained for No. 1 Al_2O_3 which supported no $FeCl_3$ showed a 95.0% recovery, which is a little low.

Effect of the Amount of Catalyst and Heating Temperature. The effect of the amount of the additional catalyst, covering the sample supported on the catalyst (1.5 g) in the boat, and that of heating temperature in the hot zone on the recovery of pyridine, *p*-dinitrobenzene, azobenzene, urea, and ammonium sulfate were studied. The results are given in Table 2. The concentration of the catalyst was 4%-Fe/Al_2O_3.

Pyridine was recovered quantitatively by the catalyst of 2 and 3 g at 800 and 900 °C, respectively. Below 700 °C the pyrolysis of pyridine could not be completed. Presumably oxidation took place to reduce the recovery at temperatures above 1000 °C.

Although nitro and N–N bonded compounds such as *p*-dinitrobenzene and azobenzene have not been determined quantitatively, 800 °C and 2—3 g of catalyst are suitable.

Ammonium sulfate required no additional covering catalyst for conversion into ammonia, low temperatures (700 °C) being suitable. Oxidation by Fe_xO_y produced on Al_2O_3 during pyrolysis supposedly causes NH_4^+ being partly converted into NO_x or N_2. A certain amount of $FeCl_3$ is necessary to release ammonia from the ammonium sulfate, since the recovery of ammonia was very low (55.1%) with use of only Al_2O_3, supporting no $FeCl_3$, as a catalyst at 800 °C.

Urea, containing one carbon atom in the molecule, requires higher temperatures for its conversion into ammonia as compared with ammonium sulfate, decreasing tendency in the recovery with an increase in the amount of catalyst being smaller than that of ammonium sulfate.

Effect of the Period of Time from Sample Insertion to Steam Supply. The method is not automatic, and sudden pyrolysis before the connection of the steam generator might cause a loss of some of the pyrolyzed products escaping out of the open end of the pyrolysis tube. A portion of the sample might burn, forming N_2 and NO_x instead of NH_3 as a result of the exposure to the air before steam is supplied.

The period of time from sample insertion to steam supply was varied using pyridine as a sample, and the effect on the recovery of nitrogen was investigated in order to estimate how long the period is allowed to determine nitrogen compounds quantitatively (Fig. 3). The concentration of $FeCl_3$ in the catalyst was 4%-Fe/Al_2O_3.

Although the boiling temperature of pyridine is

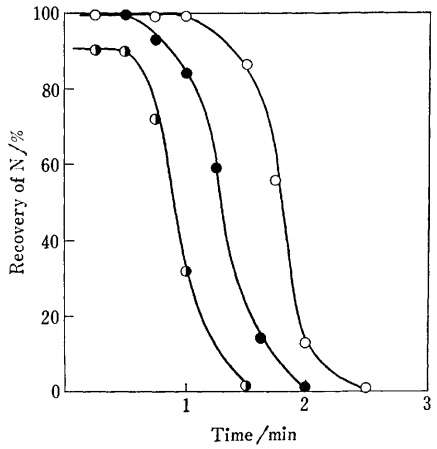

Fig. 3. Effect of the period of time from sample insertion to steam supply on the recovery of nitrogen. Reaction temperaure; ○: 800, ●: 900, ◑: 1000 °C, sample: pyridine (1 mg N), steam flow rate: 2.5 g/min.

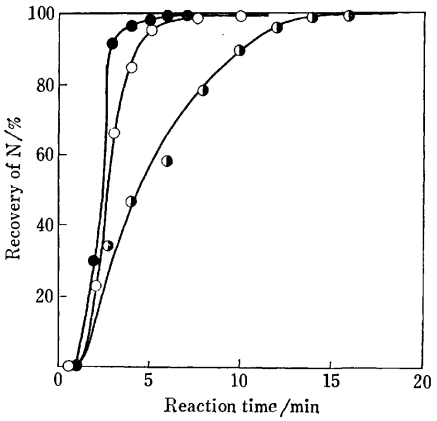

Fig. 4. Time required for pyrolysis reaction. Steam flow rate; ◑: 2.0, ○: 2.5, ●: 4.0 g/min, sample: pyridine (1 mg N), reaction temperature: 800 °C.

not high (115.5 °C), it was adsorbed on the catalyst in the hot zone of the pyrolysis tube at least for 1 min at 800 °C and 30 s at 900 °C presumably because of its adsorption to the catalyst and also the heat capacity of the sample boat and the catalyst, which prevent rapid rise in temperature.

Nitrogen in pyridine was not recovered quantitatively at 1000 °C, even when the steam was supplied immediately (5 s after insertion of the sample boat).

Similar results were obtained in the case of aniline and indole. Thus, it is not necessary to connect the steam generator quickly.

Time Required for Pyrolysis. The effect of the steam flow rate on the pyrolysis of pyridine is shown in Fig. 4. The ammonia produced by the reaction at 800 °C was recovered quantitatively within 10 min at a flow rate higher than 2.5 g/min. As compared with other methods such as the conventional Kjeldahl and Dumas method, our method is simple and rapid, even though more time is requied for the steam distillation of ammonia as in the Kjeldahl method.

Other Materials as Catalysts for Pyrolysis. Iron(III) chloride supported on porous Al_2O_3 was found to be effective for the nitrogen determination of compounds of Type I. Iron(II) sulfate and $Fe(NO_3)_3$ were examined for the effect of anion on pyrolysis.

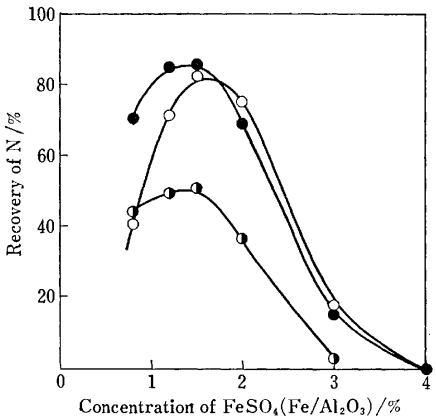

Fig. 5. Effect of $FeSO_4$ as a catalyst for pyrolysis. ○: Pyridine, ◑: *p*-dinitrobenzene, ●: azobenzene, reaction temperature: 800 °C, steam flow rate: 2.5 g/min.

Table 3. Application to various nitrogen compounds

Compound	Sample taken mg N	Found mg N
Pyridine	0.97	0.97
Quinoline	0.94	0.91
Acridine	1.01	0.98
Pyrrole	0.93	0.90
Indole	0.97	0.93
Carbazole	1.03	1.00
Aniline	1.00	0.97
Urea[a)]	1.00	0.98
Ammonium sulfate[a)]	1.00	1.00
N,N'-Diphenylthiourea	1.00	1.03
Phenazine	0.97	0.95
Imidazole	1.01	0.97
Acetanilide	0.98	0.95
p-Methoxybenzonitrile	0.97	0.95
p-Dinitrobenzene	1.00	0.76
5-Nitrosalicylic acid	0.99	0.89
Azobenzene	1.00	0.85
Benzotriazole	1.00	0.28

Reaction conditions; catalyst: 4%-Fe/Al_2O_3, reaction temp: 800 °C, steam: 2.5 g/min, reaction time: 10 min.
a) Covering catalyst: 0 g, reaction temp: 700 °C.

Plots of the concentration of $FeSO_4$ supported on Al_2O_3 (Fe/Al_2O_3) *vs.* the recovery of pyridine, *p*-dinitrobenzene, and azobenzene are given in Fig. 5. The recovery is not quantitative. As compared with chloride ion, highly concentrated sulfate ion adversely affects the pyrolysis of organic compounds.

The nitrate ion affected the reaction much more adversely, producing almost no ammonia but NO_x or N_2 releasing NO_2 due to the thermal decomposition of the nitrate ion.

Cobalt and nickel might also be useful for the reac-

tion. However, $CoCl_2$ and $NiCl_2$ supported on Al_2O_3 gave no satisfactory results.

Application to Various Nitrogen Compounds. The results of various nitrogen compounds analyzed are given in Table 3. Compounds of Type I such as pyridine and aniline were determined satisfactorily, but not those of Types II and III, nitro and N–N bonded compounds.

Reproducibility of the Method. The reproducibility of the method was examined, the average recovery of pyridine (n=8) being 98.1% with a standard deviation of 0.77%.

References

1) K. Hozumi and W. J. Kirsten, *Anal. Chem.*, **34**, 434 (1962).
2) R. L. Martin, *Anal. Chem.*, **38**, 1209 (1966).
3) A. Foutijn, A. J. Sabadell, and R. J. Ronco, *Anal. Chem.*, **42**, 575 (1970).
4) A. E. Beet and R. Belcher, *Fuel*, **17**, 175 (1938).
5) Y. Morita, *Bull. Chem. Soc. Jpn.*, **41**, 2029 (1968).
6) H. Brockmann and H. Schodder, *Chem. Ber.*, **74**, 73 (1941).

The Structure of (Hydrogen Ethylenediaminetetraacetato)antimony(III) Dihydrate $Sb(C_{10}H_{13}N_2O_8)\cdot 2H_2O$

Mamoru Shimoi, Yoshinari Orita, Takashi Uehiro, Itsuro Kita, Toschitake Iwamoto, Akira Ouchi,* and Yukichi Yoshino

Department of Chemistry, College of General Education, The University of Tokyo, Komaba, Meguro-ku, Tokyo 153

(Received February 29, 1980)

The crystal and molecular structure of the title complex has been determined by X-ray diffraction using 1882 reflections. The crystal was orthorhombic, with the space group $Pbn2_1$; $a=10.98(2)$, $b=18.496(4)$, $c=7.341(9)$, $Z=4$, $D_x=1.99$, $D_m=1.98(2)$ g cm^{-3}, μ(Mo $K\alpha$)$=19.3$ cm^{-1}, and the final R value was 0.036. A distorted ψ-pentagonal bipyramid is formed around the central antimony(III) atom by two nitrogen and two oxygen atoms, together with a lone electron pair at the equatorial positions and two oxygen atoms at the axial positions. One of the Sb–O distances, 2.78 Å, is longer than the others (2.20(2) Å on the average), and it is determined that the carbonyl oxygen is essentially of the free-acid type and that its carbonyl oxygen is weakly coordinated. The splitting of the ν_{as}(COO) band of its infrared and Raman spectra shows the existence of both free and coordinated carboxyl groups. The ^{1}H- and ^{13}C-NMR results show that the antimony(III)–edta complex does not exchange with the free ligand in an aqueous solution at pH 1.5—3.5.

There has been a growing interest in the study of antimony(III) complexes in recent years. Privalova and Ryabenhikov isolated and analyzed 1:1 edta (H_4(edta)=ethylenediaminetetraacetic acid) and other amine-*N*-polycarboxylato complexes of antimony(III).[1] Bhat and Iyer determined the formation constants of the antimony(III)–edta complex,[2] as well as those of the antimony(III)–*N*-(2-hydroxyethyl)ethylenediamine-*N,N,N'*-triacetato complex,[3] in an aqueous solution using spectrophotometric and potentiometric methods; the results were reinvestigated by Özer and Bogucki using the potentiometric titration technique.[4] The infrared spectral study was reported by Iyer and Shankar,[5] while the chelatometric titration of antimony(III) using edta was reported by Takamoto[6] and by Yurist.[7]

From these results, it seems that the antimony(III)-edta complex, Sb(Hedta)$\cdot n\,H_2O$ (n=1,2), should be a very stable compound. Accoding to Bhat,[2] the apparent formation constant of the complex ion [Sb(edta)]$^-$ in an aqueous solution shown by the following equation is about 10^{25}:

$$SbO^+ + 2H^+ + (edta)^{4-} = [Sb(edta)]^- + H_2O$$

In fact, the antimony(III)–edta complex does not decompose even in an acid medium with a pH of 2. However, the antimony in the edta chelate can easily and almost immediately be replaced by zinc, copper, or other metals in an aqueous solution over pH=4, and the back titration with a metal salt solution is possible only under limited conditions.[6,7]

To study this interesting complex, the present authors have determined the crystal and molecular structure of the acid chelate, Sb(Hedta)$\cdot 2\,H_2O$, by the X-ray diffraction method: its infrared and Raman spectra were also examined. Moreover, the state of the complex in an aqueous solution was investigated by means of the NMR technique.

Experimental

Syntheses of Chelates. (Hydrogen Ethylenediaminetetraacetato)antimony(III) Dihydrate; $Sb(C_{10}H_{13}N_2O_8)\cdot 2H_2O$: This compound was prepared by a slight modification of the method of Bhat;[2] the drop-by-drop addition of antimony(III) chloride in 1 M hydrochloric acid into 0.1 M Na_2H_2(edta) precipitates the complex (1 M=1 mol dm^{-3}). The drop-by-drop addition is essential; if the two solutions are mixed all at once, only H_4(edta) and the hydroxide of antimony(III) are obtained. The complex was partly hydrolized when it was recrystallized from water. The mixed solvent of acetonitrile and water (3:1 v/v) was good for the purpose. The analytical results support the chemical composition: $SbC_{10}H_{17}N_2O_{10}$. Found: Sb, 26.8; C, 27.01; H, 3.78; N, 6.20%. Calcd for $SbC_{10}H_{17}N_2O_{10}$: Sb, 27.23; C, 26.87; H, 3.83; N, 6.27%. Formula weight per 1 mol of edta, Found 453; Calcd, 447.

Sodium Ethylenediaminetetraacetatoantimony(III) Trihydrate: $Na[Sb(C_{10}H_{12}N_2O_8)]\cdot 3H_2O$: This salt was obtained by neutralizing the acid-form complex with a calculated quantity of sodium hydroxide, followed by the evaporation of the water. A more convenient procedure was to mix calculated quantities of Na_4(edta) in an acetic acid–sodium acetate (1:1) buffer, and of antimony(III) chloride. The salt was purified by reprecipitation from water–methanol. Found: Sb, 24.7; C, 24.58; H, 3.76; N, 5.75%. Calcd for $NaSbC_{10}H_{18}N_2O_{11}$: Sb, 25.00; C, 24.66; H, 3.73, N, 5.75%. Formula weight per one mol of edta; Found: 482; Calcd: 487.

X-Ray Measurements. The single crystals of Sb(Hedta)$\cdot$ 2 H_2O were obtained as colorless thin plates, which were stable in open air. As they were too brittle, a crystal 0.3$\times$ 0.1$\times$0.3 mm in size was used for the X-ray measurements without any more reshaping.

Formerly, this crystal was thought to be monoclinic.[8] However, we found that when new axes, a,b, and c, were chosen as follows, the new α,β, and γ were all 90°.

$$\begin{pmatrix} a \\ b \\ c \end{pmatrix} = \begin{pmatrix} 1 & 0 & 1 \\ 0 & -1 & 0 \\ 1 & 0 & 0 \end{pmatrix} \begin{pmatrix} a' \\ b' \\ c' \end{pmatrix}$$

(Where a', b', and c' are former axes of the monoclinic unit cell.[8])

The new space group was confirmed by the results of the reinvestigation of the Weissenberg photographs, as well as the systematic absence of the reflections. Consequently, the results of the present analysis are essentially identical with those of the previous paper,[8] although they are more refined. The crystallographic data are as follows: $SbC_{10}H_{17}N_2O_{10}$, F.W.=447.01, orthorhombic, space group $Pbn2_1$, $Z=4$, $a=10.98(2)$, $b=18.496(4)$, $c=7.341(9)$ Å, $D_x=1.99$, $D_m=1.98(2)$ g cm^{-3}, μ(Mo $K\alpha$)$=19.35$ cm^{-1}.

The reflections within the range of $2\theta<60°$ were collected

by Rigaku automated four-circle diffractometer, applying the ω-2θ scan technique. Independent 1882 reflections with $|F_o|>3\sigma(|F_o|)$ were used for the structure refinement. The intensities were corrected for Lorentz and polarization factors, but no correction was made for the absorption and extinction. All the calculations were carried out on a HITAC 8700/8800 computer at the Computer Center of The University of Tokyo, using the local version of UNICS.[9] The atomic scattering factors, and the corrections for the anomalous scattering of the antimony atom were taken from authentic tables.[10]

Structure Determination. The structure was solved by the heavy-atom method and refined by the block-diagonal least-squares method. The position of the antimony atom was obtained from the three-dimensional Patterson function, while the positions of all the other non-hydrogen atoms were successively located by Fourier syntheses. The positions of the hydrogen atoms were calculated and fixed. Their isotropic temperature factors were all assumed to be 5.0, which was twice the value of the average isotropic temperature factor of the bonded carbon atoms.

In the last cycle of the refinement with anisotropic temperature factors for all non-hydrogen atoms, all the parameter shifts were less than one-third of the corresponding standard deviations. The final R-value was 0.036.[11]

It was difficult to determine the chirality of the crystal from the discrepancy indices. The reversal of the sign of all the z coordinates gave the final R-value of 0.037 after the refinement. Although a slight difference between the final R-values is found between them, it is likely to be within the range of error. Therefore, the former polarity of the crystal was adopted.

The Other Measurements. The infrared spectra of the samples were obtained by means of a JASCO infrared spectrophotometer, type 403G, using Nujol and hexachloro-1,3-butadiene mull.

The Raman spectra of Sb(Hedta)·2 H_2O (crystalline powder packed in a glass capillary tube (ϕ=0.5 mm) were measured by means of a JEOL LASER Raman spectrophotometer, type JRS-409D, using the JLG-A4 argon-ion LASER.

The proton NMR spectra were obtained by means of a JEOL-JNM-MH-100 (100 MHz) NMR spectrometer, using about a 0.2 mol dm^{-3} D_2O solution of samples at 26 °C with DSS (Sodium 3-(trimethylsilyl)-1-propanesulfonate, δ= 0 ppm) and t-butyl alcohol (δ=1.27 ppm downward from DSS) as the internal standards. The carbon-13 NMR were obtained by means of a JEOL C-60-HL spectrometer (15 MHz for ^{13}C-NMR), using a ϕ=8 mm sample tube and using acetic acid and cyclohexane as the external standards. The results were obtained from 32- to 128-times accumulation of the measurements.

The pH of the solution was the direct reading of the pH-meter (HM-5A type Toa Denpa Kogyo); the pD values were not corrected, as the composition of the sample solution was not always simple.

Results and Discussion

The final atomic parameters, except those for hydrogen atoms, are listed in Table 1,[12] the interatomic distances, in Table 2, and the bond angles, in Table 3. The perspective drawing of the complex and the numbering scheme of atoms are shown in Fig. 1, and a projection of the structure along the c-axis, in Fig. 2.

The Sb, N(1), N(2), O(4), and O(6) atoms are almost on a plane; the deviations of these atoms from the calculated best plane are shown in Table 4. The bond angles, N(1)–Sb–N(2), N(1)–Sb–O(4), and N(2)–Sb–O(6), were in the range of 64—77°; however, that of O(4)–Sb–O(6) was 149.6°, almost twice the former ones. This is due to the existence of a lone electron pair in this direction. The small angles of N–Sb–N and N–Sb–O cannot be explained only by the elongated metal–O and metal–N bond lengths compared with those of the first transition-metal edta complexes.

Therefore, the central metal in this chelate is in a

Table 1. Final atomic coordinates ($\times 10^4$) and equivalent isotropic temperature factors (B/Å^2), with the estimated standard deviations of the non-hydrogen atoms

Atom	x	y	z	B_{eq}
Sb	902.0(2)	2382.8(4)	7500	1.9
O(1)	−2361(3)	3274(2)	5469(7)	3.0
O(2)	−991(3)	2513(3)	6626(8)	2.3
O(3)	2635(4)	4702(3)	7034(7)	3.6
O(4)	1717(5)	3770(2)	8353(7)	4.0
O(5)	−766(4)	313(3)	7752(10)	3.6
O(6)	349(4)	1276(2)	8405(7)	3.1
O(7)	4049(4)	1548(4)	5038(10)	4.2
O(8)	2756(4)	2237(3)	6523(7)	2.9
N(1)	947(3)	3213(3)	5021(7)	1.9
N(2)	745(4)	1648(3)	4966(7)	1.9
C(1)	1140(5)	2797(3)	3328(8)	2.1
C(2)	419(5)	2085(3)	3345(7)	2.1
C(3)	−271(4)	3575(3)	5057(8)	2.3
C(4)	−1280(5)	3084(3)	5757(8)	2.1
C(5)	1921(5)	3778(3)	5101(9)	2.6
C(6)	2046(5)	4082(3)	6985(9)	2.6
C(7)	−210(5)	1094(3)	5298(8)	2.5
C(8)	−211(5)	866(3)	7285(9)	2.4
C(9)	1949(5)	1280(3)	4735(8)	2.5
C(10)	3012(5)	1724(3)	5463(9)	2.6
O(W1)	2700(4)	5249(3)	10221(8)	3.4
O(W2)	5328(7)	304(4)	6502(11)	5.9

Table 2. Interatomic distances (l/Å), with the estimated standard deviations in parentheses

Sb–N(1)	2.382(5)	C(3)–N(1)	1.495(7)
Sb–N(2)	2.311(5)	C(5)–C(6)	1.499(9)
Sb–O(2)	2.188(5)	C(5)–N(1)	1.497(7)
Sb–O(4)	2.788(5)	C(7)–C(8)	1.519(9)
Sb–O(6)	2.236(5)	C(7)–N(2)	1.485(7)
Sb–O(8)	2.175(5)	C(9)–C(10)	1.524(8)
O(1)–C(4)	1.256(7)	C(9)–N(2)	1.497(7)
O(2)–C(4)	1.273(8)	N(1)–C(1)	1.477(8)
O(3)–C(6)	1.316(8)	C(1)–C(2)	1.538(8)
O(4)–C(6)	1.214(8)	C(2)–N(2)	1.482(7)
O(5)–C(8)	1.238(8)	O(W1)···O(3)	2.550(8)
O(6)–C(8)	1.227(7)	O(W2)···O(7)	2.902(10)
O(7)–C(10)	1.225(7)	O(W1)···O(5)^{I}	2.714(8)
O(8)–C(10)	1.259(8)	O(W1)···O(1)^{II}	2.764(6)
C(3)–C(4)	1.522(8)	O(W1)···O(W2)^{III}	2.952(10)

Key to symmetry operations: I. $0.5+x$, $0.5-y$, $0.5+z$; II. $-x$, $1.0-y$, $0.5+z$; III. $-0.5+x$, $0.5-y$, $0.5+z$.

Table 3. Bond angles (ϕ/°), with estimated standard deviations in parentheses

N(1)-Sb-N(2)	76.5(2)	C(7)-N(2)-C(9)	109.2(4)
N(1)-Sb-O(2)	74.0(2)	Sb-O(2)-C(4)	118.4(3)
N(1)-Sb-O(4)	64.7(2)	Sb-O(4)-C(6)	110.4(4)
N(1)-Sb-O(8)	79.0(2)	Sb-O(6)-C(8)	119.0(4)
N(2)-Sb-O(2)	76.0(2)	Sb-O(8)-C(10)	120.4(4)
N(2)-Sb-O(6)	71.4(2)	O(2)-C(4)-O(1)	123.5(5)
N(2)-Sb-O(8)	74.4(2)	O(2)-C(4)-C(3)	118.8(5)
O(2)-Sb-O(4)	105.6(1)	O(1)-C(4)-C(3)	117.7(5)
O(2)-Sb-O(6)	86.0(2)	O(4)-C(6)-O(3)	122.6(6)
O(2)-Sb-O(8)	143.7(2)	O(4)-C(6)-C(5)	123.9(5)
O(4)-Sb-O(6)	149.6(2)	O(3)-C(6)-C(5)	113.4(5)
O(4)-Sb-O(8)	83.5(1)	O(6)-C(8)-O(5)	123.4(6)
O(6)-Sb-O(8)	103.8(2)	O(6)-C(8)-C(7)	116.9(5)
Sb-N(1)-C(1)	108.1(3)	O(5)-C(8)-C(7)	119.8(6)
Sb-N(1)-C(3)	104.9(3)	O(8)-C(10)-O(7)	124.5(6)
Sb-N(1)-C(5)	115.8(3)	O(8)-C(10)-C(9)	116.9(5)
C(1)-N(1)-C(3)	112.1(4)	O(7)-C(10)-C(9)	118.6(5)
C(1)-N(1)-C(5)	107.1(4)	N(1)-C(3)-C(4)	113.0(4)
C(3)-N(1)-C(5)	109.0(4)	N(1)-C(5)-C(6)	111.3(5)
Sb-N(2)-C(2)	110.1(3)	N(2)-C(7)-C(8)	110.5(5)
Sb-N(2)-C(7)	109.0(3)	N(2)-C(9)-C(10)	113.0(4)
Sb-N(2)-C(9)	107.0(3)	N(1)-C(1)-C(2)	111.5(5)
C(2)-N(2)-C(7)	109.7(4)	N(2)-C(2)-C(1)	110.5(4)
C(2)-N(2)-C(9)	111.7(4)		
O(W1)···O(3)-C(6)	112.6(4)		
O(W2)···O(7)-C(10)	124.5(5)		
O(3)···O(W1)···O(5)^{I}	119.6(3)		
O(3)···O(W1)···O(1)^{II}	116.7(3)		
O(3)···O(W1)···O(W2)^{III}	97.5(2)		
O(5)^{I}···O(W1)···O(1)^{II}	114.6(3)		
O(5)^{I}···O(W1)···O(W2)^{III}	101.4(3)		
O(1)^{II}···O(W1)···O(W2)^{III}	101.7(2)		
O(7)···O(W2)···O(W1)^{IV}	125.7(3)		

Key to symmetry operations: I. $0.5+x$, $0.5-y$, $0.5+z$; II. $-x$, $1.0-y$, $0.5+z$; III. $-0.5+x$, $0.5-y$, $0.5+z$; IV. $0.5+x$, $0.5-y$, $-0.5+z$.

Table 4. Least-squares planes and the deviations of atoms (l/Å)

Plane(1) [Sb, N(1), N(2), O(4), O(6)]
$0.95973X-0.26305Y-0.098592Z+0.71985=0$
Sb −0.032, N(1) −0.209, N(2) +0.344, O(4) +0.090, O(6) −0.142

Plane(2) [C(3), C(4), O(1), O(2)]
$0.01008X-0.50894Y-0.86074Z+6.56170=0$
C(3) −0.002, C(4) +0.007, O(1) −0.002, O(2) −0.002

Plane(3) [C(5), C(6), O(3), O(4)]
$0.87836X-0.47137Y+0.07936Z+1.15408=0$
C(5) +0.010, C(6) −0.025, O(3) +0.006, O(4) +0.010

Plane(4) [C(7), C(8), O(5), O(6)]
$0.83334X-0.53324Y-0.14557Z+1.83477=0$
C(7) −0.003, C(8) +0.009, O(5) +0.003, O(6) −0.003

Plane(5) [C(9), C(10), O(7), O(8)]
$-0.05604X+0.61186Y-0.78898Z+1.41084=0$
C(9) −0.003, C(10) +0.013, O(7) −0.005, O(8) −0.005

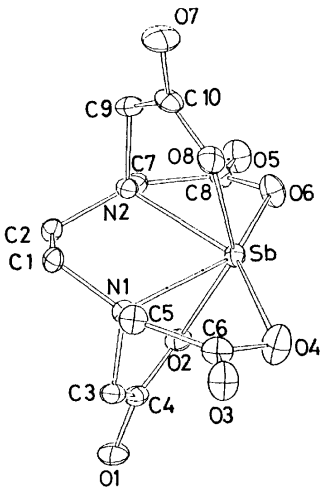

Fig. 1. The perspective drawing of $Sb(Hedta)\cdot 2H_2O$ and the numbering scheme of non-hydrogen atoms.

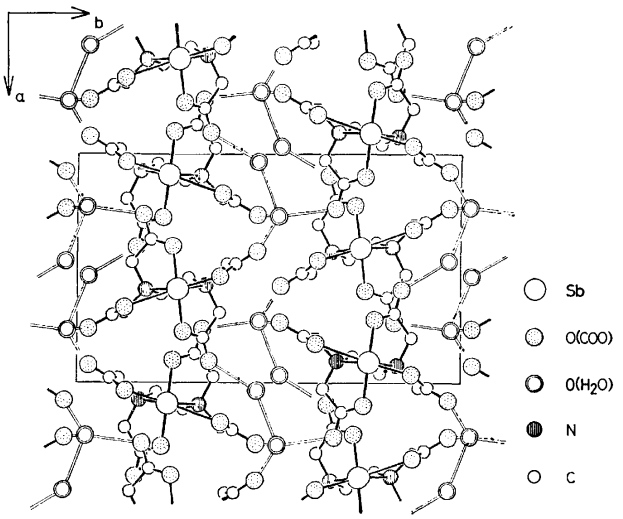

Fig. 2. The projection of the structure along the c axis.
(=: Hydrogen bonding)

ϕ-pentagonal bipyramidal environment. The hepta-coordinated pentagonal bipyramidal structure is found in several edta chelates such as $Rb[Fe^{III}(edta)(H_2O)]\cdot H_2O$,[13] $Sn[Sn^{II}(edta)(H_2O)]\cdot H_2O$,[14] and $[Mg(H_2O)_6][Mg(edta)(H_2O)]\cdot 2H_2O$.[15]

Moreover, such hexa-coordinated metal chelates, *i.e.*, ϕ-hepta-coordinated ones including a lone pair, are also found in the complexes of bivalent group IVB metals or of tervalent group VB metals.[14,17,18] In the cases of tris(oxalato)antimonate(III),[15] and of tris(diphenylthiophosphinato)antimony(III),[16] the lone pair is in the axial direction, which is more desirable from the point of view of VSEPR consideration[19] than the structure of this antimony(III)–edta complex. As the coordinating atoms of an edta cannot occupy all of the five positions of a planar pentagon because of its steric hindrance, the lone-pair electrons seem to occupy the equatorial direction. The O(2)–Sb–O(8) axis bends in the direction opposite to the lone pair, because the repulsion from the lone-pair electrons is stronger than the other bonding-pair ones. The Sb–

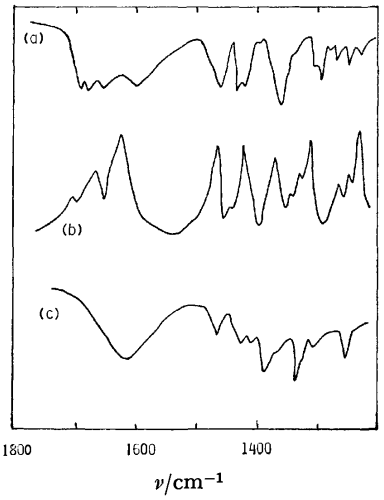

Fig. 3. Infrared (a), and Raman (b) spectra of (hydrogen ethylenediamine-*N*,*N*,*N*′,*N*′-tetraacetato)antimony(III) dihydrate, and infrared spectra of its sodium salt (c).

O(2) and Sb–O(8) bonds make angles of 65.7, and 74.4° respectively with respect to the average Sb–N(1)–N(2)–O(4)–O(6) plane.

Antimony(III), generally, does not make a strong bond with a nitrogen atom of amines. As antimony(III) has a strong affinity to a hydroxo group, when some amine is added, it reacts with the hydroxo group produced by the hydrolysis of an amine, except under a strictly dry medium. The Sb–N distances of this complex are shorter than that of the $SbCl_3$–aniline adduct (2.525 Å),[20] and the Sb–N bond of this edta complex is stronger than that of the common antimony(III)–amine complexes.

With respect to the bond lengths of Sb–O and of C–O, there are two types of carboxyl groups in the chelate: Type 1: the bond lengths of Sb–O(2), Sb–O(6), and Sb–O(8) are in the range of 2.18 and 2.24 and are normal.[17,21–26] The difference between the two C–O bond lengths of each carboxyl group of this type is in the range of 0.02 and 0.04 Å, like the usual ionized carboxyl group.[27a] Type 2: Sb–O(4) distance, 2.79 Å, is out of the ordinary. The C(6)–O(3) is longer than C(6)–O(4) by 0.10 Å, which is comparable with the value of a free carboxylic acid. Therefore, this type of carboxyl group is likely to be in a free-acid form, coordinating to an antimony atom with its carbonyl oxygen atom. This type of coordination seems to cause the especially strong acidity of Sb(Hedta) ($pK_a=1.02$).[4] Of all the carboxyl groups, the Type 2 group has the largest deviations from the best plane, as is shown in Table 4. This phenomenon is also found at the coordinated-acid-form carboxyl group in $[Cu(H_2edta)(H_2O)]$.[28]

One of the crystalline water oxygen atoms, O(W1), forms a hydrogen bond with O(3) of the Type 2 carboxyl group. This O(3)–H···O(W1) distance is 2.55 Å, and it agrees with that of a hydrogen bond between a water and an acid.[27b] The other hydrogen bonds of the crystalline-water oxygens are those between O(W1)···O(5)^{I}, O(W1)···O(1)^{II}, O(W1)···O(W2)^{III}, and O(W2)···O(7), as is shown in Table 2 and Fig. 2, where O(1), O(5), and O(7) are all Type 1 carboxyl-group oxygen atoms.

The infrared and Raman spectra of the complex have essentially the same absorption bands; almost all peaks of the infrared spectra were recognized also in its Raman spectra between 200 and 4000 cm^{-1}. The spectra between 1200 and 1800 cm^{-1} are shown in Fig. 3. In the case of $Sb(Hedta)\cdot 2H_2O$, the ν_{as}(COO) peak in the infrared spectra splits into 4 peaks, and that in the Raman spectra, into 3 peaks.

The band at 1693 cm^{-1} of the infrared spectra (1702 cm^{-1} in Raman spectra) shows the existence of a free carboxyl group, while the 1677 and 1651 cm^{-1} bands of the infrared spectra (1667 cm^{-1} band of the Raman spectra) are those of the coordinated carboxyl groups; both of them are ν_{as}(COO) bands. Although some additional splitting is recognized in the spectra of this region, it is probably due to the difference in the effects on each carboxyl group of its coordination bond, its position in the ψ-pentagonal bipyramidal configuration, and the hydrogen bonds of crystalline waters around it.

According to Nakamoto[29b,c] and Sawyer,[30–32] the ν_{as}(COO) band of metal-edta chelates appears at about 1650 cm^{-1}, when the coordinate bond is a rather covalent-dominant one. As has been shown above, the wave numbers of the band of the Sb–edta complex are higher than those of typical covalent-dominant edta complexes, such as Cr(III) (1640 cm^{-1}), Co(III) (1645 cm^{-1}), and Th(IV) (1630 cm^{-1}).[32]

The sodium salt of the antimony(III)–edta complex has a broad ν_{as}(COO) band at about 1630 cm^{-1}, lower than that of the free-acid-type complex. This effect is due to the more ionic character of the Type 2 carboxyl group in this salt.

Like the edta complexes of other metals,[29c,30–32] four bands in the 1302—1470 cm^{-1} region, which are likely ν_s(COO) or its mixing bands, were observed in the infrared as well as in the Raman spectra.

In the far-infrared region, the band near 240 cm^{-1} is tentatively assigned as the ν(Sb–O) band, and those in the 370—390 cm^{-1} region, as the ν(Sb–N) modes, by analogy to the amino-acid complexes of several metals.[29a]

This antimony(III)–edta complex can also exist even in an aqueous solution of a limited pH region, in spite of the tendency of the common antimony(III) salt to be easily hydrolyzed, a fact which is proved by the NMR spectral data to be shown below.

In the cases of covalent-dominant edta complexes, such as Co(III)–,[33] Zr(IV)–,[34] and Hf(IV)–edta,[34] the AB pattern was observed in their ^{1}H-NMR spectra due to the fixation of the ligand. In the case of the Bi(III)–edta complex, as well as of the Sb(III)-*trans*-1,2-cyclohexanediamine-*N*,*N*,*N*′,*N*′-tetraacetic acid complex, both of them can be expected to have a structure very near to that of the antimony(III)–edta complex, and the acetato-proton peak splits into an AB-pattern quartet due to the spin-spin coupling of geminal protons, as the nitrogen atoms of the ligand in these complexes bond tightly with the central metal. The typical ^{1}H-NMR spectra of $Sb(Hedta)\cdot 2H_2O$ in an aqueous solution containing a sodium acetate–

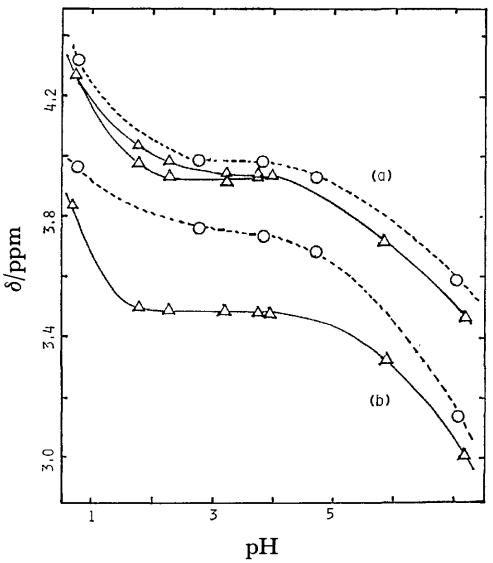

Fig. 4. Chemical shifts of acetato (a), and ethylene (b) protons of Sb(Hedta) complex (—○--) compared with those of sodium salt of edta (—△—) in D_2O solution. (δ: DSS=0, downwarp +) (pH shown is the reading of a pH meter; correction for D_2O was not applied).

acetic acid buffer show two peaks; one for the acetato-protons, and the other for ethylene-protons of the ligand. The acetato-proton peak clearly splits into two or more peaks in the pH region of 1.5—3.5, with a splitting of 3 Hz. The ethylene-proton peak also seems to have some fine structure when the pH of the solution is in the same region. However, the splitting is too small to be identified clearly.

The relations between the pH of the solution and the chemical shifts of acetato- and ethylene-protons of the ligand in the antimony(III)–edta complex are shown in Fig. 4. As is shown in the figure, when the pH of the solution was between 1.5—3.5, the chemical shifts of both peaks, especially those of the ethylene-protons, are different from those of the sodium salt of edta. This fact seems to show that the edta ligand in the antimony(III)–edta complex bonds with the metal atom only in the 1.5—3.5 pH region. This fact coincides with the result of a potentiometric titration study by Özer.[4]

When disodium salt of edta is added to the solution of the antimony(III)–edta complex in the pH region of 1.5—3.5, a new peak due to the ethylene-proton of the $[H_2(edta)]^{2-}$ ion appears, in addition to the original two peaks of the antimony complex (The acetato-proton peak of the excess salt could not be recognized; it is probably due to the accidental overlapping of the peaks of the antimony complex with that of the disodium salt.) From this fact, it can be said that the edta ligand in the antimony complex does not exchange with the free ligand ion in the aqueous solution of this pH region; this is a proof of the strong covalent character bond between the ligand and the central metal atom of the complex.

Although the ^{13}C-NMR of the acid-type complex Sb(Hedta) could not be measured by our spectrometer because of its low solubility, its sodium salt was examined by the technique. The peak for its carboxyl carbons, 176.6; for ethylene carbons, 62.0: for acetato-methylene carbons, 57.0 (δ ppm, downward from TMS). No splitting of the carboxyl carbon peak was found. The ethylene and acetato methylene carbon peaks of the antimony complex shift to a lower magnetic field than the tetra- and disodium salts of the free ligand. (Na_4(edta): 181.0, 60.4, and 53.5; Na_2H_2(edta): 171.5, 58.9, and 52.5 ppm, respectively, for carboxyl, ethylene, and acetato-methylene carbons.) As the chemical shifts of both types of ligand carbons are very different from those of the free ligand, it is likely that the edta ligand in this complex does not dissociate from the central antimony(III) atom, not even in the aqueous solution. The chemical shifts of the carboxyl carbons in some metal-edta complexes were shown by Hagen and others.[35] Compared with their data, the resonances of the carbon atoms of the antimony(III)–edta chelate appear in a relatively higher magnetic field than the corresponding peaks of common edta complexes.

The authors greatly appreciate the help of Dr. Akiko Kobayashi for the X-ray diffractometer measurements, performed under the guidance of Professor Yukiyoshi Sasaki, The University of Tokyo. A part of this work was supported by a Grant-in-Aid for Scientific Research of the Ministry of Education, Science and Culture.

References

1) M. M. Privalova and R. Ryabenhikov, *Zh. Neorg. Khim.*, **7**, 2537 (1962).
2) T. R. Bhat and R. K. Iyer, *Z. Anorg. Allg. Chem.*, **335**, 331 (1965).
3) T. R. Bhat, R. K. Iyer, and J. Shankar, *Z. Anorg. Allg. Chem.*, **343**, 329 (1966).
4) U. Y. Özer and R. F. Bogucki, *J. Inorg. Nucl. Chem.*, **33**, 4143 (1971).
5) R. K. Iyer and J. Shankar, *Indian J. Chem.*, **10**, 97 (1972).
6) S. Takamoto, *Nippon Kagaku Zasshi*, **76**, 1339 (1955).
7) I. M. Yurist, *Zavodsk Lab.*, **32**, 1050 (1966); *Chem. Abstr.*, **66**, 25750 (1967).
8) I. Kita, T. Uehiro, T. Iwamoto, A. Ouchi, and Y. Yoshino, *Chem. Lett.*, **1976**, 333.
9) The Universal Crystallographic Computation Program System (UNICS), ed by T. Sakurai, Crystallographic Society of Japan, Tokyo (1967).
10) "International Tables for X-ray Crystallography," Kynoch Press, Birmingham, U. K. (1974), Vol. IV.
11) $R=\sum||F_o|-|F_c||/\sum|F_o|$.
12) The final coordinates, including those of hydrogen atoms, their thermal parameters, and the final F_o—F_c table, are kept at the Chemical Society of Japan as Document No. 8031.
13) M. D. Lind and J. L. Hoard, *Inorg. Chem.*, **3**, 34 (1964).
14) F. P. van Remoortere, J. J. Flynn, F. P. Boer, and P. P. North, *Inorg. Chem.*, **10**, 1511 (1971).
15) A. I. Pozhiaev, T. N. Polynova, M. A. Porai-Koshit, and V. A. Logvinenko, *Zh. Strukt. Khim.*, **14**, 746 (1973).
16) M. J. Begley, D. B. Sowerby, and I. Haiduc, *J. Chem. Soc., Chem. Commun.*, **1980**, 64.
17) M. C. Poore and D. R. Russell, *J. Chem. Soc., D*, **1971**, 18.

18) S. L. Lawton and G. T. Kokotailo, *Nature*, **221**, 550 (1969).
19) R. J. Gillespie and R. S. Nyholm, *Quart. Rev.*, **11**, 339 (1957).
20) R. Hulme and J. C. Struton, *J. Chem. Soc., A*, **1968**, 2448.
21) G. A. Kiosse, N. I. Golovastikov, and N. V. Belov, *Dokl. Akad. Nauk. SSSR*, **155**, 545 (1964).
22) K. Yokoho, K. Matsumoto, S. Ooi, and H. Kuroya, *Bull. Chem. Soc. Jpn.*, **49**, 1864 (1976).
23) M. E. Gress and R. A. Jacobson, *Inorg. Chim. Acta*, **8**, 209 (1974).
24) Y. Nakayama, K. Matsumoto, S. Ooi, and H. Kuroya, *Bull. Chem. Soc. Jpn.*, **50**, 2304 (1977).
25) B. Aurivillius and C. Särnstrand, *Acta Chem. Scand., Ser. A*, **30**, 232 (1976).
26) I. Hansson, *Acta Chem. Scand.*, **22**, 509 (1968).
27) A. F. Wells, "Structural Inorganic Chemistry," 4th ed, Clarendon Press, Oxford, U.K. (1975), a) p. 731, b) p. 304.
28) F. S. Stephens, *J. Chem. Soc., A*, 1969, 1723.
29) K. Nakamoto, "Infrared Spectra of Inorganic and Coordination Compounds," 3rd ed, Wiley, New York (1978), a) p. 307, b) p. 232, c) p. 305.
30) D. T. Sawyer and P. J. Paulsen, *J. Am. Chem. Soc.*, **80**, 1597 (1958).
31) D. T. Sawyer and P. J. Paulsen, *J. Am. Chem. Soc.*, **81**, 816 (1959).
32) D. T. Sawyer and J. M. McKinnie, *J. Am. Chem. Soc.*, **82**, 4191 (1960).
33) J. L. Sudmeier, A. J. Senzel, and G. L. Blackmer, *Inorg. Chem.*, **10**, 90 (1971).
34) Y. O. Aochi and D. T. Sawyer, *Inorg. Chem.*, **5**, 2085 (1966).
35) R. Hagen, J. P. Warren, D. H. Hunter, and J. D. Roberts, *J. Am. Chem. Soc.*, **95**, 5721 (1973).

The Determination of Kojic Acid Using the Stopped-flow Method†

Hiroshi TANIGAKI, Hitoshi OBATA,* and Tai TOKUYAMA
Department of Chemistry, Faculty of Engineering, Kansai University, Suita, Osaka 564
(Received March 12, 1980)

A kinetic method of the determination of kojic acid with 2,6-dichlorophenolindophenol(DCIP) is described. The oxidized form of DCIP, reacting with kojic acid, changes to the colorless reduced form of DCIP. By spectrophotometrically measuring the rate of discoloration, the apparent first-order rate constant, k_{app}, and the second-order rate constant, k, were obtained. The determination of kojic acid in the fermentation medium is possible by using k the constant, even in the presence of various organic substances.

Recently, kojic acid has attracted considerable attention in the food industry because it can be used as a starting material for synthesizing maltol and ethylmaltol, which are flavor enhancers of foods. It is often necessary to determine exactly the kojic acid which is produced in a fermentation medium. The colorimetric analysis of kojic acid with ammonium iron(III) sulfate has been widely used as a standard method[1–6] for the determination of kojic acid in a fermentation medium because of its simplicity and convenience, however, it involves some drawbacks in that it is susceptible to interference by the turbidity or color of the samples. Recently, the reaction of reductones with 2,6-dichlorophenolindophenol(DCIP) has been studied by Hiromi *et al.*,[7] Tonomura *et al.*,[8] and our laboratory[9–13] using the stopped-flow method, and its application to the determination of L-ascorbic acid and triose reductone has been suggested, since kojic acid is a pseudo-reductone whose redox behavior is quite similar to that of L-ascorbic acid.

Experimental

Materials. The DCIP is obtained from the Merck Chemical Co. Kojic acid was produced by the fermentation method using *Aspergillus oryzae* M-128.[14] It was purified by sublimation *in vacuo* at 130 °C. The other reagents used were of an analytical grade purchased from Wako Pure Chemical Industries, Ltd.

Measurement of the Rate Constant. The apparatuses used in this study were a Hitachi spectrophotometer Model 101 with a mixing injector and a Towa Model EPR-10A recorder. The reduction of DCIP was followed by measuring the absorbance at 525 nm,[13] the light path of the cell being 10 mm. The reactions were performed at 25 °C in a 0.2 mol dm^{-3} acetate buffer or a 0.2 mol dm^{-3} sodium phosphate buffer containing both 0.2 mol dm^{-3} sodium chloride and 5% 1-butanol, the DCIP was dissolved in distilled water containing 0.2 mol dm^{-3} sodium chloride and 5% 1-butanol. The concentration of the DCIP was kept at less than 5% of the concentration of kojic acid. The DCIP solution was prepared a fresh daily. All the kinetic results presented are the average of three measurements.

Results and Discussion

If we consider that the reaction of kojic acid with DCIP proceeds in a way similar to that of L-ascorbic acid, the reaction can be expected to obey the following second-order kinetics:

$$-d[\text{DCIP}]/dt = k[\text{kojic acid}][\text{DCIP}] = k_{app}[\text{DCIP}]$$

where [kojic acid] and [DCIP] represent the concentrations of kojic acid and DCIP respectively. When [kojic acid] is greatly in excess of [DCIP], k_{app} is the apparent first-order rate constant and k_{app} equals k times the initial concentration of kojic acid.

Reaction Curve of the Reaction of Kojic Acid with DCIP. Figure 1 shows the reaction curve of the reaction of kojic acid with DCIP. The reduction of DCIP was followed by the disappearance of the color at 525 nm for DCIP. In the initial stage of the reaction, a dead time due to the apparatus was observed. The apparent first-order rate constant(k_{app}) can be calculated from the absorbance changes by means of the following equation:[15]

$$\ln (A_0 - A_\infty / A_X - A_\infty) = k_{app}t$$

where A_0, A_X, and A_∞ represent the absorbances at $t=0$, X, and ∞ (the termination of the reaction) respectively. The first-order plot is linear, as is shown in Fig. 2. The apparent first-order rate constant, k_{app}, was obtained from the slope of the plot.

k-pH *Profile.* Figure 3 shows the pH dependence of the second-order rate constant, k. The second-order rate constants were obtained by dividing the k_{app} by the concentration of kojic acid. A maximum was observed in the acidic region (pH 6.0—6.5) for fast reactions. A bluff was observed at pH 7.0 for slow reactions. The k at pH 6.3 was about 5 times as large as that at pH 8.0. The half-time of the reaction, $t_{1/2}$, was 47.9 s for the kojic-acid concentration of 12.5 mmol dm^{-3} at pH 6.3. The plot of log k

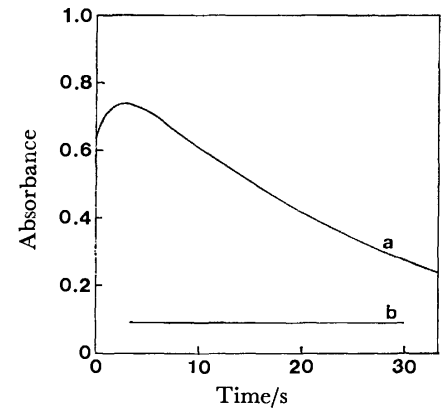

Fig. 1. Reaction curve of the reaction of kojic acid with DCIP at 25 °C.
pH 6.0, 10 mm cell, 525 nm, [kojic acid]=100 mmol dm^{-3}, [DCIP]=200 μmol dm^{-3}. a: Reaction signals, b: signals of the termination of reaction.

† This work was presented at the ACS/CSJ Chemical Congress, Honolulu, April 1979.

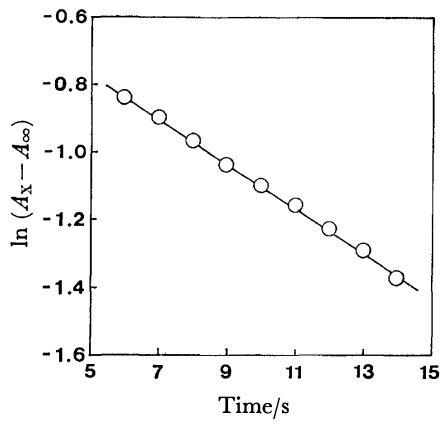

Fig. 2. First-order plot of the reaction of kojic acid with DCIP at 25 °C.
The experimental conditions were the same as in Fig. 1. A_X and A_∞ indicate the values of absorbances at time=X and ∞ (the termination of reaction). It was obtained from the slope of the plot that k_{app} was 6.81×10^{-2} s^{-1}.

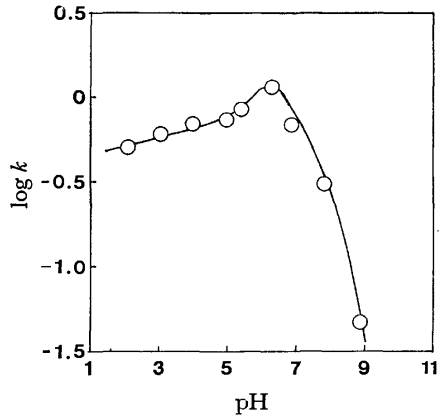

Fig. 3. The pH dependence of the second-order rate constants of the reaction of kojic acid with DCIP at 25 °C.
[Kojic acid]=12.5 mmol dm^{-3}, [DCIP]=200 μmol dm^{-3}, the ionic strength of the buffer solution was 0.10.

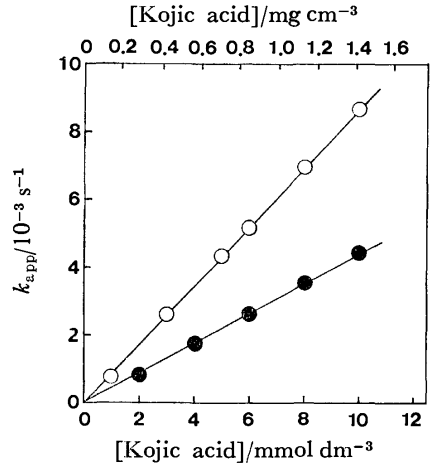

Fig. 4. Proportionally between k_{app} and kojic acid concentration at 25 °C.
[DCIP]=200 μmol dm^{-3}, ●: pH 4.0, ○: pH 6.0.

TABLE 1. EFFECTS OF VARIOUS ADDED SUBSTANCES ON THE k OF THE REACTION OF KOJIC ACID WITH DCIP AT 25 °C

Added substance	k / mol dm^{-3} s^{-1}	Relative rate constant
None	1.18	1.00
Glycine	1.13	0.96
L-Phenylalanine	1.18	1.00
L-Tryptophan	1.20	1.02
Malic acid	1.19	1.01
Succinic acid	1.19	1.01
Fructose	1.21	1.03
Glucose	1.13	0.96
Sucrose	1.19	1.01
$FeCl_3 \cdot 6H_2O$	38.6	32.7
$MgCl_2 \cdot 6H_2O$	1.21	1.03
$ZnCl_2$	1.18	1.00

pH 6.3, [kojic acid]=12.5 mmol dm^{-3}, [DCIP]=200 μmol dm^{-3}, [Added substance]=12.5 mmol dm^{-3}.

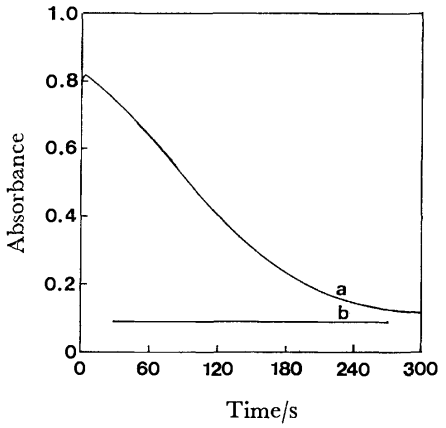

Fig. 5. Reaction curve of the reaction of DCIP with kojic acid in the fermentation medium at 25 °C. pH 6.0, [DCIP]=200 μmol dm^{-3}. a: Reaction signals, b: signals of the termination of reaction. The growth medium were glucose (10.0 g), $MgSO_4 \cdot 7H_2O$ (0.05 g), KH_2PO_4 (0.1 g), and bonito extract (0.25 g). The culture was shaken on a rotary shaker for 72 h at 25 °C.

against the pH is different from that obtained for the reaction of L-ascorbic acid with DCIP. These results suggest that the reaction mechanism of kojic acid with DCIP is considerably different from that of L-ascorbic acid over a wide pH range.

Calibration Curve of Kojic-acid Determination. Figure 4 shows the proportionality between k_{app} and the kojic-acid concentration at pH 4.0 and 6.0. It gives a straight line, suggesting the possibility of applying the reaction to the determination of kojic acid. The determination of kojic acid using the stopped-flow method was possible, even in the pH 2—7 region and in concentrations from 1 to 100 mmol dm^{-3}.

Effects of Various Substances. Table 1 shows the effects of various substances often encountered in kojic-acid determination; amino acids, organic acids, sugars, and metal ions were tested. The results show that

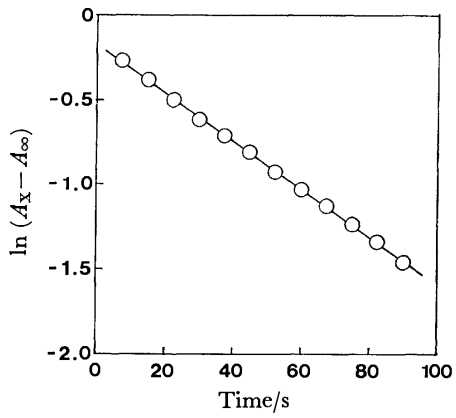

Fig. 6. First-order plot of the reaction of DCIP with kojic acid in the fermentation medium at 25 °C. The experimental conditions were the same as in Fig. 5. It was obtained from the slope of the plot that k_{app} was 1.41×10^{-2} s^{-1}.

most additives, except for iron(III) chloride, do not interfere with the determination of kojic acid. The iron(III) chloride, however, reacted with kojic acid.[1)]

Analysis of Kojic Acid in the Fermentation Medium. The growth medium of the mold strain of *Aspergillus* was prepared with glucose (10.0 g), $MgSO_4 \cdot 7H_2O$ (0.05 g), KH_2PO_4 (0.1 g), and bonito extract (0.25 g). The culture was shaken on a rotary shaker for 72 h at 25 °C. Figure 5 shows the results of the analysis of the kojic-acid fermentation medium containing various substances. The apparent first-order rate constant (k_{app}) was obtained from the slope of the apparent first-order plot of Fig. 6. In this method, the kojic-acid concentration in broth was determined to be 18.0 mg cm^{-3}. By the colorimetric method, the amount of kojic acid was determined to be 18.3 mg cm^{-3}. The analytical data obtained by the stopped-flow method is in fair agreement with the colorimetric data. The determination of kojic acid using the stopped-flow method may be recommended for use with colored and turbid samples such as the fermentation medium of molasses.

We wish to thank Professor Keitaro Hiromi, Department of Food Science and Technology, Faculty of Agriculture, Kyoto University, and Professor Masanosuke Takagi, College of Agriculture, University of Osaka Prefecture, for their valuable advice on the stopped-flow measurement of the reaction rate of kojic acid.

References

1) K. Sakaguchi, *Nippon Nōgeikagaku Kaishi*, **6**, 400 (1930).
2) H. R. V. Arnstein and R. Bentley, *Biochem. J.*, **54**, 508 (1953).
3) C. Tatsumi and M. Ameyama, *Nippon Nōgeikagaku Kaishi*, **28**, 274 (1954).
4) C. Tatsumi, M. Ameyama, and J. Gōda, *Nippon Nōgeikagaku Kaishi*, **28**, 279 (1954).
5) Chas. Pfizer and Co., "Kojic Acid," Data Sheet No. 502 (1956).
6) S. Kawate, M. Koike, and T. Fukuo, *Tech. Reports of Kansai Univ.*, **12**, 67 (1971).
7) K. Hiromi, H. Fujimori, J. Yamaguchi-Ito, H. Nakatani, M. Ohnishi, and B. Tonomura, *Chem. Lett.*, **1977**, 1333.
8) B. Tonomura, H. Nakatani, M. Ohnishi, J. Yamaguchi-Ito, and K. Hiromi, *Anal. Biochem.*, **84**, 370 (1978).
9) H. Obata, M. Tatsuno, T. Tokuyama, Y. Nitta, M. Takagi, and K. Hiromi, *Agric. Biol. Chem.*, **43**, 1021 (1979).
10) H. Obata, M. Tatsuno, T. Tokuyama, Y. Nitta, M. Takagi, and K. Hiromi, *Agric. Biol. Chem.*, **43**, 1025 (1979).
11) H. Obata, M. Tatsuno, T. Tokuyama, Y. Nitta, M. Takagi, and K. Hiromi, *Agric. Biol. Chem.*, **43**, 2191 (1979).
12) K. Shikata, H. Tanigaki, H. Obata, and T. Tokuyama, *Tech. Reports of Kansai Univ.*, **20**, 97 (1979).
13) H. Tanigaki, H. Obata, and T. Tokuyama, *Tech. Reports of Kansai Univ.*, **21**, 113 (1980).
14) K. Saito, *Bot. Mag. Tokyo*, **21**, 249 (1907).
15) K. Hiromi, "Kōsohannōkaiseki No Jissai," Kōdansha, Tokyo (1978), p. 50.

Hypochlorite Oxidation of Ammonia. Effective Removal of Ammonia from Waste Water by UV-irradiation[1)]

Makoto KIMURA, Teiichi SUZUKI, and Yoshiro OGATA*

Department of Applied Chemistry, Faculty of Engineering, Nagoya University, Chikusa-ku, Nagoya 464

(Received March 14, 1980)

The hypochlorite oxidation of ammonia giving rise to nitrogen evolution was carried out in the dark or under irradiation in order to study the reaction mechanism and application to waste water treatment. UV-irradiation accelerates remarkably the rate of decomposition of unfavorable chloramines. The acceleration covers the pH region 2—12, where corresponding dark reactions are slow. The irradiation also affects the formation of by-products such as NO_2^- and NO_3^-, the effect being a slight increase in NO_2^- formation in the pH range 2—12. These results suggest an effective industrial application to avoid eutrophication in seas and lakes. The irradiation effect is discussed in relation to reaction mechanism, in which the irradiation possibly facilitates the N–N bond formation after chloramine formation.

Hypochlorite salt, especially sodium hypochlorite, oxidizes ammonia or ammonium ion in water. Though the oxidation is useful for hydrazine synthesis, it usually leads to rapid and quantitative evolution of nitrogen in the presence of excessive oxidant.

$$2NH_3 + 3NaOCl \longrightarrow N_2 + 3H_2O + 3NaCl \quad (1)$$

Another industrial application has recently been worked out for waste water treatment.[2–4)] Ammonia together with related nitrogen compounds brings about serious eutrophication in seas and lakes, so that an effective industrial plan is required. This hypochlorite oxidation of ammonia is called break-point chlorination.[2–4)] Generally, the oxidation rate is not high enough at low NH_3 concentration as observed in ordinary waste water, so that unfavorable chlorinated products such as NH_2Cl, $NHCl_2$, and NCl_3 remain, depending on the pH as well as relative dosage of the oxidant to NH_3.[2)] As regards the elimination of chloramines, the active carbon is proposed because of its industrial availability.[4)]

On the other hand, hypochlorites are susceptible to light, decomposing to oxygen and chlorate along with chloride ion.[5)] Studies in this laboratory have shown that irradiation with hypochlorite enables complete oxidation of several organic substances which otherwise cannot be attained.[6–8)] This article describes the effect of irradiation in the hypochlorite oxidation of ammonia, and the influencing factors such as pH and the molar ratio of hypochlorite to ammonia. A probable mechanism is discussed.

Experimental

Materials. Sodium hypochlorite was prepared by taking into account the dissociation constant for HOCl.[9)] Into ice-cooled 0.20 M (1 M=1 mol dm^{-3}) aqueous NaOH (1 l) was absorbed commercial chlorine gas until the solution showed 0.10 M by iodometry and pH 10 with a glass-electrode. After its pH was adjusted to 12 by addition of NaOH, the solution was stored in a refrigerator (stable at least for several months). An ammonia solution was prepared by dissolving a weighed amount of ammonium sulfate in distilled water. Buffer solutions except for preliminary experiments were prepared by mixing each 0.02 M phosphoric, boric and acetic acids with an appropriate amount of 0.10 M NaOH (Britton-Robinsons' buffer solution). Analytical reagents were used.

Instruments. UV and visible absorption measurements were carried out on a Hitachi 124 spectrophotometer in 1 cm cells. UV-irradiation reactions were conducted in a vessel equipped with a Halos 100 W high-pressure mercury lamp. Gas chromatograms were taken on a Yanaco 550 using a column of Molecular Sieves 5A.

Analysis. Iodometric titration was carried out according to the usual procedures to determine residual concentrations of oxidants such as $OCl^-/HOCl$, Cl_2, NH_2Cl, $NHCl_2$, NCl_3, and NO_2^-/HNO_2, but not NO_3^-/HNO_3 nor $ClO_3^-/HClO_3$. Rapid titration was carried out for the sake of clear end point, since slow air oxidation causes regeneration of HNO_2.

Ammonia was determined by Nessler's method according to JIS K 0101-1976. In order to attain distinct coloration, the resulting solution should be adjusted to pH 12. The calibration curve was based on the absorbance at 450 nm, its apparent molar coefficient being 1.6×10^3 in the range 0.10—0.50 mM ammonia.

Concentrations of NO_2^-/HNO_2 and NO_3^-/HNO_3 were determined by Gries' method involving diazotization of acidified aniline and the subsequent azo-dye development with 1-naphthylamine. The determination involves the reduction of HNO_3 to HNO_2 after elimination of HNO_2. Both procedures were carried out according to JIS K 010-1976.

Dark Reaction. Examination of breakpoint was carried out in buffered 2.0 mM ammonia solutions of pH 9.5, 7.9, 7.3, 6.9, 5.1, 2.6, and 1.6 by adding an appropriate amount of aqueous NaClO. After 15 min, concentrations of residual active chlorine were determined iodometrically.

The influence of pH on reaction rate was examined as follows. To a solution of 20 mM NH_3 (10 ml) mixed with a buffer solution (80 ml) was added 25, 30, or 35 mM aqueous NaClO (10 ml) with stirring. The reaction solution was kept standing in the dark for 1 h, and an aliquot (10 ml) was titrated iodometrically. The results are given in Table 1.

Identification of chloramines formed initially is based on the following UV spectra; absorption max. (ε) OCl^-, 292 nm(392); HOCl, 235 (105); Cl_2, 315 (34); NH_2Cl, 245 (416); $NHCl_2$, 297 (265); NCl_3, 340 (255).[10)] The acidity constant of HOCl and hydrolysis constant of Cl_2[9)] were taken into consideration for assigning the species in the reaction solutions.

Irradiation Reaction. Irradiation was carried out at room temperature in the air. For the product analysis of evolved gas, it was performed under helium with the system connected to a gas burette. For detection of ClO_3^-, zinc powder reducing ClO_3^- to Cl^- was added to the ir-

Table 1. Residual active chlorine[a] in dark reactions[b]

[Ox] (mM) / [NH_3] (mM)		2.5/2.0	3.0/2.0	3.5/2.0
pH[c]	12	2.22	1.55	1.81
	11	1.93	0.95	0.65
	10	1.43	0.25	0.30
	9	1.34	0.35	0.20
	8	1.26	0.70	0.04
	7	1.18	0.85	0.00
	6	1.51	1.30	0.30
	5	1.76	1.55	0.00
	4	1.81	1.00	0.50
	3	1.88	1.70	2.30
	2	1.86	1.81	2.35

a) Concentration; mM. b) Reaction time; 1 h at 30 °C. c) Britton-Robinsons' buffer solution.

radiated solutions adjusted at pH 5, and the concentration of resulting Cl^- was determined by colorimetry of iron(III) thiocyanate after addition of ammonium iron(III) sulfate and mercury(II) thiocyanate. The color development was checked with ClO_3^- solutions, and calibrated with standard Cl^- solutions.

Comparative experiments between dark and irradiation reactions were carried out as follows. A buffer solution (320 ml) was mixed with a 20 mM NH_3 solution (40 ml) and 25 or 30 mM aqueous NaClO (40 ml) was added with stirring. Half of the resulting solution was irradiated for 5—20 min until the iodometric titer became constant. Aliquots were diluted to an appropriate concentration and adjusted to neutral to make test solutions for analysis of NH_3, NO_2^-, and NO_3^-. Their standard calibration curves were checked from time to time. The other half of the solution was kept standing in the dark for 5—10 d in a stoppered flask, then worked up by a similar analytical procedure. The results are given in Table 2.

UV absorptions of species: NO_2^-, 354 nm (ε 23); HNO_2, 371 (44); NO_3^-, 357 (12); HNO_3, 371 (19). Supplementary irradiation of 5.0 mM NH_3 was conducted in the presence of $NaNO_2$ (5.0 mM) or $NaNO_3$ (5.0 mM) at various pH for 1 h, no significant decrease being observed in the concentration of NH_3, NO_2^-, nor NO_3^-.

Results

Dark Reaction. At 2 mM concentration of ammonia, the dark reaction of ammonia with hypochlorite proceeds rapidly to a considerable extent at room temperature. The change is readily followed by iodometric titration, on addition of an appropriate amount of aqueous sodium hypochlorite to buffered ammonia solutions. Studies on breakpoint chlorination show that a plot of residual active chlorine *vs.* the amount of the oxidant added gradually reaches a maximum and then drops sharply to a minimum (breakpoint), increasing again.[2-4] The breakpoint lies at the molar ratio 3/2, hypochlorite (Ox) to ammonia (Ox/NH_3), or slightly above, which corresponds to Eq. 1. The reaction was examined over a wide range of pH at a reaction time of 15 min. Such a breakpoint was observed in the pH range 4—8. However, a solution at pH>8 and pH<4 gave no breakpoint. A curve for pH 9.5 is located at a little lower than the expected line for no ammonia oxidation. At pH 2.6, a slightly distinct minimum was observed at about 2.0 of Ox/NH_3.

In order to examine the influence of H on residual

Table 2. Comparison between dark and irradiation reactions[a]

[Ox] (mM) / [NH_3] (mM)	pH	Dark (mM)			Irradiation (mM)		
		$[NH_3]\times10$	$[NO_2^-]\times10^2$	$[NO_3^-]\times10$	$[NH_3]\times10$	$[NO_2^-]\times10^2$	$[NO_3^-]\times10$
2.5/2.0	12	7.3	0.2	0.2	4.0	6.4	0.2
	11	6.8	0.4	0.4	4.7	5.6	0.3
	10	6.8	0.4	0.9	4.0	2.4	0.2
	9	5.8	0.3	0.5	3.8	3.3	0.4
	8	6.5	0.1	2.3	4.3	2.0	0.4
	7	6.8	0.1	1.4	3.7	2.0	0.3
	6	5.8	0.1	2.3	0.3	2.0	0.4
	5	6.5	0.1	1.7	3.2	2.7	0.9
	4	6.5	0.3	1.1	4.5	2.5	0.8
	3	6.5	0.1	0.5	5.7	0.7	1.4
3.0/2.0	12	3.2	12.7	0.5	3.8	19.5	0.6
	11	2.1	0.0	0.5	3.9	10.5	0.5
	10	1.9	0.0	0.8	2.8	6.0	0.3
	9	2.2	0.0	1.8	3.0	7.0	0.4
	8	1.6	0.0	1.9	2.4	7.0	0.5
	7	1.3	0.0	1.7	2.6	6.5	0.4
	6	1.8	0.0	3.4	3.4	4.5	0.6
	5	2.5	0.0	1.7	3.4	2.0	1.7
	4	1.6	0.6	0.8	3.2	3.8	0.8
	3	1.4	0.6	1.0	3.6	2.0	1.9
	2	0.9	1.4	0.7	3.6	1.8	2.5

a) Reaction time; dark 5-10 d, irradiation 20 min (a 100 W high-pressure mercury lamp).

active chlorine, a series of runs were conducted in buffer solutions with three values of the ratio Ox/NH_3 adjusted around the stoichiometric ratio of 3/2 (Table 1).

When a sufficient amount of hypochlorite ($Ox/NH_3 > 3/2$) is used in the pH region 4—10, oxidation is completed within at least 1 h. When Ox/NH_3 is lower than 3/2, oxidation takes place sluggishly. Thus, a deviation from the neutral solution causes insufficient oxidation, even with excess oxidant.

The progress of reaction was followed by UV spectroscopy. Immediate measurements on addition of aqueous hypochlorite to buffered ammonia showed new absorptions corresponding to NH_2Cl, $NHCl_2$, and NCl_3[10] instead of OCl^-, HOCl, and Cl_2, apart from contamination of OCl^-, HOCl, and Cl_2 formed readily from sodium hypochlorite (see Experimental). The type of chloramines formed depends not only on pH,[2,10] but also on Ox/NH_3. UV measurements on various ratios of Ox/NH_3 (0.5—3.0) were carried out at several pH. At pH 12.0, the absorption of NH_2Cl alone took place up to *ca.* 1.0 of Ox/NH_3, while two absorptions of NH_2Cl and OCl^- appeared over 1.0 of Ox/NH_3. Solutions of pH 9.5 gave an absorption indicating overlap of NH_2Cl and HOCl up to 1.3 of Ox/NH_3, the absorption at 290 nm becoming distinct with an increase in Ox/NH_3. Since aqueous sodium hypochlorite at pH 9.5 exists as a form of HOCl, the absorption at 290 nm may be assigned to $NHCl_2$ rather than OCl^-. At pH 5.1, the result was similar to that at pH 9.5. At pH 2.6, the third absorption appeared at 340 nm, and was assigned to NCl_3 and/or Cl_2. These chloramines undergo rapid interconversion as well as nitrogen evolution, determination of their equilibrium constants being unsuccessful.

Effect of Irradiation. The iodometric titer decreased very rapidly when solutions containing NH_2Cl, $NHCl_2$, NCl_3 or their equilibrated species (*vide infra*) were irradiated with UV light of wavelength > 290 nm. Consumption of the oxidant was completed after 5—20 min by internal irradiation with a 100 W high-pressure mercury lamp. UV study of the resulting solutions showed transparency at 210—370 nm, indicating photo-decomposion of chloramines. The gas evolved was confirmed to be nitrogen by gas chromatography. The volumetric determination of evolved nitrogen gave an over 80% yield on the basis of NaClO assuming that the irradiation is also expressed as in Eq. 1. In order to estimate ClO_3^- which is formed in *ca.* 40% yield on irradiation of aqueous NaClO alone,[5] several attempts on Cl^- determination were made after treatment with zinc powder which reduced ClO_3^- to Cl^-. But no significant increase in Cl^- concentration was observed with this reduction treatment.

Several breakpoint chlorination studies reveal that NO_2^- and NO_3^- are accompanied as by-products in the reaction in alkaline media.[2] Such a side reaction was also observed in the irradiation reaction. Comparative experiments between dark and irradiation reactions (Table 2) were conducted by changing the ratio Ox/NH_3 as well as pH. For completion of the reaction, 5—10 d were required in the dark, while only 20 min was sufficient under irradiation. The concentrations of residual NH_3, NO_2^-, and NO_3^- were determined.

Discussion

We see from residual active chlorine in dark reactions (Table 1) that the rate of reaction depends on the relative ratio of Ox/NH_3 as well as pH of the solution. UV spectra show transient existence of chloramines such as NH_2Cl, $NHCl_2$, and NCl_3. The type of chloramine formed depends on pH,[2,10] *viz.*, alkaline or neutral solution gives NH_2Cl, while NCl_3 is favored at pH below 4, the relatively unstable $NHCl_2$ being formed in the pH range 4.5—5.0. This was confirmed by our observation. Since nitrogen evolution requires 3/2 mol of hypochlorite for 1 mol of NH_3 (Eq. 1), the chloramine formation should also depend on Ox/NH_3. One mol of NH_2Cl, $NHCl_2$, and NCl_3 requires 1, 2, and 3 mol of hypochlorite, respectively. NH_2Cl, $NHCl_2$, and NCl_3 are then in equilibrium with each other and even with OCl^-, HOCl, and Cl_2. Possible equilibria in the system of ammonia and sodium hypochlorite are as follows.

$$NH_3 + H_2O \rightleftharpoons NH_4OH \rightleftharpoons NH_4^+ + OH^- \quad (2)$$

$$Cl_2 + H_2O \rightleftharpoons HOCl + H^+ + Cl^- \quad (3a)$$

$$HOCl \rightleftharpoons H^+ + OCl^- \quad (3b)$$

$$NH_3 + HOCl \rightleftharpoons NH_2Cl + H_2O \quad (4a)$$

$$NH_2Cl + HOCl \rightleftharpoons NHCl_2 + H_2O \quad (4b)$$

$$NHCl_2 + HOCl \rightleftharpoons NCl_3 + H_2O \quad (4c)$$

By taking advantage of the low reactivity of NH_2Cl (slow nitrogen evolution) in a high alkaline solution, the equilibrium constant for $NH_2Cl + OH^- \rightleftharpoons NH_3 + OCl^-$ was estimated to be 1.6×10^{-3} at 15 °C,[12] showing the preference of NH_2Cl to free NH_3. According to our preparative attempts, generation of NCl_3 requires a highly acidic solution to suppress the nitrogen evolution and to enable ultimate chlorination of NH_3. Though $NHCl_2$ requires the ratio Ox/NH_3 of 2, a maximum amount of $NHCl_2$ is generated under the conditions where Ox/NH_3 is slightly lower than 3/2 at pH 4.0—4.5. In any event, the formation of chloramines such as NH_2Cl, $NHCl_2$, and NCl_3 is a rapid process, influencing the whole oxidation mechanism at the initial stage.

The reaction time in the dark is shortened by a factor of over 100 for the present systems, where the ratio Ox/NH_3 is less than that of stoichiometry (Table 2). The acceleration effect due to UV-irradiation would provide an effective industrial design in waste water treatment, where thermal acceleration cannot be applied. The UV-irradiation may also have an advantage over active carbon[4] because of the applicability at various pH.

The dark and irradiation reactions give essentially the same products, though the amount of by-product NO_2^- in the irradiation is larger than that in the dark. The similarity in products is of interest, since species OCl^-, HOCl and Cl_2 equilibrated with NH_2Cl, $NHCl_2$, and NCl_3 (Eq. 2) might decompose into oxygen or chlorate ion on irradiation.[5] Our results suggest that NH_3 can be oxidized in accordance with Eq. 1. The

reason is not clear why the dark and irradiation reactions differ in the by-product formation of NO_2^-. Solutions of NO_2^-, HNO_2, NO_3^-, and HNO_3 possess very weak absorptions at wavelength<400 nm (see Experimental). However, the irradiation of these species in the presence of NH_3 or NH_4^+ gave rise to neither significant evolution of nitrogen nor change in concentration of NO_2^- and NO_3^-. Thus, irrespective of by-product formation, the irradiation reaction should proceed via a path analogous to the dark reaction.

The mechanism of nitrogen evolution, in particular the process after the rapid formation of chloramines, has not been clarified. Schmitz *et al.*[13] reported in their study on the side-reaction of $NHCl_2$ that the following condensation takes place between two mol of $NHCl_2$, leading to nitrogen, as an explanation for chlorinated products of ethers.

$$NHCl_2 + OH^- \longrightarrow Cl_2N^- + H_2O \quad (5a)$$

$$Cl_2N^- + NHCl_2 \longrightarrow Cl_2N\text{-}NHCl + Cl^- \quad (5b)$$

$$Cl_2N\text{-}NHCl \xrightarrow[-HCl]{} Cl\text{-}N{=}N\text{-}Cl \longrightarrow N_2 + 2Cl \quad (5c)$$

The postulate involves deprotonation with base (Eq. 5a). On the basis of UV spectra, stepwise chlorination occurs to a greater extent with lowering in pH to give $NHCl_2$ and NCl_3. As a result, the postulate might be in line with the fact that the dark reaction is more rapid in neutral solution than in solutions of higher or lower pH (Table 1). However, species undergoing N–N bond formation do not seem to be restricted to $NHCl_2$, since irradiation enables nitrogen evolution from NH_2Cl in an alkaline solution or from NCl_3 in an acidic solution. Thus the following kinds of condensation are possible:

$$Cl_2N^- + NH_2Cl \longrightarrow Cl_2N\text{-}NH_2 + Cl^- \quad (6a)$$

$$Cl_2N^- + NCl_3 \longrightarrow C_2N\text{-}NCl_2 + Cl^- \quad (6b)$$

Even the intervention of hydrazine may be possible, since the reaction of aqueous NaOCl with NH_3 gives hydrazine which is readily oxidized to nitrogen.

As regards acceleration by irradiation, in the case of *N*-chlorinated organic compounds irradiation causes their homolytic N–Cl bond cleavage because of its low bond energy.[15] It might affect the step of decomposition of chlorinated hydrazine (Eqs. 5c and 6), assuming that it is rate-determining. The rate-determining step for nitrogen evolution might be N–N bond formation (Eq. 5a, 5b, or 6) rather than decomposition (Eq. 5c), since chloramines are detected instead of unstable chlorinated hydrazines. Irradiation can change the acid dissociation constants of phenols or amines.[16] The change of basicity of chloramines by irradiation is probable in this case. Photoexcitation energy might be changed to molecular thermal energy, *e.g.*, vibrational energy, facilitating N–N bond formation (Eqs. 5a, 5b and 6).

The authors would like to thank Dr. K. Takagi for his valuable discussions. Acknowledgement is made to Toa Gohsei Co. for the supply of chlorine gas.

References

1) Contribution No. 272.
2) T. A. Pressley, D. F. Bishop, and S. G. Roan, *Environ. Sci. Tech.*, **6**, 622 (1972) and references cited therein.
3) Y. Isomura, *Bull. Chem. Soc. Jpn.*, **40**, 835 (1967).
4) W. N. Stasiuk, Jr., L. J. Hetling, and W. W. Shuster, *J. Water Pollution Control Fed.*, **46**, 1974 (1974).
5) G. V. Buxton and M. S. Subhani, *J. Chem. Soc., Faraday Trans. 1*, **1972**, 958 and references cited therein.
6) M. Nakamura and Y. Ogata, *Bull. Chem. Soc. Jpn.*, **50**, 2205 (1977).
7) Y. Ogata, K. Takagi, and T. Suzuki, *J. Chem. Soc., Perkin Trans. 2*, **1978**, 562.
8) Y. Ogata, T. Suzuki, and K. Takagi, *J. Chem. Soc., Perkin Trans. 2*, **1979**, 1715.
9) G. Holst, *Chem. Revs.*, **54**, 169 (1954).
10) W. S. Metcalf, *J. Chem. Soc.*, **1942**, 148, and see also Ref. 11.
11) P. Bekiaroglou, A. Drusas, and G.-M. Schwab, *Z. Phys. Chem.*, **77**, 43 (1972).
12) R. E. Corbett, W. S. Metcalf, and F. G. Soper, *J. Chem. Soc.*, **1953**, 1927.
13) E. von Schmitz, S. Schramn, W. Flamme, and U. Bicker, *Z. Anorg. Allg. Chem.*, **396**, 178 (1973).
14) L. F. Audrieth and T. T. Nickles, *Inorg. Synth.*, **1**, 90 (1939).
15) A. Schoenberg, "Preperative Organic Photochemistry," Springer-Verlag, New York (1968), Chap. 6.
16) R. S. Becker, "Theory and Interpretation of Fluorescence and Phosphorescence," John Wiley and Sons (1971), Chap. 17.

Preparation of Polynuclear (Diamine)telluratocobalt(III) Complexes

Yutaka Hosokawa* and Yoichi Shimura

Department of Chemistry, Faculty of Science, Osaka University, Toyonaka, Osaka 560

(Received April 11, 1980)

Penta- and hexa-nuclear condensates of mono(diamine)cobalt(III) complexes and tellurates have been prepared and some of the optically active isomers separated. They are $[\{Co(TeO_6H_4)(diamine)\}(Te_2O_{10})\{Co(TeO_6H_4)(diamine)\}]^{6-}$ (brown complexes) and $[\{Co(TeO_6H_4)(diamine)\}(TeO_6)\{Co(TeO_6H_4)(diamine)\}]^{4-}$ (blue complexes), where diamine=ethylenediamine, (*R*)-(−)-propylenediamine, and (*R*,*R*)-(−)-1,2-cyclohexanediamine. The structures have been determined from the visible and ultraviolet absorption and circular dichroism spectra; the electrostatic repulsion between cobalt(III) and tellurium(VI) atoms is considered in detail.

Continued efforts have been made to synthesize polynuclear complexes of a hybrid type between a metal chelate and a heteropoly condensed complex. Several cobalt(III) compounds such as $[Co_2(Te_2O_{10}H_4)(en)_4]Cl_2$,[1] $H_3[Co_4I_3O_{18}(en)_3]$,[2] and $Na_5[Co(Nb_6O_{19})(dien)]$[3] were reported in previous papers. The former tetranuclear complex $[Co_2(Te_2O_{10}H_4)(diamine)_4]^{2+}$ prepared by dehydration condensation of a binuclear complex $[Co(TeO_6H_4)(diamine)_2]^+$ has a chain structure consisting of two bis(diamine)cobalt(III) and two tellurate(VI) octahedra. The present report is concerned with the preparation of similar polynuclear condensates of mono(diamine)cobalt(III) complexes and tellurates. Some pentanuclear $[Co_2Te_3O_{18}H_8(diamine)_2]^{4-}$ and hexanuclear $[Co_2Te_4O_{22}H_8(diamine)_2]^{6-}$ complexes have been obtained which also have chain structures consisting of five or six octahedra sharing edges. Ordinary compact structures, which have been found in iso- and hetero-poly oxoanions such as $Nb_6O_{19}^{8-}$ and $[CoMo_6O_{24}H_6]^{3-}$, are unfavorable for the present complexes. Reasonable chain structures have been inferred by considering the need to avoid electrostatic repulsion between cobalt(III) and tellurium(VI) atoms. The bidentate diamine ligands used are ethylenediamine (en), (*R*)-(−)-propylenediamine (*l*-pn), and (*R*,*R*)-(−)-1,2-cyclohexanediamine (*l*-chxn).

Experimental

Preparation, Separation, and Optical Resolution of Complexes. (1) $Li_4[\{Co(TeO_6H_4)(en)\}(TeO_6)\{Co(TeO_6H_4)(en)\}]\cdot 6H_2O$ (Blue en Complex): A solution of 2.3 g (10 mmol) of $Te(OH)_6$ in 20 cm³ of water was added to a solution of 1.3 g (5 mmol) of *trans*(NH_3)-$[CoCl_2(NH_3)_2(en)]Cl\cdot H_2O$[4] in 15 cm³ of water. To the mixture was added a solution of 0.8 g (20 mmol) of sodium hydroxide in 10 cm³ of water. The resulting solution was stirred mechanically at about 65 °C until the evolution of ammonia ceased. After being cooled in an ice-bath, the solution was poured into a column (3 cm × 70 cm) of anion exchanger (QAE Sephadex A-25, Cl^- form). The adsorbed band was eluted with 0.2 mol dm^{-3} lithium chloride solution (pH 10 by 1 mol dm^{-3} lithium hydroxide); during that time the column was cooled by flushing it with ice-water. Several red and blue bands eluted rapidly. To the combined eluates was added a large amount of acetone. The precipitate was then separated by a centrifuge, washed a few times with acetone, and dried in a stream of air. This solid was dissolved in a small amount of water and the solution was poured into a column of the type mentioned above, and the adsorbed band was eluted with the same eluting reagent. Three colored bands, purple, blue, and brown, were eluted in this order. The first purple eluate was discarded in this work. The last brown eluate was preserved for the treatment in (2) to obtain another complex. The blue middle eluate was concentrated at 15 °C in a rotary evaporator, and a large amount of methanol–acetone (1:10) mixture was added to the concentrated solution. After the mixture had been kept in a refrigerator overnight, the blue precipitate was collected by a centrifuge, recrystallized at 0 °C from lithium hydroxide solution (pH 10) by adding methanol–acetone mixture, and washed repeatedly with methanol and acetone. Found: C, 4.56; H, 3.45; N, 5.32; Co, 11.2; Te, 36.4%. Calcd for $Li_4[\{Co(TeO_6H_4)(en)\}(TeO_6)\{Co(TeO_6H_4)(en)\}]\cdot 6H_2O$: C, 4.78; H, 3.39; N, 5.23; Co, 10.5; Te, 36.3%. Cobalt was weighed as Co_3O_4 and tellurium as the metal.

(2) $Li_6[\{Co(TeO_6H_4)(en)\}(Te_2O_{10})\{Co(TeO_6H_4)(en)\}]\cdot 7H_2O$ (Brown en Complex): The brown eluate from the chromatography in (1) was concentrated at about 20 °C in a rotary evaporator, and a large volume of methanol–acetone mixture was added to the concentrated solution. The brown product was isolated by a similar method to that used in (1). Found: C, 3.74; H, 2.74; N, 4.19; Co, 8.8; Te, 38.3%. Calcd for $Li_6[\{Co(TeO_6H_4)(en)\}(Te_2O_{10})\{Co(TeO_6H_4)(en)\}]\cdot 7H_2O$: C, 3.76; H, 3.00; N, 4.39; Co, 9.2; Te, 40.0%.

(3) $K_4H_2[\{Co(TeO_6H_4)(en)\}(Te_2O_{10})\{Co(TeO_6H_4)(en)\}]\cdot 4H_2O$: The brown en complex obtained in (2) was dissolved in 0.001 mol dm^{-3} potassium hydroxide solution, and to this was added an appropriate amount of potassium chloride. After the resulting solution had been kept in a refrigerator overnight, the product was separated by filtration, washed a few times with cold water, methanol, and acetone, and dried in a desiccator over calcium chloride. Found: C, 3.59; H, 2.64; N, 4.20%. Calcd for $K_4H_2[\{Co(TeO_6H_4)(en)\}(Te_2O_{10})\{Co(TeO_6H_4)(en)\}]\cdot 4H_2O$: C, 3.39; H, 2.56; N, 4.19%.

(4) $Li_4[\{Co(TeO_6H_4)(l\text{-}pn)\}(TeO_6)\{Co(TeO_6H_4)(l\text{-}pn)\}]\cdot 5.5H_2O$ (Blue l-pn Complex) and $Li_6[\{Co(TeO_6H_4)(l\text{-}pn)\}(Te_2O_{10})\{Co(TeO_6H_4)(l\text{-}pn)\}]\cdot 9H_2O$ (Brown l-pn Complex): These were obtained by almost the same procedure as for the corresponding en complexes. A solution of 2.3 g (10 mmol) of $Te(OH)_6$ in 15 cm³ of water was added to a solution of 1.37 g (5 mmol) of *trans*(NH_3)-$[CoCl_2(NH_3)_2(l\text{-pn})]Cl\cdot 4H_2O$[4] in 25 cm³ of water, and to the mixture was added a solution of 0.8 g (20 mmol) of sodium hydroxide in 15 cm³ of water. The solution was concentrated to about 15 cm³ at 70 °C with mechanical stirring, and poured into a column similar to that used in (1). The column chromatography showed two colored bands, blue and brown, in this order. The blue and brown complexes were isolated as described in (1). Found: C, 6.68; H, 3.67; N, 5.23%. Calcd for $Li_4[\{Co(TeO_6H_4)(l\text{-pn})\}(TeO_6)\{Co(TeO_6H_4)(l\text{-pn})\}]\cdot 5.5H_2O$: C, 6.72; H, 3.67; N, 5.23%. Found: C, 5.41; H, 3.23; N, 4.16%. Calcd for $Li_6[\{Co(TeO_6H_4)(l\text{-pn})\}(Te_2O_{10})\{Co(TeO_6H_4)(l\text{-pn})\}]\cdot 9H_2O$: C, 5.38; H,

3.47; N, 4.18%.

The latter complex was dissolved in a small amount of water, and the solution was treated by column chromatography as described above. The adsorbed band separated gradually into two brown bands, 1 and 2 in this order, when eluted with 0.15 mol dm^{-3} lithium chloride solution (pH 10.5 by 1 mol dm^{-3} lithium hydroxide). Both eluates showed a similar absorption spectrum to that of the unseparated brown *l*-pn complex. The brown *l*-pn 1 and 2 complexes have $\Delta\varepsilon = +0.44$ and $+1.72$, respectively, at the Na D line.

(5) $Li_6[\{Co(TeO_6H_4)(l\text{-chxn})\}(Te_2O_{10})\{Co(TeO_6H_4)(l\text{-chxn})\}]\cdot 12H_2O$ (Brown l-chxn Complex): A solution in 15 cm^3 of water was made of 1.57 g (5 mmol) of *trans*(Cl)-$[CoCl_2(NH_3)_2(l\text{-chxn})]Cl$, which was obtained according to the method[4] for the corresponding en complex using *l*-chxn instead of en. To this solution was added first a solution of 2.3 g (10 mmol) of $Te(OH)_6$ in 20 cm^3 of water and then a solution of 0.8 g (20 mmol) of sodium hydroxide in 15 cm^3 of water. The resulting solution was stirred mechanically at 60 °C for 3 h, and was then poured into a column similar to that in (*1*). The column chromatography showed one brown band predominantly. Found: C, 9.53; H, 3.84; N, 3.73; Te, 33.4%. Calcd for $Li_6[\{Co(TeO_6H_4)(l\text{-chxn})\}(Te_2O_{10})\{Co(TeO_6H_4)(l\text{-chxn})\}]\cdot 12H_2O$: C, 9.79; H, 4.11; N, 3.73; Te, 34.6%.

(6) Optical Resolution of the Blue and Brown en Complexes: A solution of 0.012 g of Λ-$(+)_{589}$-$[Co(en)_3]Br_3\cdot H_2O$ in 10 cm^3 of water was added gradually to a solution of 0.15 g of the blue en complex in 20 cm^3 of lithium hydroxide solution of pH 11 at about 5 °C. After the resulting solution had been kept in a refrigerator overnight, the yellow green diastereomer was separated by filtration, and washed with cold water a few times. It was difficult to replace the $(+)_{589}$-$[Co(en)_3]^{3+}$ cation of the less soluble diastereomer by an ordinary cation such as K^+ or Na^+. Then, to the filtrate containing the more soluble diastereomer was added an appropriate amount of cation exchanger (SP Sephadex C-25, Na^+ or K^+ form) to remove $(+)_{589}$-$[Co(en)_3]^{3+}$. The cation exchanger was filtered and CD of the filtrate was measured. The blue en complex in this solution has $\Delta\varepsilon = -0.31$ at the Na D line.

The optical resolution of the brown en complex was made by the same procedure as that used for the blue en complex, using 0.13 g of the brown en complex and 0.024 g of Λ-$(+)_{589}$-$[Co(en)_3]Br_3\cdot H_2O$; the CD of the filtrate was measured after removing $(+)_{589}$-$[Co(en)_3]^{3+}$. The brown en complex has $\Delta\varepsilon = -0.52$ at the Na D line.

(7) $[\{Co(dien)(H_2O)\}(Te_2O_{10}H_4)\{Co(dien)(H_2O)\}]Cl_2\cdot 5H_2O$ (Tetranuclear dien Complex): A solution of 1.15 g (5 mmol) of $Te(OH)_6$ in 10 cm^3 of water was added, with mechanical stirring, to a solution of 1.35 g (5 mmol) of *mer*-$[CoCl_3(dien)]$ in 20 cm^3 of water at 60—70 °C (dien= diethylenetriamine). A solution of 1.12 g (20 mmol) of potassium hydroxide in 10 cm^3 of water was added to the solution by portions. After being stirred mechanically at 65 °C for *ca.* 3 h, the mixture was kept in a refrigerator overnight. The light red precipitate was filtered, and to the filtrate was added an appropriate amount of acetone. After the solution had been kept in a refrigerator overnight again, the red oily precipitate was separated by decanting the supernatant liquid. The product was recrystallized from a small amount of cold water by adding acetone, and washed with a methanol–water (5:1) mixture, methanol, and ethanol. Found: C, 10.52; H, 4.38; N, 9.22; Te, 28.0%. Calcd for $[\{Co(dien)(H_2O)\}(Te_2O_{10}H_4)\{Co(dien)(H_2O)\}]Cl_2\cdot 5H_2O$: C, 10.62; H, 4.47; N, 9.29; Te, 27.8%.

Measurements. The visible and ultraviolet absorption spectra were taken on a Shimadzu UV-200 spectrophotometer. The CD spectra were recorded on a JASCO MOE-1 spectropolarimeter. The absorption and CD measurements of the present complexes (lithium salts) were made in aqueous lithium hydroxide solutions (pH 10) over the concentration range 10^{-3} to 10^{-5} mol dm^{-3} at *ca.* 10 °C. The ^{13}C nuclear magnetic resonance spectra were measured in deuterium oxide with a Varian XL-100-15 NMR spectrometer.

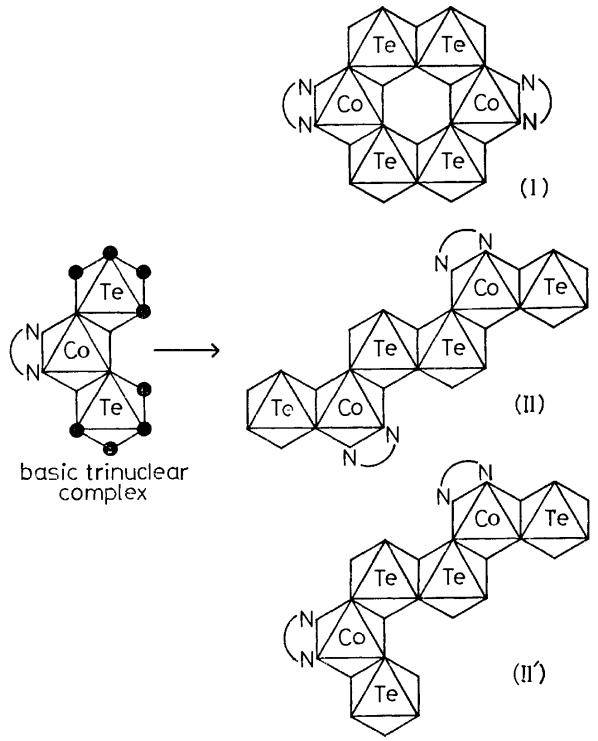

Fig. 1. Some condensation products of a basic trinuclear complex $[Co(TeO_6H_4)_2(diamine)]^-$. Hydroxo lignads of the basic complex are marked by circles.

Results and Discussion

The brown and blue complexes were separated by column chromatography from the reaction mixture of *trans*(NH_3)- or *trans*(Cl)-$[CoCl_2(NH_3)_2(diamine)]^+$, $Te(OH)_6$, and alkali in a proper molar ratio at 60—70 °C. Because all the complexes, particularly blue ones, were unstable in solution at room temperature, the solutions were carefully treated below 15 °C. The yields of blue complexes were much less than those of the brown ones.

The Brown Complexes. The composition $M_6[Co_2Te_4O_{22}H_8(diamine)_2]$ was confirmed by the preparative method and elemental analysis. A previous paper[1] reported that two binuclear complexes $[Co(TeO_6H_4)(diamine)_2]^+$ were prepared from the reaction mixture of *cis*-$[CoCl_2(diamine)_2]Cl$, $Te(OH)_6$, and alkali, the corresponding tetranuclear complexes $[Co_2(Te_2O_{10}H_4)(diamine)_2]^{2+}$ being obtained by dehydration condensation of the coordinated orthotellurate moieties of the binuclear complexes. Since the starting cobalt(III) complex used in the present study has only one diamine ligand, trinuclear complexes $[Co(TeO_6H_4)_2(diamine)]^-$ and hexanuclear condensates $[Co_2Te_4O_{22}H_8(diamine)_2]^{6-}$ may be formed in the

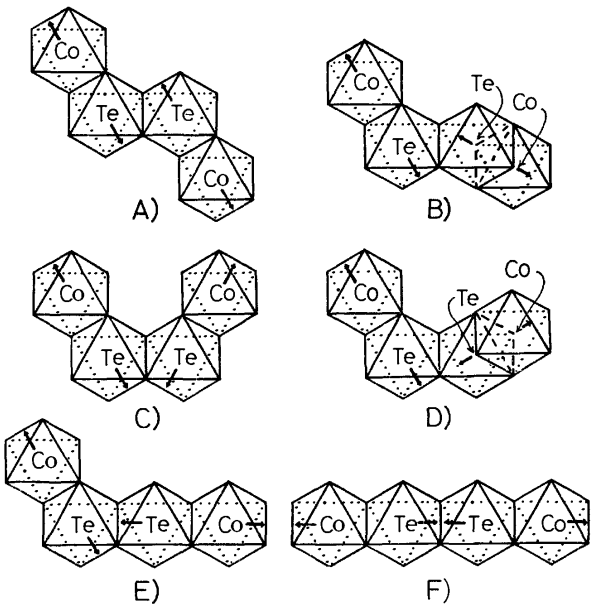

Fig. 2. Isomerism of the Co–Te–Te–Co tetra-octahedra.

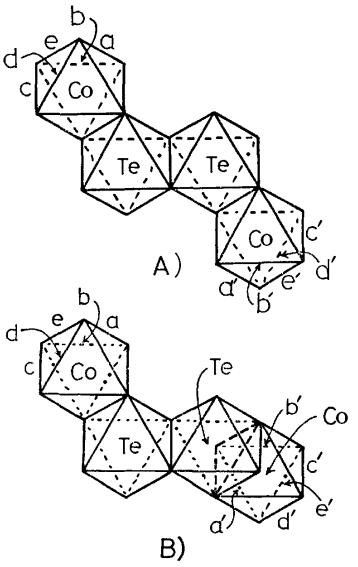

Fig. 3. Numbering for the edges of structures A) and B).

reaction mixture. As is seen in Fig. 1, when the condensation occurs by edge-sharing in two tellurate ligands of each trinuclear complex simultaneously, only a ring structure (I) is possible. This structure has a C_{2h} symmetry unsuitable for the brown complexes optically resolved. When it occurs in one tellurate ligand of each trinuclear complex, many kinds of hexanuclear chain structures, such as (II) and (II'), are possible. The isomerism of this type of chain structure (Te–Co–Te–Te–Co–Te hexa-octahedra) can be formally treated as follows by starting from a tetranuclear Co–Te–Te–Co tetra-octahedra structure. For the tetra-octahedra, the six structures shown in Fig. 2 are possible. The adjacent tellurium(VI) and cobalt(III) atoms repulse each other electrostatically in the directions of the marked arrows, and hence the

Table 1. Possible structures of hexa-octahedra derived from A) or B) structure

They are denoted by the edges to which two more TeO_6 octahedra are added in Fig. 3.

	a′	b′	c′	d′	e′
a	aa′				
b	ba′	bb′			
c	ca′	cb′	cc′		
d	da′	db′	dc′	dd′	
e	ea′	eb′	ec′	ed′	ee′

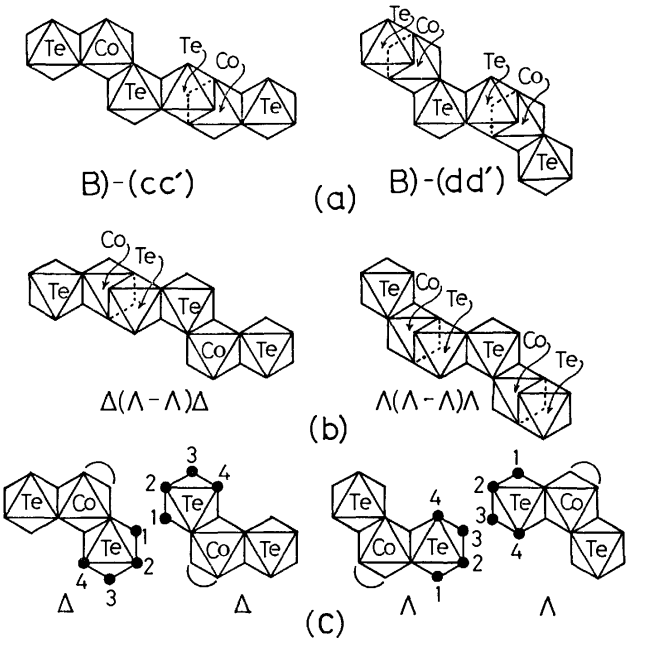

Fig. 4. Proposed structures of $[\{Co(TeO_6H_4)(diamine)\}(Te_2O_{10})\{Co(TeO_6H_4)(diamine)\}]^{6-}$.
(a) B)-(cc′) and B)-(dd′) structures. (b) Drawn along other direction. (c) Numbering of the apexes of Δ- and Λ-$[Co(TeO_6)_2(diamine)]$ groups.

tellurium(VI)-tellurium(VI) repulsion increases in the order A)<B)<D)<C)<E)<F). Furthermore, because the two cobalt(III) octahedra are more separated for A) and B) than for C) and D), the former two have a smaller repulsion between the cobalt(III) octahedra than the latter two. Since this kind of electostatic repulsion should have the primary influence upon the structure of polynuclear complexes,[5] the structures A) and B) are probable for the tetra-octahedra of present complexes. Thus far only the structure A) has been found in $[Co(diamine)_2(Te_2O_{10}H_4)Co(diamine)_2]^{2+}$ (diamine=en and *l*-chxn)[1] and $[(en)_2Cr(OH)_2Cr(en)(OH)_2Cr(en)(OH)_2Cr(en)_2]^{6+}$.[6] As shown in Fig. 3, the edges of two cobalt(III) octahedra in the structure A) (C_i symmetry) and B) (C_2 symmetry) are named a,b,c,d,e,a′,b′,c′,d′, and e′. In the cases of both structures, A) and B), fifteen hexa-octahedra structures can be formed by adding two more TeO_6 octahedra, as shown in Table 1. Among the thirty structures, A)-(cc′), -(dd′), -(dc′), B)-(cc′), -(dd′), and -(dc′) are expected to have less electrostatic

Table 2. Absorption data in the region of 14000—35000 cm^{-1}

Complex	Color	σ_{max}[a] (log ε)[b]		
		1st band	2nd band	CT band
$[\{Co(TeO_6H_4)(en)\}(TeO_6)\{Co(TeO_6H_4)(en)\}]^{4-}$	Blue	17.7 (2.33)	25 sh (2.6)	30 sh (3.2)
$[\{Co(TeO_6H_4)(l\text{-pn})\}(TeO_6)\{Co(TeO_6H_4)(l\text{-pn})\}]^{4-}$	Blue	17.4 (2.38)	25 sh (2.6)	30 sh (3.4)
$[\{Co(TeO_6H_4)(en)\}(Te_2O_{10})\{Co(TeO_6H_4)(en)\}]^{6-}$	Brown	17.6 (2.43)	c)	28 sh (3.4)
$[\{Co(TeO_6H_4)(l\text{-pn})\}(Te_2O_{10})\{Co(TeO_6H_4)(l\text{-pn})\}]^{6-}$	Brown	17.7 (2.50)	c)	28 sh (3.4)
$[\{Co(TeO_6H_4)(l\text{-chxn})\}(Te_2O_{10})\{Co(TeO_6H_4)(l\text{-chxn})\}]^{6-}$	Brown	17.5 (2.50)	c)	28 sh (3.5)

a) In units of 10^3 cm^{-1}. b) The ε values are in units of mol^{-1} dm^3 cm^{-1}. c) The second absorption band is overlapped by the CT band at 28000 cm^{-1}.

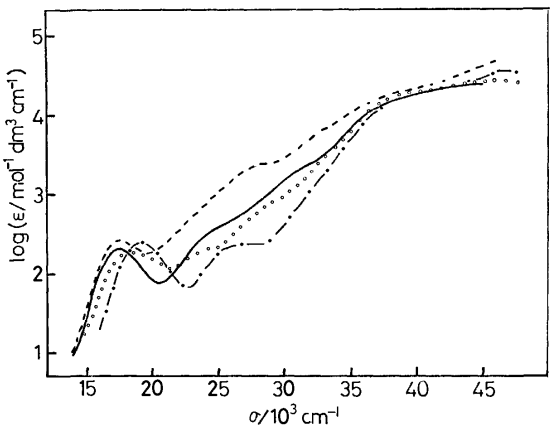

Fig. 5. Absorption spectrum of blue en complex $[\{Co(TeO_6H_4)(en)\}(TeO_6)\{Co(TeO_6H_4)(en)\}]^{4-}$ (·——), brown en complex $[\{Co(TeO_6H_4)(en)\}(Te_2O_{10})\{Co(TeO_6H_4)(en)\}]^{6-}$ (----), $[\{Co(dien)(H_2O)\}(Te_2O_{10}H_4)\{Co(dien)(H_2O)\}]^{2+}$ (○○○○), and $[Co(en)_2(Te_2O_{10}H_4)Co(en)_2]^{2+}$ (—·—).

repulsion between cobalt(III) and tellurium(VI) atoms in the local Te–Co–Te–Te tetra-octahedra units, since two such local tetra-octahedra units of these six structures have the structure A) or B). Because the brown en complex was optically resolved, the structures A)-(cc') and -(dd'), which have a center of symmetry, are excluded from consideration. The ^{13}C-NMR spectrum of the brown en complex showed only a band at *ca.* 42 ppm with respect to TMS. Thus, the structures A)-(dc') and B)-(dc'), which have no element of symmetry, are omitted. In this way it is concluded that the most probable structure is B)-(cc') or -(dd') of C_2 symmetry (Fig. 4-a). As is seen in Figs. 4-b and -c, a $\Delta(\Lambda\text{-}\Lambda)\Delta$-B)-(cc') isomer is formed by condensing the apexes 1 and 1 as well as 2 and 2 of two Δ-$[Co(TeO_6)_2(diamine)]$ groups, and the enantiomer $\Lambda(\Delta\text{-}\Delta)\Lambda$-B)-(cc') from two Λ-$[Co(TeO_6)_2(diamine)]$ groups. A $\Lambda(\Lambda\text{-}\Lambda)\Lambda$-B)-(dd') isomer is formed by condensing the apexes 1 and 1 as well as 3 and 3 of two Λ-$[Co(TeO_6)_2(diamine)]$ groups, and the enantiomer $\Delta(\Delta\text{-}\Delta)\Delta$-B)-(dd') from two Δ-$[Co(TeO_6)_2(diamine)]$ groups.

The absorption spectrum of brown en complex is characteristic of a *cis*-CoN_2O_4 type complex and similar to that of $[Co(CO_3)_2(en)]^-$ (σ_{max}=17500 and 25600 cm^{-1})[7] in the d-d absorption band region (Fig. 5). The first absorption band (at 17600 cm^{-1}) is located at a lower energy than those of $[Co(en)_2(Te_2O_{10}H_4)Co(en)_2]^{2+}$ (at 19200 cm^{-1}) of the *cis*-CoN_4O_2 type and $[\{Co(dien)(H_2O)\}(Te_2O_{10}H_4)\{Co(dien)(H_2O)\}]^{2+}$ (at 18500 cm^{-1}) of the *mer*-CoN_3O_3 type. The second absorption band is obscured by overlapping with a strong absorption band at about 28000 cm^{-1} (long ε=3.4). The latter band is not observed for the ditellurate $[Te_2O_{10}H_{8-n}]^{n-}$ and orthotellurate $[TeO_6H_{6-n}]^{n-}$ ions, and also does not appear for $[Co(ox)_x(en)_{3-x}]^{n\pm}$ (x=1[8] and 2[9]) or $[Co(CO_3)_x(en)_{3-x}]^{n\pm}$ (x=1[8] and 2[7]). The strong band shifts to higher energy in the order of complex types: *cis*-CoN_2O_4 (at 28000 cm^{-1})→*mer*-CoN_3O_3 (at *ca.* 29000 cm^{-1})→*cis*-CoN_4O_2 (at *ca.* 33000 cm^{-1}). These bands are assigned to charge-transfer (CT) transitions from the coordinated orthotellurate or ditellurate oxygen ions to cobalt(III). Table 2 shows that the same absorption behavior is observed for all the complexes of the brown type.

The CD spectra of brown en and *l*-pn complexes are shown in Figs. 6 and 7. The CD curve of $(-)^{CD}_{589}$ brown en complex, which was obtained from the more soluble diastereomer with Λ-$(+)_{589}$-$[Co(en)_3]^{3+}$, consists of a main CD band with negative sign and a weak one with positive sign (at lower energy side) in the first absorption band region (Fig. 7 and Table 3). Since the Λ-$[Co(CO_3)_2(en)]^-$ and Λ-$[Co(ox)_2(en)]^-$ complexes show a main CD band with positive sign in this region,[7,10] the $(-)^{CD}_{589}$ brown en complex will have Δ-configuration in regard to skew pairs of the orthotellurate and ethylenediamine chelate rings about local cobalt(III) atoms (see Fig. 4), provided that the CD of this complex in the first absorption band region comes mainly from chiral configurations about local cobalt(III) atoms. Thus, the configuration of $(-)^{CD}_{589}$ brown en complex is tentatively assigned to be $\Delta(\Lambda\text{-}\Lambda)\Delta$-B)-(cc') or $\Delta(\Delta\text{-}\Delta)\Delta$-B)-(dd').

Two diastereomeric isomers, 1 and 2, of $[\{Co(TeO_6H_4)(l\text{-pn})\}(Te_2O_{10})\{Co(TeO_6H_4)(l\text{-pn})\}]^{6-}$ were separated by column chromatography. The configurational and vicinal CD contributions are separable for many kinds of cobalt(III) complexes by utilizing an additivity rule for CD curves of a pair of diastereomeric isomers.[11] The calculated Δ-configurational CD curve agrees well with the observed CD curve of Δ-enantiomer of brown en complex (Fig. 7). The configurational CD ($\Delta\varepsilon_{ext}$=+0.64 at 17000 cm^{-1}) is weaker than the vicinal CD ($\Delta\varepsilon_{ext}$=+1.08 at 17000 cm^{-1}). From the sign patterns of isolated config-

Table 3. CD data in the region of 14000—35000 cm^{-1}

Complex	σ_{ext}[a] ($\Delta\varepsilon$)[b] 1st band	2nd band	CT band
$(-)_{589}^{CD}$-[{Co(TeO_6H_4)(en)}(TeO_6){Co(TeO_6H_4)(en)}]$^{4-}$	15.0 (+0.08) 17.2 (−0.32) 19.9 (+0.02)	23.5 (−0.03)	29.5 (+0.15)
[{Co(TeO_6H_4)(*l*-pn)}(TeO_6){Co(TeO_6H_4)(*l*-pn)}]$^{4-}$ [c]	15.5 (−0.15) 17.2 (+0.76) 20.0 (−0.02)	24.5 (+0.14)	30.0 (+0.17)
$(-)_{589}^{CD}$-[{Co(TeO_6H_4)(en)}(Te_2O_{10}){Co(TeO_6H_4)(en)}]$^{6-}$	15.0 (+0.13) 17.2 (−0.54)	23.5 (−0.14)	29.0 (+0.40) 30.5 (+0.49)
[{Co(TeO_6H_4)(*l*-chxn)}(Te_2O_{10}){Co(TeO_6H_4)(*l*-chxn)}]$^{6-}$ [c]	15.5 (−0.17) 19.1 (+0.74)	23.5 (+0.13)	29.0 (+0.45)
[{Co(TeO_6H_4)(*l*-pn)}(Te_2O_{10}){Co(TeO_6H_4)(*l*-pn)}]$^{6-}$: BP1	15.6 (−0.31) 17.2 (+0.51) 19.2 (−0.15)	22.0 (+0.14) 23.5 (+0.17)	28.0 (+0.20)
: BP2	15.3 (−0.61) 17.2 (+1.81) 19.4 (−0.13)	23.8 (+0.51)	28 sh (−0.8)

a) In units of 10^3 cm^{-1}. b) The $\Delta\varepsilon$ values are given in units of mol^{-1} dm^3 cm^{-1}. c) Unresolved complex.

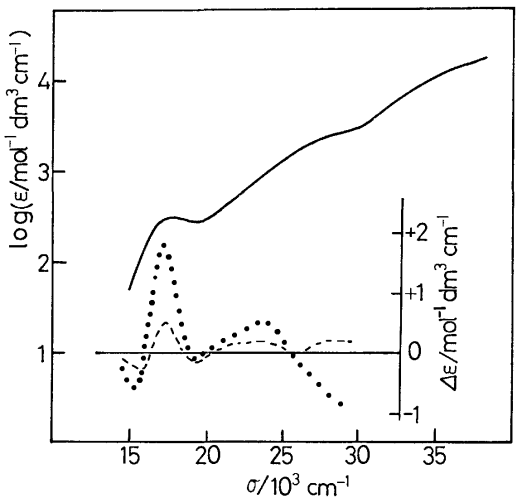

Fig. 6. Absorption spectrum of unresolved [{Co(TeO_6H_4)(*l*-pn)}(Te_2O_{10}){Co(TeO_6H_4)(*l*-pn)}]$^{6-}$ (——) and CD spectra of the resolved brown *l*-pn 1 (----) and and 2 (••••) diastereomeric isomers.

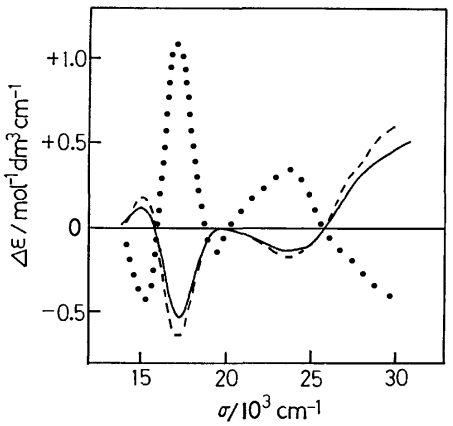

Fig. 7. Calculated configurational (----) and vicinal (••••) CD curves of [{Co(TeO_6H_4)(*l*-pn)}(Te_2O_{10})-{Co(TeO_6H_4)(*l*-pn)}]$^{6-}$, and observed CD curve (——) of $(-)_{589}^{CD}$-[{Co(TeO_6H_4)(en)}(Te_2O_{10}){Co(TeO_6H_4)(en)}]$^{6-}$.

urational CD curves it is likely that the isomer 1 has $\Delta(\Lambda\text{-}\Lambda)\Lambda$-B)-(cc') or $\Lambda(\Delta\text{-}\Delta)\Delta$-B)-(dd') configuration and the isomer 2 $\Lambda(\Lambda\text{-}\Delta)\Lambda$-B)-(cc') or $\Lambda(\Lambda\text{-}\Lambda)\Lambda$-B)-(dd').

The Blue Complexes. These were obtained as a by-product in the preparation of the brown complexes. They have the chemical composition $M_4[Co_2Te_3O_{18}H_8(diamine)_2]$ as confirmed by the preparative procedure and elemental analysis. It is supposed that the complexes have a Te–Co–Te–Co–Te penta-octahedra structure. The isomerism of the penta-octahedra can be formally treated by edge-sharing of a TeO_6 octahedron with each outer cobalt(III) octahedron of a Co–Te–Co tri-octahedra structure. Then, from the same consideration as used for the brown en complex, the most probable structure is (I) or (II) of C_2 symmetry (Fig. 8). Because these structures have no axis of rotatory reflection, a pair of enantiomers are possible. In fact, the blue en complex was optically resolved. Two diastereomeric isomers are possible for the blue *l*-pn complex, but the chromatographic separation was unsuccessful. The absorption spectrum of blue en complex is similar to that of the brown en complex in the d-d absorption band region (Fig. 5 and Table 2.) The second absorption band appears as a shoulder because of overlapping with the CT absorption band at about 30000 cm^{-1} ($\log\varepsilon=3.2$). The CT band is at higher energy than that for the brown complex. As is shown in Fig. 9 and Table 3, the CD pattern of $(-)_{589}^{CD}$ blue en complex is similar to that of $(-)_{589}^{CD}$ brown en complex (Fig. 7), though the former shows three CD

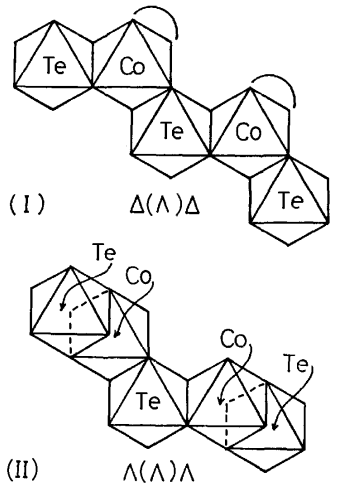

Fig. 8. Proposed structures of $[\{Co(TeO_6H_4)(diamine)\}(TeO_6)\{Co(TeO_6H_4)(diamine)\}]^{4-}$.

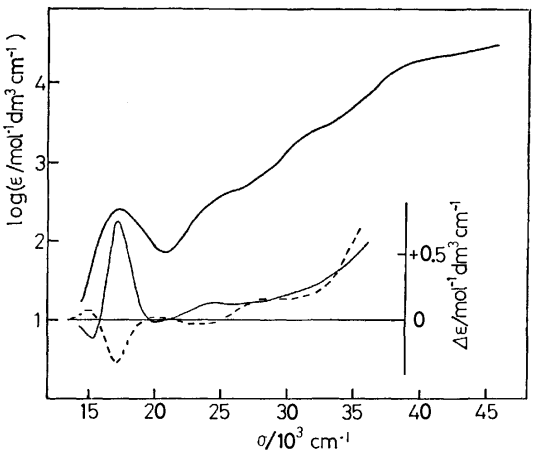

Fig. 9. Absorption and CD spectra (——) of unresolved $[\{Co(TeO_6H_4)(l\text{-pn})\}(TeO_6)\{Co(TeO_6H_4)(l\text{-pn})\}]^{4-}$ and CD spectrum (----) of $(-)^{CD}_{589}$-$[\{Co(TeO_6H_4)(en)\}(TeO_6)\{Co(TeO_6H_4)(en)\}]^{4-}$.

bands with positive, negative, and positive signs from the lower energy side in the first absorption band region. As the sign of the main CD band is negative, the configurations of local cobalt(III) octahedra will be Δ. Thus, $(-)^{CD}_{589}$ blue en complex is tentatively assigned to be $\Delta(\Delta)\Delta$-(I) or $\Delta(\Delta)\Delta$-(II) (see Fig. 8).

Tetranuclear dien Complex. This complex was isolated from the reaction mixture of *mer*-$[CoCl_3(dien)]$, $Te(OH)_6$, and alkali in a proper molar ratio at 60—70 °C. In this case, only the tetranuclear complex was obtained, which corresponds to a condensate of the binuclear complex $[Co(TeO_6H_4)(dien)(H_2O)]^+$. The second d-d absorption band is obscured by overlapping with a strong CT absorption band at 29000 cm^{-1} ($\log \varepsilon = 2.9$). The CT band is located at lower energy than that for the blue diamine complexes (Fig. 5). This reflects the existence of Te_2O_{10} unit in the structure. As the first d-d absorption band is broad, the terdentate dien ligand may be coordinated meridionally.

References

1) Y. Hosokawa and Y. Shimura, *Bull. Chem. Soc. Jpn.*, **52**, 1051 (1979); *Chem. Lett.*, **1978**, 847.
2) T. Ama, J. Hidaka, and Y. Shimura, *Bull. Chem. Soc. Jpn.*, **46**, 2145 (1973).
3) Y. Hosokawa, J. Hidaka, and Y. Shimura, *Bull. Chem. Soc. Jpn.*, **48**, 3175 (1973).
4) C. J. Hawkins, J. A. Stark, and C. L. Wong, *Aust. J. Chem.*, **25**, 273 (1972).
5) D. L. Kepert, *Inorg. Chem.*, **8**, 1556 (1969).
6) P. Anderson and T. Berg, *Acta Chem. Scand.*, A**32**, 989 (1978).
7) M. Shibata, *Nippon Kagaku Zasshi*, **87**, 771 (1966).
8) Y. Shimura and R. Tsuchida, *Bull. Chem. Soc. Jpn.*, **29**, 311 (1956).
9) J. Hidaka, Y. Shimura, and R. Tsuchida, *Bull. Chem. Soc. Jpn.*, **35**, 567 (1962).
10) B. E. Douglas, R. A. Haines, and J. G. Brushmiller, *Inorg. Chem.*, **2**, 1194 (1963).
11) N. Matsuoka, J. Hidaka, and Y. Shimura, *Bull. Chem. Soc. Jpn.*, **48**, 458 (1975); *Inorg. Chem.*, **9**, 719 (1970).

 © 1980 The Chemical Society of Japan Bull. Chem. Soc. Jpn., 53, 3208—3213 (1980) [Vol. 53, No. 11

Metal Complexes of Peptides. I. The Cobalt(III) Complexes Containing Dipeptidate and *N*-Methyliminodiacetate as Mixed Ligands

Hiroshi KAWAGUCHI,* Makoto KANEKIYO, Tomoharu AMA, and Takaji YASUI

Department of Chemistry, Faculty of Science, Kochi University, Akebono-cho, Kochi 780

(Received May 6, 1980)

The mixed-ligand complexes, $Ba[Co(mida)(dipept)]_2$ (where mida is *N*-methyliminodiacetate and dipept denotes dianions of glycyl-L-alanine, L-alanylglycine, glycyl-L-leucine, L-leucylglycine, glycyl-β-alanine, β-alanylglycine, L-alanyl-β-alanine, and β-alanyl-L-alanine) have been prepared. The structure and properties of these complexes have been characterized by their electronic absorption, CD, and NMR spectral data.

Most studies on the metal complexes with peptides have attempted to understand the behavior of metal ions in living systems.[1] However, there are not enough data on the structures and properties of the cobalt(III) complexes with peptides.

The crystal structure of the cobalt(III) complex with glycylglycinate has been determined by the X-ray method.[2] In this complex the dipeptide binds to cobalt in terdentate fashion (meridional form) through the nitrogens of amino and amide groups and the oxygen of carboxyl group. The preparation and properties of the bis(dipeptidato) complex, $[Co(\alpha_1\text{-}\alpha_2)_2]^-$ ($\alpha_1\text{-}\alpha_2$ represents the dianion of the dipeptide $H_2\alpha_1\text{-}\alpha_2$, where α_1 is the *N*-terminal residue) have been studied in detail by Boas *et al.*[3] On the other hand, little work has been done on the mixed-ligand complexes containing dipeptide and one other ligand, though the complexes $[Co(NH_3)_3(\alpha_1\text{-}\alpha_2)]^+$ and $[Co(dien)(\alpha_1\text{-}\alpha_2)]^+$ have been prepared and characterized by Browning *et al.*[4]

Recently we found that the complexes of $[Co(ida)(\alpha_1\text{-}\alpha_2)]^-$ exhibit novel spectral behavior in the region of the d-d transition band,[5] compared with that for the typical cobalt(III) chromophore of the type $[Co(N)_3(O)_3]$.[6] In the present paper we report the preparation of mono(dipeptidato) complexes of the type $[Co(mida)(\alpha_1\text{-}\alpha_2)]^-$, where mida represents the dianion of *N*-methyliminodiacetic acid, H_2mida. These complexes have been characterized by elemental analysis, ^1H-NMR, absorption, and CD spectroscopy. In order to study the influence of the chelate-ring size of dipeptide on the properties of the $[Co(mida)(\alpha_1\text{-}\alpha_2)]^-$ complexes, especially on the absorption and CD spectra, the complexes of the dipeptides containing β-alanine have been studied in detail. The effects of the pH on the absorption and CD spectra have been also examined.

Experimental

Ligands. *N*-Methyliminodiacetic acid (H_2mida) was prepared according to the literature.[7]

Glycyl-β-alanine was prepared by a combination of conventional techniques, using *N*-(benzyloxycarbonyl)glycine (z-gly) and β-alanine ethyl ester (β-ala-OEt) as the starting materials.[8] Dicyclohexylcarbodiimine coupling was used to form the dipeptide derivative from these precursors. The peptide hydrobromide (H_2gly-β-ala·HBr) was formed by the reaction of z-gly-β-ala-OEt with aqueous NaOH solution and then with HBr-acetic acid. The HBr salts of β-alanylglycine (H_2β-ala-gly), L-alanyl-β-alanine (H_2L-ala-β-ala), and β-alanyl-L-alanine (H_2β-ala-L-ala) were also prepared by the same method as that of H_2gly-β-ala·HBr. These dipeptides were used for the syntheses of the complexes without removing HBr. The other dipeptides, glycylglycine (H_2gly-gly), L-alanylglycine (H_2L-ala-gly), glycyl-L-alanine (H_2gly-L-ala), L-leucylglycine (H_2L-leu-gly), and glycyl-L-leucine (H_2gly-L-leu), were obtained commercially from Sigma Chemical Company and Protein Research Foundation. These dipeptides were used without further purification.

Preparation of Complexes. *Ba[Co(mida)(gly-L-ala)]$_2$·5H_2O*: An aqueous solution (10 cm^3) of cobalt(II) chloride hexahydrate (2.37 g, 0.01 mol) was added slowly to an aqueous solution (10 cm^3) containing glycyl-L-alanine (1.46 g, 0.01 mol) and *N*-methyliminodiacetic acid (1.47 g, 0.01 mol), adjusting the pH of the mixed solution at *ca.* 9.5 with sodium hydroxide. The resulting solution was oxidized with lead dioxide (5 g) at 40 °C for about 1 h with stirring, and then it was cooled to room temperature. After removal of insoluble material by filtration, the filtrate, which contained $[Co(gly\text{-}L\text{-}ala)_2]^-$, $[Co(mida)_2]^-$, $[Co(mida)(gly\text{-}L\text{-}ala)]^-$, and some minor products, was chromatographed on a column (4.5 cm × 90 cm) of QAE-Sephadex A-25 using 0.05 M† KCl as an eluant. After the elution of bis(dipeptidato)cobaltate(III) complex, the objective dark-gray band ($[Co(mida)(gly\text{-}L\text{-}ala)]^-$) was separated completely from the overlapped brown-violet band (*fac*-$[Co(mida)_2]^-$) by further development of another column (4.5 cm × 90 cm) connected to the original column with a teflon tube (ϕ 1 mm). The eluted solution from the dark-gray band was concentrated to a small volume (20—30 cm^3) using a rotary evaporator at *ca.* 35 °C. To the concentrated solution was added a large amount of methanol, and then potassium chloride which deposited was filtered off. The filtrate was concentrated again to a few milliliters, and the residual KCl in the solution was removed by using a Sephadex G-10 column (3 cm × 90 cm). The deliquescent potassium salt of the complex was converted to barium salt by chromatography on SP-Sephadex C-25 to give a crystalline product. The barium salt was recrystallized from an aqueous solution by addition of ethanol and acetone.

The preparations of the type $Ba[Co(mida)(\alpha_1\text{-}\alpha_2)]_2$ containing other dipeptide ligands were carried out by the same method as described above. Analytical data of the new complexes are listed in Table 1.

[Co(NH_3)$_3$(gly-β-ala)]Cl·H_2O: Preparation of this compound was performed in the same way as that for the corresponding glycylglycinato complex.[4] Concentrated aqueous ammonia (15 cm^3) was added to the solution containing glycyl-β-alanine hydrobromide (4.54 g, 0.02 mol) and cobalt(II) chloride hexahydrate (4.74 g, 0.02 mol) in water (10 cm^3). Hydrogen peroxide (30%, 2 cm^3) was added slowly to the above ammoniac solution with constant stirring and then the solution was gently warmed for 10 min. The complex, $[Co(NH_3)_3(gly\text{-}\beta\text{-}ala)]^+$, in the reactant solution

† 1 M = 1 mol dm^{-3}.

Table 1. Analytical data of the complexes

Complex	C, %		H, %		N, %	
	Found	(Calcd)	Found	(Calcd)	Found	(Calcd)
$Ba[Co(mida)(gly\text{-}gly)]_2\cdot 9H_2O$	22.73	(22.34)	4.73	(4.58)	8.24	(8.68)
$Ba[Co(mida)(gly\text{-}L\text{-}ala)]_2\cdot 5H_2O$	25.96	(26.00)	4.14	(4.36)	8.82	(9.10)
$Ba[Co(mida)(L\text{-}ala\text{-}gly)]_2\cdot 6H_2O$	25.79	(25.51)	4.18	(4.49)	8.62	(8.92)
$Ba[Co(mida)(gly\text{-}L\text{-}leu)]_2\cdot 6H_2O$	30.38	(30.36)	5.40	(5.29)	8.08	(8.17)
$Ba[Co(mida)(L\text{-}leu\text{-}gly)]_2\cdot 5H_2O$	30.70	(30.98)	4.99	(5.20)	8.14	(8.34)
$Ba[Co(mida)(gly\text{-}\beta\text{-}ala)]_2\cdot 4H_2O$	26.13	(26.52)	4.12	(4.23)	9.52	(9.28)
$Ba[Co(mida)(\beta\text{-}ala\text{-}gly)]_2\cdot 2H_2O$	27.53	(27.62)	3.81	(3.94)	10.13	(9.66)
$Ba[Co(mida)(L\text{-}ala\text{-}\beta\text{-}ala)]_2\cdot 6H_2O$	26.94	(27.25)	4.82	(4.78)	8.87	(8.68)
$Ba[Co(mida)(\beta\text{-}ala\text{-}L\text{-}ala)]_2\cdot 3H_2O$	28.81	(28.85)	4.07	(4.40)	8.87	(9.18)
$K[Co(\beta\text{-}ala\text{-}gly)_2]\cdot H_2O$	29.64	(29.71)	4.51	(4.49)	14.33	(13.83)
$[Co(NH_3)_3(gly\text{-}\beta\text{-}ala)]Cl\cdot H_2O$	19.68	(19.52)	6.30	(6.23)	23.11	(22.77)

was separated from by-products on a SP-Sephadex C-25 column (4.5 cm × 50 cm) by elution with 0.05 M KCl solution. Potassium chloride was removed by the same method as that described above. The complex obtained was recrystallized from an aqueous solution by addition of ethanol.

$K[Co(\beta\text{-}ala\text{-}gly)_2]\cdot H_2O$: β-Alanylglycine hydrobromide (2.27 g, 0.01 mol) was dissolved in water (10 cm^3). The solution was adjusted to pH *ca.* 9.5 with sodium hydroxide. An aqueous solution containing $Co(NO_3)_2\cdot 6H_2O$ (1.46 g, 5 mmol) in water (10 cm^3) was added drop-by-drop to the above solution, adjusting the pH of the solution at *ca.* 9.5 with NaOH. After an addition of activated charcoal (0.5 g) the mixed solution was oxidized by an air stream for 12 h. The reactant solution was chromatographed on a QAE-Sephadex A-25 column (4.5 cm × 90 cm). The objective complex was eluted with 0.05 M KCl, and KCl was removed by the same method as that for the $Ba[Co(mida)(gly\text{-}L\text{-}ala)]_2$ complex. The complex was recrystallized from water by addition of ethanol and acetone.

Measurements. The absorption spectra were measured by a Hitachi 557-type spectrophotometer and the CD spectra by a JASCO J-22 spectropolarimeter. The proton NMR spectra were recorded on a JEOL MH-100 spectromcter with DSS as an internal reference.

Results and Discussion

The mixed ligand complexes, $[Co(mida)(\alpha_1\text{-}\alpha_2)]^-$, were conveniently prepared by the oxidation of the aqueous solutions containing cobalt(II) chloride, dipeptide, and H_2mida with lead dioxide, but this preparative method gave also substantial quantities of by-products: $[Co(mida)_2]^-$, $[Co(\alpha_1\text{-}\alpha_2)_2]^-$, and others. The yields of the mixed ligand complexes depend very much on the pH of the reaction solutions; at low pH (*ca.* 7) a large amount of $[Co(mida)_2]^-$ and minor products were formed, and at high pH (*ca.* 11) the initially formed precipitate (presumably cobalt(II) hydroxide) prevented the formation of the mixed type complexes. The pH range of 9 to 10 was most suitable for the preparation of the mixed type complexes; the racemization of active peptides may also be ignored in this pH range.[3] With the dipeptides containing β-alanine, however, the reactions were carried out in the pH range of 8 to 9 to prevent the formation of precipitate.

The $[Co(mida)(\alpha_1\text{-}\alpha_2)]^-$ anion was separated from other uninegative complexes, $[Co(mida)_2]^-$ and $[Co(\alpha_1\text{-}\alpha_2)_2]^-$, on a QAE-Sephadex A-25 column by elution with 0.05 M KCl. The order of the elutions was: $[Co(\alpha_1\text{-}\alpha_2)_2]^-$, $[Co(mida)_2]^-$, and $[Co(mida)(\alpha_1\text{-}\alpha_2)]^-$. In the cases of the β-alanylglycine and β-alanyl-L-alanine, however, the $[Co(mida)(\beta\text{-}ala\text{-}\alpha_2)]^-$ was eluted faster than the $[Co(mida)_2]^-$ anion. For all the peptides used here, it was difficult to separate completely $[Co(mida)(\alpha_1\text{-}\alpha_2)]^-$ from $[Co(mida)_2]^-$ on a QAE-Sephadex column, but these complexes could be separated by the different solubility of their potassium salts in a mixed solvent of methanol–water. Partial separation of these complexes also occurs on a Sephadex G-10 column. The potassium salts of the $[Co(mida)(\alpha_1\text{-}\alpha_2)]^-$ could not be often obtained in crystal state, because they are very hygroscopic. Accordingly, the salts were converted to the barium salts to give crystalline products.

Proton NMR Spectra. The dipeptide containing only α-amino acids coordinates to cobalt(III) in meridional configuration, and the chelate rings of the dipeptide ligand take the coplanar form. This has been established for the bis(glycylglycinato) complex by two independent X-ray crystallographic studies.[2,9] The ^{1}H-NMR spectrum of $[Co(mida)(gly\text{-}gly)]^-$ in slightly basic D_2O shows only one AB pattern (δ_A=4.42, δ_B=4.02 ppm, J_{gem}=16.5 Hz) for the two CH_2 groups of mida, indicating that both gly-gly and mida adopt the *mer* disposition.[5] An additional support for the *mer* structure of $[Co(mida)(gly\text{-}gly)]^-$ is provided by ^{13}C-NMR data; the peaks at 66.1 and 183.1 ppm can be assigned to two methylene and two carboxyl carbons, respectively, indicating an equivalence of the two acetate groups in mida ligand. The ^{1}H-NMR data of other $[Co(mida)(\alpha_1\text{-}\alpha_2)]^-$ in slightly basic D_2O are listed in Table 2. With the dipeptides containing only α-amino acids, the structure of these complexes can be also concluded to be *mer* on the basis of the ^{1}H-NMR data of the mida ligand. In the spectra of $[Co(mida)(gly\text{-}L\text{-}ala)]^-$ and $[Co(mida)(gly\text{-}L\text{-}leu)]^-$, the signal of the C-terminal methine proton can not be assigned clearly because of the overlap of the methylene signals of mida. The same situation is also realized in $[Co(mida)(L\text{-}leu\text{-}gly)]^-$; the resonances due

TABLE 2. ^{1}H-NMR DATA OF THE TYPE [Co(mida)(α_1-α_2)]$^-$ COMPLEXES

α_1-α_2	Mida(ppm)			N-Terminal (α_1) (ppm)		C-Terminal (α_2) (ppm)	
	-CH_2-	(AB, J(Hz))	CH_3 (s)	-CH_2-(-CH-)	-CH_2-CH_2-	-CH_2-(-CH-)	-CH_2-CH_2-
gly-gly	4.42	4.02(16.5)	3.07	3.47(s)		4.35(s)	
gly-L-ala	4.42	3.99(17.0)	3.02	3.49(s)		a)	
L-ala-gly	4.42	4.00(16.5)	3.08	3.61(q, J=7.0)		4.36(s)	
gly-L-leu	4.41	3.93(16.5)	3.00	3.53, 3.38(AB, J=16.0)		a)	
L-leu-gly	4.39	3.97(16.5)	3.09	3.54(br)		4.35, 4.38 a)	b)
gly-β-ala	4.53	3.75(16.5)	2.94	3.37(s)			2.47(br), 3.61(br)
β-ala-gly	4.50	3.70(17.0)	2.74		2.58(s)	4.20(s)	
L-ala-β-ala	4.55	3.80(16.5)	3.01	a)			2.50(br), 3.63(br)
β-ala-L-ala	4.51	3.76(16.5)	2.74		2.59(br, s)	a)	

AB: AB pattern resonance, s: singlet, q: quartet, br: broad.
a) Obscured by overlap of another resonance. b) Inside components of AB pattern.

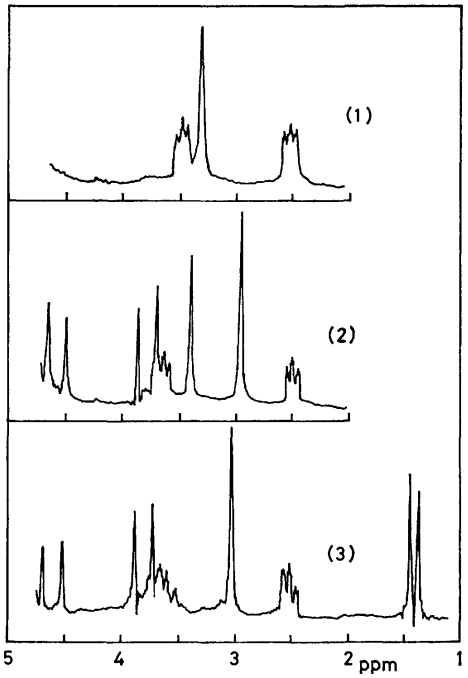

Fig. 1. The ^{1}H-NMR spectra of [Co(NH_3)$_3$(gly-β-ala)]$^+$ (1), [Co(mida)(gly-β-ala)]$^-$ (2), and [Co(mida)(L-ala-β-ala)]$^-$ (3) in alkaline D_2O.

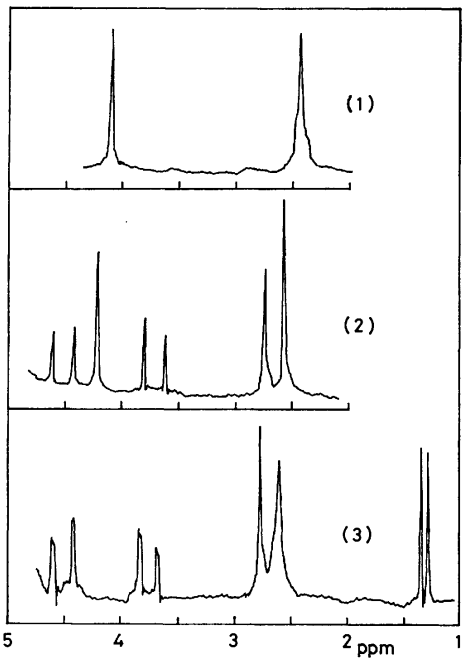

Fig. 2. The ^{1}H-NMR spectra of [Co(β-ala-gly)$_2$]$^-$ (1), [Co(mida)(β-ala-gly)]$^-$ (2), and [Co(mida)(β-ala-L-ala)]$^-$ (3) in alkaline D_2O.

to the C-terminal CH_2 which are only slightly inequivalent (4.35 and 4.38 ppm) are overlapped by one component of the resonances due to the CH_2 of mida. In the present study, the [Co(mida)(L-leu-gly)]$^-$ is the only example in which the C-terminal CH_2 protons are inequivalent at 100 MHz.

Examination of molecular models indicates that the dipeptides containing β-alanine can coordinate to cobalt(III) in both *mer* and *fac* configurations. On the other hand, the mida ligand adopts preferably the *fac* disposition, although the *mer*-K[Co(mida)$_2$] has been stably isolated.[10] Figure 1 shows the comparison among the ^{1}H-NMR spectra of [Co(NH_3)$_3$-(gly-β-ala)]$^+$, [Co(mida)(gly-β-ala)]$^-$, and [Co(mida)-(L-ala-β-ala)]$^-$ ions in slightly basic D_2O. The spectrum of [Co(NH_3)$_3$(gly-β-ala)]$^+$ exhibits three resonance peaks: a singlet signal due to the N-terminal CH_2 at 3.28 and two broad triplet-like peaks due to the C-terminal -CH_2-CH_2- at 2.50 and 3.45 ppm. In the [Co(mida)(gly-β-ala)]$^-$ complex, the resonances of the gly-β-ala ligand are analogous to those of [Co-(NH_3)$_3$(gly-β-ala)]$^+$, and an AB pattern in the range of 3.66 to 4.62 ppm can be assigned to the two CH_2 groups of mida, giving a hint of the equivalence of the two methylenes. This spectrum supports the assertion that the [Co(mida)(gly-β-ala)]$^-$ complex has the *mer* configuration. The same situation is realized in the [Co(mida)(L-ala-β-ala)]$^-$ complex, in which only one AB pattern resonance due to the two CH_2 of mida indicates that the *mer* configuration is taken.

TABLE 3. ABSORPTION AND CD SPECTRA OF THE TYPE [Co(mida)(α_1-α_2)]$^-$ COMPLEXES IN THE d-d TRANSITION REGION MEASURED IN WATER

α_1-α_2	AB_{max} $\sigma/10^3$ cm^{-1} (log ε)			CD_{ext} $\sigma/10^3$ cm^{-1} ($\Delta\varepsilon$)		
gly-gly	17.30(2.18)	21.05(2.27)	25.97(2.12)			
gly-L-ala	17.04(2.24)	20.83(2.32)	25.06(2.19)	16.81(−0.62)	20.75(−0.59)	25.19(−0.68)
L-ala-gly	17.09(2.19)	20.88(2.29)	25.13(2.15)	16.31(−0.37)	20.75(−0.19)	25.71(−0.25)
gly-L-leu	17.12(2.21)	21.19(2.30)	25.51(2.19)	16.39(−1.22)	21.28(−1.06)	*ca.* 24.50 sh (−0.90)
L-leu-gly	17.09(2.22)	20.83(2.34)	25.32(2.17)	16.37(−0.51)	*ca.* 19.50 sh (−0.26)	25.77(−0.29)
gly-β-ala	16.84(2.20)	20.24(2.19)	25.32(2.13)			
β-ala-gly	16.75(2.21)	20.41(1.85)	25.38(2.31)			
L-ala-β-ala	16.72(2.23)	20.41(2.21)	25.19(2.17)	16.39(−0.60)	20.75(+0.08)	24.69(−0.51)
β-ala-L-ala	16.67(2.20)	20.41(1.85)	25.45(2.33)	16.08(−1.13)	20.53(+1.83)	25.00(−3.71)

sh: Shoulder.

The complex, [Co(β-ala-gly)$_2$]$^-$, shows a simple NMR spectrum (Fig. 2). The two peaks with the relative intensity of 2:1 at 2.43 and 4.12 ppm can be assigned to the N-terminal $-CH_2-CH_2-$ and C-terminal CH_2 protons, respectively. In the spectrum of [Co(mida)(β-ala-gly)]$^-$, the two singlets at 2.58 and 4.20 ppm can be assigned to the N-terminal $-CH_2-CH_2-$ and C-terminal CH_2 protons, respectively, and the AB pattern (δ_A=4.50, δ_B=3.70 ppm, J_{gem}=17.0 Hz) to the two CH_2 groups of mida. It is also suggested that the configuration of [Co(mida)(β-ala-gly)]$^-$ is *mer*. A singlet resonance which arises from the $-CH_2-CH_2-$ group of the β-ala-gly in these complexes is in accordance with the data observed for the *cis*(N)*trans*-(O_g,N)-[Co(β-ala)(gly)(ox)]$^-$ complex.[11]

In the case of the dipeptide complexes containing β-alanine, the chelate rings of the coordinated dipeptide are not coplanar. Consequently, the conformational isomerism due to the puckered β-alanine ring can be expected for the [Co(mida)(α_1-β-ala)]$^-$ or the [Co(mida)(β-ala-α_2)]$^-$. However, the interconversion between the ring conformations is presumed to be easy. The simple ^{1}H-NMR spectra of β-alanyl groups in their complexes may be attributed to the rapid interconversion. The [Co(mida)(α_1-α_2)]$^-$ complex provides another problem of the conformational isomerism arising from the choice of the conformation of mida ligands: which is the methyl group of mida directed to, the C- or the N-terminal residue of dipeptide ligand? In all the [Co(mida)(α_1-α_2)]$^-$ complexes isolated in this work, the signal assigned to the methyl protons of mida exhibited a sharp singlet, suggesting an existence of only one isomer. Our present data are not sufficient to decide the conformation of the mida ligand. The possibility of the rapid interconversion between the two conformational isomers due to the methyl moiety may be ignored, because such interconversion requires the rupture of the coordinate bond.

Absorption Spectra. Figure 3 shows the absorption spectra of the [Co(mida)(gly-L-ala)]$^-$ and [Co(mida)(L-ala-gly)]$^-$ complexes together with their CD spectra. The absorption spectra of both complexes are quite similar to each other and also to that of [Co(mida)(gly-gly)]$^-$ (the spectra are little affected by the α-substituents in the N- and C-terminal residues of dipeptides). Such similarities were also observed in the spectra of [Co(mida)(gly-L-leu)]$^-$ and [Co(mida)(L-leu-gly)]$^-$ complexes. The spectral data are summarized in Table 3. The typical cobalt(III) chromophore of the type *mer*-[Co(N)$_3$(O)$_3$] shows two d-d transition bands (the lower-energy one is slightly split) with nearly equal intensity in the visible region.[6] However, the [Co(mida)(α_1-α_2)]$^-$ complexes show three bands in the visible region; two components in the lower-energy band region have enhanced intensities and are markedly separated from each other.

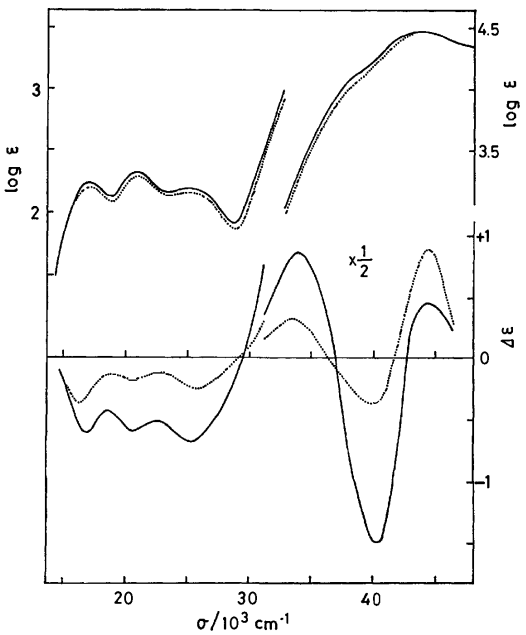

Fig. 3. The absorption and CD spectra of [Co(mida)(gly-L-ala)]$^-$ (——) and [Co(mida)(L-ala-gly)]$^-$ (·····) in water.

As shown in Fig. 4, the absorption spectrum of the [Co(mida)(L-ala-β-ala)]$^-$ complex is similar to that of the type [Co(mida)(α_1-α_2)]$^-$ complex in which both α_1 and α_2 are α-amino acid residues, though they differ from one another in the relative intensities of the two band components in the lower-energy band region. On the other hand, the [Co(mida)(β-ala-L-ala)]$^-$ (Fig. 4) shows the remarkably different absorption behavior in the d-d transition region, com-

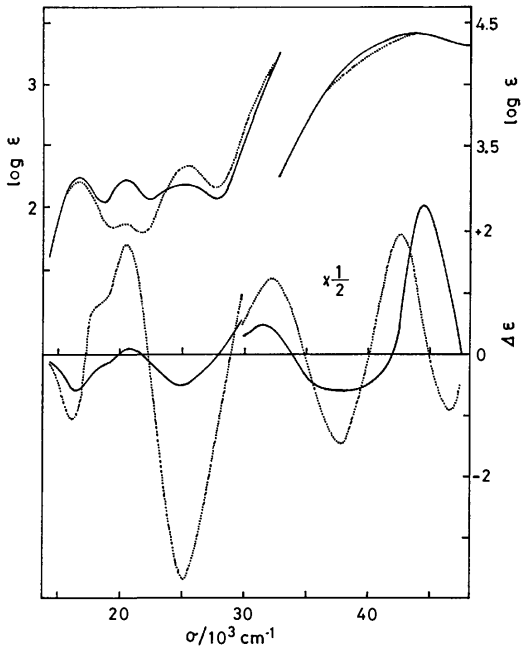

Fig. 4. The absorption and CD spectra of [Co(mida)(L-ala-β-ala)]⁻ (——) and [Co(mida)(β-ala-L-ala)]⁻ (·····) in water.

pared with those of the other [Co(mida)(α_1-α_2)]⁻ complexes; one of the split lower-energy bands has low intensity, but the higher-energy band has enhanced intensity. The spectrum of the [Co(mida)(β-ala-gly)]⁻ complex indicates quite similar behavior to that of the corresponding complex with β-ala-L-ala. Molecular models provide no obvious reasons for the difference between the spectral behaviors of the [Co(mida)(α_1-β-ala)]⁻ and [Co(mida)(β-ala-α_2)]⁻ complexes.

CD Spectra. Unlike the bis(dipeptidato)cobalt(III) complexes, the chelate rings forming the environment of the central cobalt are symmetrical in the [Co(mida)(α_1-α_2)]⁻ complex, ruling out any configurational contribution to the optical activity. Also, in the case of the dipeptide, α_1-α_2, where both α_1 and α_2 are α-amino acids, no conformational contribution to the optical activity can be invoked, because of the planarity of the entire dipeptide ligand. Therefore the sole source of optical activity in the d-d transition region is ascribed to the vicinal effect of the asymmetric carbon.[12]

Both the [Co(mida)(L-ala-gly)]⁻ and [Co(mida)(gly-L-ala)]⁻ complexes show three negative CD bands associated with three absorption bands in the visible region (Fig. 3 and Table 3). Similar CD spectra were obtained for the [Co(mida)(L-leu-gly)]⁻ and [Co(mida)(gly-L-leu)]⁻ complexes. It is remarkable that these complexes have a comparatively intense CD associated with the higher-energy d-d band. The asymmetry factor $g(=\Delta\varepsilon/\varepsilon)$ for the higher-energy d-d band is comparable to that for the lower-energy one, whereas in most optically active cobalt(III) complexes, the g value for the higher-energy band is much lower than that for the lower-energy band.[13] There is a large difference in the magnitude of $\Delta\varepsilon_{ext}$ between [Co(mida)(gly-L-ala)]⁻ and [Co(mida)(L-ala-gly)]⁻,

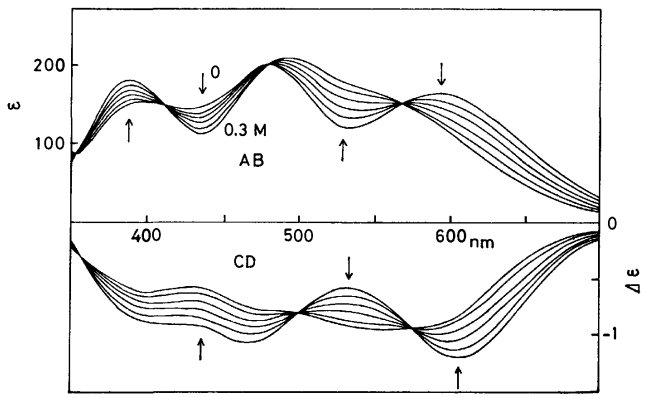

Fig. 5. The absorption (AB) and CD spectral changes of [Co(mida)(gly-L-leu)]⁻ in $HClO_4$ (0, 0.02, 0.05, 0.1, 0.2, 0.3 M).

which is not easy to explain, as the bis(dipeptidato)-complexes with these peptides have similar values of $\Delta\varepsilon_{ext}$. Also, this difference can not be attributed to the racemization of ligand during the synthesis of the complex, because in the weak alkaline solution only the C-terminal methylene or methine protons undergo the exchange reaction.[3]

As shown in Fig. 4, both the [Co(mida)(β-ala-L-ala)]⁻ and [Co(mida)(L-ala-β-ala)]⁻ complexes show the negative and positive CD bands associated with the lower-energy d-d transition and a strong negative CD band associated with higher-energy d-d transition. The CD data for these complexes also show that the magnitude of $\Delta\varepsilon_{ext}$ from the C-terminal active center is larger than that of $\Delta\varepsilon_{ext}$ from the N-terminal one. The [Co(mida)(β-ala-L-ala)]⁻ complex has extremely intense CD bands in the d-d transition region, especially in the higher-energy side. Though the puckering in the β-alanine-chelate ring of the β-ala-α_2 (or α_1-β-ala) ligand gives rise to some conformational contribution to the total CD, it is unlikely on the examination of molecular models that one conformation would be favored.

Protonation on [Co(mida)(α_1-α_2)]⁻. An example is described in detail of the protonation on the [Co(mida)(α_1-α_2)]⁻ species with glycyl-L-leucinate in acid solution. As shown in Fig. 5, on increasing the acid concentration, two components of the lower-energy d-d band approach each other and the higher-energy d-d band shifts to the higher-energy side with increasing of the intensity. The CD bands in the lower-energy d-d transition change in the same pattern as the absorption bands do, whereas the CD band in the higher-energy band region decreases in intensity. The changes of the absorption and CD spectra show isosbestic points and also are reversible, indicating that the changes are due to the protonation on the amide oxygen of the coordinated peptide,[14] and ruling out the successive protonation on the coordinated carboxyl group which has been proposed for the $[Co(NH_3)_3(\alpha_1\text{-}\alpha_2)]^+$ complexes.[4] The conjugate system of the amide group should be strikingly affected by the protonation following the spectral change. These acidic solutions were stable on standing at room temperature for several hours. The same situation was realized for

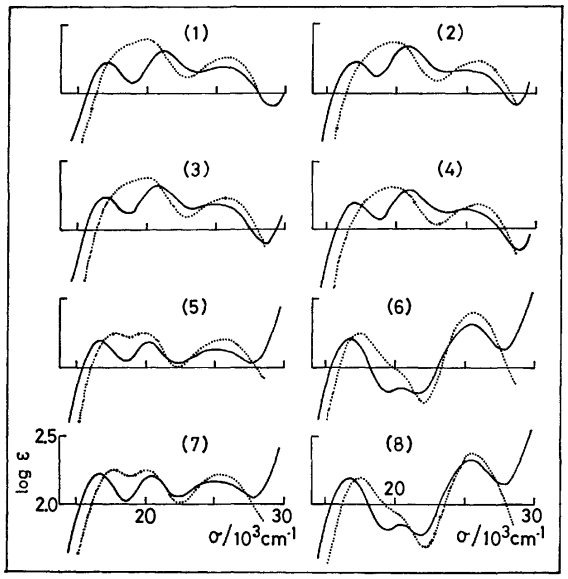

Fig. 6. The absorption spectra of the type [Co(mida)-$(\alpha_1\text{-}\alpha_2)$]$^-$ in water (——) and 60% $HClO_4$ (·····). $\alpha_1\text{-}\alpha_2$: (1) gly-L-leu, (2) L-leu-gly, (3) gly-L-ala, (4) L-ala-gly, (5) gly-β-ala, (6) β-ala-gly, (7) L-ala-β-ala, (8) β-ala-L-ala.

the other [Co(mida)$(\alpha_1\text{-}\alpha_2)$]$^-$ complexes examined. Figure 6 shows the comparison between the absorption spectra in water and in 60% $HClO_4$, *i.e.*, the spectra of the deprotonated and protonated type complexes. The spectral change caused by protonation is larger for the [Co(mida)$(\alpha_1\text{-}\alpha_2)$]$^-$ complex than for the [Co-$(\alpha_1\text{-}\alpha_2)_2$]$^-$ complex.

The protonation on the amide group intimately depends on the kind of dipeptide ligand; for the dipeptides containing β-alanine, especially N-terminal β-alanine, the protonation occurred in the weakly acidic solution, whereas for the dipeptides with N-terminal substituent, the protonation took place in the strongly acidic solution. However, it was impossible to calculate precisely the pK_a for the protonation on the amide group from the variation of ε or $\Delta\varepsilon$ with pH, because of the difficulty of the measurement of meaningful pH in strongly acidic solutions. The pK_a values estimated semi-quantitatively decreased in the following order:

[Co(mida)(β-ala-L-ala)]$^-$ ≃ [Co(mida)(β-ala-gly)]$^-$ > [Co(mida)(gly-β-ala)]$^-$ > [Co(mida)(L-ala-β-ala)]$^-$ > [Co(mida)(gly-L-leu)]$^-$ ≃ [Co(mida)(gly-L-ala)]$^-$ > [Co(mida)(gly-gly)]$^-$ > [Co(mida)(L-leu-gly)]$^-$ ≃ [Co(mida)(L-ala-gly)]$^-$.

This work was supported by a Grant-in-Aid for Scientific Research from the Ministry of Education, Science and Culture (No. 343012).

References

1) M. Fujioka, Y. Nakao, and A. Nakahara, *Bull. Chem. Soc. Jpn.*, **49**, 477 (1976); *J. Inorg. Nucl. Chem.*, **39**, 1885 (1977); Y. Nakao and A. Nakahara, *Bull. Chem. Soc. Jpn.*, **51**, 3522 (1978); T. Sakurai and A. Nakahara, *Inorg. Chem.*, **19**, 847 (1980); A. G. Lappin, C. K. Murray, and D. W. Margerum, *Inorg. Chem.*, **17**, 1630 (1978); S. T. Kirksey, Jr., T. A. Neubecker, and D. W. Margerum, *J. Am. Chem. Soc.*, **101**, 1631 (1979); N. Ueyama, M. Nakata, T. Araki, A. Nakamura, S. Yamashita, and T. Yamashita, *Chem. Lett.*, **1979**, 421; Y. Kuroda and H. Aiba, *J. Am. Chem. Soc.*, **101**, 6837 (1979); D. W. Appleton, T. P. A. Kruck, and B. Sarkar, *J. Inorg. Biochem.*, **10**, 1 (1979); R. E. Viola, C. R. Hartzell, and J. J. Villafranca, *ibid.*, **10**, 281, 293 (1979).
2) R. D. Gillard, E. D. McKenzie, R. Mason, and G. B. Robertson, *Nature*, **209**, 1347 (1966).
3) L. V. Boas, C. A. Evans, R. D. Gillard, P. R. Mitchell, and D. A. Phipps, *J. Chem. Soc., Dalton Trans.*, **1979**, 582.
4) I. G. Browning, R. D. Gillard, J. R. Lyons, P. R. Mitchell, and D. A. Phipps, *J. Chem. Soc., Dalton Trans.*, **1972**, 1815.
5) H. Kawaguchi, K. Maeda, T. Ama, and T. Yasui, *Chem. Lett.*, **1979**, 1105.
6) N. Matsuoka, J. Hidaka, and Y. Shimura, *Bull. Chem. Soc. Jpn.*, **40**, 1868 (1967).
7) G. J. Berchet, *Org. Synth.*, Coll. Vol. 2, 397 (1956).
8) N. Izumiya, M. Oono, T. Kato, and H. Aoyagi, "Peputido Goosei," Maruzen, Tokyo (1975).
9) M. T. Barnet, H. C. Freeman, D. A. Buckingham, I-Nan Hsu, and D. van der Helm, *Chem. Commun.*, **1970**, 368.
10) N. Koine, T. Tanigaki, J. Hidaka, and Y. Shimura, *Chem. Lett.*, **1980**, 871.
11) T. Ama, M. Higa, N. Koine, and T. Yasui, *Bull. Chem. Soc. Jpn.*, **50**, 2632 (1977).
12) Y. Shimura, *Bull. Chem. Soc. Jpn.*, **31**, 315 (1958).
13) W. Moffit, *J. Chem. Phys.*, **25**, 1189 (1956); L. I. Katzin, *Coord. Chem. Rev.*, **7**, 331 (1972).
14) The position of the protonation was suggested by Refs. 3 and 4.

Synthesis and Characterization of Cobalt(II), Nickel(II), and Copper(II) Complexes with 2-Furancarbaldehyde Oxime

Hiro KUMA, Kyoji MOTOBE, Wasuke MORI, and Shoichiro YAMADA*

Institute of Chemistry, College of General Education, Osaka University, Toyonaka, Osaka 560

(Received May 15, 1980)

Cobalt(II), nickel(II), and copper(II) complexes with 2-furancarbaldehyde oxime have been prepared and characterized mainly on the basis of electronic spectra and magnetic data. The cobalt(II) and nickel(II) complexes of the formula $MX_2(oxime)_4$ (X=Cl, Br) have been isolated. They are all six-coordinated, the oxime being coordinated as a unidentate through the nitrogen atom. Copper(II) forms complexes of the formula $CuX_2(oxime)_2$ (X=Cl, Br). Possible structures for these complexes are discussed.

It has recently been concluded that 2-thiophenecarbaldehyde oxime (Ia, abbreviated as tox in the present paper) forms metal complexes of the type $MCl_2(tox)_4$ and $MBr_2(tox)_4$, M being Co(II), Ni(II), and Zn(II). The ligand tox in these complexes is coordinated as a unidentate through the nitrogen atom,[1] contrary to the previous claim[2] that only complexes of the type $MCl_2(tox)_2$ could be isolated, *tox* in these complexes functioning as a bidentate through its nitrogen and sulfur atoms.

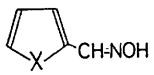

I

a: X=S, b: X=O

It was also claimed previously that 2-furancarbaldehyde oxime (Ib, abbreviated as *fox*) formed metal complexes of the type $MCl_2(fox)_2$, in which the ligand fox was coordinated as a bidentate through two oxygen atoms.[3,4] In view of our isolation of $MX_2(tox)_4$ instead of $MX_2(tox)_2$, reexamination of the metal complexes with fox is thought to be rewarding and significant. It is also interesting to examine whether or not the furan oxygen atom of fox may be coordinated with the metal ion.

Experimental

Materials. *syn*(α)- and *anti*(β)-2-Furancarbaldehyde oxime were prepared as reported previously.[5]

With *anti*-2-furancarbaldehyde oxime, all the metal complexes described below were synthesized successfully, their analytical data being given in Table1 . With *syn*-2-furancarbaldehyde oxime, however, the cobalt(II) and copper(II) complexes were synthesized in a similar manner, while attempts to isolate the nickel(II) complexes have so far been unsuccessful.

Dihalogenotetrakis(2-furancarbaldehyde oxime)cobalt(II), $CoX_2(fox)_4$ (X=Cl, Br). Cobalt(II) halide hexahydrate (10 mmol) was added to a solution of 2-furancarbaldehyde oxime (40 mmol) in ethanol (100 cm^3) at 50 °C. The reaction was continued for 2 h. A brown precipitate was recrystallized from methanol to give orange (X=Cl) and red-orange (X=Br) crystals.

$Co(NCS)_2$(fox)$_2$. A method similar to the dihalogeno complexes yielded only $Co(NCS)_2(fox)_2$ instead of $Co(NCS)_2(fox)_4$. The precipitate was recrystallized from methanol to give red-brown crystals. Attempts to isolate $Co(NCS)_2(fox)_4$ have so far been unsuccessful.

Dihalogenotetrakis(2-furancarbaldehyde oxime)nickel(II), NiX_2(fox)$_4$ (X=Cl, Br). These complexes were prepared as yellow-green crystals in a manner analogous to the corresponding cobalt(II) complexes. Recrystallization was carried out from methanol.

Ni(NCS)$_2$(fox)$_4$. A solution of nickel(II) thiocyanate (10 mmol) and fox (40 mmol) in ethanol (100 cm^3) was heated at 60 °C with stirring under reflux for 3 h. The solution was filtered and evaporated to about half the volume. A pale green precipitate was recrystallized from methanol-chloroform (3:7) to give green crystals.

The nickel(II) and cobalt(II) complexes described above are soluble in methanol, ethanol, and chloroform, but insoluble in benzene.

CuX_2(fox)$_2$ (X=Cl, Br). A suspension of anhydrous copper(II) halide (10 mmol) and fox (20 mmol) in ethanol (100 cm^3) was heated at 50 °C for 1 h. A brown precipitate was recrystallized from ethanol to yield red-brown (X=Cl) and dark brown (X=Br) needle-like crystals.

These copper(II) complexes are soluble in hot methanol and ethanol, but insoluble in chloroform.

Measurements. Electronic absorption spectra of the complexes were measured on a Shimadzu MPS-50L spectrophotometer. Infrared spectra were recorded as Nujol mulls using a Hitachi EPI-S2 infrared spectrophotometer and a Hitachi 215 infrared spectrophotometer.

Magnetic susceptibilities of the cobalt(II) and nickel(II) complexes were measured by the Gouy method at room temperature. Magnetic measurements with the copper(II) complexes were carried out in the temperature range of 4.2—300 K by the Faraday method using a Cahn balance.

Powder X-ray diffraction patterns were obtained with a Rigakudenki 4001-A2 diffractometer using Co $K\alpha$ radiation and an iron filter.

Results and Discussion

Nickel(II) Complexes. Previously a compound of composition $NiCl_2(fox)_2$ was reported and was claimed to contain the molecules of fox functioning as bidentate ligands.[3,4] In the present work, however, this complex could not be isolated, but compounds of the formula $NiX_2(fox)_4$ only were obtained, X being Cl, Br, and NCS.

The nickel(II) complexes prepared are paramagnetic and of a high spin type (Table 1). Their magnetic moments are in the range expected for the six-coordinate nickel(II) complexes.

The electronic absorption spectra of $NiCl_2(fox)_4$ and $NiBr_2(fox)_4$ are very similar to those of *trans*-$NiX_2(tox)_4$ (Fig. 1). Hence, it is presumed that $NiX_2(fox)_4$ (X=Cl, Br) have a six-coordinate *trans*-dihalogeno structure, in which the oxime molecules are bound through their nitrogen atoms as unidentate ligands with the nickel-

Table 1. Analytical data of nickel(II), cobalt(II), and copper(II) complexes with 2-furancarbaldehyde oxime

Compound	Found, %			Calcd, %			μ[a]
	C	H	N	C	H	N	
$NiCl_2(fox)_4$	41.57	3.65	9.90	41.85	3.51	9.76	3.23
$NiBr_2(fox)_4$	36.61	3.30	8.51	36.24	3.04	8.46	3.22
$Ni(NCS)_2(fox)_4$	42.82	3.26	13.57	42.67	3.22	13.52	3.23
$CoCl_2(fox)_4$	41.45	3.47	9.74	41.83	3.51	9.76	5.03
$CoBr_2(fox)_4$	36.22	3.28	8.54	36.24	3.04	8.45	5.11
$Co(NCS)_2(fox)_2$	36.03	2.81	13.90	36.27	2.54	14.10	4.90
$CuCl_2(fox)_2$	33.40	3.14	7.82	33.67	2.83	7.86	1.86
$CuBr_2(fox)_2$	27.17	2.58	6.48	26.95	2.23	6.29	1.88

a) μ: BM at room temperature.

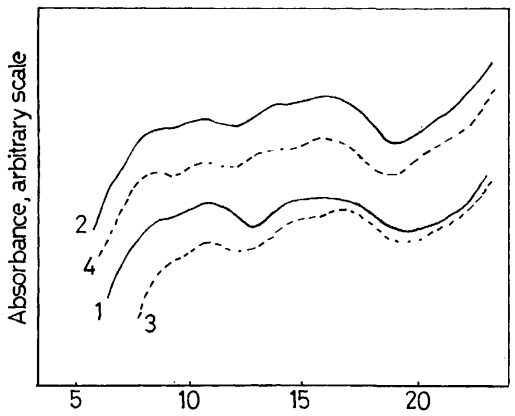

Fig. 1. Electronic absorption spectra of *trans*-$NiX_2(fox)_4$ (——) and *trans*-$NiX_2(tox)_4$ (----) in Nujol. 1: X=Cl, 2: X=Br, 3: X=Cl, 4: X=Br.

(II) ion. The powder X-ray diffraction pattern of $NiCl_2(fox)_4$ is similar to that of $NiBr_2(fox)_4$. The Ni–O (furan) vibration around 400—500 cm^{-1} previously reported for $NiCl_2(fox)_2$[4] was not observed for $NiCl_2(fox)_4$ prepared in the present work.

The approximate symmetry of *trans*-$NiX_2(fox)_4$ is D_{4h}. Six-coordinate nickel(II) complexes of O_h symmetry show three spin-allowed d-d bands, each of which is split into two components as the symmetry of the complexes changes from O_h to D_{4h}. The observed flat absorption curves are regarded as due to overlapping of split components of the d-d bands.

The complex $Ni(NCS)_2(fox)_4$ is paramagnetic with a moment of 3.2 BM, and its electronic absorption spectrum is typical of the six-coordinate nickel(II) complex (Table 2). Infrared O–N stretching, C–S stretching, and NCS bending vibrations occur at 2108, 830, and 470 cm^{-1}, respectively, indicating that the NCS^- ions are bound through the nitrogen atoms with the nickel(II) ion. Each of these bands appears as a single symmetrical peak, in agreement with the *trans*-diisothiocyanato structure.[6]

The d-d band splitting for *trans*-$Ni(NCS)_2(fox)_4$ may be small, since fox lies close to NCS^- in the spectrochemical series, both the ligands being coordinated through the nitrogen atom. The electronic spectrum

Table 2. Absorption maxima of metal(II) complexes with 2-furancarbaldehyde oxime

Compound	d-d bands 10^{-3} cm^{-1}
$Ni(NCS)_2(fox)_4$	8.9, 14.8, 25.6
$Ni(NCS)_2(py)_4$[a]	10.1, 16.7, 26.7
$Ni(NCS)_2(NH_3)_4$[b]	10.8, 17.4, 28.0
$CoCl_2(fox)_4$	9.1, 15.6 sh, 18.5
$CoBr_2(fox)_4$	8.8, 15.4 sh, 18.1
$CoCl_2(tox)_4$[c]	8.8, 15.3 sh, 18.6
$CoBr_2(tox)_4$[c]	8.7, 14.8 sh, 18.3
$Co(NCS)_2(fox)_2$	9.6, 15.1 sh, 19.2
$Co(NCS)_2(tox)_2$	9.1, 15.5 sh, 18.7

sh: Shoulder. a) O. Piovesana and C. Furlani, *J. Inorg. Nucl. Chem.*, **30**, 1249 (1968). b) Ref. 7. c) Ref. 1.

Table 3. Infrared ν(OH) and ν(C=N) frequencies of metal complexes with 2-furancarbaldehyde oxime

Compound	ν(OH) cm^{-1}	ν(C=N) cm^{-1}
$NiCl_2(fox)_4$	3225	1662
$NiBr_2(fox)_4$	3250	1662
$Ni(NCS)_2(fox)_4$	3210	1660
$CoCl_2(fox)_4$	3250	1660
$CoBr_2(fox)_4$	3260	1655
$Co(NCS)_2(fox)_2$	3430	1655
$CuCl_2(fox)_2$	3250	1660
$CuBr_2(fox)_2$	3260	1660
fox(anti-form)	3155	1645

of this complex is similar, in the shape of the whole curve as well as in the band maxima, to that of *trans*-$Ni(NCS)_2(NH_3)_4$, which also shows very slight splitting of the d-d bands.[7]

Just like the nickel(II) complexes with such a nitrogen-coordinating unidentate as tox,[1] the nickel(II) complexes with fox show hydrogen-bonded OH stretching vibrations at about 3200—3300 cm^{-1} (Table 3).

Cobalt(II) Complexes. Previously reported $CoCl_2(fox)_2$[3,4] has not been isolated, but $CoX_2(fox)_4$, X being Cl and Br, have been obtained in the present

TABLE 4. MAXIMA OF MAIN d-d BANDS OF COPPER(II) COMPLEXES WITH 2-FURANCARBALDEHYDE OXIME AND RELATED LIGANDS

Compound	d-d band 10^3 cm^{-1}
$CuCl_2(fox)_2$	14.3
$CuBr_2(fox)_2$	14.4
$CuCl_2(tox)_2$	14.3
$CuBr_2(tox)_2$	14.3
$CuCl_2(py)_2$	14.5
$CuBr_2(py)_2$	14.6

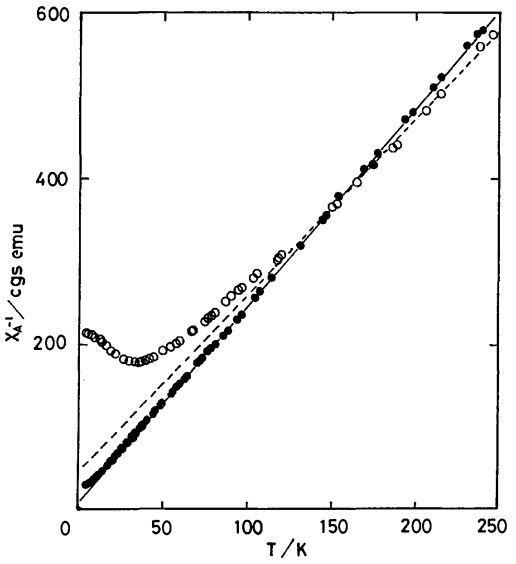

Fig. 2. Plots of reciprocal magnetic susceptibilities (corrected for the temperature-independent paramagnetism) of $CuX_2(fox)_2$ against absolute temperature. ●: Experimental for X=Cl, ○: experimental for X=Br. The solid line (X=Cl) and dashed line (X=Br) were derived theoretically from the Curie-Weiss law, θ and g being 4 K and 2.12 for X=Cl and 20 K and 2.25 for X=Br. The value for $N\alpha$ was assumed to be 60×10^{-6} cgs emu.

work. On the other hand, the complex $Co(NCS)_2(fox)_2$ has been isolated instead of $Co(NCS)_2(fox)_4$.

The complexes $CoX_2(fox)_4$ are paramagnetic with magnetic moments of 5.0—5.1 BM, which are in the range expected for the six-coordinate cobalt(II) complexes (Table 1), the d-d band maxima being nearly equal to those of *trans*-$CoX_2(tox)_4$ (Table 2). The powder X-ray pattern of $CoCl_2(fox)_4$ is very similar to that of $NiCl_2(fox)_4$, which has been presumed to have a *trans*-dihalogeno structure. It is very likely, therefore, that the complexes $CoX_2(fox)_4$ have a six-coordinate *trans*-dihalogeno structure, in which the ligands *fox* are coordinated as unidentate ligands to the cobalt(II) ion through the nitrogen atom, the oxygen atom in *fox* not being bound to the metal ion.

The complex $Co(NCS)_2(fox)_2$ is paramagnetic with a magnetic moment of 4.9 BM, which lies in the range expected for the six-coordinate cobalt(II) complex, Its electronic spectrum (Table 2) is also in agreement with this stereochemistry. Its infrared C–N stretching, C–S stretching, and NCS bending vibrations appear at 2100, 780, and 484 and 475 cm^{-1}. These values indicate the presence of the bridging NCS group on the basis of the previously proposed criteria.[8]

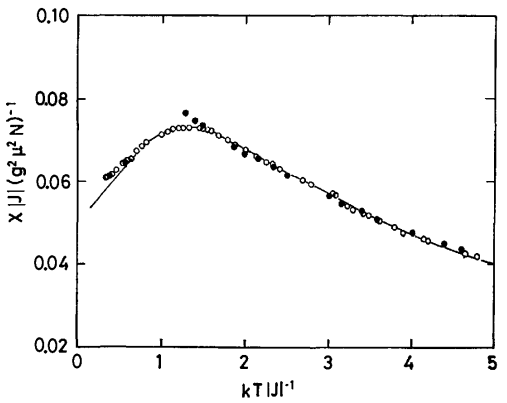

Fig. 3. Magnetic susceptibilities (corrected for the temperature-independent paramagnetism) of $CuX_2(fox)_2$. ●: Experimental for X=Cl, ○: experimental for X=Br. The solid curve was obtained by the method of Bonner and Fisher assuming the antiferromagnetic linear chain and on the basis of the Heisenberg model for the interaction between spins with $S=1/2$. For $CuCl_2(fox)_2$ $J/k=-3.5$ K, $g=2.06$, $N\alpha=60\times10^{-6}$ cgs emu and for $CuBr_2(fox)_2$ $J/k=-25$ K, $g=2.27$, $N\alpha=60\times10^{-6}$ cgs emu.

Exactly like the corresponding nickel(II) complexes,[1] $CoX_2(fox)_4$ exhibit hydrogen-bonded OH stretching vibrations at about 3200—3300 cm^{-1}, while $Co(NCS)_2(fox)_2$ shows a sharp OH band at a much higher frequency, indicative of the presence of the non-hydrogen-bonded NOH group (Table 3). When *fox* is bound with the metal ion, ν(C=N) and ν(N–O) frequencies of *fox* are found to shift toward higher frequencies. These findings are similar to those of the corresponding complexes with *acox* and *tox*, *acox* being acetaldehyde oxime. The Co–O(furan) vibration at about 400—500 cm^{-1}, which was reported previously for $CoCl_2(fox)_2$,[4] has not been observed with $CoX_2(fox)_4$ prepared in the present work.

Copper(II) Complexes. Two copper(II) complexes $CuX_2(fox)_2$, X being Cl and Br, have been obtained in the present work. In view of the results on the corresponding cobalt(II) and nickel(II) complexes and also on the metal complexes with related oximes,[1,9] it may be reasonable to assume that *fox* is coordinated as a unidentate ligand through its nitrogen atom in $CuX_2(fox)_2$.

Billing and Underhill examined correlation between electronic absorption spectra and stereochemistry of complexes of the type CuX_2L_2, L being pyridine and its derivatives.[10] On the basis of their conclusions, the stereochemistry of $CuX_2(tox)_2$ and $CuX_2(acox)_2$ was discussed with reasonable success in previous papers.[1,9] The d-d band maxima of $CuX_2(fox)_2$ are close to those of the multinuclear complexes $CuX_2(tox)_2$ and $CuX_2(py)_2$ (Table 4).[1] According to the criteria reported previously,[1,10] and in view of the present finding that *fox* lies very close to *tox*, *acox*, and *py* in the spectrochemical series, the electronic spectra

seem to indicate that $CuX_2(fox)_2$ most probably have a multinuclear structure similar to that of $CuX_2(tox)_2$, $CuX_2(acox)_2$, and $CuX_2(py)_2$, in which the copper(II) ions are six-coordinated with halide ions as bridges. The two complexes $CuCl_2(fox)_2$ and $CuBr_2(fox)_2$ have a similar structure, since they show similar powder X-ray diffraction patterns.

The copper(II) complexes with such a structure as assumed above are expected to exhibit the antiferromagnetism characteristic of the chain structure with bridges, –Cu–X–Cu–X–Cu–. Room temperature moments of $CuX_2(fox)_2$, which are 1.86 (X=Cl) and 1.88 BM (X=Br), differ very little from the normal moments. As shown in Fig. 2, the susceptibilities obey the Curie-Weiss law in the higher temperature range, the Curie-Weiss constants θ being 4 K for $CuCl_2(fox)_2$ and 20 K for $CuBr_2(fox)_2$. The temperature dependence of magnetic susceptibilities below 5 K is shown in Fig. 3. Except for deviation below 1.5 K for the chloro complex, the data are in good coincidence with the theoretical curves derived by the method of Bonner and Fisher,[11] which is based upon the assumption of an infinite one-dimensional Heisenberg spin lattice with $S=1/2$.

These findings combined may be regarded as supporting the assumption of the antiferromagnetic interaction through halide ions between copper ions in the proposed structure.

The present authors are grateful to Professor Masayoshi Obashi for powder X-ray diffraction patterns.

References

1) H. Kuma, K. Motobe, and S. Yamada, *Bull. Chem. Soc. Jpn.*, **51**, 1101 (1978).
2) M. P. Coakley and M. E. Casey, *J. Inorg. Nucl. Chem.*, **34**, 1937 (1972).
3) B. Sen and M. E. Pickerell, *J. Inorg. Nucl. Chem.*, **35**, 2573 (1973).
4) V. K. Gupta and A. N. Bhat, *Z. Naturforsch., Teil B*, **32**, 225 (1977).
5) O. L. Brady and R. F. Goldstein, *J. Chem. Soc.*, **1927**, 1960.
6) M. M. Chamberlain and J. C. Bailar, Jr., *J. Am. Chem. Soc.*, **81**, 6412 (1959).
7) C. R. Hare and C. J. Ballhausen, *J. Chem. Phys.*, **40**, 792 (1964).
8) S. M. Nelson and T. M. Shepherd, *J. Inorg. Nucl. Chem.*, **27**, 2123 (1965); R. A. Bailey, S. L. Kozak, T. W. Michelsen, and W. N. Mills, *Coord. Chem. Rev.*, **6**, 407 (1971).
9) H. Tanaka, H. Kuma, and S. Yamada, *Bull. Chem. Soc. Jpn.*, **50**, 3259 (1977).
10) D. E. Billing and A. E. Underhill, *J. Inorg. Nucl. Chem.*, **30**, 2147 (1968).
11) J. C. Bonner and M. E. Fisher, *Phys. Rev. A*, **135**, 640 (1964).

Synthesis and Characterization of Metal Complexes with Schiff Bases Obtained from *N,N'*-Bis(3-aminopropyl)piperazine and Salicylaldehyde Derivatives

Hiro KUMA and Shoichiro YAMADA*

Institute of Chemistry, College of General Education, Osaka University, Toyonaka, Osaka 560

(Received June 10, 1980)

Cobalt(II), nickel(II), cobalt(III), manganese(III), and iron(III) complexes have been synthesized with Schiff bases (abbreviated as X-sal-prpi) derived from *N,N'*-bis(3-aminopropyl)piperazine and salicylaldehyde derivatives. On the basis of electronic spectra, infrared spectra, and magnetic data, the structures of the metal complexes are discussed. Complexes of the type Co^{II}(X-sal-prpi) are five-coordinated, and M^{III}(X-sal-prpi)ClO_4 consist of six-coordinated $[M(X\text{-sal-prpi})]^+$ and free ClO_4^- ions, the ligands X-sal-prpi being quinquidentate in the former and sexadentate in the latter.

It was previously reported that the ligands X-salen-pip (Ia) with four donor atoms form cobalt(II) and nickel(II) complexes of the type M(X-salen-pip)$_2$, in which X-salen-pip serve as terdentate ligands, one of the four donor atoms not being bound to the metal ions.[1] It is now interesting to examine metal complexes with the similar ligands X-sal-prpi (Ib) having six donor atoms and compare the results with those of X-salen-pip.† The present paper describes synthesis and characterization of some 3d metal complexes with these new ligands, *i.e.*, Schiff bases obtained from *N,N'*-bis(3-aminopropyl)piperazine and salicylaldehyde derivatives.

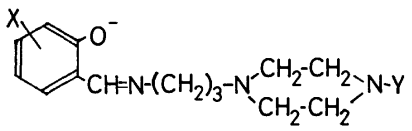

I

a: Y = H

b: Y = $-(CH_2)_3$-N=CH-

Experimental

Materials. The Schiff bases H(X-sal-prpi) (X=H, 5-Cl, 5-Br) were synthesized in the following way. *N,N'*-Bis(3-aminopropyl)piperazine (0.5 mol) was added gradually to a solution of X-salicylaldehyde (1 mol) in ethanol (300 ml), the reaction vessel being placed in an ice bath. The solution was stirred for 30 min. A yellow crystalline precipitate was collected by filtration and recrystallized from ethanol to give yellow crystals. Elemental analysis agreed with the empirical formulae of the compounds. Mp 76 (X=H), 106 (X=5-Cl), 113 °C (X=5-Br).

Ni(X-sal-prpi) (X=H, 5-Cl, 5-Br). To a solution of nickel(II) acetate tetrahydrate (10 mmol) in ethanol (100 ml) was added a Schiff base H(X-sal-prpi) (11 mmol) and the mixture was heated with stirring on a water bath at about 70 °C for 10 min, followed by addition of sodium acetate trihydrate (12.5 mmol); a green precipitate appeared in 30 min. The reaction was continued for 3 h and a green crystalline precipitate was collected by filtration and washed with hot methanol. Attempts to recrystallize the products from such solvents as chloroform and benzene have not been successful.

Co(X-sal-prpi) (X=5-Cl, 5-Br). These cobalt(II) complexes were prepared as red crystals in a manner similar to the corresponding nickel(II) complexes. Recrystallization was carried out from methanol.

[Co(X-sal-prpi)]ClO_4 (X=H, 5-Cl, 5-Br). Cobalt(II) acetate tetrahydrate (10 mmol) was added to a solution of H(X-sal-prpi) (11 mmol) in ethanol (100 ml), and the brown solution was heated on a water bath at about 65 °C for 10 min. Sodium acetate trihydrate (12.5 mmol) and sodium perchlorate (10 mmol) were added to the solution, and the reaction was continued for 3 h. A brown precipitate was recrystallized from methanol to give brown crystals. Molar conductivities (Λ/Ω^{-1} cm^2 mol^{-1}): 98.5 (X=H); 88.1 (X=5-Cl); 84.0 (X=5-Br).

[Mn(X-sal-prpi)]ClO_4 and [Fe(X-sal-prpi)]ClO_4 (X=H, 5-Cl, 5-Br). These complexes were prepared in a manner similar to the corresponding cobalt(III) complexes. The manganese(III) complexes were obtained as dark green crystals by recrystallization of the crude products from methanol or chloroform. The iron(III) complexes were isolated as dark brown crystals, recrystallization being carried out from ethanol. Λ/Ω^{-1} cm^2 mol^{-1}: 98.7 (X=H, Mn^{3+}); 102.2 (X=5-Cl, Mn^{3+}); 98.8 (X=5-Br, Mn^{3+}); 95.0 (X=H, Fe^{3+}); 89.4 (X=5-Br, Fe^{3+}).

Analytical data of the complexes prepared in the present work are shown in Table 1.

Measurements. Electronic absorption spectra of the complexes were measured on a Shimadzu MPS-50L spectrophotometer. The absorption maxima of the metal complexes in solution are almost coincident with those of the same complexes in the solid state. Infrared spectra were recorded as Nujol mulls using a Hitachi 215 infrared spectrophotometer. Magnetic measurements at room temperature were carried out by the Gouy method using $CoHg(SCN)_4$ as a calibrant. Conductivity measurements with methanolic solutions were carried out using a calibrated Toa-Electronics CG 201 PL conductivity cell and a Toa-Electronics Model CM-1DB conductivity bridge. The concentration of the solutions was 1/2000 mol dm^{-3}. The conductivity measurement with [Fe(5-Cl-sal-prpi)]ClO_4 was not carried out because of its low solubility in appropriate solvents.

Results and Discussion

Bivalent Metal Complexes. With cobalt(II) and nickel(II), complexes of the type M^{II}(X-sal-prpi) were isolated (Table 1). Since the nickel(II) complex is diamagnetic and shows a d-d band at 16.1×10^3 cm^{-1}, it is presumed that the nickel(II) ion in this complex

† For X=H, these ligands are abbreviated as salen-pip and sal-prpi, respectively.

Table 1. Analytical data of metal complexes of the types M(X-sal-prpi) and [M(X-sal-prpi)]ClO_4

Compound	Mp °C	Found, %			Calcd, %			μ[a]
		C	H	N	C	H	N	
Ni(sal-prpi)	dec	61.66	6.58	12.13	61.96	6.50	12.04	dia
Co(5-Cl-sal-prpi)	206	54.16	5.22	10.52	53.94	5.28	10.49	4.58
Co(5-Br-sal-prpi)	232	46.03	4.61	8.84	46.25	4.53	8.99	4.50
Co(sal-prpi)ClO_4	235	50.58	5.48	9.89	51.02	5.35	9.92	dia
Co(5-Cl-sal-prpi)ClO_4	206	45.16	4.83	8.33	45.48	4.75	8.54	dia
Co(5-Br-sal-prpi)ClO_4	232	40.13	4.31	7.66	39.88	3.90	7.75	dia
Fe(sal-prpi)ClO_4	214	51.28	5.45	10.00	51.30	5.38	9.97	5.94
Fe(5-Cl-sal-prpi)ClO_4	244	45.70	4.40	9.13	45.70	4.47	8.88	5.98
Fe(5-Br-sal-prpi)ClO_4	236	39.97	3.89	8.10	40.05	3.92	7.79	5.93
Mn(sal-prpi)ClO_4	dec	51.09	5.54	9.98	51.39	5.39	9.99	5.07
Mn(5-Cl-sal-prpi)ClO_4[b]	98[c]	35.92	3.59	6.41	35.95	3.48	6.45	4.95
Mn(5-Br-sal-prpi)ClO_4[b]	85[c]	32.97	3.16	5.95	32.61	3.16	5.85	4.96

a) μ: BM at room temperature. b) 2 $CHCl_3$ adduct. c) The low melting point may be due to the inclusion of the chloroform molecules.

Table 2. Main d-d absorption bands of Co(X-sal-prpi) and [M(X-sal-prpi)]ClO_4

Compound	Solvent	ν (log ε)
Co(5-Cl-sal-prpi)	$CHCl_3$	7.8(0.7)sh, 9.3(0.8), 12.0(0.7)sh, 18.2(1.5)
Co(5-Br-sal-prpi)	$CHCl_3$	7.8(0.7)sh, 9.3(0.8), 12.2(0.75)sh, 18.1(1.5)
[Co(sal-prpi)]ClO_4	CH_3OH	16.0(2.25)sh, 20.0(2.75)
[Co(5-Cl-sal-prpi)]ClO_4	CH_3OH	16.0(2.3)sh, 20.0(2.8)
[Co(5-Br-sal-prpi)]ClO_4	CH_3OH	15.9(2.3)sh, 20.0(2.8)
[Mn(sal-prpi)]ClO_4	CH_3OH	16.2(2.75)
[Mn(5-Cl-sal-prpi)]ClO_4	CH_3OH	15.9(2.77)
[Mn(5-Br-sal-prpi)]ClO_4	CH_3OH	15.7(2.77)

ν: 10^3 cm^{-1}. sh: Shoulder.

is planar four-coordinated. This complex does not show a sharp melting point, and is probably polymeric. From the experimental data so far available, it is difficult to draw a definite conclusion about its precise structure.

Contrary to the nickel(II) complex, the cobalt(II) complexes Co(X-sal-prpi) show sharp melting points. They are paramagnetic (Table 1), and their electronic spectra have d-d bands typical of the five-coordinated cobalt(II) complexes, as shown in Fig. 1 and Table 2. It is thus found that five of the six donor atoms in the ligands are coordinated to cobalt(II) ion.

Infrared C=N frequencies of the cobalt(II) complexes are at lower frequencies than those of the free ligands (Table 3), and appear as a single peak, implying that the two imine nitrogen atoms of the ligands are coordinated to the metal ion. Similarly, infrared bands of the free ligands at about 1560—1570 cm^{-1}, which are usually ascribed to C–O vibrations, appear as a single peak and are shifted toward appreciably lower frequencies as the ligands are bound to the cobalt(II) ion, implying that the two phenolic oxygen atoms of the ligands are bound to the cobalt(II) ion. These facts lead to the presumption that only one of the two tertiary nitrogen atoms of the ligands is bound to the cobalt(II) ion in these complexes.

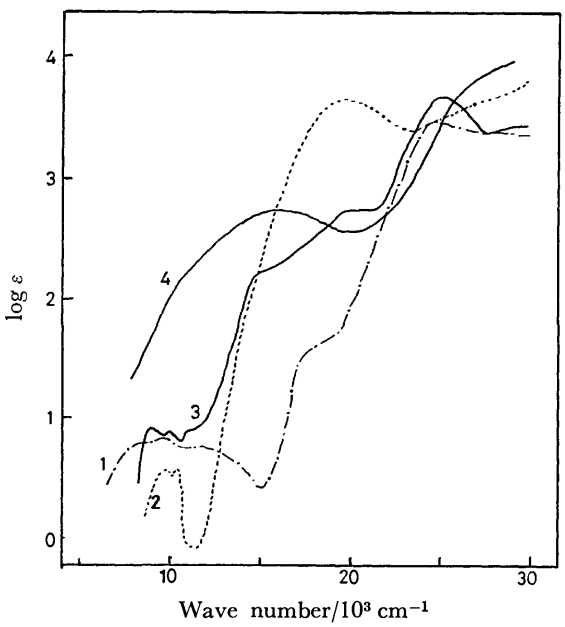

Fig. 1. Electronic absorption spectra: 1, Co(5-Cl-sal-prpi), in chloroform; 2, [Fe(sal-prpi)]ClO_4, in methanol; 3, [Co(sal-prpi)]ClO_4, in methanol; 4, [Mn(sal-prpi)]ClO_4, in methanol.

TABLE 3. MAIN INFRARED ABSORPTION BANDS OF M(X-sal-prpi) AND [M(X-sal-prpi)]ClO_4

Compound	ν(C=N) cm^{-1}	ν(C-O) cm^{-1}
H(sal-prpi)	1635	1565
H(5-Cl-sal-prpi)	1625	1570
H(5-Br-sal-prpi)	1625	1560
Ni(sal-prpi)	1615	1540
Co(5-Cl-sal-prpi)	1618	1518
Co(5-Br-sal-prpi)	1618	1512
[Co(sal-prpi)]ClO_4	1620	1540
[Co(5-Cl-sal-prpi)]ClO_4	1618	1520
[Co(5-Br-sal-prpi)]ClO_4	1618	1520
[Mn(sal-prpi)]ClO_4	1610	1545
[Mn(5-Cl-sal-prpi)]ClO_4	1600	1530
[Mn[5-Br-sal-prpi)]ClO_4	1600	1525
[Fe(sal-prpi)]ClO_4	1610	1545
[Fe(5-Cl-sal-prpi)]ClO_4	1610	1530
[Fe(5-Br-sal-prpi)]ClO_4	1610	1527

Tervalent Metal Complexes. With manganese(III), iron(III), and cobalt(III), complexes of the type M^{III}(X-sal-prpi)ClO_4 were isolated. The perchlorate ion in these complexes is not coordinated, since a broad infrared band due to the free perchlorate ion appears at about 1040 to 1110 cm^{-1}.[2] This is borne out by their electric conductivities, which are found to be in the range between 89 and 103 Ω^{-1} cm^2 mol^{-1}, showing that they are 1:1 electrolytes.[3] As shown in Table 3, stretching C=N and C–O frequencies of the complexes lie at lower frequencies than those of the free ligands, and each of them appears as a single peak, implying that the two imine nitrogen atoms and two phenolic oxygen atoms are bound to the metal ion.

The cobalt(III) complexes are diamagnetic. Judging from the general tendency of the cobalt(III) ion, the low spin cobalt(III) complexes obtained in the present work are reasonably assumed to be six-coordinated. Their electronic absorption spectra, which are similar to each other, are also in agreement with this view. Examination of the model shows that in the most favourable structure the four nitrogen atoms occupy the coordination sites at the corners of the square, the two oxygen atoms being *trans* to each other. The d-d band at about 14 to 21×10^3 cm^{-1}, which is assigned to the $^1T_{1g}\leftarrow{}^1A_{1g}$ transition in the O_h symmetry scheme, is found to be composed of two components, as may be seen in Fig. 1 and Table 2. The significant band splitting seems to support the *trans*-configuration.[4]

The manganese(III) and iron(III) complexes are of a high spin type (Table 1). Infrared spectra of M(X-sal-prpi)ClO_4, M being Mn(III) and Fe(III), are similar to those of Co(X-sal-prpi)ClO_4 in the whole region from 650 to 4000 cm^{-1}. All the infrared bands are almost coincident with the corresponding bands of the cobalt(III) complexes. It is thus very likely that the coordination mode of the multidentate ligands X-sal-prpi is similar in the manganese(III), iron(III), and cobalt(III) complexes.

The manganese(III) complexes exhibit a broad d-d band at about 16×10^3 cm^{-1}, which may be assigned, in the octahedral group, to the $^5T_{2g}\leftarrow{}^5E_g$ transition.[5]

In the spectra of the iron(III) complexes some feeble, sharp spin-forbidden d-d bands appear at about 10×10^3 cm^{-1}. However, most of the spin-forbidden bands are hidden under an intense metal-to-ligand charge transfer band, whose maximum occurs at 19.5 (X=H), 19.1 (X=5-Cl), and 19.2×10^3 cm^{-1} (X=5-Br).

All these findings combined show that the manganese(III) and iron(III) complexes most probably have a configuration similar to that of the corresponding cobalt(III) complexes, namely a *trans*-six-coordinated $(N)_4(O)_2$ configuration.

References

1) H. Kuma and S. Yamada, *Bull. Chem. Soc. Jpn.*, **49**, 2635 (1976).
2) K. Nakamoto, "Infrared Spectra of Inorganic and Coordination Compounds," Wiley-Interscience, New York (1970).
3) W. J. Geary, *Coord. Chem. Rev.*, **7**, 81 (1971).
4) S. Yamada, *Coord. Chem. Rev.*, **2**, 83 (1967).
5) A. B. P. Lever, "Inorganic Electronic Spectroscopy," Elsevier, Amsterdam (1968).

The Regiospecific Mono Tosylation of Cyclodextrins

Shigeharu Onozuka, Masayoshi Kojima, Kenjiro Hattori,† and Fujio Toda*

Department of Synthetic Chemistry, Faculty of Engineering, The University of Tokyo, Hongo, Bunkyo-ku, Tokyo 113

† *Department of Industrial Chemistry, Faculty of Engineering, Tokyo Institute of Polytechnics, Atsugi 243-02*

(Received November 8, 1979)

α- and β-Cyclodextrins were tosylated with tosyl chloride in an alkaline solution. The products were confirmed to be monotosylated compounds, and the tosyl group was introduced at the C-3 position of one glucose unit of the cyclodextrin molecule. The 1:1 complex formation of cyclodextrin with tosyl chloride was observed spectrometrically.

Cyclodextrins (CD) have been shown to form inclusion complexes with many kinds of molecules. For this reason, CD has been used to simulate an enzyme action.[1-3] Bender *et al.* showed enzyme-like actions of CD, that is, a large rate enhancement and stereospecificity in ester hydrolysis, and saturation and competitive inhibition phenomena, kinetically.[4,5]

In order to prepare a better enzyme model, several modified cyclodextrins have been synthesized. For example, Cramer and Mackensen synthesized imidazole-containing cyclodextrins by tosylation techniques in organic solvents.[6-8] In these procedures, one or more primary hydroxyl group(s) of cyclodextrins were modified, and so it was difficult to prepare regiospecific monosubstituted cyclodextrins. The introduction of an imidazole group of the primary hydroxyl side of cyclodextrins resulted in only a slight rate enhancement. It was not clearly ascertained if the formation of cyclodextrin acylate in an aqueous solution proceeded through complexation, but the benzoate group was attached on the secondary hydroxyl side.[5,9,10]

Another route to attach functionality on the secondary hydroxyl side of cyclodextrin is carboxymethylation by using the anion of dimethylsulfoxide. Bender's group introduced hydroxamic-acid derivatives on the more open face of the cyclodextrin molecule by using this method.[11,12] Imidazole-containing α-cyclodextrin, the catalytic group of which was introduced on a glucose unit, was prepared *via* monotosylated cyclodextrin in an aqueous solution.[13]

In this paper, we wish to report a simple, useful method for the preparation of regiospecific monotosylated cyclodextrins, the tosyl group of which is introduced on the secondary alcohol side of cyclodextrin accompanying 1:1 complex formation between tolylsulfonyl chloride and cyclodextrin in an aqueous solution. We also wish to suggest the mechanism of this regiospecific tosylation.

Experimental

p-Tolylsulfonyl-β-cyclodextrin. β-Cyclodextrin (1 g) was dissolved in a 0.15 M (1 M=1 mol dm^{-3}) sodium hydroxide solution (40 ml) with a pH of around 13.0. *p*-Tolylsulfonyl chloride (1 g) was dissolved in a minimum quantity of acetonitrile, after which the solution was magnetically stirred, drop by drop, into the alkaline solution. The suspension was then vigorously stirred for 1 h, adding 1 M NaOH occasionally to maintain the pH of the solution at more than 12.5. The reaction was terminated by neutralization with 1 M hydrochloric acid. The reaction mixture was filtered *in vacuo* to remove the unreacted *p*-tolylsulfonyl chloride, and then the filtrate was passed through a column with a cation-anion exchanger (Amberlite MB-3 ϕ 1.5×50 cm) and eluted with water. The desalted eluate was condensed and dried with a water bath *in vacuo*. The HPLC data, obtained using a OSD-SIL column (Tokyo Soda LS-410, ϕ 0.5×30 cm) eluted with 10% acetonitrile in water and detected by UV absorption at 254 nm, indicated there were more than 20 species in this crude product. The purity, calculated on the basis of the UV peak area, showed 70% of the main product. The present crude tosyl-CD (*ca.* 0.9 g) was dissolved in a minimum amount of water, and then the solution poured into a large amount of methanol (150 ml). The methanol solution was filtered and evaporated to dryness. The residue from the methanol (0.6 g) was dissolved again in warm water (9 ml, 60 °C) and filtered. The solution was left in a refrigerator at 5 °C for a few days. The white crystalline product was collected by filtration and dried *in vacuo* (0.4 g). In submitting the sample to elemental analysis, the present product (1 g) was further purified by a combination of various types of column chromatography. The aqueous solution was passed through porous polystyrene gel (ϕ 3×20 cm, DIAION HP-20). The column was washed with water, and the trapped component was eluated by the use of 30% aqueous methanol. The fractions containing tosylated CD were indicated by UV absorption, refractive index, and optical rotation, and were then collected and liophilized. Also, the product was purified by the use of gel chromatography (Sephadex G-15, ϕ 3×100 cm), eluated with water as well as a Lober column (ϕ 2.5×31 cm, Merck) and eluated with 10% acetonitrile in water. The yield was 0.1—0.3 g for each column chromatography. The purity was confirmed by HPLC and ^{1}H-NMR. Mp 168—170 °C (dec). Found: C, 43.66; H, 6.08%. Calcd for $C_{49}H_{76}O_{37}S\cdot 3H_2O$: C, 43.72; H, 6.14%.

p-Tolylsulfonyl-α-cyclodextrin. The tosylation of α-CD was carried out in the manner used for β-CD described above, except for the reaction medium. A carbonate buffer solution of pH 12 was used. For the purified sample: mp 160—162 °C; Found: C, 43.04; H, 6.28%. Calcd for $C_{43}H_{66}O_{32}S\cdot 3H_2O$: C, 43.16: H, 6.31%.

The R_f values of these two tosyl CD products in TLC on silica gel were 0.41 for α-CDOTs and 0.54 for β-CDOTs respectively (solvent: 1-butanol-dimethylformamide-water, 2:1:1; detecting reagent: iodine vapor or diphenylamine spray, followed by UV radiation). λ_{max} nm (logε: 274(2.40), 265 (2.70), and 263(2.78) for α-CDOTs, and 273(2.63), 265(2.71), and 262(2.73) for β-CDOTs, with referrence to 273(2.65), 265(2.75), and 262(2.75) for EtOTs at pH 6.50, 25 °C.

6-(Mono)-O-tolylsulfonyl-α-cyclodextrin. This compound was prepared by the method of Melton and Slessor.[14] The purification of the crude product was carried out by filtration through a Celite pad and by recrystalization from

95% ethanol. The total yield was 30%. Found: C, 43.46; H, 6.40%. Calcd for $C_{43}H_{66}O_{32}\cdot 3H_2O$: C, 43.16; H, 6.31%. Mp 155—157 °C (reported[14] 159—162 °C); the R_f in TLC was 0.55.

NMR Measurement. The ^{13}C-NMR measurement of tosyl CD was carried out at the concentration of 0.1—0.5 g in 1.0 ml of a D_2O or DMSO-d_6 solution, referred to dioxane as an internal standard with 2700—10000 times accumulation. The ^{1}H-NMR was observed in a 10% (g/ml) D_2O solution, using trimethylsilyl tetradeutropropionate as the internal referrence.

Partial Hydrolysis of Monotosylated β-Cyclodextrin. The present monotosylated β-CD, prepared in an aqueous solution, was partially hydrolized in a 1 M HCl solution at 80 °C for 6 h. The reaction mixture was neutralized with 1 M NaOH and then desalted with an ion exchanger, Amberlite MB-3. In the product, two components were observed with HPLC and paper chromatography (in 1-butanol–dimethylformamide–water (2:1:1), with dimethylaniline–phtalic acid as the detecting reagent). The lower spot of the R_f value (0.55) was the same as that of authentic glucose. The hydrolyzate was purified by gel chromatography using Sephadex G-15, giving a product with a higher R_f value (0.72) in the paper chromatography; the product was confirmed as monotosylated glucose by characterization by NMR; 2.22(ppm) due to the CH_3 of the tosyl group, 3.2—4.0 due to nonanomeric C–H, 5.0 due to C_1H, and 6.8—7.3 due to benzene-ring C–H. Both the R_f value (0.72) and the spectrum of ^{1}H-NMR agreed with those of authentic 3-*O*-tosyl glucose, which was prepared according to Freudenberg and Ivers.[23]

Determination of Dissociation Constants. The increase in the absorbance of the aromatic chromophore in the presence of cyclodextrin was determined by the spectrophotometric method. To suppress the disturbance due to the hydrolysis of tosyl chloride and the pH change in the solution, the UV absorbance was observed within several seconds after the mixing of tosyl chloride. With a change in CD concentration from 0—0.955×10^{-2} M, the substrate concentration was held constant at 5.0×10^{-5} M. A linear relationship was observed between the spectral change and the added concentration of CD, employing the Benesi-Hildebrand plot at 246 nm with the equation: $C_{CD}\cdot C_{TsCl}/\Delta A = K_{diss}/\Delta\varepsilon + C_{CD}/\Delta\varepsilon$, where K_{diss} indicates a dissociation constant; C_{CD}, the initial concentration of CD; C_{TsCl}, the initial concentration of TsCl; ΔA, the change in the absorbance, and $\Delta\varepsilon$, the difference between the molar extinction coefficients of the free and the complexed substrate. The slope ($1/\Delta\varepsilon$) and the intercept ($K_{diss}/\Delta\varepsilon$) were obtained by the least-squares method.

Results and Discussion

Tosylation of α-, and β-Cyclodextrins in an Aqueous Medium. The reaction of α-, and β-CD with TsCl in an alkaline solution at room temperature for an hour gave products. The products from both α-CD and β-CD were confirmed to be monotosylated compounds (α-CDOTs and β-CDOTs) by UV estimation referred to ethyl tosylate (EtOTs) as well as by ^{1}H-NMR estimation by the peak area.[15–17] It is noteworthy that only one tosyl residue was introduced to a CD molecule in spite of there being many hydroxyl groups on a CD molecule. The optimum alkaline concentrations were around pH 12 for α-CD and around pH 13 for β-CD. Prolonged (12 h) and short (6 min) reactions gave a low attachment of the tosyl residue on CD. One hour was the optimum reaction time. The optimum reaction temperature was about 20 °C in the range of 0—60 °C.

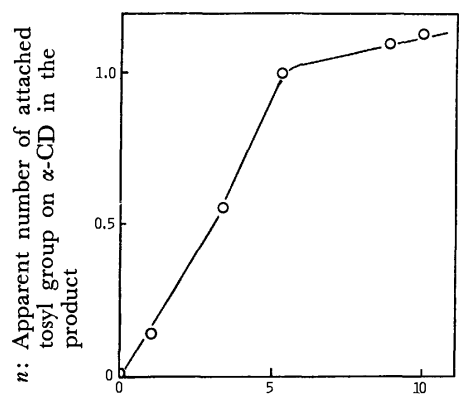

Fig. 1 The number of attached tosyl group on α-CD is plotted as a function of [TsCl]/[α-CD]. Tosylation was occured in 0.15 M NaOH solution at 25 °C for 1 h. The number (n) was calculated from the ^{1}H-NMR measurement.

As is shown in Fig. 1, when the ratio of the initial concentration of TsCl/α-CD was changed from 0 to 10, the plot of the apparent number of the tosyl group introduced on α-CD gave a saturation curve. It seemed that the number, n, increased linearly with the increase in the TsCl/α-CD ratio, which ranged 0 to 5. Hardly more than one tosyl residue to one CD molecule was introduced, even if the TsCl concentrations was 10 times larger than the CD concentration. When CD was tosylated in pyridine, in contrast, CD reacted easily with more than one TsCl and the number (n) would be stoichiometrically controlled. These facts suggest strongly there is 1:1 complex formation during the tosylation reaction in an aqueous solution.

The present product of tosyl-CD was compared with the tosyl-CD through stoichiometrically controlled monotosylation in pyridine, where the tosyl group was attached on a primary hydroxyl group of a glucose unit.[14] The R_f value of TLC was distinctly different between α-CDOTs prepared in pyridine and the α-CDOTs prepared in an aqueous solution. This fact suggested that the present monotosylated α-CD, prepared in an aqueous solution had a tosyl group at a secondary hydroxyl group of a glucose unit of a CD molecule.

The ^{13}C-NMR spectra of these tosyl CD's were observed and assigned according to the literature.[19–22] There was no evidence that each tosyl CD was a mixture of any isomers. The comparison of these spectra showed clearly that each of the tosylated cyclodextrins should have a single and particular structure as a tosyl CD. It had been reported that the amino group of amino-α-CD derived from the present tosylated α-CD was introduced at the C-3 position of a glucose of the CD molecule by means of ^{13}C-NMR spectroscopy.[13] Therefore, the tosyl group of the present tosylated α-CD may be introduced mainly at the C-3 position of the glucose ring of α-CD.

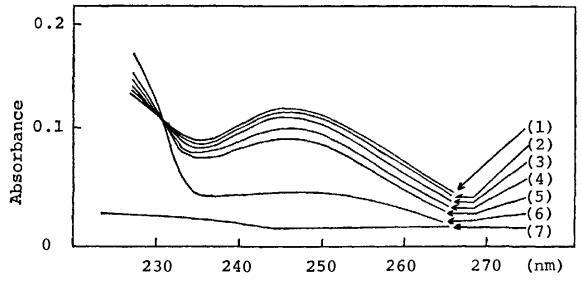

Fig. 2. Spectrum of tosyl chloride at varying α-CD concentrations; pH 6.50, 25 °C, acetonitrile/buffer= 0.5% (v/v). [TsCl] is 5.0×10^{-5} M. [α-CD] is changed at 9.55, 6.63, 3.32, 1.66, 0.332, and 0 ($\times10^{-3}$ M) from the curve 1 to 6 respectively. [TsCl] and [α-CD] are none for the curve 7.

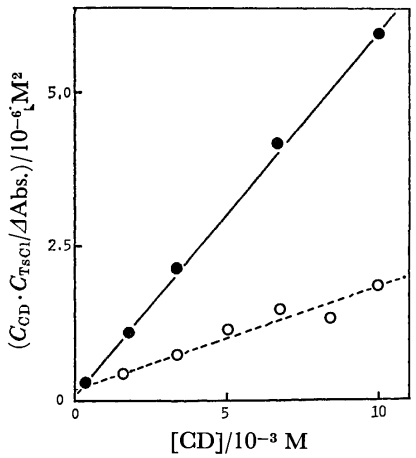

Fig. 3. Benesi-Hildebrandt plot for the mixture of CD and TsCl.
●: α-CD, ○: β-CD.

In order to get direct evidence to determine the substituted position of the tosylated β-CD group, the partial hydrolysis of β-CDOTs was carried out. The resulting hydrolyzate gave two spots in paper chromatography. The lower spot agreed with that of authentic 3-*O*-tosylglucose. The structure of the purified component with the higher R_f value was observed by ^{1}H-NMR to be monotosylglucose. The ^{1}H-NMR spectra and R_f values were coincident with the authentic sample of 3-*O*-tosylglucose. This result strongly suggested that the tosyl group of β-CDOTs was introduced at the C-3 position of glucose unit of β-CD.

Direct Evidence for a Complex Formation. The changes in the UV absorption spectra of TsCl in aqueous solutions with various amounts of the excess α-CD are shown in Fig. 2. A comparison of the UV spectra of EtOTs and TsOH with that of TsCl in an α-CD solution showed a distinct difference. Therefore, the broad absorption at around 245 nm in Fig. 2 must be due to the complex formation of CD with TsCl, and not to TsOH or tosylated CD. Moreover, the complex formation of CD with TsCl may be confirmed by the observation of the isosbestic point (Fig. 2). The Benesi-Hildebrand plots[18] for both α-CD and β-CD with TsCl gave a straight line (Fig. 3). The dissociation constants (K_{diss}) for the

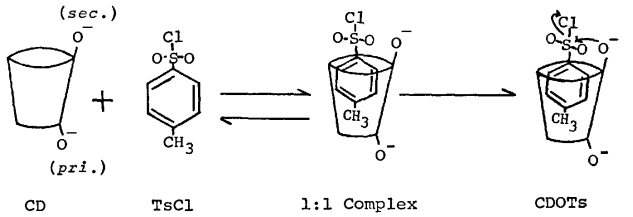

Scheme 1. The mechanism of the regiospecific monotosylation of cyclodextrin with *p*-tolylsulfonyl chloride in alkaline solution.

complexes of CD with TsCl, as calculated from the slopes of these lines, are 0.68×10^{-3} M for α-CD and 1.8×10^{-3} M for β-CD. These dissociation constants showed that the binding of α-CD to TsCl is tighter than in the case of β-CD, which may allow the alkoxide anions of α-CD more chances to attack the sulfur atom of TsCl than β-CD. This suggested that α-CD reacted with TsCl more easily than β-CD and why α-CD reacted with TsCl at a lower pH than did β-CD.

Mechanistic Scheme. The mechanistic scheme of the regiospecific tosylation of cyclodextrin with tosyl chloride in an alkaline solution is shown schematically in Scheme 1. As soon as tosyl chloride was dispersed in water, a cyclodextrin cavity should form a 1:1 complex with a tosyl chloride molecule. In that case, as the methyl group of the tosyl chloride consists of the hydrophobic part of the molecule, the methyl group should be near the primary hydroxyl group down into the cyclodextrin cavity, as is shown in the scheme. The sulfonyl chloride group should be positioned near the secondary hydroxyl group. The scale molecular model (CPK model) indicated that the distance between the sulfur atom of TsCl in the complex and the C-3 oxygen atom of the glucose unit in CD was a little shorter than the distance between the sulfur atom and the C-2 oxygen atom. This proximity effect between the sulfonyl chloride and the secondary hydroxyl group may accelerate the nucleophilic attack of a secondary hydroxyl (3-*O*) anion as the sulfur atom of the tosyl chloride molecule. This would result in a single tosylated CD on a specific secondary hydroxyl of cyclodextrin.

References

1) D. W. Griffiths and M. L. Bender, *Adv. Catal.*, **23**, 209 (1973).
2) M. L. Bender and M. Komiyama, "Bioorganic Chemistry," ed by E. E. van Tamelen, Academic Press, New York, N. Y. (1977), Vol. 1, Chap 2.
3) M. L. Bender and M. Komiyama, "Reactivity and Structure Concepts in Organic Chemistry **6**; Cyclodextrin Chemistry," Springer-Verlag, New York (1978).
4) R. L. VanEtten, J. F. Sebastian, G. A. Clowes, and M. L. Bender, *J. Am. Chem. Soc.*, **89**, 3242 (1967).
5) R. L. VanEtten, G. A. Clowes, J. F. Sebastian, and M. L. Bender, *J. Am. Chem. Soc.*, **89**, 3253 (1967).
6) F. Cramer and G. Mackensen, *Angew. Chem.*, **78**, 641 (1966).
7) F. Cramer and G. Mackensen, *Chem. Ber.*, **103**, 2138 (1970).

8) W. Lautsch, R. Wiechert, and H. Lehmann, *Kolloid-Z.*, **135**, 134 (1954).
9) R. Breslow and L. E. Overman, *J. Am. Chem. Soc.*, **92**, 1075 (1970).
10) A. Harada, M. Furue, and S. Nozakura, *Macromol.*, **9**, 701 (1976).
11) W. B. Gruhn and M. L. Bender, *Bioorg. Chem.*, **3**, 324 (1974).
12) Y. Kitaura and M. L. Bender, *Bioorg. Chem.*, **4**, 237 (1975).
13) Y. Iwakura, K. Uno, F. Toda, S. Onozuka, K. Hattori, and M. L. Bender, *J. Am. Chem. Soc.*, **97**, 4432 (1975).
14) L. D. Melton and K. N. Slessor, *Carbohydr. Res.*, **18**, 29 (1971).
15) B. Casu and M. Reggiani, *Tetrahedron*, **22**, 3061 (1966).
16) P. V. Demarco and A. L. Thakkar, *J. Chem. Soc., Chem. Commun.*, **1970**, 2.
17) K. Takeo and T. Kuge, *Agric. Biol. Chem.*, **34**, 1416 (1970).
18) H. A. Benesi and J. H. Hildebrand, *J. Am. Chem. Soc.*, **71**, 2703 (1949).
19) T. Usui, N. Yamaoka, K. Matsuda, K. Tsuzimura, H. Sugiyama, and S. Seto, *J. Chem. Soc., Perkin Trans. 1*, **1973**, 2425.
20) P. Colson, H. J. Jennings, and I. C. P. Smith, *J. Am. Chem. Soc.*, **96**, 8081 (1974).
21) K. Takeo, K. Hirose, and T. Kuge, *Chem. Lett.*, **12**, 1233 (1973).
22) L. F. Johnson and W. C. Jankowski, "Carbon-13 NMR Spectra," A Wiley-Interscience Publication, John Wiley and Sons, pp. 155, 163, and 243.
23) K. Freudenberg and O. Ivers, *Chem. Ber.*, **55**, 929 (1922).

Monochromatic Light-induced Reactions of Benzophenone Hydrazones and the *N*-Acetyl Derivatives in Carbon Tetrachloride in the Presence of Oxygen[1)]

Hiroshi SUGINOME*,** and Tsutomu UCHIDA

Department of Chemistry, Faculty of Science, Hokkaido University, Sapporo 060

(Received December 24, 1979)

Irradiation of hydrazones of benzophenone, 4-methylbenzophenone and 4-methoxybenzophenone in carbon tetrachloride with monochromatic light in the presence of oxygen afforded the corresponding azine, resulting from N–N bond cleavage, as the major product together with the hydrazone hydrochloride. In contrast to the hydrazones, benzophenone acetylhydrazone in carbon tetrachloride in the presence of oxygen afforded an unstable hydroperoxide as the only product, on photolysis with monochromatic light (288±8 nm); this product was transformed spontaneously into benzophenone on evaporation of the solvent at room temperature. 4-Methylbenzophenone acetylhydrazone and 4-methoxybenzophenone acetylhydrazone reacted in a manner similar to benzophenone acetylhydrazone. Irradiation of benzophenone diacetylhydrazone with 266±8 nm light under conditions analogous to the photo-reactions of hydrazones and acetylhydrazones resulted in loss of an acetyl group, resulting in N–CO bond cleavage to afford acetylhydrazone. The mechanism of the photooxygenation of benzophenone acetylhydrazones is interpreted in terms of chlorine radical-induced autoxidation.

In previous papers,[2)] it was reported that steroidal cyclic ketone acetylhydrazones afforded various yields of lactams on photolysis in the presence of oxygen, while the corresponding hydrazones gave the azines under similar conditions. It was of interest to compare the behavior of alicyclic ketone hydrazone and acetylhydrazone with that of aromatic ketone hydrazone and acetylhydrazone when they were irradiated in the presence of oxygen under similar conditions.

In this paper, we report results of photoinduced oxygenation of some benzophenone acetylhydrazones and diacetylhydrazones in carbon tetrachloride. A comparison is made with the behavior of the parent hydrazones under similar conditions. To avoid secondary photodecompositions[3)] as much as possible, all the photolyses were undertaken with monochromatic light.

Results

Benzophenone hydrazone (**1**),[4)] 4-methoxybenzophenone hydrazone (**3**),[5)] 4-methylbenzophenone hydrazone (**5**),[6)] their *N*-acetyl derivatives (**2**, **4**, and **6**), and *N*-diacetyl derivative (**7**) were prepared by the standard methods.

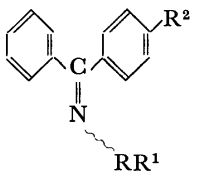

1 R=R¹=R²=H
2 R=R²=H, R¹=Ac
3 R=R¹=H, R²=OCH_3
4 R=H, R¹=Ac, R²=OCH_3
5 R=R¹=H, R²=CH_3
6 R=H, R¹=Ac, R²=CH_3
7 R=R¹=Ac, R²=H

The 4-substituted hydrazones, **3** and **5**, and their *N*-acetyl derivatives, **4** and **6**, used for the photoreactions were a mixture of *E* and *Z* isomers, as indicated by their NMR spectra (Table 1). All the hydrazones exhibited two strong absorption maxima due to $\pi\rightarrow\pi^*$ transitions in their UV spectra in dioxan, one at 277—278 nm and the other at 223—234 nm. The absorption at the longer wavelength showed a hypsochromic shift and a hyperchromic effect in methanol, as expected for the $\pi\rightarrow\pi^*$ transitions.

The acetylhydrazones also exhibited two absorption maxima, stronger than the hydrazones, attributable to $\pi\rightarrow\pi^*$ configurations.[7)] The absorptions at the longer wavelength in methanol exhibited bathochromic shifts to 285—288 nm in dioxan. As for the hydrazones, the shorter wavelength absorptions (222—231 nm) in dioxan exhibited hypsochromic shifts to 205—208 nm and a hyperchromic effect in methanol.

Photolysis. A solution of benzophenone acetylhydrazone (**2**) (30 mg in 4 ml of carbon tetrachloride containing oxygen) was irradiated with monochromatic light of 288±8 nm generated by a JASCO CRM-FA grating spectro-irradiator. The progress of the reaction was monitored by the NMR and UV spectra. The irradiation caused the gradual disappearance of the absorption maximum at 288 nm in the UV spectrum, and two singlets due to NH and acetyl protons at τ 1.82 and τ 7.74 emerged in the NMR spectrum. Irradiation for 110 h resulted in the disappearance of the UV absorption maximum at 288 nm and the replacement of the signals due to NH and acetyl protons by a 3-H singlet at τ 7.99 and a 1-H singlet at τ 7.79. In fact, examination of the solution by TLC disclosed the absence of the starting material and the formation of a single product much more polar than the starting material. The addition of aqueous potassium iodide to the solution liberated iodine immediately. The NMR spectrum of the photolyzed solution at 75° showed little change in the spectrum, indicating that the product in solution was stable at that temperature. However, the evaporation of the solvent caused a total decomposition of the product. The NMR spectrum of the residue after removal of the

** Present address: Organic Chemistry Laboratory, Department of Chemical Process Engineering, Faculty of Engineering, Hokkaido University, Sapporo 060.

Table 1. NMR parameters (100 MHz) for benzophenone hydrazones, the *N*-acetyl derivatives, and the azines in CCl_4 ($CDCl_3$) solution [chemical shifts (τ) and splittings (Hz; in parenthesis)]

Compound	NH or NH_2	Aromatic protons	$COCH_3$	OCH_3	CH_3
1	4.76(s)	2.36—2.96(m)	—	—	—
1[a]	4.63(s)	2.32—3.02(m)	—	—	—
2	1.82(s)	2.30—2.90(m)	7.74(s)	—	—
2[a]	1.65(s)	2.30—2.96(m)	7.56(s)	—	—
3a[b]	4.89 br(s)	3.24(d) (9.0) 3 and 5H; 2.36—3.06 (m) other aromatic protons	—	6.24(s)	—
3b[b]	4.7 br	3.04(d) (9.0) 3 and 5H; 2.45—2.93 other aromatic protons	—	6.31(s)	—
4	1.81(s) (0.6H) and 1.99(s) (0.4H)	3.22(d) (9.0) 3 and 5H (1.2H), 2.87(d) (9.0) 3 and 5H (0.8H), 2.27—3.00(m) other aromatic protons	7.69(s)	6.21(s) (1.8H) and 6.13(s) (1.2H)	—
5[b]	5.08 br	2.89(d) (9.0) 3 and 5-H; 2.30—2.78 (m) other aromatic protons	—	—	7.69(s)
5[b]	4.62 br	2.85(d) (9.0) 3 and 5-H; 2.40—2.80 (m) other aromatic protons	—	—	7.57(s)
6	1.87(s) (0.53H) and 1.95(d) (0.47H)	2.29(d) (9.0) 3 and 5H (1.1H), 2.75(s) (9.0) 3 and 5H (0.9H); 2.24- *ca.* 2.90(m) other aromatic protons	7.71(s)	—	7.65(s) (1.6H) and 7.55(s) (1.4H)
7	—	2.31—2.91(m)	7.80(s)	—	—
14[a]	—	3.19(d) (8.4) 3, 5, 3′ and 5′H, 2.92(d) (8.4) 2, 6, 2′ and 6′H; 2.67—3.24(m) other aromatic protons	—	6.32(s) (3.6H) and 6.08(s) (2.4H)	—
16[a]	—	2.40—2.95(m)	—	—	7.68(s) (2.5H) and 7.61(s) (3.5H)

a) Values in $CDCl_3$. b) *Z-E* configuration of these compounds are undetermined.

Table 2. The yields of benzophenones in the photolysis of benzophenone acetylhydrazones in carbon tetrachloride with monochromatic light

Compound	Wavelength of the irradiation light (nm)	Time of irradiation (h)	Yield of benzophenones (%)
2	288±8	110	60
2[a]	286±8	168	0
4	289±8	43	73
6	289±8	48	63

a) Solvent: dioxan.

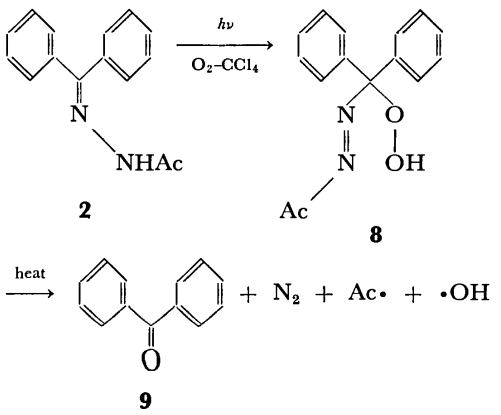

Scheme 1.

solvent disclosed that the signal due to the acetyl group had vanished, and it was actually the spectrum of benzophenone which was isolated in 79% yield by preparative TLC. These observations confirmed that a highly unstable intermediate was formed, which decomposed spontaneously to afford benzophenone upon evaporation of the solvent.

A hydroperoxide structure **8** accommodates all the NMR spectral results, the chemical properties and the result of TLC (Scheme 1). Two singlets at τ 7.99 and 7.79 are ascribable to the acetyl and the hydroperoxide protons. The hydroperoxide proton signals usually resonate at τ −0.3 to −0.75.[8,9] The considerable upfield shift is attributable to shielding by the aromatic ring.

In contrast to the benzophenone acetylhydrazone, irradiation of benzophenone hydrazone (**1**) itself with monochromatic light (270±8 nm) for 72 h under conditions comparable to the case of *N*-acetyl derivative afforded three products: **10**, **11**, and **12** (Scheme 2). Product **10**, which gradually separated as a solid on the wall of the vessel while being irradiated, was identified as benzophenone hydrazone hydrochloride[10] (25% yield). Product **11**, mp 161—163 °C, was iden-

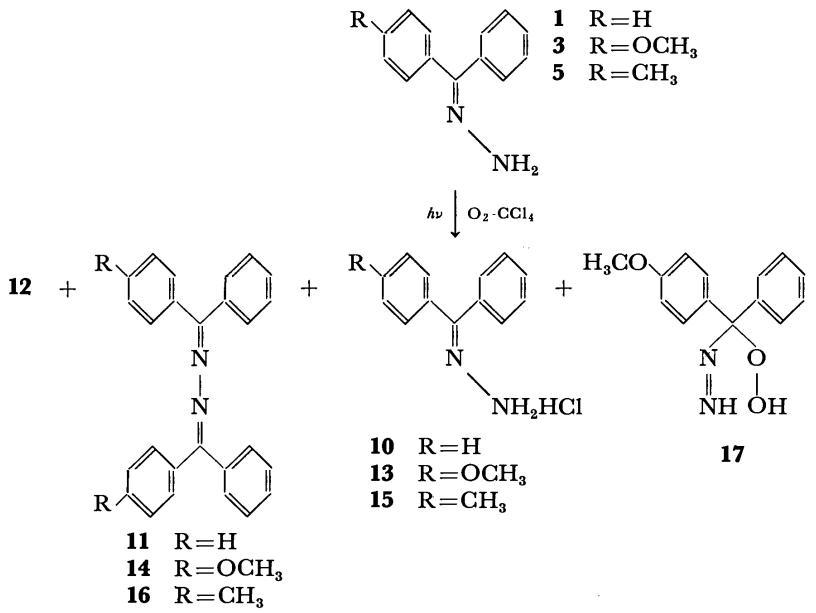

Scheme 2.

Table 3. Products and the yields in the photolysis of benzophenone hydrazones in carbon tetrachloride with monochromatic light

Compound	Wavelength of light (nm)	Time of irradiation (h)	Yields of products (%)		
			The azine	The ketone	The hydrochloride
1	277±8	72	50	0	25
3	279±8	20	7	25	32
5	276±8	11	47	0	31

tified as benzophenone azine by a comparison with a specimen prepared by the reported method.[4] The third product, **12**, mp 230—232 °C, the structure of which has not been deduced, exhibited the molecular ion at *m/e* 418 in the mass spectrum and a single absorption maximum at 307 nm in the UV spectrum.

Irradiation of other two nuclear substituted acetylhydrazones **4** and **6** in carbon tetrachloride with monochromatic light gave results parallel with those for acetylhydrazone **2**. The reaction conditions and the yields of the product ketone are shown in Table 2.

In order to obtain further information with regard to the role of the solvent, photolysis of benzophenone acetylhydrazone (**2**) in dioxan with monochromatic light (286±8 nm) was carried out under conditions similar to those in carbon tetrachloride. However, no trace of hydroperoxide was found after 168 h irradiation and the starting material was recovered.

Irradiation of nuclear substituted hydrazone **5** in carbon tetrachloride with appropriate monochromatic light provided results parallel to the case of the hydrazone **1**. It is notable, however, that while the irradiation of the hydrazones **1** and **5** did not afford any parent ketones, the irradiation of the hydrazone **3** afforded a significant amount of the parent ketone formed *via* a hydroperoxide **17**. The reaction conditions and the yields of products are shown in Table 3.

These results are in a sharp contrast with the results by Binkley,[16] who reported that irradiation of benzophenone hydrazone (**1**) in oxygen-free methanol, with Vycor-filtered light, afforded diphenylmethane (26%) and benzophenone (34%). Repetition of this photolysis in the presence of oxygen with monochromatic light showed the photoreaction in methanol to be slower than that in carbon tetrachloride and confirmed the formations of only diphenylmethane and benzophenone as the products. Photolysis in dioxan with Vycor-filtered light was also carried out. Diphenylmethane was again the major product (28%), accompanied by the azine (3%) and the parent ketone (15%). The formation of diphenylmethane by irradiation in this aprotic solvent in the presence of oxygen seems to suggest that the reaction does not involve radical species and that the methylene proton(s) of diphenylmethane may be provided by an ionic intramolecular proton transfer from the amino group, although no experiments in deuteriodioxan were undertaken.

Finally, photolysis of benzophenone diacetylhydrazone **7** in carbon tetrachloride with monochromatic light (266±8 nm) was carried out in order to define further structural requirement for the formation of the hydroperoxide. It was expected that the photoinduced transformation of **7** may be slower than that of acetylhydrazone **2**, since the former did not have a hydrogen on the nitrogen center. However, the disappearance of **7** was found to complete in a period even shorter than in the case of benzophenone acetyl-

hydrazone (90 h). The NMR spectrum of the solution exhibited four sharp singlets at τ 6.42, 7.62, 7.78, and 8.02 in 1:0.7:0.2 ratio, a broad singlet at τ 1.38, and a multiplet at τ 2.22 to 2.80. Examination of the product by TLC disclosed the formation of virtually two products, the Rf values of which were identical with those of benzophenone and benzophenone acetylhydrazone (**2**). These two compounds were isolated by preparative TLC in 77 and 20% yields. Two singlets at τ 1.38 and 7.78 in the photolyzed solution can be attributable to benzophenone acetylhydrazone (**2**). Other singlets in the solution could be due to volatile products resulting from the reaction of the acetyl radical.

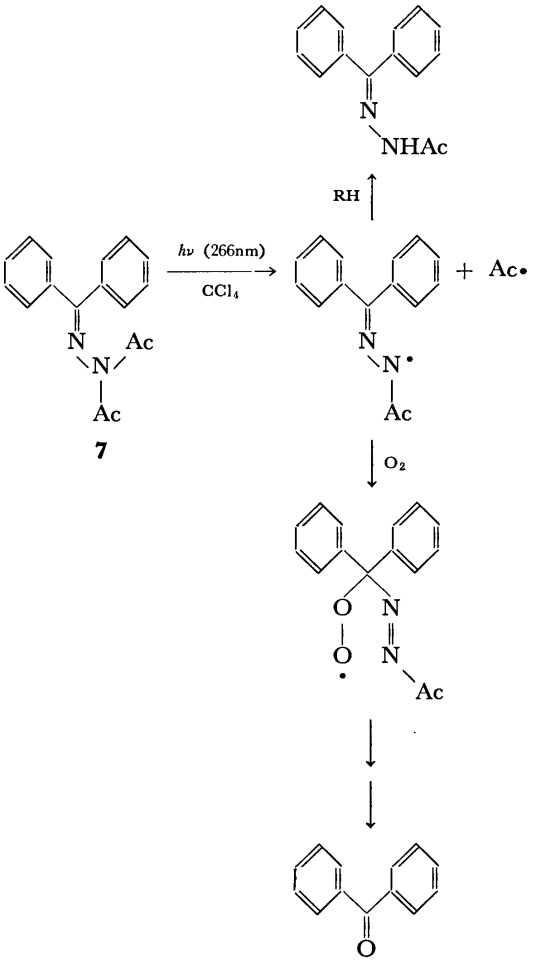

Scheme 3.

Discussion

There are at least two possible mechanistic pathways for the formation of the hydroperoxides (*e.g.*, **8**) from the acetylhydrazones. One is *via* a radical-induced autoxidation observed for benzaldehyde phenylhydrazones by Busch and Dietz.[9,11] Another is by sensitized oxygenation, as observed for acetone phenylhydrazone by Schenck and Wirth.[12] In this case, singlet oxygen is involved.[13]

Of these two mechanisms, involvement of singlet oxygen, which might be generated *via* sensitization by the acetylhydrazone itself, is ruled out, since no hydroperoxides are formed in the photolysis in dioxan. Thus, oxygenation through the autoxidation remains as a mechanistic possibility. To compare the present reaction with the autoxidation of benzaldehyde phenylhydrazone, benzophenone acetylhydrazone **2** in benzene was subjected to autoxidation under the conditions analogous to the autoxidation of benzaldehyde phenylhydrazone.[11] However, no hydroperoxide **8** was formed under these conditions and irradiation was necessary to obtain hydroperoxide **8** from acetylhydrazone **2**.

One of the probable autoxidation pathways for the hydroperoxide formation is depicted in Scheme 4. In this pathway, a chlorine atom generated from carbon tetrachloride abstracts a hydrogen attached to the amide nitrogen of the acetylhydrazone to form a stabilized amidyl radical and to initiate a chain reaction. Generation of chlorine atoms from carbon tetrachloride under the experimental conditions was confirmed by the formation of the hydrochlorides **10**, **13**, and **15** in the photolysis of the hydrazones. It should be noted that this autoxidation process for the acetylhydrazones predominates over other processes such as N–N bond cleavage, which is almost only reaction in monochromatic photolysis of benzophenone hydrazones, and N–CO bond cleavage.

In contrast to the acetylhydrazone, the parent hydrazones are virtually unreactive toward oxygen under irradiation, with the exception of 4-methoxybenzophenone hydrazone (**3**) in which 25% of the parent

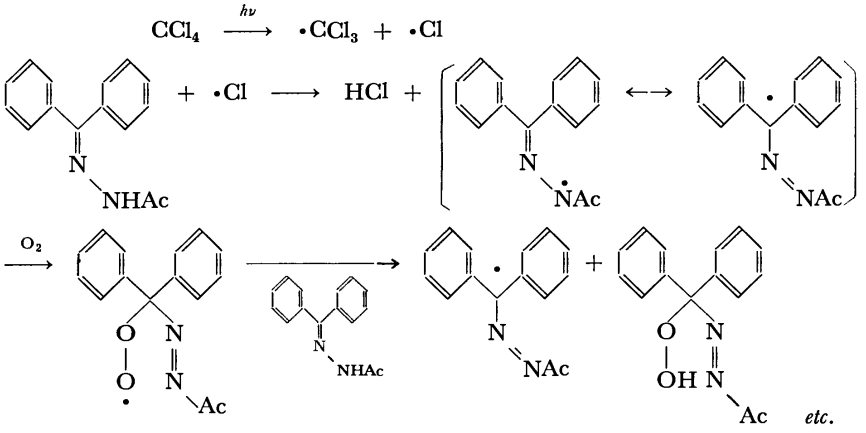

Scheme 4.

ketone was formed together with the azine (Table 3). The major reaction in the hydrazone photolysis is the homolysis of the N–N bond to afford the imino radicals. The homolysis probably takes place from the excited singlet state of the hydrazones since it occurs even in the presence of oxygen.[14] For the hydrazones, generation of a nitrogen-centered radical *via* the abstraction by electrophilic chlorine atom is probably more difficult than for the acetylhydrazones, owing to the lower stabilization of the radicals to be formed.

In this connection, it is notable that only 4-methoxybenzophenone hydrazone (**3**) afforded the hydroperoxide (as indicated by the formation of the parent ketone). We explain this in terms of the polar effects that frequently influence radical reactions.[15] The reactions involving electrophilic chlorine atom have a considerable ionic character.[15] In the present case, the electron-donating methoxyl substituent should stabilize the transition state and facilitate the hydroperoxide formation. The electron-donating effect of a methoxyl group also may play a role in accelerating the attack by the chlorine atom on the hydrogen atom attached to the nitrogen. The difference in the products in the photo-reaction of benzophenone hydrazones in carbon tetrachloride and those in methanol or dioxan is appreciable. Although the exact reason for this difference is not clear, it is likely that a photochemical N–N bond cleavage in the hydrazone is facilitated by the protonation of the amino group with the hydrogen chloride generated by irradiation.

The foregoing experiments showed that a primary photochemical reaction of the diacetylhydrazones is the cleavage of one of the N–CO bonds[17] rather than the N–N bond cleavage. The N–CO bond cleavage is followed by competitive processes: *i.e.*, the combination of the amidyl radical with oxygen or with hydrogen from another substrate or chlorine abstraction of the amidyl radical from the solvent. These processes may lead to the observed products. We noted previously[2] that in the photolysis of acetyl- and diacetylhydrazones of some steroidal alicyclic ketones, no azine resulting from N–N bond cleavage was formed. The present results with regard to acetyl- and diacetylhydrazones of aromatic ketones seem to be parallel to the previous results[2] in that no azine was found in the products.

Experimental

For instruments used and general procedure see part 30.[18] The mass spectra were taken with a Hitachi RMU-6E spectrometer (ion source temperature 200 °C; ionizing voltage 80 eV) with the exception of **5**. The mass spectrum of **5** was taken with a Hitachi JMS-D 300 spectrometer (ion source temperature 175 °C and ionizing voltage 70 eV).

*Benzophenone Hydrazone (**1**).* This hydrazone was prepared by the described procedure,[4,10] mp 97—99 °C (lit,[4] mp 97—98 °C). UV ν_{max} (dioxan) 278 nm (ε: 11500), ν_{max} (CH_3OH) 281 nm (ε: 23000), ν_{max} (CCl_4) 288 nm (ε: 24000); MS, *m/e* (rel. intensity) 196 (M^+, 100%).

*Benzophenone Acetylhydrazone (**2**).* Benzophenone hydrazone (1.8 g) and acetic anhydride (7 ml) in pyridine (10 ml) were stirred for 63.5 h at room temperature. After the addition of methanol, the solvent was removed by the addition of benzene and the residue was dissolved in chloroform. The organic layer was washed with 2 mol dm^{-3}-hydrochloric acid and water successively and dried (Na_2SO_4). After removal of the solvent, the residue was recrystallized from diethyl ether to afford benzophenone acetylhydrazone (1.64 g), mp 106—107.5 °C. Found: C, 74.84; H, 5.57; N, 11.50%. Calcd for $C_{15}H_{14}N_2O$: C, 75.60; H, 5.92; N, 11.76%. UV ν_{max} (dioxan) 286 nm (ε: 18700); ν_{max} (CH_3OH) 281 nm (ε: 23000); ν_{max} (CCl_4) 288 nm (ε: 24000); IR, 3179 (NH), 1688 (NHCO), 1332, 1311, 1290, 1127, 1020, 954, 784, and 770 cm^{-1}; MS, *m/e* (rel. intensity) 238 (M^+, 60%), 196 (100), and 195 (89).

*4-Methoxybenzophenone Hydrazone (**3**).* 4-Methoxybenzophenone (3 g) and hydrazine hydrate (15 ml) in ethanol (30 ml) were refluxed for 22 h. A part of the solvent was removed and the crystals which appeared were collected by filtration, (1.77 g). These were a 2:3 mixture of *E* and *Z* isomers, judged by the NMR spectrum, but recrystallization from ethanol twice afforded a more abundant single isomer, mp 95—96.5 °C, which gave a single peak due to the methoxyl at τ 6.24 (lit,[5] α-form, mp 95—96 °C). Found: C, 74.15; H, 6.29; N, 12.32%. Calcd for $C_{14}H_{14}N_2O$: C, 74.31; H, 6.24; N, 11.38%. UV ν_{max} (dioxan) 278 nm (ε: 15000); ν_{max} (CH_3OH) 278 nm (ε: 17400); ν_{max} (CCl_4) 279 nm (ε: 12600); IR 3422 and 3309 (NH_2), 1609, 1251, 1073, 1028, and 838 cm^{-1}. MS, *m/e* (rel. intensity) 226 (M^+, 100), 195, and 128 (50).

*4-Methoxybenzophenone Acetylhydrazone (**4**).* The hydrazone **3** (1.5 g) and acetic anhydride (5 ml) in pyridine (7.5 ml) were stirred for 18 h at room temperature. After work-up as usual, the residue was recrystallized from acetone to yield the acetylhydrazone (1.47 g), mp 98—99 °C. Found: C, 71.65; H, 6.01; N, 10.51%. Calcd for $C_{16}H_{16}N_2O_2$: C, 71.62; H, 6.01; N, 10.44%. UV ν_{max} (dioxan) 285 nm (ε: 18800); ν_{max} (CH_3OH) 287 nm (ε: 22400); ν_{max} (CCl_4) 289 nm (ε: 17500); IR 3180 (NH), 1665 (CONH), 1605, 1507, 1334, 1303, 1243, 1169, 1128, 1037, 843, 779, and 698 cm^{-1}. MS, *m/e* (rel. intensity) 268 (M^+, 79), 226 (78), and 225 (100).

*4-Methylbenzophenone Hydrazone (**5**).* 4-Methylbenzophenone (3 g) and hydrazine hydrate (15 ml) in ethanol (30 ml) were refluxed for 10 h. A part of the solvent was removed and the crystals which appeared were collected by filtration to yield the hydrazone (2.90 g). This was a 2:1 mixture of *E* and *Z* isomers, judged by the NMR spectrum. Recrystallization from ethanol twice afforded a more abundant single isomer, which showed a single peak due to the methyl (τ 7.57), mp 87.5—88.5 °C (lit,[6] mp 80—81 °C). UV ν_{max} (dioxan) 277 nm (ε: 12000); ν_{max} (CH_3OH) 272 nm (ε: 12000); ν_{max} (CCl_4) 276 (ε: 11800); IR 3360 (NH_2), 1579, 1076, and 832 cm^{-1}. MS, *m/e* (rel. intensity) 210 (M^+, 100), 195 (20), and 194 (20).

*4-Methylbenzophenone Acetylhydrazone (**6**).* The hydrazone **5** (1.5 g) and acetic anhydride (10 ml) in pyridine (15 ml) were stirred for 17 h at room temperature. After the addition of methanol, the solvent was removed by the addition of benzene. The residue was dissolved in diethyl ether. The solution was washed with water and dried (Na_2SO_4). The usual work-up gave a residue which was recrystallized from diethyl ether. (659 mg), mp 95—96 °C. Found: C, 76.37; H, 6.41; N, 11.05%. Calcd for $C_{16}H_{16}N_2O$: C, 76.16; H, 6.39; N, 11.10%. UV ν_{max} (dioxan) 288 nm (ε: 19100); ν_{max} (CH_3OH) 285 nm (ε: 19800); ν_{max} (CCl_4) 289 nm (ε: 18400). IR 3180 (NH), 1674 (NHCO), 1336, 1309, 1297, 1113, 1020, 960, 832, and 778 cm^{-1}. MS, *m/e* (rel. intensity) 252 (M^+, 71%), 210 (98), and 209 (100).

Photolysis of Benzopenone Acetylhydrazone (2) in the Presence of Oxygen with Monochromatic Light (286±8 nm). In Carbon Tetrachloride: Benzophenone acetylhydrazone (**2**) (30 mg) in purified carbon tetrachloride[19] (4 ml) saturated with oxygen in a quartz vessel was placed in the chamber of a CRM-FA grating spectro-irradiator and was irradiated. The progress of the reaction was monitored by UV spectroscopy. The intensity of the absorption maximum at 288 nm gradually diminished during irradiation and after 110 h the absorption maximum nearly vanished. The NMR spectrum also showed that the signals of the starting material were replaced by those of the product (see text). The solvent was evaporated and the residue was purified by preparative TLC with a 1:1 mixture of benzene and diethyl ether to afford benzophenone (18 mg). A small amount of a more polar unidentified compound (3 mg) was obtained.

In Dioxan: Benzophenone acetylhydrazone (100 mg) in dioxan (Dotite Spectrosol, Wako, Japan) (4 ml) was irradiated with 286±8 nm wavelength light for 168 h. The absence of the hydroperoxide in the solution was proved by TLC and the absence of the parent ketone was confirmed by the NMR spectrum of the product after evaporation of the solvent.

Photolysis of 4-Methoxybenzophenone Acetylhydrazone (4) in the Presence of Oxygen with Monochromatic Light (288±8 nm). 4-Methoxybenzophenone acetylhydrazone (**4**) (30 mg) in purified carbon tetrachloride (4 ml) saturated with oxygen in a quartz vessel was irradiated for 43 h as for benzophenone acetylhydrazone. After removal of the solvent, the residue showed two spots in TLC (benzene). This was subjected to preparative TLC to afford two fractions. The more mobile fraction (22 mg) was nearly pure 4-methoxybenzophenone. The less mobile fraction (few mg) was unidentified gum.

Photolysis of 4-Methylbenzophenone Acetylhydrazone (6) in the Presence of Oxygen with Monochromatic Light (294±8 nm). 4-Methylbenzophenone acetylhydrazone (**6**) (30 mg) in purified carbon tetrachloride (4 ml) saturated with oxygen in a quartz vessel was irradiated for 48 h, as done for benzophenone acetylhydrazone. After removal of the solvent, the residue showed two spots on TLC (benzene), but the less mobile spot was very weak. Preparative TLC of the residue afforded two fractions. The more mobile fraction (19 mg) was nearly pure 4-methylbenzophenone. The less mobile fraction (6 mg) was an unidentified gum.

Photolysis of Benzophenone Hydrazone (1) in Dioxan in the Presence of Oxygen with Vycor-filtered Light. Benzophenone hydrazone (**1**) (500 mg) in dioxan (220 ml) was irradiated with a Hanovia 450-W high pressure Hg arc with a Vycor-filter until the starting material disappeared (24 h). After removal of the solvent, the oily residue was subjected to preparative TLC with benzene to afford three fractions. The most mobile fraction (120 mg) was diphenylmethane and the next mobile fraction (28 mg) was benzophenone. The 3rd fraction (194 mg) was still a mixture, which was subjected to preparative TLC with a 3:1 benzene and hexane. Three developments afforded major two fractions. The more mobile fraction (14 mg) was the azine **11** which was recrystallized from ethanol. The less mobile fraction (40 mg) was benzophenone.

Photolysis of Benzophenone Hydrazone (1) in the Presence of Oxygen with Monochromatic Light (270±8 nm). In Carbon Tetrachloride: Benzophenone hydrazone (30 mg) in purified carbon tetrachloride (4 ml) containing oxygen in a quartz vessel was irradiated with monochromatic light for 72 h, as done for *N*-acetylbenzophenone hydrazone (**2**). During the irradiation, a solid appeared in the solution. The solid (9 mg) was collected by filtration and was recrystallized from methanol to yield hydrazone hydrochloride **10**, mp 166—167 °C (lit,[10] mp 183 °C). This was identified by its mass spectrum. Removal of the solvent from the filtrate afforded the residue (17 mg). This was subjected to preparative TLC with a 4:1 benzene–diethyl ether mixture to afford four fractions. The most mobile fraction (15 mg) was identified as benzophenone azine (**11**), which was recrystallized from methanol (5 mg), mp 161—163 °C (lit,[4] mp 162—164 °C). The second and third mobile fractions (4 mg and 3 mg) were unidentified gums. The fourth fraction (5 mg) was recrystallized from methanol to yield crystals (**12**), mp 230—232 °C. UV ν_{max} (CCl_4) 307 and 280 nm (inflexion); ν_{max} ($CHCl_3$) 1707 and 1111 cm^{-1}; MS, *m/e* (rel. intensity) 418 (M^+, 2), 223 (15), and 196 (100).

In Methanol: Benzophenone hydrazone (**1**) (2 mg) in methanol (Dotite Spectrosol, Wako, Japan) (4 ml) was irradiated with monochromatic light (273±8 nm). Irradiation for 5 h completed the photo-decomposition. After evaporation of the solvent, the residue was subjected to preparative TLC with a 4:1 benzene and diethyl ether mixture to afford seven fractions. All the fractions except the most mobile one was very minor. The most mobile fraction was again subjected to preparative TLC with a 1:3 hexane and benzene mixture to afford more mobile diphenylmethane and less mobile benzophenone. Both compounds were identified by comparisons of the UV spectra and the TLC behaviors with those of the authentic materials.

Photolysis of 4-Methoxybenzophenone Hydrazone (3) in the Presence of Oxygen with Monochromatic Light (277±8 nm). The hydrazone (20 mg) in carbon tetrachloride (3 ml) containing oxygen was photolyzed for 20 h. The solid (11 mg) which separated was collected and recrystallized from methanol–diethyl ether to afford hydrochloride **12** (2 mg), mp 127—130 °C. The residue (13 mg) obtained by evaporation of the filtrate was subjected to preparative TLC with 1:5 hexane and benzene to afford three fractions. The most mobile fraction (1.5 mg) was azine **13** which was identified by a comparison with the specimen prepared by a ground state reaction. The second mobile fraction (5 mg) was 4-methoxybenzophenone. The least mobile fraction (7.5 mg) was an unidentified gum.

Photolysis of 4-Methylbenzophenone Hydrazone (5) in the Presence of Oxygen with Monochromatic Light (287±8 nm). The hydrazone (30 mg) in carbon tetrachloride (4 ml) was photolyzed for 11 h. The solid (11 mg) which separated was collected and recrystallized from methanol to afford hydrochloride **15** (5 mg), mp 138—139 °C. The residue (20 mg) obtained by the evaporation of the filtrate of the photolyzed solution was subjected to preparative TLC with a 4:1 benzene and diethyl ether mixture to afford two fractions. The mobile fraction was again purified by preparative TLC with a 5:1 benzene and hexane mixture to afford the azine **16** (14 mg), which was identified by a comparison with the authentic specimen prepared by a ground state reaction.

Preparation of 4-Methoxybenzophenone Azine (13). 4-Methoxybenzophenone (400 mg), hydrazine hydrate (0.3 ml), and potassium hydroxide (1 g) were refluxed in ethanol (3 ml) for 20 h. A part of the solvent was removed and the solution was extracted with chloroform. The chloroform solution was neutralized with 2 mol dm^{-3} hydrochloric acid, washed with water, and dried (Na_2SO_4). Evaporation of the solvent left the residue which was purified by preparative TLC with a 1:5 hexane and benzene mixture to afford an oily azine **15** (450 mg). This azine could not be induced to crystallize. IR (CCl_4) 1614, 1516, 1398, 1458, 1308, 1249, 1176, 1042, 724, and 698 cm^{-1},

*Preparation of 4-Methylbenzophenone Azine (**15**).* 4-Methylbenzophenone (400 mg), hydrazine hydrate (0.3 ml) and potassium hydroxide (1 g) in ethanol (3 ml) were refluxed for 3 h. A part of the solvent was removed by a rotary evaporator and the solution was extracted with dichloromethane. The dichloromethane solution was worked up as done for 4-methoxybenzophenone azine. The product was purified by preparative TLC with a 1:5 hexane and benzene mixture to afford an oily azine **15** (69 mg). This was recrystallized from methanol–diethyl ether (31 mg), mp 137—138 °C. IR 1607, 1588, 1322, 1303, 1177, 823, 767, 718, and 694 cm^{-1}.

*Attempted Autoxidation of Benzophenone Acetylhydrazone (**2**). In the Presence of Hydrogen Peroxide and Oxygen.* Benzophenone acetylhydrazone (60 mg) in benzene (10 ml) and 30% hydrogen peroxide (1 drop) were stirred under air for 288 h at room temperature. TLC showed that no product other than the starting material was present in the solution.

In the Presence of Oxygen: Benzophenone acetylhydrazone (100 mg) in benzene (0.6 ml) was bubbled with oxygen and the solution was stirred for 96 h in an atmosphere of oxygen at room temperature. After removal of the solvent, the residue was recrystallized from diethyl ether to afford the starting material (26 mg). Removal of the solvent left a residue which was subjected to preparative TLC with a 1:3 benzene and dichloromethane to afford two fractions. The more mobile fraction (39 mg) was examined by the NMR spectrum, which showed no aromatic protons. The less mobile fraction (30 mg) was the starting material.

*Benzophenone Diacetylhydrazone (**7**).* Benzophenone hydrazone (2.014 g) and acetic anhydride (10 ml) in pyridine (10 ml) were stirred for 20 h at 70—80 °C. After the addition of methanol, the reaction mixture was worked up as done for the preparation of benzophenone acetylhydrazone. After removal of the solvent, the residue was subjected to column chromatography (Wako gel C-200; 45 g). Elutions with benzene and benzene containing increasing amounts of chloroform afforded two fractions. The less polar fraction (1.845 g) was recrystallized from diethyl ether to afford benzophenone diacetylhydrazone, mp 121—124 °C. Found: C, 72.86; H, 5.66; N, 9.81%. Calcd for $C_{17}H_{16}N_2O_2$: C, 72.84; H, 5.75; N, 9.99%; UV ν_{max} (MeOH) 208 nm (ε: 25000), and 245 nm (ε: 16000); ν_{max} (dioxan) 253 nm (ε: 14000).

*Photolysis of Benzophenone Diacetylhydrazone (**7**) in the Presence of Oxygen with Monochromatic Light (266±8 nm) in Carbon Tetrachloride.* Benzophenone diacetylhydrazone (**7**) (30 mg) in purified carbon tetrachloride (3 ml) in a quartz vessel was placed in the chamber of a CRM-FA grating spectroirradiator and was irradiated. The progress of the reaction was monitored by TLC, which showed the disappearance of the starting material after 90 h. After evaporation of the solvent, the residue was subjected to preparative TLC (Merck, silica gel 60F-254) with a 1:1 mixture of benzene and diethyl ether to afford two fractions. The more mobile fraction (15 mg) was benzophenone and the other (5 mg) was benzophenone acetylhydrazone.

We thank Mrs. T. Okayama for the measurements of NMR spectra.

References

1) Photoinduced Transformations, Part 49. Part 48: H. Suginome and T. Uchida, *Bull. Chem. Soc. Jpn.*, **53**, 2292 (1980).
2) H. Suginome and T. Uchida, *J. Chem. Soc., Perkin Trans. 1*, **1980**, 1356; H, Suginome, T. Uchida, K. Kizuka, and T. Masamune, *Bull. Chem. Soc. Jpn.*, **53**, 2285 (1980).
3) J. G. Gorse, III, and R. W. Binkley, *J. Org. Chem.*, **37**, 575 (1972).
4) D. H. R. Barton, R. E. O'Brien, and S. Sternhell, *J. Chem. Soc.*, **1962**, 470.
5) R. W. Johnson and J. Stegletz, *J. Am. Chem. Soc.*, **56**, 1904 (1934).
6) H. Staudinger and J. Goldstein, *Ber.*, **49**, 1923 (1916).
7) H. H. Jaffe and M. Orchin, "Theory and Applications of Ultraviolet Spectroscopy," Wiley, New York (1962), p. 276.
8) N. A. Milas and A. Golubovic, *J. Org. Chem.*, **27**, 4319 (1962).
9) H. C. Yao and P. Resnik, *J. Org. Chem.*, **30**, 2832 (1965).
10) T. Curtius and F. Rauterberg, *J. Prakt. Chem.*, **44**, 192 (1891).
11) M. Busch and W. Dietz, *Ber.*, **47**, 3277 (1914); R. Criegee and G. Lohaus, *ibid.*, **84**, 219 (1951).
12) G. O. Schenck, *Angew. Chem.*, **69**, 579 (1957); G. O. Schenck and H. Wirth, *Naturwissenschaften*, **40**, 141 (1953).
13) A. Nickon, V. T. Chuang, P. J. L. Daniels, R. W. Denny, J. B. Digiorgio, J. Tsunetsugu, H. G. Vilhuber, and E. Werstiuk, *J. Am. Chem. Soc.*, **94**, 5517 (1972).
14) Benzophenone hydrazone and the *N*-acetyl derivative showed neither detectable fluorescence nor phosphorescence in EPA matrix at 77 K as in other compounds having a C–N double bond in which *syn-anti* isomerization is possible; quantum yields of the emissions were lower than 10^{-6}. We are grateful to Drs. T. Takemura and K. Fujikawa of Research Insitute of Applied Electricity, Hokkaido University, for their help in the measurements of the emission spectra.
15) G. A. Russell and R. C. Williamson, *J. Am. Chem. Soc.*, **86**, 2357 (1964); C, Walling and B. Miller, *ibid.*, **79**, 4181 (1957); R. E. Pearson and J. C. Martin, *ibid.*, **85**, 3142 (1963).
16) R. W. Binkley, *Tetrahedron Lett.*, **1969**, 1893; *J. Org. Chem.*, **35**, 2796 (1970).
17) For review of photo-reactions of amides, see J. D. Coyle, *Chem. Rev.*, **78**, 97 (1978).
18) H. Suginome, T. Tsuneno, N. Sato, N. Maeda, T. Masamune, H. Shimanouchi, Y. Tsuchida, and Y. Sasada, *J. Chem. Soc., Perkin Trans. 1*, **1976**, 1297.
19) L. F. Fieser, "Experiments in Organic Chemistry," 3rd ed, D. C. Heath and Co., Boston (1955), p. 283.

Synthesis of Indeno[1,2-*d*]azepine Derivatives

Masaru KIMURA,* Kyosuke SATAKE, Shigeaki YONEMORI, and Shiro MOROSAWA
Department of Chemistry, Okayama University, Tsushimanaka 3-1-1, Okayama 700
(Received January 28, 1980)

4-Ethoxyindeno[1,2-*d*]azepine(**18**) and 10-bromo-4-ethoxyindeno[1,2-*d*]azepine were prepared by *O*-ethylation of indeno[1,2-*d*]azepin-4-ol(**12ab**) and 10-bromoindeno[1,2-*d*]azepin-4-ol(**13ab**) with Et_3OBF_4 in 62 and 69% yields, respectively. **12ab** was obtained by bromination of 1,2,3,4,5,10-hexahydro-4-indeno[1,2-*d*]azepine(**3**) or 1,2,3,4-tetrahydroindeno[1,2-*d*]azepin-4-one with NBS, and subsequent dehydrobromination of the corresponding bromide formed *in situ* on basic alumina in 10% yield. When the bromination time was over 20 h, only **13ab** was isolated in 20% yield. Direct dehydrogenation of **3** with DDQ gave 10-chloroindeno[1,2-*d*]azepin-4-ol in 27% yield. The NMR and electronic spectra of **18** indicated the presence of a fully conjugated 14-pi ring system in it. We also investigated the possibility for dehydrogenation of 3-ethoxycarbonyl-1,2,3,4,5,5a,10,10a-octahydroindeno[1,2-*d*]azepin-10-one.

We have derived a simple synthetic approach for benz[*a*]azulene derivatives containing a nitrogen atom in the seven-membered ring that should lead to new theoretical and practical fields. Benz[*a*]azulene is a typical nonbenzeniod aromatic compound having two $(4n+2)$pi ring systems.[1] When an electron withdrawing >C=N– bond is introduced into part of the seven-membered ring, the stable 14-pi ring system may be destabilized by the contribution of a canonical structure like **1c**. As shown here, unconventional physical and

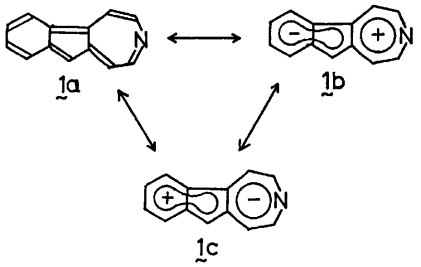

chemical properties can be anticipated to be associated with such molecules as **labc**. Although there are five basic skeletones for azabenz[*a*]azulene, *i.e.*, indeno[2,1-*b*]-, indeno[2,1-*c*]-, indeno[1,2-*d*]-, indeno[1,2-*c*]-, and indeno[1,2-*b*]azepine, only 3-ethoxycarbonyl indeno[2,1-*b*]azepine(**4**) was prepared and studied by Treibs *et al.*[2] Furthermore, most of the reported azazulenes[3] to date, such as cyclopent[*c*]azepine,[3a] 6,7,8-triphenylcyclopent[*b*]azepine,[3b] and **4** have been prepared by the method using no dehydrogenation process to furnish the ring system. The development of a general synthesis of indenoazepines by dehydrogenation of the corresponding saturated ring system is desiable. We wish to report two independent methods (methods A and B) utilized in the preparation of **1** by the use of **2** and **3**. In method A, we investigated the possibility for dehydrogenation of **2**. In method B, we wish to report the successful synthesis of novel **18** from **3**.

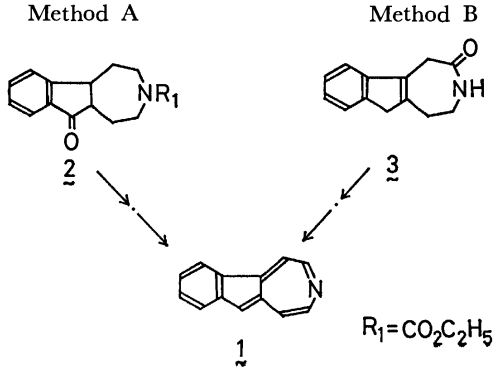

Results and Discussion

Method A. Some Attempts for Dehydrogenation of **2**: This method was characterized by the use of **2**, the structure of which was established.[4] Mono- and dibromination of **2** were effected with 1 equiv of bromine in ether solution. Upon dehydrobromination of the corresponding bromides using lithium chloride in DMF at 120 °C, there was a yellow oil obtained. Preparative column chromatography of the reaction mixture on silica gel permitted purification and isolation of 3-ethoxycarbonyl-1,2,3,4,5,10-hexahydroindeno[1,2-*d*]-azepin-10-one(**5**), and 3-ethoxycarbonyl-1,2,3,10-tetrahydroindeno[1,2-*d*]azepin-10-one(**6**). The structures of **5** and **6** were deduced from the following NMR, IR, electronic spectra, and elemental analyses. An elemental analysis suggested that **5** was formulated as $C_{16}H_{17}NO_3$ and **6** was $C_{16}H_{15}NO_3$. Therefore a new double bond and two double bonds were introduced into **2**, and **5** and **6** were prepared, respectively. The electronic spectrum of the yellow compound **5** showed strong absorption bands at 237 (log ε, 4.54) and 244 nm (4.55). This absorption pattern was similar to that of 8-methyl-1,2,3,4-tetrahydrofluoren-9-one(**7**).[10] In NMR spectrum of **5**, the resonances of methylene groups appear at 2.45—2.49 (4H, m) and 3.45—3.88 ppm (4H, m). These results support the structure of **5**. The electronic spectrum of the red compound **6** showed three absorption bands at 224 (log ε, 4.22), 277 (4.34), and 455 nm (2.93). In NMR spectrum of **6**, the resonances of methylene groups appear at 2.88 (2H, t, J=4.5 Hz), and the resonances at 5.75 (1H, d, J=9.1 Hz) and 7.02 ppm (1H, d, J=9.1 Hz)

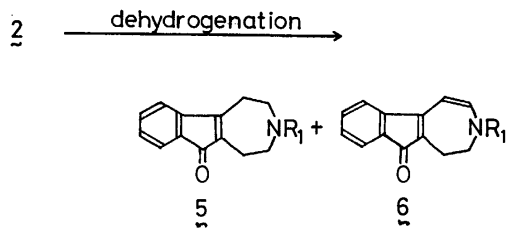

Table 1. Summary of Method A

Starting azepine	Reaction conditions: Dehydrogenation agent (Solvent/temp, °C/time)		Products and their yield (%): 5	6
2	1) Br_2	(Ether/0/20 min)	31.5	5.2
	2) LiCl	(DMF/120/7 h)		
2	DDQ	(Dioxane, N_2/Reflux/53 h)	31.0	11.0
2	Pd/C	(Decalin, N_2/Reflux/190/53 h)	3.4	2.6
2	Ph_3CBF_4	(CH_3COOH, Ar/Reflux/8.5 h)	—	8.6
5	DDQ	(Dioxane, Ar/Reflux/9 h)	Polymers	
5	Ph_3CBF_4	(CH_3COOH, N_2/Reflux/14 h)		17.0

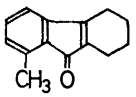

7

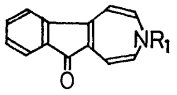

8

are corresponding to γ and δ protons of $\alpha,\beta,\gamma,\delta$-unsaturated ketone system in **6**. These results support the structure of **6**. The results of bromination and subsequent dehydrobromination of **2** are summarised in Table 1. Allylic bromination of both **5** and **6** were achieved with 1 equiv of NBS in the presence of a catalytic amount of bezoyl peroxid. The dehydrobrominations of the corresponding bromides with LiCl in DMF produced a complex and tarry mixture. Similarly, the dehydrogenation of **5** and **6** with DDQ produced a complex and tarry mixture. In the case of dehydrogenation of **5** with triphenylmethyl tetrafluoroborate, **6** was isolated by preparative TLC. Dehydrogenation of **6** with triphenylmethyl tetrafluoroborate gave no evidence for the formation of **8**. It thus became necessary to develop another method for preparing **1** by the use of more stable intermediates.

Method B. *Synthesis of **18** and **19** from **3***: Considering the difficulty of the preparation of a fully conjugated azepine system from hydroazepine(**2**), we chose **3** as an intermediate into which introduction of >C=N– bond was accomplished with the aid of tautomerism between the lactam form (**12a**) and azepinol form (**12b**). The reaction sequence is outlined in Scheme 1. The ring expansion of 1,2,3,9a-tetrahydrofluoren-3-one (**9**)[5] with sodium azide in PPA at 40 °C, followed by column chromatography on neutral alumina produced **3** in 60% yield. For the confirmation of the structure, **3** was treated successively with $LiAlH_4$ and ethyl chloroformate. The expected 1-ethoxycarbonyl-1,2,3,4,5,10-hexahydroindeno[1,2-*d*]azepine (**10**: R=$CO_2C_2H_5$) was obtained in 80% yield. **10** was identified by comparison with the NMR and IR data of the authentic sample obtained by Kimura and Morosawa.[4a] Bromination of **3** with 1.1 molar equiv of pyridinium hydrogenbromide perbromide in acetic acid at 40 °C for 4 h,

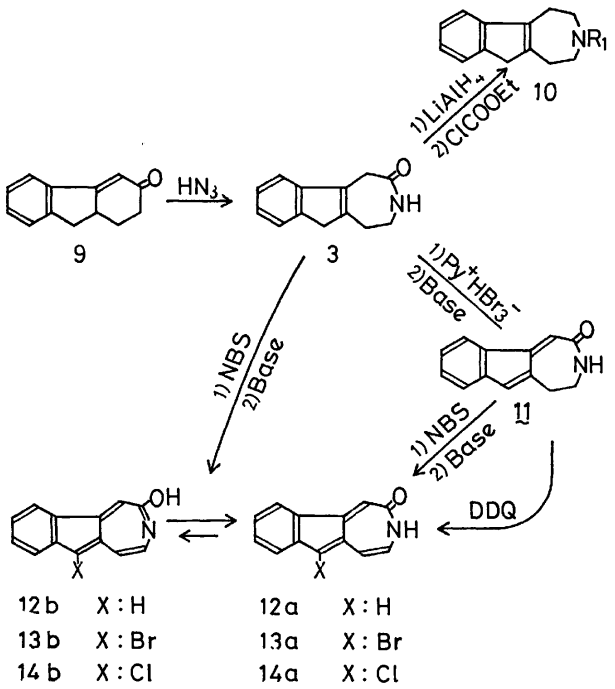

Scheme 1.

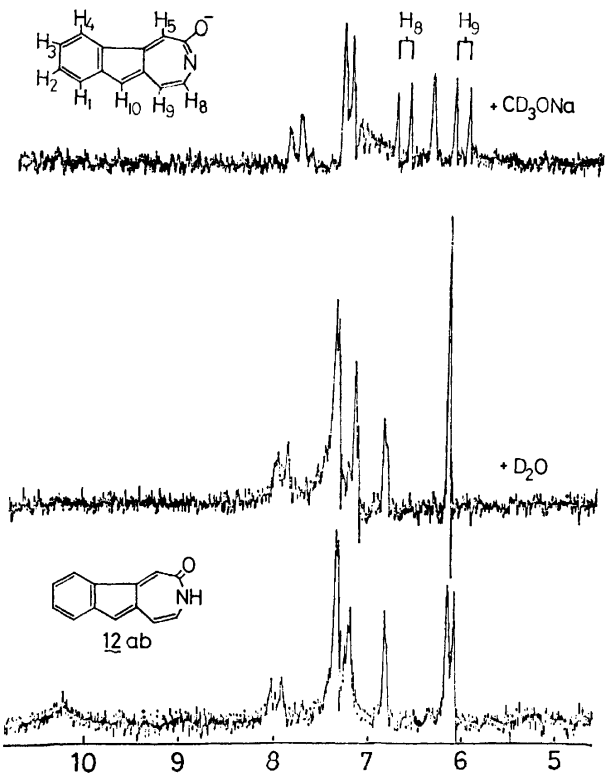

Fig. 1. NMR spectra of **12ab** in DMSO-d_6 (bottom), in the presence of few drops of D_2O (middle), and in the presence of 1 equiv of CD_3ONa (top).

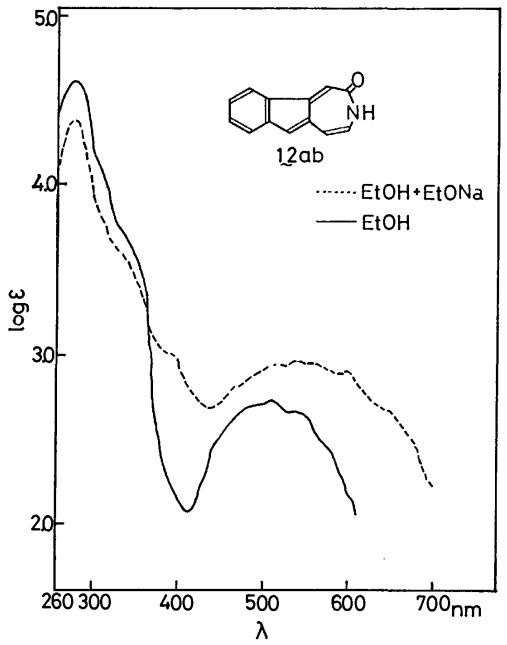

Fig. 2. Electronic spectra of **12ab** in EtOH (——) and in the presence of 1 equiv of EtONa (----).

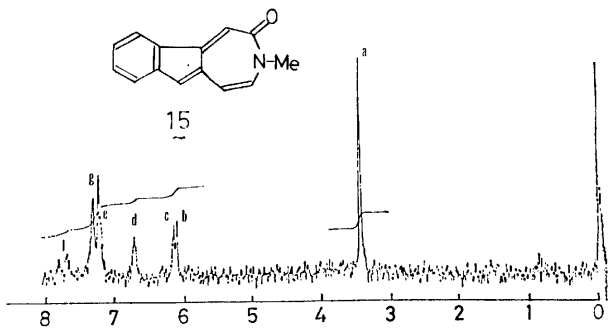

Fig. 3. NMR spectrum of **15** in $CDCl_3$.

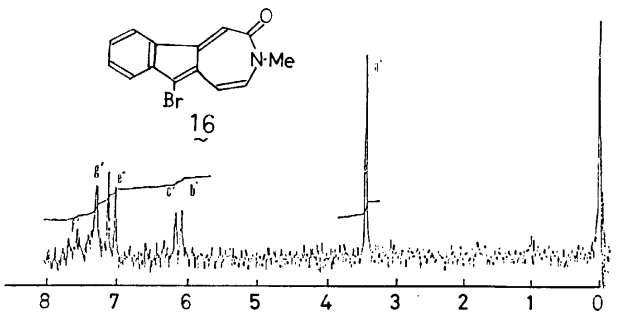

Fig. 4. NMR spectrom of **16** in $CDCl_3$.

followed by dehydrobromination of the corresponding bromide on basic alumina, produced a yellow-orange solid **11** in 83% yield. Bromination of **11** with 1.1 molar equiv of NBS in refluxing benzene in the presence of a catalytic amount of benzoyl peroxide for 10 h, followed by dehydrobromination of the corresponding bromide formed *in situ* on basic alumina, produced **12ab** in 10% yield. The NMR spectrum of the reddish purple solution of **12ab** in DMSO-d_6 showed resonance peaks at 6.25 (2H), 7.40 (1H), 7.20—7.60 (4H), 7.95 (1H), and 10.25 ppm (1H). When a few drops of D_2O were added to the solution, the resonance peak at 6.25 ppm became pseudo singlet and the resonance peak at 10.25 ppm disappeared. The resonance peak at 6.25 ppm became a pair of doublet peaks at 6.05 (1H, d, J=9 Hz, H_9) and 6.75 ppm (1H, d, J=9 Hz, H_8) with the addition of 1 equiv of CD_3ONa (shown in Fig. 1). On the basis of these findings the resonance peak at 6.25 ppm may be assigned to the adjacent 8- and 9-protons of **12ab**. The IR spectrum of **12ab** showed absorptions at 3200 and 1650 cm^{-1} for >NH and >C=O streching of the amide group, respectively. The electronic spectrum of **12ab** in EtOH showed absorptions at λ_{max} 510 (log ε, 2.9), 345(sh), 283 nm(4.7). When 1 equiv of EtONa was added to the solution, the absorptions shifted to a longer wavelength by ≈50 nm (shown in Fig. 2). The bathochromic shift in basic solution was attributable to the substantial enhancement of the double bond character of the >N(CO)– bond by the removal of the amide proton.[6]

When the refluxing time of the bromination of **3** with NBS was over 20 h, **13ab** was obtained in a 20% yield. On the other hand, the direct dehydrogenation of **3** with DDQ in refluxing benzene for 20 h, followed by chromatography on silica gel eluting with CH_2Cl_2, produced purple solids **14ab** in 20% yield. The reaction mechanisms for the formation of these unexpected products (**13ab** and **14ab**) were now under-investigation. **3** and **11** showed strong infrared absorptions at 1670 and 1650 cm^{-1}, respectively, as streching for each amide's carbonyl in their lactam rings occured. Both **13ab** and **14ab**, however, showed medium infrared absorptions at 1640 cm^{-1} as streching for the amide's carbonyl in their lactam rings occured. The electronic spectra of **13ab** and **14ab** were similar to that of **12ab**. The possition of X in **13ab** and **14ab** (Scheme 1) was determined in the following discussion.

N-Methylation of **12ab**, **13ab**, and **14ab** using an excess of 40% NaOH and CH_3I with a trace of benzyltriethylammonium chloride under phase-transfer conditions[7] at room temperature for 12 h produced high yields of **15**, **16**, and **17**, respectively. The assignment

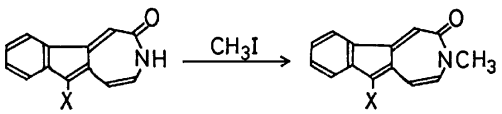

12ab	X:H	15	X:H
13ab	X:Br	16	X:Br
14ab	X:Cl	17	X:Cl

of the position of entry of the bromine atom was determined by the comparison between NMR spectra **15** and **16** in the presence of a shift reagent ($Eu(fod)_3$). The NMR spectra of **15** and **16** are shown in Figs. 3 and 4. Figures 5 and 6 show plots of the induced shifts *vs.* the shift reagent/substrate mole ratios (E/S) for the substrates **15** and **16**, respectively. In Figs. 3 and 4, the absorption labeled by a and a′ are assigned to methyl groups of **15** and **16** in terms of their integrations and chemical shifts of 3.50 and 3.45 ppm, re-

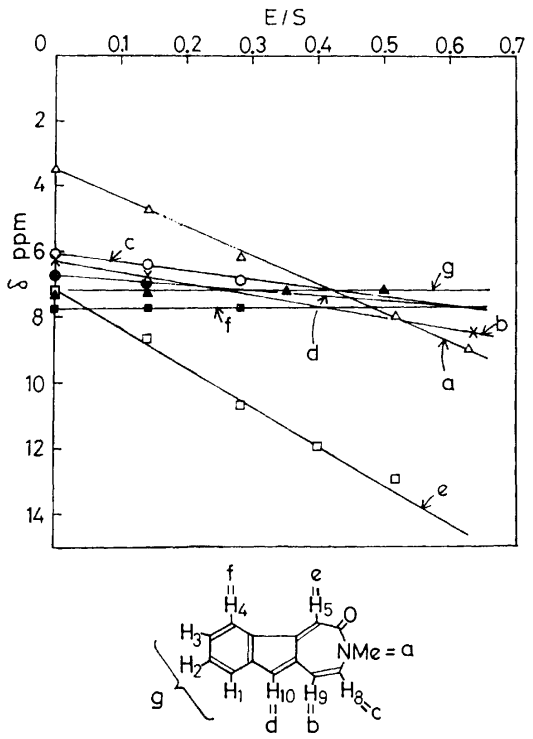

Fig. 5. δ *vs.* E/S for **15** with $Eu(fod)_3$ in $CDCl_3$.

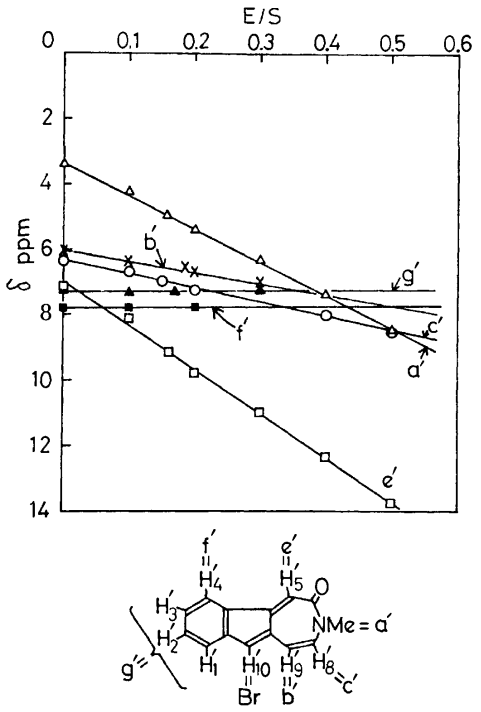

Fig. 6. δ *vs.* E/S for **16** with $Eu(fod)_3$ in $CDCl_3$.

spectively. The sizable shifts observed in their methyl protons nearest to their carbonyl groups indicate association through their carbonyl groups. The shifts of vinyl protons e and e′ were greater than the other vinyl protons in Figs. 5 and 6, respectively. Each of these should be assigned to H_5 and H_5' where the positions are nearest to each carbonyl group. Two couples of their resonances of f and g, and f′ and g′ were assigned to each benzene ring, due to the lack

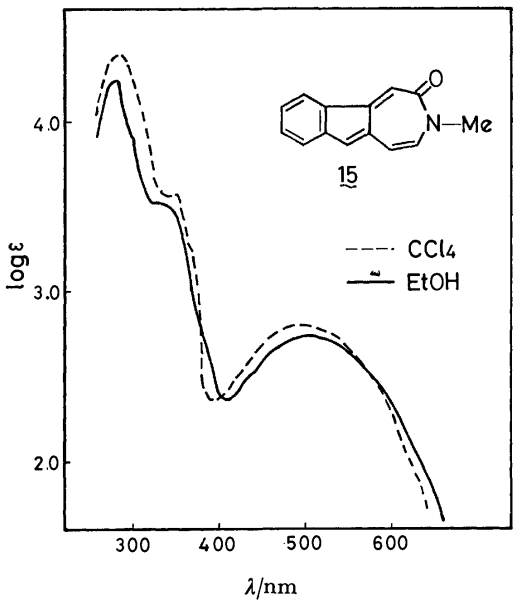

Fig. 7. Electronic spectra of **15** in EtOH (——) and in CCl_4 (----).

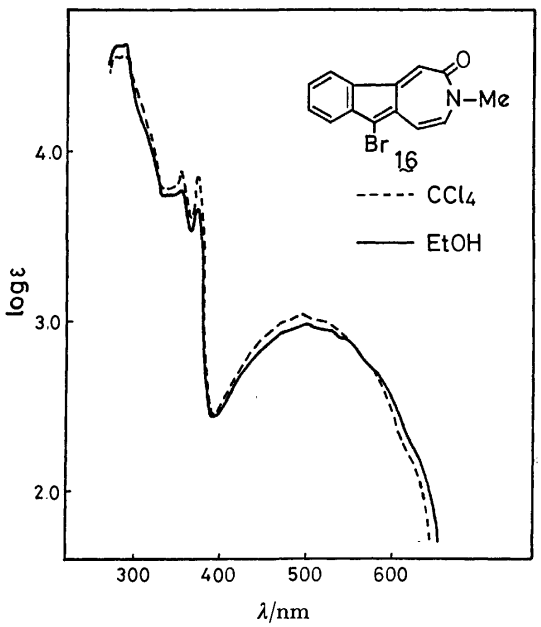

Fig. 8. Electronic spectra of **16** in EtOH (——) and in CCl_4 (----).

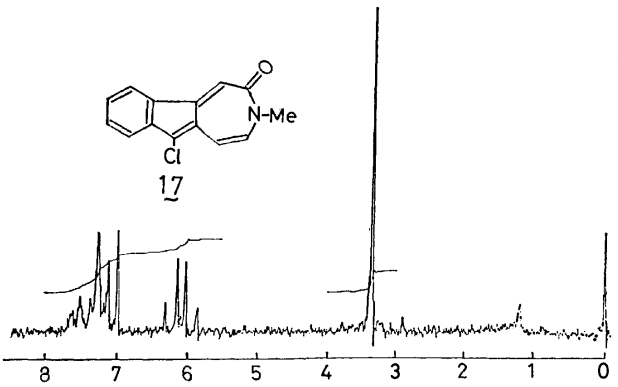

Fig. 9. NMR spectrum of **17** in $CDCl_3$.

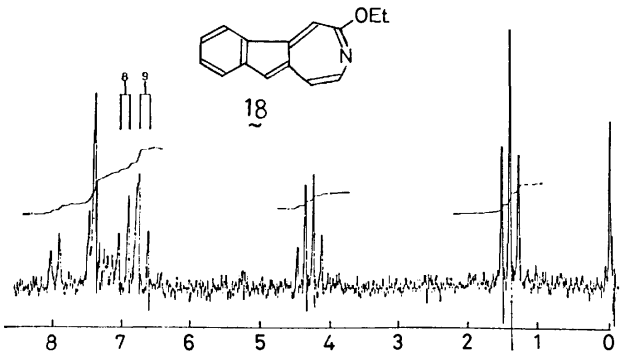

Fig. 10. NMR spectrum of **18** in CCl_4.

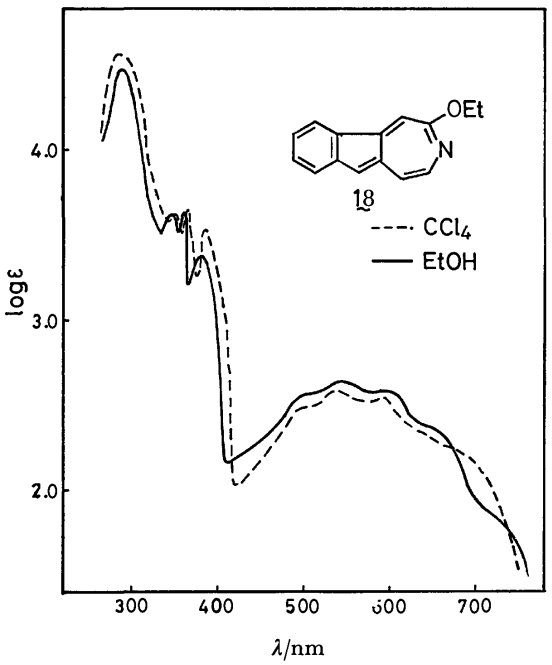

Fig. 11. Electronic spectra of **18** in EtOH (——) and in CCl_4 (----).

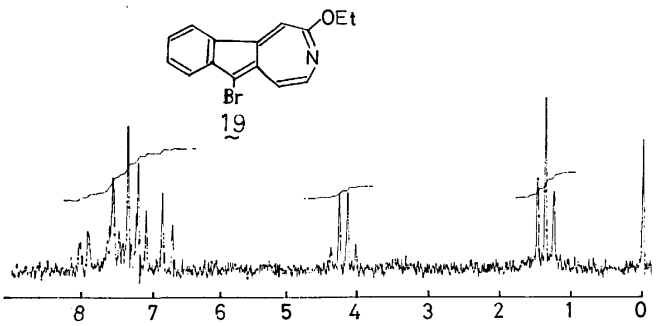

Fig. 12. NMR spectrum of **19** in $CDCl_3$.

of shifts up to equimolar ratios of **15** to $Eu(fod)_3$ and of **16** to $Eu(fod)_3$. Two pairs of b and c, and b′ and c′ were assigned to H_8 and H_9, and H_8' and H_9', respectively, with each coupling constant $J=10$ Hz. In Figs. 4 and 6, lack of the resonance corresponding to H_{10}' indicated that the position was substituted by bromine atom. The electronic spectra of **15** and **16** are shown in Figs. 7 and 8, respectively. Com-

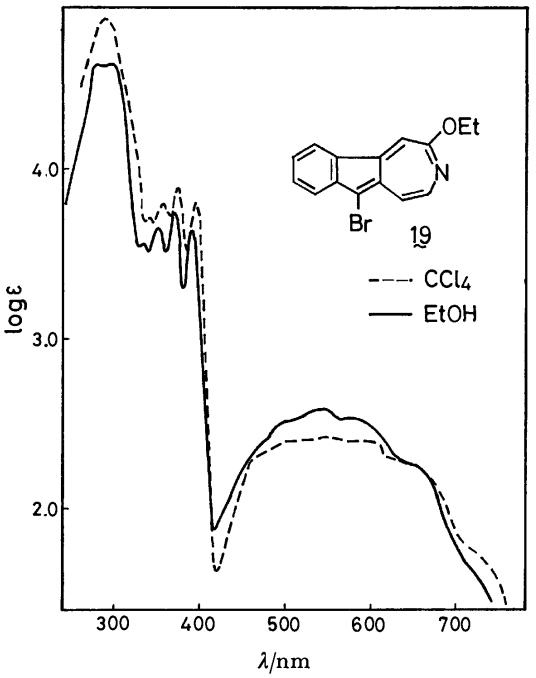

Fig. 13. Electronic spectra of **19** in EtOH (——) and in CCl_4 (----).

parison of NMR spectrum of **17** with that of **16** revealed that the position of the entry of the chlorine atom to the indeno[1,2-*d*]azepine ring was the same as that of the bromine atom in **16** (see Figs. 4 and 9).

O-Ethylation of **12ab** and **13ab** with triethyloxonium tetrafluoroborate[8] led to the isolation of the novel 4-ethoxyindeno[1,2-*d*]azepine (**18**) and 10-bromo-4-ethoxyindeno[1,2-*d*]azepine(**19**) in 53 and 60% yields,

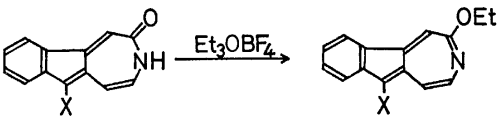

12ab X:H
13ab X:Br

18 X:H
19 X:Br

respectively. These compounds were found to be labile by treatment with base, and had to be handled with care to avoid decomposition during chromatography on alumina.[9] Their structures followed from their spectral characteristics. IR showed 1640 and 1585 cm^{-1} as representative of the streching of the >C=N– and >C=C< bonds, respectively. In Fig. 10 the resonance of hydrogens H_8 and H_9 appears at lower fields than those of **15** by $\approx$1.00 ppm. This deshielding of the ring protons in **18** indicated the aromatic character of the 14-pi ring system supporting diamagnetic anisotropy. The electronic spectrum of **18** in CCl_4 (Fig. 11) was similar to that of benz[*a*]azulene itself.[1a,4b] The longest absorption band of **18** shifted to a longer wavelength by $\approx$50 nm than that of **15** (see Figs. 7 and 11). These results also indicated the presence of a fully conjugated 14-pi ring system in **18**. **19** showed similar characteristics on NMR and electronic spectra to that of **18** (Figs. 12 and 13).

Experimental

The structures of all the new compounds were cofirmed by NMR, IR, UV, and elemental analyses. All melting points and boiling points are uncorrected. IR(nujol) spectra were determined on a JASCO IR A-1 grating infrared spectrometer. NMR($CDCl_3$/TMS, Hitachi-Perkin Elmer R-20) spectra were obtained at 60 MHz unless otherwise noted. The chemical shifts are represented in terms of δ values. UV(Hitachi UV-200) spectra were obtained in terms of nm. Column chromatography and TLC were performed using Wakogel C-200, and Kieselgel 60F 254 respectively. **2** and **9** were prepared by the method developed by M. Kimura and S. Morosawa,[4a] and E. Bergmann *et al.*[5] respectively. Triphenylmethyl tetrafluoroborate was prepared by the procedure developed by H. J. Dauben, Jr., *et al.*[11]

*3-Ethoxycarbonyl-1,2,3,4,5,10-hexahydroindeno[1,2-d]azepin-10-one(**5**) and 3-Ethoxycarbonyl-1,2,3,10-tetrahydroindeno[1,2-d]azepin-10-one(**6**).* To a stirring solution of 3-ethoxycarbonyl-1,2,3,4,5,5a,10,10a-octahydroindeno[1,2-*d*]azepin-10-one (**2**, 490 mg, 1.7 mmol) in 25 ml of ether was added a solution of bromine (310 mg, 1.9 mmol) in CCl_4 over a period of 20 min at 0 °C. After stirring for additional 10 min at room temperature, the solution was washed with 10% aqueous $NaHSO_3$, and 5% aqueous $NaHCO_3$ and dried over $MgSO_4$. The solvent was removed to give a yellow oil (670 mg). The viscous slightly yellow bromide was employed without further purification. A suspension of LiCl (720 mg, 1.7 mmol) and the crude bromide (600 mg, 1.7 mmol) in 15 ml of dry THF was heated at 120 °C for 7 h under a nitrogen atmosphere. After being cooled to room temperature, the solvent was removed *in vacuo*, and the residue was taken up in benzene. The solution was washed with saturated aqueous NaCl solution, and the solvent was removed to give a brown oil. The oil was chromatographed on silica gel (benzene as eluent) to give 21.3 mg(5.3%) of **7**, 129.3 mg(31%) of **5**. **5**: IR(KBr) 1703, 1694, 1621, 1603, 1595 cm^{-1}; NMR 1.28 (3H, t, J=7.1 Hz), 2.43—2.94 (4H, m), 3.45—3.88 (4H, m), 4.22 (2H, q, J=7.1 Hz), 6.93—7.68 ppm (4H, m); UV λ_{max} (EtOH) 237 (log ε, 4.54), 244 (4.55), 305 (2.95). Found: C, 70.74; H, 6.52; N, 4.97%. Calcd for $C_{16}H_{17}NO_3$: C, 70.83; H, 6.32; N, 5.16%. **6**: IR(KBr) 1700, 1690, 1606, 1590 cm^{-1}: NMR 1.33 (3H, t, J=7.1 Hz), 2.88 (2H, t, J=4.5 Hz), 3.92 (2H, t, J=4.5 Hz), 5.75 (1H, d, J=9.1 Hz), 7.02 (1H, d, J=9.1 Hz), 6.88—7.88 ppm (4H, m); UV λ_{max} (EtOH) 224 (log ε, 4.22), 277 (4.34), 455 (2.93). Found: C, 71.06; H, 5.61; N, 4.97%. Calcd for $C_{16}H_{15}NO_3$: C, 71.36; H, 5.61; N, 5.20%.

*Dehydrogenation of 3-Ethoxycarbonyl-1,2,3,4,5,5a,10,10a-octahydroindeno[1,2-d]azepin-10-one(**2**) with DDQ.* A solution of **2** (50 mg, 0.183 mmol) and DDQ (138 mg, 0.549 mmol) in 1 ml of dry dioxane was refluxed for 53 h under a nitrogen atmosphere. After cooling to room temperature, the solvent was removed to give a brownish residue. The residue was separated with TLC (silica gel, 50% ether in benzene) to give **6** (5.4 mg, 11%, R_f (silica gel, benzene/ether=1:1)= 0.61), **5** (15.6 mg, 31%, R_f=0.47), and **2** (17.3 mg, 35% recovered, R_f=0.38). These products were identified by comparison of their R_f values and UV data with those of each authentic sample.

*Dehydrogenation of **2** with Pd/C.* A suspension of **2** (500 mg, 1.83 mmol) and 8%-Pd/C (500 mg) in 4 ml of dry decalin was refluxed for 53 h under a nitrogen atmosphere. After cooling to room temperature, the Pd/C was filtered off and the filtrate was passed through short column (silica gel, eluting with benzene). Removing the solvent under reduced pressure, 390 mg of red oil was remained. The residue was chromatographed using a silica gel column with 50% ether in benzene as eluent. From first fraction, 8.3 mg of **6** was collected, and 7.3 mg of **5** was collected from second fraction. **5** and **6** were identified by the method shown in preceeding experiment.

*Dehydrogenation of **2** with Triphenylmethyl Tetrafluoroborate.* A mixture of **2** (20 mg, 0.073 mmol) and triphenylmethyl tetrafluoroborate (26.6 mg, 0.081 mmol) in 2 ml of dry acetic acid was refluxed for 8.5 h under an argon atmosphere. Additional 24.2 mg (0.073 mmol) of triphenylmethyl tetrafluoroborate was added and the brown solution was refluxed for additional 4.5 h under the same conditions. After cooling to room temperature, the solvent was removed under reduced pressure, and a brown residue was poured into water and extracted with ether. The ethereal extract was dried over Na_2SO_4. After removing the solvent, brown oil (16.4 mg) was obtained. This oil was chromatographed on silica gel eluting with 5% ether in benzene to give **6** (1.7 mg, 8.6%) and **2** (6.3 mg, 32%). **2** and **6** were identified by the method shown in preceeding experiment.

*Dehydrogenation of **5** with DDQ.* A solution of **5** (20 mg, 0.074 mmol) and DDQ (98%, 18.8 mg, 0.081 mmol) in 2 ml of dry dioxane was refluxed for 9 h under an argon atmosphere. Additional DDQ (17.1 mg, 0.074 mmol) was added to the mixture and the solution was refluxed for another 24.5 h. After usual workup, **5** was recovered.

*Dehydrogenation of **5** with Triphenylmethyl Tetrafluoroborate.* A solution of **5** (20 mg, 0.074 mmol) and triphenylmethyl tetrafluoroborate (51.1 mg, 0.16 mmol) in dry acetic acid was refluxed for 14 h under a nitrogen atmosphere. After usual workup, **6** (3.4 mg, 17%) was obtained and **5** (12.9 mg, 65%) was recovered. **5** and **6** were identified by the method shown in preceeding experiment.

*Dehydrogenation of **6** with DDQ.* A solution of **6** (5.0 mg, 0.019 mmol) and DDQ (13.0 mg, 0.056 mmol) in 3 ml of dry dioxane was refluxed under an argon atmosphere. The reaction was monitored by TLC and the starting material was completely disappered after 17 h. Some uncharacterized polymer was obtained.

*Dehydrogenation of **6** with Triphenylmethyl Tetrafluoroborate.* A solution of **6** (5.0 mg, 0.019 mmol) and triphenylmethyl tetrafluoroborate (12.3 mg, 0.037 mmol) in 2 ml of dry acetic acid was refluxed under an argon atmosphere and the reaction was monitored by TLC. No reaction was observed up to 6.5 h and only **6** was recovered.

*1,2,3,4,5,10-Hexahydroindeno[1,2-d]azepin-4-one (**3**).* To a stirring mixture of **9** (3.58 g, 0.036 mol) and phosphorus pentaoxide (1.7 g, 0.012 mol) in 600 g of polyphosphoric acid (105%) was added in portions sodium azide (3.5 g, 0.054 mol) over 1 h at 40—50 °C and the reaction mixture was stirred for 48 h at same temperature. After cooling to room temperature, the reaction mixture was poured onto ice–water, and extracted with chloroform. The extract was washed with 5% aqueous $NaHCO_3$, then with water, and was dried over $MgSO_4$. The residue obtained on evaporation of the solvent was solidified to give an orange solid (2.7 g, 70%). The solid was subjected to column chromatography on neutral alumina eluting with CH_2Cl_2 to give **3** (2.3 g, 60%): pale yellow prisms from C_2H_5OH, mp 207—209 °C; IR 3250, 1670 cm^{-1}; UV λ_{max} (EtOH) 207 (log ε, 4.28), 260 (4.01); NMR(CCl_4) 2.50—2.90 (2H, m), 3.28 (2H, bs), 3.45—3.75 (4H, m), 7.00—7.60 (5H, m, aromatic H and NH). Found: C, 78.21; H, 6.51; N, 7.10%. Calcd for $C_{13}H_{13}NO$: C, 78.36; H, 5.58; N, 7.03%.

*3-Ethoxycarbonyl-1,2,3,4,5,10-hexahydroindeno[1,2-d]azepine (**10**).* A suspension of $LiAlH_4$ (0.72 g, 19 mmol) in

40 ml of dry THF was stirred and refluxed for 1 h. After cooling on an ice bath, a solution of **3** (1.5 g, 7.5 mmol) in dry THF (100 ml) was added dropwise over a period of 1 h. After addition was complete, the mixture was stirred 24 h at room temperature. A sufficient amount of 3 N aqueous hydrochloric acid (10 ml) was carefully added dropwise to decompose excess $LiAlH_4$. The acidified solution was workup immediately by extraction with ether. To the ether extract was added 3% aqueous potassium carbonate (30 ml), and ethyl chloroformate (3.8 g, 35 mmol). After stirring for 1 h, the ether layer was separated. The ether was removed and the residue was distilled under reduced pressure to give the indene **10** (1.63 g, 80%), bp 214—217 °C/0.2 Torr. **10** was identified by comparison of IR and NMR spectra with those of authentic sample obtained by M. Kimura and S. Morosawa.[4a]

*1,2,3,4-Tetrahydroindeno[1,2-d]azepin-4-one (**11**).* A solution of **3** (100 mg, 0.50 mmol) and pyridinium hydrogenbromide perbromide (192 mg, 0.6 mmol) in 15 ml of dry acetic acid (passed through alumina) was heated at 40 °C for 6 h. The residue obtained on evaporation of the solvent was taken up in chloroform. Column chromatography on alumina eluting with chloroform gave **11** (60 mg, 61%): orange prisms from CH_2Cl_2, mp 201 °C; IR 3180, 1650, 1600(sh) cm^{-1}; UV λ_{max} (EtOH) 260 (log ε, 4.5), 330 (3.9), 380(sh); NMR (DMSO-d_6) 2.60—3.00 (2H, m), 3.10—3.50 (2H, m), 6.69 (2H, bs), 7.20 (3H, m), 7.65 (1H, bs), 8.10 (1H, m). Found: C, 79.10; H, 5.89; N, 6.96%. Calcd for $C_{13}H_{11}NO$: C, 79.16; H, 5.62; N, 7.10%.

*Indeno[1,2-d]azepin-4-ol (**12ab**).* 1) A solution of **3** (5 g, 26 mmol), NBS (5.1 g, 29 mmol), and benzoyl peroxide (100 mg, 0.41 mmol) was refluxed at 45 °C for 24 h. The reaction mixture was chromatographed on alumina eluting with 4% ethanol in CH_2Cl_2 to give **11** (2.0 g, 40%) and **12ab** (502 mg, 10%). **12ab**: black fine prisms from CH_2Cl_2, mp 240 °C (sublimed); IR 3200, 1650 cm^{-1}; UV λ_{max} (EtOH) 283 (log ε, 4.7), 345 (sh), 510(2.9); NMR (DMSO-d_6) 6.25 (2H, m), 6.40 (1H, s), 7.10—7.20 (4H, m), 7.95 (1H, d), 10.25 (1H, m). Found: C, 79.63; H, 4.43; N, 6.76%. Calcd for $C_{13}H_9NO$: C, 79.98; H, 4.65; N, 7.17%. **11** was identified by comparison of IR and NMR spectra with those of authentic sample obtained in preceeding experiment. 2) A solution of **11** (200 mg, 1.0 mmol) and NBS (180 mg, 1.0 mmol) in benzene was refluxed in the presence of a catalytic amount of benzoyl peroxide for 4.5 h. After cooling to room temperature, the reaction mixture was passed through alumina eluting with CH_2Cl_2, removed the solvent to give a black solid. Recrystallization of the solid from THF gave **12ab** (20 mg, 10%). **12ab** was identified by comparison of its IR and NMR spectra with those of authentic sample obtained in preceeding experiment.

*10-Bromoindeno[1,2-d]azepin-4-ol (**13ab**).* A solution of **11** (100 mg, 0.51 mmol) and NBS (100 mg, 0.56 mmol) in CH_2Br_2 was refluxed at 120 °C (bath temperature) in the presence of a catalytic amount of benzoyl peroixide for 24 h. After usual workup, **13ab** (60 mg, 43%) was obtained: black fine hair like needles from THF, mp 320 °C dec; IR 3200, 3130, 1675, 1638, 1615, 1600 cm^{-1}; NMR (DMSO-d_6) 6.00—6.55 (2H, m), 7.22—7.60 (4H, m), 8.00—8.25 (1H, m), 10.30—10.50 ppm (1H, bs); UV λ_{max} (EtOH) 286 (log ε, 4.7), 350(sh), 368(sh), 500(3.0). Found: C, 56.87; H, 2.88; N, 4.82%. Calcd for $C_{13}H_8NOBr$: C, 56.96; H, 2.94; N, 5.11%.

*10-Chloroindeno[1,2-d]azepin-4-ol (**14ab**).* A solution of **11** (1.6 g, 8.1 mmol) and DDQ (5.5 g, 24 mmol) in dry dioxane was refluxed for 24 h under a nitrogen atmosphere. After cooling to room temperature, the reaction mixture was filtered and passed through short alumina column eluting with $CHCl_3$. After removing the solvent, the residue was column chromatographed on alumina eluting with CH_2Cl_2 to give **14ab** (530 mg, 28%): black hair like needles from THF, mp 260 °C dec; IR 3200, 3130, 1675, 1640, 1620, 1598 cm^{-1}; NMR (DMSO-d_6) 6.05—6.50 (2H, m), 7.20—7.70 (4H, m), 8.25—8.95 (1H, m), 10.20—10.60 ppm (1H, m); UV λ_{max} (EtOH) 285 (log ε, 4.7), 350(sh), 368(sh), 515 (2.9). Found: C, 67.69; H, 3.27; N, 5.75%. Calcd for $C_{13}H_8NOCl$: C, 67.99; H, 3.51; N, 6.10%.

*3-Methylindeno[1,2-d]azepin-4-one (**15**).* To a 50% aqueous solution of NaOH (5 ml) was added a solution of **12ab** (30 mg, 0.15 mmol) and benzyltriethylammonium chloride (41 mg, 0.18 mmol). After 15 min stirring at room temperature, 52 mg of MeI (0.36 mmol) was added to the suspension. The reaction mixture was stirred for 40 min at room temperature. Organic layer was separated, washed with water, and dried over $MgSO_4$. The residue obtained by evaporation of the solvent was recrystallized from ethanol to give **15** (30 mg, 95%): brown needles from CH_2Cl_2, mp 149—150 °C; IR 1628, 1620, 1600(sh) cm^{-1}; UV λ_{max} (EtOH) 275 (log ε, 4.2), 330(sh), 505(2.9); NMR 3.50 (3H, s), 6.09 (1H, d, J=9 Hz), 6.29 (1H, d, J=9 Hz), 6.80 (1H, s), 7.29 (1H, s), 7.20—7.55 (3H, m, aromatic H), 7.82 ppm (1H, bs, aromatic H). Found: C, 80.01; H, 5.27; N, 6.71%. Calcd for $C_{14}H_{11}NO$: C, 80.36; H, 5.30; N, 6.69%.

*10-Bromo-3-methylindeno[1,2-d]azepin-4-one (**16**).* The reaction was carried out as described for the preparation of **14ab**. The crude product was purified by recrystallization from CH_2Cl_2: **16**, 95% yield, dark brown needles, mp 154—156 °C; IR 1655, 1640(sh), 1605(sh), 1598 cm^{-1}; UV λ_{max} (EtOH) 280 (log ε, 4.64), 354 (3.76), 372(3.66), 500 (2.98); NMR 3.42 (3H, s), 6.05 (1H, d, J=10 Hz), 6.35 (1H, d, J=10 Hz), 7.05 (1H, s), 7.22—7.62 (3H, m, aromatic H), 7.75 ppm (1H, bd, aromatic H). Found: C, 68.48; H, 3.91; N, 5.47%. Calcd for $C_{14}H_{10}NOCl$: C, 69.00; H, 4.14; N, 5.75%.

*10-Chloro-3-methylindeno[1,2-d]azepin-4-one (**17**).* The crude product, obtained in a similar way used for **14ab**, was crystallized from CH_2Cl_2: **17**, 95% yield, dark brown needles, mp 160—160.5 °C; IR 1652(sh), 1640, 1603(sh), 1596 cm^{-1}; UV λ_{max} (EtOH) 277 (log ε, 4.66), 330 (3.82), 345(3.75), 490(3.08); NMR 3.45 (3H, s), 6.10 (1H, d, J=10 Hz), 6.45 (1H, d, J=10 Hz), 7.20 (1H, s), 7.20—7.60 (3H, m, aromatic H), 7.75 ppm (1H, bs, aromatic H). Found: C, 58.45; H, 3.27; N, 4.85%. Calcd for $C_{14}H_{10}NOBr$: C, 58.36; H, 3.50; N, 4.86%.

*4-Ethoxyindeno[1,2-d]azepine (**18**).* In a dry 20 ml two-necked flask protected from atmospheric moisture was placed a solution of freshly redistilled boron trifluoride etherate (74 μl, 0.58 mmol) in 2 ml of anhydrous ether. Epichlorohydrin (36 μl, 0.45 mmol) was added dropwise at 40 °C. When the epichlorohydrin had been added, the oil which initially formed began to solidify. The mixture was stirred at room temperature for 2 h, and the solvent was decanted. The triethyloxonium tetrafluoroborate was washed well with anhydrous ether and dissolved in 1.5 ml of dry CH_2Cl_2. This solution was stirred at 10—15 °C while a solution of **12ab** (20 mg, 0.10 mmol) in 2 ml of dry CH_2Cl_2 was added dropwise. The resulting solution was stirred at room temperature for 12 h. To the stirred solution was cautiously added 2 g of a 50% aqueous potassium carbonate solution. After separation of CH_2Cl_2 layer, the solution was washed with water, and dried over $MgSO_4$. The solution was passed through silica gel to give crude **18** (14 mg, 62%): purple

fine needles from CH_2Cl_2, mp 115—117 °C; IR 1640, 1585 cm^{-1}; UV λ_{max} (EtOH) 288 (log ε, 4.5), 345(3.6), 361 (3.6), 382(3.5), 544(2.6); NMR(CCl_4) 1.38 (3H, t, J= 7 Hz), 4.29 (2H, q, J=7 Hz), 6.73 (1H, d, J=9 Hz), 6.82 (1H, s), 7.03 (1H, d, J=9 Hz), 7.15—7.60 (3H, m, aromatic H), 7.45 (1H, s), 8.07 (1H, d, aromatic H). Found: C, 80.50; H, 6.64; N, 6.17%. Calcd for $C_{15}H_{13}NO$: C, 80.69; H, 8.87; N, 6.27%.

*10-Bromo-4-ethoxyindeno[1,2-d]azepine (**19**).* The crude product, obtained in a similar way used for **18**, was crystallized from CH_2Cl_2 to give **19**: 69%, black fine prisms from CH_2Cl_2, mp 143—144 °C; IR 1650, 1640, 1600, 1580 cm^{-1}; UV λ_{max} (EtOH) 290 (log ε, 4.60), 352(3.65), 370(3.74), 390 (3.64), 544(2.59); NMR(CCl_4) 1.37 (3H, t, J=7 Hz), 4.30 (2H, q, J=7 Hz), 6.32 (1H, d, J=9 Hz), 7.17 (1H, d, J= 9 Hz), 7.36 (1H, s), 7.40—7.70 (3H, m, aromatic H), 7.99 (1H, d, aromatic H). Found: C, 59.58; H, 3.86; N, 4.54%. Calcd for $C_{15}H_{12}NOBr$: C, 59.60; H, 3.97; N, 4.64%.

References

1) a) E. Kloster-Jensen, E. Kovátis, A. Eschenmoser, and E. Heilbronner, *Helv. Chim. Acta*, **39**, 1051 (1956); b) P. A. Plattner, A. Fürst, J. Chopin, and G. Winteler, *Helv. Chim. Acta*, **31**, 501 (1948).

2) W. Treibs, H. M. Barchet, G. Bach, and W. Kirchof, *Ann. Chem.*, **574**, 54 (1951).

3) a) K. Hafner and M. Kreuder, *Angew. Chem.*, **73**, 657 (1961); b) M. K. Conner and E. LeGoff, *Tetrahedron Lett.*, **1970**, 2687; c) 6-Azazulene was reported as a rather unstable compound without data for confirming the structure except UV-visible spectrum of it. K. Hafner, *J. Heterocycl. Chem.*, **12**, (Suppl. Vol. 3) S-33 (1975).

4) a) M. Kimura and S. Morosawa, *Bull. Chem. Soc. Jpn.*, **52**, 1437 (1979); b) M. Kimura, K. Satake, and S. Morosawa, *Chem. Lett.*, **1979**, 807.

5) E. Bergmann, R. Ikan, and H. Weiler-Feilchenfeld, *Bull. Soc. Chim. Fr.*, **1957**, 290.

6) I. Yavari and J. D. Roberts, *J. Am. Chem. Soc.*, **100**, 5217 (1978).

7) C. M. Starks, *J. Am. Chem. Soc.*, **93**, 195 (1971).

8) a) H. Meerwein, W. Florian, N. Schön, and J. Stopp, *Ann.*, **641**, 1 (1961); b) L. A. Paquette, *J. Am. Chem. Soc.*, **86**, 4096 (1964).

9) **18** and **19** were purified by column chromatography on neutral alumina or silica gel.

10) H. O. House, V. Paragamian, and D. J. Wluka, *J. Am. Chem. Soc.*, **82**, 2561 (1960).

11) H. J. Dauben, Jr., L. R. Honner, and K. M. Harmon, *J. Org. Chem.*, **25**, 1442 (1960).

 © 1980 The Chemical Society of Japan Bull. Chem. Soc. Jpn., 53, 3240—3243 (1980) [Vol. 53, No. 11

Studies on the Polymerization of Acrolein Oxime. XIV.† The Structure of 2,4,7-Trimethylperhydroisoxazolo-[2,3-*a*]pyridine-2,7-dicarbaldehyde Dioxime

Tadatoshi Ota,* Seizo Masuda, and Masaru Kido**

Department of Applied Chemistry, Faculty of Engineering, Tokushima University, Minamijosanjima-cho, Tokushima 770

** *Ōtsuka Pharmaceutical Co. Ltd., Tokushima Factory, Laboratories of Natural Products Chemistry, Kawauchi-cho, Tokushima 771-01*

(Received February 18, 1980)

The thermal oligomerization of methacrylaldehyde oxime leads preferentially to two 2,4,7-trimethylperhydroisoxazolo[2,3-*a*]pyridine-2,7-dicarbaldehyde dioximes, which are comformationally isomeric with each other. The crystal structure of the α-form has been determined by means of X-ray diffraction. It is monoclinic, with the space group $P2_1/a$. The cell dimensions are $a=7.858(3)$, $b=13.186(6)$, $c=17.259(6)$ Å, $\beta=130.38(3)°$, and $Z=4$. The molecules are linked by OH···O and OH···N intermolecular hydrogen bonds, with the O···O and O···N distances of 2.794(6) and 2.760(5) Å respectively. Since attempts of the crystallization of the β-form have been unsuccessful, the determination of its chemical structure was attempted by means of ^{13}C-NMR spectroscopy and gas chromatography-mass spectrometry. The β-form is, at any rate, different from the α-form.

Methacrylaldehyde oxime undergoes spontaneous polymerization on heating to give, though in a very low yield, oligomers which consist of several products, including isomeric bicyclic trimers. A previous paper has shown that the recrystallization of the oligomers from methanol gives colorless, needle-like crystals, which are identified as 2,4,7-trimethylperhydroisoxazolo[2,3-*a*]pyridine-2,7-dicarbaldehyde dioxime(**1**).[1] The present paper will be concerned with the structure determination of two isomers (α- and β-forms) of **1**. In order to obtain detailed information on the molecular structure of the α-form, the X-ray crystal structure analysis has been carried out. Since the crystallization of the β-form has been unsuccessful, the spectroscopic determination of the chemical structure was attempted.

Experimental

Oligomerization of Methacrylaldehyde Oxime. The thermal oligomerization of methacrylaldehyde oxime was carried out at 60—90 °C for 10 h in an ampoule. The unreacted monomer was removed in a stream of nitrogen under reduced pressure, the residue was placed in a large amount of ether, and then the oligomer was precipitated. Three crystallizations from methanol gave colorless needle crystals of **1** (α-form). After the removal of these crystals, the mother liquor was condensed, and then an isomeric trimer of **1** (β-form) was fractionated by gas chromatography, silicon OV-17 (5%) supported on Gaschrom Q being used as the stationary phase.

Mass and NMR Spectroscopy. The mass spectra were measured on a Shimadzu LKB-9000 mass spectrometer, equipped with a gas-chromatographic inlet system. The ionizing potential was 70 eV, and the ionizing current was 60 μA. The ^{13}C-NMR spectra were obtained with a Hitachi R-42 FT apparatus (22.6 MHz), using DMSO-d_6 as the solvent and the internal standard.

X-Ray Diffraction. An α-form crystal, with approximate dimensions of $0.5\times0.5\times0.8$ mm, was mounted on a Syntex R_3 automated four-circle diffractometer. The unit-cell dimensions were precisely determined by the least-square method, using 11 reflections measured on the diffractometer with graphite-monochromatized Mo K_α radiation (collimator size, 1.5 mm). The crystal data are summarized in Table 1.

The intensity data were collected on the diffractometer with the same radiation, using the ω scan mode ($2\theta\leqq50°$) at a variable scan speed. Reflections with intensities below the minimum intensity (150) were collected at the minimum scan speed (3 ° min^{-1}); those with intensities above the maximum intensity (2500) were collected at the maximum scan speed (30 ° min^{-1}). Medium-range intensities were collected at a scan speed on a linear scale between the minimum and maximum speeds. The intensities of the reference reflections were measured periodically; they showed no significant fluctuation during the course of data collection. Background counts were accumulated in each 1-scan range (in degree) before and after each scan and at the same scan speed. A total of 2409 independent reflections were collected, among which 1699 ($I\geqq1.96\ \sigma\ (I)$) were classed as observed. These intensity data were corrected for Lorentz and polarization effects, but not for absorption [μ(Mo K_α)= 1.0 cm^{-1}].

Structure Determination and Refinement

The structure was solved by the direct method (MULTAN program package[2]). The atomic parameters were then refined by the block-diagonal least-squares method, using anisotropic temperature factors for all the non-hydrogen atoms and isotropic ones for hydrogen atoms. The final value of R was 0.078 for non-zero reflections. In the least-squares procedure, the function minimized was $\Sigma(|F_o|-|F_c|)^2$.

Table 1. Crystal data

$C_{12}H_{21}N_3O_3$, M.W.=255.32	
Space group $P2_1/a$ (systematic absence of reflections, $h0l$: $h=2n+1$, $0k0$: $k=2n+1$)	
a/Å 7.858(3)	Z, 4
b/Å 13.186(6)	D_x/g cm^{-3} 1.243
c/Å 17.259(6)	D_m/g cm^{-3} 1.239 (flotation
β/° 130.38(3)	in C_6H_6-CCl_4 solution, 25 °C)
U/Å^3 1362	

† Part XIII: T. Ota, Y. Mori, M. Tanaka, H. Tamai, and S. Masuda, *Polymer J.*, **12**, 751 (1980).

Table 2. Atomic co-ordinates, multiplied by 10^4 for non-hydrogen atoms and by 10^3 for hydrogen atoms, and thermal parameters, multiplied by 10^2

The anisotropic temperature factors are in this form:
$\exp[-(1/4)(B_{11}h^2a^{*2}+B_{22}k^2b^{*2}+B_{33}l^2c^{*2}+2B_{12}hka^*b^*+2B_{13}hla^*c^*+2B_{23}klb^*c^*)]$.

Atoms	x	y	z	B_{11} or B	B_{22}	B_{33}	B_{12}	B_{13}	B_{23}
O(1)	5254(5)	3716(3)	4179(3)	27(2)	36(2)	30(2)	10(2)	23(2)	7(1)
O(14)	12511(5)	3187(3)	7371(2)	17(2)	36(2)	20(1)	6(1)	6(1)	−2(1)
O(18)	−909(6)	5348(3)	2073(3)	23(2)	37(2)	36(2)	7(2)	13(2)	−2(2)
N(8)	6157(6)	2878(3)	3990(3)	19(2)	30(2)	23(2)	1(2)	13(2)	−1(2)
N(13)	11221(6)	2521(3)	6537(3)	18(2)	32(2)	16(2)	−1(2)	8(2)	−3(2)
N(17)	1460(7)	5401(3)	2853(3)	25(2)	34(2)	31(2)	4(2)	16(2)	2(2)
C(2)	4866(8)	4567(4)	3534(4)	26(2)	28(3)	24(2)	2(2)	16(2)	3(2)
C(3)	5844(9)	4210(4)	3038(4)	32(3)	36(3)	35(3)	7(2)	25(2)	4(2)
C(4)	8233(10)	2572(5)	3425(4)	48(3)	48(3)	50(3)	11(3)	41(3)	6(3)
C(5)	9733(9)	1845(5)	4333(4)	37(3)	53(4)	33(3)	15(3)	24(3)	−4(3)
C(6)	8516(9)	1421(4)	4675(4)	37(3)	35(3)	29(3)	8(2)	17(2)	−2(2)
C(7)	7548(8)	2237(4)	4922(4)	23(2)	31(3)	21(2)	2(2)	11(2)	1(2)
C(9)	7506(8)	3401(4)	3787(4)	22(2)	41(3)	29(2)	−1(2)	20(2)	1(2)
C(10)	9563(11)	3028(5)	3153(5)	62(4)	57(4)	59(4)	1(3)	47(4)	3(3)
C(11)	5982(9)	1765(5)	5073(4)	29(3)	45(3)	33(3)	−5(3)	18(2)	9(2)
C(12)	9266(8)	2863(4)	5847(3)	23(2)	36(3)	19(2)	1(2)	15(2)	−4(2)
C(15)	6075(9)	5467(5)	4234(4)	30(3)	43(3)	41(3)	−8(2)	21(3)	−6(3)
C(16)	2368(8)	4683(4)	2771(4)	26(2)	30(3)	24(2)	4(2)	15(2)	1(2)
HO(14)	1354(7)	283(3)	779(3)	50(11)					
HO(18)	−129(7)	592(3)	220(3)	60(10)					
H(31)	648(7)	478(3)	297(3)	48(10)					
H(32)	460(7)	388(3)	234(3)	50(10)					
H(4)	662(5)	222(3)	258(2)	74(8)					
H(51)	1119(7)	220(3)	494(3)	45(10)					
H(52)	997(7)	127(3)	410(3)	46(10)					
H(61)	713(7)	98(3)	404(3)	45(10)					
H(62)	964(7)	98(3)	538(3)	40(10)					
H(9)	896(7)	374(3)	452(3)	19(10)					
H(101)	828(7)	350(3)	249(3)	65(10)					
H(102)	1103(6)	344(3)	387(3)	87(10)					
H(103)	959(6)	235(3)	270(3)	74(10)					
H(111)	690(6)	123(3)	566(3)	30(10)					
H(112)	479(6)	137(3)	443(3)	46(10)					
H(113)	552(6)	237(3)	535(3)	68(10)					
H(12)	880(6)	345(3)	600(3)	79(10)					
H(151)	756(6)	535(3)	467(3)	51(9)					
H(152)	577(6)	604(3)	383(3)	47(9)					
H(153)	567(6)	559(3)	463(3)	53(9)					
H(16)	153(6)	418(3)	217(3)	37(9)					

The computer programs used were the Syntex R_3 package.*** The atomic-scattering factors were taken from "International Tables for X-Ray Crystallography," Vol IV.[3] All the calculations were carried out on the NOVA 3 belonging to the diffractometer. The atomic parameters are given in Table 2.****

Results and Discussion

Molecular Structure. Figure 1 shows the molecular structure, while the bond distances and bond angles are given in Tables 3 and 4 respectively. The six-membered ring (piperidine ring) of the α-form has a chair comformation, and the five-membered ring, which is in a half-chair form, is joined to the piperidine ring through two equatorial-type bonds (N(8)–O(1) and C(9)–C(3)). The two rings are approximately coplanar to each other. The methyl groups at the C(4) and C(7) carbons are equatorial, while the oxime group at the C(7) carbon is axial. In addition, the oxime and methyl groups at the C(2) carbon are on the same side of the average coplane of the rings, and on the opposite side, with the methyl group at the C(7) carbon, respectively. The bond distances

*** The MULTAN program is modified for the Syntex R_3 diffractometer.

**** The observed and calculated structure factors are kept as Document No. 8033 at the Chemical Society of Japan.

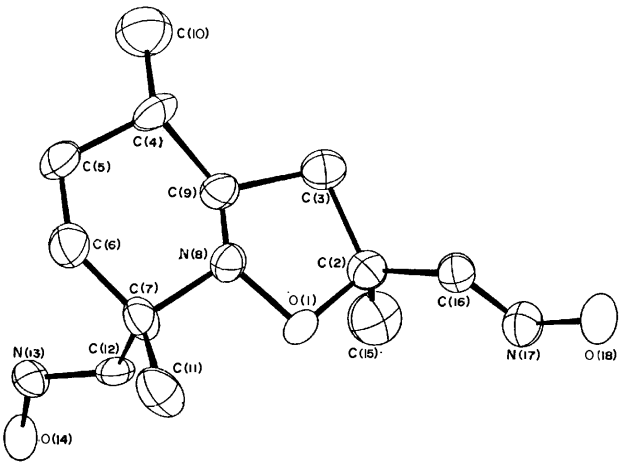

Fig. 1. A perspective view of the α-form molecule. Thermal ellipsoids of non-hydrogen atoms were drawn, at 50% probability level, by *ORTEP*.[4]

Table 3. Bond distances

Bond	Distance (l/Å)	Bond	Distance (l/Å)
O(1)-N(8)	1.460(6)	O(1)-C(2)	1.467(6)
O(14)-N(13)	1.408(5)	O(18)-N(17)	1.426(7)
N(8)-C(9)	1.484(9)	N(8)-C(7)	1.490(6)
N(13)-C(12)	1.269(7)	N(17)-C(16)	1.247(8)
C(2)-C(3)	1.548(10)	C(2)-C(15)	1.512(8)
C(2)-C(16)	1.504(9)	C(3)-C(9)	1.526(8)
C(4)-C(9)	1.541(10)	C(4)-C(5)	1.540(8)
C(4)-C(10)	1.519(13)	C(5)-C(6)	1.519(11)
C(6)-C(7)	1.529(9)	C(7)-C(11)	1.544(11)
C(7)-C(12)	1.502(7)		
O(14)-HO(14)	0.81(5)	O(18)-HO(18)	0.88(5)
C(3)-H(31)	0.95(5)	C(3)-H(32)	1.04(4)
C(4)-H(4)	1.25(3)	C(5)-H(51)	1.04(5)
C(5)-H(52)	0.94(5)	C(6)-H(61)	1.09(4)
C(6)-H(62)	1.10(4)	C(9)-H(9)	1.11(4)
C(10)-H(101)	1.11(4)	C(10)-H(102)	1.15(4)
C(10)-H(103)	1.20(5)	C(11)-H(111)	1.04(4)
C(11)-H(112)	1.02(4)	C(11)-H(113)	1.10(5)
C(12)-H(12)	0.96(5)	C(15)-H(151)	0.90(5)
C(15)-H(152)	0.94(4)	C(15)-H(153)	0.93(5)
C(16)-H(16)	1.03(4)		

Table 4. Bond angles

Bond	Angle (ϕ/°)	Bond	Angle (ϕ/°)
N(8)-O(1)-C(2)	107.5(4)	O(1)-N(8)-C(9)	103.1(4)
O(1)-N(8)-C(7)	108.1(4)	C(9)-N(8)-C(7)	112.5(4)
O(14)-N(13)-C(12)	111.7(5)	O(18)-N(17)-C(16)	110.4(5)
O(1)-C(2)-C(3)	104.7(5)	O(1)-C(2)-C(15)	106.2(5)
O(1)-C(2)-C(16)	104.7(5)	C(3)-C(2)-C(15)	113.7(5)
C(3)-C(2)-C(16)	112.4(5)	C(15)-C(2)-C(16)	114.1(5)
C(2)-C(3)-C(9)	101.8(5)	C(9)-C(4)-C(5)	105.6(5)
C(9)-C(4)-C(10)	110.8(6)	C(5)-C(4)-C(10)	109.6(6)
C(4)-C(5)-C(6)	111.5(6)	C(5)-C(6)-C(7)	113.6(5)
N(8)-C(7)-C(6)	104.3(5)	N(8)-C(7)-C(11)	107.7(5)
N(8)-C(7)-C(12)	111.2(5)	C(6)-C(7)-C(11)	110.9(5)
C(6)-C(7)-C(12)	114.5(5)	C(11)-C(7)-C(12)	108.0(5)
C(8)-C(9)-C(3)	100.0(5)	N(8)-C(9)-C(4)	106.0(5)
C(3)-C(9)-C(4)	119.4(5)	N(13)-C(12)-C(7)	120.7(5)
N(17)-C(16)-C(2)	119.8(5)		
N(8)-O(14)-HO(14)	101(4)	N(17)-O(18)-HO(18)	100(3)
C(2)-C(3)-H(31)	108(3)	C(2)-C(3)-H(32)	110(3)
C(9)-C(3)-H(31)	115(3)	C(9)-C(3)-H(32)	109(3)
H(31)-C(3)-H(32)	112(4)	C(9)-C(4)-H(4)	112(2)
C(5)-C(4)-H(4)	119(2)	C(10)-C(4)-H(4)	100(2)
C(4)-C(5)-H(51)	111(3)	C(4)-C(5)-H(52)	108(3)
C(6)-C(5)-H(51)	110(3)	C(6)-C(5)-H(52)	102(3)
H(51)-C(5)-H(52)	114(4)	C(5)-C(6)-H(61)	106(3)
C(5)-C(6)-H(62)	111(3)	C(7)-C(6)-H(61)	108(3)
C(7)-C(6)-H(62)	105(3)	H(61)-C(6)-H(62)	113(4)
N(8)-C(9)-H(9)	106(3)	C(3)-C(9)-H(9)	112(3)
C(4)-C(9)-H(9)	112(3)	C(4)-C(10)-H(101)	101(3)
C(4)-C(10)-H(102)	105(2)	C(4)-C(10)-H(103)	102(2)
H(101)-C(10)-H(102)	117(4)	H(101)-C(10)-H(103)	98(3)
H(102)-C(10)-H(103)	130(3)	C(7)-C(11)-H(111)	108(3)
C(7)-C(11)-H(112)	107(3)	C(7)-C(11)-H(113)	108(3)
H(111)-C(11)-H(112)	107(4)	H(111)-C(11)-H(113)	106(4)
H(112)-C(11)-H(113)	121(4)	N(13)-C(12)-H(12)	118(3)
C(7)-C(12)-H(12)	119(3)	C(2)-C(15)-H(151)	109(3)
C(2)-C(15)-H(152)	108(3)	C(2)-C(15)-H(153)	113(3)
H(151)-C(15)-H(152)	109(4)	H(151)-C(15)-H(153)	107(4)
H(152)-C(15)-H(153)	111(4)	N(17)-C(16)-H(16)	124(3)
C(2)-C(16)-H(16)	116(3)		

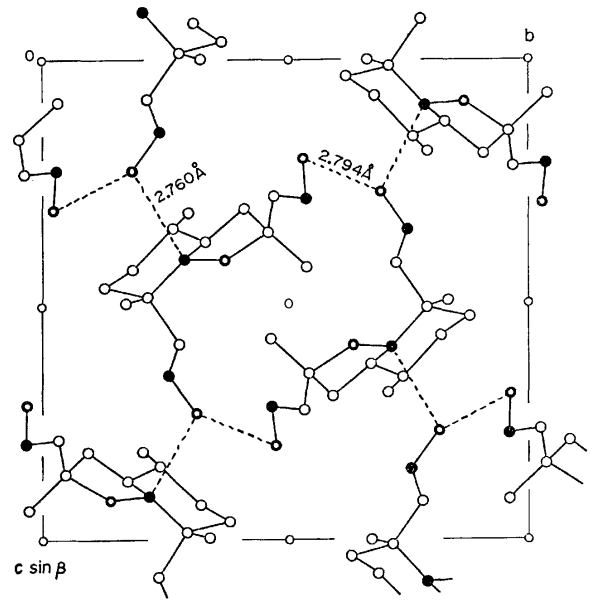

O, Carbon; ●, Nitrogen; ○, Oxygen

Fig. 2. Orthogonal projection of the crystal structure viewed along the a-axis.
Dashed lines exhibit hydrogen bonds.

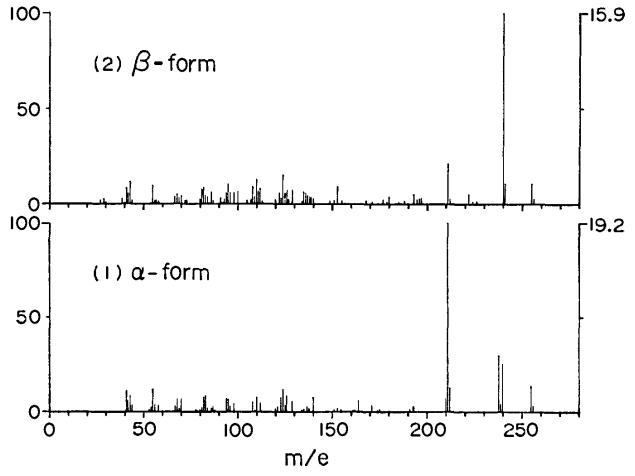

Fig. 3. Mass spectra of (1) α- and (2) β-forms.

between the skeleton atoms are in the range of 1.548 to 1.460 Å; they seem to be reasonable. The deviation of the N(8)–C(3)–C(9) angle from the tetrahedral angle corresponding to the sp^3 hybrid orbital is obviously to be ascribed to the highly-strained ring system caused by the heterobicyclic compound. On the whole, the values of the bond distances and angles shown in the tables are reasonable except that the C(4)–H(4) distance is too long.

Crystal Structure. The crystal structure is shown in Fig. 2. Both oxygen and nitrogen atoms participate in the hydrogen bond. The molecules related by a center of symmetry form a cyclic aggregate by means of O(18)–H···O(14) hydrogen bonds, 2.794(6) Å. The aggregates are linked by O(14)–H···N(8) hydrogen bonds, 2.760(5) Å, to make a three-dimensional network.

Characterization of the β-form. Since the attempts of crystallization of the β-form has been unsuccessful, the determination of the chemical structure was attempted by ^{13}C-NMR and mass spectrometric methods.

Table 5. Assignment of ^{13}C-NMR peaks of **1**

Structure	Peak position/ppm from TMS	
	α-form	β-form
$-CH_3$	18.79 24.42 27.42	10.86 12.59 24.38
$\backslash CH_2 /$	30.16 35.28 44.41	27.15 30.78 41.75
$\backslash CH /$	36.44	30.47
$\backslash CH\text{-}N /$	65.99	59.13
$\backslash C\text{-}N /$	60.75	61.41
$\backslash C\text{-}O /$	77.62	77.16
$-CH{=}N-$	150.40 154.44	154.41 156.48

As is shown in Fig. 3, the mass spectra of both α- and β-forms have a molecular ion peak at *m/e* 255, and they give similar fragmentation patterns except for the base ion peaks, which appear at *m/e* 211 (the lost of the oxime radical) for the former and at *m/e* 240 (the lost of the methyl radical) for the latter.

The NMR peak assignments are shown in Table 5, together with those of the α-form. The peak positions for the α-form were assigned by using the off-resonance technique and on the basis of the molecular structure determined by means of X-ray diffraction. The assignments for the β-form were made by comparison with those for the α-form. Carbon atoms of the β-form, particularly C(4), C(9), C(10), and C(11), resonate at a higher magnetic field compared with those of the α-form; that is due to a steric compression effect. These data reveal that the β-form is a geometrical isomer of the α-form, 2,4,7-trimethylperhydroisoxazolo[2,3-*a*]pyridine-2,7-dicarbaldehyde dioxime. The most plausible structure of the β-form is as follows. In the five-membered ring fused to the piperidine ring, the O(1) atom remains equatorial, but the C(3) atom goes to the axial position, the two rings being neither coplanar nor perpendicular to each other. Further, it can also be concluded that the methyl and oxime groups at the C(7) atom are axial and equatorial respectively, contrary to those of the α-form, because the C(11) and C(12) atoms of the β-form resonate 12 ppm higher and 4 ppm lower respectively than those of the α-form.

References

1) T. Ota, E. Matsushima, and S. Masuda, *Polymer J.*, **11**, 909 (1979).
2) G. Germain, P. Main, and M. M. Woolfson, *Acta Crystallogr., Sect., A*, **27**, 368 (1971).
3) "International Tables for X-Ray Crystallography," Kynoch Press, Birmingham (1974), Vol. IV, p. 71.
4) C. K. Johnson, *ORTEP*, ORNL-3794, Oak Ridge National Laboratory, Tennessee (1965).

Reduction by a Model of NAD(P)H. 28. Reduction of an α-Diketone in the Presence of Zinc Ion

Atsuyoshi Ohno,* Shinro Yasui, and Shinzaburo Oka
Institute for Chemical Research, Kyoto University, Uji, Kyoto 611

(Received February 22, 1980)

Reduction of 1-phenyl-2-(2-pyridyl)-1,2-ethanedione with 1-benzyl-1,4-dihydronicotinamide in acetonitrile in the presence of zinc perchlorate has been studied. The α-diketone coordinates onto zinc ion through its pyridine-ring nitrogen and benzene-side carbonyl oxygen, whereas the reduction takes place on pyridine-side carbonyl group. It is concluded that an effective ligand to a metal ion is not necessarily a facile substrate of the reduction.

Approaches to elucidate the role of bivalent metal ion in the reduction with an NAD(P)H-model compound have been tried from many aspects.[1-6] In the preceding paper, it was claimed that an effective ligand to a metal ion is not necessarily a facile substrate of the reduction with an NAD(P)H-model compound.[7]

An α-diketone, 1-phenyl-2-(2-pyridyl)-1,2-ethandione (**1**), has two carbonyl groups and can be regarded either as 2-benzoylpyridine (**2**) analog or as methyl benzoylformate (**3**) analog, both of which have been

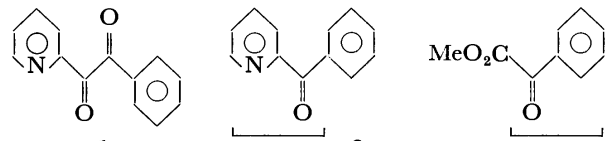

1 **2** **3**

known to be good substrates for metal ion-catalyzed reduction with an NAD(P)H-model compound.[4,5] Therefore, an interest is focused to the point whether **1** acts like **2** or **3** in the metal ion-catalyzed reduction. Note that **2** forms a complex with bivalent metal ion in a considerable amount,[8,9] whereas **3** interacts little with metal ion.[4] In this connection it is interesting to reveal which carbonyl group in **1** is subjected to the reduction and what factor governs the selectivity.

Results and Discussion

Product Analysis. The reaction of **1** with equimolar amount of 1-benzyl-1,4-dihydronicotinamide (BNAH) in the presence of equimolar amount of zinc perchlorate in acetonitrile at 50 °C for 1 h (Eq. 1) afforded a single product besides 1-benzyl-3-carbamoylpyridinium ion (BNA^+). Unfortunately, however, this

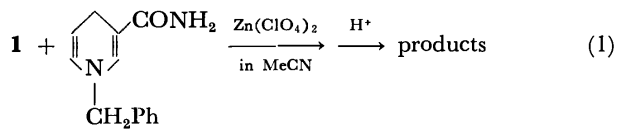

(1)

product was very unstable under the air. During the procedure to isolate the product from the reaction mixture on preparative TLC, the product was converted smoothly into the starting material **1**. Therefore, the structure of the product was elucidated after protecting the hydroxyl group in the product by trimethylsilylation.

After treatment of the reaction mixture with 1,1,1,3,3,3-hexamethyldisilazane (HMDS), gas-phase chromatography-mass spectroscopy (GC-MS) gave a fragment at $m/e=179$, which could be assigned to the ion **4** suggesting the structure **5** for the trimethylsilylated

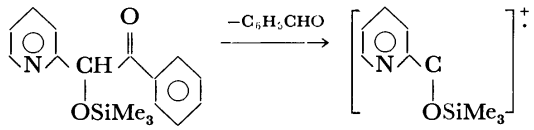

5 **4**

(2)

product. Consequently, the product from the reduction of **1** with BNAH was identified to be 2-hydroxy-1-phenyl-2-(2-pyridyl)ethanone, **6**. NMR spectrum of the product also confirmed the structure.

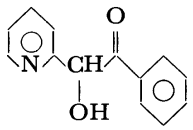

6

An attempt to synthesize the authentic **6** ended in failure. Instead, **7** afforded **1** on hydrolysis. This

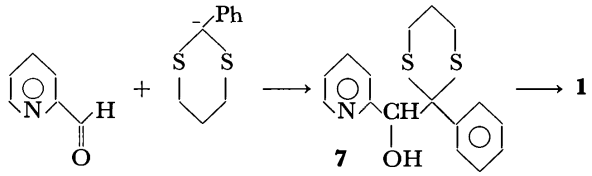

(3)

observation supports the fact that **6** is oxidized to **1** quite easily. When **1** was allowed to react for 22 h with three equivalences of BNAH in the presence of zinc ion in acetonitrile at 50 °C, the product obtained in poor yield was a mixture of *threo*- and *erythro*-diastereoisomers of 1-phenyl-2-(2-pyridyl)-1,2-ethanediol, **8**.

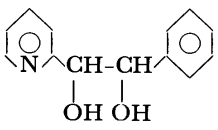

8

Complexation with Zinc Ion. Complexation of **1** with zinc ion was noted spectrophotometrically. A double reciprocal plot of the stoichiometric concentration of zinc ion present in a solution against the change in absorbance of the solution at 292 nm showed a straight line (correlation coefficient; $r>0.999$), indicating that the complexation obeys Eq. 4;

$$S + M \overset{K_S}{\rightleftharpoons} SM \qquad (4)$$

where S and M denote **1** and zinc ion, respectively. The complexation constant, K_S, at 25 °C in acetonitrile was given to be 65 M^{-1} by dividing the intercept

with the slope of the straight line.[7] Spectrometry was performed with stoichiometric concentrations of **1** and zinc perchlorate to be 2.87×10^{-5} M and (0.26—1.51) $\times 10^{-2}$ M, respectively.

On the other hand, benzil, **9**, showed no change

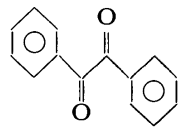

9

in spectrum even upon the addition of large excess of zinc perchlorate, which indicates that there is little interaction, if any, between **9** and zinc ion. This fact may reveal that a ring nitrogen is prerequisite to the complexation, and may rule out the possibility of bidentate complexation through two carbonyl oxygens.

To elucidate the structure of **1**–zinc ion complex, ^{1}H- and ^{13}C-NMR studies were carried out. Table 1 shows metal ion-induced shifts in ^{1}H- and ^{13}C-NMR spectra of **1** on addition of lithium, magnesium, and zinc perchlorates in CD_3CN. The fact that the shifts induced by lithium ion are the smallest among those induced by three different metal ions can be compared with the previously reported result that both chemical and optical yields in lithium ion-catalyzed reduction of **3** with a chiral NAD(P)H-model compound are remarkably lower than those catalyzed by magnesium or zinc ion.[10,11] Since ionic radii of lithium and magnesium ions are approximately the same,[12] the result indicates that the complexation depends largely on the charge density on the metal ion.

In Table 2, a comparison between zinc ion-induced maximum shifts for **1** and **2** is listed. It should be noted that the shifts of both pyridine-ring and benzene-ring carbons in **1** have similar values to those in **2**. This fact suggests that magnetic environments of pyridine and benzene rings in **1**–zinc ion complex resemble to those in **2**–zinc ion complex, inferring that the carbonyl group in **2**–zinc ion complex corresponds to the benzene-side carbonyl group in **1**–zinc ion complex. Recall that **2** coordinates bidentately onto zinc ion through pyridine-ring nitrogen and carbonyl oxygen.[7] Since **1** cannot behave as a tridentate ligand due to its structural requirement, it is reasonable to conclude that **1** coordinates onto zinc ion bidentately through pyridine ring and benzene-side carbonyl oxygen, **10**.

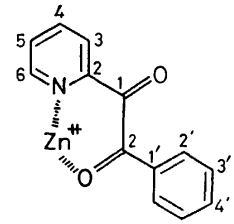

10

Although the sign in shifts of signals from carbonyl carbons are reversed in **1** and **2**, it is important that the shift of signal from benzene-side carbonyl carbon is larger than that from pyridine-side carbonyl carbon.[13]

It is interesting to point out that **1**–zinc ion complex prefer a six-membered ring structure. Although distorted octahedral geometry has been proposed for a certain pyridine derivative–zinc perchlorate complex,[14,15] the structure of 2-cinnamoylpyridine–zinc ion complex has been determined to be tetrahedral.[16,17] The six-membered ring structure presently proposed for **1**–zinc ion complex may be in accordance with tetrahedral structure, because six-membered ring is less strained in tetrahedral structure than in octahedral one.

Table 1. Metal ion-induced shifts ($\Delta\delta$) in ^{13}C- and ^{1}H-NMR spectra of 1-phenyl-2-(2-pyridyl)-1,2-ethanedione (**1**) on the addition of $M(ClO_4)_n$ in CD_3CN[a,b,c]

$\Delta\delta = \delta_{complexed} - \delta_{free}$

M^{n+}	Li^+	Mg^{2+}	Zn^{2+}
C=O-1	−0.63	−1.40	−3.80
C=O-2	−0.52	−3.99	−7.16
C-2	−1.04	−4.45	−9.44
C-3	+0.14	+3.36	+7.59
C-4	−0.22	+1.35	+4.06
C-5	−0.35	+0.70	+2.93
C-6	−0.34	−0.35	−0.11
C-1′	−0.81	−1.87	−2.22
C-2′	−0.05	−0.12	+0.95
C-3′	−0.35	−0.29	−0.39
C-4′	−0.17	+0.24	+1.06
H-3,4,5	0.0	+0.1	+0.15—0.25
H-6	+0.05	+0.26	+0.46
Ph-H	0.0	+0.1—0.2	+0.15—0.20

a) In ppm. b) [**1**]=0.4 M, $[M^{n+}]$=2.0 M. c) Corrected by considering the shift of *CN in CD_3CN ($\Delta\delta$= +0.52 for Li^+, +0.88 for Mg^{2+}, and +0.64 for Zn^{2+}).

Table 2. Comparison of maximum metal ion-induced shifts ($\Delta\delta$) in ^{13}C-NMR spectra of 1-phenyl-2-(2-pyridyl)-1,2-ethanedione (**1**) and 2-benzoylpyridine (**2**) on the addition of $Zn(ClO_4)_2$ in CD_3CN[a]

$\Delta\delta = \delta_{complexed} - \delta_{free}$

Position	**1**[b,c]	**2**[d]
C=O-1	−3.80	+2.8
C=O-2	−7.16	—
C-2	−9.44	−9.9
C-3	+7.59	+7.2
C-4	+4.06	+5.1
C-5	+2.93	+2.7
C-6	−0.11	+1.7
C-1′	−2.22	−3.0
C-2′	+0.95	+1.0
C-3′	−0.39	+0.2
C-4′	+1.06	+2.4

a) In ppm. b) [**1**]=0.4 M, $[Zn^{2+}]$=2.0 M. c) Corrected by considering the shift of *CN in CD_3CN ($\Delta\delta$= +0.64 ppm). d) [**2**]=1.67 M, $[Zn^{2+}]$=1.50 M. Ref. 8.

Kinetics. Pseudo-first-order kinetics at 25 °C in acetonitrile was followed spectrophotometrically by observing the decrease in the intensity of absorption from BNAH at 370 nm. Each run gave a good first-

Table 3. Reduction of 1-phenyl-2-(2-pyridyl)-1,2-ethanedione (**1**) in acetonitrile at 25 °C

$10^3[\mathbf{1}]_T$ / M	$10^3[Zn^{2+}]_T$ / M	$10^4[BNAH]_T$ / M	$10\,k_{obsd}$ / s^{-1}
1.99	1.00	1.01	0.281
1.99	2.00	1.01	0.446
1.99	4.00	1.01	0.566
1.99	6.00	1.01	0.585
1.99	10.1	1.01	0.549
1.99	15.3	1.01	0.465
1.99	20.8	1.01	0.414
8.01	0.412	2.00	0.765
8.09	0.824	2.00	1.18
8.01	1.64	2.00	1.64
7.91	3.30	2.00	1.18
8.06	4.94	2.00	2.13
7.87	8.02	2.00	2.38
7.87	12.2	2.00	2.37
7.98	16.3	2.00	2.02
7.98	20.1	2.00	1.83
7.98	28.1	2.00	1.43
7.98	36.1	2.00	1.33

order relationship (correlation coefficient; $r>0.999$) for more than at least two half-lives. The results are listed in Table 3. Obviously, the rate constant-zinc ion concentration profile has a maximum similarly to those of **2** and other 2-acylpyridines.[1,7] Computer-assisted simulation of the profile gave a numerical value for a constant $k_1K_B+k_2K_S$ to be 2.65×10^4 M^{-2} s^{-1},[1] where K_B, k_1, and k_2 are defined by Eqs. 5 and 6;

$$B + M \overset{K_B}{\rightleftharpoons} BM \tag{5}$$

$$\left.\begin{aligned} BM + S &\xrightarrow{k_1} \\ SM + B &\xrightarrow{k_2} \end{aligned}\right\} \text{products} \tag{6}$$

and B, S, and M denote BNAH, **1**, and zinc ion, respectively.

Role of Zinc Ion. Both kinetics and reaction site indicate that **1** behaves like **2** rather than like **3**. More striking fact revealed by the present study is that the carbonyl group which coordinates onto zinc ion is different from the one subjected to the reduction. Although reasonable explanation for this fact has not been given yet, stereochemical requirement for the carbonyl groups at the transition state should be taken into account as one of controlling factors.[18] 2-Cinnamoylpyridine is an example of a substrate where the reaction and coordination sites are different each other.[16] However, since these positions are conjugated, the result from 2-cinnamoylpyridine is not surprising.

Conjugation of two carbonyl groups in **1** is not efficient, because a canonical form with a positive charge on an oxygen is unstable. Therefore, **1** may be the first example of a substrate which has different reaction site from the coordination site. In addition, a comparison of calculated rate constants for rate-determining proton (or hydrogen atom)-transfer step shows that non-coordinated carbonyl group in **1** has larger reactivity than coordinated carbonyl group in **2**.

The present result confirms the idea that an effective ligand to a bivalent metal ion is not necessarily a facile substrate of the reduction with an NAD(P)H-model compound.

It seems likely that zinc ion plays a role to enhance the encounter of a model compound and substrate by coordinating onto both reagents. Another role of zinc ion is to catalyze the initial electron-transfer step,[19] but it interferes the following transfer of a proton (or hydrogen atom).

Experimental

1-Phenyl-2-(2-pyridyl)-1,2-ethanedione, **1** (mp; 70.5—71 °C), was prepared according to a literature procedure.[20,21] Other materials were obtained and purified as described in the preceding paper.[7] Procedures for determining rate and complexation constants were also described in the preceding paper.[7]

Product Analysis. A solution of 6.3 mg (0.030 mmol) of **1**, 6.7 mg (0.031 mmol) of BNAH, and 9.0 mg (0.034 mmol) of zinc perchlorate in 0.5 ml of acetonitrile was allowed to react at 50 °C under nitrogen atmosphere in the dark for 1 h. A 10 μl aliquot was mixed with 10 μl of 1,1,1,3,3,3-hexamethyldisilazane (HMDS), then the mixture was analyzed on a Shimadzu LKB-9000S GC-MS Spectrometer equipped with a PACK 300DG-b Computing System. Reproducibility from three times experiments was satisfactory.

The mass spectrum obtained showed a fragment at $m/e=179$ with fragments of small intensities at $m/e=180$ and 181. Such a fragmentation pattern is common to moieties that contain a silicon atom.[22] Therefore, this fragment was assigned to the cation radical **4**. Other fragments appeared at $m/e=135$, 105, and 77.

The production of 1-phenyl-2-(2-pyridyl)-1,2-ethanediol, **8**, from **1** on the reduction with BNAH was confirmed as following: a solution of 52.7 mg (0.250 mmol) of **1**, 159.9 mg (0.747 mmol) of BNAH, and 69.2 mg (0.262 mmol) of zinc perchlorate in 10 ml of acetonitrile was allowed to react at 50 °C under nitrogen atmosphere in the dark. After 22 h, complete consumption of **1** was confirmed on TLC. Then, aqueous sodium carbonate was added to the solution and the mixture was extracted three times with benzene. The organic layer was washed once with water, dried over anhydrous sodium sulfate, and concentrated *in vacuo* remaining 150 mg of solids. The solids were separated into four fractions on preparative TLC with ethyl acetate as an eluent. A NMR spectrum of each product was recorded. The first product (with the largest R_f-value) was identified to be **1** generated during the procedure of isolation (15 mg; 28% yield). The structure of the third product was determined as **8** based on comparison of its NMR spectrum with that of the authentic sample (*ca.* 5 mg; 10% yield). Unfortunately, the second (17 mg) and the fourth (10 mg) products could not be identified.

NMR Spectroscopy. Proton and carbon-13 NMR studies were carried out in CD_3CN. The concentration of **1** employed was 0.4 M for each run.[23]

The signals in ^{13}C-NMR spectrum of **1** were assigned as following: in the proton-decoupled spectrum, four signals at 134.03, 152.23, 196.73, and 197.56 ppm had low intensities. Moreover, these four signals did not split in the off-resonance spectrum, then these are attributed to C-2, C-1′, C=O-1, and C=O-2 carbons. By comparing with the chemical shifts of 2-benzoylpyridine, **2**, the signals at 134.03 and

152.23 ppm could easily be assigned to C-1′ and C-2 carbons, respectively.[8] In the non-decoupled spectrum of **1**, the signal at 197.56 ppm showed more complex coupling pattern than the signal at 196.73 ppm, indicating that the signal at 197.56 ppm was attributable to C=O-2 carbon. Long-range coupling of C=O-1 carbon with four protons on the pyridine ring would be simpler than that of C=O-2 carbon with five protons on the benzene ring. Other signals could be assigned on the basis of comparison with those of **2**,[8] benzophenone,[24] and benzil, **9**.[25]

Correlation of Physical Unit. A unit used for temperature is correlated with the SI-unit by the following equation

$$t/°C = T/K - 273.15.$$

References

1) A. Ohno, S. Yasui, R. A. Gase, S. Oka, and U. K. Pandit, *Bioorg. Chem.*, **9**, 199 (1980).

2) A. Ohno, S. Yasui, K. Nakamura, and S. Oka, *Bull. Chem. Soc. Jpn.*, **51**, 290 (1978).

3) a) M. Hughes and R. H. Prince, *J. Inorg. Nucl. Chem.*, **40**, 703 (1978); b) M. Hughes, R. H. Prince, and P. Wyeph, *ibid.*, **40**, 713 (1978).

4) A. Ohno, H. Yamamoto, T. Okamoto, S. Oka, and Y. Ohnishi, *Bull. Chem. Soc. Jpn.*, **50**, 2385 (1977).

5) R. A. Gase, G. Boxhoorn, and U. K. Pandit, *Tetrahedron Lett.*, **1976**, 2889.

6) D. J. Creighton, J. Hajdu, and D. S. Sigman, *J. Am. Chem. Soc.*, **98**, 4619 (1976).

7) A. Ohno, S. Yasui, and S. Oka, *Bull. Chem. Soc. Jpn.*, **53**, 2651 (1980).

8) R. A. Gase, Ph. D. Thesis, Univ. of Amsterdam, Amsterdam, The Netherlands (1979).

9) R. R. Osborne and W. R. McWhinnie, *J. Chem. Soc., A*, **1967**, 2075.

10) A. Ohno, T. Kimura, H. Yamamoto, S. G. Kim, S. Oka, and Y. Ohnishi, *Bull. Chem. Soc. Jpn.*, **50**, 1535 (1977).

11) Y. Ohnishi, M. Kagami, and A. Ohno, *J. Am. Chem. Soc.*, **97**, 4766 (1975).

12) J. P. Jesson and E. L. Muetterties, "Basic Chemical and Physical Data," Marcel Dekker, Inc., New York, N. Y. (1963), pp. 5, 6.

13) Paramagnetic effect of zinc ion may account for the up-field shifts of the signals from carbonyl carbons.

14) R. E. Lenkinski and J. L. Dallas, *J. Am. Chem. Soc.*, **101**, 5902 (1979).

15) E. B. Fleisher, A. E. Gebala, D. R. Swift, and P. A. Tasker, *Inorg. Chem.*, **11**, 2775 (1972).

16) R. A. Gase and U. K. Pandit, *J. Am. Chem. Soc.*, **101**, 7059 (1979).

17) Tetrahedral structure has also been proposed for dichlorobis(4-substituted pyridine)zinc(II) complexes; W. L. Steffen and G. J. Palenik, *Inorg. Chem.*, **16**, 1119 (1977).

18) F. M. Moracci, S. Tortorella, B. Di Rienzo, and F. Liberatore, *Tetrahedron*, **35**, 2591 (1979).

19) A. Ohno, S. Yasui, H. Yamamoto, S. Oka, and Y. Ohnishi, *Bull. Chem. Soc. Jpn.*, **51**, 294 (1978).

20) H. Baurath, *Ber.*, **20**, 2719 (1887).

21) C. A. Buehler, J. O. Harris, and W. F. Arendale, *J. Am. Chem. Soc.*, **72**, 4953 (1950).

22) E. Stenhangen, S. Abrahamsson, and F. W. McLafferty, "Registry of Mass Spectral Data," John Wiley & Sons, Inc., New York, N. Y. (1974), Vols. 1—4.

23) The concentration of **1** for the non-decoupled spectrum was 1 M. Concentration shift of every signal, however, was not recognized within the range of these concentrations.

24) R. Takeda, Ms. Thesis, Kyushu University, Fukuoka, Japan (1978).

25) L. F. Johnson and W. C. Jankowski, "Carbon-13 NMR Spectra," John Wiley & Sons, Inc., New York, N. Y. (1972), p. 457.

Restricted Rotation Involving the Tetrahedral Carbon. XXXIV. Stable Rotamers of 9-Arylfluorenes Carrying Oxygen-substituents in the Ortho Position of the Aryl Group[1,2]

Mikio NAKAMURA and Michinori ŌKI*,**

Department of Chemistry, School of Medicine, Toho University, Omorinishi, Ota-ku, Tokyo 143

** *Department of Chemistry, Faculty of Science, The University of Tokyo, Hongo, Bunkyo-ku, Tokyo 113*

(Received May 31, 1980)

9-(2-Hydroxy-1-naphthyl)fluorene, 9-(2-hydroxy-4,6-dimethylphenyl)fluorene, and their methyl ethers have been prepared. They give stable rotamers, *sp* and *ap*, at room temperature. *ap* forms of the hydroxylic compounds are favored over the *sp* and contrary is true for the methyl ethers. These results are attributed to the stabilization of the *ap* form of the hydroxylic compounds due to intramolecular OH···π interaction. Barriers to rotation are *ca.* 105 kJ mol^{-1}.

9-Arylfluorenes (**1**) are unique systems which exhibit high barriers to rotation about the C_9–C_{ar} bond.[3] In some special cases they give stable rotational isomers, *sp* and *ap*, at room temperature.[4] As for the equilibrium between rotamers, the bulkiness of substituents X and Y are known to be primarily important.[5] That is, the predominant conformation is the one in which a bulkier substituent proximates the hydrogen in 9 position. Since the substituent X or Y in each

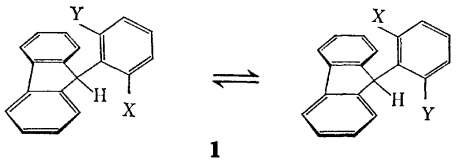

1

rotamer is quite close to the fluorene ring, electronic interaction may occur, if a substituent has a proper character, to affect the equilibria and barriers to rotation. In fact, we have found that the charge-transfer interaction has taken place between the fluorene ring and the aroyl moiety in aroates of 9-(2-hydroxy-1-naphthyl)fluorene.[6] Thus, 9-arylfluorene is a good model for investigation of the interaction between two groups. We wish to report in this paper the syntheses of the compounds **4**—**7**, which carry oxygen-substituents in an ortho position of the aryl group and thermodynamic and kinetic parameters involving the rotational isomers. The effects of the oxygen-substituents on the thermodynamic and kinetic values will be discussed in terms of molecular interactions.

Experimental

Spectral Measurement. ^{1}H NMR spectra were determined either on a Hitachi R-20B spectrometer operating at 60 MHz or on a Varian EM 390 operating at 90 MHz. The chemical shifts of the characteristic signals of 9-arylfluorenes are given in Table 1. IR spectra were obtained on a Hitachi EPI G-3 spectrometer.

Syntheses. The syntheses of methyl ethers (**4** and **6**) were carried out by the Grignard reaction between 9-fluorenone and an appropriate arylmagnesium bromide followed by reduction with hydriodic acid at room temperarure. The hydroxylic compounds (**5** and **7**) were prepared either by demethylation of the methyl ether or by a series of similar reactions used for the syntheses of the methyl ethers.

9-(2-Methoxy-4,6-dimethylphenyl)-9-fluorenol (2). To a vigorously stirred tetrahydrofuran solution of 2-methoxy-4,6-dimethylphenylmagnesium bromide, prepared from 1.02 g (0.047 mol) of 1-bromo-2-methoxy-4,6-dimethylbenzene[7] and 1.20 g (0.049 mol) of magnesium, was added 5.41 g

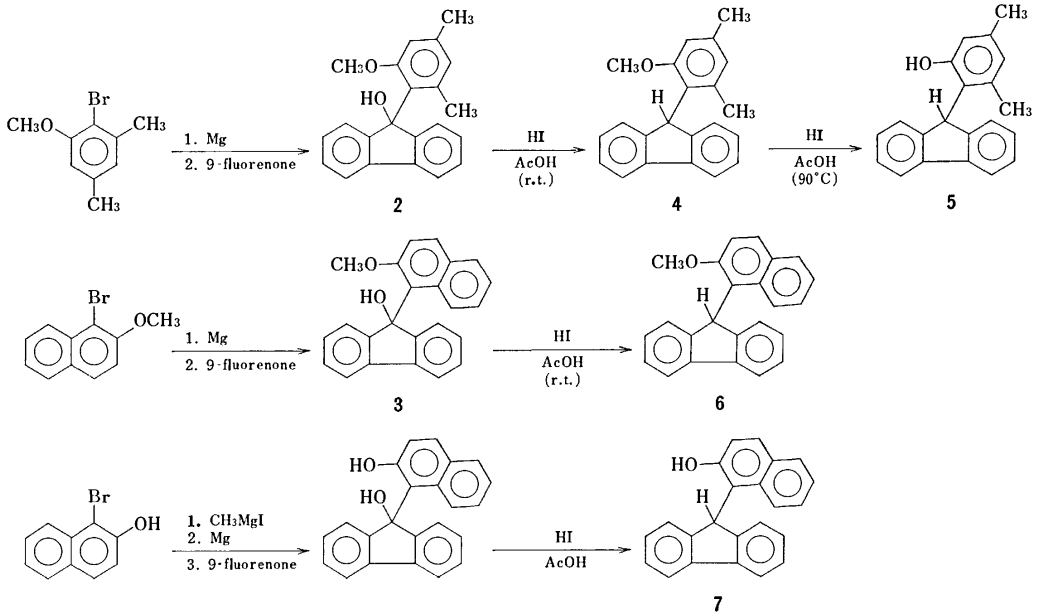

Table 1. ^{1}H NMR data of 9-arylfluorenes ($CDCl_3$, δ)

Compound	Form	2′-OCH_3	2′-OH	4′-CH_3	6′-CH_3	3′-H	5′-H	8′-H	9-H
4	*sp*	3.92	—	2.30	1.10	6.75	6.44	—	6.03
	ap	2.90	—	2.28	2.65	6.40	6.60	—	5.23
5	*sp*	—	5.0	2.20	1.10	6.51	6.36	—	5.89
	ap	—	3.6	2.22	2.62	6.35	6.72	—	5.38
6	*sp*	4.10	—	—	—	—	—	6.36	6.30
	ap	3.02	—	—	—	—	—	8.47	5.88
7	*sp*	—	5.8	—	—	—	—	6.38	6.18
	ap	—	4.1	—	—	—	—	8.40	6.02

(0.03 mol) of 9-fluorenone at 0 °C. The reaction mixture was stirred for 3 h at room temperature and was then heated with stirring for 1 h. The mixture was cooled and treated with aqueous ammonium chloride. The organic layer was dried over sodium sulfate. After evaporation of the solvent, the product was purified by chromatography on silica gel. Elution with benzene gave a pure product, mp 93.0—94.5 °C, in 78% yield based on 9-fluorenone. Found: C, 83.22; H, 6.37%. Calcd for $C_{22}H_{20}O_2$: C, 83.51; H, 6.37%. ^{1}H NMR ($CDCl_3$, δ): 1.27 (*sp*-6′-CH_3), 2.92 (*ap*-6′-CH_3), 2.27 (*sp*- and *ap*-4′-CH_3), 2.85 (*ap*-OCH_3), 4.05 (*sp*-OCH_3), 6.49 (*sp*-5′-H), 6.80 (*sp*-3′-H). The population ratio (*ap*/*sp*) was 1/9.7 in $CDCl_3$ at 34 °C.

*9-(2-Methoxy-4,6-dimethylphenyl)fluorene (**4**).* To a solution of 1.2 g (3.8 mmol) of **2** in 50 mL of acetic acid was added 10 mL of 57% hydriodic acid. The solution was stirred for 5 h at room temperature, poured into water, and then extracted with ether. The ether layer was washed with aqueous sodium hydrogencarbonate and then with aqueous sodium hydrogensulfite, and dried over sodium sulfate. After evaporation of the solvent, the products were separated by chromatography on alumina. Elution with hexane gave a pure *sp* form, mp 128—129 °C, in 55% yield. Found: C, 88.04; H, 6.59%. Calcd for $C_{22}H_{20}O$: C, 87.96; H, 6.71%. The chloroform solution of the *sp* form was heated for 5 h to make an equilibrium mixture and the *ap* form thus formed was separated by preparative thin layer chromatography on silica gel. The R_f value of the *ap* form was smaller than that of the *sp* form. The mp of the *ap* form was 131—133 °C. The identity of the *ap* form was established by the spectral data and the equilibration experiment: heating the *ap* afforded the same mixture of *sp* and *ap* forms which was obtained by heating the *sp* form.

*9-(2-Hydroxy-4,6-dimethylphenyl)fluorene (**5**).* To a solution of 1.10 g (43.7 mmol) of **4** in 50 mL of acetic acid was added 10 mL of 57% hydriodic acid. The solution was stirred for 5 h at 90 °C and then treated similarly as in the synthesis of **4**. The products were chromatographed on silica gel and eluted with benzene-hexane. The *ap* isomer was obtained as easily eluted fractions. Recrystallization from benzene-hexane gave pure *sp*, mp 144—145 °C, and *ap*, mp 102—104 °C. Found: (*sp*): C. 87.79; H, 6.20%. Calcd for $C_{21}H_{18}O$: C, 88.08; H, 6.34%. The identity of the *ap* form was established as described above.

*9-(2-Methoxy-1-naphthyl)-9-fluorenol (**3**)*, mp 130—131 °C, was prepared by treating 2-methoxy-1-naphthylmagnesium bromide with 9-fluorenone in tetrahydrofuran. The yield was 85% based on the fluorenone. Found: C, 85.37; H, 5.34%. Calcd for $C_{24}H_{18}O_2$: C, 85.18; H, 5.36%. ^{1}H NMR ($CDCl_3$, δ): 2.4 (*ap*-OH), 3.00 (*ap*-OCH_3), 4.19 (*sp*-OCH_3), 9.72 (*ap*-8′-H). The population ratio (*ap*/*sp*) was 1/3.4 in $CDCl_3$ at 34 °C.

*9-(2-Methoxy-1-naphthyl)fluorene (**6**).* To a solution of 2.1 g (6.2 mmol) of **3** in 70 mL of acetic acid was added 15 mL of 57% hydriodic acid. The solution was stirred for 5 h at room temperature and then treated similarly as in the case of **4**. The products were separated by chromatography on silica gel. Elution with hexane gave a pure *sp* form, mp 121—122 °C, in 72% yield. Found: C, 89.26; H, 5.55%. Calcd for $C_{24}H_{18}O$: C, 89.41; H, 5.63%. The chloroform solution of the *sp* form was refluxed for 5 h to make an equilibrium mixture and the *ap* form thus formed was separted by thin layer chromatography on silica gel. The *ap* form was eluted after the *sp* form and was then recrystallized from benzene-hexane, mp 125—126 °C. Found: C, 89.42; H, 5.70%. Calcd for $C_{24}H_{18}O$: C, 89.41; H, 5.63%.

*9-(2-Hydroxy-1-naphthyl)fluorene (**7**).* To a vigorously stirred tetrahydrofuran solution of 4.5 g (20 mmol) of 1-bromo-2-naphthol was added an ether solution of methylmagnesium iodide, prepared from 3.6 g (25 mmol) of methyl iodide and 0.65 g (27 mmol) of magnesium in ether. The reaction mixture was stirred for 10 min. The resulting suspension of the magnesium salt of 1-bromo-2-naphthol was put into a dropping funnel and was added dropwise to 0.48 g (20 mmol) of magnesium in tetrahydrofuran at the refluxing temperature. After the addition was completed, the reaction mixture was heated with refluxing for 2 h, cooled to room temperature, and then 2.16 g (12 mmol) of 9-fluorenone was added in small portions. The solution was refluxed for 1 h, cooled, and treated with aqueous ammonium chloride. The organic layer was dried over sodium sulfate and the solvent was evaporated completely *in vacuo*. The resulting oil was dissolved in 100 mL of acetic acid and 20 mL of 57% hydriodic acid was added. The mixture was stirred for 5 h at room temperature and then treated similarly as in the case of **4**. The products were separated by chromatography on silica gel. Elution with benzene gave 0.3 g (8%) of *ap*, mp 176—177 °C, and then 1.5 g (41%) of *sp*, mp 88—89 °C. Found (*ap*): C, 89.82; H, 5.06%. Calcd for $C_{23}H_{16}O$: C, 89.58; H, 5.23%. The identity of the *sp* form was established by equilibration.

Kinetics. A $CDCl_3$ solution of the *sp* form of **4** was put in an NMR sample tube and was heated at a given temperature. New signals attributable to the *ap* form gradually increased in their intensities. Since the features are the large chemical shift differences between two methoxyl signals ($\Delta\delta$=*ca.* 1.0 ppm), the increase and decrease in intensities of these signals were monitored. The rates of isomerization were obtained at 4 different temperatures by assuming the unimolecular reversible process. Putting these rate constants into Eyring's equation, we could obtain the activation parameters for rotation. The rates for rotation were similarly obtained with **5** and **6** by monitoring the change in intensities of 6′-methyl and 2′-methoxyl signals, respectively. In the case of **7**, the change in intensities of hydroxyl signals were monitored since the proton exchange between these hydroxyl groups was found to be frozen on

Table 2. Kinetic Parameters for the internal rotation and equilibrium constants at 56.3 °C for 9-arylfluorenes

Compound	Process	ΔH^*/kJ mol^{-1}	ΔS^*/J K^{-1} mol^{-1}	ΔG^*_{329}/kJ mol^{-1}	K
4	*sp*→*ap*	102.0±0.4	−7.9±0.4	104.6±0.4	1/3.30
	ap→*sp*	96.1±0.4	−14.5±0.4	100.9±0.4	
5	*sp*→*ap*	93.6±0.4	−29.7±1.3	103.4±0.4	1.80
	ap→*sp*	96.1±0.4	−27.2±0.8	105.0±0.4	
6	*sp*→*ap*	101.2±0.8	−21.7±2.9	108.3±0.4	1/3.56
	ap→*sp*	94.9±0.8	−30.5±2.5	110.0±0.4	
7	*sp*→*ap*	92.8±0.8	−45.1±1.7	107.7±0.4	2.30
	ap→*sp*	96.1±1.2	−42.2±3.8	110.0±0.4	

the NMR time scale.

Results and Discussion

Assignment of Stereochemistry. For the two rotamers isolated, stereochemistry was assigned with the use of ^{1}H NMR spectroscopic features as were used previously.[4] The features are a high field signal due to the 2′-substituent (OH or OCH_3) and a low field signal due to the 6′-CH_3 of **4** and **5** or the 8′-H of **6** and **7** for the *ap* form. The contrary is true for the *sp* isomers: a high field signal due to 6′-CH_3 of **4** and **5** or the 8′-H of **6** and **7** and a low field signal due to OH or OCH_3. The protons of the hydroxyl or methoxyl group is a little far from the fluorene ring but the chemical shift differences were large enough for the assignment of the structures. The chemical shifts of the characteristic protons are given in Table 1.

Conformational Equilibria. Equilibrium constants are given in Table 2 together with kinetic parameters for rotation about the C_9–C_{ar} bond. The interesting features of the data are that, in both naphthyl and phenyl series, the *ap* forms of the phenolic compounds (**5** and **7**) are favored over the corresponding *sp* forms by *ca.* 2 kJ mol^{-1} at 56.3 °C. The *ap* forms of the methyl ethers (**4** and **6**), on the contrary, are less stable than the *sp* forms by *ca.* 3 kJ mol^{-1} at the same temperature. This is rather unusual, since a hydroxyl group is considered to be almost equal to a methoxyl group in the effective size.[8] The facts that the equilibrium constants (*ap*/*sp*) of 9-(2-methylphenyl)- (**8a**) and 9-(2-ethylphenyl)fluorene (**8b**) are 1/1.6 and 1/3.3, respectively, supplement the anomaly of the results observed with **4**—**7**.[5] The reason for this anomaly

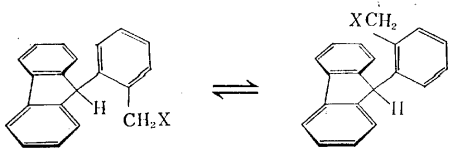

8 a) X=H b) X=CH_3

is probably the stabilization due to intramolecular OH···π interaction, involving the hydroxyl group and the fluorene ring. Thus the infrared spectra were measured and the results are given in Table 3. Clearly, the OH···phenyl interaction[9] is indicated for the *ap* forms, whereas the *sp* form is present as a free phenol in dilute solutions in carbon tetrachloride. We then measured the IR spectra by imitating the conditions of the NMR measurement: chloroform as a solvent and concentrations of *ca.* 0.3 mol L^{-1}. Although the bands are shifted a little due to the solvent effects, the *ap* forms give the monomer OH···π bonded absorption only. As for the absorption of the *sp* forms, compound **5** gives only the free OH band. Compound **7**, in contrast, shows a shoulder, probably due to the dimer.[10] Although the reason for the absence of the dimer band in *sp*-**5** is unknown at present, the absence of the dimer in the *ap* forms can be ascribed to the steric effect, since sterically crowded phenols are known to exhibit monomer bands only even at a high concentration.[11] The IR study described above clearly shows that the OH···π interaction is the main origin for the stabilization of the *ap* forms of the phenolic compounds.

Table 3. ν_{OH} absorption spectral data

Compound	Solvent	Concentration / mmol L^{-1}	ν_{OH} / cm^{-1}
sp-**5**	CCl_4	9.4	3611
	$CHCl_3$	260	3602
ap-**5**	CCl_4	5.7	3546
	$CHCl_3$	250	3535
sp-**7**	CCl_4	9.6	3610
	$CHCl_3$	250	3600, 3558(sh)
ap-**7**	CCl_4	10	3533
	$CHCl_3$	320	3521

Barriers to Rotation. The OH···π stabilization is also reflected to the barriers to rotation as shown in Table 2: the free energies of activation for rotation of the phenolic compounds are larger by *ca.* 4 kJ mol^{-1} than those of the methyl ethers in the *ap*→*sp* processes. If we assume that the energy level of the *sp* form of the phenolic compound is equal to that of the corresponding methyl ether, then the free energy profile may be written as shown in Fig. 1 for compounds **4** and **5**. The figure indicates that the energy level of the transition state of **4** is higher than that of **5** by 1.2 kJ mol^{-1}, which may be ascribed to the difference in steric effects between methoxyl and hydroxyl groups on the transition states for rotation. We read also from the figure that the difference in free energies of *ap* forms of **4** and **5** is 5.3 kJ mol^{-1}. Since this value contains the difference in energies ascribable to the steric effects of methoxyl and hydroxyl groups in the *ap* form, the net stabilization may be *ca.* 4 kJ mol^{-1}, which conforms with the OH···π interaction energy.[12,13] The same calculation was

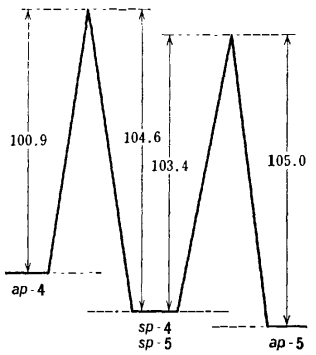

Fig. 1. Free energy profiles of **4** and **5** at 56.3 °C (kJ mol^{-1}).

applied to compounds **6** and **7** and *ca.* 3 kJ mol^{-1} was derived as the net stabilization energy of the *ap* form due to the OH$\cdots\pi$ interaction.

Comparison of the barriers to rotation of the oxygen-compounds studied here with those of the corresponding methyl or substituted methyl compound reveals that the formers exhibit lower barriers: Arrhenius activation energies for rotation of 9-(2-methyl-1-naphthyl)fluorene[14] and 9-(2-bromomethyl-6-methylphenyl)fluorene[4] are known to be 125 kJ mol^{-1} and 113 kJ mol^{-1}, respectively, for the *sp*→*ap* processes. The lowering of the barriers to rotation of compounds **4**—**7** may be attributed to lessening of the van der Waals radii of the substituents in 2′ position by going from a methyl to an oxygen, which directly affects the transition state for rotation. The difference in the barriers between the naphthyl and 2-methylphenyl analogs is smaller in the oxygen-compounds than the hydrocarbons (approximated by the bromomethyl compound). The reason for this phenomenon must further be studied.

References

1) Preceding paper: M. Nakamura and M. Ōki, *Bull. Chem. Soc. Jpn.*, **53**, 2977 (1980).
2) A preliminary note has been published: M. Nakamura and M. Ōki, *Chem. Lett.*, **1975**, 671.
3) M. Ōki, *Angew. Chem. Int. Ed. Engl.*, **15**, 87 (1976).
4) M. Nakamura and M. Ōki, *Tetrahedron Lett.*, **1974**, 505.
5) M. Nakamura, N. Nakamura, and M. Ōki, *Bull. Chem. Soc. Jpn.*, **50**, 2986 (1977).
6) M. Nakamura and M. Ōki, *Chem. Lett.*, **1976**, 651.
7) E. J. O'Bara, R. B. Balsley, and I. Starer, *J. Org. Chem.*, **35**, 16 (1970).
8) J. A. Hirsch, "Table of Conformational Energies-1967" in "Topics in Stereochemistry" ed by N. L. Allinger and E. L. Eliel, Interscience, New York (1967), Vol. 1, pp. 199—222.
9) M. Ōki and H. Iwamura, *Bull. Chem. Soc. Jpn.*, **32**, 1135 (1959).
10) R. N. Jones and C. Sandorfy, "Infrared and Raman Spectroscopy: Applications," in "Technique of Organic Chemistry" ed by W. West, Interscience, New York (1956), Vol. 9, pp. 417—420.
11) N. A. Puttnam, *J. Chem. Soc.*, **1960**, 486.
12) M. Ōki and H. Iwamura, *Bull. Chem. Soc. Jpn.*, **33**, 717 (1960).
13) M. Ōki, K. Akashi, G. Yamamoto, and H. Iwamura, *Bull. Chem. Soc. Jpn.*, **44**, 1683 (1971).
14) T. H. Siddall, III, and W. E. Stewart, *J. Org. Chem.*, **34**, 233 (1969).

Synthetic Studies of Rifamycins. II.[1] Syntheses of Methyl 2,4,6,7-Tetradeoxy-4-*C*-methyl-3-*O*-methyl-α-L-*arabino*-heptopyranosid-6-ulose and Its Derivatives Utilizable in the Construction of the Rifamycin Ansa Chain Portion

Masaya NAKATA, Yutaka IKEYAMA, Hideaki TAKAO, and Mitsuhiro KINOSHITA*

Department of Applied Chemistry, Faculty of Engineering, Keio University, Hiyoshi, Kohoku-ku, Yokohama 223

(Received February 29, 1980)

3,6-Dideoxy-3-*C*-methyl-2-*O*-methyl-D-galactopyranose(**12**) was prepared in 10 steps from methyl 4,6-*O*-benzylidene-3-deoxy-3-*C*-methyl-α-D-altropyranoside. **12** was converted into 4,5-di-*O*-acetyl-3,6-dideoxy-3-*C*-methyl-2-*O*-methyl-D-galactose, which was then condenced in ether with (methoxymethylene)triphenylphosphorane (generated from the phosphonium salt with the dimethylsulfinylmethanide anion in ether) to produce 5,6-di-*O*-acetyl-2,4,7-trideoxy-4-*C*-methyl-1,3-di-*O*-methyl-D-*galacto*-1-enoheptitol (**16**). The treatment of **16** with NBS in methanol, followed by the debromination of the resulting 2-bromo aldehyde dimethyl acetal with tributylstannane, deacetylation, and mild methanolysis afforded methyl 2,4,7-trideoxy-4-*C*-methyl-3-*O*-methyl-β-D-*galacto*-heptopyranoside(**19**), which then provided the title compound **20** upon Jones oxidation. The potential intermediates, the 1-lithio-1-(methyl 2,4-dideoxy-4-*C*-methyl-3-*O*-methyl-α-L-*arabino*-pentopyranos-5-yl)ethene and (*E*)-2-(methyl 2,4-dideoxy-4-*C*-methyl-3-*O*-methyl-α-L-*arabino*-pentopyranos-5-yl)propenylcopper intermediates, were prepared from **20** *via* the corresponding alkenyl iodide and (methyl 2,4-dideoxy-4-*C*-methyl-3-*O*-methyl-α-L-*arabino*-pentopyranos-5-yl)ethyne and were demonstrated to condense with benzaldehyde and ethylene oxide respectively.

Rifamycins are the first natural compound with an aromatic ring system spanned by a long aliphatic bridge,[2] called the ansa chain. The aliphatic chain compound, **1**, corresponding to the intact ansa chain present in rifamycin B, O, S, and SV has thus far been neither isolated from a natural source nor synthesized. Corey[3] has recently reported the highly stereoselective synthesis of some fragment intermediates for the elaboration of the ansa-chain portion of rifamycins. In the course of our synthetic studies of rifamycins, the new ansa-chain compound, **2**, the deacetylated cyclic methyl acetal derivative of **1**, has been isolated[1] on the novel degradation of 25-deacetylrifampicin. We have been interested[4] in the synthesis of the rifamycin ansa chain in the form of **2**, which is considered to be a useful intermediate in the synthesis of rifamycin. This paper deals with the synthesis of methyl 2,4,6,7-tetradeoxy-4-*C*-methyl-3-*O*-methyl-α-L-*arabino*-heptopyranosid-6-ulose (**20**), a viable synthetic intermediate containing the cyclic methyl acetal moiety of **2**, and with its conversions into the potential intermediates, **23** or **26**, utilizable in the coupling reaction with the second synthetic segments, such as **A** or **B**, with the aldehydic or epoxidic functionality (Scheme 1).

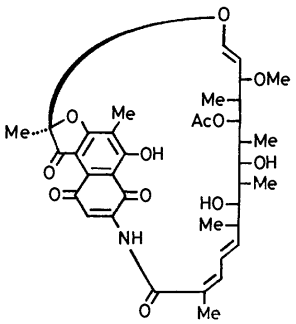

Rifamycin S

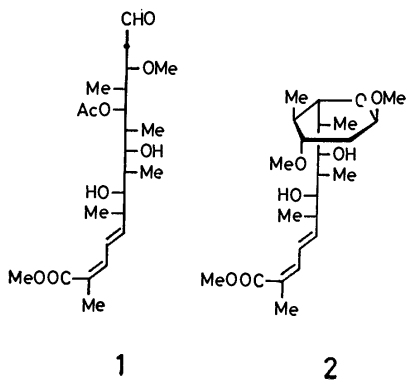

1 2

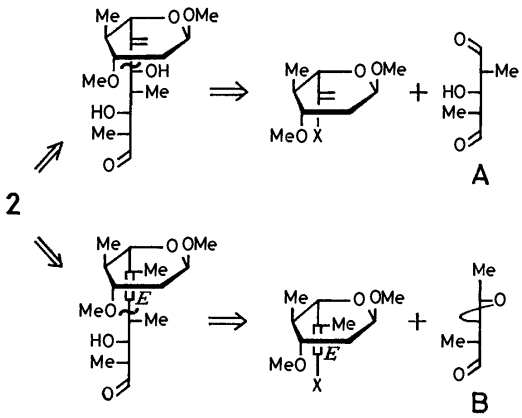

Scheme 1.

Results and Discussion

The starting material, methyl 4,6-*O*-benzylidene-3-deoxy-3-*C*-methyl-α-D-altropyranoside(**3**),[5-7] could be obtained on a large scale from methyl 2,3-anhydro-4,6-*O*-benzylidene-α-D-mannopyranoside[8] and methylmagnesium chloride by the method of Inch and Lewis.[7] The conversion of **3** into methyl 4,6-*O*-benzylidene-3-deoxy-3-*C*-methyl-α-D-glucopyranoside(**5**) was accomplished *via* the inverted keto sugar, **4**, according to

the procedure of Inch *et al.*[9] in a 74% overall yield. The *O*-methylation of **5** with sodium hydride and methyl iodide in DMF gave **6** in a 73% yield. The treatment of **6** with *N*-bromosuccinimide (NBS)

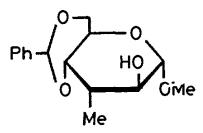

3

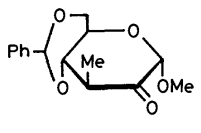

4

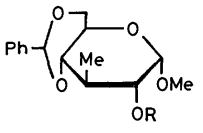

5 R = H
6 R = Me

in boiling carbon tetrachloride,[10] followed by the lithium aluminium hydride reduction of the bromo derivative, **7**, afforded methyl 3,6-dideoxy-3-*C*-methyl-2-*O*-methyl-α-D-glucopyranoside(**8**) in a 65% yield. The *O*-mesylation of **8** with mesyl chloride in pyridine, followed by the treatment of the resulting 4-mesylate, **9**, with sodium benzoate in DMSO at 120 °C, gave the inverted benzoate **10** in a 61% overall yield from **8**. The acetolysis of **10** with acetic anhydride in the presence of concd sulfuric acid afforded **11** as an anomeric mixture in a 76% yield. The hydrolysis of **11** with sodium hydroxide gave 3,6-dideoxy-3-*C*-methyl-2-*O*-methyl-D-galactose(**12**) in a 92% yield. In preparative runs, compound **12** could be obtained in about a 32% overall yield from **3** without any isolation of the intermediates (**4**—**11**).

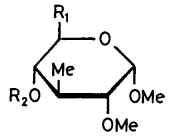

7 R_1 = CH_2Br, R_2 = Bz
8 R_1 = Me, R_2 = H
9 R_1 = Me, R_2 = Ms

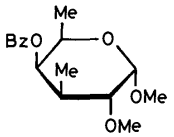

10

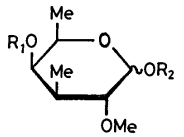

11 R_1 = Bz, R_2 = Ac
12 R_1 = R_2 = H

The conversion of **12** into **19** in a moderate overall yield (23%) was accomplished through the following eight steps. The dithioacetalization of **12** with 1,2-ethanedithiol and concd hydrochloric acid, followed by acetylation with acetic anhydride and 4-dimethylaminopyridine in ethyl acetate, gave **14** in a 70% overall yield. The demercaptalation of **14** with a 2:1 mixture of mercury(II) chloride and red mercury(II) oxide[11] afforded the aldehyde **15** in a 95% yield. The Wittig condensation[12] of **15** in ether with (methoxymethylene)triphenylphosphorane (prepared from the corresponding phosphonium chloride with phenyllithium in ether) yielded the enol ether, **16**, in a low yield (≈10%). When **15** was treated with the ylide in DMSO according to Corey's method,[13] no condensation product was obtained, but when **15** was allowed to react in ether with a two-fold excess of the ylide (prepared by the action of 4 M** methylsulfinylmethanide anion in DMSO[13a]) with the phosphonium chloride in ether), the desired enol ether, **16**, was obtained in a 72% yield as a 7.7:1 mixture of *E* and *Z* isomers. The direct conversion of **16** into the

** 1 M=1 mol dm^{-3}.

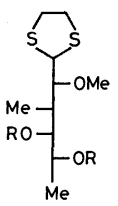

13 R = H
14 R = Ac

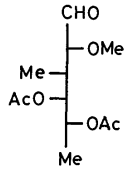

15

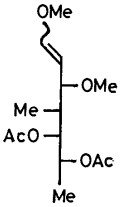

16

homolog of **15** by acid-catalyzed hydrolysis could not be accomplished because of the predominant formation of the α,β-unsaturated aldehyde by the elimination of the 3-methoxyl group, and so an indirect process was necessary. The treatment of **16** with NBS in methanol containing solid sodium hydrogencarbonate afforded the crystalline bromo dimethyl acetal **17** as an epimeric mixture in a 74% yield. The debromination of **17** with tributylstannane and α,α'-azobisisobutyronitrile gave **18** in a 96% yield. The deacetylation of **18** with sodium hydroxide, followed by mild methanolysis with 0.5% methanolic hydrogen chloride, afforded a 1:5 mixture of methyl 2,4,7-trideoxy-4-*C*-methyl-3-*O*-methyl-α-D-*galacto*-heptopyranoside and its β-anomer, which, after recrystallization, gave the major isomer, **19**, in a 63% overall yield from **18**. The Jones oxidation of **19** afforded the title compound, **20**, in a 93% yield.

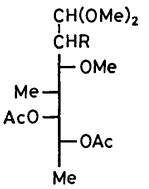

17 R = Br
18 R = H

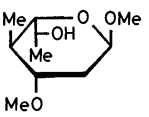

19

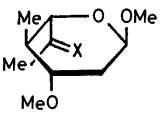

20 X = O
21 X = NNH_2

The methyl ketone, **20**, was converted into the alkenyl iodide, **22**, in a 72% yield *via* the hydrazone, **21**, according to the procedure of Barton *et al.*[14] The iodide, **22**, was convertible into the lithium compound, **23**, in ether by treatment with a 1—1.2 equiv of butyllithium[15] in hexane at −78 °C for 1 h. The lithium reagent, **23**, thus obtained was reacted with 1 equiv of benzaldehyde at −50 °C to give the addition product, **24**, in a 54% yield. The potential intermediate, **26**, was derived from **22**. The treatment[16] of **22** with potassium hydroxide in boiling ethanol afforded the alkyne, **25**, in a 74% yield. The alkyne **25** was subjected to an addition reaction[17] with the methylcopper complex which had been prepared from methylmagnesium bromide and a dimethyl sulfide complex of copper(I) bromide[18] in a mixture of ether and dimethyl sulfide according to the procedure reported by Marfat *et al.*[17] The reaction proceeded effectively in the same solvent system at −25 °C for 1 week, resulting in the almost exclusive formation of the alkenylcopper intermediate, **26**, as evidenced by the isolation of the 1-iodo-2-methylalkene, **27**, presumably with an *E*-configuration, in a 52% yield as the sole

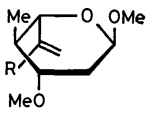
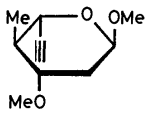
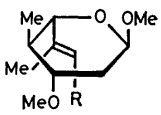

22 R = I
23 R = Li
24 R = CH(OH)Ph

25

26 R = Cu(Me$_2$S)MgBr$_2$[17]
27 R = I
28 R = CH_2CH_2OH

addition product after a reaction with iodine.[19] This result indicated that the addition reaction proceeded in a stereospecific syn manner, with copper becoming associated with the terminal carbon, as in the case of simple nonfunctionalized terminal alkyne.[20] Normant *et al.*[21,22] showed that the regioselectivity of the addition of the RCu, MgX_2 reagent to terminal alkynes was affected by the presence of such heteroatom substituents as alkoxyl groups at the propargyric position in the alkyne, and mixtures of products were frequently obtained. The coordination of the hetero atom with a copper moiety has been suggested to explain the formation of products derived from alkenylcopper intermediates with copper at the internal carbon.[23] Under our reaction conditions, the copper reagent forms complexes so strongly with dimethyl sulfide present in the solvent system that the coordination of the copper moiety with the propargyric-ring oxygen atom may be out of the question. The alkenylcopper intermediate, **26**, was converted into the mixed cuprate with 1-lithiopentyne according to the procedure proposed by McGuirk *et al.*[24] and allowed to react with ethylene oxide at −25 °C for 24 h to give the homoallylic alcohol, **28**, in a 46% yield.

Experimental

The melting points were determined on a micro hot-stage Yanaco MP-83 and are uncorrected. The specific rotations were measured with a Carl Zeiss photoelectric precision polarimeter. The ^{1}H NMR (PMR) spectra were determined with Varian A60 and EM-390 spectrometers, using TMS as the internal standard. Unless otherwise stated, the TLC and column chromatography were performed on silica gel Wakogel B-5 and Wakogel C-200 respectively. In general, the concentration was carried out under a reduced pressure of below 30 °C.

*Methyl 4,6-O-Benzylidene-3-deoxy-3-C-methyl-α-D-arabino-hexopyranosid-2-ulose (**4**).* A mixture of dry DMSO (54 ml), dry pyridine (5.5 ml), and trifluoroacetic acid (2.89 ml, 0.037 mol) was added to a solution of **3** (50.0 g, 0.178 mol) in dry benzene (350 ml). A solution of dicyclohexylcarbodiimide (44.2 g, 0.214 mol) in dry benzene (150 ml) was then added, drop by drop, to the mixture under ice-cooling. After the mixture had been stirred at room temperature for 7 h, the precipitates formed were filtered and washed with benzene. The filtrate and washings were combined and washed successively with saturated aqueous $KHSO_4$, $NaHCO_3$, and NaCl solutions, dried, and evaporated to afford a yellow syrup of crude methyl 4,6-*O*-benzylidene-3-deoxy-3-*C*-methyl-α-D-*ribo*-hexopyranosid-2-ulose (51.4 g). This syrup was dissolved in DMF (247 ml) containing triethylamine (23 ml). After being stored at room temperature for 3 d, the mixture was poured into ice water. The precipitates were collected by filtration, washed with water, and dried at 40 °C to afford pale yellow crystals of **4** (43.4 g, 87.5%); mp 127.5—129 °C. Recrystallization from ethyl acetate–hexane gave a pure sample of **4**: mp 130—131 °C; $[\alpha]_D^{27}$ +58° (*c* 1.26, $CHCl_3$); IR (0.122 M, CCl_4) 1750 cm^{-1}; PMR ($CDCl_3$) δ=1.21 (3H, d, 3-Me, J=5.9 Hz), 3.50 (3H, s, OMe), 4.63 (1H, s, H-1), and 5.53 (1H, s, benzylic H). Found: C, 64.87; H, 6.55%. Calcd for $C_{15}H_{18}O_5$: C, 64.73; H, 6.52%.

*Methyl 4,6-O-Benzylidene-3-deoxy-3-C-methyl-α-D-glucopyranoside (**5**).* Powdered $LiAlH_4$ (5.22 g, 0.138 mol) was slowly added to a stirred ice-cooled solution of **4** (38.4 g, 0.138 mol) in dry ether (1.0 l), and then the mixture was stirred at room temperature for 0.5 h. Ethyl acetate (300 ml) and water (0.5 l) were added to the cooled reaction mixture, and it was stirred at room temperature for 1 h. The organic layer thus separated was washed with a saturated aqueous NaCl solution, dried, and evaporated to afford **5** as colorless plates (35.7 g, 92.3%). Recrystallization from methanol–petroleum ether gave a pure sample: mp 150.5—151.5 °C; $[\alpha]_D^{23}$ +94° (*c* 1.04, $CHCl_3$); PMR ($CDCl_3$) δ=1.18 (3H, d, 3-Me, J=6.1 Hz), 1.91 (1H, d, OH, $J_{2,OH}$=11.1 Hz), 3.26 (1H, dd, H-4, $J_{3,4}$=10.7 Hz, $J_{4,5}$=4.7 Hz), 3.48 (3H, s, OMe), 4.71 (1H, d, H-1, $J_{1,2}$=3.6 Hz), and 5.51 (1H, s, benzylic H). Found: C, 64.53; H, 7.27%. Calcd for $C_{15}H_{20}O_5$: C, 64.27; H, 7.19%.

*Methyl 4,6-O-Benzylidene-3-deoxy-3-C-methyl-2-O-methyl-α-D-glucopyranoside (**6**).* Sodium hydride (17.1 g, 55% emulsion in mineral oil) was placed in a flask and washed free from the mineral oil with hexane. The flask was evacuated until the last traces of hexane were removed from the sodium hydride. Dry DMF (75 ml) was then introduced under stirring, and a solution of **5** (10.5 g, 37.5 mmol) in DMF (30 ml) was added dropwise to the stirred ice-cooled contents. After the sirring had been continued at room temperature for 1 h, methyl iodide (34.2 ml, 513.8 mmol) was added dropwise to the stirred ice-cooled mixture over a period of 20 min. After the mixture had been stirred for 1.5 h, the excess of hydride was then destroyed by the careful addition of methanol and the solvents were removed. The residue was taken up with chloroform, washed with water and a saturated aqueous NaCl solution, dried, and evaporated to afford **6** as a yellow crystalline solid (11.5 g). The recrystallization of the crude crystals of **6** from acetone–petroleum ether gave the pure sample (8.00 g, 73%): mp 121—122.5 °C; $[\alpha]_D^{27}$ +84° (*c* 1.10, $CHCl_3$); PMR ($CDCl_3$) δ=1.15 (3H, d, 3-Me J=6.1 Hz), 3.02 (1H, dd, H-2, $J_{1,2}$=3.2 Hz, $J_{2,3}$=10.0 Hz), 3.50 (6H, s, 1- and 2-OMe), 4.86 (1H, d, H-1), and 5.52 (1H, s, benzylic H). Found: C, 65.50; H, 7.49%. Calcd for $C_{16}H_{22}O_5$: C, 65.29; H, 7.53%.

*Methyl 4-O-Benzyl-6-bromo-3,6-dideoxy-3-C-methyl-2-O-methyl-α-D-glucopyranoside (**7**).* A mixture of **6** (8.00 g, 27.2 mmol), NBS (5.08 g, 28.8 mmol), and carbon tetrachloride (120 ml) containing barium carbonate (6.76 g, 34.7 mmol) was refluxed for 2h under stirring (argon atmosphere). The solids were filtered off and washed with carbon tetrachloride. The filtrate and washings were combined and washed with saturated aqueous $Na_2S_2O_3$, $NaHCO_3$, and NaCl solutions successively. The dried solution was evaporated to give **7** (10.0 g, 98.6%) as a colorless syrup which was suitable for the next synthesis. A portion of this product (50 mg) was chromatographyd on silica gel (3 g) with 20:1 benzene–ethyl acetate to afford a pure sample of **7** (39 mg, 78%): $[\alpha]_D^{28}$ +93° (*c* 0.81, $CHCl_3$); PMR ($CDCl_3$) δ=1.04 (3H, d, 3-Me, J=6.4 Hz), 3.12 (1H, dd, H-2, $J_{1,2}$=3.7 Hz, $J_{2,3}$=10.9 Hz), 3.48 and 3.57 (each 3H, each s, 1- and 2-OMe), 4.88 (1H, d, H-4, $J_{3,4}$=9.9 Hz, $J_{4,5}$=10.2 Hz), and 4.94 (1H, d, H-1). Found: C, 51.22; H, 5.46; Br, 21.66%. Calcd for $C_{16}H_{21}O_5Br$: C, 51.49; H, 5.67; Br,

21.41%.

Methyl 3,6-Didoxy-3-C-methyl-2-O-methyl-α-D-glucopyranoside (8). The crude sample of **7** (10.0 g) was dissolved in dry THF (650 ml) and cooled in an ice bath. Powdered $LiAlH_4$ (8.13 g, 215 mmol) was slowly added to the stirred solution. The resulting mixture was refluxed for 1.5 h and then cooled in an ice bath. Ethyl acetate (240 ml) and water (150 ml) were slowly added to the reaction mixture, and the resulting mixture was stirred at room temperature overnight. The mixture was filtered with a super cell, and the filter cake was washed with ethyl acetate. The combined filtrate and washings were washed with a saturated aqueous NaCl solution, dried, and evaporated. The residual syrup (7.30 g) was chromatographed on silica gel (360 g) with 1:1 benzene–ethyl acetate to afford a colorless syrup of **8** (4.0 g, 77%): $[\alpha]_D^{15}$ +159° (*c* 0.56, $CHCl_3$); PMR ($CDCl_3$) δ=1.11 (3H, d, 3-Me, J=6.2 Hz), 1.24 (3H, d, H-6, $J_{5,6}$=6.1 Hz), 2.92 (1H, dd, H-2, $J_{1,2}$=3.1 Hz, $J_{2,3}$=10.7 Hz), 3.43 (6H, s, 1- and 2-OMe), and 4.76 (1H, d, H-1). Found: C, 56.85; H, 9.32%. Calcd for $C_9H_{18}O_4$: C, 56.82; H, 9.54%.

Methyl 3,6-Dideoxy-4-O-mesyl-3-C-methyl-2-O-methyl-α-D-glucopyranoside (9). A mixture of **8** (4.00 g, 21.0 mmol), dry pyridine (40 ml), and mesyl chloride (2.48 ml, 32.0 mmol) was allowed to stand at room temperature for 24 h and then evaporated. The residue was taken up with ethyl acetate, washed with a saturated aqueous NaCl solution, dried, and evaporated to afford pale yellow needles of **9** (5.07 g, 90%). Some of these crystals (71 mg) were chromatographed on silica gel (2 g) with 10:1 benzene–ethyl acetate to give a pure sample (56 mg) as colorless needles: mp 81.5—83.0 °C; $[\alpha]_D^{26}$ +127° (*c* 1.67, $CHCl_3$); PMR ($CDCl_3$) δ=1.17 (3H, d, 3-Me, J=6.3 Hz), 1.32 (3H, d, H-6, $J_{5,6}$=6.0 Hz), 2.99 (1H, dd, H-2, $J_{2,3}$=10.8 Hz), 3.08 (3H, s, OMs), 3.46 (6H, s, 1- and 2-OMe), 4.16 (1H, dd, H-4, $J_{3,4}$=9.7 Hz, $J_{4,5}$=9.7 Hz), and 4.78 (1H, d, H-1, $J_{1,2}$=3.2 Hz). Found: C, 44.44; H, 7.28; S, 11.65%. Calcd for $C_{10}H_{20}O_6S$: C, 44.72; H, 7.53; S, 11.95%.

Methyl 4-O-Benzoyl-3,6-dideoxy-3-C-methyl-2-O-methyl-α-D-galactopyranoside (10). A solution of **9** (105 mg, 0.391 mmol) in DMSO (5.0 ml) was heated with dried sodium benzoate (282 mg, 1.96 mmol) at 120 °C for 6 h. After being cooled to room temperature, the reaction mixture was diluted with ethyl acetate; the solids were filtered off and washed with ethyl acetate. The filtrate and washings were combined and washed with water and a saturated aqueous NaCl solution. The dried solution was evaporated, and the residue (189 mg) was chromatographed on silica gel (5 g) with 5:1 hexane–acetone to afford a syrup of **10** (102 mg, 88.6%): $[\alpha]_D^{29}$ +153° (*c* 0.59, $CHCl_3$); IR (CCl_4) 1720 cm^{-1}; PMR ($CDCl_3$) δ=1.02 (3H, d, 3-Me, J=7.3 Hz), 1.13 (3H, d, H-6, $J_{5,6}$=6.8 Hz), 3.41 (1H, dd, H-2, $J_{1,2}$=3.1 Hz, $J_{2,3}$=10.8 Hz), 3.47 and 3.50 (each 3H, each s, 1- and 2-OMe), 4.12 (1H, dq, H-5, $J_{4,5}$=1.5 Hz), 4.94 (1H, d, H-1), and 5.27 (1H, dd, H-4). Found: C, 65.42; H, 7.45%. Calcd for $C_{16}H_{22}O_5$: C, 65.29; H, 7.53%.

1-O-Acetyl-4-O-benzoyl-3,6-dideoxy-3-C-methyl-2-O-methyl-D-galactopyranose (11). To a solution of **10** (5.30 g, 18.0 mmol) in acetic anhydride (197 ml), concd H_2SO_4 (1.9 ml) was added dropwise under ice-cooling. After being kept at room temperature for 0.5 h, the reaction mixture was poured into cold water (1.8 l), neutralized with solid $NaHCO_3$, and then extracted with chloroform. The extract was washed with a saturated aqueous NaCl solution, dried, and evaporated. The residual yellow-brown syrup (5.8 g) was chromatographed on silica gel (50 g) with 10:1 benzene–ethyl acetate to afford a semi-crystalline solid of **11** (4.41 g, 76.3%) as an anomeric mixture: PMR ($CDCl_3$) δ=1.10 (3H, d, 3-Me, J=6.9 Hz), 1.19 (3H, d, H-6, $J_{5,6}$=6.2 Hz), 2.10 and 2.21 (3H, each s, OAc), 3.38 and 3.54 (3H, each s, OMe), 5.64 and 6.2—6.3 (1H, each d, H-1 of β- and α-anomers, $J_{\beta\text{-}1,2}$=7.9 Hz). Found: C, 63.53; H, 6.88%. Calcd for $C_{17}H_{22}O_6$: C, 63.34; H, 6.88%.

3,6-Didoxy-3-C-methyl-2-O-methyl-D-galactopyranose (12). A 1 M aqueous NaOH solution (3.67 ml) was added to a solution of **11** (490 mg, 1.52 mmol) in dioxane (3.67 ml). After being kept at room temperature for 2 d, the mixture was neutralized with a 0.5 M H_2SO_4 solution and evaporated, and acetone was added to the residue. The insoluble matter was filtered off, and the filtrate was evaporated to afford crude **12** (268 mg, 100%) as a yellow syrup. A sample (60 mg) of the syrup was chromatographed on silica gel (2 g) with 1:1 benzene–ethyl acetate to give a colorless syrup of **12** (55 mg, 92%) as an anomeric mixture; PMR ($CDCl_3$) δ=1.17 (3H, d, 3-Me, J=6.2 Hz), 1.22 (3H, d, H-6, $J_{5,6}$=6.2 Hz), 3.71 (1H, dq, H-5, $J_{4,5}$=2.9 Hz), 4.62 and 5.38 (1H, each d, H-1 of two anomers, $J_{\alpha\text{-}1,2}$=4.4 Hz, $J_{\beta\text{-}1,2}$=7.9 Hz), and 3.80 (2H, s, 1- and 4-OH). Found: C, 54.27; H, 8.98%. Calcd for $C_8H_{16}O_4$: C, 54.53; H, 9.15%.

3,6-Dideoxy-3-C-methyl-2-O-methyl-D-galactose Ethylene Dithioacetal (13). To a stirred solution of the crude **12** (1.08 g) in 1,2-ethylenedithiol (2.57 ml) was added concd HCl (0.63 ml) dropwise under ice-cooling. After being stirred at room temperature for 2 h, the reaction mixture, which showed the presence of a trace amount of **12** on TLC (1:1 benzene–ethyl acetate), was treated with additional concd HCl (1.93 ml) at room temperature for 40 min. The resulting mixture was then poured into ice water and extracted with chloroform. The extract was washed successively with saturated aqueous $NaHCO_3$ and NaCl solutions, dried, and evaporated. The residual yellow syrup (3.18 g) was chromatographed on silica gel (60 g) with 2:1 benzene–ethyl acetate to afford **13** (1.17 g, 76%) as a syrup: $[\alpha]_D^{30}$ +5° (*c* 1.21, $CHCl_3$); PMR ($CDCl_3$) δ=0.98 (3H, d, 3-Me, J=7.0 Hz), 1.28 (3H, d, H-6, $J_{5,6}$=6.4 Hz), 1.7—2.5 (1H, m, H-3), 2.56 (2H, s, 4- and 5-OH), 3.24 (4H, s, S–CH_2–CH_2–S), 3.29 (1H, dd, H-4, $J_{3,4}$=8.2 Hz, $J_{4,5}$=3.0 Hz), 3.63 (1H, dd, H-2, $J_{1,2}$=9.0 Hz, $J_{2,3}$=1.9 Hz), 3.65 (3H, s, OMe), 3.93 (1H, dq, H-5), and 4.68 (1H, d, H-1). Found: C, 47.34; H, 7.76; S, 25.18%. Calcd for $C_{10}H_{20}O_3S_2$: C, 47.59; H, 7.99; S, 25.41%.

4,5-Di-O-acetyl-3,6-dideoxy-3-C-methyl-2-O-methyl-D-galactose Ethylene Dithioacetal (14). To a stirred ice-cooled solution of **13** (2.36 g, 9.35 mmol) in ethyl acetate (24 ml), acetic anhydride (2.12 ml, 22.5 mmol) and 4-dimethylaminopyridine (2.74 g, 22.5 mmol) were added successively; stirring was then continued at room temperature for 0.5 h. The resulting precipitates were filtered off and washed with ethyl acetate. The filtrate and washings were combined and washed successively with water, saturated aqueous $KHSO_4$, $NaHCO_3$, and NaCl solutions, dried, and evaporated. The residual yellow syrup (3.25 g) was chromatographed on silica gel (100 g) with 6:1 benzene–ethyl acetate to afford a practically pure sample of **14** as colorless needles (2.88 g, 91.5%). Recrystallization from ethyl acetate–hexane gave a pure sample: mp 74.5—75.5 °C; $[\alpha]_D^{19}$ +30° (*c* 1.44, $CHCl_3$); PMR ($CDCl_3$) δ=0.90 (3H, d, 3-Me, J=7.0 Hz), 1.21 (3H, d, H-6, $J_{5,6}$=6.2 Hz), 2.10 and 2.18 (each 3H, each s, 4- and 5-OAc), 2.0—2.6 (1H, m, H-3), 3.18 (1H, dd, H-2, $J_{1,2}$=9.3 Hz, $J_{2,3}$=1.7 Hz), 3.23 (4H, s, S–CH_2–CH_2–S), 3.52 (3H, s, OMe), 4.62 (1H, d, H-1), 5.00 (1H, dd, H-4, $J_{3,4}$=8.2 Hz, $J_{4,5}$=3.2 Hz), and 5.18 (1H, dq, H-5). Found: C, 50.21; H, 7.16; S, 18.83%. Calcd for $C_{14}H_{24}O_5S_2$: C, 49.98; H, 7.19; S, 19.06%.

*4,5-Di-O-acetyl-3,6-dideoxy-3-C-methyl-2-O-methyl-D-galactose (**15**).* Red mercury(II) oxide (2.83 g, 13.1 mmol) and mercury(II) chloride (7.10 g, 26.2 mmol) were added successively at room temperature to a solution of **14** (2.00 g, 5.94 mmol) in aqueous 80% acetone (150 ml). The mixture was then stirred efficiently and refluxed under argon for 17 h. The resulting suspension was cooled and filtered through a super cell, and the filter cake was washed thoroughly with acetone. The filtrate and washings were combined and concentrated to remove the acetone. The aqueous residue was extracted with ethyl acetate, and the extract was washed with water and a saturated aqueous NaCl solution, dried, and evaporated. The residual pale yellow syrup was chromatographed on silica gel (78 g) with 3:1 hexane–ethyl acetate to afford **15** as pale yellow plates (1.48 g, 95.4%): PMR ($CDCl_3$) δ=0.89 (3H, d, 3-Me, J=7.1 Hz), 1.20 (3H, d, H-6, $J_{5,6}$=6.1 Hz), 2.10 and 2.18 (each 3H, each s, 4- and 5-OAc), 2.1—2.7 (1H, m, H-3), 3.44 (3H, s, OMe), 3.3—3.6 (1H, m, H-2), 4.9—5.4 (2H, m, H-4 and H-5), and 9.75 (1H, d, H-1).

*5,6-Di-O-acetyl-2,4,7-trideoxy-4-C-methyl-1,3-di-O-methyl-D-galacto-1-enoheptitol (**16**).* A 4 M methylsulfinylmethanide anion in DMSO,[13a] prepared with sodium hydride (6.37 mmol as a 55% dispersion in mineral oil) and DMSO (1.7 ml), was added dropwise to a stirred suspension of (methoxymethyl)triphenylphosphonium chloride (2.31 g, 6.73 mmol) in dry ether (35 ml) under argon at room temperature. The mixture was stirred for 10 min and then, to the resulting red suspension of the ylide, a solution of **15** (0.88 g, 3.37 mmol) in dry ether (18 ml) was added dropwise. After the mixture had been stirred at room temperature for 15 min, the resulting orange suspension was poured into ether (100 ml), and the organic layer was washed with water and a saturated aqueous NaCl solution, dried, and evaporated to a brown syrup (2.56 g). The syrup was chromatographed on silica gel (Mallinckrodt SILICAR CC-7 special, 80 g) with 4:1 hexane–ethyl acetate to afford a practically pure sample of **16** as a pale yellow syrup (0.70 g, 72%). A part of this sample was again chromatographed on the same silica gel with the same solvent system to give an analytically pure sample as a 7.7:1 mixture of the *E*- and *Z*-isomers: PMR ($CDCl_3$) δ=0.88 and 0.91 (3H, each d, 4-Me of *E*- and *Z*-isomers, J_E=7.3 Hz, J_Z=7.0 Hz), 1.19 (3H, d, H-7, $J_{6,7}$=6.7 Hz), 2.08 and 2.17 (each 3H, each s, 5- and 6-OAc), 3.16 and 3.18 (3H, each s, 1-OMe of *E*- and *Z*-isomers), 3.41 (1H, dd, H-3, $J_{2,3}$=9.0 Hz, $J_{3,4}$=3.0 Hz), 3.61 and 3.62 (3H, each s, 3-OMe of *E*- and *Z*-isomers), 6.10 and 6.48 (1H, each d, H-1 of *E*- and *Z*-isomers). Found: C, 58.30; H, 8.24%. Calcd for $C_{14}H_{24}O_6$: C, 58.31; H, 8.39%.

*5,6-Di-O-acetyl-2,4,7-trideoxy-4-C-methyl-3-O-methyl-D-galacto-heptose Dimethyl Acetal (**18**).* To an ice-cooled solution of **16** (1.05 g, 3.63 mmol) in methanol (10 ml) were added solid $NaHCO_3$ (0.37 g, 4.41 mmol) and NBS (0.77 g, 4.41 mmol) successively. After being stirred at 0 °C for 1 h, the mixture was evaporated and the residue was extracted with ethyl acetate. The extract was washed with water and a saturated aqueous NaCl solution, dried, and evaporated to afford a crystalline solid (1.60 g). Chromatography of the solid on silica gel (Mallinckrodt, 80 g) with 3:1 hexane–ethyl acetate gave colorless needles (1.08 g, 74.4%) as an epimeric mixture, **17**, of 5,6-di-*O*-acetyl-2-bromo-2,4,7-trideoxy-4-*C*-methyl-3-*O*-methyl-D-*glycero*-L-*manno*-heptose dimethyl acetal and its D-*glycero*-L-*gluco*-epimer. Tributylstannane (0.33 ml, 1.224 mmol) and α,α'-azobisisobutyronitrile (17 mg) were added to a solution of **17** (409 mg, 1.02 mmol) in dry benzene (6.1 ml). The solution was stirred, under an argon atmosphere, at 60 °C for 1 h and then evaporated. The residual syrup was chromatographed on silica gel (Mallinckrodt, 41 g) with 3:1 hexane-ethyl acetate to give **18** (315 mg, 96% based on **17**) as a syrup: PMR ($CDCl_3$) δ=0.85 (3H, d, 4-Me, J=7.0 Hz), 1.17 (3H, d, H-7, J=6.0 Hz), 2.07 and 2.14 (each 3H, each s, 5- and 6-OAc), 3.26 (3H, s, 3-OMe), 3.34 [6H, s, CH-$(OMe)_2$], 4.42 (1H, dd, H-1, $J_{1,2}$=5.0 Hz, $J_{1,2'}$=6.0 Hz), 4.98 (1H, dd, H-5, $J_{4,5}$=7.5 Hz, $J_{5,6}$=2.5 Hz), and 5.11 (1H, dq, H-6). Found: C, 56.29; H, 8.69%. Calcd for $C_{15}H_{28}O_7$: C, 56.23; H, 8.81%.

*Methyl 2,4,7-Trideoxy-4-C-methyl-3-O-methyl-β-D-galacto-heptopyranoside (**19**).* 1 M aqueous NaOH (9.86 ml) was added to an ice-cooled solution of **18** (1.58 g, 4.93 mmol) in dioxane (9.86 ml), after wihich the mixture was kept at room temperature for 2 h. The reaction mixture was neutralized (pH 7—8) with ion-exchange resin (CG 50 H^+ type), and the filtrate was evaporated to afford a crude syrup (1.21 g) of the deacetylation product. The pure sample of this product was obtained by column chromatography, using silica gel (Mallinckrodt) with 1:2 hexane–ethyl acetate as a colorless syrup, in an 87% yield (Found: C, 55.63; H, 9.84%. Calcd for $C_{11}H_{24}O_5$: C, 55.91; H, 10.24%). A solution of the crude syrup (1.21 g) in 0.5% methanolic hydrogen chloride (59 ml) was allowed to stand at room temperature for 1 h. The reaction mixture was then neutralized with solid $NaHCO_3$ and evaporated. The residue was extracted with ethyl acetate, and the extract was washed with a saturated aqueous NaCl solution, dried, and evaporated to give a pale yellow crystalline solid (1.19 g). The product was chromatographed on silica gel (59 g) with 5:1 chloroform–acetone to afford colorless needles (839 mg, 83% from **18**) melting at 88—98 °C. The PMR analysis (in $CDCl_3$) revealed that these crystals were a 1:5 mixture of α- and β-methyl glycoside, based on the areas of the signals at δ=4.35 (dd, $J_{1,2ax}$=9.8 Hz, $J_{1,2eq}$=2.2 Hz) and δ=4.94 (dd, $J_{1,2ax}$=4.0 Hz, $J_{1,2ex}$=1.5 Hz), which are attributed to the α- and β-anomeric protons respectively. The practically pure major β-anomer, **19**, was obtained on the recrystallization of the mixture from ethyl acetate–hexane as a first crop (366 mg, mp 99.5—101 °C) and a second crop (264 mg, mp 95—100.5 °C), the total yield from **18** being 62.4%. The pure sample of **19** was obtained by the recrystallization of the first crop from the same solvent system: mp 100—101 °C; $[\alpha]_D^{15}$ −102° (*c* 1.00, $CHCl_3$); PMR ($CDCl_3$) δ=0.99 (3H, d, 4-Me, J=6.5 Hz), 1.29 (3H, d, 6-Me, J=6.5 Hz), 1.2—1.7 (1H, m, H-2ax), 1.88 (1H, d, 6-OH), 1.4—2.0 (1H, m, H-4), 2.23 (1H, ddd, H-2eq, $J_{1,2eq}$=1.5 Hz, $J_{2eq,3}$=4.5 Hz, $J_{2eq,2ax}$=12.5 Hz), 3.0—3.6 (2H, m, H-3 and H-5), 3.35 and 3.37 (each 3H, each s, 1- and 3-OMe), 3.6—4.3 (1H, m, H-6), and 4.94 (1H, dd, H-1, $J_{1,2ax}$=4.0 Hz). Found: C, 58.99; H, 9.66%. Calcd for $C_{10}H_{20}O_4$: C, 58.80; H, 9.87%.

*Methyl 2,4,7-Trideoxy-4-C-methyl-3-O-methyl-α-L-arabino-heptopyranosid-6-ulose (**20**)* A solution of **19** (0.24 g, 1.17 mmol) in acetone (4.8 ml) was cooled at −60 °C in a Dry Ice–acetone bath. After the addition of an aliquot (0.872 ml) of the Jones reagent prepared with CrO_3 (1.00 g), concd H_2SO_4 (0.861 ml), and water (2.88 ml), the mixture was allowed to warm to −10 °C and then stirred for 1.5 h; TLC analysis with 2:1 benzene–ethyl acetate then indicated the complete conversion of **19** into a single product, **20**. The reaction mixture was then neutralized with a saturated aqueous $NaHCO_3$ solution and extracted with ether. The extract was washed with a saturated aqueous NaCl solution, dried, and evaporated to a pale yellow oil of crude **20** (0.23 g), which was subsequently chromatographed on silica gel

(8 g) with 5:1 benzene–ethyl acetate to afford a pure sample of **20** (0.22 g, 93%) as a colorless oil: $[\alpha]_D^{17}$ +4° (*c* 1.33, $CHCl_3$); IR (0.168 M, $CHCl_3$) 1720 cm^{-1}; PMR ($CDCl_3$) δ=0.95 (3H, d, 4-Me J=7.0 Hz), 1.53 (1H, ddd, H-2_{ax}, $J_{2ax,3}$=11.0 Hz, $J_{1,2ax}$=3.5 Hz, $J_{2ax,2eq}$=13.0 Hz), 2.22 (3H, s, H-7), 2.26 (1H, ddd, H-2eq, $J_{1,2eq}$=1.5 Hz, $J_{2eq,3}$=4.5 Hz), 3.27 (1H, ddd, H-3, $J_{3,4}$=9.5 Hz), 3.36 and 3.38 (each 3H, each s, 1- and 3-OMe), 3.77 (1H, d, H-5, $J_{4,5}$=10.5 Hz), and 4.96 (1H, dd, H-1). Found: C, 59.41; H, 8.76%. Calcd for $C_{10}H_{18}O_4$: C, 59.38; H, 8.97%.

*Hydrazone **21** of **20**.* A mixture of **20** (0.20 g, 8.35 mmol), ethanol (2 ml), triethylamine (1.17 ml, 8.35 mmol), and 100% hydrazone hydrate (0.191 ml, 3.93 mmol) was refluxed for 1 h. After cooling, the reaction mixture was neutralized with carbon dioxide gas and extracted with chloroform (30 ml). The extract was washed with water, and the aqueous layer was again extracted with chloroform. The combined chloroform layers were washed with a saturated aqueous NaCl solution, dried, and evaporated to afford practically pure colorless needles of **21** (0.21 g, 98%). Recrystallization from chloroform–petroleum ether gave a pure sample: mp 71—72 °C; $[\alpha]_D^{18}$ −72° (*c* 1.11, $CHCl_3$); IR (KBr) 3400 (NH_2) and 1630 cm^{-1} (C=N). Found: C, 55.44; H, 9.20; N, 12.97%. Calcd for $C_{10}H_{20}N_2O_3$: C, 55.53; H, 9.32; N, 12.95%.

*Methyl 2,4,6,7-Tetradeoxy-6-iodo-4-*C*-methyl-3-*O*-methyl-α-*L*-arabino-hept-6-enopyranoside (**22**).* The hydrazone **21** (0.20 g, 0.929 mmol) in THF (9.1 ml) and triethylamine (6.48 ml) was treated with iodine (0.52 g, 2.05 mmol) in THF (1.0 ml) at room temperature with stirring under argon. Initially the iodine color was discharged, triethylamine hydroiodide being precipitated and gas evolved. The orange-colored suspension was stirred at room temperature for 45 min and then diluted with chloroform (75 ml). The mixture was washed with water, 2 M hydrochloric acid, a 5% aqueous $Na_2S_2O_3$ solution (30 ml), and a saturated aqueous NaCl solution, dried, and evaporated. The residual dark brown syrup (0.34 g) was chromatographed on silica gel (13 g) with 15:1 benzene–ethyl acetate to afford colorless needles of **22** (0.21 g, 72%). Recrystallization from ethyl acetate–hexane gave an analytical sample: mp 86—87 °C; $[\alpha]_D^{20}$ −74° (*c* 1.06, $CHCl_3$); IR (0.15 M, $CHCl_3$) 1620 cm^{-1} (C=C); PMR ($CDCl_3$) δ=0.88 (3H, d, 4-Me, J=7.0 Hz), 1.2—1.9 (1H, m, H-4), 1.51 (1H, ddd, H-2ax, $J_{1,2ax}$=3.5 Hz, $J_{2ax,3}$=11.5 Hz, $J_{2ax,2eq}$=13.0 Hz), 2.25 (1H, ddd, H-2eq, $J_{1,2eq}$=1.5 Hz, $J_{2eq,3}$=11.5 Hz), 3.23 (1H, d, with a little long range coupling with H-7′, H-5, $J_{4,5}$=10.0 Hz), 3.1—3.7 (1H, m, H-3), 3.39 (6H, s, 1- and 3-OMe), 4.94 (1H, dd, H-1), 6.01 (1H, d, H-7 or H-7′, $J_{7,7'}$=1.2 Hz), and 6.40 (1H, m, H-7′ or H-7). Found: C, 38.28; H, 5.38; I, 40.32%. Calcd for $C_{10}H_{17}O_3I$: C, 38.48; H, 5.49; I, 40.65%.

*Condensation of **22** with Benzaldehyde* via *the Lithium Compound, **23**.* A solution of **22** (30.4 mg, 0.097 mmol) in dry ether (0.25 ml) was cooled to −78 °C. To the resulting white suspension was added a 1.6 M butyllithium in hexane (0.0729 ml, 0.117 mmol) using a syringe. After the resulting pale yellow solution had been stirred at −78 °C for 2.5 h, benzaldehyde (0.0119 ml, 0.117 mmol) was added slowly *via* the syringe to the solution of the alkenyllithium, **23**, thus formed; stirring was then continued for 1.5 h. The reaction mixture was quenched at 0 °C by the addition of an aqueous saturated NH_4Cl solution, and was then extracted with ether. The organic layers were washed with a saturated aqueous NaCl solution, dried, and evaporated to a pale yellow oil (62.7 mg). The crude product was purified by chromatography on silica gel (3.1 g) with 5:1 hexane–acetone to afford a colorless syrup (15.4 mg, 54%) of the condensation product, **24**, as a 1:1.2 mixture of epimers: PMR ($CDCl_3$) δ=0.78 and 0.84 (3H, each d, 4-Me, J=7.0 Hz), 1.1—1.9 (2H, m, H-2ax H-4), 2.0—2.5 (1H, m, H-2eq), 2.7—2.9 (1H, br, OH), 2.9—3.5 (1H, m, H-3), 3.24, 3.26, 3.35, and 3.39 (6H, each s, 1- and 3-OMe), 3.93 (1H, dd, H-5, $J_{4,5}$=10.5 Hz, $J_{5,=CH}$=2.5 Hz), 4.91 (1H, dd, H-1, $J_{1,2eq}$=1.5 Hz, $J_{1,2ax}$=3.5 Hz), 5.1—5.5 (3H, m, =CH and benzylic H), and 7.42 (5H, s, ArH); M^+ 292 (20 eV).

*Methyl 2,4,6,7-Tetradeoxy-4-*C*-methyl-3-*O*-methyl-α-*D*-arabino-hept-6-enopyranoside (**25**).* The iodide, **22** (0.185 g), was added to a solution of KOH (0.66 g) in ethanol (6.5 ml), after which the mixture was refluxed with stirring for 1.5 h. After cooling, the mixture was neutralized with carbon dioxide gas and extracted with ether (30 ml). The ethereal extract was washed with water and a saturated aqueous NaCl solution, and dried. After the removal of the solvent, the residual brown oil (0.128 g) was chromatographed on silica gel (7 g) with 20:1 benzene–ethyl acetate to afford a colorless oil of **25** (80 mg, 74%): $[\alpha]_D^{19}$ −80° (*c* 0.84, $CHCl_3$; IR (0.211 M, $CHCl_3$) 3300 cm^{-1} (≡CH); PMR ($CDCl_3$) δ=1.10 (3H, d, 4-Me, J=7.0 Hz), 1.49 (1H, ddd, H-2ax, $J_{1,2ax}$=3.5 Hz, $J_{2ax,3}$=11.5 Hz, $J_{2ax,2eq}$=13.0 Hz), 1.3—2.1 (1H, m, H-4), 2.21 (1H, ddd, H-2eq, $J_{1,2ex}$=1.5 Hz, $J_{2eq,3}$=4.5 Hz), 2.45 (1H, d, H-7, $J_{5,7}$=2.5 Hz), 3.22 (1H, ddd, H-3, $J_{3,4}$=9.8 Hz), 3.36 and 3.39 (each 3H, each s, 1- and 3-OMe), 4.14 (1H, dd, H-5, $J_{4,5}$=10.5 Hz), and 4.90 (1H, dd, H-1). Found: C, 65.16; H, 8.57%. Calcd for $C_{10}H_{16}O_3$: C, 65.19; H, 8.75%.

*Methyl 2,4,6,7-Tetradeoxy-7-iodo-4,6-di-*C*-methyl-3-*O*-methyl-α-*L*-arabino-hept-6-enopyranoside (**27**).* A solution of dimethyl sulfide complex[18] of copper(I) bromide (86.6 mg, 0.42 mmol) in ether (0.5 ml) and dimethyl sulfide (0.4 ml) under argon was cooled to −45 °C, at which temperature a white solid was formed; 1.71 M methylmagnesium bromide in ether (0.246 ml, 0.42 mmol) was then added dropwise using a syringe over a period of 2 min. The resulting suspension of a yellow solid was stirred at −45 °C for 2 h, after which a solution of **25** (64.7 mg, 0.351 mmol) in ether (0.15 ml) was added and the mixture was stirred at −25 °C for 1 week. The resulting dark green reaction mixture was cooled to −50 °C, and to this stirred mixture was added iodine (0.107 g, 0.42 mmol). After the mixture had been stirred at −30 °C for 2 h, to the red-brown reaction mixture was added triethyl phosphite (0.024 ml) and 5 M hydrochloric acid (0.524 ml) at the same temperature. The resulting mixture was diluted with ether (20 ml), washed with saturated aqueous $NaHCO_3$ and NaCl solutions, and evaporated after being dried. The residue was chromatographed on silica gel (5.8 g) with 20:1 hexane–acetone to afford **27** (59.6 mg, 52%) as colorless needles and **25** (12.2 mg, 18.9%). A pure sample of **27** was obtained by recrystallization from ethyl acetate and hexane: mp 84—85 °C; $[\alpha]_D^{16}$ −75° (*c* 1.11, $CHCl_3$); IR (KBr) ν_{max}=1620 cm^{-1} (C=C); PMR ($CDCl_3$) δ=0.83 (3H, d, 4-Me, J=7.0 Hz), 1.2—1.8 (1H, m, H-4), 1.49 (1H, ddd, H-2ax, $J_{1,2ax}$=3.5 Hz, $J_{2ax,3}$=11.5 Hz, $J_{2ax,2eq}$=13.0 Hz), 1.86 (3H, d, 6-Me, J=1.2 Hz), 2.26 (1H, ddd, H-2eq, $J_{1,2ex}$=1.5 Hz, $J_{2eq,3}$=4.5 Hz), 2.9—3.5 (1H, m, H-3), 3.36 and 3.39 (each 3H, each s, 1- and 3-OMe), 3.94 (1H, d, H-5, $J_{4,5}$=10.5 Hz), 4.89 (1H, dd, H-1), and 6.34 (1H, m, H-7). Found: C, 40.68; H, 5.93; I, 38.62%. Calcd for $C_{11}H_{19}O_3I$: C, 40.51; H, 5.87; I, 38.91%.

*Reaction of Ethylene Oxide with Complexed Organocopper Reagent **26*** via *Mixed Cuprate.* By the same procedure as was used in the preparation of **27**, a dark green solution of the alkenylcopper intermediate **26** was prepared from **25** (47.4

mg, 0.257 mmol) and cooled to −78 °C. A solution of 1-lithiopentyne prepared from butyllithium (0.308 mmol) and 1-pentyne (0.308 mmol) in ether (0.37 ml), to which HMPA (0.108 ml, 0.616 mmol) had been added, was transferred to the solution of **26** mentioned above. After being stirred for 1 h, ethylene oxide (0.0153 ml, 0.308 mmol) was slowly added with a chilled syringe. The resulting mixture was stirred at −78 °C for 2.5 h, allowed to stand at −25 °C for 24 h, and worked up by the procedure described by McGuirk *et al.*[24] The resulting yellow-green oil (66.4 mg) was chromatographed on silica gel (3.5 g) with 10:1 hexane–acetone to afford a pale yellow syrup (29.2 mg, 46.5%) of the homoallylic alcohol **28**: PMR ($CDCl_3$) δ=0.84 (3H, d, 4-Me, J=7.0 Hz), 1.1—1.9 (2H, m, H-2ax and H-4), 1.69 (3H, d, 6-Me, J=1.0 Hz), 1.79 (1H, br, 9-OH), 2.0—2.6 (3H, m, H-2eq, H-8 and 8′), 3.0—3.5 (1H, m, H-3), 3.35 and 3.39 (each 3H, each s, 1- and 3-OMe), 3.5—3.9 (2H, m, H-9, 9′), 3.75 (1H, d, H-5, $J_{4,5}$=9.5 Hz), 4.88 (1H, dd, H-1, $J_{1,2eq}$=1.5 Hz, $J_{1,2ax}$=3.5 Hz), and 5.46 (1H, m, H-7). Further purification of this sample by repeated chromatography failed to give an analytically pure sample of **28**, but the acetylation of the sample with acetic anhydride in pyridine afforded the pure acetate of **28** showing *m/e* 287 (M^++1) and 286 (M^+) in its mass spectrum: PMR ($CDCl_3$) δ=0.83 (3H, d, 4-Me, J=7.0 Hz), 1.2—1.7 (1H, m, H-4), 1.46 (1H, ddd, H-2ax, $J_{1,2ax}$=3.5 Hz, $J_{2ax,3}$=9.0 Hz, $J_{2ax,2eq}$=13.0 Hz), 1.65 (3H, d, 6-Me, $J_{6\text{-}Me,7}$=1.2 Hz), 2.02 (3H, s, OAc), 2.25 (1H, ddd, H-2eq, $J_{1,2eq}$=1.5 Hz, $J_{2eq,3}$=4.5 Hz), 2.42 (2H, dt, H-8, 8′, $J_{7,8}$=6.8 Hz, $J_{8,9}$=7.2 Hz), 3.0—3.4 (1H, m, H-3), 3.32 and 3.36 (each 3H, each s, 1- and 3-OMe), 3.72 (1H, d, H-5, $J_{4,5}$=10.5 Hz), 4.09 (2H, t, H-9, 9′), 4.88 (1H, dd, H-1), and 5.41 (1H, m, H-7).

We wish to thank Dr. Kuniaki Tatsuta for his helpful discussion and Mr. Saburo Nakada for carrying out the microanalyses. The authors are also grateful to the Institute of Microbial Chemistry for its financial support.

References

1) Part I: M. Kinoshita, K. Tatsuta, and M. Nakata, *J. Antibiot.*, **31**, 630 (1978).
2) P. Sensi, A. M. Greco, and R. Ballotta, *Antibiot. Annual.*, **1959/1960**, 260 (1960); W. Oppolzer and V. Prelog, *Helv. Chim. Acta*, **56**, 2287 (1973).
3) E. J. Corey and T. Hase, *Tetrahedron Lett.*, **1979**, 335; E. J. Corey and G. Schmidt, *ibid.*, 2317 (1979).
4) M. Kinoshita, N. Nakata, T. Sakai, and K. Tatsuta, Organic Abstracts, Joint Meeting of the American Chemical Society and Chemical Society of Japan, April 1979, Abstract No. 481.
5) A. A. J. Feast, W. G. Overend, and N. R. Williams, *J. Chem. Soc.*, **1965**, 7378.
6) M. Sharma and R. K. Brown, *Can. J. Chem.*, **46**, 757 (1968).
7) T. D. Inch and G. J. Lewis, *Carbohydr. Res.*, **15**, 1 (1970).
8) G. J. Robertson and C. F. Griffith, *J. Chem. Soc.*, **1935**, 1193; L. F. Wiggins, *Methods Carbohyd. Chem.*, **2**, 188 (1963).
9) T. D. Inch, G. J. Lewis, and N. E. Williams, *Carbohydr. Res.*, **19**, 17 (1971); M. Kinoshita, S. Aburaki, and S. Umezawa, *J. Antibiot.*, **25**, 373 (1972).
10) S. Hanessian, *Carbohydr. Res.*, **2**, 86 (1966).
11) E. J. Corey and B. W. Erickson, *J. Org. Chem.*, **36**, 3553 (1971).
12) S. G. Levine, *J. Am. Chem. Soc.*, **80**, 6150 (1958); G. Wittig, W. Böll, and K-H. Krück, *Chem. Ber.*, **95**, 2514 (1962); A. Ferwanach, W. Pressler, and C. Reichardt, *Tetrahedron Lett.* **1973**, 3979.
13) a) E. J. Corey and M. Chaykovsky, *J. Am. Chem. Soc.*, **84**, 866 (1962); b) R. Greenwald, M. Chaykovsky, and E. J. Corey, *J. Org. Chem.*, **28**, 1128 (1963); c) O. S. Bhanot, and P. C. Dutta, *J. Chem. Soc., C*, **1968**, 2583.
14) P. H. R. Barton, R. E. O'Brien, and S. Sternhell, *J. Chem. Soc.*, **1962**, 470.
15) J. -C. Depezay and Y. Le Merrer, *Tetrahedron Lett.*, **1974**, 2751.
16) A. M. Krubiner, N. Gottfried, and E. P. Oliveti, *J. Org. Chem.*, **34**, 3502 (1969).
17) A. Marfat, D. R. McGuirk, and P. Helquist, *Tetrahedron Lett.*, **1978**, 1363.
18) H. O. House, C. -Y. Chu, J. M. Wilkins, and M. J. Umen, *J. Org. Chem.*, **40**, 1460 (1975).
19) J. F. Normant, G. Cahiez, and C. Chuit, *J. Organomet. Chem.*, **77**, 269 (1974).
20) J. F. Normant and M. Bourgain, *Tetrahedron Lett.*, **1971**, 2583; J. F. Normant, G. Cahiez, M. Bourgain, C. Chuit, and J. Villieras, *Bull. Soc. Chim. Fr.*, **1974**, 1656.
21) J. F. Normant, A. Alexakis, and J. Villieras, *J. Organomet. Chem.*, **57**, C99 (1973).
22) "New Application of Organometallic Reagents in Organic Synthesis," ed by D. Seyferth, Elsevier, Amsterdam (1976), pp. 219—256.
23) A. Alexakis, J. F. Normant, and J. Villieras, *J. Organomet. Chem.*, **96**, 471 (1975).
24) P. R. McGuirk, A. Marfat, and P. Helquist, *Tetrahedron Lett.*, **1978**, 2465.

The Total Synthesis of Neomycin C[1]

Sumio UMEZAWA,* Akihiko HARAYAMA, and Yoshio NISHIMURA
Institute of Bioorganic Chemistry, Ida, Nakahara-ku, Kawasaki, Kanagawa 211
(Received March 3, 1980)

The total synthesis of the pseudo-tetrasaccharides antibiotic neomycin C is described, involving condensation of 6,3′,4′,5″-tetra-*O*-acetyl-1,3,2′,6′-tetra-*N*-(benzyloxycarbonyl)ribostamycin with 3,4-di-*O*-acetyl-2-deoxy-2-(*p*-methoxybenzylideneamino)-6-*O*-tosyl-α-D-glucopyranosyl bromide by a modified Koenigs-Knorr reaction.

Neomycin,[2] a useful antibiotic, was independently discovered by H. Umezawa *et al.*[3] in 1948 and S. A. Waksman *et al.*[2] in 1949. The neomycin complex consists of neomycin A, B, and C, and neomycin C was isolated by Dutcher *et al.*[4] Neomycins are pseudo-tetrasaccharides and show broad-spectrum antibacterial activity. Elucidation of the complete structures of neomycins are achieved by Rinehart *et al.*[5,6] in 1963. We wish now describe in full the total synthesis of neomycin C. This represents the first synthesis of an antibiotic of pseudo-tetrasaccharides.

Neomycin C is composed of neosamine C (2,6-diamino-2,6-dideoxy-D-glucopyranose) and ribostamycin which is a pseudo-trisaccharide composed of D-ribose and neamine, a pseudo-disaccharide composed of neosamine C and 2-deoxystreptamine.[7] Neamine was synthesized by S. Umezawa *et al.*,[8] and ribostamycin was subsequently synthesized by Ito *et al.*[9] by ribosylation of neamine. In the present paper, we describe the synthesis of neomycin C by regio- and stereo-selective glycosylation of a pertinently protected ribostamycin (**3**) with a glycosyl halide (**11**) of glucosamine.

Ribostamycin was protected in the following manner. The selective cyclohexylidenation of 1,3,2′,6′-tetra-*N*-(benzyloxycarbonyl)ribostamycin[10] was achieved by treatment with 1,1-dimethoxycyclohexane (2 mol) in *N*,*N*-dimethylformamide (DMF) (20 h at 70 °C) in the presence of *p*-toluenesulfonic acid to give the 2″,3″-*O*-cyclohexylidene derivative (**1**) in 80% yield. Treatment of the acetal with acetic anhydride and pyridine gave the tetraacetyl derivative (**2**) in 98% yield. Decyclohexylidenation of **2** with 50% aqueous acetic acid followed by column chromatography on silica gel provided 6,3′,4′,5″-tetra-*O*-acetyl-1,3,2′,6′-tetra-*N*-(benzyloxycarbonyl)ribostamycin (**3**).

On the other hand, the synthesis of neosamine portion was carried out in the following manner. Our initial approach to the neosamine portion involved treatment of 2-(benzyloxycarbonylamino)-2-deoxy-α-D-glucopyranose[11] (**4**) with tosyl chloride in pyridine to give 2-(benzyloxycarbonylamino)-2-deoxy-6-*O*-tosyl-α-D-glucopyranose (**5**) in 51% yield. Displacement of the tosyl group of **5** with sodium azide in DMF gave 6-azido-2-(benzyloxycarbonylamino)-2,6-dideoxy-α-D-glucopyranose (**6**). Hydrolysis of **6** with 3 M (1 M= 1 mol dm^{-3}) aqueous hydrochloric acid followed by treatment with *p*-anisaldehyde in a mixture of 1 M aqueous sodium hydroxide solution and ethanol afforded 6-azido-2,6-dideoxy-2-(*p*-methoxybenzylideneamino)-β-D-glucopyranose (**7**). Acetylation with acetic anhydride in pyridine then gave 1,3,4-tri-*O*-acetyl-6-azido-2,6-dideoxy-2-(*p*-methoxybenzylideneamino)-β-D-glucopyranose (**8**). However, replacement of the anomeric acetoxyl group of **8** with bromine by treatment with hydrogen bromide in dichloromethane was unsuccessful and resulted in the formation of 1,3,4-tri-*O*-acetyl-6-bromo-2,6-dideoxy-2-(*p*-methoxybenzylideneamino)-β-D-glucopyranose (**9**), the azido group at C-6 being replaced by bromide.[12] A desired glycosyl halide, 3,4-di-*O*-acetyl-2-deoxy-2-(*p*-methoxybenzylideneamino)-6-*O*-tosyl-α-D-glucopyranosyl bromide (**11**), was successfully prepared by conversion of 1,3,4-tri-*O*-acetyl-2-deoxy-2-(*p*-methoxybenzylideneamino)-6-*O*-tosyl-β-D-glucopyranose[13] (**10**) by reaction with hydrogen bromide in dichloromethane (3 h at 0 °C) in 85% yield.

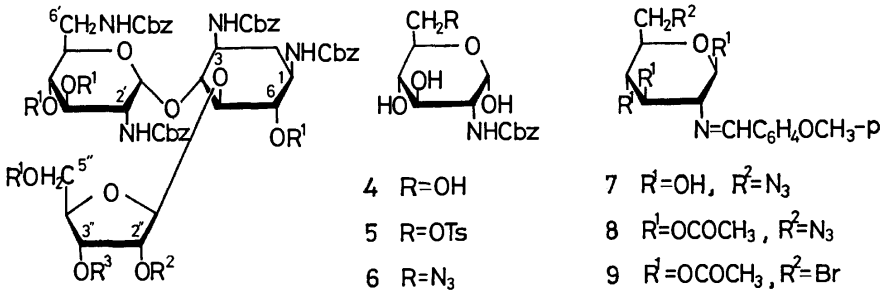

Condensation of the protected glycosyl halide (**11**) with **3** in anhydrous chloroform in the presence of silver carbonate, perchlorate, and Drierite afforded a mixture of condensation products containing the desired pseudo-tetrasaccharide as the main product. Hydrolysis of the Schiff base moiety of the mixture of condensation products at pH 2 in acetone–hydrochloric acid followed by treatment with benzyloxycarbonyl chloride in aqueous acetone in the presence of sodium carbonate and silica-gel chromatography afforde d6,3′,4′,5″,3‴,4‴-hexa-*O*-acetyl-1,3,2′,6′,2‴-penta-*N*-(benzyloxycarbonyl)-6‴-deamino-6‴-tosyl oxyneomycin C (**12**), a colorless solid, in 34% overall yield from **3**. Treatment of **12** with sodium azide in DMF gave the 6‴-azido derivative (**13**) in 85% yield. Finally, de-benzyloxycarbonylation of **13** by catalytic hydrogenolysis with palladium black followed by hydrolysis with 0.5 M barium hydroxide and purification by use of Sephadex C-25 (NH_4^+) completed the synthesis, giving neomycin C (**14**), identical with that obtained from natural source as judged by optical rotations, IR spectra, and ^{1}H-NMR and ^{13}C-NMR spectra. The antibiotic spectra and minimal inhibitory concentrations[1] of the synthetic **14** against test organisms were in agreement with those of natural neomycin C.

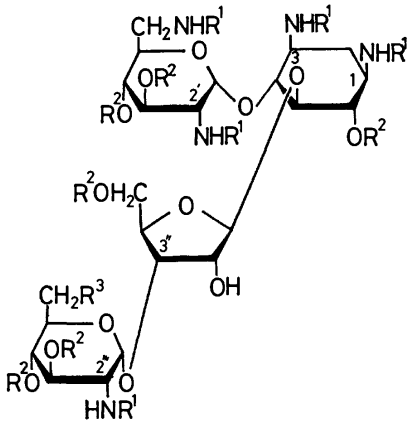

12 R^1=Cbz, R^2=Ac, R^3=OTs
13 R^1=Cbz, R^2=Ac, R^3=N_3
14 R^1=R^2=H, R^3=NH_2 (Neomycin C)

Experimental

Thin layer (TLC) and column chromatography were carried out on silica gel of Wakogel B-5 and Wakogel C-200 (Wako Pure Chemicals Co., Ltd., Osaka), and the spots on TLC were visualized with sulfuric acid. ^{1}H-NMR (PMR) spectra were recorded at 60, 90, and 100 MHz with Hitachi R-24, Varian EM-390, and Varian XL-100 spectrometers, respectively.

1,3,2′,6′-Tetra-N-*(benzyloxycarbonyl)-2″,3″*-O-*cyclohexylideneribostamycin (**1**).* To a solution of 1,3,2′,6′-tetra-*N*-(benzyloxycarbonyl)ribostamycin[10] (52 g) in dry DMF (520 ml) were added *p*-toluenesulfonic acid (0.9 g) and 1,1-dimethoxycyclohexane (15.1 g), and the mixture was stirred at 70 °C for 20 h. On TLC of silica gel with benzene–ethyl acetate (1:6), the starting material (R_f 0.01) almost disappeared, and the products of R_f 0.51 (major), R_f 0.89 (minor), and R_f 0.72 (minor) appeared. The solvent was evaporated to half volume, and then the solution was poured into a large amount of water. The resulting precipitate (56 g) was chromatographed on a column of silica gel (2 kg, 76×1040 mm) with benzene–ethyl acetate (1:6) to give a foamy solid, 45.1 g (80%), mp 119—120 °C, $[\alpha]_D^{20}$ +6° (*c* 1.0, chloroform); IR (KBr): 3400, 1700 (broad), and 1520 (broad) cm^{-1}.

Found: C, 61.95; H, 6.13; N, 4.98%. Calcd for $C_{55}H_{66}N_4O_{18}$: C, 61.67; H, 6.21; N, 5.23%.

NMR (in $CDCl_3$): δ 1.0—1.9 (10H m, cyclohexylidene), 5.10 (8H s, 4×COOC$\underline{H}_2C_6H_5$), 7.30 and 7.35 (each s, 20H in all, 4×COOC$H_2C_6\underline{H}_5$).

6,3′,4′,5″-Tetra-O-*acetyl-1,3,2′,6′-tetra*-N-*(benzyloxycarbonyl)-2″,3″*-O-*cyclohexylideneribostamycin (**2**).* To a solution of compound **1** (5 g) in dry pyridine (75 ml) was added acetic anhydride (20 ml), and the solution was allowed to stand at room temperature overnight. On TLC of silica gel with benzene–acetone (7:1), the starting material of R_f 0.01 disappeared, and the product of R_f 0.32 appeared. The mixture was poured into a large amount of water, and the resulting precipitate was filtered and dried to give a colorless solid, 5.7 g (98%), mp 101—102 °C, $[\alpha]_D^{21}$ +16.2° (*c* 1.54, chloroform); IR (KBr): 1740, 1520 cm^{-1}.

Found: C, 60.82; H, 5.92; N, 4.51%. Calcd for $C_{63}H_{74}N_4O_{22}$: C, 61.06; H, 6.02; N, 4.52%.

NMR (in $CDCl_3$): δ 1.0—2.5 (12H m, H_{ax}-2 and H_{eq}-2 and cyclohexylidene), 1.85 and 2.02 (each 6H s, 2×COCH_3) and 7.28 (20H s, 4×C$H_2C_6\underline{H}_5$).

6,3′,4′,5″-Tetra-O-*acetyl-1,3,2′,6′-tetra*-N-*(benzyloxycarbonyl)-ribostamycin (**3**).* Compound **2** (4 g) was dissolved in a hot 50% aqueous acetic acid (320 ml), and the solution was stirred at 80 °C for 12 h. On TLC of silica gel with benzene–acetone (2:1), the mixture showed five spots of R_f 0.82 (starting material, minor), 0.65 (minor), 0.47 (major), 0.32 (minor), and 0.23 (minor). The mixture was poured into a large amount of water, and the resulting precipitate was filtered. The solid was chromatographed on a column of silica gel (160 g, 28×500 mm) with benzene–acetone (2:1) to give a colorless solid, 1.38 g (35%), mp 102—103 °C, $[\alpha]_D^{20}$ +18° (*c* 1.39, chloroform); IR (KBr): 1720, 1620 cm^{-1}.

Found: C, 58.82; H, 5.69; N, 4.84%. Calcd for $C_{57}H_{66}O_{22}N_4$: C, 59.06; H, 5.74; N, 4.83%.

NMR (in $CDCl_3$): δ 1.87, 1.90, 1.94, and 2.00 (each 3H s, COC$\underline{H}_3$) and 7.28 (20H s, $CH_2C_6\underline{H}_5$).

*2-(Benzyloxycarbonylamino)-2-deoxy-6-*O-*tosyl-α-*D-*glucopyranose (**5**).* To a solution of 2-(benzyloxycarbonylamino)-2-deoxy-α-D-glucopyranose[11] (**4**) (4 g) in dry pyridine (80 ml) was added dropwise a solution of *p*-toluenesulfonyl chloride (2.8 g) in dry pyridine (80 ml) at −30 °C for 1.5 h. The solution was stirred at −20 °C for 18 h. On TLC of silica gel with benzene–acetone (2:1), the starting material (R_f 0.03) almost disappeared, and the product (R_f 0.4) appeared. After adding water (20 ml), evaporation of the solvent gave a light brown solid. The solid was chromatographed on a column of silica gel (250 g, 38×450 mm) with benzene–acetone (2:1) to give a colorless solid (3.8 g). Recrystallization from a mixture of benzene–acetone (2:1) afforded colorless crystals, 3.2 g (51%), mp 100—101 °C, $[\alpha]_D^{20}$ +47.6° (*c* 0.36, methanol); IR (KBr): 3400, 1680, 1520, 1170 cm^{-1}.

Found: C, 53.71; H, 5.29; N, 2.90; S, 6.99%. Calcd for $C_{21}H_{25}NO_9S$: C, 53.95; H, 5.39; N, 3.00; S, 6.86%.

NMR (in Py-d_5): δ 2.17 (3H s, $SO_2C_6H_4C\underline{H}_3$), 3.20 (2H s, C$\underline{H}_2C_6H_5$), 5.18 (1H d, *J* 3.5 Hz, H-1), 7.10 and 7.88 (4H ABq, *J* 9 Hz, $SO_2C_6\underline{H}_4CH_3$) and 7.21 (5H s, $CH_2C_6\underline{H}_5$).

*6-Azido-2-(benzyloxycarbonylamino)-2,6-dideoxy-α-D-glucopyranose (**6**).* Sodium azide (7.2 g) was added to a solution of **5** (14.4 g) in DMF (144 ml), and the solution was stirred at 135 °C for 20 min. On TLC of silica gel with benzene–acetone (2:1) the starting material (R_f 0.38) disappeared, and the product of R_f 0.34 (major) and 0.02 (trace) appeared. Evaporation of the solvent gave a solid which was separated into soluble and insoluble parts with dioxane. The soluble part was chromatographed on a column of silica gel (700 g, 80×200 mm) with benzene–acetone (1:1) to give a colorless solid (9.2 g). Recrystallization from a mixture of benzene–acetone (2:1) gave colorless crystals, 8.1 g (78%), mp 175—176 °C, $[\alpha]_D^{20}$ +60.9° (*c* 1.0, water–methanol (1:1)); IR (KBr): 3350 (sho), 2100, 1680, and 1545 cm^{-1}.

Found: C, 50.00; H, 5.41; N, 16.34%. Calcd for $C_{14}H_{18}N_4O_6$: C, 49.70; H, 5.36; N, 16.56%.

NMR (in Py-d_5 containing a small amount of D_2O): δ 5.15 (2H s, $C\underline{H}_2C_6H_5$), 5.7 (1H d, *J* 2 Hz, H-1), and 7.24 (5H s, $CH_2C_6\underline{H}_5$).

*6-Azido-2,6-dideoxy-2-(p-methoxybenzylideneamino)-β-D-glucopyranose (**7**).* Compound **6** (620 mg) was dissolved in 3 M hydrochloric acid (62 ml), and the solution was stirred at 90 °C for 3 h. Evaporation of the solvent and coevaporation with toluene gave a solid (458 mg). The solid was dissolved in 0.5 M aqueous sodium hydroxide (2.3 ml) in ethanol (0.45 ml), and *p*-anisaldehyde (0.3 ml) was added to the solution. The mixture was allowed to stand at room temperature for 30 min and then at 0 °C to give crystalline **7**, 260 mg (44%). Recrystallization from a mixture of acetone–methanol (1:2) gave colorless crystals, 190 mg (32%), mp 168—169 °C, $[\alpha]_D^{20}$ +32.6° (*c* 0.95, methanol); IR (KBr): 2100, 1640, 1610, and 1515 cm^{-1}.

Found: C, 52.54; H, 5.31; N, 17.05%. Calcd for $C_{14}H_{18}N_4O_5$: C, 52.17; H, 5.63; N, 17.38%.

NMR (in Py-d_5 containing a small amount of D_2O): δ 3.77 (3H s, $CHC_6H_4OC\underline{H}_3$), 5.67 (1H d, *J* 7.5 Hz, H-1), 6.95 and 7.95 (4H ABq, *J* 9 Hz, $CHC_6\underline{H}_4OCH_3$), and 8.75 (1H s, $N{=}C\underline{H}C_6H_4OCH_3$).

*1,3,4-Tri-O-acetyl-6-azido-2,6-dideoxy-2-(p-methoxybenzylideneamino)-β-D-glucopyranose (**8**).* To a solution of **7** (430 mg) in dry pyridine (5 ml) was added acetic anhydride (1.5 ml), and the solution was allowed to stand at room temperature overnight. The mixture was poured into 2% aqueous sodium hydrogencarbonate solution (70 ml), and the resulting precipitate was washed with water. Recrystallization from a mixture of ethanol–water (3:1) gave colorless crystals, 400 mg (67%), mp 115—116 °C, $[\alpha]_D^{20}$ +117.6° (*c* 1.43, chloroform); IR (KBr): 2100 and 1755 cm^{-1}.

NMR (in $CDCl_3$): δ 1.88, 2.03, and 2.05 (each 3H s, $COC\underline{H}_3$), 3.43 (1H t, *J* 9 Hz, H-2), 3.0—3.8 (2H m overlapped with OCH_3, $C\underline{H}_2N_3$), 3.86 (3H s, $-OCH_3$), 3.8—4.1 (1H m, H-5), 5.10 (1H t., *J* 9 Hz, H-4), 5.43 (1H t, *J* 9 Hz, H-3), 5.95 (1H d, *J* 9 Hz, H-1), 6.93 and 7.70 (4H ABq, $-N{=}CHC_6\underline{H}_4OCH_3$), and 8.20 (1H s, $-N{=}C\underline{H}C_6H_4OCH_3$).

*1,3,4-Tri-O-acetyl-6-bromo-2,6-dideoxy-2-(p-methoxybenzylideneamino)-β-D-glucopyranose (**9**).* A solution of **8** (100 mg) in dry dichloromethane (5 ml) was saturated with dry hydrogen bromide at −20 °C (about 2 min). Evaporation of the solvent gave a syrup, which was solidified with hexane and washed three times with a mixture of dry ether and dry hexane (4:1). The solid was dissolved in chloroform (20 ml), and the solution was washed several times with phosphate buffer solution (KH_2PO_4–Na_2HPO_4, pH 6.8) and water, and dried (Na_2SO_4). Evaporation of the solvent gave a colorless syrup which was crystallized from a mixture of chloroform, ether and hexane (1:5:20) to give colorless crystals, 50 mg (46%), mp 151—152 °C, $[\alpha]_D^{20}$ +96.8° (*c* 0.67, chloroform); IR (KBr): 1760 cm^{-1}.

Found: C, 49.22; H, 5.07; N, 2.91; Br, 16.45%. Calcd for $C_{20}H_{24}NO_8Br$: C, 49.37; H, 4.98; N, 2.88; Br, 16.44%.

NMR (in $CDCl_3$): δ 1.90, 2.03, and 2.08 (each 3H s, $COC\underline{H}_3$), 3.87 (3H s, $OC\underline{H}_3$), 5.14 (1H t, *J* 9 Hz, H-4), 5.43 (3H t, *J* 9 Hz, H-3), 5.98 (1H d, *J* 9 Hz, H-1), 6.93 and 7.70 (4H ABq, *J* 9 Hz, $N{=}CHC_6\underline{H}_4OCH_3$), and 8.20 (1H s, $N{=}C\underline{H}C_6H_4OCH_3$).

*3,4-Di-O-acetyl-2-deoxy-2-(p-methoxybenzylideneamino)-6-O-tosyl-α-D-glucopyranosyl Bromide (**11**).* A solution of **10** (5 g) in dichloromethane was saturated with anhydrous hydrogen bromide at 0 °C and allowed to stand at 0 °C for 3 h. Evaporation of the solvent gave a syrup, which was solidified with hexane and washed several times with hexane. A chloroform solution of the solid was washed with 1% aqueous sodium hydrogencarbonate solution (pH 7) and several times with phosphate buffer solution (KH_2PO_4–Na_2HPO_4, pH 6.8), dried (Na_2SO_4) and filtered. Evaporation of the filtrate gave a colorless syrup, 4.5 g (85%).

NMR (in $CDCl_3$): δ 1.83, 1.95, and 2.43 (each 3H s, $COC\underline{H}_3$), 3.43 (1H q, *J* 4.5 and 9 Hz, H-2), 3.85 (3H s, OCH_3), 4.17 (2H d, *J* 3.9 Hz, H-6), 5.13 (1H t, *J* 9 Hz, H-4), 5.57 (1H t, *J* 9 Hz, H-3), 6.15 (1H d, *J* 4.5 Hz, H-1), 6.90 and 7.68 (4H ABq, *J* 9 Hz, $N{=}CHC_6\underline{H}_4OCH_3$), 7.35 and 7.82 (4H ABq, *J* 9 Hz, $SO_2C_6\underline{H}_4CH_3$) and 8.27 (1H s, $N{=}C\underline{H}C_6H_4OCH_3$).

*6,3',4',5'',3''',4'''-Hexa-O-acetyl-1,3,2',6',2'''-penta-N-(benzyloxycarbonyl)-6'''-deamino-6'''-tosyloxyneomycin C (**12**).* A mixture of **3** (1.1 g), newly prepared Ag_2CO_3 (4 g) and Drierite (10 g) in dry chloroform was stirred at room temperature for 20 h in the dark. To the mixture was added a solution of **11** (1.8 g) in dry chloroform (20 ml) and then $AgClO_4$ under vigorous stirring. The mixture was stirred at room temperature for 20 h. On TLC of silica gel with benzene–acetone (3:1), the mixture showed four products of R_f 0.45, 0.40, 0.37, and 0.32 and some by-products. The insoluble matter was filtered, and the filtrate was thoroughly washed with chloroform. The filtrate and washings were combined, washed with three portions of 2% aqueous sodium hydrogencarbonate (20 ml), then dried (Na_2SO_4). The solution was evaporated to a syrup (2.8 g). The starting materials and by-products were removed by a short column of silica gel (120 g, 34×250 mm) with benzene–acetone (3:1). The crude product (1.7 g) thus obtained was dissolved in acetone (5 ml), and a small amount of 1 M hydrochloric acid was added to the mixture (pH 2). To the mixture was added a large amount of ether, and the resulting oily precipitate was triturated with five portions of ether (10 ml). The oil (1.5 g) was suspended in a mixture of acetone (20 ml) and water (15 ml). After adjustment of pH of the mixture with Na_2CO_3 to pH 7, Na_2CO_3 (150 mg) was added to the mixture, and then benzyloxycarbonyl chloride (0.25 ml) was added at room temperature under vigorous stirring and stirred at room temperature for 20 h. On TLC of silica gel with benzene–acetone (4:1), the mixture showed four products of R_f 0.23 (major), 0.26 (minor), 0.34 (minor), and 0.36 (minor). The insoluble matter was filtered, and the residue was washed with chloroform. The filtrate and washings were combined, and the solvent was evaporated to syrup, which was dissolved in chloroform (300 ml). The chloroform solution was washed with three portions of water (20 ml), dried (Na_2SO_4) and evaporated. The syrup (1.4 g) was chromatographed on a column of silica gel (120 g, 27×450 mm) with benzene–acetone (5:1) to give **12**, a colorless foamy solid, 555 mg (34%), mp 104—105 °C, $[\alpha]_D^{20}$ +42.2° (*c* 0.97, chloroform); IR (KBr): 3400, 1740, 1530, and 1180

cm^{-1}.

Found: C, 57.94; H, 5.56; N, 3.89; S, 2.03%. Calcd for $C_{82}H_{93}N_5O_{32}S$: C, 58.17; H, 5.54; N, 4.14; S, 1.89%.

NMR (in $CDCl_3$): δ 1.7—2.2 (18H m, $6\times COOCH_3$), 2.47 (3H s, $SO_2C_6H_4C\underline{H}_3$), 7.40 and 7.43 (10H and 15H s, respectively, $5\times CH_2C_6\underline{H}_5$), 7.77 and 7.87 (2H q, J 2 and 8 Hz, two protons of $SO_2C_6\underline{H}_4CH_3$(?)).

*6,3',4',5'',3''',4'''-Hexa-O-acetyl-6'''-azido-1,3,2',6',2'''-penta-N-(benzyloxycarbonyl)-6'''-deamino-neomycin C (**13**).* To a solution of **12** (440 mg) in dry DMF (7 ml) was added sodium azido (NaN_3, 85 mg), and the mixture was stirred at 130 °C for 15 min. On TLC of silica gel with benzene–acetone (2:1), the mixture showed two products of R_f 0.59 (major) and 0.56 (trace). Evaporation of the solvent gave a light brown solid, which was dissolved in chloroform (50 ml). The chloroform solution was washed with two portions of saturated aqueous sodium chloride (10 ml) and two portions of water (10 ml), and dried. The solvent was evaporated to give a syrup, which was chromatographed on a column of silica gel (18 g, 10×540 mm) with benzene–acetone (4:1) to give a colorless foamy solid, 350 mg (85%), $[\alpha]_D^{20}$ +64.4° (c 0.71, acetone); IR (KBr): 3400, 2100, 1740, and 1520 cm^{-1}.

Found: C, 57.46; H, 5.50; N, 7.06%. Calcd for $C_{75}H_{86}N_8O_{29}$: C, 57.61; H, 5.54; N, 7.17%.

NMR (in $CDCl_3$): δ 1.7—2.1 (18H m, $6\times COOCH_3$), 7.40 and 7.42 (15H and 10H s, $5\times COOCH_2C_6\underline{H}_5$).

*Neomycin C (**14**).* The compound **13** was hydrogenated over palladium black in a mixture of dioxane (12 ml), water (4 ml), and acetic acid (0.4 ml) at room temperature under 4 kg/cm^2 pressure of hydrogen for 14 h. After removal of the catalyst, the solution was evaporated to dryness *in vacuo*. The solid was dissolved in a hot 0.5 M aqueous barium hydroxide ($Ba(OH)_2$) (6 ml), and the mixture was stirred at 95 °C for 5 h. To the solution was introduced carbon dioxide, and the resulting precipitates were removed by centrifugation. The supernatant was evaporated to give a colorless solid (150 mg), which was chromatographed on a column of CM Sephadex C-25 (NH_4^+) (30 ml, 10×400 mm). After washing with water (40 ml), the column was eluted with an aqueous ammonia by the linear gradient from 0.0 to 0.3 M to give a colorless solid of neomycin C, 75 mg (61%), hydrochloride: $[\alpha]_D^{20}$ +78° (c 0.86, water); IR (KBr): 3400 (broad), 2950 (broad), 1980 (broad), 1600, 1500, 1030 (sh) cm^{-1}.

NMR (in D_2O): δ 5.52 (1H d, J 3.5 Hz, H-1'''), 5.88 (1H d, J 1 Hz, H-1''), and 5.94 (1H d, J 3 Hz, H-1').

^{13}C NMR (in D_2O): δ 36.4, 42.4, 42.5, 51.1 (2 carbons), 55.9, 56.3, 62.4, 72.2 (2 carbons), 73.98 (4 carbons), 74.5, 75.5, 78.4, 81.7, 82.8, 85.2, 99.7 ($C_{1'}$ and $C_{1'''}$), and 109.45 ($C_{1''}$).

The authors would like to acknowledge stimulating discussions with Professor H. Umezawa, the Institute of Microbial Chemistry. The authors also thank Dr. H. Naganawa for ^{13}C NMR measurements.

References

1) A part of this work has briefly been communicated: S. Umezawa and Y. Nishimura, *J. Antibiot.*, **30**, 189 (1977).
2) S. A. Waksman and H. A. Lechevalier, *Science*, **109**, 305 (1949).
3) H. Umezawa, S. Hayano, and Y. Ogata, *Jpn. Med. J.*, **1**, 504 (1948).
4) J. D. Dutcher, N. Hosansky, M. N. Donin, and O. Wintersteiner, *J. Am. Chem. Soc.*, **73**, 1384 (1951).
5) K. L. Rinehart, Jr., H. Hichens, A. D. Argoudelis, W. Chilton, H. Carter, M. P. Georgiadis, C. P. Schaffner, and R. T. Schillings, *J. Am. Chem. Soc.*, **84**, 3218 (1962).
6) M. Hichens and K. L. Rinehart, Jr., *J. Am. Chem. Soc.*, **85**, 1547 (1963).
7) M. Nakajima, A. Hasegawa, and N. Kurihara, *Tetrahedron Lett.*, **1964**, 967.
8) S. Umezawa, K. Tatsuta, T. Tsuchiya, and E. Kitazawa, *J. Antibiot.*, **A20**, 53 (1967).
9) T. Ito, E. Akita, T. Tsuruoka, and T. Niida, *Antimicrob. Agents Chemother.*, **1**, 33 (1970).
10) D. Ikeda, T. Suzuki, T. Tsuchiya, S. Umezawa, and H. Umezawa, *Bull. Chem. Soc. Jpn.*, **46**, 3210 (1973).
11) K. Onodera and T. Komano, *J. Org. Chem.*, **26**, 3932 (1961).
12) During the course of our work, a similar replacement was reported: S. Ogawa, H. Fujimori, and T. Suami, *Bull. Chem. Soc. Jpn.*, **49**, 2585 (1976).
13) CH. J. Morel, *Helv. Chim. Acta*, **41**, 1505 (1958).

 © 1980 The Chemical Society of Japan Bull. Chem. Soc. Jpn., 53, 3263—3265 (1980)

Photochemical Ethoxycarbonylation, Formylation, and Ethoxymethylation of Ruthenocene in Ruthenocene–Polychloromethane–Ethanol Systems

Akira Sugimori,* Masaru Matsui, Takeo Akiyama, and Masatsugu Kajitani

Department of Chemistry, Faculty of Science and Technology, Sophia University, Kioi-cho 7-1, Chiyoda-ku, Tokyo 102

(Received March 6, 1980)

Similar to ferrocene the UV-irradiation of ruthenocene–polychloromethane–ethanol systems brings about substitution (ethoxycarbonylation for CCl_4, formylation for $CHCl_3$, and ethoxymethylation for CH_2Cl_2) and oxidation. When $CHCl_3$ and CH_2Cl_2 are used, substitution is dominant. In the irradiation of ruthenocene–CCl_4–ethanol system, $[Ru(C_5H_5)_2]^+[RuCl_4]^-$ and cyclopentenes substituted by chlorine and trichloromethyl are obtained. The excitation of the CT-complex between ruthenocene and polychloromethane initiates the reaction.

We have reported the photochemical substitution (ethoxycarbonylation, formylation, ethoxymethylation, and alkylation) in ferrocene–halogenated hydrocarbon–ethanol systems.[1] As to ruthenocene, a ferrocene analog, photochemical oxidation to ruthenocenium ions has been reported.[2,3] However, in these studies the photoreactions of ruthenocene in halogenated hydrocarbon–(alcohol) solutions have been studied mainly on the basis of UV- and visible spectral changes and the product analysis has not been done completely. We report here that the UV-irradiation of ruthenocene–polychloromethane–ethanol systems brings about the substitution similar to that of ferrocene in addition to the oxidation of ruthenocene.

Experimental

Materials. Ruthenocene(**1**) was synthesized from $RuCl_3$ and cyclopentadiene according to Pertici *et al.*[4] mp 198—199 °C.

UV-irradiation. A solution of ruthenocene (4×10^{-2} mol dm^{-3}) in polychloromethane–ethanol (1:1 v/v, 40 cm^3) in a quartz vessel was deaerated by the freeze-thaw method using a vacuum system. The solution was irradiated either with a low pressure or with a high pressure mercury lamp.

Photoproducts. During the irradiation of ruthenocene–CCl_4–ethanol system, a brown precipitate was formed. Other systems gave no precipitate. After the precipitate was filtered, the solvent was distilled off. The residue was extracted with benzene and the products were separated by means of TLC (on silica gel of Merck GF_{254}; developing solvent, benzene).

Ruthenocenium tetrachlororuthenate(III) was identified by the comparison of UV- and IR-spectra with those reported by Traverso *et al.*[2] (Found: C, 25.84; H, 2.64%).

*Ethyl Ruthenocenecarboxylate (**2a**)*[5]: Brownish yellow crystal; mp 77.5—79 °C; IR(KBr disk) 3110, 2960 (C–H), 1690 (C=O), 1130 (ester C–O), 1100 and 995 cm^{-1} (C–H deformation of C_5H_5 ring); NMR (CCl_4) δ=5.01 (2H, t, J=2.0 Hz, ring H at α-position), 4.59 (2H, t, J=2.0 Hz, ring H at β-position), 4.52 (5H, s, H at unsubstituted ring), 4.13 (2H, q, J=7.0 Hz, CH_2), and 1.27 (3H, t, J=7.0 Hz, CH_3); MS (70 eV), *m/e* (rel intensity), 306(56), 304(100), 303(56), 302(42), 301(38) (M^+); 278(38), 276(68), 275(37), 274(28), 273(27) ($(M-C_2H_4)^+$); 234(22), 233(19), 232(40), 231(48), 230(31), 229(29), 228(16) ($(M-COOC_2H_5)^+$ and $(M-COOC_2H_5+H)^+$); 169(18), 167(30), 166(19), 165(15), 164(14) ($(RuC_5H_5)^+$).

A mixture of chlorinated hydrocarbons was obtained. By means of TLC technique it could not be separated completely. However, by the consideration of the results of GC-MS and NMR spectra, two major components were assigned to 3,4,5-tris(trichloromethyl)cyclopentene and 4-chloro-3,5-bis(trichloromethyl)cyclopentene.

3,4,5-Tris(trichloromethyl)cyclopentene. NMR(CCl_4) δ= 6.14 (2H, s, olefinic), 4.03 (2H, d, H=2.0 Hz, H at 3- and 5-position), 3.66 (1H, t, J=2.0 Hz, H at 4-position); MS (20 eV), *m/e* (rel intensity), 350(6), 348(9), 346(9), 344(4) ($(M-2HCl)^+$); 303(31), 301(39), 299(20) ($(M-CCl_3)^+$); 269(20), 267(58), 265(91), 263(54) ($(M-HCl-CCl_3)^+$); 233 (11), 231(31), 229(43), 227(27) ($(M-2HCl-CCl_3)^+$); 185 (6), 183(16), 181(19) ($(M-H-2CCl_3)^+$); 149(6), 147(12), 145(18), 143(16) ($(M-HCl-H-2CCl_3)^+$); 121(15), 119 (48), 117(50) ($(CCl_3)^+$); 113(12), 111(66), 109(100) ($(M-2HCl-H-2CCl_3)^+$).

4-Chloro-3,5-bis(trichloromethyl)cyclopentene. NMR (CCl_4) δ=6.25 (2H, s, olefinic), 4.21 (2H, d, J=3.0 Hz, H at 3- and 5-position), and 3.85 (1H, t, J=3.0 Hz, H at 4-position); MS (20 eV), *m/e* (rel intensity), 301(2), 299(2) ($(M-Cl)^+$); 269(3), 267(7), 265(11), 263(7) ($(M-HCl-Cl)^+$); 231(4), 229(6), 227(4) ($(M-2HCl-Cl)^+$); 223(7), 221(36), 219(78), 217(62) ($(M-CCl_3)^+$); 185(31), 183(98), 181(100) ($(M-HCl-CCl_3)^+$); 150(3), 148(14), 146(22) ($(M-HCl-Cl-CCl_3)^+$); 149(8), 147(23), 145(29) ($(M-2HCl-CCl_3)^+$); 121(3), 119(12), 117(10) ($(CCl_3)^+$); 111 (11), 109(14) ($(M-H-2CCl_3)^+$).

*Formylruthenocene (**2b**).* Mp 99—100 °C lit,[6] 103—104 °C; IR and NMR spectra agreed with reported ones.

*(Ethoxymethyl)ruthenocene (**2c**).* Yellow oil, IR 3090, 2965, 2850(CH), 1080(C–O), 1090, and 990 cm^{-1} (deformation of ring hydrogen); NMR($CDCl_3$) δ=4.63 (2H, t, J= 1.7 Hz, ring H at α-position), 4.50 (7H, H at β-position of the substituted ring and of the unsubstituted ring), 4.05 (2H, s, CH_2), 3.48 (2H, q, J=7.0 Hz, $C\underline{H}_2$–CH_3), and 1.17 (3H, t, J=7.0 Hz, CH_3); MS (70 eV) *m/e* (rel intensity), 292(55), 290(100), 289(58), 288(44), 287(39) (M^+); 264(5), 263(11), 262(9), 261(22), 260(15), 259(13), 258(11) ($(M-C_2H_4)^+$ and $(M-C_2H_5)^+$); 248(34), 247(44), 246(61), 245 (95), 244(61), 243(49), 242(31) ($(M-C_2H_5O+H)^+$ and $(M-C_2H_5O)^+$); 234(24), 233(49), 232(57), 231(39), 230(35), 229(18) ($(M-C_2H_5OCH_2+H)^+$ and $(M-C_2H_5OCH_2)^+$); 169(38), 167(66), 166(38), 165(30), 164(29) ($(RuC_5H_5)^+$).

Spectroscopic Measurements. GC-MS analysis was carried out with a Shimadzu GC-MS Model 6020 equipped with a 2 m column of OV-17 (2% on chromosorb N; column temperature, 160—240 °C).

NMR and IR spectra were recorded on a Hitachi NMR spectrometer Model R-22 and a Hitachi IR spectrometer Model 125, respectively.

Table 1. Photochemical reactions of ruthenocene–polychloromethane–ethanol systems
RcH=Ruthenocene; [RcH]=4×10^{-2} mol dm^{-3}; Solvent 1 : 1 v/v.

Solvent	Light source[a)]	Irr. time / h		Conversion / %	Photoproduct	Yield[b)] / %
CCl_4–EtOH	LP	9		27	RcCOOEt (**2a**)	5.4
					$[Ru(C_5H_5)_2]^+[RuCl_4]^-$	10.3
	LP	10	Refluxed for 3 h after irradiation	28	RcCOOEt (**2a**)	6.4
					$[Ru(C_5H_5)_2]^+[RuCl_4]^-$	9.4
	HP	10		28	RcCOOEt (**2a**)	9.5
					$[Ru(C_5H_5)_2]^+[RuCl_4]^-$	4.0
	HP	12	Pyrex-filtered	12	RcCOOEt (**2a**)	2.3
					$[Ru(C_5H_5)_2]^+[RuCl_4]^-$	12
$CHCl_3$–EtOH	LP	15		21	RcCHO (**2b**)	57
	HP	15		20	RcCHO (**2b**)	39
	HP	42	Pyrex-filtered	19	RcCHO (**2b**)	6
CH_2Cl_2–EtOH	LP	10		31	$RcCH_2OEt$ (**2c**)	51
	HP	10		26	$RcCH_2OEt$ (**2c**)	20

a) LP, Low pressure mercury lamp; HP, High pressure mercury lamp. b) Yield was measured by means of TLC and is based on the quantity of ruthenocene consumed.

Results and Discussion

Similar to ferrocene (**3**), ruthenocene (**1**) undergoes photochemical substitution, accompanying oxidation.

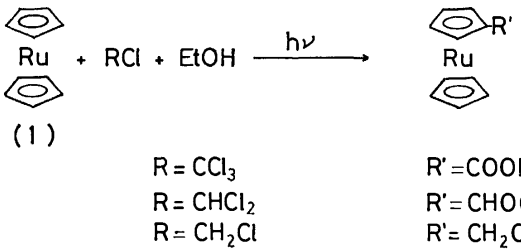

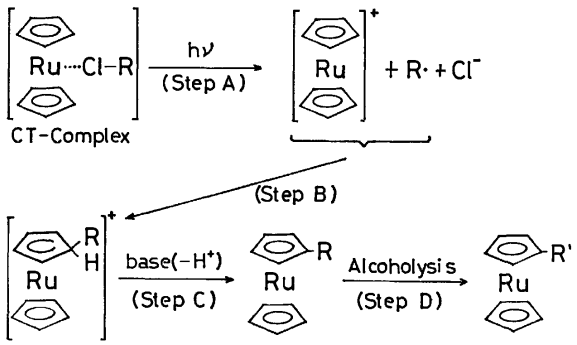

Scheme 1. Mechanism of photo-substitution.

The type of the photo-substitution in ruthenocene–polychloromethane–ethanol systems is the same as that in ferrocene–polychloromethane–ethanol systems. The yields of the products under various irradiation conditions are shown in Table 1. Formylation in $CHCl_3$–EtOH and ethoxymethylation in CH_2Cl_2–EtOH occur effectively by UV-irradiation. In these reactions the color change that indicates the formation of ruthenocenium tetrachlororuthenate(III) (**4**), an oxidation product, was not observed. On the other hand, the photoreaction of the **1**–CCl_4–EtOH system shows a feature different from that of the **3**–CCl_4–EtOH system: UV-irradiation of ferrocene in a CCl_4–EtOH solution gives effectively the ethoxycarbonylation product, whereas that of ruthenocene gives a small amount of ethyl ruthenocenecarboxylate (**2a**) and considerable amounts of ruthenocenium tetrachlororuthenate(III) and cyclopentenes substituted by chlorine and trichloromethyl group ($C_5H_5Cl(CCl_3)_2$, $C_5H_5(CCl_3)_3$ *etc.*). Under the assumption that the average molecular weight of the cyclopentenes with chlorine and trichloromethyl is 338 (the molecular weight of $C_5H_5Cl(CCl_3)_2$), the yields of the halogenated compounds are estimated to be 40 and 34% for the irradiation with a low pressure mercury lamp and that with a high pressure mercury lamp, respectively.

In the ruthenocene–polychloromethane–ethanol systems the irradiation with a low pressure mercury lamp (with shorter wavelength light) gives higher yields of the substitution products than that with a high pressure mercury lamp (with longer wavelength light) except for the **1**–CCl_4–EtOH system. The light of wavelength longer than 300 nm (pyrex-filtered light) was almost ineffective for the photo-substitution.

Similar to ferrocene, ruthenocene forms charge transfer complexes with halogenated hydrocarbons.[2,3] This fact and the similarity of the photoreactions of ruthenocene to those of ferrocene suggest the mechanism shown in Scheme 1.

The factors which determine the effectiveness of the photo-substitution are: 1) the efficiency of photo-induced electron transfer in the CT-complex between metallocene and polychloromethane (Step A), 2) the reactivity of metallocenium ions with polychloromethyl radicals (Step B), 3) the elimination of H^+ (Step C), and 4) the effectiveness of alcoholysis of chlorine on the side chain (Step D).

The fact that the CT-absorption bands are situated around 280 nm (CTTS-band for ruthenocene–CCl_4, 285 nm)[2,3] can explain the wavelength dependence of the photoreactions.

A remarkable difference between the photoreactions of the **1**–CCl_4–EtOH system and those of the **3**–CCl_4–EtOH system is the low yield of the photo-ethoxycar-

bonylated product for ruthenocene. This difference might be ascribed to the difference in the efficiencies of Step A: the CT-complex between **1** and CCl_4 is expected to be less stable than that between **3** and CCl_4 because of the higher ionization potential of **1** (I_p for ruthenocene, 7.45 eV; I_p for ferrocene, 6.88 eV[7]). However, the association constant for the CT-complex between **1** and CCl_4 was estimated to be similar to that for the complex between **3** and CCl_4 (association constant; for **1**–CCl_4, 0.012 $dm^3\,mol^{-1}$; for **3**–CCl_4, 0.015 $dm^3\,mol^{-1}$).[3] Moreover, the less stable CT-complexes of **1**–$CHCl_3$ and **1**–CH_2Cl_2 give the substitution products in good yields. These facts indicate that the low efficiency of the photo-ethoxycarbonylation in the **1**–CCl_4–EtOH system can not be ascribed to the efficiency of Step A.

Step D is not the controlling step. It has been reported that the solvolysis rate at the carbon atom attached to ruthenocenyl group is greater than that at the carbon atom attached to ferrocenyl group.[8]

The low yield of the ester in the photoreaction of the **1**–CCl_4–EtOH system accompanies the formation of ruthenocenium tetrachlororuthenate(III) and cyclopentenes substituted by chlorine and trichloromethyl. The cyclopentene derivatives are composed mainly of $C_5H_5Cl(CCl_3)_2$ and $C_5H_5(CCl_3)_3$. This result suggests that the decomposition competes with Step C. If the decomposition occurs after the elimination of H^+, the decomposition products of the type $C_5H_4Cl_n(CCl_3)_{4-n}$ should be obtained.

The cationic intermediate formed by the addition of trichloromethyl to metallocenium ions would be destabilized owing to the electron attraction of the trichloromethyl group and would undergo the decomposition. The destabilization would be greater for the more electronegative ruthenium compound than for the iron compound.

The authors are very grateful to the Shimadzu Corporation and Professor Shigeo Nishimura of Tokyo University of Agriculture and Technology for the GC-MS measurements and to Mr. Susumu Kumon of Shin-nihon Jitsugyo Co. for the MS measurements.

References

1) T. Akiyama, Y. Hoshi, S. Goto, and A. Sugimori, *Bull. Chem. Soc. Jpn.*, **46**, 1851 (1973); T. Akiyama, A. Sugimori, and H. Hermann, *ibid.*, **46**, 1855 (1973).

2) O. Traverso, S. Sostero, and G. A. Mazzocchin, *Inorg. Chim. Acta*, **11**, 237 (1974).

3) P. Borrel and E. Henderson, *J. Chem. Soc., Dalton Trans.*, **1975**, 432.

4) P. Pertici, G. Vitulli, and L. Polli, *J. Chem. Soc., Chem. Commun.*, **1975**, 846.

5) Methyl ester has been described by M. D. Rausch, E. O. Fischer, and H. Grubert (*J. Am. Chem. Soc.*, **82**, 76 (1960)).

6) S. Kamiyama, T. M. Suzuki, T. Kimura, and A. Kasahara, *Bull. Chem. Soc. Jpn.*, **51**, 909 (1978).

7) S. Evans, M. L. H. Green, B. Jewitt, A. F. Orchard, and C. F. Pygall, *J. Chem. Soc., Faraday Trans. 2*, **1972**, 1847.

8) A. Hill and J. H. Richards, *J. Am. Chem. Soc.*, **83**, 3840 (1961).

Catalysis of the Hydrolysis of *p*-Nitrophenyl 1-Adamantaneacetate by Cyclodextrins

Makoto KOMIYAMA* and Shohei INOUE

Department of Synthetic Chemistry, Faculty of Engineering, The University of Tokyo, Hongo, Bunkyo-ku, Tokyo 113

(Received March 6, 1980)

The cleavage of *p*-nitrophenyl 1-adamantaneacetate was accelerated by β- and γ-cyclodextrins, which was in contrast with their deceleration of the cleavage of a sterically analogous substrate, *p*-nitrophenyl 1-adamantanecarboxylate. The presence and absence of a methylene group in these substrates absolutely governed the directions of the rate effects of the cyclodextrins. The specificity, explicitly showing that cyclodextrins are quite good models of enzymes, was attributed to the difference of the structures of the inclusion complexes of cyclodextrins with these substrates.

Recently cyclodextrins (CDs) have been often used as an enzyme model. One of the important reasons for the increasing attention to CDs is the complex formation of these oligosaccharides with the substrates prior to their catalytic functions. Thus, the stereochemistry in the complex formation can result in the specificities in the subsequent reactions, which is similar to enzymatic reactions.[1]

This paper describes a strict specificity in the catalyses by CDs. It will be shown that the cleavage of *p*-nitrophenyl 1-adamantaneacetate (**1**) is accelerated by β- and γ-cyclodextrins (β- and γ-CDs), in spite of the retardation of the cleavage of sterically a quite analogous substrate, *p*-nitrophenyl 1-adamantanecarboxylate (**2**) by CDs.[2] The mechanism of the CD-catalyzed hydrolysis of **1** is kinetically examined. Furthermore, the difference in the effects of CDs on these two analogous substrates will be discussed in terms of the structures of the CD-substrate complexes by use of the results of absorption spectrometry.

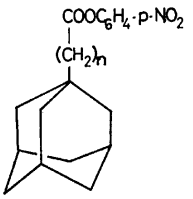

1 : n = 1
2 : n = 0

Experimental

Materials. **1** was synthesized from 1-adamantaneacetic acid and *p*-nitrophenol by use of dicyclohexylcarbodiimide as the dehydration reagent and was purified by the recrystallization from ethanol; mp 114.0—114.5 °C; Found; C, 68.35; H, 6.75; N, 4.43%. Calcd for $C_{18}H_{21}NO_4$; C, 68.54; H, 6.72; N, 4.44%. Synthesis of **2** and its characterization were described in the previous paper.[2] α-Cyclodextrin (α-CD) and β-CD were purified by the recrystallization from water. γ-CD was purchased from Nakarai Chemical Co. and was used without further purification. The 0.1 mol dm^{-3} NaOH and NaOD solutions had the factors of 1.00± 0.01 as shown by the titration with 0.1 mol dm^{-3} HCl standard solution.

Kinetics. Hydrolysis of **1** was carried out at 16 °C mostly in the 66:34 (v/v) mixture of 0.1 mol dm^{-3} NaOH aqueous solution and acetonitrile. The reaction was initiated by the addition of 30 μl stock solution of **1** in acetonitrile to the mixture of 2 ml 0.1 mol dm^{-3} NaOH aqueous solution and 1 ml acetonitrile. The initial concentration of **1** was approximately 2×10^{-5} mol dm^{-3}, and the cleavage was followed at 410 nm by the appearance of *p*-nitrophenol.

The cleavage of **1** was also examined in the 99:1 (v/v) mixture of 0.1 mol dm^{-3} NaOH aqueous solution and acetonitrile, which was prepared by the addition of 30 μl stock solution in acetonitrile to 3 ml 0.1 mol dm^{-3} NaOH aqueous solution. In this case, the initial concentration of **1** was kept as low as 5×10^{-6} mol dm^{-3}, because of the poor solubility of **1** in aqueous solution.

Absorption Spectrometry. Absorption spectra were measured at 16 °C in the 66:34 (v/v) mixture prepared similarly as described in the Kinetics section. The initial concentrations of **1** and **2** were 10^{-4} mol dm^{-3}, and that of β-CD was 3×10^{-2} mol dm^{-3}. The absorbance at a specific wavelength was determined by the extrapolation of the absorbance-time dependence to the time of the mixing (the addition of the stock solution).

Product Analyses. The reactions were initiated by the addition of 23 mg of **1** (or 22 mg of **2**) in 2 ml acetonitrile to 4 ml of 0.1 mol dm^{-3} NaOH aqueous solution containing 51 mg of β-CD. The values of $[\beta\text{-CD}]_0$, $[\mathbf{1}]_0$, and $[\mathbf{2}]_0$ were 7.5×10^{-3}, 1.2×10^{-2}, and 1.2×10^{-2} mol dm^{-3}. Considering the K_d's of the β-CD–**1** and β-CD–**2** complexes in the 66:34 mixture shown in Table 1, about 77 and 61% of β-CD in the reaction solutions should form complexes with **1** and **2**, respectively. After 16 s for **1** and 500 s for **2** (the one half-life calculated from k_c's), the reactions were stopped by the addition of a small amount of 1 mol dm^{-3} HCl solution, followed by the extraction with 6 ml ether. The aqueous layer was dried *in vacuo* and the resulting white powder was analyzed by infrared spectrometry.

Results

Figure 1 shows the dependence of the rate constant of the cleavage of **1** (k_{obsd}) on the initial concentrations of CDs ($[CD]_0$). Obviously, both β- and γ-CDs showed acceleration effects of the cleavage of **1**. The data in Fig. 1 were analyzed according to Eq. 1, which is based on the scheme involving the complex formation of CDs with **1** prior to the chemical transformation:

$$(k_{obsd}-k_{un}) = -K_d(k_{obsd}-k_{un})/[CD]_0 + (k_c-k_{un}). \quad (1)$$

Here, k_{un} and k_c are the rate constant of the cleavage of **1** in the absence of CDs and that of **1** incorporated in the CD–**1** complex, respectively, and K_d is the equilibrium constant of the dissociation of the CD–**1** complex.[1]

As shown in Fig. 2, the plots of $(k_{obsd}-k_{un})$ *vs.* $(k_{obsd}-$

k_{un})/[CD]$_0$ exhibited straight lines, from the slopes and the intercepts of which k_c and K_d were determined.

Table 1 lists the values of k_c and K_d for the CD-catalyzed cleavage of **1**. For the purpose of comparison, the values for the cleavage of an analogous substrate, **2**, determined in the previous paper,[2] are also shown.

β- and γ-CDs showed 3.0 and 2.1 fold *acceleration* of the cleavage of **1** in the 66:34 mixture of 0.1 mol dm^{-3} NaOH aqueous solution and acetonitrile, which is in contrast with the 3.3 and 1.4 fold *deceleration* of the cleavage of **2** by β- and γ-CDs. Still larger difference in the rate effects by CDs was found in the cleavages of **1** and **2** in the 99:1 mixture. Thus, the cleavage of **1** was *accelerated* by 1.8 and 1.7 fold by β- and γ-CDs, whereas the cleavage of **2** was *decelerated* by 28 and 13 fold by β- and γ-CDs. However, the effect of α-CD on the cleavages of **1** and **2** was much smaller.

Table 2 shows the D_2O solvent isotope effects on k_c and k_{un} in the 66:34 mixture. k_c's for **1** and **2** in the 66:34 D_2O–acetonitrile mixture were found to be 1.1—1.2 times those in the H_2O–acetonitrile mixture. These results indicated that the cleavages of **1** and **2** incorporated in the CD complexes proceed *via* nucleophilic catalysis by hydroxide ion, since the nucleophilicity of OD^- is 20—40% larger than that of OH^-.[3] Larger nucleophilicity of OD^- than OH^- in the present reactions is definitely shown by the 1.1 fold larger values of k_{un}'s in the D_2O–acetonitrile mixture than those in the H_2O–acetonitrile mixture.

Nucleophilic attack by hydroxide ion indicated above for the CD-accelerated cleavage of **1** and the CD-decelerated cleavage of **2** was supported by the product analyses. After the reactions of β-CD with excess amounts of **1** and **2** (see Experimental), essentially

Table 1. Values of k_c, k_c/k_{un}, and K_d for the cleavages of **1** and **2** in the presence of CDs[a]

Substrate	CD	k_c / 10^{-3} s^{-1}	k_c/k_{un}	K_d / 10^{-3} mol dm^{-3}
1[b]	α-CD	1.6	1.0	—
	β-CD	4.6	3.0	1.8
	γ-CD	3.2	2.1	2.6
1[c]	α-CD	2.3[d]	1.1	—
	β-CD	3.9[d]	1.8	—
	γ-CD	3.6[d]	1.7	—
2[b]	α-CD	0.39[d]	0.82	—
	β-CD	0.14	0.30	4.7
	γ-CD	0.35[d]	0.74	—
2[c]	α-CD	0.60	0.31	13
	β-CD	0.069	0.036	0.36
	γ-CD	0.15	0.078	0.82

a) The data for **2** were taken from Ref. 2. b) In the 66:34 (v/v) 0.1 mol dm^{-3} NaOH-acetonitrile mixture at 16 °C; k_{un}'s of **1** and **2** under these conditions were 1.54×10^{-2} and 4.75×10^{-3} s^{-1}, respectively. c) In the 99:1 (v/v) 0.1 mol dm^{-3} NaOH-acetonitrile mixture at 16 °C; k_{un}'s of **1** and **2** under these conditions were 2.17×10^{-2} and 1.93×10^{-2} s^{-1}, respectively. d) k_{obsd}'s in the presence of 3×10^{-2} mol dm^{-3} CD. These values were taken as k_c here, since they were identical with those in the presence of 2×10^{-2} mol dm^{-3} CD within experimental error.

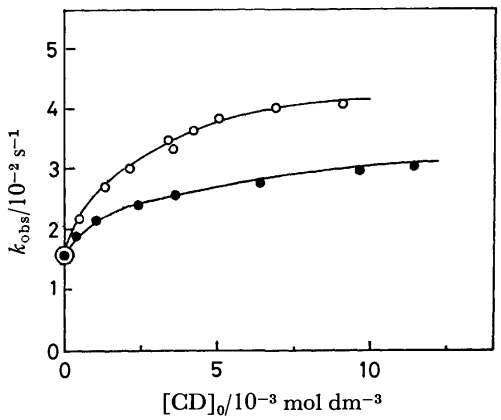

Fig. 1. Dependence of k_{obsd} of the cleavage of *p*-nitrophenyl 1-adamantaneacetate (**1**) on the concentration of cyclodextrins (CDs); ○, β-CD; ●, γ-CD; at 16 °C in the 66:34 mixture of 0.1 mol dm^{-3} NaOH aqueous solution and acetonitrile.

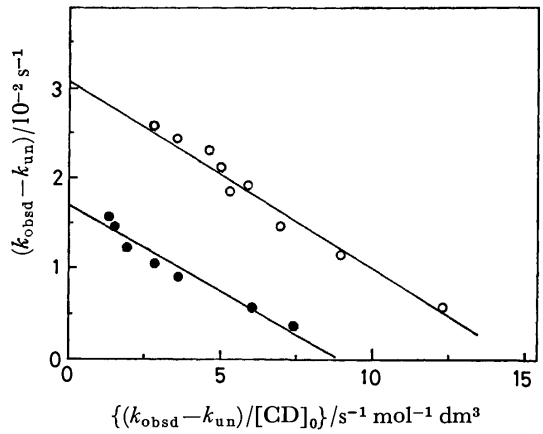

Fig. 2. Plots of $(k_{obsd}-k_{un})$ *vs.* $(k_{obsd}-k_{un})/[CD]_0$ for the β-CD (○)- and γ-CD (●)- catalyzed cleavage of **1**; at 16 °C in the 66:34 mixture of 0.1 mol dm^{-3} NaOH aqueous solution and acetonitrile; the data in Fig. 1 were used here.

Table 2. D_2O solvent isotope effects for the cleavages of **1** and **2** in the presence or absence of β- and γ-CDs[a,b]

Substrate	$k_{un}(D_2O)/k_{un}(H_2O)$	$k_c^{\beta\text{-CD}}(D_2O)/k_c^{\beta\text{-CD}}(H_2O)$	$k_c^{\gamma\text{-CD}}(D_2O)/k_c^{\gamma\text{-CD}}(H_2O)$
1	1.14±0.02	1.17±0.04	1.16±0.04
2	1.12±0.02	1.11±0.03	—

a) In a 66:34 mixture of 0.1 mol dm^{-3} NaOH H_2O solution (or 0.1 mol dm^{-3} NaOD D_2O solution) and acetonitrile. b) The k_{obsd}'s in the presence of 3×10^{-2} mol dm^{-3} CDs were taken as k_c's here. See the footnote d of Table 1.

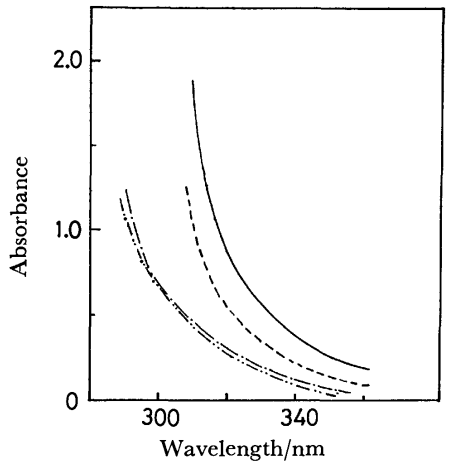

Fig. 3. Absorption spectra of **1** and **2** in the presence and absence of β-CD; —·—, **1**+β-CD; —··—, **1** only; ——, **2**+β-CD; ----, **2** only; [β-CD]=3×10^{-2} and [**1**]=[**2**]=10^{-4} mol dm^{-3} in the 66:34 mixture of 0.1 mol dm^{-3} NaOH aqueous solution and acetonitrile.

all of β-CD was recovered in its intact form as characterized by infrared spectrometry. No carbonyl stretching band due to the β-CD ester of 1-adamantanecarboxylic acid or 1-adamantaneacetic acid, the possible intermediate of nucleophilic catalysis by β-CD, was detected at all. At least some of these intermediates should be trapped by the present procedure (after one half-life of the substrates), if the reaction were involving the nucleophilic attack by β-CD, since the rates of the hydrolyses of the intermediates, which have rather poor leaving groups of pK_a 12 (β-CD),[1] should be smaller than those of **1** and **2**, which have good leaving groups of pK_a 7.1 (*p*-nitrophenol).[4] These arguments are supported by the fact that the rate constant of the alkaline hydrolysis of *p*-nitrophenyl acetate is five fold larger than that of trifluoroethyl acetate, the pK_a of the leaving group of which (12.4) is similar to that of β-CD,[4] and the rate constant of the alkaline hydrolysis of α-CD ester of *p*-nitrobenzoic acid ester is about two fold larger than that of its trifluoroethyl ester.[5]

Figure 3 shows the change in the absorption spectra of **1** and **2** due to the addition of 3×10^{-2} mol dm^{-3} β-CD. Almost all of **1** and **2** should form complexes with β-CD under the present conditions considering the K_d values shown in Table 1. Considerable change was found in the 300—360 nm region in the case of **2**, whereas much smaller change, if any, was observed in the case of **1**. These results indicated that the *p*-nitrophenyl portion of **2** is included in the cavity of β-CD to a greater extent than that of **1** is, since the change of absorption spectrum of *p*-nitrophenol on the complex formation with CDs was well known.[1] The change in the molar absorption coefficient observed for the complex formation between **2** and β-CD is a little bit smaller than the value reported for the complex formation between *p*-nitrophenol and α-CD (2.9×10^3 at 354 nm).[6]

Discussion

This paper shows that catalyses by CDs are quite specific, which is characteristic of enzymatic catalyses. β-CD and γ-CD showed deceleration of the cleavage of **2**, whereas they showed acceleration of the cleavage of **1**. Thus, the presence or absence of a methylene group in the substrate predominantly governs the catalyses by CDs. There have been few reports showing the different directions of the rate effects of CDs on the reactions of analogous substrates,[7] although the magnitudes of the rate effects of CDs (in the same directions) were in some cases strongly dependent on the structures of the substrates.[8] The specificity observed here may be associated with the specific catalysis by β-CD for the selective preparation of vitamin K analogs.[9]

In the previous paper,[2] the deceleration of the alkaline hydrolysis of **2** by β- and γ-CDs was attributed to the steric hindrance by the wall of CDs as well as the electrostatic repulsion between the negative charges of the secondary alkoxide anions of CDs and that of hydroxide ion. The steric hindrance was so important in the hydrolysis of **2** because the adamantyl portion and the carbonyl group are located in a close proximity. Therefore, both of them should be included in the cavity. In the hydrolysis of **1**, however, the methylene group between the adamantyl group and the carbonyl group makes it possible for the carbonyl group to be kept outside the cavity, when the apolar adamantyl group is included in the cavity. Thus, the steric and electrostatic hindrance by CDs is not operative so much in the hydrolysis of **1**.

Absorption spectrometry shown in Fig. 3 is consistent with the above arguments. The *p*-nitrophenyl group of **2**, which is adjacent to the adamantyl group, is partly located inside the cavity (the considerable change in the absorption spectrum), whereas that of **1**, which is located at a larger distance from the adamantyl group, is hardly included in the cavity (the negligible change in the absorption spectrum).

The acceleration of the cleavage of **1** by β- and γ-CDs, which proceeds *via* nucleophilic catalysis by hydroxide ion, is probably attributed to the functions of the primary hydroxyl group(s) of CDs. It is difficult to figure out any mechanism where the secondary hydroxyl groups, which are present in their anionic forms under the present conditions, accelerate the alkaline reactions. Rather, the electrostatic repulsion between the secondary alkoxide anion and hydroxide ion should retard the reactions. The primary hydroxyl group(s) of CDs can alter the microscopic surroundings of the ester group, resulting in the acceleration of the attack by hydroxide ion. Alternatively, the hydrogen bonding of the primary hydroxyl group(s) with the substrate in the transition state can facilitate the alkaline reaction.[10–13] In the hydrolysis of **2**, however, the attack of the hydroxide ion at the carbonyl carbon atom as well as the assistance of the primary hydroxyl groups described above should be unfavorable, since the carbonyl carbon atom is deeply included in the cavity of CDs.

The magnitude of the acceleration of the cleavage of **1** by β- and γ-CDs in the 66:34 mixture of 0.1 mol dm^{-3} NaOH aqueous solution and acetonitrile was larger than that in the 99:1 mixture. This result

is probably associated with the shallower inclusion of the carbonyl carbon atom of **1** in the cavity in the 66:34 mixture than in the 99:1 mixture, resulting in the more efficient nucleophilic attack by hydroxide ion assisted by the primary hydroxyl groups of CDs. This interpretation is supported by the fact that the magnitude of the effect of the deceleration of the cleavage of **2** by CDs was much larger in the 99:1 mixture than in the 66:34 mixture. Here, the shallower inclusion of the carbonyl carbon atom of **2** should enhance the alkaline reaction.

In conclusion, cyclodextrins showed marked specificity in the hydrolyses of analogous substrates, *p*-nitrophenyl 1-adamantaneacetate (acceleration) and *p*-nitrophenyl 1-adamantanecarboxylate (deceleration). This specificity is similar to that of the enzymatic reactions. Present finding confirmed that CDs are quite good models of enzymes.

References

1) M. L. Bender and M. Komiyama, "Cyclodextrin Chemistry," Springer-Verlag, Berlin (1978).
2) M. Komiyama and S. Inoue, *Bull. Chem. Soc. Jpn.*, **53**, 2330 (1980).
3) K. B. Wiberg, *Chem. Rev.*, **55**, 713 (1955).
4) J. F. Kirsch and W. P. Jencks, *J. Am. Chem. Soc.*, **86**, 837 (1964).
5) M. Komiyama and S. Inoue, *Chem. Lett.*, **1979**, 1101.
6) F. Cramer, W. Saenger, and H.-Ch. Spatz, *J. Am. Chem. Soc.*, **89**, 14 (1967).
7) K. Mochida, Y. Matsui, Y. Ota, K. Arakawa, and Y. Date, *Bull. Chem. Soc. Jpn.*, **49**, 3119 (1976).
8) R. L. VanEtten, J. F. Sebastian, G. A. Clowes, and M. L. Bender, *J. Am. Chem. Soc.*, **89**, 3242 (1967).
9) I. Tabushi, K. Yamamura, K. Fujita, and H. Kawakubo, *J. Am. Chem. Soc.*, **101**, 1019 (1979).
10) H. B. Henbest and B. J. Lovell, *J. Chem. Soc.*, **1957**, 1965.
11) S. M. Kupchan and C. R. Narayanan, *J. Am. Chem. Soc.*, **81**, 1913 (1959).
12) S. M. Kupchan, P. Slade, and R. J. Young, *Tetrahedron Lett.*, **1960**, 22.
13) T. C. Bruice and T. H. Fife, *J. Am. Chem. Soc.*, **84**, 1973 (1962).

Substituent Effects in Heterogeneous Catalysis. VII. Temperature Independence of the Relative Rates in Metal-catalyzed Hydrogenation of Cyclohexanone and Its 2-Alkyl Derivatives

Teiji CHIHARA and Kazunori TANAKA*

The Institute of Physical and Chemical Research, Wako, Saitama 351

(Received March 8, 1980)

The rates of hydrogenation of cyclohexanone and its 2-alkyl derivatives have been measured using decalin as the solvent in a temperature range of −5 to 68 °C over Ru/Al_2O_3, Rh/Al_2O_3, and Pt/Al_2O_3 catalysts. As predicted previously, 2-methyl-, 2-ethyl-, and 2-propylcyclohexanone have exhibited nearly identical temperature dependencies in adsorption and hydrogenation, while cyclohexanone and 2-isopropylcyclohexanone had quite different dependencies.

This is a continuation of our series of studies concerning the effects of alkyl substitution in cyclohexanone (**1**) hydrogenation catalyzed by platinum metals. Three recent papers[1-3] have dealt with **1** and its 2-alkyl derivatives, *i.e.*, 2-methyl-, 2-ethyl-, 2-propyl-, 2-isopropyl-, and 2-*t*-butylcyclohexanone (abbreviated to **2m**, **2e**, **2p**, **2ip**, **2tb**, respectively). The activity sequence for hydrogenation of each of the individual ketones is

$$\mathbf{1} > \mathbf{2m} = \mathbf{2e} = \mathbf{2p} > \mathbf{2ip} > \mathbf{2tb}, \quad (1)$$

while the activity sequence for competitive hydrogenation of a mixture of different ketones is

$$\mathbf{1} \gg \mathbf{2m} > \mathbf{2e} > \mathbf{2p} \gg \mathbf{2ip} \gg \mathbf{2tb}. \quad (2)$$

As pointed out previously,[3] sequence (1) seems to be inversely related to the steric hindrance of the alkyl substituents. With respect to the identity **2m**=**2e**=**2p** for the triad ketones having a straight side chain, it should be noted that **2e** and **2p** are viewed as being brought from **2m** by alkyl substitution of a hydrogen atom β to the carbonyl group. Thus, it is unlikely that the triad ketones are significantly different from one another in charge density of the functional group. Another important fact is that the side alkyl chains of **2e** and **2p** are flexible. Owing to this flexibility, upon adsorption of **2e** and **2p** the side chains could point away from the catalyst surface and also from the carbonyl group. In different terms, the steric hindrance of the side chain to adsorption and the subsequent surface reaction remain unchanged on going from **2m** to **2e** or **2p**. Thus, it is expected that the adsorption strength as well as the reactivity of the carbonyl group should be the same for the adsorbed triad ketones, thus, giving rise to the observed identity **2m**=**2e**=**2p** in sequence (1).

The adsorbed triad ketones, however, might be different in entropy factor. It is very likely that upon adsorption a ketone loses its translational and rotational freedom.[4] If so, the greater the substituent, the greater would be the entropy loss. As previoulsy demonstrated, the relative magnitudes of the entropy losses for different ketones can be calculated in terms of the molecular weight (m) and product of the three principal moments of inertia (I). Such calculations account quantitatively for the reactivity differences in sequence (2) between **2m**, **2e**, and **2p**.

The purpose of the present work has been to substantiate the above interpretation of the alkyl substituent effects. One of the basic assumptions involved here is that the adsorption and hydrogenation of the triad ketones (**2m**, **2e**, **2p**) are different only in entropy factor. If this assumption is valid, the heat of adsorption as well as the activation energy must be identical for the triad ketones; that is to say, the relative rates of hydrogenation of the triad ketones must be temperature independent. The present work tests this prediction. For a comparison, **1** and **2ip** are also examined; these are expected to behave quite differently from the triad.

Experimental

Materials. Commercial decalin (Wako Pure Chemical Ind., "First Grade," a mixture of cis and trans isomers) was purified by refluxing with calcium hydride (*ca.* 1 g per liter decalin) for 24 h, followed by distillation. The middle was collected and redistilled with benzoic acid (*ca.* 25 mg per liter decalin).

The catalysts used were the same as those employed previously,[2,3] *i.e.*, Ru/Al_2O_3, Rh/Al_2O_3, and Pt/Al_2O_3, each in the form of pellets (Engelhard Ind., 1/8 inch in diameter containing 0.5 wt% metal).

Kinetic Procedure. The relative rates of hydrogenation of five ketones (**1**, **2m**, **2e**, **2p**, **2ip**) were measured either separately with one of the individual ketones or competitively with an equimolar mixture of **1** and **2** (**2** represents any one of **2m**, **2e**, **2p**, and **2ip**). Hydrogenation runs were conducted by the procedures described previously,[2] with an exception that decalin was used as the solvent in place of cyclohexane. The reaction temperature ranged from −5 °C to 68 °C, and the hydrogen pressure was atmospheric. Decalin was chosen because its liquid-state temperature range is wider than that of cyclohexane and its vapor pressure is lower (9.7 mmHg at 66.1 °C for the isomeric mixture[5]).

Results and Discussion

The linearity of Arrhenius plots was satisfactory over the whole temperature range (−5 °C—68 °C) as shown in Fig. 1. The rate data obtained at both ends of this range are listed in Table 1. Before discussing these data, let us consider the physical meaning of the relative rates involved.

According to a common practice in heterogeneous catalysis, the relative rate R_2/R_1 in competitive reactions may be expressed as

$$R_2/R_1 = k_2K_2/k_1K_1, \quad (3)$$

where k is the rate constant referred to the unit fraction of the surface covered and K is the adsorption equili-

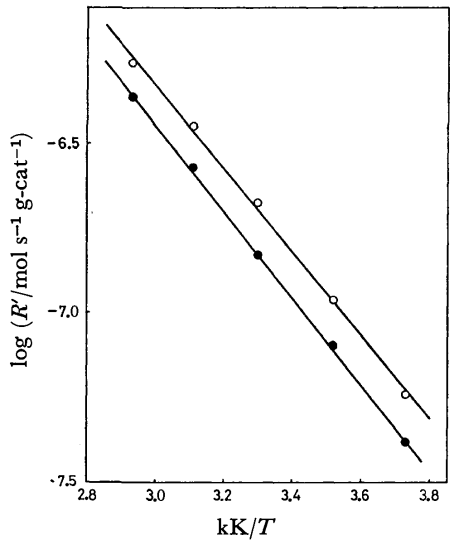

Fig. 1. Typical Arrhenius plots.
Hydrogenation of **1** and **2m** on Ru/Al_2O_3.
○: **1**, ●: **2m**.

brium constant. On the other hand, for the relative rate R_2'/R_1' in individual reactions we have

$$R_2'/R_1' = k_2/k_1, \tag{4}$$

provided that the concentrations of **1** and **2** are sufficiently high that R_2' and R_1' are concentration independent. The establishment of this prerequisite under our reaction conditions has been confirmed by preliminary experiments.[6]

Entropy Factors. Based on Eqs. 3 and 4 we obtain

$$\frac{K_{2e}}{K_{2m}} = \frac{K_{2e}}{K_1}\frac{K_1}{K_{2m}} = \frac{(R_{2e}/R_1)}{(R_{2e}'/R_1')}\frac{(R_1/R_{2m})}{(R_1'/R_{2m}')}. \tag{5}$$

Since sequence (1) indicates $R_{2e}'=R_{2m}'$, Eq. 5 is reduced to

$$\log(K_{2e}/K_{2m}) = \log(R_{2e}/R_1) - \log(R_{2m}/R_1). \tag{6}$$

Since the numerical values for the two terms of the right side are given in Table 1, we can estimate the experimental $\log(K_{2e}/K_{2m})$ values using Eq. 6. On the other hand, a theoretical $\log(K_{2e}/K_{2m})$ value has previosuly[2] been worked out based on the equation

$$\log\left(\frac{K_{2e}}{K_{2m}}\right) = \frac{3}{2}\log\left(\frac{m_{2m}}{m_{2e}}\right) + \frac{1}{2}\log\left(\frac{I_{2m}}{I_{2e}}\right) - \frac{\omega_{2e}-\omega_{2m}}{2.303\,kT}, \tag{7}$$

where ω is the heat of adsorption (negative values for exothermic). In the calculation of the theoretical $\log(K_{2e}/K_{2m})$ value, it was assumed that $\omega_{2e}=\omega_{2m}$. Both experimental and theoretical $\log(K_{2e}/K_{2m})$ values are listed in Table 2. Also for a pair **2e**+**2p**, we can write down two equations which are analogous to Eqs. 6 and 7. The experimental and theoretical $\log(K_{2p}/K_{2e})$ values obtained are also included in Table 2. It is seen that, except for a value of −0.39 for Pt, the agreement between theory and experiment is satisfactory. Since the last term in Eq. 7 has been taken as zero in the theoretical calculations, this agreement provides indirect evidence for the assumed identity in heats of adsorption between the triad ketones, *i.e.*, $\omega_{2m}=\omega_{2e}=\omega_{2p}$.

Table 1. The observed rates

Catalyst	Competitive reaction: Ketone pair	$\log_{10}(R_2/R_1)$ −5 °C	$\log_{10}(R_2/R_1)$ 68 °C	Individual reaction: Ketone	$10^8 R_1'$ mol s⁻¹ g-cat⁻¹ −5 °C	$10^8 R_1'$ mol s⁻¹ g-cat⁻¹ 68 °C
Ru/Al_2O_3				**1**	5.75	54.4
	2m/1	−1.18	−0.74	**2m**	4.16	43.4
	2e/1	−1.48	−1.01	**2e**	3.91	37.4
	2p/1	−1.76	−1.23	**2p**	3.73	39.1
Rh/Al_2O_3	**2m/1**	−0.98	−0.85			
	2e/1	−1.22	−1.10			
	2p/1	−1.49	−1.35			
Pt/Al_2O_3				**1**	5.62	59.6
	2m/1	−0.47	−0.48	**2m**	3.10	33.7
	2e/1	−0.86	−0.74	**2e**	3.26	37.4
	2p/1	−1.13	−0.98	**2p**	3.11	37.1
	2ip/1	−1.96	−1.57	**2ip**	1.02	13.1

Table 2. The experimental and theoretical values for relative equilibrium constants

Catalyst		Obsd −5 °C	Obsd 68 °C	Calcd
Ru/Al_2O_3	$\log_{10}(K_{2e}/K_{2m})$	−0.30	−0.27	−0.28
	$\log_{10}(K_{2p}/K_{2e})$	−0.27	−0.23	−0.27
Rh/Al_2O_3	$\log_{10}(K_{2e}/K_{2m})$	−0.23	−0.25	−0.28
	$\log_{10}(K_{2p}/K_{2e})$	−0.27	−0.25	−0.27
Pt/Al_2O_3	$\log_{10}(K_{2e}/K_{2m})$	−0.39	−0.26	−0.28
	$\log_{10}(K_{2p}/K_{2e})$	−0.28	−0.24	−0.27

Energy Factors. The relation between the rate constant k_i referred to adsorbed **1** or **2** and the activation energy is

$$R\frac{\mathrm{d}\ln k_i}{\mathrm{d}(1/T)} = -(\varepsilon_i-\omega_i). \tag{8}$$

Herein R with no subscript is the gas constant and ε_i is the energy required for bringing the substrate i in the bulk solution up to the activated state on the catalyst surface (apparent activation energy). The quantity $\varepsilon_i-\omega_i$, therefore, represents the energy required for bringing the adsorbed i to the activated state (true activation energy), as shown in Fig. 2. The following relation is also available:

$$R\frac{\mathrm{d}\ln K_i}{\mathrm{d}(1/T)} = -\omega_i. \tag{9}$$

From Eqs. 3, 4, 8, and 9 we obtain

$$R\frac{\mathrm{d}\ln(R_2/R_1)}{\mathrm{d}(1/T)} = -(\varepsilon_2-\varepsilon_1) \equiv -\Delta\varepsilon_{2,1} \tag{10}$$

and

$$R\frac{\mathrm{d}\ln(R_2/R_1)}{\mathrm{d}(1/T)} - \left\{R\frac{\mathrm{d}\ln R_2'}{\mathrm{d}(1/T)} - R\frac{\mathrm{d}\ln R_1'}{\mathrm{d}(1/T)}\right\} = -(\omega_2-\omega_1) \equiv -\Delta\omega_{2,1}. \tag{11}$$

TABLE 3. THE VALUES FOR ENERGETIC QUANTITIES

Catalyst	Ketone pair	$\Delta\varepsilon_{2,1}$[a] / kcal mol^{-1}	$\Delta\omega_{2,1}$ / kcal mol^{-1}	Ketone	$\varepsilon_1-\omega_1$ / kcal mol^{-1}
Ru/Al_2O_3				**1**	5.6
	2m/1	2.5	2.3	**2m**	5.8
	2e/1	2.7	2.7	**2e**	5.6
	2p/1	3.0	2.7	**2p**	5.8
Rh/Al_2O_3	**2m/1**	0.8			
	2e/1	0.7			
	2p/1	0.8			
Pt/Al_2O_3				**1**	5.9
	2m/1	−0.1	−0.1	**2m**	5.9
	2e/1	0.7	0.5	**2e**	6.1
	2p/1	0.9	0.6	**2p**	6.2
	2ip/1	2.2	1.8	**2ip**	6.3

a) 1 kcal=4.184×10^3 J.

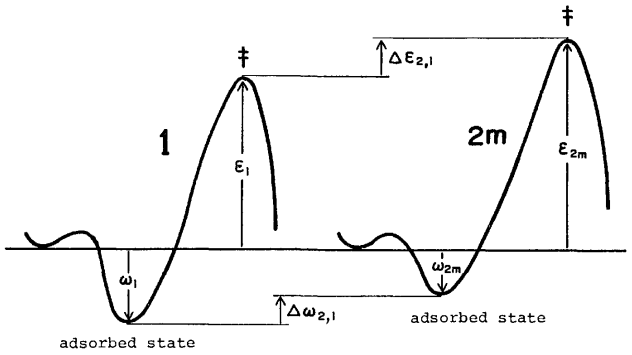

Fig. 2. Comparison of reaction coordinates between **1** and **2m**.

The values for $\Delta\varepsilon_{2,1}$ and $\Delta\omega_{2,1}$ can be estimated from Table 1 using Eqs. 10 and 11, respectively, if $\ln(R_2/R_1)$, $\ln R_2'$, and $\ln R_1'$ are linearly correlated with $1/T$. This sort of linearity has been confirmed with several representative reaction systems which are different in ketone or ketone pair. Table 3 summarizes the values for $\Delta\varepsilon_{2,1}$, $\Delta\omega_{2,1}$ and derived quantities.

Except for the **2m/1** system on Pt, the $\Delta\varepsilon_{2,1}$ values are nearly identical for **2m/1**, **2e/1**, and **2p/1** on each catalysts. This indicates that there is no significant difference in ε between **2m**, **2e**, and **2p**, as predicted in Introduction. In contrast to this near identity, a small but significant jump in ε is seen on going from **1** to **2m** and also for Pt on going from **2p** to **2ip**. Thus, the ε sequence for ketones is

$$\mathbf{1} < \mathbf{2m} \approx \mathbf{2e} \approx \mathbf{2p} < \mathbf{2ip}, \qquad (12)$$

which is the inverse of sequence (1). With respect to $\Delta\omega_{2,1}$ also, sequence (12) holds both for Ru and Pt although the value for **2m** on Pt is again exceptional. At present we cannot explain the unexpected result with **2m** on Pt.

Interestingly, little difference is seen in the true activation energy ($\varepsilon_1-\omega_1$) for **1** and **2**'s; there is no gap when going from **1** to **2m** or from **2p** to **2ip**. This indicates that there is a compensation relation between $|\varepsilon_1|$ and $|\omega_1|$, *i.e.*, the greater the $|\varepsilon_1|$ value, the lower the $|\omega_1|$ value. Although this compensation must reflect certain characteristic features of the surface reaction, they are not clear at present.

In summary, the predicted near identity in the heat of adsorption and in the activation energy for the triad ketones **2m**, **2e**, and **2p** has been confirmed. This near equivalence is understood in terms of the particular conformation of the side chains in the adsorbed state (*cf.* Introduction). Comparing **1** with the triad, the latter is more weakly adsorbed and has a higher activation barrier, as shown in Fig. 2. The same is true for a comparison of the triad with **2ip**.

The present work was partially supported by Grant-in-Aid for Scientific Research No. 454134 from the Ministry of Education, Science and Culture.

References

1) T. Chihara and K. Tanaka, *Bull. Chem. Soc. Jpn.*, **52**, 507 (1979).
2) T. Chihara and K. Tanaka, *Bull. Chem. Soc. Jpn.*, **52**, 512 (1979).
3) T. Chihara and K. Tanaka, *Bull. Chem. Soc. Jpn.*, **52**, 633 (1979).
4) S. Glasstone, K. J. Laidler, and H. Eyring, "The Theory of Rate Processes," McGraw-Hill, New York (1941), pp. 396—399.
5) J. A. Riddick and W. B. Bunger, "Organic Solvents," 3rd ed, (Vol. II of the Technique of Organic Chemistry Series), Wiley-Interscience, New York, (1970), p. 99.
6) For instance, R_1' was independent of concentration of **1** at concentrations above 1/8 mol/l for all the catalysts at both temperatures, −5 and 68 °C.

One-step Synthesis of 3-(Dialkylamino)indolizines by the Palladium-catalyzed Reaction of α-Bromopyridine, Propargyl Alcohol, and Secondary Amine[1]

Akio Ohsawa, Yoshihito Abe, and Hiroshi Igeta*
School of Pharmaceutical Sciences, Showa University, Shinagawa-ku, Tokyo 142

(Received March 10, 1980)

3-(Dialkylamino)indolizines were synthesized in one step by the reaction of 2-bromopyridine, propargyl alcohol, and secondary amines in the presence of $Pd(PPh_3)_2Cl_2$–CuI as a catalyst. 3-(2-Pyridyl)-2-propyn-1-ol and 3-(2-pyridyl)acrylaldehyde were suggested to be intermediates of the reaction. 3-Dialkylamino derivatives of pyrrolo[1,2-*a*]quinoline, pyrrolo[2,1-*a*]isoquinoline, and pyrrolo[1,2-*b*]pyridazine were obtained from the corresponding α-haloazaaromatics in a similar way.

Since the first preparation[2] of indolizine from α-picoline and acetic anhydride, various types of its derivatives have been synthesized by a number of methods undertaken from chemical,[3] pharmaceutical,[4] and physical[5] points of view.

As for aminoindolizines, Hurst *et al.* prepared some of them in several steps in order to evaluate them biologically.[6] Nevertheless, a general synthetic method for aminoindolizine derivatives has not been established. During an examination of the alkynylation of α-haloazaaromatics with propargyl alcohol according to Sonogashira's method,[7] it was found that indolizine derivatives are unexpectedly formed instead of alkynylated products. In this paper, we describe a one-step synthesis of 3-(dialkylamino)indolizines by the reaction of α-haloazaaromatics, propargyl alcohol, and secondary amines, using $Pd(PPh_3)_2Cl_2$–CuI as a catalyst.

Results and Discussion

When 2-bromopyridine (**1**) and propargyl alcohol (**2**) were heated in piperidine with $Pd(PPh_3)_2Cl_2$–CuI (**3**), a somewhat air-sensitive yellow compound (**4a**) was obtained. Its NMR spectrum indicated the presence of a piperidino group and showed signals which were assigned to the protons on the indolizine-ring carbons. The maximum of its UV spectrum appeared at 241 nm ($\varepsilon=2.4\times10^4$), similarly to that of indolizine.[8] On the basis of the elemental analysis and the above data, its structure was assumed to be piperidinoindolizine. Moreover, the position of the piperidino group in **4a** was synthetically confirmed. The product obtained from the reaction of 3-chloroindolizine(**5**)[9] with lithium piperidide was identical with **4a**, and the structure of **4a** was determined to be 3-piperidinoindolizine.

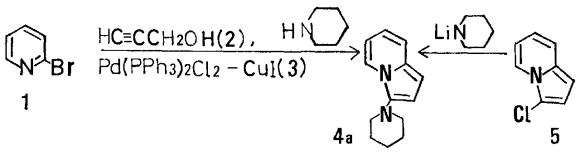

Additionally, the application and limitation of this reaction were examined. The treatment of **1**, **2**, and piperidine in the absence of the catalyst(**3**) did not afford **4a**. The reaction of **1** and **2** in the presence of **3** with other secondary amines, such as morpholine and diethylamine, afforded 3-morpholinoindolizine(**4b**) and 3-(diethylamino)indolizine(**4c**) respectively. However, the use of primary amines (*e.g.*, butylamine) did not afford the corresponding indolizines. The similar treatment of other α-haloazaaromatics, such as 2-chloroquinoline(**6**) and 1-chloroisoquinoline(**7**), in diethylamine afforded 3-(diethylamino)pyrrolo[1,2-*a*]-quinoline(**8**) and 3-(diethylamino)pyrrolo[2,1-*a*]isoquinoline(**9**) respectively. Similarly, the reaction of 3-chloropyridazines (**10**—**12**), which have substituents at the 6-positions, in secondary amines afforded 2-substituted 7-(dialkylamino)pyrrolo[1,2-*b*]pyridazines (**13a**—**c**, **14**, and **15**). These results are shown in Table 1.

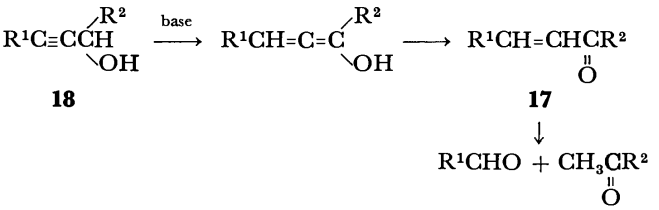

The mechanism of the formation of **4c** was investigated. It has been known that the halogen atoms of some haloazaaromatics are substituted with alkynyl groups by means of reactions with monosubstituted acetylenes, in the presence of amines and $Pd(PPh_3)_2Cl_2$–CuI (**3**) as catalysts.[7,10,11] Actually, the reaction of **1** with **2**, Et_2NH, and **3** under mild conditions (30 °C, for 16 h) afforded the 2-alkynylated pyridine, *i.e.*, 3-(2-pyridyl)-2-propyn-1-ol (**16**), in an 89% yield, although it was not obtained in the absence of **3**. When **16** was heated (80 °C, 16 h) in Et_2NH with **3**, the expected indolizine (**4c**) was obtained in a 15% yield, although heating **16** in Et_2NH in the absence of the catalyst did not give **4c** and the starting material was recovered.

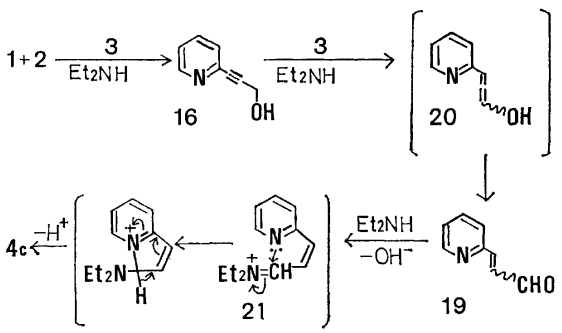

Scheme 1.

Table 1. Synthesis of 3-(dialkylamino)indolizine derivatives

	Halide	Amine	Conditions		Products	Yield (%)
			Temp/°C	Time/h		
1	2-Br-pyridine	$(CH_2)_5NH$	80	16	**4a**	36
		O NH	80	16	**4b**	12
		Et_2NH	70	3	**4c**	11
6	2-Cl-quinoline	Et_2NH	70	16	**8**	17
7	1-Cl-isoquinoline	Et_2NH	70	16	**9**	18
10	3-Cl-6-Me-pyridazine	Et_2NH	70	16	**13a**	49
		$(CH_2)_5NH$	70	16	**13b**	26
		O NH	70	16	**13c**	30
11	3-Cl-6-Ph-pyridazine	Et_2NH	70	16	**14**	13
12	3,6-Cl_2-pyridazine	Et_2NH	70	16	**15**	14

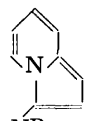

4a: $NR_2=N(CH_2)_5$
4b: $NR_2=N$ O
4c: $NR_2=NEt_2$

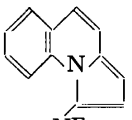

8

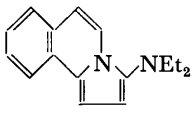

9

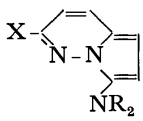

13a: X=Me, $NR_2=NEt_2$
13b: X=Me, $NR_2=N(CH_2)_5$
13c: X=Me, $NR_2=N$ O
14 : X=Ph, $NR_2=NEt_2$
15 : X=Cl, $NR_2=NEt_2$

Table 2. Properties of 3-(dialkylamino)indolizine derivatives

4	Mp (°C) or bp (°C/mm)	Found (Calcd) (%)			NMR (δ, J in Hz)
		C	H	N	
4a	58	77.45	8.19	13.78	1.4—2.0(6H, brm), 2.7—3.1(4H, brm), 6.2—6.7(4H, m),
		(77.96	8.05	13.99)	7.1—7.4(1H, m), 7.7—8.0(1H, m)
4b	85	71.48	7.07	13.65	2.8—3.1(4H, m), 3.7—4.0(4H, m), 6.2—6.7(4H, m),
		(71.26	6.98	13.85)	7.1—7.4(1H, m), 7.7—8.0(1H, m)
4c	50/3	76.25	8.41	14.69	0.94(6H, t, J=6.9), 2.98(4H, q, J=6.9), 6.2—6.7(4H, m),
		(76.55	8.57	14.88)	7.1—7.4(1H, m), 7.9—8.2(1H, m)
8	140/2	80.44	7.66	11.50	1.02(6H, t, J=6.9), 3.06(4H, q, J=6.9), 6.42(2H, s),
		(80.63	7.61	11.76)	6.78(1H, d, J=9.3), 7.18(1H, d, J=9.3), 7.1—7.7(3H, m), 9.4—9.7(1H, m)
9	210/3	80.64	7.82	11.74	0.96(6H, t, J=6.3), 3.00(4H, q, J=6.3), 6.36(1H, d, J=4.5),
		(80.63	7.61	11.76)	6.64(1H, d, J=7.5), 6.86(1H, d, J=4.5), 7.1—7.6(3H, m), 7.94(2H, m)
13a	100/1	70.40	8.41	20.67	1.00(6H, t, J=7.5), 2.38(3H, s), 3.24(4H, q, J=7.5),
		(70.90	8.43	20.67)	6.10(1H, d, J=9.0), 6.30(2H, s), 7.40(1H, d, J=9.0)
13b	54—55	72.66	7.80	19.37	1.4—2.0(6H, brm), 2.40(3H, s), 3.0—3.3(4H, brm),
		(72.52	7.96	19.52)	6.0—6.4(3H, m), 7.46(1H, d, J=9.0)
13c	53—54	66.64	6.91	19.63	2.40(3H, s), 3.0—3.4(4H, m), 3.7—4.0(4H, m),
		(66.34	6.96	19.34)	6.14(1H, d, J=8.4), 6.1—6.4(2H, m), 7.45(1H, d, J=8.4)
14	oil[a]	76.91	7.36	15.63	1.08(6H, t, J=7.2). 3.36(4H, q, J=7.2), 6.40(2H, s),
		(76.94	7.22	15.84)	6.76(1H, d, J=9.0), 7.3—7.6(3H, m), 7.64(1H, d, J=9.0), 7.8—8.1(2H, m)
15	150/2	59.96	6.52	18.86[b]	1.02(6H, t, J=7.2), 3.26(4H, q, J=7.2), 6.30(1H, J=9.0),
		(59.06	6.31	18.78)	6.3—6.6(2H, m), 7.50(1H, d, J=9.0)

a) The compound could not be distilled at 200 °C under 0.01 mm. b) Because elemental analyses of this compound did not give satisfactory data, it was derived into **13a**. See Experimental.

Lappin[12] has assumed that the conjugated ketones (**17**) were the intermediates in the degradation of β-acetylenic alcohols (**18**) with alkali to give aldehydes and methylketones.

Therefore, 3-(2-pyridyl)acrylaldehyde (**19**) was postulated as the intermediate of the reaction from **16** to **4c**; in fact, the alternatively available **19** gave **4c** (56%) on treatment with Et_2NH at room temperature.

On the basis of these observations, we propose that

the reaction proceeds as is shown in Scheme 1.

The cross-coupling between **1** and propargyl alcohol in the presence of an amine and $Pd(PPh_3)_2Cl_2$–CuI might occur to give **16**, which is then transformed into **19** through the 1,3-migration of a hydrogen atom, followed by the ketonization of the allenic alcohol (**20**). The condensation of **19** and Et_2NH then affords the iminium ion (**21**), and an intramolecular cyclization of **21** gives **4c**.

Thus, we have established a one-step synthesis of novel types of indolizines, which are difficult to obtain, using easily available starting materials.

Experimental

The properties of the products are listed in Table 2. All the melting points are uncorrected. All the boiling points are represented by the bath temperature. The NMR spectra were recorded on Hitachi R-20 and R-22 instruments.

General Procedure of One-step Synthesis. A mixture of α-haloazaaromatic (5 mmol), propargyl alcohol (0.6 g, 11 mmol), $Pd(PPh_3)_2Cl_2$ (73 mg, 0.1 mmol), CuI (5 mg), and secondary amine (3 ml) was heated at 60—70 °C for 3—16 h with stirring under a nitrogen atmosphere. The solution was then evaporated to remove the excess amine. The residue was chromatographed over basic Al_2O_3 to give a yellow oil or crystals, and the material was purified by distillation or recrystallization (from pentane or MeOH) to give 3-(dialkylamino)indolizine.

*3-Piperidinoindolizine (**4a**)*: 2-Bromopyridine (0.8 g, 5 mmol), propargyl alcohol (0.6 g, 11 mmol), $Pd(PPh_3)_2Cl_2$ (73 mg, 0.1 mmol), and CuI (5 mg) were heated in piperidine (3 ml) at 80 °C for 16 h with stirring under a nitrogen atmosphere. The solution was then evaporated, and the residue was chromatographed over basic Al_2O_3 with hexane–ether (50:1) to give yellow crystals (**4a**); yield, 0.36 g (36%); mp 58 °C (pentane).

*2-Chloro-7-(diethylamino)pyrrolo[1,2-b]pyridazine (**15**)*: 3,6-Dichloropyridazine (0.75 g, 5 mmol), propargyl alcohol (0.6 g, 11 mmol), $Pd(PPh_3)_2Cl_2$ (73 mg, 0.1 mmol), and CuI (5 mg) were heated in Et_2NH (3 ml) at 70 °C for 16 h. A work-up similar to that used before afforded 2-chloro-7-(diethylamino)pyrrolo[1,2-*b*]pyridazine (**15**) as a yellow oil [bp 150 °C (2 mmHg)] in a yield of 0.16 g (14%).

*Synthesis of 2-Methyl-7-(diethylamino)pyrrolo[1,2-b]pyridazine (**13a**) from **15***: Ni(dppp)Cl_2 (3 mg) was added to a solution of MeMgI prepared from Mg (28 mg) and MeI (150 mg) in ether (3 ml). A solution of **15** (112 mg) was stirred, drop by drop, into the reaction mixture under a nitrogen atmosphere. The oil obtained by the usual work-up[13] was found to be identical with 2-methyl-7-(diethylamino)pyrrolo-[1,2-*b*]pyridazine (**13a**) by TLC, IR, and NMR.

*Reaction of 3-Chloroindolizine (**5**) and Lithium Piperidide.* Ten ml of a solution containing BuLi (15% in hexane) was added dropwise into a solution of piperidine (0.85 g in 10 ml of THF) under a nitrogen atmosphere, with cooling in a Dry Ice–acetone bath. The mixture was allowed to stand at room temperature for 30 min and then cooled again in a Dry Ice–acetone bath. A solution of 3-chloroindolizine (**5**, 0.75 g in 10 ml of THF) was then stirred in, drop by drop. Then the mixture was allowed to stand at room temperature for 16 h, and H_2O (0.5 ml) was added dropwise to the mixture. After filtration and evaporation, the residue was purified by basic Al_2O_3 column chromatography with hexane–ether (20:1), followed by silica-gel chromatography (hexane), to give a compound which was found to be identical with **4a** by means of its NMR and IR spectra and melting point.

Reaction of 3-Chloro-6-methylpyridazine with $BuNH_2$. A mixture of 3-chloro-6-methylpyridazine (0.65 g), propargyl alcohol (0.6 g), $Pd(PPh_3)_2Cl_2$ (73 mg), CuI (5 mg), and $BuNH_2$ (3 ml) was heated at 70 °C for 16 h with stirring under nitrogen. The solution was then evaporated to give a tar. Attempts to isolate products failed.

Reaction of 2-Bromopyridine and Propargyl Alcohol in Et_2NH at 30 °C. A mixture of 2-bromopyridine (1.6 g), propargyl alcohol (1.2 g), $Pd(PPh_3)_2Cl_2$ (146 mg), CuI (10 mg), and Et_2NH (30 ml) was stirred at 30 °C for 16 h under nitrogen. After the filtration of crystals (diethylamine hydrobromide), the filtrate was evaporated and the residue was chromatographed on silica gel with CH_2Cl_2 to give crystals. Recrystallization from ether gave 3-(2-pyridyl)-2-propyn-1-ol; mp 82—83 °C (lit,[14] 82—82.5 °C); yield, 1.2 g (89%). When either $Pd(PPh_3)_2Cl_2$ or CuI was absent, the reaction did not proceed.

Reaction of 3-(2-Pyridyl)-2-propyn-1-ol and Et_2NH. A mixture of 3-(2-pyridyl)-2-propyn-1-ol (0.65 g), Et_2NH (3 ml), $Pd(PPh_3)_2Cl_2$ (73 mg), and CuI (5 mg) was heated at 80 °C for 4 h with stirring under nitrogen. The solution was evaporated, and the residue was chromatographed over basic Al_2O_3 with hexane–ether (50:1) to give 3-(diethylamino)indolizine (**4c**); yield, 0.14 g (15%). A similar operation in the absence of $Pd(PPh_3)_2Cl_2$ and CuI did not give **4c**; rather the starting material was recovered.

Reaction of 3-(2-Pyridyl)acrylaldehyde and Et_2NH. A solution of 3-(2-pyridyl)acrylaldehyde (230 mg) in Et_2NH was allowed to stand at room temperature (26 °C) for 30 min under nitrogen. The solution was then evaporated below 35 °C, and the residue was chromatographed over basic Al_2O_3 with hexane to give 170 mg (56%) of **4c**.

References

1) A preliminary communication has been reported: *Chem. Lett.*, **1979**, 241.

2) M. Scholtz, *Ber. Dtsch. Chem. Ges.*, **45**, 734 (1912).

3) E. J. Swinbourne, "Advances in Heterocyclic Chemistry," ed by A. R. Katritzky and A. J. Boulton, Academic Press, New York (1978), Vol. 23, p. 103.

4) For example, I. Antonini, F. Claudi, U. Gulini, L. Micossi, and F. Venture, *J. Pharm. Sci.*, **68**, 321 (1979).

5) For example, A. Gamba and G. Favini, *Gazz. Chim. Ital.*, **98**, 167 (1968) and the references cited therein.

6) J. Hurst, T. Melton, and D. G. Wibberley, *J. Chem. Soc.*, **1965**, 2948.

7) K. Sonogashira, Y. Tohda, and N. Hagihara, *Tetrahedron Lett.*, **1975**, 4467.

8) V. Boekelheide and W. Feely, *J. Org. Chem.*, **22**, 589 (1957).

9) K. B. Nielsen, *Acta Chem. Scand.*, **B31**, 224 (1977); 3-chloroindolizine was obtained in a very low yield from the reaction of 2-vinylpyridine and dichlorocarbene.

10) K. Edo, H. Yamanaka, and T. Sakamoto, *Heterocycles*, **9**, 271 (1978).

11) Y. Abe, A. Ohsawa, H. Arai, and H. Igeta, *Heterocycles*, **9**, 1397 (1978).

12) G. R. Lappin, *J. Org. Chem.*, **16**, 419 (1951).

13) A. Ohsawa, Y. Abe, and H. Igeta, *Chem. Pharm. Bull. (Tokyo)*, **26**, 2550 (1978).

14) M. S. Shvartsberg, I. L. Kotlyarevskii, A. N. Kozhevnikova, and V. N. Andrievskii, *Izv. Akad. Nauk SSSR, Ser. Khim.*, **1970**, 1144 [*Chem. Abstr.*, **73**, 130851w (1970)].

The Synthesis of 2-Styrylazulene and Its Derivatives by the Condensation of 2-Methylazulene Derivatives with Benzaldehydes

Motoyasu SAITO, Tadayoshi MORITA, and Kahei TAKASE*

Department of Chemistry, Faculty of Science, Tohoku University, Aramaki-aza-Aoba, Sendai 980

(Received March 10, 1980)

The reaction of 2-methylazulene derivatives, such as dimethyl 2-methylazulene-1,3-dicarboxylate, methyl 3-cyano-2-methylazulene-1-carboxylate, and 1-cyano- and 1-carbamoyl-2-methylazulenes, with benzaldehyde in the presence of alkoxide resulted in condensation to give 2-styrylazulene derivatives. 2-Styrylazulene, a parent hydrocarbon, and its *p*-nitro and *p*-dimethylamino derivatives were also synthesized.

Styrylazulenes are important azulenic compounds analogous to stilbene and interesting for their chemical and physical properties. Of the five possible position isomers, 1-,[1] 5-,[2] and 6-styrylazulenes,[2] and some derivatives of 4-,[3] and 5-styrylazulenes[4] have been synthesized.

On the other hand, we have found that 2-methylazulene derivatives with electron-withdrawing substituents, such as an alkoxycarbonyl or cyano group, at the 1 (and/or 3)-position easily condensed with benzaldehyde in the presence of alkoxide to give 2-styrylazulene derivatives; an outline of a part of these results has been reported in a preliminary communication.[5] This paper will describe the details of the synthesis of 2-styrylazulene (**1**) and its derivatives by the condensation of 2-methylazulene derivatives with benzaldehydes.

Results and Discussion

2-Methylazulene (**2**) and its derivatives, such as dimethyl 2-methylazulene-1,3-dicarboxylate (**3**), methyl 3-cyano-2-methylazulene-1-carboxylate (**4**), and 1-cyano- (**5**) and 1-carbamoyl-2-methylazulenes (**6**), were prepared, and the condensation reactions of these azulenes with benzaldehyde were examined, in order to synthesize 2-styrylazulenes. The treatment of **2** with benzaldehyde in the presence of sodium ethoxide gave no condensation product. In contrast with this, the treatment of **3** and **4** with benzaldehyde in the presence of sodium methoxide or ethoxide at room temperature resulted in condensation to give 3-methoxycarbonyl- (**7**) and 3-cyano-2-styrylazulene-1-carboxylic acids (**8**) in excellent yields respectively. In a similar manner, **5** gave 1-cyano-2-styrylazulene (**9**) in a good yield. The condensation of **6** with benzaldehyde was not easy, so it proceeded under reflux to give 1-carbamoyl-2-styrylazulene (**10**) in only a low yield of 14%. The structures of **7**, **8**, **9**, and **10** were determined on the basis of the chemical evidence described below, as well as the spectral data. Compounds **7** and **8** are acidic enough to be soluble in an aq sodium hydrogen carbonate solution and gave methyl esters (**11** and **12**) on methylation with diazomethane. The treatment of **7** and **8** with phosphoric acid[6] resulted in decarboxylation to give methyl 2-styrylazulene-1-carboxylate (**13**) and **9** respectively. Further, on treatment with concd sulfuric acid at 100 °C,[6] **9** gave **10**, together with a lactam, judging from the IR spectrum, which exhibits the $\nu_{C=O}$ of amide at 1639 cm^{-1}, compatible with that at 1642 cm^{-1} in 1-carbamoyl-2-methylazulene.[6] The NMR spectral data are also consistent with the assigned structure. The configuration of the ethylenic linkage in the 2-styrylazulenes obtained here is established to be *trans* on the basis of the IR and NMR spectral data.[5] The formation of the hydrolized carboxylic acids, **7** and **8**, even though the reaction was carried out under anhydrous media, is presumed to be *via* lactone-type intermediates.[5]

The fact that **3**, **4**, and **5** easily reacted with benzaldehyde in the presence of alkoxide to give the condensation products indicates that the methyl group at the 2-position in these compounds is acidic enough to yield the carbanion, which can react with benzaldehyde, by means of alkoxide. For this reason, it seems that the electronic effects, that is, the mesomeric and inductive effects of the electron-withdrawing methoxycarbonyl or cyano substituent at the 1 (and/or 3)position of the azulene ring, contribute to the activation of the methyl proton. Such condensation also took place when other aromatic aldehydes were used. Thus, the treatment of **5** with *p*-nitro- and *p*-dimethylaminobenzaldehydes in the presence of sodium ethoxide gave 1-cyano-2-(*p*-nitrostyryl)- (**15**) and 1-cyano-2-(*p*-dimethylaminostyryl)azulenes (**16**) respectively, although in the latter case, the reaction was not easy, but did proceed by heating under reflux.

A parent hydrocarbon, **1**, could be obtained from

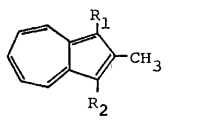

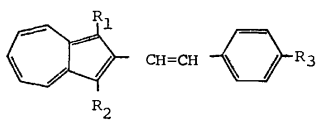

2: R_1= R_2= H
3: R_1= R_2= CO_2Me
4: R_1= CO_2Me, R_2= CN
5: R_1= CN, R_2= H
6: R_1= $CONH_2$, R_2= H

1: R_1= R_2= R_3= H
7: R_1= CO_2H, R_2= CO_2Me, R_3= H
8: R_1= CO_2H, R_2= CN, R_3= H
9: R_1= CN, R_2= R_3= H
10: R_1= $CONH_2$, R_2= R_3= H
11: R_1= R_2= CO_2Me, R_3= H
12: R_1= CO_2Me, R_2= CN, R_3= H
13: R_1= CO_2Me, R_2= R_3= H
15: R_1= CN, R_2= H, R_3= NO_2
16: R_1= CN, R_2= H, R_3= NMe_2
17: R_1= R_2= H, R_3= NO_2
18: R_1= R_2= H, R_3= NMe_2
19: R_1= $CONH_2$, R_2= H, R_3= NO_2
20: R_1= $CONH_2$, R_2= H, R_3= NMe_2

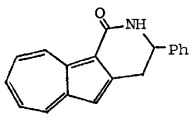

14

Fig. 1.

7 in an 88% yield on hydrolysis with aq ethanolic alkali and the subsequent decarboxylation of the resulting dicarboxylic acid by heating with phosphoric acid. Further, **1** was also obtained from **10** by decarbamoylation[6] on treatment with phosphoric acid. 2-(*p*-Nitrostyryl)- (**17**) and 2-(*p*-dimethylaminostyryl)azulene (**18**) could also be synthesized as follows: the treatment of **15** and **16** with concd sulfuric acid afforded carbamoyl derivatives (**19** and **20**), accompanied by the formation of small amounts of **17** and **18** respectively. Further, the treatment of **19** and **20** with phosphoric acid resulted in decarbamoylation to give **17** and **18** respectively in good yields.

Experimental

All the melting points are uncorrected. The IR spectra were taken on a Shimadzu IR-27 infracord spectrophotometer, and the electronic spectra, on a Hitachi EPS-3 spectrophotometer. The NMR spectra were recorded with a Varian A-60D spectrometer. Compounds **4**, **5**, and **6** were prepared according to a method previously reported.[6]

*Dimethyl 2-Methylazulene-1,3-dicarboxylate (**3**).* This compound was prepared by a procedure similar to that used for the preparation of ethyl methyl 2-methylazulene-1,3-dicarboxylate.[6] A mixture of 940 mg (5 mmol) of 3-acetyl-2*H*-cyclohepta[*b*]furan-2-one[6] and 1.32 g (10 mmol) of dimethyl malonate in a sodium methoxide solution, prepared from 460 mg of sodium and 50 ml of anhydrous methanol, was treated in a manner similar to that previously described.[6] The part insoluble in an aq potassium carbonate solution gave 160 mg (13%) of methyl 3-acetyl-2-hydroxyazulene-1-carboxylate as yellow needles; mp 201—202 °C (from benzene). IR (KBr): 3440, 1670, 1127, and 1053 cm^{-1}. Found: C, 68.62; H, 5.02%. Calcd for $C_{14}H_{12}O_4$: C, 68.84; H, 4.95%.

The part soluble in an aq potassium carbonate solution gave 640 mg (52%) of 3-methoxycarbonyl-2-methylazulene-1-carboxylic acid as pale red crystals; mp 209 °C (dec). The treatment of this acid with diazomethane in a manner similar to that previously described[6] gave 595 mg of **3** as red needles; mp 112—115 °C (from methanol). λ_{max}^{MeOH} 237 nm (log ε 4.50), 270 (4.38), 295 (4.57), 305 (4.66), 343 (3.90), 371 (3.93), and 490 (2.95); IR (KBr): 1690, 1233, and 1080 cm^{-1}. Found: C, 70.01; H, 5.51%. Calcd for $C_{15}H_{14}O_4$: C, 69.75; H, 5.46%.

*3-Methoxycarbonyl-2-styrylazulene-1-carboxylic Acid (**7**).* To a sodium methoxide solution, prepared from 300 mg of sodium and 15 ml of anhydrous methanol, 1.29 g (5 mmol) of **3** and 900 mg (8.5 mmol) of benzaldehyde were added; the mixture was stirred for 5 h and then allowed to stand overnight at room temp. The reaction mixture was diluted with 100 ml of water and shaken with ether. The ether layer was washed with water and concentrated to recover 340 mg of **3**. The combined aq solution was acidified with with 6 M (1M = 1 mol dm^{-3}) hydrochloric acid, and the crystals thus separated out were collected to give 1.10 g (90%) of **7** as red prisms; mp 177—178 °C (from methanol). λ_{max}^{MeOH} 233 nm (log ε 4.50), 295 (4.50), 338 (4.71), 404 (4.20), and 540 (2.75). Found: C, 76.19; H, 4.97%. Calcd for $C_{21}H_{16}O_4$: C, 75.89; H, 4.85%.

*3-Cyano-2-styrylazulene-1-carboxylic Acid (**8**).* A mixture of 900 mg (4 mmol) of **4** and 720 mg (6.8 mmol) of benzaldehyde in a sodium ethoxide solution, prepared from 280 mg of sodium and 20 ml of anhydrous ethanol, was treated in a manner similar to that described above to give 1.17 g (98%) of **8** as reddish brown prisms: mp 238—239 °C (from ethanol). λ_{max}^{MeOH} 230 nm (log ε 4.46), 340 (4.76), 409 (4.23), and 560 (2.72). Found: C, 79.88; H, 4.48; N, 4.69%. Calcd for $C_{20}H_{13}O_2N$: C, 80.25; H, 4.38; N, 4.68%.

*1-Cyano-2-styrylazulene (**9**). a)*: A mixture of 165 mg (1 mmol) of **5** and 180 mg (1.7 mmol) of benzaldehyde in a sodium ethoxide solution, prepared from 70 mg of sodium and 5 ml of ethanol, was stirred for 5 h and then allowed to stand overinght at room temp. The reaction mixture was subsequently diluted with 50 ml of water and extracted with chloroform. After the evaporation of the solvent from the extract, the residue was chromatographed (alumina, benzene) to give 170 mg (67%) of **9** as green needles; mp 119—120 °C (from benzene–cyclohexane). λ_{max}^{MeOH} 231 nm (log ε 4.27), 323 (4.75), 335 (4.83), 388 (4.15), 408 (4,43), 433 (4.42), 558 (2.72), 589 (2.75), and 653 (2.42). Found: C, 90.01; H, 5.15; N, 5.38%. Calcd for $C_{19}H_{13}N$: C, 89.38; H, 5.13; N, 5.49%.

b): A mixture of 220 mg o **8** and 3 ml of 85% phosphoric acid was heated at 100 °C for 30 min; then it was poured into ice water and extracted with chloroform. The extract was worked up as has been described above to give 160 mg (85%) of **9** as green needles; mp 119—120 °C.

*1-Carbamoyl-2-styrylazulene (**10**).* A mixture of 50 mg (0.27 mmol) of **6** and 80 mg (0.76 mmol) of benzaldehyde in a sodium ethoxide solution, prepared from 70 mg of sodium and 3 ml of ethanol, was heated under reflux for 5.5 h. The reaction mixture was then diluted with 20 ml of water and extracted with chloroform. After the evaporation of the solvent from the extract, the residue was chromatographed (silica gel, benzene) to give 10 mg (14%) of **10** as green needles; mp 207—208 °C (from benzene). λ_{max}^{MeOH} 318 nm (log ε 4.64), 327 (4.72), 405 (4.38), and 426 (4.26). Found: C, 83.46; H, 5.82; N, 4.85%. Calcd for $C_{19}H_{15}ON$: C, 83.49; H, 5.53; N, 5.13%.

*Dimethyl 2-Styrylazulene-1,3-dicarboxylate (**11**).* To a suspension of 300 mg of **7** in 20 ml of ether, 5 ml of an ethereal solution of diazomethane was added, after which the mixture was stirred for 3 h and allowed to stand overnight in a refrigerator. After the evaporation of the solvent, the residue was chromatographed (alumina, benzene) to give 300 mg (96%) of **11** as red scales; mp 136—137 °C (from methanol). λ_{max}^{MeOH} 233 nm (log ε 4.59), 294 (4.58), 338 (4.80), 404 (4.31), and 540 (2.81). Found: C, 76.21; H, 5.50%. Calcd for $C_{22}H_{18}O_4$: C, 76.28; H, 5.24%.

*Methyl 3-Cyano-2-styrylazulene-1-carboxylate (**12**).* The treatment of 200 mg of **8** with diazomethane in a manner similar to that described above gave 190 mg (91%) of **12** as red needles; mp 149—150 °C (from cyclohexane). λ_{max}^{MeOH} 232 nm (log ε 4.06), 291 (4.31), 342 (4.77), and 410 (4.35). Found: C, 80.54; H, 4.97; N, 4.47%. Calcd for $C_{21}H_{15}O_2N$: C, 80.49; H, 4.83; N, 4.47%.

*Methyl 2-Styrylazulene-1-carboxylate (**13**).* A mixture of 50 mg of **7** and 1 ml of 100% phosphoric acid was heated at 100 °C for 3 min; then it was poured into 10 ml of ice water and extracted with chloroform. After the evaporation of the solvent, the residue was chromatographed (alumina, benzene) to 35 mg (81%) of **13** as green needles; mp 88—89 °C (from methanol). λ_{max}^{MeOH} 335 nm (log ε 4.50), 402 (4.05), 424 (3.90), and 574 (2.86). Found: C, 83.02; H, 5.52%. Calcd for $C_{20}H_{16}O_2$: C, 83.31; H, 5.59%.

*Treatment of **9** with Sulfuric Acid.* A mixture of 510 mg of **9** and 4 ml of 80% sulfuric acid was heated at 100 °C for 1 h; then it was poured into 80 ml of ice water and extracted with chloroform. After the evaporation of the solvent from the extract, the residue was chromatographed

(alumina, benzene, and chloroform). The first fraction, eluted with benzene, recovered 32 mg of **9**. The second fraction, eluted with benzene, gave 95 mg (19%) of **14** as reddish violet prisms; mp 204—205 °C (from benzene). λ_{max}^{MeOH} 299 nm (log ε 4.65), 358 (3.91), and 376 (3.95). NMR ($CDCl_3$) δ 3.34 (d, J=8.0 Hz, $CHC\underline{H}_2$), 4.94 (t, J=8.0 Hz, $C\underline{H}CH_2$), 5.80 (br s, N$\underline{H}$), 7.05 (s, H-3), 7.4—7.8 (m H-5, -7), 7.38 (br s, C_6H_5), 8.33 (br d, J=9 Hz, H-4), 9.70 (br d, J=9 Hz, H-8). Found: C, 83.46; H, 5.54; N, 5.05%. Calcd for $C_{19}H_{15}ON$: C, 83.49; H, 5.53; N, 5.13%. The third fraction, eluted with chloroform, gave 210 mg (41%) of **10** as green needles; mp 207—208 °C.

*2-Styrylazulene (**1**).* *a)*: A solution of 1.00 g of **7** dissolved in a mixture of 10 ml of a 10% aq potassium hydroxide solution and 100 ml of ethanol, was heated under reflux for 40 min. The subsequent acidification of the solution with 1 M hydrochloric acid separated out 920 mg of 2-styrylazulene-1,3-dicarboxylic acid. A mixture of the acid and 5 ml of 85% phosphoric acid was heated at 100 °C for 15 min and then poured into 100 ml of ice water and extracted with chloroform. After the evaporation of the solvent from the extract, the residue was chromatographed (alumina, benzene) to give 610 mg (88%) of **1** as green scales; mp 207—208 °C (from cyclohexane). Found: C, 93.95; H, 6.11%. Calcd for $C_{18}H_{14}$: C, 93.87; H, 6.13%.

b): A mixture of 80 mg of **10** and 1 ml of 85% phosphoric acid was heated at 100 °C for 1 h; then it was diluted with 20 ml of water and extracted with chloroform. After the evaporation of the solvent, the residue was chromatographed (alumina, benzene) to give 40 mg (59%) of **1** as green scales; mp 207—208 °C.

*1-Cyano-2-(p-nitrostyryl)azulene (**15**).* A mixture of 166 mg (1 mmol) of **5** and 226 mg (1.5 mmol) of *p*-nitrobenzaldehyde in a sodium ethoxide solution, prepared from 53 mg of sodium and 3 ml of ethanol, was stirred for 20 h at 0—10 °C; then it was diluted with 20 ml of water and extracted with chloroform. The extract was washed with water and concentrated, and the residue was chromatographed (alumina, benzene) to give 75 mg (25%) of **15** as bluish green needles; mp 227—228 °C (from benzene). λ_{max}^{MeOH} 233 nm (log ε 4.27), 286 (4.20), 333 (4.72), 404 (4.59), and 424 (4.48). Found: C, 75.51; H, 4.07; N, 9.16%. Calcd for $C_{19}H_{12}O_2N_2$: C, 75.99; H, 4.03; N, 9.33%.

*1-Cyano-2-(p-dimethylaminostyryl)azulene (**16**).* A mixture of 167 mg (1 mmol) of **5** and 255 mg (1.7 mmol) of *p*-dimethylaminobenzaldehyde in a sodium ethoxide solution, prepared from 56 mg of sodium and 3 ml of ethanol, was heated under reflux for 7 h. The reaction mixture was then worked up in a manner similar to that described above, except for the use of chloroform in place of benzene as the solvent for chromatography, to give 113 mg (38%) of **16** as reddish brown needles; mp 196—197 °C (benzene). λ_{max}^{MeOH} 260 nm (log ε 4.17), 307 (4.63), 357 (4.45), and 490 (4.57). Found: C, 84.26; H, 5.91; N, 9.55%. Calcd for $C_{21}H_{18}N_2$: C, 84.53; H, 6.08; N, 9.39%.

*2-(p-Nitrostyryl)- (**17**) and 1-Carbamoyl-2-(p-nitrostyryl)-azulene (**19**).* *a)*: A mixture of 340 mg of **15** and 4 ml of concd sulfuric acid was heated at 100 °C for 3 h and then diluted with 50 ml of water. The crystals thus separated out were collected and chromatographed (alumina, benzene and chloroform). The first fraction, eluted with benzene, gave 10 mg (3%) of **17** as green prisms; mp 254—256 °C (from chloroform). λ_{max}^{MeOH} 231 nm (log ε 4.07), 282 (4.50), 323 (4.51), 406 (4.60), 425 (4.51), 584 (2.67), and 627 (2.64). Found: C, 78.42; H, 4.61; N, 4.89%. Calcd for $C_{18}H_{13}O_2N$: C, 78.53; H, 4.76; N, 5.09%. The second fraction, eluted with chloroform, gave 230 mg (64%) of **19** as green needles; mp 238—239 °C (from chloroform). λ_{max}^{MeOH} 230 nm (log ε 4.97), 284 (4.50), 327 (4.59), and 404 (4.55). Found: C, 71.64; H, 4.43; N, 8.60%. Calcd for $C_{19}H_{14}O_3N_2$: C, 71.69; H, 4.43; N, 8.80%.

b): A mixture of 260 mg of **19** and 3 ml of 100% phosphoric acid was heated at 100 °C for 3 h and then worked up in a manner similar to that described above to give 69 mg (31%) of **17** as green prisms; mp 254—256 °C.

*2-(p-Dimethylaminostyryl)- (**18**) and 1-Carbamoyl-2-(p-dimethylaminostyryl)azulene (**20**).* *a)*: A mixture of 310 mg of **16** and 3 ml of 80% sulfuric acid was treated in a manner similar to that described above. The first fraction from chromatography, eluted with benzene, gave 30 mg (11%) of **18** as reddish brown scales; mp 237—238 °C (from benzene). λ_{max}^{MeOH} 262 nm (log ε 4.30), 294 (4.68), 340 (4.56). Found: C, 87.76; H, 7.10; N, 5.00%. Calcd for $C_{20}H_{19}N$: C, 87.87; H, 7.01; N, 5.12%. The second fraction, eluted with benzene, gave 130 mg (40%) of **20** as brownish green prisms; mp 249—250 °C (from chloroform–ethyl acetate). λ_{max}^{MeOH} 302 nm (log ε 4.50), 352 (4.36), 468 (4.44). Found: 79.38; H, 6.05; N, 8.88%. Calcd for $C_{21}H_{20}ON_2$: C, 79.71; H, 6.37; N, 8.85%.

b): A mixture of 100 mg of **20** and 1 ml of 85% phosphoric acid was heated at 100 °C for 2 h; then it was worked up in a manner similar to that described above to give 48 mg (56%) of **18** as reddish brown scales; mp 237—238 °C.

This research has been financially supported by a Grant-in-Aid for Scientific Research from the Japanese Ministry of Education and by a grant from the Sankyo Co., Ltd.

References

1) R. N. McDonald and W. S. Stewart, *J. Org. Chem.*, **30**, 270 (1965).
2) H. Matsumura and S. Nagamura, *Nippon Kagaku Zasshi*, **85**, 901 (1964).
3) M. Scholz, L. n. Vien, G. Fisher, B. Tschapke, and M. Muhlstädt, *Chem. Ber.*, **100**, 375 (1967).
4) T. Kuraoka, *Nippon Kagaku Zasshi*, **83**, 928 (1962).
5) M. Saito, T. Morita, and K. Takase, *Chem. Lett.*, **1974**, 289.
6) T. Nozoe, K. Takase, T. Nakazawa, and S. Fukuda, *Tetrahedron*, **27**, 3357 (1971).

Acid-catalyzed Rearrangement of the *exo*-1,2-Dioxetane Derivative from 1-Isopropylidene-4,4-diphenyl-2,5-cyclohexadiene[1)]

Akira KAWAMOTO, Hisashi UDA,* and Nobuyuki HARADA

Chemical Research Institute of Non-aqueous Solutions, Tohoku University, 2-1-1 Katahira, Sendai 980

(Received March 13, 1980)

It is shown that acid-catalyzed decomposition of the 1,2-dioxetane derivative, 3,3-dimethyl-7,7-diphenyl-1,2-dioxaspiro[3.5]nona-5,8-diene, obtained from 1-isopropylidene-4,4-diphenyl-2,5-cyclohexadiene, gives 1-methyl-1-(*o*-terphenyl-4′-yl)ethyl hydroperoxide, bis[1-methyl-1-(*o*-terphenyl-4′-yl)ethyl] peroxide, 1-(1-hydroperoxy-1-methylethyl)-4,4-diphenylcyclohexa-2,5-dien-1-ol, and *o*-terphenyl-4′-ol, along with the usual dioxetane-scission product, 4,4-diphenyl-2,5-cyclohexadienone. The distribution and yield of these products depend on acidic agents and/or conditions employed.

Recent work by Zimmerman and coworkers[2)] concerning the thermal decomposition of the 1,2-dioxetane **2** derived from 1-isopropylidene-4,4-diphenyl-2,5-cyclohexadiene (**1**) prompts us to report results concerning the acid-catalyzed decomposition of **2** obtained simultaneously and independently in our laboratory.[1)] Zimmerman and coworkers reported[2)] that the thermal decomposition of **2** produced the rearranging excited state of 4,4-diphenyl-2,5-cyclohexadienone (**3**), which gave 6,6-diphenylbicyclo[3.1.0]hex-3-en-2-one (**4**),

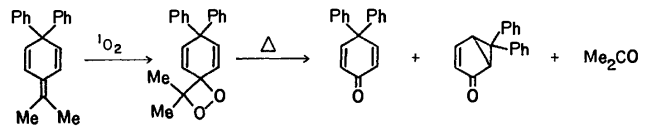

1 2 3 4

along with **3** and acetone.[3)] In our hands, the acid-catalyzed decomposition of **2** gave the *o*-terphenyl derivatives through a novel rearrangement pathway involving the scission of a carbon-oxygen bond, the migration of a phenyl group, and aromatization, which demonstrates that in the case of a special derivative the new type of cleavage of a dioxetane ring, competing with the usual dioxetane scission, may also occur.[4)]

Results and Discussion

The starting isopropylidenediphenylcyclohexadiene **1** was prepared by the Wittig reaction of the dienone **3** with isopropylidenetriphenylphosphorane.

Photooxidation. Photooxidation of **1** in anhydrous methanol at −78 °C using Rose Bengal as a sensitizer gave, after immediate separation by preparative thin-layer chromatography (TLC) on silica gel below −12 °C, a 60—90% yield of the crystalline dioxetane **2**, mp 57—61 °C (dec). The 1,2-dioxetane structure of **2** was verified by the spectral and chemical properties. A wide range of the yield of **2** depends on the reaction and/or isolation conditions: concentration, irradiation time, temperature, the nature of TLC plate, and so on. In fact, on further purification, **2** appreciably decomposed on a preparative silica gel plate to produce more polar substances (see below).

Decomposition of the 1,2-Dioxetane 2 on Silica Gel. From the observation that the dioxetane **2** is extremely sensitive to the photooxidation and isolation conditions, we have examined the reactivity of **2** to acidic agents. Re-chromatography (preparative TLC on silica gel) of **2** at 0 °C afforded, in addition to the dienone **3** (usually the major product), three crystalline products, the *o*-terphenyl hydroperoxide **5**, mp 125.5—128 °C, the dimeric *o*-terphenyl peroxide **6**, mp 148—150 °C, and the hydroxy hydroperoxide **7**, mp 124—126 °C, respectively. From a number of experiments, it was found that the decomposition of **2** on silica gel was greatly affected not only by temperature for charging and developing but also by the nature of silica gel plates used (probably due to activity, water-content, *etc*). Thus, the yields of these products were not always constant, varying appreciably from run to run; particularly, often compound **7** was not isolated due to its instability (see below).

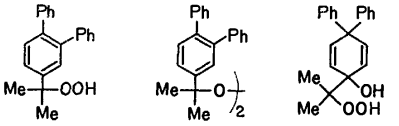

5 6 7

The structure of compound **5** was elucidated on the basis of the following spectral and chemical evidence. Compound **5** revealed the 1,3,4-trisubstituted benzene proton signals in the ^1H NMR and the absorption maxima characteristic of an *o*-terphenyl chromophor in the UV spectrum. Compound **5** showed positive potassium iodide-starch test, and treatment of **5** with various reducing reagents gave quantitatively the hydroxy compound **8**. The authentic sample of **8** was prepared by two alternative ways as shown in Scheme 1. The Diels-Alder reaction of 2,3-diphenyl-1,3-butadiene (**9**) with methyl acrylate provided the adduct **10**. Bromination of **10**, followed by dehydrobromination or direct dehydrogenation of **10** with DDQ afforded methyl *o*-terphenyl-4′-carboxylate (**11**),

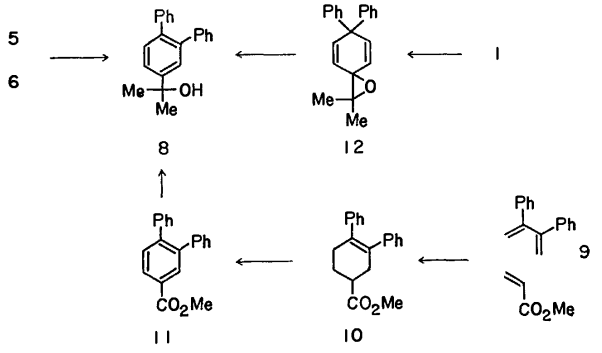

Scheme 1.

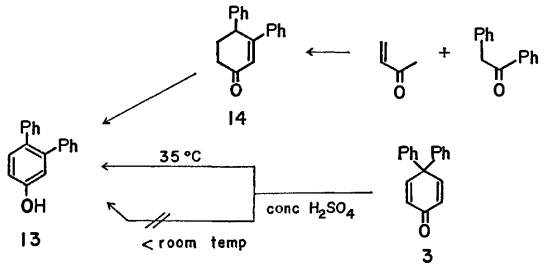

Scheme 2.

which was then transformed into **8** by the action of excess methylmagnesium iodide. Treatment of **1** with *m*-chloroperbenzoic acid gave the unstable exocyclic epoxide **12**, which was easily converted into **8** by chromatography on silica gel. The sample of **8** thus obtained was identical with that derived from **5**. The latter reaction sequence clearly indicates that the 4,4-diphenyl-2,5-cyclohexadienyl system easily undergoes a phenyl migration and aromatization.

Similarly, the product **6** also gave quantitatively the alcohol **8** on lithium aluminum hydride reduction or catalytic hydrogenation; thus, combining with the close resemblance of the spectral (^{1}H NMR and UV) properties to those of **5** or **8** and with the analytical result, the structure of **6** was assigned to be the dimeric *o*-terphenyl peroxide.

The third component **7** is the most polar compound and shows the simple ^{1}H NMR spectrum including the AB-type signal due to olefinic protons (total 4H) and the broad signal due to two protons exchangeable with deuterium oxide. These data suggests that this compound possesses a symmetrical structure having two hydroxylic functions. Furthermore, **7** is fairly unstable in solutions. The ^{1}H NMR spectrum of **7** in carbon tetrachloride or deuteriochloroform changed gradually on standing, and the final spectrum, after a few hours at 30 °C, was wholly in accord with that of the hydroperoxide **5**. From these facts, the vicinal hydroxy hydroperoxide structure **7** was assigned to this compound, and **7** meets the requirement of an intermediate in the rearrangement of **2** to **5**. The easy transformation of **7** into **5** in chlorinated solvents may be catalyzed by a trace of hydrogen (or deuterium) chloride contaminated.

Decomposition of the 1,2-Dioxetane 2 by Hydrochloric Acid. The same decomposition of **2** was also induced by hydrochloric acid, and temperature dependence on product distribution was observed. Thus, treatment of an ethereal solution of **2** with 2—6 M (1 M=1 mol dm^{-3}) hydrochloric acid at room temperature gave **3** (*ca.* 29%), **5** (*ca.* 15%), and **6** (*ca.* 34%), respectively. While below 0 °C **6** was obtained quantitatively. On treating a chloroform solution of **2** with concd hydrochloric acid below −10 °C, **6** also arose as the single product. Further, we found that these compounds **5** and **6** were not interconverted under the conditions examined, and therefore, they would be formed from **2** through different pathways subtly depending upon the environmental conditions.

Decomposition of the 1,2-Dioxetane 2 under Anhydrous Conditions. A noteworthy feature of the decomposition of **2** under the anhydrous conditions is the

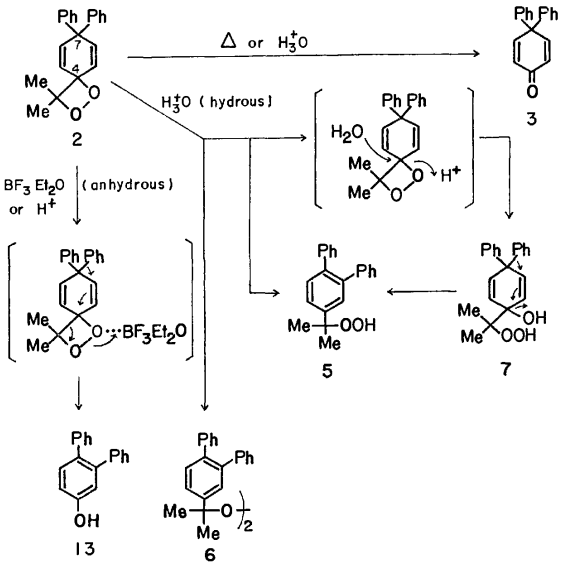

Scheme 3.

formation of a new product. Treatment of an ethereal solution of **2** with boron trifluoride etherate below −12 °C or with concd sulfuric acid below −10 °C afforded quantitatively *o*-terphenyl-4′-ol (**13**). Compound **13** was identical with a sample, which was prepared through 3,4-diphenyl-2-cyclohexenone (**14**) as shown in Scheme 2, as determined by comparison of the spectra. Since **13** corresponds to the dienone-phenol rearrangement product of the dienone **3**, **3** seems to be the most probable precursor of **13**. It was found, however, that **3** was stable even at room temperature to both of boron trifluoride etherate and concd sulfuric acid in ether. The rearrangement of **3** to **13** ultimately occurred upon prolonged refluxing. Thus, **3** would not be the precursor of **13** from **2** under the decomposition conditions examined. Acid-catalyzed decomposition of the hydroperoxide **5** to **13** corresponds to the synthetic process of phenol from cumene through cumene hydroperoxide, and therefore, the process of **2**→**5**→**13** would be an alternative pathway for the formation of **13**. However, from the fact that compound **5**, as well as compound **6**, was also inert under the decomposition conditions of **2**, this process also appears unlikely. Consequently, **13** would be formed directly from **2** through a novel fragmentation.

When wet ether was used in the decomposition of **2** by boron trifluoride etherate below −20 °C, the peroxide **6** became the sole isolable product (24%).

It is to be noted that the ionic decomposition of **2** was also observed on heating at 60—70 °C in carbon tetrachloride. The reaction was carried out in an NMR tube in the ordinary manner and followed by the ^{1}H NMR spectrum. The temporary production of the hydroxy hydroperoxide **7** could be detected, and the final product was shown to be a 1:2—5:1 mixture of **3** and **5**; there was no indication of the presence of the rearranged bicyclic ketone **4**. Traces of hydrogen chloride and water in carbon tetrachloride may cause the ionic fragmentation. Turning to the photooxidation experiment of **1**, the use of chloroform as a solvent at room temperature led to the formations

of **3**, **5**, and **6**.

As is clear from the results discussed above the reactivity of the dioxetane **2** is extremely sensitive to acidic agents and environmental conditions, and the product distribution and yield are very diverse. Although the detailed mechanisms for the formation of the products still remained unclarified, because of the low availabilities and/or the high sensitivities of both **2** and products, the results are summarized in Scheme 3.

It is conceivable that the dienone **3** arises partly from the usual thermal fission and partly from the acid (or impurities)-catalyzed one of the dioxetane ring.

The most important mode of the reaction of **2** under the hydrous conditions is the competitive cleavage of the ring carbon (C4)–oxygen bond of the dioxetane moiety. Such a cleavage of 1,2-dioxetane ring has been observed in the rearrangement of tetramethyl-1,2-dioxetane by boron trifluoride in aprotic solvents, resulted from one-oxygen coordination with boron trifluoride.[4b] In our case, easy and selective cleavage of the C4–O bond in **2** might be due to the allylic nature of C4. The ring opening and the attack of water at C4 gives the hydroxy hydroperoxide **7**. The hydroperoxide **5** is certainly formed by dehydration of **7** as discussed earlier. However, the direct pathway from **2** involving ring opening, migration of a double bond and subsequently of a phenyl group, and deprotonation can not be ruled out. The mechanism for formation of the dimeric peroxide **6** is still obscure. Anyhow, a high migratory aptitude of phenyl group and stabilization by aromatization, in addition to the allylic nature of a dioxetane carbon, should promote the formations of **5** and **6**. Among these factors, a phenyl substituent at C7 plays the most important role in the rearrangement, because the 4,4-dimethyl analogue of **1**, on sensitized photooxidation, underwent exclusively the usual 1,2-dioxetane fission to produce 4,4-dimethyl-2,5-cyclohexadienone in quantitative yield.

In view of the recent findings by Hasty and Kearns,[4a] the vicinal hydroxy hydroperoxide **7** is a unique compound as a product derived from 1,2-dioxetane derivatives. They demonstrated that the mono (epidioxide) **15** derived from 2,5-dimethyl-2,4-hexadiene can not be the intermediate in the formation of the vicinal hydroxy (or methoxy) hydroperoxide **16** which was produced by photooxidation of the above diene in basic nucleophilic solvents, as well as in the formation of the 1,4-hydroxy (or methoxy) hydroperoxide **17** in acidic media.

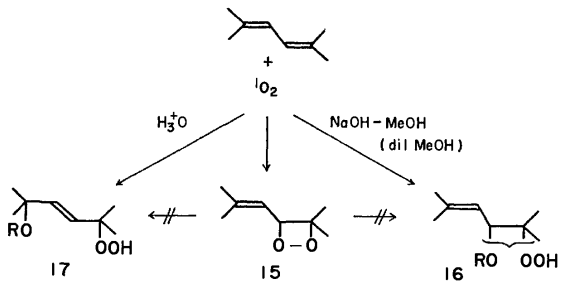

As described above, the phenol **13** would arise directly from **2**, not through **3** or **5**. An explanation for the process leading to **13** is that the coordination of acidic agents to the dioxetane oxygen atom attached to C4 might initiate the ionic fragmentation, and the simultaneous isomerization and aromatization as in the case of **5** or **6** would produce **13** as shown.

Experimental

Melting points are uncorrected. IR spectra were obtained with a Hitachi EPI-S2 or G2 and UV spectra with a Hitachi EPS-3T spectrophotometer. ^1H NMR spectra were recorded with a JEOL C-60HL (60 MHz), PMX-60 (60 MHz), or PS-100 (100 MHz) instrument with TMS as an internal standard; coupling constants are given in Hz. Mass spectra were taken with a Shimadzu LKB-9000 instrument. Silica gel (Merck GF-254) was used for analytical and preparative thin-layer chromatography (TLC); solvent systems are indicated in parentheses. Almost all of new compounds described in this paper did not give the satisfactory analytical data; the variable percentages (always low) of carbon were observed. This may be due to the thermal instabilities and/or the high contents of aromatic carbon atoms of these compounds.

*1-Isopropylidene-4,4-diphenyl-2,5-cyclohexadiene (**1**).* To a stirred suspension of isopropyltriphenylphosphonium iodide[5] (520 mg, 1.20 mmol) in anhydrous ether (15 ml) was added a solution of butyllithium in hexane (20%, 0.6 ml, 1.30 mmol) dropwise at room temperature under nitrogen. After stirring at room temperature for 15 min, a solution of 4,4-diphenyl-2,5-cyclohexadienone (**3**)[6] (250 mg, 1.00 mmol) in anhydrous ether (6 ml) and DMSO (2.5 ml) was added dropwise, and the reaction mixture was heated under reflux for 2 h. After the removal of insoluble material by filtration, the filtrate was washed with aqueous DMSO (50%, 50 ml). The water layer was extracted with a 2:1 mixture of petroleum ether and ether. The combined organic layers were washed with water and saturated brine, dried, and concentrated. The residual oil (380 mg) was chromatographed on silica gel using petroleum ether as an eluant to afford crystals. Recrystallization from petroleum ether yielded the triene **1** (180 mg, 78%): mp 90 °C (lit,[2] mp 89—91 °C); IR ($CHCl_3$) 1595, 1480, 1440, and 1375 cm^{-1}; ^1H NMR ($CDCl_3$) δ 1.89 (6H, s), 5.98 (2H, br. d, J=10.5), 6.67 (2H, d, J=10.5), and 7.42 (10H, s). Found: C, 92.33; H, 7.65%. Calcd for $C_{21}H_{20}$: C, 92.60; H, 7.40%.

*Photooxidation of **1**.* *(a) In Methanol at Low Temperature [Isolation of 3,3-Dimethyl-7,7-diphenyl-1,2-dioxaspiro[3.5]nona-5,8-diene (**2**)]*: A solution of **1** (300 mg) and Rose Bengal (5 mg) in anhydrous methanol (40 ml) and petroleum ether (5 ml) was irradiated with three 200 W tungsten lamps at −78 °C for 2.5 h. Finely dispersed stream of dry oxygen was passed through the solution continually during irradiation. The solvent was removed by vacuum distillation at −40 °C. The residue was chromatographed on two thin-layer silica gel plates (20×20 cm, 1:3 ether–petroleum ether) below −12 °C to give 300 mg (90%, the best result) of a pale yellow oil, which crystallized on standing at −12 °C. Recrystallization from petroleum ether at −12 °C gave **2**: mp 57—61 °C (lit,[2] mp 72—74 °C); IR (CCl_4) 1660, 1595, 1485, 1460, 1370, 1210, 1195, 1075, and 695 cm^{-1}; ^1H NMR (CCl_4, 100 MHz) δ 1.43 (6H, s), 6.35 (2H, d, J=10.5), 6.57 (2H, d, J=10.5), and 7.18 (10H, small split s). The dioxetane **2** could be stored as the dilute solutions in anhydrous THF, ether, benzene, and cyclohexane below −20 °C for several months.

(b) In Methanol at Room Temperature: A solution of **1** (130 mg) and Rose Bengal (5 mg) in anhydrous methanol (30 ml) was photooxidized at room temperature. After irradiation for 1.5 h, work-up in the same manner at room

temperature gave 55 mg (47%) of **2** and 50 mg (43%) of **3**, respectively.

(c) In Chloroform at Room Temperature: A solution of **1** (150 mg) and Methylene Blue (5 mg) in $CHCl_3$ (30 ml) was photooxidized at room temperature for 2.5 h and worked up in the same manner to give 40 mg (30%) of **3**, 25 mg (16%) of **5**, and 26 mg (17%) of **6**.

*Decomposition of **2** on Silica Gel and the Properties of the Products **5**, **6**, and **7***. The dioxetane **2** was re-chromatographed on thin-layer silica gel (1:3 or 1:4 ether–petroleum ether) at 0 °C to produce four UV detectable bands. Collection of these bands, followed by elution with ether and evaporation of the solvent without applying heat gave, in the order of moving, **6**, **3**, **5**, and **7** (variable yields from run to run), respectively.

1-Methyl-1-(*o*-terphenyl-4′-yl)ethyl hydroperoxide (**5**): mp 125.5—128 °C from methanol; positive KI-starch test; IR (CCl_4) 3600, 3500—3100, 1600, 1480, 1440, and 700 cm^{-1}; UV (EtOH) λ_{max} 235 (ε 31000) and 255 nm (ε 20000);[7] ^1H NMR ($CDCl_3$) δ 1.72 (6H, s), 7.24 (10H, s), around 7.30 (1H, br. s, OOH), 7.43 (1H, dd, J=8.8 and 1.9), 7.58 (1H, d, J=8.8), and 7.58 (1H, d, J=1.9); mass *m/e* 288 (parent peak, M^+-16).

Bis[1-methyl-1-(*o*-terphenyl-4′-yl)ethyl] peroxide (**6**): mp 148—150 °C (not recrystallized); IR (CCl_4) 1600, 1480, 1440, and 700 cm^{-1}; UV (EtOH) λ_{max} 235.5 (ε 60800) and 255 nm (ε 27100); ^1H NMR ($CDCl_3$) δ 1.69 (12H, s), 7.18 (20H, s), 7.41 (2H, d, J=8.5), 7.49 (2H, d, J=2.0), and 7.53 (2H, dd, J=8.5 and 2.0). Found: C, 87.20; H, 6.81%. Calcd for $C_{42}H_{38}O_2$: C, 87.77; H, 6.66%. The molecular weight could not be determined by a mass spectral or vapor pressure osmometric method, being presumably due to easy cleavage of the peroxide linkage.

1-(1-Hydroperoxy-1-methylethyl)-4,4-diphenylcyclohexa-2,5-dien-1-ol (**7**): mp 124—126 °C (not recrystallized); IR (CCl_4) 3600, 3650—3100, 1595, 1490, 1175, 865, and 700 cm^{-1}; ^1H NMR ($CDCl_3$) δ 1.18 (6H, s), 2.24 (2H, br. s, OH and OOH), 6.07 (2H, d, J=10.5), 6.32 (2H, d, J=10.5), and 7.28 (10H, s).

*Decomposition of **2** by Hydrochloric Acid. (a)*: A stock solution of **2** in ether (*ca.* 41 mg, 2.1 ml) was diluted with anhydrous ether (2 ml) at −20 °C, and then 2 M HCl (1 drop) was added to this solution. The resulting mixture was vigorously stirred at room temperature for 15 min. The mixture was washed with dilute $NaHCO_3$ solution, water, and saturated brine, dried, and evaporated. The residue was chromatographed on preparative TLC (1:3 ether–petroleum ether) to afford **3** (*ca.* 29%), **5** (*ca.* 15%), and **6** (*ca.* 34%).

(b): The reaction mixture (the same amount as above) was stirred at −18——8 °C. After the reaction was completed (4 d), the mixture was worked up in the same manner, except the use of 1:6 ethyl acetate–petroleum ether as a developing solvent in this case, to give **6** (*ca.* 90%).

(c): A stock solution of **2** in THF (*ca.* 30 mg, 3 ml) was diluted with anhydrous ether (2 ml) at −20 °C, and then 6 M HCl (0.4 ml) was added. The reaction mixture was vigorously stirred at 0 °C for 50 min. Work-up in the same manner yielded **6** (*ca.* 100%).

(d): A stock solution of **2** in cyclohexane (*ca.* 65 mg, 6.5 ml) was diluted with $CHCl_3$ (5 ml) at −10 °C, and then concd HCl (a catalytic amount) was added. The reaction mixture was vigorously stirred below 10 °C for 10 min and worked up in the same manner to give **6** (*ca.* 97%).

*Decomposition of **2** under the Anhydrous Conditions and the Product **13***. *(a)*: *By Boron Trifluoride Etherate*. A stock solution of **2** in THF (*ca.* 50 mg, 3 ml) was diluted with anhydrous ether (10 ml) at −70 °C under nitrogen, and then boron trifluoride etherate (1 drop) was added. The reaction mixture was stirred at −18——12 °C for 2.5 h. Then, the mixture was passed through a short column of silica gel with the aid of ether and evaporated. The residue was chromatographed on preparative TLC (1:7 ethyl acetate–petroleum ether) to give 40 mg (*ca.* 100%) of very viscous oily *o*-terphenyl-4′-ol (**13**): yellow ferric chloride test; IR ($CHCl_3$) 3570, 3550—3100, 3040, 3010, 1600, 1470, 1300, 1210, 890, and 700 cm^{-1}; ^1H NMR ($CDCl_3$) δ 5.60 (1H, br.s, OH), 6.73 (1H, dd, J=9.1 and 2.8), 6.77 (1H, d, J=2.8), 7.05 (10H, m), and 7.15 (1H, d, J=9.1). This compound was identical with the synthetic sample (IR, ^1H NMR, see below).

When ether saturated with water was used for dilution and the reaction was conducted below −20 °C for 15 h, only **6** (*ca.* 24%) was obtained.

(b) By Concd H_2SO_4: A stock solution of **2** in ether (*ca.* 40 mg, 2 ml) was diluted with anhydrous ether (2 ml) at −70 °C, and then concd H_2SO_4 (1 drop) was added. The reaction mixture was stirred below −10 °C for 1 h under nitrogen. Work-up in the usual manner (washing, evaporation, and chromatography) gave 30 mg (*ca.* 100%) of **13**.

*1-Methyl-1-(o-terphenyl-4′-yl)ethanol (**8**). (a) From **5***: To a solution of **5** (26 mg) in anhydrous THF (5 ml) was added lithium aluminum hydride (12 mg), and the reaction mixture was heated at 50 °C for 1 h. The cooled mixture was poured into ice–water and thoroughly extracted with ether. The combined extracts were washed with water and saturated brine, and dried. Removal of the solvent under reduced pressure gave 23 mg (94%) of **8**: mp 144.5—145.5 °C from methanol–petroleum ether; IR (CCl_4) 3500, 3400 (br.), 1600, 1480, 1395, 1360, and 700 cm^{-1}; ^1H NMR ($CDCl_3$) δ 1.70 (6H, s), 7.24 (10H, s), 7.43 (1H, dd, J=8.8 and 1.9), 7.58 (1H, d, J=8.8), and 7.58 (1H, d, J=1.9); mass *m/e* 288 (M^+). This compound was identical with the synthetic sample (see below) as determined by the mixed melting point determination and by comparison of the spectra.

Reduction of **5** with other reagents (triethyl phosphite–toluene, KI–isopropyl alcohol, dimethyl sulfide–benzene) also gave **8** in good yield.

*(b) From **6***: To a solution of **6** (25 mg) in anhydrous ether (8 ml) was added lithium aluminum hydride (5 mg) with ice-cooling under nitrogen. After being stirred for 30 min, the mixture was poured into ice–water, and the water layer was extracted with ether three times. The combined extracts were washed with water and saturated brine. Evaporation of the solvent under reduced pressure left 26 mg (100%) of **8**.

Catalytic hydrogenation of **6** over Pd–C in ethanol also gave quantitatively **8**.

*(c) From **1***: To the well-stirred mixture of a solution of **1** (250 mg, 0.92 mmol) in CH_2Cl_2 (20 ml) and 0.5 M $NaHCO_3$ solution (6 ml) was added portionwise *m*-chloroperbenzoic acid (85%, 224 mg, 1.10 mmol) at 0 °C,[8] and the reaction mixture was stirred at 0 °C for 2 h. The organic layer was separated, washed with dilute NaOH solution and saturated brine, dried, and evaporated. The ^1H NMR spectrum indicated that the crude product was a 2:1 mixture of the epoxide **12** and **8**. Preparative TLC (1:2 ether–petroleum ether) of the crude mixture showed a single UV detectable band. Collection of this band, followed by elution with ether and evaporation provided 260 mg (98%) of **8**.

(d) Synthesis: 2,3-Diphenyl-1,3-butadiene (**9**), bp 150—170 °C (bath)/10 Torr (1 Torr=133.322 Pa), mp 46—47 °C, was prepared by dehydration of 2,3-diphenylbutane-

2,3-diol with $KHSO_4$.[9]

A mixture of **9** (1.4 g, 6.5 mmol), methyl acrylate (3.3 g, 38 mmol), and hydroquinone (20 mg) was heated in a sealed tube at 140 °C (bath temperature) for 15 h. The excess acrylate was removed by distillation under reduced pressure. The residual yellow solid was dissolved in 1:6 ether–petroleum ether and passed through a short column of silica gel to afford 1.74 g (88%) of methyl 3,4-diphenyl-3-cyclohexenecarboxylate (**10**), which gradually crystallized on standing: mp 181 °C; IR (neat, before crystallized) 1735, 1595, 1485, 1430, 1170, and 700 cm^{-1}; ^1H NMR (CCl_4) δ 1.70—2.20 (2H, m), 2.20—2.80 (5H, m), 3.59 (3H, s), and 6.92 (10H, s).

A solution of **10** (584 mg, 2.0 mmol) and DDQ (1.36 g, 6.0 mmol) in toluene (10 ml) was heated under reflux for 26 h under nitrogen. The solvent was removed by distillation under reduced pressure. The brown residue was chromatographed on silica gel (30 g) using 1:1 ether–petroleum ether as an eluant to give 535 mg (92%) of methyl *o*-terphenyl-4′-carboxylate (**11**): IR ($CHCl_3$) 1715, 1600, 1435, 1120, and 700 cm^{-1}; ^1H NMR ($CDCl_3$) δ 3.93 (3H, s), 7.20 (10H, s), 7.53 (1H, d, J=9.0), and 8.00—8.21 (2H, m).

A solution of **10** (292 mg, 1.0 mmol), NBS (373 mg, 2.1 mmol), and dibenzoyl peroxide (8 mg) in CCl_4 (4 ml) was heated under reflux for 80 min under nitrogen. After removal of the insoluble precipitate by filtration, the solvent was expelled by distillation under reduced pressure. The residue was dissolved in pyridine (5 ml), and the resulting solution was heated under reflux for 1 h. The reaction mixture was poured into water and extracted with ether three times. The combined extracts were washed with water, dilute $CuSO_4$ solution, water, and saturated brine, and dried. Evaporation of the solvent left 280 mg (97%) of **11**.

To a solution of methylmagnesium iodide, prepared from magnesium (1.34 g) and methyl iodide (9.9 g) in anhydrous ether (25 ml), was added dropwise a solution of **11** (5.29 g, 18.3 mmol) in anhydrous ether–benzene (2:1, 50 ml) over a period of 15 min at room temperature under nitrogen, and the reaction mixture was stirred for 100 min. Saturated NH_4Cl solution was added, and the water layer was extracted with each 40 ml portions of ether three times. The combined extracts were washed with 2 M HCl, water, and saturated brine. Evaporation of the solvent left a dark brown oil (5.5 g). Chromatography of this oil on silica gel (160 g) using 1:1 ether–petroleum ether as an eluant afforded 5.17 g (98%) of **8**.

*o-Terphenyl-4′-ol (**13**).* *(a) From **3***: To a solution of **3** (50 mg) in anhydrous ether (3 ml) was added concd H_2SO_4 (1 drop), and the reaction mixture was heated under reflux for 48 h. When the mixture was stirred at room temperature, no reaction was observed after 12 h. The cooled mixture was diluted with more ether and washed with dilute $NaHCO_3$ solution and saturated brine, and the solvent was removed by distillation. The residue was chromatographed on preparative TLC (1:5 ethyl acetate–petroleum ether) to yield 35 mg (70%) of **13**.

The reaction of **3** (50 mg) by boron trifluoride etherate (2 drops) in boiling anhydrous ether (4 ml) proceeded extremely slowly. Even after 3.5 d, almost starting material remained unchanged.

(b) Synthesis: To a solution of deoxybenzoin (19.7 g, 0.1 mol) in anhydrous ether (300 ml) was added methyl vinyl ketone (freshly distilled, 7.1 g, 0.1 mol) at 0 °C. Then, to this solution was added dropwise a solution of KOH (1.7 g) in ethanol (15 ml) over a period of 30 min at 0 °C under nitrogen, and the resulting mixture was stirred at 0 °C for 70 min; white precipitate gradually separated. This slurry was poured into a mixture of ice (200 g) and 1 M HCl (35 ml), and the precipitate was collected by filtration, washed with water, and dried *in vacuo* over concd H_2SO_4. The organic layer of the filtrate was separated, washed with water and saturated brine, and evaporated to dryness to yield a solid material. The precipitate and the solid residue were combined and suspended in ethanol (95%, 300 ml). To this slurry was added concd HCl (20 ml), and the resulting mixture was heated under reflux. After 20 min, the mixture became a homogeneous solution, and the refluxing was continued for 2 h. The reaction mixture was poured into cold water (500 ml) and extracted with ether three times. The combined extracts were washed with water and saturated brine, and dried. Evaporation of the solvent and recrystallization of the solid residue from aqueous methanol gave 17 g (69% overall) of 3,4-diphenyl-2-cyclohexenone (**14**): mp 96—97.5 °C; IR (CCl_4) 1670, 1600, 1490, 1442, 1328, 1250, 1170, 885, and 700 cm^{-1}; ^1H NMR ($CDCl_3$) δ 2.00—2.80 (4H, m), 4.35 (1H, m), 6.75 (1H, s), and 7.30 (10H, split s). Found: C, 86.75; H, 6.54%. Calcd for $C_{18}H_{16}O$: C, 87.06; H, 6.50%.

A solution of **14** (124 mg, 0.5 mmol), DDQ (139 mg, 0.6 mmol), and fused *p*-toluenesulfonic acid (19 mg) in anhydrous benzene (12 ml) was heated under reflux for 4 h under nitrogen. The reaction mixture was poured into ice–water and extracted with ether. The combined extracts were washed with water and saturated brine, and evaporated. The residue was chromatographed on preparative TLC (1:4 ethyl acetate–petroleum ether) and distilled at 90—140 °C (bath)/0.3—0.5 Torr to afford 108 mg (88%) of viscous oily **13**, which gradually crystallized on standing: mp 48—51 °C (still adhesive, being unable to recrystallize). Found: C, 87.48; H, 5.96%. Calcd for $C_{18}H_{14}O$: C, 87.77; H, 5.73%.

Acknowledgment is made to the Ministry of Education, Science, and Culture of Japan for partial support (a Grant-in-Aid for Scientific Research, No. 147028 for HU).

References

1) A main part of this work was presented at the 32nd National Meeting of the Chemical Society of Japan, Tokyo, April 3, 1975, Abstracts of Papers, Vol. 3, p. 1158.

2) H. E. Zimmerman and G. E. Keck, *J. Am. Chem. Soc.*, **97**, 3527 (1975); H. E. Zimmerman, G. E. Keck, and J. L. Pflederer, *ibid.*, **98**, 5574 (1976).

3) For reviews of the thermal decomposition of 1,2-dioxetanes, see D. R. Kearns, *Chem. Rev.*, **71**, 395 (1971); N. J. Turro, P. Lechtken, N. E. Schore, G. Schuster, H.-C. Steinmetzer, and A. Yekta, *Acc. Chem. Rec.*, **7**, 97 (1974); "Singlet Molecular Oxygen," ed by A. P. Schaap, Dowden Hutchinson & Ross, Inc., Stroudsburg, Pennsylvania (1976), p. 290, and references cited therein.

4) For the ionic decomposition of 1,2-dioxetanes, see a) N. M. Hasty and D. R. Kearns, *J. Am. Chem. Soc.*, **95**, 3380 (1973); b) P. D. Bartlett, A. L. Baumstark, and M. E. Landis, *ibid.*, **99**, 1890 (1977), and references cited therein.

5) G. Wittig and D. Wittenberg, *Justus Liebigs Ann. Chem.*, **606**, 1 (1957).

6) H. E. Zimmerman and D. I. Schuster, *J. Am. Chem. Soc.*, **84**, 4527 (1962); H. E. Zimmerman, P. Hackett, D. F. Juers, J. M. McCall, and B. Schröder, *ibid.*, **93**, 3653 (1971).

7) UV Atlas of Organic Compounds, Vol. V, D10/81, Butterworths, London; Verlag Chemie, Weinheim (1971).

8) W. K. Anderson and T. Veysoglu, *J. Org. Chem.*, **38**, 2267 (1973).

9) K. Alder and J. Haydn, *Justus Liebigs Ann. Chem.*, **570**, 201 (1950).

Polar Effects in the Reactions of a Series of Substituted Diphenyldiazomethanes with Chloranil

Takumi OSHIMA and Toshikazu NAGAI*

Institute of Chemistry, College of General Education, Osaka University, Toyonaka, Osaka 560

(Received March 28, 1980)

The kinetics and products of the reactions of fifteen meta- and para-substituted diphenyldiazomethanes with chloranil were investigated in tetrahydrofuran. The second-order rate constants, k, increased with the electron-donating ability of the substituents, and the values could be correlated with the Yukawa-Tsuno equation: $\log k/k_0 = -1.67(\sigma^0 + 0.66\,\Delta\bar{\sigma}_R^+) + 0.009$, ($r = 0.996$). The ρ value, -1.67, indicates the large development of a positive charge at the diazo carbon in the transition state, while the R value, 0.66, confirms the considerable stabilization of the positive charge by the π-electronic contribution of the para substituents. The products of these reactions were the corresponding 2,3,5,6-tetrachlorohydroquinone poly(benzhydryl)ethers, but these polyethers were easily hydrolyzed into the corresponding benzophenones and tetrachlorohydroquinone(HQ). On the other hand, the initial presence of water or methanol as an additive changed the reaction features to give benzophenone or α,α-dimethoxydiphenylmethane, together with HQ. Reaction mechanisms which account for the results are discussed.

Continuing interest is being paid to the reactions of diazoalkanes with quinones from the synthetic and mechanistic points of view.[1] This is because diazoalkanes are typical 1,3-dipoles[1a,2] with a high electron density on the diazo carbon,[3] while quinones behave as dipolarophiles[1b,4] or electron acceptors[5] with reactive conjugated C=O and C=C bonds. For example, epoxides were obtained when diazomethane was allowed to react with tetrahalo-substituted quinones such as chloranil, because the C=O bonds are more reactive than the C=C bonds in these quinones.[6] We reported in a previous paper[7] that the reactions of several phenyldiazomethanes with chloranil gave stilbenes and spirooxetanes instead of epoxide. We will now extend the diazoalkanes–chloranil systems to a series of diaryldiazomethanes and will describe the kinetics and the mechanism.

Results and Discussion

Product Studies. The reactions of diphenyldiazomethane (DDM) and its fourteen meta- and para-substituted analogues (DDMs) (**1**) with an equimolar amount of chloranil (**2**) were conducted in tetrahydrofuran at 30 °C. The decomposition rates were found to be much more accelerated with the increase in the electron-donating abilities of the substituents. For example, the presence of *p,p'*-dimethoxy substituents instantaneously brought about the deposition of a white precipitate, accompanied by a vigorous evolution of N_2, while *p*-nitro-substituted DDM needed one week for the complete disappearance of the diazo color. All these reactions gave some precipitates or suspensions which were easily degradated into the corresponding substituted benzophenones (**3**) and tetrachlorohydroquinone (HQ) on standing in atmospheric moisture or by the addition of aqueous THF. Moreover, the crude reaction mixtures were also completely changed into almost equimolar amounts of the corresponding **3** and HQ on treatment with aqueous THF. These hydrolyses show the stoichiometry to be 1 mol of DDMs to 1 mol of **2**, while the total yields of **3** or HQ are, in most cases, greater than 93%. An elemental analysis of the precipitate obtained in the case of DDM exhibited a composition (C; 54.35, H; 2.46%) very close to the combined molecular formula, $C_{19}H_{10}Cl_4O_2$, of diphenylmethylene and **2**. The IR spectrum (KBr) of this precipitate showed a weak absorption in the OH region, but no appreciable C=O absorption was observed, indicating that the quinonoid structure of **2** has already been lost.

From this chemical and spectroscopic information, it is natural to consider that the structure of these hydrolyzable products is made up by the polyether linkage depicted in Scheme 1. These polyethers consist of an alternate combination of diarylmethylenes and a chloranil moiety with a benzenoid functionality. Accordingly, it can be suggested that intermediary diazonium betaines(I) or carbonium betaines(II) play an important role in the present polymerization process. The propagation of the polyether linkage may be terminated by the action of residual water present in the solvent, the end groups thus becoming hemiketalic OH and phenolic OH. Therefore, the polymerization degree (n) will lie at a lower value with an increase in the water content; we could not estimate the value of n because the precipitates were not soluble in common aprotic solvents and were easily hydrolyzable. The degradation of these polyethers under the influence of water is caused by the successive hydrolytic cleavage of the ether linkage; the dihydroxydiarylmethanes thus formed are easily converted into **3** with a loss of water.

On the other hand, the initial presence of a large amount of water is expected to give, exclusively, the unstable ether (**4**), capable of undergoing subsequent hydrolysis. Indeed, the presence of a five-fold excess of water (ROH, R=H) in the DDM–**2** system brought about the formation of benzophenone and HQ, in addition to small amounts of benzhydrol (**8**) and tetrachlorohydroquinone dibenzhydryl ether (**7**) (Scheme 1). These two by-products seem to be derived from the acid-induced decomposition of DDM with the resulting HQ; the formation of **8** can be ascribed to the hydrolysis of tetrachlorohydroquinone benzhydryl ether (**6**) on work-up. A similar reaction was found in the presence of methanol ($R=CH_3$), where α,α-dimethoxydiphenylmethane (**5**, $R=CH_3$) was

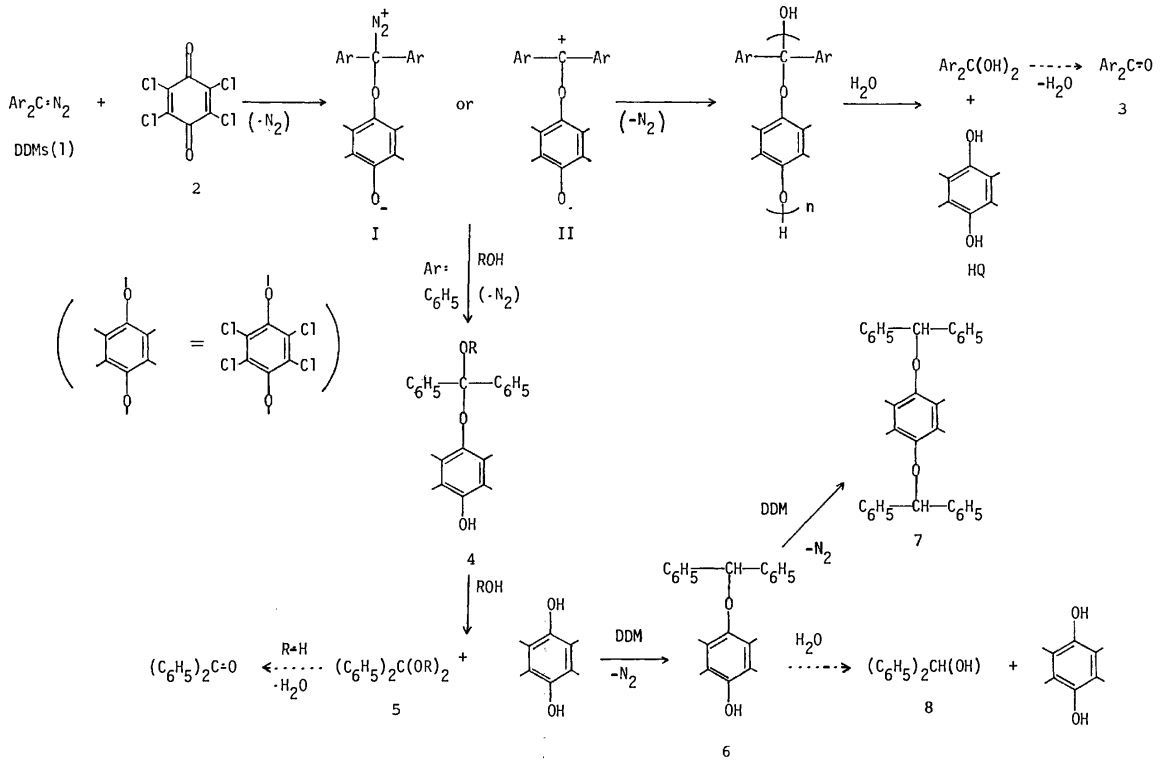

Scheme 1.

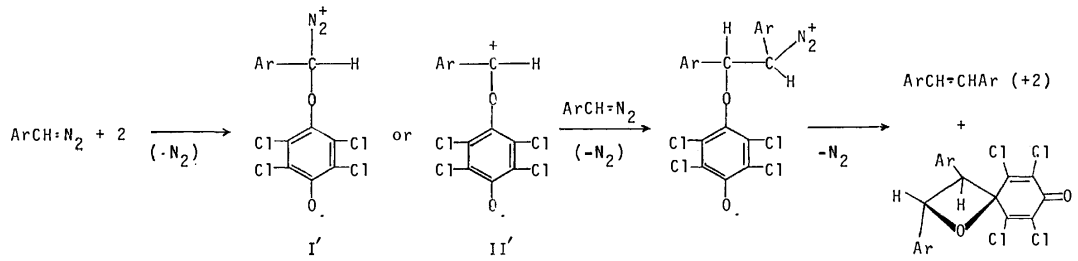

Scheme 2.

afforded instead of benzophenone.[8] These solvolysis reactions evidently confirm the occurrence of an intermediate I or II.

Interestingly, the present reactions gave neither olefins nor spirooxetanes; this is in dramatic contrast to the case of phenyldiazomethanes.[7] These products were well explained as arising from the subsequent nucleophilic attack of the diazoalkanes on the diazonium(I′) or carbonium betaine(II′) intermediate, as provided in the present system (Scheme 2). The reason why I or II reject such a nucleophilic attack is probably to be attributed to two factors. One is the steric hindrance due to the presence of two aromatic rings, which screen the central carbon atom from the nucleophilic attack of DDMs. The other is the lesser nucleophilic reactivity of the carbon atom of DDMs compared to that of phenyldiazomethanes. Consequently, the only possible behavior of I and II is to polymerize each other in the absence of strong nucleophiles.

Kinetic Studies. As was noticed in the product studies, the disappearance of the color of the DDMs was much accelerated by introducing the electron-donating substituents in the meta and the para positions of the aromatic rings of DDMs. In order to estimate these polar effects in more detail, the decompositions of fifteen meta- and para-substituted DDMs were followed spectrophotometrically in the presence of high dilute DDMs with respect to **2**; moderate reaction rates were thereby attained, thus avoiding the precipitate formation. The rates determined by monitoring the decrease in the diazo color were found to obey a simple pseudo-first order kinetic law. The rate constants (k_{obsd}) of the decomposition of DDM with various concentrations of **2** are shown in Table 1; the linear dependence of k_{obsd} on the concentration of **2** is held within the limits of experimental error: $10^5 k_{obsd}/s^{-1} = 535[\text{Chloranil}] - 0.31$. Therefore, the second-order rate constants, k, were obtained simply by dividing the k_{obsd} by the concentration of **2**. The values of k thus determined for the meta- and the para-substituted DDMs at various temperatures are given in Table 2, together with the activation parameters. It can be noted that the *p,p′*-dimethoxy substituents caused a 2500-fold increase in the rate compared with the *p*-nitro substituent at 30 °C. In the case of DDM, the rate of the decomposition was also determined by monitoring the evolved N_2, and

the second-order rate constant was nearly equal to that determined by the spectroscopic method. This means that there is no accumulation of any type of intermediate with the N_2 group in the course of the reaction.

The dependence of log k/k_0 on the Hammett σ constants[9] and the Brown σ^+ constants[10] is shown in Fig. 1. For disubstituted DDMs, the σ and the σ^+ values used are the sums of the values for the two substituents. Four meta-substituted DDMs gave an excellent linear dependence ($\rho=-1.52$), $r=0.996$ (correlation coefficient) when the simple Hammett equation and normal σ values were used. When correlating the series of fifteen meta- and para-substituted DDMs and using the normal σ values, though, we obtained substantially worse results ($r=0.933$, $\rho=-2.10$). The correlation line appears to curve upward from the meta line. The replacement of σ by σ^+ caused a considerable improvement in the correlation ($r=0.980$, $\rho=-1.37$), though a downward deviation from the meta line is still found for the methoxy-substituted DDMs. Neither the σ nor σ^+ values apparently fit the correlation of the para-substituted DDMs well.

Table 1. Observed first-order rate constants, k_{obsd}, for the decomposition of DDM(1.70×10^{-3} mol dm^{-3}) with a large excess of chloranil (**2**) in tetrahydrofuran at 40 °C

10^2[Chloranil] / mol dm^{-3}	$10^4 k_{obsd}$ / s^{-1}
8.33	4.41
6.66	3.59
5.83	3.01
5.00	2.68
4.16	2.17
3.33	1.76

Therefore, we used the two-parameter Yukawa-Tsuno equation,[11] log $k/k_0=\rho(\sigma^0+R\Delta\bar{\sigma}_R^+)$, where σ^0, R, and $\Delta\bar{\sigma}_R^+$ are the normal substituent constant, the resonance reaction constant, and the resonance substituent constant respectively. The results of regression anal-

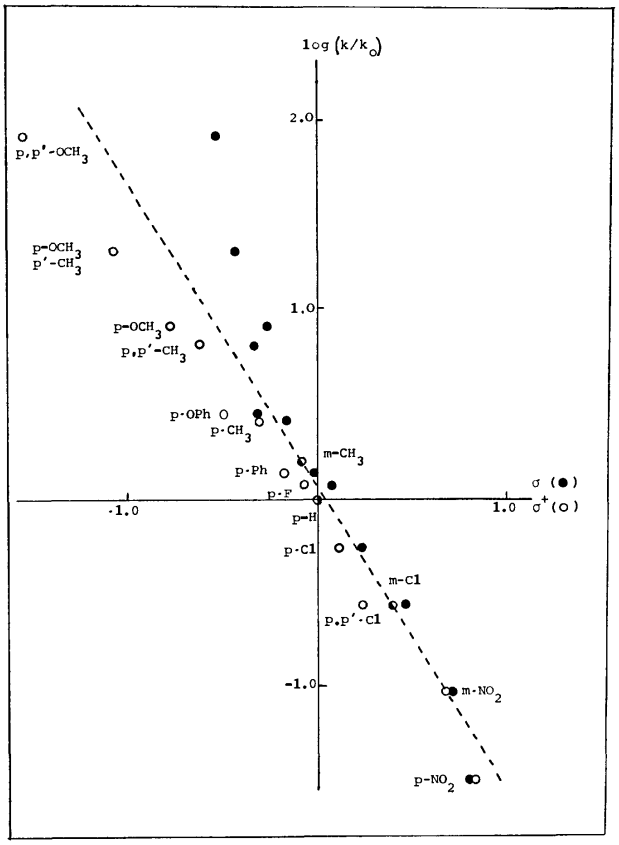

Fig. 1. The plot of log k/k_0 against the Hammett σ(●) and Brown σ^+(○) constants.

Table 2. Second-order rate constants, k, and activation parameters for the decompositions of the substituted DDMs (**1a**—**o**) with chloranil (**2**) in tetrahydrofuran

DDMs	Substituents	$10^3 k$/l mol^{-1} s^{-1} 30 °C	40 °C	50 °C	ΔH^* / kJ/mol	ΔS^* / J/mol K
1a	*p*,*p*'-OCH_3	197	—	—	—	—
1b	*p*-OCH_3, *p*'-CH_3	49.0	—	—	—	—
1c	*p*-OCH_3	19.5	38.9	69.9	49.3	−115
1d	*p*,*p*'-CH_3	15.8	33.1	62.3	53.2	−104
1e	*p*-OPh	6.67	13.8	25.7	52.3	−114
1f	*p*-CH_3	6.10	12.0	24.3	53.7	−110
1g	*m*-CH_3	3.71	7.59	14.9	54.0	−113
1h	*p*-Ph	3.38	6.03	11.2	46.2	−140
1i	*p*-F	2.80	5.63	11.3	54.2	−115
1j	*p*-H	2.43 (2.62)[a]	5.35	10.9	58.5	−102
1k	*p*-Cl	1.29	2.77	5.31	55.0	−119
1l	*p*,*p*'-Cl	0.661	1.41	2.94	58.2	−114
1m	*m*-Cl	0.623	1.38	2.85	59.3	−111
1n	*m*-NO_2	0.232	—	—	—	—
1o	*p*-NO_2	0.0790	—	—	—	—

a) The value in parentheses was determined at 30.5 °C by the volumetric method employing a 2-molar excess of **2** with respect to DDM.

Table 3. Solvent dependence of the rate constants, k, and the activation parameters for the decomposition of DDM with chloranil (**2**)

Solvent	$DN(-\Delta H_{SbCl5})$	E_T	$10^3\,k/1\,mol^{-1}\,s^{-1}$			ΔH^*	ΔS^*
			30 °C	40 °C	50 °C	kJ/mol	J/mol K
1,2-Dichloroethane	0	41.9	30.5	62.5	111	50.1	−109
Acetonitrile	14.1	46.0	23.4	49.3	85.8	50.2	−110
Ethyl acetate	17.1	38.1	5.34	10.4	20.1	51.2	−119
Benzene	0.1	34.5	2.66	6.09	12.3	59.7	−92.2
Tetrahydrofuran	20.0	37.4	2.43	5.35	10.9	58.5	−102

ysis indicate that the use of a two-parameter equation improves the correlation significantly (Eq. 1):

$$\log k/k_0 = -1.67(\sigma^0+0.66\Delta\bar{\sigma}_R^+) + 0.009, \quad (r=0.996,\ s=0.08,\ n=15) \qquad (1)$$

The negative sign and the magnitude of ρ (−1.67) are consistent with the large development of a positive charge at the diazo carbon in the activation process. The value of R=0.66 also confirms that a considerable resonance stabilization of the transition state is required in the present system.

The dependence of the rate on the solvents shows an acceleration or a retardation unexpected from the solvent parameters, *e.g.*, the E_T values (Table 3).[12] A similar unexpected tendency has been observed in the reaction of DDM with tetracyanoethylene (TCNE).[13] These phenomena seem to be ascribable to the stabilization of the initial state caused by the formation of donor–acceptor complexes between these electron acceptors and the solvents. In fact, TCNE is well known to form a strong complex with THF,[14] where the most retarded rate was observed. When the rates were examined as a function of the solvent donor number (DN),[15] the measure of the solvent donability, a decrease in the rate with the increase of DN was always found except in the case of benzene. This exception may be responsible for the lowest E_T value among these solvents, because the charge-separated transition state is not sufficiently solvated in such a nonpolar medium. In this manner, the stabilization of the initial state is so pronounced in the solvent with a high donor number that the rate is no longer directly correlated with the solvent polarities.

Mechanistically, the formation of polyether and the occurrence of the solvolysis reaction in the present system can be well explained by assuming the participation of the diazonium betaine(I) or the carbonium betaine(II) intermediate, as just as in the case of the reactions of phenyldiazomethanes with **2**.[7] The kinetic data presented in this paper provide some information concerning the transition state. The large negative entropies of activation are indicative of the highly ordered transition state usually encountered in 1,3-dipolar cycloaddition.[16] However, the magnitude of the charge separation, as revealed by the Hammett correlation as well as by the solvent effects, appears unmatched in the isopolar transition states of 1,3-dipolar additions. Therefore, the present system is postulated to proceed through the polar transition state depicted below, though the polar transition state of 1,3-dipolar addition[17] can not be ruled out.

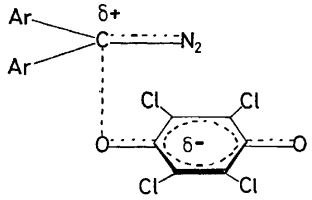

Experimental

The IR and NMR spectra were recorded on Hitachi 215 and Varian EM-360 spectrometers respectively. The UV spectra were observed with Hitachi 323 and JASCO UVIDEC 505 instruments.

Materials. The chloranil was of commercial origin and was recrystallized twice from benzene; mp 290 °C. All the diaryldiazomethanes were made by the oxidation of the corresponding hydrazones with yellow mercury(II) oxide as has been previously described.[18] The physical properties of these diazoalkanes were all listed in a previous paper[13] except for *p,p'*-dimethoxy-(mp 100—101 °C (ether) (lit,[9] mp 99—100 °C), UV: λ_{max}=540 nm (ε=85, THF)), *m*-nitro-(mp 53—54 °C(petroleum ether–ether)(lit,[20] an oil), UV: 500 nm (ε=138, THF)), and *p*-nitrodiphenyldiazomethane (mp 80—82 °C (petroleum ether–ether) (lit,[20] mp 80—83 °C), UV: 500 nm (ε=326, THF)). The THF and benzene were refluxed over lithium aluminum hydride and then fractionated. The acetonitrile and 1,2-dichloroethane were refluxed over phosphorus pentaoxide and then fractionated. The ethyl acetate was dried over anhydrous calcium carbonate and then fractionated.

Kinetic Measurements. In order to satisfy the requirements of pseudo first-order treatment, the kinetic reactions were usually carried out in the presence of a 20- to 50-fold molar excess of **2** with respect to DDMs. The change in optical density at the wavelength of the absorption maxima (524—525 nm) of DDMs (**1a—m**) was conveniently monitored because **2** in THF is transparent in this region. The procedure was similar to that described in a previous paper.[13] In the case of the nitro-substituted DDMs (**1n,o**), however, the temperature of the reaction solutions was kept at 30±0.1 °C by the use of a Haake circulator, and the absorption at 500 nm was followed over a 70-percent decomposition at certain time intervals. The pseudo first-order rate constants (k_{obsd}) were determined graphically from plots of $-\ln x$ against the time, where x is the concentration of the remaining DDMs. In all cases, excellent straight lines were obtained. Then, the second-order rate constants (k) obtained by dividing k_{obsd} with the initial concentration of **2** were reproducible to within ±3% (usually two determinations).

Reactions of Diaryldiazomethanes (DDMs) with 2 in THF. The reaction of diphenyldiazomethane (DDM) will be described below as a typical example; the reactions of the

other DDMs were carried out similarly until the characteristic color of the diazo compounds had faded. To a THF solution (40 ml) of **2** (1.0 g, 4.07 mmol) we added, all at once, a THF solution (20 ml) containing DDM (0.79 g, 4.07 mmol) at 30 °C. The purple color of DDM slowly disappeared with a slight evolution of N_2. After 6 h standing, the precipitate (0.8 g) which appeared was filtered, dried *in vacuo*, and submitted to IR measurement and elemental analysis. This white precipitate was completely hydrolyzed to benzophenone and HQ on 3 d exposure to atmosphere or by the addition of aqueous THF. The removal of the solvent, followed by the column chromatography (silica gel) of the hydrolyzed mixtures gave almost equimolar amounts of benzophenone (0.34 g, 46.0%) and HQ (0.47 g, 46.5%), with benzene and ether as the eluents. The filtrate from the white precipitate was dried *in vacuo*, and the residue was treated with a small portion of aqueous THF for 1 h. The column chromatography of the hydrolyzed mixtures also gave equimolar amounts of benzophenone (0.37 g, 50.0%) and HQ (0.52 g, 51.5%). The benzophenones (**3a**—**o**) were identified by a comparison of their IR and NMR spectra with those of authentic samples produced by the Friedel-Crafts reaction. The HQ was identified by a comparison of its IR spectrum with that of an authentic sample.[21]

Reaction of Diphenyldiazomethane (DDM) with 2 in H_2O–THF. To a THF solution (40 ml) of **2** (1.0 g, 4.07 mmol) we added, all at once, a THF solution (20 ml) containing DDM (0.79 g, 4.07 mmol) and H_2O (0.36 g, 20 mmol) at 30 °C. After 6 h standing, the removal of the solvent, followed by column chromatography, gave tetrachlorohydroquinone dibenzhydryl ether (**7**) (40 mg, 3.4% based on DDM used), recovered **2** (0.10 g, 10%), and benzophenone (0.64 g, 86%) with a petroleum ether–benzene mixture, and then HQ (0.85 g, 84%) and benzhydrol (**8**) (50 mg, 6.7%) with a benzene–ether mixture. The product, **7**, was recrystallized from benzene; mp 190—192 °C; IR (KBr): 1407, 949, and 689 cm^{-1}; NMR (δ, $CDCl_3$) 6.43 (2H, s) and 7.28 (20H, s); Found: C, 66.05; H, 3.89%. Calcd for $C_{32}H_{22}Cl_4O_2$: C, 66.23; H, 3.82%. Compound **7** was identified by a comparison of its IR and NMR spectra with those of an authentic sample given by the reaction of DDM with HQ.

Reaction of DDM with 2 in CH_3OH–THF. The reaction was carried out under conditions similar to those described in the H_2O–THF system. After 6 h standing, the removal of the solvent gave a pasty reaction mixture, the NMR spectrum of which showed the presence of large amounts of α,α-dimethoxydiphenylmethane (**5**). However, the **5** slowly hydrolyzed into benzophenone in the reaction mixture, so that the product analyses were made according to two different procedures. First, one-half of the reaction mixture was washed with 3×20 ml pentane to extract the **5**. The pentane solution was shaken with a small portion of aqueous $NaHCO_3$ (5%), washed with water, and dried over sodium sulfate. The concentration of the filtrated solution yielded crystalline **5** (0.39 g, 85%), mp 106—107 °C; IR (KBr): 1209, 1085, 1053, 987, and 689 cm^{-1}; NMR (δ, $CDCl_3$) 3.10 (6H, s, OCH_3) and 7.13—7.57 (10H, m, aromatic H); Found: C, 78.98; H, 7.01%. Calcd for $C_{15}H_{16}O_2$: C, 78.92; H, 7.06%. Second, the other half of the reaction mixture was chromatographed (silica gel). Elution with a petroleum ether–benzene mixture successively afforded **7** (25 mg, 4%), the recovered **2** (0.11 g, 11%), and benzophenone (0.31 g, 84%), while elution with a benzene–ether mixture gave HQ (0.42 g, 83%) and **8** (30 mg, 8%). Thus, **5** was completely hydrolyzed to give benzophenone during the isolation process by the chromatography.

References

1) a) G. Cowell and A. Ledwith, *Quart. Rew. Chem. Soc.*, **24**, 119 (1970); b) K. T. Finley, "The Chemistyr of the Quinonoid Compounds," ed by S. Patai, John Wiley & Sons (1974), Chap. 17.

2) a) R. Huisgen, *Angew. Chem. Int. Ed. Engl.*, **2**, 565, 633 (1963); b) S. Sorriso, "The Chemistry of Diazonium and Diazo Groups," ed by S. Patai, John Wiley & Sons (1978), Chap. 3.

3) J. Bastide, J. Hamelin, F. Texier, and Y. V. Quang, *Bull. Soc. Chim. Fr.*, **40**, 2555 (1973).

4) a) R. B. Woodward, F. Sondheimer, D. Taub, K. Heusler, and W. M. McLamore, *J. Am. Chem. Soc.*, **74**, 4223 (1952); b) G. Bianchi, C. De. Micheli, and R. Gandolfi, "The Chemistry of Double-Bonded Functional Groups," ed by S. Patai, John Wiley & Sons (1977), Chap. 6.

5) G. Briegleb, *Angew. Chem.*, **76**, 326 (1964).

6) B. Eistert, H. Fink, and A. Müller, *Chem. Ber.*, **95**, 2403 (1962).

7) T. Oshima and T. Nagai, *Bull. Chem. Soc. Jpn.*, **53**, 726 (1980).

8) This acetal is also obtained in the reaction of DDM with ninhydrin in the presence of CH_3OH; see a) A. Schönberg, K. Junghans, and E. Singer, *Tetrahedron Lett.*, **1966**, 4667; b) A. Schönberg, E. Singer, and K. Junghans, *Justus Liebigs Ann. Chem.*, **711**, 98 (1968).

9) a) H. H. Jaffé, *Chem. Rev.*, **53**, 191 (1953); b) D. H. McDaniel and H. C. Brown, *J. Org. Chem.*, **23**, 420 (1958).

10) H. C. Brown and Y. Okamoto, *J. Am. Chem. Soc.*, **79**, 1913 (1957); **80**, 4979 (1958); **81**, 3323 (1959).

11) Y. Yukawa, Y. Tsuno, and M. Sawada, *Bull. Chem. Soc. Jpn.*, **39**, 2274 (1966).

12) K. Dimroth, C. Reichardt, T. Siepmann, and F. Bohlmann, *Justus Liebigs Ann. Chem.*, **661**, 1 (1963).

13) T. Oshima, A. Yoshioka, and T. Nagai, *J. Chem. Soc., Perkin Trans. 2*, **1978**, 1283.

14) D. F. Ilten and M. Calvin, *J. Chem. Phys.*, **42**, 3760 (1965).

15) V. Gutmann, "Coordination Chemistry in Non-aqueous Solutions," Springer-Verlag (1968), Chap. 2.

16) R. Huisgen *Angew. Chem. Int. Ed. Engl.*, **2**, 633 (1963).

17) The polar transition state of 1,3-dipolar addition has already been suggested to explain the large absolute ρ values for the reactions of phenylazides with enamines; see a) R. Huisgen, G. Szeimies, and L. Möbius, *Chem. Ber.*, **100**, 2494 (1967); b) M. K. Meilahn, B. Cox, and M. E. Munk, *J. Org. Chem.*, **40**, 819 (1975).

18) L. I. Smith and K. L. Howard, *Org. Synth.*, Coll. Vol. III, 351 (1955).

19) D. Bethell and J. D. Callister, *J. Chem. Soc.*, **1963**, 3801.

20) R. Curci, F. D. Furia, and F. Marcuzzi, *J. Org. Chem.*, **36**, 3774 (1971).

21) A. Binz and C. Räth, *Ber.*, **58**, 309 (1925).

 © 1980 The Chemical Society of Japan Bull. Chem. Soc. Jpn., 53, 3289—3294 (1980)

Cyclization of Isothiosemicarbazones. III.[1] Formation of Thiazolines and Thiazoles through Potential Sulfonium Salts from *N,S*-Disubstituted Isothiosemicarbazones

Chiji YAMAZAKI

Department of Chemistry, School of Hygienic Sciences, Kitasato University, Kitasato, Sagamihara 228

(Received March 31, 1980)

The reaction of 3,4-disubstituted isothiosemicarbazones with α-bromo ketones led to the formation of 4-thiazoline derivatives, the substituents on the sulfur atom being cleaved as bromides. They are identical with the compounds obtained by the condensation of the corresponding thiosemicarbazones, having significantly lower *E*/*Z* ratios in certain products than in those from thiosemicarbazones. The yields of 4-thiazolines widely vary with the substituents on the N-4 and the sulfur atom in the isothiosemicarbazones and also with halo ketones. A mechanism has been suggested which deals with a sulfonium-formation and dissociation process at the apparently less nucleophilic sulfur atom of isothiosemicarbazone. The mechanism might explain the effect of changes in the substituents on the sulfur atom upon the yield of 4-thiazolines, the higher contents of (*Z*)-4-thiazoline from (*E*,*E*)-2,6-dichlorobenzaldehyde 3-allyl-4-methylisothiosemicarbazone, and the inertness or less reactivity of anisaldehyde 2,3-dimethylisothiosemicarbazone and salicylaldehyde 3-allyl-4-phenylisothiosemicarbazone. Differentiation between isomeric thiazole and 4-thiazoline compounds was also described.

Cyclocondensation of a number of isothiosemicarbazones with α-halo carbonyl compounds leads to the formation of 2-mercapto-1*H*-imidazole derivatives and other nitrogen-containing heterocycles.[1,2] In an attempt to improve the yield of imidazoles, an equimolar mixture of benzaldehyde *S*-allylisothiosemicarbazone (**3r**) and phenacyl bromide (**4b**) was heated in toluene at a bath temperature of 130 °C. An appreciable amount of compound was detected with a characteristic resonance at δ 6.80 ppm in chloroform-*d* together with the major product of 1-benzylideneamino-2-allylthio-4-phenyl-1*H*-imidazole (**1**). On the basis of spectral

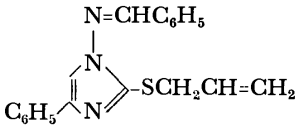

1

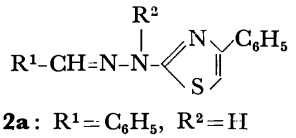

2a: $R^1=C_6H_5$, $R^2=H$
2b: $R^1=p$-$CH_3OC_6H_4$, $R^2=CH_3$

data and elemental analysis, the compound has been identified as benzaldehyde 4-phenyl-2-thiazolylhydrazone (**2a**). The formation of **2a** is of particular interest because it apparently involves an allyl-phenacyl exchange reaction on the much less nucleophilic sulfur atom of the isothiosemi-carbazone than that of alkyl sulfides,[3] probably through a sulfonium formation and dissociation process.[4] In the present work, some isothiosemicarbazones in which the N-2 or N-4 was blocked by certain substituents to prevent the imidazole formation were reacted with α-bromo ketones and the effects of substituent on the formation of sulfur-containing five-membered ring were examined in order to elucidate the reaction pathway.

Results and Discussion

An equimolar mixture of **3n** and **4b** was heated in toluene at a bath temperature of 130 °C for 90 min. A product with a characteristic resonance at δ 6.10 ppm in chloroform-*d*, having a molecular formula $C_{23}H_{19}N_3OS$ (M^+, 385) and showing no NH stretching band in the IR spectrum, was obtained by column-chromatographic separation on silica gel. It was found to be identical with a compound prepared by the condensation of anisaldehyde 4-phenylthiosemicarbazone with **4b** according to methods[5] for the preparation of 2-[alkylidene(or arylmethylene)hydrazono]-4-thiazolines and consequently assigned a structure of 2-(*p*-methoxyphenylmethylenehydrazono)-3,4-diphenyl-4-thiazoline (**5k**).

The NMR spectrum of a low-boiling portion distilled from the reaction mixture of **3o** and **4b** in toluene was found to be indentical with that of 3-bromopropene in this solvent, providing evidence for the formation of **6c** in the reaction. Similarly, a volatile compound formed by the reaction between **3b** and **4b** was identified as 1-bromopropane (**6b**). The expected high-boiling **6d** was detected by direct NMR measurement at intervals of the reaction mixture of **3p** and **4b** in toluene-d_8. No bromomethane (**6a**), which would be formed from the reaction of **3n**, was collected. The equation of the present reactions between 3,4-disubstituted isothiosemicarbazones (**3**) and α-bromo ketones (**4**) can thus be written as in Scheme 1.

The conditions for obtaining **5k** in the preliminary work can successfully be applied to the reactions of other isothiosemicarbazones, representing a general procedure[6] for carrying out the present reactions. The formation of **5** from 3,4-disubstituted isothiosemicarbazones showed considerable solvent-dependence (Table 1). Little or no formation of **5** was noted in acetic acid, 1-butanol, and dimethyl sulfoxide (DMSO),[8] a complex mixture being produced from which no identifiable materials were isolated. A polar solvent might promote the sulfonium formation, since the transition state for the reaction is more polar than the starting materials.[9] On the other hand, the starting isothiosemicarbazones and bromo ketones are not very stable in polar solvents, particularly in those having solvolytic action on the bromo ketone to generate hydrogen bromide which might destroy the starting materials or facilitate side reactions at elevated temperatures. Less polar solvents such as toluene and chlorobenzene seem to be more suitable for the 4-

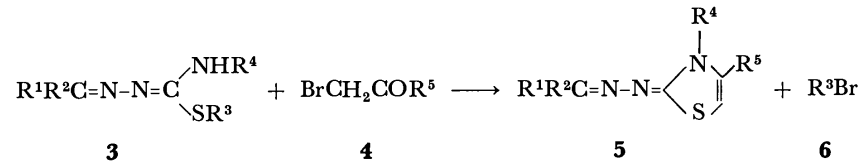

3 4 5 6

4a: $R^5=CH_3$
4b: $R^5=C_6H_5$

6a: $R^3=CH_3$
6b: $R^3=CH_2CH_2CH_3$
6c: $R^3=CH_2CH=CH_2$
6d: $R^3=CH_2C_6H_5$

	R^1	R^2	R^3	R^4
3a:	C_6H_5	H	CH_3	$CH_2CH=CH_2$
3b:	C_6H_5	H	$CH_2CH_2CH_3$	C_6H_5
3c:	C_6H_5	H	$CH_2CH=CH_2$	C_6H_5
3d:	C_6H_5	CH_3	$CH_2CH=CH_2$	CH_3
3e:	C_6H_5	C_6H_5	$CH_2CH=CH_2$	CH_3
3f:	*o*-HOC_6H_4	H	CH_3	C_6H_5
3g:	*o*-HOC_6H_4	H	$CH_2CH=CH_2$	C_6H_5
3h:	*o*-$CH_3OC_6H_4$	H	$CH_2CH=CH_2$	C_6H_5
3i:	*p*-$CH_3OC_6H_4$	H	CH_3	CH_3
3j:	*p*-$CH_3OC_6H_4$	H	$CH_2CH=CH_2$	CH_3
3k:	*p*-$CH_3OC_6H_4$	H	$CH_2C_6H_5$	CH_3
3m:	*p*-$CH_3OC_6H_4$	H	$CH_2CH=CH_2$	$CH(CH_3)_2$
3n:	*p*-$CH_3OC_6H_4$	H	CH_3	C_6H_5
3o:	*p*-$CH_3OC_6H_4$	H	$CH_2CH=CH_2$	C_6H_5
3p:	*p*-$CH_3OC_6H_4$	H	$CH_2C_6H_5$	C_6H_5
3q:	2,6-$Cl_2C_6H_3$	H	$CH_2CH=CH_2$	CH_3
3r:	C_6H_5	H	$CH_2CH=CH_2$	H

Scheme 1. The reaction of 3,4-disubstituted isothiosemicarbazones with α-bromo ketones.

TABLE 1. YIELD/%[7] OF **5** IN DIFFERENT SOLVENTS

Compd[a]/Solv.	Toluene	*N*,*N*-Dimethyl-formamide	2-Methoxy-ethanol	Chloro-benzene	Dioxane
5h	47	54	43	—	30
5k	70—68	16	13	62	44

a) From the corresponding *S*-allylisothiosemicarbazones, **3j** and **3o**, at a bath temperature of 130 °C for 20 min.

thiazoline or thiazole formation rather than highly polar ones.

When **3n** was allowed to react with **4b** in acetonitrile or ethanol at the reflux temperature, 3-(*p*-methoxyphenyl)-4-phenyl-5-methylthio-4*H*-1,2,4-triazole was the only product which could be isolated and identified,[10] its yield amounting to 30% in the latter solvent. The triazole may be formed through electrocyclic reaction[11] of the starting isothiosemicarbazone followed by autoxidation of the intermedially formed 3-methylthio-4-phenyl-5-(*p*-methoxyphenyl)-1,5-dihydro-1,2,4-triazole by analogy with oxidative cyclization of thiosemicarbazones.[12]

Since the ring closure of 3,4-disubstituted isothiosemicarbazone with loss of **6** involves displacement of R^3 by a phenacyl group, the reaction might depend primarily upon the nature of substituent on the sulfur atom. An equimolar mixture of **3i**, **3j**, **3k**, and **4b** in toluene was heated at a bath temperature of 130 °C for 15 min. **4b** disappeared and the approximate molar ratio of the remaining isothiosemicarbazones, estimated on the basis of the NMR spectrum, was found to be 1:18:30 for allyl, benzyl, and methyl compounds, respectively. Although the ratio may represent the relative reactivity of the three isothiosemicarbazones, the yield of **5h** in this reaction was only as little as 42% based on the consumed isothiosemicarbazones due to undetermined side reactions. The above order of reactivities of isothiosemicarbazones, however, is reflected in the actual yields of **5** obtained by the reaction of anisaldehyde 4-methyl- and 4-phenylisothiosemicarbazones bearing allyl, benzyl, or methyl group on the sulfur atom with **4b** in toluene (Table 2). This is in line with the order of stability of the carbocations corresponding to these substituents, the order not being affected by the nature of R^4. The higher yields of **5** from 3-allyl- and 3-benzylisothiosemicarbazones can be rationalized as a result of easy ionization of these groups by S_N1 type pathway from the positively charged

TABLE 2. YIELDS[a] OF 2-(*p*-METHOXYBENZYLIDENEHYDRAZONO)-4-THIAZOLINES FROM 3,4-DISUBSTITUTED ISOTHIOSEMICARBAZONES BEARING VARIOUS SUBSTITUENTS ON THE SULFUR ATOM

	R^3		
	CH_3[b]	$CH_2C_6H_5$	$CH_2CH=CH_2$
5h	9—11	38	47
5k	26	57	70

a) Obtained by heating an equimolar mixture of **3** and **4b** in toluene at a bath temperature of 130 °C for 20 min and isolating **5** by means of column chromatography. b) Heated for 90 min.

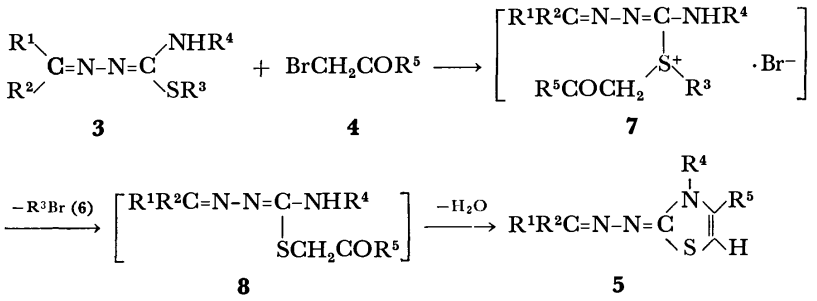

Scheme 2. Mechanism of 4-thiazoline formation.

sulfur atom of potential sulfonium salt (**7**). On the other hand, the reaction of **3b** with **4b** gave **5b** (10% yield) and **6b**, but no 2-bromopropane which would be formed if the 3-propyl group is dissociated as a free carbocation from the sulfur atom. Thus 3-propyl- and probably also 3-methylisothiosemicarbazones should react with **4b** to yield the corresponding **5** through S_N2 type dissociation of the sulfonium salt (**7**) into **6b** or **6a** and *S*-phenacylisothiosemicarbazone ($R^5=C_6H_5$) (**8**). In either case, **8** may rapidly cyclize to **5** and can be considered a common intermediate through which the same 4-thiazoline was produced from the corresponding thiosemicarbazone. A tentative mechanism for the 4-thiazoline formation is shown in Scheme 2. The reaction should involve, as the first step, nucleophilic attack of the α-carbon of the halo ketone by sulfur atom as in the simple alkylation reaction of alkyl sulfides.[4] However, the nucleophilicity of the sulfur atom of isothiosemicarbazones seems to be much lower than that of alkyl sulfides, since one of the α-carbons becomes attached to electron-withdrawing groups and the lone electron pairs on the sulfur conjugate to the 2,3-diaza-1,3-butadiene system which may further extend to R^1. Thus the thiazoline formation from isothiosemicarbazones can occur with acetonyl and phenacyl bromides (**4a** and **4b**), but not with the corresponding less reactive chlorides even under drastic conditions.

Under general reaction conditions, **9a** was unreactive and gave no expected thiazole (**2b**) upon heating with **4b** in toluene. In contrast to the inertness of 2,3-dimethyl compound (**9a**), 2-methyl-3-allylisothiosemicarbazone (**9b**) and 2-methylthiosemicarbazone (**9c**) gave **2b** in 64 and 81% yields, respectively. The

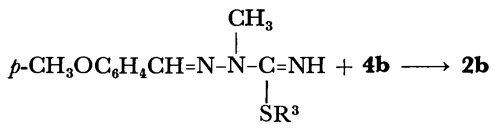

9a: $R^3=CH_3$
9b: $R^3=CH_2CH=CH_2$
9c: $R^3=H$

methyl group at the 2-position is by no means obstructive to the ring closure of the probable *S*-phenacylisothiosemicarbazone. The extremely diminished reactivity of **9a** may be explained in terms of the restraint of S_N2-type attack of the bromide ion on the methyl carbon in the sulfonium salt (**10**), presumably due to the free rotation about the N^2–C bond, which gives **10** a less rigid, fluttering structure, the methyl moiety

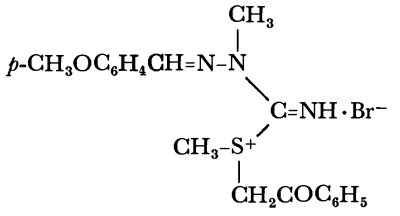

10

responsible for this reaction thus being a more elusive target for bromide ion. On the other hand, **9b** can produce *S*-phenacylisothiosemicarbazone and **6c** through S_N1 pathway from the sulfonium salt, leading to the formation of the corresponding thiazole. *o*-Hydroxybenzylidene compound (**3g**) required much longer reaction periods (5 h or more) than did the *o*-methoxy analog (**3h**) to give **5e** in comparable yields, although salicylaldehyde 4-phenylthiosemicarbazone gave **5e** in almost quantitative yield upon brief heating with **4b**. Since **3h** gave **5f** in 55% yield within 20 min, the strong intramolecular hydrogen bonding associated with the phenolic hydrogen and the N-1 atom (νOH 3060 cm^{-1} at 2×10^{-3} mol dm^{-3} in carbon tetrachloride) should account for the lower reactivity of **3g** by withdrawing electrons through 2,3-diaza-1,3-butadiene system from the sulfur atom. The unexpectedly high yield of **5d** from **3e** may be interpreted as a result of the exclusion of possible side reactions involving the azomethine double bond by virtue of the two bulky phenyl groups attached.

With bromoacetone (**4a**), major portions of the starting isothiosemicarbazones (**3j** and **3o**) remained unreacted under the general reaction conditions, **5g** and **5i** being obtained in 17 and 5% yields, respectively. Prolonged periods of time caused darkening of the reaction mixture, giving no improvement in the yield of **5**. 2-Arylmethylenehydrazono-3,4-disubstituted 4-thiazolines obtained are given in Table 3.

Compound **5m** formed through the allyl-phenacyl exchange reaction from (*E*,*E*)-**3q**[13] consists of two isomers, *E* and *Z* forms, and has higher content of *Z* (38%) than that produced by the reaction between (*E*)-2,6-dichlorobenzaldehyde 4-methylthiosemicarbazone (**11**) and **4b**, the latter route giving a mixture of *E* (91%) and *Z* (9%) forms. The higher content of *Z* compound was not the result of simple thermal isomerization of initially formed *E* isomer to *Z* form, since the pure (*E*)-**5m** isomerized to only 8% to *Z* upon heating in toluene at 130 °C for the same period of time as that for the reaction of **3q** with **4b**. Di-

TABLE 3. 2-ARYLMETHYLENEHYDRAZONO-3,4-DISUBSTITUTED 4-THIAZOLINES

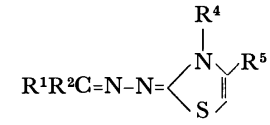

Compd No.	R^1	R^2	R^4	R^5	Yield/%[a]	Mp/°C	Formula	Found(%) C	H	N	Calcd(%) C	H	N	PMR[b] H-5
5a	C_6H_5	H	$CH_2CH=CH_2$	C_6H_5	22[c]	139.5—140.5	$C_{19}H_{17}N_3S$	71.73	5.40	13.41	71.45	5.37	13.16	5.96
5b	C_6H_5	H	C_6H_5	C_6H_5	59	189.5—190.5	$C_{22}H_{17}N_3S$	74.25	4.83	11.80	74.35	4.82	11.84	6.15
5c	C_6H_5	CH_3	CH_3	C_6H_5	55	102—104	$C_{18}H_{17}N_3S$	70.38	5.58	13.83	70.34	5.58	13.67	5.92
5d	C_6H_5	C_6H_5	CH_3	C_6H_5	98	168—169	$C_{23}H_{19}N_3S$	74.68	5.06	11.25	74.77	5.18	11.37	5.93
5e	*o*-HOC_6H_4	H	C_6H_5	C_6H_5	62	206	$C_{22}H_{17}N_3OS$	70.86	4.51	11.24	71.15	4.61	11.32	6.17
5f	*o*-$CH_3OC_6H_4$	H	C_6H_5	C_6H_5	55	178—180	$C_{23}H_{19}N_3OS$	71.63	5.01	10.94	71.67	4.97	10.90	6.08
5g	*p*-$CH_3OC_6H_4$	H	CH_3	CH_3	17	222—222.5[e]	$C_{13}H_{16}BrN_3OS$	45.53	4.74	12.34	45.62	4.71	12.28	5.65[d]
5h	*p*-$CH_3OC_6H_4$	H	CH_3	C_6H_5	47	124—125.5	$C_{18}H_{17}N_3OS$	67.16	5.33	12.99	66.86	5.30	13.00	5.95
5i	*p*-$CH_3OC_6H_4$	H	C_6H_5	CH_3	5	189—190[e]	$C_{18}H_{18}BrN_3OS$	53.54	4.36	10.32	53.47	4.49	10.39	5.65[d]
5j	*p*-$CH_3OC_6H_4$	H	$CH(CH_3)_2$	C_6H_5	57	141.5	$C_{20}H_{21}N_3OS$	68.57	6.01	12.12	68.36	6.02	11.96	5.79
5k	*p*-$CH_3OC_6H_4$	H	C_6H_5	C_6H_5	70	163—166	$C_{23}H_{19}N_3OS$	71.53	4.94	10.89	71.67	4.97	10.90	6.10
5m	2,6-$Cl_2C_6H_3$	H	CH_3	C_6H_5	58[f]	149.5—150[g]	$C_{17}H_{13}Cl_2N_3S$	56.09	3.52	11.69	56.36	3.62	11.60	5.98
						96—97.5[h]	$C_{17}H_{13}Cl_2N_3S$	56.44	3.56	11.46	56.36	3.62	11.60	5.97

a) Obtained from *S*-allylisothiosemicarbazones unless otherwise indicated. b) All the values are for free bases in deuteriochloroform. c) Obtained from *S*-methylisothiosemicarbazone. d) A poorly resolved quartet, $J=ca.$ 1.2 Hz. e) Hydrobromide salt. f) Consisting of two isomers, 62% *E* and 38% *Z*. g) *Z* form. h) *E* form.

TABLE 4. CHEMICAL SHIFTS[a] OF THIAZOLE(**2b**) AND 4-THIAZOLINE(**5h**)

	NCH_3	C_6H_5	CH=N	H-5
2b	3.69	$H^{m,p}$ 7.32	7.56	6.88
		H^{o} 7.89		
5h	3.34	7.40	8.32	5.95

a) δ ppm from internal TMS in $CDCl_3$.

minished bond order of the CH=N^1 bond in the intermediate species bearing positive charge on the sulfur atom might be responsible for the promoted isomerization. These isomers could be differentiated on the basis of the NMR spectrum in which the azomethine proton (CH=N^1) of *E* form resonated at δ 8.61 and that of *Z* form at δ 7.65 ppm in chloroform-*d*. In view of the greater difference (0.96 ppm) between the chemical shifts of the azomethine protons of these two isomers and a smaller difference (0.26 ppm) between the resonances of N-methyl protons and the substantially equivalent value for the H-5 proton on the thiazoline ring (Table 3), the isomerism should be about the C=N^1 bond rather than N^2=C bond.[14] The proximity of aldehydic proton to the electron pair of nitrogen in *Z* aldoxime caused upfield shift of that proton relative to the corresponding *E* aldoxime.[15] Thus the predominant isomer exhibiting downfield resonance should be of *E*-configuration. A trace of *Z* compound was also detected in the reaction of **3d** with **4b**, being easily removed by means of column chromatography. Recently, assignment of isomeric hydrazones of 2,6-dichlorobenzaldehyde on the basis of NOE observation[16] has been proposed and the conclusions may similarly apply to the present compounds.

A predominant tautomer has been determined by means of UV spectroscopy[17] in the 2-hydrazino-4-phenylthiazole and 2-hydrazono-4-phenyl-4-thiazoline system. An isomeric pair of thiazole (**2b**) and 4-thiazoline (**5h**) showed certain spectral differences sufficient to distinguish them from each other. In the mass spectrometry, the primary fragmentation of **5h** occurred at the N^2=C bond to produce a fragment ion, *m/e* 176, representing the base peak, whereas that of **2b** took place at the N–N bond giving an ion, *m/e* 134 (100%) (*p*-$CH_3OC_6H_4$–$C{\equiv}\overset{+}{N}H$). The former ion may be produced by hydrogen transfer from the azomethine carbon to the sulfur of thiazoline ring, probably through a six-membered transition state. This was confirmed by the spectrum of 2-(α-deuteriobenzylidenehydrazono)-3,4-diphenyl-4-thiazoline which showed a fragment ion, *m/e* 239, as compared with the value *m/e* 238 for that of the corresponding protium compound (**5b**). Further differentiation could be made on the basis of NMR spectra of **2b** and **5h** (Table 4). The resonance of H-5 proton on the heterocyclic ring seems to be of particular diagnostic value for this purpose.

Experimental

General. Melting points were determined in an open glass capillary and are uncorrected. ^1H NMR spectra, obtained with a Hitachi R-24 spectrometer (60 MHz) in chloroform-*d*, are given in δ ppm downfield from internal tetramethylsilane unless otherwise stated. IR spectra were obtained on a Hitachi EPI-G2 or 260-30 grating spectrophotometer and mass spectra (75 eV) on a Japan Electron Optics JMS-D100 mass spectrometer. Wakogel C-300 was used for column chromatography. Commercial phenacyl bromide (**4b**) was recrystallized from ethanol to give colorless prisms, mp 50 °C (lit,[18] mp 50 °C).

Thiosemicarbazones. All the thiosemicarbazones, R^1R^2C=NNHCSNHR^4, were prepared by the conventional method.[19] New ones are (R^1, R^2, R^4, % yield, mp °C, and elemental analyses given): C_6H_5, CH_3, CH_3, 78, 134.5—136. Found: C, 57.83; H, 6.39; N, 20.57%. Calcd for $C_{10}H_{13}$-

N_3S: C, 57.96; H, 6.32; N, 20.28%. *o*-$CH_3OC_6H_4$, H, C_6H_5, 87, 150—151. Found: C, 63.07; H, 5.28: N, 14.82%. Calcd for $C_{15}H_{15}N_3OS$: C, 63.15; H, 5.30; N, 14.73%. *p*-$CH_3OC_6H_4$, H, $CH(CH_3)_2$, 81, 192—193.5. Found: C, 57.26; H, 6.91; N, 16.69%. Calcd for $C_{12}H_{17}N_3OS$: C, 57.35; H, 6.82; N, 16.72%. 2,6-$Cl_2C_6H_3$, H, CH_3, 89, 190—191. Found: C, 41.11; H, 3.39; N, 16.27%. Calcd for $C_9H_9Cl_2N_3S$: C, 41.23; H, 3.46; N, 16.03%.

Isothiosemicarbazones. The compounds **3a**—**3r** were prepared according to the procedure reported previously[20] with some appropriate modifications. New ones are: **3a** (HBr salt): yellow prisms (from EtOH), mp 163—164 °C, yield 89%. Found: C, 45.99; H, 5.09; N, 13.63%. Calcd for $C_{12}H_{16}BrN_3S$: C, 45.86; H, 5.13; N, 13.37%. **3b**: colorless prisms (from hexane), mp 58—59 °C, yield 31%. Found: C, 68.55; H, 6.45; N, 13.90%. Calcd for $C_{17}H_{19}N_3S$: C, 68.66; H, 6.44; N, 14.13%. **3c** (HBr salt): pale yellow prisms (from EtOH), mp 161—162.5 °C, yield 93%. Found: C, 54.24; H, 4.80; N, 11.32%. Calcd for $C_{17}H_{18}BrN_3S$: C, 54.26; H, 4.82; N, 11.17%. **3d** (HBr salt): colorless needles (from EtOH), mp 156—157 °C, yield 87%. Found: C, 47.44; H, 5.53; N, 12.80%. Calcd for $C_{13}H_{18}BrN_3S$: C, 47.56; H, 5.53; N, 12.80%. **3e** (HCl salt): faintly yellowish needles (from aqueous *i*-PrOH), mp 128—129 °C, yield 61%. Found: C, 70.07; H, 6.15; N, 13.63%. Calcd for $C_{18}H_{19}N_3S$ (free base): C, 69.88; H, 6.19; N, 13.58%. **3f**: yellow prisms (from benzene–*i*-PrOH, 1:1 by volume), mp 137—138 °C, yield 89%. Found: C, 63.10; H, 5.29; N, 14.83%. Calcd for $C_{15}H_{15}N_3OS$: C, 63.15; H, 5.30; N, 14.73%. **3g**: pale yellow needles (from *i*-PrOH), 78—78.5 °C, yield 77%. Found: C, 65.50; H, 5.44; N, 13.56%. Calcd for $C_{17}H_{17}N_3OS$: C, 65.58; H, 5.50; N, 13.50%. **3h** (HBr salt): pale yellow fine needles (from EtOH), mp 157—158 °C, yield 88%. Found: C, 52.99; H, 4.93; N, 10.30%. Calcd for $C_{18}H_{20}BrN_3OS$: C, 53.21; H, 4.96; N, 10.34%. **3j** (HBr salt hemihydrate): yellow needles (from MeOH), mp 116.5—117 °C, yield 83%. Found: C, 44.06; H, 5.45; N, 11.72%. Calcd for $C_{13}H_{18}BrN_3OS \cdot 1/2H_2O$: C, 44.20; H, 5.42; N, 11.89%. **3k**: pale yellow fine needles (from i-Pr_2O), mp 55—56 °C, yield 96%. Found: C, 64.88; H, 6.00; N, 13.42%. Calcd for $C_{17}H_{19}N_3OS$: C, 65.16; H, 6.11; N, 13.41%. **3m** (HBr salt hemihydrate): pale yellow prisms (from EtOH), mp 98—99 °C, yield 92%. Found: C, 47.28; H, 6.13; N, 10.99%. Calcd for $C_{15}H_{22}BrN_3OS \cdot 1/2H_2O$: C, 47.25; H, 6.08; N, 11.02%. **3n**: pale yellow needles (from EtOH), mp 112 °C, yield 89%. Found: C, 64.15; H, 5.78; N, 14.13%. Calcd for $C_{16}H_{17}N_3OS$: C, 64.20; H, 5.72; N, 14.04%. **3o** (HBr salt): pale yellow needles (from EtOH), mp 157—158 °C, yield 89%. Found: C, 53.01; H, 4.91; N, 10.41%. Calcd for $C_{18}H_{20}BrN_3OS$: C, 53.21; H, 4.96; N, 10.34%. **3p**: faintly yellowish needles (from benzene–*i*-PrOH, 1:3 by volume), mp 138—138.5 °C, yield 87%. Found: C, 70.61; H, 5.52; N, 11.05%. Calcd for $C_{22}H_{21}N_3OS$: C, 70.38; H, 5.64; N. 11.19%. **3q** (HBr salt): pale yellow prisms (from EtOH), mp 167.5—168.5 °C, yield 62%. Found: C, 37.62; H, 3.65; N, 11.18%. Calcd for $C_{12}H_{14}BrCl_2N_3S$: C, 37.62; H, 3.68; N, 10.97%. **3r**: colorless needles (from hexane), mp 41—41.5 °C, yield 80%. Found: C, 60.52; H, 5.86; N, 19.28%. Calcd for $C_{11}H_{13}N_3S$: C, 60.26; H, 5.98; N, 19.15%. **9b** (HBr salt): pale yellow needles (from MeOH), 175—175.5 °C, yield 54%. Found: C, 45.46; H, 5.22; N, 12.30%. Calcd for $C_{13}H_{18}BrN_3OS$: C, 45.35; H, 5.27; N, 12.21%.

*The Reaction of Benzaldehyde 3-Allylisothiosemicarbazone (**3r**) with Phenacyl Bromide (**4b**).* A solution of **3r** (0.22 g, 1 mmol) and **4b** (0.20 g, 1 mmol) in toluene (1 ml) was heated under reflux in an oil bath at 130 °C for 20 min and then the solvent was evaporated under reduced pressure. The residue was partitioned between chloroform and a 10% aqueous sodium carbonate solution. The organic layer was washed with water, dried over anhydrous sodium sulfate and evaporated. The remaining viscous liquid (0.31 g) was subjected to column-chromatographic separation on silica gel (20 g) using a benzene–ethanol mixture (98:2 by volume). Two fractions, imidazole (0.11 g) and thiazole (0.02 g), each consisting a substantially pure compound, were obtained. Recrystallization of the former twice from ethanol gave **1** as pale yellow needles (0.02 g), mp 101—102 °C. IR (KBr): 3140 cm^{-1} (νC–H of imidazole ring[2]); NMR: 3.95 (2H, dt, $J=7$ Hz and *ca.* 1 Hz, SCH_2), 5.03—6.43 (3H, m, CH_2=CH), 7.36 (6H, m, $H^{m,p}$ of two phenyls), 7.69 (1H, s, H-5 of imidazole ring), 7.78 (4H, m, H^o of two phenyls), 8.25 (1H, s, CH=N); MS (75 eV), *m/e* (rel intensity), 319(100) (M^+), 277(29), 220(97), 215(93), 173(34), 117(51), 104(31), 103(69), 77(45), 41(22). Found: C, 71.26; H, 5.33; N, 13.05%. Calcd for $C_{19}H_{17}N_3S$: C, 71.45; H, 5.37; N, 13.16%; M, 319. This was identical with a compound obtained by the standard method.[2] The thiazole **2a** exhibited IR and NMR spectra identical with those of an authentic sample (mp 191—192 °C; Found: C, 69.03; H, 4.63; N, 14.82%; M^+, 279. Calcd for $C_{16}H_{13}N_3S$: C, 68.80; H, 4.69; N, 15.05%; M, 279) which was prepared by heating an equimolar mixture of benzaldehyde thiosemicarbazone and **4b** in 80% aqueous ethanol and neutralizing the hydrobromide formed with aqueous sodium carbonate. The hydrobromide conventionally prepared from the thiazole fraction showed no depression in melting point on mixing with the authentic sample (223 °C).

*The Reaction of Benzaldehyde 3-Allyl-4-phenylisothiosemicarbazone (**3c**) with **4b** (a Typical Example).* A mixture of **3c** (0.3 g, 1 mmol), **4b** (0.2 g, 1 mmol), and toluene (2 ml) was heated in an oil bath at 130 °C for 20 min with occasional agitating and then the solvent was removed under reduced pressure. The residue was partitioned between chloroform and a 10% aqueous sodium carbonate solution. The organic layer was washed with water, dried over anhydrous sodium sulfate and evaporated. The remaining crystalline solid (0.38 g) was subjected to column chromatography on silica gel (30 g) eluting with benzene containing 1% by volume of ethanol. A homogeneous fraction (140 ml) gave **5b** as yellow crystals (0.21 g, 59%), mp 189—190 °C. Recrystallization from an acetone–benzene mixture (1:1 by volume) gave yellow prisms, mp 189.5—190.5 °C. NMR: 6.15 (1H, s, H-5 of 4-thiazoline ring), 7.15 (5H, s, phenyl), 7.27 (5H, s, phenyl), 7.32 (3H, m, $H^{m,p}$ of benzylidene group), 7.73 (2H, m, H^o of benzylidene group), 8.22 (1H, s, CH=N); MS, *m/e* (rel intensity), 355(100) (M^+), 326(25), 238(86), 133(22), 91(15), 77(48). Under similar conditions except for a heating period of 2.5 h, **3b** gave **5b** in 10% yield. The same compound was also obtained by refluxing benzaldehyde 4-phenylthiosemicarbazone (mp 189—191 °C, lit,[19a] mp 189 °C) with **4b** in 95% ethanol for 1 h and by recrystallization of the product, after being converted into the free base by an aqueous sodium carbonate solution, from an acetone–benzene mixture, mp 190—191.5 °C. Mixed melting point with **5b** showed no depression. Similarly benzaldehyde-α-*d* 4-phenylthiosemicarbazone (C_6H_5CD=N–NHCSNHC$_6H_5$) afforded the corresponding monodeuteriothiazoline, mp 190.5—191.5 °C; IR (KBr): νC–D 2200 cm^{-1}; MS, *m/e* (rel intensity) 356(100) (M^+), 327(25), 239(70), 133(16), 91(18), 77(32).

*The Reaction of 2,6-Dichlorobenzaldehyde 3-Allyl-4-methylisothiosemicarbazone (**3q**) with **4b**.* A mixture of **3q** (0.3

g, 1 mmol), **4b** (0.2 g, 1 mmol), and toluene (1 ml) was heated under reflux for 2.5 h and then evaporated under reduced pressure. Work-up of the residue in the same way as described in the reaction of **3c** with **4b** gave a thiazoline fraction (0.21 g, 58%) consisting of 62% *E* and 38% *Z* forms. This fraction was further subjected to column chromatography on silica gel (20 g) with benzene as an eluent giving a *Z* fraction (0.045 g) which preceded an *E* fraction (0.07 g). The *Z* compound, (*Z*)-**5m**, crystallized from ethanol as yellow plates (0.04 g), mp 149.5—150 °C. NMR: 3.12 (3H, s, NCH_3), 5.98 (1H, s, H-5 of 4-thiazoline ring), 7.27 (3H, s, 2,6-dichlorophenyl), 7.38 (5H, s, phenyl), 7.65 (1H, s, CH=N); MS, *m/e* (rel intensity), 363(30), 361(41) (M^+), 326(100), 176(29), 134(7), 123(17), 102(45), 91(13), 77(10). The *E* compound, (*E*)-**5m**, was obtained as a yellow oil which gradually solidified upon standing. Recrystallization of the solid from ethanol gave fine yellow needles, mp 96—97.5 °C. NMR: 3.38 (3H, s, NCH_3), 5.97 (1H, s, H-5 of 4-thiazoline ring), 7.20 (3H, m, 2,6-dichlorophenyl), 7.35 (5H, s, phenyl), 8.61 (1H, s, CH=N); MS, *m/e* (rel intensity), 363(25), 361(35) (M^+), 326(100), 176(36), 134(32), 123(27), 102(72), 91(17), 77(18). When **5m** containing *Z* isomer was converted into the hydrobromide and the salt recrystallized from ethanol, pure (*E*)-**5m** hydrobromide was obtained as pale yellow prisms solvated with one molecule of ethanol, mp 213.5—214 °C not depressed by the authentic sample prepared by the reaction of 2,6-dichlorobenzaldehyde 4-methylthiosemicarbazone with **4b**. NMR: 1.20 (3H, t, J=7 Hz, CCH_3), 3.72 (2H, q, J=7 Hz, CCH_2), 4.01 (3H, s, NCH_3), 6.81 (1H, s, H-5 of 4-thiazoline ring), 7.35 (3H, s, 2,6-dichlorophenyl), 7.51 (5H, m, phenyl), 9.70 (1H, s, CH=N), broadly dispersed signal centered at about 14.1 ($\overset{+}{N}H$ and OH). Found: C, 46.72; H, 3.95; N, 8.70%. Calcd for $C_{19}H_{20}BrCl_2N_3OS$: C, 46,64; H, 4.12; N, 8.59%.

*The Reaction of Anisaldehyde 2-Methyl-3-allylisothiosemicarbazone (**9b**) with **4b**.* A mixture of **9b** (0.09 g, 0.34 mmol), **4b** (0.07 g, 0.35 mmol), and toluene (0.5 ml) was refluxed for 2 h and evaporated under reduced pressure. The residue was worked up by the same procedure as described for the reaction of **3c** with **4b** to give anisaldehyde 1-methyl-1-(4-phenyl-2-thiazolyl)hydrazone (**2b**) (0.07 g, 64%) as yellow plates, mp 178—180 °C. Recrystallization from an *i*-Pr_2O–AcMe mixture (1:1 by volume) raised the melting point to 186.5—187 °C. NMR: 3.69 (3H, s, NCH_3), 3.81 (3H, s, OCH_3), 6.88 (1H, s, H-5 of thiazole ring), 6.92 (2H, d, J=9.0 Hz, *p*-methoxyphenyl), 7.32 (3H, m, $H^{m,p}$ of phenyl), 7.56 (1H, s, CH=N), 7.63 (2H, d, J=9.0 Hz, *p*-methoxyphenyl), 7.89 (2H, m, H^o of phenyl). Found: C, 66.79; H, 5.29; N, 12.86%; M^+, 323. Calcd for $C_{18}H_{17}N_3OS$: C, 66.86; H, 5.30; N, 13.00%; M, 323. The same compound was obtained by refluxing anisaldehyde 2-methylthiosemicarbazone (0.22 g, 1 mmol; mp 191 °C, lit,[21] mp 192 °C) and **4b** (0.20 g, 1 mmol) in ethanol (5 ml) for 1 h and neutralizing the hydrobromide with aqueous sodium carbonate as pale yellow plates (0.26 g, 81%), mp 185—187 °C, not depressed by admixture with the compound prepared as above.

The author wishes to thank Miss Kuniko Saito and Miss Tomoko Watanabe for their helpful technical assistance in the preparation of compounds.

References

1) Part II: C. Yamazaki, *Tetrahedron Lett.*, **1978**, 1295.
2) C. Yamazaki, *Bull. Chem. Soc. Jpn.*, **51**, 1846 (1978).
3) S. Veibel and B. J. Nielsen, *Acta Chem. Scand.*, **10**, 1488 (1956).
4) F. E. Ray and I. Levine, *J. Org. Chem.*, **2**, 267 (1937).
5) a) H. Johne, K. Seifert, S. Johne, and E. Bulka, *Pharmazie*, **33**, 259 (1978); b) W. Pfeiffer, E. Dilk, and E. Bulka, *Z. Chem.*, **17**, 218 (1977).
6) Lower temperatures caused a significant reduction in the yield of **5**. For example, the reaction of **3o** with **4b** in toluene at 80 °C gave **5k** in 39% yield after the bromide had disappeared (4 h) and **3e** similarly afforded **5d** in 81% yield after heating for 7.5 h.
7) Throughout the discussion, all the yields refer to those of isolated products.
8) DMSO may act as an oxidizing agent on the halo ketone: N. Korublum, *J. Am. Chem. Soc.*, **79**, 6562 (1957).
9) C. J. M. Stirling, "Sulfonium Salts," in "Organic Chemistry of Sulfur," ed by S. Oae, Plenum Press, New York (1977), Chap. 9, p. 473.
10) Iron(III) chloride-oxidation (E. Hoggarth, *J. Chem. Soc.*, **1949**, 1160) of **3n** yielded the same 4*H*-1,2,4-triazole as obtained here. Colorless needles, mp 158 °C. Found: C, 64.66; H, 5.06; N, 14.10%. Calcd for $C_{16}H_{15}N_3OS$: C, 64.63; H, 5.09; N, 14.14%.
11) J. Elguero, *Bull. Soc. Chim. Fr.*, **1971**, 1925.
12) J. K. Landquist, *J. Chem. Soc., C*, **1970**, 63.
13) 2,6-Dichlorobenzaldehyde 3-allyl-4-methylisothiosemicarbazone (**3q**) and **11** were obtained in only one isomeric form with respect to the configuration about $C{=}N^1$ double bond. The chemical shift values of the azomethine proton, δ 8.55 for **3q** and δ 8.18 ppm for **11** in chloroform-*d*, imply *E* configuration for these compounds in the light of the conclusions of Tsujikawa *et al.*[16] In a strict sense, **3q** exists in an equilibrium mixture of 69% *E,E* and 31% *E,Z* forms in chloroform-*d*.[20] However, in view of the sharp melting point of the hydrobromide, **3q** should exist exclusively or predominantly in *E,E* configuration in that state.
14) No attempt was made to determine the configuration about $N^2{=}C$ bond.
15) a) J. V. Burakevich, A. M. Lore, and G. P. Volpp, *J. Org. Chem.*, **36**, 1 (1971); b) G. J. Karabatsos and N. Hsi, *Tetrahedron*, **23**, 1079 (1966); c) K. Shinoda, T. Shida, T. Ohtsuka, T. Uzuki, and E. Yokoyama, *Nippon Kagaku Kaishi*, **1973**, 114.
16) T. Tsujikawa, E. Mizuta, and M. Hayashi, *Yakugaku Zasshi*, **96**, 125 (1976).
17) B. Stanislaw, M. Diwa, B. Lidia, and M. Barbara, *Ann. Univ. Mariae Curie-Sklodowska, Sect. D*, **32**, 221 (1977); *Chem. Abstr.*, **89**, 107524p (1978).
18) J. B. Rather and E. E. Reid, *J. Am. Chem. Soc.*, **41**, 75 (1919).
19) a) D. Shah and J. P. Trivedi, *J. Indian Chem. Soc.*, **40**, 889 (1963); b) K. A. Jensen, U. Anthoni, B. Kaegi, C. Larsen, and C. Th. Pedersen, *Acta Chem. Scand.*, **22**, 1 (1968).
20) C. Yamazaki, *Can. J. Chem.*, **53**, 610 (1975).
21) M. E. Cattelain, *Bull. Soc. Chim. Fr.*, **1940**, 791.

Substitution and Elimination Reactions *via* One Electron Transfer Process. A New Olefin Synthesis from β-Nitro Sulfones[1]

Noboru Ono,* Rui Tamura, Tamon Nakatsuka, Jun-ichi Hayami,[2] and Aritsune Kaji

Department of Chemistry, Faculty of Science, Kyoto University, Yoshida, Sakyo-ku, Kyoto 606

(Received April 15, 1980)

gem-Bromonitro compounds or *gem*-dinitro compounds couple with carbanions derived from α-cyano sulfones or α-carbonyl sulfones to give β-nitro sulfones. The nitro and sulfonyl groups are eliminated from the coupling products on treatment with reductive one electron transfer reagents to give α,β-unsaturated carbonyl compounds or nitriles.

Reductive elimination of nitro groups from the vicinal dinitro compounds is a useful procedure for olefin synthesis, where olefins are obtained in good yields by the action of mild reducing agents such as sodium sulfide,[3] tin(II) chloride,[4] or calcium amalgam.[5] If one of the nitro groups can be replaced by a sulfonyl group in this type of elimination, synthetic utility must increase to give a wide variety of olefins from β-nitro sulfones.

In this paper we wish to report the preparation of β-nitro sulfones by the reaction of *gem*-bromonitro compounds(**1**) or *gem*-dinitro compounds(**2**) with α-sulfonyl carbanions followed by the conversion of β-nitro sulfones to olefins.

Results and Discussion

Preparation of β-Nitro Sulfones. The reaction of *gem*-bromonitro compounds(**1**) or *gem*-dinitro compounds(**2**) with α-sulfonyl carbanions was carried out in *N*,*N*-dimethylformamide (DMF) or dimethyl sulfoxide(DMSO) as shown in Eq. 1. Carbanions sta-

$$\underset{\substack{|\\ NO_2}}{R^1R^2C}\text{–X} + ArSO_2\text{–}\bar{C}(Y)R^3M^+ \longrightarrow \underset{\substack{|\\ NO_2}}{R^1R^2C}\text{—}\underset{\substack{|\\ SO_2Ar}}{C(Y)R^3} \quad (1)$$

1 X=Br; **2** X=NO_2; Y=CN, -C(=O)-; Ar=*p*-Tolyl or phenyl; M=Na, K; **4**

bilized by the sulfonyl and cyano groups or by the sulfonyl and carbonyl groups react with **1** or **2** to give the cross coupling products(**4**), but carbanions stabilized by one sulfonyl group or by the sulfonyl and nitro groups do not react with **1** or **2** at all. Results are summarized in Table 1.

Compounds **1** or **2** undergo a variety of reactions with carbanions. The following three types of reactions have been reported; 1) cross coupling reaction *via* a radical chain process, 2) cross coupling reaction *via* a radical non-chain process, 3) oxidative dimerization of carbanions.[6] Carbanions which undergo type 1 reaction are those derived from nitroalkanes, malonate esters, malonitriles, β-keto nitriles, cyanoacetates, β-keto esters, and β-diketones.[7]

It is clear that the coupling reaction of Eq. 1 proceeds *via* a radical chain process, since it is completely inhibited by the presence of 10 mol% of di-*t*-butylnitroxide. Thus, carbanions derived from α-cyano sulfones and α-carbonyl sulfones undergo type 1 reaction. A chain sequence of this type of reaction can be expressed as follows.

$$R\text{–}X + C^- \longrightarrow R\text{–}X^{\cdot-} + C\cdot$$
$$R\text{–}X^{\cdot-} \longrightarrow R\cdot + X^- \qquad X=\text{leaving groups}$$
$$R\cdot + C^- \longrightarrow R\text{–}C^{\cdot-} \qquad C^-=\text{carbanions}$$
$$R\text{–}C^{\cdot-} + R\text{–}X \longrightarrow R\text{–}C + R\text{–}X^{\cdot-}$$

It should be emphasized that the coupling reaction using α-sulfonyl carbanions involves anion radical intermediates from which a sulfonyl group can be eliminated.[8] Actually, α,β-unsaturated nitriles are formed in about 10% yield during the preparation of **4c**, **4d**, **4f**, or **4g**. This lowers the yield of the coupling products, however, this finding has an important bearing in a sense of organic synthesis.

Potassium is used as a counter cation of carbanions to prepare **4j**, **4l**, and **4m**. The reactions using sodium as a counter cation proceed very slowly. For example, it takes about 30 h to complete the reaction to prepare **4l** when sodium is a counter cation. Not much attention has been paid to counter cations of carbanions in nucleophilic substitution reaction *via* a radical chain process. Although sodium salts of carbanions have often been used, potassium salts seem to be much more reactive than sodium salts and are generally the reagent of choice.[9]

All attempts to bring about a coupling reaction of a carbanion stabilized by one sulfonyl group with **1** or **2** have failed. Starting materials were recovered unchanged (see Table 1). Simple β-nitro sulfones, the requisite starting materials to get non-functionalized olefins, have not been available by this S_{RN} route. Carbanions stabilized by one nitro group react with **1** or **2** very rapidly to afford the coupling products in good yields,[3] but highly stabilized carbanions such as those stabilized by the nitro and sulfonyl or by the nitro and carbonyl groups do not react with **1** or **2**. A possible explanation is that these highly stabilized anion is not a good electron donor to the S_{RN} acceptor.[10] Thus elimination from the vicinal dinitro compounds cannot be applied to the preparation of olefins substituted by electron-withdrawing groups at the sp^2 center.

Conversion of β-Nitro Sulfones to Olefins It is expected that the nitro and sulfonyl groups are eliminated from β-nitro sulfones on treatment with reductive one electron transfer reagents. In fact, **4a** is converted to olefin(**5a**) on treatment with various one electron transfer reagents as shown in Table 2 (Eq. 2). Inter-

$$\mathbf{4a} \longrightarrow \underset{(\mathbf{5a})}{Me_2C{=}C(CN)Me} \quad (2)$$

estingly, such a weak reducing agent as sodium

Table 1. Preparation of β-nitro sulfones (**4**)

Nitro compound	Carbanion	Solvent	Temp °C	Time h	Products	Yield[a] %
$Me_2C(Br)NO_2$ (**1a**)	$MeC^-(CN)Ts\ Na^+$ (**3a**)[b]	DMF	0	1.5	$Me_2C(NO_2)-C(CN)Me(Ts)$ (**4a**)	73
$Et(Me)C(NO_2)_2$ (**2b**)	**3a**	DMF	0	5	$Et(Me)C(NO_2)-C(CN)Me(Ts)$ (**4b**)	63
	3a	DMF	0	2	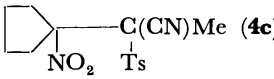 (**4c**)	45[c]
	3a	DMF	0	3	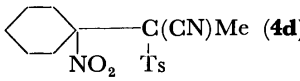 (**4d**)	40[c]
$Me_2C(NO_2)_2$ (**2a**)	$EtC^-(CN)Ts\ Na^+$	DMF	−20	5	$Me_2C(NO_2)-C(CN)Et(Ts)$ (**4e**)	65
2a	$n\text{-}C_4H_9C^-(CN)Ts\ Na^+$	DMF	−20	5	$Me_2C(NO_2)-C(CN)n\text{-}C_4H_9(Ts)$ (**4f**)	45[c]
2a	$n\text{-}C_8H_{17}C^-(CN)Ts\ Na^+$	DMF	−20	5	$Me_2C(NO_2)-C(CN)n\text{-}C_8H_{17}(Ts)$ (**4g**)	48[c]
2a	$MeC^-(CO_2Et)Ts\ Na^+$	DMF	25	3	$Me_2C(NO_2)-C(CO_2Et)Me(Ts)$ (**4h**)	80
2b	$MeC^-(CO_2Et)Ts\ Na^+$	DMSO	25	5	$Et(Me)C(NO_2)-C(CO_2Et)Me(Ts)$ (**4i**)	70
2a	$EtC^-(CO_2Et)Ts\ K^+$	DMSO	25	10	$Me_2C(NO_2)-C(CO_2Et)Et(Ts)$ (**4j**)	59
2a	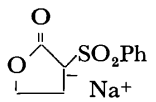	DMSO	25	5	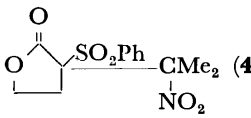 (**4k**)	62
2a	$MeC^-(CMe)Ts\ K^+$ (O)	DMSO	25	5	$Me_2C(NO_2)-C(CMe)Me(Ts)$(O) (**4l**)	49[d]
2a	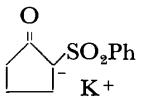	DMSO	25	10	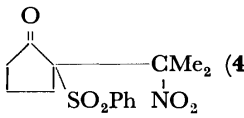 (**4m**)	54[d]
2a	$EtC^-(NO_2)Ts\ Na^+$	DMSO	25	24	No reaction	
2a	$Me_2C^-Ts\ Na^+$	DMSO	25	5	No reaction	

a) Pure isolated yield. b) Ts=*p*-CH_3-$C_6H_4SO_2$-. c) α,β-Unsaturated nitrile is obtained in about 10% yield. d) The reaction is carried out under irradiation of 150W tungsten lamp.

Table 2. Conversion of **4a** to **5a** under various conditions

Reducing reagent	Solvent	Light	Temp °C	Time h	Yield of **5a**[a]/%
$Na_2S\cdot 9H_2O$	DMF	20W[b]	25	3	92
$Na_2S\cdot 9H_2O$	DMF	dark	25	3	90
PhSNa	DMF	150W[c]	25	3	70
PhSNa	DMF	dark	25	3	5
$Me_2C(NO_2)-Li^+$	DMF	150W	25	3	53
$Me_2C(NO_2)-Li^+$	DMF	dark	25	3	2
Na	HMPA[d]		0	0.25	70
$Na_2S_2O_4$	HMPA	20W	25	168	50

a) Yields were determined by GLPC. b) Fluorescent lamp. c) Tungsten lamp. d) Hexamethylphosphoric triamide.

Table 3. Conversion of β-nitrosulfones(**4**) to olefins(**5**) on treatment with sodium sulfide

4	5	Yield[a]/%
4a	$Me_2C{=}C(CN)Me$ (**5a**)	69
4b	$Et(Me)C{=}C(CN)Me$ (**5b**)	62
4c	(**5c**)	70
4d	(**5d**)	70
4e	$Me_2C{=}C(CN)Et$ (**5e**)	62
4f	$Me_2C{=}C(CN)n\text{-}C_4H_9$ (**5f**)	71
4g	$Me_2C{=}C(CN)n\text{-}C_8H_{17}$ (**5g**)	74
4h	$Me_2C{=}C(CO_2Et)Me$ (**5h**)	79
4i	$Et(Me)C{=}C(CO_2Et)Me$ (**5i**)	60
4j	$Me_2C{=}C(CO_2Et)Et$ (**5j**)	59
4k	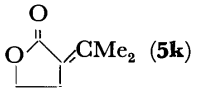 (**5k**)	62
4l	$Me_2C{=}C(\overset{\overset{O}{\|}}{C}Me)Me$ (**5l**)	48[b]
4m	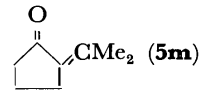 (**5m**)	65

a) Pure isolated products. b) Besides **5l**, α,β-unsaturated sulfone (**6**) was obtained in 15% yield.

benzenethiolate or the lithium salt of 2-nitropropane can induce the elimination of Eq. 2, when the reaction mixture is irradiated by a 150 W tungsten lamp. Among various reducing agents, sodium sulfide is the best one to prepare olefins in its availability, effectiveness and in the mildness of the reaction conditions. β-Nitro sulfones(**4**) listed in Table 1 are converted to olefins (**5**) on treatment with sodium sulfide in DMF at room temperature (Eq. 3). Results are summarized

$$\mathbf{4} + Na_2S \longrightarrow \underset{(\mathbf{5})}{R^1R^2C{=}C(Y)R^3} + NaNO_2 + S + ArSO_2Na \quad (3)$$

$Y = CN, -\overset{\overset{O}{\|}}{C}-$

in Table 3. The reaction proceeds very rapidly as shown in Fig. 1. The yield in the table refers to pure and isolated products. The reaction proceeds smoothly to give **5** in good yields, for example, the yield of **5a** or **5f** determined by GLPC using an internal standard is 92 and 97%, respectively. On treatment with sodium sulfide, elimination from **4h**, **4i**, or **4j** proceeds faster than hydrolysis of an ester function of these compounds. Thus, α,β-unsaturated carboxylates are obtained in good yields on treatment with **4h**, **4i**, or **4j** with sodium sulfide.

But the reaction of **4l** with sodium sulfide gives the mixture of **5l** and α,β-unsaturated sulfone(**6**) (Eq. 4).

$$\mathbf{4l} + Na_2S \longrightarrow \mathbf{5l} + \underset{(\mathbf{6})}{Me_2C{=}C(SO_2Ar)Me} \quad (4)$$

Compound **6** is formed by elimination of the nitro and acetyl groups from **4l**. This may proceed *via* one electron transfer process.[11]

It is recommended to carry out the coupling reaction

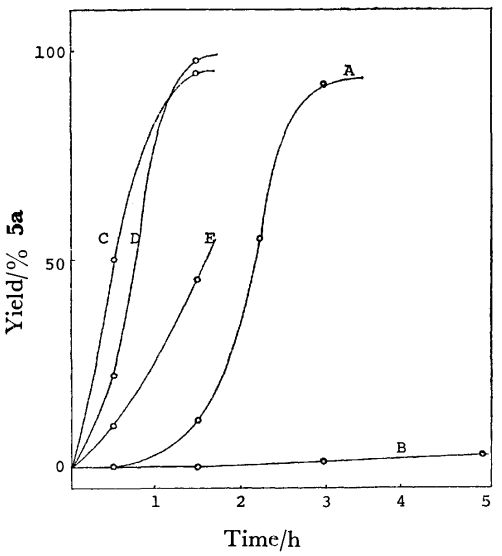

Fig. 1. Effects of di-*t*-butylnitroxide and nitro aromatics on the reaction of Eq 3. A: None, B: di-*t*-butylnitroxide (5 mol%), C: *m*-DNB (10 mol%), D: *p*-DNB (10 mol%), E: nitrobenzene (10 mol%).

Table 4. Synthesis of α,β-unsaturated nitriles by one-pot procedure

R^1	R^2	X	R^3	Products[a] (Yield/%)
CH_3	CH_3	NO_2	C_2H_5	**5e** (74)[b]
CH_3	CH_3	NO_2	$n\text{-}C_8H_{17}$	**5g** (77)[b]
$-(CH_2)_5-$		Br	CH_3	**5d** (71)[c]
CH_3	$n\text{-}C_5H_{11}$	NO_2	CH_3	**5n** (68)[c]
CH_3	$n\text{-}C_5H_{11}$	NO_2	$n\text{-}C_8H_{17}$	**5o** (62)[c]

a) $R^1R^2C{=}C(CN)R^3$. b) Yields were determined by GLPC. c) Pure isolated products.

of carbanions with **1** or **2** and the subsequent elimination by one-pot procedure to prepare α,β-unsaturated nitriles, for some amounts of olefins are already formed while the coupling reaction proceeds. Thus, α,β-unsaturated nitriles are obtained in good yields by the one-pot procedure shown in Eq. 5. Results are summarized in Table 4.

$$\mathbf{1}\text{ or }\mathbf{2} + \underset{CN}{R^3\bar{C}}\text{-}SO_2Ar\ Na^+ \xrightarrow[3\,h]{-20\text{ or }0^\circ C} \xrightarrow[3\,h]{rt} \underset{Na_2S}{R^1R^2C{=}C(CN)R^3} \quad (5)$$

The elimination of the nitro and sulfonyl groups from β-nitro sulfones is not a simple ionic process. This is clear from the data in Fig. 1, where the effect of di-*t*-butylnitroxide or nitro aromatics on the reaction of Eq. 3 is summarized. Five mol% of di-*t*-butylnitroxide inhibits this reaction completely, this fact suggests that the present elimination reaction proceeds by a free radical chain mechanism. As shown in Fig. 1, the reaction is strongly affected by nitrobenzene, *m*-dinitrobenzene (*m*-DNB), and *p*-dinitrobenzene(*p*-DNB). These nitro aromatic compounds generally retard the substitution reaction *via* one electron transfer

processes, but the present reaction is accelerated by these π-acids. These facts, and observations of other aliphatic nitro system,[3,7] suggest that the elimination reaction is initiated by the formation of anion radical of β-nitro sulfone, from which sulfinate ion and nitrogen dioxide can be split off (Eq. 6).[12]

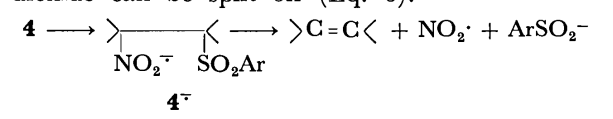

(6)

The unique olefin synthesis reported herein provides a potentially useful alternative to the classical methods using carbonyl compounds and carbanions. An important feature of the present procedure is that both the coupling and the elimination steps proceed *via* radical chain mechanism involving one electron transfer process to give highly hindered olefins under mild conditions.

Experimental

Solvents were purified by distillation. The IR spectra were recorded with a Hitachi 215 spectrophotometer. The ^{1}H-NMR spectra were recorded using a JEOL PE-100 spectrometer with TMS as an internal standard. GLPC analyses were performed with a Varian Aerograph 920 using a column containing Silicone DC-550 (20%, 1 m). The following compounds were prepared by the standard procedure; *gem*-bromonitro compounds,[13] *gem*-dinitro compounds,[14] α-cyanoalkyl sulfones.[15] Other sulfones were prepared by the reaction of the corresponding bromides with sodium *p*-toluenesulfinate or sodium benzenesulfinate in DMF. All reactions for the preparation of β-nitro sulfones (**4**) and olefins (**5**) were performed under a nitrogen atmosphere.

Preparation of β-Nitro Sulfones (4). Preparation of 4a as a Typical Procedure: Sodium hydride (44 mmol, 50% mineral oil dispersion) was placed in a 300 ml flask which was fitted with a rubber septum through which reagents can be introduced by a syringe. After sodium hydride was washed with hexane to remove mineral oil, the flask was placed under nitrogen and 50 ml of DMF was introduced *via* a syringe. A solution of 2-tosylpropionitrile (8.4 g, 40 mmol) in 50 ml of DMF was added dropwise to sodium hydride and the mixture was stirred until the evolution of hydrogen ceased. Then the DMF solution of the carbanion was cooled to 0 °C and to this solution was added 2-bromo-2-nitropropane (8.1 g, 40 mmol) in 30 ml of DMF. The resulting solution was stirred at 0 °C for 1.5 h. Working up by dilution with water, benzene extraction, followed by aqueous washing of the benzene layer, drying over anhydrous magnesium sulfate, and concentration gave a solid material. The crude material was recrystallized from ethanol to give **4a** (8.6 g, 73% yield). Other β-nitro sulfones were prepared by the similar procedure, but **4g** and **4i** were purified by column chromatography on silica gel using benzene as an eluent. Compound **4b** consisted of two diastereomers (A and B). They were separated by column chromatography on silica gel using benzene as an eluent. The ratio of A to B was unity. For the preparation of **4j**, **4k**, and **4m**, t-C_4H_9OK was used as a base instead of NaH. Reaction conditions are summarized in Table 1 and physical data of **4** are summarized in Table 5.

Inhibition Study. The reaction of the sodium salt of 2-tosylpropionitrile with 2-bromo-2-nitropropane was carried out at 0 °C. Each experiment consists of the sodium salt of the nitrile (6 mmol) and the nitro compound (7 mmol) in 15 ml of DMF and a reaction time of 1 h. Working up was carried out in the usual way. In the absence of di-*t*-butylnitroxide the crude product was subjected to column chromatography on silica gel using benzene as an eluent to give **4a** (1.0 g, 68% yield). In the presence of di-*t*-butylnitroxide (0.086 g, 0.6 mmol) **4a** was not detected on TLC. The crude product was subjected to column chromatography to give 2-tosylpropionitrile (0.85 g, 70% recovery).

Conversion of 4a to 5a under Various Conditions. Compound **4a** (1 mmol) was treated with various reducing reagents (3 mmol) under conditions listed in Table 2. After the period listed in the table, diethyl malonate (1 mmol) which is an internal standard was added. Then the reaction mixture was worked up in the usual manner and the organic materials were analyzed by GLPC. Yield of **5a** was determined from calibration curve which was made from pure **5a** and diethyl malonate. Results are summarized in Table 2.

Conversion of β-Nitro Sulfones (4) to Olefins (5) by Sodium Sulfide. General Procedure: A mixture of **4** (15 mmol) and $Na_2S \cdot 9H_2O$ (5.0 g, 18 mmol) in 30 ml of DMF was stirred at room temperature for 3 h, then 150 ml of water was added and the mixture was extracted with diethyl ether three times. The extract was washed with water, dried over magnesium sulfate, and concentrated. Distillation gave **5**. The following olefins were prepared by this procedure.

Physical Properties: **5a**: Bp 60 °C/35 Torr. (1 Torr=133.32 Pa, lit,[16] 155—157 °C). ^{1}H-NMR (CCl_4); δ 2.04 (3H, s), 1.82 (6H, s). IR (neat); 2215 cm^{-1} (CN), 1640 cm^{-1} (C=C). MS (20 eV), *m/e* (rel intensity), 95 (M^+, 100), 80(41), 68 (50).

5b: Bp 82 °C/40 Torr (lit,[17] 64 °C/17 Torr). ^{1}H-NMR (CCl_4); δ 2.44 (1H, q, J=7.5 Hz), 2.23 (1H, q, J=7.5 Hz), 2.07 (1.5H, s), 1.88 (3H, s), 1.84 (1.5H, s), 1.12 (1.5H, t, J=7.5 Hz), 1.06 (1.5H, t, J=7.5 Hz). IR (neat); 2215 cm^{-1} (CN), 1640 cm^{-1} (C=C). MS (20 eV), *m/e* (rel intensity), 109 (M^+, 14), 94(16), 67(14), 43(100).

5c: Bp 112.5 °C/32 Torr (lit,[18] 131/63 Torr). ^{1}H-NMR (CCl_4); δ 2.72—2.42 (2H, m), 2.42—2.16 (2H, m), 1.80 (3H, s), 2.0—1.6 (4H, m). IR (neat); 2215 cm^{-1} (CN), 1640 cm^{-1} (C=C). MS (20 eV), *m/e* (rel intensity), 121 (M^+, 34), 106(13), 67(80), 43(100).

5d: Bp 110 °C/15 Torr (lit,[19] 103 °C/13 Torr). ^{1}H-NMR (CCl_4); δ 2.6—2.4 (2H, m), 2.4—2.2 (2H, m), 1.87 (3H, s), 1.8—1.4 (6H, m). IR (neat); 2205 cm^{-1}(CN), 1627 cm^{-1}(C=C). MS (20 eV), *m/e* (rel intensity), 135 (M^+, 46), 120(20), 81(74), 68(100).

5e: Bp 92 °C/25 Torr. ^{1}H-NMR (CCl_4); δ 2.24 (2H, q, J=7.1 Hz), 2.07 (3H, s), 1.86 (3H, s), 1.13 (3H, t, J=7.1 Hz). IR (neat); 2210 cm^{-1}(CN), 1635 cm^{-1}(C=C). MS (20 eV), *m/e* (rel intensity), 109 (M^+, 12), 94(20), 67(12), 43(100).

5f: Bp 95 °C/25 Torr. ^{1}H-NMR (CCl_4); δ 2.19 (2H, m), 2.08 (3H, s), 1.85 (3H, s), 1.6—1.2 (4H, m), 0.97 (3H, t, J=7.1 Hz). IR (neat); 2210 cm^{-1} (CN), 1635 cm^{-1}(C=C). MS (20 eV), *m/e* (rel intensity), 137 (M^+, 25), 122(17), 96(18), 69(100).

5g: Bp 93.5 °C/0.6 Torr. ^{1}H-NMR (CCl_4); δ 2.17 (2H, m), 2.06 (3H, s), 1.84 (3H, s), 1.1—1.6 (12H, m), 0.89 (3H, t, J=7.5 Hz). IR (neat); 2210 cm^{-1}(CN), 1635 cm^{-1}(C=C). MS (20 eV), *m/e* (rel intensity), 193 (M^+, 51), 178(62), 164(80), 136(100).

5h: Bp 106 °C/100 Torr (lit,[20] 99 °C/81.5 Torr). ^{1}H-NMR (CCl_4); δ 4.10 (2H, q, J=7.0 Hz), 2.00 (3H, s), 1.77 (6H, s), 1.28 (3H, t, J=7.0 Hz). IR (neat); 1700 cm^{-1} (C=O), 1620 cm^{-1}(C=C). MS (20 eV), *m/e* 135 (M^+).

5i: Bp 95 °C/38 Torr (lit,[21] 67—72 °C/14 Torr). ^{1}H-

Table 5. Physical data of β-nitro sulfones (4)

4	Mp/°C	^{1}H-NMR: δ(CDCl$_3$, J)	IR ν̃/cm^{-1}	Found (%) (Calcd %) C	H	N	Molecular formula
4a	118.5—119.5	7.95(2H, d, 7.5 Hz), 7.40(2H, d. 7.5 Hz), 2.48(3H, s), 2.14(3H, s), 1.98(3H, s), 1.68(3H, s)	1555 1330 1160	52.52 (52.69	5.55 5.44	9.42 9.45)	$C_{13}H_{16}N_2O_4S$
4b	A 144—144.5	7.86(2H, d, 7.5 Hz), 7.40(2H, d, 7.5 Hz), 2.72(2H, q, 7.5 Hz), 2.48(3H, s), 1.92 (3H, s), 1.64(3H, s), 0.92(3H, t, 7.5 Hz)	1555 1330 1150	54.46 (54.18	5.98 5.85	8.72 9.03)	$C_{14}H_{18}N_2O_4S$
	B 129—130	7.86(2H, d, 7.5 Hz), 7.40(2H, d, 7.5 Hz), 2.48(3H, s), 2.10(2H, q, 7.5 Hz), 1.97 (3H, s), 1.81(3H, s), 0.93(3H, t, 7.5 Hz)	1555 1350 1150	53.97	5.94	9.00	
4c	121—121.5	7.91(2H, d, 7.5 Hz), 7.45(2H, d, 7.5 Hz), 2.5—2.9(4H, m), 2.52(3H, s), 1.84(3H, s), 1.0—1.9(4H, m)	1555 1335 1160	55.64 (55.89	5.25 5.36	8.40 8.69)	$C_{15}H_{18}N_2O_4S$
4d	161.5—162	7.87(2H, d, 7.5 Hz), 7.40(2H, d, 7.5 Hz), 2.3—2.8(4H, m), 2.49(3H, s), 1.63(3H, s), 1.4—1.8(6H, m)	1555 1325	57.03 (57.13	6.13 6.00	8.30 8.33)	$C_{16}H_{20}N_2O_4S$
4e	84—85	7.94(2H, d, 7.5 Hz), 7.46(2H, d, 7.5 Hz), 2.50(3H, s), 2.12(3H, s), 2.02(2H, q, 7.5 Hz), 1.96(3H, s), 0.88(3H, t, 7.5 Hz)	1550 1325 1145	54.19 (54.18	5.54 5.85	8.91 9.03)	$C_{14}H_{18}N_2O_4S$
4f	77.5—78.5	7.82(2H, d, 7.5 Hz), 7.38(2H, d, 7.5 Hz), 2.49(3H, s), 2.08(3H, s), 1.92(3H, s), 1.9—2.1(2H, m), 0.9—1.4(7H, m)	1555 1325 1145	56.98 (56.79	6.64 6.55	8.26 8.28)	$C_{16}H_{22}N_2O_4S$
4g	liquid	7.82(2H, d, 7.5 Hz), 7.36(2H, d, 7.5 Hz), 2.48(3H, s), 2.07(3H, s), 1.97(3H, s), 1.9—2.1(2H, m), 1.11(12H, m), 0.87(3H, m)	1565 1315 1160	60.51 (60.89	7.84 7.67	7.36 7.10)	$C_{20}H_{33}N_2O_4S$
4h	58—59	7.60(2H, d, 7.5 Hz), 7.24(2H, d, 7.5 Hz), 4.00(2H, q, 7.0 Hz), 2.46(3H, s), 2.24 (3H, s), 1.92(3H, s), 1.60(3H, s), 1.16 (3H, t, 7.0 Hz)	1740 1550 1160	52.30 (52.49	6.38 6.10	3.84 4.08)	$C_{15}H_{21}NO_6S$
4i	liquid	7.73(2H, d, 7.5 Hz), 7.31(2H, d, 7.5 Hz), 3.98(2H, m), 2.71(1H, q, 7.0 Hz), 2.48 (3H, s), 2.34(1H, q, 7.0 Hz), 2.20(1.5H, s), 1.90(1.5H, s), 1.71(1.5H, s), 1.50(1.5H, s), 1.04(6H, m)	1730 1540 1150	53.87 (53.77	6.63 6.49	3.95 3.92)	$C_{16}H_{23}NO_6S$
4j	83—84	7.70(2H, d, 7.5 Hz), 7.34(2H, d, 7.5 Hz), 4.16(2H, m), 2.45(3H, s), 2.40—2.10(2H, m), 2.21(3H, s), 2.03(3H, s), 1.25(3H, t, 7.0 Hz), 0.95(3H, t, 7.5 Hz)	1730 1550 1160	53.89 (53.77	6.60 6.49	3.99 3.92)	$C_{16}H_{23}NO_6S$
4k	133—134	7.89(2H, m), 7.60(3H, m), 4.06(1H, m), 3.65(1H, m), 3.22(1H, m), 2.45(1H, m), 2.00(3H, s), 1.98(3H, s)	1750 1545 1140	50.02 (49.83	4.98 4.83	4.33 4.47)	$C_{13}H_{15}NO_6S$
4l	139—140	7.65(2H, d, 7.5 Hz), 7.53(2H, d, 7.5 Hz), 2.45(3H, s), 2.07(3H, s), 1.98(3H, s), 1.96(3H, s), 1.80(3H, s)	1715 1540 1135	53.56 (53.66	6.19 6.11	4.52 4.47)	$C_{14}H_{19}NO_5S$
4m	76—77	7.89(2H, m), 7.60(3H, m), 2.2(2H, m), 2.00(3H, s), 1.82(3H, s), 1.6—2.0(4H, m)	1720 1545 1145	53.89 (54.01	5.38 5.50	4.32 4.50)	$C_{14}H_{17}NO_5S$

NMR (CCl_4); δ 4.14 (2H, q, J=7.0 Hz), 2.29 (2H, q, J=7.0 Hz), 1.94 (3H, s), 1.80 (3H, s), 1.28 (3H, t, J=7.0 Hz), 0.97 (3H, t, J=7.0 Hz). IR (neat); 1700 cm^{-1} (C=O), 1620 cm^{-1} (C=C). MS (20 eV), *m/e* 156 (M^+).

5j: Bp 54 °C/9 Torr (lit,[22] 67 °C/13 Torr). ^{1}H-NMR (CCl_4); δ 4.07 (2H, q, J=7.2 Hz), 2.25 (2H, q, J=7.2 Hz), 1.92 (3H, s), 1.78 (3H, s), 1.26 (3H, t, J=7.2 Hz), 0.95 (3H, t, J=7.2 Hz). IR (neat); 1700 cm^{-1} (C=O), 1630 cm^{-1} (C=C).

5k: Bp 109 °C/12 Torr (lit,[23] 71—73 °C/0.9 Torr). ^{1}H-

NMR (CCl_4); δ 4.20 (2H, t, J=7.5 Hz), 3.0—2.7 (2H, m), 2.21 (3H, t, J=1.5 Hz), 1.88 (3H, s). IR (neat); 1740 cm^{-1} (C=O), 1665 cm^{-1} (C=C).

5l: Bp 57 °C/49 Torr (lit,[24] 145—148 °C). ^{1}H-NMR (CCl_4); δ 2.10 (3H, s), 1.81 (6H, s), 1.73 (3H, s). IR (neat); 1690 cm^{-1} (C=O), 1610 cm^{-1} (C=C).

5m; Bp 80—82 °C/11 Torr (lit,[25] 78—79 °C/10 Torr). ^{1}H-NMR (CCl_4); δ 2.50 (2H, m), 1.9—2.1 (4H, m), 2.15 (3H, t, J=1.5 Hz), 1.80 (3H, s). IR (neat); 1700 cm^{-1} (C=O), 1610 cm^{-1} (C=C). MS (20 eV), *m/e* (rel intensity), 124 (M^+, 100), 108 (48), 96 (19), 82 (21).

Preparation of Olefins (5) by One-pot Procedure. Preparation of **5o** is described here as a typical procedure. To the 20 ml of the DMF solution of the sodium salt of 2-tosyldecanenitrile (20 mmol) which had been prepared as mentioned in the preparation of **4** was added 2,2-dinitroheptane (1.1 g, 6 mmol) in 5 ml of DMF at −20 °C, and the resulting solution was stirred at −20 °C for 3 h. Then $Na_2S \cdot 9H_2O$ (2.4 g, 9 mmol) was added to this solution. The reaction mixture was stirred at room temperature for additional 3 h. After the usual work up, the crude product was distilled to give **5o** (0.93 g, 62% yield). Bp 144.5 °C/1 Torr. ^{1}H-NMR (CCl_4); δ 2.35 (2H, t, J=7.5 Hz), 2.14 (2H, t, J=7.5 Hz), 2.02 (1.5H, s), 1.79 (1.5H, s), 1.30 (18H, m), 0.90 (6H, m). The NMR spectra show that **5o** consists of the equal amount of *E* and *Z* isomer. IR (neat); 2210 cm^{-1} (CN), 1630 cm^{-1} (C=C). MS (20 eV), *m/e* (rel intensity), 249 (M^+, 53), 234 (33), 220 (53), 206 (100), 192 (60). Found: C, 81.81; H, 12.82; N, 5.42%. Calcd for $C_{17}H_{31}N$: C, 81.86; H, 12.53; N, 5.62%. Similarly, **5n** was prepared in 68% yield. Bp 108 °C/21 Torr. ^{1}H-NMR (CCl_4); δ 2.36 (1.3H, t, J=7.5 Hz), 2.14 (0.7H, t, J=7.5 Hz), 2.02 (1H, s), 1.86 (3H, s), 1.80 (3H, s), 1.34 (6H, m), 0.92 (3H, t, J=7.5 Hz). IR (neat); 2210 cm^{-1} (CN), 1630 cm^{-1}(C=C). MS (20 eV), *m/e* (rel intensity), 151 (M^+, 38), 136 (15), 95 (85), 82 (100).

Elimination from 4l by Sodium Sulfide. The reaction of **4l** with sodium sulfide was carried out in the same way as described in a general procedure. A volatile product (**5l**) was distilled and the residue was subjected to a column chromatography to give **6** in 15% yield. Mp 60.5—61.5 °C. ^{1}H-NMR ($CDCl_3$); 7.72 (2H, d, J=7.5 Hz), 7.28 (2H, d, J=7.5 Hz), 2.42 (3H, s), 2.22 (3H, m), 1.89 (3H, m), 1.88 (3H, s). IR (Nujol); 1610 cm^{-1} (C=C). Found: C, 64.44; H, 7.12%. Calcd for $C_{12}H_{16}SO_2$: C, 64.25; H, 7.19%.

Reaction of 4a with Sodium Sulfide in the Presence of Di-t-butylnitroxide or Aromatic Nitro Compounds. The reaction of **4a** (0.888 g, 3 mmol) with sidium sulfide (2.16 g, 9 mmol) in 30 ml of DMF was carried out at room temperature in the presence of various additives, *i.e.*, A: none, B: di-*t*-butylnitroxide (0.022 g, 0.15 mmol), C: *m*-DNB (0.05 g, 0.3 mmol), D: *p*-DNB (0.05 g, 0.3 mmol), E: nitrobenzene (0.037 g, 0.3 mmol). The yield of **5a** was determined by GLPC, and the results are summarized in Fig. 1.

The present work was partially supported by a Grant-in-Aid for Scientific Research (No 447020) from the Ministry of Education, Science and Culture.

References

1) For a preliminary communication on portion of this work, see, N. Ono, R. Tamura, J. Hayami, and A. Kaji, *Tetrahedron Lett.*, **1978**, 763.

2) Present address, Department of Chemistry, College of Liberal Arts and Sciences, Kyoto University.

3) N. Kornblum, S. D. Boyd, H. W. Pinnick, and R. G. Smith, *J. Am. Chem. Soc.*, **93**, 4316 (1971).

4) K. Fukunaga and M. Kimura, *Bull. Chem. Soc. Jpn.*, **52**, 1107 (1979).

5) N. Kornblum and L. Cheng, *J. Org. Chem.*, **42**, 2944 (1977).

6) G. A. Russell, M. Jawdosiuk, and M. Makosza, *J. Am. Chem. Soc.*, **101**, 2355 (1979).

7) G. A. Russell, R. K. Norris, and E. J. Panek, *J. Am. Chem. Soc.*, **93**, 5839 (1971); N. Ono, H. Eto, R. Tamura, J. Hayami, and A. Kaji, *Chem. Lett.*, **1976**, 757; N. Ono, R. Tamura, J. Hayami, and A. Kaji, *Chem. Lett.*, **1977**, 189; Review: N. Kornblum, *Angew. Chem., Int. Ed. Engl.*, **14**, 734 (1975).

8) The sulfone group is eliminated as a sulfinate ion from anion radicals of α-nitro sulfones: N. Kornblum, S. D. Boyd, and N. Ono, *J. Am. Chem. Soc.*, **96**, 2580 (1974). So the behaviour of anion radicals of β-nitro sulfones is of interest.

9) We have found that the potassium salts of β-diketones or β-keto esters are also more reactive to **1** or **2** than the corresponding sodium salts. This finding has enabled one to prepare new coupling products of carbanions with **1** or **2** which are difficult to prepare using the sodium salts.

10) Reactivity of carbanions to **1** or **2** is an interesting problem, but complexities of chain sequence preclude a detailed discussion about this. The reaction of free radicals with carbanions to form anion radicals consists of the following equilibrium. $R\cdot + C^- \rightleftharpoons R^- + C\cdot \rightleftharpoons R\text{-}C^{\cdot}$ It is noteworthy that the chain reaction proceeds when the stability of R^- and C^- is close.

11) R. Tamura, T. Nakatsuka, N. Ono, and A. Kaji, *Chem. Lett.*, **1980**, 281, where the nitro and acetyl groups are eliminated from β-acetyl nitro compounds *via* one electron transfer processes.

12) A number of chain sequences can be envisioned, but we cannot specify the mechanism at the time being. Nitrogen dioxide may be involved in a chain sequence.

13) N. Kornblum, M. M. Kestner, S. D. Boyd, and L. C. Cattran, *J. Am. Chem. Soc.*, **95**, 3356 (1973).

14) R. B. Kaplan and H. Shecter, *J. Am. Chem. Soc.*, **83**, 3535 (1961).

15) N. Ono, R. Tamura, R. Tanikaga, and A. Kaji, *Synthesis*, **1977**, 690.

16) B. T. Brooks, U. S. Patent 2364422 (1944); *Chem. Abstr.*, **1945**, 3545.

17) E. M. Osman and A. C. Cope, *J. Am. Chem. Soc.*, **66**, 881 (1944).

18) S. F. Birch and G. A. R. Kon, *J. Chem. Soc.*, **123**, 2440 (1923).

19) A. Kandiah and R. P. Linstead, *J. Chem. Soc.*, **1929**, 2139.

20) R. C. Huston and G. L. Goerner, *J. Am. Chem. Soc.*, **68**, 2504 (1946).

21) G. A. R. Kon and K. S. Nargund, *J. Chem. Soc.*, **1932**, 2461.

22) R. C. Huston, G. L. Goerner, and H. H. György, *J. Am. Chem. Soc.*, **70**, 389 (1948).

23) K. Tanaka, H. Uneme, N. Yamagishi, N. Ono, and A. Kaji, *Chem. Lett.*, **1978**, 653.

24) P. G. Stevens, *J. Am. Chem. Soc.*, **56**, 450 (1934).

25) G. A. R. Kon and J. H. Nutland, *J. Chem. Soc.*, **1926**, 3101.

 © 1980 The Chemical Society of Japan Bull. Chem. Soc. Jpn., 53, 3301—3307 (1980)

A New and Highly Effective Aldol Synthesis[1)]

Keiji MARUOKA,† Shinsuke HASHIMOTO, Yoshizo KITAGAWA,
Hisashi YAMAMOTO,† and Hitosi NOZAKI*
Department of Industrial Chemistry, Kyoto University, Yoshida, Sakyo-ku, Kyoto 606
(Received April 26, 1980)

A new approach has been demonstrated for the regiospecific aldol synthesis by the simultaneous addition of α-halo carbonyl derivatives and aldehydes or ketones to a suspension of diethylaluminum chloride and zinc in tetrahydrofuran at low temperature. This technique is also employable under mild conditions for the Reformatsky reaction to give β-hydroxy esters in excellent yield. One of the unique synthetic applications of this process is illustrated by the intramolecular cyclization of α-bromo esters of ω-hydroxy aldehyde, which produces macrolides, an important class of compounds in the antibiotic field.

Carbon-carbon σ-bond formation, one of the most fundamental operations in organic chemistry, is often accomplished by the aldol synthesis.[2)] During the past decade numerous directed intermolecular aldol condensations have been explored with generation of the regiospecific metal enolates and interception of the initially formed aldol products as stable metal chelates.[3)] Certain regiospecifically generated, kinetic lithium enolates can retain their integrity in the aldol reaction at low temperature. The use of magnesium and zinc enolates prevents the unfavorable dissociation of the metal chelate, and boron enolates have recently been employed in stereoselective aldol syntheses.[4)]

Compared to the metals described above, aluminum shows an exceptionally high affinity for oxygen atom (138 kcal/mol for Al–O bond),[5)] and, therefore, its enolate would be one of the most attractive candidates to enhance the stability of the metal chelates in the aldol condensation. In principle, organoaluminum compounds have a vast potential as an agent of aldol reaction. However, this concept has not been generally accepted for synthesis owing to the lack of an effective procedure for converting a carbonyl compound into a reactive aluminum enolate.[6)]

Herein, we describe a new process for regioselective generation of aluminum enolate by the coupled attack of dialkylaluminum chloride and zinc on the α-halo ketone.[7)] The enolate **2**, thus obtained, is sufficiently reactive to carbonyl compound activated by trivalent aluminum producing the stable tetradentate chelate of the ketolate **3**. Aqueous work-up yields the aldol **4** in excellent yield.

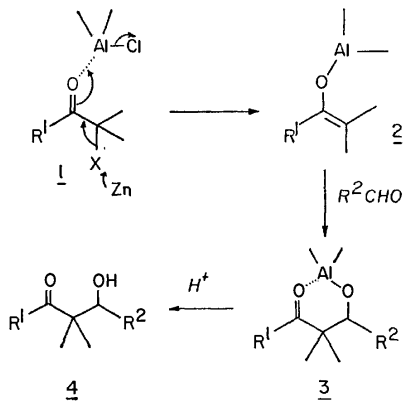

† Present address: Department of Chemistry, University of Hawaii, 2545 The Mall, Honolulu, Hawaii 96822.

Although a comparable path can be followed by two molecules of an α-halo ketone condensing each other, this would be subject to experimental control using the simultaneous addition of α-halo ketones and carbonyl compounds at low temperature provided that the reduction is sufficiently faster under acceptable conditions.[8)] This new approach has now been realized: Gradual addition (40 min) of a mixture of carbonyl compound and α-halo ketone in dry tetrahydrofuran (THF) to a suspension of zinc dust and diethylaluminum chloride (Et_2AlCl) in THF–hexane in the presence of a catalytic amount of copper(I) bromide with stirring at −20 °C under argon resulted in clean generation of the ketolate. Addition of pyridine, removal of cooling bath, and aqueous work-up afforded the desired β-hydroxy ketone in high yield (Table 1).

The regioselectivity of this reaction was demonstrated by the treatment of 2-bromo-2-methylcyclohexanone (**5**) and benzaldehyde with Et_2AlCl–Zn in THF at −20 °C to furnish the expected β-hydroxy ketone **6** in quantitative yield, without any contamination of the regioisomer (Entry 3). Since the starting bromide **5** may be prepared with high regioselectivity,[9)] the present method must be the simplest route to the β-hydroxy ketone **6**.

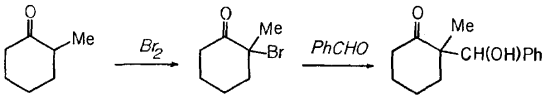

5 6

Additional examples are also summarized in Table 1. It should be noted that the use of diethylaluminum chloride and the choice of solvents and temperatures are crucial to the success of these reactions. In the absence of diethylaluminum chloride, only unchanged carbonyl compounds were recovered under these mild conditions. The relative effect of solvents and temperatures was indicated by the reaction of 2-bromocyclohexanone with isobutyraldehyde. In diethyl ether at −40 °C, only a trace amount of the desired 2-(1-hydroxy-2-methylpropyl)cyclohexanone (**7**) was produced, whereas at high temperature (25 °C) many side products were detected by TLC. The use of THF as solvent with reaction temperatures of −78 and −40 °C afforded **7** in yields of 0 and 85%, respectively. At 0 °C, the reaction proceeds as expected (86%), but with some contamination of undesired dehydrated and retro-aldol products of **7**.

Table 1. Synthesis of β-hydroxy carbonyl compounds[a)]

Entry	Bromo ketone or bromo ester	Aldehyde or ketone	Temp °C	Additive[b)]	Products	Isolated yield(%) (*erythro*/*threo*)
1	α-Bromoacetophenone	Isobutyraldehyde	−20	CuBr	$PhCOCH_2CH(OH)CH(CH_3)_2$	92
		Cinnamaldehyde	−20	CuBr	$PhCOCH_2CH(OH)CH{=}CHPh$	92
		Cyclohexanone	−20	CuBr	$PhCOCH_2C(OH)(CH_2)_5$	83
2	2-Bromocyclohexanone	Benzaldehyde	−20	CuBr	2-(α-Hydroxybenzyl)-cyclohexanone	97(1/1)[f)]
		Isobutyraldehyde	−20	CuBr	2-(1-Hydroxy-2-methylpropyl)-cyclohexanone	93[g)]
		Acetone[c)]	−20	d)	2-(1-Hydroxy-1-methylethyl)-cyclohexanone	75
3	2-Bromo-2-methyl-cyclohexanone	Benzaldehyde	−20	CuBr	2-(α-Hydroxybenzyl)-2-methylcyclohexanone	100(4/3)[f)]
4	2-Bromocamphor	Acetone	r.t.	d)	3-(1-Hydroxy-1-methylethyl)-camphor	79
5	Ethyl bromoacetate	Benzaldehyde	0	CuBr	$PhCH(OH)CH_2COOEt$	94
		Cyclohexanone	r.t.	CuBr	$(CH_2)_5C(OH)CH_2COOEt$	93
6	Methyl γ-bromo-crotonate	Benzaldehyde	−20	CuBr	$PhCH(OH)CH(CH{=}CH_2)COOMe$[e)]	100(50/44)[h)]

a) Unless specified, the reactions were carried out according to the general procedure in the experimental section. b) A catalytic amount of copper(I) bromide (0.05 equiv) was added. c) Excess acetone (5 equiv) was used for this reaction. d) Zn–Ag couple was employed without any additive. e) None of the γ-alkylation product ("normal Reformatsky ester") was detected in the reaction mixture. See Ref. 7. f) The ratio of the stereoisomers (*threo* and *erythro*) was determined by an absorption due to the benzylic proton ($CDCl_3$) as shown in the experimental section. See also Refs. 3-a and 3-b. g) *Erythro*/*threo* ratio could not be determined by NMR and TLC analyses. h) Determined by the isolated yield: See the experimental section for this compound.

Treatment of 2-bromocyclohexanone (1 equiv) and acetone (1.1 equiv) with Et_2AlCl–Zn gave the cross aldol product **8** (42%) along with the self-condensation product. Thus, with less reactive carbonyl compounds, the relative amount of self-condensation product increases. Such difficulty might be circumvented by using excess carbonyl compounds with more reactive zinc. Accordingly, the zinc–silver couple[10] was chosen with excess acetone (5 equiv) to furnish **8** in 79% yield (Entry 2).

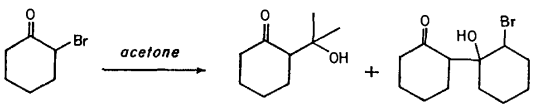

8

This new technique for the regiospecific aldol synthesis can be employed equally well under mild conditions for the Reformatsky reaction.[11] In a similar manner described above, Reformatsky products were produced from the corresponding α-halo esters and carbonyl compounds in excellent yield as were indicated in Table 1 (Entry 5, 6). In contrast with the normal Reformatsky reaction,[12] the reaction of methyl γ-bromocrotonate with benzaldehyde in the presence of Et_2AlCl–Zn afforded only the α-adduct in quantitative yield. This result suggests that the addition of aluminum enolate to the carbonyl component (initially activated by trivalent aluminum) proceeds *via* a six-membered transition state to furnish the stable aluminum chelate **3**.

Although simplicity and convenience of this aldol synthesis are appealing, the fact that the reaction proceeds in high yield with simultaneous addition of a halo ketone and an aldehyde is even more important. The highly successful application of the new method is the synthesis of macrocyclic lactones which forms the next subject of this paper.

Although the macrolide has been the attractive synthetic target in a number of laboratories, most synthetic methodologies for the macrolide are based on the internal esterification in the cyclization step (Eq. 1) and there exist a few basically different approaches.[13]

Indeed at the outset of this work there were no known synthetic methods capable of generating efficiently 3-hydroxy lactones from acyclic structures (Eq. 2). Gradual addition of the bromoacetate of

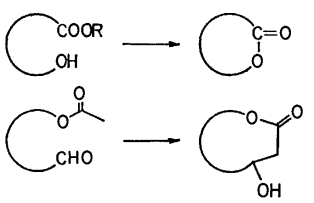

(1)

(2)

13-hydroxytridecanal **9**[14] in THF from a mechanically driven syringe over 4 h to a stirred suspension of zinc–silver couple and diethylaluminum chloride in THF at 35 °C under argon effected cyclization to 3-hydroxypentadecanolide (**10**) as the major product. Termination of the reaction with pyridine, followed by acidic

work-up gave the crude product, which was purified by column chromatography on silica gel (ether–hexane, 1:1) to afford pure lactone **10** in 48% yield. Dehydration of **10** in CH_2Cl_2 with methanesulfonyl chloride and excess triethylamine at room temperature for 11 h gave 2-pentadecenolide (**11**). Hydrogenation of **11** in ethanol–ethyl acetate over palladium on charcoal produced exaltolide (**12**).

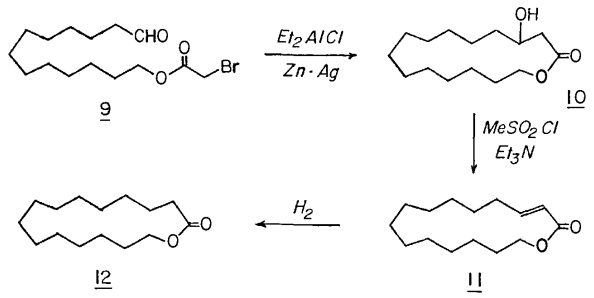

9 10 11 12

Similarly, several 3-hydroxymacrolides **13**—**16** were prepared starting from α-bromo esters of ω-hydroxy aldehyde, $BrCHRCOO(CH_2)_nCHO$ with $n=9$ or 11, and R=H or CH_3. The following list of macrolides shows the effectiveness of the new method with good yields as indicated in the parenthesis. Of crucial importance to this macrolide synthesis was the observation that the more substituted aluminum enolates derived from $BrCHRCOO(CH_2)_nCHO$ with $R=CH_3$ are substantially more reactive toward the carbonyl component to give **14** or **16** in higher yield relative to that of the unsubstituted homologs. Since the α-methyl-β-hydroxy unit in macrolides **14** or **16** is a common functionality in a variety of macrolide antibiotics including erythromycin and methymycin,[16] this method may provide a useful entry to the antibiotic field, starting with simple α,ω-diols.[17]

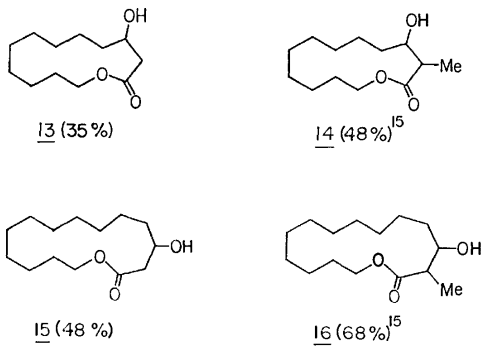

13 (35%) 14 (48%)[15]

15 (48%) 16 (68%)[15]

Experimental

Instrumentation. The infrared spectra were taken with a Shimadzu IR-27-G spectrometer; the mass spectra with a Hitachi RMU-6L mass machine; the GLPC analyses with a Yanagimoto GCG-550F; and NMR spectra with a JNM-PMX 60 or Varian EM-360 spectrometer. The chemical shifts are expressed in parts per million downfield from internal tetramethylsilane ($\delta=0$). Splitting patterns are indicated as s, singlet; d, doublet; t, triplet; q, quartet; m, multiplet. The microanalyses were performed at the Elemental Analyses Center of Kyoto University. All experiments were carried out under an atmosphere of dry argon. The products were purified by preparative thin layer chromatography on silica gel PF-254 plates (Merck), or by preparative column chromatography on silica gel E. Merck Art. 7734.

Purification or Preparation of Solvents, Metals, and Reagents. The following solvents were used: tetrahydrofuran—freshly distilled from sodium benzophenone ketyl; dichloromethane—dried over 4 Å molecular sieves. Zinc dust was washed with 5% hydrochloric acid.[17] Zinc-silver couple was obtained from zinc dust and silver acetate by a literature procedure.[10] A 1 M solution of diethylaluminum chloride was prepared by the dilution of neat diethylaluminum chloride (Ethyl Co.) with hexane under argon. Commercially available α-bromoacetophenone, 3-bromocamphor, ethyl bromoacetate, and methyl γ-bromocrotonate were used without purification. 2-Bromocyclohexanone was prepared according to the procedure in the literature.[18] 2-Bromo-2-methylcyclohexanone was obtained by the bromination of 2-methylcyclohexanone with bromine in ether at −40——50 °C.[9] 1,10-Decanediol and 1,12-dodecanediol were the commercial products of the highest purity. 1,13-Tridecanediol was prepared as follows: Reaction of cyclododecanone with diethyl carbonate and metallic sodium under reflux gave diethyl tridecanedionate, which was reduced with lithium aluminum hydride in THF to afford 1,13-tridecanediol.[19]

Preparation of β-Hydroxy Ketones. The β-hydroxy ketones were prepared by reaction of α-bromo ketones with either ketones or aldehydes according to the following general procedure: A solution of diethylaluminum chloride (1.1 mmol) in hexane was added to a slurry of zinc dust (1.5 mmol) and a catalytic amount of copper(I) bromide (0.05 mmol) in anhydrous THF (3 ml) with stirring under argon at 20 °C. The resulting mixture was cooled to −20 °C, and a solution of an α-bromo ketone (1 mmol) and an aldehyde (or a ketone) (1.1 mmol) in anhydrous THF (5 ml) was added slowly over 40 min at −20 °C. After 15 min at −20 °C, the cooling bath was removed. The reaction mixture was quenched by the addition of pyridine (0.3 ml)[20] and then poured into 2 mol dm^{-3} hydrochloric acid (10 ml). The ether extracts were washed with brine, dried over magnesium sulfate, and concentrated *in vacuo* to afford a β-hydroxy ketone after purification by preparative TLC (ether–benzene, 1:5).

3-Hydroxy-4-methyl-1-phenyl-1-pentanone. Reaction of α-bromoacetophenone with isobutyraldehyde gave the title compound as a colorless oil:[21] IR (neat) 3450 cm^{-1} (OH), 1673 cm^{-1} (C=O); NMR ($CDCl_3$) δ 7.10—8.13 (5H, m, aryl CH), 3.79—4.20 (1H, m, CH–O), 3.69 (1H, s, OH), 3.00 (2H, m, CH_2C=O), 1.78 (1H, m, CH), 0.99 (6H, d, $J=6.6$ Hz, CH_3); mass *m/e*(%) 105 (100), 174 (4, M^+-18); mp 50.5—52.0 °C (recrystallized from pentane as white crystals).

1,5-Diphenyl-3-hydroxy-4-penten-1-one. The title compound was prepared by the reaction of α-bromoacetophenone with cinnamaldehyde as a yellow oil: IR (neat) 3470 cm^{-1} (OH), 1675 cm^{-1} (C=O); NMR ($CDCl_3$) δ 6.94—8.31 (10H, m, aryl CH), 6.70 (1H, d, $J=16$ Hz, PhCH=C), 6.24 (1H, dd, $J=16$, 5.6 Hz, PhC=CH), 4.91 (1H, q, $J=5.6$ Hz, CH–O), 3.22 (2H, d, $J=6$ Hz, CH_2C=O), 2.84—3.61 (1H, s, OH); exact mass spectrum *m/e* 252.301 (Calcd for $C_{17}H_{16}O_2$ 252.313); mp 51—53 °C (recrystallized from pentane-ether as white crystals).

α-(1-Hydroxycyclohexyl)acetophenone. Reaction of α-bromoacetophenone with cyclohexanone afforded the title compound as a colorless oil;[22] IR (neat) 3513 cm^{-1} (OH), 1672 cm^{-1} (C=O); NMR ($CDCl_3$) δ 7.05—8.18 (10H, m, aryl CH), 3.88—4.01 (1H, s, OH), 3.10 (2H, s, CH_2C=O), 1.05—2.17 (10H, broad s, aliphatic CH); mass *m/e*(%) 105 (100),

200 (3, M^+-18); mp 79—80 °C (recrystallized from pentane as white crystals).

*2-(α-Hydroxybenzyl)-2-methylcyclohexanone (**6**).* Reaction of 2-bromo-2-methylcyclohexanone (191 mg, 1 mmol) with benzaldehyde (117 mg, 1.1 mmol) afforded *erythro* and *threo* mixtures of **6** (218 mg) as a pale yellow oil[21] in quantitative yield after purification by preparative TLC (ether–hexane, 1:1): NMR ($CDCl_3$) δ 7.23 (5H, s, aryl CH), 4.92, 5.00 (1H, s, CH–O), 3.53 (1H, s, OH), 2.26—266. (2H, m, $CH_2C{=}O$), 1.35—2.09 (6H, broad s, aliphatic CH), 1.00, 1.09 (3H, s, CH_3). The ratio of the *erythro* and *threo* isomers was determined by the relative intensities of the benzylic proton absorptions (NMR ($CDCl_3$) δ 4.92 (*erythro*) and 5.00 (*threo*)) to be nearly 4:3. Column chromatography of the pure **6** on silica gel (ether–hexane, 3:1) gave the fraction of pure *threo* isomer and a mixture of *erythro* and *threo* isomers (34 mg). The pure *threo* isomer has the following physical properties: IR (neat) 3503 cm^{-1}, (OH), 1690 cm^{-1} (C=O): NMR ($CDCl_3$) δ 7.15 (5H, s, aryl CH), 4.97 (1H, s, CH–O), 2.87 (1H, s, OH), 2.27—2.59 (2H, m, $CH_2C{=}O$), 1.35—2.05 (6H, broad s, aliphatic CH), 1.01 (3H, s, CH_3); mass *m/e*(%) 77 (100) 200 (0.1, M^+-18).

2-(α-Hydroxybenzyl)cyclohexanone. Condensation of 2-bromocyclohexanone with benzaldehyde yielded *erythro* and *threo* mixtures of the title compound (198 mg, 97% yield) as white solids after purification by preparative TLC (ether–hexane, 1:1). The NMR spectrum ($CDCl_3$) of the product showed the ratio of the *threo* and *erythro* isomers to be 1:1. This analysis was determined by an absorption due to the benzylic proton peak at δ 4.73 and 5.30. Column chromatography of the product on silica gel (benzene–ether, 10:1) separated two isomers. The first fraction was the *erythro* isomer: IR (neat) 3496 cm^{-1} (OH), 1697 cm^{-1} (C=O); NMR ($CDCl_3$) δ 7.27 (5H, s, aryl CH), 5.35 (1H, d, J= 2.3 Hz, CH–O), 2.90 (1H, s, OH), 1.08—2.73 (9H, broad s, aliphatic CH and CHC=O); mass *m/e*(%) 77 (100), 186 (2.5, M^+-18); mp 103—105 °C (recrystallized from hexane–ethyl acetate; lit,[21] mp 103.5—104.5 °C). From the second fraction the *threo* isomer was obtained: IR (neat) 3483 cm^{-1} (OH), 1698 cm^{-1} (C=O); NMR ($CDCl_3$) δ 7.30 (5H, s, aryl CH), 4.77 (1H, d, J=9 Hz, CH–O), 3.72 (1H, s, OH), 1.03—2.86 (9H, broad s, aliphatic CH and CHC–O); mass *m/e*(%) 77 (100), 186 (3.5, M^+-18); mp 75.5—77.5 °C (recrystallized from hexane; lit,[21] mp 75 °C).

*2-(1-Hydroxy-2-methylpropyl)cyclohexanone (**7**).* Reaction of 2-bromocyclohexanone with isobutyraldehyde produced **7** as a pale yellow oil[21]: bp 74—78 °C (bath temp, 1 mmHg); IR (neat) 3510 cm^{-1} (OH), 1688 cm^{-1} (C=O); NMR ($CDCl_3$) δ 3.47 (1H, m, CH–O), 3.03 (1H, s, OH), 1.32—2.74 (9H, broad s, aliphatic CH and CHC=O), 0.89 (6H, m, CH_3); mass *m/e*(%) 55 (100), 152 (15, M^+-18). The *erythro*/*threo* ratio of **7** could not be determined by TLC and NMR analyses.

2-(1-Hydroxy-1-methylethyl)cyclohexanone. The title compound was obtained from 2-bromocyclohexanone (1 equiv) and excess acetone (5 equiv) in the presence of diethylaluminum chloride and zinc-silver couple at −20 °C: bp 68—71 °C (bath temp, 1 mmHg (lit,[23] bp 78—80 °C/4 mmHg)); IR (neat) 3488 cm^{-1} (OH), 1690 cm^{-1} (C=O); NMR ($CDCl_3$) δ 3.95 (1H, s, CH–O), 1.42—2.62 (10H, aliphatic CH, CHC= O, and OH), 1.22 (6H, m, CH_3): mass *m/e*(%) 43 (100), 141 (5, M^+-15).

3-(1-Hydroxy-1-methylethyl)camphor. Reaction of 3-bromocamphor with acetone was performed at 20 °C using zinc-silver couple. Stirring was further continued for 1 h at 20 °C. The mixture was then quenched in a usual manner and purified by preparative TLC (ether–hexane, 1:1) to give the title compound as white crystals: mp 80—90.5 °C (recrystallized from hexane); IR (Nujol) 3473 cm^{-1} (OH), 1728 cm^{-1} (C=O); NMR ($CDCl_3$) δ 1.27, 1.46 (6H, two s, CH_3C–O); exact mass spectrum *m/e* 210.330 (Calcd for $C_{13}H_{22}O_2$ 210.317).

Preparation of β-Hydroxy Esters. The β-hydroxy esters were prepared in the same way as the β-hydroxy ketones.

Ethyl 3-Hydroxy-3-phenylpropionate. The title compound was produced from ethyl bromoacetate and benzaldehyde as a colorless oil: bp 120—123 °C (bath temp, 1 mmHg (lit,[24] bp 154 °C/12 mmHg)); IR (neat) 3435 cm^{-1} (OH), 1728 cm^{-1} (C=O); NMR ($CDCl_3$) δ 7.28 (5H, s, aryl CH), 5.06 (1H, t, J=7 Hz, CH–O), 4.08 (2H, q, J=7 Hz, CH_2–O), 3.40 (1H, s, OH), 2.65 (2H, d, J=7 Hz, $CH_2C{=}O$), 1.18 (3H, t, J=7 Hz, CH_3); mass *m/e*(%) 107 (100), 165 (5, M^+-29), 176 (4, M^+-18), 194 (22, M^+).

Ethyl 1-Hydroxycyclohexylacetate. Reaction of ethyl bromoacetate with cyclohexanone at 20 °C yielded the title compound as a colorless oil: bp 85—88 °C/2 mmHg (lit,[25] bp 89—93 °C/4 mmHg); IR (neat) 3499 cm^{-1} (OH), 1710 cm^{-1} (C=O); NMR ($CDCl_3$) δ 4.32 (2H, q, J=7 Hz, CH_2–O), 3.37 (1H, s, OH), 2.43 (2H, s, $CH_2C{=}O$), 1.52 (10H, broad s, aliphatic CH), 1.26 (3H, t, J=7 Hz, CH_3); mass *m/e* (%) 55 (100), 168 (6.8, M^+-18), 186 (6.5, M^+).

Methyl 2-(α-Hydroxybenzyl)-3-butenoate. Reaction of methyl γ-bromocrotonate (179 mg, 1 mmol) with benzaldehyde (117 mg, 1.1 mmol) at −20 °C gave the *erythro* and *threo* isomers of the title compound in quantitative yield as a colorless oil[12] after purification by preparative TLC (ether–hexane, 1:1). None of the γ-alkylation product was detected in the crude product. Column chromatography of the product on the silica gel (ether–hexane, 1:3) separated the pure *erythro* isomer (92 mg), a mixture of two isomers (16 mg), and the pure *threo* isomer (80 mg). These isomers have the following physical properties. *Erythro* isomer: IR (neat) 3549 cm^{-1} (OH), 1726 cm^{-1} (C=O); NMR ($CDCl_3$) δ 7.24 (5H, s, aryl CH), 5.96 (1H, ddd, J=8.0, 11.4, 18.8 Hz, =CH–C), 5.36—4.98 (3H, m, CH_2=C and CH–O), 3.63 (3H, s, CH_3), 3.39 (1H, dd, J=6.4, 8.0 Hz, C=C–CH), 2.92 (1H, s, OH); mass *m/e*(%) 77 (100), 188 (18.8, M^+-18): *Threo* isomer: IR (neat) 3437 cm^{-1} (OH), 1707 cm^{-1} (C=O); NMR ($CDCl_3$) δ 7.31 (5H, s, aryl CH), 5.72 (1H, ddd, J=7.8, 10.8, 17.2 Hz, =CH–C), 4.79—5.40 (3H, m, CH_2=C and CH–O), 3.77 (3H, s, CH_3), 3.50 (1H, dd, J= 8.8, 17.2 Hz, C=C–CH), 2.84 (1H, s, OH).

Preparation of Macrolides. Five hydroxy macrolides were prepared by the intramolecular aldol condensation of α-bromo esters of ω-hydroxy aldehydes. The synthesis of 3-hydroxypentadecanolide (**10**), starting from 1,13-tridecanediol is representative.

*13-Hydroxytridecyl Bromoacetate (**17**).* A solution of bromoacetyl bromide (5.18 g, 24 mmol) in anhydrous THF (20 ml) was added dropwise to a solution of 1,13-tridecanediol (4.32 g, 20 mmol) in THF (100 ml) containing *N,N*-dimethylaniline (2.79 ml, 22 mmol) under argon at 20 °C. Stirring was continued for 15 min at 20 °C. Then the solution was diluted with ether, washed with 2 mol dm^{-3} hydrochloric acid. The ether extracts were washed with brine, dried over sodium sulfate, and concentrated *in vacuo* to afford **17** (3.57 g, 53%) as white crystals after purification by column chromatography on silica gel (ethyl acetate–hexane, 2:5): IR (Nujol) 3375 cm^{-1} (OH), 1731 cm^{-1} (C=O); NMR ($CDCl_3$) δ 4.10 (2H, t, J=6 Hz, $CH_2OC{=}C$), 3.76 (2H, s, CH_2Br), 3.57 (2H, t, J=6 Hz, CH_2–O), 1.00—1.98 (23H, broad s, aliphatic CH and OH).

Found: C, 53.32; H, 8.98%. Calcd for $C_{15}H_{28}BrO_3$: C, 53.41; H, 8.67%.

Table 2. Physical properties and analytical data of macrolides and their precursors

Products	Boiling point (°C)[a] (Melting point)	IR (cm^{-1})[b]	NMR (δ)	Found, % (Calcd)
$BrCH_2COO(CH_2)_{10}OH$		3345 (OH) 1735 (C=O)	4.08 (2H, t, J=6, CH_2OC=O), 3.75 (2H, s, CH_2Br), 3.54 (2H, t, J=6, CH_2O), 1.90 (1H, s, OH), 1.30 (16H, br s, aliphatic CH)	C, 48.57(48.82) H, 7.90(7.85)
$BrCH_2COO(CH_2)_9CHO$		2733 (CHO) 1720 1735 (C=O)	9.75 (1H, t, J=1.8, CHO), 4.08 (2H, t, J=6, CH_2O), 3.75 (2H, s, CH_2Br), 2.38 (2H, td, J=1.8, 6.4, CH_2C=O), 1.30 (14H, br s, aliphatic CH)	C, 48.90(49.16) H, 7.03(7.22)
13	165/2 mm Hg	3430 (OH) 1724 (C=O)	4.02 (3H, m, CH_2O, CH-O), 2.60 (1H, s, OH), 2.07—2.57 (2H, m, CH_2C=O), 1.32 (14H, br s, aliphatic CH)	C, 67.05(67.25) H, 10.11(10.35)
$CH_3CHBrCOO(CH_2)_{10}OH$	170/1 mm Hg	3360 (OH) 1731 (C=O)	4.31 (1H, q, J=6.6, CHBr), 4.10 (2H, t, J=6.2, CH_2OC=O), 3.57 (2H, t, J=5.6, CH_2O), 1.79 (3H, d, J=6.6, CH_3), 1.66 (1H, s, OH), 1.30 (16H, br s, aliphatic CH)	C, 50.23(50.49) H, 8.32(8.15)
$CH_3CHBrCOO(CH_2)_9CHO$	(72—75)	2710 (CHO) 1731 (C=O)	9.54 (1H, t, J=1.6, CHO), 4.31 (1H, q, J=6.6, CHBr), 4.02 (2H, t, J=6.6, CH_2O), 2.33 (2H, td, J=1.6, 6, CH_2C=O), 1.76 (3H, d, J=6.6, CH_3), 1.32 (14H, br s, aliphatic CH)	C, 46.59(46.82) H, 5.35(5.59)
14		3432 (OH) 1710 1726 (C=O)	3.37—4.25 (3H, m, CH_2O, CH-O), 2.10—2.97 (2H, m, CHC=O, OH), 1.32 (16H, br s, aliphatic CH)	C, 68.43(68.38) H, 10.47(10.60)
$BrCH_2COO(CH_2)_{12}OH$	170—173/1 mm Hg	3279 (OH) 1737 (C=O)	4.15 (2H, t, J=6.2, CH_2OC=O), 3.80 (2H, s, CH_2Br), 3.60 (2H, t, J=6, CH_2O), 2.22 (1H, s, OH), 1.29 (20H, br s, aliphatic CH)	C, 52.05(52.01) H, 8.57(8.42)
$BrCH_2COO(CH_2)_{11}CHO$		2730 (CHO) 1723 1736 (COO)	9.68 (1H, t, J=2, CHO), 4.13 (2H, t, J=6.2, CH_2O), 3.79 (2H, s, CH_2Br), 2.40 (2H, td, J=6.2, CH_2C=O), 1.29 (18H, br s, aliphatic CH)	C, 52.30(52.34) H, 7.55(7.84)
15	168/2 mm Hg	3398 (OH)	3.53—4.13 (3H, m, CH_2O, CH-O) 2.47 (2H, d, J=4.8, CH_2C=O), 1.30 (21H, br s, aliphatic CH, OH)	C, 69.41(69.38) H, 10.89(10.81)
$CH_3CHBrCOO(CH_2)_{12}OH$	174—177/1 mm Hg	3352 3405 (OH)[c] 1723 (C=O)	4.28 (1H, q, J=6.6, CHBr), 4.08 (2H, t, J=6, CH_2OCO), 3.55 (2H, t, J=6, CH_2O), 1.89 (1H, s, OH), 1.76 (3H, d J=6.6, CH_3), 1.27 (20H, s, aliphatic CH)	C, 53.67(53.41) H, 8.87(8.67)
$CH_3CHBrCOO(CH_2)_{11}CHO$	(51—53)	2737 (CHO) 1733 (C=O)	9.57 (1H, t, J=1.6, CHO), 4.29 (1H, q, J=7, CHBr), 4.09 (2H, t, J=6.4, CH_2O), 2.39 (2H, td,	C, 48.58(48.93) H, 6.40(6.06)

TABLE 2. Continued

Products	Boiling point (°C)[a] (Melting point)	IR (cm^{-1})[b]	NMR (δ)	Found, % (Calcd)
			J=1.6, 6.8, CH_2C=O), 1.78 (3H, d, J=7, CH_3), 1.28 (18H, s, aliphatic CH_2)	
16	180/2 mm Hg	3425 (OH) 1725 (C=O)	3.40—4.53 (3H, m, CH_2O, CH-O), 2.80 (1H, s, OH), 2.52 (1H, q, J=6.8, CHC=O), 1.33 (23H, br s, aliphatic CH, CH_3)	C, 70.31 (70.27) H, 11.21 (11.01)

a) Bath temperature. b) Liquid film. c) Nujol mull.

Bromoacetate of 13-Hydroxytridecanal (9). Collins oxidation of **17** was slightly modified as follows: Chromium trioxide (5 g, 50 mmol) was added portionwise to a solution of pyridine (8.09 ml, 100 mmol) in dry dichloromethane (125 ml) at 0 °C, and the resulting brown suspension was stirred for 5 min at 0 °C followed by 1 h at 20 °C. Celite-545 (dried *in vacuo* for 1 h at 150 °C before use) and then **17** (1.685 g, 5 mmol) dissolved in dry dichloromethane (25 ml) were added at 0 °C. After further stirring for 10 min, the suspension was treated with powdered $NaHSO_4 \cdot H_2O$ (6.25 g). The complete removal of pyridine was checked by TLC. The suspension was diluted with hexane (200 ml), filtered through Celite-545, and washed with hexane. The filtrate was concentrated *in vacuo* to afford **9** (1.495 g, 89% yield) as a colorless oil after purification by column chromatography on silica gel (ether–hexane, 1:2): IR (neat) 2723 cm^{-1} (CHO), 1721, 1731 cm^{-1} (C=O); NMR ($CDCl_3$) δ 9.65 (1H, m, CHO), 4.06 (2H, t, J=6 Hz, CH_2O), 3.67 (2H, s, CH_2Br), 2.33 (2H, t, J=6 Hz, CCH_2C=O), 1.28 (20H, broad s, aliphatic CH).

Found: C, 53.51; H, 8.33%. Calcd for $C_{15}H_{27}BrO_3$: C, 53.74; H, 8.12%.

3-Hydroxypentadecanolide (10). A solution of diethylaluminum chloride (1.5 mmol, 1.5 ml of a 1 M solution) in hexane was added to a slurry of zinc-silver couple (3.27 g, 50 mmol) in anhydrous THF (50 ml) under argon at 20 °C. After 10 min, the suspension was warmed to 35 °C and a solution of **9** (335 mg, 1 mmol) in THF (10 ml) was added slowly over a period of 4 h. Stirring was continued for an additional 20 min, and the reaction was terminated by the addition of pyridine (0.9 ml). Then the suspension was diluted with ether, washed with iced 2 mol dm^{-3} hydrochloric acid, and brine. The organic layer and ether extracts of the aqueous washings were dried and concentrated to afford **10** (175 mg, 48% yield) as a colorless oil after purification by column chromatography on silica gel (ether–hexane, 1:1): IR (neat) 3427 cm^{-1} (OH), 1729 cm^{-1} (C=O); NMR ($CDCl_3$) δ 3.58—4.25 (1H, m, CH-O), 4.13 (2H, t, J=5 Hz, CH_2O), 2.82 (1H, s, OH), 2.53 (2H, d, J=5.5 Hz, CH_2C=O), 1.35 (22H, broad s, aliphatic CH); mass m/e(%) 238 (M^+-H_2O).

Found: C, 70.30; H, 10.88%. Calcd for $C_{15}H_{28}O_3$: C, 70.27; H, 11.01%.

2-Pentadecenolide (11). A solution of **10** (85 mg, 0.33 mmol) in dichloromethane (1.5 ml) was treated with methanesulfonyl chloride (51 μl, 0.66 mmol) in the presence of triethylamine (0.37 ml, 2.66 mmol) at −20 °C. The resulting white suspension was allowed to warm to room temperature. Further stirring was continued for one day at room temperature. The mixture was poured onto iced water and extracted with ether. Purification of the crude product by column chromatography on silica gel (ether–hexane, 1:15) gave **11** in 79% yield as a colorless oil: IR (neat) 1716 cm^{-1} (C=O), 983, 1460 cm^{-1} (C=C); NMR (CCl_4) δ 6.75 (1H, dt, J=7.2, 15.4 Hz, CH=C-C=O), 5.63 (1H, d, J=15.4 Hz, CH-C=O), 4.10 (2H, t, J=5.2 Hz, CH_2O), 2.19 (2H, m, CH_2C=C), 1.31 (20H, broad s, aliphatic CH); mass m/e(%) 238 (M^+).

Found: C, 75.31; H, 10.92%. Calcd for $C_{15}H_{26}O_2$: C, 75.58; H, 10.99%.

Synthesis of Exaltolide (12). 2-Pentadecenolide (**11**) (65 mg) was hydrogenated in ethanol–ethyl acetate over 10% palladium on charcoal at room temperature for two days to give **12** (48 mg) as colorless semi-solids: IR (neat) 1730 cm^{-1} (C=O); NMR (CCl_4) δ 4.02 (2H, t, J=5.2 Hz, CH_2O), 2.22 (2H, t, J=6.2 Hz, CH_2C=O), 1.32 (24H, broad s, aliphatic CH); mass m/e(%) 240 (M^+).

The syntheses of other hydroxy macrolides such as 3-hydroxydodecanolide (**13**), 3-hydroxy-2-methyldodecanolide (**14**), 3-hydroxytetradecanolide (**15**), and 3-hydroxy-2-methyltetradecanolide (**16**), starting from the corresponding α,ω-diols, $HO(CH_2)_nOH$ with n=10, 12 were carried out exactly as described above. The physical properties and analytical data of these four macrolides and their precursors are shown in Table 2.

The authors wish to thank the Ministry of Education, Science and Culture, Japan, for Grant-in-Aid (No. 110309, 203014).

References

1) A preliminary account of this work has appeared: K. Maruoka, S. Hashimoto, Y. Kitagawa, H. Yamamoto, and H. Nozaki, *J. Am. Chem. Soc.*, **99**, 7705 (1977).

2) For a general discussion, see (a) A. T. Nielsen and W. H. Houlihan, *Org. React.*, **16**, 1 (1968); (b) H. O. House, "Modern Synthetic Reactions," 2nd ed, W. A. Benjamin, New York, N.Y. (1972), pp. 629—682.

3) For recent synthetic methods for regiospecific aldol synthesis, see a) H. O. House, D. S. Crumrine, A. Y. Teranishi, and H. D. Olmstead, *J. Am. Chem. Soc.*, **95**, 3310 (1973); b) T. Mukaiyama, K. Banno, and K. Narasaka, *ibid.*, **96**, 7503 (1974); c) G. Stork, G. A. Kraus, and G. A. Garcia, *J. Org. Chem.*, **39**, 3459 (1974); d) T. Mukaiyama, T. Sato, S. Suzuki, T. Inoue, and H. Nakamura, *Chem. Lett.*, **1976**, 95; e) T. Mukaiyama, and T. Inoue, *ibid.*, **1976**, 559; f) R. Noyori, K. Yokoyama, J. Sakata, I. Kuwajima, E. Nakamura, and M. Shimizu, *J. Am. Chem. Soc.*, **99**, 1265 (1977); g) W. A. Kleschick, C. T. Buse, and C. H. Heathcock, *J. Am. Chem. Soc.*, **99**, 247 (1977); h) I. Kuwajima, T. Inoue, and T. Sato, *Tetrahedron Lett.*, **1978**, 4887; i) H. Nozaki, K. Oshima, K. Takai, and S. Ozawa, *Chem. Lett.*, **1979**, 379; j) A. Itoh, S. Ozawa, K. Oshima, and H. Nozaki,

Tetrahedron Lett., **21**, 361 (1980), and references cited therein.

4) a) S. Masamune, S. Mori, D. V. Horn, and D. W. Brooks, *Tetrahedron Lett.*, **1979**, 1665; b) D. A. Evans, E. Vogel, and J. V. Nelson, *J. Am. Chem. Soc.*, **101**, 6120 (1979).

5) "Lang's Handbook of Chemistry," 11th ed by, J. A. Dean, McGraw-Hill Inc., New York, N.Y. (1973), pp. 3—124.

6) E. A. Jeffery, A. Meisters, and T. Mole, *J. Organometal. Chem.*, **74**, 373 (1974).

7) This procedure has its origins in the classical Reformatsky reaction (see R. L. Shriner, *Org. React.*, **1**, 1 (1942); M. W. Rathke, *ibid.*, **22**, 423 (1975)). The combination of organoaluminum reagents and zinc is also effective for the carbonyl methylenation, see K. Takai, Y. Hotta, K. Oshima, and H. Nozaki, *Tetrahedron Lett.*, 2417 (1978).

8) In the absence of carbonyl compounds, the dimeric condensation product of the α-halo ketone was isolated as the major product: $RC(=O)CH_2Br \rightarrow RC(=O)CH_2C(OH)(CH_2Br)R$. See also T. A. Spencer, R. W. Britton, and D. S. Watt, *J. Am. Chem. Soc.*, **89**, 5727 (1967).

9) For regioselective syntheses of α-bromo ketones, see E. W. Garbisch, Jr., *J. Org. Chem.*, **30**, 2109 (1965).

10) J. M. Denis, C. Girald, and J. M. Conia, *Synthesis*, **1972**, 549.

11) The extraordinary mild reaction conditions and high efficiencies of this new process are in sharp contrast to the classical Reformatsky reaction.

12) The normal Reformatsky reaction of methyl γ-bromocrotonate with benzaldehyde gave the γ-carbonylation product predominantly. See also E. R. H. Jones, D. G. O'Suliivan, and M. C. Whiting, *J. Chem. Soc.*, **1949**, 1415.

13) a) Internal esterification: E. J. Corey and K. C. Nicolaou, *J. Am. Chem. Soc.*, **96**, 5614 (1974), and references cited therein: S. Masamune, S. Kamata, and W. Schilling, *ibid.*, **97**, 3515 (1975). b) Formation of C–C bonds in a cyclization reaction: B. M. Trost and T. R. Verhoeven, *ibid.*, **94**, 667 (1972); R. N. Hurd and D. H. Shah, *J. Org. Chem.*, **38**, 390 (1973). For a recent review, see K. C. Nicolaou, *Tetrahedron*, **33**, 683 (1977).

14) The compound **9** was conveniently prepared from 1,13-tridecanediol by: (1) Monoesterification of 1,13-tridecanediol with bromoacetyl bromide in the presence of *N,N*-dimethylaniline, followed by (2) Collins oxidation.

15) Although **14** and **16** were found to be mixtures of *erythro* and *threo* isomers ($\approx 1:1$ by TLC assay (ether–hexane, 1:2, two developments) and trimethylsilylations; attempted separation of these isomers by GLC or column chromatography was unsuccessful), the better selectivities would be expected in the naturally occurring macrolide synthesis by this methodology since such compounds were known to be conformationally rather rigid molecules. A study on the synthesis of macrolides along this possibility is under way.

16) The α-methyl-β-hydroxy unit is a common functionality in a variety of macrolide antibiotics including erythromycin and methymycin; see, for a general review, K. Nakanishi, T. Goto, S. Itoh, S. Natori, and S. Nozoe, "Natural Products Chemistry," Kodansha Ltd., Tokyo (1975) Vol. 2.

17) K. Tsuda, E. Ohki, and S. Nozoe, *J. Org. Chem.*, **28**, 783 (1963).

18) H. C. Brown, M. M. Rogic, and M. W. Rathke, *J. Am. Chem. Soc.*, **90**, 6218 (1968).

19) G. Bianchetti, *Farmaco (Pavia) Ed. Sci.*, **12**, 441 (1957).

20) Addition of pyridine might be effective to trap Zn^{2+} in the reaction mixture.

21) See Ref. 3-b.

22) E. D. Venus-Danilova, M. V. Gorelik, and T. A. Nikolaeva, *Zhur. Obshch. Khim.*, **23**, 1493 (1953).

23) J. Wolinsky, M. Senyek, and S. Cohen, *J. Org. Chem.*, **30**, 3207 (1965).

24) Andrijewski, *J. Russ. Phys. Chem. Soc.*, **40**, 1635 (1908).

25) E. Schwenk and D. Papa, *J. Am. Chem. Soc.*, **67**, 1432 (1945).

 © 1980 The Chemical Society of Japan Bull. Chem. Soc. Jpn., 53, 3308—3312 (1980) [Vol. 53, No. 11

Studies on Heteropentalenes. II.[1] Cycloaddition of Imidazo[2,1-*b*]thiazoles, Thiazolo[3,2-*a*]benzimidazole, and Imidazo[2,1-*b*]benzothiazole with a Reactive Acetylenic Ester

Noritaka Abe,* Tarozaemon Nishiwaki, and Noriko Komoto
Department of Chemistry, Faculty of Sciences, Yamaguchi University, Yamaguchi 753
(Received April 28, 1980)

Cycloaddition of imidazo[2,1-*b*]thiazoles with dialkyl acetylenedicarboxylate follows dual courses depending on the polarity of the solvent, affording pyrrolo[2,1-*b*]thiazoles in an aprotic nonpolar solvent, or imidazo[1,2-*a*]-pyridines and imidazo[3,4-*a*]pyridines, together with thiophenes, in an aprotic polar solvent. Thiazolo[3,2-*a*]-benzimidazole and imidazo[2,1-*b*]benzothiazole were also found to react with the acetylenedicarboxylate to give pyrido[1,2-*a*]benzimidazole and pyrrolo[2,1-*a*]benzothiazole, respectively. The reactions would be accounted for in light of the Diels-Alder reaction in an aprotic nonpolar solvent and the 1,4-dipolar cycloaddition in an aprotic polar solvent.

Cycloaddition of nitrogen-heterocycles with acetylenic esters has received attention.[2] Our success in the cycloaddition of azaazulenes with dimethyl acetylenedicarboxylate (DMAD)[3] prompted us to extend the study to aromatic azapentalenes.[4] A number of papers have appeared on the cycloaddition of mesoionic azapentalenes.[5] Attempts to obtain a cycloadduct by reactions of neutral azapentalenes with reactive olefins and/or acetylenes do not seem successful, the reactions of pyrrolo[2,1-*b*]thiazoles with DMAD[6] and those of imidazo[2,1-*b*]thiazoles with maleic anhydride or diethyl azodicarboxylate[7] affording only the Michael adducts. We wish to report on the cycloaddition of imidazo[2,1-*b*]thiazoles and other related 10π-electron bicyclic systems (*e.g.* thiazolo[3,2-*a*]benzimidazole and imidazo[2,1-*b*]benzothiazole) with reactive acetylenic esters.

The reaction of ethyl 3-methyl-6-phenylimidazo[2,1-*b*]thiazole-2-carboxylate (**1a**) with DMAD was carried out under various conditions (Table 1). When the reaction was carried out in boiling acetonitrile, three products, 2-ethyl 6,7-dimethyl 3-methylpyrrolo[2,1-*b*]-thiazole-2,6,7-tricarboxylate (**2a**), tetramethyl 3-phenylimidazo[1,2-*a*]pyridine-5,6,7,8-tetracarboxylate (**3a**), and 5-ethyl 2,3-dimethyl 4-methylthiophene-2,3,5-tricarboxylate (**4**), were isolated in 25, 42, and 41% yields, respectively. The reaction in *N*,*N*-dimethylformamide (DMF) at bp proceeded similarly, but the yield of **2a** in the reaction at room temperature decreased remarkably. When the solvent was replaced by hot xylene, compound **2a** was obtained as the sole product in a better yield than in hot acetonitrile or DMF, benzonitrile being detected in the reaction mixture.

The structures of **2a**, **3a**, and **4** were assigned by means of their spectroscopic data as well as their elemental analyses. The ^{1}H NMR spectrum of **2a** reveals two methyl-singlets at δ 2.75 (3H) and 3.90 (6H), ethyl-signals at δ 1.34 and 4.37, and a singlet at δ 7.58 (1H) assignable to a proton at C-5. The ^{13}C NMR spectrum displays fourteen signals in agreement with the assigned structure. The ^{1}H NMR spectrum of **3a** has a 1H-singlet at δ 7.85 (H-2) together with four methyl-singlets at δ 3.20, 3.90, 3.93, and 4.10, and a phenyl multiplet at δ 7.3—7.5. Of four methyl-singlets, the one resonating at the highest field is assigned to a CO_2Me group at C-5, which should be shielded by a phenyl group at C-3. The ^{1}H NMR spectrum of **4** shows a methyl-singlet at δ 2.49 in addition to signals for ester groups at δ 3.87 (3H, s), 3.93 (3H, s), 1.38 (3H, t, J=7 Hz), and 4.35 (2H, q, J=7 Hz).

As shown in Table 1, the reaction of **1b** with DMAD in hot xylene proceeded in a similar way to give **2b**, whereas that in hot acetonitrile or DMF afforded tetramethyl 1-phenyl-3-(1-propynylthio)imidazo[3,4-*a*]-pyridine-5,6,7,8-tetracarboxylate (**5**) in addition to **3a**. The structure of **5** was assigned on the basis of the results of elemental analysis as well as its ^{1}H NMR spectrum which has four methyl ester-singlets at δ 3.16, 3.84, 3.91, and 4.07, a methyl-singlet at δ 1.90, and a phenyl multiplet at δ 7.3—7.7. Like **3a**, the singlet at δ 3.16 is assigned to a CO_2Me group at C-8, which should be shielded by a phenyl group at C-1. Resemblance of the UV spectrum of **5** with

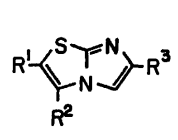
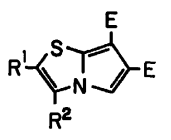
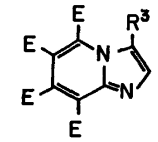

1a: R^1=CO_2Et, R^2=Me, R^3=Ph
1b: R^1=H, R^2=Me, R^3=Ph
1c: R^1=CO_2Et, R^2=Me, R^3=t-butyl
1d: R^1=H, R^2=Me, R^3=t-butyl
1e: R^1=R^2=H, R^3=Me

2a: R^1=CO_2Et, R^2=Me, E=CO_2Me
2b: R^1=H, R^2=Me, E=CO_2Me
2f: R^1=E=CO_2Et, R^2=Me
2g: R^1=H, R^2=Me, E=CO_2Et

3a: R^3=Ph, E=CO_2Me
3c: R^3=t-butyl, E=CO_2Me
3e: R^3=Me, E=CO_2Me

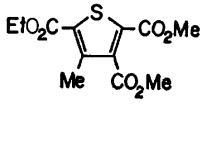
4

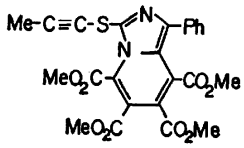
5

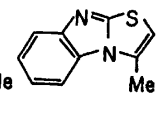
6

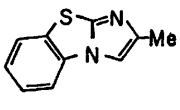
7

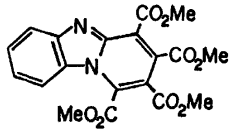
8

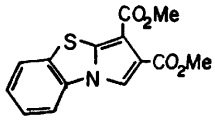
9

Table 1. Conditions and yields for reactions of **1a—e**, **6**, and **7** with the acetylenic esters

Entry	Substrate	Reagent	Solvent	Temp	Time	Products (%)[a]	Recovery (%)
1	**1a**	DMAD	MeCN	reflux	27 h	**2a** (25), **3a** (42), **4** (41)	**1a** (6)
2	**1a**	DMAD	MeCN	r.t.	11 d	**2a** (16), **3a** (44), **4** (38)	**1a** (68)
3	**1a**	DMAD	DMF	reflux	20 h	**2a** (27), **3a** (56), **4** (26)	**1a** (—)
4	**1a**	DMAD	DMF	r.t.	11 d	**2a** (9), **3a** (65), **4** (61)	**1a** (10)
5	**1a**	DMAD	Xxlene	reflux	27 h	**2a** (63)	**1a** (—)
6	**1a**	DMAD	Xylene	r.t.	27 d	**2a** (42), **3a** (48), **4** (45)	**1a** (82)
7	**1a**	DEAD	Xylene	reflux	27 h	**2f** (63)	**1a** (—)
8	**1b**	DMAD	MeCN	reflux	6 h	**3a** (43), **5** (26)	**1b** (—)
9	**1b**	DMAD	MeCN	r.t.	3 d	**3a** (26)	**1b** (5)
10	**1b**	DMAD	DMF	reflux	2 h	**3a** (42), **5** (30)	**1b** (—)
11	**1b**	DMAD	DMF	r.t.	3 d	**3a** (30)	**1b** (—)
12	**1b**	DMAD	Xylene	reflux	14 h	**2b** (50)	**1b** (—)
13	**1b**	DMAD	Xylene	r.t.	7 d	**2b** (20), **3a** (20)	**1b** (19)
14	**1b**	DEAD	Xylene	reflux	14 h	**2g** (75)	**1b** (—)
15	**1c**	DMAD	MeCN	r.t.	8 d	**3c** (29), **4** (17)	**1c** (25)
16	**1c**	DMAD	Xylene	r.t.	27 d	**2a** (17), **3c** (36)	**1c** (38)
17	**1d**	DMAD	MeCN	reflux	3 h	**3c** (44)	**1d** (—)
18	**1d**	DMAD	MeCN	r.t.	20 h	**3c** (22)	**1d** (5)
19	**1d**	DMAD	Xylene	reflux	4 h	**2b** (76)	**1d** (—)
20	**1d**	DMAD	Xylene	r.t.	7 d	**2b** (12), **3c** (15)	**1d** (32)
21	**1e**	DMAD	MeCN	r.t.	2 h	**3e** (38), **10**(5)	**1e** (—)
22	**1e**	DMAD	Xylene	r.t.	2 h	**3e** (31), **10**(12)	**1e** (—)
23	**6**	DMAD	MeCN	r.t.	3 h	**8** (24)	**6** (—)
24	**7**	DMAD	Xylene	reflux	5 h	**9** (29), **11** (4), **12**(12)	**7** (—)

a) Yields are based on consumed starting materials.

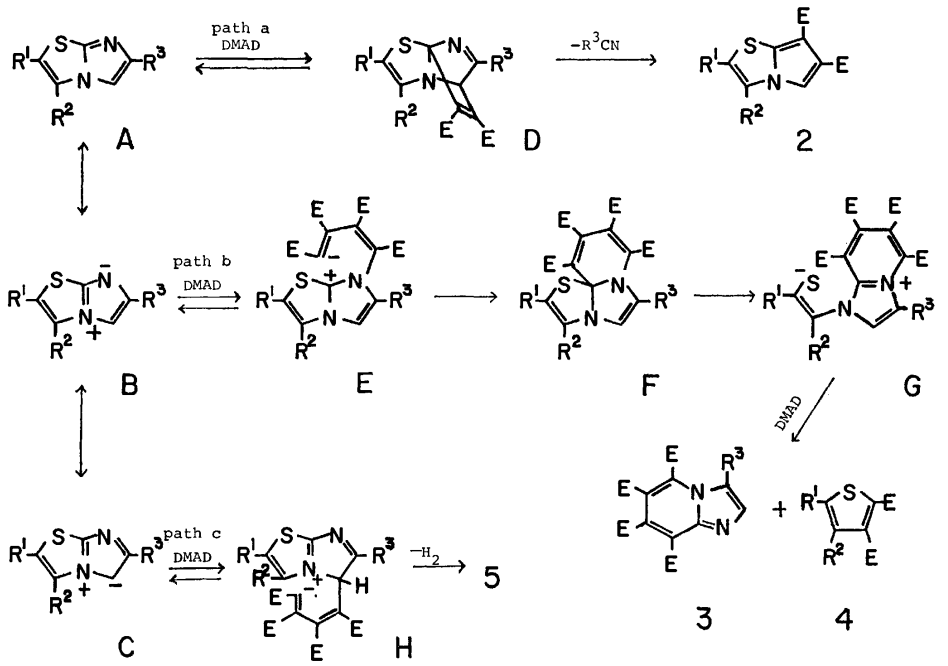

Scheme 1.

that of **3a** further supports the assigned structure.

Likewise, **1a** and **1b** react with diethyl acetylenedicarboxylate (DEAD) in hot xylene giving **2f** and **2g**, respectively, in good yields.

It appears that elimination of nitrogen- or sulfur-containing moiety from **1** highly depends on the polarity of the solvent. For the sake of clarification, 3-methylthiazolo[3,2-*a*]benzimidazole (**6**) and 2-methylimidazo[2,1-*b*]benzothiazole (**7**), respectively, were allowed to react with DMAD. The reaction of **6** in acetonitrile yielded tetramethylpyrido[1,2-*a*]benzimidazole-1,2,3,4-tetracarboxylate (**8**) with loss of the sulfur-containing moiety, whereas that of **7** in xylene gave dimethyl pyrrolo[2,1-*b*]benzothiazole-2,3-dicarboxylate (**9**) with elimination of acetonitrile and two unidentified 1:4-adducts **11** and **12**.

Plausible mechanisms for the reactions of imidazo[2,1-*b*]thiazole **1** with the reactive acetylenic ester are given in Scheme 1. In an aprotic nonpolar solvent, the reaction proceeds *via* a Diels-Alder addition of the neutral species **A** with the acetylenedicarboxylate followed by the retrogression of the adduct **D** to give **2** (path a). In an aprotic polar solvent, the ionic species **B** undergoes a 1,4-dipolar cycloaddition with DMAD to give intermediates **E**, **F**, and **G** successively. At the final stage of the reaction, **G** reacts with DMAD to give imidazo[1,2-*a*]pyridine (**3**) together with the thiophene (**4**) (path b). Potts *et al.* also postulated a zwitter ion like **G** for the reaction of thiazolium-*N*-ylides with DMAD to give 1*H*-pyrido[2,1-*c*][1,4]thiazines.[8] However, if R^1 in **1** is hydrogen, the ionic species **C** reacts with DMAD to form an intermediate **H**, from which thioether **5** is produced by loss of H_2 (path c).

In order to confirm the postulate that a bulky substituent at C-6 in the imidazo[2,1-*b*]thiazoles facilitates the isolation of intermediates **D** and **F** (Scheme 1), we examined the reactions of **1c** and **1d** with DMAD in xylene or acetonitrile. However, the products were found to be those formed by the loss of the sulfur- or nitrogen-containing moiety from the intermediates.

The reaction of **1a** with the acetylene is sluggish; over 80% yield of the starting **1a** was recovered even after being allowed to react with DMAD in xylene at room temperature for 27 d. The reaction of 6-methylimidazo[2,1-*b*]thiazole (**1e**) with DMAD in either xylene or acetonitrile was rapid and the solution boiled when DMAD was added to a solution of **1e** to give **3e** and an unidentified 1:4-adduct **10**. The results suggest that an electron-attracting substituent would decrease the electron density of the imidazole ring of **1** and hence its nucleophilic reactivity towards the acetylenedicarboxylate, whereas an electron-donating substituent would enhence its reactivity.

No such Michael-type adducts[6,7] were isolated.

Experimental

Melting points were uncorrected. ^1H and ^{13}C NMR spectra were taken with Hitachi R-24B (60 MHz) and Varian FT-80A spectrometers, respectively, for solutions in $CDCl_3$ with TMS as an internal standard. UV spectra were measured for solutions in ethanol and IR spectra for Nujol mulls. Kieselgel 60 was used for chromatography. Yields are based on the consumed starting materials. Imidazo[2,1-*b*]thiazoles (**1b** and **1e**),[9,10] thiazolo[3,2-*a*]benzimidazole (**6**),[9] and imidazo[2,1-*b*]benzothiazole (**7**)[9] were prepared as reported.

*Synthesis of Ethyl 3-Methyl-6-phenylimidazo[2,1-b]thiazole-2-carboxylate (**1a**).* A stirred mixture of ethyl 2-amino-4-methylthiazole-5-carboxylate[11] (10 g) and α-bromoacetophenone (10.6 g) in 1-butanol (40 ml) was heated under reflux for 3 h and cooled in an ice bath. Ethyl 3-methyl-6-phenylimidazo[2,1-*b*]thiazole-2-carboxylate hydrobromide (8.3 g, 40%) precipitated was recrystallized from ethanol as colorless prisms, mp 199—200 °C. A mixture of the salt (5 g) in water (150 ml) was heated under reflux for 3 h, free base precipitated on cooling, being filtered off and dried (2.3 g, 62%). Recrystallization from ethanol gave **1a** [colorless needles, mp 143—144 °C, UV_{max} 257^{sh} (log ε 4.37), 265 (4.38), 280 (4.38), 287 (4.38), 294^{sh} (4.36); IR 1690 cm^{-1} (ester C=O); ^1H NMR δ=1.38 (3H, t, *J*=7 Hz, CH_3), 2.72 (3H, s, CH_3), 4.33 (2H, q, *J*=7 Hz, OCH_2), 7.3—7.5 (3H, m, phenyl), 7.55 (1H, s, H-5), 7.7—7.9 (2H, m, phenyl). Found: C, 62.89; H, 4.97; N, 9.81; S, 11.08%. Calcd for $C_{15}H_{14}N_2O_2S$: C, 62.97; H, 4.93; N, 9.78; S, 11.20%].

*Synthesis of Ethyl 6-t-Butyl-3-methylimidazo[2,1-b]thiazole-2-carboxylate (**1c**).* Ethyl 6-*t*-butyl-3-methylimidazo[2,1-*b*]-thiazole hydrobromide was prepared in 78% yield in the same way as for **1a** from ethyl 2-amino-4-methylthiazole-5-carboxylate (17.5 g), 1-bromo-3,3-dimethyl-2-butanone[12] (16.1 g), and 1-butanol (70 ml) and recrystallized from ethanol as colorless prisms, mp 202—203.5 °C. This salt (3.2 g) was added to a sodium ethoxide solution prepared from Na (0.4 g) and abs ethanol (30 ml). The mixture was heated under reflux for 3 h and evaporated to dryness under reduced pressure, the residue being dissolved in water. Extraction with ether and evaporation of the dried (Na_2SO_4) extracts gave **1c** [1.78 g, 73%, colorless prisms (from ligroine), mp 92—93 °C. UV_{max} 274 nm (log ε 4.18); IR 1680 cm^{-1} (ester C=O); ^1H NMR δ=1.36 (9H, s, *t*-butyl), 1.38 (3H, t, *J*=7 Hz, CH_3), 2.73 (3H, s, CH_3), 4.33 (2H, q, *J*=7 Hz, OCH_2), 7.10 (1H, s, H-5). Found: C, 58.87; H, 6.76; N, 10.42; S, 12.29%. Calcd for $C_{13}H_{18}N_2O_2S$: C, 58.62; H, 6.81; N, 10.52; S, 12.04%].

*Synthesis of 6-t-Butyl-3-methylimidazo[2,1-b]thiazole (**1d**).* 6-*t*-Butyl-3-methylimidazo[2,1-*b*]thiazole hydrobromide was prepared in 83% yield in the same way as for **1a** from 2-amino-4-methylthiazole (15.8 g), 1-bromo-3,3-dimethyl-2-butanone (24.7 g) and 1-butanol (70 ml), and recrystallized from ethanol as colorless prisms, mp 242—243 °C. A mixture of this salt (5 g), NaOH (1 g), and ethanol (30 ml) was heated under reflux for 1 h and evaporated to dryness under reduced pressure. The residue was dissolved in water and extracted with ether. Evaporation of the dried (Na_2SO_4) extracts left **1d** [2.8 g, 79%, colorless prisms (from petroleum ether), mp 83—85 °C, UV_{max} 245 nm (log ε 3.80); ^1H NMR δ=1.34 (9H, s, *t*-butyl), 2.32 (3H, d, *J*=1 Hz, CH_3), 6.28 (1H, q, *J*=1 Hz, H-2), 7.04 (1H, s, H-5). Found: C, 62.02; H, 7.28; N, 14.38; S, 16.49%. Calcd for $C_{10}H_{14}N_2S$: C, 61.82; H, 7.26; N, 14.42; S, 16.50%].

*Reaction of **1a** with DMAD.* A mixture of **1a** (1.00 g), DMAD (2.48 g), and the solvent (50 ml) was allowed to react and then evaporated to dryness under reduced pressure. Chromatography of the residue with benzene and benzene–chloroform (1:1) eluted benzonitrile [IR (neat) 2200 (CN) and 700 cm^{-1} (phenyl)], compounds **4**, **1a**, **2a**, and **3a**, successively. The conditions and yields for reactions of **1a**—**e**, **6**, and **7** with acetylenic esters are given in Table 1.

2a: Colorless needles (from ethanol), mp 166.5—167 °C, UV_{max} 226 nm (log ε 4.34), 257^{sh} (4.43), 265 (4.48), 292 (3.82), 316^{sh} (3.58); IR 1730, 1705, and 1655 cm^{-1} (ester (C=O); ^1H NMR δ=1.34 (3H, t, *J*=7 Hz, CH_3), 2.75 (3H, s, CH_3), 3.90 (6H, s, 2×OCH_3), 4.37 (2H, q, *J*=7 Hz, OCH_2), 7.58 (1H, s, H-5). ^{13}C NMR δ=12.1 (q, CH_3), 14.2 (q, CH_3), 51.6 (q, OCH_3), 52.0 (q, OCH_3), 61.9 (t, OCH_2), 104.5 (s, C-7), 116.3 (d, C-5), 118.4 (s, C-6), 122.1 (s, C-2), 137.3 (s, C-3), 139.2 (s, C-7a), 161.7 (s, C=O), 162.7 (s, C=O), 163.4 (s, C=O). Found: C, 51.56; H, 4.73; N, 4.17; S, 10.09%. Calcd for $C_{14}H_{15}NO_6S$: C, 51.68; H, 4.65; N, 4.31; S, 9.85%.

3a: Yellow needles (from ethanol), mp 152—153 °C, UV_{max} 261 nm (log ε 4.41), 300^{sh} (3.69), 357 (3.53); IR 1740, 1730, and 1715 cm^{-1} (ester C=O); ^1H NMR δ=3.20 (3H, s, OCH_3), 3.90 (3H, s, OCH_3), 3.93 (3H, s, OCH_3), 4.10 (3H, s, OCH_3), 7.3—7.5 (5H, m, phenyl), 7.85 (1H, s, H-2). Found: C, 58.98; H, 4.56; N, 6.78%. Calcd for $C_{21}H_{18}N_2O_8$: C, 59.15;

H, 4.26; N, 6.57%.

4: Colorless needles (from ethanol), mp 67—68 °C, UV_{max} 275 nm (log ε 4.27); IR 1740, 1720, and 1705 cm^{-1} (ester C=O); ^1H NMR δ=1.38 (3H, t, J=7 Hz, CH_3), 2.49 (3H, s, CH_3), 3.87 (3H, s, OCH_3), 4.35 (2H, q, J=7 Hz, OCH_2). Found: C, 50.53; H, 4.99; S, 11.03%. Calcd for $C_{12}H_{14}O_6S$: C, 50.34; H, 4.93; S, 11.20%.

*Reaction of **1a** with DEAD.* A mixture of **1a** (0.70 g) and DEAD (1.66 g) in xylene (30 ml) was heated under reflux for 27 h, and worked up as above to give **2f**.

2f: Colorless needles (from ligroine), mp 109—110 °C, UV_{max} 226 nm (log ε 4.19), 257^{sh} (4.42), 265 (4.49), 292^{sh} (3.92), 316 (3.67); IR 1725, 1710, and 1650 cm^{-1} (ester C=O); ^1H NMR δ=1.40 (9H, t, J=7 Hz, 3×CH_3), 2.75 (3H, s, CH_3), 4.37 (6H, q, J=7 Hz, 3×OCH_2), 7.58 (1H, s, H-5). Found: C, 54.54; H, 5.68; N, 4.08; S, 9.27%. Calcd for $C_{16}H_{19}NO_6S$: C, 54.38; H, 5.42; N, 3.96; S, 9.07%.

*Reaction of **1b** with DMAD.* A mixture of **1b** (1.00 g), DMAD (3.32 g), and the solvent (30 ml) was allowed to react and then worked up as for **1a**. Compound **1b**, **5**, and **2b** were eluted successively.

2b: Colorless needles (from ligroine–benzene), mp 148—149 °C, UV_{max} 225 nm (log ε 4.28), 242 (4.29), 290 (4.08); IR 1725 and 1705 cm^{-1} (ester C=O); ^1H NMR δ=2.43 (3H, d, J=0.5 Hz, CH_3), 3.93 (6H, s, 2×OCH_3), 6.62 (1H, q, J=0.5 Hz, H-2), 7.62 (1H, s, H-5). Found: C, 51.99; H, 4.37; N, 5.50; S, 12.48%. Calcd for $C_{11}H_{11}NO_4S$: C, 52.16; H, 4.38; N, 5.53; S, 12.66%.

5: Yellow needles (from ethanol), mp 186—187 °C, UV_{max} 255 nm (log ε 4.14), 297^{sh} (3.74), 373 (3.59); IR 1735 and 1710 cm^{-1} (ester C=O); ^1H NMR δ=1.90 (3H, s, CH_3), 3.16 (3H, s, OCH_3), 3.84 (3H, s, OCH_3), 3.91 (3H, s, OCH_3), 4.07 (3H, s, OCH_3), 7.3—7.7 (5H, m, phenyl). Found: C, 58.14; H, 4.16; N, 5.35; S, 6.14%. Calcd for $C_{24}H_{20}N_2O_8S$: C, 58.06; H, 4.06; N, 5.46; S, 6.46%.

*Reaction of **1b** with DEAD.* A mixture of **1b** (1.00 g) and DEAD (3.18 g) in xylene (30 ml) was heated under reflux for 14 h, and then worked up as for **1a** to give **2g**.

2g: Colorless prisms (from ethanol), mp 114—115 °C, UV_{max} 225 nm (log ε 4.18), 235 (4.18), 243 (4.18), 291 (3.96); IR 1720 and 1695 cm^{-1} (ester C=O); ^1H NMR δ=1.39 (6H, t, J=7 Hz, 2×CH_3), 2.40 (3H, d, J=1 Hz, CH_3), 4.34 (4H, q, J=7 Hz, 2×OCH_2), 6.52 (1H, q, J=1 Hz, H-2), 7.52 (1H, s, H-5). Found: C, 55.53; H, 5.33; N, 4.85; S, 11.34%. Calcd for $C_{13}H_{15}NO_4S$: 55.50; H, 5.37; N, 4.98; S, 11.40%.

*Reaction of **1c** with DMAD.* A mixture of **1c** (0.90 g), DMAD (2.40 g), and the solvent (50 ml) was allowed to react and then worked up as for **1a** to give compounds **4**, **1c**, **2a**, and **3c** successively.

3c: Yellow needles (from ethanol), mp 119—120 °C, UV_{max} 261 nm (log ε 4.34), 302 (3.52), 358 (3.60); IR 1735 and 1710 cm^{-1} (ester C=O); ^1H NMR δ=1.47 (9H, s, *t*-butyl), 3.90 (6H, s, 2×OCH_3), 3.93 (3H, s, OCH_3), 4.05 (3H, s, OCH_3), 7.82 (1H, s, H-2). Found: C, 56.24; H, 5.47; N, 6.71%. Calcd for $C_{19}H_{22}N_2O_8$: C, 56.15; H, 5.46; N, 6.89%.

*Reaction of **1d** with DMAD.* A mixture of **1d** (1.00 g), DMAD (3.60 g), and the solvent (30 ml) was allowed to react and then worked up as for **1a** to give compounds **2b** and **3c** successively.

*Reaction of **1e** with DMAD.* A mixture of **1e** (1.00 g), DMAD (4.12 g), and the solvent (30 ml) was allowed to react and then worked up to give **3e** as a yellow oil, identified as a picrate, and an unidentified 1:4-adduct **10**.

3e: Picrate of **3e**, yellow prisms (from ethanol), mp 153—154 °C, UV_{max} 255 nm (log ε 4.56), 315^{sh} (4.03), 354 (4.31); IR 3350 (OH) and 1740 cm^{-1} (ester C=O); ^1H NMR (DMSO-d_6) δ=1.07 (3H, t, J=7 Hz, CH_3), 2.42 (3H, d, J=0.5 Hz, CH_3), 3.45 (2H, q, OCH_2), 3.87 (6H, s, 2×OCH_3), 3.95 (3H, s, OCH_3), 4.03 (3H, s, OCH_3), 7.13 (1H, bs, OH), 7.45 (1H, q, J=0.5 Hz, H-2), 7.95 (1H, bs, OH), 8.53 (2H, s, phenyl). Found: C, 45.44; H, 3.84; N, 10.85%. Calcd for $C_{22}H_{20}N_5O_{15}\cdot C_2H_5OH$: C, 45.08; H, 3.94; N, 10.95%.

10: Yellow prisms (from ethanol), mp 235—236 °C, UV_{max} 298 nm (log ε 4.20), 420 (4.06); IR 1730, 1705, and 1685 cm^{-1} (ester C=O); ^1H NMR δ=1.57 (3H, s), 3.62 (3H, s), 3.67 (3H, s), 3.75 (6H, s), 3.76 (3H, s), 3.83 (3H, s), 3.85 (3H, s), 3.88 (3H, s), 5.26 (1H, d, J=8 Hz), 6.43 (1H, s), 6.45 (1H, d, J=8 Hz). Found: C, 50.89; H, 4.40; N, 3.86; S, 4.50%. Calcd for $C_{30}H_{30}N_2O_{16}S$: C, 50.99; H, 4.28; N, 3.96; S, 4.54%.

*Reaction of **6** with DMAD.* A mixture of **6** (1.00 g) and DMAD (3.87 g) in acetonitrile (30 ml) was left to stand at room temperature for 3 h, and worked up as described for **1a** to give **8** (0.51 g).

8: Yellow needles (from ligroine–benzene), mp 146—147 °C, UV_{max} 277 nm (log ε 4.60), 285^{sh} (4.56), 326 (3.68), 375 (3.45); IR 1740 and 1730 cm^{-1} (ester C=O); ^1H NMR δ=3.90 (3H, s, OCH_3), 3.92 (3H, s, OCH_3), 4.08 (3H, s, OCH_3), 4.20 (3H, s, OCH_3), 7.3—7.8 (3H, m, H-7,8,9), 8.07 (1H, dm, J=8 Hz, H-6). Found: C, 57.12; H, 3.97; N, 6.92%. Calcd for $C_{19}H_{16}N_2O_8$: C, 57.00; H, 4.03; N, 7.00%.

*Reaction of **7** with DMAD.* A mixture of **7** (0.94 g) and DMAD (2.13 g) in xylene (30 ml) was heated under reflux for 5 h, and worked up as described for **1a** to give **9** (0.213 g) and two unidentified 1:4-adducts **11** (0.138 g) and **12** (0.47 g).

9: Colorless needles (from ethanol), mp 147—149 °C, UV_{max} 241 nm (log ε 4.62), 268^{sh} (4.13), 288 (4.13); IR 1740 and 1710 cm^{-1} (ester C=O); ^1H NMR δ=3.95 (6H, s, 2×OCH_3), 7.2—7.8 (4H, m, H-5,6,7,8), 7.98 (1H, s, H-1). Found: C, 58.07; H, 3.98; N, 4.98; S, 11.38%. Calcd for $C_{14}H_{11}NO_4S$: C, 58.12; H, 3.83; N, 4.84; S, 11.08%.

11: Yellow prisms (from ethanol), mp 234—235 °C, UV_{max} 291 nm (log ε 4.37), 414 (4.28); IR 1750, 1735, and 1700 cm^{-1} (ester C=O); ^1H NMR δ=1.72 (3H, s), 2.92 (3H, s), 3.48 (3H, s), 3.67 (3H, s), 3.68 (3H, s), 3.72 (3H, s), 3.78 (3H, s), 3.83 (3H, s), 3.86 (3H, s), 5.05 (1H, s), 7.2—7.6 (4H, m). Found: C, 53.98; H, 4.45; N, 3.50; S, 4.51%. Calcd for $C_{34}H_{32}N_2O_{16}S$: C, 53.96; H, 4.27; N, 3.70; S, 4.24%.

12: Orange needles (from ethanol), mp 163—165 °C, UV_{max} 265 nm (log ε 4.15), 435 (3.80); IR 1735, 1725, and 1670 cm^{-1} (ester C=O); ^1H NMR δ=1.67 (3H, s), 3.37 (3H, s), 3.50 (6H, s), 3.61 (3H, s), 3.71 (3H, s), 3.80 (3H, s), 3.84 (3H, s), 3.88 (3H, s), 5.95 (1H, s), 7.05—8.0 (4H, m). Found: C, 54.02; H, 4.41; N, 3.33; S, 4.35%. Calcd for $C_{34}H_{32}N_2O_{16}S$: C, 53.96; H, 4.27; N, 3.70; S, 4.24%.

We thank Dr. Masafumi Yasunami, Tohoku University, for NMR spectral determination.

References

1) Part I. N. Abe, T. Nishiwaki, and N. Komoto, *Chem. Lett.*, **1980**, 223.

2) R. M. Acheson and N. F. Elmore, *Adv. Heterocyclic Chem.*, **23**, 263 (1978).

3) N. Abe, Y. Tanaka, and T. Nishiwaki, *J. Chem. Soc., Perkin Trans. 1*, **1978**, 429; N. Abe and T. Nishiwaki, *Bull. Chem. Soc. Jpn.*, **53**, 1406 (1980).

4) J. Elguero, R. M. Claramunt, and A. J. H. Summers, *Adv. Heterocyclic Chem.*, **22**, 183 (1978).
5) C. A. Ramsden, *Tetrahedron*, **33**, 3203 (1977); K. Matsumoto and T. Uchida, *Chem. Lett.*, **1978**, 1093; K. T. Potts, S. K. Datta, and J. L. Marshall, *J. Org. Chem.*, **44**, 622 (1979); H. Gotthordt and F. Reiter, *Chem. Ber.*, **112**, 266 (1979).
6) O. Ceder and B. Beijer, *Tetrahedron*, **28**, 4341 (1972).
7) L. Pentimalli, G. Cogo, and A. M. Guerra, *Gazz. Chim. Ital.*, **97**, 488 (1967); L. Pentimalli and A. M. Guerra, *ibid.*, **97**, 1286 (1967).
8) K. T. Potts, D. R. Choudhury, and T. R. Westby, *J. Org. Chem.*, **41**, 187 (1976).
9) I. Iwai and T. Hiraoka, *Chem. Pharm. Bull.*, **12**, 813 (1964).
10) S. Kano, *Yakugaku Zasshi*, **92**, 51 (1972).
11) R. M. Dodson and L. C. King, *J. Am. Chem. Soc.*, **67**, 2242 (1945).
12) M. Ch-Morize, *Bull. Soc. Chim. Fr.*, **1962**, 920.

Silver(I) Ion-catalyzed Rearrangement of 3,5-Dehydronoriceane (Pentacyclo[5.3.1.$0^{2,6}$.$0^{3,5}$.$0^{4,9}$]undecane). Empirical Force-field Calculations and Behavior of 3-Noricyl (Tetracyclo[5.3.1.$0^{2,6}$.$0^{4,9}$]undec-3-yl) Cation[1]

Takeo KATSUSHIMA, Ryohei YAMAGUCHI, Mituyosi KAWANISI,* and Eiji ŌSAWA**

Department of Industrial Chemistry, Faculty of Engineering, Kyoto University, Yoshida, Sakyo-ku, Kyoto 606

***Department of Chemistry, Faculty of Science, Hokkaido University, Sapporo 060*

(Received April 30, 1980)

Treatment of 3,5-dehydronoriceane (**1**) with a catalytic amount of silver tetrafluoroborate results in a novel skeletal rearrangement to afford tetracyclo[5.3.1.$0^{2,6}$.$0^{3,9}$]undec-4-ene (2,4-ethenonoradamantane) (**5**) in 85% yield. Empirical force-filed calculations suggest that there is no substantial difference in strain energies between **1** and bicyclo[2.1.0]pentane which is inert toward silver(I) ion. Acetolysis of *endo*-3-noricyl (*endo*-tetracyclo[5.3.1.$0^{2,6}$.$0^{4,9}$]undec-3-yl) tosylate (**7**) gives *exo*-3-acetoxynoriceane (*exo*-3-acetoxytetracyclo[5.3.1.$0^{2,6}$.$0^{4,9}$]undecane) (**11**), *exo*-4-acetoxytetracyclo[5.3.1.$0^{2,6}$.$0^{3,9}$]undecane (**12**), and **5** in a ratio of 36:42:22. Similar acetolysis of the *exo*-isomer of **7** gives the same products but in a different ratio (**11**:**12**:**5**=9:47:44). A stepwise carbocation mechanism is proposed for the above mentioned silver(I) ion-catalyzed rearrangement.

Transition metal-catalyzed rearrangement of strained organic molecules has become one of the most exciting and intriguing fields of chemistry in a past decade and a number of unexpected and interesting isomerizations have been reported.[2] Among them, silver(I) ion-catalyzed rearrangements of strained σ-bonds have demonstrated remarkable and unique carbon-carbon σ-bond reorganization reactions.[2-4] Meanwhile, in spite of their high strain energies, bicyclo[2.1.0]pentane (**2**) and the even more strained spiro compound (**3**) have been found to be inert toward silver(I) ion.[5-7] We have recently reported the synthesis of 3,5-dehydronoriceane (**1**),[8] which possesses the partial bicyclo[2.1.0]pentane structure constrained within a rigid cage molecule. Although **1** has shown

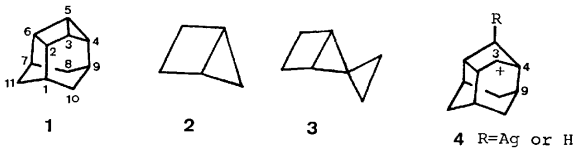

Scheme 1.

similar reactivities in hydrogenation[8] and other reactions[9] to bicyclo[2.1.0]pentane (**2**) itself,[10] we have found that **1**, unlike **2**, does react with silver(I) ion to follow a skeletal rearrangement.[11] Since nonconcerted mechanism involving carbocation intermediate has been strongly suggested to account for the hitherto known silver(I) ion-catalyzed rearrangements,[2-4] behavior of the supposed carbocation intermediate such as **4** may deserve to be investigated. In this paper, we would like to describe a new silver(I) ion-catalyzed rearrangement of bicyclo[2.1.0]pentane system together with empirical force-field calculations of strain energies of **1** and **2**, and acetolyses of *exo*- and *endo*-3-noricyl tosylates (**7** and **8**).

Results and Discussion

When **1** was treated with 3.6 mol% of silver tetrafluoroborate in chloroform at room temperature for 18 h, a novel skeletal rearrangement similar to those of cubyl systems[2,3] took place to give tetracyclo[5.3.1.$0^{2,6}$.$0^{3,9}$]undec-4-ene (2,4-ethenonoradamantane) (**5**) in 85% yield. Catalytic hydrogenation of **5** gave known tetracyclo[5.3.1.$0^{2,6}$.$0^{3,9}$]undecane (**6**),[12] confirming the structure of **5**.

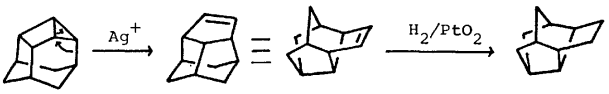

Scheme 2.

Primarily we anticipated that the strain around the central bond of **1** would be higher than that of the corresponding bond of **2** in order to explain the observed different reactivity toward silver(I) ion between **1** and **2**. Despite the acknowledged inadequacy of the presently available force-field models for cyclopropane derivatives,[13] we hoped that errors due to the force-field would cancel each other when closely related molecules were compared in molecular mechanics calculations (Table 1). The force-field[13] reproduces the geometry of **2** well, though it overestimates the strain in **2** by *ca.* 30 kcal/mol. Attention should be directed to the small difference in energy terms between **1** and **2**.[14] For **1** and **2** there appears to be no substantial difference in strain around the central bonds as well as in the whole molecule. In addition, the bow-and-stern C···C as well as flagpole H···H nonbonded interactions in the boat cyclohexane ring of **1** amount to only *ca.* 2 kcal/mol. Thus, any rationalization of the observed reactivity of **1** toward silver(I) ion compared with **2** must be based on something besides strain.

Although two mechanisms, concerted [$_{\sigma}2_{a}+_{\sigma}2_{a}$][15] and step-wise carbocation rearrangements, have been considered for silver(I) ion-catalyzed rearrangements, many experiments strongly favor the latter.[2-4] If so, 3-noricyl cation such as **4** (R=Ag) should be a supposed intermediate in the present reaction. There are two possibilities for 1,2-alkyl shift. Migration of the C_1–C_2 bond to C_3 gives again the noriceane skeleton, while shift of the C_4–C_9 bond leads to the more stable tetracyclo[5.3.1.$0^{2,6}$.$0^{3,9}$]undecane system.[12] However, our calculation has shown that there is

TABLE 1. MOLECULAR MECHANICS CALCULATIONS ON **1** AND **2** USING THE ENGLER FORCE-FIELD

	1	**2**	
	Calcd	Calcd	Exp.[a]
Length of the central bond (Å)	1.514	1.530	1.525(8) X[b]
			1.536(1) M.W.[c]
Dihedral angle around the central bond (deg)	115.6	124.7	112.5(3) X[b]
			112.74(18) M.W.[c]
Sum of strain around bridgehead carbons (kcal/mol)	88.87(C-3)	84.45(C-5)	
	59.93(C-4)	56.43(C-5)	
ΔH_f° (g, 25 °C) (kcal/mol)	74.50	73.01	37.6[d]
Strain energy (kcal/mol)	107.17	92.72	57.3[e]
Heat of the central bond hydrogenolysis (kcal/mol)	−81.92[f]	−91.45	−55.14(36)[g]

a) Standard deviations in parentheses. b) X-Ray analysis of *exo*-5-tosylate: W. Saenger, C. H. Schwalbe, K. Fellenberger, and U. Schollkopf, *Chem. Ber.*, **106**, 2883 (1973). c) Microwave analysis of hydrocarbon: R. D. Suenram and M. D. Harmony, *J. Chem. Phys.*, **56**, 3837 (1972). d) Taken from: S. W. Benson, F. R. Cruickshank, D. M. Golden, R. G. Haugen, H. E. O'Neal, A. S. Rodgers, R. Show, and R. Walsh, *Chem. Rev.*, **69**, 279 (1969). e) P. von R. Schleyer, J. E. Williams, and K. Blanchard, *J. Am. Chem. Soc.*, **93**, 2377 (1970). f) $\Delta H_f^\circ - \Delta H_f^\circ$(noriceane)(Ref. 12). g) R. B. Turner, P. Goebel, B. J. Mallon, W. von E. Doering, J. F. Coburn, Jr., and M. Pomerantz, *J. Am. Chem. Soc.*, **90**, 4315 (1968).

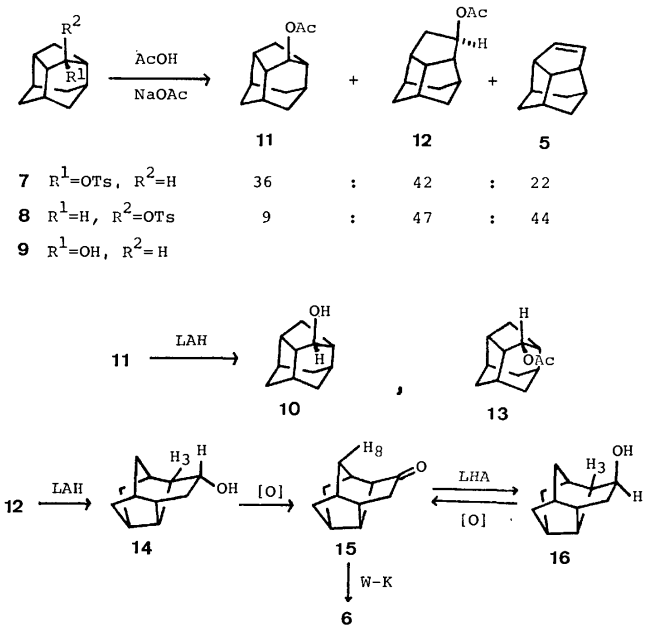

Scheme 3.

a large dihedral angle (45°) between sp^2-vacant orbital at C_3 of **4** (R=H) and the migrating C_4–C_9 bond, suggesting that such a rearrangement would be unfavorable. We, therefore, have studied the behavior of 3-noricyl cation (**4**, R=H) generated under solvolytic conditions in order to know whether the rearrangement is feasible or not.

Two isomeric *endo*- and *exo*-3-noricyl tosylates (**7** and **8**), prepared from the corresponding alcohols (**9** and **10**) by the usual way, were solvolyzed in acetic acid containing sodium acetate as a buffer. Acetolysis of the *endo*-tosylate (**7**) gave *exo*-3-acetoxynoriceane (**11**), *exo*-4-acetoxytetracyclo[5.3.1.$0^{2,6}$.$0^{3,9}$]undecane (**12**), and **5** in 95% yield in a ratio of 36:42:22. A similar acetolysis of the *exo*-isomer (**8**) gave the same products but in a different ratio (**11**:**12**:**5**=9:47:44). Lithium aluminum hydride reduction of **11** gave *exo*-3-noriceanol (**9**), which was shown to be identical with the one obtained in the reduction of 3-noriceanone with lithium in liquid ammonia.[16] Reduction of **12** with lithium aluminum hydride gave the alcohol, *exo*-tetracyclo[5.3.1.$0^{2,6}$.$0^{3,9}$]undecan-4-ol (**14**), which was oxidized with CrO_3–pyridine complex to afford tetracyclo[5.3.1.$0^{2,6}$.$0^{3,9}$]undecan-4-one (**15**).[12,17] Wolff-Kishner (W-K) reduction of **15** gave **6** confirming the parent skeleton. Lithium aluminum hydride reduction of **15** gave exclusively the isomeric *endo*-tetracyclo[5.3.1.$0^{2,6}$.$0^{3,9}$]undecan-4-ol (**16**), which reproduced **15** upon treatment with CrO_3–pyridine complex. The ^{1}H-NMR (PMR) spectra of **14** and **16** showed a doublet of doublet (J=6.9 and 2.7 Hz) at 4.33 ppm and the quintet (J=10.5, 6.3, and 4.8 Hz) at 4.58 ppm due to C_4-protons, respectively. Model investigations (Dreiding model) tell us that the *endo*-proton should not couple with the adjacent bridg-head proton (H_3) because of the large dihedral angle (*ca.* 90°). Accordingly, **14** and **15** were assigned to be *exo*- and *endo*-tetracyclo[5.3.1.$0^{2,6}$.$0^{3,9}$]undecan-4-ols, respectively. This elucidation does not contradict the exclusive formation of **16** due to the steric hindrance of H_8 in the reduction of **15** with lithium aluminum hydride.

No formation of *endo*-3-acetoxynoriceane (**13**)[16] in either acetolysis of *endo*- or *exo*-3-tosylate (**7** or **8**) may be due to large steric hindrance of the "bowsprit" hydrogen (*viz.* *endo*-H_{10}) in the boat conformation. The same steric hindrance is shown in the hydride reduction of 3-noriceanone giving exclusively *endo*-3-noriceanol (**9**).[16] The steric effect can be also responsible for the exclusive formation of **12**, as is seen in the hydride reduction of **15** (*vide supra*). More interesting is the difference in the ratio of the rearranged products (*viz.* **12** and **5**) to the unrearranged one (*viz.* **11**) between the two tosylates (**7** and **8**). The ratio is 1.8 for the *endo*-tosylate (**7**), while that is 9.1 for the *exo*-one (**8**). The stereoelectronic control can give rise to the large difference; the leaving group (*viz.* tosyloxyl group) in **8** is arranged in an almost perfect antiperiplanar position with reference to the migrating C_4–C_9 bond, where the rearrangement can

take place most easily. Furthermore, it should be also noted that almost twice as much the rearranged products as the unrearranged one are formed even in the acetolysis of the *endo*-tosylate (**7**), in which the orientation of the leaving group is not favorable for the rearrangement. Thus, 3-noricyl cation (**4**, R=H) is decisively a mutable entity into tetracyclo[5.3.1.$0^{2,6}$.$0^{3,9}$]undecane system; this implies that a stepwise carbocation mechanism is quite possible in the present silver(I) ion-catalyzed rearrangement of **1**.

An attempt was also made to trap the supposed carbocation intermediate (**4**, R=Ag) by a nucleophilic solvent. Treatment of **1** with silver(I) ion in methanol caused no rearrangement and **1** was recovered almost quantitatively.[18] Furthermore, in order to make it clear whether proton can induce the same rearrangement, **1** was treated with a catalytic amount of *p*-toluensulfonic acid in refluxing benzene. However, no substantial change was observed; this indicates that proton is far from effective for the rearrangement.

The following scheme can be delineated for a stepwise carbocation mechanism. The strain energy difference between **1** and **5** is estimated to be *ca.* 40 kcal/mol[19] sufficient for the rearrangement.[2,3] In addition, the recently proposed stabilizing interaction between silver and a carbocation center[4] appears to be more efficient in the rearranged carbocation (**17**) than in the unrearranged one (**4**, R=Ag). Judging from the fact that halonium ion and certain metal ions approach the central bond of the bicyclo[2.1.0]pentane system of **1** from the front side,[9] it is highly probable that silver(I) ion also behaves in a similar manner and, consequently, the silver takes the suitable orientation for the interaction with the carbocation center, as is shown in the scheme.

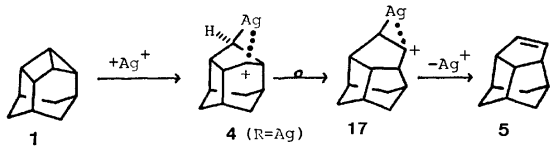

Scheme 4.

In conclusion, the present results have clearly demonstrated that both of ring strain and suitable geometry are equally important in silver(I) ion-catalyzed rearrangements of strained polycylic molecules.[3,4]

Experimental

All the temperatures were uncorrected. The melting points were measured in sealed capillaries. The IR spectra were obtained on a Shimadzu IR-27 spectrometer. The conventional mass spectra were taken by using a Hitachi RMS-4 mass spectrometer and the exact mass spectrum was obtained on a Hitachi RMU-8GN mass spectrometer. The PMR and ^{13}C-NMR (CMR) spectra were obtained on Varian EM-390 and CFT-20 spectrometers, TMS being chosen as the internal standard. The microanalyses were performed by Kyoto University Elemental Analysis Center. All the reactions were carried out under nitrogen unless otherwise noted.

*Silver(I) Ion-catalyzed Rearrangement of Pentacyclo[5.3.1.$0^{2,6}$.$0^{3,5}$.$0^{4,9}$]undecane (**1**) to Tetracyclo[5.3.1.$0^{2,6}$.$0^{3,9}$]undec-4-ene (**5**).* A solution of **1** (1.00 g; 6.88 mmol) in $CHCl_3$ (7 ml) was stirred in the presence of $AgBF_4$ (48 mg; 0.25 mmol) at room temperature for 18 h in the dark. After evaporation of the solvent, the residue was dissolved in hexane and insoluble materials were removed by filtration. The solvent was evaporated and the residue was chromatographed on silica gel. Elution by hexane gave **5** (0.86 g, 85%): mp 150—153 °C. MS *m/e* (rel intensity): 146 (M^+, 43), 92 (53), 80 (100), 79 (56), 68 (70). IR (CCl_4): 2930, 1470, 1450, 1340, 1305, 1080, 1025, 710 cm^{-1}. PMR δ (CCl_4): 5.68 (2H, t, J=1.5 Hz), 3.10 (1H, q, J=6.3 Hz), 2.60 (2H, br. s), 2.23 (1H, br. s), 2.00—1.20 (8H, complex m). CMR δ ($CDCl_3$): 128.0 (CH), 59.2 (CH), 55.8 (CH), 44.9 (CH_2), 35.9 (CH), 35.1 (CH), 31.2 (CH_2). Found: *m/e* 146.1095. Calcd for $C_{11}H_{14}$: M, 146.1095.

*Reduction of **5** to Tetracyclo[5.3.1.$0^{2,6}$.$0^{3,9}$]undecane (**6**).* A solution of **5** (148 mg; 1.01 mmol) and a small amount of PtO_2 in ethyl acetate (7 ml) was vigorously stirred under hydrogen. After one equivalent of hydrogen was absorbed, the catalyst was removed by filtration and the solvent was evaporated. The residue was chromatographed on silica gel. Elution by hexane gave **6** (118 mg, 79%), which was identical with the authentic specimen.[12]

endo-*Tetracyclo[5.3.1.$0^{2,6}$.$0^{4,9}$]undec-3-yl* p-*Toluenesulfonate (**7**).* To a solution of *endo*-tetracyclo[5.3.1.$0^{2,6}$.$0^{4,9}$]-undecan-3-ol (**10**)[16] (429 mg; 2.62 mmol) in pyridine (10 ml) was added *p*-toluenesulfonyl chloride (1003 mg; 5.26 mmol) at 0 °C. The mixture was allowed to stand overnight at room temperature and then poured onto ice–water. The organic materials were extracted with ether and washed with cold 5% HCl aq and brine, and dried (Na_2SO_4). After filtration, the solvent was evaporated to give a solid (816 mg). Recrystallization from hexane afforded **7** (745 mg, 89%): mp 89—92 °C. IR (KBr): 2930, 1350, 1180, 1165, 1095, 1020, 1015, 975, 960, 895, 850, 840, 820, 670 cm^{-1}. PMR δ (CCl_4): 8.73 (2H, d, J=8.4 Hz), 7.27 (2H, d, J=8.4 Hz), 4.32 (1H, s), 2.43 (3H, s), 2.53—0.77 (14H, br. complex m). CMR δ ($CDCl_3$): 144.5 (C), 134.5 (C), 129.8 (CH), 127.7 (CH), 85.0 (CH), 42.9 (CH), 41.3 (CH), 41.0 (CH_2), 38.3 (CH), 36.7 (CH), 31.2 (CH_2), 30.3 (CH), 23.2 (CH), 21.6 (CH_3). Found: C, 67.61; H, 7.11%. Calcd for $C_{18}H_{22}O_3S$: C, 67.89; H, 6.96%.

exo-*Tetracyclo[5.3.1.$0^{2,6}$.$0^{4,9}$]undec-3-yl* p-*Toluenesulfonate (**8**).* The reaction of *exo*-tetracyclo[5.3.1.$0^{2,6}$.$0^{4,9}$]undecan-3-ol (**9**) (62 mg; 0.38 mmol) with *p*-toluenesulfonyl chloride (145 mg; 0.76 mmol) in a similar manner to the above gave **8** (88 mg, 74%) after recrystallization from hexane. **8**: mp 62—64 °C. IR (KBr): 2930, 1600, 1355, 1180, 950, 925, 860, 845, 820, 670 cm^{-1}. PMR δ(CCl_4): 7.71 (2H, d, J=8.4 Hz), 7.28 (2H, d, J=8.4 Hz), 4.90 (1H, s), 2.47 (3H, s), 2.60—0.80 (13H, br. complex m). CMR δ($CDCl_3$): 144.6 (C), 135.1 (C), 130.0 (CH), 127.6 (CH), 85.7 (CH), 48.5 (CH), 41.3 (CH+CH_2), 38.8 (CH), 38.7 (CH), 37.6 (CH), 31.7 (CH), 30.9 (CH_2), 29.7 (CH_2), 21.6 (CH_3). Found: C, 67.63; H, 6.59%. Calcd for $C_{18}H_{22}O_3S$: C, 67.89; H, 6.96%.

*Acetolysis of **7**.* A solution of **7** (842 mg; 2.64 mmol) and sodium acetate (328 mg; 4.00 mmol) in glacial acetic acid (26 ml) was refluxed for 4 h. The reaction mixture was poured onto water and extracted with CH_2Cl_2. The organic layer was washed with brine, aqueous $NaHCO_3$ and brine, and dried (Na_2SO_4). After filtration, the solvent was evaporated to give a colorless oil (519 mg) which was chromatographed on silica gel. Elution by hexane gave **5** (82 mg, 21%) and the subsequent elution by hexane and CH_2Cl_2 (4:1) afforded a mixture of **11** and **12** (401 mg, 74%) in a ratio of 23:27 [GLC (PEG 20 M, 180 °C)]. The calculated ratio of **11**:**12**:**5** was 36:42:22. Each of the

acetates was isolated by preparative GLC. *exo*-3-Acetoxytetracyclo[5.3.1.$0^{2,6}$.$0^{4,9}$]undecane (**11**): bp 85—90 °C (bath temp)/2000 Pa. MS *m/e* (rel intensity): 206 (M^+, 4), 164 (11), 146 (100). IR (neat): 2930, 1735, 1370, 1245, 1055, 1025 cm^{-1}. PMR $\delta(CCl_4)$: 5.07 (1H, s, $W_{1/2}$=3.0 Hz), 1.95 (3H, s), 2.60—0.90 (14H, br. complex m). CMR $\delta(CDCl_3)$: 170.7 (C), 76.8 (CH), 47.9 (CH), 41.5 (CH_2) 41.3 (CH), 38.4 (CH), 37.9 (CH), 37.7 (CH), 31.5 (CH), 31.0 (CH_2), 30.1 (CH_2), 23.2 (CH_2), 21.4 (CH_3). Found: C, 75.50; H, 8.72%. Calcd for $C_{13}H_{18}O_2$: C, 75.69; H, 8.80%. *exo*-4-Acetoxytetracyclo[5.3.1.$0^{2,6}$.$0^{3,9}$]undecane (**12**): bp 90—97 °C (bath temp)/3066 Pa. IR (neat): 2930, 1740, 1360, 1250, 1020 cm^{-1}. PMR $\delta(CCl_4)$: 5.05 (1H, dd, J=7.5 and 3.0 Hz), 1.93 (3H, s), 2.87—1.37 (14H, br. complex m). CMR $\delta(CDCl_3)$: 170.8 (C), 78.2 (CH), 56.9 (CH), 51.2 (CH), 49.0 (CH), 44.0 (CH_2), 39.9 (CH), 83.4 (CH), 36.9 (CH_2), 30.6 (CH_2), 21.4 (CH_3). Found: C, 75.55; H, 9.06%. Calcd for $C_{13}H_{18}O_2$: H, 75.69; H, 8.80%.

Acetolysis of ***8***. A solution of **8** (71 mg; 0.22 mmol) and sodium acetate (28 mg: 0.34 mmol) in glacial acetic acid (2.5 ml) was refluxed for 4 h. Similar work-up and subsequent column chromatography to the above gave **5** (8 mg, 24%) and a mixture of **11** and **12** (14 mg, 30%) in a ratio of 3:17 [GLC (PEG 20 M, 180 °C)]. The calculated ratio of **11**:**12**:**5** was 9:47:44.

exo-*Tetracyclo*[*5.3.1.*$0^{2,6}$*0.*^{4,9}]*undecan-3-ol* (***10***). To a suspension of $LiAlH_4$ (59 mg; 1.55 mmol) in dry ether (5 ml) was added dropwise a solution of **11** (110 mg; 0.53 mmol) in dry ether (2 ml). The mixture was stirred under reflux for 1 h and quenched with saturated aqueous Na_2SO_4. The organic layer was washed with brine and dried (Na_2SO_4). After filtration, the solvent was evaporated and the residue was chromatographed on silica gel. Elution by a mixture of hexane and CH_2Cl_2 (4:1) gave **10** (78 mg, 89%): mp 243—244 °C. MS *m/e* (rel intensity): 164 (M^+, 80), 146 (49), 135 (57), 92 (45), 91 (46), 79 (89), 68 (100). IR (KBr): 3260, 2925, 1075 cm^{-1}. PMR $\delta(CDCl_3)$: 4.30 (1H, s, $W_{1/2}$=3.0 Hz), 2.70—0.80 (15H, br. complex m). CMR $\delta(CDCl_3)$: 72.6 (CH), 50.5 (CH), 41.7 (CH_2), 41.0 (CH), 40.0 (CH), 38.2 (CH), 37.6 (CH), 31.5 (CH), 31.3 (CH_2), 30.0 (CH_2), 22.5 (CH_2). Found: C, 80.30; H, 10.09%. Calcd for $C_{11}H_{16}O$: C, 80.44; H, 9.83%.

exo-*Tetracyclo*[*5.3.1.*$0^{2,6}$.$0^{3,9}$]*undecan-4-ol* (***14***). The reduction of **12** (34 mg; 0.17 mmol) with $LiAlH_4$ (41 mg; 1.08 mmol) in a similar manner to the above gave **14** (24 mg, 99%): mp 128—132 °C. MS *m/e* (rel intensity): 164 (M^+, 65), 146 (57), 80 (95), 79 (100), 68 (91). IR (KBr): 3300, 2925, 1025 cm^{-1}. PMR $\delta(CDCl_3)$: 4.33 (1H, dd, J=6.9 and 2.7 Hz), 2.78 (1H, q, J=6.0 Hz), 2.63—1.30 (14H, br. complex m). CMR $\delta(CDCl_3)$: 75.2 (CH), 60.4 (CH), 51.5 (CH), 48.4 (CH), 43.1 (CH_2), 42.9 (CH_2), 40.0 (CH), 39.7 (CH_2), 38.5 (CH), 30.6 (CH_2). Found: C, 80.31; H, 10.05%. Calcd for $C_{11}H_{16}O$: C, 80.44; H, 9.83%.

Tetracyclo[*5.3.1.*$0^{2,6}$.$0^{3,9}$]*undecan-4-one* (***15***). To a solution of pyridine (0.7 ml) in CH_2Cl_2 (3.5 ml) was added portionwise CrO_3 (169 mg; 1.69 mmol) under stirring. After 10 min, a solution of **14** (27 mg; 0.16 mmol) in CH_2Cl_2 (2 ml) was added to the above mixture and stirred for 1.5 h. The reaction mixture was washed with 5% aqueous NaOH, 5% aqueous HCl and brine, and dried (Na_2SO_4). After filtration, the solvent was evaporated and the residue was chromatographed on silica gel. Elution by a mixture of hexane and CH_2Cl_2 (9:1) gave **15** (24 mg, 90%): mp 180—182 °C. MS *m/e* (rel intensity): 162 (M^+, 100), 120 (33), 92 (30), 79 (62). IR (KBr): 2925, 1750, 1180 cm^{-1}. PMR $\delta(CDCl_3)$: 3.00—1.10 (14H, br. complex m). CMR δ ($CDCl_3$): 221.0 (C), 60.4 (CH), 49.2 (CH), 46.5 (CH), 44.0 (CH_2), 43.1 (CH_2), 42.2 (CH_2), 41.5 (CH), 39.8 (CH), 30.1 (CH_2). Found: C, 81.39; H, 8.83%. Calcd for $C_{11}H_{14}O$: C, 81.44; H, 8.70%.

Wolff-Kishner Reduction of ***15***. A solution of **15** (12 mg; 0.07 mmol), KOH (68 mg), and 100% $NH_2NH_2 \cdot H_2O$ (0.07 ml) in diethylene glycol (0.5 ml) was stirred at 110 °C for 30 min and subsequently at 180 °C for 3 h. The materials on the condenser was dissolved in pentane and washed with brine, and dried (Na_2SO_4). After filtration, the solvent was evaporated to give **6** (5 mg, 44%), which was shown to be identical with the authentic specimen.[12]

endo-*Tetracyclo*[*5.3.1.*$0^{2,6}$.$0^{3,9}$]*undecan-4-ol* (***16***). The reduction of **15** (23 mg; 0.14 mmol) with $LiAlH_4$ (26 mg; 0.68 mmol) in a similar manner to the above gave **16** (22 mg, 94%): mp 178—180 °C. MS *m/e* (rel intensity): 164 (M^+, 5), 146 (57), 80 (90), 79 (67), 68 (100). IR (KBr): 3300, 2925, 1100, 1050, 1015 cm^{-1}. PMR $\delta(CDCl_3)$: 4.58 (1H, quintet, J=10.5, 6.3, and 4.8 Hz), 2.75—1.20 (br. complex m). CMR $\delta(CDCl_3)$: 76.0 (CH), 55.9 (CH), 50.1 (CH), 49.0 (CH), 43.6 (CH_2), 41.1 (CH), 38.8 (CH), 37.3 (CH), 36.6 (CH_2), 30.8 (CH_2). Found: C, 80.61; H, 10.08%. Calcd for $C_{11}H_{16}O$: C, 80.44; H, 9.83%. The oxidation of **16** (13 mg; 0.08 mmol) with CrO_3 (77 mg; 0.77 mmol)–pyridine (0.38 ml)–CH_2Cl_2 (2 ml) in a similar manner to the above reproduced **15** (12 mg, 93%).

We thank Professor P. von R. Schleyer for a copy of the program Strain and Dr. R. Konaka of Shionogi Phamaceutical Co. Ltd. for obtaining the exact mass spectrum of **5**. Calculations were performed at Hokkaido University Computing Center. This work was partially supported by a Grant-in-Aid for Scientific Research from the Ministry of Education, Japan (No. 434025).

References

1) In cases where there is no ambiguity, we have used trivial nomenclatures for simplicity. The IUPAC names are described in Experimental Section.

2) For recent review; K. C. Bishop III, *Chem. Rev.*, **76**, 461 (1976). See also A. Greenberg and J. F. Liebman, "Strained Organic Molecules," Academic Press, New York (1978), p. 245.

3) L. A. Paquette, *Acc. Chem. Res.*, **4**, 280 (1971).

4) P. E. Eaton, L. Cassar, R. A. Hadson, and D. R. Hwang, *J. Org. Chem.*, **41**, 1445 (1976) and references cited therein.

5) L. A. Paquette and R. C. West, unpublished observation, quoted in Ref. 3.

6) Compound **2** undergoes rapid isomerization to cyclopentene upon treatment with a rhodium complex: P. G. Gassman, T. J. Atkins, and J. T. Lumb, *J. Am. Chem. Soc.*, **94**, 7757 (1972).

7) 1-Phenylbicyclo[2.1.0]pentane was reported to be isomerized to cyclopentene derivatives when reacted with Zn(II), Rh(I), and Ag(I) salts: M. A. Mckinney and S. K. Chou, *Tetrahedron Lett.*, **1974**, 1145.

8) T. Katsushima, R. Yamaguchi, and M. Kawanisi, *J. Chem. Soc., Chem. Commun.*, **1975**, 692.

9) See two succeeding papers.

10) R. M. Moriarty, "Topics in Stereochemistry," ed by E. L. Eliel and N. L. Allinger, Wiley, New York (1974), Vol. VIII, p. 347.

11) For preliminary report: T. Katsushima, R. Yamaguchi, M. Kawanisi, and E. Ōsawa, *J. Chem. Soc., Chem. Commun.*,

1976, 39.
12) S. A. Godleski, P. von R. Schleyer, and E. Ōsawa, *J. Chem. Soc., Chem. Commun.*, **1976**, 38; S. A. Godleski, P. von R. Schleyer, E. Ōsawa, Y. Inamoto, and Y. Fujikura, *J. Org. Chem.*, **41**, 2596 (1976).
13) E. M. Engler, J. D. Andose, and P. von R. Schleyer, *J. Am. Chem. Soc.*, **95**, 8005 (1973).
14) The Allinger 1971 force-field [N. L. Allinger, M. T. Tribble, M. A. Miller, and D. H. Wertz, *J. Am. Chem. Soc.*, **93**, 1673 (1971)] gave essentially the same conclusions.
15) R. B. Woodward and R. Hoffmann, "The Conservation of Orbital Symmetry," Verlag Chemie, Weinheim/Bergstr., Germany, 1970.
16) See the succeeding paper.
17) Although **16** has been mentioned in literature,[12] it has never been isolated in a pure form.
18) It was found that a trace amount of moisture significantly retarded the rearrangement in chloroform.
19) Since the present force-filed calculations overestimate the strain energy in **2** by 35 kcal/mol (Table 1), the corrected strain energy in **1** can be *ca.* 72 kcal/mol. The strain energy in **5** is estimated to be *ca.* 30 kcal/mol by adding the calculated strain energy in **6** (25.4 kcal/mol)[12] to 4.6 kcal/mol for the introduction of the double bond [*cf.* 22.8 kcal/mol (norbornene) −18.2 kcal/mol (norbornane)].

Synthesis of 3-Mono- and 3,5-Difunctionalized Noriceanes (Tetracyclo-[5.3.1.$0^{2,6}$.$0^{4,9}$]undecanes) *via* Oxymetallation of 3,5-Dehydronoriceane (Pentacyclo[5.3.1.$0^{2,6}$.$0^{3,5}$.$0^{4,9}$]undecane).[1] Oxidation of Bicyclo-[2.1.0]pentane System by Mercury(II), Thallium(III), and Lead(IV) Acetates.

Takeo KATSUSHIMA, Ryohei YAMAGUCHI, Satoshi IEMURA, and Mituyosi KAWANISI*

Department of Industrial Chemistry, Faculty of Engineering, Kyoto University, Yoshida, Sakyo-ku, Kyoto 606

(Received April 30, 1980)

Oxymercuration of 3,5-dehydronoriceane (**1**) followed by sodium borohydride reduction gives exclusively *endo*-3-noriceanol in 80% yield. The *trans*-1,3-addition organomercury intermediate is isolated as *endo*-3-acetoxy-*exo*-5-(chloromercurio)noriceane. Oxidation of **1** with thallium(III) acetate gives three diacetates, *exo,exo*- and *endo,exo*-3,5-diacetoxynoriceanes [(**9**) and (**10**)] and *endo,exo*-4,5-diacetoxytetracyclo[5.3.1.$0^{2,6}$.$0^{3,9}$]undecane (**11**) in a ratio of 6:61:27 in 68% combined yield. The analogous oxidation of **1** with lead(IV) acetate gives **9**, **10**, and **11** in a ratio of 50:25:25 in 80% combined yield. On the basis of the stereochemistry of the products as well as the products distribution, we propose that 1,3-bridged metal ion intervenes and plays an important role in the oxymetallation reaction of bicyclo[2.1.0]pentane system.

Electrophilic or radical-type cleavage of cyclopropane ring in a cage molecule has proved to become one of the powerful methods of functionalizing a cage compound.[2] Oxidative cleavages of cyclopropane rings by mercury(II), thallium(III), and lead(IV) salts give mono- and difunctionalized compounds *via* oxymetallations. We have recently reported the synthesis of 3,5-dehydronoriceane (**1**),[3] which incorporates bicyclo-[2.1.0]pentane moiety in its cage structure. Since oxidations of highly strained bicyclo[2.1.0]pentane with the metal salts have been reported to rupture the central bond exclusively,[4] we anticipate that **1** can give hitherto unknown 3-mono- and 3,5-difunctionalized noriceanes when allowed to react with the metal salts. In addition to this synthetic possibility, the bicyclo-[2.1.0]pentane system fixed in the cage structure is expected to provide some mechanistic insight which is concerned with the stereochemistry of the initial attack of the metal ion and remains to be explored.[5]

Results

*Oxidation of **1** with Mercury(II) Acetate.* When **1** was treated with mercuric acetate in aqueous THF and subsequently reduced with sodium borohydride, *endo*-3-noriceanol (**2**) was obtained as a sole product in 80% yield. The structure of **2** was determined as follows. Oxidation of **2** with CrO_3–pyridine complex gave a keto compound, 3-noriceanone (**3**), which was reduced to afford noriceane (**4**)[3] by Wolff-Kishner (W-K) method, confirming a parent skeleton of **2**. Whereas reduction of **3** with lithium aluminum hydride reproduced **2**, a treatment of **3** with lithium in liquid ammonia gave **2** and its stereoisomer, *exo*-3-noriceanol (**5**) in 85% combined yield (**2**:**5**=1:2 by ^{1}H-NMR (PMR) analysis). Although the separation of **5** from **2** was unsuccessful, the regeneration of **3** in the oxidation of the mixture indicated that **5** and **2** were stereoisomeric with each other in reference to the 3-position.[6] An inspection of molecular model (Dreiding) suggests us that *exo*-H on the 3-position should couple more with the adjacent protons in PMR spectroscopy than the *endo*-one does. Since the PMR spectra of **2** and **5** show a broad singlet with half-width of 8.0 Hz at 3.90 ppm and a singlet with half-width of 3.4 Hz at 4.30 ppm, respectively, we conclude that **2** is *endo*-3-noriceanol and that **5** is the *exo*-isomer.

In addition to the above elucidation, we inspected the PMR spectra of **2** and 3-noriceanol-5-*d* (**6**), which was prepared by the oxymercuration of **1** followed by the reduction with sodium borodeuteride, by using NMR shift reagent [Eu(dpm)$_3$]. As is shown in Fig. 1, the results of PMR shift experiment for **2** are compatible with the assigned structure of **2**. Figure 2 shows partial PMR spectra of **2** and **6** in the presence of Eu(dpm)$_3$. The signal shown as a doublet of doublet (J=5.5 and 12.0 Hz) at *ca.* 6.6 ppm (*viz.* H_{5X}) in Fig. 2a disappears in Fig. 2b and the signal shown as a doublet (J=12.0 Hz) at *ca.* 5.9 ppm (*viz.* H_{5N}) in Fig. 2a appears as a singlet in Fig. 2b. Since Fig. 1 indicates that the slope for H_{5X} is slightly steeper than that for H_{5N}, H_{5X}, and H_{5N} must be *exo*- and *endo*-protons, respectively. These results imply that deuterium is exclusively located on the *exo*-5-position and, therefore, **6** is determined to be *endo*-3-hydroxy-*exo*-5-deuteronoriceane.

In order to gain further insight about the stereochemistry of the oxymercuration of the bicyclo[2.1.0]-

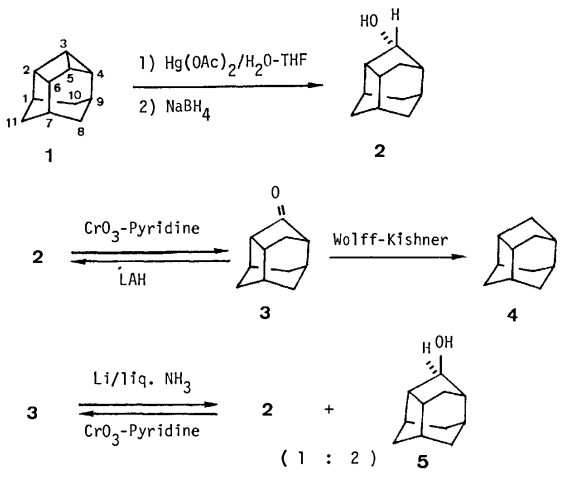

Scheme 1.

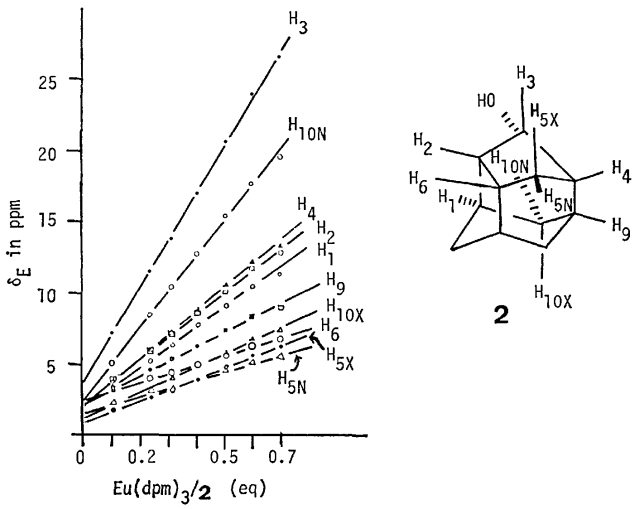

Fig. 1. Variation of chemical shift, δ_E, with molar ratio $Eu(dpm)_3$/**2**.

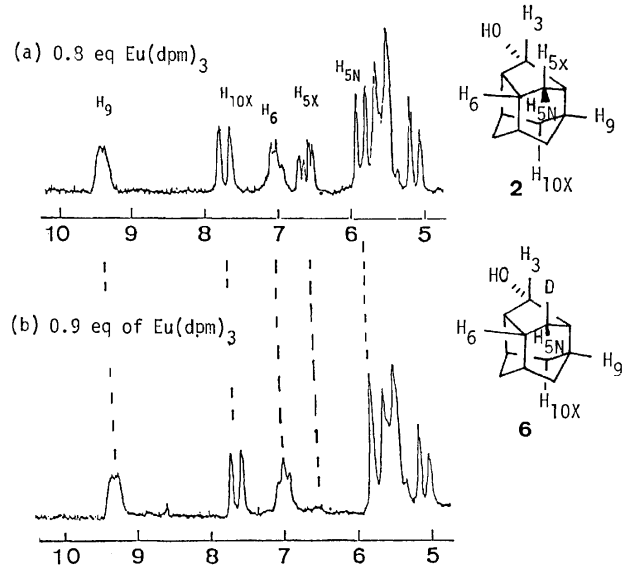

Fig. 2. Partial PMR spectra of **2** and **6** in the presence of $Eu(dpm)_3$; a for **2**, b for **6**.

pentane system, a organomercury intermediate was intentionally isolated and examined. A reaction of **1** with mercury(II) acetate in glacial acetic acid followed by an addition of sodium chloride gave an organomercury compound (**7**) in 95% yield. The compound, **7**, was reduced with sodium borohydride to give *endo*-3-acetoxynoriceane (**8**), which was also obtained by acetylation of the alcohol, **2**. A similar PMR shift experiments with **7** and **8** to the above led to the conclusion that **7** is *endo*-3-acetoxy-*exo*-5-(chloromercurio)noriceane (Scheme 2); this implies that the oxymercuration must proceed in a *trans*-fashion.

Oxidations of **1** *with Thallium(III) and Lead(IV) Acetates.* When **1** was oxidized with thallium(III) acetate in glacial acetic acid at room temperature for 4 h, three diacetates, *exo,exo*-3,5- and *endo,exo*-3,5-diacetoxynoriceanes (**9** and **10**) and *endo,exo*-4,5-diacetoxytetracyclo-[5.3.1.$0^{2,6}$.$0^{4,9}$]undecane (**11**), were obtained along with a small amount of an unidentified product (**12**) (**9**:**10**:

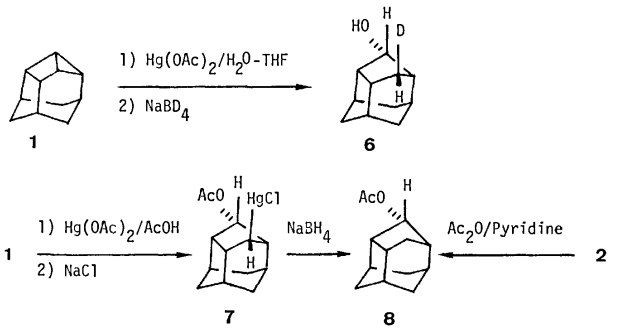

Scheme 2.

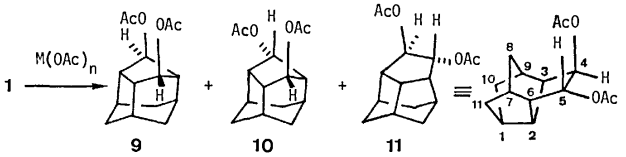

$Tl(OAc)_3$;	6	:	61	: 27
$Pb(OAc)_4$;	50	:	25	: 25

Scheme 3.

11:**12**=6:61:27:6, estimated from the area ratio in GLC analysis) in 68% combined yield. A similar oxidation of **1** with lead(IV) acetate at room temperature for 24 h gave the same three products, **9**, **10**, and **11** (**9**:**10**:**11**=50:25:25 by GLC analysis) in 80% combined yield.

The structures of **9** and **10** were determined as follows. The diacetates, **9** and **10**, were separated by preparative GLC and reduced to the corresponding diols (**13** and **14**) with lithium aluminum hydride, respectively. Oxidations of **13** and **14** with CrO_3–pyridine complex gave one kind of diketone, 3,5-noriceanedione (**16**), which afforded noriceane (**4**) on base-catalyzed reduction of the semicarbazone of **16**. Accordingly, it is evident that **9** and **10** are stereoisomeric 3,5-diacetoxynoriceanes. Out of three possible isomers, *endo,endo*-3,5- and *exo,exo*-3,5-isomers have a plane of symmetry, whereas *endo,exo*-one does not. Since ^{13}C-NMR (CMR) and PMR spectra of **10** showed a lack of the symmetry, **10** was determined to be *endo, exo*-3,5-diacetoxynoriceane. On the other hand, CMR spectrum of **9** indicated the presence of symmetry and its PMR spectrum showed a singlet with a half-width of 2.7 Hz at 5.17 ppm, indicating the *exo*-configuration of the substituents at 3- and 5-positions (*vide supra*). Thus, **9** was determined to be *exo,exo*-3,5-diacetoxynoriceane.

The structure of **11** was determined by the following chemical transformations. Reduction of **11** followed by oxidation with Fetizon's reagent[7] gave *exo*-5-hydroxytetracyclo[5.3.1.$0^{2,6}$.$0^{3,9}$]undecan-4-one (**17**).[8] Acetylation of **17** with acetic anhydride in pyridine gave *exo*-5-acetoxytetracyclo[5.3.1.$0^{2,6}$.$0^{3,9}$]undecan-4-one (**18**). Reductive cleavage of **18** with lithium in liquid ammonia gave a mixture of stereoisomeric tetracyclo[5.3.1.$0^{2,6}$.$0^{3,9}$]undecan-4-ols (**19a** and **19b**).[6] Subsequent oxidation of the mixture gave tetracyclo-[5.3.1.$0^{2,6}$.$0^{3,9}$]undecan-4-one (**20**).[6] As the PMR and

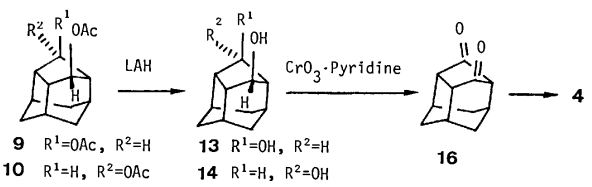

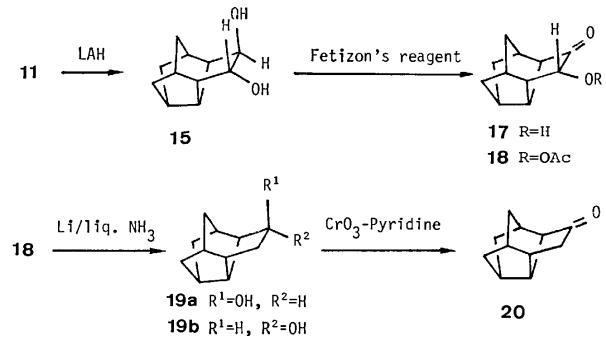

Scheme 4.

CMR spectra of **11** showed a lack of a plane of symmetry, **11** was determined to be *endo,exo*-4,5-diacetoxytetracyclo[5.3.1.$0^{2,6}$.$0^{3,9}$]undecane.

Discussion

The structures of **6** as well as **7** allow us to delineate the following scheme as a possible reaction pathway (Scheme 5). An initial electrophilic attack on the bicyclo[2.1.0]pentane system by mercury(II) ion must take place from the front side of the central bond with retention of configuration to produce the 1,3-bridged acetoxymercurium ion (**21**).[9] This is subsequently captured by nucleophilic solvent with complete inversion of configuration. By taking account of the fact that solvolyses of 3-noricyl tosylates give nothing but *exo*-3-noricyl acetate and a considerable amount of the rearranged products,[6] we can safely conclude that the 1,3-bridged ion (**21**) intervenes significantly in the oxymercuration reaction of bicyclo-[2.1.0]pentane system. Although Levina *et al.* reported that the oxymercuration of bicyclo[2.1.0]pentane itself gave 3-hydroxycyclopentylmercury(II) acetate,[4b] the stereochemistry of the product was not studied. We believe that the present result is the first example which clarifies a stereochemical course and provides a strong evidence for an intervention of an 1,3-bridged mercurium ion in oxymercuration reaction of bicyclo-[2.1.0]pentane system. In addition, it is noteworthy that reduction of the organomercury compound with sodium borohydride proceeds with retention of configuration.

In the cases of oxidations with thallium(III) and lead(IV) acetates, the reaction pathways are more speculative than the above because an isolation of the corresponding organometallic intermediates has been impossible and, accordingly, their decomposition modes are unknown. Judging from the fact that the reactions lack the stereoselectivity and that some amount of the rearranged product, **11**, is obtained, it is highly

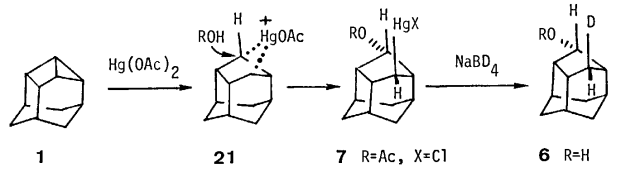

Scheme 5.

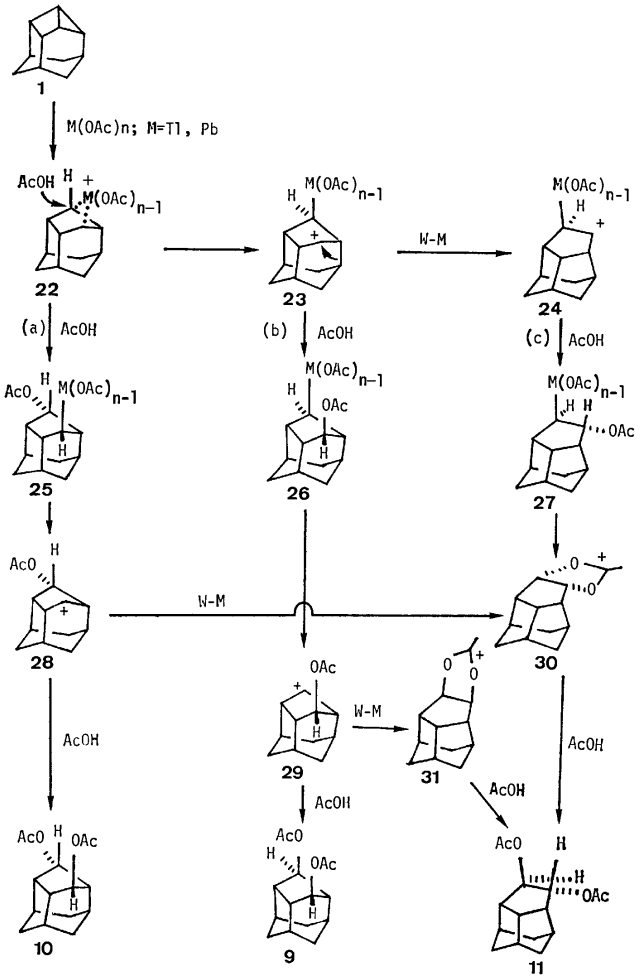

Scheme 6.

probable that a free carbocation character is involved in the reactions. The following rather simple scheme (Scheme 6) may reasonably explain the results. The initial attack on the bicyclo[2.1.0]pentane system by the metal ion would take place from the front-side to produce the 1,3-bridged metal ion (**22**) analogous to **21** in the case of the oxymercuration. Nucleophilic capture of **22** with the solvent gives an *endo*-acetoxyorganometallic intermediate (**25**), which, on decomposition, could produce a "free" carbocation intermediate (**28**). The *endo,exo*-diacetates (**10**) is the expected product in nucleophilic capture of **28** with the solvent, because, as described before, 3-noricyl cation formed in the solvolysis is attacked by nucleophile exclusively from the *exo*-side[6] (path a in Scheme 6).

When the 1,3-bridged metal ion (**22**) is so unstable as to convert into a "free" carbocation (**23**), an *exo*-acetoxyorganometallic intermediate (**26**) may be formed by the same reason as described above. Subsequent

decomposition and nucleophilic capture could afford the *exo,exo*-diacetate (**9**) (path b in Scheme 6). The "free" carbocation (**23**) is also possibly subjected to Wagner-Meerwein rearrangement into tetracyclo[5.3.1.$0^{2,6}$.$0^{3,9}$]undecane system (**24**), which could give the *trans*-diacetate (**11**) *via* 1,2-acetoxyl-participation (path c). The diacetate (**11**) could be also formed from **28** as well as **29** through the pathways shown in the Scheme.

Thus, it can be safely said that the amount of the *endo,exo*-diacetate (**10**) depends on the stability of the 1,3-bridged metal ion (**22**). The fact that the yield of **10** is higher with thallium(III) acetate than with lead(IV) acetate implies that **22** (M=Tl) is more stable than **22** (M=Pb). In addition, it is evident that **22** (M=Hg, namely **21**) is much more stable than the both (**22**, M=Tl and Pb). This order of stability of the 1,3-bridged metal ions (Hg>Tl>Pb) is consistent with the order of the stability of C–M bonds (Hg>Tl>Pb).[10]

In conclusion, it has been found that oxymetallations of 3,5-dehydronoriceane (**1**) with mercury(II), thallium(III), and lead(IV) acetates give 3-mono- and 3,5-difunctionalized noriceanes in good yields along with a small amount of *trans*-4,5-difunctionalized tetracyclo[5.3.1.$0^{2,6}$.$0^{3,9}$]undecane. The present results also provide the first evidence for an intervention of an 1,3-bridged metal ion in oxymetallation reaction of bicyclo[2.1.0]pentane system.

Experimental

All the temperatures were uncorrected. The melting points were measured in sealed capillaries. The IR spectra were obtained on a Shimadzu IR-27 spectrometer. The mass spectra were taken by using a Hitachi RMS-4 mass spectrometer. The PMR and CMR spectra were obtained on Varian EM-390 and CFT-20 spectrometers, TMS being chosen as the internal standard. The microanalyses were performed by Kyoto University Elemental Analysis Center.

endo-*Tetracyclo*[*5.3.1.*$0^{2,6}$.$0^{4,9}$]*undecan-3-ol* (*2*). To a solution of $Hg(OAc)_2$ (478 mg; 1.5 mmol) in THF (3 ml) and water (3 ml) was added pentacyclo[5.3.1.$0^{2,6}$.$0^{3,5}$.$0^{4,9}$]-undecane (**1**) (219 mg; 1.5 mmol) and the mixture was stirred for 1 h at room temperature. Then, 3 M aqueous NaOH (3 ml) and subsequently 3 ml of a solution of 0.5 M $NaBH_4$ in 3 M aqueous NaOH were added and the mixture was stirred for additional 1 h. After the precipitated mercury was removed by filtration, organic materials were extracted with CH_2Cl_2, washed with brine, and dried (Na_2SO_4). After filtration, the solvent was evaporated and the residue was chromatographed on silica gel. Elution by hexane and ether (1:1) gave **2** (198 mg, 80%): mp 270 °C. MS *m/e* (rel intensity): 164 (M^+, 70), 146 (45), 135 (51), 92 (50), 91 (46), 80 (99), 79 (95), 68 (100). IR (KBr): 3200, 2930, 1465, 1300, 1290, 1160, 1090, 1055 cm^{-1}. PMR δ ($CDCl_3$): 3.90 (1H, br. s, $W_{1/2}$=8.0 Hz), 2.67—0.80 (15H, br, complex m). CMR δ ($CDCl_3$): 76.9 (CH), 44.8 (CH), 42.1 (CH), 41.4 (CH_2), 38.5 (CH), 38.4 (CH), 36.7 (CH), 31.9 (CH_2), 31.4 (CH_2), 30.7 (CH), 24.4 (CH_2). Found: C, 80.51; H, 9.89%. Calcd for $C_{11}H_{16}O$: C, 80.44; H, 9.83%.

Tetracyclo[*5.3.1.*$0^{2,6}$.$0^{4,9}$]*undecan-3-one* (*3*). To a solution of pyridine (5 ml) in CH_2Cl_2 (25 ml) was added gradually CrO_3 (730 mg; 7.3 mmol) and then a solution of **2** (195 mg; 1.2 mmol) in CH_2Cl_2 (20 ml). The reaction mixture was stirred for 1 h at room temperature and washed with 5% aqueous NaOH, 5% aqueous HCl, and brine, and dried (Na_2SO_4). After filtration, the solvent was evaporated and the residue was chromatographed on silica gel. Elution by hexane and ether (3:1) afforded **3** (183 mg, 95%): mp 259—261 °C. MS *m/e* (rel intensity): 162 (M^+, 98), 134 (92), 92 (99), 79 (100). IR (Nujol): 2925, 1750, 1460, 1370 cm^{-1}. PMR δ ($CDCl_3$): 2.95—1.10 (14H, br. complex m). CMR δ ($CDCl_3$): 221.7 (C=O), 51.5 (CH), 45.7 (CH), 43.5 (CH), 41.8 (CH_2), 41.4 (CH), 38.6 (CH), 34.0 (CH), 32.3 (CH_2), 30.2 (CH_2), 21.6 (CH_2). Found: C, 81.31; H, 8.69%. Calcd for $C_{11}H_{14}O$: C, 81.44; H, 8.70%.

Wolff-Kishner Reduction of ***3*** *to Tetracyclo*[*5.3.1.*$0^{2,6}$.$0^{4,9}$]-*undecane* (*4*). A solution of **3** (120 mg; 0.74 mmol), KOH (600 mg; 10.7 mmol), 100% $NH_2NH_2 \cdot H_2O$ (470 mg; 9.4 mmol) in diethylene glycol (3 ml) was stirred at 110 °C for 30 min and then at 180 °C for 3 h. Sublimate on the condenser was dissolved in hexane and washed with brine, and dried (Na_2SO_4). After filtration, the solvent was evaporated to give almost pure **4** (96 mg, 88%), which was identical with the authentic specimen[3] in all respects (GLC retention time, mass, PMR, and CMR spectra).

Reduction of ***3***. (*a*): To a suspension of $LiAlH_4$ (146 mg; 3.8 mmol) in dry ether (5 ml) was added dropwise a solution of **3** (125 mg; 0.77 mmol) in dry ether (5 ml). The reaction mixture was stirred at room temperature for 30 min and then quenched with sat aqueous Na_2SO_4. The organic layer was separated, washed with brine, and dried (Na_2SO_4). After filtration, the solvent was evaporated to give **2** (118 mg, 97%) as a sole product (PMR analysis). (*b*): A solution of **3** (230 mg; 1.4 mmol) in dry ether (10 ml) was added to dry liq ammonia (50 ml) at −78 °C. To this mixture were added NH_4Cl (6.15 g; 115 mmol) and then Li (559 mg; 80 mmol) in small pieces over 30 min. The reaction mixture was refluxed until the blue color disappeared. The ammonia was evaporated and water (50 ml) was added. The aqueous solution was acidified with 5% aqueous HCl and extracted with ether. The ethereal solution was washed with sat aqueous $NaHCO_3$ and brine, and dried (Na_2SO_4). After filtration, the solvent was evaporated and the residue was chromatographed on silica gel. Elution by hexane and ether (1:1) gave a mixture of **2** and *exo*-tetracyclo[5.3.1.$0^{2,6}$.$0^{4,9}$]undecan-3-ol (**5**) (197 mg, 85%). Although **5** could not be separated from **2** by either column chromatography or GLC, a comparison of the PMR spectrum of the mixture with that of pure **5**[6] indicated that a ratio of **2** to **5** was 1:2. Furthermore, the mixture (39 mg; 0.24 mmol) was oxidized with CrO_3 (204 mg; 2.0 mmol) and pyridine (0.8 ml) in CH_2Cl_2 (5 ml) reproduced **3** (32 mg, 83%).

endo-*3-Hydroxy*-exo-*5-deuterotetracyclo*[*5.3.1.*$0^{2,6}$.$0^{4,9}$]*undecane* (*6*). A similar oxymercuration reaction of **1** (292 mg; 2.0 mmol) to the above followed by reduction with $NaBD_4$ gave **6** (200 mg, 61%). The extent of monodeuteration was shown to be 90% by mass spectroscopic analysis. ***6***: Mp >270 °C. MS *m/e* (rel intensity): 165 (M^+, 76), 147 (32), 136 (40), 93 (44), 92 (50), 80 (100), 79 (82), 69 (82). IR (KBr): 3320, 2940, 1485, 1385, 1295, 1160, 1095, 1055 cm^{-1}. PMR δ ($CDCl_3$): 3.88 (1H, br. s, $W_{1/2}$=7.8 Hz), 2.70—1.20 (12H, br. complex m), 1.03 (2H, d, J=12.0 Hz). CMR δ ($CDCl_3$): 76.9 (CH), 44.7 (CH), 42.0 (CH), 41.4 (CH_2), 38.4 (2CH), 36.7 (CH), 31.9 (CH_2), 31.4 (CH_2), 30.6 (CH), 25.0, 24.0, 23.0 (CHD). Found: C, 79.93; H(D), 10.53%. Calcd for $C_{11}H_{15}DC$: C, 79.95; H(D), 10.37%.

endo-*3-Acetoxy*-exo-*5-(chloromercurio)tetracyclo*[*5.3.1.*$0^{2,6}$.$0^{4,9}$]-*undecane* (*7*). A solution of $Hg(OAc)_2$ (118 mg; 0.37

mmol) and **1** (50 mg; 0.34 mmol) in glacial AcOH (1 ml) was stirred at room temperature for 1 h. To the mixture was added a solution of NaCl (242 mg; 4.1 mmol) in ice-water (10 ml). After 20 min, white precipitates were collected by filtration and washed with water, and dried over P_2O_5 at reduced pressure to give **7** (144 mg, 95%): mp 183—186 °C. IR (KBr): 2925, 1735, 1370, 1455, 1065 cm^{-1}. PMR δ ($CDCl_3$): 4.58 (1H, dd, J=5.5 and 2.5 Hz), 2.08 (3H, s), 3.00—0.85 (13H, br. complex m). Found: C, 35.65; H, 4.15%. Calcd for $C_{13}H_{17}ClHgO_2$: C, 35.38; H, 3.88%.

endo-*3-Acetoxytetracyclo*[*5.3.1.0*^{2,6}*.0*^{4,9}]*undecane* (***8***).

(a): A solution of **2** (51 mg; 0.31 mmol) in pyridine (0.5 ml) and acetic anhydride (0.25 ml) was kept at room temperature overnight. The mixture was poured onto 5% aqueous HCl and extracted with CH_2Cl_2. The organic layer was washed with aqueous Na_2CO_3 and brine, and dried (Na_2SO_4). After filtration, the solvent was evaporated and the residue was chromatographed on silica gel. Elution by hexane and CH_2Cl_2 (4:1) afforded **8** (59 mg, 91%): bp 90 °C (bath temp)/1995 Pa. MS *m/e* (rel intensity): 206 (M^+, 7), 146 (100). IR (neat): 2930, 1745, 1365, 1245, 1070, 1055 cm^{-1}. PMR δ (CCl_4): 4.55 (1H, br. s), 2.00 (3H, s), 2.70—0.85 (14H, br. complex m). CMR δ ($CDCl_3$): 170.9 (C=O), 78.2 (CH), 42.7 (CH), 41.7 (CH), 41.3 (CH_2), 38.4 (CH), 36.8 (CH), 36.3(CH), 31.6 (CH_2), 31.5 (CH_2), 30.6 (CH), 23.9 (CH_2), 21.5 (CH_3). Found: C, 75.74; H, 8.86%. Calcd for $C_{13}H_{18}O_2$: C, 75.69; H, 8.80%.

(b): To a solution of **7** (42 mg; 0.10 mmol) in THF (2 ml) was added a solution of $NaBH_4$ (23 mg; 0.61 mmol) in 3 mol dm^{-3} aqueous NaOH (1 ml) and the mixture was stirred at room temperature. After 1 h, CH_2Cl_2 was added to the mixture and the mercury was removed by filtration. The organic solution was washed with brine and dried (Na_2SO_4). After filtration, the solvent was evaporated and the residue was chromatographed on silica gel. Elution by hexane and CH_2Cl_2 (4:1) gave **8** (10 mg, 50%) which was identical with that prepared above.

Oxidation of ***1*** *with Thallium(III) Acetate.* A solution of **1** (147 mg; 1.0 mmol) and $Tl(OAc)_3$ (572 mg, 1.5 mmol) in glacial AcOH (10 ml) was stirred at room temperature for 4 h under argon. Then, CH_2Cl_2 and water was added to the mixture. After filtration, the organic layer was washed with brine and aqueous $NaHCO_3$, and dried (Na_2SO_4). After filtration, the solvent was evaporated and the residue was chromatographed on silica gel. Elution by hexane and CH_2Cl_2 (7:3) gave a mixture of the three diacetates (**9**, **10**, and **11**) along with a small amount of an unidentified product (**12**) (181 mg, 68%). A ratio of **9**, **10**, **11**, and **12** was estimated to be 6:61:27:6 (GLC analysis, AP 180 °C). Each of **9**, **10**, and **11** was isolated by preparative GLC. *exo,exo*-3,5-Diacetoxytetracyclo[5.3.1.0^{2,6}.0^{4,9}]undecane (**9**): mp 77—79 °C. MS *m/e* (rel intensity): 264 (M^+, 5), 221 (26), 162 (100). IR (neat): 2925, 1730, 1370, 1270, 1240, 1050 cm^{-1}. PMR δ (CCl_4): 5.17 (2H, s), 1.95 (6H, s), 2.80—1.40 (10H, br. complex m), 1.07 (2H, d, J=13.5 Hz). CMR δ ($CDCl_3$): 170.5 (C=O), 76.8 (CH), 47.9 (CH), 41.2 (CH), 40.4 (CH_2), 39.8 (CH), 33.5 (CH), 31.0 (CH_2), 21.3 (CH_3). Found: C, 68.06; H, 7.50%. Calcd for $C_{15}H_{20}O_4$: C, 68.16; H, 7.63%. *endo,exo*-3,5-Diacetoxytetracyclo[5.3.1.0^{2,6}.0^{4,9}]undecane (**10**): mp 71—73 °C. MS *m/e* (rel intensity): 264 (M^+, 10), 221 (37), 162 (100). IR (neat): 2930, 1740, 1730, 1365, 1245, 1080, 1050, 1025 cm^{-1}. PMR δ (CCl_4): 5.20 (1H, dd, J=5.7 and 2.0 Hz), 5.02 (1H, d, J=1.2 Hz). 2.02 (6H, s), 2.80—1.40 (10H, br. complex m), 1.08 (2H, d, J=13.5 Hz). CMR δ ($CDCl_3$): 170.7 (C=O), 74.1 (CH), 72.9 (CH), 47.8 (CH), 42.5 (CH), 42.0 (CH_2), 40.5 (CH), 38.8 (CH), 36.6 (CH), 32.1 (CH+CH_2), 30.9 (CH_2), 21.4 (CH_3). Found: C, 68.16; H, 7.45%. Calcd for $C_{15}H_{20}O_4$: C, 68.16; H, 7.63%. *endo,exo*-4,5-Diacetoxytetracyclo[5.3.1.0^{2,6}.0^{3,9}]undecane (**11**): bp 90—100 °C (bath temp)/133 Pa. MS *m/e* (rel intensity): 204 (M^+—AcOH, 17), 162 (100). IR (neat): 2935, 1750, 1735, 1370, 1240, 1045, 1025 cm^{-1}. PMR δ (CCl_4): 5.20 (1H, dd, J=3.0 and 6.0 Hz), 5.07 (1H, d, J=3.0 Hz), 2.03 (3H, s), 2.00 (3H, s), 2.93—1.20 (12H, br. complex m). CMR δ ($CDCl_3$): 170.4 (C=O), 83.5 (CH), 80.8 (CH), 54.5 (CH), 53.9 (CH), 47.6 (CH), 43.0 (CH_2), 42.8 (CH_2), 39.3 (CH), 39.1 (CH), 37.1 (CH), 31.0 (CH_2), 21.1 (CH_3), 20.9 (CH_3). Found: C, 68.11; H, 7.73%. Calcd for $C_{15}H_{20}O_4$: C, 68.16; H, 7.63%.

Oxidation of ***1*** *with Lead(IV) Acetate.* A solution of **1** (219 mg; 1.5 mmol) and $Pb(OAc)_4$ (665 mg; 1.5 mmol) in glacial AcOH (22 ml) was stirred at room temperature for 24 h. The mixture was poured onto water and extracted with CH_2Cl_2. The organic layer was washed with aqueous $NaHCO_3$ and brine, and dried (Na_2SO_4). After filtration, the solvent was evaporated to give a crude mixture of **9**, **10**, and **11** (430 mg, **9**:**10**:**11**=50:25:25), which was purified by preparative TLC (silica gel, hexane:ether=1:1) to afford a mixture of **10** and **11** (153 mg, 39%) and **9** (161 mg, 41%).

exo,exo-*3,5-Dihydroxytetracyclo*[*5.3.1.0*^{2,6}*.0*^{4,9}]*undecane* (***13***). To a suspension of $LiAlH_4$ (268 mg; 7.1 mmol) in dry ether (10 ml) was added dropwise a solution of **9** (155 mg; 0.59 mmol) in dry ether (10 ml). The mixture was refluxed overnight and quenched with AcOEt and sat aqueous Na_2SO_4, and the organic layer was separated and dried (Na_2SO_4). After filtration, the solvent was evaporated to give **13** (103 mg, 97%): mp 186—190 °C. MS *m/e* (rel intensity): 180 (M^+, 8), 162 (59), 134 (100). IR (KBr): 3225, 2920, 1235, 1095, 1070, 1045 cm^{-1}. PMR δ ($CDCl_3$): 5.10 (2H, s, 20H), 4.48 (2H, s), 2.75—2.20 (6H, br. complex m), 1.95—1.40 (4H, br. complex m), 0.98 (2H, d, J=13.5 Hz). CMR δ ($CDCl_3$): 75.4 (CH), 50.6 (CH), 42.8 (CH), 41.4 (CH), 38.8 (CH), 33.0 (CH), 30.9 (CH_2). Found: C, 73.01; H, 9.10%. Calcd for $C_{11}H_{16}O_2$: C, 73.30; H, 8.95%.

endo,exo-*3,5-Dihydroxytetracyclo*[*5.3.1.0*^{2,6}*.0*^{4,9}]*undecane* (***14***). A similar reduction of **10** (87 mg; 0.33 mmol) with $LiAlH_4$ (150 mg; 3.9 mmol) to the above gave **14** (58 mg, 98%): mp >270 °C. MS *m/e* (rel intensity): 180 (M^+, 7), 162 (40), 134 (98), 91 (100). IR (KBr): 3300, 2925, 1085, 1065, 1040, 1020 cm^{-1}. PMR δ (DMSO-d_6): 4.57 (2H, s, 20H), 4.40 (1H, dd, J=3.2 Hz), 3.97 (1H, s), 2.67 (1H, d, J=12.0 Hz), 2.45—1.07 (9H, br. complex m), 0.90 (2H, d, J=12.0 Hz). CMR δ (DMSO-d_6): 69.2 (CH), 67.9 (CH), 49.9 (CH), 44.1 (CH), 43.6 (CH), 41.9 (CH_2), 37.9 (CH), 36.1 (CH), 31.7 (CH_2), 31.5 (CH), 30.7 (CH_2). Found: C, 73.44; H, 9.24%. Calcd for $C_{11}H_{16}O_2$: C, 73.30; H, 8.95%.

endo,exo-*4,5-Dihydroxytetracyclo*[*5.3.1.0*^{2,6}*.0*^{3,9}]*undecane* (***15***). A similar reduction of **11** (56 mg; 0.21 mmol) with $LiAlH_4$ (143 mg: 3.8 mmol) to the above gave **15** (37 mg, 96%): mp 197—199 °C. MS *m/e* (rel intensity): 180 (M^+, 40), 162 (41), 96 (100), 83 (94), 82 (91). IR (KBr): 3330, 2925, 1090, 1035, 1015, 1005 cm^{-1}. PMR δ (DMSO-d_6): 4.60 (2H, s, 20H), 4.10 (1H, br. s), 3.87 (1H, s), 2.85—1.10 (12H, br. complex m). CMR δ (DMSO-d_6): 84.2 (CH), 80.1 (CH), 57.5 (CH), 56.4 (CH), 46.8 (CH), 42.8 (CH_2), 42.5 (CH_2), 39.0 (CH), 38.3 (CH), 36.3 (CH), 30.8 (CH_2). Found: C, 73.00; H, 9.08%. Calcd for $C_{11}H_{16}O_2$: C, 73.30; H, 8.95%.

Tetracyclo[*5.3.1.0*^{2,6}*.0*^{4,9}]*undecane-3,5-dione* (***16***). Oxida-

tion of **13** (134 mg; 0.74 mmol) with CrO_3 (1350 mg; 13.5 mmol)-pyridine complex in a similar manner to the above gave **16** (80 mg, 61%): mp 184—187 °C. MS *m/e* (rel intensity): 176 (M^+, 93), 166 (66), 79 (50), 66 (100). IR (KBr): 2935, 1770, 1735, 1215, 1145, 1080 cm^{-1}. PMR δ (CCl_4): 3.30—2.50 (6H, br. complex m), 2.20—1.50 (6H, br. complex m). CMR δ ($CDCl_3$): 210.3 (C=O), 63.5 (CH), 59.9 (CH), 46.9 (CH), 44.7 (CH), 42.6 (CH_2), 33.0 (CH_2). Found: C, 74.71; H, 7.12%. Calcd for $C_{11}H_{12}O_2$: C, 74.97; H, 6.86%. A similar oxidation of **14** (52 mg; 0.29 mmol) with CrO_3 (515 mg; 5.2 mmol)-pyridine complex also afforded **16** (43 mg, 85%).

*Reduction of **16** to **4**.* Semicarbazide hydrochloride (300 mg; 2.7 mmol) and KOAc (300 mg; 3.1 mmol) were dissolved in a mixture of water (1 ml) and methanol (3 ml), and undissolved materials were removed by filtration. The diketone (**16**) (52.8 mg; 0.30 mmol) was dissolved in the above solution (1 ml) and kept at room temperature for one week. The precipitates (61 mg) were collected by filtration and dissolved in diethylene glycol (2 ml) containing KOH (153 mg; 2.7 mmol). The mixture was heated at 110 °C for 1 h and subsequently at 180 °C for 20 h. Sublimate on the condenser was dissolved in pentane and washed with brine, and dried (Na_2SO_4). After filtration, the solvent was evaporated and the residue was chrmatographed on silica gel. Elution by pentane gave **4** (4 mg, 9%) as a sole product, which was identical with authentic specimen.[3]

exo-*5-Hydroxytetracyclo[5.3.1.0^{2,6}.0^{3,9}]undecan-4-one (**17**).* A suspension of **15** (37 mg; 0.21 mmol) and Fetizon's reagent (1.2 g)[7] in dry benzene (50 ml) was stirred under reflux for 1 d. After filtration, the solvent was evaporated to give **17** (31 mg, 85%): mp 141—143 °C. MS *m/e* (rel intensity): 178 (M^+, 100), 150 (32), 79 (42). IR (KBr): 3375, 2930, 2880,1735, 1175, 1035 cm^{-1}. PMR δ ($CDCl_3$): 4.03 (1H, s), 3.30—1.15 (13H, br. complex m). CMR δ ($CDCl_3$): 221.5 (C=O), 75.5 (CH), 60.3 (CH), 53.6 (CH), 47.2 (CH), 44.2 (CH_2), 43.0 (CH_2), 42.2 (CH), 39.7 (CH), 39.3 (CH), 31.0 (CH_2). Found: C, 74.28; H, 8.08%. Calcd for $C_{11}H_{14}O_2$: C, 74.13; H, 7.92%.

exo-*5-Acetoxytetracyclo[5.3.1.0^{2,6}.0^{3,9}]undecan-4-one (**18**).* A solution of **17** (31 mg; 0.17 mmol) and acetic anhydride (0.2 ml) in pyridine (0.4 ml) was kept at room temperature overnight and poured onto 5% aqueous HCl. The mixture was extracted with CH_2Cl_2 and washed with aqueous Na_2CO_3 and brine, and dried (Na_2SO_4). After filtration, the solvent was evaporated to give **18** (33 mg, 73%): bp 90—100 °C (bath temp)/133 Pa. MS *m/e* (rel intensity): 220 (M^+, 13), 178 (100), 160 (20), 91 (14). IR (neat): 2930, 2880, 1745, 1370, 1225, 1175, 1035 cm^{-1}. PMR δ (CCl_4): 4.48 (1H, s), 2.07 (3H, s), 3.20—1.15 (12H, br. complexm). CMR δ ($CDCl_3$): 216.5 (C=O), 169.9 (C=O), 76.5 (CH), 60.9 (CH), 52.2 (CH), 47.3 (CH), 44.1 (CH_2), 42.8 (CH_2), 42.1 (CH), 39.7 (CH), 39.5 (CH), 30.8 (CH_2), 20.8 (CH_3). Found: C, 71.04; H, 7.28%. Calcd for $C_{13}H_{16}O_2$: C, 70.89; H, 7.32%.

*Chemical Transformation of **18** to Tetracyclo[5.3.1.0^{2,6}.0^{3,9}]undecan-4-one (**20**).* To liquid ammonia (10 ml) was added at −78 °C a solution of **18** (33 mg; 0.15 mmol) in dry ethyl ether (3 ml) and subsequently small pieces of lithium (112 mg; 16 mmol). The mixture was refluxed for 5 h and ammonia was evaporated. After an addition of water, the mixture was extracted with ether, washed with brine, and dried (Na_2SO_4). After filtration, the solvent was evaporated to give a mixture of tetracyclo[5.3.1.0^{2,6}.0^{3,9}]-undecan-4-ols (**19a** and **19b**, *ca.* 1:1 by PMR analysis, 20 mg, 81%),[6] which, on oxidation with CrO_3–pyridine complex, afforded **20** as a sole product (13 mg, 63%). The ketone (**20**) was identical with that prepared by the different route.[6]

This work was partially supported by a Grant-in-Aid for Scientific Research from the Ministry of Education, Japan (No. 434025).

References

1) In cases where there is no ambiguity, we have used trivial nomenclatures for simplicity. The IUPAC names are described in Experimental Section.

2) For example, a) A. C. Udding, J. Strating, and H. Wynberg, *Tetrahedron Lett.*, **1968**, 1345; b) D. Farcasiu and P. v. R. Schleyer, *ibid.*, **1973**, 1835; c) R. Yamaguchi, T. Katsushima, and M. Kawanisi, *Bull. Chem. Soc. Jpn.*, **48**, 2328 (1975); d) R. Yamaguchi and M. Kawanisi, *Chem. Lett.*, **1975**, 649; e) D. F. Covey and A. Nickon, *J. Org. Chem.*, **42**, 794 (1977).

3) T. Katsushima, R. Yamaguchi, and M. Kawanisi, *J. Chem. Soc., Chem. Commun.*, **1975**, 692.

4) a) R. Criegee and A. Rimmelin, *Chem. Ber.*, **90**, 414 (1957); b) R. Y. Levina, V. N. Kostin, and T. K. Ustynyuk, *Zhur. Obshch. Khim.*, **30**, 359 (1960), *Chem. Abstr.* **54**, 24457c (1960); c) R. J. Quellette, A. South, Jr., and D. L. Shaw, *J. Am. Chem. Soc.*, **87**, 2602 (1965).

5) We have used **1** as a model compound for a mechanistic investigation of halogenation of bicyclo[2.1.0]pentane system; see the succeeding paper.

6) See the preceding paper.

7) M. Fetizon and M. Golfier, *C. R. Acad. Sci.*, **267**, 900 (1968); M. Fieser and L. Fieser, "Reagents for Organic Synthesis," **2**, 363 (1969).

8) The configuration of the substituent at 5-position was determined to be *exo* by comparison of its PMR spectrum with those of **19a** and **19b** (see the preceding paper).

9) An intervention of 1,2-bridged acetoxymercurium ion is strongly suggested in oxymercuration reaction of olefin. See H. O. House, "Modern Synthetic Reactions," 2nd ed., Benjamin, Menlo Park (1972), p. 387.

10) a) R. J. Quellette, "Oxidation in Organic Chemistry, Part B," ed by W. S. Trahanovsky, Academic Press, New York (1973), p. 135; b) A. Lethbridge, R. O. C. Norman, and C. B. Thomas, *J. Chem. Soc., Perkin Trans. 1*, **1974**, 1929.

Halogenation of 3,5-Dehydronoriceane (Pentacyclo[5.3.1.$0^{2,6}$.$0^{3,5}$.$0^{4,9}$]undecane.[1] Front Side Attack on the Bicyclo[2.1.0]pentane System by Halonium Ion and Corner Side Attack by Halogen Radical[2]

Takeo KATSUSHIMA, Ryohei YAMAGUCHI, Satoshi IEMURA, and Mituyosi KAWANISI*

Department of Industrial Chemistry, Faculty of Engineering, Kyoto University, Yoshida, Sakyo-ku, Kyoto 606

(Received April 30, 1980)

Halogenations of 3,5-dehydronoriceane (**1**) in dichloromethane in the dark exclusively or predominantly give *endo,exo*-4,5-dihalotetracyclo[5.3.1.$0^{2,6}$.$0^{3,9}$]undecanes; these results provide a decisive evidence for the front side attack on the bicyclo[2.1.0]pentane system by halonium ion. On the other hand, the corner side attack on the bicyclo[2.1.0]pentane system by halogen radicals takes place in photohalogenations of **1**, which give *endo,endo*- and *endo,exo*-3,5-dihalonoriceanes. In addition, the halogenation of **1** in the dark is found to be sensitive to the solvent polarity and the ionic nature of the halogen used. Bromination of **1** in nonpolar solvents in the dark likely proceeds through intervention of the 1,3-bridged bromonium ion.

In 1965 LaLond[3] reported that halogenation of bicyclo[2.1.0]pentane gave predominantly *trans*-1,2-dihalocyclopentane. On the basis of the results, he postulated the mechanism that consisted of conversion of an initially formed 1,3-bridged halonium ion into 1,2-bridged one *via* 1,2-hydride migration. To our knowledge, there has been no further report on the mechanism of halogenation of bicyclo[2.1.0]pentane system. Either the validity of the above mechanism or mechanistic details including the stereochemical fate of the halogen (*i.e.*, whether front side attack with retention of configuration or corner side attack with inversion of configuration) remains unexplored.[4] We have recently reported the synthesis of 3,5-dehydronoriceane (**1**)[5] and expect that **1** is a likely model compound for solving the above problems to some extent, because **1** has the partial bicyclo[2.1.0]pentane structure constrained within a rigid cage structure. We now wish to desribe here our results on the stereochemical aspects of the halogenation reaction of bicylo-[2.1.0]pentane system as well as the susceptibility of the reaction to the solvent and the halogen used.[6]

Results and Discussion

*Halogenation of **1** in the Dark.* When **1** was treated with bromine in dichloromethane at −78 °C in the dark, *endo,exo*-4,5-dibromotetracylo[5.3.1.$0^{2,6}$.$0^{3,9}$]undecane (**2a**) was obtained predominantly along with a small amount of *endo,exo*-3,5-dibromonoriceane (**8a**) (*vide infra*) and an unidentified compound (**2a**:**8a**=90:5).[7,8] The structure of **2a** was determined by elemental analysis, spectroscopic data ^{1}H-NMR (PMR) and ^{13}C-NMR (CMR) which showed a lack of a plane of symmetry, and the debromination to tetracyclo-[5.3.1.$0^{2,6}$.$0^{3,9}$]undec-4-ene (**3**)[9] with lithium aluminium hydride. A similar treatment of **1** with iodine gave predominantly *endo,exo*-4,5-diiodotetracyclo[5.3.1.$0^{2,6}$.-$0^{3,9}$]undecane(**2b**), along with **3** and *endo,endo*- and *endo,exo*-3,5-diiodonoriceanes (**7b** and **8b**, *vide infra*) (**2b**:**3**:**7b**:**8b**=73:12:4:11). Although **2b** has never been isolated in a pure form because of its rapid decomposition to the olefin (**3**), the structure of **2b** has been elucidated by a resemblance between the PMR spectra of **2a** and **2b** as well as the chemical trans-formation to **3**.

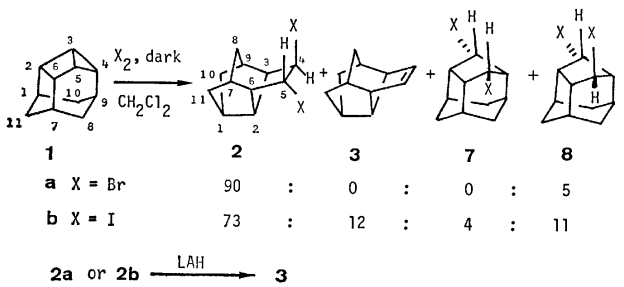

Scheme 1.

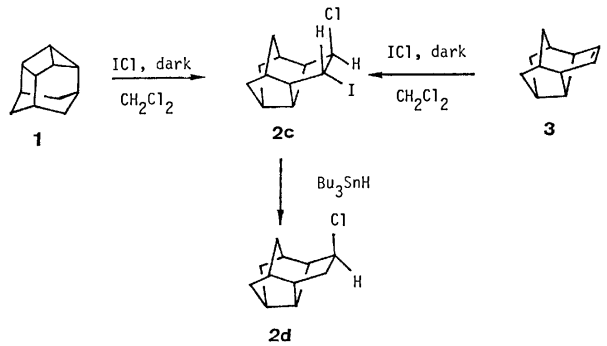

Scheme 2.

In order to investigate the stereochemistry of these halogenations, the reaction of **1** was effected with iodine chloride, the attacking species of which was the iodonium ion, under a similar conditions to the above. This gave exclusively *endo*-4-chloro-*exo*-5-iodotetracyclo-[5.3.1.$0^{2,6}$.$0^{3,9}$]undecane (**2c**) in 78% yield. The configurations of halogens in **2c** were determined as follows. (i) As the coupling patterns of H_4 and H_5 in the PMR spectrum resemble those of **2a** and **2b**, the stereochemistry of the halogens should be trans. (ii) The selective reduction **2c** with Bu_3SnH gave 4-chlorotetracyclo[5.3.1.$0^{2,6}$.$0^{3,9}$]undecane (**2d**), the PMR spectrum of which showed a quintet at 4.55 ppm due to H_4. Since PMR spectra of *exo*- and *endo*-4-tetracyclo-[5.3.1.$0^{2,6}$.$0^{3,9}$]undecanols have shown a doublet of doublet at 4.33 ppm and a quintet at 4.58 ppm, respectively, due to H_4,[10] the configuration of the chlorine substituent in **2d** is determined to be *endo*. (iii) Furthermore, the reaction of **3** with iodine chloride afforded the same chloro iodo compound (**2c**).

Scheme 3 can best explain the above results. The

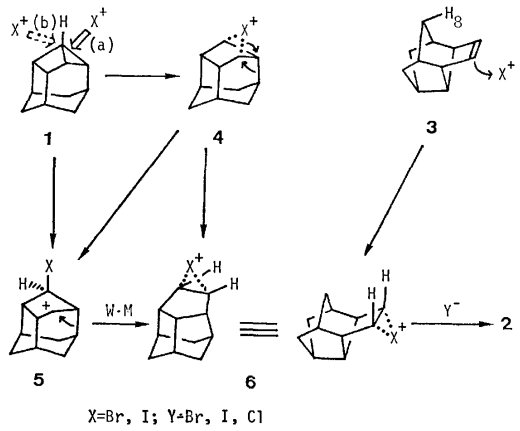

Scheme 3.

initial attack on the bicyclo[2.1.0]pentane group by halonium ion (X^+) must take place from the front side (a) with retention of configuration, but not from the corner side (b) with inversion of configuration. The resulting carbocation intermediate (**5**) may undergo Wagner-Meerwein (W-M) rearrangement to give an 1,2-bridged halonium ion (**6**). It would be also possible that **6** is produced through an 1,3-bridged halonium ion (**4**), as is shown in Scheme 3. A nucleophile (Y^-) captures **6** to afford the *trans*-dihalides (**2**). The same 1,2-bridged halonium ion (**6**, X=I) is also generated from the olefin (**3**) because of the steric hindrance due to H_8. Thus, it has been established that halonium ions may participate with the central bond of the bicyclo[2.1.0]pentane system in an edge fashion and we believe that this is the first decisive experimental evidence for front side attack on the bicyclo[2.1.0]pentane system by halonium ions.

Photohalogenation of ***1***. While halogenations of **1** in dichloromethane in the dark give predominantly or exclusively the rearranged products (**2**), a small amount of unrearranged 1,3-addition products (**7** and **8**) is also produced, especially in the iodination. We, therefore, have investigated photohalogenations of **1**, because it has been known that photohalogenations of cyclopropanes take place in a radical fashion to give 1,3-dihalides.[11] When **1** was allowed to react with bromine in carbon tetrachloride under the irradiation through soft glass filter by means of 300 W medium-pressure mercury arc, *endo,endo*- and *endo,exo*-3,5-dibromonoriceanes (**7a** and **8a**) were obtained in 72% combined yield (**7a**:**8a**=46:54). Similarly, a photoiodination of **1** under the daylight[12] gave *endo,endo*- and *endo,exo*-3,5-diiodonoriceans (**7b** and **8b**) in 96% combined yield (**7b**:**8b**=44:56).

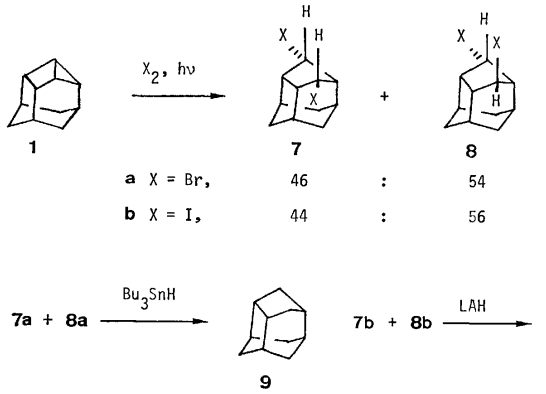

Scheme 4.

The structures of **7** and **8** were determined as follows. Reduction of the mixture of **7a** and **8a** with Bu_3SnH gave noriceane (**9**)[5] and deiodination of **7b** and **8b** with lithium aluminium hydride reproduced **1**. Since **8a** and **8b** have been shown to have to symmetry by NMR analyses, these must be *endo,exo*-3,5-dihalonoriceanes. The PMR spectra of **7a** and **7b** showed only one kind of a broad singlet with half-width of 8.5 Hz due to H_3 and H_5. In noriceane system, the *exo*-H_3 (or H_5) appears as a broad singlet with half-width of *ca.* 8.5 Hz and *endo*-one does as a sharp singlet with half-width of *ca.* 3 Hz.[13] Consequently, **7a** and **7b** were determined to be *endo,endo*-3,5-dihalonoriceanes.

Thus, it has been found that photohalogenations of **1** give *endo,endo*- and *endo,exo*-3,5-dihalonoriceanes in a ratio of *ca.* 1:1. No *exo,exo*-isomer has been detected. These results are compatible with the mechanism which has been suggested for photohalogenations of cyclopropanes.[11] According to the mechanism, the initial attack on the bicyclo[2.1.0]pentane system by halogen radical takes place from the corner side with inversion of configuration to give *endo*-3-halonoricyl radical (**10**). The subsequent non-stereoselective abstraction of a halogen atom from a halogen molecule can give a mixture of an almost equal amount of **7** and **8** (Scheme 5).

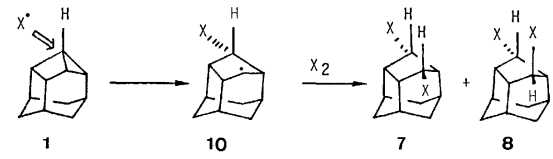

Scheme 5.

Solvent Effects on the Halogenation of ***1***. In addition to the new insight mentioned above on the halogenation of **1**, we have found that considerable amount of the unrearranged dihalides (**7** and **8**) are produced even in the dark when the solvent is changed from dichloromethane to carbon tetrachloride (Table 1). As shown in Table 1, the iodination did not give the rearranged product (**2b**) but the unrearranged ones (**7b** and **8b**). In the case of the bromination, both of the rearranged and unrearranged dibromides were formed. Furthermore, it is interest-

Table 1. Halogenation of **1** in CCl_4 in the dark

	Halogens	Yield/%	Products ratio/%[a] 2 : 7 : 8
a	X=Y=Br	77	52 : 1 : 33[b]
b	X=Y=I	59	0 : 42 : 58
c	X=I, Y=Cl	95	100 : 0 : 0

a) Determined by GLC and/or PMR analyses.
b) An identified product was also obtained.

TABLE 2. BROMINATION OF **1** IN VARIOUS SOLVENTS IN THE DARK

Run	Solvent	E_T-value[a]	Temp/°C	Products ratio/%[b,c]			
				2a :	**7a** :	**8a**	**7a/8a**
1	CH_2Cl_2	41.1	−78	91	0	5	0
2			15[d]	90	0	5	0
3	$CHCl_3$	39.1	−78	89	0	6	0
4			15[d]	80	0	12	0
5			61[e]	74	0	22	0
6	Et_2O	34.6	−78	19	30	37	0.81[f]
7			15[d]	51	12	26	0.46[f]
8	CCl_4	32.5	−23[g]	85	0	10	0
9			15[d]	52	1	33	0.03
10	Cyclohexane	31.2	6[g]	39	14	41	0.34
11			15[d]	51	11	32	0.34

a) Taken from Ref. 14. b) Determined by GLC analysis. c) In all cases except for ether, a small amount of an unidentified product was formed.[8] d) Room temperature. e) Reflux temperature. f) Two unidentified products were formed. g) Freezing point of the solvents.

ing that the iodochlorination gave only the rearranged product (**2c**). These results strongly suggest that the iodination of **1** in carbon tetrachloride proceeds in a radical fashion even in the dark and that the iodochlorination takes place in an ionic fashion regardless of the polarity of the solvent. In addition, attention should be paid to the predominant formation of the *endo,exo*-isomer (**8a**) over the *endo,endo*-one (**7a**) in the bromination; this indicates the possibility of another non-radical reaction pathway. We, therefore, have investigated the solvent effects on bromination of **1** in more detail.

Table 2 summarizes the results. Two major distinctive features should be mentioned as follows. (i) As the polarity (E_T-value)[14] of the solvent decreases, the formation of the unrearranged products (**7a** and **8a**) increases. (ii) More *endo,exo*-isomer (**8a**) is always formed than the *endo,endo*-one (**7a**). Especially in runs of 1—5, 8, and 9, **8a** is exclusively produced over **7a**. This is in a marked contrast to the bromination of bicyclo[3.1.0]hexane in chloroform in the dark which gives *cis*- and *trans*-1,3-dibromocyclohexane in an almost 1:1 ratio.[4] The predominant or exclusive formation of the *endo,exo*-isomer (**8a**) can be best rationalized by assuming that a 1,3-bridged bromonium ion such as **4** (X=Br) mentioned before is captured by bromide ion (Scheme 6). It is highly probable that a lifetime of **4a** is longer in nonpolar solvents than in polar ones becasue the latters can stabilize a carbocation character by solvation in greater extent than the formers. In other words, the 1,3-bridging can be stronger in nonpolar solvents than polar ones. As a result, more rearranged product (**2a**) is formed in polar solvents; this is compatible with the fact that, in general, rearrangements during halogenations of alkenes are enhanced by utilizing polar solvents.[15] Although we do not think that the limited data available here can permit to discuss a further precise mechanism, the present results give a strong support for the intermediacy of the 1,3-bridged halonium ion such as **4** in halogenations of bicyclo[2.1.0]pentane system and reveal that halogenations of bicyclo[2.1.0]pentane system are sensitive to the solvent polarity as well as nature of the halogen used.[16]

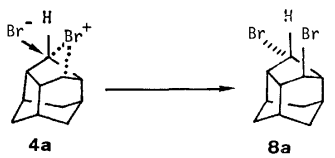

Scheme 6.

Experimental

All the temperatures were uncorrected. The melting points were measured in sealed capillaries. The IR spectra were obtained on a Shimadzu IR-27 spectrometer. The mass spectra were taken by using a Hitachi RMS-4 mass spectrometer. The PMR and CMR spectra were obtained on Varian EM-390 and CFT-20 spectrometers, TMS being chosen as the internal standard. The microanalyses were performed by Kyoto University Elemental Analysis Center. All the reactions were carried out under nitrogen unless otherwise noted.

*Bromination of Pentacyclo[5.3.1.0^{2,6}.0^{3,5}.0^{4,9}]undecane (**1**) in CH_2Cl_2.* To a solution of **1** (292 mg; 2.0 mmol) in CH_2Cl_2 (15 ml) was added a solution of Br_2 (320 mg; 2.0 mmol) in CH_2Cl_2 (10 ml) at −78 °C in the dark. The reaction mixture was stirred for 1 h and washed with aqueous $Na_2S_2O_3$ and brine, and dried ($CaCl_2$). After filtration, the solvent was evaporated and the residue was chromatographed on silica gel. Elution by hexane gave a mixture of *endo,exo*-4,5-dibromotetracyclo[5.3.1.0^{2,6}.0^{3,9}]undecane (**2a**), **8a** (*vide infra*), and an unidentified compound in a ratio of 91:5:4 (estimated from GLC analysis, AP 170 °C) (525 mg, 86%). Pure **2a** was obtained by preparative GLC. **2a**: mp 58—61 °C. MS *m/e* (rel intensity): 227, 225 (M^+−Br, 94, 100), 145, (63). IR (KBr): 2925, 1465, 1305, 1265, 1200, 1155, 785, 770, 725 cm^{-1}. PMR δ (CCl_4): 4.70 (1H, dd, J=6.5 and 4.5 Hz), 4.47 (1H, d, J=4.5 Hz), 2.97 (1H, q, J=6.0 Hz), 2.82—2.42 (3H, complex m), 2.37—1.20 (8H, br. complex m). CMR δ ($CDCl_3$): 61.5 (CH), 58.0 (CH), 67.8 (CH), 47.8 (CH), 42.2 (CH_2), 41.0 (CH), 39.4 (CH), 39.4 (CH), 30.1 (CH_2). Found: C, 42.87; H, 4.88%. Calcd for $C_{11}H_{14}Br_2$: C, 43.17; H, 4.61%.

*Debromination of **2a** with $LiAlH_4$.* To a suspension of $LiAlH_4$ (54 mg; 1.42 mmol) in ether (5 ml) was added a solution of **2a** (84 mg; 0.27 mmol) in ether at room temperature. The reaction mixture was stirred for 1.5 h and quenched with sat aqueous Na_2SO_4. The organic layer was separated by decantation and dried (Na_2SO_4). After filtration, the solvent was evaporated and the residue was chromatographed on silica gel. Elution by hexane gave tetracyclo[5.3.1.$0^{2,6}$.$0^{3,9}$]undec-4-ene (**3**) (22 mg, 55%) which was identical with the authentic specimen.[9]

*Iodination of **1** in CH_2Cl_2.* To a solution of **1** (73 mg; 0.50 mmol) in CH_2Cl_2 (5 ml) was added a solution of iodine (127 mg; 0.50 mmol) in CH_2Cl_2 (5 ml) at room temperature in the dark. The reaction mixture was stirred for 1 h and washed with aqueous $Na_2S_2O_3$ and brine, and dried ($CaCl_2$). After filtration, the solvent was evaporated to give a mixture of *endo,exo*-4,5-diiodotetracyclo[5.3.1.$0^{2,6}$.$0^{3,9}$]undecane (**2b**), **3**, **7b** and **8b** (*vide infra*) in a ratio of 73:12:4:11 (PMR analysis) (187 mg). The diiodide (**2b**) has never been isolated in a pure form because of its rapid decomposition to **3** and iodine. The following data for **2b** were deduced from the measurement of the mixture. **2b**: PMR δ (CCl_4): 4.72 (1H, dd, J=6.3 and 5.4 Hz), 4.45 (1H, d, J=5.4 Hz), 3.18—1.18 (12H, br. complex m). CMR δ ($CDCl_3$): 64.2 (CH), 58.4 (CH), 47.0 (CH), 41.8 (CH_2), 41.7 (CH), 41.4 (CH_2), 41.2 (CH), 39.8 (CH), 39.5 (CH), 34.7 (CH), 29.6 (CH_2). To a suspension of $LiAlH_4$ (61 mg) in ether (5 ml) was added a solution of the above products mixture (127 mg) in ether (3 ml) at room temperature and the mixture was stirred for 1 h. Usual work-up followed by column chromatography on silica gel gave a mixture (39 mg) of **3** and **1** in a ratio of 3:1.

*Iodochlorination of **1** in CH_2Cl_2.* To a solution of **1** (219 mg; 1.50 mmol) in CH_2Cl_2 (10 ml) was added a solution of iodine chloride (244 mg; 1.50 mmol) in CH_2Cl_2 (10 ml) at room temperature in the dark. The reaction mixture was stirred for 45 min, washed with aqueous $Na_2S_2O_3$ and brine, and dried (Na_2SO_4). After filtration, the solvent was evaporated and the residue (400 mg) was distilled to give *endo*-4-chloro-*exo*-5-iodotetracyclo[5.3.1.$0^{2,6}$.$0^{3,9}$]undecane (**2c**) (361 mg, 78%): bp 90 °C (bath temp)/67 Pa. MS *m/e* (rel intensity): 183, 181 (M^+—I, 33, 100), 145 (30). IR (neat): 2950, 2875, 1310, 770, 750 cm^{-1}. PMR δ (CCl_4): 4.80 (1H, dd, J=6.5 and 4.5 Hz), 4.40 (1H, d, J=4.5 Hz), 3.03 (1H, q, J=6.0 Hz), 2.87—1.20 (11H, br. complex m). CMR δ ($CDCl_3$): 73.8 (CH), 63.3 (CH), 57.3 (CH), 48.1 (CH), 42.5 (CH_2), 42.3 (CH_2), 41.5 (CH), 38.9 (CH), 38.3 (CH), 32.5 (CH), 29.7 (CH). Found: C, 43.04; H, 4.78%. Calcd for $C_{11}H_{14}ClI$: C, 42.9; H, 4.57%.

endo-*4-Chlorotetracyclo[5.3.1.$0^{2,6}$.$0^{3,9}$]undecane (**2d**).* A solution of **2c** (97 mg; 0.26 mmol) and Bu_3SnH (84 mg; 0.29 mmol) in dry benzene (3 ml) was refluxed for 1 h washed with brine, and dried (Na_2SO_4). After filtration, the solvent was evaporated and the residue was sublimed (62 °C/1729 Pa) to give **2d** (29 mg, 62%): mp 79—82 °C. MS *m/e* (rel intensity): 184, 182 (M^+, 20, 61), 146 (77), 80 (88), 79 (83), 68 (100). PMR δ (CCl_4): 4.45 (1H, dt, J=10.8 and 5.7 Hz), 2.72—1.25 (14H, br. complex m). CMR δ ($CDCl_3$): 61.8 (CH), 56.6 (CH), 50.2 (CH), 49.7 (CH), 43.1 (CH_2), 43.0 (CH_2), 41.1 (CH), 39.5 (CH), 38.9 (CH), 37.8 (CH_2), 30.3 (CH_2). Found: C, 72.56; H, 8.51%. Calcd for $C_{11}H_{15}Cl$: C, 72.32; H, 8.28%.

*Iodochlorination of **3**.* To a solution of **3** (77 mg; 0.53 mmol) in CH_2Cl_2 (5 ml) was added a solution of iodine chloride (120 mg; 0.74 mmol) in CH_2Cl_2 (5 ml) at room temperature in the dark. The reaction mixture was stirred for 2 h, washed with aqueous $Na_2S_2O_3$ and brine, and dried (Na_2SO_4). After filtration, the solvent was evaporated and the residue was distilled to give **2c** (53 mg, 33%) which was identical with that described above.

*Photobromination of **1**.* To a solution of **1** (59 mg; 0.47 mmol) in CCl_4 (10 ml) was added dropwise a solution of bromine (124 mg, 0.04 ml; 0.78 mmol) in CCl_4 (4 ml) at 0 °C under irradiation through soft glass filter by 300 W medium-pressure mercury arc over 2 min and the mixture was washed with aqueous $Na_2S_2O_3$ and brine, and dried (Na_2SO_4). After filtration, the solvent was evaporated and the residue was chromatographed on silica gel. Elution by hexane gave a mixture of *endo,endo*-3,5-dibromotetracyclo[5.3.1.$0^{2,6}$.$0^{4,9}$]undecane (**7a**) and *endo,exo*-3,5-dibromotetracyclo[5.3.1.$0^{2,6}$.$0^{4,9}$]undecane (**8a**) in a ratio of 46:54 (PMR analysis) (89 mg, 72%). Each of the products was isolated by preparative GLC (AP, 180 °C). **7a**: mp 98—101 °C. MS *m/e* (rel intensity): 308, 306, 304 (M^+, 2, 5, 2), 227 (97), 225 (100), 145 (66). IR (KBr): 2925, 1480, 1295, 1210, 865, 815, 670 cm^{-1}. PMR δ (CCl_4): 4.00 (2H, s, $W_{1/2}$=8.5 Hz), 3.00 (2H, d, J=13.5 Hz), 2.85—2.30 (6H, br. complex m), 1.65 (2H, s), 1.00 (2H, d, J=13.5 Hz). CMR δ ($CDCl_3$): 48.5 (CH), 47.6 (CH), 44.3 (CH), 40.9 (CH_2), 37.9 (CH), 30.8 (CH), 30.1 (CH_2). Found: C, 43.18; H, 4.59%. Calcd for $C_{11}H_{14}Br_2$: C, 43.16; H, 4.61%. **8a**: mp 74—77 °C. MS *m/e* (rel intansity): 308, 306, 304 (M^+, 5, 10, 5), 227 (97), 225 (100), 145 (73). IR (KBr): 2930, 790, 680 cm^{-1}. PMR δ (CCl_4): 5.00 (1H, s, $W_{1/2}$=8.5 Hz), 4.63 (1H, s, $W_{1/2}$=3.0 Hz), 3.08 (1H, d, J=13.5 Hz), 2.28—1.40 (9H, br. complex m), 1.12 (1H, d, J=13.5 Hz). CMR δ ($CDCl_3$): 53.6 (CH), 53.5 (CH), 49.4 (CH), 46.6 (CH), 45.1 (CH), 41.5 (CH), 40.8 (CH_2), 36.8 (CH), 33.7 (CH), 30.6 (CH_2), 30.0 (CH_2). Found: C, 43.17; H, 4.69%. Calcd for $C_{11}H_{14}Br_2$: C, 43.16; H, 4.61%.

*Reduction of a Mixture of **7a** and **8a** with Bu_3SnH.* A mixture of **7a** and **8a** (166 mg; 0.54 mmol), Bu_3SnH (189 mg; 0.65 mmol), and $NaBH_4$ (20 mg; 0.53 mmol) in THF (10 ml) was refluxed overnight and quenched with 5% aqueous HCl. The mixture was poured onto water and extracted with hexane. The organic layer was washed with brine and dried (Na_2SO_4). After filtration, the solvent was evaporated to give **9** as a sole hydrocarbon product. The product, **9** (30 mg), was isolated by preparative GLC and shown to be identical with the authentic specimen[5] by GLC and PMR analyses.

*Photoiodination of **1**.* To a solution of **1** (73 mg; 0.50 mmol) in CH_2Cl_2 (5 ml) was added a solution of iodine (127 mg; 0.50 mmol) in CH_2Cl_2 under daylight at room temperature. The mixture was stirred for 1.5 h, washed with aqueous $Na_2S_2O_3$ and brine, and dried (Na_2SO_4). After filtration, the solvent was evaporated to give a mixture of *endo,endo*-3,5- and *endo,exo*-3,5-diiodotetracyclo[5.3.1.$0^{2,6}$.$0^{4,9}$]undecanes (**7b** and **8b**) (191 mg, 96%) in a ratio of 45:56 (GLC and PMR analyses). Each of the products was isolated by preparative GLC (HVSG, 165 °C). **7b**: mp 123—125 °C. MS *m/e* (rel intensity): 400 (M^+, 4), 273 (100), 146 (88). IR (KBr): 2925, 1480, 1200, 860, 620 cm^{-1}. PMR δ (CCl_4): 3.98 (2H, s, $W_{1/2}$=8.5 Hz), 3.20 (2H, d, J=13.5 Hz), 2.90—2.25 (6H, complex m), 1.65 (2H, s), 0.95 (2H, d, J=13.5 Hz). CMR δ ($CDCl_3$): 48.3 (CH), 44.0 (CH), 40.8 (CH_2), 38.4 (CH), 30.3 (CH), 29.5 (CH_2), 18.9 (CH). Found: C, 33.01; H, 3.54%. Calcd for $C_{11}H_{14}I_2$: C, 33.02; H, 3.53%. **8b**: 115—118 °C, MS *m/e* (rel intensity): 400 (M^+, 8), 273 (100), 146 (89). IR (KBr): 2925, 1475, 1200, 765, 690, 650 cm^{-1}. PMR δ (CCl_4): 4.97 (1H, s, $W_{1/2}$=8.5 Hz), 4.63 (1H, s, $W_{1/2}$=3.0 Hz), 3.27 (1H, d, 13.5 Hz), 2.90—2.25 (6H, complex m),

2.05–1.35 (complex m), 1.08 (1H, d, J=13.5 Hz), 1.04 (1H, d, J=13.5 Hz). CMR δ ($CDCl_3$): 54.3 (CH), 47.4 (CH), 45.8 (CH), 42.6 (CH), 40.1 (CH_2), 37.5 (CH), 33.2 (CH), 32.0 (CH), 30.2 (CH_2), 29.6 (CH_2), 24.7 (CH). Found: C, 32.98; H, 3.51%. Calcd for $C_{11}H_{14}I_2$: C, 33.02; H, 3.53%.

Deiodination of a Mixture of ***7b*** *and* ***8b*** *with* $LiAlH_4$. To a suspension of $LiAlH_4$ (91 mg; 2.4 mmol) in dry ether (5 ml) was added dropwise a solution of a mixture of **7b** and **8b** (190 mg; 0.48 mmol) in dry ether (5 ml) at room temperature. The mixture was stirred overngiht and quenched with sat aqueous Na_2SO_4. Usual work-up gave **1** (60 mg, 87%).

Bromination of ***1*** *in Various Solvents in the Dark.* To a solution of **1** (10—29 mg; 0.07—0.20 mmol) in each of the solvents (2 ml) described in Table 2 was added bromine (17—50 mg; 0.11—0.31 mmol) in the solvent (1 ml) in the dark. The mixture was stirred for 1 h and analyzed by GLC (AP, 170 °C) before and/or after usual work-up. The results were summarized in Table 2.

Iodination of ***1*** *in* CCl_4 *in the Dark.* To a solution of **1** (69 mg; 0.47 mmol) in CCl_4 was added a solution of iodine (138 mg; 0.54 mmol) in CCl_4 (10 ml) in the dark at room temperature. The reaction mixture was stirred for 25 h, washed with aqueous $Na_2S_2O_3$ and brine, and dried (Na_2SO_4). After filtration, the solvent was evaporated to give a mixture of products (111 mg, 59%) which was shown to consist of **7b** and **8b** in a ratio of 42:58 by GLC and PMR analyses.

Iodochlorination of ***1*** *in* CCl_4 *in the Dark.* To a solution of **1** (128 mg; 0.88 mmol) in CCl_4 (5 ml) was added a solution of ICl (171 mg; 1.05 mmol) in CCl_4 (2 ml) in the dark at room temperature. The mixture was stirred for 1 h, washed with aqueous $Na_2S_2O_3$ and brine, and dried (Na_2SO_4). After filtration, the solvent was evaporated and the residue was chromatographed on silica gel. Elution by hexane gave **2c** (256 mg, 95%).

This work was partially supported by a Grant-in-Aid for Scientific Research from the Minsitry of Education, Japan (No. 434025).

References

1) In cases where there is no ambiquity, we have used trivial nomenclatures for simplicity. The IUPAC names are described in Experimental Section.

2) Front side attack means that attacking species participates with the front lobe of the central bond of bicyclo[2.1.0]pentane system and the initial attack proceeds with retention of configuration. Corner side attack means that attacking species participates with the back lobe and the attack proceeds with inversion of configuration.

3) R. T. LaLonde, *J. Am. Chem. Soc.*, **87**, 4217 (1965).

4) Lambert *et al.* have reported that there is no evidence which requires a 1,3-bridged bromonium ion in bromination of bicyclo[3.1.0]hexane; J. B. Lambert, R. D. H. Black, J. H. Shun, and J. J. Papay, *J. Org. Chem.*, **35**, 3214 (1970).

5) T. Katsushima, R. Yamaguchi, and M. Kawanisi, *J. Chem. Soc., Chem. Commun.*, **1975**, 692.

6) Preliminary report; T. Katsushima, R. Yamaguchi, S. Iemura, and M. Kawanisi, *J. Chem. Soc., Chem. Commun.*, **1980**, 133.

7) In the preliminary experiments, these by-products could not be detected. However, an extensive search in larger scale as well as modification of GLC analysis led to the detection of trace amount of the by-products by GLC.

8) The mass spectroscopic analysis indicated that this unidentified compound has its molecular weight more than $C_{11}H_{14}Br_2$. Because of its small quantity which was available, an extensive structural determination was not performed.

9) T. Katsushima, R. Yamaguchi, M. Kawanisi, and E. Osawa, *J. Chem. Soc., Chem. Commun.*, **1976**, 39.

10) See the first preceding paper.

11) K. J. Shea and P. S. Skell, *J. Am. Chem. Soc.*, **95**, 6728 (1973).

12) Use of UV-light resulted in a considerable decomposition of the products.

13) See the second preceding paper.

14) K. Dimroth, C. Reichardt, T. Spiepmann, and F. Bohlmann, *Ann. Chem.*, **661**, 1 (1963); **669**, 95 (1963).

15) H. O. House, "Modern Synthetic Reactions," 2nd ed, Benjamin, Menlo Park (1972), p. 426.

16) It should be noted that in the case of bicyclo[1.1.0]-butane system, 1,3-dihalocyclobutanes are the predominant products; K. B. Weiber, G. M. Lampman, R. P. Ciula, D. S. Connor, P. Schertler, and J. Lavanish, *Tetrahedron*, **21**, 2749 (1965); S. Masamune, *Tetrahedron Lett.*, **1965**, 949; S. Mazur, A. H. Schroder, and M. C. Weiss, *J. Chem. Soc., Chem. Commun.*, **1977**, 262.

Reaction of Dialkyl-substituted Alkynes with Carbon Dioxide Catalyzed by Nickel(0) Complexes. Incorporation of Carbon Dioxide in Alkyne Dimers and Novel Cyclotrimerization of the Alkynes

Yoshio INOUE,* Yoshio ITOH, Haruo KAZAMA, and Harukichi HASHIMOTO

Department of Applied Chemistry, Faculty of Engineering, Tohoku University, Aoba, Aramaki, Sendai 980

(Received May 16, 1980)

$Ni(cod)_2$–$Ph_2P(CH_2)_4PPh_2$ system (cod=1,5-cyclooctadiene) catalyzed the reaction of 3-hexyne, for example, with CO_2 to give a CO_2 incorporated product, *i.e.*, tetraethyl-2-pyrone, in a fairly good yield together with novel two cyclotrimers of the alkyne having cyclopentadiene structures, *i.e.*, pentaethyl-5-(1-propenyl)-1,3-cyclopentadiene and pentaethyl-5-allyl-1,3-cyclopentadiene. The novel two cyclotrimers were formed selectively on $Ni(cod)_2$–PPh_3 system under CO_2, whereas under N_2 the main trimer was hexaethylbenzene. A nickelacyclopentadiene intermediate has been proposed for the pyrone formation. The novel two cyclotrimers were also formed on the oligomerization catalyzed by a cationic nickel hydride complex, $[HNi(Ph_2PCH_2CH_2PPh_2)_2]OCOCF_3$, together with a novel dimer having a methylenecyclobutene structure, *i.e.*, 1,2,4-triethyl-3-ethylidenecyclobutene. The effect of phosphine added and that of active-hydrogen compounds on the novel oligomerization are mentioned.

We are currently studying the CO_2 chemistry for the purpose of using it as a raw material for organic syntheses. There are many reports on the reaction of metal compounds with CO_2 in recent years but only a few examples of the catalytic fixation of CO_2 in organic compounds by transition metals have been known. Earlier papers in this series have dealt with novel reactions of CO_2 with dialkyl-substituted alkynes like 3-hexyne and 4-octyne to form pyrone derivatives (**1**) catalyzed by $Ni(cod)_2$–tertiary phosphine system.[1] This reaction is interesting because CO_2 can be catalytically linked in an alkyne dimer. In addition to the pyrone (**1**) we got two novel cyclotrimers having cyclopentadiene structures, **2** and **3**, which were accompanied by hydrogen migration together with a usual cyclotrimer, hexaalkylbenzene (**4**). Small amounts of several other products including two tetramers of the alkynes were also formed.

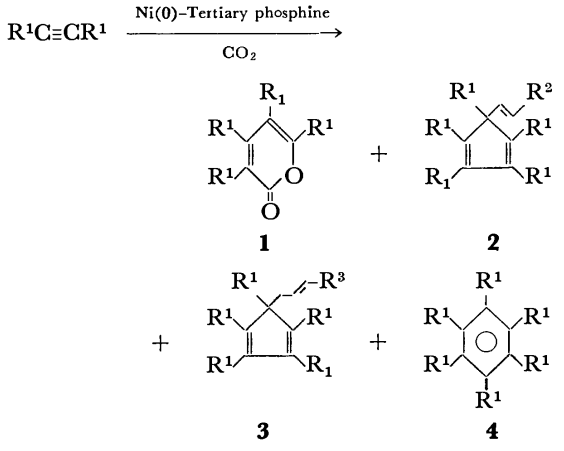

a; R^1=Et, R^2=Me, R^3=H
b; R^1=Pr^n, R^2=Et, R^3=Me

The course of the reaction between CO_2 and alkynes was quite sensitive to the phosphine added, resulting in significantly altered products distributions.

It has also been found that a cationic nickel hydride complex$[HNi(Ph_2PCH_2CH_2PPh_2)_2]OCOCF_3$ catalyzed the novel cyclotrimerization of alkynes to afford **2** and **3**. In this system a novel dimer (**5**) having a methylenecyclobutene structure was also formed.[2]

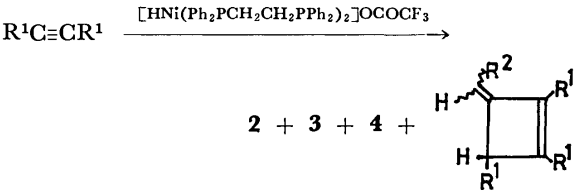

a; R^1=Et, R^2=Me
b; R^1=Pr^n, R^2=Et

5

Although cyclotrimerization of internal alkynes to benzene derivatives has been catalyzed by various kinds of nickel complexes, cyclotrimerization accompanied by hydrogen migration seems rather rare.[3]

In this paper we wish to describe the effect of phosphine added on the CO_2-alkyne reaction and that of active-hydrogen compounds on the novel oligomerization of the alkyne.

Results and Discussion

The results of the reaction between CO_2 and 3-hexyne and 4-octyne employing a variety of tertiary phosphines are summarized in Tables 1 and 2, respectively. Almost the same effects of the phosphine

TABLE 1. REACTION OF 3-HEXYNE CATALYZED BY $Ni(cod)_2$–PHOSPHINE SYSTEM UNDER CO_2 PRESSURE[a]

Phosphine	Conversion %	Yield/%[b] 1a	2a	3a	4a
$Ph_2P(CH_2)_4PPh_2$	96	57	23	2	2
	21[c]	7	2	0.2	trace
	99[d]	54	25	4	2
$Ph_2P(CH_2)_3PPh_2$	—[e]	2	2	1	0.3
$Ph_2P(CH_2)_2PPh_2$	82	13	46	6	2
PPh_3	99	9	66	7	3
$Me_2P(CH_2)_2PMe_2$	71	1	4	1	trace

a) 3-Hexyne; 8.8 mmol, $Ni(cod)_2$; 0.4 mmol, $R_2P(CH_2)_nPR_2$ (R=Ph, n=4,3,2; R=Me, n=2); 0.8 mmol, PPh_3; 1.6 mmol, benzene; 5 ml, CO_2; 50 kg cm^{-2} at 25 °C: 120 °C, 20 h. b) Based on 3-hexyne charged (by GLC). c) 0.5 h. d) 0.06 mmol of water was added. e) Not analyzed.

TABLE 2. REACTION OF 4-OCTYNE CATALYZED BY $Ni(cod)_2$–PHOSPHINE SYSTEM UUNDER CO_2 PRESSURE[a)]

Phosphine	Conversion (%)	Yield/%[b)] 1b	2b	3b	4b
$Ph_2P(CH_2)_4PPh_2$	98	60	21	3	1
$Ph_2P(CH_2)_2PPh_2$	96	12	72	6	3
	96[c)]	11	58	7	—[d)]
	56[e)]	3	23	23	3
PPh_3	100	14	75	4	4

a) 4-Octyne; 6.8 mmol, and the other conditions were the same as those in Table 1. b) Based on 4-octyne charged (by GLC). c) 0.4 mmol of water was added. d) Not analyzed. e) 6.5 mmol of water was added.

were observed in 3-hexyne and 4-octyne reactions. The ditertiary phosphine, $Ph_2P(CH_2)_4PPh_2$, was found to be the most effective for the formation of the pyrone (**1**), whereas the novel cyclotrimer (**2**) was obtained as the main product in the $Ph_2PCH_2CH_2PPh_2$ and PPh_3 systems. In case of $Ph_2P(CH_2)_3PPh_2$, 3-hexyne reacted only scarcely. In the $Me_2PCH_2CH_2PMe_2$ system, higher oligomers of 3-hexyne were the main products with a low conversion of 3-hexyne.

A possible mechanism for the pyrone formation involves a nickelacyclopentadiene as an intermediate (Scheme 1).[4)] The formation of the nickelacyclopentadiene complex from two moles of alkyne and a nickel complex is followed by CO_2 insertion into a nickel-carbon bond to give a carboxylated complex, which then eliminates the pyrone with intramolecular C–O coupling (Route A). Another route involving [4+2]cycloadditions of the cyclopentadiene complex with CO_2 in the sense of Diels-Alder reaction (Route B) cannot be eliminated but is less probable because CO_2 does not undergo [4+2]cycloaddition with dienes.[5)] Attack of another alkyne molecule to the nickelacyclopentadiene complex will result in the formation of a benzene derivative.

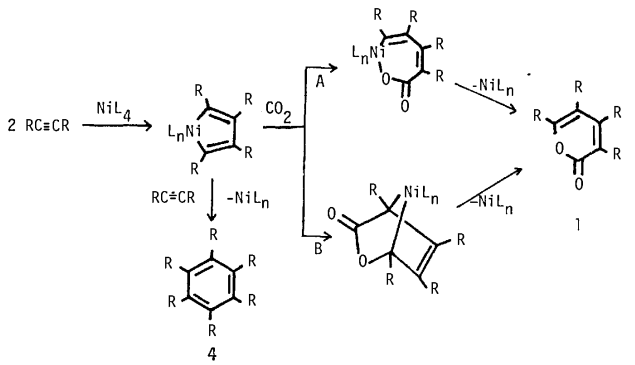

Scheme 1.

The diphosphines of the type $Ph_2P(CH_2)_nPPh_2$ have high coordinating ability by chelation. ^{31}P NMR studies[6)] show that the bonding ability to Ni(0) is in the order

$$Ph_2P(CH_2)_3PPh_2 \approx Ph_2P(CH_2)_2PPh_2 > Ph_2P(CH_2)_4PPh_2.$$

In case of $Ph_2P(CH_2)_3PPh_2$, the reaction took place with great difficulty. This diphosphine has such a high coordinating ability that blocks active sites of nickel to stop the reaction almost completely.

In the proposed scheme above, CO_2 is acting as an electrophile. So a nickel complex bearing more basic ligands is expected to react profitably with CO_2. But the experimental result showed that the diphosphine $Me_2PCH_2CH_2PMe_2$, which is more basic than the corresponding phenyl derivative $Ph_2PCH_2CH_2PPh_2$, was scarcely effective for the formation of the pyrone. This may be ascribed to the steric bulkiness of the phenyl groups in the latter phosphine: CO_2 is competing with an alkyne molecule in reacting with the nickelacyclopentadiene intermediate. Smaller molecule (CO_2) can preferencially react with the intermediate in the $Ph_2P(CH_2)_nPPh_2$ system.

The marked effect of the diphosphine $Ph_2P(CH_2)_4PPh_2$ on the pyrone formation can be ascribed to its adequate coordinating ability and the steric bulkiness.

The reactivity of the other internal alkynes toward CO_2 was also examined. 2-Hexyne gave possible four isomers of 2-pyrone with ill selectivity and also gave many isomers of cyclopentadiene derivatives on $Ni(cod)_2$–$Ph_2P(CH_2)_4PPh_2$ system. 2-Butyne did not react with CO_2 at 120 °C on 20 h reaction by the same (or $-PPh_3$) system in benzene only giving a higher oligomer in very small amount. A reaction mixture of 2-butyne after 40 h reaction at 120 °C by $Ni(cod)_2$–PPh_3 system, however, showed a carbonyl stretching vibration at 1705 cm^{-1} in its IR chart indicating that 2-butyne reacted with CO_2. But the amount of the product was too small to decide the structure. Diphenylacetylene did not react at all under these reaction conditions.

Various kinds of organometallic compounds are known to oligomerize acetylenic compounds into cyclic trimers. The product is hexasubstituted benzene in case of a disubstituted alkyne. The other type of catalytic cyclotrimerization has not been observed for disubstituted alkynes.

In the present reaction of disubstituted alkynes under CO_2, novel cyclotrimerization accompanied by hydrogen migration occurred: $Ni(cod)_2$–$Ph_2PCH_2CH_2PPh_2$ system afforded a novel trimer (**2b**) in 72% yield on the reaction of 4-octyne under CO_2 pressure as shown in Table 2. So the further investigation on the oligomerization of disubstituted alkynes was made. Results of the oligomerization of 3-hexyne and 4-octyne by nickel complexes are summarized in Table 3. The effect of CO_2 was remarkable because $Ni(Ph_2PCH_2CH_2PPh_2)_2$ complex or $Ni(cod)_2$–$Ph_2PCH_2CH_2PPh_2$ (1:1) system scarcely catalyzed the oligomerization of 3-hexyne. $Ni(Ph_2PCH_2CH_2PPh_2)_2$–AcOH (or –PhOH) system afforded a small amount of the cyclopentadiene derivatives. When PPh_3 was used **2a** was formed selectively under CO_2 as shown in Table 1. Under N_2, however, the main product was **4a**. Such effect of CO_2 to alter the catalyst properties has been also observed in the dimerization of butadiene catalyzed by transition metal complexes. For example, $Pt(PPh_3)_3$ converts butadiene to a cyclic dimer, 4-vinylcyclohexene, under N_2 or Ar atmosphere. However a linear dimer, 1,3,7-octatriene, becomes the

Table 3. Oligomerization of 3-hexyne and 4-octyne by nickel catalysts[a)]

Alkyne	Catalyst	Additive	Conversion %	Yield/%[b)] 2	3	4	5
3-Hexyne	$Ni(Ph_2PCH_2CH_2PPh_2)_2$	—	*ca.* 0	0	0	trace	0
		AcOH	9	2	2	trace	1
		PhOH	10	3	5	trace	1
		MeOH	*ca.* 0	0	0	trace	0
	$Ni(cod)_2$–$Ph_2PCH_2CH_2PPh_2$ (1:1)	—	5	1	0	1	0
	$Ni(cod)_2$–PPh_3 (1:4)	—	72[c)]	9	4	39	0
	H-Ni^+	—	99[d)]	4	16	3	36
4-Octyne	H-Ni^+	—	87[d,e)]	4	9	trace	18
	H-Ni^+ [f)]	—	21[d,e)]	1	1	trace	7

a) 3-Hexyne 8.8 mmol, 4-octyne 6.8 mmol, nickel complex 0.4 mmol, additive 0.4 mmol, benzene 5 ml: 120 °C, 5 h. H-Ni^+–$[HNi(Ph_2PCH_2CH_2PPh_2)_2]OCOCF_3$. b) Based on alkyne charged(by GLC). c) 20 h. d) In these reactions considerable amounts of oily products were also formed, the IR spectra of which indicated the existence of CF_3COO– group. e) 90 °C. f) 0.08 mmol.

predominant product when CO_2 is introduced.[7)] In this case a direct effect of CO_2 on the catalyst has been suggested.

It is necessary to make a complex in a coordinately unsaturated state for the occurrence of the reaction. It has been said that a protic acid such as PhOH has an effect to liberate the ligand around the metal atom to place the complex in such a state.[8)] Even if a protic acid or CO_2 has such a function, the product will be as benzene derivative.

The intermediacy of transition metal hydride complexes in the catalytic oligomerization of olefins and diolefins accompanied by hydrogen migration has been recognized. Various nickel hydride complexes have been obtained from the reaction of zerovalent nickel with acids such as H_2SO_4, HCl, CF_3COOH, $HClO_4$, C_6H_5OH, and CH_3COOH by protonation or oxidative addition. Although the starting nickel complex is not a hydride one, carbonic acid from a catalytic amount of water and CO_2 may be a candidate for producing a nickel hydride species in the present system. Water was added to examine the effect on the product distribution in alkyne oligomerization catalyzed by $Ni(cod)_2$–$Ph_2PCH_2CH_2PPh_2$ system under CO_2. 0.15 Equivalent of water to nickel had a slight effect for the formation of **2a** and **3a** under CO_2 as shown in Table 1. The possibility that **2a** was derived from **3a** by isomerization might be excluded because with a short reaction time of 0.5 h rather than the usual 20 h, the distribution of the products did not significantly change. One or excess molar equivalent of water brought about the lowering of the catalytic activity, decreasing the selectivity for **1b** and **2b**, and increased the selectivity for **3b** as shown in Table 2. The preferencial formation of **3** over **2** resembled the results in the nickel hydride complex system (*vide infra*).

In order to clarify the role of hydride species on the alkyne oligomerization, the catalytic action of a cationic hydride complex, $[HNi(Ph_2PCH_2CH_2PPh_2)_2]$-$OCOCF_3$, which was prepared from $Ni(Ph_2PCH_2CH_2PPh_2)_2$ and CF_3COOH,[9)] was examined. Actually this complex oligomerized 3-hexyne (and 4-octyne) into **2**, **3**, and **4**, and in this case a novel dimer, 1,2,4-triethyl-3-ethylidenecyclobutene (**5a**), which was not yielded in the CO_2-concerned system, was also obtained as the main product. This is a rare example of the catalytic dimerization of internal alkynes involving the migration of hydrogen. There is a possibility that the oligomerization of 3-hexyne was catalyzed by traces of acid.[10)] But it could be excluded by a control experiment. The products of these types were formed in reactions catalyzed by metallic species.

It is not certain at the present time whether CO_2 has a direct effect on the catalyst or has a tendency to produce a hydride species. But at least a certain nickel hydride complex can catalyze the novel cyclotrimerization.

Although we could not get positive data by NMR study (see the experimental part), we tentatively propose the following scheme for the novel cyclotrimerization and dimerization of 3-hexyne as a possible one by analogy with the one proposed by Maitlis on the palladium induced cyclotrimerization of alkynes.[3)] The σ-butadienyl (n=2) and the σ-hexatrienyl (n=3) complex can ring close to the cyclobutenyl and the cyclopentadiene complex which is then converted into **5** and **2**, respectively. If **6** isomerizes into another cyclopentadiene complex (**7**) with 1,2-hydride shift,[3)] **3** is formed.

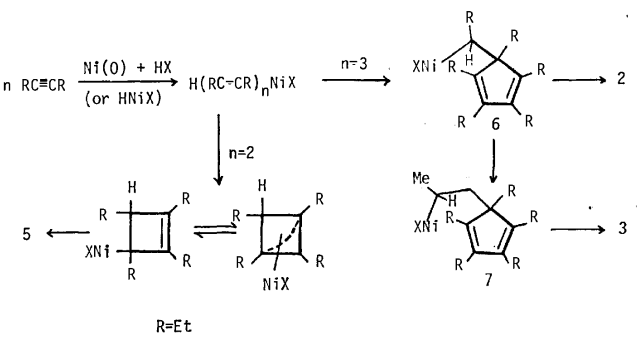

Scheme 2.

Certainly other mechanisms are possible but one other possibility for the formation of the dimer **5** is mentioned here: That is the isomerization of a cyclobutadiene compound to the dimer (**5**).[11,12)]

Experimental

IR, ^{1}H NMR (coupled with spin decoupling method), ^{13}C NMR (coupled with off-resonance technique), mass, and UV spectra were recorded on following apparatus, respectively; Shimadzu IR-430, Hitachi R-24A (60 MHz), JNM MH-100, JMS 06H, and Shimadzu UV 200. Quantitative analyses were performed by GLC on a Shimadzu GC-3AH instrument equipped with a FFAP column with helium as a carrier gas. Preparative GLC was performed on a Shimadzu GC-2H instrument equipped with a FFAP column with hydrogen as a carrier gas.

Materials. 2-Butyne, 2- and 3-hexyne, and 4-octyne were commercially obtained. Diphenylacetylene was prepared according to the published method.[14] The diphosphines $Ph_2P(CH_2)_nPPh_2$ (n=2,3,4)[15] and $Me_2P(CH_2)_2PMe_2$[16] were synthesized according to the methods reported previously. The synthesis of the cationic nickel hydride complex $[HNi(Ph_2PCH_2CH_2PPh_2)_2]OCOCF_3$ was reported previously.[1]

Reaction of 3-Hexyne with CO_2 Catalyzed by Nickel Complexes. To a 100 ml stainless steel autoclave equipped with a magnetic agitator, benzene (5 ml), 3-hexyne (1 ml, 8.8 mmol), $Ni(cod)_2$ (110 mg, 0.4 mmol), and $Ph_2P(CH_2)_4PPh_2$ (341 mg, 0.8 mmol) were added under N_2 atmosphere. Then CO_2 was introduced to the pressure of 50 kg·cm^{-2}. The autoclave was heated to 120 °C and agitated for 20 h. The reaction mixture was analyzed by GLC. The other alkynes were reacted with CO_2 similarly.

Oligomerization of 3-Hexyne Catalyzed by the Cationic Nickel Hydride Complex. To a 20 ml glass ampoule, benzene (5 ml), 3-hexyne (1 ml, 8.8 mmol), and $[HNi(Ph_2PCH_2CH_2PPh_2)_2]OCOCF_3$ (0.387 g, 0.4 mmol) were added under N_2 atmosphere. After the ampoule was cooled in liquid N_2, it was evacuated, sealed, and then agitated for 5 h at 120 °C. The reaction products were analyzed by GLC. Oligomerization of alkynes in other systems was performed similarly.

Identification of Products. Volatile products were flash distilled from the reaction mixtures (oil bath temperature of ≈200 °C) at 1 mmHg,* and were purified by preparative GLC.

*Tetraethyl-2-pyrone (**1a**)*: IR (neat): 1700 (C=O), 1630 (C=C), and 1550 cm^{-1} (C=C). ^{1}H NMR (C_6D_6): δ 0.5—1.3 (12H, m, CH_3), 1.6—2.2 (6H, m, CH_2), and 2.4 (2H, q, J=5.4 Hz, CH_2). MS: *m/e* (rel intensity), 208 (M^+, 16), 180 (27), 165 (100), and 57 (18). UV_{max} (EtOH): 304 nm.

*Tetrapropyl-2-pyrone (**1b**)*: IR (neat): 1705 (C=O), 1635 (C=C), and 1550 cm^{-1} (C=C). ^{1}H NMR (C_6D_6): δ 0.5—2.7 (m, CH_3 and CH_2). Found: C, 77.83; H, 11.62%. Calcd for $C_{17}H_{28}O_2$: C, 77.22; H, 10.67%.

*Pentaethyl-5-(1-propenyl)-1,3-cyclopentadiene (**2a**)*: IR (neat): 972 cm^{-1} (*trans* C=C). ^{1}H NMR (C_6D_6): δ 0.44 (3H, t, J=7.0 Hz, $C_{(5)}$-$CH_2\underline{CH_3}$), 0.96 (12H, m, CH_3), 1.50 (3H, d, J=6.0 Hz, $\underline{CH_3}CH$=), 1.60 (2H, q, J=7.0 Hz, $C_{(5)}$-$\underline{CH_2}CH_3$), 1.85—2.34 (8H, m, CH_2), 4.81 (1H, d, J=15.6 Hz, $\underline{HC}$=CHCH$_3$), and 5.33 (1H, m, HC=C$\underline{H}$CH$_3$). ^{13}C NMR (CD_3COCD_3): δ 144.9 (s), 143.0 (s), 136.2 (d),122.1 (d) 64.2 (s), 22.9, 19.5, 19.2, 18.4, 15.6, 15.2, and 7.8. MS: *m/e* (rel intensity), 246 (M^+, 60), 217 (100), 189 (24), and 161 (22). UV_{max} (EtOH): 206, 239, and 265 nm. Both the large spin coupling constant J=15.6 Hz in the ^{1}H NMR spectrum and the strong absorption at 972 cm^{-1} in the IR spectrum indicate that the double bond in the propenyl group has the *trans* configuration.

*Pentapropyl-5-(1-butenyl)-1,3-cyclopentadiene (**2b**)*: IR (neat): 970 cm^{-1} (*trans* C=C). ^{1}H NMR (C_6D_6): δ 0.7—1.1 (18H, m, CH_3), 1.2—1.9 (12H, m, CH_2), 1.9—2.5 (10H, m, CH_2C=), 4.81 (1H, d, J=15.4 Hz, $\underline{HC}$–CHEt), and 5.47 (1H, dt, J=15.4 and 6.5 Hz, HC=C$\underline{H}$Et). The olefinic proton at δ 5.47 ppm appeared as a doublet by irradiation of the methylene proton centered at δ 2.15 ppm. This indicates the existence of the –CH=CHCH$_2$–group. Both the large spin coupling constant J=15.4 Hz and the strong absorption at 970 cm^{-1} in the IR spectrum indicate that the double bond in the 1-butenyl group has the trans configuration.

*Pentaethyl-5-allyl-1,3-cyclopentadiene (**3a**)*: IR (neat): 1640 (C=C), 990 (C=C), and 910 cm^{-1} (C=C). ^{1}H NMR (C_6D_6): δ 0.37 (3H, t, J=7.0 Hz, $C_{(5)}$-$CH_2\underline{CH_3}$), 0.75—1.15 (12H, m, CH_3), 1.38 (2H, q, J=7.0 Hz, $C_{(5)}$-$\underline{CH_2}CH_3$), 1.70—2.35 (10H, m, CH_2), and 4.50—5.50 (3H, m, CH_2=CH). ^{13}C NMR (CD_3COCD_3): δ 143.4 (s), 143.1. (s), 135.9 (d), 114.7 (t), 61.6 (s), 39.9, 27.9, 19.3, 18.7, 15.5, 14.3, and 8.0.

*Pentapropyl-5-(2-butenyl)-1,3-cyclopentadiene (**3b**)*: IR (neat): 965 cm^{-1} (*trans* C=C). ^{1}H NMR (C_6D_6): δ 0.6—1.1 (15H, m, CH_3), 1.2—1.7 (15H, m, CH_2 and CH_3C=), 1.8—2.4 (10H, m, CH_2C=), and 4.9—5.6 (2H, m, CH=CH). The existence of the CH_3CH=C group was confirmed by a spin decoupling experiment; The methyl group which absorbed at δ 1.40 ppm as an indistinct doublet in the array of the methylene proton peaks collapsed to a singlet by irradiation of the olefinic protons. The strong absorption at 965 cm^{-1} in the IR spectrum suggests that the double bond in the 2-butenyl group has the *trans* configuration.

*1,2,4-Triethyl-3-ethylidenecyclobutene (**5a**)*: IR (neat): 800 cm^{-1} (CH=C$\diagup$). ^{1}H NMR (CD_3COCD_3): δ 0.7—1.2 (9H, m, CH_3), 1.2—1.7 (2H, m, CH_2), 1.59 (3H, d, J=7.4 Hz, $\underline{CH_3}CH$=), 1.8—2.4 (4H, m, $CH_3C\underline{H_2}C$=), 2.72 (1H, t, J=5.7 Hz, –$\underline{C}$H–), and 4.58 (1H, q, J=7.4 Hz, $CH_3C\underline{H}$=). ^{13}C NMR (CD_3COCD_3): δ 152.9 (s), 144.0 (s), 143.8 (s), 102.8 (d), 48.5 (d), 24.8, 20.7, 20.4, 14.0, 13.7, 12.6, and 11.9. UV_{max} (n-hexane): 256 nm (ε 6500). We could not determine the geometry of the ethylidene moiety.

*1,2,4-Tripropyl-3-propylidenecyclobutene (**5b**)*: IR (neat): No characteristic peaks were observed other than those due to the propyl groups. ^{1}H NMR (C_6D_6): δ 0.5—2.5 (26H, m, CH_3 and CH_2), 2.90 (1H, t, J=5.3 Hz, –$\underline{C}$H–), and 4.72 (1H, t, J=8.1 Hz, Et$\underline{H}$C=). This compound gave a very similar NMR spectrum to the ethyl counterpart (**5a**). The geometry of the exocyclic double bond could not be determined.

In these experiments it was difficult to assign the multiplicities of the methyl and methylene carbons in **2a**, **3a**, and **5a** by the off-resonance proton-decoupled technique mainly due to the overlap of the bands.

The Study of the Reaction between the Cationic Nickel Complex and 3-Hexyne by ^{1}H NMR. To a solution of 0.484 g (0.5 mmol) of the cationic nickel hydride complex $[HNi(Ph_2PCH_2CH_2PPh_2)_2]OCOCF_3$ in 5 ml of benzene, 113 μl (1 mmol) of 3-hexyne was added with stirring at room temperature. Orange oil was formed immediately at the bottom of the reaction vessel. So this system was unsuitable for NMR study unfortunately. Then the solvent was switched from benzene to CH_2Cl_2. To a solution of 0.1938 g (0.2 mmol) of the nickel complex in 0.5 ml of CH_2Cl_2 was added 45.4 μl (0.4 mmol) of 3-hexyne at room temperature. The homogeneous orange solution was quickly transferred into a NMR tube under N_2, then it was placed in the spectrometer of probe temperature 35 °C. The spectrum showed resonances of 3-hexyne δ 1.0 (CH_3) and 2.0 (CH_2) and

* 1 mmHg=133.322 Pa.

those characteristic of the hydride complex, a broad triplet and a broad singlet due to the ligand at δ 2.4 and 7.1, respectively and a quintet of the hydride at δ −13.0. In 2 h the initial resonances at δ 7.1 and −13.0 disappeared almost completely and those at δ 1.0, 2.0, and 2.4 became broad with appearence of two new resonances at δ 7.5 (broad singlet) and 0.5 (triplet). During the experiment the color of the sample changed into dark red and finally into deep blue. Although GLC analysis showed the formation of **5a** in a low yield, we might not observe the exact course of the reaction because the color change did not seem normal.

References

1) Y. Inoue, Y. Itoh, and H. Hashimoto, *Chem. Lett.*, **1977**, 855; **1978**, 633.

2) Y. Inoue, Y. Itoh, and H. Hashimoto, *Chem. Lett.*, **1978**, 911.

3) There are several reports on the non-catalytic trimerization of 2-butyne to cyclopentadiene derivatives by palladium compounds: T. R. Jack, C. J. May, and J. Powell, *J. Am. Chem. Soc.*, **99**, 4707 (1977); P. M. Maitlis, *Acc. Chem. Res.*, **9**, 93 (1976), and references cited therein.

4) We tried to provide such an example by making a complex analogous to the proposed cyclopentadiene intermediate. A 2,3,4,5-tetraphenylnickelacyclopentadiene complex was synthesized by the Eisch's method[13] by reaction of $NiCl_2(PPh_3)_2$ with (*E*,*E*)-1,4-dilithio-1,2,3,4-tetraphenylbutadiene. But this complex did not react with CO_2 under the reaction conditions. This system was not adequate because diphenylacetylene did not react with CO_2 (See the text). A similar reaction of CS_2 with cobaltacyclopentadiene complexes to give 2*H*-thiopyran-2-thiones has been reported; Y. Wakatsuki and H. Yamazaki, *J. Chem. Soc., Chem. Commun.*, **1973**, 280.

5) J. Hamer and J. A. Turner, "1,4-Cycloadditions," ed by J. Hamer, Academic Press, New York (1967), p. 205.

6) C. A. Tolman, *Chem. Rev.*, **77**, 313 (1977).

7) J. F. Kohnle, L. H. Slaugh, and K. L. Nakamaye, *J. Am. Chem. Soc.*, **91**, 5904 (1969).

8) Y. Iwamoto and S. Yuguchi, *Kogyo Kagaku Zasshi*, **71**, 233 (1968).

9) R. A. Schunn., *Inorg. Chem.*, **9**, 394 (1970).

10) P. E. Peterson and J. E. Duddey, *J. Am. Chem. Soc.*, **88**, 4990 (1966); **85**, 2865 (1963).

11) G. Criegee, J. Dekker, W. Engel, P. Ludwig, and K. Noll, *Chem. Ber.*, **96**, 2362 (1963).

12) E. M. Arnett and J. M. Bollinger, *J. Am. Chem. Soc.*, **86**, 4729 (1964).

13) J. J. Eisch and J. E. Galle, *J. Organomet. Chem.*, **96**, C23 (1975).

14) L. I. Smith and M. M. Falkof, *Org. Synth.*, **22**, 50 (1942).

15) W. Hewertson and H. R. Watson, *J. Chem. Soc.*, **1962**, 1490.

16) H. Niebergall and B. Langelfeld, *Chem. Ber.*, **93**, 1852 (1960).

α-Cyclodextrin-catalyzed Hydrolysis of 2,2,2-Trifluoroethyl 4-Nitrobenzoate

Makoto KOMIYAMA* and Shohei INOUE

Department of Synthetic Chemistry, Faculty of Engineering, The University of Tokyo, Hongo, Bunkyo-ku, Tokyo 113

(Received May 21, 1980)

The hydrolysis of 2,2,2-trifluoroethyl 4-nitrobenzoate (**1**) was catalyzed by α-cyclodextrin at pH 8.6, 16 °C. The reaction, involving the complex formation of **1** with α-cyclodextrin, proceeded mostly (80%) *via* the general base catalysis by the secondary alkoxide ion of α-cyclodextrin with 20% contribution of the nucleophilic catalysis. This is the first finding of the general base catalysis of the hydrolyses of esters by cyclodextrins. The rate constants of the cleavage of **1** by the general base catalysis and the nucleophilic catalysis, respectively, of α-cyclodextrin were 5.3×10^{-2} and 1.5×10^{-2} min^{-1}, whereas the value in the absence of α-cyclodextrin was 1.2×10^{-2} min^{-1}. The hydrolysis of an analogous substrate, 2,2,2-trifluoroethyl 3-methyl-4-nitrobenzoate, however, was little affected by α-cyclodextrin, showing that **1** included the cavity of α-cyclodextrin with the nitro group first.

Recently the attention to the catalyses by cyclodextrins (CDs) as enzyme models has been increasing. This is mostly attributable to the fact that the reactions catalyzed by CDs proceed *via* the complex formation of the substrates with the catalysts preceding the catalytic functions, which is consistent with enzymatic reactions.[1]

In spite of so many examples of nucleophilic catalyses by CDs,[1] reports on general base catalyses, which are important in enzymatic reactions, by CDs have been scanty. In the previous paper,[2] however, general base catalysis by CDs was found for the first time in the α-cyclodextrin (α-CD)-catalyzed hydrolysis of 2,2,2-trifluoroethyl 4-nitrobenzoate (**1**), which was accompanied by some contribution of nucleophilic catalysis by α-CD.

In the present study, both the rate constant of the general base catalysis and that of the nucleophilic catalysis for the α-CD-catalyzed hydrolysis of **1** will be determined. Furthermore, the effect of α-CD on the hydrolysis of 2,2,2-trifluoroethyl 3-methyl-4-nitrobenzoate (**2**), which is sterically analogous to **1** but has a methyl substituent in the *ortho* position to the nitro group, will be also shown. The comparison of the results on the reactions of **1** and **2** provides structural information on the binding of **1** with α-CD.

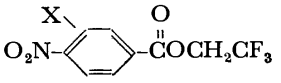

1: X=H
2: X=CH_3

Experimental

Materials. α-CD was purified by the recrystallization from water. The synthesis of **1** and its characterization were described previously.[2] **2** was synthesized by the reaction of 3-methyl-4-nitrobenzoyl chloride, prepared from the corresponding acid and thionyl chloride, with 2,2,2-trifluoroethanol and was purified by the recrystallization from the ethanol-water solution; mp 54.0—54.2 °C.

Kinetics. The hydrolyses of **1** and **2** were carried out at 16 °C in a pH 8.6 borate buffer and in a pH 11.6 carbonate buffer, respectively. The initial concentrations of **1** and **2** were approximately 10^{-4} mol dm^{-3} and the appearance of the corresponding benzoate anions was followed at 296 nm.[3]

The concentration of 4-nitrobenzoyl-α-CD (**4**), the intermediate of the nucleophilic catalysis of the hydrolysis of **1** by α-CD, was determined in the following way. At a predetermined time, sampling of an aliquot of the reaction solution was made, followed by its acidification with small amount of hydrochloric acid. Then, the aliquot was extracted three times with diethyl ether, and the aqueous layer containing **4** as well as α-CD was dried into a white powder *in vacuo*. The amount of **4** in the white powder was determined by measuring the absorbance at 270 nm, after dissolving it in pH 7 buffer.

The rate constant of the hydrolysis of **4** was determined to be 3.1×10^{-3} min^{-1} by the measurement of the change of the absorbance at 260 nm (due to the liberation of 4-nitrobenzoate ion) in the α-CD-accelerated hydrolysis of 3-chlorophenyl 4-nitrobenzoate.[2]

For the D_2O solvent isotope effect experiment, the pD was determined by using the equation: pD=pH meter reading +0.4.[4]

Results

Figure 1 shows the time course of 4-nitrobenzoate ion (**3**) for the hydrolysis of **1** at pH 8.6 in the presence and the absence of 5.0×10^{-2} mol dm^{-3} α-CD. Obviously α-CD showed acceleration of the hydrolysis of **1**.

The appearance of **3** in the absence of α-CD fol-

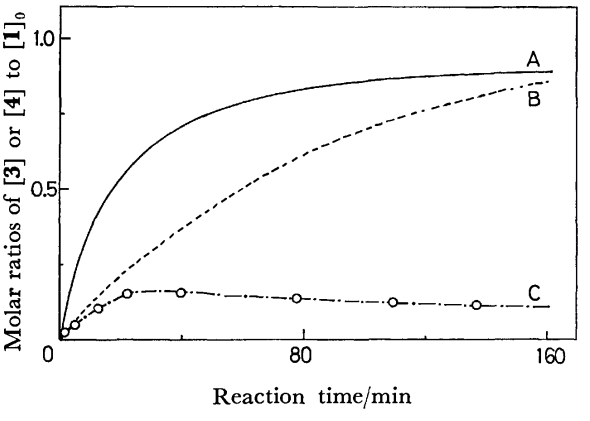

Fig. 1. Time courses of the hydrolysis of 2,2,2-trifluoroethyl 4-nitrobenzoate (**1**) in the presence and the absence of 5×10^{-2} mol dm^{-3} α-CD at pH 8.6, 16 °C; A, ——, 4-nitrobenzoate ion (**3**) in the presence of α-CD; B, ----, **3** in the absence of α-CD; C, —·—, 4-nitrobenzoyl-α-CD (**4**) in the presence of α-CD, where the circles shows the experimental results; the amounts of **3** and **4** are represented by the molar ratios of their concentrations to the initial concentration of **1**.

lowed the first-order kinetics, the rate constant k_{un} being 1.2×10^{-2} min^{-1}. On the other hand, the reaction in the presence of α-CD did not follow the first-order kinetics. This deviation from the first-order kinetics is attributable, as shown later, to the small contribution of nucleophilic catalysis in addition to the major participation of the general base catalysis. Thus, the analysis of the major catalysis was first made by use of the initial slope of the plot of the concentration of **3** *vs.* reaction time, since the initial slope is essentially free from the contribution of the nucleophilic catalysis (see Fig. 4).

As depicted in Fig. 2, the rate constant of the appearance of **3** in the initial stage (k_{obsd}) asymptotically increased with the initial concentration of α-CD ([α-CD]$_0$), indicating the formation of the complex of **1** with α-CD prior to the catalysis. The equilibrium constant of the dissociation of the α-CD-**1** complex (K_d) and the rate constant of the hydrolysis of **1** incorporated in the α-CD–**1** complex (k_c) were determined to be 3.4×10^{-3} mol dm^{-3} and 5.0×10^{-2} min^{-1}, respectively, by plotting the date in Fig. 2 according to Eq. 1;[1]

$$(k_{obsd}-k_{un}) = -K_d(k_{obsd}-k_{un})/[\alpha\text{-CD}]_0+(k_c-k_{un}) \quad (1)$$

The k_c (5.0×10^{-2} min^{-1}) is much larger than the rate constant of the hydrolysis of 4-nitrobenzoyl-α-CD (**4**) (3.1×10^{-3} min^{-1}), the reaction intermediate of the nucleophilic catalysis by the secondary alkoxide ion of α-CD. On the basis of this result, the nucleophilic catalysis by α-CD is definitely ruled out as the major catalysis associated with k_c.

The logarithm of k_{obsd} in the presence of 5×10^{-2} mol dm^{-3} α-CD, where about 94% of **1** form complexes with α-CD, increased linearly with pH (Fig. 3). This fact is consistent with participation of alkoxide ion of α-CD in the catalysis.

The k_{obsd} in the presence of 5×10^{-2} mol dm^{-3} α-CD in D_2O was 1.7 fold smaller than that in H_2O. Here, the difference between the pK_a of the secondary hydroxyl group of α-CD in H_2O and that in D_2O was taken as 0.6.[5] This D_2O solvent isotope effect, considerably different from unity, indicates the general

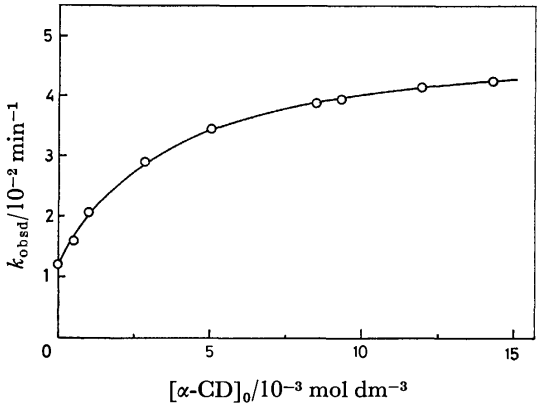

Fig. 2. Dependence of the rate constant of the hydrolysis of **1** (k_{obsd}) on the initial concentration of α-CD at pH 8.6, 16 °C; the k_{obsd}'s were determined from the rate of the appearance of 4-nitrobenzoate ion in the initial stage and are mostly associated with the general base catalysis by α-CD (see the text.).

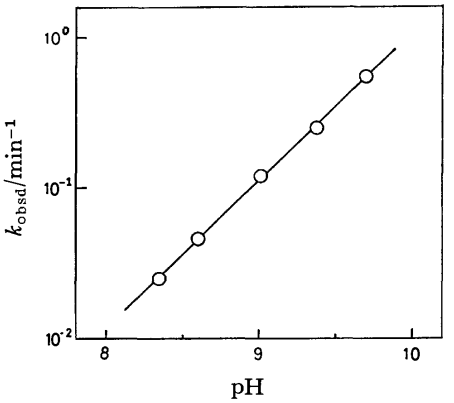

Fig. 3. pH-rate constant profile in the hydrolysis of **1** in the presence of the 5×10^{-2} mol dm^{-3} α-CD at 16 °C.

base catalysis by α-CD. The alkaline hydrolysis assisted by α-CD, which is kinetically indistinguishable from the general base-catalyzed reaction, is unlikely, since the alkaline hydrolysis should show an inverse D_2O solvent isotope effect because of larger nucleophilicity of OD^- than OH^- by 20—40%.[6]

In Fig. 1, the time course of [**4**] in the α-CD-catalyzed hydrolysis of **1**, determined as described in the Experimental Section, is also shown (the C curve). [**4**] first increased with time, showing a maximum around 30 min. The rate constant of the subsequent decrease of the C curve was identical with the independently determined value of the hydrolysis of 4-nitrobenzoyl-α-CD (**4**), 3.1×10^{-3} min^{-1} (see Experimental).

The appearance of **3** due to the nucleophilic catalysis by α-CD was shown by the C curve in Fig. 4, which was estimated by using [**4**] in Fig. 1 and the rate constant of its hydrolysis (3.1×10^{-3} min^{-1}). The amount of **3** due to the nucleophilic catalysis gradually increased with time after being essentially zero for around 30 min.

The B curve in Fig. 4 corresponds to the appearance of **3** due to the general base catalysis by α-CD. This curve is determined by subtracting the appearance of **3** due to the nucleophilic catalysis (the C curve) from the total appearance of **3** measured photometrically (the A curve).

The B curve in Fig. 4 fits well with the first-order kinetics. Table 1 lists the rate constant of the general base-catalyzed hydrolysis of **1** by α-CD as well as that of the nucleophile-catalyzed hydrolysis by α-CD. The second value was determined by using the rate of the appearance of **4** (the C curve in Fig. 1) and the concentration of the residual **1** at a certain time, estimated from the total consumption of **1** (the sum of

Table 1. Rate constants of the cleavage of **1**[a]

Catalysis	Rate constant/10^{-2} min^{-1}
General base catalysis by α-CD	5.3
Nucleophilic catalysis by α-CD	1.5
Uncatalyzed	1.2

a) pH 8.6, 16 °C.

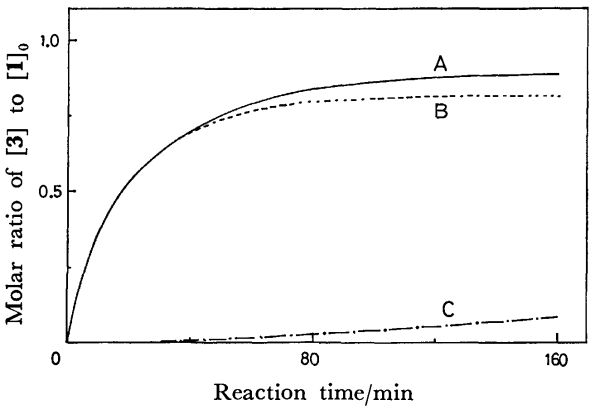

Fig. 4. Time courses of the hydrolysis of **1** in the presence of 5×10^{-2} mol dm^{-3} α-CD at pH 8.6, 16 °C; A, ——, the total amount of **3**; B, ----, **3** due to the general base catalysis by α-CD; C, —·—, **3** due to the nucleophilic catalysis by α-CD; the amount of **3** is represented by the molar ratio of its concentration to the initial concentration of **1**.

the B curve in Fig. 4 and the C curve in Fig. 1). The rate constant of the general base catalysis determined by the first-order plot of the curve B in Fig. 4 (5.3×10^{-2} min^{-1}) is almost identical with the value determined from the initial rate constants (k_{obsd}'s) in Fig. 2 (5.0×10^{-2} min^{-1}).

In contrast with the acceleration of the hydrolysis of **1** by α-CD, α-CD showed little effect on the hydrolysis of an analogous substrate, **2**. The rate constant of the hydrolysis of **2** at pH 11.5 (carbonate buffer), 16 °C in the presence of 5×10^{-2} mol dm^{-3} α-CD (1.4×10^{-2} min^{-1}) was virtually the same as that in its absence (1.3×10^{-2} min^{-1}). No deviation from the first-order kinetics was observed here.

Discussion

The present paper showed that about 80% of the hydrolysis of **1** complexed with α-CD proceeded *via* the general base catalysis by the secondary alkoxide ion of α-CD. This is the first finding of the general base catalysis of the hydrolysis of an ester by CD.

On the complex formation of **1** with α-CD, the nitrophenyl group of **1** included in the cavity with the nitro group first, since no catalysis of α-CD was observed in the hydrolysis of **2** in contrast with the considerable acceleration of the hydrolysis of **1**. The predominant role of the steric hindrance by the adjacent methyl group in the complex formation of **2** with α-CD is consistent with the previous finding that the complex formation of 4-nitrophenol with α-CD is totally inhibited by the methyl substitution of 4-nitrophenol at the 3 position.[7] The structure of the α-CD–**1** complex, where the nitrobenzene group of **1** locates inside the cavity of α-CD, is further supported by the fact that the K_d of this complex (3.4×10^{-3} mol dm^{-3}) is close to that of α-CD–4-nitrophenol complex (5.2×10^{-3} mol dm^{-3}).[7]

The mechanism of the general base catalysis of the hydrolysis of **1** by α-CD is schematically depicted in Fig. 5. A secondary alkoxide ion of α-CD enhances

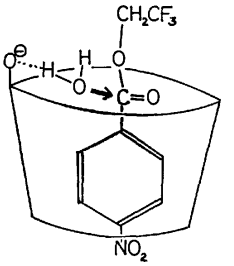

Fig. 5. Mechanism of the general base catalysis of the hydrolysis of **1** by α-CD.

the nucleophilic attack of a water molecule at the carbonyl carbon atom of **1** by partially abstracting a hydrogen atom from the water molecule.

The effectiveness of the general base catalysis by α-CD is attributable to the complex formation of **1** with α-CD, where the secondary alkoxide ion of α-CD functions as an intracomplex catalyst. The rate constant of the intermolecular general base catalysis of the hydrolysis of **1** by the alkoxide ion of α-CD, a base of pK_a 12,[1] was estimated as follows. First the rate constant of the general base-catalyzed hydrolysis of 2,2,2-trifluoroethyl acetate by *N*-methylimidazole (2.3×10^{-4} mol^{-1} dm^3 min^{-1})[8] was converted to the corresponding value of **1** (6.2×10^{-3} mol^{-1} dm^3 min^{-1}) by multiplying the ratio of the rate constant of the alkaline hydrolyses of these two substrates (2.7×10^2).[9] The conversion of the rate constant of the general base-catalyzed hydrolysis of **1** by *N*-methylimidazole (pK 7.0)[10] to that by the secondary alkoxide ion of α-CD (pK_a 12) was made by use of the Brønsted relationship, taking the α for this reaction as 0.5.[11] Consequently, the rate constant of the intermolecular general base-catalyzed hydrolysis of **1** by the secondary alkoxide ion of α-CD was estimated to be 2 mol^{-1} dm^3 min^{-1}. On the other hand, the rate constant of the general base-catalyzed hydrolysis of **1** in the α-CD–**1** complex, referring to the total ionization of α-CD, is calculated to be 1.3×10^2 mol dm^{-3} from the observed value at pH 8.6 (5.3×10^{-2} min^{-1}) and the pK_a of α-CD (12). Thus, the intracomplex general base catalysis of the secondary alkoxide ion of α-CD in the hydrolysis of **1** is equivalent to the catalysis by as large as 65 mol dm^{-3} [12] of the corresponding intermolecular catalyst.

Two reasons are responsible for the small contribution of the nucleophilic catalysis of α-CD in the hydrolysis of **1** in spite of effective nucleophilic catalyses in the hydrolyses of phenyl acetates[13] and *S*-ethyl thiobenzoate.[14] The first reason is that the pK_a of the leaving group, 2,2,2-trifluoroethanol (12.37)[15] is a little bit larger than the pK_a of the secondary hydroxyl group of α-CD (12). Thus, the tetrahedral intermediate, formed by the nucleophilic attack of the secondary alkoxide ion of α-CD at the carbonyl carbon atom of **1**, should return to α-CD and **1** more favorably than produce the products, **3** and **4**. The second reason comes from the structure of the α-CD–**1** complex, in which the nitrobenzene group is located inside the cavity of α-CD. In order for the nucleophilic catalysis to take place, the nitrobenzene group must be taken out of the cavity in the course of the

catalysis, since 4-nitrobenzoyl–α-CD with the nitrobenzene group inside the cavity is too much sterically strained to be formed. This structural change should reduce the rate constant.

In conclusion, the hydrolysis of 2,2,2-trifluoroethyl 4-nitrobenzoate (**1**) catalyzed by α-cyclodextrin (α-CD) proceeds mostly (80%) *via* general base catalysis with 20% contribution of nucleophilic catalysis. The complex formation of **1** with α-CD involves the inclusion of the nitrobenzene group with the nitro group first.

The authors wish to thank Prof. Hidefumi Hirai at The University of Tokyo for his valuable comments.

References

1) M. L. Bender and M. Komiyama, "Cyclodextrin Chemistry," Springer-Verlag, Berlin (1978).
2) M. Komiyama and S. Inoue, *Chem. Lett.*, **1979**. 1101.
3) The absorption spectrum of 4-nitrobenzoyl-α-CD (**4**), prepared from 3-chlorophenyl 4-nitrobenzoate and α-CD, is virtually identical with that of **1**.
4) P. K. Glasoe and F. A. Long, *J. Phys. Chem.*, **64**, 188 (1960).
5) M. Komiyama, E. J. Breaux, and M. L. Bender, *Bioorg. Chem.*, **6**, 127 (1977).
6) K. B. Wiberg, *Chem. Rev.*, **55**, 713 (1955).
7) R. J. Bergeron, M. A. Channing, G. J. Gibeily, and D. M. Pillor, *J. Am. Chem. Soc.*, **99**, 5146 (1977).
8) J. F. Kirsch and W. P. Jencks, *J. Am. Chem. Soc.*, **86**, 837 (1964).
9) The rate constants of the alkaline hydrolyses of 2,2,2-trifluoroethyl acetate and **1**, respectively, are 1.1×10^2 (Ref. 7) and 3×10^3 (this study) $mol^{-1}\,dm^3\,min^{-1}$.
10) M. L. Bender and B. W. Turnquest, *J. Am. Chem. Soc.*, **79**, 1656 (1957).
11) This value is reasonable in the general base-catalyzed hydrolyses of alkyl esters. For example, the α in the general base-catalyzed hydrolysis of ethyl dichloroacetate was 0.47; W. P. Jencks and J. Carriuolo, *J. Am. Chem. Soc.*, **83**, 1743 (1961).
12) The value is 210 and 21 mol dm^{-3}, respectively, when the value of α is taken as 0.4 and 0.6.
13) R. L. VanEtten, J. F. Sebastian, G. A. Clowes, and M. L. Bender, *J. Am. Chem. Soc.*, **89**, 3242 (1967).
14) M. Komiyama and M. L. Bender, *Bull. Chem. Soc. Jpn.*, **53**, 1073 (1980).
15) P. Ballinger and F. A. Long, *J. Am. Chem. Soc.*, **82**, 795 (1960).

Coordinative Role of Alkali Cations in Organic Reactions. V. The Perkin Reaction

Narinder S. Poonia,* Swagata Sen, Prafulla K. Porwal, and A. Jayakumar
Department of Chemistry, University of Indore, Indore-1, India

(Received October 1, 1979)

The Perkin condensation of benzaldehyde (PhCHO) and acetic anhydride (Ac_2O) in the presence of an alkali acetate (M^+OAc^-) involves extensive participation of M^+ and takes place best with K^+OAc^-. Employing an excess of meticulously dehydrated K^+OAc^-, a record high yield of cinnamic acid ($\approx$75%) can be obtained in a 60 min reaction. The product of the reaction before hydrolysis is not PhCH=CHCOOCOCH$_3$ as usually believed but potassium cinnamate plus K^+(OAc, HOAc)$^-$. Conductometric solution stability studies on M^+-ligand (M^+=Na^+ and K^+; Ligand=PhCHO, *o*-$NO_2C_6H_4CHO$, *o*-HOC_6H_4CHO) systems in 2-propanol show that stability sequences for PhCHO and *o*-$NO_2C_6H_4CHO$ are NaOAc<KOAc and KOAc<NaOAc, respectively. These are in line with the catalytic efficiency these salts displayed during the condensation reaction. *o*-HOC_6H_4CHO, for which the Perkin condensation is extremely poor, is practically non-complexing with M^+OAc^- in 2-propanol.

It is a rather established belief[1] that in the organic reactions involving caustic alkalis (M^+OH^-) and alkali salts (M^+X^-) the anion of the inorganic reactant is the only or the main participant in the reaction. Because of our experience in the coordination chemistry of these cations,[2] we initiated work on some such reactions and found that M^+ is very important in determining the route[3,4] as well as the efficiency[3-7] of the reaction and discussed such features of alkali and alkaline earth cations as one of the main themes related to their coordination chemistry.[8] In the course of our work we noticed that participation of M^+ was discussed in the nineteen fifties and sixties with respect to reactions such as the aldol condensation of esters with ketones,[9] certain displacement reactions[10] and the benzil-benzilic acid rearrangement[11] but these reports do not appear to have stimulated other workers.

In this article we discuss the role of M^+ during the Perkin reaction, in particular with respect to the synthesis of cinnamic acid. The Perkin reaction is one of the most general organic reactions[12] and has also been reviewed repeatedly.[13-16] Of the various conflicting views about its mechanism the most accepted is that for a system such as PhCHO–Ac_2O–M^+OAc^-, the OAc^- works as a nucleophile and eliminates the α-proton of Ac_2O to produce the carbanion which condenses with PhCHO (Scheme 1).

In the absence of an ionising medium, however, it is difficult to visualize how the chelating OAc^- can be charge-separated from the formally charged M^+ in preference for a feebly charged α-proton of Ac_2O unless M^+ is effectively stabilized through coordinative interactions with PhCHO and Ac_2O. Detailed studies on cinnamic acid synthesis employing K^+OAc^- reveal that K^+ is extensively involved in the reaction and that the product of the reaction before hydrolysis is not A (Scheme 1) but potassium cinnamate plus K^+(OAc, HOAc)$^-$. A record high yield of cinnamic acid ($\approx$75% for a condensation period of 60 min as against 60% and 72% for condensation periods of five[17] and eight[18] hours, respectively) is obtained by using excess potassium acetate. The results of the Perkin reaction with respect to PhCHO, *o*-$NO_2C_6H_4CHO$, and *o*-HOC_6H_4CHO are discussed in the light of their complexing ability toward M^+OAc^- in a medium of low polarity (2-propanol).

Results and Discussion

Synthetic Studies. For the synthesis of cinnamic acid it is known that the yield of the reaction product is drastically decreased when K^+OAc^- in the reaction is replaced by Na^+OAc^-.[19] We confirm this and show further (see Table 1) that the reaction almost fails when Li^+OAc^- is used. This is, obviously, because the M^+OAc^- ion pair is increasingly tight in the order $K^+<Na^+<Li^+$ so that the activity of OAc^-, the complexation of M^+ with PhCHO and Ac_2O, and hence the dissolution of M^+OAc^- in the latter reactants all become increasingly unfavored.

Detailed work with K^+OAc^- revealed that the primary products of the reaction are potassium cinnamate and the acid salt, K^+(OAc, HOAc)$^-$ as evident from the spectra of the reaction products (d to f) in comparison with those of the standard samples (a to c) in Fig. 1. Comparison of the spectra d to f with that of the 1:1 K^+Cin^-–K^+(OAc, HOAc)$^-$ (spectrum c) reveals that the K^+Cin^- contribution dominates when less K^+OAc^- is used in the reaction (spectrum d) and that the K^+(OAc, HOAc)$^-$ contribution dominates

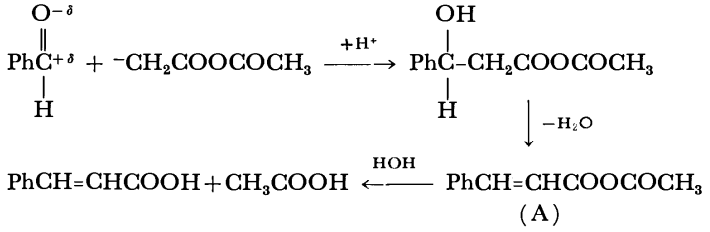

Scheme 1.

Table 1. Enlisting selected experimental results; reaction time 5 h, reaction temperature, 180±2 °C

PhCHO : Ac_2O : M^+OAc^- [a]	Percentage yield[b] of cinnamic acid
Reaction mixture involving different M^+OAc^-	
1 : 1.5 : 0.63[c] (Li^+OAc^-)	nil
1 : 1.5 : 0.63[d] (Na^+OAc^-)	24
1 : 1.5 : 0.63[d,e] (K^+OAc^-)	56
Reaction mixture involving varying proportions of K^+OAc^-	
1 : 1.5 : 1.25	58
1 : 1.5 : 2.00	63
1 : 1.5 : 2.25	70
1 : 1.5 : 2.50	75
1 : 1.5 : 2.50 (1 h)[f]	75
1 : 1.5 : 2.75	65
Reaction mixture involving varying proportions of PhCHO and Ac_2O with K^+OAc^-	
1 : 1 : 1	63
1.5 : 1 : 1	51[g]
1 : 1.5 : 1	45[g]
2 : 1 : 1	49[h]
1 : 2 : 1	39[h]
2 : 2 : 1[i]	48

a) All experiments were carried out under nitrogen atmosphere. b) Average of three experimental results, the reaction yield of which varied within ±1%. c) This particular proportion of the reactants has usually been recommended.[17] d) The Perkin condensation is a typically time-dependent and a slow reaction; with this proportion of the reactants the yield is increased to 39% and 72% with Na^+OAc^- and K^+OAc^- respectively, when reaction time was increased to 8 h. e) On addition of the reation product to water, free cinnamic acid is insolubilized in low yield (2—5%) as observed earlier,[1] but this byproduct gradually disappears as K^+OAc^- in the reaction is increased. This may be attributed to partial hydrolysis of potassium cinnamate with the residual amount of AcOH which can persist in reaction mixtures offering insufficient K^+OAc^- for its conversion into $K^+(OAc, HOAc)^-$. f) The yield of cinnamic acid decreases if reaction time is decreased any further but is practically constant if the time is increased even to as long as 8 h. g) The yield of cinnamic acid decreased because of displacement of one reactant from K^+ by the other which is used in excess; the effect is pronounced when the bidentate and hence strongly complexable Ac_2O is used in excess. h) The benzene wash of the reaction product was found to contain potassium cinnamate which was, obviously, carried into this non-polar phase through complexation with Ac_2O. i) The amount of potassium cinnamate in the benzene phase increased further which indicates that PhCHO acts as a co-ligand during complexation (and hence benzene solubilization) of potassium cinnamate with Ac_2O.

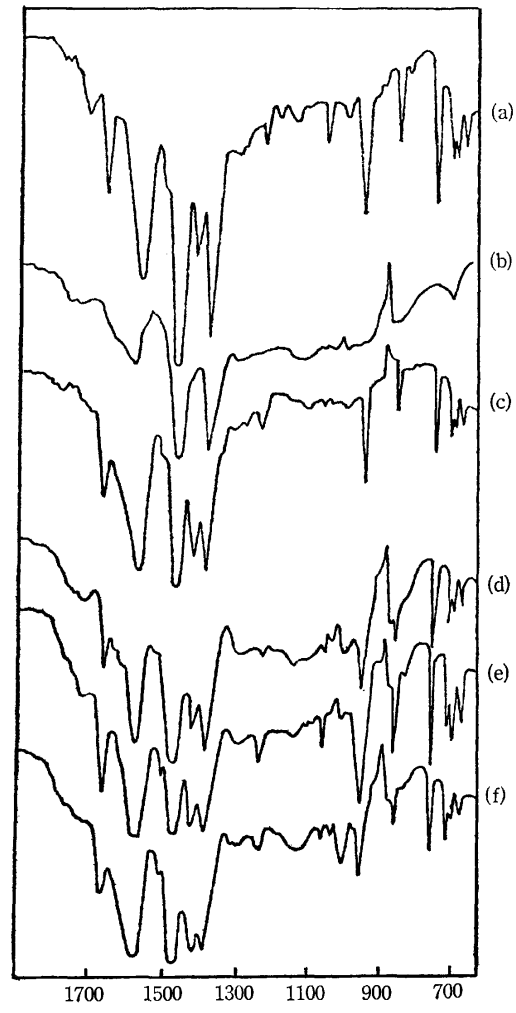

Fig. 1. Showing infrared features (1700—700 cm^{-1}) of some authentic samples [a, potassium cinnamate, b, $K^+(OAc,HOAc)^-$, and c, a 1:1 physical mixture of potassium cinnamate and $K^+(OAc,HOAc)^-$ which was heated at ≈180 °C for 30 min] and products of the Perkin condensation employing different proportions of PhCHO, Ac_2O, and K^+OAc^- [d, 1:1:1; e, 1:1.5:0.6 and f, 1:1.5:2.5].

when excess K^+OAc^- is used (spectrum f).

Direct production of potassium cinnamate may be attributed to an interactive organisation[8] of the reactants as shown in Scheme 2. This interactive mode helps (i) PhCHO to develop the required carbonium character, (ii) Ac_2O to have its α-proton cationized, and (iii) K^+OAc^- to become the loose ion pair required to make OAc^- an available nucleophile. Above all, the energy of coordinative interaction of PhCHO and Ac_2O with K^+OAc^- should help the thermodynamically unfavorable processes, *viz.*, charge separation of K^+OAc^- and cleavage of the $C–H_\alpha$ covalent bond. That the alkali cation is required for such an interactive organisation is evidenced by the failure of the condensation when the cation in the reaction is concealed through sandwich encapsulation using benzo-15-crown-5.[20] Simultaneous interaction of PhCHO and Ac_2O with K^+OAc^- is evidenced by the observation that the yield of the reaction is drastically lowered when either PhCHO or Ac_2O is displaced from K^+OAc^- by using the other in excess (see Table 1).

Coordination of K^+OAc^- with PhCHO and Ac_2O

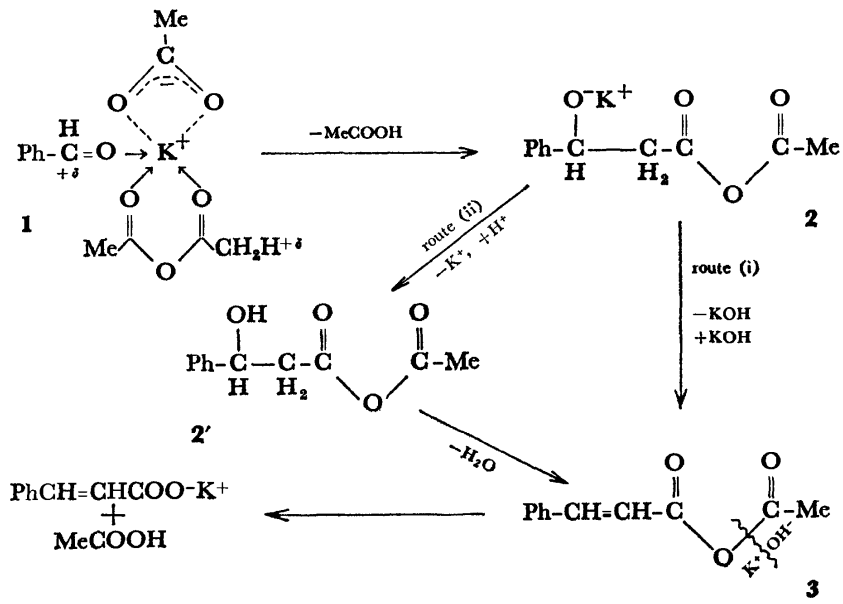

Scheme 2.

is also supported by the observation that the salt can be solubilised just in PhCHO and particularly when Ac_2O is also present. When PhCHO and Ac_2O are used in excess during condensation, even the reaction product, potassium cinnamate, gets complexed and rendered benzene-soluble (see Experimental). Stable solid solvates of alkali and alkaline earth salts involving coordinated PhCHO[21,22] acetone,[21,23] and other ketones[23] have long been characterised.

Accurate kinetic work on this reaction cannot be carried out because it is a high temperature reaction and each organic reactant is unstable with time. Synthesis of a stoichiometric PhCHO–Ac_2O–K^+OAc^- complex is also not possible for it requires a coordinative ligation of a ligand with the cation to be of a particular minimum strength which is apparently not so with PhCHO and Ac_2O.

During the reaction, Ac_2O is susceptible to hydrolysis by moisture which can be incorporated in the system through the hygroscopic K^+OAc^-. AcOH produced by hydrolysis reduces also the effective concentration of K^+OAc^- through the formation of $K^+(OAc, HOAc)^-$. If, on the contrary, an excess of meticulously dehydrated K^+OAc^- is used (see Table 1) a record high yield of cinnamic acid (≈75%) can be obtained by refluxing the reactants just for 60 min. This may in part be because excess K^+OAc^- serves to bind the deleterious byproduct of the reaction, AcOH, and partly because it may help shift the reaction equilibria toward the complexation required for "cationization" of PhCHO and carbanion formation of Ac_2O. In condensation reactions employing M_2CO_3, the favorable role of the alkali has been attributed to its neutralizing action toward HOAc.

Solution Studies. Conductometric studies in the feebly polar 2-propanol reveal (Figs. 2 and 3, Table 2) that K^+OAc^- undergoes a 1:1 interaction with PhCHO ($\log K=2.48$) and Ac_2O ($\log K=3.23$). Na^+OAc^-, which is less favorable for Perkin condensations, interacts relatively weakly with PhCHO ($\log K=2.08$) as well as Ac_2O ($\log K=2.35$). Li^+OAc^-, which does not aid the condensation, behaves insoluble and hence tightly ion-paired in 2-propanol. The most facilitated complexation of K^+ may be attributed to its large size (low charge density) because of which it is comparatively loosely paired with OAc^- (see K_d values in Table 2), and gets effectively polarized by the donor atoms of the neutral ligands. The fact that Ac_2O complexes K^+ more strongly than does PhCHO explains why, in reactions employing a dis-

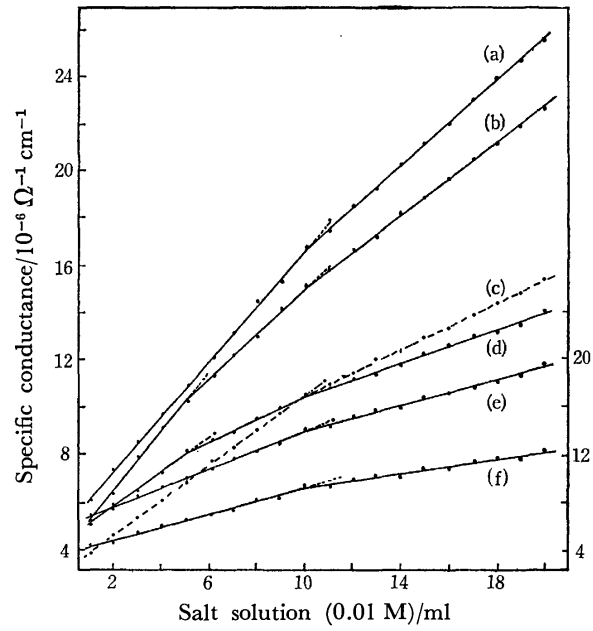

Fig. 2. Specific conductance *versus* salt concentration plots for K^+OAc^- in presence of (a) $NO_2C_6H_4CHO$, (b) Ac_2O, and (c) PhCHO, and for Na^+OAc^- in presence of (d) $NO_2C_6H_4CHO$, (e) Ac_2O and (f) PhCHO. Conductance scale on the right refers to Na^+–OAc^- systems.

Table 2. Dissociation constants (K_d) of M^+OAc^- and log of formation constants (log K) of their complexes with aromatic aldehydes and acetic anhydrides; medium, 2-propanol; temperature 25±1 °C

Salt	K_d mol l^{-1}	System	Stoichiometry	log K
KOAc	2.19×10^{-6}	KOAc-PhCHO	1 : 1	2.48
		KOAc-$NO_2C_6H_4CHO$	1 : 1	2.03
		KOAc-Ac_2O	1 : 1	3.23
			1 : 2	—
NaOAc	5.49×10^{-8}	NaOAc-PhCHO	1 : 1	2.08
		NaOAc-$NO_2C_6H_4CHO$	1 : 1	2.47
			1 : 2	—
		NaOAc-Ac_2O	1 : 1	2.35

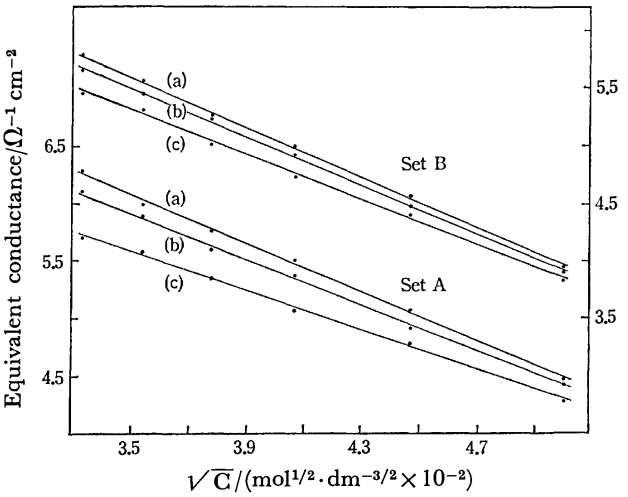

Fig. 3. Equivalent conductance versus salt concentration plots which were used to determine the solution stability values. Set A (K^+OAc^-–PhCHO systems); (a) K^+OAc^-, (b) K^+OAc^-–PhCHO (1:1), and (c) K^+OAc^-–PhCHO (1:10). Set B (K^+OAc^-–Ac_2O systems); (a) K^+OAc^-, (b) K^+OAc^-–Ac_2O (1:1), and (c) K^+OAc^-–Ac_2O (1:10). Conductance scale on the right refers to Ac_2O systems.

proportionately high amount of either of these two, Ac_2O is more effective in reducing the efficiency of the condensation (through displacement of PhCHO from K^+). *o*-HOC_6H_4CHO, which yields only traces of *o*-hydroxycinnamic acid by Perkin reactions,[24] has been found to be practically non-interacting with Na^+-OAc^- or K^+OAc^-.[25]

o-$NO_2C_6H_4CHO$ shows a strong complexation with Na^+OAc^- as well as K^+OAc^- (Table 2) and synthesis of *o*-nitrocinnamic acid is also possible with both.[26] Contrary to what has been noted for PhCHO, however, the stability value is high for Na^+OAc^- and, interestingly, yields of *o*-nitrocinnamic acid in Perkin reaction is also higher for Na^+OAc^-. One of the possible interacting sites of the nitroaldehyde with M^+ is the nitro oxygen which, being linked to the electronegative nitrogen, can be visualized as "reinforced"[8] or "anionic" and hence a more preferable site for the comparatively anionphilic Na^+.[27]

The Condensation Mechanism. Detailed studies on PhCHO–Ac_2O–M^+OAc^- reveal that even before the water treatment the product of the reaction is potassium cinnamate. Obviously, the reaction intermediate (*e.g.*, A in Scheme 1 or **3** in Scheme 2) undergoes molecular degradation right during condensation through some bond cleavage process. Understandably, therefore, **2** loses MOH (*cis*-elimination of M^+ and OH^-) to produce an unsaturated intermediate **3** and MOH molecule then causes bond cleavage of **3** as shown in Scheme 2. That MOH and not M^+OAc^-, is involved in bond cleavage, appears to be supported by the observation that the alkali cinnamate can be produced from a reaction mixture containing less than an equivalent amount of M^+OAc^- such as from PhCHO:Ac_2O:M^+OAc^- (1:1.5:0.6) (see Fig. 1).

There is a likelihood of K^+/H^+ exchange between **2** and MeCOOH so that **2′** is produced (Route (ii)). The water molecule which gets eliminated from the latter, however, has the only recourse of hydrolyzing MOAc and especially Ac_2O. The hydrolysis of the latter appears evidenced by the observation that for obtaining maximum efficiency of the reaction, use of some excess Ac_2O is a requirement (see Table 1).

The suggested mechanism involving simultaneous coordinative organization of the three reactants sorts out earlier conflicts wherein either AcO^-–Ac_2O[28,29] or AcO^-–PhCHO[28,30] interaction has been argued to be a possible triggering step for the condensation. Since alkali cinnamate is the product of the reaction the Perkin's original diacetate mechanism,[31] which has already been disputed[30,32] becomes even less acceptable.

During the *o*-$NO_2C_6H_4CHO$–Ac_2O condensation in the presence of $PhCH_2COONa$, ML, the acid salt $Na^+(PhCH_2COO, PhCH_2COOH)^-$, MLHL, has been detected and considered to be an intermediate of the reaction[33a] because reaction of this acid salt with a mixture of *o*-$NO_2C_6H_4CHO$ and Ac_2O yielded the α,β-unsaturated acid. This view, however, does not present anything new and infact creates confusion because use of this MLHL (wherein L and HL are only hydrogen bonded) at a high reaction temperature amounts to the use of ML plus HL and ML as a participating species. We have failed to synthesize cinnamic acid by the reaction of $K^+(AcO, AcOH)^-$ and PhCHO. Detection of the acid salt as a product (infact byproduct), however, is understandable as we, too, detected in the present work.

The rather "modern view" involving the formation

and participation of alkali salt of enolic acetic anhydride[13] appears unlikely because we failed to synthesize an alkali enolate by the direct reaction of Ac_2O and Na^+OAc^- or K^+OAc^- at 180 °C.[33] Since the condensation temperature (180 °C) is well below the fusion temperature of Na^+OAc^- (324 °C) and K^+OAc^- (299 °C), possible reaction routes involving $^-CH_2COO^-$ (which is believed to exist in fused M^+OAc^-) are also ruled out.

Experimental

Synthesis Procedure. Using 22.5 mmol (2.39 g) as a unit of weight for PhCHO, the PhCHO–Ac_2O–K^+OAc^- mixtures were fused at 180±2 °C in different proportions for different time periods (see Table 1) under a nitrogen atmosphere. The fused solid product was cooled and divided into two equal parts. One part was subjected to the recovery of cinnamic acid to determine its yield following the conventional procedure. The other part was subjected to qualitative examination for which the residue was first scrubbed with benzene or acetone (50 ml) and filtered. The washed residue was subjected to hot stage microscopy and infrared spectroscopy which indicated it to be potassium cinnamate plus $K^+(OAc, HOAc)^-$ (see Fig. 1). The organic filtrate, which contains the polymeric material and the unused PhCHO and Ac_2O plus potassium cinnamate complex involving PhCHO and Ac_2O, was evaporated to dryness in the open to destroy the unused reactant and to decompose the complex. The organic matter from this residue was eliminated by washing with benzene or acetone. The clarified residue was found to be pure potassium cinnamate, the amount of which was found to be in accordance with the amount of PhCHO and Ac_2O used in the reaction.

Condensation in Absence of Alkali Cation. Potassium acetate (1 mmol, 0.098 g) was scrubbed in the absence of moisture with benzo-15-crown-5 (2 mmol, 0.536 g). The solid mixture was treated with PhCHO (1 mmol, 0.106 g) and Ac_2O (1 mmol, 0.102 g). The reaction mixture was subjected to condensation at 180±2 °C for five hours and then processed for the recovery of cinnamic acid following the conventional procedure. A polymeric product instead of cinnamic acid was obtained.

Conductometric Solution State Studies. Stock solutions of the salt (10 mmol) and the ligands (2.5 mmol) were prepared in anhydrous 2-propanol. Complexation and stoichiometry of the resultant complex was followed adopting the conductometric monovariation titration technique[34] while solution stability of each complex was determined following the Matsuura's conductometric dilution technique.[35] For the monovariation technique 40 ml of the ligand solution was titrated with the salt solution (1—25 ml) while applying volume correction.[36] Since for each system which indicated complexation, the initially formed biligand (1:2) complex was converted to a 1:1 complex on the addition of more salt, Matsuura's method was followed to determine the stability of the apparently more stable 1:1 species only. Figure 2 shows the stoichiometry of the selected complexes while Fig. 3 displays the exemplary sets of the phoreograms obtained for the systems K^+OAc^-–PhCHO and K^+OAc^-–Ac_2O.

One of us (NSP) is thankful to the UGC (India) for financial support and others for Research Fellowships.

References

1) P. Sykes, "A Guidebook to Mechanism in Organic Chemistry," Longman, London (1965); E. S. Gould, "Mechanism and Structures in Organic Chemistry," Holt, Reinhart and Winstin, New York (1959).
2) N. S. Poonia, *J. Am. Chem. Soc.*, **96**, 1012 (1974); *J. Inorg. Nucl. Chem.*, **37**, 1855 (1975); *Inorg. Chim. Acta*, **23**, 5 (1977); *J. Sci. Ind. Res.*, **36**, 268 (1977).
3) Part I: N. S. Poonia, B. P. Yadav, G. C. Kumar, and V. W. Bhagwat, *J. Org. Chem.*, **42**, 2030 (1977).
4) Part III: N. S. Poonia and B. P. Yadav, *J. Org. Chem.*, **43**, 2842 (1978).
5) Part II: N. S. Poonia, K. Chhabra, G. C. Kumar, and V. W. Bhagwat, *J. Org. Chem.*, **42**, 3311 (1977).
6) Part IV: N. S. Poonia, A. K. Arora, and A. V. Bajaj, *Bull. Chem. Soc. Jpn.*, **53**, 569 (1980).
7) N. S. Poonia, P. K. Porwal, and S. Sen, unpublished data.
8) N. S. Poonia and A. V. Bajaj, *Chem. Rev.*, **79**, 389 (1979).
9) C. R. Hauser and W. H. Puterbaugh, *J. Am. Chem. Soc.*, **75**, 1068, 4756 (1953).
10) W. H. Puterbaugh and C. R. Hauser, *J. Org. Chem.*, **24**, 416 (1959); W. H. Puterbaugh and R. L. Readshaw, *J. Am. Chem. Soc.*, **82**, 3635 (1960).
11) W. H. Puterbaugh and W. S. Gaugh, *J. Org. Chem.*, **26**, 3513 (1961).
12) W. H. Perkin, *J. Chem. Soc.*, **21**, 53, 181 (1868).
13) J. R. Johnson, "Organic Reactions," ed by R. Roger Adams, John Wiley & Sons, Inc., New York (1942), Vol. I, p. 210.
14) T. I. Crowell, "The Chemistry of Alkenes," ed by S. Patai, Wiley Interscience, New York (1964), p. 260.
15) H. O. House, "Modern Synthetic Reactions," Benzamin, Menlopark (1965), p. 234.
16) R. C. Reeves "The Chemistry of Carbonyl Groups," ed by S. Patai, Wiley Interscience, New York (1966), p. 598.
17) A. I. Vogel, "Practical Organic Chemistry," Longman, London (1971); F. G. Mann and B. C. Saunders, " A Text Book of Practical Organic Chemistry," Longman, London (1971).
18) P. Kalnin, *Helv. Chim. Acta.*, **11**, 977 (1928).
19) R. Meyer and H. Beer, *Monatsh*, **34**, 649 (1913).
20) P. R. Mallinson and M. R. Truter, *J. Chem. Soc., Perkin Trans. 2*, **1972**, 1818.
21) B. N. Menschutkin, *Z. Anorg. Allg. Chem.*, **52**, 9, 155; **53**, 26 (1907).
22) E. Pfeil, *Chem. Ber.*, **84**, 229 (1951).
23) W. R. G. Bell, C. B. Rowlands, I. J. Bamford, W. G. Thomas, and W. J. Jones, *J. Chem. Soc.*, **1930**, 1927.
24) Tiemann and Herzfeld, *Ber.*, **10**, 285 (1877).
25) The experimental temperatures for the solution and synthesis studies are different, and in the former studies a degree of solvent effect is also incorporated, the parallelism between the results may be taken just to appreciate the trends of the reaction.
26) S. Gabriel, *Ber.*, **49**, 1608 (1916); I. Tanasesu, *Bull. Soc. Chim.*, **41**, 1075 (1927).
27) N. S. Poonia, "Progress in Macrocyclic Chemistry," ed by R. M. Izatt and J. J. Christensen, Wiley Interscience, New York (1979), Vol. I, Chap. 3.
28) Fittig, *Ann.*, **195**, 169 (1879); *Ber.*, **27**, 2658 (1897).
29) A. Michael and Hartman, *Ber.*, **34**, 918 (1901); A. Michael, *Am. Chem. J.*, **50**, 411 (1913).
30) D. S. Breslow and C. R. Hauser, *J. Am. Chem. Soc.*, **61**, 786 (1939).

31) W. H. Perkin, *J. Chem. Soc.*, **31**, 44 (1877); **49**, 317 (1886).
32) Nef, *Ann.*, **298**, 302 (1897); F. Bock, G. Lock, and K. Schmidt, *Monatsh*, **64**, 401 (1934).
33) The M^+OAc^-–Ac_2O solution containing excess Ac_2O yielded a small amount of $K^+(OAc, HOAc)^-$ in the case of K^+OAc^- the amount depending upon the water contamination incorporated through this salt.
33a) M. Bakunin and D. Peccerillo, *Gazz. Chim. Ital.*, **65**, 1145 (1935).
34) P. Job, *Ann. Chim.*, **9**, 113 (1928).
35) N. Matsuura, K. Umemoto, Y. Takeda, and A. Sasaki, *Bull. Chem. Soc. Jpn.*, **49**, 1246 (1976).
36) J. Bassett, R. C. Denney, G. H. Jeffery, and J. Mendham, "Vogels Text Book of Quantitative Inorganic Analysis including Elementary Instrumental Analysis," 4th ed, Longman, London (1978), p. 618.

Configuration Analysis and Electronic State Properties. III. Ten-π-electron Systems

Giuseppe Buemi
Istituto Dipartimentale di Chimica e Chimica Industriale, Università di Catania, Viale A. Doria 8, 95125 Catania, Italy

(Received November 8, 1979)

The electronic state properties of the nonbenzenoid hydrocarbons fulvalene, heptatriafulvalene, dimethylenebenzocyclobutene, [5]radialene, 8-vinylheptafulvene, 1,2-benzofulvene and 2,3-benzofulvene have been studied by means of MIM and PPP-configuration analyses. The resonance integrals evaluated by Kon's equation are satisfactory for the MIM method but not for PPP. On the whole the general spectral trend is fairly predicted by both approximations, the wavefunction composition being in line with the first electronic transitions. The lower energy electronic transitions are found to be a mixture of locally excited and charge transfer states while those computed at higher energy have prevailing charge transfer character.

The electronic state properties of several nonbenzenoid hydrocarbons having four, six and eight π-electrons have been studied[1,2] by means of PPP[3] and MIM methods,[3,4] employing the configuration analysis procedure[5] to interpret the results of PPP calculations directly in terms of the locally excited (Λ) and charge transfer (T_m^k) configurations of the localized orbital model. In this paper the same procedure is extended to the following molecules, having a ten-π-electron system: fulvalene (I), heptatriafulvalene (II), dimethylenebenzocyclobutene (III), [5]radialene (IV), 8-vinylheptafulvene (V), 1,2-benzofulvene (VI) and 2,3-benzofulvene (VII).

Ethylene, *cis*- or *trans*-butadiene and benzene were considered as component systems in MIM model. Their SCF-MOs excited states composition and all the parameters required by the adopted methods are the same as in previous papers.[1,2] The experimental transition energies of ethylene are taken from Ref. 6. Both in MIM and PPP approximations all the monoexcited configurations were considered in the configuration interaction treatment, but in the former method the lowest occupied and highest vacant molecular orbitals of the benzene systems were excluded since they are not necessary for its UV spectrum description.

The topology of the compounds examined is shown in Fig. 1. The ground state charge densities and bond orders obtained are given in Table 1.

Fulvalene (1,1'-Bicyclopentadienylidene) (I). This molecule has been the subject of numerous studies at different level of calculations[7–13] including CNDO/CI;[14] its negative topological resonance energy (TRE) indicates that it is an antiaromatic and very reactive compound.[15] The UV spectrum shows a weak absorption band at 2.9—3.0 eV and an intense band at 3.9—4.0 eV.[7,14] My calculation for which the molecular geometry reported by Brown et Coll.[7] was adopted has been performed by assuming, at MIM level, five ethylene molecules (MIM/A) or two *cis*-butadiene and one ethylene molecules (MIM/B) as component systems. The results obtained are compared with those of PPP-configuration analysis (Table 2). PPP correctly predicts the experimental order of the electronic transitions in contrast to MIM, by which the lowest energy electronic transition was obtained as the most intense one. From the energy order of PPP results, the first electronic transition having prevailing charge transfer character is computed at 3.63 eV (calculated

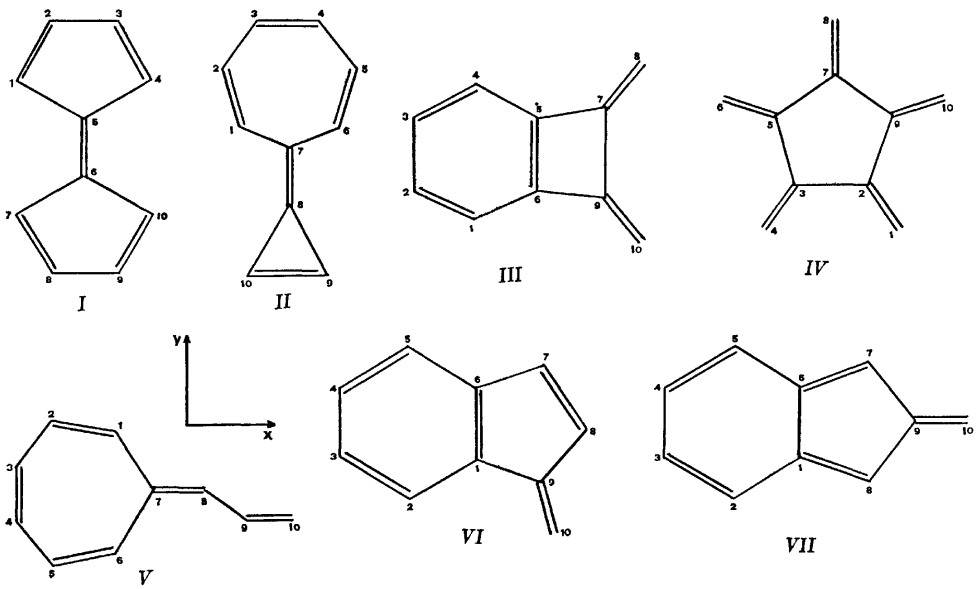

Fig. 1. Topology of the studied molecules.

TABLE 1. GROUND STATE CHARGE DENSITIES (q_i) AND BOND ORDERS (p_{ij}) OF THE STUDIED COMPOUNDS

q_i	PPP	MIM/A	MIM/B	MIM/C	p_{ij}	PPP	MIM/A	MIM/B	MIM/C
					Fulvalene (I)				
1	1.028	1.001[a]	1.013[b]		1—2	0.926	0.962[a]	0.945[b]	
2	0.998	1.013	1.007		2—3	0.296	0.179	0.247	
5	0.948	0.971	0.960		1—5	0.244	0.173	0.205	
					5—6	0.882	0.928	0.902	
					Heptatriafulvalene (II)				
1	0.967	1.001[a]			1—2	0.898	0.966[a]		
2	1.040	1.007			2—3	0.330	0.160		
3	1.002	0.998			3—4	0.893	0.967		
7	1.168	1.141			6—7	0.300	0.166		
8	0.995	0.955			7—8	0.822	0.910		
9	0.910	0.946			8—9	0.299	0.217		
					9—10	0.910	0.946		
					Dimethylenebenzocyclobutene (III)				
1	1.000	1.000[c]	1.002[d]		1—2	0.662	0.665[c]	0.651[d]	
2	1.000	1.000	1.002		2—3	0.665	0.656	0.671	
6	1.000	1.000	1.000		1—6	0.658	0.664	0.671	
9	1.000	1.000	1.000		5—6	0.637	0.657	0.651	
10	1.000	1.000	0.996		6—9	0.188	0.129	0.134	
					7—9	0.154	0.166	0.222	
					9—10	0.970	0.971	0.958	
					[5]Radialene (IV)				
1	1.000	1.000[a]			1—2	0.945	0.965[a]		
					2—3	0.230	0.171		
					8-Vinylheptafulvene (V)				
1(=6)	0.991	1.001[a]			1—2(=5—6)	0.939	0.961[a]		
2(=5)	0.999	0.997			2—3(=4—5)	0.261	0.185		
3(=4)	0.997	0.997			3—4	0.934	0.960		
7	1.000	1.001			1—7(=6—7)	0.233	0.177		
8	1.022	1.007			7—8	0.920	0.946		
9	0.997	1.000			8—9	0.229	0.171		
10	1.007	1.001			9—10	0.973	0.982		
					1,2-Benzofulvene (VI)				
1	1.010	1.000[c]	1.005[d]		1—2	0.647	0.664[c]	0.663[d]	
2	1.002	0.998	0.998		2—3	0.672	0.664	0.663	
3	1.001	1.000	1.006		3—4	0.658	0.654	0.650	
4	1.003	1.006	1.005		4—5	0.674	0.665	0.665	
5	0.997	1.000	0.997		5—6	0.644	0.663	0.661	
6	1.005	1.005	1.004		1—6	0.631	0.654	0.651	
7	1.004	1.008	1.003		6—7	0.255	0.153	0.175	
8	1.014	1.000	1.004		7—8	0.941	0.956	0.950	
9	1.001	1.000	1.003		8—9	0.231	0.213	0.228	
10	0.965	0.982	0.976		1—9	0.230	0.141	0.159	
					9—10	0.944	0.957	0.952	
					2,3-Benzofulvene (VII)				
1	1.004	1.015[a]	1.010[b]	1.020[e]	1—2	0.249	0.168[a]	0.216[b]	0.238[e]
2	0.999	1.000	1.001	1.000	2—3	0.936	0.965	0.942	0.947
3	1.004	1.001	1.001	1.003	3—4	0.273	0.173	0.257	0.212
8	1.024	1.000	1.012	1.002	1—6	0.272	0.184	0.242	0.219
9	1.000	0.999	1.007	0.998	1—8	0.902	0.944	0.918	0.919
10	0.938	0.968	0.947	0.951	8—9	0.238	0.171	0.198	0.194
					9—10	0.940	0.963	0.951	0.952

a) Five ethylene molecules considered as component systems. b) Two *cis*-butadiene molecules and ethylene as component systems. c) Benzene and two ethylenes as component systems. d) Benzene *trans*-butadiene as component systems. e) Two *trans*-butadiene molecules and ethylene as component systems.

Table 2. First excited

	Ψ_3		Ψ_4		Ψ_6		Ψ_8	
	MIM	PPP	MIM	PPP	MIM	PPP	MIM	PPP
							MIM/A: Five ethylene	
Γ	—	—	0.04	0.16	0.04	0.10	—	—
$(1/2)(\Lambda_a+\Lambda_b+\Lambda_d+\Lambda_e)$	—	—	0.12	—	0.04	0.01	—	—
Λ_c	0.27	0.17	—	—	—	—	0.13	0.12
$(1/2)(\Lambda_a+\Lambda_b-\Lambda_d-\Lambda_e)$	0.05	0.03	—	—	—	—	0.01	0.03
$(1/2)(T^b_a+T^a_b+T^e_d+T^d_e)$	—	—	0.28	0.28	0.26	0.08	—	—
$(1/2)(T^b_a+T^a_b-T^e_d-T^d_e)$	0.09	0.11	—	—	—	—	0.85	0.44
$(1/2)(T^c_a+T^c_b+T^c_d+T^c_e)$	0.14	0.09	—	—	—	—	—	0.03
$(1/2)(T^c_a+T^c_b-T^c_d-T^c_e)$	—	—	0.34	0.12	0.06	0.13	—	—
$(1/2)(T^d_a+T^e_b+T^a_d+T^b_e)$	—	—	—	—	0.07	0.09	—	—
$(1/2)(T^d_a+T^e_b-T^a_d-T^b_e)$	0.03	0.03	—	—	—	—	—	—
$(1/2)(T^e_a+T^d_b+T^a_e+T^b_d)$	—	—	—	—	0.08	0.08	—	—
$(1/2)(T^e_a+T^d_b-T^a_e-T^b_d)$	0.02	0.02	—	—	—	—	—	—
$(1/2)(T^a_c+T^b_c+T^d_c+T^e_c)$	—	—	0.22	0.08	0.46	0.20	—	—
$(1/2)(T^a_c+T^b_c-T^d_c-T^e_c)$	0.40	0.30	—	—	—	—	0.01	0.06
Total weight (%)	100	75	100	64	100	69	100	70
E	3.11	4.76	5.31	6.44	6.11	6.83	6.22	7.23
Polarization	y	y	—	—	—	—	y	y
Symmetry	$^1B_{2u}$		$^1A_{1g}$		$^1A_{1g}$		$^1B_{2u}$	
f	0.60	1.13	0	0	0	0	0.16	0.43
							MIM/B: Two *cis*-butadiene molecules	
Γ	—	—	0.01	0.03	0.14	0.15	—	—
$(1/\sqrt{2})(\Lambda_{2a}+\Lambda_{2c})$	—	—	0.37	0.52	0.03	0.03	—	—
$(1/\sqrt{2})(\Lambda_{3a}+\Lambda_{3c})$	—	—	0.07	—	—	0.01	—	—
$(1/\sqrt{2})(\Lambda_{2a}-\Lambda_{2c})$	0.07	0.12	—	—	—	—	0.36	0.49
$(1/\sqrt{2})(\Lambda_{3a}-\Lambda_{3c})$	0.04	0.03	—	—	—	—	0.01	0.03
Λ_b	0.26	0.20	—	—	—	—	0.03	0.15
$(1/\sqrt{2})(T^b_{1a}+T^b_{1c})$	0.15	0.11	—	—	—	—	0.32	0.04
$(1/\sqrt{2})(T^{3c}_{1a}-T^{3a}_{1c})$	0.06	0.06	—	—	—	—	0.01	0.01
$(1/\sqrt{2})(T^{4c}_{2a}-T^{4a}_{2c})$	—	—	—	—	—	—	—	—
$(1/\sqrt{2})(T^{3a}_b-T^{3c}_b)$	0.42	0.33	—	—	—	—	0.27	0.08
$(1/\sqrt{2})(T^{3c}_{1a}+T^{3a}_{1c})$	—	—	—	—	0.42	0.20	—	—
$(1/\sqrt{2})(T^b_{1a}-T^b_{1c})$	—	—	0.25	0.09	0.15	0.15	—	—
$(1/\sqrt{2})(T^{4c}_{2a}+T^{4a}_{2c})$	—	—	—	—	—	—	—	—
$(1/\sqrt{2})(T^{3a}_b+T^{3c}_b)$	—	—	0.30	0.16	0.26	0.19	—	—
Total weight (%)	100	85	100	80	100	73	100	80
ΔE	2.77	4.76	4.66	6.44	6.24	6.83	5.92	7.23
Polarization	y	y	—	—	—	—	y	y
Symmetry	$^1B_{2u}$		$^1A_{1g}$		$^1A_{1g}$		$^1B_{2u}$	
f	0.60	1.13	0	0	0	0	<0.01	0.43

a) a, b, c, d, and e denote the ethylenic fragments C_1=C_2, C_3=C_4, C_5=C_6, C_7=C_8, and C_9=C_{10}, respectively.

at 3.57—2.91 eV by MIM/A and MIM/B, respectively) and should be assigned to the forbidden $^1B_{1g}\leftarrow{}^1A_{1g}$ transition.

The second electronic transition, polarized along the short molecular axis (x) and computed at 3.81 eV by PPP and at 3.39—3.03 eV (in agreement with experimental result) by MIM/A and MIM/B, is assigned to a $^1B_{3u}\leftarrow{}^1A_{1g}$ transition. It shows noticeable percentage of locally excited states but the largest weights are those due to electronic transfers partially localized inside the two cyclopentadienyl systems and partially directed towards the "external" molecular ethylenic fragment joining the two pentatomic rings. This composition closely resembles that of the lowest energy $^1B_2\leftarrow{}^1A_1$ transition in fulvene, calculated in the range 2.9—3.3 eV.[1]

The most intense third electronic transition, corresponding to the strong absorption band at ≃4.0 eV, is predicted at 4.76 eV by PPP, very close to the value of 4.93 eV obtained by Marschner and Pohle,[10] and at 3.11—2.77 eV by MIM/A and MIM/B. It is a $^1B_{2u}\leftarrow{}^1A_{1g}$ transition polarized along the y molecular axis and results principally from the electronic transfer from the "external" ethylene fragment to the two cyclopentadienyl rings. A similar situation is encountered in the $^1A_1\leftarrow{}^1A_1$ transition of fulvene,[1]

SINGLET STATES OF FULVALENE

	Ψ_1		Ψ_2		Ψ_5		Ψ_7	
	MIM	PPP	MIM	PPP	MIM	PPP	MIM	PPP
molecules as component systems[a]								
$(1/2)(\Lambda_a-\Lambda_b+\Lambda_d-\Lambda_e)$	—	—	0.37	0.16	—	—	0.17	0.30
$(1/2)(\Lambda_a-\Lambda_b-\Lambda_d+\Lambda_e)$	0.30	0.20	—	—	0.14	0.28	—	—
$(1/2)(T^b_a-T^a_b+T^d_e-T^e_d)$	0.34	0.14	—	—	0.19	0.08	—	—
$(1/2)(T^b_a-T^a_b-T^d_e+T^e_d)$	—	—	0.32	0.13	—	—	0.11	0.10
$(1/2)(T^d_a-T^e_b+T^a_d-T^b_e)$	—	—	0.01	0.04	—	—	0.14	0.12
$(1/2)(T^d_a-T^e_b-T^a_d+T^b_e)$	0.02	0.04	—	—	0.14	0.09	—	—
$(1/2)(T^e_a-T^d_b+T^a_e-T^b_d)$	0.02	0.03	—	—	0.15	0.11	—	—
$(1/2)(T^e_a-T^d_b-T^a_e+T^b_d)$	—	—	0.02	0.04	—	—	0.15	0.07
$(1/2)(T^c_a-T^c_b+T^c_d-T^c_e)$	0.32	0.26	—	—	0.38	0.17	—	—
$(1/2)(T^c_a-T^c_b-T^c_d+T^c_e)$	—	—	0.28	0.29	—	—	0.43	0.12
$(1/2)(T^a_c-T^b_c+T^d_c-T^e_c)$	—	—	—	—	—	—	—	0.03
$(1/2)(T^a_c-T^b_c-T^d_c+T^e_c)$	—	—	—	—	—	0.01	—	—
	100	67	100	66	100	74	100	74
	3.57	3.63	3.39	3.81	5.86	6.69	5.78	7.02
	—	—	x	x	—	—	x	x
	$^1B_{1g}$		$^1B_{3u}$		$^1B_{1g}$		$^1B_{3u}$	
	0	0	0.08	0.06	0	0	0.15	0.30
(a and c) and ethylene (b) as component systems.								
$(1/\sqrt{2})(\Lambda_{1a}+\Lambda_{1c})$	—	—	0.22	0.33	—	—	0.55	0.42
$(1/\sqrt{2})(\Lambda_{4a}+\Lambda_{4c})$	—	—	—	—	—	—	—	0.03
$(1/\sqrt{2})(\Lambda_{1a}-\Lambda_{1c})$	0.28	0.39	—	—	0.55	0.37	—	—
$(1/\sqrt{2})(\Lambda_{4a}-\Lambda_{4c})$	—	—	—	—	—	0.04	—	—
$(1/\sqrt{2})(T^c_{1a}-T^a_{1c})$	—	—	—	—	—	—	—	—
$(1/\sqrt{2})(T^b_{2a}+T^b_{2c})$	0.58	0.31	—	—	0.05	0.20	—	—
$(1/\sqrt{2})(T^c_{2a}-T^a_{2c})$	0.14	0.09	—	—	0.40	0.21	—	—
$(1/\sqrt{2})(T^a_b-T^c_b)$	—	—	—	—	—	0.01	—	—
$(1/\sqrt{2})(T^c_{1a}+T^a_{1c})$	—	—	—	—	—	—	—	0.01
$(1/\sqrt{2})(T^c_{2a}+T^a_{2c})$	—	—	0.16	0.10	—	—	0.44	0.22
$(1/\sqrt{2})(T^b_{2a}-T^b_{2c})$	—	—	0.62	0.36	—	—	0.01	0.14
$(1/\sqrt{2})(T^a_b+T^c_b)$	—	—	—	—	—	—	—	0.03
	100	79	100	79	100	83	100	85
	2.91	3.63	3.03	3.81	5.35	6.69	5.61	7.02
	—	—	x	x	—	—	x	x
	$^1B_{1g}$		$^1B_{3u}$		$^1B_{1g}$		$^1B_{3u}$	
	0	0	0.01	0.06	0	0	0.21	0.30

computed by MIM at 3.6—4.0 eV shifting to lower energy in fulvalene by the higher percentage of charge transfer states.

Three electronic transitions, all with predominant charge transfer character and theoretically forbidden, were calculated at 6.44, 6.69 and 6.83 eV by PPP and at 5.31—4.66 eV, 5.86—5.35 eV and 6.11—6.24 eV by MIM/A and MIM/B, respectively. They are assigned to $^1A_{1g}\leftarrow{}^1A_{1g}$, $^1B_{1g}\leftarrow{}^1A_{1g}$, and $^1A_{1g}\leftarrow{}^1A_{1g}$ transitions, in order of sequence.

Two other allowed transitions follow at 7.02 and 7.23 eV calculated by PPP, and at 5.78—5.69 and 6.22—5.92 eV by MIM (the first figure refers to MIM/A, the second to MIM/B). The former, of $^1B_{3u}\leftarrow{}^1A_{1g}$ type, x-polarized, is the predicted charge transfer if MIM/A results are taken into account, a mixture of locally excited (Λ_{1a}, Λ_{1c}) and charge transfer states if the MIM/B results are considered. In both cases, however, its composition resembles that of the $^1B_2\leftarrow{}^1A_1$ transition in fulvene at 6.45 eV[1] with some percentage variation due to the presence of two pentatomic rings in fulvalene. The latter, $^1B_{2u}\leftarrow{}^1A_{1g}$, y-polarized transition, is nearly exclusively due to charge transfers between the ethylene molecules constituting the cyclopentadienyl rings (MIM/A results), and to charge transfers involving the whole π-system with a greater

percentage of locally excited states (MIM/B results). The composition is similar in the corresponding $^1A_1 \leftarrow {}^1A_1$ transition at 6.28 eV in fulvene.[1] It is evident that all the allowed transitions found in fulvalene correspond to the electronic transitions of fulvene as well as in energy and composition.

Heptatriafulvalene (II). The PPP results[16] subjected to configuration analysis are compared with the MIM ones, the energies and oscillator strengths obtained by using Kon's resonance integrals being given (Table 3). Since no experimental spectrum of heptatriafulvalene has been found in the literature a comparison with the theoretical data is not possible, however a discussion about the theoretical transitions is possible with reference to the heptafulvene and triafulvene molecules. The first electronic transition,

Table 3. First singlet excited states of heptatriafulvalene. Five ethylene molecules as component systems[a]

States of $^1A_1$ symmetry	Ψ_3		Ψ_5		States of $^1B_2$ symmetry	Ψ_1		Ψ_2		Ψ_4	
	MIM	PPP	MIM	PPP		MIM	PPP	MIM	PPP	MIM	PPP
Γ	0.01	—	0.02	0.15	$(1/\sqrt{2})(\Lambda_a-\Lambda_c)$	0.21	0.09	—	—	0.05	0.11
$(1/\sqrt{2})(\Lambda_a+\Lambda_c)$	0.06	0.02	0.25	0.06	Λ_b	0.15	0.05	—	—	0.14	0.11
Λ_d	0.28	0.14	0.10	0.08	Λ_e	0.01	—	0.33	0.11	—	—
$(1/\sqrt{2})(T_c^a+T_a^c)$	0.06	0.08	—	0.10	$(1/\sqrt{2})(T_c^a-T_a^c)$	0.05	0.04	—	—	0.01	—
$(1/\sqrt{2})(T_a^d+T_c^d)$	0.18	0.10	—	0.02	$(1/\sqrt{2})(T_a^b+T_c^b)$	0.20	0.09	—	—	0.01	—
$(1/\sqrt{2})(T_a^b-T_c^b)$	—	0.02	0.24	0.10	$(1/\sqrt{2})(T_a^e+T_c^e)$	—	—	0.06	0.11	—	—
$(1/\sqrt{2})(T_a^e-T_c^e)$	—	—	—	—	$(1/\sqrt{2})(T_a^d-T_c^d)$	—	—	—	—	0.02	0.05
$(1/\sqrt{2})(T_b^a+T_b^c)$	0.06	0.06	0.14	0.02	$(1/\sqrt{2})(T_b^a-T_b^c)$	0.12	0.05	—	—	0.12	0.13
T_b^d	0.03	0.04	0.03	—	T_b^e	—	—	—	0.03	—	—
$(1/\sqrt{2})(T_d^a+T_d^c)$	0.14	0.10	0.05	—	$(1/\sqrt{2})(T_d^a-T_d^c)$	0.15	0.13	—	—	0.36	0.11
$(1/\sqrt{2})(T_e^a+T_e^c)$	0.05	0.03	—	—	T_d^b	0.06	0.06	—	—	0.09	0.08
T_e^d	0.13	0.06	0.17	0.01	T_d^e	0.01	—	0.61	0.30	—	—
					$(1/\sqrt{2})(T_e^a-T_e^c)$	0.03	0.03	—	—	0.15	0.04
					T_e^b	0.01	0.02	—	—	0.05	0.03
Total weight (%)	100	65	100	54		100	56	100	55	100	66
ΔE[b]	3.22	4.27 (5.07)	5.36	5.96 (6.58)		3.37	2.38 (3.68)	4.15	3.45 (5.05)	4.94	5.91 (6.43)
f[b]	0.53	0.91 (0.97)	0.10	0.74 (0.54)		0.02	0.01 (0.02)	0.09	0.05 (0.07)	0.14	0.13 (0.13)
Polarization	y	y	y	y		x	x	x	x	x	x

a) a, b, c, d, and e denote the fragments C_1=C_2, C_3=C_4, C_5=C_6, C_7=C_8, and C_9=C_{10}, respectively. b) Values obtained by using Kon's resonance integrals given in parentheses.

Table 5. First singlet excited states of [5] radialene.

	Ψ_1		Ψ_2		Ψ_3		Ψ_4	
	MIM	PPP	MIM	PPP	MIM	PPP	MIM	PPP
Γ	—	—	—	—	—	—	—	—
$(1/\sqrt{2})(\Lambda_a+\Lambda_b)$	0.03	0.03	0.25	0.22	0.01	—	0.01	0.02
$(1/\sqrt{2})(\Lambda_c+\Lambda_e)$	0.24	0.21	0.04	0.03	0.03	0.01	—	—
Λ_d	0.18	0.17	0.19	0.17	0.02	0.01	0.01	0.02
$(1/\sqrt{2})(T_a^b+T_b^a)$	—	—	—	—	0.21	0.18	0.28	0.21
$(1/\sqrt{2})(T_a^c+T_b^e)$	—	—	0.02	0.02	0.08	0.07	0.08	0.08
$(1/\sqrt{2})(T_a^e+T_b^c)$	0.05	0.04	0.16	0.10	0.16	0.12	0.03	0.02
$(1/\sqrt{2})(T_c^a+T_e^b)$	0.02	0.01	0.01	0.01	0.17	0.13	0.01	—
$(1/\sqrt{2})(T_e^a+T_c^b)$	0.08	0.06	0.17	0.12	0.12	0.11	0.02	0.02
$(1/\sqrt{2})(T_c^e+T_e^c)$	0.03	0.02	0.02	0.02	0.03	0.03	0.02	0.02
$(1/\sqrt{2})(T_a^d+T_b^a)$	0.01	0.01	—	—	—	—	0.06	0.05
$(1/\sqrt{2})(T_c^d+T_e^d)$	0.15	0.12	0.08	0.06	0.03	0.02	0.18	0.13
$(1/\sqrt{2})(T_d^a+T_d^b)$	0.04	0.02	0.01	0.01	0.13	0.10	0.11	0.09
$(1/\sqrt{2})(T_d^c+T_d^e)$	0.17	0.12	0.05	0.03	0.01	0.02	0.19	0.14
Total weight (%)	100	81	100	79	100	80	100	80
ΔE	3.57	5.09	4.81	5.95	5.32	6.24	6.04	7.05
f	0	0	0.84	1.34	0	0	0.03	0.08
Polarization	—	—	y	y	—	—	y	y

a) a, b, c, d, and e denote the C_1=C_2, C_3=C_4, C_5=C_6, C_7=C_8, and C_9=C_{10} fragments respectively.

TABLE 4. FIRST SINGLET EXCITED STATES OF DIMETHYLENEBENZOCYCLOBUTENE

States of $^1A_1$ symmetry	Ψ_1		Ψ_3		Ψ_5		States of $^1B_2$ symmetry	Ψ_2		Ψ_4	
	MIM	PPP	MIM	PPP	MIM	PPP		MIM	PPP	MIM	PPP
	MIM/A: Benzene (a) and two ethylenes (b, c) as component systems										
Γ	—	—	—	—	0.01	0.02	Λ_{2a}	0.01	0.78	0.53	0.02
Λ_{1a}	0.82	0.84	—	—	0.12	0.03	Λ_{4a}	—	0.01	0.10	0.46
Λ_{3a}	—	—	0.25	0.46	—	—	$(1/\sqrt{2})(\Lambda_b-\Lambda_c)$	0.54	0.01	—	0.02
$(1/\sqrt{2})(\Lambda_b+\Lambda_c)$	—	—	0.23	0.18	—	—	$(1/\sqrt{2})(T^b_{1a}+T^c_{1a})$	0.08	0.01	—	0.05
$(1/\sqrt{2})(T^b_{1a}-T^c_{1a})$	0.03	0.02	0.03	0.04	—	—	$(1/\sqrt{2})(T^b_{2a}-T^c_{2a})$	0.01	0.03	0.15	0.05
$(1/\sqrt{2})(T^b_{2a}+T^c_{2a})$	0.05	0.01	0.22	0.09	0.28	0.27	$(1/\sqrt{2})(T^{3a}_b+T^{3a}_c)$	0.01	0.03	0.15	0.05
$(1/\sqrt{2})(T^{4a}_b+T^{4a}_c)$	0.03	0.02	0.04	0.04	—	—	$(1/\sqrt{2})(T^{4a}_b-T^{4a}_c)$	0.08	0.01	—	0.05
$(1/\sqrt{2})(T^{3a}_b-T^{3a}_c)$	0.05	0.01	0.23	0.09	0.28	0.27	$(1/\sqrt{2})(T^c_b-T^b_c)$	0.27	0.01	0.07	0.18
$(1/\sqrt{2})(T^c_b+T^b_c)$	0.02	—	—	—	0.31	0.26					
Total weight (%)	100	90	100	90	100	85		100	89	100	88
ΔE	4.34	4.60	4.93	6.08	5.65	6.73		4.68	4.84	5.36	6.38
f	$\simeq 0$	$\simeq 0$	1.17	1.67	$\simeq 0$	$\simeq 0$		0.46	0.03	0.10	0.31
Polarization	—	—	x	x	—	—		y	y	y	y
	MIM/B: Benzene (a) and *cis*-butadiene (b) as component systems										
Γ	—	—	0.01	—	0.03	0.07	Λ_{2a}	0.06	0.79	0.33	0.02
Λ_{1a}	0.60	0.86	0.12	—	0.20	0.03	Λ_{4a}	0.02	0.01	0.12	0.47
Λ_{3a}	—	—	0.11	0.46	0.04	—	Λ_{1b}	0.40	—	0.09	0.17
Λ_{2b}	0.07	—	—	—	0.29	0.22	Λ_{4b}	—	0.02	0.06	0.04
Λ_{3b}	—	—	0.10	0.18	0.02	—	T^{3b}_{1a}	0.08	0.01	—	0.05
T^{4b}_{1a}	0.04	0.02	—	0.04	0.01	—	T^{4b}_{2a}	—	0.03	0.13	0.05
T^{3b}_{2a}	0.02	0.01	0.19	0.09	0.32	0.25	T^{3a}_{1b}	0.01	0.04	0.27	0.05
T^{4a}_{1b}	0.04	0.02	0.06	0.04	0.01	—	T^{4a}_{2b}	0.43	0.01	—	0.05
T^{3a}_{2b}	0.23	0.01	0.41	0.09	0.08	0.25					
Total weight (%)	100	92	100	90	100	82		100	90	100	90
ΔE	4.16	4.60	4.57	6.08	5.22	6.73		4.56	4.84	4.92	6.67
f	0.04	$\simeq 0$	0.82	1.67	0.14	$\simeq 0$		0.15	0.03	0.08	0.31
Polarization	x	x	x	x	x	x		y	y	y	y

FIVE ETHYLENES AS COMPONENT SYSTEMS[a)]

	Ψ_1		Ψ_2		Ψ_3		Ψ_4	
	MIM	PPP	MIM	PPP	MIM	PPP	MIM	PPP
$(1/\sqrt{2})(\Lambda_a-\Lambda_b)$	0.33	0.31	0.13	0.12	0.04	0.02	0.01	0.01
$(1/\sqrt{2})(\Lambda_c-\Lambda_e)$	0.13	0.12	0.35	0.31	0.02	0.01	0.02	0.03
$(1/\sqrt{2})(T^b_a-T^a_b)$	0.18	0.13	0.19	0.12	—	—	—	—
$(1/\sqrt{2})(T^c_a-T^a_b)$	0.03	0.02	—	—	0.08	0.06	0.03	0.02
$(1/\sqrt{2})(T^e_a-T^a_b)$	0.14	0.09	0.03	0.02	0.06	0.06	0.25	0.19
$(1/\sqrt{2})(T^a_c-T^b_c)$	0.02	0.01	0.02	0.03	—	—	0.11	0.09
$(1/\sqrt{2})(T^a_e-T^b_c)$	0.10	0.08	0.01	—	0.09	0.06	0.26	0.19
$(1/\sqrt{2})(T^e_c-T^e_e)$	—	—	—	0.01	0.13	0.11	0.09	0.08
$(1/\sqrt{2})(T^d_a-T^d_b)$	0.03	0.01	0.02	0.02	0.16	0.13	0.05	0.05
$(1/\sqrt{2})(T^d_c-T^d_e)$	0.03	0.02	0.11	0.06	0.18	0.16	0.10	0.08
$(1/\sqrt{2})(T^a_d-T^b_d)$	—	—	0.01	0.01	0.03	0.03	—	—
$(1/\sqrt{2})(T^c_d-T^e_d)$	0.01	0.01	0.13	0.10	0.21	0.16	0.08	0.06
	100	80	100	80	100	80	100	80
	3.57	5.09	4.81	5.95	5.32	6.24	6.04	7.05
	0	0	0.84	1.34	0	0	0.03	0.08
	—	—	x	x	—	—	x	x

having $^1B_2$ symmetry, is calculated by PPP at 2.38 eV[16] or at 3.68 eV (2.09 eV according to CNDO/CI calculations[14]), whilst MIM predicts it at 3.37 eV. Its prevailing charge transfer tendency is evident, but the ethylenic fragment *e* (component of the cyclopropenyl ring) does not appreciably participate to the wavefunction composition. The transition seems to be the same as that at 3.46—3.98 eV (MIM-PPP)[2] and experimentally observed at 2.91 eV[16] in heptafulvene. It would lie at *ca.* 2.8—2.9 eV in the heptatriafulvalene absorption spectrum, probably as a shoulder.

The second electronic transition, computed at 4.15 eV by MIM, at 3.45 eV[16] or 5.05 eV by PPP and at 3.45 eV by CNDO/CI[14] corresponds to the analogous $^1B_2 \leftarrow ^1A_1$ transition found in triafulvene at 4.83—5.48 eV (standard MIM and PPP calculations respectively[1]) and at 4.08 eV in calicene.[2] Even if a consistent percentage of the locally excited state Λ_e is present, the remarkable electronic transfer from ethylene *d* to ethylene *e* determines a spectral shift of about 2 eV with respect to the component molecules.

The third theoretical transition, of $^1A_1 \leftarrow ^1A_1$ type, polarized along the y axis, is the most intense, showing conjugative character. It was calculated at 3.91 eV by CNDO/CI[14] and at 4.27 eV[16] or 5.07 eV by PPP. By MIM it is predicted at 3.22 eV as the lowest energy transition with a strong bathochromic shift with respect to the corresponding transition in heptafulvene (3.94 eV[2]).

The fourth ($^1B_2 \leftarrow ^1A_1$) and fifth ($^1A_1 \leftarrow ^1A_1$) electronic transitions, computed by PPP at 5.91 and 5.96 eV[16] or 6.43 and 6.58 eV (Kon's resonance integrals) and by MIM at 4.94 and 5.36 eV, still have predominating charge transfer character involving the whole π-system shifted at lower energy with respect to the analogous transitions found in heptafulvene.

As in calicene,[2] the triatomic ring is positively charged and the total weight of the PPP-CA states is found to be rather low.

Dimethylenebenzocyclobutene (III). Theoretical and experimental geometrical data concerning the dimethylenebenzocyclobutene molecule are lacking. An improved LCAO method,[17] taking into account both σ and π energy applied to determine the molecular structure and the UV spectrum, shows that the benzene bond lengths are not appreciably different from their standard value of 1.397 Å, the cyclobutene ring being nearly square. The PPP-SCF-MO-LCAO method, modified to take into account the effect of neighbouring atoms[18] gives different results depending on the starting geometry. Since in planar molecules slight differences in bond angles of bond lengths do not appreciably affect the calculated spectra, the benzene ring was chosen as a regular hexagon with all bond lengths equal to 1.4 Å while the values found by electron diffraction studies[19] were taken for the remaining bond lengths and bond angles relative to the dimethylenecyclobutane fragment. At MIM level benzene and two ethylene molecules (MIM/A), or benzene and *cis*-butadiene (MIM/B) were considered as component systems. Similar results obtained in the two cases are compared with the PPP ones (after application of configuration analysis) in Table 4.

The experimental UV absorption spectrum in ethanol[20] exhibits very close maxima in the range 3.7—4.0 eV which would be partially due to bond vibrations. The first weak electronic transition, calculated at 4.34—4.16 eV by MIM and at 4.60 eV by PPP, could be correlated with the absorption in the above region. It closely resembles the bonzenic α band as supported by the large weight relative to the benzenic configuration Λ_{1a} and it is assigned to a $^1A_1 \leftarrow ^1A_1$ transition.

The second, $^1B_2 \leftarrow ^1A_1$, y-polarized transition, calculated at 4.68—4.56 eV by MIM/A and MIM/B, respectively, and at 4.84 eV by PPP, corresponds to the absorption band experimentally observed at 4.52 eV.[20] According to MIM results the predominating weights in its wavefunction composition are those due to locally excited ethylenic (MIM/A) or butadienic (MIM/B) configurations together with electronic transfers between the two ethylenic component systems (MIM/A) or from butadiene to benzene (MIM/B). PPP results, on the contrary, attributes to this transition a benzenic nature. This on the basis that the predominant weight in the relative wavefunction is that of the Λ_{2a} configuration which corresponds to the benzenic p-band.

The third electronic transition is predicted as the most intense transition and is polarized along the x-axis ($^1A_1 \leftarrow ^1A_1$). It is estimated by MIM at 4.93—4.57 eV and by PPP at higher energy (6.08 eV) as a mixture of locally excited and charge transfer states and should be correlated with the intense absorption band observed at 5.4 eV ($\log \varepsilon = 4.8$).

The fourth is a $^1B_2 \leftarrow ^1A_1$, y-polarized, weak transition calculated at 5.36—4.92 eV (MIM/A and MIM/B) and 6.38 eV (PPP). It originates from locally excited and charge transfer configurations involving all the component systems.

The fifth $^1A_1 \leftarrow ^1A_1$ transition is predicted at 5.65—5.22 eV (MIM) and 6.76 eV (PPP) as a forbidden transition, even though an oscillator strength of 0.14 is given by MIM/B. MIM/A points out the charge transfer character of this transition in contrast with MIM/B results predicting an equilibrium between charge transfer and locally excited configurations. The transitions having $^1B_2$ symmetry show different compositions in MIM and PPP approaches. Particularly, while the $^1B_2 \leftarrow ^1A_1$ transitions exhibit a comparable energy calculated by the MIM and PPP methods, the composition of their wavefunctions seem to be interchanged, *i.e.* the composition calculated by the MIM for the transition at 4.56—4.84 eV agrees better with the one calculated by PPP for the transition at $\simeq$6.6 eV, and *vice versa*. In any case however, the agreement is scarcely satisfactory. The second and third electronic transitions of $^1A_1$ symmetry have a composition approximatively comparable with that of the corresponding ones of dimethylenecyclobutene.

The biexcited configurations calculated by configuration analysis (not included in PPP and MIM calculations) have negligible weight (each of them appears with a percentage lower than 1%) so that they should not affect the results. From PPP results,

in which all the monoexcited configurations were included some wavefunctions relative to transitions at energies higher than those given in Table 4, show a noticeable percentage of configurations involving the lowest occupied and the highest vacant benzenic molecular orbitals. A calculation at MIM level in which these configurations were taken into account gave no appreciable variation in energy or composition of the first excited states.

[5]Radialene(Pentamethylenecyclopentane) (IV). The [5]radialene molecule, not known as yet, has been assumed as a regular pentagon with single bond lengths of 1.467 Å and double bonds of 1.366 Å.[21]

The first degenerate electronic transition calculated at 3.57—5.09 eV (MIM-PPP) is a mixture of locally excited and charge transfer configurations (Table 5). Calculations show it is forbidden.

The second ($E_1' \leftarrow A_1'$) transition has a strong intensity and a composition similar to that of the first one. It is predicted at 4.81—5.95 eV (MIM-PPP), *i.e.* very near the theoretical value found for [4]radialene[2] (4.77—6.41 eV (MIM-PPP)) and experimentally observed at 4.59 eV.

The third (forbidden) and fourth (weak) electronic transitions are calculated at 5.32—6.24 eV and 6.04—7.05 eV (MIM-PPP) and originate exclusively from charge transfer configurations. On the whole the results confirm what Heilbronner predicted for this compound.[22]

8-Vinylheptafulvene(7-Methylene-1,3,5-cycloheptatriene) (V). The geometry postulated by Lo and Whitehead was adopted for calculations.[23] The results are given in Table 6.

The UV trend is fairly reproduced by MIM and PPP, even though the latter method gives rather high energy values. The first electronic transition, roughly polarized along the short axis (y), is computed at 3.55—4.17 eV (MIM-PPP) and is to be associated with the weak absorption band experimentally observed at 2.8 eV.[24] PPP predicts it is prevailingly due to charge transfer states while MIM indicates it is a mixture of locally excited and charge transfer configurations. However both methods show that it is localized in the seven-membered ring, corresponding

Table 6. First singlet excited states of 8-vinylheptafulvene
Five ethylene molecules as component systems.[a]

	Ψ_1		Ψ_2		Ψ_3		Ψ_4		Ψ_5	
	MIM	PPP	MIM	PPP	MIM	PPP	MIM	PPP	MIM	PPP
Γ	—	—	—	0.03	0.01	0.08	—	—	—	—
Λ_a	0.11	0.09	0.06	0.02	0.06	0.01	0.05	0.06	0.02	0.02
Λ_b	0.19	0.11	—	—	—	—	0.03	0.09	0.12	0.05
Λ_c	0.13	0.09	0.03	0.02	0.04	0.02	0.06	0.05	0.03	0.02
Λ_d	—	—	0.25	0.17	0.07	0.06	—	—	—	—
Λ_e	—	—	0.04	0.05	0.14	0.09	—	—	—	—
T_a^b	0.11	0.07	0.01	—	0.01	0.03	0.01	—	—	—
T_a^c	0.03	0.03	0.02	0.03	0.03	0.07	0.08	0.03	0.02	0.06
T_a^d	—	—	0.09	0.07	0.02	—	0.19	0.09	0.10	0.11
T_a^e	—	—	0.01	0.01	—	—	0.01	0.01	0.01	0.01
T_b^c	0.08	0.05	0.01	0.02	0.11	0.04	0.01	0.03	0.08	0.10
T_b^d	—	—	0.03	0.05	0.03	0.04	—	—	—	—
T_b^e	—	—	—	0.01	—	—	—	—	—	—
T_c^d	0.01	—	0·09	0.07	0.01	—	0.19	0.09	0.10	0.11
T_c^e	—	—	0.01	0.01	—	—	0.01	0.01	0.01	0.01
T_d^e	—	—	0.04	0.04	0.20	0.07	—	—	—	—
T_b^a	0.07	0.04	0.03	0.02	0.10	0.05	0.01	0.02	0.09	0.10
T_c^a	0.03	0.03	0.03	0.03	0.02	0.06	0.08	0.04	0.01	0.06
T_d^a	0.03	0.06	0.10	0.05	—	—	0.08	0.08	0.16	0.03
T_e^a	—	—	0.01	0.01	—	—	0.01	0.01	0.01	0.01
T_c^b	0.11	0.07	—	—	0.02	0.06	0.01	0.01	—	—
T_d^b	0.04	0.06	—	—	—	—	0.07	0.08	0.07	0.05
T_e^b	—	0.01	—	—	—	—	0.01	0.02	0.01	0.01
T_d^c	0.05	0.07	0.07	0.04	—	—	0.08	0.09	0.14	0.04
T_e^c	—	0.01	0.01	0.01	—	—	0.01	0.02	0.02	0.01
T_e^d	—	—	0.06	0.05	0.10	0.04	—	—	—	—
Total weight (%)	100	79	100	81	100	75	100	83	100	80
ΔE	3.55	4.17	3.69	4.97	5.28	6.43	5.51	6.51	5.76	7.32
f	0.07	0.05	0.82	1.24	0.01	0.58	<0.01	0.02	0.32	0.42
Polarization[b]	−70	−85	−0.2	−2	−28	−3	70	73	88	89

a) a, b, c, d, and e denote fragments $C_1=C_2$, $C_3=C_4$, $C_5=C_6$, $C_7=C_8$, and $C_9=C_{10}$ respectively. b) Angles with respect to x axis.

Table 7. First excited singlet states of 1,2-benzofulvene. Benzene (a) and two

MIM/A	MIM/B	Ψ_1				Ψ_2			
		MIM/A	PPP	MIM/B	PPP	MIM/A	PPP	MIM/B	PPP
Γ	Γ	—	—	—	—	—	—	—	—
Λ_{1a}	Λ_{1a}	0.22	0.09	0.30	0.10	0.11	0.58	0.11	0.62
Λ_{2a}	Λ_{2a}	—	0.30	0.01	0.32	0.17	0.08	0.13	0.08
Λ_{3a}	Λ_{3a}	0.03	0.03	0.04	0.03	0.06	—	0.04	—
Λ_{4a}	Λ_{4a}	0.02	—	0.01	—	0.02	0.01	0.02	0.01
Λ_b	Λ_{1b}	0.10	0.08	0.15	0.11	0.09	0.01	0.01	—
Λ_c	Λ_{2b}	0.11	—	—	0.03	0.02	0.01	0.07	0.01
T^b_{1a}	Λ_{3b}	0.01	0.02	—	0.02	0.20	0.06	0.02	—
T^c_{1a}	Λ_{4b}	0.01	0.05	—	—	0.16	0.04	—	—
T^b_{2a}	T^{3b}_{1a}	0.06	0.05	0.01	0.07	0.04	—	0.49	0.10
T^c_{2a}	T^{4b}_{1a}	0.06	0.04	—	—	0.01	0.02	—	—
T^c_b	T^{3b}_{2a}	0.11	0.07	0.24	0.10	0.03	—	0.05	0.01
T^{3a}_b	T^{4b}_{2a}	0.02	0.03	—	—	0.05	0.01	0.01	0.01
T^{3a}_c	T^{3a}_{1b}	0.02	0.01	—	—	—	0.01	0.02	0.02
T^{4a}_b	T^{3a}_{2b}	0.10	0.05	0.05	0.03	0.02	0.01	0.01	—
T^{4a}_c	T^{4a}_{1b}	0.06	—	0.02	0.04	0.01	0.01	0.02	—
T^b_c	T^{4a}_{2b}	0.07	—	0.17	0.01	0.01	0.01	—	0.03
Total weight (%)		100	82	100	86	100	86	100	89
ΔE		3.80	4.35	3.82	4.35	4.35	4.47	4.10	4.47
f		0.41	0.06	0.30	0.06	0.08	0.03	0.08	0.03
Polarization[a]		−39	−3	−22	−3	59	−63	73	−63

a) Angle with respect to x-axis.

in energy as well in composition and intensity, to the first electronic transition found in heptafulvene at 3.46—3.98 eV (MIM-PPP) and experimentally observed at 2.9 eV.[2]

The most intense second absorption band occurs at 3.81 eV,[24] the corresponding band in heptafulvene lying at 4.4 eV.[8,24] The bathochromic shift was fairly predicted by calculations. The associated electronic transition, in fact, computed at 3.69—4.97 eV (MIM-PPP) and polarized along the x axis (3.94—5.31 eV in heptafulvene[2]) has prevailing charge transfer character involving the whole π-system with consistent interaction of the vinyl group with the heptafulvene nucleus.

A very similar composition is found for the weak third theoretical electronic transition, computed at 5.28—6.43 eV (where Λ_e is the most consistent among the locally excited states) which appears shifted at lower energy with respect to the corresponding one in heptafulvene (5.62—6.66 eV, MIM-PPP).[2] A lower bathochromic shift is predicted by PPP approach because less interaction is predicted between the vinyl group and the remaining heptafulvene fragment.

Next two transitions, both roughly polarized along the y-axis, are calculated at 5.51—6.51 eV (weak) and 5.76—7.32 eV (intense) by MIM and PPP respectively, being nearly exclusively originated by charge transfers involving principally the heptafulvene π-system.

*1,2-Benzofulvene(1-Methylene-1*H*-indene) (VI).* The bond lengths calculated by the LCAO-MO-SCF-PPP ($\pi+\sigma$) method[23] were adopted for the fulvene ring, benzene being assumed to be a regular hexagon. The most recent UV spectrum[25] shows a great number of absorption bands and shoulders, often very near each other, giving results very difficult to interpret. Three distinct absorption bands were reported by Bloor *et al.*,[13] where reference is made to the spectrum in heptane solution reported by Pullman *et al.*[26] My MIM and PPP-CA results are discordant (Table 7) principally as regards the composition and oscillator strengths of the first and fourth electronic transitions so that the relative assignment is uncertain. Probably this situation is partially due to the molecular asymmetry of this compound. However, the first electronic transition computed at 3.80—3.82 eV by MIM and at 4.35 eV by PPP seems to be associated with the experimental absorption observed at $\simeq$3.6 eV. The second theoretical transition at 4.35—4.10 eV (MIM/A-MIM/B) and 4.47 eV (PPP) corresponds to the absorption band at about 4 eV. The third and fourth calculated transitions might be correlated with the strong absorption at about 4.8 eV. If a comparison is made between the composition of these transitions and the composition of the transitions found in fulvene[1] no resemblance is observed.

*2,3-Benzofulvene(2-Methylene-2*H*-indene) (VII).* As regards 2,3-benzofulvene no spectroscopic data seem to have appeared. Calculations have been performed adopting the molecular geometry of Lo and Whitehead.[23] Three different approaches at MIM level were examined. The molecule was considered to be five interacting ethylene molecules (MIM/A) or two *cis*-butadienes and ethylene (MIM/B) or two *trans*-butadienes and ethylene (MIM/C). The results are given in Tables 8 and 9, together with those of PPP-CA for comparison. In each case a y-polarized $^1B_2 \leftarrow {}^1A_1$

ETHYLENES (b, c) OR BENZENE (a) AND *trans*-BUTADIENE (b) AS COMPONENT SYSTEMS

Ψ_3				Ψ_4				Ψ_5			
MIM/A	PPP	MIM/B	PPP	MIM/A	PPP	MIM/B	PPP	MIM/A	PPP	MIM/B	PPP
—	—	0.01	0.01	—	0.01	—	—	0.01	0.06	0.05	0.05
0.53	0.06	0.42	0.06	—	0.03	—	0.03	—	—	0.02	—
0.03	0.23	0.02	0.24	0.14	0.13	0.08	0.14	—	—	—	—
—	0.11	0.02	0.11	0.04	—	0.04	—	0.10	0.04	0.02	0.04
0.04	0.01	0.07	0.01	0.05	0.16	0.03	0.17	0.15	0.11	0.05	0.11
0.02	0.08	0.14	0.29	0.01	—	—	0.06	0.02	—	0.01	0.04
0.15	0.09	0.01	—	—	0.12	0.01	0.08	—	—	—	—
—	0.01	—	0.01	0.04	0.07	0.03	0.06	—	0.01	—	0.01
0.06	—	0.01	—	0.04	0.11	—	—	0.04	0.01	—	0.01
0.01	0.01	0.07	—	0.03	—	0.06	0.19	0.26	0.19	0.03	—
0.02	0.02	0.04	0.01	0.01	—	—	—	0.12	0.13	—	0.02
0.02	0.10	—	0.02	0.03	0.01	—	—	0.10	0.02	0.46	0.34
0.01	0.01	—	—	0.21	0.05	—	—	—	0.03	—	—
0.01	—	0.03	0.01	0.15	0.02	—	—	0.11	0.05	0.01	—
—	0.03	0.05	—	0.11	—	0.49	0.07	0.04	0.08	0.16	0.08
0.06	0.06	0.02	—	0.10	0.02	—	0.02	—	0.01	0.03	0.02
0.04	0.02	0.09	0.09	0.04	0.06	0.26	—	0.05	0.04	0.16	0.08
100	83	100	86	100	79	100	82	100	78	100	80
4.50	5.36	4.71	5.36	5.34	5.75	5.00	5.75	5.77	6.54	5.50	6.54
0.33	0.41	0.55	0.41	0.09	0.72	0.02	0.72	0.39	0.24	0.04	0.24
−50	−23	−34	−23	−60	−50	−68	−50	25	21	14	21

TABLE 8. FIRST SINGLET EXCITED STATES OF 2,3-BEAZOFULVENE. MIM/A—FIVE ETHYLENE MOLECULES AS COMPONENT SYSTEMS[a)]

States of $^1A_1$ symmetry	Ψ_2		Ψ_5		States of $^1B_2$ symmetry	Ψ_1		Ψ_3		Ψ_4	
	MIM	PPP	MIM	PPP		MIM	PPP	MIM	PPP	MIM	PPP
Γ	0.02	0.11	0.01	0.04	$(1/\sqrt{2})(\Lambda_a-\Lambda_b)$	0.08	0.04	0.30	0.29	—	—
$(1/\sqrt{2})(\Lambda_a+\Lambda_b)$	0.01	0.01	0.12	0.03	$(1/\sqrt{2})(\Lambda_c-\Lambda_d)$	0.25	0.18	0.09	0.03	0.02	0.03
$(1/\sqrt{2})(\Lambda_c+\Lambda_d)$	0.10	0.01	0.09	0.05	$(1/\sqrt{2})(T_a^b-T_b^a)$	0.06	0.03	0.26	0.15	—	—
Λ_e	0.20	0.10	—	0.13	$(1/\sqrt{2})(T_a^c-T_b^d)$	0.06	0.04	0.01	0.01	0.17	0.11
$(1/\sqrt{2})(T_a^b+T_b^a)$	—	0.01	0.04	0.14	$(1/\sqrt{2})(T_a^b-T_b^c)$	0.10	0.06	0.03	0.04	0.28	0.16
$(1/\sqrt{2})(T_a^c+T_b^a)$	0.01	0.02	0.06	0.08	$(1/\sqrt{2})(T_a^e-T_b^a)$	0.03	0.04	—	—	0.09	0.10
$(1/\sqrt{2})(T_a^d+T_b^c)$	0.06	0.01	0.08	0.04	$(1/\sqrt{2})(T_c^a-T_d^b)$	0.04	0.03	0.02	0.01	0.14	0.11
$(1/\sqrt{2})(T_a^e+T_b^a)$	0.01	0.01	—	—	$(1/\sqrt{2})(T_c^b-T_d^a)$	0.07	0.04	0.03	0.04	0.28	0.21
$(1/\sqrt{2})(T_c^a+T_d^b)$	0.01	0.04	0.05	0.06	$(1/\sqrt{2})(T_c^d-T_d^c)$	0.21	0.11	0.12	0.07	0.01	0.01
$(1/\sqrt{2})(T_c^b+T_d^a)$	0.01	0.01	0.30	0.01	$(1/\sqrt{2})(T_c^e-T_d^a)$	0.10	0.17	0.14	0.09	0.01	—
$(1/\sqrt{2})(T_c^d+T_d^c)$	0.11	0.11	0.21	0.04	$(1/\sqrt{2})(T_e^a-T_e^b)$	—	—	—	—	—	—
$(1/\sqrt{2})(T_c^e+T_d^a)$	0.16	0.07	0.03	—	$(1/\sqrt{2})(T_e^c-T_e^d)$	—	—	—	—	—	—
$(1/\sqrt{2})(T_e^a+T_e^b)$	0.02	0.04	0.01	—							
$(1/\sqrt{2})(T_e^c+T_e^d)$	0.28	0.13	—	0.09							
Total weight (%)	100	68	100	71		100	74	100	73	100	73
ΔE	3.83	5.31	5.30	6.56		2.67	3.79	4.18	5.44	5.18	6.36
f	0.69	0.62	0.46	0.99		0.09	0.12	0.05	0.12	0.01	0.02
Polarization	x	x	x	x		y	y	y	y	y	y

a) a, b, c, d, and e denote fragments C_2=C_3, C_4=C_5, C_6=C_7, C_1=C_8, and C_9=C_{10}, respectively.

transition of weak intensity is predicted as first electronic transition at 2.67, 2.40 and 2.38 eV (MIM/A, MIM/B and MIM/C respectively) and at 3.79 eV (PPP). With respect to the first calculated electronic transition in 1,2-benzofulvene a greater charge transfer character is found, the calculated transition shifting at lower energy. Moreover the composition of the wavefunction relative to this transition is very similar to that of the first transition in fulvene,[1)] where it was computed at 3.3 eV.

The second ($^1A_1 \leftarrow {}^1A_1$) transition is predicted to be very intense and polarized towards the long molecular axis (x). It is calculated by MIM in the range 3.4—3.8 eV and by PPP at 5.32 eV, the result being pre-

Table 9. First excited singlet states of 2,3-benzofulvene

States of $^1A_1$ symmetry	Ψ_2		Ψ_5		States of $^1B_2$ symmetry	Ψ_1		Ψ_3		Ψ_4	
	MIM	PPP	MIM	PPP		MIM	PPP	MIM	PPP	MIM	PPP
MIM/B: Two *cis*-butadiene (a, b) and ethylene (c) as component systems											
Γ	0.01	0.04	—	—	$(1/\sqrt{2})(\Lambda_{1a}-\Lambda_{1b})$	0.08	0.07	0.22	0.46	—	—
$(1/\sqrt{2})(\Lambda_{1a}+\Lambda_{1b})$	0.01	0.01	0.08	0.03	$(1/\sqrt{2})(\Lambda_{2a}-\Lambda_{2b})$	—	—	—	0.01	—	—
$(1/\sqrt{2})(\Lambda_{2a}+\Lambda_{2b})$	0.01	0.03	0.06	0.20	$(1/\sqrt{2})(\Lambda_{3a}-\Lambda_{3b})$	0.25	0.33	0.06	0.11	0.06	0.04
$(1/\sqrt{2})(\Lambda_{3a}+\Lambda_{3b})$	0.08	0.02	0.06	0.05	$(1/\sqrt{2})(\Lambda_{4a}-\Lambda_{4b})$	—	—	0.01	0.01	—	—
$(1/\sqrt{2})(\Lambda_{4a}+\Lambda_{4b})$	0.14	0.19	0.12	0.08	$(1/\sqrt{2})(T^{3b}_{1a}-T^{3a}_{1b})$	—	—	—	—	—	—
Λ_c	0.15	0.12	—	0.15	$(1/\sqrt{2})(T^{4b}_{1a}-T^{4a}_{1b})$	0.30	0.12	0.02	0.06	0.46	0.31
$(1/\sqrt{2})(T^{3b}_{1a}+T^{3a}_{1b})$	0.08	0.04	0.02	—	$(1/\sqrt{2})(T^{c}_{1a}-T^{c}_{1b})$	0.06	0.04	0.01	—	0.05	0.12
$(1/\sqrt{2})(T^{4b}_{1a}+T^{4a}_{1b})$	0.02	0.01	—	—	$(1/\sqrt{2})(T^{3b}_{2a}-T^{3a}_{2b})$	0.17	0.20	0.38	0.11	0.07	0.01
$(1/\sqrt{2})(T^{c}_{1a}+T^{c}_{1b})$	—	—	0.34	0.15	$(1/\sqrt{2})(T^{4b}_{2a}-T^{4a}_{2b})$	0.14	0.07	0.29	0.06	0.35	0.34
$(1/\sqrt{2})(T^{3b}_{2a}+T^{3a}_{2b})$	0.15	0.07	0.01	—	$(1/\sqrt{2})(T^{c}_{2a}-T^{c}_{2b})$	—	—	0.01	0.01	0.01	0.01
$(1/\sqrt{2})(T^{4b}_{2a}+T^{4a}_{2b})$	0.05	0.06	0.08	0.02	$(1/\sqrt{2})(T^{3a}_{c}-T^{3b}_{c})$	—	—	—	—	—	—
$(1/\sqrt{2})(T^{c}_{2a}+T^{c}_{2b})$	0.02	0.04	—	—	$(1/\sqrt{2})(T^{4a}_{c}-T^{4b}_{c})$	—	—	—	—	—	—
$(1/\sqrt{2})(T^{3a}_{c}+T^{3b}_{c})$	—	0.01	0.22	0.03							
$(1/\sqrt{2})(T^{4a}_{c}+T^{4b}_{c})$	0.28	0.18	0.01	0.03							
Total weight (%)	100	82	100	82		100	83	100	83	100	83
ΔE	3.42	5.32	4.61	6.56		2.40	3.79	3.85	5.44	3.97	6.35
f	0.62	0.70	0.39	0.98		0.05	0.12	0.04	0.12	$\simeq 0$	0.02
Polarization	x	x	x	x		y	y	y	y	y	y
MIM/C: Two *trans*-butadienes (a, b) and ethylene (c) as component systems											
Γ	0.05	0.10	0.02	0.02	$(1/\sqrt{2})(\Lambda_{1a}-\Lambda_{1b})$	0.30	0.31	0.04	0.15	0.02	0.02
$(1/\sqrt{2})(\Lambda_{1a}+\Lambda_{1b})$	0.06	0.04	0.01	0.13	$(1/\sqrt{2})(\Lambda_{2a}-\Lambda_{2b})$	0.01	0.03	0.31	0.28	—	0.01
$(1/\sqrt{2})(\Lambda_{2a}+\Lambda_{2b})$	0.02	—	—	—	$(1/\sqrt{2})(\Lambda_{3a}-\Lambda_{3b})$	—	—	—	—	0.22	0.40
$(1/\sqrt{2})(\Lambda_{3a}+\Lambda_{3b})$	—	0.01	—	0.02	$(1/\sqrt{2})(\Lambda_{4a}-\Lambda_{4b})$	—	0.01	—	—	—	0.01
$(1/\sqrt{2})(\Lambda_{4a}+\Lambda_{4b})$	—	—	—	—	$(1/\sqrt{2})(T^{3b}_{1a}-T^{3a}_{1b})$	0.01	—	0.21	0.12	0.30	0.14
Λ_c	0.18	0.12	0.06	0.14	$(1/\sqrt{2})(T^{4b}_{1a}-T^{4a}_{1b})$	0.01	—	—	—	0.02	—
$(1/\sqrt{2})(T^{3b}_{1a}+T^{3a}_{1b})$	0.04	0.02	0.01	0.01	$(1/\sqrt{2})(T^{c}_{1a}-T^{c}_{1b})$	0.01	0.02	0.06	0.06	—	0.04
$(1/\sqrt{2})(T^{4b}_{1a}+T^{4a}_{1b})$	—	—	—	—	$(1/\sqrt{2})(T^{3b}_{2a}-T^{3a}_{2b})$	0.51	0.22	0.06	0.22	0.08	—
$(1/\sqrt{2})(T^{c}_{1a}+T^{c}_{1b})$	0.04	0.02	—	—	$(1/\sqrt{2})(T^{4b}_{2a}-T^{4a}_{2b})$	0.02	0.01	0.24	0.12	0.06	0.10
$(1/\sqrt{2})(T^{3b}_{2a}+T^{3a}_{2b})$	0.13	0.17	0.68	0.36	$(1/\sqrt{2})(T^{c}_{2a}-T^{c}_{2b})$	0.13	0.21	0.08	0.04	0.23	0.07
$(1/\sqrt{2})(T^{4b}_{2a}+T^{4a}_{2b})$	0.04	0.01	—	—	$(1/\sqrt{2})(T^{3a}_{c}-T^{3b}_{c})$	—	—	—	—	0.06	0.01
$(1/\sqrt{2})(T^{c}_{2a}+T^{c}_{2b})$	0.17	0.07	0.02	—	$(1/\sqrt{2})(T^{4a}_{c}-T^{4b}_{c})$	—	—	—	—	0.01	—
$(1/\sqrt{2})(T^{3a}_{c}+T^{3b}_{c})$	0.23	0.18	0.13	0.06							
$(1/\sqrt{2})(T^{4a}_{c}+T^{4b}_{c})$	0.04	0.02	0.07	0.04							
Total weight (%)	100	76	100	78		100	81	100	79	100	80
ΔE	3.54	5.32	4.70	6.56		2.38	3.79	3.94	5.44	5.33	6.35
f	0.50	0.70	0.17	0.98		0.10	0.12	0.05	0.12	0.04	0.02
Polarization	x	x	x	x		y	y	y	y	y	y

valently charge transfer in nature.

Next transition, $^1B_2 \leftarrow {}^1A_1$, found at *ca.* 4.2 eV by MIM and at 5.44 eV by PPP shows charge transfer character if MIM results are taken into account, in contrast with PPP composition where the greatest contribution is given by locally excited states. Since the calculated energy values for the second and the third transition are very close each other it is probable that the third transition (weak) might appear as a shoulder of the second one on higher energy side.

The fourth electronic transition is predicted having $^1B_2$ symmetry with very low intensity and exclusively charge transfers configurations. Both MIM/A and PPP predict that it is lying very near to the fifth $^1A_1 \leftarrow {}^1A_1$ intense electronic transition, probably as a shoulder on lower energy side. On the contrary MIM/C results predict the fourth transition to be forbidden and lying at about 4 eV, in disagreement with the above results.

Conclusion

If [5]radialene and the two benzofulvenes are excluded, the spectra of the molecules studied can be correlated with those of the smaller cyclic compounds which constitute them, by means of the nature, energy and intensity as well as the composition of the corresponding electronic transitions. The principal feature which can be noted by analysing the theoretical electronic transitions energies is the difference between MIM and PPP results. The latter gives values higher than those of MIM and experiment, even if the general

spectral trend is acceptable. The main cause seems to be the resonance integrals. When β_{ij} values are evaluated by the exponential formula

$$\beta_{ij} = -2.38 \exp 1.586 (r_0 - r_{\mu\nu})$$

where r_0 is the C–C bond length in benzene (for details Ref. 16, method I), the energy values calculated by PPP are lower than those obtained with Kon's resonance integrals and nearer to the experimental ones. On the other hand MIM values became too low. For a more reliable comparison of the theoretical results we have chosen Kon's integrals in both methods since calculations on some compounds showed that wavefunction compositions do not appreciably differ in the two cases. The nature of the first electronic transitions, among which those experimentally observed are included, are generally concordant in the two methods while mutual shifts are noted for higher energy wavefunctions. However this behaviour is usual and independent of the molecules. Generally the lowest energy transitions are a mixture of locally excited and charge transfer configurations with nearly exclusively Λ character in compounds including benzene ring, while prevalently charge transfer transitions are found at higher energy values. For all the compounds the calculated ground state bond orders are satisfactory.

References

1) G. Favini and G. Buemi, *Theor. Chim. Acta (Berl.)*, **24**, 61 (1972).
2) G. Buemi, *Z. Phys. Chem. Neue Folge*, **119**, 1 (1980).
3) R. G. Parr, "The Quantum Theory of Molecular Electronic Structure," W. A. Benjamin, New York (1963).
4) H. C. Longuet-Higgins and J. N. Murrell, *Proc. Phys. Soc.*, **A68**, 601 (1955).
5) H. Baba, S. Suzuki, and T. Takemura, *J. Chem. Phys.*, **50**, 2078 (1969).
6) N. L. Allinger, J. C. Tai, and T. W. Stuart, *Theor. Chim. Acta (Berl.)*, **8**, 101 (1967).
7) R. D. Brown, F. R. Burden, and G. R. Williams, *Aust. J. Chem.*, **21**, 1939 (1968).
8) Z. Yoshida and T. Kobayashi, *Bull. Chem. Soc. Jpn.*, **45**, 316 (1972).
9) T. Nakajima and S. Katagiri, *Bull. Chem. Soc. Jpn.*, **35**, 910 (1962).
10) F. Marschner and H. Pohle, *Tetrahedron*, **34**, 105 (1978).
11) K. D. Warren and J. R. Yandle, *Theor. Chim. Acta (Berl.)*, **12**, 279 (1968).
12) O. W. Adams and R. L. Miller, *Theor. Chim. Acta (Berl.)*, **12**, 151 (1968).
13) J. E. Bloor, B. R. Gilson, and N. Brearley, *Theor. Chim. Acta (Berl.)*, **8**, 35 (1967).
14) A. Tajiri, N. Ohmichi, and T. Nakajima, *Bull. Chem. Soc. Jpn.*, **44**, 2347 (1971).
15) I. Gutman, M. Milun, and N. Trinajstic, *J. Am. Chem. Soc.*, **99**, 1692 (1977).
16) H. Yamaguchi, T. Nakajima, and T. L. Kunii, *Theor. Chim. Acta (Berl.)*, **12**, 349 (1968).
17) P. Francois, *J. Chim. Phys. Phys. Chim. Biol.*, **67**, 1063 (1970).
18) A. Skancke and P. N. Skancke, *Acta Chem. Scand.*, **22**, 175 (1968).
19) A. Skancke, *Acta Chem. Scand.*, **22**, 3239 (1968).
20) M. P. Cava, R. J. Pohl, and M. J. Mitchell, *J. Am. Chem. Soc.*, **85**, 2080 (1963).
21) V. Buss and H. D. Försterilng, *Tetrahedron*, **29**, 3001 (1973).
22) E. Heilbronner, *Theor. Chim. Acta (Berl.)*, **4**, 64 (1966).
23) D. H. Lo and M. A. Whitehead, *Tetrahedron*, **25**, 2615 (1969).
24) D. J. Bertelli, *J. Am. Chem. Soc.*, **86**, 3320 (1964).
25) M. Neuenschwander, R. Vögeli, H. P. Fahrni, H. Lehmann, and J. P. Ruder, *Helv. Chim. Acta*, **60**, 1073 (1977).
26) A. Pullman, B. Pullman, E. D. Bergmann, G. Berthier, Y. Hirshberg, and Y. Spirinzak, *Bull. Soc. Chim. Fr.*, **1951**, 702.

New Type of Active Carbon Catalyst for Simultaneous Removal of SO_x and NO_x

Akio NISHIJIMA,* Minoru KURITA, Yoshimichi KIYOZUMI, Rikio KOBAYASHI, Hiroyuki HAGIWARA, Akifumi UENO, Toshio SATO, and Naoyuki TODO

National Chemical Laboratory for Industry, 2-19-19, Mita, Meguro-ku, Tokyo 153 †

(Received April 16, 1979)

Active carbons prepared from nitrogen containing compounds were found to show high activity for SO_2 removal. Enhancement of the activity for NO reduction was realized by supporting vanadium ions on these active carbons. Regeneration of the catalyst was examined with various reducing agents. The activity for SO_2 removal was recovered by removing sulfate ions on the catalyst with NH_3 at 350 °C. The 200 h life test of the present catalyst was carried out for the simultaneous removal of SO_x and NO_x.

Development of the technique for removal of sulfur oxides (SO_x) and nitrogen oxides (NO_x) in a flue gas emitted from a stationary combustion equipment involves complicated problems. Recently, active carbons have been used for the simultaneous removal of SO_x and NO_x in a flue gas.[1,2] SO_x is removed by adsorption on a catalyst as sulfate compounds, NO_x being reduced by NH_3 added in a flue gas as a reducing agent. However, active carbon (AC) developed so far are applied at a low space velocity below 1000 h^{-1} because of lower activities at the temperature range in which AC is of use. Development of active catalysts which can be used at a higher space velocity is desirable. According to studies by Sano and Ogawa[3] on new types of catalysts with higher activity for SO_2 removal, certain impurities such as surface nitrogen species seem to have a good effect on activity. Investigation was carried out in order to improve the activity for simultaneous removal of NO and SO_2. Develpoment of technique for regeneration is also important in connection with the simultaneous reduction. In this paper, the method of regeneration and result of the life test for 200 h are described.

Experimental

Catalyst. As raw materials for active carbons, nitrogen-containing compounds such as polyacrylonitrile or urea resin, a sulfur-containing compound (ashaltene) and a silica-containing compound (chaff) were used. Materials were put into a reactor made of quartz (length 500 mm, diam 60 mm) and were carbonized at *ca.* 250 °C in N_2 flow (1 *l*/h). Activation was carried out in the temperature range 600—1000 °C using water vapor or $ZnCl_2$ as an activating reagent. Some commercial AC were also used as a reference. The nitrogen-containing AC preapred from polyacrylonitrile was found to show superior activity for SO_2 removal and was selected as a carrier for the simultaneous removal of SO_2 and NO. Metal salts were supported by the impregnation method. Impregnation was carried out at 30 °C for 5 h, and the catalysts obtained were dried at 120 °C for 3 h, and then calcined at 250 °C in N_2 stream (1 *l*/h). Catalysts prepared are summarized in Table 1.

Activity Measurement. Activity measurements were carried out at 200 °C at a space velocity of 5000 h^{-1} using a conventional flow reactor made of stainless steel (length 300 mm, diam 25 mm). A gas mixture consisting of SO_2 500 ppm, NH_3 500 ppm, O_2 5 vol%, H_2O 10 vol%, and N_2 was used as standard feed, 300 ppm of NO being added in the case of simultaneous removal. The activities for SO_2 removal and NO reduction were determined by measurements of the concentrations before and after the reaction. Analyses of SO_2 and NO were made with a NDIR type SO_x analyzer and a chemiluminescence type NO_x analyzer, respectively. The analysis of NH_3 was performed by the chemical method (JIS-K-0099).

Measurement of Catalyst Property. Measurement of surface areas and elemental analysis of C and N were carried out by the BET method and CHN corder (Yanaco MT-2), respectively. An X-ray photoelectron spectrometer (Dupont 650B) was used to examine surface properities of the catalysts. An ion microanalyzer (Hitachi IMA-2) and an electron microprobe (Hitachi HU-12) were also used to estimate the line profile of each element and the despersion of supported vanadium ions, respectively.

Results and Discussion

Comparison of AC as Regards Activity for SO_2 Removal. The activities of various AC for SO_2 removal are shown in Fig. 1. AC prepared from nitrogen-containing compounds showed superior activity to other AC, while

Table 1. Preparation of AC from raw material

Raw material	Activating conditions	Surface area	Nitrogen content
Polyacrylonitrile	600—1000 °C	300—1000 m^2/g	2—12 wt %
Urea resin	800 °C	525 m^2/g	6.4 wt %
Melamine resin	800 °C	517 m^2/g	8.1 wt %
Aniline-formaldehyde resin	800 °C	662 m^2/g	5.2 wt %
m-Phenylenediamine-formaldehyde resin	800 °C	420 m^2/g	5.5 wt %
Asphaltene	800 °C	520 m^2/g	—
Chaff	800 °C	625 m^2/g	—

† Present address: 1-1, Higashi, Yatabe, Ibaraki 305.

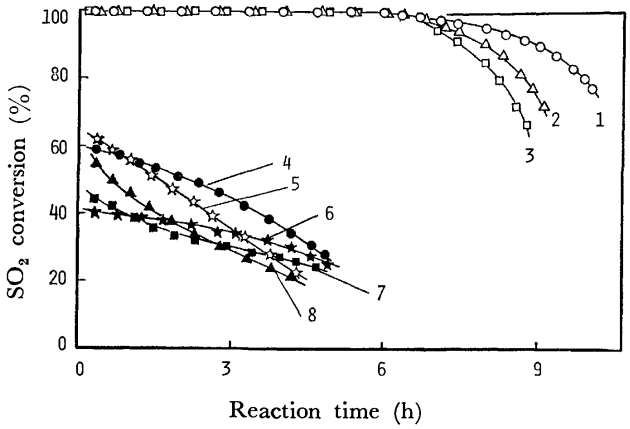

Fig. 1. Comparison of performance of various AC for SO_2 removal. Raw materials;
1 ○: Polyacrylonitrile, 2 △: *m*-phenylenediamine-formaldehyde resin, 3 □: urea resin, 4 ●: commerical type A, 5 ☆: commercial type B, 6 ★: commercial type C, 7 ■: asphaltene, 8 ▲: chaff.
Reaction conditions;
Reaction temp: 200 °C, SV: 5000 h^{-1}, SO_2: 500 ppm, NH_3: 500 ppm, O_2: 5 vol%, H_2O: 10 vol% N_2: balance.

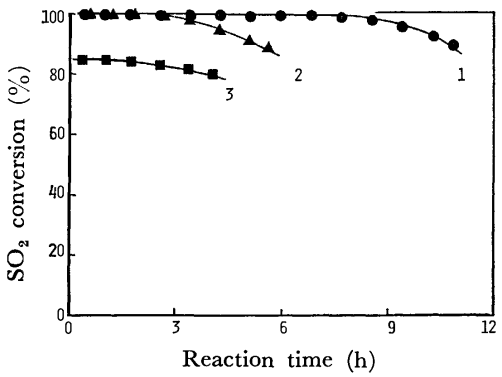

Fig. 2. Effect of space velocity on activity for SO_2 removal.
Space velocities;
1 ●: 5000 h^{-1}, 2 ▲: 10000 h^{-1}, 3 ■: 15000 h^{-1}.
Reaction conditions;
Reaction temp 200 °C,
SO_2: 500 ppm, NH_3: 500 ppm, O_2: 5 vol%, H_2O: 10 vol%, N_2: balacne.

those prepared from asphaltene and chaff showed lower activity than commercial ones. Figure 2 shows the effect of space velocity on activity for the removal of SO_2. AC prepared from polyacrylonitrile (PAN) showed high activity at space velocity higher than 10000 h^{-1}, indicating the merit of the AC prepared from nitrogen-containing compounds.

Effect of Preparation Conditions on the Catalytic Activity for SO_2 Removal. Figure 3 shows the effect of activating conditions on activities and capacities of active carbons from PAN for SO_2 removal. When $ZnCl_2$ was used as an activating agent, the catalysts obtained were not active, probably due to the blocking of SO_2 adsorption sites by zinc atom. In fact, the results obtained with the ion micronalyzer showed that the surface concentration of Zn on AC with lower

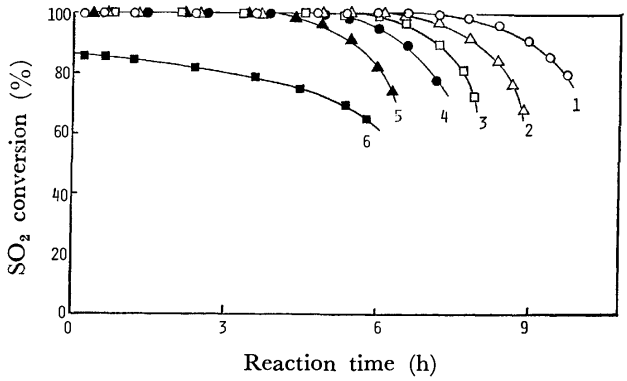

Fig. 3. Effect of preparation conditions on the catalytic activity for SO_2 removal.
Activating conditions;
1 ○: 800 °C, 30 min, water vapor, 2 △: 900 °C, 15 min, water vapor, 3 □: 900 °C, 30 min, water vapor, 4 ●: 700 °C, 30 min, water vapor, 5 ▲: 1000 °C, 20 min, water vapor, 6 ■: $ZnCl_2$, 700 °C, 30 min, N_2.
Reaction conditions;
Reaction temp: 200 °C, SV: 5000 h^{-1}, SO_2: 500 ppm, NH_3: 500 ppm, O_2: 5 vol%, H_2O: 10 vol%, N_2: balance.

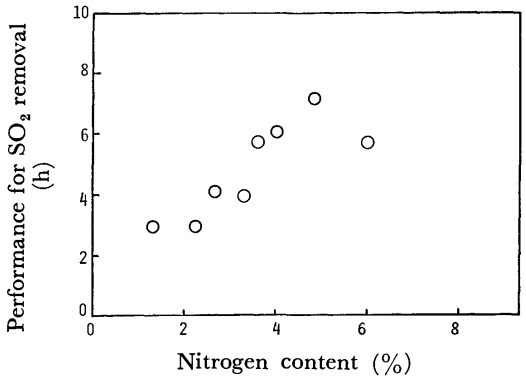

Fig. 4. Relation between performance of SO_2 removal and nitrogen content in present AC.
Performance of SO_2 removal: hours to keep 100% of SO_2 removal.

activity for SO_2 removal is higher than that on AC with higher activity. Though highly active ones were obtained when activated by H_2O, capacity performance of SO_2 removal was found to be deeply dependent on activating conditions. The specific surface area of the AC prepared under various conditions is in the range 300—1000 m^2/g, the activity of these AC being superior to that of commerical ones whose specific surface area is 700—1000 m^2/g. Surface functional groups of carriers play an important role in the catalysis.[4,5] It seems that some kinds of surface species contribute to the performance of SO_2 removal. A few percent of nitrogen atom remained after activation. Nitrogen species seem to exist in the state of C–N or N–N.[6] Thus the nitrogen species existing on the surface of the AC seem to be effective for the SO_2 removal. The amount of SO_2 adsorbed on AC was enhanced when nitrogen species were formed on the usual AC by impregnation with aqueous solutions of

Table 2. Binding energy of photoelectron spectra for N 1s, V $2p_{3/2}$, and S 2p on catalyst

	N 1s (eV)	V $2p_{3/2}$ (eV)	S 2p (eV)
Fresh catalyst	396.1	517.7	—
	397.5		
Deactivated catalyst	396.1	517.2	169.0
	397.6		

Binding energies were obtained based on C 1s spectra of contaminant carbon (285.0 eV).

nitrogen-containing compounds.[3] The amount of nitrogen in the AC we prepared was in the range 2—12 wt%. The relation between the amount of nitrogen and the performance is shown in Fig. 4. The increase in the amount of nitrogen seems to be correlated with activity. We thus examined the nitrogen species on the surface of AC in order to study the chemical states. Two peaks of N ls spectra were observed on the surface (Table 2), their binding energies being 396.1 and 397.5 eV, respectively. This indicates that two different chemical states of nitrogen atoms exist on the surface of the AC (probably C–N and C–N–N) and that one of them would be more effective for the removal of SO_2.

Effect of Coexisting Gas on Activity for SO_2 Removal. In the removal of SO_2 with NH_3, the following reactions are considered as the mechanism:[1]

$$SO_2 + 1/2O_2 \longrightarrow SO_3 \quad (1)$$

$$SO_3 + H_2O \longrightarrow H_2SO_4 \quad (2)$$

$$H_2SO_4 + NH_3 \longrightarrow NH_4HSO_4 \quad (3)$$

$$NH_4HSO_4 + NH_3 \longrightarrow (NH_4)_2SO_4 \quad (4)$$

Figure 5 shows the effect of coexisting gases on the activity for SO_2 removal. When O_2 or H_2O was removed from the feed gas, the activity decreased rapidly, indicating that the existence of both O_2 and H_2O is indispensable for the removal of SO_2 (Reactions 1 and 2). The activity for SO_2 removal increased to some extent in the absence of NO in the feed gas (Fig. 5). In the case of commercial AC, the activity increased when NO was added to the feed gas. This might be explained by the catalysis of NO for the formation of SO_3. On the other hand, in the AC prepared from polyacrylonitrile, the activity for SO_2 removal was higher in the absence of NO. This is also one of the features of AC from polyacrylonitrile, suggesting that the activity for SO_2 removal depends on C–N–N and/or C–N species on AC. When NH_3 was removed from the feed gas, the activity was found to decrease gradually because of the lack of NH_3 for SO_2 removal (Reactions 3 and 4). The effect of the amount of NH_3 in the feed gas for SO_2 removal is shown in Fig. 6. The capacity SO_2 removal increased with increase in the amount of NH_3 added. Leak of NH_3 was observed at the outlet of the reactor when the concentration of NH_3 in the feed gas exceeded 500 ppm. Thus in the present work, 500 ppm of NH_3 was introduced in the feed gas.

Enhancement of Activity for NO Reduction. Activities of AC for NO reduction do not differ much

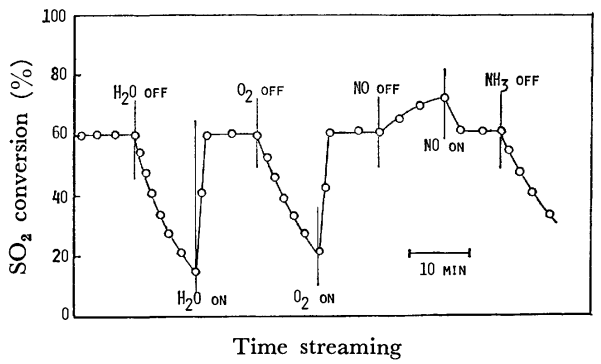

Fig. 5. Effect of coexisting gas on acetivity for SO_2 removal.
Reaction conditions;
Reaction temp: 230 °C, SV: 15000 h^{-1}, SO_2: 500 ppm, NO: 300 ppm, NH_3: 500 ppm, O_2: 5 vol%, H_2O: 10 vol%, N_2: balance.

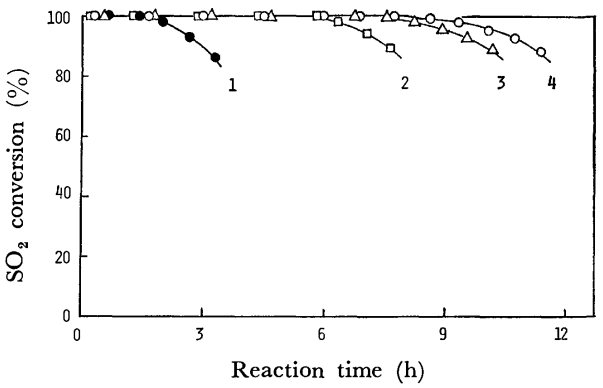

Fig. 6. Effect of amount of NH_3 on performance of SO_2 removal.
Amounts of NH_3;
1 ●: 0 ppm, 2 □: 300 ppm, 3 △: 500 ppm, 4 ○: 700 ppm.
Reaction conditions;
Reaction temp. 200 °C, SV: 5000 h^{-1}, SO_2: 500 ppm, O_2: 5 vol%, H_2O: 10 vol%, N_2: balance.

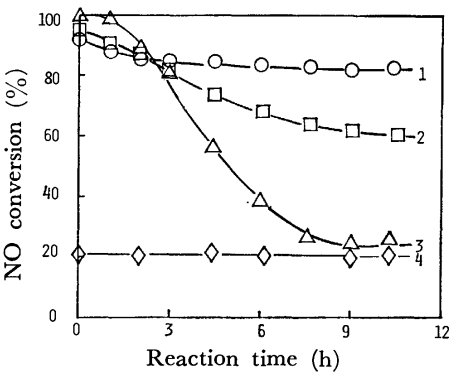

Fig. 7. Enhancement of activity for NO reduction.
1 ○: 5 wt% V_2O_5–AC, 2 □: 5 wt% CeO-AC, 3 △: 5 wt% MnO_2–AC, 4 ◇: AC
Reaction conditions;
Reaction temp: 220 °C, SV: 5000 h^{-1}, SO_2: 500 ppm, NO: 300 ppm, NH_3: 600 ppm, O_2: 5 vol%, H_2O: 10 vol%, N_2: balance.
AC used in this study was prepared from polyacrylonitrile.

from those of commercial ones. Under the reaction conditions, the activity of AC was so low that only 20% of NO was removed. Enhancement of activity for NO reduction was attempted by supporting various metal salts. Metals such as V or Mn which were found effective for NO reduction when supported on Al_2O_3 or TiO_2[7] were loaded on AC for the enhancement of the activity for NO reduction. Cerium, vanadium and manganese oxides supported catalysts were found to be highly active (Fig. 7). However, the activity of manganese or cerium supported catalyst decreased gradually with formation of the sulfate, regeneration of activity being difficult by the conventional technique. Since vanadium oxide supported catalyst exhibits a high activity for more than 10 h, vanadium ions were supported on the AC to improve the activity. The effect of the content of vanadium ions on both SO_2 removal ability and NO reduction activity was investigated in order to know the optimum content. The activity of the AC for SO_2 removal decreased with increase in the amount of vanadium supported (Fig. 8). On the contrary, the activity for NO reduction increased with increase in the amount of vanadium, apporaching a ceiling value at a certain vanadium content. AC with 2 wt% of vanadium supported showed optimum performance for the simultaneous removal.

Regeneration of Catalyst. The activity of catalyst for SO_2 removal decreases over a certain reaction time (Fig. 1 or 6); that for NO reduction does not decrease over 10 h. Sulfuric acid or ammonium sulfates formed during the course of reaction would diminish the number of active sites for successive adsorption of SO_2. Thus the removal of these compounds from the catalyst is indispensable for the regeneration of the catalyst. Deactivated catalysts were usually regenerated by (a) heating above 400 °C in nitrogen or (b) washing with water. In (a) surface compounds seem to react with AC as follows.

$$2H_2SO_4 + C \longrightarrow 2SO_2 + 2H_2O + CO_2 \quad (5)$$

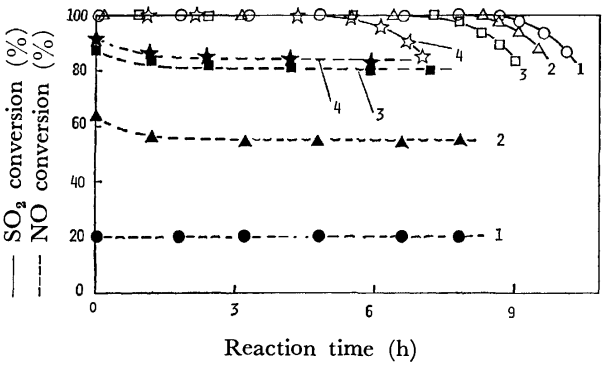

Fig. 8. Effect of amount of vanadium on activity for SO_2 removal and NO reduction.
Amounts of vanadium;
1 ○●: 0 wt%, 2 △▲: 1 wt%, 3 □■: 2 wt%, 4 ☆★: 4 wt%.
Reaction conditions;
Reaction temp: 220 °C, SV: 5000 h^{-1}, SO_2: 500 ppm, NO: 300 ppm, NH_3: 600 ppm, O_2: 5 vol%, H_2O; 10 vol%, N_2: balance.

$$NH_4HSO_4 + C \longrightarrow 2NH_3 + 2H_2O + 2SO_2 + CO_2 \quad (6)$$

Consumption of AC is unavoidable. In (b) elusion of vanadium salt takes place because of its change from oxide to soluble sulfate state in water. A new method free from the loss of active components is desirable.

In an industrial SO_2 removal process using $Cu–Al_2O_3$ catalyst, H_2, CO or low molecular HC is effective.[8] We have found that CO and H_2 are effective and that the consumption of AC caused by the regeneration with H_2 or CO was less than that by heating in nitrogen. When deactivated catalysts are treated with NH_3 gas, however, H_2SO_4 on the deactivated catalyst changes to NH_4HSO_4 or $(NH_4)_2SO_4$ (Reactions 3 and 4), and the consumption of the catalyst (Reactions 5 and 6) decrease as compared with the case in which other reducing agents are used.

Figure 9 shows the variation of photoelectron spectra for S 2p and V $2p_{3/2}$ on the catalyst. The intensity of S 2p peak increased with reaction time, that of V $2p_{3/2}$ peak decreasing gradually. No S 2p peak was observed after regeneration with NH_3. Analysis of sulfate ions (JIS-K-0101) showed no sulfate ions after the regeneration. The results show that sulfur was removed perfectly from the catalyst by regenerating with NH_3 gas. The electronic state of vanadium ions turned electronegative with reaction time (Fig. 9). The change of the electronic state of the active component would affect the activity for NO reduction. The activity of the AC catalyst was found to decrease at the initial state of the reaction (Fig. 8). After regeneration with NH_3 gas, both the electronic state of vanadium ions and the activity for NO reduction were recovered. For practical purposes, repeated regeneration is desirable.

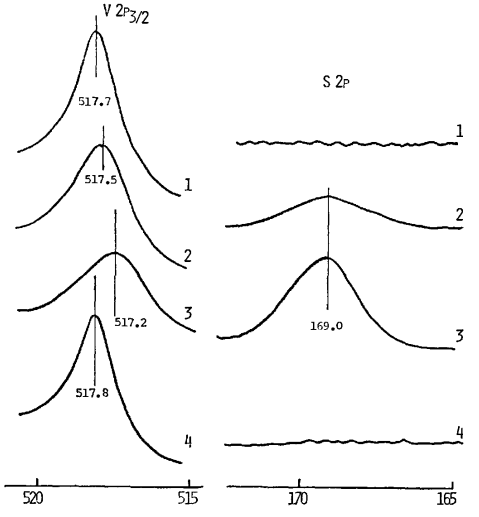

Fig. 9. Variation of photoelectron spectra for S 2p and V $2p_{3/2}$.
1: Fresh catalyst, 2: used for 2 h, 3: deactivated (used for 10 h), 4: regenerated with NH_3 at 350 °C. Catalyst: 2 wt% on AC prepared from polyacrylonitrile. Binding energies were referenced to C ls of contaminant carbon (285.0 eV).

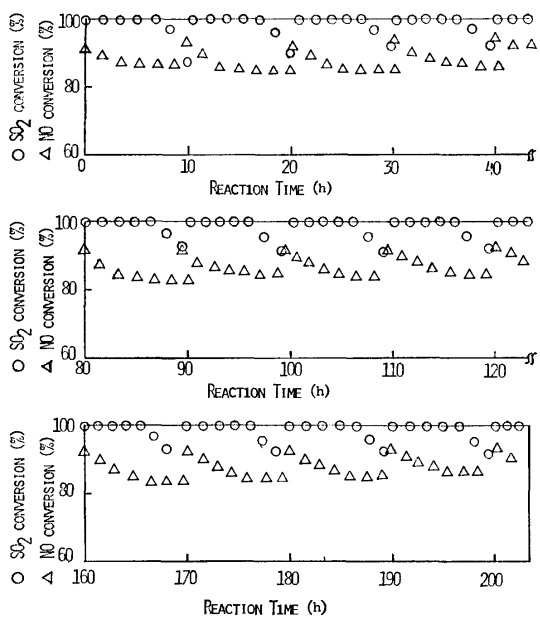

Fig. 10. Life test of simultaneous removal of SO_2 and NO.
Reaction conditions;
Reaction temp: 220 °C, SV: 5000 h^{-1}, SO_2: 500 ppm, NO: 300 ppm, NH_3: 600 ppm, O_2: 10 vol%, H_2O: 10 vol%, N_2: balance.
Regeneration conditions;
Reaction temp: 350 °C, Reaction time: 2 h, SV: 130 h^{-1}, NH_3: 2 vol%, N_2: balance.

Life Test of AC Catalyst for Simultaneous Removal. Figure 10 shows the result of the life test of AC catalyst for the simultaneous removal of SO_2 and NO. After every 10 h, regeneration was performed using NH_3 gas at 350 °C for 2 h. Steady activities over 90% of SO_2 removal and 80% of NO reduction were achieved. The consumption of the catalyst for 200 h of the life test was less than 0.1 ml (20 ml of the catalyst). After the life test, the dispersion of vanadium ions on regenerated catalysts was examined. The particle size of vanadium (smaller than 20 Å) and the highly dispersed state did not change after 20 repetitions of regeneration.

The results indicate that the simultaneous removal of SO_2 and NO with space velocity higher than 5000 h^{-1} is feasible.

References

1) H. Nishino, *Kankyo Sozo*, **4**, 25 (1976).
2) R. Yamada, 4th Symposium of Environmental Techniques, Tokyo, March 1977, 7—35.
3) H. Sano and H. Ogawa, *Sangiyo Kogai*, **10**, 2245 (1974).
4) A. N. Sidorov, *Zh. Fiz. Khim.*, **30**, 995, (1956).
5) J. B. Peri, 2nd Int. Congr. on Catalysis, Paris, 1960, Proc. 1333.
6) R. Kobayashi, 25th Summer Seminar of the Society of Polymer Science, Japan, 1977, Abstr. 155.
7) N. Todo, M. Kurita, H. Hagiwara, A. Ueno, and T. Sato, The Japan-U.S.A. Seminar on Catalytic NO_x Reactions, November 1975, Preprints 3-1.
8) F. M. Davtzenberg, J. E. Nader, and A. J. J. Van Ginneken, *Chem. Eng. Prog.*, **67**, 8—86 (1971).

CO Shift Reaction on the Potassium Polyaluminate Catalyst

Seiji KIHARA,†,** Kunihito KOUMOTO,* Yasuo NISHIKAWA,†† and Hiroaki YANAGIDA

Department of Industrial Chemistry, Faculty of Engineering, The University of Tokyo, Hongo, Bunkyo-ku, Tokyo 113

† *Engineering Research Institute, Faculty of Engineering, The University of Tokyo, Yayoi, Bunkyo-ku, Tokyo 113*

†† *Kyushu Taika Renga Co. Ltd., Urainbe, Bizen, Okayama 705*

(Received September 17, 1979)

Synopsis. Potassium polyaluminate (β_K''-alumina) has been employed as a catalyst for CO shift reaction ($CO+H_2O=CO_2+H_2$). The dependence of catalytic activity on the K^+ content was investigated. The initial reaction rate abruptly increased above 11 wt% K_2O.

Alkali polyaluminates, of which β-alumina has been classified into β, β', and β'',[1] have the characteristic layer structure[2] and are solid electrolytes with high ionic conductivity.[3] Alkali polyaluminates are also effective as catalysts for the steam reforming reaction of hydrocarbons;[4,5] fuel gas of good quality and rich in hydrogen gas can be produced. They are also applicable to atmospheric and vacuum residue oil of inferior quality, and considered to be important materials in view of effective utilization of petroleum energy sources. The catalytic ability of alkali polyaluminates lies mainly in enhancement of water gas shift reaction and gasification of carbon.[4,5] This is characteristic of basic catalysts and is exibited in the steam reforming reaction of inferior hydrocarbons. In the present study, potassium polyaluminate (β_K''-alumina) has been employed as a catalyst for CO shift reaction ($CO+H_2O=CO_2+H_2$) in order to investigate the dependence of catalytic activity on the K^+ content.

Experimental

The powder of β_K''-alumina (Kyushu Taika Renga Co. Ltd.) was pressed into cylindrical pellets, diam 20 mm and thickness 3 mm, under the pressure of 500 kg/cm^2. After the pellets had been calcined at 1300 °C for 1 h in an electric furnace, they were crushed into particles, 1—3 mm in diam Samples with lower K^+ content were obtained by eluting K^+ with purified water, HCl solution, and H_2SO_4 solution. Those with higher K^+ content were prepared by calcining β_K''-alumina pellets containing excess K_2CO_3. The procedure and K_2O content of the samples obtained are given in Table 1. For determination of the K_2O content by flame photometry, the sample was dried at 300 °C for 1 h and dissolved in H_2SO_4–$(NH_4)_2SO_4$ aqueous solution.

The initial rate of the CO shift reaction was measured at 600 °C under differential conditions using a reaction vessel of the normal-pressure flow system. 0.8 g of the catalyst (particle size 14—20 mesh) was diluted with 17.2 g fused alumina (particle size 12—20 mesh) which had been confirmed to be non-active as a catalyst. The volume of the catalyst bed was 10 ml and its height 2 cm. The center of the catalyst bed was placed at the highest temperature region in the reaction tube. The stainless sheath thermocouple (chromel-alumel, JIS 0.75 grade) protected by a high alumina tube was inserted in the center of the catalyst bed, the temperature being controlled by a proportional position temperature regulator (CHINO, NS 141). The temperature fluctuation in the catalyst bed was within ±2.5 °C, the prescribed temperature being controlled within ±5 °C.

Gas sampling was performed after the reaction reached steady state, and the composition of the gas was analyzed by means of a gas chromatograph (Gasukuro Kogyo, KOR-70). Molecular sieves of 5A, 13X, and silica gel were used as separating columns for CO, H_2, and CO_2, respectively. The area under the chromatogram was measured with a digital integrator (Shimadzu, ITG 4A), the gas composition being determined by the absolute calibration method. The error of mass balance of the reaction was within *ca.* ±3%.

Table 1. Specimens

Specimen NO.	Preparation process	Phase[a]	K_2O content[b] wt%
1	$+K_2CO_3$	β''-alumina	14.5
2	$+K_2CO_3$	β''-alumina	14.4
3	$+K_2CO_3$	β''-alumina	12.1
4	No Treatment	β''-alumina	11.4
5	Elution (H_2O)	β''-alumina	11.0
6	Elution (H_2O)	β''-alumina	10.4
7	Elution (H_2O, boiled)	β''-alumina	9.1
8	Elution (HCl, boiled)	β''-alumina	4.1
9	Elution (H_2SO_4, 200 °C)	β''-alumina	1.2

a) Determined by X-ray diffraction method. b) By flame photometry.

Results and Discussion

The initial reaction rate generally depends on the feed gas composition.[6] However, no dependence was observed in a preliminary experiment with use of specimen NO. 4. Thus, the feed gas composition was fixed as $P_{H_2O}/P_{CO}=1$, the total pressure being 1 atm.

The initial rate of the CO shift reaction obtained at 600 °C as a function of K_2O content in β_K''-alumina is shown in Fig. 1. The abrupt variation in the initial rate was found at *ca.* 11 wt% K_2O content. The result indicates that the surface state of β_K''-alumina with over 11 wt% K_2O differs from that with less than 11 wt% K_2O. The samples with less than 11 wt% K_2O also show the X-ray diffraction pattern of β_K''-alumina structure (Table 1), suggesting that H^+ or H_3O^+ ions undergo exchange with K^+ ions in the solid structure. However, the ions might not have been distributed homogeneously in the bulk, the concentration of K^+ ions near the surface being assumed

** Present address: Kyushu Taika Renga Co. Ltd., Urainbe, Bizen, Okayama 705.

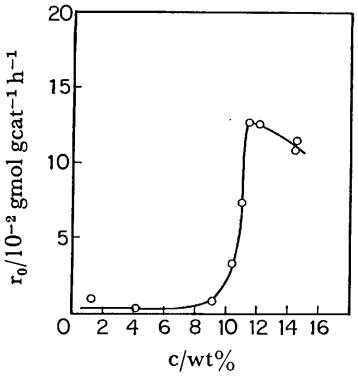

Fig. 1. Initial reaction rate *vs.* K_2O content obtained at 600 °C.

to be lower than expected. If this was the case, the result suggests that K^+ ion on the catalyst surface acts as an active center for the reaction.

The abrupt variation in the initial rate is also understandable if two kinds of K^+ ions exist, one as an active center but easily eluted by water or acid, the other being non-active but stable against elution.

References

1) G. Yamaguchi and K. Suzuki, *Bull. Chem. Soc. Jpn.*, **41**, 93 (1963).
2) C. A. Beevers and M. A. Ross, *Z. Kristallogr.*, **97**, 59 (1937).
3) Yung-Fang Yu Yao and J. T. Kummer, *J. Inorg. Nucl. Chem.*, **29**, 2453 (1967).
4) S. Komatsu and G. Yamaguchi, *Sekiyu Gakkai Shi*, **17**, 1038 (1974).
5) S. Komatsu and G. Yamaguchi, *Sekiyu Gakkai Shi*, **17**, 662 (1974).
6) K. H. Yang and O. A. Hougan, *Chem. Eng. Prog.*, **46**, 146 (1950).

ESR Studies of Temperature Dependent Zero-field Splitting in Yang's Biradical

Kazuo MUKAI,* Kazuhiko ISHIZU, Mizue NAKAHARA, and Yasuo DEGUCHI**
Department of Chemistry, Faculty of Science, Ehime University, Matsuyama 790
***College of Liberal Arts and Science, Kyoto University, Kyoto 606*
(Received March 27, 1980)

Synopsis. The ESR absorptions of Yang's biradical in a few organic solvents have been studied in detail as a function of temperature, and the effect of temperature on the symmetry of the biradical molecule has been discussed on the basis of the temperature dependence of the zero-field splitting parameters.

Yang's biradical is known as a stable π-conjugated phenoxyl biradical, having a structural three-fold symmetrical axis in the molecule.[1] In the previous work, the **D**-tensor values of Yang's biradical have been determined from an analysis of its asymmetric frozen ESR spectrum.[2] The results have provided direct experimental evidence for the asymmetrical molecular distortion in Yang's biradical. On the other hand, in fluid solution the biradical molecule still retains a three-fold symmetry; the results of ESR, NMR, and ENDOR studies[3–5] in solution indicate that the six meta-ring protons are magnetically equivalent, giving a hyperfine splitting attributable to the six meta-ring protons. In the present work, the ESR absorptions of Yang's biradical in a few organic solvents have been studied in detail as a function of temperature, and the effect of temperature on the symmetry of the biradical molecule has been discussed on the basis of the temperature dependence of the zero-field splitting (ZFS) parameters.

Results and Discussion

The toluene rigid matrix ESR spectrum of Yang's biradical shows a characteristic spectrum of a non-axially symmetrical triplet, with $|D|=34.1$ G and $|E|=1.9$ G at 77 K (see Fig. 1(c)).[2] In the low temperature region between −196 and −140 °C, the ESR spectra remain almost unchanged upon variation of the temperature. When the samples were warmed to the higher temperatures, the decrease in the separation between the Z and Z′ lines and the sharpening of both the XY and X′Y′ lines have been observed until the typical triplet spectra become unobservable, as shown in Figs. 1(a) and (b). By recooling the samples to 77 K, it was confirmed that the change in the ESR spectra is reversible. A similar temperature effect on the triplet ESR spectra has also been observed in ethanol and 2-MTHF (2-methyltetrahydrofuran). The ZFS parameters $|D|$ and $|E|$ calculated from the observed spectra[2] are given in Table 1 and Fig. 2. In the low temperature region, the ZFS parameters show no detectable change. At higher temperature, the decrease in D is 10—20% and the decrease in E is 50—60% for the organic solvents used in the present work.

The Yang's biradical is thought to have a fixed structure in the low temperature region, because the ZFS parameters D and E show no detectable change. On warming with a consequent softening of the matrix, the D value decreases, for instance, from 34.1 G at −196 °C to 30.1 G at −110 °C in toluene. We think that one possible reason for the temperature dependence of D may be the rotation of the phenyl rings in Yang's biradical.[6] If one considers the rotation of the three phenyl rings, the average twist angle of each phenyl ring is increased as the temperature is raised. This would result in an increased average separation between the two unpaired electrons and a consequent decrease in the value of D.

At 77 K where Yang's biradical is trapped rigidly in the organic solvent matrices, the molecule has a distorted propeller structure with a non-zero E value,

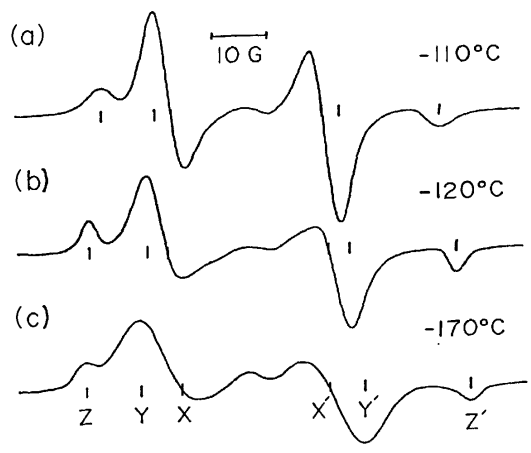

Fig. 1. Temperature dependence of the ESR absorption of Yang's biradical in toluene.
(a): −110 °C, (b): −120 °C, (c): −170 °C.

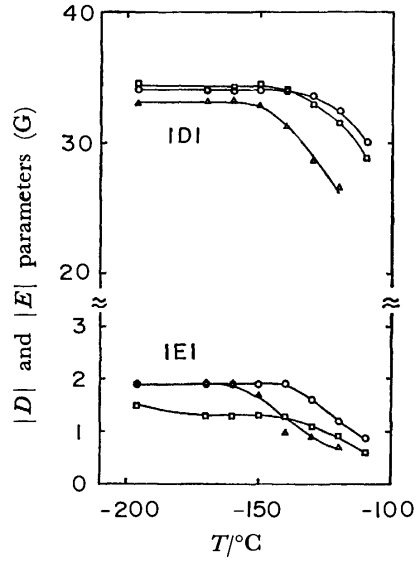

Fig. 2. Temperature dependence of the ZFS parameters $|D|$ and $|E|$ of Yang's biradical in toluene (○), ethanol (□), and 2-MTHF (△).

Table 1. The $|D|$ and $|E|$ values of Yang's biradical in toluene, ethanol and 2-MTHF at various temperatures

T/°C	Toluene		Ethanol		2-MTHF	
	$\|D\|$[a]/G	$\|E\|$[a]/G	$\|D\|$/G	$\|E\|$/G	$\|D\|$/G	$\|E\|$/G
−110	30.1	0.9	28.9	0.6	—	—
−120	32.5	1.2	31.5	0.9	26.6	0.7
−130	33.6	1.6	33.0	1.1	28.7	0.9
−140	34.0	1.9	34.1	1.3	31.3	1.0
−150	34.0	1.9	34.5	1.3	32.9	1.7
−160	34.0	1.9	34.2	1.3	33.4	1.9
−170	34.0	1.9	34.0	1.3	33.2	1.9
−196	34.1	1.9	34.6	1.5	33.1	1.9

a) The $|D|$ and $|E|$ values were calculated from the $ZZ'=2D$ and $YY'=D+3E$ separations. The E value thus calculated is smaller than the true value, considering the overlaping of the inner two pairs of lines.[2] The experimental errors in the values of $|D|$ and $|E|$ are ± 0.2 and 0.4 G, respectively. $1\,G=10^{-4}\,T$.

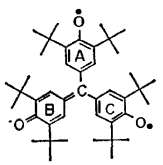

Yang's Biradical

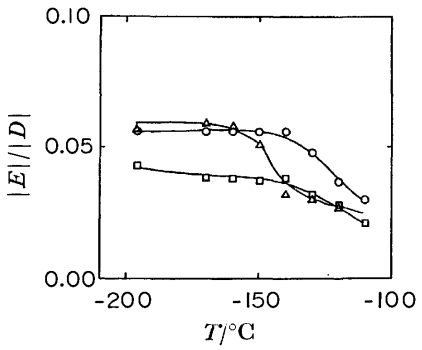

Fig. 3. Temperature dependence of the ratio of $|E|/|D|$ of Yang's biradical in toluene (○), ethanol (□), and 2-MTHF (△).

because of the asymmetric environment due to the frozen-solvent molecules. Although both the D and E values decrease with increasing temperature, the 50—60% decrease in E with increasing temperature is large compared with the 10—20% decrease in D. Among the ZFS parameters, D measures the average distance between electrons. On the other hand, E measures the deviation of the molecule from three-fold or higher symmetry weighted by this distance. Therefore, the ratio E/D provides a measure of the deviation from a structure of high symmetry. In Fig. 3, the ratio E/D is plotted as a function of temperature. The ratio E/D is constant in the low temperature region, but decreases rapidly with increasing temperature at higher temperature region (approaching the melting point of the solvent). This result may be explained by assuming that the degree of molecular asymmetry was decreased with increasing temperature. At the higher temperatures, the decrease in the rigidity of solvent matrix should allow the guest biradical molecule to assume its preferred geometry. This fact corresponds well to the fact that the molecular asymmetry of the Yang's biradical observed at the low temperature is eliminated at room temperature.[3-5]

Yang's biradical is thought to be a derivative of trimethylenemethane (TMM) $(\cdot CH_2)_2C{=}CH_2$, which also has structural three-fold symmetry. Therefore, in TMM biradical, we can expect similar temperature dependent variation in the D and E parameters. However, in the low temperature matrices, TMM shows the characteristic spectrum of an axially symmetrical triplet molecule, with $D=254$ G and $E=0$ G.[7] On the other hand, the decrease in D value of TMM with increasing temperature has been found,[8] and, in addition, the splitting of the XY lines at temperatures above 77 K has been observed,[9] using the deuterium derivative of the TMM, $(\cdot CD_2)_2C{=}CD_2$; the results suggest that the TMM molecule lacks a three-fold symmetry at the high temperature region. Recently, Claesson *et al.*[10] have proposed that the change in D value and the deviation from axial symmetry can be attributed to an anisotropic temperature dependent oscillation about a preferred axis in the TMM plane, from the results of the single crystal study of the triplet TMM molecule. Such a difference in the temperature dependence of the ZFS parameters between the small TMM molecule and the large Yang's biradical molecule is interesting.

References

1) N. C. Yang and A. J. Castro, *J. Am. Chem. Soc.*, **82**, 6208 (1960).
2) K. Mukai, T. Mishina, and K. Ishizu, *J. Chem. Phys.*, **66**, 1680 (1977).
3) R. Kreilick, *J. Chem. Phys.*, **43**, 308 (1965).
4) P. W. Kopf and R. W. Kreilick, *J. Am. Chem. Soc.*, **91**, 6569 (1969).
5) H. V. Willigen, M. Plato, K. Möbius, K. -P. Dinse, H. Kurreck, and J. Reusch, *Mol. Phys.*, **30**, 1359 (1975).
6) C. Steelink, J. D. Fitzpatrick, L. D. Kispert, and J. S. Hyde, *J. Am. Chem. Soc.*, **90**, 4354 (1968).
7) T. Yamaguchi, M. Irie, and H. Yoshida, *Chem. Lett.*, **1973**, 975.
8) H. Yoshida and O. Edlund, *Chem. Phys. Lett.*, **42**, 107 (1976).
9) P. Dowd and M. Chow, *J. Am. Chem. Soc.*, **99**, 2825 (1977).
10) O. Claesson, A. Lund, T. Gillbro, T. Ichikawa, O. Edlund, and H. Yoshida, unpublished data.

Purification of Methylthymol Blue and Methylxylenol Blue by High-Performance Liquid Chromatography†

Shoji NAKADA, Mutsuo YAMADA, Tasuku ITO,†† and Masatoshi FUJIMOTO*

Department of Chemistry, Faculty of Science, Hokkaido University, Sapporo 060

(Received April 17, 1980)

Synopsis. Relatively large amounts of 3,3′-bis[bis(carboxymethyl)aminomethyl]thymolsulfonphthalein (Methylthymol Blue, MTB) and 3,3′-bis[bis(carboxymethyl)aminomethyl]-*p*-xylenolsulfonphthalein (Methylxylenol Blue, MXB) are easily purified by high-performance liquid chromatography (HPLC).

Multidentate ligands of triphenylmethane complexon (TPMC) series, MTB and MXB, are metallochromic indicators for the complexometric titration of a number of metal ions in aqueous solutions.[1] However, only a few quantitative data on the complex formation of these ligands have been reported. These data show serious discrepancies resulting from the use of specimens of low purity.

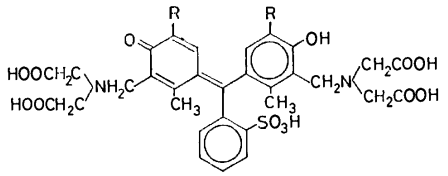

MTB : R = $CH(CH_3)_2$

MXB : R = CH_3

The purity of synthesized or commercial specimens of these ligands is low. MTB usually contains the starting materials, iminodiacetic acid (IDA) and Thymol Blue (TB), and a by-product, Semi-Methylthymol Blue (SMTB). Similarly, MXB contains IDA, *p*-Xylenol Blue (*p*-XB), and Semi-Methylxylenol Blue (SMXB). Since the monosubstituted products, SMTB and SMXB, and IDA also form stable metal complexes, the use of MTB or MXB free of these impurities is essential for quantitative studies of metal complex formation. However, the separation of IDA, SMTB or SMXB, and TB or *p*-XB from MTB or MXB was not easy; the method of purification reported for MTB[2] is incomplete, and that for MXB has not been established.

In a previous paper we reported the purification of Xylenol Orange (XO) by preparative HPLC.[3] We have applied the method to the purification of MTB and MXB, and succeeded in preparing relatively large amounts of MTB and MXB of high purity.

Ten grams of crude sample of synthesized MTB or MXB was preliminarily purified by cellulose column chromatography (CCC) using a 45 × 1000 mm column packed with 600 g of Whatman CC-31 cellulose powder and 1-butanol saturated with 1% aqueous acetic acid as an eluent. The last fraction of three colored bands clearly separated on the chromatogram was used as a sample for HPLC. In the case of MXB, the yield of the last fraction by CCC was very low as compared with that of MTB. Paper partition chromatography (PPC) of the pre-treated sample gave no spots of SMTB (or SMXB) and TB (or *p*-XB), but a considerable amount of IDA still remained unremoved.

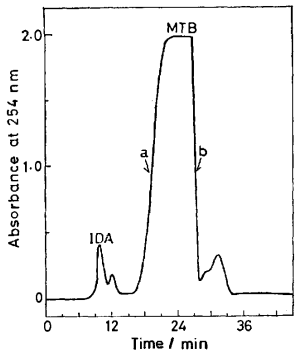

Fig. 1. Elution curve of the pre-purified sample of MTB.

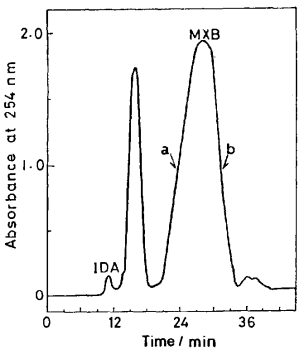

Fig. 2. Elution curve of the pre-purified sample of MXB.

Figure 1 shows a typical elution curve of preparative HPLC for the pre-purified sample of MTB. One gram of the sample pre-purified on CCC was dissolved in 5 cm^3 of water. One cubic centimeter of the sample solution was injected for each run. The separation was accomplished with an eluent, 5% aqueous acetic acid–methanol (60/40, v/v),** at a flow rate 6.0 $cm^3\,min^{-1}$ and at 1500 psi. MTB was clearly separated from the impurities on a preparative scale, a small peak of an unknown substance being observed in the tail portion of the MTB peak. After elution of MTB the column was regenerated by washing with methanol for 20 min. An unknown reddish yellow material probably containing a trace amount of SMTB was flushed out. The column thus regenerated was used repeatedly.

Figure 2 shows an elution curve for the pre-purified sample of MXB under the same conditions as those for MTB except for the use of 5% aqueous acetic acid–methanol (80/20, v/v)** as an eluent. The peak

† Presented in part at the 1980 Winter Meeting of the Chemical Society of Japan and the Japan Society for Analytical Chemistry, Sapporo, Hokkaido, February 1, 1980, Abstract, p. 36.

†† Present address: Institute for Molecular Science, Okazaki 444.

** Preliminary experiments showed that the retention time for the parent triphenylmethane dyes is much longer than that of the corresponding TPMC and IDA as in the case of XO,[3] and that the retention time for TB-series is much longer than that for *o*-CR- and *p*-XB-series. With increase in methanol content in the given eluent, the retention times of *o*-CR, TB, and *p*-XB become shorter. Thus in the case of MTB we applied the eluent of higher methanol content (40%, v/v). The difference in retention time among the three series can be ascribed to the difference in the alkyl substituents in the triphenylmethane skeleton.

Table 1. Elemental analyses and DSC measurements of MTB and MXB

Compound	Formula		Elemental analyses C, %	H, %	N, %	S, %	S/N	Mp/°C
MTB	$C_{37}H_{44}O_{13}N_2S\cdot 3H_2O$	Found	54.80	6.02	3.37	3.93	1.17	201
		Calcd	54.80	6.21	3.46	3.95	1.14	
MXB	$C_{33}H_{36}O_{13}N_2S\cdot 3H_2O$	Found	53.72	5.52	3.59	4.20	1.17	270
		Calcd	52.52	5.61	3.71	4.24	1.14	(dec)

of MXB is much smaller than that of MTB. A colorless component giving a large frontal peak was assigned to an unreactive form of formaldehyde, which was revealed by ultraviolet spectra and chromatographic behavior. As in the case of MTB, a small peak was observed in the tail portion of the MXB peak. This was not assigned to that of the corresponding monosubstituted product, SMXB. The results indicate that the purification of MTB and MXB is not complete by means of a single HPLC even under the best conditions; repeated HPLC is necessary for complete purification.

The effluent between **a** and **b** for each run in Figs. 1 and 2 was collected as the portions of MTB and MXB, respectively. Each effluent was combined, concentrated, and injected again for repeated HPLC. For the effluent after the second HPLC treatment, almost complete purification of MTB or MXB was confirmed by analytical HPLC with a column of Microbondapak C_{18}, 4×300 mm, and a solvent, 5% aqueous acetic acid–methanol (60/40, v/v). The purified MTB or MXB was converted into acid form, concentrated, and dried. For MTB about 300 mg of the acid form of pure specimen was obtained from 1 g of a pre-purified sample. For MXB, however, only 160 mg was obtained from 1 g of a pre-purified sample. The reason for the low yield of MXB can be attributed to structural requirements in MXB.

Experimental

Materials. The solvents used as eluents were purified beforehand. Acetic acid of analytical grade was filtered through a glass filter G4, methanol was distilled, and water was deionized and redistilled. The crude sample of MTB or MXB was synthesized by Mannich condensation from TB or *p*-XB, IDA, and formaldehyde.[4] The sample solutions for HPLC were filtered through a Toyo membrane filter TM-2.

Instruments. A Waters liquid chromatograph Model ALG/GPC 204 equipped with three 7×610 mm columns of Bondapak C_{18}/Porasil B in series and an ultraviolet detector ($\lambda=254$ nm).

Free-Acid Form of Purified MTB and MXB. Aqueous solutions of the sodium salts of purified MTB and MXB were passed through a column of Dowex 50W-X8 in the hydrogen form. The effluents were concentrated at 40 °C in a rotary evaporator and dried in a vacuum desiccator. The purity of the specimens of MTB and MXB was confirmed by elemental analyses and DSC measurements (Table 1). The values of pK_a, λ_{max}, and the molar absorptivity of the aqueous solutions of the pure ligands, MTB and MXB, will be reported.[5]

The authors wish to thank Prof. Yoshio Matsunaga for the kindness in the DSC measurements. The present work was supported by a Grant-in-Aid for Scientific Research from Ministry of Education, Science, and Culture (No. 347031).

References

1) B. Buděšínský, "Chelates in Analytical Chemistry," ed by H. A. Flaschka and A. J. Barnard, Jr., Marcel Dekker, New York, N. Y. (1967), Vol. 1, pp. 15—47.
2) T. Yoshino, H. Imada, T. Kuwano, and K. Iwasa, *Talanta*, **16**, 151 (1969).
3) S. Nakada, M. Yamada, T. Ito, and M. Fujimoto, *Bull. Chem. Soc. Jpn.*, **50**, 1887 (1977).
4) J. Kŏrbl and R. Přibil, *Chem. Ind. (London)*, **1957**, 233.
5) S. Nakada, M. Yamada, T. Ito, and M. Fujimoto, *Bull. Chem. Soc. Jpn.*, **53**, 2252 (1980).

The Stereo-differentiating (Asymmetric) Hydrogenation of the C=O Double Bond with a Modified Nickel Catalyst. XXXV. A Facile Method for the Preparation of Optically Pure β-Diols

Kazuhisa Ito, Tadao Harada, and Akira Tai*

Institute for Protein Research, Osaka University, Yamada-kami, Suita, Osaka 565

(Received April 4, 1980)

Synopsis. The hydrogenation of $RCOCH_2COR$ over a Raney nickel catalyst modified with a mixture of tartaric acid and NaBr gave (*R**, *R**)-$RCH(OH)CH_2CH(OH)R$ selectively with a high optical purity. The substrates with R=CH_3-, CH_3CH_2-, $CH_3CH_2CH_2$-, $CH_3(CH_2)_4CH_2$-, and Ph- were employed in this study. In all cases, the recrystallization of the hydrogenation product gave an optically pure (*R**,*R**)-isomer which was free from the (*R**,*S**)-isomer.

Optically pure β-diols and their derivatives are potentialy useful chiral compounds as chiral solvents, chiral ligands, and chemicals for the preparation of optically active compounds. Althgouh a small amount of (+)-(2*S*,4*S*)-2,4-pentanediol has been prepared by the tedious optical resolution,[1] no practical methods for the large-scale preparation of optically pure compounds have been reported.

In a previous communication, we have briefly reported that the Raney nickel catalyst (RNi) modified with a solution containing tartaric acid (TA) and NaBr (TA–NaBr–MRNi) is an excellent catalyst for the hydrogenation of acetylacetone (Ia) to 2,4-pentanediol (Ib), giving (2*R**,4*R**)-Ib selectively with a high optical purity.[2] The catalyst was also found to be effective for the hydrogenation of other symmetric β-diketones to a mixture of (*R**,*R**)- and (*R**,*S**)-diol.

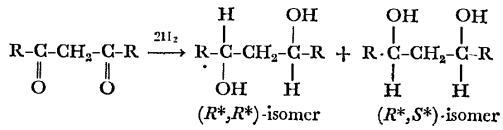

R=CH_3-, acetylacetone (Ia) 2,4-pentanediol (Ib)
R=CH_3CH_2-, 3,5-heptanedione (IIa) 3,5-heptanediol (IIb)
R=$CH_3CH_2CH_2$-, 4,6-nonanedione (IIIa) 4,6-nonanediol (IIIb)
R=$CH_3(CH_2)_4CH_2$-, 7,9-pentadecanedione (IVa) 7,9-pentadecanediol (IVb)
R=Ph-, dibenzoylmethane (Va) 1,3-diphenyl-1,3-propanediol (Vb)

The results are listed in Table 1. The major product, the (*R**,*R**)-isomer, can be separated from the (*R**,*S**)-isomer by the recrystallization of the reaction product. In all cases, the isolated (*R**,*R**)-isomer was found to be already optically pure. All substrates gave (−)-(*R**,*R**)-isomers in excess when (*R*,*R*)-TA–NaBr–MRNi was used.

As is found in the table, the ratio of the (*R**,*R**)-isomer to the (*R**,*S**)-isomer in the hydrogenation product is slightly decreased with an increase in the chain length of R in the substrate. Consequently, the isolation yield of the (*R**,*R**)-isomer decreases with the increase in the chain length of the substrate. However, the advantage of the present method is that optically pure β-diols are easily obtained by the recrystallization of the hydrogenation products. Furthermore, the preparation of TA–NaBr–MRNi is very simple, and the cost of the catalyst is negligibly low. Therefore, the present method would be easily applicable for the large-scale production of β-diols.

The optical purity of the (*R**,*R**)-isomers listed in Table 1 can be determined by means of the NMR of the diacetate derived from each diol. The chemical shifts for the acetyl group (singlet) of (−)- and (+)-diacetate were separated by 3 to 5 Hz in the presence of 2 molar eqivalents of $Eu(hfmc)_3$ to the acetate. In all cases, the signals of the diacetates derived from (+)-diols appeared at a high field.

The absolute configurations of the diols have not yet been determined except for the case of (−)-(2*R*, 4*R*)-Ib. However, the configurations of the (−)-isomer can be expected to be (*R*,*R*) for the following reasons: 1) the lanthanid-induced shifts of all the (−)-diols in NMR show the same tendency as that of Ib, and 2) the analogues of the substrates thus far examined are hydrogenated to (−)-(*R*)-products over (*R*,*R*)-TA–NaBr–MRNi; *i.e.*, Ia, 4-hydroxy-2-butanone, and methyl acetoacetate are converted to (−)-(2*R*, 4*R*)-Ib, (−)-(*R*)-1,3-butanediol,[3] and (−)-(*R*)-methyl 3-hydroxybutyrate[4] respectively.

Experimental

The ^{1}H-NMR and IR spectra were taken with a JELO FX-100 spectrometer and a Shimadzu IR 27G spectrometer respectively. The optical rotation was measured with a Perkin Elmer 241 polarimeter. The analytical GLC was carried out with a Shimadzu GC 4A-PF gas chromatograph, using a 3 m—5 mm o.d. glass column packed with 15% Ucon 50 HB-2000 on Chromosorb W (Ucon) or 2% Silicone OV-17 on Chromosorb W (OV-17) at the stated temperature. The preparative GLC was carried out with a Shimadzu 3A instrument using a 6 m—6 mm o.d. stainless column packed with OV-17. The preparative TLC was carried out on a Silicagel F plate (Merck Co.) with a solvent of ether/hexane=1/1.

All the chemicals except those listed below were obtained from commercial sources. 3,5-Heptanedione (IIa), 4,6-nonanedione (IIIa), and 7,9-pentadecanedione (IVa) were prepared from an appropriate ester, $RCOOCH_3$, and the 2-alkanones, CH_3COR, by a previously reported method.[5] The physical constants of the products were identical with those previously reported.[5] The GLC analysis indicated that the purity of each compound was more than 97%.

The preparation of TA–NaBr–MRNi and the hydrogenation of each substrate were carried out by a procedure reported before.[2]

Determination of the Ratio of Diastereomers in the Hydrogenation Product. The hydrogenation products of Ia and IIa were directly subjected to the GLC (Ucon) analysis. The GLC data (retention time and column temperature) are as follows: (2*R**,4*R**)-Ib, 170 min/80 °C; (2*R**,4*S**)-Ib, 159 min/80 °C; (3*R**,5*R**)-IIb, 109 min/120 °C; (3*R**,5*S**)-IIb, 99.6 min/120 °C. The GLC analyses of the hydrogenation products of IIIa to Va were carried out after the products had been converted to its trimethylsilyl (TMS) ether. A 0.1-g portion of the sample was treated with 0.2 ml each

Table 1. Hydrogenations of β-diketones over (*R,R*)-TA-NaBr-MRNi[a)]

Substrate	Proportion of diastereomers (%) in the hydrogenation product		Isolation of (*R*, R**)-diol from the hydrogenation product	
	(*R*, R**)-diol	(*R*, S**)-diol	Yield/%	$[\alpha]_D^{20}$ of diol
Ia	87	13	65 (57)	−54.5 (+53.6)
IIa	80	20	30 (25)	−39.1 (+39.0)
IIIa	85	15	11 (13)	−21.4 (+21.2)
IVa	80	20	21 (20)	−10.8 (+11.1)
Va	77	23	20 (23)	−72.7 (+72.3)

a) Figures in parenthese show the results of (*S,S*)-TA-NaBr-MRNi.

of $(CH_3)_3SiCl$ and $(CH_3)_3Si$–NH–$Si(CH_3)_3$ in 20 ml of pyridine at 90 °C for 10 min. After the removal of volatiles under reduced pressure at 90 °C, the residue was mixed with 1 ml of hexane and then centrifuged. The TMS ether in the supernatant was subjected to GLC analysis. The GLC data (retention time, packings of column, and column temperature) are as follows: (4*R**,6*R**)-TMS-IIIb, 58.4 min/Ucon/150 °C; (4*R**,6*S**)-TMS-IIIb, 54.4 min/Ucon/150 °C; (7*R**,9*R**)-TMS-IVb, 89.6 min/Ucon/150 °C; (7*R**,9*S**)-TMS-IVb, 83.6 min/Ucon/150 °C; (1*R**,3*R**)-TMS-Vb, 122 min/OV-17/140 °C; (1*R**,3*S**)-TMS-Vb, 116 min/OV-17/140 °C. The ratio of the diastereomers was evaluated from the ratio of the peak areas of the GLC.

*Isolation of the (*R*,R**)-Isomers from the Hydrogenation Product. (−)-(2*R*,4*R*)-2,4-Pentanediol (Ib)*: A 9-g portion of the hydrogenation product of Ia over (*R,R*)-TA-NaBr-MRNi was dissolved in 10 ml of ether, after which the solution was cooled at −50 °C for 1 h. The crystals precipitated from the solution were taken out and recrystallized from 10 ml of ether at −5 °C to give 5 g of (*2R,4R*)-Ib (bp 111—113 °C/19 mmHg; mp 50.5 °C). The analytical GLC (Ucon, 120 °C) showed a single peak. The crystals were too hygroscopic for the elemental analysis to be performed with a completely dried sample. The results of a partially dried sample were as follows; Found: C, 56.50; H, 11.70%. Calcd for $C_5H_{12}O_2 \cdot (0.1\ H_2O)$: C, 56.70; H, 11.62%. The NMR and IR spectra of the sample were consistent with the structure of Ib. The optical rotation of the sample was as follows; $[\alpha]_D^{20}$ −53.7° (*c* 10, ethanol), $[\alpha]_D^{25}$ −41.2° (*c* 10, $CHCl_3$) (lit,[1)] −41.3° ($CHCl_3$, *c* not stated)). As a large-scale preparation, the hydrogenation of 200 g of Ia over 26 g of (*R,R*)-TA-NaBr-MRNi was carried out in an autoclave with a capacity of 2000 ml. From the hydrogenation products, 131 g of (*2R,4R*)-Ib was obtained.

*(−)-(3*R**,5*R**)-3,5-Heptanediol (IIb)*: A 9 g portion of the hydrogenation product of IIa over (*R,R*)-TA-NaBr-MRNi was dissolved in 20 ml of ether, after which the solution was cooled at −50 °C for 3 h. The crystals thus precipitated were separated from the supernatant solution by decantation at −50 °C. Two successive recrystallizations of the crystals from 20-ml portions of ether at −10 °C gave optically pure (−)-(3*R**,5*R**)-IIb in a yield of 2.7 g (30% based on the crude product) (bp 110 °C/12 mmHg; mp 52—53 °C; Found: C, 62.64; H, 12.21%. Calcd for $C_7H_{16}O_2 \cdot (0.1\ H_2O)$: C, 62.73; H, 12.18%, $[\alpha]_D^{20}$ −39.1° (*c* 10, ethanol)). The analytical GLC (Ucon, 120 °C) showed a single peak. The NMR and IR spectra of the sample were consistent with the structure of IIb.

*(−)-(4*R*,6*R**)-4,6-Nonanediol (IIIb)*: A solution of 9 g of the hydrogenation product of IIIa over (*R,R*)-TA-NaBr-MRNi in 20 ml of ether was kept overnight at −50 °C. The crystals thus precipitated were taken out by filtration in a cold room. Three successive recrystallizations from 20 ml of ether at −10 °C gave 1.4 g of an optically pure (−)-(4*R**,6*R**)-IIIb (16% based on the crude product); mp 58—59 °C; Found: C, 67.05; H, 12.56%. Calcd for $C_9H_{20}O_2 \cdot (0.05\ H_2O)$: C, 67.07; H, 12.57%, $[\alpha]_D^{20}$ −21.4° (*c* 10, ethanol). The NMR and IR spectra of the sample were consistent with the structure of IIIb.

*(−)-(7*R*,9*R**)-7,9-Pentadecanediol (IVb)*: A solution of 9 g of the hydrogenation product of IVa over (*R,R*)-TA-NaBr-MRNi in 20 ml in 20 ml of ethyl acetate was allowed to stand at −50 °C for 1 h. The crystals thus precipitated were taken out at −50 °C and recrystallized three times from 20 ml of ethyl acetate at 5 °C to give 1.9 g of optically pure (−)-(7*R**,9*R**)-IVb (21% based on the crude product); mp 73—74 °C, Found: C, 72.89; H, 13.10%. Calcd for $C_{15}H_{32}O_2$ (0.05 H_2O): C, 73.17; H, 13.18%, $[\alpha]_D^{20}$ −10.8° (*c* 10, ethanol). The NMR and IR of the sample were consistent with the structure of IVb.

*(−)-(1*R*,3*R**)-1,3-Diphenyl-1,3-propanediol (Vb)*: A solution of 9 g of the hydrogenation product of Va over (*R,R*)-TA-NaBr-MRNi in 10 ml of ethyl acetate was allowed to stand at −10 °C overnight. The crystals thus precipitated were separated by filtration and then recrystallized three times from 20 ml of (ether/ethyl acetate)=(8/2) to give 1.8 g of optically pure (−)-(1*R**,3*R**)-Vb (20% based on the crude product); mp 145—147 °C; Found: C, 78.40; H, 7.21%. Calcd for $C_{15}H_{16}O_2 \cdot (0.05\ H_2O)$: C, 78.30; H, 7.45%, $[\alpha]_D^{20}$ −72.7° (*c* 10, ethanol). The NMR and IR spectra of the sample were consistent with the structure of Vb.

Determination of the Optical Purity of the Purified Sample. The optical purities of the purified diols were determined by means of NMR after the diols had been converted to diacetates. Into a solution of 0.5 g of diol in 5 ml of pyridine were added 2 ml of acetic anhydride. The solution was heated at 60 °C for 3 h and then worked up in the usual manner to give the crude diacetate of the diol. The purification of the diacetate was carried out by either preparative GLC (diacetates of Ib and IIb) or preparative TLC (diacetates of IIIb, IVb, and Vb). The NMR spectra were measured with a solution of diacetate (10 mg) and $Eu(hfmc)_3$ (2 molar equvalents to the acetate) in $CDCl_3$ (0.4 ml) at 50 °C. None of the diacetates derived from purified products showed any detectable signal of the antipode.

The autors would like to thank Professor Yoshiharu Izumi for his helpful suggestions and discussions. Thanks are also due to Mrs. Aiko Kobatake for the elemental analyses and Mr. Yuji Hiraki for measuring the NMR spectra.

References

1) A. J. Fry and W. E. Britton, *J. Org. Chem.*, **38**, 4016 (1973).
2) K. Ito, T. Harada, A. Tai, and Y. Izumi, *Chem. Lett.*, **1979**, 1049.
3) H. Murakami, T. Harada, and A. Tai, *Bull. Chem. Soc. Jpn.*, **53**, 1356 (1980).
4) T. Harada and Y. Izumi, *Chem. Lett.*, **1978**, 1195.
5) J. T. Adams and R. Hauser, *J. Am. Chem. Soc.*, **66**, 1220 (1944).

The Synthesis of 1,3,5-Thiadiazinylium Salts

Isao SHIBUYA

National Chemical Laboratory for Industry, Yatabe, Ibaraki 305

(Received February 4, 1980)

Synopsis. 1,3,5-Thiadiazinylium salts were synthesized in good yields by the reaction of *N*-acyl imidoyl chlorides with thioamides or the treatment of 4*H*-1,3,5-thiadiazines with trityl salts.

Heteroaromatic cation compounds, such as pyrylium, 1,3-oxazinylium salts, and their S-analogs, have been synthesized, and the reactions of these salts with various nucleophiles have been investigated to afford numerous derivatives. In these salts, the S-analog is stabler or less reactive than the corresponding O-analog. The present author has been studying the reaction of the 2,4,6-triphenyl-substituted compounds of these salts with active methylenes in order to ascertain the reactivity of these hetero rings.[1] 2,4,6-Triphenyl-1,3,5-oxadiazinylium salt has been known previously as the adduct of benzonitrile–benzoyl chloride–alminium chloride (2:1:1); since this salt is very hygroscopic, however, it is almost impossible to isolate as a pure salt.[2] On the other hand, the S-analog, 2,4,6-triphenyl-1,3,5-thiadiazinylium salt, has not yet been found, though this salt is supposed to be stabler than the corresponding O-analog. Therefore, it is expected that this salt may be obtained in a good purity if a synthetic route is found. 2-Amino-4,6-diphenyl-1,3,5-thiadiazinylium salts have been synthesized by Liebscher *et al.*[3] but his method is specific and almost impossible to apply to other 1,3,5-thiadiazinylium salts. In order to find the general synthetic method of 1,3,5-thiadiazinylium salts, several probable paths were offered by analogy with those of other known heteroaromatic cations, and their reaction conditions were checked. As a result, it was found that a number of 1,3,5-thiadiazinylium salts (**1**—**11**) were given by the paths, (**A**) and (**B**), shown in Scheme 1.

In Path **A**, *N*-acyl imidoyl chlorides reacted with thioamides in a strong acidic medium to produce cycloization products, **1**—**6**. In Path **B**, the starting

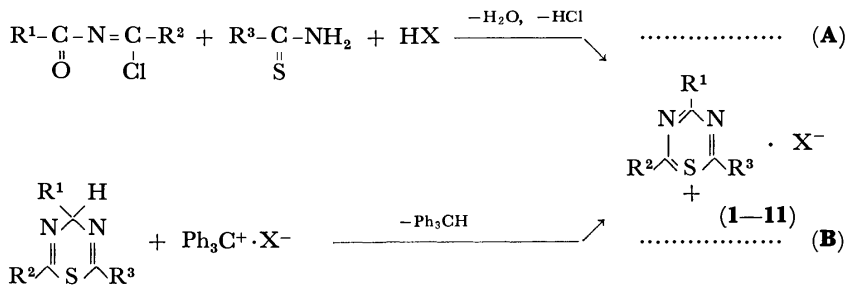

Scheme 1.

TABLE 1. 1,3,5-THIADIAZINYLIUM SALTS (**1**—**11**)

Compd	R^1	R^2	R^3	X^-	Yield/% Mp(dc)/°C	Found (Calcd) (%) C	H	N	S	IR(KBr)/cm^{-1}
1	C_6H_5-	C_6H_5-	C_6H_5-	ClO_4^-	87 242	58.93 (59.09)	3.55 (3.54)	6.56 (6.56)	7.26 (7.51)	1530, 1490, 1450, 1390, 1340, 1080.
2	$(CH_3)_2N$-	$(CH_3)_2N$-	$(CH_3)_2N$-	ClO_4^-	81 >300	32.92 (32.98)	5.53 (5.53)	21.44 (21, 36)	9.78 (9.78)	1570, 1550, 1390, 1370, 1080.
3	C_6H_5-	C_6H_5-	2-C_4H_3S-	ClO_4^-	78 223	52.57 (52.72)	3.04 (3.03)	6.47 (6.47)	14.85 (14.81)	1530, 1490, 1360, 1330, 1080.
4	C_6H_5-	C_6H_5-	$C_6H_5CH_2S$-	ClO_4^-	60 179	55.58 (55.87)	3.71 (3.67)	5.81 (5.92)	13.74 (13.56)	1510, 1480, 1370, 1330, 1080.
5	C_6H_5-	C_6H_5-	$(CH_3)_2N$-	ClO_4^-	46 211	51.90 (51.84)	4.11 (4.10)	10.70 (10.67)	8.07 (8.14)	1530, 1470, 1400, 1340, 1080.
6	*p*-$CH_3C_6H_4$-	*p*-$CH_3C_6H_4$-	*p*-$CH_3C_6H_4$-	BF_4^-	63 148	62.88 (63.17)	4.64 (4.64)	6.14 (6.14)	7.04 (7.03)	1530, 1500, 1390, 1330, 1170, 1050.
7	C_6H_5-	C_6H_5-	C_6H_5-	BF_4^-	81 246	60.73 (60.89)	3.70 (3.65)	6.85 (6.76)	7.95 (7.74)	1530, 1490, 1450, 1390, 1350, 1050.
8	*p*-ClC_6H_4-	C_6H_5-	C_6H_5-	BF_4^-	56 176	56.60 (56.22)	3.44 (3.14)	5.98 (6.24)	7.02 (7.15)	1530, 1490, 1390, 1350, 1050.
9	*p*-ClC_6H_4-	*p*-ClC_6H_4-	*p*-ClC_6H_4-	BF_4^-	40 128	48.81 (48.73)	2.59 (2.34)	5.40 (5.41)	6.21 (6.19)	1510, 1490, 1390, 1340, 1220, 1050.
10	*p*-$CH_3OC_6H_4$-	C_6H_5-	$C_6H_5^-$	ClO_4^-	60 148	57.53 (57.83)	3.75 (3.75)	6.08 (6.13)	7.26 (7.06)	1510, 1480, 1450, 1340, 1270, 1080.
11	*p*-$CH_3OC_6H_4$-	*p*-$CH_3OC_6H_4$-	*p*-$CH_3OC_6H_4$-	ClO_4^-	92 261	55.65 (55.76)	4.14 (4.09)	5.48 (5.42)	6.20 (6.20)	1530, 1500, 1440, 1400, 1270, 1080.

materials, 4*H*-thiadiazines, were obtained by treating a mixture of aldehyde–nitrile–thioamide (1:1:1) with the BF_3–ether complex in chloroform[4] and then treated with trity salt to lead to **7**—**11**.

Satisfactory analytical data were obtained for all the compounds. Their IR spectra have four common characteristic absorptions at 1530–1330 cm^{-1} except for **2**. These salts are not so stable in a dilute solution, and consequently do not show exact UV spectra. The reaction of **1** or **7** with ammonia, hydrazine, or hydroxylamine gave 2,4,6-triphenyl-1,3,5-triazine, 3,5-dipenyl-1,2,4-triazole, or 3,5-diphenyl-1,2,4-oxadiazole respectively in good yields. These results show that the behavior of **1** or **7** toward these nucleophiles is in the same manner as the 2,4,6-triphenyl-1,3,5-oxadiazinylium salt.[5] It is thus confirmed that **1**—**11** are 1,3,5-thiadiazinylium salts.

Experimental

The Reaction of N-*Acyl Imidoyl Chloride with Thioamide.* Into a solution of *N*-acyl imidoyl chloride (0.011 mol) and thioamide (0.010 mol) in 15 ml of acetic anhydride, 1.2 ml of 70% perchloric acid or 2.4 ml of 40% tetrafluoroboric acid was stirred drop by drop, at room temperature for 10 min, the mixture was then allowed to stand at 0—5 °C for 2 d. The resulting precipitate was collected by filtration and then recrystallized from acetonitrile to give **1**—**6**. The data thus obtained are summarized in Table 1.

The Reaction of 4H-*Thiadiazine with Trityl Salt.* Into a stirred solution of 4*H*-thiadiazine (0.010 mol) in 20 ml of acetic anhydride, 0.012 mol of trityl perchlorate or tetrafluoroborate was added at room temperature for 15 min. The mixture was added to dry ether (10 ml), after which the mixture was allowed to stand 3 d at 0—5 °C. The resulting precipitate was collected by filtration and then washed with dry ether to give **7**—**11**. Their data are also given in Table 1.

The Reaction of ***1*** *or* ***7*** *with Ammonia, Hydrazine, or Hydroxylamine.* Into 10 ml of 28% ammonium hydroxide, 30% aqueous hydrazine, or a solution of $NH_2OH \cdot HCl$ (1.5 g) in 10 ml of 5 mol dm^{-3} NaOH, 1 mmol of **1** or **7** was stirred in small portions at 0—5 °C, after which the mixture allowed to stand at room temperature for 2 h. The resulting precipitate was filtered and recrystallized from acetic acid, ethanol, or methanol to give 2,4,6-triphenyl-1,3,5-triazine (87%, mp 233 °C), 3,5-diphenyl-1,2,4-triazole (78%, mp 192 °C), or 3,5-diphenyl-1,2,4-oxadiazole (71%, mp 108 °C) respectively. Their IR spectra were completely superimposed on those of the respective authentic samples.[2,6]

References

1) I. Shibuya and M. Kurabayashi, *Bull. Chem. Soc. Jpn.*, **46**, 3902 (1973); **48**, 73 (1975); I. Shibuya, *ibid.*, **52**, 3767 (1979).
2) P. Eitner and F. Kraft, *Ber.*, **25**, 2266 (1892).
3) J. Liebscher and H. Hartmann, *Z. Chem.*, **15**, 438 (1975).
4) C. Giordano, A. Belli, and V. Bellotti, *Synthesis*, **1975**, 266.
5) R. R. Schmidt, *Chem. Ber.*, **98**, 334 (1965).
6) I. Shibuya, *Nippon Kagaku Kaishi*, **1979**, 389.

A ^{13}C NMR and CNDO/2 Calculation Study of the Transannular Interaction in [2.2]Metacyclophanes

Kazushi TOKITA, Shoichi KONDO, and Nobuo MORI*

Department of Chemistry, Science University of Tokyo, Kagurazaka, Shinjuku-ku, Tokyo 162

(Received February 8, 1980)

Synopsis. The substituent effects on the chemical shifts and CNDO/2 total electron densities of the facing aryl carbons, C-8 and C-16, in [2.2]metacyclophanes are reported.

In the course of ^{13}C NMR and electron density studies of [2.2]cyclophanes, we found that there is neither detectable transmission of spin information[1] nor detectable charge transfer *via* a transannular route in the ground electronic state.[2] Furthermore, we explained[3] the known paramagnetic proximity effect on aryl carbon resonances in [2.2]cyclophanes[4] by assuming a local decrease in the excitation energy term of the paramagnetic shielding expression by Karplus and Pople.

In the present work, we have studied the relationships between the chemical shifts (δ) and the total electron densities (q^t) of the facing inner aryl carbons, C-8 and C-16, in the nine [2.2]metacyclophanes, **1**—**9**, shown in Table 1. This study has been undertaken mainly in an attempt to explain the recent results by Atobe and Sato[5] that in substituted [2.2]metacyclophanes the resonance of C-8 (or C-16) moves downfield with an increase in the Hammett σ_p constant of a substituent at the 13 (or 5)-position, respectively.

Table 1 gives the excess total electron densities (Δq^t: $4-q^t$) on C-8 and C-16 in **1**—**9** together with the δ values observed in $CDCl_3$. The q^t values were calculated using the CNDO/2-MO method.[6] In these calculations,[7] the geometry of each substituted cyclophane was assumed to be the same as that of the parent hydrocarbon, **1**,[8] but with the hydrogen replaced by a substituent. As for the substituents, X and Y, the standard geometry parameters[9] were used.

TABLE 1. CHEMICAL SHIFTS AND EXCESS TOTAL ELECTRON DENSITIES OF C-8 AND C-16 IN THE CYCLOPHANES

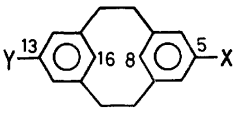

Compound	X	Y	C-8 $\delta(\Delta q^t \times 10^3)$	C-16 $\delta(\Delta q^t \times 10^3)$
1	H	H	136.3[a] (−22)	136.3 (−22)
2	F	H	132.6[b] (−44)	136.2 (−22)
3	NO_2	H	142.1[c] (+1)	136.9 (−25)
4	CH_3O	CH_3	130.0[d] (−53)	133.6 (−32)
5	CH_3	CH_3	133.9[a] (−32)	133.9 (−32)
6	CN	CH_3	140.6[d] (−17)	134.2 (−34)
7	NO_2	CH_3	142.3[d] (+1)	134.4 (−36)
8	CH_3O	CH_3O	129.3[d] (−52)	129.3 (−52)
9	NO_2	CH_3O	141.9[d] (+2)	130.0 (−56)

a) Data taken from Ref. 4. b) From Ref. 3. c) From Ref. 2. d) From Ref. 5.

The δ and the Δq^t values in Table 1 bear a fairly good linear relationship, as Fig. 1 shows. It should be noticed that X (or Y) has small, but significant, effects for both values of C-16 (or C-8), respectively. These effects can be confirmed by inspecting the data for the following groups of compounds, each having either X or Y as a fixed substituent (A) and the other as an unfixed one (B): **1**—**3** (H as A), **4**—**7** (CH_3 as A), **4**, **8**, and **9** (CH_3O as A), and **3**, **7**, and **9** (NO_2 as A).

For example, in the group of **4**—**7** having a methyl as Y (= A), an electron-withdrawing X (= B) causes a decrease in Δq^t (increase in q^t) and an increase in δ (downfield shift of the resonance) for C-16. In the other groups, the same can be found. From this result it is evident that, in spite of the increase in q^t, the resonance of C-16 is shifted downfield. A possible explanation for this downfield shift may be obtained by assuming that the introduction of the electron-withdrawing X causes a decrease in the diamagnetic anisotropy effect of the X-bearing ring, resulting from the decreased electron density, and a local decrease in the electronic excitation energy[10] by a transannular interaction between C-8 and C-16.[3]

The above results give additional support to our previous proposal[3] that the known paramagnetic proximity effect in [2.2]cyclophanes is not due to a decrease in electron density.

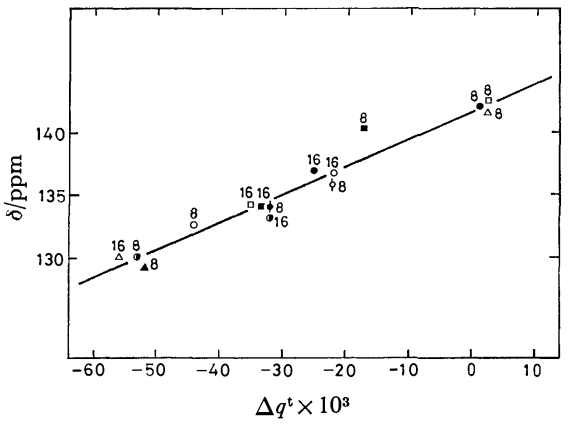

Fig. 1. Plots of δ *vs.* Δq^t for C-8 and C-16 of Compounds **1**—**9**.
○: **1**, ○: **2**, ●: **3**, ◑: **4**, ◖: **5**, ■: **6**, □: **7**, ▲: **8**, △: **9**. The least-squares relationship: $\delta = 229\,\Delta q^t + 141.9$ (correlation coefficient: 0.978; standard deviation: 0.86).

References

1) T. Takemura and N. Mori, *Chem. Lett.*, **1978**, 857.
2) T. Takemura, K. Tokita, S. Kondo, and N. Mori, *J. Chem. Res.* (S), **1978**, 452.

3) T. Takemura, K. Tokita, S. Kondo, and N. Mori, *Chem. Lett.*, **1977**, 865; K. Tokita, T. Takemura, S. Kondo, and N. Mori, *Bull. Chem. Soc. Jpn.*, **53**, 450 (1980).
4) T. Sato, T. Takemura, and M. Kainosho, *J. Chem. Soc., Chem. Commun.*, **1974**, 97; T. Takemura and T. Sato, *Can. J. Chem.*, **54**, 3412 (1976).
5) H. Atobe and T. Sato, 37th National Meeting of the Chemical Society of Japan, Yokohama, April 1978, Abstract No. 1A27.
6) J. A. Pople and D. L. Beveridge, "Approximate Molecular Orbital Theory," McGraw-Hill, New York (1970).
7) All computations were performed on a HITAC-8800/8700 Computer at the Computer Centre of the University of Tokyo.
8) C. J. Brown, *J. Chem. Soc.*, **1953**, 3278.
9) J. A. Pople and M. Gordon, *J. Am. Chem. Soc.*, **89**, 4253 (1967).
10) M. Karplus and J. A. Pople, *J. Chem. Phys.*, **38**, 2803 (1963).

The Preparation of Pyrrolotropones from Furotropones

Hitoshi TAKESHITA,* Atsuko CHISAKA, and Hiroaki MAMETSUKA
Research Institute of Industrial Science, 86, Kyushu University, Hakozaki, Fukuoka 812
(Received March 18, 1980)

Synopsis. Furotropones were transformed into a series of pyrrolotropones by heating with amines. The methine proton of 1-isopropyl-2-methylcyclohepta[1,2-*b*]-pyrrol-8-one was found to appear at an unusually low field.

Recently, we have developed a new method of synthesizing furotropones, 8*H*-cyclohepta[1,2-*b*]furan-8-ones,[1] and difurotropones, 6*H*-cyclohepta[1,2-b:3,4-b']difuran-6-ones.[2] This prompted us to investigate a new method of synthesizing pyrrolotropones,[3,4] 8*H*-cylohepta[1,2-*b*]pyrrol-8-ones, by condensation with amines.[5]

2-Methyl-8*H*-cyclohepta[1,2-*b*]furan-8-one (**1**)[6] was heated with methylamine in a sealed tube to give a single product (**2**). The NMR spectra of **2** clearly showed it to be 1,2-dimethyl-8*H*-cyclohepta[1,2-*b*]pyrrol-8-one. Similarly, products (**3**, **4**, **5**, and **6**) were obtained from reaction with ethylamine, propylamine, isopropylamine, and cyclohexylamine respectively. When bulky amines were used, 2-alkylamino-3-(2-oxopropyl)tropones (**7**, **8**, and **9**) were obtained as by-products. However, **1** did not react with ammonia or *t*-butylamine under comparable conditions.

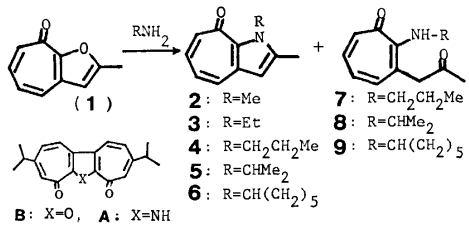

The structures of these products were deduced from their NMR spectra. The signal arising from the methine proton of the isopropyl group of 1-isopropyl-2-methyl-8*H*-cyclohepta[1,2-*b*]pyrrol-8-one (**5**) was found to appear at an unusually low field (δ[7]: 6.33).

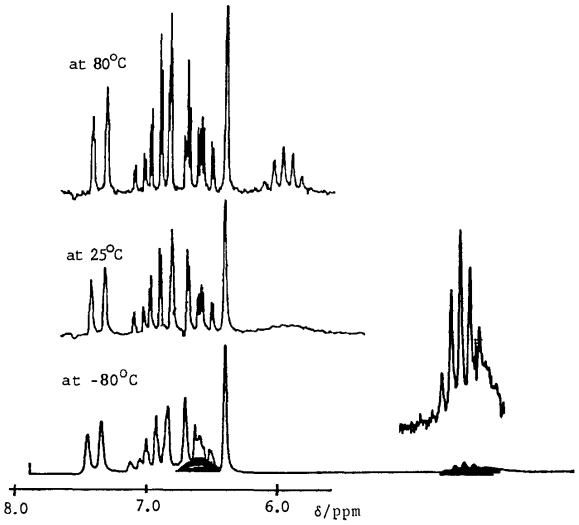

Fig. 1. The temperature dependent NMR spectrum of **5**.

Moreover, although the methine proton appeared as a broad and unsolved signal at room temperature, it became a sharp septet (J=7 Hz) at 80 and 120 °C with almost the same chemical shift (Fig. 1). This extraordinary low-field shift can be explained in terms of the anisotropy of the carbonyl group, which is in the near vicinity of the methine group. This was further confirmed by a low-temperature measurement of the NMR spectrum; although above −40 °C, the NMR features were not very different, at −80 °C, the NMR disclosing the presence of the isomerism by showing pairs of signals, isopropyl methyl doublets, vinyl methyl singlets, and the methine broad multiplets [$\delta^{(CD_3)_2CO}$: 4.7 and 6.6], in a ratio of *ca.* 1:2.[8]

On the other hand, although the methine proton of the 1-cyclohexyl derivative (**6**) could not be identified in the room-temperature NMR spectrum, it was observed as a very broad multiplet at δ *ca.* 5.9 by heating the sample over 80 to 120 °C. Furthermore, a pair of broad, methine-proton signals due to the occurrence of rotational isomerism, as well as other signals, began to appear at $\delta^{(CD_3)_2CO}$: 4.6 and 6.4 (1:2) at −80 °C. The behavior is thus the same as that of **5**.

As we have mentioned, **1** was unreactive with ethanolic ammonia. However, we thought that a dihydrofurotropone, 3-ethylidene-2,3-dihydro-8*H*-cyclohepta[1,2-*b*]furan-8-one (**10**), might be more reactive than the fully conjugated furans such as **1**. Again, no reaction took place when **10** was heated with ethanolic ammonia in a sealed tube, but we found that, with methylamine, **10** yielded, when heating at 100 °C, 1,2,3-trimethylcyclohepta[1,2-*b*]pyrrol-8-one (**11**), 3-ethyl-1-methylcyclohepta[1,2-*b*]pyrrol-8-one (**12**), 3-ethylcyclohepta[1,2-*b*]furan-8-one (**13**), and two other by-products, 3-hydroxymethyl-1,2-dimethyl-2,3-dihydrocyclohepta[1,2-*b*]pyrrol-8-one and 2-methylamino-3(1-hydroxymethylpropen-1-yl)tropone (**14** and **15**). The **11**, product which was also obtained by the thermolysis of **14**, may be formed by the sequence depicted in Scheme 2.

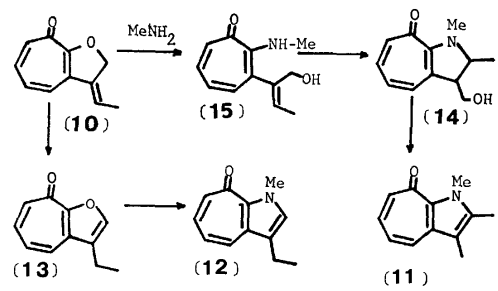

Experimental

Reaction of 1 with Methylamine. A mixture of **1**[6] (80 mg) and methylamine (30% in water, 4 cm³) was heated in a sealed tube at 160 °C for 6 h. The mixture was then chromatographed on a silica-gel column, using hexane–

ethyl acetate as the eluent. The sole product identified was **2**; colorless needles; mp 76—77 °C (from hexane–benzene); 66 mg (76%) [Found: C, 76.29; H, 6.35; N, 8.00%. Calcd for $C_{11}H_{11}ON$: C, 76.27; H, 6.40; N, 8.00%. δ: 2.32 (3H, d, J=1 Hz), 4.14 (3H, s), 6.25 (1H, qm, J=1 Hz), 6.58 (1H, ddd, J=10.5, 5.5, 3.5 Hz), 6.97 (1H, dd, J=3.5, 1 Hz), 6.98 (1H, dd, J=5.5, 1 Hz), and 7.33 (1H, dt, J=10.5, 1 Hz)].

Reaction of ***1*** *with Ethylamine.* Similarly, a mixture of **1** (75 mg) and ethylamine (70% in water, 4 cm³) was heated in a sealed tube at 120 °C for 14 h to give **3** (colorless needles; mp 85—87 °C (from hexane–benzene); 57 mg (65%) [Found: C, 76.95; H, 7.08; N, 7.45%. Calcd for $C_{12}H_{13}ON$: C, 76.97; H, 7.00; N, 7.48%. δ: 1.37 (3H, t, J=7 Hz), 2.41 (3H, s), 4.71 (2H, q, J=7 Hz), 6.33 (1H, s), 6.62 (1H, ddd, J=10.5, 5.5, 4.5 Hz), 7.0 (2H, m), and 7.36 (1H, dt, J=10.5, 1 Hz)]), together with a colorless oil (≈1 mg) which showed spectral features similar to those of uncyclized products, but no further characterization was carried out.

Reaction of ***1*** *with Propylamine.* A mixture of **1** (83 mg) and propylamine (33% in water, 4 cm³) was heated in a sealed tube at 160 °C for 24 h. Subsequently, silica gel chromatography of the mixture gave **7** (a colorless oil; 4.5 mg (4%) [Found: *m/e*, 219(M⁺). δ: 1.05 (3H, t, J=7 Hz), 1.77 (2H, m), 2.28 (3H, s), 3.26 (2H, tm, J=7 Hz), 3.80 (2H, s), 6.54 (1H, dd, J=10, 1 Hz), 6.62 (1H, td, J=9.5, 1 Hz), 7.21 (1H, ddd, J=10, 8.5, 1 Hz), and 7.34 (1H, dd, J=9.5, 1 Hz)]) and **4** (colorless needles; mp 57—58 °C (from hexane–benzene); 89 mg (85%) [Found: C, 77.47; H, 7.53; N, 6.94%. Calcd for $C_{13}H_{15}ON$: C, 77.58; H, 7.51; N, 6.96%. δ: 0.96 (3H, t, J=7 Hz), 1.77 (2H, m), 2.39 (3H, s), 4.59 (2H, t, J=7 Hz), 6.32 (1H, s), 6.61 (1H, ddd, J=10.5, 5.5, 4 Hz), 6.99 (2H, m), and 7.35 (1H, dt, J=10.5, 1 Hz)]).

Reaction of ***1*** *with Isopropylamine.* A mixture of **1** (85 mg) and isopropylamine (33% in water, 4 cm³) was heated in a sealed tube at 160 °C for 23 h to give **8** (a colorless oil; 21 mg (18%) [Found: *m/e*, 219 (M⁺). δ: 1.30 (6H, d, J=7 Hz), 2.27 (3H, s), 3.77 (2H, s), 3.80 (1H, m), 6.52 (1H, dd, J=10.5, 1 Hz), 6.60 (1H, td, J=8, 1 Hz), 7.20 (1H, td, J=10.5, 1 Hz), and 7.33 (1H, dd, J=8, 1 Hz)]) and **5** (colorless needles; mp 78—79 °C (from hexane); 48 mg (45%) [Found: C, 77.17; H, 7.61; N, 6.55%. δ: 1.37 (6H, d, J=7 Hz), 2.51 (3H, d, J=1 Hz), 6.3 (1H, qm, J=1 Hz), 6.1—6.4 (1H, br. m), 6.60 (1H, ddd, J=10.5, 5, 4 Hz), 6.97 (2H, m), and 7.33 (1H, dt, J=10.5, 1 Hz)]).

Reaction of ***1*** *with Cyclohexylamine.* A neat mixture of **1** (96 mg) and cyclohexylamine (200 mg) was heated in a sealed tube at 160 °C for 6 h to give **9** (a colorless oil; 18 mg (12%) [Found: *m/e*, 259(M⁺). δ: 1.1—2.2 (10H, m), 2.28 (3H, s), 3.45 (1H, m), 3.78 (2H, s), 6.57 (1H, dt, J=9, 1 Hz), 6.59 (1H, td, J=9, 1 Hz), 7.18 (1H, td, J=9, 1 Hz), 7.32 (1H, dd, J=9, 1 Hz), and 7.2—7.5 (1H, br., N*H*)]) and **6** (a colorless oil; 20 mg (14%) [Found: M.W., 241.1471. Calcd for $C_{16}H_{19}ON$: 241.1567. δ: 1.1—2.4 (11H, m), 2.53 (3H, d, J=1 Hz), 6.30 (1H, qm, J=1 Hz), 6.60 (1H, ddd, J=10.5, 5, 4.5 Hz), 6.98 (2H, m), and 7.33 (1H, dt, J=10.5, 1 Hz)]).

*Reaction of 3-Ethylidene-8*H*-2,3-dihydrocyclohepta[1,2-*b*]furan-8-one (****10****) with Methylamine.* A mixture of **10** (90 mg) and methylamine (30% in water, 4 cm³) was heated in a sealed tube at 100 °C for 4 h. The mixture was then diluted with water and extracted with ether. Subsequent silica gel column chromatography of the extracts gave **11** (pale yellow prisms; mp 106—107.5 °C (from hexane–methanol); 9.6 mg (9.9%) [Found: C, 76.85; H, 7.22; N, 7.33%. Calcd for $C_{12}H_{13}ON$: C, 76.97; H, 7.00; N, 7.48%. δ: 2.23 (3H, s), 2.34 (3H, s), 4.20 (3H, s), 6.65 (1H, ddd, J=10.7, 6, 3 Hz), 6.9—7.1 (2H, m), and 7.43 (1H, dt, J=10.7, 1 Hz)]), **12** (pale yellow needles; mp 73—74 °C (from hexane–benzene); 5.2 mg (5.4%) [Found: 76.72; H, 6.90; N, 7.59%. δ: 1.26 (3H, t, J=7 Hz), 2.68 (2H, q, J=7 Hz), 4.20 (3H, s), 6.60 (1H, ddd, J=11, 7, 2.5 Hz), 6.85 (1H, s), 7.00 (2H, m), and 7.42 (1H, dt, J=11, 1 Hz)]), **14** (a yellow liquid; 75 mg (70%) [Found: M.W., 205.1103. Calcd for $C_{12}H_{15}O_2N$: 205.1103. δ: 1.28 (3H, d, J=6 Hz), 2.89 (1H, q, J=6 Hz), 3.16 (1H, br. m), 3.51 (3H, s), 3.70 (2H, d, J=6 Hz), 6.44 (1H, ddd, J=10, 8, 2 Hz), and 6.8—7.1 (3H, m)]), and **15** (a yellow liquid; 5.5 mg (5.3%) [Found: *m/e*, 205 (M⁺). δ: 1.92 (3H, d, J=7 Hz), 3.06 (3H, d, J=5.5 Hz), 4.2 (2H, m), 4.5—4.8 (1H, br. s), 5.76 (1H, q, J=7 Hz), 6.57 (1H, d, J=10 Hz), 6.67 (1H, td, J=10, 1 Hz), 7.25 (1H, td, J=10, 1 Hz), 7.39 (1H, dd, J=10, 1 Hz), and 7.2—7.6 (1H, br., N*H*))].

Thermal Dehydration of ***14*** *to* ***11****.* A dimethyl sulfoxide solution (0.3 cm³) of **14** (20 mg) was heated in a sealed tube at 185 °C for 4 h. The NMR analysis indicated the formation of **11** in a 60% yield, together with unchanged **14** (40%).

*Reaction of 3-Ethyl-8*H*-cyclohepta[1,2-*b*]furan-8-one (****13****)*[1] *with Methylamine.* A mixture of **13** (45 mg) and an aqueous solution of methylamine (30%, 4 cm³) was heated in a sealed tube at 120 °C for 7 h. Subsequent silica gel chromatography of the mixture afforded **12** (40 mg; 83%).

References

1) a) H. Takeshita, I. Kouno, and K. Miyake, *Kyushu Daigaku Seisan Kagaku Kenkyusho Hokoku*, **66**, 1 (1977); b) H. Takeshita, K. Tajiri, and I. Kouno, *Bull. Chem. Soc. Jpn.*, **52**, 223 (1979).

2) a) H. Takeshita, K. Tajiri, and I. Kouno, *Heterocycles*, **6**, 1101 (1977); b) H. Takeshita, K. Tajiri, and I. Kouno, *Kyushu Daigaku Seisan Kagaku Kenkyusho Hokoku*, **70**, 65 (1979).

3) T. Nozoe, Y. Kitahara, and T. Arai, *Proc. Jpn. Acad.*, **30**, 478 (1954).

4) M. Muhlstadt and W. Treibs, *Ann. Chem.*, **608**, 38 (1957).

5) Previously, a dicycloheptapyrroledione (**A**) was obtained by the amination of the corresponding dicycloheptafurandione(**B**); see T. Nozoe, K. Doi, and Y. Kitahara, *Proc. Jpn. Acad.*, **32**, 480 (1956).

6) A. Pryde, J. Zsindely, and H. Schmid, *Helv. Chim. Acta*, **57**, 1598 (1974).

7) The NMR spectra were obtained in $CDCl_3$ solutions unless otherwise stated, and the chemical shifts were expressed in terms of the δ value (Me_4Si as the internal standard).

8) Assuming the coalescent temperature as *ca.* 30 °C, the observed $\Delta\delta$=190 led to an estimation for the activation barrier of rotatomers as 13.7 kcal/mol.

The Chemical Shifts of the Bridge Methylene Protons of 1,6-Methano-[11]annulene Systems. Positive Evidence for the Assignments

Tadao UYEHARA* and Akito ICHIDA

Department of Chemistry, Faculty of Science, Tohoku University, Aoba, Aramaki, Sendai 980

(Received March 21, 1980)

Synopsis. The assignments of the chemical shifts to the bridge methylene protons of 1,6-methano[11]annulen-9-one (**3**) were established on the basis of their lanthanoid-induced shifting. Those of the protonated cation of **3** were proven from the spectrum of a mixture of 12-d_1 derivatives of **3** in trifluoroacetic acid.

The ^{1}H-NMR chemical shifts of the bridge protons are key indices to know the tropicity of bridged annulenes. Thus, the assignments of the chemical shifts to the bridge protons are quite important, especially those of asymmetrical bridged-annulenes such as 1,6-methano[11]annulene systems.

During the course of our investigations of the condensed pi-electron systems containing the methano-[11]annulene part (**1**) and its protonated species (**2**),[1] we noticed that the chemical shifts of the bridge methylene protons of methano[11]annulenes had been assigned without positive proof. This paper will deal with the evidence for the assignments to the bridge protons of 1,6-methano[11]annulen-9-one (**3**) and its protonated cation (**4**).[2]

Results and Discussion

The chemical shifts of the bridge methylene protons of 1,6-methano[11]annulenes (mainly bicyclo[5.4.1]-dodeca-2,5,7,9,11(1)-pentaen-4-ylidenes), except those of **3**, were previoulsy assigned without any explanation.[3] The assignments to the bridge protons (H_s and H_a, the *syn* and *anti*-protons to the cycloheptatriene system respectively) of **3** by Vogel and his co-workers[2] were based on an assumption of long-range couplings (W-shape couplings) between H_2, (H_5), and H_a (δ= 1.68, (dt), $J_{a,s}$=11.4 Hz, and $J_{a,2}$=$J_{a,5}$=1.5 Hz). The assignment may be reasonable because, in the spectrum most 1,6-methano[11]annulenes,[3] the center of the signals (a doublet) due to the other bridge proton (H_s) appears in the δ=0.2—0.0 range; the chemical shifts of H_s may not be affected greatly by substituents on the C_5-bridge. However, one can point out that the long-range couplings might be replaced by allylic couplings between H_2, (H_5), and H_s, since the allylic angles of H_a (θ=0°, from a molecular model) indicate $J_{allylic}$=0 Hz, while those of H_s (θ=60°) indicate $J_{allylic}$=1.5 Hz. Thus, we can not apply the assignments of the bridge methylene protons of **3** to those of more complicated systems such as **1** without any positive evidence for the W-shape coupling. In order to distinguish the signals for H_a and those for H_3 of **3**, we used lanthanoid-shift reagents ($Eu(fod)_3$ and $Pr(fod)_3$). The lanthanoid-induced shifting (given in Table 1) of the peripheral protons is normal pseudo-contact shifting. Now, the signals appearing as the doublet of triplets at δ=1.68 and as the doublet at δ=0.04 are for H_a and H_s respectively, since the former are shifted more than the latter. *The long-range couplings are exactly due to the W-shape coupling between H_2, (H_5), and H_a.*

Table 1. Chemical shifts (δ) and lanthanoid-induced shifts ($\Delta\delta$, ppm) of 1,6-methano[11]annulen-9-one (**3**)

Proton	δ[a]	$\Delta\delta$ Concn of $Eu(fod)_3$[b] 0.047	0.063	0.104	$\Delta\delta$ Concn of $Pr(fod)_3$[b] 0.019	0.06
$H_{8,10}$	6.02	c)	−2.01	−2.92	+1.08	+2.78
$H_{7,11}$	7.18	c)	−0.55	−0.78	+0.26	+0.73
$H_{2,5}$	6.90	c)	−0.37	−0.51	+0.12	+0.39
$H_{3,4}$	7.21	c)	−0.37	−0.47	+0.03	+0.14
H_a-(dt)	1.68	−0.68	−0.96	−1.34	+0.57	+1.55
H_s-(d)	0.04	−0.26	−0.36	−0.53	+0.17	+0.59

a) Ref. 2. b) Mole ratios to the substrate. c) Overlapping each other.

The crucial difference between the multiplicities of H_a and H_s should be generally found in the specta of other 1,6-methano[11]annulenes containing the cycloheptatriene system, such as **1** and the hydrocarbon (**5**).[4]

The spectrum of cation **2** shows a broad-doublet at δ=−0.21 (J=11.4 Hz, $W_{1/2}$=5 Hz) and a doublet at δ=0.45 (J=11.4 Hz, $W_{1/2}$=1 Hz) for the bridge protons.[1] Similarly, the signals for those of **4**[2] and the cation (**6**)[5] are seen as broad-doublets in the higher-field and doublets in the lower-field: **4**: δ=−0.6 (bd) and δ=−0.4 (d); **6**: δ=−1.8 (bd) and δ=−0.3 (d). For those, the high-field- and low-field protons were assigned tentatively

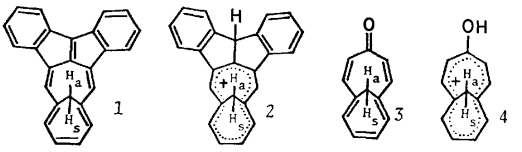

to H_a and H_s respectively.[2,6]

In order to establish the assignments, we chose the 12-monodeuterated derivatives of **4** as the models. A mixture of the ketones (**7** and **8**) was prepared from the acetal (**9**) based on a modification of the method of Vogel.[2] The ^{1}H-NMR spectra of the mixture in CCl_4 and in trifluoroacetic acid (TFA) are shown in Fig. 1. The spectrum in CCl_4 indicates that **7** and **8** are formed in a ratio of 3 to 1. In TFA, the cations (**12** and **13**) should be formed in a 3-to-1 ratio respectively.

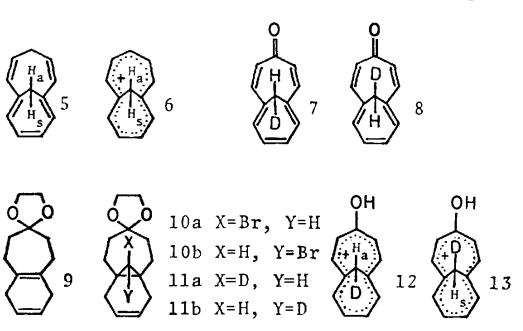

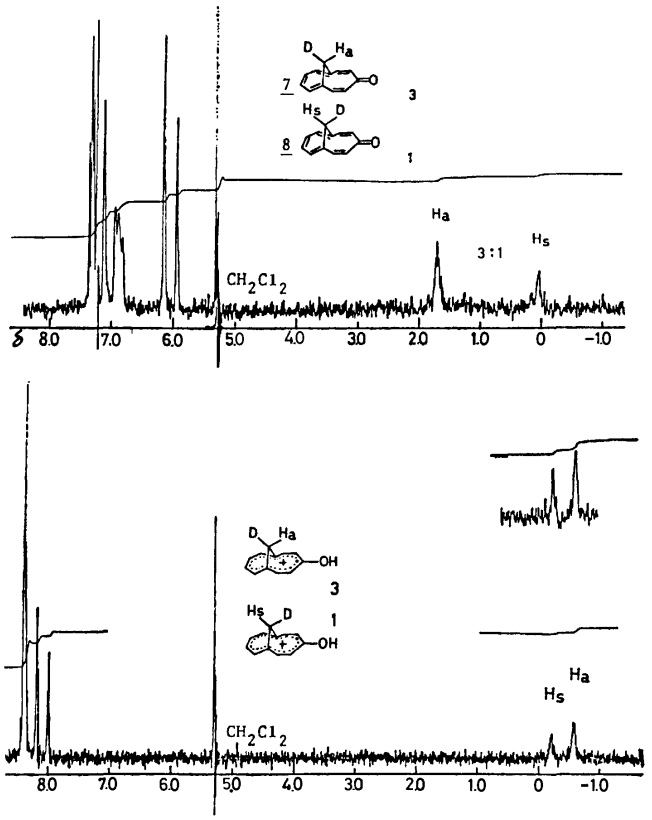

Fig. 1. ^{1}H-NMR spectra of 1,6-methano[11]annulen-9-one-12-d_1 (**7** and **8**) in CCl_4 (upper) and in TFA (lower).

Now, the high-field bridge proton of **4** is H_a, and the other is H_s. Thus, it is true that the line-broadening of the signals for H_a of **4** is due to the W-shape coupling between H_2, (H_5), and H_a. This assignment can aslo be applied to each bridge proton of **2** and **6**.

Experimental

General. Melting points were determined on a Thomas Hoover MP apparatus and are uncorrected. Infrared spectra were recorded on a Hitachi Model 215 spectrometer. NMR spectra were obtained on Varian A-60 or JEOL JNM-PMX 60 spectrometers, using tetramethylsilane and/or dichloromethane as internal standards. Mass spectral studies were conducted using a Hitachi M-52 spectrometer.

*12,12-Dibromotricyclo[5.4.1.0^{1,7}]dodeca-9-en-4-one Ethylene Acetal (**9a**).* To a mixture of the acetal (**9**, 2.0 g) and *t*-BuOK (1.41 g) in dry ether (25 ml) was added a solution of bromoform (1.3 ml) in ether (1.3 ml) at 0 °C under a nitrogen atmosphere over a period of 1 h. After 19 h stirring at 0 °C, the mixture was diluted with water (60 ml) and extracted with CH_2Cl_2 (3×40 ml). The extracts were combined, dried ($MgSO_4$), concentrated, and subjected to chromatography on alumina. The adduct, **9a**, was isolated in a 28.3% yield (1.04 g). **9a**: colorless prisms, mp 95—122 °C; NMR ($CDCl_3$) δ=1.62—1.93 (m, 8H), 2.28 (bd, 4H), 3.88 (s, 4H), and 5.58 (bt, 2H). Found: C, 44.23; H, 4.86%; M$^+$, 380 (1.24%), 378 (2.49%), and 376 (1.58%). Calcd for $C_{14}H_{18}Br_2O_2$: C, 44.47; H, 4.80%.

*12-Bromotricyclo[5.4.1.0^{1,7}]dodeca-9-en-4-one Ethylene Acetal (**10a** and **10b**).* A mixture of **9a** (2.63 g), tributyltin hydride (2.22 g), AIBN (13 mg), and dry cyclohexane (18 ml) was heated at 60 °C for 2.5 h and then at 80 °C for 1.5 h while being stirred under an argon atmosphere. Carbon tetrachloride (5 ml) was then added to the solution, and the mixture was concentrated *in vacuo*. The resulting oil was chromatographed on alumina, and eluted with hexane–benzene. A colorless, amorphous powder (1.61 g) was thus obtained. A mixture of **10a** and **10b**: NMR (CCl_4) δ= 1.53—1.83 (m, 8H), 2.16 and 2.23 (bs each, 4H), 2.88 (s, 0.6H), 3.18 (s, 0.4H), 3.80 and 3.85 (s each, 4H), and 5.48 (bs, 2H). Found: M$^+$, 300 (10.2%) and 298 (11.7%).

*Tricyclo[5.4.1.0^{1,7}]dodeca-9-en-4-one-12-*d$_1$ *Ethylene Acetal (**11a** and **11b**).* To a solution of a mixture of **10a** and **10b** (1.0 g) in THF (dry, oxygen free) was added *n*-BuLi (1.56 M in hexane, 2.9 ml) at −78 °C under argon. After 1.5 h stirring, the solution was allowed to warm to room temperature. After having 0.5 ml of methanol-d_4 syringed in, stirred for 10 min, poured onto brine, and extracted with ether (3×50 ml), the combined organic solutions were dried ($MgSO_4$) and evaporated, yielding a pale yellow oil (728 mg, 98.6%). NMR (CCl_4) δ=0.13 (bs, 0.75H), 0.66 (bs, 0.25H), 1.38—1.78 (m, 8H), 2.20 (bs, 4H), 3.84 (s, 4H), and 5.45 (bs, 2H). The crude **11a** and **11b** thus obtained were used without further purification.

*Bicyclo[5.4.1]dodeca-2,5,7,9,11(1)-pentaen-4-one-12-*d$_1$ *(**7** and **8**).* A solution of bromine (527 mg) in CH_2Cl_2 (7 ml) was added to a mixture of **11a** and **11b** (728 mg) in CH_2Cl_2 (20 ml) at −78 °C over a period of 20 min. The subsequent evaporation of the solvent gave a pale yellow solid, which was then heated under reflux with 15% KOH in methanol (20 ml) for 2 h. After the solvent had then been removed and the mixture had been diluted with water (50 ml) and extracted with ether (3×40 ml), the extracts were combined, dried ($MgSO_4$), and concentrated, yielding a colorless oil (714 mg). To a solution of the crude products in THF (20 ml) were added perchloric acid (60%, 0.4 ml) and water (4 ml), after which the mixture was heated at 50 °C for 5 h. After most of the THF had been removed *in vacuo*, and the mixture had been diluted with water (50 ml), and extracted with ether (3×25 ml), the combined organic solutions were washed with aqueous $NaHCO_3$, water, and brine, dried ($MgSO_4$), and evaporated, thus yielding a pale yellow oil (580 mg). It was chromatographed on silica gel (30 g) and eluted with hexane–benzene, thus yielding bicyclo[5.4.1]-dodeca-7,9,11(1)-trien-4-one-12-d_1 as a pale yellow oil (320 mg, 52%). IR (film) 1716 cm^{-1}; NMR (CCl_4) δ=1.57 (bs, 0.3H), 2.85—3.10 (m, 8.7H), 5.98 (m, 2H), and 6.46 (m, 2H). The dehydrogenation of the ketones (90 mg) with DDQ (418 mg) in benzene (4.5 ml) at 115 °C for 12 h in a sealed tube gave a mixture of **7** and **8** (26 mg, 30%, mp 69.5—71.8 °C) after repeated chromatography on alumina (15 g). IR (CCl_4) 1624 cm^{-1}; MS *m/e* (%) 171(29.7), 170 (4.5), 143 (53.2), and 142 (100).

References

1) T. Uyehara and A. Ichida, 11th Symposium on Non-benzenoid Aromatic Compounds, Osaka, October 1978, Abstr. No. N-26.

2) W. Grimme, J. Reisdorff, W. Jünemann, and E. Vogel, *J. Am. Chem. Soc.*, **92**, 6335 (1970).

3) W. M. Jones, R. A. LaBar, U. H. Brinker, and P. H. Gebert, *J. Am. Chem. Soc.*, **99**, 6379 (1977), and the references cited therein.

4) E. Vogel, R. Feldmann, and H. Düwel, *Tetrahedron Lett.*, **1970**, 1941.

5) W. Grimme, H. Hoffmann, and E. Vogel, *Angew. Chem. Int. Ed. Engl.*, **4**, 354 (1965).

6) A. V. Kemp-Jones, A. J. Jones, M. Sakai, C. P. Beeman, and S. Masamune, *Can. J. Chem.*, **51**, 767 (1973), and the references cited therein.

The Reaction of Thiocumulenes with Fulvene

Takao Saito, Teruhiko Musashi, and Shinichi Motoki*

Department of Chemistry, Faculty of Science, Science University of Tokyo, Kagurazaka, Shinjuku-ku, Tokyo 162

(Received March 25, 1980)

Synopsis. *S*-(9-Fluorenylidene)-*N*-(*p*-tolylsulfonyl)-sulfimide and bis(*p*-tolylsulfonyl)sulfur diimide reacted as 1,3-dipoles with fulvenes to form (2+3)cycloadducts.

Thiocumulenes add readily to a great variety of multiple bond compounds, giving rise to stable or unstable cycloadducts. *N*-Sulfinylamines (R–N=S=O), sulfur diimides (R–N=S=N–R′), thione *S*-oxides (RR′C=S=O), and sulfimides (RR′C=S=N–R″) react as 2π-components with acyclic dienes to give stable (2+4)-cycloadducts.[1–4] In the reaction with cyclopentadiene, thione *S*-oxides react also as 2π-components,[3] whereas sulfimides react as 1,3-dipoles to give (2+3)cycloadducts.[4] The (2+4)adduct of cyclopentadiene and *N*-sulfinylbenzenesulfonamide can be isolated only at low temperatures, but decomposes into its components at room temperature.[5] Accordingly we took an interest in the reactions of these thiocumulenes with fulvene because fulvene is one of the model compounds which undergo periselective cycloaddition reactions.[6]

The reaction of sulfimide (**1**) with dimethylfulvene (**2a**) under mild conditions produced a single adduct **3a** in nearly quantitative yield. The mass spectra and the elemental analyses suggested that the product was a 1:1-adduct. The IR spectrum showed the presence of νC=C absorption at 1670 cm^{-1} and the absence of any strong νS=N absorption band in the region of 900—1000 cm^{-1}. The ^{1}H NMR spectrum displayed three methyls as singlets at δ 0.57, 1.49 and 2.47 (Ts) and two olefinic and two methine protons (δ 6.59 (H_A, dd), 5.96—5.76 (H_B, H_C, m), 4.04 (H_D, d)). The chemical shifts of H_A-H_D and the coupling constants (J_{AB}=5.3, J_{AC}=1.9, J_{CD}=7.0 Hz) determined by spin-decoupling measurements centered at H_A, H_{B-C}, and H_D are consistent with structure **3** or **4** rather than with **5** or **6**, indicating that H_A and H_B are vicinal olefinic protons and that H_C and H_D are vicinal *cis*-methine protons. In the two methyls of the fulvene moiety, the resonance for the inside methyl group (δ 0.57) appeared at a higher field than that of the outside methyl group (δ 1.49) due to the shielding effect exerted by the diamagnetic anisotropy of the adjacent fluorenylidene ring. This excludes the possibility of the regioisomer **4**. The structure **3** was also supported by the ^{13}C NMR spectroscopy (see Experimental). Treatment of **1** with **2b** and **2c** also gave (2+3)cycloadducts (**3b** and **3c**) in fairly good yields.

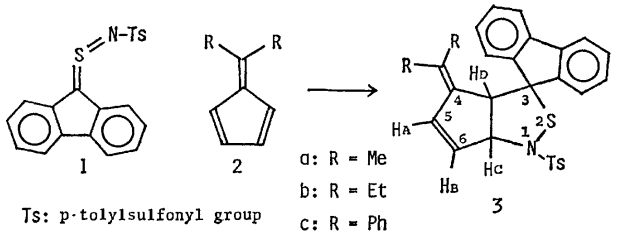

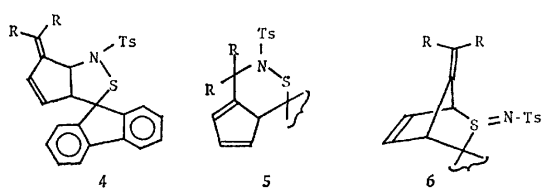

When the mixture of bis(*p*-tolylsulfonyl)sulfur diimide (**7**) and **2a** in 1,2-dichloroethane was stirred for a day at room temperature, a minor cycloadduct (**8a**) was obtained together with a major polymeric black tar and *p*-toluenesulfonamide, which might be derived from **7** (the unreacted **7** or **9**) during the column chromatography operation.[7] The IR spectrum of the adduct showed νC=C at 1660 cm^{-1}. In the ^{1}H NMR spectrum, four sets of methyl protons were observed, at δ 1.80, 1.83, 2.42 and 2.44, as singlets. Obviously the two methyls of higher field were those of the substituents at C-6 of the fulvene, and the others arose from the megnetically unequivalent *p*-tolylsulfonyl groups. The four resonances at δ 6.56 (dd, H_A, J_{AB}=5.8, J_{AC}=1.0 Hz), 5.69 (dt, H_D, J_{CD}=6.0, J_{BD}=1.0 Hz), 5.38 (d of m, H_B, J_{AB}=5.8 Hz), and 5.23 (d of m, H_C, J_{CD}=6.0, J_{AC}=1.0 Hz) were assigned to the protons attached to the fulvene frame in **8a** by means of spin-decoupling measurements. These coupling patterns exclude the other peri-isomeric cycloadducts such as the Diels-Alder type (2+4)cycloadduct **9a**. The treatment of **2a** with *N*-sulfinyl-*p*-toluenesulfonamide (**10**) also gave **8a** in a low yield (6%), along with the major decomposed products. Partial conversion of **10** into **7** can account for this anomalous result.[8] As in the reaction between *N*-sulfinylbenzenesulfonamide and cyclopentadiene,[5] it has been considered that **7** and **10** can also interact with **2** to give (2+4)-cycloadducts (**9, 11**), but the adducts would be unstable and decomposed under the reaction conditions.

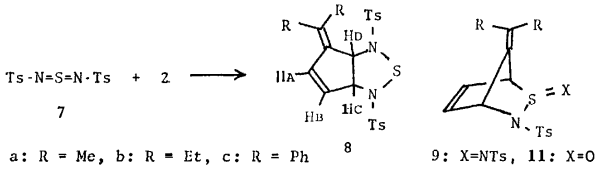

Reactions of 9-fluorenethione *S*-oxide or 9-xanthenethione *S*-oxide with **2** were unsuccessful, and only decomposed products were formed.[9]

In summary, the thiocumulenes[10] (**1**, **7**) with the preferential 1,3-dipolar nature were found to react with **2** to give the stable (2+3)cycloadducts regio- and siteselectively, whereas the dienophilic thiocumulenes[10] (**10** and thione *S*-oxide) underwent only decomposition reactions, presumably *via* unstable (2+4)cycloadducts.

Experimental

Reaction of Sulfimide (1) with Fulvenes (2). To a partially suspended solution of **1** (914 mg, 2.5 mmol) in

dry 1,2-dichloroethane (30 ml) was added a solution (10 ml) of dimethylfulvene (**2a**) (318 mg, 3 mmol) with stirring at temperature 0—5 °C under a nitrogen atmosphere. The red suspension of **1** gradually disappeared and the solution turned orange-yellow within 1 h. After the reaction mixture was stirred overnight at room temperature, the solvent was evaporated and the residue was recrystallized from benzene–hexane to give spiro[fluorene-9,3′-1′,2′,3′,3′a,4′,6′a-hexahydro-4′-isopropylidene-1′-(*p*-tolylsulfonyl)-2′-thia-1′-azapentalene] (**3a**) as colorless needles (99% yield). None of the other adducts was obtained from the reaction mixture by a chromatography, and the excess of the fulvene was recovered. The adduct **3b** was obtained by a similar treatment and column chromatography (silica gel, benzene and/or dichloromethane). The reaction of **1** with diphenylfulvene (**2c**) was carried out at a temperature of *ca.* 30 °C for 3 h. After the mixture was stirred overnight at room temperature, the solvent was evaporated and the residue was subjected to a column chromatography (silica gel, benzene) to give **3c** as colorless crystals (benzene–hexane, 87%).

3a: 99% yield; mp 210—211 °C; IR (KBr) 1670 cm^{-1} (C=C); ^1H NMR δ 0.57, 1.49 (s, CH_3), 2.47 (s, CH_3(Ts)), 4.04 (d, H_D, J_{CD}=7.0 Hz), 5.76—5.96 (m, H_B, H_C), 6.59 (dd, H_A, J_{AB}=5.3, J_{AC}=1.9 Hz), 7.00—7.92 (m, 12H, arom); ^{13}C NMR δ 20.2 ,21.6 (q, CH_3), 21.7 (q, CH_3(Ts)), 59.2 (d, C-5), 72.3 (s, C-4), 77.0 (d, C-1); MS *m/e* 471 (30, M^+). Found: C, 71.35; H, 5.44; N, 2.97%. Calcd for $C_{28}H_{25}NO_2S_2$: C, 71.32; H, 5.34; N, 2.97%.

3b: 74% yield; mp 166—167 °C; IR (KBr) 1660 cm^{-1} (C=C); ^1H NMR δ 0.26 (t, CH_3 (inside Et)), 0.64 (t, CH_3 (outside Et)), 0.7—1.3 (m, CH_2 (inside Et)), 1.7—2.1 (m, CH_2 (outside Et)), 2.49 (s, CH_3 (Ts)), 4.07 (d, H_D, J_{CD}=7.0 Hz), 5.80—5.96 (m, H_B, H_C), 6.61 (dd, H_A, J_{AB}=5.3, J_{AC}=2.0 Hz), 7.03—7.96 (m, 12H, arom); ^{13}C NMR δ 11.4, 13.1 (q, CH_3), 21.6 (s, CH_3(Ts)), 23.6 25.7 (t, CH_2), 58.7 (d, C-5), 72.4 (s, C-4), 76.8 (d, C-1); MS *m/e* 499 (33, M^+). Found: C, 72.22; H, 5.90; N, 2.76%. Calcd for $C_{30}H_{29}NO_2S_2$: C, 72.13; H, 5.85; N, 2.80%.

3c: 87% yield; mp 215—216 °C; IR (KBr) 1660 cm^{-1} (C=C); ^1H NMR δ 2.45 (s, CH_3(Ts)), 4.66 (d, H_D, J_{CD}=6.8 Hz), 5.89 (ddd, H_C, J_{CD}=6.8, J_{AC}=2.1, J_{BC}=2.1 Hz), 6.07 (dd, H_B, J_{AB}=5.7, J_{BC}=2.1 Hz), 6.14—6.30 (m, 2H, arom), 6.46—6.70 (m, H_A, 3H-arom), 6.77—7.03 (m, 12H, arom); MS *m/e* 595 (39, M^+). Found: C, 76.67; H, 5.03; N, 2.27%. Calcd for $C_{38}H_{29}NO_2S_2$: C, 76.62; H, 4.91; N, 2.35%.

*Reaction of Sulfur Diimide (**7**) with Fulvene (**2**).* The sulfur diimide (**7**) was prepared from *N*-sulfinyl-*p*-toluenesulfonamide (**10**) by the method in the literature.[2,8] A freshly prepared sulfur diimide (**7**) (1.15 g, 3.11 mmol) in a 1,2-dichloroethane solution (15 ml) was dropwise added over a period of 1.5 h to a solution of **2a** in 1,2-dichloroethane (10 ml) with stirring at a temperature of −10—−15 °C. After being stirred overnight at room temperature, the solvent was evaporated and the residue was subjected to column chromatography twice (silica gel, benzene and dichloromethane) to give crude **8a**, which was recrystallized from benzene–ligroin. Consequent elution with methanol gave *p*-toluenesulfonamide (0.69 g, 65%).

8a: Colorless crystals (14% yield); mp 179—180 °C; IR (KBr) 1660 (weak, C=C); ^1H NMR δ 1.80, 1.83 (s, CH_3), 2.42, 2.44 (s, CH_3(Ts)), 5.23 (d of m, H_C, J_{CD}=6.0, J_{AC}=1.0 Hz), 5.38 (d of m, H_B, J_{AB}=5.8 Hz), 5.69 (dt, H_B, J_{CD}=6.0 Hz), 6.56 (dd, H_A, J_{AB}=5.8, J_{AC}=1.0 Hz), 7.20—7.88 (m, 8H, arom); ^{13}C NMR δ 20.9, 22.0 (q, CH_3), 21.6, 21.7 (q, CH_3(Ts)), 70.0, 72.0 (d, C-1, C-5); MS *m/e* 476 (7, M^+). Found: C, 55.59; H, 5.10; N, 5.77; S, 20.06%. Calcd for $C_{22}H_{24}N_2O_4S_3$: C, 55.44; H, 5.08; N, 5.88; S, 20.18%.

8b: Colorless crystals (12% yield); mp 129—131 °C; IR (KBr) 1655 cm^{-1} (weak, C=C); ^1H NMR δ 0.88, 0.96 (t, CH_3), 1.9—2.5 (m, 4H, CH_2), 2.42 ,2.45 (s, CH_3(Ts)), 5.19 (ddd, H_C, J_{CD}=6.0, J_{BC}=2.4, J_{AC}=1.0 Hz), 5.44 (dd, H_B, J_{AB}=6.0, J_{BC}=2.4 Hz), 5.69 (d, H_D, J_{CD}=6.0 Hz), 6.54 (dd, H_A, J_{AB}=6.0, J_{AC}=1.0 Hz), 7.2—7.9 (m, 8H, arom); ^{13}C NMR δ 13.0 ,13.6 (q, CH_3), 21.6, 21.7 (q, CH_3 (Ts)), 24.6, 25.6 (t, CH_2), 70.3, 71.5 (d, C-1, C-5); MS *m/e* 504 (5, M^+). Found: C, 57.13; H, 5.76; N, 5.38; S, 18.92%. Calcd for $C_{24}H_{28}N_2O_4S_3$: C, 57.12; H, 5.59; N, 5.55; S, 19.06%.

8c: Colorless crystals (27% yield); mp 209—210 °C; IR (Nujol) 1670 cm^{-1} (weak, C=C); ^1H NMR δ 2.36 ,2.42 (s, CH_3 (Ts)), 5.29 (ddd, H_C, J_{CD}=6.0, J_{BC}=2.5, J_{AC}=0.8 Hz), 5.65 (dd, H_B, J_{AB}=5.8, J_{BC}=2.5 Hz), 6.31 (d, H_D, J_{CD}=6.0 Hz), 6.49 (dd, H_A, J_{AB}=5.8, J_{AC}=0.8 Hz), 6.9—7.8 (m, 18H, atom); ^{13}C NMR δ 21.6 (q, CH_3 (Ts)), 70.0, 71.7 (d, C-1, C-5); MS *m/e* 600 (2, M^+). Found: C, 64.01; H, 4.69; N, 4.67; S, 15.98%. Calcd for $C_{32}H_{28}N_2O_4S_3$: C, 63.98; H, 4.70; N, 4.66; S, 16.01%.

Reaction of N-*Sulfinyl*-p-*toluenesulfonamide (**10**) with Dimethylfulvene (**2a**).* To a solution of **10** (1.09 g, 5 mmol) in 1,2-dichloroethane (20 ml) was added dropwise a solution of **2a** (0.53 g, 5 mmol) in 1,2-dichloroethane (15 ml) with stirring at 0 °C. The reaction mixture was stirred for 4 h and gradually became darker. After removal of the solvent, the residue was chromatographed (silica gel, benzene, dichloromethane and methanol) to give 72 mg (6%) of **8a**, 20 mg of unidentified material, 0.7 g (82%) of *p*-toluenesulfonamide, and a black tar. The **8a** was identified by comparisons of the IR and NMR spectra with those of the previously mentioned **8a**.

References

1) G. Kresze, A. Maschke, R. Albrecht, K. Bederke, H. P. Patzschke, H. Smalla, and A. Trede, *Angew. Chem., Int. Ed. Engl.*, **1**, 89 (1962).

2) G. Kresze and W. Wucherpfenning, *Angew. Chem., Int. Ed., Engl.*, **6**, 149 (1967).

3) B. Zwanenburg, L. Thijs, J. B. Broens, and J. Strating, *Recl. Trav. Chim. Pays-Bas*, **1972**, 443.

4) T. Saito and S. Motoki, *J. Org. Chem.*, **44**, 2493 (1979).

5) J. Hamer and A. Macaluso, *J. Org. Chem.*, **31**, 3049 (1966).

6) a) K. N. Houk, J. K. George, and R. E. Duke, Jr., *Tetrahedron*, **30**, 523 (1974); b) K. N. Houk and L. J. Luskus, *J. Org. Chem.*, **38**, 3836 (1973); c) I. Fleming, "Frontier Orbitals and Organic Chemical Reactions," Wiley, London (1976).

7) On the contrary, a (2+3) adduct between **7** and cyclopentadiene was quantitatively obtained (92%; mp 189—191 °C).

8) W. Wucherpfenning and G. Kresze, *Tetrahedron Lett.*, **1966**, 1671. *N*-Sulfinylarenesulfonamides easily produce the corresponding sulfur diimides even by the action of a catalytic weak base such as pyridine.

9) Zwanenburg *et al.* reported that the reaction of thione S-oxides with cyclopentadiene and acyclic dienes yielded Diels-Alder type (2+4)cycloadducts, which were relatively unstable (Ref. 3).

10) According to the proposal by Inagaki and Okazaki, the order of 1,3-dipolar nature is as follows:

>CSN- > -NSN- > >CSO > -NSO.

Y. Inagaki and R. Okazaki, *Yuki Gosei Kagaku Kyokai Shi*, **36**, 1 (1978).

Michael Addition of *p*-Styrenesulfinate to Acrylic Compounds

Hiroyoshi KAMOGAWA,* Hiroyuki KUSAKA, and Masato NANASAWA
Department of Applied Chemistry, Yamanashi University, Takeda 4, Kofu 400

(Received April 11, 1980)

Synopsis. Acrylic compounds CH_2=CHX, where X represents -COOH, $-CONH_2$, -CN, and $-COOCH_2CH_2OH$, were converted into the corresponding 3-(*p*-vinylphenylsulfonyl)- and 3-(*p*-tolylsulfonyl)propionic acids and their derivatives by the Michael addition with *p*-styrene- and *p*-toluenesulfinates, respectively, in the presence of acid as proton source.

In the course of studies on the syntheses of functional vinyl monomers and polymers by the application of the nucleophilic reactions of *p*-styrenesulfinate and its polymer, a number of reactions were reported including simple displacement with halides, reductive addition to quinonoid compounds, and replacement of aromatic nitro group.[1)]

In this note, we wish to report the Michael addition of sodium *p*-styrenesulfinate and its model compound, *p*-toluenesulfinate, to acrylic compounds. A paper describing the Michael addition of arenesulfinates such as *p*-toluenesulfinate to α,β-unsaturated ketones such as methyl vinyl ketone in the presence of acid as proton source[2)] prompted us to undertake this study.

By use of acid either as Michael acceptor itself or as simple proton source we have synthesized a number of novel Michael addition products not obtained under conventional alkaline conditions as follows.

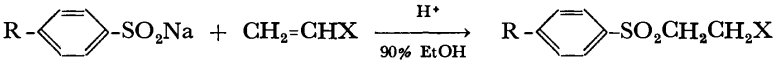

1a: R=CH_2=CH- **1b**: R=CH_3

2a: X=-COOH **2b**: X=$-CONH_2$ **2c**: X=-CN **2d**: X=$-COOCH_2CH_2OH$

3a: R=CH_2=CH-; X=-COONa
3b: R=CH_2=CH-; X=$-CONH_2$
3c: R=CH_2=CH-; X=-CN
3d: R=CH_2=CH-; X=$-COOCH_2CH_2OH$
4a: R=CH_3; X=-COONa
4b: R=CH_3; X=$-CONH_2$
4c: R=CH_3; X=-CN
4d: R=CH_3; X=$-COOCH_2CH_2OH$

It was found that acrylic Michael acceptors employed (**2a—d**) reacted with arenesulfinates (**1a—b**) at room temperature in the presence of an acid. The kind of R considerably affects both yield and mp of product (Table 1). However, weight losses during the course of isolation of products were greater in the case of **3a—d** than in the corresponding **4a—d**; no exact discussion can be made on the yield.

Use of the Michael addition gave rise to easy conversion of the acrylic double bond of a functional monomer to the 2-(*p*-vinylphenylsulfonyl)ethyl group, keeping the functional portion intact. Novel monomers **3a—d** thus synthesized may indicate polymerization behavior differing from that of **2a—d** leading to vinyl polymers with longer side chains, the terminal functional groups of which are more accessible.

Table 1. Yield of Michael-addition products

Compd	Yield/%[a)]	Mp/°C	AcOH
3a	38	179—180	none
3b	20	123—126	added
3c	38	87— 88	added
3d	63	liquid	added
4a	76	300<	none
4b	50	166—168	added
4c	80	93— 96	added
4d	77	liquid	added

a) For products isolated and purified, when required, after 12 h-reaction at room temperature.

Experimental

The infrared, ^{1}H-NMR, and mass spectra were recorded on a Hitachi 215 spectrophotometer, a JNM-PMX 60 spectrometer, and a Hitachi RMU-6 MG spectrometer, respectively, under standard conditions. The elemental analyses were carried out using a Perkin-Elmer 250 instrument.

*Sodium 3-(*p*-Vinylphenylsulfonyl)propionate (**3a**).* A solution of sodium *p*-styrenesulfinate (**1a**; 1.9 g, 10 mmol), synthesized according to the procedure reported,[1)] and acrylic acid (**2a**; 0.72 g, 10 mmol) in 90% ethanol (20 ml) was stirred at room temperature (20 °C) for 12 h to afford a pale pink precipitate, analytically pure without further purification. Found: C, 50.23; H, 4.38%. Calcd for $C_{11}H_{11}O_2SNa$: C, 50.38; H, 4.23%. IR (KBr) 2920, 2850 (CH_2), 1630 (vinyl), 1600 ($-COO^-$, Ar), 1305, 1140 (SO_2), 990, 910 (vinyl) cm^{-1}; NMR (DMSO-d_6+$CDCl_3$) δ 2.5 (t, 2H, CH_2), 3.5 (t, 2H, CH_2), 5.5 (d, 1H, $C\underline{H}_2$=CH–), 6.0 (d, 1H, $C\underline{H}_2$=CH–), 6.8 (q, 1H, CH_2=C$\underline{H}$–), 7.3—8.1 (m, 4H, ArH) ppm.

*Sodium 3-(*p*-Tolylsulfonyl)propionate (**4a**).* The same procedure as that for **2a** was applied to **1b** (4.2 g, 20 mmol) and **2a** (1.5 g, 20 mmol) in 90% ethanol (25 ml) to afford white crystals. Found: C, 48.19; H, 4.22%. Calcd for $C_{10}H_{11}O_2SNa$: C, 47.99; H, 4.43%. IR (KBr) 2960, 2930 (CH_3, CH_2), 1600 ($-COO^-$, Ar), 1280, 1150 (SO_2) cm^{-1}; NMR (D_2O) δ 2.4 (s, 3H, CH_3), 2.7 (t, 2H, CH_2), 3.6 (t, 2H, CH_2), 7.3—7.9 (q, 4H, ArH) ppm.

*3-(*p*-Vinylphenylsulfonyl)propionamide (**3b**).* A solution of **1a** (1.9 g, 10 mmol), **2b** (0.71 g, 10 mmol), and acetic acid (0.6 g, 10 mmol) in 90% ethanol (20 ml) was stirred at room temperature for 12 h. The reaction mixture with a small amount of precipitate was extracted with $CHCl_3$.

The extreact was washed with satd aq $NaHCO_3$, dried over anhyd Na_2SO_4, and evaporated *in vacuo* below 50 °C to leave a solid, which was recrystallized from ethanol to afford light yellow crystals. Found: C, 55.13; H, 5.92; N, 6.13%. Calcd for $C_{11}H_{13}NO_3S$; C, 55.21; H, 5.48; N, 5.85%. IR (KBr) 3420, 3180 (NH_2), 2900 (CH_2), 1690 (C=O), 1600 (Ar), 1300, 1140 (SO_2), 990, 930 (vinyl) cm^{-1}; NMR (DMSO-d_6+$CDCl_3$) δ 2.5 (t, 2H, CH_2), 3.4 (t, 2H, CH_2), 5.5 (d, 1H, $C\underline{H}_2$=CH–), 6.0 (d, 1H, $C\underline{H}_2$=CH–), 6.8 (q, 1H, CH_2=C$\underline{H}$–), 7.3—8.1 (m, 6H, ArH+NH_2) ppm: Mass (*m/e*) 239 (M^+).

*3-(*p-*Tolysulfonyl)propionamide (**4b**).* The same reaction procedure as that for **3b** was applied to **1b** (20 mmol) and **2b** (20 mmol) in the presence of AcOH (30 mmol). The reaction mixture provided a white precipitate upon cooling, which was analytically pure without further purification. Found: C, 52.94; H, 5.94; N, 6.40%. Calcd for $C_{10}H_{13}NO_3S$: C, 52.90; H, 5.70; N, 6.17%. IR (KBr) 3420, 3180, (NH_2), 2950 (CH_2), 1700 (C=O), 1600 (Ar), 1325, 1305 (SO_2) cm^{-1}; NMR (DMSO-d_6+$CDCl_3$) δ 2.5 (s, 3H, CH_3), 2.5 (t, 2H, CH_2), 3.4 (t, 2H, CH_2), 7.1—8.1 (m, 6H, ArH+NH_2) ppm; Mass (*m/e*) 227 (M^+, 1), 91 (100).

*3-(*p-*Vinylphenylsulfonyl)propionitrile (**3c**).* The same procedure as that for **3b** was applied to **1a** (10 mmol) and **2c** (10 mmol) in the presence of AcOH (10 mmol). The clear reaction mixture, when subjected to the same purification procedure except for recrystallization from ethanol–ether, provided pale yellow crystals. Found: C, 59.04; H, 4.96; N, 6.16%. Calcd for $C_{11}H_{11}NO_2S$: C, 59.71; H, 4.56; N, 6.33%. IR (KBr) 2990, 2950 (CH_2), 2250 (CN), 1635 (vinyl), 1600 (Ar), 1305, 1140 (SO_2), 1000, 920 (vinyl) cm^{-1}; NMR (DMSO-d_6+$CDCl_3$) δ 2.8 (t, 2H, CH_2), 3.6 (t, 2H, CH_2), 5.5 (d, 1H, $C\underline{H}_2$=CH–), 6.0 (d, 1H, $C\underline{H}_2$=CH–), 6.8 (q, 1H, CH_2=C$\underline{H}$–), 7.4—8.1 (m, 4H, ArH) ppm; Mass (*m/e*) 221 (M^+, 26), 104 (100).

*3-(*p-*Tolylsulfonyl)propionitrile (**4c**).* The same procedure as that for **3b** was applied to **1b** (20 mmol) and **2c** (20 mmol) in the presence of AcOH (30 mmol). The reaction mixture provided white crystals upon cooling, which were analytically pure without further purification. Found: C. 57.17; H, 5.34; N, 6.69%. Calcd for $C_{10}H_{11}NO_2S$: C, 57.40; H, 5.30; N, 6.69%. IR (KBr) 2990, 2930, 2850 (CH_3, CH_2), 2250 (CN), 1600 (Ar), 1300, 1120, (SO_2) cm^{-1}; NMR (DMSO-d_6+$CDCl_3$) δ 2.5 (s, 3H, CH_3), 2.8 (t, 2H, CH_2), 3.5 (t, 2H, CH_2), 7.3—8.0 (m, 4H, ArH) ppm; Mass (*m/e*) 209 (M^+).

*2-Hydroxyethyl 3-(*p-*Vinylphenylsulfonyl)propionate (**3d**).* The same procedure as that for **3b** was applied to **1a** (10 mmol) and **2d** (10 mmol) in the presence of AcOH (10 mmol) to afford a viscous liquid, which was purified by silica gel column chromatography using ethanol for elution (a viscous pale yellow liquid). Found: C, 54.20; H, 5.80%. Calcd for $C_{13}H_{16}O_5S$: C, 54.92; H, 5.32%. IR ($CHCl_3$) 3500 (OH), 2940, 2900 (CH_2), 1740 (ester), 1640 (vinyl), 1600 (Ar), 1310, 1140 (SO_2), 980, 920 (vinyl) cm^{-1}; NMR ($CDCl_3$) δ 2.6 (s, 1H, OH), 2.8 (t, 2H, CH_2), 3.3—4.0 (m, 4H, $2CH_2$), 4.2 (t, 2H, CH_2), 5.5 (d, 1H, $C\underline{H}_2$=CH–), 5.9 (d, 1H, $C\underline{H}_2$=CH–), 7.8 (q, 1H, CH_2=C$\underline{H}$–), 7.3—8.0 (m, 4H, ArH) ppm; Mass (*m/e*) 284 (M^+, 1), 254 (100).

*2-Hydroxyethyl 3-(*p-*Tolylsulfonyl)propionate (**4d**).* The same procedure as that for **3b** was applied to **1b** (20 mmol) and **2d** (20 mmol) in the presence of AcOH (30 mmol) to afford a viscous yellowish green liquid. Found: C, 52.74; H, 5.89%. Calcd for $C_{12}H_{16}O_5S$: C, 52.93; H, 5.92%. IR ($CHCl_3$) 3450 (OH), 2950, 2900 (CH_3, CH_2), 1740 (ester), 1600 (Ar), 1310, 1145 (SO_2) cm^{-1}; NMR ($CDCl_3$) δ 2.5 (s, 3H, CH_3), 2.5 (s, 1H, OH), 2.7 (t, 2H, CH_2), 3.2—4.0 (m, 4H, 2 CH_2), 4.2 (t, 2H, CH_2), 7.2—8.0 (q, 4H, ArH) ppm; Mass (*m/e*) 254 (M^+-H_2O).

References

1) H. Kamogawa, H. Inoue, H. Fukuyama, and M. Nanasawa, *Bull. Chem. Soc. Jpn.*, **52**, 3010 (1979).

2) J. Fayos, J. Clardy, L. T. Dolby, and T. Farnham, *J. Org. Chem.*, **42**, 1349 (1977).

Carbon-13 NMR Chemical Shifts of Some Ruthenocenophanes and Ferrocenophanes

Yasuhisa SENDA,* Shin-ichi KAMIYAMA,** Akira KASAHARA,***
Taeko IZUMI,*** and Satoshi MURAKAMI***

Department of Applied Science, Faculty of Engineering, Tohoku University, Aoba, Sendai 980
***Government Industrial Research Institute, Tohoku, Nigatake, Haranomachi, Sendai 983*
****Department of Applied Chemistry, Faculty of Engineering, Yamagata University, Yonezawa 992*

(Received April 18, 1980)

Synopsis. The ^{13}C NMR spectra of ruthenocenophanes, ferrocenophanes and their precursors were measured. The examination of molecular models for metallocenophanes and the spectral data offer some hints about the conformation of the molecules.

We wish to report the carbon chemical shift data of the title compounds and their precursors. The structures of these metallocenophanes are discussed, using the spectral data together with molecular models which were constructed by using the data from X-ray crystallography.[1]

The assignments of the carbon signals were based on standard methods, *i.e.*, the relative intensities, the off-resonance CW decoupling, and a comparison of the signal shift between closely related compounds. In addition, the bridged methylene carbons of [3]- and [4]ruthenocenophanes, and their ferrocenophane homologs were assigned by comparison of their spectra with those of the deuterated compounds which were obtained by the reduction of the corresponding oxo-compounds with $LiAlD_4$ and $AlCl_3$ combination. The chemical shifts are collected in Table 1.

Both proton and carbon signals of ruthenocene (**1**)[2] shifted to lower fields than those of ferrocene (**2**).[2,3] Since a linear correlation between the ^{13}C chemical shift and charge density has been established for a series of monocyclic aromatic systems,[4] such a shift difference suggests that the ruthenium atom pulls the π-electrons from cyclopentadienyl rings more than the iron atom does. This is supported by the fact that electrophilic substitutions *e.g.*, Friedel-Crafts reactions, occur to a lesser extent with **1** than with **2**.[5]

The carbon signals of ruthenocenophanes also appeared at a lower field than those of ferrocenophanes, except for the carbonyl carbon signals. The chemical shifts for carbonyl groups of [4]ruthenocenophan-2-one (**5**) and [4]ferrocenophan-2-one (**6**) show almost equal values. The carbonyl carbon signal of [3]ruthenocenophan-1-one (**3**) shifted to a higher field than that of [3]ferrocenophan-1-one (**4**). The upfield shift of the carbonyl carbon signal is observed by an introduction of the electron-withdrawing substituents at the neighboring position. The simplest interpretation of this trend would attribute the increase in shielding to decreased polarization of the π-bond, because the electron-withdrawing effect of the substituent decreases the contribution of the polarized form.[6] Such a difference in the chemical shifts for the carbonyl carbons may be correlated to the resonance contribution of the carbonyl group; $Cp-\underset{|}{C}=O \leftrightarrow Cp-\overset{+}{\underset{|}{C}}-\bar{O}$. In infrared spectra,[7] however, the absorption band of **3** is at 1656 cm^{-1} and that of **4** at 1681 cm^{-1}. The carbonyl stretching band generally shifts to the shorter wavelength by an introduction of the electron-withdrawing group at the neighboring position.[8] We assume that the chemical shift difference of the carbonyl carbons between **3** and **4** is primarily due to the electron delocalization by the conjugation of this carbonyl group with the cyclopentadienyl ring. Since the cyclopentadienyl rings of **4** are tilted to about 9°,[9] the longer distance between the two rings of **3**[7] results in an appreciable strain on the bridge of the carbon chain connecting these two rings, which are supposed to be tilted to a greater extent. The molecular model for [3]oxophanes indicates that the dihedral angle between the plane of the carbonyl group and the adjacent cyclopentadienyl ring becomes small when the cyclopentadienyl rings are tilted to a greater extent (see Fig. 2; θ_2 is smaller than θ_1). The π-orbital of the carbonyl group can effectively conjugate with the π-system of the cyclopentadienyl ring. As a consequence, the carbonyl carbon signal of **3** shifts to higher field and the carbonyl stretching band shifts to longer wavelengths than those of **4**. Lentzner and Watts reported that in the acylation of [3]-, [4]-, and [5]ferrocenophan-1-ones, the product ratio, (acylated product at the ring opposite side to the carbonyl group)/(acylated product at the ring adjacent to the carbonyl group), was found to be much higher for [5]oxophane than for other homologs. The finding that the ratio for [3]oxophane is approximately twice that for [4]-oxophane was perplexing. They commented that the distortion of the ferrocene nucleus occasioned by a 4-carbon bridge may be greater than that occasioned by a 3-carbon bridge.[5] The molecular model used in the present investigation indicates that the dihedral

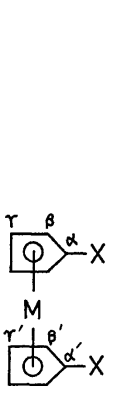

Fig. 1.

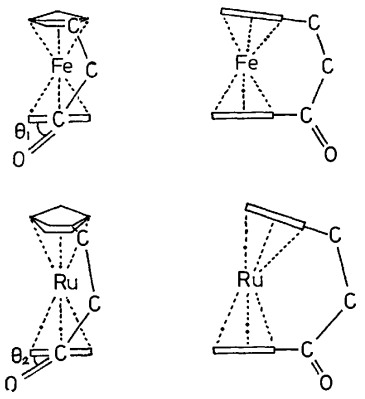

Fig. 2. Conformation models for [3]-ruthenocenophan-1-one and [3]ferrocenophan-1-one.

TABLE 1. CARBON-CHEMICAL SHIFTS OF RUTHENOCENOPHANES, FERROCENOPHANES, AND THEIR PRECURSORS[a)]

X	M	Compd No.	α	α′	β,β′,γ,γ′				1	2	3	4
H	Ru	1			70.0							
	Fe	2			67.7[b)]							
α-$\overset{1}{C}O\overset{2}{C}H_2\overset{3}{C}H_2$-α′	Ru	3	138.8	92.2	71.1,	72.9,	73.6,	75.4	208.5	46.2	32.0	
	Fe	4	128.3	88.0	69.2,	70.3,	71.1,	72.5	211.9	44.1	31.6	
			87.6	74.0	68.8,	69.8,	70.2,	72.0	210.1	43.8	31.1[c)]	
α-$\overset{1}{C}H_2\overset{2}{C}O\overset{3}{C}H_2\overset{4}{C}H_2$-α′	Ru	5	93.4	81.6	70.0,	70.4,	72.3,	72.4	45.3	206.7	42.1	27.3
	Fe	6	86.5	76.6	68.3,	68.9			(41.5)[d)]	206.5	(41.3)	25.7
α-$\overset{1}{C}H_2\overset{2}{C}H_2\overset{3}{C}H_2$-α′	Ru	7	85.7	85.7	71.4,	71.6			38.2	24.6	38.2	
	Fe	8	85.4	85.4	68.1,	69.3			35.0	24.5	35.0	
			85.2	85.2	67.9,	69.1			35.1	24.2	35.1[c)]	
α-$\overset{1}{C}H_2\overset{2}{C}H_2\overset{3}{C}H_2\overset{3}{C}H_2$-α′	Ru	9	91.6	91.6	69.7,	71.7			30.6	29.1	29.1	30.6
	Fe	10	88.0	88.0	65.7,	65.9			29.3	27.0	27.0	29.3
					β	γ	α′,β′,γ′					
α-CHO	Ru	11	84.8		71.0	74.4	72.2		189.6			
	Fe	12	79.6		68.2	72.9	69.6		192.9			
			79.2		68.0	72.6	69.2		192.2[b)]			
α-$\overset{1}{C}H$=$\overset{2}{C}H\overset{3}{C}OOH$	Ru	13	82.8		70.2	71.9	71.2		143.1	115.4	167.3	
(in DMSO-d_6)	Fe	14	78.5		68.3	70.4	69.2		144.7	115.6	167.3	
α-$\overset{1}{C}H_2\overset{2}{C}H_2\overset{3}{C}OOH$	Ru	15	91.7		69.0	70.2	70.1		23.7	35.7	173.6	
(in DMSO-d_6)	Fe	16	87.1		66.7	67.5	68.1		24.3	34.9	174.5	

a) In $CDCl_3$ unless otherwise indicated. b) Ref. 3. c) A. N. Nesmeyanov, G. B. Shul'pin, and M. I. Rybinskaya, *Dokl. Akad. Nauk. SSSR*, **218**, 1107 (1974). d) Values in parentheses may be interchanged.

angle between the plane of the carbonyl group and the adjacent cyclopentadienyl ring becomes small when the number of carbon of the bridge diminishes from 4 to 3. In consequence, the carbonyl-cyclopentadienyl conjugation would be stronger for the latter ketone. The product ratio which they obtained seems quite reasonable.

The ^{13}C NMR spectra of precursors of phane compounds: formylruthenocene (**11**), ruthenocenylacrylic acid (**13**), ruthenocenylpropionic acid (**15**) and their ferrocene homologs, **12**, **14**, and **16**, were also measured. Similarly to the case of the parent and phane compounds, the carbon signals of cyclopentadienyl rings of ruthenocenes are located at lower fields than those of ferrocenes.

Experimental

NMR Spectra. The ^{13}C FT-NMR spectra were obtained at 25.15 MHz with a JEOL JNM-MH-100 instrument equipped with a JNM-MFT-100 Fourier transform accessory; the instrument was controlled with a JEC-6 spectrum computer. Samples were observed in 5 mm spinning tubes at 15±5% solutions in $CDCl_3$ or DMSO-d_6 at 28 °C. The solvent provided the internal lock signal. The measurement conditions were as follows: pulse width, 27.5 μs (*ca.* 45°); repetition time, 4 s; spectral width, 6.25 kHz; data points, 8192; acquistion time, 0.65 s. Noise modulated proton decoupling was carried out at a nominal power of 20 W and the off-resonance was carried out at a nominal power of 7 W. All chemical shifts are expressed in δ (ppm; downfield from internal Me_4Si). Each observed chemical shift is estimated to be accurate to δ±0.1.

Materials. The compounds employed in this work have been previously prepared: ferrocenophanes and ferrocenes,[10)] ruthenocenophanes, and ruthenocenes.[7)]

References

1) E. A. Siebold and L. E. Sutton, *J. Chem. Phys.*, **23**, 1967 (1955); J. D. Dunitz, L. E. Orgel, and A. Rich, *Acta Crystallogr.*, **9**, 373 (1956); R. K. Bohn and A. Haaland, *J. Organomet. Chem.*, **5**, 470 (1966); G. L. Hardgrove and D. H. Templeton, *Acta Crystallogr.*, **12**, 28 (1959); M. D. Rausch, E. O. Fischer, and H. Grubert, *J. Am. Chem. Soc.*, **82**, 76 (1960).

2) M. D. Rausch and V. Mark, *J. Org. Chem.*, **28**, 3225 (1963).

3) A. A. Koridze, P. V. Petrovskii, A. I. Mokhov, and A. I. Lutsenko, *J. Organomet. Chem.*, **136**, 57 (1977).

4) H. Spiesecke and W. G. Schneider, *Tetrahedron Lett.*, **1961**, 468; E. A. LaLancette and R. E. Benson, *J. Am. Chem. Soc.*, **87**, 4941 (1965).

5) H. L. Lentzner and W. E. Watts, *Tetrahedron*, **28**, 121 (1972).

6) J. B. Stothers, "Carbon-13 NMR Spectroscopy," Academic Press, New York (1972), p. 279.

7) S. Kamiyama, T. M. Suzuki, T. Kimura, and A. Kasahara, *Bull. Chem. Soc. Jpn.*, **51**, 909 (1978).

8) L. J. Bellamy, "The Infrared Spectra of Complex Molecules," Wiley, New York (1958), p. 132.

9) N. D. Jones, R. E. Marsh, and J. H. Richards, *Acta Crystallogr.*, **19**, 330 (1965).

10) M. Rosenblum, A. K. Banerjee, N. Danieli, R. W. Fish, and V. Schlatter, *J. Am. Chem. Soc.*, **85**, 316 (1963); G. D. Broadhead, J. M. Osgerby, and P. L. Pauson, *J. Chem. Soc.*, **1958**, 650; K. L. Rinehart, Jr., R. J. Curby, Jr., D. H. Gustafson, K. G. Harrison, R. E. Bozak, and D. E. Bublitz, *J. Am. Chem. Soc.*, **84**, 3263 (1962).

Synthetic Studies on Terpenic Compounds. XII.[1] Selective Degradation of the Side Chain in Portulal[2]

Takashi TOKOROYAMA,* Keizo MATSUO,† and Reizo KANAZAWA††
Faculty of Science, Osaka City University, Sumiyoshi-ku, Osaka 558
(Received May 6, 1980)

Synopsis. Stepwise degradation of the side chain in portulal has been investigated in connection with synthetic studies. Selective cleavage of the double bond in the side chain was achieved by ozonolysis after protection of the endo-double bond by iodoetherification of the corresponding alcohol. Further degradation led to the formation of the γ-lactone *via* the δ-lactone.

Portulal (**1**), a diterpene isolated from *Portulaca grandflora* Hook as a plant growth regulator, has a unique perhydroazulenoid skeleton with clerodane substitution.[3] In connection with the total synthesis of **1**,[1,4] we examined the products derived from **1** by degradation of its side chain since they might be utilized for confirming the stereochemistry of synthetic intermediates and also as relay compounds. The results of the investigation are given herewith.

The key problem for selective degradation of the side chain lies in the preferential cleavage of the $\Delta^{13,14}$ double bond, since its reactivity and that in the ring hardly differ. We found a solution to this problem by protecting the ring double bond with internal addition of the angular functional group. After several preliminary experiments the iodoetherification of portulol (**2**), obtained by lithium aluminium hydride reduction of **1**,[5] was found to be feasible. Treatment of **2** under specified conditions (Scheme 1) afforded the iodo ether **3** quantitatively. It was found that the latter can be reverted to the former by the reaction with zinc–silver couple[6] or chromium(II) chloride.[7] Ozonolysis of **3** and subsequent treatment of the product with zinc–silver couple gave an α-ketol **4** which was cleaved by periodic acid to yield the δ-lactone **5**, its IR spectrum showing carbonyl absorption at 1740 cm^{-1}. Further degradation of **5** to **6** was effected by formylation and subsequent treatment with alkaline hydrogen peroxide. The product showed the carbonyl peak at 1770 cm^{-1} in its IR spectrum. A salient feature in the NMR spectrum was the presence of signals due to vinyl methyl and vinylic protons (δ 1.71 and 5.38, respectively), a singlet (δ 2.39) and an AB quartet (δ 4.09 and 4.23) due to the methylene protons of the spiro-γ-lactone and an AB quartet (δ 3.35 and 3.57) due to the hydroxymethyl protons. A counterpart of the latter AB quartet (δ 3.57) split further with coupling constant of 1.5 Hz, this being observable also in the NMR spectrum of the δ-lactone **5**. The extra splitting might be ascribed to the W-letter coupling with 5α proton, indicating that the free rotation of the angular hydroxylmethyl group is sufficiently restricted and stays in the most stable conformation. Oxidation of **6** with Jones' reagent followed by acid treatment afforded the dilactone **7** which has been correlated with the synthetic intermediate of portulal synthesis.[1] Compound **6** was found to be a pertinent relay compound.

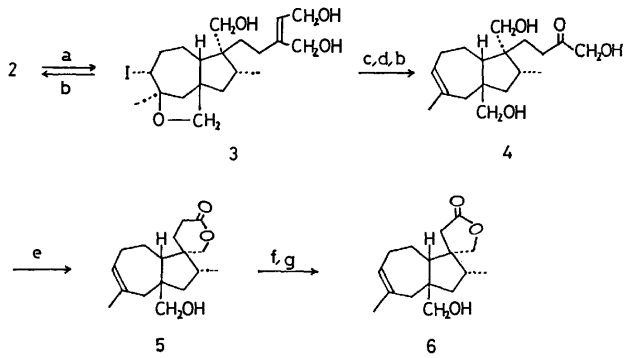

3 4 5 6

Scheme 1. (a) I_2, $NaHCO_3$, THF; (b) Zn–Ag; (c) O_3; (d) Me_2S; (e) HIO_4; (f) HCO_2Et, NaH; (g) H_2O_2, KOH, MeOH

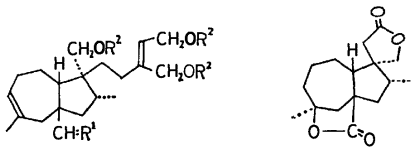

1 R^1 = O, R^2 = H
2 R^1 = H, OH, R^2 = H

7

Fig. 1.

Experimental

Melting points are uncorrected. IR spectra were taken on a JASCO IRA-1 spectrometer as films (liquid) or Nujol mulls (solid), ^1H NMR spectra in $CDCl_3$ on a JEOL PS-100 spectrometer and mass spectra on a Hitachi M-52 spectrometer.

Extraction of Portulal (1). Portulal was extracted from *Portulaca grandiflora* Hook by essentially the same procedure as that reported.[5] The cut aerial part of the plant was extracted with methanol and the extract concentrated *in vacuo* to about one-fourth of the original volume. The concentrated solution was washed with petroleum ether and then extracted continuously with ether. The ether layer was washed with saturated aq $NaHCO_3$ and dried with anhydrous Na_2SO_4, the solvent being removed. The neutral extract thus obtained was chromatographed on a silica-gel column. The crystalline material, eluted with benzene-ethyl acetate (1:1) followed by ethyl acetate, was recrystallized from aq methanol giving portulal **1** as needles, mp 119.5—120 °C.

Iodo Ether 3. A solution of $LiAlH_4$ (220 mg, 5.8 mmol) in tetrahydrofuran (20 ml) was added to a solution of **1** (1.359 mg, 4.05 mmol) in anhydrous tetrahydrofuran (30 ml) over a period of 10 min under ice-cooling, After the mixture had been stirred at room temperature for 80

† Present address: Faculty of Pharmaceutical Sciences, Kinki University, Higashiosaka, Osaka 577.

†† Present address: Daiichi Isotope Laboratories, Ltd, Chuo-ku, Tokyo 103.

min, excess reagent was destroyed by the addition of ethyl acetate, water (1.5 ml) and anhydrous $MgSO_4$. Filtration with the aid of Celite and evaporation of the solvent from the filtrate followed by chromatography on a column of silica gel (30 g) afforded portulol (**2**) as a colorless oil (1.388 g), which solidified when cooled. The substance dissolved in a mixture of tetrahydrofuran (30 ml) and water (22 ml) was mixed with aq $NaHCO_3$ (2.298 g, 27.35 mmol) and KI-I_2 solution prepared from KI (3.978 g), I_2 (1.934 g, 7.61 mmol), and water (25 ml). The mixture was stirred at ambient temperature for 4.5 h. Saturated aq $NaHCO_3$ solution was added to reduce excess iodine, the product isolated by ether extraction giving the iodo ether **3** as a pale yellow oil (1.831 g, 98% overall yield): IR 3360 cm^{-1}; ^1H NMR 0.98 (3H, d, J=6 Hz, $-\underset{|}{C}HC\underline{H}_3$), 1.51 (3H, s, $-O\underset{|}{C}CH_3$). 3.61 (2H, s, $-\underset{|}{C}C\underline{H}_2OH$), 3.79, 3.87 (2H, AB q, J=7 Hz, $-CH_2O-$), 4.15 (2H, s, $-\underset{|}{C}=\underset{|}{C}C\underline{H}_2OH$), 4.16 (2H, d, J=7 Hz, $-\underset{|}{C}=C\underline{H}CH_2OH$), 4.38 (1H, br s, $-CH_2C\underline{H}I-$), 5.58 (1H, t, J=7 Hz, $-\underset{|}{C}=C\underline{H}CH_2OH$).

*Reversion of Iodo Ether **3** to Portulol (**2**).* *(a) With Zinc-Silver Couple*: A solution of **3** (54 mg, 0.116 mmol) in dry ether (1.5 ml) was treated with zinc-silver couple prepared[6] from silver acetate (0.2 mg) and zinc dust (25 mg) with addition of ethanol (0.25 ml) and acetic acid (1 drop) under reflux for 1.5 h. After filtration, the filtrate was washed successively with dil. HCl saturated aq $NaHCO_3$ and brine, and dried with anhydrous $MgSO_4$. Evaporation of the solvent and purification of the product by silica gel chromatography gave portulol (**2**) (32 mg, 81% yield).

(b) With $CrCl_2$: A $CrCl_2$ solution (9 ml, *ca.* 3.7 mmol) was added to an ice-cooled solution of **3** (70 mg, 0.151 mmol) in *N,N*-dimethylformamide (8 ml), the mixture being stirred for 1 h. The product was extracted with $CHCl_3$ and the organic layer washed with saturated aq $NaHCO_3$ and brine. Removal of the solvent gave a product which was purified by chromatography (silica gel) to give portulol (**2**) (33 mg, 65% yield).

*δ-Lactone **5**.* The iodo ether **3** (2.47 g, 5.32 mmol) dissolved in methanol (100 ml) was ozonized at −70 °C until blue coloration was observed. After the mixture had been left to stand at −70 °C for 15 min, excess ozone was expelled by bubbling of nitrogen gas. Dimethyl sulfide (390 mg, 6.29 mmol) was then added. The mixture was kept at −70 °C for 30 min, the temperature then being allowed to rise by removal of the cooling bath. Evaporation of the solvent gave a crude product which was dissolved in absolute ether (25 ml) and treated with zinc-silver couple (prepared from silver acetate, 14 mg and zinc dust, 2.4 g), ethanol (3 ml) and acetic acid (2 drops) with stirring at room temperature for 16 h. Work-up afforded the ketol **4** as colorless oil (1.6 g). The product dissolved in a mixture of dioxane (40 ml) and water (20 ml) was treated with $HIO_4 \cdot 2H_2O$ (1.7 g, 7.46 mmol) overnight at room temperature. Chloroform extraction and the washing of the extract solution with saturated aq $NaHCO_3$ followed by evaporation of the solvent gave an oil which was purified by silica-gel chromatography. Elution with chloroform-methanol (25:1) gave δ-lactone **5** as a colorless oil: IR ($CHCl_3$) 3470, 1740 cm^{-1}; ^1H NMR 1.07 (3H, d, J=7 Hz, $-\underset{|}{C}HC\underline{H}_3$), 1.71 (3H, br s, $-CH=\underset{|}{C}C\underline{H}_3$), 2.52 (2H, t, J=7.5 Hz, $-CH_2C\underline{H}_2CO_2-$), 3.33 (1H, d, J=10.5 Hz, $-C\underline{H}_2OH$), 3.56 (1H, dd, J=1.5, 10.5 Hz, $-C\underline{H}_2OH$), 4.25 (2H, s, $-CH_2OCO-$) 5.36 (1H, m, $-\underset{|}{C}=C\underline{H}CH_2-$)

*Conversion of δ-Lactone **5** into γ-Lactone **6**.* NaH (53 mg, 50% oil dispersion) and ethyl formate (0.5 ml) were added to a solution of **5** (50 mg, 0.18 mmol) in dry benzene (3 ml). After addition of a drop of methanol, the mixture was stirred overnight at room temperature. The reaction mixture was diluted with benzene and shaken with water. The aqueous layer was separated and acidified with dil HCl. Isolation of the product with chloroform extraction gave a yellow oil (50 mg). The formyl derivative thus obtained was dissolved in a mixture of methanol (0.7 ml), water (0.5 ml) and 3 M (1 M=1 mol dm^{-3}) NaOH (0.1 ml) and mixed with 3 M NaOH (2 ml) and 30% H_2O_2 (0.8 ml). The mixture was stirred at ambient tempearture, 3 M NaOH (2 ml and 3 ml) and 30% H_2O_2 (0.4 ml and 2.5 ml) being added after 1.5 and 2.5 h, respectively. The reaction was continued overnight and then worked up. Acidification with dil HCl followed by chloroform extraction and chromatographic purification (silica gel) gave the γ-lactone **6** (25 mg, 53% yield) as a colorless oil: IR ($CHCl_3$) 3500, 1770, 1180, 1030 cm^{-1}; ^1H NMR 0.97 (3H, d, J=6.5 Hz, $-\underset{|}{C}HC\underline{H}_3$), 1.71 (1H, br s, $-CH=\underset{|}{C}C\underline{H}_3$), 2.39 (2H, s, $-CH_2CO_2-$), 3.35 (1H, d, J=11 Hz, $-C\underline{H}_2OH$), 3.57 (1H, dd, J=1.5, 11 Hz, $-C\underline{H}_2OH$), 4.09, 4.23 (2H, AB q, J=10 Hz, $-CH_2OCO-$), 5.38 (1H, m, $-\underset{|}{C}=C\underline{H}CH_2-$).

References

1) Part XI; T. Tokoroyama, K. Matsuo, H. Kotsuki, and R. Kanazawa, *Tetrahedron*, in press.

2) This work was taken from the doctorate thesis of R. Kanazawa.

3) S. Yamazaki, S. Tamura, F. Marumo, and Y. Saito, *Tetrahedron Lett.*, **1969**, 359.

4) T. Tokoroyama, K. Matsuo, R. Kanazawa, H. Kotsuki, and T. Kubota, *Tetrahedron Lett.*, **1975**, 3651.

5) Y. Abe, E. Taniguchi, M. Eto, and Y. Oshima, *Nogeikagaku-zasshi*, **45**, 169 (1971).

6) J. M. Denis, C. Girrard, and J. M. Conia, *Synthesis*, **1972**, 549.

7) G. Rosenkranz, O. Mancera, J. Gatica, and C. Djerassi, *J. Am. Chem. Soc.*, **72**, 4077 (1950).

8) M. Fieser and L. F. Fieser, "Reagents for Organic Synthesis," John Wiley and Sons, New York (1967), Vol. 1, p. 143.

Studies on Biologically Active Pteridines. V.[1] Synthesis of (6*S*)-5,6,7,8-Tetrahydro-1,3,5,6-tetramethyllumazine

Takashi SUGIMOTO* and Sadao MATSUURA

Department of Chemistry, College of General Education, Nagoya University, Chikusa-ku, Nagoya 464

(Received May 12, 1980)

Synopsis. (+)-5,6,7,8-Tetrahydro-1,3,5,6-tetramethyllumazine, a compound derived from enzymically reduced (−)-5,6,7,8-tetrahydro-6-methylpterin, was shown to be of (*S*)-configuration at the C-6 chiral center by a synthesis, which was performed by condensation of 5-bromo-6-chloro-1,3-dimethyluracil and (2*S*)-1-amino-2-(methylamino)propane. The structure of the condensation product was determined unequivocally by an independent synthesis using a regioselective methylation of 5,6,7,8-tetrahydro-1,3,6-trimethyllumazine.

(−)-5,6,7,8-Tetrahydrobiopterin[2] is an essential cofactor for phenylalanine,[3] tyrosine,[4] and tryptophan hydroxylases,[5] all of which play important roles in the biosynthesis of neurotransmitting dopamine or serotonine. Thus, deficiency of tetrahydrobiopterin causes severe neurological disturbance such as atypical phenylketonuria.[6] Tetrahydrobiopterin is produced stereospecifically referring to the C-6 chiral center from 7,8-dihydrobiopterin by dihydrofolate reductase and NADPH; chemical reduction gives a mixture of diastereomers. Since the two diastereomers show different biological properties,[7,8] determination of the C-6 configuration of natural (−)-tetrahydrobiopterin is essential for understanding its properties in biological systems. 5,6,7,8-Tetrahydro-6-methylpterin is also produced stereospecifically from the 7,8-dihydro precursor by the action of the same enzyme, and thus formed (−)-tetrahydro-6-methylpterin and (−)-tetrahydrobiopterin were shown to have same L-configuration at C-6 in a rather indirect manner by comparison with 1,2,3,4-tetrahydro-2-methylquinoxaline.[8]

As an alternative and more direct approach to confirm the C-6 configuration of these pterins, we studied the C-6 configuration of (+)-5,6,7,8-tetrahydro-1,3,5,6-tetramethyllumazine, a compound recently derived from (−)-tetrahydro-6-methylpterin by methylation and deamination without altering the configuration.[9]

We synthesized (6*S*)-5,6,7,8-tetrahydro-1,3,5,6-tetramethyllumazine (**3**) from 5-bromo-6-chloro-1,3-dimethyluracil(**1**) and (2*S*)-1-amino-2-(methylamino)propane (**2**). Heating of **1** and **2** in ethanol gave a tetrahydrolumazine as a main product, which showed a weak basicity (pK_a 5.39) and λ_{max} at 235(sh.) and 286 (pH 8.0) and at 263 (pH 3.0). Its ^{13}C-NMR spectrum showed signals at the following chemical shifts (ppm): 160.3(C-4), 150.7(C-2), 144.1(C-8a), 99.5(C-4a), 50.7 (C-6), 40.0(C-7), 41.4, 28.9, 27.9 (three N–CH_3), and 17.1(C–CH_3). We tentatively assigned the compound as **3**, because it showed resistance toward air oxidation, an important characteristic of N-5 substituted tetrahydropteridines. However, the observed chemical and physical properties could not exclude the possibility that the compound might have the isomeric structure, *i.e.*, 5,6,7,8-tetrahydro-1,3,7,8-tetramethyllumazine. In order to confirm the above assignment, we synthesized racemic **3** by an independent method: 1,3,6-trimethyllumazine[10] was hydrogenated over platinum oxide into 5,6,7,8-tetrahydro derivative, which was subsequently hydrogenated in the presence of formaldehyde over the same catalyst. A methyl group was introduced regioselectively at N-5 to produce (±)-**3**, whose spectral data allowed to confirm the condensation product as (6*S*)-**3**.

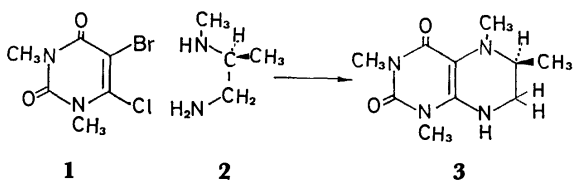

1 **2** **3**

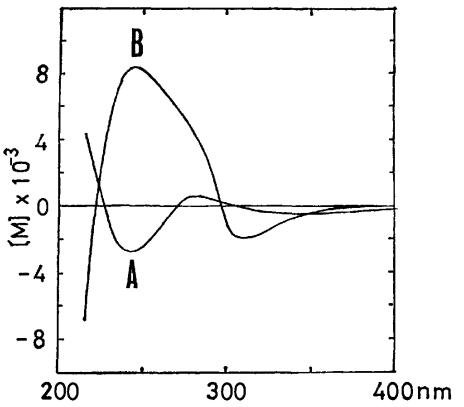

Fig. 1. The ORD curves of (6*S*)-**3**: **A**, at pH 3.0 (cation) and **B**, at pH 8.0 (neutral molecule).

The cation of (6*S*)-**3** showed, as expected, positive Cotton effect in ORD with a peak at 283 nm and trough at 242 nm (Fig. 1), though neutral (6*S*)-**3** gave opposite sign of rotation. The present results confirmed that (+)-**3**, derived from (−)-tetrahydro-6-methylpterin, has (6*S*)-configuration. Consequently, it is concluded that the enzymically reduced (−)-tetrahydro-6-methylpterin has (6*S*)-configuration and the (−)-tetrahydrobiopterin the same (6*R*)-configuration.

Experimental

The elemental analyses were carried out at the Analytical Section, Meijo University. The pK_a values were determined spectroscopically on a Shimadzu UV-300 spectrometer. The ORD curves were measured on a JASCO ORD/UV-5 spectropolarimeter in appropriate pH buffer solutions and the ^{13}C-NMR spectra on a JEOL JNM-PFT-60 NMR spectrometer in $CDCl_3$. The chemical shifts are expressed in terms δ (ppm downfield from the internal TMS).

(2S)-1-Amino-2-methylaminopropane (2). L-Alaninamide[11] (60 g) was formylated by acetic formic anhydride

at 20 °C to give (2*S*)-2-(formamino)propanamide (45 g), mp 112—113 °C (from ethanol) (Found: C, 41.59; 7.11; N, 23.84%. Calcd for $C_4H_8N_2O_2$: C, 41.37; H, 6.94; N, 24.13%). The amide (30 g) and $LiAlH_4$ (45 g) in tetrahydrofuran (1.5 l) was refluxed for 24 h and the excess reagent was decomposed by water. The filtered solution was fractionally distilled twice to give **2** (10 g) boiling at 112—122 °C; ^{13}C-NMR: at δ 58.0 (CH_2), 55.4 (CH), 36.7 (N-CH_3), 24.0 (N-CH_3), and 18.2 (C-CH_3).

*(6S)-5,6,7,8-Tetrahydro-1,3,5,6-tetramethyllumazine (**3**).* A solution of **1**[12] (7.0 g), **2** (2.5 g), and triethylamine (7 g) in ethanol (100 ml) was heated under reflux and nitrogen for 7 h. The solution was evaporated and the residue was dissolved in water (50 ml). The solution was adjusted to pH 1—2 with HCl and extracted continuously with chloroform for 2 h. The aqueous solution was adjusted to pH 7—8 with $NaHCO_3$ and again extracted continuously with chloroform for 1 h. The latter extract was fractionated on a silica gel column (4.5 cm × 40 cm) developed by ethanol and ethyl acetate (1:9). The fraction of the main product was chromatographed once more as above. Evaporation of the eluate gave an oily residue, which was mixed with ethanol (0.5 ml). Dilution with ether (10 ml) and chilling gave colorless prisms (4.85 g) of **3**, mp 164—166 °C (dec), (Found: C, 53.58; H, 7.34; N, 24.90%. Calcd for $C_{10}H_{16}N_4O_2$: C, 53.55; H, 7.19; N, 24.99%); pK_a 5.39±0.01; λ_{max} (log ε) in nm at pH 8.0: 235 (sh., 3.72) and 286 (4.11); at pH 3.0: 263 (4.22).

*Racemic **3**.* 1,3,6-Trimethyllumazine (1.5 g) was hydrogenated over platinum oxide (0.5 g) in methanol (100 ml) at atmospheric pressure and temperature for 1 h. Formalin (37%, 2.5 g) was added to the mixture and hydrogenation was continued over night. The filtered solution was evaporated and chromatographed as above to give colorless prisms (1.24 g) of (±)-**3**, mp 200—202 °C (dec), (from ethanol) (Found: C, 53.63; H, 7.42; N, 24.64%. Calcd for $C_{10}H_{16}N_4O_2$: C, 53.55; H, 7.19; N, 24.99%); pK_a 5.36±0.01; λ_{max} nm (log ε) at pH 8.0: 235 (sh., 3.73) and 286 (4.10); at pH 3.0: 263 (4.22); ^{13}C-NMR at δ 160.3, 150.7, 143.9, 99.6, 50.8, 41.4, 40.1, 28.9, 28.0, and 17.1.

The authors thank Prof. H. Nakata for measuring the NMR spectra, Mrs. N. Nishioka for measuring the pK_a values and UV spectra, and Dr. W. L. F. Armarego, The Australian National University, for sending a pre-publication paper and discussion.

References

1) Part IV: T. Sugimoto, S. Matsuura, and T. Nagatsu, *Bull. Chem. Soc. Jpn.*, **53**, 2334 (1980).

2) Because of general instability of tetrahydropteridines toward air oxidation at a pH value forming the neutral molecules, the signs of Cotton effects in CD or ORD of these compounds are compared among their N-5 protonated cations measured in an acidic solution in this paper.

3) S. Kaufman, *Pcoc. Natl. Acad. Sci. U. S. A.*, **50**, 1085 (1963).

4) T. Nagatsu, M. Levitt, and S. Undenfriend, *J. Biol. Chem.*, **239**, 2910 (1964).

5) A. Ichiyama, S. Nakamura, Y. Nishizuka, and O. Hayaishi, *J. Biol. Chem.*, **245**, 1699 (1970).

6) D. M. Danks, R. G. H. Cotton, and P. Schlesinger, *Lancet i*, 1236 (1976).

7) S. W. Bailey and J. E. Ayling, *J. Biol. Chem.*, **253**, 1598 (1978).

8) H. Hasegawa, S. Imaizumi, A. Ichiyama, T. Sugimoto, S. Matsuura, K. Oka, T. Kato, T. Nagatsu, and M. Akino, "Chemistry and Biology of Pteridines," ed by Kisliuk and Brown, Elsevier North Holland (1979), p. 183.

9) W. L. F. Armarego, P. Waring, and J. W. Williams, *J. Chem. Soc., Chem. Commun.*, **1980**, 334.

10) H. Zondler, H. S. Forrest, and J. M. Lagowski, *J. Heterocycl. Chem.*, **4**, 124 (1967).

11) P. S. Yang and M. M. Rising, *J. Am. Chem. Soc.*, **53**, 3183 (1931).

12) W. Pfleiderer and H. Deiss, *Israel J. Chem.*, **6**, 603 (1968).

A One Step Transformation of a 7-Oxo Steroid into a 7-Oxa Steroid. A New Photo-oxidation of Cyclic Ketone[1)]

Hiroshi SUGINOME*,** and Chi- Ming SHEA

Department of Chemistry, Faculty of Science, Hokkaido University, Sapporo 060

(Received May 15, 1980)

Synopsis. Irradiation of 3α,5-cyclo-5α-cholestan-7-one in methanol saturated with oxygen gives a novel cyclo-7-oxa steroid, 3α,5-cyclo-7-oxa-5α-cholestane, together with methyl 3α,5-cyclo-7,8-seco-5α-cholestan-7-oate.

We report here a one-step transformation of 7-oxo-3α,5-cyclo-5α-cholestan-7-one (**1**)[2,3)] into a novel cyclo-7-oxa steroid, 3α,5-cyclo-7-oxa-5α-cholestane (**3**), by irradiation in the presence of oxygen. The ketone **1** in methanol saturated with oxygen was irradiated with a Hanovia 450-W mercury arc through a Pyrex filter for 96 h. Preparative TLC of the reaction mixture gave two major crystalline products, **2** (12%) and **3** (18%), together with several minor products. Product **2** was identified as methyl 3α,5-cyclo-7,8-seco-5α-cholestan-7-oate,[3)] which was an exclusive product when **1** in methanol was photolyzed in the absence of oxygen,[3)] by a direct comparison. The less mobile compound **3** was a new compound; the structure was confirmed to be 3α,5-cyclo-7-oxa-5α-cholestane (**3**) by the analysis of the spectra. The molecular formula $C_{26}H_{44}O$ was determined by high resolution mass spectrometry. The low resolution mass spectrum showed an intense molecular ion peak at *m/e* 372 (14.4%), a M^+-CH_3 peak at *m/e* 357 (5.2%), and the base peak at *m/e* 317. The IR spectrum showed a strong band at 1087 cm^{-1} arising from C–O stretching of a cyclic ether. The NMR spectrum showed a 1H double doublet at τ 9.87 (J=8 and 6 Hz, a cyclopropyl proton) a 1H triplet at τ 9.62 (J=4.5 Hz, a cyclopropyl proton), a 3H singlet at τ 9.26 (18-H) and a 3H singlet at τ 9.01 (19-H). It also showed an AB quartet centred at τ 6.89 and 6.05 (J=12.0 Hz) and a 1H diffused triplet at τ 6.69 (J=7.5 Hz); these are assigned to the C-6 methylene protons and the 8β-H. Assuming the ring B of **3** to be in a chair conformation, the 6α-H should be shielded by the cyclopropane ring, and the doublet at τ 6.89 is thus assigned to the 6α-H.

The photochemical transformation of an oxo steroid into an oxa steroid in the presence of oxygen appears to be a new type of reaction of excited cyclic ketones. The pathway from the excited ketone (A) to cyclic ether **3** is not clear at the present stage. However, the process outlined in Scheme 2 may explain the formation of cyclic ether **3**: here a β-scission of the resulting biradical (B)[4)] could lead to a peroxylactone (C) which photodecarboxylates[5)] to give cyclic ether **3**.

Experimental

For instruments used and general procedures see Ref. 3. Mass spectra were recorded with a Hitachi JMS-D 300 spectrometer (70 eV) by Miss Yuko Chiba of the Faculty of Agriculture.

Photo-oxidation of 3α,5-Cyclocholestan-7-one (1).[2,3)] Ketone **1** (200 mg) in methanol (200 ml) saturated with oxygen was irradiated with a Hanovia 450-W mercury arc through a Pyrex glass filter for 96 h. After the evaporation of the solvent, the product (213 mg) was subjected to preparative TLC (Merck, silica gel 60 F254) with a 1:1 benzene and hexane mixture to give nine fractions: A (35 mg), B (35 mg), C (17 mg), D (4 mg), E (2 mg), F (2 mg), G (2 mg), H (6 mg), and I (77 mg), in the order of decreasing mobility. The fraction (A) was recrystallized from methanol to give seco ester **2**,[3)] mp 72—73 °C. The fraction B was recrystallized from methanol to yield 3α,5-cyclo-7-oxa-5α-cholestane (**3**), mp 144—145 °C. (Found: *m/e* 372.3412. Calcd for $C_{26}H_{44}O$: M^+, 372.3390); for mass, IR, and NMR spectra see text.

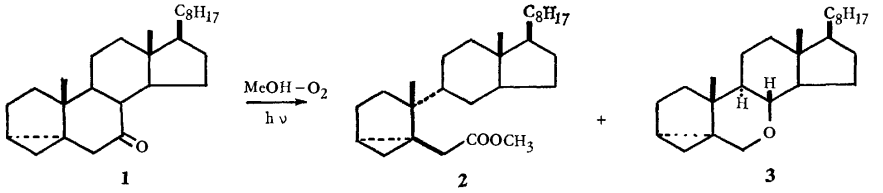

1 2 3

Scheme 1.

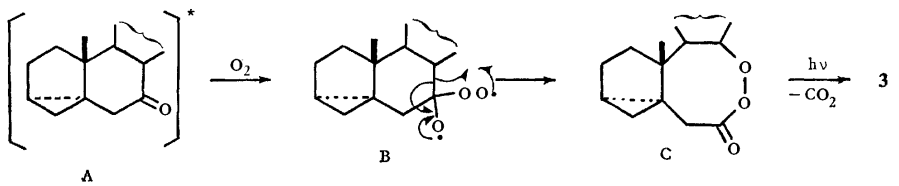

A B C

Scheme 2.

** Present address: Organic Chemistry Laboratory, Department of Chemical Process Engineering, Faculty of Engineering, Hokkaido University, Sapporo 060.

References

1) Photoinduced Transformations. Part 54. Previous paper in this series. H. Suginome and N. Maeda, *Bull. Chem. Soc. Jpn.*, **53**, 2626 (1980).
2) V. Cerny, *Collect. Czech. Chem. Commun.*, **38**, 1563 (1973).
3) H. Suginome and Chi-Ming Shea, *J. Chem. Soc.' Perkin Trans. 1*, **1980**, 2268.
4) N. Shimizu and P. D. Bartlett, *J. Am. Chem. Soc.*, **98**, 4193 (1976); P. D. Bartlett, *Chem. Soc. Rev.*, **5**, 154 (1976).
5) W. Adam and G. S. Aponte, *J. Am. Chem. Soc.*, **93**, 4300 (1971).

Catalysis by Heteropolyacid. III. Acylation and Sulfonylation of Aromatic Compounds Catalyzed by Keggin-structure Heteropolyacids

Kenji NOMIYA, Yoshio SUGAYA, and Makoto MIWA*

Department of Industrial Chemistry, Faculty of Engineering, Seikei University, Musashino-shi, Tokyo 180

(Received June 19, 1980)

Synopsis. Catalytic acylation and sulfonylation reactions of aromatic compounds by Keggin-structure heteropolyacids, $H_4[SiMo_{12}O_{40}]$, $H_3[PMo_{12}O_{40}]$ and $H_4[SiW_{12}O_{40}]$, have been studied. Tungsten is more effective than molybdenum for the reactions.

Brønsted acidity of Keggin-structure heteropolyacid is a key factor in the catalysis for polycondensation of benzyl alcohols[1] and Friedel-Crafts-type reaction.[2] These reactions proceed *via* a carbonium ion mechanism. The constitutional metal of the Keggin-unit is another important factor, molybdenum, rather than tungsten, being effective for the alkylation reaction.[3] We have examined the role of the metal and the hetero atom in the catalytic acylation and sulfonylation for aromatic compounds.

The heteropolyacids, $H_4[SiMo_{12}O_{40}]$, $H_3[PMo_{12}O_{40}]$ and $H_4[SiW_{12}O_{40}]$, were prepared according to the usual method. The mononuclear complex, H_2MO_4 (M=Mo, W), was prepared by heating a hydrochloric aqueous solution of MO_3 at 40—60 °C and cooling. All organic reagents were purified by the usual methods. Acylation was carried out with acetyl chloride and sulfonylation with *p*-tolylsulfonyl chloride (tosyl chloride). Dried toluene, anisole, thiophene and furan were used as aromatic substrates. The reaction mixture was refluxed in the presence of heteropolyacid or mononuclear complex. After refluxing, the cata-

TABLE 1. ACYLATION AND SULFONYLATION REACTIONS CATALYZED BY HETEROPOLYACIDS

Heteropolyacid	Reactant A (mol)	Reactant B (mol)	Amount of catalyst (10^{-5} mol)	Reflux time (h)	Products	Turn-over number per hour
$H_4[SiMo_{12}O_{40}]$	Toluene	Tosyl chloride				
	(0.24)	(0.01)	2.75	20	23% DTS	4
	(0.91)	(0.026)	5.49	19	13% DTS	3
	Anisole	Tosyl chloride				
	(0.23)	(0.026)	5.49	23	14% MMXDPS	3
	(0.23)	(0.026)	5.49	22	11% MMXDPS	2
	Anisole	Acetyl chloride				
	(0.23)	(0.1)	5.49	20	19% MXAP	17
	(0.23)	(0.1)	5.49	24	17% MXAP	13
	Thiophene	Acetyl chloride				
	(0.06)	(0.1)	5.49	30	44% AT	16
	(0.06)	(0.1)	5.49	17	36% AT	23
$H_3[PMo_{12}O_{40}]$	Toluene	Tosyl chloride				
	(0.094)	(0.01)	2.74	18	27% DTS	5
	(0.141)	(0.01)	2.74	19	37% DTS	7
	Anisole	Tosyl chloride				
	(0.14)	(0.01)	2.74	18	29% MMXDPS	6
	(0.14)	(0.01)	2.74	18	21% MMXDPS	4
	Anisole	Acetyl chloride				
	(0.093)	(0.056)	2.74	20	15% MXAP	15
	(0.14)	(0.056)	2.74	20	19% MXAP	19
	Thiophene	Acetyl chloride				
	(0.038)	(0.07)	2.74	17.5	22% AT	17
	(0.05)	(0.056)	2.74	5	6% AT	22
$H_4[SiW_{12}O_{40}]$	Toluene	Tosyl chloride				
	(0.094)	(0.01)	1.74	20.5	38% DTS	11
	(0.141)	(0.01)	1.74	19	48% DTS	15
	Anisole	Tosyl chloride				
	(0.14)	(0.01)	1.74	21	36% MMXDPS	10
	(0.14)	(0.01)	1.74	21	26% MMXDPS	8
	Anisole	Acetyl chloride				
	(0.23)	(0.1)	3.47	18	16% MXAP	26
	(0.14)	(0.056)	1.91	17	18% MXAP	31
	Thiophene	Acetyl chloride				
	(0.063)	(0.1)	3.47	3	6% AT	36
	(0.05)	(0.056)	1.74	5	5% AT	32

Abbreviation; DTS: 4,4'-di-*p*-tolyl sulfone, MMXDPS: 4-methyl-4'-methoxydiphenyl sulfone, MXAP: 4-methoxyacetophenone, AT: 2-acetylthiophene.

lyst was removed by filtration and acylated products were isolated by distillation under reduced pressure and sulfonylated products by recrystallization from ethanol.[4] They were identified by IR, ^{1}H-NMR and their melting points.

Three heteropolyacids showed effective activity, but the mononuclear complexes showed hardly any. The acylated compounds were obtained from anisole and thiophene, not from toluene and furan, and the sulfonylated compounds from toluene and anisole, not from thiophene and furan. Products were para-substituted for six-membered ring and oriented to 2-position for five-membered ring.

Reaction conditions, yields and turn-over numbers per hour are given in Table 1. The turn-over number per hour, conveniently estimated by a molar ratio of the amount of catalyst used and that of the product obtained per hour, is interpreted not only as a diagnostic parameter of whether the reaction proceeds catalytically or stoichiometrically, but also as a criterion for efficiency of the catalyst. The results are summarized as follows. (1) All the reactions are catalyzed by each heteropolyacid. (2) Acylation proceeds more easily than sulfonylation. (3) The reactions are largely influenced by the kind of metal constituting the Keggin unit, rather than the kind of hetero atom. (4) Of constitutional metals, tungsten, rather than molybdenum, is effective in the reactions; this aspect is contrary to the case of alkylation of toluene with benzyl chloride.[3]

Since the Keggin formula is designated by twelve sexivalent metals, forty bivalent oxygens and one hetero atom, the number of protons as counter ion is determined by the charge of hetero atom, *e.g.*, four for Si, three for P and As. Thus the difference in the number of protons between $H_4[SiMo_{12}O_{40}]$ and $H_3[PMo_{12}O_{40}]$ is not important in the catalysis.

References

1) K. Nomiya, T. Ueno, and M. Miwa, *Bull. Chem. Soc. Jpn.*, **53**, 827 (1980).
2) K. Nomiya, Y. Sugaya, S. Sasa, and M. Miwa, *Bull. Chem. Soc. Jpn.*, **53**, 2089 (1980); *Chem. Lett.*, **1980**, 1075.
3) K. Nomiya, H. Saijoh, and M. Miwa, *Bull. Chem. Soc. Jpn.*, **53**, (1980) in press.
4) J. F. White and M. F. Farona, *J. Organomet. Chem.*, **63**, 329 (1973).

 © 1980 The Chemical Society of Japan Bull. Chem. Soc. Jpn., 53, 3391—3394 (1980)

The Acidity and Basicity of Bi_2O_3-based Binary Oxides

Mamoru Ai

Research Laboratory of Resources Utilization, Tokyo Institute of Technology, 4259 Nagatsuta, Midori-ku, Yokohama 227

(Received January 26, 1980)

The numbers of both acidic and basic sites in a series of Bi_2O_3–X_nO_m binary oxides, with different kinds and amounts of the second component, X_nO_m, were systematically determined by means of the adsorption of NH_3 and CO_2 from the gas phase, using the static method. Pure Bi_2O_3 has both acidic and basic sites, much like TiO_2, SnO_2, and Fe_2O_3, and it is more basic than these oxides. The generation of an unexpectedly high acidity or basicity was not observed in the combination of Bi_2O_3 with 11 kinds of oxides, and the acid-base properties of the binary oxides can be understood in terms of the nature of the second component. The order of ability for the promotion of the acidity and the diminution of the basicity is: MoO_3, SO_3, $WO_3 > V_2O_5$, $P_2O_5 > Sb_2O_4 > TiO_2$, SnO_2, Fe_2O_3. The addition of K_2O decreases the acidity and increases the basicity. The relationship between the acid-base properties and the catalytic activities for the isomerization of 1-butene, the dehydration and dehydrogenation of 2-propanol, and the oxidative decomposition of formic acid was investigated. It was proposed that the basic sites of the Bi_2O_3-based mixed oxides originate from Bi_2O_3 and that the nature remains approximately the same, regardless of any change in the kind and amount of the second component. However, the acidic sites are generated by the combination with second component; therefore, the nature varies widely depending on the nature of the second component.

Recently, it has been proposed that acid-base-type interaction between the catalyst surface and the organic substance to be oxidized plays the determining role in mild oxidation, and that the combination of metal oxides contributes to a modification of the acid-base properties.[1-3] On this basis, it is of decisive importance to know the acid-base properties of the oxidation catalysts. However, there have been very few reports dealing with the acid-base properties of mixed transition-metal oxides.

The purpose of the present study is to determine systematically the acid-base properties of the Bi_2O_3–X_nO_m (where X_nO_m consists of different kinds and amounts of oxides) binary system and to demonstrate how the incorporation of foreign oxides into Bi_2O_3 modifies the acid-base properties.

Experimental

Catalysts. The catalysts used in this study were a series of Bi_2O_3–X_nO_m with different X/Bi ratios (X/Bi= 0—1.0), where X_nO_m refers to 11 different kinds. They were prepared as follows. The required quantities of bismuth nitrate were dissolved in concentrated nitric acid, and to this was added an aqueous solution or a slurry of the second metallic component; thereafter, 10- to 20-mesh pumice (surface area$<$0.3 m^2/g) originating from volcanic rocks was mixed with the solution, and the mixture was evaporated with vigorous stirring. The amount of pumice was 500 ml in a stream of oxygen at 500 °C for 4 to 5 h. As the starting materials, the following compounds were used: nitrate for Fe; ammonium salts of oxy acids for V, Mo, and W; chlorides (converted to hydroxides by dilute ammonia) for Ti and Sn; hydrate for K; H_2SO_4 for S; H_3PO_4 for P; and Sb powder (converted to oxide by concentrated nitric acid) for Sb. The surface areas were measured by the BET method using nitrogen at −196 °C.

Acidity and Basicity Measurements. Since the Bi_2O_3-based oxides are colored, the determination of the acidity and basicity by an ordinary titration method[4] seems to be difficult; therefore, it was attempted to measure the acidity and basicity by means of the adsorption of the basic and acidic molecules respectively from the gas phase, using the static method.[5-7] NH_3 and CO_2 were chosen as the adsorbates. The amount of adsorption at a pressure of 300 mmHg was measured volumetrically using an ordinary BET apparatus. Subsequently, the catalyst was pumped out for 30 min at the same temperature. Then, similar adsorption procedures were repeated and the amount of readsorption was measured. The amount of irreversible adsorption was obtained as the difference between the amount of readsorption and that of the first adsorption. This was adopted as the measure of the acidity and basicity. The details of the procedures were the same as those described in the previous papers.[5-7]

Catalytic Activity Measurements. The dehydration and dehydrogenation of 2-propanol (IPA), the isomerization of 1-butene, and the oxidative decomposition of formic acid were carried out in an ordinary continuous-flow system. The reactor was a steel tube, 50 cm in length and 1.8 cm in internal diameter. It was immersed in a lead bath, the temperature of which was controlled within ±1 °C. The concentrations of 2-propanol, 1-butene, and formic acid were 1.65, 0.67, and 1.2 mol% in air respectively. The total flow rate was kept constant at 1.5 l/min (at 25 °C), and the amount of catalyst used weighed 1 to 20 g. The details of the experimental procedures were the same as those employed in the previous works.[5-7]

Results

Acidity. The acidity (number of acidic site) per unit of the surface area of the Bi_2O_3–X_nO_m catalysts, as determined by the amount of NH_3 irreversibly adsorbed at 200 °C, is plotted as a function of the X_nO_m content in Figs. 1 and 2.

The acidity of pure Bi_2O_3 is relatively low. The acidity increases markedly upon the incorporation of acidic compounds. The order of this promoting ability is found to be: $SO_3 > MoO_3 > WO_3 > P_2O_5 > V_2O_5 > Sb_2O_4$. The abilities of amphoteric oxides such as SnO_2, TiO_2, Al_2O_3, and Fe_2O_3 are less prominent. The acidic sites are extinguished by the addition of a small amount of K_2O.

Basicity. The basicity (number of basic site) per unit of the surface area of the Bi_2O_3–X_nO_m catalysts, as

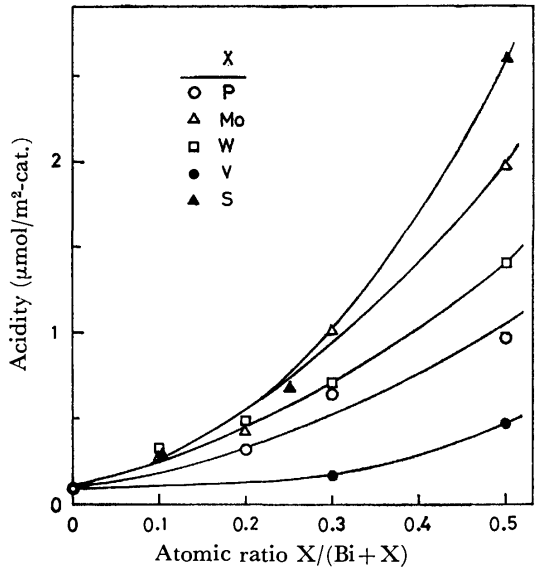

Fig. 1. Acidity of Bi_2O_3–X_nO_m (I).

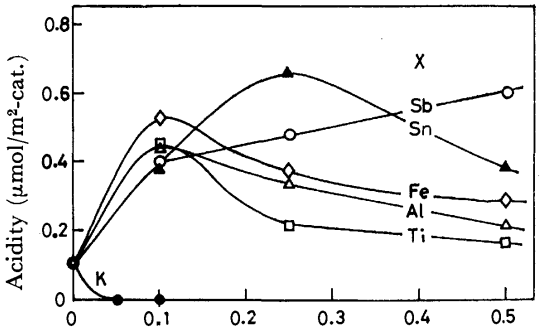

Fig. 2. Acidity of Bi_2O_3–X_nO_m (II).

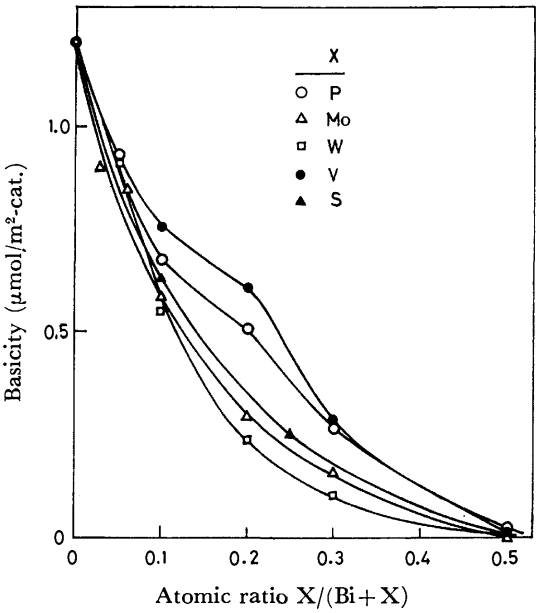

Fig. 3. Basicity of Bi_2O_3–X_nO_m (I).

determined by the amount of CO_2 irreversibly adsorbed at 25 °C, is plotted in Figs. 3 and 4.

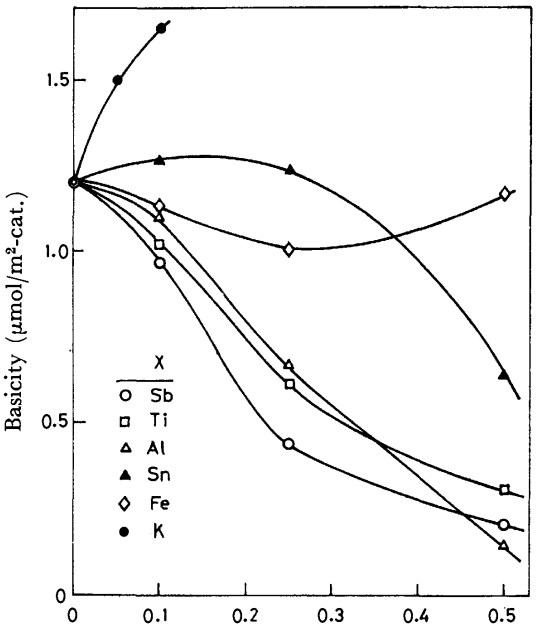

Fig. 4. Basicity of Bi_2O_3–X_nO_m (II).

Bi_2O_3 by itself is fairly basic. The basicity decreases upon the addition of more acidic compounds. The ability to diminish basicity is found to be in this order: $WO_3 > MoO_3 > SO_3 > V_2O_5 = P_2O_5 > Sb_2O_4 > TiO_2 = Al_2O_3 > SnO_2$. The ability of Fe_2O_3 is small, and the addition of K_2O increases the basicity.

Correlation between Acidity and Catalytic Activity. In order to confirm the validity of the acidity data, their correlation with the catalytic activity for certain acid-catalyzed reactions was checked. The dehydration of 2-propanol to propylene and the isomerization of 1-butene to 2-butenes were chosen as the model reactions, since it has been shown with various kinds of mixed metal oxides that the catalytic activity for the two reactions, as measured in a continuous-flow experiment in an atmosphere of air, can be tied with the acidity.[1,5-8]

Dehydration Activity for 2-Propanol: A gaseous mixture of 2-propanol and air was passed through a bed of the catalyst under the above-mentioned conditions. The main products were propylene and acetone, and the amounts of the other products were negligibly small. The rate of dehydration at 242 °C, r_p (mole per hour m^2 of catalyst), was measured for certain binary systems with relatively high acidities. Following the principle of the differential reactor, the conversion was held at a slow level, *i.e.*, usually below 10%.

The results are plotted in Fig. 5 as a function of the acidity of the catalysts. It is found that, so long as the second component, X_nO_m, is the same, the values of r_p vary in the same direction as the acidity.

Isomerization Activity for Butene: The activity for the isomerization of 1-butene to 2-butenes under the circumstances of the oxidation reaction at 473 °C, r_i (mole per hour m^2 of catalyst), was studied for certain binary systems with relatively high acidities.[1,6-8]

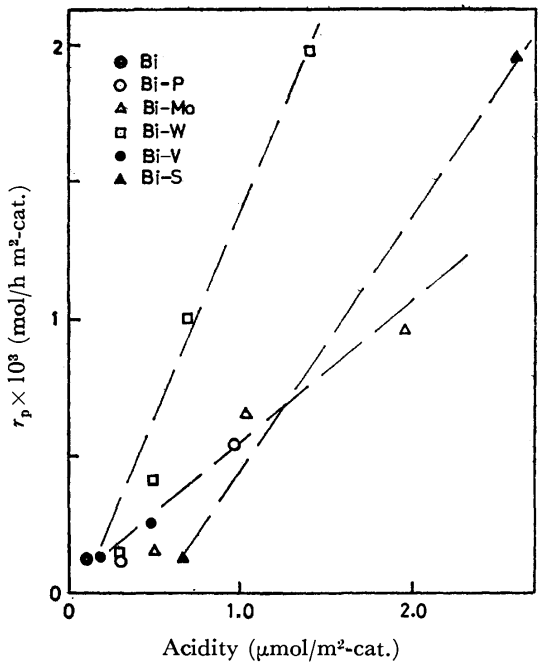

Fig. 5. Relation between the dehydration activity for 2-propanol at 242 °C (r_p) and the acidity of catalyst.

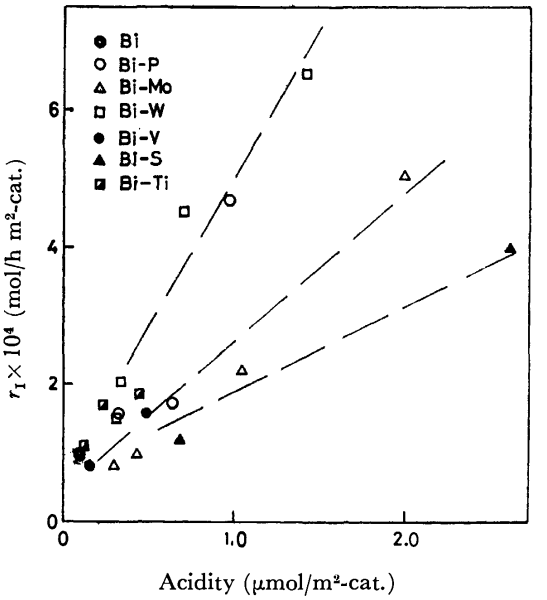

Fig. 6. Relation between the isomerization activity for 1-butene at 473 °C (r_I) and the acidity of catalyst.

It is plotted in Fig. 6 as a function of the acidity of the catalysts. Much as with the dehydration activity for 2-propanol, the isomerization activity changes in the same direction as the acidity, so long as the second component, X_nO_m, is the same.

Correlation between Basicity and Catalytic Activity. Next, the basicity data were confirmed by studying the correlation with the catalytic activity for certain base-catalyzed reactions. It has been shown that the catalytic activity for the oxidative decomposition of formic acid to CO_2[8] and the r_a/r_p ratio, where r_p and r_a are the initial rates of 2-propanol dehydration and dehydrogenation respectively,[1,6,9] are effective as measures of the basicity of the oxidation catalysts.

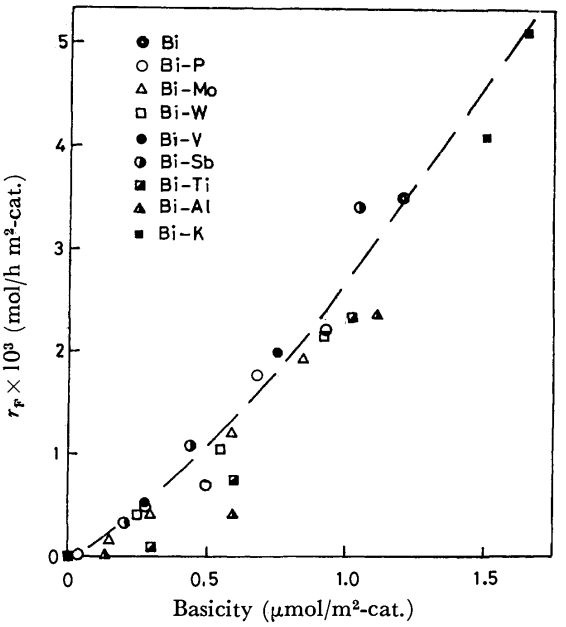

Fig. 7. Relation between the activity for oxidative decomposition of formic acid to CO_2 155 °C (r_F) and the basicity of catalyst.

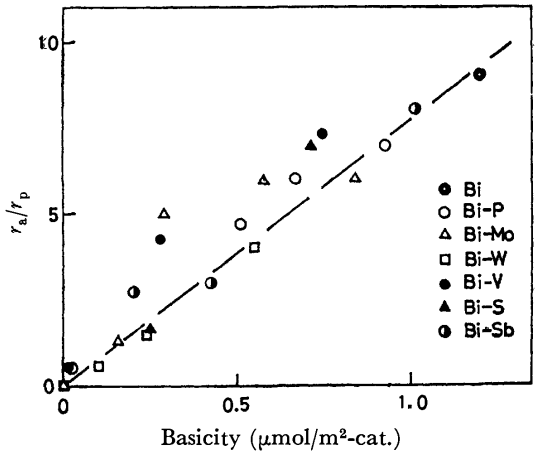

Fig. 8. Relation between the r_a/r_p ration and the basicity of catalyst.

Oxidative Decomposition of Formic Acid: As has been mentioned in a previous paper,[8] the reaction products were CO_2 and H_2O, and the amounts of CO and H_2 were negligibly small. The rate of CO_2 formation at 115 °C, r_F (mole per hour m^2 of catalyst), was measured for each catalyst. It is plotted in Fig. 7 as a function of the basicity of the catalysts. A very good correlation is observed between the activity and the basicity.

(Dehydrogenation Activity)/(Dehydration Activity) Ratio in the Reaction of 2-Propanol: The r_a/r_p ratio is plotted in Fig. 8 as a function of the basicity. A relatively good correlation is obtained between the r_a/r_p ratio and the basicity.

Discussion

It was found that Bi_2O_3 by itself has both acidic and

basic sites, much like TiO_2, SnO_2, and Fe_2O_3, and that Bi_2O_3 is more basic than the latter oxides; this is in conformity with the earlier results.[6,7,9-11] It was also demonstrated in a direct way that the Bi_2O_3-based mixed oxides are, more or less, acid-base bifunctional and that the generation of an unexpectedly high acidity or basicity, which often occurs in combination of metal oxides, was not observed. Therefore, the acid-base properties can be understood relatively easily in terms of the nature of the second components, X_nO_m.[1,2,9] The more acidic the second component, the more acidic and the less basic become the binary oxides. The order of the ability to promote acidity and diminish basicity is found to be: MoO_3, SO_3, $WO_3 > V_2O_5$, $P_2O_5 > Sb_2O_4 > TiO_2$, SnO_2, Fe_2O_3. The effect of the amphoteric oxides, such as TiO_2, SnO_2, Fe_2O_3, and Al_2O_3, is less prominent. Contrary to the acidic compounds, the addition of K_2O decreases the acidity and increases the basicity. In the case of oxidation catalysts, the valence of metal is varied by the combination of oxides, so it seems difficult to predict the acidity generation basing on the hypothesis proposed by Tanabe *et al.*[12]

We would like to propose the following view. When Bi_2O_3 is combined with a more acidic oxide, the basic sites of the mixed oxides originate from Bi_2O_3 and some of the basic sites are extinguished by the combination of the acidic compound, as can be reasonably expected in the case of a liquid acid-base. Accordingly, the natures of the basic sites remain approximately the same, regardless of the changes in kind and amount of the second component, X_nO_m. This may be the main reason why the plots of the activity for base-catalyzed reactions against the basicity give a straight line extraporated through the point of origin.

On the other hand, the acidic sites of the binary oxides do not originate from Bi_2O_3 but are generated by the combination with second components. Consequently, the natures of the acidic sites vary widely depending on the nature of the second components, X_nO_m. This may be the reason why the correlation between the catalytic activity and the acidity is obtained only when the second component is of the same kind.

References

1) M. Ai, *Yuki Gosei Kagaku Kyokai Shi*, **35**, 201 (1977).
2) M. Ai, *Shokubai*, **20**, 292 (1978).
3) M. Ai, *Shokubai*, **21**, 316 (1979).
4) K. Tanabe, "Solid Acids and Bases," Kodansha, Tokyo, and Academic Press, New York (1970).
5) M. Ai and T. Ikawa, *J. Catal.*, **40**, 203 (1975).
6) M. Ai, *J. Catal.*, **40**, 318 (1975).
7) M. Ai, *Bull. Chem. Soc. Jpn.*, **49**, 1328 (1976).
8) M. Ai, *J. Catal.*, **50**, 291 (1977).
9) M. Ai and S. Suzuki, *Shokubai*, **15**, 159 (1973).
10) M. Ai, *J. Catal.*, **52**, 16 (1978).
11) M. Ai, *J. Catal.*, **60**, 306 (1979).
12) K. Tanabe, "Kinzoku-sankabutsue To Sono Shokubai-sayo," Kodansha, Tokyo (1978), p. 407.

Structure Determination of the 1,4-Cycloadduct Quenched after the High-pressure Reaction of Tetracyanoethylene with Styrene and Its Derivatives

Masaru NAKAHARA,* Yasuhiro UOSAKI, Muneo SASAKI, and Jiro OSUGI

Department of Chemistry, Faculty of Science, Kyoto University, Oiwake-cho, Kitashirakawa, Sakyo-ku, Kyoto 606

(Received February 4, 1980)

The electronic, ^{13}C NMR, ^{1}H NMR, and IR spectra of the 1,4-cycloadducts of TCNE with styrene, styrene-α-d_1, *p*-chlorostyrene, *p*-methylstyrene, α-methylstyrene, and 1,1-diphenylethylene were taken at low temperatures at 1 bar after the high-pressure reaction; the ^{13}C NMR spectra were of decisive importance in determining the structure; the other kinds of spectra were consistent with the established structure. They have an electronic absorption band around 320 nm, which is assigned to the π-π^* transition of the triene system in the adducts. Neither *cis*- nor *trans*-stilbene, which have a lower ionization potential, provides the 1,4-cycloadduct even at high pressure.

Tetracyanoethylene (TCNE) is one of the strongest electron acceptors to give the EDA (electron-donor-acceptor) complexes with electron donors; it undergoes the 1,2-cycloaddition to electron-rich olefins and the 1,4-cycloaddition to dienes.[1-3] Styrene, which is composed of vinyl and phenyl groups conjugated together, has been considered to yield neither 1,2- nor 1,4-cycloadduct of TCNE under mild conditions,[4] while its derivatives with an electron-donating substituent at *para*-, α-, or β-position are known to afford the 1,2-cycloadducts.[4-7] Actually, a number of papers[8-11] have been published on the formation constant and molar absorption coefficient of the EDA complex between TCNE and styrene without noticing the coexistence of the 1,4-cycloadduct confirmed here.

The present authors found a strong piezochromism in the dichloromethane solution of TCNE and styrene, and showed that a new species having an absorption band around 320 nm was formed reversibly in the solution.[12] The concentration of the new species at atmospheric pressure is too low to provide its IR and NMR spectra, which are required for determining spectroscopically the molecular structure. But the concentration can be increased sufficiently by pressure and decomposition after pressure release can be prevented at a low temperature well below 0 °C. The striking influences of high pressure and low temperature on the unstable species fortunately allows the molecular structure to be clarified unambiguously from the ^{13}C NMR and other spectra.

Experimental

Materials. Styrene and α-methylstyrene were purified by the usual method and distilled immediately before use. Styrene-α-d_1 (98% D atom, Merck Sharp and Dohme Canada Ltd.) and commercial *p*-chlorostyrene (guranteed reagent grade, Nakarai Chemicals Co., Ltd.) were used without further purification. *p*-Methylstyrene and 1,1-diphenylethylene were synthesized according to the methods in the literature[13,14] and purified by repeated distillation at reduced pressure. *trans*-Stilbene was recrystallized twice from ethanol and *cis*-stilbene was distilled at reduced pressure before use. TCNE was sublimed three times or more *in vacuo* at 50—60 °C. Dichloromethane was purified by the usual method and distilled before use. Dichloromethane-d_2 (99.3% D atom) was supplied by CEA (France).

Apparatus and Procedure. Electronic absorption spectra were recorded on a Shimadzu UV-200S spectrophotometer at 1 bar (1 bar = 10^5 Pa) and on a Union RA-405 spectrophotometer at high pressure. IR, ^{1}H NMR, and ^{13}C NMR spectra at 1 bar were measured with JASCO DS-402G, JEOL JNNM-PS-100, and JEOL FX-100 spectrometers, respectively. A high-pressure optical cell[15] with two sapphire windows of 1-cm thickness was used to measure electronic spectra at high pressure. Pressure was measured with a calibrated manganin-coil gage which was put in a flexible teflon capsule filled with silicone oil. The small teflon capsule was fixed on a plug inside the high-pressure optical cell. Thermostatted water was circulated around the cell to keep the temperature at 25±0.1 °C.

Sample solutions of the reaction mixtures of TCNE with styrene and its derivatives were prepared for the spectroscopic investigation in a special way as follows. Styrene or its derivatives were put together with TCNE in a flexible teflon capsule containing (deuterated) dichloromethane (≈1.6 cm^3). The amount of TCNE which was mixed was 2 or 3 times as much as the solubility (<0.1 mol dm^{-3}) in the solvent at room temperature at 1 bar, because pressure markedly enhanced its conversion into the adduct. The capsule was sealed with a teflon plug and a rubber O-ring, and placed in a usual piston-cylinder device having a jacket for thermal control. A pressure of ≈8 kbar was applied to the capsule for several hours at room temperature using silicone oil as a pressure-transmitting fluid, and ice-cold water was circulated through the jacket for an hour. As soon as pressure was released at 0 °C, the cold capsule was taken out from the piston-cylinder device and immersed in liquid N_2 to stock the quenched sample for a long time. Just before a spectroscopic study, the solid solution was melted again at about −95 °C and transferred by a previously chilled syringe to a cell. Cells for electronic and IR spectra were cooled at around 0 °C during the course of the measurements, while NMR glass tubes 10 mm in diameter were kept at −50 °C by circulating cold N_2 vapor around the tubes.

Results and Discussion

Electronic Spectra. On mixing the dichloromethane solutions of styrene and TCNE, a red color appears instantaneously because the EDA-complex formation is a diffusion-controlled reaction. Figure 1 shows the time dependence of the absorption spectrum of the reaction mixture at 1 bar. The absorption peaks at 396 and 480 nm are due to the EDA complex between styrene and TCNE; styrene and TCNE have no absorp-

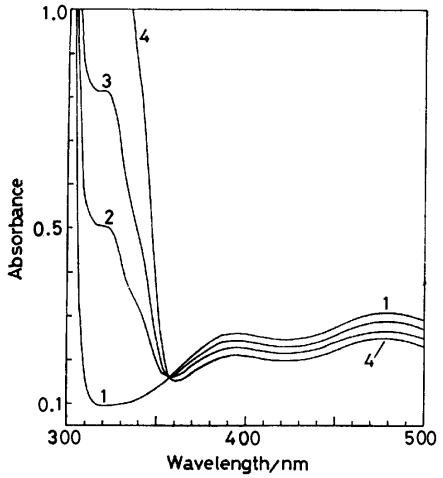

Fig. 1. Time dependence of the electronic spectra of TCNE–styrene mixture in CH_2Cl_2 at room temperature at 1 bar. Concentration (mol dm^{-3}): TCNE, 1.5×10^{-3}; styrene, 0.5. 1, 30 s after mixing; 2, 18.5 min; 3, 47.5 min; 4, 14 h.

tions in the visible region. The absorption of the EDA complex decreases slowly with time, while a new band develops around 320 nm. The absorption spectrum reaches a stationary state after a long time, leaving an isosbestic point at 357 nm. These facts suggest that a new species assigned to the 320-nm band (confirmed later as the 1,4-cycloadduct) is in equilibrium with the EDA complex as

$$D + A \underset{}{\overset{K_1}{\rightleftharpoons}} C \overset{K_2}{\rightleftharpoons} P, \qquad (1)$$

where D, A, C, and P are the donor (styrene), acceptor (TCNE), EDA complex, and new species, respectively, and K_1 and K_2 are equilibrium constants.

Although we could not measure at 1 bar the electronic, IR, and NMR spectra dominated by the new species P, a large pressure effect on the formation equilibrium (K_2) of P was found. The spectra A, B, C, D, and E (except B′) in Fig. 2 were taken at each pressure after they changed no more with time. The decrease with pressure in the absorption of the EDA complex is tremendous, especially at 8 kbar. If only a single equilibrium K_1 were involved in the solution as assumed

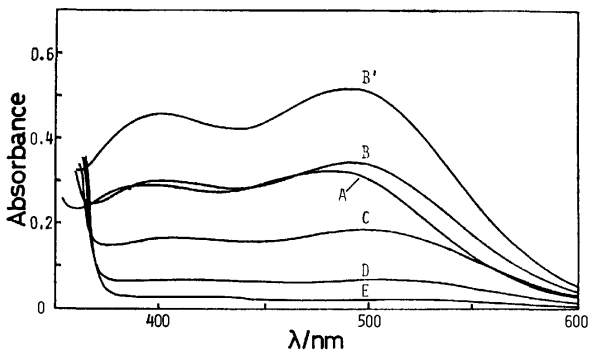

Fig. 2. Effect of pressure on the charge-transfer band of TCNE–styrene mixture in CH_2Cl_2 at 25 °C. Concentration (mol dm^{-3}): TCNE, 6.5×10^{-3}; styrene, 0.26. Path length, 5 mm. A, 1 bar; B and B′ (see the text), 2 kbar; C, 4 kbar; D, 6 kbar; E, 8 kbar.

elsewhere,[8–11] the absorbance would increase with pressure owing to the increase with pressure in the molar absorption coefficient and in the concentration of the EDA complex.[16,17] As a matter of fact, the trend exists transiently in Fig. 2; at 2 kbar, the initial absorbance B′ is larger than the equilibrium one B. The difference indicates that the EDA complex is slowly converted into the new species. The backward reaction from the new species to the complex is also slow, above all at 1 bar, so that the new species can be quenched in the solution.

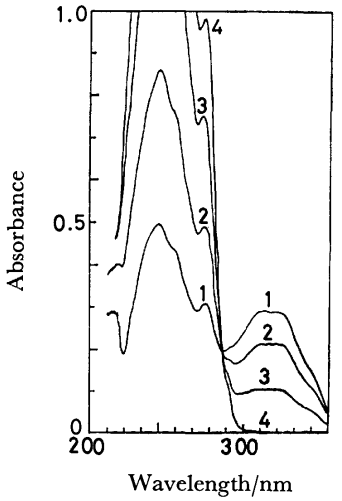

Fig. 3. UV spectra of the decomposing TCNE–styrene adduct in CH_2Cl_2 at room temperature at 1 bar. 1, 10 s after the quenched solution was diluted; 2, 10 min; 3, 30 min; 4, 16 h.

The UV spectra in Fig. 3 are taken at 1 bar after diluting the quenched reaction mixture. The well resolved spectrum of the new species is seen above the isosbestic point at 288 nm; it has a broad maximum between 310 and 325 nm with a shoulder at the longer wavelength. The spectrum below the isosbestic point corresponds to the parent molecules; when we denote the molar absorption coefficient of X at the wavelength λ by $\varepsilon_\lambda(X)$, ε_{250}(styrene) and ε_{250}(TCNE) are, respectively, 1.48×10^4 and 1.10×10^4 cm^{-1} mol^{-1} dm^3 and ε_{278}(TCNE) and ε_{278}(styrene) are, respectively, 1.26×10^4 and 1.2×10^2 cm^{-1} mol^{-1} dm^3. Thus, the variation with time of the absorbances in Fig. 3 discloses that the new species is an adduct between styrene and TCNE. The adduct is composed of an equal number of the parent molecules, because the quantity

$$\frac{A^2_{250}-A^1_{250}}{\varepsilon_{250}(\text{styrene})+\varepsilon_{250}(\text{TCNE})} = 1.36\times10^{-5} \qquad (2)$$

agrees well with

$$\frac{A^2_{278}-A^1_{278}}{\varepsilon_{278}(\text{styrene})+\varepsilon_{278}(\text{TCNE})} = 1.40\times10^{-5}, \qquad (3)$$

where A^1 and A^2 are the absorbances of spectra 1 and 2, respectively. In the dilute solution, the EDA complex is negligible. Hence, if the adduct has the stoichiometry expressed by reaction 1, ε of the adduct at 320 nm is given by the equation:

$$\frac{A^1_{320}-A^i_{320}}{A^i_\lambda-A^1_\lambda}\{\varepsilon_\lambda(\text{styrene})+\varepsilon_\lambda(\text{TCNE})\}=(5.5\pm0.1)\times10^3, \quad (4)$$

where λ=250 and 278 nm and i=2, 3, and 4. Adducts of the same type are found for the substituted styrenes except for the stilbenes, as shown in Table 1. It is unknown at present why neither *cis*- nor *trans*-stilbene provides the adduct under the same condition despite the fact that the ionization potentials are lower than those of the other electron donors.[18]

Table 1. Electronic absorptions of EDA complexes and adducts formed by the reaction of TCNE with styrene and its derivatives in CH_2Cl_2 at 25 °C

Donor	EDA complex λ_{max}/nm	Adduct[a] λ_{max}/nm
Styrene	480±1, 396±1	320±3
p-Chlorostyrene	483±1, 362±1	318±3
p-Methylstyrene	525±1, 401±1	317±3
α-Methylstyrene	495±1, 399±1	325±3
1,1-Diphenylethylene	507±1, ≈400	329±3
trans-Stilbene	597±1, ≈390	—[b]
cis-Stilbene	528±1, 389±1	—[b]

a) Obtained by diluting reaction mixtures quenched after pressurization. b) Adducts are not formed.

^{13}C and ^1H NMR spectra. The ^{13}C NMR spectra of the quenched reaction mixtures of TCNE with styrene, styrene-α-d_1, and *p*-chlorostyrene are of great use in proving that the adduct is really composed of one molecule of styrene and one molecule of TCNE, as in reaction 1, and in deciding how the donor molecule is combined with the acceptor. The ^{13}C NMR spectrum of the 1,4-cycloadduct is anticipated to give fourteen separate signals for the nonequivalent carbons. As a matter of fact, fourteen separate signals are found for the adduct, besides those for the parent molecules (Fig. 4), and the peaks in Fig. 4 are assigned to the carbon atoms numbered in the structural formula for the 1,4-cycloadduct, as summarized in Table 2.[19] The

Table 2. Assignment of the ^{13}C NMR peaks of the 1,4-cycloadducts[a]

Carbon No. (C-X)	Styrene adduct	Styrene-α-d_1 adduct	*p*-Chloro-styrene adduct
X=1	131.47	131.27	133.52
2[b]	128.54	128.50	129.17
3[b]	126.94	126.84	126.25
4[b]	124.21	124.11	127.96
5	119.82	119.77	120.75
7	118.31	118.2	115.24
6	43.02	42.93	43.85
10	41.12	41.07	41.03
9	39.03	38.98	38.69
8	32.60	32.40	32.64

a) The 4 peaks between 111 and 108 ppm are due to the cyano carbons. b) The distinction among these is less reliable.

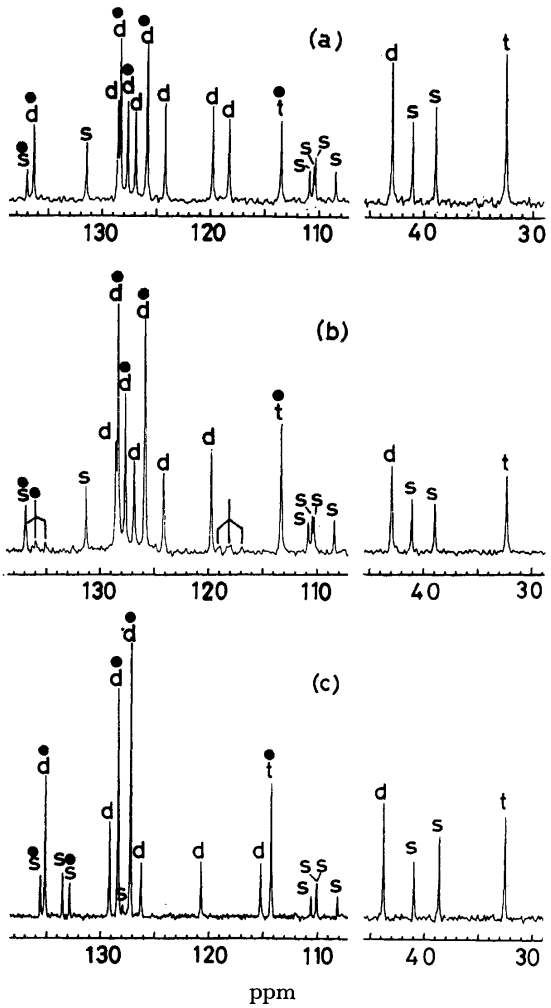

Fig. 4. ^{13}C NMR (complete decoupling) spectrum of the 1,4-cycloadduct in CD_2Cl_2 at −50 °C at 1 bar. (a), TCNE+styrene; (b), TCNE+styrene-α-d_1; (c), TCNE+*p*-chlorostyrene. Symbols s, d, and t denote singlet, doublet, and triplet in off-resonance decoupling, respectively. ●, Due to free styrene or its derivatives. The solubility of TCNE at the low temperature is too low to give signals. Chemical shifts are relative to the TMS reference.

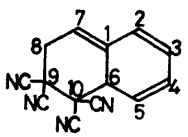

deuteration experiment elegantly reveals that the α-carbon in styrene remains in the sp^2 state in the adduct. This is compatible with the conjugated triene system in the 1,4-cycloadduct. Although it is reported that two acceptor (maleic anhydride) molecules combine with one styrene molecule after the reaction in benzene at 80 °C,[20] such a kind of cycloadduct has not been recognized in the present system. Actually, there is no other possibility than the present one that is consistent with the number, multiplicity, and position of the peaks found in the ^{13}C NMR spectra.

All the information from the ^1H NMR spectra[19] of

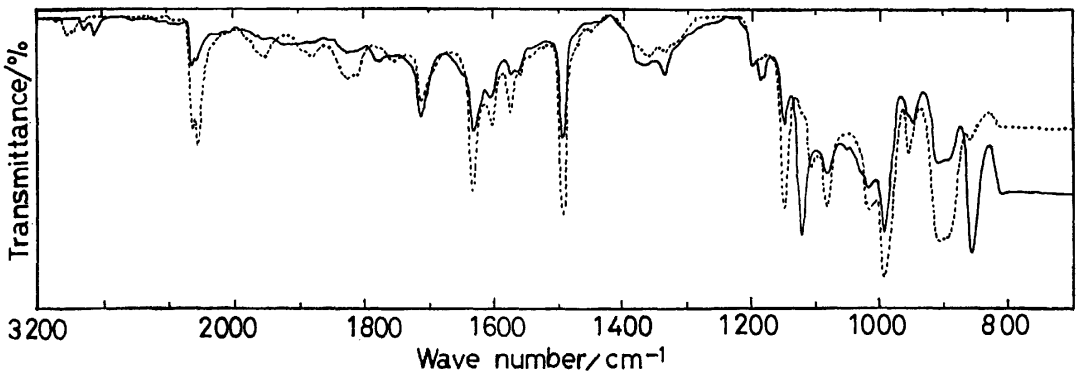

Fig. 5. IR spectra of TCNE–styrene mixture in CH_2Cl_2 around 0 °C at 1 bar.
——, Dominated by the adduct; ----, after the adduct being decomposed.

the quenched reaction mixtures of TCNE with styrene, styrene-α-d_1, and *p*-chlorostyrene is consistent with the conclusion reached above. There are three peaks, at 3.2—3.4, 4.4—4.6, and 5.5—5.7 ppm (internal TMS reference), whose peak ratio is 2 : 1 : 1; they are assigned to H_2C-8, HC-6, and HC-7, respectively. The facts that the styrene-α-d_1 adduct loses the peak at 5.5—5.7 ppm and that the *p*-chlorostyrene adduct does not lose the peaks at 3.2—3.4 and 4.4—4.6 ppm support the 1,4-cycloadduct. The complicated peaks in the range of 5.8 to 6.3 ppm are due to the protons involved in the conjugated triene system. Although a spin-decoupling experiment was attempted to reaffirm the above assignment, the low S/N ratio in the spectra due to the low concentration of the adduct made it difficult to see changes in the signal multiplicity.

IR Spectra. IR spectra tell us more about the molecular structure of the found adduct than do the electronic spectra. Vibrational spectra of the symmetric molecule TCNE have been well studied,[21-24] and the group frequencies related to the complicated molecule of styrene are available.[25,26] Figure 5 shows the IR spectra of the reaction mixture of styrene and TCNE, which is taken by using the quenching technique described in the experimental section. In the adduct, the bands at 2245 and 2220 cm^{-1} characteristic of the C≡N stretches in TCNE decrease in intensity, accompanied by a shift (≈15 cm^{-1}) to the higher frequencies. These changes indicate the loss of the conjugation of the double and triple bonds in TCNE; as a result, the C≡N bonds become stronger in the adduct than in TCNE. The C–C stretching vibrations at 1150 and 955 cm^{-1} in TCNE also decrease in intensity, and the corresponding bands in the adduct appear at the lower frequencies 1123 and 945 cm^{-1}, respectively. Thus, the loss of the conjugation makes also the C–C bonds weaker. The following bands of styrene decrease in intensity as reaction 1 proceeds; the vinylic C–H deformation bands at 990 and 890—910 cm^{-1}, the vinylic C–C stretching band at 1632 cm^{-1}, the aromatic C=C stretching bands at 1600, 1580, and 1500 cm^{-1}, and the combinations and overtones characteristic of the benzene ring[27] at 2000—1700 cm^{-1}. These spectral features of styrene show that both vinyl and phenyl groups are modified by the addition of TCNE; that is to say, the new species found is not the 1,2-cycloadduct. Thus, the IR spectral information supports the structure determination based on the ^{13}C NMR spectra.

Chromophore of the Band around 320 nm. It has been proved that the new species having the band around 320 nm is the 1,4-cycloadduct formed by the reaction of TCNE with styrene and its derivatives. The absorption band is attributed to the conjugated triene system rather than the C≡N group, because the 1,4-cycloadduct is predicted to have a band at 303 nm according to the additivity rule for the conjugated trienes.[28]

There is a short communication[29] which states that styrene derivatives benzylidenecyclopropane and (diphenylmethylene)cyclopropane having the exocyclic or strained double bond, 1,4-cycloadduct thermally to TCNE. In the latter case, the UV absorption at 333 nm with log ε=3.91 is comparable with the present results; moreover, the ^1H NMR signals agree well with those of the 1,4-cycloadduct confirmed here. In the former case, however, two strong peaks at 269 (log ε=4.23) and at 278 nm (log ε=4.21) are reported, although a bathochromic shift is anticipated because of the presence of the electron-donating three-membered ring.[28]

Recent studies on the thermal polymerization of styrene in bulk showed the existence of an absorption band with a maximum at 325 nm. This band is attributed to a Diels-Alder adduct of two styrene molecules, which is considered to be responsible for the initiation of the spontaneous polymerization.[30-32] The present thorough studies on the 1,4-cycloadduct between styrene and TCNE are in favor of the suggestion of the styrene adduct based on the UV spectrum.

References

1) D. N. Dhar, *Chem. Rev.*, **67**, 611 (1967).
2) E. M. Kosower, "Progress in Physical Organic Chemistry," ed by S. G. Cohen, A. Streitwieser, Jr., and R. W. Taft, Interscience Publishers, New York (1965), Vol. 3, p. 81.
3) R. Foster, "Organic Charge-Transfer Complexes," Academic Press, London (1969).
4) J. K. Williams, D. W. Wiley, and B. C. McKusick, *J. Am. Chem. Soc.*, **84**, 2210 (1962).
5) P. D. Bartlett, *Quart. Rev.*, **24**, 473 (1970).
6) S. Nishida, I. Moritani, and T. Teraji, *J. Org. Chem.*, **38**, 1878 (1973).

7) H. Yamaoka, Y. Yamada, S. Ono, and T. Hanafusa, *Chem. Lett.*, **1979**, 523.
8) A. R. Cooper, C. W. P. Crowne, and P. G. Farrell, *Trans. Faraday Soc.*, **62**, 18 (1966).
9) T. Arimoto and J. Osugi, *Chem. Lett.*, **1974**, 271.
10) B. Tonchéva, R. Vélichkova, and I. M. Panayotov, *Bull. Soc. Chim. Fr.*, **1974**, 1033.
11) K. Hayashi, P. A. Marchese, S. Munari, and S. Russo, *Chim. Ind. (Milan)*, **56**, 187 (1974).
12) M. Nakahara, Y. Tsuda, M. Sasaki, and J. Osugi, *Chem. Lett.*, **1976**, 731.
13) M. Sulzbache and E. Bergmann, *J. Org. Chem.*, **13**, 303 (1948).
14) C. F. H. Allen and S. Converse, *Org. Synth.*, Coll. Vol. 1, 226 (1941).
15) J. Osugi and Y. Kitamura, *Rev. Phys. Chem. Jpn.*, **35**, 25 (1965).
16) A. H. Ewald, *Trans. Faraday Soc.*, **64**, 733 (1968).
17) T. Nakayama and J. Osugi, *Rev. Phys. Chem. Jpn.*, **45**, 79 (1975).
18) J. P. Maier and D. W. Turner, *J. Chem. Soc., Faraday Trans. 2*, **69**, 196 (1975).
19) Readers who are interested in the detailed discussion on the assignment are referred to the previous note on the NMR spectra; M. Nakahara, Y. Uosaki, M. Sasaki, and J. Osugi, *Rev. Phys. Chem. Jpn.*, **47**, 119 (1977).
20) K. Alder and R. Schmitz-Josten, *Ann. Chem.*, **595**, 1 (1955); K. Alder and H. Niklas, *ibid.*, **585**, 97 (1954).
21) D. A. Long and W. O. George, *Spectrochim. Acta*, **19**, 1717 (1963).
22) T. Takenaka and S. Hayashi, *Bull. Chem. Soc. Jpn.*, **37**, 1216 (1964).
23) F. A. Miller, O. Sala, P. Devlin, J. Overend, E. Lippert, W. Lüder, H. Moser, and J. Varchmin, *Spectrochim. Acta*, **20**, 1233 (1964).
24) A. Rosenberg and J. P. Devlin, *Spectrochim. Acta*, **21**, 1613 (1965).
25) G. Hertzberg, "Infrared and Raman Spectra of Polyatomic Molecules," D. Van Nostrand Company, Inc., Toronto (1945).
26) S. Mizushima and T. Shimanouchi, "Sekigaisen Kyushu To Raman Koka (IR Absorption and Raman Effect)," Kyoritsu Shuppan, Tokyo (1955).
27) C. W. Young, R. E. Duyall, and N. Wright, *Anal. Chem.*, **23**, 709 (1951).
28) H. H. Jaffè and M. Orchin, "Theory and Applications of Ultraviolet Spectroscopy," John Wiley & Sons, Inc., New York (1962).
29) R. Noyori, N. Hayashi, and M. Kato, *J. Amer. Chem. Soc.*, **93**, 4948 (1971).
30) K. Buchholz and K. Kirchner, *Makromol. Chem.*, **177**, 935 (1976).
31) H. F. Kauffmann, O. F. Olaj, and J. W. Breitenbach, *Makromol. Chem.*, **177**, 939 (1976).
32) H. F. Kauffmann, *Makromol. Chem.*, **178**, 3007 (1977).

Kinetics of the Reactions of Ni(II) with Several Ligands in Water-*t*-Butyl Alcohol Mixtures

Tatsuo TAKAHASHI* and Takefumi KOISO
Department of Chemistry, Fukushima Technical College, Iwaki 970
(Received February 19, 1980)

The kinetics of the complex-formation reactions of Ni(II) with 4-phenylpyridine, isoquinoline, 2,2′-bipyridine, 1,10-phenanthroline, and 2,2′: 6′,2″-terpyridine in water–*t*-butyl alcohol mixtures were investigated by means of stopped-flow measurement. With an increase in the *t*-butyl alcohol content of mixtures for all ligands, the rate constants for the reactions decrease monotonically, while the activation parameters, $\Delta H_f^{\ddagger}$ and $\Delta S_f^{\ddagger}$, pass through distinct minimum values, and the minima occur at the same concentration of *t*-butyl alcohol. The results are briefly discussed in terms of the stability of the outer-sphere complex of Ni(II) with the ligands, and the structural properties of the solvents.

In an aqueous solution, the rate constants and activation parameters for the complex-formation reactions of many metal ions depend only slightly on the nature of ligand and are approximately equal to those quantities for the exchange of the water molecule from the first coordination sphere of metal ions. In such a case, the reaction is best represented by the Eigen dissociative mechanism (I_d), in which the rate-determining step of the reaction is the dissociation of a water molecule from the coordination sphere of the metal ions.[1,2] On the other hand, it was found that the kinetic parameters in certain nonaqueous solutions exhibit a marked ligand dependence, and some solvent properties influencing the kinetic behavior have been discussed.[3-6] Meanwhile, it may be expected that the change from a single-to a two-component solvent increases the number of factors influencing the kinetic behavior. In fact, a few studies[7-9] have revealed that the kinetic behavior of a mixed solvent depends on the composition of the inner-sphere of the metal ions, the steric requirement of the ligands, and the structures of the solvents.

As a part of an investigation aiming at identifying the mixed solvent properties influencing the kinetics, we wish to report here the results of the complex-formation reactions of Ni(II) with pyridine-type ligands in water–*t*-butyl alcohol mixtures.

Experimental

Materials. *t*-Butyl alcohol (Baker analyzed reagent) was purified by distillation from sodium metal (Baker) through a 25 mm ID × 1219 mm-long glass column packed with 6 mm OD × 6 mm-glass tubes. Ni(II) was introduced as the perchlorate. Ni(II) solutions were standardized by EDTA titration, using Murexide as the indicator. Isoquinoline (Eastman) was distilled alone under a vacuum in a Perkin Elmer Model 251 Auto Annular Still with a Teflon spinning band at a reflux ratio of 200 : 1, with a pot temperature of 126 °C and a head temperature of 62 °C. All the other chemicals used were of reagent quality.

Instrumentation and Experimental Procedure. The kinetic measurements were made with a Dionex Corporation (Sunnyvale, Calif.) Model D-110 stopped-flow spectrophotometer equipped with a Kel-F flow system, observing the precautions necessary for adequate temperature control (±0.5 °C). The reactions were monitored at wavelengths where the complexes and free ligands show the largest difference in absorptivity, *viz.*, 272—275 nm, 322—325 nm, 305—310 nm, 270—275 nm, and 334—338 nm for 4-phenylpyridine, isoquinoline, 2,2′-bipyridine, 1,10-phenanthroline, and 2,2′:6′,2″-terpyridine respectively. All the measurements were made under pseudo-first-order conditions with the total ligand concentration (C_L, after mixing) kept constant at 2.5×10^{-5} mol dm^{-3} for 2,2′-bipyridine and 2,2′:6′,2″-terpyridine, and 10^{-4} mol dm^{-3} for 1,10-phenanthroline, while the Ni(II) concentrations (C_{Ni}) were varied in the range from 1×10^{-3} to 5×10^{-3} mol dm^{-3}. In the cases of 4-phenylpyridine and isoquinoline, the complexes are relatively unstable, so that it was necessary to increase C_L to 2.1×10^{-4} mol dm^{-3}, and C_{Ni} to 0.8—2.4×10^{-2} mol dm^{-3} for isoquinoline, and C_L to 2.5×10^{-5} mol dm^{-3}, and C_{Ni} to 0.6—2.0×10^{-2} mol dm^{-3} for 4-phenylpyridine. The absorbancy measurements were made with a Shimadzu Model UV-200 double-beam recording spectrophotometer equipped with temperature control to ±0.5 °C.

Results and Discussion

The observed pseudo-first-order rate constant, k_{obsd}, is given by Eq. 1:[6]

$$k_{obsd} = k_f[Ni^{2+}] + k_d, \quad (1)$$

where k_f and k_d are the overall second-order and first-

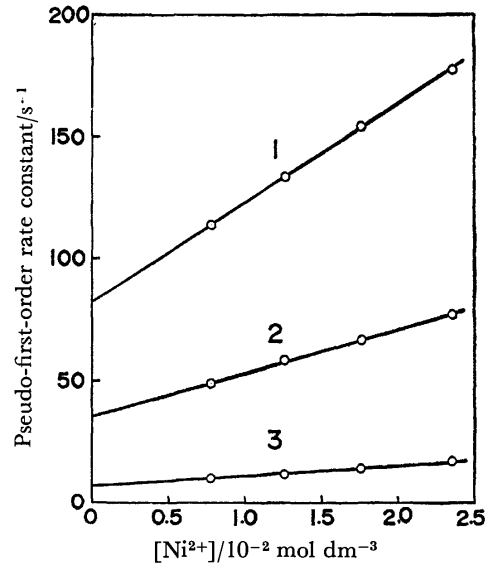

Fig. 1. Pseudo-first-order rate constants for the reaction of Ni(II) with 4-phenylpyridine in water.
Temperature (°C): (1) 35.0, (2) 25.0, (3) 10.0. Concn of 4-phenylpyridine: 2.5×10^{-5} mol dm^{-3}.

order rate constants for a complex-formation reaction and a dissociation reaction respectively. Equation 1 shows that a plot of k_{obsd} *vs.* $[Ni^{2+}]$ should be linear with a slope and an intercept equal to k_f and k_d. A typical result obtained in this study is shown in Fig. 1.

The rate constants at various temperatures for the reactions of Ni(II) with pyridine-type ligands studied in water–*t*-butyl alcohol mixtures are listed in Table 1. In Table 2, the rate constants at 25.0 °C and the activation parameters for the ligands are given for each solvent. The changes in the activation parameters with the solvent composition are shown in Figs. 2 and 3. These are the values of ΔH_f^*, $-T\Delta S_f^*$, and ΔG_f^* relative to pure water. Figures 2 and 3 show that the minima in ΔH_f^* and ΔS_f^* for all ligands occur at the same concentration of *t*-butyl alcohol, and that the rate constants decrease with a substantial compensation of the changes in ΔH_f^* by those in $-T\Delta S_f^*$ over the whole range of solvent compositions studied. Analogous extrema have been found for other properties, such as the partial molal heat of solution of a variety of salts[10] and the limiting cation-transference number[11] in a mixed solvent.

The k_d values can, in principle, be obtained from

Table 1. Rate constants for the complex-formation reactions of Ni(II) in water–*t*-butyl alcohol mixtures at various temperatures

Solvent[a]	Ligand	Rate constant $(k_f)/10^3$ dm^3 mol^{-1} s^{-1} 10 °C	15 °C	20 °C	25 °C	30 °C	35 °C	40 °C
0	2,2′-Bipyridine	0.64_5	0.94_0		2.4_4			7.5_6
2		0.54_3	0.78_0		1.7_1			4.8_5
5		0.41_0	0.59_9		1.2_4			3.3_9
8		0.18_0	0.29_2		0.71_8			1.9_9
0	2,2′:6′,2″-Terpyridine	0.47_2	0.74_3		1.6_7			5.5_1
2		0.41_3	0.58_1		1.3_4			3.7_5
5		0.18_4	0.26_3		0.53_1			1.3_7
8		0.08_0	0.11_5		0.26_5			0.76_8
0	1,10-Phenanthroline	1.6_2	2.4_6		6.0_1		$12._6$	
5		1.1_9	1.8_7		4.0_7		7.7_7	
0	4-Phenylpyridine	0.4_8	0.7_9	1.1_5	$1._9$	$2._5$	$4._0$	
2		0.4_4	0.6_7		1.3_5			
5		0.3_6	0.4_8	0.6_7	0.8_9			
8		0.2_2	0.3_2	0.4_9	0.6_5			
0	Isoquinoline		1.1_8	$1._9$	$2._6$	$3._8$		
2		0.7_8	1.1_1	1.6_0	$2._2$			
5		0.8_0	1.0_6	1.5_1	$2._0$			
8		0.3_8	0.5_5	0.7_6	$1._1$			

a) Mol % *t*-butyl alcohol.

Table 2. Rate constants and activation parameters for the complex-formation reactions of Ni(II) in water–*t*-butyl alcohol mixtures at 25.0 °C

Solvent[a]	Ligand	$\log k_f$ (dm^3 mol^{-1} s^{-1})	ΔH_f^* (kJ mol^{-1})	ΔS_f^* [b] (J K^{-1} mol^{-1})	ΔG_f^* (kJ mol^{-1})
0	2,2′-Bipyridine	3.3_9	59.0±1.6	+17	$53._6$
2		3.2_3	51.9±0.5	− 8	$54._4$
5		3.0_9	49.4±0.3	−21	$55._2$
8		2.8_6	56.5±2.3	0	$56._9$
0	2,2′:6′,2″-Terpyridine	3.2_2	57.7±0.5	+13	$54._8$
2		3.1_3	52.3±1.2	− 8	$55._2$
5		2.7_3	46.9±0.1	−34	$57._3$
8		2.4_2	53.6±0.9	−21	$59._0$
0	1,10-Phenanthroline	3.7_8	57.7±1.2	+21	$51._5$
5		3.6_1	51.9±1.4	0	$52._3$
0	4-Phenylpyridine	3.3	58.0±1.8	+13	$54._4$
2		3.1	49.5±1.4	−21	$55._2$
5		3.0	40.2±0.9	−54	$56._1$
8		2.8	48.8±2.5	−29	$56._9$
0	Isoquinoline	3.4	53.8±2.0	0	$53._6$
2		3.3	46.4±0.5	−25	$54._0$
5		3.2	40.0±1.7	−46	$54._4$
8		3.0	46.1±0.7	−34	$55._6$

a) Mol % *t*-butyl alcohol. b) Reliability is about ±4 J K^{-1} mol^{-1}.

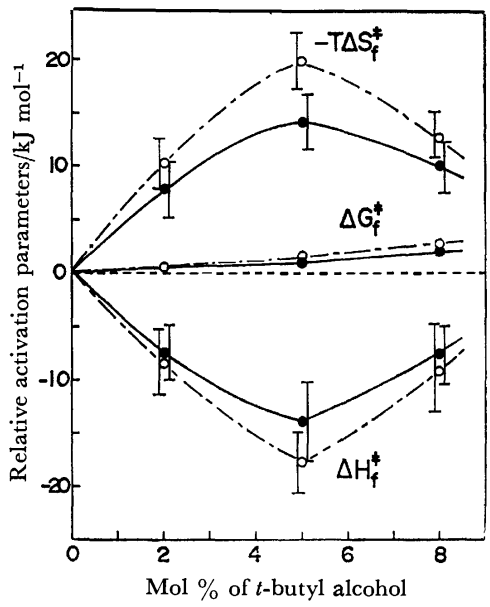

Fig. 2. Activation parameters for the reactions of Ni(II) with 4-phenylpyridine (-○-○-) and isoquinoline (-●-●-) in water–*t*-butyl alcohol mixture, normalized with respect to those in pure water (25.0 °C).

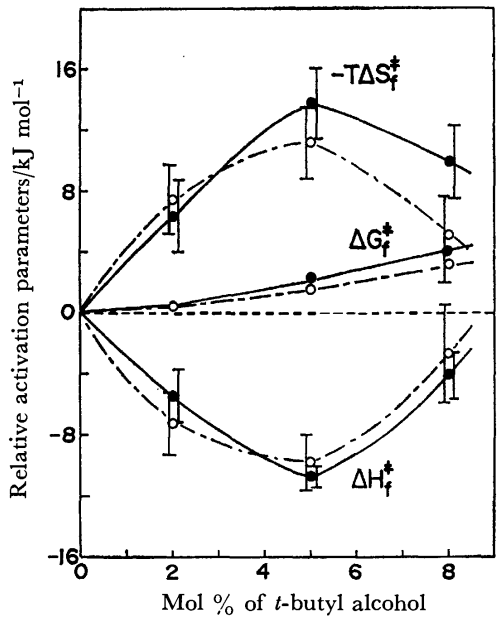

Fig. 3. Activation parameters for the reactions of Ni(II) with 2,2′-bipyridine (-○-○-) and 2,2′:6′,2″-terpyridine (-●-●-) in water–*t*-butyl alcohol mixture, normalized with respect to those in pure water (25.0 °C).

the analysis of the plots of Fig. 1. However, it should be noted that the intercept in Fig. 1 does not always give a correct dissociation-rate constant.[3] At present, it is, therefore, impossible to discuss strictly the solvent dependence on the dissociation reactions of metal complexes using the k_d values obtained by means of Eq. 1. In testing whether or not the complex-formation reaction proceeds through an I_d mechanism, the following equation presented by Chattopadhyay and Coetzee[7] was used:

$$R_1 = (4/3)k_f/K_{ass}k_s, \quad (2)$$

where K_{ass} and k_s are the formation constant of the outer-sphere complex and the rate constant for solvent exchange respectively, and where a dimensionless ratio, R_1, should have a value near unity. The log R_1 values calculated for the reactions in water at 25.0 °C are as follows: 4-phenylpyridine, −0.6; isoquinoline, −0.5; 2,2′-bipyridine, −0.5; 1,10-phenanthroline, −0.1; 2,2′:6′,2″-terpyridine, −0.7. The log k_s value for Ni(II) used was 4.5,[12] and the K_{ass} values were estimated by the Eigen-Fuoss equation.[13,14] Furthermore, the activation parameters, ΔH_s^* and ΔS_s^*, for Ni(II) in water were as follows: $\Delta H_s^* = 58.6$ kJ mol^{-1} and $\Delta S_s^* = +38$ J K^{-1} mol^{-1}.[12] From these results, it may be concluded that the complex-formation reactions of Ni(II) in water proceed through an I_d pathway.

It is probable that the Ni(II) species is solvated by only water molecules in the aqueous mixtures containing a small amount of *t*-butyl alcohol, taking into consideration the results on the form of Ni(II) in methyl alcohol–water mixtures.[15] Moreover, it has been shown that the water structure in mixtures containing a small amount of alcohol is both stiffer and more ordered than in pure water.[3,8,11] As has been assumed by previous workers,[7,8] the sharp decrease in the kinetic parameters shown in Figs. 2 and 3 may, therefore, be interpreted with the framework of an I_d mechanism. That is, the decrease in ΔH_f^* and ΔS_f^* may be caused by the passage of a water molecule from the disordered region near the Ni(II) into a bulk solvent which is more structured than water itself.

The enthalpy of activation should be related to that for solvent exchange as follows:

$$\Delta H_f^* = \Delta H_s^* + \Delta H_{ass}, \quad (3)$$

where ΔH_{ass} is the standard enthalpy for the formation of the outer-sphere complex and will usually be negligible when the ligand is uncharged. In previous papers,[16–18] we ourselves reported that the specific interactions between the inner-sphere and the outer-sphere (*e.g.*, hydrogen-bonding) should be considered in the formation of the outer-sphere complex. The decrease in the dielectric constant of media upon the addition of *t*-butyl alcohol will result in a stronger hydrogen-bonding interaction, and the outer-sphere complex is assumed to be stabilized. The increased stability of the outer-sphere complex may cause the remaining coordinated water molecule to be labilized as a result of the partially ionic character imparted to the water molecule involved in the hydrogen bond. The type of interaction introduced here is similar to the "internal conjugate base" mechanism proposed by Rorabacher.[19] In conclusion, we assume that the decrease in ΔH_f^* and ΔS_f^* upon the addition of *t*-butyl alcohol to water could arise mainly from the combined effects by stiffening the solvent structure and promoting the specific interaction between the inner-sphere and the outer-sphere. The increase in ΔH_f^* and ΔS_f^* upon the further addition of *t*-butyl alcohol to water remains unexplained, but a dramatic change in the solvation shell of Ni(II) and a breakdown of the water structure are expected to be of the greatest importance.

This work has been undertaken at the Department of Chemistry, University of Pittsburgh. We wish to express our deep gratitude to Professor J. F. Coetzee for his kind guidance in the course of this work.

References

1) M. Eigen, "Advances in the Chemistry of Coordination Compounds," ed by S. Kirschner, Macmillan, New York (1961), p. 371.
2) M. Eigen, *Pure Appl. Chem.*, **6**, 97 (1963).
3) H. P. Bennetto and E. F. Caldin, *J. Chem. Soc., A*, **1971**, 2191, 2198.
4) P. K. Chattopadhyay and J. F. Coetzee, *Anal. Chem.*, **46**, 2014 (1974).
5) J. F. Coetzee and C. G. Karakastanis, *Inorg. Chem.*, **15**, 3112 (1976).
6) J. F. Coetzee, *Pure Appl. Chem.*, **49**, 27 (1977).
7) P. K. Chattopadhyay and J. F. Coetzee, *Inorg. Chem.*, **12**, 113 (1973).
8) H. P. Bennetto and E. F. Caldin, *J. Chem. Soc., A*, **1971**, 2207.
9) H. P. Bennetto, *J. Chem. Soc., A*, **1971**, 2211.
10) E. M. Arnett and D. R. McKelvey, *J. Am. Chem. Soc.*, **87**, 1393 (1965).
11) T. L. Broadwater and R. L. Kay, *J. Phys. Chem.*, **74**, 3802 (1970).
12) J. W. Neely and R. E. Connick, *J. Am. Chem. Soc.*, **94**, 3419, 8646 (1972).
13) M. Eigen, *Z. Phys. Chem. (Frankfurt am Main)*, **1**, 176 (1954).
14) R. M. Fuoss, *J. Am. Chem. Soc.*, **80**, 5059 (1958).
15) W. J. MacKellar and D. B. Rorabacher, *J. Am. Chem. Soc.*, **93**, 4379 (1971).
16) T. Takahashi, T. Koiso, and N. Tanaka, *Nippon Kagaku Kaishi*, **1974**, 65.
17) T. Takahashi and T. Koiso, *Bull. Chem. Soc. Jpn.*, **49**, 2784 (1976).
18) T. Takahashi and T. Koiso, *Bull. Chem. Soc. Jpn.*, **51**, 1307 (1978).
19) D. B. Rorabacher, *Inorg. Chem.*, **5**, 1891 (1966).

Full-range Bond-order Dependence of Intramolecular Vibrations: Ethylene and Tetracyanoethylene

Jun-ichi AIHARA

Department of Chemistry, Faculty of Science, Hokkaido University, Sapporo 060

(Received March 10, 1980)

For analogous normal vibrations in conjugated systems of a similar type a linear relationship often exists between vibrational frequencies and bond orders. We find that this linearity can, in principle, be extended to include conjugated systems in both excited electronic states and ionic states. This indicates that the linearity covers a full range of bond order conceivable for conjugated systems. Such an aspect of molecular vibrations gives a concise and sometimes decisive clue not only to vibrational assignments but also to structural analyses of conjugated systems in various electronic states. Symmetric C=C stretching vibrations of ethylene and tetracyanoethylene nicely illustrate this situation.

Although most of the constituent atoms contribute to every vibrational mode of a molecule, many of the modes behave as if they were properties of individual functional groups.[1] This effect leads to a characteristic infrared band which appears within a relatively narrow energy range for such functional groups as methyl, hydroxyl, and carbonyl. For conjugated systems vibrational energies have both σ- and π-components. Detailed analysis by Coulson and Longuet-Higgins showed that a force constant for a π bond is a function of π bond order and π bond polarizability.[2] However, the use of bond order alone often suffices to estimate the vibrational frequency.[3] Berthier *et al.* found that a characteristic frequency for a variety of aldehydes and ketones typically gives an excellent linear correlation with a bond order of the carbonyl group.[4]

It is widely known that, when a conjugated compound forms a molecular ion, its infrared and Raman spectra change markedly;[5-9] so do the bond orders. When a conjugated system is electronically excited, such vibrational frequencies as found in the electronic absorption bands often change from those of the ground-state species.[9] However, attempts to correlate these frequencies with the corresponding bond orders have scarcely been made. This kind of study has been restricted to neutral conjugated systems in the ground state, where a change in bond order is rather modest.[3] In this paper, I would like to show that a linear relationship between vibrational frequencies and π bond orders can, in principle, be extended to cases where both quantities change much more widely. Recall that a wide variation in π bond order can usually be realized in the following three ways: exciting a conjugated system of a molecule, removing one or more π electrons from a molecule, and attaching one or more π electrons to a molecule.

Results and Discussion

Ethylene is the simplest conjugated hydrocarbon. A vibrational frequency of the symmetric C=C stretching mode can be detected in the Raman spectrum. It is 1623 cm^{-1} in the ground electronic state.[10] This frequency is reduced to 850 cm^{-1} in the excited electronic state,[10] which is observed as a vibrational component of the first electronic absorption band around 45000 cm^{-1}. Some vibrational frequencies can be seen in a photoelectron spectrum of ethylene.[11] They are ascribed to the molecular cation $C_2H_4^+$. The first photoelectron band corresponds to a removal of a π electron from the single π-valence orbital. This band exhibits a 1230 cm^{-1} vibrational progression, which has been assigned to a symmetric C=C stretching mode of $C_2H_4^+$.

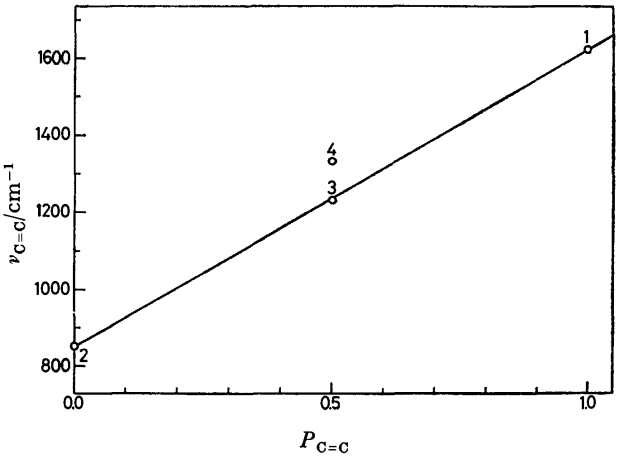

Fig. 1. Plot of $\nu_{C=C}$ *vs.* $P_{C=C}$ for ethylene: 1, C_2H_4; 2, C_2H_4*; 3, $C_2H_4^+$; 4, $C_2H_4^-$.

In order to see if these frequencies ($\nu_{C=C}$) correlate with the corresponding C=C π bond orders ($P_{C=C}$), the former quantities are plotted against the latter ones in Fig. 1. The C=C π bond orders are 1.000 for C_2H_4, 0.000 for C_2H_4*, and 0.500 for $C_2H_4^+$, where C_2H_4 and C_2H_4* denote the ground and excited electronic states of ethylene, respectively. C_2H_4 and C_2H_4* are chosen to draw a reference line in Fig. 1 because the number of π electrons are kept constant. This line is expressed as

$$\nu_{C=C} = 773.0\,P_{C=C} + 850.0. \quad (1)$$

Here, it is surprising to see that this linear relationship can exactly be applied to $C_2H_4^+$. Note that C=C π bonds of C_2H_4, C_2H_4*, and $C_2H_4^+$ cover the full range of π bond order conceivable for conjugated systems.

In 1973 Sanche and Schultz reported an electron transmission spectrum of ethylene in the gas phase.[12] The first band exhibits an average vibrational spacing of 1330 cm^{-1}, which most likely results from a symmetric

C=C stretching vibration of an ethylene anion ($C_2H_4^-$). The C=C π bond order of $C_2H_4^-$ must be the same as that of $C_2H_4^+$. However, this anion is placed about 100 cm^{-1} above the reference line in Fig. 1. This implies that the C=C bond in $C_2H_4^-$ is a bit more stabilized than expected from Eq. 1.

An analogous symmetric C=C stretching mode of tetracyanoethylene (TCNE) gives another good example which supports a wide-range π-bond-order dependence of vibrational frequencies. A Raman spectrum of this compound shows that the vibrational frequency of 1569 cm^{-1} can be assigned to the symmetric C=C stretching mode.[13,14] This frequency is nearly comparable to that of C_2H_4. TCNE exhibits the first electronic absorption band in the energy range 35000—43000 cm^{-1} in the gas phase. Spacings of the vibrational components are irregular, and the 0-1 level seems to be shifted, probably due to an intersection of the two potential surfaces.[15] Its average 1128 cm^{-1} spacing was assigned to the symmetric C=C stretching mode of the excited TCNE molecule (TCNE*).

TCNE is a typical electron acceptor with an electron affinity of 2.89 eV.[16] Therefore, its monoanion ($TCNE^-$) is considerably stabilized,[17] forming many anion radical salts[18] in the form M^+TCNE^-. For these salts it is striking that there appears intense absorption at about 1370 cm^{-1} in a region barren of significant absorption by TCNE.[19] This has been assigned to the totally symmetric C=C stretch which became infrared active by the Ferguson-Matsen mechanism.[20] This interpretation was later justified by a Raman spectroscopic study.[14] The C=C stretch of $TCNE^-$ is influenced by the cation to some extent. Thus C=C stretching frequencies are 1387 cm^{-1} for the lithium, 1390 cm^{-1} for the sodium, 1371 cm^{-1} for the potassium, and 1358 cm^{-1} for the cesium salt.[21] The first absorption band of $TCNE^-$ in solution exhibits numerous vibrational maxima. Unfortunately, the average spacing of 530 cm^{-1} should rather be assigned to the symmetric C–C stretch.[22]

Recently, Khatkale and Devlin prepared $TCNE^{2-}$ and $TCNE^{3-}$ by vacuum condensation methods[23] and measured infrared and Raman spectra of the four molecule series TCNE, $TCNE^-$, $TCNE^{2-}$, and $TCNE^{3-}$. Symmetric C=C stretching frequencies are 1392, 1256, and 1346 cm^{-1} for the sodium salts of $TCNE^-$, $TCNE^{2-}$, and $TCNE^{3-}$, respectively. A photoelectron spectrum of TCNE has been reported by three research groups.[24-26] Stafast and Bock analyzed it[26] and attributed the 1360 cm^{-1} progression of the first band to the symmetric C=C stretch of $TCNE^+$. An uncertainty of $\pm$100 cm^{-1} may be included in this experimental frequency.[24-26]

π Bond orders of the TCNE series were calculated using Coulomb and resonance integrals suggested by Orgel and coworkers.[27] A Coulomb integral for a cyano nitrogen was set equal to $\alpha+\beta$, and a resonance integral for the C≡N bond to 1.2β. The C=C π bond orders thus calculated are 0.700 for TCNE, 0.314 for TCNE*, 0.491 for $TCNE^+$, 0.523 for $TCNE^-$, and 0.347 for $TCNE^{2-}$ and $TCNE^{3-}$. The C=C stretching frequencies are then plotted against the corresponding

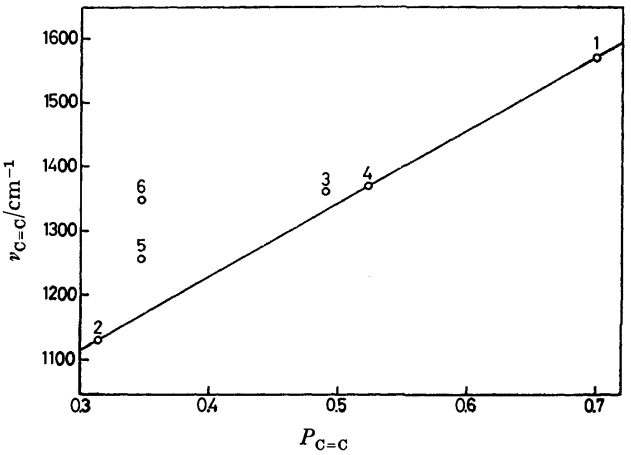

Fig. 2. Plot of $\nu_{C=C}$ *vs.* $P_{C=C}$ for tetracyanoethylene: 1, TCNE; 2, TCNE*; 3, $TCNE^+$; 4, $TCNE^-$; 5, $TCNE^{2-}$; 6, $TCNE^{3-}$.

bond orders in Fig. 2, where a reference line crosses two points representing TCNE and TCNE*. This line is expressed as

$$\nu_{C=C} = 1142.5\,P_{C=C} + 769.6. \quad (2)$$

As seen from Fig. 2, both $TCNE^+$ and $TCNE^-$ are also located near this line. Some other cyanoethylenes appear to behave analogously, although data for the electronically excited species are lacking. The C=C stretching frequencies are 1615 cm^{-1} for acrylonitrile (0.886), 1360 cm^{-1} for its cation (0.515), 1594 cm^{-1} for 1,1-dicyanoethylene (0.806), and 1360 cm^{-1} for its cation (0.523).[26] Here, values in parentheses are the appropriate π bond orders.

We hence feel confident that a linear bond-order dependence of the C=C stretching frequency exists among a variety of electronic states. Note that the C=C π bond order in our case changes within a range of 0.000—1.000, while in the case of aldehyde and ketones[3,4] the C=O π bond order changes modestly, in the range 0.819—0.958. Khatkale and Devlin reported that a plot of the empirical force constant *vs.* bond order is nearly linear for tetracyanoquinodimethane anions ($TCNQ^{n-}$).[28] This fact also supports a universality of such linearity as Eqs. 1 and 2 indicate.

Unfortunately, some exceptional species are found in Fig. 2. As in the case of $C_2H_4^-$, higher anions of TCNE show considerably larger frequencies than expected from Eq. 2. The C=C stretching frequency of $TCNE^{2-}$ deviates upward from the reference line by 90 cm^{-1} and that of $TCNE^{3-}$ by 180 cm^{-1}. It is especially noticeable that the C=C stretching frequency of $TCNE^{3-}$ is somewhat larger than that of $TCNE^{2-}$. The effect of the third π electron added is apparently quite different. This electron is expected to enter an orbital which is nonbonding in the C=C region, so an apparent strengthening of the C=C bond was not anticipated.[23] Accordingly, it is quite natural to consider some possible mechanism which intensifies the C=C bond strength.

We have assumed that skeletal structures of all molecular species are identical with that of a neutral molecule. This may be true for TCNE* and $TCNE^+$ since the 0-0 vibrational component of the first band

is strongest in the electronic absorption spectrum of TCNE[15] and in its photoelectron spectrum.[26] The same situation applies to the ethylene cation.[11] However, there is no reason to believe that the same situation must apply to the other species, especially to higher anions of TCNE.

On the other hand, it is not difficult to imagine that additional π electrons in the TCNE anions are highly delocalized with high polarizability. Perhaps more reasonable is the assumption that the structures of the dianion and the trianion are strongly distorted by asymmetric cation polarization fields, such that the original TCNE D_{2h} symmetry is no longer useful for the purpose of vibrational analyses.[23] According to Jeanmaire *et al.*,[22] the electrogeneration of $TCNE^{2-}$ in acetonitrile containing tetrabutylammonium perchlorate seemed to be electrochemically quasireversible. They speculated that the cause of the quasireversible electron transfer to form the dianion is due to a geometry change and that $TCNE^{2-}$ is a nonplanar species even in solution.[22] Such a tendency toward nonplanarity may be enhanced in $TCNE^{3-}$. For these reasons, we cannot always take the premise that the molecular ion series might constitute such a set of molecular ions that vibrational assignments for the other members would follow smoothly from a firm assignment of the modes of one member of the series. Significant deviation of a vibrational frequency from the reference line should be interpreted as due to a molecular deformation or some other geometry change. However, this does not deny our view that the bond-order dependence of vibrational frequencies holds widely because bond orders are necessarily modified for the deformed species.

A conjugated system of TCNE is fairly large compared with that of ethylene, so $TCNE^-$ appears to retain the geometry of its neutral species. However, it may be impossible for the ethylene monoanion to retain the ground-state geometry of the neutral species because of its compact conjugated system. The deviation of 100 cm^{-1} apparently indicates the degree of extra stabilization of the C=C bond.

I previously observed a vibrational structure in the charge-transfer (CT) absorption band of the naphthalene–TCNE complex in various saturated hydrocarbons.[29] The vibrational frequency was 1300—1400 cm^{-1}. Similar frequencies are found in the solid-state absorption spectra of several aromatic hydrocarbon–TCNE complexes.[30,31] According to Kadhim and Offen,[30] such vibrational frequencies might be characteristic of the acceptor molecule because a CT transition is naively viewed as an electron jump to the lowest unoccupied orbital of the acceptor. The appearance of a 1300—1400 cm^{-1} vibration thus indicates that the TCNE component in the complex is almost completely ionized in the CT excited state since the frequency is close to that of $TCNE^-$ in Fig. 2. On the other hand, the resonance Raman spectrum of TCNE in benzene[32] exhibits a strong line at 1565 cm^{-1}, and that of TCNE in anisole[33] at 1556 cm^{-1}. These frequencies suggest that the ground-state TCNE complexes with benzene and anisole are essentially nonionic, in accord with the prediction by simple CT theory.[34]

Concluding Remarks

As has been examined above, a linear bond-order dependence of vibrational frequencies can, in principle, be extended to a conjugated system in any electronic state. This aspect of intramolecular vibrations can be used to assign not only electronic absorption bands but also photoelectron bands of various conjugated systems. In this connection, Ikemoto *et al.* observed a 1530 cm^{-1} vibrational component in the first photoelectron band of TCNE,[24] and assigned it to the symmetric C=C stretch. However, the frequency of this mode is predicted from Eq. 2 to be close to 1330 cm^{-1}. In this sense the frequency read by Stafast and Bock (1360 cm^{-1})[26] appears more reasonable. If a given vibrational mode deviates to a higher energy side, this should be regarded as a significant indication of a geometry change, and some possible stabilizing mechanism must be considered for the species concerned. Thus the relationship established between π bond orders and vibrational frequencies will give an important and sometimes decisive clue to structural chemistry of conjugated systems, especially when other experimental data are scanty.

The use of the facilities of the Hokkaido University Computing Center is gratefully acknowledged.

References

1) See, *e.g.*, L. J. Bellamy, "Advances in Infrared Group Frequencies," Methuen, London (1968).
2) C. A. Coulson and H. C. Longuet-Higgins, *Proc. R. Soc. London, Ser. A*, **193**, 456 (1948).
3) A. Streitwieser, Jr., "Molecular Orbital Theory for Organic Chemists," Wiley, New York, N. Y. (1961), Chap. 8.
4) G. Berthier, B. Pullman, and J. Pontis, *J. Chim. Phys.*, **49**, 367 (1952); J. Baudet, G. Berthier, and B. Pullman, *ibid.*, **54**, 282 (1957).
5) Y. Matsunaga, *Can. J. Chem.*, **38**, 1172 (1960); *J. Chem. Phys.*, **41**, 1609 (1963).
6) J. Stanley, D. Smith, B. Latimer, and J. P. Devlin, *J. Phys. Chem.*, **70**, 2011 (1966).
7) Y. Iida, *J. Phys. Soc. Jpn.*, **27**, 1371 (1969); *Bull. Chem. Soc. Jpn.*, **43**, 345 (1970).
8) K. Ohno, *J. Mol. Spectrosc.*, **72**, 238 (1978); **77**, 329 (1979). See also many references cited in these papers.
9) See, *e.g.*, K. Ohno, *Chem. Phys. Lett.*, **64**, 560 (1979).
10) G. Herzberg, "Molecular Spectra and Molecular Structure III. Electronic Spectra and Electronic Structure of Polyatomic Molecules," D. van Nostrand, Princeton, N. J. (1967), pp. 533—535 and 629.
11) D. W. Turner, C. Baker, and C. R. Brundle, "Molecular photoelectron Spectroscopy," Wiley-Interscience, London (1970).
12) L. Sanche and G. J. Schultz, *J. Chem. Phys.*, **58**, 479 (1973); P. D. Burrow and K. D. Jordan, *Chem. Phys. Lett.*, **36**, 594 (1975).
13) F. A. Miller, O. Sala, P. Devlin, J. Overend, E. Lippert, W. Luder, H. Moser, and J. Varchmin, *Spectrochim. Acta*, **20**, 1233 (1964); P. Devlin, J. Overend, and B. Crawford, Jr., *ibid.*, **20**, 23 (1964); T. Takenaka and S. Hayashi, *Bull. Chem. Soc. Jpn.*, **37**, 1216 (1964).
14) Y. Iida, *Bull. Chem. Soc., Jpn.*, **46**, 423 (1973); J. J. Hinkel and J. P. Devlin, *J. Chem. Phys.*, **58**, 4750 (1973).

15) J. Prochorov and A. Tramer, *Bull. Acad. Polon. Sci., Ser. Sci. Math. Astr. et Phys.*, **12**, 429 (1964).
16) A. L. Farragher and F. M. Page, *Trans. Faraday Soc.*, **63**, 2369 (1967).
17) W. D. Phillips, J. C. Rowell, and S. I. Weissman, *J. Chem. Phys.*, **33**, 626 (1960).
18) O. W. Webster, W. Mahler, and R. E. Benson, *J. Am. Chem. Soc.*, **84**, 3678 (1962).
19) J. Stanley, D. Smith, B. Latimer, and J. P. Devlin, *J. Phys. Chem.*, **70**, 2011 (1966).
20) E. E. Ferguson and F. A. Matsen, *J. Chem. Phys.*, **29**, 105 (1958); *J. Am. Chem. Soc.*, **82**, 3268 (1960); E. E. Ferguson, *J. Chim. Phys.*, **61**, 257 (1964).
21) J. C. Moore, D. Smith, Y. Youhne, and J. P. Devlin, *J. Phys. Chem.*, **75**, 325 (1971).
22) D. L. Jeanmaire, M. R. Suchanski, and R. P. Van Duyne, *J. Am. Chem. Soc.*, **97**, 1699 (1975).
23) M. S. Khatkale and J. P. Devlin, *J. Phys. Chem.*, **83**, 1636 (1979).
24) I. Ikemoto, K. Samizo, T. Fujikawa, K. Ishii, T. Ohta, and H. Kuroda, *Chem. Lett.*, **1974**, 785.
25) K. N. Houk and L. L. Munchausen, *J. Am. Chem. Soc.*, **98**, 937 (1976).
26) H. Stafast and H. Bock, *Tetrahedron*, **32**, 855 (1976).
27) L. E. Orgel, T. L. Cottrell, W. Dick, and L. E. Sutton, *Trans. Faraday Soc.*, **47**, 113 (1951); L. R. Melby, "The Chemistry of the Cyano Group," ed by Z. Rappoport, Wiley-Interscience, London (1970), Chap. 10.
28) M. S. Khatkale and J. P. Devlin, *J. Chem. Phys.*, **70**, 1851 (1979).
29) J. Aihara, *Bull. Chem. Soc. Jpn.*, **44**, 1174 (1971).
30) A. H. Kadhim and H. W. Offen, *Mol. Cryst.*, **3**, 311 (1968).
31) H. Kuroda, I. Ikemoto, and H. Akamatu, *Bull. Chem. Soc. Jpn.*, **39**, 1842 (1966); H. Kuroda, T. Kunii, S. Hiroma, and H. Akamatu, *J. Mol. Spectrosc.*, **22**, 60 (1967).
32) K. Kaya, A. Nakatsuka, N. Kubota, and M. Itoh, *J. Raman Spectrosc.*, **1**, 595 (1973).
33) P. W. Jensen, *Chem. Phys. Lett.*, **39**, 138 (1976).
34) R. S. Mulliken, *J. Am. Chem. Soc.*, **74**, 811 (1952); *J. Phys. Chem.*, **56**, 801 (1952).

Cotton Effect Induced in Optically Inactive Molecules and Molecular Complexes by Optically Active Environment. III. Circular Dichroism Induced by Association of α-Chymotrypsin and Dyes

Yasumasa J. I'HAYA,* Yasunobu OIKAWA, and Tomoyasu NAKAMURA†

Department of Materials Science and Laboratory of Magneto-Electron Physics, The University of Electro-Communications, Chofu, Tokyo 182

(Received April 4, 1980)

Two types of circular dichroism (CD) spectra are found to be induced in the solution systems of α-chymotrypsin (αCT) and dyes. One is a single positive CD band which is due to a 1 : 1 αCT–dye complex (Type I; proflavine, Acridine Yellow G, acriflavine), and the other consists of one positive and one negative CD bands which are mainly due to a complex of the composition, one αCT to two dye molecules (Type II; Pyronin B, Rhodamine 6G). Mechanisms of CD induction tentatively proposed are that in Type I complexes a single dye molecule is bound to an asymmetric environment of the active site of αCT while in Type II complexes two dye molecules are bound at a specific site exerting a dipole-dipole interaction with one another.

There have been published a number of physicochemical and biochemical works on the interaction between biopolymers and dyes, of which the most elegant means may be the measurement of the Cotton effect induced in the corresponding visible absorption region of the dye. This is because once an accurate analysis is accomplished the bound dye molecules play a role as probes in determining the geometrical and electronic structures of the partner, biomacromolecules. Biopolymers that have been hitherto investigated in this way are nucleic acids,[1,2] polypeptides,[3] and polysuccharides,[4] and in all cases the primary cause of circular dichroism (CD) induction is recognized as a complex formation between polymer and dyes, though less quantitative description of such complexes has been found.

We have reported in a previous paper[5] that the Cotton effect is induced in the absorption region of a dye molecule embedded in cellulose diacetate film and proposed a mechanism of CD induction that the dyes are imprisoned in a cage formed by an assembly of the folded chains of cellulose diacetate and the Cotton effect is induced by an electrostatic interaction between electronic transition moments of the dye and of the chromophores involved in the cage. In the present paper, we set our eyes on a system of enzyme and dyes. The concept that an enzyme molecule forms an intermediate complex with a substrate or substrates in an early stage of enzymic action has been well established. It is also well known that each enzymic action has its specificity with respect to a single substrate. In the study of enzyme-dye interactions, whether some sort of specificity appears in a complex formation is an interesting subject. We measured CD spectra induced in a variety of combination systems of enzymes and dyes and tried to find out some interrelation between a way of grouping and whether and what sort of Cotton effects are induced in the visible absorption region of the dyes. We report in what follows the CD spectral features of α-chymotrypsin–dye solutions, the truth being that α-chymotrypsin was found to be the only enzyme to interact overnicely with some specific dyes.

Experimental

Commercial α-chymotrypsin, bovine pancreas (Nutritional Biochemicals, 3X crystallized and lyophilized) was purified by recrystallization three times. Proflavine, Acridine Yellow G, acriflavine, Pyronin B, and Rhodamine 6G were all commercial reagert grade and used without further purification. Stock aqueous solutions of α-chymotrypsin and the dyes were dissolved in 0.1 mol dm^{-3} Tris buffer (pH 8.1—8.5). In order to avoid aggregation of dye molecules, concentrations of the dyes were held in the range of $1—5\times10^{-5}$ mol dm^{-3}. The molar concentration of α-chymotrypsin was calculated from its molecular weight which was assumed to be 25,000.

The absorption spectra were measured with a Hitachi model 124 spectrophotometer, the CD spectra by a JASCO J-40 polarimeter, and the optical rotatory dispersion (ORD) spectra by a JASCO ORD-UV-5 spectrophoto and polarimeter. All the measurements were performed at room temperature.

The ORD measurement (molecular rotation [ϕ]) had such a disadvantage that accurate determination became difficult when the concentration of α-chymotrysin was high, because the ordinanry dispersion of α-chymotrypsin extended over the absorption region of the dyes. For this reason, our primary attention was focused on the CD measurements. The molecular ellipticity [θ] of an induced CD (ICD) band was calculated by using the concentration of a dye involved.

Results

ICD spectra observed for the α-chymotrypsin (αCT)–dye systems may be divided into two classes; Type I consists of a single positive CD band, to which the αCT–proflavine (PF), Acridine Yellow G (AY), and acriflavine (AF) systems belong, and Type II is formed of a longer wavelength negative band and a shorter wavelength positive band, to which the αCT–Pyronin B (PB) and Rhodamine 6G (RG) systems belong. Since the ICD spectra of the same type (Types I and II) are not very much different from one another, we mention in detail only about the representative systems, αCT–PF and αCT–PB.

† Present address: Senshu University, Ikuta, Kawasaki, Kanagawa 214.

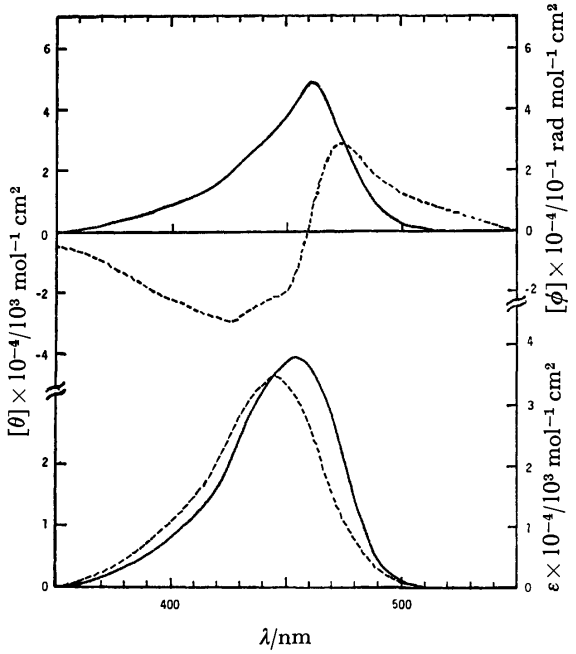

Fig. 1. CD (solid line, upper), ORD (broken line, upper), and visible absorption (solid line, lower) spectra of the α-chymotrypsin–proflavine complex dissolved in Tris buffer. [D]=4.0×10⁻⁵ mol dm⁻³ and [E]/[D]=3.8. The broken line in the lower half is the absorption spectrum of free proflavine of the same concentration.

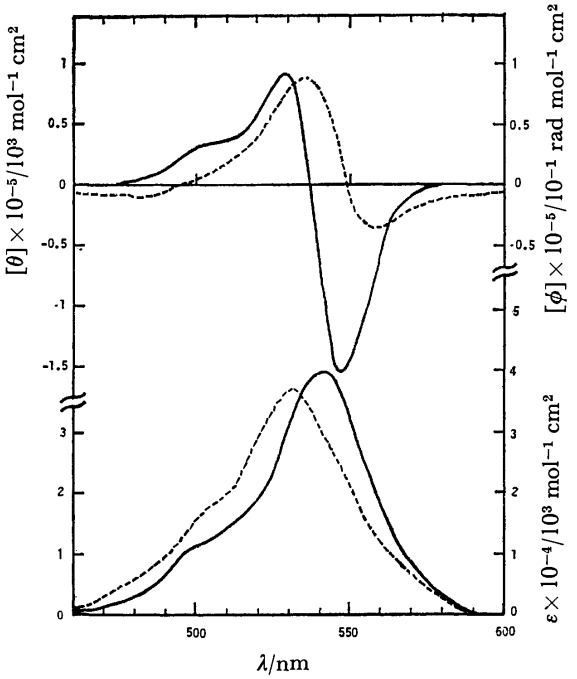

Fig. 3. CD (solid line, upper), ORD (broken line, upper), and visible absorption (solid line, lower) spectra of the α-chymotrypsin–Pyronin B complex dissolved in Tris buffer. [D]=5.0×10⁻⁵ mol dm⁻³ and [E]/[D]=4.0. The broken line in the lower half is the absorption spectrum of free Pyronin B of the same concentration.

α-Chymotrypsin–Proflavine. Figure 1 shows the CD, ORD, and visible absorption spectra of the αCT–PF system where the concentration of PF is 4.0×10^{-5} mol dm^{-3} and the molar concentration ratio of αCT to PF, [E]/[D], is 3.8. The single positive ICD band peaked at 462 nm corresponds to the broad absorption band of PF (peak: 456 nm; *cf.* peak of free PF: 445 nm), its molar ellipticity [θ] being 4.9×10^{4}. The corresponding ORD spectrum shows a positive Cotton effect. The peak intensity of the ICD spectrum was found to increase as [E]/[D] increases, while the peak wavelength and the spectral shape remained unchanged. Beyond [E]/[D]=8, the peak intensity itself remained constant, the corresponding [θ] value being 5.5×10^{4}. The relationship between [θ] and [E]/[D] is shown in Fig. 2.

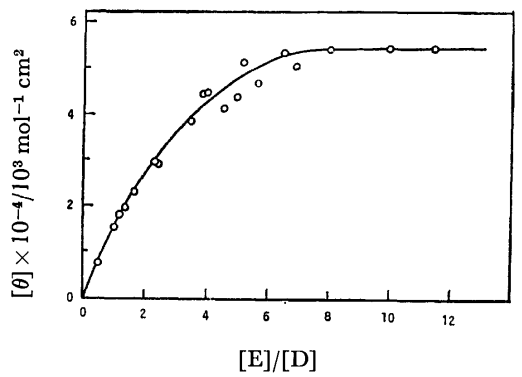

Fig. 2. Concentration dependence of the peak intensity of the induced CD band (462 nm) of the α-chymotrypsin–proflavine complex.

The absorption spectrum of PF shifts to the red and gains its intensity with the addition of αCT. The further shift of the absorption peak is not observed when [E]/[D]≧5, the peak converging to the value 460 nm. Furthermore, we found an isosbestic point at 443 nm.

α-Chymotrypsin–Pyronin B. Figure 3 illustrates the visible absorption and the induced CD and ORD spectra of the αCT–PB system, where the concentration of PB is 5.0×10^{-5} mol dm^{-3} and [E]/[D]=4. Contrary to the αCT–PF system, there appeared both positive and negative CD bands at the absorption region of the dye. The positive maximum lies at 529 nm with $[\theta]=9.1\times10^{4}$ and the negative maximum at 547 nm with $[\theta]=-1.54\times10^{5}$. Furthermore, a shoulder appeared at about 500 nm. As in the case of αCT–PF,

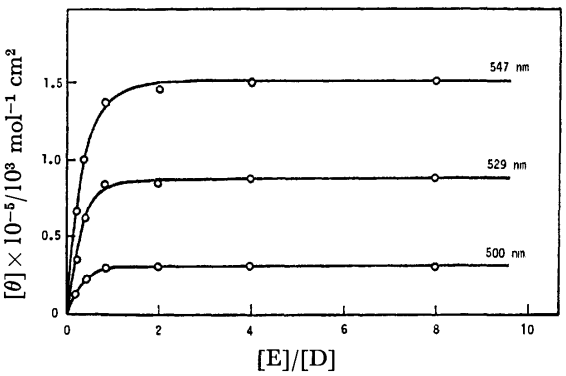

Fig. 4. Concentration dependence of the molecular ellipticities of the positive (529 nm), negative (547 nm), and shoulder (500 nm) CD bands of the α-chymotrypsin–Pyronin B complex.

the peak intensity was concentration dependent but the whole CD spectral feature remained unchanged. In Fig. 4 are plotted the molecular ellipticities of the positive, negative, and shoulder CD peaks against [E]/[D]. It is seen that in excess of [E]/[D]=4 the [θ] values tend to be concentration independent. The converged [θ] value for the positive band is 9.1×10^4, that for the negative band is -1.54×10^5, and that for the positive shoulder is 3.3×10^4.

The absorption spectrum of the αCT–PB system was quite similar to that of the αCT–PF system. The red shift of the absorption peak came to be over at 541 nm when [E]/[D]≧2. Contrary to the αCT–PF system, however, an isosbestic point was not observed explicitly.

The followings are brief descriptions of the results for the other systems.

α-Chymotrypsin–Acridine Yellow G. The positive ICD band was observed as in the case of αCT–PF. The peak of the CD band lies at 461 nm and its concentration dependence closely resembles the αCT–PF system; the [θ] value converges to 8.6×10^3 when [E]/[D]>4. The peak of the visible absortion spectrum of the system shifts from 435 nm (free dye) to 445 nm when [E]/[D] is varied, the latter being the converged value for [E]/[D]>4.

α-Chymotrypsin-Acriflavine. The spectral features of the ICD and visible absorption bands were just a copy of αCT–PF and/or αCT–AY.

α-Chymotrypsin–Rhodamine 6G. Like the αCT–PB system, the positive and negative ICD bands were observed. The whole spectral features of the CD bands are very much like those of αCT–PB, together with the similarity in the appearance of a weak shoulder in the shorter wavelength side. The corresponding ORD curve also resembles the case of αCT–PB. The molecular ellipticities of the negative (548 nm), the positive (529 nm), and the shoulder (505 nm) bands increase with the values of [E]/[D] and tend to converge to the value -5.3×10^5, 3.1×10^5, and 1.2×10^5, respectively, in excess of [E]/[D]=4. The visible absorption spectrum of αCT–RG behaves in the same fashion as that of αCT–PB upon concentration variation.

Finally, we like to add that no ICD spectra were observed with the solution systems of αCT and the following chromophores, though their molecular shapes are more or less analogous to those of the species described above: 9-aminoacridine, Methylene Blue, Toluidine Blue 0, thionine, Pyronin G, Rhodamine B, phenosafranine, Erythrosin B, Eosin B, Eosin Y, and Methyl Orange. Neither spectral shifts were observed in the visible absorption spectra of these solution systems.

Discussion

The observations described above for the αCT-specific dye systems clearly show a complex formation between αCT and the dyes. The appearance and the general features of the induced CD spectra in the aforementioned systems closely resemble those in the systems of nucleic acids, polypeptides, and polysuccharides with a variety of dye molecules.[1–4] Schlessinger and Steinberg[6] reported the appearance of CD absorption induced and circular polarization of fluorescence emitted in αCT–substrate complexes in which the substrates had been proven to bind at specific sites of αCT. However, the appearance of ICD in a system of an enzyme and a molecule which is understood not to receive specific enzymic actions has not been reported before.

As can be seen from the results described before, the ICD spectra and/or the modes of interaction of αCT and the dyes are discriminated into two classes without doubt. The following discussions will be divided into the Type I and Type II complexes.

Type I Complexes. From the shift of the visible absorption spectrum observed in the αCT–PF system, Bernhard *et al.*[7] concluded that a 1 : 1 complex is formed between αCT and PF and the binding site is the enzymic active site of αCT. The latter was deduced from the fact that PF behaves like a competitive inhibitor in enzymic reactions. Bearing in mind that the visible absorption spectrum of the αCT–PF complex resembles the spectrum of PF in various dioxane–water mixtures, a hydrophobic environment of αCT seems to be the primary cause for the formation of the complex. As can be seen in Fig. 2, the [θ] value increases with [E]/[D] until [E]/[D] ≈8 where almost all of the dye molecules are guessed to bind to αCT. The corresponding [θ] value for these saturated states, 5.5×10^4, is considered to be the molecular ellipticity for the αCT–PF complex. Moreover, it is possible that a specific binding site of PF is unique as evidenced from the fact that the shape of ICD spectrum remains unchanged with the increase of [E]/[D].

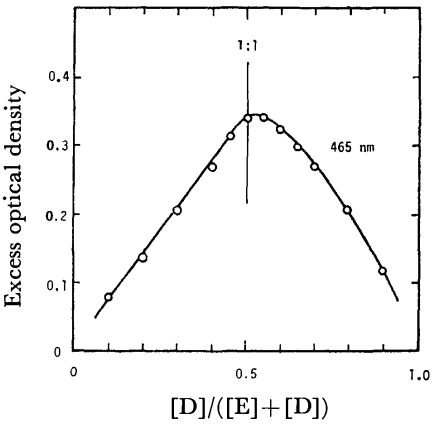

Fig. 5. Demonstration of formation of α-chymotrypsin-proflavine complex by method of continuous variations. [E]+[D]=2.0×10^{-4} mol dm^{-3}.

In order to find out a stoichiometric formula for the complex, we used the method of continuous variations.[8] In Fig. 5 is plotted the difference optical density at 465 nm as a function of [D]/([E]+[D]). From this, it is clear that one PF molecule binds to one αCT molecule in accordance with the conclusion made by Bernhard *et al.*[7]

In previous papers,[2] we proposed two mechanisms of CD induction in the system of DNA- and RNA–dye complexes; one which appears in high P/D (nucleic

acid phosphate to dye ratio) complexes is due to a static asymmetric perturbation caused in a dye monomer (referred to as optical activity I) and the other which appears in low P/D complexes results from an interaction between two dye molecules bound to the nucleic acid helices in the form of a dimer (optical activity II). In other words, the former arises from a one-electron mechanism in a perturbed single dye molecule and/or from an interaction between electric dipole transition moments of a single dye molecule and of neighboring chromophores involved in a macromolecule, and the latter from the exciton-type coupling mechanism between the two dye molecules bound to the biopolymer side by side. The general features of the single positive CD spectrum (Type I) of the αCT–PF complex and optical activity I above are not very much different from one another, so that the mechanism of CD induction in the αCT–PF complex is deduced to be a one-electron origin or the like. That is, αCT and PF form a 1 : 1 complex in which PF is bound near the asymmetric environment of αCT and CD is induced by the interaction of an electrically allowed transition of the dye with magnetically and electrically allowed transitions of the nearby asymmetric perturbers. The very same discussion will apply to the αCT–AY and αCT–AF systems, though we have not shown data of stoichiometric measurements for these complexes.

The questions still remaining are two fold; a definite site of the dyes binding in αCT and a reason why no CD spectra are induced in αCT and analogous dye systems mentioned before. These two problems are related to one another. First of all, it is certain that there is only one dye-binding site per one αCT molecule in the Type I complexes because the absorption spectral shift and the induced CD are like one another. Another basis for this deduction is that many other molecular homologues which have the acridine and phenothiazine rings do not form molecular complexes with αCT, as evidenced from the finding that there is no visible spectral shift in these systems. That is, the acridine and phenothiazine dyes can be classified into two as for the complex formation with αCT; one forms a 1 : 1 complex (Type I) and the other does not, the fashion of complex formation being unique and once a complex is formed CD being induced.

Secondly, it is quite possible that the site of dye binding is the enzyme active site of αCT, since that there exists only one substrate binding site per enzyme molecule has been well established with αCT. Bernhard *et al.*[7] demonstrated that monoacylation of αCT completely displaces the PF molecule from the enzyme active site. It seems therefore that the specific enzyme-dye interaction is restricted to the conformation of the enzyme active site. In fact, we found that no complexes were formed between the same dyes as studied in this paper and pepsin and/or papain.

As will be reported in a forthcoming paper,[9] a dye molecule has to be imprisoned in a certain segment of a partner macromolecule in order to induce optical activity. At the active site of αCT, there is a spatial blank of moderate size surrounded with Histidyl 57, Seryl 195, and Methionyl 192. Whether an enzyme–dye

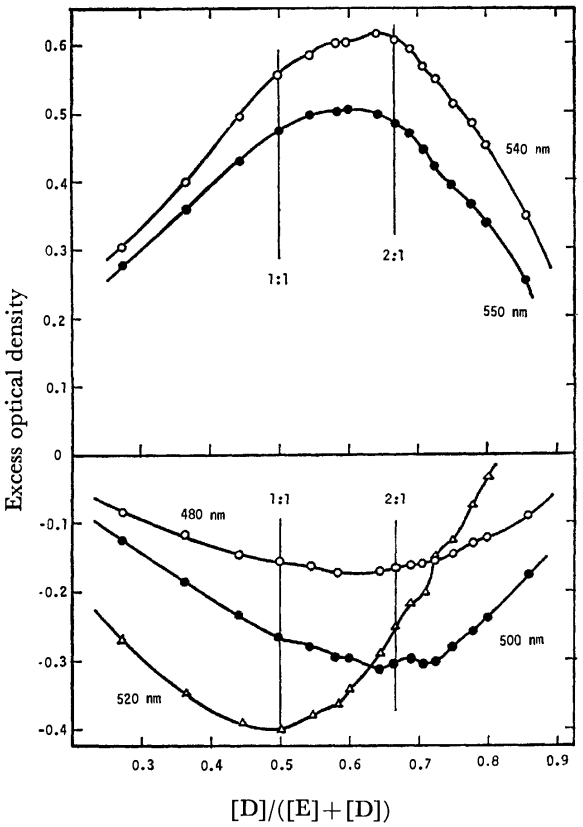

Fig. 6. Demonstration of formation of α-chymotrypsin–Pyronin B complex by method of continuous variations. $[E]+[D]=1.0\times10^{-4}$ mol dm^{-3}.

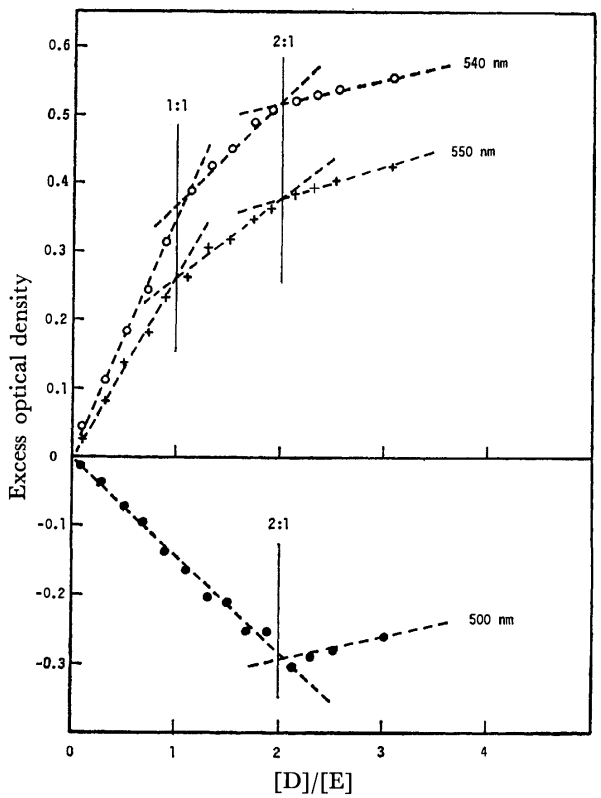

Fig. 7. Demonstration of formation of α-chymotrypsin–Pyronin B complex by molar ratio method. $[E]=3.6\times10^{-5}$ mol dm^{-3}.

complex is formed then depends upon a specific hydrophobic environment of the enzyme active site. This situation looks something like the well-known "lock-and-key" theory in the mechanism of enzyme action.

Type II Complexes. We will discuss the αCT–PB system as a Type II complex in which both positive and negative CD bands are induced. As in the case of the Type I complexes, the visible absorption spectrum of PB shifts to longer wavelength side upon addition of αCT, its general feature resembling closely to that of the absorption spectrum of PB brought about by the decrease of solvent polarity. It is clear therefore that the change in the visible spectral region of the αCT–PB system is due to the binding of PB to αCT which is less polar than water. The reason why a definite isosbestic point is not obtained is probably that there are more than two species of complexes in which stoichiometric compositions of αCT *vs.* PB are different from one another. The experiment of continuous variations revealed that there exists a complex formed by one αCT molecule and two PB molecules in addition to a 1 : 1 complex (Fig. 6). The same result was obtained by using the molar ratio method (Fig. 7).

It is hard to estimate the composition ratio of these two-type complexes. However, one can utilize the following experimental findings in order to guess whether 1 : 1 or 1 : 2 complexes is predominate to induce CD bands: (i) The variation of [E]/[D] with keeping [D] constant does not yield even slight change of the ICD spectral pattern; (ii) the molecular ellipticity becomes constant when [E]/[D] is in excess of 4 (*cf.* Fig. 4); the $[\theta]$ values of the Type II complexes are larger by an order of magnitude than those of the Type I complexes. We may thus conclude that the ICD spectrum shown in Fig. 3 is mainly due to the 1 : 2 complex.

When two dye molecules of the same species are brought together somewhere not far from one another, there occurs a rather strong dipole-dipole coupling. The leading term of the rotatory strength in this case is proportional to $\mathbf{R}\cdot(\boldsymbol{\mu}_1\times\boldsymbol{\mu}_2)$, $\boldsymbol{\mu}_1$ and $\boldsymbol{\mu}_2$ being the electric dipole transition moments of dye 1 and dye 2 respectively and $\mathbf{R}$ being the separation between $\boldsymbol{\mu}_1$ and $\boldsymbol{\mu}_2$.[10] If this is the case in the Type II complexes, the ICD spectrum may be resolved into four components, since in acridine dyes there exist two electric dipole transition moments, one along the molecular long axis and the other along the molecular short axis, both being in the molecular plane. We have carried out a Kronig-Kramers type analysis for the ICD spectrum and the observed optical rotatory dispersion curve of the αCT–PB system (Fig. 3). A resolution of the ICD bands is demonstrated in Fig. 8 which shows that two rotatory strength "couplets" are characteristic forms of dispersion. That is, the observed ICD spectrum is understood as a sum of the two Cotton effects of equal but opposite rotatory strength which are centered at 540 nm and lie less than a band width from one another, and of the other two Cotton effects of similar but smaller type centered at 520 nm. From the coincidence between the recomposed curve and the observed ICD spectrum (the recomposed and observed rotatory dispersion

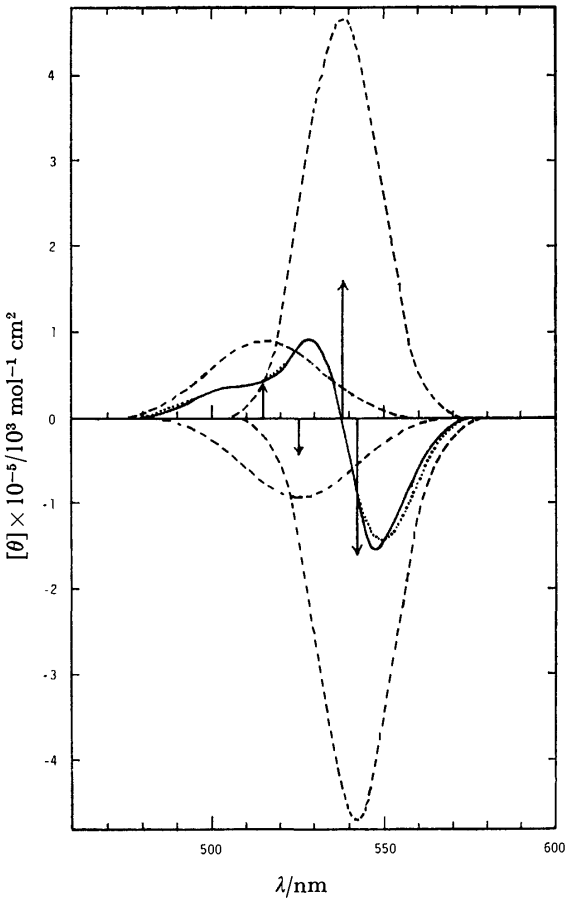

Fig. 8. Resolution of induced CD bands of α-chymotrypsin–Pyronin B complex assuming dipole-dipole coupling. The arrows show the positions and the strengths of electric dipole transition moments, the broken lines the component CD bands, the dotted line resultant CD bands, and the solid line observed CD bands.

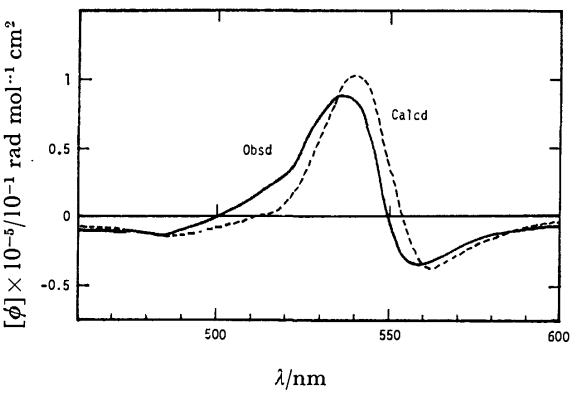

Fig. 9. Recomposed and observed rotatory dispersion curves of α-chymotrypsin–Pyronin B complex.

curves are compared in Fig. 9), a contribution from the 1 : 1 complex is unable to be taken into account. It is possible to speculate that the single dye molecule binds at the active site of αCT and the dye dimer binds at some other specific site, the contribution of the former to CD induction being negligibly small. On the other hand, our feeling at present is that a dye molecule

in the Type II complex is bound at a specific site which is not the active site of αCT and is therefore unable to act as a perturber for CD induction, the second dye molecule getting close to and keeping in a favorable direction side by side with the first dye molecule. If this is the case, the observations described above are well explained and it turns out that by some reason Pyronin G and/or Rhodamine B neither forms a complex with αCT nor associates one another in the neighborhood of the αCT molecule. No answer is possible to a question why there are two species of dyes, one forms a complex with αCT and the other does not.

Conclusion and Remark

The results and interpretation on the induced optical activity of the αCT–dye systems are summarized as follows:

(1) Some dyes form complexes with αCT with the appearance of CD and others do not.

(2) There are two ways of complex formation; whether a dye monomer is bound to αCT (Type I) or a dimer-like dye aggregate (Type II) is.

(3) To the Type I complex, proflavine, Acridine Yellow G, and acriflavine belong, yielding a single positive CD band. Composition of the complex is 1 : 1.

(4) To the Type II complex, Pyronin B and Rhodamine 6G belong, yielding one positive and one negative CD bands. Composition of the complex is mainly two dye molecules to one αCT.

(5) In the Type I complex, the site of dye binding is probably the enzyme active site of αCT which acts as an asymmetric perturber to induce CD in the visible absorption region of the dye.

(6) In the Type II complex, a dye molecule is bound at a specific site which is probably not the active site of αCT, and the second dye molecule combines with the first one in a fashion of forming a dimer. The coupling between the electric dipole transition moments of the two dye molecules is a leading term of the induced rotatory strength.

There are a lot of remaining questions: What is the reason for item (1)? Why any other enzyme does not form complexes with dyes such as those studied in this paper? Is there anything wrong with the reasoning for the site of dye binding? Experiments of the circular polarization of fluorescence and the fluorescence detected circular dichroism in the visible region are in progress, being aimed at the examination of the interaction mechanism in excited states of enzymes and dye chromophores.

The authors thank M. Miyake, K. Ogawa, H. Sakurai, and Y. Tsuboi for their technical assistance.

References

1) A. R. Peacoke and J. N. H. Skrett, *Trans. Faraday Soc.*, **52**, 261 (1956); K. Yamaoka, *Biopolymers*, **11**, 2537 (1972).

2) Y. J. I'Haya and T. Nakamura, *Bull. Chem. Soc. Jpn.*, **44**, 951 (1971); T. Nakamura and Y. J. I'Haya, *ibid.*, **45**, 2720 (1972).

3) R. E. Ballard, A. J. McCaffery, and S. F. Mason, *Biopolymers*, **4**, 97 (1966).

4) B. Chakrabarti and E. A. Balazs, *Biochem. Biophys. Res. Commun.*, **52**, 1170 (1973).

5) Y. J. I'Haya, T. Aoi, and T. Sano, *Bull. Chem. Soc. Jpn.*, **53**, 616 (1980).

6) J. Schlessinger and I. Z. Steinberg, *Proc. Natl. Acad. Sci. U.S.A.*, **69**, 769 (1972).

7) S. A. Bernhard, B. F. Lee, and Z. H. Tashijian, *J. Mol. Biol.*, **18**, 405 (1966).

8) P. Job, *Ann. Chim. Phys.*, **9**, 113 (1928); L. I. Katzin and E. Gebert, *J. Am. Chem. Soc.*, **72**, 5455 (1950).

9) Y. J. I'Haya and M. Miyake, to be published.

10) J. A. Schellman, *Acc. Chem. Res.*, **1**, 144 (1968).

Thermodynamic Study on Mixed Monolayers of Butyl Eicosanedioate and Tetradecanoic Acid

Yoshiteru HAYAMI, Takeshi YANO, Kinsi MOTOMURA, and Ryohei MATUURA*

Department of Chemistry, Faculty of Science, Kyushu University 33, Hokozaki, Fukuoka 812

(Received April 25, 1980)

In order to clarify the behavior of mixed monolayers of butyl eicosanedioate and tetradecanoic acid, the surface pressure was measured as a function of mean area at various compositions and temperatures. Four types of phase transition were observed. By use of the thermodynamic treatment previously developed, the apparent molar entropy and energy changes associated with the phase transition were evaluated. It was concluded on thermodynamic considerations that the butyl eicosanedioate and tetradecanoic acid monolayers are immiscible in condensed states and their phase diagram has a two-dimensional eutectic point.

It seems valuable to relate the states of monolayers with the molecular structure of film-forming substances by the thermodynamic approach.[1,2] It has been clarified through the study on mixed monolayers that the monolayer systems reveal the ideal,[3,4] eutectic,[5] azeotropic,[6-8] and other behaviors,[9] depending upon their molecular interactions. Now it seems useful to investigate the mixed monolayers of bipolar substances because they are expected to show a two-step transformation. While many works have been reported on the monolayer of dibasic substances since those of Adam *et al.*,[10-12] they are insufficient to make clear the state of the monolayers.

In this paper, the system consisting of tetradecanoic acid and butyl eicosanedioate was employed and the state of monolayers was clarified thermodynamically. Butyl eicosanedioate is a bipolar substance which contains a long carbon chain between two relatively large polar groups.

Experimental

Tetradecanoic acid was purified by vacuum distillation and recrystallization from ether. Butyl eicosanedioate was synthesized by the Fischer method from 1-butanol and eicosanedioic acid (presented by the courtesy of Okamura Seiyu Co.), and its purity was checked by gas-liquid chromatography and elemental analysis. Benzene purified by the standard procedure was used as the spreading solvent. Monolayers were spread on 0.5 mol kg^{-1} sodium chloride solution which was prepared from twice distilled water and sodium chloride (Wako special grade) as done in the previous papers.[6-9]

Surface pressure was measured by a Wilhelmy type electrosurface balance and automatically recorded on the chart paper. Temperature was kept constant within 0.1 K by circulating thermostated water. The surface pressure *vs.* area curve was reproducible within an experimental error.

Results and Discussion

The surface pressure of mixed monolayers consisting of butyl eicosanedioate and tetradecanoic acid was measured at various compositions and temperatures. The surface pressure π *vs.* surface area per monolayer molecule A curves of butyl eicosanedioate obtained at temperatures 290.7, 293.2, 295.7, and 298.2 K are shown in Fig. 1. It is seen that the π *vs.* A curves have two break points which represent phase transitions. The surface pressure of the second transition point

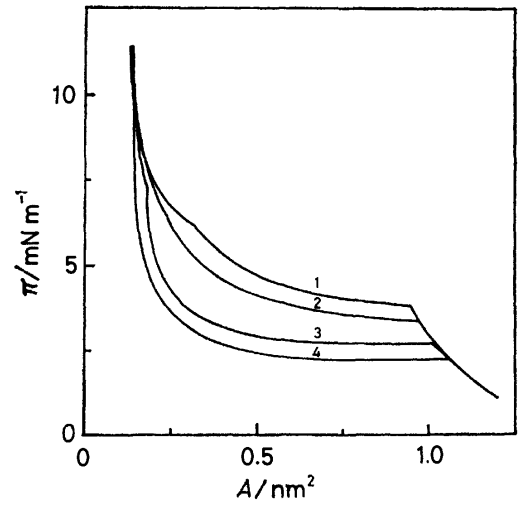

Fig. 1. Surface pressure π *vs.* mean area A curves of butyl eicosanedioate monolayer: (1) 298.2 K, (2) 295.7 K, (3) 293.2 K, (4) 290.7 K.

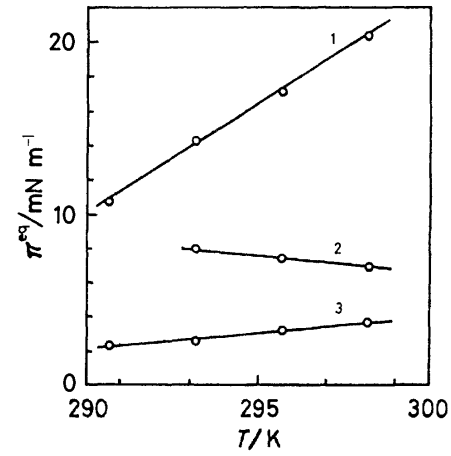

Fig. 2. Transition pressure π^{eq} *vs.* temperature curves: (1) tetradecanoic acid, (2) the second break point, (3) the first break point.

decreases, while that of the first transition point increases, with increasing temperature. This is shown clearly in Fig. 2. Comparing these temperature dependences of the transition pressure π^{eq} with those of tetradecanoic acid, the first break point is found to correspond to the transformation from an expanded to a

condensed film. On the other hand, the π^{eq} *vs.* T curve of the second break point has a negative slope greater than that of substrate with regard to the absolute value. This might suggest that the phase transition is accompanied by a positive entropy change, which leads us to the conclusion that the transformation takes place from the first condensed film (indicated by c(1,I)), in which both polar groups of butyl eicosanedioate molecule are in contact with the substrate, to the second condensed film (indicated by c(1,II)), in which one of them is in contact with the substrate.

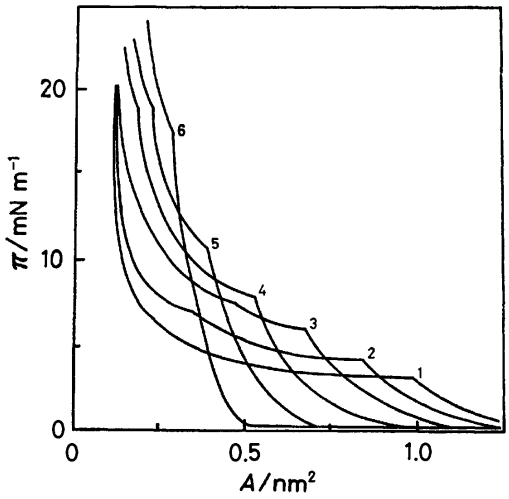

Fig. 3. Surface pressure π *vs.* mean area A curves of butyl eicosanedioate–tetradecanoic acid monolayers at 295.7 K: (1) $x_2^{\pi}=0$, (2) 0.2, (3) 0.4, (4) 0.6, (5) 0.8, (6) 1.

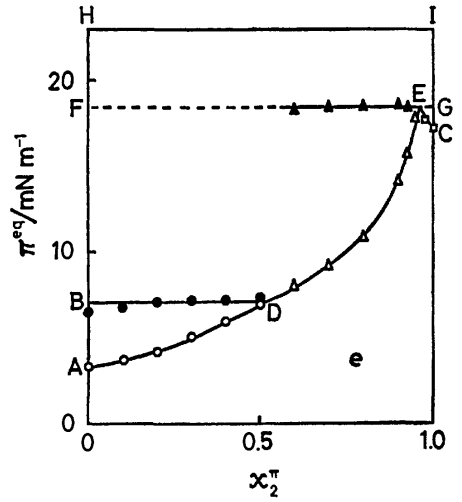

Fig. 4. Phase diagram of butyl eicosanedioate–tetradecanoic acid monolayer at 295.7 K.
Type of transition: ○, (e, c(1, I)); △, (e, c(1, II)); ●, (c(1, I), c(1, II)); □, (e, c(2)); ▲, (e, c(1, II) and c(2)).

The π *vs.* A curves of mixed monolayers obtained at various compositions at 295.7 K are shown in Fig. 3. These curves seem to have several kinds of break point. In Fig. 4, the surface pressure at the break point is plotted against the mole fraction of tetradecanoic acid defined by

$$x_2^{\pi} = n_2/(n_1+n_2), \tag{1}$$

where n_i is the number of moles of film-forming component i. It is seen that the first transition pressure of butyl eicosanedioate increases with addition of tetradecanoic acid (curve AE), whereas the second transition pressure remains approximately constant (curve BD). Similarly, the transition pressure of tetradecanoic acid increases with addition of butyl eicosanedioate (curve CE). These symmetrical π^{eq} *vs.* x_2^{π} curves appear to meet with each other at the point E which lies on the π^{eq} *vs.* x_2^{π} curve (curve FG) of the second break point observed in the concentration range from $x_2^{\pi}=0.50$ to 0.95. It is easily understood that the curves AE and CE express the equilibrium between expanded and condensed films.

Taking into account that the second transition pressure of mixed monolayer at low concentration is approximately equal to that of butyl eicosanedioate monolayer, it may be expected that the line BD in Fig. 4 represents the transformation from the first condensed film c(1,I) to the second condensed film c(1,II). This expectation is realized by consulting the temperature dependence of transition pressure. By measuring the surface pressure of mixed monolayers at 290.7, 293.2, and 298.2 K, the linear π^{eq} *vs.* T plots were obtained. As shown by the curve BD in Fig. 5, their slopes have about the same value. This result supports the above view.

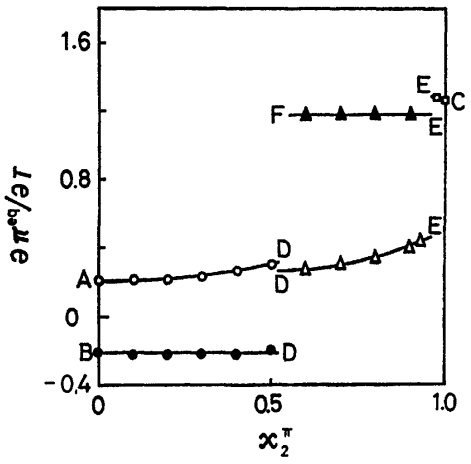

Fig. 5. $\partial\pi^{eq}/\partial T$ *vs.* x_2^{π} curves at 295.7 K.
Type of transition: ○, (e, c(1, I)); △, (e, c(1, II)); ●, (c(1, I), c(1, II)); □, (e, c(2)); ▲, (e, c(1, II) and c(2)).

Inspecting closely Fig. 4, on the other hand, the π^{eq} *vs.* x_2^{π} curve AE of the first break point seems to be divided into two parts at the point D where the curve is intersected by that of the second break point. This is substantiated by the fact that the value of $\partial\pi^{eq}/\partial T$ in Fig. 5 is discontinuous at that point. Thus we are led to the conclusion that the point D is the one where the condensed films c(1,I) and c(1,II) of butyl eicosanedioate and the expanded film, denoted by the

letter e, composed of butyl eicosanedioate and tetradecanoic acid coexist in equilibrium at 295.7 K under atmospheric pressure. Now we may say that the curve AD represents the equilibrium between the films c(1,I) and e and the curve DE the equilibrium between the films c(1,II) and e.

Let us next consider the point E on Fig. 4. Consulting Figs. 4 and 5, we immediately notice that the values of the second transition pressure in the concentration range $x_2^{\pi}=0.50$ to 0.95 are on the straight line FG parallel to the abscissa and their derivatives with respect to temperature are nearly equal. Furthermore, the temperature dependences of the curves DE and CE are found to be significantly different. Taking into consideration that the curve DE refers to the equilibrium of the expanded phase e of mixed monolayer with the condensed phase c(1,II) of butyl eicosanedioate monolayer, therefore, we can assign the curve CE to the equilibrium of the expanded state e with the condensed phase c(2) of tetradecanoic acid monolayer. The above results lead us to the conclusion that the point E represents the state where the films c(1,II), c(2), and e coexist in equilibrium and is called a two-dimensional eutectic point.

Now it is possible to say that the areas ADB, BDEF, CEG, and HFGI in Fig. 4 are the heterogeneous regions composed of the condensed film c(1,I) and expanded film e, the condensed film c(1,II) and expanded film e, the condensed film c(2) and expanded film e, and the condensed films c(1,II) and c(2), respectively. It is needless to say that the area denoted by e is the stable region of expanded film e. Therefore, Fig. 4 can be regarded as a phase diagram of the mixed monolayer of butyl eicosanedioate and tetradecanoic acid at 295.7 K under atmospheric pressure.

Let us now consider to evaluate the apparent molar entropy change $\Delta s^{\gamma}(\alpha,\beta)$ associated with the transition from phase α to phase β. For a pure monolayer, we have the equation[1,13]

$$\Delta s^{\gamma}(\alpha,\beta) = \bar{s}_i^{\gamma,\beta} - \bar{s}_i^{\gamma,\alpha} = N_A(A^{\beta}-A^{\alpha})[(\partial\pi^{eq}/\partial T)_p - (\partial\gamma^{\circ}/\partial T)_p], \quad i = 1, 2, \qquad (2)$$

where s_i^{γ} is the apparent partial molar entropy of component i, γ° the surface tension of substrate, and N_A Avogadro's number. On the other hand, the apparent molar entropy of transition from the expanded phase of mixed monolayer to the condensed phase c(1,I), c(1,II), or c(2) is evaluated with the aid of the relation

$$\Delta s^{\gamma}(e,\beta) = \bar{s}_i^{\gamma,\beta} - \bar{s}_i^{\gamma,e} = N_A[A^{\beta}-A^{e}-(\delta_{i2}-x_2^{\pi,e})(\partial A^{e}/\partial x_2^{\pi,e})_{T,p,\pi}] \times [(\partial\pi^{eq}/\partial T)_{p,x_i^{\gamma,e}} - (\partial\gamma^{\circ}/\partial T)_p], \quad i = 1, 2, \qquad (3)$$

where

$$\delta_{i2} = 0, \quad i = 1; \qquad = 1, \quad i = 2. \qquad (4)$$

The value of $\Delta s^{\gamma}(e,c(2))$ may be calculated by making use of the value of $\partial\pi^{eq}/\partial T$ given in Fig. 5 on the assumption that the area of tetradecanoic acid in the condensed film is replaced by the corresponding one of octadecanoic acid and the value of γ° is approximated by that of pure water. The values obtained are depicted as a function of $x_2^{\pi,e}$ in Fig. 6. In evaluating $\Delta s^{\gamma}(e,c(1,I))$ and $\Delta s^{\gamma}(e,c(1,II))$, however, it is necessary to estimate the values of $A^{c(1,I)}$ and $A^{c(1,II)}$. With the aid of the thermodynamics, we can easily derive the equation which holds at the eutectic point E:

$$(\partial\pi^{eq}/\partial T)_p^{FE} - (\partial\gamma^{\circ}/\partial T)_p = [x_1^{\pi,e}\Delta s^{\gamma}(e, c(1, II)) + x_2^{\pi,e}\Delta s^{\gamma}(e, c(2))]/N_A[(x_1^{\pi,e}A^{c(1,II)} + x_2^{\pi,e}A^{c(2)}) - A^{e}], \qquad (5)$$

where the superscript FE on $(\partial\pi^{eq}/\partial T)_p$ means that its value is the extrapolated one of the curve FE to the point E in Fig. 5. Substituting Eq. 3 and rearranging the resulting equation, Eq. 5 is rewritten in the form

$$A^{c(1,II)} = A^{e} + \{x_2^{\pi,e}(A^{c(2)}-A^{e})[(\partial\pi^{eq}/\partial T)_{p,x_i^{\gamma,e}}^{CE} - (\partial\pi^{eq}/\partial T)_p^{FE}] + x_1^{\pi,e}x_2^{\pi,e}[(\partial A^{e}/\partial x_2^{\pi,e})_{T,p,\pi}^{DE}(\partial\pi^{eq}/\partial T)_{p,x_i^{\gamma,e}}^{DE} - (\partial A^{e}/\partial x_2^{\pi,e})_{T,p,\pi}^{CE}(\partial\pi^{eq}/\partial T)_{p,x_i^{\gamma,e}}^{CE}]\}/x_1^{\pi,e}[(\partial\pi^{eq}/\partial T)_p^{FE} - (\partial\pi^{eq}/\partial T)_{p,x_i^{\gamma,e}}^{DE}]. \qquad (6)$$

The superscripts CE and DE have the same meaning as FE concerning the respective curve. Thus the value of $A^{c(1,II)}$ at the eutectic point can be estimated experimentally; $A^{c(1,II)}=1.68\,A^{c(2)}$ was obtained. By assuming the relation

$$A^{c(1,II)}(\pi')/A^{c(2)}(\pi') = A^{c(1,II)}(\pi)/A^{c(2)}(\pi), \qquad (7)$$

we can now evaluate $\Delta s^{\gamma}(e,c(1,II))$. The value obtained is also shown in Fig. 6.

Further, the following equation is proved to hold at the point D where the three phases e, c(1,I), and c(1,II) coexist in equilibrium:

$$\Delta s^{\gamma}(c(1, I), c(1, II)) = \Delta s^{\gamma}(e, c(1, II)) - \Delta s^{\gamma}(e, c(1, I)). \qquad (8)$$

Substitution of Eqs. 2 and 3 into Eq. 8 and rearrange-

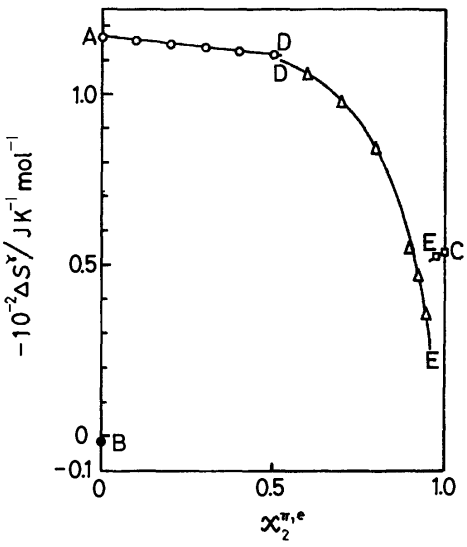

Fig. 6. Apparent molar entropy change Δs^{γ} *vs.* mole fraction of tetradecanoic acid $x_2^{\pi,e}$ curves at 295.7 K. Type of transition: ○, (e, c(1, I)); △, (e, c(1, II)); ●, (c(1, I), c(1, II)); □, (e, c(2)).

ment yield the expression

$$A^{c(1,I)} = A^{e} + \{(A^{c(1,II)} - A^{e})[(\partial\pi^{eq}/\partial T)^{ED}_{p,x_1^{\pi,e}} - (\partial\pi^{eq}/\partial T)^{BD}_{p}] - x_2^{\pi,c}[(\partial A^{e}/\partial x_2^{\pi,e})^{AD}_{T,p,\pi}(\partial\pi^{eq}/\partial T)^{AD}_{p,x_1^{\pi,e}} - (\partial A^{e}/\partial x_2^{\pi,e})^{ED}_{T,p,\pi}(\partial\pi^{eq}/\partial T)^{ED}_{p,x_1^{\pi,e}}]\}/[(\partial\pi^{eq}/\partial T)^{AD}_{p,x_1^{\pi,e}} - (\partial\pi^{eq}/\partial T)^{BD}_{p}]. \quad (9)$$

Thus the value of $A^{c(1,I)}$ was estimated to be $1.86A^{c(2)}$. In a similar manner as above, we can evaluate the values of $\Delta s^{\gamma}(e,c(1,I))$ and $\Delta s^{\gamma}(c(1,I), c(1,II))$ by virtue of Eqs. 2 and 3. The results are also shown in Fig. 6.

It is seen from Fig. 6 that the apparent molar entropy change $\Delta s^{\gamma}(e,c(1,I))$ of butyl eicosanedioate monolayer has an appreciably large negative value as compared with the corresponding one $\Delta s^{\gamma}(e,c(2))$ of tetradecanoic acid monolayer. The value of $\Delta s^{\gamma}(c(1,I), c(1,II))$ is found to be small but definitely positive. These results are compatible with the view that butyl eicosanedioate is a bipolar molecule of which the hydrocarbon chain is long enough to take a bent conformation in the first condensed film. Further, Fig. 6 reveals that the apparent molar entropy change associated with the transformation of component i from expanded to condensed film increases with decreasing $x_1^{\pi,e}$. In cases of the mixed monolayers of tetradecanoic acid with pentadecanoic acid and ethyl heptadecanoate which form homogeneous condensed phases, we have observed that the corresponding apparent partial molar entropy changes of these film-forming substances are approximately constant over the whole range of concentrations.[6] Therefore it is supported by the above results that butyl eicosanedioate and tetradecanoic acid are immiscible in the condensed state.

Now let us evaluate the apparent molar energy changes $\Delta u^{\gamma}(\alpha,\beta)$ and $\Delta u^{\gamma}(e,\beta)$ related, respectively, to $\Delta s^{\gamma}(\alpha,\beta)$ and $\Delta s^{\gamma}(e,\beta)$ (Eqs. 2 and 3) by the expressions[6]

$$\Delta u^{\gamma}(\alpha,\beta) = -(\pi^{eq}-\gamma^{\circ})N_A(A^{\beta}-A^{\alpha}) + T\Delta s^{\gamma}(\alpha,\beta), \quad i = 1, 2 \quad (10)$$

and

$$\Delta u^{\gamma}(e,\beta) = -(\pi^{eq}-\gamma^{\circ})N_A[A^{\beta}-A^{e}-(\delta_{12}-x_2^{\pi,e}) \times (\partial A^{e}/\partial x_2^{\pi,e})_{T,p,\pi}] + T\Delta s^{\gamma}(e,\beta), \quad i = 1, 2 \quad (11)$$

where we have neglected contribution of the apparent molar volume change. Evidently they can be calculated by making use of the experimental results. The numerical values are shown in Fig. 7. It is observed, as expected, that the values of apparent molar energy of transition deviate from the straight line connecting the values of Δu^{γ} for the pure components. Comparing with Fig. 6, we notice that the Δu^{γ} *vs.* $x_2^{\pi,e}$ and Δs^{γ} *vs.* $x_2^{\pi,e}$ curves behave similarly except that the value of $\Delta u^{\gamma}(c(1,I), c(1,II))$ is negative while that of $\Delta s^{\gamma}(c(1,I), c(1,II))$ is positive. It is of importance to note that the value of $\Delta u^{\gamma}(c(1,I), c(1,II))$ is responsible for the difference between $\Delta u^{\gamma}(e,c(1,I))$ and $\Delta u^{\gamma}(e,c(1,II))$ at the discontinuous point D.

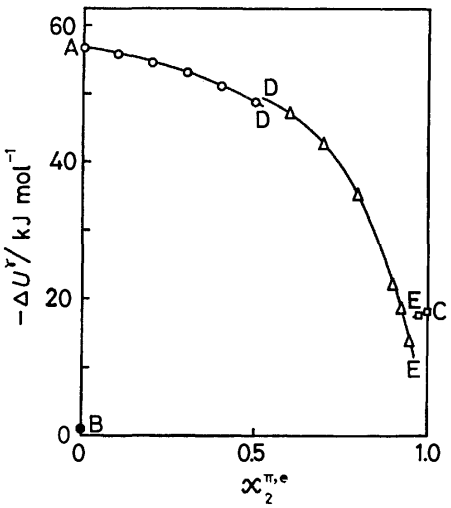

Fig. 7. Δu^{γ} *vs.* $x_2^{\pi,e}$ curves for butyl eicosanedioate–tetradecanoic acid system at 295.7 K.
Type of transition: ○, (e, c(1, I)); △, (e, c(1, II)); ●, (c(1, I), c(1, II)); □, (e, c(2)).

References

1) K. Motomura, *J. Colloid Interface Sci.*, **48**, 307 (1974).
2) K. Motomura, K. Sekita, and R. Matuura, *J. Colloid Interface Sci.*, **48**, 319 (1974).
3) K. Sekita, M. Nakamura, K. Motomura, and R. Matuura, *Mem. Fac. Sci. Kyushu Univ., Ser. C*, **10**, 51 (1976).
4) H. Matuo, K. Hiromoto, K. Motomura, and R. Matuura, *Bull. Chem. Soc. Jpn.*, **51**, 690 (1978).
5) K. Motomura, T. Terazono, H. Matuo, and R. Matuura, *J. Colloid Interface Sci.*, **57**, 52 (1976).
6) K. Motomura, T. Yano, M. Ikematsu, H. Matuo, and R. Matuura, *J. Colloid Interface Sci.*, **69**, 209 (1979).
7) H. Matuo, N. Yosida, K. Motomura, and R. Matuura, *Bull. Chem. Soc. Jpn.*, **52**, 667 (1979).
8) H. Matuo, K. Motomura, and R. Matuura, *J. Colloid Interface Sci.*, **69**, 192 (1979).
9) H. Matuo, K. Motomura, and R. Matuura, *Bull. Chem. Soc. Jpn.*, **52**, 673 (1979).
10) N. K. Adam, and G. Jessop, *Proc. R. Soc. London, Ser. A*, **112**, 376 (1926).
11) N. K. Adam, J. F. Danielli, and J. B. Harding, *Proc. R. Soc. London Ser. A*, **147**, 491 (1934).
12) P. M. Jeffers and J. Daen, *J. Phys. Chem.*, **69**, 2368 (1965).
13) K. Motomura, *Adv. Colloid Interface Sci.*, **12**, 1 (1980).
14) J. J. Jasper, *J. Phys. Chem. Ref. Data*, **1**, 841 (1972).

Use of Propagators in the Hückel Model

Shigeyuki Aono* and Kiyoshi Nishikawa
Department of Chemistry, Faculty of Science, Kanazawa University, Marunouchi, Kanazawa 920
(Received May 6, 1980)

The electronic structures of molecules composed of identical atoms are investigated in terms of propagators under the Hückel approximation. General rules to get propagators for systems under considerations are presented. Then some physical quantities (the charge densities, the bond orders and the total energies) are obtained by making the analysis of the propagators. Expressions for the mutual polarizabilities are also exactly derived. Some discussions about the approximate natures of current results are made.

Quantum mechanical calculations are usually carried out as follows: First, the Shrödinger equation for a system under consideration is solved under a certain approximation, and then the observed quantities are estimated as the expectation values of the corresponding operators by the use of the wave function. It has been pointed out by Coulson and Longuet-Higgins[1] that even in the quantum chemical calculations the procedure mentioned above is not always necessary. They stressed that once the Hückel determinant is given, any physical quantity is directly calculated without solving the secular equation, by making the analysis of this determinant:

Let

$$\Delta(\omega) \equiv \begin{vmatrix} \alpha_1-\omega & \beta_{12} & \beta_{13} & \cdots & \beta_{1n} \\ \beta_{21} & \alpha_2-\omega & \beta_{23} & \cdots & \beta_{2n} \\ \vdots & \vdots & \vdots & & \vdots \\ \beta_{n1} & \beta_{n2} & \beta_{n3} & \cdots & \alpha_n-\omega \end{vmatrix} \quad (1)$$

where α_i, β_{ik}, and ω are the coulomb integral, resonance integral and energy parameter respectively. Then the bond order q_{rs} (its diagonal term is the charge density) and the total energy E are obtained as

$$q_{rs} = \frac{1}{2\pi i}\int_C dz \frac{\Delta_{rs}(z)}{\Delta(z)}, \quad (2)$$

$$E = \frac{1}{2\pi i}\int_C dz\, z\frac{\partial}{\partial z} \ln \Delta(z). \quad (3)$$

where $\Delta_{rs}(z)$ is the (r,s) cofactor of $\Delta(z)$ and integration with respect to the complex variable z is performed along the so-called Coulson contour shown in Fig. 1. Integration is assumed to include the spin summation.

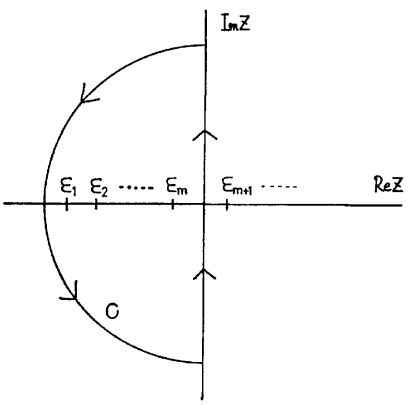

Fig. 1. Coulson contour: ε_1—ε_m are occupied energies and ε_{m+1}.... are unoccupied.

Coulson and Longuet-Higgins have also given similar expressions for mutual polarizabilities. It is needless to say that for these quantities the expressions with LCAO coefficients are commonly used, and that the use of these approximate expressions is only for the convienience of numerical calculations.

In the present work, a theory with propagator is developed in the Hückel model. This is related very closely to the idea of Coulson and Longuet-Higgins. The processes of constructing propagators, however, make clear the physical content of the Hückel model.

Propagator

The Green's function (propagator), corresponding to the linear Hermitian time-independent differential operator $L(r)$ and the complex variable z, is defined as the solution of the equation

$$(z-L(r))G(r,r';z) = \delta(r-r'), \quad (4)$$

subject to certain boundary conditions on the surface of the domain of r and r'. Equation 4 can be considered as the coordinate representation of the operator equation

$$(z-L)G = 1. \quad (5)$$

If $\{|n\rangle\}$ is the complete orthonormal set of the operator L, *i.e.*,

$$L|n\rangle = \lambda_n|n\rangle, \quad (6)$$

$$\langle n|m\rangle = \delta_{nm}, \quad (7)$$

$$\sum_n |n\rangle\langle n| = 1, \quad (8)$$

then one can write

$$G = (z-L)^{-1} = \sum_n \frac{|n\rangle\langle n|}{z-\lambda_n}. \quad (9)$$

$G(r,r';z)$ in Eq. 4 may be regarded as the (r,r') matrix element of the operator G.

Hückel Model. The Hückel Hamiltonian (the tight-binding approximation in the solid state physics) is written as

$$H = \sum_s |s\rangle\varepsilon_s\langle s| + \sum_{st}{}' |s\rangle v_{st}\langle t|, \quad (10)$$

where s and t are site indices. Keeping in mind that we are dealing with molecules which consist of the same kind of atoms, we put $\varepsilon_s=0$, $v_{st}=v$ and the second summation in Eq. 10 is carried out as usual only for the nearest neighbors. Thus the Hamiltonian becomes simply

$$H = v\sum_{st}{}' |s\rangle\langle t|. \quad (11)$$

In order to perform the forthcoming analysis in the present work, we investigate the diatomic molecule a—b in Fig. 2a in terms of propagators. The diagonal term of the Green's function in the zeroth-order approximation, $G_0(a,a;z)$ is simply obtained from Eq. 9 and the first term of Eq. 10 as

$$G_0(a,a;z)=\sum_s \frac{\langle a|s\rangle\langle s|a\rangle}{z-\varepsilon_s}=\frac{1}{z}, \quad (\varepsilon_s=0), \tag{12}$$

where the completeness condition (8) has been used.

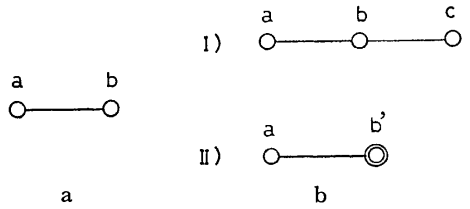

Fig. 2. Schematic diagrams of molecules. a: Diatomic molecule, b: triatomic molecule.

Now we consider the exact propagator $G(a,a;z)$ fully dressed by interactions:

$$\begin{aligned}G(a,a)=&G_0(a,a)+G_0(a,a)vG_0(b,b)vG_0(a,a)\\&+G_0(a,a)vG_0(b,b)vG_0(a,a)vG_0(b,b)vG_0(a,a)+\cdots,\end{aligned} \tag{13}$$

where the first term is the bare propagator, the second includes the interaction twice, the third four times and so on. Equation 13 is rewritten as

$$\begin{aligned}G(a,a)&=G_0(a,a)+G_0(a,a)vG_0(b,b)v[G_0(a,a)\\&\quad+G_0(a,a)vG_0(b,b)vG_0(a,a)+\cdots\\&=G_0(a,a)+G_0(a,a)vG_0(b,b)vG(a,a)\\&=[G_0(a,a)^{-1}-vG_0(b,b)v]^{-1}.\end{aligned} \tag{14}$$

The last expression is the Dyson equation for our simplest case. Substituting Eq. 12 into Eq. 14, we obtain

$$G(a,a;z)=z/(z^2-v^2). \tag{15}$$

It is obvious that the poles of Eq. 15, *i.e.*, the roots of $z^2-v^2=0$, give us the Hückel orbital energies.

The charge density q_a at site a, the bond order q_{ab} and the total energy E are obtained with the propagators as,

$$q_a=\frac{1}{2\pi i}\int_C dz\, G(a,a;z), \tag{16}$$

$$\begin{aligned}q_{ab}&=\frac{1}{2\pi i}\int_C dz\, G(a,b;z)\\&=\frac{1}{2\pi i}\int_C dz\, G(a,a;z)vG_0(b,b;z),\end{aligned} \tag{17}$$

$$E=\frac{1}{2\pi i}\sum_a\int_C dz\, zG(a,a;z), \tag{18}$$

where the integration is made along the Coulson contour and is assumed to include the spin summation. Thus we can easily get the well-known results, $q_a=q_{ab}=1$ and $E=2v$.

General Rules to Get Propagators

We generalize the method in the previous section to the arbitrary finite network. This procedure is called the renormalization perturbation expansion which has been investigated by Anderson[2,3] for the infinite lattice. Generalization will be done step by step in the following.

End Point Propagator. Consider the edge atom a in the triatomic molecule shown in Fig. 2b. If we replace b and c in (I) by b' as in (II), the propagator $G(a,a)$ can be immediately obtained as has been done in the previous section:

$$G(a,a)=[G_0(a,a)^{-1}-vG(b',b')v]^{-1} \tag{19}$$

in which $G(b',b')$ is the propagator dressed only by the interaction between b and c, since the interaction between a and b is already taken into account, that is,

$$G(b',b')=[G_0(b,b)^{-1}-vG_0(c,c)v]^{-1}. \tag{20}$$

In this sense, $G(b',b')$ is rewritten as $G(b,b[a])$ indicating that the effect of site a should be excluded. We rewrite Eq. 19 as

$$G(a,a)=[G_0(a,a)^{-1}-vG(b,b[a])v]^{-1}. \tag{21}$$

This relation is itself a generalized expression for an arbitrary chain molecule, as seen from Fig. 3.

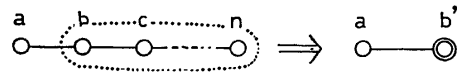

Fig. 3. Renormalization of the propagator of a linear molecule.

The off-diagonal term $G(a,c)$ in Fig. 2b is given by

$$G(a,c)=G(a,a)vG(b,b[a])vG(c,c[a,b]), \tag{22}$$

where it is apparent that $G(c,c[a,b])=G_0(c,c)$. Generalization of Eq. 22 to an arbitrary path is straightforward.

Branching Point Propagator. Consider the propagator $G(b,b)$ at site b in Fig. 2b. Since we have two paths arrived at site b, $G(b,b)$ can be expressed as

$$G(b,b)=[G_0(b,b)^{-1}-vG_0(a,a)v-vG_0(c,c)v]^{-1}. \tag{23}$$

This result is easily generalized to the branching point at which many paths end as shown in Fig. 4:

$$G(b,b)=[G_0(b,b)^{-1}-\sum_i vG(a_i,a_i[b])v]^{-1}. \tag{24}$$

It should be noted that there is no interactions among branches in this case.

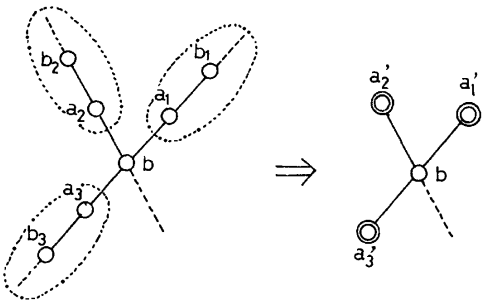

Fig. 4. Schematic diagram of a branched molecule and renormalization of its propagator.

Ring Propagator. We consider a ring of three members as shown in Fig. 5a. In order to obtain $G(a,a)$, we first follow the path $a\rightarrow b\rightarrow c\rightarrow a$. If there were no

interaction between a and c, we would simply have

$$G(a,a) = [G_0(a,a)^{-1} - vG(b,b[a])v]^{-1}. \quad (25)$$

Actually we need a new term $G(b,c[a])$ to enclose the loop, and obtain

$$G(a,a) = [G_0(a,a)^{-1} - vG(b,b[a])v - vG(b,c[a])v]^{-1}. \quad (26)$$

This procedure should be performed also along the path $a \to c \to b \to a$. Thus we obtain

$$G(a,a) = [G_0(a,a)^{-1} - vG(b,b[a])v - vG(b,c[a])v - vG(c,c[a])v - vG(c,b[a])v]^{-1}, \quad (27)$$

where for example

$$G(b,c[a]) = G(b,b[a])vG(c,c[a,b]) \quad (28)$$

is the off-diagonal term of the b—c subsystem.

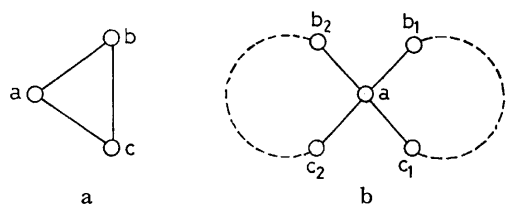

Fig. 5. Schematic diagrams of ring molecules. a: Triatomic ring molecule, b: two rings joinning at site a.

The physical meanings of Eq. 27 are as follows: The propagator $G(a,a)$ is the sum of the quantum mechanical probability amplitude for all the possible ways the electron can propagate in a ring from site a to itself interacting with various sites on the way. The first term is the free propagator given by Eq. 12. The second term represents the process that the electron interacts with site b, propagates many times in the b—c subsystem and finally returns to site a through site b. This process is schematically shown in Fig. 6a. The third term represents a new process due to the ring character. The electron propagates in the b—c subsystem as before, but comes back to site a through site c. This process is also shown in Fig. 6b. The last two terms are the counterparts of the above processes.

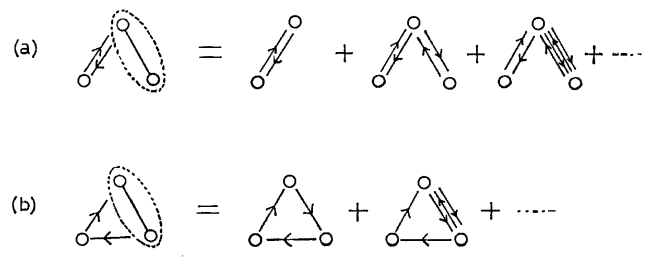

Fig. 6. Renormalization of the interactions between a and b—c subsystem.

The generalization to a more complicated ring shown in Fig. 5b is straightforward. The three types of the processes mentioned above suffice to obtain the propagator for an arbitrary network.

Illustrative Examples

Triatomic Linear Molecule. Substituting Eqs. 12 and 15 into Eqs. 21 and 23, we have

$$G(a,a;z) = G(c,c;z) = \frac{z^2-v^2}{z^3-2zv^2}, \quad (29)$$

$$G(b,b;z) = \frac{z^2}{z^3-2zv^2}, \quad (30)$$

The off-diagonal elements are also easily estimated as

$$G(a,b;z) = \frac{zv}{z^3-2zv^2}, \quad (31)$$

$$G(a,c;z) = \frac{v^2}{z^3-2zv^2}. \quad (32)$$

The Hückel orbital energies are obtained from the poles of these propagators, as $z=\pm\sqrt{2}v$, 0. We can estimate the bond order matrix and the total energy, using Eqs. 17 and 18, respectively, as

$$q = \begin{pmatrix} 1 & 1/\sqrt{2} & 0 \\ 1/\sqrt{2} & 1 & 1/\sqrt{2} \\ 0 & 1/\sqrt{2} & 1 \end{pmatrix}, \quad (33)$$

$$E = 2\sqrt{2}v. \quad (34)$$

It is noted that in this case the Coulson contour has to include the origin.

Triatomic Ring Molecule (Positive Ion). We consider only the case of positive ion for the sake of simplicity. Using Eqs. 12 and 20 in Eq. 27, we get

$$G(a,a;z) = \frac{z^2-v^2}{z^3-3zv^2-2v^2}. \quad (35)$$

The off-diagonal element, $G(a,b)$, can be calculated by taking into account two paths, that is, $a \to b$ and $a \to c \to b$:

$$G(a,b;z) = G(a,a)vG(b,b[a]) + G(a,a)vG(c,c[a])vG(b,b[a,c])$$

$$= \frac{zv+v^2}{z^3-3zv^2-2v^2}. \quad (36)$$

The poles of these propagators determine the Hückel orbital energies as $z=2v$, $-v$(doubly degenerate). If we consider the positive ion case, the contour goes around only the pole, $z=2v$. Then we obtain the bond order and total energy as

$$q_{ij} = 2/3 \text{ for all } i,j, \qquad E = 4v. \quad (37)$$

Chain Molecule; Recurrence Formulae. We have seen in the preceding treatment that any kind of matrix element of the propagator can be constructed from the diagonal elements at the edge of the chain molecule. It is useful at this stage to provide a simple way to obtain them. In this section, G_N denotes the diagonal matrix element at the edge of the chain molecule of N atoms.

It is a simple task to estimate G_N as a continued fraction, *i.e.*,

$$G_N(z)^{-1} = z - \cfrac{1}{z - \cfrac{1}{z - \cfrac{1}{z - \cdots}}}$$

$$\equiv z - \frac{1}{z} + \frac{1}{z} - \frac{1}{z} + \cdots, \quad (38)$$

where we put $v=1$. If there is a more general continued fraction

$$S_N = b_1 + \frac{1}{b_2} + \frac{1}{b_3} + \cdots + \frac{1}{b_N}, \quad (39)$$

this is expressed as

$$S_N = P_N/Q_N, \tag{40}$$

where, for P_N and Q_N, the following recurrence relations hold:

$$\begin{aligned} P_N &= b_N P_{N-1} + P_{N-2}, \\ Q_N &= b_N Q_{N-1} + Q_{N-2}, \end{aligned} \tag{41}$$

with

$$\begin{aligned} P_0 &= 1, \quad P_{-1} = 0, \\ Q_0 &= 0, \quad Q_{-1} = 1. \end{aligned} \tag{42}$$

In the case of Eq. 38, observing that $b_N=(-1)^{N-1}z$, we can easily calculate the first few series for P_N and Q_N. Then we use the mathematical induction to obtain the general formula and get

$$\begin{aligned} P_N &= \varepsilon_N p_N \\ &= \varepsilon_N\left[\sum_k (-1)^k \binom{N-k}{k} z^{N-2k}\right] \end{aligned} \tag{43}$$

where ε_N is the phase factor defined by

$$\varepsilon_N = \begin{cases} (-1)^{(N-1)/2} & \text{for odd } N, \\ (-1)^{N/2} & \text{for even } N. \end{cases} \tag{44}$$

We also obtain

$$Q_N = (-1)^{N-1} P_{N-1}. \tag{45}$$

Combining Eqs. 43 and 45, we have

$$G_N(z)^{-1} = p_N(z)/p_{N-1}(z). \tag{46}$$

It is obvious that p_N is nothing but the Hückel determinant. We list up some p_N in the following:

$$\begin{aligned} p_1 &= z, \\ p_2 &= z^2 - 1, \\ p_3 &= z^3 - 2z, \\ p_4 &= z^4 - 3z^2 + 1, \\ p_5 &= z^5 - 4z^3 + 3z, \\ p_6 &= z^6 - 5z^4 + 6z^2 - 1. \end{aligned} \tag{47}$$

Perturbation Theory

In order to express the various polarizabilities in terms of propagators, we provide an alternative method in the perturbation expansion of the propagator. In the matrix notation,

$$\begin{aligned} \boldsymbol{G}(z) &= \boldsymbol{G}_0(z) + \boldsymbol{G}_0(z)\boldsymbol{v}\boldsymbol{G}_0(z) + \boldsymbol{G}_0(z)\boldsymbol{v}\boldsymbol{G}_0(z)\boldsymbol{v}\boldsymbol{G}_0(z) + \cdots \\ &= \boldsymbol{G}_0(z) + \boldsymbol{G}_0(z)\boldsymbol{T}(z)\boldsymbol{G}_0(z), \end{aligned} \tag{48}$$

where

$$\begin{aligned} \boldsymbol{T}(z) &= \boldsymbol{v} + \boldsymbol{v}\boldsymbol{G}_0(z)\boldsymbol{v} + \boldsymbol{v}\boldsymbol{G}_0(z)\boldsymbol{v}\boldsymbol{G}_0(z)\boldsymbol{v} + \cdots \\ &= \boldsymbol{v}[1-\boldsymbol{G}_0(z)\boldsymbol{v}]^{-1}. \end{aligned} \tag{49}$$

In the above, $\boldsymbol{v}$ is the perturbation whose magnitude is arbitrary in our treatment, so that the full propagators previously obtained are rewritten $\boldsymbol{G}_0$ in this section.

The Perturbation of the Coulomb Potential at Site m. In this case, the perturbation becomes

$$v_{ij} = \begin{cases} \varepsilon_m & \text{for } i=j=m, \\ 0 & \text{for others,} \end{cases} \tag{50}$$

so that $\boldsymbol{T}(z)$ is given by

$$T(i,j;z) = \begin{cases} \varepsilon_m/(1-G_0(m,m;z)\varepsilon_m) & \text{for } i=j=m \\ 0 & \text{for others.} \end{cases} \tag{51}$$

Substituting this into Eq. 48, we get

$$G(a,a) = G_0(a,a) + G_0(a,m)T(m,m)G_0(m,a). \tag{52}$$

Hence, the change in charge density at site a becomes

$$\begin{aligned} \delta q_a &= \frac{1}{2\pi i}\int_C dz(G(a,a;z)-G_0(a,a;z)) \\ &= \varepsilon_m \frac{1}{2\pi i}\int_C dz|G_0(a,m;z)|^2/(1-G_0(m,m;z)\varepsilon_m) \\ &\equiv \varepsilon_m \cdot \Pi_{a;m}, \end{aligned} \tag{53}$$

where the last equation defines the atom-atom polarizability. Remember that we have assumed the integration includes the spin summation. If we neglect $G_0(m,m)\varepsilon_m$ as a small quantity compared to unity, Eq. 53 reproduces the result of the elementary perturbation theory:

$$\Pi^0_{a;m} = \frac{1}{2\pi i}\int_C dz|G_0(a,m;z)|^2. \tag{54}$$

It should be noted that in our exact expression, ε_m is replaced by the effective interaction

$$\begin{aligned} \tilde{\varepsilon}_m &= T(m,m;z) \\ &= \varepsilon_m/(1-G_0(m,m)\varepsilon_m). \end{aligned} \tag{55}$$

Next, evaluating the off-diagonal element of Eq. 48, we get

$$G(a,b) = G_0(a,b) + G_0(a,m)T(m,m)G_0(m,b), \tag{56}$$

from which the change in bond order is derived;

$$\begin{aligned} \delta q_{ab} &= \frac{1}{2\pi i}\int_C dz(G(a,b;z)-G_0(a,b;z)) \\ &= \varepsilon_m \frac{1}{2\pi i}\int_C dz G_0(a,m;z)G_0(m,b;z)/(1-G_0(m,m;z)\varepsilon_m) \\ &\equiv \varepsilon_m \cdot \Pi_{ab;m}, \end{aligned} \tag{57}$$

where the last equation defines the bond-atom polarizability. If we replace $\tilde{\varepsilon}_m$ by ε_m as before, we get

$$\Pi^0_{ab;m} = \frac{1}{2\pi i}\int_C dz\, G_0(a,m;z)G_0(m,b;z). \tag{58}$$

The Perturbation of the Resonance Energy at the Bond (m,n). Here we consider the case that

$$v_{ij} = \begin{cases} v & \text{for } (i,j) = (n,m) \text{ or } (m,n) \\ 0 & \text{otherwise.} \end{cases} \tag{59}$$

In this case, as seen from Eq. 49, non-vanishing part of $\boldsymbol{T}$ becomes a 2×2 matrix and its explicit form may be calculated as follows:

$$\begin{aligned} \boldsymbol{T}(z) &= (\boldsymbol{v}^{-1}-\boldsymbol{G}_0(z))^{-1} \\ &= \begin{pmatrix} -G_0(m,m) & 1/v-G_0(m,n) \\ 1/v-G_0(n,m) & -G_0(n,n) \end{pmatrix}^{-1} \\ &= \frac{\tilde{v}}{1-\tilde{v}^2 G_0(m,m)G_0(n,n)} \begin{pmatrix} \tilde{v}G_0(n,n) & 1 \\ 1 & \tilde{v}G_0(m,m) \end{pmatrix}, \end{aligned} \tag{60}$$

where

$$\tilde{v}(z) = v/(1-G_0(m,n)v). \tag{61}$$

Substituting Eq. 60 into Eq. 48, we obtain

$$\begin{aligned} G(a,a) &= G_0(a,a) + \sum_{k,l}^{m,n} G_0(a,k)\,T(k,l)G_0(l,a) \\ &= G_0(a,a) + \frac{\tilde{v}}{1-\tilde{v}^2 G_0(m,m)G_0(n,n)} \\ &\quad \times [G_0(a,m)\tilde{v}G_0(n,n)G_0(m,a) + G_0(a,m)G_0(n,a) \\ &\quad + G_0(a,n)G_0(m,a) + G_0(a,n)\tilde{v}G_0(m,m)G_0(n,a)]. \end{aligned} \tag{62}$$

Thus, the change in the charge density at site a is

$$\begin{aligned}\delta q_a = v\frac{1}{2\pi i}\int_C dz \frac{1}{(1-vG_0(m,n))(1-\bar{v}^2G_0(m,m)G_0(n,n))} \\ \times[G_0(a,m)\bar{v}G_0(n,n)G_0(m,a)+G_0(a,m)G_0(n,a) \\ +G_0(a,n)G_0(m,a)+G_0(a,n)\bar{v}G_0(m,m)G_0(n,a)] \\ \equiv v\Pi_{a:mn}, \end{aligned} \quad (63)$$

where the final equation defines the atom-bond polarizability.

Comparing Eq. 57 with Eq. 63, we see

$$\Pi_{a:mn} \neq 2\Pi_{mn:a} \quad (64)$$

which is aginst the result of Coulson and Longuet-Higgins.[1] However, if we neglect $vG_0(m,n)$ and $vG_0(n,m)$ as very small quantities compared to unity, the relation $\Pi_{a:mn}=2\Pi_{mn:a}$ approximately holds. (We assume propagators here are real).

Next, by evaluating $G(a,b)$, the similar calculation yields the bond-bond polarizability as

$$\begin{aligned}\Pi_{ab:mn} = \frac{1}{2\pi i}\int_C dz \frac{1}{(1-vG_0(m,n))(1-\bar{v}^2G_0(m,m)G_0(n,n))} \\ \times[G_0(a,m)\bar{v}G_0(n,n)G_0(m,b)+G_0(a,m)G_0(n,b) \\ +G_0(a,n)G_0(m,b)+G_0(a,n)\bar{v}G_0(m,m)G_0(n,b)] \\ \cong \frac{1}{2\pi i}\int_C dz(G_0(a,m)G_0(n,b)+G_0(a,n)G_0(m,b)). \end{aligned} \quad (65)$$

The Poles of T Matrix. It should be noted that the poles of the $\boldsymbol{T}$ matrix exactly give new eigenvalues, since the present theory takes into account the effect of the perturbation to the infinite order. As an illustrative example, we put the perturbation v between a and c in the triatomic linear molecule (see Fig. 7). Then the poles of $\boldsymbol{T}$ matrix in this case are given by the roots of the equation

$$1-\left[\frac{1}{1-vG_0(a,c;z)}\right]^2 G_0(a,a;z)G_0(c,c;z)=0. \quad (66)$$

Using Eqs. 29 and 32, we obtain $z=2v$, $-v$ (degenerate). Thus, we successfully reproduce the eigenvalues of the triatomic ring molecule.

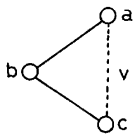

Fig. 7. Interaction v between a and c in the triatomic linear molecule.

Double Perturbations at Site m *and* n. Let us consider a couple of perturbation, ε_m and ε_n at sites m and n. In this case the required interaction is given by

$$\boldsymbol{v} = \begin{pmatrix}\varepsilon_m & 0\\ 0 & \varepsilon_n\end{pmatrix}. \quad (67)$$

For this system we obtain

$$\begin{aligned}\boldsymbol{T}(z) &= \begin{pmatrix}1/\varepsilon_m-G_0(m,m) & -G_0(m,n)\\ -G_0(n,m) & 1/\varepsilon_n-G_0(n,n)\end{pmatrix}^{-1} \\ &= \frac{1}{1-\bar{\varepsilon}_m\bar{\varepsilon}_n|G_0(m,n)|^2}\begin{pmatrix}\bar{\varepsilon}_m & \bar{\varepsilon}_m\bar{\varepsilon}_nG_0(m,n)\\ \bar{\varepsilon}_n\bar{\varepsilon}_mG_0(n,m) & \bar{\varepsilon}_n\end{pmatrix}, \end{aligned} \quad (68)$$

where $\bar{\varepsilon}_m$ is defined in Eq. 55. Thus we can estimate the change of the bond order by evaluating the (a,b) element of Eq. 48, as

$$\begin{aligned}\delta q_{ab} &= \frac{1}{2\pi i}\int_C dz[G(a,b;z)-G_0(a,b;z)] \\ &= \frac{1}{2\pi i}\int_C dz\frac{1}{1-\bar{\varepsilon}_m\bar{\varepsilon}_n|G_0(m,n)|^2}[\bar{\varepsilon}_mG_0(a,m)G_0(m,b) \\ &+\bar{\varepsilon}_nG_0(a,n)G_0(n,b)+\bar{\varepsilon}_m\bar{\varepsilon}_n\{G_0(a,m)G_0(m,n)G_0(n,b) \\ &+G_0(a,n)G_0(n,m)G_0(m,b)\}]. \end{aligned} \quad (69)$$

The first two terms of the square bracket are direct effects separately arisen from two sites, while the remaining terms are indirect ones caused by the perturbation at site $m(n)$ *via* site $n(m)$. If $G_0(m,n)\varepsilon_m$ and $G_0(n,m)\varepsilon_n$ are negligibly small compared to unity, it follows that

$$\delta q_{ab} \cong \frac{1}{2\pi i}\int_C dz[\varepsilon_mG_0(a,m)G(m,b)+\varepsilon_nG_0(a,n)G(n,b)]. \quad (70)$$

This shows the additivity of two perturbing effects in a crude approximation.

Discussion

In the present work, the renormalized perturbation theory had been used to build up propagators for the Hückel model. If we confine ourselves to discuss the obtained results, we have nothing new more than the simple LCAO MO theory does. However, in the course of constructing propagators, we visualize how interactions work in the Hückel model.

Recently, Hosoya[4-8] introduced the topological index as a quantity characterizing the physical properties of hydrocarbons. This is, simply speaking, the sum of absolute values of the Hückel polynomials corresponding to the molecule in question. The value of the topological index increases almost monotonously with the molecular size, and varies as molecular shapes change. Hosoya displayed some parallel trends between topological indices and physical properties. He also found a convenient procedure to calculate the topological indices other than the simple summation mentioned above. His rule which is found in Eq. 7 in reference 5 is almost analogous to the rules indicated by Eqs. 21, 24, and 27. Therefore we are inclined to say that our work has presented some physical basis for Hosoya's intuition, though we have not yet obtained any direct physical interpretation of the topological index.

We turn to discussion of the polarizabilities. The pioneering work of Coulson and Longuet-Higgins has been followed by Fukui *et al.*[9-11] These works including Coulson's are manipulated mainly by the use of properties of the Hückel determinant, but the final expressions of polarizabilities are given in terms of the LCAO coefficients of the zeroth order molecular orbitals. Their results are not beyond the elementary perturbation theory. Here we rewrite the treatment of Coulson and Longuet-Higgins to derive the relationship

$$\Pi_{a:mn} = 2\Pi_{mn:a}. \quad (71)$$

The orbital energy ε_i is given by

$$\varepsilon_i = \sum_a c_{ia}^2\alpha_a + \sum_{mn}c_{im}c_{in}\beta_{mn}, \quad (72)$$

with the optimized LCAO coefficients c_{im} (assumed to

be real). Then it follows that

$$\frac{\partial \varepsilon_i}{\partial \alpha_a} = c_{ia}^2, \quad \frac{\partial \varepsilon_i}{\partial \beta_{mn}} = c_{im}c_{in}. \tag{73}$$

The charge density q_a at site a, and the bond order q_{mn} are given as

$$q_a = 2\sum_i^{\text{occ}} c_{ia}^2 = 2\sum_i^{\text{occ}} \frac{\partial \varepsilon_i}{\partial \alpha_a} = \frac{\partial E}{\partial \alpha_a}, \tag{74}$$

$$q_{mn} = 2\sum_i^{\text{occ}} c_{im}c_{in} = 2\sum_i^{\text{occ}} \frac{\partial \varepsilon_i}{\partial \beta_{mn}} = \frac{\partial E}{\partial \beta_{mn}}, \tag{75}$$

where the factor 2 arises from the spin sum, and E is the total energy. Now we get the polarizabilities

$$\Pi_{a;mn} \equiv \frac{\partial q_a}{\partial \beta_{mn}} + \frac{\partial q_a}{\partial \beta_{nm}} = 2\frac{\partial}{\partial \beta_{mn}}\left(\frac{\partial E}{\partial \alpha_a}\right) \quad (\beta_{mn}=\beta_{nm}), \tag{76}$$

$$\Pi_{mn;a} \equiv \frac{\partial q_{mn}}{\partial \alpha_a} = \frac{\partial}{\partial \alpha_a}\left(\frac{\partial E}{\partial \beta_{mn}}\right). \tag{77}$$

From these expressions, we can conclusively get Eq. 71. The above derivation looks quite general, but is not beyond the elementary perturbation theory, since Eq. 73 is valid only for infinitesimal variations of α or β.

On the other hand, the present theory works even for an arbitrary magnitude of perturbing interaction. The resultant expressions are exact in the Hückel model, so that we can perform any order of perturbation expansion. In order to explain what we mean, we give a simple example shown by Eq. 53. As was mentioned there, the bare interaction ε_m is replaced by the effective interaction $\tilde{\varepsilon}_m$ which is obtained by the infinite repetition of interaction with site m. From the viewpoint of practical use, our theory is not so bad, since propagators in our expressions are easily obtainable from the simple algebra by means of the recurrence formula.

References

1) C. A. Coulson and H. C. Longuet-Higgins, *Proc. R. Soc. London, Ser. A*, **191**, 39 (1947).
2) P. W. Anderson, *Phys. Rev.*, **105**, 1388 (1957).
3) E. N. Economou, "Green's Functions in Ouantum Physics," Springer-Verlag (1979), p. 230.
4) H. Hosoya, *Bull. Chem. Soc. Jpn.*, **44**, 2332 (1971).
5) H. Hosoya, K. Hosoi, and I. Gutman, *Theoret. Chim. Acta (Berl.)*, **38**, 37 (1975).
6) H. Hosoya and M. Murakami, *Bull. Chem. Soc. Jpn.*, **48**, 3512 (1975).
7) H. Hosoya and K. Hosoi, *J. Chem. Phys.*, **64**, 1065 (1976).
8) I. Gutman, T. Yamaguchi, and H. Hosoya, *Bull. Chem. Soc. Jpn.*, **49**, 1811 (1976).
9) K. Fukui, C. Nagata, T. Yonezawa, H. Kato, and K. Morokuma, *J. Chem. Phys.*, **31**, 289 (1959).
10) K. Fukui, C. Nagata, T. Yonezawa, and A. Imamura, *Bull. Chem. Soc. Jpn.*, **32**, 450 (1959).
11) K. Fukui, K. Morokuma, T. Yonezawa, and C. Nagata, *Bull. Chem. Soc. Jpn.*, **33**, 963 (1960).

Electrochemical Aspects of a NADH/FAD Model System

Kazuo SASAKI,* Akira KITANI, Atsutaka KUNAI, and Hitoshi MIYAKE
Department of Applied Chemistry, Hiroshima University, Senda-machi, Hiroshima 730
(Received May 6, 1980)

A model system of the NADH/FAD redox couple has been studied by the use of electrochemical techniques. The system studied was composed of 1-benzyl-1,4-dihydronicotinamide (BNAH) and riboflavin (RF), which were used in place of NADH and FAD respectively, dissolved in a DMSO solution. The results obtained were as follows. RF is reduced either by BNAH or sodium borohydride, obeying a second-order rate law, presumably by the mechanism of hydride-ion transfer. The resultant product is inactive to the electrochemical reduction at a mercury-pool electrode. Entirely different products were produced when RF was reduced electrochemically. RF was reduced at a rate of 1 *F*/mol at the initial stage of controlled potential electrolysis to form, probably, a dimeric compound, but the latter product underwent further reduction and the total quantity of electricity necessary for the complete reduction exceeded 10 *F*/mol. Interestingly, the electrolytic reduction gives the same product as that obtained by BNAH when electrolysis is performed in the presence of a sufficient amount of BNAH, indicating that the initial product of electrochemical reduction receives the hydride ion rather than further electrons.

$$2RF + 2e \rightleftharpoons (RF)_2^{2-} \xrightarrow{+H^-,\ +H^+} 2RFH^-$$

The Zn^{2+} added to the BNAH/RF system was found to act as the oxidizing agent of RFH^- and regenerated the neutral RF. This is markedly different from the case of BNAH/organic carbonyl compounds, where the metal ions behave as catalysts to promote the reaction.

In a series of papers,[1-4] we have reported on our electrochemical studies of the reaction of 1-benzyl-1,4-dihydro-nicotinamide (BNAH) with several aromatic compounds. The results may be outlined as follows:

1) Metal cations, which catalyze the redox reactions between BNAH and organic substrates, act as bridging agents in a ternary Michaelis complex composed of BNAH, a substrate, and a metal catalyst.

2) The force sustaining the ternary complex is mainly due to ion-pairing stabilization (Coulomic force between the organic anion and the metal ion).

3) Zinc exhibits the highest catalytic activity.

In the present paper, we should like to report the somewhat different behavior of metal ions observed in the redox reaction between BNAH and riboflavin (Vitamin B_2).

Riboflavin, which will hereafter be abbreviated as RF, is known as a constituent of flavocoenzymes. An excellent review article on the nature and reactions of flavins and flavocoenzymes is available.[5] Electrochemical studies of the same subject were reviewed extensively by Elving.[6]

Studies hitherto reported were done in aqueous media, and only a little is known about nonaqueous systems. By means of cyclic voltammetry, Sawyer[7] studied the qualitative behavior, including the metal-ion interactions, of several flavin compounds in DMF, acetonitrile, and DMSO.

Yoshinaga[8] also studied the electrochemistry of RF in DMF solutions using cyclic voltammetry and a.c. and d.c. polarography. According to these works, RF is reduced exhibiting two one-electron waves the first electron transfer being quasi-reversible, and the second, irreversible.

Experimental

Reagents. The solvent used in this experiment was dimethyl sulfoxide (DMSO). In some preliminary experiments, *N,N*-dimethylformamide (DMF) was also tested. Although the basic behavior of RF was found to be more or less similar in the two solvents, a slight advantage was found with DMSO in the solubility of RF. Commercial DMSO was first treated with Molecular Sieve 3A overnight and then distilled under reduced pressure in a nitrogen atmosphere. The supporting electrolyte was tetraethyl ammonium perchlorate (TEAPC). The RF of Katayama Chemicals was used as purchased. BNAH and its oxidized form BNA^+ were supplied by Dr. Ohnishi of the Sagami Chemical Research Center. The zinc salt was in the form of perchlorate.

Equipment and Procedures. The polarograph used was a Yanagimoto P-8 type, and the basic conditions of measurements were as follows:

Height of mercury column: 63.5 cm

Drop rate: 1.84 mg s^{-1} (at −1.0 V in DMSO)

Drop life: 3.81 s (at −1.0 V in DMSO)

Scan rate: 0.2 V s^{-1}.

The reference electrode was a SCE in a DMSO solution.

The homogeneous reaction of BNAH with RF was studied in a 20-ml polarographic cell in which 10 ml of a test solution had been placed. The test solution, initially composed of 0.1 M (1M=1 mol dm^{-3}) TEAPC and 1 mM RF, was first deoxygenated with bubbling nitrogen, and then BNAH equivalent to 30 mM was dissolved in it. The progress of the reaction was monitored periodically by means of d.c. polarography.

Electrolysis was carried out in a two-compartment cell separated by a glass frit. The working electrode was a mercury pool, and the counter electrode, a platinum foil. In the mercury-pool compartment, a dropping mercury electrode was also inserted to monitor the advance of the electrolysis.

Results

Electrochemical Behavior of RF in DMSO. The electrochemical behavior of RF has been studied by means of a.c. and d.c. polarography as well as by means of cyclic voltammetry.[8] Here, we shall cite only a part of our results.

The d. c. polarogram of 1 mM of RF in DMSO is

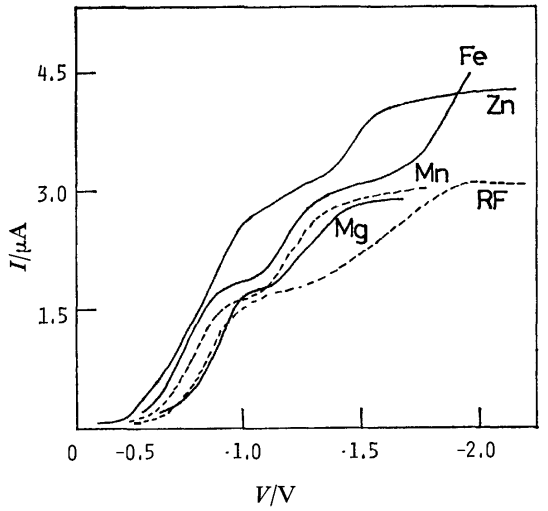

Fig. 1. D. c. polarograms of riboflavin (1 mM) in the presence of equimolar amount of several metal cations.

shown by the dotted curve in Fig. 1. As may be seen, the first one-electron wave appears at $E_{1/2}=-0.90$, and the second, at -1.56 V. Both of the waves are diffusion-limiting, the first one being quasi-reversible, and the second, totally irreversible.

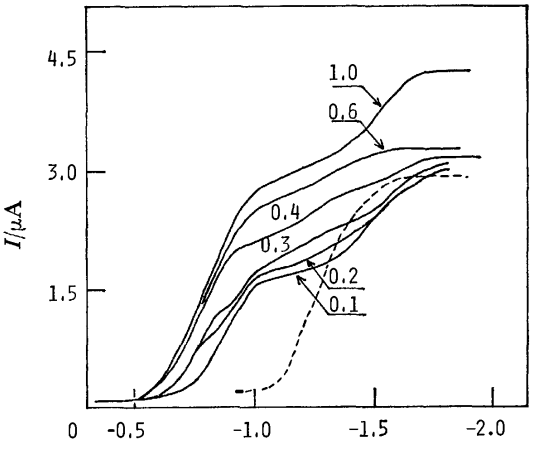

Fig. 2. Effect of zinc ion concentration on the polarogram of riboflavin (1 mM). Numbers indicate Zn^{2+} concentration in mM. Broken curve stands for 1 mM Zn^{2+}.

When equimolar amount of various metal salts are added, the wave shifts in a more positive direction, indicating the existence of ion-pair formation (Fig. 1). Figure 2 shows the effect of the zinc ion at a variety of concentrations. When the concentration of the zinc ion exceeds 0.6 mM, the wave corresponding to Zn^{2+} itself appears and the change in the wave form of RF almost ceases. This may be an indication that, in the ion-pair formed, two molecules of reduced RF are fixed per Zn^{2+} ion, on the average.

Reduction of RF by BNAH in Homogeneous DMSO Solutions. When RF is reacted with a large excess of BNAH in DMSO solutions containing 0.1 M TEAPC, the following reaction proceeds:

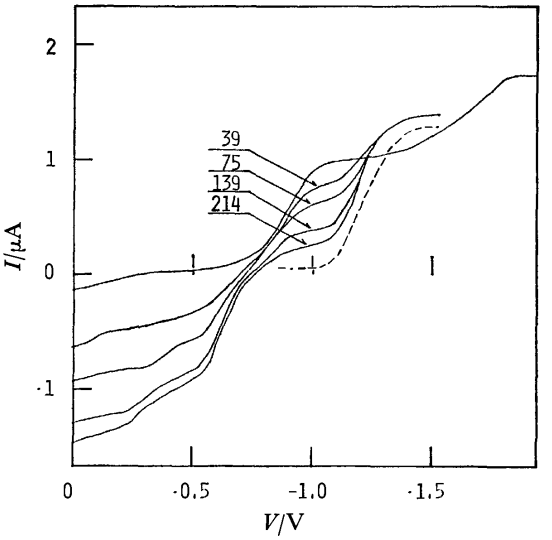

Fig. 3. Change in polarograms with the progress of reaction between BNAH and RF. Numbers indicate reaction time in minutes. The uppermost curve stands for RF before adding BNAH, and broken curve for BNA^+ (1 mM). RF: 1 mM, BNAH: 30 mM.

$$RF + BNAH \xrightarrow{k_{II}} RFH^- + BNA^+. \quad (1)$$

The progress of the reaction was monitored periodically by the aid of polarography with the reacting solution. Figure 3 shows a part of the results, where the initial concentrations of the reactants were 1 mM for RF and 30 mM for BNAH respectively. When the cathodic wave height at -1.1 V, as a measure of the amount of RF remaining unreacted, and the anodic wave height at -0.2 V, for the amount of reduced product, are plotted against each other, Curve A in Fig. 4 is obtained. The slope of the curve is exactly 2, indicating that the reduction occurring is equivalent to a two-electron transfer per molecule of RF. The reaction as a whole can be expressed by Eq. 1. The apparent rate constant was determined to be $(3.7\pm0.2)\times10^{-3}$ M^{-1} s^{-1}.

Westheimer[9] showed that the reaction between NAD^+ and certain organic substrates occurs *via* a hydride-ion mechanism. We are inclined to conclude

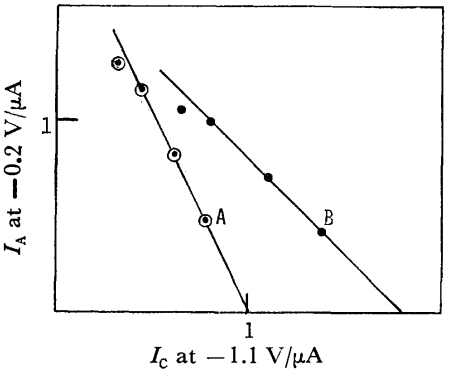

Fig. 4. Equivalency between RF and its reduced product. The abscissa stands for the concentration of RF remained unreacted and the ordinate for reduced RF. A: Without additives, B: with 0.7 mM Zn^{2+}.

that the present reaction, as expressed by Eq. 1, proceeds by the same mechanism, *i.e.*, hydride-ion transfer.[10]

The product, BNA^+, is polarographically reactive and gives a cathodic wave with the half-wave potential at -1.5 V. The curve of the broken line in Fig. 3 stands for the solution of 1 mM BNA^+ observed separately. The curves in Fig. 3 clearly indicate that the wave corresponding to the BNA^+ reduction increases progressively with the reaction time. In this figure, there are two facts worthy of note. The first is that the limiting current at the BNA^+ wave remains constant, regardless of the reaction time, and the second, that the second wave of RF itself disappears completely.

The reason why the second wave disappears can be explained by assuming that the following sequence of reactions is taking place at the dme surface:

$$RF + e \rightleftarrows RF^{\cdot} \quad (2)$$

$$2RF^{\cdot} \longrightarrow (RF)_2^{2-} \quad (3)$$

$$(RF)_2^{2-} + BNAH + H^+ \longrightarrow BNA^+ + 2\,RFH^-. \quad (4)[11]$$

If both the reactions, (3) and (4), are assumed to occur in the closest vicinity of dropping mercury, and if they are assumed to proceed sufficiently rapidly, there may be no $RF^{\cdot}$ which is responsible for the second wave.

The constancy of the wave height at the plateau of the BNA^+ wave also supports the occurrence of Reaction 4. The species responsible for the wave height concerned should be both the RF remaining unreacted and the BNA^+ formed by the homogeneous reaction (1). If the RF remaining unreacted undergoes a series of reactions, (2) to (4), rapidly and quantitatively, the concentration of BNA^+ at the electrode surface will be equal to the sum of those due to the homogeneous reaction (Eq. 1) and produced by the follow-up chemical reaction (Eq. 4). Accordingly, the concentration of BNA^+ should always be equal to the initial concentration of RF itself, 1 mM in this case.

It is worthy of note that RF gives the same product, RFH^-, even when the reaction is initiated by electronation (Eq. 2) as long as a sufficient amount of BNAH is present in the system. In other words, $(RF)_2^{2-}$ reacts more easily with BNAH than it receives further electrons. Very similar behavior was observed when sodium borohydride was used in place of BNAH. This suggests that the role of BNAH is as a hydride-ion source rather than as an electron donor.[10]

Behavior of Zn^{2+} in the Redox Reaction between BNAH and RF. As has been reported previously, BNAH reduces various aromatic carbonyl compounds, and several metal ions have been found to accelerate the rate of the reaction. In contrast to this, the existence of some metal ions apparently retards the reduction of RF with BNAH.

Figure 5 shows the results of a measurement similar to that of Fig. 3. The only difference was that the starting solution contained 0.7 mM Zn^{2+} besides 1 mM of RF and 30 mM of BNAH. Because of the ion-pairing phenomena, the polarogram of RF changed to one two-electron wave. As had been done before the cathodic wave height was plotted against the anodic one to get Curve B in Fig. 4. The slope is exactly unity.

Since the cathodic wave was two-electron, the anodic

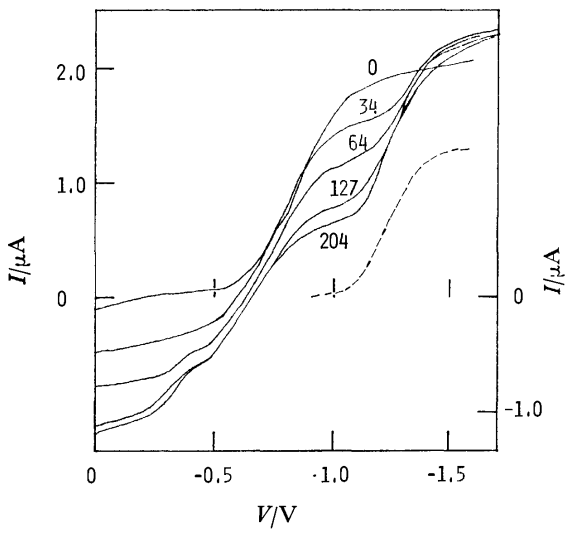

Fig. 5. Change in polarograms with progress of reaction between BNAH and RF in the presence of 0.7 mM Zn^{2+}. RF: 1 mM, BNAH: 30 mM.

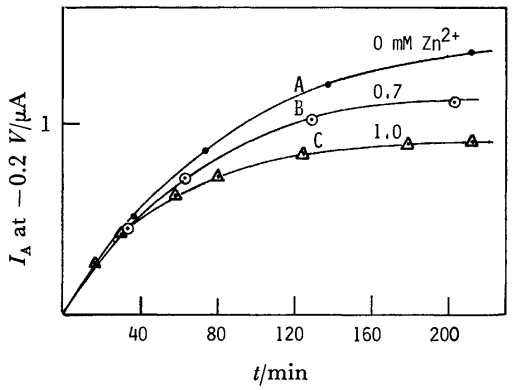

Fig. 6. Accumlation of reduced RF and the effect of Zn^{2+} ion on it.

wave corresponds to a two-electron reaction. The shape of the anodic wave is indistinguishable from that in Fig. 3. Accordingly, one may conclude that the presence of Zn^{2+} does not affect the production of RFH^-.

The anodic wave appearing in the polarograms of Figs. 3 and 5 is due to the reoxidation of the reduction product, RFH^-. Therefore, its wave height can be used as a measure of the concentration of RFH^-. This is examined in Fig. 6, where Curve A stands for the measurement in the absence of Zn^{2+}, and B and C for those in the presence of 0.7 mM and 1.0 mM Zn^{2+} respectively. It is clearly indicated that the accumulation of RFH^- is retarded by the presence of Zn^{2+}.

In Fig. 5, the limiting current at the second plateau, where BNA^+ is reduced, is roughly constant, irrespective to the reaction time. However, the value is much greater than that observed in Fig. 3. This requires an additional explanation. The species responsible for the total wave height of interest are, of course, the BNA^+ produced homogeneously and the RF remaining unreacted, the latter gives a two-electron wave in this case[12] owing to the presence of the Zn^{2+} ion. Accordingly, the difference in the heights of the first and second

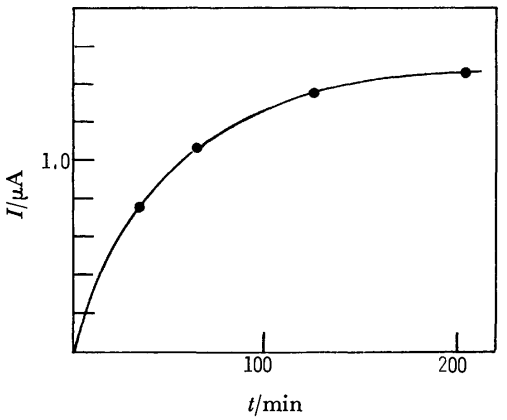

Fig. 7. Increase of BNA^+ concentration with reaction time observed by polarography.
1.5 μA corresponds to 1.2 mM roughly.

waves must correspond to the concentration of BNA^+ produced by the homogeneous reaction. This is plotted in Fig. 7 against the reaction time. It should be noted that the final value is approximately 1.5 μA, which corresponds to a BNA^+ concentration of 1.2 mM or more. Undoubtedly, this value exceeds the initial concentration of RF. This is a result of the following regeneration reaction:

$$RFH^- + Zn^{2+} \xrightarrow{k_{reg}} RF + H^+ + Zn^\circ. \quad (6)$$

In order to confirm the occurrence of Reaction 6, we carried out the analysis of the zinc ion in the solution phase by means of atomic-absorption spectrometry. If Reaction 6 actually takes place, the Zn^{2+} ion will disappear from the solution. The first measurement was made with 1.0 mM of Zn^{2+} added to a solution of DMSO containing 1 mM of RF and 30 mM of BNAH, and the second with 1.5 mM of Zn^{2+}. The reaction mixture was stirred by means of a magnetic stirrer and kept for several hours at room temperature (*ca.* 22 °C). When the resultant solution was subjected to atomic-absorption spectrometry without any additional treatment, 75 to 80% of the Zn^{2+} was recovered, indicating that the major part of the metallic zinc was still in the solution. Therefore, the solution was brought into contact with mercury and the whole system was vigorously agitated. By this treatment, the metallic zinc can be transferred into the mercury phase.

For the two solutions tested, the initial zinc concentrations of which were 1.0 and 1.5 mM, the values were reduced to 0.05 mM and 0.1 mM respectively. This means, on the average, that, during a period of homogeneous reaction of several hours, each molecule of reduced riboflavin had a chance to return to the oxidized form (RF).

The above findings indicate the following combination of redox cycles:

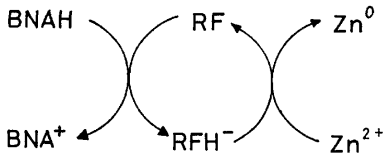

This is a fact unexpected at the beginning of the present study, some comments will be made below.

Electrochemical Reduction of RF. The controlled potential electrolysis of RF was also studied with a mercury-pool electrode. The change in solution composition was studied also by means of polarography.

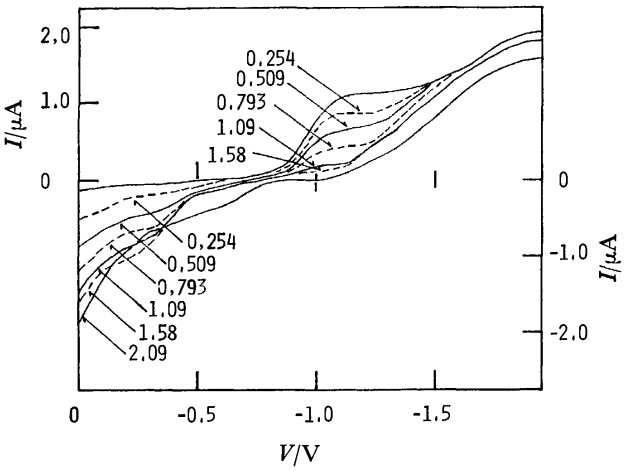

Fig. 8. Progress of controlled potential electrolysis of RF as observed by polarography. Electrolysis was made at −1.90 V. Numerical figures indicate *F*/mol.

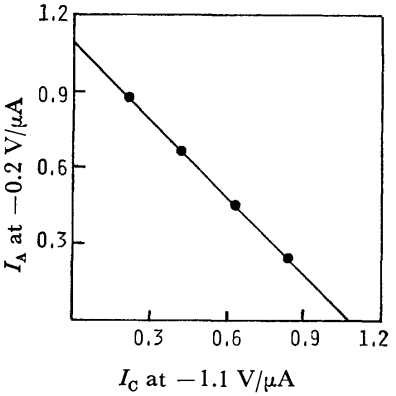

Fig. 9. Coulometric correlation in the electrolytic reduction of RF. The ordinate stands for the amount of reduced product and the abscissa for RF remained.

As is shown in Fig. 8, the first wave of RF reduction decreases with the progress of electrolysis and disappears after passing the electricity of *ca.* 1 *F*/mol. The decreasing cathodic wave and the increasing anodic one are compared in Fig. 9. The slope of this curve is unity, in contrast to Curve A in Fig. 4, where the slope was 2. Since the cathodic wave under consideration is of one-electron, the product which is responsible for the anodic wave seems to be a dimeric compound. The reaction taking place at the cathode electrode may thus be written as:

$$RF + e \rightleftharpoons RF^{\cdot} \quad (7)$$

$$2RF^{\cdot} \longrightarrow (RF)_2^{2-}. \quad (8)$$

Unexpectedly, the wave height at the potential region where RF gives the second wave does not show a marked decrease.

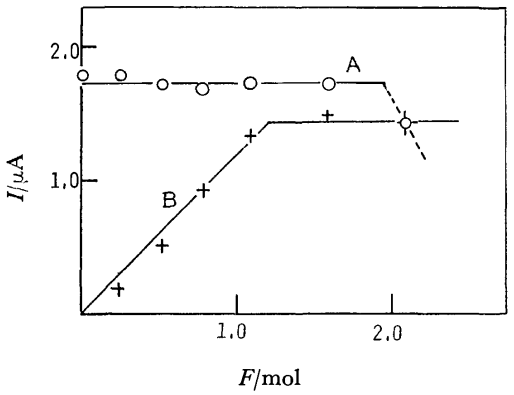

Fig. 10. Analysis of polarograms during the controlled potential electrolysis. Curve A is the wave height at −1.9 V, where not only neutral RF but also several reduced products may contribute to the wave height. Curve B may be considered as the concentration of dimeric product, $(RF)_2^{2-}$.

When the change in wave height measured at −1.9 V is plotted against the quantity of electricity consumed, Curve A of Fig. 10 is obtained. It may be seen that the decrease begins after 2 *F*/mol or so of electricity is consumed. This suggests that the dimer anion $(RF)_2^{2-}$ produced by Eq. 8 is further reduced to contribute to the wave height. The rest of the wave height is, of course, due to the RF remaining. Since the contribution of the latter is simply twice the height of the first wave, the difference will give the concentration of the dimer anion. Curve B in Fig. 10 shows this. The linear increase ceases at a point corresponding to 1 *F*/mol, supporting the foregoing estimation that the initial electrode product is a dimeric compound.[13]

It should be noted that the constant potential coulometry made at −1.9 V indicated that the number of electrons involved exceeds 10. This indicates that, upon electrochemical reduction, RF undergoes a complete reduction for almost all of the reducible groups.

Anodic Oxidation of Reduced Riboflavin (Preliminary Report). From the foregoing descriptions, it is clear that there are at least two types of reduction products. One is the BNAH-product, which is assumed to be the so-called leucoflavin,[14] while the other consists of electrode products. The latter is, in general, a mixture of compounds differing in their stages of reduction. In order to avoid confusion, we will hereafter confine the meaning of "electrode product" to the "dimer compound" which is obtained within the limit of an applied charge of 1 *F*/mol.

The BNAH-product gives a two-stage anodic wave in polarograms, with half-wave potentials at −0.65 (Wave A1) and −0.35 V (A2). The former is much higher than the latter amounting to 85% of the total height. The reoxidation of the electrode product also exhibits a two-stage wave, but the half-wave potentials appear at −0.35 V (A2) and 0 V (A3).

The BNAH-product is sensitive to oxygen, and, if a sufficient amount of oxygen is introduced, the polarogram of the original RF recovers quantitatively. Similarly, RF is regenerated, at least polarographically, when the BNAH-product is subjected to the anodic oxidation at the mercury-pool electrode at −0.5 V.

On the other hand, the electrode product behaves somewhat complicatedly in response to the anodic oxidation. When the electrode product is reoxidized at −0.2 V, Wave A2 disappears after passing a charge of 0.5 *F*/mol, but at this same stage Wave A3 remains unchanged. The disappearance of Wave A2 gives rise to the regeneration of the reduction wave of RF. However, the recovery is, atmost, 60% of the original RF wave.

A tentative explanation for these findings is that the electrode product, which is assumed to be a dimer anion, undergoes one-electron oxidation to give half the original RF:

$$(RF)_2^{2-} + e \xrightarrow{A1} RF + (RF^{\tau})'.$$

One of the products $(RF^{\tau})'$ is solely an assumption in order to explain both the one-electron behavior of the A2 wave and the 50% recovery of the RF wave. When the electrode product is anodically oxidized at +0.2 V, all of the anodic wave disappears, but the reaction is complicated.

The A2 wave appeared in the reoxidation of both the BNAH and electrode products. If the active species responsible for this wave is the same, it should be the dimer anion. As a possibility, the following reaction seems to operate:

$$RFH^- \xrightarrow[A1]{-e} RFH\cdot \xrightarrow[A1]{-e} RF + H^+$$
$$\downarrow \times 2,\ -2H^+$$
$$(RF)_2^{2-} \xrightarrow[A1]{-e} RF + (RF^{\tau})'.$$

References

1) A. Kitani, N. Hashimoto, and K. Sasaki, *Nippon Kagaku Kaishi*, **1977**, 1108.
2) A. Kitani and K. Sasaki, *Nippon Kagaku Kaishi*, **1978**, 817.
3) K. Sasaki and A. Kitani, *J. Electroanal. Chem.*, **94**, 201 (1978).
4) A. Kitani and K. Sasaki, *Bioelectrochem. Bioenerg.*, in press.
5) P. Hemmerich, C. Veeger, and H. C. S. Wood, *Angew. Chem., Int. Ed. Engl.*, **4**, 671 (1965).
6) B. Janik and P. J. Elving, *Chem. Rev.*, **68**, 295 (1968).
7) D. T. Sawyer and R. L. McCreery, *Experimentia*, Suppl., No. 18, **1971**, 563.
8) H. Yoshinaga, Master Thesis, Hiroshima University (1977).
9) F. H. Westheimer, H. F. Fisher, E. E. Conn, and B. Vennesland, *J. Am. Chem. Soc.*, **73**, 2403 (1951).
10) The electrochemical behavior of BNAH is totally irreversible. Its anodic oxidation exhibits a two-electron wave at +0.6 V and produces BNA^+, while the reduction of BNA^+ takes place at about −1.0 V. This means that the electron-transfer reaction of BNA^+/BNAH couple is much hindered. Taking into account the result of Westheimer,[9] who indisputablly verified the hydride-ion mechanism for the NAD^+/NADH couple, the homogeneous reaction between BNAH and RF seems to proceed by means of a hydride mechanism. We have found that sodium borohydride, known as a typical hydride-ion source, also reduces RF.

11) There is another way to describe the reaction:

$$2RF^{\cdot} + BNAH + H^{+} \longrightarrow BNA^{+} + 2RFH^{\cdot}. \quad (5)$$

This insists that BNAH attacks the $RF^{\cdot}$ radical anion, but not the dimer anion $(RF)_2^{2-}$. We, however, prefer the mechanism of Eq. 4.

12) The latter species might produce BNA^{+} as a result of a follow-up chemical reaction, as in the manner of Eq. 4. However, this does not affect the total wave height.

13) After passing 1 *F*/mol, the current appears to be constant until *ca.* 2 *F*/mol. This constancy is, however, meaningless for discussion, since the species responsible for this current can not be uniquely specified.

14) Spectrometric identification has not yet been attempted, because the absorption of BNAH masks the flavin spectra.

Absorption and Reflection Spectra of Pure and $ClSO_3H$ Doped Polyacetylene Films

Masashi TANAKA,* Atsushi WATANABE, and Jiro TANAKA
Department of Chemistry, Faculty of Science, Nagoya University, Chikusa-ku, Nagoya 464
(Received May 8, 1980)

Optical absorption and reflection measurements are carried out on pure and $ClSO_3H$ doped polyacetylene films over a wide wavelength region (350—35000 cm^{-1}). In the doped polymer, the transition from the valence band to the impurity level is observed at 870 cm^{-1} and the free carrier absorption band appears over the wide region of 350 to 20000 cm^{-1}, while the interband transition located in the region of 15000 cm^{-1} disappears. This means that doping removes the bond alternation leading to a uniform bond length and all π-electrons contribute to the transport. For the heavily doped films, the d.c. conductivity of polyacetylene films is obtained by the optimum fit of the theoretical curve to the observed absorption and reflection spectra. The obtained values are comparable with the d. c. conductivity ($\sigma \simeq 280$—$250\ \Omega^{-1}\ cm^{-1}$) obtained by the four probe method.

Polyacetylene, $(CH)_x$, is one of the simplest linear conjugated polymers with a single chain structure. The theoretical studies upon the electronic structure of pure $(CH)_x$ polymer showed that the alternant structure was found to have the lowest energy and the energy gap between the π and π^* bands was too high.[1-4] The observation[5,6] of the $\pi \rightarrow \pi^*$ transition band at about 16000 cm^{-1} also showed that the bond alternation is present in the polymer and $(CH)_x$ would be expected to make semiconducting behavior.[7] However, Shirakawa, Heeger, and MacDiarmid and co-workers found that AsF_5 doped $(CH)_x$ films have the high conductivity of about $10^3\ \Omega^{-1}\ cm^{-1}$ [8] and they observed the new absorption bands in the lower frequency region by the absorption and reflection measurements.[9-11] Tanaka *et al.* estimated the optical conductivity by measuring the free carrier absorption band of BF_3 doped film[12] and also showed that $ClSO_3H$ is a good dopant by the d.c. conductivity measurement of $ClSO_3H$, H_2SO_4, and BF_3 doped films.[13]

In the present paper, we report the absorption and reflection spectra in the 350—35000 cm^{-1} region of $(CH)_x$ films doped with $ClSO_3H$ and discuss about the electronic structure of the heavily doped $(CH)_x$ films.

Experimental

The polyacetylene films were prepared from acetylene gas by treatment of the Ziegler catalyst in hexane at −80 °C as described by Shirakawa, Ikeda, and co-workers.[14-16] The films were doped by exposure to the vapor of $ClSO_3H$ *in vacuo*. The dopant level were determined by the measurement of the four probe d.c. conductivity.

After the thin $(CH)_x$ films were polymerized on the KBr plate or the polyethylene film and doped with $ClSO_3H$, the absorption spectra of $(CH)_x$ films were measured with Hitachi IR 260-50 (350—4000 cm^{-1}) and Carl Zeiss M4Q (4000—35000 cm^{-1}) spectrophotometers. For the study of the *cis-trans* isomerization of $(CH)_x$ films, the thin films were polymerized on the inner surface of the 1 cm quartz cell and the absorption spectra of the films kept *in vacuo* were measured with a Carl Zeiss spectrophotometer after heating at 60 °C. The reflection measurement of pure and doped thick films were taken with Hitachi IR 260-50 and a microscopic spectrophotometer (4000—35000 cm^{-1}) made in our laboratory. It consists of an Olympus microscope, a Carl Zeiss Ultrafluar lens (×10), a Nikon crystal mount, a HTV 928 photomultiplier and a PbS tube, and an Intel 8080 microcomputer for data processing.

The Kramers-Kronig (K-K) transformation[17,18] of the reflection spectra of pure $(CH)_x$ films and the best fit of the calculated absorption and reflection spectra of $ClSO_3H$ doped films to the observed spectra were made on a FACOM M-200 computer of Nagoya university.

Results and Discussion

Absorption and Reflection Spectra of Pure $(CH)_x$ Films. The thin $(CH)_x$ film polymerized at −80 °C shows the reddish cupric color and the film becomes blue on heating it *in vacuo*. This color change was explained by the analysis of IR-vibration spectra[14-16] to be due to the *cis-trans* isomerization of $(CH)_x$. In Fig. 1 is shown the visible absorption spectral change of the thin $(CH)_x$ film at 60 °C and *in vacuo*. *cis*-Rich $(CH)_x$ has two vibronic peaks at 17100 and 18300 cm^{-1} and the second peak (18300 cm^{-1}) is the most intense. On heating the *cis*-rich thin film at 60 °C, the broad band in the region of 15000 cm^{-1} becomes more intense and the

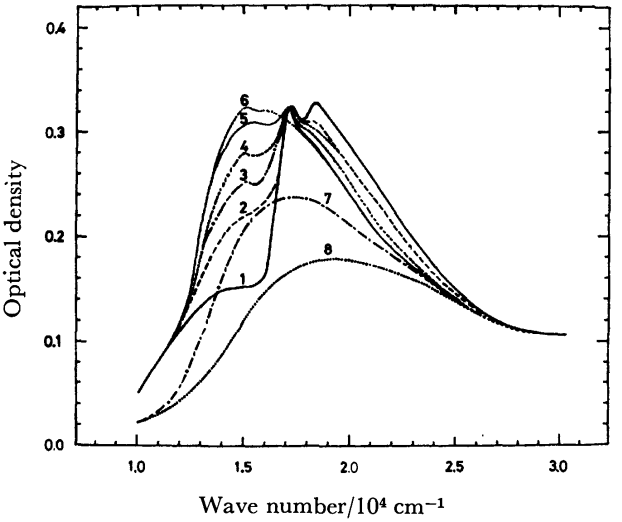

Fig. 1. The visible absorption spectral change due to the *cis-trans* isomerization of the thin $(CH)_x$ film at 60 °C and *in vacuo*. 1) 0.0 h, 2) 3.2 h, 3) 8.2 h, 4) 14.5 h, 5) 2.0 d, 6) 4.9 d 7) 16.3 d, 8) 22.2 d.

18300 cm^{-1} peak of *cis*-$(CH)_x$ becomes weaker. Finally, the 15000 cm^{-1} band of *trans*-$(CH)_x$ has the same absorption intensity as that of the 17000 cm^{-1} band of *cis*-$(CH)_x$ before heating. This means that *cis*-$(CH)_x$ transforms completely to *trans*-$(CH)_x$. After that, the absorption intensity of *trans*-$(CH)_x$ becomes weaker and the maximum peak shifts to the higher frequency region. This fact seems to be due to the formation of the bridge between the $(CH)_x$ chains and the decrease in the C=C conjugated system.

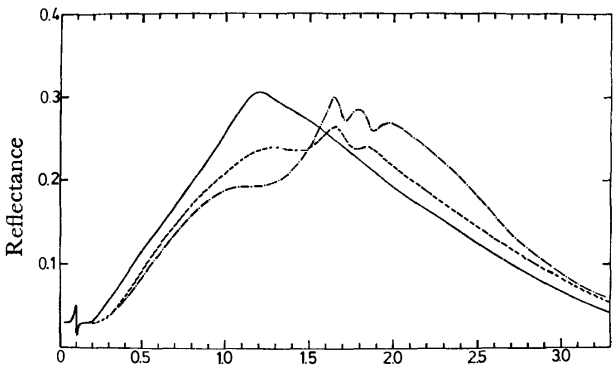

Fig. 2. The reflection spectra of the thick $(CH)_x$ films. ·—·—: 80% *cis*-$(CH)_x$, – – –: 55% *cis*-$(CH)_x$, ——: 85% *trans*-$(CH)_x$.

In Fig. 2 is shown the reflection spectral change of the thick $(CH)_x$ films at about 200 °C. The *cis,trans*-content of $(CH)_x$ films was determined by measuring the optical density of *cis* (740 cm^{-1}) and *trans* (1015 cm^{-1}) C–H out-of-plane vibrations.[16] The reflection spectrum of 80% *cis*-$(CH)_x$ film has the vibronic structures at 16400 and 18000 cm^{-1} as is observed in the absorption spectra of thin $(CH)_x$ films and the 16400 cm^{-1} peak has a reflectivity of 30%. For the 85% *trans*-$(CH)_x$ film, the reflection spectrum has the broad band at 12000 cm^{-1} and the sharp peak at 1015 cm^{-1} corresponding to the C–H out-of-plane mode of *trans*-$(CH)_x$. The main band at 12000 cm^{-1} has a reflectivity of 30.6%. The absorption spectra of $(CH)_x$ film are obtained by the K-K transformation of the reflection spectra as is shown in Fig. 3. The 16400 cm^{-1} band of 80% *cis*-$(CH)_x$ has the maximum absorption coefficient, α, of 2.59×10^5 cm^{-1} and the 12000 cm^{-1} band of 85% *trans*-$(CH)_x$ has $\alpha=2.33\times10^5$ cm^{-1}. On comparison between Figs. 1 and 3, the absorption maxima of thick $(CH)_x$ films are shifted to the lower frequency region than those of the thin films. This may be explained by the difference of the conjugated system length.

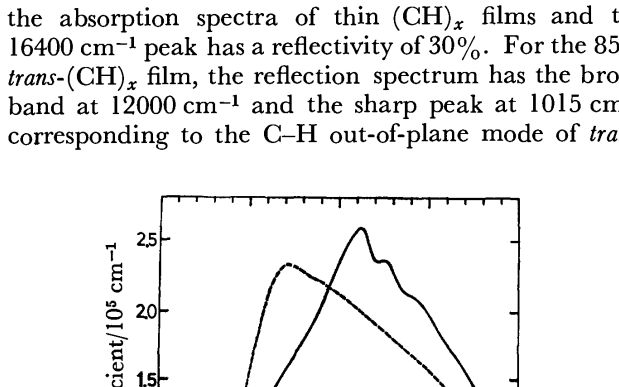

Fig. 3. The absorption spectra obtained from the K-K transformation of the reflection spectra of the thick $(CH)_x$ films. ——: 80% *cis*-$(CH)_x$, – – –: 85% *trans*-$(CH)_x$.

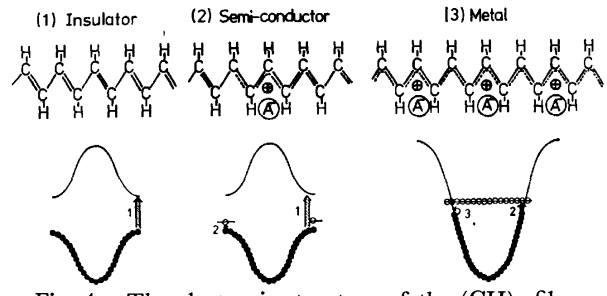

Fig. 4. The electronic structure of the $(CH)_x$ film.

$(CH)_x$ is one of the simplest linear conjugated polymers with a single chain structure and has the configuration of alternating the single and double bonds. Then, the π-electrons on each carbon atom form two separate bands as shown in Fig. 4-1. The one is the bonding π band (valence band) and the other is the antibonding π^* band (conduction band). Accordingly, the complex dielectric constant of $(CH)_x$ is given by the following equation,[19]

$$\varepsilon(\omega)=\varepsilon_{\text{core}}+\sum_{k}\frac{(4\pi Ne^2/m)\hbar^2 f_{\pi k,\pi^* k+q}}{(\varepsilon_{\pi^*}(k+q)-\varepsilon_{\pi}(k))^2-\hbar^2\omega^2-i\hbar^2\omega/\tau_0} \quad (1)$$

where N is the number density of π-electrons, m is the electron mass, and $f_{\pi k,\pi^* k+q}$ is the oscillator strength of the $\pi k\rightarrow\pi^* k+q$ transition. $\varepsilon_{\pi^*}(k+q)$ and $\varepsilon_{\pi}(k)$ are the energy of π and π^* bands. When the momentum of photon, q, is neglected, the imaginary part $\varepsilon_2(\omega)$ of the complex dielectric constant is derived from Eq. 1 as follows,

$$\varepsilon_2(\omega)=\frac{\pi}{2}\frac{4\pi Ne^2}{m}\bar{f}_{\pi,\pi^*}\sum_{k}\frac{\hbar}{\omega}\delta(\varepsilon_{\pi^*}(k)-\varepsilon_{\pi}(k)-\hbar\omega). \quad (2)$$

Here, $\bar{f}_{\pi,\pi^*}$ is the average of the oscillator strength of the $\pi k\rightarrow\pi^* k$ transition. The sum rule of $\varepsilon_2(\omega)$ is defined for a finite range from the absorption edge $E_g=\hbar\omega_g$ to the energy $E_0=\hbar\omega_0$,

$$\int_{\omega_g}^{\omega_0}\omega\varepsilon_2(\omega)d\omega=\frac{\pi}{2}\frac{4\pi Ne^2}{m}\bar{f}_{\pi,\pi^*}\sum_{k}\int_{E_g}^{E_0}\delta(\varepsilon_{\pi^*}(k)-\varepsilon_{\pi}(k)-E)dE$$

$$=\frac{\pi}{2}\frac{4\pi Ne^2}{m}\bar{f}_{\pi,\pi^*}G(E_0) \quad (3)$$

where $G(E_0)$ is the integral of the joint density of state $\rho(E)$ over the energy region of E_g to E_0,

$$G(E_0)=\int_{E_g}^{E_0}\rho(E)dE \quad (4)$$

and

$$\rho(E)=\sum_{k}\delta(\varepsilon_{\pi^*}(k)-\varepsilon_{\pi}(k)-E). \quad (5)$$

In the typical one-dimensional system of the length L,

the band energy $\varepsilon_\pi(k)$ and $\varepsilon_\pi^*(k)$ can be approximated by the parabolic function,

$$\varepsilon_\pi(k) = -\frac{\hbar^2}{2m_\pi}\left(k-\frac{\pi}{2a}\right)^2 \quad (6)$$

and

$$\varepsilon_{\pi^*}(k) = E_g + \frac{\hbar^2}{2m_\pi}\left(k-\frac{\pi}{2a}\right)^2. \quad (7)$$

Then, the joint density of state near the gap edge varies as

$$\rho(E) = \frac{L\sqrt{m_\pi}}{h}(E-E_g)^{-1/2} \quad (8)$$

and the integral of the joint density of state rises toward the square root as follows

$$G(E_0) = \frac{2L\sqrt{m_\pi}}{h}(E_0-E_g)^{1/2}. \quad (9)$$

In this case, $\varepsilon_2(\omega)$ is calculated from the K-K transformation of the reflection spectra (Fig. 2) of $(CH)_x$ films and the sum rule of Eq. 10 is found by integrating $\varepsilon_2(\omega)$,

$$\frac{m}{2\pi^2 Ne^2}\int_{\omega_g}^{\omega_0}\omega\varepsilon_2(\omega)d\omega = f_{\pi,\pi^*}G(E_0), \quad (10)$$

where the number of π-electrons per unit volume of the medium is taken to be $N\approx 2\times 10^{22}$ cm^{-3} from the measured density of $(CH)_x$ (0.4 g/cm^3).[20] The obtained sum rule curves are shown in Fig. 5 together with the

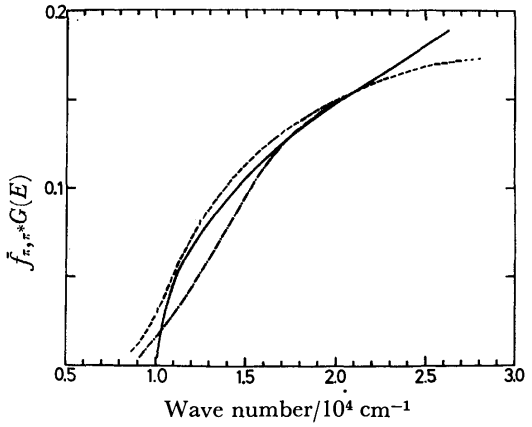

Fig. 5. The sum rule of $\varepsilon_2(\omega)$ obtained from the K-K transformation of the reflection spectra of the thick $(CH)_x$ films. ·—·—·: 80% *cis*-$(CH)_x$, ------: 85% *trans*-$(CH)_x$, ——: $G(E)=A(E-E_g)^{1/2}$.

theoretical curve of $G(E_0)=A(E_0-E_g)^{1/2}$. The good agreement between the observed and theoretical curves indicates that $(CH)_x$ can be treated as the one-dimensional system and that the top of π band and the bottom of π^* band can be approximated as the parabolic function. Accordingly, the absorption band observed in the visible region can be assigned to the direct interband transition (type 1 shown in Fig. 4-1) from the π band to the π^* band.

Absorption Spectra of Thin $(CH)_x$ Films Doped with $ClSO_3H$. In the lightly doped $(CH)_x$ film ($\sigma\simeq 2\times 10^{-2}\ \Omega^{-1}$ cm^{-1}) polymerized on the KBr plate, two infrared peaks of the additional absorption are

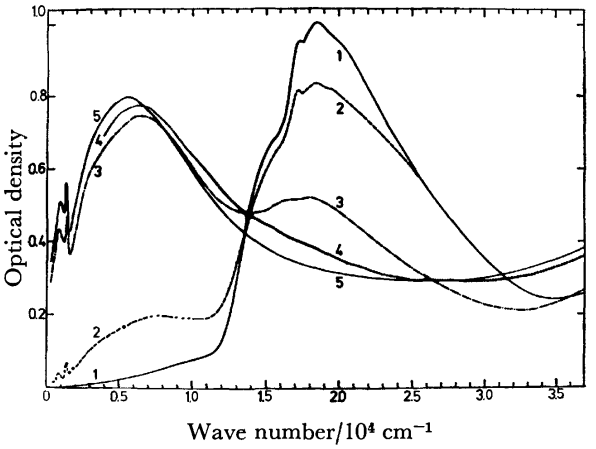

Fig. 6. The absorption spectra of *cis*-rich thin $(CH)_x$ films doped with $ClSO_3H$.
1) Pure $(CH)_x$, 2) $\sigma_0\simeq 2\times 10^{-2}\ \Omega^{-1}$ cm^{-1}, 3) $\sigma_0\simeq 2.6\ \Omega^{-1}$ cm^{-1}, 4) $\sigma_0\simeq 10^2\ \Omega^{-1}$ cm^{-1}, 5) $\sigma_0\simeq 250\ \Omega^{-1}$ cm^{-1}.

observed at 1370 and 870 cm^{-1} as shown in Fig. 6. In doping $(CH)_x$ with $ClSO_3H$, the π-electrons transfer from $(CH)_x$ chain to $ClSO_3H$. The resulting hole (cation) on the polymer chain is bound by the Coulomb potential to the region of the chain near the acceptor ion and the impurity state appears in the energy gap (Fig. 4-2). The band at 870 cm^{-1} can be assigned to the transition (type 2 shown in Fig. 4-2) from the valence band to the impurity 1s level according to Fincher *et al.*[9] and Tanaka *et al.*[12] In this model, the cation on the $(CH)_x$ chain delocalizes near the acceptor ion and a region of the uniform bond lengths occurs. This phenomenon is called "Soliton" and the possibility of the existence of soliton was theoretically recognized.[21,22] The 1370 cm^{-1} mode appears at a frequency approximately intermediate between the single bond (C–C, 950 cm^{-1}) and double bond (C=C, $\simeq$1650 cm^{-1}) stretching mode and may be assigned to the stretching mode of the bond order 1.5 corresponding to the uniform bond lengths, while Harada *et al.*[23] and Rabolt *et al.*[24] concluded that the 870 and 1370 cm^{-1} peaks were the molecular vibration mode.

In addition to the 870 and 1370 cm^{-1} bands, a broad band appears in the region of 8000 cm^{-1} and the absorption intensity of the interband transition at about 17000 cm^{-1} decreases (Fig. 6). The fact that there is an isosbestic point at about 14000 cm^{-1} in the spectra clearly indicates that there is an equilibrium between two absorbing species of the 8000 and 17000 cm^{-1} bands.

In heavily doped $(CH)_x$ films polymerized on the polyethylene films, the 870 and 1370 cm^{-1} bands remain clearly. Furthermore, the absorption band corresponding to the interband transition disappears in the visible region and the broad band observed in the near IR region becomes more intense. The broad band has the maximum peak at about 5500 cm^{-1} and the absorption edge in the region of less than 300 cm^{-1}. This fact suggests that the energy gap between the π and π^* bands becomes zero in the heavily doped $(CH)_x$ and doping removes the bond alternation leading to a

unform bond lengths. Accordingly, the electronic structure of heavily doped $(CH)_x$ consists of one π band and one impurity band. Figure 4-3 shows the observed intraband transition (type 3) and impurity band (type 2), although the transition energy to the impurity level seems to become zero due to the electron screening effect in the metallic state.

In the system, the complex dielectric constant of heavily doped $(CH)_x$ can be easily derived from Eq. 1 by substituting the zero energy gap between the π and π^* bands

$$\varepsilon_{\pi^*}(k+q) - \varepsilon_{\pi}(k) \simeq 0 \tag{11}$$

and the oscillator strength of the intraband transition[19,25]

$$\lim_{q\to 0} \sum_k f_{\pi k, \pi^* k+q} = \lim_{q\to 0} f_{\pi k_F, \pi^* k_F+q} = \frac{m}{\hbar^2}\left(\frac{\partial^2 \varepsilon_\pi(k)}{\partial k^2}\right) = \frac{m}{m^*}. \tag{12}$$

Here, m^* is the effective mass of the free carrier. The obtained dielectric constants are given in the following equations,

$$\varepsilon(\omega) = \varepsilon_{core} - \frac{\omega_p^2}{\omega^2 + i\omega/\tau_0}, \tag{13}$$

$$\varepsilon_1(\omega) = \varepsilon_{core} - \frac{\omega_p^2 \tau_0^2}{1+\omega^2\tau_0^2}, \tag{14}$$

and

$$\varepsilon_2(\omega) = \frac{1}{\omega}\frac{\omega_p^2 \tau_0}{1+\omega^2\tau_0^2}, \tag{15}$$

where the plasma frequency ω_p is defined as follows

$$\omega_p^2 = \frac{4\pi N e^2}{m^*}, \tag{16}$$

and N is the number density of the free carrier. Then, the extinction coefficient $k(\omega)$ and the absorption coefficient $\alpha(\omega)$ are expressed by the next equations,[19]

$$k(\omega) = \{(\sqrt{\varepsilon_1^2+\varepsilon_2^2} - \varepsilon_1)/2\}^{1/2} \tag{17}$$

and

$$\alpha(\omega) = \frac{2\omega}{c}k(\omega) = \frac{\sqrt{2}\,\omega}{c}\{\sqrt{\varepsilon_1^2+\varepsilon_2^2} - \varepsilon_1\}^{1/2}. \tag{18}$$

The maximum absorption coefficient of the interband transition is determined to be 2.58×10^5 cm^{-1} near 17000 cm^{-1} by the K-K transformation of the reflection spectra as is shown in Fig. 3. Accordingly, the absorption coefficient of the intraband transition of the heavily doped film ($\sigma \simeq 250\ \Omega^{-1}$ cm^{-1}) can be estimated as is shown in Fig. 7. Then, the parameters of Eqs. 14 and 15 were determined by the optimum fit of Eq. 18 to the experimental data. The fit was obtained with $\hbar\omega_p = 31000$ cm^{-1}, $\tau_0 = 0.48\times10^{-15}$ s and $\varepsilon_{core} = 6$ (see Table 1). The calculated absorption spectrum based on these values is plotted for comparison with the experimental curves in Fig. 7.

Reflection Spectra of 85% trans-$(CH)_x$ Films Doped with $ClSO_3H$. Reflection spectra of 85% *trans*-$(CH)_x$ films doped with $ClSO_3H$ are shown in Figs. 8 and 9.

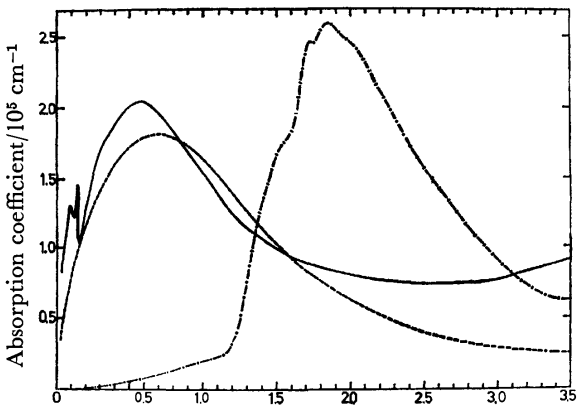

Fig. 7. Comparison between the observed and calculated absorption spectra of the thin $(CH)_x$ film ($\sigma_0 \simeq 250\ \Omega^{-1}$ cm^{-1}) heavily doped with $ClSO_3H$. ——: Observed, ------: theoretical, ·—·—·: pure $(CH)_x$.

Table 1. Optical parameters obtained from the best fit of the absorption and reflection spectra of the heavily doped $(CH)_x$ films

Optical parameter	Absorption spectra	Reflection spectra
ε_{core}	6	1.81
$\hbar\omega_p$/cm^{-1}	31000	28200
τ_0/s	0.48×10^{-15}	0.277×10^{-15}
N/cm^{-3}	1.2×10^{22}—1.8×10^{22}	1.0×10^{22}—1.5×10^{22}
σ_0/Ω^{-1} cm^{-1}	1450	690

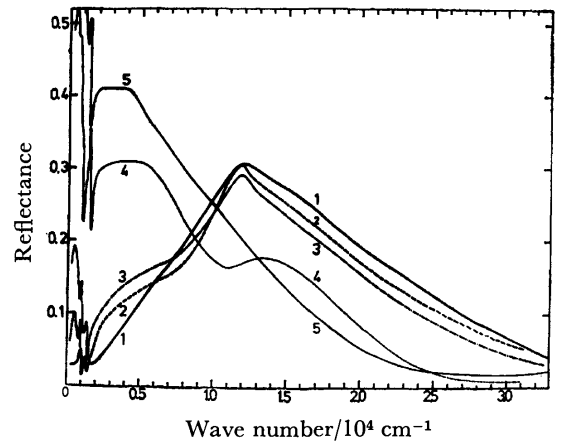

Fig. 8. The reflection spectra of thick 85% *trans*-$(CH)_x$ films doped with $ClSO_3H$. 1) pure $(CH)_x$, 2) $\sigma_0 \simeq 0.1\ \Omega^{-1}$ cm^{-1}, 3) $\sigma_0 \simeq 0.6\ \Omega^{-1}$ cm^{-1}, 4) $\sigma_0 \simeq 20\ \Omega^{-1}$ cm^{-1}, 5) $\sigma_0 \simeq 280\ \Omega^{-1}$ cm^{-1}.

Pure *trans*-$(CH)_x$ has the sharp dispersion peak of C–H out-of-plane mode at 1015 cm^{-1} in addition to the interband transition located in the visible region. Lightly doping of the film with $ClSO_3H$ increases the reflectance below 10000 cm^{-1} and decreases the reflectance over the region of the interband transition. The shoulder at 800 cm^{-1}, the peak at 1400 cm^{-1} and the broad band in the region of 8000 cm^{-1} correspond to those observed in the absorption spectra of thin films

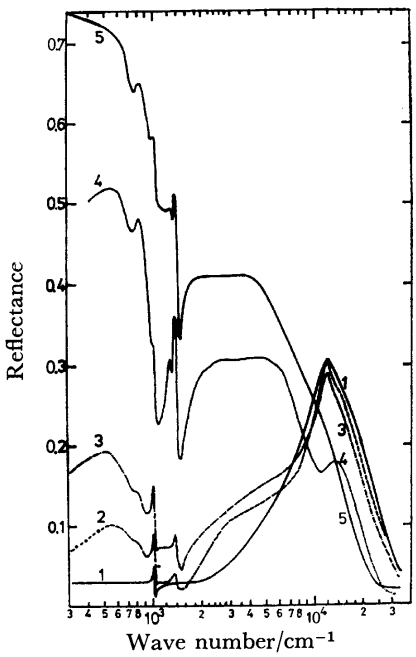

Fig. 9. The plot for the logarithmic wave number of the reflection spectra of thick 85% *trans*-$(CH)_x$ films doped with $ClSO_3H$. 1) Pure $(CH)_x$, 2) $\sigma_0 \simeq 0.1\ \Omega^{-1}\ cm^{-1}$, 3) $\sigma_0 \simeq 0.6\ \Omega^{-1}\ cm^{-1}$, 4) $\sigma_0 \simeq 20\ \Omega^{-1}\ cm^{-1}$, 5) $\sigma_0 \simeq 280\ \Omega^{-1}\ cm^{-1}$.

as shown in Fig. 6. The appearance of the peak below 800 cm^{-1} seems to show that the hole carriers occur in the $(CH)_x$ chain and the $(CH)_x$ film becomes the p-type semiconductor. In heavily doped samples, the reflectance becomes larger and larger below 10000 cm^{-1} and the reflectivity reaches to 70% in the frequency region of lower than 500 cm^{-1} although the interband transition disappears in the visible region. It looks like the metallic reflection spectrum. Furthermore, the 1400 and 800 cm^{-1} bands can be also clearly observed. The increase in the intensity of the 1400 cm^{-1} band means that the region of the uniform bond lengths expands in the $(CH)_x$ chain and the observation of the 800 cm^{-1} implies that the impurity band exists in the metallic π band as shown in Fig. 4-3. The behavior of the reflection spectra of doped thick films is in good agreement with that of the absorption spectra of doped thin films.

The reflectance is given by the following equation[19,26]

$$R = \frac{|\varepsilon|+1-\sqrt{2(|\varepsilon|+\varepsilon_1)}}{|\varepsilon|+1+\sqrt{2(|\varepsilon|+\varepsilon_1)}} \tag{19}$$

and

$$|\varepsilon| = \sqrt{\varepsilon_1^2+\varepsilon_2^2}. \tag{20}$$

Accordingly, the best fit of Eq. 19 to the observed reflection spectrum of the heavily doped film ($\sigma \simeq 280\ \Omega^{-1}\ cm^{-1}$) can be obtained by using the parameters of $\hbar\omega_p = 28200\ cm^{-1}$, $\tau_0 = 0.277 \times 10^{-15}$ s and $\varepsilon_{core} = 1.81$ (see Table 1). The calculated reflection spectrum based on these values is depicted for comparison with the experimental curve in Fig. 10.

Relation of the Obtained Optical Parameters with the Conductivity. The effective mass, m^*, of the free carrier in the $(CH)_x$ chain can be given in the tight

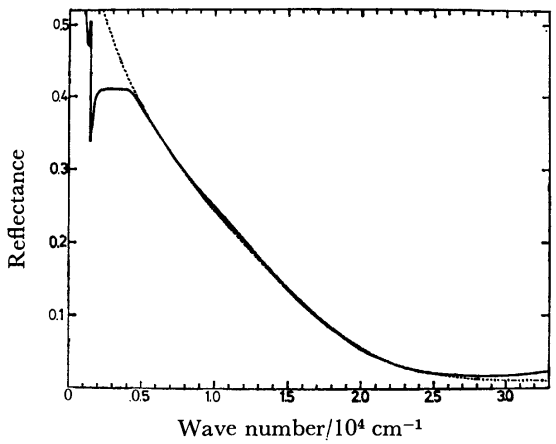

Fig. 10. Comparison between the observed and calculated reflection spectra of the thick $(CH)_x$ film heavily doped with $ClSO_3H$. ——: Observed, ------: theoretical.

binding approximation as follows,[26]

$$\frac{m}{m^*} = \frac{m}{\hbar^2}\left(\frac{\partial^2\varepsilon_x(k)}{\partial k^2}\right) = \frac{4ta^2m}{\pi\hbar^2} \tag{21}$$

and can be estimated to be $0.6 < m/m^* < 0.9$ by using $a = 1.4$ Å and $t = 2.0$—2.5 eV. Then, the number density, N, of the free carrier contributing to the metallic conductivity is given as follows,

$$N = \omega_p^2 m^*/(4\pi e^2). \tag{22}$$

The number density of the free carrier in the metallic $(CH)_x$ film can be extracted by substituting the observed plasma frequency and the effective mass, m^*, into Eq. 22 and is shown in Table 1. The observed number density, N, is comparable with the total π-electron number density ($N \simeq 2 \times 10^{22}\ cm^{-3}$) in the $(CH)_x$ film. This means that all π-electrons contribute to the transport and that heavily doping removes the bond alternation leading to a uniform bond lengths.

Furthermore, the d.c. conductivity, σ_0, is given by Eq. 23,[19]

$$\sigma_0 = \frac{\omega_p^2\tau_0}{4\pi} \tag{23}$$

and is calculated by using the observed plasma frequency, ω_p, and relaxation time, τ_0. The obtained values are comparable with the observed value ($\sigma \simeq 280$—$250\ \Omega^{-1}\ cm^{-1}$) of the d.c. conductivity of the heavily doped films as is shown in Table 1.

References

1) C. B. Duke, A. Paton, W. Salaneck, H. Thomas, E. W. Plummer, A. J. Heeger, and A. G. MacDiarmid, *Chem. Phys. Lett.*, **59**, 146 (1978).

2) P. M. Grant and I. P. Batra, *Solid State Commun.*, **29**, 225 (1979).

3) A. Karpfen and J. Petkov, *Solid State Commun.*, **29**, 251 (1979).

4) T. Yamabe, K. Tanaka, H. Terama-e, K. Fukui, A. Imamura, H. Shirakawa, and S. Ikeda, *Solid State Commun.*, **29**, 329 (1979).

5) H. Shirakawa, T. Sasaki, and S. Ikeda, *Chem. Lett.*, **1978**, 1113.

6) C. R. Fincher, Jr., D. L. Peebles, A. J. Heeger, M. A. Druy, Y. Matsumura, and A. G. MacDiarmid, *Solid State Commun.*, **27**, 489 (1978).
7) H. Shirakawa, T. Ito, and S. Ikeda, *Makromol. Chem.*, **179**, 1565 (1978).
8) C. K. Chiang, C. R. Fincher, Jr., Y. W. Park, A. J. Heeger, H. Shirakawa, E. J. Louis, S. C. Gau, and A. G. MacDiarmid, *Phys. Rev. Lett.*, **39**, 1098 (1977).
9) C. R. Fincher, Jr., M. Ozaki, A. J. Heeger, and A. G. MacDiarmid, *Phys. Rev. B*, **19**, 4140 (1979).
10) C. R. Fincher, Jr., M. Ozaki, M. Tanaka, D. Peebles, L. Lauchlan, A. J. Heeger, and A. G. MacDiarmid, *Phys. Rev. B*, **20**, 1589 (1979).
11) M. Tanaka, C. R. Fincher, Jr., A. J. Heeger, and A. G. MacDiarmid, to be published.
12) M. Tanaka, A. Watanabe, and J. Tanaka, *Bull. Chem. Soc. Jpn.*, **53**, 645 (1980).
13) A. Watanabe, M. Tanaka, and J. Tanaka, *Chem. Lett.*, **1980**, 575.
14) H. Shirakawa and S. Ikeda, *Polym. J.* ,**2**, 231 (1971).
15) H. Shirakawa, T. Ito, and S. Ikeda, *Polym. J.*, **4**, 460 (1973).
16) T. Ito, H. Shirakawa, and S. Ikeda, *J. Polym. Sci., Part A-1*, **12**, 11 (1974), **13**, 1943 (1975).
17) H. J. Bowlden and J. K. Wilmshurst, *J. Opt. Soc. Am.*, **53**, 1073 (1963).
18) D. M. Roessler, *Brit. J. Appl. Phys.*, **16**, 1119 (1965).
19) F. Wooten, "Optical Properties of Solids," Academic press, New York (1972).
20) G. E. Wnek, J. C. W. Chien, F. E. Karasy, M. A. Druy, Y. W. Park, A. G. MacDiarmid, and A. J. Heeger, *J. Polym. Sci., Polymer Lett. Ed.*, **17**, 779 (1979).
21) M. J. Rice, *Phys. Lett. A*, **71**, 152 (1979); M. J. Rice and J. Timonen, *ibid.*, **73**, 368 (1979).
22) W. P. Su, J. R. Schrieffer, and A. J. Heeger, *Phys. Rev. Lett.*, **42**, 1698 (1979).
23) I. Harada, M. Tasumi, H. Shirakawa, and S. Ikeda, *Chem. Lett.*, **1978**, 1411.
24) J. F. Robolt, T. C. Clarke, and G. B. Street, *J. Chem. Phys.*, **71**, 4614 (1979).
25) D. Pines, "Elementary Excitations In Solids," Benjamin, New York (1964); R. Brout and P. Carruthers, "Lectures On The Many-Electron Problem," John Wiley & Sons, New York (1963), p. 155; H. Ehrenreich and M. Cohen, *Phys. Rev.*, **115**, 786 (1959).
26) A. A. Bright, A. F. Garito, and A. J. Heeger, *Phys. Rev. B*, **30**, 1328 (1974).

 © 1980 The Chemical Society of Japan Bull. Chem. Soc. Jpn., 53, 3436—3438 (1980) [Vol. 53, No. 12

The Preparation and ^{13}C-NMR Spectra of Alkoxymethyltriphenylphosphonium Salts

Yoshihisa YAMAMOTO* and Zenjiro KANDA

Faculty of Pharmaceutical Science, Higashi Nippon Gakuen University, Ishikari-Tobetsu, Hokkaido 061-02

(Received May 12, 1980)

Alkoxymethyltriphenylphosphonium salts, $[(C_6H_5)_3PCH_2OR]X$, X: Cl, Br, and I, R: CH_3, C_2H_5, and i-C_3H_7, have been obtained from the reaction of the triphenylphosphine and the corresponding alkyl halomethyl ether. In the ^{13}C-NMR spectra of these salts, the coupling constant (J_{CP}) is 68—71 Hz, which is larger than that (J_{CP}: 48—56 Hz) of $[(C_6H_5)_3PCH_2R]Br$, R: H, CH_3, and i-C_3H_7, Me_3P=S and Me_3P=Se, while it is close to that (66—69 Hz) of Me_3P=O and Et_3P=O. The coupling constant (J_{CP}) of these salts can be caused by the oxygen atom in the salts.

Although the ^{1}H-NMR spectra of methoxymethyltriphenylphosphonium chloride[1] has already been described, the ^{13}C-NMR spectra of alkoxymethyltriphenylphosphonium salts and alkyltriphenylphosphonium salts, except for methyltriphenylphosphonium salt,[2,3] have been the subject of little research.

Previously we have reported on several ylides and Ib-group (Cu,[4] Ag,[4] and Au[5]) or IIb-group[6] (Zn, Cd, and Hg) metal complexes. The present paper will deal with the preparation and ^{13}C-NMR measurements of alkoxymethyltriphenylphosphonium salts, $[(C_6H_5)_3PCH_2OR]X$, X: $[Ag(CN)_2]$, $[Au(CN)_2]$, Cl, Br, and I, R: CH_3, C_2H_5, and i-C_3H_7, and with the ^{13}C-NMR measurements of alkyltriphenylphosphonium salts, $[(C_6H_5)_3PCH_2R]Br$, R: H, CH_3, and i-C_3H_7.

Results and Discussion

Synthesis and Properties. Methoxymethyltriphenylphosphonium salt[1,7] (**1a**, **1b**, and **1c**) and ethoxymethyltriphenylphosphonium salt (**1d**) were prepared by the reaction of triphenylphosphine and the corresponding alkyl halomethyl ether. Isopropoxymethyltriphenylphosphonium bromide (**1e**) was prepared by the reaction of the triphenylphosphine and the bromomethyl isopropyl ether. The alkoxymethyltriphenylphosphonium dicyanoargentate(I) (**2a**—**2c**) and alkoxymethyltriphenylphosphonium dicyanoaurate(I) (**3a**—**3c**) were synthesized by the reaction of **1b**, **1d**, or **1e** and potassium dicyanoargentate(I)[8] or potassium dicyanoaurate-(I)[9] respectively.

$$[(C_6H_5)_3PCH_2OR]Br \xrightarrow{K[M(CN)_2]} [(C_6H_5)_3PCH_2OR][M(CN)_2]$$

R	CH_3	C_2H_5	i-C_3H_7
	1b	**1d**	**1e**

M: Ag, Au

M	R: CH_3	C_2H_5	i-C_3H_7
Ag	**2a**	**2b**	**2c**
Au	**3a**	**3b**	**3c**

$$\xrightarrow{NaNH_2 \text{ or } NaH} (C_6H_5)_3P{=}CHOR$$

4 (in solution)

These salts are soluble in most organic solvents, but are insoluble in ether, ethyl acetate, and benzene.

Attempts at the isolation of the alkoxymethylidenetriphenylphosphorane (**4**) from the reaction mixture of **1a**—**1e** and $NaNH_2$ or NaH in dry THF have been unsuccessful, probably because the electron density of ylide carbanion of **4** is too high, as compared with other unstable alkylidenetriphenylphosphoranes,[4,10] to allow its existence. At present, the ylide **4**[7,11,12] can never be isolated from the solution.

NMR Spectra. The ^{1}H-NMR spectra of **1a**—**1e**, **2a**—**2c**, and **3a**—**3c** were measured in $CDCl_3$ at room temperature. In the ^{1}H-NMR spectrum of **3a**, the signal (3.67 ppm) at the highest field is assigned to the methyl protons of the OCH_3 group. The signal of 5.28 ppm is assigned to the methylene protons of the PCH_2 group. The multiplet signal of 7.8 ppm at the lowest field is assigned to the protons of the phenyl groups. The coupling constants (J_{HCP}: 4 Hz) of the methylene protons of **1a**—**1e**, **2a**—**2c**, and **3a**—**3c** are much smaller than those ($J_{HCP} \approx 13$ Hz) of the alkyltriphenylphosphonium salts, $[(C_6H_5)_3\overset{+}{P}CH_2R]$, R: H (**5a**),[3,13] CH_3 (**5b**),[13] and i-C_3H_7 (**5c**),[13] of tetracovalent phosphorus, as is shown in Table 1. Hendrickson, *et al.*[1] explained the small coupling constant (4 Hz) of **1b** by assuming that the oxygen was partially bound to the positive phosphorus. The coupling constant (J_{HCP}) of $[(C_6H_5)_3PCH_2SeC_6H_5]Br$ (**6**) is 7 Hz,[14] which is also small. The selenium atom in **6** may interact with the positive phosphorus center, but the interaction can be weaker than that of **1a**—**1e**, **2a**, and **3a**, because the coupling constant of **6** is larger than those of these salts.

The ^{13}C-NMR spectra of **1a**—**1e**, **2a**, **3a**, and **5b**—**5c** have also been measured in $CDCl_3$ at room temperature. The doublet signals (10.1—29.2 ppm) at the highest field of **5a**—**5c** are assigned to the carbon of the $PCH_{2(3)}$ group. The chemical shift (10.1 ppm) of the methyl carbon of **5a** is much higher than that (29.2 ppm) of the methylene carbon of **5c**, while the coupling constant (J_{CP}: 56.6 Hz) of the methyl carbon of **5a** is larger than that (47.9 Hz) of the methylene carbon of **5c**. These changes seem to be due to the substituent (R) effect of $[(C_6H_5)_3\overset{+}{P}CH_2R]$; *i.e.*, the isopropyl group of the substituent in **5c** has a greater electron-donating effect than does the hydrogen of **5a**. In the ^{13}C-NMR spectra of **3a**, the doublet signal of 62.9 ppm is assigned to the carbon of the OCH_3 group, and the doublet signal of 66.3 ppm is assigned to the carbon of the PCH_2 group, while the singlet signal of 151.2 ppm is assigned to the cyano carbon of the $[Au(CN)_2]$ ion. The chemical shifts (δ CH_2P: 62—66 ppm) of **1a**—**1e**, **2a**, and **3a** are much lower than those of **5a**—**5c**. The coupling constants (J_{CP}) of these salts are 68—71 Hz, larger than those (48—56 Hz) of **5a**—**5c**, Me_3P=S,[15] and Me_3P=Se,[15] but close to that (66—69 Hz) of

Table 1. ^{1}H-NMR spectra of alkoxymethyltriphenylphosphonium salts

	OH_2P δ/ppm	J_{HCP}/Hz	OCH_{1-3} δ/ppm	CH_3 δ/ppm	J_{HCCH}/Hz	C_6H_5 δ/ppm
1a	5.83 d (2H)	4.0	3.67 s (3H)			7.80m(15H)
1b	5.80 d (2H)	4.0	3.73 s (3H)			7.83m(15H)
1c	5.70 d (2H)	4.0	3.73 s (3H)			7.83m(15H)
1d	5.80 d (2H)	4.0	3.93 q (2H)	1.17 t (3H)	7.2	7.80m(15H)
1e	5.75 d (2H)	4.0	4.13m(1H)	1.20 d (6H)	6.0	7.80m(15H)
2a	5.28 d (2H)	4.5	3.64 s (3H)			7.80m(15H)
2b	5.28 d (2H)	4.0	3.83 q (2H)	1.24 t (3H)	7.2	7.80m(15H)
2c	5.24 d (2H)	5.0	3.94m(1H)	1.23 d (6H)	6.0	7.80m(15H)
3a	5.28 d (2H)	4.5	3.67 s (3H)			7.80m(15H)
3b	5.31 d (2H)	4.0	3.89 q (2H)	1.25 t (3H)	7.2	7.80m(15H)
3c	5.23 d (2H)	5.0	3.94m(1H)	1.22 d (6H)	6.0	7.80m(15H)

Solvent and standard: $CDCl_3$ (int. TMS).

Table 2. ^{13}C-NMR spectra of **1a—1e**, **2a**, **3a**, and **5a—5c**

No.	PCH_{2-3} δ/ppm	$^{1}J_{CP}$/Hz	OCH_{1-3} [CH] δ/ppm	$^{3}J_{COCP}$/ Hz	$^{2}J_{CCP}$/ Hz	CH_3 δ/ppm	C_6H_5 δ/ppm (J_{CP}/Hz) c-l	*o*	*m*	*p*	CN δ/ppm
1a	65.7 d	68.4	62.5 d	13.7			116.3 (85.9)	133.9 (11.7)	130.2 (11.7)	135.2 (—)	
1b	65.1 d	70.3	61.8 d	13.7			115.4 (85.9)	133.1 (9.8)	129.6 (13.7)	134.4 (—)	
1c	66.0 d	69.3	62.5 d	13.7			115.8 (86.9)	133.7 (10.7)	127.2 (12.7)	135.2 (2.9)	
1d	63.3 d	68.4	69.8 d	13.7		13.9 s	115.4 (85.9)	132.9 (9.8)	129.9 (13.7)	134.4 (3.9)	
1e	62.0 d	70.3	76.3 d	11.7		21.2 s	116.1 (85.8)	133.6 (9.8)	129.9 (11.7)	134.8 (—)	
2a	66.2 d	71.3	62.7 d	13.7			115.8 (86.9)	133.8 (9.8)	130.8 (12.7)	135.9 (2.9)	153.4s
3a	66.3 d	70.3	62.9 d	13.7			115.8 (86.9)	133.8 (9.8)	130.7 (12.7)	135.9 (2.9)	151.2s
5a	10.1 d	56.6					118.5 (87.9)	132.7 (11.7)	130.0 (11.7)	134.7 (—)	
5b	16.1 d	51.8			4.9	5.9 d	116.9 (85.9)	132.6 (10.7)	129.6 (12.7)	134.2 (2.9)	
5c	29.2 d	47.9	[23.0 d]		3.9	23.4 s	117.4 (85.9)	132.4 (10.7)	129.4 (12.7)	133.9 (2.9)	
$K[Ag(CN)_2]$[a]											149.7s
$K[Au(CN)_2]$[a]											154.1s

Solvent and standard: $CDCl_3$ (δ=77.1 ppm). a) D_2O and internal dioxane (δ=67.4 ppm).

$Me_3P{=}O$[16] and $Et_3P{=}O$.[16] The large coupling constants (J_{CP}) of these salts can be caused by the highly electronegative[17] oxygen in salts. As the oxygen atom and the positive phosphorus center in these salts come close to each other and interact, the 2p electrons of the oxygen atom are partially bound to the 3d-orbital of the positive phosphorus. Thus, the positive charge is delocalized over the P——C system, and the phosphorus is considered to be formally pentacovalent (Formulae II and III) with the dsp^3 configuration from the Formulae I—III. The chemical shifts and the coupling constants of **1a—1e**, **2a**, and **3a** receive less influence from the substituent. The anion in these salts has no effect on the chemical shift or the coupling constant. The ^{13}C-NMR data of these salts are collected in Table 2.

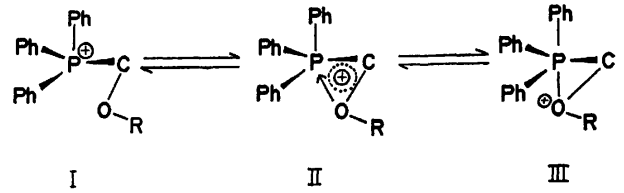

I II III

Experimental

Measurements. The NMR spectra were measured with an FX-60 spectrometer (JEOL) for ^{13}C-NMR, and with JNMPMX-60 (JEOL) and R-40 (Hitachi) spectrometers for ^{1}H-NMR.

Starting Materials. Alkyl halomethyl ether were prepared by Vousi,[18] Lapkina,[19] and Marvel's[20] methods.

*Methoxymethyltriphenylphosphonium Chloride, $[(C_6H_5)_3PCH_2O\text{-}CH_3]Cl$ (**1a**), Methoxymethyltriphenylphosphonium Bromide (**1b**), Methoxymethyltriphenyl phosphonium Iodide $[(C_6H_5)_3PCH_2OCH_3]I$ (**1c**), Ethoxymethyltriphenylphosphonium Bromide (**1d**), and Isopropoxymethyltriphenylphosphonium Bromide (**1e**)*: The correspond-

ing alkyl halomethyl ether (7.55 g (95 mmol dm^{-3}) for **1a**. 39.0 g (314 mmol dm^{-3}) for **1b**, 1.83 g (10.7 mmol dm^{-3}) for **1c**, 14.00 g (101 mmol dm^{-3}) for **1d**, and 18.00 g (118 mmol dm^{-3}) for **1e**) was added to a benzene solution of triphenylphosphine (25 g (95 mmol dm^{-3}) for **1a**, 82.1 g (312 mmol dm^{-3}) for **1b**, 2.8 g (10.7 mmol dm^{-3}) for **1c**, 26.4 g (101 mmol dm^{-3}) for **1d** and 31.0 g (118 mmol dm^{-3}) for **1e**). The solution was then stirred for 24 h at room temperature. The white salt thus precipitated was filtered off, washed with benzene, and dried under vacuum. The crude products were recrystallized from chloroform and ethyl acetate. Yield: 30.0 g (92.1%) for **1a**, 106.0 g (87.7%) for **1b**, 3.47 g (74.7%) for **1c**, 37.1 g (91.5%) for **1d**, and 41.0 g (83.7%) for **1e**. Found: C, 69.89; H, 5.80% for **1a**, C, 61.84; H, 5.06% for **1b**, C, 55.40; H, 4.50% for **1c**, C, 62.73; H, 5.83% for **1d**, and C, 63.54; H, 5.70% for **1e**. Calcd for $C_{20}H_{20}OClP$ (MW 342.81) C, 70.07; H, 5.88 for **1a**, $C_{20}H_{20}OBrP$ (MW 387.26) C, 62.03; H, 5.21 for **1b**, $C_{20}H_{20}OIP$ (MW 434.26) C, 55.32; H, 4.64 for **1c**, $C_{21}H_{22}OBrP$ (MW 401.28) C, 62.87; H, 5.53 for **1d**, and $C_{22}H_{24}OBrP$ (MW 415.33) C, 63.62; H, 5.82% for **1e**. Mp: 198—199 for **1a**, 208—210 for **1b**, 189—190 for **1c**, 227—229 for **1d**, and 190—191 °C for **1e**.

Methoxymethyltriphenylphosphonium Dicyanoargentate (I) (2a), Ethoxymethyltriphenylphosphonium Dicyanoargentate (I) (2b), and Isopropoxymethyltriphenylphosphonium Dicyanoargentate (I) (2c): **1b** (0.387 g, 1.0 mmol dm^{-3}), **1d** (0.40 g, 1.0 mmol dm^{3}), and **1e** (0.415 g, 1.0 mmol dm^{-3}) were dissolved in 1 cm^3 of methanol. Potassium dicyanoargentate (I) (0.2 g, 1.0 mmol dm^{-3}) was dissolved in 0.7 cm^3 of water. The methanol solution was added to an aqueous solution, and the new mixture was stirred; the white complex thus precipitated was filtered, washed with cooled water, and dried. Yield: 0.38 g (81.4%) for **2a**, 0.40 g (83.2%) for **2b**, and 0.40 g (80.8%) for **2c**. Found: C, 56.54; H, 4.52 for **2a**, C, 57.26; H, 4.59 for **2b**, and C, 58.32; H, 4.88% for **2c**. Calcd for $C_{22}H_{20}N_2OAgP$ (MW 467.28) C, 56.55; H, 4.31 for **2a**, $C_{23}H_{22}N_2OAgP$ (MW 481.31) C, 57.40; H, 4.01 for **2b**, and $C_{24}H_{24}N_2OAgP$ (MW 495.33) C, 58.20; H, 4.88% for **2c**. Mp: 122—124 for **2a**, 133—135 for **2b** and 126—127 °C for **2c**.

Methoxymethyltriphenylphosphonium Dicyanoaurate (I) (3a), Ethoxymethyltriphenylphosphonium Dicyanoaurate (I) (3b), and Isopropoxymethyltriphenylphonium Dicyanoaurate (I) (3c): 0.194 g (0.5 mmol dm^{-3}) of **1b**, 0.20 g (0.5 mmol dm^{-3}) of **1c**, and 0.207 g (0.5 mmol dm^{-3}) of **1d** was soluble in 0.5 cm^3 methanol. Potassium dicyanoaurate (I) (0.15 g, 0.5 mmol dm^{-3}) was soluble in water of 0.7 cm^3. The above methanol solution was added to an aqueous solution, the mixture was stirred; the white complex thus precipitated was filtered, washed with cooled water, and dried. Yield: 0.2 g (71.9%) for **3a**, 0.2 g (70.1%) for **3b** and 0.23 g (78.7%) for **3c**. Found: C, 47.52; H, 3.84 for **3a**, C, 48.44; H, 3.99 for **3b**, and C, 49.76; H, 4.30% for **3c**. Calcd for $C_{22}H_{20}N_2OAuP$ (MW 556.38) C, 47.49; H, 3.62 for **3a**, $C_{23}H_{22}N_2OAuP$ (MW 570.41) C, 48.43; H, 3.89 for **3b**, and $C_{24}H_{24}N_2OAuP$ (MW 584.43) C, 49.32; H, 4.14% for **3c**. Mp: 143—145 for **3a**, 150—152 for **3b**, and 143—146 °C for **3c**.

Methyltrihpenylphosphonium Bromide[21] *(5a), Ethyltriphenylphosphonium Bromide*[21a,22] *(5b), and Isobuthyltriphenylphosphonium Bromide*[23] *(5c)*: They were prepared from triphenylphosphine and the corresponding alkyl bromide.

The Reaction of 1b and Base: **1b** (4.20 g, 10.8 mmol dm^{-3}) and sodium amide (0.42 g, 10.8 mmol dm^{-3}) were suspended in dry THF (12 ml) at room temperature, and the mixture was stirred for approximately 1 h. The orange solution[11] was filtered under nitrogen. Dry pentane was added to the solution and cooled. The yellow crystal was filtered under nitrogen and dried. The ^{1}H-NMR spectrum of that crystal in benzene-d_6 did not show the expected signal of the ylide carbanion at room temperature. ^{1}H-NMR spectrum of yellow crystals: δ 3.07 (s, 3H, OCH_3), 4.0 (d, 2H, J=6, PCH_2), 7.2—8.1 (m, 15H, C_6H_5), in C_6D_6.

A solution of 0.13 g of phLi (1.15 mmol dm^{-3}) in toluene-d_8 (5 ml) was slowly added to a suspension of **1b** (0.95 g, 2.45 mmol dm^{-3}) in 2 ml of toluene-d_8 at −70 °C under helium. The orange solution was filtered after 4 h at −70 °C under helium. The orange filtrate did not show the signal of the ylide carbanion from the ^{1}H-NMR spectrum.

The orange solutions from NaH and **1b** in solvents (THF or toluene) at the present temperatures (r.t. or −70 °C) did not show the signals of the ylide carbanion from the ^{1}H-NMR spectra.

References

1) J. B. Hendrickson, M. L. Maddox, J. J. Sims, and H. D. Kaesz, *Tetrahedron* **20**, 449 (1964).

2) Y. Yamamoto and H. Schmidbaur, *J. Chem. Soc., Chem. Commun.*, **1975**, 668.

3) T. A. Albright, W. J. Freeman, and E. E. Schweizer, *J. Am. Chem. Soc.*, **97**, 940 (1975).

4) a) Y. Yamamoto and H. Schmidbaur, *J. Organomet. Chem.*, **96**, 133 (1975); b) Y. Yamamoto and H. Schmidbaur, *ibid.*, **97**, 479 (1975); c) W. Richter, Y. Yamamoto, and H. Schmidbaur, *Chem. Ber.*, **110**, 1312 (1977).

5) a) Y. Yamamoto and Z. Kanda, *Bull. Chem. Soc. Jpn.*, **52**, 2560 (1979); b) Y. Yamamoto, *Chem. Lett.*, **1980**, 311.

6) Y. Yamamoto and H. Sugimoto, *Bull. Chem. Soc. Jpn.*, **53**, 3176 (1980).

7) G. Wittig and M. Schlosser, *Chem. Ber.*, **94**, 1373 (1961).

8) a) "Shin Jikken Kagaku Koza," ed by Tachibana, Maruzen, Tokyo (1976), Vol. 8 (III), p. 1370; b) "Muki Seizo Jikken," ed by Inoue, Shokabo, Tokyo (1939), p. 578.

9) "Shin Jikken Kagaku Koza," ed by Tachibana, Maruzen, Tokyo (1976), Vol. 8 (III), p. 1372.

10) a) H. Schmidbaur, H. Stuhler, and W. Vornberger, *Chem. Ber.*, **105**, 1084 (1972); b) R. Koster, D. Simic, and M. A. Grassberger, *Liebigs Ann. Chem.*, **739**, 211 (1970).

11) a) G. Wittig and W. Böll, *Chem. Ber.*, **95**, 2526 (1962); b) G. Wittig, W. Böll, and K. H. Krück, *ibid.*, **95**, 2514 (1962); c) G. Wittig and M. Schlosser, *Angew. Chem.*, **72**, 324 (1960).

12) S. G. Levine, *J. Am. Chem. Soc.*, **80**, 6150 (1958).

13) C. E. Griffin and M. Gordon, *J. Organomet. Chem.*, **3**, 414 (1965).

14) N. Petragnani, R. Rodrigues, and J. V. Comasseto, *J. Organomet. Chem.*, **114**, 281 (1976).

15) a) J. B. Stothers, "Carbon-13 NMR Spectroscopy," Academic Press (1972), Chap. 10; b) W. McFarlane, *Proc. R. Soc. London, Ser. A*, **306**, 185 (1968).

16) G. A. Gray and S. E. Cremer, *J. Org. Chem.*, **37**, 3458 (1972).

17) H. O. Pritchard and H. A. Skinner, *Chem. Rev.*, **55**, 745 (1955).

18) B. A. Vovsi and A. A. Petrov, *Zh. Obshch. Khim.*, **28**, 1426 (1958) [*Chem. Abstr.*, **53**, 1105f (1959)].

19) I. I. Lapkin and O. M. Lapkina, *Zh. Obshch. Khim.*, **22**, 1602 (1952) [*Chem. Abstr.*, **47**, 9293f (1953)].

20) C. S. Marvel and P. K. Parter, *Org. Synth.*, Coll Vol. 1, 377 (1956).

21) a) L. Horner and A. Mentrup, *Justus Liebigs Ann. Chem.*, **646**, 65 (1961); b) G. Wittig and U. Scholköpf, *Chem. Ber.*, **87**, 1318 (1954).

22) G. Wittig and D. Wittenberg, *Justus Liebigs Ann. Chem.*, **606**, 1 (1957).

23) H. J. Bestmann and O. Kratzer, *Chem. Ber.*, **96**, 1899 (1963).

A Contribution to the Theory of Pulse Polarography. I. Theory of Current-Potential Curves

Hiroaki MATSUDA

Department of Electronic Chemistry, Graduate School at Nagatsuta, Tokyo Institute of Technology, Nagatsuta, Midori-ku, Yokohama 227

(Received May 19, 1980)

A general theory of pulse polarographic current-potential curves is developed for a simple electrode reaction proceeding at the expanding plane electrode. It is shown that when the ratio of the sampling time to the pre-electrolysis time is smaller than 1/30, this condition being satisfied in usual pulse polarographic practice, the equation of current-potential curves can be greatly simplified. The theory developed is applied to the three modes of pulse polarography nowadays practically employed, *i.e.*, normal pulse, scan-reversal pulse and differential pulse polarography. For each mode, the dependence of current-potential curves on the kinetic parameters of electrode reaction as well as on the experimental variables is discussed.

Pulse polarography, originally devised by Barker[1] as an outcome of his work on square wave polarography, has become one of the most powerful and widely used electroanalytical techniques. Nowadays, this technique is successfully employed in routine works for chemical analysis of both inorganic and organic compounds, especially for trace analysis because of its high sensitivity.

A great potentiality of pulse polarography has been recognized also for the characterization of the mechanism of electrode reactions. Thus, the theoretical studies have been made extensively by Los and coworkers[2] and Galvez and Serna[3] for various types of limiting currents, *i.e.*, the diffusion-controlled, kinetic and catalytic currents. However, the theory of current-potential curves has not yet made significant progress and so pulse polarography seems not to realize sufficiently its great potentiality for the study of electrode kinetics. Oldham[4] reported a general theory of the potential pulse electrolysis for the stationary plane electrode and thus his results can not be applied quantitatively to the pulse polarographic conditions using the dropping mercury electrode (DME). Recently, Ruzic[5] has developed a general theory of pulse polarography, but the explicit equations derived by him hold only for the case, in which the pulse duration is short enough so that the d.c. component does not change appreciably during the pulse application. Birke[6] also published a theory of differential pulse polarography, in which he made, however, some simplifying assumption which were not well justified.

In view of the great potentiality of pulse polarography in studies of electrode kinetics, it is desirable to complete the theory of pulse polarographic waves, *i.e.*, to derive the explicit general equation of current-potential curves. In the present paper, we shall attempt such an approach and present explicit equations for several modes of pulse polarography nowadays practically used.

General Equation of Current-Potential Curves

Consider a simple electrode reaction, designated by

$$\mathrm{Ox} + ne \rightleftharpoons \mathrm{Red} \tag{1}$$

where both reactants Ox and Red are assumed to be soluble in solution or in DME. It is also assumed that (a) the electrode reaction (1) proceeds at the expanding plane electrode, which has been recognized as a good mathematical model of DME, and (b) the bulk of the solution contains only the reactant Ox. Then, the concentrations of Ox and Red at the electrode surface, C_O^s and C_R^s, can be expressed by[7]

$$C_O^s = C_O^\circ - \sqrt{\frac{7}{3\pi}}\frac{1}{\sqrt{D_O}}\int_0^t \frac{(i/nFq)u^{2/3}}{\sqrt{t^{7/3}-u^{7/3}}}\mathrm{d}u \tag{2}$$

$$C_R^s = \sqrt{\frac{7}{3\pi}}\frac{1}{\sqrt{D_R}}\int_0^t \frac{(i/nFq)u^{2/3}}{\sqrt{t^{7/3}-u^{7/3}}}\mathrm{d}u \tag{3}$$

where C_O° is the bulk concentration of Ox, D_O, and D_R denote the diffusion coefficients of Ox and Red, respectively, t is the time elapsed after the drop growth has begun, i the instantaneous faradaic current and q the surface area of DME. The faradaic current density is expressed as a function of the electrode potential and of the concentrations of Ox and Red at the electrode surface. According to the usual kinetic theory of electrode processes,[8] we have

$$i = nFq\{\vec{k}C_O^s - \overleftarrow{k}C_R^s\} \tag{4}$$

with

$$\begin{aligned}\vec{k} &= k_0 \exp\left[-(\alpha nF/RT)(E-E^\circ)\right]\\ \overleftarrow{k} &= k_0 \exp\left[\{(1-\alpha)nF/RT\}(E-E^\circ)\right]\end{aligned} \tag{5}$$

where E is the electrode potential, E° the formal standard potential of the reaction (1), α the cathodic transfer coefficient, k_0 the standard rate constant and F, R and T have their usual significance. Introducing Eqs. 2 and 3 into Eq. 4 yields

$$(i/nFq) = \vec{k}C_O^\circ - \sqrt{\frac{7}{3\pi}}\lambda\int_0^t \frac{(i/nFq)u^{2/3}}{\sqrt{t^{7/3}-u^{7/3}}}\mathrm{d}u \tag{6}$$

with

$$\lambda = (\vec{k}/\sqrt{D_O}) + (\overleftarrow{k}/\sqrt{D_R}) = (k_0/\sqrt{D})[\exp(-\alpha\zeta) + \exp\{(1-\alpha)\zeta\}] \tag{7}$$

$$\zeta = (nF/RT)(E - E_{1/2}^r) \tag{8}$$

$$E_{1/2}^r = E^\circ - (RT/nF)\ln\sqrt{D_O/D_R} \tag{9}$$

$$D = D_O^{1-\alpha}D_R^{\alpha} \tag{10}$$

where $E_{1/2}^r$ denotes the polarographic reversible half-wave potential. Equation 6 is the Volterra integral equation of second kind with respect to (i/nFq), whose solution gives the general expression for the current-

potential-time relationship of the potential-controlled electrolysis.

In the pulse polarographic conditions, the potential of DME is set on a constant value E_1 from the beginning of the drop growth to some time τ, and at $t=\tau$ it is stepped up from E_1 to the other constant value E_2. Therefore, if we write the current intensities during the periods $0<t<\tau$ and $\tau<t$ as i_1 and i_2, respectively, the electrolysis condition can be expressed as

$$0<t<\tau: E=E_1,\ i=i_1(t) \tag{11a}$$

$$\tau<t \quad : E=E_2,\ i=i_2(t) \tag{11b}$$

First, consider the electrolysis during the period $0<t<\tau$. Introducing Eq. 11a into Eqs. 6—8 yields

$$(i_1/nFq)=\vec{k}_1C_0^\circ-\sqrt{\frac{7}{3\pi}}\lambda_1\int_0^t\frac{(i_1/nFq)u^{2/3}}{\sqrt{t^{7/3}-u^{7/3}}}du \tag{12}$$

with

$$\lambda_1=(\vec{k}_1/\sqrt{D_O})+(\overleftarrow{k}_1/\sqrt{D_R})$$
$$=(k_0/\sqrt{D})[\exp(-\alpha\zeta_1)+\exp\{(1-\alpha)\zeta_1\}] \tag{13}$$

$$\zeta_1=(nF/RT)(E_1-E_{1/2}^r) \tag{14}$$

The solution of the Volterra integral Eq. 12 was already obtained in a previous paper.[9] We have

$$i_1=\frac{(i_d^c)_{Ilk}}{1+\exp(\zeta_1)}\sqrt{3\pi/7}(\lambda_1\sqrt{t})\psi(\lambda_1\sqrt{t}) \tag{15}$$

where

$$\psi(\lambda_1\sqrt{t})=\sum_{\nu=0}^{\infty}(-1)^\nu a_\nu(\sqrt{3/7}\ \lambda_1\sqrt{t})^\nu \tag{16a}$$

with

$$a_0=1,\ a_\nu=\prod_{\mu=1}^{\nu}\left\{\Gamma\left(\frac{3\mu+7}{14}\right)\Big/\Gamma\left(\frac{3\mu+14}{14}\right)\right\} \tag{16b}$$

and

$$(i_d^c)_{Ilk}=\sqrt{7/3}nFq\sqrt{D_O}C_0^\circ/\sqrt{\pi t} \tag{17}$$

In the above equations, Γ denotes Euler's Gamma function and $(i_d^c)_{Ilk}$ the instantaneous diffusion current of d.c. polarography given by the Ilkovic equation. For numerical calculations of the function $\psi(\lambda_1\sqrt{t})$, it is convenient to use the following approximate equation derived previously,[10] which holds in the whole range of the argument within an error of 0.2%:

$$\psi(\lambda_1\sqrt{t})=\sqrt{\frac{7}{3\pi}}\frac{g(\lambda_1\sqrt{t})/(\lambda_1\sqrt{t})}{1+g(\lambda_1\sqrt{t})} \tag{18}$$

with

$$g(\lambda_1\sqrt{t})=0.293(\lambda_1\sqrt{t})$$
$$\times[\tanh\{1.3\log(\lambda_1\sqrt{t}/1.61)\}+4.96] \tag{19}$$

Next, we shall obtain the solution of the Volterra integral Eq. 6 for the period $t>\tau$. We write, thereafter, $\tau+\theta$ instead of t. Then, introducing Eqs. 11a and 11b into Eq. 6, we have

$$(i_2/nFq)=\vec{k}_2C_0^\circ-\sqrt{7/3\pi}\ \lambda_2(I_1+I_2) \tag{20}$$

with

$$I_1=\int_0^\tau\frac{(i_1/nFq)u^{2/3}}{\sqrt{(\tau+\theta)^{7/3}-u^{7/3}}}du \tag{21}$$

$$I_2=\int_\tau^{\tau+\theta}\frac{(i_2/nFq)u^{2/3}}{\sqrt{(\tau+\theta)^{7/3}-u^{7/3}}}du \tag{22}$$

where

$$\lambda_2=(\vec{k}_2/\sqrt{D_O})+(\overleftarrow{k}_2/\sqrt{D_R})$$
$$=(k_0/\sqrt{D})[\exp(-\alpha\zeta_2)+\exp\{(1-\alpha)\zeta_2\}] \tag{23}$$

$$\zeta_2=(nF/RT)(E_2-E_{1/2}^r) \tag{24}$$

In appendix, the integrals I_1 and I_2 will be evaluated as a power series of $\sqrt{\theta/\tau}$ under the assumption that $\theta/\tau<1$. Thus, introducing Eqs. A-8 and A-9 into Eq. 20, we obtain, after some rearrangements,

$$(i_2/nFq)=\sqrt{D_O}C_O^\circ\left[\frac{1}{1+\exp(\zeta_2)}-\frac{1}{1+\exp(\zeta_1)}\right]\lambda_2$$
$$+\left[\frac{i_1(\tau)}{nFq(\tau)}\right]\left[\frac{\lambda_2}{\lambda_1}\right]\left\{1+\left[\frac{d\ln\psi}{d\ln\tau}\right]\left[\frac{\theta}{\tau}\right]+O([\theta/\tau]^2)\right\}$$
$$+\left[\frac{i_1(\tau)}{nFq(\tau)}\right]\frac{2}{\sqrt{\pi}}(\lambda_2\sqrt{\theta})$$
$$\times\left\{1-\frac{2}{3}\left[\frac{1}{6}-\frac{d\ln\psi}{d\ln\tau}\right]\left[\frac{\theta}{\tau}\right]+O([\theta/\tau]^2)\right\}$$
$$-\frac{\lambda_2}{\sqrt{\pi}}\int_0^\theta\frac{(i_2/nFq)}{\sqrt{\theta-u}}\left\{1-\frac{1}{3}\left[\frac{\theta-u}{\tau}\right]+O([\theta/\tau]^2)\right\}du \tag{25}$$

where $O([\theta/\tau]^2)$ denotes the sum of the second and higher order terms with respect to (θ/τ). Now, we expand (i_2/nFq) into a power series of $\sqrt{\theta/\tau}$. Thus

$$(i_2/nFq)=\phi_0+\phi_1+\phi_2+\phi_3+\cdots\cdots \tag{26}$$

where the function ϕ_j (j=0, 1, 2, 3, ···) corresponds to the order of $(\theta/\tau)^{j/2}$. Substituting Eq. 26 into Eq. 25 and equating the coefficients of like powers of $\sqrt{\theta/\tau}$ yields the following set of integral equations:

$$\phi_0=\sqrt{D_0}\,C_0^\circ\left[\frac{1}{1+\exp(\zeta_2)}-\frac{1}{1+\exp(\zeta_1)}\right]\lambda_2$$
$$+\left[\frac{i_1}{nFq}\right]\left[\frac{\lambda_2}{\lambda_1}\right]-\frac{\lambda_2}{\sqrt{\pi}}\int_0^\theta\frac{\phi_0(u)}{\sqrt{\theta-u}}du \tag{27}$$

$$\phi_1=\frac{2}{\sqrt{\pi}}\left[\frac{i_1}{nFq}\right](\lambda_2\sqrt{\tau})\sqrt{\theta/\tau}-\frac{\lambda_2}{\sqrt{\pi}}\int_0^\theta\frac{\phi_1(u)}{\sqrt{\theta-u}}du \tag{28}$$

$$\phi_2=\left[\frac{\lambda_2}{\lambda_1}\right]\left[\frac{i_1}{nFq}\right]\left[\frac{d\ln\psi}{d\ln\tau}\right]\left[\frac{\theta}{\tau}\right]+\frac{1}{3\tau}\frac{\lambda_2}{\sqrt{\pi}}$$
$$\times\int_0^\theta\sqrt{\theta-u}\,\phi_0(u)du-\frac{\lambda_2}{\sqrt{\pi}}\int_0^\theta\frac{\phi_2(u)}{\sqrt{\theta-u}}du \tag{29}$$

$$\phi_3=-\frac{4}{3\sqrt{\pi}}\left[\frac{i_1}{nFq}\right](\lambda_2\sqrt{\tau})\left[\frac{1}{6}-\frac{d\ln\psi}{d\ln\tau}\right](\theta/\tau)^{3/2}$$
$$+\frac{1}{3\pi}\frac{2}{\sqrt{\pi}}\int_0^\theta\sqrt{\theta-u}\,\phi_1(u)du$$
$$-\frac{\lambda_2}{\sqrt{\pi}}\int_0^\theta\frac{\phi_3(u)}{\sqrt{\theta-u}}du \tag{30}$$

This set of integral equations can easily be solved by applying the method of Laplace transformation.[11] Thus, we obtain for (i_2/nFq), after performing some calculations,

$$(i_2/nFq)=\frac{(i_d^c)_{Cott}}{nFq}\left[\frac{1}{1+\exp(\zeta_2)}-\frac{1}{1+\exp(\zeta_1)}\right]\Phi(\lambda_2\sqrt{\theta})$$
$$\times\left\{1-\frac{1}{3}\left(\frac{\theta}{\tau}\right)\left[1+\frac{F_2(\lambda_2\sqrt{\theta})}{F_0(\lambda_2\sqrt{\theta})}\right]+O([\theta/\tau]^2)\right\}$$
$$+\left[\frac{i_1(\tau)}{nFq(\tau)}\right]\{(\lambda_2/\lambda_1)-1\}F_0(\lambda_2\sqrt{\theta})$$
$$\times\left\{1-\frac{1}{3}\left(\frac{\theta}{\tau}\right)\left[1+\frac{F_2(\lambda_2\sqrt{\theta})}{F_0(\lambda_2\sqrt{\theta})}\left(1+3\frac{d\ln\psi}{d\ln\tau}\right)\right]\right.$$
$$\left.+O([\theta/\tau]^2)\right\}$$
$$+\left[\frac{i_1(\tau)}{nFq(\tau)}\right]\left\{1+\left(\frac{\theta}{\tau}\right)\left[\frac{d\ln\psi}{d\ln\tau}\right]+O([\theta/\tau]^2)\right\} \tag{31}$$

with

$$(i_d^c)_{Cott} = nFq(\tau+\theta)\sqrt{D_0}C_0^\circ/\sqrt{\pi\theta} \quad (32)$$

$$F_0(\xi) = \exp(\xi^2)\,\mathrm{erfc}(\xi) \quad (33)$$

$$F_2(\xi) = \xi^{-2}[1-(2/\sqrt{\pi})\,\xi - \exp(\xi^2)\mathrm{erfc}(\xi] \quad (34)$$

$$\Phi(\xi) = \sqrt{\pi}\,\xi\,F_0(\xi) = \sqrt{\pi}\,\xi\exp(\xi^2)\,\mathrm{erfc}(\xi) \quad (35)$$

where $(i_d^c)_{cott}$ denotes the diffusion current at the stationary plane electrode given by the Cottrell equation and erfc the complementary error function. The pulse polarographic current is in general measured as a difference between i_2 at $t=\tau+\theta_s$ (θ_s: sampling time) and i_1 at $t=\tau$. Therefore, taking into account the fact that the ratio of the surface area of DME at $t=\tau+\theta_s$ to that of $t=\tau$ can be expanded into the following power series of (θ_s/τ):

$$q(\tau+\theta_s)/q(\tau) = 1 + (2/3)(\theta_s/\tau) + O([\theta_s/\tau]^2), \quad (36)$$

we obtain for the pulse polarographic current, i_{pulse},

$$\begin{aligned} i_{pulse} &= i_2(\tau+\theta_s) - i_1(\tau) \\ &= (i_d^c)_{Cott}\left[\frac{1}{1+\exp(\zeta_2)} - \frac{1}{1+\exp(\zeta_1)}\right]\Phi(\lambda_2\sqrt{\theta_s}) \\ &\quad\times\left\{1-\frac{1}{3}\left[\frac{\theta_s}{\tau}\right]\left[1+\frac{F_2(\lambda_2\sqrt{\theta_s})}{F_0(\lambda_2\sqrt{\theta_s})}\right] + O([\theta_s/\tau]^2)\right\} \\ &\quad + i_1(\tau)\{(\lambda_2/\lambda_1) - 1\}F_0(\lambda_2\sqrt{\theta_s}) \\ &\quad\times\left\{1+\frac{1}{3}\left[\frac{\theta_s}{\tau}\right]\left[1-\frac{F_2(\lambda_2\sqrt{\theta_s})}{F_0(\lambda_2\sqrt{\theta_s})}\left(1+3\frac{\mathrm{d}\ln\phi}{\mathrm{d}\ln\tau}\right)\right]\right. \\ &\quad\left. + O([\theta_s/\tau]^2)\right\} \\ &\quad + i_1(\tau)\left\{\left[\frac{\theta_s}{\tau}\right]\left[\frac{2}{3}+\frac{\mathrm{d}\ln\phi}{\mathrm{d}\ln\tau}\right] + O([\theta_s/\tau]^2)\right\} \end{aligned} \quad (37)$$

In usual pulse polarographic practice, the values of τ and θ_s employed are of the orders of second and millisecond, respectively, *i.e.*, $\tau\simeq$ 1—6 s and $\theta_s\simeq$ 1—100 ms. Furthermore, the following relations hold in the whole range of the corresponding arguments:

$$-1 \geqq \frac{F_2(\lambda_2\sqrt{\theta_s})}{F_0(\lambda_2\sqrt{\theta_s})} \geqq -2 \text{ and } 0 \geqq \frac{\mathrm{d}\ln\phi(\lambda_1\sqrt{\tau})}{\mathrm{d}\ln\tau} \geqq -\frac{1}{2}.$$

Therefore, for $(\theta_s/\tau)\leqq 1/30$, which may be satisfied in usual experimental conditions, Eq. 37 can be greatly simplified, as follows:

$$\begin{aligned} i_{pulse} &= (i_d^c)_{Cott}\left[\frac{1}{1+\exp(\zeta_2)} - \frac{1}{1+\exp(\zeta_1)}\right]\Phi(\lambda_2\sqrt{\theta_s}) \\ &\quad + i_1(\tau)\{(\lambda_2/\lambda_1) - 1\}F_0(\lambda_2\sqrt{\theta_s}) \end{aligned} \quad (38)$$

This equation provides a general expression of the current-potential profiles for pulse polarography. Several modes of pulse polarography, nowadays practically used, are incorporated in this general equation. In the following, we shall further simplify Eq. 38 by introducing the experimental conditions corresponding to the mode employed.

Normal Pulse Polarography

In normal pulse polarography, the initial potential E_1 is anodic of the reduction wave and the scan of the potential E_2 is made to the cathodic direction. Therefore, we have E_1→sufficiently more anodic potential than $E_{1/2}^r$. Thus

$$\zeta_1 \longrightarrow +\infty,\ \lambda_1 \longrightarrow +\infty \text{ and } i_1(\tau) \longrightarrow 0.$$

Introducing the above conditions into Eq. 38 yields

$$i_{n\text{-}pulse}^c = \frac{(i_d^c)_{Cott}}{1+\exp(\zeta_2)}\Phi(\lambda_2\sqrt{\theta_s}) \quad (39)$$

where $i_{n\text{-}pulse}^c$ denotes the normal pulse polarographic current. This is the general equation of current-potential curves for normal pulse polarography. For the variations of current-potential curves with the kinetic parameters of electrode reaction, see Fig. 1. Equation 39 is exactly the same as derived by a number of authors[12] for the potentiostatic experiments at the stationary plane electrode. In the potentiostatic method, the variation of faradaic current with time at a constant potential is examined, whereas in pulse polarography the faradaic current at a given time θ_s is measured as a function of the electrode potential. Therefore, in order to examine the behavior of pulse polarographic waves, it is convenient to derive the expression similar to the log-plot in d.c. polarography.

First, consider the limiting case of reversible waves. The function $\Phi(\xi)$ is equal to unity within an error of 2%, when $\xi\geqq 5$. Therefore, if the condition

$$(k_0\sqrt{\theta_s}/\sqrt{D}) \geqq 5\times\alpha^\alpha(1-\alpha)^{1-\alpha} \quad (40)$$

is satisfied, Eq. 39 can be simplified into

$$i_{n\text{-}pulse}^c = (i_d^c)_{Cott}/[1+\exp(\zeta_2)] \quad (41a)$$

or solving the above equation with respect to E_2 yields

$$E_2 = E_{1/2}^r - (RT/nF)\ln[x/(1-x)] \quad (41b)$$

with

$$x = i_{n\text{-}pulse}^c/(i_d^c)_{Cott} \quad (42)$$

This is the equation for the log-plot of reversible waves, which is of the same form as for d.c. polarography.

Next, consider the case, $(k_0\sqrt{\theta_s}/\sqrt{D})\leqq 5\times\alpha^\alpha(1-\alpha)^{1-\alpha}$, in which the irreversibility appears in the pulse polarograms. Fortunately, Oldham and Parry[13] derived the convenient approximate equation for the inverse function of $\Phi(\xi)$, as follows:

$$\xi = \frac{\sqrt{3}}{4}\left\{\frac{1.75+\Phi^2}{1-\Phi}\right\}^{1/2}\Phi \quad (43)$$

Therefore, after combining Eq. 39 with Eq. 43 and performing some rearrangements, we obtain

$$E_2 = E^* - \frac{RT}{\alpha nF}\ln\left\{x\left[\frac{1.75+x^2(1+\exp\zeta_2)^2}{1-x(1+\exp\zeta_2)}\right]^{1/2}\right\} \quad (44)$$

with

$$E^* = E_{1/2}^r + \frac{RT}{\alpha nF}\ln\left[\frac{4}{\sqrt{3}}\frac{k_0\sqrt{\theta_s}}{\sqrt{D}}\right] \quad (45)$$

Equation 44 suggests a new log-plot for the normal pulse polarographic waves.

Now consider the pulse-polarographically quasi-reversible waves, for which the condition

$$5\times\alpha^\alpha(1-\alpha)^{1-\alpha} \geqq (k_0\sqrt{\theta_s}/\sqrt{D}) \geqq \exp[-4(1+\alpha)] \quad (46)$$

is satisfied. In general, the d.c. polarographic wave exhibits higher reversibility than the corresponding pulse polarographic wave does, because of the difference in electrolysis time scales employed in two methods. Therefore, from the analysis of d.c. polarographic wave corresponding to the pulse-polarographically quasi-

reversible wave, we can determine the reversible half-wave potential $E^{r}_{1/2}$ by using the extrapolation methods.[14,15] Then, the log-term in Eq. 44 becomes the experimentally accessible quantity. Thus, if we plot $\log (x[\{1.75+x^2(1+\exp\zeta_2)^2\}/\{1-x(1+\exp\zeta_2)\}]^{1/2})$ against E_2, we obtain a straight line, which has the reciprocal slope of $(2.3RT/\alpha nF)$ and intersects with the zero-line at $E_2=E^*$, provided that the transfer coefficient α may be regarded as constant in the potential region concerned. Therefore, we can determine the kinetic parameters of electrode reaction from the values of the reciprocal slope and of the potential E^*.

For the irreversible waves, which satisfy the condition

$$(k_0\sqrt{\theta_s}/\sqrt{D}) \leqq \exp[-4(1+\alpha)], \tag{47}$$

the term $\exp(\zeta_2)$ in Eq. 44 can be neglected compared with unity in the whole potential region concerned. Therefore, Eq. 44 can be reduced to

$$E_2 = E^* - \frac{RT}{\alpha nF} \ln\left\{x\left(\frac{1.75+x^2}{1-x}\right)^{1/2}\right\} \tag{48}$$

where E^* is the half-wave potential of irreversible wave. This is the same equation as that previously proposed by Oldham and Parry[13] for totally irreversible waves. Equation 48 indicates that the plot of $\log [x\{(1.75+x^2)/(1-x)\}^{1/2}]$ *vs.* E_2 can be made without any knowledge of $E^{r}_{1/2}$ and thus the kinetic parameters of electrode reaction can be determined from this plot in the same way as described above.

According to the modern theory of electron transfer at electrodes,[16] it is shown that the transfer coefficient may depend on the electrode potential. In such cases, it is better to rewrite Eq. 44 as

$$\ln \vec{k}_2 = -\ln\left[\frac{4}{\sqrt{3}}\frac{\sqrt{\theta_s}}{\sqrt{D_0}}\right] + \ln\left\{x\left[\frac{1.75+x^2(1+\exp\zeta_2)^2}{1-x(1+\exp\zeta_2)}\right]^{1/2}\right\} \tag{49}$$

which can be derived from Eq. 44 by taking into account the relations given by Eqs. 5, 9, and 10. Equation 49 indicates that the plot of $\log (x[\{1.75+x^2(1+\exp\zeta_2)^2\}/\{1-x(1+\exp\zeta_2)\}]^{1/2})$ *vs.* E_2 manifests the potential dependence of the cathodic rate constant $\vec{k}_2$. Thus, this log-plot may appear as bent toward the potential axis, if the transfer coefficient shows such a potential dependence as predicted by the modern theory of electron transfer at electrodes.[17]

Scan-reversal Pulse Polarography

In order to examine the reversibility of electrode reactions, Oldham and Parry[18] presented the scan-reversal pulse polarographic technique and discussed two limiting cases, *i.e.*, the behavior of reversible and totally irreversible waves. Since the general case is incorporated in Eq. 38, we shall derive a general equation for the scan-reversal pulse polarographic current, $i^{a}_{r\text{-pulse}}$.

In scan-reversal pulse polarography, the initial potential E_1 is set on the cathodic diffusion current plateau and the potential E_2 is scanned from the cathodic plateau to the anodic direction. Hence we have

$E_1 \longrightarrow$ sufficiently more cathodic potential than $E^{r}_{1/2}$.

Thus

$$\zeta_1 \longrightarrow -\infty,\ \lambda_1 \longrightarrow +\infty \text{ and } i_1(\tau) \longrightarrow (i^{c}_{d})_{IIk}.$$

Substituting the above conditions into Eq. 38 yields

$$i^{a}_{r\text{-pulsd}} = -\frac{(i^{c}_{d})_{Cott}}{1+\exp(-\zeta_2)}\Phi(\lambda_2\sqrt{\theta_s}) - (i^{c}_{d})_{IIk}F_0(\lambda_2\sqrt{\theta_s}) \tag{50}$$

This is the general expression of current-potential curves in scan-reversal pulse polarography. The first term on the right hand side of Eq. 50 manifests the anodic normal pulse polarographic wave, as can readily be seen from the comparison with Eq. 39, whereas the second term indicates the effects of the pre-electrolysis at the potential corresponding to the cathodic diffusion current plateau during the period 0—τ.

In order to visualize the variations of wave-shapes in dependence of the kinetic parameters of electrode reaction, the normalized current-potential curves, *i.e.*, $i^{a}_{r\text{-pulse}}/(i^{c}_{d})_{Cott}$ *vs.* E_2 curves, were calculated numerically for a series of values of $(k_0\sqrt{\theta_s}/\sqrt{D})$ under the assumption that $n=2$, $\alpha=0.5$, $\theta_s/\tau=0.01$ and $T=25$ °C. The results obtained are shown in Fig. 1, in which the cathodic normal pulse polarographic waves are also given for comparison.

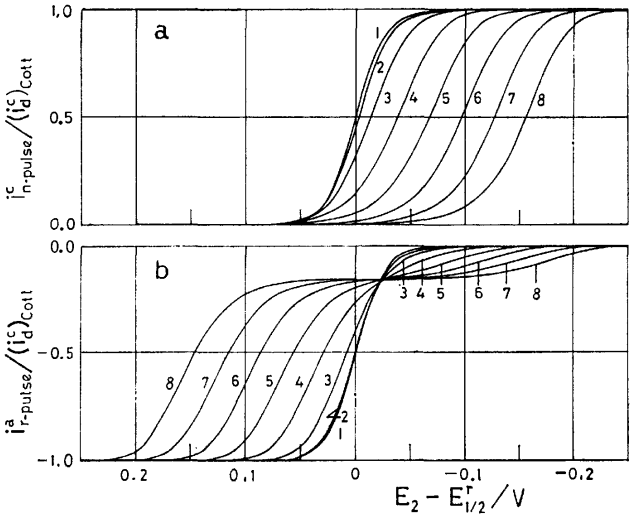

Fig. 1. Current-potential curves of normal pulse and scan-reversal pulse polarography.
(a) Normal, (b) scan-reversal. Values of $\log(k_0\sqrt{\theta_0}/\sqrt{D})$: (1)$\geqq$0.5 (reversible), (2) 0.0, (3) −0.5, (4) −1.0, (5) −1.5, (6) −2.0, (7) −2.5, (8) −3.0.

In the following, we shall examine the general Eq. 50. First, consider the reversible case, in which the condition (40) is fulfilled. In this case, the function $\Phi(\lambda_2\sqrt{\theta_s})$ in the first term on the right hand side of Eq. 50 is reduced to unity and the second term can be neglected within an error of *ca.* 3%. Hence we have for the reversible waves of scan-reversal pulse polarography

$$i^{a}_{r\text{-pulse}} = -(i^{c}_{d})_{Cott}/[1+\exp(-\zeta_2)] \tag{51}$$

Equation 51 indicates that the reversible scan-reversal pulse polarographic wave has the same wave-height

and the same half-wave potential as the reversible normal pulse polarographic wave does.

When values of the parameter $(k_0\sqrt{\theta_s}/\sqrt{D})$ are decreased, both the irreversibility and the effect of the second term on the right hand side of Eq. 50 appear and hence the portions of the wave, which are lower than or higher than $(i_d^c)_{Ilk}$, shift toward the more cathodic or the more anodic potential, respectively, as can readily be seen from Fig. 1. Thus the wave appears to have a drawn-out shape. Finally, when values of $(k_0\sqrt{\theta_s}/\sqrt{D})$ become so small that the condition (47) is fulfilled, the wave splits definitely into two waves. This behavior of the wave can readily be understood if recalling the fact that the pulse polarographic current is measured as the difference between the currents before and after the pulse application. Thus, the first wave does not correspond to the true anodic process but to the cathodic one, and in the potential region of the second wave occurs the anodic process.

Now such irreversible cases will be examined in some detail. The first and second waves appear at the potentials sufficiently more cathodic and more anodic than $E_{1/2}^r$, respectively, so that in the potential region corresponding to the first wave Eq. 50 can be reduced to

$$i_{r\text{-pulse}}^a = -(i_d^c)_{Ilk} F_0(\lambda_2\sqrt{\theta_s}) \tag{52}$$

This is the equation for the current-potential curve of the first wave. When the potential E_2 is placed near $E_{1/2}^r$, the values of $(\lambda_2\sqrt{\theta_s})$ become very small and thus the function $F_0(\lambda_2\sqrt{\theta_s})$ approarches to unity. Hence the limiting current of the first wave, $(i_1^a)_{1st}$, can be given by

$$(i_1^a)_{1st} = -(i_d^c)_{Ilk}. \tag{53}$$

This equation indicates that the height of the first wave is equal to that of d.c. polarographic wave, expressed by the Ilkovic equation. The half-wave potential of the first wave $(E_{1/2}^r)_{1st}$, can be obtained by equating $i_{r\text{-pulse}}^a$ to $-(1/2)(i_d^c)_{Ilk}$. Thus, by recalling the facts that the function $F_0(\xi)$ is equal to 1/2 at $\xi=0.770$ and that in this potential region $(\lambda_2\sqrt{\theta_s})$ can be written as $(k_0\sqrt{\theta_s}/\sqrt{D})\exp[-(\alpha nF/RT)(E_2-E_{1/2}^r)]$, we have

$$(E_{1/2}^a)_{1st} = E_{1/2}^r + \frac{RT}{\alpha nF}\ln[1.30\,(k_0\sqrt{\theta_s}/\sqrt{D})] \tag{54}$$

Hence the half-wave potential of the first wave shifts toward the cathodic direction with decreasing values of $(k_0\sqrt{\theta_s}/\sqrt{D})$. On the other hand, the potential region corresponding to the second wave is sufficiently more anodic than $E_{1/2}^r$, so that Eq. 50 can be reduced to

$$i_{r\text{-pulse}}^a = -(i_d^c)_{Cott}\Phi(\lambda_2'\sqrt{\theta_s}) - (i_d^c)_{Ilk}F_0(\lambda_2'\sqrt{\theta_s}) \tag{55}$$

with

$$\lambda_2'\sqrt{\theta_s} = (k_0\sqrt{\theta_s}/\sqrt{D}) \times \exp[\{(1-\alpha)\,nF/RT\}(E_2-E_{1/2}^r)] \tag{56}$$

where it should be kept in mind that $i_{r\text{-pulse}}^a$ in Eq. 50 denotes the total anodic current measured from the zero-line. If the current of the second wave is measured from the limiting current plateau of the first wave, we may write the equation for the current-potential curves of the second wave, as follows:

$$(i_{r\text{-pulse}}^a)_{2nd} = -(i_d^c)_{Cott}\Phi(\lambda_2'\sqrt{\theta_s}) + (i_d^c)_{Ilk}[1-F_0(\lambda_2'\sqrt{\theta_s})] \tag{57}$$

The limiting current of the second wave, $(i_1^a)_{2nd}$, can be derived by inserting the condition $(nF/RT)(E_2-E_r^{1/2})\to+\infty$ into Eq. 57. Hence

$$(i_1^a)_{2nd} = -[(i_d^c)_{Cott} - (i_d^c)_{Ilk}]. \tag{58}$$

The half-wave potential of the second wave, $(E_{1/2}^a)_{2nd}$, may be obtained by substituting the condition $(i_{r\text{-pulse}}^a)_{2nd}=(1/2)(i_1^a)_{2nd}$ into Eq. 57. Thus, we have, after performing some rearrangements,

$$[1-2\,\Phi(\gamma)]/[2F_0(\gamma)-1] = (i_d^c)_{Ilk}/(i_d^c)_{Cott} \tag{59}$$

with

$$\gamma = (k_0\sqrt{\theta_s}/\sqrt{D})\exp[\{(1-\alpha)nF/RT\} \times \{(E_{1/2}^a)_{2nd} - E_{1/2}^r\}] \tag{60}$$

The values of γ, which satisfy Eq. 59, may be calculated numerically as a function of $[(i_d^c)_{Ilk}/(i_d^c)_{Cott}]$. Since $(\theta_s/\tau)<1/30$ for usual pulse polarographic conditions, numerical calculations were performed for the range:

$$0 < (i_d^c)_{Ilk}/(i_d^c)_{Cott} < 0.3$$

The results obtained indicates that γ can be expressed by the following equation within errors of ±0.001 in the absolute values of γ:

$$\gamma = 0.433 - 0.205\,[(i_d^c)_{Ilk}/(i_d^c)_{Cott}] - 0.16\,[(i_d^c)_{Ilk}/(i_d^c)_{Cott}]^2 \tag{61}$$

Taking the logarithms of both sides of Eq. 60 yields for the half-wave potential of the second wave

$$(E_{1/2}^a)_{2nd} = E_{1/2}^r - \frac{RT}{(1-\alpha)nF}\ln[(1/\gamma)(k_0\sqrt{\theta_s}/\sqrt{D})], \tag{62}$$

where γ is given by Eq. 61. Hence, the half-wave potential of the second wave shifts toward the anodic direction with decreasing values of $(k_0\sqrt{\theta_s}/\sqrt{D})$.

Comparison of Eq. 58 with Eq. 53 yields for the ratio of the height of the first wave to that of the second wave

$$(i_1^a)_{1st}/(i_1^a)_{2nd} = (i_d^c)_{Ilk}/[(i_d^c)_{Cott} - (i_d^c)_{Ilk}] = 1/[\sqrt{(3/7)(\tau/\theta_s)}-1] \tag{63}$$

Thus, for usual pulse polarographic conditions, *i.e.*, $(\tau/\theta_s)\sim100$, we have $(i_1^a)_{1st} : (i_1^a)_{2nd}\approx1 : 6$. Further, the difference between the half-wave potentials of the first and second waves can be obtained from Eqs. 54 and 62, as follows:

$$(E_{1/2}^a)_{2nd} - (E_{1/2}^a)_{1st} = -\frac{RT}{\alpha(1-\alpha)nF}\ln\left[\frac{1.30^{1-\alpha}}{\gamma^\alpha}\,\frac{k_0\sqrt{\theta_s}}{\sqrt{D}}\right] \tag{64}$$

Equation 64 indicates that the difference between two half-wave potentials is increased with decreasing values of $(k_0\sqrt{\theta_s}/\sqrt{D})$ and thus it can be employed as an index indicating the degree of irreversibility of the electrode reaction concerned.

Differential Pulse Polarography

In differential pulse polarography, both the potentials E_1 and E_2 are scanned simultaneously toward the cathodic direction with their difference, $E_1-E_2\equiv\Delta E$, being kept constant. Hence, after performing some calculations by taking into account Eqs. 15, 17, 32, and 35, Eq. 38 can be transformed into

$$i_{\text{dif-pulse}} = (i_d^c)_{\text{Cott}} \frac{\sinh(\Delta\zeta/2)}{\cosh(\zeta_m)+\cosh(\Delta\zeta/2)} F_{\text{dcp}}\,\Phi(\lambda_2\sqrt{\theta_s}) \tag{65}$$

with

$$F_{\text{dcp}} = 1 + \frac{\exp(-\zeta_m)\sinh(\alpha\Delta\zeta/2)-\sinh([1-\alpha]\Delta\zeta/2)}{\exp(\alpha\Delta\zeta/2)\sinh(\Delta\zeta/2)} \times \psi(\lambda_1\sqrt{\tau}) \tag{66}$$

$$\Delta\zeta = \zeta_1 - \zeta_2 = (nF/RT)(E_1 - E_2) = (nF/RT)\Delta E \tag{67}$$

$$\zeta_m = (\zeta_1 + \zeta_2)/2 = (nF/RT)(E_m - E^r_{1/2}) \tag{68}$$

$$E_m = (E_1 + E_2)/2 = E_1 - (\Delta E/2) \tag{69}$$

where $\psi(\lambda_1\sqrt{\tau})$ is defined by Eq. 16 and can be evaluated with sufficient accuracy by using the approximate Eq. 18. Further it should be noticed that the potential E_m defined by Eq. 69 is by $(\Delta E/2)$ more negative than the potential E_1 which is frequently employed as the potential axis of differential pulse polarograms. Equation 65 is the general expression for the differential pulse polarographic waves, which holds for any values of the pulse height ΔE. If ΔE is smaller than *ca.* $5/n$ mV, Eq. 65 can be simplified into

$$i_{\text{dif-pulse}} = \frac{(i_d^c)_{\text{Cott}}\Delta\zeta}{4\cosh^2(\zeta_m/2)} F_{\text{dcp}}\Phi(\lambda_m\sqrt{\theta_s}) \tag{70}$$

with

$$F_{\text{dcp}} = 1 + [\alpha\exp(-\zeta_m) - (1-\alpha)]\psi(\lambda_m\sqrt{\tau}) \tag{71}$$

$$\lambda_m = (k_0/\sqrt{D})[\exp(-\alpha\zeta_m) + \exp\{(1-\alpha)\zeta_m\}] \tag{72}$$

In order to visualize the behavior of differential pulse polarographic waves in dependence of the kinetic parameters of electrode reaction, numerical calculations using the general Eq. 65 were performed for a series of values of $(k_0\sqrt{\theta_s}/\sqrt{D})$ and α under the assumption that $n=2$, $\Delta E=10$ mV, $\theta_s/\tau=0.01$ and $T=25$ °C. In Fig. 2, the normalized differential pulse polarographic currents obtained for $\alpha=0.5$ and 0.3 are plotted against the potential E_m. It can be seen from Fig. 2 that the $i_{\text{dif-pulse}}$—E_m curves have generally one peak, but when $\alpha<0.5$ and $(k_0\sqrt{\theta_s}/\sqrt{D})\approx 0.1-0.02$, they show some anomaly, *i.e.*, they have a shoulder or two peaks, as can be seen from the curves 4, 5, and 6 in Fig. 2(b). Further, we can see that the peak currents decrease at first very rapidly with decreasing the value of $(k_0\sqrt{\theta_s}/\sqrt{D})$ and then approach to a limiting value which does not depend on the standard rate constant k_0 (see Eq. 88). This behavior of differential pulse polarographic waves in dependence of the kinetic parameters is quite similar to that of square wave polarographic waves, which are given in Fig. 3 of Ref. 19.

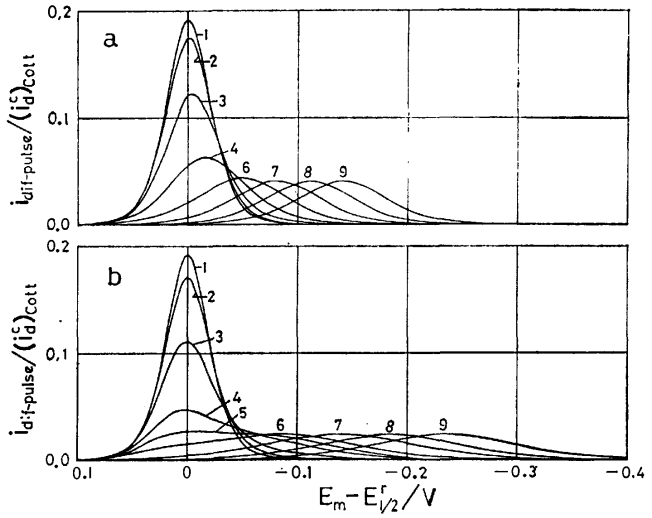

Fig. 2. Current-potential curves of differential pulse polarography.
(a) $\alpha=0.5$, (b) $\alpha=0.3$. Values of log $(k_0\sqrt{\theta_s}/\sqrt{D})$: (1)$\geqq$0.5 (reversible), (2) 0.0, (3) −0.5, (4) −1.0, (5) −1.25, (6) −1.5, (7) −2.0, (8) −2.5, (9) −3.0.

In the following, we shall examine the two limiting cases in some detail. First, consider the reversible limiting case, in which the condition (40) is fulfilled. In this case, the functions F_{dcp} and $\Phi(\lambda_2\sqrt{\theta_s})$ both approarch to unity. Hence Eq. 65 can be reduced to

$$i_{\text{dif-pulse}} = (i_d^c)_{\text{Cott}} \frac{\sinh(\Delta\zeta/2)}{\cosh(\zeta_m)+\cosh(\Delta\zeta/2)}. \tag{73}$$

This is the equation for the reversible waves of differential pulse polarography, which should be compared with Eq. 75 or 76 of Ref. 7 for the reversible square wave polarographic waves. Now we determine the three parameters which characterize the wave-shape, *i.e.*, the peak potential $(E_m)_p$, the peak current $(i_{\text{dif-pulse}})_p$ and the half-peak width $\Delta(E_m)_{p/2}$. As can easily be seen from Eq. 73, a maximum appears at $\zeta_m=0$. Hence, the peak potential can be given by

$$(E_m)_p = E^r_{1/2}. \tag{74}$$

Thus the peak potential coinsides with the reversible half-wave potential. The peak current can be derived by inserting Eq. 74 into Eq. 73, as follows:

$$(i_{\text{dif-pulse}})_p = (i_d^c)_{\text{Cott}}\tanh(\Delta\zeta/4) = (i_d^c)_{\text{Cott}}\tanh(nF\Delta E/4RT) \tag{75}$$

Equation 75 reveals that the normalized peak current, $(i_{\text{dif-pulse}})_p/(i_d^c)_{\text{Coff}}$, is increased in proportion to the pulse height ΔE for $(nF\Delta E/RT)<1$ and it approarches to the limiting value of unity when $(nF\Delta E/RT)>10$. The half-peak width can be defined as the difference between two potentials which satisfy the condition:

$$i_{\text{dif-pulse}} = (1/2)(i_{\text{dif-pulse}})_p.$$

Thus, introducing Eqs. 73 and 75 into the above condition and performing some calculations yields for such potentials

$$(E_m)_{p/2} = E^r_{1/2} \pm (RT/nF) \times \cosh^{-1}[2 + \cosh(nF\Delta E/2RT)]. \tag{76}$$

Hence the half-peak width $\Delta(E_m)_{p/2}$ can be expressed as

$$\Delta(E_m)_{p/2} = (2RT/nF) \times \cosh^{-1}[2 + \cosh(nF\Delta E/2RT)]. \tag{77}$$

For $(nF\Delta E/RT)<0.8$, Eq. 77 can be reduced to

$$\Delta(E_m)_{p/2} = 3.53(RT/nF), \tag{78}$$

On the other hand, when $(nF\Delta E/RT)>8$, we have

$$\Delta(E_m)_{p/2} = \Delta E \tag{79}$$

Equations 78 and 79 indicate that the half-peak width has the constant value of $90/n$ mV at 25 °C when $\Delta E<20/n$ mV, whereas it becomes to be equal to the pulse height ΔE for $\Delta E>200/n$ mV.

Next, consider another limiting case, in which the condition:

$$(k_0\sqrt{\tau}/\sqrt{D}) \leqq \exp[-4(1+\alpha)] \tag{80}$$

is fulfilled. In this case, the electrode process becomes d.c. polarographically irreversible[9] and thus, of course, pulse-polarographically irreversible. Then the corresponding wave appears in the potential region sufficiently more cathodic than $E^{r}_{1/2}$. Therefore, the general Eq. 65 can be transformed into

$$i_{\text{dif-pulse}} = (i^{c}_{d})_{\text{Cott}}[1-\exp(-\alpha\Delta\zeta)]\psi(\kappa^{-1}\chi)\Phi(\kappa\chi) \tag{81}$$

where κ and χ are defined as

$$\kappa = \sqrt[4]{\theta_s/\tau}\,\exp(\alpha\Delta\zeta/2) \tag{82}$$

$$\chi = (k_0\sqrt[4]{\theta_s\tau}/\sqrt{D})\exp(-\alpha\zeta_m) \tag{83}$$

Equation 81 provides the expression of irreversible waves. We shall now derive the equations for the peak potential, the peak current and the half-peak width of irreversible waves. As can be seen from Eqs. 81—83, the dependence of $i_{\text{dif-pulse}}$ on E_m can be given by $\psi(\kappa^{-1}\chi)\Phi(\kappa\chi)$ *vs.* $\ln\chi$ curves. Thus, the values of $\psi(\kappa^{-1}\chi)\Phi(\kappa\chi)$ in dependence of $\ln\chi$ were numerically calculated for a series of values of κ. The results obtained for the range of $0.1<\kappa<30$ are summarized as follows:

(1) The values of $\ln\chi_p$, at which $\psi(\kappa^{-1}\chi)\Phi(\kappa\chi)$ shows a maximum, can be given by

$$\ln\chi_p = -0.27 - 0.40\,\mathrm{sech}(2.2-0.8\ln\kappa) \tag{84}$$

(2) The maximum values of $\psi\Phi$, *i.e.*, $\psi(\kappa^{-1}\chi_p)\Phi(\kappa\chi_p)$, can be given by

$$\psi(\kappa^{-1}\chi_p)\Phi(\kappa\chi_p) = \frac{(\ln\kappa)^{1.62}}{1.50+(\ln\kappa)^{1.62}} \tag{85}$$

(3) The difference between the two values of $\ln\chi$, $\ln\chi'_{p/2}$ and $\ln\chi''_{p/2}$, which satisfy the algebraic equation:

$$\psi(\kappa^{-1}\chi)\Phi(\kappa\chi) = (1/2)\psi(\kappa^{-1}\chi_p)\Phi(\kappa\chi_p),$$

can be given by

$$\Delta\ln\chi_{p/2} = \ln\chi'_{p/2} - \ln\chi''_{p/2} = 3.21+0.522\,|\ln\kappa|^{1.77} \tag{86}$$

Equations 84—86 hold with errors of less than 2%. Therefore, by taking into account Eqs. 81—86, we obtain the following equations for the peak potential, the peak current and the half-peak width of the irreversible wave:

$$\begin{aligned}(E_m)_p = E^{r}_{1/2} + (RT/\alpha nF)\{&\ln(k_0\sqrt[4]{\theta_s\tau}/\sqrt{D}) + 0.27\\ &+ 0.40\,\mathrm{sech}[2.2-0.2\ln(\theta_s/\tau)\\ &- 0.4(\alpha nF/RT)\Delta E]\}\end{aligned} \tag{87}$$

$$\begin{aligned}(i_{\text{dif-pulse}})_p = (i^{c}_{d})_{\text{Cott}}&[1-\exp\{-(\alpha nF/RT)\Delta E\}]\\ &\times \frac{[(\alpha nF/2RT)\Delta E+(1/4)\ln(\theta_s/\tau)]^{1.62}}{1.50+[(\alpha nF/2RT)\Delta E+(1/4)\ln(\theta_s/\tau)]^{1.62}}\end{aligned} \tag{88}$$

$$\begin{aligned}\Delta(E_m)_{p/2} = (RT/\alpha nF)\{&3.21\\ &+0.522|(\alpha nF/2RT)\Delta E+(1/4)\ln(\theta_s/\tau)|^{1.77}\}\end{aligned} \tag{89}$$

From Eqs. 87—89 we can readily see how the shape of irreversible waves varys in dependence of the kinetic parameters of electrode reaction. The standard rate constant k_0 is not contained in the equations of the peak current and the half-peak width and hence it has no influence on the shape of irreversible waves, while the peak potential shifts in proportion to $\ln k_0$. On the other hand, the transfer coefficient α has a great influence both on the wave-shape and the peak potential in somewhat complicated ways, as can be seen from Eqs. 87—89.

Remark for Applying the Theory to Analysis of Experimental Data

In the pulse polarographic practice, in order to increase the S/N ratio, the pulse polarographic current is frequently integrated over some short period, $\Delta\theta$, at the end of the pulse duration, and it is expressed as the value averaged over $\Delta\theta$. In the theoretical considerations developed above, however, it is the instantaneous value at $\theta=\theta_s$. Thus, one problem may arise: what magnitude of error is introduced when the instantaneous value at $\theta=\theta_s$ is replaced by the value averaged over the time-duration from $\theta_s-(1/2)\Delta\theta$ to $\theta_s+(1/2)\Delta\theta$? If the current may vary linearly with time, the average current is precisely equal to the instantaneous one at the middle point of the time duration concerned. The case, in which the variation of current with time most greatly deviates from the linearity, is that of reversible waves. As can be seen from Eqs. 32, 41a, 51, and 73, the pulse polarographic current of reversible waves is proportional to $1/\sqrt{\theta}$. Therefore, the current, $\bar{i}_{\text{pulse}}$, averaged over the time-duration from $\theta_s-(\Delta\theta/2)$ to $\theta_s+(\Delta\theta/2)$ is given by

$$\begin{aligned}\bar{i}_{\text{pulse}} &= \text{const.}\frac{1}{\Delta\theta}\int_{\theta_s-\Delta\theta/2}^{\theta_s+\Delta\theta/2} d\theta/\sqrt{\theta}\\ &= \text{const.}\frac{2\sqrt{\theta_s}}{\Delta\theta}\left\{\left[1+\frac{\Delta\theta}{2\theta_s}\right]^{1/2}-\left[1-\frac{\Delta\theta}{2\theta_s}\right]^{1/2}\right\}\end{aligned}$$

For $\Delta\theta/2\theta_s<1$, we have

$$\bar{i}_{\text{pulse}} = \text{const.}\frac{1}{\sqrt{\theta_s}}\left\{1+\frac{1}{8}\left[\frac{\Delta\theta}{2\theta_s}\right]^2+\frac{7}{128}\left[\frac{\Delta\theta}{2\theta_s}\right]^4+\cdots\right\}$$

On the other hand, the instantaneous value of the pulse polarographic current at $\theta=\theta_s$ is given by

$$i_{\text{pulse}}(\theta=\theta_s) = \text{const.}\,(1/\sqrt{\theta_s})$$

Hence

$$\left|\frac{i_{\text{pulse}}(\theta=\theta_s)-\bar{i}_{\text{pulse}}}{i_{\text{pulse}}(\theta=\theta_s)}\right| = \frac{1}{8}\left[\frac{\Delta\theta}{2\theta_s}\right]^2\left\{1+\frac{7}{16}\left[\frac{\Delta\theta}{2\theta_s}\right]^2+\cdots\right\} \tag{90}$$

Equation 90 reveals that when the condition:

$$\Delta\theta/\theta_s \leqq 1/2 \tag{91}$$

is satisfied, the average current is equal to the instantaneous one at the middle point of the integration range with errors of less than 1%. This statement holds well also for the quasi-reversible and irreversible waves. Hence, we can derive the following conclusion: Let the current be integrated over the time-duration from θ_1 to $\theta_1+\Delta\theta$. Then θ_1 should be selected to be larger than $(3/2)\Delta\theta$, and in such a case the average value may be replaced by the instantaneous one at $\theta=\theta_1+(\Delta\theta/2)$.

Appendix

In this appendix, the integrals I_1 and I_2 will be evaluated. Introducing Eq. 15 with Eq. 16a into Eq. 21 yields

$$I_1 = \frac{\sqrt{D_0}C_0^\circ}{1+\exp(\zeta_1)}\lambda_1\sum_{\nu=0}^{\infty}(-1)^\nu a_\nu(\sqrt{3/7}\,\lambda_1)^\nu \times\int_0^\tau \frac{u^{(3\nu+4)/6}\mathrm{d}u}{\sqrt{(\tau+\theta)^{7/3}-u^{7/3}}} \quad \text{(A-1)}$$

Substituting $u=(\tau+\theta)\,v^{3/7}$ into the above equation and performing the indicated integration, we obtain

$$I_1 = \sqrt{\frac{3}{7}}\,\frac{\sqrt{D_0}C_0^\circ}{1+\exp(\zeta_1)}\sum_{\nu=0}^{\infty}(-1)^\nu a_\nu(\sqrt{3/7}\,\lambda_1\sqrt{\tau+\theta})^{\nu+1} \times\left\{\frac{\sqrt{\pi}\,\Gamma([3\nu+10]/14)}{\Gamma([3\nu+17]/14)} - B\left[1-(1+[\theta/\tau])^{-7/3};\ \frac{1}{2},\frac{3\nu+10}{14}\right]\right\} \quad \text{(A-2)}$$

where $B\,(\xi;\,a,\,b)$ is the incomplete beta function, defined by

$$B(\xi;a,b) = \int_0^\xi \xi^{a-1}(1-\xi)^{b-1}\mathrm{d}\xi$$

Taking into account Eqs. 16a, 16b, and 17, we obtain

$$I_1 = \sqrt{\frac{3\pi}{7}}\,\frac{\sqrt{D_0}C_0^\circ}{1+\exp(\zeta_1)}\left\{1-\psi(\lambda_1\sqrt{\tau+\theta}) - \frac{1}{\sqrt{\pi}}\sum_{\nu=0}^{\infty}(-1)^\nu a_\nu\,(\sqrt{3/7}\,\lambda_1\sqrt{\tau+\theta})^{\nu+1} \times B\left[1-(1+[\theta/\tau])^{-7/3};\ \frac{1}{2},\frac{3\nu+10}{14}\right]\right\} \quad \text{(A-3)}$$

For $(\theta/\tau)<1$, the functions B, ψ and $(\tau+\theta)^{(\nu+1)/2}$ can be expanded into the power series of (θ/τ), as follows:

$$B\left[1-(1+[\theta/\tau])^{-7/3};\ \frac{1}{2},\frac{3\nu+10}{14}\right] = 2\sqrt{\frac{7\theta}{3\tau}} \times\left\{1-\frac{3\nu+11}{18}\left(\frac{\theta}{\tau}\right)+O\left(\left[\frac{\theta}{\tau}\right]^2\right)\right\} \quad \text{(A-4)}$$

$$\psi(\lambda_1\sqrt{\tau+\theta}) = \psi(\lambda_1\sqrt{\tau}) + \frac{\mathrm{d}\psi(\lambda_1\sqrt{\tau}}{\mathrm{d}\ln\tau}\left(\frac{\theta}{\tau}\right)+O\left(\left[\frac{\theta}{\tau}\right]^2\right) \quad \text{(A-5)}$$

$$(\tau+\theta)^{(\nu+1)/2} = \tau^{(\nu+1)/2}\left\{1+\frac{\nu+1}{2}\left[\frac{\theta}{\tau}\right]+O([\theta/\tau]^2)\right\} \quad \text{(A-6)}$$

Further, from Eq. 16a we obtain the following relation:

$$\frac{\mathrm{d}\psi(\lambda_1\sqrt{\tau})}{\mathrm{d}\ln\tau} = \frac{1}{2}\sum_{\nu=0}^{\infty}(-1)^\nu\nu a_\nu(\sqrt{3/7}\,\lambda_1\sqrt{\tau})^\nu \quad \text{(A-7)}$$

Therefore, taking into account Eqs. A-4—A-7, the integral I_1 can be expanded into the following power series of $\sqrt{\theta/\tau}$:

$$I_1 = \sqrt{\frac{3\pi}{7}}\,\frac{\sqrt{D_0}C_0^\circ}{1+\exp(\zeta_1)}\left\{[1-\psi(\lambda_1\sqrt{\tau})] - \frac{2}{\sqrt{\pi}}[(\lambda_1\sqrt{\tau})\psi(\lambda_1\sqrt{\tau})]\sqrt{\theta/\tau} - \left[\frac{\mathrm{d}\psi}{\mathrm{d}\ln\tau}\right](\theta/\tau) + \frac{4}{3\sqrt{\pi}}[(\lambda_1\sqrt{\tau})\,\psi(\lambda_1\sqrt{\tau})]\left[\frac{1}{6}-\frac{\mathrm{d}\ln\psi}{\mathrm{d}\ln\tau}\right](\theta/\tau)^{3/2} + O([\theta/\tau]^2)\right\} \quad \text{(A-8)}$$

On the other hand, the integral I_2 can be evaluated as follows: Rewriting $\tau+u$ insted of u in Eq. 22 yields

$$I_2 = \frac{1}{\sqrt{\tau}}\int_0^\theta \frac{(i_2/nFq)(1+[u/\tau])^{2/3}\mathrm{d}u}{\sqrt{(1+[\theta/\tau])^{7/3}-(1+[u/\tau])^{7/3}}} = \sqrt{\frac{3}{7}}\int_0^\theta \frac{(i_2/nFq)}{\sqrt{\theta-u}}\left\{1-\frac{1}{3}\left[\frac{\theta-u}{\tau}\right]+O([\theta/\tau]^2)\right\}\mathrm{d}u. \quad \text{(A-9)}$$

The present work was partially supported by a Grand-in-Aid for Scientific Research No. 247065 from the Ministry of Education. The author is indebted to Dr. K. Tokuda for his help for numerical calculations.

References

1) G. C. Barker and A. W. Gardner, *Z. Anal. Chem.*, **173**. 70 (1960); G. C. Barker, "Progress in Polarography," ed by P. Zuman and I. M. Kolthoff, Wiley-Interscience, New York-London (1962), Vol. 2, p. 423.

2) A. A. A. M. Brinkman and J. M. Los, *J. Electroanal. Chem.*, **7**, 171 (1964); **14**, 269, 285 (1967); L.F. Loeleveld, B. J. C. Wetsema, and J. M. Los, *ibid.*, **75**, 839 (1977).

3) J. Galvez and A. Serna, *J. Electroanal. Chem.*, **69**, 133, 145, 157 (1976); J. Galvez, A. Serna, and T. Fuente, *ibid.*, **96**, 1 (1979).

4) K. B. Oldham, *Anal. Chem.*, **40**, 1024 (1968).

5) I. Ruzic, *J. Electroanal. Chem.*, **75**, 25 (1977).

6) R. L. Birke, *Anal. Chem.*, **50**, 1489 (1978).

7) H. Matsuda, *Z. Elektrochem.*, **61**, 489 (1957).

8) K. J. Vetter, "Electrochemical Kinetics," Academic, New York-London (1967), p. 107.

9) H. Matsuda and Y. Ayabe, *Bull. Chem. Soc. Jpn.*, **28**, 422 (1955).

10) C. Nishihara and H. Matsuda, *J. Electroanal. Chem.*, **73**, 261 (1976).

11) "Tables of Integral Transforms," ed by A. Erdelyi, McGraw-Hill, New York-Toronto-London (1954), Vol. 1, p. 227; G. E. Roberts and H. Kaufman, "Table of Laplace Transforms," W. B. Saunders, Philadelphia-London (1966).

12) M. Smutek, *Chem. Listy*, **45**, 241 (1951); P. Delahay and J. E. Strassner, *J. Am. Chem. Soc.*, **73**, 5218 (1951); T. Kambara and I. Tachi, *Bull. Chem. Soc. Jpn.*, **25**, 135 (1952); M. G. Evans and N. S. Hush, *J. Chim. Phys.*, **49**, 159 (1952); P. Delahay, *J. Am. Chem. Soc.*, **75**, 1430 (1953); H. Gerischer and W. Vielstich, *Z. Phys. Chem. (Frankfurt)*, **3**, 16 (1955).

13) K. B. Oldham and E. P. Parry, *Anal. Chem.*, **40**, 65 (1968).

14) H. Matsuda, Y. Ayabe and K. Adachi, *Ber. Bunsenges. Phys. Chem.*, **67**, 593 (1963); H. Matsuda, *Tokyo Kogyo Shikensho Hokoku*, **61**, 315 (1966).

15) R. Tamamushi and N. Tanaka, *Z. Phys. Chem. (Frankfurt)*, **39**, 117 (1963).

16) R. A. Marcus, *Ann. Rev. Phys. Chem.*, **15**, 155 (1964); V. G. Levich, "Advances in Electrochemistry and Electrochemical Engineering," ed by P. Delahay, Interscience, New York (1966), Vol. 4, p. 249; R. R. Dogonadze, A. M. Kuznetsov and T. A. Marsagishvili, *Electrochim. Acta*, **25**, 1 (1980).

17) J. M. Saveant and D. Tessier, *J. Phys. Chem.*, **81**, 2192 (1977); V. Marecek, Z. Samec, and J. Weber, *J. Electroanal. Chem.*, **94**, 169 (1978).

18) K. B. Oldham and E. P. Parry, *Anal. Chem.*, **42**, 229 (1970).

19) H. Matsuda, *Z. Elektrochem.*, **62**, 977 (1958).

Infrared Multiple Photon Dissociation of Cyclobutanone

Seiichiro KODA,† Yasushi OHNUMA, Tadashi OHKAWA, and Soji TSUCHIYA*

Department of Pure and Applied Sciences, College of General Education, The University of Tokyo, Komaba, Meguro-ku, Tokyo 153

†*Department of Reaction Chemistry, Faculty of Engineering, The University of Tokyo, Hongo, Bunkyo-ku, Tokyo 113*

(Received May 21, 1980)

The multiple photon dissociation of cyclobutanone was discussed on the basis of the observed relative significance of two reaction channels. Cyclobutanone was irradiated by a TEA CO_2 laser beam of 9.6 μm R(14) line in a parallel and a focussed geometry. The detected products were ethylene, ketene, and cyclopropane under parallel geometry irradiation. Propylene and acetylene were also produced in focussed geometry irradiation. The kind of the products as well as the effects of reaction conditions on their yields led to the conclusion that the dissociation proceeds along two channels, in one of which ethylene and ketene are produced and in the other cyclopropane and CO. The experimental results agreed almost with the result simulated by a statistical model calculation based on the hypothesis that the energy absorbed in cyclobutanone molecules is statistically distributed among all vibrational degrees-of-freedom.

During the last decade, there has been a lot of interest in the mechanism of chemical reactions induced by a strong infrared laser field through multiple photon excitation.[1] A variety of polyatomic molecules are found to dissociate *via* the infrared multiple photon dissociation (MPD) even under a collisionless condition. The mechanism of MPD, at least its outline, is now well established, particularly for several pet molecules such as SF_6.[2,3] In MPD of relatively simple polyatomic molecules, the energy pumped into a molecule by a laser field is more or less randomly distributed in all vibrational degrees-of-freedom before decomposition, and most of the excited molecules decompose along the lowest possible thermal decomposition channel. Sometimes, however, apparently unexpected processes from the hypothesis of energy randomization are reported, such as a direct formation of C_2 fragment from ethylene.[4] Thus, more studies on variety of molecules are needed for full understanding of the MPD mechanism.

The events associated with MPD might be complex, particularly when the process is to be studied by means of conventional product analyses. The chemical reactions subsequent to MPD would be simplest for the case that the expected mode of dissociation involves only stable molecular products, thereby minimizing the possibilities of post-pulse chemical reactions. The thermal unimolecular dissociation process[5-9] as well as single photon photochemistry[10] is relatively well known for cyclobutanone. The thermal decomposition of this molecule occurs along two channels; the major one yields ethylene and ketene, and the minor one, cyclopropane and CO; *i.e.*,

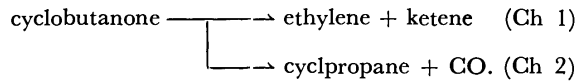

These two channels seem to proceed in a concerted molecular elimination manner, though the detailed mechanism of the minor process is still open to debate. Provided that the decomposition of this molecule in MPD occurs along the above thermal channels, the dependency of the branching ratio as well as the yield of each channel on the laser energy would help understanding the inter- and intramolecular energy distributions of the excited molecules through multiple photon absorption. The branching ratio of the MPD reaction was studied very recently by Back and Back[11] and also by Harrison *et al.*[12] mainly as a function of pressure. Though these two data are quite contradictory to each other, both of them found that the branching ratio remained constant at pressures above 3 Torr, and concluded that the MPD at higher pressures was essentially the same as the thermal decomposition reaction. In the present paper, we will describe our experimental determination of the reaction yield as well as the branching ratio mainly against laser fluence at around 1 Torr. The result will be compared with calculations by a stochatic model for the excitation and reaction. Similar discussions on branching ratios were reported for several other molecules such as 1-bromo-2-fluoroethane,[13] ethylchloride-2d_1,[14] and 1-chloro-2-fluoroethylene.[15]

Experimental

A grating tuned TEA laser (Lumonics Research Ltd. Type 102, multimode) was employed as the irradiation source. The laser medium was the mixture of He and CO_2 without adding N_2 and the ouput pulse was about 80 ns fwhm with no appreciable longer tail as measured with a photon drag detector (Rofin Ltd., Model 7425/7400). Shot-to-shot fluctuations in the pulse energy were within ±5%. The laser energy was selectively attenuated by polyethylene sheets and was monitored by an energy meter (Gentic, ED-500).

Two different ways of irradiation were adopted. (1) A cylindrical (2.6 cm inner diameter × 10 cm length) Pyrex cell sealed with NaCl windows at both ends was used for the following focussed gemetry irradiation. The CO_2 laser beam was focussed inside the cell by use of a Ge lens of a 25 cm focal length. The radial distribution of the laser intensity at the focal point was determined by scanning a pin hole (90 μm dia.) to be a near Gaussian with an effective diameter of 0.1 cm; thus the effective irradiation area at the focus was estimated to be 8×10^{-3} cm^2. (2) A disc type (2.6 cm inner diameter × 1 cm length) Pyrex cylinder sealed with two NaCl windows was employed for the following parallel geometry irradiation. The cell was placed between a 25 cm focal length Ge lens and its focal point, around 19 cm distant from the lens. The effective irradiation area was determined to be 0.36 cm^2 on the basis of the burnt area measurement on thermal paper by

the laser irradiation. Within this area, the laser intensity was assumed to be constant. The field intensity or the fluence varied over 1.4 times between the two NaCl windows along the laser beam according to the geometric consideration. In both of the above geometries, precise determination of the effective area was difficult due to the multimode laser pattern. Errors introduced by the overall procedure might give a 40% uncertainty in the absolute value of the laser fluence, but much less than this for relative values.

Commercially obtained cyclobutanone of extra pure grade from Nakarai Kagaku Co. Ltd. was used after several freeze-thaw cycles. It proved to contain no detectable impurities identical to the irradiation products by gas-chromatography and infrared spectroscopy.

The gaseous materials were treated in a conventional vacuum line equipped with a MKS baratron pressure meter (170-6B/310BHS). Cyclobutanone was introduced into the irradiation cell manometrically. After the irradiation of a necessary number of laser shots (repetition rate was less than 0.3 Hz), the resultant gas mixture, or sometimes, a part of it, was transferred into a gas-sampler for a gas-chromatographic analysis. The products were analysed by use of a Shimadzu GC-4C gas-chromatograph with a flame ionization detector. The products (ethylene, acetylene, cyclopropane, and propylene) were identified in terms of their retention times by use of a Porapak Q and activated charcoal columns. Authentic samples were commercially obtained. Quantitative analyses were carried out with an activated charcoal column. Whether the products were totally recovered or not was checked with model mixture gases. The quantitative analyses were reliable within 10% for C_2 and C_3 hydrocarbons. Sometimes, the 10 cm irradiation cell itself was used as a sample cell for the double beam infrared spectrometer (Japan Spectroscopic Co. Ltd., IRA-1). The infrared spectra of cyclobutanone and the reaction mixture were thus obtained.

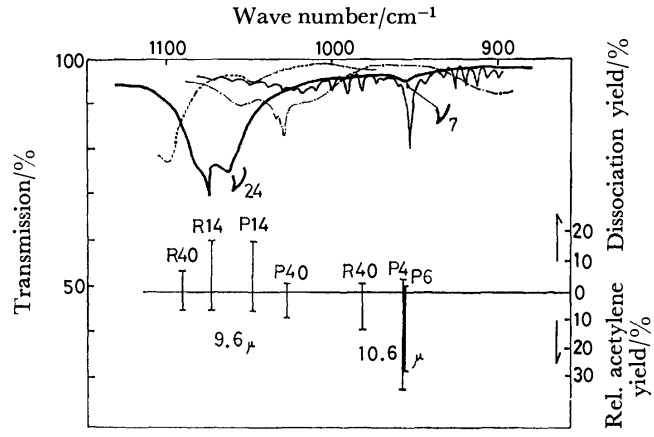

Fig. 1. Dissociation yield and relative acetylene yield with various laser lines, and the IR absorption spectra of cyclobutanone, ethylene, cyclopropane, and ketene. The dissociation yield is the consumed cyclobutanone per 100 shots divided by the initial cyclobutanone, and the relative acetylene yield is the fraction of acetylene among the summed yield of ethylene, acetylene, cyclopropane, and propylene. The irradiation was carried out in focussed gemoetry with 0.37—0.52 J incident laser pulses. The pressure of cyclobutanone was 1 Torr. The conventional IR absorption spectra were measured at 5 Torr (10 cm optical length) in the present work except for ketene. Its spectrum is from the Ref. 17.
Cyclobutanone (——), ethylene (——), cyclopropane (·—·—·), ketene (------).

Results

Product Analyses. The 9.6 μm R(14) line of the TEA CO_2 laser at 1075 cm^{-1} was usually employed in the present work. This line is approximately resonant with the Q branch of the cyclobutanone ν_{24} band (A type, rocking mode of the CH_2 groups, see Fig. 1),[16] which is the strongest absorption band in accord with the CO_2 laser lines. The linear absorption cross section was measured to be 3×10^{-19} cm^2 $molecule^{-1}$ by means of a conventional infrared spectrometer with a 2 cm^{-1} slit width.

The identified products in focussed geometry irradiation were ethylene, cyclopropane, propylene, acetylene, and ketene. The products except ketene were quantitatively analysed gas-chromatographically. In the gas chromatograms with an activated charcoal column, three other peaks were found at the retention times corresponding to methane, ethane, and propane. One unidentified peak was also observed between the cyclopropane and the propylene peak. These products were, however, found to be very minor, less than 1% of the total products even under the strongest irradiation conditions. No other gas chromatographic peaks were recognized before the effusion of cyclobutanone. Ketene gave no gas chromatographic peak, probably because of its reaction with column materials. Thus it was identified by its characteristic infrared absorption peak at 2150 cm^{-1}.[17] Furthermore, the identification was confirmed by the fact that the infrared peaks disappeared when the reaction mixture was kept with 50 Torr methanol for 30 min,[18] and that the resultant production of methyl acetate was proved gas chromatographically.

In parallel geometry irradiation, ethylene and cyclopropane were almost the exclusive products found by gas chromatographic analyses; acetylene, propylene, and other minor products gave only trace gas chromatographic peaks if any.

If the MPD proceeds *via* the two reaction channels similar to the thermal decomposition, ethylene, cyclopropane, and ketene are the expected products. We did not try to detect one other expected product, CO, because of its low sensitivity for the gas chromatographic and infrared analyses. In agreement with the assumption that the major channel is Ch 1, the observed amount of ethylene was 80% or more of the decomposed cyclobutanone under various irradiation conditions. At the same time, the infrared peak intensity of the band assigned to ketene were found to be approximately proportional to the peak intensity at 950 cm^{-1} of the product ethylene. Cyclopropane must not be produced by a secondary reaction such as CH_2+ethylene→ cyclopropane, in which CH_2 is supplied by MPD of ketene or other primary products, because the cyclopropane formed *via* the insertion of CH_2 to ethylene possesses too large internal energy to be stabilized under the present low pressure.[19] Acetylene and propylene,

which are not primary products of the above two channels, were found only in focussed geometry irradiation. As will be discussed later, acetylene is formed through MPD of a primary product and propylene through isomerization of the energy-excess cyclopropane. Thus, we will assume that the MPD of cyclobutanone proceeds *via* the two dissociation channels which are the same as those in the thermal decomposition. The product ethylene or ethylene+acetylene represents an extent of the Ch 1 decomposition, while cyclopropane or cyclopropane+propylene does that of the Ch 2. The products and the reaction mechanism coincide with the results of Back and Back[11] and of Harrison *et al.*,[12] who irradiated cyclobutanone with the laser light of 1047 cm^{-1} P(20) and 1073 cm^{-1} R(12) lines, respectively.

Effect of Irradiation Wavelength. Several preliminary experimental runs were carried out with various laser lines in focussed geometry. The kind of products did not change, but the dissociation yield and the relative yield of acetylene varied considerably as shown in Fig. 1. The dissociation yield is the highest at the 9.6 μm R(14) line among the examined laser lines, and decreases towards both sides of this line being approximately proportional to the linear absorption of cyclobutanone. The relatively high yield compared with the linear absorption at the 9.6 μm P(14) line may be reasonable, because the multiple photon absorption has the tendency to extend to the red compared with the single photon absorption.[1]

Ethylene[4,20,21] and cyclopropane[22] are known to give acetylene in high yields *via* CO_2 laser MPD. The high yield of acetylene in irradiation with the laser line of smaller wavenumber is understandable, because the primary products could absorb the laser lights of these wavenumber lines effectively. The absence of dissociation of ketene with 1080 cm^{-1} CO_2 laser irradiation is reported at a ketene pressure lower than 5 Torr. Only H_2 and CO with trace amount of acetylene is reported as gas phase products at higher ketene pressures.[23]

Thus we selected the 9.6 μm R(14) line as the most adequate for the present purpose to find out the dependence of the ratio of the two different channels on the irradiation conditions, because the dissociation yields were high and the interference by possible undesirable secondary reactions was small with this line. We confirmed, however, almost the same mechanism in the primary dissociation with other laser lines, including the 10.6 μm P(4) and P(6) lines which are resonant to the ν_7 ring mode band[16] of cyclobutanone.

Effect of the Number of Laser Shots. Figure 2 shows the dissociation yield as a function of the laser shot number in focussed geometry irradiation. Let $P_{CB(0)}$ mean the initial pressure of cyclobutanone and $P_{CB(N)}$, the pressure after N repetitive shots. log $[P_{CB(N)}/P_{CB(0)}]$ is plotted against the number of laser shots in Fig. 2 to show that a good proportionality exists between the two variables. The proportionality relation is readily derived, if the dissociation yield per one laser shot $W(=[P_{CB(N)}-P_{CB(N-1)}]/P_{CB(N-1)})$, is independent of the consumption of cyclobutanone and the gas mixture becomes uniform before the subsequent laser shot. The following proportionality relation is equated,

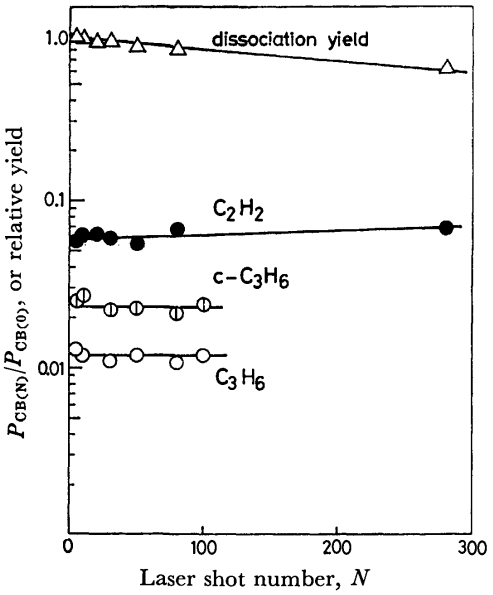

Fig. 2. Variations of dissociation yield and relative yields of acetylene, cyclopropane, and propylene with laser shot numbers. Cyclobutanone of 1.0—1.7 Torr was irradiated in focussed geometry with 0.46—0.47 J incident energy pulses.
△: $P_{CB(N)}/P_{CB(0)}$, ●: relative yield of acetylene, ①: relative yield of cyclopropane, ○: relative yield of propylene.

$$\log(P_{CB(N)}/P_{CB(0)}) = N\cdot\log(1-W). \quad (1)$$

When the dissociation yield is kept small enough (for example less than 10%), Eq. 1 is approximated by the equation,

$$W = [(P_{CB(0)} - P_{CB(N)})/P_{CB(0)}]/N, \quad (2)$$

which makes it possible to obtain W by dividing the yield after N shots by number N.

The relative yields of acetylene, cyclopropane, and propylene against the number of laser shots are also shown in Fig. 2. The relative yields of cyclopropane and propylene are independent of the laser shot number as is expected from the proposed reaction mechanism if no appreciable secondary dissociation of these products occurs. The yield of acetylene shows a slight increase with the laser shot number. Most of acetylene is considered to be produced *via* some secondary dissociation of the primary products, probably ethylene, as will be described in the next section. The fact that the observed dependence of the acetylene yield on shot numbers is small implies that the secondary dissociation proceeds mainly during the same laser pulse when the primary products are still vibrationally hot.

Effect of Laser Energy in Focussed Geometry Irradiation. Figure 3 shows the effect of laser energy (which is proportional to laser fluence in the present work) upon the product yields. The total yield is proportional to the 3/2 power of the laser energy. In focussed geometry irradiation, the 3/2 power dependence could be explained based on a conical geometry of the laser beam incorporating saturation effects.[24] In this treatment, the volume inside of which the laser intensity exceeds a

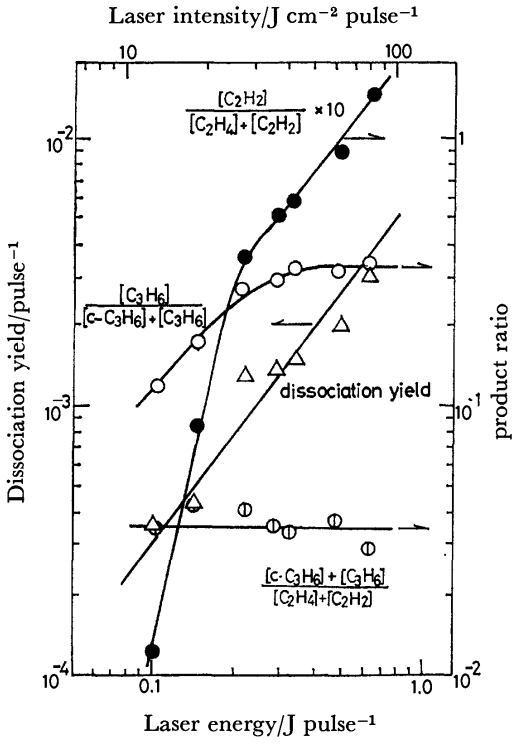

Fig. 3. The dependence of the dissociation yield, the fraction of acetylene, the branching ratio, and the degree of isomerization of the cyclopropane on the laser pulse energy in focussed geometry irradiation.
The laser energy (along the *absissa*) means the incident laser energy per pulse and the laser intensity means the field intensity which is defined as the energy of one pulse divided by the effectively irradiated area normal to the laser beam in the focal region.
△: Dissociation yield per pulse. The straight line shows the 3/2 power law, ●: ratio of acetylene *vs.* ethylene+acetylene (multiplied by 10), ⦶: ratio of cyclopropane+propylene *vs.* ethylene+acetylene, ○: ratio of propylene *vs.* cyclopropane+propylene.

certain value increases proportional to the 3/2 power of the incident laser energy. If the dissociation yield is effectively described by the relation $W=\alpha(I/I_{th})^n$ with a large n when $I<I_{th}$ and is constant α when $I\geq I_{th}$, the 3/2 power law holds over a broad intensity range, masking the effect of the order n of the process. The experimental finding in Fig. 3 is understandable in this context.

The ratio of acetylene *vs.* the sum of ethylene and acetylene increases proportional to the power of 3/2 or higher of the laser energy. This fact shows that acetylene is not a primary reaction product from cyclobutanone. Most of acetylene must be produced through MPD of some primary products during the same laser pulse. A theoretical model calculation will show in Discussion that the dissociation of cyclobutanone is complete far before the end of the laser pulse of a large power, and thus it is possible that the primary products absorb enough laser energy within the same laser pulse to dissociate. Under stronger irradiation conditions with a focussed geometry, visible luminescence was observed at the focal region. This suggests that radicals such as C_2 and CH_x are produced *via* some secondary MPD of primary products and may be intermediates for production of acetylene and other minor hydrocarbon species. Most of the acetylene should come from ethylene and/or ketene, which are the primary products capable of yielding a considerable amount of acetylene *via* the subsequent multiple photon absorption. The yield of acetylene under irradiation of a stronger laser pulse exceeds considerably the yield of C_3 hydrocarbons, which is almost independent of the laser energy. This shows that the C_3 hydrocarbons could not be the main primary product to yield acetylene. It is not determined conclusively which is the main primary product to produce acetylene, ethylene or ketene. Though ketene is reported not to produce acetylene through the MPD at 1080 cm^{-1},[23] the possibility may not be denied that the primary ketene, when it is still hot, could be the starting material for some secondary MPD. In spite of this, we prefer a view that the primary hot ethylene is the main precursor, judging from the fact that the relative acetylene yield decreased with increasing the irradiation wavenumber, roughly in agreement with the change of the linear absorption of ethylene, but reverse to that of ketene (see Fig. 1). The possibility that the primarily produced ethylene dissociates directly to yield acetylene without absorbing subsequent laser photons is considered to be very small on the basis of energetics.

It is important to note that the ratio of the sum of cyclopropane and propylene *vs.* that of ethylene and acetylene is independent of the laser energy. This is probably caused by the fact that, in focussed geometry irradiation, most of the dissociation occurs in the region where the laser intensity is equal to or slightly exceeds I_{th} in the context of the previous explanation of the geometric effect. Moreover, the later theoretical model calculation shows that the branching ratio does not strongly depend on the laser intensity so long as it is strong enough. The slight decrease in the experimental plots with increasing laser energy may mean some occurrence of secondary dissociations of the C_3 hydrocarbons.

The ratio of propylene *vs.* the sum of cyclopropane and propylene increases with the laser energy to a certain plateau value as shown in Fig. 3. This behaviour is consistent with the hypothesis that most of propylene is produced *via* unimolecular isomerization of the primary product cyclopropane.[25] The energetical threshold for the isomerization is much higher than those for Ch 1 and Ch 2 (see Discussion, Fig. 8). Thus the increase of the ratio until a certain plateau value does not conflict with the observed constancy in the branching ratio over the examined laser energy range. The fact that the certain plateau value is reached indicates that most of propylene is not produced *via* secondary MPD of primary products. If so, the ratio should increase with the laser energy similarly to the yield of acetylene.

Pressure Effects in Focussed and in Parallel Geometry Irradiations. Figure 4 shows the effect of the cyclobutanone pressure on the dissociation yield, the branching ratio, and also the degree of the isomerization of the primary product cyclopropane. The yield is pressure dependent, which may mean that the dissocia-

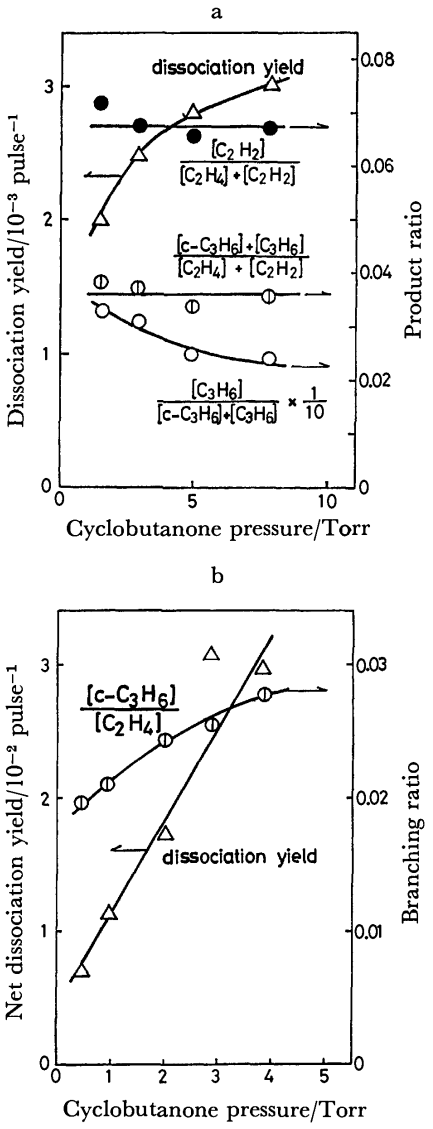

Fig. 4. The dependences of dissociation yield, the branching ratio, and the degree of isomerization of the cyclopropane on the pressure of cyclobutanone in focussed (4a) and in parallel (4b) geometry irradiations.
4a) △: Dissociation yield per pulse, ●: ratio of acetylene *vs.* ethylene+acetylene, ⓘ: ratio of cyclopropane +propylene *vs.* ethylene+acetylene, ○: ratio of propylene *vs.* cyclopropane+propylene (multiplied by 1/10). The incident energy per pulse was 0.47 J.
4b) △: Dissociation yield per pulse in the effectively irradiated volume (=net dissociation yield), ⓘ: ratio of cyclopropane *vs.* ethylene. The incident laser intensity was 6.0 J cm^{-2} pulse^{-1}.

tion partly proceeds collision free and is partly supported by a certain kind of collisional events. It is difficult to extrapolate the dissociation yield to zero pressure to find out the percentage of the contribution of collision free dissociation without doubt, but it seems to be less than 50% even under 1 Torr of cyclobutanone. The branching ratio is pressure dependent in the parallel geometry irradiations. The dependence in the present experiments are in agreement with the observation by Harrison *et al.*,[12] but reverse to the result by Back and Back.[11] The increase in the branching ratio with increasing the pressure suggests that the collisional events result in producing cyclobutanone molecules with a relatively larger internal energy. In focussed geometry irradiation, the pressure effects are rather small, as is expected from the geometric consideration explained in the previous section. The fraction of propylene among C_3 products decreases with increasing pressure. This is due to the collisional stabilization of the primary hot cyclopropane.

In practice, full analysis of collisional effects is very difficult.[26] There must be many factors to be discussed such as rotational relaxation, redistribution of the energies of laser excited molecules, retardation of the diffusion loss of active species, collisional deactivation, and so forth. The data under lower pressures are thus desirable in order to elucidate the MPD mechanism, so long as a detection technique allows. However, our subsequent discussions are limited to the data taken at around 1 Torr due to the detectivity of the present analytical method.

Laser Intensity Effect on Product Yields in Parallel Geometry Irradiation. As has been already described, the exclusive products in parallel geometry irradiation are ethylene (Ch 1) and cyclopropane (Ch 2). The laser intensity dependence of the ethylene yield is plotted in Fig. 5. In these experiments, the yield is corrected for the fact that the effectively irradiated volume

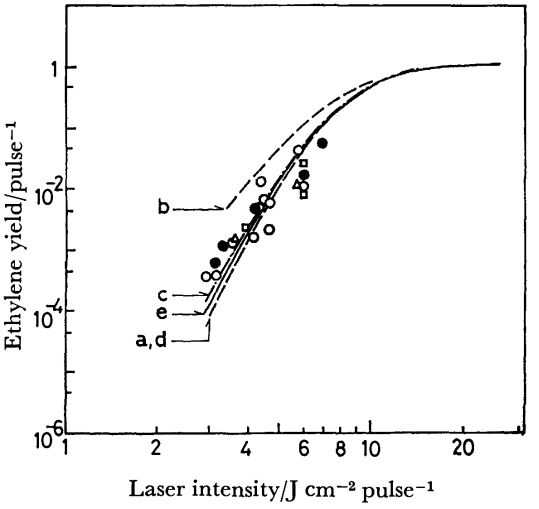

Fig. 5. Yield of ethylene *vs.* laser intensity in parallel geometry irradiation. Experimental data were from experiments with 2 (●), 1 (○), 0.5 (□), and 0.25 Torr (△) cyclobutanone. The yield means the yield per pulse in the effectively irradiated volume. The laser intensity means the incident energy of one pulse divided by the effectively irradiated area. The curves show model calculation results.
a: Calculations with $s=27$ for 1 Torr cyclobutanone. The effective dissociation threshold is at $n=18$ for Ch 1, and $n=21$ for Ch 2, b: calculations with $s=6$. The other conditions are the same as a, c: calculations for 0.25 Torr cyclobutanone. Other conditions are the same as a, d: calculations with $s=27$ for 1 Torr cyclobutanone. The effective dissociation threshold is at $n=18$ for Ch 1, and at $n=20$ for Ch2, e: revised relationship calculated by incorporating the inhomogeneity effect of the field intensity along the laser beam. The data are from curve a.

($0.36\ cm^3$) is much smaller than the total cell volume ($6.77\ cm^3$). The yield increases apparently proportional to around 7 power of the laser intensity. This trend is qualitatively in agreement with that observed by Back and Back[11] at 9.5 Torr pressure. The dissociation yield in the present experiment is, however, considerably smaller comparing at the same fluence. This is partly because of the pressure difference between the two experiments. At the same time, the P(20) line might be more efficient than the present R(14) line.

The ratio of the yield of cyclopropane over that of ethylene, which is the branching ratio of the two channels, is plotted against the laser intensity in Fig. 6. The range of the branching ratio (=[cyclopropane+propylene]/[ethylene+acetylene]) from focussed geometry irradiation is also indicated in the figure by hatching.

The experimental results in Figs. 5 and 6 are open to theoretical discussions on the basis of statistics in Discussion. The curves drawn in the figures show such theoretically predicted relationships.

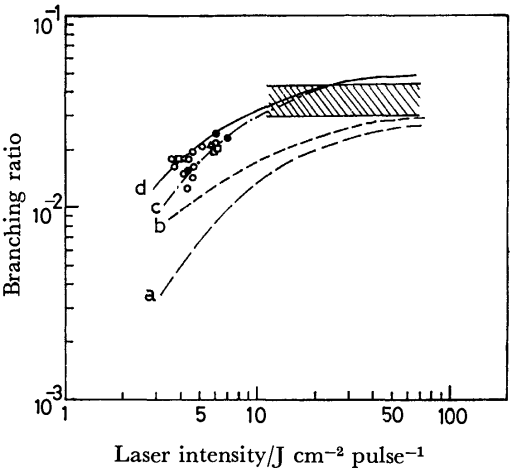

Fig. 6. The branching ratio *vs.* laser intensity. The branching ratio is the ratio of cyclopropane+propylene *vs.* ethylene+acetylene. The experimental results are plotted for 2 (●), 1 (○), 0.5 (□), and 0.25 Torr (△) cyclobutanone pressures. The hatching shows the range from focussed geometry irradiation. In this case, the laser intensity is that one at focal point. The curves show model calculation results. a, b, c, and d have the same meaning as those described in the figure caption of Fig. 5.

Discussion

Model Calculation of MPD Process. There have been reported a lot of theoretical treatments of multiple photon absorption and dissociation of polyatomic molecules. This complex process is analysed[2,3,27-34] based on a rather phenomenological view point by classifying the process into three regions: the first one is a coherent interaction region until some photons are absorbed, the second is an incoherent quasicontinuum region, and the third is a region where dissociation competes with absorption of laser photons. In the first region, the laser power is the deciding factor, and in the second, the laser fluence. In most polyatomic molecules, the dissociation yield as well as other observed phenomena are found to be dependent on the laser fluence, not on the laser power.[31] Thus the absorption of the laser photons in the second quasicontinuum region and the dissociation mechanism are considered to determine almost completely the total MPD process.

In this paper, the MPD process of cyclobutanone will be simulated on the method described by Black *et al.*,[31] whose validity has been proved in the analysis of the MPD of SF_6. We will expand their way to the case of the present two channels dissociation. The first coherent absorption region is neglected. In the quasicontinuum region, the energy pumped into a molecule by the laser field is assumed to be randomly distributed among all available internal degrees-of-freedom, owing to a very fast intramolecular energy migration. Molecules above the threshold of dissociation decompose at RRKM rates. The formulation is as follows.

The probability W_n of being in the state having the energy $n\hbar\omega$ above the starting level is described by use of the following rate equations,

$$dW_n/dt = K_n^a I W_{n-1} + K_n^e I W_{n+1} - (K_{n+1}^a + K_{n-1}^e) I W_n - K_n^{d1} W_n - K_n^{d2} W_n, \quad (3)$$

where K_n^a and K_n^e are absorption and stimulated-emission coefficients into that group, K_n^{d1} and K_n^{d2} are the dissociation rate constants along the two dissociation channels, and I is the laser intensity. The absorption and stimulated-emission coefficients in Eq. 3 represent up and down transitions. Assuming that the transition rates are governed by Fermi's Golden rule, the ratio of transition rates is given by the ratio of density of final states,

$$K_n^e/K_{n+1}^a = \rho_n/\rho_{n+1}, \quad (4)$$

where ρ_n is the density of vibrational states at a vibrational energy of $n\hbar\omega$ above the starting state. The net absorption cross section σ_n is equated as,

$$\sigma_n = (K_{n+1}^a - K_{n-1}^e)\hbar\omega. \quad (5)$$

In this treatment, the possible collisional effect on the distribution is neglected. In fact under stronger irradiation, the dissociation proceeds very rapidly and may not be interfered by collisional events seriously. But in weak irradiation, the dissociation occurs mainly after the laser pulse with a relatively slow rate. Dissociation must compete with some sort of collisional deactivation, and not every molecule with an energy in excess of the dissociation energy may react. The fractional dissociation from level n after the laser pulse is assumed to be written as,

$$f_n^i = K_n^{di}/(\sum_i K_n^{di} + D) \quad (i = 1, 2), \quad (6)$$

where D is the collisional deactivation rate constant with which K_n^{di} competes. The total fraction yield F^i after the laser pulse is the convolution of the fractional deactivation with the distribution function $W_{n(f)}$ at the end of the laser pulse,

$$F^i = \sum_n f_n^i W_{n(f)}. \quad (7)$$

These values should be added to the dissociation yields during the laser pulse.

According to the above procedure, the calculation was carried out with a Gear package for ordinary differential equations.[35] The necessary factors are selected as follows. (1) The time profile for the laser pulse was assumed to be an isoscales triangle of 80 ns fwhm. (2) The internal energy was quantized by $\hbar\omega$ of the adopted laser line, which is 3.07 kcal mol^{-1}. (3) ρ_n was calculated mostly by a RRK formula with $s=27$, the total number of the degrees-of-freedom of internal motion. Sometimes different s values were adopted. The density was once calculated according to the Whitten-Rabinovitch method[36] by adopting the internal vibrational frequencies summarized by E. K. C. Lee *et al.*[37] The result fairly agreed with calculations based on a RRK formula with $s=27$. (4) The net absorption cross section σ_n was assumed to be a constant independent of the internal energy. The value was selected so as to result in a fair agreement between the calculated and experimental results. The selected value was 4.5×10^{-20} cm^2 molecule^{-1}, which was about an order of magnitude smaller than the linear absorption cross section. Because the MPD process is described by the product $\sigma_n\times I$ as the first approximation, but not by the individual σ_n or I, the possible experimental error in the estimation of the laser intensity up to 40% may result in the estimation error in σ_n up to the same amount. (5) The RRKM dissociation rates were taken from the work of E. K. C. Lee *et al.*[37] The values were from their OSA and MP models respectively. No serious differences were expected by selecting other models. In accordance with the artificial quantization of the internal energy of cyclobutanone, the effective threshold for the two channels were selected at $n=18$ ($K_{18}^{d1}=3\times10^6$ s^{-1}), and $n=21$ ($K_{21}^{d2}=3\times10^5$ s^{-1}), respectively. (6) The collisional stabilization rate constant D was selected as 1.1×10^7 s^{-1} based on the collision diameter of 5.07 A for cyclobutanone.[38]

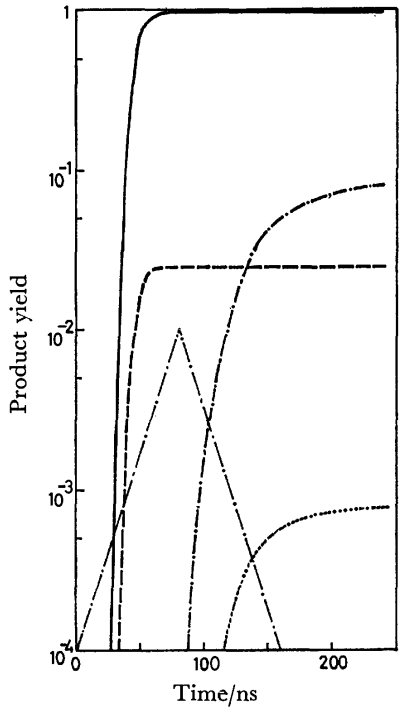

Fig. 7. Calculated time evolution of products of Ch 1 and Ch 2 under irradiations of several laser intensity. The isoscales triangle shows the time evolution of the model laser pulse (linear scale). Calculations were carried out by assuming $s=27$, and the absorption cross section$=4.5\times10^{-20}$ cm^2 molecule^{-1}, and by using the RRKM specific rates. The effective dissociation threshold is at $n=18$ (Ch 1) and at $n=21$ (Ch 2). Laser intensity, 67 J cm^{-2} pulse^{-1} (——; Ch 1, ——; Ch 2), or 6.7 J cm^{-2} pulse^{-1} (·—·—·; Ch 1, ------; Ch 2).

Comparison between the Calculated and Experimental Results. Figure 7 shows the time evolution of the dissociation yields. In this figure, no collision effect is taken into account even after the laser pulse. One important fact is that almost all molecules are dissociated shortly after the beginning of the laser pulse under a such intense irradiation as is met in focussed geometry irradiation. It is then understandable that the secondary multiple photon dissociation of the primary product occurs. Another fact to note is that the dissociation continues long after the end of the laser pulse, particularly under weaker irradiations.

Figure 8 shows the calculated dissociation yields from various levels above the dissociation energy during the laser pulse and also after the laser pulse. The average energy of the distribution of the yield is about 65 kcal mol^{-1} for Ch 1 dissociation under 4.7 J cm^{-2} pulse^{-1} irradiation, and is high as 85 kcal mol^{-1} for Ch 1 under 67 J cm^{-2} pulse^{-1} irradiation.

As has been already described in Results, the yield of Ch 1 as well as the branching ratio depend somewhat on the cyclobutanone pressure even at 1 Torr or less.

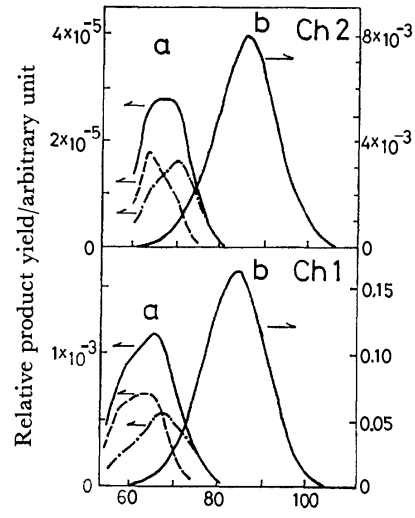

Fig. 8. The calculated dissociation yields from various levels above the dissociation energy.
a shows the results under a 4.7 J cm^{-2} pulse^{-1} irradiation. ·—·—·: The yields during the pulse, ——; the yields after the pulse, ——: the summation.
b shows the results under a 67 J cm^{-2} pulse^{-1} irradiation. In this case, dissociation is complete dur ing the laser pulse.
The pressure of cyclobutanone was 1 Torr. $s=27$, and the RRKM specific rates with the threshold for Ch 1 at $n=18$, and that for Ch 2 at $n=20$ were adopted.

This might correspond to the gradual change from the intrinsic MPD at a lower pressure to the thermal reaction at a higher pressure as are suggested by previous researchers.[11,12] The present model calculation does not take into account the collisional events rigorously. It is worthy to note that Eq. 3 is originally derived for collision-free MPD, and the vibrational-translational energy transfer is disregarded. When the absorption cross section σ_n is assumed to be independent of n, the analytic solution of Eq. 3 with neglecting the dissociation process turns out to be a thermal distribution,

$$W_n = (1/Q)\exp(-n\hbar\omega/kT)(n + s - 1)!/[n!(s - 1)!]. \quad (8)$$

Here, the state density is estimated by a RRK type calculation, and Q is an appropriate partition function. In the actual MPD, the distribution may be somewhat different from the one in Eq. 8 because of the effect of the dissociation process. Anyhow in this case of the constant σ_n, collisions are expected not to affect the distribution seriously. When the cross section σ_n is different in each energy state, the distribution reached by the absorption of laser photons might be quite different from the thermal one, and may change to a large extent through collisions towards the thermal distribution. That is, the collisional events play an important role. We have not any information about the individual σ_n values, and assumed a constant cross section. We consider that the treatment on the basis of Eq. 3 with the constant σ_n is valid as a zeroth approximation, and the following comparison between the present experimental results at around 1 Torr and the model calculations should be taken rather qualitatively.

The curves drawn in Fig. 5 show the yield of Ch 1 *vs.* the laser intensity. Curve b shows the result with $s=6$ for the state density calculation. As has been stated in Experimental, the field intensity varies over 1.4 times along the laser beam between the two NaCl windows even in parallel geometry irradiation. The curve e is estimated from the data in the curve a with taking into account the inhomogeneous distribution of the field intensity. This curve should be compared with the experimental results directly. The agreement between the experimental and calculated results is good, though the theoretically predicted pressure effect is overwhelmed by the data scattering. Unfortunately, we could explain the experimental results by an alternative choice of a larger absorption cross section with a smaller s value. Thus it is impossible to decide whether the vibrational freedom is all available or not by the analysis of this kind, unless the absorption cross section is exactly known.

The curves in Fig. 6 show the dependence of the branching ratio on the laser intensity. The inhomogeneity in the field intensity does not affect the theoretical curves to any appreciable extent. The calculation could not reproduce the experimental results, even by selecting a very small s value. Thus a faster dissociation along Ch 2 than that is predicted by the previous model must be assumed in order to reproduce the experimental results. This was achieved by lowering the effective threshold energy of Ch 2 by one unit, thus from $n=21$ to $n=20$. The results are shown in the figure. The experimental results both from parallel and focussed geometry irradiations seem to be relatively well reproduced. The change in the effective threshold must not be taken so serious, because of the unrealistic, but unavoidable, quantization of energy in the present model calculation, and also because of some ambiguity in the set of the RRKM calculation. The latter is caused by the fact that the thermal decomposition experiments of cyclobutanone by previous researchers are limited to a rather small temperature range with a very small yield of Ch 2 (about 0.5%).[5-9] At the same time, the theoretical curves are affected by the way of estimation of the collisional deactivation rate constant, D, under weaker irradiation. The change of the energy threshold of Ch 2 does not affect the curves in Fig. 5 to any appreciable extent.

Isomerization of the Primarily Produced Cyclopropane. If the cyclopropane possesses an excess internal energy of more than 63 kcal mol^{-1} immediately after its production, the unimolecular process to form propylene starts to compete with the collisional stabilization.[25] The energy content of the cyclopropane may be estimated by the following relation on the assumption that the excess energy along the dissociation is equally divided to all degrees-of-freedom,

$$\varepsilon_{CP} = (\varepsilon_{CB} - Q_{endo}) \times (3M - 6)/(3N - 6), \quad (9)$$

where ε_{CB} is the internal energy of cyclobutanone dissociating along Ch 2 and Q_{endo}, the endothermisity of Ch 2 (6.8 kcal mol^{-1} at 298 K[25]). N and M are the number of atoms in cyclobutanone and cyclopropane, respectively. The specific isomerization rates were taken from the work of Lin and Laidler,[39] and the strong collision was assumed with adopting the collisional deactivation rate constant as 1.1×10^7 s^{-1} Torr^{-1} from the collision diameters, 5.07 Å for cyclobutanone[38] and 4.17 Å for cyclopropane.[39]

The calculated fraction of isomerization is plotted

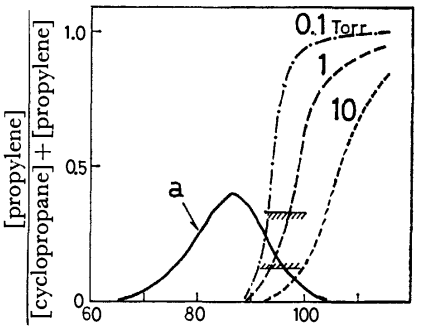

Fig. 9. The calculated degree of isomerization of the primary cyclopropane against the interanal energy of the dissociating cyclobutanone along Ch 2.
The cyclobutanone pressures of 0.1 (-·-·-), 1 (——), and 10 Torr (------) were employed. The hatching shows the range of the experimental results. The bold line of a mountain shape is the dissociation yield distribution against the internal energy of the dissociating cyclobutanone under 67 J cm^{-2} pulse^{-1} irradiation. This is taken from Fig. 8.

against the internal energy of cyclobutanone in Fig. 9. The experimental fraction is about 0.3 in focussed geometry irradiation, which leads to the conclusion that the average internal energy of the dissociating cyclobutanone is around 95 kcal mol^{-1}, with the aid of the curve in Fig. 9. This average values seems to be somewhat higher than the average energy content of the dissociating cyclobutanone obtained in the previous model calculation under 67 J cm^{-2} $pulse^{-1}$ irradiation, but the difference is not so large. It is also understandable that no propylene is observed in parallel geometry irradiation, where the energy of the dissociating cyclobutanone along Ch 2 is estimated to be lower than 80 kcal mol^{-1} as is shown in Fig. 8. Thus the degree of the cyclopropane isomerization does not contradict the hypothesis of the statistical molecular energy distribution in the MPD process.

The possibility of the unimolecular formation of acetylene from the primary hot ethylene without absorbing any subsequent laser photon is denied, because the process requires more than an excess energy of 70 kcal mol^{-1} [40,41] in ethylene. As an average, the ethylene possesses only a 36 kcal mol^{-1} excess energy after its formation from the cyclobutanone of 100 kcal mol^{-1} internal energy, according to the analogous estimation procedure to Eq. 9. No thermal unimolecular dissociation is known for ketene.

Table 1. Branching ratios under various excitation methods

Excitation	Ch 2/Ch1	Ref.
Pyrolysis at 350 °C	*ca.* 0.005	6
IR-MPD		
parallel ($\simeq$1 Torr)	0.015—0.03	this work
focus ($\simeq$1 Torr)	0.03—0.045	
IR-MPD		
parallel ($>$3 Torr)	*ca.* 0.01	11
parallel ($>$3 Torr)	*ca.* 0.033	12
Triplet sensitization	$>$*ca.* 100	42
Direct photolysis at		
334.3 nm	3.4	
313.0 nm	0.4	43
253.7 nm	0.8	

The Branching Ratio under a Variety of Excitation Procedures. The ratio of Ch 2/Ch 1 under various excitation methods are summarized in Table 1. In the photochemistry of cyclobutanone, it was established[10,42] that the triplet state (T_1, about 80 kcal mol^{-1} above S_0) of cyclobutanone decomposes exclusively to cyclopropane and CO. It was also established[10,43] that the singlet excited state (S_1, about 87 kcal mol^{-1} above S_0) undergoes $S_1 \rightarrow T_1$ intersystem crossing at a low photoexcitation energy and $S_1 \rightarrow S_0$ internal conversion at a high photoexcitation energy. The resulting hot ground state decomposes unimolecularly along the thermal dissociation channels. A molecular predissociation is also supposed to set on below 313 nm. The observed branching ratios in the photochemistry of cyclobutanone are understood according to the above scheme.

If a certain inverse intersystem crossing (or internal conversion) proceeds following the multiple photon absorption, a relatively large branching ratio is expected according to the above discussion. The observed small branching ratio in the MPD experiments denies the possibility. The fast intramolecular energy randomization and the very large difference in state densities between the ground and excited electronic states do not allow the excitation of the upper electronic states. Until now, the observation of the inverse intersystem crossing seems to be limited to the relatively simple molecule, F_2CO.[44]

Conclusion

(1) Multiple photon dissociation of cyclobutanone with 9.6 μm R(14) TEA CO_2 laser line proceeds along the same two channels as those observed in the thermal decomposition; the major one yields ethylene and ketene, and the minor one, cyclopropane and CO. Under stronger irradiations, the primary produced cyclopropane partly isomerizes to propylene, and some subsequent multiple photon absorptions of the primary products result in the formation of secondary products, particularly acetylene.

(2) From the comparison between the experimental results and a statistical model calculation concerning the laser energy effect on the product yields, the branching ratio, and the degrees of the subsequent isomerization from the primary produced cyclopropane, no sound evidence is found to reject the hypothesis that, during the laser pulse, the cyclobutanone molecules remain in external and also internal equilibria and dissociates at rates which are predicted from the unimolecular rates observed in conventional thermal experiments.

We acknowledge the Grant-in-Aid of the Ministry of Education, Science and Culture (No. 311606) given to this work.

References

1) R. V. Ambartzmian and V. S. Letokhov, "Chemical, and Biological Applications of Lasers III," ed by C. B. Moore, Academic Press, New York (1977), p. 167.
2) E. R. Grant, M. J. Coggiola, Y. T. Lee, P. A. Schulz, Aa. S. Sudbø, and Y. R. Shen, *Chem. Phys. Lett.*, **52**, 595 (1977).
3) E. R. Grant, P. A. Schulz, Aa. S. Sudbø, Y. R. Shen, and Y. T. Lee, *Phys. Rev. Lett.*, **40**, 115 (1978).
4) J. H. Hall, Jr., M. L. Lesiecki, and W. A. Guillory, *J. Chem. Phys.*, **68**, 2247 (1978).
5) M. N. Das, F. Kern, T. D. Coyle, and W. D. Walters, *J. Am. Chem. Soc.*, **76**, 6271 (1954).
6) A. T. Blades, *Can. J. Chem.*, **47**, 615 (1969).
7) T. H. McGee and A. Schleifer, *J. Phys. Chem.*, **76**, 963 (1972).
8) A. T. Blades and H. S. Sandhu, *J. Phys. Chem.*, **77**, 1316 (1973).
9) T. H. McGee and A. Schleifer, *J. Phys. Chem.*, **77**, 1317 (1973).
10) E. K. C. Lee, *Acc. Chem. Res.*, **10**, 319 (1977).
11) M. H. Back and R. A. Back, *Can. J. Chem.*, **57**, 1511 (1979).
12) R. G. Harrison, H. L. Hawkins, R. M. Leo, and P. John, *Chem. Phys. Lett.*, **70**, 555 (1980).

13) T. H. Richardson and D. W. Setser, *J. Phys. Chem.*, **81**, 2301 (1977).
14) A. J. Colussi, S. W. Benson, and R. J. Hwang, *Chem. Phys. Lett.*, **52**, 349 (1977).
15) A. V. Baklanov, Yu. N. Molin, and A. K. Petrov, *Chem. Phys. Lett.*, **68**, 329 (1979).
16) R. Cataliotti, M. G. Giorgini, G. Paliani, and A. Poletti, *Spectrochim. Acta, Part A*, **31**, 1879 (1975).
17) W. R. Harp, Jr. and R. S. Rasmussen, *J. Chem. Phys.*, **15**, 778 (1947).
18) G. M. Breuer, F. J. Grieman, and E. K. C. Lee, *J. Phys. Chem.*, **79**, 542 (1975).
19) H. M. Frey and G. B. Kistiakowski, *J. Am. Chem. Soc.*, **79**, 6373 (1957).
20) N. V. Chekalin, V. S. Dolzhikov, V. S. Letokhov, V. N. Lokhman, and H. N. Shibanov, *Appl. Phys.*, **12**, 191 (1977).
21) K. Nagai and M. Katayama, *Bull. Chem. Soc. Jpn.*, **51**, 1269 (1978).
22) M. L. Lesiecki and W. A. Guillory, *J. Chem. Phys.*, **66**, 4317 (1977).
23) W. A. Jalenak, D. Schultz, M. Fisher, and N. S. Nogar, *Chem. Phys. Lett.*, **64**, 457 (1979).
24) S. Speiser and J. Jortner, *Chem. Phys. Lett.*, **44**, 399 (1976).
25) S. W. Benson and H. E. O'Neal, "Kinetic Data on Gas Phase Unimolecular Reactions," United States Department of Commerce, NSRDS-NBS-21 (1970).
26) J. C. Jang and D. W. Setser, *J. Phys. Chem.*, **83**, 2809 (1979).
27) J. L. Lyman, *J. Chem. Phys.*, **67**, 1868 (1977).
28) M. J. Shultz and E. Yablonovitch, *J. Chem. Phys.*, **68**, 3007 (1978).
29) C. C. Jensen, J. I. Steinfeld, and R. D. Levine, *J. Chem. Phys.*, **69**, 1432 (1978).
30) Aa. S. Sudbø, P. A. Schulz, Y. R. Shen, and Y. T. Lee, *J. Chem. Phys.*, **69**, 2312 (1978).
31) J. G. Black, P. Kolodner, M. J. Shultz, E. Yablonovitch, and N. Bloembergen, *Phys. Rev. Part A*, **19**, 704 (1979).
32) Aa. S. Sudbø, P. A. Schulz, E. R. Grant, Y. R. Shen, and Y. T. Lee, *J. Chem. Phys.*, **70**, 912 (1979).
33) J. C. Stephenson, D. S. King, M. F. Goodman, and J. Stone, *J. Chem. Phys.*, **70**, 4496 (1979).
34) J. Stone and M. F. Goodman, *J. Chem. Phys.*, **71**, 408 (1979).
35) A. C. Hindmarsh, USID Computer Documentation, 30001, Rev. 3, Lawrence Livermore Lab., Univ. of California (1974).
36) R. J. Robinson and K. A. Holbrook, "Unimolecular Reactions," Wiley-Interscience (1972).
37) G. M. Breuer, R. S. Lewis, and E. K. C. Lee, *J. Phys. Chem.*, **79**, 1985 (1975).
38) R. J. Campbell and E. W. Schlag, *J. Am. Chem. Soc.*, **89**, 5103 (1967).
39) M. C. Lin and K. J. Laidler, *Trans. Faraday Soc.*, **64**, 927 (1968).
40) I. D. Gray, R. D. Kern, and G. B. Kistiakowski, *J. Chem. Phys.*, **45**, 2371 (1966).
41) Y. Ogata, K. Obi, H. Akimoto, and I. Tanaka, *Bull. Chem. Soc. Jpn.*, **44**, 2671 (1971).
42) H. O. Denschlag and E. K. C. Lee, *J. Am. Chem. Soc.*, **90**, 5294 (1968).
43) J. C. Hemminger, C. F. Rusbult, and E. K. C. Lee, *J. Am. Chem. Soc.*, **93**, 1867 (1971).
44) J. W. Hudgens, J. L. Durant, Jr., D. J. Bogan, and R. A. Coveleskie, *J. Chem. Phys.*, **70**, 5906 (1979).

The Fraction of Bound Segments and the Chain Motion of Adsorbed Poly(methyl methacrylate) at the Solution-Solid Interface as Studied by Electron Spin Resonance

Harutoshi SAKAI,* Toshihiko FUJIMORI, and Yoshio IMAMURA

Department of Chemistry, Faculty of Science, Science University of Tokyo, Kagurazaka, Shinjuku-ku, Tokyo 162

(Received May 23, 1980)

The configuration of poly(methyl methacrylate) adsorbed on silica from dilute solution (CCl_4, benzene, and $CHCl_3$) was studied from the point of view of the chain motion by a spin-labeling technique. The ESR spectrum of the adsorbed polymer was found to be composed of three portions, which had considerably different degrees of the motional freedom of the local chain segments. The rotational correlation times corresponding to the three portions were estimated by the line shape analysis and the rapid passage technique. These times were 1×10^{-9}, 5×10^{-9}, and longer than 10^{-6} s, and were attributed to the motions in the long loop, short loop, and train, respectively. The large fractions of the bound segments, obtained in all the cases of low surface coverage, showed highly flattened structures of the adsorbed chain molecules. In the adsorption from a poor solvent (CCl_4), a strongly compressed structure with a large number of the short loops was found. The adsorbed layer thickness, indicated by the fraction of the segments in the three states, became much smaller with an increase in the solvent power and a decrease in the surface coverage.

In recent years, the configurational properties of chain polymer molecules adsorbed at the solution-solid interface have attracted the interest of many investigators. From the experimental results as well as the theoretical treatments, it is commonly accepted that an adsorbed molecule consists of sequences of segments restrained in the surface layer (train) and of other sequences that extend into the bulk solution phase (loop or tail).

More recently, experimental techniques such as IR, ESR, NMR, ellipsometry, *etc.*, have been applied to estimate the train and loop contents and the thickness of the adsorbed polymer layer.[1-6] However, each technique was thought to result in uncertainties both in the evaluating methods and in the data interpretation. For example, Robb and Smith pointed out the advantageous and disadvantageous aspects inherent in the ESR technique, by comparing their ESR results with the published data obtained by IR and NMR techniques.[3] In our previous study, we made a direct comparison of the ESR method with the IR method using an identical solution–adsorbent system (PMMA–CCl_4–silica).[4] Based on the experimental results, we pointed out a disagreement: the ESR method gave much larger values of p (fraction of the train segments of the adsorbed polymer) than the IR values.

In the same paper, we reported the new finding that the ESR spectrum of the adsorbed PMMA (nitroxide-labeled) was composed of three portions which were easily distinguishable by the degrees of the motional freedom of the segments. The three spectral components were assigned to the signals from the train, short loop, and long loop segments. These assignments in the previous study, however, had been qualitatively performed by the comparison of the observed line shape with those of three model spectra, obtained from a free polymer solution of low viscosity, a cooled solution to the frozen state, and a highly viscous polymer in the molten state.

In the present study, the rotational correlation times of the three components of the adsorbed PMMA and the model systems were quantitatively estimated. A rapid passage technique was used to examine the very slow motion of the bound segments. The detailed behavior of the train and loop segments is discussed in relation to the solvent effects and the degree of adsorption.

Experimental

The spin-labeled PMMA was prepared by an anionic polymerization, as described in a previous paper.[4] The procedure basically followed the method of Goode, *et al.*[7] A single fraction of the polymer used was obtained by the fractional precipitation from an acetone–water system. M_n/M_w was determined to be about 1.3 by GPC analysis, and M_n was 1.2×10^5 by membrane osmometry. The spin concentration was three labels per polymer molecule. The polymer was essentially isotactic, which gave the IR J-value of 26, and was more soluble in CCl_4 than the atactic PMMA.

Cabosil M-5 (Cabot) with a specified surface area of 220 m^2/g for nitrogen adsorption was used as the adsorbent. The silica was essentially nonporous and had an average particle size of 14 nm.

The polymer solution was added to silica, and the mixture was stirred for 4 h with a magnetic stirrer. The adsorption isotherms, shown in Fig. 1, were determined as follows. The silica dispersions were centrifuged, and the polymer concentrations in the supernatant solutions were determined by means of the infrared spectroscopy at the normal carbonyl stretching band near 1740 cm^{-1}. In the case of the benzene solutions, the concentrations were determined by using a calibration curve obtained with the plots of the solution viscosity *vs.* the concn. The amount of adsorption was calculated from the changes in the concn before and after the adsorption.

The ESR spectra were recorded on a JEOL JES FE 3-X spectrometer utilizing 100 kHz field modulation and X-band microwaves. Temperature was controlled by a cooled and rewarmed nitrogen-gas-flow system. To detect the spectrum of the adsorbed polymer itself, the silica was washed before the measurements with pure solvent to eliminate the free polymer. In the regions of unsaturated adsorption, the measurements were made without the washing, since the contribution from the unadsorbed polymer into the spectrum was negligible.

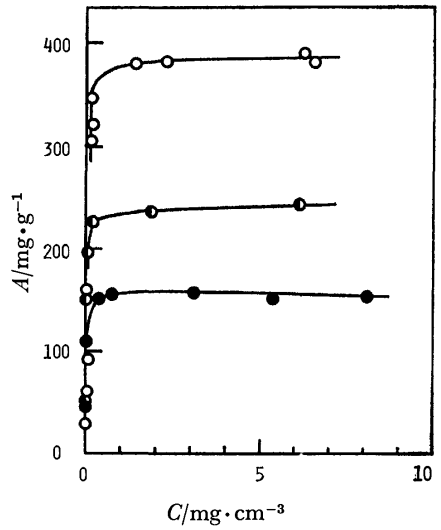

Fig. 1. Adsorption isotherms of PMMA at 25 °C.
From ○: CCl_4 solution, ◐: benzene, ●: $CHCl_3$.

An adiabatic rapid passage technique, developed by Hyde, *et al.*,[8] was also applied to the examination of the very slow tumbling motion of the adsorbed chain segments. The first harmonic of the dispersion signal was detected at 90° out-of-phase with respect to the Zeeman modulation. The saturation-transfer spectra were observed under the conditions of moderately saturating microwave field.

Calculation of Rotational Correlation Times. For the region of motionally narrowed line shape, 10^{-9} to 10^{-11} s, the correlation times (τ_c) were calculated by the equation:[9,10]

$$\tau_c = c\,\Delta H_{msl}[(h_0/h_{-1})^{1/2} - (h_0/h_{+1})^{1/2}]. \quad (1)$$

Here, ΔH_{msl} is the maximum slope width of the center field line, and h_{-1}, h_0, and h_{+1} are the signal heights of high, center and low field lines, respectively. The constant c is a parameter depending on the anisotropies of the hyperfine interaction and the g-factor.

In the region of relatively slow motion from 10^{-7} to 10^{-9} s, τ_c was estimated by the expression of Goldman, *et al.*:[11]

$$\tau_c = a(1 - S)^b, \quad (2)$$

where $S=A'_z/A_z$, A'_z is one-half the separation width of the hyperfine extrema (W), and A_z corresponds to the rigid limit value (W_{max}). The parameters, a and b, are dependent on the rotational diffusion model and the intrinsic line width in the spectrum. In this work, the values for the moderate jump diffusion model, $a=1.1\times10^{-9}$ and $b=-1.01$, was used for the calculation.

Results and Discussion

ESR Spectra. Figure 2 shows the ESR spectra of PMMA adsorbed on silica from CCl_4 solution. The line shapes indicate the diverse motion of the adsorbed chain. The ESR signals from the nitroxide labels attached to the polymer chain reflect sensitively the changes in the motion of the adsorbed chain segments arising from the differences in the configurational states, whether in the loop or the train. The spectral intensity ratio of the wings (marked with * in Fig. 2) to the inner parts (**) decreased with an increase in the surface coverage: the amount of adsorption relative to the saturated adsorption. This shows an increase in the

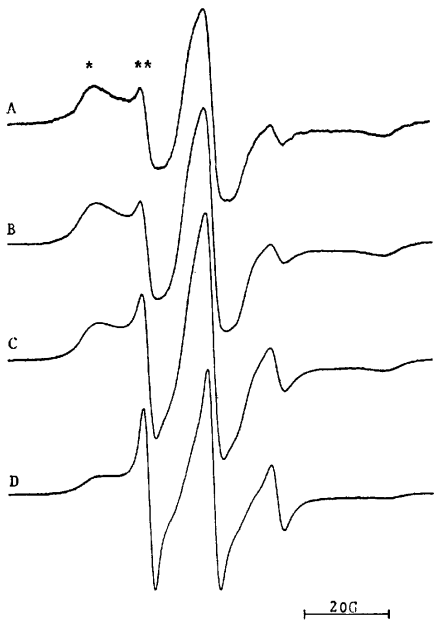

Fig. 2. ESR spectra of the adsorbed PMMA on silica from CCl_4 at 25°C.
A: θ=0.07, B: 0.15, C: 0.28, D: 0.89.

content of the mobile segments. These ESR spectra are composed of three portions which have different mobilities of the local chain, as described in a previous publication.[4] In conclusion, the three portions were attributed to the signals from train, short loop, and long loop parts of the adsorbed chain. As shown in Fig. 3 for an example, an ESR spectrum of the adsorbed PMMA could be synthesized by superposing three reference spectra, obtained from the following model systems in which each polymer chain had different degrees of the motional freedom. The spectrum A was observed in the unadsorbed polymer in CCl_4 solution at 10 °C, and consisted of three motional-narrowing lines due to the rapid rotational motion of the segments in the low viscosity medium. The spectrum B was obtained from the cooled polymer solution in the frozen state at −120 °C, and showed a typical powder pattern due to a rigid immobilization. The solid polymer in the molten state at 146 °C gave an incompletely averaged pattern due to an intermediate restriction of the chain motion (spectrum C). These three model spectra were superimposed upon one another on a computer to match the observed spectrum of the adsorbed polymer. As a result of the repeated runs, spectrum D gave a good fit to the line shape of the observed spectrum E. Thus, it was decided that the adsorbed polymer chain was constructed with three portions.

The Motion of the Adsorbed Chain Segments. The rotational motion of the loop segments is somewhat restricted by the fixing of the two loop ends by the surface, and will strongly depend on the length and the distance from the surface. The value of τ_c of the most mobile component was 1×10^{-9} s, while that of the intermediate portion was approximately 5×10^{-9} s. Therefore, resonable assignments for the relatively mobile components are as follows: the most freely

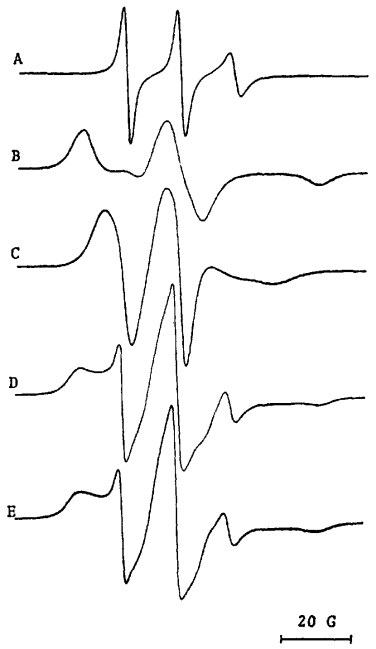

Fig. 3. ESR spectra of the spin-labeled PMMA.
A: Unadsorbed in CCl_4 at 10°C, B: unadsorbed in CCl_4 at −120 °C, C: in the molten state at 146 °C, D: reproduced by superposition of above three model spectra, E: adsorbed on silica in CCl_4 at 25 °C.

rotating segments are in long loops, while the intermediately restricted segments are in short loops. The value of τ_c of the long loop segments was about twice as long as the unadsorbed polymer in solution at the same temperature, 25 °C. The sequences of the detached segments were considered to be long enough to allow the rapid tumbling motion, although each segment behaves in a less mobile way than does the free polymer in solution. The intermediate restriction of the short loop segments, 5×10^{-9} s, should be caused by a close neighboring with the train segments. Robb and Smith demonstrated the presence of short loops of about 2 or 3 segments, from a comparison of their ESR results with the IR.[3] They thought that the ESR counted the short loops as the train. However, we suggest that the intermediately restricted portion of the adsorbed chain corresponds to the short loops of a few segments.

On the other hand, the most immobilized portion could be attributed to the train segments. Their motion was examined by the dependence of the extreme separation width (W) upon the temperature and the rapid-passage experiments. In Fig. 4, the values of W in various systems are plotted *vs.* the temperature. In the case of the adsorbed polymer, W values remained constant over the wide temperature range of −120 to 70 °C. The value of 68.5 G is in good agreement with the rigid limit (W_{max}) of the unadsorbed polymer in CCl_4 or benzene in the frozen states at −120 °C. These results mean that τ_c of the most immobilized component is at least longer than 10^{-7} s, since this time is the useful rigid limit for the motion of the nitroxide-spin labels to be detected by normal ESR measurements. In addition, W_{max} values of the adsorbed systems were significantly smaller than those in hydrogen-bonding

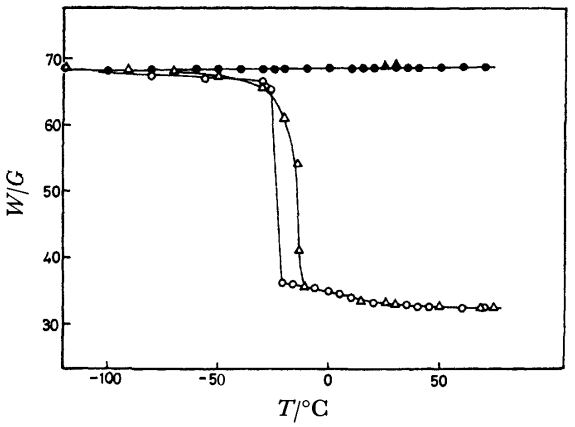

Fig. 4. Extreme separation width (W) of the ESR spectra *vs.* temperature.
●: Adsorbed in CCl_4, ▲: adsorbed in benzene,
○: unadsorbed in CCl_4, △: unadsorbed in benzene.

media.[12] For example, the polymer solutions containing methanol or phenol gave the values of 73 and 76 G, respectively. Therefore, in the case of the adsorbed polymer phase, the direct H-bonding between the nitroxide labels and the surface silanol groups was negligible, and any specific adsorption through the nitroxide labels was not predominant over that between the original polymer segments and the surface. From the adsorption experiments using the unlabeled PMMA and the monomeric species (MMA and the labeled MMA), the same conclusion was obtained.

When the first harmonics of the dispersion mode were detected at 90° out-of-phase with respect to the field modulation under the conditions of a moderately saturating-microwave field, the rapid passage spectra could be observed. The spectrum A shown in Fig. 5 was obtained from the unadsorbed polymer in benzene solution in the frozen state at −50 °C. The spectrum B was obtained from the adsorbed polymer in benzene solution at 25 °C, and showed a slight effect of the saturation transfer. These spectra were quite similar

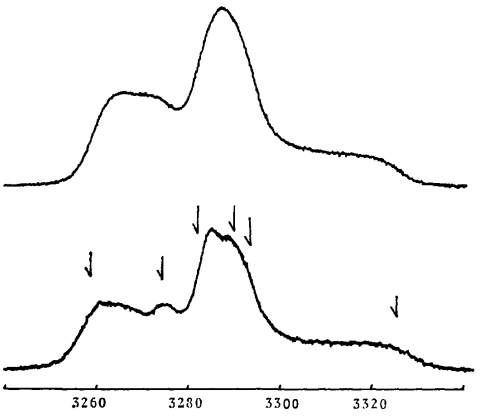

Fig. 5. Rapid passage dispersion spectra detected at 90° out-of-phase with respect to the field modulation of 5 G. Top: Unadsorbed in benzene at −50 °C, bottom: adsorbed on silica in benzene at 25 °C. The arrows show the turning points. Full scale is an interval of 100 G.

to the undifferentiated absorption spectra in the shape of the actual spectral distribution of spins. When τ_c is close to the reciprocal of the modulation frequency, approximately 10^{-6} s in this case, the spectral response is most sensitive to changes in τ_c.[8] The signal intensity would remarkably reduce with decreasing τ_c, in the regions between the turning points shown with arrows in Fig. 5. These turning points are the resonance fields where the magnetic principal axis of the nitroxide is oriented parallel or perpendicular to the applied field direction. The observed line shapes showed a very strong immobilization of the adsorbed polymer chain. If one neglects any contribution from a small amount of the mobile components on the spectrum, τ_c of the most immobile portion can be taken as longer than 10^{-6} s. Such a strong restriction demonstrates a rigid binding of the train segments by the surface sites. The motion was considerably slower than in the case of adsorbed monomeric species (labeled MMA) on silica. In general the rearrangements of the conformation of adsorbed polymeric molecules requires a relatively long period.[13] Such a strong restriction, due to the strict binding by the surface as described above, would disturb the rearrangement and consequently prevent the desorption process.

Miyamoto and Cantow studied the adsorption of isotactic PMMA onto silica from $CHCl_3$ solution using high-resolution NMR spectroscopy.[5] Since all of the signals from the adsorbed PMMA on the solid surface could not be detected, they concluded that the chain motion was strongly restricted at most of the segments, and the adsorbed molecule had an uniform and relatively compressed structure. In the present case of the ESR method, however, the spectrum seems to be composite, because the monitor attached to the polymer chain reflects sensitively the changes in the local segment motion over the wide range of τ_c from 10^{-7} to 10^{-11} s. The slow motional region in the long time scale is important in the case of the adsorbed chain. The considerable change in the motion arising from the differences in the configurational states of the adsorbed polymer segments, whether they are in train or loop, can be detected individually. The presence of three portions in the ESR spectrum was revealed by the line shape analysis in our study.

Effects of Solvent and Surface Coverage. The segment fractions in the three states were estimated from the integrated intensities of the signal components divided into three parts. Figures 6 and 7 show the fractions of the train, short loops and long loops as a function of the surface coverage (θ). At relatively low θ, most of the segments were highly localized near the surface. Consequently, the adsorbed polymer was flattened and formed a thin adsorbed layer. All of the theoretical treatments predict that a flexible chain polymer molecule will be strongly attracted by a solid surface and have an appreciably flat structure with a large fraction of train segments, in the case of a high level of the adsorption energy between the segments and the surface. In the present case, the adsorption is regarded to be caused by a strong attractive force much above 1 kT; the solvents used would not seriously perturb the adsorption energy, since H-bonding is the predominant interaction between the polymer and the surface. The revealed structures roughly agree with the theoretical prediction.

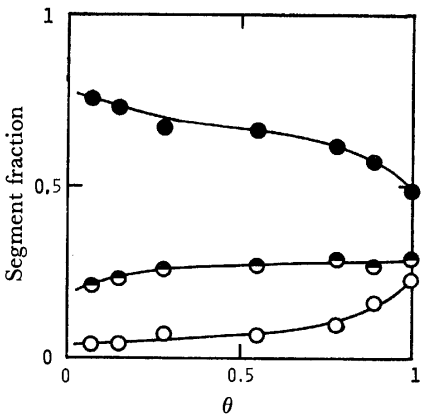

Fig. 6. The segment fractions of adsorbed PMMA in CCl_4 at 25 °C as a function of the surface coverage (θ).
●: In train, ◓: short loop, ○: long loop.

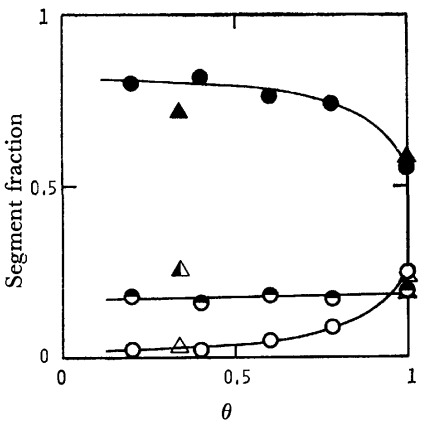

Fig. 7. The segment fractions of adsorbed PMMA on silica at 25 °C.
From benzene, ●: train, ◓: short loop, ○: long loop;
from $CHCl_3$, ▲: train, ◭: short loop, △: long loop.

The thickness of the adsorbed layer increased moderately with an increase in θ. The intermolecular interactions such as the adsorption competition among the molecules were encountered at the high concentration of the adsorbed polymer, and would cause the thickening. However, even at the saturation adsorption, a flat configuration still remained. In a previous publication, we reported that one adsorbed PMMA molecule had 24% of the H-bonded carbonyls. The surface area occupied by one molecule was estimated to be approximately 1.2×10^2 nm^2 at the saturation. This value is much smaller than the cross section of the random coil in solution estimated from the unperturbed dimension of PMMA.[14] Therefore, the adsorbed molecule seems to have a "compressed structure" at the CCl_4-silica interface.

The thickness was smaller in the good solvents (benzene and $CHCl_3$) than in the poor solvent (CCl_4). On the other hand, the maximum amount of adsorption (A_s) was appreciably decreased with increasing solvent

power, in the order of CCl_4, benzene, and $CHCl_3$. The decrease in A_s can be explained by the fact that a randomly coiled polymer is so extended in a good solvent that it occupies a larger surface area than in a poor solvent. The extension results in the decrease in the thickness under a strongly attractive force field. Particularly, there was a higher tendency of the short loop formation in the case of adsorption from CCl_4. In a poor solvent, such as CCl_4, the polymer molecule coiled and tended to form a large number of short loops. This tendency is consistent with the results from the computational statistical study by Clark *et al.*[15]

References

1) B. J. Fontana and J. R. Thomas, *J. Phys. Chem.*, **65**, 480 (1961).
2) K. K. Fox, I. D. Robb, and R. Smith, *J. Chem. Soc., Faraday Trans., 1*, **70**, 1186 (1974).
3) I. D. Robb and R. Smith, *Polymer*, **18**, 500 (1977).
4) H. Sakai and Y. Imamura, *Bull. Chem. Soc. Jpn.*, **53**, 1749 (1980).
5) T. Miyamoto and H. J. Cantow, *Makromol. Chem.*, **162**, 43 (1972).
6) P. Peyser, D. J. Tutas, and R. R. Stromberg, *J. Polym. Sci., A-1*, **5**, 651 (1967).
7) W. E. Goode, F. H. Owens, R. P. Fellman, W. H. Snyder, and J. E. Moore, *J. Polym. Sci.*, **46**, 317 (1960).
8) J. S. Hyde and L. R. Dalton, *Chem. Phys. Lett.*, **16**, 568 (1972): D. D. Thomas, L. R. Dalton, and J. S. Hyde, *J. Chem. Phys.*, **65**, 3006 (1976).
9) D. Kivelson, *J. Chem. Phys.*, **33**, 1094 (1960).
10) R. N. Rogers and G. E. Pake, *J. Chem. Phys.*, **33**, 1107 (1960).
11) S. A. Goldman, G. V. Bruno, and J. H. Freed, *J. Phys. Chem.*, **76**, 1858 (1972).
12) G. P. Lozos and B. M. Hoffman, *J. Phys. Chem.*, **78**, 2110 (1974).
13) W. H. Grant, L. E. Smith, and R. R. Stromberg, *Faraday Discuss. Chem. Soc.*, **1975**, 209.
14) R. Kirste and G. V. Schulz, *Z. Phys. Chem. (Frankfurt)*, **30**, 171 (1961).
15) A. T. Clark, M. Lal, M. A. Turpin, and K. A. Richardson, *Faraday Discuss. Chem. Soc.*, **1975**, 189.

 © 1980 The Chemical Society of Japan Bull. Chem. Soc. Jpn., 53, 3462—3467 (1980) [Vol. 53, No. 12

^{1}H NMR Study of Interaction of Probe Molecules with the Phosphate Ion on the Iron Core of Horse Spleen Ferritin

Noboru IMAI,* Yoji ARATA, and Shizuo FUJIWARA

Department of Chemistry, Faculty of Science, The University of Tokyo, Hongo, Bunkyo-ku, Tokyo 113

(Received June 10, 1980)

The surface of the iron core of ferritin was investigated by ^{1}H NMR using small probe molecules which have different sizes and charges. It was shown that the parameter k, which is the linewidth for each NMR probe normalized by the total concentration of iron in ferritin, is dependent on the content of phosphorus in ferritin. At pH 7.4, the k values are 1—10 for positively charged probes, 2×10^{-2}—8×10^{-2} for negatively charged probes and 0.1—0.2 for neutral probes. Above pH 7, the k values for positively charged probes increase with an increase in pH, whereas those for negatively charged probes decrease. By contrast, the k values for neutral probes remain constant over the entire pH range. It was concluded that the k values reflect the mode of interactions of small molecules with the phosphate which exists on the surface on the iron core of ferritin, and that these interactions are determined primarily by the electrostatic force between the small molecules and the negative charge of the phosphate of ferritin. Furthermore, it was shown by using t-butylamine as a probe that K^+ ion binds strongly to ferritin and that chelating agents interact with ferritin in a wide concentration range.

Ferritin is an iron storage protein consisting of a shell of protein subunits surrounding the iron core which contains up to approximately 4000 iron atoms.[1,2] It has been shown that the iron core contains about 1 to 1.5% phosphate[3] and the concentration is much higher on the surface than in the inner part of the iron core.[4,5] It has also been reported that the ratio of phosphate to iron decreases with an increase in the iron content of ferritin.[5] Treffry and Harrison showed that ferritin, which had been reconstituted from iron(II) ion and apoferritin followed by incubation of the product in the presence of phosphate, resembles native ferritin with respect to the concentrations of phosphate incorporated per molecule or per Fe atom, and suggested that in the native ferritin most of the phosphate is adsorbed on the surface of the ferritin iron core after it is formed in the absence of phosphate.[6] May and Fish reported that the diffusion of acetic acid into apoferritin is much slower than that of methanol, glucose, and methylammonium ion.[7] Jones *et al.* showed that iron release from ferritin by polyanionic dihydroflavins is much slower than that by other dihydroflavins.[8]

In a previous paper, we have reported an NMR probe method where small molecules such as solvent water, tetramethylammonium ion and glycylglycylglycylglycine were used to study magnetic properties of the iron core of ferritin and to determine the pK_a values of the phosphate group on the surface of the iron core.[10] Because of the large size of the protein (molecular weight of the protein part, 445000),[1,2] any NMR signal from the protein shell of the native ferritin cannot be detected. It has been confirmed that the linewidth of the NMR probe examined is not influenced even if a high concentration of apoferritin (10 mg/ml) is present, indicating that the probe molecules are little influenced, if any, by the protein part of ferritin. It is unlikely that the paramagnetism of the ferritin iron can contribute to the line broadening of the probe molecules which exist outside the ferritin molecule; the effect of the iron core would decrease with the inverse of the sixth power of the distance.[9] Therefore only a direct interaction between ferritin iron core and the probe molecules, which contact with the iron core inside the protein shell, can be observed by the NMR method.

In the present experiment, the charge and size of the probe molecules were changed systematically. From these results, the state of the phosphate in the iron core will be discussed in detail. The interaction between ferritin and chelating agents, which are known to play an improtant role in the release of iron from ferritin, was also studied by the NMR probe method; the concentration range in which the chelating agents strongly interact with ferritin will be determined.

Experimental

Horse spleen ferritin was purchased from Nutritional Biochemicals Corporation (crystallized twice, Cd free, lot No. 4871, 4493). All chemicals used were of reagent grade. The concentration of iron in ferritin solutions were determined by atomic absorption.[10] Protein concentrations were measured by the Lowry method[11] and phosphorus concentrations were measured by a colorimetric method using ammonium molybdate and ascorbic acid.[12] The pH and concentration of ferritin in sample solutions were adjusted as follows: A stock solution of ferritin was prepared at concentrations of 0.2—0.4 M (as iron), and the pH of the solution was adjusted by dialyzing it against a buffer solution at a desired pH. The buffer solutions used were 10 mM glycine–HCl below pH 3.5; 0.1 M acetate in the pH range 3.5—6.2; 0.1 M Tris–HCl above pH 6.8. The stock solution thus prepared was added to a 10 mM probe solution just before each measurement. Before and after this treatment, very little pH change was observed; precipitation did not occur either. The pH of ferritin solutions was varied from 2 to 10. ^{1}H NMR spectra were recorded using a JEOL PS-100 spectrometer operating at 100 MHz in the conventional cw mode.

Results

Figure 1A shows how the linewidths of the methyl protons of methylamine and acetic acid are influenced differently with increasing concentrations of ferritin. At pH 7.4, the linewidth for methylamine is broadened 4—5 times at a concentration of 0.36 mM (as iron), whereas that for acetic acid remained almost unchanged even in the presence of 3.6 mM ferritin. Figure 1B

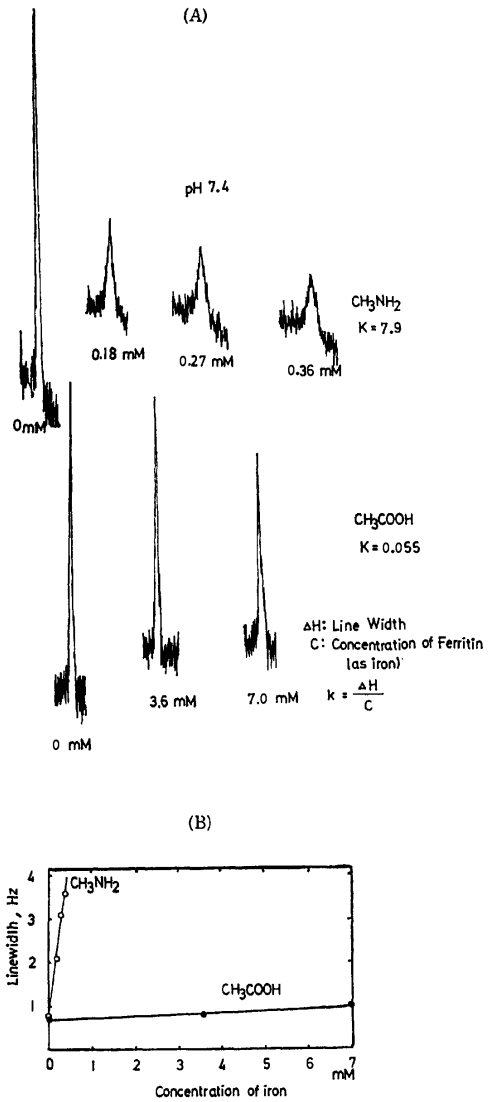

Fig. 1. (A) ^1H NMR spectra of methylamine (10 mM) and acetic acid (10 mM) at pH 7.4 in the presence of ferritin. The concentration (as iron) of ferritin added is shown in the figure. (B) The linewidths of the methyl peaks of methylamine and acetic acid as a function of the concentration of ferritin added.
○: Methylamine, ●: acetic acid.

shows the plots of the iron added *vs.* the linewidth of the peak. As shown in this figure, the slope for methylamine obtained from the plot is much larger than that for acetic acid.

We define the k value which is the linewidth normalized by the concentration of ferritin added and represents the line broadening of each peak. The observed linewidth ΔH_{obs} may be given as

$$\Delta H_{obsd} = \Delta H_0 + \Delta H_p \quad (1)$$

where ΔH_0 is the linewidth observed in the absence of ferritin and ΔH_p is a contribution from ferritin. When exchange between molecules which are under the influence of the iron core and those which are free in solution is fast enough, ΔH_p should increase linearly with the ferritin concentration (C) added. Therefore, $k(=\Delta H_p/C)$ should be constant, and

$$\Delta H_{obsd} = \Delta H_0 + kC. \quad (2)$$

The k value for methylamine is 8, whereas that for acetic acid is 6×10^{-2}; the former is two orders of magnitude larger than the latter. In view of the fact that at pH 7.4 methylamine and acetic acid exist as cation and anion, respectively, it appears that this large difference is caused by the difference in interaction between each of these probes and the negative charge of the phosphate group on the surface of iron core.[10] In fact, when ferritin containing less phosphate (phosphate : iron ratio (P/Fe) 0.08) is used, the k value of methylamine is 2.2, which is one fourth of that for ferritin with a larger P/Fe ratio of 0.10. This suggests that the k value is a sensitive parameter for the difference of the content of the phosphate of ferritin, and that the NMR probe method is useful to investigate the phosphate of ferritin.

The k *Values for Various Probes. Effects of the Charge and Size of the Probes*: The interaction of various probes with ferritin were investigated systematically. The probes which have the amino, hydroxyl, and carboxyl groups were used as representatives of positively charged, neutral and negatively charged probes, respectively. In addition, probe molecules which have the methyl and *t*-butyl groups were compared to study effects of the size of the probes. Probes with aromatic rings were also used to investigate the effect of the aromatic ring. Results are shown at two different pH values, 7.4 and 3.2 in Figs. 2A and 2B, respectively, where abscissa

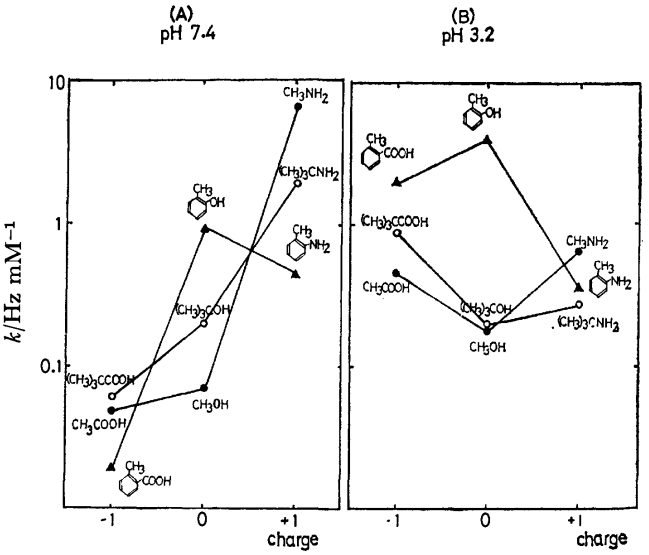

Fig. 2. The k values for probes with the amino, hydroxyl, and carboxyl groups. (A): pH 7.4, (B): pH 3.2.

represents the number of the charge of the probes used. The k values for neutral probes having the hydroxyl groups were about 0.1. The results for probes with the aromatic ring is quite different from those with the amino or carboxyl groups. It should also be noted that the k value for *o*-cresol is abnormally large and that *o*-toluidine is small compared with those of methylamine and *t*-butylamine.

At pH 3.2, the pattern of each curve in Fig. 2B

becomes quite different from that observed at pH 7.4; the k values for probes with the carboxyl group are much larger, whereas those for methylamine and t-butylamine are much smaller. By contrast, the k values for the neutral probes with the hydroxyl group remain constant. When the carboxyl groups of the probes lose their charges at low pH, electrostatic repulsion should decrease. Since the neutral probe has no charge, it is quite conceivable that the k value is not influenced by the change of pH.

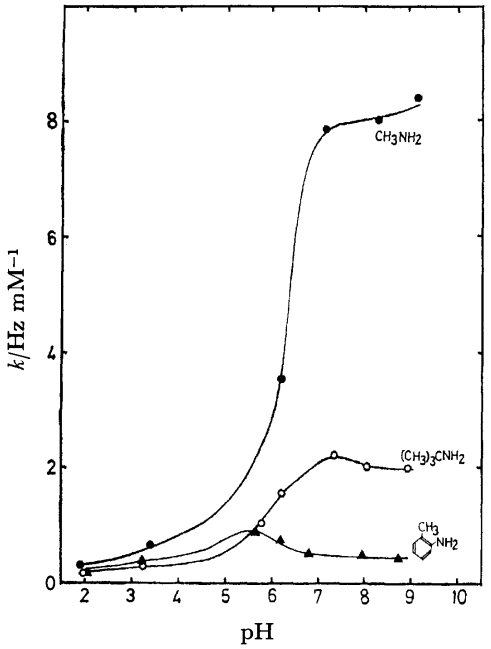

Fig. 3. The pH dependence of the k values for probes with the amino groups.
●: Methylamine, ○: t-butylamine, ▲: o-toluidine.

The pH *Dependence of the* k *Values. Positively Charged Probes with the Amino Group*: The pH dependence of the k values for various probes was investigated over a wide pH range in order to discuss in detail the results obtained above. The pH dependence of the k values for probes with the amino group is shown in Fig. 3. The pK_a of the phosphate in the iron core may be estimated from this curve.[10] It is seen in Fig. 3 that the k value for t-butylamine is one fourth of that for methylamine. The curve for o-toluidine has a maximum at pH 5—6. The charge of the amino group of o-toluidine with a pK_a of the amino group of 4.5 is lost at high pH; at the same time, the phosphate dissociates from the monoanion to the dianion in this pH range, suggesting that the maximum is due to a superposition of these two effects.

Neutral Probes with the Hydroxyl Groups: The pH dependence of the k values for methanol, t-butyl alcohol, and o-cresol is shown in Fig. 4. The k values for methanol and t-butyl alcohol are independent of pH. By contrast, the k value for o-cresol is much larger than those for methanol and t-butyl alcohol and has a maximum at low pH.

Negatively Charged Probes with the Carboxyl Group: As

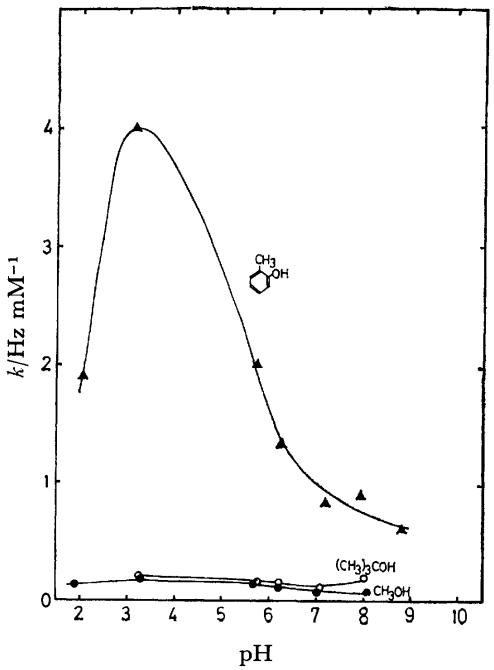

Fig. 4. The pH dependence of the k values for probes with the hydroxyl groups.
●: Methanol, ○: t-butyl alcohol, ▲: o-cresol.

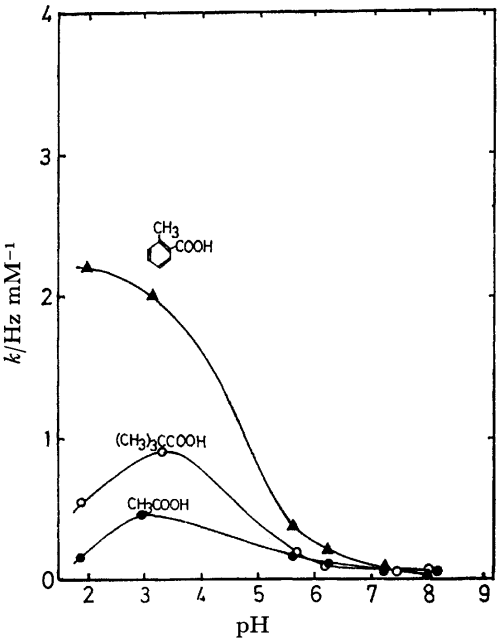

Fig. 5. The pH dependence of the k values for probes with the carboxyl groups.
●: Acetic acid, ○: pivalic acid, ▲: o-toluic acid.

Fig. 5 shows, the k values are quite small at pH 5 and increase below pH 5.

The affinity of Li^+, Na^+, and K^+ with Ferritin. Silk and Breslow[13] reported the effect of KCl and NaCl on the pH at which ferritin or apoferritin have no net charge, and suggested that K^+ ion binds with ferritin strongly. In the following we will show the usefulness of the NMR probe method in investigating interactions

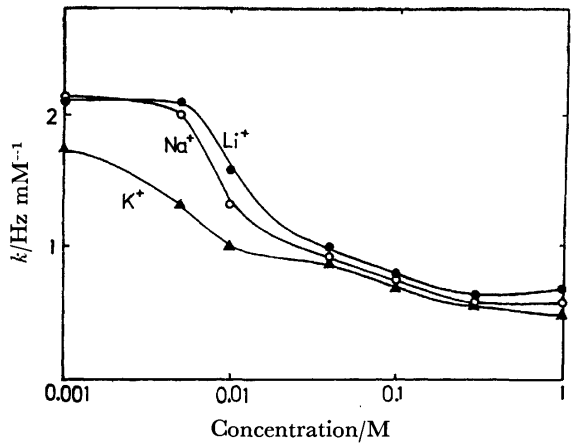

Fig. 6. The k values of t-butylamine as a function of the logarithmic concentration of Li^+, Na^+, and K^+ ions.
●: Li^+, ○: Na^+, ▲: K^+.

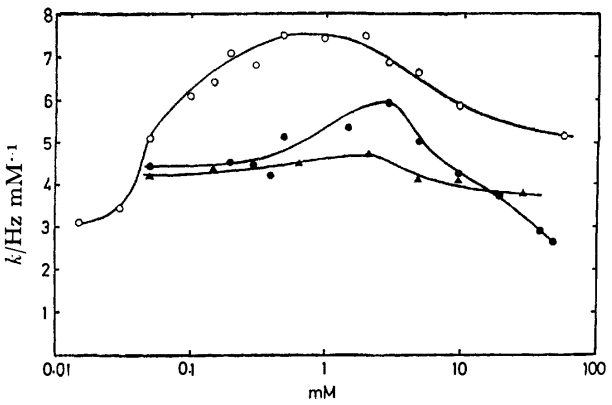

Fig. 7. The k values for t-butylamine as a function of the logarithmic concentrations of chelating agents.
▲: Acetic acid, ●: Citric acid, ○: EDTA.

between ferritin and various kinds of ions, alkali cations being taken as an example. In Fig. 6, the k values for t-butylamine were plotted against the logarithmic concentration of each of the alkali ions. From a decrease in the k value for t-butylamine, it may be concluded that the interaction of t-butylamine with ferritin becomes weak with the increasing concentration of the cations added. When the concentration of the cations is high, there is little difference among k values for the three kinds of cations. In the concentration range below 10 mM, the k values for Na^+ and Li^+ become identical and equal to those observed in the absence of these ions (k=2.1). This result suggests that, in this concentration range of the cations, the broadening of linewidth is not affected by these ions. However, in the case of K^+ ion, the k value was still small even at a quite low concentration of 1 mM. This appears to indicate that the affinity of K^+ to ferritin is much stronger than those of Na^+ and Li^+.

The Interaction of Chelating Agents with Ferritin. It is well-known that chelating agents, as well as reducing agents, are capable of releasing iron from ferritin.[1,2] It has been reported that the rate, at which iron is released from ferritin by chelating agents, is generally quite slow; for example, only a small amount of iron can be released from ferritin by EDTA.[14] The NMR probe method may be used to investigate whether or not the poor iron releasing ability of EDTA is due to a weak interaction between EDTA and ferritin. In the present experiment, we use EDTA, citric acid, and acetic acid with four (pK_1 2.0, pK_2 2.67, pK_3 6.16, pK_4 10.26), three (pK_1 3.09, pK_2 5.49, pK_3 6.15), and one (pK 4.67) carboxyl groups, respectively. As expected from the negative charges which all these molecules have, the k values are quite small. Therefore, the interaction between the chelating agents and ferritin was investigated by using more sensitive second probes such as t-butylamine as described previously. The results are shown in Fig. 7. The k values for t-butylamine are plotted against the logarithmic concentrations of the chelating agents. The k value for acetic acid remains almost constant in the whole concentration range examined, whereas the curve for citric acid has a maximum at about a concentration of 3 mM and the curve for EDTA has a large value in a wide concentration range 0.03 to 10 mM. These results suggest that acetic acid which has no chelating ability does not interact with ferritin, whereas citric acid interacts with ferritin strongly in the narrow concentration range 1 to 10 mM and EDTA interacts more strongly in a much wider concentration range.

Discussion

Interaction of the Probe Molecules with the Phosphate on the Iron core of Ferritin. In the previous paper[10] we have suggested that the probe molecules interact with ferritin through the phosphate on the iron core. In order to confirm this, we compare interaction on the probe molecules with two types of ferritin, ferritin I (Fe/protein ratio 0.20; P/Fe ratio 0.10) and ferritin II (Fe/protein ratio 0.30; P/Fe ratio 0.08). Ferritin II contains more iron and less phosphate than ferritin I.

We first consider the broadening of neutral probes (for example, solvent water) in a solution which contains each of these two types of ferritin. The k values for ferritins I and II are designated as k_I and k_{II}, respectively. It was observed that at the same iron concentrations, the ratio k_I/k_{II} for neutral probes is 1.1, whereas k_I/k_{II} for positively charged probes is 3—5.

The broadening of the linewidths may be assumed to be proportional to the exposed area of the iron core which probe molecules can freely contact with. This area may be calculated as follows: The size and surface area of iron core are estimated using Fe/protein ratio (the number of iron atoms per molecule) and X-ray data (the size of unit cell)[15] on the basis of the assumption that each ferritin molecule contains one spherical iron core. At a given amount of iron, *i.e.*, at the same iron concentration, the number of iron core contained in a solution increases and the product of the number and the surface area of one iron core (total surface area) increases as the particle size decreases. Therefore, the surface area increases as the size of iron core (iron content of ferritin) decreases. Figure 8 shows the calculated surface area of iron core as a function of the

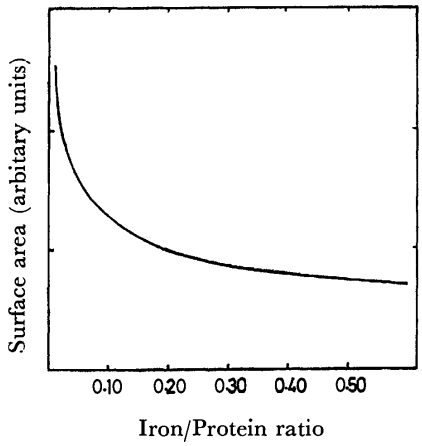

Fig. 8. The surface area of iron core as a function of the iron content of ferritin.

iron content of ferritin. This means that the linewidth should decrease as the iron content increases. This result is consistent with the report by Hoy *et al.*,[16,17] who reported that the rate of iron release from ferritin is closely related to the iron content.

In the above model, the ratio of the surface area of the iron core of ferritin I to that of ferritin II is about 1.1. This is consistent with the observation for the k values of the neutral probes. In view of these results, it may be concluded that the linewidth of the neutral probes is influenced only by the size of the iron core and not by the presence of the phosphate.

However, the line broadening for the positively charged probes in a ferritin I solution is quite different from that in a ferritin II solution. As mentioned above, the k_I/k_{II} ratio for the two solutions is 3—5. The large difference in k for the charged probes appears to be caused by the difference of the phosphate content. If the phosphate exists exclusively on the surface of the iron core,[4,5] the surface charge density of the phosphate for ferritin I should be larger than that for ferritin II. This would mean that the positively charged probe in the ferritin I solution is attracted to the iron core more strongly than in a ferritin II solution, and the k value for the ferritin I solution becomes larger than that for the ferritin II solutions. Since the protein part of ferritin I is presumably the same as that of ferritin II, it is likely that these differences are caused most probably by the phosphate on the iron core.

The Affinity of Li^+, Na^+, and K^+ with the Phosphate of Ferritin. The reason that the k values for t-butylamine decrease when the concentration of alkali ions becomes higher than 10 mM in Fig. 6 may be considered as follows: The alkali ions as well as t-butylamine have positive charges at pH$<$10 and presumably attracted to the negative charge of the phosphate of the iron core of ferritin. When the concentrations of the Li^+, Na^+, and K^+ ions are higher than that of t-butylamine (10 mM), it is probable that the alkali ions neutralize the negative charge of the phosphate; this would weaken the interaction of t-butylamine with ferritin and result in the narrowing of the linewidth of t-butylamine. On the other hand, when the concentration of alkali ions is lower than that of t-butylamine, the interaction of t-butylamine with the phosphate of ferritin would dominate and the linewidth of t-butylamine remain unchanged.

Interaction between Chelating Agents and Ferritin. Several chelating agents with the carboxyl groups were used to investigate how these molecules interact with ferritin. As mentioned previously, these molecules are subject to strong repulsing force from the negative charge of the phosphate on the core of ferritin and therefore should be insensitive as NMR probe. Thus, t-butylamine which is a sensitive NMR probe is added to the solutions, and the interaction between chelating agents and ferritin was investigated through the linewidth of t-butylamine. In this experiment, the linewidth of t-butylamine in a ferritin solution increases when the chelating agents are added. Possible reasons for the broadening of the linewidth of t-butylamine are as follows: 1) As mentioned previously, when the concentration of alkali ions increases, the negative charge of the phosphate of the iron core of ferritin is neutralized and the linewidth of t-butylamine decreases at a high concentration range of alkali ions as shown in Fig. 6. In the present experiment, this seems to be one of the reasons that each k value of EDTA, citric acid and acetic acid decreases in a high concentration range as shown in Fig. 7. 2) The negative charge of the chelating agents would cancel the positive charge of t-butylamine, resulting in a decrease in the k value of t-butylamine. 3) It is possible that the chelating agents strongly interact with ferritin and bind to the iron core of ferritin. The number of negative charges per ferritin molecule increases when the negatively charged chelating agents bind to the iron core of ferritin. This would also increase the k value of t-butylamine.

Conclusion

It has been shown that the NMR probe method is useful in obtaining information about ferritin and, in particular, the mode of interaction between the small molecules and ferritin. It was suggested that this interaction was determined primarily by the electrostatic repulsion and attraction which arise from the negative charge of the phosphate on the iron core of ferritin. It was also concluded that K^+ ion interacts strongly with the phosphate of the iron core even below a concentration of 1 mM and that EDTA binds strongly with ferritin in a wide concentration range 0.1—10 mM.

References

1) R. R. Crichton, *Struct. Bonding (Berlin)*, **17**, 67 (1973).
2) P. M. Harrison, R. J. Hoare, T. G. Hoy, and I. G. Macara, "Iron in Biochemistry and Medicine," ed by A. Jacobs and M. Worwood, Academic Press, London (1974), p. 73.
3) S. Granick and P. F. Hahn, *J. Biol. Chem.*, **155**, 661 (1944).
4) S. Granick, *J. Biol. Chem.*, **146**, 451 (1942).
5) F. A. Fishbach, P. M. Harrison, and T. G. Hoy, *J. Mol. Biol.*, **39**, 235 (1969).
6) A. Treffry and P. M. Harrison, *Biochem. J.*, **171**, 313

(1978).
7) M. E. May and W. W. Fish, "Proteins of Iron Metabolism," ed by E. B. Brown, P. Aisen, J. Fielding, and R. R. Crichton, Grune and Stratton, New York (1977), p. 31.
8) T. Jones, R. Spencer, and C. Walsh, *Biochemistry*, **17**, 4011 (1978).
9) T. J. Swift, "NMR of Paramagnetic Molecules," ed by G. N. La Mar, W. D. Horrocks, Jr., R. H. Holm, Academic Press, London (1973), p. 53.
10) N. Imai, H. Terada, Y. Arata, and S. Fujiwara, *Bull. Chem. Soc. Jpn.*, **51**, 2538 (1978).
11) O. H. Lowry, N. J. Rosebrough, A. L. Farr, and R.J. Randall, *J. Biol. Chem.* **193**, 265 (1951).
12) P. S. Chen, Jr., T. Y. Tribara, and H. Warner, *Anal. Chem.*, **28**, 1756 (1956).
13) S. T. Silk and E. Breslow, *J. Biol. Chem.*, **251**, 6963 (1976).
14) L. Pape, J. S. Multani, C. Stitt, and P. Saltman, *Biochemistry*, **7**, 613 (1968).
15) P. M. Harrison, F. A. Fishbach, T. G. Hoy, and G. H. Haggis, *Nature*, **216**, 1188 (1967).
16) T. G. Hoy, P. M. Harrison, M. Shabbir, and I. G. Macara, *Biochem. J.*, **137**, 67 (1974).
17) P. M. Harrison, T. G. Hoy, I. G. Macara, and R. J. Hoare, *Biochem. J.*, **143**, 445 (1974).

 © 1980 The Chemical Society of Japan Bull. Chem. Soc. Jpn., 53, 3468—3473 (1980) [Vol. 53, No. 12

Fluorescence Decay Studies of 9-Aminoacridine Bound to Polyriboadenylic Acid

Yukio KUBOTA* and Yuko MOTODA

Department of Chemistry, Faculty of Science, Yamaguchi University, Yamaguchi 753

(Received June 16, 1980)

The interaction of the mutagenic dye 9-aminoacridine (9AA) with polyriboadenylic acid (poly rA) was studied by both steady-state and transient fluorescence measurements. It was found that the fluorescence decay of 9AA bound to poly d(A-T) follows a single-exponential decay law but that the decay data of 9AA bound to poly rA can be well described as a sum of two-exponential functions. The fact that nanosecond time-resolved fluorescence spectra are independent of time suggests that the double-exponential decay may be attributed to different microenvironments at the binding sites. The decay parameters, fluorescence emission maxima, and fluorescence quantum yields obtained at acid pH differ from those obtained at neutral pH. The fluorescence behavior of 9AA is discussed in connection with the conformational change of poly rA.

The dye 9-aminoacridine (9AA) is one of a number of acridines that are mutagenic[1] and that interact with DNA *in vitro*.[2] In previous work,[3,4] we have reported that guanine–cytosine base pairs completely quench the fluorescence of 9AA, upon binding to DNA, while adenine–thymine base pairs are responsible for its fluorescence and that the emitting sites of 9AA on DNA exhibit fluorescence decay curves which can be resolved into three-exponential components. The result has been attributed to the heterogeneity of the emitting sites.[4]

Studies on binding interactions between the dye and DNA are considerably complicated due to the content and the stereochemical arrangement of DNA bases.[2] Two approaches have been shown to be very useful in understanding the nature of interactions between the dye and DNA; one is to study using synthetic polynucleotides which contain simple types of binding sites, compared with DNA[3-6] and the other is to study complex formation between the dye and mononucleotides.[7-9] We have found that, upon binding to poly d(A-T) which contains only one type of site, the fluorescence quantum yield of 9AA is not substantially altered and its fluorescence decay follows a single-exponential decay law.[4] We have also found that the fluorescence of 9AA is markedly quenched by purine mononucleotides and that the weak fluorescence arises from 9AA complexed with adenosine 5′-monophosphate (AMP).[7,9] These findings suggest that the fluorescence behavior of 9AA may depend on whether the 6-amino group of adenine is hydrogen-bonded or free.

It is well established that the conformation of polyriboadenylic acid (poly rA) in solution changes from the hydrogen-bonded double-strand helix at low pH to the ordered single-strand structure of stacked bases at neutral pH.[10] Therefore, it is of great interest to study the fluorescence behavior of 9AA bound to poly rA in connection with its conformational change. Such a study may give a clue to the nature of interactions between 9AA and adenine residues.

In the present study, we investigated the fluorescence of 9AA bound to poly rA at various pH's by both steady-state and transient decay measurements. The decay behavior was found to be rather complex and possible interpretations are discussed.

Experimental

Materials. All chemicals were of reagent-grade purity or better. Poly rA was obtained from Miles, and, according to the manufacturer, had a molecular weight greater than 10^5. Poly d(A-T) was purchased from Miles. 9AA was the same sample as used before.[3,4] Poly rA solutions were prepared by first dissolving the required amounts of poly rA in 0.005 M† phosphate buffer (pH=6.9) and then dialyzing against the buffer solution to yield the desired pH. Concentrations of poly rA solutions were determined spectrophotometrically.[10] All measurements were carried out in 0.005 M phosphate buffer (pH=6.9) or 0.01 M acetate buffer (pH=4.1—5.9) solutions at (25±0.1)°C.

Absorption and Flow Dichroism Measurements. Absorption spectra were recorded using a Shimadzu UV-200S spectrophotometer. Flow dichroism measurements were made as described elsewhere.[11]

Steady-state Fluorescence Measurements. Steady-state fluorescence spectra were measured with a Hitachi MPF-2A spectrophotofluorometer. Correction was applied for the unequal quantum response of the detector system. The fluorescence quantum yield of the poly rA–9AA complex was determined by comparing the area under the fluorescence spectrum of the complex with the corresponding area of 9AA and by taking the quantum yield of 9AA to be 0.96.[3] For quantum yield measurements, the excitation monochromator was set at 408 nm with a 2—3 nm band pass, and the emission was recorded with a 2 nm band pass.

Transient Fluorescence Measurements. Transient fluorescence decay curves and time-resolved fluorescence spectra were measured with an Ortec nanosecond spectrophotofluorometer.[4,8,9] All decay measurements were performed under single photon counting conditions. The flash lamp was thyratron-triggered, air-filled (0.5 atm), and operated at 5.5 kV with a repetition rate of 25 kHz. The excitation wavelength at 375 nm was selected with an interference filter (Japan Vacuum Optics). The emission was observed by an RCA 8850 photomultiplier tube through a grating monochromator (Applied Photophysics Ltd.) whose bandpasses were varied from 2 to 10 nm according to the fluorescence intensity of the sample. Care was taken to eliminate anisotropic contributions to the observed decay according to the method described elsewhere.[4]

The observed decay curve $i(t)$ is represented by the convolution integral:

† 1 M=1 mol dm^{-3}.

$$i(t) = \int_0^t g(u)I(t-u)\mathrm{d}u \quad (1)$$

where $g(t)$ is the apparatus response function and $I(t)$ is the fluorescence decay which would be obtained with the δ-pulse excitation. It has been shown that the response function $g(t)$ depends on the energy of the photon impinging on the photocathode.[12] According to the method of Wahl *et al.*,[12] the true $g(t)$ was determined from the fluorescence decay curve of 1,1,4,4-tetraphenyl-1,3-butadiene in deaerated cyclohexane ($\tau = 1.72 \pm 0.02$ ns at 25 °C).

Deconvolution of Eq. 1 was achieved by the methods of Laplace transformation[13] and nonlinear least-squares[14] on the assumption that the fluorescence decay $I(t)$ is given by a sum of exponential functions:

$$I(t) = \sum_{i=1}^{n} \alpha_i \exp(-t/\tau_i) \quad (2)$$

where the α_i's and τ_i's are the amplitudes and lifetimes, respectively, of the ith component. Both methods yielded very similar results. The parameters obtained by analyses were convolved with the apparatus response function $g(t)$ and goodness of the fit between the observed and calculated decay curves was judged by inspection of the reduced χ^2, the weighed residuals, and the autocorrelation function of the residuals.[13,14] Data analysis was accomplished using a PDP 11/04 minicomputer (Digital Equipment Corp.) interfaced with an Ortec 6240B multichannel analyzer.

Results

Absorption and Steady-state Fluorescence Spectra. It is well established that the conformation of poly rA in solution changes from the double-strand helix at acid pH to the ordered single-strand structure of stacked bases at neutral pH.[10] The conformational transition depends on pH, temperature, and ionic strength.[10,15] Under the present conditions (ionic strength of 0.01 and 25 °C), the transition pH was found to be 6.0 in agreement with the previous finding.[10,15]

Since little is known about the optical properties of acridine dyes bound to poly rA,[16,17] absorption and steady-state fluorescence spectra at various pH's were first examined in order to obtain information on the

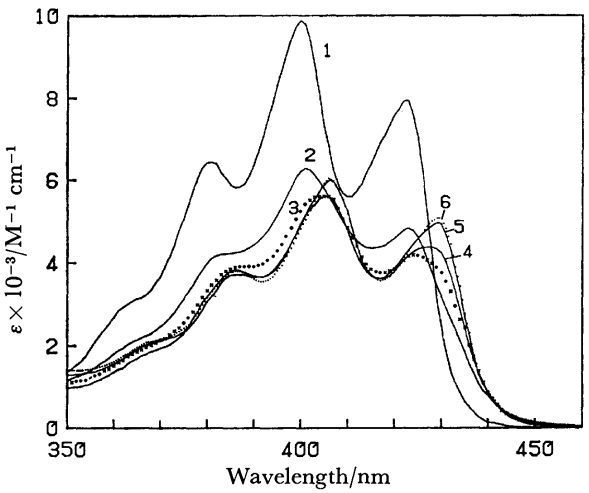

Fig. 1. Absorption spectra of poly rA–9AA complexes in 0.01 M acetate buffer (pH=4.9). 9AA: 3.8×10^{-5} M. P/D: (1) 0; (2) 4; (3) 10; (4) 20; (5) 150; (6) 193.

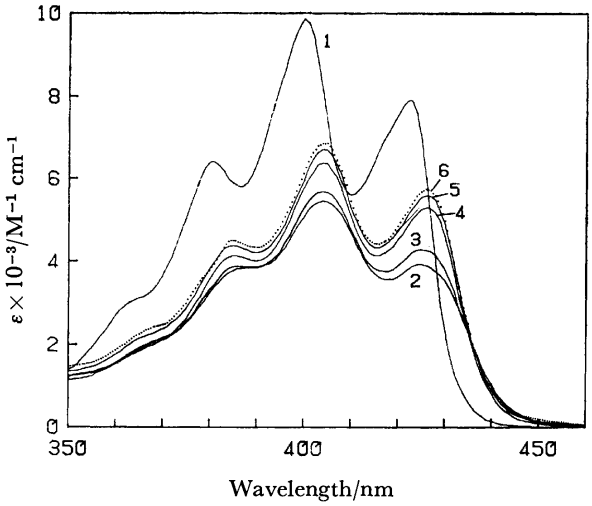

Fig. 2. Absorption spectra of poly rA–9AA complexes in 0.005 M phosphate buffer (pH=6.9). 9AA: 3.8×10^{-5} M. P/D: (1) 0; (2) 4; (3) 10; (4) 50; (5) 150; (6) 200.

binding state of 9AA. Figures 1 and 2 show absorption spectra of 9AA in the presence of poly rA, respectively, at pH=4.9 and pH=6.9. Absorption changes at low P/D** values ($P/D<4$), although spectra are not shown in Figs. 1 and 2 to avoid the complication due to overlaping, were found to result from the contributions of the bound and free 9AA. With increasing P/D, isosbestic points (425 nm at pH=4.9 ($P/D>20$) and 435 nm at pH=6.9 ($P/D>4$)) appear in the absorption spectra, and absorption bands can be seen to shift progressively toward a limit at high P/D values ($P/D>200$) (Figs. 1 and 2.) This finding suggests that the bound 9AA is transformed gradually from one type of complex (complex I) to a different type of complex (complex II). The limiting spectra at pH=4.9 and pH=6.9 ($P/D>200$), respectively, resemble closely the spectra of 9AA intercalated into DNA[4] and of 9AA complexed with AMP;[7] both spectra show hypochromicity and red shift, compared with the spectrum of the free dye. As Dourlent *et al.*[17] first inferred from absorption spectra of proflavine bound to poly rA and their similarity to its spectra upon binding to DNA, complex I may be attributed to electrostatic interactions of the 9AA cation with the phosphate group, followed by cooperative binding along the phosphate backbone of poly rA, whereas complex II may be ascribed to stacking interactions between 9AA and adenine residues.

In order to avoid the complication due to the presence of different binding processes, the following fluorescence studies were performed at sufficiently high P/D values ($P/D>400$) where complex II predominates and the concentration of the free dye is negligible.

Figure 3 shows steady-state fluorescence spectra of the poly rA–9AA complexes obtained at acid and neutral pH's and also shows their comparison with spectra of 9AA complexed with AMP or poly d(A-T). As can be seen from Fig. 3, the spectrum at pH=6.9 is very similar to that of the AMP–9AA complex, and the

** Molar ratio of DNA Phosphate to Dye.

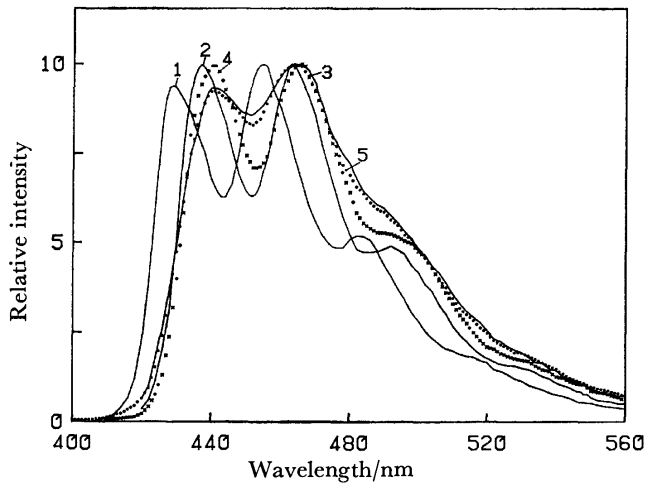

Fig. 3. Normalized fluorescence quantum spectra of 9AA in: (1) 0.005 M phoshpate buffer (pH=6.9); (2) poly rA (P/D=502, pH=4.9); (3) poly rA (P/D=503, pH=6.9); (4) poly d(A-T) (P/D=132, pH=4.9); (5) AMP (0.1 M, pH=6.9). The excitation wavelength was 390 nm, and the dye concentration was $7.4—12\times10^{-6}$ M.

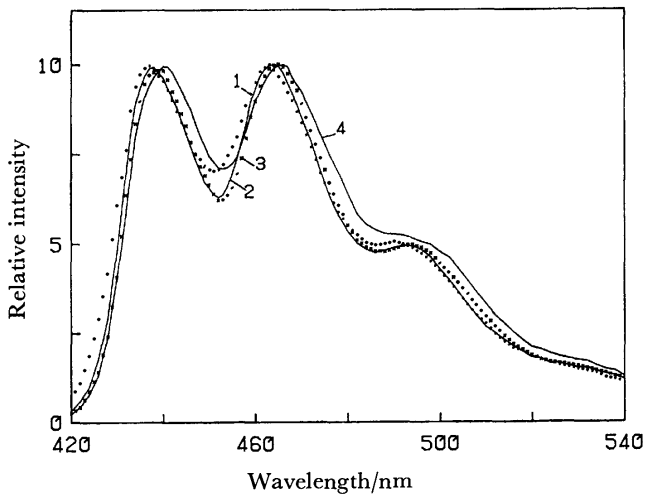

Fig. 4. Normalized fluorescence quantum spectra of poly rA–9AA complexes as a function of pH: (1) P/D=512, pH=4.1; (2) P/D=524, pH=5.3; (3) P/D=533, pH=5.9; (4) poly d(A-T)–9AA complex (P/D=132, pH=4.9). The excitation wavelength was 408 nm, and dye concentration was 1.2×10^{-5} M.

spectra at pH=4.9 and of the poly d(A-T)–9AA complex are similar in shapes except that the fluorescence bands of the poly d(A-T)–9AA complex are shifted toward longer wavelengths compared to those of the poly rA–9AA complex. Figure 4 indicates fluorescence spectra obtained at other acid pH's; a gradual red shift of the spectra can be seen upon going from pH=4.1 to pH=5.9. On the other hand, the fluorescence quantum yield (Φ_F) in this pH region (pH=4.1—5.9) was almost constant, while the Φ_F value at neutral pH was smaller than that at acid pH (Table 1).

Flow Dichroism. The poly rA–9AA complexes at acid pH showed negative flow dichroism in both the visible and ultraviolet regions; the reduced flow dichroism at a velocity gradient of 3200 s^{-1} was found to be −0.23 at 260 nm and −0.18 at 400 nm under conditions of P/D=20, [9AA]=5×10^{-5} M, and pH=5.0. This finding suggests that the acridine ring is oriented rather perpendicularly to the helix axis of poly rA like adenine residues.[11,18]

Fluorescence Decay Curves. Since fluorescence spectra of 9AA bound to poly rA depended on pH, fluorescence decay studies were undertaken to investigate further the nature of interactions between the dye and the binding sites. Decay curve measurements were made at high P/D values (P/D>400) and at low ionic strength (0.01). Under these conditions, the contribution of the free dye and energy transfer between bound dye molecules were negligibly small.

Figures 5 and 6 display typical decay data obtained at pH=4.9 and pH=6.9, respectively; the fit between the observed and theoretical convolved decay curves for a double-exponential decay law can be seen to be excellent. Sets of decay parameters obtained at various pH's are summarized in Table 1. In all cases, the χ^2, the weighed

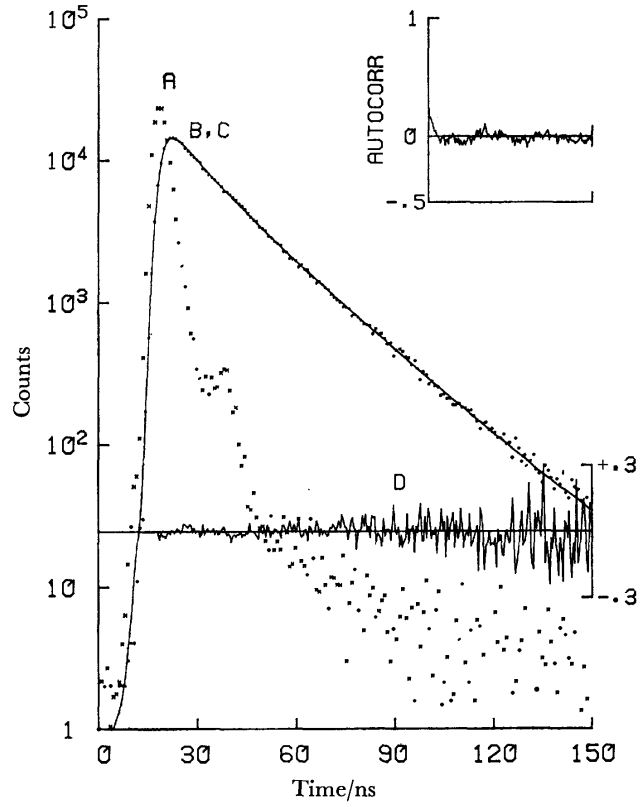

Fig. 5. Experimental decay curves and the results of a two-component analysis for poly rA–9AA complex (P/D=502) in 0.01 M acetate buffer (pH=4.9). 9AA: 7.4×10^{-6} M. The excitation and emission wavelengths were 375 and 455 nm, respectively. A: Apparatus response function. B: Observed decay curve. C: Best theoretical decay curve (smooth curve). D: Weighed residuals. The inset is the autocorrelation function of the residuals. Parameters obtained: τ_1=21.2 ns, τ_2=8.4 ns, α_1=0.088, α_2=0.077, and χ^2=1.71. The amplitudes normalized to unity are α_1=0.54 and α_2=0.46.

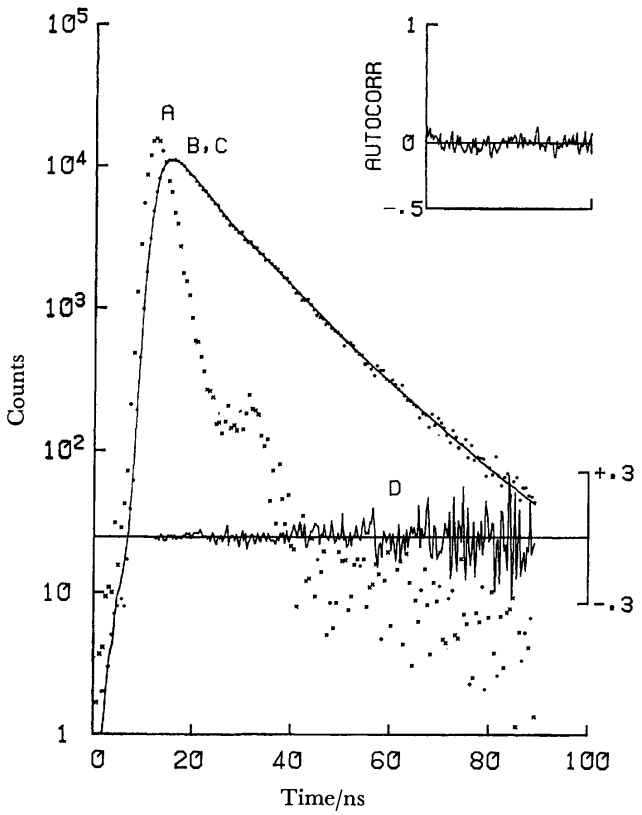

Fig. 6. Experimental decay curves and the results of a two-component analysis for poly rA–9AA complex (P/D=503) in 0.005 M phosphate buffer (pH=6.9). 9AA: 7.4×10^{-6} M. The excitation and emission wavelengths were 375 and 460 nm, respectively. Legends to each curve are as described for Fig. 5. The theoretical curve is based on the following parameters: τ_1=12.9 ns, τ_2=5.1 ns, α_1=0.111, α_2=0.123, and χ^2=1.19. The amplitudes normalized to unity are α_1=0.47 and α_2=0.53.

residuals, and the autocorrelation function of the residuals indicated that the data cannot be explained in terms of a single-exponential decay law but can be explained in terms of a double-exponential decay law. However, it must be emphasized that other more complex decay laws are not precluded because it is hard to analyze decay data in which two decay times are very close or one of amplitudes is very small.[13,19]

The decay parameters at acid pH differ from those at neutral pH, reflecting the differences in fluorescence spectra (Fig. 3) and quantum yields (Table 1). It should be noted that, at acid pH (pH=4.1—5.9), the value of τ_1 (long lifetime) increases with increasing pH, whereas that of τ_2 (short lifetime) is nearly constant in this pH range (Table 1). The implications of this finding are discussed below.

In contrast, the fluorescence decay of 9AA upon binding to poly d(A-T) at both acid and neutral pH's followed a single-exponential decay law (Table 1) in agreement with our previous finding.[4]

Nanosecond Time-resolved Fluorescence Spectra. Time-resolved fluorescence spectra in the nanosecond scale were measured in order to study any time-dependent interactions between the dye and its environments at the binding sites. The spectra were taken at time intervals ranging from 0 to 70 ns after the peak of exciting pulse. It was found that spectra showed no time dependence and were nearly identical with the steady-state fluorescence spectra. In agreement with this finding, there were no significant changes in the decay parameters when the decay was observed at emission wavelengths ranging from 430 to 510 nm.

Discussion

It is found in the present study that, at both acid and neutral pH's, the fluorescence decay of 9AA bound to poly d(A-T) obeys a single-exponential decay law, while that of 9AA bound to poly rA does not. The fluorescence decay curves of 9AA upon binding to poly rA can be well resolved into two-exponential components corresponding to the long (τ_1) and short (τ_2) lifetimes (Table 1).

Energy transfer between bound dye molecules might be possible as an explanation for the deviation of decay curves from single exponentiality.[6] On the basis of the Förster critical transfer distance (23±1 Å),[20] however, this appears unlikely at high P/D values. It is well

Table 1. Fluorescence decay parameters and quantum yields for 9AA bound to poly rA and poly d(A-T)[a]

System	pH	P/D	τ_1	α_1	τ_2	α_2	χ^2	Φ_F
Poly rA–9AA	4.10	512	20.2	0.63	9.0	0.37	1.11	0.47
	4.90	400	20.9	0.54	8.7	0.46	1.65	0.42
	4.90	502	21.2	0.54	8.4	0.46	1.71	0.42
	5.05	524	21.5	0.54	8.4	0.46	1.72	0.41
	5.30	524	22.4	0.54	8.3	0.46	1.50	0.41
	5.72	533	23.3	0.59	8.2	0.41	1.30	0.41
	5.90	533	23.8	0.58	8.5	0.42	1.31	0.43
	6.90	407	13.2	0.48	5.1	0.52	1.25	0.29
	6.90	503	12.9	0.47	5.1	0.53	1.19	0.28
Poly d(A-T)–9AA	4.90	132	30.3	1.00			1.38	0.71
	6.90	136	31.3	1.00			1.11	0.73

a) The dye concentration was $7.4—12\times10^{-6}$ M. The decay was observed at 455 or 460 nm; the results obtained here are not dependent on the emission wavelength. τ is given in nanoseconds, and the amplitudes (α's) are normalized to unity. Uncertainties in τ's and α's are within ±0.15 ns and ±1%, respectively.

established that the photophysics of excited-state reactions such as excimer or exciplex formation can easily lead to double-exponential decay kinetics.[21] If we focus our attention on such an excited-state system, the double-exponential decay of the poly rA–9AA complexes might be attributed to two distinct emitting species. This is unlikely, however, since the decay parameters do not show a significant dependence on the emission wavelength. The decay parameters obtained at acid and neutral pH's are seen to be quite different (Table 1). A conformational change at the binding sites may play an important role in the decay behavior of the bound 9AA. We suggest here that two lifetimes are related to different microenvironments at the binding sites.

If we assume that bound 9AA molecules are all fluorescent and that the radiative lifetime of the bound dye (τ_r) is independent of the nature of the binding sites, we obtain

$$\Phi_F = \frac{1}{\tau_r}(\alpha_1\tau_1 + \alpha_2\tau_2). \quad (3)$$

We observe that the absorption and fluorescence spectral behavior of the poly rA–9AA complexes at pH=4.9 and pH=6.9, respectively, is very similar to that of the poly d(A-T)–9AA and AMP–9AA complexes (Fig. 3).[4,7] It therefore seems reasonable to assume that the τ_r value of the poly rA–9AA complex at pH=4.9 or pH=6.9 is approximately equal to that of the poly d(A-T)–9AA or AMP–9AA complex. Using the observed lifetimes and quantum yields for the poly d(A-T)–9AA (Table 1) and AMP–9AA complexes (τ=1.45 ns and Φ_F=0.058),[9] the τ_r values for the poly d(A-T)–9AA and AMP–9AA complexes are evaluated to be 42.7 and 25.0 ns, respectively. Substituting the decay parameters given in Table 1 into Eq. 3 yields the following Φ_F values; $\Phi_F \approx 0.36$ at pH=4.9 and $\Phi_F \approx 0.35$ at pH=6.9. Taking into account the experimental error, both observed and calculated Φ_F values seem to be in reasonable agreement. This result and the double-exponential decay imply that there are at least two different microenvironments at the binding sites.

From the absorption and fluorescence spectral behavior at neutral pH and its similarity to that of the AMP-9AA complex, it seems likely that complex II at pH=6.9 results from stacking interactions between 9AA and adenine residues in a way very similar to the partial intercalation which predominantly occurs in single-strand denatured DNA;[22] the positive ring nitrogen of the dye is closely associated with the polynucleotide phosphate group and the dye lies between successive nucleotide bases. In such binding, greater contact between the acridine and adenine rings is expected to cause more effective quenching interactions.[9] Thus we propose that it is the mutual orientation or the extent of overlap between the dye and adenine residue which is responsible for the decay behavior. We attribute the component τ_1 (long lifetime) or τ_2 (short lifetime) to stacking interactions resulting in less or greater contact between the dye and adenine rings. It should be noted, however, that the actual decay law might be more complex since there would be many possibilities for the geometry of the bound dye; unfortunately more detailed decay analysis is beyond the present method.[13,19]

At acid pH, complex II shows the fluorescence spectrum similar to that of the poly d(A-T)–9AA complex and also shows negative flow dichroism. Furthermore, we observed that the decay of fluorescence anisotropy of the poly rA–9AA complex is very similar to that of ethidium bromide[23] or acridine dyes[24] intercalated between adjacent DNA base pairs. From these results it may be reasonably thought that the bound 9AA lies between hydrogen-bonded adenine-adenine pairs in a way similar to the intercalation into double-helical DNA.[25] We postulate that the above binding is responsible for the component τ_1 (long lifetime). Due to hydrogen bonding between the 6-amino group of adenine and the phosphate group and due to the protonation of 1-nitrogen (N_1) of adenine,[10,18,26] some steric hindrance may occur for the intercalation of 9AA. It is likely that 9AA binds rather outside the helix. In such binding sites (less hydrophobic ones), a part of the acridine ring would be exposed to solvent molecules, and hence the possibility of radiationless transition would be increased by collisions with the surrounding solvent. This explains why the τ_1 value is smaller than the lifetime of the poly d(A-T)–9AA complex (Table 1). The fraction of protonated N_1 is gradually decreased with increasing pH.[26] This allows 9AA to bind more interior areas of the helix, that is, more hydrophobic areas. This interpretation is consistent with a red shift of the fluorescence spectra (Fig. 4) and the increase of τ_1 with an increase in pH (Table 1).

Surprisingly there is an additional component τ_2 (short lifetime), in contrast with the poly d(A-T)–9AA complex (Table 1). The results in Table 1 show that the values of τ_2 and α_2 are almost independent of pH (pH=4.1—5.9). This means that the protonation of N_1 may not be so significant for the component τ_2. One possible explanation would assume that this component results from 9AA bound in the vicinity of discontinuities or ends of the helix,[10] in which adenine residues free from hydrogen bonding may cause some quenching of the 9AA fluorescence. However, the proportion of this component (α_2) seems to be rather high (Table 1). It is unlikely that there are a degree of strand discontinuities. Perhaps both sites corresponding to the components τ_1 and τ_2 may possess unequal binding affinity for 9AA owing to a conformational difference.

In conclusion, the results obtained here indicate that the decay behavior of 9AA bound to poly rA is rather complex. It is apparent that the 6-amino group of adenine free from hydrogen bonding plays a role in the quenching of the 9AA fluorescence. At present, however, there is no convincing evidence for the quenching mechanism. Indeed the study of transient intermediates by laser photolysis may answer the problem.

This work was supported by a Grant-in-Aid for Scientific Research from the Ministry of Education, Science and Culture (243002).

References

1) A. Orgel and S. Brenner, *J. Mol. Biol.*, **3**, 762 (1961).
2) A. R. Peacocke, "Heterocyclic Compounds: Acridines," ed by R. M. Acheson, Interscience, New York (1973), Vol. 9, p. 723.
3) Y. Kubota, K. Hirano, and Y. Motoda, *Chem. Lett.*, **1978**, 123.
4) Y. Kubota, Y. Motoda, and Y. Fujisaki, *Chem. Lett.*, **1979**, 237; Y. Kubota and Y. Motoda, *Biochemistry*, **19**, 4189 (1980).
5) J. P. Schreiber and M. P. Daune, *J. Mol. Biol.*, **83**, 487 (1974).
6) Y. Kubota and R. F. Steiner, *Biophys. Chem.*, **6**, 279 (1977).
7) Y. Kubota, *Chem. Lett.*, **1977**, 311.
8) Y. Kubota, Y. Motoda, Y. Shigemune, and Y. Fujisaki, *Photochem. Photobiol.*, **29**, 1099 (1979).
9) Y. Kubota and Y. Motoda, *Chem. Lett.*, **1979**, 1375; Y. Kubota and Y. Motoda, *J. Phys. Chem.*, in press.
10) D. N. Holcomb and I. Tinoco, Jr., *Biopolymers*, **3**, 121 (1965).
11) Y. Kubota, K. Hashimoto, K. Fujita, M. Wakita, E. Miyanohana, and Y. Fujisaki, *Biochim. Biophys. Acta*, **478**, 23 (1977).
12) Ph. Wahl, J. C. Auchet, and B. Donzel, *Rev. Sci. Instrum.*, **45**, 28 (1974).
13) A. Gafni, R. L. Modlin, and L. Brand, *Biophys. J.*, **15**, 263 (1975).
14) A. Grinvald and I. Z. Steinberg, *Anal. Biochem.*, **59**, 583 (1974).
15) J. R. Fresco and E. Klemperer, *Ann. N. Y. Acad. Sci.*, **81**, 730 (1959).
16) A. Gafni, J. Schlessinger, and I. Z. Steinberg, *Isr. J. Chem.*, **11**, 423 (1973).
17) M. Dourlent and C. Hélène, *Eur. J. Biochem.*, **23**, 86 (1971); M. Dourlent, J. F. Hogrel, and C. Hélène, *J. Am. Chem. Soc.*, **96**, 3398 (1974); M. Dourlent and J. F. Hogrel, *Biopolymers*, **15**, 29 (1976).
18) A. Rich, D. R. Davies, F. H. C. Crick, and J. D. Watson, *J. Mol. Biol.*, **3**, 71 (1961).
19) I. Isenberg, *J. Chem. Phys.*, **59**, 5708 (1973).
20) Th. Förster, *Discuss. Faraday Soc.*, **27**, 7 (1959).
21) J. B. Birks, "Photophysics of Aromatic Molecules," Wiley-Interscience, New York (1970), Chap. 7; W. R. Ware, D. Watt, and J. D. Holmes, *J. Am. Chem. Soc.*, **96**, 7853 (1974).
22) N. J. Pritchard, A. Blake, and A. R. Peacocke, *Nature*, **212**, 1360 (1966).
23) Ph. Wahl, J. Paoletti, and J. B. Le Pecq, *Proc. Natl. Acad. Sci. U.S.A.*, **65**, 417 (1970).
24) Y. Kubota and R. F. Steiner, *Bull. Chem. Soc. Jpn.*, **50**, 1502 (1977).
25) L. S. Lerman, *J. Mol. Biol.*, **3**, 18 (1962); L. S. Lerman, *Proc. Natl. Acad. Sci. U.S.A.*, **49**, 94 (1963).
26) R. F. Steiner and R. F. Beers, Jr., *J. Polymer Sci.*, **31**, 53 (1958).

Laser Induced Biphotonic Dissociation of Nitrobenzene Derivatives in Solution

Kenji YOKOYAMA, Junko NAKAMURA, Takayoshi KOBAYASHI, and Saburo NAGAKURA*
The Institute of Physical and Chemical Research, Wako, Saitama 351
(Received June 20, 1980)

By irradiation with a focused laser beam, *p*-nitroanisole and *N*-[2-(*p*-nitrophenoxy)ethyl]aniline (**2**) in acetonitrile were found to show new reactions yielding nitroso compounds different from the case of the defocused laser beam irradiation. The laser intensity dependence of the product yield shows that the new reaction of **2** proceeds *via* a biphotonic process. The quenching effects of oxygen and *cis*-1,3-pentadiene upon the reaction rate indicate that the intermediate state is an excited singlet state.

Recently, laser induced chemical reactions have been studied by many authors, importance being attached to such multiphoton processes in the gas phase as unimolecular dissociation, ionization and sequential reactions.[1] However, reports on laser induced multiphoton reactions in the solution (at room temperature) are limited to the process with unstable products.[2]

In the present study, we have found a new phenomenon that two different kinds of stable products are obtained with the photochemical reaction of nitrobenzene derivatives in acetonitrile by changing the focusing degree of laser beam for excitation. The result seems to be a typical example of switching of laser photoreactions to yield different kinds of stable products in the solution.

Experimental

Acetonitrile (Wako, Spectroscopic grade) was used as solvent without further purification. *p*-Nitroanisole (compound **1**) (Tokyo Kasei, Extra pure) was used after recrystallization from ethanol. *N*-[2-(*p*-nitrophenoxy)ethyl]aniline (compound **2**) was offered by Prof. K. Mutai, The University of Tokyo.

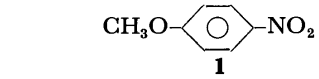

1

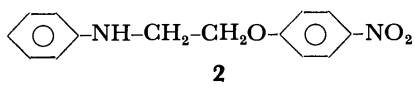

2

p-Nitrosoanisole was prepared by the method of Mijs *et al.*[3]

An N_2 laser (Molectron UV-24, peak power 900 kW, pulse duration 10 ns) was used as a source of irradiation. When a laser beam is defocused, the minimum cross section of beam, S, is about 1.0×0.3 cm^2 and $S\leq0.5\times0.1$ cm^2 when the laser beam is focused inside a sample cell. The incident energy per pulse was kept constant (10^{16} photons) for both cases. The repetition rate (20 Hz) and peak intensity of the exciting laser pulse were monitored with a photodiode throughout the reaction. Calibrated neutral density filters were used to attenuate the laser intensity.

Absorption spectra were measured with a Hitachi 320 spectrophotometer. Transient absorptions were measured by the apparatus reported previously.[4] Experiments were carried out at room temperature. Dielectric break down in the sample solution was not observed even for the maximum laser intensity.

Results and Discussion

The spectral change of **1** in acetonitrile by irradiation with defocused and focused beams of the N_2 laser were measured with the spectrophotometer and the results are shown in Figs. 1a) and 1b), respectively. The absorption intensity of **1** at 305 nm shows a slight decrease by the irradiation with a defocused beam, while the irradiation with a focused beam results in a large decrease of the absorption intensity and growing up of a new absorption band around 335 nm. These results show that the reactivity of **1** depends on the focusing degree of laser beam.

Similar experiments were made for **2** and the results are shown in Figs. 2a) and 2b). Mutai *et al.* concluded that a photo-Smiles rearrangement reaction occurs when **2** is irradiated with a defocused beam.[4,5] The absorption band of the photo-Smiles reaction product grows up at 390 nm (Fig. 2a)). By focusing the laser beam, however, a new band turns out to appear at 335 nm as is shown in Fig. 2b). This implies that a high density excitation induces a new reaction and produces a photoproduct other than that of the photo-Smiles rearrangement.

Both products from **1** and **2** by the irradiation with the focused laser beam have the band at 335 nm. This suggests that both products are similar to each other

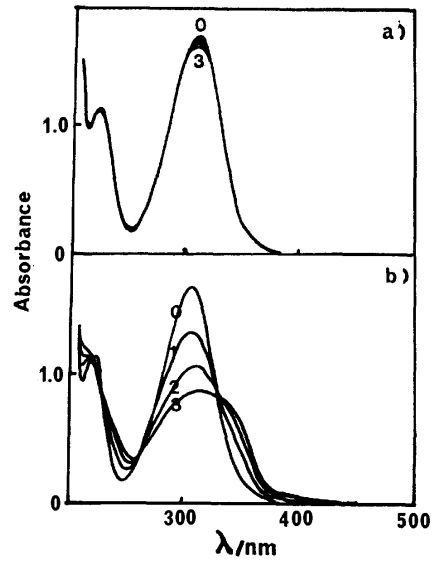

Fig. 1. Absorption spectra of **1** in acetonitrile after the irradiation with a) a defocused beam and b) a focused beam. Curves 0, 1, 2, and 3 represent the spectra after the irradiation for 0, 20, 40, and 60 min, respectively.

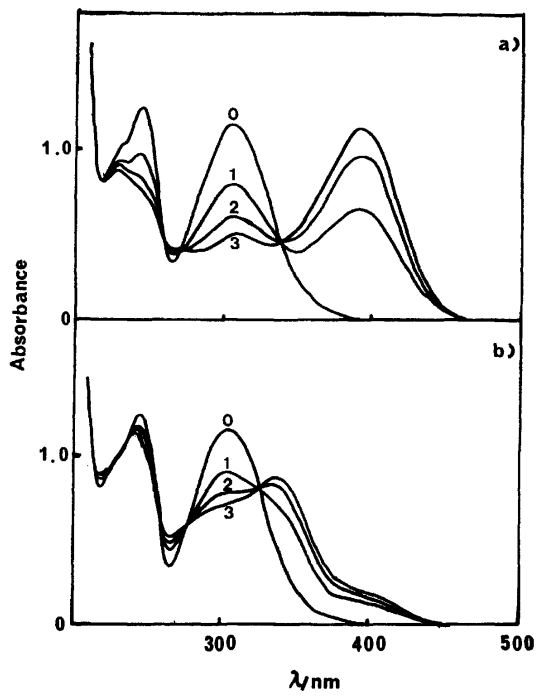

Fig. 2. Absorption spectra of **2** in acetonitrile after the irradiation with a) a defocused beam and b) a focused beam. Curves 0, 1, 2, and 3 represent the spectra after the irradiation for 0, 10, 20, and 30 min, respectively.

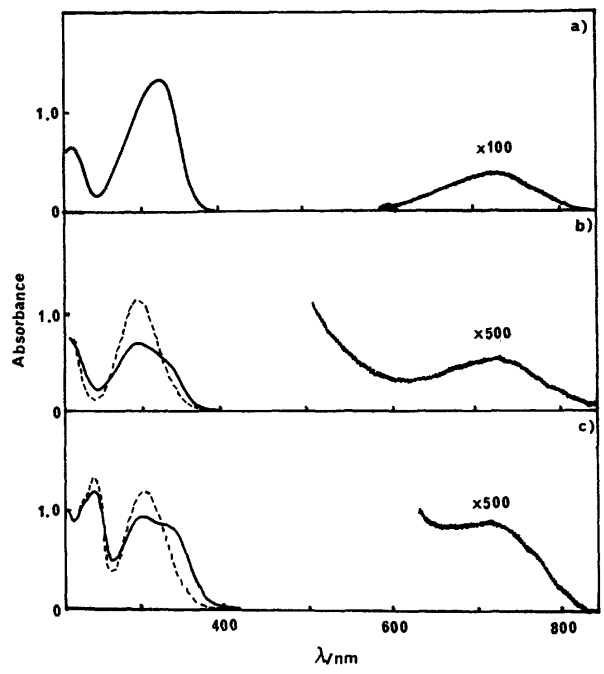

Fig. 3. Absorption spectra of *p*-nitrosoanisole and the new photoproducts from **1** and **2**. Cell thickness; 1 mm for the range of 200—500 nm and 100 mm for the range of 500—800 nm. a) The spectrum of *p*-nitrosoanisole. b) The spectrum of **1** after the irradiation. c) The spectrum of **2** after the irradiation. (Broken lines; the spectra before the irradiation.)

in their electronic structures. Since the 335 nm bands remain unchanged by addition of O_2 to the sample solutions or storing them in air for a few days, the new products responsible for the 335 nm bands are stable compounds. The process is unimolecular because the relative rate of the reaction is independent of the concentrations of the parent molecules.

In order to identify the new products which have the band at 335 nm, their spectra were measured in the wavelength region of 850—200 nm and a weak band was observed at 730 nm (Fig. 3). This finding suggests that the new products are nitroso compounds. For the purpose of comparison, the absorption spectrum of *p*-nitrosoanisole chemically prepared was measured and the result is shown in Fig. 3a). The spectrum is similar to the spectra of the products from **1** and **2** by the irradiation with the focused laser beam. This leads us to the conclusion that nitroso compounds are produced by the dissociation of an oxygen from the nitro group. Similarity of the absorption spectrum of the nitroso compound produced from **2** to that of *p*-nitrosoanisole is explained by the fact that conjugation between the ON-⟨○⟩-O-CH_2- and -HN-⟨○⟩ moieties is prohibited by the alkyl bridge.

The laser intensity dependence of the yield of the nitroso compound produced from **2** was studied. The

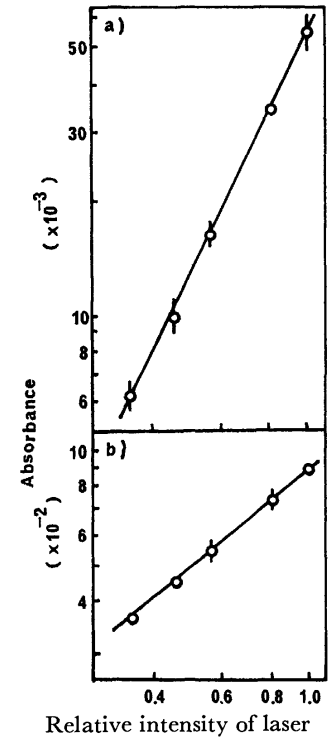

Fig. 4. The dependence of the yield of the photoproducts from **2** on the laser intensities. a) A plot of the logarithm of the absorbance of the nitroso compound at 335 nm *vs.* the laser intensity. The acetonitrile solution of **2** was irradiated with a focused beam for 5 min after bubbling with O_2 gas for 30 min. b) A plot of the logarithm of the absorbance of the final product of the photo-Smiles reaction at 390 nm *vs.* the laser intensity. The acetonitrile solution of **2** was irradiated with a defocused beam for 3 min.

logarithmic plot of the absorbance at 335 nm against the laser beam intensity shows a straight line with a slope of 2.0 (Fig. 4a)). This shows that the reaction proceeds *via* a biphotonic process. On the other hand, the laser intensity dependence of the yield of the final product in the photo-Smiles reaction shows a straight line with a slope of about 0.8, indicating that the reaction proceeds *via* a one photon process.

Considering the fact that the molar extinction coefficients of the nitroso compound at 335 nm and the final product of the photo-Smiles reaction at 390 nm are nearly equal, comparison between Figs. 2a) and 2b) induces the conclusion that the relative yield for the biphotonic process exceeds that for the one photon process when the laser beam is focused. This indicates that the new reaction proceeds *via* a consecutive two step process rather than a simultaneous two-photon process, since the transition probability of simultaneous two-photon absorption is much smaller than that of one photon absorption even in the resonance condition.[6]

The rate of reaction by the irradiation with a focused laser beam was not affected markedly by the addition of triplet quenchers (O_2 gas bubbled for 30 min or *cis*-1,3-pentadiene (0.1 mol dm^{-3})). This indicates that the intermediate state for the two step process is not the lowest triplet state with the lifetime of about 70 ns,[7] but an excited singlet state.

The biphotonic dissociation caused by the irradiation of the 337 nm laser beam indicates that an excited state existing at 6—7 eV above the ground state is responsible for the reaction. According to the calculation based on the CNDO/S-CI method[8] or the composite molecule method,[9] a state locally excited within the NO_2 group is located at 6.6 eV for nitrobenzene. This state has large transition component from a nonbonding MO to an antibonding MO on the NO bond as is shown in Fig. 5.

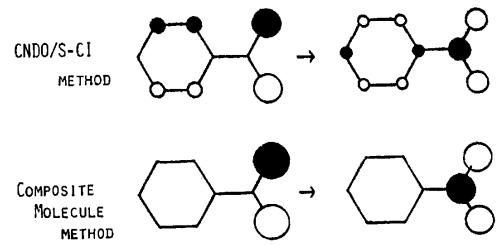

Fig. 5. The lower and upper MO corresponding to the local excitation within the nitro group.

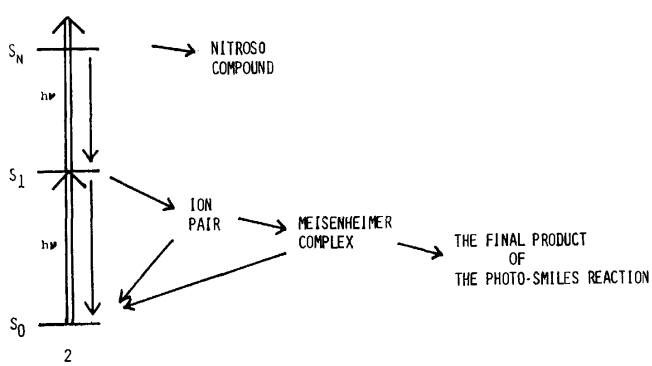

Fig. 6. The reaction scheme of **2**.

The antibonding character of the NO bond is expected to result in the cleavage of the bond.

Figure 6 shows the most probable scheme of photoreaction of **2**. The photo-Smiles reaction initiated with a defocused beam starts from the S_1 state and proceeds *via* an ion pair and a Meisenheimer complex to the final product.[4] This conclusion is confirmed by the fact that the yields of the two intermediates show linear dependences on laser intensity. By the irradiation with a focused laser beam, an effective excitation from S_1 to S_n state competes with the process of the photo-Smiles reaction and results in the production of the nitroso compound.

Nitrobenzene derivatives are known to have a large decay rate of the excited singlet state resulting in a nonfluorescent character. Thus, the focusing of laser beam seems to be necessary for the occurrence of the second absorption in a very short time of picosecond order. In turn, the short lifetime of intermediate state is consistent with the fact that the observed dependence of the amount of the produced nitroso compound on the laser intensity is quadratic, because a long lifetime of intermediate state would bring an approximately linear dependence on laser intensity.

Hasting and Matsen reported that nitrobenzene was converted into nitrosobenzene in the vapor phase by the irradiation of d.c. arcs with metal electrodes.[10] The detailed experimental conditions including the wavelength distribution of the irradiating source are not shown in their paper and the reaction mechanism is not clear. The present study has confirmed that nitro compounds can be converted into relating nitroso compounds *via* a two step process by the irradiation with light at 337 nm with the photon density of about 10^{17} photon cm^{-2} $pulse^{-1}$ and has presented a typical example of switching between different chemical reactions in solution by changing the focusing degree of a laser beam.

The authors express their sincere thanks to Prof. Kiyoshi Mutai, The University of Tokyo, for favorable offering of compound **2**.

References

1) N. Bloembergen and E. Yablonovitch, *Physics Today*, **1978**, May 23; V. S. Letokhov, *ibid.* **1977**, May 23; M. Katayama, *Bunko Kenkyu*, **27**, 269 (1978).

2) M. Martin, E. Bréhéret, F. Tfibel, and B. Lacourbas, *J. Phys. Chem.*, **84**, 70 (1980); A. Matsuzaki, T. Kobayashi, and S. Nagakura, *J. Phys. Chem.*, **82**, 1201 (1978); T. W. Scott, A. J. Twarowski, and A. C. Albrecht, *Chem. Phys. Lett.*, **66**, 1 (1979).

3) W. J. Mijs, S. E. Hoekstra, R. M. Ulman, and E. Havinga, *Recl. Trav. Chim. Pays-bas*, **77**, 746 (1958).

4) K. Yokoyama, R. Nakagaki, J. Nakamura, K. Mutai, and S. Nagakura, *Bull. Chem. Soc. Jpn.*, **53**, 2472 (1980).

5) K. Mutai, S. Kanno, and K. Kobayashi, *Tetrahedron Lett.*, **1978**, 1273.

6) According to a rough numerical estimation, when laser intensity is about 10^{17} photon cm^{-2} $pulse^{-1}$, the number of photons absorbed by a sample molecule at an ordinary simultaneous two-photon absoption band is about 10^{-10} photon $pulse^{-1}$, but that at a one photon absorption band is about

one photon pulse^{-1} (I. Webman and J. Jortner, *J. Chem. Phys.*, **50**, 2706 (1969)). Thus, the transition probability of two-photon process is much smaller than that of one photon process, although the former becomes about 7 orders larger when excitation energy coincides with a transition energy of one photon absorption band (J. E. Bjorkholm and P. F. Liao, *Phys. Rev. Lett.*, **33**, 128 (1974)).

7) D. A. Duddel and J. T. Richards, "Lasers in Chemistry," ed by M. A. West, Elsevier, Amsterdam (1977), pp. 349—353.

8) Ts. Kobayashi, private communication.

9) S. Nagakura, M. Kojima, and Y. Maruyama, *J. Mol. Spectrosc.*, **13**, 174 (1964).

10) S. H. Hasting and F. A. Matsen, *J. Am. Chem. Soc.*, **70**, 3514 (1948).

Proton Magnetic Resonance Study of Interaction between Penicillin G and Hen Egg White Lysozyme

Fumiyuki MITSUMORI,*,† Yoji ARATA, and Shizuo FUJIWARA

Department of Chemistry, Faculty of Science, The University of Tokyo, Hongo, Tokyo 113

(Received July 14, 1980)

Interaction between penicillin G and hen egg white lysozyme has been studied using NMR and gel chromatography. It has been demonstrated that the stoichiometry of the interaction is one to one with an association constant of approximately 1.9×10^2 M^{-1} (1M=1mol dm^{-3}). It has also been shown that the phenacyl side chain of penicillin G is interacting with the tryptophan-123 residue of the lysozyme molecule.

Study of interaction of penicillin with proteins is important in order to elucidate the behavior of penicillin in biological systems such as its transportation, antibacterial activity and allergy. Proteins such as serum albumin are known to function as a transport carrier of drugs in the blood circulation.[1] The antibacterial activity of penicillin is closely related to the fact that penicillin becomes an inhibitor of enzymes which synthesize the cell wall of bacteria.[2] As for the allergy, penicillin conjugates with proteins as a hapten, acquires immunogenicity, and at the antibody-antigen reaction penicillin interacts with its antibody protein selectively with high sensitivity, causing anaphylactic shock.[3] In each case, penicillin-protein interaction plays a decisive role.

Penicillin-serum albumin interaction has been examined using NMR.[4] However, very little is known about the binding site of albumin. It was also reported that in the complex between penicillin and carboxypeptidase, the C2-H proton of one of histidine residues of the protein shows a downfield shift.[5]

In the present paper, interaction between penicillin and lysozyme, one of the best characterized proteins, will be discussed on the basis of NMR measurements. Several studies have already been published on the penicillin-lysozyme interaction by means of X-ray diffraction,[6] inhibition of lysozyme activity,[7] equilibrium dialysis,[8] radioisotope labeling[9], and pulse radiolysis.[10] It has been reported that penicillin V binds to lysozyme in the ratio of one to one in the crystalline state,[6] and that hydrolytic action of lysozyme is inhibited 50% by the presence of 24 mM penicillin G.[7] It has been reported that an irreversible binding of penicillin G with lysine-116 of lysozyme occurs when a mixture of penicillin G and lysozyme is incubated for 48 h at 37 °C.[9] It has also been reported that no complex formation between penicillin G and lysozyme can be detected by means of equilibrium dialysis, whereas naphthylazopenicillin strongly interacts with lysozyme.[8]

In the present work, stoichiometry and the binding constant of the interaction between penicillin G and lysozyme are determined, and the binding sites on both sides will be discussed on the basis of NMR and gel chromatography results.

† Present address: National Institute for Environmental Studies, Yatabe, Tsukuba, Ibaraki 305.

Experimental

Penicillin G potassium salt (Sigma, Lot No. 24C-2130) and hen egg white lysozyme (Seikagaku Kogyo, Lot No. E5210) were used without further purification. All other reagents were of analytical grade.

For NMR measurements of the NH proton of tryptophan residues, lysozyme were dissolved in H_2O (5 mM in 0.1 M NaCl, pH 5.5), to which penicillin G was added. For other NMR measurements, penicillin G and lysozyme were dissolved in 0.3 M deuterated acetate buffer in D_2O (pH 5.5). NMR measurements at 100 MHz were performed using a JEOL PS-100 spectrometer operating in the correlation[11] and in the CW mode, and 360 MHz spectra were recorded on a Bruker HXS-360 in the correlation and in the FT mode. Chemical shift values are from either external DSS or internal HDO in D_2O.[12]

Gel chromatography was performed at 25 °C on a column (1×25 cm) of Sephadex G-25 by following the procedure described by Hummel and Dreyer.[13,14] Before use, the column was equilibrated with 0.1 M acetate buffer solution (pH 5.5) containing penicillin G (0.8—8.3 mM). About 50 mg of lysozyme was dissolved in 0.5 ml of the same eluting solution, and elution was performed at flow rate of 0.25 ml/min. The effluent was collected in 2.0-ml fractions and diluted to fit the concentration of penicillin G for UV measurements. The concentration of penicillin G was determined by the color development at 325 nm.[15]

Results and Discussion

Stoichiometry and Binding Constant of the Interaction between Penicillin G and Lysozyme. Figure 1 shows a typical elution profile at 325 nm. The amount of penicillin G bound to lysozyme is estimated from the area of trough displayed in the elution profile. The extent of binding of penicillin G to lysozyme was also measured at varying concentrations of penicillin G and the result is shown as a Scatchard plot in Fig. 2. This result clearly indicates that the stoichiometry of interaction between penicillin and lysozyme is one to one. The binding constant obtained from the plot is approximately 1.9×10^2 M^{-1}.

Binding Site in Penicillin G. Fischer and Jardetzky used the broadening of the phenyl and methylene peaks of penicillin G in the presence of albumin and concluded that the phenyl part of the penicillin molecule is involved in the interaction between penicillin G and albumin.[4] The phenyl and methylene peaks, which they treated as single peaks, are actually of AB and A_2B_2C spin systems, and are no longer singlet at 360 MHz. They

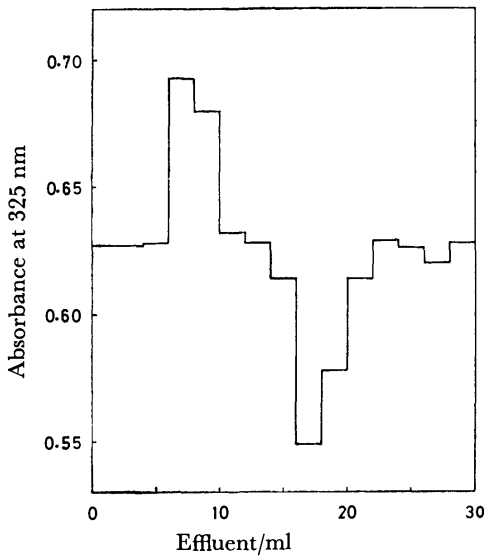

Fig. 1. Elution profile of the 325 nm absorbance accompanying the passage of lysozyme (50 mg) through a column of Sephadex G-25 which was equilibrated with 1.73 mM penicillin G at 25 °C. The collected effluent was diluted by 12.5-fold before the color development.

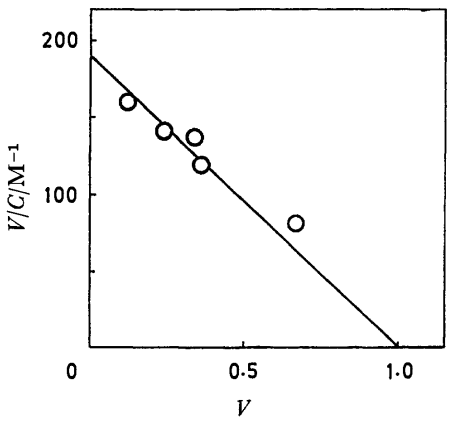

Fig. 2. Scatchard plot for the binding of penicillin G and lysozyme. C: The concentration of penicillin G in the eluting buffer, V: moles of penicillin G bound per mole of lysozyme.

have also shown that the chemical shift values of these peaks are dependent on the concentration of penicillin G. Thakkar and Wilham concluded that this concentration dependence of chemical shift values was caused by the self association of penicillin G.[16]

In the present experiment, the concentration of penicillin G is fixed at 32 mM, whereas that of lysozyme is varied from 0 to 10 mM. The change in spectrum of penicillin G under these conditions are shown in Fig. 3. With an increase in concentration of lysozyme from 0 to 10 mM, the phenyl peak shows an upfield shift of 0.098 ppm, the methylene peak an upfield shift of 0.079 ppm, and the β-CH_3 and 6-H peaks small upfield shifts of 0.035 ppm and 0.022 ppm, respectively. On the other hand, very little shift is observed in the α-CH_3, 3-H and 5-H protons. The result that 3-H is not affected by the presence of lysozyme suggests that no electrostatic

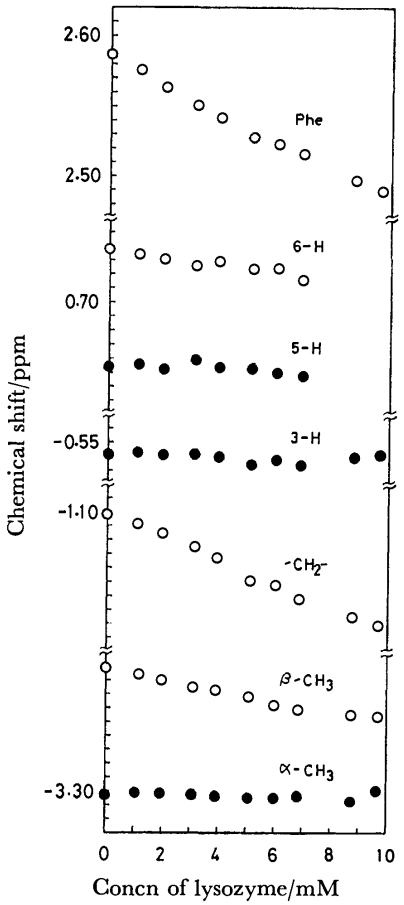

Fig. 3. A change in chemical shift values of penicillin G at varying concentrations of lysozyme in 0.3 M deuterated acetate buffer (pH 5.5). 28 °C. The concentration of penicillin G: 32 mM. Chemical shift values are in ppm from internal HDO whose chemical shifts are independent of the concentration of lysozyme within experimental error.

interaction involving the carboxyl group at C-3 of penicillin G occurs between penicillin G and lysozyme.

Among the groups of protons affected by the addition of lysozyme, the shifts observed for the phenyl and methylene peaks in the side chain are probably caused by the interaction with lysozyme; small shift in the β-CH_3 protons appears to be due to a change in intramolecular interaction of penicillin G molecule caused by interaction with lysozyme. This is supported by the experiments of the temperature dependence of the chemical shifts of penicillin G. As shown in Fig. 4, the β-CH_3 signal shows large temperature dependent shift. In contrast to this, 6-aminopenicillanic acid (6-APA), which has no side chain, does not show any such temperature dependent shift. Therefore, it may be concluded that the temperature dependent shift of β-CH_3 of penicillin G is primarily caused by the phenacyl side chain. Furthermore, the temperature dependent shift is much larger in the β-CH_3 group as compared to the α-CH_3 group. This result suggests that in an aqueous solution the penicillin G molecule tends to be less extended in shape, with the phenacyl side chain approaching from the side of the β-CH_3 group to the heterocyclic ring.

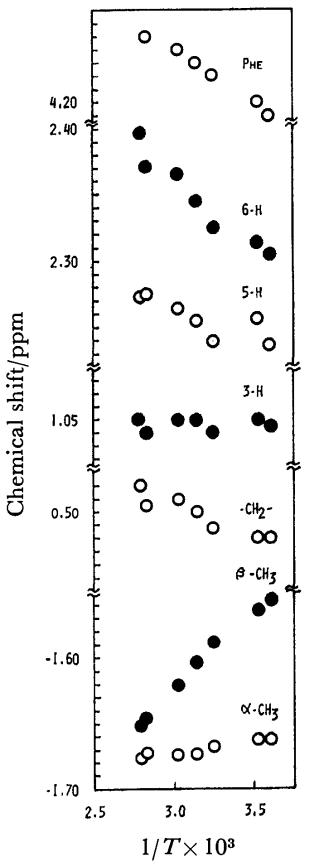

Fig. 4. Temperature dependence of chemical shift values of penicillin G in 0.3 M deuterated phosphate buffer (pH 7.0). Chemical shift values are in ppm from internal tetramethylammonium.

We assume that the shift caused by the addition of lysozyme is due to the fast exchange between the free and bound penicillin molecules. Then, the binding constant (K) and the chemical shift difference between the two states can be estimated by a least-squares method;[17] K was estimated to be in the range 10—250 M^{-1}, and the chemical shift differences for the phenyl and methylene groups in the ranges 0.4—1.3 ppm and 0.3—1.1 ppm, respectively.

In the presence of lysozyme, broadening of the methylene peak of penicillin G is observed at 100 MHz as Fischer and Jardetzky have already reported.[4] This peak is observed as an AB quartet at 360 MHz. Therefore, the broadening observed at 100 MHz is not quite helpful in obtaining information about the interaction of penicillin G with lysozyme.

Binding Site in Lysozyme. The result that the aromatic side chain of penicillin G molecule is the binding site suggests that aromatic amino acid residues of lysozyme may be involved in this interaction. Even in a relatively small protein such as lysozyme (M.W. 14300), proton signals observed separately are limited at the present resolving power of an NMR spectrometer.[18] Among those, C2-H proton of histidine-15 and NH protons of the indole ring of tryptophan residues can be used as probes for the investigation of the interaction site of lysozyme. The C2-H proton of His-15 does not show any change in chemical shift in the presence and absence of penicillin G, indicating that this histidine residue is not responsible for the interaction of penicillin G with lysozyme.

Correlation NMR technique is employed to observe exchangeable NH protons in H_2O. As shown in Fig. 5, the indole NH protons of five among six tryptophan residues are resolved. Peak I which is at the lowest field shows an upfield shift in the presence of penicillin G. Figure 6 gives chemical shift values of these five NH protons at varying concentrations of penicillin G. Only peak I shows an upfield shift with an increasing concentration of penicillin G. This result indicates that the tryptophan residue giving rise to peak I is involved in the interaction with penicillin G. Glickson, Phillips, and Rupley have reported that peaks III and V show a large shift in the presence of N-acetylglucosamine (NAG), an inhibitor of lysozyme.[19] The result of the present experiment suggests that penicillin G is different from NAG in its way of interaction with lysozyme.

On the basis of experiments such as chemical modification, binding of paramagnetic ions, inhibitors, and spin labels and solvent exchange, Cassels, Dobson, Poulsen, and Williams assigned the NH proton peaks from downfield as Trp-123, Trp-111 (or Trp-28), Trp-63, Trp-62, and Trp-108. In addition to this, they found the sixth peak in the upper field and assigned it as Trp-28 (or Trp-111).[20-22] Lenkinski, Dallas, and Glickson independently reported the assignments which agree with one of the two possibilities reported by Cassels *et al.*[23] Following the above assignments, Trp-123 is

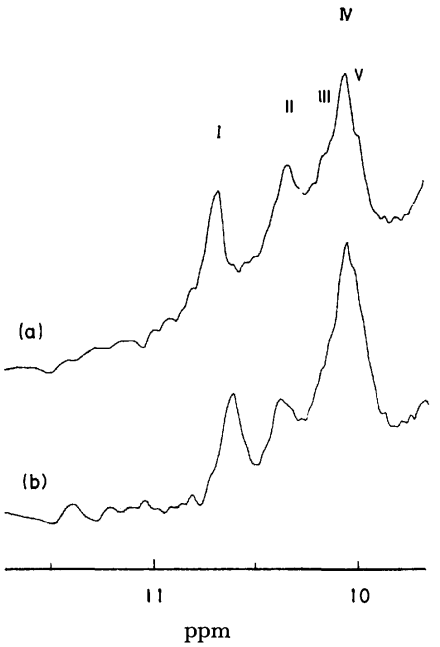

Fig. 5(A). Correlation NMR spectra (100 MHz) of indole NH protons of tryptophan residues of hen egg white lysozyme in the absence (a) and presence (b) of penicillin G. (a): 5.0 mM lysozyme in H_2O (0.1 M NaCl), pH 5.5, 48 °C. (b): 5.0 mM lysozyme in H_2O (0.1 M NaCl) containing 31 mM penicillin G. pH 5.5, 48 °C. Chemical shift values are in ppm from external DSS in H_2O. sweep rate: 417 Hz/s, sampling time: 0.512 s, repetition time: 0.8 s, sampling point: 512, number of accumulation: 2048, filter: 125 Hz.

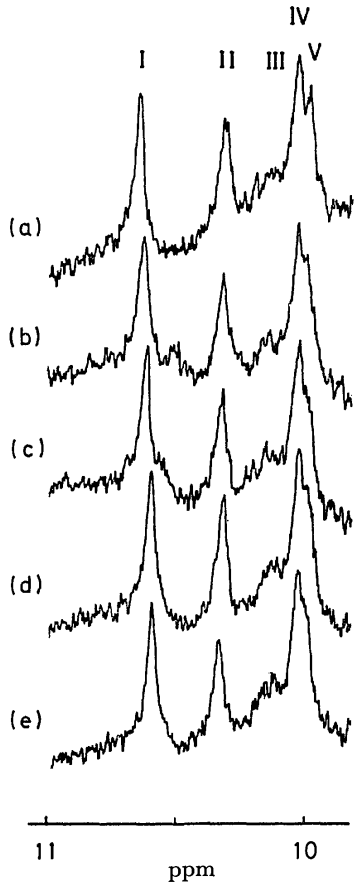

Fig. 5(B). Correlation NMR spectra (360 MHz) of indole NH protons of tryptophan residues of hen egg white lysozyme in the absence (a) and presence (b—e) of penicillin G. 5.0 mM lysozyme in H_2O (0.1 M NaCl). pH 5.5, 53 °C. The concentration of penicillin G: (b) 6 mM, (c) 12 mM, (d) 17 mM, (e) 26 mM. Chemical shift values are in ppm from external DSS in H_2O. sweep width: 1200 Hz, sampling interval: 0.2 ms, sampling point: 4096, number of accumulation: 256.

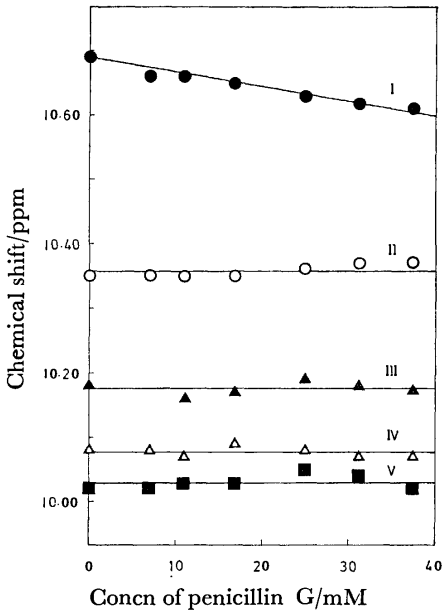

Fig. 6. A change in chemical shift values of indole NH protons of tryptophan residues of lysozyme (5.0 mM) at varying concentrations of penicillin G (pH 5.5, 48 °C).

the one which is involved in the interaction with penicillin G. Measurements of solvent exchange rates and X-ray structure studies have shown that Trp-123 is exposed to solvent;[20,24] penicillin G is presumably interacting with the Trp-123 residue on the surface of the lysozyme molecule.

Felsenfeld and Handschumacher have suggested that penicillin G binds to all tryptophan residues.[7] On the contrary, the present experiment indicates that penicillin G-lysozyme binding is more specific. Corran and Waley have reported that penicillin G is irreversibly bound to Lys-116 of lysozyme at its ε-amino group. However, this irreversible binding was observed after incubation of both substances for 48 h at pH 7.4 and 37 °C,[9] under which condition penicillin G is known to degrade forming various products.[25] In the present experiments, NMR measurements were performed immediately after penicillin G and lysozyme were mixed, so that it is quite unlikely that the covalent bond is formed.

The binding constant of $1.9\times10^2\,M^{-1}$ obtained for penicillin G is larger than that for NAG ($K=39\,M^{-1}$) and other saccharide monomers; however, it is smaller than those for dimers and trimers such as $(NAG)_2$ and $(NAG)_3$.[26] It is known that various pigments such as Biebrich scarlet, which have aromatic rings in the molecular structure, bind to lysozyme with high affinity.[27] Our result that the aromatic side chain of penicillin G is interacting with lysozyme with higher affinity than monosaccharides is consistent with these facts.

On the basis of an X-ray structural study of lysozyme which is diffused by penicillin V, Johnson has concluded that penicillin V binds specifically to the cleft on the surface of lysozyme. He has also shown that the penicillin binding site is apart $\approx$12 Å from the binding site of NAG and suggested that the binding is weaker than in the case of NAG.[6] Our results are not consistent with the conclusion reached by Johnson; *i.e.*, Trp-123 is not in the cleft of lysozyme molecule and the binding of penicillin G is stronger than that of NAG. There are two possibilities for this discrepancy. One is the difference in the molecular structure of penicillin G and penicillin V; in the penicillin V molecule the phenoxymethyl side chain is substituted for the benzyl side chain of penicillin G. All of our experiments were carried out in solution, whereas the X-ray structure was obtained in the crystalline state. This difference is another possibility for the above discrepancy. It is likely that in the crystalline state, where the lysozyme molecules are presumably more closely packed than in the case of solution, the penicilline molecule is hindered from approaching to Trp-123, which is in the dominant binding site of lysozyme.

In conclusion, interaction between penicillin G and lysozyme is one to one with a binding constant of approximately $1.9\times10^2\,M^{-1}$, and the phenacyl side chain of penicillin G and tryptophan-123 in lysozyme are involved in the binding.

The authors gratefully acknowledge a support from the Ministry of Health and Welfare (Special Research Grant #160). 360 MHz spectra were measured at Stanford Magnetic Resonance Laboratory which is supported by NIH grant #RR00711 and NSF grant #GP23633.

References

1) G. Sudlow, D. J. Birkett, and D. N. Wade, *Mol. Pharmacol.*, **11**, 824 (1975).
2) "Cephalosporins and Penicillins," ed by E. H. Flynn, Academic Press (1972).
3) H. E. Eisen, "Immunology," Harper and Row, Haugerstown (1974).
4) J. J. Fischer and O. Jardetzky, *J. Am. Chem. Soc.*, **87**, 3237 (1965).
5) J. Degelaen, J. Feeney, G. C. K. Roberts, A. S. V. Burgen, J. M. Frère, and J. M. Ghuysen, *FEBS Lett.*, **98**, 53, (1979).
6) L. N. Johnson, *Proc. R. Soc. London, Ser. B*, **167**, 439 (1967).
7) H. Felsenfeld and R. E. Handschumacher, *Mol. Pharmacol.*, **3**, 153 (1967).
8) I. M. Klotz, J. M. Urguhart, and W. W. Weber, *Arch. Biochem.*, **26**, 420 (1950).
9) P. H. Corran and S. G. Waley, *Biochem. J.*, **149**, 357 (1975).
10) G. O. Phillips, D. M. Power, and J. T. Richards, *Isr. J. Chem.*, **11**, 517 (1973).
11) Y. Arata and H. Ozawa, *J. Magn. Reson.*, **21**, 67 (1976).
12) S. Ono, F. Mitsumori, Y. Arata, and S. Fujiwara, *Bunseki Kagaku*, **26**, 766 (1977).
13) J. P. Hummel and W. J. Dreyer, *Biochem. Biophys. Acta*, **63**, 530 (1962).
14) K. Takahashi, *J. Biochem.*, **72**, 1469 (1972).
15) H. Bundgaard and K. Ilver, *J. Pharm. Pharmacol.*, **24**, 790 (1972).
16) A. L. Thakkar and W. L. Wilham, *Chem. Commun.*, **1971**, 320.
17) M. A. Raftery, F. W. Dahlquist, S. M. Parsons, and R. G. Wolcott, *Proc. Natl. Acad. Sci.*, **62**, 44 (1969).
18) S. J. Perkins and R. A. Dwek, *Biochemistry*, **19**, 245 (1980).
19) J. D. Glickson, W. D. Phillips, and J. A. Rupley, *J. Am. Chem. Soc.*, **93**, 4031 (1971).
20) R. Cassels, C. M. Dobson, F. M. Poulsen, and R. J. P. Williams, *Eur. J. Biochem.*, **92**, 81 (1978).
21) R. Cassels, C. M. Dobson, F. M. Poulsen, and R. J. P. Williams, *J. Magn. Reson.*, **37**, 141 (1980).
22) I. D. Campbell, C. M. Dobson, and R. J. P. Williams, *Proc. R. Soc. London, Ser. B*, **189**, 485 (1976).
23) R. E. Lenkinski, J. L. Dallas, and J. D. Glickson, *J. Am. Chem. Soc.*, **101**, 3071 (1979).
24) C. C. F. Blake, G. A. Mair, A. C. T. North, D. C. Phillips, and V. R. Sarma, *Proc. R. Soc. London, Ser. B*, **167**, 365 (1967); C. C. F. Blake, L. N. Johnson, G. A. Mair, A. C. T. North, D. C. Phillips, and V. R. Sarma, *ibid.*, **167**, 378 (1967).
25) F. Mitsumori, Y. Arata, S. Fujiwara, M. Muranaka, and Y. Horiuchi, *Bull. Chem. Soc. Jpn.*, **50**, 3164 (1977).
26) T. Imoto, L. N. Johnson, A. C. T. North, D. C. Phillips, and J. A. Rupley, "Enzymes," 3rd ed, Academic Press (1972), Vol. 7, p. 665.
27) G. L. Rossi, E. Holler, S. Kumar, J. A. Rupley, and G. P. Hess, *Biochem. Biophys. Res. Commun.*, **37**, 757 (1969).

The Crystal and Molecular Structure of the Copper(I) Chloride Complex Containing *p*-Benzoquinone as a Ligand

Tetsuo UECHI,* Hiroko YAMAGUCHI,† Ikuhiko UEDA, and Kazuo YASUKOUCHI†

College of General Education, Kyushu University 01, Ropponmatsu, Fukuoka 810

†*Department of Industrial Chemistry, Faculty of Engineering, Kumamoto University, Kurokami, Kumamoto 860*

(Received April 26, 1979)

The crystal and molecular structure of the red compound, $[(NH_4)Cu_3Cl_4(C_6H_4O_2)_{1.5}\cdot H_2O]$, has been determined from 2115 X-ray diffraction data collected on an automated four-circle diffractometer. The crystals are monoclinic, with space group $P2_1/c$, and with four formula units in a unit cell of dimensions; $a=7.308(5)$, $b=11.593(7)$, $c=18.359(9)$ Å, and $\beta=90.16(3)°$. The structure was solved by direct methods, and block-diagonal least-squares refinements led to a final discrepancy index, R, of 0.035. The crystal structure is characterized by polymeric, beehive-like layers composed of $Cu_3Cl_4^-$ anions, and centro- and pseudocentrosymmetric *p*-benzoquinone molecules. Each of the *p*-benzoquinone molecules acts as a bridging ligand to the two *trans* $Cu_3Cl_4^-$ anions, with the Cu–C closest distances falling in the range from 2.047(5) to 2.086(5) Å. The NH_4^+ cations and the water molecules are accommodated by a roughly coplanar arrangement within the tunnel-like holes of the beehives, and the NH_4^+ cations are joined to the layers by intra- and interlayer hydrogen bonds of the N–H···O type. The $Cu_3Cl_4^-$ has a distorted cubane-type structure with one corner missing, and each Cu atom has a distorted tetrahedral coordination.

Yamaguchi *et al.* have synthesized a new compound with the composition of $[(NH_4)Cu_3Cl_4(C_6H_4O_2)_{1.5}\cdot H_2O]$ (hereafter abbreviated as BQ-Red), from $CuCl_2$, hydroquinone, and NH_4Cl in an aqueous solution. They have found, on the basis of spectroscopic studies, that this compound in the solid state is a polynuclear π-complex between $Cu_3Cl_4^-$ and *p*-benzoquinone (*p*-BQ).[1] It seems to have been reported few X-ray structural studies of metallic complexes containing *p*-BQ molecules as ligands, and so BQ-Red was expected to be a *p*-BQ complex of Cu(I) chloride of a novel type. The study of the crystal structure of BQ-Red has been carried out by the X-ray diffraction method to reveal the interactions between the $Cu_3Cl_4^-$ anions and the *p*-BQ molecules.

Experimental

Single crystals of this compound were prepared by one of the authors. Preliminary Weissenberg photographs showed the systematic absences of $0k0$, k odd and $h0l$, l odd, indicating the space group $P2_1/c$. The unit-cell parameters were obtained by a least-squares procedure using the 2θ values of 15 reflections measured on a Syntex $P\bar{1}$ four-circle diffractometer with Mo $K\alpha$ radiation. The density was measured by flotation in a methyl-iodide solution. The crystal used for X-ray work was ground to a sphere of 0.38 mm in diameter. The crystal data are given in Table 1.

TABLE 1. CRYSTAL DATA[a]

Formula unit	$Cu_3C_9H_{12}NO_4Cl_4$
Formula weight	530.65
Space group	$P2_1/c$
Density:	
D_m	2.27 g cm^{-3}
D_x	2.266 g cm^{-3}
Cell parameters:	
$a=7.308(5)$ Å	
$b=11.593(7)$ Å	
$c=18.359(9)$ Å	
$\beta=90.16(3)°$	
$V=1555.4(16)$ Å^3	
Number of formula units per unit cell:	$Z=4$
Linear absorption coefficient: (for Mo $K\alpha$ Radiation)	$\mu=49.1$ cm^{-1}

a) The numbers in parentheses, here and elsewhere in this paper, are the e.s.d.'s in the last significant digits.

Intensity data were collected by the θ-2θ scan technique at rates varying from 5.0 to 12.0° min^{-1} and with Mo $K\alpha$ radiation monochromated by a graphite crystal. 2115 independent reflections with 2θ values less than 45° were collected. Of these, 155 reflections with $I<0.7\sigma(I)$ were assigned values of $I=0.7\sigma(I)$ and were given zero weight in the initial refinement. The intensity data were corrected for Lorentz-polarization and absorption effects. The over-all temperature factor and the initial scale factor were obtained by the method of Wilson and were then used to compute the normalized structure factors, $|E|$.

Structure Determination and Refinement

The structure was solved by direct methods using the automatic phasing program MULTAN.[2] An E map calculated using 289 reflections with $|E|>1.5$ revealed the positions of all the Cu and Cl atoms. The other non-hydrogen atoms were obtained from a subsequent Fourier synthesis. Refinement was carried out by block-diagonal least-squares calculations in which the function minimized was $\Sigma\omega(|F_o|-|F_c|)^2$, initially with the unit weight and later with Cruickshank's weighting schemes for all reflections.[3] After refinement with anisotropic temperature factors, the H-atom positions were deduced from the difference Fourier syntheses, and the 35 most intense low-order reflections affected by the second extinction were corrected according to the method described by Stout and Jensen.[4] Refinement including the H atoms was terminated when the shifts of the parameters for the non-hydrogen atoms became less than a quarter of their estimated standard deviations. The final discrepancy index, R, was 0.035 for all reflections. A list of observed and calculated structure factors has been deposited with the office of the Chemical

TABLE 2. FRACTIONAL ATMIC COORDINATES AND TEMPERATURE FACTORS

(a) Non-hydrogen atoms.

All values have been multiplied by 10^4. The anisotropic temperature factors are expressed in the form: $\exp\{-(h^2B_{11}+k^2B_{22}+l^2B_{33}+2hkB_{12}+2hlB_{13}+2klB_{23})\}$.

Atom	x	y	z	B_{11}	B_{22}	B_{33}	B_{12}	B_{13}	B_{23}
Cu(1)	2173(1)	−301(1)	717(0)	94(1)	45(1)	15(0)	5(1)	5(0)	2(0)
Cu(2)	2157(1)	828(1)	2323(0)	96(1)	39(0)	17(0)	−9(1)	−3(0)	−1(0)
Cu(3)	2187(1)	−1980(1)	2092(0)	98(1)	39(0)	18(0)	6(1)	−7(0)	2(0)
Cl(1)	619(2)	1182(1)	1236(1)	96(2)	49(1)	19(0)	20(1)	−6(1)	−2(1)
Cl(2)	721(2)	−683(1)	2893(1)	110(2)	44(1)	19(0)	−5(1)	11(1)	2(1)
Cl(3)	673(2)	−2033(1)	1008(1)	108(2)	48(1)	19(0)	−13(1)	−11(1)	3(1)
Cl(4)	4457(2)	−486(1)	1728(1)	73(2)	37(1)	14(0)	0(1)	−1(1)	2(0)
O(1)	4339(5)	2270(3)	−113(2)	156(8)	38(3)	27(1)	18(4)	9(3)	3(2)
C(1)	4626(6)	1239(4)	−58(3)	84(10)	49(4)	12(1)	1(5)	10(3)	−1(2)
C(2)	3240(7)	364(4)	−246(3)	92(10)	53(4)	12(1)	23(5)	5(3)	6(2)
C(3)	3579(7)	−792(4)	−208(3)	90(10)	54(4)	10(1)	−10(5)	5(3)	−3(2)
O(2)	4558(6)	3143(4)	1445(2)	214(10)	79(4)	19(1)	−29(5)	−21(3)	14(2)
O(3)	5441(6)	646(4)	3865(3)	228(11)	71(4)	30(2)	−19(5)	−22(3)	18(2)
C(4)	4748(7)	2570(5)	2008(3)	118(10)	40(4)	16(2)	−17(5)	−10(3)	−5(2)
C(5)	3264(6)	2437(4)	2532(3)	99(9)	25(3)	19(2)	6(5)	−13(3)	−3(2)
C(6)	3469(7)	1766(4)	3138(3)	100(10)	43(4)	17(2)	−14(5)	4(3)	−10(2)
C(7)	5234(7)	1209(4)	3314(3)	158(12)	27(4)	18(2)	−11(5)	−22(4)	0(2)
C(8)	6739(7)	1364(4)	2787(3)	94(10)	35(4)	23(2)	15(5)	−18(3)	−8(2)
C(9)	6495(6)	1986(4)	2172(3)	78(9)	45(4)	19(2)	−11(5)	5(3)	−16(2)
O(W)	7595(6)	4005(4)	333(2)	191(10)	85(4)	28(2)	−7(5)	−2(3)	−9(2)
N	1666(7)	3856(4)	442(3)	140(10)	60(4)	32(2)	16(5)	−8(4)	5(2)

(b) Hydrogen atoms.

The hydrogen atoms are labelled in terms of the atom to which they are attached. The coordinate values have been multiplied by 10^3. The average e.s.d. of the isotropic temperature factors is 1.4 Å^2.

Atom	x	y	z	B/Å^2	Atom	x	y	z	B/Å^2
H(C2)	233(7)	66(4)	−50(3)	2.0	H(W)1	709(10)	361(7)	−1(4)	7.0
H(C3)	291(6)	−136(4)	−40(3)	2.5	H(W)2	693(11)	433(7)	64(5)	7.8
H(C5)	228(6)	288(4)	248(3)	2.3	H(N)1	207(9)	327(5)	19(4)	5.1
H(C6)	275(7)	175(5)	347(3)	3.2	H(N)2	203(10)	384(6)	88(4)	6.8
H(C8)	771(7)	90(4)	286(3)	2.3	H(N)3	202(8)	452(5)	26(3)	3.9
H(C9)	728(6)	200(4)	182(3)	2.0	H(N)4	53(9)	376(6)	42(4)	6.2

Society of Japan as a Document No. 8036. The atomic scattering factors for Cu^+, Cl^-, O, N, and C_{cov}, and also the anomalous dispersion factors for the first two atoms, were taken from International Tables for X-ray Crystallography,[5] and those for H atom, from Stewart, Davidson, and Simpson.[6] All the calculations were carried out on a FACOM 230-75 computer in the Computer Center of Kyushu University, mainly by the use of the UNICS-II program system.[7] The figures were drawn by the use of the *ORTEP* program.[8] The final atomic parameters are listed in Table 2, along with their estimated standard deviations.

Results and Discussion

Crystal Structure. A projection of the crystal structure down the c axis is shown in Fig. 1, along with the atomic nomenclature scheme, while a stereoscopic illustration viewed along the a axis is shown in Fig. 2. The crystal structure consists of $Cu_3Cl_4^-$ anions, *p*-BQ molecules, NH_4^+ cations, and water molecules. The bond distances(l) and angles(θ) are listed in Table 3.

The $Cu_3Cl_4^-$ anions are arranged with an approximate $\bar{3}$ symmetry around the axis parallel to the a axis and passing through the inversion center at (1/2,1/2,0). Each of the *p*-BQ molecules is sandwiched between these anions in such a mode that the molecular plane is tilted about 99° in relation to the planes defined by the two C atoms and the one Cu atom, as shown in Fig. 3. These *p*-BQ molecules are also in an approximately threefold symmetric arrangement around each anion, with the Cu–C closest distances ranging from 2.047(5) to 2.086(5) Å. Inspection of these Cu–C distances and dihedral angles suggests that π-complexing occurs in BQ-Red. These Cu–C closest distances are shorter than the sum of the relevant Pauling's covalent radii, 2.12 Å.[9] This is indicative of strong interaction between the Cu atoms and the *p*-BQ molecules. It appears that this interaction plays an important role in the stability of the crystal. The distances from the Cu atoms to the centers of their nearest C–C bonds were found to be in the range from 1.953(5) to 1.960(5) Å, with an average value of 1.957 Å. BQ-Red is, to the best of our knowledge, the first reported π-complex

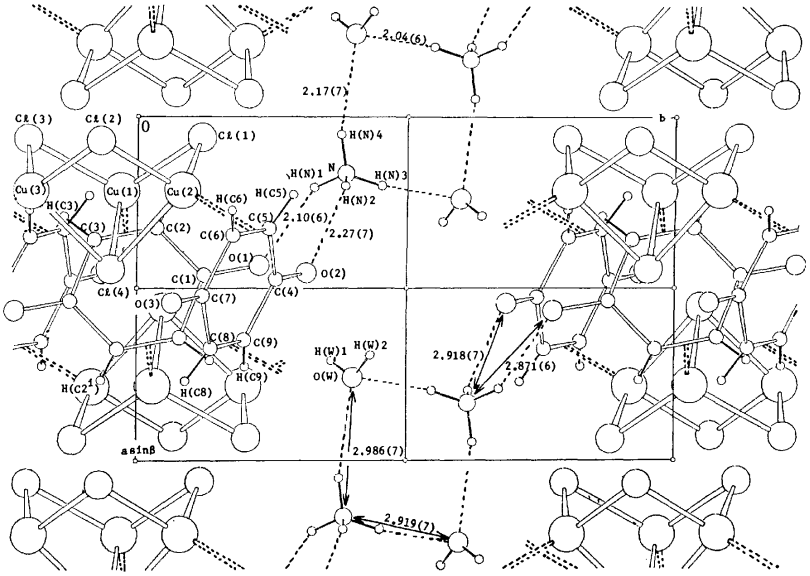

Fig. 1. Crystal structure projected down the c axis. Dashed and double-dashed lines indicate hydrogen bonds and Cu(I)-olefin bonds respectively, and distances in Å. The atoms in (1−x, 1/2+y, 1/2−z) and (x, 1/2−y, 1/2+z) have been omitted for clarity.

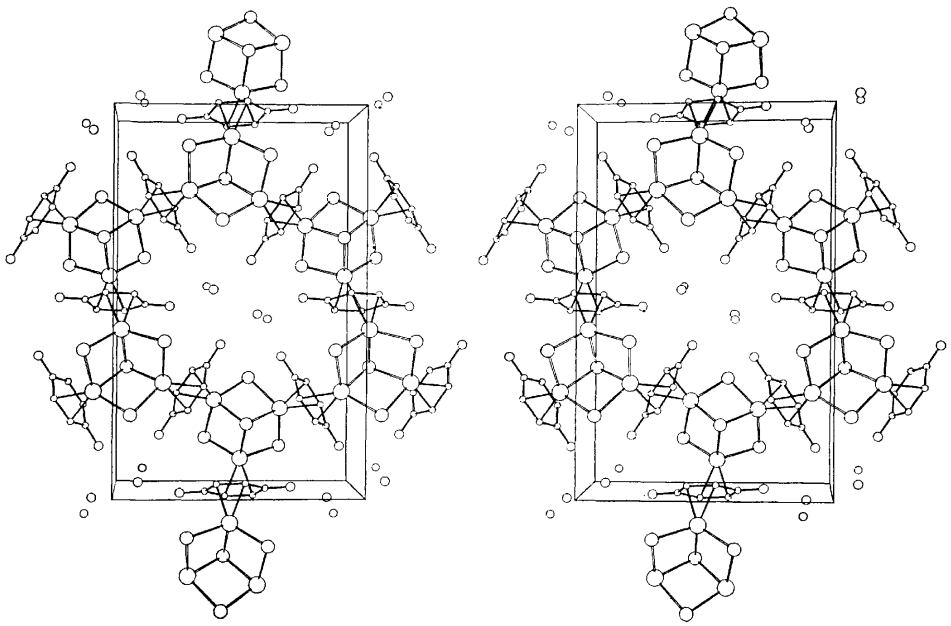

Fig. 2. Stereoscopic view of the crystal structure along the a axis. The center of the cell outline is at the inversion point (1/2, 1/2, 0). The b axis is horizontal, left to right, and the c axis points upward. The H atoms have been omitted for clarity.

where the *p*-BQ molecule bridges two *trans* Cu(I) cations as a di-olefinic ligand, although similar π-complexing has been found in $C_6H_6 \cdot (CuOSO_2CF_3)_2$, where the benzene molecule acts as a bridging ligand to two *trans* Cu(I) cations, with the Cu–C closest distances ranging from 2.09(2) to 2.30(2) Å.[10]

As shown in Fig. 2, each of the $Cu_3Cl_4^-$ anions is surrounded by three *p*-BQ molecules acting as bridging ligands, and these anions and molecules form a polymeric, two-dimensional, beehive-like network extended all over the bc plane. The beehive-like layers are stacked along the a axis, and the holes of the beehive look like tunnels running almost normal to the bc plane.

As shown in Fig. 1, the NH_4^+ cations and the water molecules are accommodated with a roughly coplanar arrangement within the tunnel-like holes of the beehive. The NH_4^+ is linked by hydrogen bonds to two *p*-BQ molecules and one water molecule within a layer, and the NH_4^+ cations and the water molecules in pairs bridge the layers with the hydrogen bonds across the centers of symmetry.

The crystal structure, thus, consists of polymeric,

Table 3. Bond distances and angles[a)]

(a) Bond distances (l/Å)

Cu(1)–Cl(1)	2.271(2)	Cu(2)–Cl(2)	2.295(2)	Cu(3)–Cl(3)	2.275(2)
Cu(1)–Cl(3)	2.350(2)	Cu(2)–Cl(1)	2.325(2)	Cu(3)–Cl(2)	2.363(2)
Cu(1)–Cl(4)	2.502(2)	Cu(2)–Cl(4)	2.520(1)	Cu(3)–Cl(4)	2.491(1)
Cu(1)–C(3)	2.068(5)	Cu(2)–C(5)	2.069(5)	Cu(3^{ii})–C(9)	2.047(5)
Cu(1)–C(2)	2.082(5)	Cu(2)–C(6)	2.082(5)	Cu(3^{ii})–C(8)	2.086(5)
Cu(1)–C(23)[b)]	1.959(5)	Cu(2)–C(56)[b)]	1.960(5)	Cu(3^{ii})–C(89)[b)]	1.953(5)
O(1)–C(1)	1.218(6)	O(2)–C(4)	1.236(6)	O(3)–C(7)	1.214(7)
C(1)–C(2)	1.474(7)	C(4)–C(5)	1.460(7)	C(6)–C(7)	1.477(7)
C(2)–C(3)	1.364(7)	C(5)–C(6)	1.366(7)	C(8)–C(9)	1.351(7)
C(3)–C(1^{i})	1.491(7)	C(6)–C(7)	1.477(7)	C(9)–C(4)	1.475(7)
C(2)–H(C2)	0.88(5)	C(6)–H(C6)	0.81(5)	C(9)–H(C9)	0.87(5)
C(3)–H(C3)	0.89(5)	C(5)–H(C5)	0.89(5)	C(8)–H(C8)	0.90(5)
O(W)–H(W)1	0.86(8)	N–H(N)1	0.87(6)	N–H(N)3	0.88(6)
O(W)–H(W)2	0.83(8)	N–H(N)2	0.85(7)	N–H(N)4	0.84(7)

(b) Bond angles (θ/°)

Cl(1)–Cu(1)–Cl(3)	108.50(6)	Cl(2)–Cu(2)–Cl(1)	107.77(6)	Cl(3)–Cu(3)–Cl(2)	109.98(6)
Cl(1)–Cu(1)–Cl(4)	95.00(5)	Cl(2)–Cu(2)–Cl(4)	92.44(5)	Cl(3)–Cu(3)–Cl(4)	96.14(5)
Cl(3)–Cu(1)–Cl(4)	93.95(5)	Cl(1)–Cu(2)–Cl(4)	93.19(5)	Cl(2)–Cu(3)–Cl(4)	91.58(5)
C(2)–Cu(1)–C(3)	38.4(2)	C(5)–Cu(2)–C(6)	38.4(2)	C(8)–Cu(3^{ii})–C(9)	38.2(2)
Cu(1)–C(2)–C(3)	70.3(3)	Cu(2)–C(6)–C(5)	70.3(3)	Cu(3^{ii})–C(8)–C(9)	69.3(3)
Cl(1)–Cu(1)–C(23)	124.4(2)	Cl(2)–Cu(2)–C(56)	124.3(2)	Cl(3)–Cu(3^{ii})–C(89)	123.2(2)
Cl(3)–Cu(1)–C(23)	117.5(2)	Cl(1)–Cu(2)–C(56)	119.7(2)	Cl(2)–Cu(3^{ii})–C(89)	117.4(2)
Cl(4)–Cu(1)–C(23)	110.6(2)	Cl(4)–Cu(2)–C(56)	111.3(2)	Cl(4)–Cu(3^{ii})–C(89)	111.5(2)
Cu(1)–Cl(1)–Cu(2)	89.18(5)	Cu(2)–Cl(2)–Cu(3)	89.63(6)	Cu(3)–Cl(3)–Cu(1)	87.10(5)
Cu(1)–Cl(4)–Cu(2)	79.96(5)	Cu(2)–Cl(4)–Cu(3)	81.88(5)	Cu(3)–Cl(4)–Cu(1)	79.35(5)
O(1)–C(1)–C(2)	122.6(4)	O(2)–C(4)–C(9)	120.8(5)	O(3)–C(7)–C(6)	121.6(5)
O(1)–C(1)–C(3^{i})	121.3(4)	O(2)–C(4)–C(5)	121.7(5)	O(3)–C(7)–C(8)	121.4(5)
C(2)–C(1)–C(3^{i})	116.1(4)	C(5)–C(4)–C(9)	117.5(4)	C(6)–C(7)–C(8)	117.1(4)
C(1)–C(2)–C(3)	122.7(4)	C(5)–C(6)–C(7)	121.4(5)	C(4)–C(9)–C(8)	121.8(4)
C(2)–C(3)–C(1^{i})	121.2(4)	C(4)–C(5)–C(6)	121.1(4)	C(7)–C(8)–C(9)	121.0(4)
C(1)–C(2)–H(C2)	112(3)	C(7)–C(6)–H(C6)	113(4)	C(4)–C(9)–H(C9)	114(3)
C(3)–C(2)–H(C2)	123(3)	C(5)–C(6)–H(C6)	125(4)	C(8)–C(9)–H(C9)	123(3)
C(1^{i})–C(3)–H(C3)	111(3)	C(4)–C(5)–H(C5)	118(3)	C(7)–C(8)–H(C8)	114(3)
H(N)1–N–H(N)2	113(7)	H(N)2–N–H(N)3	107(6)	H(N)3–N–H(N)4	113(6)
H(N)1–N–H(N)3	112(6)	H(N)2–N–H(N)4	110(7)	H(N)1–N–H(N)4	102(7)
H(W)1–O(W)–H(W)2	119(7)				

a) The superscripts, here and elsewhere in this paper, refer to the following equivalent positions: none) x, y, z; i) $1-x$, $-y$, $-z$; ii) $1-x$, $1/2+y$, $1/2-z$. b) C(23), C(56), and C(89) are the centers of the C(2)–C(3), C(5)–C(6), and C(8)–C(9) bonds respectively.

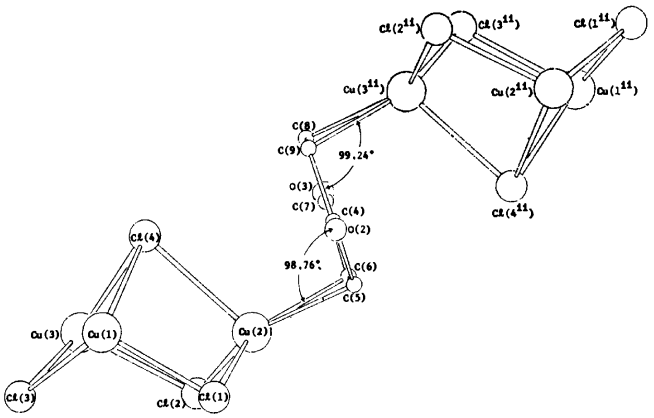

Fig. 3. Edge-on view of the p-BQ molecule lying at the general position. Similarly, the p-BQ molecule lying at the center of symmetry is coordinated to Cu(1) and Cu(1^{i}) so that its molecular plane makes an angle of 98.31° with the plane defined by C(2), C(3), and Cu(1).

beehive-like layers formed by $Cu_3Cl_4^-$ anions and p-BQ molecules, and of intra- and interlayer hydrogen bonds of the N–H···O type within the tunnel-like holes of the beehives.

Molecular Structure. The Cu_3Cl_4 moiety has a cap-like structure with an approximate threefold symmetry axis passing through the apex, Cl(4), and the midpoint of the three Cu atoms. The bond distances in the ring of the six-membered zigzag Cu–Cl chain range from 2.271(2) to 2.363(2) Å, while the three Cu–Cl(4) bonds bridging to the ring have distances ranging from 2.491(1) to 2.520(1) Å. The former and latter values are comparable respectively to the distances of the bidentate- and tridentate-chlorine-to-copper bonds found in other Cu(I) chloride complexes.[11,12] The bond angles within the Cu_3Cl_4 moiety fall into three groups; angles of about 109° between the ring Cl atoms subtended at each Cu atom, angles of about 80° at Cl(4), and the other angles of about 90°. Inspection

of these bond distances and angles suggests that the geometry of the Cu_3Cl_4 moiety may be described also as a distorted cubane-type with one corner missing. It has been found that the Cu_4Cl_4 core of $(P\cdot Ph_3CuCl)_4$ has a cubane-type structure in which each of the four Cu atoms has a distorted tetrahedral coordination, with Cu–Cl bond distances ranging from 2.362(2) to 2.505(2) Å.[13] In BQ-Red, each of the three Cu atoms has a distorted tetrahedral geometry coordinated by three Cl atoms and one *p*-BQ molecule, and the angles at the Cu atoms between the centers of their nearest C–C bonds and Cl atoms vary from 110.6(2) to 124.4(2)°. Such an environment around the Cu atom has also been found in $C_6H_6\cdot CuAlCl_4$, where the Cu atom has a distorted tetrahedral geometry coordinated by three Cl atoms and one benzene molecule acting as a mono-olefinic ligand.[14]

There are two crystallographically independent *p*-BQ molecules, one lying at an inversion center and the other at a general position. The latter has an approximate center of symmetry, though O(3) is the only oxygen atom not involved in hydrogen-bond formation. None of the bond distances or angles in either molecule is significantly different from the values obtained by gaseous electron diffraction.[15] Both molecules are also substantially planar, within the maximum deviations of 0.015 and 0.024 Å from their best-fit planes, despite that each of these molecules bridges two $Cu_3Cl_4^-$ anions with strong interactions.

The thermal-motion analysis has been applied to the three moieties of the $Cu_3Cl_4^-$ and the two independent *p*-BQ molecules in terms of the rigid-body model of translation and libration. The results suggest that both the *p*-BQ molecules behave as non-rigid bodies, in contrast with the Cu_3Cl_4 moiety, which behaves as a rigid body. This may be attributable to the polymeric structure. The thermal-motion corrections of the bond distances and angles were not applied in this work.

The authors are grateful to Professor Kawasaki at the Faculty of Pharmaceutical Sciences of Kyushu University for allowing them to use the automated diffractometer, and to Asst. Professor Kawano at the College of General Education of this university for his advice on the computation process.

References

1) H. Yamaguchi, H. Kimura, and K. Yasukouchi, *Bull. Chem. Soc. Jpn.*, **52**, 2056 (1979).
2) P. Main, M. M. Woolfson, and G. Germain, "MULTAN, A Computer Program for the Automatic Solution of Crystal Structures," Univ. of York, England (1971).
3) D. W. J. Cruickshank, "Computing Methods in Crystallography," ed by J. S. Rollett. Pergamon Press, Oxford (1965), p. 112.
4) G. H. Stout and L. H. Jensen, "X-Ray Structure Determination," Macmillan, London (1968).
5) "International Tables for X-Ray Crystallography," Kynoch Press, Birmingham (1974), Vol. IV, p. 72.
6) R. F. Stewart, E. R. Davidson, and W. T. Simpson, *J. Chem. Phys.* **42**, 3175 (1965).
7) T. Sakurai, H. Iwasaki, Y. Watanabe, K. Kobayashi, Y. Bando, and Y. Nakamichi, *Rep. Inst. Phys. Chem. Res.*, (in Japanese), **50**, 75 (1972).
8) C. K. Johnson, "ORTEP," Oak Ridge National Laboratory Report ORNL-3794 (1965).
9) L. Pauling, "The Nature of the Chemical Bond," 3rd ed, Cornell Univ. Press, Ithaca (1960).
10) M. B. Dines and P. H. Bird, *J. Chem. Soc., Chem. Commun.*, **1973**, 12.
11) A. Camus, G. Nardin, and L. Randaccio, *Inorg. Chim. Acta*, **12**, 23 (1975), and the references cited therein.
12) J. T. Gill, J. J. Mayerle, P. S. Welcker, D. F. Lewis, D. A. Ucko, D. J. Barton, and D. Stowens, *Inorg. Chem.*, **15**, 1155 (1976), and the references cited therein.
13) M. R. Churchill and K. L. Karla, *J. Am. Chem. Soc.*, **95**, 5772 (1973).
14) R. W. Terner and E. L. Amma, *J. Am. Chem. Soc.*, **88**, 1877 (1966).
15) K. Hagen and K. Hedberg, *J. Chem. Phys.*, **59**, 158 (1973).

The Kinetics of the Polymerization of Silicic Acid

Kanichi SHIMADA and Toshikazu TARUTANI*

Department of Chemistry, Faculty of Science, Kyushu University, Hakozaki, Higashi-ku, Fukuoka 812

(Received July 16, 1979)

The process of the polymerization of silicic acid can be divided into three steps: (1) a reaction between monosilicic acids, (2) a reaction between monosilicic and polysilicic acids, and (3) a reaction between polysilicic acids. The rates of the reactions between monomer-monomer, monomer-polymer and polymer-polymer are most rapid at pH values around 9.3, 8.5, and 6.8 respectively. It is concluded that, above about pH 4, the polymerization due to Reactions 1, 2, and 3 proceeds mainly by a reaction between ionized and un-ionized silanol groups.

The rate of the polymerization of silicic acid differs with the pH values of the solution.[1-4] The polymerization of silicic acid is rapid in weakly alkaline and strongly acidic solutions, but very slow in the pH range of 1—3. The kinetics of polymerization of silicic acid have been studied by colorimetry,[1,4] because monosilicic acid reacts with a molybdate reagent in an acidic solution to give a yellow color, whereas polysilicic acid does not react with a molybdate reagent. However, no information is available on the change in particle size of the polymers with time. From a gel chromatographic study of the polymerization of silicic acid, it has been suggested that the mechanism of the growth of particles of polysilicic acid differs with the pH.[5]

The process of the polymerization of silicic acid may be divided into three steps.

(1): A reaction between monosilicic acids.
(2): A reaction between monosilicic and polysilicic acids.
(3): A reaction between polysilicic acids.

The first step of the polymerization of monosilicic acid is to form disilicic acid by the Reaction 1. If it can be assumed that, in the early stage of polymerization, the decrease in the concentration of monosilicic acid in solutions of various pH values is due mainly to Reaction 1, it may be possible to obtain the relationship between the rate of Reaction 1 and the pH.

When the concentration of monosilicic acid is higher than the solubility of amorphous silica at a given pH, monosilicic acid generally polymerizes, but the rate of polymerization depends on the concentration of monosilicic acid. In a solution with an adequate concentration of monosilicic acid, Reaction 1 does not occur within a certain period of time. Therefore, when monosilicic acid solution in which Reaction 1 does not occur within a certain period of time is mixed with a polysilicic acid solution and the concentration of monosilicic acid decreases with time from the moment of mixing the solutions, it is concluded that the decrease in the concentration of monosilicic acid is due mainly to Reaction 2.

When the concentration of monosilicic acid is close to the solubility of amorphous silica at a given pH, Reactions 1 and 2 virtually do not occur. As Reaction 3 proceeds regardless of the presence of monosilicic acid, the effect of the pH on the reaction between polysilicic acids can be measured by gel chromatography from the change in elution curves for silicic acid in the solutions of various pH values.

The present paper describes the effect of the pH on the rate of Reactions 1, 2, and 3. The term "monosilicic acid" here indicates the total sum of monosilicic acid (H_4SiO_4) and its conjugate base ($H_3SiO_4^-$), unless otherwise specified, while the term "polysilicic acid" indicates the dimer and larger polymer species.

Experimental

Sample Solution and Reagents. All the reagents used were of an analytical reagent grade. The monosilicic acid stock solution was prepared by fusing 0.500 g of anhydrous silica with 2.5 g of sodium carbonate, dissolving the melt in distilled water, and diluting the solution to 500 cm^3. A solution of Blue Dextran 2000 (Pharmacia Fine Chemicals, 0.4%) was used for the measurement of the void volume of gel bed in gel chromatography. The eluent for elution of silicic acid and Blue Dextran 2000 was a 0.1 mol/dm^3 sodium chloride solution of pH 2.

Preparation of Sephadex Column. Sephadex G-100 (Pharmacia Fine Chemicals) was suspended in the solution to be used as an eluent and was allowed to swell for three days. The column was a 1.0×45 cm or 1.5×45 cm glass tube with a porous polystyrene disc at the bottom. The Sephadex G-100 column was prepared as has been described in the literature.[6]

Procedure for Determination of Reaction 1. The monosilicic acid solution (500 ppm SiO_2) was adjusted to the desired pH with hydrochloric acid. After 5, 10, and 15 min, the concentration of monosilicic acid was measured by colorimetry.

Procedure for Determination of Reaction 2. The pH of the monosilicic acid solution (500 ppm) was adjusted to 8.3 with hydrochloric acid. After the solution had stood for 5 h, the pH of this solution was adjusted to 2 with hydrochloric acid, because polymerization and depolymerization do not occur for a short period at pH 2.[4] The concentration of monosilicic acid in this solution (Solution A) was 205 ppm, with the remainder being polysilicic acid. Several sample solutions containing 314 ppm of monosilicic acid and 187 ppm of polysilicic acid were prepared by mixing aliquots of Solution A and a 1000 ppm monosilicic acid solution. At the same time, the sample solutions were adjusted to the pH range of 6.9—9.6. After the solution had stood for 30 min, the concentration of monosilicic acid was measured by colorimetry and the silicic acid was chromatographed on Sephadex G-100 column. Elution was performed with a procedure similar to one previously reported.[5]

Procedure for Determination of Reaction 3. The pH of the monosilicic acid solution (500 ppm) was adjusted to 8 with hydrochloric acid. After the solution had stood for 5 h, the pH of this solution was adjusted to 2 with hydrochloric acid. The polysilicic acid was concentrated by the addition of dried Sephadex G-25 gel to the solution. After this treatment, the concentrations of monosilicic acid and polysilicic acid in

Table 1. The concentrations of monosilicic acid in initial sample solutions of various pH values

pH	SiO_2(ppm)	pH	SiO_2(ppm)
1	150	6	115
2	190	7	110
3	190	8	120
4	140	9.5	210
5	120	10	320

the solution (Solution B) were 179 and 536 ppm respectively. Ten sample solutions of various pH values containing 350 ppm polysilicic acid and monosilicic acid, in concentrations of various pH values shown in Table 1, were prepared by mixing solution B, a 1000 ppm monosilicic acid solution, distilled water, and a sodium hydroxide solution or hydrochloric acid. After the solutions had stood for 48 h, the pHs of these sample solutions were adjusted to 2 and the silicic acid was chromatographed.

All the experiments were carried out at 20 ± 1 °C.

Results

Effect of pH *on the Reaction between Monosilicic Acids.* The kinetics of polymer formation obtained by monitoring the concentration of monosilicic acid as functions of time and the pH is shown in Fig. 1. As it can be assumed that the decrease in the concentration of monosilicic acid is due mainly to the formation of disilicic acid by a Reaction 1 in an early stage of the polymerization, it is considered that the pH of the maximum of the decrease in the concentration of monosilicic acid after a few minutes may close to the pH at which the rate of the formation of disilicic acid is maximal. The pH giving the maximum rate of decrease in the concentration of monosilicic acid slightly shifted to a lower pH with lapse of time. This may be due to the effect of polymer formation by Reaction 2 as will be discussed later. The results indicate that the reaction between monosilicic acids is most rapid at a pH value around 9.3.

Effect of pH *on the Reaction between Monosilicic and Polysilicic Acids.* When the pHs of 330 ppm monosilicic acid solutions were adjusted to 8.6 and 9.0, the concentration of monosilicic acid in these solutions did not decrease within 30 min. That is, the monosilicic acid does not polymerize within this short period of time under these conditions. If the concentration of monosilicic acid decreases from the moment of mixing after polysilicic acid is introduced into the monosilicic acid solution of about 300 ppm, it may be concluded that the decrease in monosilicic acid is caused by the reaction between monosilicic and polysilicic acids. The procedure for the determination of Reaction 2 has been done under these conditions. The results are shown in Fig. 2. The decrease in the concentration of monosilicic acid was maximal at a pH value around 8.5.

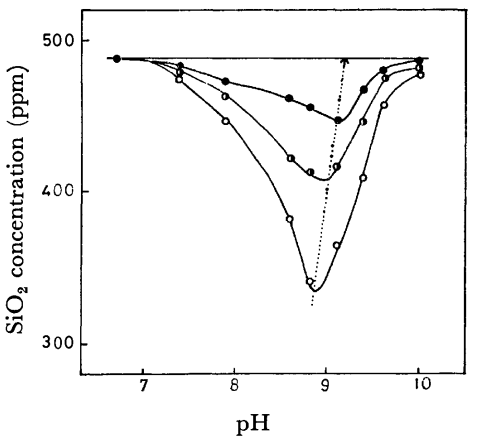

Fig. 1. Variation of the concentration of monosilicic acid as a function of pH. Time after ajusting pH: 5 min (—●—), 10 min (—◑—), 15 min (—○—).

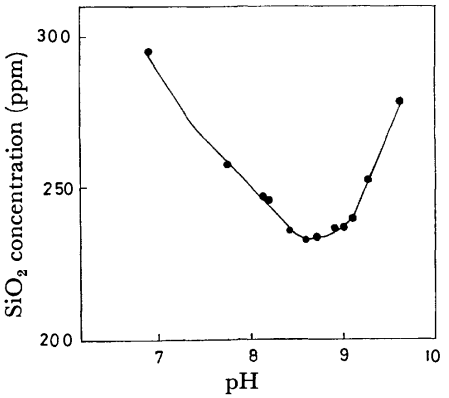

Fig. 2. Change in the concentration of monosilicic acid with pH after 30 min when polysilicic acid was added in monosilicic acid solutions.

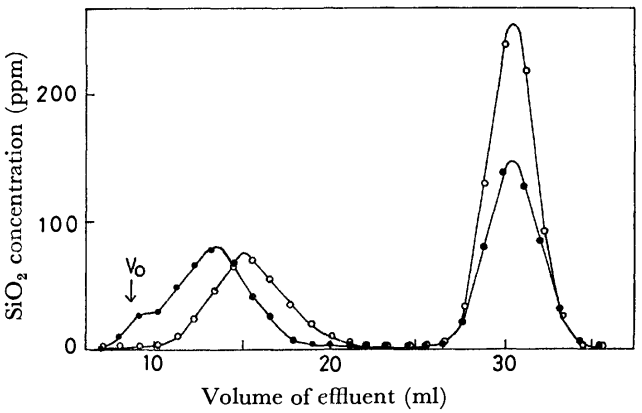

Fig. 3. Variation of elution curves for silicic acid in the solution of pH 8.9 with time. (Column, 1×45 cm). Initial solution: (—○—), solution after 30 min: (—●—).

The variation in elution curves for silicic acid with time is shown in Fig. 3. The position shown as V_0 is the elution volume of Blue Dextran 2000, which is considered not to be able to diffuse in the gel phase. It can be assumed that the elution volume of Blue Dextran is equal to the void volume of the bed. The peaks on the right are due to monosilicic acid, while the peaks on the left are due to polysilicic acid. The elution curve for silicic acid in the initial solution is symmetrical. The elution curve for the polysilicic acid in the solution shifts to the left after 30 min, but the shape of the elution curve, except shoulder at the V_0 position, is almost the same as that obtained from the initial solution. The shoulder of the elution curve at the V_0

position means that polysilicic acids larger in size than the possible separation range of the gel are eluted together at the V_0 position. If the growth of particles of polymers is due mainly to polymerization between monomer and polymer, the elution curves for polysilicic acid are symmetrical, and this symmetry is maintained in spite of the lapse of time.[5] The results shown in Fig. 3 reveal that the growth of the particles of the polymers is due mainly to the polymerization between monomer and polymer. From the results shown in Figs. 2 and 3, it is concluded that the polymerization between monomer and polymer is most rapid at a pH value around 8.5.

Effect of pH *on the Reaction between Polysilicic Acids.*

The concentrations of monosilicic acid shown in Table 1 are close to the solubility of amorphous silica at a given pH.[1,7,18] Reactions 1 and 2 did not occur in 1.0—10.0 pH range within 48 h. As the reaction between polymers proceeds regardless of the presence of monosilicic acid, the results obtained by the procedure used for the determination of Reaction 3 give the relationship between Reaction 3 and the pH. The elution curves for silicic acid in solutions of various pH values after they have stood for 48 h are shown in Fig. 4. The elution curve for silicic acid in the solution of pH 2 did not change within 48 h. This elution curve represents the distribution of particle sizes of silicic acids in initial solutions of various pH values. In the solutions above pH 4, the elution curves due to polymers shifted to the left after 48 h compared with that at pH 2. This means that the particle sizes of polymers became larger than in the initial solutions. The elution curve for silicic acid in the solution of pH 3 after 48 h was identical with that in the initial solution.

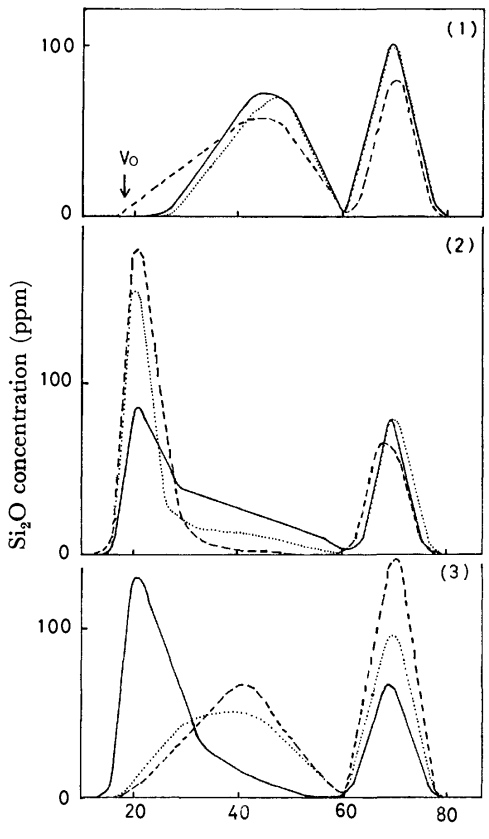

Fig. 4. Variation of elution curves for silicic acid in the solutions of various pH. (Column, 1.5×45 cm).
(1): pH 1 (——), pH 2 (·····), pH 4 (– – –), (2): pH 5 (——), pH 6 (·····), pH 7 (– – –), (3): pH 8 (——), pH 9.5 (·····), pH 10 (– – –).

Laurent and Killander[8] defined a constant, K_{av}, for a given gel in gel chromatography:

$$K_{av} = \frac{V_e - V_o}{V_t - V_o}$$

where V_0 is the void volume; V_t, the total bed volume, and V_e, the elution volume. Here, V_0, V_t, and V_e are easily measured. As the K_{av} value is correlated to V_e, it is a measure of the particle size and decreases with an increase in the particle size. As the elution volumes of polymers can not be obtained directly from the elution curves shown in Fig. 4, the mean elution volumes must be calculated using the following relationship;

$$V_e = \sum C_i V_i / \sum C_i$$

where V_e is the mean elution volume, C_i is the concentration in the i-th fraction, and V_i is the volume of the i-th fraction. The relationship between the pH and the K_{av} values of polysilicic acids in the solutions of various pHs after 48 h is shown in Fig. 5. It appears that the K_{av} value of polysilicic acid is at its minimum at a pH around 6.8. The results show that the rate of reaction between polysilicic acids is most rapid at a pH around 6.8.

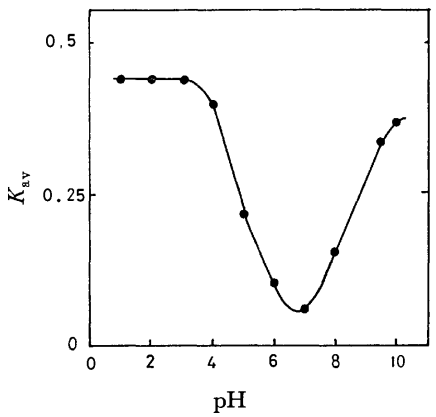

Fig. 5. Plot of K_{av} against pH.

Discussion

The rates of the reactions between monomer-monomer, monomer-polymer, and polymer-polymer are most rapid at pH values around 9.3, 8.5, and 6.8 respectively. From the variation in ammonium molybdate reactive monosilicic acid, Richardson and Waddams[9] found that the polymerization is most rapid between pH 8—9. Merrill and Spencer[10] reported that the pH at the minimum gel time is about 7; Ray and Gangly[11] obtained similar results for gelation reactions. This discrepancy in the pH at which the maximum polymerization takes place can be explained by the facts that Richardson and Waddams measured the rate of polymerization caused by Reactions 1 and 2,

while, on the other hand, Merrill and Spencer measured the rate of Reaction 3.

As singly ionized monosilicic acid forms in a basic solution, the concentration of the singly ionized form becomes higher with an increase in the pH. Ashley and Innes[12] proposed that the polymerization of silicic acid proceeds by a reaction between singly ionized and un-ionized silicic acids. Reaction 1 does have its maximum

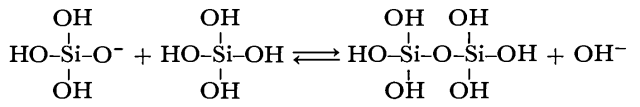

rate at a pH around 9.3 (Fig. 1). At this pH the concentration of un-ionized silicic acid and the singly ionized form is reasonably high; Greenberg and Sinclair[13] calculated the $(H_3SiO_4^-)/(H_4SiO_4)$ ratio based on the reported ionization constant of silicic acid and obtained the ratio of 1/1 at pH 9.5. As the pH giving the maximum rate of Reaction 1 is almost the same as that giving the $(H_3SiO_4^-)/(H_4SiO_4)$ ratio of 1/1, it is concluded that Reaction 1 mainly proceeds by the reaction of singly ionized silicic acid and un-ionized silicic acid, and that the rate of the formation of disilicic acid reaches its maximum at the pH at which the $(H_3SiO_4^-)/(H_4SiO_4)$ ratio is unity.

Komura *et al.*[15] have reported that the point of the zero charge of colloidal silica is pH 3.5 and that the negative charge of colloidal silica increases with an increase in the pH. If it can be assumed that the reaction between monosilicic acid and polysilicic acid is a reaction between a negatively charged site on the surface of polysilicic acid and un-ionized monosilicic acid, the rate of the polymerization due to Reaction 2 will reach its maximum at the pH at which the concentration of the negative ionic charge of polysilicic acids and un-ionized monosilicic acid is reasonably high. It is expected that the pH giving the maximum rate of polymerization by Reaction 2 is lower than that giving that by Reaction 1 because of the high concentration of un-ionized monosilicic acid at low pHs. The results show that the rate of polymerization due to Reaction 2 is most rapid at a pH around 8.5 (Fig. 2). At pH 8.5, the concentration of the negative charge of polysilicic acids is high and monosilicic acid mainly exists as an un-ionized form. Above pH 8.5, the concentration of the negative charge of polysilicic acids increases, and the concentration of un-ionized monosilicic acid decreases, with an increase in the pH. Below pH 8.5, the concentration of the negative charge of polysilicic acids decreases, and the concentration of un-ionized monosilicic acid increases, with a decrease in the pH. As is shown in Fig. 2, the rate of Reaction 2 becomes slow below and above pH 8.5. This means that Reaction 2 mainly proceeds by the reaction between an ionized silanol group of polysilicic acids and un-ionized monosilicic acid.

The isoelectric point of colloidal silica is between pH 1 and 2,[14] while the point of the zero charge of colloidal silica is pH 3.5.[15] However, below pH 3.5, the stability of polysilicic acid is very high in spite of these being no charge of polysilicic acids (Fig. 5). The DLVO theory can not be applied to this system. As negative ionic charges of silica particles increase with an increase in the pH, and as, above pH 9, a sufficient concentration of the negative charge is developed on the surface of the particles, causing mutual repulsion, the rate of Reaction 3 becomes very slow.[5] When it can be assumed that the growth of polymer particles due to Reaction 3 is mainly caused by the formation of Si–O–Si bonds by the reaction of $Si–O^-$ and Si–OH, and that the concentrations of Si–OH and $Si–O^-$ on the surface of polymer particles are suitable, there may be an optimum pH at which the rate of growth of particles is at its maximum. The rate of Reaction 3 is maximal at a pH around 6.8 (Fig. 5), for at this pH polysilicic acids have a negative charge and there may be a repulsive force between polymers. However, as Reaction 3 is most rapid at pH 6.8, it is suggested that repulsive force between polymers is weak at this pH and that polymers can collide. As the value of the acidity constant of the silanol group, Si–OH, on the surface of colloidal silica is around $pK_a=7$,[14–16] the ratio of Si–OH and $Si–O^-$ on the surface of polymers may be unity at a pH of about 7. As the rate of Reaction 3 is at its maximum at pH 6.8, it is concluded that the rate of Reaction 3 is controlled by the concentrations of ionized and un-ionized silanol groups in the same manner as in Reaction 1. From the experimental evidence of this study, it is concluded that, above about pH 4, the polymerization due to Reactions 1, 2, and 3 mainly proceeds by a reaction between ionized and un-ionized silanol groups.

References

1) T. Tarutani, *Nippon Kagaku Zasshi*, **77**, 1721 (1956).
2) T. Kojima and T. Tarutani, *Mem. Fac. Sci., Kyushu Univ., Ser. C, Chem.*, **9**, 1 (1974).
3) R. K. Iler, "The Colloid Chemistry of Silica and Silicate," Cornell Univ. Press, Ithaca, N. Y. (1955).
4) T. Tarutani, *J. Chromatogr.*, **50**, 523 (1970).
5) K. Shimada and T. Tarutani, *J. Chromatogr.*, **168**, 401 (1979).
6) L. Fisher, "An Introduction to Gel Chromatography," North-Holland, Amsterdam (1969).
7) G. B. Alexander, W. M. Heston, and R. K. Iler, *J. Phys. Chem.*, **58**, 453 (1954).
8) T. C. Laurent and J. Killander, *J. Chromatogr.*, **14**, 317 (1964).
9) E. Richardson and J. A. Waddams, *Research*, **7**, S42 (1954).
10) R. C. Merrill and R. W. Spencer, *J. Phys. Chem.*, **54**, 806 (1950).
11) R. C. Ray and P. B. Gangly, *J. Phys. Chem.*, **34**, 352 (1930).
12) K. D. Ashley and W. B. Innes, *Ind. Eng. Chem.*, **44**, 2857 (1952).
13) S. A. Greenberg and D. Sinclair, *J. Phys. Chem.*, **59**, 435 (1955).
14) K. Mushiake and N. Masuko, *Seisankenkyu*, **29**, 2 (1977).
15) A. Komura, K. Hatsutori, and H. Imanaga, *Nippon Kagaku Zasshi*, **1978**, 779.
16) D. N. Strazhesko, V. B. Strelko, V. N. Belyakov, and S. C. Rubanik, *J. Chromatogr.*, **102**, 191 (1974).
17) M. L. Hair and W. Hertle, *J. Phys. Chem.*, **74**, 91 (1970).
18) W. F. Linke, "Seidell's Solubilities," 4th ed, Am. Chem. Soc., Washington, D. C. (1965), Vol. 2, p. 1452.

Mass Spectrometric Studies of Some Carboxylic Acid Dimers Produced by a Nozzle Beam: HCO_2H, CH_3CO_2H, $C_2H_5CO_2H$, and n-$C_3H_7CO_2H$

Yoshihiro MORI,* Taiji KITAGAWA, Tomoki YAMAMOTO, Kazuo YANADA, and Shigeru NAGAHARA

Department of Pharmaceutical Sciences, Toyama Medical and Pharmaceutical University, Sugitani, Toyama 930-01

(Received December 10, 1979)

Characteristic ions $(M+1)^+$ and $(M+45)^+$, assigned to be the protonated monomer ion MH^+ and $(M\cdot CO_2H)^+$ respectively, have been detected in the mass spectrometric measurements of the dimer molecules M_2 and the higher clusters M_n of some carboxylic acids produced in their nozzle beams. It has been shown from the dependences of their relative intensities on the stagnation conditions that these ions are mainly formed through the fragmentation of the dimer ions. The MH^+ ion plays the most important role in these fragmentation processes of the dimers, while no dimer ion M_2^+ was observed. These results are discussed in terms of the enthalpy changes for the unimolecular decomposition reactions of M_2^+.

Protonated cluster ions $M_{n-1}H^+$ as well as $M_n^+(n\geq 2)$ have been observed in some hydrogeneous molecules, such as H_2O,[1] NH_3,[2] hydrogen halides,[3] and alcohols,[4] through electron or photon impact ionization of their cluster molecules produced using supersonic nozzle beams. The reactions to form these protonated ions have been explained by the unimolecular decomposition reaction of M_n^+.[5] However the detailed mechanisms vary with different molecules[3b] and the degree of their association,[5] and also depend on the impact energy of the electron or photon.[2]

A variety of new fragment ions other than the protonated ones have been observed in the ionization of van der Waals clusters of butane[6] and ethylene.[7] Some of them have been regarded as the key species in the ion-molecule reactions. These findings on the electron or photon impact induced fragmentations of the weakly bound clusters have enabled us to discuss the mechanisms of ion-molecule reactions[5,7] and the solvation of ions in the gas phase[1,2,5] from some different viewpoints. So it is of great interest to make clear such fragmentation processes of these cluster molecules and ions.

In this paper we report several common features observed in the electron impact induced fragmentations of the dimers of some aliphatic carboxylic acids produced in their nozzle beams. These acids have been well known to form a stable cyclic dimer through intermolecular hydrogen bonds even in the usual vapor phase.[8]

Experimental

The nozzle beam system in this experiment is shown in Fig. 1. A 60° conical nozzle source which has a 0.015 cm diameter orifice at the apex of this cone was used. The nozzle was fastened to the reservoir with a thin teflon gasket. No skimmer was used. Some copper plates with a circular opening of 1 cm diameter for the beam, cooled by liquid nitrogen, were used as a cryopump. This nozzle source has previously been employed in the optical measurements of naphthalene beams and has been compared with other nozzles having different shapes and orifice diameters.[9] Using this source, we could observe reasonable cooling effects and mach numbers, accompanied by the adiabatic expansion of pure naphthalene vapor.

The temperature T_0 at the nozzle throat was measured with a Fe-Constantan thermocouple mounted on the external face of the nozzle plate. The stagnation pressure P_0 behind the nozzle was determined by adjusting the temperature of the liquid carboxylic acid in the reservoir F according to the published data of vapor pressure.[10] Within the range of T_0 and P_0 in this work, the dimer fraction evaluated from the observed equilibrium constant[11] could be covered over the wide range from 0.1 to 0.6 in the stagnation conditions.

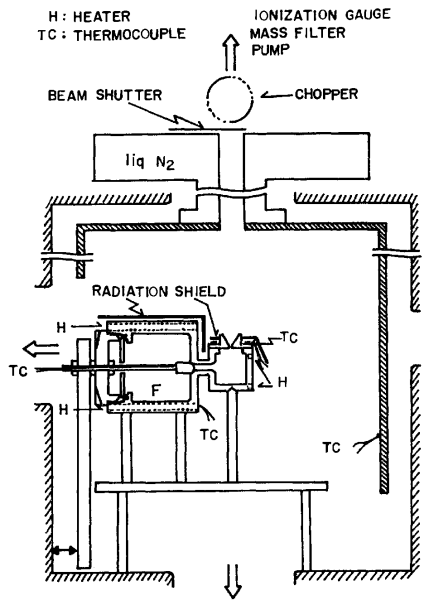

Fig. 1. Experimental apparatus for the measurements of mass spectra in the nozzle beam.

The beams were mechanically modulated at a frequency of 20—100 Hz and then directed into the ionizer of a quadrupole mass filter (Nichiden Varian model 531) equipped with a Bayard-Alpert gauge-type ionizer. Most measurements were carried out at the electron energy of 30 eV and the emission current of 1.0 mA. No marked dependences of mass spectra on the electron energy were observed in the range of 20 eV to 100 eV. To get the corrected intensities for the relative sensitivity of the secondary electron multiplier, the observed intensities of the ions with $m/e\geq 28$ were multiplied by the dimensionless factor $(m/28)^{1/2}$.[12]

Commercially available extra pure CH_3CO_2H, $C_2H_5CO_2H$, n-$C_3H_7CO_2H$, and HCO_2H were used after a distillation *in vacuo*. Deuterated CH_3CO_2D and CD_3CO_2D enriched more than 97—98% were commercially supplied.

Results and Discussion

Mass spectra of the four carboxylic acids RCO_2H (R=H, CH_3, C_2H_5, and n-C_3H_7) were measured in the nozzle beams as a function of T_0 and P_0 in stagnation conditions in the mass range from 1 up to 310. Two peaks, corresponding to the mass numbers of $(M+1)^+$ and $(M+45)^+$, were observed for all the acids, in addition to the previously reported mass spectrum of each monomer acid (M).[13]

Table 1. Mass shifts of MH^+ and $(M\cdot CO_2H)^+$ fragment ions in the deuterated acetic acid beams

Beam		CH_3CO_2H	CH_3CO_2D	CD_3CO_2D
T_0/K		374	369	381
P_0/Torr		100	120	160
Ion	m/e	Relative intensity		
M^+ and MH^+	60	1.0	0.028	
	61	0.35	1.0	
	62	0.008	0.044	
	63		0.39	0.025
	64		0.009	1.0
	65			0.025
	66			0.40
	67			0.010
$(M\cdot CH_3CO)^+$ and $(M\cdot CO_2H)^+$	103	0.0007		
	104		0.0005	
	105	0.0048	0.0001	
	106	0.0002		
	107		0.0058	
	108		0.0002	
	109		0.0001	0.0002
	110			0.0054
	111			0.0002

In order to assign these ions, mass spectra were measured in the nozzle beams of deuterated acetic acid, CD_3CO_2D and CH_3CO_2D. According to the results of the corresponding mass shift, these ions were assigned to the protonated monomer ion MH^+ and the adduct ion $(M\cdot CO_2H)^+$ ions, respectively. Table 1 summarizes the results of the mass shift and their relative intensities around the mass ranges of MH^+ and $(M\cdot CO_2H)^+$ ions in CH_3CO_2H, CH_3CO_2D, and CD_3CO_2D beams.

Figure 2 shows the temperature dependences of the relative intensities of MH^+ and $(M\cdot CO_2H)^+$ ions. It is clearly shown in the figure that MH^+ ion as well as $(M\cdot CO_2H)^+$ ion increases with decreasing T_0. From Fig. 2 the intensity ratios between MH^+ and $(M\cdot CO_2H)^+$ ions were obtained to be about 100, 2000, and 5000 for CH_3CO_2H, $C_2H_5CO_2H$, and n-$C_3H_7CO_2H$, respectively. In the case of the formic acid beam, it is difficult to obtain quantitative results for a long period of experimental runs because of a gradual corrosive reaction inside the nozzle source. But the results were qualtatively in accord with those obtained in the other acids and the intensity ratio $I_{MH^+}/I_{(M\cdot CO_2H)^+}$ was about 500.

Similar behaviors were observed in their pressure P_0

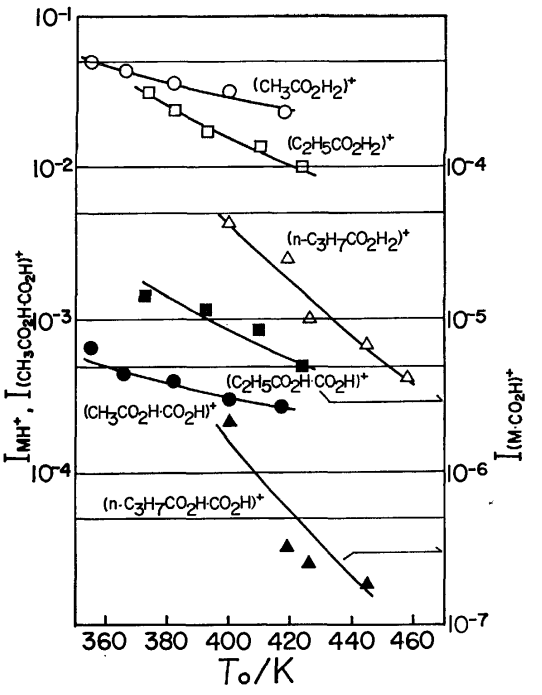

Fig. 2. Temperature dependences of the relative intensities of MH^+ and $(M\cdot CO_2H)^+$, I_{MH^+} and $I_{(M\cdot CO_2H)^+}$, normalized to the sum of each ion intensity, in CH_3CO_2H, $C_2H_5CO_2H$, and n-$C_3H_7CO_2H$ nozzle beams. The stagnation pressures were kept at about 140, 100, and 110 Torr, respectively. Open and full symbols represent MH^+ and $(M\cdot CO_2H)^+$, respectively. (1 Torr=133.322 Pa)

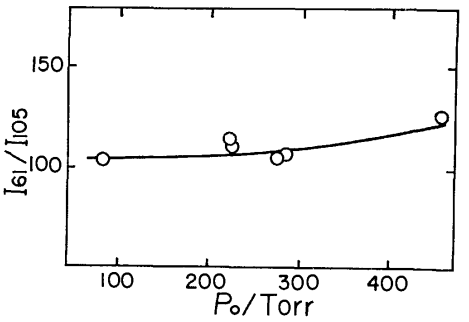

Fig. 3. Pressure dependence of intensity ratio between MH^+ and $(M\cdot CO_2H)^+$, I_{61}/I_{105}, at T_0=410 K for acetic acid. (1 Torr=133.322 Pa)

dependences. For acetic acid, this intensity ratio I_{61}/I_{105} was found to be nearly constant or slightly increasing with increasing P_0 as shown in Fig. 3.

Other fragment ions than MH^+ and $(M\cdot CO_2H)^+$ did not show such marked T_0 dependences within the range of T_0 in this study. Only RCO^+ ions (R=CH_3, C_2H_5, and n-C_3H_7) were found to slightly increase with decreasing T_0. Some portion of these acyl ion intensities might be ascribed to the dehydration reaction of MH^+ ion with excess energy.[14]

From such similar dependences of MH^+ and $(M\cdot CO_2H)^+$ ions on the stagnation conditions, both ions are considered to be formed by the electron impact fragmentation of the same molecular species, namely

the cluster molecules $M_n(n\geq 2)$, produced in their nozzle beams. However no traces of the dimer ion M_2^+ or of $M_n^+(n=3,4,5)$ were observed within the limit of the detection sensitivity, 10^{-6} of M^+. For these carboxylic acids, M_2H^+ ions with very weak intensities (10^{-4}—10^{-6} of M^+) were observed. But we could not definitely ascribe them to the fragmentation from $M_n^+(n\geq 3)$ because of the nearly equal contribution of ion-molecule addition reaction which presumably occurred in the ionizer. Only a small contribution of the higher clusters is suggested by the slight increase of MH^+ ion relative to $(M\cdot CO_2H)^+$ when P_0 increases, as can be seen in Fig. 3. This could be explained by the result that MH^+ fragment, not $M_{n-1}H^+$, is predominantly formed in the fragmentation processes of the parent cluster ion M_n^+.[15] Another reason for such an apparent small contribution of the higher clusters to these mass spectra is that some portion of the higher clusters and the dimer could be decomposed down to the dimer or the monomer on the electrode surface of the ionizer.

Thus we can conclude in this study that the observed MH^+ and also $(M\cdot CO_2H)^+$ ions are mainly formed through spontaneous decomposition of the dimer ions M_2^+, which can initially be generated in their vibrationally or electronically excited states by the electron impacts at 20—100 eV. The fragmentation to the protonated monomer ion is characteristic for these carboxylic acid dimer ions. These fragmentation behaviors resemble the case in $(HF)_2$,[3a] but are quite different from those in $(CH_3OH)_2$ and $(CH_3NH_2)_2$, where the intensity ratios $I_{M_2^+}/I_{MH^+}$ have been observed to be about 0.5.[4] Such differences can qualitatively be interpreted from some thermodynamical considerations about reaction (1):

$$M_2^+ \longrightarrow NH^+ + (M\text{-}H). \qquad (1)$$

The enthalpy change ΔH_2 for this unimolecular decomposition reaction can be estimated using the binding energy of M_2^+ ion, $-\Delta H_s(M_2^+)$, or the solvation energy of MH^+ by M, $-\Delta H_s(M_2H^+)$, and several thermodynamical parameters for a monomer molecule. The values of $\Delta H_s(M_2^+)$ have recently been obtained from the ionization potential measurements of the dimers by means of photoionization ($(H_2O)_2$[1c] and $(NH_3)_2$[2b]) and photoelectron spectroscopy ($(CH_3CO_2H)_2$[16]). The calculated values of ΔH_2 are shown in Table 2. It is shown that $(HF)_2^+$ ion spontaneously decomposes into H_2F^+ and F, while the decompositions of $(H_2O)_2^+$, $(NH_3)_2^+$, and $(CH_3OH)_2^+$ are rather endothermic. These trends are consistent with the observations of their M_2^+ ions in the eletron or photon impact ionization.[1-5] The decomposition of acetic acid dimer ion seems to be more endothermic, although this endothermicity may be reduced by the contribution of the entropy terms $T\Delta S_2$ for this reaction (1).[17] Nevertheless, no dimer ions of acetic acid nor of the other carboxylic acids were observed in this study. This fact suggests that there exist very effective channels to promote proton transfer along the hydrogen bond in the excited states of the dimer ions which strongly couple with MH^+ ion formation. At the present stage we can't explore these channels further, because we lack the experimental evidence about the state selected ionization or fragmentation. But these channels must greatly depend upon the cyclic structure of the dimer ion, which includes two hydrogen bonds.

Furthermore, we note that the dominant fragmentation is to $(M\cdot CO_2H)^+$ rather than to the $(M\cdot RCO)^+$ in the dimer ions. Indeed the observed intensity of $(M\cdot CH_3CO)^+$ ion for acetic acid was so weak (0.1 of $(M\cdot CO_2H)^+$) that the origins of this adduct ion were undecided for the same reasons as in M_2H^+. For propionic and butyric acids, no $(M\cdot RCO)^+$ ions could be detected. This trend contrasts with the observations in ion-molecule reactions, in which the $(M\cdot RCO)^+$ adduct ions have often been observed.[14,18]

Concerning $(M\cdot CO_2H)^+$ ions, the hydrogen bonded cyclic ion $(HCO_2H\cdot CO_2H)^+$ has been theoretically predicted from the β^- decay processes of monotritiated formic acid dimer $(HCO_2H\cdot {}^3HCO_2H)$.[19] It has been shown that in this ion the proton transfer occurs along the hydrogen bond with no activation energy to produce $HCO_2H_2^+$ and CO_2. This process could not be confirmed

Table 2. Estimated enthalpy changes ΔH_2 at 298 K for the reaction $M_2^+ \longrightarrow MH^+ + (M\text{-}H)$ (in kcal/mol) (1 kcal = 4.184 kJ)

ΔH_2[a]	$(H_2O)_2$	$(NH_3)_2$	$(CH_3OH)_2$	$(CH_3CO_2H)_2$	$(HF)_2$
	10 (6)[b]	2 (2—11)[b]	(15)[b]	26—29	(−7)[b]
D(H-XY)[c]	120[h]	107[j]	101[k]	110—112[n]	136[q]
ΔH_I(M)[d]	291[h]	235[j]	251[l]	246—247[o,p]	369[q]
ΔH_{PA}(M)[e]	169[i]	202[i]	182[i]	187[p]	112[r]
$-\Delta H_s(M_2^+)$[f]	36[h]	18[j]		36[p]	
$-\Delta H_s(M_2H^+)$[g]	(32)[i]	(18—27)[j]	(33)[m]		(25)[q]

a) $\Delta H_2 = D(H-XY) + I(H-H^+) - \Delta H_I(M) - \Delta H_{PA}(M) - \Delta H_s(M_2^+)$ (or $\Delta H_s(M_2H^+)$), where $I(H-H^+)$ = 314 kcal/mol. b) The ΔH_2 values in parentheses are estimated by assuming that $\Delta H_s(M_2^+)$ can be approximated to $\Delta H_s(M_2H^+)$.[5] c) Bond dissociation energy of the H–X bond (X=O, N, or F). d) Ionization potential of M. e) Proton affinity of M. f) Binding energy of M_2^+, where the values of $\Delta H_s(M_2^+)$ at 298 K are nearly equal to those at 0 K within the experimental errors in the determinations of $\Delta H_s(M_2^+)$ (a few kcal/mol). g) Solvation energy of MH^+ by M. h) Ref. 1c. i) P. Kebarle, *Ann. Rev. Phys. Chem.*, **28**, 445 (1977). j) Ref. 2b. k) K. J. Reed and J. I. Brauman, *J. Am. Chem. Soc.*, **97**, 1625 (1975). l) F. M. Benoit and A. G. Harrison, *J. Am. Chem. Soc.*, **99**, 3980 (1977). m) E.P. Grimsrud and P. Kebarle, *J. Am. Chem. Soc.*, **95**, 7939 (1973). n) K. W. Egger and A.T. Cocks, *Helv. Chim. Acta*, **56**, 1516 (1973); J. A. Kerr, *Chem. Rev.*, **66**, 465 (1966). o) D. J. Knowles and A. C. Nicholson, *J. Chem. Phys.*, **60**, 1180 (1974). p) Ref. 16. q) Ref. 3b. r) M.S. Foster and J. K. Beauchamp, *Inorg. Chem.*, **14**, 1229 (1975).

as the main channel of MH^+ ion formation in the present study, but our results suggest that the $(M \cdot CO_2H)^+$ ions are stable species.

Another point shown in this work is that the transferable proton in an M_2^+ ion to yield MH^+ fragment ion is the hydroxyl proton, not the alkyl ones. The proofs are given by comparing the amounts of $CH_3CO_2DH^+$ ion in the CH_3CO_2D beam. The relative intensity of $CH_3CO_2DH^+$ ion ($m/e=62$) to M^+ ($m/e=61$) was obtained to be 0.044 in Table 1. This value never exceeds the value estimated from the natural abundances of the isotopes (0.024) and the contribution of $CH_3CO_2DH^+$ ion produced from an impurity of CH_3CO_2H (0.025). Thus, no proton transfer can occur from those of acetyl group to the other M in a dimer ion in the fragmentation processes from the M_2^+. This result does not contradict the fact that $(M \cdot CH_3CO)^+$ ion has rarely been observed *via* fragmentation of M_2^+ ion, as mentioned above.

The present work was partially supported by Grants-in-Aid for Scientific Research No. 354134 and also No. 247004 from the Ministry of Education, Science and Culture. The authors gratefully thank Dr. K. Nomoto for helpful discussions.

References

1) a) J. Fricke, W. M. Jackson, and W. L. Fite, *J. Chem. Phys.*, **57**, 580 (1972); b) T. R. Dyke and J. S. Muenter, *ibid.*, **57**, 5011 (1972); c) C. Y. Ng, D. J. Trevor, P. W. Tiedemann, S. T. Ceyer, P. L. Kronebusch, B. H. Mahan, and Y. T. Lee, *ibid.*, **67**, 4235 (1977).

2) a) J. A. Odutola, T. R. Dyke, B. J. Howard, and J. S. Muenter, *J. Chem. Phys.*, **70**, 4884 (1979); b) S. T. Ceyer, P. W. Tiedemann, B. H. Mahan, and Y. T. Lee, *ibid.*, **70**, 14 (1979).

3) a) T. R. Dyke, B. J. Howard, and W. Klemperer, *J. Chem. Phys.*, **56**, 2442 (1972); b) P. W. Tiedemann, S. L. Anderson, S. T. Ceyer, T. Hirooka, C. Y. Ng, B. H. Mahan, and Y. T. Lee, *ibid.*, **71**, 605 (1979).

4) J. A. Odutola, R. Viswanathan, and T. R. Dyke, *J. Am. Chem. Soc.*, **101**, 4787 (1979).

5) C. E. Klots and R. N. Compton, *J. Chem. Phys.*, **69**, 1644 (1978).

6) T. A. Milne, J. E. Beachey, and F. T. Greene, *J. Chem. Phys.*, **56**, 3007 (1972).

7) S. T. Ceyer, P. W. Tiedemann, C. Y. Ng, B. H. Mahan, and Y. T. Lee, *J. Chem. Phys.*, **70**, 2138 (1979).

8) G. Allen and E. F. Caldin, *Quart. Rev.*, **7**, 255 (1953); P. A. Kollman and L. C. Allen, *Chem. Rev.*, **72**, 283 (1972).

9) K. Mawatari, H. Minami, Y. Mori, T. Kitagawa, and S. Nagahara, *Progress Report Studies of Atomic Collisions and Related Topics in Japan*, **3**, 96 (1977).

10) T. Boublik, V. Fried, and E. Hara, "The Vapour Pressure of Pure Substances," Elsevier, Amsterdam (1973).

11) CH_3CO_2H: J. R. Barton and C. C. Hsu, *J. Chem. Eng. Data*, **14**, 1841 (1969), $C_2H_5CO_2H$ and HCO_2H: M. D. Taylor and J. Bruton, *J. Am. Chem. Soc.*, **74**, 4151 (1952), n-$C_3H_7CO_2H$: R. E. Lundin, F. E. Harris, and L. K. Nash, *J. Am. Chem. Soc.*, **74**, 743 (1952).

12) J. Q. Searcy and J. B. Fenn, *J. Chem. Phys.*, **61**, 5282 (1974); sensitivity at $m/e \leq 28$ was regarded as constant.

13) G. P. Happ and D. W. Stewart, *J. Am. Chem. Soc.*, **74**, 4404 (1952).

14) G. I. Mackay, A. C. Hopkinson, and D. K. Bohme, *J. Am. Chem. Soc.*, **100**, 7460 (1978).

15) Y. Mori, T. Kitagawa, T. Yamamoto, and S. Nagahara, XIth International Conference on Physics of Electronic and Atomic Collisions, Kyoto, 1979, Abstr. 394.

16) K. Nomoto, Doctor thesis, Hokkaido University, Sapporo, 1978.

17) The largest term in $T\Delta S_2$ is given by $T\Delta S_s$ (M_2^+) for the reaction $M^+ + M \rightarrow M_2^+$. This contribution is estimated to be about -10 kcal/mol at 298 K, assuming that the entropy change ΔS_s (M_2^+) can be approximated by the entropy change for the neutral dimer formation of acetic acid. W. Weltner, Jr., *J. Am. Chem. Soc.*, **77**, 3941 (1955).

18) J. Long and B. Munson, *J. Chem. Phys.*, **95**, 2427 (1973).

19) S. Hashimoto, S. Ikuta, and M. Imamura, *Chem. Phys. Lett.*, **62**, 567 (1979); S. Ikuta, S. Hashimoto, and M. Imamura, *Chem. Phys.*, **42**, 269 (1979).

Is $O_2^*(a^1\Delta_g)$ Formed in the $O+O_3$, $H+O_3$, and $NO+O_3$ Reactions?

Nobuaki WASHIDA,* Hajime AKIMOTO, and Michio OKUDA
The National Institute for Environmental Studies, P.O. Tsukuba-gakuen, Tsukuba, Ibaraki 305
(Received March 11, 1980)

An attempt was made to detect $O_2^*(a^1\Delta_g)$ in the reactions of $O+O_3$, $H+O_3$, and $NO+O_3$ using a photoionization mass spectrometer. No significant signals for $O_2^*(a^1\Delta_g)$ were observed in these reactions. From the results, it is concluded that less than 0.06, 0.001, and 0.002 of the reactive collisions result in the production of $O_2^*(a^1\Delta_g)$ in the reactions of $O+O_3$, $H+O_3$ and $NO+O_3$ respectively, all at 298 K. The failure to observed $O_2^*(a^1\Delta_g)$ in these reactions was discussed by means of correlation diagrams and GVB model representations.

Recently, the observation of the singlet oxygen formed in the reaction of hydrogen atoms with molecular oxygen was reported in our laboratory.[1] In this system it was determined that the singlet oxygen was produced by the reaction of hydrogen atoms with hydroperoxyl radicals, which had themselves been formed by the recombination reaction of hydrogen atoms with molecular oxygen:

$$H + O_2 + M \rightarrow HO_2 + M \quad (1)$$

$$HO_2 + H \rightarrow H_2 + O_2^*(a^1\Delta_g) \quad (2)$$

A photoionization mass spectrometer was used to detect the singlet oxygen. When an argon lamp with a LiF window is used as a light source to photoionize the molecules, singlet oxygen can be photoionized by the argon resonance lines (11.83 and 11.62 eV), but ground-state molecular oxygen can not be ionized by these lines,[1,2] since the ionization potential for ground-state molecular oxygen is 12.06 eV, and the $O_2^*(a^1\Delta_g)$ and $O_2^*(b^1\Sigma_g^+)$ states are 0.98 and 1.63 eV higher than the ground-state respectively. The detection sensitivity of the photoionization mass spectrometer to singlet oxygen is quite high in comparison with the photometric detection by means of the forbidden $O_2^*(a^1\Delta_g) \rightarrow O_2(X^3\Sigma_g^-)$ transition. The detection limit is about 10^9—10^{10} molecules cm^{-3} for singlet oxygen in the reactor under good conditions (very low background signals and in the absence of the large signals around mass 32). Further, when photoionization mass spectrometry was used to detect singlet oxygen, the interference by the chemiluminescence in the reaction system was eliminated. For example, in the $H+O_2$ reaction system, singlet oxygen in the $a^1\Delta_g$ state could not be observed by the photometric method,[3] since the emission from $O_2^*(a^1\Delta_g)$ was overlapped by the strong chemiluminescence by HO_2. Therefore, photoionization mass spectrometry is a useful method to detect singlet oxygen in the chemiluminescent reaction system.

The reactions of $O+O_3$, $H+O_3$ and $NO+O_3$ can produce singlet oxygen according to the exothermicity and the spin correlation of the reactions. Nevertheless, this possibility has been ignored.[4] In this work, the fractions for the formation of singlet oxygen in the above reactions were determined by the use of the photoionization mass spectrometer; it seemed that this would be useful because strong chemiluminescence by OH and NO_2 has been observed in the near-IR region in all the above reactions except the $O+O_3$ reaction. After that, the reaction processes will be discussed using correlation diagrams and GVB model representations.

Experimental

The experimental set-up of the fast-flow reactor is shown in Fig. 1. The photoionization mass spectrometer coupled to the fast-flow reactor is as has been described previously.[5] The inner diameter of the cylindrical Pyrex reactor tube is 12.6 mm, and the length of the reaction zone can be varied from 10 to 200 mm by sliding the inlet tube (4 mm o.d.) in an O-ring seal. Ozone enters the main flow through six radially directed holes at the end of the inlet tube.

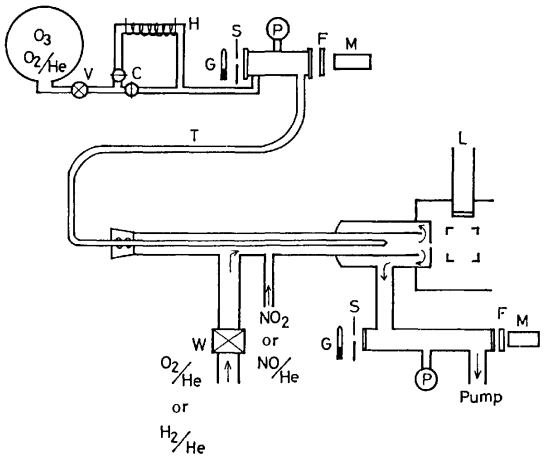

Fig. 1. Schematic diagram of the fast-flow reactor for the reactions of O, H, and NO with O_3.
V: Variable leak, C: Teflon stopcock, H: heater, G: Hg lamp, S: slit P: MKS baratron gauge, F: filter M: photomultiplier L: Ar lamp, T: Teflon tube, W: microwave cavity.

Hydrogen and oxygen atoms were produced in a microwave discharge (2450 MHz) in a helium mixture. The concentrations of both atoms were determined by titration with NO_2 according to the $H+NO_2 \rightarrow OH+NO$, and $O+NO_2 \rightarrow NO+O_2$ reactions, using the signals for NO at mass 30 as an indicator of the titration endpoint. NO_2 was added at a point 200 mm upstream from the sampling pinhole (the reaction time is about 10 ms under total pressure of 4 Torr (1 Torr = 133.3 Pa)). The method of determining the hydrogen-atom concentration is as has been described previously.[5] The known partial pressures of NO were added to calibrate the instrument sensitivity, typically about 2×10^4 counts/s for 1 mTorr of NO when two new argon lamps were used. Since the intensity of the argon lamps decreased slowly as a result of the origination of a color center in the LiF windows, the lamps were changed every 20 h. The measurements were then done between 10 to 20 h after the start of the discharge

of the new lamps, because in this period the intensity of the lamp was fairly stable.

The total and partial pressures of the gases were measured with an MKS Baratron gauge and were corrected to the values at the pinhole, considering the effect of the small pressure drop down the reactor tube.[5] Furthermore, the partial pressures of each component gas were corrected by means of the flow equation.[5] The linear-flow velocity, as measured with a bubble meter, was 16.5 m s^{-1} at 2 Torr, 19.9 m s^{-1} at 4 Torr, and 21.4 m s^{-1} at 6 Torr at 298 K. In this case, the flow in the flow tube, F (Torr l s^{-1}), as a function of the total pressure, P (Torr), was given by this equation: $F(P)=0.192+2.001P+0.0919P^2$. In this study, experiments were done under a total pressure of about 4 Torr.

The gases, H_2 (Nippon Sanso, 99.9999%), O_2 (Nippon Sanso, 99.99%), He (Nippon Sanso, 99.9999%), and NO_2 (Matheson, 99.5%), were used without further purification. The NO (Matheson, 99.0%) was purified by passing it through a column of Ascarite and was then distilled bulb-to-bulb using liquid nitrogen traps. After this purification, the amount of NO_2 present in this purified NO was less than 0.01%.[5] The ozone was prepared from a commercial ozonizer and was trapped on 500 grams of liquid nitrogen-cooled silica gel (5—10 mesh). After pumping, the adsorbed mixture of O_3 and O_2 on silica gel was heated up to room temperature and stored in a 50-l flask with a helium diluent. The mixture obtained usually consisted of 2—10% ozone and 10—20% oxygen in helium. The concentration of ozone was measured by absorption photometry at positions upstream and downstream of the flow reactor using a quartz cell, a Hg lamp coupled with a 2540 Å filter, and a photomultiplier.

The ozone was added to the reactor through a movable inlet. The measurements were done in both the presence and absence of ozone. In the case without O_3, the mixture of O_3–O_2–He was passed through a heated quartz tube (about 800 °C). In this case, the ozone was decomposed completely and converted to O_2 (no O atoms or no O_3 were detected by mass spectrometry and UV absorption). Switching the conditions with ozone and without ozone by means of Teflon stopcocks, the change in the signal at mass 32 was measured. The concentration of O_2 which was contained initially in the O_3–O_2–He mixture, $[O_2]_I$, was determined as follows. The O_3–O_2–He mixture was passed through the heated quartz tube. Under the condition without ozone, molecular oxygen was reacted with hydrogen atoms, and the singlet oxygen was produced as has been described before. Since the fraction of Reaction 2 in the total reaction of HO_2+H was determined[1] to be 0.015 ± 0.003, the concentration of O_2,

$$[O_2] = [O_2]_I + 3/2[O_3], \quad \text{(I)}$$

could be calculated using the rate constant for Reaction 1, the concentration of the hydrogen atoms, the total pressure, the reaction time, and the concentration of the singlet oxygen produced:

$$[O_2] = \frac{[O_2^*(a^1\Delta_g)]}{0.015\,k_1[H]t}, \quad \text{(II)}$$

where it is assumed that the rate for Reaction 2 is very rapid and that the concentration of HO_2 is in a steady-state concentration.[1] When the value for $[O_2]$ is determined, the $[O_2]_I$ can be calculated by means of Eq. I.

The flowing gases were sprayed through a conical Pyrex pinhole (0.2 mm in diameter) into the ionization region of a quadrupole mass spectrometer, where a collimated light beam from a microwave-powerd discharge lamp was intersected. In this work, an argon lamp with a LiF window was used photoionize the molecules. The concentration of singlet oxygen was calculated from the relative ionization cross section for NO and $O_2^*(a^1\Delta_g)$ by means of argon-resonance lines,[6] *i.e.*, $\sigma_{O_2^*}/\sigma_{NO}=0.5$. Since the sensitivity of NO to this instrument is 2×10^4 counts/s for 1 mTorr of NO, 10^{-4} m Torr of $O_2^*(a^1\Delta_g)$ could theoretically be detected.

The ions formed by photoionization were accelerated and focused into a quadrupole mass filter (UTi Model 100C). After mass selection, the ions were counted by means of a Daly-type detector[7] operated at −20 kV, a thin aluminum-coated plastic scintillator, and pulse-counting electronics (Canberra, Multichannel Analyzer, Omega-1). A working pressure of 2×10^{-5} Torr or less was maintained in the vacuum can by means of a 1200-l s^{-1} oil-diffusion pump with a liquid nitrogen trap. All the measurements were done at room temperature, 298±3K.

Results and Discussion

1) $O+O_3$ Reaction. The reaction of atomic oxygen with ozone is known to produce two ground-state oxygen molecules:

$$O(^3P) + O_3(X^1A_1) \rightarrow 2O_2(X^3\textstyle\sum_g^-) \quad \text{(3a)}$$
$$\Delta H = -93.7 \text{ kcal/mol.}$$

The vibrational excitation of ground-state oxygen[7] has been observed in levels up to $v=20$ or up to $v=25$ due to the exothermicity of Reaction 3a. However, the existence of singlet oxygen ($a^1\Delta_g$ and $b^1\textstyle\sum_g^+$) has never been observed, although the processes to form $O_2(X^3\textstyle\sum_g^-)+O_2^*(a^1\Delta_g)$ or $O_2^*(b^1\textstyle\sum_g^+)$ are accessible energetically and spin-allowed:

$$O(^3P) + O_3(X^1A_1) \rightarrow O_2(X^3\textstyle\sum_g^-) + O_2^*(a^1\Delta_g) \quad \text{(3b)}$$
$$\rightarrow O_2(X_3\textstyle\sum_g^-) + O_2^*(b^1\textstyle\sum_g^+). \quad \text{(3c)}$$

Measurements of the signals at mass number 32 were made by the addition of ozone to the oxygen atoms/He flow, which was produced in the microwave discharge of the O_2/He mixture. In this case, singlet oxygen was produced initially through the microwave discharge of the O_2/He mixture. This singlet oxygen initially produced disturbs the measurement of the signals at $m/e=32$ as a background. Therefore, measurements under the conditions of a high concentration of oxygen atoms and a low singlet-oxygen concentration in the

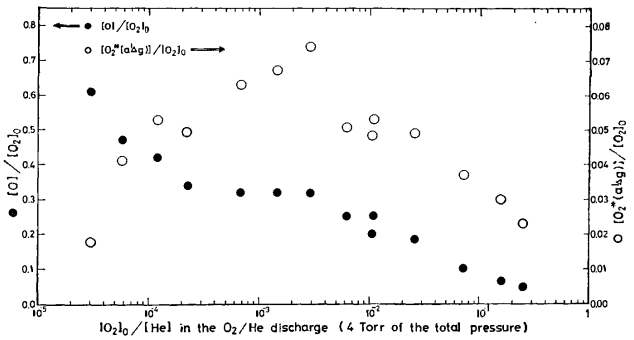

Fig. 2. The ratio of oxygen atoms produced to the initial concentration of O_2 in the O_2/He discharge, $[O]/[O_2]_0$ (●), and the ratio of singlet oxygen produced to the initial concentration of O_2 in the O_2/He discharge, $[O_2^*(a^1\Delta g)]/[O_2]_0$ (○), are plotted against the $[O_2]_0$/[He] in the O_2/He mixture. Discharge was done at total pressure of 4 Torr.

O_2/He discharge were desired. The concentrations of the oxygen atoms and singlet oxygen produced in the discharge were measured under a variety of ratios of O_2 to He in the O_2/H_2 discharge. Figure 2 shows that the absolute concentrations of both the oxygen atoms and the singlet oxygen increased at higher values of $[O_2]_0/[He]$, but the ratio of the concentration of the oxygen atoms produced to the initial concentration of O_2 is larger at lower values of $[O_2]_0/[He]$ (*i.e.*, oxygen atoms were produced effectively at a low "initial concentration of O_2," $[O_2]_0$). On the other hand, the ratio of the concentration of the singlet oxygen produced to the initial concentration of O_2 is smaller at lower values of $[O_2]_0/[He]$. The value of $[O_2^*]/[O_2]_0$ then passed through a maximum and, after that, decreased as the value of $[O_2]_0/[He]$ in increased. This decrease can be explained by the quenching of the singlet oxygen by oxygen atoms and ozone because the mixture of O_2 and He is discharged very far upstream of the reactor and the contact time of the discharged gases is about 50 ms. According to the results shown in Fig. 2, the condition of a low $[O_2]_0/[He]$ ratio should be good for measurement because the ratio of the atomic oxygen to the singlet oxygen formed is the largest.

The mass spectra measured in the $O+O_3$ reaction system are shown in Fig. 3. As is shown in Fig. 3, the singlet oxygen was produced in the O_2/He discharge and the increment of the signal at $m/e=32$ was not clear when ozone was added. The signal observed at $m/e=30$ may be the signal for NO, which is produced by the nitrogen present in the O_2/He mixture as an impurity. The small signal at $m/e=32$ when only the O_3–O_2–He mixture was introduced ((d) in Fig. 3) can be explained by the surface ionization in the ionization chamber. The mass spectrometer was fixed at $m/e=32$, and the signals at $m/e=32$ were accumulated. The results are shown in Table 1. In this case, measurements were

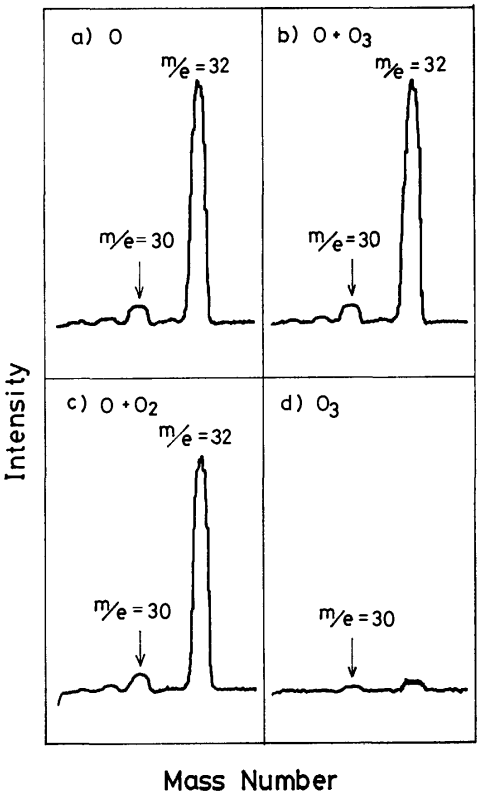

Fig. 3. Mass spectra in the $O+O_3$ reaction system. a): Only O_2/He discharge. b): O_3–O_2–He mixture was added to the O_2/He discharge. c): O_3–O_2–He mixture was passed through the heated quartz tube. Ozone was converted to O_2. d): Discharge was turned off. Only O_3–O_2–He mixture flowed Conditions: total pressure=4.032 Torr, $[O]_0$=4.6 m Torr $[O_3]$= 28.6 mTorr, reaction time =10.05 ms.

TABLE 1. RESULTS IN THE MEASUREMENT OF THE SIGNALS AT $m/e=32$ IN THE $O+O_3$ REACTION

Conditions				Signals at $m/e=32$ counts/5 s ($\pm$ was derived from the standard deviation in the 50 measurements)		
O_2/He discharge	Sensitivity of NO for 1 mTorr of NO	Reaction time (ms)	O_3–O_2–He Mixture added	O_2/He Discharge	Addition of O_3 (O_3–O_2–He mixture)	O_3 converted to O_2 (O_2–He mixture)
[a] Total pressure, 4.043 Torr $[O_2]_0$ 0.16 mTorr $[O]_0$ 0.095 mTorr $O_2^*(a^1\Delta_g)$ 0.003 mTorr	18326 counts/s	10.05	Total: 338 mTorr $[O_3]$ 29.4 mTorr $[O_2]_I$ 62.5 mTorr	d. 207.3±18.1 nd. 69.7±10.0 d.—nd. 137.6±12.4	d. 216.3±19.4 nd. 84.2± 9.7 d.—nd. 132.1±11.9	d. 216.7±16.2 nd. 74.9± 8.4 d.—nd. 141.8±10.6
[b] Total pressure, 4.032 Torr $[O_2]_0$ 13.8 mTorr $[O]_0$ 4.6 mTorr $O_2^*(a^1\Delta_g)$ 0.86 mTorr	17458 counts/s	10.05	Total: 329 mTorr $[O_3]$ 28.6 mTorr $[O_2]_I$ 60.9 mTorr	d. 37638.9±390.6 nd. 103.3±9.9 d.—nd. 37535.6±389.5	d. 37496.2±370.3 nd. 135.1±11.1 d.—nd. 37361.1±369.0	d. 37594.4±353.5 nd. 111.3±8.5 d.—nd. 37483.1±352.3

done under two different conditions: the $[O_2]_0/[He]$ ratios in the O_2/He discharge were 4.0×10^{-5} and 3.4×10^{-3}. As is shown in Fig. 2, the former is the case when the value for the ratio of the singlet oxygen to the oxygen atoms produced in the O_2/He discharge is small, while the latter is the case when the ratio of the singlet oxygen to the atomic oxygen has its maximum value. All the experimental conditions and signals at $m/e=32$ (counts/5 s) in the presence and absence of ozone are listed in Table 1. All the signals at $m/e=32$ were accumulated for 5 s per channel, and 50 channels were used for one measurement. The error limits ($\pm$) were derived from the standard deviation in these 50 signals. The signals at mass 32 were measured with the discharge on (d.) and off (nd.), (*i.e.*, in the presence and absence of oxygen atoms) and the difference (d. $-$nd.) used as the real signal for each measurement. The concentration of the singlet oxygen formed initially in the O_2/He discharge, listed in the first column in Table 1, was calculated from the signals at $m/e=32$ in the O_2/He discharge and the sensitivity of the instrument to NO. The small increment in the background (signals for nd.) when the O_3–O_2–He mixture was added can be explained by the effect of the field emission from the -20 kV stainless-steel target. As is shown in Table 1, the increase in the signals at $m/e=32$ could not be observed when the O_3–O_2–He mixture was added to the O_2/He discharged gases.

The rate constants for the reactions of $O+O_3$, k_3, have been reported to be 7.5, 8.3, and 10.6×10^{-15} cm^3 $molecule^{-1}$ s^{-1} at 300 K.[8-10] If the reaction proceeds only to produce singlet oxygen (Reactions 3b or 3c), the singlet oxygen produced should be given by $k_3[O][O_3]t$. The values for $k_3[O][O_3]t$ calculated are 2.5×10^{11} and 1.2×10^{13} molecule/cm^3 in the (a) and (b) measurements respectively in Table 1. In this case, 8.3×10^{-15} cm^3 $molecule^{-1}$ s^{-1} was used at the value for k_3. The detectable limit, if the increment of the signals occurred in the addition of the O_3–O_2–He mixture, can be estimated to be 20 counts/5 s for the (a) measurement and 1000 counts/5 s for the (b) measurement. These values (counts/5 s) correspond to 1.4×10^{10} molecule/cm^3 and 7.6×10^{11} molecule/cm^3 respectively. The value for the detectable $O_2^*(a^1\Delta_g)$, divided by the value for $k_3[O]_0[O]_3t$, gives the upper limit of the fraction for the formation of singlet oxygen, Reactions 3b or 3c, in the total reaction of $O+O_3$. The fractions were calculated to be less than 0.06 in both measurements, (a) and (b). No advantage was obtained in the accuracy of the value of the fraction in the (a) measurement (with the small initial signal of $O_2^*(a^1\Delta_g)$), because the ratio of the counting error to the signal was larger in the smaller signal in this equipment.

The deactivation rate constants of $O_2^*(a^1\Delta_g)$ by $O(^3P)$, O_2 and O_3 previously reported are $\leq1.3\times10^{-16}$,[11] 0.4—2.2×10^{-18},[12] and 4.4×10^{-15} cm^3 $molecule^{-1}$ s^{-1} [13] respectively. These deactivation rates are quite slow. The quenching of $O_2^*(a^1\Delta_g)$ by $O(^3P)$ and O_2 is negligibly small, and that by O_3 is less than 5% of the $O_2^*(a^1\Delta_g)$ supposed to be formed in Reaction 3b. Therefore, it was concluded that the fraction for the formation of $O_2^*(a^1\Delta_g)$, Reaction 3b, in the total reaction of $O+O_3$ is less than 0.06. The deactivation rate constant of $O_2^*(b^1\Sigma_g^+)$ by O_3 was been reported to be fast, 7×10^{-12} cm^3 $molecule^{-1}$ s^{-1},[14] This rate shows that the $O_2^*(b^1\Sigma_g^+)$ should be quenched completely under our experimental conditions if the $O_2(b^1\Sigma_g^+)$ is produced *via* Reaction 3c. Therefore, the conclusion is given only for the formation of $O_2^*(a^1\Delta_g)$, and only $O_2^*(a^1\Delta_g)$ will be dealt with in the following experiments and discussions.

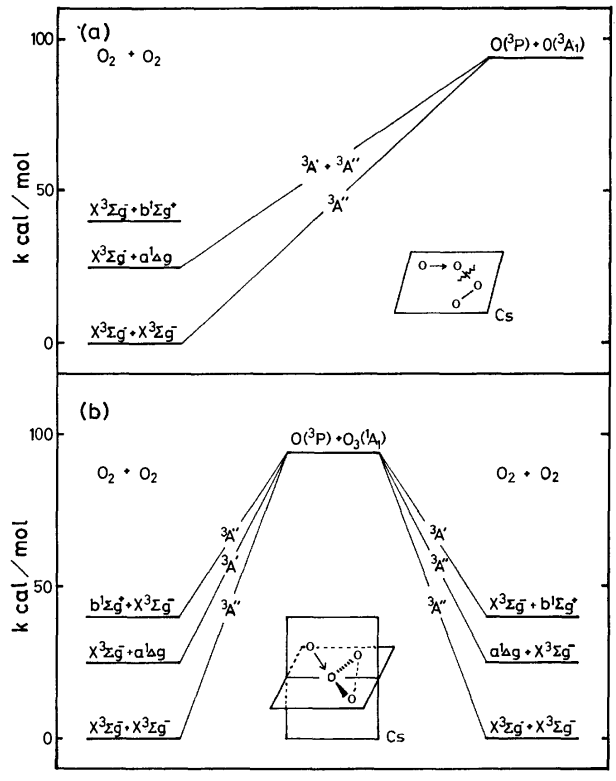

Fig. 4. Minimal state correlation diagrams in the $O+O_3$ reaction system when all atoms lie in a plane (a) and when $O(^3P)$ approaches O_3 in the plane which bisects the O_3 bond angle (b).

As has been mentioned before, vibrationally excited ground-state oxygen molecules were observed in the flash-photolysis absorption experiment.[7] According to the measurement by McGrath and Norrish,[7] the maximum in the population distribution of vibrationally excited O_2 is when $v=12$, 13, or 14, and both higher and lower levels have progressively lower populations. However, since the absorption cross-section in the Schumann-Runge band system in O_2 is smaller at lower v levels, population distributions lower than $v=11$ could not be measured in their observation. The energy for $v=12$, 13, or 14 is about a half of the exothermic energy for the $O+O_3$ reaction, 3a, that is about 4 eV. Therefore, the formation of singlet oxygen is energetically acceptable except when the two oxygen molecules formed in Reaction 3a are equally vibrationally excited. The minimal-state correlation diagrams when all atoms lie on a plane (Cs symmetry), and when $O(^3P)$ approaches O_3 on the plane which bisects the O_3 bond angle, are shown in Fig. 4. In these cases, the correla-

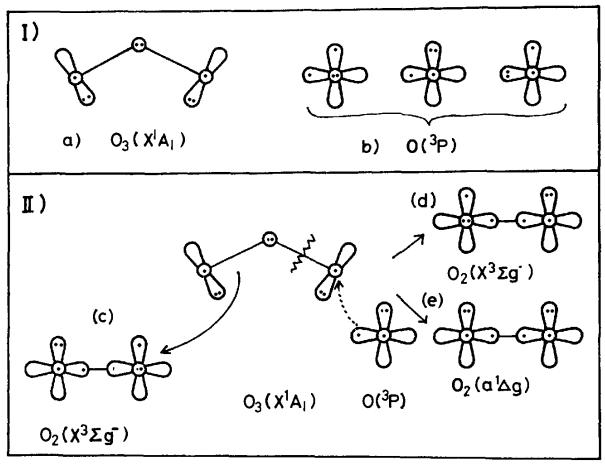

Fig. 5. GVB model representation in the $O+O_3$ reaction system.

tions with other upper states are abridged. As is shown in Fig. 4, the formation of the $a^1\Delta_g$-state molecular oxygen is possible in both the coplanar and bisecting plane models.

According to the valence-bond model which was explained by Goddard,[15] ground-state ozone and atomic oxygen are represented by (a) and (b) respectively in Fig. 5 (I). Figure 5 (II) shows the case in which an $O(^3P)$ approaches the side oxygen atom of ozone perpendicular to the ozone plane and in which each p-orbital having one electron makes a σ-bond. According to Goddard, this mechanism probably occurs in the lowest energy. In this case, O_4 in the transition state has no symmetry (C_1). When this O_4 complex is cleaved into two oxygen molecules, the electronic state of the O_2 on the left-hand side is in the ground state ($^3\Sigma_g^-$), while the O_2 in the right-hand side is the ground state (d) or the $a^1\Delta_g$ state (e). However, the O–O bond distance is expected to be shorter for the states with three oxygen π electrons than for those with four π electrons. This means that the energy of O_4 of the state of three π electrons is lower than that of four electrons. Therefore, (d) in Case (II), the formation of the ground-state O_2, should give the lowest energy to the O_4 complex. It can be considered that the energy of the transition-state complex of O_4 is lowest in the case of the formation of two ground-state molecular oxygens (probably vibrationally excited) after cleavage.

2) $H+O_3$ Reaction. This reaction is wellknown as the source of the vibrationally excited OH radicals. Recent work[16] has shown that the OH-product vibrational distribution peaks strongly in the highest accessible vibrational level, $v=9$, and that the mean fractions of the total energy entering the vibration and rotation in the OH are $\langle f'v\rangle \approx 0.90$ and $\langle f'r\rangle \approx 0.03$.

$$H(^2S) + O_3(X^1A_1) \rightarrow OH(^2\pi) + O_2(X^3\Sigma_g^-) \quad (4a)$$

$$\Delta H = -76.9 \text{ kcal/mol}$$

However, OH is distributed in the lower levels, although it has progressively lower populations. Therefore, it is possible that singlet oxygen can be formed due to the exothermicity:

$$H(^2S) + O_3(X^1A_1) \rightarrow OH(^2\pi) + O_2{}^*(a^1\Delta_g) \quad (4b)$$

$$\rightarrow OH(^2\pi) + O_2{}^*(b^1\Sigma_g^+). \quad (4c)$$

There have been no reports on the singlet oxygen produced in the reaction of $H+O_3$. Measurements of the signals at mass number 32 were attempted by the method described above. The mass spectra measured in the $H+O_3$ reaction system are shown in Fig. 6. As is shown in Fig. 6, the signals at mass 32 are not changed in the $H+O_3+O_2$ and $H+O_2$ systems (O_3/O_2 was passed through the heater). The signals at mass 32 measured under a variety of O_3/O_2 concentrations are shown in Fig. 7. As is shown in Fig. 7, the signals for mass 32 did not increase in the presence of ozone. In this case, 4.6% of an O_3/O_2 mixture (without He as a diluent) was added. The concentration of ozone in the O_3/O_2 mixture and the absolute concentration of

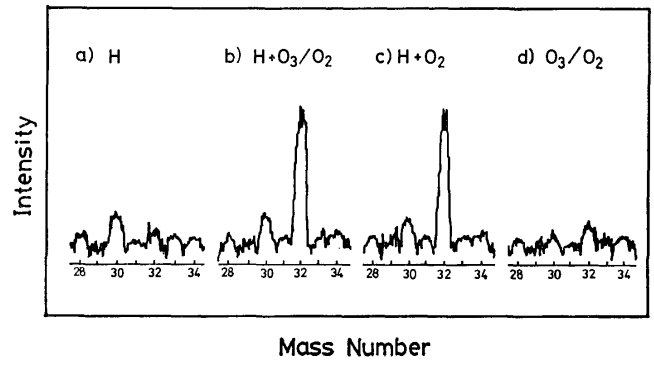

Fig. 6. Mass spectra in the $H+O_3$ reaction system. a): Only H_2/He discharge. b): O_3/O_2 mixture was added to the H_2/He discharge. c): O_3/O_2 mixture was passed through the heated quartz tube. Ozone was converted to O_2. d): Discharge was turned off. Only O_3/O_2 mixture flowed. Conditions: total pressure=4.6 Torr, [H]=8.69 mTorr, O_3+O_2=52 mTorr, O_3/O_2=7.5%, reaction time=6.1 ms.

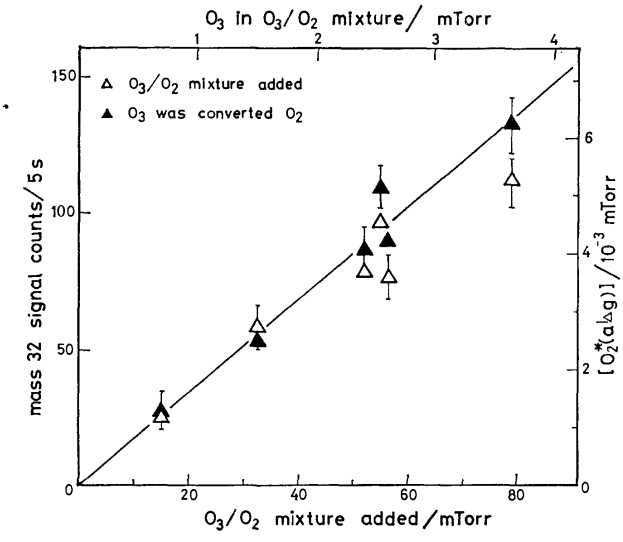

Fig. 7. Signals at $m/e=32$ *vs.* O_3/O_2 mixture added. △: Signals when O_3/O_2 mixture was added, ▲: signals when O_3/O_2 mixture was passed through the heated quartz tube. Conditions: total pressure=4.44 Torr, [H]=11.95 mTorr, reaction time=6.08 ms.

$O_2^*(a^1\Delta_g)$, as calculated from the sensitivity of NO, are shown in Fig. 7. When O_3 was converted to O_2 through the heater, the increase in the pressure of the O_3/O_2 mixture was about 2% ($O_3 \rightarrow 3/2O_2$). This is negligibly small compared with the counting error. The lack of increase in the signals for $O_2^*(a^1\Delta_g)$ in the presence of ozone showed that the $O_2^*(a^1\Delta_g)$ was formed only by Reactions 1 and 2. The absolute value for $O_2^*(a^1\Delta_g)$ agreed well with that of a previous work,[1] in which the fraction of Reaction 2 was about 0.015 of the total reaction of HO_2+H.

The deactivation of $O_2^*(a^1\Delta_g)$ by O_2 and O_3 can be neglected during the contact time of this work, 6.08 ms. The deactivation rate constant of $O_2^*(a^1\Delta_g)$ by hydrogen atoms has been reported to be 2.5×10^{-14} cm^3 molecule^{-1} s^{-1} [17]. This rate was also slow enough to neglect under those conditions, [H]=11.95 mTorr. The deactivation rate of $O_2^*(a^1\Delta_g)$ by OH is unknown. However, the nearly linear increase in the $O_2^*(a^1\Delta_g)$ signal in the presence of O_3 in Fig. 7 shows that the deactivation of $O_2^*(a^1\Delta_g)$ by OH does not affect the $O_2^*(a^1\Delta_g)$ signals.

The rate constant for Reaction 1 previously reported[18] is 1.57×10^{-32} cm^6 molecule^{-2} s^{-1} (M=He). This means that the second-order rate for Reaction 1 is 2.3×10^{-15} cm^3 molecule^{-1} s^{-1} under 4.44 Torr of He. On the other hand, the rate for Reaction 4 is very rapid. The rate constant for Reaction 4 was reported most recently[19] to be 2.8×10^{-11} cm^3 molecule^{-1} s^{-1} at 300 K. Therefore, the ozone should be consumed completely in the reactor under these experimental conditions, and the concentration of hydrogen atoms to react with O_2 might decrease with the addition of O_3. This effect is evident in Fig. 7. As is shown in Fig. 7, since the increment in the 1×10^{-3} mTorr of $O_2^*(a^1\Delta_g)$ should be detectable in both the presence and absence of O_3, it was concluded that the fraction of the formation of $O_2^*(a^1\Delta_g)$, Reaction 4b, in the total reaction of $H+O_3$ must be less than 0.001.

The reaction of OH with O_3 produces HO_2:

$$OH + O_3 \rightarrow HO_2 + O_2. \quad (5)$$

The rate constant for Reaction 5 reported most recently[20] is 8.2×10^{-14} cm^3 molecule^{-1} s^{-1} at 298 K. Three possible reaction paths have been suggested[21] for the reaction of vibrationally excited OH with O_3:

$$OH^* + O_3 \rightarrow HO_2 + O_2 \quad (6a)$$
$$\rightarrow H + 2O_2 \quad (6b)$$
$$\rightarrow OH + O + O_2. \quad (6c)$$

The reactions of OH^* (v=2—9) with O_3 have been shown to proceed with rate constants of $(2—11)\times10^{-12}$ cm^3 molecule^{-1} s^{-1} [21]. These rates for Reaction 5 and 6 are not fast enough to compete with Reaction 4 under these experimental conditions ($[H]\gg[O_3]$).

In the correlation in the reaction of $H(^2S)+O_3(X^1A_1)$, the ground states $OH(X^2\pi)+O_2(X^3\Sigma_g^-)$, can be correlated through the $^2A'$-state HO_3 complex (in both Cs planar and Cs bisecting complex) to the $H(^2S)+O_3(X^1A_1)$. However the $OH(X^2\pi)+O_2^*(a^1\Delta_g)$ or $O_2^*(b^1\Sigma_g^+)$ can not be correlated to it. This fact is consistent with the finding of this experiment in which the production of singlet oxygen can not be observed and is a result of the production of highly vibrationally excited OH radicals.[16]

3) $NO+O_3$ Reaction. The reaction of $NO+O_3$ is well known to emit the so-called "air afterglow" by means of the NO_2 formed, and this chemiluminescent reaction has been used by the chemiluminescent NO_x analyzer:

$$NO(X^2\pi) + O_3(X^1A_1) \rightarrow NO_2(X^2A_1) + O_2(X^3\Sigma_g^-) \quad (7)$$
$$\Delta H = -47.74 \text{ kcal/mol.}$$

In this case, the reaction produces visible and infrared emissions from electronically ($^2B_2$, $^2A_2$) and vibrationally excited ground-state NO_2.[22] Recent works using seeded beams[23,24] suggest that the cross-section of this chemiluminescent reaction increases very rapidly with an increase in the collision energy and is influenced by the electronic fine-structure states of NO ($\pi_{1/2}$, $\pi_{3/2}$). The enhancement of the reaction rate and chemiluminescence in this reaction by selective vibrational excitation with IR lasers has also been investigated.[25]

A puzzling feature of the reaction is the failure to observe excited $O_2^*(a^1\Delta_g)$ and $O_2^*(b^1\Sigma_g^+)$, energetically accessible and favored by the correlation diagram, since $O_2^*(a^1\Delta_g)$ lies lower than any other excited states of NO_2. The failure to observe $O_2^*(a^1\Delta_g)$ has also been reported by Gauthier and Snelling[26] in the reaction of O_3 with NO, where no $a^1\Delta_g$ emission was detected, and places an upper limit of 0.003 on the fraction of reactive collisions. A re-examination to observe

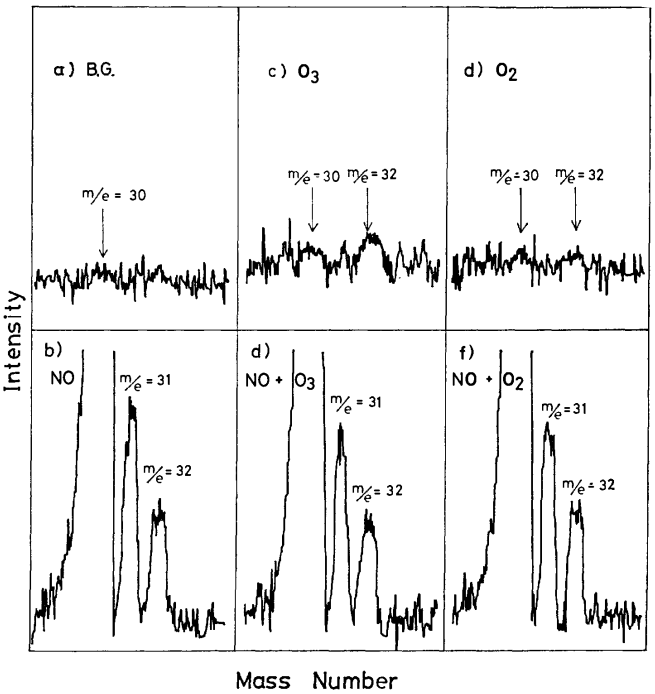

Fig. 8. Mass spectra in the $NO+O_3$ reaction system. a) Background. b) Only NO flowed. c) Only O_3–O_2–He mixture flowed. d) $NO+O_3$–O_2–He mixture. e) O_3–O_2–He mixture passed through the heated quartz tube. f) $NO+O_3$–O_2–He mixture passed through the heated quartz tube. Conditions: total pressure=3.8 Torr, $[O_3]$=18.2 mTorr, [NO]=2.3 mTorr, $[O_2]_1$=56.31 mTorr, reaction time=10.05 ms.

TABLE 2. SIGNALS AT $m/e=32$ IN THE O_3+NO REACTION SYSTEM UNDER THESE CONDITIONS TOTAL PRESSURES=3.782 Torr, $[O_3]=18.23$ mTorr, $[NO]=2.30$ mTorr, $[O_2]_I=56.31$ mTorr, REACTION TIME=10.05 ms

Run	Condition	Mass 32 signal, counts/5 s averaged over 128 measurements	
A	Background	28.9± 8.9	
B	Only O_3	31.7± 9.1	
C	Only O_2 (through heater)	30.2± 9.8	
D	Only NO	615.5±27.8	
E	O_3+NO	561.2±21.7	E−B=529.5±20.5
F	O_2+NO (through heater)	566.2±25.7	F−C=535.9±24.3

$O_2^*(a^1\Delta_g)$ was undertaken in the reaction of O_3+NO by means of the photoionization mass spectrometer used in this study.

The mass spectra measured in the $NO+O_3$ reaction system are shown in Fig. 8. The signals at $m/e=32$ are overlapped by the isotope signals of NO. The signals accumulated at $m/e=32$ are shown in Table 2. The difference between the signals in the O_3+NO (E—B) and O_2+NO (F—C) reactions is −6.44 counts/5 s, which means that the increment in the signal at $m/e=32$ can not be observed in the O_3+NO reaction. The rate constant for Reaction 7 reported most recently[27] is 1.80×10^{-14} cm^3 molecule^{-1} s^{-1} at 298 K. Therefore, the O_2 formed in Reaction 7 can be calculated to be $k_7[NO][O_3]t=0.250$ mTorr under the conditions listed in Table 2. On the other hand, 30 counts/5 s of the increment of the signal should be detectable under the conditions listed in Table 2 if $O_2^*(a^1\Delta_g)$ is produced. The 30 counts/5 s of the $O_2^*(a^1\Delta_g)$ signal can be calculated to be 4.8×10^{-4} mTorr because of the sensitivity of NO, 2.5×10^4 counts/s for 1 mTorr. Therefore, the fraction for the formation of $O_2^*(a^1\Delta_g)$ in the total reaction of O_3+NO should be less than 0.002.

The deactivation of $O_2^*(a^1\Delta_g)$ by NO and NO_2 have been reported[14] to be very slow, 4.5×10^{-17} and 5.0×10^{-18} cm^3 molecule^{-1} s^{-1} respectively. Therefore, the quenching of $O_2^*(a^1\Delta_g)$ by the reacting gases can be neglected. It has been suggested[2,28] that $O_2^*(a^1\Delta_g)$ can be formed in the energy-transfer reaction by electronically excited NO_2 with O_2.

$$NO_2^* + O_2 \rightarrow NO_2 + O_2^*(a^1\Delta_g). \quad (8)$$

According to a report by Clough and Thrush,[22] the formation of electronically excited NO_2 emitting light shorter than 875 nm is 6.5% of the total reaction of $NO+O_3$ at 300 K. Jones and Bayes[2] have determined the efficiency for Reaction 8, which decreases from 3.5 to 0.5% as the NO_2 excitation wavelength increases from 420 to 620 nm. Therefore, if NO_2^* is quenched completely only by O_2, the amount of $O_2^*(a^1\Delta_g)$ formed by Reaction 8 should be less than 0.002 of the total reaction of $NO+O_3$. Therefore, it is reasonable that the $O_2^*(a^1\Delta_g)$ produced in Reaction 8 could not be detected in this study. The above finding that less than 0.002 of the $NO+O_3$ reactive collisions result in the production of $O_2^*(a^1\Delta_g)$ is in good agreement with the result by Gauthier and Snelling.[26]

Redpath, Menzinger, and Carrington[23] preferred

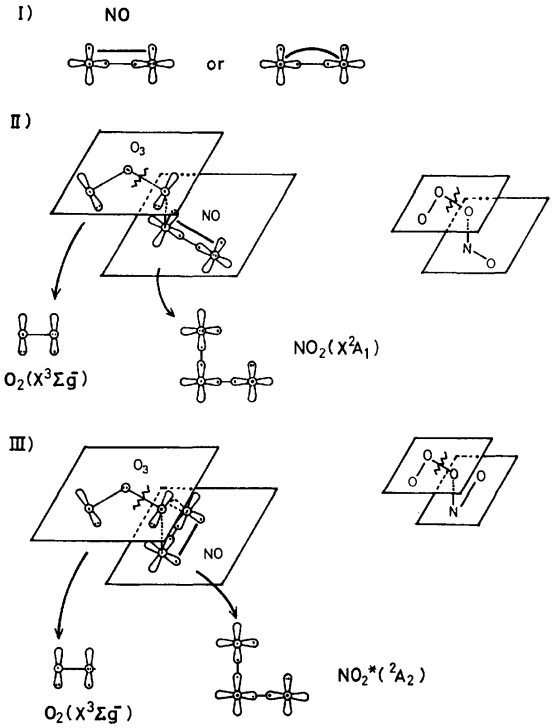

Fig. 9. GVB model representation in the $NO+O_3$ reaction system.

the bisecting-plane model in the $NO+O_3$ reaction, in which the NO approaches O_3 on the plane bisecting the O_3-bond angle (Cs symmetry); the formation of electronically excited NO_2 rather than the energetically preferred $O_2^*(a^1\Delta_g)$ can be explained by this model. However, the reaction on such a bisecting plane requires a very high energy, since ozone has the form of Ia) in Fig. 5.

According to the GVB-model representation, the NO molecule is shown by I) in Fig. 9. The cases in which O_3 reacts with NO with the lowest energy are Cases (II) and (III) in Fig. 9. In these cases, NO approaches the side oxygen atom of O_3 parallel to the ozone plane and makes a N–O σ-bond perpendicular to the ozone plane. After this stage, the NO_4 complex cleavages to O_2 and NO_2. Two types of NO_2 are produced: NO_2 with 4π electrons, Case (II), corresponds to $NO_2(X^2A_1)$ and $NO_2^*(^2B_2)$, and that having 3π electrons, Case (III), corresponds to $NO_2^*(^2A_2)$ and $NO_2^*(^2B_1)$. Since it can be expected that molecules with a lower energy are predominantly produced, the

NO_2 formed in Case (II) should be in the ground state ($^2A_1$) while that in Case (III) should be in the $^2A_2$ state. On the other hand, the O_2 formed is in the ground state in both cases.

The formation of electronically excited NO_2^* rather than the energetically preferred $O_2^*(a^1\Delta_g)$ can be explained by the GVB-model representation. However, the formation of the $^2B_1$ and the $^2B_2$ states of NO_2 can not be explained thus. It might be possible that the $^2B_1$ and the $^2B_2$ states of NO_2 are populated by vibronic interaction[29] with the $^2A_1$ and the $^2A_2$ states of the NO_2 produced initially after the O_2 has departed.

Further exact theoretical calculations are needed in order to clarify these reactions.

The authors wish to thank Professor Shigeru Nagase of Yokohama National University for his helpful discussions.

References

1) N. Washida, H. Akimoto, and M. Okuda, *J. Phys. Chem.*, **82**, 18 (1978).
2) I. T. N. Jones and K. D. Bayes, *J. Chem. Phys.*, **59**, 3119 (1973).
3) J. R. Hislop and R. P. Wayne, *J. Chem. Soc., Fraday Trans. 2*, **73**, 506 (1977).
4) M. A. A. Clyne, "Physical Chemistry of Fast Reactions," ed by B.P. Levitt, Plenum Press (1973), Vol. 1, Chap. 4.
5) N. Washida, H. Akimoto, and M. Okuda, *J. Phys. Chem.*, **82**, 2293 (1978).
6) I. D. Clark and R. P. Wayne, *Mol. Phys.*, **18**, 523 (1970).
7) W. D. McGrath and R. G. W. Norrish, *Proc. R. Soc. London, Ser. A*, **242**, 265 (1957); W. D. McGrath and R. G. W. Norrish, *Nature*, **182**, 235 (1958); N. Basco and R. G. W. Norrish, *Can. J. Chem.*, **38**, 1769 (1960); W. M. Jones and N. Davidson, *J. Am. Chem. Soc.*, **84**, 2868 (1962); T. Carrington and D. Garoin, "Comprehensive Chemical Kinetics," ed by C. H. Barnford and C. F. H. Tipper, Elsevier Pub. (1969), Vol. 3, Chap. 4.
8) G. A. West, R. E. Weston, Jr., and G. W. Flynn, *Chem. Phys. Lett.*, **56**, 429 (1978).
9) D. D. Davis, W. Wong, and J. Lephardt, *Chem. Phys. Lett.*, **22**, 273 (1973).
10) J. L. McCrumb and F. Kaufman, *J. Chem. Phys.*, **57**, 1270 (1972).
11) I. D. Clark and R. P. Wayne, *Chem. Phys. Lett.*, **3**, 405 (1969).
12) I. D. Clark and R. P. Wayne, *Chem. Phys. Lett.*, **3**, 93 (1969); F. D. Findlay, C. J. Fortin, and D. R. Snelling, *Chem. Phys. Lett.*, **3**, 204 (1969); P. Borrell, P. M. Borrell, and M. D. Pedley, *Chem. Phys. Lett.*, **51**, 300 (1977); A. Leiss and U. Schurath, *J. Photochem.*, **8**, 211 (1978).
13) R. J. Collins, D. Husain, and R. J. Donovan, *J. Chem. Soc., Faraday Trans. 2*, **69**, 149 (1973).
14) K. H. Becker, W. Groth, and U. Schurath, *Chem. Phys. Lett.*, **8**, 259 (1971).
15) W. R. Wadt and W. A. Goddard, III, *J. Am. Chem Soc.*, **97**, 3004 (1975); P. J. Hay, T. J. Dunning, Jr., and W. A. Goddard III, *J. Chem. Phys.*, **62**, 3912 (1975); P. J. Hay and T. H. Dunning, Jr., *J. Chem. Phys.*, **67**, 2290 (1977); L. B. Harding and W. A. Goddard, III, *J. Am. Chem. Soc.*, **100**, 7180 (1978).
16) J. C. Polany and J. J. Sloan, *Int. J. Chem. Kinet. Symp.*, **1**, 51 (1975).
17) C. Schmidt and H. I. Schiff, *Chem. Phys. Lett.*, **23**, 339 (1973).
18) M. J. Kurylo, *J. Phys. Chem.*, **76**, 3518 (1972); W. Wong and D. D. Davis, *Int. J. Chem. Kinet.*, **6**, 401 (1974).
19) L. F. Phillips and H. E. Schiff *J. Chem. Phys.*, **37**, 1233 (1962); M. A. A. Clyne and P. B. Monkhouse, *J. Chem. Soc., Faraday Trans. 2*, **73**, 298 (1977); J. H. Lee, J. V. Michael, W. A. Payne, and L. J. Stief, *J. Chem. Phys.*, **69**, 350 (1978); L. F. Keyser, *J. Phys. Chem.*, **83**, 645 (1979).
20) A. R. Ravishankara, P. H. Wine, and A. O. Langford, *J. Chem. Phys.*, **70**, 984 (1979).
21) G. E. Streit and H. S. Johnston, *J. Chem. Phys.*, **64**, 95 (1976); R. N. Coltharp, S. D. Worley, and A. E. Potter, *Appl. Opt.*, **10**, 1786 (1971).
22) M. A. A. Clyne, B. A. Thrush, and R. P. Wayne, *Trans. Faraday Soc.*, **60**, 359 (1964); P. N. Clough and B.A. Thrush, *Trans. Faraday Soc.*, **63**, 915 (1967); P. N. Clough and B. A. Thrush, *Trans. Farday Soc.*, **65**, 23 (1969); M. F. Golde and F. Kaufman, *Chem. Phys. Lett.*, **29**, 480 (1974).
23) A. E. Redpath, M. Menzinger, and T. Carrington, *Chem. Phys.*, **27**, 409 (1978).
24) S. L. Anderson, J. Fite, O. V. Nguyen, and P. R. Brooks, "Molecular Beam Reaction of NO with O_3," Paper Presented at the ACS/CSJ Chemical Congress, Honolulu, Hawaii, April 1979; D. Van den Ende and S. Stolte, *Chem. Phys.*, **45**, 55 (1980).
25) M. J. Kurylo, W. Braun, A. Kaldor, S. M. Freund, and R. P. Wayne, *J. Photochem.*, **3**, 71 (1974); W. Braun, M. J. Kurylo, A. Kaldor, and R. P. Wayne, *J. Chem. Phys.*, **61**, 461 (1974); M. J. Kurylo, W. Braun, C. N. Xuan, and A. Kaldor, *ibid.*, **62**, 2065 (1975); **63**, 1042 (1975); R. J. Gordon and M. C. Lin, *ibid.*, **64**, 1058 (1976); J. Moy, E. Bar-Ziv, and R. J. Gordon, *ibid.*, **66**, 5439 (1977); *J.* C. Stephenson and S. M. Freund, *ibid.*, **65**, 4303 (1976); E. Bar-Ziv, J. Moy, and R. J. Gordon, *ibid.*, **68**, 1013 (1978); K. Hui and T. A. Cool, *ibid.*, **68**, 1022 (1978).
26) M. Gauthier and D. R. Snelling, *Chem. Phys. Lett.*, **20**, 178 (1973).
27) J. W. Birks, B. Schoemaker, T. J. Leck, and D. M. Hinton, *J. Chem. Phys.*, **65**, 5181 (1976).
28) T. C. Frankiewicz and R. S. Berry, *J. Chem. Phys.*, **58**, 1787 (1973).
29) J. C. D. Brand, W. J. Chan, and J. L. Hardwick, *J. Mol. Spectry.*, **56**, 309 (1975); C. G. Stevens and R. N. Zare, *ibid.*, **56**, 167 (1975); T. Tanaka, R. W. Field, and D. O. Harris, *ibid.*, **56**, 188 (1975).

Phase Transitions in *N*-Propylpyridinium-TCNQ Ion-radical Complex Salts

Mutsuaki MURAKAMI* and Susumu YOSHIMURA
Matsushita Research Institute Tokyo, Inc., Ikuta, Tama-ku, Kawasaki 214
(Received March 27, 1980)

N-Propylpyridinium $(TCNQ)_x$ crystallized in two complex salts ($x=2$, 2.5), both of which displayed initial irreversible and subsequent reversible first-order phase transitions with a sharp discontinuity in the electrical conductivity. The reversible transitions of both salts are essentially the same in spite of their differences in stoichiometry. The transitions were accompanied by crystal structure changes; the changes in the physical properties were ascribed to the crystalline distortion in both the one-dimensional TCNQ chain and the motion of the cation molecules. The high-temperature phase was metallic, with a zero activation energy for conduction; the source of the metallic behavior was also discussed. The electronic and infrared absorption spectra suggest that the high-temperature modification has a less distorted stacking of TCNQ molecules in the column.

The phase transitions and metallic conductivity in a quasi-one-dimensional system based on 7.7.8.8-tetracyanoquinodimethane (TCNQ) ion-radical salts have been the subject of extensive investigation. The highly conducting salts of TCNQ with *N*-methylphenazinium (NMP(TCNQ)),[1,2] quinolinium $(Q(TCNQ)_2)$[3,4] and acridinium $(Ad(TCNQ)_2)$[5] display a metal-insulator (M-I) transition characterized by a smooth maximum in the conductivity. The metallic behavior of these salts has been explained in various manners: a mobility model in which the conductivity is defined as the product of the concentration of charge carriers and the mobility of the carriers,[6] diffusion through the localized state by means of a disorder effect,[7-9] inter-strand hopping due to the finite length of the conducting chains,[10,11] and an M-I transition with a single particle gap going to zero.[1]

On the other hand, there are some examples of first-order phase transitions which display a discrete change in the electrical conductivity. Reversible transitions are found in alkali-metal (TCNQ),[12,13] methyltriphenylphosphonium $(TCNQ)_2$,[14] and *N*-ethyl·*N*·methylmorpholinium $(TCNQ)_2$,[15,16] $(MEM(TCNQ)_2)$, while monotropic transitions are found in *N*-methylquinolinium $(TCNQ)_x$[17] and methyldiethylcyclohexylammonium $(TCNQ)_2$.[18] They have been understood on the basis of crystallographic change, Adler-Brooks transition,[19,20] spin Peierls transition, or transition from a metastable to a stable form.[21]

In a previous paper, we reported that substituted pyridinium and picolinium–TCNQ complex salts exhibited a variety of first-order phase transitions.[22] The irreversible transition was correlated to the appearance of multiple forms, while the reversible one manifested itself for specific cations. *N*-propylpyridinium $(TCNQ)_x$, $(NPPy(TCNQ)_x)$ complex salts crystallized in two forms ($x=2.5$ and 2.0) displayed two kinds of first-order phase transitions, *viz.*, an initial irreversible transition, and subsequent reversible transitions. In this paper, we will report on the electrical, optical, and magnetic properties of the transitions, and will discuss the transition mechanism and the source of the metallic behavior in the high-temperature phase.

Experimental

Preparation of NPPy(TCNQ)$_x$ Complex Salts. NPPy-$(TCNQ)_x$ complex Salt II was synthesized from *N*-propylpyridinium iodide and three-halves molar excess of TCNQ using one of the methods generally described by Melby *et al.*[23] After the salt had been synthesized, recrystallization was done in highly purified acetone at 0 °C. The formation of the two salts was controlled by the crystallization conditions: the Salt I was obtained from a concentrated solution (50 mmol dm^{-3}) with rapid crystallization as a fine needle form, while the Salt II was recrystallized by slow crystallization from a dilute solution (30 mmol dm^{-3}) as a rod or triclinic prism form.

The cation-to-TCNQ ratio of the complex salts was estimated by the spectral analysis from a simple salt of NPPy-(TCNQ) and neutral TCNQ.[21] The value of the molar excitation coefficient for TCNQ in highly purified acetonitrile was 67000 mol^{-1} dm^3 cm^{-1} at the wavelength of 395 nm, while the coefficients of $TCNQ^-$ were 26300 and 46100 mol^{-1} dm^3 cm^{-1} at 420 and 842 nm respectively; the coefficient at 395 nm was 21200 mol^{-1} dm^3 cm^{-1}. From the analysis, the cation-to-TCNQ ratio of I is estimated to be 2.48, and that of II, to be 1.94. The elemental analysis values for I were; Found: C, 72.32; H, 3.43; N, 24.43%, calcd for $(C_8H_{12}N)_2(C_{12}H_4N_4)_5$: C, 72.15; H, 3.48; N, 24.36%, while those for II were; Found: C, 72.62; H, 3.70; N, 23.48%, calcd for $(C_8H_2N)(C_{12}H_4N_4)_2$: C, 72.45; H, 3.77; N, 23.77%. From these results, considering the experimental error, we decided the cation-to-TCNQ ration to be 2.5 for I and 2.0 for II.

Electrical Measurements. The specific resistivities of compactions were determined with a resistivity measuring apparatus, Kokusai Electric Co., Ltd., Model VR4. The temperature dependence of the electrical resistivity along three crystallographic directions of a single crystal was measured with an ordinary four-point method with gold wires (0.05 mmϕ) and silver paste (duPont conductive silver coating material No. 4929). The sample was mounted in an evacuated glass cell sealed with a hermetic seal (NEC No. S110). The temperature was regulated with thermostat equipment (Sigma Electric Co., Ltd., Model TE-307S) and a temperature sweeper (Model SP-9D) at the sweep rate of 0.1—2.0 °C/min in the temperature range of 210—430K.

Other Measurements. The infrared absorption spectra were measured at various temperature with a Hitachi grating infrared spectrometer Model No. 215, in the wave number range between 4000 and 650 cm^{-1}. The solid state electronic absorption spectra were measured in the range between 5000 and 44000 cm^{-1} with a Cary spectrometer, Model No. 14. Samples were fully ground and carefully rubbed on a substrate; a quartz plate for measurements in the electronic region or a sodium chloride plate, for those in the infrared region.

Measurements of differential scanning calorimetry (DSC) were made with a Shimadzu thermoflex apparatus, SC-20, in a nitrogen atomosphere at the sweeping rate of 0.5—2.0 °C/

min in the temperature range of 293—430K. The data employed were an average value of ten measurements.

The powder X-ray diffraction patterns were measured with a Philips PW-1051 X-ray diffractometer by the use of the Cu·$K\alpha$ line.

The magnetic susceptibility was measured on a magnetic balance using Faraday's method in the temperature range of 100—430K. The sample, a pressed pellet about 100 mg, was placed in a quartz cell, and measurement was made under a vaccum. The absolute value of the susceptibility was estimated from gadrinium oxide ($\chi = 135 \times 10^{-6}$ emu/g) placed in the same quartz cell. The paramagnetic contribution (χ_{para}) to the susceptibility was determined from the difference of $\chi - \chi_{dia}$, while the diamagnetic contribution, χ_{dia}, was estimated from Pascal's rule.

Results and Discussion

Electrical Properties of NPPy(TCNQ)$_x$ Salts. The most typical difference between the two salts, besides stoichiometry and morphology, is the resistivity at room temperature; the specific resistivity of the powder smaple I (x=2.5) was 1.4 Ω cm, while that of the II (x=2.0) was 2000 Ω cm. In the Salt II, the lowest resistivity is found in the direction of the a-axis (1000 Ω cm), and the resistivity anisotropy ratio of the a, b, and c axes was 1 : 24 : 4.5. On the other hand, the lowest resistivity of I was found in the long axis (0.12 Ω cm) and its anisotropy ratio is expected to be larger than that of II.

The Temperature Dependence of the Resistivity of II. The temperature dependence of the electrical resistivity along each crystallographic direction of II was measured; the results are shown in Fig. 1. The resistivity abruptly changed at three temperatures; the resistivity jump observed at 383 K by initial heating was irreversible, while the other two jumps, at 370 K and 376 K, were the portions of a hysteresis loop of a reversible transition. We recognized two kinds of phase transitions and three distinct phases; it will be convenient to identify the phases as α_{II}, β', β as is indicated in the figure.

For example, in the c-direction, the inclination of the log ρ-T^{-1} curve in the semiconducting α_{II} phase increased with the temperature, from 0.18 eV in the temperature range of 200—230 K to 0.42 eV in the range of 330—370 K. On the other hand, the β' phase was metallic in the sense that it had a zero temperature coefficient of resistivity. The β phase was semiconducting, with an activation energy of 0.54 eV between 320 and 350 K, which was larger than that of the α_{II} phase in the same temperature range. A decrease in the activation energy was also observed at lower temperatures; the value was 0.16 eV in the temperature range of 200—230 K.

The features of the ρ-T characteristic for the three crystallographic directions closely resembled each other. Some quantitative differences between these crystal axes are summarized as follows: 1) The magnitudes of the resistivity jumps at the irreversible transitions were factors of 23, 140, and 45 for the a, b, and c axes respectively. 2) In the high-temperature β' phase, the resistivities were 2, 8, and 4 Ω cm for the a, b, and c axes respectively. The maximal anisotropy ratio in this phase was only 4, which is to be compared with that of the α_{II} phase, 24. 3) The a- and c-axis conductivity in the β' phase had a zero activation energy, while the b-axis one had a small positive value of 0.09 eV. 4) The magnitudes of the resistivity jumps in the reversible transition at 376 K were factors of about 12, 20, and 8 for the a, b, and c axes respectively. The maximal anisotropy ratio in the β phase at 293 K was reduced to about 20.

Crystal Structure Change of II. The very sharp resistivity change shown in Fig. 1 suggests a first-order phase transition, and, in fact, latent heat was observed at three temperatures with the DSC experiment. The results for ΔH were +13.81, −9.83, and +10.13 kJ mol^{-1} for the $\alpha_{II} \rightarrow \beta'$, $\beta' \rightarrow \beta$, and $\beta \rightarrow \beta'$ transitions respectively, and the corresponding entropy changes (ΔS) were +35.98, −26.57, and +26.69 J K^{-1} mol^{-1}.

Powder X-ray experiments were made at three temperatures corresponding to the three phases: the α_{II}

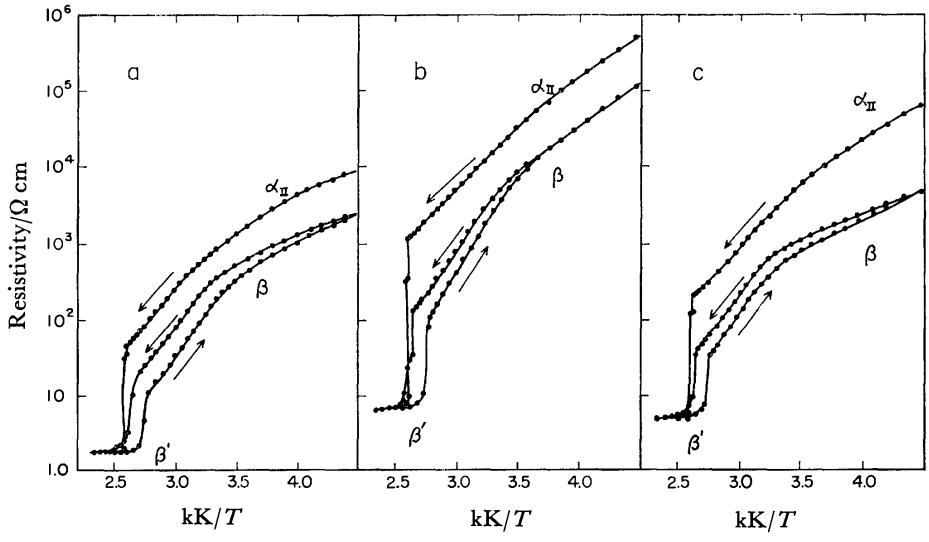

Fig. 1. Temperature dependence of the electrical resistivity of Salt-II along the a, b, c-directions.

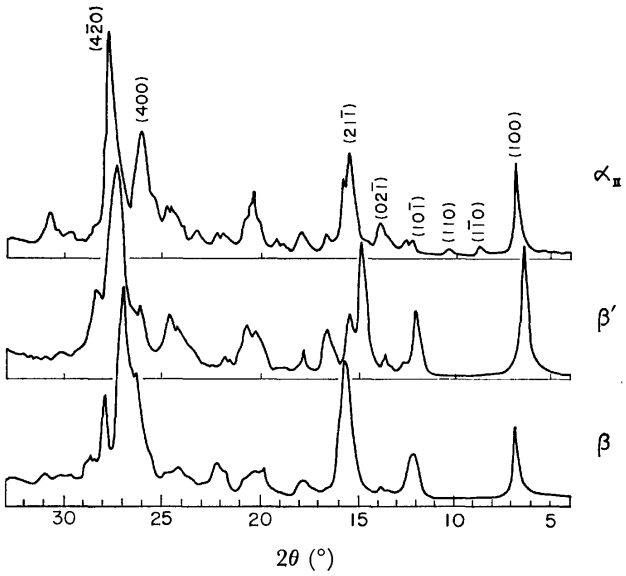

Fig. 2. Powder X-ray diagrams of α_{II} (293 K), β' (393 K), and β (293 K) modifications of Salt-II.

phase, 293 K, the β' phase, 399 K, and the β phase, 293 K. The results are shown in Fig. 2. The three X-ray diagrams of the α_{II}, β', and β phases were entirely different form each other, which confirms that the transitions are crystallographic phase transitions. Though a detail discussion of the crystal structure change must await a full crystal structure analysis of the β' and β phases, we can provide a rough view of the structure change as inferred from the shifts of the characteristic lines on the powder X-ray patterns. The most remarkable change at the $\alpha_{II}\rightarrow\beta'$ transition is observed in the lower angle region than 10°. From the crystal structure analysis of the α_{II} phase,[24] the relation between the lines and the reflection plane was calculated. The α_{II} belongs to the triclinic system with the space group P1 or P$\bar{1}$ and the lattice constants $a=$ 14.542, $b=13.723$, $c=7.802$ Å, $\alpha=104.06°$, $\beta=110.72°$, $\gamma=94.08°$ and $z=2$. The intense line at the lowest angle, 6.60°, is a (100) reflection, while the lines at 8.6° and 10.2° are reflections from (1$\bar{1}$0) and (110) respectively. In the β' phase, the lines corresponding to (1$\bar{1}$0) and (110) reflections disappeared, and only an intense line at 6.08° was observed in this region. The results indicate the change in the crystal symmetry: from a triclinic crystal (α_{II} phase) to a monoclinic crystal (β' phase). On the contrary, the crystal symmetry did not change at the $\beta'\leftrightarrows\beta$ transition, because the β phase had only a new line appearing at 6.55°. If these lines correspond to the (100) reflection, it means that the β' phase has the largest (100) spacing. The average inter-TCNQ column distance increased during the $\alpha_{II}\rightarrow\beta'$ transition and decreased during the $\beta'\rightarrow\beta$ transition. The large change in the interchain distance suggests that the rotation of cation molecules plays an important role at these transitions.

The most intense line in the α_{II} phase at 27.7° or the distance of about 3.2 Å originates from a spacing or paired TCNQ[24] in the TCNQ column. If the most intense reflection in the β' phase at 27.2° also comes from a plane nearly parallel to the TCNQ planes, the shift of this line with the $\alpha_{II}\rightarrow\beta'$ transition corresponds to a 1.8% increase in the inter-planar spacing of paired TCNQ molecules. Therefore the resistivity change at the $\alpha_{II}\rightarrow\beta'$ transition can be explained by the change in the stacking mode of TCNQ molecules from diadic to monadic configurations. In the β phase, the reflection appears at 27.0°; it undergoes an increase of about 0.7% in the spacing at the $\beta'\rightarrow\beta$ transition. The change in the interplanar spacing of TCNQ molecules at the reversible transition well explains the resistivity change.

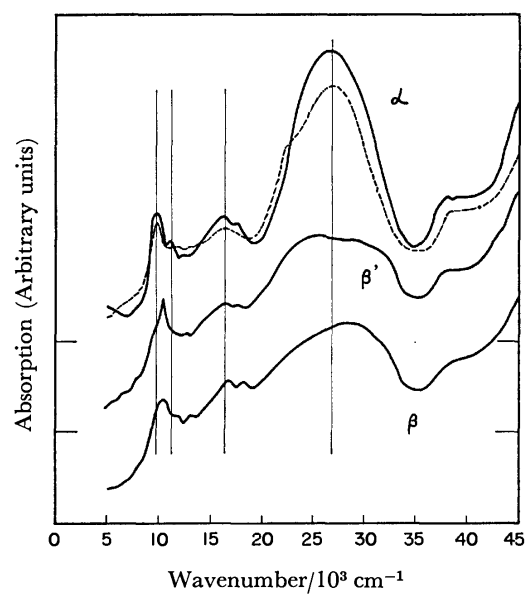

Fig. 3. Electronic absorption spectra of α (293 K), β' (393 K), and β (293 K) modifications of Salt-II (——) and Salt-I (-----).

Change in TCNQ Column Structure of II. Figure 3 shows the electronic absorption spectra of a powder film rubbed over a quartz plate at three temperatures corresponding to the α_{II}, β', and β phases. The spectrum of the α_{II} phase was characterized by a strong intramolecular absorption centered at 26800 cm^{-1} (local excitation band, LE_2)[25] and a relatively strong absorption at about 16000 cm^{-1}. The latter may be interpreted as an intramolecular transition of a TCNQ molecule (LE_1) and/or an absorption of associated TCNQ molecules.[26] In general, the absorption band at around 10000 cm^{-1} has been interpreted in various manners: as an intermolecular charge transfer transition of $TCNQ^-$ to $TCNQ^-$,[27] as a transition to an upper band distinguished from a near infrared absorption which is due to an intraband transition, or as an interaction between LE_1 and CT_1. The doubly splitting band at 10000 cm^{-1} and 11300 cm^{-1} may be due to an interaction of LE_1 and CT_1 by analogy of the electronic spectra of $TEA(TCNQ)_2$; the band splitting suggests the crystallographic inequivalence of the TCNQ molecules in the column.

The absorption spectrum of the β' phase differed from those of the α phase, in which it had a weaker absorption in the intramolecular excitation regions at around 25000

cm^{-1} and in which the absorption located at around 10000 cm^{-1} had a single sharp peak at 10400 cm^{-1}. The remarkable change in the intramolecular absorption may explain the increase in the conductivity in the β' phase. The change of the spectrum around 10000 cm^{-1} shows the change of the TCNQ column, namely, the structure at the β' phase is almost equivalent which implies that the negative charge may delocalize throughout the TCNQ column. In the case of such a column structure, the CT_1 absorption band does not appear; in fact, $Q(TCNQ)_2$ and NMP(TCNQ) show only a single LE_1 peak at around 10000 cm^{-1}. The spectrum of the β phase was characterized by an intramolecular absorption band at 28000 cm^{-1} and splitting bands at 10100 cm^{-1} and 11400 cm^{-1} (shoulder). The latter bands indicate the presence of crystallographic inequivalency in the TCNQ column.

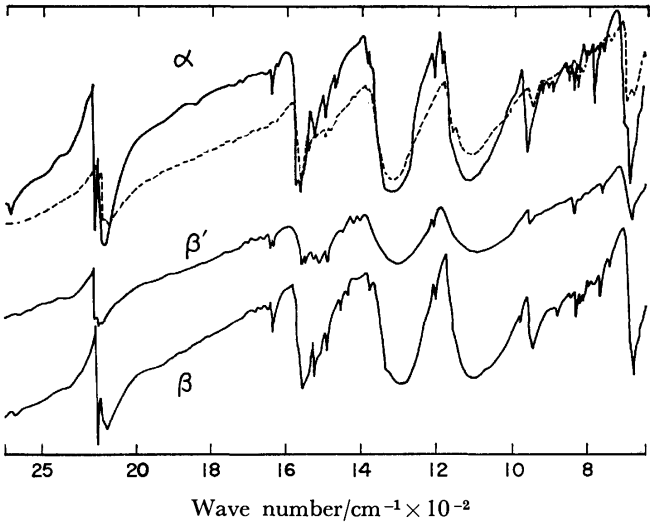

Fig. 4. Infrared absorption spectra of α (293 K), β' (393 K), and β (293 K) modifications of Salt-II (——) and Salt-I (------).

Similar results for the arrangement of TCNQ molecules were obtained from the infrared measurement.[28,29] The results are shown in Fig. 4. The α_{II} and β phases had sharp molecular absorption bands of TCNQ in the C≡N stretching regions around 2200 cm^{-1}, which indicates the presence of localized TCNQ molecules in the column. In the β' phase, sharp C≡N stretching absorptions were absent and the C–H bending band centered at 1290 cm^{-1} and the C–CN stretching band (1100 cm^{-1}) were broader and located at lower energies as compared with the α_{II} and β phases. The shift of the bands shows the decreased intermolecular repulsion or contraction of the electronic band gap, while the broadening of the bands may be due to the increased electronic band, which broadened to the infrared region. Thus, we concluded that the α_{II} and β phases have a disordered arrangement of TCNQ molecules, whereas the β' phase has an almost ordered stack of TCNQ molecules.

Metallic Nature of II in the β' Phase. The results of the ρ-T characteristics for the reversible $\beta \rightleftarrows \beta'$ transition are similar to those found in VO_2, which has offered a good example of a crystalline distortion or Adler-Brooks model.[30,31] The optical data which have suggested a pairing of TCNQ molecules at low temperatures are consistent with the increased resistivity of the β phase, because such a pairing opens an energy gap, as in the case of VO_2. The rough coincidence in both the transition temperature, T_0, and the activation energy for conduction just below, T_0, is noteworthy: II, 376 K and 0.51 eV, and VO_2 339 K and 0.50 eV.[32] However, a more exact examination may lead to the conclusion that the phase transition of our salt cannot be described by this mode. The Adler-Brooks model predicts that the energy gap, E_{g0}, due to a crystalline distortion is proportional to T_0, provided that the band widths are not very different. If we take $E_{g0}/kT_0=10$ as a rough estimate, the measured T_0 (376 K) gives an energy gap of 0.32 eV. Note that the observed activation energy, 0.51 eV (c-axis), is considerably larger than the predicted one, 0.16 eV. This discrepancy indicates the inapplicability of the Adler-Brooks model.

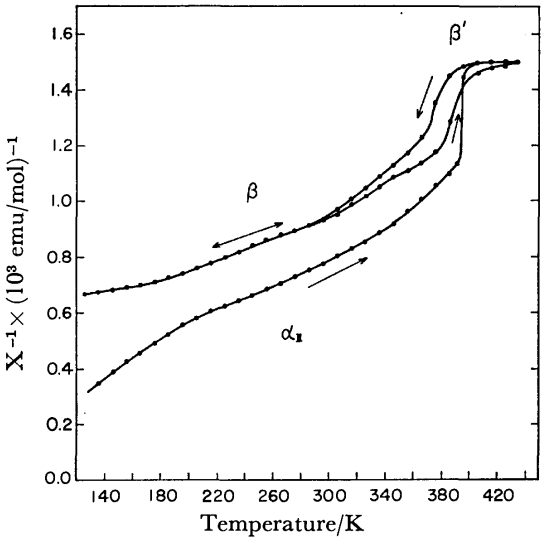

Fig. 5. Temperature dependence of the inverse paramagnetic susceptibility of Salt-II.

Figure 5 shows the temperature dependence of the paramagnetic susceptibility for the temperature range of 100—430 K. The results show discrete changes in χ which correspond to the resistivity jumps found in Fig. 1. The β' phase had a temperature independent susceptibility of about 5.0×10^{-4} emu/mol. The low-temperature α_{II} and β phases, on the other hand, exhibited Curie-Weiss like behavior, with a marked increase in the paramagnetic susceptibility at low temperatures.

The observed magnetic behavior cannot be described by ferromagnetic impurities, for the low-temperature α_{II} and β phases did not have the same magnitude of susceptibility. Indeed, the effective Curie-Weiss behavior may be explained by an array of disordered paramagnetic moments. The reason for this speculation is that the hopping motion of a localized electron is suggested by the fact that the activation energy around

370—300 K is considerably larger than that predicted by the Adler-Brooks model. Other reasons are that the NPPy cation is assymmetric and II was crystallized as a metastable crystal. The decrease in the magnitude of χ with the $\alpha_{II} \rightarrow \beta$ transition indicated that the crystal structure was made less ordered with the irreversible transition, which is consistent with the crystallographic and optical data.

The observed behavior of the paramagnetic susceptibility of the β' phase is likely to be connected with the Pauli spin susceptibility of the free electron system, and this seems to provide evidence that the β' phase is indeed metallic. However, the weak temperature dependence of the paramagnetic susceptibility of highly conducting TCNQ salts can also be described by the properties of a one-dimensional Mott insulator[33] or by those of a tight binding band.[34] In these cases, the electronic states have been thought to be localized at a lattice point in the one-dimensional TCNQ chain. Moreover, the disorder model can explain the observed behavior with an expression in the form of $\chi = \chi_{para} + \chi_{curie\text{-}weiss}$. Several data presented above suggest that the β' phase may also be described by a localized electronic model. For example, the intramolecular absorption band at 16000 cm^{-1} (Fig. 3) has a doublet peak, which indicates that the β' phase does not have a completely uniform stacking of the TCNQ molecule. This may be understood on the basis of the highly asymmetric structure of the cation molecule, which makes a major contrast to the case of MEM-$(TCNQ)_2$.[15,16] At this stage, we surmise that the β' phase is described by the phonon-assisted hopping between localized states. The relatively high and temperature-independent conductivity agrees well with the expected values of the minimum resistivity by hopping (order of 1 Ω cm) and the small temperature slope of the resistivity ($(\partial\rho/\partial T = 1.2 \times 10^{-3}$ Ω cm K^{-1}).[5]

Phase Transitions of I. The temperature dependence of the electrical resistivity of a powder sample of I ($x=2.5$) is shown in Fig. 6. An irreversible transition appeared in a broad temperature range starting at about 390 K, where the resistivity increased by a factor of about 5. Since the transition temperature was varied by the rate of the rise in the temperature or by the crystal perfection, the transition is a polymorphic transition from an unstable to a stable form. After the irreversible transition was completed, the salt displayed a reversible transition similar to that of II. We can also recognize three phases, so we indicates the phases as α_I, β', and β, as is indicated in the figure.

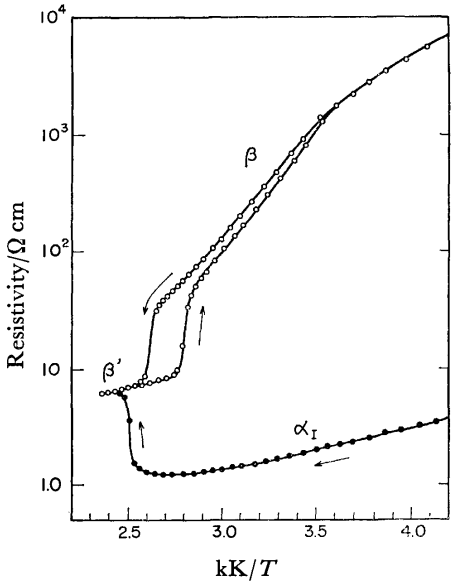

Fig. 6. Temperature dependence of the electrical resistivity of Salt-I (pressed rod), irreversible change (-●-●-), reversible change (-○-○-).

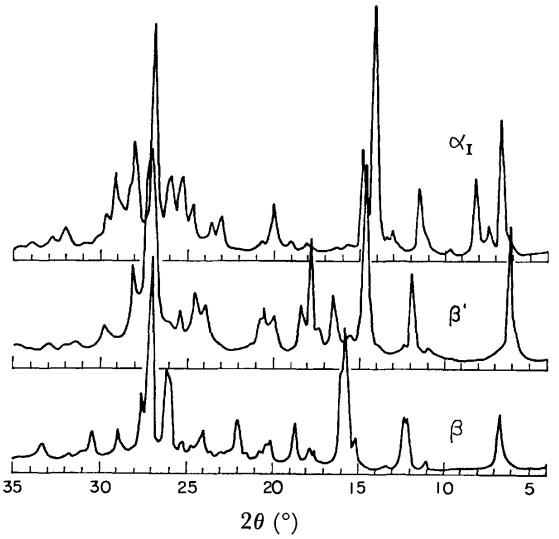

Fig. 7. Powder X-ray diagrams of α_I (293 K), β' (393 K), and β (293 K) modifications of Salt-I.

The powder X-ray diffraction patterns of I are shown in Fig. 7. The pattern of the α_I phase is quite different from that of the α_{II} phase, but the patterns of the β' or β phase of I and II are identical. During the $\alpha_I \rightarrow \beta'$ transition, a distinct change was observed at the most intense line around 26.8°, which implies that the average distance between TCNQ molecules expanded at the $\alpha_I \rightarrow \beta'$ transition. The electronic and infrared absorption spectra of I are shown by dotted lines in Figs. 3 and 4 respectively. The infrared spectrum of the α_I phase was characterized by broader bands located at a lower energy region as compared with the characteristic bands of TCNQ of the α_{II} phase. The electronic spectrum of the α_I phase was characterized by an absorption located at around 10000 cm^{-1}, in which the band splitting was not clear and the second peak was shouldered. The results indicate that the TCNQ column at the α_I phase is less distorted than that of the α_{II} phase and that TCNQ molecules are stacked almost uniformly. The conductivity change of the $\alpha_I \rightarrow \beta'$ transition is well explained by these results.

A difference in the ρ-T characteristic of I from that of II was the activation energy for conduction in the β' phase: 0 eV for II and 0.10 eV for I. Although I has quite a different stoichiometry from that of II, the same crystal structure may be realized by discarding one cation out of the five cation molecules from the structure of II.

If the crystal structure of I is characterized by such large defects in the cation column, the difference in the activation energies in the β' phase may be explained by such defects.

The authors offer their thanks to Dr. Ichimin Shirotani of Tokyo University and to Prof. Hayao Kobayashi of Tōhō University for their stimulating discussions. They are also indebted to Dr. Michiko Konno of Tokyo University for providing them with the details of the crystal structure of NPPy(TCNQ)$_x$, II.

References

1) L. B. Coleman, J. A. Cohen, A. F. Garito, and A. J. Heeger, *Phys. Rev. B*, **7**, 2122 (1973).
2) A. J. Epstein, E. M. Conwell, D. J. Sandman, and J. S. Miller, *Solid State Commun.*, **23**, 355 (1977).
3) L. I. Buravov, D. N. Fedutin, and I. F. Schegolev, *Sov. Phys. JETP.*, **32**, 612 (1971).
4) K. Holczer, G. Mihaly, A. Janossy, and G. Grüner, *Mol. Cryst. Liq. Cryst.*, **32**, 199 (1976).
5) G. Mihaly, K. Ritvay-Emandity, and G. Grüner, *J. Phys. Chem.*, **8**, L361 (1975).
6) A. J. Epstein, E. M. Conwell, and J. S. Miller, *Ann. N. Y. Acad. Sci.*, **313**, 183 (1978).
7) A. N. Bloch, R. B. Weisman, and C. M. Varma, *Phys. Rev. Lett.*, **28**, 753 (1972).
8) E. Ehrenfreund, S. Etemad, L. B. Coleman, E. F. Rybaczewski, A. F. Garito, and A. J. Heeger, *Phys. Rev. Lett.*, **29**, 269 (1972).
9) Gogolin, A. A., S. P. Zolotuhin, V. I. Melnikov, E. I. Rashba, and I. F. Shchgolev, *JETP Lett.*, **22**, 278 (1975).
10) E. Ehrenfreund, E. F. Rybaczewski, A. F. Garito, and A. J. Heeger, *Phys. Rev. Lett.*, **28**, 873 (1972).
11) M. J. Rice and J. Bernasconi, *J. Phys. F*, **3**, 55 (1973).
12) J. G. Vegter and J. Kommandeur, *Mol. Cryst. Liq. Cryst.*, **30**, 11 (1975).
13) M. Konno, T. Ishii, and Y. Saito, *Acta Crystallogr., Sect. B*, **33**, 763 (1977).
14) Y. Iida, *J. Chem. Phys.*, **59**, 1607 (1973).
15) S. Huizinga, J. Kommandeur, G. A. Sawatzky, B. T. Thole, K. Kopinga, W. J. M. de Jonge, and J. Roos, *Phys. Rev. B*, **19**, 4723 (1979).
16) A. Bosh and B. Van Bodegom, *Acta Crystallogr., Sect. B*, **33**, 3013 (1977).
17) M. Murakami and S. Yoshimura, *J. Phys. Soc. Jpn.*, **38**, 488 (1975).
18) J. C. Giuntini, D. Jullien, and J. V. Zanchetta, *Mol. Cryst. Liq. Cryst.*, **32**, 203 (1976).
19) D. Adler and H. Brooks, *Phys. Rev.*, **155**, 826 (1967).
20) J. G. Vegter and J. Kommandeur, *The AIP Conf. Proc.*, **No. 10**, 1525 (1972).
21) M. Murakami and S. Yoshimura, *Bull. Chem. Soc. Jpn.*, **48**, 157 (1975).
22) M. Murakami and S. Yoshimura, *Chem. Lett.*, **1977**, 929.
23) L. R. Melby, R. J. Harder, W. R. Hertler, W. Mahler, R. E. Benson, and W. E. Mochel, *J. Am. Chem. Soc.*, **84**, 3374 (1962).
24) M. Konno and Y. Saito, *Proc. Symp. Molecular Structure*, Tokyo, Oct. 9—12 (1979), p. 20.
25) J. Tanaka, M. Tanaka, T. Kawai, T. Takabe, and O. Maki, *Bull. Chem. Soc. Jpn.*, **49**, 2358 (1976).
26) J. G. Vegter and J. Kommandeur, *Phys. Rev. B*, **9**, 5150 (1974).
27) J. B. Torrance, B. A. Scott, and F. B. Kaufman, *Solid State Commun.*, **17**, 1369 (1975).
28) K. Kondow and T. Sakata, *Phys. Status Solidi A*, **6**, 551 (1971).
29) B. Lunelli and C. Pecile, *J. Chem. Phys.*, **52**, 2375 (1970).
30) D. Adler, "Solid State Physics," ed by F. Seitz, D. Turnbell, and H. Ehrenreich, Acad. Press, New York (1968), Vol. 21.
31) A. Zylbersztejn and N. F. Mott, *Phys. Rev. B*, **11**, 4383 (1975).
32) D. Adler, J. Feinleib, H. Brooks, and W. Paul, *Phys. Rev.*, **155**, 851 (1967).
33) L. N. Bulaeuskii, A. V. Zvarykina, Yu. S. Karimov, R. B. Lyubouskii, and I. F. Schegolev, *Zh, Eksp. Teor. Fiz.*, **62**, 725 (1972); [*Soviet Phys. JETP*, **35**, 384 (1972)].
34) A. H. Kahn, G. A. Candela, V. Waltka, Jr, and J. H. Perlstein, *J. Chem. Phys.*, **60**, 2264 (1974).

The Heats of Solution of Optically Active Compounds and the Corresponding Racemic Compounds

Masayuki MATSUMOTO† and Kazuo AMAYA*

National Chemical Laboratory for Industry, 1-1, Azuma, Yatabe-Machi, Tsukuba-Gun, Ibaragi 305

(Received March 31, 1980)

The heats of solution of crystalline amino acids and hydroxy acid in water at 298.15 K were measured with a twin isoperibol calorimeter. It was found, as was expected from the theory, that the difference in the heat of solution between optically active compounds and their corresponding racemic compounds was appreciably large compared with the heat of mixing of concentrated aqueous solutions of *d*- and *l*-optical isomers.

According to the statistical thermodynamic theory for solutions containing *d*- and *l*-optical isomers, it was previously found by one of the present authors that first term of the excess enthalpy of the system was proportional to the inverse of the absolute temperature, $1/T$.[1,2] Takagi *et al.* measured the heat of mixing of aqueous solutions of *d*- and *l*-optical isomers at 298.75 K, but the values they obtained were too small to test the relation.[3] This may be attributed to the free rotation of optical isomers in solution, resulting in an averaging out, of the difference in interaction energy for each configuration.

However, in the solid state each molecule is confined in the cage formed by the surrounding molecules and is fixed to the most favorable configuration, and difference in configuration energy between an optically active compound and the corresponding racemic compound can be expected to be appreciably large.

In order to test this experimentally, the heats of solution of crystalline optically active compounds and the corresponding racemic compounds were measured.

Experimental

Materials. The alanine, D-glutamic acid, histidine, threonine, and L-valine were purchased from the Takara Kohsan Co., Ltd., the DL-glutamic acid, DL-valine and tartaric acid were also purchased, but from the Tokyo Kasei Co., Ltd. Their purities were certified by these makers and were guaranteed to be more than 99%.

These samples were dried over silica gels in a desiccator at room temperature for at least 3 d before use and were then used without further purification.

Apparatus and Procedures. The calorimeter used in this experiment was a Model TIC-2D twin isoperibol calorimeter manufactured by the Tokyo Riko Co., Ltd.; it is shown in Fig. 1.

It consists of two identical transparent Dewar vessels, about 0.15 dm³ in inner volume and equipped with a pair of thermistors with equal temperature coefficients, a pair of identical calibrating heaters, a pair of ampoule-breaking devices, and a pair of stirres driven by outside, rotating, permanent magnets. All these parts are installed in an aluminum block, which can be thermostatted within ±0.004 °C at any desired arbitrary temperature between −10 °C and 80 °C. Precise results can easily obtained by the employment of this twin system. During the experiment, the calorimeter was kept

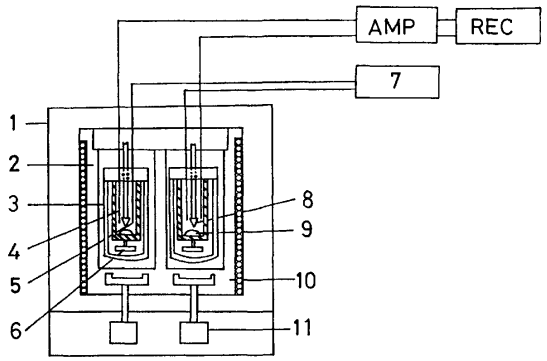

Fig. 1. Twin isoperibol calorimeter.
1): Case, 2): aluminum block, 3): Dewar vessel, 4): thermistor, 5): heater, 6): magnetic stirrer, 7): heater power source, 8) ampoule breaking device, 9): ampoule, 10): temperature controller, 11): motor for stirring, AMP: d.c.-amplifier, REC: recorder.

at 298.15±0.004 K. In each measurement, from 50 to 100 mg of the sample were sealed in a glass ampoule, and the sample and the blank ampoule were, respectively, set in the measurering and reference Dewar vessels, filled with 0.1 dm³ of distilled water.

The calorimeter was left for 24 h to reach thermal equilibrium, after which the sample and the blank ampoule were broken simultaneously with the ampoule-breaking devices. The dissolution was complete within 3 to 20 min, according to the sample. The difference in temperature between the two Dewar vessels was recorded on a chart recorder. The temperature change on dissolution was obtained by extrapolating the fore and after linear parts of the calorimetric curves (Challoner Method).[4] Electrical calibration was also made after the solution experiment, while the temperature change was obtained by the same procedure. The heat of solution, q_s, was derived by means of the following equation:

$$q_s = q_c \frac{\Delta t_s}{\Delta t_c}$$

where q_c is the heat quantity for electrical calibration, and where Δt_s and Δt_c are the temperature changes in solution and in the calibration experiment respectively.

Calibration of the Calorimeter. The calorimeter was calibrated with the NBS standard reference material 724a, tris(hydroxymethyl)aminomethane (THAM), and a 0.1 N (f=1.008) hydrochloric acid solution at 298.15 K.

Before use, THAM was dried *in vacuo* at room temperature for 1 h.

About 500 mg of THAM was sealed in a glass ampoule and set in the Dewar vessel filled with a 0.1 dm³ hydrochloric acid solution, and then the heat of solution was measured by the procedure described above. The mean value of the molar

† Present address: Department of Nutrition, Sagami Women's University, Bunkyo, Sagamihara, Kanagawa 228.

enthalpy of solution obtained by 3 runs was -29.32 ± 0.09 kJ/mol.

The value recommended by Hill *et al.* was -29.744 ± 0.003 kJ/mol.[5] Accordingly, the systematic error of our calorimeter was 1.4%, and the precision was 0.34%.

Results and Discussion

The values of the heat of solution of crystalline optically active compounds and their corresponding racemic compounds, and the difference between the two, are shown in Tables 1 and 2 respectively. This experiment was carried out under the conditions described above, so that these relative amounts gave final concentrations of about 0.01 mol/kg. Therefore, the heat of solution is considered to be the value at infinite dilution obtained by Spink and Auker.[6]

Table 1. Heats of solution of amino acids and tartaric acid in water at 298.15 K

Substance	Sample weight (g)	Observed heats of solution (J)	Heats of solution (kJ/mol)	
DL-Alanine	0.1001	10.60	9.44	
	0.1004	10.44	9.27	9.35±0.09
	0.1003	10.51	9.34	
L-Alanine	0.1000	8.41	7.49	
	0.1004	8.37	7.43	7.35±0.21
	0.1001	8.06	7.14	
DL-Glutamic acid	0.0512	10.0	28.8	
	0.0543	10.5	28.6	28.6±0.2
	0.0510	9.84	28.4	
D-Glutamic acid	0.0499	8.32	24.5	
	0.0497	8.29	24.5	24.5±0.0
	0.0490	8.17	24.5	
DL-Histidine	0.1005	9.78	15.1	
	0.1010	9.96	15.3	15.1±0.2
	0.0979	9.38	14.9	
L-Histidine	0.1006	8.90	13.7	
	0.1006	8.79	13.6	13.6±0.1
	0.1011	8.86	13.6	
DL-Threonine	0.1001	8.12	9.66	
	0.1000	8.10	9.65	9.61±0.08
	0.1012	8.09	9.53	
L-Threonine	0.1009	8.36	9.87	
	0.1011	8.32	9.81	9.78±0.13
	0.1004	8.14	9.65	
DL-Valine	0.1010	4.44	5.15	
	0.1002	4.41	5.16	5.16±0.01
	0.1006	4.43	5.16	
L-Valine	0.1009	2.46	2.86	
	0.1006	2.46	2.87	2.87±0.01
	0.1010	2.48	2.88	
(±)-Tartaric acid	0.0987	16.9	25.7	
	0.1000	17.1	25.6	25.6±0.1
	0.1003	17.1	25.6	
(+)-Tartaric acid	0.1002	11.0	16.5	
	0.1007	10.7	15.9	16.2±0.3
	0.1002	10.9	16.3	

Table 2. Differences in the heat of solution between optically active compounds and their corresponding racemic compounds

Substance	Differences in the heat of solution at 298.15 K (kJ/mol)
Alanine	2.00±0.21
Glutamic acid	4.1±0.2
Histidine	1.5±0.2
Threonine	0.17±0.13
Valine	2.29±0.01
Tartaric acid	9.4±0.3

It may be seen from Table 2 that the difference in the heat of solution between optically active compounds and their corresponding racemic compounds, which corresponds to the heat of mixing of optical isomers and their optical antipodes in the solid state, is appreciably large.[7]

On the other hand, the heat of mixing of optical isomers and their optical antipodes in the liquid state was nearly zero.[3]

This fact may be explained qualitatively as follows by employing simplified model of optical isomers.[1,8]

We assume that the optically active molecule is a cylindrical rod with circular planes at both ends, and that the circular planes are composed of three different elements a, b, and c.

For the *d*-isomer, the arrangement of these three elements is in the order a, b, and c clockwise as viewed from the top, while for its antipode, the *l*-isomer, it is a, b, and c anticlockwise, the peripheral part is composed of a uniform element, n, as is shown in Fig. 2.

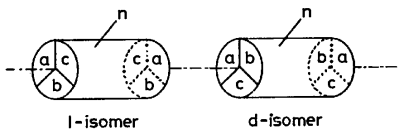

Fig. 2. A model of optical isomers.

Two neighboring molecules on the same axis can take three different states, which are obtained by rotating one of the molecules around the axis, with interacting pairs of elements $\begin{bmatrix} a & b & c \\ a & c & b \end{bmatrix}$, $\begin{bmatrix} a & b & c \\ c & b & a \end{bmatrix}$, and $\begin{bmatrix} a & b & c \\ b & a & c \end{bmatrix}$, whose interaction energies are $U_{aa}+2U_{bc}$, $U_{bb}+2U_{ac}$, and $U_{cc}+2U_{ab}$ respectively.

For the give of simplicity, we further assume that, in a system consisting of a large number of molecules, these molecules are arranged in such a way that their cylindrical axes lie on a straight line, and that each axis is surrounded by z nearest axes, as is shown in Fig. 3.

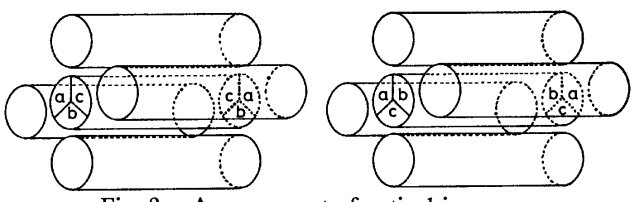

Fig. 3. Arrangement of optical isomers.

In the solid state, the relative angular positions of two neighboring molecules which lie on the same axis, are fixed and take the most stable position among the three states.

In the system of a pure *d*- or *l*-isomer, the interaction energy of the pair of circular planes for each of the three states takes such values as:

$$U_{aa} + 2U_{bc},\ U_{bb} + 2U_{ac},\ \text{and}\ U_{cc} + 2U_{ab}$$

respectively, where U_{ij} denotes the interaction energy of a pair of i and j elements.

The total configurational energy of the system consisting of N molecules of the pure isomer, U^{s}_{TA}, is expressed as:

$$U^{s}_{TA} = \frac{z}{2} NU_{nn} + NU_{Amax}$$

where U_{nn} and U_{Amax} denote the interaction energy between peripheral elements, n, and the interaction energy of the most stable position, respectively.

For a racemic system which consists of $N/2$ molecules of the *l*-isomer and $N/2$ molecules of the *d*-isomer, we may assume that the *l*-isomer and *d*-isomer lie alternately along the axis. Therefore, the interaction energy of pair of circular planes for each of the three states takes these values:

$$U_{aa} + U_{bb} + U_{cc},\ U_{ab} + U_{ac} + U_{bc},\ \text{and}$$
$$U_{ab} + U_{ac} + U_{bc}.$$

Two of them have equal values.

In the solid state, the relative angular position around the axes of two neighboring molecules is fixed. The total configurational energy of the system is, then expressed as:

$$U^{s}_{TR} = \frac{z}{2} NU_{nn} + NU_{Rmax}$$

where U_{Rmax} denotes the interaction energy of the most stable state among the three.

Therefore, the heat of mixing of *l*- and *d*-optical isomers in the solid state, ΔH^{s}_{m}, is expressed as: $\Delta H^{s}_{m} = N(U_{Rmax} - U_{Amax})$.

In general, U_{Rmax} and U_{Amax} have different values, and the heat of mixing has a finite value. However, in the liquid state each molecule can rotate freely around the axis. The average interaction energy is, then the mean of three states, and the total configurational energy of N pure optical isomers, U^{l}_{TA}, may be expressed as:

$$\begin{aligned} U^{l}_{TA} &= \frac{z}{2} NU_{nn} + \frac{N}{3}\{(U_{aa} + 2U_{bc}) + (U_{bb} + 2U_{ac}) \\ &\quad + (U_{cc} + 2U_{ab})\} \\ &= \frac{z}{2} NU_{nn} + \frac{N}{3}\{(U_{aa} + U_{bb} + U_{cc}) \\ &\quad + 2(U_{ab} + U_{ac} + U_{bc})\}. \end{aligned}$$

Similarly, for racemic systems, the total configurational energy, U^{l}_{TR}, may be expressed as:

$$\begin{aligned} U^{l}_{TR} &= \frac{z}{2} NU_{nn} + \frac{N}{3}\{(U_{aa} + U_{bb} + U_{cc}) \\ &\quad + 2(U_{ab} + U_{ac} + U_{bc})\}. \end{aligned}$$

Accordingly, the heat of mixing in the liquid state, $(U^{l}_{TR} - U^{l}_{TA})$ becomes zero in this approximation.

References

1) K. Amaya, *Bull. Chem. Soc. Jpn.*, **34**, 1689 (1961).
2) K. Amaya, *Bull. Chem. Soc. Jpn.*, **34**, 1803 (1961).
3) S. Takagi, R. Fujishiro, and K. Amaya, *Chem. Commun.*, **1968**, 480.
4) A. R. Challoner, H. A. Gundry, and A. R. Meetham, *Phil. Trans. R. Soc. London, A*, **247**, 553 (1955).
5) J. O. Hill, G. Ojelund, and I. Wadsö, *J. Chem. Thermodyn.*, **1**, 111 (1969).
6) C. H. Spink and M. Auker, *J. Phys. Chem.*, **74**, 1742 (1970).
7) M. Matsumoto and K. Amaya, *Chem. Lett.*, **1978**, 87.
8) J. A. Barker, *J. Chem. Phys.*, **20**, 1526 (1952).

 © 1980 The Chemical Society of Japan Bull. Chem. Soc. Jpn., 53, 3513—3516 (1980)

Electron Spin Resonance Study of Cu(II)-Crown Ether Complexes with $3d_{z^2}$ Ground State Doublet in Solution

Kazuhiko Ishizu,* Tokuhiro Haruta, Yuji Kohno, Kazuo Mukai, Kiyonori Miyoshi,† and Yukio Sugiura††

Department of Chemistry, Faculty of Science, Ehime University, Matsuyama 790
†Department of Metallurgical Engineering, Niihama Technical College, Niihama 792
††Faculty of Pharmaceutical Science, Kyoto University, Sakyo-ku, Kyoto 606

(Received December 11, 1979)

Copper(II) chloride and crown ethers (12-crown-4, 15-crown-5 and 18-crown-6) formed orange or orange-yellow complexes in dry chloroform. We found that the ESR g-anisotropy of the complexes was greatly dependent on the numbers of donor oxygens and the ring-numbers. The complexes obtained from 12-crown-4 and 18-crown-6 showed g-anisotropy ($g_{//}>g_{\perp}$); these are well characterized by the $3d_{x^2-y^2}$ or $3d_{xy}$ ground state. On the other hand, the complexes of 15-crown-5 and its benzo derivatives exhibited the reverse g-anisotropy ($g_{//}<g_{\perp}$); these are characterized by the $3d_{z^2}$ ground state with $S=1/2$. The electron nuclear dipolar term and the Fermi's isotropic term were estimated from the ESR parameters based on Bleaney's calculation. The chlorine superhyperfine splittings were observed in the $g_{//}$- component. The MO bonding parameters were estimated by assuming the compressed octahedral, the trigonal bipyramidal, and pentagonal bipyramidal geometry at the paramagnetic site. The bonding nature was studied on the basis of the observed ligand spin densities.

Many synthetic macrocyclic polyethers, polyamines, and other related molecules have been known to possess very interesting and unusual binding properties. They show a pronounced ability to bind a wide variety of cations and anions with marked conformational changes during binding. In addition, their hydrophobic exterior allows them to solubilized ionic substances in nonaqueous solvents.[1] These novel properties of crown ethers and polyamines resulted in their use as model ligands for ion transport systems, biological macrocycles, and the active chromophore of enzyme systems. It has been shown that the spectroscopic parameters of various model Cu(II)–polyamine or –macrocyclic complexes are useful in studying the paramagnetic active sites of Cu(II)–enzyme systems.

The ESR parameters of some cyclic polyamine–Cu(II) complexes have already been compared with those of the type (II)-Cu(II) protein.[2] Some model studies of the type (I)-Cu(II) protein have been performed using some thioether macrocyclic ligands.[3] Several investigators have also extensively studied the Cu(II)–proteins with model ligands such as nitrogen heterocyclics,[4] histidine and cystein containing oligo peptide.[5,6] In fact, the ESR parameters as well as the optical absorption character of these model complexes showed the excellent agreement with those of the square planar ($3d_{x^2-y^2}$ ground state) and of the tetrahedral type ($3d_{xy}$ ground state) paramagnetic active sites in copper proteins, where the g-anisotropy has been shown to be $g_{//}>g_{\perp}$ everywhere.

The possibility of the trigonal bipyramidal active site has also been proposed; the importance of the model studies with the $3d_{z^2}$ ground state in solution has been pointed out by Miskowski.[7] Several ESR studies of copper complexes with the $3d_{z^2}$ ground state have been reported for the compressed tetragonal, compressed trigonal bipyramidal, and *cis*-distorted octahedral site doped in solid matrices.[8] In solutions, however, formations of copper complexes with an axially compressed coordination require quite exceptional conditions, because the coordination geometries are usually fixed by the strong equatorial coordination of the polar functional groups and of the solvent molecules. In order to reveal unusual coordinations, we have chosen the crown ethers as the ligand. ESR investigations have been made for several Cu(II)–crown ether ligands with 12, 15, and 18 ring members in dry chloroform solutions (shown in Fig. 1).

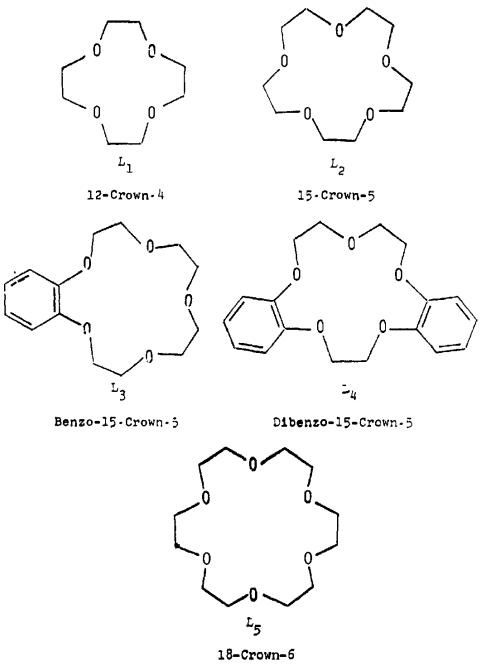

Fig. 1.

We found that the g-anisotropy of the crown ether Cu(II) complexes is strictly dependent on the numbers of ligand oxygen atoms. Cu(II) complexes with the L_2, L_3, and L_4 ligands reveal the inverted g-anisotropy ($g_{//}<g_{\perp}$), while the L_1 and L_5 complexes show the usual g-anisotropy ($g_{//}>g_{\perp}$). The bonding parameters in the copper-ligand bond of the L_2, L_3, and L_4 complexes were determined from the g and A tensors as well as

from the superhyperfine couplings of the chlorine atoms which are axially coordinated. The analysis of the ESR spectra confirmed that the L_2, L_3, and L_4 complexes are in the $3d_{z^2}$ ground state doublet. The electron nuclear dipolar term P and the Fermi isotropic term were determined based on Bleaney's calculation. The MO bonding parameters were estimated assuming the compressed octahedral, the trigonal, and the pentagonal bipyramidal geometry at the paramagnetic site. The bonding nature was characterized on the basis of the ligand spin densities.

Experimental

Benzo-15-crown-5 (L_3) and dibenzo-15-crown-5 (L_4) were synthesized according to Pedersen's procedure.[9] The pure materials were obtained by recrystallization in hexane; L_3: mp 80—82 °C (uncorrected). Found: C, 62.48; H, 7.46%. Calcd for $C_{14}H_{20}O_5$: C, 62.69; H, 7.46%. L_4: mp 114—115 °C (uncorrected). Found: C, 67.95; H, 6.33%. Calcd for $C_{18}H_{20}O_5$: C, 68.34; H, 6.37%. 12-Crown-4 (L_1), 15-crown-5 (L_2), and 18-crown-6 (L_5) purchased from Aldrich Chemicals were used without further purification.

Sample solutions were prepared as follows: commercial anhydrous cupric chloride, dried by heating the material at 110 °C for 6 h (0.04 mmol), and crown ether (0.4 mmol) were mixed with dry $CHCl_3$ (4 ml) under vacuum. The ESR spectra of the orange-to-yellow colored solutions were measured at 77 K. The details of the preparation and the ESR operating conditions were described in the previous paper.[10]

Results and Discussion

ESR Spectra. ESR spectra (Fig. 2) measured at 77 K for the L_1 and L_5 complexes showed the usual g-anisotropy with axial symmetry ($g_{//}>g_{\perp}$), whereas those of the L_2 and L_3 complexes[10] contained a typical line shape for nonoriented systems ($S=1/2$, $g_{//}>g_{\perp}$) (Fig. 3). The ligand superhyperfine splittings due to the two equivalent chlorine atoms can be clearly detected in the g_z component of the ESR spectra of the L_2, L_3, and L_4 complexes. The ESR parameters

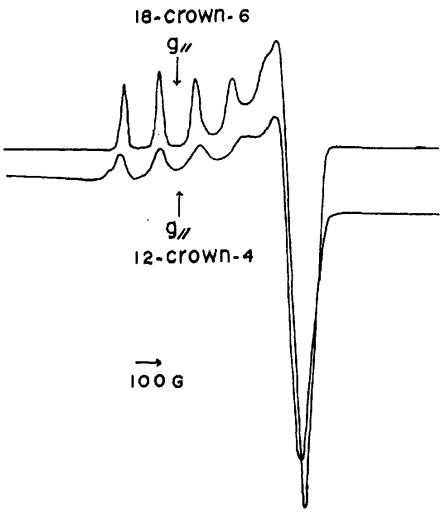

Fig. 2. ESR spectra of $CuCl_2$-12-crown-4 and $CuCl_2$-18-crown-6 measured at 77 K.

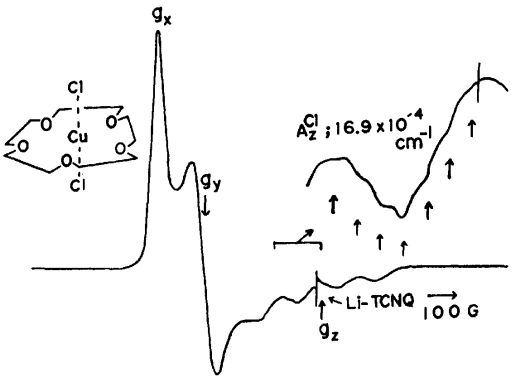

Fig. 3. ESR spectrum of $CuCl_2$-15-crown-5 measured at 77 K.

Table 1. ESR parameters of crown ether $CuCl_2$ complexes

Ligand		g_z	g_x	g_y	A_z	A_x	A_y	A_z^{Cl}
L_2	Obsd	2.000	2.372	2.265	121	—	—	16.9
	Calcd	—	—	—	+126	−8	−39	—
L_3	Obsd	1.995	2.321		130	—	—	16.9
	Calcd	—	—		+125	−23		—
L_4	Obsd	1.992	2.323		137	—		16.5
	Calcd	—	—		+124	−22		—
L_1	Obsd	2.335	2.081		147	—		
L_5	Obsd	2.345	2.077		126	—		

A in 10^{-4} cm^{-1}. Calcd values are obtained using $P=319\times10^{-4}$ cm^{-1} and $K=0.127$, based on Bleaney's method.

determined are summarized in Table 1. The X-ray analysis of the L_1–$CuCl_2$ complex has already been performed. In this case, the copper atom binds with the two equatorial chlorine atoms and takes a distorted octahedral geometry, with the apical Cu–O (2.343 and 2.403 Å) distance much longer than the equatorial bond length (Cu–Cl=2.214, Cu–O=2.128 and 2.113 Å).[11] The ESR parameters of the L_1 and L_5 complexes shown in Table 1 suggest that the unpaired electron occupies either $d_{x^2-y^2}$ or d_{xy} type orbitals in the axially elongated octahedral ligand field. In fact, this conclusion is consistent with the results of the X-ray analysis of the L_1-complex. The structure of the L_5-complex has not been determined yet, but an analogous coordination scheme can be assumed based on the similarity in the observed ESR parameters.[12] In both cases, one will see that the equatorial chlorine atoms play an important role in stabilizing the in-plane bonding ($d_{x^2-y^2}$ or d_{xy}) in the octahedral geometry. The inverted g-anisotropy observed for the L_2, L_3, and L_4 complexes indicates that the unpaired electrons mainly occupy the $3d_{z^2}$ orbital of the metal in the ground state, because their Δg_z-value (g_z-g_e) has a small negative value (see Table 2).[13] The ultimate value of Δg_z is −0.02 for the pure $3d_{z^2}$ ground state, according to the theory.[14] The L_3 and L_4-complexes showed g-anisotropy with nearly axial symmetry. The L_2-complex had rhombic symmetry, which is supposedly due to the distortion arising from some steric requirement

in coordinating the metal ions with crown ether.[15] The ligand hyperfine splitting due to the chlorine atoms associated with the g_z-component suggests an apical perturbation on the Cu ions due to the two chlorine atoms coordinated above and below the pentagonal crown ring (Fig. 4).

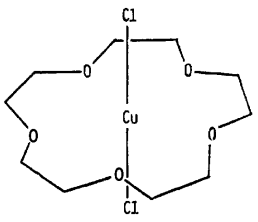

Fig. 4. The structure of $CuCl_2$-15-crown-5.

Characterization of the Bonding Parameters of L_2, L_3, and L_4 Complexes. The observed ESR spectra can be fitted by the spin Hamiltonian:

$$\hat{H} = \sum_{i=x,y,z} (g_i \beta H_i S_i + A_i \hat{S}_i \hat{I}_i) \quad (1)$$

if we neglect the copper nuclear Zeeman effect and the quadrupole interactions. A detailed discussion of the hyperfine tensor and its relation to the g-factors of the Cu(II) with the $3d_{z^2}$ ground state has already been given in the work of Bleaney.[14] For rhombic symmetry of the paramagnetic site, the relations between the g and the hyperfine tensor elements are given as follows:

$$A_x = P[-K + \Delta g_x + \frac{1}{14}\Delta g_y - \frac{2}{7}] \quad (2)$$

$$A_y = P[-K + \Delta g_y + \frac{1}{14}\Delta g_x - \frac{2}{7}] \quad (3)$$

$$A_z = P[-K + \Delta g_z - \frac{1}{14}(\Delta g_x + \Delta g_y) + \frac{4}{7}] \quad (4)$$

$$\Delta g_z = g_z - g_e,\ \Delta g_x = g_x - g_e,\ \Delta g_y = g_y - g_e$$

where K is the Fermi isotropic term and P defines the dipolar interaction of the copper nucleus with the unpaired electron, which is proportional to the average value of the inverse cubic power of the metal-unpaired electron distance. In the previous paper, P and K values were evaluated for the L_3 complex based on Swalen's calculation:[16]

$$P = 319 \times 10^{-4}\ cm^{-1} \text{ and } K = 0.127.^{10}$$

With the tentative use of these P and K values, the hyperfine tensor elements of the copper nucleus (A_x, A_y, and A_z) were calculated by using Bleaney's simple treatment; this gave satisfactory agreement between the observed and the calculated values for the L_2 and L_3 complexes, provided that $A_z > 0$ and A_x, $A_y < 0$ (see Table 1).

The considerable discrepancy between the observed and the calculated A_z values seen for the L_4 complex would be attributed to the overestimation of the K value; this will be revised in the following section. For nearly axially symmetry (L_3 and L_4) $\Delta g_\perp (g_\perp - g_e)$ can be expressed as a function of the ^2A-^2E, d-d transition energy $\Delta E_{xz,yz}$ and of the effective spin-orbital interaction parameter λ', which gives a measure of the extent of the electron delocalization into the ligand; $\lambda' = \alpha^2 \lambda_0$, $\Delta g_\perp = 6\lambda'/\Delta E_{xz,yz}$, where α^2 is the spin density on the copper $3d_{z^2}$ orbital. The effective value of spin-orbit interaction $\lambda'(-733.7\ cm^{-1})$ can be obtained based on the assumption that $\lambda' = (P/P_0)\lambda_0$,[17] where $P_0(360 \times 10^{-4}\ cm^{-1})$ and $\lambda_0(-828\ cm^{-1})$ are the dipolar-term and the spin-orbit interaction parameter of a Cu(II) free ion, respectively.

The value of α^2 was ≈ 0.89, and the corresponding d-d band transition energy $\Delta E_{xz,yz}$ was roughly 13800 cm^{-1} for the L_3 and the L_4 complex. A more rigorous value of α^2 was estimated from the ligand superhyperfine structures.

MO Scheme of the Bonding Parameters. According to ligand field theory, the unpaired electron occupies the molecular orbital involving the metal ion $3d_{z^2}$ and the ligand orbital.

The appropriate σ-unpaired orbital, ψ_{z^2}, can be expressed as follows:

$$\psi_{z^2} = \alpha d_{3z^2} - \frac{\alpha'}{2\sqrt{3}}(2Z_1 + 2Z_2 - Z_3 - Z_4 - Z_5 - Z_6) \quad (5)$$

$$\psi_{z^2} = \alpha d_{3z^2} - \frac{\alpha'}{2\sqrt{6}}(\sqrt{6}Z_1 + \sqrt{6}Z_2 - 2Z_3 - 2Z_4 - 2Z_5) \quad (6)$$

$$\psi_{z^2} = \alpha d_{3z^2} - \frac{\alpha'}{2\sqrt{10}}(\sqrt{10}Z_1 + \sqrt{10}Z_2 - 2Z_3 - 2Z_4 - 2Z_5 - 2Z_6 - 2Z_7) \quad (7)$$

for the octahedral (5), the trigonal bipyramidal (6), and the pentagonal bipyramidal (7) geometry, where Z_1 and Z_2 denote the AO's in the axial ligands, and Z_3—Z_6 and Z_7 are those in the equatorial ligands.[18]

The detailed structures of the L_2, L_3, and L_4 complexes are unknown. In order to obtain a qualitative view of the structure, however, some idealized calculations were carried out based on the chlorine hyperfine splitting. We used the assumption that the atomic orbitals of the two axially coordinated chlorine atoms can be described in term of the hybridization expressed as $Z_i = np \pm \sqrt{1-n^2}\,S$. For the maximum bonding of the ligand, the ideal sp hybridization may be assumed for

Table 2. Bonding parameters of 15-crown-5 copper complexes

	Octahedral				Pentagonal bipyramidal / Trigonal bipyramidal					A_z^{Cl}
	α^2	P	K	β^2	α^2	P	K	β^2	Δg_z	
L_2	0.936	337	0.1648	0.0864	0.914	329	0.1561	0.0875	−0.0023	16.9
L_3	0.936	337	0.1328	0.0984	0.914	329	0.1235	0.0995	−0.0073	16.9
L_4	0.937	337	0.1082	0.1078	0.916	330	0.0995	0.1085	−0.0103	16.5

A_z^{Cl} and P in $10^{-4}\ cm^{-1}$.

the chlorine atoms ($n^2=1/2$). The hyperfine tensor of the chlorine atoms ($A_{//}$) for unit spin density is thus given as follows:

$$A_{//} = (1 - n^2)[A_f + 2A_p],\ n^2 = \frac{1}{2} \text{ for sp chlorine atoms}$$

$$A_f = g_N\beta_N g\beta[\frac{8}{9}\pi|\psi_{3s}(0)|^2],\ A_p = \frac{2}{5}g_N\beta_N g\beta < r^{-3} >_{3p} \quad (8)$$

where A_f and A_p are isotropic and anisotopic hyperfine constants, respectively. The effective values of A_f (1490×10^{-4} cm^{-1}) and A_p (44×10^{-4} cm^{-1}) were obtained from the parameters of ^{35}Cl and ^{37}Cl based on their natural abundance ratio.[19] The net spin densities ($\rho_{Cl}=0.011$) on the chlorine atoms are determined from the superhyperfine splittings due to the chlorine atoms listed in Table 1. The total ligand spin densities thus obtained are 0.066 for the octahedral ligand geometry and 0.088 for the trigonal and pentagonal bipyramidal geometry. The magnitudes of the spin density on the 3d orbital ($\alpha^2\simeq0.912$—0.934) were estimated by neglecting the overlap integral between the copper and ligand orbitals. Based on the α^2 values thus determined, the electron-nuclear dipolar term P and the Fermi contact term K were calculated from the A_z values using Bleaney's equation (4). The calculated bonding parameters are given in Table 2. Both P and K values evaluated from the ligand spin densities are in excellent accord with the previous assumption; $P=319\times10^{-4}$ cm^{-1} and $K=0.127$. Of interest is the anomalously small K value estimated for the Cu(II)–crown complexes in the $3d_{z^2}$ ground state, which is of the correct symmetry to mix with the 4s orbital.[20]

The isotropic interaction term measures the sum of the spin polarization due to 3d and 4s electrons, as is expressed below; $-PK=A_{3d}\alpha^2+A_{4s}\beta^2$, where $A_{3d}=-142\times10^{-4}$ cm^{-1} and $A_{4s}=+896\times10^{-4}$ cm^{-1}.[21] The β^2 values thus obtained are cited in Table 2. One will see that contribution of about 10% from 4s reduces the K value to a large extent in the present complexes. From the inspection of the bonding parameters listed in Table 2, several important aspects of the bonding nature of the L_2, L_3, and L_4 complexes can be clarified. The α^2-values assumed here are more or less qualitative, but at least it may be concluded that the natures of the copper-ligand bonds are rather ionic and that the unpaired electron weakly delocalizes into the ligand orbitals in these complexes. The Δg_z value, a measure of the admixture of $d_{x^2-y^2}$ into the ground state, decreases with increasing numbers of the fused benzene rings.

This means that the planar fused benzene restricts a conformational change in the crown ring during the optimum binding at the equatorial positions. The A_z value also shows a concomitant change with the Δg_z-value. The lower g_z value gives a larger A_z value, which is reflected in the K value. The smallest K-value can be calculated for the L_4-complex, where the 4s admixture parameter increases with increasing z character due to the octahedral Jahn-Teller distortion.

The ^{1}H, ^{14}N, and ^{63,64}Cu ENDOR spectra of stellacyanin have been measured recently. The unusual copper hyperfine tensor was explained by assuming a flattened tetrahedral geometry.[22] To our knowledge, the Cu(II)–chromophors or the complexes with the $3d_{z^2}$ ground state have not been clearly characterized in the biological systems. Nevertheless, the present work will present some fundamental knowledge for the ESR studies of Cu(II)-complexes with the $3d_{z^2}$ ground state as studied in solutions.

References

1) J. J. Christensen, D. J. Eatough, and R. M. Izatt, *Chem. Rev.*, **74**, 351 (1974).

2) M. C. Styka, R. C. Smieriak, E. L. Blinn, R. E. Desimone, and J. V. Passariello, *Inorg. Chem.*, **17**, 82 (1978).

3) T. E. Jones, D. B. Rorabachor, and L. A. Ochrymowycz *J. Am. Chem. Soc.*, **97**, 7485 (1975).

4) H. Yokoi and A. W. Addison, *Inorg. Chem.*, **16**, 1341 (1977).

5) Y. Sugiura and Y. Hirayama, *J. Am. Chem. Soc.*, **99**, 1581 (1977).

6) Y. Sugiura and Y. Hirayama, H. Tanaka, and K. Ishizu, *J. Am. Chem. Soc.*, **97**, 5577 (1975).

7) V. Miskowsky, S. P. W. Tang, T. G. Spiro, and T. H. Moss, *Biochemistry*, **14**, 1244 (1975).

8) R. Hirasawa and H. Kon, *J. Chem. Phys.*, **56**, 4467 (1972).

9) C. J. Pedersen, *J. Am. Chem. Soc.*, **89**, 7017 (1967).

10) K. Ishizu, T. Haruta, K. Nakai, K. Miyoshi, and Y. Sugiura, *Chem. Lett.*, **1978**, 579.

11) F. P. Van Remoorte, F. P. Boer, and E. C. Steiner, *Acta. Crystallogr.*, **31**, 1420 (1975).

12) The ESR g-parameters ($g_{//}=2.18$, $g_{\perp}=2.05$) were reported for the L_5–$2CuCl_2$ complex. Preparation of the complex was carried out using the hydrated metal salt. The complex is assigned to different paramagnetic species. D. E. Vos, J. Van Daalen, A. C. Knegt, Th. C. Van Heyningen, L. P. Otto, M. W. Vonk, A. J. Mijsman, and W. L. Driessen, *J. Inorg. Nucl. Chem.*, **37**, 1319 (1975).

13) A. Abragam and B. Bleaney, "Electron Paramagnetic Resonance," Clarendon Press, Oxford (1970), p. 456.

14) B. Bleaney, K. D. Bower, and M. H. L. Pryce, *Proc. R. Soc. London*, **228**, 147 (1955).

15) D. H. Bush, *Acc. Chem. Res.*, **11**, 392 (1978).

16) J. D. Swalen, B. Johnson, and H. M. Gladney, *J. Chem. Phys.*, **52**, 4078 (1970).

17) B. B. Wayland, J. V. Minkiewicz, and M. E. Abd-Elmageed, *J. Am. Chem. Soc.*, **96**, 2797 (1974).

18) C. E. Schäffer and C. K. Jørensen, *Mol. Phys.*, **9**, 401 (1965).

19) J. E. Wertz and J. R. Bolton, "Electron Spin Resonance," McGraw-Hill, N. Y. (1972). Table C. Nuclear spins, abundances, moments and hyperfine coupling for some common magnetic nuclei.

20) R. E. Watson, *Phys. Rev.*, **119**, 1934 (1960).

21) A. F. Garito and B. B. Wayland, *J. Am. Chem. Soc.*, **91** 866 (1969).

22) J. E. Roberts, T. G. Brown, B. M. Hoffman, and J. Peisach, *J. Am. Chem. Soc.*, **102**, 825 (1980).

Paramagnetic Cobalt(III) Complexes with Organic Ligands. V. The Isolation and Properties of Salts of the Paramagnetic Bis(2,2'-bipyridine)(5-nitrosalicylato)cobalt(III) and of the Paramagnetic "β_1 and β_2"-Isomers of the 5-Nitrosalicylato(triethylenetetramine)-cobalt(III) and Their Derivatives[1]

Yoshihisa YAMAMOTO,* Eiko TOYOTA, and Naoto MITSUDERA
Faculty of Pharmaceutical Sciences, Higashi Nippon Gakuen University, Ishikari-Tobetsu, Hokkaido 061-02
(Received February 4, 1980)

The picrate of the paramagnetic, $[Co(5\text{-}NO_2sal)(bpy)_2]^{2+}$, has been isolated from a reaction mixture of picric acid, 60% nitric acid, and bis(2,2'-bipyridine)(salicylato)cobalt(III) chloride trihydrate, $[Co(sal)(bpy)_2]Cl\cdot 3H_2O$, which had been prepared from salicylic acid and *cis*-bis(2,2'-bipyridine)dichlorocobalt(III) chloride dihydrate. The absorption spectrum and the stability of an aqueous solution of the picrate of the paramagnetic, $[Co(5\text{-}NO_2sal)(bpy)_2]^{2+}$, were somewhat different from those of complexes of the paramagnetic, $[Co(5\text{-}NO_2sal\text{-}R)(NH_3)_4]^{2+}$ (R: H, CH_3). Several complexes of the paramagnetic, β_1-5-nitrosalicylato-, β_2-5-nitrosalicylato-, and β_2-3-methyl (and 4-methyl)-5-nitrosalicylato(triethylenetetramine)cobalt(III) have, analogously, been isolated from reaction mixtures of 60% nitric acid and β_1-salicylato-, β_2-salicylato, or β_2-methylsalicylato(triethylenetetramine)cobalt(III) chloride hydrate respectively. Their β_1 and β_2-isomeric forms were proved by a study of their IR and ^{1}H-NMR spectra. From the IR, NMR, and the magnetic susceptibility measurement results, these compounds are considered to have the paramagnetic complex, $[Co(5\text{-}NO_2sal)L]^{2+}$ (L: $(NH_3)_4$, $(en)_2$, $(bpy)_2$, and trien), and the electron hole is considered to delocalize over the chelate ring containing the cobalt atom and the 5-nitrosalicylato ligand.

Previously we have reported on several green paramagnetic cobalt(III) complexes with organic ligands, which are formally tetravalent. Various physicochemical measurements have showed, however, that the compounds contain radical cations and that the cobalt is trivalent.[2] In the paramagnetic cobalt(III) complexes, the paramagnetic cobalt(III) complex of an aromatic amine ligand such as bipyridine and the isomers of the paramagnetic cobalt(III) complex such as the triethylenetetramine ligand have not yet been described.

The present paper deals with the isolation and properties of complexes of the paramagnetic bis(2,2'-bipyridine)(5-nitrosalicylato)cobalt(III) and of the isomers of the paramagnetic β_1 and β_2-5-nitrosalicylato-(triethylenetetramine)cobalt(III); also, their properties are compared with those of 5-nitrosalicylato(tetraammine)cobalt(III) complexes.[2]

Results and Discussion

*Bis(2,2'-bipyridine)(salicylato)cobalt(III) Chloride Trihydrate, $[Co(sal)(bpy)_2]Cl\cdot 3H_2O$ (**1**) and Paramagnetic Bis(2,2'-bipyridine)(5-nitrosalicylato)cobalt(III) Picrate, $[Co(5\text{-}NO_2sal)(bpy)_2](pic)_2$ (**2**).* Although many studies of bis(2,2'-bipyridine)cobalt(III) complexes with aliphatic organic ligands[3-6] or inorganic ligands[5-8] have already been reported, the bis(2,2'-bipyridine)-cobalt(III) complex with an aromatic organic ligand has never been described. Complex **1** was prepared by the reaction of the salicylic acid and *cis*-$[CoCl_2(bpy)_2]Cl\cdot 2H_2O$. Complex **1** can also be prepared from the corresponding *trans* dichloro complex. It is soluble in water, methanol, or dimethyl sulfoxide and is insoluble in most organic solvents. The color of an aqueous solution of **1** is reddish brown, while that of a methanolic solution is green. This color change is reversible.[9] Complex **1** decomposes in an aqueous solution. Complex **2** has been isolated from the reaction mixture of Complex **1**, 60% nitric acid, and picric acid. In an aqueous solution, **2** is much more unstable than paramagnetic 5-nitrosalicylato(tetraammine)cobalt(III) complexes, $[Co(5\text{-}NO_2sal\text{-}R)(NH_3)_4]^{2+}$ (R: H, CH_3) (**3**).

The absorption spectrum of **1** in methanol has three absorption bands at 301, 313, and 587 nm. The absorption bands at 301 and 313 nm are the specific absorption bands[3c] of **1**. The absorption band at 587 nm is based on the d-d transition ($^1T_{1g}\leftarrow{}^1A_{1g}$) of the cobalt ion. The absorption spectrum of **2** in 65% nitric acid has two absorption bands, at 577 and 645 nm, in the 450—700 nm region. The ε at 645 nm of **2** is much weaker than that[10] at 660 nm of **3**, while the peak at 577 nm is stronger than that at 587 nm of **1**.

In the ^{1}H-NMR spectra, the signals (6.1—7.5 ppm) of the salicylato protons of the coordinated salicylato ligand of **1** were observed in dimethyl-d_6 sulfoxide, but those of **2** were not observed.[2] The signals (7.3—9.1 ppm) of the bipyridine protons of the coordinated bipyridine ligand of **1** and **2** were observed. In the ^{13}C-NMR spectrum of **1** in heavy water we observed fifteen signals for the bis(2,2'-bipyridine) ligand and seven signals for the salicylato ligand, which were assigned on the basis of the chemical shifts of salicylato-(tetraammine)cobalt(III) chloride monohydrate,[2] $[Co(sal)(NH_3)_4]Cl\cdot H_2O$ (**4**). The spectrum of **2** did not show the expected signals because of paramagnetism.[2]

The effective magnetic moment was 1.6 B.M., and the Curie-Weiss constant was -10 K for **2**.

In the IR spectra, the rocking deformation vibration was observed at 764 cm^{-1} for **1** and at 766 cm^{-1} for **2**. The cobalt atom of these complexes is considered to contain trivalent cobalt.[2]

From the IR, ^{1}H- and ^{13}C-NMR spectra and the magnetic susceptibility, an aromatic amine complex (**2**) was found to show the same properties as those of the

TABLE 1. THREE ISOMERIC FORMS AND THE ABBREVIATIONS OF THE SALICYLATO (TRIETHYLENETETRAMINE)COBALT COMPLEXES

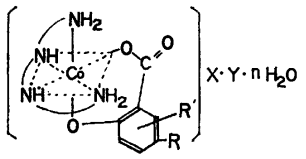

β_1

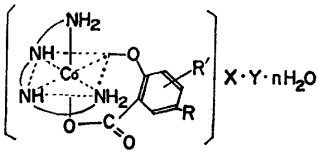

β_2

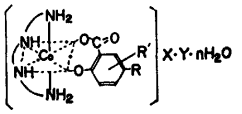

α

Complex	5	6	7	8	9	10	11	12	13	14	15	16	17	18	19
Form	β_1	β_1	β_2	β_2	β_1	β_2	β_2	β_2	β_2	β_1	β_2	β_2	β_2	β_1	β_2
R	H	H	H	H	H	H	NO_2	NO_2	NO_2	NO_2	NO_2	NO_2	NO_2	NO_2	NO_2
R'	3-CH_3	4-CH_3	3-CH_3	4-CH_3	H	H	H	3-CH_3	4-CH_3	H	H	3-CH_3	4-CH_3	H	H
X	Cl	Cl	Cl	Cl	Cl	Cl	NO_3	NO_3	NO_3	Cl	Cl	Cl	Cl	Cl	Cl
Y	—	—	—	—	—	—	—	—	—	NO_3	NO_3	NO_3	NO_3	Cl	Cl
n	2	2	1	1	1	1	3	2	2	2	2	2	2	3	3

TABLE 2. SOME PHYSICAL PROPERTIES OF COMPLEXES **3**—**6** AND **9**—**15**

Complex No.	IR spectra			Absorption bands		Magnetic moments	Mp [dec]	Electro conductivity of aqueous solutions
	3000—3300 cm^{-1}	990—1100 cm^{-1}	$\rho_r(NH_2)_r$ cm^{-1}	λ/nm	ε	μ_{eff}(B.M.)	°C	$S \cdot cm^2\ eq^{-1}$
5	2950, 3100, 3220	995, 1030	860	335	3330[1]		238—240	110
	3250, 3270	1062(vs), 1080		524	291			
6	2950, 3080, 3180	998, 1030	857	328	3100[1]		236—239	105
	3230, 3270	1058(vs), 1072		525	287			
7	2880, 2940, 3055	993, 1033	860	338	3370[1]		245—247	106
	3150, 3220, 3270	1055, 1078(vs)		510	288			
8	2880, 2940, 3060	990, 1035	860	331	3060[1]		247—248	104
	3150, 3240, 3270	1052, 1078(vs)		511	275			
11	2870, 3100	995, 1030,	830	378	13550[1]		[229—231]	91
	3200, 3270	1050, 1070(vs)		498	316			
12	2870, 3120	995, 1030	835	382	15000[1]		[255—258]	120
	3230, 3270	1053, 1078(vs)		496	340			
13	2870, 3120	995, 1028	830	374	13450[1]		[249—251]	107
	3230, 3270	1050, 1070(vs)		500	307			
14	2900, 3100	1000, 1035	835	345	4100[2]	1.68	[124—125]	283
	3200, 3250	1070, 1090		460	4250			
				660	12900			
15	2870, 3080	995, 1030	835	360	3240[2]	1.70	[183—184]	254
	3180, 3260	1055, 1078		455	3300			
				663	11800			
16	2880, 3120	995, 1030	838	340	3980[2]	1.66	[182—183]	271
	3180, 3260	1052, 1075		455	2900			
				667	7850			
17	2880, 3120	996, 1030	830	360	3600[2]	1.64	[182—183]	272
	3200, 3260	1055, 1075		452	3940			
				633	7400			

Mp: **9**; 238—241, **10**; 240—243 °C. Solvents: 1) H_2O, 2) 60% HNO_3.

aliphatic amine complexes (**3**) except for the absorption spectra and the stability of the aqueous solutions.

β-Salicylato(triethylenetetramine)cobalt(III) Complexes and Paramagnetic β-5-Nitrosalicylato(triethylenetetramine)cobalt-(III) Complexes. The paramagnetic properties of these isomers have been the subject of little research. We expect that the delocalization of a radical cation of these isomers will differs from that of **3**. Three isomeric forms and the abbreviations of the salicylato (triethylenetetramine)cobalt(III) complexes studied in this paper are listed in Table 1. The color and solubility of **5**—**8** are similar to those of **9**[11] and **10**.[11] Complexes **14**—**19** are insoluble in most organic solvents, but are soluble in nitric acid, hydrochloric acid, and dimethyl sulfoxide. Aqueous solutions of the **14**—**19** complexes are somewhat more unstable than that of **3**, while that of **14** is more unstable than that of **15**.

The IR spectra of the **5**—**7** and **11**—**17** complexes have four strong peaks in the 990—1100 and 3000—3300 cm^{-1} regions respectively, as is shown in Table 2;

Table 3. ^{1}H-NMR spectra of complexes **3**—**6** and **9**—**15**

Complex No.	$NH_2CH_2CH_2NHCH_2CH_2NHCH_2CH_2NH_2$[a]				[N(2)H+salicylato]		CH_3
	CH_2 δ/ppm	N(1)H_2 δ/ppm	N(4)H_2 δ/ppm	N(3)H δ/ppm	N(2)H δ/ppm	salicylato δ/ppm	δ/ppm
5	2.38—3.87(12H)	4.34(1H) 4.53(1H)	4.70(1H) 5.20(1H)	b)	6.49(1H)	6.50—7.80(3H)	2.26(3H)[1]
6	2.39—3.86(12H)	4.34(1H) 4.48(1H)	4.69(1H) 5.21(1H)	6.12(1H)	6.52(1H)	6.52—7.81(3H)	2.30(3H)[1]
7	2.38—2.85 (3H) 2.85—3.75 (9H)	4.35(2H)	4.60(1H) 5.18(1H)	6.12(1H)	[6.40—7.83(4H)]		2.30(3H)[1]
8	2.37—2.82 (3H) 2.82—3.74 (9H)	4.32(2H)	4.62(1H) 5.13(1H)	6.05(1H)	[6.37—7.78(4H)]		2.29(3H)[1]
11	2.35—2.85 (3H) 2.85—3.85 (9H)	4.53(2H)	4.97(1H) 5.35(1H)	6.34(1H)	6.87(1H)	7.13—8.85(3H)	— [1]
12	2.47—2.81 (3H) 2.81—3.88 (9H)	4.47(2H)	4.89(1H) 5.34(1H)	6.31(1H)	6.85(1H)	7.96—8.67(2H)	2.30(3H)[1]
13	2.42—2.87 (3H) 2.87—3.87 (9H)	4.52(2H)	4.92(1H) 5.39(1H)	6.35(1H)	6.89(1H)	7.29—8.74(2H)	2.25(3H)[1]
14	2.42—3.92(12H)	4.40(1H) 4.70(1H)	5.27(1H) 5.48(1H)	6.52(1H)	b)		— [2]
	2.45—3.98(12H)	4.43(1H) 4.70(1H)	c)	6.60(1H)	7.00(1H)		— [1]
15	2.33—2.82 (3H) 2.82—3.84 (9H)	4.48(2H)	5.14(1H) 5.38(1H)	6.35(1H)	b)		— [2]
	2.34—2.83 (3H) 2.83—3.88 (9H)	4.54(2H)	c)	6.36(1H)	7.13(1H)		— [1]
16	2.46—2.90 (3H) 2.90—3.88 (9H)	4.60(2H)	c)	6.51(1H)	7.21(1H)		2.25(3H)[1]
17	2.46—2.84 (3H) 2.84—3.92 (9H)	4.56(2H)	c)	6.45(1H)	7.15(1H)		2.27(3H)[1]

Solvents: 1) 1.8 mol dm^{-3} D_2SO_4. 2) 3.6 mol dm^{-3} D_2SO_4. Standard: internal DSS.

a) N(1), N(2), N(3), and N(4) of the coordinated triethylenetetramine ligand.

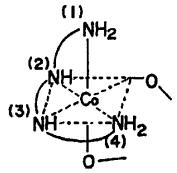

b) This signal overlapped with the solvent. c) This signal overlapped with the side band of the solvent.

Table 4. ^{13}C-NMR spectra of complexes **1**, **5**—**8**, and **11**

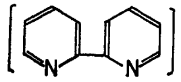

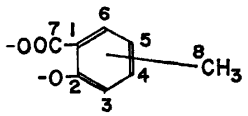

Complex No.	$NH_2CH_2CH_2NHCH_2CH_2NHCH_2CH_2NH_2$ δ/ppm						c-1	c-2	c-3	c-4	c-5	c-6	c-7	c-8
							δ/ppm							
1	123.1	125.6	125.8	125.9	129.3		118.1	165.9	117.8	134.8	124.5	132.1	173.2	—
	129.5	142.7	142.8	143.5	151.4									
	152.0	152.2	157.1	157.4	157.9									
5	56.3	53.8	52.4	52.1	45.9	43.7	115.3	167.0	133.1	135.1	116.4	129.9	175.1	17.3
6	56.3	53.9	52.3	52.0	45.9	43.7	115.3	168.0	119.0	146.1	124.1	132.3	174.8	21.2
7	52.7	51.9	50.1	48.5	47.6	42.0	116.2	167.0	133.0	134.4	115.7	130.0	174.7	17.9
8	52.8	52.2	49.7	48.3	47.4	42.0	118.8	168.3	118.4	145.7	124.0	132.4	174.2	21.1
11	52.9	52.3	50.1	48.5	47.8	42.4	116.0	172.3	125.1	136.8	128.5	130.7	176.1	—

Solvent: D_2O. Standard: internal dioxane (δ=67.4 ppm).

therefore, they are assigned the β-form.[12] The rocking deformation vibrations[2] of these complexes were observed at 830—860 cm^{-1}.

The absorption spectra of the **14**—**17** complexes in 60% nitric acid showed three absorption bands at about 345, 460, and 660 nm. In the **14** and **15** complexes, although these spectra show similar forms, the second absorption band of **14** is shorter than that of **15**. The ε at 660 nm of these complexes is similar to that[10a] at 660 nm of **3**. In the **15**—**17** complexes, the second absorption band of **16** is shorter than that of **15**, while the ε at 667 nm of **16** and that at 633 nm of **17** are

weaker than that at 663 nm of **15**. These properties seem to be due to the substituent effect of the methyl group.[10b] In the **11**—**13** complexes, the second absorption bands are longer than those of **7**, **8**, and **10** respectively, while the ε's of those bands of the **11**—**13** complexes are much stronger than those of **7**, **8**, and **10** respectively. Those properties seem to be due to the substituent effect of the nitro group. The first absorption bands of **7**, **8**, and **10** shift to a shorter wavelength area than those of **5**, **6**, and **9** respectively. The absorption spectra of **18** and **19** could not be obtained because they turned dark green in 35% hydrochloric acid.

In the ^{1}H-NMR spectra, the protons of the coordinated triethylenetetramine and methylsalicylato ligands of these complexes were assigned on the basis of the results in earlier papers,[11,13] as is shown in Table 3. The signals of the 5-nitrosalicylato protons of the coordinated 5-nitrosalicylato ligands of **14** and **15**—**17** were not observed, either. The spectra of **5**, **6**, and **14** are similar to that of β_1-complex[11] (**9**) while those of **7**, **8**, and **15**—**17** are similar to that of the β_2-complex[11] (**10**). They are assigned the β_1 and β_2-forms respectively. The chemical shifts of the NH and NH_2 protons of coordinated trien in **11**, **14**, and **15** shifted to a lower field than those of **9** and **10**. This could be due to the nitro group in the coordinated 5-nitrosalicylato ligand. In the ^{13}C-NMR spectra of **5**—**8** and **11** in heavy water, we observed eight signals for the methylsalicylato ligand and six signals for the triethylenetetramine ligand. The chemical shifts of the methylsalicylato ligand are assigned on the basis of the chemical shift of **4**.[2] Those of the trien ligand are difficult to assign to the individual carbon atom. The ^{13}C-NMR spectra of **14**—**19** did not show the expected signals because of paramagnetism.

The effective magnetic moments of the **14**—**19** complexes were 1.7 B.M.

The above data show that the paramagnetic properties of the **14** and **15** isomers are little different from each other, while their properties are in agreement with those of **3**. The properties of **16** and **17** are only a little different from those of **15**. They can thus be grouped together as paramagnetic 5-nitrosalicylato-(amine)cobalt(III) complexes, $[Co(5\text{-}NO_2sal)L]^{2+}$ (L: $(NH_3)_4$, $(en)_2$, $(bpy)_2$, trien), with a radical cation delocalized over the chelate ring containing the cobalt atom and the 5-nitrosalicylato ligand, from the results of the IR spectra,[2] ^{1}H-, and ^{13}C-NMR spectra,[2] the magnetic susceptibility,[14] and the electric resistivity.[14] The properties of these complexes are collected in Tables 2—4.

Experimental

Measurements. The NMR spectra were recorded with an FX-60 apparatus (JEOL) for ^{13}C-NMR and an R-40 apparatus (Hitachi) for ^{1}H-NMR. The IR spectra were recorded on potassium bromide disks with a IR-27G apparatus (Shimadzu). The visible absorption spectra were recorded with a Shimadzu MPS-5000 recording spectrophotometer. The magnetic susceptibilities were measured by the Gouy method using a magnetic balance (Shimadzu) from liq.N_2 to r.t. The pH was measured with a Corning pH-meter M-125. The electro conductivity of an aqueous solution was determined by the use of a conductometer, CM-30 (Shimadzu) at room temperature.

Preparation of Complexes. Bis(2,2'-bipyridine)(salicylato)cobalt(III) Chloride Trihydrate (1): *cis*-Bis(2,2'-bipyridine)-dichlorocobalt(III) chloride dihydrate[15] (2.0 g, 3.89 mmol dm^{-3}) was added to AgOH, which had been made from silver nitrate (1.33 g, 7.83 mmol dm^{-3}) and potassium hydroxide. The mixture was stirred for about 30 min at 60 °C and then filtered. To the filtrate we then added salicylic acid (0.53 g, 3.84 mmol dm^{-3}) in a 10% ammonia solution of 5 ml. The mixture was concentrated at 60 °C. The black complex thus precipitated was filtered off, washed with a 3% ammonia solution, dried, and recrystallized from a 2—3% ammonia solution. Complex **1** was dried in a desiccator over diphosphorus pentaoxide. Yield: 1.70 g (73.2%). Found: C, 54.56; H, 4.07; N, 9.82; Cl, 5.23%. Calcd for $CoC_{27}H_{26}N_4O_6Cl$ (MW 596.91) C, 54.33; H, 4.39; N, 9.39; Cl, 5.94%. mp 240—243 °C. IR spectrum: $\rho_r(Co\text{–}N)_r$: 764 cm^{-1}. Absorption bands: 301 (ε=25600), 313 (ε=24200), and 587 nm (ε=330) in MeOH.

Paramagnetic Bis(2,2'-bipyridine)(5-nitrosalicylato)cobalt(III) Dipicrate (2): About 1 cm^3 of 60% nitric acid was added to **1** of 1.0 g (1.68 mmol dm^{-3}). The color of the solution was thus changed to green. Then several cm^3 of 60% nitric acid were added to it. An aqueous solution of picric acid (0.77 g, 3.36 mmol dm^{-3}) was added to the green solution, and it was stirred. The yellowish-green complex (**2**) thus precipitated was filtered off, washed with ice water, and dried. Yield: 1.34 g (79.1%). Found: C, 46.82; H, 2.40; N, 14.94%. Calcd for $CoC_{39}H_{23}N_{11}O_{19}$ (MW 1008.61) C, 46.44; H, 2.30; N, 15.28%. Dec 163—167 °C. IR spectrum: $\rho_r(Co\text{–}N)_r$: 766 cm^{-1}. Absorption bands: 577 (ε=867) and 645 nm (ε=675) in 65% DNO_3.

β-Salicylato(triethylenetetramine)cobalt(III) Chloride Monohydrate, β-3-Methylsalicylato(triethylenetetramine)cobalt(III) Chloride Monohydrate, and β-4-Methylsalicylato(triethylenetetramine)-cobalt(III) Chloride Monohydrate: These complexes were prepared by the reaction of the α-dichloro(triethylenetetramine)-cobalt(III) chloride[16] and salicylic acid, 3-methylsalicylic acid, or 4-methylsalicylic acid at pH 10—11 by Morgan's method.[17] Yields: 3-methylsalicylato(triethylenetetramine)-cobalt(III) chloride monohydrate, 64.4%; 4-methylsalicylato-(triethylenetetramine)cobalt(III) chloride monohydrate, 67.1%.

Separation of β_1-3-Methylsalicylato(triethylenetetramine)cobalt(III) Chloride Dihydrate (5), β_1-4-Methylsalicylato(triethylenetetramine)-cobalt(III) Chloride Dihydrate (6), β_2-3-Methylsalicylato(triethylenetetramine)cobalt(III) Chloride Monohydrate (7), and β_2-4-Methylsalicylato(triethylenetetramine)cobalt(III) Chliorde Monohydrate (8): The separation of β_1 and β_2 complexes was achieved by the use of ion-exchange resin.[18] Complexes **5** and **6** are changed to the corresponding β_2-complexes in an alkali solution. Yields: 0.033 g (6.6%) for **5**; 0.028 g (5.6%) for **6**; 0.43 g (86%) for **7**; 0.42 g (84%) for **8**. Found **5**: C, 39.88; H, 6.66; N, 13.48; Cl, 9.08%. **6**: C, 39.10; H, 6.39; N, 12.89; Cl, 8.95%. **7**: C, 41.35; H, 6.68; N, 13.59; Cl, 9.16%. **8**: C, 40.81; H, 6.14; N, 13.80; Cl, 9.39%. Calcd for **5** and **6**: $CoC_{14}H_{28}N_4O_5Cl$ (MW 426.79) C, 39.40; H, 6.61; N, 13.13; Cl, 8.31%. **7** and **8**: $CoC_{14}H_{26}N_4O_4Cl$ (MW 408.78) C, 41.14; H, 6.41; N, 13.71; Cl, 8.67%.

β_2-5-Nitrosalicylato(triethylenetetramine)cobalt(III) Nitrate Trihydrate (11): Complex **11** was prepared according to the procedure of a previous paper.[2] An orange-colored solution of **11**, acetone, and 60% nitric acid was set aside to crystallize at room temperature for several days. The orange complex thus separated was filtered off, washed with ice-water, and

dried. It was recrystallized several times from water, while it did not turn green in the 60% nitric acid. Yield: 0.54 g (14.1%). Found: C, 30.87; H, 5.07; N, 17.16%. Calcd for $CoC_{13}H_{27}N_6O_{11}$ (MW 502.33) C, 31.08; H, 5.42; N, 16.73%.

β_2-3-Methyl-5-Nitrosalicylato(triethylenetetramine)cobalt(III) Nitrate Dihydrate (12) and β_2-4-Methyl-5-Nitrosalicylato(triethylenetetramine)cobalt(III) Nitrate Dihydrate (13): Complexes **12** and **13** were prepared according to the procedure used for Complex **11**. Yields: 0.26 g (21.3%) for **12**; 0.20 g (16.4%) for **13**. Found **12**: C, 33.54; H, 5.22; N, 17.26%. **13**: C, 33.47; H, 5.26; N, 16.86%. Calcd for $CoC_{14}H_{27}N_6O_{10}$ (MW 498.34) C, 33.74; H, 5.46; N, 16.86%.

Paramagnetic β_1-5-Nitrosalicylato(triethylenetetramine)cobalt(III) Chloride Nitrate Dihydrate (14): Three cm^3 of 60% nitric acid were added to **9** (1.0 g, 2.53 mmol dm^{-3}). After the reaction,[16b] the solution was filtered using a glass filter (G-4), and the green filtrate was added to acetone. The green complex thus precipitated was filtered off, washed with acetone, and dried. It was then reprecipitated twice more by dissolution in 60% nitric acid and by the addition of acetone. Yield: 0.46 g (35.5%). Found: C, 30.64; H, 5.18; N, 15.90; Cl, 6.86%. Calcd for $CoC_{13}H_{25}N_6O_{10}Cl$ (MW 519.77) C, 30.04; H, 4.85; N, 16.17; Cl, 6.82%.

Paramagnetic β_2-5-Nitrosalicylato(triethylenetetramine)cobalt(III) Chloride Nitrate Dihydrate (15): Complex **15** was prepared from **10** (3.0 g, 7.60 mmol dm^{-3}) and 60% nitric acid (9 cm^3), according to the procedure used for Complex **14**. Yield: 1.87 g (47.3%). Found: C, 30.23; H, 5.03; N, 16.02, Cl, 7.25%. Calcd for $CoC_{13}H_{25}N_6O_{10}Cl$ (MW 519.77) C, 30.04; H, 4.85; N, 16.17; Cl, 6.82%.

Paramagnetic β_2-3-Methyl-5-Nitrosalicylato(triethylenetetramine)-cobalt(III) Chloride Nitrate Dihydrate (16) and Paramagnetic β_2-4-Methyl-5-Nitrosalicylato(triethylenetetramine)cobalt(III) Chloride Nitrate Dihydrate (17): Complexes **16** and **17** were prepared from **7** (1 g, 2.45 mmol dm^{-3}) or **8** (1 g, 2.45 mmol dm^{-3}) and 60% nitric acid (3 cm^3), according to the procedure used for Complex **14**. Yields: 0.56 g (42.8%) for **16**; 0.44 g (33.6%) for **17**. Found **16**: C, 31.11; H, 5.40; N, 16.01; Cl, 6.19%. **17**: C, 31.82; H, 5.15; N, 16.09; Cl, 6.70%. Calcd for **16** and **17** $CoC_{14}H_{27}N_6O_{10}Cl$ (MW 533.80) C, 31.50; H, 5.10; N, 15.74; Cl, 6.64%.

Paramagnetic β_1-5-Nitrosalicylato(triethylenetetramine)cobalt(III) Chloride Trihydrate (18) and Paramagnetic β_2-5-Nitrosalicylato-(triethylenetetramine)cobalt(III) Chloride Trihydrate (19): Complexes **18** and **19** were prepared from **14** (0.30 g, 0.52 mmol dm^{-3}) or **15** (0.50 g, 0.96 mmol dm^{-3}) and 35% hydrochloric acid (1 cm^3 for **14** and 1.5 cm^3 for **15**) respectively. Yields: 0.17 g (62.9%) for **18**; 0.31 g (63.1%) for **19**. Found **18**: C, 30.56; H, 5.52; N, 13.50; Cl, 13.10%. **19**: C, 29.97; H, 5.27; N, 13.42; Cl, 13.46%. Calcd for $CoC_{13}H_{27}N_5O_8Cl_2$ (MW 511.23) C, 30.54; H, 5.32; N, 13.70; Cl, 13.87%. Magnetic moments, μ_{eff}: 1.66 for **18**, 1.70 B.M. for **19**.

The authors wish to express their gratitude to Professor Masayasu Mori of Osaka City University for his discussions.

References

1) Part IV; Ref. 2. Presented at the 29th Symposium on Coordination Chemistry of the Chemical Society of Japan, Hamamatsu, 1979.

2) Y. Yamamoto, *Bull. Chem. Soc. Jpn.*, **51**, 2894 (1978).

3) a) M. Murakami, S. Senoh, N. Matsusato, H. Itatani, and J-W Kang, *Nippon Kagaku Zasshi.*, **83**, 734 (1962); b) M. Murakami, S. Senoh, N. Matsusato, H. Itatani, and J-W Kang, *ibid.*, **83**, 737 (1962); c) M. Murakami, S. Senoh, N. Matsusato, H. Itatani, and J-W Kang, *ibid.*, **83**, 741 (1962); d) M. Murakami, S. Senoh, N. Matsusato, H. Itatani, and J-W Kang, *ibid.*, **83**, 819 (1962); e) M. Murakami, S. Senoh, N. Matsusato, H. Itatani, and J-W Kang, *ibid.*, **83**, 823 (1962)

4) D. A. Palade and T. N. Volokh, *Zh. Neorg. Khim.*, **15**, 1872 (1970).

5) "Advances in Inorganic Chemistry and Radiochemistry," ed by H. J. Emeleus and A. G. Sharpe, Academic Press, New York and London (1969), Vol. 12, p. 135.

6) a) D. M. Palade, *Ukr. Khim. Zh. (Russ. Ed.)*, **37**, 319 (1971); b) D. M. Palade, *Zh. Neorg. Khim.*, **14**, 3029 (1969).

7) D. M. Palade, A. V. Ablov, and V. N. Zubarev, *Zh. Neorg. Khim.*, **14**, 445 (1969).

8) M. P. Hancock, J. Josephsen, and C. E. Schaffer, *Acta. Chem. Scand.*, **A30**, 79 (1976).

9) "Shin Jikken Kagaku Koza," ed by T. Tachibana Maruzen, Tokyo (1976), Vol. 8 (III), p. 1470; b) S. Herzog, R. Klausch, and J. Lantos, *Z. Chem.*, **4**, 150 (1964).

10) a) Y. Yamamoto, K. Ito, H. Yoneda, and M. Mori, *Bull. Chem. Soc. Jpn.*, **40**, 2580 (1967); b) Y. Yamamoto, M. Mori, H. Yoneda, S. Misumi, and K. Ito, *ibid.*, **42**, 984 (1969).

11) Y. Yamamoto and E. Toyota. *Bull. Chem. Soc. Jpn.*, **52**, 2540 (1979).

12) a) D. A. Buckingham, M. Dwyer, G. J. Gainsford, V. Janson Ho, L. G. Marzilli, Ward T. Robinson, A. M. Sargeson, and K. R. Turnbull, *Inorg. Chem.*, **14**, 1739 (1975); b) L. G. Marzilli and D. A. Buckingham, *Inorg. Chem.*, **6**, 1042 (1967); c) D. A. Buckingham and D. Jones, *Inorg. Chem.*, **4**, 1387 (1965).

13) Y. Yamamoto and E. Toyota, *Chem. Pharm. Bull.*, **26**, 2275 (1978).

14) Y. Yamamoto, *Bull. Chem. Soc. Jpn.*, **42**, 999 (1969).

15) a) F. M. Jaeger and J. A. van Dijk, *Z. Anorg. Allg. Chem.*, **227**, 273 (1936); b) F. M. Jaeger and J. A. van Dijk, *Proc. Acad. Sci. Amsterdam.*, **39**, 164 (1936).

16) A. M. Sargeson and G. H. Searle, *Inorg, Chem.*, **6**, 787 (1967).

17) G. T. Morgan and J. D. M. Smith, *J. Chem. Soc.*, **1956**, 1922.

18) D. A. Buckingham, P. J. Cresswell, R. J. Dellaca, M. Dwyer, G. J. Gainsford, L. G. Marzilli, I. E. Maxwell, Ward T. Robinson, A. M. Sargeson, and K. R. Turnbull, *J. Am. Chem. Soc.*, **96**, 1713 (1974).

The *trans-cis* Isomerization of the Diaquabis(malonato)chromate(III) Ion in Various Organic Solvent-Water Mixtures

Kengo UCHIDA* and Yoshinobu TAKINAMI

Department of Chemistry, Faculty of Science, Hirosaki University, Bunkyo-cho, Hirosaki 036

(Received March 7, 1980)

The kinetics of the *trans-cis* isomerization of $[Cr(mal)_2(H_2O)_2]^-$ have been investigated in binary mixed solvents, including methanol–, ethanol–, dioxane–, and acetone–water mixtures. The first-order rate constant increases with a decrease in the volume percentage of the water, but is independent of the kind of organic solvent. The rate is not affected by the addition of any cation to an aqueous solution. These results are in contrast to those for the analogous oxalato complex, and are interpreted in terms of a dissociation mechanism in which the rate-determining step is the dissociation of the coordinating water molecule.

Many studies[1-14] have been made of various reactions of potassium diaquabis(oxalato)chromate(III), $K[Cr(ox)_2(H_2O)_2]$. Much less information is, though, available on the analogous complex of diaquabis(malonato)chromate(III). Some aquation,[15,16] anation,[17] and isomerization[8,18,19] have been investigated, though, and the behavior of the malonato complex seems to be rather different from that of the oxalato complex. For example, the isomerization of the malonato complex is much slower, but the aquation takes place more easily than that of the oxalato complex in an acid solution. With respect to the isomerization mechanism, Frank and Huchital[19] suggested a ring-opening mechanism and Casula *et al.*[8] proposed a primary dissociation of the water molecule.

In this work, we have studied the effects of mixed aqueous solvents, the addition of some kinds of salts, and the pH value of the solution on the *trans-cis* isomerization, and have proposed an aqua-ligand dissociation mechanism.

Experimental

Materials. Potassium *trans*-diaquabis(malonato)chromate(III), *trans*-$K[Cr(mal)_2(H_2O)_2]$, was prepared in a manner similar to that described by Chang.[20] The product was recrystallized twice from water. The other inorganic salts were of a guaranteed reagent grade and were recrystallized from water. Redistilled water and organic solvents of an ultraspecial grade or a guaranteed reagent grade were used as the solvents.

Procedures. The rates of the reactions were determined spectrophotometrically[8] at the wavelength of 565 nm using a Shimadzu double-beam spectrophotometer, UV 200S, with a temperature-controlled cell holder. The first-order rate constants, k, were obtained from the slopes of the plots of $\ln(A_\infty - A)$ *vs.* t, where A is the absorbance at time t and where A_∞ is the absorbance after the reaction is complete. These plots were straight, with very little scatter, in every case. The reaction cell was a quartz cell ($1 \times 1 \times 4.5$ cm) for a spectrophotometer with a branch. The concentration of the complex was 1.50×10^{-2} mol dm^{-3} in all cases. Most of the kinetic experiments were performed at 50 °C.

The pH values of the solution, which were not adjusted unless otherwise noted, were 4.4—4.6. When the pH value was varied, 0.1 mol dm^{-3} of NaOH or 0.05 mol dm^{-3} of HCl was added. The pH values were measured by means of a Hitachi-Horiba pH meter, M5, before and after the reaction. The pH values did not change during the reactions.

Results

Absorption Spectra. The wavelengths and the molar absorption coefficients, ε, of the absorption maxima of the complexes are collected in Table 1, where the subscript "eq" indicates the equilibrated mixture of the *trans*- and the *cis*-isomer after the reaction has stopped.

TABLE 1. SPECTRAL DATA FOR SOME COMPLEX IONS

Complex	λ_{1max}/nm[a]	λ_{2max}/nm[a]
trans-$[Cr(mal)_2(H_2O)_2]^-$	402(23.0)	556(18.6)
	401(20.3)[b]	555(17.6)[b]
	405(22)[c]	560(21)[c]
$[Cr(mal)_2(H_2O)_2]^-_{eq}$	418(40)	565(45.6)
cis-$[Cr(mal)_2(H_2O)_2]^-$	418(42.1)[b]	565(50.8)[b]
	415(41)[c]	565(51)[c]
trans-$[Cr(mal)_2(OH)(H_2O)]^{2-}$	414(38)	570(26)
	420(41)[c]	570(26)[c]
cis-$[Cr(mal)_2(OH)(H_2O)]^{2-}$	416(44)	574(39)
	425(48)[c]	575(43)[c]

a) Values in parentheses are the molar absorption coefficients (dm^3 mol^{-1} cm^{-1}). b) Ref. 19. c) Ref. 8.

Kinetics. When the *trans*-isomer is dissolved in water, *trans-cis* isomerization occurs and the reaction comes to an end at an equilibrium. The equilibrium lies close to the *cis*-form, and it has been reported[18] that 95% is of the *cis*-form at the equilibrium. The isomerization obeys good first-order kinetics even after 90% reaction, and a constant A_∞ value is always obtained. Aquation can be neglected in this work.

As the complex does not dissolve in such organic solvents as methanol, ethanol, dioxane, and acetone, mixtures of the organic solvent and water were used as the solvents. In such mixtures, the kinetic behavior was very similar to that in an aqueous solution which contained no organic solvent. The k values increased with an increase in the concentration of the organic solvent in every case, as is shown in Fig. 1. The values at higher concentrations of the organic solvent could not be obtained because of the low solubility of the complex. It may be clear that the specificity of the solvents is very small, and the variation in k values can not be elucidated individually by the mole fraction of the organic solvents, the relative permittivity, or the

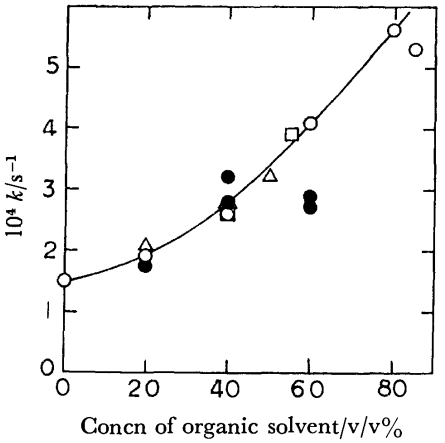

Fig. 1. Effect of concentration of organic solvent on the rate constant.
○: Methanol, ●: ethanol, □: dioxane, △: acetone.

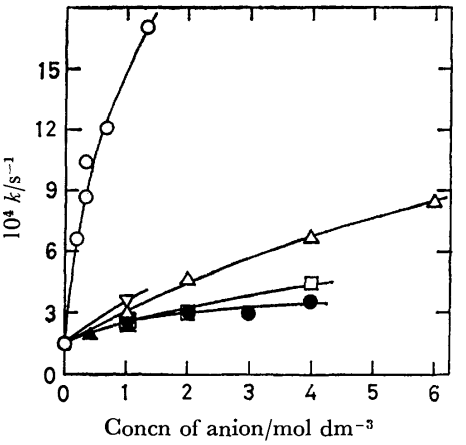

Fig. 2. Effect of concentration of various anion on the rate constant.
○: SO_4^{2-}, ▽: I^-, △: NO_3^-, □: ClO_4^-, ●: Br^-, ▲: Cl^-.

viscosity of the solution. The k values seem to depend on only the volume percentage of the water, namely, the molarity of water, and to increase with a decrease in the molar concentration of the water. For example, the k values at 40 v/v% remain approximately constant ($(2.6—3.2)\times10^{-4}\ s^{-1}$) in every solvent. Some deviations do, however, occur near the limits of the solubility in the systems of alcohol and water. In these solvents, some structural effect due to a hydrogen bond between solvent molecules might play a special role.[21]

Effect of Added Salts on the k *Values. In an Aqueous Solution*: The effect of added salts on the k values was investigated. At first, several chlorides were added in order to examine the cationic effect. As the rate depends on the ionic strength, I, the concentration of the salts was adjusted to $I=1.0$. The k values were 2.5×10^{-4}, 2.6×10^{-4}, 2.8×10^{-4}, and $2.4\times10^{-4}\ s^{-1}$ for NaCl, $CaCl_2$, $SrCl_2$, and $LaCl_3$ respectively. Also, it is obvious that the values are approximately constant and independent of the kind of cation, in contrast to the case of the analogous oxalato complex, $[Cr(ox)_2(H_2O)_2]^-$.[4,11] As the reaction was not accelerated by the addition of a bivalent or tervalent cation, which has a great effect in the case of $[Cr(ox)_2(H_2O)_2]^-$, it is concluded that cations have no catalytic effect on the isomerization of the malonato complex.

On the other hand, Frank and Huchital[19] have found the accelerating effect of the nitrate ion. However, we found that this effect is general for the other anions and that the bivalent anion seems to be more effective. The effects of the concentration of the anions on the rate constants are shown in Fig. 2, where sodium salts are used. The sulfate ion has the greatest effect, and the order of the k values seems to be as follows:

$$SO_4^{2-} \gg I^- > NO_3^- > ClO_4^- \approx Br^- \geqslant Cl^-.$$

In Organic Solvent–Water Mixtures: A similar anionic effect was investigated in organic solvent–water mixtures. Ethanol of a protic solvent and acetone and dioxane of an aprotic solvent were used. The volume percentage of the organic solvent was adjusted to 50%, and sodium salts were used. As has been mentioned above, no solvent effect was observed in the absence of added salts, but a distinct solvent effect appeared in the presence of the added salts. The results are listed in Table 2. The order of k values is as follows:

$$\text{dioxane–}H_2O > \text{acetone–}H_2O > \text{ethanol–}H_2O.$$

Although the effect is not great, evidently some interaction between the anions and the organic solvents is present. The order of the catalytic effect by the anions also seems to change to $Cl^- > I^- > Br^-$, whereas the order is $Cl^- \leqslant Br^- < I^-$ in an aqueous solution containing no organic solvent.

pH Effect. The k values measured at various pH values are shown in Fig. 3. The rate increases rapidly above pH 5. All the spectra after the equilibrium is reached are very similar in the pH region of 3—6.

Table 2. Effect of added anion on k values in organic solvent–water mixtures
(50 v/v%, [anion] = 1.0 mol dm^{-3})

Solvent	$10^4\ k/s^{-1}$		
	Cl^-	Br^-	I^-
H_2O	2.5	2.7	3.7
Ethanol–H_2O	4.9	3.9	5.1
Acetone–H_2O	5.9	4.4	5.2
Dioxane–H_2O	6.1	4.9	6.1

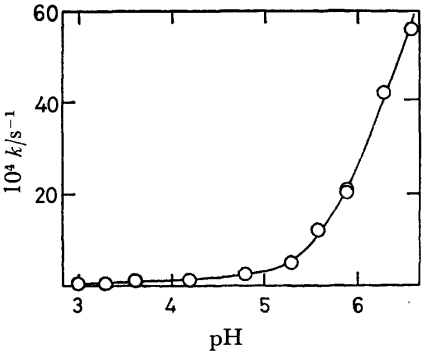

Fig. 3. Effect of pH on the rate constant.

Slight shifts of the absorption maxima can be seen above pH 6, but the molar absorption coefficients do not change so much. The spectral changes are probably due to the formation of a hydroxo complex of $[Cr(mal)_2(OH)(H_2O)]^{2-}$, spectral data of which are also shown in Table 1.

In the higher pH region, k values were obtained at 25.0 °C and $I=0.015$, because the rates were too fast to measure at 50.0 °C. The k values are 14.8×10^{-4} s^{-1} at pH 8.3 and 15.9×10^{-4} s^{-1} at pH 10.5.

Effect of the Temperature. The k values were measured at five different temperatures over the range from 307.2 K to 323.2 K. The activation parameters, listed in Table 3, were calculated from plots of $\ln k$ *vs.* $1/T$.

TABLE 3. ACTIVATION PARAMETERS

Solution	ΔH^*/kJmol^{-1}	ΔS^*/J mol^{-1}
Aqueous solution	116	42
Aqueous solution at pH 5.7	103	20
Aqueous solution containing Na_2SO_4	135	114
60%methanol-H_2O	163	195

Discussion

The rate of the isomerization of the malonato complex is much slower than that of the analogous oxalato complex. The orders of magnitude of the k values of the malonato and the oxalato complex are 10^{-6} and 10^{-4} s^{-1} respectively at 25 °C; the difference is about 100 times. The mechanism of the reaction has been studied for the oxalato complex,[6,8,22] and two main mechanisms have been proposed. At first, the added cation, such as Na^+, Ca^{2+}, or La^{3+}, forms an ion-pair, and a bond rupture takes place at a Cr–oxalato bond; then, the isomerization proceeds *via* a five-coordinated trigonal bipyramidal intermediate. Next is the twist mechanism, in which the rate is not affected by the cations and a proton.

In the malonato complex, the next four mechanisms could be considered in general: (a) a water-association mechanism, (b) a twist mechanism, (c) a ring-opening mechanism, and (d) an aqua-ligand dissociation mechanism.

Of these mechanisms, (a) can be eliminated because the k values increase with a decrease in the concentration of water and are independent of the kind of organic solvent, and it would be more difficult for solvent water to enter the complex when the concentration of the water decreases. Moreover, a seven-coordinated intermediate could hardly be considered, since the entropy of activation, ΔS^*, is positive. If a water molecule coordinates to the Cr atom, ΔS^* would be negative because of the decrease in the degree of freedom.

The twist mechanism (b) is also not reasonable, because the positive and great ΔS^* value, the anionic effect, and the increase in the k value with an increase in the volume percentage of the organic solvents could not be explained by this mechanism. Although the viscosity of the solvent may affect the twist, there is no close relation between the k value and the viscosity. However, it seems impossible to deny the possibility of this mechanism, since the oxalato complex may isomerize *via* a twist mechanism in the absence of any added salts.[22] A malonato chelate is larger and might be more easily distorted. Thus, the twist intermediate might be stabilized.

Mechanism (c) could be removed since the isomerization is not catalyzed by cations in the case of the malonato complex. On the other hand, in the oxalato complex the apparent rate constants are 5.5×10^{-4} s^{-1} and 1.3×10^{-2} s^{-1} in the presence of Na^+ and La^{3+} respectively,[11] these values differ by about 24 times. From these results, it seems that the cation may not play an important part in breaking the Cr–malonato bond, contrary to the case of the oxalato complex. Frank and Huchital[19] suggested the ring-opening mechanism because of the positive ΔS^*, the analogy to the oxalato complex, and the stability of the malonato complex referred to the second formation constants of the *cis*-oxalato and the *cis*-malonato complexes. However, they did not neglect the dissociation mechanism and proposed a combination of the ring-opening and water-dissociation mechanisms. However, Banerjea and Chatterjee[15] reported that the rate of the dissociation (aquation) of the *cis*-malonato complex in an aqueous acidic solution is about 70 times faster than that of the oxalato complex, and that the former is much more labile. If the malonato chelate is labile, the other mechanism should be proposed because the k value of the malonato is about 100 times smaller than that of the oxalato complex. An ion-pair formation would be important in the catalytic effect by cations in the oxalato complex, which is given by:

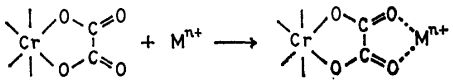

(1)

In the malonato complex, however, the methylene group seems to prevent the ion-pair formation, as given by:

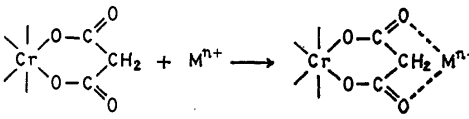

(2)

Mechanism (d) seems to be most plausible. In the mechanism accompanying a dissociation of a ligand water molecule, ΔS^* would have a large positive value. Then, a five-coordinated intermediate may be formed after the dissociation. Moreover, the k value may increase with the decrease in the concentration of water, since the ligand water molecule could be removed more easily when the concentration of the water decreases. After the release of the water molecule, the chance of the recombination of the intermediate complex and a water molecule may decrease, while the possibility of the isomerization may increase as the concentration of the organic solvent increases. Although the organic solvent molecule may coordinate to the intermediate,

the bond may be weak, and so the isomerization would take place easily. Consequently, the isomerization could be accelerated. A catalytic effect by a nitrate ion has been found,[19] but a sulfate ion has an even more remarkable effect. A bivalent anion coming close to the ligand water molecule may assist the release of the water molecule effectively. The effects of univalent anions are less significant, and the difference in the effects in organic solvents could not be elucidated clearly. Hunt *et al.*[23] reported that the rate constant of the exchange of a water molecule, k_{ex}, is 7×10^{-7} s^{-1} and that the activation energy, E_a, is 112 kJ mol^{-1} [24] for $[Cr(H_2O)_6]^{3+}$ at 25 °C, while k_{ex} is less than 10^{-6} s^{-1} for *cis*-$[Cr(ox)_2(H_2O)_2]^-$.[3] It may tentatively be assumed from these values that the k_{ex} is 10^{-6}—10^{-7} s^{-1} for $[Cr(mal)_2(H_2O)_2]^-$. The observed k is 1.5×10^{-6} s^{-1}, and E_a is 119 kJ mol^{-1}, for the malonato complex in an aqueous solution. The similarity of these values may also support the theory that the rate-determining step is the dissociation of the ligand water molecule.

In the higher pH region, $[Cr(mal)_2(OH)(H_2O)]^{2-}$ is formed and the k values become larger. These values at 25 °C, which are very close to the values obtained by Casula *et al.*,[8] can be reduced to $k=0.040$ s^{-1} at pH 8.3 and $k=0.043$ s^{-1} at pH 10.5 at 50 °C by using the activation parameters. The two values are approximately the same as the rate constant for the hydroxo complex. In general, a hydroxo complex is more labile than a conjugate acid complex, as well as a cobalt(III) complex, since the charge of the central metal atom decreases partially upon the addition of a negative OH group and the bond of $Cr–OH_2$ becomes weak. The rate constant of the *trans-cis* isomerization of $[CrCl(en)_2(H_2O)]^{2+}$ is less than 6×10^{-6} s^{-1} at 35.0 °C.[25] If the isomerization occurs *via* water exchange, the rate might be expected to be similar for the malonato complex. The isomerization rate constant of the conjugate base, $[CrCl(OH)(en)_2]^+$, is less than 6×10^{-5} s^{-1}.[26] This value is not large, but it may be a little larger than that of $[CrCl(en)_2(H_2O)]^{2+}$.

The authors are sincerely grateful to Professor Taro Isobe for his continuing interest and encouragement.

References

1) K. R. Ashley and R. E. Hamm, *Inorg. Chem.*, **4**, 1120 (1965).
2) H. Kelm and G. M. Harris, *Inorg. Chem.*, **6**, 706 (1967).
3) J. Aggett, I. Mawston, A. L. Odell, and B. E. Smith, *J. Chem. Soc., A*, **1968**, 1413.
4) H. Kelm, H. Stieger, and G. M. Harris, *Z. Phys. Chem. (Frankfurt am Main)*, **67**, 98 (1969).
5) H. Kelm, H. Stieger, and G. M. Harris, *Ber. Bunsenges. Phys. Chem.*, **73**, 939 (1969).
6) M. W. Rophael and M. A. Malati, *J. Chem. Soc., A*, **1971**, 1903.
7) H. Kelm, H. Stieger, and G. M. Harris, *Chem. Ber.*, **104**, 2743 (1971).
8) M. Casula, G. Illuminati, and G. Ortaggi, *Inorg. Chem.*, **11**, 1062 (1972).
9) S. N. Choi and D. W. Carlyle, *Inorg. Chem.*, **11**, 1718 (1972).
10) M. B. Davies and J. W. Lethbridge, *J. Inorg. Nucl. Chem.*, **37**, 141 (1975).
11) Y. Harada and K. Uchida, *Sci. Rep. Hirosaki Univ.*, **23**, 68 (1976).
12) T. W. Kallen, *Inorg. Chem.*, **15**, 440 (1976).
13) L. Goswami, S. Sarkar, and D. Banerjea, *Z. Anorg. Allg. Chem.*, **435**, 301 (1977).
14) P. L. Kendall, G. A. Lawrance, and D. R. Stranks, *Inorg. Chem.*, **17**, 1166 (1978).
15) D. Banerjea and C. Chatterjee, *J. Inorg. Nucl. Chem.*, **29**, 2387 (1967).
16) C. Furlani and E. Mantovani, *J. Inorg. Nucl. Chem.*, **31**, 1213 (1969).
17) R. E. Hamm and R. H. Perkins, *J. Am. Chem. Soc.*, **77**, 2083 (1955).
18) K. R. Ashley and K. Lane, *Inorg. Chem.*, **9**, 1795 (1970).
19) M. J. Frank and D. H. Huchital, *Inorg. Chem.*, **11**, 776 (1972).
20) J. C. Chang, *J. Inorg. Nucl. Chem.*, **30**, 945 (1968).
21) E. M. Arnett, W. G. Bentrude, J. J. Burke, and P. McC. Duggleby, *J. Am. Chem. Soc.*, **87**, 1541 (1965), *etc.*
22) Y. Takinami and K. Uchida, The Tohoku District Meeting of the Chemical Society of Japan, Yamagata, Oct., 1978, Abstr. No. 1B05. A fuller discussion will be published in the near future.
23) J. P. Hunt and H. Taube, *J. Chem. Phys.*, **19**, 602 (1951).
24) J. P. Hunt and R. A. Plane, *J. Am. Chem. Soc.*, **76**, 5960 (1954).
25) D. J. MacDonald and C. S. Garner, *Inorg. Chem.*, **1**, 20 (1962).
26) D. C. Olson and C. S. Garner, *Inorg. Chem.*, **2**, 558 (1963).

A Kinetic Study on the Proton-transfer Reactions of Bis(dimethylglyoximato)cobalt(III) Complex Ions in Dioxane-Water Media†

Noboru Yoshida and Masatoshi Fujimoto*

Department of Chemistry, Faculty of Science, Hokkaido University, Sapporo 060

(Received March 15, 1980)

The proton-transfer reactions of bis(dimethylglyoximato)cobalt(III) complex ions, $[Co^{III}(dmgH)_2X_2]^n$, with hydroxide ion, OH^-, were studied in dioxane–water media by means of a temperature-jump method. The rate constant, k_f, for the direct proton-transfer from $[Co^{III}(dmgH)_2X_2]^n$ to OH^- was found to be 1.6×10^5—2.9×10^6 mol^{-1} dm^3 s^{-1} in aqueous solution. The value of k_f for $[Co^{III}(dmgH)_2(CN)_2]^-$ anion decreased gradually from 1.6×10^5 to 4.0×10^4 mol^{-1} dm^3 s^{-1} for the change in the mole fraction of dioxane, x_{diox}, from 0 to 0.174. On the other hand, with increase in x_{diox}, the value of k_f for $[Co^{III}(dmgH)_2(NH_3)_2]^+$ cation gradually decreased from 2.9×10^6 to 1.1×10^6 mol^{-1} dm^3 s^{-1} in a region of lower x_{diox}, and then increased from 1.1×10^6 to 1.6×10^7 mol^{-1} dm^3 s^{-1} in a region of higher x_{diox}. The dependence of k_f on x_{diox} is interpreted in connection with reaction mechanism.

A large number of fast proton-transfer reactions in aqueous solutions have been investigated by relaxation techniques,[1] but only a few measurements have been reported for the reactions in non-aqueous media such as dioxane–water,[2-5] DMSO–water,[6] chlorobenzene,[7] and acetonitrile.[8]

We have studied the proton-transfer reactions of the univalent[4] and bivalent[5] anions of *o*-hydroxy azo compounds with hydroxide ion in dioxane–water media using a temperature-jump method. From the change in k_f of these Brønsted acids with increasing x_{diox} the dependency of k_f on x_{diox} was explained by both the change of the dielectric constant of medium and the solute-solvent interactions.

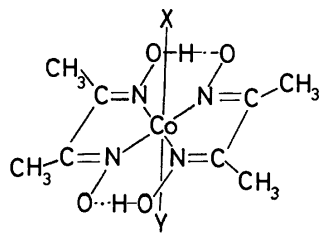

Fig. 1. Structural formulae of $[Co^{III}(dmgH)_2XY]^n$.

It has been established that dimethylglyoxime ($dmgH_2$) forms a stable square planar complex, $[Co^{III}(dmgH)_2X_2]Y$, on the basis of NMR[9] and IR[10] spectroscopic studies, chemical characteristics,[11] and syntheses,[12] where dmgH, X, and Y denote the coordinated univalent dimethylglyoximate anion, the axial ligand, and the counter ion, respectively. The structure of complexes having axial ligands is shown in Fig. 1. They constitute a series which enables us to design systematic variations in acid-dissociation constant and charge type of complexes. The acid-dissociation of bis(dimethylglyoximato)cobalt(III) complex ions can generally be represented by

$$[Co^{III}(dmgH)_2X_2]^n \rightleftharpoons [Co^{III}(dmg)(dmgH)X_2]^{n-1} + H^+, \quad (1)$$

where dmg denotes the coordinated bivalent dimethylglyoximate anion.[13,14] The values of pK_a of these weak Brønsted acids are in the order of magnitude 10—12 due to the strong intramolecular hydrogen-bond, OH···O⁻.

In the present paper, we report a kinetic study on the proton-transfer reactions in dioxane–water media of diamminebis(dimethylglyoximato)cobalt(III) cation ($[Co^{III}(dmgH)_2(NH_3)_2]^+$; DGA cation) and dicyanobis(dimethylglyoximato)cobaltate(III) anion ($[Co^{III}(dmgH)_2(CN)_2]^-$; CDG anion). DGA cation and CDG anion are relatively stable in both aqueous and dioxane–water media. The values of pK_a were determined spectrophotometrically ($pK_a^c(s)$) and kinetically ($pK_a^c(k)$), the $pK_a^c(s)$ and $pK_a^c(k)$ values being in good agreement with each other at each dioxane content. The rate constants, k_f and k_r, for the reaction

$$[Co^{III}(dmgH)_2X_2]^n + OH^- \underset{k_r}{\overset{k_f}{\rightleftharpoons}} [Co^{III}(dmg)(dmgH)X_2]^{n-1} + H_2O \quad (2)$$

were measured by the temperature-jump method. The dependency of the value of k_f on x_{diox} was found to differ considerably from each other due to the difference in the signs of their charge and the solute-solvent interactions. The dependency is discussed in connection with reaction mechanism.

Experimental

Materials. Water was deionized and distilled. Guaranteed grade dioxane (Wako) was distilled over sodium.

Bis(dimethylglyoximato)diamminecobalt(III) chloride, $[Co^{III}(dmgH)_2(NH_3)_2]Cl\cdot5H_2O$, was prepared from purpureo salt, $[Co^{III}Cl(NH_3)_5]Cl_2$, and dimethylglyoxime in the presence of ammonium acetate, and recrystallized from hot water.[15] Found: C, 21.28; H, 6.78; N, 18.90; Cl, 7.77%. Calcd for $C_8H_{30}N_6O_9CoCl$: C, 21.41; H, 6.74; N, 18.73; Cl, 7.90%.

Potassium dicyanobis(dimethylglyoximato)cobaltate(III), $K[Co^{III}(dmgH)_2(CN)_2]\cdot3/2\cdot H_2O$, was prepared from $[Co^{III}(dmgH)_2(NH_3)_2]Cl\cdot5H_2O$ and potassium cyanide.[16] Found: C, 28.30; H, 3.97; N, 19.86%. Calcd for $K[Co(C_8H_{14}O_4N_4)(CN)_2]\cdot3/2\cdot H_2O$: C, 29.49; H, 3.96; N, 20.63%.

† Presented in part at the 37th National Meeting of the Chemical Society of Japan, Tokyo, April 1, 1978, Abstracts Vol. 1, p. 275 and the 28th Annual Meeting on Coordination Chemistry, Matsuyama, October 11, 1978, Abstract, p. 337.

The metal complex $[Co^{III}(dmgH)_2(NH_3)_2]Cl$ at pH 4.3—9.5 was strongly adsorbed on the cation-exchange resin (Dowex 50W-X8) but not on the anion-exchange resin (Dowex 1-X4), indicating that the metal complex exists in a cationic form at pH 4—9. In the pH region higher than 10.17, the pK_a^c of the complex, a neutral species, $[Co^{III}(dmg)(dmgH)(NH_3)_2]$ is formed. On the other hand, the metal complex $K[Co^{III}(dmgH)_2(CN)_2]$ at pH 4.0—8.0 was strongly adsorbed on the anion-exchange resin but not on the cation-exchange resin.

Measurements. Measurements of pH in dioxane–water media were reported in a previous paper.[2] The acid-dissociation constants were determined spectrophotometrically with a Hitachi recording spectrophotometer Model EPS-3T. Kinetic measurements were carried out with a Union Giken co-axial-cable temperature-jump apparatus Model RA-105. The reactions were followed on the screen of an oscilloscope Tektronix Type 545B at a wavelength in the range 400—500 nm. All the measurements were carried out at 25.0±0.1 °C and at a constant ionic strength 0.10 adjusted with potassium nitrate.

Results and Discussion

The metal complex ions (Fig. 1) have two equivalent strong intramolecular hydrogen-bonds, OH···O⁻. An infrared absorption band around 1775 cm^{-1} for Ni(dmgH)$_2$ complex has been assigned to an intramolecular hydrogen bonding.[17] The absorption band for O–H stretching appears at 3170 cm^{-1} in the free ligand dimethylglyoxime. The bond length of the intramolecular hydrogen-bond, OH···O⁻, was reported to be 2.44 Å from the data of X-ray crystallography.[18] In some $[Co^{III}(dmgH)_2XY]$ complexes the O–H stretching frequency lies in the range 1770—1680 cm^{-1}.[19] As regards the complexes with X, Y=NH_3, a planar chelate structure was confirmed based on the data of X-ray crystallography.[20]

The absorption spectra of an aqueous solution of the cationic complex DGA at various pH values, at 25 °C, and at I=0.1 mol dm^{-3} ($NaClO_4$),[21] gave an isosbestic point at 246 nm (Fig. 2), indicating that the presence of only two absorbing species involved. In the pH region studied only one proton is dissociated from the Co(III) complex ion. The first acid-dissociation constant, K_a^c(s), of the reaction for DGA cation

$$[Co^{III}(dmgH)_2(NH_3)_2]^+ \rightleftarrows [Co^{III}(dmg)(dmgH)(NH_3)_2]^0 + H^+, \quad (3)$$

and that for CDG anion

$$[Co^{III}(dmgH)_2(CN)_2]^- \rightleftarrows [Co^{III}(dmg)(dmgH)(CN)_2]^{2-} + H^+, \quad (4)$$

are determined by the change in absorbance at 285 nm, ΔA_{285}, the equilibrium concentration of proton, $\bar{C}_H$, and the total concentration of the complex ion, C.[5] The plot of $C/\Delta A_{285}$ against $\bar{C}_H$ gives a straight line at each solvent composition. The values of K_a^c(s) determined spectrally at various dioxane contents are summarized in Table 1. The value of pK_a^c(s) increases with the increase in x_{dlox} irrespective of the difference in the sign of the charge of DGA cation and CDG anion (Fig. 3). The values of pK_a^c(s) of CDG anion at x_{dlox}=0 and 0.174 are 1.53 and 2.79 larger than those of DGA cation, respectively. These differences in pK_a^c(s) are attributed to the difference in the basicity of the axial ligands, NH_3 and CN^-.

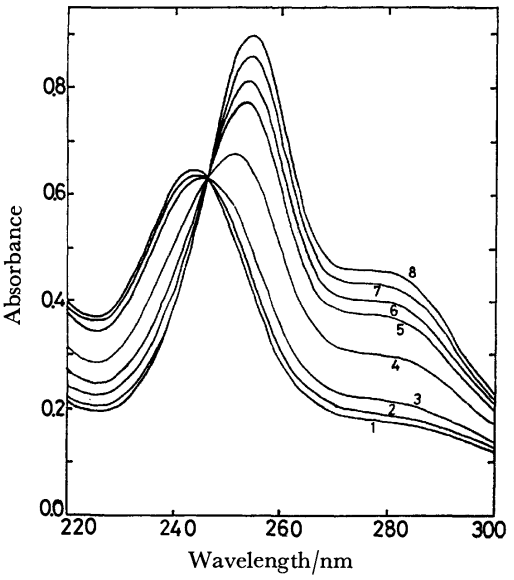

Fig. 2. Absorption spectra of the solution containing 2.59×10^{-5} mol dm^{-3} $[Co^{III}(dmgH)_2(NH_3)_2]^+$ ion at 25 °C and I=0.1 mol dm^{-3} ($NaClO_4$).
pH: (1) 5.85; 6.70, (2) 9.02, (3) 9.33, (4) 10.07, (5) 10.45, (6) 10.75, (7) 10.96, and (8) 11.11.

Table 1. Acid-dissociation constants of $[Co^{III}(dmgH)_2(CN)_2]^-$ and $[Co^{III}(dmgH)_2(NH_3)_2]^+$ in dioxane–water media at 25 °C and I=0.1 mol dm^{-3} ($NaClO_4$)

x_{dlox}	pK_a^c(s) = $-\log(K_a^c(s)/\text{mol dm}^{-3})$	
	CDG	DGA
0.000	11.70	10.17[a]
0.023	12.13	10.39
0.050	12.67	10.59
0.083	13.13	10.76
0.128	13.62	11.05
0.174	13.96	11.17

a) This value was reported to be 10.5 at room temperature, see Ref. 13.

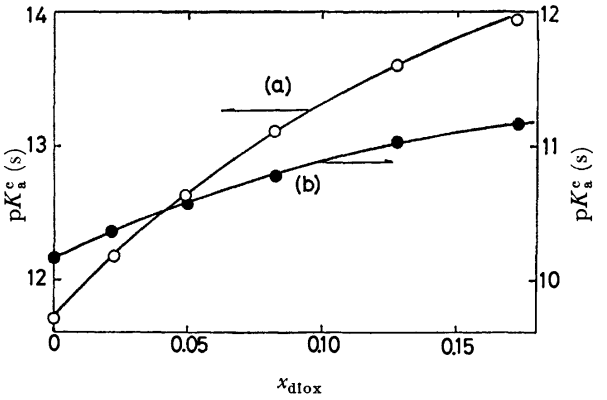

Fig. 3. Dependence of pK_a^c(s) on x_{dlox} at 25 °C and I=0.1 mol dm^{-3} ($NaClO_4$).
(a): $[Co^{III}(dmgH)_2(CN)_2]^-$ anion. (b): $[Co^{III}(dmgH)_2(NH_3)_2]^+$ cation.

Table 2. Rate and equilibrium constants for the proton-transfer reactions of $[Co^{III}(dmgH)_2(CN)_2]^-$ and $[Co^{III}(dmgH)_2(NH_3)_2]^+$ in dioxane–water media at 25 °C and I=0.1 mol dm^{-3} (KNO_3)

x_{diox}	k_f/mol^{-1} dm^3 s^{-1}	k'_r/s^{-1}	K^c_b/mol^{-1} dm^3	pK^c_a(k)	k_f/mol^{-1} dm^3 s^{-1}	k'_r/s^{-1}	K^c_b/mol^{-1} dm^3	pK^c_a(k)
	CDG				DGA			
0.000	1.6×10^5 a)	1.3×10^3	120	11.66	2.9×10^6 b)	6.0×10^2	4.8×10^3	10.1
0.023	1.3×10^5	2.1×10^3	62	12.26	1.1×10^6	3.4×10^2	3.2×10^3	10.5
0.050	9.5×10^4	2.0×10^3	48	12.59	1.3×10^6	1.6×10^2	8.1×10^3	10.4
0.083	7.0×10^4	2.0×10^3	35	13.00	1.1×10^6	1.2×10^2	9.2×10^3	10.6
0.128	6.5×10^4	2.1×10^3	31	13.48	5.1×10^6	3.0×10^2	1.7×10^4	10.7
0.174	4.0×10^4	1.3×10^3	31	13.82	1.6×10^7	9.0×10^2	1.8×10^4	11.1

a, b) See Ref. 28.

For the proton-transfer reactions in the dioxane–water media of DGA cation,[22]

$$[Co^{III}(dmgH)_2(NH_3)_2]^+ + OH^- \rightleftharpoons [Co^{III}(dmg)(dmgH)(NH_3)_2]^0 + H_2O \quad (6)$$

and those of CDG anion,[23]

$$[Co^{III}(dmgH)_2(CN)_2]^- + OH^- \rightleftharpoons [Co^{III}(dmg)(dmgH)(CN)_2]^{2-} + H_2O, \quad (8)$$

the observed relaxation time, τ, is expressed by

$$\tau^{-1} = k_f(\bar{C}_{H_2A} + \bar{C}_{OH}) + k'_r, \quad (8)$$

where $\bar{C}$, suffix H_2A, and k'_r denote the equilibrium concentration, the acid form of Co(III) complex ions, and $k_r[H_2O]$, respectively. The plot of τ^{-1} against the sum of equilibrium concentrations gives a straight line at each dioxane content (Fig. 4). The values of k_f and

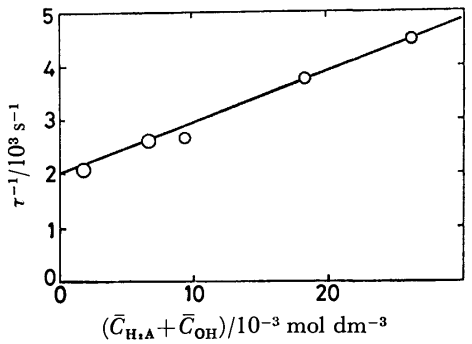

Fig. 4. Plot of the reciprocal relaxation time *vs.* $\bar{C}_{H_2A}+\bar{C}_{OH}$ at x_{diox}=0.050, 25 °C, and I=0.1 mol dm^{-3} (KNO_3). $[Co^{III}(dmgH)_2(CN)_2]^-$–$OH^-$ system.

k_r thus obtained are summarized in Table 2. The values of k_f are several orders of magnitude smaller than those for the diffusion-controlled proton-transfer reactions due to the strong intramolecular hydrogen-bond, OH···O$^-$. The values of log k_f of DGA cation are 1.26 and 2.60 larger than those of CDG anion at x_{diox}=0 and 0.174, respectively. The rate constant for the recombination of CDG anion with OH^- ion, k_f, decreases linearly with the increase in x_{diox}, *viz.*, from 1.6×10^5 to 4.0×10^4 mol^{-1} dm^3 s^{-1} for the change in x_{diox} from 0 to 0.174, similar to the changes observed in the univalent anions of *o*-hydroxy azo compounds.[4] However, the value of k_f of DGA cation decreases in a region of lower x_{diox} from 2.9×10^6 to 1.1×10^6 mol^{-1} dm^3 s^{-1} and increases in a region of higher x_{diox} from 1.1×10^6 to 1.6×10^7 mol^{-1} dm^3 s^{-1}.

The value of pK^c_a(k) was evaluated by the relationship, $K^c_a(k)=(k_f/k'_r)\cdot K^c_w=K^c_b\cdot K^c_w$, where K^c_w denotes the apparent ionic product of water.[5] The values of pK^c_a(k) are summarized in Table 2.

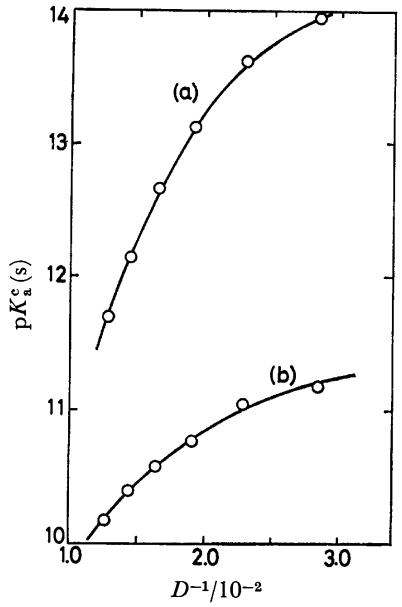

Fig. 5. Dependence of pK^c_a(s) on the inverse dielectric constant of the medium, D^{-1}.
(a): $[Co^{III}(dmgH)_2(CN)_2]^-$ anion. (b): $[Co^{III}(dmgH)_2(NH_3)_2]^+$ cation.

In Fig. 5 the values of pK^c_a(s) are plotted against D^{-1}, the inverse macroscopic dielectric constant of the medium. The dependence is not linear. A simple Born-type electrostatic effect is not observed. According to the Born theory[24] the change in pK^c_a of a Brønsted acid, H_2A, is expressed as

$$\Delta pK^c_a = pK^c_a(\text{in dioxane-water}) - pK^c_a(\text{in aqueous solution}) = (0.215Ne^2/RT)(1/r_H + Z^2_{HA}/r_{HA} - Z^2_{H_2A}/r_{H_2A})(1/D_{II} - 1/D_I), \quad (9)$$

where Z_{HA} and Z_{H_2A} denote the charge of the base (HA) and the acid form (H_2A), D is the macroscopic dielectric constant of the medium, r the radius of the species, R the gas constant, T the absolute temperature, e the elementary charge, and N the Avogadro number. From

Eq. 9 ΔpK_a^c of the univalent cation ($Z_{H_2A}=+1$ and $Z_{HA}=0$) is expected to be small. However, in the case of DGA cation the value of $\Delta pK_a^c(s)$ is as large as 1.00 for the change in x_{diox} from 0 to 0.174. The corresponding value of $\Delta pK_a^c(s)$ of CDG anion is 2.26. The value of $\Delta pK_a^c(s)$ of univalent anions of *o*-hydroxy azo compounds, 4-(2-hydroxy-5-ethylphenylazo)benzenesulfonic acid (HEB) and 4-(2-pyridylazo)resorcinol (PAR), were reported to be +1.77 and +1.83[5] and bivalent anions of *o*-hydroxy azo compounds, 4-(2,4-dihydroxyphenylazo)benzenesulfonic acid (TPO) and 7-hydroxy-8-phenylazo-1,3-naphthalenedisulfonic acid (HPN), +2.27 and +2.31.[4]

A reaction mechanism

$$H_2A \underset{k_{21}}{\overset{k_{12}}{\rightleftharpoons}} H_2A^* \quad (10)$$

$$H_2A^* + OH^- \underset{k_{32}}{\overset{k_{23}}{\rightleftharpoons}} H_2A^*\cdots(H_2O)_n\cdots OH^- \quad (11)$$

$$H_2A^*\cdots(H_2O)_n\cdots OH^- \underset{k_{43}}{\overset{k_{34}}{\rightleftharpoons}} HA + H_2O, \quad (12)$$

postulated previously[5] for the proton-transfer reactions of *o*-hydroxy azo compounds in dioxane–water media might be applied also to those of DGA cation and CDG anion. Equation 10 denotes the equilibrium between two isomeric Co(III) complex ions, *viz.*, an H_2A species having an intramolecular hydrogen-bond and an intermediate species H_2A^* having no intramolecular hydrogen-bond. The rate constant for the recombination of Brønsted acid with OH^-, k_f, is expressed as the product of the rate constant, k_{23}, for the diffusion-controlled encounter between H_2A^* and OH^-, and the equilibrium constant, $K_{12}=[H_2A^*]/[H_2A]$, for the breaking of the intramolecular hydrogen-bond and the interaction with the surrounding water molecules.[5]

$$k_f = K_{12}k_{23} = (k_{12}/k_{21})k_{23} \quad (13)$$

As regards the ion-ion reactions the Christiansen-Scatchard equation is proposed[25]

$$\ln(k_f/k_f^\circ) = -z_1z_je^2/kTr^*D, \quad (14)$$

where k is the Boltzmann's constant, r^* the reaction distance, and k_f° the rate constant at infinite dielectric constant.

Since the proton-transfer reaction of CDG anion and OH^- ion is a reaction between the same charge-type ions, the negative slope is expected in the plot of log k_f against D^{-1} (Fig. 6). From the slope the value of r^* is calculated to be 4.6 Å. This value is the intermediate one between the values for the slightly water-soluble Brønsted acid, (4-(*p*-nitrophenylazo)resorcinol; $r^*=2.9$ Å)[3] and a water-soluble Brønsted acid (4-(2-hydroxy-5-ethylphenylazo)benzenesulfonic acid; $r^*=7.2$ Å).[4] In the case of CDG anion having hydrophobic groups (four methyl groups) as in 4-(*p*-nitrophenylazo)-resorcinol (one nitro group), the inflection is observed in the plot as shown in Fig. 6.

The following reaction mechanism is proposed for the case of intramolecularly hydrogen-bonded dicarboxylic acid monoanions, AH^-, in aqueous solution.[26]

$$AH^- + OH^- \rightleftharpoons A^-\cdots H\cdots OH^- \rightleftharpoons A^{2-} + H_2O, \quad (15)$$

where $A^-\cdots H\cdots OH^-$ denotes an encounter complex with a weakened intramolecular hydrogen-bond. The mechanism shown in Eqs. 10—12 would be reasonable for the explanation of the solvent effects. From Eq. 14 the slope in Fig. 6 is expected to be positive in the case of DGA cation. However, with increasing D^{-1} the value of log k_f decreases at higher value of D (78—52) and then increases at lower value of D (52—35). This behavior is explained by the solute-solvent interactions and not by the simple electrostatic law (Eq. 14) nor by the reaction mechanism (Eq. 15). The rate constant, k_f, is equal to $K_{12}k_{23}$ (Eq. 13). The equilibrium constant, K_{12}, is a parameter which denotes the solute-solvent interactions, *viz.*, interactions with the surrounding water molecules. Thus the value of K_{12} gradually decreases with the increase in x_{diox}, *viz.*, decrease in D. If the contribution of the decrease of K_{12} to the value of k_f is larger than that of the increase of k_{23}, the rate constant k_f decreases at higher D where solute-solvent interaction is predominant, and then increases at lower D where the electrostatic effect is predominant.

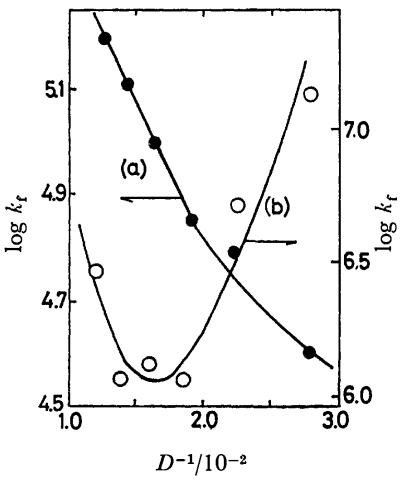

Fig. 6. Dependence of log k_f on the inverse dielectric constant of the medium, D^{-1}.
(a): $[Co^{III}(dmgH)_2(CN)_2]^-$ anion. (b): $[Co^{III}(dmgH)_2(NH_3)_2]^+$ cation.

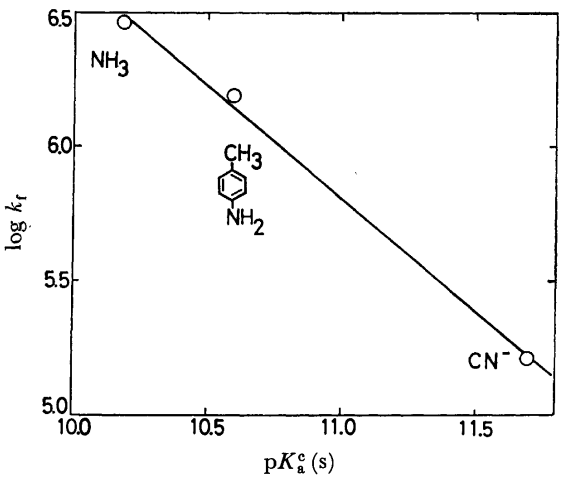

Fig. 7. Plot of log k_f *vs.* pK_a^c(s) in bis(dimethylglyoximato)cobalt(III) complex–OH^- system.

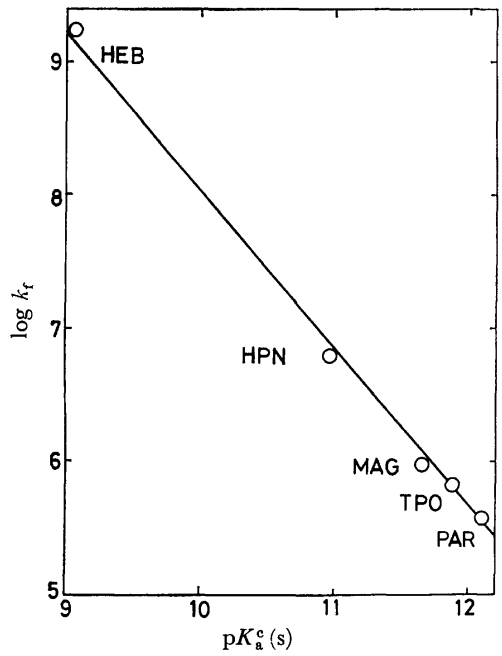

Fig. 8. Plot of log k_f *vs.* pK_a^c(s) in *o*-hydroxy azo compound–OH^- system.

Figure 7 shows the Brønsted plot with the slope −0.85 in aqueous solution,

$$\log k_f = -0.85\,pK_a^c(s) + 15.15. \quad (16)$$

The value is the intermediate one between −0.5 for the substituted malonic acids[27] and −1.2 for *o*-hydroxy azo compounds (log $k_f = -1.2$ pK_a^c(s)+20.05) (Fig. 8).[1-5] Masuda *et al.* reported the relationship of pK_a^c(s) and the basicity of an axial ligand and pointed out the importance of the transmittance of an electronic effect of the axial ligand to the oximato radical.[13] The rate constant k_f does reflect the thermodynamic stability of the intramolecular hydrogen-bond, namely the values of pK_a^c. This fact indicates that the axial ligand with larger electronic effect on the increase in the proton-dissociation of the in-plane oximato group tends to accelerate the dissociation of proton in the intramolecular hydrogen-bond of the Co(III) complex ion.

References

1) M. Eigen, *Angew. Chem.*, **75**, 489 (1963).
2) N. Yoshida and M. Fujimoto, *Bull. Chem. Soc. Jpn.*, **49**, 1557 (1976).
3) N. Yoshida and M. Fujimoto, *Bull. Chem. Soc. Jpn.*, **50**, 1328 (1977).
4) N. Yoshida and M. Fujimoto, *Bull. Chem. Soc. Jpn.*, **52**, 2527 (1979).
5) N. Yoshida and M. Fujimoto, *Bull. Chem. Soc. Jpn.*, **53**, 101 (1980).
6) F. Hibbert and H. J. Robbins, *J. Am. Chem. Soc.*, **100**, 8239 (1978).
7) E. F. Caldin and J. F. Crooks, *J. Chem. Soc., B*, **1967**, 959.
8) F. Strohbusch, D. B. Marshall, and E. M. Eyring, *J. Phys. Chem.*, **82**, 2447 (1978).
9) H. A. O. Hill, K. G. Morallee and R. E. Collis, *Chem. Commun.*, **1967**, 888; Y, Yamano, I. Masuda, and K. Shinra, *Inorg. Nucl. Chem. Lett.*, **4**, 581 (1968); R. D. Gillard and G. Wilkinson, *J. Chem. Soc.*, **1963**, 6041.
10) A. Nakahara, J. Fujita, and R. Tsuchida, *Bull. Chem. Soc. Jpn.*, **29**, 296 (1956).
11) Y. Nakatsuka and H. Iinuma, *Bull. Chem. Soc. Jpn.*, **11**, 48 (1936).
12) L. Tschugaeff, *Z. Anorg. Chem.*, **46**, 144 (1905).
13) I. Masuda, H. Sakano, and K. Shinra, *Bull. Chem. Soc. Jpn.*, **42**, 2296 (1969).
14) A. V. Ablov and M. D. Fillipov, *Russ. J. Inorg. Chem.*, **5**, 1311 (1960).
15) L. Tschugaeff, *Z. Anorg. Chem.*, **46**, 160 (1905). The salt, NH_4Cl, formed during the course of reaction, $[CoCl(NH_3)_5]Cl_2 + 2\,dmgH_2 \rightleftharpoons [Co(dmgH)_2(NH_3)_2]Cl + 2\,NH_4Cl + NH_3$, should be removed carefully from the reaction mixture.
16) N. Maki, *Bull. Chem. Soc. Jpn.*, **38**, 2013 (1965). In the course of the reaction, $[Co(dmgH)_2(NH_3)_2]Cl + 2\,KCN \rightleftharpoons K[Co(dmgH)_2(CN)_2] + 2\,NH_3 + KCl$, an insoluble yellow powder was deposited. The deposit should be removed quickly in a hot state.
17) R. E. Rundle and M. Parasol, *J. Chem. Phys.*, **20**, 1487 (1952).
18) L. E. Godycki and R. E. Rundle, *Acta Crystallogr.*, **6**, 487 (1953).
19) J. Fujita, A. Nakahara, and R. Tsuchida, *J. Chem. Phys.*, **23**, 1541 (1955).
20) K. S. Viswanathan and N. R. Kunchur, *Acta Crystallogr.*, **14**, 675 (1961).
21) Sodium perchlorate was used for the adjustment of ionic strength in equilibrium measurements in order to avoid the disturbance by the intense absorption of KNO_3 in 280—340 nm.
22) The absorption in the range 400—500 nm of the base form of DGA cation rapidly increases in the time region of 2 μs div^{-1}. The reciprocal relaxation time of this fast step does not depend on the sum of the equilibrium concentrations of H_2A^+ and OH^- ions at each dioxane content. The signal-amplitude of the fast step depends only on the equilibrium concentration of the base form, HA^0. This indicates that the fast step would be an intramolecular structural change in the base form. The sum of the rate constants, k_1+k_{-1}, for this fast step is determined to be 4.5×10^4—2.3×10^5 s^{-1}. Since the concentration of the intermediate species accompanied by this fast step is very low, the value of K_a^c(s) is in good agreement with that of K_a^c(k) at each dioxane content.
23) Three relaxation phenomena were observed in the CDG anion–OH^- system. The signal amplitude of a very fast step is small as compared with that of DGA cation. The values of k_1+k_{-1} are found to be 1.3×10^5—2.0×10^5 s^{-1}. The very slow step would be the intramolecular step accompanied by the motion of axial ligands, since the value of τ^{-1} (3—5 s^{-1}) does not depend on the equilibrium concentrations. The values of k_2+k_{-2} for this slow step are found to be in the range 3.0—5.5 s^{-1}.
24) M. Born, *Z. Phys.*, **1**, 45 (1920); H. Ohtaki, *Denki Kagaku*, **41**, 674 (1973).
25) J. A. Christiansen, *Z. Phys. Chem.*, **113**, 35 (1924); G. Scatchard, *Chem. Rev.*, **10**, 229 (1932).
26) M. H. Miles, E. M. Eyring, W. W. Epstein, and R. E. Ostlund, *J. Phys. Chem.*, **69**, 467 (1965).
27) M. H. Miles, E. M. Eyring, W. W. Epstein, and M. T. Anderson, *J. Phys. Chem.*, **70**, 3490 (1966).
28) For CDG anion, $k_f = 1.9\times10^5$ mol^{-1} dm^3 s^{-1}, $k_r' = 1.35\times10^3$ s^{-1}, and $K_b^c = 140$ mol^{-1} dm^3 at 15 °C and $I = 0.1$ mol dm^{-3} ($NaClO_4$) in aqueous solution. For DGA cation, $k_f = 1.33\times10^6$ mol^{-1} dm^3 s^{-1}, $k_r' = 1.5\times10^3$ s^{-1}, and $K_b^c = 900$ mol^{-1} dm^3 at 15 °C and $I = 0.1$ mol dm^{-3} ($NaClO_4$) in aqueous solution. See J. P. Birk, P. B. Chock, and J. Halpern, *J. Am. Chem. Soc.*, **90**, 6959 (1968).

The Hydrothermal Preparation and Characterization of Platinum Metal Complexes with Ethylenediaminetetraacetic Acid and Propylenediaminetetraacetic Acid

Masami SAITO, Takashi UEHIRO,** and Yukichi YOSHINO*

Department of Chemistry, College of General Education, The University of Tokyo, Komaba, Meguro-ku, Tokyo 153

(Received March 19, 1980)

A new method for hydrothermal syntheses of osmium(III), ruthenium(III), iridium(III), and rhodium(III) complexes with ethylenediaminetetraacetic acid (EDTA) and propylenediaminetetraacetic acid (PDTA) has been developed. More than ten new complexes have been obtained in good yields and characterized by measuring their magnetic susceptibilities, infrared and electronic spectra, and acid-base properties. The stereochemical behavior of the iridium(III) and rhodium(III) complexes has also been described.

It is well known that most of the platinum metal ions are kinetically inert in aqueous solution,[1] that the preparation of their complexes with ethylenediaminetetraacetic acid and propylenediaminetetraacetic acid is not always reproducible, and that the yields are generally low. In order to improve this, the present authors have tried to prepare these complexes at temperatures higher than 100 °C using a Teflon bucket with a stainless-steel holder.[2]

In the present study attention was focused on the complexes of the less familiar platinum metals, *i.e.*, osmium, ruthenium, iridium, and rhodium, and efficient methods of the hydrothermal preparation of their EDTA and PDTA complexes involving some new complexes have been developed. The complexes thus obtained were characterized by measurements of their magnetic susceptibilities, infrared and electronic spectra, and acid-base properties.

Experimental

Materials. Osmium(VIII) oxide from Degussa, ruthenium(IV) oxide from the Japan Engelhard Co., iridium(IV) chloride from the Tanaka Noble Metals Co. and rhodium(III) chloride trihydrate from the Koso Chemicals Co. were employed. The other chemicals were of a reagent grade from the Wako Pure Chemicals Co. and were purified by recrystallization or distillation when necessary. Twice-distilled water was used throughout the experiment. For the hydrothermal preparation, a "Uniseal" with capacity of 23 ml from Uniseal Decomposition Vessels, Ltd., was used.

Physical Measurements. The infrared spectra were recorded on a JASCO Model 403G spectrophotometer, using the nujol or hexachlorobutadiene mull technique. The electronic spectra were obtained on a Hitachi Model 124 spectrophotometer, and the CD spectra, on a JASCO Model J-20 recording spectropolarimeter. The optical rotations were measured by means of a Yanaco Model OR-50 photoelectric polarimeter, and the NMR spectra, on a JEOL JUN-MH-100 spectrometer (100 MHz) at an ambient temperature (*ca.* 20 °C). The magnetic measurements were carried out with a Gouy balance at room temperature. Toa Dempa Digital pH-meters, Types HM-8 and HM-20B, were used for the acid-base titrations.

Preparation of Complexes. The general scheme of hydrothermal syntheses was as follows: the platinum metal halide or halogeno complex (1—4 mmol) and EDTA or PDTA (free acid or disodium salt) were mixed in a ratio of 1 : 1.05 in a bucket. To the mixture we then added 15 ml of water, and the resulting mixture was stirred for a while. Then, the bucket and the sealing lid were set in a stainless-steel holder, and the assembly was heated in an electric oven at temperatures from 100 to 150 °C for several hours or overnight. After the vessel has been cooled, a small amount of insoluble matter was filtered off, and the filtrate was evaporated to a small volume on a water bath. The addition of ethanol is often effective for crystallization.

*$NH_4[OsCl_2(H_2edta)]$ (**1a**).* The starting material, $(NH_4)_2[OsCl_6]$ was prepared by the reduction of OsO_4 with iron(II) in a methanol–HCl solution.[3] A mixture of 1.8 g of $(NH_4)_2[OsCl_6]$ (4 mmol) and 1.2 g of H_4edta (4.1 mmol) was suspended in 15 ml of water in a Teflon bucket, and the apparatus was heated at 150 °C for 5 h. Then, the filtrate was evaporated to a smaller volume. The crystals thus deposited were washed with ethanol and air-dried. Yield, 1.5 g.

*$H[OsCl_2(H_2edta)]\cdot 2.5H_2O$ (**1b**).* The filtrate obtained by the hydrothermal reaction in **1a** was directly passed through a column of cation-exchange resin in the hydrogen form (Dowex 50W, X8, 50—100 mesh). The effluent was concentrated by evaporation on a water bath, and the deposited crystals were washed with cold ethanol. Yield, 1.7 g.

*$NH_4[OsBr_2(H_2edta)]$ (**2a**).* OsO_4 was converted to $(NH_4)_2[OsBr_6]$ by Dwyer's method.[4] Then, a suspension of 2.8 g of $(NH_4)_2[OsBr_6]$ (4 mmol) and 1.2 g of H_4edta (4.1 mmol) in 15 ml of water was heated at 150 °C for 5 h. From the filtrate, yellowish brown crystals were obtained. Yield, 1.0 g.

*$H[OsBr_2(H_2edta)]$ (**2b**).* The above-mentioned filtrate containing **2a** was passed through a column of cation-exchange resin (H^+-form). Yield, 1.0 g.

*$H[RuCl_2(H_2edta)]\cdot 3.5H_2O$ (**3**).* One gram of $RuO_2\cdot nH_2O$ ($n=3$—4) was dissolved in 20 ml of concd HCl by heating. After repeated heating to dryness, the residue was dissolved in 15 ml of water. To this we added 1.7 g of H_4edta (5.7 mmol), after which the mixture was heated on a water bath to give a clear solution. The resulting solution was heated at 120 °C for 5 h. The filtrate was cooled in an ice bath to give yellow crystals. The crystals were washed with a small amount of cold ethanol and acetone successively. Yield, 2.5 g.

*$Na[RuCl(Hpdta)]\cdot 3H_2O$ (**4**).* To a $RuCl_3$ solution (5.5 mmol) obtained from $RuO_2\cdot nH_2O$ and concd HCl, 5.8 mmol of NaH_3pdta was added. The mixture was heated at 120 °C for 10 h. The filtrate from the reaction mixture was then concentrated to *ca.* 10 ml, and twice the volume of ethanol was added. The fine crystals thus obtained were

** Present address: National Institute for Environmental Studies, Yatabe, Tsukuba-gun, Ibaraki 305.

washed with ethanol. Yield, 1.5 g.

Na[IrCl(Hedta)]·2H$_2$O (5). A suspension of 0.68 g of $IrCl_4$ (2 mmol) and 0.75 g of Na_2H_2edta·2H$_2$O (2 mmol) in 15 ml of water was heated at 150 °C for 24 h. The filtrate from the reaction mixture was evaporated to *ca.* 5 ml. When the solution was cooled, yellow crystals separated out. Yield, 0.7 g.

Na[IrCl(Hpdta)]·3H$_2$O (6). A procedure similar to that described in **5** was applied, using Na_2H_2pdta in place of Na_2H_2edta. Yield, 0.7 g.

NH$_4$[RhCl$_2$(H$_2$edta)] (7). An aqueous suspension of 1.3 g of $RhCl_3·3H_2O$ (5 mmol) and 2.0 g of Na_2H_2edta·2H$_2$O (5.4 mmol) was heated at 120 °C for 5 h. To the filtrate we then added 8 ml of concd HCl, and the solution was evaporated to 10 ml. In this solution, 0.5 g of NH_4Cl was dissolved, after which the solution was cooled in an ice bath. Yellowish brown crystals were collected and washed with 50% ethanol and diethyl ether successively. Yield, 2.1 g.

[Os(edta)(H$_2$O)]·H$_2$O (8). An aqueous solution (20 ml) containing 1.5 g of H[OsCl$_2$(H$_2$edta)]·2.5H$_2$O (**1b**) was aerated for 20 h. The black, lustrous crystals thus deposited were collected and washed with water until free from chloride ions, and then with diethyl ether. Yield, 1.1 g.

H[OsI(Hedta)]·2.5H$_2$O (9a). One gram of **8** was added to 10 ml of concd HI (7.5 mol dm^{-3}), after which the mixture was stirred for 1 h. The I_2 liberated during the procedure was removed by extraction with diethyl ether. The crystals thus deposited were filtered and washed with a small amount of ethanol. Yield, 1.0 g.

NH$_4$[OsI(Hedta)] (9b). One gram of **9a** (1.5 mmol) was dissolved in 10 ml of warm water (*ca.* 40 °C). To this we then added 1.5 g of NH_4I. The crystals thus obtained were washed with a small amount of cold water and with ethanol successively. Yield, 0.9 g.

[Ir(Hedta)(H$_2$O)]·1.5H$_2$O (10). To an aqueous solution containing 3 mmol of **5** (10 ml) we added 3.1 mmol of $AgNO_3$ dissolved in 10 ml of water; the excess Ag^+ in the filtrate was removed by passing the solution through a column of hydrogen-form cation-exchange resin. After the effluent had been concentrated by evaporation, ethanol was added to give a precipitate. The precipitate was washed with ethanol and diethyl ether. Yield, 1.4 g.

(−)$_{589}$- and (+)$_{589}$-Na[IrCl(Hedta)]·2H$_2$O (11a). One millimole of **5** was dissolved in 10 ml of a warm solution containing 0.5 mmol of (+)$_{589}$-*cis*-[Co(NO$_2$)$_2$(en)$_2$]Cl. When the solution was cooled, yellowish brown crystals of the diastereoisomer separated out, the molar rotion being $[M]_{589}=-84°$. The diastereoisomer was mixed with 1 g of NaI paste and then minimum amount of water was added and filtration was done. The addition of ethanol led to the crystallization of (−)$_{589}$-Na[IrCl(Hedta)]·2H$_2$O; $[M]_{589}=-350°$. The (+)$_{589}$-isomer was obtained similarly by using (−)$_{589}$-*cis*-[Co(NO$_2$)$_2$(en)$_2$]Cl; $[M]_{589}=+350°$.

(+)$_{589}$- and (−)$_{589}$-Na[Ir(Hedta)(H$_2$O)]·1.5H$_2$O (11b). These were prepared by treating **11a** with $AgNO_3$ in the way described earlier for **10**. $[M]_{589}=\pm526°$.

(+)$_{589}$- and (−)$_{589}$-Na[IrCl((S)-Hpdta)]·3H$_2$O (12). These complexes were obtained in the same way as in the case of the active Na[IrCl(Hedta)]·2H$_2$O (**11a**) except that the molar ratio of the racemate to the resolving agent was 1 : 1. $[M]_{589}=\pm380°$. The optically active complex (−)$_{589}$-Na[IrCl((*R*)-pdta)]·3H$_2$O could be prepared directly by using (*R*)-PDTA under somewhat milder conditions, *i.e.*, 120 °C and 20 h. $[M]_{589}=-380°$.

(−)$_{589}$-[Rh(Hedta)(H$_2$O)] (13). The reacmic Na[RhCl(Hedta)]·2H$_2$O was resolved by using (+)$_{589}$-*cis*-[Co(NO$_2$)$_2$(en)$_2$]Br; the resulting (−)$_{589}$-[RhCl(Hedta)]$^-$ was converted into (−)$_{589}$-[Rh(Hedta)(H$_2$O)] by treating it with $AgNO_3$. $[M]_{589}=-260°$.

Results and Discussion

Hydrothermal Preparation. The analytical data for the complexes are presented in Table 1. In Table 2, the results of the hydrothermal preparation of the EDTA and PDTA complexes of osmium(III), ruthenium(III), iridium(III), and rhodium(III) are summarized. Of these, the osmium(III) complexes of EDTA were synthesized for the first time.[5] As may be seen from the table, the yields of the known complexes increased remarkably; for example, the yield of the iridium(III) complex (**5**) increased from 35% to 60%.[6] In the case of rhodium(III), both EDTA and PDTA complexes were obtained nearly quantitatively. As for ruthenium(III), the PDTA complex was obtained for the first time. It is noteworthy that, in the case of the iridium(III)-PDTA complex, (−)$_{589}$-Na[IrCl((*R*)-Hpdta)]·3H$_2$O can be prepared hydrothermally using optically active (*R*)-PDTA as a ligand, without any accompanying

Table 1. Analyses of platinum metal complexes with EDTA and PDTA

Complex	Found (%)					Calcd (%)				
	M	C	H	N	X	M	C	H	N	X
NH$_4$[OsCl$_2$(H$_2$edta)]	33.97	21.06	3.21	7.47	12.31	33.41	21.08	3.19	7.38	12.45
H[OsCl$_2$(H$_2$edta)]·2.5H$_2$O	31.73	20.03	3.37	4.69	11.99	31.81	20.11	3.38	4.63	11.57
NH$_4$[OsBr$_2$(H$_2$edta)]	28.64	18.10	2.27	6.33	24.00	28.95	18.28	2.76	6.39	24.32
H[OsBr$_2$(H$_2$edta)]	29.43	18.83	2.38	4.42	24.50	29.67	18.77	2.34	4.38	24.93
NH$_4$[OsI(Hedta)]	28.39	18.19	3.16	6.34	19.20	28.64	18.20	3.21	6.37	19.11
H[OsI(Hedta)]·2.5H$_2$O	29.23	18.35	3.06	4.32	19.36	29.17	18.42	2.94	4.30	19.46
[Os(edta)(H$_2$O)]H$_2$O	36.92	23.29	3.14	5.54		36.98	23.35	3.14	5.45	
H[RuCl$_2$(H$_2$edta)]·3.5H$_2$O		22.99	4.21	5.36	12.80		22.85	4.13	5.48	12.91
Na[RuCl(Hpdta)]·3H$_2$O		25.63	3.81	5.46	6.98		25.58	3.68	5.42	6.87
Na[IrCl(Hedta)]·2H$_2$O	33.09	20.88	2.77	4.93	6.53	33.38	20.85	2.97	4.89	6.15
Na[IrCl(Hpdta)]·3H$_2$O		21.41	3.36	4.64	6.00		21.71	3.49	4.61	5.84
[Ir(Hedta)(H$_2$O)]·1.5H$_2$O		22.43	3.41	5.38			22.79	3.45	5.32	
NH$_4$[RhCl$_2$(H$_2$edta)]		24.79	3.69	8.61	14.49		24.90	3.76	8.72	14.73
Na[RhCl(Hpdta)]·3H$_2$O		25.73	3.67	5.40	5.25		25.43	4.04	5.39	5.19

Table 2. Hydrothermal syntheses of platinum metal complexes

Metal	Complex	Temp/°C	Time/h	Yield/%
Os(III)	$NH_4[OsCl_2(H_2edta)]$	150	7	70
	$H[OsCl_2(H_2edta)]\cdot 2.5H_2O$	150	7	70
	$NH_4[OsBr_2(H_2edta)]$	150	7	70
	$H[OsBr_2(H_2edta)]$	150	7	70
Ru(III)	$H[RuCl_2(H_2edta)]\cdot 3.5H_2O$	120	5	85
	$Na[RuCl(Hpdta)]\cdot 3H_2O$	120	12	50
Ir(III)	$Na[IrCl(Hedta)]\cdot 2H_2O$	150	24	60(35)[a]
	$Na[IrCl(Hpdta)]\cdot 3H_2O$	150	24	60
Rh(III)	$NH_4[RhCl_2(H_2edta)]$	120	5	90(50)[a]
	$Na[RhCl(Hpdta)]\cdot 3H_2O$	120	5	90(50)[a]

a) Figures in parentheses are literature values.

racemization.

Osmium(III), (IV), and Ruthenium(III) Complexes. All the osmium complexes except **8** were found to be paramagnetic, with magnetic moments ranging from 1.73 to 1.82 B.M. which is to be expected for a spin-only atom with one unpaired electron spin. Hence, together with the analytical data in Table 1, the oxidation state of the osmium was presumed to be +3 with a low-spin $5d^5$ configuration. Some typical examples of the infrared spectra of the osmium-EDTA complexes in the region from 1200 to 1800 cm^{-1} are shown in Fig. 1. In the trivalent osmium complexes, there appear two characteristic CO stretching bands, one in the region of 1600 cm^{-1} and the other in the region higher than 1700 cm^{-1}. The former is assigned to the carboxylate coordinated to the metal, and the latter, to the free carboxylic acid. The frequencies of these bands are tabulated in Table 3. The appearance of these two bands indicates that, in all the complexes of osmium(III), the EDTA is bonded to the octahedral sites as a quinque- or quadridentate ligand. Such an interpretation may be supported by the examination of the pH-titration curves of the complexes with an alkali solution (Fig. 2). In the case of dihalogeno complex acid (**1b** or **2b**), 3 mol of alkali were consumed for 1 mol of osmium(III), indicating the presence of two carboxylic acid radicals. On the other hand, in the case of monohalogeno complex acid (**9a**), 2 mol of alkali were required for 1 mol of osmium(III), indicating the presence of one carboxylic acid radical.

Figure 3 presents some typical examples of the electronic spectra of the osmium(III) complexes. Strong and broad absorption bands are seen in the ultraviolet region.

The **8** complex was found to react with potassium

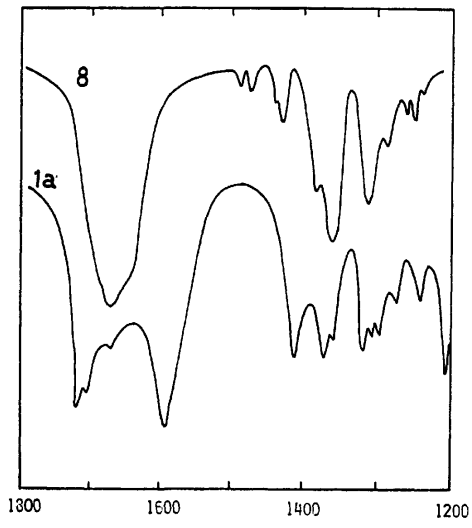

Fig. 1. Infrared spectra of osmium(III) and osmium-(IV) complexes with EDTA.
1a: $NH_4[OsCl_2(H_2edta)]$, **8**: $[Os(edta)(H_2O)]\cdot H_2O$.

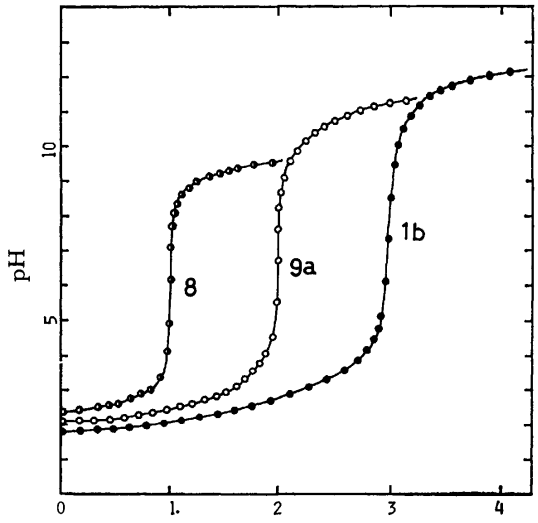

Fig. 2. Titration curves of osmium (III) and osmium (IV) complexes with EDTA at 20 °C.
1b: $H[OsCl_2(H_2edta)]\cdot 2.5H_2O$, 1.0×10^{-2} mol dm^{-3}, **8**: $[Os(edta)(H_2O)]\cdot H_2O$, 4.7×10^{-3} mol dm^{-3}, **9a**: $H[OsI(Hedta)]\cdot 2.5H_2O$, 5.6×10^{-3} mol dm^{-3}, NaOH, 1.2×10^{-1} mol dm^{-3}.

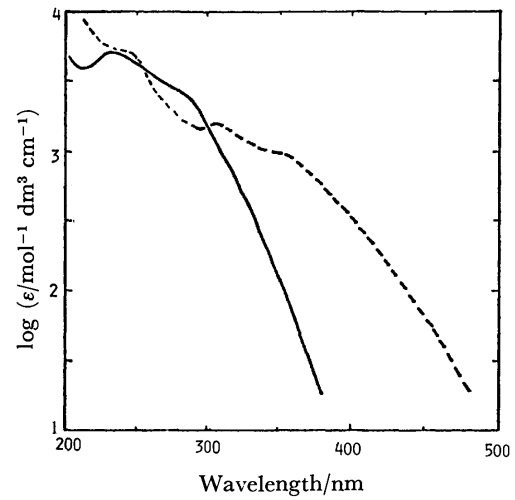

Fig. 3. Electronic spectra of osmium (III) complexes with EDTA.
——: $H[OsCl_2(H_2edta)]\cdot 2.5H_2O$, ------: $H[OsBr_2(H_2edta)]$.

Table 3. Magnetic moments, IR absorption bands, and pK values of Os(III), Os(IV), and Ru(III) complexes with EDTA and PDTA

Complex	μ/B.M.	IR absorption bands ν(COO$^-$)	ν(COOH)	pK_{av} at 20 °C
$NH_4[OsCl_2(H_2edta)]$	1.80	1590	1735	
$H[OsCl_2(H_2edta)]\cdot 2.5H_2O$	1.79	1590	1723	2.8
$NH_4[OsBr_2(H_2edta)]$	1.82	1585	1720	
$H[OsBr_2(H_2edta)]$	1.74	1600	1717	3.0
$NH_4[OsI(Hedta)]$	1.73	1620	1725	
$H[OsI(Hedta)]\cdot 2.5H_2O$	1.78	1620	1725	2.6
$[Os(edta)(H_2O)]\cdot H_2O$	dia	1675		2.6
$H[RuCl_2(H_2edta)]\cdot 3.5H_2O$	1.90	1590	1740	2.7
$Na[RuCl(Hpdta)]\cdot 3H_2O$	1.90	1635	1750	2.3[a]

a) The value for H[RuCl(Hpdta)] obtained by cation exchange.

iodide to give **1** equivalent of iodine per mole of osmium; this supports the idea that the oxidation state of the osmium atom is +4. As may be seen from Table 3 and Figs. 1, 2, and 3, the behavior of the tetravalent osmium complex is very different from that of the osmium(III) complexes described above. In the IR spectrum, a strong band was observed at 1675 cm^{-1}, too low to attribute it to a free COOH. In the acid-base titration (Fig. 2), the complex behaves as a rather strong monobasic acid, and deprotonation from a coordinated water molecule can be expected to take place. Furthermore, the magnetic susceptibility of the tetravalent osmium complex was determined to be -140×10^{-6} emu mol^{-1}. This observation seems rather unexpected because, in general, the tetravalent osmium complexes have been known to be paramagnetic, the magnetic moments ranging from 1.2 to 1.8 B.M. at room temperature.[7]

The question was finally solved by the X-ray structure analysis of a single crystal of the complex. The results revealed that the osmium(IV) complex is seven-coordinate (one edta^{4-} and one water molecule), and so the diamagnetism of the complex could be interpreted in terms of the 18-electron rule.[8]

The EDTA complexes of ruthenium(III) were prepared for the first time by Mukaida *et al.* in 1965;[9] since they have been well characterized by other workers as well.[10,11] In our study, we have attempted the hydrothermal preparation of other ruthenium complexes with EDTA and PDTA; two new complexes, $H[RuCl_2(H_2edta)]\cdot 3.5H_2O$ and $Na[RuCl(Hpdta)]\cdot 3H_2O$ were obtained in good yields. The characteristic properties of these complexes are shown in Table 3.

Iridium(III) and Rhodium(III) Complexes. The iridium complexes, **5**, **6**, and **10** were found to be diamagnetic. With reference to the analytical data (Table 1), the oxidation state of iridium was assumed as +3. In the IR spectra, besides ν_{asym}(COO$^-$) at 1650 cm^{-1}, ν_{asym}(COOH) in the region higher than 1700 cm^{-1} was observed in all the complexes. Therefore, in the solid states of these complexes, EDTA and PDTA may act as quinquedentate ligand, and one Cl$^-$ ion or H_2O molecule may occupy the sixth coordination site.

However, for the monochloro or monoaqua complex, two geometrical isomers are possible; the Cl$^-$ ion or the H_2O molecule may be *trans* to either a nitrogen or oxygen atom. In order to determine the structure, the deuteration of the acetate protons of $[IrCl(Hpdta)]^-$ in D_2O was studied by ^{1}H-NMR. It was observed that the only one AB-pattern with J=16.5 Hz survived after the other acetate signals had diminished upon deuteration. The remaining AB-pattern may be assigned to the in-plane acetate methylene protons.[12] Therefore, in the present complex, Cl$^-$ ion should be *trans* to a nitrogen atom. This structure is the same as that of the result of the X-ray structure analysis of the corresponding $[Rh(Hedta)(H_2O)]$.[13]

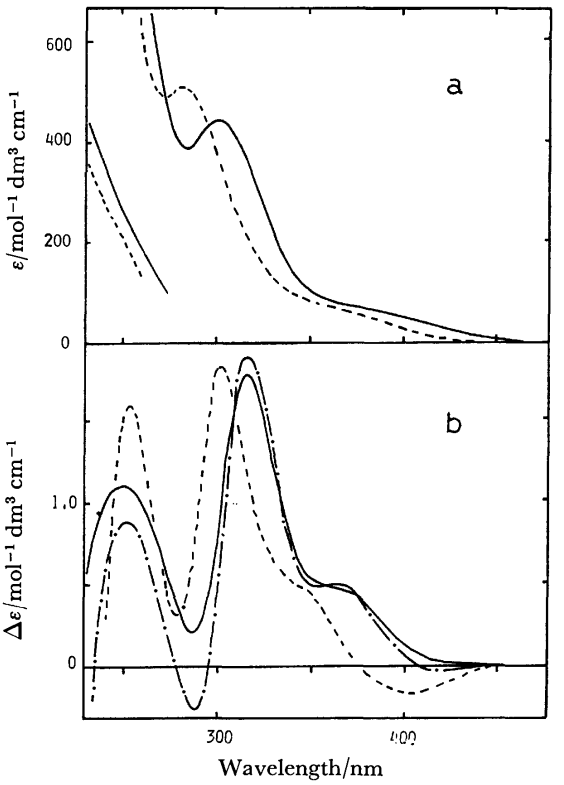

Fig. 4. Electronic and CD spectra of iridium(III) complexes with EDTA and PDTA.
(a): Absorption spectra. ——: $Na[IrCl(Hedta)]\cdot 2H_2O$ or $Na[IrCl(Hpdta)]\cdot 3H_2O$, ------: $[Ir(Hedta)(H_2O)]\cdot 1.5H_2O$.
(b): CD spectra. ——: $(-)_{589}$-$Na[IrCl(Hedta)]\cdot 2H_2O$, —·—: $(-)_{589}$-$Na[IrCl(Hpdta)]\cdot 3H_2O$, ------: $(-)_{589}$-$[Ir(Hedta)(H_2O)]\cdot 1.5H_2O$.

Figure 4 shows the electronic spectra and CD curves. The aqueous solution of $Na[IrCl(Hedta)]\cdot 2H_2O$ and $Na[IrCl(Hpdta)]\cdot 3H_2O$ exhibited a very similar spectral pattern; ε=440 at 303 nm and a shoulder (ε=70) at *ca.* 385 nm. These peaks are tentatively assigned to the d-d transitions, though a possible overlapping of charge-transfer bands in the shorter-wavelength region must be taken into consideration. The spectrum of

[Ir(Hedta)(H_2O)] shifts to shorter wavelengths as compared with that of the parent complex, [IrCl(Hedta)]$^-$, *i.e.*, from 303 nm (ε=440) for the monochloro complex to 290 nm (ε=510) for the monoaqua complex. This is consistent with the spectrochemical series.

Since the sexidentate (*R*)-PDTA complexes of cobalt(III) and rhodium(III) have the *Δ* configuration,[14,15] the corresponding complex of iridium(III) can be expected to have the same configuration. As may be seen from Fig. 4, the CD spectra of the $(-)_{589}$-isomer of EDTA- and PDTA complexes are quite similar. Therefore, it is presumed that $(-)_{589}$-[IrCl(Hedta)]$^-$ has the same structure as that of the sexidentate EDTA complex of the *Δ* configuration, in which one carboxyl group coplanar with the N–C–C–N chelate is free. This is consistent with the presumption presented by Ezerskaya *et al.* on the basis of the Cotton effects of the iridium(III)–EDTA complexes.[16]

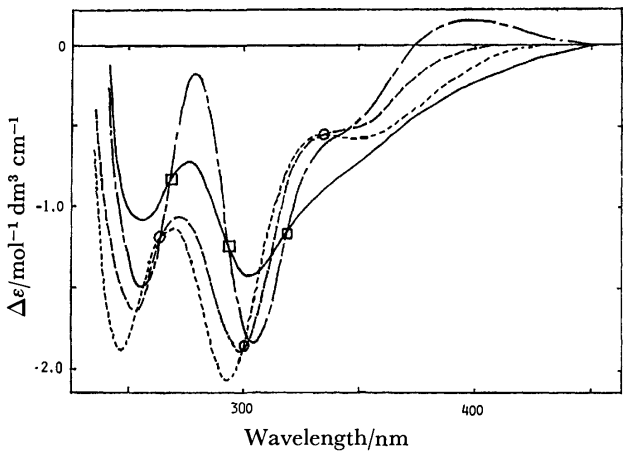

Fig. 5. pH dependence of CD spectra of $(+)_{589}$-[Ir(Hedta)(H_2O)]·1.5H_2O.
·····: pH=1.6, ----: pH=2.6, —·—: pH=7.6, ——: pH=10.0.

It was found that the CD spectra of monoaqua complexes of iridium(III) and rhodium(III) shows a remarkable pH dependence, while those of monochloro complexes change little with the pH of the solution (Fig. 5 and Fig. 7). In the case of the iridium(III) complex, in the acidic region three isosbestic points appear at 335, 309, and 264 nm, while in the basic region they shift to 319, 294, and 268 nm. A plot of $\Delta\varepsilon$ values at 280 nm against the pH gives the curve in Fig. 6, while the curve in Fig. 8 was obtained by a similar plot at 315 nm for $(-)_{589}$-[Rh(Hedta)(H_2O)]. This behavior implies that there exist stepwise acid-base equilibria between species, I, II, and III, of the Ir(III)- and Rh(III) complexes:

$$\mathrm{I} \underset{pK_1}{\rightleftharpoons} \mathrm{II} \underset{pK_2}{\rightleftharpoons} \mathrm{III}$$

From the curves in Fig. 6 and Fig. 8, the pK values are evaluated as:

pK_1=2.5 and pK_2=9.1 for the Rh(III) complex, and pK_1=2.9 and pK_2=8.4 for the Ir(III) complex.

The pK values for the Rh(III)–EDTA complex may be

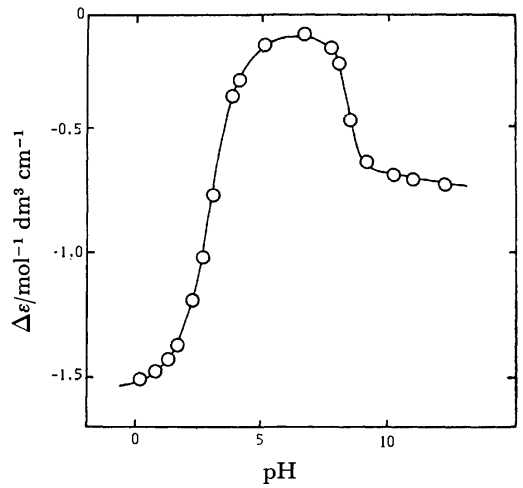

Fig. 6. The plot of $\Delta\varepsilon$ values for $(+)_{589}$-[Ir(Hedta)(H_2O)]·1.5H_2O against pH at 280 nm.

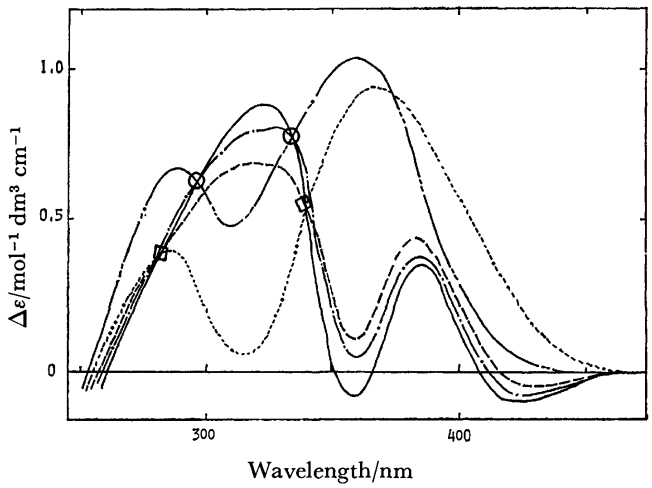

Fig. 7. pH dependence of CD spectra of $(-)_{589}$-[Rh(Hedta)(H_2O)].
—··—: pH=0.8, —·—: pH=2.6, ——: pH=3.5, ----: pH=8.9, ·····: pH=12.1.

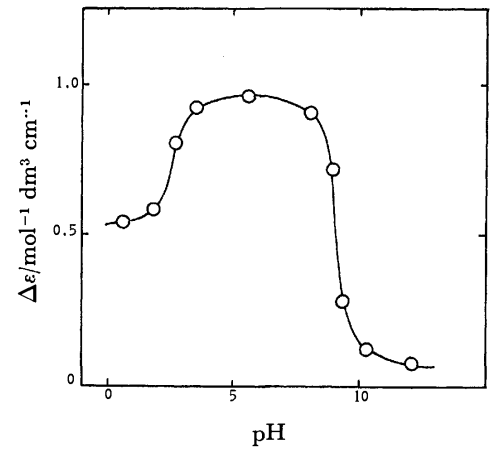

Fig. 8. The plot of $\Delta\varepsilon$ values for $(-)_{589}$-[Rh(Hedta)(H_2O)] against pH at 315 nm.

compared with the values of $pK_1=2.32$ and $pK_2=9.12$ reported by Dwyer and Garvan.[17] Furthermore, the remarkable pH dependence of the CD spectra of the Rh(III) complex may be responsible for the formation of a sexidentate complex, $[Rh(edta)]^-$, in the intermediate pH region (pH=4—8), as has been suggested by Smith and Sawyer on the basis of their PMR study.[18] A similar interpretation should be applicable to the pH dependence of the CD spectra of the iridium(III) complexes, but further study is necessary to elucidate the nature of this observation.

The authors wish to thank Professor Iwao Taminaga of the Tokyo University of Commerce and Navigation for helping with the hydrothermal preparation of the iridium(III) complexes. We also would like to thank Professor Tatsujiro Ishimori of St. Paul's University for his helpful suggestions regarding the chemistry of ruthenium and rhodium.

References

1) For example, H. Taube, *Chem. Rev.*, **50**, 69 (1952).
2) B. Bernas, *Anal. Chem.*, **40**, 1682 (1968).
3) F. P. Dwyer and J. W. Hogarth, *Inorg. Synth.*, **5**, 206 (1957).
4) F. P. Dwyer and J. W. Hogarth, *Inorg. Synth.*, **5**, 204 (1957).
5) M. Saito, T. Uehiro, and Y. Yoshino, *Chem. Lett.*, **1977**, 809.
6) N. A. Ezerskaya, T. P. Solovykh, and L.K. Shubockim, *Zh. Neorg. Khim.*, **17**, 2227 (1972).
7) E. König, "Magnetische Eigenschaften der Koordinations und Metallorganischen Verbindungen der Übergangselemente," in Landolt-Bernstein Tabellen, Neue Serie, ed by K. -H. Hellwege, Springer-Verlag, Berlin (1966), Vol. 2, Group II, pp. 141—143.
8) M. Saito, T. Uehiro, F. Ebina, T. Iwamoto, A. Ouchi, and Y. Yoshino, *Chem. Lett.*, **1979**, 997,.
9) M. Mukaida, H. Okuno, and T. Ishimori, *Nippon Kagaku Zasshi*, **86**, 598 (1965).
10) K. Shimizu, T. Matsubara, and G. P. Sato, *Bull. Chem. Soc. Jpn.*, **50**, 2921 (1977).
11) T. Uehiro, Dr. Sc. Thesis, The University of Tokyo, Tokyo, Japan (1977).
12) G. L. Blackmer and J. L. Sudmeier, *Inorg. Chem.*, **10**, 209 (1973).
13) G. H. Y. Lin, J. D. Leggett, and R. M. Wing, *Acta Crystallogr., Sect. B*, **29**, 1023 (1973).
14) F. P. Dwyer and F. L. Garvan, *J. Am. Chem. Soc.*, **81**, 2955 (1959).
15) F. P. Dwyer and F. L. Garvan, *J. Am. Chem. Soc.*, **83**, 2610 (1961).
16) P. A. Chel'tsov, O. N. Adriamova, and N. A. Ezerskaya, *Koord. Khim.*, **3**, 1220 (1977).
17) F. P. Dwyer and F. L. Garvan, *J. Am. Chem. Soc.*, **82**, 4823 (1960).
18) B. B. Smith and D. T. Sawyer, *Inorg. Chem.*, **7**, 2020 (1968).

The Stereochemistry and Reactivity of Metal-Schiff Base Complexes. III. The Kinetic and Thermodynamic Stereoselectivities in the Formation of *N,N'*-Ethylenebis(α-methylsalicylideneaminato)cobalt(III) Complexes with L-Proline, Hydroxy-L-proline, and *allo*-Hydroxy-L-proline

Yuki Fujii,* Katsuji Shiono, Kuniko Ezuka, and Takashi Isago
Department of Chemistry, Faculty of Science, Ibaraki University, Bunkyo-cho, Mito, Ibaraki 310
(Received March 25, 1980)

Under air-oxidation conditions, the reaction of [Co(α-Me-sal$_2$en)] with L-aaH, where α-Me-sal$_2$en represents the dianion of *N,N'*-ethylenebis(α-methylsalicylideneamine) and where L-aaH denotes L-proline, hydroxy-L-proline, or *allo*-hydroxy-L-proline, proceeded rapidly to yield *Λ-cis*-β_2-[Co(α-Me-sal$_2$en)(L-aa)] stereoselectively, followed by the slow isomerization of the *Λ-cis*-β_2-isomer thus formed to give the corresponding *Δ-cis*-β_2-isomer in a yield of almost 100% under equilibrium conditions. The complexes thus formed were isolated and characterized by the use of their absorption, circular dichroism, and ^{1}H-NMR spectra. The preferential formation of the *Λ-cis*-β_2-isomer in the initial reaction was found to be kinetic in origin. The kinetic stereoselectivity was determined to be 87% for L-proline, 56% for hydroxy-L-proline, and 23% for *allo*-hydroxy-L-proline by the measurement of the rotation at 435 nm of the reaction solutions. On the other hand, no kinetic differentiation was observed for the formation of the similar *cis*-β_2-complexes with L-alanine, L-valine, L-methionine, L-phenylalanine, L-tryptophan, *N*-benzyl-L-alanine, and *N*-methyl-L-alanine. On the basis of these data, the mechanism of the initial complexation was discussed. The high thermodynamic stereoselectivity for *Δ-cis*-β_2-isomer was explained in terms of the intramolecular steric interaction between the pyrrolidine ring of the coordinated L-aa and the distorted α-Me-sal$_2$en ligand in the complex.

The asymmetric reaction of metal complexes with chiral amino acid is an attractive problem, and many studies have been directed toward the stereoselectivity or stereospecificity of cobalt(III)–amino acid complexes. However, almost all of the asymmetric reactions reported have been those for the first-order[1-6] or second-order[7] transformations of the diastereoisomers thus formed. For the asymmetric reaction under kinetically controlled conditions, there are few studies, and no kinetic differentiation has been conclusively demonstrated for the formation of the diastereoisomers of cobalt(III) complexes containing chiral amino acid. A kinetic stereoselective formation of *Λ*-[Co(L-glu)(en)$_2$]$^+$ from racemic-[Co(CO_3)(en)$_2$]$^+$ and L-glutamic acid had been proposed by Gillard and his co-workers,[8-11] but subsequently disproven.[12,13] Kinetic differentiation has been claimed in the complexation of racemic-[Co(CO_3)(en)$_2$]$^+$ with the *N*-terminus of chiral peptides,[14] but no evidence has been presented to preclude a thermodynamic equilibrium upon the hydrolysis of the peptide linkage to produce *Λ*- and *Δ*-[Co(L-amino acidato)(en)$_2$]$^{2+}$. Little stereospecificity was found in the synthesis of β_2-[Co(L-pro)(trien)]$^{2+}$ from β-[Co(OH)(H_2O)(trien)]$^{2+}$ and L-proline under kinetically controlled conditions.[15,16] The selective formation of *Λ*-β_2-[Co(L-ala)(tetramine)]$^{2+}$ by the decarboxylation of the α-methyl-α-amino-malonato ligand (AMM) bound to the *Λ*-β_2-Co(tetramine)-complex should be kinetic in origin,[17,18] but it is a kind of ligand reaction of the coordinated AMM and not the direct complexation of chiral amino acid.

On the other hand, we have recently found that the reaction of [Co(α-Me-sal$_2$en)] with L-proline produces, stereoselectively, *Λ-cis*-β_2-[Co(α-Me-sal$_2$en)(L-pro)] under air-oxidation conditions, followed by the slow isomerization of the *Λ-cis*-β_2-isomer to give the corresponding *Δ-cis*-β_2-isomer in a high stereoselectivity (almost 100% at the equilibrium conditions).[19,20] This reaction is very interesting because 1) the preferential formation of the *Λ*-β_2-isomer in the initial reaction seems to be kinetic in origin, and 2) the stereoselectivity for the final product, the *Δ*-β_2-isomer, is quite high as compared with that for cobalt(III)-tetramine complexes with L-proline.[15,21-24] In this paper, the initial complexations between [Co(α-Me-sal$_2$en)] and various L-amino acids[25] are studied in detail, and the kinetic stereoselectivity in the formation of *Λ*- and *Δ-cis*-β_2-isomers of their complexes will be discussed, together with the formation mechanism. The high stereoselectivity for the *Δ*-β_2-isomer of the L-pro-complex will also be discussed from the stereochemical point of view.

Experimental

The Isolation of the Reaction Products. The starting material, [Co(α-Me-sal$_2$en)], was prepared by the method of Bigotto *et al.*[26]

(1) [Co(α-Me-sal$_2$en)(L-pro)]: In a previous communication,[19] methanol was used as the solvent for the reaction between [Co(α-Me-sal$_2$en)] and L-proline; however, in the present study a mixture of chloroform, methanol, and water was used as the solvent. This is mainly done to increase the solubilty of the reactants. L-Proline (1.4 g, 0.012 mol), in a mixed solvent of methanol (20 cm^3) and water (2 cm^3), was added to a chloroform solution (200 cm^3) of [Co(α-Me-sal$_2$en)] (3.7 g, 0.01 mol). The solution was stirred in the open air for about 15 min, until the color of the solution became green. The solution was then filtered to eliminate a trace amount of a brownish by-product.

(a) $(-)_{435}$-Product(2 : 1 Mixture of Λ- *and* Δ-cis-β_2-*Isomers)*: The green filtrate was concentrated as soon as possible to near dryness at room temperature. The green powder thus obtained was washed with a mixture of ether and methanol (9 : 1) and then air-dried. Yield, about 4.9 g (96%). Found:

C, 54.46; H, 6.29; N, 8.20%. Calcd for $CoC_{23}H_{26}N_3O_4 \cdot 2H_2O$: C, 54.87; H, 6.01; N, 8.34%. $[M]_{435} = -10700$ °m mol^{-1} dm^3 in chloroform. When the green product was dissolved in chloroform and the solution was concentrated to near dryness, a green powder with a $[M]_{435}$ value of $-10700°$ was obtained. Found: C, 54.35; H, 6.39; N, 8.25%. However, when this product was slowly recrystallized from methanol, green crystals with a plus rotation were obtained. Found: C, 54.72; H, 5.83; N, 8.31%. $[M]_{435} = +30500°$ in chloroform.

(b) $(\pm)_{435}$-Product (1 : 1 Mixture of Λ- and Δ-cis-β_2-Isomers): The green filtrate obtained above was stirred for a further 3—4 h and then slowly concentrated to a small volume at room temperature. The green powder so obtained was washed with a mixture of ether and methanol (9 : 1) and then air-dried. Yield, about 4.5 g. Found: C, 54.98; H, 5.89; N, 8.33%. Calcd for $CoC_{23}H_{26}N_3O_4 \cdot 2H_2O$: C, 54.87; H, 6.01; N, 8.34%. $[M]_{435} = -600°$ in chloroform. The $(\pm)_{435}$-product was sometimes obtained in the form of no-crystalline water, and the latter was scarcely soluble in various solvents. Found: C, 58.89; H, 5.74; N, 8.85%. Calcd for $CoC_{23}H_{26}N_3O_4$: C, 59.10; H, 5.61; N, 8.99%. When the soluble $(\pm)_{435}$-product was reprecipitated from chloroform by reducing the solution to near dryness, a green powder with $[M]_{435}$ value of $-600°$ (in chloroform) was obtained. However, when it was recrystallized from methanol, green crystals with a plus rotation ($[M]_{435} = +30500°$) were isolated.

(c) $(+)_{435}$-Product (Δ-cis-β_2-Isomer): The green filtrate obtained above was warmed for 1 d at about 40 °C, and then it was concentrated to a small volume. Green crystals with a plus rotation were thus obtained in about a 90% yield. Found: C, 54.98; H, 6.15; N, 8.51%. Calcd for $CoC_{23}H_{26}N_3O_4 \cdot 2H_2O$: C, 54.87; H, 6.01; N, 8.34%. $[M]_{435} = +30500°$ in chloroform.

(2) [Co(α-Me-sal$_2$en)(HO-L-pro)]: Hydroxy-L-proline (0.8 g, 6.1×10^{-3} mol), in a mixed solvent of water (3 cm^3) and methanol (25 cm^3), was added to a chloroform solution (150 cm^3) of [Co(α-Me-sal$_2$en)] (1.85 g, 5.0×10^{-3} mol). The solution was stirred in the open air for about 13 min. After a trace amount of hydroxy-L-proline had then been filtered off, the filtrate was concentrated to dryness as soon as possible at room temperature. A green powder (about 2.5 g) was thus obtained and was treated as follows.

(a) $(-)_{435}$-Product (3 : 2 Mixture of Λ- and Δ-cis-β_2-Isomers): The green powder (2.5 g) was partially dissolved in chloroform (70 cm^3), and the chloroform-soluble component was evaporated to dryness at room temperature. The green powder thus obtained was washed with ether and air-dried. Yield, about 0.3 g. Found: C, 52.92, H, 5.69; N, 7.92%. Calcd for $CoC_{23}H_{26}N_3O_5 \cdot 2H_2O$: C, 53.18; H, 5.82; N, 8.09%. $[M]_{435} = -7500°$ in chloroform.

(b) $(\pm)_{435}$-Product (1 : 1 Mixture of Λ- and Δ-cis-β_2-Isomers): The green powder (2.5 g) was dissolved in methanol (about 100 cm^3), and an equal volume of water was added. The solution was concentrated as soon as possible to a small volume at room temperature. Green crystals with a small rotation ($[M]_{435} = -700°$ in chloroform) were thus obtained in about a 70% yield. Found: C, 54.30; H, 5.91; N, 8.10%. Calcd for $CoC_{23}H_{26}N_3O_5 \cdot 1.5H_2O$: C, 54.12; H, 5.73; N, 8.23%.

(c) $(+)_{435}$-Product (Δ-cis-β_2-Isomer): The green powder (2.5 g) was dissolved in 200 cm^3 of methanol, and then water (20 cm^3) was added. The solution was heated at about 60 °C for 1 h, and then it was allowed to stand at room temperature for 1 d. Green crystals with a plus rotation ($[M]_{435} = +34000°$ in chloroform) were thus obtained in about an 80% yield. Found: C, 54.36; H, 5.90; N, 7.99%. Calcd for $CoC_{23}H_{26}N_3O_5 \cdot 1.5H_2O$: C, 54.12; H, 5.73; N, 8.23%.

(3) [Co(α-Me-sal$_2$en)(allo-HO-L-pro)]: *(a) $(\pm)_{435}$-Product (1 : 1 Mixture of Λ- and Δ-cis-β_2-Isomers)*: [Co(α-Me-sal$_2$en)] (0.7 g, 1.9×10^{-3} mol) was partially dissolved in chloroform (50 cm^3), and then *allo*-hydroxy-L-proline (0.25 g, 1.9×10^{-3} mol) in a mixed solvent of water (2 cm^3) and methanol (5 cm^3) was added. The mixture was stirred vigorously in the open air for about 15 min. After a trace amount of unreacted materials had been filtered off, the green solution was reduced as soon as possible nearly to dryness at room temperature. The green powder thus obtained was washed with ether and air-dried. Yield, about 0.9 g. Found: C, 50.80; H, 5.91; N, 7.65%. Calcd for $CoC_{23}H_{26}N_3O_5 \cdot 3.5H_2O$: C, 50.55; H, 6.09; N, 7.79%. $[M]_{435} = +600°$ in chloroform.

(b) $(+)_{435}$-Product (Δ-cis-β_2-Isomer): The $(\pm)_{435}$-product (0.5 g) obtained above was dissolved in methanol (100 cm^3) and then the solution was slowly concentrated to a small volume. Green crystals with a plus rotation ($[M]_{435} = +48000°$ in chloroform) were thus obtained in about a 70% yield. Found: C, 55.05; H, 5.58; N, 8.19%. Calcd for $CoC_{23}H_{26}N_3O_5 \cdot H_2O$: C, 55.09; H, 5.63; N, 8.38%.

Measurements. The electronic absorption spectra were recorded with a Hitachi EPS-3 Spectrophotometer at 23 °C. The CD spectra were measured with a JASCO J-20 Automatic Recording Spectropolarimeter at room temperature. The optical rotation at 435 nm was measured with a JASCO DIP-180 Automatic Polarimeter at 23 °C. The PMR spectra were recorded with a Hitachi R-20 Spectrometer (60 MHz) at 35 °C, using TMS as the internal reference. The solution for the measurement of the kinetic stereoselectivity was prepared as follows: an amino acid (5.5×10^{-5} mol) was dissolved in a mixed solvent (6 cm^3) of methanol and water (11 : 1 in volume), and this solution was added to a freshly prepared chloroform solution of [Co(α-Me-sal$_2$en)] (2.5×10^{-3} mol dm^{-3}, 20 cm^3). The solution was made up to 50 cm^3 with chloroform as soon as possible and stirred in the open air for 1 or 2 min. After this, the rotation at 435 nm and the absorption at 595 nm of the solution were measured.

Results and Discussion

The Isolation and Properties of the Reaction Products. When [Co(α-Me-sal$_2$en)] (orange in color) was allowed to react with L-proline under air-oxidation conditions, the reaction solution immediately became green in color and exhibited a minus rotation at 435 nm. After this, the absorption spectrum of the green solution scarcely varied any more; however, the rotation at 435 nm slowly increased to show a plus rotation under the equilibrium conditions. The time dependence of the absorption at 595 nm and the mutarotation at 435 nm for the reaction solution are shown in Fig. 1. In order to get informations about the above phenomena, the isolation of the reaction products was attempted. As has been mentioned in the Experimental section, depending upon the reaction time, three green complexes with different rotations could be isolated from the solution: the initial product with a minus rotation at 435 nm (represented by $(-)_{435}$-product), the second with almost no rotation ($(\pm)_{435}$-product), and the final product with a plus rotation ($(+)_{435}$-product). They all had the same composition, corresponding to [Co(α-Me-sal$_2$en)(pro)]$\cdot 2H_2O$.

Also from the reaction solutions of [Co(α-Me-sal$_2$en)] with hydroxy-L-proline and *allo*-hydroxy-L-proline, similar products were obtained. Since the properties

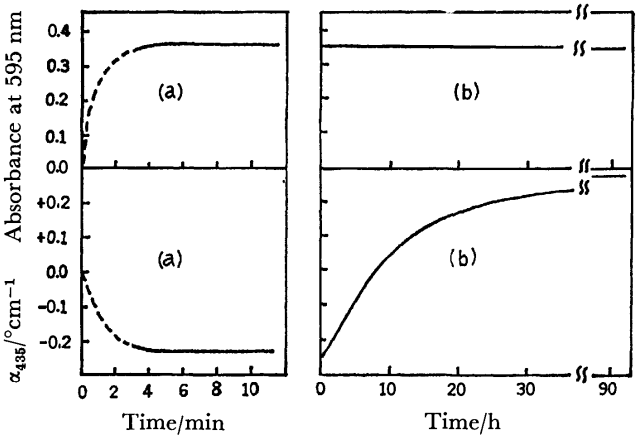

Fig. 1. The time dependences of the absorption (595 nm) and the rotation (435 nm) of the reaction solution between [Co(α-Me-sal$_2$en)] (1.0×10^{-3} M) and L-proline (1.1×10^{-3} M) in the mixed solvent of $CHCl_3$, CH_3OH, and H_2O (88: 11: 1 in volume).
Cell length: 1.0 cm, (a): those for the initial reaction solution, (b): those for full time.

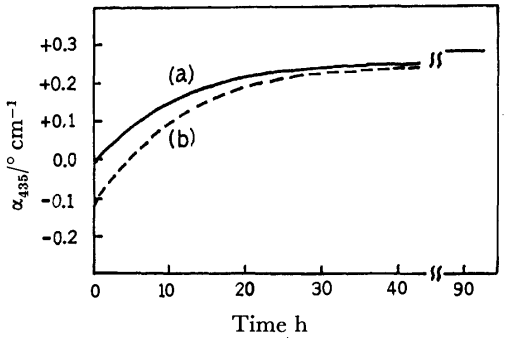

Fig. 2. The mutarotation of [Co(α-Me-sal$_2$en)(L-pro)] complex (1.0×10^{-3} M) in the mixed solvent of $CHCl_3$, CH_3OH, and H_2O (88: 11: 1 in volume).
Cell length: 1.0 cm, (a) (——): $(\pm)_{435}$-product, (b) (------): $(-)_{435}$-product.

of the L-pro-, HO-L-pro-, and *allo*-HO-L-pro-complexes resemble each other quite closely, the L-pro-complex will be used here for an example.

Both the $(-)_{435}$- and $(\pm)_{435}$-products of the L-pro-complex exhibited mutarotation in methanol or in a mixed solvent containing methanol, to show plus rotations under the equilibrium conditions, although the $(+)_{435}$-product showed no observable mutarotation. The mutarotation curves for both the $(-)_{435}$- and $(\pm)_{435}$-products are shown in Fig. 2. From both the equilibrated solutions, the $(+)_{435}$-product was isolated. As may be seen in Fig. 2, the mutarotation curves for both products are quite similar: the plots of $\ln(\alpha_\infty-\alpha_t)$ *vs.* the time for both mutarotation curves give straight lines with the same slope. Accordingly, it is clear that the $(-)_{435}$-product isomerizes to the $(+)_{435}$-product by way of the $(\pm)_{435}$-product. Since the mutarotation curve for the reaction solution of [Co(α-Me-sal$_2$en)] with L-proline in Fig. 1 closely resembles that for the $(-)_{435}$-product in Fig. 2, it can be concluded that the reaction between [Co(α-Me-sal$_2$en)] and L-proline produces $(-)_{435}$-[Co(α-Me-sal$_2$en)(L-pro)] preferentially, followed by its isomerization to give the corresponding $(+)_{435}$-isomer.

The rates of mutarotation for the $(-)_{435}$- and $(\pm)_{435}$-products depend strongly on the nature of the solvent: the rate is comparatively fast in methanol, but it is quite slow in chloroform. Therefore, the molar rotations of the $(-)_{435}$- and $(\pm)_{435}$-products scarcely varied between before and after their recrystallizations from chloroform.

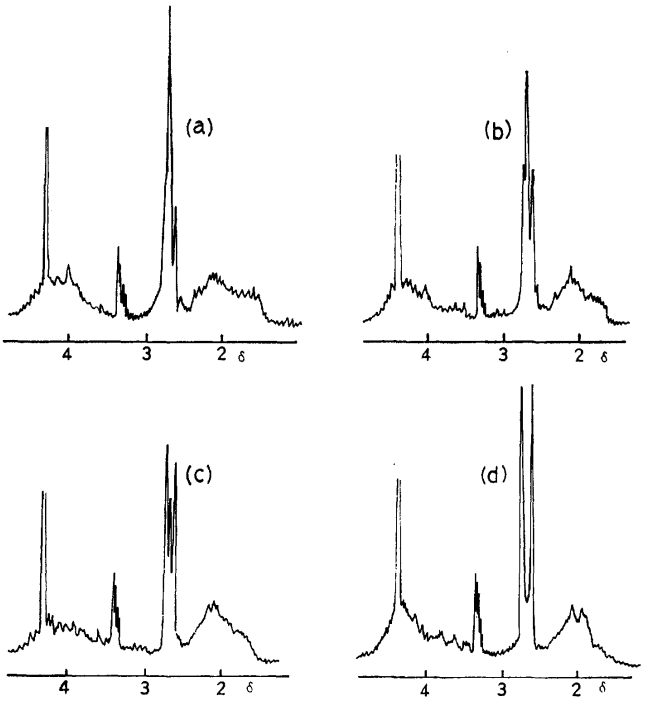

Fig. 3. The ^{1}H-NMR spectra of [Co(α-Me-sal$_2$en)-(L-pro)] complex in the mixed solvent of $CDCl_3$ and CD_3OD (4 : 1) at 35 °C.
(a): $(-)_{435}$-product, (b): $(\pm)_{435}$-product, (d): $(+)_{435}$-product. The ^{1}H-NMR spectra of $(-)_{435}$- and $(\pm)_{435}$-products exhibit time dependence. Those for $(-)_{435}$-product about 40 min and 240 min after dissolution correspond to (b) and (c), respectively, and that at the equilibrium conditions to (d). The ^{1}H-NMR spectra for $(\pm)_{435}$-product about 180 min after dissolution and at the equilibrium conditions correspond to (c) and (d), respectively.

Figure 3 shows the ^{1}H-NMR spectra of the isolated L-procomplexes soon after dissolution. The numerical data are listed in Table 1. The ^{1}H-NMR spectra of the $(-)_{435}$- and $(\pm)_{435}$-products each exhibited a clear time dependence in the methyl signal of the coordinated α-Me-sal$_2$en ligand, and each ^{1}H-NMR spectrum at the equilibrium conditions coincided with that of the $(+)_{435}$-product. However, the $(+)_{435}$-product showed no observable time dependence in its ^{1}H-NMR spectrum. From the time dependence of the methyl signal, the central peak at 2.76 ppm can safely be ascribed to $(-)_{435}$-[Co(α-Me-sal$_2$en)(L-pro)], and the two peaks with an equal intensity at 2.72 and 2.82 ppm, to $(+)_{435}$-[Co(α-Me-sal$_2$en)(L-pro)]. No other shoulders or peaks were observed in the methyl signal. These facts clearly

Table 1. ^{1}H-NMR spectral data for [Co(α-Me-sal$_2$en)((L-aa)][a] (δ)

L-aa and solvent	Products	φ-Protons[b]	$-CH_2-CH_2-$[b]	$-CH_3$[c]		$-CH_2-$[b] (Pyrrolidine ring)
L-pro $CDCl_3+CD_3OD$[d] (4 : 1)	$(-)_{435}$-	6.5—7.7	3.5—4.5	2.71 2.81	(doublet) [1 : 1]	1.6—2.4
	$(\pm)_{435}$-	6.5—7.7	3.5—4.5	2.76 2.72 2.82	[4] (doublet) [1 : 1]	1.6—2.4
	$(+)_{435}$-	6.5—7.7	3.5—4.5	2.77 2.72 2.82	[2] (doublet) [1 : 1]	1.6—2.4
HO-L-pro DMSO-d_6+$CDCl_3$[e] +CD_3OD (3 : 1 : 1)	$(-)_{435}$-	6.4—7.8	3.5—4.6	2.68 2.75	(doublet) [1 : 1]	1.7—2.4
	$(\pm)_{435}$-	6.4—7.8	3.5—4.6	2.75 2.68 2.75	[3] (doublet) [1 : 1]	1.7—2.4
	$(+)_{435}$-	6.4—7.8	3.5—4.4	2.75 2.68 2.75	[2] (doublet) [1 : 1]	1.7—2.4
allo-HO-L-pro $CDCl_3$+DMSO-d_6[f] +CD_3OD (6 : 2 : 1)	$(\pm)_{435}$-	6.5—7.7	3.5—4.5	2.70 2.72	(doublet) [1 : 1]	1.8—2.5
	$(+)_{435}$-	6.5—7.7	3.5—4.4	2.70 2.76 2.70 2.76	(doublet) [1 : 1] (doublet) [1 : 1]	1.9—2.4

a) The data are those soon after dissolution. b) Multiplet. c) [ ] represents the relative peak area. d) Signals of the solvent: MeOH (3.32 ppm), HDO (4.20 ppm), $CHCl_3$ (7.45 ppm). e) Signals of the solvent: DMSO (2.55), MeOH (3.23), HDO (4.11), $CHCl_3$ (overlap with φ-protons). f) Signals of the solvent: DMSO (2.59), MeOH (3.30), HDO (3.85), $CHCl_3$ (7.75).

Table 2. Isomer ratios for the isolated products

Complex	Products	Λ-β_2-Isomer : Δ-β_2-Isomer
[Co(α-Me-sal$_2$en)-(L-pro)]	$(-)_{435}$-	6.6 : 3.3
	$(\pm)_{435}$-	5 : 5
	$(+)_{435}$-	0 : 10
[Co(α-Me-sal$_2$en)-(HO-L-pro)]	$(-)_{435}$-	6 : 4
	$(\pm)_{435}$-	5 : 5
	$(+)_{435}$-	0 : 10
[Co(α-Me-sal$_2$en)-(*allo*-HO-L-pro)]	$(\pm)_{435}$-	5 : 5
	$(+)_{435}$-	0 : 10

indicate that only two species are involved in the isomerization of the $(-)_{435}$- and $(\pm)_{435}$-products.

From the relative peak area of the methyl signal in the ^{1}H-NMR spectra of the isolated products soon after dissolution, the existing ratio between $(-)_{435}$- and $(+)_{435}$-isomers in each product can be estimated; the values are listed in Table 2. In the case of the L-pro-complex, it becomes clear that the $(-)_{435}$- and $(\pm)_{435}$-products are 2 : 1 and 1 : 1 mixtures of $(-)_{435}$- and $(+)_{435}$-[Co(α-Me-sal$_2$en)(L-pro)] respectively, but the $(+)_{435}$-product is the pure $(+)_{435}$-isomer of [Co(α-Me-sal$_2$en)(L-pro)]. Since the $(+)_{435}$-product shows no time dependence in its ^{1}H-NMR spectrum, its thermodynamic stereoselectivity can be concluded to be almost 100%.

Similar results have also been obtained for the HO-L-pro- and *allo*-HO-L-pro-complexes.

The Structure and the Thermodynamic Stereoselectivity of the Complexes. The electronic absorption (AB) and the circular dichroism (CD) spectra of the L-pro-complexes are shown in Fig. 4. The numerical data are listed in Table 3. The CD spectra of the $(-)_{435}$- and $(\pm)_{435}$-products for the L-proline varied gradually in methanol or in a mixed solvent containing methanol, and their CD spectra under the equilibrium conditions coincided with the CD spectrum of the $(+)_{435}$-product, although the variation in their AB spectra was negligibly small. Further, as may be seen in Fig. 4, an isosbestic point is observed at 21.4 k cm^{-1} in their CD spectra. These facts strongly support that only two species, $(-)_{435}$- and $(+)_{435}$-isomers of [Co(α-Me-sal$_2$en)(L-pro)], are involved in the mutarotation of the L-pro-complex. The CD spectrum of the $(+)_{435}$-product showed no observable time dependence.

The AB spectrum of the $(-)_{435}$-product closely resembles that of the $(+)_{435}$-product, and the CD spectrum of the $(-)_{435}$-product is quite similar to that of the $(+)_{435}$-product, except for the reversed CD sign. Therefore, it seems that the $(-)_{435}$- and $(+)_{435}$-isomers take the same geometrical structure with respect to the coordinated atoms. The AB and CD spectra of the $(+)_{435}$-product closely resemble those of $(-)_{435}$-*Λ-cis-*β_2-[Co(α-Me-sal$_2$en)(L-ileu)]·1.5H$_2$O,[3,20] except for the reversed CD sign. Accordingly, the *Δ-cis-*β_2-structure can be assigned to the $(+)_{435}$-isomer of [Co(α-Me-sal$_2$en)(L-pro)], and the *Λ-cis-*β_2-structure, to the $(-)_{435}$-isomer.

Similar results have also been obtained for the HO-L-pro- and *allo*-HO-L-pro-complexes.

Generally, the stereoselectivity under the equilibrium conditions is thermodynamic in origin. The Co(α-Me-sal$_2$en)-complexes with L-pro, HO-L-pro, and *allo*-HO-

Table 3. Absorption and CD spectral data[a)]

Complex	Products	Absorption $\bar{\nu}/10^3$ cm^{-1} (log ε)	CD $\bar{\nu}/10^3$ cm^{-1} ($\Delta\varepsilon$)
[Co(α-Me-sal$_2$en)-(L-pro)]	$(-)_{435}$-	16.7(2.55) 26.4(3.78)	16.3(+3.52), 19.2(+1.38) 22.7(−2.80), 24.1(−3.31) 25.3(−3.83), 30.8(−3.19)
	$(\pm)_{435}$-	16.7(2.54) 26.4(3.77)	14.3(+0.07), 15.8(−0.27) 17.8(+0.32), 21.2(−0.94) 23.0(+0.28), 24.5(−1.33) 27.2(+2.80), 29.4(−0.20) 31.0(+0.47)
	$(+)_{435}$-	16.7(2.54) 26.4(3.76)	16.3(−9.99). 19.2(−4.15) 23.2(+10.2), 27.2(+17.9) 30.8(+8.84)
[Co(α-Me-sal$_2$en)-(HO-L-pro)]	$(-)_{435}$-	16.8(2.58) 26.7(3.83)	16.6(+4.21), 18.5(+2.20) 22.7(−3.47), 25.6(−4.44) 30.3(−3.74)
	$(\pm)_{435}$-	16.8(2.59) 26.7(3.84)	16.9(+1.58), 18.5(+1.29) 21.7(−1.05), 24.9(−3.11) 27.4(+1.90), 30.3(−1.59)
	$(+)_{435}$-	16.9(2.57) 26.7(3.84)	16.3(−11.8), 19.2(−4.53) 23.3(+12.8), 27.2(+21.3) 30.8(+10.1)
[Co(α-Me-sal$_2$en)-(*allo*-HO-L-pro)]	$(\pm)_{435}$-	16.8(2.62) 26.9(3.78)	14.6(+0.22), 16.2(−0.67) 17.7(+0.29), 20.5(−1.72) 23.6(+0.41), 25.5(−0.71) 27.4(+1.40), 31.4(+0.71)
	$(+)_{435}$-	16.9(2.63) 27.1(3.85)	16.3(−15.4), 19.7(−8.08) 23.5(+15.2), 27.3(+22.6) 31.1(+13.9)

a) Soon after dissolution in a mixed solvent of $CHCl_3$+MeOH+H_2O (88 : 11 : 1 in volume).

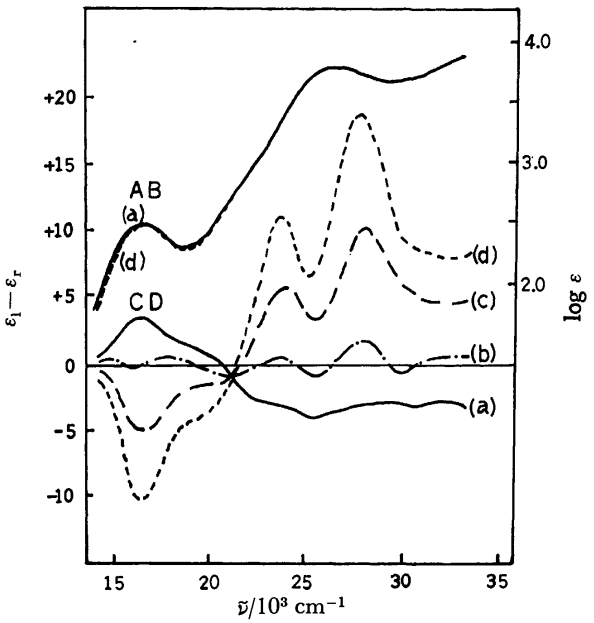

Fig. 4. The AB and CD spectra of [Co(α-Me-sal$_2$en)-(L-pro)] complex in the mixed solvent of $CHCl_3$, CH_3OH, and H_2O (88: 11: 1 in volume) at room temperature.
(a) (——): $(-)_{435}$-product, (b) (-·-·-): $(\pm)_{435}$-product, (d) (----): $(+)_{435}$-product. The CD spectra of $(-)_{435}$- and $(\pm)_{435}$-products exhibit time dependence. Those for $(-)_{435}$-product about 4 and 16 h after dissolution correspond to (b) and (c), respectively, and that at the equilibrium conditions to (d). The CD spectra for $(\pm)_{435}$-product about 12 h after dissolution and at the equilibrium conditions correspond to (c) and (d), respectively.

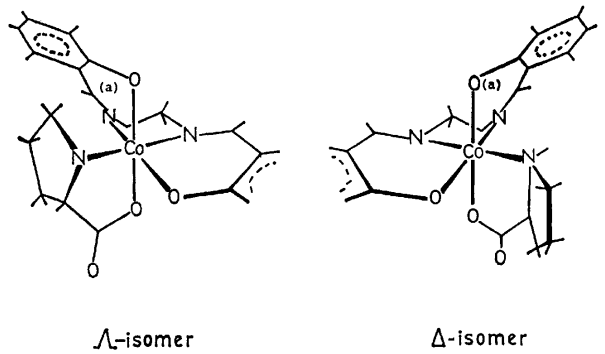

Fig. 5. The steric structure of *Λ-cis-*β_2- and *Δ-cis-*β_2-isomers of [Co(α-Me-sal$_2$en)(L-pro)] complex.

L-pro take the *Λ-cis-*β_2-structure almost always under the equilibrium conditions, as has been mentioned above. This implies that the *Δ-cis-*β_2-isomer is more stable than the corresponding *Λ-cis-*β_2-isomer at about 11.3 kJ mol^{-1} ($-\Delta G$ value of 1 : 100 equilibrium mixture) or more in each complex. On the other hand, in the cases of $[Co(en)_2(L\text{-pro})]^{2+}$ and β_2-$[Co(trien)(L\text{-pro})]^{2+}$, although they favor the *Δ*-configuration, the ratio between the *Δ*- and *Λ*-isomers under the equilibrium conditions is about 3 : 1 ($\Delta G = -2.7$ kJ mol^{-1}) in both complexes. From these facts, it can be said that the stereoselectivity of the Co(α-Me-sal$_2$en)-complexes is much higher than that of the Co(tetramine)-complexes. This high thermodynamic stereoselectivity of the Co(α-Me-sal$_2$en)-complexes comes from the characteristic steric structure of the coordinated α-Me-sal$_2$en ligand. As is shown in Fig. 5, when it takes the *cis-β*-configuration, a chelate ring (a) inclines toward the

side of the coordinated amino acid about 30° from the N–Co–O plane of (a).[3,20] In the case of the L-pro-complex, the molecular model suggests that this inclination of the chelate ring (a) brings about an extreme steric closeness (1.4—1.6 Å) between the distorted chelate ring (a) and the pyrrolidine ring of the L-proline when it has the *Λ-cis-*β_2-structure. However, when it has the *Δ-cis-*β_2-structure, there is no abnormal closeness between them. In the case of the *Δ-cis-*β_2-structure, the pyrrolidine ring somewhat approaches the two phenolic oxygen atoms of α-Me-sal$_2$en (about 2.5 Å), but the steric repulsion in the *Δ-cis-*β_2-structure seems to be much weaker than that between the pyrrolidine ring and the chelate ring (a) in the *Λ-cis-*β_2-structure. Thus, the *Δ-cis-*β_2-structure may be favored under equilibrium conditions.

In the cases of the HO-L-pro- and *allo*-HO-L-pro-complexes, their molecular models indicate that the hydroxy group on each pyrrolidine ring brings about no intramolecular steric interaction with the coordinated α-Me-sal$_2$en ligand, whether it has the *Λ-* or *Δ-cis-*β_2-structure. Therefore, they may also favor the *Δ-cis-*β_2-structure almost always, as is observed in the L-pro-complex.

Kinetic Stereoselectivity. In spite of the thermodynamic advantage of the *Δ-cis-*β_2-structure, the initial reaction between [Co(α-Me-sal$_2$en)] and L-proline produced the thermally unstable *Λ-cis-*β_2-isomer of [Co(α-Me-sal$_2$en)(L-pro)] preferentially. This fact can be explained only when the kinetic advantage in the formation of *Λ-cis-*β_2-isomer is considered. In fact, it has been observed in another of our experiments that the formation rate of *Λ-cis-*β_2-[Co(sal$_2$-(*S,S*)-chxn)(L-pro)] from [Co(sal$_2$-(*S,S*)-chxn)] and L-proline is much faster than that of *Δ-cis-*β_2-[Co(sal$_2$-(*R,R*)-chxn)(L-pro)] from [Co(sal$_2$-(*R,R*)-chxn)] and L-proline, where sal$_2$chxn represents the dianion of *N,N'*-1,2-cyclohexylenebis(salicylideneamine).[4,27] Hence, the initial formation of the *Λ-cis-*β_2-isomer for the Co(α-Me-sal$_2$en)-complex can be regarded as a kinetically controlled reaction. Here, the initial complexations between [Co(α-Me-sal$_2$en)] and various L-amino acids were studied in detail in order to estimate the values of the kinetic stereoselectivity for their reactions. In order to follow the initial reactions, a mixture of chloroform, methanol, and water (88 : 11 : 1 in volume) was used as the solvent. This solvent is used mainly because it will increase the solubiltiy of the reactants, but also partly because it will slow the isomerization rate of the formed complexes. Since the manner of the reactions is quite similar for all the amino acids investigated here, the reactions with L-proline and L-phenylalanine will be given as examples.

Figure 6 shows the absorption spectra of the complexes before and after the reaction. Figure 7 shows the time dependence of the absorbance at 595 nm and the mutarotation at 435 nm of the reaction solution with L-phenylalanine; those for L-proline are shown in Fig. 1. In each case, the absorbance became constant within a few minutes after the initiation of the reaction, and the absorption spectra a few minutes after the initiation of the reaction closely resembled those under equilibrium

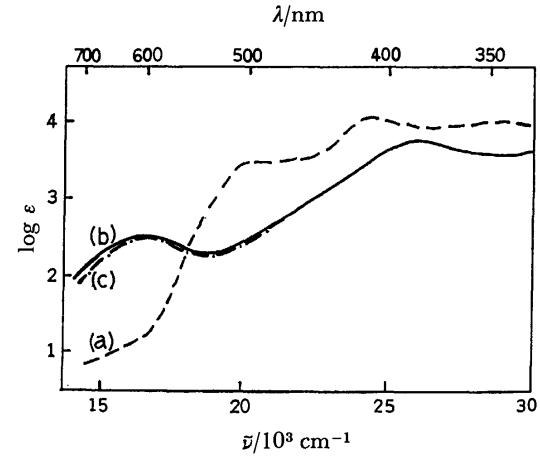

Fig. 6. The absorption spectra of [Co(α-Me-sal$_2$en)] in chloroform (1.0×10^{-3} M) and of the reaction solution between [Co(α-Me-sal$_2$en)] (1.0×10^{-3} M) and L-proline (1.1×10^{-3} M) in the mixed solvent of $CHCl_3$, CH_3OH, and H_2O (88: 11: 1 in volume).
(a): [Co(α-Me-sal$_2$en)], (b): few min after initiation of the reaction, (c) : at the equilibrium conditions.

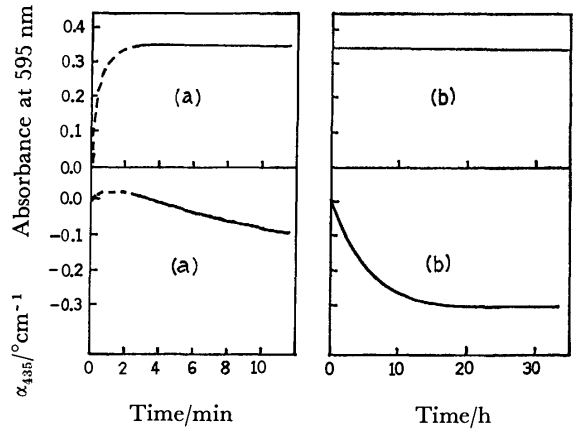

Fig. 7. The time dependences of the absorption (595 nm) and the rotation (435 nm) of the reaction solution between [Co(α-Me-sal$_2$en)] (1.0×10^{-3} M) and L-phenylalanine (1.1×10^{-3} M) in the same solvent with that in Fig. 1.
(a) : Those for the initial reaction solution, (b) : those for full time.

conditions. Further, the absorption spectrum under equilibrium conditions coincided with that of the corresponding complex, *cis-*β_2-[Co(α-Me-sal$_2$en)(L-pro)] or *cis-*β_2-[Co(α-Me-sal$_2$en)(L-phe)].[3,20] From these facts, it is concluded that the complexation of [Co(α-Me-sal$_2$en)] with L-amino acid proceeds quite rapidly under air-oxidation conditions to form *cis-*β_2-[Co(α-Me-sal$_2$en)-(L-aa)] quantitatively.

The plots of $\ln|\alpha_\infty-\alpha_t|$ *vs.* the time for each mutarotation gave a straight line, and the slope coincided with the observed isomerization rate constant between the *Λ-* and *Δ-cis-*β_2-isomers of the corresponding complex (see Table 4). Accordingly, the mutarotation of each reaction solution can safely be ascribed to the isomerization of the *cis-*β_2-complex formed between the *Λ-* and *Δ-*isomers. As is shown in Fig. 7 and Table 4, the

TABLE 4. THE ROTATION OF REACTION SOLUTIONS OF [Co(α-Me-sal$_2$en)] WITH L-AMINO ACIDS AND THAT OF THE ISOLATED COMPLEXES, [Co(α-Me-sal$_2$en)(L-aa)][a]

Amino acid[25]	Reaction solution[b]			Isolated complex[c]		
	α_{435} (°cm^{-1}) (soon after reaction)	α_{435} (°cm^{-1}) (at equilibrium conditions)	k_{obsd} (s^{-1})	α_{435} (°cm^{-1}) (soon after dissolution)	α_{435} (°cm^{-1}) (at equilibrium conditions)	k_{obsd} (s^{-1})
L-ala	+0.011	−0.086	6.2×10^{-4}	+0.013[d]	−0.085	6.1×10^{-4}[g]
L-val	+0.016	−0.160	6.9×10^{-4}	+0.011[d]	−0.165	6.8×10^{-4}[g]
L-ileu	+0.028	−0.148	7.0×10^{-4}	−0.425[e]	−0.153	
L-met	0.000	−0.089	7.7×10^{-4}	−0.416[e]	−0.088	
L-phe	+0.018	−0.310	5.6×10^{-4}	+0.020[d]	−0.312	5.8×10^{-4}[g]
L-trp	+0.008	−0.349	6.3×10^{-4}	−0.510[e]	−0.352	
N-benzyl-L-ala	+0.016	−0.363	3.2×10^{-4}		−0.364[f]	
N-methyl-L-ala	−0.038	−0.355	1.2×10^{-5}		−0.355[f]	
L-pro	−0.235	+0.275	2.2×10^{-5}	−0.006[d]	+0.285	2.2×10^{-5}[h]
HO-L-pro	−0.185	+0.330	2.0×10^{-5}	−0.007[d]	+0.335	2.0×10^{-5}[h]
allo-HO-L-pro	−0.110	+0.485	6.1×10^{-5}	+0.006[d]	+0.480	6.2×10^{-5}[h]

a) Rotations with a 1 cm cell at 23 °C in a mixed solvent of $CHCl_3+CH_3OH+H_2O$ (88 : 11 : 1 in volume). b) The concentration of [Co(α-Me-sal$_2$en)]$=1.0\times10^{-3}$ mol dm^{-3}; the concentration of L-aaH$=1.1\times10^{-3}$ mol dm^{-3}. c) The concentration of the complex$=1.0\times10^{-3}$ mol dm^{-3}. d) 1 : 1 mixture of *Λ*- and *Δ*-*cis*-β_2-isomers.[3] e) *Λ*-*cis*-β_2-isomer. f) Unpublished data. g) Observed isomerization rate from *Λ*- to *Λ*-*cis*-β_2-isomers. h) Observed isomerization rate from *Λ*- to *Δ*-*cis*-β_2-isomers.

initial rotation of the reaction solution for L-phenylalanine is very small, and it is nearly identical with that of the 1 : 1 mixture of *Λ*- and *Δ*-*cis*-β_2-[Co(α-Me-sal$_2$en)(L-phe)]. Therefore, it is concluded, for L-phenylalanine, that the formation ratio between the *Λ*- and *Δ*-*cis*-β_2-isomers in the initial complexation is about 1 : 1; the kinetic stereoselectivity is estimated to be nearly zero. Similar results have also been obtained for L-ala, L-val, L-met, L-ileu, and L-trp. In the cases of *N*-benzyl-L-ala and *N*-methyl-L-ala, since the rotations of their initial reaction solutions are also very small, their kinetic stereoselectivities are both estimated to be almost zero, although four *cis*-β_2-isomers are possible in the *N*-alkyl-amino acidato complex.

On the other hand, in the cases of L-pro, HO-L-pro, and *allo*-HO-L-pro, each reaction solution initially exhibited a large minus rotation. Since the rotations of the free amino acids were negligibly small under the experimental conditions employed (1×10^{-3} mol dm^{-3}), it is clear that the large minus rotation of each reaction solution comes from the $(-)_{435}$-isomer of the formed complex. Generally, the vicinal effect of the coordinated chiral amino acid is additive in nature. In the cases of the L-pro-, HO-L-pro-, and *allo*-HO-L-pro-complexes, it can be regarded that the rotation of each $(\pm)_{435}$-product corresponds to the vicinal effect of each L-amino acid, because the $(\pm)_{435}$-product is a 1 : 1 mixture of the *Λ*- and *Λ*-*cis*-β_2-isomers of the corresponding L-amino acidato complex. Therefore, the kinetic stereoselectivity for these complexes can be estimated by the use of the following equation:

$$\{([\Lambda]-[\Delta])/([\Lambda]+[\Delta])\}\times100(\%) = |([M]^{A}_{435}-[M]^{B}_{435})/([M]^{C}_{435}-[M]^{B}_{435})|\times100$$

where $[\Lambda]$ and $[\Delta]$ represent the concentrations of the *Λ*- and *Λ*-*cis*-β_2-isomers of the formed complex respectively; $[M]^{A}_{435}$ and $[M]^{C}_{435}$ represent the molar rotations at 435 nm of the complexes in the initial reaction solution (A) and in the equilibrium reaction solution (C) respectively, $[M]^{C}_{435}$ corresponds to the molar rotation of the $(+)_{435}$-isomer, and $[M]^{B}_{435}$ indicates the molar rotation of the $(\pm)_{435}$-product. The estimated values are listed in Table 5. Figure 8 shows the CD spectra for the reaction solutions of L-pro and *allo*-HO-L-pro. From these CD spectra, it is confirmed that: 1) the CD spectrum for the initial reaction solution of L-pro and that for the $(+)_{435}$-*Λ*-*cis*-β_2-isomer of the L-pro-complex are almost mirror images of each other; 2) the *Λ*-*cis*-β_2-isomer is formed with a high kinetic stereoselectivity; 3) the CD-intensity of the initial reaction solution for *allo*-HO-L-pro is much smaller than that for L-pro, while the kinetic stereoselectivity for the *allo*-HO-L-pro-complex is much lower than that for L-pro-complex, and 4) the CD spectrum of the reaction solution under equilibrium conditions coincides with that of the $(+)_{435}$-isomer of the corresponding isolated complex.

TABLE 5. KINETIC STEREOSELECTIVITY IN THE FORMATION OF *Λ*- AND *Δ*-*cis*-β_2-[Co(α-Me-sal$_2$en)(L-aa)]

Amino acid[25]	$([\Lambda]-[\Delta])/([\Lambda]+[\Delta])\times100(\%)$
L-ala, L-val, L-met L-ileu, L-phe, L-trp	≈0
N-benzyl-L-ala, *N*-methyl-L-ala	≈0
L-pro	87
HO-L-pro	56
allo-HO-L-pro	23

From these results and discussion, it can be concluded that 1) the kinetic differentiation in the formation of the *Λ*- and *Λ*-*cis*-β_2-diastereoisomers is characteristic of

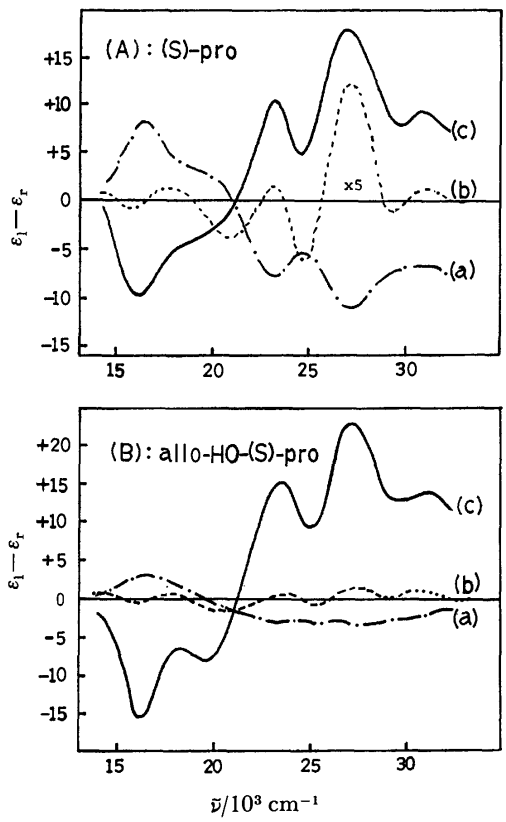

Fig. 8. The CD spectra of the reaction solutions of [Co(α-Me-sal$_2$en)] with L-proline (A) and *allo*-OH-L-proline (B) in the same solvent with that in Fig. 1. The reaction molar ratio=1 : 1.1.
(a) : Soon after reaction, (c) : at the equilibrium conditions, (b) : the CD spectrum of the corresponding $(\pm)_{435}$-product, which corresponds to the vicinal effect of the coordinated L-proline or *allo*-HO-L-proline.

the amino acids with a pyrrolidine ring, but 2) the kinetic stereoselectivity decreases in the order of: L-pro>HO-L-pro>*allo*-HO-L-pro.

The Reaction Mechanism. As has been mentioned above, the reaction between [Co(α-Me-sal$_2$en)] and L-amino acid under air-oxidation conditions proceeded quite rapidly to form *cis*-β_2-[Co(α-Me-sal$_2$en)(L-aa)] quantitatively. However, no reaction occurred under nitrogen. When the L-amino acid neutralized with LiOH was used, the formation of [Co(α-Me-sal$_2$en)-(L-aa)] was rather slow. Further, the rate of the air oxidation of [Co(α-Me-sal$_2$en)] was quite slow in the absence of L-amino acid. On the other hand, it is well known that the planar Co(II)–Schiff base complexes adsorp O_2 to give [Co(Schiff base)(O_2)] or [Co(Schiff base)]$_2O_2$.[28,29] Further, in the presence of a base, *trans*-[Co(Schiff base)(O_2)(Base)][30,31] and *trans*-[Co(Schiff base)(Base)$_2$][+][26,32] are formed. Thus, the formation reaction of [Co(α-Me-sal$_2$en)(L-aa)] from [Co(α-Me-sal$_2$en)] and L-aaH by air-oxidation can be thought to proceed as follows:

$$[\text{Co}(\alpha\text{-Me-sal}_2\text{en})] + O_2 + {}^-\text{OOC-CHR-NH}_3^+ \longrightarrow \textit{trans}\text{-}[\text{Co}(\alpha\text{-Me-sal}_2\text{en})(O_2)(\text{OOC-CHR-NH}_3^+)] \quad (1)$$

$$\textit{trans}\text{-}[\text{Co}(\alpha\text{-Me-sal}_2\text{en})(O_2)(\text{OOC-CHR-NH}_3^+)] \longrightarrow \textit{cis}\text{-}\beta_2\text{-}[\text{Co}(\alpha\text{-Me-sal}_2\text{en})(\text{OOC}\diagdown\diagup\text{NH}_2\text{CHR})] + HO_2. \quad (2)$$

The first reaction (1) is the formation of the O_2-adduct in the presence of amino acid. Since the amino acid exists as a zwitter-ion in solution, here it may coordinate to cobalt, with its carboxylato group as a unidentate ligand. The second reaction (2) is the chelation of the unidentate amino acid, which includes the deprotonation from the ammonium group of amino acid and the subsequent coordination of the amino group to the central cobalt ion, with the departure of O_2 from the O_2-adduct as O_2^- or HO_2.

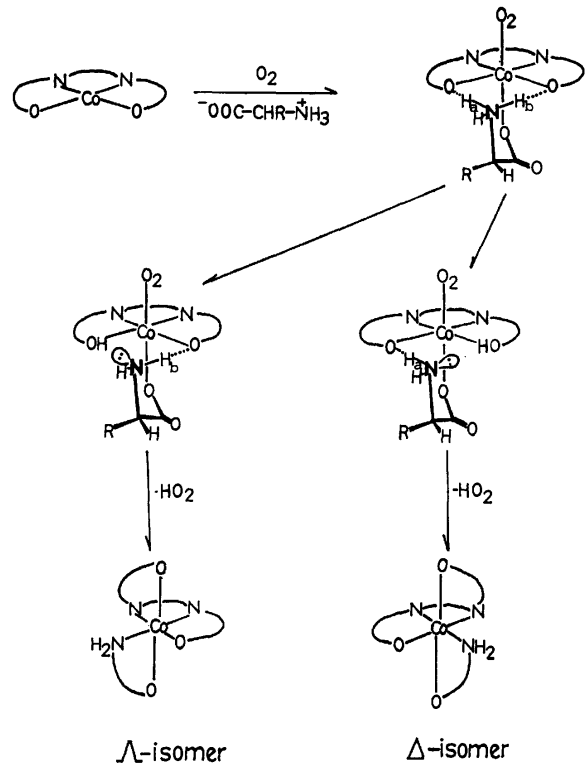

Fig. 9. The proposed reaction mechanism for the formation of *cis*-β_2-[Co(α-Me-sal$_2$en)(L-aa)] complex from [Co(α-Me-sal$_2$en)] and L-aaH under air-oxidation conditions.

In the intermediate, [Co(α-Me-sal$_2$en)(O_2)(OOC-CHR-NH_3^+)], the ammonium group of the amino acid has a positive charge and the phenolic oxygen atoms of the coordinated α-Me-sal$_2$en ligand have a negative charge. Thus, a hydrogen bonding can be expected to exist between them. Further, it has been reported recently that the phenolic oxygen atoms act as proton acceptors.[33] Accordingly, the deprotonation in Reaction (2) may take place by the transfer of one of the protons on the ammonium group to one of the phenolic oxygen atoms through the hydrogen bonding. A plausible reaction mechanism is shown in Fig. 9. In order to explain the kinetic stereoselectivities for various amino acids in Table 5, it is assumed in this mechanism that, when H_a in Fig. 9 is deprotonated, the *Λ-cis*-β_2-isomer is

produced, but when H_b is deprotonated, the *Δ-cis-*β_2-isomer is formed.

In the cases of such amino acids as L-ala, L-phe, and L-ileu, the molecular models indicate that the two protons, H_a and H_b, are sterically equivalent in the intermediate, [Co(α-Me-sal$_2$en)(O_2)(OOC–CHR–NH_3^+)]. This corresponds to the finding that the probability of the deprotonation of H_a and H_b is 50 : 50; the formation ratio between *Λ-* and *Δ-cis-*β_2-isomers is 1 : 1. In fact, as may be seen in Table 5, the kinetic stereoselectivity for such amino acids complexes as L-ala, L-phe, and L-ileu is nearly zero.

In the case of L-pro, the two protons are not equivalent, because L-proline can coordinate as a chelating ligand only when the configuration of the nitrogen atom is in the (*S*)-form. That is, only the deprotonation of H_a is effective in the chelation of L-proline. Therefore, the *Λ-cis-*β_2-isomer may be formed preferentially in the case of the L-pro-complex. On the other hand, in the case of HO-L-pro, because of the equatorial orientation of the hydroxyl group, the conformation of the pyrrolidine ring is not the same as that of L-pro. Hence, the intermediate of the HO–L-pro-complex is not able to take the same hydrogen-bonding structure as that of the L-pro-complex. The most plausible hydrogen bonding in the HO-L-pro-complex is shown in Fig. 10, together with that of the L-pro-complex. In the case of the HO-L-pro-complex, the proton, H_a in Fig. 10, can transfer either of the two phenolic oxygen atoms. Thus, the kinetic stereoselectivity becomes lower than that for the L-pro-complex. In the case of *allo*-HO-L-pro, as is shown in Fig. 11, since an intramolecular hydrogen bonding between the hydroxyl group and the carboxylato group is possible, its pyrrolidine ring takes the same conformation as that for the HO-L-pro-complex. Therefore, the kinetic stereoselectivity for the *allo*-HO-L-pro-complex may become much lower than that for the L-pro-complex.

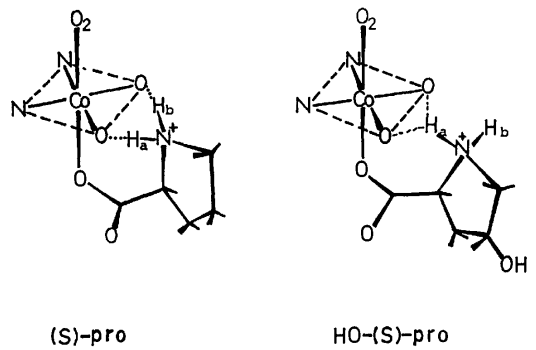

Fig. 10. The hydrogen bonding structure of the reaction intermediates for L-proline and HO-L-proline.

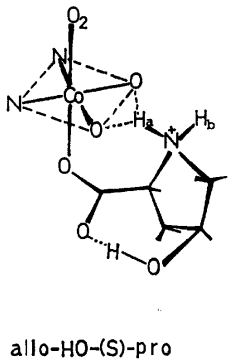

Fig. 11. The proposed structure of the reaction intermediate for *allo*-HO-L-proline.

Regarding the isomerization mechanism between *Λ-* and *Δ-cis-*β_2-isomers, a study is now underway; we have already obtained the reliable experimental result that the isomerization proceeds through a five-coordinated intermediate, [Co(α-Me-sal$_2$en)(OOC–CHR–NH_2)]. This study will be reported in the near future.

The authors wish to express their deep thanks to Professor J. Hidaka of Tsukuba University and to Professor K. Sone and Dr. Y. Fukuda of Ochanomizu University for their kind assistance in the CD spectral measurements. This work was supported in part by a Science Research Grant from the Ministry of Education, Science and Culture, Japan (No. 547038).

References

1) M. Saburi, S. Yoshikawa, and M. Shibata, "The Coordination Stereochemistry of Octahedron," Kagaku Sosetsu, **13**, Gakkai Shuppan Center, pp. 109 and 134 (1976). Other references are cited therein.

2) H. Takenaka and M. Shibata, *Bull. Chem. Soc. Jpn.*, **49**, 2133 (1976).

3) Y. Fujii, T. Isago, M. Sano, N. Yanagibashi, S. Hirasawa, and S. Takahashi, *Bull. Chem. Soc. Jpn.*, **49**, 3509 (1976).

4) Y. Fujii, M. Sano, and Y. Nakano, *Bull. Chem. Soc. Jpn.*, **50**, 2609 (1977).

5) S. Yoshikawa, M. Saburi, and M. Yamaguchi, *Pure Appl. Chem.*, **50**, 915 (1978); M. Yamaguchi, S. Yamamatsu, T. Furusawa, S. Yano, M. Saburi, and S. Yoshikawa, *Inorg. Chem.*, **19**, 2010 (1980).

6) M. Okabayashi, K. Igi, and J. Hidaka, *Bull. Chem. Soc. Jpn.*, **52**, 753 (1979).

7) R. C. Job and T. C. Bruice, *J. Am. Chem. Soc.*, **100**, 5089 (1978).

8) J. H. Dunlop, R. D. Gillard, N. C. Payne, and G. B. Robertson, *J. Chem. Soc., Chem. Commun.*, **1966**, 784.

9) J. H. Dunlop, R. D. Gillard, and N. C. Payne, *J. Chem. Soc., A*, **1967**, 1469.

10) R. D. Gillard, N. C. Payne, and G. B. Robertson, *J. Chem. Soc., A*, **1970**, 2579.

11) R. D. Gillard, R. Maskill, and A. Pasini, *J. Chem. Soc., A*, **1971**, 2268.

12) J. I. Legg and J. Steele, *Inorg. Chem.*, **10**, 2177 (1971).

13) D. A. Buckingham, J. Dekkers, A. M. Sargeson, and L. G. Marzilli, *Inorg. Chem.*, **12**, 1207 (1973).

14) D. E. Allen and R. D. Gillard, *J. Chem. Soc., Chem. Commun.*, **1967**, 1091.

15) D. A. Buckingham, I. E. Maxwell, and A. M. Sargeson, *J. Chem. Soc., Chem. Commun.*, **1969**. 581.

16) D. A. Buckingham, L. G. Marzilli, I. E. Maxwell, A. M. Sargeson, and H. C. Freeman, *J. Chem. Soc., Chem. Commun.*, **1969**, 583; D. A. Buckingham, I. E. Maxwell, A. M. Sargeson, and M. R. Snow, *J. Am. Chem. Soc.*, **92**, 3617 (1970).

17) R. G. Asperger and C. F. Liu, *Inorg. Chem.*, **6**, 796 (1967).

18) R. C. Job and J. C. Bruice, *J. Am. Chem. Soc.*, **96**, 809 (1974).

19) Y. Fujii, T. Isago, and M. Sano, *Chem. Lett.*, **1975**, 1299.

20) In previous papers,[3,4,19] the *cis*-β_1-structure was assigned tentatively to the [Co(Schiff base)(amino acid)] complex; however, it has been found recently, in our X-ray study for $(-)_{435}$-[Co(α-Me-sal$_2$en)(L-ileu)]·1.5H$_2$O, that the complex takes the *cis*-β_2-structure: Y. Kushi, R. Tamura, M. Kuramoto, T. Yoshizawa, H. Yoneda, and Y. Fujii, *J. Chem. Soc., Chem. Commun.*, **1978**, 266. Since the CD spectrum of the complex in solution is identical with that in the solid state, the *cis*-β_2-structure can be assigned also to the complex in solution.

21) M. Saburi, M. Homma, and S. Yoshikawa, *Inorg. Chem.*, **8**, 367 (1969).

22) C. T. Lin and B. E. Douglas, *Inorg. Chem. Acta*, **4**, 3 (1970).

23) M. H. Ghandehari, T. N. Anderson, D. R. Boone, and H. Eyring, *J. Am. Chem. Soc.*, **92**, 6466 (1970).

24) D. A. Buckingham, J. Dekkers, A. M. Sargeson, and M. Wein, *Inorg. Chem.*, **12**, 2019 (1973).

25) In this paper, the following abbreviations are used: L-ala=L-alanine, L-val=L-valine, L-met=L-methionine, L-ileu=L-isoleucine, L-phe=L-phenylalanine, L-trp=L-tryptophan, L-pro=L-proline, HO-L-pro=hydroxy-L-proline, *allo*-HO-L-pro=*allo*-hydroxy-L-proliue, N-benzyl-L-ala=*N*-benzyl-L-alanine, and *N*-methyl-L-ala=*N*-methyl-L-alanine.

26) A. Biggoto, G. Costa, G. Mestroni, G. Pellizer, A. Puxeddu, E. Reisenhofer, L. Stefani, and G. Tauzher, *Inorg. Chem. Acta Reviews*, **4**, 41 (1970).

27) Will be published elsewhere.

28) H. Ogino and K. Ogino, "Coordination Chemistry of Metalloenzymes," Nankodo, Tokyo (1974), p. 55.

29) A. Nishinaga, "Bioinorganic Chemistry," Kagakudojin, Kyoto (1974), p. 179.

30) G. Amiconi, M. Brunori, E. Autonini, G. Tauzer, and G. Costa, *Nature*, **228**, 549 (1970).

31) A. L. Crumbliss and F. Basolo, *J. Am. Chem. Soc.*, **92**, 55 (1970).

32) Y. Fujii, A. Osawa, Y. Furukawa, F. Ebina, and S. Takahashi, *Bull. Chem. Soc. Jpn.*, **45**, 2459 (1972).

33) J. R. Thornback and G. Wilkinson, *J. Chem. Soc., Dalton Trans.*, **1978**, 110.

Configurations of Solvated Complex Ions of First Transition Metals in Hexamethylphosphoric Triamide as Inferred from Their Absorption Spectra and Stokes Radii

Yuriko ABE* and Goro WADA
Department of Chemistry, Nara Women's University, Nara 630
(Received April 10, 1980)

The absorption spectra and Stokes radii of solvated complex ions of first transition metals (Mn(II), Fe(II), Co(II), Ni(II), Cu(II), and Zn(II)) were observed in hexamethylphosphoric triamide (HMPA) in order to determine their configurations. It seems that the Stokes radii of complex ions are sensitive to the configurational change, since the diameter of an HMPA molecule is very large as compared with the crystallographic diameters of central metal ions. As to the result, metal ions are tetrahedrally solvated in the cases of Mn(II), Fe(II), Co(II), and Cu(II), while in the case of Ni(II), equilibria are established among octahedral, square planar and tetrahedral solvated species. Zn(II) forms probably a complex ion solvated octahedrally by HMPA.

Syntheses of the transition metal complexes with hexamethylphosphoric triamide (HMPA), and their solid state stereochemistries have been investigated by many workers.[1] In these solid complexes HMPA tends to form tetrahedral configuration around metal ions, when anions such as ClO_4^-, $B(C_6H_5)_4^-$, SCN^-, NO_3^-, SO_4^{2-}, and halide ions, are outside of the coordination sphere, or when some of them are in the coordination sphere as unidentate ligands.[1-4] But when metal ions are coordinated with anions such as NO_3^-, SO_4^{2-}, and CH_3COO^- ions as multidentate ligands, octahedral or square planar configurations are mostly preferred according to the nature of metal ions.[1,4] On the other hand, in nitromethane solution,[2,3,5] the complexes $[M^{II}(hmpa)_4](ClO_4)_2$ formed are mostly tetrahedral when M^{II} is Mn^{II}, Fe^{II}, Co^{II}, Cu^{II}, or Zn^{II}, but not so when it is Ni^{II}.

In HMPA solutions, the stereochemistry of the solvated complex ions of the first transition metals has not been reported yet except for the case of Co(II).[6] In the present study, the absorption spectra and Stokes radii of solvated complex ions of the first transition metals in HMPA were observed in order to determine their configurations. It seems that the Stokes radii are sensitive to the configurational change of solvated complex ions, since the diameter of an HMPA molecule is very large as compared with the crystallographic radii of the central metal ions.

Experimental

Materials. Commercial HMPA of guaranteed reagent grade was distilled under a reduced nitrogen atmosphere of 3 mmHg at 70—80 °C after it had been dried over barium oxide and a small amount of peroxide accidentally contained in HMPA had been decomposed by iron(II) chloride. The distilled HMPA was deoxygenated by passing nitrogen, and then stored in a dark and cool room. Nitromethane was dried over calcium chloride and distilled under atmospheric pressure. Complexes of various metal ions $[M^{II}(hmpa)_4](ClO_4)_2$ ($M^{II}=Mn^{II}$, Fe^{II}, Co^{II}, Ni^{II}, Cu^{II}, or Zn^{II}) were synthesized according to the methods reported by Donoghue and Drago.[2,3] Stock solutions of these metal complexes were prepared, and portions of them were used for the spectrophotometric or conductivity determinations. Anhydrous sodium perchlorate was prepared by heating monohydrous salt which had been recrystallized twice from water.

Procedure. For the determination of absorption spectra, a Hitachi Recording Spectrophotometer Model EPS-3T was used with a thermostated cell. The metal ion concentrations in stock solutions were determined spectrophotometrically by the following methods; Mn(II): formaldoxime method[7] (molar absorptivity $\varepsilon=1.040\times10^4$ M^{-1} cm^{-1} at 450 nm); Fe(II): 2,2'-bipyridine method[8] ($\varepsilon=9.205\times10^3$ M^{-1} cm^{-1} at 522 nm); Co(II): nitroso-R salt method[8] ($\varepsilon=9.350\times10^3$ M^{-1} cm^{-1} at 550 nm); Ni(II): dimethylglyoxime method[8] ($\varepsilon=1.457\times10^4$ M^{-1} cm^{-1} at 450 nm); Cu(II): sodium diethyldithiocarbamate method[8] ($\varepsilon=9.223\times10^3$ M^{-1} cm^{-1} at 430 nm); Zn(II): zincone method[7] ($\varepsilon=2.341\times10^4$ M^{-1} cm^{-1} at 620 nm). (1 M = 1 mol dm^{-3}.)

The measurements of electric conductivities of HMPA solutions containing complex ions were performed with a Yanagimoto Conductivity Apparatus Model MY-8. The cell used was calibrated with a 0.01 M aqueous KCl solution.

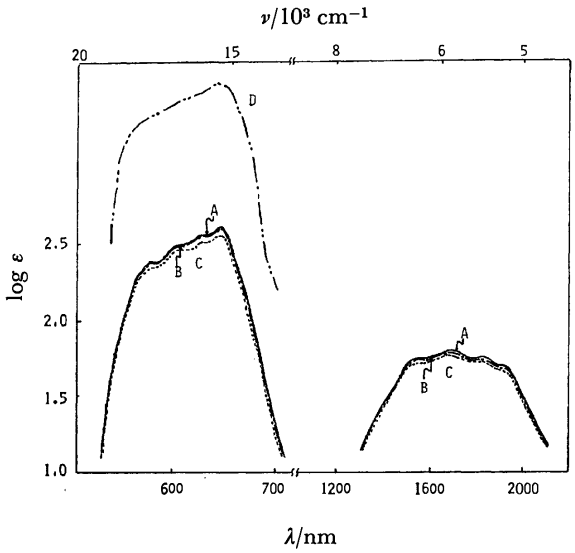

Fig. 1. Absorption spectra of solvated Co^{2+} ion in HMPA and $[Co(hmpa)_4]^{2+}$ ion in nitromethane at 25 °C.
A(——): $[[Co(hmpa)_4]^{2+}]=8.0\times10^{-4}$ M in HMPA, B(---): $[[Co(hmpa)_4]^{2+}]=8.0\times10^{-4}$ M and $[HMPA]_0=0.5$ M in nitromethane, C(——): $[[Co(hmpa)_4]^{2+}]=8.0\times10^{-4}$ M in nitromethane,[2] D(----): the solid reflectance spectrum[2] of $[Co(hmpa)_4](ClO_4)_2$, ordinate in arbitrary scale.

Results

The absorption spectra of the solvated Co^{2+} ion in HMPA, and $[Co(hmpa)_4]^{2+}$ in nitromethane are shown in Fig. 1. Figure 2 shows the absorption spectra of solvated Ni^{2+} ion, which change remarkably with temperature. The absorption spectra of the solvated Cu^{2+} ion in HMPA, and $[Cu(hmpa)_4]^{2+}$ in nitromethane are shown in Fig. 3.

The plots of the equivalent conductivities of various

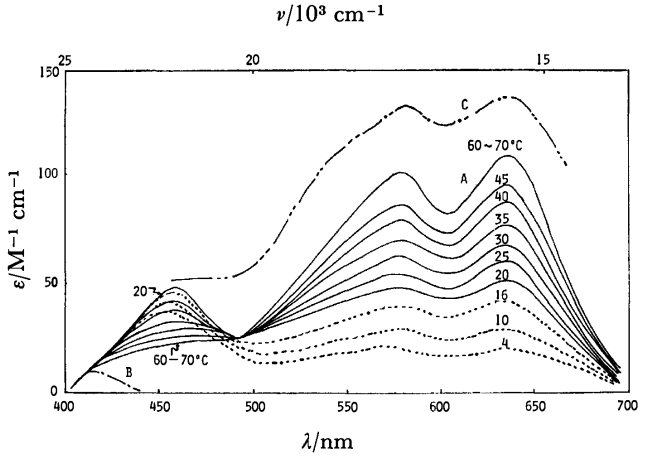

Fig. 2. Absorption spectra of solvated Ni^{2+} ion in HMPA at various temperatures.
A(—— and ----): $[Ni(II)]=4.1\times10^{-3}$ M in HMPA, B(— — —): $[[Ni(dmso)_6]^{2+}]=4.1\times10^{-3}$ M in DMSO. C(—·—·—): the solid reflectance spectrum[2] of $[Ni(hmpa)_4](ClO_4)_2$, ordinate in arbitrary scale.

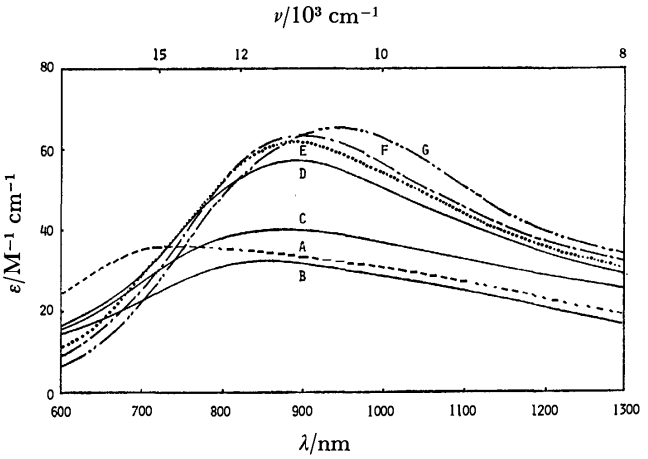

Fig. 3. Absorption spectra of solvated Cu^{2+} ion in HMPA and $[Cu(hmpa)_4]^{2+}$ ion in nitromethane.
A(----): $[[Cu(hmpa)_4]^{2+}]=2.0\times10^{-3}$ M in nitromethane, B(——): $[[Cu(hmap)_4]^{2+}]=2.0\times10^{-3}$ M and $[HMPA]_0=1.0\times10^{-2}$ M in nitromethane, C(——): $[[Cu(hmpa)_4]^{2+}]=2.0\times10^{-3}$ M and $[HMPA]_0=1.0\times10^{-1}$ M in nitromethane, D(——): $[[Cu(hmpa)_4]^{2+}]=2.0\times10^{-3}$ M and $[HMPA]_0=5.0\times10^{-1}$ M in nitromethane, E(——): $[[Cu(hmpa)_4]^{2+}]=2.0\times10^{-3}$ M and $[HMPA]_0=1.0$ M in nitromethane, F(——): $[[Cu(hmpa)_4]^{2+}]=2.0\times10^{-3}$ M and $[HMPA]_0=2.0$ M in nitromethane, G(— — —): $[[Cu(hmpa)_4]^{2+}]=2.0\times10^{-3}$ M in HMPA (5.8 M).

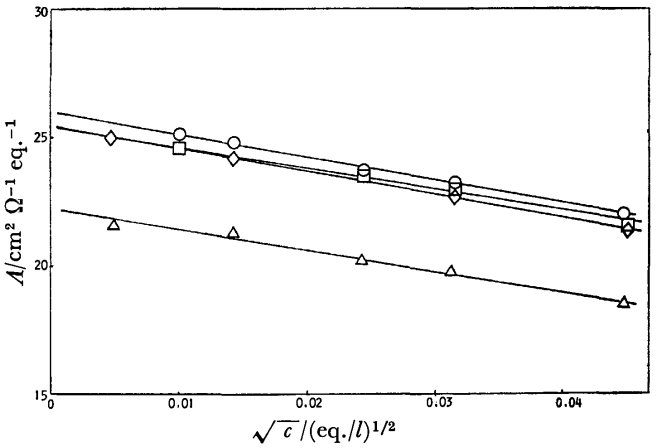

Fig. 4. Relationships of equivalent conductivities of complex perchlorates *vs.* square roots of equivalent concentrations in HMPA at 25 °C.
◇: Solvated Co^{2+} ion, ○: solvated Fe^{2+} ion, □: solvated Cu^{2+} ion, △: solvated Zn^{2+} ion.

complex perchlorates in HMPA (Λ) against the square roots of the equivalent concentrations ($\sqrt{c}$) give straight lines with negative slopes as shown in Fig. 4. Consequently, Eq. 1 holds for these salts;

$$\Lambda = \Lambda_0 - k\sqrt{c}, \tag{1}$$

where Λ_0 is a limiting equivalent conductivity and k is an empirical constant. The limiting equivalent ionic conductivity of a solvated cation (λ_0^+) is obtained by subtracting that of perchlorate ion ($\lambda_0^-=15.5$ cm² Ω^{-1} eq.$^{-1}$)[9] from Λ_0. Then, the Stokes radius of the solvated cation (r^+) can be calculated by Eq. 2:

$$r^+ = \frac{0.82|z|}{\lambda_0^+\eta} \tag{2}$$

where η is the viscosity of HMPA ($\eta=0.0323$ poise at 25 °C)[10,11] and z is the number of electric charges on the solvated cation ($z=2$). The values of Λ_0, λ_0^+, and r^+ thus obtained are listed in Table 1.

Table 1. Limiting equivalent conductivities and Stokes radii of solvated metal ions in HMPA at 25 °C

Ion	Λ_0[a] / cm² Ω^{-1} eq.$^{-1}$	λ_0^+ / cm² Ω^{-1} eq.$^{-1}$	Stokes radius r^+ / Å
Mn^{2+}	24.80	9.30	5.47
Fe^{2+}	25.65	10.15	5.00
Co^{2+}	25.58	10.08	5.03
Ni^{2+}	23.40	7.90	6.43
Cu^{2+}	25.31	9.81	5.17
Zn^{2+}	22.20	6.70	7.59

a) Values for complex perchlorates.

Discussion

Configuration of Solvated Co^{2+} Ion in HMPA. In Fig. 1 are shown the absorption spectra of solvated Co^{2+} ion in pure HMPA (Curve A) and of $[Co(hmpa)_4]^{2+}$ in nitromethane at $[[Co(hmpa)_4]^{2+}]=8.0\times10^{-4}$ M and $[HMPA]_0=0.5$ M (Curve B). The

latter absorption spectrum is in good agreement with that obtained in nitromethane by Donoghue and Drago,[2] which is also shown (Curve C) in Fig. 1. These three spectral patterns are similar to that of the solid reflectance spectrum of $[Co(hmpa)_4](ClO_4)_2$ (Curve D), which was reported to be tetrahedral.[2] Therefore, it can be reasonably deduced that the solvated Co^{2+} ion in HMPA is regularly tetrahedral.

In general,[12] the absorption bands due to $\nu_2(^4T_1(F)\leftarrow{}^4A_2)$ and $\nu_3(^4T_1(P)\leftarrow{}^4A_2)$ transitions of tetrahedral cobalt(II) complexes appear in the near-infrared and visible regions, respectively. The molar absorptivities of these bands are of the magnitude of 10—100 M^{-1} cm^{-1} for ν_2 and 100—2000 M^{-1} cm^{-1} for ν_3, respectively. But bands of octahedral cobalt(II) complexes such as $[Co(H_2O)_6]^{2+}$, $[Co(dmso)_6]^{2+}$, $[Co(pyo)_6]^{2+}$ (pyo= pyridine oxide), and $[Co(NH_3)_6]^{2+}$ are observed in the visible region near 500 nm (ε=5—40 M^{-1} cm^{-1}). These bands allow a fairly clear-cut distinction between tetrahedral and octahedral cobalt(II) complexes. Thus, the characteristics of the absorption spectrum of solvated Co^{2+} ion in HMPA coincide with those of the tetrahedral Co(II) complexes. Moreover, the absorption spectrum in HMPA is not affected by temperature. Therefore, it is deduced that no tetrahedral↔octahedral configurational transition of the complex ion exists. Accordingly, it is concluded that the only solvated Co^{2+} ion in HMPA is the tetrahedral $[Co(hmpa)_4]^{2+}$ ion.

The conductivity measurements of HMPA solutions containing $[Co(hmpa)_4]^{2+}$ in the concentration range 10^{-5}—10^{-3} M give the linear relationships as shown in Fig. 4. This shows clearly that $[Co(hmpa)_4]^{2+}$ in HMPA forms no ion-pair, because no deviation from the linearity is seen to occur. The perchlorates $[M^{II}(hmpa)_4](ClO_4)_2$ of other first transition metals also dissociate completely in HMPA.

The value of the Stokes radius (r^+) of tetrahedral $[Co(hmpa)_4]^{2+}$ ion was found to be 5.03 Å. Since an HMPA molecule coordinated to a divalent metal ion is very bulky as compared with the central metal ion, small differences of the crystallographic radii among the divalent metal ions would have little influence on the Stokes radii of the complexes $[M^{II}(hmpa)_4]^{2+}$. Accordingly, when HMPA molecules are tetrahedrally coordinated to the metal ions, it will be reasonable to assume that the values of their Stokes radii are all about 5 Å, irrespective of the kind of the central metal ions.

Configuration of Solvated Ni^{2+} Ion in HMPA. Figure 2 shows the temperature dependence of the absorption spectra of solvated Ni^{2+} ion in HMPA. The spectral change is no longer observed above 60 °C and the final spectrum agrees very closely with that of the solid reflectance spectrum of the tetrahedral $[Ni(hmpa)_4](ClO_4)_2$.[2] Since an isosbestic point appears at 490 nm above 20 °C, the solvated Ni^{2+} ion is supposed to be in equilibrium between two different configurations in HMPA. At 60—70 °C, the solvated Ni^{2+} ions are completely tetrahedral. Below 20 °C, the spectra do not pass through the isosbestic point which appears above 20 °C but approach to that of the octahedral $[Ni(dmso)_6]^{2+}$.[12] Accordingly, the following equilibria seem to exist.

$$\underset{\text{octahedral}}{[Ni(hmpa)_6]^{2+}} \overset{K_2}{\rightleftharpoons} \underset{\text{square planar}}{[Ni(hmpa)_4]^{2+}} \overset{K_1}{\rightleftharpoons} \underset{\text{tetrahedral}}{[Ni(hmpa)_4]^{2+}} \quad (3)$$

The value of ΔH_1 of the reaction from the square planar to tetrahedral configuration is obtained by Eq. 4;

$$\frac{d \ln K_1}{d\ T^{-1}} = d \ln \frac{c\Delta\varepsilon - \Delta A}{\Delta A} \Big/ d\ T^{-1} = -\frac{\Delta H_1}{R} \quad (4)$$

$$\Delta\varepsilon = \varepsilon_t^{633} - \varepsilon_p^{633}$$

$$\Delta A = A_t - A$$

in which ε_t^{633}(=106 M^{-1} cm^{-1}) and ε_p^{633} stand for the molar absorptivities of the tetrahedral and square planar complexes at 633 nm, respectively, A_t and A are absorbances at 60—70 °C and at a certain temperature between 20 °C and 60 °C at 633 nm, respectively, and c is total concentration of Ni(II).

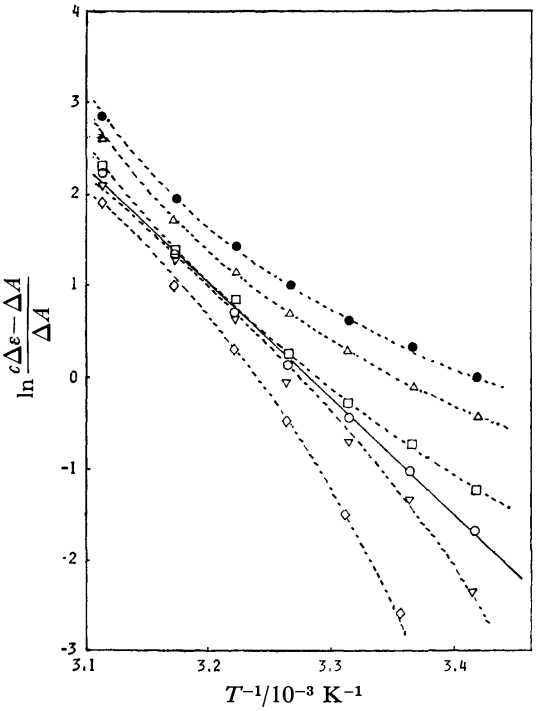

Fig. 5. The plots of $\ln\frac{c\Delta\varepsilon-\Delta A}{\Delta A}$ *vs.* T^{-1} with various values for ε_p^{633}.
ε_p^{633}: ●; 0 M^{-1} cm^{-1}, △; 20 M^{-1} cm^{-1}, □; 40 M^{-1} cm^{-1}, ○; 45 M^{-1} cm^{-1}, ▽; 50 M^{-1} cm^{-1}, ◇; 60 M^{-1} cm^{-1}.

Figure 5 shows the linear relationship between $\ln[(c\Delta\varepsilon-\Delta A)/\Delta A]$ *vs.* T^{-1} according to Eq. 4. When ε_p^{633}=45 M^{-1} cm^{-1} is used, a straight line which satisfies Eq. 4 best can be drawn. Thus, the following results are obtained: ΔH_1=25.1 kcal mol^{-1}, ΔS_1=83 cal K^{-1} mol^{-1}, and ΔG_1=0.6 kcal mol^{-1} at 25 °C (1 cal=4.2 J).

The value of ΔH_2 for the reaction from the octahedral to the square planar configuration is obtained by Eq. 5;

$$\frac{d \ln K_2}{d\ T^{-1}} = d \ln \frac{-(c\varepsilon_o^{633} - A)}{K_1(c\varepsilon_t^{633} - A) + (c\varepsilon_p^{633} - A)} \Big/ d\ T^{-1}$$

$$= -\frac{\Delta H_2}{R} \quad (5)$$

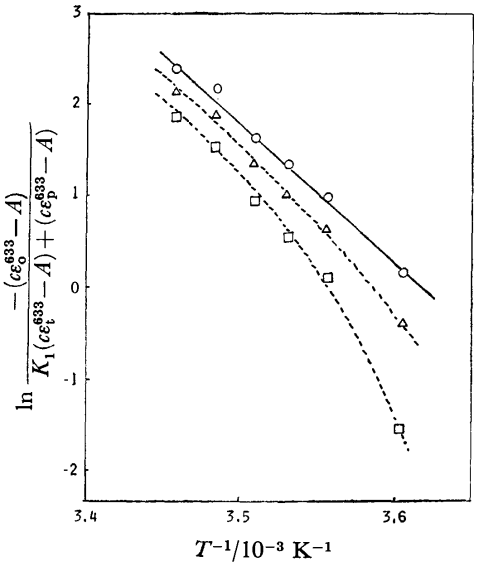

Fig. 6. The plots of $\ln \frac{-(c\varepsilon_o^{633}-A)}{K_1(c\varepsilon_t^{633}-A)+(c\varepsilon_p^{633}-A)}$ *vs.* $1/T$ with various values for ε_o^{633}.
ε_o^{633}: ○; 0 M^{-1} cm^{-1}, △; 10 M^{-1} cm^{-1}, □; 20 M^{-1} cm^{-1}.

where ε_o^{633} is the molar absorptivity of the octahedral configuration at 633 nm. A value $\varepsilon_o^{633}=0$ M^{-1} cm^{-1} satisfies Eq. 5 best as shown in Fig. 6. Therefore, the thermodynamic functions are obtained as follows: $\Delta H_2=27.8$ kcal mol^{-1}, $\Delta S_2=101$ cal K^{-1} mol^{-1}, and $\Delta G_2=0.8$ kcal mol^{-1} at 25 °C.

In general,[12] tetrahedral Ni(II) complexes exhibit a visible band near 600—700 nm (ε: 100—200 M^{-1}cm^{-1}) assignable to $^3T_1(P)\leftarrow{}^3T_1(\nu_3)$ transition and a near-infrared band near 1250 nm (ε: 20 M^{-1} cm^{-1}) assignable to $^3A_2\leftarrow{}^3T_1$ (ν_2) transition. On the other hand, octahedral Ni(II) complexes exhibit visible absorption bands of lower molar absorptivities, (ε: about 1—10 M^{-1} cm^{-1}), while square planar Ni(II) complexes show stronger bands in the visible region (ε: 50—500 M^{-1} cm^{-1}). Consequently, the spectral patterns of the tetrahedral, square planar and octahedral complexes observed are quite reasonable ones, and support the explanation of the solution equilibria proposed above.

The Stokes radius of the solvated Ni^{2+} ion in HMPA is 6.43 Å at 25 °C, at which temperature, the equilibrium of the solvated Ni^{2+} ion between the square planar and tetrahedral configurations is established. Since ΔS_1 value of this reaction is a large positive one, the tetrahedral complex seems to be less strongly solvated than the square planar complex is, although the coordination numbers of both complexes are the same. This may be the reason why the average value of the Stokes radius of solvated Ni^{2+} ion in HMPA at 25 °C is larger than 5 Å expected from the tetrahedral configuration.

ΔS_2 value for the reaction from the octahedral to square planar configuration is a larger positive one than that observed in a similar reaction from the octahedral to square planar configuration,[13] since the HMPA molecules are so closely packed in the coordination sphere of the octahedral complex that the rotational degree of freedom of HMPA is much reduced.

Configuration of Solvated Cu^{2+} Ion in HMPA. A broad absorption maximum near 720 nm in the spectrum at $[[Cu(hmpa)_4]^{2+}]=2.0\times10^{-3}$ M in nitromethane (Curve A) agrees with that obtained by Donoghue and Drago[2] in Fig. 3. In nitromethane at $[HMPA]_0=1.0\times10^{-2}$ M (Curve B), the absorption maximum appears near 850 nm and its peak is lower than that in pure nitromethane. In the $[HMPA]_0$ range 0.1—0.5 M, the absorption maxima shift to longer wavelength, and their peaks become higher (Curves C and D). In nitromethane of the $[HMPA]_0$ range 1.0—2.0 M and in pure HMPA (5.8 M), the absorption spectra shift further to longer wavelength with only slight absorbance changes (Curves E, F, and G).

In nitromethane, $[Cu(hmpa)_4]^{2+}$ is square planar because its absorption spectrum resembles that[14] of square planar $[Cu(Ph_3PO)_4]^{2+}$. When a small amount of HMPA is added to nitromethane, the Cu(II) complex in the solution seems to become tetragonal with HMPA molecules coordinated along the z axis of the square planar complex. The changes in the absorption spectra in the $[HMPA]_0$ range 0.1—0.5 M suggest that a tetragonal↔distorted tetrahedral transition is in equilibrium, and that the changes in the solvent properties due to excess HMPA merely shift this equilibrium. According to Wayland and Drago,[5] the NMR contact shifts are independent of HMPA concentrations in the $[HMPA]_0$ range 0.5—1.5 M. Consequently, $[Cu(hmpa)_4]^{2+}$ becomes only distorted tetrahedral at $[HMPA]_0=1.0$ M. In nitromethane of the HMPA concentrations higher than 1.0 M and in pure HMPA, it seems that the change in the absorption spectrum is not due to the change in the coordination number or in the configuration, but due to that in the degree of distortion of the complex. Liehr theoretically predicted[15] that regularly tetrahedral Cu(II) complexes would show an electronic transition in the near-infrared region but not in the visible one. Accordingly, the distorted tetrahedral $[Cu(hmpa)_4]^{2+}$ at $[HMPA]_0=1.0$ M is gradually liberated from distortion at the HMPA concentrations higher than 1.0 M in nitromethane and finally becoming nearly regular tetrahedral in pure HMPA (5.8 M). The Stokes radius of $[Cu(hmpa)_4]^{2+}$ ion in HMPA, 5.17 Å, supports this deduction. If the solvated Cu^{2+} ion is either square planar or tetragonal in HMPA, the Stokes radius would be larger than 5 Å expected from the tetrahedral configuration. This problem has been discussed at the previous section on the solvated Ni^{2+} ion.

Configurations of Solvated Fe^{2+}, Mn^{2+}, and Zn^{2+} Ions in HMPA. The values of log ε of solvated Fe^{2+} and Mn^{2+} ions in HMPA are 2.6 at 400 nm and −0.002 at 412 nm, respectively, while those of $[Fe(hmpa)_4]^{2+}$ and $[Mn(hmpa)_4]^{2+}$ in nitromethane are 2.6 and −0.002 at the same wavelengths, respectively. These values agree with those of the tetrahedral $[Fe(hmpa)_4]^{2+}$ and the tetrahedral $[Mn(hmpa)_4]^{2+}$ ions in nitromethane reported by Donoghue and Drago.[3] Therefore, it is concluded that solvated Fe^{2+} and Mn^{2+} ions in HMPA are $[Fe(hmpa)_4]^{2+}$ and $[Mn(hmpa)_4]^{2+}$ ions. Stokes radii of solvated Fe^{2+} and Mn^{2+} ions in HMPA are 5.00 Å and 5.47 Å, respectively (Table 1), suggesting

that they are both tetrahedral.

The configuration of solvated Zn^{2+} ion in HMPA can not be decided from the absorption spectrum. The Stokes radius of solvated Zn^{2+} ion in HMPA is 7.5 Å which is 2.5 Å larger than 5 Å expected for the tetrahedral configuration. Consequently, solvated Zn^{2+} ion in HMPA is probably octahedral. This is supported by the complex formation constants of Zn^{2+} ion with HMPA and with bpy; the details on this point will be published later.

General Discussion. Complexes of the first transition metal ions $[M^{II}(hmpa)_4](ClO_4)_2$ (M^{II}=Mn^{II}, Fe^{II}, Co^{II}, Ni^{II}, Cu^{II}, or Zn^{II}) are tetrahedral in nitromethane except for Ni(II) and Cu(II) complexes, although they are all known to be tetrahedral in the solid states.[2,3,5] In HMPA, the Mn(II), Fe(II), Co(II), and Cu(II) ions are tetrahedrally solvated by HMPA, while Ni(II) establishes equilibria among solvated complexes of the octahedral, square planar and tetrahedral configurations. Zn(II) forms probably an octahedrally solvated complex.

In dimethyl sulfoxide (DMSO) and *N,N*-dimethylformamide (DMF), solvated complex ions of the first transition metals are mostly octahedral. Since an HMPA molecule is very bulky as compared with DMSO and DMF, it seems that solvated complex ions in HMPA prefer the tetrahedral configurations to the octahedral ones.

Although Libuś and Uruska describe that the first transition metal complexes tend to be tetrahedral in solutions according to the differences between the crystal field stabilization energies (c.f.s.e.) of the octahedral and the tetrahedral configurations in the following order: Mn(II)~Zn(II)>Fe(II)>Co(II)>Cu(II)>Ni(II),[16] Zn(II) prefers the octahedral configuration in HMPA. Since Zn(II) has no c.f.s.e. in its complexes, it may be better to put it at the last in the sequence in the present case.

References

1) M. W. G. De Bolster and W. L. Groeneveld, *Recl. Trav. Chim. Pays-Bas*, **90**, 477 (1971).
2) J. T. Donoghue and R. S. Drago, *Inorg. Chem.*, **1**, 866 (1962).
3) J. T. Donoghue and R. S. Drago, *Inorg. Chem.*, **2**, 1158 (1963).
4) J. T. Donoghue and R. S. Drago, *Inorg. Chem.*, **2**, 572 (1963).
5) B. B. Wayland and R. S. Drago, *J. Am. Chem. Soc.*, **87**, 2372 (1965).
6) V. Gutmann, A. Weisz, and W. Kerber, *Monatsh. Chem.*, **100**, 2096 (1969).
7) "Japanese Industrial Standards; Testing Methods for Industrial Waste Water," ed by M. Tahara, Japanese Standards Association, Tokyo (1974), pp. 113 and 136.
8) G. Muto, "Hishoku Bunseki-ho," Kyoritsu Shuppan, Tokyo (1952), Chap. 8.
9) C. Atlani, J. C. Justice, M. Quintin, and J. E. Dubois, *J. Chim. Phys.*, **66**, 180 (1969).
10) T. Fujinaga, K. Izutsu, and S. Sakura, *Nippon Kagaku Zasshi*, **1973**, 191.
11) T. Fujinaga and S. Sakura, *Nippon Kagaku Zasshi*, **1977**, 135.
12) A. B. P. Lever, "Inorganic Electronic Spectroscopy," Elsevier Publishing Company, Amsterdam (1968), Chap. 9.
13) N. Iwasaki, K. Sone, and Y. Fukuda, *Z. Anorg. Allg. Chem.*, **412**, 170 (1975).
14) E. Bannister and F. A. Cotton, *J. Chem. Soc.*, **1960**, 1878.
15) A. D. Liehr, *J. Phys. Chem.*, **64**, 43 (1960).
16) W. Libuś and I. Uruska, *Inorg. Chem.*, **5**, 256 (1966).

 © 1980 The Chemical Society of Japan Bull. Chem. Soc. Jpn., 53, 3552—3559 (1980)

Studies of Inorganic Ion Exchangers. V.[1] The Preparation of the Granulated Product from Titanium(IV) Bis(hydrogenphosphate) and Carbonaceous Materials, and Its Ion-exchange Properties

Etsuro KOBAYASHI* and Tadao KANAYAMA

National Chemical Laboratory for Industry, Yatabemachi, Tsukuba-gun, Ibaraki 305

(Received April 12, 1980)

In order to develop an inorganic ion exchanger for industrial use, a mixture of titanium(IV) bis(hydrogenphosphate), a carbonaceous material (sugar, flour, or sodium ligninsulfonate), and an additive (H_2SO_4 or H_3PO_4) was sintered, and the resultant sintered product was crushed to obtain a granulated product, the ion-exchange property of which was then investigated. The mixing ratio of the titanium phosphate to the carbonaceous material has an influence on the ion-exchange capacity and the durability of the granulated product. In consideration of this influence, the weight ratio of the titanium phosphate to carbon included in the carbonaceous material was expediently chosen as 1 : 0.5. The acid additives promoted the carbonization of the carbonaceous material, whereby the sintered product of porosity was obtained. The weight ratio of the carbonaceous part to the titanium phosphate in the product decreased with an increase in the temperature within the range from 185 to 350 °C. In a batch method, a granulated product including $Ti(HPO_4)_2 \cdot H_2O$ adsorbed Na^+, but not K^+. A granulated product including $Ti(HPO_4)_2 \cdot 1/2H_2O$, however, adsorbed these ions, the equilibrium ion-exchange capacities toward Na^+ and K^+ being 1.28—1.78 and 1.56—2.34 meq/g respectively, and the selectivity quotient and the distribution coefficient toward K^+ showed larger values than those toward Na^+. In a column method, when a NaCl (26.66 g/l)-KCl (0.67 g/l) aqueous solution flowed into a column which had been packed with the granulated product (5 g) including the hemihydrate, the ion-exchange capacities of this granulated product toward Na^+ and K^+ were 1.1—1.2 and 0.38—0.58 meq/g, respectively, showing the separation factor (α_{Na}^{K}) of 18—25. When artificial brackish water also flowed into the column, very small quantities of the Mg^{2+} and Ca^{2+} were adsorbed; consequently, a selective ion-exchange property of the granulated product toward K^+ was recognized. Also, the carbonaceous part in the granulated product adsorbed such coloring matter as Methylene Blue.

Some phosphates of multivalent metals are known as inorganic ion-exchangers; among them, zirconium phosphate is used as a typical inorganic ion-exchanger in the field of analytical chemistry. With a view to developing inorganic ion-exchangers for industrial use, our attention was paid to titanium phosphate, which is almost equivalent in stability to zirconium phosphate and which is rather cheap as a raw material. Our studies revealed that titanium(IV) bis(hydrogenphosphate) 0—1/2 hydrate [$Ti(HPO_4)_2 \cdot 0—1/2H_2O$],[2] with an X-ray diffraction pattern quite different from that of the known titanium(IV) bis(hydrogenphosphate) monohydrate [$Ti(HPO_4)_2 \cdot H_2O$],[3] could be prepared by refluxing various titanium compounds with concentrated phosphoric acid and that titanium(IV) bis(hydrogenphosphate) 0—1/2 hydrate had a unique ion-exchange property.[4] In order to establish an industrial method of producing $Ti(HPO_4)_2 \cdot 0—1/2H_2O$, this compound was synthesized by refluxing a sulfuric acid solution of $TiOSO_4$, as an intermediate in the production of titanium(IV) oxide, with concentrated phosphoric acid.[5] In the previous report,[1] the ion-exchange equilibria between titanium(IV) bis(hydrogenphosphate) and an aqueous solution of NaCl–KCl under various conditions were investigated. As a result of the investigation, it was found that K^+ was separated more effectively than Na^+ when the anhydride was added to a solution containing equivalents of NaCl and KCl, but trouble occurred in the separation of the solid phase from the liquid phase because the crystals of the titanium(IV) bis(hydrogenphosphate) were too small. In the batch method, on the other hand, it was not easy to effect the elution of K^+ adsorbed on the microcrystals. These difficulties constituted a great obstacle for the practical use of the compound. Generally, inorganic ion-exchangers of a hydrated oxide or hydroxide formed as a gel have been used for analytical use after a dry solid of the gel has been crushed into particles of an adequate size, but an ideal strength can not be expected for them. In case a column is packed with an inorganic ion-exchanger obtained by further pulverizing the dry solid or supplied in microcrystalline form, water can not pass through the column smoothly. Reported in this paper is a result of our investigations with an eye to granulating the inorganic ion-exchanger. A mixture of microcrystalline titanium(IV) bis(hydrogenphosphate), a viscous carbonaceous material, such as sugar or wheat flour, and some of an additive such as an inorganic acid was sintered at a given temperature, the sintered product was then so crushed as to have a granule size proper for an ion-exchanger. The ion-exchange capacities of the resultant granulated product toward K^+ and Na^+ were examined according to the batch method and compared with those when titanium(IV) bis(hydrogenphosphate) was used as the raw material. A result of the test made to separate K^+ from Na^+ by the column method is also reported in this paper.

Experimental

Preparation and Analysis of Ion-exchangers. Titanium(IV) bis(hydrogenphosphate) as an ion-exchanger was synthesized in accordance with the refluxing method described in previous report.[2,5] The synthetic conditions and the composition of the products are shown in Table 1.

Preparation of Granulated Products. In a 50-ml porcelain crucible was placed given amounts of titanium (IV) bis(hydro-

TABLE 1. SYNTHESIS AND ANALYSIS OF TITANIUM(IV) BIS(HYDROGENPHOSPHATE)

No.	Reaction conditions: Raw material ATiP[a] (g)	Raw material $TiOSO_4$[b] (ml)	Mother liquid H_3PO_4 (mol/l)	Mother liquid H_2SO_4 (mol/l)	Mother liquid Volume (ml)	Temp (°C)	Time (h)	Reaction products: TiO_2 (%)	P_2O_5 (%)	H_2O (%)	$TiO_2 : P_2O_5 : H_2O$ (mole ratio)	Empirical formula
1	—	30.0	6.76	3.08	900	135	50	32.1	54.4	14.5	1.05 : 1.00 : 2.10	$Ti(HPO_4)_2 \cdot H_2O$
2	25.0	—	8.08	3.39	900	160	50	12.1	25.8	62.1	(1.00 : 1.17 : 51.3)	
						(dry product)		31.9	57.4	10.8	0.99 : 1.00 : 1.48	$Ti(HPO_4)_2 \cdot 1/2H_2O$
3	—	30.0	8.03	3.40	900	160	50	32.6	57.7	9.0	1.01 : 1.00 : 1.23	$Ti(HPO_4)_2 \cdot 0—1/2H_2O$
4	75.0	—			2850	160	50	34.2	57.9	7.9	1.04 : 1.00 : 1.07	$Ti(HPO_4)_2$

a) Amorphous titanium phosphate containing TiO_2 42.4%, P_2O_5 33.8%, H_2O 23.3%. b) Solution containing TiO_2 250 and H_2SO_4 1044 g/l.

genphosphate) or a hydrate thereof (a product not as yet rinsed in the production of titanium(IV) bis(hydrogenphosphate), and a carbonaceous material (a reagent-grade saccharoseas sugar, commercially available wheat flour, or a reagent-grade sodium ligninsulfonate). When anhydrous titanium(IV) bis(hydrogenphosphate) was used, 9 M H_2SO_4, 7 M H_3PO_4, and an adequate amount of water were added; the mixture was stirred homogeneously and then dried at 105 °C for about 3 h until it became a dark brown solid. Next, a lid cap was put on the crucible, which was then placed in an electric furnace kept at a given temperature in order to sinter the content of the crucible. After allowing the content to stand and cool, the sintered brown-black product was weighed, crushed so as to have an adequate granule size, sived, throughly washed with water until the acids in the granulated product could no longer be detected, and then dried at 50—60 °C for 24 h. The size distribution of the typical granulated product was found to be as follows; 16—32 mesh 16 w%, 32—42 mesh 52 w%, 42—65 mesh 29 w%, 65—100 meash 3 w%. The strength of the granulated product was determined to be 87—94% with the testing method (JIS-K 1474) used for granular activated carbon.

Measurement of Ion-exchange Capacities by the Batch Method. The equilibrium ion-exchange capacity (Q^A, meq/g) between the granulated product and an aqueous solution of the chloride (NaCl, KCl), and the saturated ion-exchange capacity (Q°, meq/g) at pH 4.5 were both measured in accordance with the method previously reported,[4] such ion-exchange characteristics as a selectivity quotient (K_H^M) and a distribution coefficient (K_D) were derived from the above ion-exchange capacities.

Adsorption of Na^+ and K^+ by the Column Method. A column of Pyrex glass (9 mm in inner diameter and 200 mm in height) was packed with 5.0 g of the dried granulated product (60—100 mesh) previously moistened with water. A given volume (500 ml, 1000 ml, or 1500 ml) of a sample solution (the aqueous solution of NaCl–KCl or artificial brackish water; the compositions and concentrations of these solutions are shown in Table 4) was permitted to flow through the column at a flow rate of 0.4—0.5 ml/min. Every 10-ml portion of the effluent from the column was collected in a fraction-collector. The pH value of each fraction was measured, and the Na^+ and K^+ contained therein were determined by flame photometry, while the Mg^{2+} and Ca^{2+} were determined by atomic absorptiometry, thereby estimating the quantity of each ion adsorbed on the granulated product. The cations adsorbed on the granulated product were subjected to complete elution with 30 ml of 6 M hydrochloric acid and an adequate amount of water; each ion in the eluate was determined, whereby the ion-exchange capacity of the granulated product, the distribution coefficient (K_D^M), and the separation factor (α_{Na}^K) were also then calculated.

Adsorption Test of Coloring Matter. To 100 ml of a solution of methylene blue with a concentration of 1 ppm were added 1 g of the granulated product (0.33 g in carbon content) or 0.33 g of active carbon (Pittsburg Co.). The mixture was stirred occasionally, and the coloring matter in the supernatant liquid was determined at a given time interval, using a spectrophotometer at the wave length of 660 nm in order to examine the change in the concentration of methylene blue in the solution with the lapse of time.

Results and Discussion

Titanium(IV) Bis(hydrogenphosphate) as Microcrystals. The titanium(IV) bis(hydrogenphosphate) monohydrate and 0—1/2 hydrate, formed by refluxing various titanium compounds with phosphoric acid, were all microcrystalline. Electron microscope photographs of both hydrates are shown in Fig. 1.

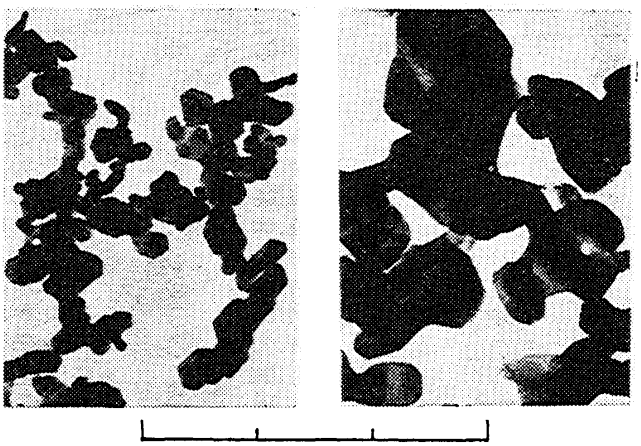

$Ti(HPO_4)_2 \cdot H_2O$ $Ti(HPO_4)_2 \cdot 0—1/2H_2O$

Fig. 1. Electron microscope photographs of titanium (IV) bis(hydrogenphosphate).

As has already been reported,[5] the crystals of these hydrates were quite different in their X-ray diffraction patterns. Besides, they were different in their appearances in the electron-microscope photographs; the monohydrate, showing a good crystallinity, had a crystal structure of hexagonal plates, with a particle size of 0.3—0.6 μ, while the 0—1/2 hydrate has a particle size of 1—2 μ. Since it was very difficult to flow water through a column packed with such microcrystalline hydrates, therefore, the granulation of these microcrystalline hydrates was contemplated.

Granulation of Titanium(IV) Bis(hydrogenphosphate) with The Aid of a Carbonaceous Material. The use of a binder, such as silicic acid gel, poly(vinyl alcohol), or gelatin, came into question for the production of a granulated product of titanium(IV) bis(hydrogenphosphate). Although a composite material of titanium(IV) bis(hydrogenphosphate) and silicic acid gel was expected to have a good stability to heat, it was impossible to produce the composite material possessing satisfactory strength in water according to our present techniques. The granulated product obtained by using poly(vinyl alcohol) or gelation as a binder had good strength, but was devoid of the stability required for inorganic ion-exchangers capable of withstanding use at a high temperature. Hence, an attempt has been made the granulation of titanium(IV) bis(hydrogenphosphate) with the aid of a carbonaceous material as a binder. The conditions for preparing the product and composition thereof are summarized in Table 2.

The carbonaceous material was selected from among saccharose, wheat flour, and sodium ligninsulfonate. A mixture containing saccharose was melted by heating, and the viscous melt was carbonized while bubbling. A mixture containing wheat flour gave a relatively hard sintered product containing nitrogen of proteins. These materials are carbohydrates with a definite carbon content. Sodium ligninsulfonate was chosen from the view point of utilizing pulp-waste liquor. In addition to these materials, a pitch is also regarded as a promising carbonaceous material.

Regarding the proportion of titanium(IV) bis(hydrogenphosphate) to the carbonaceous material in the preparation of the ion-exchanger, the use of a larger amount of the latter increases the strength of the granulated product, but naturally results in decrease in the ion-exchange capacity.

Taking the balance of these effects into consideration, the raw materials were so mixed that the ratio by weight of titanium(IV) bis(hydrogenphosphate) to C was 1 : 0.5. Sulfuric acid or phosphoric acid as an additive served to accelerate the carbonization of the carbonaceous materials by virtue of its dehydration effect and gave a relatively porous sintered product. In Table 2, Nos. 1—5 show the results obtained by using Titanium(IV) bis(hydrogenphosphate) monohydrate and sugar as carbonaceous material, and by sintering the mixture at 185—300 °C. As the carbonization proceeded rapidly at 300 °C, the heating time in this case was shortened. Nevertheless, a decrease in the weight of the granulated product was observed. The ratio by weight of Carb. (carbonaceous part formed by heating) to titanium(IV) bis(hydrogenphosphate) decreased as the temperature was elevated. Accordingly, the product sintered at a relatively lower temperature was not carbonized completely. The same tendency was observed in the cases of Nos. 6—10, wherein titanium(IV) bis(hydrogenphosphate) 0—1/2 hydrate was used.

TABLE 2. PREPARATION OF GRANULATED PRODUCTS FROM TITANIUM PHOSPHATE WITH CARBONACEOUS MATERIAL AND THEIR ANALYSIS

No.	Preparation conditions										Products		
	TiP $Ti(HPO_4)_2 \cdot H_2O$ (△) $Ti(HPO_4)_2$ 0—1/2 H_2O (▲) (g)[c]		Carbonaceous material Sugar(○), Flour(⊙), Sodium ligninsulfonate (●) (g)		TiP : C[a]	Addition agents 7 M H_3PO_4 (g)	9 M H_2SO_4 (g)	H_2O (g)	Temp (°C)	Time (min)	Yield (g)	TiP (%)	Carb.[b] (%)
1	3.20	△	4.00	○	1.00:0.50	0.90	0.10	1.00	185	120	5.59	61.9	38.1
2	3.20	△	4.00	○	1.00:0.50	0.90	0.10	1.00	200	90	5.48	63.4	36.6
3	3.20	△	4.00	○	1.00:0.50	0.90	0.10	1.00	220	60	5.43	64.1	37.9
4	3.20	△	4.00	○	1.00:0.50	0.90	0.10	1.00	250	60	5.20	67.1	32.9
5	3.20	△	4.00	○	1.00:0.50	0.90	0.10	1.00	300	30	5.03	69.5	30.5
6	9.00(3.20)	▲	4.00	○	1.00:0.50	—	—	—	185	90	5.98	53.5	46.5
7	9.00(3.20)	▲	4.00	○	1.00:0.50	—	—	—	200	60	5.83	54.9	45.1
8	9.00(3.20)	▲	4.00	○	1.00:0.50	—	—	—	250	60	5.46	58.6	41.4
9	9.00(3.20)	▲	4.00	○	1.00:0.50	—	—	—	300	30	5.33	60.0	40.0
10	9.00(3.20)	▲	4.00	○	1.00:0.50	—	—	—	350	30	5.26	60.8	39.2
11	3.20	▲	4.00	○	1.00:0.50			1.50	220	90	5.64	56.7	43.3
12	3.20	▲	4.00	○	1.00:0.50	0.90	0.10	1.00	220	90	5.61	61.7	38.3
13	3.20	▲	4.00	⊙	1.00:0.50	0.90	0.10	15.0	220	90	5.50	65.0	35.0
14	3.20	▲	3.60	●	1.00:0.50	0.90	0.10	15.0	220	90	5.85	57.8	42.2
15	64.00	△	80.00	○	1.00:0.50	18.00	2.00	42.0	220	300	95.6	62.4	37.6
16	64.00	▲	80.00	○	1.00:0.50	18.00	2.00	26.0	220	300	108	64.4	35.6

a) C: Carbon contained in the used carbonaceous material. b) Carb.: Carbonaceous part formed by heating.
c) The values in parentheses indicate the TiP content in the wet sample.

In these cases, a solid centrifuged from the mother liquor in the course of synthesis was directly used as titanium(IV) bis(hydrogenphosphate), so that it contained some phosphoric acid and sulfuric acid, which also functioned as additives. Nos. 11 and 12 show the influence of the additives on the sintered product. As is evident from the above discussion, the carbonization was remarkably promoted by the addition of phosphoric acid and sulfuric acid; the Carb./titanium(IV) bis(hydrogenphosphate) ratio (by weight) was decreased from 0.76 (No. 11 in the case of adding no additive) to 0.62 (No. 12 in the case of adding the additive). In Nos. 12, 13, and 14, the sintering experiments were performed using different kinds of the carbonaceous material. The use of wheat flour or sodium ligninsulfonate as carbonaceous material required a relatively greater amount of water than the case of using saccharose for the kneading of the raw material. No remarkable difference was found in the weights of the sintered products, but the Carb./titanium(IV) bis(hydrogenphosphate) ratio (by weight) was 0.54 in the case of wheat flour, 0.62 in the case of saccharose, and 0.73 in the case of sodium ligninsulfonate. (In the case of the sintered product using sodium ligninsulfonate, the sodium contained therein was extracted with hydrochloric acid, and the product was then dried to obtain the yield. Thus, "Carb." was free from sodium.). For reference's sake, Nos. 15 and 16 show the conditions for the preparation of the granulated products used in the column method and their compositions.

Ion-exchange Capacities of The Granulated Products. The ion-exchange titration curves of the granulated products containing the monohydrate and the 0—1/2 hydrate toward Na^+ and K^+, obtained according to

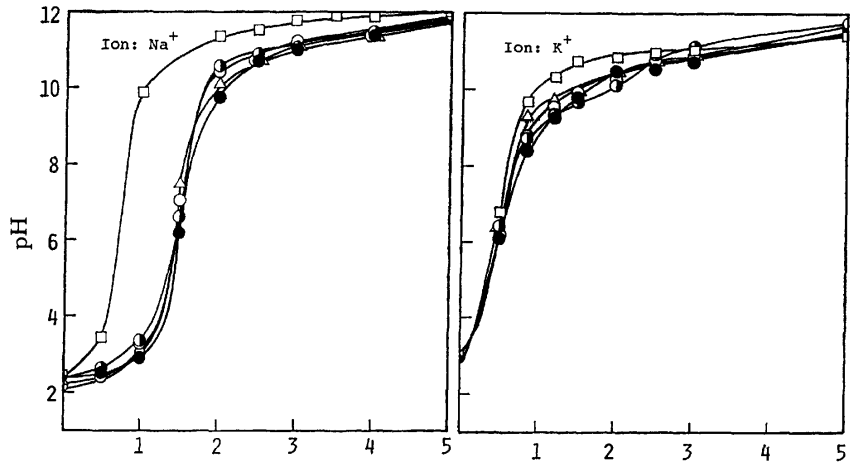

Fig. 2. Ion-exchange titration curves of the product granulated from $Ti(HPO_4)_2 \cdot H_2O$ with carbonaceous material.
Carbonaceous material: Sugar.
Heating temperature: △; 185, ○; 200, ◑; 220, ●; 250, □; 300.

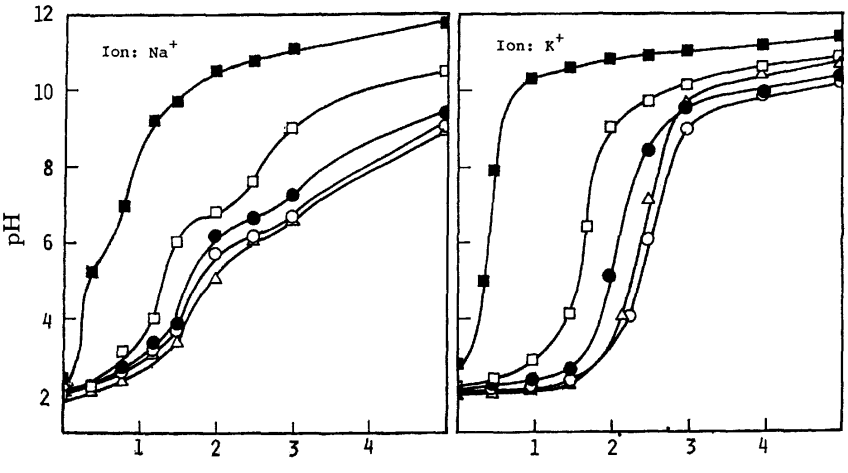

Fig. 3. Ion-exchange titration curves of the product granulated from $Ti(HPO_4)_2 \cdot 0—1/2\ H_2O$ with carbonaceous material.
Carbonaceous material: Sugar.
Heating temperature: △; 185, ○; 200, ●; 250, □; 300, ■; 350.

the method of the previous report,[4] are shown in Figs. 2 and 3 respectively.

In Fig. 2, the ion-exchange capacities toward Na^+ of the granulated products containing the monohydrate were 1.22—1.35 and 1.45—1.55 meq/g at the pH values of 4.5 and 7.0 respectively, except for the case wherein the product was sintered at 300 °C. These values were quite small as compared with those of the ion-exchange capacities of the monohydrate itself given in the previous reports[3,4] (3.6 and 7.5 meq/g at pH values of 4.5 and 7.0 respectively). The noticeable decrease in the ion-exchange capacity of the sintered product at pH 7.0 is considered to be a response to the change in the crystal structure of the monohydrate contained in the granulated product in the course of heating. It may also be considered that the surface of the crystals of titanium(IV) bis(hydrogenphosphate) was coated with the formed Carb. to slow down the speed of ion-exchange; thereafter Na^+ was hydrated in a neutral to alkaline solution to form a hydrated ion which was not adsorbed into the cavities of the ion-exchanger. This resulted, as is shown in Fig. 2, in a rapid rise in the titration curves at the point where the quantities of ion-exchange were small.

The ion-exchange capacities toward K^+ of the granulated product containing the monohydrate were 0.18—0.26 and 0.6 meq/g at pH values of 4.5 and 7.0 respectively. These values were half the values of the ion-exchange capacity of the monohydrate itself.

In Fig. 3, the ion-exchange capacities toward Na^+ of the granulated products containing the 0—1/2 hydrate, were 0.30—1.78 and 0.75—3.25 meq/g at pH of 4.5 and 7.0 respectively. The ion-exchange capacities of the granulated product varied remarkably according to the sintering temperature; these values decreased in the range of 185—350 °C with the elevation of the sintering temperature. This is probably ascribable to the same reason as in the case discussed above wherein the granulated product containing the monohydrate was used.

The ion-exchange capacities toward K^+ of the granulated products containing the 0—1/2 hydrate were 0.40—2.34 and 1.7—2.6 meq/g at pH 4.5 and 7.0 respectively. These values were extremely small as

TABLE 3. ION-EXCHANGE PROPERTIES OF GRANULATED PRODUCTS TOWARD Na AND K IONS

Iox-exchanger				Ion-exchange properties					
Sample No.	Row material	Heating temp (°C)	Ion	Equilibrium capacity (Q^A, meq/g)	Saturation capacity at pH 4.5 (Q°, meq/g)	Selectivity quotient (K_H^M)	Mole fraction (Q^A/Q°)	Adsorption quantity (A, %)	Distribution coefficent (K_D, ml/g)
1	△ + ○	185	Na	0.73	1.25	0.58	0.584	29.2	20.6
2	△ + ○	200	Na	0.90	1.30	1.27	0.692	36.0	28.1
3	△ + ○	220	Na	0.92	1.22	1.81	0.754	36.8	29.1
4	△ + ○	250	Na	0.95	1.35	1.45	0.704	38.0	30.6
5	△ + ○	300	Na	0.43	0.68	0.37	0.632	17.2	10.4
1	△ + ○	185	K	0.24	0.26	1.28	0.923	9.6	5.30
2	△ + ○	200	K	0.19	0.20	1.57	0.950	7.6	4.11
3	△ + ○	220	K	0.22	0.24	1.06	0.917	8.8	4.82
4	△ + ○	250	K	0.24	0.26	1.28	0.923	9.6	5.30
5	△ + ○	300	K	0.14	0.18	0.21	0.778	5.6	2.96
6	▲ + ○	185	Na	1.08	1.77	1.19	0.610	43.2	38.1
7	▲ + ○	200	Na	1.10	1.78	1.27	0.618	44.0	39.3
8	▲ + ○	250	Na	1.05	1.70	1.17	0.618	42.0	36.2
9	▲ + ○	300	Na	0.86	1.28	1.07	0.672	34.4	26.3
10	▲ + ○	350	Na	0.28	0.30	1.96	0.933	11.2	6.31
6	▲ + ○	185	K	1.90	2.28	15.8	0.833	76.0	158.3
7	▲ + ○	200	K	1.98	2.34	20.6	0.846	79.2	190.4
8	▲ + ○	250	K	1.72	1.93	18.5	0.891	68.8	110.1
9	▲ + ○	300	K	1.46	1.56	20.5	0.936	58.4	70.4
10	▲ + ○	350	K	0.35	0.40	1.12	0.875	14.0	8.14
11	▲ + ○	220	K	2.07	2.50	23.1	0.828	82.8	240.7
12	▲ + ○	220	K	2.12	2.72	19.7	0.779	84.8	278.9
13	▲ + ⊙	220	K	1.90	2.31	14.7	0.823	76.0	158.3
14	▲ + ●	220	K	1.24	1.60	3.42	0.775	49.6	163.2

△: $Ti(HPO_4)_2 \cdot H_2O$, ▲: $Ti(HPO_4)_2 \cdot 1/2\ H_2O$, ○: sugar, ⊙: flour, ●: sodium ligninsulfonate. Equilibrium capacity: ion-exchange capacity at pH 4.5 in Fig. 4. Saturation capacity: ion-exchange capacity at pH 4.5 in Figs. 2 and 3.

Selectivity quotient: $K_H^M = \frac{(M^+)I}{(H^+)I} \cdot \frac{(H^+)S}{(M^+)S} = \frac{Q^A}{Q^\circ - Q^A} \cdot \frac{Q^A}{C - Q^A}$

Adsorption quantity: $Q^A/C \times 100 = A$

Distribution coefficient: $K_D = A/I \cdot (100 - A)$

C: Initial quantity of MCl (2.5 meq)

S: MCl solution (25 ml)

I: Ion-exchanger (0.5 g)

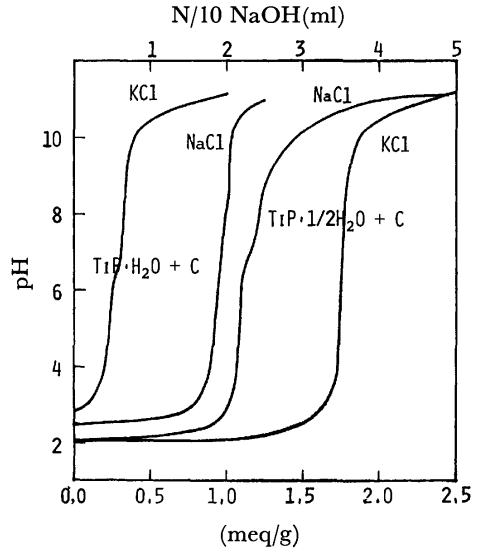

Fig. 4. Titration curves for equilibrium solution of granulated product with sodium and potassium chlorides.

compared with those of the 1/2 hydrate itself, determined to be 4.1 and 6.7 meq/g at pH 4.5 and 7.0 respectively. However, the ion-exchange capacities within such ranges are almost equal to those of commercially available cation-exchange resins; thus they can be utilized satisfactorily as ion-exchangers.

Ion-exchange Characters of The Granulated Products. The titration curves drawn for the estimation of the quilibrium ion-exchange capacity are shown in Fig. 4. The ion-exchange characters of the granulated product toward Na^+ and K^+ are summarized in Table 3.

The equilibrium ion-exchange capacities (Q^A) toward K^+ and Na^+ of the granulated products containing the monohydrate (Nos. 1—5) were 0.43—0.95 and 0.14—0.24 meq/g respectively.

Although the saturation ion-exchange capacities (Q°) toward Na^+ show significantly large values at pH 4.5, as has been described above, the satisfactory results expected for the separation between Na^+ and K^+ were not obtained in connection with the selectivity quotient (K_H^M) and the distribution coefficient (K_D). On the other hand, the values of Q^A toward Na^+ and K^+ of the granulated product containing the 0—1/2 hydrate were 0.86—1.10 and 1.46—1.98 meq/g respectively, except for those obtained for the product sintered at 350 °C. The values of Q° toward Na^+ and K^+ of the same product were 1.28—1.78 and 1.56—2.34 meq/g respectively, except for those obtained for the product sintered at 350 °C. The values of Q^A and Q° were at their maximum for the granulated product sintered at 200 °C, and these values decreased with the elevation in the sintering temperature. Especially, the values of the ion-exchange capacity for the product sintered at 350 °C decreased to 1/6 of the values for the product sintered at 200 °C. It is considered that, at high temperatures, some changes occurred in the structure of the 1/2 hydrate contained in the sintered product. The values of K_H^M and K_D toward K^+ were extremely large as compared with those toward Na^+, thus proving that the granulated products containing the 1/2 hydrate had an excellent adsorption selectivity toward the K^+ ion. As is evident from the previous paper,[4] the value of K_D toward K^+ was 15.7 for the 1/2 hydrate itself, a value almost equal to that of the granulated product. The value of K_D toward K^+ for the 1/2 hydrate itself was 607.0 ml/g, while the values of K_D for the granulated products decreased to about 1/3—1/5 of the above value, probably becouse the products contained the Carb. These results indicate that the sintering temperature for the granulated products influencing the ion-exchange capacity is most suitably within the range of 200—250 °C. Accordingly, the granulated products sintered at 220 °C were used in the subsequent samples of Nos. 11—14. In Nos. 11 and 12, the influence on the ion-exchange character of the additive at the time of sintering was observed. In the case of the sample of No. 12, wherein the additive was added, a slight increase was observed in the ion-exchange capacity. This phenomenon was probably caused by the fact that the carbonization of the carbonaceous material was promoted by the addition of the inorganic acids; then, the value of the titanium(IV) bis(hydrogenphosphate)/Carb. increased, as is shown in Table 2.

The influence of the carbonaceous material on the ion-exchange properties was examined in Nos. 12, 13, and 14. In these results, the Q^A and Q° values decreased in the order of sugar, wheat flour, and sodium lignin-sulfonate. A similar tendency also appeared in other ion-exchange properties, such as K_H^M and K_D. Among the carbonaceous materials used, sugar showed the best result.

Selective Adsorption toward K^+ as Determined by The Column Method. As has already been reported,[1,4] the values of K_H^M toward Na^+ and K^+ of $Ti(HPO_4)_2 \cdot 0—1/2H_2O$ showed a sufficient value for the separation of the two ions. As the value of K_H^M toward K^+ was large, the elution of adsorbed K^+ on the batch method using hydrochloric acid was not easy. Since titanium-(IV) bis(hydrogenphosphate) was microcrystalline, as has been described above, this compound was quite inappropriate for the column method. Accordingly, the selective adsorption toward K^+ in an aqueous solution of NaCl–KCl and in artificial brackish water was investigated according to the column method, using the granulated product prepared in this study. The results obtained are shown in Table 4.

In the table, the distribution coefficients, K_D^{Na} and K_D^K, are obtained as the values of $\bar{m}Na/mNa$ and $\bar{m}K/mK$ respectively, wherein $\bar{m}Na$ and $\bar{m}K$ stand for the amounts (meq) of Na^+ and K^+ respectively adsorbed on 1 g of the ion exchanger, and mNa and mK, for the amount (meq) of Na^+ and K^+ respectively existing in 1 ml of the solution under the equilibrium adsorption conditions. The separation factor, α_M^K, between K^+ and $M^{1+ \text{ or } 2+}$ (M=Na, Mg, or Ca) is indicated by the following formula:[6]

$$\alpha_M^K = (\bar{m}K \cdot mM)/(\bar{m}M \cdot mK) = k_D^K/k_D^M.$$

In Nos. 1 and 2, the concentration of KCl–NaCl in water was about twice as much as that of natural sea water, and the atomic ratio of Na/K was 50.8. As the

TABLE 4. SELECTIVE ADSORPTION OF POTASSIUM ION BY A COLUMN METHOD FROM A NaCl–KCl MIXED SOLUTION AND ARTIFICIAL BRACKISH WATER

No.	Granulated product Kind	(g)	NaCl–KCl solution (Artificial brackish water) NaCl (g/l) KCl (g/l)	(ml)	Ion-exchange Na (meq/g)	Ion-exchange K (meq/g)	Ion-exchange properties Na/K (atomic ratio)	Distribution coefficient K_D^{Na}	Distribution coefficient K_D^{K}	Separation factor α_{Na}^{K}
1	$Ti(HPO_4)_2 \cdot H_2O + C$	5	53.32 / 1.34	1000	0.483	0.068	7.11	0.530	3.78	7.13
2	$Ti(HPO_4)_2 \cdot 1/2H_2O + C$	5	53.32 / 1.34	1000	1.05	0.577	1.83	1.15	32.1	27.9
3	$Ti(HPO_4)_2 \cdot 1/2H_2O + C$	5	26.66 / 0.67	500	1.05	0.337	2.79	2.30	41.9	18.2
4	$Ti(HPO_4)_2 \cdot 1/2H_2O + C$	5	26.66 / 0.67	1000	1.12	0.526	2.13	2.45	58.5	23.9
5	$Ti(HPO_4)_2 \cdot 1/2H_2O + C$	5	26.66 / 0.67	1500	1.15	0.575	2.00	2.52	64.0	25.4
6	$Ti(HPO_4)_2 \cdot 1/2H_2O + C$	5	41.26 / 13.40	1000	0.856	1.05	0.814	1.18	5.84	4.95
7	$Ti(HPO_4)_2 \cdot 1/2H_2O + C$	5	(26.66) / (0.67) / ($MgCl_2 \cdot 6H_2O$ 7.19) / ($MgSO_4 \cdot 7H_2O$ 4.24) / ($CaSO_4$ 1.55)	1000	0.938 (Mg; 0.0423 M mol/g) (Ca; 0.00343 M mol/g)	0.440 (Mg/K; 0.0961) (Ca/K; 0.0078)	2.13	2.06 (K_D^{Mg} 0.809) (K_D^{Ca} 0.394)	45.5 (α_{Mg}^{K} 56.2) (α_{Ca}^{K} 115)	22.1

granulated product containing the monohydrate (No. 1) which was packed into a column adsorbed only a little K^+, the product was not suitable as an ion-exchanger for K^+. On the other hand, the granulated product containing the 0—1/2 hydrate (No. 2) showed an ion-exchange capacity of 0.557 meq/g toward K^+, an atomic ratio of the adsorbed Na^+ to the adsorbed K^+ of 1.83, and a separation factor, α_{Na}^{K}, of 27.9. In Nos. 3, 4, and 5, an aqueous solution of NaCl–KCl was used in which the concentrations of NaCl and KCl were almost equal to those in sea water. When this solution was permitted to flow through the column, the amounts of Na^+ and K^+, and the α_{Na}^{K} value were increased according to the increase in the flow. In No. 6, the sum of the concentrations of NaCl and KCl was equal to that in No. 2 (54.66 g), but the concentration of KCl in No. 6 was increased ten times as much as that of No. 2, decreasing the concentration of NaCl accordingly. As a result, the ion-exchange capacity toward Na^+ was decreased from 1.05 to 0.856 meq/g, while the ion-exchange capacity toward K^+ was increased from 0.577 meq/g to 1.05 meq/g. As the concentration of K^+ in the sample solution was comparatively high in this case, the α_{Na}^{K} value was about 5. Artificial brackish water was used as the sample solution in No. 7. As a result, the ion-exchange capacities toward Na^+ and K^+ were both somewhat decreased as compared with the case of No. 4, wherein an aqueous solution of NaCl–KCl with the same concentrations of NaCl and KCl was used. However, the atomic ratio of Na to K in No. 7 was equal to 2.13 in the case of No. 4. Although considerable amounts of Mg^{2+} and Ca^{2+} were contained in the artificial brackish water, those ions were adsorbed very little on the granulated product containing the 0—1/2 hydrate, and both the α_{Mg}^{K} and α_{Ca}^{K} values showed a large number. The pH values of the effluents and the

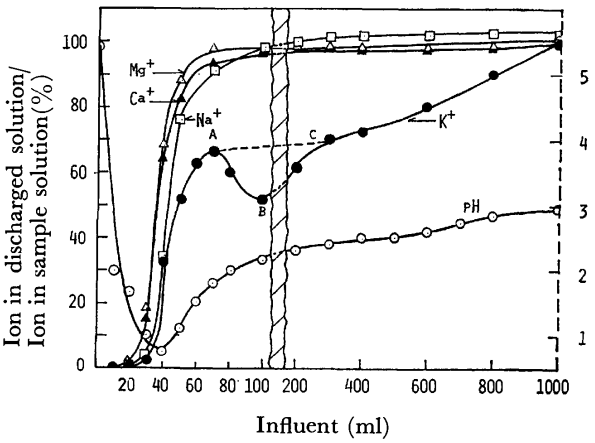

Fig. 5. The concentration of each ion containing in the discharged solution from the column.
Ion-exchanger: glanulated product of $Ti(HPO_4)_2 \cdot 1/2\ H_2O + C$ (5 g), sample solution: artificial brackish water (see Table 4).

changes in the concentration of the individual ions were examined in order to check the behavior of the individual ions adsorbed on the granulated product in the column. The result obtained are shown in Fig. 5.

As soon as the aqueous solution of NaCl–KCl or the artificial brackish water, each having a pH value of 5—6, was passed through the column as a sample solution, an ion-exchange reaction took place whereby the pH value of the effluent decreased so rapidly that the pH value dropped to the minimum value of 0.75 when the volume of the effluent reached 30—40 ml. Thereafter, the pH value gradually increased as the volume of the effluent became larger, shown about 2, 2.5, and 3 at the stages where the volumes of the effluent reached 100, 500, and 1000 ml respectively. As a large amount of

Na^+ was contained in the sample solution, the concentration of Na^+ in the effluent rapidly increased to the same level as that of the sample solution when 30 ml of the effluent discharged from the column. The concentration of Na^+ in the effluent eventually reached 102—103% of that in the sample solution supplied. This phenomenon was considered to show that the Na^+ initially adsorbed on granulated product was gradually replaced by K^+ in the following sample solution. Although K^+ was also contained together with Na^+ in the effluent, the concentration of K^+ showed a peak at Point, A, in Fig. 4 where the volume of the effluent reached about 70 ml. With the increase in the volume of the effluent, the concentration of K^+ was decreased to a valley, B, and then again increased to Point C. This phenomenon was also observed in Nos. 3—5, wherein the concentration of K^+ in the sample solution was low, but it not observed in Nos. 1, 2, and 6, wherein the concentration of K^+ was comparatively high. In the latter case, the concentration of K^+ increased, as is shown by the dotted line connecting Points A and C in Fig. 4. Before Na^+ began to appear in the effluent, Mg^{2+} and Ca^{2+} were contained therein, and their concentrations were increased rapidly. In view of the facts that the α^{K}_{Na} value reached 22.1 by passing the artificial brackish all at once through a column in which the granulated products containing the 0—1/2 hydrate had been placed, and that K^+ could be separated effectively from Mg^{2+} and Ca^{2+}, the effective separation of K^+ from sea water can be expected by further improvement in the technical problems.

Adsorption of Coloring Matter by The Granulated Products. In the preparation of the granulated products, the carbonaceous material used as a binder was converted by heating it into substances composed predominantly of carbon. If this carbonaceous part had an adsorbing effect like active carbon, the granulated products would have the functions of both ion-exchange and adsorption. Using methylene blue as the material to be adsorbed, the granulated product was added to an aqueous solution of methylene blue and the change in the color density with the lapse of time was examined, the resulting being shown in Fig. 6.

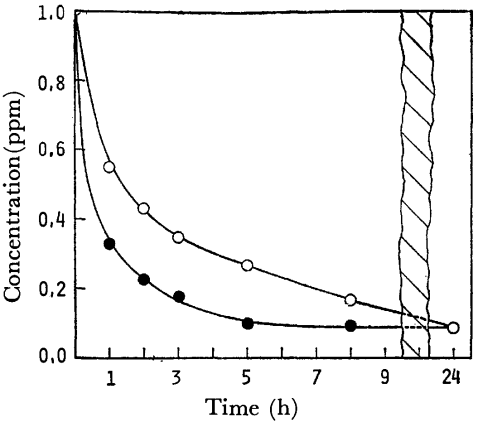

Fig. 6. Adsorption of methylene blue by granulated product and active carbon. 1 g (C; 0.33 g) of granulated product or 0.33 g of active carbon were added to 100 ml of methylene blue aqueous solution (1 ppm), respectively.
○: Granulated product, ●: active carbon.

Since the sintering temperature for preparing the granulated products was as low as 200—250 °C, we were unable to obtain a product with an adsorbing capacity equivalent to active carbon, but the product could adsorb coloring matter to some extent.

References

1) a) Presented at the 41st National Meeting of the Chemical Society of Japan, Osaka, April 1980; b) Part IV of this series; E. Kobayashi, *Bull. Chem. Soc. Jpn.*, **52**, 1359 (1979).
2) E. Kobayashi, *Bull. Chem. Soc. Jpn.*, **48**, 3114 (1975); *Tokyo Kogyo Shikensho Hokoku*, **72**, 177 (1977).
3) G. Alberti, P. Cardini-Galli, U. Constantion, and E. Torrasca, *J. Inorg. Nucl. Chem.*, **29**, 571 (1967).
4) E. Kobayashi, *Bull. Chem. Soc. Jpn.*, **52**, 1351 (1979).
5) E. Kobayashi, *Bull. Chem. Soc. Jpn.*, **51**, 2306 (1978); *Kagaku Gijutsu Kenkyusho Hokoku*, **74**, No. 9 (1979).
6) H. Matsushita, T. Takayanagi, and K. Iida, *Bull. Soc. Sea Water Sci. Jpn.*, **25**, 247 (1972).

The Thermal Decomposition of Ammonium Chloride Tetrachlorozincate and the Formation of Tetrachlorozincate Complexes of Alkali Metal by Means of Solid Reactions with Alkali Chlorides

Sumio Ichiba,* Satoshi Oshima, Hisao Negita, and Haruhiko Tanaka†

Department of Chemistry, Faculty of Science, Hiroshima University, Naka-ku, Hiroshima 730

†Faculty of School Education, Hiroshima University, Minami-ku, Hiroshima 734

(Received April 14, 1980)

Ammonium chloride tetrachlorozincate, $(NH_4)_3Cl[ZnCl_4]$, decomposes to $ZnCl_2$ in two stages through an intermediate phase $(NH_4)_2[ZnCl_4]$. In the first stage, 1 mol of NH_4Cl is lost by one-dimensional diffusion mechanisms with the activation energy of 138 kJ mol^{-1}, and in the second stage the release of two moles of NH_4Cl is controlled by a random nucleation reaction with the activation energy of 126 kJ mol^{-1}, corresponding to the bond-breaking. Anhydrous alkali metal tetrachlorozincate complexes, $M_2[ZnCl_4]$(M=Na, K, Rb, Cs), are obtained by solid reactions with alkali chlorides when $(NH_4)_3Cl[ZnCl_4]$ decomposes. A dry chemical method using $(NH_4)_3Cl[ZnCl_4]$ as a starting material is proposed for the preparation of the anhydrous chlorozincate complexes, which have thus far been difficult to synthesize.

Ammonium chloride tetrachlorozincate, $(NH_4)_3Cl[ZnCl_4]$, is known to decompose to zinc chloride upon heating.[1] However, the mechanisms and kinetics of the thermal decomposition are not well understood. In this study, the mechanisms and kinetics of the decomposition were examined by thermogravimetry (TG), differential scanning calorimetry (DSC), and X-ray diffraction.

The solid reaction which took place in the mixtures of $(NH_4)_3Cl[ZnCl_4]$ and MCl (M=Na, K, Rb, Cs) simultaneously when $(NH_4)_3Cl[ZnCl_4]$ decomposed was also studied by TG, DSC, and X-ray diffraction. The products are interesting because the preparation of the anhydrous chlorozincate complexes is difficult on account of the deliquescence of $ZnCl_2$ and hydrolysis in water, and the anhydrous complexes have yet to be examined. That is, the stereochemistry of the chlorozincate complexes is not obvious other than that of the tetrahedral anion $[ZnCl_4]^{2-}$, though a number of other halogenozincate complexes, such as fluorozincate complexes, $M^{I}ZnX_3$, $M^{I}_2ZnX_4$, $M^{I}_3ZnX_5$, and $M^{I}_4ZnX_6$, have been reported.[2]

Experimental

Materials. Ammonium chloride tetrachlorozincate was prepared by a published method.[3] Commercial alkali chlorides were used without further purification. The samples for the solid reaction were prepared by mixing alkali chloride and $(NH_4)_3Cl[ZnCl_4]$ in a 2 : 1 molar ratio in an agate mortar in a nitrogen atomosphere. For the X-ray diffraction measurements, the samples were prepared by heating pure $(NH_4)_3Cl[ZnCl_4]$ or the mixture powder in a furnace with a nitrogen gas flow for two hours at the temperature where the reaction occurs in the DSC curve.

Measurements. The TG and DSC curves were recorded simultaneously using a Rigaku Thermoflex TG-DSC M8085 by heating the sample in flowing nitrogen gas at a rate of 2 K min^{-1}. About a 10-mg of the sample was placed in a platinum crucible, and α-alumina was used as the reference material. The TG curves were analysed by the method of Šatava and Škvára[4] to obtain the parameters of the reaction mechanisms and kinetics.

Results and Discussion

Thermal Decomposition of $(NH_4)_3Cl[ZnCl_4]$. The TG-DSC curves of $(NH_4)_3Cl[ZnCl_4]$ are shown in Fig. 1. $(NH_4)_3Cl[ZnCl_4]$ decomposed to $ZnCl_2$ in two stages. From the weight loss, the stages are confirmed as:

$$(NH_4)_3Cl[ZnCl_4](s) \longrightarrow (NH_4)_2[ZnCl_4](s) + NH_4Cl(g) \quad (1)$$

$$(NH_4)_2[ZnCl_4](s) \longrightarrow ZnCl_2(s) + 2NH_4Cl(g). \quad (2)$$

The existence of $(NH_4)_2[ZnCl_4]$ as an intermediate phase was also confirmed by X-ray diffraction. The endothermic peak at 313 °C corresponded to the

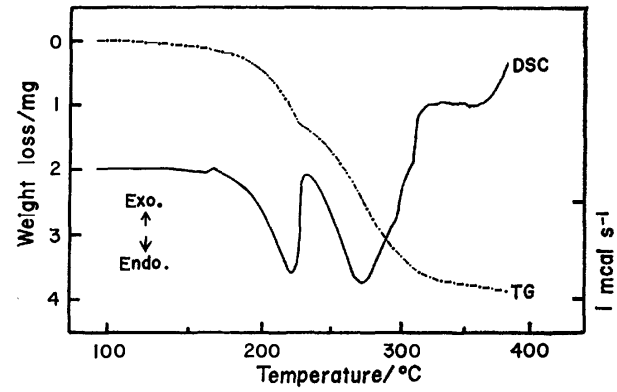

Fig. 1. TG–DSC curves of $(NH_4)_3Cl[ZnCl_4]$. Sample weight: 6.38 mg.

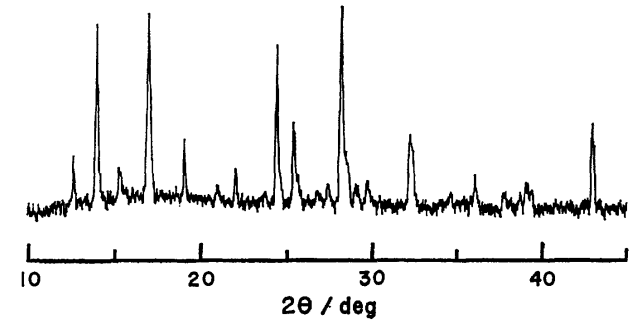

Fig. 2. X-Ray diffraction pattern of $ZnCl_2$ produced by thermal decomposition of $(NH_4)_3Cl[ZnCl_4]$.

melting point of $ZnCl_2$. The $ZnCl_2$ produced was mainly in the β-form, but containing a small amount of α-form, as determined by X-ray diffraction (Fig. 2). The compositions of the two forms changed according to the cooling conditions: the α-form is obtained by the rapid cooling of the melt, and the β-form, by the slow cooling.

The decomposition reaction mechanisms and kinetic parameters are deduced from the TG curve by the method of Šatava and Škvára. This method was used because it allows a fairely quick estimation of the parameters.

The thermogravimetric curve of a decomposition reaction can be expressed by this equation: $\log g(\alpha) - \log p(x) = B$. In this equation, the $g(\alpha)$ function requires a knowledge of the reaction mechanism and can be calculated from the experimental data of α, the fraction of the initial compound reacted. Šatava and Škvára gave data for $\log g(\alpha)$ which cover nine common reaction models.[4] Graphs of $\log p(x)$ can be computed for various activation energies, E, over a given range of temperature. The B values depend only upon the nature of the compound studied and upon the heating rate, not upon the temperature. A graphical comparison of the curves of both $\log g(\alpha)$ and $\log p(x)$ over the known experimental temperature range allows the reaction mechanisms and reaction parameters to be determined. The evaluation of the TG curve of the decomposition of $(NH_4)_3Cl[ZnCl_4]$ by the method of Šatava and Škvára is shown in Fig. 3 as an example. The enthalpy change for the reaction was obtained from the DSC curve.

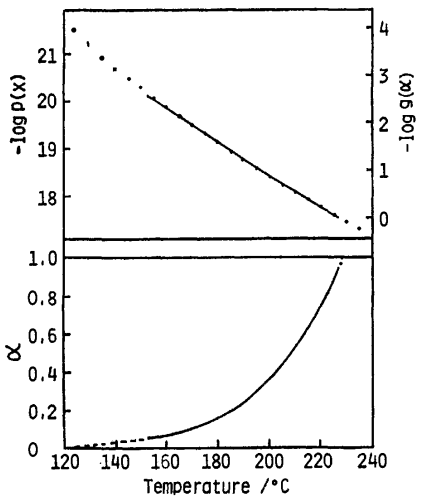

Fig. 3. The evaluation of the TG curve of the first decomposition stage of $(NH_4)_3Cl[ZnCl_4]$. The upper solid line is a plot of $-\log g(\alpha)$ *vs.* T calculated from TG curve (lower curve) for the reaction kinetic equation of one-dimensional diffusion. The dotted line is a plot of $\log p(x)$ *vs.* T for $E=138$ kJ mol^{-1}.

The best fits between experimental and calculated thermogravimetric curves and ΔH for each stage are as follows:

The First Stage: The loss of one mole of NH_4Cl occurs through a one-dimensional diffusion process following the parabolic law ($\alpha^2=kt$). The activation energy of the diffusion process, E, is 138 kJ mol^{-1}, the frequency factor, Z, 4.8×10^{13} s^{-1} mol$^{1/2}$, and ΔH, 85 kJ mol^{-1}.

The Second Stage: The loss of two moles of NH_4Cl is controlled by a random nucleation of one nucleus on each particle, with the activation energy of 126 kJ mol^{-1} corresponding to a bond breaking. The value of Z is 1.2×10^{11} s^{-1} mol$^{1/2}$, and that of ΔH, 134 kJ mol^{-1}.

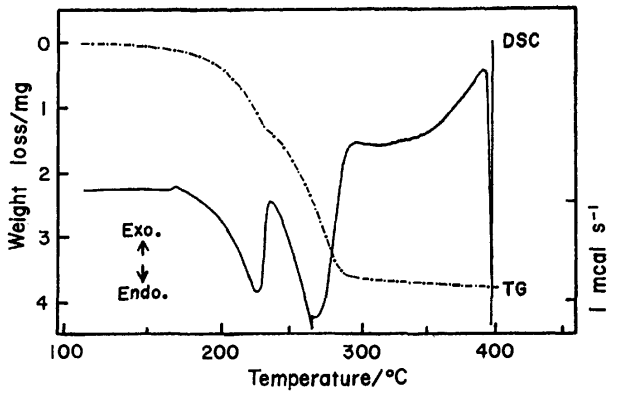

Fig. 4. TG–DSC curves of the mixture powder of $(NH_4)_3Cl[ZnCl_4]$ and NaCl with a 1 : 2 molar ratio. Sample weight: 9.31 mg.

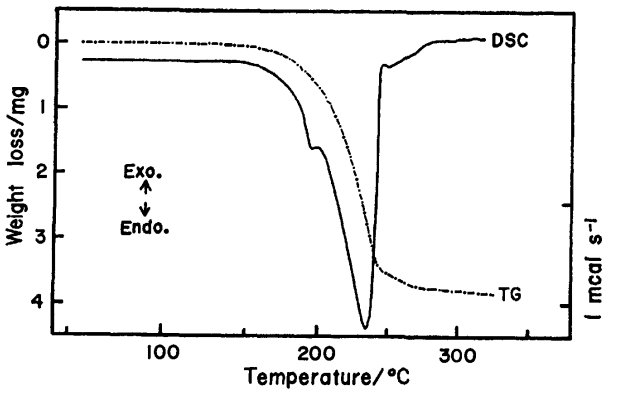

Fig. 5. TG–DSC curves of the mixture powder of $(NH_4)_3Cl[ZnCl_4]$ and CsCl with a 1 : 2 molar ratio. Sample weight: 14.36 mg.

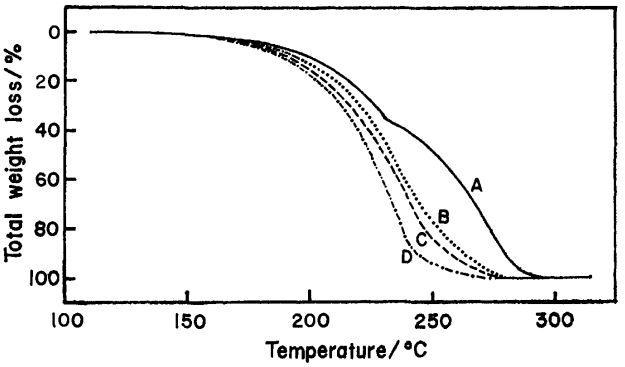

Fig. 6. Weight loss curves of the mixtures of $(NH_4)_3Cl[ZnCl_4]$ and MCl (M=Na, K, Rb, Cs) with a 1 : 2 molar ratio.
A: NaCl, B: KCl, C: RbCl, D: CsCl.

Those results are not inconsistent with the structure of $(NH_4)_3Cl[ZnCl_4]$, in which tetrahedral $[ZnCl_4]^{2-}$ ions are contained.

Solid Reaction between $(NH_4)_3Cl[ZnCl_4]$ and Alkali Chloride. A solid reaction took place between $(NH_4)_3Cl[ZnCl_4]$ and alkali chloride simultaneously when $(NH_4)_3Cl[ZnCl_4]$ decomposed upon the heating of the mixture in a 1 : 2 molar ratio. The mechanisms and kinetics of this reactions were followed in the usual way. The TG-DSC curves of the mixtures of 2NaCl–$(NH_4)_3Cl[ZnCl_4]$ and 2CsCl–$(NH_4)_3Cl[ZnCl_4]$ are shown in Figs. 4 and 5 respectively. The weight-loss curves of the mixtures of MCl (M=Na, K, Rb, Cs) and $(NH_4)_3Cl[ZnCl_4]$ with a 2 : 1 molar ratio are arranged in Fig. 6. The tail parts of the curves were sensitive to the sample properties, such as the paritcle-size distribution, and the contact condition of the reactants.

2NaCl–$(NH_4)_3Cl[ZnCl_4]$: Figure 4 shows that the reaction proceeds in two stages, in the same way as the decomposition reaction of pure $(NH_4)_3Cl[ZnCl_4]$. When the TG-DSC curves in Fig. 4 are compared with the curves in Fig. 1, the first stages of the reactions coincided with each other well, but in the second stage the loss of two moles of NH_4Cl occurs well below the temperature of the pure compound. In Fig. 1 the melting point of $ZnCl_2$ is observed at 313 °C, in accordance with the literature value, whereas in Fig. 4 a large peak is observed at 390 °C, which corresponds to the melting point of the product compound of $Na_2[ZnCl_4]$. Thus, the reaction pattern of the 2NaCl–$(NH_4)_3Cl$-$[ZnCl_4]$ mixture is as follows:

$$(NH_4)_3Cl[ZnCl_4](s) + 2NaCl(s) \longrightarrow (NH_4)_2[ZnCl_4](s) + 2NaCl(s) + NH_4Cl(g) \longrightarrow Na_2[ZnCl_4](s) + 2NH_4Cl(g) \xrightarrow{390°C} Na_2[ZnCl_4](l). \quad (3)$$

$(NH_4)_3Cl[ZnCl_4]$–2MCl (M=K, Rb, Cs): In these mixtures three moles of NH_4Cl were lost at one stage of the reaction, as is shown in Fig. 5. The reaction temperatures at which the loss of NH_4Cl occurs in these mixtures are well below the temperature of the pure compound of $(NH_4)_3Cl[ZnCl_4]$, as is shown in Fig. 6. The product of $Cs_2[ZnCl_4]$ was identified by means of X-ray diffraction. The other products were also confirmed to be $K_2[ZnCl_4]$ and $Rb_2[ZnCl_4]$, though the X-ray data were not available. The melting point of $K_2[ZnCl_4]$ was observed at 450 °C in the DSC curve.

Table 1. Mechanisms and kinetic parameters for the solid reactions between $(NH_4)_3Cl[ZnCl_4]$ and alkali chlorides

MCl	Mechanisms	E / kJ mol^{-1}	Z / s^{-1} mol$^{1/2}$	ΔH / kJ mol^{-1}	Products
KCl	One-dimensional diffusion	159	1.0×10^{15}	226	$K_2[ZnCl_4]$
RbCl	One-dimensional diffusion	159	1.7×10^{15}	231	$Rb_2[ZnCl_4]$
CsCl	One-dimensional diffusion	159	1.8×10^{15}	263	$Cs_2[ZnCl_4]$

The reaction mechanisms and kinetic parameters derived from the TG curves are shown in Table 1, along with the values of ΔH. These results show that the reaction pattern in these mixtures is as follows:

$$(NH_4)_3Cl[ZnCl_4](s) + 2MCl(s) \longrightarrow M_2[ZnCl_4](s) + 3NH_4Cl(g). \quad (4)$$

The mechanisms exhibit one-dimensional diffusion, so that the alkali chloride diffuses over the surface of the $(NH_4)_3Cl[ZnCl_4]$ particles prior to the formation of alkali metal tetrachlorozincate. No difference in the values of the activation energy was distinguished in those mixtures, but the reaction temperatures fall in accordance with the lattice energy of the alkali chlorides, as is shown in Fig. 6. The values of ΔH, as estimated from the DSC curves, changed considerably with the ending part of the curves. However, the values of ΔH were much larger than the values of the activation energy. This disagreement between ΔH and E seems to be ascribable to the contributions to ΔH from the fast reaction stages other than the rate-controlling diffusion process.

A solid reaction which occurs simultaneously when $(NH_4)_3Cl[ZnCl_4]$ decomposes is proposed for the synthesis of the other chlorozincate complexes.

References

1) "Shin Jikken Kagaku Koza," ed by the Chemical Society of Japan, Maruzen Co. (1977), Vol. 8, p. 933.
2) *E.g.*, A. F. Wells, "Structural Inorganic Chemistry," 4th ed, Clarendon Press, Oxford (1975), p. 394.
3) H. P. Klug and L. Alexander, *J. Am. Chem. Soc.*, **66**, 1056 (1944).
4) V. Šatava and Škvára, *J. Am. Ceram. Soc.*, **52**, 591 (1961).

 © 1980 The Chemical Society of Japan Bull. Chem. Soc. Jpn., 53, 3563—3566 (1980)

Studies on High-pressure Reaction of Er_2O_3 or Yb_2O_3 with VO_2

Tsutomu SHIN-IKE,* Gin-ya ADACHI,** Jiro SHIOKAWA,**
Masahiko SHIMADA,*** and Mitsue KOIZUMI***

Department of Chemistry, Osaka Dental University, Makino-honmachi, Hirakata, Osaka 573
**Department of Applied Chemistry, Faculty of Engineering, Osaka University, Yamadakami, Suita, Osaka 565*
***The Institute of Scientific and Industrial Research, Osaka University, Yamadakami, Suita, Osaka 565*

(Received April 22, 1980)

The reaction of erbium sesquioxide (Er_2O_3) or ytterbium sesquioxide (Yb_2O_3) with vanadium dioxide (VO_2) at 1400 °C and 50 kbar and 30 kbar pressures was studied. Quadrivalent vanadium ions were reduced to the trivalent state, erbium vanadite ($ErVO_3$) or ytterbium vanadite ($YbVO_3$) being obtained. The crystal structure of $ErVO_3$ obtained at 50 kbar pressure was vaterite-type isostructural with $ErBO_3$ belonging to a hexagonal system, and that obtained at 30 kbar calcite-type belonging to a rhombohedral (pseudo-hexagonal) system. In the reaction of Yb_2O_3 with VO_2 at high pressure, a perovskite-type crystal was obtained. The electrical and magnetic properties of the vaterite- and the calcite-type $ErVO_3$ were studied.

Success in the synthesis of a diamond has encouraged studies on high-pressure syntheses for the development of new functional materials. In general, increase in pressure tends to stabilize dense phase and lower valence state.[1] It is considered that the most dense ABO_3 phase has cubic-perovskite structure. Rare-earth vanadites ($LnVO_3$) obtained by the reaction of rare-earth sesquioxides (Ln_2O_3) and divanadium trioxide (V_2O_3) at atmospheric pressure are perovskite-type compounds isostructural with orthorhombic $GdFeO_3$.[2] When the reactions were carried out at high pressures, the products were perovskites isomorphous with those obtained by synthesis at atmospheric pressure, their density not depending on pressure.[3]

Pyrochlore-type ytterbium vanadite ($Yb_2V_2O_7$) was obtained by the reaction of ytterbium sesquioxide (Yb_2O_3) and vanadium dioxide (VO_2) at 1400 °C in a vacuum. However, a mixture of perovskite-type $ErVO_3$ and zircon-type $ErVO_4$ was obtained under the same conditions by the reaction between erbium sesquioxide (Er_2O_3) and vanadium dioxide.[4] When the reaction of Er_2O_3 or Yb_2O_3 with VO_2 is carried out at high pressure, the quadrivalent vanadium ions are expected to be reduced to form a type of erbium or ytterbium vanadite ($ErVO_3$ or $YbVO_3$) differing from that of perovskite compounds.

Experimental

Materials. Erbium and ytterbium sesquioxides (Er_2O_3 and Yb_2O_3) (minimum purity 99.9%, Shin-etsu Kagaku Co. Ltd.) were ignited at 1200 °C in order to remove volatile constituents. Divanadium trioxide (V_2O_3) and divanadium pentaoxide (V_2O_5) of special reagent grade were used without further purification. Vanadium dioxide (VO_2) was prepared by heating V_2O_3–V_2O_5 1 : 1 mixture at 1000 °C in a vacuum furnace for 4 h.[5]

Procedure. Er_2O_3 or Yb_2O_3 and VO_2 in 1 : 2 mixtures were weighed and ground with an aluminum mortar and then placed in a cell (Fig. 1). The reactions were carried out at 1400 °C and 50 and 30 kbar pressures with a 15 mm diam. cubic anvil-type apparatus.[6] The samples were subjected to pressure before the temperature was raised. After being kept at 1400 °C for a certain time, the samples were cooled under pressure. The pressure was then released and the products were subjected to X-ray powder-diffraction analysis.

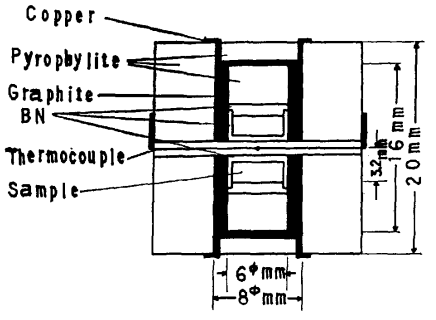

Fig. 1. Cell assemblage for a cubic anvil type high pressure apparatus.

Analysis. The analysis was carried out with a Rigaku Denki Geiger-Flex D-6C diffractometer, using Ni-filtered Cu-K_α radiation ($\lambda = 1.5418$ Å) at a scanning rate of 0.25° (2θ)/min. The diffractometer was calibrated with high-purity silicon.

The atomic ratio of rare-earth to vanadium in the products was determined by fluorescent X-ray analysis with a Rigaku Denki Fluorescent X-ray Analysis Unit.

The valence states of vanadium in the products were inferred from oxygen analysis, which was carried out by igniting the samples in an oxygen stream in order to oxidize all the vanadium ions in the products completely to V^{5+} and calculating their oxygen contents from the weight gain.

Measurements of the Physical Properties. The electrical conductivity measurements were carried out at room temperature (18±1 °C) using polycrystalline pellets, diam. *ca.* 4 mm and thickness 1 mm, by a d.c. two-probe method.

The magnetic suceptibility was measured with a Shimadzu magnetic balance MB-11 equipped with a low temperature apparatus built by members of the Shiokawa Laboratory in the temperature range 4—300 K.

Results and Discussion

The Reaction Products of Er_2O_3 or Yb_2O_3 with VO_2 at High Pressures. Er_2O_3 or Yb_2O_3–VO_2 1 : 2 mixtures were heated at 1400 °C and 50 or 30 kbar pressure. The atomic ratio of erbium or ytterbium to vanadium in the products was determined to be 1.0 by fluorescent X-ray analysis. The valence states of vanadium in the products were inferred from oxygen analysis. The results of oxygen analysis, valence states of vanadium ions and formulas of products obtained by high-pressure

TABLE 1. RESULTS OF OXYGEN ANALYSIS

Starting materials	Reaction conditions	Weight gain %	Valence state of V	Formula
$Er_2O_3+2VO_2$	1400 °C 50 kbar 30 min	5.93	3.0	$ErVO_{3.0}$
$Er_2O_3+2VO_2$	1400 °C 30 kbar 30 min	5.88	3.0	$ErVO_{3.0}$
$Yb_2O_3+2VO_2$	1400 °C 50 kbar 30 min	4.71	3.4	$YbVO_{3.2}$
$Yb_2O_3+2VO_2$	1400 °C 30 kbar 30 min	4.34	3.5	$YbVO_{3.3}$
$Yb_2O_3+2VO_2$	1400 °C 50 kbar 60 min	5.86	3.0	$YbVO_{3.0}$
$Yb_2O_3+2VO_2$	1400 °C 30 kbar 60 min	5.45	3.1	$YbVO_{3.1}$

synthesis are given in Table 1. We see that quadrivalent vanadium ions are reduced gradually to the trivalent states, formulas of the products being eventually $ErVO_3$ or$YbVO_3$.

X-Ray Diffraction Results. X-Ray diffraction data for vaterite (μ-$CaCO_3$)-type $ErBO_3$[7] and the reaction product of 1 : 2 mixtures of Er_2O_3 and VO_2 at 50 kbar are given in Table 2. The fact that the X-ray diffraction pattern for $ErVO_3$ is similar to that of the vaterite-type compound suggests that the compound crystallizes in the hexagonal space group $P6_3/mmc$, $a_0=3.762$ Å and $c_0=8.790$ Å.

X-Ray diffraction data for calcite-type $LuBO_3$[7] and $ErVO_3$ at 30 kbar are given in Table 3. Since the X-ray diffraction pattern for $ErVO_3$ is similar to that of calcite-type $LuBO_3$, the compound seems to crystallize in the rhombohedral (pseudo-hexagonal) space group $R\bar{3}c$-D_{3d}^6, $a_0=4.929$ Å and $c_0=16.429$ Å.

The density of $ErVO_3$ calculated from X-ray diffraction data was 7.99 g/cm³ for the perovskite-type,[8] 7.68 g/cm³ for the calcite-type and 8.25 g/cm³ for the vaterite-type structure. It is the first time that $ErVO_3$ with

TABLE 2. X-RAY DIFFRACTION DATA DOR VATERITE-TYPE $ErBO_3$ AND $ErVO_3$

	$ErBO_3$[7] Vaterite-type hexagonal $a_0=3.761$ Å $c_0=8.790$ Å		$ErVO_3$ $a_0=3.762$ Å $c_0=8.790$ Å		
hkl	d	I	d_{obsd}	d_{calcd}	I
002	4.38	30	4.39	4.40	90
100	3.25	100	3.25	3.26	100
101	3.05	12	3.05	3.05	5
102	2.62	75	2.62	2.62	70
004	2.20	8	2.20	2.20	20
103	2.18	2	—		—
110	1.880	40	1.880	1.881	42
104	1.821	30	1.820	1.821	30
112	1.729	30	1.728	1.729	20
200	1.629	14	1.629	1.629	15
202	1.527	18	1.527	1.527	12
006	1.462	2	1.465	1.465	5
114	1.429	8	1.429	1.429	7
106	1.335	6	1.335	1.336	11
204	1.309	8	1.308	1.309	4
210	1.231	8	1.232	1.231	5
212	1.186	12	1.186	1.186	8
116	1.155	4	1.156	1.156	2
008	—	—	1.099	1.099	6
300	1.086	6	1.087	1.086	7
214	1.074	6	1.073	1.074	5
302	1.055	4	1.055	1.054	3

TABLE 3. X-RAY DIFFRACTION DATA FOR CALCITE-TYPE $LuBO_3$ AND $ErVO_3$

	$LuBO_3$[7] Calcite-type pseudo-hexagonal $a_0=4.913$ Å $c_0=16.214$ Å		$ErVO_3$ $a_0=4.929$ Å $c_0=16.429$ Å		
hkl	d	I	d_{obsd}	d_{calcd}	I
012	3.76	95	3.78	3.79	80
104	2.933	100	2.96	2.96	100
006	2.699	10	2.73	2.74	10
110	2.453	55	2.47	2.47	30
113	2.235	8	2.25	2.25	7
022	2.057	45	2.07	2.07	32
024	1.883	25	1.890	1.894	15
018	1.828	30	1.850	1.851	20
116	1.817	55	1.833	1.832	30
122	1.577	25	1.585	1.583	10
$10\bar{1}0$	1.515	10	1.534	1.533	8
214	1.495	25	1.504	1.502	10
208	1.468	12	—		—
300	1.418	14	1.425	1.423	5
$00\bar{1}2$	1.351	4	—		—
$02\bar{1}0$	1.290	6	1.302	1.302	4
128	1.260	10	1.269	1.269	4
306	1.256	12	1.262	1.263	5
220	1.228	6	1.232	1.232	2
$11\bar{1}2$	1.184	8	1.197	1.197	8
$31\bar{2}$	1.168	8	—		—
$21\bar{1}0$	1.142	8	1.153	1.151	4
134	1.133	8	1.139	1.138	5

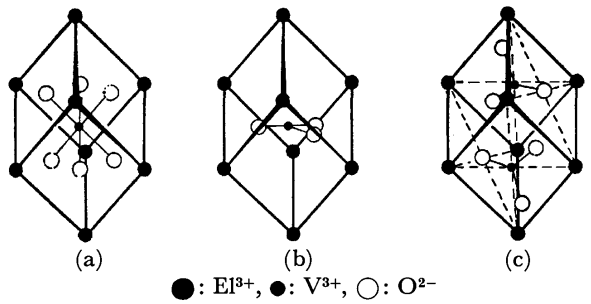

Fig. 2. Comparison of the three structure types of $ErVO_3$.
(a): Perovskite, (b): calcite, (c) vaterite.

density greater than that of perovskite has been obtained. The coordination of atoms in these three structure types is given in Fig. 2. In the vaterite-type structure (Fig. 2(c)), two vanadium ions and two of six oxygen ions are at the center of the faces, two of the oxygen ions in the unit cell, the remainder being out of the cell of the hexahedron consisting of eight erbium ions. $ErVO_3$ having calcite-type or vaterite-type structure, is a salt of Er^{3+} with VO_3^{3-}, rather than a mixed oxide of Er_2O_3 with V_2O_3 as in the perovskite-type $ErVO_3$.

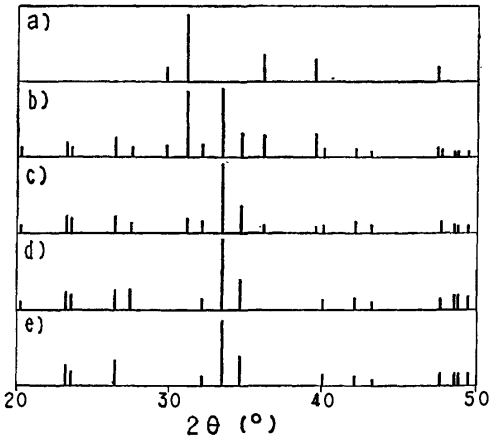

Fig. 3. X-Ray diffraction patterns.
a): Pyrochlore-type $Yb_2V_2O_7$, b): product obtained at 50 kbar for 30 min, c): product obtained at 50 kbar for 60 min, d): product obtained by reheating of c) at 1400 °C in a vacuum for 3 h, e): perovskite-type $YbVO_3$.

The X-ray diffraction patterns of the products obtained by the reaction of Yb_2O_3–VO_2 1 : 2 mixtures along with that of the pyrochlore-type $Yb_2V_2O_7$ and the perovskite-type $YbVO_3$ are shown in Fig. 3. When the reaction was carried out at 1400 °C and 50 kbar pressure for 30 min, a mixture of pyrochlore-type $Yb_2V_2O_7$ and perovskite-type $YbVO_3$ was obtained (Fig. 3(b)). It can be seen that the longer reaction time results in a decrease in $Yb_2V_2O_7$ and an increase in $YbVO_3$. In the reaction of Yb_2O_3 with VO_2, pyrochlore-type $Yb_2V_2O_7$ would be formed first and then transformed into a perovskite-type crystal gradually evolving its oxygen.

Crystal-structures Consideration. Rare-earth vanadites obtained from the reaction of rare-earth sesquioxides and divanadium trioxide at atmospheric or high pressure are perovskite-type compounds isomorphous with orthorhombic $GdFeO_3$. In the case of the reaction of Yb_2O_3 with VO_2 at high pressure, a pyrochlore-type compound $Yb_2V_2O_6O'$ (Fig. 4) is formed first. In this structure, V^{4+} ions occupy corner-shared octahedra and Yb^{3+} ions occupy an eightfold, hexagonal-bipyramid interstice. Two types of tetrahedrally coordinated anions can be distinguished: O^{2-} anions having two Yb^{3+} and two V^{4+} ions as near-neighbors; and O'^{2-} anions having four Yb^{3+} as near-neighbours. The O'^{2-} anions are located at the top and bottom of the apex-shared hexagonal bipyramids. The unique O'^{2-} anion might disappear at high pressure.

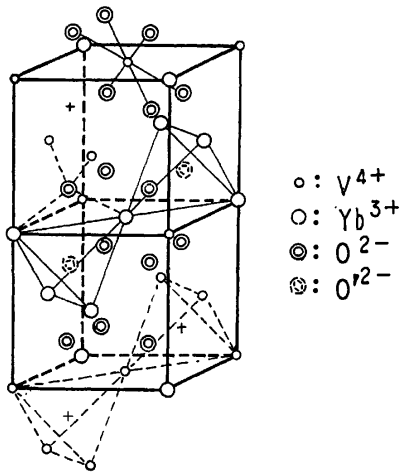

Fig. 4. Idealized crystal structure of a pyrochlore-type $Yb_2V_2O_6O'$ derived from a fluorite-type structure.

The defect pyrochlore $Yb_2V_2O_6$, in which a large electrostatic repulsion between Yb^{3+} cations facing each other across the anion vacancy is introduced, would be transformed easily into a perovskite-type $YbVO_3$ as the tolerance factor of the former was within the limit of perovskite-forming. The reaction product between Yb_2O_3 with VO_2 was a pyrochlore at atmospheric pressure and a perovskite at high pressure. However, in the case of the erbium sesquioxide, the radius ratio, r_{Er}/r_V is so great that no pyrochlore-type structure is formed.[4] It seems that the intermediate phase in the reaction of Er_2O_3 with VO_2 contains no octahedral-site vanadium as in the pyrochlore structure but V_2O_7 clusters of corner-shared tetrahedra or chains of paired trigonal bipyramidal sites sharing corners along a chain and between pairs. Elimination of shared O^{2-} ions would produce VO_3^{3-} clusters, leading to a calcite or vaterite structure.

Physical Properties of $ErVO_3$. The electrical conductivity at 18 °C was 1×10^{-3}, 2×10^{-7} and 1×10^{-7} $\Omega^{-1}\,cm^{-1}$ for perovskite-, calcite- and vaterite-type $ErVO_3$, respectively. The conductivity for calcite- or vaterite-type $ErVO_3$ was much lower than that for perovskite-type $ErVO_3$. This can be interpreted as follows: for perovskite-type $ErVO_3$ electrons are conducted by small polarons produced by anion defects,[8] while calcite- and vaterite-type $ErVO_3$ are salts of Er^{3+} with VO_3^{3-}.

Magnetic susceptibility measurements were carried out in the temperature range 4—300 K. Data for perovskite-type $ErVO_3$ and products obtained by high-pressure synthesis are summarized in Table 4. The

Table 4. Summary of magnetic properties

	Magnetic moment (μ_B)		T_N (K)
Perovskite-type $ErVO_3$	10.0	$T>110$ K	109
	9.3	$T<50$ K	
Calcite-type $ErVO_3$	8.9	$T>70$ K	65
	9.3	$T<50$ K	
Vaterite-type $ErVO_3$	8.8	$T>65$ K	65
	9.3	$T<50$ K	

fact that all the observed values of the magnetic moment for $ErVO_3$ at low temperatures are close to that for Er^{3+} ($\mu_{Er}{}^{3+}=9.4\ \mu_B$) shows that V^{3+} ions order antiferromagnetically at low temperature, and therefore, the observed transitions are attributable to antiferromagnetic ordering of the V^{3+} ions. The perovskite-type $ErVO_3$ is an antiferromagnet with a weak ferromagnetism because of antisymmetric exchange interaction below the transition temperature.[9] All the compounds were paramagnetic, the magnetic susceptibility following the Curie-Weiss law above the transition temperature.

The observed value of the magnetic moment for the perovskite-type $ErVO_3$ above the transition temperature is in good agreement with the calculated value ($\mu_{cal}=9.8\ \mu_B$), if we assume that there was no magnetic interaction between Er^{3+} ions and V^{3+} ions. However, the values for the calcite-type and the vaterite-type

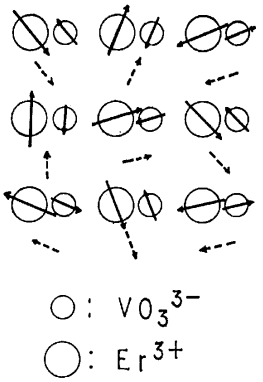

Fig. 5. Proposed orientation of the magnetic moment for the vaterite- or the calcite-type $ErVO_3$ above the transition temperature.

$ErVO_3$ are smaller than the calculated ones. The value of μ_{cal} was calculated by

$$\mu_{cal}=\sqrt{\mu^2_{Er}{}^{3+}+\mu^2_V{}^{3+}}$$

where $\mu_{Er}{}^{3+}=9.4\ \mu_B$ and $\mu_V{}^{3+}=2.8\ \mu_B$. The peculiar magnetic property of these compounds would be interpreted by means of the following. There is a magnetic interaction between an Er^{3+} ion and a V^{3+} ion to make their spins align antiparallel in a unit of $ErVO_3$ (Fig. 5). The net magnetic moment takes the value shown by dotted lines in the figure. The value calculated by $\mu_{cal}=\sqrt{\mu^2_{Er}{}^{3+}-\mu^2_V{}^{3+}}$ is $8.9\ \mu_B$, being in good agreement with the observed one for the calcite- and vaterite-type $ErVO_3$.

References

1) J. B. Goodenough, J. A. Kafalas, and J. M. Longo, "High-Pressure Synthesis," Academic Press, Inc., New York (1972).
2) G. J. McCarthy, C. A. Sipe, and K. E. McIlvried, *Mater. Res. Bull.*, **9**, 1279 (1974).
3) T. Shin-ike, unpublished data.
4) T. Shin-ike, G. Adachi, and J. Shiokawa, *Mater. Res. Bull.*, **12**, 1149 (1977).
5) T. Horlin, T. Niklewski, and M. Nygren, *Chim. Commun., Univ. Stockholm*, **1973**, 9; *Chem. Abstr.*, **79**, 26599h (1973).
6) M. Shimada, N. Ogawa, M. Koizumi, F. Dachile, and R. Roy, *Am. Ceram. Soc. Bull.*, **58**, 519 (1979).
7) E. M. Levin, R. S. Roth, and J. B. Martin, *Am. Min.*, **46**, 1030 (1960).
8) T. Sakai, G. Adachi, J. Shiokawa, and Shin-ike, *Mater. Res. Bull.*, **11**, 1295 (1976).
9) T. Sakai, G. Adachi, J. Shiokawa, and T. Shin-ike, *J. Appl. Phys.*, **48**, 379 (1977).

Anodic Stripping Semidifferential Electroanalysis of Mercury(II) at Gold Disk Electrode and Its Application to Environmental Analysis

Masashi GOTO,* Kazuhiko IKENOYA, and Daido ISHII

Department of Applied Chemistry, Faculty of Engineering, Nagoya University, Chikusa-ku, Nagoya 464

(Received April 26, 1980)

Anodic stripping semidifferential electroanalysis using a gold disk working electrode was proposed for the trace determination of mercury(II) ion, theoretical predictions being verified. A gold electrode was steeped in aqua regia, activated electrochemically before use, and rotated during the course of pre-electrolysis. A hydroxylamine hydrochloride medium was selected as supporting electrolyte. The detection limit was found to be *ca.* 0.5 nM under the pre-electrolysis conditions of 10 min at 0 V *vs.* Ag/AgCl. The relative standard deviation was *ca.* ±4% for the measurement at 2 nM level. Removal of the oxygen dissolved in sample solutions was not necessary. Experiments were carried out to examine the feasibility of the technique to environmental analysis. The method consists of only the following procedure: sample acidification, standard mercury(II) ion addition, UV irradiation pretreatment, and medium exchange for stripping. It was successfully applied to river water and sea water to separately evaluate ionic mercury, mercury occluded in organic matter, and total mercury (excluding mercury occluded in inorganic matter).

Environmental scientists realize the increasing nead for reliable methods which can differentiate and determine the chemical forms of trace toxic metals such as mercury in natural waters.[1] Sensitive analytical techniques such as neutron activation analysis and atomic absorption spectrophotometry are not applicable to speciation studies since they deal only with total metal concentration. Anodic stripping voltammetry determines only the labile ionic metal and might be utilized in speciation studies.

Voltammetric methods reported so far for the determination of mercury(II) ion make use of carbon electrodes such as wax-impregnated graphite,[2,3] glassy carbon,[4,5] and carbon paste.[6] However, the methods provide no satisfactory sensitivity for the environmental analysis of mercury(II) ion because of a relatively small affinity of the carbon electrodes with metallic mercury. Recently gold electrodes have drawn renewed attention for trace mercury analysis because of the large solubility of mercury in gold.[7] Sipos *et al.*[8,9] successfully applied the voltammetric method using one or two gold electrodes for the simultaneous determination of total copper and mercury in environmental samples. All the voltammetric methods reported so far for mercury analysis make use of the conventional linear sweep voltammetry at a slow potential scan rate, potentiometry, or differential pulse voltammetry for stripping process. No report seems to have appeared on the systematic speciation analysis of mercury in natural waters.

Goto and Ishii[10] and Dalrymple-Alford *et al.*[11,12] developed a new voltammetric technique "*semidifferential electroanalysis.*" It was applied to anodic stripping analysis of heavy metal ions except mercury(II) ion at a hanging mercury drop[13] and a thin mercury film electrode.[14] Semidifferential electroanalysis has been applied to detection in anodic stripping process at a gold electrode, facilitating the analysis of trace mercury-(II) ion. The method is recommended for simple speciation analysis of mercury in natural waters.

Theoretical

Consider a solution of reduced species in a thin layer of electrode. On oxidation the oxidized species diffuses into a solution of infinite thickness. The trace mercury deposited on a gold disk electrode from a mercury(II) ion solution may be regarded as a solution of mercury in a thin layer of gold. The electrode reaction is considered to be reversible without pre- or post-kinetics. In this case, the same approximate equation between the semiderivative of current, e, with respect to time, t, and the electrode potential, E, as that derived in anodic stripping process at thin mercury film electrode[14] holds under the conditions defined by the dimmentionless parameter, H, less than 1.6×10^{-3}. H is equal to $l^2\sigma/D'$ and $\sigma=nFv/RT$, l is the thickness of gold into which mercury diffuses, D' the diffusion coefficient of mercury in gold and v the potential scan rate, other symbols having their usual meanings. The theoretical e *vs.* E curve for anodic stripping process of mercury from a gold electrode has a maximum and a minimum (Fig. 1).[14] The height from the negative peak to the positive one is given by

$$e_{pp}=\frac{0.429n^{2.5}F^{2.5}Av^{1.5}t_pD^{2/3}N^{1/2}C}{\nu^{1/6}R^{1.5}T^{1.5}}, \quad (1)$$

the negative peak potential by

$$E_{np}=E_{1/2}-\frac{0.656RT}{nF}+\frac{1.15RT}{nF}\log H, \quad (2)$$

and the width between the negative peak and the positive one in the e *vs.* E curve for re-dissolution process of mercury accumulated on a rotating gold disk electrode by pre-electrolyzing trace mercury(II) ion in sample solution by

$$W_{pp}=\frac{2.52RT}{nF}, \quad (3)$$

where A is the electrode area, t_p the pre-electrolysis time, D the diffusion coefficient of mercury(II) ion in solution, N the revolution rate of electrode, C the concentration of mercury(II) ion, ν the kinematic viscosity, and $E_{1/2}$ the d.c. polarographic half-wave

potential. We see that the height is proportional to the mercury(II) ion concentration in sample, the one half powers of the potential scan rate, the square root of the revolution rate of electrode during pre-electrolysis, and the pre-electrolysis time.

Experimental

Apparatus and Reagents. The same apparatus as that reported[14] was used. The working electrode, a gold disk of thickness 0.5 cm and diam. 0.3 cm, was sealed into glass tubing, length 15 cm and i. d. 0.3 cm. The exposed surface of the disk was metallographically polished with emery paper, then with Al_2O_3 powder (0.05 μm) on an acrylic resin plate. The surface had been dipped in aqua regia for 1 min, rinsed with distilled and deionized water, and then kept in 0.5% $HCl \cdot NH_2OH$ solution until use. A rotating electrode assembly (Yanagimoto Co., model P8-RE) was used to rotate the gold disk electrode. The Ag/AgCl (satd KCl) and platinum spiral were used as reference and counter electrodes, respectively, and separated from the sample solution by an agar salt bridge.

The stock solution of 100 mM** $Hg(NO_3)_2$ was prepared by dissolving mercury (99.9999%) in nitric acid. The solution or the mercury standard solution of 1000 ppm for atomic absorption spectrophotometry was used as the standard mercury(II) solution. The stock solutions of 5 M H_2SO_4 and 5% $HCl \cdot NH_2OH$ were prepared for one of supporting electrolytes. All the reagents were of special grade, the solutions being diluted with distilled and deionized water. The cell and all vessels used for sample preparation were filled with 1 M HNO_3 or 0.5 M H_2SO_4 for 1 d, rinsed out, and then filled with distilled and deionized water before use.

Procedure. *Standard Sample*: 25 ml of a standard mercury(II) solution with excess supporting electrolyte was poured into the cell, three electrodes being set. First, the working electrode was rotated, a potential of 0.8 V (*vs.* Ag/AgCl) applied for 30 s to clean the surface of the working electrode, and the required deposition potential of mercury(II) ion was applied for certain time. After this, the rotation was stopped, the potential set to 0 V, and the potential anodically swept at a definite scan rate following a rest period of 30 s. For the re-dissolution process of deposited mercury, the *e vs. E* curve was measured at room temperature (≈20 °C). Next, the working electrode was rotated, a potential of 0.8 V being applied for 30 s, after which the rotation was stopped, the potential of electrode set to 0 V, and the potential anodically swept again at the same scan rate following a rest period of 30 s, to measure the blank *e vs. E* curve. The net *e vs. E* curve was corrected by means of the blank curve.

Environmental Sample: Inland water and sea water were collected in polyethylene bottles and immediately acidified to pH 1 with concd. H_2SO_4. An aliquot of 25 ml of the sample was placed in an open weighing vessel, spiked 25 μl of 30% H_2O_2, and irradiated for a certain time with UV light from a 18 W lamp. The sample was then cooled and the volume adjusted to 25 ml by supplying water to compensate the loss caused by irradiation. The gold disk electrode was activated electrochemically in 0.25 M H_2SO_4 containing 0.5% $HCl \cdot NH_2OH$ by cyclic polarization in the range 0.8—1.6 V at a scan rate of 100 mV/s and again at 0.8 V for 1 min. The electrode was set in the sample solution and electrolysis of mercury(II) ion was carried out at 0 V for 10 min under rotation (rpm 1800) without deaeration of solution. The electrode was then transferred promptly to a medium of 0.25 M H_2SO_4 containing 0.5% $HCl \cdot NH_2OH$. The potential was anodically swept from 0 V to 0.8 V at a scan rate of 100 mV/s following quiet polarization for 30 s at 0 V . The blank *e vs. E* curve was constructed in the same way as in the case of standard sample, electrochemical activation of the electrode being carried out in the same medium. 10 μl of mercury(II) standard solution was then added to the sample solution, the above procedure being repeated to determine mercury.

** 1 M = 1 mol dm^{-3}.

Results and Discussion

e vs. E *Curve in Anodic Stripping Process.* Figure 1 shows a typical *e vs. E* curve of the re-dissolution process of mercury deposited on the gold disk electrode, the corresponding *i vs. E* curve being given for comparison. The dotted *e vs. E* and *i vs. E* curves indicate the blank curves measured after cleaning the gold electrode at 0.8 V for 30 s under rotation. As predicted theoretically, a maximum and a minimum were observed in the *e vs. E* curve for stripping process. We see that the *e vs. E* curve has the following advantages over the ordinary *i vs. E* curve. It is easy to estimate the height from the negative peak to the positive one rather than the peak height from the base line. From a comparison of both blank curves, the semidifferentiation of the *i vs. E* curve seems to reduce the interference of charging current.

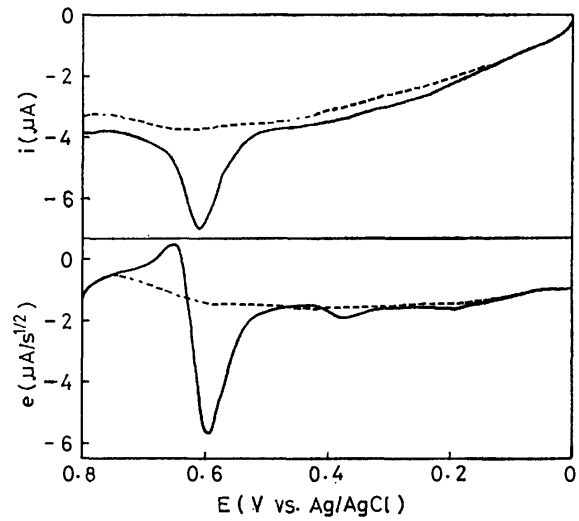

Fig. 1. Typical *e vs. E* curve for the re-dissolution of mercury deposited on the gold disk electrode. Sample: 98.4 nM Hg (II) in 0.25 M H_2SO_4 plus 0.5% $HCl \cdot NH_2OH$, potential scan rate: 100 mV/s, electrode area: 7.07 mm^2, pre-electrolysis potential: 0 V *vs.* Ag/AgCl, pre-electrolysis time: 5 min at rotating electrode and then 30 s at standing one, revolution rate of electrode: 1800 rpm. Dotted lines show the blank curves.

Effect of Supporting Electrolyte. Various supporting electrolytes including sulfuric acid, hydrochloric acid, potassium chloride, potassium thiocyanate, and hydroxylamine hydrochloride were investigated. In a sulfuric acid medium, the anodic stripping waves of mercury appeared at *ca.* 0.9 V, its reproducibility not being

satisfactory. The oxidation of thiocyanate started from *ca.* 0.6 V in thiocyanate medium. A nice stripping wave of mercury was observed in all chloride media (Fig. 1). Since the hydroxylamine hydrochloride medium gave the most reproducible wave in the three chloride media, hydroxylamine hydrochloride was chosen as the supporting electrolyte in addition to 0.25 M H_2SO_4.

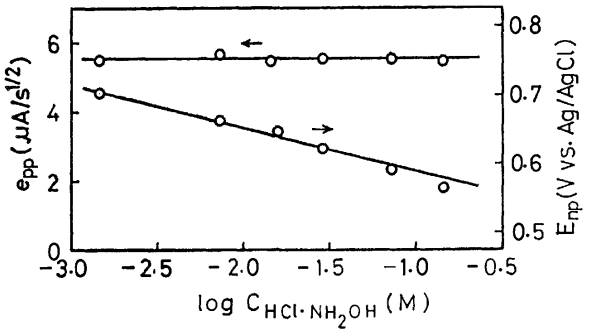

Fig. 2. Dependence of height from the negative peak to the positive one and negative peak potential of *e vs. E* curve for the re-dissolution process on concentration of $HCl \cdot NH_2OH$. Conditions except concentration of $HCl \cdot NH_2OH$ are the same as in Fig. 1.

Figure 2 shows the effect of $HCl \cdot NH_2OH$ concentration in the supporting electrolyte on e_{pp} and E_{np} in the *e vs. E* curve for anodic stripping process. e_{pp} was found to be independent of $HCl \cdot NH_2OH$ concentration. E_{np} shifted to negative potential side with increase in concentration, being linear with its logarithm. This indicates that mercurous ion forms complex with chloride ion:

$$Hg_2^{2+} + pCl^- \rightleftarrows Hg_2Cl_p^{(2-p)-} \quad (4)$$

the electrode reaction being

$$2Hg + pCl^- \rightleftarrows Hg_2Cl_p^{(2-p)-} + 2e \quad (5)$$

where p is the number of ligands involved in the complex. The d.c. polarographic half-wave potential for the electrode reaction of Eq. 5 is given by

$$E_{1/2} = E_s - \frac{RT}{2F} \ln \beta - \frac{pRT}{2F} \ln [Cl^-] \quad (6)$$

where E_s is the standard redox potential of $Hg_2^{2+}/2Hg$ couple and β the stability constant of the chemical reaction of Eq. 4. Thus E_{np} in the *e vs. E* curve should vary linearly with the logarithm of chloride concentration, since E_{np} is the simple function of $E_{1/2}$ (Eq. 2). The slope of the line for E_{np} *vs.* log $C_{HCl \cdot NH_2OH}$ was -62 mV, being comparable with the value -58 mV calculated from $-2.303\ RT/F$. The number of ligand involved in the complex is thus two.

For mercury analysis, the concentration of 0.5% $HCl \cdot NH_2OH$ seems to be most suitable, since the gold electrode itself starts to dissolve from about 0.8 V. A small unknown peak appears at *ca.* 0.4 V, the re-dissolution wave of mercury at this concentration appearing at *ca.* 0.6 V, not overlapping with the undesirable waves.

Pre-electrolysis Potential. The dependence of pre-electrolysis potential on e_{pp} in anodic stripping process was examined. e_{pp} was constant, independent of the pre-electrolysis potentials from 0.4 to -0.9 V. The pre-electrolysis potential of 0 V was chosen for mercury analysis. No influence of dissolved oxygen was observed, removal of oxygen in the solution thus being unnecessary.

Dependence of e_{pp} *on* t_p, v, N, *and* C. The relationship between e_{pp} and t_p at different concentrations was measured by keeping all other parameters constant (Fig. 3). e_{pp} was linear with pre-electrolysis time at rotating electrode up to 5 min at concentration of *ca.* 100 nM and 10 min at that of 10 nM. The positive intersepts with ordinate correspond to the pre-electrolysis for 30 s under standing electrode. Figure 4 shows the relationship between e_{pp} and v, and N. The line of e_{pp} *vs.* $v^{1.5}$ passed through the origin, e_{pp} being

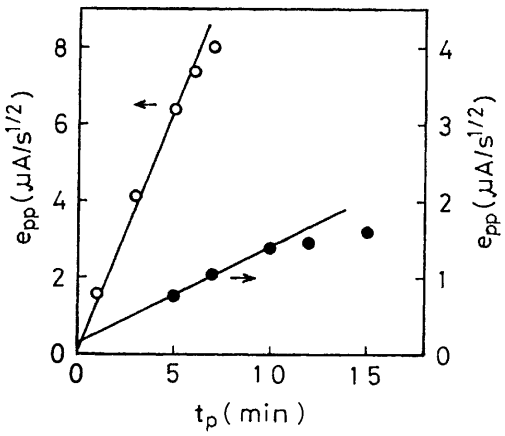

Fig. 3. Relationship between height from the negative peak to the positive one of *e vs. E* curve for the re-dissolution process and pre-electrolysis time at the rotating electrode. Concentration of Hg (II): ○ 98.4 nM, ● 9.8 nM, other conditions are the same as in Fig. 1.

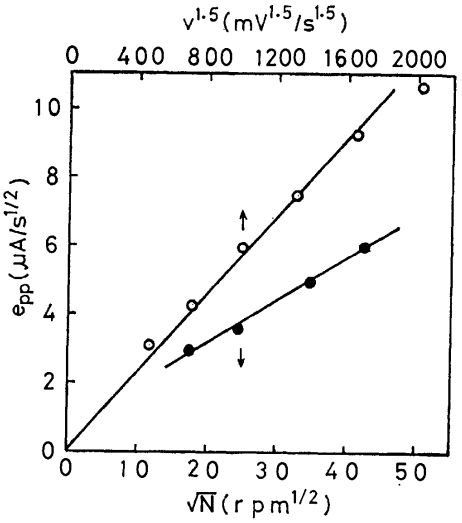

Fig. 4. Relationship between height from the negative peak to the positive one of *e vs. E* curve for the re-dissolution process and potential scan rate (○), and revolution rate of electrode (●). Conditions except potential scan rate (○), and revolution rate of electrode (●) are the same as in Fig. 1.

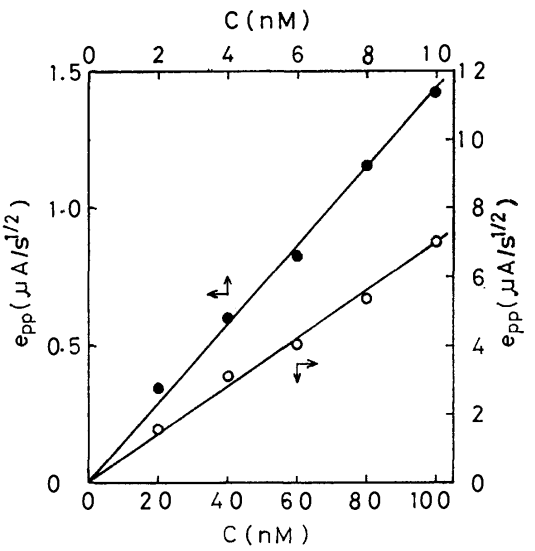

Fig. 5. Relationship between height from the negative peak to the positive one of *e vs. E* curve for the redissolution process and concentrations of Hg (II) present in original solution. Pre-electrolysis time: 5 min for (○), 10 min for (●) at rotating electrode and then 30 s at standing one, other conditions are the same as in Fig. 1.

linear with $N^{1/2}$. Figure 5 shows the relationship between e_{pp} and C at different concentration levels. The pre-electrolysis time employed was 5 min at 10 nM level and 10 min at 1 nM level, respectively. In both cases, e_{pp} was linear with C, the lines passing through the origin.

The results indicate that Eq. 1 applies in the anodic stripping process of mercury from the gold disk electrode.

Dependence of E_{np} *and* W_{pp} *on* C *and* v. The results are given in Table 1. E_{np} is independent of mercury(II) ion concentration to average 0.594 V at the scan rate of 100 mV/s, shifting towards the positive side with increasing scan rate as seen from Eq. 2. W_{pp} averaged *ca.* 52 mV, as compared with the theoretical value of 29 mV for two-electron transfer calculated by means of Eq. 3. This indicates that the electrode reaction (Eq. 5) is not completely reversible.

Table 1. Negative peak potential and width between negative and positive peak of *e vs. E* curve for redissolution process at different concentrations and potential scan rates[a)]

C(nM)	v(mV/s)	E_{np}(V *vs.* Ag/AgCl)	W_{pp}(mV)
19.7	100	0.590	49
39.4	100	0.593	50
59.0	100	0.596	51
78.7	100	0.592	51
98.4	100	0.597	52
98.4	60	0.592	52
98.4	80	0.596	52
98.4	120	0.600	53
98.4	140	0.603	59
98.4	160	0.600	57

a) Supporting electrolyte: 0.25 M H_2SO_4 plus 0.5% $HCl \cdot NH_2OH$, electrode area: 7.07 mm^2, pre-electrolysis potential: 0 V *vs.* Ag/AgCl, pre-electrolysis time: 5 min at rotating electrode and then 30 s at standing one, revolution rate of electrode: 1800 rpm.

Table 2. Relationship between height from negative to positive peak of *e vs. E* curve for re-dissolution process and sweep number at different concentrations[a)]

Sweep number	e_{pp}(μA/s$^{1/2}$) (A)	e_{pp}(μA/s$^{1/2}$) (B)[b)]
1	1.43	0.33
2	1.46	0.32
3	1.41	0.33
4	1.41	0.30
5	1.50	0.32
6		0.33
7		0.30
8		0.33
av.	1.44	0.32
r.s.d.	±3%	±4%

a) Sample: (A) 9.8 nM, (B) 2.0 nM Hg (II), pre-electrolysis time: 10 min at rotating electrode and then 30 s at standing one, other conditions are the same as in Table 1. b) Working electrode was dipped in aqua regia for 1 min befor each measurement.

Analytical Aspects. Table 2 gives the reproducibility for successive measurements of e_{pp} on the same aliquot at different concentrations. The relative standard deviations were ±3% for 10 nM and ±4% for 2 nM. The detection limit of mercury(II) ion was 0.5 nM at the potential scan rate of 100 mV/s and pre-electrolysis time of 10 min.

Application to Environmental Analysis. In order to examine the applicability of the gold electrode for the determination of mercury(II) ion in natural waters, experiments were carried out to see whether the stripping process can be directly performed in natural water

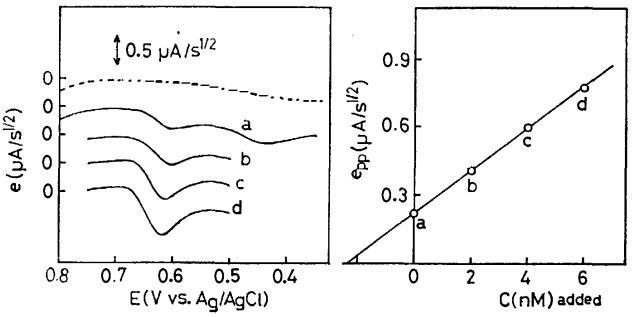

Fig. 6. Performance of anodic stripping semidifferential electroanalysis after medium exchange for 0.25 M H_2SO_4 plus 0.5% $HCl \cdot NH_2OH$ before stripping and regression line for mercury determination by the standard addition method in river water without UV irradiation pretreatment. a: unspiked, b: 2 nM spiked, c: 4 nM spiked, d: 6 nM spiked, pre-electrolysis time: 10 min at rotating electrode and 30 s at standing one after medium exchange, other conditions are the same as in Fig. 1.

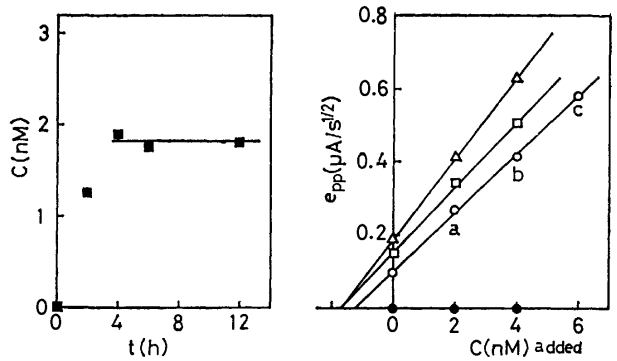

Fig. 7. Effect of pretreatment by UV irradiation on mercury determination in river water by anodic stripping semidifferential electroanalysis after medium exchange. UV irradiation time, t, (h): ● 0, ○ 2, □ 6, △ 12, other conditions are the same as in Fig. 6.

spiked with 0.25 M H_2SO_4 and 0.5% $HCl \cdot NH_2OH$. We were unable to establish the conditions including various electrode pretreatment to get a definite stripping peak of mercury. However, satisfactory results were obtained when the medium was exchanged for the supporting electrolyte solution of 0.25 M H_2SO_4 containing 0.5% $HCl \cdot NH_2OH$ after pre-electrolysis and the gold electrode was electrochemically activated before each run (see Experimental).[9] Figure 6 shows the e *vs.* E curves for the re-dissolution process of mercury after medium exchange following pre-electrolysis in the river water spiked with only 0.05 M H_2SO_4 at different standard mercury(II) ion additions, and the regression line for the determination of mercury in the river water with no pretreatment. The relationship between mercury(II) ion concentration added and e_{pp} remained linear. Samples from river waters frequently contain a large amount of dissolved, colloidal, and particulate organic matter. They must be subjected to UV irradiation to release trace mercury bound to, adsorbed on, and occuluded in components of organic matter by photolytic decomposition by addition of a small amount of H_2O_2. Figure 7 shows the effect of UV irradiation on e_{pp} for mercury analysis at different irradiation times. When the sample was not subjected to UV irradiation, no anodic stripping wave was observed even after standard mercury(II) ion addition. UV irradiation for 2 h with a 18 W lamp gave a regression line similar to that in Fig. 6, the slope increasing with increase in irradiation time. This indicates that the photolytic decomposition of organic matter progresses with irradiation time. The regression concentrations coincide with each other at irradiation times longer than 6 h (Fig. 7), the regression concentration indicating concentration at the intercept of regression line with abscissa.

Mercury Speciation in Natural Waters. The chemical forms of trace heavy metals in natural waters can be classified into the following groups with a slight modification of those given by Florence and Batley:[1] (1) simple hydrated metal ions, (2) labile metal-inorganic complexes, (3) labile metal-organic complexes, (4) stable metal-inorganic complexes, (5) stable metal-organic complexes, (6) metal adsorbed on inorganic colloids and particulate matter, (7) metal adsorbed on organic colloids and particulate matter, (8) metal occluded in inorganic colloids and particulate matter, (9) metal occluded in organic colloids and perticulate matter.

Anodic stripping voltammetry measures only the labile metal ions in (1)—(3) detecting no metal in other chemical form. UV irradiation with H_2O_2 oxidizes organic matter in solution to liberate metal in (5), (7), and (9). The metal-complexing and adsorbing capacity of natural water[15-18] can be determined by the standard addition method in anodic stripping voltammetry. When all metal-complexing and adsorbing material has been consumed, there will be a sudden increase in the slope of regression line. The break point represents the complexing and adsorbing capacity of the water. The slope before the break point would depend on the complexing and adsorbing ability of natural water, while the slope after it should agree with that in pure water.

In the chemical speciation analysis of mercury in river water and sea water by the standard addition method with and without UV irradiation pretreatment (Fig. 8), filtration of natural waters was not carried out in order to eliminate the contamination or loss of mercury. The total labile mercury(II) ions in (1)—(3) can be estimated from e_{pp} obtained with no standard addition and without UV irradiation and the slope of calibration curve in Fig. 5. The regression concentration without UV irradiation may represent the total mercury in (1)—(7), while that with UV irradiation the total mercury in (1)—(7) and (9). The coinciding

Table 3. Examples of mercury concentrations in some forms existing in natural waters

Species of mercury	Sample	
	River water	Sea water
Total ionic mercury	0.2 nM	1.0 nM
Mercury occluded in organic matter	0.9 nM	3.9 nM
Total mercury (excluding mercury occluded in inorganic matter)	1.2 nM	6.0 nM

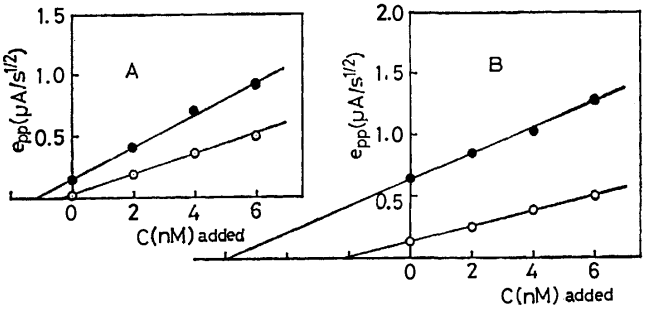

Fig. 8. Typical chemical speciation analysis of mercury in natural waters by the standard addition method with and without UV irradiation pretreatment. Sample: (A) river water, (B) sea water, UV pretreatment: ○ non, ● 12 h at 18 W lamp, other conditions are the same as in Fig. 6.

regression concentrations (Fig. 7) indicate that total mercury excluding (8) can be estimated so far as all mercury in (9) has been liberated, even though the decomposition of organic matter in solution is not complete. The difference between the regression concentrations with and without UV irradiation corresponds to the mercury in (9). When the decomposition of organic matter is complete, e_{pp} obtained with no standard addition and UV irradiation reflects roughly the total mercury in (1)—(3), (5), (7), and (9). Table 3 gives the analytical results of river water and sea water (Fig. 8). The proposed technique for chemical speciation of mercury is applicable to not only inland waters but also sea water.

References

1) T. M. Florence and G. E. Batley, *Talanta*, **24**, 151 (1977).
2) S. P. Perone and W. J. Kretlow, *Anal. Chem.*, **37**, 968 (1965).
3) R. Fukai and L. Huynh-Ngoc, *Anal. Chim. Acta*, **83**, 375 (1976).
4) T. Miwa and A. Mizuike, *Jpn. Analyst*, **17**, 448 (1968).
5) D. Jagner, *Anal. Chim. Acta*, **105**, 33 (1979).
6) L. Ulrich and P. Ruegsegger, *Fresenius Z. Anal. Chem.*, **277**, 349 (1975).
7) R. W. Andrews, J. H. Larochelle, and D. C. Johnson, *Anal. Chem.*, **48**, 212 (1976).
8) L. Sipos, P. Valenta, H. W. Nurnberg, and M. Branica, *J. Electroanal. Chem.*, **77**, 263 (1977).
9) L. Sipos, J. Golimmowski, P. Valenta, and H. W. Nurnberg, *Fresenius Z. Anal. Chem.*, **298**, 1 (1979).
10) M. Goto and D. Ishii, *J. Electroanal. Chem.*, **61**, 361 (1975).
11) P. Dalrymple-Alford, M. Goto, and K. B. Oldham, *J. Electroanal. Chem.*, **85**, 1 (1977).
12) P. Dalrymple-Alford, M. Goto, and K. B. Oldham, *Anal. Chem.*, **49**, 1390 (1977).
13) M. Goto, K. Ikenoya, M. Kajihara, and D. Ishii, *Anal. Chim. Acta*, **101**, 131 (1978).
14) M. Goto, K. Ikenoya, and D. Ishii, *Anal. Chem.*, **51**, 110 (1979).
15) R. G. Smith, *Anal. Chem.*, **48**, 74 (1976).
16) T. M. Florence and G. E. Batley, *J. Electroanal. Chem.*, **75**, 791 (1977).
17) E. A. Schonberger and W. F. Pickering, *Talanta*, **27**, 11 (1979).
18) K. Matsunaga, H. Tsujioku, S. Fukasa, and K. Hasebe, *Bull. Chem. Soc. Jpn.*, **51**, 3519 (1978).

 © 1980 The Chemical Society of Japan Bull. Chem. Soc. Jpn., 53, 3573—3576 (1980)

Thermal Decomposition Reactions of Analogous Penta-amminenitrosylcobalt(III) Complexes

Kikuo Miyokawa,* Hakaru Masuda, and Isao Masuda

Department of Chemistry, Faculty of Science, Fukuoka University, Nanakuma, Nishi-ku, Fukuoka 814

(Received April 30, 1980)

The thermal behavior of five complexes, $[Co(NH_3)_6]Cl_3$ (**1**), $[Co(NH_3)_5NO_2]Cl_2$ (**2**), $[Co(NH_3)_5NO]Cl_2$ (**3**), $[(NH_3)_5Co\text{–}N(O)\text{–}NO\text{–}Co(NH_3)_5]Cl_4\cdot 2H_2O$ (**4**), and $[(NH_3)_5Co\text{–}NO\text{–}ON\text{–}Co(NH_3)_5]Cl_4\cdot 4H_2O$ (**5**), has been investigated. The pyrolysis-gaschromatographic technique has been successfully applied to the N_2- and N_2O-analyses of the gases evolved on the pyrolysis of the complexes. The thermal decomposition of these complexes is characterized predominantly by the reduction process of Co(III) to Co(II). In the simple nitrosyl **3**, the NO^- group reduces the Co(III) ion and dissociates as NO. As for the remaining complexes, a thermally induced transient-state tends to dissociate H^+ from the coordinated ammonia as follows: $Co^{III}\text{–}NH_3 \rightarrow [Co^{III}\text{–}NH_2^{\delta-}\cdots H^{\delta+}] \rightarrow Co^{II} + NH_2 + H^+$. The NH_2 species is subsequently decomposed as $NH_2 \rightarrow 2/3NH_3 + 1/6N_2$. Moreover, H^+ is captured by an anionic species and/or the NH_3 present in the system, that is, by Cl^- and NH_3 forming NH_4Cl in the case of **1**, by NO_2^- and NH_3 forming NH_4NO_2, which then decomposes to N_2 and H_2O, in **2**, and by $N_2O_2^{2-}$ forming $H_2N_2O_2$, which then decomposes to N_2O and H_2O, in **4**. The **5** complex undergoes an exothermic decomposition, affording a larger amount of N_2 and N_2O than those to be expected from the above stoichiometry, suggesting an oxidative behavior of the bridged, dimeric $(\text{–NO–ON–})^{2-}$ group towards ammonia.

Three isomeric compounds with the unitary composition of $[Co(NH_3)_5NO]X_2$, where X=Cl or NO_3, have so far been isolated by the reaction of gaseous NO with an ammoniacal solution of cobalt(II) salt.[1,2] X-Ray diffraction studies have confirmed that the black isomer (Black salt), obtained when the reaction is carried out at −10 °C, is a monomeric nitrosyl complex in which a NO^- group is bound to the cobalt atom in a bent manner,[3] while the red isomer (Red-I salt), obtainable by a similar reaction carried out at room temperature, is a binuclear complex in which two of the $Co(NH_3)_5$ groups are bridged through a *cis*-hyponitrite group, $(\text{–N(O)–NO–})^{2-}$.[4] Recently Miki and Ishimori[2] have isolated another red isomer (Red-II salt) by reacting NO at *ca.* 0 °C with an ammoniacal cobalt(II) solution which had previously been exposed to air for 20 h at *ca.* 20 °C. On the basis of IR and ^{15}N-NMR spectral investigations, they have identified this isomer as a binuclear complex including a $(\text{–NO–ON–})^{2-}$ group bridging two cobalt atoms of $Co(NH_3)_5$ groups.

As these isomers are thought to include intermediary forms of the NO group in a variety of compounds, it seems that it would be interesting to clarify the chemical properties of these isomers. In this work, their pyrolytic behavior in the solid state has been investigated.

Experimental

Materials. $[Co(NH_3)_6]Cl_3$,[5] $[Co(NH_3)_5NO_2]Cl_2$,[6] $[Co(NH_3)_5NO]Cl_2$ (Black salt),[1] $[(NH_3)_5Co\text{–}N(O)\text{–}NO\text{–}Co(NH_3)_5]Cl_4\cdot 2H_2O$ (Red-I salt),[2] and $[(NH_3)_5Co\text{–}NO\text{–}ON\text{–}Co(NH_3)_5]Cl_4\cdot 4H_2O$ (Red-II salt)[2] were prepared according to the published procedure; they were identified by means of cobalt analyses and a study of their infrared spectra.

Measurements. Thermogravimetric (TG) and differential scanning calorimetric (DSC) curves were recorded on a Rigaku Denki thermal analyzer, Model 8002. The measurements were carried out in a nitrogen atomosphere and at a heating rate of 5 °C/min. A 20-mg aliquot of the sample was used. The analyses of the gases evolved were carried out by means of TCD-gaschromatography using a YANAKO G 80 instrument equipped with a YANAKO G 1018 pyrolysis pippeter.[7] A 2.0-mg aliquot of the sample was injected into the pyrolysis pippeter, whose furnace had been kept at the desired temperature; the sample was pyrolyzed rapidly in a helium gas, and the gaseous products were then swept by the helium-gas carrier into the separation column. A stainless steel column (size, 1.5 m×3 mm i.d.; packing, Molecular Sieve 5A, 60/80 mesh or Porapak S, 50/80 mesh) was used. The column and TCD temperature were maintained at 50 °C and 60 °C respectively. The flow rate of carrier gas was 25 cm³/min. The calibration curves for the N_2 and N_2O determinations were made by means of the direct injection of pure gas (0 to 0.25 cm³) into the separation column using a microsyringe; the peak area was measured by means of an integrator. The amount of ammonia evolved was determined by trapping it through bubbling into a standard 0.05 M-sulfuric acid solution and by then titrating the excess acid with a standard 0.1 M-sodium hydroxide solution. The magnetic susceptibility measurements were carried out by the Faraday method. The instrument was calibrated using $[Ni(en)_3]S_2O_3$ as the standard.[8] The IR spectra were recorded on a KBr disk using a Hitachi 345 infrared spectophotometer.

Results

The TG and DSC curves of three isomers are reproduced in Fig. 1, while the analytical results of the gaseous products on pyrolysis are shown in Table 1 and Fig. 2.

As Fig. 1-a shows, Black salt exhibits three endothermic DSC peaks, with maximum temperatures at 135, 230, and 295 °C. Step-by-step weight-losses of 32.2, 6.2, and 7.1% are observed in the TG curve; these seem to correspond to the above DSC peaks. These losses are comparable to those of 31.1, 6.9, and 6.9% calculated by assuming the elimination of 3 mol of ammonia and 1 mol of nitrogen monoxide, of 1 mol of ammonia, and of one further mole of ammonia, respectively. Black salt is well characterized by the IR absorption due to the coordinated NO^- group at 1620 cm^{-1},[9] while the pyrolysis of Black salt at 180 °C resulted in leaving a compound which showed no characteristic absorption in the same range. The results of gas analyses are considered to indicate that,

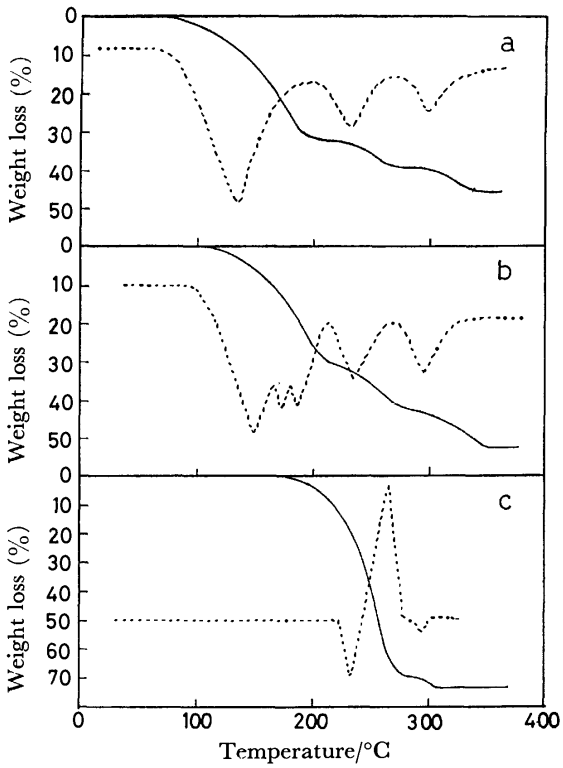

Fig. 1. TG and DSC curves obtained in nitrogen atmosphere.
a: $[Co(NH_3)_5NO]Cl_2$ (Black salt), b: $[Co_2(NH_3)_{10}N_2O_2]Cl_4 \cdot 2H_2O$ (Red-I salt), c: $[Co_2(NH_3)_{10}N_2O_2]Cl_4 \cdot 4H_2O$ (Red-II salt), TG:——, DSC: ——.

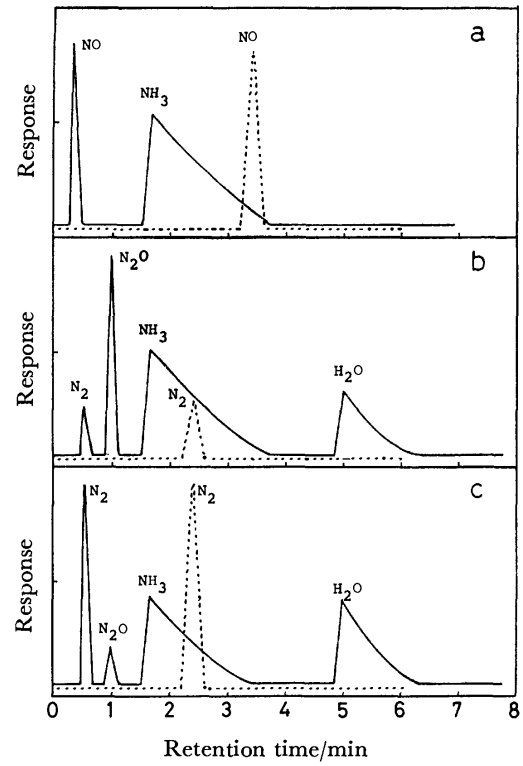

Fig. 2. Pyrolysis gaschromatograms.
a: $[Co(NH_3)_5NO]Cl_2$ (Black salt), pyrolyzed at 200 °C, b: $[Co_2(NH_3)_{10}N_2O_2]Cl_4 \cdot 2H_2O$ (Red-I salt), pyrolyzed at 290 °C, c: $[Co_2(NH_3)_{10}N_2O_2]Cl_4 \cdot 4H_2O$ (Red-II salt), pyrolyzed at 310 °C. Adsorbent: Porapak S: ——, molecular Sieve 5A: -·-·-.

upon pyrolysis at 290 °C, 1 mol of Black salt produces almost quantitatively 1 mol of nitrogen monoxide and 5 mol of ammonia.

The DSC curve of Red-I salt is rather more complicated than that of Black salt, being composed of five endothermic peaks at 150, 170, 185, 230, and 290 °C. The apparent total weight-loss up to 350 °C in the TG curve is 52.3%, which is close to the value of 50.7%, calculated by assuming the final product to be cobalt(II) chloride. The gas-analytical data in Table 1 show that, on the pyrolysis of Red-I salt at 170 °C, only *ca.* 2 mol of ammonia are dissociated, accompanied by water of crystallization. However, pyrolysis at 220 °C causes the evolution of nitrogen and dinitrogen oxide besides ammonia and water. The compound obtained by pyrolyzing Red-I salt at 220 °C contained 27.2% of cobalt and 31.1% of chloride, and showed a magnetic susceptibility of 37.7 cgs. The apparent magnetic moment for the compound is, then, calculated as 4.4 B.M. on the basis of the cobalt content; it falls in the range of the magnetic moments of the high-spin-type Co(II) complexes.[10] By taking these observations into account, the DSC curve of Red-I salt may be interpreted as follows: the first endothermic peak, at 150 °C, corresponds mainly to the dehydration process; the second one, at 170 °C, to the elimination process of a part of the coordinated ammonia, and the third one, at 185 °C, to the decomposition of the coordinated hyponitrite group to dinitrogen oxide and the oxidation process of a coordinated ammonia to nitrogen, as will be discussed later.

The DSC curve of Red-II salt shown in Fig. 1-c is composed of an endothermic peak with a maximum temperature at 230 °C and a large exothermic peak at

Table 1. Analytical data of gaseous products evolved on pyrolysis

Complex	Temp °C	N_2	N_2O	NO[a]	NH_3	H_2O[a]
		(Mol of evolved gas/mol of complex)				
Black salt	200	0.00	0.00	1[b]		
	290	0.07	0.00	1[b]	4.91	
Red-I salt	150	0.00	0.00	—	0.30	○
	170	0.00	0.00	—	1.81	○
	220	0.32	0.96	—		○
	290	0.39	0.96	—		○
Red-II salt	230	0.00	0.00	—		○
	310	2.70	0.21	—		○
$[Co(NH_3)_6]Cl_3$	310	0.17	0.00	—	4.66	
$[Co(NH_3)_5NO_2]Cl_2$	280	1.16	0.00	—	3.62	○

a) Since the calibration curves for these gases could not be obtained under the present experimental conditions, only qualitative data are given for NO and H_2O. Observation of the GC-peak due to H_2O is noted with ○; no observation of the GC-peak due to NO is noted with —. b) The apparent GC-peak of NO is ascribed to a quantitative elimination of NO, for the complex gives no, or only a minor quantity of N_2 and/or N_2O.

265°C, followed by a small endothermic peak at 280 °C. The weight-loss up to 350 °C in the TG curve is 71.0%. Miki and Ishimori[2] have reported, on the basis of the DTA data, that Red-II salt undergoes endothermic dehydration at 220 °C and then vigorous exothermic decomposition at 260 °C. The gas-analytical results shown in Table 1 reveal that only water is evolved on pyrolysis at 230 °C. The IR characteristic bands at 1480, 1280, and 1020 cm^{-1} assigned to the coordinated $(-NO-ON-)^{2-}$ group were observed for the product obtained after pyrolyzing Red-II salt at 230 °C, but not for the product at 265 °C. Nitrogen, dinitrogen oxide, ammonia, and water were detected in the gaseous product evolved on the pyrolysis of this salt at 280 °C; ammonium chloride was also found to be produced. The pyrolysis at 350 °C resulted in leaving a mixture of cobalt(II) chloride and cobalt(III) oxide, which were identified by means of the IR spectrum.

Discussion

The experimental results are indicative of the following pyrolysis process of Black salt:

$$[Co^{III}(NH_3)_5NO]Cl_2 \longrightarrow Co^{II}(NH_3)_2Cl_2 + (3NH_3 + NO)\uparrow$$
$$Co(NH_3)_2Cl_2 \longrightarrow Co(NH_3)Cl_2 + NH_3\uparrow$$
$$Co(NH_3)Cl_2 \longrightarrow CoCl_2 + NH_3\uparrow.$$

Black salt has been depicted formally as having the bonding unit Co(III)–NO^-. Thus, the thermal decomposition in the first stage may be initiated by the electron transfer from the NO^- group to the central Co(III) ion, accompanied by the concomitant elimination of nitrogen monoxide and ammonia. Moreover, the sequence of dissociating ammonia is analogous with that of hexaamminecobalt(II) chloride, which subsequently gives diamminecobalt(II) chloride, monoamminecobalt(II) chloride, and finally cobalt(II) chloride, dissociating ammonia.[11]

Red-I salt includes a *cis*-hyponitrite group bridging two $Co(NH_3)_5$ groups. As is shown in Table 1, the pyrolysis of Red-I salt at $\geqslant$220 °C evolves nitrogen and dinitrogen oxide, besides ammonia and water; the total amount of the former two is more than one mole per mole of the complex. These facts indicate that the nitrogen in these two gases does not originate only from the hyponitrite group. Miki and Ishimori[2] have confirmed that the ammonia groups do not participate in the formation reaction of dinitrogen oxide, for the characteristic $^{14}N^{15}NO$ absorption is not observed in the IR spectrum of the gaseous product obtained by the pyrolysis of Red-I salt, which contains the ^{15}N-substituted hyponitrite group. The formation of nitrogen has not been taken into consideration.

In the investigations of pyrolytic behavior, it has been known that hexaamminecobalt(II) chloride decomposes liberating ammonia and gives cobalt(II) chloride,[11] whereas hexaamminecobalt(III) chloride decomposes in a different manner, depending on the conditions employed.[12-14] On the basis of the results obtained by means of the GEA method, where pyrolysis was carried out in a helium atmosphere and at a heating rate of 1 °C/min, Onodera[12] has recently demonstrated that the latter cobalt(III) complex produces nitrogen and ammonia, following a stoichiometric relation indicated by Eq. 1, which had been proposed by Clark *et al.*:[13]

$$[Co(NH_3)_6]Cl_3 \longrightarrow CoCl_2 + NH_4Cl + 1/6N_2 + 28/6NH_2. \quad (1)$$

However, the reaction mechanism forming nitrogen and/or ammonium chloride still remains obscure. Tanaka and Nagase[14] have pointed out the electron-transfer process involved in the reaction, and they determined, by means of a polarographic technique, the reduction rate of Co(III) to Co(II) on the pyrolysis reaction proceeding *in vacuo*, under isothermal conditions. For a series of the complexes, $[Co(NH_3)_{6-n}X_n]X_{3-n}$ (X=Cl or Br; n=0 or 1), the rates have been found to depend on the nature of X and on the number of n. The results have been interpreted in terms of the reductive behavior of the halide anion. As to the hexaammine complex, then, the following overall reaction has been presented:

$$[Co^{III}(NH_3)_6]X_3 \longrightarrow CoX_2 + 6NH_3 + 1/2X_2. \quad (2)$$

In order to verify nitrogen formation under the present experimental conditions, hexaamminecobalt(III) chloride has been analyzed by pyrolysis-gaschromatography. The results, shown in Table 1, indicate that the amounts of nitrogen and ammonia in the evolved gases are fairly consistent with the stoichiometric relation given in Eq. 1. It should be noticed that the amount of nitrogen is equivalent to that in the one-electron oxidation reaction of ammonia to nitrogen, with a change in the oxidation number from −3 to 0.

By taking the above evidence into consideration, the formation of nitrogen and dinitrogen oxide by Red-I salt can be explained as follows. After dehydrating and dissociating two moles of the coordinated ammonia, the complex is thermally induced to a transient state such as is shown in Eq. 3. Also, the dissociation of this transient species to H^+ and NH_2 species can be accelerated by a concomitant electron-transfer from the NH_2^- moiety to the cobalt(III) and by a subsequent nitrogen-forming reaction (Eq. 4) and dinitrogen oxide-forming reaction (Eq. 5).

$$[Co^{III} - NH_2] \longrightarrow \underbrace{[Co^{III} - NH_2^{\delta-} \cdots H^{\delta+}]}_{\text{transient state}} \longrightarrow$$
$$Co^{II} + NH_2 + H^+ \quad (3)$$
$$NH_2 \longrightarrow 1/6N_2 + 2/3NH_3 \quad (4)$$
$$[H^+ \cdots O-N=N-O \cdots\cdots H^+] \longrightarrow N_2O + H_2O \quad (5)$$

The fact that an ammonia group in the hexaamminecobalt(III) cation readily exchanges the hydrogen atom with deuterium in a D_2O solution is not contrary to the above assumption.[15] The reduced cobalt(II) would release the bonding towards the hyponitrite group. Also, free hyponitrous acid is known to be thermally unstable, and it decomposes at −6 °C.[16]

On the pyrolysis of hexaamminecobalt(III) chloride, the proton expelled by Reaction 3 may be captured by ammonia and the chloride anion, thus forming thermally stable ammonium chloride.

The above assumption can well explain the facts that dinitrogen oxide, one mole per mole of Red-I salt, is produced exclusively from the coordinated hyponitrite

group, and that nitrogen, 1/6 mol per mole of cobalt(III), is produced from a coordinated ammonia.

On the pyrolysis of Red-II salt, the nitrogen evolution is 8—9 times as much as that of Red-I salt. Moreover, the DSC curve in Fig. 1-c shows a large exothermic peak ascribable to the process forming nitrogen and dinitrogen oxide. The proposed structure of Red-II salt includes NO groups in a dimeric $(-NO-ON-)^{2-}$ form, which implies an oxidative behavior of the peroxo moiety. This probably causes an unpredictable oxidation-reaction of ammonia other than that described above.

As for pentaamminenitrocobalt(III) chloride, the gas-analytical data shown in Table 1 are in good agreement with the stoichiometric relation in the following, overall reaction:

$$[Co(NH_3)_5NO_2]Cl_2 \longrightarrow CoCl_2 + 7/6N_2 + 22/6NH_3 + 2H_2O.$$

In this reaction, 1/6 mol of nitrogen can be attributed to the oxidation of the coordinated ammonia by the cobalt(III) ion, and one more mole to the following decomposition of ammonium nitrite, formed by the reaction of the H^+ in Eq. 3 and ammonia and the nitrite anion:

$$NH_4NO_2 \longrightarrow N_2 + 2H_2O.$$

This nitrogen-forming reaction may be understood in terms of an oxidation of ammonia by the nitrite anion. This implies that the nitrogen evolution from Red-II salt would be attributable not only to Reaction 4, but also to an oxidation reaction of ammonia by the dimeric, $(-NO-ON-)^{2-}$ group.

References

1) J. Sand and O. Genssler, *Ber.*, **36**, 2083 (1903).
2) E. Miki and T. Ishimori, *Bull. Chem. Soc. Jpn.*, **49**, 987 (1976).
3) C. S. Pratt, B. A. Coyle, and J. A. Ibers, *J. Chem. Soc., Inorg. Phys. Theor.*, **1971**, 2146.
4) B. F. Hoskins and F. D. Whillans, *J. Chem. Soc., Dalton Trans.*, **1973**, 607.
5) J. Bierrum and J. P. McReynold, *Inorg. Synth.*, **2**, 216 (1946).
6) S. M. Jorgensen, *Z. Anorg. Chem.*, **5**, 169 (1894).
7) T. Takeuchi and S. Tsuge, "Kobunshi no Netsubunkai-gaschromatography," Kagaku-Dojin, Kyoto (1977), pp. 47—54.
8) N. F. Curtis, *J. Chem. Soc.*, **1961**, 3147.
9) P. Gans, *J. Chem. Soc. Inorg. Phys. Theor.*, **1967**, 943.
10) B. N. Figgis and J. Lewis, *Progr. Inorg. Chem.*, **6**, 37 (1964).
11) W. W. Wendlandt and J. P. Smith, *J. Inorg. Nucl. Chem.*, **25**, 985 (1963).
12) S. Onodera, *Bull. Chem. Soc. Jpn.*, **50**, 123 (1977).
13) G. L. Clark, A. J. Quick, and W. D. Harkins, *J. Am. Chem. Soc.*, **42**, 2483 (1920); W. W. Wendlant, *J. Inorg. Nucl. Chem.*, **25**, 545 (1963); G. W. Watt, *Inorg. Chem.*, **3**, 325 (1964).
14) N. Tanaka and K. Nagase, *Bull. Chem. Soc. Jpn.*, **40**, 546 (1967); W. W. Wendlandt and J. P. Smith, *J. Inorg. Nucl. Chem.*, **25**, 1267 (1963).
15) J. S. Anderson, N. L. Spoor, and H. V. A. Briscoe, *J. Chem. Soc.*, **1943**, 361.
16) A. Hantzsch and L. Kaufman, *Lieb. Ann.*, **292**, 324 (1896).

Solubility Isotherms of Systems Containing Optically Active Tris(ethylenediamine)cobalt(III) Ion. I. Reciprocal Salt-pairs, (*Λ*-$[Co(en)_3]^{3+}$, *Δ*-$[Co(en)_3]^{3+}$)-(Br^-, (*R,R*)-$C_4H_4O_6^{2-}$), at 25 °C

Akira Fuyuhiro,* Kazuaki Yamanari, and Yoichi Shimura
Department of Chemistry, Faculty of Science, Osaka University, Toyonaka, Osaka 560
(Received May 17, 1980)

A four-component solubility isotherm consisting of (*Λ*-$[Co(en)_3]^{3+}$, *Δ*-$[Co(en)_3]^{3+}$)-(Br^-, (*R,R*)-$C_4H_4O_6^{2-}$)-H_2O was determined at 25 °C. It was found that three double salts, *rac*-$[Co(en)_3]Br_3\cdot 3H_2O$, *Λ*-$[Co(en)_3]Br(d\text{-}C_4H_4O_6)\cdot 5H_2O$, and *Λ*-$[Co(en)_3]_{0.48}\cdot$*Δ*-$[Co(en)_3]_{0.52}(d\text{-}C_4H_4O_6)_{1.5}\cdot 5H_2O$ and a gelatinous precipitate exist, six invariant points appearing. Application of this phase diagram to practical optical resolutions is discussed. The solubility of each salt in the system was measured in the range 5—65 °C in water, that of *Λ*- and *Δ*-$[Co(en)_3](d\text{-}C_4H_4O_6)_{1.5}\cdot nH_2O$ being found to be reversed at 42 °C.

A multi-component solubility isotherm containing chiral compounds is important for optical resolution, and those for some systems of metal complexes have been determined.[1,2] In the four-component systems of (*Λ*-$[Co(ox)(en)_2]^+$, *Δ*-$[Co(ox)(en)_2]^+$)-(Cl^-, R^-)-H_2O, where R^- denotes *d*-H_3tart^-, *Δ*-$[Co(edta)]^-$, or *d*-bcs^-((*R,R*)-$C_4H_6O_6\equiv d\text{-}H_4tart$ and (1*R*,3*S*,4*S*,7*R*)-$C_{10}H_{14}OBrSO_3^-\equiv d\text{-}bcs^-$), optically inactive chloride ion does not participate in the formation of diastereomers or pseudoracemates, its introduction thus not playing any part in making optical resolution possible. On the other hand, in the system of $[Co(en)_3]^{3+}$ ion, optical resolution becomes possible by precipitating the diastereomer of double salt, *Λ*-$[Co(en)_3]Br(d\text{-}H_2tart)\cdot 5H_2O$.[3] It would be of interest to find the particular role of the fourth component, Br^-, in this optical resolution.

This paper deals with the determination of the solubility isotherm of reciprocal salt-pairs, (*Λ*-$[Co(en)_3]^{3+}$, *Δ*-$[Co(en)_3]^{3+}$)-(Br^-, *d*-H_2tart^{2-})-H_2O, at 25 °C, and of the solubility of *rac*-$[Co(en)_3]Br_3$, *Λ*-$[Co(en)_3]Br_3$, *Λ*- and *Δ*-$[Co(en)_3](d\text{-}H_2tart)_{1.5}$, and *Λ*-$[Co(en)_3]Br(d\text{-}H_2tart)$ at 5—65 °C.

Experimental

Materials. *Λ*-$[Co(en)_3]X$, $X=Br_3\cdot H_2O$, $Br(d\text{-}H_2tart)\cdot nH_2O$, *and* $(d\text{-}H_2tart)_{1.5}\cdot nH_2O$: The *Λ*-$[Co(en)_3]Br(d\text{-}H_2tart)\cdot 5H_2O$ diasteromer was prepared by the method of Werner,[3] partial asymmetric synthesis,[4] HCl being replaced by HBr, and by addition of equimolar amounts of HBr and *d*-H_4tart to a *rac*-$[Co(en)_3](OH)_3$ solution obtained by treating *rac*-$[Co(en)_3]Br_3$ with an anion exchange resin of OH^- form. Found: C, 21.44; H, 6.85; N, 15.08%. Calcd for *Λ*-$[Co(en)_3]Br(d\text{-}H_2tart)\cdot 5H_2O$: C, 21.55; H, 6.87; N, 15.08%. When a solution of the diastereomer was concentrated at *ca.* 60 °C, a monohydrated sample was obtained. Found: C, 24.67; H, 6.24; N, 17.32%. Calcd for *Λ*-$[Co(en)_3]Br(d\text{-}H_2tart)\cdot H_2O$: C, 24.75; H, 6.23; N, 17.32%. The *Λ*-$[Co(en)_3]Br_3\cdot H_2O$ complex was obtained by the method of Werner.[3] Found: C, 14.47; H, 5.30; N, 17.01%. Calcd for *Λ*-$[Co(en)_3]Br_3\cdot H_2O$: C, 14.50; H, 5.27; N, 16.91%. The diastereomer *Λ*-$[Co(en)_3](d\text{-}H_2tart)_{1.5}\cdot nH_2O$ was prepared from *Λ*-$[Co(en)_3]Br(d\text{-}H_2tart)\cdot 5H_2O$ and $Ag_2(d\text{-}H_2tart)$.[5] At first a paste-like solid precipitated from the solution, gradually turning into needles at room temperature. With a dilute solution the needles deposited directly. The needles are highly efflorescent. Crystallization from a solution at *ca.* 60 °C gave a hygroscopic 1.5-hydrated diastereomer. Found: C, 29.63; H, 6.83; N, 17.30%. Calcd for *Λ*-$[Co(en)_3](d\text{-}H_2tart)_{1.5}\cdot 1.5H_2O$: C. 29.51; H, 6.81; N, 17.21%.

Δ-$[Co(en)_3]X$, $X=Br_3\cdot H_2O$ *and* $(d\text{-}H_2tart)_{1.5}\cdot nH_2O$: The *Δ*-bromide monohydrate was prepared by adding 8 mol dm^{-3} HBr to the filtrate of the less soluble diastereomer *Λ*-$[Co(en)_3]Br(d\text{-}H_2tart)\cdot 5H_2O$. The bromide was optically purified by extraction into water at *ca.* 5 °C and repeated crystallization. Found: C, 14.51; H, 5.33; N, 16.96%. Calcd for *Λ*-$[Co(en)_3]Br_3\cdot H_2O$: C, 14.50; H, 5.27; N, 16.91%. The diastereomer *Δ*-$[Co(en)_3](d\text{-}H_2tart)_{1.5}\cdot nH_2O$ was prepared from *Δ*-$[Co(en)_3]Br_3\cdot H_2O$ and $Ag_2(d\text{-}H_2tart)$.[5] The prismatic crystals, highly efflorescent, have *ca.* 1.5—8 crystal waters. Found: C, 26.84; H, 7.11; N, 15.68%. Calcd for *Δ*-$[Co(en)_3](d\text{-}H_2tart)_{1.5}\cdot 4H_2O$: C, 27.02; H, 7.18; N, 15.76%.

rac-$[Co(en)_3]Br_3\cdot nH_2O$: Racemic bromide trihydrate was prepared by the method of Werner.[3] Found: C, 13.43; H, 5.69; N, 15.66%. Calcd for *rac*-$[Co(en)_3]Br_3\cdot 3H_2O$: C, 13.52; H, 5.67; N, 15.77%. Crystallization of the complex at *ca.* 60 °C gave a very hygroscopic monohydrate. Found: C, 14.40; H, 5.38; N, 16.97%. Calcd for *rac*-$[Co(en)_3]Br_3\cdot H_2O$: C, 14.50; H, 5.27; N, 16.91%.

Λ-$[Co(en)_3]_{0.48}\cdot$*Δ*-$[Co(en)_3]_{0.52}(d\text{-}H_2tart)_{1.5}\cdot 5H_2O$: An apparent nonstoichiometric compound (not a mixture, see Results and Discussion) was prepared from *rac*-$[Co(en)_3]Br_3\cdot 3H_2O$ and $Ag_2(d\text{-}H_2tart)$ in a 2 : 3 mole ratio. Found: C, 26.16; H, 7.25; N, 15.26%. Calcd for $[Co(en)_3](d\text{-}H_2tart)_{1.5}\cdot 5H_2O$: C, 26.14; H, 7.31; N, 15.24%. The exact composition of the cations was determined by circular dichroism(CD)

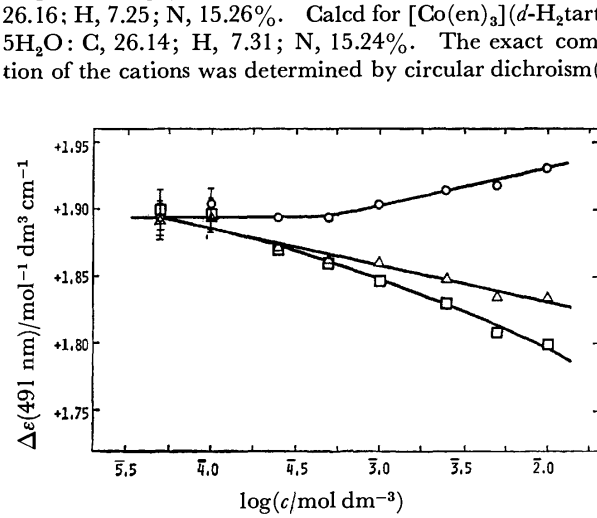

Fig. 1. Concentration dependence of Δε(491 nm) in water.
○: *Λ*-$[Co(en)_3]Br_3$, △: *Λ*-$[Co(en)_3]Br(d\text{-}H_2tart)$, □: *Λ*-$[Co(en)_3](d\text{-}H_2tart)_{1.5}$.

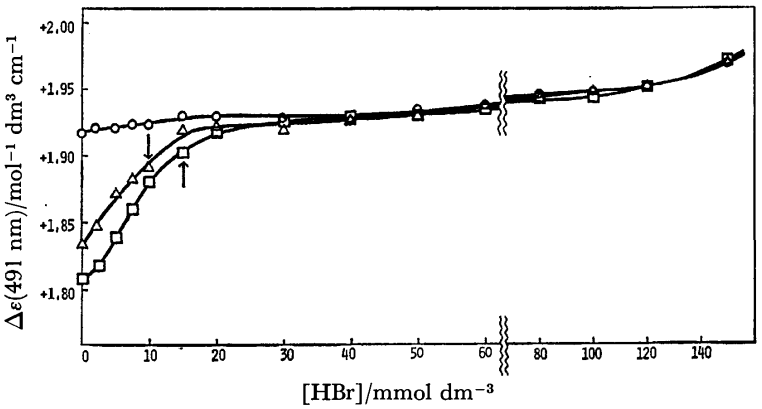

Fig. 2. CD in HBr aqueous solution. The concentration of Λ-$[Co(en)_3]^{3+}$ is 5 mmol dm^{-3}.
○: Λ-$[Co(en)_3]Br_3$, △: Λ-$[Co(en)_3]Br(d\text{-}H_2tart)$, □: Λ-$[Co(en)_3](d\text{-}H_2tart)_{1.5}$.

measurement in solution. The composition ($\Lambda : \Delta = 48\pm1 : 52\mp1$) was reproducible even by repeated recrystallization. Rapid cooling of the solution of $[Co(en)_3](d\text{-}H_2tart)_{1.5}$ sometimes provided a Λ-rich precipitate.

Measurements. *Calibrations of CD:* The molar absorption coefficient of $[Co(en)_3]^{3+}$ at the first d-d band(466 nm) was almost constant in spite of the presence of H^+, Br^-, and/or $d\text{-}H_2tart^{2-}$ in the concentration range 5×10^{-5}—10^{-2} mol dm^{-3} of the complex ion. Since the CD spectrum is considerably affected by the presence of $d\text{-}H_2tart^{2-}$ ion,[6] the influence of this ion on CD intensity was examined in water and in HBr solutions. The Λ-diastereomers, Λ-$[Co(en)_3]Br(d\text{-}H_2tart)$ and Λ-$[Co(en)_3](d\text{-}H_2tart)_{1.5}$, showed a gradual decrease in CD intensity with increase of complex concentration, and the $\Delta\varepsilon$ values at 10^{-2} mol dm^{-3} became 3 and 5% lower than the authentic value ($|\Delta\varepsilon(491\text{ nm})|=1.89$), respectively, the Λ-$[Co(en)_3]Br_3$ complex showing the reversed change (Fig. 1). The corresponding Δ-diastereomers, Δ-$[Co(en)_3]Br(d\text{-}H_2tart)$ and Δ-$[Co(en)_3](d\text{-}H_2tart)_{1.5}$, showed about half decreases in absolute values of $\Delta\varepsilon$ as compared with Λ-diastereomers in the concentration range 5×10^{-5}—10^{-2} mol dm^{-3}. The CD intensities depend a great deal upon the complex concentration in water. Figure 2 shows the variations of CD intensity at 491 nm in HBr solutions. In both systems of Λ-$[Co(en)_3]Br(d\text{-}H_2tart)$ and Λ-$[Co(en)_3](d\text{-}H_2tart)_{1.5}$, the CD intensities were almost constant in HBr solutions (2×10^{-2}—10^{-1} mol dm^{-3}) in Fig. 2, where the arrows indicate the points at which $d\text{-}H_2tart^{2-}$ should exist in acid form $d\text{-}H_4tart$ if we neglect the acid dissociations. The corresponding Δ-diastereomers showed about 2/3 increase in absolute values of $\Delta\varepsilon$ between [HBr]=0 and the plateau as compared with the Λ-diastereomers. Figures 3 and 4 show the concentration dependence of induced CD of *rac*-$[Co(en)_3](d\text{-}H_2tart)_{1.5}$ in water and in HBr solutions, respectively. Since the complex could not be obtained as a solid, the reaction mixture was used in solution, its concentration being determined by optical density. The induced CD peak appears at 461 nm,[6] but the measurements were carried out at 491 nm. Measurements in HBr solutions were found to be more favorable than in water because the CD intensities are almost zero in an appropriate HBr solution irrespective of the complex concentration. Beer's law holds in the concentration range 0—10^{-2} mol dm^{-3} in a 5×10^{-2} mol dm^{-3} HBr aqueous solution.

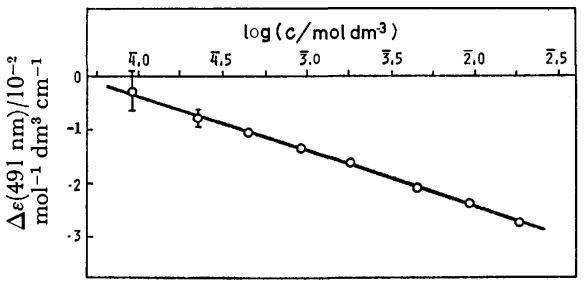

Fig. 3. Concentration dependence of induced CD of *rac*-$[Co(en)_3](d\text{-}H_2tart)_{1.5}$ in water at 491 nm.

Analyses of Saturated Solutions: Solubility in water was determined in molality.[1] Saturated solution weighed was diluted with a 5×10^{-2} mol dm^{-3} HBr aqueous solution to a certain volume. Optical densities and CD were measured under the conditions described above. The concentrations of $\{\Lambda\text{-}[Co(en)_3]^{3+}+\Delta\text{-}[Co(en)_3]^{3+}\}$ were determined from the

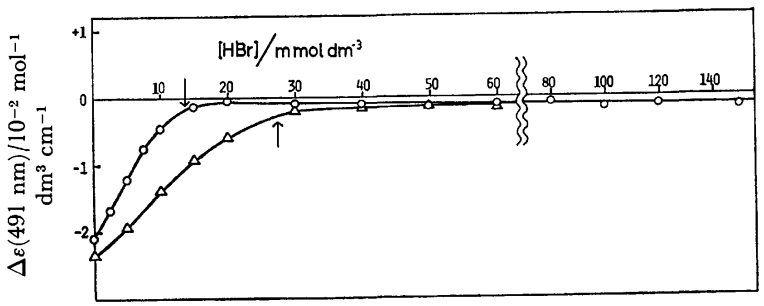

Fig. 4. Induced CD of *rac*-$[Co(en)_3](d\text{-}H_2tart)_{1.5}$ (○; 4.62 mmol dm^{-3} and △; 9.17 mmol dm^{-3}) in HBr aqueous solution.

observed optical densities, referring to the calibrated molar absorption coefficient of $[Co(en)_3]^{2+}$, $\varepsilon(466\,nm)=91.0$, the concentrations of $\{\Lambda\text{-}[Co(en)_3]^{3+}-\Delta\text{-}[Co(en)_3]^{3+}\}$ being obtained from CD intensities calibrated above; $\Delta\varepsilon(491\,nm)=+1.93$ and -1.93 for Λ- and Δ-$[Co(en)_3]^{3+}$, respectively. The concentrations of Λ- and Δ-$[Co(en)_3]^{3+}$ were separately calculated from the concentrations of $\{\Lambda\text{-}[Co(en)_3]^{3+}+\Delta\text{-}[Co(en)_3]^{3+}\}$ and $\{\Lambda\text{-}[Co(en)_3]^{3+}-\Delta\text{-}[Co(en)_3]^{3+}\}$. In the presence of both Br^- and d-H_2tart^{2-} ions, a titration method was combined with the spectral one in order to determine the amount of Br^-. A saturated solution was taken, weighed and diluted with an appropriate amount of water. The solution was titrated with a 0.03 mol dm^{-3} $AgNO_3$ solution till the end point of precipitation of AgBr, which was followed by the electromotive force(e.m.f.) of the following chemical cell: Ag|sample||KNO_3 soln.||3.33 mol dm^{-3} KCl soln.|AgCl(s)|Ag. The e.m.f. jumped distinctly between the precipitation of AgBr and $Ag_2(d\text{-}H_2tart)$, and the end point was calibrated by the known amounts of NaBr, Λ- and *rac*-$[Co(en)_3]Br_3\cdot nH_2O$, Λ-$[Co(en)_3]Br(d\text{-}H_2tart)\cdot 5H_2O$, and Λ- and Δ-$[Co(en)_3](d\text{-}H_2tart)_{1.5}\cdot nH_2O$. In the binary systems the concentration could be derived from only the optical densities. In this way, the amounts of all cations and anions and then the amount of water in the saturated solution were obtained and given in molality.

Analyses of Solid Phases: The solid phases were identified from elemental analyses, absorption and CD spectra, gravimetric analyses, and differential thermal analyses(DTA). The DTA were performed under dry or suspended (in water) conditions at atmospheric pressure. Optical densities were measured with a JASCO UVIDEC-1 spectrophotometer and CD with a JASCO MOE-1 spectropolarimeter.

Results and Discussion

The solubility data are given in Tables 1 and 2, and Figs. 5—11. A saturated solution is expressed as a point defined by summing up the position vectors of the solubilities of the component salt(s) contained.[1)]

Binary Systems between 5 and 65 °C. Figure 5 shows the binary solubility curves of the complexes, a few points of solubility of which have been reported.[5,7)] The more the tartrate ion share in the counter ions, the steeper the slopes of solubility curves. The solubility of Λ-$[Co(en)_3](d\text{-}H_2tart)_{1.5}$ at 60 °C in particular is about 90 times greater than that at 5 °C. The solubility of a pair of diastereomers, Λ- and Δ-$[Co(en)_3](d\text{-}H_2tart)_{1.5}$ is reversed at 42 °C; the Λ-diastereomer is less soluble at temperatures below 42 °C and the Δ above 42 °C. Inflection points were observed in *rac*-[Co-

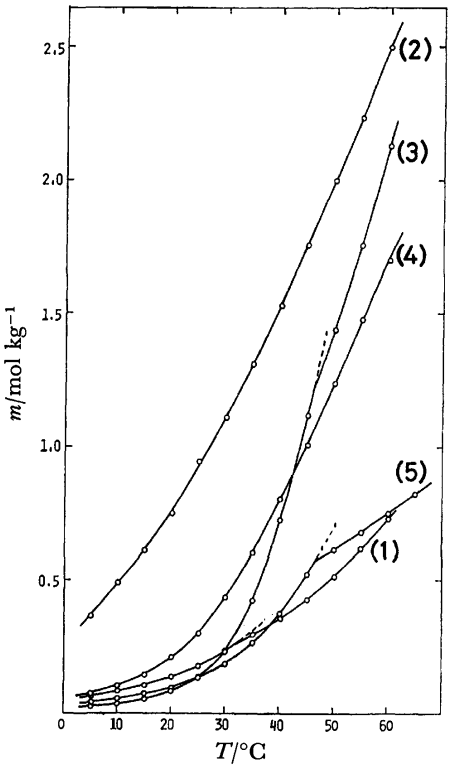

Fig 5. Solubility curves, where solubility is presented in molality m of anhydrous salt. (1): *rac*-$[Co(en)_3]Br_3\cdot nH_2O$, $n=3(\lesssim 32\,°C)$ and $n\simeq 1(\gtrsim 32\,°C)$, (2): Λ-$[Co(en)_3]Br_3\cdot H_2O$, (3): Λ-$[Co(en)_3](d\text{-}H_2tart)_{1.5}\cdot nH_2O$, $n\gtrsim 7(\lesssim 47\,°C)$ and $n\simeq 1.5(\gtrsim 47\,°C)$, (4): Δ-$[Co(en)_3](d\text{-}H_2tart)_{1.5}\cdot nH_2O$, $n\simeq 8$, (5): Λ-$[Co(en)_3]Br(d\text{-}H_2tart)\cdot nH_2O$, $n=5(\lesssim 47\,°C)$ and $n=1(\gtrsim 47\,°C)$.

Table 1. Solubility of the $[Co(en)_3]^{3+}$ salts in water (molality m/mol kg^{-1} of anhydrous salt)

T/°C	No. of salt[a)]							
	(1)-α	(1)-β	(2)	(3)-α	(3)-β	(4)	(5)-α	(5)-β
5	0.0629		0.363	0.0236		0.0729	0.0402	
10	0.0820		0.491	0.0351		0.103	0.0540	
15	0.107		0.613	0.0538		0.145	0.0736	
20	0.138		0.751	0.0847		0.210	0.0981	
25	0.178		0.947	0.138		0.299	0.135	
30	0.231		1.11	0.237		0.436	0.187	
35		0.295	1.31	0.422		0.604	0.263	
40		0.356	1.53	0.727		0.807	0.374	
45		0.428	1.76	1.12		1.01	0.522	
50		0.514	2.00		1.44	1.24		0.619
55		0.622	2.24		1.76	1.49		0.681
60		0.734	2.50		2.13	1.70		0.750
65		—	—		—	—		0.825

a) (1) *rac*-$[Co(en)_3]Br_3\cdot nH_2O$, $n=3(\alpha)$ and $n\simeq 1(\beta)$; (2) Λ-$[Co(en)_3]Br_3\cdot H_2O$; (3) Λ-$[Co(en)_3](d\text{-}H_2tart)_{1.5}\cdot nH_2O$, $n\gtrsim 7(\alpha)$ and $n\simeq 1.5(\beta)$; (4) Δ-$[Co(en)_3](d\text{-}H_2tart)_{1.5}\cdot nH_2O$, $n\simeq 8$; (5) Λ-$[Co(en)_3]Br(d\text{-}H_2tart)\cdot nH_2O$, $n=5(\alpha)$ and $n=1(\beta)$.

TABLE 2. EQUILIBRIUM OF (Λ-$[Co(en)_3]^{3+}$, Δ-$[Co(en)_3]^{3+}$)-(Br^-, d-H_2tart^{2-})-H_2O SYSTEM AT 25 °C

In liquid phases, solubility is presented in molality m of the component ions. Abbreviations are as follows: Λ-$[Co(en)_3]^{3+}=\Lambda^{3+}$, Δ-$[Co(en)_3]^{3+}=\Delta^{3+}$, Λ-$[Co(en)_3]Br_3\cdot H_2O=\Lambda Br_3$, Δ-$[Co(en)_3]Br_3\cdot H_2O=\Delta Br_3$, *rac*-$[Co(en)_3]Br_3\cdot 3H_2O=\Lambda\Delta Br_6$, Λ-$[Co(en)_3]Br(d\text{-}H_2tart)\cdot 5H_2O=\Lambda Br(tart)$, Λ-$[Co(en)_3](d\text{-}H_2tart)_{1.5}\cdot nH_2O$ ($n\gtrsim 7$)$=\Lambda(tart)_{1.5}$, Δ-$[Co(en)_3](d\text{-}H_2tart)_{1.5}\cdot nH_2O$ ($n\simeq 8$)$=\Delta(tart)_{1.5}$, and Λ-$[Co(en)_3]_{0.48}\cdot\Delta$-$[Co(en)_3]_{0.52}$-$(d\text{-}H_2tart)_{1.5}\cdot 5H_2O=(\Lambda,\Delta)(tart)_{1.5}$. The gelatinous precipitate(Gela) is treated as solid.

Position of points (Figs. 6—11)	No. of components	Liquid phase[a] $m/10^{-1}$ mol kg^{-1} Λ^{3+}	Δ^{3+}	Br^-	Solid phase
A	2	9.47 (±0.08)		28.4 (±0.2)	ΛBr_3
E_3	2	0.892 (±0.010)	0.892 (±0.010)	5.35 (±0.06)	$\Lambda\Delta Br_6$
E_3 ↕ E_1	3	1.01 1.15 1.38 2.20 3.59 5.29 6.06 7.52	0.77 0.70 0.52 0.22 0.08 0.08 0.00 0.00	5.36 5.53 5.69 7.25 11.0 15.9 18.2 22.6	$\Lambda\Delta Br_6$
E_1	3	9.63 (±0.16)	0.00	28.9 (±0.5)	ΛBr_3 + $\Lambda\Delta Br_6$
E_3 ↕ E_2	3	0.808 0.70 0.48 0.14 0.03 0.01 0.00 0.00	0.990 1.14 1.47 2.56 4.26 6.11 7.00 8.75	5.39 5.52 5.86 8.10 12.9 18.4 21.0 26.3	$\Lambda\Delta Br_6$
E_2	3	0.00	9.63 (±0.16)	28.9 (±0.5)	ΛBr_3 + $\Lambda\Delta Br_6$
B	2		9.47 (±0.08)	28.4 (±0.2)	ΔBr_3
C	2		2.99 (±0.04)		$\Delta(tart)_{1.5}$
D	2	1.38 (±0.02)			$\Lambda(tart)_{1.5}$
D ↕ G_1	3	1.39 1.42 1.45	0.07 0.12 0.16		$\Lambda(tart)_{1.5}$
G_1	3	1.47 (±0.02)	0.20 (±0.02)		$(\Lambda,\Delta)(tart)_{1.5}$ + $\Lambda(tart)_{1.5}$
G_1 ↕ G_2	3	1.36 1.28 1.12 1.00 0.967 0.964 0.956 0.916 0.832 0.810 0.774 0.731 0.626 0.500 0.468	0.20 0.20 0.21 0.23 0.252 0.250 0.246 0.248 0.268 0.277 0.280 0.295 0.340 0.414 0.450		$(\Lambda,\Delta)(tart)_{1,5}$
G_1 ↕ G_2	3	0.430 0.368 0.369 0.305 0.252 0.21 0.20 0.18 0.17 0.16 0.14 0.14 0.13 0.12 0.11 0.11 0.10 0.11	0.479 0.550 0.568 0.689 0.856 1.05 1.20 1.37 1.47 1.66 1.81 2.03 2.26 2.45 2.59 2.71 2.74 2.83		$(\Lambda,\Delta)(tart)_{1.5}$
G_2	3	0.10 (±0.01)	3.09 (±0.07)		$(\Lambda,\Delta)(tart)_{1.5}$ + $\Delta(tart)_{1.5}$
D ↕ H_1	3	1.45 1.57 1.71 1.84 2.00		0.09 0.25 0.44 0.62 0.81	$\Lambda(tart)_{1.5}$
H_1	3	2.15 (±0.02)		1.02 (±0.04)	$\Lambda(tart)_{1.5}$ + $\Lambda Br(tart)$
H_1 ↕ H_3	3	2.07 2.00 1.99 1.80 1.72 1.65 1.64 1.52 1.43 1.39 1.37		1.02 1.05 1.03 1.08 1.16 1.12 1.14 1.19 1.24 1.29 1.32	$\Lambda Br(tart)$
H_3	2	1.35 (±0.01)		1.35 (±0.01)	$\Lambda Br(tart)$
H_3 ↕ H_2	3	1.30 1.28 1.28 1.26 1.24 1.23 1.21 1.24 1.27 1.24 1.38 1.50		1.42 1.46 1.49 1.54 1.57 1.68 1.79 1.91 2.24 2.23 2.72 3.19	$\Lambda Br(tart)$

TABLE 2. (Continued)

Position of points (Figs. 6—11)	No. of components	Liquid phase[a] $m/10^{-1}$ mol kg^{-1} A^{3+}	Δ^{3+}	Br^-	Solid phase
		1.66		3.78	
		1.98		4.79	
		2.31		5.78	
		2.39		5.95	
		2.47		6.21	
H_3		2.72		6.96	
↑		3.37		8.85	
	3	4.03		10.8	ABr(tart)
		5.09		13.8	
↓		5.66		15.6	
H_2		6.09		16.5	
		6.40		17.5	
		7.40		20.1	
		7.42		20.4	
		8.30		22.9	
		8.89		24.7	
H_2	3	10.9 (±0.2)		30.3 (±0.7)	ABr(tart) + ABr$_3$
A		9.67		28.4	
↑	3	9.91		28.7	ABr$_3$
↓		9.99		28.8	
H_2		10.3		29.5	
E_1	4	10.5	0.0	29.9	ABr$_3$
↕		11.2	0.0	31.0	+ $A\Delta$Br$_6$
P_1					
P_1	4	10.9 (±0.2)	0.0	30.6 (±0.9)	ABr(tart) + ABr$_3$ + $A\Delta$Br$_6$
		8.11	0.02	22.3	
		7,32	0.01	20.1	
		6.92	0.03	19.0	
		4.91	0.05	13.4	
		4.24	0.11	11.7	
		3.80	0.13	10.3	
		3.00	0.24	8.32	
		2.64	0.33	7.48	
		2.27	0.50	6.78	
		2.19	0.54	6.70	
		2.16	0.64	6.81	
P_1		2.06	0.65	6.51	
↑		2.02	0.76	6.62	ABr(tart)
	4	1.84	0.98	6.53	
		1.69	1.18	6.53	+ $A\Delta$Br$_6$
↓		1.61	1.39	6.53	
P_4		1.54	1.58	6.65	
		1.50	1.73	6.68	
		1.48	1.85	6.85	
		1.44	2.18	7.08	
		1.41	2.44	7.36	
		1.43	2.35	7.24	
		1.42	2.39	7.20	
		1.40	2.73	7.56	
		1.37	3.46	8.37	
		1.38	3.87	8.73	
		1.40	3.97	8.87	
P_1		1.41	4.38	9.19	
↕	4	1.43	4.82	9.64	ABr(tart) + $A\Delta$Br$_6$
P_4		1.45	5.83	10.7	
P_4	4	1.51 (±0.01)	6.89 (±0.08)	11.8 (±0.3)	ABr(tart) + $A\Delta$Br$_6$ + Gela
G_1		1.61	0.21	0.20	(A,Δ)(tart)$_{1.5}$
↕	4	2.07	0.27	0.87	+ A(tart)$_{1.5}$
P_2					
H_1		2.23	0.18	1.06	A(tart)$_{1.5}$
↕	4	2.23	0.19	1.07	+ ABr(tart)
P_2					
P_2	4	2.28 (±0.03)	0.29 (±0.01)	1.12 (±0.03)	(A,Δ)(tart)$_{1.5}$ + A(tart)$_{1.5}$ + ABr(tart)
		2.06	0.33	1.20	
		2.02	0.33	1.20	
		1.91	0.36	1.23	
		1.79	0.40	1.30	
		1.73	0.42	1.36	
		1.73	0.43	1.40	
		1.72	0.44	1.38	
		1.69	0.45	1.39	
		1.68	0.47	1.44	
		1.65	0.47	1.46	
		1.62	0.49	1.48	
		1.59	0.52	1.52	
P_2		1.55	0.55	1.61	
↑		1.52	0.57	1.62	(A,Δ)(tart)$_{1.5}$
	4	1.47	0.64	1.72	
		1.43	0.72	1.81	+ ABr(tart)
↓		1.41	0.75	1.87	
P_5		1.37	0.82	2.00	
		1.35	0.91	2.14	
		1.33	1.01	2.27	
		1.30	1.15	2.49	
		1.30	1.17	2.60	
		1.30	1.19	2.55	
		1.29	1.32	2.77	
		1.27	1.46	3.01	
		1.26	1.89	3.63	
		1.26	2.30	4.25	
		1.29	2.66	4.77	
		1.30	3.09	5.42	
P_5	4	1.36 (±0.02)	4.12 (±0.19)	6.99 (±0.27)	(A,Δ)(tart)$_{1.5}$ + ABr(tart) + Gela
				9.89	29.1	
B				10.4	29.8	
↑				11.4	31.3	
				12.5	33.0	
	3			13.4	34.0	ΔBr$_3$
				14.1	35.0	
↓				14.7	35.7	
F_2				14.5	35.0	
				14.4	35.2	

Table 2. (Continued)

Position of points (Figs. 6—11)	No. of components	Liquid phase[a] $m/10^{-1}$ mol kg^{-1} Λ^{3+}	Δ^{3+}	Br^-	Solid phase
F_2	3		15.4 (±0.4)	36.5 (±0.7)	ΔBr_3 +Gela
E_2	4	0.0	10.4	29.8	
		0.0	11.3	31.4	
		0.0	12.1	32.5	
		0.0	12.8	33.4	ΔBr_3
		0.0	13.5	34.1	$+\Lambda\Delta Br_6$
P_3		0.0	14.0	34.6	
		0.0	14.8	36.2	
		0.0	15.5	36.5	
P_3	4	0.0	15.8 (±0.2)	36.0 (±0.2)	ΔBr_3 $+\Lambda\Delta Br_6$ +Gela
C	3		3.39	0.41	
			3.82	0.90	
			4.59	1.65	$\Delta(tart)_{1.5}$
			5.66	2.88	
F_1			6.62	4.02	
F_1	3		6.91 (±0.29)	4.40 (±0.35)	$\Delta(tart)_{1.5}$ +Gela
G_2	4	0.11	3.57	0.60	
		0.13	4.33	1.42	
		0.16	5.09	2.33	$(\Lambda,\Delta)(tart)_{1.5}$ $+\Delta(tart)_{1.5}$
P_6		0.17	5.70	3.08	
		0.18	6.55	3.93	
P_6	4	0.21 (±0.03)	7.11 (±0.24)	4.66 (±0.31)	$(\Lambda,\Delta)(tart)_{1.5}$ $+\Delta(tart)_{1.5}$ +Gela

a) Values in parentheses are estimated errors and calculated from twice the standard deviations of measurements repeated 3—14 times.

$(en)_3]Br_3$, Λ-$[Co(en)_3]Br(d\text{-}H_2tart)$, and Λ-$[Co(en)_3]$-$(d\text{-}H_2tart)_{1.5}$ at about 32, 47, and 47 °C, respectively. The points were also clearly observed by DTA. Under dry conditions these three complexes provided no DTA peak at the inflection points, the peaks being observed under suspended conditions in water. The *rac*-$[Co(en)_3]Br_3\cdot nH_2O$ salt showed the peak in both heating and cooling processes, Λ-$[Co(en)_3]Br(d\text{-}H_2tart)\cdot nH_2O$ and Λ-$[Co(en)_3](d\text{-}H_2tart)_{1.5}\cdot nH_2O$ only in heating process. The Λ-$[Co(en)_3]Br(d\text{-}H_2tart)$ salt in high temperature form were gradually transformed into low temperature form in 1—3 h at room temperature, the latter giving the DTA peak again on heating. It took a few days for Λ-$[Co(en)_3](d\text{-}H_2tart)_{1.5}$ to be transformed into low temperature form, the change corresponding to the transfer of the paste-like precipitate to the needles (see Experimental).

The Ternary System, Λ-$[Co(en)_3]Br_3$–Δ-$[Co(en)_3]Br_3$–H_2O. The solubility isotherm of this type determines whether the racemate is spontaneously resolved or not.[8,9] Figure 6 shows the solubility isotherm of the ternary system, Λ-$[Co(en)_3]Br_3$–Δ-$[Co(en)_3]Br_3$–H_2O, at 25 °C. Points A, B, and E_3 indicate the binary solubility of Λ-, Δ-, and *rac*-$[Co(en)_3]Br_3\cdot nH_2O$, respectively, no spontaneous resolution taking place. In this system, two invariant points, E_1 and E_2, appear and the widely spread curve, $E_1E_3E_2$, represents the solubility isotherm of the racemic compound, *rac*-$[Co(en)_3]Br_3\cdot 3H_2O$. Point $E_1(E_2)$ lies extremely close to the left(right) axis, optical purity of the liquid phase at E_1 and E_2 being almost perfect. A similar ternary system, Λ-$[Co(ox)(en)_2]I$–Δ-$[Co(ox)(en)_2]I$–H_2O,[9] is not so extreme as the present system.

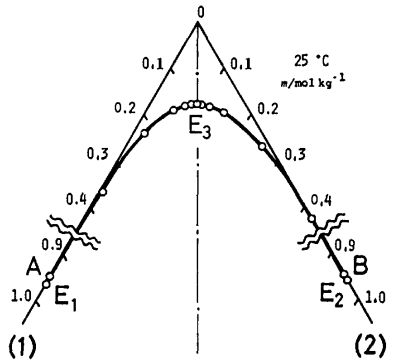

Fig. 6. Solubility isotherm of the ternary system, Λ-$[Co(en)_3]Br_3$–Δ-$[Co(en)_3]Br_3$–H_2O, at 25 °C.
Solubility is presented in molality m of anhydrous salt. (1): Λ-$[Co(en)_3]Br_3$, (2): Δ-$[Co(en)_3]Br_3$.

The Ternary System, Λ-$[Co(en)_3](d\text{-}H_2tart)_{1.5}$–$\Delta$-$[Co(en)_3](d\text{-}H_2tart)_{1.5}$–$H_2O$. The solubility isotherm of this type which consists of a pair of diastereomers and solvent is the simplest one for discussion of optical resolution. Figure 7 shows the system, Λ-$[Co(en)_3]$-$(d\text{-}H_2tart)_{1.5}$–Δ-$[Co(en)_3](d\text{-}H_2tart)_{1.5}$–$H_2O$, at 25 °C. This resembles those of the following systems, Λ-$[Co(ox)(en)_2]R$–Δ-$[Co(ox)(en)_2]R$–H_2O (25 °C); $R^- = 1/2\text{-}[Sb_2(d\text{-}tart)_2]^{2-}$ and *d*-bcs^-, in which the pseudoracemic compounds, Λ-$[Co(ox)(en)_2]\cdot\Delta$-$[Co(ox)(en)_2]\cdot[Sb_2(d\text{-}tart)_2]\cdot 5H_2O$ and Λ-$[Co(ox)(en)_2]\cdot\Delta$-$[Co(ox)(en)_2](d\text{-}bcs)_2\cdot 2H_2O$, respectively, are formed between

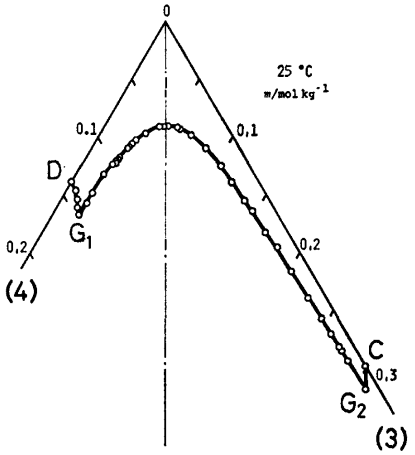

Fig. 7. Solubility isotherm of the ternary system, Λ-$[Co(en)_3](d\text{-}H_2tart)_{1.5}$–$\Delta$-$[Co(en)_3](d\text{-}H_2tart)_{1.5}$–$H_2O$, at 25 °C.
Solubility is presented in molality m of anhydrous salt. (4): Λ-$[Co(en)_3](d\text{-}H_2tart)_{1.5}$, (3): Δ-$[Co(en)_3]$-$(d\text{-}H_2tart)_{1.5}$.

the two diastereomers.[9,10] However, the ratio of *Λ*: *Δ* in the central solid phase of the present system is not 50 : 50% but (48±1) : (52∓1)% on the curve G_1G_2 (Fig. 7). Since the effect of induced CD exerts less than 0.1% for deviation of this ratio (see Experimental), it is reasonable to conclude that the compound is a nonstoichiometric substance with the composition *Λ*-$[Co(en)_3]_{0.48}$·*Δ*-$[Co(en)_3]_{0.52}$(*d*-H_2tart)$_{1.5}$·$5H_2O$. The compound (not mixture) might correspond to the precipitate prepared from a mixed solution of *rac*-$[Co(en)_3]X_3$ (X=Cl and Br) and KNa(*d*-H_2tart) by addition of ethanol.[11] If we attempt optical resolution with this ternary system, *viz.*, a solution of $[Co(en)_3]$-(*d*-H_2tart)$_{1.5}$ is concentrated at 25 °C, only a partially resolved *compound* will be obtained. Thus we must treat a four-component system to resolve the $[Co(en)_3]^{3+}$ complex perfectly.

The Ternary System, Λ-*[Co(en)$_3$](d-H$_2$tart)$_{1.5}$*–Λ-*[Co(en)$_3$]Br$_3$–H$_2$O.* Figure 8 shows the isotherm at

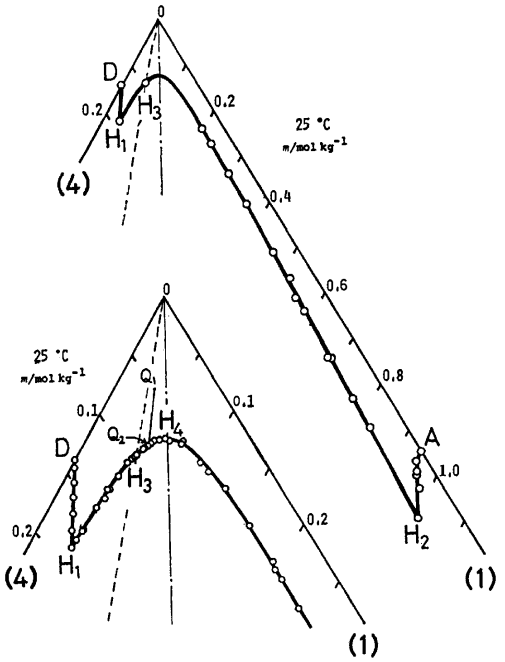

Fig. 8. Solubility isotherm (upper) and its magnification of the ternary system, *Λ*-$[Co(en)_3]$(*d*-H_2tart)$_{1.5}$–*Λ*-$[Co(en)_3]Br_3$–H_2O, at 25 °C.
Solubility is presented in molality *m* of anhydrous salt. (4): *Λ*-$[Co(en)_3]$(*d*-H_2tart)$_{1.5}$, (1): *Λ*-$[Co(en)_3]Br_3$.

25 °C which is irrelevant to a successful optical resolution. Points D, H_3, and A denote the solubility of binary systems, *Λ*-$[Co(en)_3]$(*d*-H_2tart)$_{1.5}$, *Λ*-$[Co(en)_3]$Br-(*d*-H_2tart), and *Λ*-$[Co(en)_3]Br_3$, respectively. Since the central solid has the composition *Λ*-$[Co(en)_3]$Br(*d*-tart)·$5H_2O$, the point of this solid exists on the elongation of line OH_3. The liquid phase composition of minimum solubility of *Λ*-$[Co(en)_3]^{3+}$ corresponds to point H_4 where the ratio of *Λ*-$[Co(en)_3]$(*d*-H_2tart)$_{1.5}$: *Λ*-$[Co(en)_3]Br_3$ is equal to 1 : 1, or (*d*-H_2tart)$^{2-}$: Br^- to 1 : 2, but not to 1 : 1 which agrees with point H_3. When an unsaturated solution of Q_1 is concentrated at 25 °C, the salt *Λ*-$[Co(en)_3]$Br(*d*-H_2tart)·$5H_2O$ will deposit at Q_2 and the composition of the saturated solution will concomitantly move toward the minimum solubility of *Λ*-$[Co(en)_3]^{3+}$(H_4), and in turn, to the point H_2 where two solids, *Λ*-$[Co(en)_3]$Br(*d*-H_2tart)·$5H_2O$ and *Λ*-$[Co(en)_3]Br_3$·H_2O, coexist.

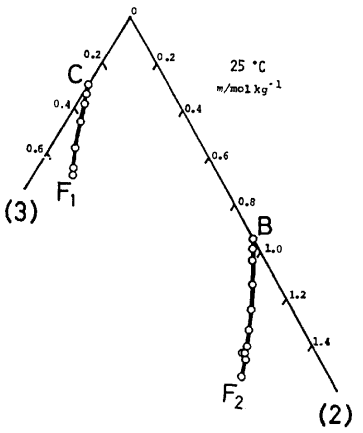

Fig. 9. Solubility isotherm of the ternary system, *Δ*-$[Co(en)_3]$(*d*-H_2tart)$_{1.5}$–*Δ*-$[Co(en)_3]Br_3$–H_2O, at 25 °C.
Solubility is presented in molality *m* of anhydrous salt. (3): *Δ*-$[Co(en)_3]$(*d*-H_2tart)$_{1.5}$, (2): *Δ*-$[Co(en)_3]Br_3$.

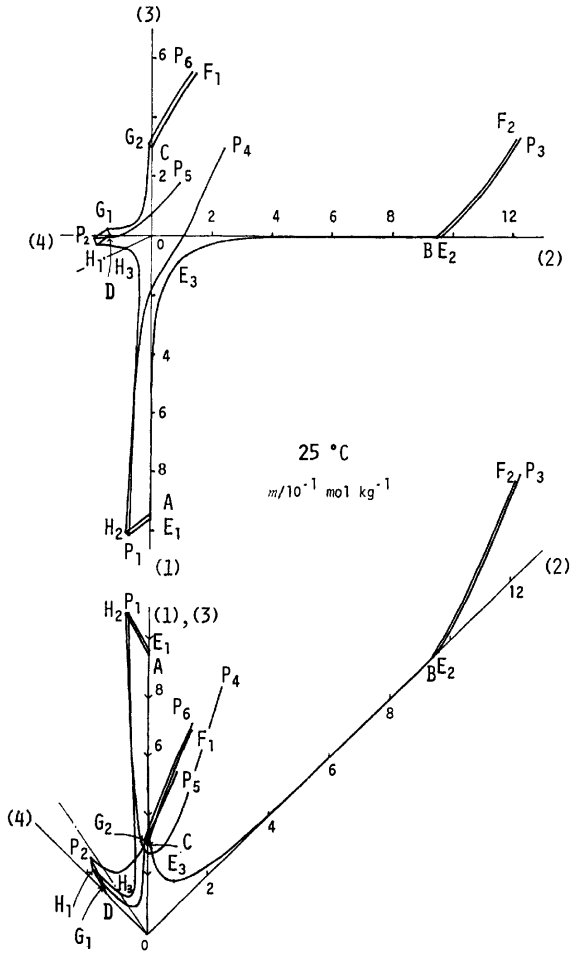

Fig. 10. The plane projection(upper) and the side elevation of solubility isotherm of the system, (*Λ*-$[Co(en)_3]^{3+}$, *Δ*-$[Co(en)_3]^{3+}$)-(Br^-, *d*-H_2tart^{2-})-H_2O, at 25 °C.
Solubility is presented in molality *m* of anhydrous salt. (1): *Λ*-$[Co(en)_3]Br_3$, (2): *Δ*-$[Co(en)_3]Br_3$, (3): *Δ*-$[Co(en)_3]$(*d*-H_2tart)$_{1.5}$, (4): *Λ*-$[Co(en)_3]$(*d*-H_2tart)$_{1.5}$.

The Ternary System, Δ-[Co(en)$_3$](d-H$_2$tart)$_{1.5}$–Δ-[Co(en)$_3$]Br$_3$–H$_2$O. As shown in Fig. 9, the central part of the isotherm is blank owing to the appearance of gelatinous substances; when measurements of the saturated solutions from points C and B were carried out to points F_1 and F_2, respectively, the liquid phase turned into a gelatinous substance. This was obtained from the filtrate of the optical resolution and reported as Δ-[Co(en)$_3$]Br(*d*-H$_2$tart)·5H$_2$O,[3] but the composition and structure have not been determined clearly.

The lines DG_1, CG_2, DH_1, AH_2, CF_1, and BF_2 in Figs. 7—9 go down almost vertically. The situation differs significantly from the one expected from the common ion effect, suggesting that the activity coefficient of each salt becomes very small because of the association between $[Co(en)_3]^{3+}$ and *d*-H_2tart^{2-}.

The Solubility Isotherm of Reciprocal Salt-pairs, (Λ-[Co(en)$_3$]$^{3+}$, Δ-[Co(en)$_3$]$^{3+}$)–(Br$^-$, d-H$_2$tart^{2-})–H$_2$O. The solubility isotherm of reciprocal salt-pairs consisting

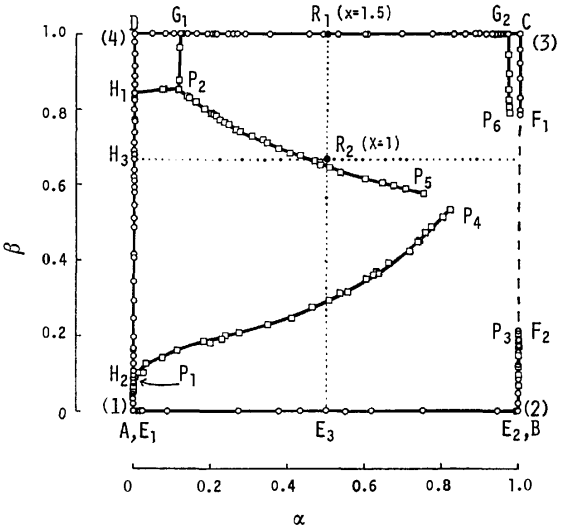

Fig. 11. The clinographic projection of solubility isotherm of the system, (Λ-[Co(en)$_3$]$^{3+}$, Δ-[Co(en)$_3$]$^{3+}$)–(Br$^-$, *d*-H$_2$tart^{2-})–H$_2$O, at 25 °C.
α: mole fraction of Δ-[Co(en)$_3$]$^{3+}$ to all the cations, β: mole fraction of (*d*-H$_2$tart)$_{1.5}^{3-}$ to {(Br$_3$)$^{3-}$+(*d*-H$_2$tart)$_{1.5}^{3-}$}, (1): Λ-[Co(en)$_3$]Br$_3$, (2): Δ-[Co(en)$_3$]Br$_3$, (3): Δ-[Co(en)$_3$](*d*-H$_2$tart)$_{1.5}$, (4): Λ-[Co(en)$_3$](*d*-H$_2$tart)$_{1.5}$, □: solubilities of four-components, ○: solubilities of two- or three-components.

of two cations, two anions, and solvent can be drawn in space and projected on three planes according to the definition[1] in which solubility is expressed in molality of component ions and then the molality of three salts. In the present system, the charges of the component anions differ, molalities of Br^- and *d*-H_2tart^{2-} being calculated as those of $(Br_3)^{3-}$ and (*d*-H$_2$tart)$_{1.5}^{3-}$, respectively. The four-component system includes the ternary systems in the above sections. The plane projection and side elevation are shown in Fig. 10 and the clinographic projection of the isotherm at 25 °C in Fig. 11. The left, right, lower, and upper sides in Fig. 11 correspond to Figs. 8, 9, 6, and 7, respectively. There are three double salts, Λ-[Co(en)$_3$]·Δ-[Co(en)$_3$]Br$_6$·6H$_2$O(=*rac*-[Co(en)$_3$]Br$_3$·3H$_2$O), Λ-[Co(en)$_3$]Br(*d*-H$_2$tart)·5H$_2$O, and Λ-[Co(en)$_3$]$_{0.48}$·Δ-[Co(en)$_3$]$_{0.52}$(*d*-H$_2$tart)$_{1.5}$·5H$_2$O and one gelatinous precipitate in the areas $E_1E_3E_2P_3P_4P_1E_1$, $H_1H_3H_2P_1P_4P_5P_2H_1$, $G_1P_2P_5P_6G_2G_1$, and $F_2F_1P_6P_5P_4P_3F_2$, respectively. In this system six invariant points, P_1—P_6, having four components exist at 25 °C. Since the Λ-[Co(en)$_3$]Br(*d*-H$_2$tart)·5H$_2$O diastereomer covers the area across the "racemic line" R_1E_3 (Fig. 11), the perfect optical resolution of $[Co(en)_3]^{3+}$ ion is possible by using Br^- and *d*-H_2tart^{2-} as resolving agents at 25 °C. However, it should be noted that the saturated solution of *rac*-[Co(en)$_3$]Br(*d*-H$_2$tart) prepared from 1 mol of *rac*-[Co(en)$_3$]Br$_3$ and x mol (x=1) of Ag$_2$(*d*-H$_2$tart) lies on R_2 (Fig. 11), in equilibrium with the partially resolved compound Λ-[Co(en)$_3$]$_{0.48}$·Δ-[Co(en)$_3$]$_{0.52}$(*d*-H$_2$tart)$_{1.5}$·5H$_2$O, but not with the solid Λ-[Co(en)$_3$]Br(*d*-H$_2$tart)·5H$_2$O. In the case of $0.43<x<0.97$, the isothermal concentration in equilibrium at 25 °C would enable us to attain perfect optical resolution.

The authors are grateful to Dr. Takasuke Matsuo and Mr. Yoshichika Yoshioka, Osaka University, for their advice and use of the DTA apparatus.

References

1) A. Fuyuhiro, K. Yamanari, and Y. Shimura, *Bull. Chem. Soc. Jpn.*, **52**, 90 (1979).
2) A. Fuyuhiro, K. Yamanari, and Y. Shimura, *Bull. Chem. Soc. Jpn.*, **52**, 2261 (1979).
3) A. Werner, *Chem. Ber.*, **45**, 121 (1912).
4) J. A. Broomhead, F. P. Dwyer, and J. W. Hogarth, *Inorg. Synth.*, **6**, 186 (1960).
5) H. Yoneda, K. Miyoshi, S. Suzuki, and T. Taura, *Bull. Chem. Soc. Jpn.*, **47**, 1661 (1974).
6) B. Norden, *Acta. Chem. Scand.*, **26**, 111 (1972).
7) A. Werner and M. Basyrin, *Chem. Ber.*, **46** 3230 (1913).
8) K. Yamanari, J. Hidaka, and Y. Shimura, *Bull. Chem. Soc. Jpn.*, **46**, 3724 (1973).
9) Y. Shimura and K. Tsutsui, *Bull. Chem. Soc. Jpn.*, **50**, 145 (1977).
10) A. Fuyuhiro, K. Yamanari, and Y. Shimura, *Chem. Lett.*, **1978**, 1393; A. Fuyuhiro, K. Yamanari, and Y. Shimura, *Bull. Chem. Soc. Jpn.*, **52**, 1420 (1979).
11) H. Yoneda, G. Takemoto, and U. Sakaguchi, *Bull. Chem. Soc. Jpn.*, **47**, 513 (1974).

 © 1980 The Chemical Society of Japan Bull. Chem. Soc. Jpn., 53, 3585—3589 (1980)

Polarographic Study on the Transportation of Oxygen by Perfluorocarbon Emulsion as Artificial Blood

Katsumi HAYASHI and Masanosuke TAKAGI*

Department of Agricultural Chemistry, College of Agriculture, University of Osaka Prefecture, Sakai, Osaka 591

(Received May 19, 1980)

Restrictive factors of oxygen release from dispersed particles of perfluorocarbon (PFC) in a form of emulsion have been studied by polarographic reduction currents of oxygen in the emulsion. The oxygen reduction currents in PFC emulsion in open system increased linearly with the volume fraction of PFC component, and were diffusion-controlled. The increase of current was ascribed to the increase of oxygen supply to the electrode from PFC particles in the emulsion. Analyzing the oxygen reduction current due to PFC particles, the ratio of diffusion coefficients of oxygen inside and outside PFC particle (D_i/D_o) and the oxygen partition coefficient between the both sides (C_i/C_o) were obtained. The release of oxygen from PFC particle was rate-determined by oxygen diffusion in the particle and the diffusion itself was determined by inner viscosity of PFC particle. The surfactant layer of PFC particle did not play any appreciable role such as permeability barrier for oxygen transportation.

Clark and Gollan[1] suggested that perfluorocarbons (PFC) with high oxygen solubility were useful materials for artificial blood. Later, the emulsification of PFC developed this kind of investigations,[2-5] since bio-availability of PFC emulsion so far been demonstrated.[6-9] However, few physicochemical studies on uptake or release of oxygen by the dispersed particles in PFC emulsion have been known,[8-10] though relatively many kinetic studies on oxygen transport by erythrocyte were reported by different investigators.[11-14] In order to evaluate the effectiveness of PFC emulsion as artificial blood, the limiting step of uptake or release of oxygen by PFC particle should be clarified and compared with that of erythrocyte. In addition, for better understanding of oxygen transporting capacity of erythrocyte, it may be useful that the PFC particle can be regarded as a simplified model of erythrocyte under some experimental conditions. However, spectroscopic methods, which are advantageous for erythrocytes, are inapplicable to PFC emulsion which exhibits no specific color change in uptaking or releasing oxygen. Consequently, for the estimation of oxygen binding character of such systems, electrochemical methods may be recommended.[15] Especially polarographic techniques seem to have several advantages for PFC emulsion, further for real blood or general oxygen carriers, since the electrode *e.g.*, dropping mercury electrode (DME), to which an appropriate potential is applied, works as a model of biological surface on which oxygen is consumed immediately when it arrives at. The total limiting current due to oxygen discharge then is the value corresponding to the rate of the transport of oxygen from the bulk.

In this study, we applied d.c.-polarographic method to PFC emulsion. Then, the restrictive factors of the release of oxygen from the dispersed particles in PFC emulsion were discussed based on the behavior of the reduction currents of oxygen in PFC emulsion.

Experimental

Materials. Perfluorocarbon emulsion was a product of Green Cross Corporation (Osaka) named Fluosol-43 which is an emulsion of FC-43 (perfluorotributylamine) with a surfactant Pluronic F-68 [poly(oxypropylene)-poly(oxyethylene) copolymer, M.W.=8350]. The average diameter of dispersed particle is 860 Å.[16] Pluronic F-68 and FC-43 were products of Asahi Denka, Inc. (Tokyo) and Dainippon Ink and Chemicals, Inc. (Tokyo), respectively. All other reagents used were of analytical grade unless otherwise stated.

Apparatus and Procedures. Polarograph used was a Yanagimoto Polarograph Model PA 101. The dropping mercury electrode had the following characteristics: $m=1.91$ mg s^{-1}, $t=5.87$ s at open circuit in distilled water with 60 cm height of mercury reservoir. As for oxygen electrode, a Teflon covered gold electrode (TCGE) whose electrode surface area was *ca.* 3 mm^2, was employed for the determination of dissolved oxygen with an applied potential -0.7 *V* (*vs.* SCE). Saturated calomel electrode (SCE) was used as a reference electrode. The viscometer used was a cone and plate viscometer, made by Tokyo Keiki, Ltd. (Tokyo).

Most experiments were carried out in test solutions thermostated and under the oxygen partial pressure equilibrated with open atmosphere. For some experiments with a constant total oxygen amount in solution, a simple vessel designed as presented in Fig. 1 was used. In this vessel no gas phase is

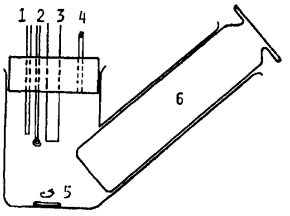

Fig. 1. Electrolytic vessel for oxygen measurement in closed system.
(1): Reference electrode, (2): working electrode, (3): indicater electrode, (4): inlet of sample solution, (5): magnetic stirrer, (6) syringe.

left over the liquid surface and when a given amount of test solution previously deoxygenated by nitrogen streaming, is added, the syringe moves by the increase of volume of the solution.

Results and Discussion

Effects of Pluronic F-68 on Oxygen Reduction Waves. Surfactants usually affect the electrode reaction due to the adsorption to the electrode surface.[17] As is well known, oxygen gives two reduction waves at DME in supporting electrolyte solutions, corresponding to Eqs. 1 and 2.[18]

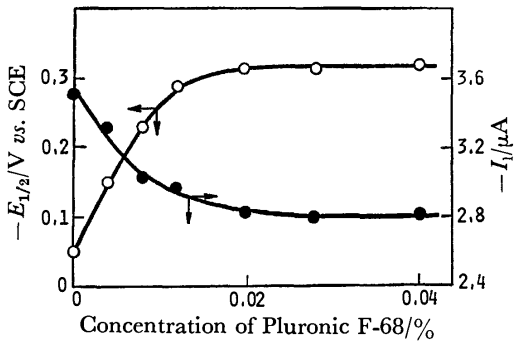

Fig. 2. Effect of Pluronic F-68 on half wave potential ($E_{1/2}$) and limiting current (I_l) of the first wave of oxygen reduction waves.
Medium: 0.1 mol dm^{-3} KNO_3 equilibrated with atmospheric oxygen, ○: $E_{1/2}$, ●: I_l.

$$O_2 + 2e + 2H^+ \longrightarrow H_2O_2 \quad (1)$$

$$H_2O_2 + 2e + 2H^+ \longrightarrow 2H_2O \quad (2)$$

Figure 2 shows the effects of Pluronic F-68 on limiting currents (I_l) and half-wave potential ($E_{1/2}$) of the first wave of oxygen reduction waves. The increase of the concentration of Pluronic F-68 results in a lowering of I_l value and a shift of $E_{1/2}$ to a more negative potential. Electrocapillary curves in Fig. 3 revealed the adsorption

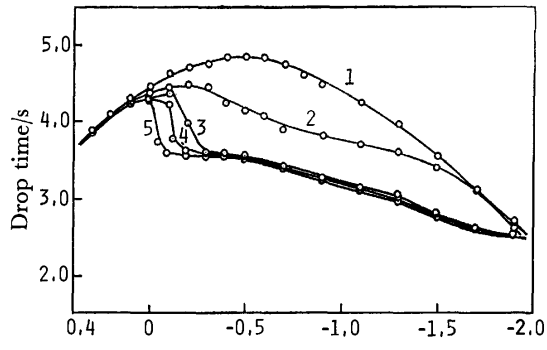

Fig. 3. Effect of Pluronic F-68 on electrocapillary curve.
Medium: the same as for Fig. 2.
Concentration of Pluronic F-68 (w/v %): (1) 0, (2) 0.004, (3) 0.008, (4) 0.016, (5) 0.04.

of the surfactant on the electrode surface corresponding to the decrease of I_l and the shift of $E_{1/2}$ in Fig. 2. Consequently, to study the effect of the volume fraction of PFC component (ϕ) on oxygen reduction waves, experiments must be carried out without changing the concentration of Pluronic F-68. In this study, 3.2% Pluronic F-68, which was the same concentration as that in Fluosol-43, was employed. pH was maintained to be 7.4 with Tris–HCl buffer (ionic strength 0.1 mol dm^{-3}).

Oxygen Reduction Current in PFC Emulsion. The reduction current increased linearly with PFC emulsion in the electrolytic solution, when the system was open to the atmosphere (Fig. 4). Since the ratio of the 1st wave height and the 2nd did not change by adding

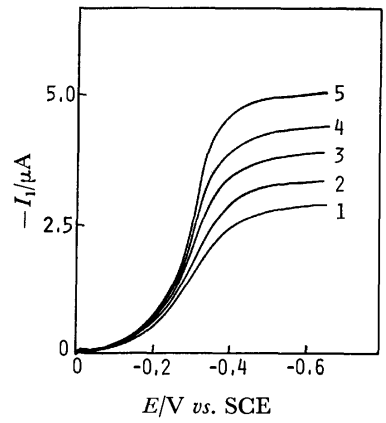

Fig. 4. Change of the oxygen reduction wave (1st wave) with volume fraction of PFC component in the electrolyte solution at 25 °C in open system.
Medium: pH 7.4, Tris–HCl buffer (ionic strength 0.1) with Pluronic F-68 3.2%. Volume fraction of PFC component (ϕ): (1) 0, (2) 0.024, (3) 0.059, (4) 0.083, (5) 0.119.

emulsion, I_l of the 1st wave was examined in most cases. The increase in this I_l with ϕ (as seen in Fig. 4) may be attributed to the reduction of oxygen included in PFC particle, since the concentration of free oxygen in dispersion medium except PFC particles should be constant, equilibrated with atmospheric oxygen, in spite of the change of ϕ. The character of fully diffusion-controlled current was confirmed from the dependence of I_l on mercury head. Similar diffusion-controlled limiting currents of oxygen were also observed in the electrolyte solution containing 3.2% Pluronic F-68 *i.e.* the dispersion medium without PFC particles. As a consequence, the increase of current due to added PFC emulsion must also be diffusion-controlled. Then, the significance of this diffusion-controlled oxygen wave due to PFC component was considered for two possibilities: 1) Diffusion of PFC particle to the electrode and discharge of oxygen involved in PFC at the contact of the particle to the electrode: for example, Hayano and Shinozuka[19-20] reported the reduction current of a dye solubilized in surfactant micelles and concluded that the limiting step of the observed reduction current was the diffusion of surfactant micelle.

If the diffusion of the PFC particle is not adequate for the rate-determining step, other diffusion factors should be considered. 2) Direct contribution of oxygen diffusion in PFC in the particles: since our experimental conditions were sufficiently simple, the diffusion of oxygen in space other than disparsion medium would only be possible in PFC inside the dispersed particles. To simplify the treatment of problem on this assumption, we may assume that PFC particles occupy a relative space on the electrode surface, corresponding to ϕ and the remaining space ($1-\phi$) is covered by the dispersion medium.

The first assumption of the above two was examined as follows: estimating the concentration of PFC particle, its diffusion coefficient calculated from the particle size[16] and Stokes' equation, and the number of oxygen molecules in the particle, Ilkovic equation was applied

to obtain the expected diffusion current due to PFC particles (I_{dem}). The calculation† revealed that the observed diffusion current (I_d) was too large to accept the first assumption. This suggests that I_{dem} is not determined by the diffusion of PFC particle, but by the diffusion of oxygen inside PFC particle. Present case is therefore different from that of the reduction of dye solubilized in micelle.[19-21] For PFC emulsion, it seems reasonable to consider the latter assumption of the above two.

Analysis of Oxygen Diffusion Current in Open System. If we assume that the diffusion of oxygen can be observed only in the direction perpendicular to the electrode surface, but in horizontal direction the diffusion between the particles and the medium can be neglected, the observed diffusion current (I_d) may be written as

$$I_d = I_{do,} + I_{dem}, \tag{3}$$

where $I_{do,}$ and I_{dem} are diffusion current of free oxygen and that due to PFC particles, respectively.
Then,

$$I_{do,} = \kappa\sqrt{D_o}C_o\,(1-\phi), \tag{4}$$

$$I_{dem} = \kappa\sqrt{D_i}C_i\cdot\phi, \tag{5}$$

where D and C are diffusion coefficient and concentration of oxygen, respectively and $\kappa=607\,n\,m^{2/3}\,t^{1/6}$ (at 25 °C) with $n=2$, and ϕ is volume fraction of PFC in the system. Suffix o and i represent outside and inside of the particle, respectively. Equation 3 now can be written as

$$I_d = \kappa\sqrt{D_o}C_o\,(1-\phi) + \kappa\sqrt{D_i}C_i\cdot\phi. \tag{6}$$

Dividing this equation by I_{do}

$$I_d/I_{do} = 1 + (K\sqrt{D_i/D_o} - 1)\phi \tag{7}$$

can be obtained, where I_{do} is I_d at $\phi=0$ ($I_{do}=\kappa\sqrt{D_o}C_o$)†† and $K=C_i/C_o$. Then, the value K should be the partition coefficient of oxygen between FC-43 and water. As seen in Fig. 5, a linear relation between I_d/I_{do} and ϕ was obtained. From the slope, $K\sqrt{D_i/D_o}$ was found to be 8.9 ± 0.2. The evaluation of this value is interesting to prove the validity of the assumption presented as the possibility (2) in the above section. Namely, we must evaluate our K value involved in Eq. 7 on the basis of experimental results, and compare it with that obtained by other methods. Because no further information could be independently obtained with the open system, experiments with closed system were then carried out, in order to estimate K and D_i/D_o.

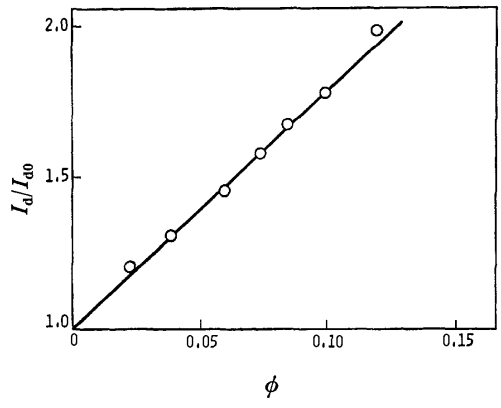

Fig. 5. Plot of I_d/I_{do} against volume fraction of PFC component (ϕ) in electrolyte solution. Explanation in text.

† See Appendix.

†† The diffusion coefficient D_o may change with concentration of emulsion particles. However, for the sake of simplifying the treatment of problem, it was neglected for this study, since the experiments were carried out only in relatively dilute emulsion system, that is $\phi<0.12$. Namely, D_o in emulsion was regarded to be always equal to that in dispersion medium ($\phi=0$).

Evaluation of K *and* D_i/D_o *with Closed System.* Using the vessel shown in Fig. 1, experiments were carried out both with TCGE and DME, but the latter enabled us more intimate analysis than TCGE. So, we introduce here the method with DME more in detail and for TCGE only some discussion will be added.

The above Eq. 6 for open system is also valid for the present closed system. However, since the absolute oxygen content in closed system is constant, the following equation can be added.

$$C_o(1-\phi)V + C_i\phi V = C^0V_0, \tag{8}$$

where V is the volume of the test solution closed against atmosphere and V_0 is V at $\phi=0$. C^0 is the oxygen concentration at $\phi=0$. The experiment starts with a requisite volume of electrolyte solution equilibrated with atmospheric oxygen but now closed against the atmosphere. Then, a small constant volume of deoxygenated PFC emulsion of known concentration may be added. Each I_d can be measured from its polarogram and, ϕ and V are easily calculated.
From Eqs. 6 and 8 the following relation can be derived.

$$I_dV/(I_{do}V_0) = [1 + (K\sqrt{D_i/D_o} - 1)\phi]/[1 + (K-1)\phi] \tag{9}$$

Further, modifying the Eq. 9,

$$\frac{1}{1-(I_dV)/(I_{do}V_0)} = \frac{1}{K(1-\sqrt{D_i/D_o})}\cdot\frac{1}{\phi} + \frac{K-1}{K(1-\sqrt{D_i/D_o})} \tag{10}$$

is available.

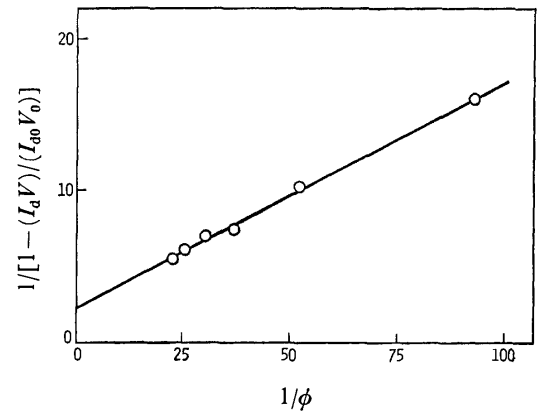

Fig. 6. Graphical treatment for estimation of partition coefficient of oxygen between inside and outside PFC particle $K=C_i/C_o$ and D_i/D_o using the experimental results in closed system. Medium: the same as for Fig. 4. Explanation in text.

As seen in Fig. 6, plot of $1/[1-(I_dV)/(I_{d0}V_0)]$ against $1/\phi$ gave a straight line. From the slope and intercept on ordinate, $K=16.4\pm0.7$ and $\sqrt{D_i/D_o}=0.61\pm0.03$ could be obtained. The D_i value was 7.4×10^{-6} $cm^2\,s^{-1}$, assuming that D_o was 2.0×10^{-5} $cm^2\,s^{-1}$.†††[22,23] Consequently, $K\sqrt{D_i/D_o}=10.0$ which is not identical with the value 8.9 obtained from the experiment in open system. However, The value $\sqrt{D_i/D_o}$ is interesting, since according to Stokes' equation, D should be reciprocally proportional to the viscosity. The validity of 0.61 can be confirmed by measuring the viscosities (η) of both the dispersion medium and that of dispersed substance separately. Our measurement of η for pure FC-43 and that for the electrolyte solution containing the surfactant employed, gave a satisfactory result, *i.e.* $\sqrt{\eta_o/\eta_i}=0.57$. The reciprocal relationship between D_i/D_o and η_i/η_o suggests that the release of oxygen from PFC particles was rate-determined by the viscosity of dispersed phase, and surfactant layer of PFC particle does not play any appreciable role such as the permeability barrier for oxygen release. This favorable permeability of the surfactant layer for oxygen is not due to the dimensions of thickness of surfactant layer of PFC particle, but it may arise from the oxygen-philic property of Pluronic F-68. Because the thickness of surfactant layer of PFC particle, which can be estimated to be *ca.* 70 Å**, is close to that of common biomembranes such as erythrocyte.[24] The K value obtained was nearly equal to the calculated one from the solubility of oxygen in FC-43[25] and in water.[26] The validity of this K value estimation was again proved by applying TCGE to the closed system as described in the following part.

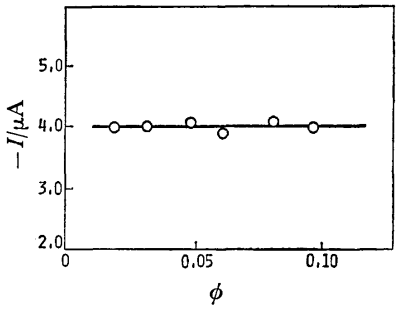

Fig. 7. Effect of PFC emulsion on reduction current of oxygen at Teflon covered gold electrode (TCGE) in open system. Medium: the same as for Fig. 4. Current was measured at −0.7 V (*vs.* SCE).

††† As diffusion coefficient of oxygen in buffer solution pH 7.4, 2.0×10^{-5} $cm^2\,s^{-1}$ was used for the present study, since several investigators have reported similar values with minor deviations for various electrolyte solution at 20—25 °C.

** For the calculation of this value, first we obtained volume fraction of PFC particle (ϕ_p) in the emulsion by centrifugation. This ϕ_p is comprised of both inside PFC component (ϕ) and surfactant layer component. Since the average particle diameter ($2r$) was known experimentally,[16] and ϕ of the stock emulsion was given by the manufacturer, the thickness of the surfactant layer (δ) can be readily obtained by the following equation,

$$\delta = r[1-(\phi/\phi_p)^{1/3}]$$

Estimation of K *by Oxygen Electrode.* Figure 7 shows that in open system the cathodic current obtained by TCGE as oxygen electrode at a fixed applied potential in a relatively low concentration range seems to be constant and proportional to the oxygen concentration in the dispersion medium, irrespective of the change of ϕ in system, while in the same PFC concentration range I_d at DME exhibits an apparent increase. The current obtained by TCGE (I) may be expressed as

$$I = \alpha C_o(1-\phi) \qquad \alpha: \text{const.} \tag{11}$$

For closed system, Eq. 8 is also valid. Then, the following equation can be derived from Eq. 8 and 11.

$$I_0V_0/(IV) = 1 + K\phi/(1-\phi), \tag{12}$$

where I_0 is I at $\phi=0$ and equal to αC_o.

With the experiments similar to those with DME in closed system, $I_0V_0/(IV)$ can be plotted against $\phi/(1-\phi)$ and K can be estimated as a slope of the obtained straight line, which intercepts the ordinate at 1.0, as shown in Fig. 8. Our result gave $K=15.3$ which should

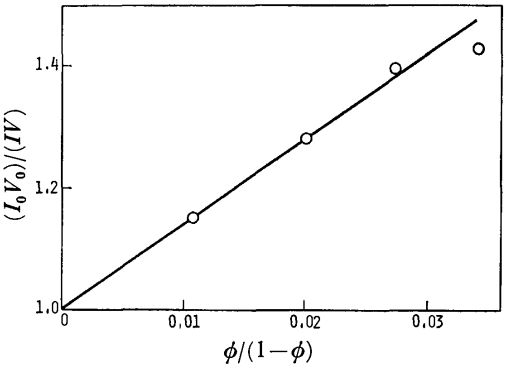

Fig. 8. Graphical treatment for the estimation of partition coefficient of oxygen between inside and outside PFC particle by TCGE in closed system. Medium: the same as for Fig. 4. Explanation in text.

be theoretically equal to that obtained from DME. The disagreement of the values may be partly due to the difficulty of experiment in closed system. Especially the work with oxygen electrode, may require a larger caution for stability of electrode surface under the present conditions. For this reason, we recommend DME method rather than solid electrode method.

Concluding Remarks. The above results may support the validity of the second possibility of the two assumptions presented. Consequently, the restrictive factor of the release of oxygen from PFC particle is the diffusion rate of oxygen inside PFC particle. The oxygen equilibrium between inside and outside of PFC particle seems to attain sufficiently fast. Further, the particle size is not the factor to change I_{dem}, as Ohyanagi and Mitsuno[8] reported that the rate of uptake and release of oxygen by PFC particle was independent of the particle size. The DME method may be expected to give some quantitive informations on the behavior of oxygen inside a larger particle such as erythrocyte. The application will be reported elsewhere.

Appendix

According to the first assumption, the diffusion current of

oxygen due to PFC particles (I_{dem}) is limited by the diffusion of PFC particle itself. Applying Ilkovic equation to I_{dem}, it can be written as

$$I_{dem} = \kappa^* \sqrt{D_p} C_p,$$
$$\kappa^* = 607 n^* m^{2/3} t^{1/6},$$

where D_p and n^* are the diffusion coefficient of PFC particle and the number of electrons transferred at the electrode reaction per PFC particle, respectively. Assuming all of oxygen molecules inside PFC particle might simultaneously discharge at the contact of the particle to the electrode, n^* would be given by multiplying the number of electrons transferred at the reduction of oxygen (n) by the number of oxygen molecules inside PFC particle, that is,

$$n^* = n \cdot C_1 \cdot v \cdot N,$$

where C_1, v, and N are concentration of oxygen dissolved in PFC, the average volume of a PFC particle and Avogadro's number, respectively. C_p is molar concentration of PFC particle, and can be written as

$$C_p = \phi/(v \cdot N).$$

From the above relations, I_{dem} can be rewritten as

$$I_{dem} = \kappa \sqrt{D_p} C_1 \phi,$$
$$\kappa = 607 n m^{2/3} t^{1/6}.$$

On the other hand, the diffusion current due to free oxygen (I_{do_1}) can be written as

$$I_{do_1} = \kappa \sqrt{D_o} C_o$$

The observed diffusion current (I_d) is given by Eq. 3. Therefore, the ratio I_d/I_{do_1} can be written as

$$I_d/I_{do_1} = 1 + K \sqrt{D_p/D_o} \cdot \phi,$$
$$K = C_1/C_o.$$

Now, we can estimate D_p in water to be 4.5×10^{-8} cm^2 s^{-1} at 25 °C, using Stokes' equation, $D = RT/(N \cdot 6\pi\eta r)$, with the average diameter ($2r$) reported: 860 Å,[16] and the viscosity of water as dispersion medium (η): 0.890 cp (1cp$=1 \times 10^{-3}$ N s m^{-2}) at 25 °C. Since 2.0×10^{-5} cm^2 s^{-1} is taken as D_o value, $\sqrt{D_p/D_o} = 4.7 \times 10^{-2}$ can be obtained. At $\phi = 0.12$, I_d/I_{do_2} value can be calculated to be 1.1 with the above obtained values, that is, the diffusion current would increase only by one tenth at this ϕ. In fact, the diffusion current observed was twice that at $\phi = 0$. This result allows us to eliminate the first assumption to explain the increase of diffusion current with ϕ.

The authors thank Green Cross Corporation in Osaka for the kind supply of perfluorocarbon emulsion Fluosol-43 and a surfactant Pluronic F-68.

References

1) L. C. Clark Jr., and F. Gollan, *Science*, **152**, 1755 (1966).
2) H. A. Sloviter and T. Kamimoto, *Nature*, **216**, 458 (1967).
3) H. A. Sloviter, M. Petkovic, S. Ogoshi, and H. Yamada, *J. Appl. Physiol.*, **27**, 666 (1969).
4) T. H. Mauth, *Science*, **179**, 669 (1973).
5) R. P. Geyer, "Proc. the Xth Intern. Conger. Nutrition: Symposium on Perfluorochemical Artificial Blood," ed and published by Igakushobo, Kyoto (1975), p. 3.
6) R. Watanabe, H. Inahara, and Y. Motoyama, "Proc. the Xth Intern. Congr. Nutrition: Symposium on Perfluorochemical Artificial Blood," ed and published by Igakushobo, Kyoto (1975), p. 113.
7) H. Okamoto, M. Iwai, Y. Tsuda, and K. Yokoyama, "Proc. the Xth Intern. Conger. Nutrition: Symposium on Perfluorochemical Artificial Blood," ed and published by Igakushobo, Kyoto (1975), p. 73.
8) H. Ohyanagi and T. Mitsuno, "Proc. the Xth Intern. Conger. Nutrition: Symposium on Perfluorochemical Artificial Blood," ed and published by Igakushobo, Kyoto (1975), p. 21.
9) K. Yamanouchi, R. Murashima, and K. Yokoyama, *Chem. Pharm. Bull.*, **23**, 1363 (1975).
10) H. Ohyanagi, T. Itoh, M. Sekita, M. Okamoto, and T. Mitsuno, *Artificial Organs*, **2**, 90 (1978).
11) R. Benesch, R. E. Benesch, and C. Bauer, "The Red Blood Cell," 2nd ed, ed by D. M. Surgener, Academic Press, New York (1975), Vol. 2, p. 825.
12) F. J. W. Roughton, *Prog. Biophys. Biophysical Chem.*, **9**, 55 (1959).
13) J. P. Harrington, D. Elbaum, R. M. Bookchin, J. B. Wittenberg, and R. L. Nagel, *Proc. Natl. Acad. Sci. U.S.A.*, **74**, 203 (1977).
14) J. T. Coin and J. S. Olson, *J. Biol. Chem.*, **254**, 1178 (1978).
15) T. Koyama and M. Mochizuki, *Rev. Polarogr. (Kyoto)*, **14**, 405 (1967).
16) K. Yokoyama, A. Suzuki, I. Utsumi, and R. Naito, *Chem. Pharm. Bull.*, **22**, 2966 (1974).
17) J. Heyrovsky and J. Kuta, "Principles of Polarography," Academic Press, New York and London (1966), p. 287.
18) I. M. Kolthoff and J. J. Lingane, "Polarography," Interscience Publishers, New York (1952), Vol. 2, p. 552.
19) S. Hayano and N. Shinozuka, *Bull. Chem. Soc. Jpn.*, **42** 1469 (1969).
20) S. Hayano and N. Shinozuka, *Bull. Chem. Soc. Jpn.*, **43**, 2083 (1970).
21) S. Hayano and N. Shinozuka, *Bull. Chem. Soc. Jpn.*, **44**, 1503 (1971).
22) V. S. Griffiths and M. I. Jackman, *Talanta*, **9**, 205 (1962).
23) S. L. Phillips, *Anal. Chem.*, **38**, 1714 (1966).
24) J. D. Robertson, *Biochem. Soc. Symp.*, **16**, 3 (1959).
25) J. W. Sargent and R. J. Seffl, *Fed. Proc.*, **29**, 699 (1970).
26) "Intern. Critical Tables," Nat. Res. Council U.S.A., McGraw Hill, New York (1933), Vol. 1, p. 393.

 © 1980 The Chemical Society of Japan Bull. Chem. Soc. Jpn., 53, 3590—3595 (1980) [Vol. 53, No. 12

Kinetic Studies of Fast Equilibrium by High-performance Liquid Chromatography I. Ternary Complex Formation of *N,N*-Disubstituted Dithiocarbamate Chelates of Ni(II) and Cu(II)

Masataka MORIYASU* and Yohei HASHIMOTO

Kobe Women's College of Pharmacy, Motoyamakita-machi, Higashinada-ku, Kobe 658

(Received May 23, 1980)

The equilibrium of labile ternary complex formation of metal dialkyldithiocarbamate chelates ($MA_2 + MB_2 \underset{k-}{\overset{k}{\rightleftharpoons}} 2MAB$, $K=[MAB]^2/[MA_2][MB_2]$) has been investigated by high-performance liquid chromatography, the separation process of which is so fast that kinetically unstable ternary complexes can be eluted with no disproportionation during the course of chromatography. High-performance liquid chromatography makes it possible to halt the progress of considerably fast reactions at the moment when the solution of reaction system is injected into the column. Thus, chromatograms obtained indicate the concentration of each species before chromatography, facilitating the determination of equilibrium constant K of Ni(II) and Cu(II) chelates. The equilibrium constants obtained are always 4.0, suggesting that ternary complex formation is controlled by a statistical factor. Disproportionation takes place by collision of two ternary metal chelates, the rate constants being of the order 10^1—10^2 M^{-1} s^{-1} (Ni(II) chelates) and 10^3 M^{-1} s^{-1} (Cu(II) chelates). The activation parameters of ternary complex formation have been obtained.

Study of fast reactions in solution has drawn the attention of investigators, the flow and relaxation methods being utilized. The conventional method, in which two reactants are mixed and then the change of concentration of reactants or products is measured, was found to be ineffective because of the lack of appropriate means of rapid analysis. High-performance liquid chromatography (HPLC) developed in recent years has been successfully applied to microdetermination of various substances. The merit of rapid separation in HPLC might be hopeful for determining kinetic characteristics of considerably fast reactions in solution.

Since the first report on metal acetylacetonates by Huber and Kraak,[1] only a few reports have appeared on HPLC separation of metal chelates, many of them being on HPLC of metal diethyldithiocarbamates.[2-9] We carried out quantitative determination of various metal diethyldithiocarbamates.[7] This article deals with the applicability of HPLC to kinetical investigation of relatively fast equilibrium of labile ternary complex formation.

Experimental

Reagents. Commercial sodium salts of diethyldithiocarbamic acid and dibenzyldithiocarbamic acid were used. Sodium salts of other *N,N*-disubstituted dithiocarbamic acid were prepared by the usual procedure from dialkylamine, carbon disulfide and sodium hydroxide. They were recrystallized from either chloroform–methanol or chloroform–hexane. Standard solutions of Ni(II) and Cu(II) were prepared by dissolving $NiCl_2 \cdot 6H_2O$ and $CuSO_4 \cdot 5H_2O$ in water. The concentrations of these metal ions were determined by colorimetry as diethyldithiocarbamate chelates.

Apparatus. An HPLC apparatus we constructed was used.[7] The two plunger reciprocal pump (Model KHD-W-294, Kyowa Seimitsu Co. Ltd.), damper, sample injector (5 μl or variable) and column were combined . A single-beamed spectrometer (Model Spectra 20, Toshiba Beckmann Co. Ltd., 210—700 nm) equipped with a flow cell was used as a detector. Since the detector is not designed for HPLC use, its sensitivity is not so high. The upper limit of rate constants determined by the present method is restricted by the sensitivity of the detector. Silica gel packings (LiChrosorb SI 100, 5 μ, E. Merck Darmstadt and Wako gel LC-5H, 5 μ, Wako Pure Chemicals Co. Ltd.) were packed into stainless steel columns (diameter 2 mm, length 25 cm) by a balanced slurry packing technique.[10] A pre-packed silica gel column (Shodex silipak, 5 μ, diameter 4 mm, length 15 cm, Showa Denko Co. Ltd.) was used. Absorption spectra of metal chelates were observed with a double-beamed spectrometer (Model 124, Hitachi Co. Ltd.).

Procedure. In adsorption chromatography, adjustment of column is important as regards the mode of elution and reproducibility, and the water content on silica gel was controlled as follows. *Ca.* 100 cm^3 of water containing acetone (3%) was pumped through the column. At least 200 cm^3 of water saturated hexane flowed out, the activity of silica gel column being reduced. Reproducible results were obtained when water saturated eluent was used. Before use each organic solvent was saturated with water by shaking the mixture of the solvent and water vigorously, followed by standing for 1 d. Since it is desirable in some cases to perform chromatography at low temperature, column temperature was kept low by plunging solvent reservoir and column into an ice bath when necessary.

Metal chelates were prepared by mixing the corresponding metal ion and sodium dialkyldithiocarbamate. The metal chelates produced were extracted with chloroform under conditions of complete extraction (at pH 4.0 in acetate buffer). In order to avoid any effects of residual free ligands in chloroform, the extract was washed with water four times. The standard solutions of each metal chelate (0.1 to 2 mM) thus prepared were used for HPLC after being diluted to proper concentration. Measurements of rate constants were carried out as follows. Two dilute solutions of binary complexes were mixed under thermostated conditions. After the lapse of a certain time, a portion of the mixture was supplied to HPLC. All the measurements were carried out three times.

Theoretical

Possible chromatogram patterns of a mixture of two

different binary complexes, MA_2 and MB_2, will be considered first. It is assumed that no decomposition of each chelate takes place during the course of chromatography. If no interaction exists between the two binary complexes, two peaks corresponding to each complex should appear. However, the chromatogram patterns would be complicated if a mixed ligand complex is formed in the mixture as follows.

$$MA_2 + MB_2 \underset{k_-}{\overset{k}{\rightleftharpoons}} 2MAB \quad (1)$$

$$K = [MAB]^2/[MA_2][MB_2] \quad (2)$$

Equilibrium is hardly attained when M is a metal ion which forms very inert complexes. In such a case, a ternary complex will be formed when the mixture is left to stand for a long time or brought to elevated temperature. The ternary complex formed can be separated by the conventional method without disproportionation. If M is a metal ion which forms very labile complexes, the ternary complex undergoes disproportion into two binary complexes, as soon as it is separated from binary complexes. Studies have been carried out on the equilibrium by mixing two solutions of MA_2 and MB_2 and observing the resulting remarkable change of physico-chemical properties such as UV absorption. The separation process of HPLC is so fast that it might compete with the progress of disproportionation in the column. Possible chromatogram

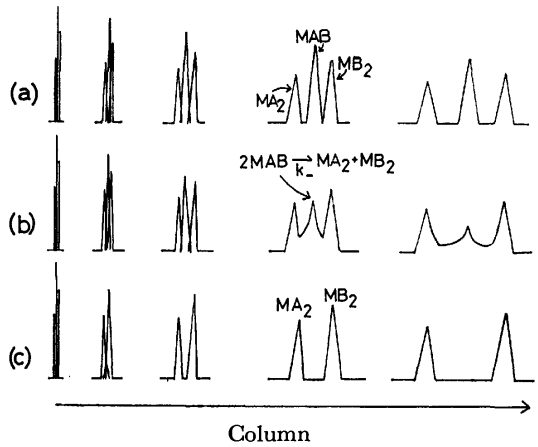

Fig. 1. Possible chromatogram patterns of the system of labile ternary complex formation.

patterns are shown in Fig. 1. When the separation process is so fast that disproportionation of the ternary complex during chromatography can be neglected, three peaks corresponding to MA_2, MB_2, and MAB would appear on the chromatograms (Fig. 1(a)), the chromatograms obtained directly indicating the concentration of each species before chromatography was carried out. When disproportionation is much faster than the separation process, peaks of only two binary complexes would appear on the chromatograms (Fig. 1(c)). In case of the intermediate of these two extremes, the peak of a ternary complex would appear accompanied by disproportionation in the column (Fig. 1(b)). In this case disproportionation is retarded with increase in flow rate, bringing about a change of chromatogram patterns. Thus, if the peak height of the ternary complex remains unchanged with flow rate, disproportionation is negligible.

In HPLC there are some favorable factors to retard disproportionation in the column. (1) Each species is diluted rapidly during the course of chromatography, suppressing disproportionation which is anticipated to occur by the bimolecular collisional process of two ternary complexes. Actual concentration in the liquid phase will be low since a considerable part of each species is retained on the column, collision of two ternary complexes adsorbed on silica gel surface being unlikely to occur. (2) The rate of disproportionation can be controlled by a suitable choice of initial concentrations of MA_2 and MB_2, disproportionation being slow when initial concentrations are low. (3) Control of column temperature is useful, disproportionation being retarded when column temperature is kept low. Thus a combination of high speed separation, rapid dilution, suitable choice of initial concentrations and low temperature, similar to the case of the rapid quenching method,[11] might halt the progress of the reaction in the column. If these conditions are fulfilled, the equilibrium constant K will be determined by direct measurements of peak heights appearing on chromatograms.

Rate constants k and k_- are determined as follows. Two dilute solutions of MA_2 and MB_2 are mixed. A ternary complex is produced gradually and the equilibrium Eq. 1 will be attained. After the lapse of a certain time a portion of the mixed solution is supplied to HPLC. The progress of the reaction ceases when the solution is injected into the column. Thus, concentrations of each species at a definite time after mixing can be determined by HPLC. The rates of formation of ternary complex and decrease of binary complexes are expressed as follows.

$$\frac{d[MA_2]}{dt} = \frac{d[MB_2]}{dt} = k_-[MAB]^2 - k[MA_2][MB_2] \quad (3a)$$

$$\frac{d[MAB]}{dt} = k[MA_2][MB_2] - k_-[MAB]^2 \quad (3b)$$

Assuming that the initial concentrations of MA_2 and MB_2 are the same ($=a_0$), we have

$$\frac{dx}{dt} = 4k_-(a_0 - x)^2 - kx^2$$
$$= (4/K - 1)kx^2 - 8a_0kx/K + 4a_0^2k/K \quad (4a)$$

$$\frac{dy}{dt} = k(a_0 - y/2)^2 - k_-y^2$$
$$= -(ky^2/4)(4/K - 1) - a_0ky + a_0^2k, \quad (4b)$$

where x and y are concentrations of MA_2 (or MB_2) and MAB, respectively. Rate constants k and k_- are determined by means of Eq. 4a or 4b. When $K=4.0$, we have the following equations by integrating Eqs. 4a and 4b.

$$-\ln(1 - 2x/a_0) = ka_0t \quad (5a)$$

$$-\ln(1 - y/a_0) = ka_0t \quad (5b)$$

When $K \neq 4.0$, k and k_- are determined by means of the following equation.[12]

$$k = (2/mt)\left\{\ln\left(\frac{\left(\frac{2a_0-m}{1-4/K}\right)-y}{\left(\frac{2a_0+m}{1-4/K}\right)-y}\right)+\left(\ln\frac{(2a_0-m)}{(2a_0+m)}\right)\right\} \quad (6)$$

$$m = 4a_0\sqrt{1/K}$$

Results and Discussion

Determination of Equilibrium Constant. By use of a well deactivated silica gel-column, various metal chelates of *N,N*-disubstituted dithiocarbamic acid gave chromatograms with no decomposition of chelates. Metal chelates of Cu(II), Hg(II), Ni(II), Pd(II), and Co(III) *etc.* gave linear calibration graphs (detection limit, few μg-few ng). A mixed solution of two different *N,N*-disubstituted dithiocarbamate chelates of Ni(II) always gave three peaks[13,14] (Fig. 2(c)). Peak heights of these three peaks remained unchanged in the flow rate range of the pump 3.0—0.4 cm³/min (Figs. 2(c)—2(f)). This indicates that the conditions shown in Fig. 1(a) are satisfied. When the initial concentrations of two binary complexes were chosen to be the same ($=a_0$), the equilibrium concentrations of the chelates were both $a_0/2$. Thus the equilibrium concentration of ternary complex was equal to a_0. Exactly half of the initial binary complexes was transformed into a ternary complex, the equilibrium constant K being 4.0. Formation of the ternary complex is controlled by a statistical factor. In all the systems of a mixture of two binary complexes K was always equal to 4.0, suggesting that the lack of the factor either stabilizes of destabilizes the ternary complex.[15]

Cu(II) chelates showed different chromatogram

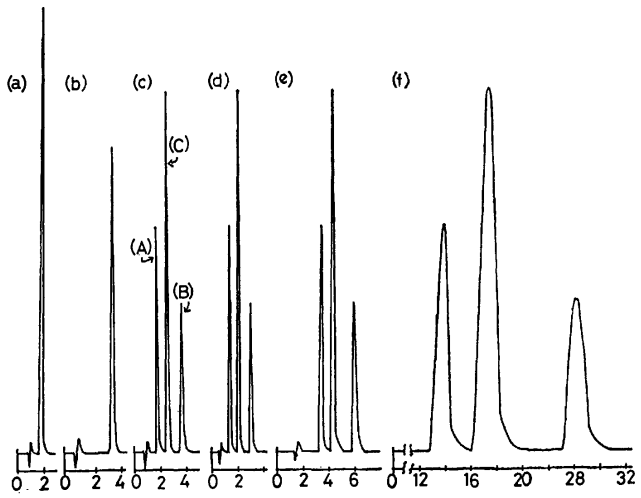

Fig. 2. Chromatogram patterns of two different dithiocarbamate chelates of nickel.
Column: Shodex silipak (4 mm × 15 cm), eluent: hexane : ethyl acetate = 100 : 7 (water saturated), flow rate: (a)—(c) 2.5 cm³/min; (d) 3.0 cm³/min; (e) 1.5 cm³/min; (f) 0.4 cm³/min, detector: 325 nm, sample: (a) 0.4 mM $Ni[(CH_3CH_2CH_2)_2NCSS]_2$ in $CHCl_3$; (b) 0.4 mM $Ni[(CH_3CH_2CH_2)_2NCSS]_2$ in $CHCl_3$; (c) 0.4 mM $Ni[(CH_3CH_2CH_2)_2NCSS]_2$ + 0.4 mM $Ni[(CH_3CH_2)_2NCSS]_2$ in $CHCl_3$, sample size: 5 μl.
(A): $Ni[(CH_3CH_2CH_2)_2NCSS]_2$, (B): $Ni[(CH_3CH_2)_2NCSS]_2$, (C): $Ni[(CH_3CH_2CH_2)_2NCSS][(CH_3CH_2)_2NCSS]$.

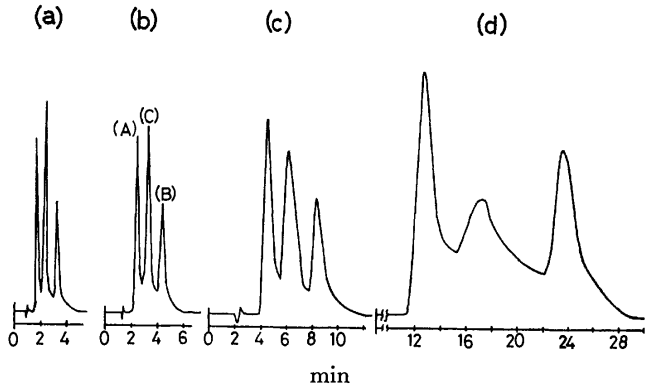

Fig. 3. Chromatogram patterns of two different dithiocarbamate chelates of copper at relatively higher concentrations.
Column: LiChrosorb SI 100 (2 mm × 25 cm), eluent: hexane : cyclohexane : isopropyl acetate = 50 : 50 : 4 (water saturated), flow rate: (a) 1.3 cm³/min; (b) 0.9 cm³/min; (c) 0.5 cm³/min; (d) 0.2 cm³/min, detector: 440 nm, sample: 1 mM $Cu[(CH_3CH_2CH_2)_2NCSS]_2$ + 1 mM $Cu[(CH_3CH_2)_2NCSS]_2$ in $CHCl_3$, sample size: 5 μl.
(A): $Cu[(CH_3CH_2CH_2)_2NCSS]_2$, (B): $Cu[(CH_3CH_2)_2NCSS]_2$, (C): $Cu[(CH_3CH_2CH_2)_2NCSS][(CH_3CH_2)_2NCSS]$. The broadening of this peak (C) is due to disproportionation of this ternary chelate in the column.

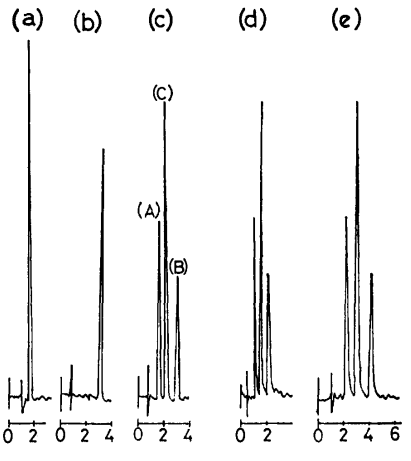

Fig. 4. Chromatogram patterns of two different dithiocarbamate chelates of copper at low concentrations.
Column: Shodex silipak (4 mm × 15 cm), eluent: hexane : ethyl acetate = 100 : 15 (water saturated), flow rate: (a)—(c) 2.5 cm³/min; (d) 3.0 cm³/min; (e) 1.5 cm³/min, detector: 280 nm, sample: (a) 4.0×10^{-6} M $Cu[(CH_3CH_2)_2NCSS]_2$; (b) 4.0×10^{-6} M $Cu[(CH_3)_2NCSS]_2$; (c) 4.0×10^{-6} M $Cu[(CH_3CH_2)_2NCSS]_2 + 4.0 \times 10^{-6}$ $Cu[(CH_3)_2NCSS]_2$; these samples are solutions in hexane : chloroform : ethyl acetate = 8 : 1 : 1, sample size: 50 μl.
(A): $Cu[(CH_3CH_2)_2NCSS]_2$, (B): $Cu[(CH_3)_2NCSS]_2$, (C): $Cu[(CH_3CH_2)_2NCSS][(CH_3)_2NCSS]$.
No disproportionation was observed in this case.

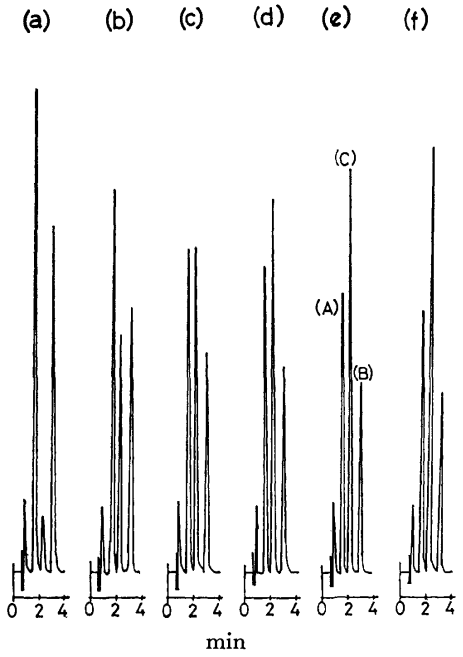

Fig. 5. Change of chromatogram patterns of the mixture of two different dithiocarbamate chelates of nickel.
Column: Shodex silipak (4 mm × 15 cm), eluent: hexane : ethyl acetate = 100 : 20 (water saturated), flow rate: 2.5 cm³/min, detector: 325 nm, sample: 2.5×10^{-5} M $Ni[(CH_3CH_2)_2NCSS]_2$ + 2.5×10^{-5} M $Ni[(CH_3)_2NCSS]_2$ (a) After mixing 0.5 min; (b) 4.0 min; (c) 7.5 min; (d) 11.0 min; (e) 18.0 min; (f) 60.0 min (equilibrium); these samples are solutions in hexane : chloroform : ethyl acetate = 3 : 1 : 1 at 25 °C, sample size: 50 μl.
(A): $Ni[(CH_3CH_2)_2NCSS]_2$, (B): $Ni[(CH_3)_2NCSS]_2$, (C): $Ni[(CH_3CH_2)_2NCSS][(CH_3)_2NCSS]$.

patterns. When a relatively high a_0 was chosen ($a_0 = 1.0\times10^{-3}$ M), chromatogram patterns were seriously affected by the flow rate, suggesting the disproportionation of the ternary complex in the column. On the other hand, when a very low a_0 was chosen ($a_0 = 4.0\times10^{-6}$ M), they were unaffected by the flow rate (from 1.5 to 3.0 cm³/min) (Fig. 4). In order to compensate the decrease of concentration of the sample, it was necessary to inject a large volume of sample. The composition of the solvent of the injected sample should be similar to that of the eluent, otherwise serious broadening of each peak takes place. About 200 μl of sample volume could be injected into the column without remarkable broadening of each peak. For Cu(II) chelates the chromatogram patterns were also sensitive to column temperature. At ambient temperature, when a_0 was chosen 4.0×10^{-5} M, chromatogram petterns were affected slightly by flow rate. However, when column temperature was low, no disproportionation in the column was observed. The values K were also always equal to 4.0 for all the systems of Cu(II) chelates.

Determination of Rate Constants. As shown in Fig. 5, a trace peak of the ternary complex appeared on chromatograms immediately after mixing of two solutions. With the lapse of time the peak of the ternary complex rose while the peaks of binary complexes fell. The rate constants k and k_- were determined by means of Eq. 5b. The results are summarized in Tables 1 and 2 (for Ni(II) and Cu(II) chelates, respectively). The values of k and k_- were sensitive to temperature and composition of solvent of the mixture. Since k and k_- were affected by the water content of the mixed solution, experimental conditions were so chosen that each solution of MA_2 and MB_2 was saturated with water before mixing. Disproportionation was slow when solvent was not saturated with water. Column temperature and composition of eluent play insignificant role. By use of HPLC we can promptly separate various species including kinetically unstable ones and elute them. Varying chromatographic conditions such as composition of eluent, column temperature and flow rate does not change the values of k and k_- if disproportionation can be neglected during the course of chromatography.

The rate constants k of Ni(II) chelates are of the order 10^1—10^2 M^{-1} s^{-1}. Since Cu(II) chelates are more labile than Ni(II) chelates, values of k of Cu(II) chelates are larger and of the order 10^3 M^{-1} s^{-1}. Values of k seems to be small when molecular weights of two

Table 1. Rate constants of formation and disproportionation of labile ternary dithiocarbamate chelates of Ni(II)

$$NiA_2 + NiB_2 \underset{k_-}{\overset{k}{\rightleftharpoons}} 2NiAB, \qquad K = [NiAB]^2/[NiA_2][NiB_2] = k/k_- = 4.0$$

B	k (M^{-1} s^{-1})	k_- (M^{-1} s^{-1})	Retention time (min)			Eluent
			MA_2	MAB	MB_2	
$(CH_3)_2NCSS$	$(1.3\pm0.1)\times10^2$	$(3.3\pm0.4)\times10^1$	1.2	2.2	3.1	A
$(CH_3CH_2CH_2)_2NCSS$	$(2.4\pm0.2)\times10^2$	$(6.0\pm0.6)\times10^1$	3.9	2.7	1.8	C
$(CH_2)_4NCSS$	$(1.1\pm0.07)\times10^2$	$(2.8\pm0.2)\times10^1$	3.1	4.2	5.9	B
$(CH_2)_5NCSS$	$(9.7\pm0.5)\times10^1$	$(2.4\pm0.15)\times10^1$	4.4	5.1	5.7	D
$(C_6H_5CH_2)_2NCSS$	$(1.9\pm0.2)\times10^2$	$(4.8\pm0.5)\times10^1$	3.9	2.8	1.8	C
$(CH_2CH_2OCH_2CH_2)NCSS$	$(7.3\pm0.5)\times10^1$	$(1.8\pm0.1)\times10^1$	1.2	2.4	4.1	A

A: $(CH_3CH_2)_2NCSS$, $a_0 = 2.5\times10^{-5}$M. Chromatographic conditions: column: Shodex silipak (4 mm × 15 cm), eluent: hexane: ethyl acetate (water saturated) = 100: 20 (A), 100 : 8 (B), 100 : 6 (C), 100 : 5 (D), flow rate: 2.5 cm³/min, detector: 325 nm, sample size: 50 μl, column temperature: ambient, Equal amounts of NiA_2 and NiB_2 dissolved in the mixed solvent system, chloroform : ethyl acetate : hexane = 3 : 1 : 1 (water saturated), were mixed at 25 °C.

Table 2. Rate constants of formation and disproportionation of labile ternary dithiocarbamate chelates of Cu(II)

$$CuA_2 + CuB_2 \underset{k_-}{\overset{k}{\rightleftharpoons}} 2CuAB, \qquad K = [CuAB]^2/[CuA_2][CuB_2] = k/k_- = 4.0$$

B	k ($M^{-1}s^{-1}$)	k_- ($M^{-1}s^{-1}$)	Retention time (min)			Eluent
			MA_2	MAB	MB_2	
$(CH_3)_2NCSS$	$(3.5\pm0.4)\times10^3$	$(8.8\pm1.0)\times10^2$	1.5	2.0	2.8	A
$(CH_3CH_2CH_2)_2NCSS$	$(6.4\pm0.8)\times10^3$	$(1.6\pm0.2)\times10^3$	3.0	2.1	1.5	B
$(CH_2)_5NCSS$	$(1.2\pm0.05)\times10^3$	$(3.0\pm0.15)\times10^2$	3.7	4.3	5.1	C
$(C_6H_5CH_2)_2NCSS$	$(3.4\pm0.3)\times10^3$	$(8.5\pm0.8)\times10^2$	3.0	2.5	1.8	B

A: $(CH_3CH_2)_2NCSS$, $a_0=4.0\times10^{-6}$M. Chromatographic conditions: column: Shodex silipak (4 mm × 15 cm), eluent: hexane : ethyl acetate (water saturated) = 100 : 15 (A), 100 : 4 (B), 100 : 3(C), flow rate: 2.5 cm³/min, detector: 270 nm, sample size: 50 μl, column temperature: 0 °C (Column and solvent reservoir were plunged into an ice bath). Equal amounts of CuA_2 and CuB_2 dissolved in the mixed solvent system, chloroform : ethyl acetate : hexane = 8 : 1 : 1 (water saturated), were mixed at 25 °C.

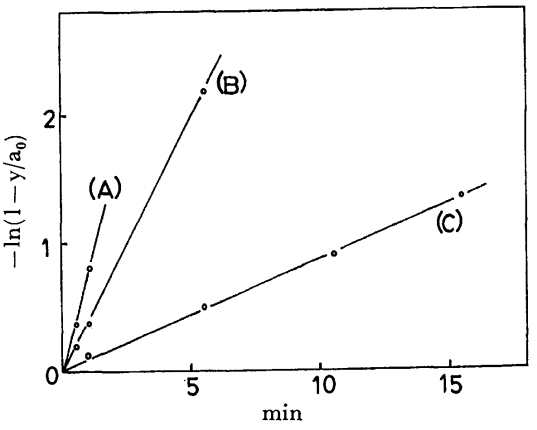

Fig. 6. Plot of Eq. 5a at different a_0.
Chromatographic conditions: column: Shodex silipak (4 mm × 15 cm), eluent: hexane : ethyl acetate = 100 : 7 (water saturated), flow rate: 2.5 cm³/min, detector: 325 nm, sample: the mixed solution of Ni[$(CH_3CH_2CH_2)_2NCSS]_2$ and Ni[$(CH_3CH_2)_2NCSS]_2$ in hexane : chloroform : ethyl acetate = 3 : 1 : 1 were subjected to HPLC after mixing a definite time at 25 °C, (A): $a_0=5.0\times10^{-5}$ M, (B) $a_0=2.5\times10^{-5}$ M, (C): $a_0=6.25\times10^{-6}$ M.

Table 3. Activation parameters of ternary complex formation of *N*,*N*-disubstituted dithiocarbamate chelates

$$M[(CH_3CH_2)_2NCSS]_2 + M[(CH_3CH_2CH_2)_2NCSS]_2 \rightleftharpoons M[(CH_3CH_2)_2NCSS][(CH_3CH_2CH_2)_2NCSS]$$

M	$H^{\ddagger}$ (kJ mol⁻¹)	$G^{\ddagger}$ (25 °C) (kJ mol⁻¹)	$S^{\ddagger}$ (kJ K⁻¹ mol⁻¹)
Ni(II)[a]	65±5	60±3	$(1.7\pm2.7)\times10^{-2}$
Cu(II)[b]	24±5	51±4	$(9.1\pm3.0)\times10^{-2}$

a) In chloroform : ethyl acetate : hexane = 1 : 1 : 3 (water saturated). b) In chloroform : ethyl acetate : hexane = 1 : 1 : 8 (water saturated).

dithiocarbamates are close to each other. Validity of the bimolecular collisional process of disproportionation was confirmed by changing a_0 (Fig. 6). When a_0 exceeds this range, the rate of disproportionation does not increase in proportion to a_0.

The activation parameters of disproportionation was determined by measuring k values at various temperatures. This was carried out by mixing two solutions of MA_2 and MB_2 under thermostated conditions at various temperatures. Results of the system consisting of diethyldithiocarbamic acid, dipropyldithiocarbamic acid and metal ion are given in Table 3. The activation enthalpy of Cu(II) chelates is smaller than that of Ni(II) chelates.

Conclusion

Fast bimolecular reactions can be traced by HPLC. Chromatographic conditions should be so chosen that no decomposition of species occurs during the course of chromatography. This can be done to a certain extent by choice of column packings and solvent systems. The upper limit of the rate constants is restricted by the sensitivity of the detector. Absorption of 0.05 units could be extended to a full scale without serious noise with the spectrometer we used. It seems that rate constants of the order $10^4\ M^{-1}s^{-1}$ can be determined. Since the sensitivity of a commercial UV detector for HPLC is about ten times larger than that of the present one, fast reactions with rate constants of the order $10^5\ M^{-1}s^{-1}$ might be traced by HPLC if absorption coefficient of the detected species is large ($\log\varepsilon>4$). The present method will also be useful for investigation of physicochemical properties of kinetically unstable species in solution.

References

1) J. F. K. Huber and J. C. Kraak, *Anal. Chem.*, **44**, 1554 (1972).
2) P. Heizmann and K. Ballschmiter, *J. Chromatogr.*, **137**, 153 (1977).
3) P. C. Uden and I. E. Bigley, *Anal. Chim. Acta*, **94**, 29 (1977).
4) G. Schwedt, *Chromatographia*, **11**, 145 (1978).
5) G. Schwedt, *Chromatographia*, **12**, 289 (1979).
6) J. W. O'Laughlin and T. P. O'Brien, *Anal. Lett.*, **A11**, 829 (1978).
7) M. Moriyasu and Y. Hashimoto, *Anal. Lett.*, **A11**, 593 (1978).

8) O. Liska, J. Lehotay, E. Brandstererova, G. Guichon, and H. Colin, *J. Chromatogr.*, **172**, 384 (1979).
9) J. Lehotay, E. Brandstererova, O. Liska, and G. Guichon, *J. Chromatogr.*, **172**, 379 (1979).
10) R. F. Majors, *Anal. Chem.*, **44**, 1722 (1972).
11) R. C. Bray, *Biochem. J.*, **81**, 189 (1961).
12) M. Bodenstein, *Z. Phys. Chem.*, **13**, 56 (1894); **22**, 1 (1897); **29**, 295 (1898).
13) M. Moriyasu and Y. Hashimoto, *Chem. Lett.*, **1980**, 117.
14) O. Liska, G. Guichon and H. Colin, *J. Chromatogr.*, **171** 145 (1979).
15) H. Sioge, *Angew. Chem. Int. Ed. Engl.*, **14**, 397 (1975).

The Reduction of Hexakis(urea)chromium(III) Ions at the Dropping Mercury Electrodes

Akifumi YAMADA,* Yasuo NAKABAYASHI, Tadatsugu YOSHIKUNI, and Nobuyuki TANAKA

Department of Chemistry, Faculty of Science, Tohoku University, Sendai 980

(Received June 5, 1980)

The polarographic reduction of hexakis(urea)chromium(III) ions at the dropping mercury electrode has been studied in various supporting electrolyte solutions. This complex exhibits two irreversible reduction waves; the first corresponds to Cr(III)→Cr(II), and the second, to Cr(II)→Cr(0). The kinetic parameters of the electrode reactions were determined in various supporting electrolyte solutions and at varied ionic strengths by means of Tast polarography. The differential-pulse polarographic characteristics of this complex are also given.

The cyclic voltammetry of hexakis(urea)chromium-(III) ions (abbreviated hereafter as $[Cr(urea)_6]^{3+}$) has been briefly reported in dimethyl sulfoxide solutions.[1] This complex exhibits two irreversible reduction waves; the first corresponds to Cr(III)→Cr(II), and the second, to Cr(II)→Cr(0). The present investigation was undertaken to ascertain the electrochemical behavior in aqueous solutions in the hope of gaining further insight into the mechanism of the electroreduction of $[Cr(urea)_6]^{3+}$ ions. The kinetic parameters of the electrode reaction of $[Cr(urea)_6]^{3+}$ ions were also examined by means of Tast polarography.

Experimental

The Tast polarograms were recorded by a Yanagimoto voltammetric analyzer, P-1000. A National digital tester, Model VP-2521A, was used; the current and the the potential were thus measured precisely. A three-electrode cell equipped with a saturated calomel electrode (Yanagimoto MR-P_2-05-1) and a platinum-wire electrode was employed. The DME with a flow rate of 1.10 mg s^{-1} and a drop time of 2.99 s in 0.4 M (1 M=1 mol dm^{-3}) of NaCl containing a 0.1 M acetate buffer solution and 20 μM LEO was used. Poly-(oxyethylene) dodecyl ether (LEO: mean molecular weight, 862) was used as the maximum suppressor.

The complex, $[Cr(urea)_6]Cl_3$, was prepared according to the literature[2] and converted to perchlorate salt. This complex is stable in aqueous solutions.[3] All the other chemicals used were of a guaranteed reagent-grade.

The dissolved oxygen was removed by bubbling purified nitrogen gas through the solution. All the measurements were made at 25 °C unless otherwise stated.

Results

Effects of Surface-active Substances. In the polarographic measurements, the $[Cr(urea)_6]^{3+}$ ions were found not to give a well-defined polarographic wave, but to give two well-defined waves in the presence of a small amount of surface-active substances. The effects of the surface-active substances on the Tast polarogram were examined; the results are shown in Fig. 1.

The addition of 20 μM of LEO to a solution containing 1 mM of complex ions gave satisfactory results; the maximum was suppressed without causing a decrease in the diffusion current. The addition of other surface-active substances, such as 0.0015% Triton X-100, 0.015% PAA (polyacrylamide) and 0.005% gelatin, caused a distortion of the Tast polarogram. The

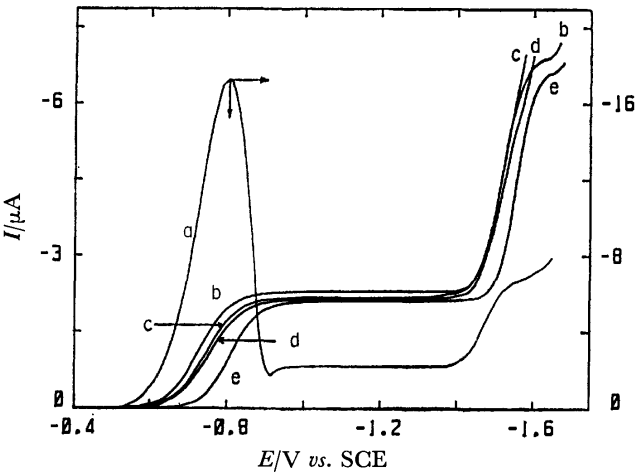

Fig. 1. Effects of surface active substances on the Tast polarogram of 1 mM $[Cr(urea)_6](ClO_4)_3$ in 0.4 M NaCl containing 0.1 M acetate buffer (pH 4.6).
(a) without maximum suppressor, with (b) 20 μM LEO, (c) 0.005% gelatin, (d) 0.015% polyacrylamide and (e) 0.0015% Triton X-100.

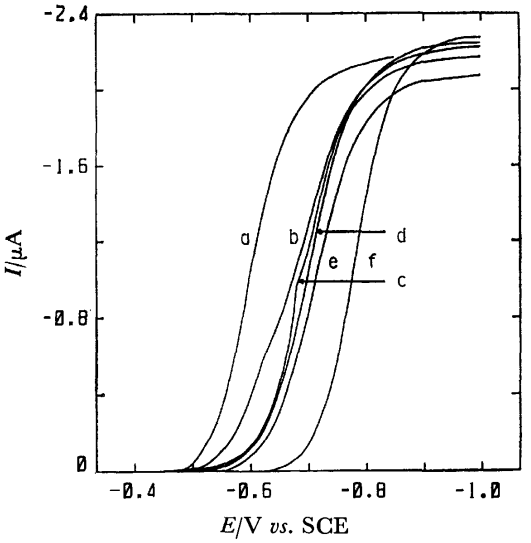

Fig. 2. Tast polarograms for the first wave of 1 mM $[Cr(urea)_6](ClO_4)_3$ obtained in various supporting electrolyte solutions containing 0.1 M acetate buffer and 20 μM LEO (μ=0.5) at 25 °C.
(a) NaI, (b) NaBr, (c) $NaNO_3$, (d) NaCl, (e) Na_2SO_4, (f) NaSCN.

current-potential curves were shifted to more negative potentials by the presence of Triton X-100. Also, the Tast polarogram in the presence of PAA and gelatin did not exhibit a second wave.

Effects of the Supporting Electrolytes. Measurements were made in various supporting electrolyte solutions. Figure 2 shows a Tast polarogram of the first waves of the 1 mM $[Cr(urea)_6]^{3+}$ ions obtained in various supporting electrolyte solutions (ionic strength $\mu=0.5$) containing 0.1 M of an acetate buffer and 20 μM of LEO at 25 °C. The Tast polarogram obtained in the solution containing NaSCN or $NaNO_3$ did not exhibit a second wave.

Conventional polarographic log-plots[4] were tested for the current-potential curves of the $[Cr(urea)_6]^{3+}$ ions. The value of the log-plot slope was found to be far different from the one predicted for a reversible electrode process indicating that the electrode reaction proceeds irreversibly.

The modified log-plots for an irreversible electrode process proposed by Oldham and Parry[5] were examined.

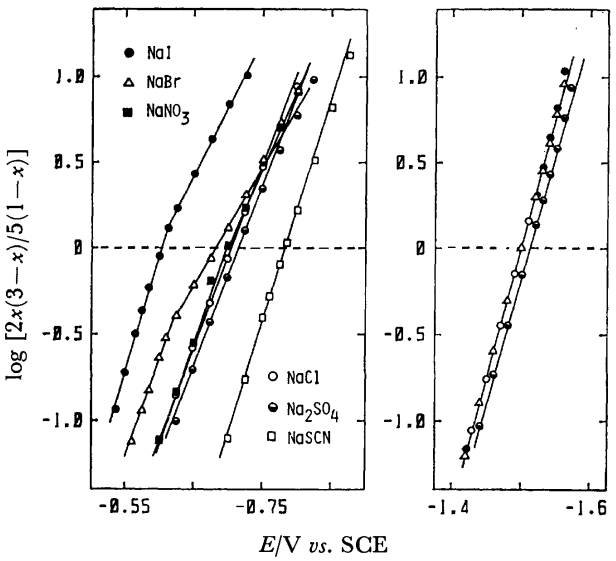

Fig. 3. Log-plots for the first (left) and the second (right) waves of 1 mM $[Cr(urea)_6](ClO_4)_3$ obtained in various supporting electrolyte solutions containing 0.1 M acetate buffer and 20 μM LEO at 25 °C.
(●) NaI, (△) NaBr, (■) $NaNO_3$, (○) NaCl, (◒) Na_2SO_4, (□) NaSCN.

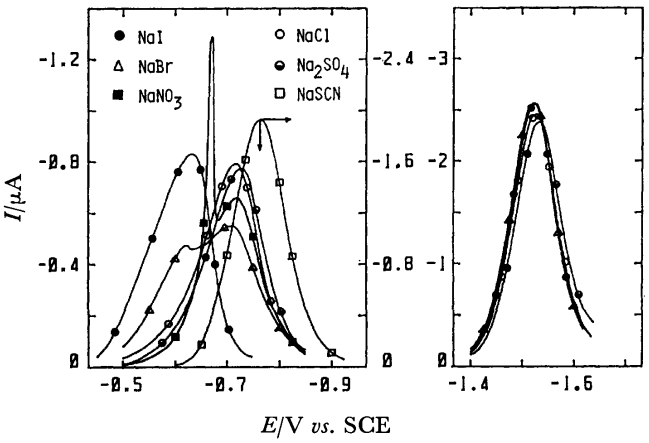

Fig. 4. Differential pulse polarograms of 1 mM $[Cr(urea)_6](ClO_4)_3$ in various supporting electrolyte solutions containing 0.1 M acetate buffer and 20 μM LEO (pH 4.6, $\mu=0.5$) at 25 °C.
(●) NaI, (△) NaBr, (■) $NaNO_3$, (○) NaCl, (◒) Na_2SO_4, (□) NaSCN.

The results for the first and the second waves are given in Fig. 3 (see also Discussion). The log-plots for the first wave in NaBr, NaI, and $NaNO_3$ did not give a straight line.

Differential Pulse Polarogram. Figure 4 shows the differential pulse polarograms of the 1 mM $[Cr(urea)_6]^{3+}$ ions obtained in several media at 25 °C. Much as in the results of the Tast polarography, the first waves appeared over a wide range of potentials, while the second waves appeared in a rather narrow potential range. The peak current for NaSCN was about twice as large as in the other cases.

The peak potential(E_p), the half-width(ΔW), and the peak current(I_p) of the differential pulse polarogram, which were obtained in several media, are given in Table 1. These results suggest that the electroreduction of $[Cr(urea)_6]^{3+}$ to the Cr(II) species proceeds irreversibly.

Measurements were also made at varied ionic strengths. Various parameters which characterize a differential pulse polarogram were obtained; they are shown in Table 2. The peak currents for the first and the second waves decreased with an increase in the ionic strength. The half-width of the first wave increased

Table 1. Differential-pulse polarographic characteristics of 1 mM $[Cr(urea)_6](ClO_4)_3$ in various supporting electrolyte solutions containing 0.1 M of an acetate buffer and 20 μM of LEO at 25 °C

Medium	First wave			Second wave		
	E_p / V vs. SCE	ΔW / mV	I_p / μA	E_p / V vs. SCE	ΔW / mV	I_p / μA
0.4 M NaCl	−0.717	125	−0.792	−1.528	90	−2.500
0.4 M NaBr	−0.705	206	−0.547	−1.525	90	−2.580
0.4 M NaI	−0.632	134	−0.836	−1.526	88	−2.590
0.4 M $NaNO_3$	−0.717		−0.644	—	—	—
	(−0.672)[a]		(−1.260)[a]			
0.4 M NaSCN	−0.764	115	−1.880	—	—	—
0.13 M Na_2SO_4	−0.727	128	−0.755	−1.536	94	−2.340

a) Corresponds to the prewave.

TABLE 2. DIFFERENTIAL-PULSE POLAROGRAPHIC CHARACTERISTICS OF 1 mM $[Cr(urea)_6](ClO_4)_3$ IN VARIED IONIC STRENGTHS IN SOLUTIONS CONTAINING SODIUM CHLORIDE, 0.1 M OF AN ACETATE BUFFER AND 20 μM OF LEO AT 25 °C.

Ionic strength	First wave			Second wave		
	E_p / V *vs.* SCE	ΔW / mV	I_p / μA	E_p / V *vs.* SCE	ΔW / mV	I_p / μA
0.1	−0.702	93	−0.904	−1.489	88	−2.700
0.3	−0.715	110	−0.842	−1.516	89	−2.600
0.5	−0.717	125	−0.792	−1.528	90	−2.500
1.0	−0.730	143	−0.673	−1.548	92	−2.460
2.0	−0.690	190	−0.615	−1.560	94	−2.270

with an increase in the ionic strength, while that of the second wave scarcely changed. The shifts in $E_{1/2}$ and E_p were rather complicated.

Discussion

The hexakis(urea)chromium(III) ions gave two well-defined current-potential curves, as may be seen in Fig. 1. The limiting currents of both the first and second waves were diffusion-controlled and were proportional to the concentration of the complex. The limiting current of the second wave was twice that of the first one. The first wave corresponds to the reduction of $[Cr(urea)_6]^{3+}$ to $[Cr(urea)_6]^{2+}$ species.[1] The tervalent chromium species is stable,[3] but the divalent one, produced on the surface of the electrode, is unstable and may undergo hydrolysis. The overall electrode reaction was considered by a comparison of its electrode reaction with that of other chromium(III) complexes.[6-11] Thus,

$$[Cr(urea)_6]^{3+} + e \longrightarrow [Cr(urea)_6]^{2+}, \quad (1)$$

$$[Cr(urea)_6]^{2+} + pH_2O \longrightarrow [Cr(urea)_{6-p}(H_2O)_p]^{2+} + p\text{urea}, \quad (2)$$

for the first wave, and

$$[Cr(urea)_{6-p}(H_2O)_p]^{2+} + 2e \longrightarrow Cr(0) + (6-p)\text{urea} + pH_2O, \quad (3)$$

for the second wave.

The diffusion coefficient of the $[Cr(urea)_6]^{3+}$ ions was measured by means of a method previously reported[12] by using $[Co(NH_3)_6]^{3+}$ as the reference substance; the results are summarized in Table 3.

The reduction of $[Cr(urea)_6]^{3+}$ to chromium(II) species in an acid solution was considered to be irreversible from the facts described above (Fig. 3 and Table 1). For a totally irreversible electrode reaction, the following relations of the Tast polarography are derived:[5]

$$(RT/\alpha nF) \ln [2x(3-x)/5(1-x)] = E_{1/2} - E, \quad (4)$$

with:

$$x = I/I_d, \quad (5)$$

and:

$$E_{1/2} = (RT/\alpha nF) \ln [1.35k_c^\circ (t_d/D)^{1/2}], \quad (6)$$

where I is the current at the potential, E; I_d, the diffusion-controlled current; D, the diffusion coefficient; t_d, the drop time; α, the transfer coefficient; k_c°, the cathodic rate constant at $E=0$; n, the number of electrons; R, the gas constant; F, the Faraday constant, and T the absolute temperature. According to Eq. 4, a plot of $\ln[2x(3-x)/5(1-x)]$ *vs.* E should be a straight line. The transfer coefficient, α, can be obtained from the slope, and the half-wave potential, $E_{1/2}$, from the intersection. The rate constant, k_c°, can be obtained from $E_{1/2}$ by applying Eq. 6. An example of the plots for Eq. 4 has been shown above (Fig. 3).

The kinetic parameters of the electrode reactions thus obtained are given in Table 3. These kinetic parameters obtained were checked by calculating the current according to this relation:

$$2x(3-x)/5(1-x) = 1.35k_c^\circ (t_d/D)^{1/2} \exp(-\alpha nFE/RT). \quad (7)$$

The calculated currents were in agreement with the observed ones except for the cases of NaBr, NaI, and $NaNO_3$.

It has been reported that the interaction reaction between the reduced chromium(II) complex and the nitrate ions occurs to a considerable extent.[13,14] The abnormality of the current-potential curve in a nitrate medium may, therefore, be understood in termes of this effect.

TABLE 3. KINETIC PARAMETERS OF ELECTRODE REACTIONS OF $[Cr(urea)_6](ClO_4)_3$ OBTAINED IN VARIOUS SUPPORTING ELECTROLYTE SOLUTIONS CONTAINING 0.1 M OF AN ACETATE BUFFER AND 20 μM OF LEO AT 25 °C

Medium	D / 10^{-6} cm^2 s^{-1}	First wave			Second wave		
		$E_{1/2}$ / V *vs.* SCE	α	k_c° / cm s^{-1}	$E_{1/2}$ / V *vs.* SCE	α	k_c° / cm s^{-1}
0.4 M NaCl	5.16	−0.705	0.62	3.78×10^{-11}	−1.500	0.44	7.11×10^{-26}
0.4 M NaBr	5.26	−0.685	0.72	1.18×10^{-11}	−1.500	0.45	2.62×10^{-26}
			(0.47)[a]	(3.79×10^{-9})[a]			
0.4 M NaI	5.13	−0.600	0.86	1.97×10^{-12}	−1.500	0.46	6.50×10^{-27}
			(0.53)[a]	(1.28×10^{-8})[a]			
0.4 M $NaNO_3$	5.07	−0.699	0.67	1.34×10^{-11}	—	—	—
			(0.53)[a]	(5.01×10^{-10})[a]			
0.4 M NaSCN	5.11	−0.783	0.73	2.50×10^{-13}	—	—	—
0.13 M Na_2SO_4	4.40	−0.716	0.63	1.94×10^{-11}	−1.510	0.43	9.32×10^{-26}

a) The values in parentheses were obtained from the more negative potential range.

Table 4. Kinetic parameters of electrode reactions of $[Cr(urea)_6](ClO_4)_3$ obtained at varied ionic strengths in solutions containing 0.1 M of an acetate buffer and 20 μM of LEO at 25 °C

Ionic strength	D	First wave			Second wave		
		$E_{1/2}$	α	k_c°	$E_{1/2}$	α	k_c°
	10^{-6} cm^2 s^{-1}	V *vs.* SCE		cm s^{-1}	V *vs.* SCE		cm s^{-1}
0.1	5.33	−0.681	0.77	1.34×10^{-12}	−1.463	0.50	1.73×10^{-28}
0.3	5.27	−0.696	0.69	7.62×10^{-12}	−1.488	0.46	1.18×10^{-26}
0.5	5.16	−0.705	0.62	3.78×10^{-11}	−1.500	0.44	7.11×10^{-26}
1.0	5.03	−0.718	0.56	1.54×10^{-10}	−1.516	0.43	1.37×10^{-25}
1.5	4.83	−0.693	0.52	8.59×10^{-10}	−1.519	0.42	3.77×10^{-25}
2.0	4.70	−0.682	0.49	2.41×10^{-9}	−1.525	0.41	4.82×10^{-25}
3.0	3.72	−0.663	0.40	2.74×10^{-8}	−1.526	0.39	6.14×10^{-24}

On the other hand, the distortion of the Tast polarogram obtained in solutions containing NaBr or NaI may be explained by the double-layer effect. It is a well-known fact that Br^- and I^- are specifically adsorbed on mercury and change the double-layer potentials.[15] The potential of PZC (point of zero charge) in the presence of Br^- and I^- lies[16] near the potential where the half-wave potential of the Tast polarogram appears. Therefore, the effect of the double layer on the current-potential curves may be more pronounced,[17] since the charge of $[Cu(urea)_6]^{3+}$ ions is high and its electroreduction process is irreversible. This causes a distortion of the current-potential curves. Such a double-layer effect has also been reported for the reduction of $[Cr(NH_3)_6]^{3+}$ ions in the presence of Br^- and I^-.[18]

Kinetic parameters are also obtained at varied ionic strengths in solutions containing 0.1 M of an acetate buffer and 20 μM of LEO at 25 °C. The results are shown in Table 4. The rate constants, k_c°, for the first and the second waves increased with an increase in the ionic strength. The transfer coefficient varied drastically, indicating the presence of a specific adsorption of the complex ions.

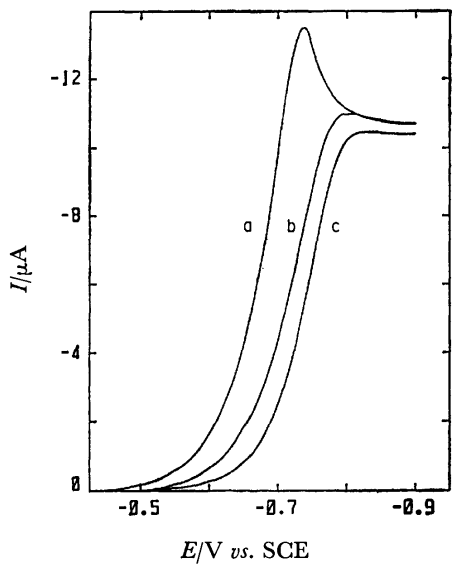

Fig. 5. Normal pulse polarograms of 1 mM $[Cr(urea)_6](ClO_4)_3$ in various halogenide solutions containing 0.1 M acetate buffer and 20 μM LEO (pH 4.6, $\mu=0.5$) at 25 °C.
(a) NaI, (b) NaBr, (c) NaCl.

Anion-induced adsorption[19-21] has been reported for the reduction of some cations, such as Pb(II), Cd(II), and Zn(II), in the presence of I^-, Br^-, Cl^-, *etc.* A similar situation will hold good for the reduction of $[Cr(urea)_6]^{3+}$ ions: the charge of the complex ions is tripositive, and, therefore, the extensive adsorption of $[Cr(urea)_6]^{3+}$ ions on mercury electrodes might be induced from iodide and bromide media. This prediction might be supported by the results of the normal-pulse polarography. Usually, the maximum diminishes at a longer sampling time of the current, but in the present case the maximum still appears at a shorter sampling time ($t_d=50$ ms), as is shown in Fig. 5. For the case of the anion-induced adsorption, the possibility that current-potential curves obtained at shorter sampling times shows a maximum at intermediate potentials has been suggested by Oka and Matsuda.[22]

The diffusion current in Na_2SO_4 was found lower by about 15% than those in other clectrolytes. This is considered to be a result of the formation of ion pairs between $[Cr(urea)_6]^{3+}$ and SO_4^{2-}, by analogy with the electrode reactions of other tervalent complexes.[23,24]

The authors are indebted to Dr. Yoshikiyo Kato for technical assistance. They also wish to thank the Ministry of Education, Science and Culture for the financial support granted for this research.

References

1) M. Prügel and P. Janietz, *Z. Chem.*, **16**, 113 (1976).
2) P. Pfeiffer, *Chem. Ber.*, **36**, 1926 (1903).
3) K. B. Yatsimirskii and E. I. Yasinskene, *Zh. Obshch. Khim.*, **24**, 55 (1954); *Chem. Abstr.*, **49**, 7346c (1955).
4) I. M. Kolthoff and J. J. Lingane, "Polarography," Interscience Publishers, New York (1964), Vol. 1, Chap. 11.
5) K. B. Oldham and E. P. Parry, *Anal. Chem.*, **40**, 65 (1968).
6) N. Tanaka, K. Ebata, and G. Sato, *Bull. Chem. Soc. Jpn.*, **36**, 912 (1963).
7) N. Tanaka, A. Yamada, and R. Tamamushi, *Bull. Chem. Soc. Jpn.*, **37**, 1821 (1964).
8) J. A. Friend and P. W. Smith, *J. Phys. Chem.*, **63**, 314 (1959).
9) N. Tanaka, Y. Sato, R. Tamamushi, and G. Sato, *Bull. Chem. Soc. Jpn.*, **36**, 1059 (1963).
10) N. Tanaka, T. Ito, and R. Tamamushi, *Bull. Chem. Soc. Jpn.*, **37**, 1430 (1964).

11) N. Tanaka and A. Yamada, *Bull. Chem. Soc. Jpn.*, **39**, 920 (1966).
12) A. Yamada, Y. Kato, T. Yoshikuni, Y. Tanaka, and N. Tanaka, *Anal. Chim. Acta*, **112**, 55 (1979).
13) N. Tanaka and T. Ito, *Bull. Chem. Soc. Jpn.*, **39**, 1043 (1966).
14) N. Tanaka, T. Kano, and A. Yamada, *Chem. Lett.*, **1974**, 231.
15) P. Delahay, "Double Layer and Electrode Kinetics," Interscience Publishers, New York (1965), Chap. 4.
16) M. A. V. Devanathan and P. Peries, *Trans. Faraday Soc.*, **50**, 1236 (1954).
17) M. Breiter, M. Kleinerman, and P. Delahay, *J. Am. Chem. Soc.*, **80**, 5111 (1958).
18) A. Yamada, Doctoral Thesis, Tohoku University, Sendai, 1968.
19) F. C. Anson and D. J. Barclay, *Anal. Chem.*, **40**, 1791 (1968).
20) D. J. Barclay and F. C. Anson, *J. Electroanal. Chem.*, **28**, 71 (1970).
21) F. C. Anson, *Acc. Chem. Res.*, **8**, 400 (1975).
22) S. Oka and H. Matsuda, "Potential-step Method—Theory, Instrumentation and Application," in "Polarography, Part 2," ed by T. Fujinaga and M. Maruyama, Nankodo, Kyoto (1963), pp. 81—101.
23) N. Tanaka, K. Ogino, and G. Sato, *Bull. Chem. Soc. Jpn.*, **39**, 366 (1966).
24) N. Tanaka and A. Yamada, *Z. Anal. Chem.*, **224**, 117 (1967).

Potentiometric Study on the Complex Formation of Cobalt(II) Ion with Ethylenediamine-*N*-acetic Acid, Diethylenetriamine, and Iminodiacetic Acid

Takeo OHSAKA, Noboru OYAMA, and Hiroaki MATSUDA*

Department of Electronic Chemistry, Graduate School at Nagatsuta, Tokyo Institute of Technology, Nagatsuta, Midori-ku, Yokohama 227

(Received June 6, 1980)

The formation constants of Co(II)–ethylenediamine-*N*-acetate (edma), –diethylenetriamine (dien) and –iminodiacetate (ida) complexes were determined by potentiometric titration in 1.0 M $NaClO_4$ solution at 25 °C. The following results were obtained. Edma: $\log \beta_{101}=7.51$, $\log \beta_{102}=14.05$; dien: $\log \beta_{101}=9.34$, $\log \beta_{102}=16.89$; ida: $\log \beta_{101}=6.54$, $\log \beta_{102}=11.95$, β_{pqr} being the overall formation constant defined in the text. The relative effects of amino and carboxyl groups on the affinity of ligands to Co(II) ion are discussed.

Ethylenediamine-*N*-acetic acid (edma) is a simple, artificial and basic amino acid in products formed during the carboxymethylation of ethylenediamine;[1] Nevertheless, only a few papers have appeared on the complex formation equilibria between metal ions and $edma^-$ anion, in contrast to those of ethylenediaminetetraacetic acid (EDTA). Fujii *et al.*[2-6] have prepared this ligand by a new, simple method and studied the complex formation with Cd(II), Pb(II), Cu(II), and Tl(I) ions by d.c. polarography and with Ni(II) by spectrophotometry. Oyama *et al.*[7] reexamined the Cd(II)–edma system in detail by means of potentiometric titration as well as the d.c. polarographic method. However, no data of complex formation equilibria between Co(II) ion and $edma^-$ anion seem to have been reported.

We have examined the electrode kinetics of the redox couples of Co(II)/Co(III) complexes with tridentate ligands which contain nitrogen and/or oxygen as coordinating atoms, *e.g.*, edma, diethylenetriamine (dien), iminodiacetate (ida). For analysis of electrode kinetics, it is necessary to obtain the equilibrium data of Co(II)–edma, –dien, and –ida complexes under the same conditions as for the examination of electrode kinetics. We have determined the stepwise formation constants of (a) Co(II)–edma, (b) –dien, and (c) –ida complexes in 1.0 M (1 M=1 mol dm^{-3}) $NaClO_4$ solution by potentiometric titration. The formation constants of (b) and (c) for different solution compositions have been reported.[8-10] On the basis of the formation constants, relative effects of amino and acetate groups on the affinity of ligands to Co(II) ion are discussed.

Symbols

- h Concentration of hydrogen ion at equilibrium
- c_{Co} Total concentration of Co(II) ion
- L Ligand ($edma^-$, dien or ida^{2-})
- c_L Total concentration of L
- l Concentration of free ligand
- X Degree of neutralization of ligand, defined by $(-H+h-K_w/h)/c_L$, where H denotes the analytical excess of hydrogen ion in a test solution and K_w the autoprotolysis constant of water in 1.0 M $NaClO_4$ solution ($10^{-13.95}$ mol^2 dm^{-6})[11]
- $\bar{n}$ Average number of protons bound to one L
- $\bar{Z}$ Average number of ligand anions bound to one Co(II) ion
- β_{pqr} Equilibrium constant for the reaction: $pCo^{2+}+qH^+ + rL^{a-} = Co_pH_qL_r^{(2p+q-ra)+}$

Experimental

Reagents. *Cobalt(II) perchlorate* was purified by recrystallizing $Co(ClO_4)_2$ three times, which was prepared from $HClO_4$ and $CoCO_3$, the latter being precipitated from $Co(NO_3)_2$ solution with Na_2CO_3 and then thoroughly decanted. The stock solution contained a small amount of $HClO_4$ to prevent the hydrolysis of Co(II) ion, where the amount of excess $HClO_4$ was determined from the location of end point of neutralization by means of a Gran-plot. The concentration of Co(II) ion in the stock solution was determined by EDTA titration using a murexide indicator. *Diethylenetriamine* was vacuumdistilled twice at ca. 59 °C. *Iminodiacetic acid* was purified by recrystallization twice from water. All other chemicals used were prepared and purified by the method described previously.[7,12]

Potentiometric Measurements. The measurements were performed in a paraffin oil thermostat at 25.00±0.02 °C with use of a glass electrode. Sodium perchlorate was used as an indifferent salt to keep the perchlorate concentration at 1.0 mol dm^{-3} in all runs. The titration vessel and burets were filled with Ar gas before the test, solutions being then introduced. The solutions were deaerated with Ar gas, a vigorous stream of Ar gas being passed through the solution during the course of titration. The Ar gas was freed from O_2 by being passed through hot activated copper and then led through three washing bottles filled with 10% NaOH, 10% $HClO_4$ and 1.0 M $NaClO_4$ solutions, respectively. The apparatus and experimental procedure for potentiometric titration were reported.[12]

Results and Discussion

Evaluation of Protonation Constants of Ligands. The potentiometric titration curves of the Hedma, dien and H_2ida solutions are given in Figs. 1, 2, and 3, respec-

TABLE 1. PROTONATION CONSTANTS OF edma, dien, AND ida BASES IN 1.0 M $NaClO_4$ SOLUTION AT 25 °C

Base	$\log \beta_{011}$	$\log \beta_{021}$	$\log \beta_{031}$
edma	9.97±0.02	16.71±0.02	18.76±0.02
dien	10.76±0.02	20.56±0.02	25.40±0.02
ida	9.05±0.02	11.60±0.02	13.58±0.02

tively. Overall protonation constants of these ligand bases, β_{0q1}, were determined from the formation function, $\bar{n}$, by means of the generalized least squares method.[12] The results are given in Table 1. The values for the edma base are the same as obtained previously.[7] For the dien base Evtimova *et al.*[13] obtained the values log $\beta_{011}=10.03$, log $\beta_{021}=19.39$, and log $\beta_{031}=24.26$ in 1 M NH_4NO_3 solution at 25 °C. Grenthe and Gardhammar[14] obtained log $\beta_{011}=9.32$, log $\beta_{021}=11.89$ and log $\beta_{031}=13.77$ for the ida base under the same experimental conditions as in the present work.

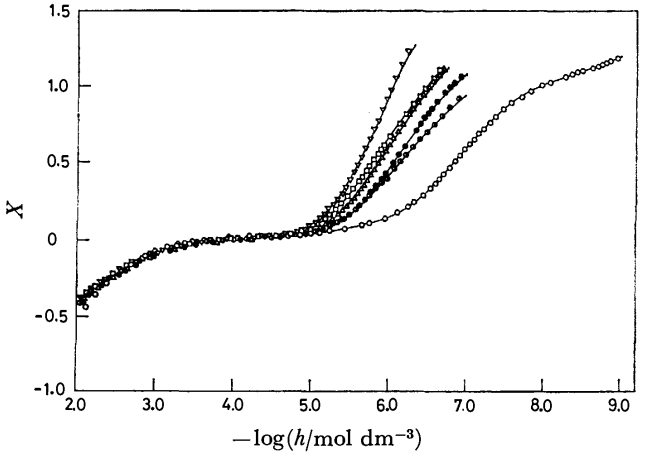

Fig. 1. Degree of neutralization, X, of edma solutions for the Co(II)–edma system.
(○): $c_{Co}=0.0$ mol dm^{-3}, $c_L=0.002200$ mol dm^{-3},
(▽): $c_{Co}=0.004381$ mol dm^{-3}, $c_L=0.008462$ mol dm^{-3},
(□): $c_{Co}=0.004504$ mol dm^{-3}, $c_L=0.01979$ mol dm^{-3},
(△): $c_{Co}=0.003079$ mol dm^{-3}, $c_L=0.01355$ mol dm^{-3},
(●): $c_{Co}=0.001503$ mol dm^{-3}, $c_L=0.008135$ mol dm^{-3},
(◑): $c_{Co}=0.001852$ mol dm^{-3}, $c_L=0.01360$ mol dm^{-3}.
Solid lines are the values of X calulated by the use of the for mation constants given in Table 2.

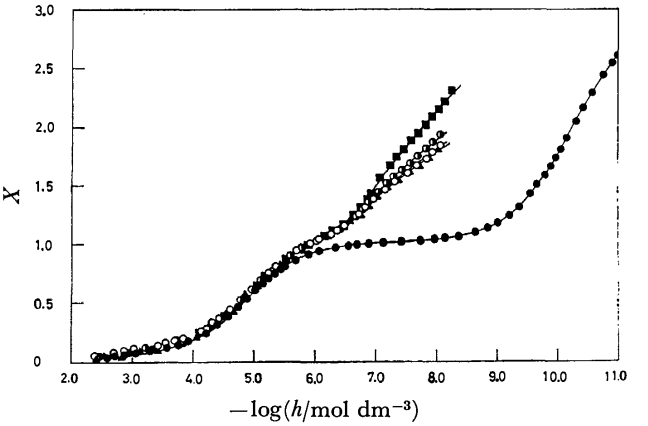

Fig. 2. Degree of neutralization, X, of dien solutions for the Co(II)–dien system.
(●): $c_{Co}=0.0$ mol dm^{-3}, $c_L=0.02000$ mol dm^{-3},
(■): $c_{Co}=0.003639$ mol dm^{-3}, $c_L=0.01086$ mol dm^{-3},
(◑): $c_{Co}=0.002898$ mol dm^{-3}, $c_L=0.01165$ mol dm^{-3},
(○): $c_{Co}=0.003139$ mol dm^{-3}, $c_L=0.01581$ mol dm^{-3},
(▲): $c_{Co}=0.002388$ mol dm^{-3}, $c_L=0.01259$ mol dm^{-3}.
Solid lines are the values of X calculated by the use of the formation constants given in Table 2.

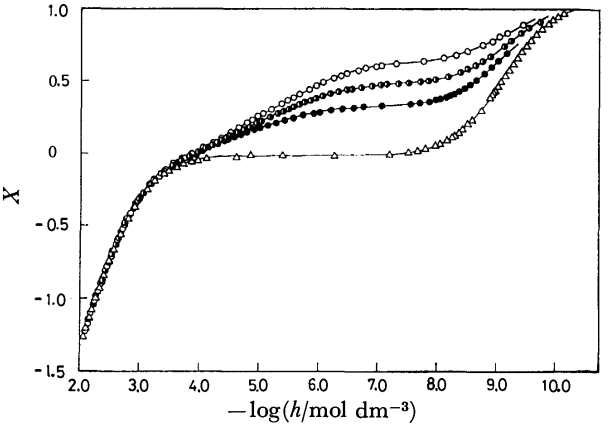

Fig. 3. Degree of neutralization, X, of ida solutions for the Co(II)–ida system.
(△): $c_{Co}=0.0$ mol dm^{-3}, $c_L=0.01004$ mol dm^{-3},
(○): $c_{Co}=0.002945$ mol dm^{-3}, $c_L=0.008965$ mol dm^{-3},
(◑): $c_{Co}=0.002990$ mol dm^{-3}, $c_L=0.01193$ mol dm^{-3},
(●): $c_{Co}=0.003051$ mol dm^{-3}, $c_L=0.01791$ mol dm^{-3}.
Solid lines are the values of X calculated by the use of the formation constants given in Table 2.

We see that the third protonation constant of edma, log $(\beta_{031}/\beta_{021})=2.05$, is almost equal to the average value of the second and third ones of ida, log $(\beta_{021}/\beta_{011})=2.57$ and log $(\beta_{031}/\beta_{021})=1.88$, indicating that these constants correspond to protonation of the carboxyl group. The carboxyl group bound to the imino group of edma and ida is acidic to a greater extent than the acetate (log $\beta_{011}=4.6$).

Determination of the Composition and Formation Constants of the Complexes. Titration curves for the Co(II)–edma, –dien, and –ida solutions are shown in Figs. 1, 2, and 3, respectively. The experiments were performed with the c_L/c_{Co} ratio in the range 2—7, c_{Co} and c_L being varied from 1.5 to 4.5 mmol dm^{-3} and from 8 to 27 mmol dm^{-3}, respectively. In high pH regions above pH 7.5 for the edma system and above pH 8.5 for the dien system, the potential of glass electrode becomes unstable. Thus measured points corresponding to such pH regions are not given in the figures. The instability of glass electrode might result from the interaction of Co(II)L_2 with a very small amount of oxygen remaining in the solutions. Miller *et al.*[15] reported that for Co(II)–dien complexes this interaction may occur even at oxygen concentration below 10^{-8} mol dm^{-3}.

In the pH range 2—5 the values of X for edma system are independent of c_{Co} and c_L, no proton being released from the ligand by complex formation (Fig. 1). On the other hand, above pH 5 the titration curves of solution containing Co(II) ion deviate from that of solution containing only the ligand, indicating that some protons are released from the ligand by the complex formation. As a first approximation for analyzing data we assumed that neither protonated nor polynuclear species are formed, since this was found to be the case for the Cd(II)–edma system.[7] The concentration of the free ligand l and the complex formation function $\bar{Z}$ can be expressed by Eqs. 8 and 9 of Ref. 7, respectively. The plot of $\bar{Z}$ *vs.* log l is shown by curve II in

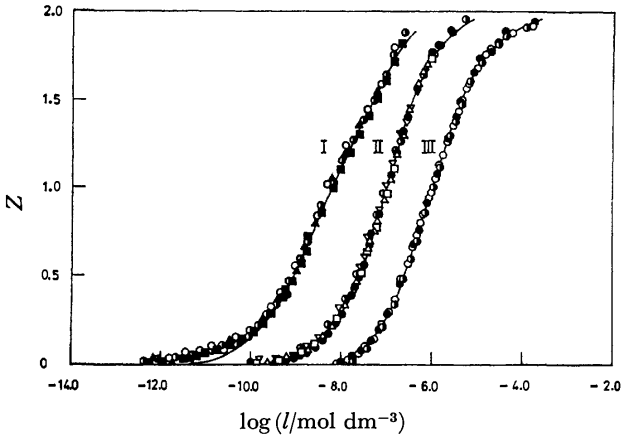

Fig. 4. Relationships between the complex formation function $\bar{Z}$ and log l for the Co(II)–dien, –edma, and –ida systems.
(I): Co(II)–dien, (II): Co(II)–edma, (III): Co(II)–ida. Solid lines are the best fit curves calculated by Eq. 11 of Ref. 7.

Fig. 4. We see that a single curve is obtained regardless of variation of c_L/c_{Co}, c_{Co}, and c_L, satisfying the above assumption, and also that the values of $\bar{Z}$ approach to 2 when the values of log l increase, showing that the complex species of Co(edma)$^+$ and Co(edma)$_2^0$ are formed in the pH range 5—7.

Similarly, for the dien and ida systems, the following conclusion may be deduced from the behavior of curves I and III (Fig. 4): the complex species of 1 to 1 and 1 to 2 compositions are formed in the pH ranges 6—8 (for dien) and 4—10 (for ida). No evidence of the formation of protonated complex species was detected for both systems, although for the dien system a slight deviation from the best fit curve (solid curve) was observed in the region $\log l = -12 - -10.5$. This suggests the formation of protonated complex species. For dien complexes, Miller *et al.*[15] postulated the formation of monoprotonated species such as Co(II)-(dien)(Hdien)$^{3+}$ for interpreting the pH dependence of the rate constant for oxygen uptake by the bis species.

The formation constants of the Co(II)–edma, –dien, and –ida complexes were evaluated by curve fitting using the generalized least squares method.[7] The results are summarized in Table 2. The solid curves in Figs. 1—4 represent the theoretical curves calculated by using these formation constants, which are seen to reproduce the experimental results.

Table 2 indicates that the first step formation constants, K_1 ($=\beta_{101}$), are somewhat larger than the second ones, K_2 ($=\beta_{201}/\beta_{101}$), and also that the coordinating ability of the ligands to Co(II) ion is reduced with

Table 2. Formation constants of Co(II)–edma, –dien, and –ida complexes in 1.0 M $NaClO_4$ solution at 25 °C

Complex	log β_{101}	log β_{102}
Co(II)–edma	7.51±0.02	14.05±0.05
Co(II)–dien	9.34±0.02	16.89±0.05
Co(II)–ida	6.54±0.02	11.95±0.05

increase in the number of replacement of amino group in dien by carboxyl group. Further we see that the following relation holds approximately among the successive formation constants, K_n ($n=1, 2$):

$$\log K_n(\text{edma}) = \frac{1}{2}[\log K_n(\text{dien}) + \log K_n(\text{ida})]. \quad (1)$$

This can be understood from the following consideration: The ligands we used are typical tridentate ones of (N,N,N)-, (N,N,O)-, and (O,N,O)-types, forming the five-membered chelate rings. Their chelate entropy effect[16] as well as steric effect on complex formation may be almost the same. If we assume that the contributions of amino, imino and carboxyl groups to the free energy change, ΔG_n°, of succesive complex formation are constitutive and additive, and denote them by ΔG_n(amino), ΔG_n(imino), and ΔG_n(carboxyl), respectively, ΔG_n° can be given by

$$\Delta G_n^\circ(\text{dien}) = \Delta G_n(\text{imino}) + 2\Delta G_n(\text{amino}) \quad (2)$$

$$\Delta G_n^\circ(\text{edma}) = \Delta G_n(\text{imino}) + \Delta G_n(\text{amino}) + \Delta G_n(\text{carboxyl}) \quad (3)$$

$$\Delta G_n^\circ(\text{ida}) = \Delta G_n(\text{imino}) + 2\Delta G_n(\text{carboxyl}). \quad (4)$$

Combining Eqs. 2—4, we obtain

$$\Delta G_n^\circ(\text{edma}) = \frac{1}{2}[\Delta G_n^\circ(\text{dien}) + \Delta G_n^\circ(\text{ida})]. \quad (5)$$

Equation 5 is identical with Eq. 1. By using the values of successive formation constants available,[8,9] we can show that Eq. 1 holds for Ni(II) and Cu(II) (only for $n=1$) complexes with dien, edma and ida, with somewhat larger deviations, partly because the conditions relevant to each measurement are not the same. A similar relation can be deduced for complexes of some divalent metal ions, such as Co(II), Ni(II), and Cu(II) ions, with the bidentate ligands containing amino and/or carboxyl groups, *e.g.*, ethylenediamine, glycinate and oxalate.[8,9]

The present work was partially supported by a Grand-in-Aid for Scientific Research No. 247065 from the Ministry of Education.

References

1) M. A. Doran, *Anal. Chem.*, **33**, 1752 (1961).
2) Y. Fujii, E. Kyuno, and R. Tsuchiya, *Bull. Chem. Soc. Jpn.*, **43**, 786 (1970).
3) Y. Fujii, T. Ueda, and M. Kodama, *Bull. Chem. Soc. Jpn.*, **43**, 409 (1970).
4) Y. Fujii and M. Kodama, *Bull. Chem. Soc. Jpn.*, **42**, 3172 (1969).
5) Y. Fujii, *Nippon Kagaku Zasshi*, **91**, 671 (1970).
6) M. Kodama, Y. Fujii, and T. Ueda, *Bull. Chem. Soc. Jpn.*, **43**, 2085 (1970).
7) N. Oyama, M. Horie, H. Matsuda, and H. Ohtaki, *Bull. Chem. Soc. Jpn.*, **50**, 1945 (1977).
8) L. G. Sillen and A. E. Martell, "Stability Constants," Chemical Society, London (1964); "Supplement No. 1," 1971.
9) D. D. Perrin, "Stability Constants of Metal-Ion Complexes, Part B Organic Ligands," Pergamon, Oxford-New York-Toronto-Sydney-Paris-Frankfurt (1979).
10) T. Arishima, K. Hamada, and S. Takamoto, *Nippon Kagaku Zasshi*, **1973**, 1119.

11) G. Anderegg, *Helv. Chim. Acta*, **50**, 2333 (1967).
12) N. Oyama, T. Shirato, H. Matsuda, and H. Ohtaki, *Bull. Chem. Soc. Jpn.*, **49**, 3047 (1976).
13) B. Evtimova, J. P. Scharf, and M. R. Paris, *Bull. Soc. Chim. Fr.*, **1969**, 81.
14) I. Grenthe and G. Gardhammar, *Acta Chem. Scand.*, **25**, 1401 (1971).
15) F. Miller, J. Simplicio, and R. G. Wilkins, *J. Am. Chem. Soc.*, **91**, 1962 (1969).
16) H. Irving, R. J. P. Williams, D. J. Ferrett, and A. E. Williams, *J. Chem. Soc.*, **1954**, 3494.

Preparation and Characterization of Dinuclear Cobalt(III) Complexes Bridged by Quadridentate Ligand with Thioether Donor Atoms

Kazuaki YAMANARI* and Yoichi SHIMURA

Department of Chemistry, Faculty of Science, Osaka University, Toyonaka, Osaka 560

(Received June 21, 1980)

From the reaction of (2-aminoethanethiolato)bis(ethylenediamine)cobalt(III)(2+) complex with α,ω-dibromoalkanes $Br(CH_2)_nBr$, a series of novel monobridged dinuclear cobalt(III) complexes $[(en)_2Co\{NH_2(CH_2)_2S(CH_2)_nS(CH_2)_2NH_2\}Co(en)_2]^{6+}$ ($n=1$, 2, 3, 4, 5, 6, 8, and 10) were prepared and characterized on the basis of their absorption, circular dichroism, and infrared spectra and elemental analyses. In the case of $n=2$, two geometrical isomers, *meso* and *rac*, were isolated and identified.

Thiolato group retains its strong nucleophilic property even after coordinating to a metal ion. This characteristic has been utilized to prepare a variety of new metal complexes containing coordinated thioether,[1] sulfenato,[2] and sulfinato ligands.[3] In particular, alkylation reactions of dithiolato complexes with difunctional alkylating agents have been known to lead to the concomitant formation of two thioether donor atoms and a chelate ring joining them, that is, the formation of macrocyclic ligands.[4] Similar reactions are applicable to the synthesis of bridged complexes.

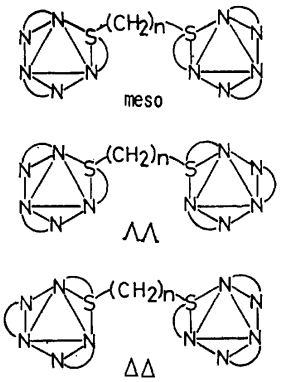

Fig. 1. Three isomers of monobridged dinuclear cobalt(III) complex.

The present report describes the synthesis of monobridged dinuclear cobalt(III) complexes by the reaction of (2-aminoethanethiolato)bis(ethylenediamine)cobalt(III) complex $[Co(aet)(en)_2]^{2+}$ with α,ω-dibromcalkane $Br(CH_2)_nBr$ as bridging agents. As one of advantages of this method, the direct synthesis of optically active bridged complexes becomes possible by starting from the optically active $[Co(aet)(en)_2]^{2+}$ complex.[5] Since the dinuclear complex consists of two optically active octahedral units, a meso (*ΔΛ*) and two optically active (*ΔΔ* and *ΛΛ*) forms are possible (Fig. 1), the latter two of which form a racemate in practice. The isolation of two geometrical isomers of this kind, *meso* and *rac*, has so far been limited to only two cases of $[(en)_2Cr(OH)_2Cr(en)_2]Cl_4\cdot 2H_2O$[6] and $[(en)_2Co(OH)(O_2)Co(en)_2]^{3+}$[7] with double bridged structure, no report being published for the monobridged dinuclear complexes.

Experimental

Preparation and Separation of Complexes. rac- *and/or* meso-$[(en)_2Co\{NH_2(CH_2)_2S(CH_2)_nS(CH_2)_2NH_2\}Co(en)_2]Cl_6$ *($n=1$, 2, 3, 4, 5, 6, 8, and 10)*: A general procedure was developed by using α,ω-dibromoalkanes $Br(CH_2)_nBr$ and *N,N*-dimethylformamide (DMF) as bridging agents and reaction solvent, respectively. To a black solution of four millimoles of *rac*-$[Co(aet)(en)_2](ClO_4)_2$[5] dissolved in 5 cm^3 of DMF was added an excess (2.2 mmol) of α,ω-dibromoalkane. The mixture was allowed to stand for about 20 d at room temperature, leading to a deep-red solution. The DMF and unreacted dibromoalkane were extracted into diethyl ether for several times. The resulting dark red oil was dissolved in water, adsorbed on an SP-Sephadex C-25 cation exchange column (Na^+ form), and eluted with a 0.8 M NaCl solution (1 M= 1 mol dm^{-3}). Five colored bands were eluted in the order, a yellow one of $[Co(en)_3]^{3+}$, a dark brown one of $[Co(aet)(en)_2]^{2+}$, and three orange ones A, B, and C. Each of the orange bands was concentrated to a small volume in a rotary evaporator and after repeated removal of NaCl deposited out the solution was treated with a small amount of ethanol to give orange crystals of the desired chloride salt. Analytical data (Table 1) for the complexes A, B, and C corresponded to $[Co(en)_2\{NH_2(CH_2)_2S(CH_2)_nOH\}]Cl_3$, $[Co(en)_2\{NH_2(CH_2)_2S(CH_2)_nBr\}]Cl_3$, and $[Co_2(en)_4\{NH_2(CH_2)_2S(CH_2)_nS(CH_2)_2NH_2\}]Cl_6$, respectively. This characterization is agreed with the column chromatographic behavior; when developed with a 0.3 M NaCl solution, only the last band C remains on the top of Sephadex resin and therefore seems to be the proposed bridge structure with a hexapositive charge.

For the dinuclear complexes prepared from a racemic starting material *rac*-$[Co(aet)(en)_2]^{2+}$, two geometrical isomers, *meso* and *rac*, are possible. In the case of $n=2$, fractional crystallization of the eluate C produced two different orange crystals: the eluate C was evaporated to a small volume using a rotary evaporator, and the deposit, NaCl, was filtered off. The filtrate was cooled to give first crop of orange crystals (C-1). After filtration the filtrate was further evaporated, a small amount of methanol being added to the concentrated solution, and the deposit, NaCl, was again filtered off. The final filtrate was cooled in an ice bath to give another kind of orange crystals (C-2). Both complexes showed the dinuclear composition, $[Co_2(en)_4\{NH_2(CH_2)_2S(CH_2)_2S(CH_2)_2NH_2\}]Cl_6$, the less soluble C-1 being 3-hydrate and the more soluble C-2 5.5-hydrate.

In order to elucidate the structures, optical resolution was attempted. An aqueous solution containing 0.03 g of the complex C-1 or C-2 was poured into a column of SP-Sephadex C-25 (Na^+ form, 3×80 cm). The adsorbed band was eluted with a mixed solution of 0.5 M NaCl and 0.15 M $Na_2[Sb_2(d-$

TABLE 1. ANALYTICAL DATA OF THE COMPLEXES

n	X	C, % Found(Calcd)	H, % Found(Calcd)	N, % Found(Calcd)
$[(en)_2Co\{NH_2(CH_2)_2S(CH_2)_nS(CH_2)_2NH_2\}Co(en)_2]Cl_6\cdot X$(complex C or C′)				
rac and/or *meso*				
1	$0.25C_2H_5OH$	19.69(19.54)	6.87(6.86)	16.92(16.88)
2	$3H_2O$(C-1)	20.79(20.88)	6.81(6.76)	17.26(17.39)
2	$5.5H_2O$(C-2)	19.74(19.77)	6.81(6.99)	16.20(16.47)
3	$8.5H_2O$	19.45(19.62)	7.30(7.35)	15.20(15.25)
4	$5.5H_2O$	21.91(21.88)	7.27(7.23)	15.95(15.94)
5	$7H_2O$	22.12(22.21)	7.44(7.45)	14.92(15.23)
6	$5.5H_2O$	23.83(23.85)	7.35(7.45)	15.39(15.45)
8	$4.5H_2O$	26.61(26.21)	7.69(7.59)	15.27(15.28)
active($\Delta\Delta$)				
2	$5H_2O$	19.88(19.99)	6.92(6.95)	16.61(16.65)
3	$8H_2O$	19.83(19.81)	7.32(7.31)	15.30(15.40)
4	$5.5H_2O$	21.83(21.88)	7.16(7.23)	15.89(15.95)
5	$5.5H_2O$	22.85(22.89)	7.21(7.34)	15.70(15.69)
6	$5.5H_2O$	23.75(23.85)	7.40(7.45)	15.38(15.45)
8	$5H_2O$	26.08(25.95)	7.57(7.62)	15.15(15.13)
10	$0.75NaCl\cdot0.75-C_2H_5OH\cdot2.5H_2O$	28.65(28.60)	7.69(7.66)	14.26(14.19)
rac-$[Co(en)_2\{NH_2(CH_2)_2S(CH_2)_nBr\}]Cl_3\cdot X$(complex B)				
2	H_2O	19.76(19.71)	5.91(5.79)	14.45(14.36)
3	$2.5H_2O$	20.68(20.45)	6.23(6.29)	12.85(13.25)
4	$2.5H_2O$	22.37(22.13)	6.47(6.50)	12.92(12.91)
5	$0.5H_2O$	25.35(25.37)	6.50(6.39)	13.26(13.45)
6	$1.5H_2O$	26.31(26.08)	6.86(6.75)	12.53(12.67)
8	H_2O	29.61(29.41)	7.12(7.05)	12.42(12.25)
10	$0.5H_2O$	32.38(32.53)	7.45(7.34)	12.06(11.85)
rac-$[Co(en)_2\{NH_2(CH_2)_2S(CH_2)_nOH\}]Cl_3\cdot X$(complex A)				
4	$0.5C_2H_5OH\cdot2H_2O$	26.48(26.76)	7.58(7.76)	14.23(14.18)
5	$2H_2O$	27.20(27.25)	7.37(7.69)	13.63(14.45)
6	$1.5H_2O$	29.79(29.43)	7.56(7.82)	13.96(14.30)
8	H_2O	32.90(33.04)	7.94(8.12)	13.52(13.76)

tart)$_2$]$\cdot2H_2O$, which produced a broad band. The eluate was separated into fractions of 5 cm^3 each. The fractions of complex C-1 showed no optical activity, while the first fractions of complex C-2 exhibited a positive dominant CD band in the first absorption band region which is completely enantiomeric to that of the last fractions. Thus, the two orange complexes are geometrical isomers, C-1 and C-2 corresponding to *meso* and racemic forms, respectively. In all cases other than $n=2$, the band C could not be splitted into two or more kinds of orange complexes.

Active-$[(en)_2Co\{NH_2(CH_2)_2S(CH_2)_nS(CH_2)_2NH_2\}Co(en)_2]Cl_6$ *($n=2$, 3, 4, 5, 6, 8, and 10)*: Optically active complexes were prepared and separated in the same manner as described above with use of active-$[Co(aet)(en)_2](ClO_4)_2$[5] instead of the racemic starting material. When eluted with a 0.8 M NaCl solution, the column gave the following five band regardless of the kind of $Br(CH_2)_nBr$ used; a yellow bands of $[Co(en)_3]^{3+}$, a dark brown one of $[Co(aet)(en)_2]^{2+}$, and three orange ones A′, B′, and C′. Each orange band was concentrated to a small volume and the chloride salt was crystallized out. Elemental analyses (Table 1) and absorption spectra of the complexes A′, B′, and C′ confirmed their compositions $[Co(en)_2\{NH_2(CH_2)_2S(CH_2)_nOH\}]Cl_3$, $[Co(en)_2\{NH_2(CH_2)_2S(CH_2)_nBr\}]Cl_3$, and $[Co_2(en)_4\{NH_2(CH_2)_2S(CH_2)_nS(CH_2)_2NH_2\}]Cl_6$, respectively.

The distribution of products A′, B′, and C′ under above conditions changed considerably depending upon the number of methylene groups. The yields of the bridged complexes decreased in the following order; $n=3$ and 4 (*ca.* 75%)$>n=5$ (*ca.* 70%)$>n=6$ (*ca.* 65%)$>n=8$ (*ca.* 50%)$>n=10$ (*ca.* 40%)$>n=2$ (*ca.* 20%)$\gg n=1$ (below 5%). The yields of complexes B′ were inversely proportional to those of the corresponding bridged complexes C′ but the total yields of complexes B′ and C′ were almost constant. The yields of complexes A′ were about 5% irrespective of the number of methylene groups, though the products in the case of $n=1$ were so complicated that the yields of the complexes except the bridged one could not be determined.

Measurements. The electronic absorption spectra were measured on a Shimadzu UV-200 spectrophotometer and CD spectra with a JASCO MOE-1 spectropolarimeter in aqueous solution. The infrared spectra were obtained on a JASCO DS-402G spectrophotometer with NaCl prism nsing Nujol mull or KBr disk. All measurements were made at room temperature.

Results and Discussion

Preparation and Characterization of the Complexes. Several preparative methods have been developed for the alkylation of coordinated thiols. It has been noted that DMF is a superior medium for the alkylation

reactions because most alkyl halides and metal perchlorate salts are soluble in this medium.[8] The use of DMF as a reaction solvent in the present study permitted the formation of the alkylated products in a high yield which were not accessible by the use of other solvents such as methanol–water. The formation of $[Co_2(en)_4\{NH_2(CH_2)_2S(CH_2)_nS(CH_2)_2NH_2\}]^{6+}$ is more favorable in a high concentration of reactants than in a dilute one. The concentration dependence can be elucidated from the following mechanism;[9] the reaction of $[Co(aet)(en)_2]^{2+}$ with $Br(CH_2)_nBr$ gives at first an intermediate $[Co(en)_2\{NH_2(CH_2)_2S(CH_2)_nBr\}]^{3+}$ species and then an intermolecular reaction leads to the formation of the bridged complex. In fact, when the reaction mixture was diluted twenty times no orange complexes were detectable under the same condition as described above. The yield of the bridged complexes depends upon the number of methylene groups, being especially low in the cases of $n=1$ or 2 (see Experimental). The low yield seems to be ascribed to the steric and electrostatic repulsion between two tripositive

Table 2. Absorption and CD data of the complexes

n		Absorption[a] σ_{max}(log ε)		CD[a] $\sigma_{ext}(\Delta\varepsilon)$
$[(en)_2Co\{NH_2(CH_2)_2S(CH_2)_nS(CH_2)_2NH_2\}Co(en)_2]^{6+}$		*rac* and/or *meso*	active($\Delta\Delta$)	active($\Delta\Delta$)
1		20.3(2.44)		
		30 (3.5)[b]		
		35.9(4.06)		
		45.7(4.59)		
2	C-1	20.4(2.57)		
		29 (2.8)[b]		
		35.4(4.35)		
		45.7(4.52)		
2	C-2	20.3(2.59)	20.3(2.60)	19.9(−4.83)
				23.5(+0.02)
		29 (2.8)[b]	29 (2.8)[b]	26 (−0.3)[b]
				29 (−1.1)[b]
		35.2(4.33)	35.3(4.34)	34.9(−26.7)
		45.9(4.55)	46.0(4.56)	46.1(+55.7)
3		20.4(2.59)	20.4(2.59)	19.9(−4.52)
				23.5(+0.03)
		29 (2.8)[b]	29 (2.8)[b]	26 (−0.3)[b]
				29 (−1.0)[b]
		35.2(4.33)	35.2(4.33)	34.5(−30.2)
		45.4(4.55)	45.4(4.55)	46.4(+53.6)
4		20.5(2.60)	20.4(2.60)	20.0(−5.19)
		29 (2.8)[b]	29 (2.8)[b]	26.7(−0.17)
				29 (−0.6)[b]
		35.2(4.33)	35.2(4.33)	34.8(−23.0)
		45.1(4.54)	45.0(4.55)	46.1(+50.8)
5		20.5(2.60)	20.5(2.60)	19.9(−4.98)
		29 (2.8)[b]	29 (2.8)[b]	26.2(−0.17)
				29 (−0.7)[b]
		35.2(4.32)	35.2(4.33)	34.8(−21.9)
		45.0(4.54)	44.9(4.54)	45.8(+48.0)
6		20.5(2.61)	20.5(2.61)	20.0(−5.09)
		29 (2.8)[b]	29 (2.8)[b]	26.3(−0.15)
				29 (−0.5)[b]
		35.1(4.33)	35.1(4.32)	34.8(−18.8)
		44.9(4.55)	44.9(4.55)	45.9(+47.4)
8		20.5(2.59)	20.5(2.60)	20.0(−4.91)
		29 (2.8)[b]	29 (2.8)[b]	26.3(−0.07)
				29 (−0.4)[b]
		35.2(4.31)	35.1(4.33)	35.0(−17.5)
		45.0(4.51)	45.1(4.55)	46.1(+43.9)
10			20.5(2.62)	20.1(−5.31)
			29 (2.8)[b]	26.3(−0.07)
				29 (−0.04)[b]
			35.1(4.32)	35.0(−17.9)
			45.1(4.54)	46.1(+45.7)
$[Co(en)_2\{NH_2(CH_2)_2S(CH_2)_nBr\}]^{3+}$		*rac*		active (Δ)[c]
2		20.4(2.26)		19.9(−2.63)
		29 (2.4)[b]		26.3(−0.12)
		35.5(3.99)		35.3(−8.68)
		45.9(4.27)		46.5(+22.7)
3		20.5(2.26)		20.0(−2.62)
		29 (2.5)[b]		26.0(−0.08)
		35.5(3.97)		35.3(−8.83)
		45.5(4.24)		46.1(+24.5)
4		20.4(2.29)		
		29 (2.5)[b]		
		35.3(3.96)		
		45.2(4.28)		
5		20.5(2.27)		20.0(−2.83)
		29 (2.5)[b]		26.1(−0.06)
		35.3(3.98)		35.1(−9.43)
		45.1(4.23)		45.8(+25.0)
6		20.5(2.28)		20.0(−2.64)
		29 (2.5)[b]		25.9(−0.07)
		35.2(4.00)		35.1(−8.24)
		45.1(4.24)		45.9(+21.8)
8		20.5(2.30)		
		29 (2.5)[b]		
		35.2(4.01)		
		45.1(4.25)		
10		20.5(2.30)		20.0(−2.95)
		29 (2.5)[b]		25.9(−0.06)
		35.1(4.01)		35.0(−9.64)
		45.0(4.23)		45.9(+25.3)
$[Co(en)_2\{NH_2(CH_2)_2S(CH_2)_nOH\}]^{3+}$		*rac*		active (Δ)[c]
4		20.5(2.28)		
		29 (2.5)[b]		
		35.3(3.99)		
		45.1(4.24)		
6		20.5(2.27)		19.9(−2.51)
		29 (2.5)[b]		26.0(−0.06)
		35.2(3.98)		35.0(−7.59)
		45.0(4.22)		46.0(+20.0)
8		20.5(2.27)		
		29 (2.5)[b]		
		35.2(3.97)		
		45.1(4.22)		

a) Wave numbers are given in 10^3 cm^{-1} unit and log ε or $\Delta\varepsilon$ values (in parentheses) in mol^{-1} dm^3 cm^{-1}.
b) Shoulder. c) CD intensity was calculated by applying molar absorption coefficient of the corresponding racemate.

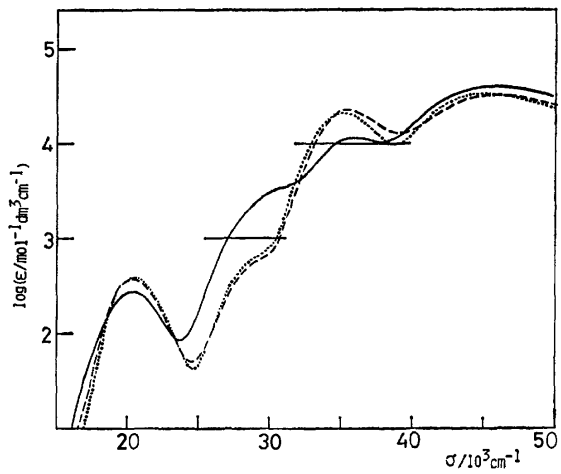

Fig. 2. Absorption spectra of the bridged complexes. $[(en)_2Co\{NH_2(CH_2)_2S(CH_2)_nS(CH_2)_2NH_2\}Co(en)_2]^{6+}$: $n=1$, ——; $n=2$, – – –; $n=8$, ·····.

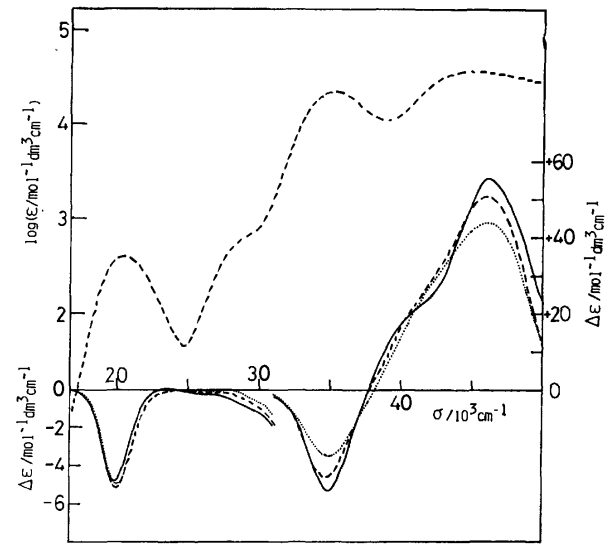

Fig. 3. CD spectra of the bridged complexes $[(en)_2Co\{[NH_2(CH_2)_2S(CH_2)_nS(CH_2)_2NH_2\}Co(en)_2]^{6+}$: $n=2$, ——; $n=4$, – – –; $n=8$, ·····.

groups which must be tied with the shortest methylenic chain.

Absorption Spectra. Figure 2 and Table 2 show the absorption spectra of the present complexes. The bridged complexes exhibit their first d-d absorption bands at about 20400 cm^{-1} which quite agree with those of the $[Co(N)_5(S)]$ type complexes containing a thioether donor atom.[5] The first d-d absorption band shifts slightly to higher energy side with increasing the number of methylene groups, while two charge transfer absorption bands in the near-ultraviolet region reversely.

As for the bridged complex of $n=1$, another intense band appears at *ca.* 30000 cm^{-1} with diminishing the intensity of the charge transfer band characteristic of the coordinated sulfur atoms at 35000 cm^{-1}. This new band seems to be also of charge transfer character judging from its intensity ($\log\varepsilon=3.5$). The other bridged complexes of $n=2$—10 did not show such an intense band but the second d-d absorption band in the same region. Thus, the new band may be due to the *geminal*-sulfur interaction like that observed in organic compounds such as bis(methylthio)methane and 2,2-bis(butylthio)propane,[10] because the interaction reduces the promotion energy of lone-pair electrons. A similar absorption band has been reported in a cobalt(III) complex containing a disulfide ligand, $[Co(en)_2\{S(SCH_2CH_2NH_3)CH_2CH_2NH_2\}]^{4+}$.[11]

Both monomeric complexes, $[Co(en)_2\{NH_2(CH_2)_2S(CH_2)_nBr\}]^{3+}$ and $[Co(en)_2\{NH_2(CH_2)_2S(CH_2)_nOH\}]^{3+}$, show almost the same absorption spectra as those of the corresponding bridged complexes except that their molar extinction coefficients are reduced to one-half the values of dinuclear complexes (Table 2).

CD Spectra. In the preparations of optically active bridged complex, the Δ-$[Co(aet)(en)_2]^{2+}$ complex was used as the starting material whose absolute configuration had been assigned on the basis of the CD sign in the first d-d absorption band region.[5] As shown in Fig. 3, all the bridged complexes exhibit nearly the same CD spectra irrespective of n values, a negative CD band being dominant in the first absorption band region. The spectral pattern is very analogous to that of Δ-$[Co(en)_2(NH_2CH_2CH_2SR)]^{3+}$ ($R=CH_3$ or C_2H_5).[5] Therefore, it is concluded that the alkylation reaction proceeds with retention of the initial absolute configuration and the bridged complexes obtained have the $\Delta\Delta$ absolute configuration.

Both monomeric complexes, $[Co(en)_2\{NH_2(CH_2)_2S(CH_2)_nBr\}]^{3+}$ and $[Co(en)_2\{NH_2(CH_2)_2S(CH_2)_nOH\}]^{3+}$, show a similar CD pattern to that of the bridged complexes, being also assigned to the Δ absolute configuration.

The CD intensities of the bridged complexes are approximately 2 times larger than those of the monomeric $[Co(en)_2\{NH_2(CH_2)_2S(CH_2)_nBr\}]^{3+}$ complexes in almost all regions. However, the CD intensities of $[Co_2(en)_4\{NH_2(CH_2)_2S(CH_2)_2S(CH_2)_2NH_2\}]^{6+}$ and $[Co_2(en)_4\{NH_2(CH_2)_2S(CH_2)_3S(CH_2)_2NH_2\}]^{6+}$ in the thioether charge transfer band region are 3.1 and 3.4 times larger than those of the corresponding monomeric complexes, respectively. This increase of CD intensity seems to represent an additional chirality which arises on the thioether donor atoms of bridged complexes of only $n=2$ or 3 because of a rather short bridge chain and the resulting unbalance of the *R* and *S* chiralities of the asymmetric sulfur atoms. In fact, the CD intensity per one cobalt(III) ion of the dinuclear complex of $n=10$ becomes almost the same as that of the monomeric complex, the increase in the number of methylene groups reducing such interaction between the two coordination centers.

Characterization of Geometrical Isomers. In the case of $n=2$, fractional crystallization of the bridged complex prepared from the racemic starting complex led to the isolation of the two orange crystals, C-1 and C-2. The chromatographic separation with a mixed solution of 0.5 M NaCl and 0.15 M $Na_2[Sb_2(d\text{-tart})_2]\cdot 2H_2O$ as an eluent indicated that only the complex C-2 is resolvable into the optical antipodes. Therefore, it is concluded that the complexes C-1 and C-2 are *meso* and *rac* forms, respectively. As shown in Table

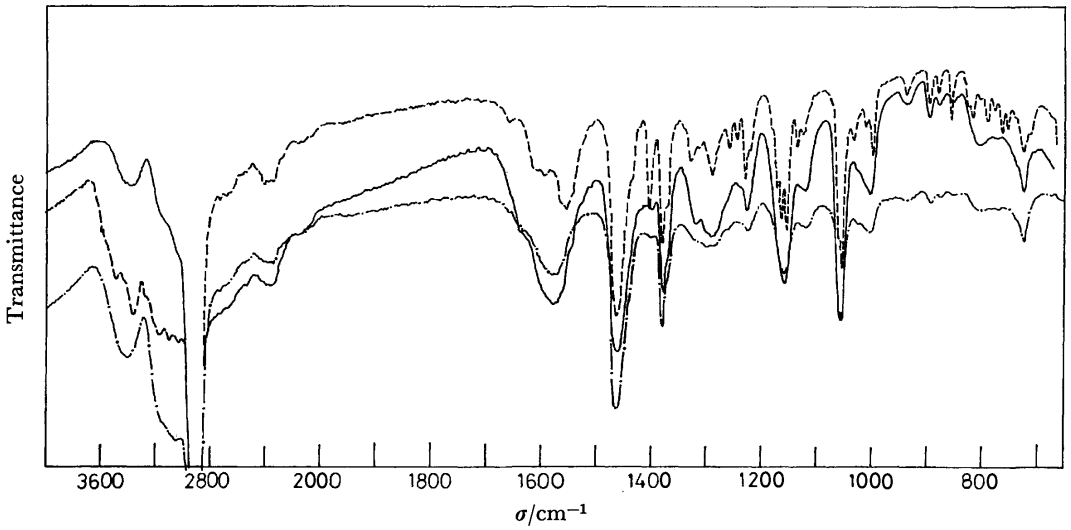

Fig. 4. Infrared spectra of $[(en)_2Co\{NH_2(CH_2)_2S(CH_2)_2S(CH_2)_2NH_2\}Co(en)_2]Cl_6$: C-1, ——; C-2, ——; ΔΔ, ·–·–·.

2, the optically active *ΔΔ* isomer of the bridged complex of $n=2$ exhibits the analogous absorption spectra to that of the racemate C-2 rather than the *meso* form C-1 with respect to both the spectral position and intensity. A similar trend was also observed in the infrared spectra of these complexes (Fig. 4). The chlorides of complexes C-1 and C-2 gave significantly different spectra in the region 4000—400 cm^{-1}. However, the spectrum of active *ΔΔ* isomer is nearly identical to that of the racemate C-2.

In the case of $n=3$, the complex C obtained from *rac*-$[Co(aet)(en)_2]^{2+}$ showed a similar IR spectrum to that of the optically active *ΔΔ* isomer in the region 4000—700 cm^{-1}. Since there appear no other absorption peaks besides those of the active isomer, this complex consists of a single species and could be assigned to the racemic form.

References

1) D. H. Busch, D. C. Jicha, M. C. Thompson, J. W. Wrathall, and E. Blinn, *J. Am. Chem. Soc.*, **86**, 3642 (1964); V. M. Kothari and D. H. Busch, *Inorg. Chem.*, **8**, 2276 (1969).

2) C. P. Sloan and J. H. Krueger, *Inorg, Chem.*, **14**, 1481 (1975); M. Kita, K. Yamanari, and Y. Shimura, *Chem. Lett.*, **1980**, 275.

3) M. P. Schubert, *J. Am. Chem. Soc.*, **55**, 3336 (1933); B. A. Lange, K. Libson, E. Deutsch, and R. C. Elder, *Inorg. Chem.*, **15**, 2985 (1976).

4) M. C. Thompson and D. H. Busch, *J. Am. Chem. Soc.*, **86**, 3651 (1964).

5) K. Yamanari, J. Hidaka, and Y. Shimura, *Bull. Chem. Soc. Jpn.*, **50**, 2299 (1977).

6) H. Toftlund and J. Springborg, *J. Chem. Soc., Chem. Commun.*, **1976**, 1017.

7) M. Zehnder and S. Fallab, *Helv. Chim. Acta*, **58**, 2312 (1975).

8) R. C. Elder, G. J. Kennard, M. D. Payne, and E. Deutsch, *Inorg. Chem.*, **17**, 1296 (1978).

9) H. Ogino and J. Fujita, *Bull. Chem. Soc. Jpn.*, **48**, 1836 (1975).

10) H. H. Jaffe and M. Orchin, "Theory and Applications of Ultraviolet Spectroscopy," John Wiley and Sons (1962), Chap. 17.

11) M. Woods, J. Karbwang, J. C. Sullivan, and E. Deutsch, *Inorg. Chem.*, **15**, 1678 (1976).

 © 1980 The Chemical Society of Japan Bull. Chem. Soc. Jpn., 53, 3610—3614 (1980) [Vol. 53, No. 12

On the Enhancement of the Selectivity of Organic Sulfonate Ion Electrode by Alkylphenols†

Hirokazu HARA, Satoshi OKAZAKI, and Taitiro FUJINAGA*

Department of Chemistry, Faculty of Science, Kyoto University, Sakyo-ku, Kyoto 606

(Received June 23, 1980)

An enhancing effect of alkylphenols on the selectivity of the liquid membrane electrode responsive to organic sulfonate ion has been investigated. The interference of perchlorate ion expressed in terms of the selectivity coefficient decreased to one eighthundredth in the presence of *p*-*t*-octylphenol. This effect was attributed to the formation of the hydrogen bonding between the phenol and sulfonate. The dependence of the potentiometric behavior, paticularly with respect to the selectivity on the membrane components was examined. The optimum composition of the ion-exchanger for sulfonate was found to be 0.05 mol dm^{-3} trioctylmethylammonium *p*-toluenesulfonate with 0.5 mol dm^{-3} *p*-*t*-octylphenol in *o*-dichlorobenzene. The decrease of the selectivity coefficient for perchlorate due to the phenol was also discussed in relation to ion-exchange equilibrium constants, ionic parameters, and dissociation constants of the ion-pair. The effect of the membrane solvents was also discussed in terms of their solubility parameters.

To date, in a liquid membrane electrode, more interest has been shown in the membrane solvent rather than in the ion-exchange site as an effectual dominant of selectivity. Though several useful solvents having wide selectivity ranges, such as nitrobenzene and 1,2-dichloroethane have been recommended,[1,2] the selectivity of the liquid membrane electrode is generally insufficient. Particularly, in the case of an anion sensitive electrode, an ion-exchanger such as a neutral carrier for cation selective electrode has not been developed.

In the previous papers,[3,4] the authors have reported on an organic sulfonate ion selective electrode of a coated wire type and a solid solvent membrane type. In the course of the study on the selectivity characteristics of *p*-toluenesulfonate (pTS) ion selective electrode, the authors found an enhancing effect of an alkylphenol on the selectivity, *i.e.*, the interferences of the inorganic anions such as perchlorate, tetrafluoroborate ions decreased remarkably by the addition of some alkylphenols into the liquid membrane; for example, the logarithmic selectivity coefficient of perchlorate decreased from +2.3 to −0.6 in the presence of 0.5 M† *p*-*t*-octylphenol(*p*-(1,1,3,3-tetramethylbutyl)phenol; ptOP). This effect of the phenol was attributed to the formation of hydrogen bonding between the phenol and pTS anion.

In this paper, the influences of the concentration of ion-pair and phenols upon the membrane response and selectivity were examined. This phenomenon was interpreted on the basis of Sandblom-Eisenman-Walker theory.[5] The effect of some alkylphenols on the selectivity was studied in relation to their hydrogen bonding ability. The effect of the membrane solvents was also discussed with reference to their hydrogen bonding parameters.

Experimental

Reagents. All chemicals were of analytical reagent grade and used without further purification unless otherwise noted. Ion-pair of trioctylmethylammonium(abbreviated as TOMA) with *p*-toluenesulfonate was synthesized as follows: trioctylmethylammonium chloride (commercially available as Capriquat from Dojin Chemicals, Kumamoto) dissolved in chloroform was shaken with an aqueous solution of 0.1 M sodium pTS for 10 min. The extraction was repeated several times until chloride was not detected any more in the aqueous phase. After chloroform was evaporated by a rotary evaporator, the deposit was recrystallized from ethyl acetate. *o*-Dichlorobenzene used for the conductivity measurements was purified by distillation after the dehydration with calcium hydride. Its water content was estimated as 0.02% (v/v) by gas chromatography. A series of the following phenols were examined: *p*-*t*-octylphenol (*p*-(1,1,3,3-tetramethylbutyl)phenol; ptOP), *p*-*t*-pentylphenol (ptPP), *p*-*t*-butylphenol (ptBP) 2,3,5-trimethylphenol, 2,4,6-trimethylphenol, and 2,6-di-*t*-butyl-4-methylphenol.

Preparation of Membranes. A liquid membrane was prepared by dissolving the ion-pair of TOMA pTS into *o*-dichlorobenzene, which was held in a Corning probe with a hydrophobic ceramic junction. A solid solvent membrane[4] was prepared by dissolving the ion-pair in phenol at elevated temperature and then powdered. *Ca.* 30 mg of the ion-exchanger was pressed at a pressure of 3×10^8 Pa on a silver disk of 1 cm in diameter. The electrical contact was taken directly from the silver disk.

Apparatus. Membrane potentials were measured against SCE at 25 °C with an Orion Digital Ionalyzer Model 601 equipped with a Matsushita Pen Recorder Model VP654-A. IR spectra were measured by a JASCO Infrared Spectrophotometer Model DS-402G using a NaCl cell having a light pass length of 0.1 mm. The conductivity was measured at 25 °C by a Yokogawa Universal Bridge Type BV-Z-13B with a cell having a cell constant of 0.1060 s cm^{-1}.

Estimation of Various Parameters. Logarithmic selectivity coefficient, log K^{pot} was measured by the separate solution method; the potential difference between a solution of 10^{-2} M pTS^- and that of interfering anion was divided by the slope of the calibration curve for pTS^-. For the measurement of ion-exchange equilibrium constant, K^{ex}, 50 cm^3 of 10^{-2} M organic solution of TOMA pTS was shaken with the equivolume of 10^{-2} M aqueous solution of sodium perchlorate for 1 h at 25 °C. After the ion-exchange equilibrium in Eq. 1 was reached,

$$(\text{TOMA pTS})_{org} + (ClO_4^-)_{aq} \overset{K^{ex}}{\rightleftharpoons} (\text{TOMA } ClO_4)_{org} + (pTS^-)_{aq}, \quad (1)$$

† A preliminary report has been published: T. Fujinaga, S. Okazaki, and H. Hara, *Chem. Lett.*, **1978**, 1201.

†† Throughout this paper 1 M = 1 mol dm^{-3}.

$$K^{ex} = \frac{[\text{TOMA ClO}_4]_{org}[\text{pTS}^-]_{aq}}{[\text{TOMA pTS}]_{org}[\text{ClO}_4^-]_{aq}}, \quad (2)$$

the concentrations of pTS^- and ClO_4^- in the aqueous phase were measured with the liquid membrane electrodes, the ion-exchanger of which were TOMA pTS plus ptOP and TOMA ClO_4 in *o*-dichlorobenzene for *p*-toluenesulfonate and perchlorate electrodes, respectively. For the associated ion-pair, the mole fractions of ions extracted in the organic phase were assumed to be equal to those of ions eluted inversely into the aqueous phase. Thus, after the equilibrium was reached, following relationships hold; $[\text{TOMA pTS}]_{org}=[\text{ClO}_4^-]_{aq}$, $[\text{TOMA ClO}_4]_{org}=[\text{pTS}^-]_{aq}$. Then, Eq. 2 is simplified as follows,

$$K^{ex} = [\text{pTS}^-]_{aq}^2/[\text{ClO}_4^-]_{aq}^2. \quad (2)'$$

The molar conductivities of ClO_4^- and $TOMA^+$ at infinite dilution were obtained using tetrabutylammonium tetraphenylborate as a reference electrolyte.[6] The dissociation constant, K^D of TOMA ClO_4 in the absence of ptOP was estimated by the Shedlovsky method.[7] Being considered small the interactions between the phenol and $TOMA^+$ or ClO_4^-, the molar conductivity of $TOMA^+$, $\lambda^\circ(\text{TOMA}^+)_p$ in the presence of ptOP, was assumed to have the same magnitude as that in the absence of the phenol. Also $\lambda^\circ(\text{ClO}_4^-)_p$ was estimated so that the K^D values in the presence and absence of the phenol were of the same magnitude. Here, K^D in the presence of the phenol was calculated by Eq. 3,

$$K^D = C(\Lambda/\Lambda_0)^2/(1 - \Lambda/\Lambda_0), \quad (3)$$

where Λ is the conductivity at the concentration $C(10^{-5}\ M < C < 10^{-4}\ M)$ and Λ_0 is the molar conductivity given by the sum of $\lambda^\circ(\text{TOMA}^+)_p$ and $\lambda^\circ(\text{ClO}_4^-)_p$. The $\lambda^\circ(\text{pTS}^-)$ and $\lambda^\circ(\text{pTS}^-)_p$ were obtained assuming that Walden's rule holds in these systems,[8] *i.e.*,

$$\lambda^\circ(\text{pTS}^-) = 0.7 \times \lambda^\circ(\text{ClO}_4^-),$$
$$\lambda^\circ(\text{pTS}^-)_p = 0.7 \times \lambda^\circ(\text{ClO}_4^-)_p. \quad (4)$$

The dissociation constants for TOMA pTS were calculated from Eq. 3 using these relations.

The formation constants, K_1^F between pTS^- and alkylphenols were estimated according to the method reported by Aitken and Gilkerson.[9] The dissociation constant, K^D for TOMA pTS in the absence of a phenol is assumed to be given in Eq. 3. If the dissociation constant varies from K^D to K_p^D by the addition of phenol, then,

$$K_p^D/K^D = (C_p/C)(\Lambda_p/\Lambda_{0p})^2(\Lambda/\Lambda_0)^{-2}(1 - \Lambda/\Lambda_0) \times (1 - \Lambda_0/\Lambda_{0p})^{-1}. \quad (5)$$

This equation can be reduced to Eq. 6, provided that the concentration of ion-pair is constant, *i.e.*, $C_p=C$, and the molar conductivities Λ and Λ_p at concentration C and C_p are much smaller than those at infinite dilution.

$$K_p^D/K^D = (\Lambda_p/\Lambda)^2 \equiv R \quad (6)$$

Those simplifying assumptions are reasonable in a solvent of low dielectric constant such as *o*-dichlorobenzene. The following interactions were assumed to exist between pTS^- or ion-pair and the phenol (denoted by P),

$$\text{pTS}^- + \text{P} \rightleftarrows \text{pTS}\cdot\text{P}^-,\ K_1^F = [\text{pTS}\cdot\text{P}^-]/[\text{pTS}^-][\text{P}] \quad (7)$$

$$\text{TOMA pTS} + \text{P} \rightleftarrows \text{TOMA pTS}\cdot\text{P},$$
$$K_2^F = [\text{TOMA pTS}\cdot\text{P}]/[\text{TOMA pTS}][\text{P}]. \quad (8)$$

Then the ratio, K_p^D/K^D was given by Eq. 9,[9,10]

$$K_p^D/K^D = (1 + K_1^F[\text{P}])/(1 + K_2^F[\text{P}]). \quad (9)$$

The lefthand side of Eq. 9 is approximated by R and the righthand side by $(1+K_1^F[\text{P}])$ at low concentration of the phenol. Consequently, K_1^F can be obtained from the slope of the plot of R *vs.* [P].[9]

Results and Discussion

Effect of ptOP on the Sensitivity and Selectivity. The effects of the concentrations of the ion-pair, TOMA pTS and the phenol on the sensitivity and selectivity of the sulfonate electrode were examined. The potential difference between the pTS^- solutions of 10^{-1} M and 10^{-5} M was defined as a sensitivity factor, $\Delta E_{1\text{-}5}$. In the absence of the phenol, both the sensitivity and selectivity were independent of the ion-pair concentration over the experimental range from 1.5 mM to 50 mM; *i.e.*, $\Delta E_{1\text{-}5} \approx 200$ mV and $\log K^{pot} \approx 2.3$, 0.6, -0.5, -1.0, and -2.0 for perchlorate, iodide, nitrate, bromide, and chloride ions, respectively. When the concentration of the ion-pair was below 0.5 mM, the sensitivity decreased to 170 mV, owing to the decrease of the ion-exchange current density due to the dilution of the ion-exchanger. In the case of the diluted ion-exchanger membrane, as shown in Fig. 1-a, the values of $\log K^{pot}$ were decreased in proportion to the logarithm of the ptOP concentration and also the value $\Delta E_{1\text{-}5}$ was decreased more significantly. When the concentration of the ion-pair was sufficiently high, the membrane maintains still high sensitivity even at high concentration of ptOP, as shown in Fig. 1-b. In conclusion, the optimum concentration of ptOP was chosen at 0.5 M. Figure 2 shows the relationships between the concentration of the ion-pair and the sensitivity factor or logarithmic selectivity coefficients in the presence of 0.5 M

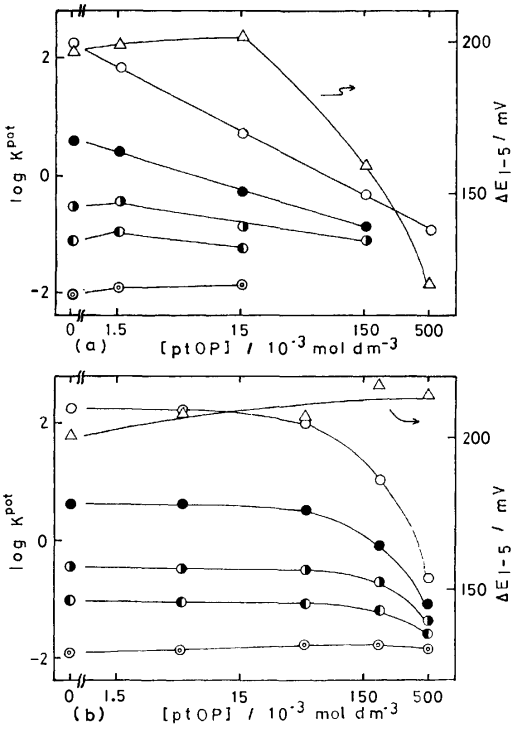

Fig. 1. Effect of concentration of *p-t*-octylphenol on selectivity coefficients and sensitivity factor $\Delta E_{1\text{-}5}$.
(a): $[\text{TOMA pTS}]=1.5\times10^{-3}$ mol dm^{-3}, (b): $[\text{TOMA pTS}]=50\times10^{-3}$ mol dm^{-3}.
○ ClO_4^-, ● I^-, ◑ NO_3^-, ◐ Br^-, ◎ Cl^-.

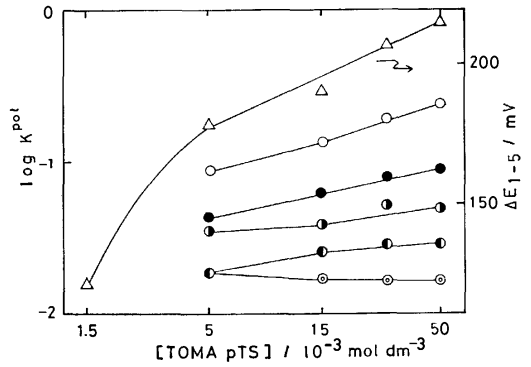

Fig. 2. Effect of concentration of TOMA pTS on selectivity coefficients and sensitivity factor $\Delta E_{1\text{-}5}$. [ptOP]=0.5 mol dm^{-3}, ○: ClO_4^-, ●: I^-, ◑: NO_3^-, ◐: Br^-, ◎: Cl^-.

ptOP. The concentration of the ion-pair should be higher than 0.03 M to keep the sensitivity sufficiently high.

As shown in Figs. 1 and 2, the interference of perchlorate decreased remarkably by the addition of ptOP, though perchlorate is one of the most serious interferent against the conventional liquid membrane electrodes. It seems to be noteworthy that the selectivity coefficient for perchlorate is reduced to one eight-hundredth and becomes smaller than one, in other words, perchlorate becomes a "weaker" anion than pTS anion. This remarkable change in selectivity against perchlorate by ptOP can be explained on the basis of Sandblom-Eisenman-Walker theory[5,11] for the liquid membrane potential. In the case of a strongly associated ion-pair, the membrane potential E is given by Eq. 10[11]

$$\frac{F}{RT}E = (1-\tau)\ln\frac{a_i'+\bar{P}a_j'}{a_i''+\bar{P}a_j''} + \tau\ln\frac{a_i'+\bar{K}a_j'}{a_i''+\bar{K}a_j''}, \quad (10)$$

where a_i', a_j', a_i'', and a_j'' are activities of ions i and j in the phases denoted with suffixes (′) and (″). Three selectivity factors $\bar{P}$, $\bar{K}$, and τ are defined by Eqs. 11—13;

$$\bar{P} = \frac{(u_j+u_s)k_j}{(u_i+u_s)k_i} = \frac{u_j+u_s}{u_i+u_s}K^{ex}\frac{K_{js}^p}{K_{is}^p}, \quad (11)$$

$$\bar{K} = \frac{u_{js}}{u_{is}}K^{ex}, \quad (12)$$

$$\tau = \frac{u_s[(u_{js}/K_{js}^p)-(u_{is}/K_{is}^p)]}{(u_i+u_s)(u_{js}/K_{js}^p)-(u_j+u_s)(u_{is}/K_{is}^p)} \quad (0<\tau<1), \quad (13)$$

where u_i, u_j, u_{is}, u_{js} are the mobilities of ions i, j, and ion-pairs in liquid membrane, k_i and k_j are the partition coefficients and K_{is}^p K_{js}^p, are the ion-pair dissociation constants and K^{ex} is the ion-exchange equilibrium constant. Therefore, $\bar{P}$ is governed by the mobilities of ions in the membrane and their partition equilibria, whereas $\bar{K}$ is governed by the mobilities of the ion-pair and the ion-exchange equilibrium constant of Eq. 1. A parameter τ indicates the relative weight between $\bar{P}$ and $\bar{K}$, and depends on the ion dissociation phenomena in the membrane. These parameters estimated with respect to ions pTS^-(i) and ClO_4^-(j) in the presence and absence of ptOP are summarized in Table 1 together with the potentiometric selectivity constant, K^{pot}.

The observed selectivity coefficients in the presence and absence of ptOP agree fairly well with the mean values between $\bar{P}$ and $\bar{K}$. This indicates that the variation of the selectivity coefficient can be interpreted well by this theory. The factors of the mobility ratio and the dissociation constant ratio in Eqs. 11 and 12 vary at most three times by the addition of ptOP. Therefore, it seems that these factors are not responsible for the lowering of the selectivity of perchlorate. Judging from the variation of τ caused by the addition of ptOP, the contribution of the associated species to the selectivity is large in the absence of ptOP, whereas the contribution of the diffusion of free ions becomes important in the presence of ptOP, namely, this variation results from

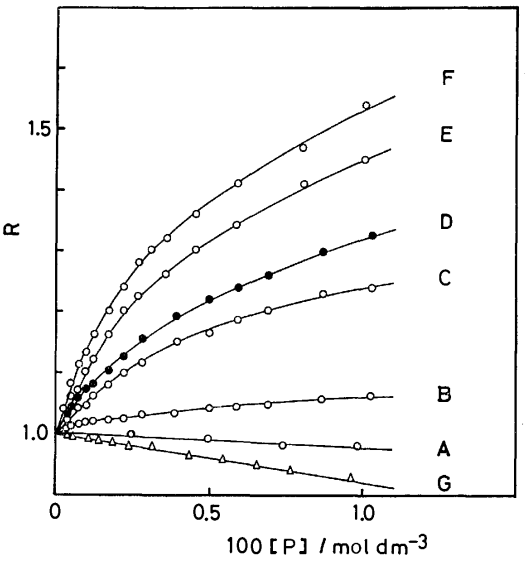

Fig. 3. R *vs.* [P] plots for alkylphenols.
10^{-4} mol dm^{-3} TOMA pTS+alkylphenol in *o*-dichlorobenzene.
(A): 2,6-Di-*t*-butyl-4-methylphenol, (B): 2,4,6-trimethylphenol, (C): 2,3,5-trimethylphenol, (D): *p*-*t*-octylphenol, (E): *p*-*t*-pentylphenol, (F): *p*-*t*-butylphenol, (G): 10^{-4} mol dm^{-3} TOMA ClO_4+*p*-*t*-octylphenol.

Table 1. Effects of ptOP on the selectivity parameters of TOMA pTS/*o*-dichlorobenzene membrane

Solvent	K^{pot}	τ	$\bar{P}$	$\bar{K}$	λ_s°	λ_i°	λ_j°	K_{is}^p ($\times 10^{-6}$)	K_{js}^p ($\times 10^{-6}$)	K^{ex}
o-Dichlorobenzene										
without PtOp	200[a]	0.69	520	60	9.9	17.2	24.6	1.1	8.5	53
with 0.5 M ptOP	0.25[a]	0.44	0.26	0.11	9.9	7.1	10.1	3.5	8.6	0.091

Subscript i, j, and s refer to pTS^-, ClO_4^-, and $TOMA^+$, respectively. a) Concentration of ion-pair is 0.05 M.

the promotion of the dissociation of ion-pair by the formation of hydrogen bonding between the ptOP and sulfonate.

Relationship between the Hydrogen Bonding Abilities of Alkylphenols and Selectivity of Sulfonate Electrode. As a measure of the hydrogen bonding abilities of alkylphenols used, the formation constants, K_1^F between pTS^- and the phenols were evaluated from the slopes of the extrapolation of the plot of R *vs.* [P] back to the zero concentration of the phenols, as shown in Fig. 3. In the figure, when the concentration of the phenols becomes high, the plots are curving convexly. This indicates the formation of the associated species between the phenols and the ion-pair. It can be seen in the Figure, that the more sterically hindered the hydroxyl group of the phenols is, the smaller the K_1^F value becomes (A—D). The phenols having small *p*-alkyl substituent were likely to show the large values of K_1^F (D—F). This result does not necessarily indicate that the hydrogen bonding ability increases in the order, D<E< F in *p*-alkyl-substituted phenols, because the molar conductivities of the associated species between pTS^- and these phenols vary with their sizes. Namely, the larger the phenol is, the more slowly the associated species move. In the case of TOMA ClO_4 (curve G), the decrease of R was observed. The result is explained that only the free perchlorate anion is associated with ptOP and the molar conductivity of the associated species decreases in comparison with that of the free perchlorate.

These results obtained by conductometry were confirmed by the IR spectra of these phenols in *o*-dichlorobenzene in the presence of pTS^- or ClO_4^-. The stretching band ν(OH) of phenols near 3600 cm^{-1} shifted to the longer wavelength by the addition of pTS^-, the shift of which was in proportion to the hydrogen bonding abilities of the phenols with sulfonate.[12,13] As shown in Table 2, a good correlation was obtained between the frequency shift of the ν(OH) band and the formation constants measured by conductmetry (A—D). The difference was not entirely observed among the hydrogen bonding abilities of the *p*-alkyl-substituted phenols (D—F), in spite of the remarkable difference in their formation constants. The shift of the ν(OH) band was also observed when ptOP was added to the solution of TOMA ClO_4, and this shift shows the formation of associated species between ptOP and perchlorate. Figure 4 shows the relationships between log K^{pot} and log K_1^F with respect to the liquid membrane(upper) and to the solid solvent membrane (lower), respectively. It can be said that the more sterically hindered the phenols are, the less selective the electrode is in both the liquid and solid solvent

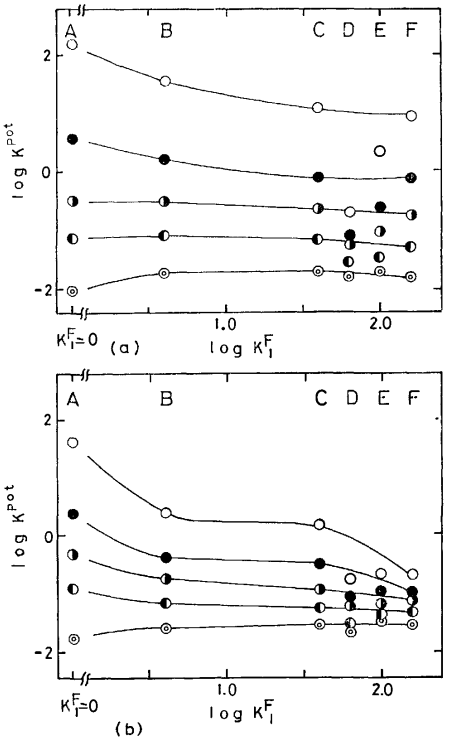

Fig. 4. Relationship between formation constant and selectivity coefficients.
(A)—(F): Same as in Fig. 3.
(a): Liquid membrane (0.03 mol dm^{-3} TOMA pTS+ 0.5 mol dm^{-3} ptOP in *o*-dichlorobenzene), (b): Solid solvent membrane (0.05 mol dm^{-3} TOMA pTS in alkylphenol).

membranes (A—C,F). The effect of the size of *p*-alkyl substituent was significant in the liquid membrane in contrast with the solid solvent membrane (D—F). This result can be explained by the fact that in the liquid membrane the surface concentration of the phenols decreased with decreasing the size of *p*-alkyl substituent by the dissolution of phenol into the aqueous phase. Consequently, the highest selectivity was observed with ptOP having the largest *p*-alkyl substituent among the phenols D,E,F. The lowering tendency of the selectivity in the liquid membrane in comparison with that in the solid solvent membrane can be interpreted in the same way.

Effect of the Membrane Solvents on the Selectivity. The solvent effect on the selectivities of the sulfonate electrode was examined in the presence and absence of ptOP. Jyo *et al.*[2] examined the solvent effects in the liquid membrane electrode and reported that chloroform enhanced the selectivity for halide ion and 1-decanol decreased the selectivity of perchlorate and

Table 2. Comparison between infrared frequency shift of alkylphenols and logarithmic formation constant

Phenol	2,6-Di-*t*-butyl-4-methylphenol	2,4,6-Tri-methylphenol	2,3,5-Tri-methylphenol	ptOP	ptPP	ptBP
$\Delta\nu$(OH)[a] cm^{-1}	0	330	380	400	400	400
log K_1^F [b]	—[c]	0.6	1.6	1.8	2.0	2.2

a) Frequency shift caused by pTS^- in *o*-dichlorobenzene. b) Formation constant between pTS^- and phenol measured by conductometry. c) No formation was observed.

TABLE 3. SOLVENT EFFECTS ON THE SELECTIVITY COEFFICIENTS IN THE PRESENCE AND ABSENCE OF ptOP
Ion-exchanger: 0.05 M TOMA pTS without(or with 0.5 M) ptOP in each solvent.

Solvent	δ_h[a] ($MPa^{1/2}$)	log K^{pot}											
		ClO_4^-	BF_4^-	SCN^-	RSO_3^-[b]	I^-	ClO_3^-	ϕSO_3^-	NO_3^-	Br^-	NO_2^-	BrO_3^-	Cl^-
o-Dichlorobenzene	3.3	2.3	1.6[c]	1.2	1.1	0.6	−0.2	−0.3	−0.4	−1.0	−1.3	−1.5	−1.9
with 0.5 M ptOP	—	−0.6	−1.2[c]	−0.3	0.8	−1.1	−1.5	−0.5	−1.3	−1.5	−1.2	−2.0	−1.8
Nitrobenzene	4.1	2.0	1.4	1.1	0.8	0.7	−0.1	−0.3	−0.2	−0.8	−1.0	−1.1	−1.6
with 0.5 M ptOP	—	0.0	−0.6	0.1	0.7	−1.0	−1.3	−0.5	−1.0	−1.4	−1.1	−1.8	−1.7
Chloroform	5.7	1.8	1.1	1.1	1.0	1.1	−0.1	−0.3	−0.3	−0.6	−1.2	−1.2	−1.5
with 0.5 M ptOP	—	−0.7	−1.2	−0.3	0.7	−0.9	−1.3	−0.5	−1.1	−1.4	−1.1	−1.6	−1.6
1-Octanol	11.9	0.1	−0.5	0.3	0.7	−0.2	−0.8	−0.5	−0.9	−1.0	−1.2	−1.7	−1.5
with 0.5 M ptOP	—	−0.3	−0.9	0.1	0.7	−0.5	−1.0	−0.5	−1.0	−1.1	−1.1	−1.7	−1.5

a) Hydrogen bonding component of solubility parameter. See Ref. 14. b) 1-Naphthalenesulfonate. c) The values in the preliminary report were corrected here.

tetrafluoroborate, in contrast to the increasing effect of this solvent to the selectivity of organic anions. The hydrogen bonding ability of the solvents seems also to play an important role in the selectivity characteristics of the sulfonate electrode. Table 3 summarizes the solvent effect on the selectivities of the sulfonate electrode in the presence and absence of ptOP. In the table, the hydrogen bonding component δ_h of solubility parameters[14] is also listed. The interference of the inorganic anions such as perchlorate, tetrafluoroborate and others decreased with increasing δ_h. In the presence of ptOP, however, no remarkable effect of the solvents is observed. This shows that the selectivity is primarily determined by ptOP. The effect of ptOP in nitrobenzene was not so significant as that in the other solvents. This result is due to the relatively high dielectric constant of nitrobenzene. No effect of solvents on the selectivity of 1-naphthalenesulfonate and benzenesulfonate was observed. Namely, these organic sulfonates seem to interact with solvent or ptOP in the same way as the objective ion like *p*-toluenesulfonate. The interference of ions such as perchlorate and tetrafluoroborate which interact weakly with proton was decreased remarkably by the addition of ptOP. On the other hand, the interference of ions such as nitrite and chloride which strongly interact with proton did not always decrease but even increased in some cases.

Conclusion

From the above discussion, it is concluded that the phenol primarily governs the selectivity of the sulfonate electrode and the membrane solvent influences in a minor extent. For the optimum selection of phenol in order to obtain the high selectivity, the hydroxyl group of the phenol should be little hindered sterically, and the solubility of the phenol should be large in a membrane solvent and small in a aqueous sample solution.

In conclusion, it was found that the recommended ion-exchanger for *p*-toluenesulfonate was 0.05 M TOMA pTS with 0.5 M ptOP in *o*-dichlorobenzene. The potentiometric response characteristics of this ion-exchanger were as follows: (1) the linear response range is 10^{-1} M—$10^{-3.8}$ M, (2) the usable response range is 10^{-1} M—10^{-5} M, (3) the slope is 61 mV/decade, and (4) the response time at 10^{-2} M is within 3 min.

The authors are grateful to Dr. Ikko Sakamoto in their laboratory for his offer of the samples used in the conductivity measurements and also for his helpful discussions on the results.

References

1) N. Ishibashi, H. Kohara, and K. Horinouchi, *Talanta*, **20**, 867 (1973).
2) A. Jyo, M. Torikai, and N. Ishibashi, *Bull. Chem. Soc. Jpn.*, **41**, 2862 (1974).
3) T. Fujinaga, S. Okazaki, and H. Freiser, *Anal. Chem.*, **46**, 1842 (1974).
4) T. Fujinaga, S. Okazaki, and H. Hara, *Rev. polarogr.*, **21**, Nos 1/6, 99 (1975).
5) J. Sandblom, G. Eisenman, and J. Walker, Jr., *J. Phys. Chem.*, **71**, 3862, (1967).
6) C. Fabiani, P. R. Danesi, G. Scibona, and B. Scuppa, *J. Phys. Chem.*, **78**, 2370 (1974).
7) R. M. Fuoss and T. Shedlovsky, *J. Am. Chem. Soc.*, **71**, 1496 (1947).
8) T. Fujinaga and I. Sakamoto, *J. Electroanal. Chem.*, **67**, 201 (1976).
9) H. W. Aitken and W. R. Gilkerson, *J. Am. Chem. Soc.*, **95**, 8551 (1973).
10) J. Macau, L. Lamberts, and P. Huyskens, *Bull. Soc. Chim. Fr.*, **7**, 2387 (1971).
11) C. Fabiani, *Anal. Chem.*, **48**, 865 (1976).
12) A. T. Lemley, "The Chemistry of Nonaqueous Solvents," ed by J. J. Lagowski, Academic Press, (1976), Vol. IV, Chap. 2.
13) M. Miyamae and T. Kagiya, *Nippon Kagaku Kaishi*, **1976**, 211.
14) A. M. F. Barton, *Chem. Rev.*, **75**, 731 (1975).

Neighboring Group Participation in the Oxidation of Hydroxy Sulfides. Control of the Reaction Courses and Products

Yoshio Ueno,* Tadaaki Miyano, and Makoto Okawara

Research Laboratory of Resources Utilization, Tokyo Institute of Technology, Nagatsuta, Midori-ku, Yokohama 227

(Received December 20, 1979)

Oxidation of the hydroxy sulfides [$PhS(CH_2)_nCH(OH)R$] with hexabutyldistannoxane (HBD)–bromine system was studied in order to clarify neighboring group participation during the course of reaction. The oxidation products were found to be highly dependent on the positions of the two functional groups [sulfide and hydroxyl group]. Thus hydroxy sulfoxides [$PhSO(CH_2)_nCH(OH)R$] were obtained as the main product when $n=1$ or 2, bromo sulfones [$PhSO_2(CH_2)_nCHBrR$] being predominant when $n=3$ or 4. Keto sulfoxide [$PhSO(CH_2)_nCOR$] was exclusively formed when $n=6$. The results are discussed in terms of the different intramolecular interactions depending on the positions of the two functional groups.

Neighboring group participation is an important factor controlling reactions. For example, neighboring group participation in biological systems operates to fix and activate the substrates in an unequivocal manner particularly in enzymatic reactions.[1]

Studies have been carried out to explore the neighboring group participation or intramolecular interactions in static state by means of spectroscopic methods such as IR, UV, Fluorescence, NMR, or ESR spectroscopy.[2] However, no study seems to have been carried out on these subjects during the course of reaction.

In order to investigate neighboring group participation as a function controlling the reaction courses and products, it is important to choose suitable model compounds having two functional groups. We chose hydroxy sulfides, in which both hydroxyl and sulfide groups are isolated systematically by different methylene-chain lengths ($n=1$—6). It was shown that a hexabutyldistannoxane (HBD)–bromine system is an effective oxidant for alcohols[3] or sulfides.[4] Especially this oxidant has one advantage over the existing ones, since sulfides are oxidized selectively to the corresponding sulfoxides without overoxidation to sulfones even in the presence of excess HBD–Br_2. These observations enable us to investigate the oxidation of these two functional groups existing in the same molecule with HBD–Br_2.

Results and Discussion

The hydroxy sulfides were prepared by the usual methods (see Experimental). Oxidation was carried out in dichloromethane at room temperature. Bromine solution (2.4 equiv.) was added to a solution of HBD (2.4 equiv.) and hydroxy sulfides (1 equiv.). The results of oxidation are given in Table 1.

The products were hydroxy sulfoxides (Type A), bromo sulfones (Type B), and Keto sulfoxides (Type C). In some cases, one of the three was formed exclusively.

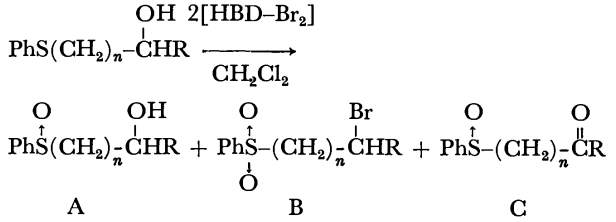

Distribution of the products depends on the methylene-chain length, Type A being predominant when the two functional groups are located in relatively closer positions ($n=1$ or 2), and Type B when $n=3$ or 4. Keto sulfoxide was formed exclusively when $n=6$. The differences in product distribution should arise from the different neighboring group participations during the course of reaction depending on the distance between the two functional groups. This is discussed in terms of the most fovorable cyclic intermediate in each substrate.

Hydrogen Bonding between Hydroxyl and Sulfoxide Group. Hydroxy sulfoxides (Type A) exibited in their IR spectra an ultimate shift to lower wave numbers of both νO–H (3320—3380 cm^{-1}) and νS–O (990—1020 cm^{-1}) streching frequencies, indicating a strong hydrogen bonding between OH and SO groups. The figures in parentheses indicate isolated yields of hydroxy sulfoxides. The hydrogen bondings seem to prevent the hydroxyl group from further oxidation to the corresponding carbonyl group.

The hydrogen bondings are composed of six-, seven- or eight-membered (less effective) ring systems. Larger ring systems should be extremely unfavorable, since no hydroxy sulfoxides were obtained from **4** and **5**, which should undergo cyclization to nine- and eleven-membered ring, respectively, for the sake of intramolecular hydrogen bonding.

A bulky substituent such as the phenyl group in compound **9** might contribute to the more rigid hydrogen bonding formation by the restriction of the free rotation of the molecule, resulting in a higher yield of hydroxy sulfoxides.

Intramolecular Oxygen Transfer via *Cyclic Alkoxysulfoxonium Ions.* Bromo sulfones (Type B) were obtained unexpectedly, since HBD–Br_2 gave no sulfones. Since both oxidation and work-up were carried out under anhydrous conditions, it is unlikely that the one oxygen atom of the sulfones is derived from the external sources such as water. The formation of bromo sulfones may be best explained by the intramolecular oxygen atom transfer mechanism (Scheme 1).

The detailed mechanism for the formation of the alkoxysulfoxonium bromide (**17**) is not clear. However, a possible scheme is the intramolecular cyclization by the attack of hydroxyl group towards stannyloxysulfonium ion (**16**).[5] This cyclic alkoxysulfoxonium bromide

Table 1. Oxidation of hydroxy sulfides

Hydroxy sulfide	Products (%)		
	Hydroxy sulfoxide	Bromo sulfone	Keto sulfoxide
1a 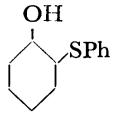	**6** 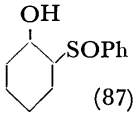 (87)		
1b 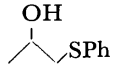	**7** 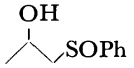 (49)	**8** 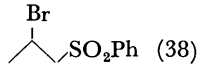 (38)	
2a 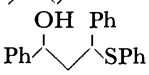	**9** 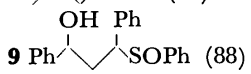 (88)		
2b 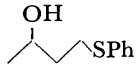	**10** (18)	t[a]	**11** 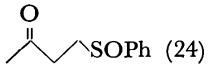 (24)
3 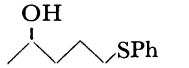	**12** 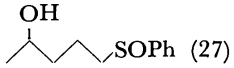 (27)	**14** 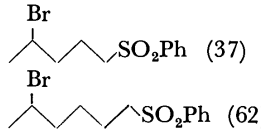 (37) (62)	t[a]
4 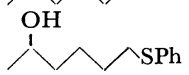			
5 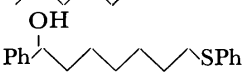			**15** 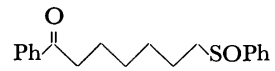 (97)

a) Formation of a trace amount of the corresponding products was observed.

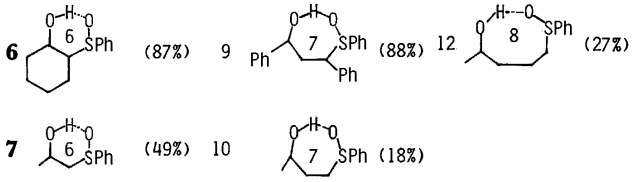

(**17**)[6] may be a key intermediate, which undergoes cleavage to a bromo sulfone by the attack of bromide ion. This is supported by the fact that the yield of bromo sulfone (**13**) increases (37%→66%), when lithium bromide is added as an additive.

The alkoxysulfoxonium ions again fall into mainly six- and seven-membered rings except one four-membered intermediate.

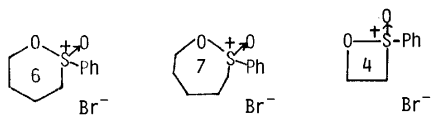

Keto Sulfoxide Formation. When the hydroxyl and sulfide groups were isolated by six methylene-chains (compound **5**), oxidation proceeded to give keto sulfoxide almost quantitatively. This indicates no appreciable interaction, either hydrogen bonding (eleven-membered ring) or cyclic alkoxysulfoxonium ion formation (nine-membered ring) during the course of reaction, *viz.*, no possible cyclic intermediates more than eight-membered rings opperate, two functional groups behaving independently.

A plausible reaction scheme for the formation of the Type A, B and C products is shown in Scheme 1. Oxidation is assumed to proceed by consumption of twice the molar amount of HBD and bromine except for the formation of Type A product.

In conclusion, mainly more favorable six- and seven-membered cyclic intermediates determine the reaction courses and the products.

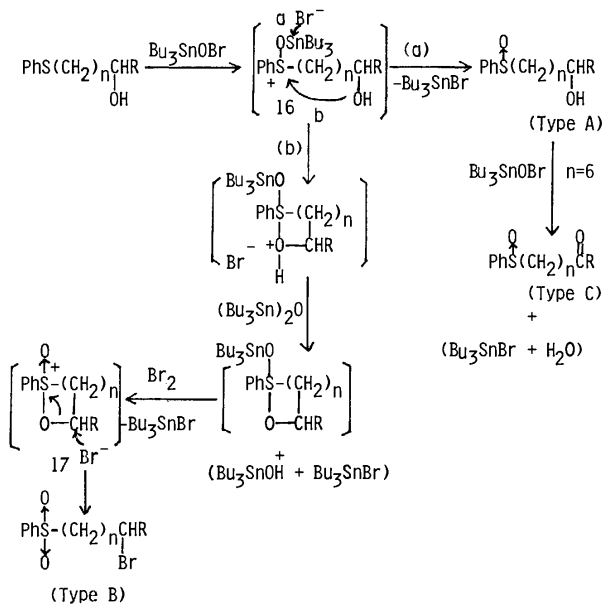

Scheme 1.

Experimental

General. Infrared spectra were taken in a film for liquids and KBr pellets for solids using a Hitachi EPI-S2 IR

spectrometer. All NMR spectra were measured with a TMS internal standard using a Varian EM-360 or JEOL JNM-C 100.

Materials. Hydroxy sulfides were prepared by the usual process by means of sodium borohydride reduction of the corresponding keto sulfides in methanol. *trans*-2-Phenylthiocyclohexanol (**1a**) was prepared by the reaction of sodium benzenethiolate with cyclohexene oxide.[7]

1-Phenylthio-2-propanol (1b). This was obtained in 71% yield from 1-phenylthio-2-propanone; bp 100—120 °C/2 mmHg (1 mmHg=133.322 Pa); NMR (CCl_4) δ=1.20 (d,3, J=6 Hz, CH_3), 2.87 (d, 2, J=6 Hz, SCH_2), 3.43 (s, 1, OH), 3.53—4.07 (m, 1, OCH), and 7.00—7.50 (m, 5, C_6H_5).

3-Phenylthio-1,3-diphenyl-1-propanol (2a). This was similarly obtained in 96% yield as an oil from 3-phenylthio-1,3-diphenyl-1-propanone: NMR (CCl_4) δ=2.10 (m, 2, CH_2), 2.93 (s, 1, OH), 4.26 (m, 1, OCH), 4.67 (t, 1, J=6 Hz, SCH), and 6.83—7.37 (m, 15, C_6H_5). Found: C, 78.88; H, 6.23%. Calcd for $C_{22}H_{20}OS$: C, 78.70; H, 6.30%.

4-Phenylthio-2-butanol (2b). This was similarly obtained in 62% yield: bp 105—106 °C/2 mmHg; NMR (CCl_4) δ=1.17 (d, 3, J=6 Hz, CH_3), 1.70 (q, 2, J=6 Hz, CH_2), 2.93—2.97 (m, 3, SCH_2 and OH), 3.87 (m, 1, OCH), and 7.07—7.40 (m, 5, C_6H_5). Found: C, 66.22; H, 8.18; S, 17.45%. Calcd for $C_{10}H_{14}OS$: C, 65.91; H, 7.74; S, 17.56%.

5-Phenylthio-2-pentanol (3). To a solution of pyridinium chlorochromate (14.7 g, 68 mmol) in dichloromethane (90 ml) was added a solution of 4-phenylthiobutanol (6.2 g, 34 mmol) in the same solvent (15 ml) at room temperature. After being stirred for 2 h, dry ether was added to the mixture, the organic layer being decanted three times. The combined etheral solution was washed with saturated aqueous sodium hydrogencarbonate and aqueous sodium chloride. 4-(Phenylthio)butanal was obtained as a colorless oil after the usual work-up in 43% yield: bp 113—115 °C/1 mmHg; IR 1720 cm^{-1} (νC=O). NMR (CCl_4) δ=1.80 (q, 2, J=6 Hz, CH_2), 2.56 (t, 2, J=6 Hz, CH_2CO), 2.93 (t, 2, J=6 Hz, CH_2S), 7.13—7.17 (m, 5, C_6H_5), and 9.53 (t, 1, J=1.2 Hz, CHO), 2,4-dinitrophenylhydrazone; mp 103—105 °C. Found: C, 53.39; H, 4.40; N, 15.73; S, 8.92%. Calcd for $C_{16}H_{16}N_4O_4S$: C, 53.32; H, 4.48; N, 15.55; S, 8.90%.

To a solution of methylmagnesium iodide prepared from methyl iodide (27 mmol) and magnesium (27 mg atom) in dry ether was added a solution of 4-(phenylthio)butanal (1.14 g, 8 mmol) in dry ether (15 ml). After being stirred at room temperature for 3 h, the mixture was treated with water (30 ml) and 0.5 mol/l sulfuric acid for 1 h. After the usual work-up, 5-phenylthio-2-pentanol (**3**) was obtained by distillation in 93% yield as a colorless oil: bp 120—125 °C/2 mmHg; NMR (CCl_4) δ=1.06 (d, 3, J=6 Hz, CH_3), 1.56 (m, 4, CH_2CH_2), 2.83 (t, 2, J=6 Hz, SCH_2), 3.26 (broad s, 1, OH), 3.63 (m, 1, OCH), and 6.96—7.33 (m, 5, C_6H_5). Found: C, 67.30; H, 8.37%. Calcd for $C_{11}H_{16}OS$: C, 67.31; H, 8.23%.

6-Phenylthio-2-hexanol (4). 5-Acetoxyhexyl phenyl sulfide was prepared by the reaction of sodium benzenethiolate and 5-acetoxy-1-bromohexane[8] in 76% yield as an oil. This was treated with 30% aqueous potassium hydroxide (40 ml) and dioxane (40 ml) under reflux for 5 h. The usual work-up gave 6-phenylthio-2-hexanol (**4**) in 95% yield as a colorless oil: bp 135—138 °C/2 mmHg; NMR (CCl_4) δ=1.25 (d, 3, J=7 Hz, CH_3), 1.37—1.86 (m, 6, $(CH_2)_3$), 2.70—3.26 (m, 3, SCH_2 and OH), 3.33—3.37 (m, 1, OCH), and 7.03—7.53 (m, 5, C_6H_5). Found: C, 68.61; H. 8.52%. Calcd for $C_{12}H_{18}OS$: C, 68.51; H, 8.64%.

7-Phenylthio-1-phenyl-1-heptanol (5). 1-Bromo-6-(Phenylthio)hexane (2.28 g, 8 mmol) was treated with magnesium (0.20 g, 8 mg atom) in the presence of a catalytic amount of iodine in dry ether for 70 min under argon atmosphere. Benzaldehyde (0.85 g, 8 mmol) was added dropwise to the mixture. The resulting mixture was refluxed for 1 h. The usual work-up gave 7-phenylthio-1-phenyl-1-heptanol (**5**) in 13% yield: mp 50.5—51.5 °C (pentane); NMR (CCl_4) δ=1.1—2.0 (m, 10), 1.7 (m, 1), 2.9 (t, 2, J=6 Hz), 4.6 (t, 1, J=6 Hz), and 7.2 (m, 10). Found: C, 76.16; H, 7.97%. Calcd for $C_{19}H_{24}OS$: C, 75.97; H, 8.05%.

Oxidation of Hydroxy Sulfides. General Procedure: To a mixture of hydroxy sulfide (6 mmol) and hexabutyldistannoxane (HBD, 13 mmol) in dichloromethane (15 ml) was added dropwise a solution of bromine (13 mmol) in dichloromethane (10 ml). The red color of bromine was immediately discharged and the reaction mixture was stirred at room temperature for 2—3 h. The solvent was removed under reduced pressure and the residue was separated by chromatography on silica gel. Tributyltin bromide was isolated by elution with hexane. Type B and C products were then obtained by elution with chloroform, the type A product being finally eluted with chloroform–ethanol (2 : 1).

2-(Phenylsulfinyl)cyclohexanol (6). After evaporation of dichloromethane the residue was treated with a small amount of pentane with cooling (Dry Ice–acetone bath) to give white solid **6** in 87% yield: mp 154—155 °C (benzene); IR 1008, 990 cm^{-1} (νS–O), 3320 cm^{-1} (νOH), Found: C, 63.80; H, 7.42, S, 14.01%. Calcd for $C_{12}H_{16}O_2S$: C, 64.25, H, 7.19: S, 14.29%. 2-(Phenylsulfinyl)cyclohexanol **6** obtained seems to be trans isomer, since its melting point is close to that reported (mp 156.0—156.6 °C[7]). When the same reaction was carried out in methanol or tetrahydrofuran in place of dichloromethane, hydroxy sulfoxide **6** was obtained in 57 or 60% yield, respectively.

2-Bromopropyl Phenyl Sulfone (8). This was obtained in 38% yield as an oil: IR 1300, 1150 cm^{-1} (νSO_2). NMR ($CDCl_3$), δ=1.88 (d, 3, J=6.9 Hz, CH_3), 3.53—3.70 (m, 2, SO_2CH_2), 4.13—4.67 (m, 1, BrCH), and 7.40—8.10 (m, 5, C_6H_5). This compound is too unstable to be satisfactorily purified for elemental analysis. Found: C, 42.07: H, 4.65; S, 12.45%. Calcd for $C_9H_{11}BrO_2S$: C, 41.07; 4.22; S, 12.18%.

3-Phenylsulfinyl-2-propanol (7).[9] This was obtained as an oil in 49% yield. IR: 3330 cm^{-1} (νOH), 1014, 990 cm^{-1} (νS–O). NMR ($CDCl_3$) δ=1.29, 1.35 (each d, 3, J=6 Hz, CH_3), 2.58—3.25 (m, 2, CH_2), 4.00—4.63 (m, 1, CH), 4.73—5.08 (broad s, 1, OH), and 7.30—7.85 (m, 5, C_6H_5). Found: C, 58.28; H, 6.25%. Calcd for $C_9H_{12}O_2S$: C, 58.69; H, 6.57%.

3-Phenylsulfinyl-1,3-diphenyl-1-propanol (9). This was isolated as a white solid in 88% yield in a similar way as that for compound **6**: mp 148—150 °C (CH_2Cl_2–hexane); IR 3380 (νOH), 1010, 990 cm^{-1} (νS–O). NMR (DMSO-d_6) δ=2.28 (m, 2, CH_2), 3.84 (t, 1, J=3.4 Hz, SOCH), 4.68 (broad s, 1, OH), 5.60 (m, 1, OCH), and 6.76—7.47 (m, 15, C_6H_5). Found: C, 74.62, H, 6.01; S, 10.01%. Calcd for $C_{21}H_{20}O_2S$: C, 74.96; H, 6.00; S, 9.53%.

4-Phenylsulfinyl-2-butanol (10). This was obtained as an oil in 18% yield. IR 3360 cm^{-1} (νOH), 1020 cm^{-1} (νS–O). NMR ($CDCl_3$) δ=1.17 (d, 3, J=6 Hz, CH_3), 1.50—1.98 (m, 2, CH_2), 2.97 (t, 2, J=8 Hz, $SOCH_2$), 3.37—4.10 (m, 2, OH and O–CH), and 7.33—7.73 (m, 5, C_6H_5). Found: C, 60.34; H, 7.23%. Calcd for $C_{10}H_{14}O_2S$: C, 60.59; H, 7.12%.

4-Phenylsulfinyl-2-butanone (11). This was isolated as oil in 24% yield. IR 1720 cm^{-1} (νC=O), 1010 cm^{-1} (νS–O). NMR (CCl_4) δ=2.00 (s, 3, CH_3), 2.40—2.73 (m, 2, CH_2), 2.83—3.17 (m, 2, $SOCH_2$), and 7.00—7.04 (m, 5, C_6H_5), Found: C, 60.86; H, 6.23%. Calcd for $C_{10}H_{12}O_2S$: C, 61.19;

H, 6.17%.

5-Phenylsulfinyl-2-pentanol (12). An oil, 27%. IR 3380 cm^{-1} (νOH), 1010 cm^{-1} (νS–O). NMR ($CDCl_3$) δ=1.15 (d, 3, J=6 Hz, CH_3), 1.32—2.15 (m, 4, CH_2CH_2), 2.62—3.12 (m, 2, $SOCH_2$), 3.45—4.15 (m, 2, OH and OCH), and 7.32—7.82 (m, 5, C_6H_5). The procuct **12** was identified by comparison with the authentic sample prepared by sodium periodate oxidation of hydroxy sulfide **3**.

5-Bromopentyl Phenyl Sulfone (13). This was obtained as an oil in 37% yield. IR 1310, 1150 cm^{-1} (νSO_2). NMR ($CDCl_3$)=δ 1.72 (d, 3, J=4 Hz), 1.96 (m, 4, CH_2CH_2), 3.20 (m, 2, SO_2CH_2), 4.10 (m, 1, BrCH), and 7.60—7.78 (m, 5, C_6H_5). Found: C, 45.51; H, 5.31; S, 11.65%. Calcd for $C_{11}H_{15}BrO_2S$: C, 45.36; H, 5.15; S, 11.00%.

5-Bromohexyl Phenyl Sulfone (14). This was obtained as an oil in 62% yield. IR 1300, 1140 cm^{-1} (νSO_2). NMR ($CDCl_3$)=δ 0.87—2.37 (m, 9, $(CH_2)_3$ and CH_3), 2.92—3.37 (m, 1, BrCH), 3.53 (t, 2, J=7 Hz, SO_2CH_2), and 7.47—8.30 (m, 5, C_6H_5). Found: C, 47.48; H, 5.54%. Calcd for $C_{12}H_{17}BrO_2S$: C, 47.21; H, 5.62%.

1-Phenyl-7-phenylsulfinyl-1-heptanone (15). The oxidation of **5** was carried out at −75 °C. After evaporation of methylene chloride, the residue was treated with ether (50 ml) and aqueous ammonium fluoride (4 g/50 ml) with stirring. The resulting solid was filtered and the filtrate was washed with water and dried over magnesium sulfate. Evaporation of ether followed by cooling with a small amount of hexane gave white solids **15** (97%): mp 62—63 °C (hexane). IR 1675 cm^{-1} (νC=O), 1030 cm^{-1} (νS–O). NMR (CCl_4) δ= 1.1—2.0 (m, 8), 2.6—3.0 (m, 4), 7.2—7.7 (m, 8), and 7.8—8.0 (m, 2). Found: 72.36: H, 7.14; S; 10.40%. Calcd for $C_{19}H_{22}O_2S$: C, 72.57; H, 7.05; S, 10.18%. When the same reaction was carried out at room temperature, keto sulfoxide (**15**) was obtained in 99% yield.

Oxidation in the Presence of Lithium Bromide. To a mixture of hydroxy sulfide **3** (0.35 g, 1.8 mmol), HBD (2.3 ml, 4.5 mmol), and lithium bromide (0.16 g, 1.8 mmol) in chloroform (10 ml) was added dropwise a solution of bromine (3.96 mmol) in chloroform (10 ml) at −70 °C. Stirring was continued at −70 °C for 30 min and then at room temperature for 1 h. The usual work-up gave bromo sulfone **13** in 66% yield.

References

1) N. P. Jencks, "Catalysis in Chemistry and Enzymology," Mcgraw-Hill Book Co., New York (1969), Chap. 1.

2) For example, F. C. De Schryver, N. Boens, and J. Put, "Advances in Photochemistry," ed by J. N. Pitts, Jr., G. S. Hammond, and K. Golinick, John Wiley and Sones, New York (1977), Vol. 10, pp. 359—465.

3) Y. Ueno and M. Okawara, *Tetrahedron Lett.*, **1976**, 4597.

4) Y. Ueno, T. Inoue, and M. Okawara, *Tetrahedron Lett.*, **1977**, 2413.

5) In the oxidation using HBD–Br_2, Bu_3SnOBr might be a possible active oxidizing reagent. See, Refs. 3 and 4.

6) T. Durst, K. C. Tin, and M. J. V. Marcil, *Can. J. Chem.*, **51**, 1704 (1973).

7) D. J. Pasto, C. C. Cumbo, and P. Balasubramaniyan, *J. Am. Chem. Soc.*, **88**, 2187 (1966).

8) D. E. Ames, *J. Chem. Soc.*, **1963**, 4863.

9) M. Cinquini, S. Colonna, *Boll. Sci. Fac. Chim. Ind. Bologna*, **27**, 157 (1969).

Lithiation of Alkoxyalkyl Phenyl Sulfones. New Approach to Acyl Anion Synthesis

Kazuhiko TANAKA,* Syuichi MATSUI, and Aritsune KAJI
Department of Chemistry, Faculty of Science, Kyoto University, Sakyo-ku, Kyoto 606
(Received January 9, 1980)

(1-Ethoxyethoxy)methyl and 1-(1-ethoxyethoxy)ethyl phenyl sulfones undergo metalation with LDA in THF in the presence of HMPA. The resulting lithium salts were easily alkylated with various alkyl halides and hydrolyzed under mild conditions to give the corresponding carbonyl compounds. The new synthetic method for the preparation of aldehydes and ketones employing these carbanions has been developed.

The potential usefulness of sulfur-stabilized carbanions as acyl anion equivalents has been widely recognized.[1] The commonly used "umpolung" reagents include 1,3-dithianes,[2] alkyl alkylthiomethyl sulfoxides,[3,4] vinyl sulfides,[5] dithioesters,[6] and ketene dithioacetals.[7] Few methods exist, however, for the analogous acyl anion equivalents involving an α-sulfonyl carbanion.[8] Recently, Kondo *et al.* and Julia *et al.* reported a route to α,β-unsaturated carbonyl compounds employing the lithium salts of sulfonyl ketone acetals as β-acylvinyl anion equivalents.[9] Most recently, Gokel *et al.* found that the lithio derivative of 4,4-dimethyl-1,3-oxathiolane 3,3-dioxide reacted with alkyl halides to give aldehydes by pyrolysis.[10] An α-hydroxy sulfone, as well as α,β-epoxy sulfones and cyanohydrins, gives readily a carbonyl compounds under basic conditions.[11]

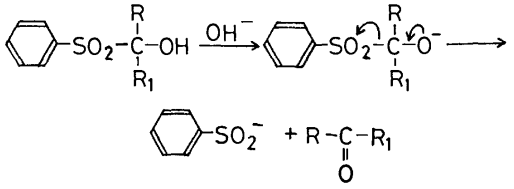

Therefore, the alkylation of the carbanion of α-alkoxy sulfone (**1**) might provide a new method for the syntheses of aldehydes and ketones from alkyl halides.

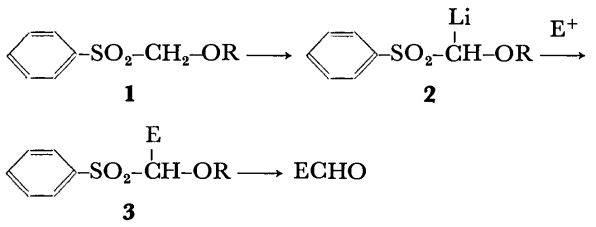

Unfortunately, Magnus and Schank have failed in the alkylation of the carbanion **2** except deuteration and methylation,[8,12] while we have found that the hitherto unknown lithium salts of (1-ethoxyethoxy)methyl phenyl sulfone (**4a**) and 1-(1-ethoxyethoxy)ethyl phenyl sulfone (**4b**) can be successfully generated and are reactive towards alkyl halides. Presumably, the carbanions of **4a** and **4b**, the ethoxyethoxyl group of which was introduced to protect the hydroxyl group, would be advantageously stabilized by the internal lithium chelation.[13] In this report we shall describe the results of our recent work on the use of lithium derivatives (**5a** and **5b**) as acyl anion equivalents.

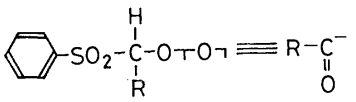

Results and Discussion

Alkylation of Carbanion **5**. Treatment of α-alkoxyalkyl phenyl sulfone (**4**) with lithium diisopropylamide (LDA) in THF at −78 °C in the presence of HMPA produced the yellow solution of carbanion (**5**).

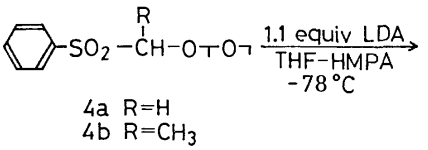

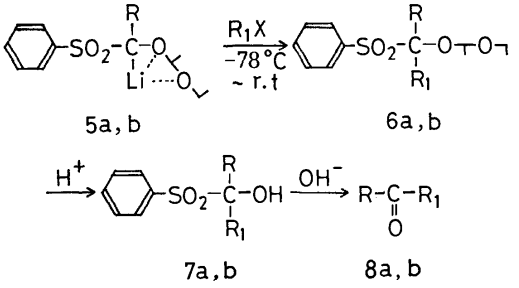

The anion of sulfone (**4**) was efficiently trapped with alkyl halides to provide the monoalkylated product (**6**), which was hydrolyzed to afford aldehydes or ketones in moderate to good isolated yields (Table 1).

Since the elimination of benzenesulfinic acid from the product (**7**) occurs under mild basic conditions and does

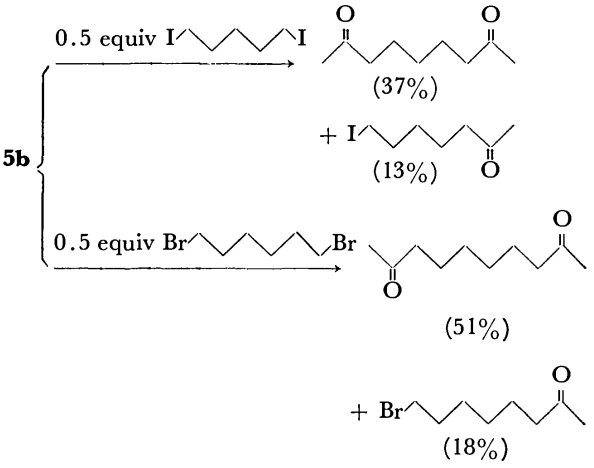

TABLE 1. PREPARATION OF ALDEHYDES AND KETONES FROM CARBANIONS (**5**) AND ALKYL HALIDES (R_1X)

Sulfone (5)	Halide R_1X	Product (8)	Yield %	Bp °C/Torr[a]	IR cm^{-1}	NMR (CCl_4, ppm)	Found(Calcd) C%	Found(Calcd) H%
5a	1-Iodohexane	$CH_3(CH_2)_5CHO$	71[b]	72.0/30	1720 (neat)	0.80—1.00 (m, 3H), 1.00—1.76 (m, 8H), 2.35 (t, J=7.0 Hz, 2H), 9.62 (t, J=2.0 Hz, 1H)	73.34 (73.63)	12.59 (12.36)
5a	1-Bromoheptane	$CH_3(CH_2)_6CHO$	54[b]		1710 (neat)	0.50—1.00 (m, 3H), 1.00—1.80 (m, 10H), 2.05 (t, J=7.0 Hz, 2H), 9.54 (t, J=2.0 Hz, 1H)	74.78 (75.00)	12.61 (12.50)
5a	1-Bromooctane	$CH_3(CH_2)_7CHO$	48[b,c]	92.0/32	1710 (neat)	0.69—0.90 (m, 3H), 1.00—1.40 (m, 12H), 2.17 (t, J=7.5 Hz, 2H), 9.60 (t, J=2.0 Hz, 1H)	75.74 (76.00)	13.15 (12.76)
5a	1-Bromononane	$CH_3(CH_2)_8CHO$	51[d]		1720 (neat)	0.76—1.02 (m, 3H), 1.02—1.82 (m, 14H), 2.43 (t, J=7.0 Hz, 2H), 9.70 (t, J=2.0 Hz, 1H)	76.83 (76.92)	12.92 (12.82)
5a	1-Bromodecane	$CH_3(CH_2)_9CHO$	53[b,e]	78.0/1	1720 (neat)	0.80—1.00 (m, 3H), 1.10—1.60 (m, 16H), 2.35 (t, J=7.0 Hz, 2H), 9.56 (t, J=2.0 Hz, 1H)	77.28 (77.65)	13.19 (12.94)
5b	1-Iodobutane	$CH_3C(=O)(CH_2)_3CH_3$	47[b]	40.0/32	1720 (neat)	0.80—1.00 (m, 3H), 1.12—1.68 (m, 4H), 2.04 (s, 3H), 2.40 (t, J=7.0 Hz, 2H)	71.73 (71.95)	12.11 (12.08)
5b	1-Iodohexane	$CH_3C(=O)(CH_2)_5CH_3$	53[b]	56.0/22	1710 (neat)	0.80—1.00 (m, 3H), 1.16—1.64 (m, 8H), 2.04 (s, 3H), 2.35 (t, J=7.5 Hz, 2H)	74.63 (75.00)	12.94 (12.50)
5b	1-Bromohexane	$CH_3C(=O)(CH_2)_5CH_3$	46[b] (31)[d,f]					
5b	1-Bromoheptane	$CH_3C(=O)(CH_2)_6CH_3$	55[b]		1720 (neat)	0.40—1.10 (m, 3H), 1.10—1.80 (m, 10H), 2.04 (s, 3H), 2.35 (t, J=7.0 Hz, 2H)	75.69 (76.06)	12.81 (12.68)
5b	1-Bromooctane	$CH_3C(=O)(CH_2)_7CH_3$	51[b]	49.5—50.0/4	1720 (neat)	0.80—1.00 (m, 3H), 1.12—1.68 (m, 12H), 2.06 (s, 3H), 2.34 (t, J=7.0 Hz, 2H)	77.05 (76.92)	12.69 (12.82)
5b	1-Bromononane	$CH_3C(=O)(CH_2)_8CH_3$	66[b,d]	88.0—89.0/10	1720 (neat)	0.70—0.95 (m, 3H), 0.95—1.60 (m, 14H), 2.04 (s, 3H), 2.35 (t, J=8.0 Hz, 2H)	77.69 (77.65)	13.43 (12.94)
5b	1-Bromodecane	$CH_3C(=O)(CH_2)_9CH_3$	51[b]		1720 (neat)	0.70—1.04 (m, 3H), 1.04—2.00 (m, 16H), 2.04 (s, 3H), 2.24 (t, J=7.5 Hz, 2H)	77.58 (78.26)	13.15 (13.04)

a) 133.322 Pa. b) Isolated yields. c) $CH_3(CH_2)_7C(=O)(CH_2)_7CH_3$ was isolated in 26% yield. d) GLPC yields. e) $CH_3(CH_2)_9C(=O)(CH_2)_9CH_3$ was isolated in 14% yield. f) Without HMPA.

not require the use of heavy metal, this sequence constitutes a useful preparation of aldehydes and ketones from alkyl halides. However, the overall yields of these syntheses are insufficient for a synthetic method, and secondary and cyclic halides could not be used successfully in these synthesis. It seems to be attributed to the steric hindrance of sulfonyl group.

The ketone synthesis employing **5b** is also applicable to certain α,ω-diketones. For example, 1,5-diiodopentane and 1,6-dibromohexane were converted to 2,8-nonanedione and 2,9-decanedione, respectively.

t-Butyl 1-bromooctanoate prepared from *t*-butyl acetate and 1,6-dibromohexane was converted to *t*-butyl 9-oxodecanoate, *i.e.*, a key intermediate of 9-oxodec-(*E*)-2-enoate.[14]

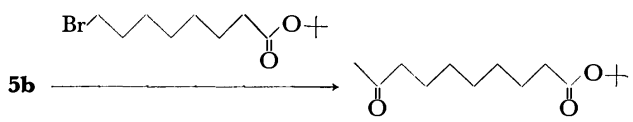

(27%)

Furthermore, the monoanion **9a** generated by potassium diisopropylamide–lithium *t*-butoxide (KDA)[15] reacted with ketone to afford hydroxy aldehyde,

Table 2. Preparation of symmetrical ketones from dianions (**10**) and alkyl halides (R_1X)

Halide R_1X	Product (**12**)	Yield %	Mp(Bp) °C(°C/Torr[a])	IR cm^{-1}	NMR (CCl_4, ppm)	Found(Calcd) C%	Found(Calcd) H%
1-Bromobutane	$CH_3(CH_2)_3C(CH_2)_3CH_3$ ‖ O	52[b]	(78.0/30)	1720 (neat)	0.64—0.96 (m, 6H), 1.08—1.64 (m, 8H), 2.30 (t, J=7.5 Hz, 4H)	76.32 (76.06)	12.77 (12.68)
1-Bromohexane	$CH_3(CH_2)_5C(CH_2)_5CH_3$ ‖ O	55[b]	31.5	1720 (KBr)	0.70—1.00 (m, 6H), 1.00—2.10 (m, 16H), 2.28 (t, J=7.0 Hz, 4H)	78.52 (78.79)	13.38 (13.13)
1-Bromoheptane	$CH_3(CH_2)_6C(CH_2)_6CH_3$ ‖ O	72[b]	40.0—40.5	1710 (KBr)	0.70—1.10 (m, 6H), 1.10—1.80 (m, 20H), 2.32 (t, J=7.0 Hz, 4H)	79.83 (79.65)	13.15 (13.27)
1-Bromooctane	$CH_3(CH_2)_7C(CH_2)_7CH_3$ ‖ O	52[b]	52.0—53.0	1710 (KBr)	0.80—1.00 (m, 6H), 1.00—1.80 (m, 24H), 2.30 (t, J=7.0 Hz, 4H)	80.02 (80.31)	13.47 (13.39)
1-Bromodecane	$CH_3(CH_2)_9C(CH_2)_9CH_3$ ‖ O	72[b]	61.0—62.0	1710 (KBr)	0.80—1.00 (m, 6H), 1.16—1.72 (m, 32H), 2.28 (t, J=7.5 Hz, 4H)	80.88 (81.29)	13.71 (13.55)
1,5-Dibromopentane	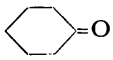	70[b]	(65.0/36)	1700 (neat)	1.50—2.10 (m, 6H), 2.20—2.50 (m, 4H)	73.27 (73.47)	10.12 (10.20)

a) 133.322 Pa. b) Isolated yields.

whereas the monoanion **5a** generated by LDA could not be used successfully in the reaction. For example, treatment of **9a** with 4-heptanone in THF produced 2-hydroxy-2-propylpentanal in 63% yield.

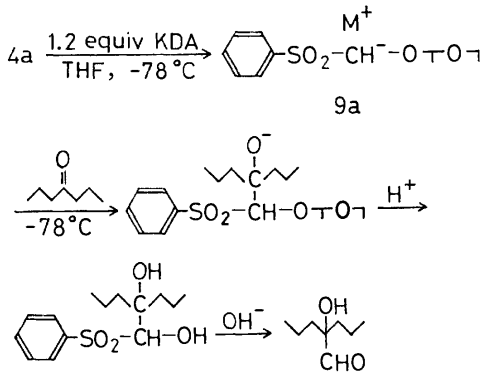

Formation and Alkylation of Dianion ***10***. The dianion of (1-ethoxyethoxy)methyl phenyl sulfone (**4a**) was successfully generated on treatment with 2.2 equiv. of LDA in THF in the presence of HMPA. The dianion thus formed reacted with alkyl halides to give symmetrical ketones **13** in good yields (Table 2).

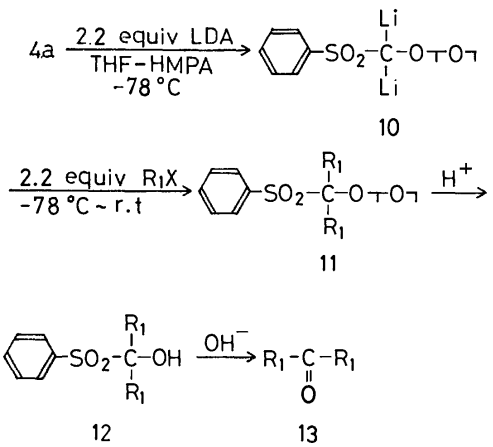

Since it was expected that **4a** is alkylated stepwise with the different kinds of alkyl halides, the unsymmetrical ketone synthesis from **4a** was carried out according to the following route.

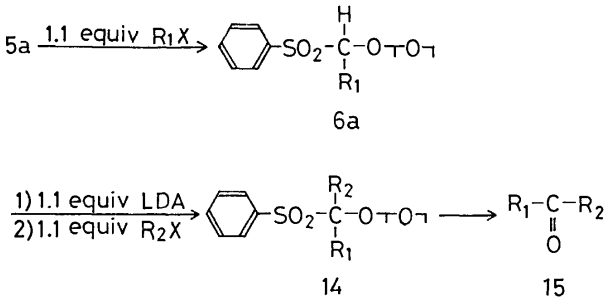

The use of 1-bromohexane as R_1X and bromoethane as R_2X afforded a mixture of ethyl hexyl ketone (14%), diethyl ketone (14%) and dihexyl ketone (37%). The low yield of the desired ketone **15** may be attributable to a predominant deprotonation of **6a** with **5a** followed by alkylation with R_1X.

Experimental

Melting points were determined with a Yanagimoto melting point apparatus and are uncorrected. Boiling points were determined during distillation and are uncorrected, Infrared data were obtained using a Hitachi Model 215 spectrophotometer. The proton magnetic resonance spectra were determined on a JEOL PS-100 spectrometer. Chemical shifts are given in δ units, part per million relative to tetramethylsilane as an internal standard.

*(1-Ethoxyethoxy)methyl Phenyl Sulfone (**4a**).* Hydroxymethyl phenyl sulfone was prepared from formaldehyde and benzenesulfinic acid by the reported procedure.[16] To a solution of hydroxymethyl phenyl sulfone (68.0 g, 0.40 mol) in the presence of *p*-toluenesulfonic acid (0.40 g) in 200 ml of dichloromethane at 0 °C was added dropwise a solution of ethyl vinyl ether (0.53 mol) in 100 ml of dichloromethane. The reaction mixture was stirred at 0 °C for 3 h and extracted

with dichloromethane. The combined organic layers were washed successively with water, saturated aqueous solution of sodium hydrogencarbonate, and water, and dried (Na_2SO_4). Removal of the solvent under reduced pressure gave a yellow oil (90.0 g, 92%). Purification by alumina (Woelm B-Super 1) column chromatography (benzene) gave **4a** (50.8 g, 52%) as a colorless oil; IR (neat): 1070, 1140, and 1300 cm^{-1}. ^1H-NMR (CCl_4): δ 1.08 (t, J=6.8 Hz, 3H), 1.20 (*d*, J=6.8 Hz, 3H), 3.20—3.70 (m, 2H), 4.50 (s, 2H), 4.90 (q, J=6.8 Hz, 1H), 7.40—8.00 (aromatic, 5H). Found: C, 54.32; H, 6.69%. Calcd for $C_{11}H_{16}O_4S$: C, 54.08; H, 6.60%.

1-(1-Ethoxyethoxy)ethyl Phenyl Sulfone (4b). 1-Hydroxyethyl phenyl sulfone was prepared by stirring an ethereal solution of benzenesulfinic acid with excess acetaldehyde at 0 °C for 9 h. A solution of ethyl vinyl ether (18.5 g, 0.26 mol) in dichrolomethane (20 ml) was added to a solution 1-hydroxyethyl phenyl sulfone (37.2 g, 0.20 mol) in the same solvent (100 ml) in the presence of catalytic amount of *p*-toluenesulfonic acid (0.20 g). The reaction mixture was stirred at 0 °C for 3 h and extracted with dichloromethane. The subsequent work-up was carried out by the same procedure as described in the preparation of **4a** to give a yellow oil. Purification by alumina (Woelm B-Super 1) column chromatography (benzene) gave **4b** (30.0 g, 60%) as a pale yellow oil; IR (neat): 1300, 1140, and 1080 cm^{-1}. ^1H-NMR (CCl_4): δ 1.12 (t, J=6.8 Hz, 3H), 1.32 (d, J=6.7 Hz, 6H), 3.30—4.00 (m, 2H), 4.38 (q, J=6.7 Hz, 1H), 4.90 (q, J=6.7 Hz, 1H), 7.30—7.90 (aromatic, 5H). Found: C, 55.53; H, 6.44%. Calcd for $C_{12}H_{18}O_4S$: C, 55.82; H, 6.98%

General Procedure. Reaction of the Carbanion 5a with 1-Iodohexane: To a solution of LDA (22 mmol) in a mixture of 80 ml of THF and 4 ml of HMPA at −78 °C was added dropwise under nitrogen a solution of **4a** (20 mmol) in 10 ml of dry THF. After stirring for 1 h, a solution of 1-iodohexane (30 mmol) in 10 ml of dry THF was added dropwise. The reaction mixture was stirred at −78 °C for 2 h and at room temperature for 16 h. After quenching with methanol, the reaction mixture was treated with 2 mol dm^{-3} hydrochloric acid (150 ml) for 1 h and extracted with ether. The combined ethereal layers were treated with an aqueous sodium hydrogencarbonate solution (40 mmol) for 4 h and dried (Na_2SO_4). Removal of the solvent and distillation under reduced pressure gave 1.62 g (71%) of heptanal.

2,9-Decanedione: Mp 57.0—57.5 °C. IR (KBr): 1710 cm^{-1}. ^1H-NMR (CCl_4): δ 1.10—1.70 (m, 8H), 2.06 (s, 6H), 2.36 (t, J=7.8 Hz, 4H). Found: C, 70.31; H, 10.77%. Calcd for $C_{10}H_{18}O_2$: C, 70.59; H, 10.59%.

2,8-Nonanedione: Mp 47.5—48.0 °C. IR (KBr): 1720 cm^{-1}. ^1H-NMR (CCl_4): δ 1.00—1.70 (m, 6H), 2.08 (s, 6H), 2.38 (t, J=7.0 Hz, 4H).

t-*Butyl 9-Oxodecanoate*: Bp 97.0—98.0 °C/146.7 Pa. IR (neat): 1720 cm^{-1}. ^1H-NMR (CCl_4): δ 1.10—1.70 (m, 19H), 2.00 (s, 3H), 2.16 (t, J=7.0 Hz, 2H), 3.34 (t, J=7.0 Hz, 2H). Found: C, 69.17; H, 11.08%. Calcd for $C_{14}H_{26}O_3$: C, 69.42; H, 10.74%.

2-Hydroxy-2-propylpentanal: To a solution of potassium *t*-butoxide (2.52 g, 22 mmol) and diisopropylamine (3.1 ml, 22 mmol) in dry THF (60 ml) at −78 °C under nitrogen was added butyllithium (18 mmol). The mixture was stirred for 10 min at −78 °C, and a solution of **4a** (3.66 g, 15 mmol) in dry THF (10 ml) was added. After stirring at −78 °C for 10 min, a solution of 4-heptanone (2.57 g, 22 mmol) in dry THF (5 ml) was added, and the mixture was maintained at −78 °C for 1 h. The reaction was quenched with methanol (50 ml). The subsequent aqueous work-up was carried out by the same procedure as described previously to give a yellow oil. Chromatography on silica-gel column (hexane–benzene, 1 : 1, v/v) gave 1.36 g (63%) of 2-hydroxy-2-propylpentanal as a colorless oil; IR (neat): 3450 and 1720 cm^{-1}. ^1H-NMR (CCl_4): δ 0.60—1.90 (m, 14H), 3.45 (s, 1H), 9.40 (s, 1H). Found: C, 67.02; H, 10.90%. Calcd for $C_8H_{16}O_2$: C, 66.67; H, 11.11%.

Dihexyl Ketone: To a solution of LDA (44 mmol) in 80 ml of dry THF in the presence of HMPA (8 ml) at −78 °C was added dropwise under nitrogen a solution of **4a** (20 mmol) in 10 ml of dry THF. After stirring for 1 h, a solution of 1-bromohexane (44 mmol) in 10 ml of dry THF was added dropwise and the reaction mixture was stirred at −78 °C for 2 h and at room temperature for 16 h. The subsequent work-up was carried out by the same procedure to give yellow crystals. Recrystallization from ethanol gave 2.18 g (55%) of pure dihexyl ketone as white needles.

S. Matsui wishes to thank the Ministry of Education of Japan for a grant supporting his stay at Kyoto University.

References

1) D. Seebach and M. Kolb, *Chem. Ind. (London)*, **1974**, 687; B. T. Gröbel and D. Seebach, *Synthesis*, **1977**, 357; D. Seebach, *Angew. Chem.*, **81**, 690 (1969); D. Seebach, *Angew. Chem., Int. Ed., Engl.* **18**, 239 (1979); E. Block, "Reactions of Organosulfur Compounds," AcademicPress, New York (1978), p. 36; O. W. Lever, Jr., *Tetrahedron*, **32**, 1943 (1976).

2) D. Seebach and E. J. Corey, *J. Org. Chem.*, **40**, 231 (1975); D. Seebach, *Synthesis*, **1969**, 17, and references cited therein.

3) K. Ogura, N, Katoh, I. Yoshimura, and G. Tsuchihashi, *Tetrahedron Lett.*, **1978**, 375; K. Ogura and G. Tsuchihashi, *J. Chem. Soc., Chem. Commun.* **1970**, 1689; For excellent review see, K. Ogura, *J. Syn. Org. Chem. (Japan)*, **37**, 903 (1979).

4) J. E. Richman, J. L. Herrmann, J. E. Richman, and R. H. Schlessinger, *Tetrahedron Lett.*, **1973**, 3271; K. Ogura and G. Tsuchihashi, *Bull. Chem. Soc. Jpn.*, **45**, 2203 (1972); K. Ogura and G. Tsuchihashi, *Tetrahedron Lett.*, **1971**, 3151; K. Ogura and G. Tsuchihashi, *J. Am. Chem. Soc.*, **96**, 1960 (1974).

5) K. Oshima, K. Shimoji, H. Tsukashi, H. Yamamoto, and H. Nozaki, *J. Am. Chem. Soc.*, **95**, 2694 (1973).

6) A. I. Meyers, T. A. Tait, and D. L. Comins, *Tetrahedron Lett.*, **1978**, 4657.

7) M. Braun and D. Seebach, *Chem. Ber.*, **109**, 669 (1976).

8) P. D. Magnus, *Tetrahedron*, **33**, 2019 (1977).

9) K. Kondo and D. Tsunemoto, *Tetrahedron Lett.*, **1975**, 1007; M. Julia and B. Badet, *Bull. Soc. Chim. Fr.*, **1974**, 1363.

10) G. W. Gokel, H. M. Gerdes, D. E. Miles, J. M. Hufnal, and G. A. Zerby, *Tetrahedron Lett.*, **1979**, 3375.

11) F. de Reinach-Hiztzbuch and T. Durst, *Tetrahedron Lett.*, **1976**, 3677; A. D. Barone, D. L. Snitman, and D. S. Watt, *J. Org. Chem.*, **43**, 2066 (1978); G. Stork and L. Maldonaldo, *J. Am. Chem. Soc.*, **93**, 5286 (1971).

12) K. Schank, H. -G. Schmitt, F. Schroeder, and A. Weber, *Justus Liebigs Ann. Chem.*, **1977**, 1116.

13) A. I. Meyers and P. J. Reider, *J. Am. Chem. Soc.*, **101**, 2501 (1979).

14) B. M. Trost, T. N. Salzmann, and K. Hiroi, *J. Am. Chem. Soc.*, **98**, 4887 (1976).

15) S. Raucher and G. A. Koolpe, *J. Org. Chem.*, **43**, 3794 (1978).

16) H. Bredereck and E. Bäder, *Chem. Ber.*, **87**, 129 (1954).

The Conformations of Several Aliphatic Alcohols. The General Occurrence of the Attractive Alkyl/Phenyl Interaction

Jun UZAWA,† Shoji ZUSHI, Yoshio KODAMA, Yoshimasa FUKUDA, Ken NISHIHATA, Koshiro UMEMURA, Motohiro NISHIO,* and Minoru HIROTA††

Central Research Laboratories, Meiji Seika Kaisha, Ltd., Morooka, Kohoku, Yokohama 222
†*The Institute of Physical and Chemical Research, Wako 351*
††*Department of Applied Chemistry, Faculty of Engineering, Yokohama National University, Tokiwadai, Hodogaya, Yokohama 240*

(Received February 16, 1980)

The conformation has been studied, by means of NMR spectroscopy, for diastereoisomeric pairs of a series of alcohols having the following general structure:

$$CH_3CH(C_6H_5)CH(OH)\text{-}R$$

where R is a methyl, ethyl, isopropyl, or a *t*-butyl group. It has been demonstrated that the alkyl group (R) is oriented close to the phenyl group in the most preferred conformations; this conclusion is essentially in accord with the results obtained for the structurally related sulfoxides. The general occurrence of an attractive interaction (the CH/π interaction) has, therefore, been suggested between an alkyl and a phenyl group.

In recent years it has become clear that an alkyl group often prefers to be close to a phenyl group in certain molecular environments.[1-3] Thus, in compounds having the general structure of $C_6H_5CH(CH_3)$-X-Bu^t, the *t*-butyl group has been found to orient itself *gauche* to the phenyl group, and *anti* to the methyl group, present in the molecule (Fig. 1). The examples include a sulfide[4] (**1**, X=S), a diastereoisomeric pair of sulfoxides[5,6] (X=SO) and alcohols[2] (X=CHOH), a sulfone[4,7] ($X=SO_2$), a ketone[8,9] (X=CO), and a hydrocarbon[9] ($X=CH_2$). Evidence for the hydrocarbon rests on an empirical force-field calculation. The conclusions regarding the other compounds have, in every case, experimental bases (X-ray,[5,7] NMR,[2,5a,8,10] ORD/CD,[5a] dipole moment,[6] IR,[2,9] or product analysis in the stereoselective reactions[1,3,4,11]). We further studied the conformation of a series of diastereoisomeric sulfoxides (**2**), where the *t*-butyl group in the above structure (**1**, X=SO) is replaced by a methyl, ethyl, or isopropyl group.[12] In these cases also, the alkyl group has been shown to be *gauche* to the phenyl group and *anti* to the methyl group in their most preferred conformation (Fig. 2, rotamer **a**). In addition to this, a considerable fraction of the second stable rotamer (rotamer **b**) has been suggested to contribute, whereby the alkyl group is flanked by the phenyl and methyl group; the rotamer **c** seems to be least important.

To account for these findings, an attractive force has been suggested to operate between an alkyl and a phenyl group (CH/π interaction).[1-3] The nature of the weak secondary force remains open, however, we believe this to originate from a hydrogen-bond like interaction of a CH group with the π-system; this might also be regarded as a through-space hyperconjugation. In order to explore the generality of the phenomenon and to obtain insight into the nature of the interactions, the conformation has been studied for diastereoisomeric

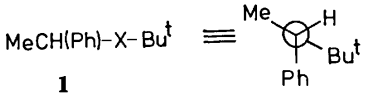

Fig. 1.

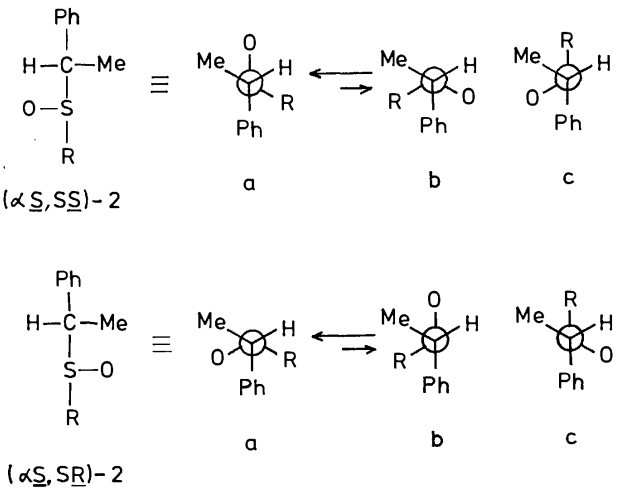

Fig. 2.

(a) *erythro* series

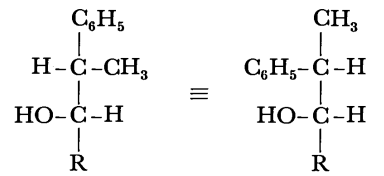

R = CH_3 (2*R*, 3*R*/2*S*, 3*S*: **3**-*er*)
C_2H_5 (2*R*, 3*R*/2*S*, 3*S*: **4**-*er*)
i-C_3H_7 (3*R*, 4*R*/3*S*, 4*S*: **5**-*er*)
t-C_4H_9 (3*R*, 4*S*/3*S*, 4*R*: **6**-*er*)

(b) *threo* series

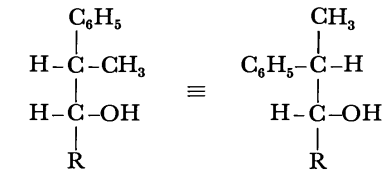

R = CH_3 (2*R*, 3*S*/2*S*, 3*R*: **3**-*th*)
C_2H_5 (2*R*, 3*S*/2*S*, 3*R*: **4**-*th*)
i-C_3H_7 (3*R*, 4*S*/3*S*, 4*R*: **5**-*th*)
t-C_4H_9 (3*R*, 4*R*/3*S*, 4*S*: **6**-*th*)

Fig. 3.

pairs of a series of alcohols (**3**—**6**), where the sulfoxide function in **2** is replaced by a CHOH group (Fig. 3).

Results

Tables 1 and 2 list the proton and carbon NMR data respectively for the diastereoisomeric pairs of alcohols;

Table 1. Proton NMR parameters[a] for the alcohol diastereoisomers $CH_3CH(C_6H_5)CHOH$–R

	Ar	H_a	Me	H_x	H_y	H_z	OH[b]	J_{ax}[c]
erythro								
3-*er*	7.23	2.63 (2.58)	1.30 (1.22)	3.82 (3.74)	1.07 (0.93)	—	1.82	6.5 (6.7)
4-*er*	7.21	2.75	1.30	3.54	1.39	0.91	1.93	6.5
5-*er*	7.20	2.85	1.28	3.35	1.54	0.88 0.90	1.93	6.5
6-*er*	7.18	2.97	1.27	3.37	—	0.92	2.03	3.7
threo								
3-*th*	7.26	2.66 (2.61)	1.26 (1.22)	3.82 (3.68)	1.19 (1.08)	—	1.57	6.5 (6.3)
4-*th*	7.28	2.74	1.25	3.55	1.54	0.97		6.5
5-*th*	7.30	2.83	1.23	3.39	1.75	0.93 1.01		6.5
6-*th*	7.23	2.98	1.36	3.34	—	0.84		3.9

a) The chemical shifts are reported in ppm downfield from internal TMS ($CDCl_3$). The data in parentheses are those reported in Ref. 14 for CCl_4 solutions. b) The peaks attributed to the OH proton (δ as well as the line shape) are sensitive to the conditions. c) Approximate values; the data are reported in Hz.

Table 2. Carbon NMR parameters for the diastereoisomeric alcohols $CH_3CH(C_6H_5)CH(OH)$–R

	1	2,6	3,5	4	7	8	9	10		11	Δ[a]
erythro series											
3-*er*	144.3	127.8	128.3	126.3	47.2	72.3	16.2			21.0	
4-*er*	144.7	127.7	128.3	126.2	45.4	77.6	27.6	10.4		15.8	
5-*er*	145.2	127.6	128.4	126.1	42.8	81.0	30.1	16.6	20.0	15.8	
6-*er*[b]	148.0	127.4	128.3	125.9	41.1	82.9	36.1	26.8		16.5	
threo series											
3-*th*	143.5	128.0	128.5	126.6	47.9	72.3	17.8			20.5	(+0.5)
4-*th*	143.5	128.1	128.5	126.5	45.6	77.2	27.2	10.0		17.9	(−2.1)
5-*th*	144.0	128.1	128.5	126.5	43.4	80.4	29.9	15.3	20.4	18.6	(−2.8)
6-*th*[b]	144.1	128.8	128.2	126.3	41.7	83.4	35.9	26.7		22.4	(−5.9)

a) $\Delta = \delta(erythro) - \delta(threo)$. b) Taken from Ref. 2.

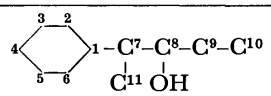

Table 3. The lanthanoid-induced shifts (LIS)[a] for the alcohol diastereoisomers $CH_3CH(C_6H_5)CH(OH)$–R

	Protons							Carbons								
	H_o	H_m	H_a	Me	H_x	H_y	H_z	1	2,6	3,5	4	7	8	9	10	11
erythro series																
3-*er*	0.18	0.07	0.39	0.20	0.61	0.35	—	0.27	0.21	0.11	0.09	0.47	(1.00)	0.49	—	0.27
4-*er*	0.17	0.06	0.39	0.21	0.63	0.38 0.32	0.21	0.27	0.20	0.10	0.09	0.48	(1.00)	0.48	0.28	0.29
5-*er*	0.14	0.06	0.41	0.24	0.64	0.31	0.28 0.20	0.24	0.16	0.10	0.08	0.51	(1.00)	0.48	0.32 0.28	0.34
6-*er*	0.17	0.01	0.35	0.32	0.65	—	0.25	0.25	0.16	0.05	0.04	0.52	(1.00)	0.47	0.28	0.39
threo series																
3-*th*	0.19	0.05	0.34	0.22	0.63	0.35	—	0.30	0.20	0.10	0.08	0.44	(1.00)	0.51	—	0.26
4-*th*	0.22	0.06	0.32	0.25	0.64	0.34	0.16	0.32	0.24	0.11	0.09	0.47	(1.00)	0.48	0.24	0.30
5-*th*	0.25	0.05	0.32	0.26	0.63	0.36	0.17 0.16	0.34	0.25	0.12	0.09	0.50	(1.00)	0.47	0.28 0.21	0.33
6-*th*	0.29	0.06	0.29	0.26	0.65	—	0.18	0.35	0.26	0.13	0.11	0.50	(1.00)	0.43	0.24	0.33

a) The chemical shifts induced by the addition of $Yb(fod)_3$ to $CDCl_3$ solutions. The data are normalized to the value for C(8) carbon ($LIS_{rel} = 1.00$). See Tables 1 and 2 for the numbering of the nuclei.

3-phenyl-2-butanols (**3**), 2-phenyl-3-pentanols (**4**), and 2-methyl-4-phenyl-3-pentanols (**5**). Table 3 lists the lanthanoid-induced shifts (LIS) determined for the proton and carbon resonances. The data for the diastereoisomers of 2,2-dimethyl-4-phenyl-3-pentanol (**6**)[2] are also included for the purpose of comparison. In Figs. 4—6 are reproduced parts of the proton NMR spectra of these alcohols (**3**—**5**).

An inspection of the NMR spectra reveals several interesting features. First, the peaks attributed to the proton α to the hydroxyl group (labeled H_x) are broader in the *threo*[13] alcohols (Figs. 5b and 6b) than in the *erythro* series, and in these cases we did not find any signal appropriate to the hydroxyl proton. Quite a similar result has also been reported for the *t*-butyl homologues (**6**; see Fig. 8 in Ref. 2). The spectrum for a methyl homologue (**3**-*th*; Fig. 4b) is the only exception; here we found a quintet for H_x and a sharp singlet for the hydroxyl proton (sharper than that in **3**-*er*). Second, the peaks assignable to the benzylic proton (H_a) appear, in all cases, as a quintet with an intensity ratio of 1 : 4 : 6 : 4 : 1. This implies that the spin-spin coupling constants between H_x and H_a ($^3J_{H_aH_x}$) are similar to each other among the alcohols examined and that they are not far from the value of 6.5 Hz.[14] This is quite in contrast to the observation for the *t*-butyl homologues (**6**-*er* and **6**-*th*), where $^3J_{HH}$ has been found to be *ca.* 4 Hz in both

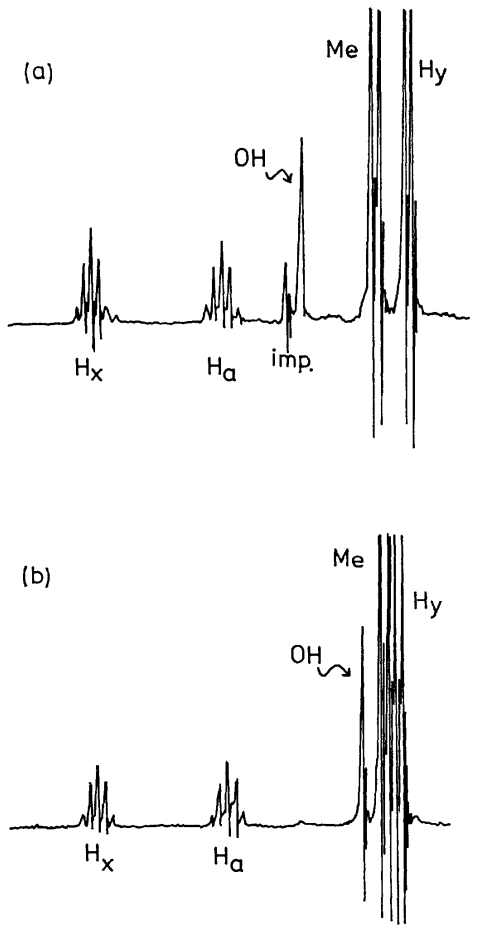

Fig. 4. Proton NMR spectra of (a) **3**-*er* and (b) **3**-*th* obtained for CCl_4 solutions.

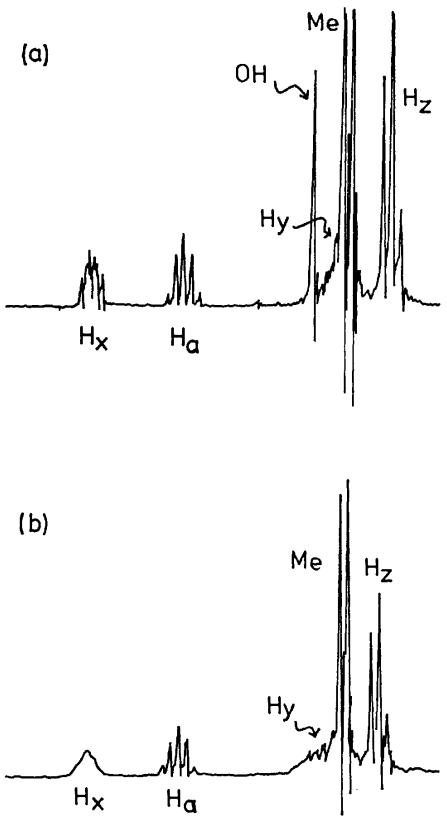

Fig. 5. Proton NMR spectra of (a) **4**-*er* and (b) **4**-*th* obtained for CCl_4 solutions.

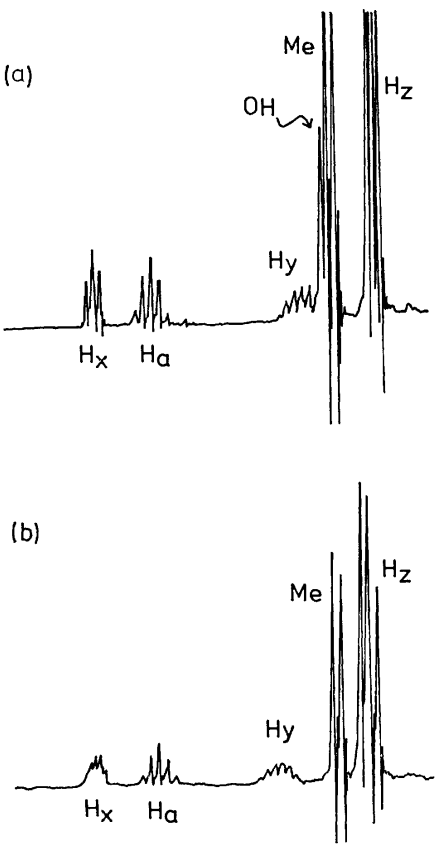

Fig. 6. Proton NMR spectra of (a) **5**-*er* and (b) **5**-*th* obtained for CCl_4 solutions.

cases.[2]

We then carried out the computer-simulation of the LIS[15] for these alcohols; the procedure has been outlined in earlier papers.[2,10,12] The structural parameters were assumed to have the usual values. After several trials and a literature survey, the lanthanoid (Ln)–O–C angle was fixed at 130°.[16,17] The index, A, represents the degree of the distribution of the metal in a mixture of the lanthanoid–substrate complexes (at a given geometry of the substrate) in this equation: $w(\theta)=A/\sqrt{\pi}\ \exp[-A^2\ (\theta-\theta_0)^2]$. On steric grounds, θ_0 was set so that the LSR was always farthest from the phenyl group. A higher value of A, therefore, corresponds to a more localized lanthanoid distribution (centered at θ_0), while the free rotation of Ln in a complex is represented by $A=0$. The Ln–O distance (R) and the torsional angle around the C(7)–C(8) bond were then allowed to vary incrementally at a constant A, in order to search for a reasonable fit of the calculated LIS set [assuming the $(3\cos^2\chi_i-1)/r_i^3$ proportionality] with the observed ones. Figure 7 is a brief illustration of the above procedure; see Ref. 12 for the details.

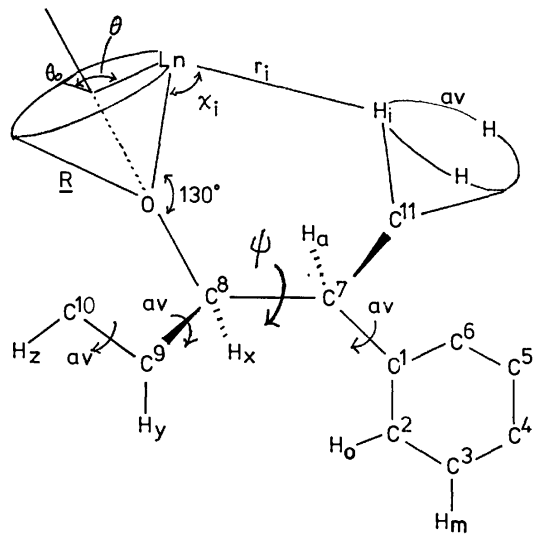

Fig. 7. The procedure for calculating the LIS; av. means the averaging about its rotation (30° increment).

The number of probes which can be used in this program (PSCONT) is limited to 9 nuclei. Therefore, we selected the LIS data which are most appropriate for the present purpose. The data for C(8), which is adjacent to the coordination site, were omitted in view of possible contamination from the contact shift.[18] The data for the β carbons (C7 and C9) should also be used with caution for a similar reason. In order to obtain a reliable result, it is better to use the LIS for the nuclei, the geometrical dispositions of which to the complexation site (OH group) vary with the rotation around the C(7)–C(8) bond. These include the aromatic protons and carbons, H_a, Me, and C(11). Thus, the data which we used for the computation are those for 5—6 protons (H_o and/or H_m; H_a, Me, H_x; H_y and/or H_z) and 3—4 carbons (Cl and/or C2, C3, C4; C9 or C10; and C11). The results have been shown to be rather insensitive to the choice of the probes if an appropriate precaution was taken. The deletion of the carbon LIS, for example, did not significantly affect the qualitative nature of the computed result. The inclusion of the data for C(7), C(8), and/or C(9) did not affect the results appreciably, either, suggesting that the contact shift is unimportant with an ytterbium complex.[18] The Hamilton reliability factor, $AF=[\sum_i(\mathrm{LIS}_i^{\mathrm{obsd}}-\mathrm{LIS}_i^{\mathrm{calcd}})^2/\sum_i(\mathrm{LIS}_i^{\mathrm{obsd}})^2]^{1/2}$, has been used to assess the agreement between the calculated and the observed LIS sets.[19] Figures 8 and 9 plot the AF against the R–C(8)–C(7)–C_6H_5 dihedral angle (ϕ) for these alcohols.[20] The data in Table 4 were extracted from an AF map (R *vs.* ϕ) for a representative case of Compound **5**-*er*.

It should be noted first that, for alcohols having the *erythro* configuration, the essential features of the curve are not significantly affected by a change in the value of A. The minimum AF has invariably been found at ϕ around 60°, accompanied with shallow minima at ϕ *ca.* 160° and 320°. The AF/ϕ profile for the *t*-butyl homologue (**6**-*er*) shows a distinct difference from those of the lower alkyl homologues. Thus, the R/Ph torsional angle at the best agreement is slightly shifted to a larger value ($\phi\approx80°$), while another, rather profound minimum appears at ϕ *ca.* 135°.

For the *threo* alcohols, **4**-*th*, **5**-*th*, and **6**-*th*, on the other hand, the shape of the profile has been shown to be rather sensitive to the value of A. There is a general tendency for a more reasonable agreement to be found with a higher value of the distribution index; this trend is reasonable on steric grounds.[2,10] In view of this,

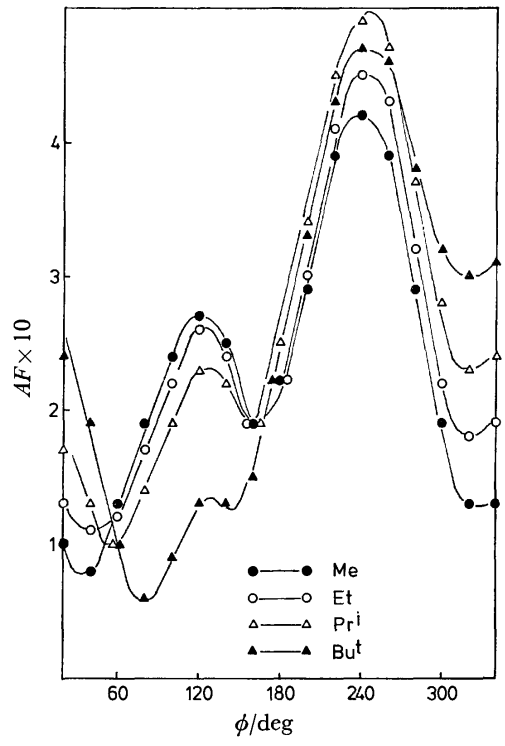

Fig. 8. Plots of AF *vs.* the R/Ph dihedral angle (ϕ) for the *erythro* alcohols, **3**-*er*, **4**-*er*, **5**-*er*, and **6**-*er*. The lanthanoid distribution index (A) and the Ln–O distance (R) are kept constant at 0.8 and 0.30 nm, respectively.

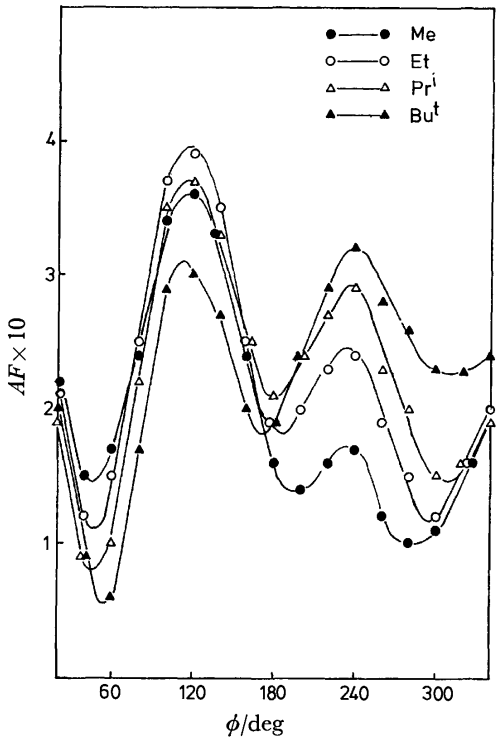

Fig. 9. Plots of *AF vs.* the R/Ph dihedral angle (ϕ) for the *threo* alcohols, **3**-*th*, **4**-*th*, **5**-*th*, and **6**-*th*. The LSR distribution index (A) and the Ln–O distance (R) are kept constant at 0.8 and 0.30 nm, respectively.

Table 4. A part of the *AF* (in %) maps for **5**-*er* (A=0.8; the monitor nuclei were H_a, Me, H_o, H_m, H_z, H_x, C4, C10, and C11)

	ϕ/deg				
R(nm)	20	40	60	80	100
0.26	45	43	28	21	25
0.28	28	25	18	16	21
0.30	17	13	10	14	19
0.32	11	6	7	12	18
0.34	11	7	8	12	18
0.36	14	12	11	13	19
0.38	17	16	13	14	19

we took the results obtained with a higher value of A as relevant; this is consonant with the experience with the sulfoxide analogues.[12] It is interesting that, in these cases also, the curves are always accompanied by three minima of unequal importance. The best fit has been recorded at ϕ *ca.* 50° for **5**-*th* and **6**-*th*, while the profile of **4**-*th* is accompanied with two minima of *ca.* an equal *AF* at $\phi \approx 45°$ and 300°. The profile for the methyl homologue (**3**-*th*) represents an exception. The curve is, in essence, insensitive to the change in A, and the best fit has been found at *ca.* 290°.

Discussion

Consideration of the LIS Results. It should be noted at first that the simulated conformations of the molecules represent the weighted-average geometries of the lanthanoid–substrate complex. A possibility remains that the complexation perturbs the rotameric equilibrium of the free substrate. However, for the presently studied alcohols, the vicinal coupling constant, $^3J_{H_aH_x}$, remained practically unchanged on the addition of the lanthanoid species. This clearly demonstrates that these molecules are conformationally unperturbed by the coordination.

The computation was carried out on the basis of the assumption that there is an unique contribution from a single conformer. Of course, this is not a correct description of the fact in general, but it represents an approximation. It should be noted that the *AF* in a profile corresponds to the reliability for the average geometry at a given ϕ and by no means represents the potential energy (or population) of the respective rotamer. A good fit may result, even with this simplest model, if a single, highly preferred rotamer is present in solution. A significant change for the *AF* would be accompanied, in such a case, with a slight modification in the substrate geometry. However, a geometry corresponding to the minimum *AF* does not necessarily reflect the most stable one if there are several conformers separated by a low free-energy barrier(s). In such a case, an *AF* minimum may represent the weighted-average geometry of the possible rotamers. In view of this, it is noteworthy that the *AF*/ϕ profiles (Figs. 8 and 9) have, in every case, three distinct minima, at ϕ around 60°, 180°, and 300° (*i.e.*, at the staggered geometries of the groups). It is likely that the location of ϕ and the goodness of fit at the respective minimum reflect, though in an indirect manner, the probable geometries of the substrates and the relative importance of the rotamers.

It is suggested that, for all of the alcohols with the *erythro* configuration, the rotamer with $\phi \approx 60°$ (rotamer **a** in Fig. 10) is most populated. In this rotamer, the alkyl group positions itself *gauche* to the phenyl and *anti* to the methyl group. A somewhat twisted conformation ($\phi \approx 80°$) is more plausible for the *t*-butyl homologue. The second stable one is suggested to be the rotamer **c** for **5**-*er* and **6**-*er*, while this is the rotamer **b** in the cases of the lower alkyl homologues (**3**-*er* and **4**-*er*). Note that, in the rotamer **b** the alkyl group is flanked by the methyl and phenyl groups.

In the case of the *threo* alcohols, **5**-*th* and **6**-*th*, the most stable conformation has been suggested to have an R/Ph dihedral angle of *ca.* 60°; the second most stable one seems to be the rotamer **b** for **5**-*th*, but the rotamer **c** for **6**-*th*. The rotamers **a** and **b** can be said to be equally stable for **4**-*th*. The conclusion, in essence, is the same as for the *erythro* alcohols. Thus, the alkyl group, in the preferred conformations, tends to be oriented close to the phenyl group in every case.

The methyl homologue with the *threo* configuration (**3**-*th*) represents an exceptional case. The *AF*/ϕ profile of this compound suggests that the rotamer **b** is most stable. The rotamers **a** and **c** seem to be relatively unimportant and to have an about equal stability. This trend is different from that of the other alcohols having the same (*threo*) configuration.[21] Consonant with this fact is the observation that the hydroxyl proton in **3**-*th* gives rise to a sharp singlet in the NMR

spectrum (*vide supra*). For the *threo* alcohols other than **3**-*th*, the OH peak is absent and the peaks assignable to H_x are broader than those for the *erythro* isomers. The disappearance of the OH proton signal as well as the broadening of the H_x peaks can be ascribed to the presence of the OH/π interaction for the *threo* alcohols.[2,22] Thus, for the *threo* isomers (**4**-*th*, **5**-*th*, and **6**-*th*) where the rotamer **a** (OH/Ph *gauche*) is the most important contributor, the exchange rate of the hydroxyl proton is expected to be slowed down. This likely causes the line broadening (and then disappearance) of the OH signal and the observance of the OH/H_x coupling. For the *erythro* alcohols, on the other hand, the OH group is mostly free from the OH/π complexation (OH/Ph *anti* in the rotamer **a**), thus giving rise to an observable peak. The above exceptional observation for the proton NMR of **3**-*th*, therefore, is in line with the conclusion that the most stable conformer has its OH group *anti* to the phenyl group (rotamer **b**). A question remains, however, as to the reconciliation of the present results with the IR finding[2,22] that the (seemingly) π-bonded OH peak at *ca.* 3595 cm^{-1} is very intense for **3**-*th* relative to those for the other alcohols. It is interesting, at all events, that the findings suggest that the alkyl (methyl) group lies close to the phenyl group in this case also.[23] Figure 10 summarizes the order of stability for the rotamers thus speculated. Note that the relative importance of the rotamers **a** : **b** : **c** varies systematically with a change in the alkyl substituent, R.

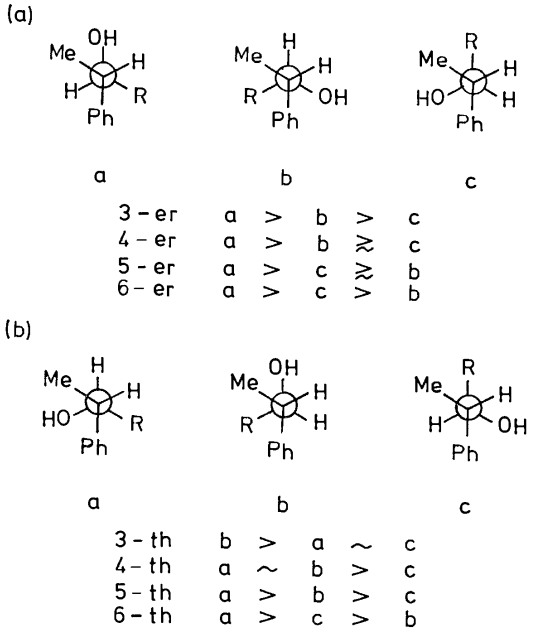

Fig. 10. Possible conformations and the proposed order of the rotamer stability for (a) *erythro* alcohols and (b) *threo* alcohols.

Consideration of the C-13 γ-Effect.[24] The methyl carbon (labeled C11) in **6**-*er* has been shown to be considerably more shielded relative to that in **6**-*th* [$\Delta = \delta(erythro) - \delta(threo) = 16.5 - 22.4 = -5.9$ ppm]. The above phenomenon has been interpreted in terms of the γ-*gauche* effect.[2] In the *erythro* alcohol, the OH group has been shown to be closer to the methyl group (OH/Me dihedral angle *ca.* 40° in the rotamer **a**) than in the *threo* isomer (*ca.* 60°) in their most preferred conformation (see Figs. 8 and 9); thus, the γ-*gauche* effect should be greater for the *erythro* alcohol (**6**-*er*). The result can also be understood in terms of the involvement of a second stable rotamer.[12] For **6**-*th*, the γ-effect (and therefore the shielding) would well be expected to decrease if an appreciable fraction of the rotamer **c** (OH/Me *anti*) is contributing, but this is not so for **6**-*er* (OH/Me *gauche* in the rotamer **c**).

An inverse trend would be expected to be observed for the lower alkyl homologues, for which the relative importance of the rotamer **b** has been suggested. In the rotamer **b**, the OH group is *anti* to Me for the *erythro* alcohols, but is *gauche* to Me for the *threo* isomers. Thus, an involvement of the rotamer **b** would result in the deshielding of the methyl carbon for the *erythro* alcohols, whereas the effect would be not significant for the *threo* alcohols. Therefore, a reversal in the sign of Δ may be observed; this is what we have found for the lower alkyl sulfoxides.[12] This, however, is not the case for the present cases of the ethyl and isopropyl-substituted alcohols. The chemical-shift difference between the isomers (Δ) has, in fact, been found to decrease for the ethyl and isopropyl homologues; however, a reversal in the sign of the shift difference has been recorded only in the case of the methyl homologues (see Table 2). This probably reflects an involvement of the rotamer **c**, but we must reserve further comment until more exact knowledge about the rotameric equilibria becomes available.

Consideration of the Vicinal Spin-Spin Coupling Constants. It has been shown that the spin coupling constant, $^3J_{H_aH_x}$, is about 6.5 Hz in all of the alcohols except the *t*-butyl homologues. The foregoing conclusion regarding the rotameric equilibria should be compatible with these data. A simple consideration of the Karplus relationship would require the vicinal coupling constant to be, *e.g.*, *ca.* 11 and 2 Hz respectively[25] for the **a** rotamers of the *erythro* alcohols (H/H *anti*) and of the *threo* ones (H/H *gauche*). A high preference of these conformers, therefore, cannot be an exact description of the fact. The rotamer **a** is, undoubtedly, the most populated one, but the contributions from the other rotamers should also be taken into account. In view of the limitation of the present methodology, only the perfectly staggered rotamers are considered in Fig. 10. As may be perceived by an inspection of the profiles, however, somewhat twisted versions of these conformations must be the real contributors. The above considerations are in line with the results obtained from the LIS-simulation and the C-13 γ-effect.

Possibility of the Attractive Alkyl/π-system Interaction. The importance of the attractive alkyl/phenyl interaction (CH/π interaction) and the consequences thereof have been argued in previous papers.[1-3,26] The suggestion has been made on the basis of some experimental findings and of a MO calculation. We believe that the findings reported here provide strong support for the above suggestion. Thus, in the conformations

which are found to be preferred, the alkyl group always orients itself close to the phenyl group, irrespective of the nature of the alkyl group and irrespective of the configuration. We feel further that the OH/π interaction is comparatively unimportant in controlling the conformation of these molecules. The van der Waals (repulsive as well as attractive[27]) and the CH/π interaction seem to be more important in the consideration of these problems.[28] The suggestion that the CH/π interaction may be more important than the OH/π interaction is in line with the HSAB (hard and soft acids and bases) principle[29] that a soft acid prefers to interact with a soft base. Thus, a phenyl group (more generally, a π-system) is a soft base, and the CH hydrogen is softer than OH as an acid. The stabilization energy has been estimated to be very small (*ca.* 3.5 kJ mol^{-1} or less)[1-3] for a single CH/π interaction. In spite of this, we suggest the possibility that the CH/π interaction plays an important role in determining molecular shapes and in controlling the subtle behavior of dynamically interacting systems. Generally, a CH group is present in a structure with some kinds of symmetry (methyl, isopropyl, long-chain alkyl groups, *etc.*). The total stabilization energy would thus become important by an accumulation of multiple CH/π bonds. Further, for obvious reasons, an interaction of this type (CH_3/π as well as CH_3/*n*; *n*=lone pair electrons) is entropically advantageous as compared to, *e.g.*, the OH/π interaction. In order to find support for the above suggestion and to ascertain the possible implication, efforts are currently being made in these laboratories.

Experimental

Materials. The alcohols studied in the present work were prepared as has been described in the literature.[14,22] The configurations of these alcohols have been elucidated by Cram,[30] Felkin,[22,31] Kingsbury,[14] and their groups.

NMR Measurements. The proton NMR spectra were recorded on a JEOL MH-100 spectrometer for *ca.* 0.2 M solutions in carbon tetrachloride. The LIS data (^1H and ^{13}C) were determined on a JEOL FX-100 instrument for *ca.* 0.2 M solutions in deuteriochloroform, using $Yb(fod)_3$[18] as the LSR. These values were found to be directly proportional to the LSR/substrate ratio up to a value of *ca.* 0.2 eq mol^{-1}.

References

1) M. Nishio, *Kagaku No Ryoiki*, **31**, 834, 998 (1977).

2) Y. Kodama, K. Nishihata, S. Zushi, M. Nishio, J. Uzawa, K. Sakamoto, and H. Iwamura, *Bull. Chem. Soc. Jpn.*, **52**, 2661 (1979).

3) Y. Kodama, K. Nishihata, M. Nishio, and N. Nakagawa, *Tetrahedron Lett.*, **1977**, 2105.

4) K. Nishihata and M. Nishio, *Tetrahedron Lett.*, **1977**, 1041.

5) a) Y. Kodama, K. Nishihata, M. Nishio, and Y. Iitaka, *J. Chem. Soc., Perkin Trans. 2*, **1976**, 1490; b) Y. Iitaka, Y. Kodama, K. Nishihata, and M. Nishio, *J. Chem. Soc., Chem. Commun.*, **1974**, 389.

6) M. Hirota, Y. Takahashi, M. Nishio, and K. Nishihata, *Bull. Chem. Soc. Jpn.*, **51**, 2358 (1978).

7) Y. Kodama, K. Nishihata, and M. Nishio, unpublished results.

8) S. Zushi, Y. Kodama, K. Nishihata, K. Umemura, M. Nishio, J. Uzawa, and M. Hirota, *Bull. Chem. Soc. Jpn.*, **53**, 3631 (1980).

9) M. Hirota, T. Sekiya, M. Nishio, and K. Nishihata, CSJ-ACS Meeting, Honolulu, April 1979, ORGN 091.

10) Y. Kodama, K. Nishihata, and M. Nishio, *J. Chem. Res. (S)*, **1977**, 102.

11) See also K. Nishihata and M. Nishio, *J. Chem. Soc., Perkin Trans. 2*, **1973**, 758; *Chem. Commun.*, **1969**, 51, **1970**, 1485.

12) Y. Kodama, S. Zushi, K. Nishihata, M. Nishio, and J. Uzawa, *J. Chem. Soc., Perkin Trans. 2*, **1980**, 1306.

13) To avoid confusion, we employ here the *threo/erythro* notations. The sequence-rule symbols do not necessarily relate to the stereochemically corresponding structures (see Fig. 3). Configurationally, the *threo* alcohols correspond to the *erythro* sulfoxides in Ref. 12.

14) C. A. Kingsbury and W. B. Thornton, *J. Org. Chem.*, **31**, 1000 (1966).

15) For the leading references on this subject, see a) "NMR Shift Reagents," ed by R. E. Sievers, Academic Press, New York (1973) and b) O. Hofer, *Top. Stereochem.*, **9**, 111 (1976).

16) J. D. Roberts, G. E. Hawkes, J. Husar, A. W. Roberts, and D. W. Roberts, *Tetrahedron*, **30**, 1833 (1974).

17) K. L. Williamson, D. R. Clutter, R. Emch, M. Alexander, A. E. Burroughs, C. Chua, and M. E. Bogel, *J. Am. Chem. Soc.*, **96**, 1471 (1974).

18) a) O. A. Gansow, P. A. Loeffler, R. E. Davis, M. R. Willcott, III, and R. E. Lenkinski, *J. Am. Chem. Soc.*, **95**, 3389, 3390 (1973); b) G. E. Hawkes, D. Leibfritz, D. W. Roberts, and J. D. Roberts, *ibid.*, **95**, 1661 (1973).

19) M. R. Willcott, III, R. E. Lenkinski, and R. E. Davis, *J. Am. Chem. Soc.*, **94**, 1742 (1972). The calculated shifts were normalized to the average experimental LIS in the computational process. In earlier papers,[2,10,12] we used a simpler function, $AF=\sum_i|LIS_i^{obsd}-LIS_i^{calcd}|/\sum_i LIS_i^{obsd}$, for the assessment of the agreement (the calculated LIS's were scaled to the largest experimental LIS). The results have been shown, in essence, to be independent of the error function used.

20) In these figures, the Ln–O distance was fixed at 0.30 nm, since the reasonable fit has invariably been found at *ca.* this value (if there are any solutions). We do not mean this to be the most correct one, but the above value is compatible with the available evidence.[15,16]

21) Note, however, that the relative importance of the rotamers varies systematically with a change in the substituent R; see Fig. 9.

22) J. Sicher, M. Chérest, Y. Gault, and H. Felkin, *Collect. Czech. Chem. Commun.*, **28**, 72 (1963).

23) The above conclusion regarding the conformational preferences of these alcohols agrees, in essence, with those of Felkin,[22] Kingsbury[14] and their groups.

24) D. M. Grant and B. V. Cheney, *J. Am. Chem. Soc.*, **89**, 5315 (1967); J. D. Roberts, F. J. Weigert, J. I. Kroschwitz, and H. J. Reich, *ibid.*, **92**, 1338 (1972).

25) M. Karplus, *J. Chem. Phys.*, **30**, 11 (1959); L. M. Jackman and D. P. Kelly, *J. Chem. Soc., B*, **1970**, 102.

26) M. Nishio, *Kagaku No Ryoiki*, **33**, 422 (1979).

27) R. E. Carter, B. Nilsson, and K. Olsson, *J. Am. Chem. Soc.*, **97**, 6155 (1975); R. E. Carter and P. Stilbs, *ibid.*, **98**, 7515 (1976).

28) The empirical force-field calculations for the above molecules are currently being made; the results will appear in a forthcoming paper.

29) R. G. Pearson, *Science*, **151**, 172 (1966); R. G. Pearson and J. Songstad, *J. Am. Chem. Soc.*, **89**, 1827 (1967).
30) J. L. Mateos and D. J. Cram, *J. Am. Chem. Soc.*, **81**, 2756 (1959).
31) M. Chérest, H. Felkin, and N. Prudent, *Tetrahedron Lett.*, **1968**, 2201; Y. Gault and H. Felkin, *Bull. Soc. Chim. Fr.*, **1965**, 742; H. E. Audier, H. Felkin, M. Fetizon, and W. Vetter, *ibid.*, **1965**, 3236.

The Conformations of 2-Phenylpropionaldehyde and Some Aliphatic Ketones. The Possible Importance of the CH/π and CH/n Interactions in Determining the Molecular Geometry of a Mobile System

Shoji Zushi, Yoshio Kodama, Ken Nishihata, Koshiro Umemura, Motohiro Nishio,* Jun Uzawa,† and Minoru Hirota††

Central Research Laboratories, Meiji Seika Kaisha, Ltd., Morooka, Kohoku, Yokohama 222
†*The Institute of Physical and Chemical Research, Wako, Saitama 351*
††*Department of Applied Chemistry, Faculty of Engineering, Yokohama National University, Tokiwadai, Hodogaya, Yokohama 240*

(Received April 19, 1980)

The conformations have been studied by means of NMR spectroscopy, largely by the computer simulation of the lanthanoid-induced shifts, for a series of aliphatic carbonyl compounds with the following structures: $CH_3CH(C_6H_5)CO$–R; R=H, CH_3, C_2H_5, i-C_3H_7, and t-C_4H_9. It has been suggested that two rotamers are important in the conformational equilibria of these ketones, in which the R–C–C–C_6H_5 dihedral angle is *ca.* 30° and *ca.* 90°. The relative stability of the above two rotamers has been found to depend on the nature of the alkyl group, R. The results have been discussed in light of the possible weak attractive forces, the CH/π and CH/n interactions.

In connection with the interest described in the preceding paper,[1] we have now studied the conformation of a series of acyclic carbonyl compounds with the following structures:

$$CH_3CH(C_6H_5)CO\text{–}R$$

R = H(**1**), CH_3(**2**), C_2H_5(**3**), i-C_3H_7(**4**), t-C_4H_9(**5**).

Results

Tables 1 and 2 list the proton and carbon NMR data, respectively, for 2-phenylpropionaldehyde (**1**), 2-phenyl-3-butanone (**2**), 2-phenyl-3-pentanone (**3**), 2-methyl-4-phenyl-3-pentanone (**4**), and 2,2-dimethyl-4-phenyl-3-pentanone (**5**).

Table 1. Proton chemical shifts[a] for the $CH_3CH(C_6H_5)CO$–R ketones

R		H_z	H_y	Me	H_a	H_m	H_o	H_{ald}[b]
H	(**1**)	—	—	1.40	3.58	7.44	7.32	9.63
Me	(**2**)	—	2.01	1.37	3.70	7.21	7.19	—
Et	(**3**)	0.95	2.35	1.38	3.73	7.20	7.20	—
Pr^i	(**4**)	0.90 1.06	2.66	1.36	3.89	7.20	7.20	—
Bu^t	(**5**)	1.09	—	1.38	4.26	7.26	7.26	—

a) Ppm downfield from internal TMS in $CDCl_3$.
b) The aldehydic proton. $^3J_{H_aH_{ald}} \approx 1.4$ Hz.

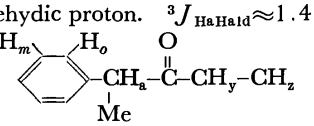

The Computer Simulation of the Lanthanoid-induced Shifts. The conformations of these compounds have been studied according to the method described in the preceding paper. For the present purpose of simulating the conformation of a ketone, a modification is necessary for the lanthanoid-distribution parameter. In the case of a carbonyl compound, the LSR can be assumed to be distributed, practically, only in the plane of the C=O double bond and to orient itself toward the lone-pair electrons on the carbonyl oxygen atom; the rationale for this approach has been presented by Montaudo and his co-workers.[2] Here, we used an index, p, the molar fraction of the Type **a** complex in Fig. 1, for describing the proportions of the diastereoisomeric LSR-ketone complexes. The input data were the atomic coordinates (standard values) and the experimental LIS's (Table 3) for the appropriate nuclei. The lanthanoid (Ln)–O–C angle (ω) was fixed at 140.[2b] The Ln–O distance (R) and the R–C(8)–C(7)–Ph dihedral angle (ϕ) were then varied, step by step, at a given LSR-distribution parameter (p) in order to search for the most reasonable fit of the computed LIS's with the observed ones. The number of the monitor nuclei were 9.[1]

Figure 2 plots the agreement factors (AF) against

Table 2. Carbon chemical shifts[a] for the $CH_3CH(C_6H_5)CO$–R ketones

R		1	2,6	3,5	4	7	8	9	10	11
H	(**1**)	137.7	128.3	129.0	127.4	52.9	200.8	—	—	14.6
Me	(**2**)	140.6	127.8	129.0	127.1	53.7	208.5	28.3	—	17.2
Et	(**3**)	140.9	127.8	128.8	127.0	52.7	211.2	34.2	8.0	17.5
Pr^i	(**4**)	140.7	127.9	128.8	127.0	51.1	214.4	39.2	18.3 19.2	18.2
Bu^t	(**5**)	141.4	127.6	128.5	126.7	46.4	215.7	45.1	26.6	21.1

a) Ppm downfield from internal TMS in $CDCl_3$.

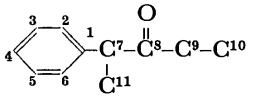

Table 3. The lanthanoid-induced shifts[a] for the $CH_3CH(C_6H_5)CO$–R ketones

R		H_o	H_m	H_a	Me	H_{ald}	H_y	H_z	1	2,6	3,5	4	7	8	9	10	11
H	(**1**)	0.11		0.27	0.22	0.52	—	—	0.22	0.15	0.11	0.08	0.39	1.00	—	—	0.24
Me	(**2**)	0.16		0.27	0.23	—	0.31	—	0.23	0.15	0.1	0.08	0.38	1.00	0.46	—	0.27
Et	(**3**)	0.13	0.06	0.27	0.23	—	0.26	0.20	0.25	0.22	0.19	0.11	0.44	1.00	0.44	0.36	0.31
Pr^i	(**4**)	0.13	0.06	0.26	0.22	—	0.25	0.20 0.16	0.26	0.18	0.1	0.06	0.42	1.00	0.42	0.26 0.25	0.32
Bu^t	(**5**)	0.22	0.03	0.26	0.25	—	—	0.18	0.27	0.20	0.09	0.07	0.46	1.00	0.44	0.24	0.32

a) The chemical shifts induced by the addition of $Yb(fod)_3$ in $CDCl_3$ solutions. The data are normalized to the value for C(8) carbon ($LIS_{rel}=1.00$). See Tables 1 and 2 for the numbering of the nuclei.

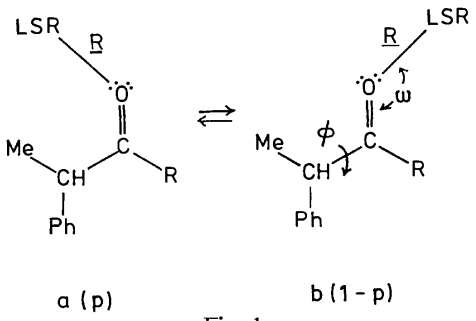

Fig. 1.

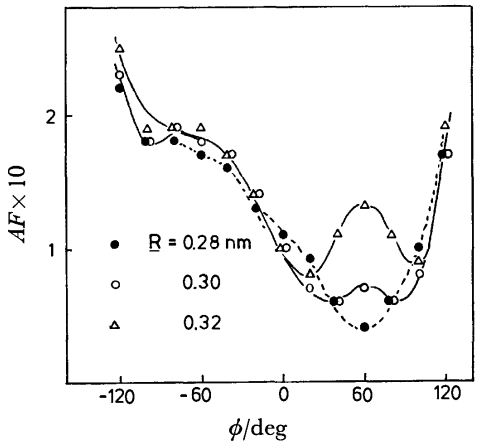

Fig. 2.

the R/Ph dihedral angle (ϕ) for the representative case of Compound **2** (R=Me). Here, the value of p is fixed at 0.4, while the Ln–O distance (R) is varied from 0.28 to 0.32 nm. For R=0.28 nm, the profile shows a single minimum at ϕ=60°, accompanied by a shoulder at *ca.* ϕ=−80°. For a longer Ln–O distance, this minimum splits into two shallow minima at ϕ=40° and 80° (R=0.30 nm), and then into more distinct minima at ϕ=20° and 100° (R=0.32 nm). The agreements have been found to become poorer for R=0.26 and 0.34 nm. A similar trend has also been found to exist for the other ketones and aldehyde. Thus, at a certain Ln–O distance (0.30—0.32 nm) the agreements become reasonably good, and the presence of a second minimum or an inflection becomes most clear. To illustrate this, parts of the *AF* maps for Compounds **4** and **5** (R=Pr^i and Bu^t) are shown in Table 4. The shape of the AF/ϕ profile has been found to be rather insensitive to the population index in the range of *ca.* p=0.2—0.6 in the case of the **2** ketone. The most satisfactory results have been obtained at around p=0.4, 0.4, 0.3, and 0.2 respectively for **2**, **3**, **4**, and **5**.[3]

Table 4. Parts of the *AF* (in %) maps for compounds **4** and **5**

	ϕ/deg							
R/nm	0	20	40	60	80	100	120	140
(a) Compound **4** (p=0.3)								
0.26	25	23	20	18	17	18	23	39
0.28	21	17	14	12	9	9	16	32
0.30	19	15	14	14	10	6	12	28
0.32	19	16	16	17	13	8	11	27
0.34	19	17	19	20	17	11	12	27
(b) Compound **5** (p=0.2)								
0.26	44	42	40	38	37	37	39	58
0.28	27	24	22	21	18	16	18	46
0.30	20	17	16	15	11	6	11	41
0.32	22	19	18	17	14	11	15	40
0.34	26	24	23	22	20	18	21	41

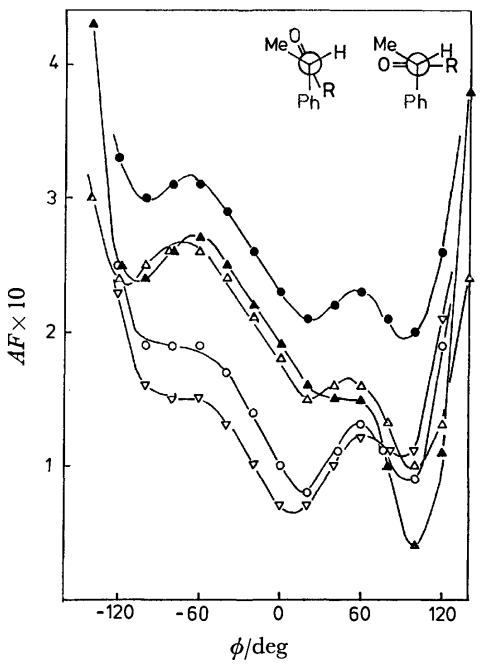

Fig. 3. Plots of *AF vs.* the R/Ph dihedral angle (ϕ) for Compounds **1**—**5**.
The Ln–O distance (R) is kept constant at 0.32 nm. ▽: R=H (**1**), ○: R=Me (**2**), ●: R=Et (**3**), △: R=Pr^i(**4**), ▲: R=Bu^t(**5**).

Figure 3 gives the AF/ϕ plots for all of the compounds presently studied (R is fixed at 0.32 nm). We may note at first that there are three minima (or two minima and an inflection) in these figures. The above finding is consonant with the general understanding that there is a three-fold barrier to rotation about the carbon-carbon bond for aliphatic aldehydes and ketones. The agreements are better in the $\phi=0°$—$120°$ range and worst at around $\pm 180°$. The most impressive is perhaps the fact that two AF minima are found at *ca.* $\phi=30°$ and 90° for all of the compounds examined here. The relative importance of these minima appears to be dependent on the nature of the alkyl group, R.[4]

The Relevance of the Present Results to the Conformational Problem of Carbonyl Compounds. A change in the conformational equilibrium may be brought about by the addition of a LSR. This has been found to be negligible in the case of **1**. The vicinal coupling constant between the aldehydic proton and the benzylic proton was found to be *ca.* 1.4 Hz; this was shown to be insensitive to the addition of the lanthanoid species. It is assumed, by analogy, that the rotameric equilibria are not appreciably perturbed by the complex formation for the other compounds in this series, either. This is supported by the fact that the perturbation to the conformational equilibria has been found to be unimportant in the cases of the structurally related sulfoxides[5] and alcohols.[1,6] Except for some particular cases,[2b,7] the conformation of a molecule has been shown not to be influenced by the complexation with a LSR. The internal consistency of the simulated result (*vide infra*) is an additional support for the above assumption.

It has become clear, from earlier studies, that the Ln–O distance (R) at which the best agreement is obtained varies with the nature of the functional group in the substrate molecules. Thus, in the case of the sulfoxides we have noted that the goodness of fit reached its maximum at $R=0.34$—0.38 nm.[5b,8] The best fit has been recorded at $R=0.30$—0.32 nm in the case of alcohols.[1,9] This is illustrated in Table 5 for some representative cases. This does not imply that the above values are necessarily the most correct ones for the Ln–O distance. It is likely, however, that these values reflect the complexing abilities of the SO, OH, and C=O groups. Among these groups, the carbonyl oxygen is intermediate as a base, and it is reasonable to expect that the value of R falls between the above two cases. In view of this, the results computed at around $R=0.32$ nm have been taken to be pertinent to the present problem of the conformational preferences of the ketones. The agreements are, indeed, reasonably good in this range of the Ln–O distance. It is noteworthy that the AF/ϕ plots (for $R=0.30$—0.32 nm) have two distinct minima, at $\phi=20°$—$40°$ and $80°$—$100°$, in all of the cases studied.[10] We believe that this phenomenon is relevant to the present problem of the conformational behavior of these compounds. It is likely that there are two rotamers which correspond approximately

Table 5. The R-dependence of AF[a] for $CH_3(Ph)CH$–X–R compounds

R	Bu^t	Me	Bu^t	Me	Bu^t(5)	Me (2)	
X[d]	SO	SO	CHOH	CHOH	CO	CO	
p (or A[b])	0.4	0.4	0.4	0.4	0.2	0.4	0.4
Dihedral angle/deg[c]	70	60	80	60	100	20	100
R/nm							
0.24	376	82	31	22	71	21	25
0.26	125	46	19	16	37	14	16
0.28	59	25	10	12	16	9	10
0.30	31	13	6	11	6	7	8
0.32	16	7	7	11	11	8	9
0.34	8	7	10	13	18	11	12
0.36	3	10	13	15	23	13	15
0.38	3	12	15	16	27	15	17
0.40	5	13	17	18	30	16	19
0.42	7	14	19	19	32	18	20

a) $AF\times 10^2$. b) Index for the LSR distribution (see text). c) The R–X–C–Ph dihedral angle. d) The X group in $CH_3(Ph)CHX$–R. The Ln–O–C angle was set at 120°, 130°, and 140° respectively for sulfoxides, alcohols, and ketones.

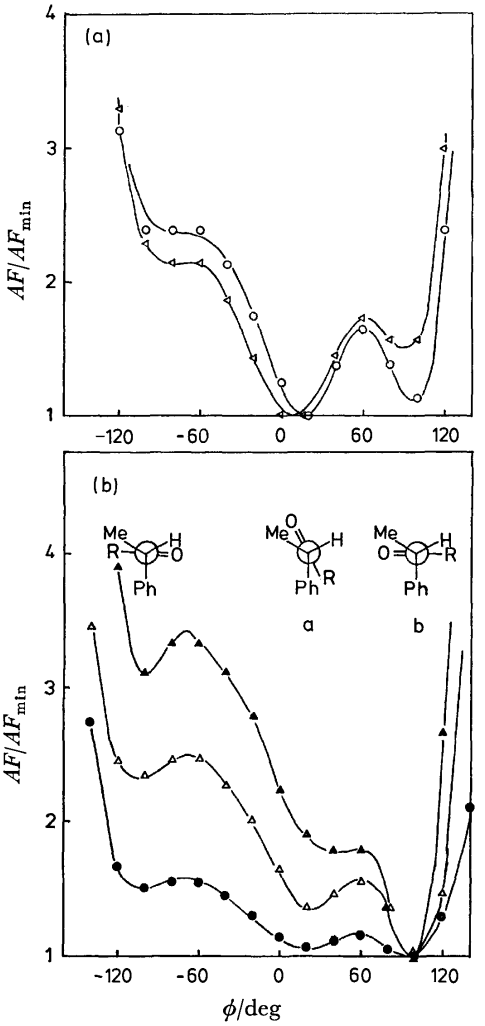

Fig. 4. Plots of the relative AF (AF/AF_{min}) *vs.* the R/Ph dihedral angle (ϕ) for (a) **1** and **2**, and (b) **3**—**5**. The parameters p and R are kept constant at 0.4 and 0.32 nm, respectively. ◁—◁: R=H (**1**), ○—○: R=Me (**2**), ●—●: R=Et (**3**), △—△: R=Pr^i (**4**), ▲—▲: R=Bu^t (**5**).

to these ϕ-values.[11]

The Preferred Rotamers in the Conformational Equilibria of 1—5. In order to see the effect of the alkyl substitution on the conformational preference, the relative *AF* (AF/AF_{min}) was plotted against the R/Ph torsional angle (ϕ).[12] It is clear from Fig. 4 that the relative *AF* values at $\phi \approx 30°$ and $\phi \approx 90°$ (these correspond to the rotamers **a** and **b** in Fig. 5, respectively) vary regularly with the change in the R group. Judging from the shapes of the curves, the contribution of the rotamer **a** appears to be largest for 2-phenylpropionaldehyde (R=H, **1**). The proportion of the rotamer **a** to the rotamer **b** seems to decrease as the aldehydic hydrogen in **1** is replaced by the methyl, ethyl, isopropyl, and then *t*-butyl groups. The two types of rotamers appear to be equally probable in the cases of **2** and **3**; the rotamer **b** is suggested to prevail in the rotameric mixture of **5**.[13]

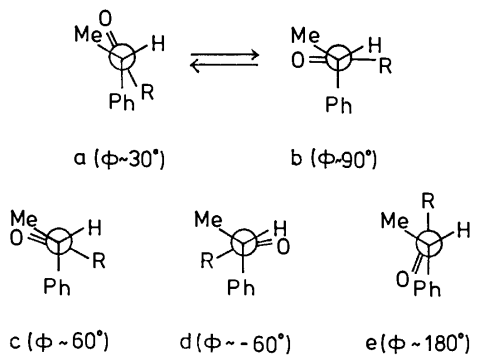

Fig. 5.

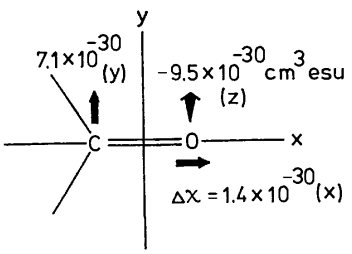

Fig. 6.

Support for the above suggestion regarding the conformational preferences of these compounds is provided by the proton NMR data. The peaks attributed to the benzylic hydrogen (H_a) appear at 3.58 ppm for **1**. They gradually move to a lower magnetic field upon the alkyl sustitution, and finally to a value of 4.26 ppm for the *t*-butyl homologue (**5**). This trend can be well understood in terms of the magnetic anisotropy of the C=O double bond (Fig. 6). Table 6 summarizes the computed data ($\Delta\sigma$ for H_a) for various conformations of a ketone.[15] Thus, in the most preferred conformations, the H_a in **1** positions itself in the shielding region of the carbonyl group, whereas H_a in **5** does not (Fig. 7a). The intermediate data found for the other ketones, **2**, **3**, and **4**, correspond to the suggested change in the conformational equilibria.[17] For the conformation of **1**, another support is provided by the fact that the aromatic protons in this compound are significantly shifted to lower magnetic fields relative to those in other compounds. According to the suggested conformation (Fig. 7b), H_o and H_m in **1** are well positioned in the deshielding region of the carbonyl group. The coupling constant found for the aldehyde is compatible with this conformation.

Table 6.

ψ	ϕ	$\Delta\sigma \times 10^{-30}$/cm^3 esu
150°	90°	−0.40
120°	60°	−0.42
90°	30°	−0.46
60°	0°	−0.81

a) For the meaning of the angles, see Fig.7 (a). $d_{C=O}$, 0.14 nm; d_{C-C}, 0.152 nm; ∠C-C=O, 120°, ∠C-C-H, 110°.

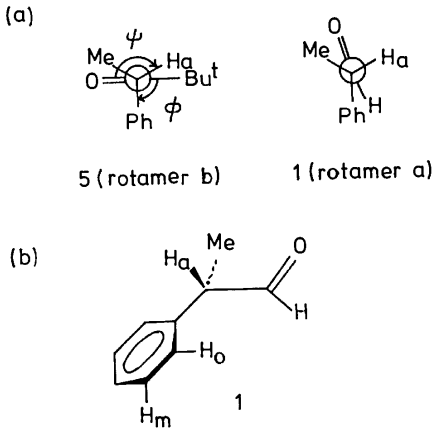

Fig. 7.

The suggestion that these conformations are important for the **1**—**5** ketones is in line with our thesis that an alkyl group prefers to lie close to a phenyl group; this again indicates the necessity to invoke an attractive force between these groups. The above conformation is compatible with the molecular geometries of some carbonyl compounds previously proposed for describing the transition state of the diastereoface-differentiating reactions.[18] We believe that the present results have an obvious implication in this problem.

Discussion

A Possible Role of the Weak CH···O Hydrogen Bond in Determining the Conformational Preferences of Carbonyl Compounds. The above conclusion is consonant with the general understanding that a methyl group interacts favorably with a carbonyl group. Thus, for a number of aldehydes and ketones, it has been established that a methyl group is nearly eclipsed by the carbonyl oxygen in the preferred conformations. The examples include microwave and NMR studies of propionaldehyde (**6**),[19] an electron-diffraction study of isobutyraldehyde (**7**),[20] and NMR studies of substituted acetaldehydes (**8**),[21] ethyl alkyl ketones (**9**),[22] and 2-substituted 3-pentanones (**10**).[23] For the sake of simplicity, and in

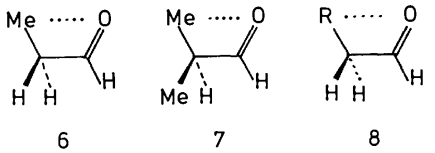

6 7 8

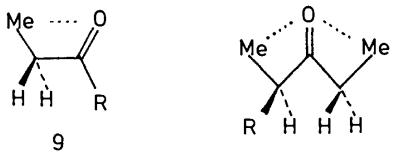

9 10

view of the limitation of the methods as well, the conformations for **6**—**10** are drawn as completely eclipsed. A somewhat twisted conformation, however, is more likely to exist in reality.[21,24] We suggest that such conformations as the above two types (rotamers **a** and **b** in Fig. 5; CH_3/O torsional angle *ca.* $\pm 30°$) are both important in the consideration of the conformational problems of these molecules (**1**—**5**). An inspection of the Dreiding models suggests that it would be easier for a hydrogen-bond like interaction involving the CH_3 and O (*vide infra*) to take place with a slightly distorted conformation. By twisting from the completely eclipsed conformation, a molecule comes to be capable of avoiding the energetically unfavorable vicinal H/H interaction (Fig. 8)[25] and simultaneously participating in a CH/O hydrogen bonding.

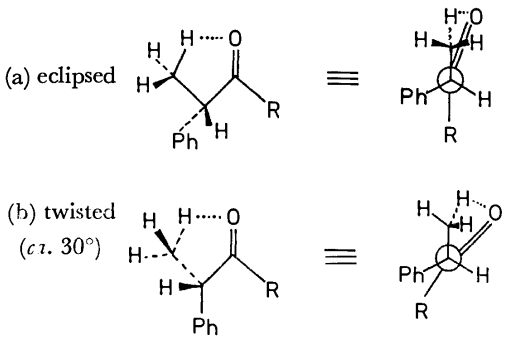

Fig. 8.

There is ample evidence in the literature that a methyl group prefers to be *gauche* or nearly (but not completely) eclipsed to a group with unshared electrons. Figure 9 illustrates some representative cases.[26,27] Several workers have interpreted these phenomena (the favored *gauche* or eclipsed interaction) in terms of the nonbonded van der Waals attraction or the London dispersion force.[28] However, we think it more probable that the favored CH_3/O (more generally CH_3/X, X=O, N, or halogens) interaction traces its origin in a kind of weak hydrogen bond.[6,29] In virtually all cases reported so far, it seems easy for the formation of a 5- or 6-membered intramolecular hydrogen bonding to take place (see **6**—**10**, Figs. 9 and 10). We would refer this hypothetical secondary force to the CH/*n* interaction[29,30] (*n*: unshared electrons).

Supports for the above suggestion have been provided by a number of experimental and theoretical studies.

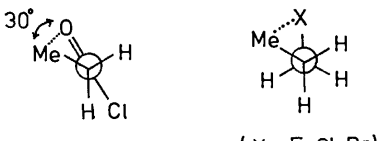

Fig. 9.

In particular, Sutor presented good evidence, from an extensive X-ray study, that there is strong possibility that a CH (CH_2, CH_3) group participates in a weak hydrogen bond with an oxygen atom.[31] Her proposal has since found a number of supports in X-ray[6,32] and NMR[5b,33] studies of a variety of molecules. Some representative examples are illustrated in Fig. 10. The presence of such a weak, hydrogen-bond like interaction has also been suggested by the MO (semi-empirical[34] as well as *ab initio*[35]) calculations of several model systems.

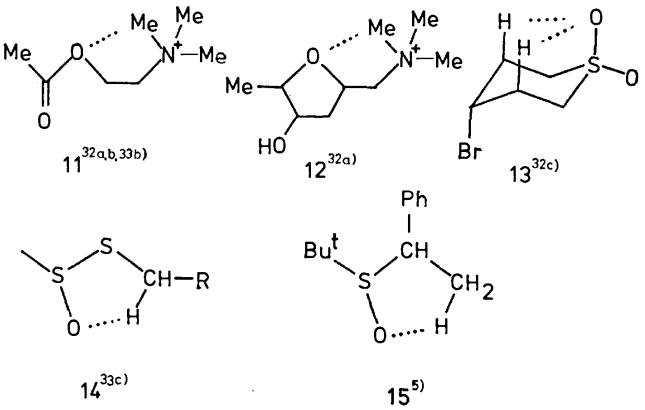

11[32a,b,33b] 12[32a] 13[32c]

14[33c] 15[5]

Fig. 10.

Karabatsos and his co-workers studied, by NMR, the conformation of a number of substituted acetaldehydes (**8**).[21] They reported that the relative stability of the rotamer **a** to the rotamer **b** (Fig. 11) decreases as the "size" of the alkyl group (R) increases, and explained this in the framework of the bulk-repulsive concept. We prefer to interpret this differently; this may be a proof for the presence of a CH/O hydrogen bond. It seems likely that it is the "number" of the CH group (which can effectively interact with the carbonyl group) which is more important in determining the relative stabilities of the respective rotamers. The factors responsible for the rotamer stability might thus be the number, the nature (5- or 6-membered, the orientation of the CH bond, the kind of X-group, *etc.*), and the probability of participating in the interaction. In fact, it has been reported that, if one of the substituents in **16** is a methyl group (Fig. 11), the most stable rotamer has always its methyl group which is eclipsed by the carbonyl oxygen.[21] The relative stability of the rotamer **a** in relation to the **b** has been reported to decrease when the methyl group is replaced by another alkyl group. This is reasonable, in our view, since the "number" of the CH groups, which can form a 5-membered H-bond with the carbonyl group,[36] decreases

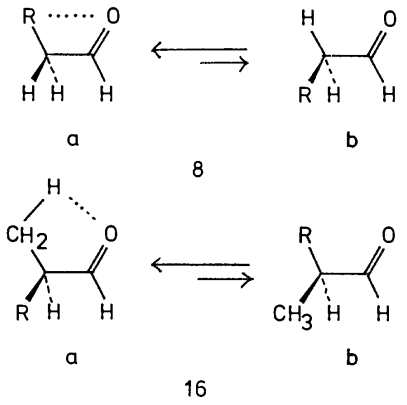

Fig. 11.

on the replacement of the methyl group by another alkyl group.

The Factors Controlling the Relative Stability of the Rotamers ***a*** *and* ***b***; *5- and 6-Membered Intramolecular H-Bond.* With regard to the stability of the rotamer **a** relative to that of the rotamer **b** in Fig. 5, we would invoke the importance of the CH/π interaction. This is a weak attractive force likely to be operative between an alkyl and a π-system,[33a,37,38] the nature of which is ascribed to a kind of weak hydrogen bond. On the basis of experimental and theoretical evidence, the interaction has been suggested to be most effective at a C–H···C(sp^2) interatomic distance of approximately 0.20—0.25 nm.[37,39] An inspection of the Dreiding models (Fig. 12) suggests that such an interaction is likely to occur in the rotamer **a** with the use of a hydrogen (H_y) attached to C9 (Type **a** interaction). If the CH/π interaction is operative with the use of the C-1 carbon, the Type **a** interaction is a kind of 5-membered intramolecular H-bond. Another type of interaction is possible with the use of H_z (Fig. 12; Type **b** interaction). This type of interaction forms a 6-membered H-bond and is most likely to occur with the rotamer **b** (Dreiding model). The 5-membered, Type **a** interaction decreases as the alkyl group changes from being a methyl to an ethyl and then to an isopropyl group; in the case of a *t*-butyl group, it is absent. On the other hand, a 6-membered, Type **b** interaction increases in this order.[40]

To explain the present results, one may argue in the framework of the bulk-repulsive concept. It is conceivable that the London dispersion force[41] is responsible, at least in part. We believe, however, that the present finding is better accommodated by considering the effects of the above two types of CH/π interaction involved there. The basic geometries of the respective rotamers are determined by the more dominant CH_3/n interaction, which we feel to be somewhat stronger than the CH/π bond. It would be pertinent, in this respect, to cite a recent finding of Inamoto and his group in an X-ray study of a very crowded molecule, bis(2,4,6-tributylphenyl)phosphinic chloride (Fig. 13).[32d] Some of the intramolecular distances found in this compound ($CH_3/C_{aromatic} \approx 0.32$, $CH_3/Cl \approx 0.33$, and $CH_3/O \approx$ 0.30 nm) are shorter by 0.04—0.05 nm than the respective van der Waals distances.

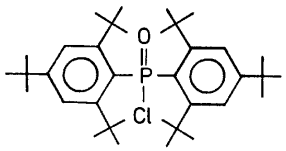

Fig. 13.

Possible Importance of the CH/π *Interaction in the Conformational and Selectivity Problems of Various Systems; CH/*π *Interaction Hypothesis.* The stabilization energy for a unit CH/π bonding is very small (*ca.* 3.5 kJ mol^{-1} or less).[6,37] However, we suggest that this type of interaction may contribute to bringing about an appreciable difference between the free-energy levels of a competitive interaction (intramolecular or intermolecular) system. The CH groups (as well as π-system) are generally arranged in a chemical structure with a certain symmetry. The difference in the interaction energies might thus become remarkable, since the "number" and the "chance" for the interaction may be expected to increase in such a case.

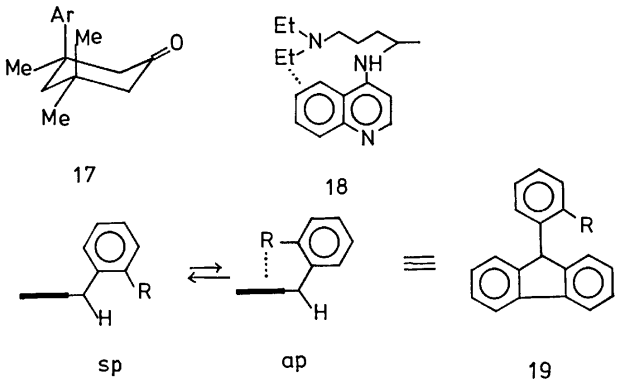

Intramolecular Interactions: To cite a few possible cases, Shapiro and his group have reported a remarkable preference for the axial aromatic (as opposed to the methyl) group in **17**.[7a,42] The conformation of an antimalarial substance, chloroquine (**18**), was studied by the LIS method; the side-chain alkyl group in this compound has been shown to be curled over the plane of the quinoline ring.[43] Nakamura, Nakamura, and Ōki recently studied the conformational problem of 9-(2-alkylphenyl)fluorenes (**19**).[44] The free-energy

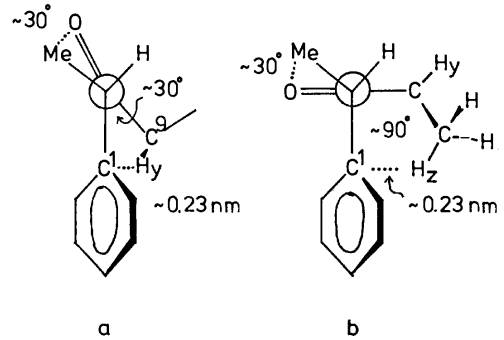

Fig. 12.

differences between the rotamers have been reported to be 0.3, 0.6, and 0.4 kcal mol^{-1} at 0° (in favor of the sp-rotamer) for the methyl, ethyl, and isopropyl derivatives respectively. The above unusual behavior of the isopropyl homologue might be an indication of the involvement of the CH/π interaction.

$RCOCOOC_{10}H_{19} \longrightarrow RCH(OH)COOC_{10}H_{19}$
(**20**)

$C_{10}H_{19}$=menthyl

R	CH_3	C_6H_5
% e.e.	14, 18	22—30

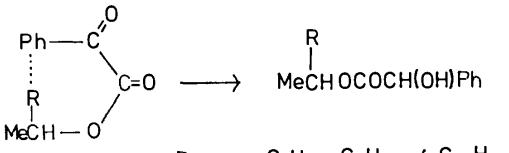

21

R	n-C_6H_{13}	C_6H_5	α-$C_{10}H_7$
% e.e.	18	3	12

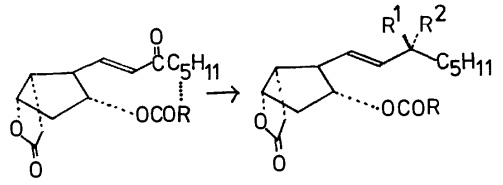

22 23S R^1=OH, R^2=H
23R R^1=H, R^2=OH

R	$(CH_2)_7CH_3$	PhPh(*p*)	PhC_5H_{11}(*p*)	NHPh
S/*R*-ratio	≈55/45	82/18	82/18	89/11

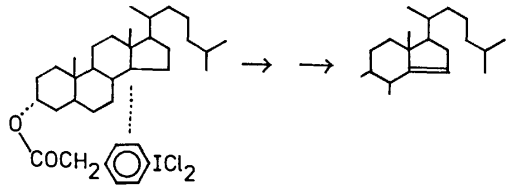

24

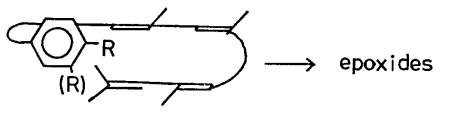

25

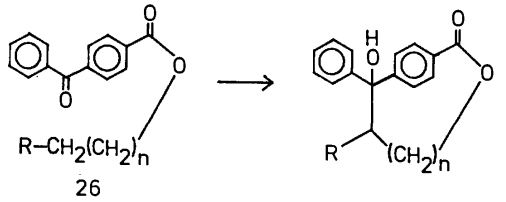

26

Evidence about the conformations of flexible molecules is well reflected in the selectivities in certain reactions (see **20**—**26**). The extent of asymmetric synthesis in a Prelog reaction system (**20**) has been shown to be greater for the benzoyl formate ester (R=Ph) than for the pyruvate ester (R=Me).[45] A similar result has been observed for **21** in the case of a 1-methylheptyl ester (R=*n*-C_6H_{13}) *vs.* a 1-phenylethyl (R=C_6H_5) or 1-(1-naphthyl)ethyl (R=$C_{10}H_7$) ester, the former giving rise to the highest optical yield.[46] Corey and his coworkers have reported that the stereoselective reduction of **22** (a prostaglandin precursor) was better accomplished when they used an ester with an aromatic substituent.[47] The examples from **24** to **26** are extracted from the template-directed functionalizations of Breslow and his group;[48] they have presented good evidence that these molecules are extensively folded in solution. Note that, in all of the reactions cited thus far where remarkable selectivities were observed, the reacting species have an aromatic group on one side, and a long-chain (or branched) alkyl group on the other end of the molecule; an alkyl/alkyl or aromatic/aromatic interaction does not seem to yield a good result in a selective reaction. Therefore, we think it very probable that an attractive interaction of the CH/π type plays an important part in determining the molecular shapes of flexible molecules.

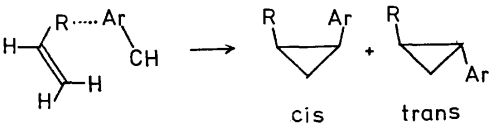

R	Me	Et	Pr^i	Bu^t
cis/*trans*	3.1	2.1	1.4	0.45

Fig. 14.

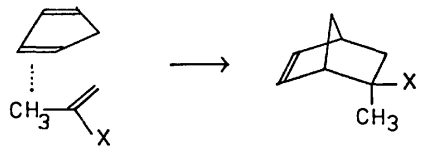

(X = CN, COOMe, CHO)

Fig. 15.

Intermolecular Interactions: We feel further that the attractive CH/π interaction plays a more important role in controlling the subtle aspects of the dynamically interacting systems,[49] *e.g.*, the efficacy of molecular recognition[50] and the selectivity problems in certain multimolecular reactions. Thus, Closs and Moss reported a remarkable effect of the alkyl substitution on the stereochemical outcome in a carbene addition to a series of olefins (Fig. 14).[51] A similar result has recently been presented in another case.[52] The *endo*-orienting tendency of the methyl group has been demonstrated for a Diels-Alder reaction (Fig. 15).[53] A steroidal enzyme model has been studied by Guthrie and his group;[54] the enolization of **27** has been shown to be most effectively catalyzed when a large aromatic group is incorporated in the substrate molecule. The rate enhancement has been reported to increase regularly when a phenyl group in **27** is replaced by a naphthyl and then by a phenanthryl group. In an enantioface-differentiat-

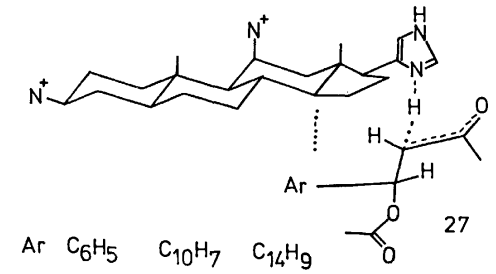

27

Ar	C_6H_5	$C_{10}H_7$	$C_{14}H_9$
k_{rel}	9	27	110

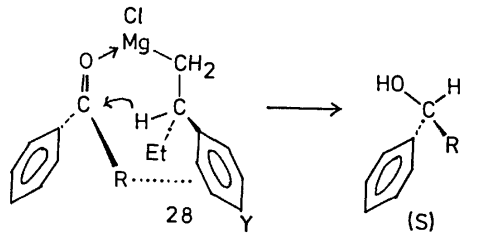

28 (S)

R \ Y	H	OMe	CF_3
C_2H_5	50	57	22 % e.e.
i-C_3H_7	81	84	58

ing reduction of phenyl alkyl ketones with a chiral Grignard reagent (**28**), Guétté and Capillon[55] have found that the introduction of a methoxyl group to the aromatic moiety of **28** results in an increase (slight but distinct) in the optical yield. The extent of the asymmetric synthesis decreases, in contrast, on substitution with an electron-withdrawing group such as CF_3.

In all of the cases cited above, the free-energy level at the transition state (which leads to the favored product) seems to be stabilized by the interaction of an alkyl group with an aromatic system. Certain of the above results were explained in terms of the van der Waals (repulsive as well as attractive) and the so-called hydrophobic interaction.[56] We feel that the substituent dependence of the product ratio (*cis/trans*) in the cyclopropane formation (Fig. 14) can better be understood by considering the involvement of the CH/π interaction. The effective "number" of the CH group, which can participate in the stabilization of the activated complex, might thus decrease upon a successive α-methylation ($CH_3 \rightarrow CH_2Me \rightarrow CHMe_2 \rightarrow CMe_3$). In fact, a significant increase in the *cis/trans* ratio has been observed upon the replacement of the olefinic hydrogen with a second *cis*-methyl group.[52] The London dispersion force and the hydrophobic interaction[56] perhaps play important parts in the selective enolization of **27**.[54] However, we think it likely that the CH/π interaction plays a role, since the probability of the interaction can be expected to increase with an increase in the surface area of the aromatic ring (phenyl→naphthyl→phenanthryl). At any event, we see no good reason why a compound becomes a good substrate only with an aromatic substituent, if the so-called nonpolar interaction is solely responsible for the observed selectivity.[57] A similar argument may apply to the selectivity problem reported for the reduction of **22** to **23**.[47] Alkyl substituents such as CH_3 and $CH_3(CH_2)_7$ have been reported to be by far less effective than aromatic ones; this is to be anticipated since we have an aliphatic moiety (C_5H_{11}) on the other terminal of the molecule. The results reported for the last example[55] seem to demonstrate that the interaction involved here, in stabilizing the favored transition state, is CH/π in type. The π-donating property of the phenyl group should increase upon the introduction of an electron-donating group, such as CH_3 or CH_3O; the inverse is true for CF_3.

Possibilities of Biological Importance: It is tempting to speculate about the possibilities that the interactions of the above kind play an important role also in the biological system.[29,58] These possibilities include the problems of biopolymer folding [59] and the substrate specificities of some globular proteins, such as enzymes and immunoglobulins. As was emphasized by Watson some 15 years ago,[60] the interactions which determine the subtle behavior of the dynamically interacting, complex biomolecules *should be weak* and orientation-dependent. Our knowledge about the important, weak chemical interactions, however, is still far from complete. We suggest that the CH/π (as well as CH/n) interaction is a good candidate for the above important secondary forces in view of its *weakness* and flexibility. Our study is thus being oriented toward an understanding of the nature and the characteristics of these forces, the biological implications of which will form the subject of a future paper.

Experimental

Materials. The 2-phenylpropionaldehyde (**1**) was obtained from a commercial source. The ketones (**2**—**5**) were prepared by treating **1** with appropriate Grignard reagents, followed by the oxidation of the resulting alcohols. The samples were purified chromatographically and gave correct analytical and spectral data.

NMR Measurements. The NMR spectra and the LIS data were determined as has been described in the preceding paper.[1]

We wish to thank Professors Tadashi Endo (Aoyama Gakuin University) and Naoya Nakagawa (University of Electro-communications) for their discussions, Professor Naoki Inamoto (University of Tokyo) for providing information prior to publication, and Dr. Teiichiro Ito (Meiji Seika Kaisha) for his encouragement.

References

1) J. Uzawa, S. Zushi, Y. Kodama, Y. Fukuda, K. Nishihata, K. Umemura, M. Nishio, and M. Hirota, *Bull. Chem. Soc. Jpn.*, **53**, 3623 (1980).

2) a) G. Montaudo, S. Caccamese, V. Librando, and P. Maravigna, *Tetrahedron*, **29**, 3915 (1973); b) P. Finocchiaro, A. Recca, P. Maravigna, and G. Montaudo, *ibid.*, **30**, 4159 (1974).

3) This trend of the Ln-distribution is reasonable in view of the steric consideration.

4) The agreements are very poor for Compound **2** (R=Et). This may be attributed to the absence of $C3$ symmetry for the alkyl group in this molecule. In the above procedure, the contributions from all of the rotamers (regarding the rotation

around the C8–C9 bond) were computed and then averaged. This is a good approximation for compounds with a symmetric group (R=H, Me, or Bu^t), but not for Compounds **3** and **4**. The deletion of the LIS data for H_y, H_z, and/or C10 has, in fact, improved the agreements.

5) a) Y. Kodama, K. Nishihata, M. Nishio, and Y. Iitaka, *J. Chem. Soc., Perkin Trans. 2*, **1976**, 1490; b) Y. Kodama, S. Zushi, K. Nishihata, M. Nishio, and J. Uzawa, *ibid.*, **1980**, 1306.

6) Y. Kodama, K. Nishihata, S. Zushi, M. Nishio, J. Uzawa, K. Sakamoto, and H. Iwamura, *Bull. Chem. Soc. Jpn.*, **52**, 2661 (1979).

7) a) B. L. Shapiro, M. D. Johnston, Jr., and M.J. Shapiro, *J. Org. Chem.*, **39**, 796 (1974); b) K. L. Williamson, D. R. Clutter, R. Emch, M. Alexander, A. E. Burroughs, C. Chua, and M. E. Bogel, *J. Am. Chem. Soc.*, **96**, 1471 (1974); c) P. Finocchiaro, A. Recca, W. G. Bentrude, H. W. Tan, and K. C. Yee, *ibid.*, **98**, 3537 (1976).

8) Y. Kodama, K. Nishihata, and M. Nishio, *J. Chem. Res. (S)*, **1977**, 102.

9) R. E. Davis and M. R. Willcott, III, *J. Am. Chem. Soc.*, **94**, 1744 (1972); S. Farid, A. Ateya, and M. Maggio, *Chem. Commun.*, **1971**, 1285; G. Hawkes, D. Leibfrits, D. W. Roberts, and J. D. Roberts, *J. Am. Chem. Soc.*, **95**, 1659 (1973).

10) The presence of a single rotamer (ϕ *ca.* 60°; rotamer **c** in Fig. 5) may be suggested for **2** if one considers the results obtained with R=0.28 nm to be more appropriate in this case. We, however, feel this to be an artefact which is brought about by the use of an improper Ln–O distance. The above single minimum probably corresponds to the time-averaged geometries of the two rotamers, **a** and **b**, in Fig. 5. It is difficult to believe that the above computational procedure will produce the wrong, artificial conclusion that there is a mixture of two rotamers if, in reality, there is only an unique rotamer prevailing in the solution.

11) The usefulness (as well as the limitations) of the LIS method in studying the conformational problems of carbonyl compounds has been demonstrated by Montaudo *et al.* in the cases of unsaturated ketones and amides.[2)]

12) The position and the goodness of fit at the respective *AF*-minimum reflect, although in an indirect manner, the plausible geometry and the relative importance of a substrate–LSR complex.

13) Impressive also is the fact that the rotamer corresponding to ϕ *ca.* −60° (rotamer **d** in Fig. 5) seems to be rather unimportant for all of the compounds studies here. Another notable feature of the above results is the (suggested) nonexistence of the rotamer corresponding to $\phi \approx 180°$ (rotamer **e** in Fig. 5); this latter conclusion differs significantly from that of a preliminary force-field calculation of these molecules.[14)]

14) M. Hirota, T. Sekiya, M. Nishio, and K. Nishihata, CSJ-ACS Meeting, Honolulu, 1979, Abstr. ORGN 091.

15) Calculation was made on the basis of the available data for the magnetic susceptibility[16)] and standard geometry of a carbonyl compound.

16) P. T. Narasimhan and M. T. Rogers, *J. Phys. Chem.*, **63**, 1388 (1959); J. A. Pople, *J. Chem. Phys.*, **37**, 60 (1962); J. W. ApSimon, W. G. Craig, P. V. Demarco, D. W. Mathieson, A. K. G. Nasser, L. Saunders, and W. B. Whalley, *Chem. Commun.*, **1966**, 754.

17) The geometrical disposition of the methyl group with respect to the carbonyl group does not differ significantly from the rotamer **a** to the rotamer **b**; the time-averaged geometry of CH_3 *vs.* C=O is not substantially affected by a shift in the rotameric equilibrium. This is, in fact, reflected in the insensitivity of the respective proton resonance to the structural variation (Table 1).

18) D. J. Cram and F. A. Abd. Elhafez, *J. Am. Chem. Soc.*, **74**, 5828 (1952); G. J. Karabatsos, *ibid.*, **89**, 1367 (1967); M. Chérest, H. Felkin, and N. Prudent, *Tetrahedron Lett.*, **1968**, 2199. See also L. Salem, *J. Am. Chem. Soc.*, **95**, 94 (1973); R. A. Auerbach and C. A. Kingsbury, *Tetrahedron*, **29**, 1457 (1973); K. Nishihata and M. Nishio, *Tetrahedron Lett.*, **1977**, 1041.

19) S. S. Butcher and E. B. Wilson, Jr., *J. Chem. Phys.*, **40**, 1671 (1964); R. J. Abraham and J. A. Pople, *Mol. Phys.*, **3**, 609 (1960).

20) L. S. Bartell, B. L. Carroll, and J. P. Guillory, *Tetrahedron Lett.*, **1964**, 705.

21) G. J. Karabatsos and N. Hsi, *J. Am. Chem. Soc.*, **87**, 2864 (1965).

22) G. J. Karabatsos, G. C. Sonnichsen, N. Hsi, and D. J. Fenoglio, *J. Am. Chem. Soc.*, **89**, 5067 (1967).

23) T. E. Gough, W. S. Lin, and R. G. Woolford, *Can. J. Chem.*, **45**, 2529 (1967).

24) G. J. Karabatsos and D. J. Fenoglio, *Top. Stereochem.*, **5**, 167 (1970).

25) D. H. Wertz and N. L. Allinger, *Tetrahedron*, **30**, 1579 (1974).

26) S. Mizushima, "Structure of Molecules and Internal Rotation," Academic Press, New York (1954); Y. Morino and K. Kuchitsu, *J. Chem. Phys.*, **28**, 175 (1958); E. Hirota, *ibid.*, **37**, 283 (1962).

27) E. L. Eliel, N. L. Allinger, S. J. Angyal, and G. A. Morrison, "Conformational Analysis," Wiley-Interscience, New York (1965), Chap. 1.

28) *Cf.* Refs. 24 and 27, and the references cited therein.

29) M. Nishio, *Kagaku No Ryoiki*, **33**, 422 (1979).

30) N. Inamoto, *Kagaku No Ryoiki*, **33**, 495 (1979).

31) D. J. Sutor, *Nature*, **195**, 68 (1962); *J. Chem. Soc.*, **1963**, 1105.

32) a) F. G. Canepa, P. Pauling, and H. Sorum, *Nature*, **210**, 907 (1966); b) J. K. Herdklotz and R. L. Sass, *B. B. R. C.*, **40**, 583 (1970); c) N. Nogami, Thesis, Univ. of Tokyo (1977); see also R. J. Abraham and Z. L. Rossetti, *J. Chem. Soc., Perkin Trans. 2*, **1973**, 582; d) M. Yoshifuji, I. Shima, N. Inamoto, K. Hirotsu, and T. Higuchi, *Angew. Chem. Int. Ed. Engl.*, **92**, 399 (1980).

33) a) N. Nakagawa, *Nippon Kagaku Zasshi*, **82**, 141 (1961); b) C. C. J. Culvenor and N. S. Ham, *Chem. Commun.*, **1966**, 537; c) T. Takata, Y. H. Kim, S. Oae, and K. T. Suzuki, *Tetrahedron Lett.*, **1978**, 4303. For other possible cases, see F. G. Riddell and M. J. T. Robinson, *Tetrahedron.*, **23**, 3417 (1967); E. L. Eliel and M. C. Knoeber, *J. Am. Chem. Soc.*, **90**, 3444 (1968).

34) N. Nakagawa, personal communications; *cf.* Ref. 29.

35) H. Umeyama and K. Morokuma, *J. Am. Chem. Soc.*, **99**, 1316 (1977); K. Morokuma, *Acc. Chem. Res.*, **10**, 294 (1977).

36) This may be, entropically as well as enthalpywise, more favorable than a 6-membered CH/X hydrogen bond. The same applies to the 5- and 6-membered, intramolecular CH/π interactions.

37) Y. Kodama, K. Nishihata, M. Nishio, and N. Nakagawa *Tetrahedron Lett.*, **1977**, 2105.

38) T. Aoyama, O. Matsuoka, and N. Nakagawa, *Chem. Phys. Lett.*, **67**, 508 (1979).

39) M. Nishio, *Kagaku No Ryoiki*, **31**, 834, 998 (1977).

40) We feel that the Type **b** interaction is of minor enthalpy for a unit bond as compared to the Type **a** interaction. In fact, H_y is α to C=O (more acidic) and is, therefore, more prone to participate in the interaction with the phenyl group. H_z is also capable of participating in a 5-membered CH/*n* interaction with the carbonyl oxygen; this is, in fact, reflected in the chemical shifts for C10 (*γ-gauche* effect).

41) R. E. Carter, B. Nilsson, and K. Olsson, *J. Am. Chem. Soc.*, **97**, 6155 (1975); R. E. Carter and P. Stilbs, *ibid.*, **98**,

7515 (1976).
42) B. L. Shapiro, M. J. Gattuson, N. F. Hepfinger, R. L. Shone, and W. L. White, *Tetrahedron Lett.*, **1971**, 219.
43) N. S. Angerman, S. S. Danyluk, and T. A. Victor, *J. Am. Chem. Soc.*, **94**, 7137 (1972).
44) M. Nakamura, N. Nakamura, and M. Ōki, *Bull. Chem. Soc. Jpn.*, **50**, 2986 (1977).
45) J. D. Morrison and H. S. Mosher, "Asymmetric Organic Reactions," Prentice-Hall, Englewood Cliffs, New Jersey (1971), Table 2-2.
46) V. Prelog, E. Philbin, E. Watanabe, and M. Wilhelm, *Helv. Chim. Acta*, **39**, 1086 (1956). *Cf.* Ref. 45, Table 2-1.
47) E. J. Corey, K. B. Becker, and R. K. Varma, *J. Am. Chem. Soc.*, **94**, 8616 (1972).
48) R. Breslow, R. Corcoran, J. A. Dales, S. Lieu, and P. Kaliky, *J. Am. Chem. Soc.*, **99**, 905 (1977); R. Breslow, J. Rothbard, F. Herman, and M. Rodoriguez, *ibid.*, **100**, 1213 (1978); R. Breslow and L. M. Maresca, *Tetrahedron Lett.*, **1978**, 887. See also M. A. Winnik, A. Mar, W. F. Reynolds, Ph. Dais, B. Clin, and B. Caussade, *Macromolecules*, **12**, 257 (1979).
49) The possible importance of the CH/π interaction in some dynamically interacting systems has been discussed in Refs. 6, 29, and 39. See also M. Nishio, 6th Symposium on Biomimetic Chemistry, Tokyo, 1978, Abstr. p. 55.
50) A remarkable example has been presented by Endo *et al.*; T. Endo, A. Kuwahara, H. Tasai, T. Murata, M. Hashimoto, and T. Ishigami, *Nature*, **268**, 74 (1977). *Cf.* Ref. 6.
51) R. A. Moss, *J. Org. Chem.*, **30**, 3261 (1965); G. L. Closs and R. A. Moss, *J. Am. Chem. Soc.*, **86**, 4042 (1964).
52) C. P. Casey, S. W. Polinchnowski, A. J. Shusterman, and C. R. Jones, *J. Am. Chem. Soc.*, **101**, 7282 (1979).
53) Y. Kobuke, T. Fueno, and J. Furukawa, *J. Am. Chem. Soc.*, **92**, 6548 (1970).
54) J. P. Guthrie and S. O'Leary, *Can. J. Chem.*, **53**, 2150 (1974); J. P. Guthrie and Y. Ueda, *ibid.*, **54**, 2745 (1976).
55) J. Capillon and J. P. Guétté, *Tetrahedron*, **35**, 1817 (1979). See also Ref. 45, Sec. 5-2, and Ref. 6.
56) For criticisms of the concept of "hydrophobic bonding," see K. Shinoda, *Kagaku To Kogyo*, **21**, 1400 (1968); K. Shinoda and M. Fujiwara, *Bull. Chem. Soc. Jpn.*, **41**, 2612 (1968); J. H. Hildebrand, *J. Phys. Chem.*, **72**, 1841 (1968); *Proc. Natl. Acad. Sci. U.S.A.*, **76**, 194 (1979); K. Shinoda, "Yoeki To Yokaido," 2nd ed, Maruzen, Tokyo (1974), Chap. 10; K. Shinoda and P. Becher, "Principles of Solution and Solubility," Marcel Dekker, New York (1978), Chap. 7.
57) One might also ask why aromatic compounds are so often good substrates for an inclusion complex with cyclodextrin, which has a "hydrophobic "cavity in the molecule.
58) a) M. Nishio, "The Molecular Basis of Recognition," Chap. 6 in "Stereochemistry of Molecular Interactions," Nankodo, Tokyo (1978); b) M. Nishio, 29th Symposium on Protein Structure, Osaka, 1978, Abstr. p. 161.
59) M. F. Perutz and H. Lehmann, *Nature*, **219**, 902 (1968); C. C. McDonald, W. D. Phillips, and J. D. Glickson, *J. Am. Chem. Soc.*, **93**, 235 (1971).
60) J. D. Watson, "The Importance of Weak Chemical Interactions," Chap. 4 in "Molecular Biology of the Gene," W. A. Benjamin, Menlo Park, Calif. (1965).

Synthetic Photochemistry. XIX.[1] The Synthesis of Protoilludanes by Photocycloadditions. Protoillud-7-ene and Several Oxygenated Derivatives

Hitoshi TAKESHITA,* Isao KOUNO, Mitsuaki IINO, Hisakatsu IWABUCHI,** and Danji NOMURA**

Research Institute of Industrial Science, 86, Kyushu University, Hakozaki, Fukuoka 812

***Faculty of Agriculture, 46, Kyushu University, Hakozaki, Fukuoka 812*

(Received February 27, 1980)

Unlike ethylene, 1,1-dimethoxyethene, an electron-rich olefin, has been photocycloadded to a *cis*-hexahydroindenone to form a norprotoilludane derivative with a correct stereostructure. Methylation and subsequent chemical transformations yielded several oxygenated derivatives, from which the parent hydrocarbon, protoillud-7-ene, was obtained by deoxygenation. Independent evidence for the stereostructures of the synthetic derivatives has been provided by the X-ray crystallographic analysis of a dihydroxy acetal.

In previous papers,[2] we have described a new approach to obtaining several oxygenated protoilludanes, biogenetic precursors of *gem*-dimethylcyclopentane sesquiterpenoids[3] from various organisms,[4] by the application of two-fold photocycloadditions, followed by methylation. However, this approach has a practical limitation; that is, with ethylene (**A**), only the *trans*-isomer (**B**) of the hexahydroindenones, *trans*-2-methoxycarbonyl-8,8-dimethylbicyclo[4.3.0]non-2-en-4-ones, is photochemically reactive, while the stereochemistry of natural protoilludanes possesses the *cis*-relationship. In this paper, we will describe a facile synthesis of the protoilludane derivatives from the *cis*-hexahydroindenones, *cis*-2-methoxycarbonyl-8,8-dimethylbicyclo-[4.3.0]non-2-en-4-one (**1**) and 2,8,8-trimethylbicyclo-[4.3.0]non-2-en-4-one (**2**), with an electron-rich olefin, 1,1-dimethoxyethene (**3**). According to a preliminary study, 1,1-dichloroethene was also photochemically unreactive to **1**, but vinyl acetate gave a complex product mixture.

Results and Discussion

The reaction of **1** with **3** was neat and gave only one adduct, 3,3-dimethoxy-2-methoxycarbonyl-10,10-dimethyltricyclo[6.3.0.$0^{2,5}$]undecan-6-one (**4**). This stereoselective formation itself may be an indication of the desired *cis-transoid-cis*-structure. With regard to this concept, we have decided to carry out further transformations. Thus, by Grignard methylation, **4** was converted to a pair of epimers, 3,3-dimethoxy-2-methoxycarbonyl-6,10,10-trimethyltricyclo[6.3.0.$0^{2,5}$]-

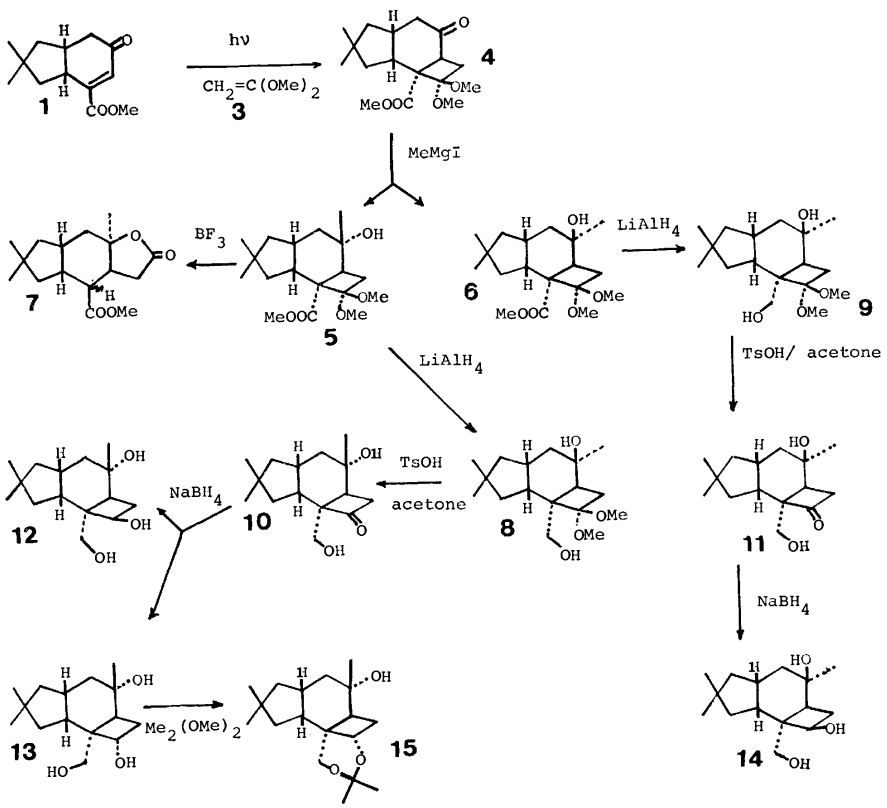

Scheme 1.

undecan-6-ols, **5**, the major product, and **6**. Against the attack of the reagent, the methoxycarbonyl group at the quarternary carbon was intact, as in the case of **B**.[3] Although **5** and **6** could be separated by silica-gel column chromatography, their cyclobutane rings were acid-sensitive; for example, the treatment of **5** with *p*-toluenesulfonic acid (TsOH) caused a ring-cleavage to yield a *seco*-γ-lactone, 4-hydroxy-2-methoxycarbonyl-4,8,8-trimethylbicyclo[4.3.0]non-3-ylacetic acid lactone (**7**), which has the same carbon skeleton as the pterosins.[5] To avoid this, the acetal group was hydrolyzed after an LAH reduction of the methoxycarbonyl group, *via* dihydroxy acetals, 2-hydroxymethyl-3,3-dimethoxy-6,10,10-trimethyltricyclo[6.3.0.$0^{2,5}$]-undecan-6-ols (**8** and **9**), to dihydroxy ketones, 6-hydroxy-2-hydroxymethyl-6,10,10-trimethyltricyclo-[6.3.0.$0^{2,5}$]undecan-3-ones (**10** and **11**). Subsequently, **10** was reduced with sodium borohydride to give isomeric 6-hydroxymethyl-6,10,10-trimethyltricyclo-[6.3.0.$0^{2,5}$]undecan-3,6-diols (**12** and **13**), while **11** yielded only **14**, the isomer of **12** and **13**, on the same treatment. The configuration of the methyl group can be deduced by NMR analysis; *i.e.*, the signals at δ: 1.22 in **6** ascribable to the newly introduced methyl groups have been changed by the reduction of the ester group to 1.12 in **9**, but the 1.12 in **5** has remained unaffected, as appears at 1.12 in **8**. Therefore, from the difference in the chemical shifts, $\Delta\delta_{(5-8)}=0.00$ and $\Delta\delta_{(6-9)}=0.10$, the methyl groups of **5** and **8** may be considered to be *trans* to the substituents carrying oxygen at the quarternary carbon (C-2), while those of **6** and **9** are *cis*. The NMR spectra of **12**, **13**, and **14** also disclosed a stereochemical point: only **13** revealed the methine proton signal (a triplet), which is ascribable to the secondary alcohol on the cyclobutane ring, coupled with the adjacent methylene group, at δ; 4.07 (J=7 Hz); on the other hand, **12**, at 4.10 (br. m), and **14**, at 4.03 (br. m), disclosed a further splitting due to a long-range coupling with the C-6 methine proton. Since such long range couplings arise from the *W*-letter-like geometry, the hydroxyl group of the cyclobutanol of **13** must be *cis* to the methine proton at the ring juncture (C-5), but those of **12** and **14** are *trans*. Independently, an attempted formation of the acetals of **12**, **13**, and **14** with 2,2-dimethoxypropane established the correctness of the assumption; only **13** yielded a cyclic acetal 5,5,10,14,14-pentamethyl-4,6-dioxatetracyclo[10.3.0.-$0^{2,7}$.$0^{2,9}$]pentadecane (**15**), at room temperature, while **12** or **14** resulted in the recovery of the respective starting material, plus unidentified products. The stereochemistry shows that the reduction has occurred preferentially from the same side of the oxygen functions in the molecules, which can form the metal-coordinated intermediate.

This strategy on the synthesis can be extended to the parent protoilludene from **2**. To prepare **2**, a primary choice must be a well known procedure,[6] *i.e.*, the photoaddition of acetylacetone with 4,4-dimethylcyclopentene, followed by the cyclization. However, the photoaddition in this case has been shown to be impractical because of its slow rate. Consequently, **2** was prepared by derivation from **1** as follows: The reaction of **1** with 1,2-ethanediol afforded a 1,3-dioxolane, **16**, which was then reduced by LAH and hydrolyzed by TsOH to give a hydroxy derivative (**17**). An acetate of **17**, *cis*-2-acetoxymethyl-8,8-dimethylbicyclo[4.3.0]-non-2-en-4-one (**18**), was reduced with zinc in acetic acid to form **2**. The photochemical cycloaddition of **2** with **3** produced two photocycloadducts, 3,3-dimethoxy-2,10,10-trimethyltricyclo[6.3.0.$0^{2,5}$]undecan-6-ones (**19** and **20**). Thus, the replacement of the ester group on the quaternary carbon with a methyl group resulted in an inferior stereoselectivity. The Grignard methylation, followed by a mild hydrolysis of **19** and **20**, produced cyclobutanone derivatives, 2,6,10,10-tetramethyl-3-oxotricyclo[6.3.0.$0^{2,5}$]undecan-6-ols (**21** and **22** respectively). By reduction with sodium borohydride, **21** produced an epimeric pair of glycols, 2,6,10,10-tetramethyltricyclo[6.3.0.$0^{2,5}$]undecan-6-ols (**23** and **24**), while **22** produced **25**, the isomer of **23** and **24**, as the

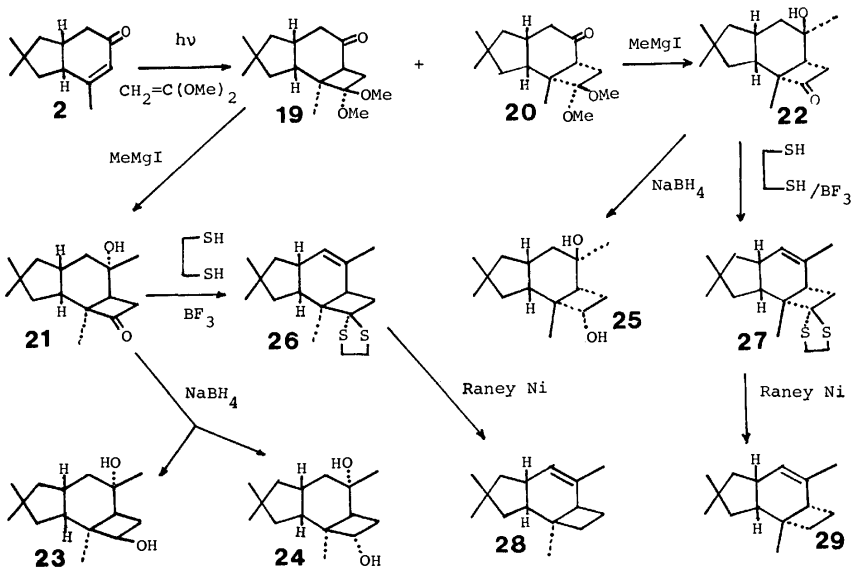

Scheme 2.

sole product. The configurations of their hydroxyl groups were again obtained by means of the NMR spectra: **24** showed a triplet at δ: 4.15 (t, J=8 Hz), but **23** (at 3.68) and **25** (at 3.89) showed multiplets. Therefore, only **24** has a *trans*-relationship to two methine protons on the cyclobutane ring. Both **21** and **22** were converted into 1,3-dithiolanes, **26** and **27**, accompanied by the dehydration of the tertiary alcohol function.[7] The Raney nickel desulfurization of these thio-acetals afforded the parent protoillud-7-ene (**28**), *cis-transoid-cis*-2,6,10,10-tetramethyltricyclo[6.3.0.$0^{2,5}$]undec-6-ene, and epi-protoillud 7-ene (**29**). The identity of **28** with the previous sample was proved by NMR comparison with the reported data.[8,9] Consequently, this constitutes an alternative total synthesis of **28** and its related derivatives.

Although the above synthesis of the derivatives with the correct stereochemistry left no doubt as to the working hypothesis, we have also carried out an X-ray crystallographic analysis in order to provide independent evidence. Since every trial of the halogenated derivatives has failed, a halogen-free derivative, **9**, was submitted to the analysis. The single crystal of **9**, monoclinic, belongs to the space group C2/c, and its crystal data showed the following features: a=15.138, b=11.486, c=20.744$\times 10^{-8}$ cm, β=112.2°, d_x=1.186 g/cm^3, and Z=8. The 1278 non-zero reflections with (F_o) $-2.3\,\sigma$ (F_o) were collected on a Syntex P$\bar{1}$ four-circle diffractometer with graphite-monochromated Mo K_α radiations in the θ-2θ scanning mode. The structure was solved by the direct method.[10] After several cycles of block diagonal least-squares refinement with anisotropic thermal parameters for non-hydrogen atoms and with isotropic ones for hydrogen atoms, except for one of the hydroxyl hydrogens, the final R value was 0.05. Figure 1 shows the structure views along the β-axis.

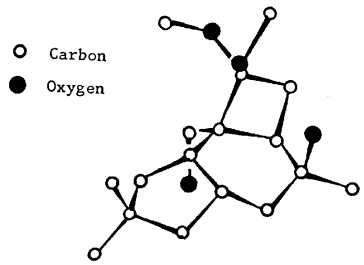

Fig. 1.

Meanwhile, we have carried out some deoxygenation reactions of the previously obtained protoilludanone, 2-acetoxymethyl-6,10,10-trimethyltricyclo[6.3.0.$0^{2,5}$]-undecan-7-one (**30**).[3] The LAH reduction of **30** afforded 2-hydroxymethyl-6,10,10-trimethyltricyclo-[6.3.0.$0^{2,5}$]undecan-7-ol (**31**), an oil. The acetylation of **31** occurred at only the primary alcohol group to give a monoacetate (**32**), but a chromium(VI) oxide oxidation in pyridine gave a keto aldehyde, 2-formyl-6,10,10-trimethyltricyclo[6.3.0.$0^{2,5}$]undecan-7-one (**33**), in a good yield. Upon treatment with 1,2-ethanedithiol and boron trifluoride etherate, **33** formed a mono(ethylenedithioacetal) (**34**). The Raney nickel desulfurization of **34** gave 2,6,10,10-tetramethyltricyclo[6.3.0.$0^{2,5}$]-undecan-7-one (**35**), which corresponds to 8-oxoprotoilludane; it was then converted to a hydroxy derivative, **36**. An acetate (**37**) of **36** could be prepared only under forced conditions, in acetic anhydride with boron trifluoride, showing the sterically hindered environment of the hydroxyl group.

Finally, we would like to make a comment on the biogenesis of the pterosines (*seco*-protoilludanes).[11] Sakan *et al.*[12] have pointed out that, based on the actual *in vitro* transformation, hypacrone (**C**), a congener *seco*-illudane derivative from brackens, must be a precursor. However, as is shown in the present experiments, oxygenated protoilludanes, like **5** or **6**, caused a retro-aldol cleavage into a pterosane skeleton. Therefore, the oxygenated protoilludanes and their relatives are likely to give these widely distributed aromatic metabolites *in vivo*.

Experimental

The mp's, determined with a Yanagimoto Model apparatus, are uncorrected. The ^{1}H- and ^{13}C-NMR spectra were measured, unless otherwise stated, in $CDCl_3$ by means of an FX 100 Model spectrometer, Nippon Denshi Co. (JEOL), while the chemical shifts expressed are the δ values from the internal standard, Me_4Si. The IR spectra were taken by an A-102 Model spectrometer, Nippon Bunko Kogyo Co. (JASCO), in CCl_4 solutions or KBr disks. The mass spectra were taken by means of an OS G1 Model spectrometer, JEOL, and the high-resolution figures were obtained by visual readings on the photographic plates. The high-pressure liquid chromatography was performed by means of an ALC 440/110 Model Apparatus, Nippon Waters Co. The elemental analyses were performed at The Elemental Analyses Center, The Faculty of Science, Kyushu University.

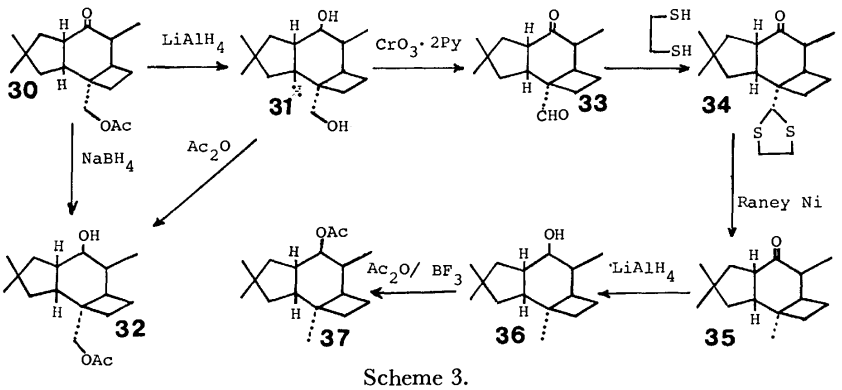

Scheme 3.

*An Attempted Photoreaction of **1** with 1,1-Dichloroethene.* A mixture of **1** (50 mg) and 1,1-dichloroethene (0.3 cm³) was externally irradiated by means of a high-pressure mercury lamp for 6 h. The NMR analysis revealed only signals ascribable to the recovered materials.

*Photocycloaddition of **1** with Vinyl Acetate.* A mixture of **1** (30 mg) and vinyl acetate (0.5 cm³) was externally irradiated for 6 h. The NMR spectral analysis indicated the occurrence of at least three photoadducts. A silica-gel column fractionation showed an extensive decomposition to aldehydic compounds. No further work was carried out.

*Photocycloaddition Reaction of **1** with **3**.* The freshly prepared **3**, from 2-chloro-1,1-dimethoxyethane (8 g) and potassium *t*-butoxide, was mixed with **1** (1.2 g) and then externally irradiated through a Pyrex glass filter by means of a 400 W high-pressure mercury lamp at 15—20 °C for 20 h under a nitrogen atmosphere. After the evaporation of the volatile material, the residue was purified on a silica-gel column; subsequent elution from ethyl acetate–hexane (1 : 9) yielded a colorless oil, **4**, 1.2 g (67%) [Found: C, 65.81%; H, 8.47%. Calcd for $C_{17}H_{26}O_5$: C, 65.78; H, 8.44%. δ: 1.05 (3H, s), 1.10 (3H, s), 1.2—2.9 (11H, m), 3.20 (3H, s), 3.27 (3H, s), and 3.76 (3H, s). δ (C): 31.9, 32.2 (2C), 35.6, 39.1 (2C), 40.1, 42.6, 43.0, 47.8, 49.3, 50.1, 51.8, 65.7, 103.2, 172.4, and 211.3], which was homogeneous in respect to NMR and gas-liquid chromatography.

*The Grignard Methylation of **4**.* To methylmagnesium iodide prepared from methyl iodide (2.3 g) in ether (20 cm³), an ethereal solution (20 cm³) of **4** (610 mg) was added, drop by drop, over a 3-h period at 0—5 °C; the mixture was then refluxed for 3 h. The mixture was then hydrolyzed and extracted by ether. The extracts were dried ($MgSO_4$) and chromatographed on a silica-gel column to give a colorless oil (420 mg), which was further fractionated by a pre-packed silica-gel column to give colorless crystals, **5** (mp 95—96 °C (from ethyl acetate–hexane); 300 mg (47%) [Found: C, 65.99; H, 9.21%. Calcd for $C_{18}H_{30}O_5$: C, 66.23; H, 9.26%. δ: 0.99 (3H, s), 1.03 (3H, s), 1.12 (3H, s), 1.4—1.9 (7H, m), 1.90 (1H, br. s), 2.1—2.7 (4H, m), 3.19 (3H, s), 3.35 (3H, s), and 3.71 (3H, s). δ (C): 27.6, 30.4, 30.9, 31.3, 34.6, 36.0, 36.6, 40.3 (2C), 44.1, 48.8, 49.6, 50.6, 51.6, 59.8, 70.1, 102.1, and 174.7]), and a colorless oil, **6** (80 mg (12%)[Found: C, 65.95; H, 9.33%. δ: 0.99 (3H, s), 1.01 (3H, s), 1.22 (3H, s), 1.2—2.7 (12H, m), 2.82 (1H, br. s), 3.30 (3H, s), and 3.69 (3H, s). δ (C): 29.7, 30.9, 31.0, 31.4, 34.2, 36.1, 36.8, 37.2, 41.3, 43.7, 47.5, 49.9, 50.3, 51.4, 61.6, 68.5, 103.7, and 173.7]).

*An Acid-catalyzed Formation of a γ-Lactone (**7**) from **5**.* An anhydrous benzene solution (10 cm³) of **5** (10 mg) and BF_3 etherate (60 mg) was kept at room temperature for 5 h. After hydrolysis, the mixture was extracted (ether) and chromatographed on silica gel to give **7** (colorless needles, mp 90—91 °C (from hexane), 7 mg [Found: C, 68.08; H, 8.49%. Calcd for $C_{16}H_{24}O_4$: C, 68.54; H, 8.63%. δ: 0.99 (3H, s), 1.09 (3H, s), 1.42 (3H, s), 3.64 (3H, s), and 1.1—3.1 (12H, m). δ (C): 28.5, 30.2, 31.4, 34.4, 35.9, 36.7, 37.3, 37.5, 38.0, 40.7, 45.7, 46.5, 51.8, 85.2, 174.1, and 175.9]).

*Conversion of **5** to a Keto Glycol, **10**.* An anhydrous ether solution (20 cm³) of **5** (100 mg) was refluxed with LAH (12 mg) for 3 h. Then, a few drops of water were added to the mixture, and the resultant supernatant was collected by decantation. The rest of the solution was acidified and extracted with ether. The combined extract was purified on a silica-gel column to give a colorless oil (68 mg, 75%), **8** [δ: 0.96 (3H, s), 1.04 (3H, s), 1.12 (3H, s), 1.2—2.6 (12H, m), 3.22 (3H, s), 3.23 (3H, m), 3.51 (1H, d, J=11 Hz), and 3.76 (1H, d, J=11 Hz). δ (C): 27.7, 27.9, 29.8, 31.7, 34.8 (2C), 37.7, 38.3, 39.1, 42.8, 49.4, 49.6, 50.0, 54.4, 66.6, 71.7, and 104.2]. Subsequently, an acetone solution (30 cm³) of **8** (50 mg) and TsOH (2 mg) was stirred at room temperature for 2 h. Subsequent silica-gel chromatography of the mixture, using ethyl acetate–hexane (2 : 3), afforded colorless needles, **10** (mp 152—153.5 °C (from ethyl acetate–hexane), 39 mg (94%) [Found: C, 71.32; H, 9.55%. Calcd for $C_{15}H_{24}O_3$: C, 71.39; H, 9.59%. δ: 0.89 (3H, s), 1.02 (3H, s), 1.24 (3H, s), 1.1—1.9 (9H, m), 2.2—2.6 (2H, m), 3.64 (1H, d, J=10 Hz), and 3.79 (1H, d, J=10 Hz). δ (C): 27.0, 29.3, 29.8, 31.9, 35.5, 35.8, 38.1, 38.6, 42.6, 47.8, 49.8, 65.5, 69.4, 72.2, and 216.2]).

*Conversion of **6** to **11**.* Much as in the above conversion of **5** to **10**, **6** (36 mg) was reduced with LAH to yield **9** (colorless plates, mp 128.5—129.5 °C (from ethyl acetate–hexane), 30 mg (86%) [δ: 0.99 (3H, s), 1.07 (3H, s), 1.12 (3H, s), 1.2—1.8 (8H, m), 2.2—2.8 (4H, m), 3.27 (3H, s), 3.34 (3H, s), and 3.60 (2H, m). δ (C): 29.7, 30.3, 30.5, 31.5, 33.7, 35.4, 35.8, 36.3, 41.9 (2C), 47.3, 49.9, 50.4, 53.9, 67.9, 68.3, and 106.1]). Subsequently, an acetone solution (30 cm³) of **9** (28 mg) and TsOH (2 mg) was kept at room temperature for 3 h. The mixture was then chromatographed (silica gel) to give colorless needles, **11** (mp 137—138 °C (from ethyl acetate–hexane), 22 mg (91%) [Found: C, 71.27; H, 9.68%. Calcd for $C_{15}H_{24}O_3$: C, 71.39; H, 9.59%. δ: 0.96 (3H, s), 1.04 (3H, s), 1.31 (3H, s), 1.15—2.0 (6H, m), 2.3—2.75 (2H, m), 2.18 (1H, t, J=7 Hz), 3.10 (2H, d, J=7 Hz), 3.61 (1H, d, J=12 Hz), and 3.84 (1H, d, J=12 Hz). δ (C): 29.1, 30.5, 31.5, 33.3, 34.7, 36.6, 37.2, 41.1, 41.7, 45.1, 47.5, 65.9, 69.1, 69.4, and 213.1]).

*The Sodium Borohydride Reduction of **10**: The Formation of Triols (**12** and **13**).* A methanol solution (20 cm³) of **10** (28 mg) was treated with $NaBH_4$ (5 mg) at 0—5 °C for 3 h. The mixture was then diluted with water, acidified with dil HCl, and extracted with ether. Subsequent silica-gel chromatography of the extracts yielded colorless needles, **13** (mp 95—96 °C (from ethyl acetate), 27 mg (95%) [Found: C, 70.70; H, 10.30%. Calcd for $C_{15}H_{26}O_3$: C, 70.83; H, 10.30%. δ: 1.00 (3H, s), 1.07 (3H, s), 1.15 (3H, s), 1.2—1.95 (8H, m), 2.2—2.7 (3H, m), 3.58 (2H, s), and 4.07 (1H, t, J=7 Hz). δ (C): 27.8, 29.0, 29.7, 30.4, 31.6, 33.3, 35.2, 37.6, 40.2, 40.6, 42.4, 49.4, 68.1, 68.5, and 72.0]), together with a colorless solid, **12** (1.4 mg (5%) [*m/e*, 254 (M^+). δ: 0.90 (3H, s), 1.00 (3H, s), 1.12 (3H, s), 1.2—2.9 (14H, m), 3.78 (2H, m), and 4.10 (1H, m). δ (C): 27.2, 29.3, 29.4, 32.2, 32.3, 37.1, 38.2, 39.2, 40.1, 43.0, 48.3, 50.1, 67.1, 72.4, and 92.6]), which was homogeneous with respect to high-pressure liquid chromatography.

*The Reduction of **11** to **14**.* A methanol solution (20 cm³) of **11** (22 mg) was treated with $NaBH_4$ (5 mg) for 3.5 h. The product mixture was then extracted with ethyl acetate and purifed by silica-gel chromatography to yield colorless needles, **14** (mp 171—172 °C (from ethyl acetate), 21 mg (95%) [Found: 70.64; H, 10.27%. Calcd for $C_{15}H_{26}O_3$: C, 70.83; H, 10.30%. δ: 1.00 (3H, s), 1.05 (3H, s), 1.10 (3H, s), 1.37—2.05 (8H, m), 2.25—2.65 (3H, m), 3.52 (1H, d, J=11 Hz), 3.65 (1H, d, J=11 Hz), and 4.03 (1H, m). δ (C): 29.8, 29.9, 31.1, 31.7, 34.9, 35.0, 37.0, 41.4, 42.3, 42.7, 48.5, 50.8, 67.3, 68.2, and 70.4]).

*Formation of an Acetal (**15**) from **13**.* A mixture of **13** (12 mg) and 2,2-dimethoxypropane (30 cm³) was kept at room temperature for 20 d. The mixture was then heated in *vacuo* to remove the volatile material. The NMR spectrum [δ: 0.98 (3H, s), 1.06 (3H, s), 1.12 (3H, s), 1.2—2.8 (11H, m), 3.11 (3H, s), 3.22 (3H, s), 3.30 (2H, m), and 3.98 (1H, t, J=8 Hz)] confirmed the formation of **15**. Every attempt to purify the material caused hydrolysis into **13**.

*An Attempted Acetal Formation of **12** or **14**.* Similarly, solutions of 2,2-dimethoxypropane (30 cm³) of both **12** and **14** (10 mg) were kept at room temperature for 20 d. The residues subsequently obtained by the evaporation of the volatile material were shown by NMR spectrometry to consist of only the recovered **12** and **14**.

*Conversion of **1** to **17**.* A sample of **1** (1.2 g) and TsOH (50 mg) were dissolved in a mixture of anhydrous benzene (150 cm³) and 1,2-ethanediol (3.1 g), and then the solution was heated for 5 h with an azeotropic removal of water. Subsequently, the mixture was washed with water and extracted by benzene. Silica-gel chromatography of the mixture yielded a colorless oil, **16** (1.5 g (quantitative) [Found: C, 67.47; H, 8.32%. Calcd for $C_{15}H_{22}O_4$: C, 67.64; H, 8.33%. δ: 1.02 (3H, s), 1.06 (3H, s), 1.2—1.4 (2H, m), 1.6—2.0 (4H, m), 2.50 (1H, m), 2.95 (1H, m), 3.71 (3H, s), 4.01 (4H, m), and 6.59 (1H, br. s). δ (C): 30.6, 31.2, 36.0, 36.8, 38.1, 38.8, 45.8, 46.4, 51.6, 64.5, 64.7, 105.5, 135.3, 136.3, and 167.1]). Subsequently, an anhydrous ether solution (50 cm³) of **16** (1.4 g) was refluxed with LAH (490 mg) for 2 h. After hydrolysis, the mixture was extracted with ether, dried (Na_2SO_4), and evaporated to remove the solvent. The residue was then dissolved in acetone (50 cm³) and treated with TsOH (10 mg). A colorless oil thus obtained, **17**, was purified (silica gel) to yield 790 mg (75%) [Found: C, 74.42; H, 9.29%. Calcd for $C_{12}H_{18}O_2$: C, 74.19; H, 9.34%. δ: 1.05 (3H, s), 1.10 (3H, s), 1.2—1.9 (3H, m), 2.3—2.4 (2H, m), 2.6—2.8 (3H, m), 4.22 (2H, br. s), and 6.08 (1H, s). δ (C): 30.6, 31.0, 38.0, 39.0, 39.8, 41.1, 45.8, 46.6, 64.0, 121.5, 166.4, and 200.3].

*Conversion of **17** to **2**.* An acetic anhydride solution (6 cm³) of **17** (755 mg) was kept at room temperature for 12 h. The residue obtained by removal of the volatile material *in vacuo* was chromatographed on silica gel to give a colorless oil, **18** (790 mg (86%) [Found: 71.26; H, 8.50%. Calcd for $C_{14}H_{20}O_3$: C, 71.16; H, 8.53%. δ: 1.05 (3H, s), 1.12 (3H, s), 1.2—1.8 (3H, m), 2.12 (3H, m), 2.3—2.5 (2H, m), 2.6—2.8 (3H, m), 4.65 (2H, br. s), and 5.95 (1H, s). δ (C): 20.5, 30.5, 30.9, 37.8, 38.8, 39.9, 40.8, 45.6, 46.4, 64.3, 122.9, 159.0, 170.0, and 198.2]). Subsequently, this **18** was dissolved in acetic acid (80 cm³) and reduced with activated zinc dust (8 g) for 6 h under reflux. The mixture was then filtered, washed with dil NaOH and $NaHCO_3$, and extracted with hexane. By silica-gel chromatography, the extract yielded a colorless oil, **2** (292 mg (50%) [Found: C, 80.69; H, 10.17%. Calcd for $C_{12}H_{18}O$: C, 80.85; H, 10.18%. δ: 1.04 (3H, s), 1.09 (3H, s), 1.2—2.0 (4H, m), 1.91 (3H, d, J=1 Hz), 2.3—2.4 (2H, m), 2.5—2.8 (2H, m), and 5.79 (1H, q, J=1 Hz). δ (C): 23.2, 30.5, 30.9, 37.5, 38.5, 40.5, 43.9, 45.6, 46.6, 125.4, 163.1, and 199.3]).

*The Photochemical Cycloaddition of **2** with **3**: The Formation of Epimeric 1 : 1-Adducts (**19** and **20**).* A benzene solution (100 cm³) of **2** (680 mg) and **3**, prepared from 2-chloro-1,1-dimethoxyethane (5 g), was irradiated externally by means of a 400-W high-pressure mercury lamp through a Pyrex glass filter for 60 h at 0—5 °C. After the evaporation of the volatile materials, the residue was chromatographed on silica gel to afford an isomeric mixture of photoadducts (**19** and **20**), which was then separated by means of a pre-packed silica-gel column to give two colorless oils, **19** (152 mg (15%) [Found: C, 71.90; H, 9.73%. Calcd for $C_{16}H_{26}O_3$: C, 72.14; H, 9.84%. δ: 1.01 (3H, s), 1.11 (3H, s), 1.28 (3H, s), 1.5—2.0 (4H, m), 2.1—2.9 (7H, m), 3.08 (3H, s), and 3.19 (3H, s). δ (C): 21.8, 31.3, 31.5, 32.3, 35.4, 41.6, 41.7, 42.9, 43.7, 43.9, 47.9, 48.6, 50.1, 54.8, 104.5, and 213.3]) and **20** (48 mg (5%) [Found: C, 71.91; H, 9.80%. δ: 0.94 (3H, s), 1.0—1.9 (5H, m), 1.08 (3H, s), 1.33 (3H, s), 2.0—2.9 (6H, m), 3.18 (3H, s), and 3.20 (3H, s). δ (C): 25.3, 28.0, 29.9, 32.0, 38.5, 40.1, 42.8, 43.0, 43.6, 44.7, 48.6, 48.7, 49.8, 55.1, 104.0, and 216.6]).

*The Grignard Methylation Reaction of **19**: The Formation of **21**.* To an ether solution (15 cm³) of methylmagnesium iodide (prepared from 500 mg of methyl iodide), an ethereal solution of **19** (82 mg) was added, drop by drop. The mixture was refluxed for 2 h and then extracted with ether. The extract was dissolved in acetone (30 cm³) containing TsOH (5 mg) and kept at room temperature for 1 h. After the removal of the solvent, the residue was chromatographed on a silica-gel column to yield **21** (81 mg (85%), colorless crystals, mp 62—63.5 °C [Found: C, 75.94; H, 10.27%. Calcd for $C_{15}H_{24}O_2$: C, 76.22; H, 10.24%. δ: 0.96 (3H, s), 1.05 (3H, s), 1.19 (3H, s), 1.1—2.0 (2H, m), 1.28 (3H, s), 2.2—2.7 (8H, m), and 3.0—3.2 (2H, m). δ (C): 22.5, 29.4, 30.6, 31.6, 33.4, 36.4, 37.0, 41.2, 41.7, 42.5, 43.9, 47.8, 63.3, 69.3, and 213.3]).

*The Grignard Methylation of **20** to **22**.* Similarly, **20** (39 mg) was methylated by methylmagnesium iodide and hydrolyzed in acetone with TsOH to give colorless plates, **22** (33 mg (80%), mp 135—136 °C [Found: C, 75.99; H, 10.18%. δ: 0.89 (3H, s), 1.05 (3H, s), 1.11 (3H, s), 1.37 (3H, s), 1.4—1.75 (5H, m), 1.8—2.5 (5H, m), and 3.0—3.1 (2H, m). δ (C): 24.8, 27.2, 28.9, 29.7, 36.4, 38.3, 38.8, 41.6, 42.6, 43.4, 43.5, 48.7, 65.7, 71.9, and 216.7]).

*The Sodium Borohydride Reduction of **21**: The Formation of **23** and **24**.* A methanol solution (20 cm³) of **21** (18 mg) was treated with $NaBH_4$ (10 mg) for 3 h at 0—5 °C. After the hydrolysis (dil HCl) of the mixture, the product was extracted with ethyl acetate and chromatographed on a silica-gel column to give colorless needles, **23** (mp 116.5—117 °C, 17 mg (93%) [Found: C, 75.37; H, 10.94%. Calcd for $C_{15}H_{26}O_2$: C, 75.58; H, 11.00%. δ: 0.99 (3H, s), 1.04 (3H, s), 1.09 (3H, s), 1.19 (3H, s), 1.2—2.0 (10H, m), 2.05—2.6 (3H, m), and 3.68 (1H, m). δ: (C): 26.4, 28.7, 30.1, 31.1, 31.2, 34.3, 36.5 (2C), 41.6, 42.9, 44.7, 46.5, 48.0, 69.3, and 76.6]), together with an epimer, **24** (colorless needles, mp 106—107 °C, ≈1 mg [Found: *m/e*, 238 (M^+). δ: 0.96 (3H, s), 1.04 (3H, s), 1.05 (3H s), 1.13 (3H, s), 1.1—2.6 (13H, m), and 4.15 (1H, t, J=8 Hz). δ (C): 19.5, 30.1, 31.1, 31.9, 32.1, 33.1, 36.2, 41.5, 42.0, 42.7, 43.2, 45.8, 47.3, 69.3, and 71.8]).

*The Sodium Borohydride Reduction of **22** to **25**.* A methanol solution (20 cm³) of **22** (15 mg) was treated with $NaBH_4$ (9 mg) for 3 h at 0—5 °C. The mixture was then acidified (dil HCl), extracted (ethyl acetate), and chromatographed (silica gel) to yield colorless needles, **25** (mp 170—171 °C (from hexane–ethyl acetate), 14.4 mg (95%) [Found: C, 75.31; H, 11.13%. δ: 0.95 (3H, s), 1.06 (3H, s), 1.14 (3H, s), 1.22 (3H, s), 1.2—2.4 (13H, m), and 3.89 (1H, m). δ (C): 28.7, 29.6, 30.8, 30.9, 37.3, 38.0, 39.1, 42.7 (3C), 46.4, 46.8, 47.2, 71.6, and 74.0]).

*The Formation of a Dithiolane (**26**) from **21**.*[7] To a glacial acetic acid solution (2 cm³) of **21** (44 mg) and 1,2-ethanedithiol (75 mg), BF_3 etherate (50 mg) was added, after which the mixture was kept at room temperature for 12 h. The mixture was then diluted with water and extracted with hexane. The extract was chromatographed (silica gel) to give a colorless oil, **26** (30 mg (55%) [δ: 0.99 (3H, s), 1.00 (3H, s), 1.39 (3H, s), 1.60 (3H, s), 1.0—2.0 (5H, m), 2.0—2.4 (3H, m), 2.70 (1H, m), 3.0—3.3 (4H, m), and 5.29 (1H, br. s)]).

*The Thio-acetal Formation of **22** to **27**.*[7] Similarly, a glacial acetic acid solution (2 cm³) of **22** (15 mg) and 1,2-ethanedithiol (50 mg) was kept at room temperature for 12 h. The mixture was then hydrolyzed (dil HCl), extracted (ethyl acetate), and chromatographed (silica gel) to give colorless oils, **27** (14 mg (93%) [δ: 1.01 (3H, s), 1.03 (3H, s), 1.29 (3H,

s), 1.58 (3H, br. s), 1.1—3.1 (8H, m), 3.05—3.3 (4H, m), 3.44 (1H, m), and 5.13 (1H, s)]).

The Raney-nickel Desulfurization of ***26****: The Formation of Protoillud-7-ene (****28****).* An ethanol solution (30 cm³) of **26** (30 mg) was refluxed with Raney nickel (W-1) (2 g) for 5 h. Then, the catalyst was removed by filtration and washed several times with ethanol. The solvent was evaporated *in vacuo* to leave a colorless oil, which was subsequently chromatographed (silica gel) to give **28** (6.3 mg (30%) [δ (C): 21.3, 24.4, 26.3, 29.7, 30.2, 32.1, 37.5, 38.5, 39.3, 40.8, 41.7, 45.5, 48.2, 125.6, and 132.1]). The ^{1}H-NMR [δ: 0.98 (6H, s), 1.17 (3H, s), 1.59 (3H, br. s), 1.9—2.8 (11H, m), and 5.11 (1H, br. s)] was identical with that of the authentic sample.

The Raney-nickel Desulfurization of ***27****.* Similarly, **27** (19 mg) and Raney nickel (W-1) (1 g) were mixed in ethanol (30 cm³) and then refluxed for 5 h to give and *epi*-protoillud-7-ene, **29** (3 mg (20%) [Found: *m/e*, 204 (M^+). δ: 0.98 (3H, s), 1.01 (3H, s), 1.11 (3H, s), 1.2—2.2 (11H, m), 1.61 (3H, br. s), and 5.42 (1H, br. s). δ (C): 20.7 (2C), 28.5, 28.8, 29.2, 29.8, 38.1, 39.2, 40.5, 42.0, 42.3, 43.5, 48.6, 123.9, and 134.0]).

The LAH Reduction of ***30****.* A sample of **30** (120 mg), prepared by a previously described method,[3] was dissolved in anhydrous ether (120 cm³) and reduced by LAH (20 mg) at 35 °C. The reaction mixture was then hydrolyzed, extracted with ether, and chromatographed (silica gel) to give **31** (a colorless oil, 110 mg (95%) [Found: M. W., 238.1959. Calcd for $C_{15}H_{26}O_2$: 238.1933. δ: 0.92 (3H, s), 0.97 (3H, d, J=7 Hz), 1.01 (3H, s), 1.2—2.6 (14H, m), 3.49 (1H, br. s), 3.50 (1H, d, J=10 Hz), and 3.64 (1H, d, J=10 Hz). δ (C): 14.8, 17.7, 26.5, 26.9, 29.4, 30.0, 36.6, 37.3, 40.0, 41.7, 43.1, 44.7, 47.9, 69.6, and 77.5]) as the sole product.

The Reduction of ***30*** *with Sodium Borohydride.* A methanol solution (10 cm³) of **30** (20 mg) was treated with $NaBH_4$ (10 mg) at 0—15 °C for 2 h. The mixture was then acidified by dil HCl and extracted with ether. Subsequent silica-gel chromatography of the extract yielded a colorless oil, **32** (15 mg (74%) [Found: M. W., 280.2040. Calcd for $C_{17}H_{28}O_3$: 280.2038. δ: 0.92 (3H, s), 0.99 (3H, d, J=5 Hz), 1.02 (3H, s), 1.0—2.6 (13H, m), 2.07 (3H, s), 3.51 (1H, br, s), 3.91 (1H, d, J=11.5 Hz), and 4.15 (1H, d, J=11.5 Hz). ν: 3640—3500, 2940, 1735, and 1240 cm^{-1}]).

The Acetylation of ***31****.* A sample of **31** (10 mg) was treated with acetic anhydride (0.5 cm³) and pyridine (0.3 cm³) at room temperature for 12 h. The usual work-up of the mixture on a silica-gel column subsequently yielded a colorless oil (10 mg, 85%), which was identical with the authentic **32** obtained by the $NaBH_4$ reduction of **30**.

The Chromium(VI) Oxide Oxidation of ***31****: The Formation of 8,13-Dioxoprotoilludane (****33****).* A dichloromethane solution (5 cm³) of **31** (10 mg) was treated with the complex prepared from CrO_3 (30 mg) and pyridine (47 mg) at room temperature for 15 min. The supernatant was collected by decantation, and the residue was washed with ether. The combined organic solution was washed with dil NaOH and dil HCl. The extract was then chromatographed (silica gel) to yield a colorless oil, **33** (8.5 mg (86%) [Found: M. W., 234.1698. Calcd for $C_{15}H_{22}O_2$: 234.1620. δ: 0.96 (3H, d, J=7 Hz), 0.98 (3H, s), 1.09 (3H, s), 1.2—2.2 (8H, m), 2.4—3.4 (4H, m), and 9.57 (1H, s). δ (C): 10.4, 16.9, 25.2, 27.8, 29.5, 39.3 (2C), 40.9, 44.5, 44.7, 44.8, 51.2, 51.3, 201.0, and 215.8]).

The Reaction of 1,2-Ethanedithiol with ***33****.* To a benzene solution (10 cm³) of **33** (50 mg), 1,2-ethanedithiol (400 mg) was added, together with the BF_3 etherate (0.2 cm³). The mixture was kept at room temperature for 20 min, and then it was diluted with water and extracted by ether. The extracts was chromatographed (silica gel) to give a colorless oil, **34**, (52 mg (75%) [δ: 0.88 (3H, d, J=7 Hz), 0.98 (3H, s), 1.06 (3H, s), 1.2—3.2 (12H, m), 3.26 (4H, s), and 4.85 (1H, s)]).

The Raney-Nickel Desulfurization of ***34*** *to* ***35****.* An ethanol solution (50 cm³) of **34** (50 mg) was treated with Raney nickel (W-1) (2 g) for 1 h. The mixture was then filtered, the residue was washed, and the extract was purified on a silica-gel column; the colorless oil thus obtained (25 mg, 74%) was **35** [Found: M.W., 220.1799. Calcd for $C_{15}H_{24}O$: 220.1827. δ: 0.88 (3H, d, J=6 Hz), 0.97 (3H, s), 1.08 (3H, s), 1.19 (3H, s), and 1.2—3.2 (12H, m). δ (C): 10.6, 15.9, 27.1, 27.6, 29.7, 30.6, 37.6, 39.4, 40.3, 45.4 (2C), 47.8, 50.3, 50.6, and 218.0].

The LAH Reduction of ***35*** *to* ***36****.* A sample of **35** (10 mg) was dissolved in ether (15 cm³) and reduced with LAH (5 mg) at room temperature for 3 h. The mixture was then acidified with dil HCl and extracted with ether. The chromatography (silica gel) of the extract afforded a colorless oil, **36** (8.5 mg (84%) [Found: M. W., 222.1994. Calcd for $C_{15}H_{26}O$: 222.1984. δ: 0.93 (3H, s), 0.97 (3H, d, J=7 Hz), 1.01 (3H, s), 1.08 (3H, s), 0.9—2.5 (13H, m), and 3.47 (1H, br. s). δ (C): 14.0, 16.9, 27.1, 28.6, 29.6, 30.8, 32.0, 37.7, 37.8, 42.2, 43.1, 43.5, 44.6, 47.9, and 76.7]).

An Acetylation of ***36*** *under Forced Conditions. The Formation of* ***37****:* A sample of **36** (5 mg) was dissolved in acetic anhydride (0.3 cm³) and the BF_3 etherate (0.03 cm³) for 1 h at room temperature. The mixture was then diluted with water and extracted with ether. Subsequent silica-gel chromatography of the extract gave a colorless oil, **37** (3 mg (50%) [Found: *m/e*, 264 (M^+). δ: 0.88 (3H, s), 0.91 (3H, d, J=6.5 Hz), 0.96 (3H, s), 1.08 (3H, s), 0.8—2.4 (12H, m), 2.10 (3H, s), and 4.57 (1H, br. s). ν: 2950, 1740, 1240, and 1120 cm^{-1}]).

An attempted acetylation, under ordinary conditions (acetic anhydride with pyridine at room temperature) gave only the recovered starting materials.

References

1) Part XVIII; T. Hatsui and H. Takeshita, *Bull. Chem. Soc. Jpn.*, **53**, 2655 (1980).

2) a) H. Takeshita, H. Iwabuchi, I. Kouno, M. Iino, and D. Nomura, *Chem. Lett.*, **1979**, 649; b) H. Takeshita, I. Kouno, H. Iwabuchi, M. Iino, and D. Nomura, *Kyushu Daigaku Sogo Rikogaku Kenkyuka Hokoku*, **1**, 25 (1979).

3) J. R. Hanson, T. Martin, and R. Nyfeler, *J. Chem. Soc., Perkin Trans. 1*, **1976**, 876.

4) a) A. Banerji, G. Ramakrishnan, and M. S. Chadha, *Tetrahedron Lett.*, **1974**, 1369; b) A. Konitz, M.B.-Ledochowska, Z. Dauter, A. Hempel, and B. Borowski, *ibid.*, **1977**, 3401; c) G. Magnusson, S. Thoren, and B. Wicberg, *ibid.*, **1972**, 1105; d) T. J. King, *J. Chem. Soc., Chem. Commun.*, **1977**, 727. The last paper suggested a non-farnesyl pyrophosphate route for alliacolide, a unique γ-lactone.

5) M. Fukuoka, M. Kuroyanagi, M. Toyama, K. Yoshihira, and S. Natori, *Chem. Pharm. Bull.*, **20**, 2282 (1972).

6) P. de Mayo and H. Takeshita, *Can. J. Chem.*, **40**, 440 (1963).

7) From **27**, two fluoro ketones, **D** [δ: 0.90 (3H, s), 1.05 (3H, s), 1.38 (3H, d, J=22 Hz), 1.2—2.2 (8H, m), 2.7—2.9 (2H, m), and 3.15 (1H, m). ν: 2990, 1775 cm^{-1}] and **E** [δ: 0.92 (3H, s), 1.06 (3H, s), 1.2—2.2 (11H, m), 1.25 (3H, s), and 1.29 (3H, d, J=7 Hz). ν: 2990, 1778 cm^{-1}], were obtained as by-products. Similarly, **26** formed a fluoro acetal, **F** [δ: 1.05 (3H, s), 1.12 (3H, d, J=24 Hz), 1.13 (3H, s), 1.19 (3H, s), 0.9—3.1 (11H, m), and 3.13 (4H, br. s)].

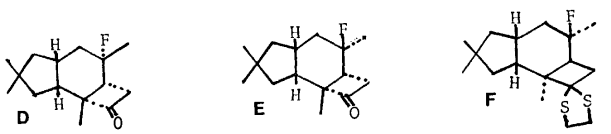

Scheme 4.

8) Y. Ohfune, H. Shirahama, and T. Matsumoto, *Tetrahedron Lett.*, **1975**, 4377.

9) S. Nozoe, H. Kobayashi, S. Urano, and J. Furukawa, *Tetrahedron Lett.*, **1977**, 1381.

10) We wish to thank The Computaion Center of Kyushu University for providing with the MULTAN '74 Program.

11) For the recent accounts; see "Terpenoids and Steroids," ed by K. H. Overton (Series of Specialist Periodical Reports, The Chemical Society, London, 1978), Vol. 8, p. 89.

12) Y. Hayashi, M. Nishizawa, and T. Sakan, *Chem. Lett.*, **1973**, 63.

The Stereochemical Course of the Photochemical Berson-Willcott Rearrangement of *exo*-1-Methoxycarbonylmethyl-3-*t*-butyl-1a,7b-dihydro-1*H*-cyclopropa[*a*]naphthalene to 7-Methoxycarbonylmethyl-5-*t*-butyl-7*H*-benzocycloheptene

Masahiko KATO,* Keizo TAKATOKU, Satoru ITO, Mitsuru FUNAKURA, and Toshio MIWA
Faculty of Science, Osaka City University, Sugimoto-cho, Sumiyoshi-ku, Osaka 558
(Received February 27, 1980)

The photolysis of (1*S*)-*exo*-1-methoxycarbonylmethyl-3-*t*-butyl-1a,7b-dihydro-1*H*-cyclopropa[*a*]naphthalene gave (7*S*)-5-*t*-butyl-7-methoxycarbonylmethyl-7*H*-benzocycloheptene by a 1,5-sigmatropic shift, proving the rearrangement to proceed with the inversion of the configuration of the migrating center.

The photochemical Berson-Willcott rearrangement of 1a,7b-dihydro-1*H*-cyclopropa[*a*]naphthalenes has been studied by Pomerantz,[1] Swenton,[2,3] and by us.[4-6] The rearrangement has thus been clarified to proceed *via* two 1,5-shift intermediates[2,3,6] (*e.g.* **2** and **3**).

In the earlier communication,[4] we clarified the rearrangement of methoxycarbonylmethyl derivative (**1**) along the path i proceeded *via* a mechanism with inversion of the configuration of C-1. Because of the molecular symmetry of **3**, it was impossible to establish the stereochemical course of path ii by using this starting material, and accordingly we chose 3-substituted derivative of **1** as a starting material. In a previous paper, we reported the photochemistry of 1a,7b-dihydro-1*H*-cyclopropa[*a*]naphthalenes (**5**) substituted with an isopropyl group at the C-3. In the present study we investigated the photolysis of the *t*-butyl homologue (**6**), with a hope to obtain much larger amount of an unsymmetrical rearrangement product of the path ii,[7] which would allow us to establish the stereochemistry of the reaction.

The starting acid, 3-*t*-butyl-1a,7b-dihydro-1*H*-cyclopropa[*a*]naphthalene-1-*exo*-carboxylic acid (**7**) was prepared from 1-*t*-butylnaphthalene (**8**) through the reaction with ethyl diazoacetate in the presence of copper powder. The acid **7** was transformed by Arndt-Eistert reaction to the next higher homologue (**6**), which was found to be thermally stable below 100 °C.[8] The methyl ester **6** in methanol was photolysed with the aid of a high pressure mercury arc (UM-452) through a Pyrex filter. The products were, in addition to **8** and a small amount of a cyclobut[*a*]indene (**9**) (*exo* : *endo*= 1 : 1), a 5*H*-benzocycloheptene (**10**) and a 7*H*-benzocycloheptene (**11**).[7]

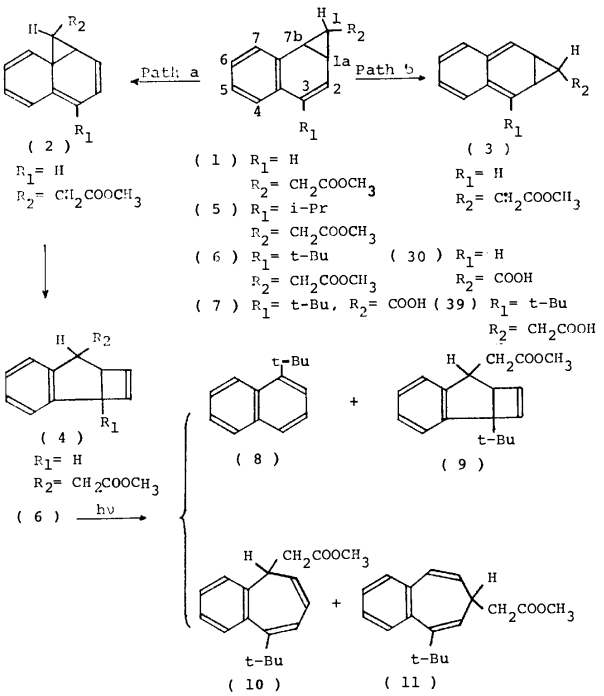

Scheme 1.

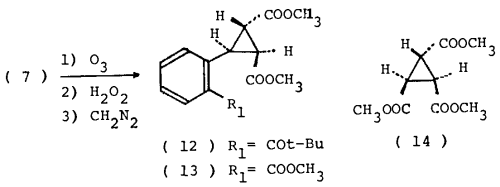

Scheme 2.

The acid **7** was carefully resolved into optically active components *via* its brucine salt. The absolute configuration of (+)-**7** was established as (1*R*) by ozonization, oxidative cleavage of the ozonide and subsequent esterification of the product with diazomethane. Of three products, (**12**—**14**), **13** was identical with a sample of known stereochemistry, (1*S*,2*S*)-3-[*o*-(methoxycarbonyl)phenyl]-1,2-bis(methoxycarbonyl)cyclopropane.[4] The optical purity of **7** was estimated, after transformation to its methyl ester, by NMR measurement with use of a chiral shift reagent, tris[3-(2,2,3,3,-4,4,4-heptafluoro-1-hydroxybutylidene)-*d*-camphorato]-europium(III). In the NMR spectra, the racemic ester showed two proton signals for the methoxycarbonyl group in equal intensities, but the (+)-ester showed one strong signal without accompanying signal more intense than 5% of the main one (Fig. 1).

The independent photolysis of each optically active ester **6** under the same conditions as described above gave the optically active esters, **9**, **10**, and **11** as shown in Table 1.

The 7*H*-benzocycloheptene, (+)-**11**, $[\alpha]_D$+127°, was hydrogenated over 10% Pd-C to give (−)-dihydro derivative (**15**), $[\alpha]_D$−61.2°, which was oxidized with purple benzene and was esterified to give a (+)-keto diester (**16**), $[\alpha]_D$+16°. In the same way, (−)-**11**, $[\alpha]_D$−89.9°, was transformed to (−)-**16**, $[\alpha]_D$−15.6°.

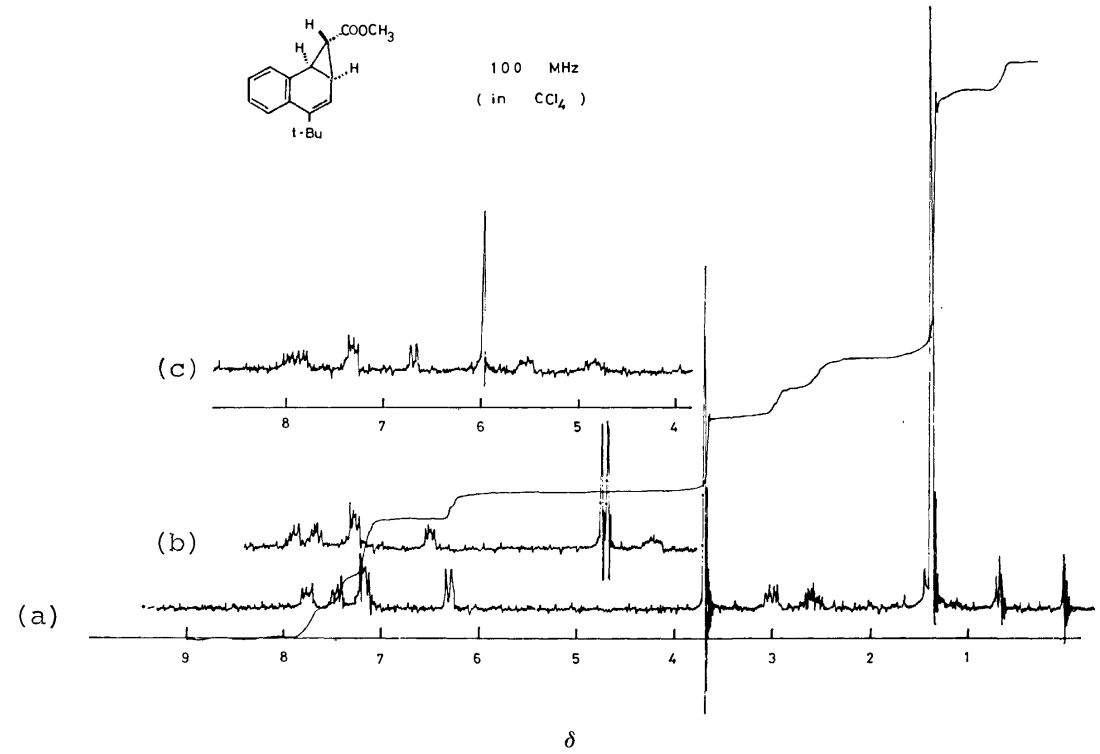

Fig. 1. ^{1}H NMR spectra of the methyl ester of **7**.
(a) Original spectrum of the racemic ester, (b) after addition of a chiral shift reagent to the above ester, (c) after addition of a chiral shift reagent to the optically active ester, obtained from (+)-acid **7**, $[\alpha]_D = +14.3°$.

Table 1. Specific rotation relationships between optically active ester **6** and the photolysis products

Starting materials		Products			
Acid **7**	Ester **6**		**9**	**10**	**11**
+14.3°	+44.7°	(**9a**)	−55°	−88.3°	+127°
		(**9b**)	+4.2°		
−13.7°	−38.6°	(not measured)			−89.9°

The molecular formula ($C_{19}H_{26}O_5$) of (+)-keto diester **16** was established by elementary analysis and the mass spectrum (M^+ 334). In the proton NMR spectrum, it showed an intense singlet of *t*-butyl at 1.24 ppm, two sharp singlets of methoxycarbonyl group at 3.65 and 3.70 ppm, and 4H broad multiplet of aromatic proton signal centered at 7.2 ppm. All the signals for aliphatic protons, except *t*-butyl one, are very similar both in the shape and the chemical shifts to those of dimethyl 2-phenylethylsuccinate **17**. In the IR spectrum, it showed two carbonyl stretching bands at 1733 and 1689 cm^{-1}, in which the former was assigned to two ester-carbonyl groups and the latter to a keto-carbonyl bound to a phenyl group. A similarity of the NMR spectrum to that of **17** and the exsistence of a disubstituted benzene ring, in addition to a consideration of the structure of the starting material **15**, lead to the structure **16** for the keto diester. The UV spectrum of **16** showed no absorption maximum near 242 nm, the λ_{max} commonly observed in the alkyl phenyl ketones, but only shoulder of ε 2200 at 242 nm. This means that the conjugation between carbonyl and phenyl groups is hindered by a bulky *t*-butyl group (dihedral angle between carbonyl sp^2 and aromatic ring planes is calculated to be 65°).[9] Because the effect of carbonyl function on the ORD curves is believed to be small when the function is located far apart from the optically active center,[10] it would be possible to determine the absolute configuration of dimethyl 2-(*o*-pivaloylphenyl)ethylsuccinate (**16**) by comparing its ORD curve with that of optically active dimethyl 2-phenylethylsuccinate (**17**) of known configuration. In general, it has been shown that L-series of the alkyl or aralkylsuccinic acid show the minus Cotton effect or minus plain curves as follows.[11]

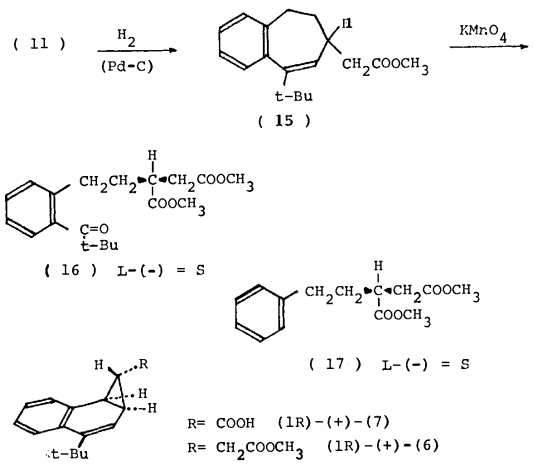

Scheme 3.

Compound	$[M]_{MeOH}$	Observed at	Type
(L)-(−)-Phenylsuccinic acid	−15450°	231 nm	minimum
(L)-(−)-Benzylsuccinic	−5260°	227 nm	minimum
(L)-(−)-2-Phenylethylsuccinic (**17**)	−4180°	222 nm	end absp.
(L)-(−)-3-Phenylpropylsuccinic	−2550°	221 nm	end absp.

The negative rotation of the ORD curve of (−)-**16** supports the (*S*)-configuration. The result shows that (−)-**11** gave (+)-**15**, which was transformed into (*S*)-(−)-**16** by oxidation.

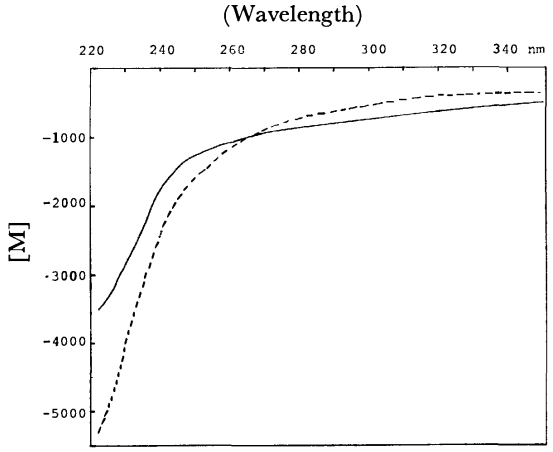

Fig. 2. ORD curves of the oxidation product **16**, $[\alpha]_D$ = −15.4° (solid line) and an authentic **17**, $[\alpha]_D$ −39.7° (dotted line), dissolved in methanol.

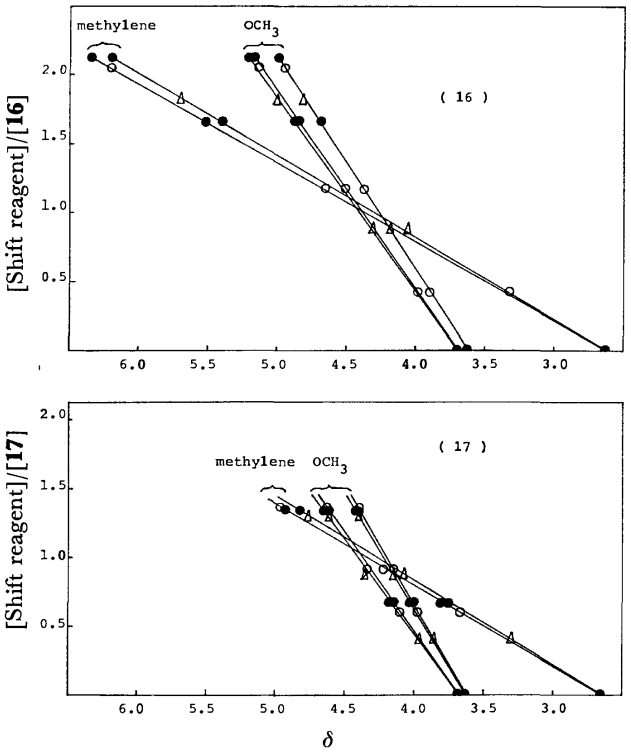

Fig. 3. Chemical shift changes of two methoxyl proton signals and one of methylene proton signal caused by the addition of a chiral shift reagent for compounds **16** and **17**.
△: (*S*)-(−)-Series, ○: (*R*)-(+)-series, ●: (±)-series.

In order to obtain information about the relationship between absolute configurations and the NMR signal shifts caused by a chiral shift reagent,[12] we compared the NMR spectra between the optically active dimethyl 2-phenylethylsuccinates with and without substituent on the phenyl group.

We found that there is a regularity on the shift caused by *tris*-[3-(2,2,3,3,4,4,4-heptafluoro-1-hydroxybutylidene)-*d*-camphorato]europium(III), *i.e.*, the methoxyl-proton signal of lower field of the two methoxyl-proton signals of *S*-(−)-series shifted to the lower field more profoundly than those of *R*-(+)-series, but the signals assigned to one of methylene-protons adjacent to methoxycarbonyl group in the *S*-(−)-series shifted to a lesser extent than those in the *R*-(+)-series (Fig. 3).

From the above results, the two series of correlations among the optically active products of the above transformations were established: *S*-(−)-**16**→*S*-(+)-**15**→*R*-(−)-**11**→(1*S*)-(−)-**6**→(1*S*)-(−)-**7**; *R*-(+)-**16**→*R*-(−)-**15**→*S*-(+)-**11**→(1*R*)-(+)-**6**→(1*R*)-(+)-**7**. Based on these experimental results, we can conclude that the photo-induced rearrangement of **6** to **11** must have proceeded with inversion of the configuration at C-1 in agreement with the prediction of the Woodward-Hoffmann rule.[13,14]

Discussion

The photochemical 1,3-sigmatropic rearrangement of **18** was established to proceed with retention of the configuration at the migrating carbon atom.[15,16] The thermal and photochemical rearrangements including cyclopropane ring are complicated because of the accompanying opening-reclosure process of three membered ring.[17–20] The thermal 1,4-shift in bicyclo-[3.1.0]hexenyl cation (**20**) is a rare example in which such an *exo-endo* isomerization does not accompanied by, and was found to proceed *via* slither motion with inversion of the configuration at C-6.[21]

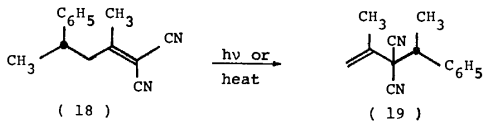

Scheme 4.

Scheme 5.

Furthermore, Zimmerman established that 4-methylene-2,6-*exo*-diphenylbicyclo[3.1.0]hept-2-ene(**22**) undergoes photoinduced skeletal rearrangement in a manner of slither motion with inversion of the configuration of the shifting carbon center, for which he proposed to rename "bicycle reaction."[22,23]

The Berson-Willcott rearangement of cycloheptatrienes is thought to proceed *via* interconversion among its norcaradiene valence tautomers.[24] The stereochemi-

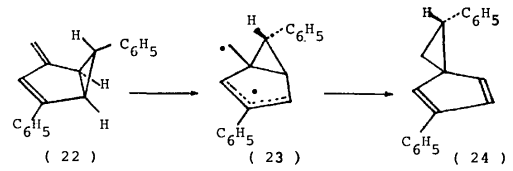

Scheme 6.

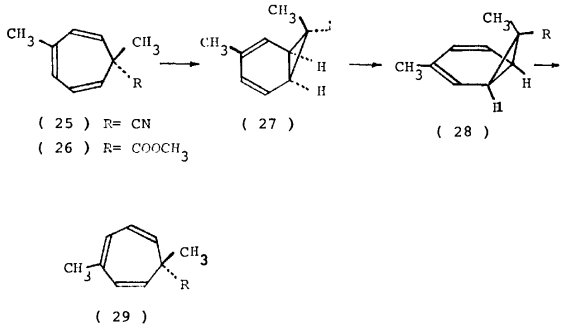

Scheme 7.

cal course of the benzophenone sensitized photochemical rearrangements of **25** and **26** had been studied by Klärner who found that the rearrangement is highly stereoselective (**25** 92% and **26** 76%) and proceeds with inversion at the migrating carbon C-7 similarly to the corresponding thermal rearrangement.[25–28] He proposed a stereoselective diradical process of the triplet states to account for the observed partial racemization.[29] These results are in line with the stereochemical course for path i of our previous results on the direct irradiation of 1a,7b-dihydro-1*H*-cyclopropa[*a*]-naphthalene derivative **1**. The rearrangement *via* path i was highly stereoselective as to configuration at C-1, even when an *exo-endo* mixture, after thermal equilibration of the methyl ester **1** obtained from optically active acid **30**, was used for the photolysis: That is, the product **4** (R_2=CH_2COOCH_3(*exo*)) retained the optical activity in high degree.

Furthermore, we found earlier that, when the *exo* and *endo* isomers of isopropyl derivative **5** were independently photolysed, they gave, without mutual interconversion, the same products each in so different rates as to support a mechanism of "bicycle reaction."[22]

From the above mentioned results, it is unlikely to assume a different stereochemical course for the *endo* isomer from that for the *exo* one. If the *exo*-**1** rearranges into *exo*-**4** *via* a course leading to an inversion at the migrating center and the *endo*-**1** does into *exo*-**4** *via* a course leading to a retention at the migrating center owing to some stereochemical reasons of the reaction, and *vice versa*, the optically active *exo-endo* mixture of **1** would give *exo*-**4** with considerable racemization. But this was not the case.

In the present case, the photochemical isomerization of optically active *exo*-1-ester **6** (optical purity>95%) to *endo*-1-ester was not observed during the reaction and the product **11** *via* path ii after photolysis retained its optical activity in high degree (>95%). For these reasons, we can conclude that the Berson-Willcott rearrangement of 1-methoxycarbonylmethyl-1a,7b-dihydro-1*H*-cyclopropa[*a*]naphthalenes by direct irradiation, in general, takes place by way of 1,5-shift to both directions in a manner of "bicycle reactions," as shown in Scheme 8, in line with the prediction of the Woodward-Hoffmann rule [*Cf.* (**36**)].[6,14]

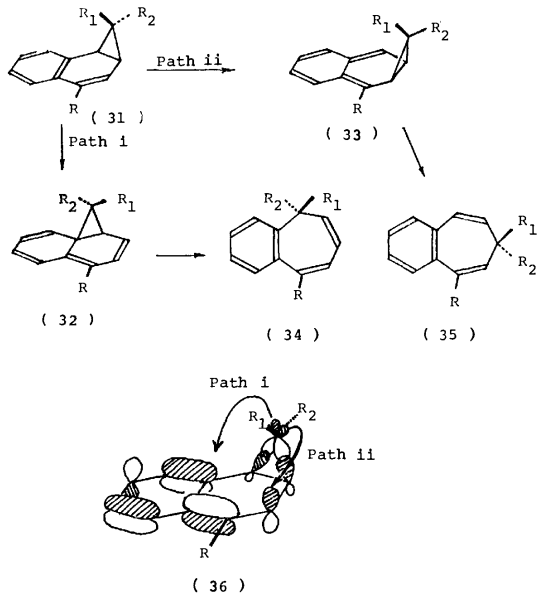

Scheme 8.

Experimental

The NMR spectra were taken on a JEOL Model PS-100 spectrometer with carbon tetrachloride as the solvent and TMS as the internal standard, unless otherwise specified. The chemical shifts are expressed in ppm from TMS. The IR spectra were recorded on a JASCO spectrometer Model IRE and the UV on a Hitachi Recording Spectrometer Model 323 with 95% ethanol as the solvent. GLC analysis was carried out on a Varian Aerograph Model 90P gas chromatograph under quoted conditions. The light source for photolysis, used throughout the experiments, was a Ushio High Pressure Mercury Lamp, UM-452, with Pyrex filter. The polarimeter used was a Rex Photoelectric one, type NEP-2, and the CD/ORD curves were recorded on a JASCO J-20 Automatic Recording Spectropolarimeter.

*3-t-Butyl-1a,7b-dihydro-1*H*-cyclopropa*[a]*naphthalene-1-carboxylic Acid* (**7**). To a melt of 1-*t*-butylnaphthalene (**8**) (37 g, 0.201 mol) containing 200 mg of copper powder, maintained at 145—150 °C, was added dropwise ethyl diazoacetate (5.14 g, 0.045 mol) over a period of 70 min with vigorous stirring. The mixture was further stirred at 145 °C for 1 h, and then 33.4 g of **8** was recovered by distillation under reduced pressure. The experiment was repeated six times with use of recovered **8**, and the collected residue in CH_2Cl_2 was filtered from copper powder and subsequently distilled to give 23 g of a mixture of three isomeric mono-esters, bp 120—143 °C (0.035 mmHg), contained 50% of ethyl ester of **7**. The oily product (11.8 g, 43.7 mmol) dissolved in 1 M 85% aq ethanolic KOH (130 ml) was refluxed for 20 h. The resulting solution was then diluted with water (130 ml) and reduced to a half volume under reduced pressure. After being washed with ether, the ice-cooled aq solution was acidified carefully with cold 2 M HCl in the presence of ether (100 ml) with stirring. The separated aq solution was extracted three times with ether. Usual work-up[6] of the combined ether solution gave **7** as

colorless crystals (3.31 g: 24% from **8**), mp 199—200 °C. IR ν_{max} (Nujol): 2670, 2580, 1690, 1321, 1214, 965, 897, 879, 771 cm^{-1}. NMR ($CDCl_3$): δ=0.75 (1H, dd, J=3.5, 3.5 Hz, H_1), 1.35 (9H, s), 2.72 (1H, m, H_{1a}), 3.16 (1H, dd, J=3.5 8.5 Hz, H_{7b}), 6.27 (1H, d, J=5.5 Hz), 7.0—7.9 (4H, m, Ar-H). Found: C, 79.37; H, 7.48%. Calcd for $C_{16}H_{18}O_2$: C, 79.37; H, 7.49%.

Optical Resolution of the Carboxylic Acid **7**. A solution of freshly crystallized brucine (8.12 g, 18.8 mmol) and the carboxylic acid **7** (4.06 g, 16.8 mmol) dissolved in 50% aq methanol was allowed to stand for 36 d in a refrigerator, when crystals of the brucine salt have developed. Repeated fractional crystallization of the salt from aq methanol gave colorless prisms (1.06 g), mp 108—111 °C, $[\alpha]_D^{26}$ −44° (c= 1.1, $CHCl_3$). Extraction of this salt dissolved in $CHCl_3$ with 2 M aq NaOH, acidification of the extracts, and extraction with ether followed by recrystallization of the residue, gave colorless amorphous powder (580 mg), $[\alpha]_D^{27}$ −13.7° (c=1.0, $CHCl_3$). Similar treatment of the brucine salt obtained from the filtrate of recrystallization gave the (+)-acid; $[\alpha]_D^{19}$ +14.3° (c=1.1, $CHCl_3$), mp 84.5—86 °C as a colorless amorphous solid. The IR spectra of these optically active acids were identical with those of the racemic acid except for the absorptions at 965 and 879 cm^{-1}, which the active forms lacked. The optical purity of the (+)-acid was estimated to be more than 95% by comparison of the NMR spectrum of its methyl ester with that of the racemic one, using a chiral shift reagent, tris[3-(2,2,3,3,4,4,4-heptafluoro-1-hydroxybutylidene)-*d*-camphorato]Eu(III), as shown in Fig. 1.

The Absolute Configuration of (+)-Acid **7**. Ozone generated from an ozonizer was passed through the carboxylic acid **7** suspended in 75% aq acetic acid (20 ml) for 3 h at room temperature. After addition of 10% aq H_2O_2 (12 ml), the resulting solution was kept at room temperature overnight and subsequently concentrated to dryness. The residue was then dissolved in 5% aq sodium hydrogen carbonate and washed with ether. The acidic fraction obtained from acidified aq solution was then treated with ethereal diazomethane. The GLC separation of the products gave three main peaks; (1) **14**, (4 mg; retention time (r.t.), 2 min); (2) **13** (10 mg; r.t. 10 min); (3) **12** (6 mg; r.t. 14 min). The compound **13** showed an identical NMR spectrum with that of a sample obtained from permanganate-oxidation and subsequent esterification of **30**. **12** NMR δ: 1.25 (9H, s), 2.2—3.1 (3H, m), 3.48 (3H, s), 3.67 (3H, s), 7.17 (4H, bs). IR ν_{max} (liq. film): 1688, 1725 cm^{-1}. Dimethyl *c*-3-[*o*-(methoxycarbonyl)phenyl]-*r*-1,*t*-2-cyclopropanedicarboxylate **13** NMR δ: 2.60 (2H, AB part of ABX), 3.37 (1H, X part of ABX), 3.44 (3H, s), 3.76 (3H, s), 3.89 (3H, s), 7.2—8.0 (4H, m). IR ν_{max} (liq. film): 1723, 1600, 1440, 1308, 1260, 1200, 1175, 1090, 1028, 908, 756 cm^{-1}. Found: C, 62.06; H, 5.67%. Calcd for $C_{15}H_{16}O_6$: C, 61.64; H, 5.52%.

Similar experiment with the (+)-acid **7**, $[\alpha]_D$ +11.7° (c= 1.2, $CHCl_3$), gave the triester **13**, $[\alpha]_D$ −55.8°, which had been previously related to the (+)-acid **30**, $[\alpha]_D$ +150°, of known stereochemistry (1*R*-(+)).[4]

rac- *and (+)-3-t-Butyl-1a,7b-dihydro-1-exo-methoxycarbonylmethyl-1H-cyclopropa[a]naphthalene (6)*. To a stirred and cooled solution of racemic acid **7** (1.45 g, 6.0 mmol), dissolved in anhydrous benzene (120 ml), was added oxalyl dichloride (3.05 g, 24 mmol) at below 15 °C. After stirring the solution for 4.5 h at 6—10 °C, it was evaporated below 20 °C and the residue was evaporated with benzene (three times each 15 ml), under reduced pressure to give the acid chloride (**37**) as a yellow liquid [IR $\nu_{c=o}$: 1760 cm^{-1}]. To a dried ether solution (20 ml) of diazomethane, prepared from *N*-nitroso-*N*-methylurea (6.08 g), was added dropwise **37** dissolved in benzene (10 ml) over a period of 15 min with cooling (ice-water). After further stirring for 14 h at room temperature, the white floatings were filtered off, and the filtrate was concentrated to dryness to give the diazo ketone **38** as a yellow liquid (2.01 g) which solidified soon. The diazo ketone **38**, dissolved in methanol (2.01 g/650 ml) was divided into two portions. Each portion was independently irradiated under nitrogen atmosphere with an HPL for 16 min with external cooling (ice). The solutions were combined and subsequent evaporation of the solvent left an orange liquid (1.82 g), which was chromatographed on silica gel (70 g) with hexane–ether (93 : 3 v/v) as the solvent to give a pale yellow liquid (**6**) (1.02 g; 61% yield). IR ν_{max} (liq. film): 2956, 1736, 1489 1440, 1372, 1251, 1197, 1176, 766, 758 cm^{-1}. NMR δ: 0.22 (1H, m, H_1), 1.36 (9H, s), 1.84 (1H, m, H_{1a}), 2.24 (1H, dd, J=4, 8 Hz, H_{7b}), 3.68 (3H, s), 6.24 (1H, d, J=6 Hz), 7.0—7.8 (4H, m).

For elementary analysis, **6** (173 mg, 0.64 mmol) was hydrolyzed with 1 M 85% aq ethanolic KOH (10 ml) by refluxing for 2 h. The crystalline acid **39** (74 mg, 47%), was obtained by usual work-up and subsequent recrystallization from aq ethanol, mp 154.5—155.5 °C. IR ν_{max} (Nujol): 1700 cm^{-1}. Found: C, 79.61; H, 7.77%. Calcd for $C_{17}H_{20}O_2$: C, 79.65; H, 7.86%.

The same experiment was carried out with the optically active acid **7** (442 mg, 1.83 mmol), $[\alpha]_D$ +14.3°, to give the ester **6** (233 mg; 43%), $[\alpha]_D^{24}$ +44.7° (c=1.03, $CHCl_3$). IR ν_{max} (liq. film): 2956, 1736, 1489, 1440, 1372, 1251, 1197, 1176, 766, 758 cm^{-1}. The spectral data (IR, UV, and NMR) were identical with those of racemic ester **6**.

Photolysis of 3-t-Butyl-1a,7b-dihydro-1-exo-methoxycarbonylmethyl-1H-cyclopropa[a]napthalene (6). The methyl ester **6** (250 mg), dissolved in methanol (300 ml), was irradiated with an HPL through a Pyrex filter for 1 h under nitrogen atmosphere. After evaporation of the solvent, the residue was separated with use of GLC (10% Apiezone L on Chromosorb WAW, column temperature 203 °C): (1) **8** (r.t. 7 min), (2) *exo*- and *endo*-2a,7b-dihydrocyclobut[*a*]indenes **9** (r.t. **9a**, 13.6 min, **9b**, 16 min), (3) methyl 5-*t*-butyl-7*H*-benzocyclohepten-7-acetate (**11**) (r.t. 17 min), (4) methyl 9-*t*-butyl-5*H*-benzocycloheptene-5-acetate (**10**) (r.t. 21 min). The structures of these compounds were assigned based on the spectral data by comparing with those of the corresponding isopropyl derivatives.[6,30] **9a**: NMR δ: 1.08 (9H, s), 2.1—2.74 (2H, m), 2.98 (1H, bd, J= 1.5 Hz), 3.28 (1H, bddd, J=10, 5.5, 1.5 Hz), 3.68 (3H, s), 6.10 (1H, dd, J=2.7, 1.0 Hz), 6.38 (1H, d, J=2.7 Hz), 7.0—7.5 (4H, m). **9b**: NMR δ: 1.03 (9H, s), 2.2—2.8 (2H, m), 3.4—3.7 (2H, m), 3.68 (3H, s), 5.98 (1H, d, J=2.8 Hz), 6.48 (1H, d, J=2.8 Hz), 6.9—7.4 (4H, m) [contaminated with a small amount of aromatic impurities]. **10**: UV λ_{max} (EtOH): 262; λ_{min}: 243 nm. NMR δ: 1.36 (9H, s), 2.8—3.0 (3H, b), 3.62 (3H, s), 5.44 (1H, dd, H_6), 5.96 (1H, dd, H_7), 6.66 (1H, bd, H_8), 7.0—7.1 (3H, m), 7.5—7.66 (1H, m) [double irradiation: $J_{5,6}$=5 Hz, $J_{6,7}$=10 Hz, $J_{7,8}$=5 Hz; contaminated with a small amount of impurities]. **11**: UV λ_{max} (EtOH): 227, 247 (infl.) nm. NMR δ: 1.16 (9H, s), 2.24 (1H, m), 2.54 (2H, bd, J=7.5 Hz), 3.62 (3H, s), 5.75 (1H, d, J=10 Hz), 5.93 (1H, dd, J=10, 5 Hz), 6.48 (1H, dd, J=10, 1.8 Hz), 7.03—7.35 (3H, m), 7.6—7.8 (1H, m). Mass spectrum: *m/e* (%); 270 (40(M^+)), 255 (61), 214 (60), 197 (55), 181 (74), 171 (100), 141 (50), 57 (79). Found: C, 79.96; H, 8.26%. Calcd for $C_{18}H_{22}O_2$: C, 79.96; H, 8.20%. Mp 51.5—52 °C.

The similar photolysis of the (+)-ester **6** (365 mg/430 ml; 16 min) gave **9** (50 mg, 14%), **11** (72 mg, 20%; $[\alpha]_D^{18.5}$ +127° (c=1.0, $CHCl_3$)), **10** (117 mg, 32%) in addition to **8** (41 mg). The optical purity of (+)-**11** was estimated to be more than 95% by applying the chiral shift reagent to its

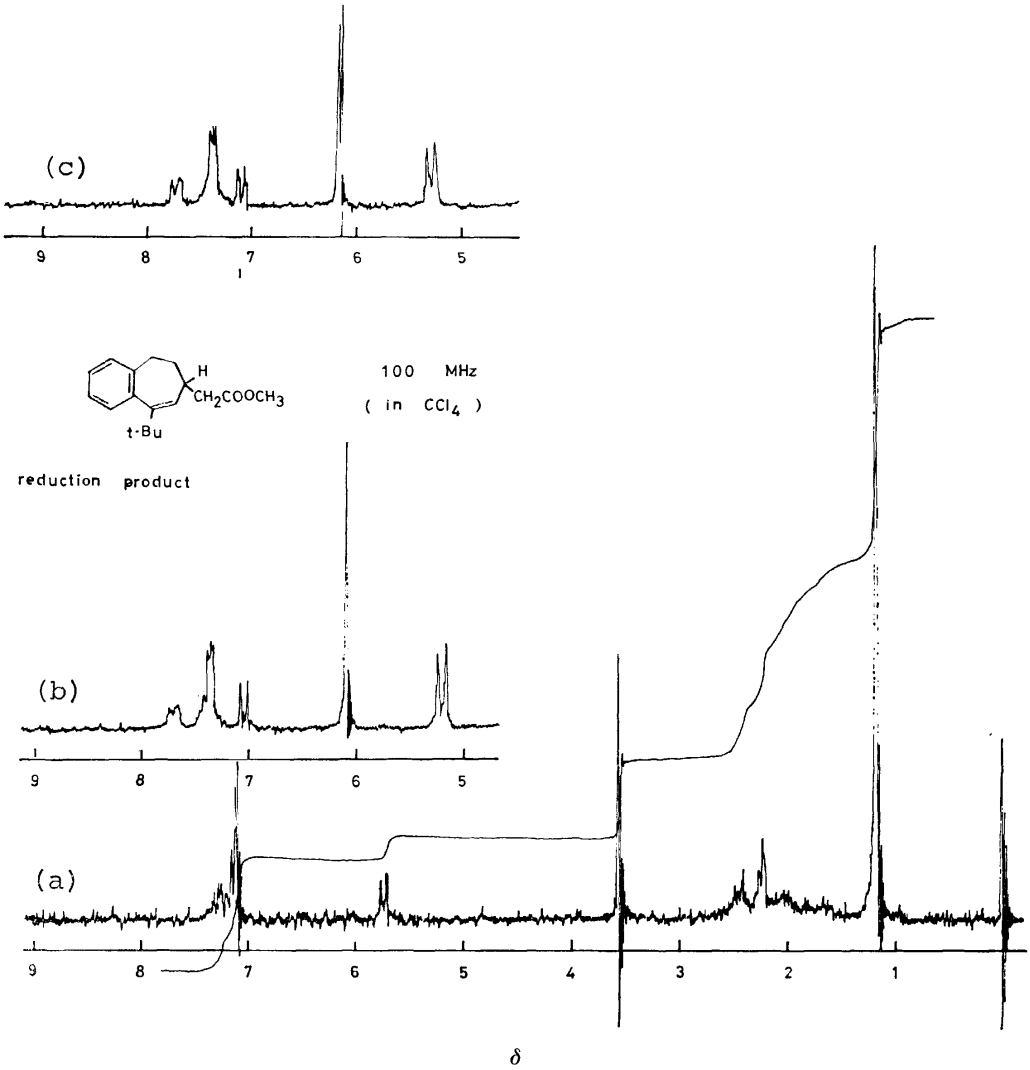

Fig. 4. ^1H NMR spectra of the hydrogenation product **15**.
(a) Original spectrum of optically active **15**, $[\alpha]_D = -61.2°$,
(b) after addition of a chiral shift reagent to the above, (c) after addition of a chiral shift reagent to the racemic ester **15**.

dihydro derivative **15** similarly as mentioned above.

Hydrogenation of the 7H-Benzocycloheptene ***11***. The *7H*-benzocycloheptene **11** (70 mg, 0.26 mmol), dissolved in ethyl acetate (10 ml), was hydrogenated over 10% Pd-C (20 mg) for 3.3 h until one molar equivalent of hydrogen was absorbed. Filtration from the catalyst and subsequent evaporation of the solvent left a yellow liquid (72 mg), which was revealed by NMR to contain **11**, 8,9-dihydro derivative of **11** (**15**), and tetrahydro derivative of **11** in a ratio of 13 : 80 : 7. The dihydro derivative **15** was separated by GLC (10% Apiezone L on Chromosorb WAW, column temperature 205 °C; r.t. 10 min). **15**: $[\alpha]_D$ −61.2° (c=1.0, $CHCl_3$). IR ν_{max} (liq. film): 2960, 1740, 1367, 1175, 1156, 849, 791, 760 cm^{-1}. UV λ_{max} (EtOH): 237 (log ε 3.90) nm, λ_{min} 225 (3.81). NMR δ: 7.25 (1H, m), 7.08 (3H, m), 5.73 (1H, d, J=6 Hz), 3.56 (3H, s), 2.76—1.60 (7H, m), 1.20 (9H, s). Mass spectrum: *m/e* (%); 272 (1.5 (M^+)), 215 (3), 183 (3), 155 (19), 141 (26.6), 128 (13.6), 115 (15.1), 57 (100), 41 (67.2). Found: C, 79.35; H, 8.94%. Calcd for $C_{18}H_{24}O_2$: C, 79.37; H, 8.88%.

Permanganate Oxidation of Methyl 5-t-Butyl-8,9-dihydro-7H-benzocycloheptene-7-acetate ***15***. To a stirred solution of perhydrodibenzo-18-crown-6 (156 mg, 0.42 mmol) in benzene (8 ml) was added potassium permanganate (66 mg, 0.42 mmol). After stirring for 1 h, **15** was added to the purple benzene solution and stirring was continued further for 2 d, until the purple color had beed discharged. Filration from the precipitates, and concentration of the filtrate gave a residue which was taken in benzene and chromatographed on silica gel to give 69% recovery of the starting material. Collected precipitates from repeated oxidation of the recovered ester **15** were combined with the initial precipitates and then extracted with hot water. The aqueous extracts were washed once with ether, acidified with 6 M hydrochloric acid, and extracted with ether to give colorless crystals (47 mg), which were esterified with ethereal diazomethane. Purification by TLC method (silica gel; ether–hexane=1 : 1) gave dimethyl (+)-2-[*o*-(2,2-dimethylpropanoyl)phenyl]ethylsuccinate **16**, $[\alpha]_D^{13.5}$ +16.0° (c=1.28, $CHCl_3$). **16** NMR δ: 7.2 (4H, m), 3.70 (3H, s), 3.65 (3H, s), 2.2—2.9 (5H, m), 1.6—2.0 (2H, m), 1.24 (9H, s). IR ν_{max} (liq. film): 2960, 1733, 1689, 1443, 1170, 969, 763 cm^{-1}. UV λ_{max} (EtOH): 233 (log ε 3.42), 251 (3.08), 271 nm (2.75). Mass spectrum: *m/e* (%); 334 (1.7 (M^+)), 303 (4.2), 277 (56.7), 245 (62.5), 217 (14.7), 185 (100), 57 (38). Found: C, 68.13; H, 7.85%. Calcd for $C_{19}H_{26}O_5$: C, 68.24; H, 7.84%.

The authors wish to thank Professor Hisao Kuroya and Dr. Keiji Matsumoto of our University for measure-

ment of the ORD curves, and Mr. Jun-ichi Goda for the elementary analysis. The authors also indebted to Mr. Masakazu Tsuji for the preliminary experiments on the photo-induced reaction of **6**.

References

1) G. W. Gruber and M. Pomerantz, *J. Am. Chem. Soc.*, **91**, 4004 (1969).
2) M. D. Madigan and J. S. Swenton, *J. Am. Chem. Soc.*, **93**, 6316 (1971).
3) J. S. Swenton, K. A. Burdett, D. M. Madigan, T. Johnson, and P. D. Rosso, *J. Am. Chem. Soc.*, **97**, 3428 (1975).
4) M. Kato, M. Funakura, M. Tsuji, and T. Miwa, *J. Chem. Soc., Chem. Commun.*, **1976**, 63.
5) M. Kato, M. Kawamura, Y. Okamoto, and T. Miwa, *Tetrahedron Lett.*, **1972**, 1171.
6) M. Kato, M. Tsuji, and T. Miwa, *Bull. Chem. Soc. Jpn.*, **51**, 1450 (1978).
7) The ratios of the 7*H*-benzocycloheptenes to the corresponding 5*H*-benzocycloheptenes after photolysis were found to be 1 : 2 for 3-isopropyl and 3 : 5 for 3-*t*-butyl derivatives.
8) The thermal *exo-endo* equilibration was completed in the substituted methyl 1a,7b-dihydro-1*H*-cyclopropa[*a*]naphthalene-1-*exo*-acetates as follows: Substituent/heating temperature and period (ratio of *exo* to *endo*); 3-H/90 °C, 5 min (2: 1); 2,6-dimethyl/100 °C, 1.25 h (1.9 : 1); 1a,5-dimethyl/100 °C, 1 h (0.72 : 1); 3-isopropyl/130 °C, 30 min (1.5 : 1); 3-*t*-butyl/145 °C, 4 h (2.7 : 1).
9) E. A. Braude and F. J. Sondheimer, *J. Chem. Soc.*, **1955**, 3754.
10) N. J. Leonard, D. F. Morrow, and M. T. Rogers, *J. Am. Chem. Soc.*, **79**, 5476 (1957).
11) A. Fredga, J. D. Jerrings, W. Klyne, P. M. Scopes, and B. Sjoberg, *J. Chem. Soc.*, **1965**, 3928.
12) It is well known that the determination of the absolute configuration by NMR method using chiral shift reagents leads sometimes erroneous results. [C. Kutal, "NMR Shift Reagents," ed by R. E. Sivers, Academic Press, New York (1973), p. 87; A. F. Cockerill, G. L. O. Davies, R. C. Harden, and D. M. Rackham, *Chem. Revs.*, **73**, 553 (1973)].
13) J. A. Berson, *Acc. Chem. Res.*, **1**, 152 (1964).
14) R. B. Woodward and R. Hoffmann, "The Conservation of Orbital Symmetry," Verlag Chemie, Weinheim, Germany (1970) pp. 132—140.
15) R. C. Cookson, J. Hudee, and M. Sharma, *J. Chem. Soc., Chem. Commun.*, **1971**, 107, 108.
16) R. C. Cookson and J. E. Kemp, *J. Chem. Soc., Chem. Commun.*, **1971**, 385.
17) H. E. Zimmerman and G. A. Epling, *J. Am. Chem. Soc.*, **94**, 3647 (1972).
18) S. S. Hixson and J. Borovsky, *J. Am. Chem. Soc.*, **98**, 2840 (1976).
19) W. A. Gros, T. Luo, and J. C. Gilbert, *J. Am. Chem. Soc.*, **98**, 2019 (1976).
20) a) H. E. Zimmerman and D. S. Crumrine, *J. Am. Chem. Soc.*, **90**, 5612 (1968); b) T. M. Brennan and R. K. Hill, *J. Am. Chem. Soc.*, **90**, 5614 (1968).
21) H. E. Zimmerman, D. S. Crumrine, D. Dopp, and P. S. Huyffer, *J. Am. Chem. Soc.*, **91**, 434 (1969).
22) H. E. Zimmerman, T. P. Gannett, and G. E. Keck, *J. Am. Chem. Soc.*, **100**, 323 (1978).
23) H. E. Zimmerman and T. P. Cutler, *J. Chem. Soc., Chem. Commun.*, **1978**, 232.
24) J. A. Berson and M. R. Willcott, III, *Rec. Chem. Progr.*, **27**, 139 (1966); *J. Am. Chem. Soc.*, **88**, 2494 (1966).
25) F.-G. Klärner and S. Yaslak, *Angew. Chem.*, **86**, 270 (1970).
26) F.-G. Klärner, S. Yaslak, and M. Wette, *Chem. Ber.*, **111**, 1168 (1978).
27) J. E. Baldwin and B. M. Broline, *J. Am. Chem. Soc.*, **100**, 4599 (1978).
28) F.-G. Klärner and B. Brassel, *J. Am. Chem. Soc.*, **102**, 2469 (1980).
29) F.-G. Klärner and S. Yaslak, *Chem. Ber.*, **112**, 2286 (1979).
30) The fact that **10** is converted cleanly into a mixture of **9a** and **9b** (7 : 5) under the irradiation conditions supports the assignments. The photochemistry of **10** will be reported in due time together with photo-induced reaction of other 5*H*-benzocycloheptene derivatives.

Modification of Aminocyclitol Antibiotics. 8. Preparation of 5,6″-Dideoxykanamycin B[1]

Tetsuo SUAMI* and Katsumi NAKAMURA

Department of Applied Chemistry, Faculty of Engineering, Keio University, Hiyoshi, Kohoku-ku, Yokohama 223

(Received March 18, 1980)

In order to obtain an effective antibiotic against a resistant strain of bacteria, two hydroxyl groups on C-5 and 6″ of kanamycin B were removed. 5,6″-Dideoxykanamycin B thus prepared was subjected to antimicrobial tests, its structure being established by mass and ^{13}C NMR spectroscopy.

In connection with the preceding paper,[2] a report is given on the preparation and antimicrobial activity of 5,6″-dideoxykanamycin B.

5-Deoxygentamicin complex[3] and 5-deoxysisomicin[4] exhibit improved activity against resistant strains of bacteria, as compared to gentamicin complex and sisomicin, respectively. Considering the structural similarity between these antibiotics and kanamycin B, 5-deoxykanamycin B[5] can be considered to have improved activity against kanamycin resistant strains of bacteria, but this is not the case. This might be attributed to a complicated structural feature of kanamycin B. The characteristic feature of kanamycin B is the existence of a hydroxymethyl group on C-5″, in contrast with gentamicin complex and sisomicin. If the hydroxyl group is removed from 5-deoxykanamycin B, the resulting 5,6″-dideoxykanamycin B (**5**) might show improved activity.

Results and Discussion

When 1,3,2′,6′,3″-pentakis-*N*-(ethoxycarbonyl)kanamycin B[6] (**1**) reacted with trityl chloride in pyridine and subsequently acylated with benzoyl chloride, tetra-*O*-benzoyl-*O*-trityl derivative (**2**) was obtained in 77% yield. Since trityl chloride attacks a primary hydroxyl group preferentially,[7] and a hydroxyl group on C-5 in kanamycin B is highly hindered against the acylation,[5] the structure of **2** is assigned to a 3′,4′,2″,4″-tetra-*O*-benzoyl-6″-*O*-trityl derivative. The assignment would be verified by the establishment of the structure of **5** by mass and ^{13}C NMR spectrometries.

Detritylation of **2** with hydrogen bromide, followed by halogenation with sulfuryl chloride in pyridine afforded a 5,6″-dichloro-5,6″-dideoxy derivative (**3**) in 50% yield.

Dehalogenation of **3** with tributylstannane gave a

Table 1. The ^{13}C NMR chemical shifts[a] of 5,6″-dideoxykanamycin B

	5,6″-Dideoxykanamycin B (**5**)	
	pD 11	pD 1
C-1	53.4	52.2
C-2	36.9	29.0
C-3	52.6	51.7
C-4	78.0	71.8
C-5	34.7	32.6
C-6	83.9	78.4
C-1′	96.1	91.4
C-2′	54.9	53.9
C-3′	76.1	71.2[b]
C-4′	72.9[b]	71.5[b]
C-5′	74.8	69.8
C-6′	42.5	41.0
C-1″	100.9	100.0
C-2″	72.4[b]	69.5
C-3″	55.7	55.6
C-4″	73.9	69.5
C-5″	68.9	69.0
C-6″	17.6	17.3

a) In parts per million downfield from tetramethylsilane. b) The signals may be reversed.

Table 2. Antimicrobial activity of 5,6″-dideoxykanamycin B (**5**) and kanamycin B

Test organisms	MIC (mcg/ml)	
	Compound **5**	Kanamycin B
Staphylococcus aureus ATCC 6538P	0.39	0.78
Staphylococcus epidermidis ATCC 12228	<0.025	0.1
Diplococcus pneumoniae Type 3	0.1	0.05
Bacillus subtilis ATCC 6633	<0.025	<0.025
Escherichia coli NIH JC-2	6.25	6.25
Klebsiella pneumoniae 602	0.78	1.56
Pseudomonas aeruginosa IAM 1007	100	25
Proteus vulgaris OX-19	0.2	0.2
Salmonella paratyphi A 1015	0.78	0.39
Salmonella paratyphi B	1.56	0.78
Shigella flexneri 2a·SH-74-1	6.25	3.12
Staphylococcus aureus Apo-1[a]	0.28	0.39
Staphylococcus epidermidis 109[a]	50	50
Salmonella sp. D-0001[a]	200	200
Proteus rettgeri J-0026[a]	400	200
Klebsiella pneumoniae 22 #3038[a]	200	400
Klebsiella pneumoniae MB-3841[a]	400	>800
Serratia marcescens MB-3848[a]	12.5	3.13
Serratia marcescens I-0087[a]	25	12.5
Pseudomonas aeruginosa M-0086[a]	>800	200
Escherichia coli K-12 57R391 JJ53[a]	200	400
Escherichia coli K-12 CSH-2 R-6[a]	200	200
Escherichia coli JR66/W677[a]	200	400
Escherichia coli (M) Cast. and Chalm. NIHJ JC-2[a]	0.28	0.28

a) A resistant strain of bacteria.

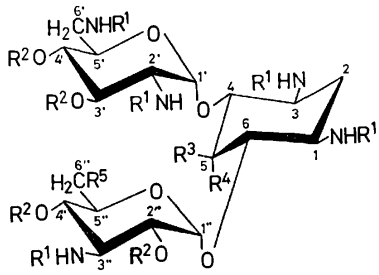

1 R^1=Cbe, R^2=R^3=H, R^4=R^5=OH
2 R^1=Cbe, R^2=Bz, R^3=OH, R^4=H, R^5=OTr
3 R^1=Cbe, R^2=Bz, R^3=H, R^4=R^5=Cl
4 R^1=Cbe, R^2=Bz, R^3=R^4=R^5=H
5 R^1=R^2=R^3=R^4=R^5=H
6 R^1=Ac, R^2=R^3=R^4=R^5=H

Scheme 1.

5,6″-dideoxy derivative (**4**) in 81% yield.

Hydrolysis of **4** in a sodium hydroxide solution gave **5** in 73% yield. *N*-Acetylation of **5** by the conventional method afforded penta-*N*-acetyl-5,6″-dideoxykanamycin B (**6**).

The structure of **5** was established by mass spectroscopy. The mass spectrum of **5** shows $[M+1]^+$ peak at *m/e* 452, corresponding to $[M+1]^+$ of kanamycin B-32. The other peaks are also consistent with the proposed structure of **5** (Scheme 1).

The ^{13}C NMR spectrum of **5** shows eighteen carbon signals (Table 1). In comparison with the spectra of 5-deoxykanamycin B and kanamycin B,[5] large shifts of the signals of C-5 and C-6″, we see in the spectrum of **5**, confirming the structure of **5**.

Compound **5** was subjected to the determination of antimicrobial activity against microorganisms by a dilution method. The MIC (minimum inhibition concentration) values are given in Table 2. As compared to kanamycin B, **5** exhibited improved activity against *Staphylococcus epidermidis* ATCC 12228 and *Klebsiella pneumoniae* 602. Compound **5** was slightly more active than kanamycin B against resistant strains of bacteria: *Staphylococcus aureus* Apo-1, *Klebsiella pneumoniae*, and *Escherichia coli*. Compound **5** showed a marked decrease in activity against *Pseudomonas aeruginosa*.

Experimental

General Method. Melting points were determined in open capillaries in a liquid bath and are uncorrected. Solutions were concentrated under reduced pressure below 40 °C. Optical rotations were measured on a Japan Spectroscopic DIP-SL polarimeter. ^{13}C NMR spectra were determined on a Varian FT-80 spectrometer at 20 MHz, D_2O being used as a solvent with an internal standard of dioxane. The resonance signals are expressed in ppm down-field from the signal of tetramethylsilane ($\delta_c^{TMS}=\delta_c^{dioxane}+67.4$). Mass

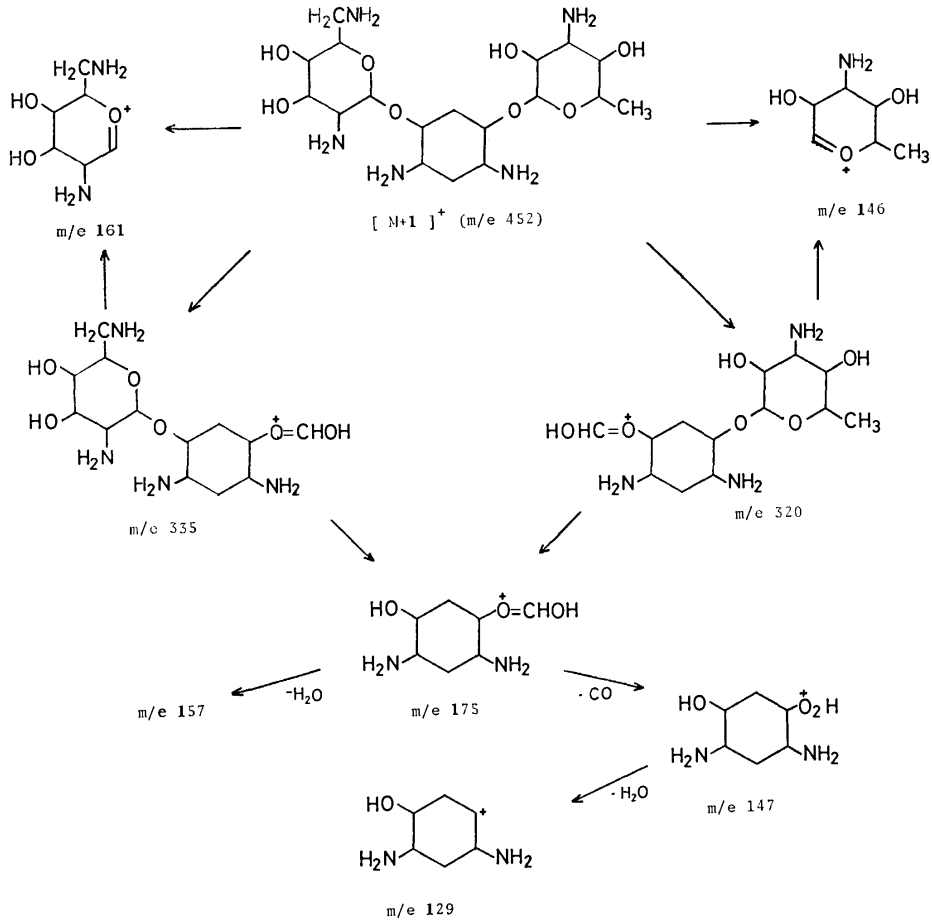

Scheme 2.

spectra were recorded with a Hitachi RMU-6M single focusing mass spectrometer. TLC was performed on Wakogel B-10 plates, silica gel (Wakogel C-300) being used in column chromatography.

3',4',2'',4''-Tetra-O-*benzoyl-1,3,2',6',3''-pentakis*-N-*(ethoxycarbonyl)-6''*-O-*tritylkamycin B (2).* Trityl chloride (1.7 g) was added to a stirred solution of 1,3,2',6',3''-pentakis-*N*-(ethoxycarbonyl)kanamycin B[8] (**1**, 1.0 g) in pyridine (50 ml). After 69 h, benzoyl chloride (3 ml) was added to the solution under ice cooling with agitation. After 24 h, the solution was poured into cold water containing $NaHCO_3$. The aqueous mixture was repeatedly extracted with $CHCl_3$, the $CHCl_3$ layers being washed with water, dried over Na_2SO_4 and concentrated. The residue was chromatographed on a SiO_2 column with 1 : 5 (v/v) 2-butanone–$CHCl_3$. From the fractions homogeneous on TLC (R_f 0.72) in 7 : 1 (v/v) benzene–methanol, 1.37 g (77%) of **2** was obtained as amorphous powder, mp 125—131 °C, $[\alpha]_D^{21}$ +85° (*c* 0.56, chloroform).

Found: C, 63.65; H, 5.85; N, 4.66%. Calcd for $C_{80}H_{87}N_5O_{24}$: C, 63.95; H, 5.84; N, 4.66%.

3',4',2'',4''-Tetra-O-*benzoyl-5,6''-dichloro-5,6''-dideoxy-1,3,2',6',3''-pentakis*-N-*(ethoxycarbonyl)-5-epikanamycin B (3).* Glacial acetic acid (3 ml) containing 30% HBr was added to a solution of **2** (1.33 g) in $CHCl_3$ (3 ml) and glacial acetic acid (6 ml) under ice cooling with agitation. After 2 min, the resulting mixture was quenched on ice and repeatedly extracted with $CHCl_3$. The combined organic layers were washed with a $NaHCO_3$ solution, water, dried over Na_2SO_4, and concentrated. Sulfuryl chloride (1.5 ml) was added to a solution of the residue in pyridine (15 ml) under ice cooling with agitation. After 19 h, the solution was poured into ice cold water, precipitates being collected by filtration. The product was chromatographed on SiO_2 with 1 : 5 (v/v) 2-butanone–$CHCl_3$. The fractions homogenous on TLC (R_f 0.47) in 7 : 1 (v/v) benzene–methanol were combined and concentrated to give 0.57 g (50%) of **3**, mp 143—149 °C, $[\alpha]_D^{25}$ +69.4° (*c* 0.54, $CDCl_3$).

Found: C, 56.47; H, 5.52; N, 5.27; Cl, 5.61%. Calcd for $C_{61}H_{71}N_5Cl_2O_{22}$: C, 56.48; H, 5.52; N, 5.40; Cl, 5.47%.

3',4',2'',4''-Tetra-O-*benzoyl-5,6''-dideoxy-1,3,2',6',3''-pentakis* N-*(ethoxycarbonyl)kanamycin B (4).* A solution of **3** (460 mg) and tributylstannane (2.0 ml) in toluene (20 ml) was heated at 80 °C in the presence of α,α'-azobisisobutyronitril (20 mg). After 24 h, the resulting solution was concentrated and the residue was chromatographed on SiO_2 with 15 : 1 (v/v) benzene–methanol. The fractions homogeneous on TLC (R_f 0.38) in the same solvent were combined and concentrated to give 350 mg (80%) of **4**, mp 144—150 °C, $[\alpha]_D^{25}$ +87.8° (*c* 0.47, $CHCl_3$).

Found: C, 59.59; H, 5.95; N, 5.43%. Calcd for $C_{61}H_{73}N_5O_{22}$: C, 59.65; H, 5.99; N, 5.70%.

5,6''-Dideoxykanamycin B (5). A solution of **4** (304 mg) in methanol (6 ml) was added to a 2 M NaOH solution (20 ml) the solution being heated under reflux. After 12 h, the solution was neutralized with HCl and concentrated. The residue was purified on a CG-50 (NH_4^+) resin column. The fractions eluted with 0.3 M NH_4OH gave 81 mg (73%) of **5**, mp 172—175 °C (dec), $[\alpha]_D^{23}$ +136° (*c* 0.44, H_2O). The product showed a single spot (R_f 0.2) on TLC in 5 : 8 : 10 : 7 (v/v) 28% NH_4OH–1-butanol–ethanol–water.

1,3,2',6',3''-Penta-N-*acetyl-5,6''-dideoxykanamycin B (6).* Acetic anhydride (0.1 ml) was added to a solution of **5** (11 mg) in methanol (2 ml), precipitates being collected by filtration to give 13 mg (79%) of **6**, mp 250 °C, $[\alpha]_D^{25}$ +113° (*c* 0.35, H_2O).

Found: C, 48.00; H, 6.67; N, 10.01%. Calcd for $C_{28}H_{47}N_5O_{13}\cdot 2H_2O$: C, 48.20; H, 7.36; N, 10.04%.

References

1) A part of the work was presented at the 5th Anniversary Meeting of the Institute of Bioorganic Chemistry, Nov. 5th, 1979, Tokyo.

2) T. Suami and K. Nakamura, *Bull. Chem. Soc. Jpn.*, **52**, 955 (1979).

3) D. Rosi, W. A. Goss, and S. J. Daum, *J. Antibiot.*, **30**, 88 (1977).

4) M. J. Weinstein, P. J. L. Danields, G. H. Wagman, and R. Testa, Jpn. Patent, 75-42092 (1975); G. B. Patent, 2437159 (1975).

5) T. Suami, S. Nishiyama, Y. Ishikawa, and E. Umemura *Bull. Chem. Soc. Jpn.*, **51**, 2354 (1978).

6) S. Umezawa, H. Umezawa, Y. Okazaki, and T. Tsuchiya, *Bull. Chem. Soc. Jpn.*, **45**, 3624 (1972).

7) B. Helferich, *Adv. Carbohydr. Chem.*, **3**, 79-111 (1948).

8) P. J. L. Daniels, M. Kugelman, A. K. Mallams, R. W. Tkach, H. F. Vernay, M. J. Weinstein, and A. Yehaskel, *Chem. Commun.*, **1971**, 1629; P. J. L. Danils, A. K. Mallams, M. J. Weinstein, J. J. Wright, and G. W. A. Milne, *J. Chem. Soc., Perkin Trans. 1*, **1976**, 1078.

Nucleophilic Substitution on Dialkoxy Disulfides. III.[1] Reaction with Thioureas

Hiroaki KAGAMI, Takashi HANZAWA, Nobuo SUZUKI, Shoso YAMAGUCHI, Masami SAITO, and Shinichi MOTOKI*

Department of Chemistry, Faculty of Science, Science University of Tokyo, Kagurazaka, Shinjuku-ku, Tokyo 162

(Received March 26, 1980)

1,3- and 1,1-Disubstituted thioureas reacted with diethoxy disulfide to give carbodiimides and 1,2,4-thiadiazoles respectively. 1,1,3-Trisubstituted thioureas and diethoxy disulfide afforded trialkyl(trialkylamidino)-thioureas.

The alkoxyl group of dialkoxy disulfide (**1**) is readily displaced by various nucleophiles. The reactions of **1** and amines, thiols,[2] thiocarboxylic acids,[3] or *N*-arylhydrazines[1] proceeded readily to give a variety of products. In the case of the reaction of thiobenzamide and diethoxy disulfide (**1a**), hydrogen sulfide was eliminated and benzonitrile was obtained in 80% yield.[2] This interesting dehydrosulfurization by **1** suggested that carbodiimides might be produced by the reaction of **1** and thiourea derivatives.

$$\mathrm{ROSSOR} \xrightarrow[-\mathrm{ROH}]{\mathrm{XH}} \mathrm{ROSSX} \xrightarrow[-\mathrm{ROH}]{\mathrm{YH}} \mathrm{YSSX}$$

(XH, YH; R'_2NH, R'SH, $R'\overset{O}{\overset{\|}{C}}SH$)

$$\mathrm{Ph\text{-}\overset{S}{\overset{\|}{C}}\text{-}NH_2} + \mathrm{EtOSSOEt} \xrightarrow[-\mathrm{EtOH},\ -\mathrm{S}]{} \mathrm{Ph\text{-}C{\equiv}N}$$

1a

Results and Discussion

When 1,3-disubstituted thioureas (**2**) were treated with **1a** at room temperature or in refluxing CH_2Cl_2 in the presence of molecular sieves (type 4A), carbodiimides (**3**) were obtained in 19—66% yield. The results are shown in Table 1. Molecular sieves (type 4A) were good absorbents of ethanol and promoted the elimination reaction.

$$\mathrm{R^1NH\text{-}\overset{S}{\overset{\|}{C}}\text{-}NHR^2} + \mathrm{EtOSSOEt} \xrightarrow[-\mathrm{EtOH},\ -\mathrm{S}]{} \mathrm{R^1N{=}C{=}NR^2}$$

2 **1a** **3**

The reaction of 1,1,3-trisubstituted thiourea (trimethylthiourea) (**4a**) and **1a** in refluxing toluene gave a light yellow liquid. The IR spectrum of the product showed an absorption at 1645 cm^{-1} assignable to the C=N stretching band, but no N–H absorption. The NMR spectrum exhibited four methyl singlets; the two signals at 3.27 and 2.88 ppm were assigned to $N(CH_3)_2$ protons. The mass spectrum allowed detection of the typical fragment (M^+—SH) of thiourea. On the basis of these data the product was formulated to be trimethyl(trimethylamidino)thiourea (**5a**). Similarly, *N,N*-diethyl-*N'*-methylthiourea (**4b**) and **1a** gave *N,N*-diethyl-*N'*-methyl-*N'*-(*N*^{1},*N*^{1}-diethyl-*N*^{2}-methylamidino)thiourea (**5b**).

$$2\ \mathrm{R^1_2N\text{-}\overset{S}{\overset{\|}{C}}\text{-}NHR^2} + \mathbf{1a} \longrightarrow \mathrm{R^1_2N\text{-}\overset{R^2N}{\overset{\|}{C}}\text{-}N(R^2)\text{-}\overset{S}{\overset{\|}{C}}\text{-}NR^1_2}$$

4 **5**

On the other hand, 1,1-disubstituted thioureas (**6**) reacted with **1a** in refluxing carbon tetrachloride to give 3,5-bis(disubstituted amino)-1,2,4-thiadiazoles (**7**) with a small amount of disubstituted cyanamides (**8**). The results are shown in Table 2.

$$\mathrm{R_2N\text{-}\overset{S}{\overset{\|}{C}}\text{-}NH_2} + \mathbf{1a} \longrightarrow \mathbf{7} + \mathrm{R_2N\text{-}C{\equiv}N}$$

6 **7** **8**

The thiadiazole systems comprise 1,2,3-, 1,2,4-, 1,2,5-, and 1,3,4-thiadiazoles. However, the structure of the product was identified as 1,2,4-thiadiazole by the ^{13}C-NMR and mass spectra. For example, the off-resonance ^{13}C decoupled spectrum of **7a** was as follows: (1) 12.7 ppm (q), (2) 13.6 (q), (3) 43.2 (t), (4) 45.7 (t), (5) 167.5 (s), (6) 186.6 (s). The four upfield signals correspond to the ethyl carbons, and the two downfield signals correspond to ring carbons. The mass spectrum of the product showed the thiazirene fragment formed by the loss of Et_2NCN from the molecular ion,[4] but no thiirene fragment.[5] All of the evidence supports the

$$\mathbf{7a}^{\ddagger} \longrightarrow \mathrm{N{=}C^{\ddagger}\text{-}S\text{-}NR_2}$$

proposed structure.

The formation of these products can be rationalized by assuming the reaction path shown in Scheme 1. First, the ethoxyl group of **1a** was replaced by **2** to give ethoxy amidino trisulfide (**9**). The trisulfide then

Table 1. Carbodiimide $R^1\text{–}N{=}C{=}N\text{–}R^2$ (**3**)

R^1	R^2	Bp/°C (mmHg)	Yield / %	Reaction time/h (Refluxing in CH_2Cl_2)
i-Pr	*i*-Pr	44(15)	66	4
Cyclohexyl	Cyclohexyl	110(0.15)	63	7
Ph	Ph	170(13)	62	5
2-$CH_3C_6H_4$	2-$CH_3C_6H_4$	121(0.07)	43	2
Ph	Cyclohexyl	114(0.5)	41	8[a]
Et	Cyclohexyl	54(1)	42	23
2-ClC_6H_4	Cyclohexyl	130(0.5)	19	3[a]
Allyl	Cyclohexyl	72(5)	20	6

a) Standing at room temperature [d].

Table 2. 1,2,4-Thiadiazole (**7**), and cyanamide (**8**)

	R	Reaction time/h	**7** Bp/°C (mmHg), or Mp/°C	**7** Yield %	**8** Bp/°C (mmHg)	**8** Absorption of $\nu_{C\equiv N}$/cm^{-1}	**8** Yield %
a	Et	7	117(4)	75	65(9)[a]	2210	5
b	Pr	7	145(3)	72	91(11)[b]	2210	3
c	Bu	8	165(5)	48	120(10)[c]	2210	5
d	R_2N=Morpholino	11[d]	102.5—103.5	51	—	2210	0
e	Ph	6	158.0[e]	69	—	2230	0

a) Lit, 68(10).[6] b) Lit, 88—90(10).[7] c) Lit, 147—151(35).[8] d) CH_3CN was used as the solvent. e) Lit, 155 °C.[a]

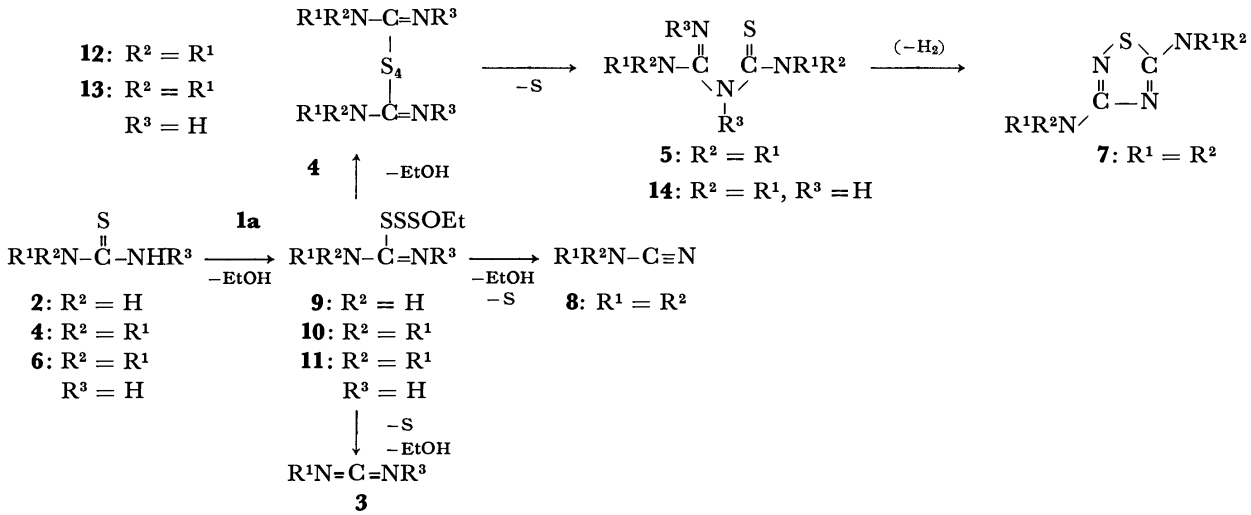

Scheme 1.

underwent intramolecular substitution by the remaining –NHR group, followed by the elimination of sulfur to give **3**.[2]

The reaction of **4** and **1a** proceeded by successive substitution of **1a** by 2 mol of **4** to give the tetrasulfide (**12**), which then rearranged to yield **5** with elimination of sulfur. In the case of the reaction of **1a** and **2**, intramolecular substitution of **9** would predominate over intermolecular substitution by **2**.

Similarly, **1a** reacted with 2 mol of **6** to give amidinothiourea (**14**). Unlike **5**, however, **14** could cyclize to form **7** with a loss of hydrogen. Presumably **1a** would participate in this step, as in the case of the reaction of **1a** and hydrazine.[1]

The formation of the cyanamide (**8**) as a by-product is considered to be due to the intramolecular substitution of **11**, followed by the loss of sulfur. However, this reaction would not proceed effectively owing to the low nucleophilicity of the imino nitrogen atom in **11**.

Experimental

All melting points and boiling points are uncorrected. Column chromatography was performed on Wako gel C-200 column by eluting with benzene. ^{1}H-NMR spectra were recorded at 100 MHz on a JEOL JNM-FX 100 spectrometer using Me_4Si as the internal standard. The ^{13}C-NMR spectrum was recorded at 25 MHz on a JEOL JNM-FX 100 spectrometer using Me_4Si as the internal standard. Infrared spectra were obtained on a Hitachi model 260-10 infrared spectrometer. Mass spectral data were obtained with a Hitachi Double Focusing Mass spectrometer, RMU-7M.

Diethoxy disulfide (**1a**) was prepared by the method of the literature.[10] Unsymmetrical 1,3-disubstituted thioureas and trialkylthioureas were prepared from isothiocyanates and amines. Molecular sieves (type 4A 1/16 in. pellets) was purchased from Nakarai Chemicals (UCC subdivision). 1,1-Dialkylthioureas were prepared by the methods of the literature.[11] All other reagents were obtained commercially.

Reactions of ***1a*** *with 1,3-Disubstituted Thiourea.* To a solution of 1,3-disubstituted thiourea (**2**, 0.05 mol) and **1a** (0.05 mol) in 100 ml of CH_2Cl_2, 30 g of molecular sieves was added and the mixture was refluxed for 4—23 h. At the end of the reaction the mixture was cooled and the resulting sulfur and molecular sieves were filtered off. The filtrate was evaporated and the residue was distilled to obtain carbodiimide. The carbodiimides (**3**) were identified by their IR spectra and boiling points.[12–16]

Reactions of ***1a*** *with Trialkylthiourea.* A solution of 5.9 g (0.05 mol) of trimethylthiourea and 7.7 g (0.05 mol) of **1a** in 150 ml of toluene was refluxed for 20 h. The toluene was evaporated, the precipitated sulfur was filtered off, and the filtrate was distilled to give 2.8 g (55%) of trimethyl (trimethylamidino)thiourea (**5a**): bp 103 °C (0.6 mmHg); Found: C, 40.45; H, 10.20; N, 31.32; S, 18.01%. Calcd for $C_6H_{18}N_4S$: C, 40.43; H, 10.18; N, 31.44; S, 17.95%. IR (neat): $\nu_{C=N}$ 1645 cm^{-1}; NMR ($CDCl_3$) δ, 3.27 (s, 3H), 3.11 (s, 6H), 2.88 (s, 3H), 2.82 (s, 6H); MS *m/e* 202 (M^+, 4), 187 ($M^+ - CH_3$, 15), 169 ($M^+ - SH$, 4), 158 ($M^+ - NMe_2$, 9), 108 (29), 85 (100). *N,N*-Diethyl-*N*-′

methyl-N'-(N^1,N^1-diethyl-N^2-methylamidino)thiourea (**5b**) was obtained similarly: yield 40%; bp 123 °C (0.5 mmHg); Found: C, 51.20; H, 11.21; N, 24.01; S, 13.65%. Calcd for $C_{10}H_{26}N_4S$: C, 51.24; H, 11.18; N, 23.90; S, 13.68%. IR (neat): $\nu_{C=N}$ 1650 cm^{-1}; NMR ($CDCl_3$) δ, 3.48 (q, 4H), 3.15 (s, 3H), 2.86 (s, 3H), 1.16 (t, 6H), 1.07 (t, 6H); MS *m/e* 258 (M^+, 5), 243 ($M^+ - CH_3$, 4), 225 ($M^+ - SH$, 3), 186 ($M^+ - NEt_2$, 15), 146 (4), 113 (100).

Reactions of ***1a*** *with 1,1-Disubstituted Thiourea.* A suspension of 1,1-disubstituted thiourea (**6**, 0.05 mol) and **1a** (0.05 mol) in carbon tetrachloride was refluxed for 6—11 h. At the end of the reaction the mixture was cooled and the resulting sulfur was filtered off. The filtrate was evaporated and the residue was distilled to obtain 3,5-bis(disubstituted amino)thiadiazole (**7**) and disubstituted cyanamide (**8**). In the cases of *N*-thiocarbamoylmorpholine (**6d**) and 1,1-diphenylthiourea (**6e**), the reaction mixture was evaporated and the residue was chromatographed on Wako gel C-200, using benzene as the eluent. The solvent was evaporated and the residue was recrystallized from ethanol, giving **7d** and **7e**. 3,5-Bis(diethylamino)-1,2,4-thiadiazole (**7a**); Found: C, 52.58; H, 8.80; N, 24.32; S, 13.87%. Calcd for $C_{10}H_{20}N_4S$: C, 52.60; H, 8.83; N, 24.53; S, 14.04%. IR (neat): 1570, 1540, 1420 cm^{-1}. ^{1}H-NMR ($CDCl_3$): δ, 1.19 (m, 12H), 3.43 (m, 8H). ^{13}C-NMR ($CDCl_3$): δ, 12.7, 13.6, 43.2, 45.7, 165.5, 181.6. MS (70 eV): *m/e* 228 (M^+, 80), 213 (100), 130 (9). Found: *m/e* 228.1390. Calcd for $C_{10}H_{20}N_4S$: 228.1409. 3,5-Bis(dipropylamino)-1,2,4-thiadiazole (**7b**); Found: C, 59.59; H, 10.06; N, 19.34; S, 11.32%. Calcd for $C_{14}H_{28}N_4S$: C, 59.11; H, 9.92; N, 19.70; S, 11.27%. IR (neat): 1565, 1530, 1420 cm^{-1}. ^{1}H-NMR ($CDCl_3$): δ, 0.92 (m, 12H), 1.64 (m, 8H), 3.36 (m, 8H). MS (70 eV): *m/e* 284 (M^+, 36), 255 (100). Found: *m/e* 284.2013. Calcd for $C_{14}H_{28}N_4S$: 284.2035. 3,5-Bis(dibutylamino)-1,2,4-thiadiazole (**7c**); Found: C, 63.73; H, 10.79; N, 16.09; S, 9.57%. Calcd for $C_{18}H_{36}N_4S$: C, 63.48; H, 10.65; N, 16.45; S, 9.41%. IR (neat): 1570, 1535, 1420 cm^{-1}. ^{1}H-NMR ($CDCl_3$): δ, 0.90 (t, 12H, J=3.5 Hz), 1.30 (m, 8H), 1.58 (m, 8H), 3.36 (m, 8H). MS (70 eV): *m/e* 340 (M^+, 62), 297 (100). Found: *m/e* 340.2690. Calcd for $C_{18}H_{36}N_4S$: 340.2661. 3,5-Dimorpholino-1,2,4-thiadiazole (**7d**); Found: C, 46.27; H, 6.24; N, 21.70; S, 12.56%. Calcd for $C_{10}H_{16}N_4O_2S$: C, 46.86; H, 6.29; N, 21.86; S, 12.51%. IR (KBr): 1560, 1510, 1410, 1120 cm^{-1}. ^{1}H-NMR ($CDCl_3$): δ, 3.30—3.80 (m). MS (70 eV): *m/e* 256 (M^+, 100), 144 (11). Found: *m/e* 256.0980. Calcd for $C_{10}H_{16}N_4O_2S$: 256.0994. 3,5-Bis(diphenylamino)-1,2,4-thiadiazole (**7e**); Found: C, 74.77; H, 4.81; S, 7.62%. Calcd for $C_{26}H_{20}N_4S$: C, 74.27; H, 4.79; S, 7.62%. IR (KBr): 1590, 1535, 1495, 1450, 1370 cm^{-1}. MS (70 eV): *m/e* 420 (M^+, 100), 226 (8). Found: *m/e* 420.1377. Calcd for $C_{26}H_{20}N_4S$: 420.1409.

References

1) The previous paper in this series: H. Kagami and S. Motoki, *Bull. Chem. Soc. Jpn.*, **52**, 3463 (1979).
2) H. Kagami and S. Motoki, *J. Org. Chem.*, **42**, 4139 (1977).
3) H. Kagami and S. Motoki, *J. Org. Chem.*, **42**, 958 (1977).
4) K. T. Potts and R. Armbruster, *J. Heterocyclic Chem.*, **9**, 651 (1972).
5) B. J. Millard and D. L. Pain, *J. Chem. Soc., C*, **1970**, 2043.
6) W. Traube and A. Engelhardt, *Chem. Ber.*, **44**, 3149 (1911).
7) J. V. Braun, *Chem. Ber.*, **40**, 3941 (1907).
8) E. B. Vliet, *J. Am. Chem. Soc.*, **46**, 1306 (1924).
9) G. Kresze, A. Horn, R. Philipson, and A. Trede, *Chem. Ber.*, **98**, 3401 (1965).
10) Q. E. Thompson, M. M. Crutchfield, M. W. Dietrich, and E. Pierron, *J. Org. Chem.*, **30**, 2692 (1965).
11) H. Horst and I. Reuter, *J. Prakt. Chem.*, **351**, 144 (1973).
12) G. D. Meakins and R. J. Moss, *J. Chem. Soc.*, **1957**, 993.
13) K. Hartke, *Angew. Chem.*, **74**, 214 (1962).
14) H. Z. Lecher, R. P. Parker, and R. S. Long, *U. S. Patent*, 2479498 (1950).
15) E. Schmidt, F. Hitzler, and E. Lahde, *Chem. Ber.*, **71**, 1933 (1938).
16) H. G. Khorana, *J. Chem. Soc.*, **1952**, 2081.

Studies of Unusual Amino Acids and Their Peptides. XIII. The Chemistry of *N*-(Carboxymethyl)amino Acids. II. The Synthesis of Peptides Containing *N*-(Carboxymethyl)amino Acids

Toshifumi MIYAZAWA

Department of Chemistry, Faculty of Science, Kōnan University, Okamoto, Higashinada-ku, Kobe 658

(Received April 4, 1980)

The basic problems in the synthesis of peptides with *N*-carboxymethyl(Cm-)amino acids were investigated. Several kinds of *N*-protected derivatives of a free Cm-amino acid and the *N*-benzyloxycarbonyl (Z) derivative of its monoester were obtained by the conventional methods used for the parent amino acid. The peptide-bond formation at either carboxyl group of a Cm-amino acid proved to be achievable by the usual methods, such as the carbodiimide, dicyclohexylcarbodiimide–1-hydroxybenzotriazole, or mixed anhydride method, as illustrated by the examples using the Z–Cm-amino acid derivatives as the carboxyl components. On the other hand, a peptide using a Cm-amino acid diester as the amino component could not be prepared by the usual methods mentioned above. The desired compound was eventually obtained by the acid chloride method. A peptide containing a Cm-amino acid with the free imino group was also prepared by the condensation of a bromoacetylated amino acid ester with an amino acid or peptide ester.

In the previous paper,[1] the author has reported on the preparation and properties of a number of *N*-carboxymethyl(Cm-)amino acids and their mono- and diesters. Such polyfunctional amino acids are incorporated in most of the known biologically active peptides. The additional functional groups always pose special problems for the synthesis of peptides and necessitate detailed studies of the amino acids in question. However, nothing is known about the chemistry of peptides containing Cm-amino acids, though bottromycin, an antibiotic, has recently proved to be an example of such a peptide occurring in nature.[2] The present paper will deal with the basic problems in the preparation of peptides containing Cm-amino acids.

Protection of the Carboxyl Groups. The use of a Cm-amino acid[3] for peptide synthesis may involve many types of its *C*-protected derivatives, according to the synthetic routes. Among them, the diester carrying two selectively removable *C*-protecting groups may be the most useful intermediate. The direct preparation of this type of diester from the parent amino acid ester is preferable to the ordinary approach, *i.e.*, the esterification of the free Cm-amino acid prepared beforehand. Thus, as described previously,[1] any derivative of a Cm-amino acid carrying two different ester groups ($R^1 \neq R^2$) can be prepared by condensing an amino acid ester with a haloacetic acid ester (Scheme 1). On the other hand, the esterification of a Cm-amino acid, for example with an alcohol–thionyl chloride, tends to afford its dialkyl ester ($R^1=R^2$). The diester of this type may be utilized for the preparation of a peptide having a Cm-amino acid at the *C*-terminal position.

$$\text{H–AA–OR}^1 + \text{XCH}_2\text{CO}_2\text{R}^2 \longrightarrow \text{H–}\underset{\displaystyle \text{OR}^2}{\underset{|}{\text{C}}}\text{mAA–OR}^1$$

(X = Br or Cl; R^1, R^2 = Me (Et), Bzl, or Bu^t)

Scheme 1.

Protection of the Imino Group. As described in the previous paper,[1] Cm-amino acids are eluted from the strongly acidic cation-exchange resin with water as an eluent. Since this indicates the low basicity of the imino group of a Cm-amino acid, the acylation of this group is presumed to be difficult. Actually, Abderhalden and Haase[4] took advantage of this poor reactivity for the purification of Cm-valine contaminated with valine: Cm-valine was isolated unchanged even after treating the reaction mixture with benzoyl chloride. No other reports concerning the acylation of a free Cm-amino acid have been found. But the *N*-ethylthiocarbonothioyl (ETCT) derivatives of Cm-amino acids were accessible, as described previously.[1] Consequently, the applicability of the conventional methods[5] of *N*-protection to the Cm-amino acid was examined. Cm-alanine, Cm-phenylalanine, and Cm-valine were chosen as model compounds for this purpose.

Contrary to the results reported by Abderhalden and Haase, the benzyloxycarbonyl (Z) group could be introduced by the Schotten-Baumann reaction using the corresponding chloride, though the yields were somewhat poorer than those with the parent amino acids. The *p*-toluenesulfonyl (Tos) derivatives were obtained by the usual method using *p*-toluenesulfonyl chloride as an acylating agent, though in rather low yields. The *o*-nitrobenzenesulfenyl (Nps) derivatives could also be obtained by the use of the corresponding chloride under the Schotten-Baumann conditions. As another type of acylating agent, ethyl trifluoroacetate–1,1,3,3-tetramethylguanidine[6] was tried in the introduction of the trifluoroacetyl (CF_3CO) group. In this case, however, the acylation proceeded quite slowly compared with the case of the parent amino acid and with that of the acylation using a reagent of the acyl chloride type. Interestingly, the formylation using formic acid–acetic anhydride was an exceptional case: the reaction was accomplished in quite a short time. The yields and physical constants of the *N*-protected Cm-amino acids thus obtained are summarized in Table 1. The above examples show that the *N*-protection of a Cm-amino acid can be achieved without any greater difficulty than expected.

Most of the *N*-protected Cm-amino acids were obtained at first as oily substances, and crystallized as the bis(dicyclohexylamine) or bis(cyclohexylamine) salts. Repeated recrystallization and/or prolonged heating of the DCHA salts caused the unsatisfactory

TABLE 1. *N*-PROTECTED Cm-AMINO ACIDS

Compound	Yield %	Salt	Mp[c] °C	$[\alpha]_D^{25}$ (*c* 1.0, MeOH)	Found (Calcd) (%) C	H	N
Z–CmAla	74	2DCHA	150—151 (A)	−3.7°	68.41 (69.01	9.61 9.55	6.33 6.53)
Z–CmPhe	76	2CHA	189.5—190 (B)	−77.6°	66.98 (67.00	8.12 8.16	7.26 7.56)
Z–CmVal	50	2CHA	169.5—171 (C)	−27.2°	63.60 (63.88	9.10 8.94	8.06 8.28)
Tos–CmAla	49	—[b]	157.5—159 (A)	−33.7°[d]	47.77 (47.84	5.07 5.02	4.59 4.65)
Tos–CmPhe	53	—[b]	173.5—174.5 (A)	0.0°[e]	57.39 (57.29	5.10 5.08	3.69 3.71)
Tos–CmVal	29	—[b]	179.5—181 (D)	−55.6°	50.95 (51.05	5.81 5.81	4.23 4.25)
Nps–CmAla	56[a]	2DCHA	159.5—160.5 (E)	+81.6°	63.64 (63.42	8.73 8.82	8.59 8.45)
Nps–CmPhe	57[a]	2DCHA	174.5—175 (E)	+41.6°	65.97 (66.64	8.66 8.46	7.30 7.58)
Nps–CmVal	52	—[b]	140—143 (D)	+96.7°[f]	47.89 (47.56	5.01 4.91	8.35 8.53)
CF_3CO–CmAla	69[a]	2DCHA	168—168.5 (A)	−8.6°	60.98 (61.47	8.87 8.98	6.82 6.94)
CF_3CO–CmPhe	81	2DCHA	174—174.5 (A)	−46.1°	64.99 (65.17	8.63 8.57	6.08 6.16)
CF_3CO–CmVal	90[a]	2DCHA	175—175.5 (A)	−18.0°	62.27 (62.53	9.22 9.22	6.52 6.63)
HCO–CmAla	73[a]	2CHA	173—175 (F)	−14.6°	57.35 (57.88	9.32 9.45	11.08 11.25)
HCO–CmPhe	64	—[b]	177.5—178 (G)	−63.3°	57.71 (57.37	5.57 5.22	5.68 5.58)
HCO–CmVal	81[a]	2DCHA	175.5—176 (D)	−10.2°	67.75 (67.92	10.46 10.51	7.40 7.43)

a) Yield of the salt based on the Cm-amino acid used. b) Physical and analytical data for the free *N*-protected compound. c) Solvents for recrystallization: A, EtOAc; B, EtOH; C, $CHCl_3$–petroleum ether; D, EtOAc–petroleum ether; E, $CHCl_3$–ether; F, EtOH–ether; G, H_2O. d) *c* 0.82. e) ORD: $[\phi]_{300}^{23}$ +184° (*c* 0.34, MeOH). f) *c* 0.40.

results in elemental analyses, probably due to the partial release of the amine. The melting point of an *N*-protected Cm-amino acid is higher than that of the corresponding derivative of the parent amino acid, while the reverse is the case with their DCHA salts.[7]

The *N*-protection of the monoester of a Cm-amino acid was examined next. A typical example is the benzyloxycarbonylation of the monoester (**2e**) of Cm-valine, prepared from ethyl valinate according to Scheme 2. To avoid the hydrolysis of the ester group, the method using Z–Cl and sodium hydrogencarbonate was chosen. Since the addition of the total amount of the chloride at the beginning had not as usual afforded a good result, its portion by portion addition was tried. By the excessive use of the chloride by 20%, the desired compound (**3e**) was obtained in a yield comparable to the cases of the monoesters of the usual monoamino dicarboxylic acids.

To shorten the synthetic route to the desired compound (**3e**), the direct benzyloxycarbonylation of the reaction mixture obtained by the condensation of ethyl valinate with bromoacetic acid was attempted. (As described previously,[1] the isolation of the monoester (**2e**) from the above mixture was unsuccessful.) The overall yield by this route, however, was no more than 28%; consequently, the route shown in Scheme 2 is more desirable.

The Z derivatives of other Cm-amino acid monoesters could likewise be obtained. These also showed no tendency to crystallize and were characterized as the DCHA or CHA salts (Table 2). As can be seen from Table 2, the DCHA salts of Z derivatives with the free carboxyl group at the glycine moiety (**3a**·DCHA and **3e**·DCHA) have lower melting points than those of their isomers (**3b**·DCHA and **3f**·DCHA).[8]

Formation of the Peptide Bond at the Carboxyl Groups. The peptide-bond formation at the two sorts of carboxyl groups of a Cm-amino acid was investigated, using Cm-valine as a model compound. First, in order to try the coupling at the carboxyl group in the glycine moiety, Z–CmVal–OEt (**3e**) obtained above was used as the carboxyl component, and H–Pro–OBu^t, H–Phe–OBzl,

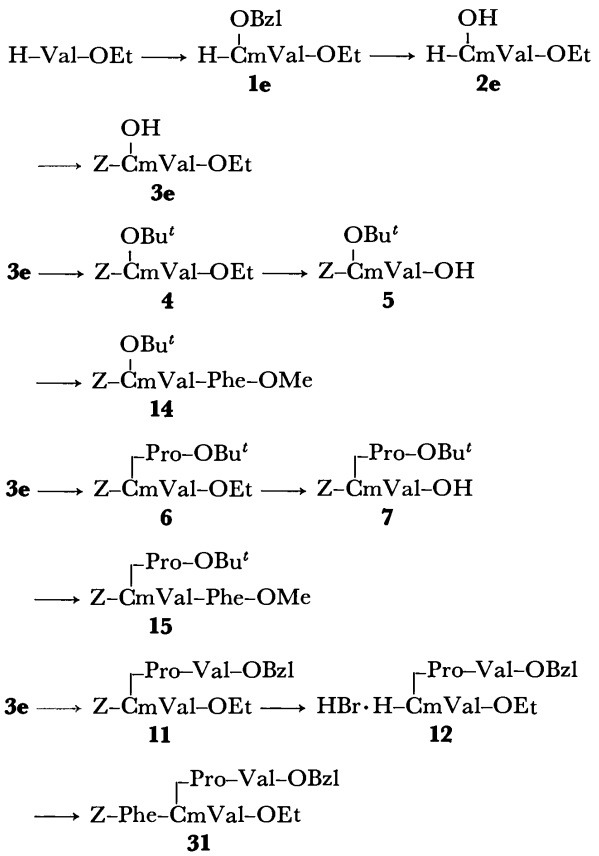

Scheme 2.

H–Gly–Gly–OEt, H–Phe–Phe–OMe, H–Pro–Val–OBzl, or H–Pro–Val–Val–OBzl as the amino component. The desired di- or tripeptides, or tetrapeptide could be obtained without too much difficulty by the carbodiimide, DCC–HOBt, or mixed anhydride method.[5] All the products were isolated as viscous oils by preparative TLC on silica gel.

The coupling at the carboxyl group in the valine moiety was tried next. Two sorts of carboxyl components (**5** and **7**) were prepared for this purpose, as shown in Scheme 2. Z–CmVal–OEt (**3e**) was converted into the *t*-butyl ester (**4**) with isobutylene in the presence of sulfuric acid. Then the ethyl ester group was cleaved by saponification, to afford **5**. Similarly, the selective removal of the ethyl ester group from the dipeptide **6** afforded **7**. By the DCC–HOBt or mixed anhydride method the desired di- and tripeptide (**14** and **15**)[9] could be obtained, using H–Phe–OMe as the amino component.

When a Z–Cm-amino acid listed in Table 1 was used as the carboxyl component, as illustrated in the case of Z–Cm-phenylalanine, the amino acid ester reacted at both the carboxyl groups and afforded a tripeptide, though in a rather low yield. Cm-proline itself also gave a similar tripeptide (**18**). The yield was better than those with Z–Cm-phenylalanine, though the reaction was heterogeneous, due probably to some remaining zwitter-ionic character of the amino acid.

As illustrated by the above examples, the peptide-bond formation at either carboxyl group of a Cm-amino acid proved to be achievable by the conventional methods. The peptides obtained here are listed in Table 3.

Formation of the Peptide Bond at the Imino Group. As already stated, the acylation of a free Cm-amino acid or its monoester was achieved without too much difficulty. The applicability of the usual coupling methods[5] to the peptide-bond formation at the imino group of a Cm-amino acid was investigated. However, the attempted couplings of Z–Phe–OH with the diester (**1e**) of Cm-valine by such common methods as the mixed anhydride, carbodiimide, DCC–HOBt, or *p*-nitrophenyl ester method all ended in failure. Both the diphenyl phosphorazidate (DPPA) method (a modified azide method) and the carbonyldiimidazole (CDI) method were unsuccessful. This was also the case with the phosphoryl chloride method, or with the phosphazo method, which involves the activation of the

Table 2. *N*-Benzyloxycarbonyl derivatives (**3**) of Cm-amino acid monoesters

Compound	Yield %	Mp[a] °C	$[\alpha]_D^{25}$ (*c* 1.0, $CHCl_3$)	Found (Calcd) (%) C	H	N
Z–CmAla–OMe·DCHA (**3a**·DCHA)	78	99—100 (A)	−14.9°	65.65 (65.52	8.62 8.46	5.62 5.88)
Z–CmAla–OH·DCHA (**3b**·DCHA)	81	155—155.5 (B)	−12.5°	65.25 (65.52	8.72 8.46	5.86 5.88)
Z–CmPhe–OMe·CHA (**3c**·CHA)	72	155—156 (C)	−56.0°	66.34 (66.36	7.38 7.28	5.89 5.95)
Z–CmPhe–OH·DCHA (**3d**·DCHA)	58	137—138 (B)	−28.3°	69.26 (69.54	8.18 8.02	5.06 5.07)
Z–CmVal–OEt·DCHA (**3e**·DCHA)	79	109.5—110 (D)	−39.8°	66.95 (67.15	9.15 8.94	5.07 5.40)
Z–CmVal–OH·DCHA (**3f**·DCHA)	68	142—143 (D)	−29.6°	67.12 (67.15	9.21 8.94	5.39 5.40)

a) Solvents for recrystallization: A, acetone–hexane; B, acetone; C, EtOAc; D, hexane.

TABLE 3. PREPARATION OF PEPTIDES USING Cm-AMINO ACID DERIVATIVES AS THE CARBOXYL COMPONENTS

Compound	Carboxyl component; Amino component	(Coupling method[a])	Yield[h] %	$[\alpha]_D^{25}$	TLC, R_f[i]	Found (Calcd) (%) C	H	N
Z-CmVal-(Pro-OBu^t)-OEt (**6**)	**3e**; Pro-OBu^t	(A)	82	−86.7° (*c* 1.0, MeOH)	0.48	63.53 (63.65	7.77 7.80	5.96 5.71)
Z-CmVal-(Phe-OBzl)-OEt (**8**)	**3e**·DCHA; Phe-OBzl·TosOH	(B)[b]	53 (E)	−24.8° (*c* 1.5, $CHCl_3$)	0.59	69.10 (68.97	6.75 6.67	4.89 4.88)
	3e·DCHA; Phe-OBzl·TosOH	(C)	70 (E)	−24.2° (*c* 0.95, $CHCl_3$)	0.59			
	3e; Phe-OBzl·TosOH[c]	(D)	55 (E)	−23.7° (*c* 2.1, $CHCl_3$)	0.59			
Z-CmVal-(Gly-Gly-OEt)-OEt (**9**)	**3e**·DCHA; Gly-Gly-OEt·HBr[d]	(C)	66 (F)	−23.7° (*c* 1.0, MeOH)	0.10	57.56 (57.61	7.16 6.94	8.56 8.76)
Z-CmVal-(Phe-Phe-OMe)-OEt (**10**)	**3e**; Phe-Phe-OMe·HCl[c,e]	(C)	47 (E,G)	−26.6° (*c* 0.90, $CHCl_3$)	0.47	67.08 (66.96	6.78 6.71	6.58 6.51)
Z-CmVal-(Pro-Val-OBzl)-OEt (**11**)	**3e**·DCHA; Pro-Val-OBzl·HBr	(C)	51 (H)	−94.7° (*c* 1.1, $CHCl_3$)	0.49	65.23 (65.47	7.39 7.27	6.72 6.74)
Z-CmVal-(Pro-Val-Val-OBzl)-OEt (**13**)	**3e**·DCHA; Pro-Val-Val-OBzl·HBr[f]	(C)	37 (H)	−92.6° (*c* 0.99, $CHCl_3$)	0.25	64.39 (64.80	7.71 7.53	7.85 7.75)
Z-CmVal-(OBu^t)-Phe-OMe (**14**)	**5**; Phe-OMe·HCl[c]	(A)	69 (G)	+6.1° (*c* 1.4, $CHCl_3$)	0.63	66.17 (66.14	7.51 7.27	5.34 5.32)
	5; Phe-OMe·HCl[c]	(D)	52 (E)	+4.9° (*c* 1.9, $CHCl_3$)	0.63			
Z-CmVal-(Pro-OBu^t)-Phe-OMe (**15**)	**7**;[g] Phe-OMe·HCl[c]	(A)	46 (H)	−31.8° (*c* 1.6, $CHCl_3$)	0.40	65.91 (65.47	7.43 7.27	6.20 6.74)
Z-CmPhe-(Ala-OBzl)-Ala-OBzl (**16**)	Z-CmPhe·2CHA; Ala-OBzl·TosOH	(B)[b]	30 (G)	−74.0° (*c* 0.90, $CHCl_3$)	0.56	69.03 (68.91	6.41 6.08	5.90 6.18)
Z-CmPhe-(Val-OBzl)-Val-OBzl (**17**)	Z-CmPhe; Val-OBzl·TosOH	(B)	25 (I)	−75.5° (*c* 1.1, $CHCl_3$)	0.63	70.37 (70.19	6.84 6.71	5.65 5.71)
CmPro-(Phe-OBzl)-Phe-OBzl (**18**)	CmPro; Phe-OBzl·TosOH[c]	(A)	57 (F,G)	−49.0° (*c* 1.7, MeOH)	0.22	71.79 (72.31	6.43 6.38	6.12 6.49)

a) A, DCC–HOBt method; B, EDC method; C, DCC method; D, mixed anhydride method (using isobutyl chloroformate). b) An equimolar amount of TosOH·H_2O to EDC was added. c) An equimolar amount of TEA was added. d) Ref. 18. e) Prepared by the debenzyloxycarbonylation of Z–Phe–Phe–OMe[19] with 5% Pd–C in MeOH containing concd HCl. f) Prepared by the debenzyloxycarbonylation of Z–Pro–Val–Val-OBzl.[21] g) Prepared by the saponification of **6**. h) Solvents for preparative TLC: E, benzene–EtOAc (9 : 1); F, $CHCl_3$–EtOAc (1 : 1); G, benzene–EtOAc (3 : 1); H, benzene–EtOAc (1 : 1); I, $CHCl_3$–EtOAc (9 : 1). i) Benzene–EtOAc (1 : 1).

amino component.

The acid chloride is considered to be the most reactive acylating agent, and has often been employed in the coupling with *N*-methylamino acids, in the synthesis of peptolides, and in the cases where other methods give only poor yields. Fortunately, by the use of Z–Phe–Cl[10] in the presence of *N*-ethyldiisopropylamine (or TEA), the desired dipeptide (**27**) was obtained also in the present case, though in a moderate yield (41%) after several successive purification procedures. In the preparation of dehydropeptides, which has recently been reported,[11] the isolation of an acid chloride was omitted and the reaction mixture was directly used for the coupling with the pyridine solution of the amino component. In the present case, however, the yield by this convenient procedure was no more than 17%. This was also the case with the related method using *N*,*N*-dimethylchloroformimidium chloride, the yield being only 13%. Recently the peptide synthesis using 2-fluoro-1,3,5-trinitrobenzene has been reported:[12] the acid fluoride was supposed to be the reactive acylating agent, and the method was applied to the condensation of amino acids containing rather bulky substituents. The coupling in question, however, resulted in a much poorer yield (12%).

A number of other dipeptides could be obtained by the acid chloride method using the diester of Cm-alanine, Cm-phenylalanine, or Cm-valine as the amino component and the phthalyl (Pht) or Z derivative of glycine, alanine, phenylalanine, or valine as the carboxyl component. The results are summarized in Table 4. A considerable amount of the unchanged amino component remaining even after acid washings was removed by treatment with the cation-exchange resin

Table 4. Preparation of dipeptides using Cm-amino acid diesters as the amino components

Compound	Carboxyl component; Amino component[b,c]	Yield[g] %	$[\alpha]_D^{25}$ ($CHCl_3$)	TLC, R_f[h]	Found (Calcd) (%) C	H	N
Pht-Gly-CmAla(OBzl)-OMe (**19**)	Pht-Gly-Cl; **1a**·TosOH[d]	48 (A)	−33.4° (*c* 2.1)	0.30	62.48 (63.01	4.99 5.06	6.14 6.39)
Pht-Gly-CmVal(OBzl)-OEt (**20**)[a]	Pht-Gly-Cl; **1e**[e]	44	−16.5° (*c* 1.0)	0.46	65.19 (64.99	5.87 5.87	5.58 5.83)
Pht-Val-CmAla(OBzl)-OMe (**21**)	Pht-Val-Cl; **1a**·TosOH[d]	58 (A)	−131.6° (*c* 2.2)	0.38	64.55 (64.99	5.87 5.87	5.59 5.83)
Pht-Val-CmVal(OBzl)-OEt (**22**)	Pht-Val-Cl; **1e**[e]	22 (B)	−186.5° (*c* 1.0)	0.47	66.72 (66.65	6.77 6.56	5.17 5.36)
Z-Ala-CmPhe(OBzl)-OMe (**23**)	Z-Ala-Cl; **1c**·TosOH[d]	28 (B)	−67.9° (*c* 0.68)	0.44	67.62 (67.65	6.18 6.06	5.10 5.26)
Z-Ala-CmVal(OBzl)-OEt (**24**)	Z-Ala-Cl; **1e**·TosOH[d]	21 (B)	−52.6° (*c* 1.0)	0.48	65.02 (65.04	7.04 6.87	5.43 5.62)
Z-Phe-CmAla(OBzl)-OMe (**25**)	Z-Phe-Cl; **1a**·TosOH[d]	29 (A,B)	−30.0° (*c* 1.0)	0.43	67.79 (67.65	6.26 6.06	5.06 5.26)
Z-Phe-CmPhe(OBzl)-OMe (**26**)	Z-Phe-Cl; **1c**·TosOH[d]	28 (B)	−57.2° (*c* 0.72)	0.52	71.14 (71.03	6.14 5.96	4.31 4.60)
Z-Phe-CmVal(OBzl)-OEt (**27**)	Z-Phe-Cl; **1e**[f]	41 (B)	−43.9° (*c* 1.1)	0.57	68.95 (68.97	6.87 6.67	4.60 4.88)
Z-Val-CmAla(OBzl)-OMe (**28**)	Z-Val-Cl; **1a**·TosOH[d]	13 (B)	−33.2° (*c* 0.88)	0.43	64.74 (64.45	6.86 6.66	5.42 5.78)
Z-Val-CmPhe(OBzl)-OMe (**29**)	Z-Val-Cl; **1c**·TosOH[d]	8 (B)	−71.0° (*c* 0.62)	0.52	68.60 (68.55	6.65 6.47	4.81 5.00)
Z-Val-CmVal(OBzl)-OEt (**30**)	Z-Val-Cl; **1e**·TosOH[d]	7 (C)	−66.7° (*c* 0.54)	0.55	66.52 (66.14	7.50 7.27	4.83 5.32)

a) Mp 112.5—114 °C (benzene). b) **1a**, H–CmAla(OBzl)–OMe; **1c**, H–CmPhe(OBzl)–OMe. c) An equimolar amount of *N*-ethyldiisopropylamine or TEA was added when the amino component was used in the form of salt. d) Molar ratio of the carboxyl component to the amino component, 2 : 1. e) Molar ratio, 1.1 : 1. f) Molar ratio, 1 : 1. g) Solvents for preparative TLC: A, benzene–EtOAc (3 : 1); B, benzene–EtOAc (9 : 1); C, benzene–EtOAc (99 : 1). h) Benzene–EtOAc (3 : 1).

Table 5. Preparation of peptides containing Cm-amino acids with the free imino group

Compound	Starting materials	Yield[d] %	$[\alpha]_D^{25}$ (MeOH)	TLC, R_f[e]	Found (Calcd) (%) C	H	N
H–CmVal(Phe-OBzl)-OMe (**32**)[a]	$BrCH_2CO$–Phe–OBzl, Val–OMe·TosOH	30 (A)	−37.5° (*c* 0.88)	0.55	67.87 (67.58	7.25 7.09	6.36 6.57)
H–CmVal(Val-OBzl)-OMe (**33**)[a]	$BrCH_2CO$–Val–OBzl, Val–OMe·TosOH	47 (A,B)	−50.3° (*c* 1.5)	0.54	63.31 (63.47	8.16 7.99	7.18 7.40)
H–CmPhe(Phe-OBzl)–Phe–OMe (**34**)[b]	$BrCH_2CO$–Phe–OBzl, Phe–Phe–OMe·HCl	28 (A,C)	−21.3° (*c* 0.46)	0.31	71.44 (71.48	6.33 6.32	6.51 6.76)
H–CmPhe(Val-OBzl)–Phe–OMe (**35**)[c]	$BrCH_2CO$–Val–OBzl, Phe–Phe–OMe·HCl	40 (A,C)	−30.1° (*c* 2.6)	0.34	69.45 (69.09	7.04 6.85	7.19 7.33)

a) Syrup. b) Glassy. c) Mp 104—106 °C (with sintering at *ca.* 78 °C) (acetone). d) Solvents for preparative TLC: A, $CHCl_3$–EtOAc (9 : 1); B, benzene–EtOAc (3 : 1); C, $CHCl_3$–EtOAc (3 : 1). e) $CHCl_3$–EtOAc (3 : 1).

(Amberlyst 15). The final stage of purification required successive chromatographic separations on silica gel, to afford the desired compound as a viscous oil, except **20**. In the cases where the acid chlorides used were relatively stable, the desired compounds were obtained in moderate yields. On the other hand, the yields of the couplings using Z–Val–Cl[13] were extremely unsatisfactory. This is presumably attributable to both the

instability and the bulkiness of the chloride. In general, the difficulty in the separation of the desired product from the starting Cm-amino acid diester was another factor which affected the yield.

The elongation of the peptide chain from a peptide having a Cm-amino acid at the *N*-terminal position was examined next. As an example, the tetrapeptide **31** could be obtained in a yield comparable to those of the above dipeptides by the reaction of Z–Phe–Cl with **12**, prepared by the debenzyloxycarbonylation of the tripeptide **11** with hydrogen bromide in acetic acid, as shown in Scheme 2.

As an example of the coupling using a Cm-amino acid with the free carboxyl group as the amino component, the reaction of Z–Phe–Cl with the DCHA salt of the monoester (**2e**) of Cm-valine in dichloromethane was attempted.[14] The desired dipeptide was found to be produced in a *ca.* 20% yield. However, the isolation of the purified product was extremely troublesome, and this approach had to be abandoned.

Preparation of Peptides Containing Cm-amino Acids with the Free Imino Group. As an extension of the method for preparing Cm-amino acid diesters shown in Scheme 1, the condensation of a bromoacetylated amino acid ester or peptide ester with the other amino acid ester or peptide ester might be employed for preparing a peptide containing a Cm-amino acid in the middle of the molecule. In practice, the imino-free di- and tripeptides listed in Table 5 were prepared by this approach, though the yields were lower than those of the preparation of the Cm-amino acid diesters. Benzyl *N*-(bromoacetyl)phenylalaninate and benzyl *N*-(bromoacetyl)valinate were prepared by treatment of the corresponding amino acid benzyl esters with bromoacetyl bromide in the presence of TEA. The condensation with an amino acid or peptide ester was conducted in the presence of TEA at room temperature. The products did not form crystalline salts with *p*-toluenesulfonic or picrolonic acid, unlike the diesters of Cm-amino acids, but they changed to a similar blue coloration when sprayed with cobalt(II) thiocyanate.[15]

In conclusion, the results obtained here indicate that, in the synthesis of peptides containing Cm-amino acids, such routes starting from the parent amino acids as shown in Scheme 2 are highly recommendable. In the case where a new peptide bond is to be built at the imino group of a Cm-amino acid, the acid chloride method or an alternative, equally potent method should be employed.

Experimental

All melting points are uncorrected. Optical rotations were measured with a JASCO DIP-4 polarimeter, and ORD curves recorded on a JASCO ORD/UV-5 spectropolarimeter. TLC and preparative TLC were performed on Merck Kieselgel 60 F_{254} and Kieselgel GF_{254} (Type 60), respectively. The amino acids and their derivatives used here are all of the L-configuration.

Preparation of N-*Protected Cm-amino Acids.* The introduction of each *N*-protecting group is illustrated by a typical example below. When the desired compound was obtained as a syrup, it was crystallized as the DCHA or CHA salt. The results are summarized in Table 1.

Z–CmPhe: To a solution of Cm-phenylalanine (1.00 g) in 2 M NaOH (4.5 ml) were added Z–Cl (0.85 g) in ether (3 ml) and 2 M NaOH (2.5 ml) simultaneously with vigorous stirring at 0—5 °C, and the mixture was stirred at room temperature overnight. The turbid reaction mixture was washed with ether and acidified to pH 2 with 2 M HCl. The precipitated oil was extracted with EtOAc, and the extract was washed with water and dried over Na_2SO_4. Evaporation of the solvent afforded a syrup; yield, 1.22 g (76%). Upon the addition of double molar amounts of CHA the corresponding salt separated out; mp 189.5—190 °C (EtOH).

Nps–CmVal: To a solution of Cm-valine (250 mg) in 2 M NaOH (1.4 ml) and dioxane (2 ml) were added *o*-nitrobenzenesulfenyl chloride (300 mg) and 2 M NaOH (0.85 ml) simultaneously with vigorous stirring, and the mixture was stirred at room temperature overnight. After addition of water and filtration, the reaction mixture was acidified to pH 2 with 0.5 M H_2SO_4. The precipitated oil was treated in a manner similar to that described for the preparation of Z–CmPhe, to afford crystals; yield, 244 mg (52%); mp 140—143 °C (EtOAc–petroleum ether).

Tos–CmPhe: To a solution of Cm-phenylalanine (1.00 g) in 1 M NaOH (13.5 ml) was added a solution of *p*-toluenesulfonyl chloride (1.29 g) in ether (6 ml) in five portions at intervals of 1 h, and the mixture was stirred at room temperature overnight. The reaction mixture was washed with ether and acidified to Congo Red with 2 M HCl. (The unchanged amino acid occasionally separated out at a lower pH.) The precipitated oil was extracted with EtOAc, and the extract was washed with 2 M HCl and water, and dried over Na_2SO_4. Evaporation of the solvent afforded crystals; yield, 895 mg (53%) (33%, in a run where an equimolar amount of the chloride was used); mp 173.5—174.5 °C (EtOAc).

CF_3CO–CmAla: A suspension of Cm-alanine (200 mg), ethyl trifluoroacetate (970 mg), and 1,1,3,3-tetramethylguanidine (390 mg) was stirred for 3 d (until an almost clear solution was obtained). After evaporation of excess ethyl trifluoroacetate, the residue was dissolved in water and acidified to pH 2 with 4 M HCl. The precipitated oil was treated in a manner similar to that described for the preparation of Z–CmPhe. Upon the addition of double molar amounts of DCHA to the residual syrup the corresponding salt separated out; yield, 569 mg (69%); mp 168—168.5 °C (EtOAc).

HCO–CmPhe: To a chilled solution of Cm-phenylalanine (500 mg) in 99% formic acid (4.7 ml) was added acetic anhydride (1.6 ml) at 0—3 °C, and the mixture was stirred at this temperature for 30 min and then at room temperature for *ca.* 4 h. After the addition and successive evaporation of water to the reaction mixture had been repeated, the residual crystals were filtered, and washed with water; yield, 360 mg (64%); mp 177.5—178 °C (H_2O).

Preparation of the Z Derivatives of Cm-amino Acid Monoesters. A typical example illustrating the preparation of these compounds is shown below.

OH
|
Z–CmVal–OEt (3e): a) To a stirred solution of H–CmVal–OEt (**2e**) (2.03 g) and $NaHCO_3$ (2.10 g) in water (17.5 ml) was added a solution of Z–Cl (2.70 g) in ether (3 ml) portion by portion, after each consumption, over a period of 4—6 h. Then the mixture was stirred below 5 °C overnight. The reaction mixture was filtered, and the filtrate acidified to pH 2 with 4 M HCl. The deposited oil was extracted with EtOAc, and the extract was washed with water and dried over Na_2SO_4. After evaporation of the solvent, the residual syrup was treated with DCHA (1.81 g), to afford the corresponding

salt; yield, 4.08 g (79%); mp 109.5—110 °C (hexane).

b) A mixture of H–Val–OEt·TosOH (3.17 g), bromoacetic acid (1.53 g), and TEA (2.12 g) was refluxed in THF (30 ml) for 50 h with occasional filtration of the precipitates. After the solvent had been removed under reduced pressure, the residue was mixed with the above precipitates, and benzyloxycarbonylated using Z–Cl and $NaHCO_3$ as described above, to afford 0.95 g of the desired compound (**3e**) (28% yield based on H–Val–OEt·TosOH).

Other Z derivatives were obtained in the same manner as used in Method a), and crystallized as the DCHA or CHA salts. The results are summarized in Table 2.

OBu^t
|
Z–CmVal–OEt (*4*). A mixture of Z–CmVal–OEt (**3e**) (recovered from the DCHA salt by treatment in EtOAc with 1.5 M HCl as usual) (667 mg), liquid isobutylene (*ca.* 2 ml), concd H_2SO_4 (0.02 ml), and dichloromethane (4 ml) was allowed to stand in a pressure vessel at room temperature overnight. The syrup (662 mg), obtained by the usual work-up,[16] was chromatographed on preparative layers of silica gel with benzene–EtOAc (98 : 2); yield, 566 mg (73%); syrup, $[\alpha]_D^{25}$ −48.2° (*c* 1.0, MeOH). TLC: R_f 0.52 (benzene–EtOAc (9 : 1)). Found: C, 64.15; H, 8.16; N, 3.32%. Calcd for $C_{21}H_{31}NO_6$: C, 64.10; H, 7.94; N, 3.56%.

Preparation of Peptides Using Cm-amino Acid Derivatives as the Carboxyl Components. The desired protected peptides were obtained as syrups. The final purification of all of these compounds, except **6**, was performed by preparative TLC on silica gel. The results are summarized in Table 3. Typical examples illustrating the procedures for the preparation of these compounds are shown below.

┌*–Pro–OBu^t*
|
Z–CmVal–OEt (*6*), *by the DCC–HOBt Method*: Z–CmVal–OEt (**3e**) (650 mg), H–Pro–OBu^t (prepared through the debenzyloxycarbonylation of Z–Pro–OBu^t [16,17] (650 mg) by hydrogenation), and HOBt (270 mg) were dissolved in THF (7 ml). To the chilled solution was added DCC (400 mg), and the resulting mixture was stirred at 0 °C for 2.5 h and then at room temperature overnight. After *N,N′*-dicyclohexylurea had been removed by filtration, the filtrate was evaporated under reduced pressure. The residue was dissolved in EtOAc, washed successively with 5% citric acid, water, 5% $NaHCO_3$, and water, and dried over Na_2SO_4. Removal of the solvent afforded a pure product as a syrup; yield, 776 mg (82%); $[\alpha]_D^{25}$ −86.7° (*c* 1.0, MeOH).

┌*–Phe–OBzl*
|
Z–CmVal–OEt (*8*), *by the EDC Method*: To a chilled mixture of Z–CmVal–OEt·DCHA (**3e**·DCHA) (311 mg), H–Phe–OBzl·TosOH (256 mg), TosOH·H_2O (114 mg), and dioxane (6 ml) was added EDC (93 mg). The resulting mixture was stirred at 0 °C for *ca.* 2 h and then at room temperature overnight. After the mixture had been evaporated under reduced pressure, the residue was distributed between EtOAc and water, and the organic layer was further washed with 2% (or 5%) HCl, water, 5% $NaHCO_3$, and water again, and dried over Na_2SO_4. Removal of the solvent afforded a syrup (305 mg), which was chromatographed on preparative layers of silica gel with benzene–EtOAc (9 : 1); yield, 183 mg (53%); syrup, $[\alpha]_D^{25}$ −24.8° (*c* 1.5, $CHCl_3$).

The tripeptides (**16** and **17**) were prepared using double molar amounts of the amino component and EDC in a manner similar to that described above.

┌*–Pro–Val–OBzl*
|
Z–CmVal–OEt (*11*), *by the DCC Method*: To a chilled mixture of Z–CmVal–OEt·DCHA (**3e**·DCHA) (1036 mg), H–Pro–Val–OBzl·HBr (prepared by the debenzyloxycarbonylation of Z–Pro–Val–OBzl[20] (876 mg) with 25% HBr in AcOH (2.64 g) as usual), and CH_3CN (24 ml) was added DCC (415 mg) at 0 °C. The reaction mixture was stirred at this temperature for 2 h and then at room temperature overnight. After filtration of *N,N′*-dicyclohexylurea and a work-up similar to that described for the preparation of **8**, the residual syrup was chromatographed on preparative layers of silica gel with benzene–EtOAc (1 : 1); yield, 640 mg (51%); syrup, $[\alpha]_D^{25}$ −94.7° (*c* 1.1, $CHCl_3$).

OBu^t
|
Z–CmVal–Phe–OMe (*14*), *by the Mixed Anhydride Method*: To a chilled solution of **5** (obtained by the saponification of **4** with 0.5 M NaOH in aq EtOH) (417 mg) and TEA (115 mg) in THF (3 ml) was added isobutyl chloroformate (156 mg) with vigorous stirring below −10 °C. After 5 min a mixture of H–Phe–OMe·HCl (246 mg) and TEA (115 mg) in $CHCl_3$ (3 ml) was added at *ca.* −10 °C. The resulting mixture was stirred below 0 °C for *ca.* 3 h and then at room temperature overnight. After a work-up similar to that described for the preparation of **6**, the residual syrup was chromatographed on preparative layers of silica gel with benzene–EtOAc (9 : 1); yield, 311 mg (52%); syrup, $[\alpha]_D^{25}$ +4.9° (*c* 1.9, $CHCl_3$).

┌*–Phe–OBzl*
|
CmPro–Phe–OBzl (*18*), *by the DCC–HOBt Method*: To a chilled suspension of Cm-proline (157 mg), H–Phe–OBzl·TosOH (778 mg), TEA (184 mg), and HOBt (245 mg) in $CHCl_3$–THF–DMF (6 ml each) was added DCC (374 mg), and the resulting mixture was stirred at 0 °C for *ca.* 2 h and then at room temperature for 2 d. After *N,N′*-dicyclohexylurea had been removed by filtration, the filtrate was treated in a manner similar to that described for the preparation of **8**, to afford a syrup (502 mg). It was chromatographed on preparative layers of silica gel with $CHCl_3$–EtOAc (1 : 1) and then with benzene–EtOAc (3 : 1); yield, 333 mg (57%); syrup, $[\alpha]_D^{25}$ −49.0° (*c* 1.7, MeOH).

Preparation of Dipeptides Using Cm-amino Acid Diesters as the Amino Components. All the desired protected peptides were prepared by the acid chloride method. They were obtained as syrups, except **20**. The final purification of all of these compounds, except **20**, was performed by preparative TLC on silica gel. The results are summarized in Table 4. The carboxyl components, Pht–Gly–Cl,[22] Pht–Val–Cl,[23] Z–Ala–Cl,[24] and Z–Phe–Cl,[10] were prepared according to the literature. Z–Val–Cl[13] was prepared in a manner similar to the case of Z–Ala–Cl as follows: to a stirred solution of Z–Val–OH (350 mg) in dry Et_2O (3 ml) was added PCl_5 (310 mg) portion by portion at 0 °C. After 25 min the resulting solution was filtered, and the filtrate concentrated under reduced pressure below 10 °C. The residual syrup was washed well with dry petroleum ether, and dissolved in dry THF (1.5 ml). The solution was directly used for the coupling reaction. Typical examples are shown below.

OBzl
|
Z–Phe–CmVal–OEt (*27*): To a stirred solution of **1e** (980 mg) and *N*-ethyldiisopropylamine (430 mg) (or TEA (337 mg)) in dry THF (5 ml) was added Z–Phe–Cl (freshly prepared by the reaction of Z–Phe–OH (1.00 g) with PCl_5 (800 mg) in dry ether) in dry THF (2 ml) at 0 °C. The mixture was stirred at this temperature for *ca.* 3 h and then at room temperature for 2 d. The precipitates were filtered off, and the filtrate evaporated under reduced pressure. The residue was distributed between EtOAc (or Et_2O) and water, and the organic layer washed successively with 10% (w/w) HCl, water, 5% $NaHCO_3$, and water. After the dried (over

Na_2SO_4) solution had been evaporated under reduced pressure, the residue was treated batchwise with Amberlyst 15 (*ca.* 2 g) in MeOH, and then chromatographed on preparative layers of silica gel with benzene–EtOAc (9 : 1), to afford a syrup; yield, 787 mg (41%); $[\alpha]_D^{25}$ −43.9° (*c* 1.1, $CHCl_3$).

*Pht–Gly–CmVal(OBzl)–OEt (**20**)*: A mixture of **1e** (2.03 g), *N*-ethyldiisopropylamine (0.89 g), Pht–Gly–Cl (1.70 g), and dry THF (16 ml) was stirred at 0 °C for a few hours and then at room temperature for 2 d. After washing with 10% (w/w) HCl and 0.5 M $NaHCO_3$ the crude product (2.31 g) was obtained as crystals; mp 107—113 °C. It was recrystallized from benzene; yield, 1.44 g (44%); prisms, mp 112.5—114 °C, $[\alpha]_D^{25}$ −16.5° (*c* 1.0, $CHCl_3$).

*Z–Ala–CmPhe(OBzl)–OMe (**23**)*: A solution of **1c**·TosOH (350 mg) and TEA (142 mg) in dry THF (5 ml) was allowed to react with a solution of Z–Ala–Cl (freshly prepared by the reaction of Z–Ala–OH (310 mg) with PCl_5 (310 mg) in dry ether as a syrup and then dissolved in dry THF (1.5 ml)) in a manner similar to that described for the preparation of **27**. The final purification by preparative TLC with benzene–EtOAc (9 : 1) afforded the desired compound (**23**) as a syrup; yield, 104 mg (28%); $[\alpha]_D^{25}$ −67.9° (*c* 0.68, $CHCl_3$).

*Z–Phe–CmVal(Pro–Val–OBzl)–OEt (**31**)*. The tripeptide **11** (310 mg) was treated with 25% HBr in AcOH (0.7 g) for 1 h, and worked up as usual, to afford **12** in a 72% yield. This product (204 mg) was mixed with *N*-ethyldiisopropylamine (107 mg) in dry THF (3 ml), and allowed to react with Z–Phe–Cl (freshly prepared from Z–Phe–OH (238 mg) as described above), at 0 °C for 5 h and then at room temperature for 2 d. After washing in a manner similar to that described for the preparation of **27**, the residual syrup (174 mg) was chromatographed on preparative layers of silica gel with benzene–EtOAc (1 : 1); yield, 84 mg (30%); syrup, $[\alpha]_D^{25}$ −126.1° (*c* 0.62, $CHCl_3$). TLC: R_f 0.09 (benzene–EtOAc (3 : 1)), 0.46 (benzene–EtOAc (1 : 1)). Found: C, 66.34; H, 7.12; N, 7.24%. Calcd for $C_{43}H_{54}N_4O_9$: C, 66.99; H, 7.06; N, 7.27%.

Preparation of Peptides Containing Cm-amino Acids with the Free Imino Group. The final purification of the desired peptides was performed by preparative TLC on silica gel. The results are summarized in Table 5. The general procedure for the preparation of these compounds is illustrated by the following example.

*H–CmVal(Val–OBzl)–OMe (**33**)*: To an ice-chilled solution of H–Val–OBzl·TosOH (3.75 g) and TEA (2.00 g) in THF (30 ml) was added bromoacetyl bromide (2.00 g) in THF (10 ml) drop by drop. Then the mixture was stirred below 5 °C overnight. The usual work-up afforded benzyl *N*-(bromoacetyl)valinate as a syrup; yield, 2.85 g (88%). (Benzyl *N*-(bromoacetyl)phenylalaninate was prepared in a similar manner in an 89% yield.) This product was used for the next reaction without further purification.

To a stirred solution of H–Val–OMe·TosOH (750 mg) and TEA (500 mg) in THF (6 ml) was added the bromoacetylated compound (870 mg) obtained above in THF (4 ml) drop by drop. Then the reaction mixture was stirred at room temperature for a week, with occasional filtration of the precipitates. After the solvent had been removed under reduced pressure, the residue was distributed between EtOAc and water, and the organic layer was washed with water and dried over Na_2SO_4. Removal of the solvent afforded a syrup, which was chromatographed on preparative layers of silica gel successively with $CHCl_3$–EtOAc (9 : 1) and benzene–EtOAc (3 : 1); yield, 442 mg (47%); syrup, $[\alpha]_D^{25}$ −50.3° (*c* 1.5, MeOH).

The author would like to express his deep gratitude to Professors (the late) Hiroshi Watanabe, Shigeru Kuwata (Kōnan University), and Kazuhiro Maruyama (Kyoto University) for their invaluable suggestions and continuous encouragement.

References

1) T. Miyazawa, *Bull. Chem. Soc. Jpn.*, **53**, 2555 (1980).
2) Y. Takahashi, H. Naganawa, T. Takita, H. Umezawa, and S. Nakamura, *J. Antibiot.*, **29**, 1120 (1976).
3) a) The following abbreviations are used for Cm-amino acids and their derivatives: CmAA for a Cm-amino acid derived from an amino acid (AA), and X–CmAA–Z for its derivative (X–NCH(R)CO–Z). In these abbreviations, H of the imino group and/or OH of the carboxyl group are sometimes omitted. b) Abbreviations given by the IUPAC-IUB Commission (*J. Biol. Chem.*, **247**, 977 (1972)) are used throughout. Additional abbreviations: TEA, triethylamine; Bzl, benzyl; Bu^t, *t*-butyl; DCHA, dicyclohexylamine; CHA, cyclohexylamine; Z–Cl, benzyloxycarbonyl chloride; DCC, dicyclohexylcarbodiimide; HOBt, 1-hydroxybenzotriazole; TosOH, *p*-toluenesulfonic acid; EDC, 1-ethyl-3-(3-dimethylaminopropyl)carbodiimide; THF, tetrahydrofuran; DMF, *N*,*N*-dimethylformamide.
4) E. Abderhalden and E. Haase, *Hoppe-Seyler's Z. Phys. Chem.*, **202**, 54 (1931).
5) a) M. Bodanszky, Y. S. Klausner, and M. A. Ondetti, "Peptide Synthesis," 2nd ed, John Wiley & Sons, New York (1976); b) "Synthese von Peptiden," ed by E. Wünsch, Part I and II, in Houben-Weyl, "Methoden der Organischen Chemie," 4th ed, Thieme-Verlag, Vol. 15/1 and 2, Stuttgart (1974); c) E. Schröder and K. Lübke, "The Peptides," Academic Press, New York (1965), Vol. 1, and others.
6) Methyl trifluoroacetate was originally employed; W. Steglich and S. Hinze, *Synthesis*, **1976**, 399.
7) *Cf.* Ref. 5b.
8) The Z derivative **3c** did not form a crystalline salt with DCHA.
9) In the peptides obtained here as well as **4** and **6**, the *t*-butyl ester group was selectively removable with 4.4 M HCl in EtOAc.
10) M. Bergmann, L. Zervas, H. Rinke, and H. Schleich, *Hoppe-Seyley's Z. Phys. Chem.*, **224**, 37 (1934).
11) C. Shin, Y. Yonezawa, and J. Yoshimura, *Tetrahedron Lett.*, **1979**, 4085.
12) H. Kinoshita, K. Inomata, O. Miyano, and H. Kotake, *Bull. Chem. Soc. Jpn.*, **52**, 2619 (1979).
13) Purification of this chloride through quick washing of the reaction mixture with ice water did not give a good result; *cf.* R. L. M. Synge, *Biochem. J.*, **42**, 101 (1948).
14) *Cf.* A. Kapoor, E. J. Davis, and M. J. Graetzer, *J. Pharm. Sci.*, **57**, 1514 (1968). The DCHA salt of a Cm-amino acid itself was sparingly soluble in such a solvent as dichloromethane.
15) E. S. Lane, *J. Chromatogr.*, **18**, 426 (1965).
16) G. W. Anderson and F. M. Callahan, *J. Am. Chem. Soc.*, **82**, 3359 (1960).

17) H. L. Maia, K. G. Orrell, and H. N. Rydon, *J. Chem. Soc., Perkin Trans. 2*, **1976**, 763.
18) B. Halpern and L. B. James, *Aust. J. Chem.*, **17**, 1282 (1964).
19) P. G. Katsoyannis, J. Ginos, G. P. Schwartz, and A. Cosmatos, *J. Chem. Soc., Perkin Trans. 1*, **1974**, 1315.
20) This compound was prepared from Z–Pro–OH and H–Val–OBzl·TosOH by the DCC method in a 73% yield; mp 87—88 °C (EtOAc–petroleum ether), $[\alpha]_D^{25}$ −82.6° (*c* 1.0, MeOH). Found: C, 68.61; H, 6.99; N, 6.45%. Calcd for $C_{25}H_{30}N_2O_5$: C, 68.47; H, 6.90; N, 6.39%.
21) This compound was prepared from Z–Pro–OH and H–Val–Val–OBzl·HBr (prepared by the debenzyloxycarbonylation of Z–Val–Val–OBzl[25] with 25% HBr in AcOH) by the mixed anhydride method using ethyl chloroformate in an 84% yield; mp 108—110 °C (EtOAc–petroleum ether), $[\alpha]_D^{25}$ −95.4° (*c* 1.0, MeOH). Found: C, 67.03; H, 7.48; N, 7.78%. Calcd for $C_{30}H_{39}N_3O_6$: C, 67.02; H, 7.31; N, 7.82%.
22) J. C. Sheehan and V. S. Frank, *J. Am. Chem. Soc.*, **71**, 1859 (1949).
23) G. Losse and G. Müller, *Chem. Ber.*, **94**, 2777 (1961).
24) M. Bergmann and L. Zervas, *Ber.*, **65**, 1195 (1932).
25) E. Schröder and K. Lübke, *Justus Liebigs Ann. Chem.*, **655**, 216 (1962).

 © 1980 The Chemical Society of Japan Bull. Chem. Soc. Jpn., 53, 3670—3677 (1980) [Vol. 53, No. 12

Studies on Nucleosides and Nucleotides. VIII.[1] Preparation and Reactions of Triphenylphosphoranediylnucleosides

Junji KIMURA, Kentaro YAGI, Hideyuki SUZUKI, and Oyo MITSUNOBU*

Department of Chemistry, College of Science and Engineering, Aoyama Gakuin University, Chitosedai, Setagaya-ku, Tokyo 157

(Received May 12, 1980)

The reaction of uridine, N^4-benzoylcytidine, guanosine, and N^6-*p*-toluoyladenosine with diethyl azodicarboxylate and triphenylphosphine resulted in the formation of the corresponding 2′,3′-*O*-(triphenylphosphoranediyl)-cyclonucleosides. On the other hand, adenosine afforded, under similar conditions, 3′,5′-*O*-(triphenylphosphoranediyl)adenosine (**19**). The difference can be explained in terms of the acidity of base moieties of the nucleosides. The reaction of 2′,3′-*O*-(triphenylphosphoranediyl)-O^2,5′-cyclouridine, N^4-benzoyl-2′,3′-*O*-(triphenylphosphoranediyl)-O^2,5′-cyclocytidine, 2′,3′-*O*-(triphenylphosphoranediyl)-N^3,5′-cycloguanosine, or N^6-*p*-toluoyl-2′,3′-*O*-(triphenylphosphoranediyl)-N^3,5′-cycloadenosine with nucleophiles and with electrophiles addorded the corresponding nucleoside derivatives with free 2′- and 3′-hydroxyl groups. Thus the 2′,3′-*O*-triphenylphosphoranediyl group serves as a protecting group which is readily removed during work-up of the reaction products. **19** reacted with phenyl isocyanate to give 5′-*O*-phenylcarbamoyladenosine and N^6,5′-*O*-bis(phenylcarbamoyl)adenosine. The reaction of **19** with diphenylketene also afforded acyladenosines with free 2′- and 3′-hydroxyl groups. These results suggested that 3′,5′-*O*-triphenylphosphoranediyl group activates the 5′-carbon atom of adenosine.

Since the discovery of 2′,3′-*O*-isopropylidene-N^3,5′-cycloadenosine by Todd and his coworkers, many cyclonucleosides have been synthesized and utilized in synthetic organic chemistry and pharmaceutical as well as in genetic studies.[2] Cyclonucleosides are generally prepared by two stage reactions which involve transformation of a hydroxyl group of the sugar moiety into a leaving group and subsequent intramolecular displacement. Recent study in this laboratory has shown that 2′,3′-*O*-isopropylideneuridine reacts with diethyl azodicarboxylate (**1**) and triphenylphosphine (**2**) giving 2′,3′-*O*-isopropylidene-O^2,5′-cyclouridine (**3**).[3]

In the present paper, we describe the synthesis of triphenylphosphoranediylnucleosides and the use of these compounds in the preparation of nucleoside derivatives.[4]

2′,3′-O-(Triphenylphosphoranediyl)-O²,5′-cyclouridine. In order to obtain unprotected O^2,5′-cyclouridine (**4**), the reaction of uridine with 3 molar equivalents each of **1** and **2** was carried out at room temperature, 2′,3′-*O*-(triphenylphosphoranediyl)-O^2,5′-cyclouridine (**5**) and not the expected **4** being isolated in 65% yield. An alternative structure, **6**, or its position isomer was ruled out by NMR study. A signal is observed in the ^{31}P-NMR spectrum at $\delta = +27.60$, lying in the region characteristic for a phosphorane and not for a phosphonium salt (Table 1).[5] Further support for the structure **5** was provided by the following reactions.

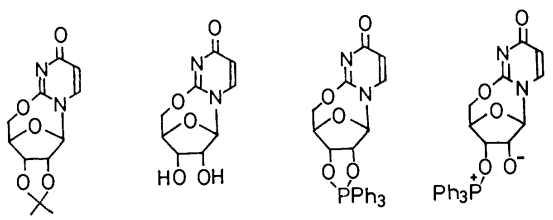

3 4 5 6

Acid or alkaline hydrolysis of **5** afforded uridine and triphenylphosphine oxide in a *ca.* 1 : 1 ratio, **4** being obtained in 70% yield[6] on treatment with H_2O–tetrahydrofuran (THF) at room temperature for 3 d. **4** reacted with **1** and **2** to regenerate **5** in 73% yield. When **5** was treated with ammonia in methanol, isocytidine (**7a**) was isolated which was subsequently converted into 2′,3′-*O*-isopropylideneisocytidine. The results indicate that the removal of triphenylphosphine oxide proceeds smoothly with retention of the configuration of 2′- and 3′-hydroxyl groups.

Bartlett *et al.* reported that 2,2,2-triphenyl-4,4,5,5-tetramethyl-1,3,2-dioxaphospholane (**8**) decomposes into tetramethyloxirane even at room temperature.[7] Unlike **8**, **5** is thermally stable and can be recrystallized from *N*,*N*-dimethylformamide (DMF) at 80 °C. As compared with the isopropylidene group, the –O–P–O– bond of the phosphoranediyl group is somewhat more labile but still stable enough to be treated without difficulty under ordinary atmosphere. **5** could therefore be utilized as a protected O^2,5′-cyclouridine.

The reaction of **5** with methanol under reflux for 10 h afforded O^2-methyluridine (**7b**) in 80% yield. As in the case of **3**,[8] **5** reacted smoothly with benzoyl bromide and with acetyl bromide to give 5′-bromo-5′-deoxy-N^3-benzoyluridine (**9a**; 72%) and 5′-bromo-5′-deoxyuridine (**9b**; 60%), respectively. The fact that no 2′- and/or 3′-acylated products could be detected in these reactions indicates that the phosphoranediyl group is stable under the reaction conditions used.

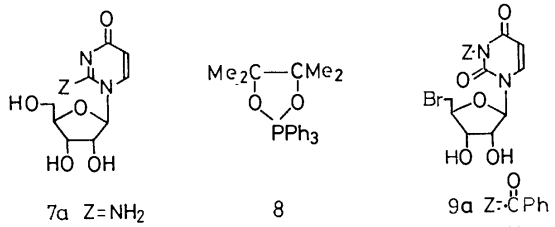

7a Z=NH₂ b Z=OMe 8 9a Z=C(=O)Ph b Z=H

In the reactions of triphenylphosphoranediyl nucleosides with nucleophiles and electrophiles, the isolated

products has no phosphorane ring, presumably because triphenylphosphine oxide was eliminated during the work-up.

N^4-Benzoyl-2′,3′-O-(triphenylphosphoranediyl)-O′,5′-cyclocytidine. When cytidine was allowed to react with **1** and **2** in a similar manner to that described above, unidentified products were formed. The reaction of N^4-benzoylcytidine with **1** and **2**, however, gave N^4-benzoyl-2′,3′-*O*-(triphenylphosphoranediyl)-O^2,5′-cyclocytidine (**10**) in 71% yield.

The O^2,5′-anhydro bond of 2′,3′-*O*-isopropylidene-O^2,5′-cyclocytidine methanesulfonate is known to be more reactive than that of **3**.[9] This is also the case with phosphoranediylcyclonucleosides **5** and **10**. Thus when **10** was treated with acetonitrile–H_2O at room temperature for 2 d, N^4-benzoylcytidine and triphenylphosphine oxide were formed in a *ca.* 1 : 1 ratio. **10** reacted smoothly at room temperature with benzoic acid giving N^4,5′-*O*-dibenzoylcytidine quantitatively.[10] By the reaction with **1** and **2**, N^4,5′-*O*-dibenzoylcytidine afforded N^4,5′-*O*-dibenzoyl-2′,3′-*O*-(triphenylphosphoranediyl)cytidine (**11**) in 49% yield. The configuration of 2′- and 3′-hydroxyl group was thus retained during the migration of the phosphoranediyl group.

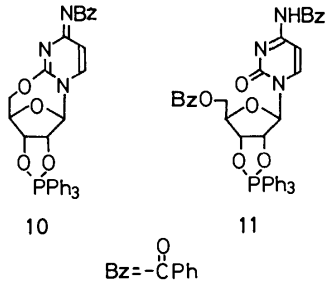

Both the anhydro and glycosidic bonds were cleaved by treatment of **10** in methanol at room temperature overnight, O^2-methylcytosine being obtained in 65% yield. Attempts to isolate and identify the products from the sugar moiety were unsuccessful. On the other hand, no glycosidic bond cleavage took place when N^4-benzoyl-2′,3′-*O*-isopropylidene-O^2,5′-cyclocytidine was treated in methanol under the same conditions.

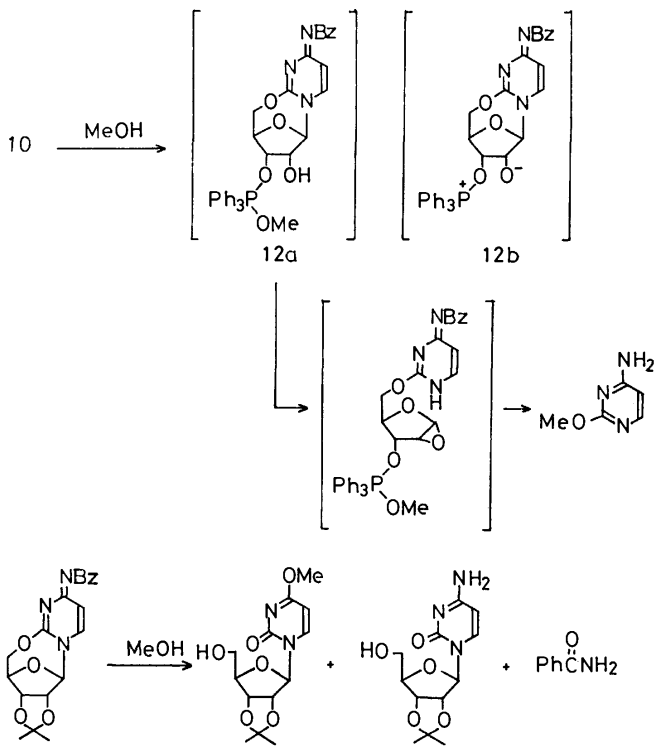

Scheme 1.

In this case O^4-methyl-2′,3′-*O*-isopropylideneuridine, 2′,3′-*O*-isopropylidenecytidine, and benzamide were isolated in 33, 23, and 36% yields, respectively (Scheme 1).

The formation of O^2-methylcytosine might be explained by the initial formation of phosphorane (**12a**) or betaine (**12b**). The glycosidic and O^2,5′-anhydro bonds were successively cleaved by intramolecular nucleophilic displacement and methanolysis as shown in Scheme 1.

The reaction of **10** with phosphoric diesters was studied. As expected, **10** reacted with tetrabutylammonium dibenzyl phosphate at room temperature to afford N^4-benzoylcytidin-5′-yl dibenzyl phosphate (**14a**; 35% isolated yield) which was converted into the corresponding isopropylidene derivatives. Similarly the reaction

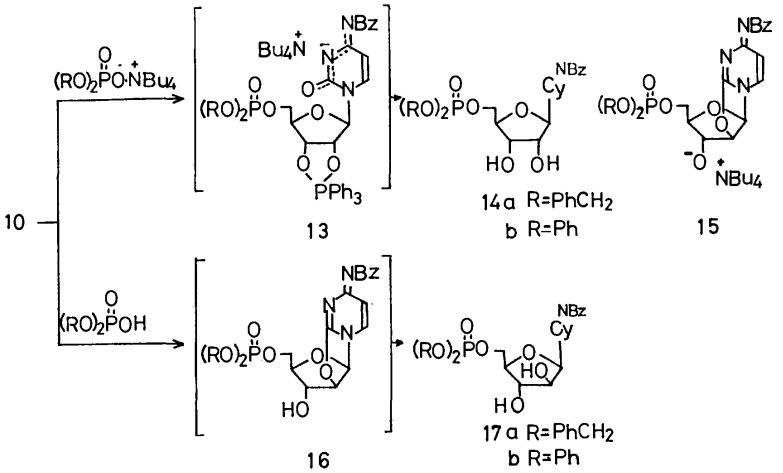

Scheme 2.

of **10** with tetrabutylammonium diphenyl phosphate gave **14b** in 15% isolated yield (Scheme 2). On the other hand, when **10** was allowed to react with dibenzyl hydrogenphosphate or diphenyl hydrogenphosphate under the same conditions, neither **14a** nor **14b** could be isolated, but 1-(β-D-arabinofuranosyl)-N^4-benzoylcytosin-5′-yl dibenzyl phosphate (**17a**) and 1-(β-D-arabinofuranosyl)-N^4-benzoylcytosin-5′-yl diphenyl phosphate (**17b**) were isolated in 38 and 52% yields, respectively (Scheme 2).[11] The structure of **17b** was determined by comparison of physical properties with those of an authentic sample prepared by the reaction of 1-(β-D-arabinofuranosyl)-N^4-benzoylcytidine with diphenyl phosphorochloridate.

The difference between the reaction of **10** with a phosphoric diester and with its tetrabutylammonium salt might be explained by the mechanism illustrated in Scheme 2. When a phosphoric diester attacks the 5′-carbon atom of **10**, rearrangement of O^2,5′-anhydro bond takes place with liberation of triphenylphosphine oxide, forming O^2,2′-cyclocytidine 5′-phosphate (**16**) which is hydrolyzed to **17** during the course of manipulation.[12] Since no evidence of the formation of O^2,2′-anhydro bond was obtained in the reaction of **10** with benzoic acid, the anhydro bond rearrangement would be an acid catalyzed process. Since no proton source exists in the reaction of **10** with a tetrabutylammonium salt of phosphoric diester, the anhydro bond rearrangement is unfavorable because of instability of the resulting alkoxide (**15**). The reaction stops at the stage of the formation of **13**.

2′,3′-O-(Triphenylphosphoranediyl)-N^3,5′*-cycloguanosine.* Guanosine also reacted with **1** and **2** at 70 °C to give 2′,3′-*O*-(triphenylphosphoranediyl)-N^3,5′-cycloguanosine (**18**) which was readily hydrolyzed to N^3,5′-cycloguanosine and triphenylphosphine oxide in a 1 : 1 ratio. ^{31}P-NMR spectrum also supports the phosphorane structure (Table 1).

TABLE 1. YIELD AND PHYSICAL CONSTANTS OF TRIPHENYLPHOSPHRANEDIYLNUCLEOSIDES

Compound	**5**	**10**	**18**	**19**	**29**
Yield/%	62	71	67	75	24
Mp/°C	>250	200—201	>250	171—172	200—204
UV_{max} (MeCN)/nm	232	235^{sh}, 318	259	260	
$\varepsilon \times 10^{-4}$	2.65	1.46	1.25	0.74	
^{31}P-NMR(δ)[a]	+27.60	+27.54	+26.58	+29.33	

a) Recorded on a Hitachi R-22 spectrometer at 36.414 MHz±1 Hz (^{1}H decoupled; solvent, DMF). Triphenylphosphine sulfide (δ −42.07; Ref. 85% H_3PO_4) was used as an internal standard, the reported chemical shift being relative to 85% H_3PO_4.

3′,5′-O-(Triphenylphosphoranediyl)adenosine. When adenosine was allowed to react with **1** and **2** in dioxane at 70 °C, a phosphorus-containing compound was obtained, showing UV_{max} 260 nm, and a ^{31}P-NMR singlet at +29.33 ppm (Table 1). This compound was hydrolyzed to adenosine and triphenylphosphine oxide in a 1 : 1 ratio. As the structure of the product, both 3′,5′-*O*-(triphenylphosphoranediyl)- and 2′,3′-*O*-(triphenylphosphoranediyl)adenosine (**19** and **20**) are conceivable.

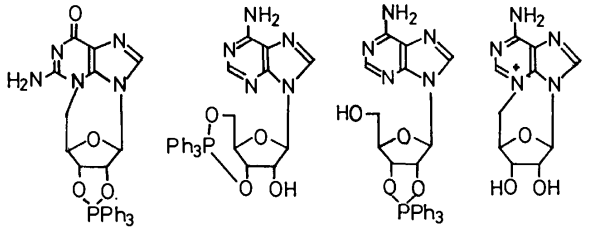

18 19 20 21

In order to confirm the structure, the product was allowed to react with benzoic acid to form 5′-*O*-benzoyladenosine and N^3,5′-cycloadenosine (**21**) in 59 and 16% yields, respectively. A similar treatment with thiobenzoic acid gave 5′-benzoylthio-5′-deoxyadenosine in 63% yield. It can be concluded that the product obtained by the reaction of adenosine with **1** and **2** is **19** rather than **20**.

The fact that **19** is readily hydrolyzed to adenosine under mild conditions suggests that the compound can be utilized as a starting material for the protection of 2′-hydroxyl group of adenosine. Contrary to expectation, reactions of **19** with acyl halide, acid anhydride or dihydropyran were complicated, giving rise to significant side reactions and affording unidentified products.

The reaction of **19** with phenyl isocyanate (**22**) and diphenylketene (**23**), however, led to definite products. **19** reacted with **22** in pyridine to give 5′-*O*-phenylcarbamoyladenosine (**25**) and N^6,5′-*O*-bis(phenylcarbamoyl)adenosine (**26**) in 34 and 45% yields, respectively. The products were identified by comparison with samples prepared by the reaction of **22** with 2′,3′-*O*-isopropylideneadenosine, followed by removal of the protecting group.

Similarly, **19** reacted with **23** to give 5′-*O*-(diphenylacetyl)adenosine and N^6,5′-*O*-bis(diphenylacetyl)-adenosine in 21 and 41% yields, respectively.

In the reaction of **19** with **22** and with **23**, no 2′- and/or 3′-*O*-carbamoyl- or acyladenosine could be obtained. The results lead to the hypothesis that the 3′,5′-*O*-triphenylphosphoranediyl group "activates" the 5′-carbon atom of **19**. The electrophilic attack at the 5′-carbon atom accompanies 5′-O–P bond rearrangement giving 2′,3′-*O*-(triphenylphosphoranediyl)-

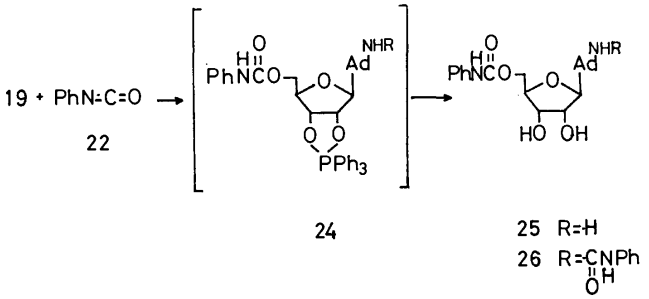

22 24 25 R=H 26 R=CNPh

Scheme 3.

adenosine derivative (**24**) in which the phosphoranediyl group protects 2'- and 3'-hydroxyl groups from further attack of the electrophiles (Scheme 3).[13]

On the basis of NMR studies, Mengel and Bartke have demonstrated that the product obtained by the reaction of adenosine with **1** and **2** is not **19** but **20**.[14] However, it is difficult to explain the formation of 5'-*O*-benzoyladenosine and N^3,5'-cycloadenosine by the structure **20**. A plausible interpretation might be given if we assume equilibrium between **19** and **20** in which the former is reactive species.

Reaction Mechanism. 2'(or 3'),5'-*O*-Bis(triphenylphosphonio)nucleoside (**27**) can be assumed to be a key intermediate for the formation of 2',3'-*O*-(triphenylphosphoranediyl)cyclonucleoside.[1,4] *N,N'*-Bis(ethoxycarbonyl)hydrazinide anion subsequently abstracts hydrogen atoms from the base and the hydroxyl group to form **5**, **10**, and **18** (Scheme 4).

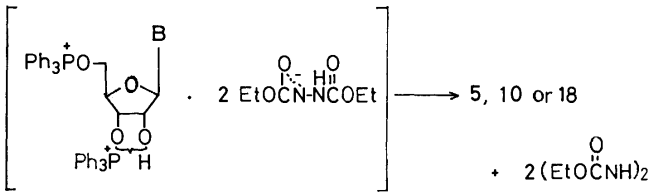

27

Scheme 4.

5 was obtained as the sole product derived from the nucleoside when the reaction of uridine with equimolar amounts of **1** and **2** was carried out with the intention of preparing **4**. This suggests that phosphorane ring formation is essential for the formation of the anhydro bond.[15]

The reaction of adenosine with **1** and **2** would also proceed through the initial formation of 5'-*O*-(triphenylphosphinio)adenosine (**28**). Since the hydrogen atom of the adenine ring is not so acidic as to be abstracted by hydrazinide anion, the 3'-hydroxyl group of **28** attacks the phosphorus atom giving **19**. Whether anhydro bond is formed or not would depend on the relative acidity of the base moiety of nucleoside and *N,N'*-bis(ethoxycarbonyl)hydrazine. In order to confirm the assumption, we carried out the reaction of N^6-*p*-toluoyladenosine in which N^6-hydrogen atom was expected to become more acidic than *N,N'*-bis(ethoxycarbonyl)hydrazine by the electron withdrawing effect of the *p*-toluoyl group.

The reaction of N^6-*p*-toluoyladenosine with **1** and **2** resulted in the formation of N^6-*p*-toluoyl-2',3'-*O*-(triphenylphosphoranediyl)-N^3,5'-cycloadenosine (**29**) in 24% isolated yield. Since purification of the product was difficult, the crude products obtained under separate experiment were treated with water under reflux to afford N^5,5'-anhydro-5-formamido-4-(*N*-*p*-toluoylamidino)-1-(β-D-ribofuranosyl)imidazole (**30a**) in 74% yield. By treatment with ammonia in methanol, **30a** was converted into **31a** which was hydrolyzed to **32a** under mild acidic conditions.

N^3,5'-Anhydro bond formation also took place when N^6-*p*-toluoyl-2',3'-*O*-isopropylideneadenosine was used. Thus the reaction of the fully protected nucleoside with **1** and **2** afforded imidazole nucleoside (**30b**) in a nearly quantitative yield rather than N^6-*p*-toluoyl-2',3'-*O*-isopropylidene-N^3,5'-cycloadenosine. Thus the precursor of **30b** should be N^6-*p*-toluoyl-2',3'-*O*-isopropylidene-N^3,5'-cycloadenosine which was hydrolyzed to **30b** during the work-up involving preparative layer chromatography. By subsequent treatment with ammonia in methanol, **30b** was converted into deformylated imidazole nucleoside (**31b**).

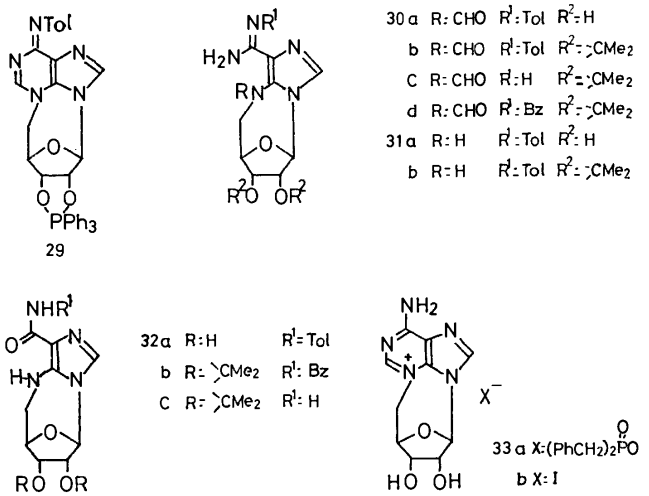

Reports have been given on the cleavage of N(1)–C(2) bond of N^3,5'-cycloadenosine derivatives. Anzai and Matsui[16] reported that treatment of 2',3'-*O*-isopropylidene-N^3,5'-cycloadenosine methanesulfonate and 5'-*O*-methylsulfonyl-N^6,N^6-dibenzoyl-2',3'-*O*-isopropylideneadenosine with alkali leads to imidazole cyclonucleoside **30c** and **30d**, respectively; they also reported the transformation of **30d** into **32b** and **32c**.

When the reaction of adenosine with **1** and **2** is carried out in the presence of dibenzyl hydrogenphosphate, N^3,5'-cycloadenosine dibenzyl phosphate (**33a**) is formed in good yield.[1] The reaction of adenosine with methyltriphenylphosphonium iodide gave N^3,5'-cycloadenosine iodide (**33b**).[17] It can thus be concluded that the N^3,5'-anhydro bond of adenosine is formed only when the reaction system involves a conjugate base of strong acid which stabilizes the N^3,5'-cycloadenosine cation.

The methods described make phosphoranediylnucleosides readily available. That the phosphoranediyl function serves as a protecting group as well as an activating group suggests a number of possibilities for the transformation of nucleosides.

Experimental

Methods. Preparative layer chromatography (TLC) was carried out on 20 cm × 20 cm or 20 cm × 30 cm glass plates coated with Merck silica gel PF_{254}. ^{1}H-Nuclear magnetic resonance (NMR) spectra were measured on a Hitachi R-20 spectrometer (60 MHz) using tetramethylsilane as an internal standard. We are grateful to Dr. G. Miyajima of Hitachi Co. Ltd. for the measurement of ^{31}P-NMR spectra. Ultraviolet absorption spectra were obtained with a Hitachi EPS-3T

recording spectrometer. Elemental analyses were carried out at the Institute of Physical and Chemical Research, Wako-shi, Saitama.

2′,3′-O-(Triphenylphosphoranediyl)-O²,5′-cyclouridine (5). A solution of **1** (2.61 g, 15 mmol) in THF (2 ml) was added to a mixture of uridine (1.22 g, 5 mmol) and **2** (3.93 g, 15 mmol) in THF (10 ml) at room temperature. The nucleoside dissolved on addition of **1**, precipitation taking place shortly afterwards. After the mixture had been kept stirred at room temperature overnight, the precipitate was collected by centrifugation, washed successively with THF and ether. Recrystallization from DMF (80 °C) gave **5** not melting below 250 °C; UV_{max} (MeCN) 232 nm; NMR (DMSO-d_6) δ=4.32, 4.50, 4.70 (m, 5, $C_{2'}H$, $C_{3'}H$, $C_{4'}H$, $C_{5'}H$), 5.86 (br. s, 1, $C_{1'}H$), 7.28 (15, aromatic H). Found: C, 66.65; H, 4.82; N, 5.81%. Calcd for $C_{27}H_{23}N_2O_5P$: C, 66.67; H, 4.76; N, 5.76%.

When **5** was treated with AcOH–H_2O or dil aqueous ammonia, uridine and triphenylphosphine oxide were formed in a 1 : 1 ratio.

O²,5′-Cyclouridine (4). A solution of **5** (486 mg, 1 mmol) in THF–H_2O (1 : 1 v/v, 10 ml) was stirred over a period of 3 d at room temperature and then evaporated. The residue was washed with acetone in order to remove triphenylphosphine oxide giving **4** (70%), which melted with decomposition at *ca.* 265 °C (lit,[6] dec 212—214 °C). UV_{max} (MeOH) 238 nm. Found: C, 47.75; H, 4.54; N, 12.34%. Calcd for $C_9H_{10}N_2O_5$: C, 47.79; H, 4.46; N, 12.39%.

When **4** was allowed to react with 1.5 molar equivalent each of **1** and **2** in THF at room temperature overnight, **5** was obtained in 73% yield.

O²-Methyl- and O²-Ethyluridine. **5** (1.458 g, 3 mmol) was treated with methanol (100 ml) under reflux for 10 h and then evaporated. The residue was washed with acetone, recrystallization from methanol giving *O²*-methyluridine with mp 171—172 °C (lit,[18] mp 173 °C). UV_{max} (H_2O) 229, 253 nm, UV_{min} 213, 238 nm.

Similarly, *O²*-ethyluridine was isolated in 41% yield, mp 176—177 °C. UV_{max}(H_2O) 228, 253 nm; UV_{min} 213, 237 nm.

Isocytidine. A solution of **5** (120 mg, 0.125 mmol) in saturated methanolic ammonia (10 ml) was left to stand at room temperature for 5 d and then separated by TLC using $CHCl_3$–MeOH (10 : 1) to give isocytidine as a glass almost quantitatively. UV_{max}(MeOH) 230^{sh}, 255 nm, UV_{min} 250 nm. Found: C, 44.23; H, 5.39; N, 17.28%. Calcd for $C_9H_{13}N_3O_5$: C, 44.44; H, 5.72; N, 17.10%.

Isocytidine (100 mg, 0.41 mmol) dissolved in 2,2-dimethoxypropane (2 ml) in the presence of a catalytic amount of *p*-toluenesulfonic acid was stirred for 2 h at room temperature and then neutralized with sodium methoxide. The resulting mixture was separated by TLC using $CHCl_3$–MeOH (10 : 1), giving 50% of 2′,3′-*O*-isopropylideneisocytidine which was purified by re-precipitation from ethanol–ether, mp 191—192 °C (lit,[18] mp 206—207 °C).

Reaction of 5 with Acyl Bromide. A mixture of **5** (484 mg, 1 mmol) and acetyl bromide (492 mg, 4 mmol) in THF (5 ml) was kept stirred at room temperature for 3 h and then evaporated. The residue was separated by TLC using $CHCl_3$–MeOH (95 : 5) giving 173 mg (73%) of **9b** with mp 183—185 °C (lit,[19] mp 180—183 °C).

In a similar way, **5** was treated with benzoyl bromide to give **9a** (300 mg, 73%). The substance softens at 78 °C, showing no definite mp. UV_{max}(MeOH) 255 nm, UV_{min} 226 nm. Found: C, 46.62; H, 3.53; N, 6.60%. Calcd for $C_{15}H_{15}N_2O_5Br$: C, 46.73; H, 3.77; N, 6.81%.

N⁴-Benzoyl-2′,3′-O-(triphenylphosphoranediyl)-O²,5′-cyclocytidine (10). A solution of **1** (4 mmol) in THF (2 ml) was added to a mixture of *N⁴*-benzoylcytidine (694 mg, 2 mmol) and **2** (4 mmol) in THF (4 ml) at room temperature. The nucleoside dissolved as **1** was added and shortly afterwards pale yellow solid began to precipitate. After the mixture had been stored at room temperature for 2 d, the precipitate was collect and recrystallized from dry acetonitrile, giving 830 mg (71%) of **10** which decomposed at 200—201 °C. UV_{max} (MeCN) 235^{sh}, 318 nm (ε 14600), UV_{min} 290 nm; NMR ($CDCl_3$) δ=4.16—4.66 (m, 5, $C_{2'}H$, $C_{3'}H$, $C_{4'}H$, $C_{5'}H$), 5.17 (d, 1, $C_{1'}H$), 6.60 (d, 1, C_5H), 8.20—8.30 (m, 21, aromatic-H, C_6H). Found: C, 69.27; H, 4.79; N, 6.93%. Calcd for $C_{34}H_{28}N_3O_5P$: C, 69.26; H, 4.79; N, 7.13%.

A solution of **10** in MeCN–H_2O (1 : 1) was kept stirred at room temperature for 2 d and then evaporated. The residue was washed with acetone to remove triphenylphosphine oxide, giving *N⁴*-benzoylcytidine in nearly quantitative yield with mp 222—225 °C (lit,[20] mp 219—220 °C). The substance was identical with an authentic sample as confirmed by IR analysis.

N⁴-Benzoyl-2′,3′-O-isopropylidene-O²,5′-cyclocytidine. A solution of **1** (4.5 mmol) in THF (2 ml) was added dropwise at room temperature to a solution of *N⁴*-benzoyl-2′,3′-*O*-isopropylidenecytidine (1.161 g, 3 mmol) and **2** (4.5 mmol) in THF (5 ml). After the mixture had been kept stirred overnight, the precipitate was filtered and recrystallized from $CHCl_3$ giving 484 mg (44%) of the compound with mp 290 °C. UV_{max} (MeCN) 252, 316 nm, UV_{min} 220, 290 nm; NMR (DMF-d_7 and acetone-d_6) δ=1.32 and 1.55 (two s, 6, isopropylidene methyl), 4.02—4.70 (m, 3, $C_{4'}H$, $C_{5'}H$), 5.06 (m, 2, $C_{2'}H$, $C_{3'}H$), 5.55 (d, 1, $C_{1'}H$), 6.51 (d, 1, C_5H), 7.36—8.11 ppm (m, 6, aromatic-H, C_6H).

N⁴,5′-O-Dibenzoylcytidine. *a) With Use of Benzoic Acid*: **10** (589 mg, 1 mmol) was allowed to react with benzoic acid (366 mg, 3 mmol) in THF (8 ml) at room temperature overnight or under reflux for 2.5 h. The TLC of the crude reaction mixture showed that **10** was completely converted into *N⁴*,5′-*O*-dibenzoylcytidine. The solvent was evaporated and the residue was purified by TLC ($CHCl_3$–MeOH= 10 : 1) giving the compound (70%) with mp 187—189 °C (lit,[21] mp 186—190 °C). UV_{max}(EtOH) 229, 261, 305 nm, UV_{min} 245, 289 nm.

b) With Use of Tetrabutylammonium Benzoate: Benzoic acid (1.5 mmol) was added to a 10% solution of tetrabutylammonium hydroxide in methanol (3 ml) and evaporated to dryness. The salt was rendered anhydrous by repeated evaporation of added portion of dry benzene. To the salt was added **10** (1 mmol) and THF (5 ml), and the mixture was kept stirred overnight. The mixture was then worked up as above giving the compound in nearly quantitative yield.

N⁴,5′-O-Dibenzoyl-2′,3′-O-(triphenylphosphoranediyl)cytidine (11). A solution of **1** (3 mmol) in THF (2 ml) was added dropwise at room temperature to a mixture of *N⁴*,5′-*O*-dibenzoylcytidine (910 mg, 2 mmol) prepared as described above and **2** (3 mmol) in THF (8 ml). The nucleoside dissolved as **1** was added, precipitation taking place shortly afterwards. The mixture was kept stirred overnight and filtered to give crude product (1.12 g, 80%) which was dissolved in acetone–$CHCl_3$ and concentrated to small volume *in vacuo*. The concentrated solution was kept standing to precipitate 700 mg (49%) of pure phosphorane which was collected by filtration, mp 183—184 °C (dec). UV_{max}(MeCN) 231, 259, 311 nm, UV_{min} 222, 246, 288 nm. NMR (DMSO-d_6) δ=4.1—4.8 (m, 5, $C_{2'}H$, $C_{3'}H$, $C_{4'}H$, $C_{5'}H$), 5.85 (d, 1, $C_{1'}H$), 7.1—8.2 (m, 27, aromatic-H, C_5H, C_6H), 11.25 ppm (br. s, 1, NH). Found: C, 68.74; H, 4.85; N, 5.44%. Calcd for $C_{40}H_{34}N_3O_7P$: C, 69.19; H, 4.87; N, 5.90%.

The phosphorane was hydrolyzed by treatment with THF–H_2O for 24 h to give N^4,5′-*O*-dibenzoylcytidine and triphenylphosphine oxide in a *ca.* 1 : 1 ratio.

Methanolysis of N⁴-*Benzoyl-2′,3′-O-(triphenylphosphoranediyl)-*O²,*5′-cyclocytidine (10).* One mmol of **10** was treated with methanol (50 ml) under reflux for 5 h or kept stirred at room temperature overnight and then evaporated. O^2-Methylcytosine was isolated in 65% yield (81 mg) by TLC using ethyl acetate. UV_{max} (H_2O) 228, 264 nm, UV_{min} 243 nm. NMR (DMSO-d_6) δ=3.82 (s, 3, CH_3O), 6.16 (d, 1, C_5H), 7.00 (br. s, 2, NH_2), 7.96 ppm (d, 1, C_6H).

Methanolysis of N⁴-*Benzoyl-2′,3′-O-isopropylidene-*O²,*5′-cyclocytidine.* When the title compound was treated with methanol as in the methanolysis of **10**, O^4-methyl-2′,3′-*O*-isopropylideneuridine with mp 235—236 °C was isolated in 33% yield (80 mg) by TLC using $CHCl_3$–MeOH (10 : 1). UV_{max} (MeOH) 276 nm, UV_{min} 240 nm. Found: C, 51.80; H, 6.05; N, 9.37%. Calcd for $C_{13}H_{18}N_2O_6$: C, 52.34; H, 6.08; N, 9.37%. Benzamide (53 mg, 36%, mp 125—128 °C) and 2′,3′-*O*-isopropylidenecytidine (36 mg, 23%, glass) were also obtained.

N⁴-Benzoylcytidin-5′-yl Dibenzyl Phosphate (14a) and Diphenyl-Phosphate (14b). Tetrabutylammonium dibenzyl phosphate was prepared from dibenzyl hydrogenphosphate (417 mg, 1.5 mmol) and tetrabutylammonium hydroxide (3 ml of 10% solution in methanol) by a procedure similar to that for N^4,5′-*O*-dibenzoylcytidine. The salt was allowed to react with **10** (489 mg, 1 mmol) at room temperature overnight, and then evaporated. The residue was purified by TLC using $CHCl_3$–MeOH (10 : 1) giving 210 mg (35%) of **14a** which was recrystallized from MeCN, melting at 136—137 °C. UV_{max} (MeOH) 262 (ε 24100), 306 nm, UV_{min} 235.5, 288 nm. NMR ($CDCl_3$+D_2O) δ=4.0—4.5 (m, 5, $C_2'H$, $C_3'H$, $C_4'H$, $C_5'H$), 5.07 (d, 4, $PhC\underline{H}_2$), 5.92 (d, 1, $C_1'H$), 7.3—8.3 ppm (m, 17, aromatic-H, C_5H, C_6H). Found: C, 59.31; H, 4.98; N, 6.92%. Calcd for $C_{30}H_{30}N_3O_9P$: C, 59.22; H, 5.03; N, 7.06%.

14a (58 mg) was converted into 2′,3′-*O*-isopropylidene derivative by treatment with acetone (1 ml) and 2,2-dimethoxypropane (2 ml) in the presence of *p*-toluenesulfonic acid (20 mg). The NMR spectrum of the product was identical with that of N^4-benzoyl-2′,3′-*O*-isopropylidenecytidin-5′-yl dibenzyl phosphate prepared by the procedure described below.

A similar treatment of **10** with tetrabutylammonium diphenyl phosphate afforded **14b** (15%) with mp 191—192 °C (from MeCN). NMR (DMSO-d_6) δ=5.35, 5.60 (2, 2′-OH, 3′-OH), 5.81 (d, 1, $C_1'H$), 11.10 ppm (br. s, 1, NH).

N⁴-Benzoyl-2′,3′-O-isopropylidenecytidin-5′-yl Dibenzyl Phosphate. Dibenzyl hydrogenphosphate (417 mg, 1.5 mmol) was converted into tetrabutylammonium salt and allowed to react with N^4-benzoyl-2′,3′-*O*-isopropylidene-O^2,5′-cyclocytidine (484 mg, 1 mmol) in THF (5 ml) at room temperature overnight. After being evaporated, the products were separated by TLC ($CHCl_3$–MeOH=19 : 1), giving 422 mg (65%) of the compound which was recrystallized from petroleum ether, melting at 123—124 °C. Found: C, 61.20; H, 5.29; N, 6.49%. Calcd for $C_{33}H_{34}N_3O_9P$: C, 61.14; H, 5.32; N, 6.51%.

*1-(β-D-Arabinofuranosyl)-*N⁴*-benzoylcytosin-5′-yl Dibenzyl Phosphate (17a).* Dibenzyl hydrogenphosphate (1.5 mmol) was allowed to react with **10** (1 mmol) in THF (5 ml) at room temperature overnight and then evaporated. **17a** (233 mg, 38%) was isolated by TLC using $CHCl_3$–MeOH (10 : 1). After recrystallization from MeCN, mp 166—169 °C. UV_{max} (EtOH) 261 (ε 24500), 308 nm, UV_{min} 235, 288 nm. NMR (DMSO-d_6) δ=3.86—4.38 (m, 5, $C_2'H$, $C_3'H$, $C_4'H$, $C_5'H$), 5.03 (d, 4, $PhC\underline{H}_2$), 5.70 (2, 2′-OH, 3′-OH), 6.20 (d, 1, $C_1'H$), 7.0—8.2 ppm (m, 17, aromatic-H, C_5H, C_6H).

*1-(β-D-Arabinofuranosyl)-*N⁴*-benzoylcytosin-5′-yl Diphenyl Phosphate (17b).* *a) Reaction of **10** with Diphenyl Hydrogenphosphate*: The compound was prepared in 52% yield by a procedure similar to that for **17a**. This compound was recrystallized from MeCN, melting at 196—197 °C. NMR (DMSO-d_6) δ=5.78 (2, 2′-OH, 3′-OH), 6.25 (d, 1, $C_1'H$), 11.15 ppm (br. s, 1, NH). Found: C, 58.08; H, 4.61; N, 7.39%. Calcd for $C_{28}H_{26}N_3O_9P$: C, 58.03; H, 4.52; N, 7.25%.

*b) Reaction of 1-(β-D-Arabinofuranosyl)-*N⁴*-benzoylcytosine with Diphenyl Phosphorochloridate*: 1-(β-D-Arabinofuranosyl)-N^4-benzoylcytosine[22] (80 mg, 0.23 mmol) was treated with diphenyl phosphorochloridate (100 mg, 0.37 mmol) in pyridine (1 ml) at room temperature overnight. After the work-up as described in a), **17b** was obtained in 51% yield. The products prepared by procedures a) and b) were identical.

*2′,3′-O-(Triphenylphosphoranediyl)-*N³,*5′-cycloguanosine (18).* A solution of **1** (6 mmol) in dioxane (2 ml) was added dropwise to a suspension of guanosine (566 mg, 2 mmol) and **2** (6 mmol) in dioxane (5 ml) at 70 °C. Guanosine dissolved as **1** was added. The homogeneous solution was kept stirred at 70 °C for 3 h and then allowed to cool to room temperature. The resulting precipitate was filtered. The solid was dissolved in DMF (15 ml) and reprecipitated by the addition of THF (60 ml) giving 700 mg (67%) of **18**, not melting below 250 °C. UV_{max} (MeCN) 235 (ε 26500), 258 (ε 13300) nm, UV_{min} 223, 253 nm. NMR (DMSO-d_6) δ=3.95 (m, 2, $C_5'H$), 4.58—5.00 (m, 3, $C_2'H$, $C_3'H$, $C_4'H$), 6.37 (s, 1, $C_1'H$), 7.00—7.95 ppm (m, 18, aromatic-H, NH_2, C_6H). Found: C, 63.41; H, 4.68; N, 12.80%. Calcd for $C_{28}H_{24}N_5O_4P$: C, 64.00; H, 4.60; N, 13.33%.

18 (400 mg, 0.76 mmol) was treated with 0.1 mol dm^{-3} HCl for 1 h at room temperature, triphenylphosphine oxide (187 mg, 94%) precipitated being filtered off. The filtrate was neutralized with aqueous ammonia and then evaporated. The residue was washed with acetone and recrystallized from H_2O giving N^3,5′-cycloguanosine (177 mg, 88%); mp 265 °C. UV_{max} (H_2O, pH 1) 249 nm, UV_{min} 222 nm. UV_{max} (H_2O, pH 11) 268 nm, UV_{min} 250 nm.

3′,5′-O-(Triphenylphosphoranediyl)adenosine (19). A solution of **1** (15 mmol) in dioxane (10 ml) was added to a mixture of adenosine (2.67 g, 10 mmol) and **2** (15 mmol) suspended in dioxane (20 ml) at 70 °C. Adenosine dissolved as **1** was added. The solution was stirred at 70 °C for 3 h, and then allowed to cool to room temperature. The precipitate thus formed was filtered and recrystallized from dioxane giving 3.95 g (75%) of **19** with mp 171—172 °C. UV_{max} (MeCN) 260 (ε 7400) nm, UV_{min} 245 nm. NMR (DMSO-d_6) δ=4.10—4.84 (m, 5, $C_2'H$, $C_3'H$, $C_4'H$, $C_5'H$), 6.01 (d, 1, $C_1'H$), 7.59 ppm (m, 15, aromatic-H). Found: C, 63.66; H, 5.08; N, 13.20%. Calcd for $C_{28}H_{26}N_5O_4P$: C, 63.75; H, 4.98; N, 13.28%.

On treatment with AcOH–H_2O or dil aqueous ammonia, **19** was hydrolized to adenosine and triphenylphosphine oxide in a 1 : 1 ratio.

*Reaction of **19** with Benzoic Acid.* A mixture of **19** (1 mmol) and benzoic acid (3 mmol) in dioxane (5 ml) was heated at 70 °C for 5 h. The solution was made up to 50 ml. A certain volume of the resulting solution was chromatographed on Toyo Roshi 51A paper using solvent system of 1-BuOH–AcOH–H_2O=5 : 2 : 3 (v/v), the spots and blank areas of the paper being eluted by soaking in water of standard volume and their concentrations determined spectrophotometrically. The yields of 5′-*O*-benzoyladenosine (UV_{max} (H_2O) 238, 260 nm, UV_{min} 224, 252 nm) and N^3,5′-cycloadenosine (**21**; UV_{max} (H_2O) 273 nm, UV_{min} 229 nm) were

determined to be 59 and 16%, respectively. The following molar extinction values of the compounds were used: 5′-*O*-benzoyladenosine, 11000 (260 nm) and N^3,5′-cycloadenosine, 13500 (273 nm).

5′-Thiobenzoyl-5′-deoxyadenosine. Thiobenzoic acid (414 mg, 3 mmol) and **19** (529 mg, 1 mmol) in pyridine (5 ml) was kept stirred under N_2 at room temperature overnight, and then evaporated. The compound was obtained by TLC using $CHCl_3$–MeOH (10 : 1), followed by recrystallization from MeCN–MeOH; 244 mg (63%), mp 159—160 °C. UV_{max} (H_2O) 248, 262 (ε 13800) nm, UV_{min} 225 nm. Found: C, 52.33; H, 4.54; N, 18.10%. Calcd for $C_{10}H_{13}N_5O_3S$: C, 52.71; H, 4.42; N, 18.08%.

*Reaction of **19** with Phenyl Isocyanate.* A mixture of **19** (1 mmol) and phenyl isocyanate (357 mg, 3 mmol) in pyridine (5 ml) was kept stirred at room temperature overnight and then evaporated. 5′-*O*-Phenylcarbamoyladenosine (**25**; 134 mg, 34%) and N^6,5′-*O*-bis(phenylcarbamoyl)adenosine (**26**; 225 mg, 45%), isolated by TLC using ethyl acetate, had the following physical properties.

25 was recrystallized from MeOH, mp 181—183 °C. UV_{max} (H_2O) 237, 259 (ε 12100) nm, UV_{min} 223, 252 nm. Found: C, 50.49; H, 4.99; N, 20.78%. Calcd for $C_{17}H_{18}N_6O_5 \cdot H_2O$: C, 50.75; H. 4.86; N, 20.79%.

26 was recrystallized from MeOH, softing at 145 °C, but showing no definite melting point. UV_{max} (MeOH) 235, 280 (ε 29900)[23] nm, UV_{min} 225, 253 nm.

Reaction of 2′,3′-O-Isopropylideneadenosine with Phenyl Isocyanate. A mixture of 2′,3′-*O*-isopropylideneadenosine (307 mg, 1 mmol) and phenyl isocyanate (3 mmol) in pyridine (5 ml) was kept stirred for 1 d and then evaporated. Ethanol was added to the residue which was evaporated. The residue was treated with 10% aqueous AcOH (40 ml) under reflux for 1.5 h in order to remove isopropylidene group. The products were separated by TLC using MeOH–$CHCl_3$ (10 : 1) giving N^6,5′-*O*-bis(phenylcarbamoyl)adenosine (374 mg, 69%) which was identical with **26** obtained by the procedure described above.

*Reaction of **19** with Diphenylketene.* A mixture of **19** (1 mmol) and diphenylketene (582 mg, 3 mmol) in pyridine (5 ml) was kept stirred at room temperature overnight and then evaporated. The following products were isolated by TLC using $CHCl_3$–MeOH (10 : 1).

5′-*O*-(Diphenylacetyl)adenosine was obtained in 20% (94 mg) yield and recrystallized from MeCN. It began to soften at 180 °C but showed no definite melting point. UV_{max} (MeOH) 260 (ε 12600) nm, UV_{min} 235 nm. Found: C, 62.46; H, 4.69; N, 14.94%. Calcd for $C_{24}H_{23}N_2O_5$: C, 62.46; H, 5.02; N, 15.18%.

N^6,5′-*O*-Bis(diphenylacetyl)adenosine was obtained in 46% (298 mg) yield and recrystallized from benzene–ether. It began to soften at 95 °C. UV_{min} (MeOH) 278 (ε 17500) nm, UV_{min} 240 nm. Found: C, 68.55; H, 5.09; N, 10.32%. Calcd for $C_{38}H_{33}N_5O_6$: C, 69.60; H, 5.07; N, 10.68%.

Reaction of N⁶-p-*Toluoyladenosine with **1** and **2**. a)* N⁶-p-*Toluoyl-2′,3′-O-(triphenylphosphoranediyl)-*N³,5′-*cycloadenosine (**29**).* A solution of **1** (4.1 mmol) in dioxane (1.5 ml) was added dropwise over a period of 1 h to a mixture of N^6-*p*-toluoyladenosine (577 mg, 1.5 mmol) and **2** (4 mmol) in dioxane (1.5 ml) at 70 °C. After the nucleoside had dissolved, the mixture was allowed to cool to room temperature and then kept stirred overnight. The precipitate formed was filtered and washed with ether and dioxane to give **29** (201 mg, 24%). An analytical sample was prepared by recrystallization twice from dioxane–ether. It turned brown above 190 °C, melting at 200—204 °C. UV_{max} (dioxane) 243^{sh}, 307 nm, UV_{min} 289 nm. NMR ($CDCl_3$) δ=2.2 (s, 3, CH_3), 3.7—5.0 (m, 5, $C_{2'}H$, $C_{3'}H$, $C_{4'}H$, $C_{5'}H$), 5.92 (s, 1, $C_{1'}H$), 6.6—8.0 ppm (m, 21, aromatic-H, C_2H, C_8H). Found: C, 67.55; H, 4.82; N, 11.57%. Calcd for $C_{36}H_{30}N_5O_4P \cdot 1/2H_2O$: C, 67.91; H, 4.91; N, 11.00%.

b) N⁵,*5′-Anhydro-5-formamido-4-(*N-p-*toluoylamidino)-1-(β-*D-*ribofuranosyl)imidazole (**30a**)*: N^6-*p*-Toluoyladenosine (770 mg, 2 mmol) was allowed to react with 6 mmol each of **1** and **2** in dioxane (15 ml) in a similar manner to that described in a). The resulting mixture was treated with H_2O (2 ml) under reflux for 1 h, and then evaporated. The residue was separated by TLC ($CHCl_3$–MeOH=10 : 1) giving **30a** in 74% (532 mg) yield. This was recrystallized from acetone, mp 181—183 °C (dec). UV_{max} (MeOH) 270, 309 nm, UV_{min} 245, 290 nm.

N⁵,*5′-Anhydro-5-amino-4-(*N-p-*toluoylamidino)-1-(β-*D-*ribofuranosyl)imidazole (**31a**).* **30a** (162 mg, 0.42 mmol) was treated with saturated methanolic ammonia (15 ml) at room temperature for 1 d and evaporated. **31a** was isolated in 64% yield and recrystallized from acetone–ethanol; dec at 214—216 °C. UV_{max} (MeOH) 255^{sh}, 273, 337 nm, UV_{min} 234, 296 nm.

N⁵,*5′-Anhydro-5-amino-4-(*N-p-*toluoylcarbamoyl)-1-(β-*D-*ribofuranosyl)imidazole (**32a**).* **31a** (90 mg, 0.27 mmol) was treated with *p*-toluenesulfonic acid hydrate (190 mg, 1 mmol) in THF (3 ml) at room temperature for 8 h. The solution was neutralized with triethylamine. The precipitate was collected by filtration and washed with water and methanol giving **32a** in 64% yield. The product was recrystallized from acetone, mp 215—217 °C (dec). UV_{max} (MeOH) 252, 314 nm, UV_{min} 237, 275 nm. Found: C, 56.21; H, 5.13; N, 15.37%. Calcd for $C_{17}H_{18}N_4O_5$: C, 56.98; H, 5.06; N, 15.64%.

N⁵,*5′-Anhydro-5-formamido-4-(*N-p-*toluoylamidino)-1-(2,3-*O-*isopropylidene-β-*D-*ribofuranosyl)imidazole (**30b**).* A solution of **1** (1.5 mmol) in THF (1 ml) was added dropwise at room temperature over a period of 1 h to a mixture of N^6-*p*-toluoyl-2′,3′-*O*-isopropylideneadenosine (425 mg, 1 mmol) and **2** (1.5 mmol) in THF (2 ml). The homogeneous solution was kept standing overnight and then evaporated. **30b** was obtained nearly quantitatively by TLC using ethyl acetate–benzene (1 : 1). It was recrystallized from MeOH, mp 240—242 °C. UV_{max} (MeOH) 270, 310 nm, UV_{min} 253, 290 nm. Found: C, 59.11; H, 5.41; N, 16.71%. Calcd for $C_{21}H_{23}N_5O_5$: C, 59.28; H, 5.45; N, 16.46%.

N⁵,*5′-Anhydro-5-amino-4-(*N-p-*toluoylamidino)-1-(2,3-*O-*isopropylidene-β-*D-*ribofuranosyl)imidazole (**31b**).* **30b** (558 mg, 1.31 mmol) was treated with saturated methanolic ammonia (120 ml) at room temperature for 8 h and then evaporated. The residue was separated by TLC ($CHCl_3$–MeOH=10 : 1) giving **31b** (52%) with mp 250—251 °C (lit,[16a] mp 245—247 °C). UV_{max} (MeOH) 250^{sh}, 272 (ε 18500), 336 (ε 16800) nm, UV_{min} 244, 296 nm (lit,[16a] UV_{max} (MeOH) 270 (ε 18500), 333 (ε 16800) nm. NMR ($CDCl_3$) δ=1.32, 1.43 (two s, 6, isopropylidene-CH_3), 2.37 (s, 3, CH_3), 3.38 (m, 2, $C_{5'}H$), 4.53, 4.94 (a pair of d, 2, $C_{2'}H$, $C_{3'}H$), 4.6 (m, 1, $C_{4'}H$), 5.71 (s, 1, $C_{1'}H$), 7.11, 7.85 ($A'_2B'_2$, 4, aromatic-H), 7.07 ppm (s, 1, C_2H). Found: C, 60.34; H, 5.86; N, 17.74%. Calcd for $C_{20}H_{23}N_5O_4$: C, 60.44; H, 5.83; N, 17.62%.

References

1) Part VII: J. Kimura, Y. Fujisawa, T. Yoshizawa, K. Fukuda, and O. Mitsunobu, *Bull. Chem. Soc. Jpn.*, **52**, 1191 (1979).

2) V. M. Clark, A. R. Todd, and J. Zussman, *J. Chem. Soc.*, **1951**, 2952. For reviews of cyclonucleosides, see M. Ikehara and T. Ueda. *Yuki Gosei Kagaku Kyokai Shi*, **32**, 403

(1974); M. Ikehara, T. Ueda, and E. Ohtsuka, "Kakusan Yuki Kagaku," Kagaku Dojin Co., Kyoto (1979).

3) M. Wada and O. Mitsunobu, *Tetrahedron Lett.*, **1972**, 1279.

4) Preliminary communications: J. Kimura, Y. Fujisawa, T. Sawada, and O. Mitsunobu, *Chem. Lett.*, **1974**, 691; J. Kimura, Y. Hashimoto, and O. Mitsunobu, *ibid.*, **1974**, 1473.

5) J. Emsley and D. Hall, "The Chemistry of Phosphorus," Harper and Row, Publishers, London (1976), pp. 77—91.

6) Direct synthesis of pyrimidine O^2,5′-cyclonucleosides was made by the reaction of nucleosides with **1** and **2**, followed by treatment with water: S. Shibuya, A. Kuninaka, and H. Yoshino, *Chem. Pharm. Bull.*, **22**, 719 (1974); S. Shibuya, A. Kuninaka, and H. Yoshino, Japan Kokai, 7562993-7562995; *Chem. Abstr.*, **83**, 131895g, 131896h, 131897j (1975).

7) P. D. Bartlett, A. L. Baumstark, and M. E. Landis, *J. Am. Chem. Soc.*, **95**, 6486 (1973), and references therein.

8) Y. Fujisawa and O. Mitsunobu, *J. Chem. Soc., Chem. Commun.*, **1973**, 201.

9) J. Zemlicka and J. Smrt, *Tetrahedron Lett.*, **1964**, 2081.

10) When **5** was treated with benzoic acid in THF, **4** and not 5′-*O*-benzoyluridine was obtained. **4** would be formed by the hydrolysis of **5** with a trace of water. The reaction of **5** with tetrabutylammonium benzoate, however, afforded 5′-*O*-benzoyluridine.

11) The thin layer chromatography of the crude reaction mixture resulting from the reaction of **10** with the tetrabutylammonium salt of phosphate diester indicates the presence of a trace of **17a** and of **17b**. Similarly, a small amount of **14a** or **14b** was also formed in the reaction of **10** with free phosphate diesters.

12) The hydrolysis of pyrimidine O^2,2′-cyclonucleosides generally affords the corresponding arabino epimers. J. J. Fox, *Pure Appl. Chem.*, **18**, 223 (1969). K. K. Ogilvie and D. J. Iwacha, *Can. J. Chem.*, **52**, 1787 (1974) and references cited therein.

13) The stannylene function of 2′,3′-*O*-stannylenenucleosides acts as a protecting group and an activating group. D. Wagner, J. P. H. Verheyden, and J. G. Moffatt, *J. Org. Chem.*, **39**, 24 (1974).

14) R. Mengel and M. Bartke, *Angew. Chem., Int. Ed. Engl.*, **17**, 679 (1978).

15) 2′,3′-*O*-Isopropylideneuridine and its derivatives give O^2,5′- and 5′,6-cyclouridines more readily than uridine itself. D. V. Santi and C. F. Brewer, *J. Am. Chem. Soc.*, **90**, 6236 (1968); B. A. Otter, E. A. Falco, and J. J. Fox, *J. Org. Chem.*, **34**, 1390 (1969); Y. Kondo, J-L. Fourrey, and B. Witkop, *J. Am. Chem. Soc.*, **93**, 3527 (1971); K. Isono and T. Azuma, *Chem. Pharm. Bull.*, **20**, 193 (1972), and references cited therein.

16) a) K. Anzai and M. Matsui, *Agric. Biol. Chem.*, **37**, 301 (1973); b) K. Anzai and M. Matsui, *ibid.*, **37**, 2431 (1973); K. Anzai, *ibid.*, **40**, 373 (1976).

17) J. P. H. Verheyden and J. G. Moffatt, *J. Org. Chem.*, **35**, 2319 (1970).

18) B. M. Brown, A. R. Todd, and S. Varadarajan, *J. Chem. Soc.*, **1957**, 868.

19) J. P. H. Verheyden and J. G. Moffatt, *J. Org. Chem.*, **37**, 2289 (1972).

20) R. H. Rammler and H. G. Khorana, *J. Am. Chem. Soc.*, **84**, 2112 (1962).

21) H. P. M. Fromageot, B. E. Griffin, C. B. Reese, and J. E. Sulston, *Tetrahedron*, **23**, 2315 (1967).

22) This compound was prepared by the reaction of 1-(β-D-arabinofuranosyl)cytosine (243 mg, 1 mmol) with benzoic anhydride (399 mg, 1.5 mmol) in DMF (2 ml) at room temperature and recrystallized from H_2O–ethanol, mp 180—182 °C.

23) N^6,3′,5′-*O*-Tris(phenylcarbamoyl)deoxyadenosine is reported to have UV_{max} (EtOH) 278 nm. K. L. Agarwal and H. G. Khorana, *J. Am. Chem. Soc.*, **94**, 3578 (1972).

 © 1980 The Chemical Society of Japan Bull. Chem. Soc. Jpn., 53, 3678—3682 (1980) [Vol. 53, No. 12

A Catalytic Effect of Amines on the Reaction of Arenesulfinic Acids with *N,N'*-Thiodiphthalimide[1]

Yasuo ABE,* Toyokazu HORII, Kunio OKA, Shunichi KAWAMURA, and Takeshige NAKABAYASHI

Radiation Center of Osaka Prefecture, Shinke-cho, Sakai 593

(Received May 19, 1980)

In the presence of catalytic amounts of several amines, *N,N'*-thiodiphthalimide has been allowed to react with one or two equiv. of arenesulfinic acids in dichloromethane, thus giving *N*-(arylsulfonylthio)phthalimides or bis(arenesulfonyl) sulfides respectively in good yields. The arenesulfinate anion seems to be a better nucleophile against *N,N'*-thiodiphthalimide than arenesulfinic acid. The mechanism of the catalytic reaction will be discussed.

N,N'-Thiodiphthalimide (**1**) has been known to be a useful sulfur-transfer reagent, giving symmetrical trisulfides[2] and *N,N'*-thiodiamines[3] by reactions with two equiv. of thiols and secondary amines respectively. Unsymmetrical trisulfides and *N*-(alkyldithio- or aryldithio)amines are prepared by the reactions of the intermediates derived from **1** with one equiv. of thiols and amines respectively.[3] It has previously been reported that **1** reacts with one equiv. of arenesulfinic acids (**2**) to give *N*-(arylsulfonylthio)phthalimides (**3**) and with two equiv. of **2** to give bis(arenesulfonyl) sulfides (**4**).[4] In a preceding paper,[5] it was shown that catalytic amounts of amines accelerate the reaction of α-toluenethiol with **1** in benzene or dichloromethane.

We wish now to report our examination to confirm that amines and their ammonium salts catalyze the reaction of **1** with **2** in dichloromethane, and to elucidate the mechanism of the catalyzed reaction. In addition, we will show the IR characteristic absorptions of the S–N bond in the compounds **3a—g** produced in the present reaction.

Results and Discussion

The reaction of **1** with **2** in the presence of catalytic amounts of amines was performed in dichloromethane at the boiling point for 1 h. Representative authentic arenesulfinic acids are stable at the same temperature for several hours in the same solvent. The product **3** was isolated from the reaction mixture by fractional dissolution in benzene and ethanol, and **4**, by column chromatography using silica gel. Preliminary work indicated that Compound **4** was recovered quantitatively from the column; Compound **3** was recovered in a 60—70% yield, but Compound **4** was not detected in the remaining eluate. These experiments suggest that **3** do not give **4** through the column.

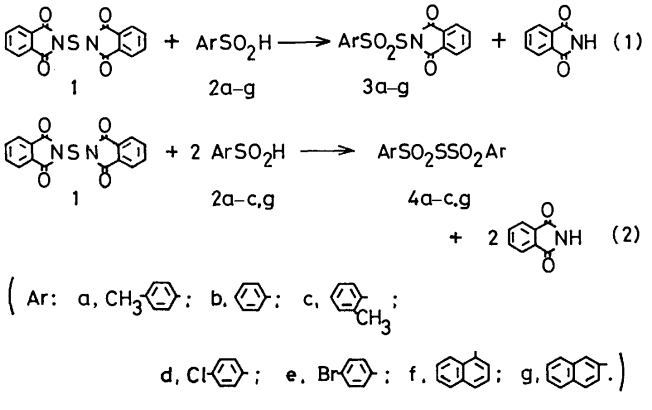

Table 1. Effects of amines on the reaction of **1** with **2a**[a]

Entry	Amine	pK_a	Yield of products **3a**(%)	Yield of products **4a**(%)
1	None		24	2
2	Aniline	4.60	91	0
3	*N*-Methylaniline	4.85	84	0
4	*p*-Toluidine	5.12	75	1
5	Pyridine	5.17	70	4
6	2,6-Lutidine	6.75	80	2
7	2,4-Lutidine	6.79	79	6
8	Imidazole	6.95	84	0
9	*N*-Methylmorpholine	7.41	78	4
10	Morpholine	8.36	88	3
11	Butylamine	10.60	81	2
12	Triethylamine	10.67	88	2
13	Tributylamine	10.87	77	6
14	Piperidine	11.22	81	7
15	DBU		59	1

a) All the reactions were performed by the use of **1** (5 mmol), **2** (5 mmol), and an amine (0.5 mmol) in dichloromethane (100 ml) at the boiling point for 1 h.

The Reaction of 1 with One Equiv. of 2. Regardless of the functional group (*i.e.*, primary, secondary, or tertiary), all the amines used here accelerated the reaction of **1** with *p*-toluenesulfinic acid (**2a**). The results of the reactions are summarized in Table 1. The yield of *N*-(*p*-tolylsulfonylthio)phthalimide (**3a**) did not vary significantly with the amine. Previously, the catalytic ability of amine in the reaction of **1** with α-toluenethiol was explained by the S–H–N-type hydrogen bonding.[5] It is more reasonable, however, to expect that the catalytib ability of amine in the present reaction is due to the formation of the corresponding ammonium sulfinate from amine and arenesulfinic acid, since the arenesulfinate anion is generally more nucleophilic to the sulfur atom than the arenesulfinic acid is. The fact that the yield of **3a** increases upon the addition of amine, independent of the pK_a value, compared with that in the reaction without amine, suggests that amine forms a salt with **2a** in dichloromethane. Therefore, a reaction mechanism in which amine revives as a catalyst is

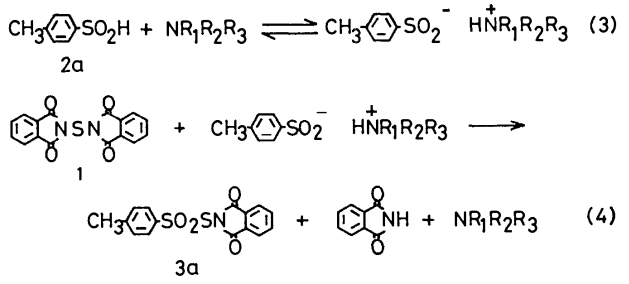

described by Eqs. 3 and 4. When DBU was used, the yield of **3a** was not so good as those with other amines, indicating that DBU would form a very tight salt with **2a**, thus, the migration of the sulfinate anion would be restrained.

To confirm the mechanism proposed above, ammonium salts were first examined as catalysts. When each 0.1 equiv. of pyridinium, imidazolium, or piperidinium *p*-toluenesulfinate was added to the reaction system, **3a** was obtained in yields of 69, 81, and 70% respectively. Comparing the yields with those of the corresponding amines in Table 1, it is clear that the two results are not significantly different.

Second, we examined the catalytic effect of amine hydrochloride and tetraalkylammonium halides, the anions of which are exchangeable. When 0.1 equivalents of each of these salts were used, **3a** was formed in yields of 85%(triethylammonium hydrochloride), 60%(tetraethylammonium chloride), 63%(tetraethylammonium bromide), and 78%(tetraethylammonium iodide). The halide anion is expected to form a hydrogen bonding with the acidic hydrogen atom of arenesulfinic acid and, consequently, to activate the acid in a manner similar to the condensation reactions of a number of organic compounds with alkyl halides in the presence of potassium fluoride.[6] As may be seen in the results with the three tetraethylammonium halides, however, the chloride anion which is more electron-rich and nucleophilic[7] has less catalytic activity than the iodide anion. In other words, the salt with a weaker ionic bonding force has a larger catalytic ability. This fact also suggests that the catalytic ability is due to the formation of a sulfinate anion *via* anion exchange rather than to the activation by hydrogen bonding between a halide anion and sulfinic acid.

The reaction of aqueous sodium *p*-toluenesulfinate with **1** in dichloromethane was performed with the aid of a phase-transfer reagent. Unfortunately, the yield of **3a** was very poor. The decrease in the yield may be a result of the decomposition of the product, **3a**. Therefore, the stability of **3a** was examined; **3a** was recovered quantitatively after having been boiled for 1 h in a mixture of water and dichloromethane, but it was found to be unstable in an alkaline solution. Since slightly basic sodium phthalimide should be formed by the reaction of sodium *p*-toluenesulfinate with **1**, the product, **3a**, had to decompose. Accordingly, it seems hard to prepare **3** from an aqueous solution of the sulfinate.

The relationship between the amount of imidazole or triethylamine and the yield of **3a** was examined for the reaction of **1** with one equiv. of **2a**; the results are summarized in Table 2. In the case of triethylamine, **3a** was isolated in a considerable yield even if the ratio of triethylamine to **1** was 1. The yield of **3a**, however, decreased with the addition of a 0.2 equiv. of imidazole. With the addition of one equiv. of imidazole, **3a** was not isolated from the reaction mixture, but 1-(*p*-tolylsulfonyl)imidazole and elemental sulfur were isolated. It has been reported that *N*-(alkyldithio)phthalimides react with secondary amine[3] and that the S–N bond of 1,1'-thiodiimidazole is very reactive.[8] The reactivity of the S–N bonds seems to indicate that **3a** reacted with imidazole to give the undesirable products by the course shown by Eqs. 5—7. Equation 5 shows that

Table 2. Effects of the amount of imidazole or triethylamine[a]

Entry	Amine	Ratio[b]	Yield of **3a**(%)
1	None	0	24
2	Imidazole	0.05	78
3	Imidazole	0.1	84
4	Imidazole	0.2	28
5	Imidazole	1	0[c]
6	Triethylamine	0.05	85
7	Triethylamine	0.1	88
8	Triethylamine	0.2	73
9	Triethylamine	1	62

a) All the reactions were performed by the use of **1** (5 mmol), and **2a** (5 mmol) in dichloromethane (100 ml) at the boiling point for 1 h. b) Molar ratio of amine to **1**. c) 1-(*p*-Tolylsulfonyl)imidazole and elemental sulfur were isolated.

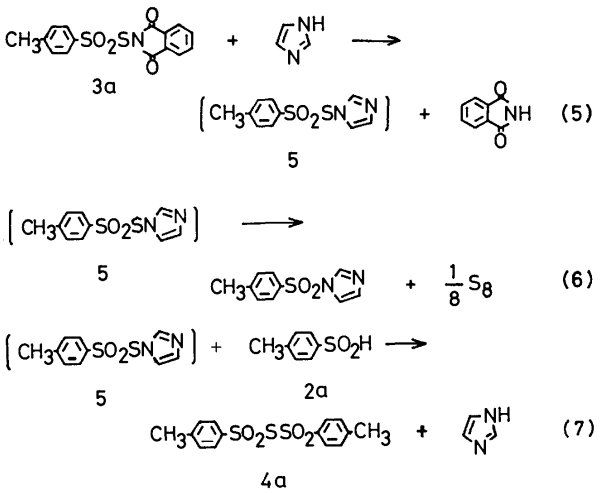

imidazole reacted with **3a** to give 1-(*p*-tolylsulfonylthio)-imidazole (**5**), which is an unstable intermediate. The acid, **2a**, still remaining in the reaction mixture would react with it to give **4a** and regenerate imidazole (Eq. 7). However, in the absence of **2a** in the reaction mixture, **5** must be desulfurated to give stable 1-(*p*-tolylsulfonyl)imidazole (Eq. 6). When authentic **3a** was treated with one equiv. of imidazole, 1-(*p*-tolylsulfonyl)imidazole was isolated in a 51% yield.

Taking into account the results obtained above, a series of **3** were prepared by the reactions of **1** with

Table 3. Preparation[a] and IR spectra of *N*-(arylsulfonylthio)phthalimides (**3**)

Substance	Aryl group in **3**	Yield/%	Mp/°C	IR (cm^{-1}) $\nu_{C=O}$	ν_{SO_2}	ν_{SN}
3a	*p*-Tolyl	83	166—167	1756,	1341, 1143,	870
3b	Phenyl	69	171—172	1750,	1327, 1147,	870
3c	*o*-Tolyl	79	165—166	1755,	1321, 1125,	867
3d	*p*-Chlorophenyl	73	168—169	1754,	1335, 1142,	868
3e	*p*-Bromophenyl	57	166—169	1743,	1341, 1144,	867
3f	1-Naphthyl	82	201—202	1752,	1344, 1153,	866
3g	2-Naphthyl	75	222—223	1751,	1326, 1127,	866
1				1760		866

a) All the reactions were performed by the use of **1** (5 mmol), **2** (5 mmol), and imidazole (0.5 mmol) in dichloromethane (100 ml) at the boiling point for 1 h.

Table 4. Effects of amines on the reaction of **1** with 2 equivalents of **2a**[a]

Entry	Amine	pK_a	Yield/% **4a**	Yield/% Phthalimide
1	None		46[b]	—
2	Aniline	4.60	88	93
3	Pyridine	5.17	85	86
4	Imidazole	6.95	81	93
5	*N*-Methylmorpholine	7.41	90	87
6	Morpholine	8.36	89	93
7	Triethylamine	10.67	86	92
8	Tributylamine	10.87	84	91
9	DBU		77	92

a) All the reactions were performed by the use of **1** (2.5 mmol), **2** (5 mmol), and an amine (0.5 mmol) in dichloromethane (50 ml) at the boiling point for 1 h. b) This value is cited from Ref. 4, and the reaction was performed for 24 h.

Table 5. Bis(arenesulfonyl) sulfides (**4**)[a]

Substance	Aryl group in **4**	Reaction time/h	Yield/%	Mp (lit, mp)
4a	*p*-Tolyl	3	76	135—136(131)[9]
4b	Phenyl	3	73	132—133(133)[9]
4c	*o*-Tolyl	1	80	136—137 (138—139)[10]
4d	*p*-Chlorophenyl	3	0[b]	
4e	*p*-Bromophenyl	3	0[c]	
4f	1-Naphthyl	3	0[d]	
4g	2-Naphthyl	1	63	158—159(153)[10]

a) All the reactions were performed by the use of **1** (2.5 mmol), **2** (5 mmol), and imidazole (0.5 mmol) in dichloromethane (50 ml) at the boiling point. b) Bis(*p*-chlorobenzenesulfonyl)disulfide was isolated in a 39% yield; mp 153—154 °C. c) Bis(*p*-bromobenzenesulfonyl) disulfide was isolated in a 47% yield; mp 175 °C. d) **3f** was isolated in a 95% yield.

several arenesulfinic acids in the presence of catalytic amounts of imidazole, which was chosen as a catalyst because of its convenience. The results are summarized in Table 3. The yields of **3** were improved significantly compared with those in reactions without any catalysts.[4]

The Reaction of 1 with Two Equiv. of 2. The reaction of **1** with two equiv. of **2a** in the presence of 0.2 equiv. of amines was performed in dichloromethane at the boiling point for 1 h. Only **4a** was produced, no **3a**. All the amines also accelerated the reaction. The results are summarized in Table 4. The yield of **4a** increased by the use of amine compared with that in the reaction without amine. This trend is similar to that of the yield of **3a** in Table 1; it implies that, at an early stage of the reaction, **3a** had appeared as an intermediate in the mechanism mentioned above, but reacted quickly with the ammonium salt of the excess **2a** to give **4a** (Eq. 8). A series of **4** were prepared by the

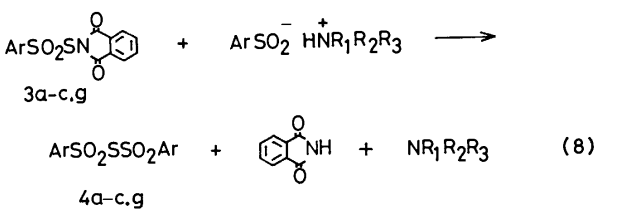

(8)

reaction of **1** with two equiv. of some arenesulfinic acids in the presence of imidazole. The results are summarized in Table 5. The yields of **4** were improved significantly,[4] but **2d—f** did not give **4**. In the case of **2f**, **3f** was isolated in a 95% yield, but no **4f** was. On the other hand, the desired **4g** was obtained in a moderate yield. The difference in the results could be due to the difference in the steric factor of the naphthyl groups. When **2d** or **2e** was used in the reaction, no **4** was formed, but the corresponding bis(arenesulfonyl) disulfide was obtained in a yield of less than 50%. Two possible explanations for the formation of the compound are as follows: (1) the arenethiosulfonate anion, which could be formed by the reaction of the arenesulfinate anion with elemental sulfur in the reaction mixture, reacted with the corresponding **3** to give bis(arenesulfonyl) disulfide, or (2) the arylsulfonylthio group dimerized after the scission of the S–N bond in **3d** or **3e**. In order to confirm these processes, a solution of **3d** or **3e** in dichloromethane was refluxed for 3 h in the presence of imidazole. The compounds, **3d** and **3e**, were stable under these conditions and were recovered quantitatively from the solution. When a solution of **3d** and one equiv. of **2d** in dichloromethane was refluxed for 3 h in the presence of imidazole, **4d** was not formed, but the starting **3d** was recovered from the mixture. The real mechanism for the formation of the bis-

Table 6. Reactions of **3** with **2** in the presence of imidazole[a)]

Entry	Aryl group in **3** and **4**	Reaction time/h	Yield of **4** %
1	Phenyl	2	71
2	*p*-Tolyl	2	94
3	*o*-Tolyl	3	80
4	*p*-Chlorophenyl	3	0[b)]

a) All the reactions were performed by the use of **2** (5 mmol), **3** (5 mmol), and imidazole (0.1 mmol) in dichloromethane (50 ml) at the boiling point. b) The starting material, **3d**, was recovered quantitatively.

(arenesulfonyl) disulfide remains mysterious.

Four authentic **3** were allowed to react with each equiv. of the corresponding **2** to give **4**; the results are summarized in Table 6.

IR Spectra. The IR spectra of **3a**—**g** showed the characteristic bands at 1750 ± 7 cm^{-1} (C=O stretching) and 1139 ± 15 and 1332 ± 12 cm^{-1} (SO_2 stretching), as may be seen in Table 3. Although a few observations have been made on the IR spectra of several organic sulfonamides and sulfenamides near 900 cm^{-1} [11a)] and at 900—985 cm^{-1},[11b)] which are assigned to the S–N stretching, no one has yet reported on the S–N stretching assignment in the IR spectra of *N*-(alkylthio and arylthio)imides. The IR spectra of **1** and **3** showed no conspicuous band in the region of 900—1000 cm^{-1}. Although, the nitrogen atom of organic sulfenamides is able to give its unpaired electron to the vacant *d* orbital of the adjacent sulfur atom, thus forming a stable $\bar{S}=\overset{+}{N}$ canonical structure, the unpaired electrons of the nitrogen atoms of **1** and **3**, which are withdrawn by the two adjacent carbonyl groups, seem not to interact with the *d* orbital of the sulfur atom. Therefore, the S–N absorptions in **3a**—**g** and **1** shift to lower frequencies compared with those of the sulfenamide and sulfonamide; a sharp band at 868 ± 2 cm^{-1} in the IR spectra of those compounds can be assigned to the S–N group.

Experimental

The *N,N'*-thiodiphthalimide (**1**) was prepared according to a previously reported method.[12)] The arenesulfinic acids, **2**, were prepared from the corresponding arenesulfonyl chloride by either of two methods reported in the literature.[13)] The benzene was purified by distillation before use. The other chemical reagents were obtained from commercial sources and were used directly. The IR spectra were recorded on a JASCO-701G grating spectrometer with KBr disks. The elemental analyses were performed by microanalytical laboratories of this Institute and the Osaka Chemical Analytical Center, Sakai, Osaka.

(1) Reaction of 1 with One Equiv. of 2. General Procedure: A solution of **1** (1.62 g, 5 mmol), **2** (5 mmol), and amine or ammonium salt (0.5 mmol) in dichloromethane (100 ml) was refluxed for 1 h. The solution was then evaporated under reduced pressure, and the residue was washed with water and dried. To the residue, 100 ml of benzene was added. After the mixture had stood for 30 min, the remaining solids were removed by filtration . The benzene filtrate was evaporated on a rotary evaporator, and the residue was washed with 50 ml of ethanol to give **3** as white crystals, which were later recrystallized from ethanol or benzene.

The analytical data of the compounds newly obtained here, except for **3a, b, d, e**,[4)] will be presented below:

N-*(o-Tolylsulfonylthio)phthalimide (3c)*: Found: C, 54.22; H, 3.19; N, 4.17; S, 18.92%. Calcd for $C_{15}H_{11}NO_4S_2$: C, 54.04; H, 3.33; N, 4.20; S, 19.24%.

N-*(1-Naphthylsulfonylthio)phthalimide (3f)*: Found: C, 58.55; H, 2.84; N, 3.60; S, 17.05%. Calcd for $C_{18}H_{11}NO_4S_2$: C, 58.53; H, 3.00; N, 3.79; S, 17.36%.

N-*(2-Naphthylsulfonylthio)phthalimide (3g)*: Found: C, 58.93; H, 2.79; N, 3.55; S, 16.80%. Calcd for $C_{18}H_{11}NO_4S_2$: C, 58.53; H, 3.00; N, 3.79; S, 17.36%. The ethanol washings were evaporated, and the residue was chromatographed on silica gel (Wakogel C-200, eluent: benzene). The first fraction gave **4**.

Procedure for a Heterogeneous Reaction: A mixture of **1** (0.811 g, 2.5 mmol), sodium *p*-toluenesulfinate (0.536 g, 2.5 mmol), benzyltriethylammonium chloride (0.144 g, 0.5 mmol), water (50 ml), and dichloromethane (50 ml) was refluxed for 1 h. The mixture was evapotated to remove the dichloromethane under reduced pressure. The aqueous mixture was then filtered, and the residue was washed with water and treated as has been described above, giving **3a** in an 18% yield.

Stability of 3a: A mixture of **3a** (0.834 g, 2.5 mmol), benzyltriethylammonium chloride (0.144 g, 0.5 mmol), water (50 ml), and dichloromethane (50 ml) was refluxed for 1 h. The mixture was treated as has been described above, giving **3a** in a 94% yield.

A mixture of **3a** (0.834 g, 2.5 mmol), potassium phthalimide (0.338 g, 2.5 mmol), benzyltriethylammonium chloride (0.114 g, 0.5 mmol), water (50 ml), and dichloromethane (50 ml) was refluxed for 1 h. The mixture was treated as has been described above, giving **3a** in a 76% yield.

Reaction of 1 with One Equiv. of 2a and Imidazole: A solution of **1** (6.5 g, 20 mmol), **2a** (3.1 g, 20 mmol), and imidazole (1.3 g, 20 mmol) in dichloromethane (100 ml) was refluxed for 2 h. The mixture was then filtered to give 5.3 g (90%) of phthalimide. The filtrate was evaporated under reduced pressure, and the residue was washed with acetone to give 0.4 g (65%) of elemental sulfur. The acetone solution was evaporated, and the residue was washed with water and dried. The residue was extracted with ethanol. The extract was then evaporated to give 1.8 g crude 1-(*p*-tolylsulfonyl)-imidazole (mp 75—95 °C). Recrystallization from hexane gave 1.7 g (39%) of a pure sample (mp 76—78 °C).

Reaction of 3a with Imidazole. A solution of **3a** (1.67 g, 5 mmol) and imidazole (0.34 g, 5 mmol) in dichloromethane (50 ml) was refluxed for 1 h. The solution was then evaporated, and the residue was extracted with benzene to give 0.66 g (90%) of phthalimide. The benzene extract was chromatographed on silica gel (eluent: benzene). The first fraction gave elemental sulfur (0.083 g, 52%). The polar substances remaining in the column were eluted with methanol. The eluate was evaoprated, and the residue was recrystallized from petroleum ether, giving 0.56 g (51%) of 1-(*p*-tolylsulfonyl)-imidazole.

(2) Reaction of 1 with Two Equiv. of 2. A solution of **1** (0.81 g, 2.5 mmol), **2** (5 mmol), and amine (0.5 mmol) in dichloromethane (50 ml) was refluxed for 1—3 h. The solution was treated as the same way described in the reaction of **1** with one equiv. of **2**. The products thus obtained, **4a**—**c**, **g**, were identified by means of their mixed melting points.[9,10)] The analytical data of bis(arenesulfonyl) disulfides obtained unexpectedly are shown below.

Bis(p-chlorobenzenesulfonyl) Didulfide. Found: C, 34.30;

H, 1.76; S, 30.8; Cl, 16.8%. Calcd for $C_{12}H_8Cl_2O_4S_4$: C, 34.70; H, 2.08; S, 30.88; Cl, 17.07%.

Bis(p-Bromobenzenesulfonyl) Disulfide. Found: C, 28.67; H, 1.61; S, 24.4; Br, 31.1%. Calcd for $C_{12}H_8Br_2O_4S_4$: C, 28.59; H, 1.60; S, 25.43; Br, 31.69%.

Reaction of 3 with 2. A solution of **3** (5 mmol), the corresponding **2** (5 mmol), and imidazole (0.068 g, 1 mmol) in dichloromethane (50 ml) was refluxed for 2—3 h. The solution was then treated as has been described in the reaction of **1** with one equiv. of **2**.

References

1) Chemistry of *N*-(Alkylthio- and Arylthio)imides VII. For Part VI of this series, see Ref. 5.

2) a) D. N. Harpp and D. K. Ash, *Int. J. Sulfur Chem., A*, **1**, 57, 211 (1971); b) A. B. Sullivan and K. S. Boustany, *ibid.*, **1**, 207 (1971).

3) D. N. Harpp and T. G. Back, *Tetrahedron Lett.*, **1972**, 1481.

4) Y. Abe and J. Tsurugi, *Chem. Lett.*, **1972**, 811.

5) Y. Abe, T. Horii, S, Kawamura, and T. Nakabayashi, *Bull. Chem. Soc. Jpn.*, **52**, 3461 (1979).

6) J. H. Clark and J. M. Miller, *J. Am. Chem. Soc.*, **99**, 498 (1977).

7) S. Winstein, L. G. Savedoff, S. Smith, I. D. R. Stevens, and J. S. Gall, *Tetrahedron Lett.*, **1960**, No. 9, 24.

8) D. N. Harpp, K. Steliou, and T. H. Chan, *J. Am. Chem. Soc.*, **100**, 1222 (1978).

9) S. Hayashi, M. Furukawa, J. Yamamoto, and K. Hamamura, *Chem. Pharm. Bull.*, **15**, 1310 (1967).

10) Troeger and Hornung, *J. Prakt. Chem.*, [**2**], **60**, 125; *Cf.* Beilsteins Handbuch der Organischen Chemie, Vol. 11, pp. 94, 190.

11) a) Y. Tanaka and Y. Tanaka, *Chem. Pharm. Bull.*, **13**, 399 (1965); b) Y. Tanaka and Y. Tanaka, *Yakugaku Zasshi*, **89**, 837 (1969).

12) M. V. Kalnins, *Can. J. Chem.*, **44**, 2111 (1966).

13) H. Gilman, *Org. Synth.*, Coll. Vol. 1, pp. 7, 492.

New Monoterpene Lactones of the Iridane Type from *Actinidia polygama* Miq.

Tsutomu SAKAI,* Kimiko NAKAJIMA, and Takeo SAKAN

**Suntory Institute for Bioorganic Research, Shimamoto-cho, Mishima-gun, Osaka 618

(Received May 29, 1980)

Fourteen iridoid monoterpene lactones including eight new compounds were isolated from the volatile oil of fresh fruits of the cat- and lacewing-attracting plant *Actinidia polygama* Miq., and their structures were established on the basis of spectral evidence and chemical transformation.

In continuous investigation of the constituents of the cat- and lacewing-attracting plant *Actinidia polygama* Miq.,[1,2] we isolated from the volatile oil of its fresh fruits eight new iridoid monoterpene lactones, which we named dihydroepinepetalactone (**1a**), isodihydroepinepetalactone (**1b**), isoepiiridomyrmecin (**2b**), isoneonepetalactone (**3b**), dehydroiridomyrmecin (**4a**), isodehydroiridomyrmecin (**4b**), actinidialactone (**5a**), and isoactinidialactone (**5b**), together with five previously isolated lactones.[3] The known compounds were identified as neonepetalactone (**3a**),[2] dihydronepetalactone (**6a**), isodihydronepetalactone (**6b**), iridomyrmecin (**7a**), and isoiridomyrmecin (**7b**). In addition, nepetalactone (**8**)[4] was also isolated from this oil.

The present paper deals with the structural elucidation of these new compounds.

*Structures of Three New Saturated Lactones **1a**, **1b**, and **2b**.* These new saturated lactones **1a**, **1b**, and **2b** were isolated by repeated preparative gas chromatography. They have the molecular formula $C_{10}H_{16}O_2$ according to high resolution mass spectra, and a characteristic IR band at 1740—1735 cm^{-1} indicated the presence of a saturated δ-lactone group. The mass spectra of **1a**, **1b**, and **2b** were almost identical to those of **6a**, **6b**, and **7b**, respectively. In their NMR spectra, the C-1 methyl protons signals were observed at δ 1.01, 1.01, and 0.83, while the analogous protons of natural **6a**, **6b**, and **7b** had signals at δ 1.19, 1.19, and 1.05. By comparison of the chemical shifts of the new lactones with those of lactones **6a**, **6b**, and **7b**, we deduced that they were the C-2 epimers of **6a**, **6b**, and **7b**.

The structures and stereochemistry of these new saturated lactones were confirmed by the following chemical evidence. When the lactones **1a** and **1b** were refluxed with sodium methoxide in methanol or potassium carbonate in xylene and followed by acidification with dil HCl, they were converted into **6a** and **6b**. As these conversions were analogous to that of epinepetalactone (**9**) into nepetalactone (**8**),[5] the lactones **1a** and **1b** were assigned as the dihydro derivatives of epinepetalactone, for which we proposed the names dihydroepinepetalactone (**1a**) and isodihydroepinepetalactone (**1b**). LAH reduction of **1a** and **1b** gave the corresponding saturated diols **10a** and **10b**. Their optical rotation data were in accord with those of β-iridodiol (**10a**) and γ-iridodiol (**10b**).[6] The lactone **2b** was also reduced with LAH to give γ-iridodiol (**10b**). From the above spectral and chemical evidence, **2b** was confirmed as the C-2 epimer of isoiridomyrmecin (**7b**) and named isoepiiridomyrmecin.

No epiiridomyrmecin (**2a**) was detected by GC-MS analysis of the oil.

*Structures of Five New Unsaturated Lactones **3b**, **4a**, **4b**, **5a**, and **5b**.* These new unsaturated lactones were also isolated by preparative gas chromatography. They were an α-unsaturated δ-lactone **3b** (MS: M^+ 166, $C_{10}H_{14}O_2$; IR: 1710, 1638 cm^{-1}), a pair of diastereomers of the unsaturated δ-lactones **4a** and **4b** (MS: M^+ 166; IR: 1730 cm^{-1}), and a pair of diastereomers of the unsaturated γ-lactones **5a** and **5b** (MS: M^+ 166; IR: 1770—1760 cm^{-1}). The mass spectrum of **3b** agreed with that of **3a**. The mass spectra of **4a** and **4b** and of **5a** and **5b** were almost identical to each other.

The α-unsaturated δ-lactone **3b** was reduced with LAH to give the corresponding unsaturated diol **11b**, which was identified as isodehydroiridodiol of known absolute configuration.[2] Catalytic hydrogenation of **3b** with Adams catalyst or Raney nickel catalyst gave a mixture of 1-epi-isodihydronepetalactone (**12b**) and the double bond migrated product **13b**, which were characterized on the basis of spectral data. The IR spectrum of **12b** was similar to that of **6b** and the NMR spectrum of **12b** closely resembled that of **6b**, except for the signals of the C-1 methyl protons: the (1*R*)-methyl signals of **12b** appeared at about 0.20 ppm higher field than the (1*S*)-methyl signals of **6b**. The IR, NMR, and mass spectra of **13b** closely resembled those of the lactone **13a** obtained from **3a**.[2] Spectral and chemical evidence showed that the lactone **3b** was the C-8 epimer of neonepetalactone (**3a**) and it was named isoneonepetalactone.

The unsaturated δ-lactones **4a** and **4b** were reduced with LAH to give dehydroiridodiol (**11a**) and isodehydroiridodiol (**11b**), respectively. Catalytic hydrogenation of **4b** gave an unsaturated carboxylic acid.[7] Lactonization of this acid with *p*-toluenesulfonic acid in benzene afforded a mixture of two new saturated γ-lactones **14b** and **15b** in a ratio of 3 : 4, which were determined by spectral analysis. Thus, the lactones **4a** and **4b** were assigned as the $\Delta^{1,2}$-dehydro derivatives of **7a** and **7b**, and designated as dehydroiridomyrmecin (**4a**) and isodehydroiridomyrmecin (**4b**).

The NMR spectra of the new unsaturated γ-lactones **5a** and **5b** showed the presence of a secondary methyl group, a methyl group on a tertiary carbon-bearing oxygen, and a trisubstituted olefinic proton. Spectral characteristics and biogenetic consideration show these compounds to be a pair of diastereomers having an

** The previous name: The Institute of Food Chemistry.

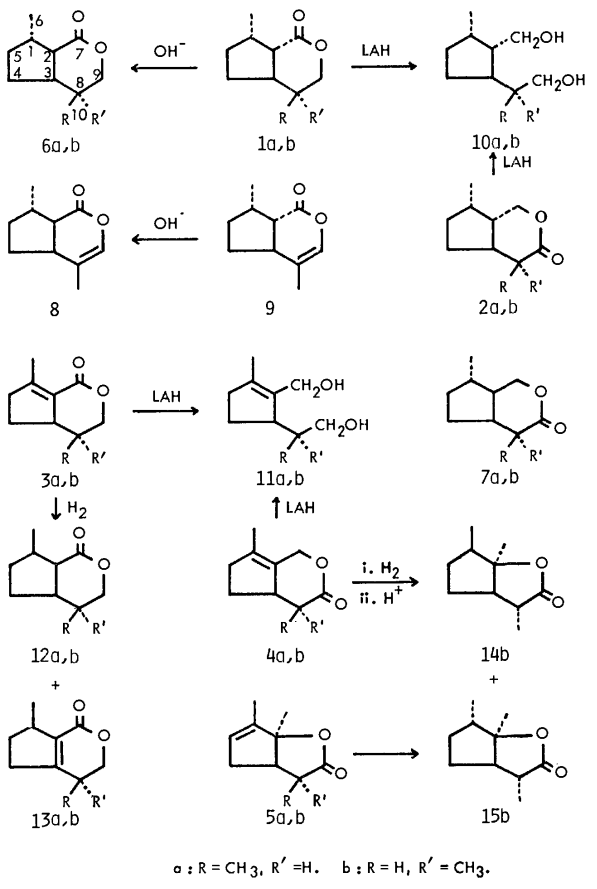

iridane skeleton with a γ-lactone group and a double bond, *i.e.*, structures **5a** and **5b**, for which we propose the names actinidialactone (**5a**) and isoactinidialactone (**5b**). The stereochemistry of **5a** and **5b** was established by the following evidence. (a) Reduction of **5b** with Adams catalyst in ether yielded a mixture of two saturated γ-lactones in a ratio of 12 : 1, which were identical in all respects (IR, NMR, MS, and CD) to the lactones **14b** and **15b** derived from **4b** with the (3*R*,8*R*)-configuration. (b) The CD spectrum of the new lactone **5a** exhibited a positive Cotton curve while **5b** showed a negative one. According to Snatzke's rule,[8] the molecules corresponding to **5a** and **5b** are supposed to show positive and negative Cotton effects, respectively. (c) Close correspondence of the ^{1}H- and ^{13}C-NMR spectra of **5a** and β-episantonin derivatives and of **5b** and α-episantonin derivatives[9,10] definitely confirmed the stereochemistry of the α-methyl-γ-lactone moiety in **5a** and **5b**.[11]

These newly isolated lactones have not yet evaluated for their bioactive effects against Felidae animals.

Experimental

NMR spectra were recorded in $CDCl_3$ with TMS as the internal standard on a JEOL JNM-FX100 instrument. IR spectra were taken as thin films between NaCl plates on a Hitachi EPI-G2 spectrometer equipped with a beam condenser. Optical rotations were measured in $CHCl_3$ on a Perkin-Elmer Model 141 polarimeter. Mass spectra were obtained on a Hitachi RMU-6 mass spectrometer (for GC-MS) or a JEOL JMS-01SG (for high resolution mass spectra) instrument. Gas liquid chromatography (GLC) was performed on a Hitachi 163 (for analytical work) or a Varian aerograph 920 (for preparative work) instrument, using a 40 m × 0.25 mm glass capillary column coated with Thermon 600T (analytical and GC-MS) or a 3 m × 10 mm aluminum column packed with 5% Thermon 1000 on Chromosorb W (preparative).

Isolation of Lactones. Fresh fruits (5.5 kg, collected in Toyama Pref. in August 1979) were steam distilled to give the volatile oil (4.5 g). Figure 1 shows its gas chromatogram.

Its components were separated by repeated preparative GLC (column temp, 180 °C; injector temp., 220 °C; helium flow rate, 40 ml/min). Eight new oily substances and six known lactones were isolated in their pure states. The known lactones were identified by direct comparison with authentic samples.

*Dihydroepinepetalactone (**1a**).* Content: 0.31%;[12] Relative retention time: 1.49;[13] $[\alpha]_D^{25}$ +31.3° (*c* 0.55); IR: 1740 cm^{-1}; NMR: δ 1.00, 1.03 (each 3H, d, J=7 Hz, C-8 Me and C-1 Me), 4.02, 4.35 (each 1H, AB q of ABX, J_{AX}=3 Hz, J_{BX}=4 Hz, J_{AB}=11 Hz, C-9 H_2); MS: 168 (22%, M$^+$), 153 (41), 139 (7), 126 (31), 113 (70), 95 (45), 81 (100), 67 (60), 55 (22), and 41 (36). [Found, M$^+$ 168.1142. $C_{10}H_{16}O_2$ requires, M$^+$ 168.1148].

*Isodihydroepinepetalactone (**1b**).* Content: 0.30%; RRT: 1.16; $[\alpha]_D^{25}$ +90.3° (*c* 0.74); IR: 1740 cm^{-1}; NMR: δ 1.01 (6H, d, J=7 Hz, C-8 Me and C-1 Me), 3.81, 4.35 (each 1H, AB q of ABX, J_{AX}=9 Hz, J_{BX}=5 Hz, J_{AB}=11 Hz, C-9 H_2); MS: 168 (17%, M$^+$), 153 (53), 139 (5), 126 (18), 123 (15), 113 (100), 109 (25), 95 (56), 81 (81), 69 (30), 67 (54), 55 (20), and 41 (30). [Found, M$^+$ 168.1145].

*Isoepiiridomyrmecin (**2b**).* Content: 0.73%; RRT: 1.47; $[\alpha]_D^{25}$ +6.17° (*c* 0.47); IR: 1730 cm^{-1}; NMR: δ 0.86, 1.31 (each 3H, d, J=7 Hz, C-1 Me and C-8 Me), 4.21, 4.48 (each 1H, AB q of ABX, J_{AX}=8 Hz, J_{BX}=5 Hz, J_{AB}=11 Hz, C-7 H_2); MS: 168 (8%, M$^+$), 109 (33), 95 (48), 81 (100), 68 (55), 67 (64), 55 (19), and 41 (25). [Found, M$^+$ 168.1146].

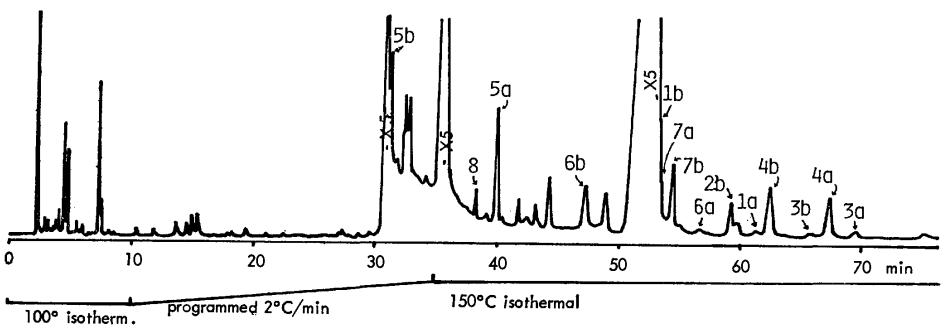

Fig. 1. The gas chromatogram of the volatile oil of fresh fruits.

*Isoneonepetalactone (**3b**).* Content: 0.003%; RRT: 1.77; $[\alpha]_D^{23}$ −66.2° (*c* 0.34); IR: 1710, 1638 cm^{-1}; NMR: δ 0.94 (3H, d, J=7 Hz, C-8 Me), 2.20 (3H, t, J=1 Hz, C-1 Me), 3.89, 4.24 (each 1H, AB q of ABX, J_{AX}=11 Hz, J_{BX}=5Hz, J_{AB}=11 Hz, C-9 H_2); MS: 166 (93%, M^+), 151 (21), 136 (8), 124 (90), 121 (30), 107 (24), 105 (13), 93 (60), 91 (26), 87 (42), 79 (100), 77 (30), 67 (15), 65 (10), 55 (12), 53 (14), 41 (30), and 39 (26). [Found, M^+ 166.0995. $C_{10}H_{14}O_2$ requires: M^+ 166.0993].

*Dehydroiridomyrmecin (**4a**).* Content: 0.80%; RRT: 1.79; $[\alpha]_D^{25}$ −105.6° (*c* 0.90); IR: 1730, 1650 cm^{-1}; NMR: δ 1.14 (3H, d, J=7 Hz, C-8 Me), 1.73 (3H, t, J=1 Hz, C-1 Me), 4.91 (2H, br s, C-7 H_2); MS: 166 (20%, M^+), 151 (1), 138 (5), 122 (22), 121 (18), 107 (57), 105 (26), 93 (100), 91 (42), 81 (21), 79 (36), 77 (34), 67 (12), 55 (14), and 41 (30). [Found, M^+ 166.0998].

*Isodehydroiridomyrmecin (**4b**).* Content: 1.40%; RRT: 1.59; $[\alpha]_D^{25}$ −79.2° (*c* 1.06); IR: 1730 cm^{-1}; NMR : δ 1.27 (3H, d, J=7 Hz, C-8 Me), 1.68 (3H, t, J=1 Hz, C-1 Me), 4.96 (2H, br s, C-7 H_2); MS: 166 (32%, M^+), 151 (2), 138 (9), 121 (6), 109 (12), 107 (13), 98 (14), 93 (100), 81 (25), 67 (7), 55 (11), and 41 (6). [Found, M^+ 166.0993].

*Actinidialactone (**5a**).* Content: 1.38%; RRT: 0.70; $[\alpha]_D^{25}$ −18.3° (*c* 1.15); IR: 1760 cm^{-1}; NMR: δ 1.23 (3H, d, J=7 Hz, C-8 Me), 1.47 (3H, s, C-2 Me), 1.75 (3H, t, J=1 Hz, C-1 Me), 5.56 (1H, br s, C-5H); MS: 166 (3%, M^+), 151 (2), 122 (50), 107 (100), 105 (16), 95 (10), 93 (22), 91 (44), 79 (28), 67 (6), 55 (6), and 43 (4). [Found, M^+ 166.0993].

*Isoactinidialactone (**5b**).* Content: 0.51%; RRT: 0.40; $[\alpha]_D^{25}$ −13.9° (*c* 0.94); IR: 1770 cm^{-1}; NMR: δ 1.29 (3H, d, J=7 Hz, C-8 Me), 1.46 (3H, s, C-2 Me), 1.73 (3H, t, J=1 Hz, C-1 Me), 5.41 (1H, br s, C-5 H); MS: 166 (5%, M^+), 151 (4), 122 (51), 107 (100), 95 (16), 93 (11), 91 (30), 79 (20), 67 (8), 55 (7), and 43 (11). [Found, M^+ 166.1009].

*Conversion of Dihydroepinepetalatone (**1a**) into Dihydronepetalactone (**6a**).* A mixture of 8 mg of **1a**, 10 mg of Na_2CO_3, and 0.5 ml of xylene was heated at 230 °C in a sealed tube for 2 h. The mixture was separated by preparative GLC to give an oily substance (6 mg), $[\alpha]_D^{25}$ +40.8° (*c* 0.60); IR: 1725 cm^{-1}; NMR: δ 0.90, 1.19 (each 3H, d, J=7 Hz, C-8 Me and C-1 Me); MS: 168 (17%, M^+), 153 (36), 139 (6), 126 (23), 113 (42), 95 (46), 81 (100), 67 (75), 55 (32), and 41 (68). The spectral data and the retention time in GLC were identical to those of natural lactone **6a**.

*Conversion of Isodihydroepinepetalactone (**1b**) into Isodihydronepetalactone (**6b**).* A solution of 28 mg of **1b** in 4 ml of methanol containing sodium methoxide (240 mg) was refluxed with stirring for 17 h. Next, 2 ml of water was added to the cooled solution and it was refluxed for another 4 h then acidified with dil HCl. After the usual work-up, the resulting oily material (18 mg) was separated by preparative GLC into two components. The major product (13 mg) showed $[\alpha]_D^{25}$ +1.6° (*c* 0.94); IR: 1725 cm^{-1}; NMR: δ 0.97, 1.18 (each 3H, d, J=7 Hz, C-8 Me and C-1 Me); MS: 168 (17%, M^+), 153 (58), 139 (12), 126 (21), 123 (18), 113 (100), 95 (36), 81 (79), 67 (53), 55 (20), and 41 (37). The spectral data and the GLC retention time were identical to those of natural lactone **6b**.

*LAH Reduction of Dihydroepinepetalactone (**1a**), Isodihydroepinepetalactone (**1b**), and Isoepiiridomyrmecin (**2b**).* Each lactone was refluxed in ether with LAH for 2 h. After the usual work-up, the residual oil was chromatographed over silicic acid. Elution with ether afforded a pure saturated diol. The diol **10a** derived from **1a** showed $[\alpha]_D^{22}$ −49.4° (*c* 0.66); IR: 3320 cm^{-1}; NMR: δ 0.85, 0.95 (each 3H, d, J=7 Hz, C-8 Me and C-1 Me), 3.38, 3.72 (each 1H, AB q of ABX, J_{AX}=5 Hz, J_{BX}=5 Hz, J_{AB}=10 Hz, C-7 H_2), 3.51 (2H, d, J=7 Hz, C-9 H_2), 4.12 (2H, br s, 2×OH); MS: 154 (0.1%, M^+ −18), 123 (38), 109 (10), 95 (60), 81 (100), 67 (45), 55 (77), and 41 (75). This diol had the same $[\alpha]_D$ as authentic β-iridodiol ($[\alpha]_D^{23}$ −62°).[6] The diol **10b** derived from **2b** was identical in all respects to the diol prepared from **1b**. The diol **10b** showed $[\alpha]_D^{24}$ −19.5° (*c* 0.64); IR: 3320 cm^{-1}; NMR: δ 0.91, 0.93 (each 3H, d, J=7 Hz, C-8 Me and C-1 Me), 3.41, 3.70 (each 2H, m, C-7 and C-9 H_2); MS: 154 (0.5%, M^+ −18), 139 (2), 136 (2). 123 (81), 109 (16), 95 (72), 81 (100), 67 (34), 55 (39), and 41 (23). The diol was identical to authentic γ-iridodiol ($[\alpha]_D^{23}$ −19°).[6]

*LAH Reduction of Isoneonepetalactone (**3b**), Dehydroiridomyrmecin (**4a**), and Isodehydroiridomyrmecin (**4b**).* Each lactone was refluxed in ether with LAH for 2 h. The lactone **4a** was reduced with LAH to yield the diol **11a**, $[\alpha]_D^{24}$ −20.7° (*c* 2.28), which was identical in all respects to the authentic sample of dehydroiridodiol.[2] The lactones **3b** and **4b** were reduced with LAH to yield the same diol **11b**, $[\alpha]_D^{24}$ −15.6° (*c* 1.08), which was identical in all respects to the authentic sample of isodehydroiridodiol.[2]

*Catalytic Hydrogenation of Isoneonepetalactone (**3b**).* A mixture of 100 mg of **3b** in 3 ml of ether and 25 mg of PtO_2 catalyst was stirred under a hydrogen pressure of 1 atm at room temp for 5 min. Filtration of the catalyst and evaporation of the solvent afforded a mixture of the reduction products. GLC indicated the presence of 84% of **12b** and 16% of **13b**. A pure sample of **12b** showed $[\alpha]_D^{28}$ −66.1° (*c* 0.46); IR: 1725 cm^{-1}; NMR: δ 0.98 (6H, d, J=7 Hz, C-8 Me and C-1 Me), 3.85, 4.19 (each 1H, AB q of ABX, J_{AX}=10 Hz, J_{BX}=4 Hz, J_{AB}=11 Hz, C-9 H_2); MS: 168 (6%, M^+), 153 (5), 126 (7), 123 (7), 113 (100), 95 (27), 81 (35), 67 (35), 55 (20), and 41 (34). A pure sample of **13b** showed $[\alpha]_D^{24}$ −89.1° (*c* 1.94); IR: 1720, 1640 cm^{-1}; UV: λ_{max}^{EtOH} 235 nm (log ε 4.10); NMR: δ 1.14 (3H, d, J=7 Hz, C-8 Me), 1.18 (3H, d, J=7 Hz, C-1 Me), 4.06, 4.37 (each 1H, AB q of ABX, J_{AX}=6 Hz, J_{BX}=5 Hz, J_{AB}=11 Hz, C-9 H_2); MS: 166 (100%, M^+), 151 (50), 136 (49), 123 (25), 121 (61), 107 (58), 95 (36), 93 (40), 91 (38), 81 (18), 79 (40), 77 (30), 67 (18), 65 (13), 53 (13), 41 (25), and 39 (26).

*Transformation of Isodehydroiridomyrmecin (**4b**) into the New Saturated γ-Lactones **14b** and **15b**.* The lactone **4b** (40 mg) was hydrogenated in ether over PtO_2 catalyst for 40 min. After the usual work-up, the residue was purified by preparative GLC to give a single product. It showed the following spectral data; IR: 3500—2500, 1700 cm^{-1} (COOH); NMR: δ 0.95 (3H, d, J=7 Hz, C-8 Me), 1.61, 1.64 (each 3H, s, C-1 Me and C-2 Me); MS: 168 (10%, M^+), 113 (13), 95 (100), 81 (10), 67 (17), 55 (13), and 41 (9). A solution of 38 mg of the acid in 4 ml of benzene containing 30 mg of *p*-toluenesulfonic acid was refluxed with stirring for 40 min. The solution was washed with 10% $NaHCO_3$ aq and water, then dried over Na_2SO_4. After the solvent was removed, the mixture was separated by preparative GLC into two saturated γ-lactones **14b** and **15b** in a ratio of 3 : 4. A pure sample of **14b** showed $[\alpha]_D^{19}$ +43.3° (*c* 0.09); IR: 1760 cm^{-1}; NMR: δ 1.05 (3H, d, J=6 Hz, C-1 Me), 1.37 (3H, d, J=7 Hz, C-8 Me), 1.48 (3H, s, C-2 Me); MS: 168 (23%, M^+), 153 (1), 140 (6), 125 (100), 109 (22), 95 (23), 81 (6), 72 (23), 69 (15), 55 (31), and 43 (22). A pure sample of **15b** showed $[\alpha]_D^{19}$ +13.8° (*c* 0.08); IR: 1760 cm^{-1}; NMR: δ 0.99 (3H, d, J=6 Hz, C-1 Me), 1.34 (3H, d, J=7 Hz, C-8 Me), 1.35 (3H, s, C-2 Me); MS: 168 (21%, M^+), 153 (1), 140 (5), 125 (100), 109 (22), 95 (28), 81 (7), 72 (32), 69 (18), 55 (45), and 43 (30).

*Catalytic Hydrogenation of Isoactinidialactone (**5b**).* The lactone **5b** (20 mg) was hydrogenated in ether over PtO_2 catalyst for 1.5 h. The reaction mixture was worked up in the usual manner to give a mixture of the lactones **14b** and **15b**

in a ration of 12 : 1. These lactones were identical in all respects to the lactones prepared from **4b** as described above.

References

1) K. Yoshihara, T. Sakai, and T. Sakan, *Chem. Lett.*, **1978**, 433.

2) T. Sakai, K. Nakajima, K. Yoshihara, T. Sakan, and S. Isoe, *Tetrahedron*, **36**, 3115 (1980).

3) T. Sakan, F. Murai, S. Isoe, S. B. Hyeon, and Y. Hayashi, *Nippon Kagaku Zasshi*, **90**, 507 (1969).

4) F. E. Regnier, E. J. Eisenbraun, and G. R. Waller, *Phytochem.*, **6**, 1271 (1967).

5) T. Sakan, S. Isoe, S. B. Hyeon, R. Katsumura, T. Maeda, J. Wolinsky, D. Dickerson, M. Slabaugh, and D. Nelson, *Tetrahedron Lett.*, **1965**, 4097.

6) E. J. Eisenbraun, A. Bright, and H. H. Appel, *Chem. Ind. (London)*, **1962**, 1242.

7) Spectral data confirmed that this acid was (1*R*, α*R*)-2,3,α-trimethyl-2-cyclopenteneacetic acid.

8) G. Snatzke, H. Ripperger, C. Horstmann, and K. Schreiber, *Tetrahedron*, **22**, 3103 (1966).

9) P. S. Pregosin, E. W. Randall, and T. B. H. McMurry, *J. Chem. Soc., Perkin Trans. 1*, **1972**, 299.

10) G. P. Moss, P. S. Pregosin, and E. W. Randall, *J. Chem. Soc., Perkin Trans. 1*, **1974**, 1525.

11) ^{13}C-NMR data of **5a** and **5b**.

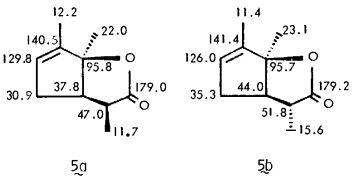

5a 5b

Cf. ^{13}C chemical shifts of the α- and β-episantonin derivatives.[9,10]

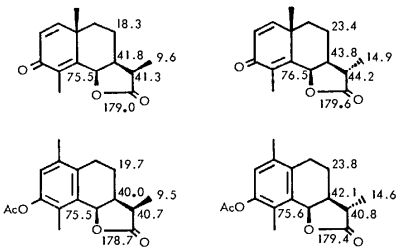

12) The content of lactone was calculated using a GC/computer system from the peak area of GLC.

13) Relative retention time was evaluated with isodihydronepetalactone (**6b**) as the standard substance.

Synthesis and Stereochemistry of 2,3,4,6-Tetra-*O*-benzyl-D-glucopyranosylidene Acetals of α-Diols and Monosaccharides

Masatoshi TAMARU,† Shigeomi HORITO, and Juji YOSHIMURA*

Laboratory of Chemistry for Natural Products, Faculty of Science, Tokyo Institute of Technology, Nagatsuta, Midori-ku, Yokohama 227

(Received June 26, 1980)

The title compounds were synthesized by addition of 2,3,4,6-tetra-*O*-benzyl-D-glucono-1,5-lactone to epoxides and by direct dehydration between the lactone and diols in the presence of concentrated sulfuric acid as a catalyst. Stereochemistry of these spiro cyclic acetals was discussed.

The unique type of acetal interlinkage between a glycosylidene(1-dehydroglycosyl) group and a glycose has been found in such oligosaccharide antibiotics as everninomicins,[1] flambamycin,[2] hygromycin B,[3] destomycins,[4] A-396-I,[5] and SS-56C.[6] Recently, these antibiotics were designated as "orthosomycins,"[2] because the spiro cyclic ortho ester at the anomeric carbon is quite different from well-known fused-ring type ortho esters in the carbohydrate chemistry.[7] In general, two configurations are possible in this interlinkage depending on whether the anomeric carbon is (*R*) or (*S*). However, it is left ambiguous except for one of the two linkages in everninomicin D.[8] Moreover, no synthetic anologs have thus far been reported except a communication[9] from our laboratory.

This paper describes in detail the synthesis of the spiro cyclic ortho esters from 2,3,4,6-tetra-*O*-benzyl-D-glucono-1,5-lactone (**1**)[10] and the stereochemistry of their ring-systems.

Results and Discussion

As the applicable methods for the preparation of spiro cyclic ortho esters from **1**, addition of **1** to epoxides[11] and the dehydration condensation of **1** with diols[12] were examined.

Reaction of **1** in dichloromethane with equivalent amount of 1-chloro-2,3-epoxypropane or 1,2-epoxypropane at 28—30 °C for 1 h in the presence of boron trifluoride etherate gave the corresponding spiro cyclic ortho esters (**2** and **3**) as syrups in 45 and 65% yields, respectively. The presence of both of the isomers possible was indicated by the ^{1}H NMR spectra of **2** and **3**, respectively. A similar reaction of **1** with 5,6-anhydro-1,2-*O*-isopropylidene-3-*O*-methyl-α-D-glucofuranose[13] for 1 h gave only one of two possible isomers, 1,2-*O*-isopropylidene-3-*O*-methyl-5,6-*O*-(2,3,4,6-tetra-*O*-benzyl-D-glucopyranosylidene)-α-D-glucofuranose (**4**) in 26% yield. The presence of the ortho ester linkage in **4** was proved by the characteristic signal of ortho ester carbon at δ 110.8 ppm (from Me_4Si) in the ^{13}C NMR spectrum. However, this method was unsuccessful in the case of such epoxides including two secondary carbons as 1,2-epoxycyclohexane and methyl 2,3-anhydro-4,6-*O*-benzylidene-α-D-mannopyranoside.[14]

On the other hand, azeotropic dehydration of a solution of equimolar amounts of **1** and ethylene glycol in benzene containing a catalytic amount of concd sulfuric acid during 10 h gave the corresponding spiro cyclic othro ester (**5**) in 43% yield. On continuation of the dehydration for 24 h, **1** disappeared and the yield of **5** rose to 77%. Compound **3** was also obtained quantitatively from **1** and 1,2-propanediol by the same method. Catalytic hydrogenation of **5** in methanol in the presence of palladium-on-charcoal and a few drops of acetic acid gave the de-*O*-benzylated product as a syrup, this was acetylated with acetic anhydride in pyridine to give the corresponding tetraacetate (**6**) in 73% overall yield.

Similar dehydration of a mixture of **1** and *cis*-1,2-cyclohexanediol for 3 h gave a mixture of two isomers of the corresponding ortho esters (**7**) which was separated on a silica gel column to give **7a** and **7b** in 45 and 28% yields, respectively. Similar reaction of *trans*-1,2-cyclohexanediol for 37 h also gave two products (**8a** and **8b**) in 21 and 22% yields, respectively. Reaction of **1** and methyl 2,3-di-*O*-methyl-α-D-glucopyranoside[15] or -α-D-mannopyranoside[16] gave only one of the two possible isomers (**9** and **10**) in 20 and 8% yields, respectively. Reaction of **1** and erythritol gave 1,2 : 3,4-di-*O*-(2,3,4,6-tetra-*O*-benzyl-D-glucopyranosylidene)-erythritol (**11**) in 80% yield. Dehydration of a mixture of **1** and methyl 4,6-di-*O*-benzyl-α-D-mannopyranoside gave unsuccessful result. However, a similar reaction with methyl 4,6-di-*O*-methyl-α-D-mannopyranoside gave a trace amount of 1 : 1 mixture of two possible isomers of methyl 4,6-di-*O*-methyl-2,3-*O*-(2,3,4,6-tetra-*O*-benzyl-D-glucopyranosylidene)-α-D-mannopyranoside (**12**) as a syrup. The separation of these two isomers was unsuccessful, but the presence was indicated by the two characteristic signals assigned to the ortho ester carbon in the ^{13}C NMR spectrum.

Examination of acidic catalysts indicated that *p*-toluenesulfonic acid, phosphorus pentaoxide, and ortho- and polyphosphoric acids were uneffective, while the super acid ($SbF_5 \cdot FSO_3H$) showed the effectiveness of the same level as concd sulfuric acid.

The chemical shifts of ortho ester carbons of glucosylidene acetals synthesized here were summarized in Table 1. The chemical shifts of the ortho ester carbons with 1,3-dioxolane rings (**2,4—8,12**), were 118—122 ppm, whereas that with 1,3-dioxane rings (**9** and **10**) 110.7—110.9 ppm. This difference in the chemical shifts of ortho ester carbons is diagnostic for the ring-size. Consequently, the chemical shift of the carbon in **11** clearly shows that the structure is 1,2 : 3,4-di-*O*-glucosylidene derivative having two 1,3-dioxolane

† Present address: Kumiai Chemical Industry Co. Ltd., Laboratory of Chemical Research, Shibukawa, Shimizu 424.

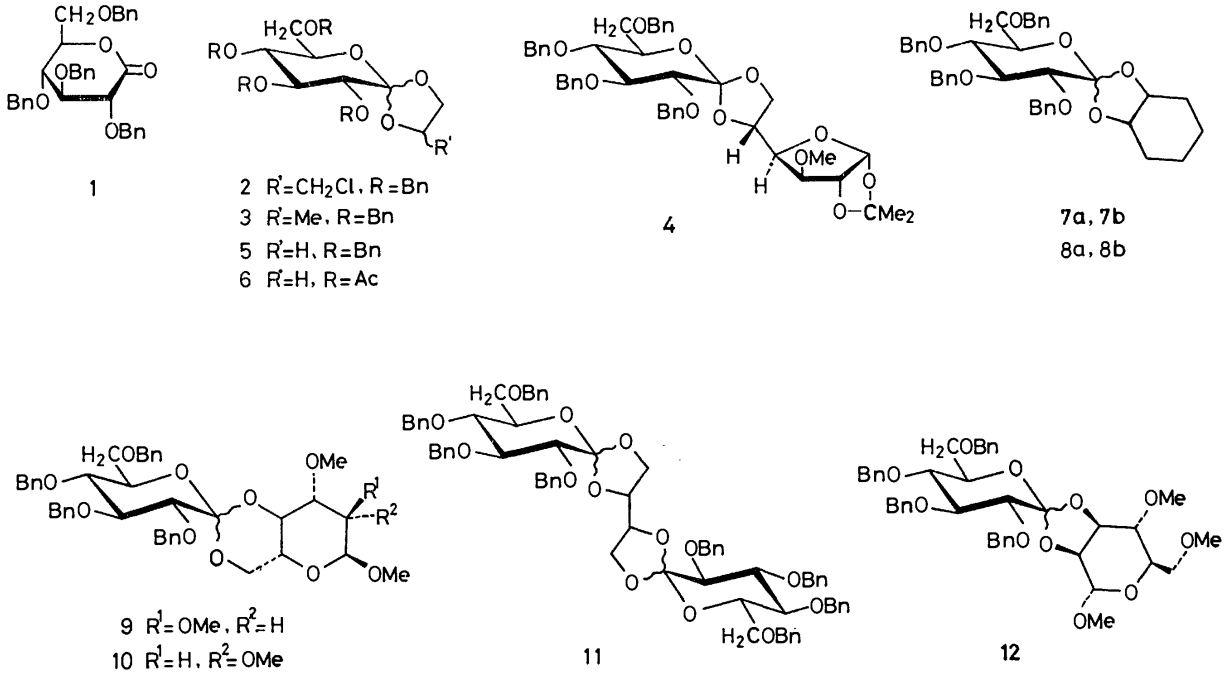

Scheme 1.

TABLE 1. THE CHEMICAL SHIFTS OF ORTHO ESTER CARBONS

Compound	Chemical shifts, δ (ppm)
2	120.5, 120.6
4	119.6
5	119.6
6	118.0
7	118.5, 119.6
8	119.1, 119.2
9	110.7
10	110.9
11	121.9
12	119.1, 120.5

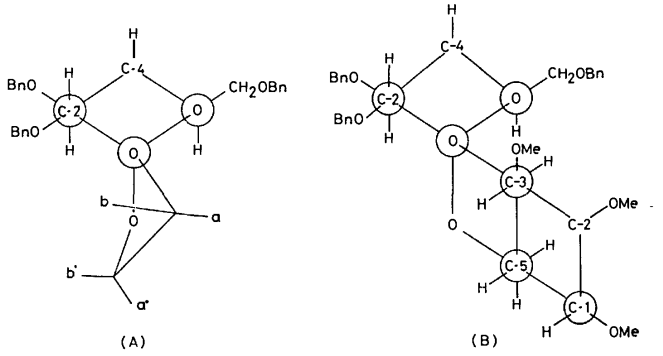

Fig. 1.

rings, but not 1,3 : 2,4-di-*O*-substituted derivative with two 1,3-dioxane rings, indicating the former ring is thermodynamically more stable than the latter.

The above results provide interesting problems in stereochemistry. In the case of five-membered spiro cyclic compounds [(A) in Fig. 1], the non-bonded interaction between groups attached to C-2 of the pyranosylidene ring and to the acetal ring can be avoided by a twist conformation of the latter, as was shown in the X-ray analysis of the olgose.[8] For example, in the case of **8** the conformation of the cyclohexane ring with a→b′ bonds will be a less-hindered one than that including b→a′ bonds. In possible formulations of **4**, the bulky D-glucofuranose ring should be attached to either b or a′ position, and therefore, the latter, the (1*R*)-pyranosylidene isomer shown by the structural formula in Scheme 1, will be much the more stable. This trend will be also true in the configuration of **11** from erythritol. In cases of **7** and **12** in which the five-membered acetal ring includes a→a′ bonds or b→b′ bonds, there was no significant difference in the yields of isomers, indicating the dispense of the strain of the two isomers by the direction of twisting of the five-membered ring. The Newman projection of the stable, (1*R*)-isomer of **9** or **10** having a six-membered acetal ring is presented in (B). It is obvious that the ring oxygen side of the glucopyranosylidene moiety is less hindered, though the absolute configuration is not yet determined.

Experimental

General Methods. Melting points were determined on a Yanagimoto micro melting-point apparatus and are uncorrected. ^{1}H and ^{13}C NMR spectra were recorded with a JNM-PS-100 and a JNM FX-100 spectrometers, respectively, in chloroform-*d* containing tetramethylsilane as the internal reference. The chemical shifts and coupling constants were recorded in δ(ppm) and Hz units. Optical rotations were measured in 0.5-dm tubes with a Carl Zeiss LEP-A1 polarimeter. Solvents were evaporated under diminished pressure.

1,2-O-(2,3,4,6-Tetra-O-benzyl-D-glucopyranosylidene)-3-chloro-1,2-propanediol (2). To a solution of tetra-*O*-benzyl-D-glucono-1,5-lactone (**1**) (1.8 g, 3.34 mmol) and boron trifluoride etherate (0.5 g) in dichloromethane (40 ml) was

added dropwise 3-chloro-1,2-epoxypropane (0.4 g, 4.32 mmol) with stirring, at 28—30 °C, during 1 h. The reaction mixture was stirred for 1 h, washed successively with 2.5 M sodium hydroxide and water, then dried and evaporated to give a syrup which was purified on a silica-gel column (7 : 2 hexane–ethyl acetate, R_f 0.41) to give **2** as a syrup in 45.0% yield. Found: C, 70.21; H, 6.61%. Calcd for $C_{37}H_{39}O_7Cl$: C, 70.41; H, 6.23%.

1,2-O-(2,3,4,6-Tetra-O-benzyl-D-glucopyranosylidene)-1,2-propanediol (3). *i*): A similar reaction of **1** (1.8 g, 3.34 mmol) with 1,2-epoxypropane (0.2 g, 3.44 mmol) as above in the presence of boron trifluoride etherate (0.5 g) gave **3** as a syrup (7 : 2 hexane–ethyl acetate, R_f 0.43) in 65.2% yield.

ii): Azeotropic dehydration of a solution of **1** (3 g, 5.57 mmol) and 1,2-propanediol (0.5 g, 6.57 mmol) in dry benzene (60 ml) containing a catalytic amount of concentrated sulfuric acid for 24 h gave **3** (3.2 g) in 96.2% yield. Found: C, 74.47; H, 7.16%. Calcd for $C_{37}H_{40}O_7$: C, 74.47; H, 6.76%.

5,6-O-(2,3,4,6-Tetra-O-benzyl-D-glucopyranosylidene)-1,2-O-isopropylidene-3-O-methyl-α-D-glucofuranose (4). A similar reaction of **1** (1.5 g, 2.78 mmol) and 5,6-anhydro-1,2-*O*-isopropylidene-3-*O*-methyl-α-D-glucofuranose (0.65 g, 3.01 mmol) as **2** in the presence of boron trifluoride etherate (0.4 g), and purification of the product (9 : 1 benzene–acetone, R_f 0.68) gave **4** as prisms (petroleum ether) in 25.9% yield. Mp 131—132 °C, $[\alpha]_D^{22}$ +17.4° (*c* 0.62, $CHCl_3$); Found: C, 70.00; H, 6.78%. Calcd for $C_{44}H_{50}O_{11}$: C, 70.01; H, 6.68%.

Signals of two C-Me groups (δ 1.21 and 1.30), and one OMe (3.42), could be distinguished in the ^1H NMR spectrum, and in addition, those of four benzyl methylene carbons (73.4, 74.8, 75.4, and 75.7 ppm), 6- and 6′-carbons (66.6 and 69.0) and the ortho ester carbon (119.6) in the ^{13}C NMR spectrum.

1,2-O-(2,3,4,6-Tetra-O-benzyl-D-glucopyranosylidene)ethanediol (5). A solution of **1** (2 g, 3.71 mmol) and ethylene glycol (340 mg, 5.45 mmol) in benzene (40 ml) containing a few drops of concentrated sulfuric acid was refluxed for 10 h, and the water formed was removed azeotropically. The benzene solution was successively washed with sodium hydroxide solution and water, then evaporated to give a syrup, which was purified on a silica-gel column (1 : 1 hexane–ether, R_f 0.42). Yield, 0.93 g (43%), mp 51—52 °C (petroleum ether), $[\alpha]_D^{22}$ +51° (*c* 1.0, $CHCl_3$). Found: C, 73.59; H, 6.52%. Calcd for $C_{36}H_{38}O_7$: C, 74.20; H, 6.57%. On continuation of the dehydration for 24 h, **5** was obtained in 77% yield.

1,2-O-(2,3,4,6-Tetra-O-acetyl-D-glucopyranosylidene)ethanediol (6). Catalytic hydrogenation of **5** (1 g, 1.72 mmol) in methanol (20 ml) in the presence of palladium–charcoal (10%, 1 g) and a few drops of acetic acid consumed theoretical amount of hydrogen (170 ml) during 8 h. The reaction mixture was filtered, and the filtrate was neutralized with lead carbonate and concentrated to give a syrup (350 mg, 93%). The syrup in pyridine was acetylated with acetic anhydride by the usual manner to give **6** as needles (toluene). Yield, 0.49 g (73%), mp 143—145 °C, $[\alpha]_D^{22}$ +51° (*c* 1.0, $CHCl_3$). ^1H NMR: 5.7—5.28 (H_2, H_3, H_4 : m), 4.52 (H_6 : q, $J_{5,6}$=4.2, $J_{6,6'}$=12.5), 4.40 ($H_{6'}$: q, $J_{5,6'}$=2.4), 4.32—6.00 (H_5, CH_2CH_2 : m), 2.31, 2.17, 2.10, 2.08 (4×OAc). Found: C, 49.35; H, 5.63%. Calcd for $C_{16}H_{22}O_{11}$: C, 49.23; H, 5.68%.

*1,2-O-(2,3,4,6-Tetra-O-benzyl-D-gluropyranosylidene)-*cis*-1,2-cyclohexanediol (7a and 7b).* Azeotropic dehydration of **1** (2.0 g, 3.7 mmol) and *cis*-1,2-cyclohexanediol (0.8 g, 6.9 mmol) for 30 h as **5**, and separation of the product on a silica gel colume (1 : 1 hexane–ether) gave two isomers of **7a** (650 mg, R_f 0.53) and **7b** (1070 mg, R_f 0.50) as needles in 28 and 45% yields, respectively.

7a: mp 58—60 °C, $[\alpha]_D^{22}$ +45° (*c* 0.90, $CHCl_3$), ortho ester ^{13}C: 119.6 ppm. Found: C, 75.72; H, 7.03%. Calcd for $C_{40}H_{44}O_7$: C, 75.45; H, 6.97%.

7b: mp 98—100 °C, $[\alpha]_D^{22}$ +55° (*c* 1.1, $CHCl_3$), ortho ester ^{13}C: 118.5 ppm. Found: C, 75.80; H, 7.12%. Calcd for $C_{40}H_{44}O_7$: C, 75.45; H, 6.97%.

*1,2-O-(2,3,4,6-Tetra-O-benzyl-D-glucopyranosylidene)-*trans*-1,2-cyclohexanediol (8a and 8b).* A similar azeotropic dehydration of **1** (2.0 g, 3.7 mmol) and *trans*-cyclohexane-1,2-diol (0.8 g, 6.9 mmol) as above gave two isomers of **8a** (490 mg, R_f 0.43, 1 : 1 hexane–ether) and **8b** (470 mg, R_f 0.50) in 21.9 and 21.0% yields, respectively.

8a: syrup, $[\alpha]_D^{22}$ +7.9° (*c* 0.5, $CHCl_3$), ortho ester ^{13}C: 119.1 ppm. Found: C, 75.00; H, 7.11%. Calcd for $C_{40}H_{44}O_7$: C, 75.45; H, 6.97%.

8b: mp 91—93 °C, (prism, petroleum ether), $[\alpha]_D^{22}$ +65° (*c* 0.8, $CHCl_3$), ortho ester ^{13}C: 119.2 ppm. Found: C, 75.43; H, 7.02%. Calcd for $C_{40}H_{44}O_7$: C, 75.45; H, 6.97%.

From the rotational values of **8a** and **8b**, it is deduced that **8a** is the condensation product of (1*R*,2*R*)-cyclohexanediol and **8b** that of (1*S*,2*S*)-isomer.[17]

Methyl 4,6-O-(2,3,4,6-Tetra-O-benzyl-D-glucopyranosylidene)-2,3-di-O-methyl-α-D-glucopyranoside (9). Azeotropic dehydration of **1** (2.0 g, 3.7 mmol) and methyl 2,3-di-*O*-methyl-α-D-glucopyranoside (1.24 g, 5.58 mmol), for 8 h, and purification of the product on a silica-gel column (6 : 1 benzene–ethyl acetate, R_f 0.47) gave **9** in 19.6% (0.54 g) yield. Mp 63—64 °C (prism, peteroleum ether), $[\alpha]_D^{22}$ +93° (*c* 0.92, $CHCl_3$), ortho ester ^{13}C: 110.7 ppm. Found: C, 69.79; H, 6.88%. Calcd for $C_{43}H_{50}O_{11}$: C, 69.52; H, 6.78%.

Methyl 4,6-O-(2,3,4,6-Tetra-O-benzyl-D-glucopyranosylidene)-2,3-di-O-methyl-α-D-mannopyranoside (10). Azeotropic dehydration of **1** (1.0 g, 1.85 mmol) and methyl 2,3-di-*O*-methyl-α-D-mannopyranoside (0.35 g, 1.57 mmol) for 65 h, and purification of the product on a silica-gel column (6 : 1 benzene–ethyl acetate, R_f 0.48), gave **10** (0.10 g) as a syrup in 8.6% yield. $[\alpha]_D^{22}$ +56.4° (*c* 0.5, CH_2Cl_2), ortho ester ^{13}C: 110.9 ppm. Found: C, 69.11; H, 6.98%. Calcd for $C_{43}H_{50}O_{11}$: C, 69.52; H, 6.78%.

1,2 : 3,4-Di-O-(2,3,4,6-tetra-O-benzyl-D-glucopyranosylidene)-erythritol (11). Azeotropic dehydration of **1** (1.5 g, 2.77 mmol) and erythritol (1.3 g, 10.6 mmol) for 24 h gave only one product (9 : 1 benzene–ethyl acetate, R_f 0.30) in 61.7% (1.05 g) yield. Mp 69—74 °C $[\alpha]_D^{22}$ +53° (*c* 0.3, $CHCl_3$), ortho ester ^{13}C: 121.9 ppm. Found: C, 73.95; H, 6.38%. Calcd for $C_{72}H_{74}O_{14}$: C, 74.34; H, 6.41%.

Methyl 2,3-O-(2,3,4,6-Tetra-O-benzyl-D-glucopyranosylidene)-4,6-di-O-methyl-α-D-mannopyranoside (12). Azeotropic dehydration of **1** (1.5 g, 2.77 mmol) and methyl 4,6-di-*O*-methyl-α-D-mannopyranoside (1.5 g, 6.75 mmol), and purification of the product on a silica-gel column (1 : 1 hexane–ether, R_f 0.42) gave a syrup (40 mg) in 0.15% yield. Syrup, ortho ester ^{13}C: 119.1 and 120.5 ppm. Found: C, 69.15; H, 6.62%. Calcd for $C_{43}H_{50}O_{11}$: C, 69.52; H, 6.78%.

One of us (J.Y.) is grateful to the Ministry of Education, Science and Culture, Japan, for a Scientific Research Grant-in-Aid (No. 347023).

References

1) A. K. Ganguly, "Topics in Antibiotic Chemistry," ed by P. G. Sammes, Wiley, New York (1978), Vol. 2, p. 59.

2) W. D. Ollis, C. Smith, and D. E. Wright, *Tetrahedron*, **35**, 105 (1979).

3) N. Neuss, K. F. Koch, B. B. Molloy, W. Day, L. L. Huckstep, D. E. Dorman, and J. D. Roberts, *Helv. Chim. Acta*,

53, 2314 (1970), and papers cited therin.

4) a) S. Kondo, K. Iinuma, H. Naganawa, M. Shimura, and Y. Sekizawa, *J. Antibiotics*, **28**, 79 (1975); b) M. Shimura, Y. Sekizawa, K. Iinuma, H. Naganawa, and S. Kondo, *Agric. Biol. Chem.*, **40**, 611 (1976); c) M. Shimura, Y. Sekizawa, K. Iinuma, H. Naganawa, and S. Kondo, *J. Antibiotics*, **28**, 83 (1975).

5) J. Shoji, S. Kozuki, M. Miyama, Y. Kawamura, and K. Matsumoto, *J. Antibiotics*, **23**, 291 (1970).

6) S. Inouye, T. Shomura, H. Watanabe, K. Totsugawa, and T. Niida, *J. Antibiotics*, **26**, 374 (1973).

7) a) E. Pacsu, *Adv. Carbohydr. Chem.*, **1**, 77 (1945); b) S. S. Bhattacharjee and P. A. J. Gorin, *Carbohydr. Res.*, **12**, 57 (1970).

8) A. K. Ganguly, O. Z. Sarre, A. T. McPhall, and R. W. Miller, *J. Chem. Soc., Chem. Commun.*, **1979**, 22.

9) J. Yoshimura and M. Tamaru, *Carbohydr. Res.*, **72**, C9 (1979).

10) H. Kuzuhara and H. G. Fletcher, Jr., *J. Org. Chem.*, **32**, 2531 (1967).

11) K. Bodenbenner, *Ann. Chem.*, **623**, 611 (1959).

12) R. A. Lemahieu and R. W. Kierstead, *Tetrahedron Lett.*, **1970**, 5111.

13) E. Vischer and T. Reichstein, *Helv. Chim. Acta.*, **27**, 1332 (1944).

14) G. J. Robertson and C. F. Griffith, *J. Chem. Soc.*, **1935**, 1193.

15) J. W. H. Oldham and J. K. Rutherford, *J. Am. Chem. Soc.*, **54**, 366 (1932).

16) G. J. Robertson, *J. Chem. Soc.*, **1934**, 330.

17) D. M. Jerina, H. Ziffer, and W. Daly, *J. Am. Chem. Soc.*, **92**, 1056 (1970).

The *in Situ*-generated Nickel(0)-catalyzed Reaction of Aryl Halides with Potassium Iodide and Zinc Powder

Kentaro TAKAGI,* Naomi HAYAMA, and Saburo INOKAWA†
College of Liberal Arts and Science, Okayama University, Tsushima, Okayama 700
(Received April 12, 1980)

The *in situ*-generated nickel(0) species, presumably atomic nickel, from nickel(II) salt and zinc powder has been proved to be an effective catalyst for the Finkelstein-type displacement reaction of aryl bromides with potassium iodide to give aryl iodides under mild conditions. This species was also effective for the Ullmann-type coupling of bromides or aryl iodides by the use of zinc powder to give biaryls. Furthermore, in the presence of excess nickel(II) salt, the coupling reaction proceeded smoothly, even at an ambient temperature, to give various biaryls in very good yields.

The chemistry of activated metal species has attracted much attention recently from the standpoint of their great affinity for various substrates, including aryl halides.[1] We have found that nickel(II) salt was readily reduced to elemental nickel with zinc powder in the presence of potassium iodide in hexamethylphosphoric triamide (HMPA). On the other hand, if the reaction was conducted in the presence of aryl halides, such as aryl bromides or aryl iodides, aryl iodides and/or biaryls were produced instead of elemental nickel. This implied that not only a Finkelstein-type displacement reaction (Eq. 1),[2] but also an Ullmann-type coupling reaction using zinc powder (Eq. 2)[3] took place, with the aid of the nickel catalyst, with otherwise inert substrates:

$$ArBr + KI \xrightarrow{Ni^0} ArI + KBr \quad (1)$$

$$2ArI + Zn \xrightarrow{Ni^0} Ar_2 + ZnI_2 \quad (2)$$

Here in this paper, we will report the detailed results of the facile synthesis of aryl iodides or biaryls from aryl halides by means of *in situ*-generated nickel(0) species.[4]

Results and Discussion

Synthesis of Aryl Iodides from Aryl Bromides. At the beginning of this study, some attempts were made to seek a favorable system for the catalytic displacement reaction of bromobenzene with potassium iodide under mild conditions. The results are shown in Table 1. *In situ*-generated nickel(0) species from nickel(II) salt and zinc powder[5] exhibited a great reactivity among the catalysts examined.[6] Some preformed nickel(0) complexes were also reactive catalysts, but preformed elemental nickel exhibited little reactivity. HMPA was the most suitable solvent. Nickel(II) complexes revealed reactivities only at such an elevated temperature as 140 °C.

The results from various aryl bromides with *in situ*-generated nickel(0) species are listed in Table 2. Aryl bromides containing a meta or para substituent afforded the corresponding aryl iodides in fair yields, accompanied by rather large quantities of biaryls. Aryl bromides containing an ortho electron-withdrawing substituent and aryl chlorides were less reactive, and in such runs elemental nickel soon appeared.

Further investigations were undertaken to improve the selectivity (aryl iodide/(aryl iodide+biaryl) ratio); the results are listed in Table 3 and Fig. 1. Table 3 shows that the selectivity depends on the amount of zinc powder: a decreased amount of zinc powder is favorable, but it simultaneously reduces the conversion. Figure 1 shows that biaryl is produced consecutively from aryl bromide *via* aryl iodide and that the transformation of aryl iodide into biaryl proceeds in preference to the desired transformation of aryl bromide into aryl iodide near the end of the reaction. Therefore, in order to enhance the selectivity, the reaction must be interrupted prior to reaching completion.

From the viewpoint of synthetic utility, a nickel(II)-catalyzed displacement reaction at elevated temperatures might bepreferable to a nickel(0)-catalyzed one, since, in the former case, the resulting product is not contaminated with any biaryl (Runs 39 and 40 and Table 1).

Synthesis of Biaryls from Aryl Iodides. The above-mentioned displacement reaction with the aid of *in situ*-generated nickel(0) species was accompanied by a coupling reaction which probably consumed the zinc powder, judging from the results in Table 3. Then, in the presence of an adequate amount of zinc powder,

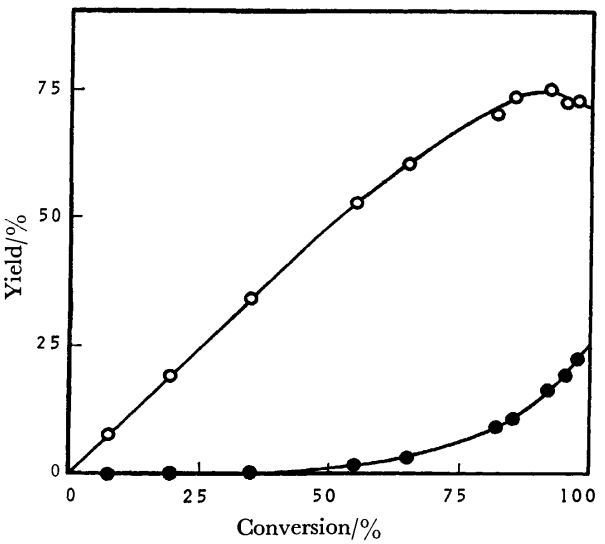

Fig. 1. Plots of conversion of bromobenzene *vs.* yield of iodobenzene or biphenyl.
—○—: Iodobenzene, —●—: biphenyl.

† Department of Chemistry, Faculty of Science, Okayama University, Tsushima, Okayama 700.

TABLE 1. EFFECTS OF VARIOUS CONDITIONS ON THE NICKEL-CATALYZED DISPLACEMENT OF BROMOBENZENE WITH POTASSIUM IODIDE[a]

Run	Catalyst	Solvent	Temp °C	Time h	Conv[b] %	Yield[b] %
1	$NiBr_2$	DMF[c]	150	24	38	34(0)
2	$NiBr_2$–PBu_3[d]	DMF	150	3	95	88(0)
3	$NiBr_2$–PEt_3[e]	DMF	150	3	59	51(0)
4	$NiBr_2$–NBu_3[f]	DMF	150	3	57	51(0)
5	$NiBr_2$–PCy_3[g]	DMF	150	3	24	19(0)
6	$NiBr_2$–TMED[h]	DMF	150	3	12	12(0)
7	$NiBr_2$–PBu_3	NMP[i]	150	3	91	89(0)
8	$NiBr_2$–PBu_3	NMP	180	3	89	87(0)
9	$NiBr_2$–PBu_3	NMP	150	1	77	76(0)
10	$NiBr_2$–PBu_3	TMU[j]	150	1	63	58(0)
11	$NiBr_2$–PBu_3	DMAc[k]	150	1	59	56(0)
12	$NiBr_2$–PBu_3	PC[l]	150	1	58	53(0)
13	$NiBr_2$–PBu_3	HMPA	150	1	31	25(0)
14	$NiBr_2$–PBu_3	DGDE[m]	150	1	10	10(0)
15	$NiBr_2$–PBu_3	DMSO[n]	150	1	7	0(0)
16	$NiBr_2$–PBu_3	DMF	140	12	93	89(0)
17	$NiBr_2$–PBu_3	DMF	80	12	—[o]	0(0)
18	Ni[p]	HMPA	50	1.5	96	77(15)
19	Ni	NMP	50	1.5	87	59(30)
20	Ni	DMF	50	1.5	38	36(2)
21	Ni	Pyridine	50	1.5	—[o]	6(0)
22	Ni	THF[q]	50	1.5	—[o]	4(0)
23	Ni	AN[r]	50	1.5	—[o]	1(0)
24	$Ni(COD)_2$	HMPA	50	4	60	52(8)
25	$Ni(PPh_3)_3$	HMPA	50	4	20	10(10)
26	Ni-$[P(OPh)_3]_4$	HMPA	50	4	—[o]	0(0)
27	Ni–PBu_3	HMPA	50	3	80	74(5)
28	Ni-$P(OBP)_3$[s]	HMPA	50	3	35	33(3)

a) The molar ratios of the components were as follows: PhBr/$NiBr_2$/Ligand/KI = 1.0/0.025/0.050/3.0 for Runs 1—17. PhBr/$NiBr_2$/Zn/Ligand(when used)/KI = 1.0/0.02/0.17/0.04/2.5 for Runs 18—23, 27, and 28. PhBr/Ni/KI = 1.0/0.05/2.5 for Runs 24—26. The reactions were carried out on a 0.5—1.0 mmol scale under nitrogen. b) GLC analysis using internal standards. Yields based on bromobenzene. Yields in parentheses were those of biphenyl. c) DMF = *N*,*N*-dimethylformamide. d) PBu_3 = tributylphosphine. e) PEt_3 = triethylphosphine. f) NBu_3 = tributylamine. g) PCy_3 = tricyclohexylphosphine. h) TMED = *N*,*N*,*N*′,*N*′-tetramethylethylenediamine. i) NMP = *N*-methyl-2-pyrrolidone. j) TMU = tetramethylurea. k) DMAc = *N*,*N*-dimethylacetamide. l) PC = propylene carbonate. m) DGDE = diethylene glycol dimethyl ether. n) DMSO = dimethyl sulfoxide. o) Not determined. p) Ni = *in situ*-generated nickel from nickel(II) bromide and zinc powder. q) THF = tetrahydrofuran. r) AN = acetonitrile. s) $P(OBP)_3$ = tris(2-biphenylyl)phosphite.

TABLE 2. CATALYTIC SYNTHESIS OF ARYL IODIDES[a]

Run	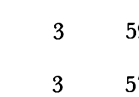 X	Y	Time h	Aryl iodide[b] %	Biaryl[b] %
18	Br	H	1.5	77	15
29	Br	4-OCH_3	1.5	78	16
30	Br	4-$COCH_3$	1.5	76	22
31	Br	4-Cl	1.5	81	9
32	Br	4-NO_2	1.5	0	0
33	Br	3-CO_2CH_3	5	81	11
34	Br	2-CH_3	3	66	23
35	Br	2-OCH_3	1.5	47	6
36	Br	2-CO_2CH_3	4	0	9
37	Cl	H	20	0	0
38	Cl	4-$COCH_3$	20	0	0
39	Br	4-OCH_3	2	(80)	
40	Br	4-$COCH_3$	2	(66)	

a) Conditions of Runs 29—38 were same as those of Run 18. Conditions of Runs 39 and 40 were same as those of Run 2, except for the reaction temperature of 153 °C. b) GLC analysis using internal standards. Yields based on aryl halides. Yields in parentheses were isolated ones.

TABLE 3. EFFECT OF ZINC POWDER ON PRODUCT DISTRIBUTION[a]

Run	Zn/$NiBr_2$ molar ratio	Time h	Conv[b] %	PhI/Ph–Ph[b] molar ratio	Ph–Ph[c] %
41	0	12	0	—	—
42	1	12	92	44	100
43	3	12	98	14	100
44	7	5	99	6	86
45	75	3	100	0.15	60

a) Conditions were same as those of Run 18, except for the amount of Zn powder. b) GLC analysis using internal standards. c) Yields based on Zn powder.

the Ullmann-type coupling of aryl iodides by the use of zinc powder (Eq. 2) was considered feasible. Actually, the coupling reaction proceeded smoothly under mild conditions with the aid of *in situ*-generated nickel(0) species.

The results from various aryl iodides are listed in Table 4. The reaction mixture was green during the reaction, but it turned black near the end of the reaction. A stoichiometric amount of zinc powder sufficed for the reaction, but the use of excess zinc powder was desirable. The presence of potassium iodide promoted the reaction efficiently.[7] Preformed elemental nickel exhibited little reactivity for this reaction, either. Aryl iodides containing a meta or para substituent afforded

Table 4. Catalytic synthesis of biaryls[a]

Run	X	Y	Time h	Yield[b] %
46	I	H	3.5	94
47[c]	I	H	3.5	(98)
48[d]	I	H	3.5	(0)
49	I	4-$COCH_3$	3	98
50	I	4-CH_3	10	92
51	I	4-OCH_3	30	87
52	I	4-NO_2	3	0
53	I	3-CO_2CH_3	3	96
54	I	2-CH_3	7	83
55	I	2-Cl	17	(25)[e]
56	I	2-CO_2CH_3	10	(22)[f]
57[g]	Br	H	7	(98)
58	Cl	H	7	(0)

a) Molar ratio of the components was as follows: ArX/Zn/$NiBr_2$/KI=1.0/1.25—1.85/0.025/1.25. The reaction was carried out on a 0.4—10 mmol scale in HMPA at 50 °C under nitrogen. b) Isolated Yields. Yields in parentheses were determined by GLC. c) PhI/Zn/$NiBr_2$/KI=1.0/0.6/0.05/1.25. d) KI was not added. e) Chlorobenzene 39%. f) Methyl benzoate 67%. g) Two times as much KI was used.

Table 5. Biaryl synthesis at ambient temperature[a]

Run	Y	Z	Time h	Yield[b] %
59	H	H	8	100
60	2-CO_2CH_3	H	6	95
61[c]	2-CO_2CH_3	H	7	28
62	2-CO_2CH_3	4-CH_3	28	(98)
63	2-$COCH_3$	H	6	96(68)[d]
64[e]	2-Cl	H	3.5	84(59)[f]
65[e]	2-CF_3	H	6	75(29)[g]

a) Molar ratio of the components was as follows: ArI/$NiCl_2$/Zn/KI=1.0/1.1/1.0/1.25. The reactions were carried out on a 0.4—8 mmol scale in HMPA at 20 °C under nitrogen. b) GLC analysis using internal standards. Yields in parentheses were isolated ones. c) $PdCl_2$ was used in the place of $NiCl_2$. d) Reaction for 16 h. e) Reaction at 35 °C. f) Reaction at 20 °C for 18 h. g) Reaction at 20 °C for 100 h.

the corresponding biaryls in good yoelds. Biaryls were also produced from aryl bromides under conditions almost identical with those in aryl iodides: this is clearly due to the rapid formation of aryl iodide from aryl bromide under this catalyst system.

Aryl iodides containing an ortho electron-withdrawing substituent afforded large quantities of dehaloprotonated products, which probably arose from organozinc compounds,[8] by-products of the combination of aryl iodides and zinc powder, upon an aqueous workup. The addition of palladium(II) or nickel(II) salt to a prepared mixture including organozinc compounds afforded the biaryls containing electron-withdrawing substituents at the 2,2′-positions, presumably *via* the well-known transfer of organo groups from zinc(II) to palladium(II) or nickel(II).[9,10] A convenient

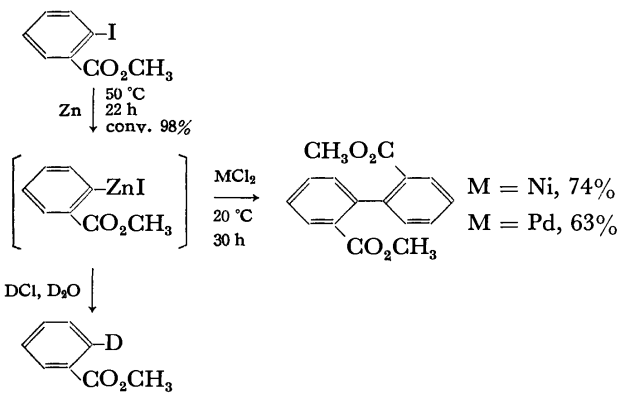

batch method could be used for the system. That is, in the presence of excess nickel(II) salt, the coupling reaction proceeded smoothly even at an ambient temperature to give various biaryls in very good yields. The results are shown in Table 5. The intermediate use of organozinc compounds in these reactions was, however, omitted on the basis of the fact that the reaction between aryl iodides and zinc powder was by far slower than the present coupling reaction.[11]

Reaction Path. The results and discussion presented above lead to the following equations as the most plausible sequences of the reaction. The atomic nickel which comes from nickel(II) salt and zinc powder (Eq. 3) readily reacts with aryl halide (bromide

$$NiX_2 + Zn \longrightarrow Ni + ZnX_2 \quad (3)$$

$$Ni + ArBr \rightleftarrows \underset{\mathbf{1}}{Ar\text{–}Ni\text{–}Br} \quad (4)$$

$$Ar\text{–}Ni\text{–}Br + KI \rightleftarrows \underset{\mathbf{2}}{Ar\text{–}Ni\text{–}I} + KBr \quad (5)$$

$$Ar\text{–}Ni\text{–}I \rightleftarrows ArI + Ni \quad (6)$$

$$2Ar\text{–}Ni\text{–}I \rightleftarrows \underset{\mathbf{3}}{Ar\text{–}Ni\text{–}Ar} + NiI_2 \quad (7)$$

$$Ar\text{–}Ni\text{–}Ar \longrightarrow Ar_2 + Ni \quad (8)$$

or iodide) to give an oxidative-addition adduct, **1** or **2** (Eqs. 4 and 6).

In a catalytic displacement reaction, the metathetical replacement of **1** with potassium iodide produces another organonickel(II) species **2** (Eq. 5), which subsequently yields aryl iodide and regenerates the atomic nickel to ensure the catalytic reaction (Eq. 6). This is the well-known sequence of oxidative addition, metathesis, and reductive elimination in transition metal chemistry.[12] It is noteworthy that the equilibrium in Eq. 5 is presumed to lie so far to the right, because the concentration of potassium iodide is much higher than that of potassium bromide in our solvent (see Experimental).[13]

In a coupling reaction, the disproportionation of **2** takes place to give nickel(II) salt and a diorganonickel(II) species, **3** (Eq. 7), which subsequently yields biaryl (Eq. 8). This type of decomposition is well-established and is not catalytic by nature.[14] To ensure the catalytic

cycle, the original atomic nickel must be regenerated from the nickel(II) salt thus formed, and then zinc powder in at least a stoichiometric quantity is required.

Some aryl halides, such as aryl chlorides, or aryl bromides and aryl iodides containing an ortho electron-withdrawing substituent, do not undergo either reaction. Presumably, these aryl halides can not trap a generated atomic nickel efficiently; consequently, they condense to form a slurry that no longer exhibits reactivity, even for reactive aryl halides, as has been described above.

Experimental

All reagents were used directly as obtained commercially, unless otherwise noted. The solvents were distilled under nitrogen and were dried over a molecular sieve (3A). The $RhCl(PPh_3)_3$[15] and $Ni[P(OPh)_3]_4$[16] were prepared by previously reported methods. Some aryl iodides were prepared according to a procedure in the literature.[17] The ^1H NMR spectra were obtained on JOEL PMX 60 apparatus. A Hitachi 160 gas chromatograph was used for the GLC analyses.

Reduction of Nickel(II) Chloride by Zinc Powder. A mixture of zinc powder (65 mg, 1.0 mmol), nickel(II) chloride (38 mg, 0.3 mmol), potassium iodide (83 mg, 0.5 mmol), and HMPA (0.5 ml) was evacuated, flushed with nitrogen, and kept at 20 °C with stirring. The initial blue-green solution gradually turned black. After 10 h, the resulting black solid was filtered off and washed with aqueous ammonia and water until the wash was free of the nickel(II) ion. The amount of elemental nickel was determined by the dimethylglyoxime method, which showed that 93% of the nickel(II) chloride had been reduced to elemental nickel.

Preparation of Aryl Iodides. *Preparation of* p-*Iodoanisole*: A mixture of *p*-bromoanisole (0.32 ml, 2.5 mmol), potassium iodide (2.07 g, 12 mmol), a 0.17 mol dm^{-3}-DMF solution of nickel(II) bromide (0.59 ml, 0.10 mmol), tributylphosphine (0.059 ml, 0.20 mmol), and DMF (1.90 ml) was heated to reflux for 2 h with stirring under nitrogen. To the resulting mixture, aqueous sodium chloride (20 ml) was added, and the organic materials, extracted with three 10-ml portions of pentane, were washed successively with three 5- ml portions of concd hydrochloric acid, aqueous sodium chloride (15 ml), aqueous sodium carbonate (15 ml), and aqueous sodium thiosulfate (15 ml), and then dried over anhydrous sodium sulfate. The evaporation of the solvent gave 0.52 g of crude *p*-iodoanisole (87%). Recrystalization from hexane gave the pure iodide. Mp 47—48 °C (lit,[18] 51—52 °C). Found: C, 35.68; H, 3.04%. Calcd for C_7H_7IO: C; 35.92; H, 3.01%. p-*Iodoacetophenone*: Mp 83.5—84 °C (lit,[19] 85 °C). Found: C, 39.21; H, 2.88%. Calcd for C_8H_7IO: C, 39.05; H 2.87%.

Preparation of Biaryls. *Preparation of Dimethyl 3,3'-Biphenyldicarboxylate*: A mixture of methyl *m*-iodobenzoate (524 mg, 2 mmol), a 0.17 mol dm^{-3}-DMF solution of nickel(II) bromide (0.30 ml, 0.05 mmol), zinc powder (164 mg, 2.5 mmol), potassium iodide (415 mg, 2.5 mmol), and HMPA (2.2 ml) was frozen at −78 °C, evacuated, flushed with nitrogen, and then kept at 50 °C for 3 h with stirring. To the resulting mixture, dilute hydrochloric acid (0.4 mol dm^{-3}, 16 ml) was added, and the organic materials, extracted with 15-ml portions of ether–dichloromethane (7 : 1), were washed with aqueous sodium sulfite (15 ml) and three 15-ml portions of aqueous sodium chloride, and dried over anhydrous sodium sulfate. The subsequent evaporation of the solvent gave 260 mg of crude dimethyl 3,3'-biphenyldicarboxylate (96%). Recrystalization from ether gave the pure biaryl. Mp 103—103.5 °C (lit,[20] 104 °C). Found: C, 70.93; H, 5.13%. Calcd for $C_{16}H_{14}O_4$: C, 71.10; H, 5.22%.

Biphenyl: Mp 68—69 °C (lit,[21] 71 °C). Found: C, 92.90; H, 6.48%. Calcd for $C_{12}H_{10}$: C, 93.46; H, 6.54%.

4,4'-Dimethylbiphenyl: Mp 117.5—119 °C (lit,[22] 121 °C). Found: C, 91.96; H, 7.85%. Calcd for $C_{14}H_{14}$: C, 92.26; H, 7.74%.

4,4'-Dimethoxybiphenyl: Mp 169—171 °C (lit,[23] 173 °C). Found: C, 78.36; H, 6.60%. Calcd for $C_{14}H_{14}O_2$: C, 78.48; H, 6.59%.

4,4'-Diacetylbiphenyl: Mp 191—192 °C (lit,[24] 192 °C). Found: C, 80.62; H, 5.91%. Calcd for $C_{16}H_{14}O_2$: C, 80.65, H, 5.92%.

2,2'-Dimethylbiphenyl: Bp 69 °C/67 Pa (lit,[25] 258 °C/98400 Pa). Found: C, 92.31; H, 7.79%. Calcd for $C_{14}H_{14}$: C, 92.26; H, 7.74%.

Preparation of Dimethyl 4,4'-Dimethyl-2,2'-biphenyldicarboxylate: A mixture of methyl 2-iodo-5-methylbenzoate (1.32 ml, 8 mmol), nickel(II) chloride (1.16 g, 9 mmol), zinc powder (1.04 g, 16 mmol), potassium iodide (1.66 g, 10 mmol), and HMPA (10 ml) was evacuated, flushed with nitrogen, and kept at 20 °C for 28 h with stirring. To the resulting mixture, aqueous sodium chloride (80 ml) was added, and the organic materials, extracted with two 60-ml portions of ether, were washed with four 120-ml portions of aqueous sodium chloride and then dried over anhydrous sodium sulfate. The subsequent evaporation of the solvent gave a crude dimethyl 4,4'-dimethyl-2,2'-biphenyldicarboxylate, which was triturated with a small amount of hexane to leave 1.10 g of the pure biaryl (98%). Mp 90—91 °C. Found: C, 72.29; H, 6.00%. Calcd for $C_{18}H_{18}O_4$: C, 72.46; H, 6.08%.

2,2'-Dichlorobiphenyl: Mp 54—55 °C (lit,[26] 59 °C). Found: C, 64.52; H, 3.45%. Calcd for $C_{12}H_8Cl_2$: C, 64.60; H, 3.61%.

2,2'-Diacetylbiphenyl: Mp 90.5—91.°C (lit,[27] 93—94 °C). Found: C, 80.57; H, 5.79%. Calcd for $C_{16}H_{14}O_2$: C, 80.65; H, 5.92%.

2,2'-Bis(trifluoromethyl)biphenyl: Bp 119—121 °C/2130 Pa (lit,[28] 236—237 °C). NMR: 7.1—7.9 (*m*).

Reaction of Methyl o-*Iodobenzoate with Zinc Powder.* A mixture of methyl *o*-iodobenzoate (0.059 ml, 0.4 mmol), zinc powder (52 mg, 0.8 mmol), potassium iodide (83 mg, 0.5 mmol), and HMPA (0.5 ml) was stirred at 50 °C for 22 h under nitrogen. To the resulting mixture, dilute hydrochloric acid was added, and the organic materials were extracted with ether. Subsequent analysis by GLC revealed the presence of 53 mg (0.39 mmol) of methyl benzoate. Atmospheric oxygen inhibited the reaction completely. A similar work-up by means of deuterium oxide–hydrochloric acid-d_1 gave methyl benzoate-d_1. NMR: 7.85—8.07 (*m*, 1H), 7.15—7.62 (*m*, 3H), 3.87 (s, 3H). Found: C, 69.97; H, 5.91%. Calcd for $C_8H_7DO_2$: C, 70.06; H, 5.84%.

An alternative treatment of the resulting mixture with palladium(II) chloride (177 mg, 1.0 mmol) at 20 °C for 30 h under nitrogen, followed by GLC analysis, gave 35 mg (0.13 mmol) of dimethyl 2,2'-biphenyldicarboxylate (63%) and 16 mg (0.12 mmol) of methyl benzoate (30%).

Solubility of Potassium Iodide or Potassium Bromide in HMPA–DMF. After a suspension of potassium iodide (9.0 g, 54 mmol) or potassium bromide (6.4 g, 54 mmol) in HMPA–DMF (22 : 3, 10 ml) has been stirred at 50 °C for 1.5 h, the concentration of the iodide ion or the bromide ion in the solution was determined by the Mohr method. One liter of mixed solvents dissolved about 0.11 mol of potassium iodide or 0.001 mol of potassium bromide respectively.

References

1) K. J. Klabunde, *Angew. Chem. Int. Ed. Engl.*, **14**, 287 (1975); R. D. Rieke, *Acc. Chem. Res.*, **10**, 301 (1977); V. M. Akhmedov, M. T. Anthony, M. L. H. Green, and D. Young, *J. Chem. Soc., Chem. Commun.*, **1974**, 777; R. D. Rieke, W. J. Wolf, and N. Kujndzic, *J. Am. Chem. Soc.*, **99**, 4159 (1977); R. D. Rieke, A. V. Kavaliunas, L. D. Rhyne, and D. J. J. Fraser, *ibid.*, **101**, 246 (1979); A. A. Millard and M. W. Rathke, *ibid.*, **99**, 4833 (1977).

2) For this type of displacement reaction of non-activated aryl halides, copper(I) salts are generally used as the source of halide ions, but aryl iodides are not obtained from the reaction: C. A. Ruehler and D. E. Pearson, "Survey of Organic Syntheses," Wiley, New York (1970), p. 339; R. G. R. Bacon and H. A. O. Hill, *J. Chem. Soc.*, **1964**, 1097.

3) A. S. Kende, L. S. Liebeskind, and D. M. Braitsch, *Tetrahedron Lett.*, **1975**, 3375; M. Zembayashi, K. Tamao, J. Yoshida, and M. Kumada, *ibid.*, **1977**, 4098.

4) For preliminary communications on a portion of this work, see K. Takagi, N. Hayama, and T. Okamato, *Chem. Lett.*, **1978**, 191; K. Takagi, N. Hayama, and S. Inokawa, *ibid.*, **1979**, 917.

5) No catalytic reaction occurred when Cr powder, Mn powder, or Na(Hg) was used in place of Zn powder.

6) No reaction occurred when other complexes, such as $(PPh_3)_2PdCl_2$, $(dibenzylideneacetone)_3Pd_2(CHCl_3)$, $(PPh_3)_2$-RhCl, $(PPh_3)_3RuCl_2$, or CuBr–$2PBu_3$, were used in place of nickel complexes. *Cf.* R. Cramer and D. R. Coulson, *J. Org. Chem.*, **40**, 2267 (1975).

7) The exact role of the iodide ion remains to be clarified. One assumption is that the coordination of the iodide ion to the atomic nickel facilitates the oxidative addition of aryl halides by increasing the electron density of the atomic nickel: T. T. Tsou and J. K. Kochi, *J. Am. Chem. Soc.*, **101**, 6319 (1979); D. Forster, *ibid.*, **97**, 951 (1975). See also M. Zembayashi, K. Tamao, J. Yoshida, and M. Kumada, *Tetrahedron Lett.*, **1977**, 4098.

8) The direct synthesis of organozinc compounds from aryl iodides and zinc powder has been believed to be difficult: C. W. Blewett, R. Schmid, and H. Zimmer, "Methodicum Chimicum," ed by K. Niedenzu and H. Zimmer, Academic Press, New York (1976), Vol. 8, p. 36; R. D. Rieke, S. J. Uhm, and P. M. Hudnall, *J. Chem. Soc., Chem. Commun.*, **1973**, 269.

9) E. Negishi, N. Okukado, A. O. King, and D. E. Vanhorn, *J. Am. Chem. Soc.*, **100**, 2254 (1978), and the references cited therein.

10) The preparation of this type of biaryl under mild conditions is somewhat troublesome and difficult; P. F. Fanta, *Synthesis*, **1974**, 9; T. Cohen and I. Cristea, *J. Org. Chem.*, **25**, 3649 (1975); F. E. Ziegler, K. W. Fowler, and S. Kanfer, *J. Am. Chem. Soc.*, **98**, 8282 (1978); M. F. Semmelhack, P. M. Helquist, and L. D. Jones, *ibid.*, **93**, 5908 (1971); A. McKillop, L. F. Elson, and E. C. Taylor, *ibid.*, **90**, 2423 (1968).

11) Only 6% of methyl benzoate was obtained by the reaction of methyl *o*-iodobenzoate with zinc powder at 20 °C for 6 h, followed by an aqueous work-up.

12) R. Noyori, "Transition Metal Organometallics in Organic Synthesis," ed by H. Alper, Academic Press, New York (1976), Vol. 1, p. 112.

13) Both halide ions appear to exhibit comparable reactivities in the reaction of Eq. 5. For example, the rate constants of the reaction of *trans*-$[Ni(PEt_3)_2(o\text{-tolyl})(X)]$ with Y^- to give *trans*-$[Ni(PEt_3)_2(o\text{-tolyl})(Y)]$ are 17.5 $dm^3\ mol^{-1}\ s^{-1}$ for X=Br and Y=I and 34.1 $dm^3\ mol^{-1}\ s^{-1}$ for X=I and Y=Br: M. Cusumano and V. Ricevuto, *J. Chem. Soc., Dalton Trans.*, **1978**, 1682.

14) A. Nakamura and S. Otsuka, *Tetrahedron Lett.*, **1974**, 463; See also T. T. Tsou and J. K. Kochi, *J. Am. Chem. Soc.*, **101**, 7547 (1979).

15) J. A. Osborn and G. Wilkinson, *Inorg. Synth.*, **10**, 67 (1967).

16) J. J. Levison and S. D. Robinson, *J. Chem. Soc., A*, **1970**, 96.

17) F. G. Mann and E. J. Chaplin, *J. Chem. Soc.*, **1937**, 527.

18) F. Reverdin, *Ber.*, **29**, 1000 (1896).

19) R. Schweizer, *Ber.*, **24**, 551 (1891).

20) F. Ullmann and O. Lowenthal, *Justus Liebigs Ann. Chem.*, **332**, 72 (1904).

21) M. Gomberg and W. E. Bachmann, *J. Am. Chem. Soc.*, **46**, 2343 (1924).

22) T. Zincke, *Ber.*, **4**, 396 (1871).

23) F. Ullmann and O. Lowenthal, *Justus Liebigs Ann. Chem.*, **332**, 67 (1904).

24) H. Finger and W. Schott, *J. Prakt. Chem.*, **115**, 289 (1927).

25) F. Ullmann and G. M. Meyer, *Justus Liebigs Ann. Chem.*, **332**, 42 (1904).

26) J. J. Dobbie, J. J. Fox, and A. J. H. Gauge, *J. Chem. Soc.*, **99**, 1619 (1911).

27) D. M. Hall, J. E. Lodbury, M. S. Lesslie, and E. E. Turner, *J. Chem. Soc.*, **1956**, 3475.

28) M. R. Pettit and J. C. Tatlow, *J. Chem. Soc.*, **1954**, 1071.

Synthesis of 2-Formylazulene and Its Derivatives by Oxidative Cleavage of 2-Styrylazulenes

Motoyasu SAITO, Tadayoshi MORITA, and Kahei TAKASE*

Department of Chemistry, Faculty of Science, Tohoku University, Aramaki-aza-Aoba, Sendai 980

(Received April 24, 1980)

2-Formylazulene and its derivatives were prepared by the oxidative cleavage of styrylazulenes with $NaIO_4$–OsO_4. 1,2-Diformyl-, 1,2,3-triformylazulenes, and 5-formylazulene derivative were also synthesized. The reaction of dimethyl 2-methylazulene-1,3-dicarboxylate with *p*-nitroso-*N*,*N*-dimethylaniline in the presence of NaOR (R=Me or Et) gave the corresponding 3-alkoxycarbonyl-2-[*p*-(dimethylamino)phenyliminomethyl]-azulene-1-carboxylic acids followed by hydrolysis with hydrochloric acid to give 3-alkoxycarbonyl-2-formylazulene-1-carboxylic acids. Acetylation of 2-formylazulene-1-carboxylic acids with acetic anhydride gave five membered lactol acetates.

Formylazulenes are useful for synthesizing various azulene derivatives because of their functional formyl groups. Of five possible positional isomers, 1-formylazulene and its derivatives were easily obtained by formylation of azulenes according to the Vilsmeier-Haack method,[1–3] Gatterman reaction,[4] and with use of triethyl orthoformate–tetrafluoroboric acid[5] or perchloric acid,[6] the properties of which have been investigated.[1,2,7] The oxidation of some 1-methylazulenes with selenium dioxide or potassium permanganate also gave 1-formylazulenes.[8,9] However, preparation of the other isomeric formylazulenes is difficult. Sato[10] reported that 2-formylazulene is derived from 2-cyanoazulene by hydrolysis, esterification, reduction with lithium aluminum hydride, and subsequent oxidation of the resulting alcohol with manganese dioxide.

Arnold and Pahls[11] reported that 6-formyl-4,8-dimethylazulene is obtained from ethyl 4,8-dimethylazulene-6-carboxylate by reduction with lithium aluminum hydride, followed by oxidation by means of the Kröhnke-Karrer method. Hafner and Moritz[12] reported that the formylation of some 1,3-dialkylazulenes by the Vilsmeier-Haack method gives 2-formyl- and 5-formyl derivatives, together with 1-formylazulenes. The oxime of 6-formylazulene derivative was obtained by treatment of diethyl 2-amino-6-methylazulene-1,3-dicarboxylate with isopentyl nitrite.[13] This paper describes a useful method of synthesizing 2-formylazulene and its derivatives by oxidative cleavage of 2-styrylazulenes obtained by the condensation of 2-methylazulene derivative with benzaldehyde in good yields.[14]

Results and Discussion

The Lemieux-Johnson oxidation[15] is effective for oxidative cleavage of the ethylenic linkage of 2-styrylazulenes. Thus, on treatment with sodium periodate in aq dioxane in the presence of a catalytic amount of osmium tetroxide, 2-styrylazulenes (**1a—j**) gave the corresponding 2-formylazulenes (**2a—j**), respectively. A lower yield (13%) of the parent 2-formylazulene (**2a**) may be due to its instability: it changes into a brown, hardly soluble substance on being heated or allowed to stand for a long time. The other 2-formylazulene derivatives, having substituents at the 1-(and 3-)positions, are stable and were obtained in good yields.

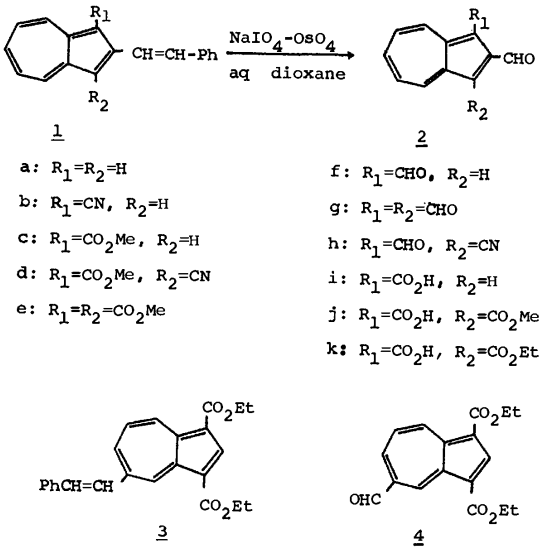

Scheme 1.

1,2-Diformyl[16] and 1,2,3-triformylazulenes (**2f,g,h**), not obtained by formylation of 2-formylazulenes (**2a,b,f**) by means of the Vilsmeier-Haack method, were obtained, in a similar manner, from 1-formyl- and 1,3-diformyl-2-styrylazulenes (**1f,g,h**) which were prepared by formylation of 2-styrylazulenes. The Lemieux-Johnson oxidation could be applied to the synthesis of not only 2-formylazulenes but also 5-formylazulenes. Thus, treatment of diethyl 5-styrylazulene-1,3-dicarboxylate (**3**) obtained by condensation of diethyl 5-methylazulene-1,3-dicarboxylate[17] and benzaldehyde with sodium periodate–osmium tetroxide afforded diethyl 5-formylazulene-1,3-dicarboxylate (**4**). The IR spectra (KBr) of 2-formylazulenes show absorptions corresponding to $\nu_{C=O}$ of the 2-formyl groups within the range 1672—1701 cm^{-1} in somewhat lower frequency region than that (1708—1699 cm^{-1})[18] of benzaldehydes; that of 1-formylazulenes appear in a lower frequency region 1610—1650 cm^{-1}.[7b,8] The electronic spectra of 2-formylazulenes conform to the extended Plattner rule.[19] The NMR spectra of 2-formylazulenes, as expected, show a singlet due to the formyl proton at δ 10—11 ppm, as well as signals due to the other protons. 2-Formylazulenes easily gave carbonyl derivatives, such as oximes and hydrazones, and were converted into the corresponding alcohols or carboxylic acids by reduction

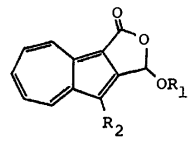

5a: $R_1=R_2=H$

5b: $R_1=H$, $R_2=CO_2Me$

6a: $R_1=COMe$, $R_2=CO_2Me$

6b: $R_1=COMe$, $R_2=CO_2Et$

Fig. 1.

with sodium borohydride or oxidation with silver oxide, respectively. 2-Formylazulene-1-carboxylic acids (**2i,j**) possess a structure analogous to that of *o*-formylbenzoic acid which undergoes cyclization easily into the lactol, and existing as a mixture of ring-chain tautomers, the acid and lactol (13 : 87) in dioxane.[20] In the case of **2i** and **2j**, however, the ring tautomers (**5a,b**) could not be detected by either IR (KBr, $CHCl_3$) or NMR ($CDCl_3$), **2i** and **2j** exist predominantly in the acid chain structure. This can be explained by resonance stabilization of the formyl group at position 2 and also by the larger bond angle between two substituents in **2i** and **2j** than in *o*-formylbenzoic acid. On the other hand, the acetylation of **2j** gave a lactol acetate (**6a**), whose structure was established on the basis of spectral data. The IR (KBr) shows an absorption at 1767 cm^{-1} due to the five-membered lactone, and the NMR spectrum ($CDCl_3$) shows singlets at δ 2.20 ($COCH_3$), 3.90 (OCH_3), and 7.78 ppm (methine), as well as signals due to the ring protons at δ 7.6—8.3 (3H,m), 9.10 (1H, bd), and 9.90 ppm (1H, bd).

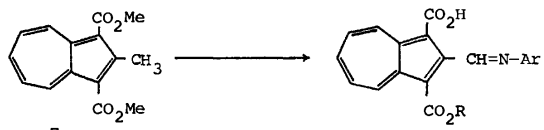

7

8a: R=Me, Ar=p-$(Me)_2NC_6H_5$-

8b: R=Et, Ar=p-$(Me)_2NC_6H_5$-

Scheme 2.

Reactive methyl or methylene groups are convertible into carbonyl groups by condensation with *p*-nitroso-*N,N*-dimethylaniline (**NDA**)[21] and subsequent hydrolysis of the resulting Shiff base. Such a reaction was carried out for synthesizing 2-formylazulenes from 2-methylazulene derivatives directly. The reaction of dimethyl 2-methylazulene-1,3-dicarboxylate (**7**) with **NDA** proceeded easily in the presence of sodium methoxide or ethoxide to give condensation products **8a** and **8b**. Hydrolysis of non-purified **8a** with acid gave an acidic compound identical with **2j**. **8a** could not be isolated in a pure form since it was easily hydrolyzed to **2j**; **8b** was isolated in pure form. Hydrolysis of **8b** gave 3-ethoxycarbonyl-2-formylazulene-1-carboxylic acid (**2k**). Acetylation of **2k** gave a lactol acetate (**6b**). The structures of **8b**, **2k**, and **6b** were established on the basis of spectral data (IR and NMR).

The fact that **8b** is acidic enough to be soluble in aq $NaHCO_3$ solution also supports the half ester structure of **8b**. The mechanism of the formation of the half ester **8b** is assumed to be similar to that of the formation of the half ester of 2-styrylazulene-1,3-dicarboxylic acid by condensation of **7** and benzaldehyde.[14]

Experimental

All melting points were determined in a capillary and are uncorrected. Electronic spectra were measured on a Hitachi EPS-3 spectrometer, and IR spectra on a Shimadzu IR-27 infracord, and NMR spectra on a Varian A-60 spectrometer in $CDCl_3$ containing TMS.

General Procedure for the Oxidation of 2-Styrylazulenes to 2-Formylazulenes. Finely ground $NaIO_4$ (2—4 molar equivalents) was added in portions to a stirred solution of 2-styrylazulenes and OsO_4 (1—2% by weight) dissolved in aq dioxane (dioxane : H_2O=7 : 3) at room temp over a period of 30—60 min. Stirring was continued for 4—8 h. The reaction mixture was diluted with water and extracted with $CHCl_3$, the extract being washed with H_2O and dried over Na_2SO_4. After evaporation of the solvent the residue was chromatographed over a silica-gel column and eluted with benzene. The first colorless effluent gave benzaldehyde, the second and third colored portions giving 2-styrylazulenes and 2-formylazulenes, respectively.

2-Formylazulene (2a). 2-Styrylazulene (**1a**) (460 mg, 2 mmol) was treated according to the general procedure to give **1a** (30 mg) and **2a** (40 mg, 13% yield) as blue scales (from cyclohexane), mp 62—63 °C (reported[10] mp 63 °C); IR (KBr): 1675 cm^{-1}; $\lambda_{max}^{cyclohexane}$ 244 nm (log ε 4.23), 275 sh (4.50), 288 (4.69), 296 (4.70), 335 (3.68), 346 (3.72), 360 (3.80), 613 (2.61), 664 (2.19); NMR ($CDCl_3$): δ 7.13 (br t, J=10 Hz, H-5,7), 7.67 (br t, J=10 Hz, H-6), 7.70 (s, H-1,3), 8.42 (br d, J=10 Hz, H-4,8), 10.37 (s, CHO). Found: C, 84.63; H, 5.23%. Calcd for $C_{11}H_8O$: C, 84.59; H, 5.16%.

Phenylhydrazone: Green needles (from benzene), mp 197 °C. Found: C, 82.63; H, 5.80; N, 11.08%. Calcd for $C_{17}H_{14}N_2$: C, 82.90; H, 5.73; N, 11.37%.

1-Cyano-2-formylazulene (2b). 1-Cyano-2-styrylazulene (**1b**) (2.25 g, 10 mmol) was treated according to the general procedure to give **1b** (340 mg) and **2b** (1.17 g, 75% yield) as green needles (from benzene), mp 184—185 °C; IR (KBr): 1686, 2217 cm^{-1}; λ_{max}^{MeOH} 233 nm (log ε 4.25), 287 (4.57), 298 (4.79), 345 (3.69), 362 (3.64); NMR ($CDCl_3$): δ 7.2—7.8 (m, H-5,7), 7.96 (br t, J=9 Hz, H-6), 8.58 (br t, J=11 Hz, H-4), 8.78 (br d, J=11 Hz, H-8), 10.48 (s, CHO). Found: C, 79.59; H, 3.80; N, 7.60%. Calcd for $C_{12}H_7ON$: C, 79.55; H, 3.89; N, 7.73%.

Oxime: Brown blue crystals (from $CHCl_3$), mp 264—266 °C. Found: 73.78; H, 3.66; N, 13.92%. Calcd for $C_{12}H_8O_2N_2$: C, 73.46; H, 4.11; N, 14.28%.

Hydrazone: Green crystals (from benzene), mp over 300 °C. Found: C, 73.78; H, 4.46; N, 21.00%. Calcd for $C_{12}H_9N_3$: C, 73.83; H, 4.65; N, 21.53%.

p-*(Dimethylamino)phenylimino Derivative*: Reddish brown crystals (from benzene–cyclohexane), mp 194—196 °C. Found: C, 79.89; H, 5.58; N, 13.88%. Calcd for $C_{20}H_{17}N_3$: C, 80.24; H, 5.72; N, 14.04%.

Methyl 2-Formylazulene-1-carboxylate (2c). Methyl 2-styrylazulene-1-carboxylate (**1c**) (1.30 g, 4.5 mmol) was treated in the usual way to give **1c** (130 mg) and **2c** (560 mg, 64% yield) as green needles (from ethanol), mp 119—120 °C; IR (KBr): 1701, 1678 cm^{-1}; λ_{max}^{MeOH} 238 nm (log ε 4.32), 291

(4.61), 301 (4.68), 335 sh (3.79), 350 (3.84), 369 (3.75), 573 (2.98), 606 (3.02), 650 sh (2.70); NMR ($CDCl_3$): δ 3.98 (s, OCH_3), 7.2—7.6 (m, H-5, 7), 7.63 (s, H-3), 7.83 (tm, J=9 Hz, H-6), 8.47 (br d, J=10 Hz, H-4), 9.62 (br d, J=10 Hz, H-8), 10.92 (s, CHO). Found: C, 72.90; H, 4.82%. Calcd for $C_{13}H_{10}O_3$: C, 72.89; H, 4.71%.

Methyl 3-Cyano-2-formylazulene-1-carboxylate (2d). Methyl 3-cyano-2-styrylazulene-1-carboxylate (**1d**) (3.13 g, 10 mmol) was treated in the usual way to give **1d** (1.02 g) and **2d** (1.29 g, 80% yield) as reddish violet needles (from MeOH), mp 221—223 °C; IR (KBr): 2865, 2219, 1698, 1678, 1115, 1064 cm^{-1}; λ_{max}^{MeOH} 235 nm (log ε 4.55), 267 (4.34), 293 (4.63), 303 (4.73), 340 (3.90), 367 (3.89). Found: C, 70.22; H, 3.82; N, 5.79%. Calcd for $C_{14}H_9O_3N$: C, 70.29; H, 3.79; N, 5.86%.

Dimethyl 2-Formylazulene-1,3-dicarboxylate (2e). Dimethyl 2-styrylazulene-1,3-dicarboxylate (**1e**) (1.38 g, 4 mmol) was treated in the usual way to give **1e** (120 mg) and **2e** (810 mg, 82% yield) as red needles (from MeOH), mp 167—168 °C; IR (KBr): 2865, 1698, 1215, 1192, 1088, 1064 cm^{-1}; λ_{max}^{MeOH} 234 nm (log ε 4.53), 275 sh (4.43), 292 (4.62), 302 (4.70), 340 (3.89), 368 (4.00); $\lambda_{max}^{CHCl_3}$ 525 nm (log ε 2.97); NMR ($CDCl_3$): δ 3.92 (s, 2 OCH_3), 7.5—8.1 (m, H-5—7), 9.73 (dm, J=10 Hz, H-4,8), 10.75 (s, CHO). Found: C, 66.34; H, 4.50%. Calcd for $C_{15}H_{12}O_5$: C, 66.17; H, 4.44%.

1,2-Diformylazulene (2f). 1-Formyl-2-styrylazulene (**1f**) (1.03 g, 4 mmol) was treated in a similar manner to that above to give **2f** (660 mg, 90% yield) as bluish green needles (from cyclohexane), mp 155—156 °C; IR (KBr): 1672, 1643 cm^{-1}; $\lambda_{max}^{chloroform}$ 290 nm (log ε 4.48), 315 (4.60), 325 (4.57), 350 (4.08), 370 (4.08), 390 (4.04), 540 (2.63), 600 (2.94), 640 sh (2.75); NMR ($CDCl_3$): δ 7.3—8.3 (m, H-5—7), 7.83 (s, H-3), 8.75 (br d, J=10 Hz, H-4), 9.87 (br d, J=10 Hz, H-8), 10.87 (s, CHO), 11.00 (s, CHO). Found: C, 78.22; H, 4.39%. Calcd for $C_{12}H_8O_2$: C, 78.25; H, 4.38%.

1,2,3-Triformylazulene (2g). 1,3-Diformyl-2-styrylazulene (**1g**) (600 mg, 2.1 mmol) was treated in the usual way to give **2g** (380 mg, 86% yield) as reddish violet needles (from $CHCl_3$), mp 242—243 °C; IR (KBr): 1689, 1658 cm^{-1}; $\lambda_{max}^{chloroform}$ 304 nm (log ε 4.64), 315 (4.66), 351 (3.98), 377 (3.84), 560 (3.14); NMR ($CDCl_3$): 8.05 (t, J=9 Hz, H-5—7), 8.33 (t, J=9 Hz, H-6), 9.90 (d, J=9 Hz, H-4,8), 10.75 (s, 2 CHO), 11.13 (s, CHO on C-2). Found: C, 73.58; H, 3.69%. Calcd for $C_{13}H_8O_3$: C, 73.58; H, 3.80%.

1-Cyano-2,3-diformylazulene (2h). 1-Cyano-3-formyl-2-styrylazulene (**1h**) (1.42 g, 5 mmol) was treated in the usual way to give **2g** (920 mg, 88% yield) as reddish violet needles (from $CHCl_3$), mp 242—245 °C; IR (KBr): 2212, 1692, 1661 cm^{-1}; $\lambda_{max}^{chloroform}$ 303 nm (log ε 4.64), 312 (4.64), 350 (3.98), 377 (3.84), 570 (3.18); NMR ($CDCl_3$): δ 7.8—8.3 (m, H-5—7), 9.05 (dm, J=10 Hz, H-4), 10.07 (dm, J=10 Hz, H-8), 10.85 (s, CHO), 10.92 (s, CHO). Found: C, 74.48; H, 3.46; N, 6.69%. Calcd for $C_{13}H_7O_2N$: C, 74.64; H, 3.37; N, 6.70%.

2-Formylazulene-1-carboxylic Acid (2i). 2-Styrylazulene-1-carboxylic acid (**1i**) (280 mg, 1 mmol) was treated according to the general procedure to give **2i** (90 mg, 44% yield) as blue needles (from ethanol), mp above 300 °C; IR (KBr): 3200—2857, 1672, 1640 cm^{-1}; $\lambda_{max}^{dichloromethane}$ 308 nm (log ε 4.54), 355 (3.98), 610 (2.99); NMR ($CDCl_3$+DMSO-d_6 (2 : 1)): δ 7.3—8.2 (m, H-5—7), 7.73 (s, H-3), 8.63 (br d, J=10 Hz, H-4), 9.83 (br d, J=10 Hz, H-8), 11.00 (s, CHO). Found: C, 71.82; H, 4.11%. Calcd for $C_{12}H_8O_3$: C, 71.99; H, 4.03%.

2-Formyl-3-(methoxycarbonyl)azulene-1-carboxylic Acid (2j). 3-Methoxycarbonyl-2-styrylazulene-1-carboxylic acid (**1j**) (405 mg, 1.2 mmol) was treated according to the general procedure. Crystals obtained on dilution with water were collected to give **2j** (205 mg, 65% yield) as red prisms (from MeOH), mp 242—245 °C; IR (KBr): 3030—2857, 1701, 1658, 1221, 1092 cm^{-1}. Found: C, 64.82; H, 3.78%. Calcd for $C_{14}H_{10}O_5$: C, 65.12; H, 3.90%.

Diethyl 5-Formylazulene-1,3-dicarboxylate (4). Diethyl 5-styrylazulene-1,3-dicarboxylate (**3**) (100 mg, 0.27 mmol) was treated according to the general procedure to give **4** (52 mg, 64.9% yield) as red needles (from ethanol), mp 137—138 °C; IR (KBr): 1700 sh, 1690, 1205, 1025 cm^{-1}: $\lambda_{max}^{chloroform}$ 275 nm (log ε 4.39), 308 (4.53), 333 (4.11), 406 (4.23), 520 (3.13); NMR ($CDCl_3$): δ 1.47 and 1.49 (t, J=7.0 Hz, 2 OCH_2CH_3), 4.45 and 4.48 (q, J=7.0 Hz, 2 OCH_2CH_3), 7.82 (t, J=10 Hz, H-7), 8.48 (dt, J=1.5 and 10 Hz, H-6), 8.83 (s, H-2), 9.83 (dd, J=1.5 and 10 Hz, H-8), 10.15 (d, J=1.5 Hz, H-4), 10.20 (s, CHO). Found: C, 66.40; H, 4.40%. Calcd for $C_{15}H_{12}O_5$: C, 66.17; H, 4.44%.

1-Formyl-2-stryrylazulene (1f). $POCl_3$ (320 mg) was added to a stirred solution of 2-styrylazulene (**1a**) (480 mg, 2 mmol) in DMF (5 ml) under ice-cooling. After being stirred for 30 min, the mixture was poured into ice-water (200 ml) containing 1 M KOH solution (10 ml). The product was extracted with $CHCl_3$, washed with water and dried over Na_2SO_4. The solvent was evaporated and the residue was chromatogtaphed over an alumina column and eluted with benzene. Recrystallization from cyclohexane gave **1f** (500 mg, 93% yield) as reddish violet needles, mp 125—127 °C; IR (KBr): 2762, 1626, 1610sh, 979 cm^{-1}; $\lambda_{max}^{dichloromethane}$ 345 nm (log ε 4.67), 365sh (4.58), 405 (4.02); NMR ($CDCl_3$): δ 7.0—7.8 (10 H, m, H-5—7, CH=CH–, and C_6H_5), 7.97 (s, H-3). 8.30 (complex d. J=9,Hz, H-4), 9.33 (complex d. J=10 Hz, H-8), 10.73 (s, CHO). Found: C, 88.10; H, 5.38%. Calcd for $C_{19}H_{14}O$: C, 88.34; H, 5.46%.

1,3-Diformyl-2-styrylazulene (1g). A solution of **1f** (510 mg, 2 mmol) in DMF (15 ml) was treated with $POCl_3$ (530 mg) in a manner similar to that described above. Recrystallization from benzene gave **1g** (540 mg, 95% yield) as red needles, mp 174—175 °C; IR (KBr): 1660—1620 (br), 979 cm^{-1}; $\lambda_{max}^{dichloromethane}$ 317 nm (log ε 4.59), 340 (4.59), 500 (2.80): NMR ($CDCl_3$): δ 6.93 (d, J=8.0 Hz, =CH–), 7.2—8.0 (m, H-5—7 and C_6H_5), 7.97 (d, J=8.0 Hz, =CH–), 9.7—9.9 (m, H-4, 8), 10.48 (s, 2 CHO). Found: C, 83.71; H, 4.81%. Calcd for $C_{20}H_{14}O_2$: C, 83.90; H, 4.93%.

1-Cyano-3-formyl-2-styrylazulene (1h). A solution of 1-cyano-2-styrylazulene (**1b**) (1.90 g, 6.7 mmol) in DMF (50 ml) was treated with $POCl_3$ (2 ml) in a similar manner to that described above. Recrystallization of the crude product from benzene gave **1h** (1.96 g, 93% yield) as red needles, mp 222—224 °C; IR (KBr): 2203, 1645, 1613, 952 cm^{-1}; NMR ($CDCl_3$): δ 7.27—8.03 (10 H, m, H-5—7, and protons of styryl group), 8.60—8.83 (m, H-4), 9.57—9.80 (m, H-8), 10.67 (s, CHO). Found: C, 84.86; H, 4.77; N, 4.85%. Calcd for $C_{20}H_{13}NO$: C, 84.78; H, 4.63; N, 4.94%.

Reduction of 2f with $NaBH_4$. To a stirred solution of **2f** (50 mg) in dioxane (2 ml) was added a solution of $NaBH_4$ (6 mg) in MeOH (1 ml) at room temp. After being stirred for 5 min, acetic acid was added in order to decompose excess $NaBH_4$. The reaction mixture was diluted with water and extracted with chloroform. The extract was washed with water and dried (Na_2SO_4). The solvent was evaporated and the residue was chromatographed (silica gel) and eluted with chloroform to give 40 mg of 1-formyl-2-(hydroxymethyl)-azulene as red needles, mp 117—118 °C (from ethanol); IR (KBr); 3400, 1621 cm^{-1}; $\lambda_{max}^{dichloromethane}$ 265 nm (log ε 4.24), 269 (4.29), 315 (4.85), 365 (4.10), 3.80 (4.22), 514 (2.69); NMR ($CDCl_3$): δ 5.13 (s, CH_2OH), 6.2 (br s, OH), 7.32 (s, H-3), 7.38—7.90 (m, H-5—7), 8.45 (br d, J=10 Hz,

H-4), 9.05 (br d, J=10 Hz, H-8), 10.60 (s, CHO). MS: *m/e* (rel intensity), 186 (M^+, 100), 168 (M^+-CO, 28), 157 (48), 139 (42).

1-Cyano-2-(hydroxymethyl)azulene was obtained by the reduction of **2b** with $NaBH_4$ in 93% yield in a similar manner to that described above, violet needles, mp 124—125 °C (from cyclohexane–dichloromethane); IR (KBr): 3460, 2200 cm^{-1}; NMR ($CDCl_3$): δ 2.37 (br s, OH), 5.17 (s, CH_2OH), 7.32 (s, H-3), 7.2—7.9 (m, H-5—7), 7.33 (d, J=9 Hz, H-4), 8.50 (d, J=9 Hz, H-8). MS (25 eV, at 120 °C): *m/e* (rel intensity), 183 (M^+, 83), 167 (83), 166 (100%).

Oxidation of 2b with Ag_2O. To a stirred solution of **2b** (205 mg) in ethanol (5 ml) was added freshly prepared Ag_2O (650 mg). After being stirred for 5 h, the mixture was diluted with water. The resulting crystals were collected and dissolved in a 1 M $NaHCO_3$ solution. The solusion was shaken with benzene and acidified with 6 M HCl to give crystals. Recrystallization from ethanol gave 1-cyanoazulene-2-carboxylic acid (86 mg, 38% yield) as dark green crystals, mp over 300 °C; IR (KBr): 2860 (br), 2217, 1686, 926 cm^{-1}. Found: C, 72.79; H, 3.68; N, 6.96%. Calcd for $C_{12}H_7O_2N$: 73.09; H, 3.58; N, 7.10%.

Diethyl 5-Styrylazulene-1,3-dicarboxylate (3). A mixture of 1.0 g (3.5 mmol) of diethyl 5-methylazulene-1,3-dicarboxylate[17] and 1.86 g (17.5 mmol) of benzaldehyde in a sodium ethoxide solution prepared from 403 mg (17.5 matom) of sodium and 50 ml of anhydrous ethanol was stirred at room temp for 4 d. The reaction mixture was diluted with water and acidified with dilute HCl and then extracted with chloroform. After evaporation of the solvent from the organic extract the residue was chromatographed (alumina, benzene) to give 114 mg of the unreacted diethyl 5-methylazulene-1,3-dicarboxylate from the first effluent and 116 mg (8.9%) of **3** from the second effluent as red needles (from ethanol); mp 127—128 °C (lit,[22] 122.5—123 °C); IR (KBr): 1690—1670 (br), 1200, 950 cm^{-1}; NMR ($CDCl_3$): δ 1.46 and 1.48 (t, J=7.0 Hz, 2 OCH_2CH_3), 4.48 and 4.50 (q, J=7.0 Hz, 2 OCH_2CH_3), 7.3—7.7 (m, C_6H_5), 7.76 (t, J=10 Hz, H-7), 8.23 (dd, J=10, 2 Hz, H-6), 8.93 (s, H-2), 9.76 (d, J=10 Hz, H-8), 10.30 (d, J=2 Hz, H-4). Found: C, 76.59; H, 6.18%. Calcd for $C_{24}H_{22}O_4$: C, 76.98; H, 5.92%. From the third effluent with chloroform, 380 mg (27.7%) of diethyl 5-(2-hydroxy-2-phenylethyl)azulene-1,3-dicarboxylate was obtained as reddish violet needles (from ethanol), mp 159.5—161 °C; IR (KBr): 3450, 1690, 1660, 770, 750 cm^{-1}; NMR ($CDCl_3$): δ 1.41 (t, J=7.0 Hz, 2 OCH_2CH_3), 2.65 (br s, OH), 3.30 (d, J=6.5 Hz, $CH(OH)CH_2$), 4.35 and 4.40 (q, J=7.0 Hz, 2 OCH_2CH_3), 5.50 (t, J=6.5 Hz, $CH(OH)CH_2$), 7.28 (br s, C_6H_5), 7.50 (t, J=9.0 Hz, H-7), 7.73 (br d, J=9.0 Hz, H-6), 8.75 (s, H-2), 9.41 (dd, J=9.0, 2 Hz, H-8), 9.75 (d, J=2 Hz, H-4). Found: C, 73.52; H, 6.35%. Calcd for $C_{24}H_{24}O_5$: C, 73.47; H, 6.16%.

Dehydration of Diethyl 5-(2-Hydroxy-2-phenylethyl)azulene-1,3-dicarboxylate. A mixture of 100 mg of diethyl 5-(2-hydroxy-2-phenylethyl)azulene-1,3-dicarboxylate, $POCl_3$ (3 ml), and pyridine (5 ml) was allowed to stand at room temp for 18 h. The reaction mixture was diluted with water and extracted with ether. The extracts were washed with dilute HCl and dried (Na_2SO_4) and worked up to give 93 mg (98% yield) of **3**.

The Lactol Acetate (6a). A drop of concd H_2SO_4 was added to a suspension of **2j** (100 mg) in Ac_2O (2 ml). After being stirred at room temp for 20 min, the mixture was diluted with water and extracted with $CHCl_3$, the extract being washed with water and dired (Na_2SO_4). The solvent was evaporated and the residue dissolved in benzene and passed through a short alumina column. Recrystallization from benzene gave **6a** (85 mg) as red needles, mp 220—222 °C; IR (KBr): 1767, 1706 cm^{-1}; λ_{max}^{MeOH} 234 nm (log ε 4.73), 271 (4.66), 300 (4.87), 327 (3.93), 355 (4.09), 367 (4.17), 492 (2.96); NMR ($CDCl_3$): δ 2.20 ($COCH_3$), 3.90 (OCH_3), 7.78 (methine), 7.6—8.3 (3H, m), 9.10 (1H, br d), 9.90 (1H, br d). Found: C, 64.37; H, 4.32%. Calcd for $C_{16}H_{12}O_6$: C, 64.00; H, 4.03%.

The Lactol Acetate (6b). The acid **2k** (50 mg) was treated with Ac_2O–concd H_2SO_4 in a silimar manner to that described above. Recrystallization from benzene gave **6b** (40 mg) as red needles, mp 198—200 °C; IR (KBr): 1770, 1701 cm^{-1}; λ_{max}^{MeOH} 235 nm (log ε 4.72), 271 (4.66), 292 (4.76), 301 (4.84), 326 (3.90), 355 (4.09), 368 (4.18). Found: C, 69.61, H, 4.28%. Calcd for $C_{17}H_{14}O_6$: C, 64.96; H, 4.49%.

Reaction of Dimethyl 2-Methylazulene-1,3-dicarboxylate (7) with p-Nitiroso-N,N-dimethylaniline (NDA). *a) In MeOH*: To a stirred solution of NaOMe were added 102 mg (0.39 mmol) of **7** and 100 mg (0.67 mmol) of NDA at room temp. After being stirred for 12 h, the reaction mixture was diluted with water and left to stand for 5 h. The precipitate formed was collected by filtration and chromatographed (silica gel, C_6H_6) to give 12 mg of **7**. The filtrate was acidified with 6 M HCl to give precipitate which was collected by filtration to give 60 mg of **2j** as red crystals.

b) In EtOH: 500 mg (3.3 mmol) of NDA was added to a stirred solution of NaOEt prepared from 150 mg of Na and anhydrous EtOH (3 ml). After being stirred for 12 h, the reaction mixture was diluted with water and extracted with chloroform. The organic layer was washed with water, dried (Na_2SO_4), and concentrated to a small volume. The residue was chromatographed (silica gel) to give 40 mg of **7** from the fraction eluted with C_6H_6. From the fraction eluted with chloroform 400 mg (53% yield) of **8b** was obtained as reddish brown needles; mp 228—229 °C (from benzene). IR (KBr): 1669, 1616, 1587, 813 cm^{-1}; λ_{max}^{MeOH} 239 nm (log ε 4.51), 308 (4.49), 540 (4.25); NMR ($CDCl_3$): δ 1.52 (t, J=7.0 Hz, OCH_2CH_3), 2.97 (s, $N(CH_3)_2$), 4.55 (q, J=7.0 Hz, OCH_2CH_3), 6.67 (2H, d, J=9.5 Hz, $=NC_6H_4N(Me)_2$), 7.45 (2H, d, J=9.5 Hz, $=NC_6H_4N(Me)_2$), 7.5—8.0 (m, H-5—7), 9.48 (br d, J=10 Hz, H-8), 9.70 (s, COOH), 10.50 (dm, J=10 Hz, H-4). Found: C, 70.94; H, 5.75; N, 7.23%. Calcd for $C_{23}H_{22}O_4N_2$: C, 70.75; H, 5.68; N, 7.18%.

3-Ethoxycarbonyl-2-formylazulene-1-carboxylic Acid (2k). A solution of 100 mg of **8b** and 6 M HCl (2 drops) in EtOH (10 ml) was heated at 80 °C for 15 min. The mixture was diluted with water and extracted with chloroform. The organic layer was worked up to give 35 mg of **2k** as red needles, mp 222—223 °C (from benzene). IR (KBr): 3030—2778, 1706, 1654, 1212, 1088, 901 cm^{-1}. Found: C, 65.80; H, 4.43%. Calcd for $C_{15}H_{12}O_5$: C, 66.17; H, 4.44%.

The present work was partially supported by a Grant-in-Aid for Scientific Research from the Ministry of Education, Science and Culture.

References

1) K. Hafner and C. Bernhard, *Angew. Chem.*, **69**, 533 (1957); *Justus Liebigs Ann. Chem.*, **625**, 108 (1959).

2) W. Treibs, H.-J. Neupert, and J. Hiebsch, *Naturwissenschaften*, **44**, 352 (1957); *Chem. Ber.*, **92**, 141 (1959); **92**, 606 (1959).

3) T. Ukita, M. Miyazaki, and M. Hashi, *Chem. Pharm. Bull.*, **6**, 223 (1958).

4) D. H. Reid, W. H. Stafford, and W. L. Stafford, *J. Chem. Soc.*, **1958**, 1118.

5) K. Hafner, H. Pelster, and J. Schneider, *Justus Liebigs*

Ann. Chem., **650**, 62 (1961).
6) E. C. Kirby, *Org. Prep. Proced. Int.*, **6**, 215 (1974); *Chem. Abstr.*, **82**, 111824j (1975).
7) a) D. Meuche, D. Dreyer, K. Hafner, and E. Heilbronner, *Helv. Chim. Acta*, **50**, 1178 (1967); b) E. C. Kirby and D. H. Reid, *J. Chem. Soc.*, **1960**, 494.
8) T. Amemiya, M. Yasunami, and K. Takase, *Chem. Lett.*, **1977**, 587.
9) K. Kohara, *Bull. Chem. Soc. Jpn.*, **42**, 3229 (1969); W. Treibs, *Chem. Ber.*, **90**, 761 (1957); W. Treibs and R. Vogt, *ibid.*, **94**, 1739 (1961).
10) A. Sato, *D. Sc. Thesis of Tohoku University* (1963).
11) H. Arnold and K. Pahls, *Chem. Ber.*, **87**, 257 (1954).
12) K. Hafner and K.-L. Moritz, *Justus Liebigs Ann. Chem.*, **656**, 40 (1962).
13) T. Morita, T. Fujita, T. Nakadate, and K. Takase, *Sci. Repts. Tohoku Univ. Ser. I*, **62**, 91 (1980); N. Kato, Y. Fukazawa, and S. Ito, *Tetrahedron Lett.*, **1976**, 2045.
14) M. Saito, T. Morita, and K. Takase, *Chem. Lett.*, **1974**, 289; *Bull. Chem. Soc. Jpn.*, **53**, 3276 (1980).
15) R. Pappo, D. S. Allen, Jr., R. U. Lemieux, and W. S. Johnson, *J. Org. Chem.*, **21**, 478 (1956).
16) M. Saito, T. Morita, and K. Takase, *Chem. Lett.*, **1974**, 955.
17) H. Akino, *Sci. Repts. Hirosaki Univ.*, **11**, 18 (1964); *Chem. Abstr.*, **63**, 1754h (1965).
18) L. J. Bellamy, "Advances in Infrared Group Frequencies," Methuen, London (1968), p. 157.
19) E. Heilbronner, "Non-benzenoid Aromatic Compounds," ed by D. Ginsburg, Interscience Publishers Inc., New York (1959), p. 171.
20) K. Bowden and G. R. Taylor, *J. Chem. Soc., B*, **1971**, 1390.
21) G. M. Bennett and E. V. Bell, *Org. Synth.*, Coll. Vol. II, 223 (1943).
22) H. Matsumura and S. Nagamura, *Nippon Kagaku Zasshi*, **85**, 901 (1964).

Analysis of the Heat of Breaking Glass Ampoules

Tetsuo MORIMOTO* and Masafumi KIRIKI

Department of Chemistry, Faculty of Science, Okayama University, Tsushima, Okayama 700

(Received March 21, 1980)

Synopsis. The heat of breaking was measured on three series of ampoules, containing N_2 at various pressures, N_2 at various pressures as well as saturated H_2O vapor, or different amounts of liquid H_2O as well as the saturated vapor in the unfilled space, respectively. This report gives the method to analyze the heat of breaking of ampoules into three factors: the release of mechanical strain stored in the ampoule under a pressure, heat of evaporation of immersion liquid, and rush-in effect of the liquid.

The heat of breaking of glass ampoules is one of the most troublesome problems in microcalorimetry such as for heat of immersion measurements, and it is quite serious when the solid has low surface energy or small surface area. Three causes have been considered for the heat of ampoule breaking:[1-3] (1) release of mechanical strain stored in the ampoule under a pressure, (2) heat of evaporation of immersion liquid due to the volume change on breaking, and (3) rush-in effect of the liquid, called the PV effect, when the ampoule is filled with the liquid after breaking. It has been reported that a major part of the heat of ampoule breaking is caused by the last effect;[4] it can be much reduced by filling up the ampoule with an inert gas like He.[1,5]

Here, we report the results of an experimental analysis of these three heat effects, from which we can establish the correction of the heat of breaking in microcalorimetry.

Experimental

The ampoules used here were commercial ones, which are cylindrical, having fairly uniform capacity of about 3 cm^3. Three series of sealed ampoules were prepared. The first series contained N_2 at various pressures, and the second series N_2 at various pressures which was saturated with H_2O. The third series contained different amounts of liquid H_2O and its vapor. Special precautions were taken for sealing off the ampoules so as to keep their volumes contant as close as possible. The average volume was 3.2 ± 0.1 cm^3. Measurements were made in H_2O at 28 ± 0.1 °C, in an adiabatic calorimeter equipped with a quartz thermometer as a temperature sensing element.[6] In order to avoid random breaking of ampoules, they were edged uniformly by a file around their circumference, and then were broken between steel knife edges, by using a screw.

Results and Discussion

Figure 1 shows the relationship between the heat of breaking and the N_2 pressure in the ampoule. For a series of ampoules containing N_2 and saturated H_2O vapor, the heat is plotted against the partial pressure of N_2. It is seen from Fig. 1 that heats of breaking of the ampoules containing both N_2 and saturated H_2O vapor are higher than those containing N_2 only, and both series of heat decreased linearly with increasing

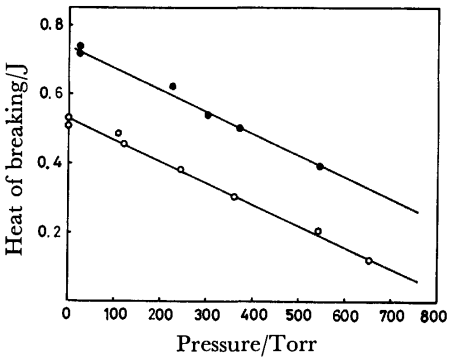

Fig. 1. Heat of breaking glass ampoules as a function of pressure of N_2, in the presence of N_2 only ○, and N_2 and saturated H_2O ●.

pressure of N_2 and in parallel with each other. This fact suggests that a constant amount of H_2O evaporates on breaking the ampoules containing N_2 only, which leads to a decrease in heat generation. This endothermic effect is 0.21 J, which is obtained from the difference between the two straight lines in Fig. 1. The heat of vaporization of H_2O into the space of 3.2 cm^3 at 28 °C can be calculated to be 0.212 J, which is in good agreement with the experimental value. Thus, it is understood that breaking of an ampoule in a liquid is accompanied by evaporation of the liquid, the volume of vapor formed being equal to that of the ampoule, except in the case where the ampoules contain saturated vapor of the immersion liquid, which results in partial cancellation of the heat evolved.

Figure 2 represents the heat of breaking when ampoules having different amounts of liquid H_2O were broken in H_2O. It is seen from Fig. 2 that the heat evolution decreases linearly with increasing amount of H_2O or decreasing space volume. Since the space in these ampoules always contains saturated H_2O, evapora-

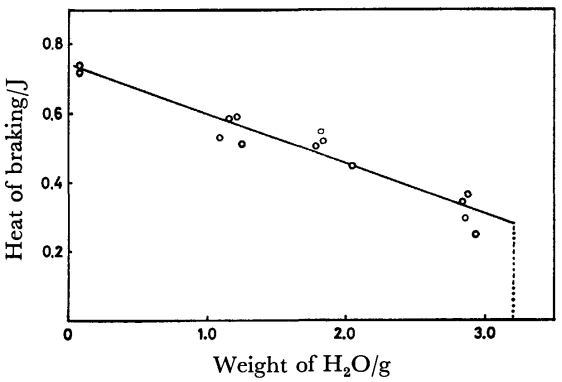

Fig. 2. Heat of breaking glass ampoules as a function of weight of H_2O contained.

tion of H_2O should not occur. Admittedly, both evaporation of H_2O and the rush-in effect of the liquid will disappear when the space volume is zero. In other words, we may consider the heat evolved in this limiting case to be equal to the heat due to the release of mechanical strain stored in the ampoule. This heat value can be obtained by extrapolating the straight line in Fig. 2 to the zero space volume and is found to be 0.28 J. It is easy to understand that the heat value changes with the variety of ampoules and also with the breaking modes.

As determined from Fig. 1, the heat of breaking of an ampoule, when it is empty, is 0.53 J. This value contains of course all the three effects of heat generation. By subtracting the heats due to evaporation of H_2O and the release of mechanical strain from the total heat effect 0.53 J, we obtain the heat due to the rush-in effect, 0.46 J. If we estimate the product of pressure difference between outside and inside the ampoule and its volume, we obtain 0.324 J, which is much less than the rush-in heat. This result suggests that the rush-in effect, formerly called the PV effect, is not only a static effect, but it also includes dynamic processes such as collision of the liquid stream with the glass wall, and of liquid masses with each other and friction of liquid when it rushes into the ampoule.

Further consideration leads to the conclusion that when ampoules containing both N_2 of 1 atm and saturated H_2O vapor are broken, only the effect of release of mechanical strain appear, because the rush-in effect disappears. In fact, the value 0.26 J from Fig. 1 is close to the value, 0.28 J, described above as the heat due to the release of mechanical strain. Thus, it can be understood that the difference of heat evolved under the conditions at both ends of every series of measurements, *i.e.*, at both ends of three straight lines (Figs. 1 and 2), represents the heat due to the rush-in effect; experimental values thus obtained from the three series of experiments are 0.48, 0.47, and 0.47 J, being quite close to each other. Therefore, the enclosure of He at 1 atm into an ampoule can avoid the rush-in effect of liquid in microcalorimetry, but does not eliminate the evaporation effect of the liquid.

Here, it is interesting to remember an ingenious method of Young and Bursh,[7] who broke several glass bulbs containing different weights of sample and extrapolated the results to zero sample content; the intercept was considered to be the heat of breaking the glass bulb, and the slope of the straight line to be the heat of immersion of sample. Strictly speaking, however, on the basis of the present analysis, the slope of the straight line should be the sum of three effects: the heat of immersion of the sample, the decreasing rush-in effect, and the decreasing evaporation effect, the last of which is endothermic.

References

1) A. C. Zettlemoyer, *Ind. Eng. Chem.*, **57**, 27 (1965).
2) A. C. Makrides and N. Hackerman, *J. Phys. Chem.*, **63**, 594 (1959).
3) H. F. Holmes and C. H. Secoy, *J. Phys. Chem.*, **69**, 151 (1965).
4) C. A. Guderjahn, D. A. Paynter, P. E. Berghausen, and R. J. Good, *J. Chem. Phys.*, **28**, 520 (1958).
5) A. C. Zettlemoyer, R. D. Iyenger, and P. Scheidt, *J. Colloid Interface Sci.*, **22**, 172 (1966).
6) T. Morimoto and H. Muraishi, *J. Phys. Chem.*, **80**, 1876 (1976).
7) G. J. Young and T. P. Bursh, *J. Colloid Sci.*, **15**, 361 (1960).

The Effect of Fatty Alcohols on the Dodecane-Water and the Dodecane-SDS Solution Interfaces

Fumitake MIENO and Keizo OGINO*

Faculty of Science and Technology, Science University of Tokyo, Yamazaki, Noda, Chiba 278

(Received October 1, 1979)

Synopsis. The effects of fatty alcohols ($C_mH_{2m+1}OH$, $m=1$—12) at the dodecane–water and the dodecane–sodium dodecyl sulfate (SDS)-solution interfaces has been investigated by measuring the interfacial tension and by observing the stability of the emulsion. The following results have been obtained: the addition of lower alcohols ($m=1$—3) increases the interfacial tension at the dodecane–SDS-solution interface, and they are considered as emulsion breakers. With regard to middle and higher alcohols, though, the interfacial tension decreases with the increase in the carbon number. They can thus be used as emulsion stabilizers.

The effects of additives on spontaneous emulsification and on the stability of emulsion have been investigated by many investigators.[1-5] We[6] ourselves have previously reported that 1-dodecanol in dodecane and sodium dodecyl sulfate (SDS) in water form emulsions spontaneously in the presence of surfactants or alcohols above certain concentrations. Vold and Mittal[7] have reported that, in a Nujol–water–0.2% SDS emulsion, the stability of the emulsion increases with the addition of 1-dodecanol up to 56%, on the basis of SDS.

In this study, the effect of the carbon-chain length of fatty alcohols has been investigated at the dodecane–water and the dodecane–SDS-solution interfaces.

Experimental

Materials. *Surfactant*: The sodium dodecyl sulfate (SDS) was supplied by Wako Pure Chemical Ind. Ltd., and was extracted with ether and recrystallized from ethanol.

Fatty Alcohols: The methanol, 1-dodecanol (Wako Pure Chemical Ind. Ltd.,), ethanol, 1-propanol, 1-butanol, 1-pentanol, 1-hexanol, 1-heptanol, 1-octanol, 1-nonanol, 1-decanol, and 1-undecanol (Tokyo Kasei Ind. Ltd.,) were of a reagent grade and were used without further purification.

Water and Oil: The distilled water and dodecane (Nikko Petrochemical Co.,) were of a commercial grade and were used without purification.

Apparatus. The interfacial tension and its variation with the time were measured at 30 °C with a Wilhelmy tensiometer, Shimadzu ST-1.

Procedure. Dodecane (8.0 ml) was used as an oil phase. Distilled water (8.0 ml) and 8×10^{-3} M† SDS solution (8.0 ml) were used as a water phase. After the equilibrium of the oil–water interface has been established, fatty alcohol was added to the oil phase with a syringe, and the change in the interfacial tension with the course of time was measured.

The dodecane, fatty alcohols, and 2×10^{-2} M SDS solution were emulsified by stirring. These emulsions were observed and photographed.

Results and Discussion

The Behavior of Fatty Alcohols at the Dodecane–Water Interface. In Fig. 1, the solid line shows the effect of fatty alcohols on the interfacial tension at the dodecane–water interface. The interfacial tension is lowered by the addition of alcohols, the extent of which is the largest in the case of 1-butanol.

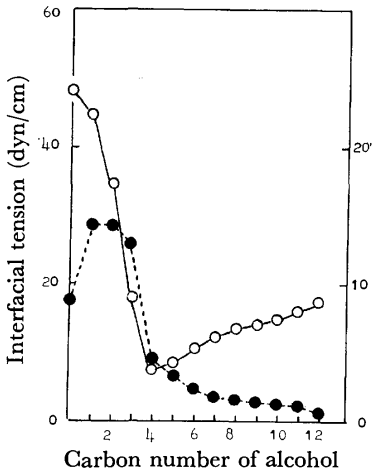

Fig. 1. The effect of carbon number of fatty alcohol on the interfacial tension at the dodecane–water interface. Oil phase : dodecane 8.0 ml, water phase : solid line-distilled water 8.0 ml; ○, dotted line-SDS soln. 8.0 ml; ●, additives : fatty alcohols ($m=1$—12) 0.8 ml.

We tried to calculate the HLB number of alcohols by the Davies method, and the concentration ratio of alcohol in the water phase and the oil phase (C_w/C_o), by means of the following equations:

$$\Delta G_{o\to w} = 800n - \Delta G_{o\to w}(\text{hydrophilic groups}) \quad (1)$$

$$C_w/C_o = \exp(-\Delta G_{o\to w}/RT) \quad (2)$$

where $\Delta G_{o\to w}$ is the free energy when alcohol is transferred from the oil phase to the water phase, n is the number of $-CH_2-$ groups in an alcohol, the increment of

Table 1. Hydrophilic and lipophilic properties of fatty alcohols

m[a)]	H.L.B.	$\Delta G_{o\to w}$ / cal mol^{-1}	C_w/C_o
1	8.4	−2400	53.9
2	8.0	−1600	14.3
3	7.5	− 800	3.7
4	7.0	0	1.0
5	6.5	800	0.26
6	6.1	1600	7.0×10^{-2}
7	5.6	2400	1.8×10^{-2}
8	5.1	3200	4.9×10^{-3}
9	4.6	4000	1.3×10^{-3}
10	4.2	4800	3.4×10^{-4}
11	3.7	5600	9.1×10^{-5}
12	3.2	6400	2.4×10^{-5}

a) m is the carbon number of fatty alcohol.

† Throughout this paper, 1 M = 1 mol dm^{-3}.

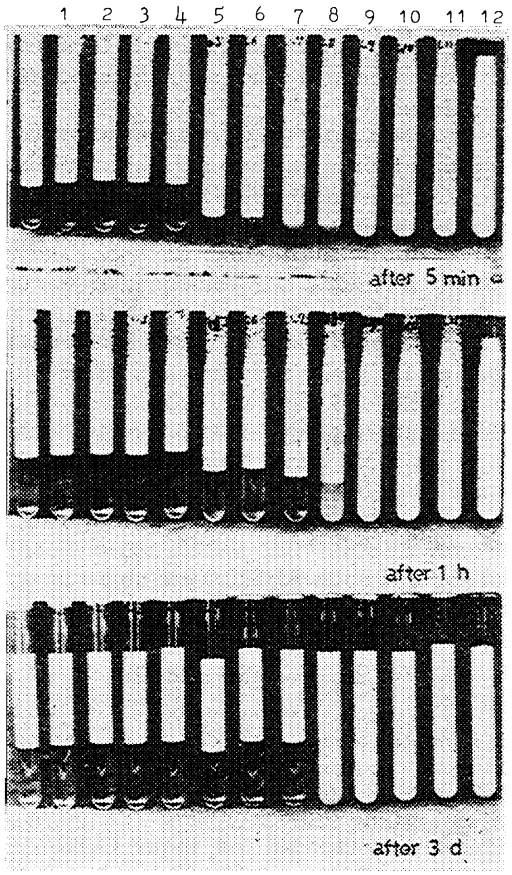

Fig. 2. The observation ofdo decane–water–SDS–fatty alcohol emulsions.
Oil phase : dodecane 3.0 ml, water phase : 2×10^{-2} M SDS soln. 3.0 ml, additives : fatty alcohols ($m=1$—12) 0.1 M in emulsion.

$\Delta G_{o \to w}$ per $-CH_2-$ groups is 800 cal/mol, and $\Delta G_{o \to w}$ (–OH group) is −3200 cal/mol.[1] C denotes the concentration of alcohol, and the subscripts o and w refer to oil and water. The results are shown in Table 1.

The results of calculation and Fig. 1 suggest that 1-butanol is well balanced in hydrophilic and lipophilic properties, and that lower alcohols ($m=1$—3) become more hydrophilic, while alcohols which have more than 4 carbon atoms become more lipophilic.

The Effect of Fatty Alcohols at the Dodecane–SDS-solution Interface. In Fig. 1, the dotted line shows the effect of alcohol on the interfacial tension at the dodecane–SDS-solution interface (right ordinate). From this results, it is considered that lower alcohols ($m=1$—3) have an emulsion-breaking effect, as is shown in Fig. 2. In the cases of the other higher alcohols, the reason for the decrease in the interfacial tension is considered to be as follows. It is well known that a complex is formed by the van der Waals force and a polar force between higher alcohol and the SDS molecule.[8] Thus, the adsorption of alcohol and the SDS molecule at the dodecane–water interface is further increased, and the interfacial tension decreases. Therefore, it may be considered that the stabilizing power of SDS is increased in the presence of alcohols which have a long chain. Figure 2 shows photographs of emulsions which are composed of dodecane, alcohols, SDS, and water. The emulsion without alcohol is at the far left of the photographs. From the left to the right of the photographs, the carbon numbers of the alcohols added increase. We ascertained by the dilution method that these emulsions were of the oil-in-water type. As can be seen from Fig. 2, it is clear that lower alcohols act as emulsion-breakers, while higher alcohols act as emulsion-stabilizers.

References

1) J. T. Davies and E. K. Rideal, "Interfacial Phenomena," Academic Press, New York and London (1963), pp. 360—377.
2) J. T. Davies and D. A. Haydon, Proc. 2nd Internat. Congr. Surface Activity, 1, 417, Butterworths, London (1957).
3) J. H. Schulman and E. G. Cockbain, *Trans. Faraday Soc.*, **36**, 651 (1940).
4) K. Ogino and M. Ota, *Yukagaku*, **23**, 28 (1974).
5) K. Ogino and M. Ota, *Bull. Chem. Soc. Jpn.*, **49**, 1187 (1976).
6) K. Ogino and H. Umetsu, *Bull. Chem. Soc. Jpn.*, **51**, 1543 (1978).
7) R. D. Vold and K. L. Mittal, *J. Colloid Interface Sci.*, **38**, 451 (1972).
8) Y. Moroi, K. Motomura, and R. Matsuura, *Bull. Chem. Soc. Jpn.*, **44**, 2078 (1971).

The Dehydration of D-Fructose to 5-Hydroxymethyl-2-furaldehyde

Yoshio NAKAMURA* and Shunichi MORIKAWA
The Noguchi Institute, 8-1, Kaga 1-Chome, Itabashi-ku, Tokyo 173
(Received April 4, 1980)

Synopsis. The continuous dehydration of D-fructose is carried out under mild conditions, using the strongly acidic ion-exchange resin with a low divinylbenzene content as the catalyst and dimethyl sulfoxide as the solvent, to give 5-hydroxymethyl-2-furaldehyde in a high yield.

Because of its potential versatility as a starting material for industrial chemicals and polymers,[1] 5-hydroxymethyl-2-furaldehyde (HMF) has been expected to be a staple chemical derived from such renewable raw materials as farm and wood products. The present authors have now investigated the procedure for obtaining HMF from D-fructose, since marked progress in the production of D-fructose from D-glucose is being made.[2]

Bonner *et al.* obtained HMF in a 71 mol% yield (based on the fructose portion) by the iodine-catalyzed dehydration of sucrose in *N,N*-dimethylformamide.[3] On the other hand, HMF has been reported to be obtained in an 80 mol% yield by the acid-catalyzed dehydration of D-fructose in tetrahydrofurfuryl alcohol, but about 40% of the HMF thus formed was found as the ether of the solvent.[4] Recently, the continuous dehydration of D-fructose catalyzed by such homogeneous acids as hydrochloric acid and phosphoric acid has been reported.[5,6] However, a continuous dehydration using a solid catalyst has never been reported.

The dehydration of D-fructose catalyzed by a strongly acidic ion-exchange resin in dimethyl sulfoxide (DMSO) was found to give HMF in a high yield under mild conditions.

TABLE 1. DEHYDRATION OF D-FRUCTOSE CATALYZED BY DIAION PK-216
Fructose, 0.5 M; catalyst, 10 meq.; solvent, DMSO; reaction mixture, 50 ml; 80 °C.

Reaction time / min	Yield of HMF (mol%)
40	30
100	57
200	81
300	89
500	90

The results of the batch-by-batch dehydration of D-fructose with Diaion PK-216 in DMSO are shown in Table 1. As shown in Table 1, HMF is obtained in a 90 mol% yield, based on the D-fructose, after 500 min.

Analyses of the reaction mixture by TLC[7] and GPC (Chromosorb 101, 1 m, 220 °C) showed that only a trace amount of by-products, such as bis(5-formylfurfuryl) ether and levulinic acid, were formed. The total amount of the acids formed during dehydration was found to be 0.34 mmol (1.4 mol% based on the D-fructose) by the titration of the reaction mixture. The dehydration product was identified as HMF by means of its IR and NMR spectra, and the dehydration of D-fructose catalyzed by the resin catalyst in DMSO is quite selective to HMF.

The effect of the divinylbenzene (DVB) content in various ion-exchange resins on the rate of the dehydration of D-fructose to HMF in DMSO was investigated. The rate of HMF formation can be given by;

$$\frac{d[HMF]}{dt} = k([F^\circ]-[HMF])$$

where [HMF], [F°], and k are the concentration of HMF, the initial concentration of D-fructose, and the rate constant, respectively.[8] A plot of the value of $\log [[F^\circ]/([F^\circ]-[HMF])]$ against t gave a straight line at an earlier stage of the reaction. The values of k for the batch-by-batch dehydration were obtained for various resins; they are shown in Table 2, which shows that the dehydration rate depends markedly on the DVB content in the resin used and that the porous resin is more effective than the gel-type ones when the DVB content in the resins is the same.

The apparent volume(V) of the resin containing 10 meq. of the sulfo group was measured after dipping overnight in DMSO. Then the values of k/V (activity per unit volume of the resin catalyst) were calculated; they are also shown in Table 2, with the values of V. Table 2 shows that even the value of k/V increases as the DVB content in the resin decreases.

The stability of the catalytic activity of the resin for the continuous dehydration of D-fructose to HMF in DMSO was examined using Amberlite IR-118 with

TABLE 2. EFFECT OF DVB CONTENT ON THE RATE CONSTANT, k, AND THE VALUE OF k/V
Solvent, DMSO; resin catalyst, 10 meq.[a]

	Resin	DVB content (%)	k (s^{-1})	V (ml)	k/V (s^{-1} ml^{-1})
Porous type	Diaion PK-208	4	3.01×10^{-4}	8.3	3.6×10^{-5}
	Diaion PK-216	8	1.46×10^{-4}	6.3	2.3×10^{-5}
	Diaion PK-228	14	0.17×10^{-4}	3.7	0.46×10^{-5}
Gel type	Amberlite IR-118	4	2.74×10^{-4}	8.9	3.1×10^{-5}
	Amberlite IR-120	8	0.58×10^{-4}	5.6	1.0×10^{-5}
	Lewatit SC-108	8	0.36×10^{-4}	5.2	0.68×10^{-5}

a) Other conditions as given in Table 1.

Table 3. Continuous dehydration of D-fructose using amberlite IR-118 as the catalyst
D-Fructose in feed, 0.5 M.

Elapsed time (h)	Concentration of HMF (M)
50	0.4
100	0.45
200	0.47
400	0.45
900	0.45

a low DVB content. After the feed solution had begun to be supplied into the column reactor containing the resin and DMSO, the concentration of HMF in the eluted solution was measured at varying times. As shown in Table 3, after about 100 h the concentration of HMF reached 0.45 M and stayed there even after 900 h.

The catalytic activity and acidity of the resin used for the continuous dehydration for 900 h were re-examined; no decrease was found in these catalytic properties.

Experimental

Preparation of Catalyst. The resins were washed with distilled water and conditioned by converting them to the sodium form and by then reconverting them to the hydrogen form. Samples were dried under a vacuum (1—2 mmHg) at 60 °C for about 6 h and used after dipping overnight in DMSO. The acidity of the resin was measured by titration.

Batch-by-batch Dehydration. A DMSO solution (50 ml) containing D-fructose (25 mmol) and the resin catalyst (10 meq. as the sulfo group) were added to a 200-ml glass flask, which was then immersed in a bath thermostated at 80±0.1 °C and the solution was stirred by a magnetic stirrer. The quantity of HMF formed was determined by means of UV absorption (λ=284 nm; Hitachi Spectrophotometer-124) after dilution (1×10^2—2×10^2 times) by distilled water. Samples (about 0.1 ml) were withdrawn at varying times.

Continuous Dehydration. Continuous dehydration was carried out using a glass column (inner diameter, 20 mm) packed with the catalyst (74 ml, 86.6 meq. as the sulfo group). The temperature of the column was kept at 60±0.1 °C by the use of a ribbon heater equipped with a thermoregulator. A DMSO solution containing D-fructose (0.5 M) and water (5 vol%)[9] was charged (mean rate=3.7 ml/h) continuously to the top of the column by means of a perista-pump (Atto Corp. SJ-1215), and the content of HMF in the eluted solution was measured as has been described above.

The authors are grateful to Professor Hidefumi Hirai of Tokyo University for his helpful discussion, and to Mr. Katsuyuki Sekino and Mr. Shigenobu Hiraiwa for their experimental assistance.

References

1) For example, C. J. Moye, *Rev., Pure Appl. Chem.*, **14** 161 (1964); J. A. Moore and J. E. Kelley, *Macromolecules*, **11**, 568 (1978); J. M. Kimko, S. S. Moore, D. M. Walba, P. C. Hiberty, and D. J. Cram, *J. Am. Chem. Soc.*, **99**, 4209 (1977).

2) K. Yoritomi, "Denpun Kagaku Hand Book," ed by J. Nikuni, Asakura Shoten (1977), p. 476; Y. Fujii and B. Okamura, *Kagaku To Kogyo*, **31**, 537 (1978).

3) T. G. Bonner, E. J. Bourne, and M. Ruszkiewicz, *J. Chem. Soc.*, **1960**, 787.

4) C. J. Moye and R. J. Goldsack, *J. Appl. Chem.*, **16**, 206 (1966).

5) B. F. M. Kuster and H. J. C. Van der Steen, *Staerke*, **29**, 99 (1977).

6) B. F. M. Kuster and J. Laurens, *Staerke*, **29**, 172 (1977).

7) C. J. Moye, *Aust. J. Chem.*, **19**, 2317 (1966).

8) B. F. M. Kuster and Hessel S. van der Baan, *Carbohydr. Res.*, **54**, 165 (1977); B. F. M. Kuster, *ibid.*, **54**, 177 (1977).

9) Water was added to prevent the DMSO solution in the line from freezing. It has been found, by the batch-by-batch dehydration of D-fructose, that the addition of 5 vol% of water to the DMSO solution decreases the reaction rate ($k=2.4\times10^{-4}$ s^{-1}, for Diaion PK-208 under the reaction conditions given in Table 2), but scarcely interferes at all with the selectivity to HMF.

The Dynamical Behavior of the Sodium Cation in Some Crown Ether-Na^+-$TCNE^-$ Ternary Complexes as Studied by ESR

Hiroyuki KOHAMA, Mayumi YOSHINAGA, and Kazuhiko ISHIZU*

Department of Chemistry, Faculty of Science, Ehime University, Matsuyama 790

(Received April 25, 1980)

Synopsis. ESR observations were performed for the ternary complexes formed with Na^+–$TCNE^-$ and 5*O*-crown ethers. The temperature dependence of the observed Na hyperfine line width was analyzed by applying Bloch's two-jump model, and the thermodynamical parameters of the complex formation were determined. The stability of the ternary complexes were found to be much affected by the substitution of either the fused benzene ring or the 2,2′-biphenyldiyl group, which acts as a steric restriction during the optimum metal binding to the flexible crown ring.

Usually, the alkali metal salts of tetracyanoethylene (M–TCNE) are insoluble in nonpolar solvents. In the presence of crown ether (CR), however, these salts can be solubilized by the complex formation between the alkali metal cation and the crown ether. Based on the ESR observation of the TCNE–crown ether complexes, Eastman *et al.*[1] previously suggested that the ternary complex, CR–M^+–$TCNE^-$, can be formed in these solutions, but the details of the dynamical behavior of alkali metal cations are not well known in these complexes. In this paper, the ESR measurements were applied to the ternary complexes composed of TCNE and 5*O*-crown ether solubilized in a nonpolar solvent. From the analysis of the temperature dependent line width alterations detected in the Na hyperfine splitting, the thermodynamical parameters of the complex formation were determined. The thermodynamical behavior of the metal cation, which will undergo a thermal vibration in the double minimum electric potential involving TCNE and crown ethers, was discussed with the aid of Bloch's equations for the two-jump processes.

Experimental

The 5*O*-crown ethers shown in Table 1 and NaTCNE were prepared according to the methods described in previous works.[2,3] Pure benzo-15-crown-5 was obtained by recrystallization in hexane; mp 80—82 °C (uncorrected). Elementary analysis: Calcd for $C_{14}H_{20}O_5$: C, 62.69; H, 7.46. Found: C, 62.48; H, 7.46%. 5,8,11,14-Pentaoxa-1,2,3,4-dibenzo-1,3-cycloheptadecadiene was purified by recrystallization using a benzene–hexane mixture (1 : 1); mp 107—109 °C (uncorrected). Elementary analysis: Calcd for $C_{20}H_{24}O_5$: C, 69.77; H, 6.98. Found: C, 69.62; H, 7.07%. 15-Crown-5 purchased from Aldrich Chemicals were used without further purification. The sample was made according to the following procedure: 2 mg of NaTCNE and an excess of CR were placed in the quartz sample tube and the desired amount of the purified solvent was brought into the cell in vacuum.

ESR spectra were measured with a JES-ME-3X spectrometer. The ESR splitting were determined by using $(KSO_3)NO$ ($a^N = 1.305 \pm 0.003$ mT) as a standard.

Table 1 Thermodynamical Parameters of CR–Na^+–$TCNE^-$ Complexes

		Toluene	o-Xylene	m-Xylene
L1	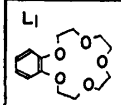	ΔH −14.6	−13.0	−17.6
		ΔS 62.8	50.6	71.6
L2	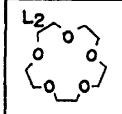	ΔH −26.4	−26.0	−27.2
		ΔS 98.4	99.6	100.0
L3	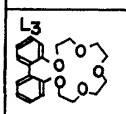	ΔH −9.2	−22.2	−15.9
		ΔS 40.6	93.8	70.3

ΔH: K J/mol ΔS: J/mol deg

Results and Discussion

The ESR spectra were measured in the temperature range from −50 to 50 °C. The alkali metal hyperfine

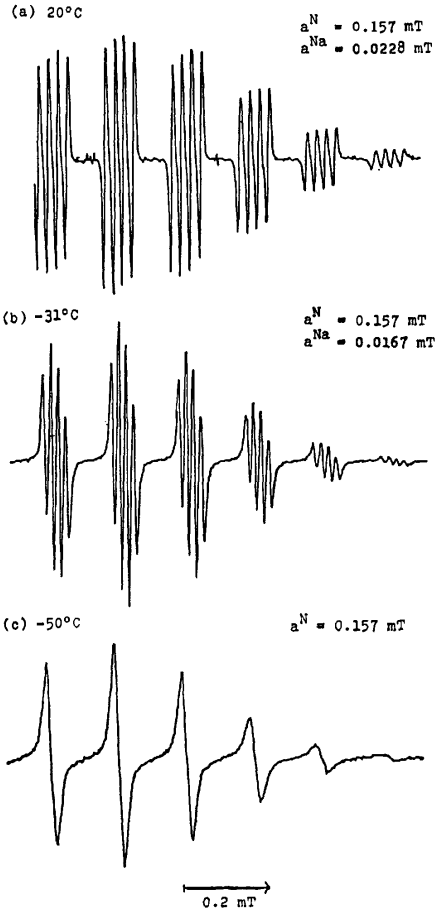

Fig. 1. The higher field halves of ESR spectra of benzo-15-crown-5–Na^+–$TCNE^-$ complex recorded in toluene solution.

line revealed a typical line width variation due to the rapid exchange between the two different paramagnetic species. The observed hyperfine structure measured at room temperature exhibits well resolved hyperfine lines composed of nine lines due to the equivalent four nitrogens ($a^{N}=0.157$ mT), which further split into the Na hyperfine lines ($a^{Na}=0.023$ mT) with equal line intensity [Fig. 1(a)].

Upon lowering the temperature, the magnitude of the alkali metal hyperfine splitting begins to decrease slightly. In addition, the line width corresponding to the alkali metal magnetic quantum number for $M_z=\pm 3/2$ increases in comparison with that for $M_z=\pm 1/2$ [Fig. 1(b)].

At -50 °C, the alkali metal splitting which had decreased by lowering the temperature merges into a single line [Fig. 1(c)].

We assume that the alkali metal cation undergoes a thermal vibration in two different electric potential minima, V_A and V_B which can be defined to CR and $TCNE^-$ respectively. At a lower temperature, a stronger ionic interaction can be expected between the Na^+ and CR, than occurs between Na^+ and $TCNE^-$; that is, $V_A<V_B$, where the alkali metal cation can be so closely accessible to the minimum potential of the CR as to reduce the magnitude of a^{Na}. At room temperature or above, the thermal activation moves the metal cation away from the CR potential; thus the contribution of the V_B could be enhanced, and the larger a^{Na} value was observed.

The equilibrium constant, K, at any temperature T is given by

$$K=\frac{a(T)-a_A}{a_B-a(T)},\quad \underset{A}{CR\text{–}Na^+\cdots TCNE^-} \underset{k_{-1}}{\overset{k_1}{\rightleftharpoons}} \underset{B}{CR\cdots Na^+\text{–}TCNE^-}$$

where a_A and a_B are the a^{Na} values of two different ion pairs at the energy minimum for V_A and V_B; $a_A=0$ mT, $a_B=0.0257$ mT, $a(T)$ is the Na splitting measured at the temperature T.

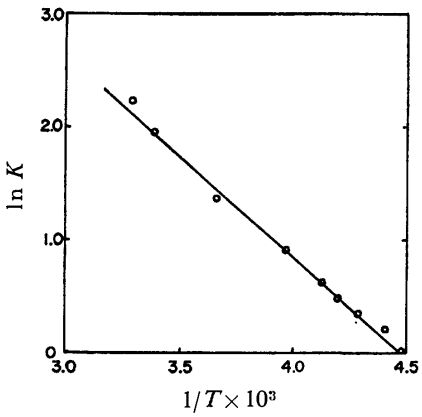

Fig. 2. Plot of ln K *vs.* $1/T$ for benzo-15-carown-5–Na^+–$TCNE^-$ complex in toluene.

The plots for ln K *vs.* $1/T$ gave an excellent straight line over the observed temperature range, as shown in Fig. 2. The value of ΔH and ΔS were calculated from the least-squares fits of the plots; $\Delta H=-14.6$ K J/mol, $\Delta S=62.8$ J/mol deg, respectively.

The rate constants k_1 and k_{-1} were also estimated by using the following equation:[4]

$$k_1=(2.03\times 10^7)\frac{K^2(a_B-a_A)^2(M_z^2-M_{z'}^2)}{(1+K)^3[(I_{M_{z'}}/I_{M_z})^{1/2}-1)\Delta H_{M_{z'}}}\ (s^{-1})$$

$$k_{-1}=\frac{k_1}{K}\ (s^{-1})$$

where I_{Mz} and $I_{Mz'}$ denote the line intensity corresponding to the alkali metal magnetic quantum number ($M_z=\pm 3/2$, $M_{z'}=\pm 1/2$), and $\Delta H_{Mz'}$ is the line width for Mz' peak. The linear plots are obtained between the logarithm of the rate constants ($\ln k_1$, $\ln k_{-1}$) and $1/T$.

The activation energy E_1 and E_{-1} thus estimated are 25.1 and 11.3 K J/mol for the TCNE–15-crown-5 complex. In order to obtain the more detailed view of these ternary complexes, the thermodynamical parameters (ΔH and ΔS) were obtained for several crown ethers, which have different steric factors upon incorporation of the alkali metal cation.

From the inspection of the thermodynamical parameters ΔH and ΔS measured in the different solvents (Table 1), some important features are found concerning the alkali metal complex formation of crown ethers containing five chelating oxygens, L_1, L_2, and L_3. No important difference in the thermodynamical parameters can be recognized by changing the solvent in each complex. This means that ternary complexes are essentially tight ion pairs. The largest values of both ΔH and ΔS are obtained for the L_2 complexes everywhere, while the ΔH values as well as the ΔS values are considerably reduced for the L_2 and L_3 complexes. This will be probably due to the fact that the planar fused benzene ring or sterically hindered 2,2′-biphenyldiyl groups act as restrictions toward any conformational change in the crown ring during the optimum binding of the alkali metal cation.

References

1) M. P. Eastman, D. A. Ramlrez, C. D. Jaeger, and M. T. Watts, *J. Phys. Chem.*, **80**, 182 (1976).
2) C. J. Pedersen, *J. Am. Chem. Soc.*, **89**, 7017 (1967).
3) O. W. Webster, W. Mahler, and R. E. Benson, *J. Am. Chem. Soc.*, **84**, 3678 (1962).
4) K. S. Chem, S. W. Mao, K. Nakamura, and N. Hirota, *J. Am. Chem. Soc.*, **93**, 6004 (1971).

Dynamic Behavior and Nature of Active Sites Directly Observed by Means of Photoluminescence Spectroscopy

Yasuhiro IWASAWA* and Sadao OGASAWARA

Department of Applied Chemistry, Faculty of Engineering, Yokohama National University, Hodogaya-ku, Yokohama 240

(Received May 13, 1980)

Synopsis. The dynamic behavior and properties of the active sites (Types I, II, and III) of SiO_2-supported Mo catalysts during a redox reaction with H_2 or O_2 (in connection with a general two-stage redox mechanism) were observed directly by means of a photoluminescence technique.

It has been demonstrated that photoluminescence is a sensitive technique for obtaining useful information on the surface structures and environments of solid catalysts.[1,2] The tetrahedral dioxo-Mo^{6+} structure of the fixed Mo catalysts (a supported molecular catalyst) has been found to have a spectroscopically uniform nature, but it was found by means of photoluminescence[2] that there were at least three different molybdenum species (Types I, II, and III) in a conventional impregnation catalyst ($Mo/SiO_2=1.7$ wt%). However, it does not naturally follow that the behavior of an individual molybdenum site during a catalytic reaction reflects the static, spectroscopic nature. The reactivities of all the active sites, with different environments, distributed on the SiO_2 surface could not be followed by conventional methods, such as adsorption, kinetics, UV diffuse reflectance spectroscopy, or IR spectrometry. In the present paper the direct observation of the dynamic behavior and the energy aspect of active sites will be reported in connection with the catalysis of Mo catalysts involving a two-stage redox mechanism; the following reaction sequence was chosen as a model process of the catalytic oxidation:

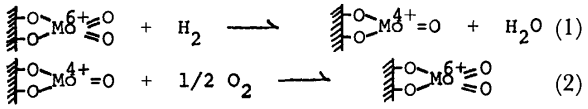

where H_2O was removed from the system by means of a liq.N_2 trap.

Experimental

The photoluminescence spectra of the fixed and impregnation catalysts were taken in a thin quartz cell connected to a vacuum system (base pressure: 1×10^{-5} Torr) at room temperature on a JASCO FP-4 spectrometer. The fixed Mo catalysts with the tetrahedral dioxostructure, $\gtrless$Si–O, O, Mo, $\gtrless$Si–O, O (XPS B.E.(eV): Mo $3d_{3/2}$=235.7, $3d_{5/2}$=232.7), were synthesized by taking advantage of the facile reaction between $Mo(\pi\text{-}C_3H_5)_4$ and OH groups of silica surface, as has previously been described;[2] $Mo/SiO_2=1.7$ wt%. The molybdenum ions fixed on silica were found to be molecularly distributed, with no interaction with one another (the average distance of Mo–Mo: *ca.* 20 Å). The impregnation catalyst was obtained by a conventional impregnation method using an aqueous ammonium paramolybdate solution.

Results and Discussion

The photoexcitation ($3t_2\leftarrow t_1$) of the charge transfer band of a $Mo^{6+}=O^{2-}$ bond in the fixed catalyst (Curve 1 of Fig. 1) and an impregnation catalyst (Curve 1 of Fig. 2) was followed by a strong luminescence from the lowest triplet T_1 state, as has previously been reported.[2] The fixed Mo^{6+} catalyst showing Spectrum 1 of Fig. 1

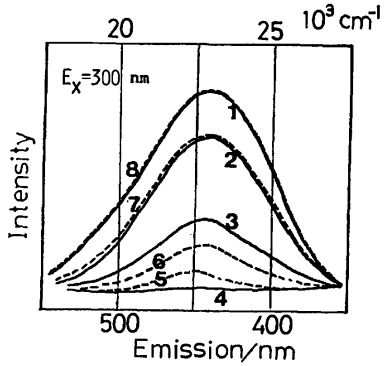

Fig. 1. Behavior of luminescence of the fixed Mo catalyst in the following consecutive redox processes; 1: oxidized catalyst, 2: after reduction of 1 with H_2 (50 Torr) at 723 K for 5 min, 3: H_2 (723 K, 17 min), 4: H_2 (733 K, 1 h), 5: after oxidation of 4 with O_2 (40 Torr) at 473 K for 5 min, 6: O_2 (513 K, 5 min), 7: O_2 (673 K, 5 min), 8: O_2 (823 K, 15 min).

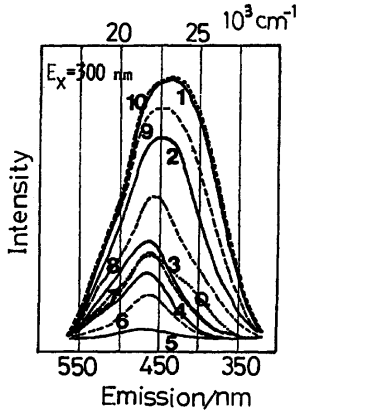

Fig. 2. Behavior of emission of the impregnation catalyst in the following consecutive steps; 1: oxidized catalyst, 2: after reduction of 1 with H_2 (50 Torr) at 673 K for 10 min, 3: H_2 (723 K, 1 h), 4: H_2 (723 K, 45 min), 5: H_2 (863 K, 2.5 h), 6: after oxidation of 5 with O_2 (40 Torr) at 463 K for 15 min, 7: O_2 (513 K, 10 min), 8: O_2 (563 K, 10 min), 9: O_2 (563 K, 20 min), 10: O_2 (823 K, 15 min), Q(quenching by CO_2): after exposure of catalyst (curve 1) to CO_2 (293 K, 280 Torr).

contained no Mo^{5+} ion, according to ESR at 77 and 295 K. The quadrivalent molybdenum with the oxostructure and the bivalent molybdenum showed no emission. Thus, the luminescence observed at 22.9 10^3 cm^{-1} directly illustrates the behavior of the tetrahedral $>Mo^{6+}\langle^{O}_{O}$ species (Type I). Figure 1 shows the variation in the emission of the fixed catalyst in the course of Reactions 1 and 2. The peak position and the shape were invariable during the redox process. On the other hand, the heterogeneous reactivity of the molybdenum species in the impregnation catalyst was observed in Fig. 2. The same emitting species (Type I) as that of the fixed catalyst reacted with hydrogen more rapidly than the molybdenum species (Type II), with an emission of 21.8 10^3 cm^{-1}. Type III, whose luminescence (21.8 10^3 cm^{-1}, Curve Q in Fig. 2) is not quenched by CO, CO_2, O_2, H_2, *etc.*, was also reduced with H_2 at 720 K. The order of ease of the reduction for molybdenum was Type I>Type II$\gg$Type III. The reduced species of the Type I-molybdenum was less reactive in the oxidation (2) (in contrast to the reduction (1)) than the other two types, although the difference among three types was not so large as the difference observed in the reduction, judging from the shapes of the emission spectra. The tetrahedral dioxomolybdenum structure obtained by the straightforward fixation of molybdenum using a reactive Mo $(\pi\text{-}C_3H_5)_4$ complex may be highly distorted and/or located on a coordination-unsaturation site of the SiO_2 surface; these structural factors would raise the T_1 state and also increase the covalency of the Mo=O double bond as active sites. The more the covalency of the Mo=O site, the more the hydrogen pulling step may be promoted.[2-4] The fixed catalyst was kinetically found to be much more active than the impregnation catalyst in the hydrogen-abstraction step in the oxidations of hydrogen,[5] ethyl alcohol,[2] and propylene.[3] Photoluminescence clearly monitored the behavior of active sites during reaction, where the fixed catalyst was found to have an active molybdenum of Type I with a uniform nature, which gave an emission of a relatively high energy.

References

1) G. T. Pott and W. H. J. Stork, Catalysis Rev., **12**, 163 (1975); G. T. Pott and B. D. McNicol, *Discuss. Faraday Soc.*, **52**, 121 (1971); S. Coluccia, M. Deane, and A. J. Tench, Proc. 6th Int. Congr. Catalysis (London, 1976), The Chemical Society, London (1977), Vol. **1**, p. 171; S. Coluccia, J. F. Hemidy, and A. J. Tench, *J. Chem. Soc., Faraday Trans. 1*, **74**, 2763 (1978); A. M. Gritscov, V. A. Shvets, and V. B Kazansky, *Chem. Phys. Lett.*, **35**, 511 (1975); C. Yun, M. Anpo, and Y. Kubokawa, *J. Chem. Soc., Chem. Commun.*, **1977**, 665.

2) Y. Iwasawa, Y. Nakano, and S. Ogasawara, *J. Chem. Soc., Faraday Trans. 1*, **74**, 2968 (1978); Y. Iwasawa and S. Ogasawara, *ibid.*, **75**, 1465 (1979).

3) Y. Iwasawa, T. Nakamura, K. Takamatsu, and S. Ogasawara, *J. Chem. Soc., Faraday Trans. 1*, **76**, 939 (1980).

4) G. K. Boreskov, *Proc. 5th Int. Congr. Catal.*, **2**, 981 (1972).

5) Y. Iwasawa, unpublished data.

Energy Transfer in γ-Irradiated Cyclohexane-Benzene Mixture Studied by Spin Trapping-ESR Technique

Takahisa DOBA, Susumu NISHIMURA, Tsuneki ICHIKAWA, Shoji NODA,* and Hiroshi YOSHIDA

Faculty of Engineering, Hokkaido University, Kita-ku, Sapporo 060

(Received May 29, 1980)

Synopsis. Cyclohexyl and phenyl radicals were detected in γ-irradiated cyclohexane–benzene mixtures by a spin trapping-ESR technique. The dependence of the radical yields upon mixture composition showed that energy transfer occurs efficiently from cyclohexane to benzene with the transfer efficiency of *ca.* 0.5 dm^3 mol^{-1}.

The rate of energy transfer in cyclohexane solutions is equal to or larger than that expected for a diffusion process,[1,2] so that the energy transfer will play an important role in the radiation chemistry of the cyclohexane–benzene mixture. The cyclohexane–benzene mixture is one of the typical systems in which the role of the energy transfer in radiation-chemical reactions has been the most extensively studied.[3] However, there still remains an ambiguity about the efficiency of the energy transfer from an excited cyclohexane to benzene.[2-4]

In this study, the spin trapping technique was utilized to detect cyclohexyl and phenyl radicals produced from cyclohexane and benzene, respectively, and to elucidate further the energy transfer in γ-irradiated cyclohexane-benzene mixture. The spin trapping has been demonstrated to be a pertinent technique to study free radicals in γ-irradiated systems not only qualitatively but also quantitatively.[5,6] The present spin trapping study will supplement the conventional product analysis methods,[3] and the fluorescence spectroscopic method[7] which have been used in the previous studies on the energy transfer. Pentamethylnitrosobenzene (PMNB) is an efficient spin-trap for carbon-centered radicals[8] and is used in this study.

Experimental

Cyclohexane and benzene of spectrograde were used as received. PMNB was synthesized and purified as described previously.[8] Each solution was degassed by the freeze-pump-thaw technique at a vacuum of 10^{-3} Pa and sealed in a quartz ESR tube. The sample was γ-irradiated and the ESR spectrum was recorded by a conventional x-band ESR spectrometer, both at ambient temperature.

Results and Discussion

The spin adduct of cyclohexyl radical was detected from the γ-irradiated cyclohexane solution containing PMNB; its *G*-value (yield for 100 eV energy absorbed) was 2.9, as reported previously.[5] The spin adduct of phenyl radical was detected from the γ-irradiated benzene solution containing PMNB; its *G*-value was found to be 0.06. The spin adducts of both the radicals were observed from cyclohexane–benzene mixtures. A typical ESR signal is shown in Fig. 1; the signal is the superposition of a broad six-line spectrum due to the cyclohexyl radical-spin adduct and a sharp multiplet one due to the phenyl radical-spin adduct.[8,9]

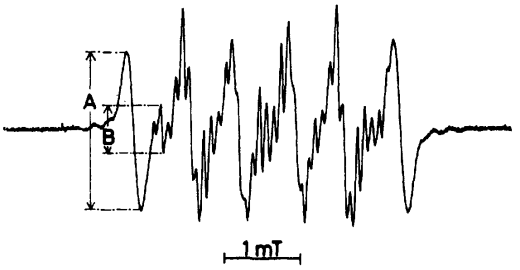

Fig. 1. ESR spectrum recorded from γ-irradiated cyclohexane–benzene mixture (benzene mole fraction, f_B= 0.55) containing 10^{-2} mol dm^{-3} PMNB at room temperature. *G*-values of cyclohexyl and phenyl radicals were calculated from the line intensities, A and B, in referring to the spectra due to the spin adducts of these radicals recorded from cyclohexane or benzene solution.

Although the yield of the spin adducts depended on the PMNB concentration, 10^{-2} mol dm^{-3} of PMNB was found to be sufficient to trap all the scavengeable radicals in the γ-irradiated cyclohexane–benzene mixtures. The yields of spin adducts increased linearly with dose up to ≈200 Gy. Therefore, the *G*-values were determined by irradiating 10^{-2} mol dm^{-3} PMNB solutions to a dose of 100 Gy. The decay of the spin adducts was so slow that it need not to be taken into account for the present determination of the yields of the free radicals by the spin trapping technique.

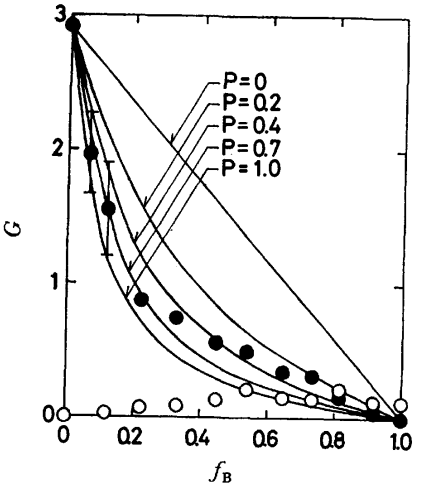

Fig. 2. Dependence of *G*-values of (●) cyclohexyl radical and (○) phenyl radical in γ-irradiated cyclohexane–benzene mixture on the mole fraction of benzene, f_B, at room temperature. The dependence was calculated from Eq. 2 for cyclohexyl radical, and shown by curves for the energy transfer efficiency, *P*, of 0, 0.2, 0.4, 0.7, and 1.0.

Figure 2 shows the G-values of cyclohexyl and phenyl radicals as a function of the mole fraction of benzene, f_B, in cyclohexane–benzene mixtures. The experimental points without error bars in Fig. 2 have an uncertainty of 20%, which comes from the rapid decay of the spin adducts due to a very minute amount of impurities. The larger error in the low benzene fraction region comes from the steep variation of a yield curve in this region. The addition of a small amount of benzene remarkably reduced the cyclohexyl radical yield, and the further addition of benzene reduced it only slowly. A similar dependence of f_B has been reported for the yields of products[3] and of the emission from excited cyclohexane.[7] The yield of phenyl radical increased with the increasing of f_B, passed a maximum at f_B of about 0.7, and decreased to the value in the pure benzene. These results indicate that the excitation energy transfer occurs efficiently from cyclohexane to benzene.

The relevant reaction scheme will be as follows:

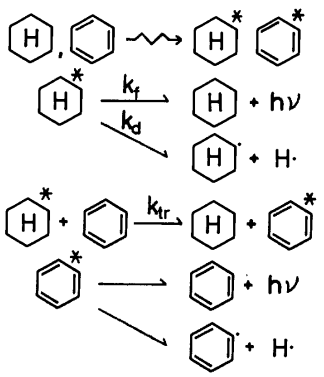

The cyclohexyl and phenyl radicals were spin-trapped and detected. H atoms will form simultaneously and react either with PMNB or with benzene to result in the formation of spin adducts of H or cyclohexadienyl radicals. However, they could not be detected, because the former are unstable[10] and the latter are not reactive with PMNB.[11]

Based on the reaction scheme, the yield of cyclohexyl radical, $G(C_6H_{11}\cdot)$, is given by the following relationship:

$$G(C_6H_{11}\cdot) = G_0(C_6H_{12}^*)\frac{k_d(1-f_B)}{k_f+k_d+k_{tr}[C_6H_6]}, \quad (1)$$

where $G_0(C_6H_{12}^*)$ represents the yield of singlet-excited cyclohexane in pure cyclohexane. Equation 1 leads to:

$$G(C_6H_{11}\cdot)/G_0(C_6H_{11}\cdot) = (1-f_B)/(1+P[C_6H_6]), \quad (2)$$

were $G_0(C_6H_{11}\cdot)$ is the yield of cyclohexyl radical in pure cyclohexane ($f_B=0$) and P is the energy transfer efficiency, $k_{tr}/(k_f+k_d)$. The curves expected from Eq. 2 are also shown in Fig. 2 for selected values of P. Although experimental points do not fall on a single curve, they show that $P=0.5\pm0.3$ mol^{-1} dm^3. The apparent deviation from the additive law (from the straight line for $P=0$) shows that some energy transfer occurs from cyclohexane to benzene.

The energy transfer efficiency has been determined to be 4[2] and 0.65—0.84 mol^{-1} dm^3 [3] by means of the conventional product analysis and 2.8 mol^{-1} dm^3 by using a radical scavenger such as DPPH and the fluorescence spectroscopic method.[7] The P values obtained in the present and previous steady-state studies are in satisfactory agreement. In contrast, a P value of as large as 60 mol^{-1} dm^3 has been reported based on the pulse radiolysis-transient optical emission study.[4] The reason for such a big difference between steady-state and transient methods is not known at the moment.

The yield of the phenyl radical, $G(C_6H_5\cdot)$, shows a peak at about 0.7 of f_B. The peak should appear if $G_0(C_6H_{12}^*)$ is larger than the yield of the singlet excited benzene in pure benzene ($f_B=1$), $G_1(C_6H_6^*)$, and P is larger than $G_1(C_6H_6^*)/\{G_0(C_6H_{12}^*)-G_1(C_6H_6^*)\}[C_6H_6]_1$ ($[C_6H_6]_1$ is the benzene concentration at $f_B=1$). $G_1(C_6H_6^*)$ has been reported to be 1.6.[12] On the other hand, the value of $G_0(C_6H_{12}^*)$ has not been unequivocally determined; it has been reported to be 1.4—1.7[13] and 0.3.[14] The latter value seems to be far too small to fulfill the condition for the $G(C_6H_5\cdot)$ peak to appear.

In conclusion, the spin trapping technique has provided a new approach to the energy transfer in the γ-irradiated cyclohexane–benzene mixture based on the G-values of free radicals involved. This study will show the validity of the quantitative, kinetic utilization of the spin trapping technique.

References

1) T. Wada and Y. Hatano, *J. Phys. Chem.*, **79**, 2210 (1975).
2) T. Wada and Y. Hatano, *J. Phys. Chem.*, **81**, 1057 (1977).
3) R. A. Holroyd, "Fundamental Processes in Radiation Chemistry," ed by A. Ausloos, Interscience, New York (1968), Chap. 7.
4) G. Beck and J. K. Thomas, *J. Phys. Chem.*, **76**, 3856 (1972).
5) T. Doba, S. Noda, and H. Yoshida, *Bull. Chem. Soc. Jpn.*, **52**, 21 (1979).
6) M. Shiotani, S. Murabayashi, and J. Sohma, *Int. J. Radiat. Phys. Chem.*, **8**, 483 (1976); F. P. Sargent and E. M. Gardy, *J. Phys. Chem.*, **80**, 854 (1976).
7) S. Horikiri and T. Saigusa, *Bull. Inst. Chem. Res. Kyoto Univ.*, **43**, 45 (1965).
8) T. Doba, T. Ichikawa, and H. Yoshida, *Bull. Chem. Soc. Jpn.*, **50**, 3124 (1977).
9) S. Noda, Y. Ohta, and H. Yoshida, *Bull. Chem. Soc. Jpn.*, **52**, 1916 (1979).
10) F. P. Sargent, E. M. Gardy, and H. R. Falle, *Chem. Phys. Lett.*, **24**, 120 (1974).
11) T. Ichikawa and H. Yoshida, *Bull. Chem. Soc. Jpn.*, **53**, 1169 (1980).
12) J. K. Thomas, *Int. J. Radiat. Phys. Chem.*, **8**, 1 (1976).
13) L. Walter and S. Lipsky, *Int. J. Radiat. Phys. Chem.*, **7**, 175 (1975).
14) J. H. Baxendale and J. Mayer, *Chem. Phys. Lett.*, **17**, 458 (1972).

The Ultraviolet Spectrophotometric Determination of Iron with 2-Thenoyltrifluoroacetone in an Aqueous Solution Containing α-Hydro-ω-dodecyloxynona(oxyethylene)

Tomitsugu TAKETATSU* and Atsuko SATO

College of General Education, Kyushu University, Ropponmatsu, Chuo-ku, Fukuoka 810

(Received April 21, 1980)

Synopsis. 2-Thenoyltrifluoroacetone is used as a spectrophotometric reagent for the iron(III) ion (0—1.5 μg ml^{-1}) in a 0.5% α-hydro-ω-dodecyloxynona(oxyethylene) aqueous solution at pH 3.2—3.8. The molar absorptivities of the iron(III) complex at 338, 388, and 500 nm are 4.75×10^4, 2.30×10^4, and 4.85×10^3 l mol^{-1} cm^{-1} respectively. Many diverse ions do not interfere.

The solvent extraction-spectrophotometric determination of the iron(III) ion with 2-thenoyltrifluoroacetone (TTA) is not practical because the extraction rate of the complex is slow.[1] Many investigators have, therefore, examined the effects of trioctylphosphine oxide (TOPO),[2] tributyl phosphate,[3] the thiocyanate ion,[4] pyridine,[5] and methyltrioctylammonium chloride[6] on the extraction of the iron (III)–TTA complex for the purpose of accelerating the extraction rate.

Recently, we have reported that Eu- and Sm–TTA–TOPO ternary complexes are readily soluble in an aqueous solution containing Triton X-100 and that the strong fluorescence originating from the ternary complexes can be applied to the determination of rare earths.[7] In the present paper, it is shown that iron(III) ions can be determined spectrophotometrically with TTA in an aqueous solution containing α-hydro-ω-dodecyloxynona(oxyethylene), $CH_3(CH_2)_{11}-O\{CH_2-CH_2-O\}_9H$, (BL-9EX). A constant absorption intensity is obtainable within a practical length of time, and the analytical sensitivity is considerably stronger than that of the corresponding extraction method, since the absorption maxima in the ultraviolet region are applicable to the measurement in the present method.

Experimental

Reagent and Apparatus. A standard solution of iron(III) ions was prepared by dissolving the analytical reagent-grade iron(III) chloride in 0.1 mol dm^{-3} hydrochloric acid. The concentration of the metal ions was determined by EDTA titration. A 1×10^{-2} M (1 M=1 mol dm^{-3}) TTA reagent solution was prepared by dissolving a known amount of the reagent (Dojin Co., Ltd.) in 100 ml of a 5% BL-9EX (Nikko Chemical Co., Ltd.) aqueous solution. An acetate buffer solution (pH 3.6) was prepared by adding 10 ml of a 0.1 M sodium acetate solution to 160 ml of 0.1 M acetic acid. All the other chemicals used were of an analytical reagent grade.

A Hitachi 200-20 automatic recording spectrophotometer and a Hitachi 100-10 manual spectrophotometer were used.

Procedure. A dilute hydrochloric acid solution containing 2—30 μg of iron(III) ions was transferred into a beaker. A 2-ml portion of the buffer solution and 2 ml of the TTA reagent solution were added to the beaker. After the pH of the solution had been adjusted to 3.2—3.8 with a dilute hydrochloric acid solution or a sodium hydroxide solution, the solution was transferred into a 20-ml volumetric flask and made up to volume with water. The absorbance was measured at 338 or 388 nm using 10-ml quartz cells. All experiments were done at 20—25 °C.

Results and Discussion

Absorption Spectra. Figure 1 shows the absorption spectrum of the iron(III)–TTA complex in the 0.5% BL-9EX aqueous solution (pH 3.3). The prominent wavelengths of the maxima of the spectrum are at 338 and 388 nm.

Effects of Reaction Variables. The variation in the absorbances at 338, 388, and 500 nm was investigated as a function of the pH. All the intensities at these wavelengths gave constants over the pH range of 3.0—4.0. The variation in the absorbance at 338 nm was examined as a function of the mole ratio of TTA to the iron(III) ion and as a function of the concentration of BL-9EX. The intensity was almost constant

TABLE 1. DETERMINATION OF FERRIC ION IN SYNTHETIC SAMPLES CONTAINING DIVERSE IONS

Diverse ions added,	μg	Fe^{3+} found, μg	error, μg	Diverse ions added,	μg	Fe^{3+} found, μg	error, μg
Mg^{2+}	111.0	1.16	+0.04	Cd^{2+}	11.1	1.11	−0.01
Ca^{2+}	111.0	1.09	−0.03	Pb^{2+}	11.9	1.09	−0.03
Mn^{2+}	11.2	1.07	−0.05	UO_2^{2+}	11.3	Serious interference	
Co^{2+}	11.2	1.18	+0.06	UO_2^{2+}	1.1	1.21	+0.09
Co^{2+}	1.1	1.08	−0.04	Al^{3+}	11.6	Serious interference	
Ni^{2+}	11.2	1.26	+0.15	Al^{3+}	1.2	1.78	+0.68
Ni^{2+}	1.1	1.10	−0.02	Al^{3+}	1.2	1.13	+0.01[a]
Cu^{2+}	11.2	Serious interference		Cr^{3+}	11.3	1.44	+0.33
Cu^{2+}	1.1	1.55	+0.43	Cr^{3+}	1.1	1.14	+0.02
Cu^{2+}	1.1	1.19	−0.07[a]	NO_3^-	113.3	1.09	−0.03
Zn^{2+}	11.1	1.16	+0.05	SO_4^{2-}	113.0	1.08	−0.04
Zn^{2+}	1.1	1.09	−0.03				

Fe^{3+} taken, 1.12 μg. a) Measured at 388 nm.

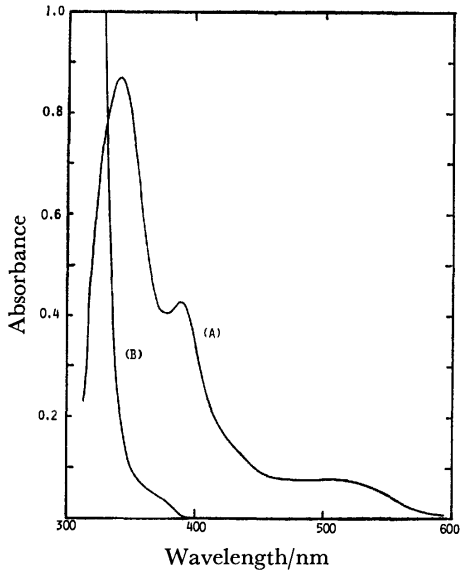

Fig. 1. Absorption spectrum of Fe(III)–TTA complex. (A) Fe(III)–TTA complex: Fe^{3+} 2×10^{-5} M, TTA 1×10^{-3} M, BL-9EX 0.5%, pH 3.3. (B) Reagent blank.

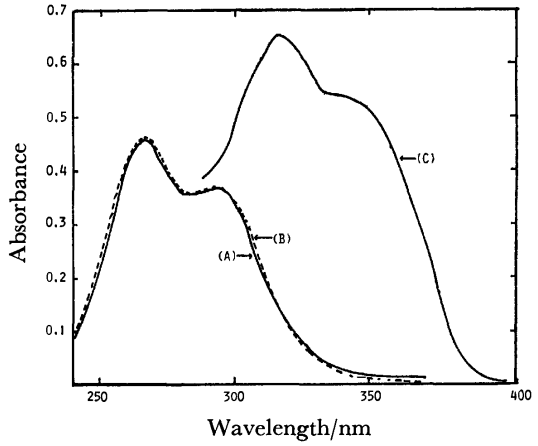

Fig. 2. Absorption spectra of TTA in aqueous solution containing BL-9EX, water, and organic solvents. (A) 0.5% BL-9EX, (B) water (pH 3.4), (C) *n*-heptane or carbon tetrachloride: TTA 5×10^{-5} M.

over the mole-ratio range of 20—100 for TTA to the iron(III) ion and also in the range of 0.2—1% of BL-9EX. With less than about 0.01%, the aqueous solution became turbid because of the precipitating of the complex. The intensity of the absorbance remained constant for 24 h after the preparation of the complex at 25 °C.

Calibration Curve. The absorbances at 338, 388, and 500 nm were linear functions of the concentration in the range of 0—1.5 μg ml^{-1} for the iron(III) ion. The molar absorptivities at the maximum wavelengths of 338, 388, and 500 nm are 4.75×10^4, 2.30×10^4, and 4.85×10^3 l mol^{-1} cm^{-1} respectively.

Effects of Diverse Ions. The effects of diverse ions on the absorbance (Fe^{3+}, 1.12 μg ml^{-1}) were investigated under the optimum conditions. Table 1 shows that 100-fold amounts of magnesium, calcium, nitrate, and sulfate ions, 10-fold amounts of manganese, cobalt, zinc, cadmium, lead, and cerium(III) ions, and equiamounts of nickel and chromium ions do not interfere with measuring the absorbance at 338 nm. However, equiamounts of copper, uranyl, and aluminum ions interfere seriously. The interference of the copper and aluminum ions can, though, be eliminated by measuring the absorbance at 388 nm.

Usually, 0.1—0.2 M TTA solutions in organic solvents are used for the extraction of the iron(III) complex, and so the ultraviolet absorption maxima (at 338 or 388 nm) adopted in the present method are inapplicable to the solvent-extraction method because the concentration of TTA in the reference solution is too high for the ultraviolet spectrum to be drawn. Therefore, the analytical sensitivity obtained by the present method is about ten times larger than that by the corresponding solvent-extraction method. Also, it is a convenience of the present method that the intensity of the absorption spectrum in the range of 320 to 390 nm of the TTA aqueous solution containing BL-9EX is considerably weak in comparison with that in the organic solvents, as is shown in Fig. 2. Also, the figure shows that the pattern of the absorption spectrum of TTA in an aqueous solution (pH 3.4) is scarcely affected by the exsistence of BL-9EX; on the other hand, the pattern of the spectra of these aqueous solutions is quite different from that in heptane or carbon tetrachloride. These facts indicate that most of the TTA exists outside the micelles, *i.e.*, in the bulk phase. After the complexation of the iron(III) ion with TTA, the metal complex can be easily taken in the micellar phase through the large micellar surface.

References

1) S. M. Khopkar and A. K. De, *Anal. Chim. Acta*, **22**, 223 (1960).
2) A. J. Fischman, H. L. Finston, and D. E. Goldberg, *J. Inorg. Nucl. Chem.*, **35**, 2497 (1973).
3) D. M. Raphael, H. L. Finston, and A. J. Fischman, *J. Inorg. Nucl. Chem.*, **35**, 2507 (1973).
4) H. L. Finston and Y. Inoue, *J. Inorg. Nucl. Chem.*, **29**, 199 (1967).
5) H. Akaiwa, H. Kawamoto, and M. Hara, *Anal. Chim. Acta.*, **43**, 297 (1968).
6) H. Kawamoto and H. Akaiwa, *Bunseki Kagaku*, **23**, 495 (1974).
7) T. Taketatsu and A. Sato, *Anal. Chim. Acta*, **108**, 429 (1979).

Optical Resolution of (2-Aminoethyl)butylphenylphosphine and the Absolute Configuration Assigned on the Basis of Circular Dichroism Spectra of Its Palladium(II) Complexes

Isamu KINOSHITA,† Kazuo KASHIWABARA, and Junnosuke FUJITA*

Department of Chemistry, Faculty of Science, Nagoya University, Chikusa, Nagoya 464

(Received May 27, 1980)

Synopsis. (2-Aminoethyl)butylphenylphosphine was resolved with $(+)_D$-di-μ-chlorobis[(*S*)-*N*,*N*-dimethyl-α-methylbenzylamine-2*C*,*N*]dipalladium(II), and the absolute configuration of the chiral phosphorus atom was assigned on the basis of the circular dichroism spectra of dichloro palladium(II) complexes with the resolved aminophosphine.

In recent years, chiral metal phosphine complexes have been widely utilized in various asymmetric syntheses for organic compounds.[1] While a tertiary aminoalkylphosphine also would be an effective ligand for such purposes, one with a chiral phosphorus atom has little been reported. We have succeeded in resolving (2-aminoethyl)butylphenylphosphine with a chiral palladium(II) complex which was developed for the optical resolution of monodentate[2] and bidentate[3] tertiary phosphines.

There has been no convenient way to assign the absolute configuration of a chiral phosphorus atom. In a previous paper,[4] we found a correlation between the absolute configuration of a pair of diastereomers of (*S*(C))-2-(butylphenylphosphinomethyl)pyrrolidine and the circular dichroism (CD) spectra of their palladium(II) complexes. In this note, we have assigned the absolute configuration of (2-aminoethyl)butylphenylphosphine by applying the correlation to the CD spectra of dichloro palladium(II) complexes with the resolved aminophosphine.

Experimental

Free aminophosphines were handled under nitrogen atmosphere until they formed palladium(II) complexes which were stable to air. Solvents were dried in the usual way and degassed by distillation in a stream of pure nitrogen. Absorption, CD, and ^{1}H and ^{13}C NMR spectra were recorded on a Hitachi 323 spectrophotometer, a JASCO J-40 spectropolarimeter, and JEOL PMX-60 and FX-60 spectrometers, respectively.

(2-Aminoethyl)butylphenylphosphine. Preparation: To liquid ammonia (250 cm^3) was added small pieces of sodium (2.3 g, 0.1 mol) and then (2-aminoethyl)diphenylphosphine (11.5 g, 0.05 mol)[5] with vigorous stirring. After 2 h, butyl bromide (14 cm^3, 0.11 mol) was added to the resulting deep red solution, the color of the solution turning gradually orange yellow. Liquid ammonia was evaporated off and the aminophosphine formed was extracted with diethyl ether. The extract was evaporated and distilled under reduced pressure to give colorless liquid, bp *ca.* 115°C/*ca.* 80 Pa. Yield: *ca.* 4.5 g (40%). Issleib and Oehme[6] prepared this aminophosphine from phenylphosphine.

Optical Resolution: To a benzene solution (15 cm^3) of $(+)_D$-di-μ-chlorobis[(*S*)-*N*,*N*-dimethyl-α-methylbenzylamine-2*C*,*N*]-dipalladium(II) (2.06 g)[2] was added a benzene solution (3 cm^3) of *rac*-(2-aminoethyl)butylphenylphosphine (1.49 g) with stirring. After a while, acetone was added to the solution to yield white precipitate which was filtered and washed with acetone. The precipitate was found from the ^{1}H NMR spectrum to be a pure diastereomer of [(*S*)-*N*,*N*-dimethyl-α-methylbenzylamine-2*C*,*N*][(2-aminoethyl)butylphenylphosphine]plladium(II) chloride, (**1a**). Yield: 1.26 g. Found: C, 52.97; H, 6.82; N, 5.58%. Calcd for $PdC_{22}H_{34}N_2PCl$: C, 52.91; H, 6.87; N, 5.61%. The filtrate was evaporated to dryness. The residue was mixed with boiling water (300 cm^3) and filtered. To the filtrate was added an aqueous solution (200 cm^3) of sodium hexafluorophosphate (1.8 g). This was stirred at 40 °C for 4 h and then at room temperature for 18 h. The resulting white precipitate was found from the ^{1}H NMR spectrum to be another optically pure diastereomer of the palladium(II) hexafluorophosphate, (**1b**). Yield: 2.0 g. Found: C, 43.42; H, 5.92; N, 4.54%. Calcd for $PdC_{22}H_{34}P_2F_6$: C, 43.39; H, 5.64; N, 4.60%.

The optically active free aminophosphines were obtained from **1a** and **1b** by adding excess sodium cyanide to the aqueous solutions and by extracting with diethyl ether.

Dichloro[(2-aminoethyl)butylphenylphosphine]palladium(II). Sodium cyanide (100 mg) was added to an aqueous solution (3 cm^3) of the less soluble diastereomer, **1a** (87 mg). The liberated aminophosphine was extracted with diethyl ether (3 cm^3) three times. The extract was mixed with an acetonitrile solution (30 cm^3) of $PdCl_2$ (30 mg) and filtered. The filtrate was evaporated to dryness and the residue was dissolved in a small amount of acetonitrile. The solution was chromatographed with an acidic alumina column and a mixture of acetonitrile and ethanol (4 : 1) for an eluent. The main yellow eluate was evaporated to dryness to give yellow residue which was recrystallized from a mixture of acetonitrile, diethyl ether, and petroleum ether. Yield: 29 mg. Found: C, 36.18; H, 5.20; N, 3.90%. Calcd for $PdC_{12}H_{20}NPCl_2 \cdot 1/2H_2O$: C, 36.43; H, 5.35; N, 3.54%.

[(S)-N,N-dimethyl-α-methylbenzylamine-2C,N][(2-aminoethyl)-diphenylphosphine]palladium(II) Chloride. This complex was prepared by the same method as that for the corresponding (2-aminoethyl)butylphenylphosphine complex. Found: C, 55.11; H, 5.79; N, 5.33%. Calcd for $PdC_{20}H_{38}N_2PCl$: C, 55.50; H, 5.83; N, 5.39%.

Results and Discussion

(2-Aminoethyl)butylphenylphosphine was resolved by forming a pair of diastereomers, **1a** and **1b**. The $(+)_D$-di-μ-chlorobis[(*S*)-*N*,*N*-dimethyl-α-methylbenzylamine-2*C*,*N*]dipalladium(II) complex is known to be a useful resolving reagent for various tertiary phosphines.[2,3] The separation of **1a** and **1b** was complete as evidenced by ^{1}H NMR spectra and both diastereomers were obtained in good chemical yields. For the planar [(*S*)-*N*,*N*-dimethyl-α-methylbenzylamine-2*C*,*N*][(2-aminoethyl)butylphenylphosphine]palladium(II) ion, there are two possible geometrical isomers; one has two

† Present address: Department of Chemistry, Faculty of Science, Osaka City University, Sumiyoshi, Osaka 558.

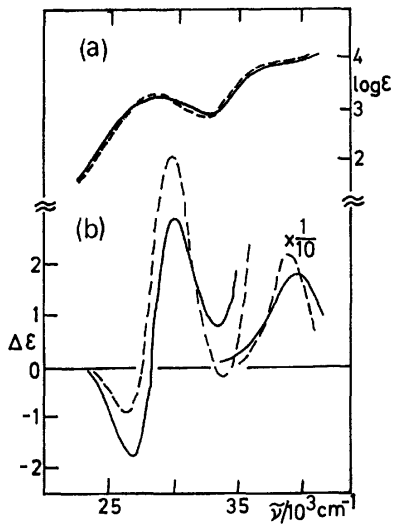

Fig. 1. (a) Absorption spectra of [$PdCl_2$-{(2-aminoethyl)-butylphenylphosphine}] (——) and [$PdCl_2$-{(*S*)-2-(butylphenylphosphinomethyl)pyrolidine}] (---). (b) CD spectrum of [$PdCl_2$-{(2-aminoethyl)butylphenylphosphine}] derived from diastereomer **1a** (——) and calculated vicinal CD curve due to the (*S*)-phosphorus atom in [$PdCl_2$-{(*S*)-2-(butylphenylphosphinomethyl)-pyrrolidine}] (----).[4]

nitrogen donor atoms in the trans positions, and the other those atoms in the cis positions. The **1a** and **1b** isomers show a similar pattern in the ^1H or ^{13}C NMR spectra, in which the long-range couplings between the phosphorus atom and the *N*-methyl protons or the *N*-methyl carbons are observed, respectively. Thus both isomers would have the phosphorus atom trans to the *N*-methyl nitrogen donor atom, the cis(*N*,*N*) configuration. The optically active free aminophosphine can be obtained from **1a** and **1b** by treating with sodium cyanide in water. The aminophosphines obtained from **1a** and **1b** form a pair of enantiomers of the dichloro palladium(II) complex.

In order to assign the absolute configuration of the chiral phosphorus atom, the CD spectrum of the dichloro palladium(II) complex of the aminophosphine obtained from the less soluble chloride, **1a** was compared with the vicinal CD curve for the (*S*)-phosphorus atom calculated from a pair of diastereomers of [$PdCl_2$-{(*S*(C)-2-(butylphenylphosphinomethyl)pyrrolidine}][4] (Fig. 1). The absolute configuration of the *R*(P)-isomer of the latter complex has been determined by the X-ray analysis.[4] Both curves in Fig. 1 are very similar and the absolute configuration of the phosphorus atom in the (2-aminoethyl)butylphenylphosphine complex given can

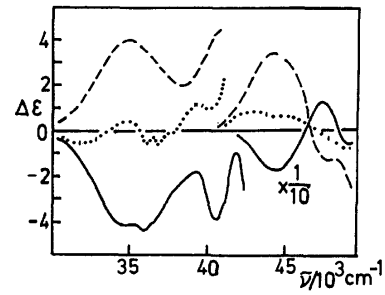

Fig. 2. CD spectra of diastereomers **1a** (——) and **1b** (------) of [Pd-{(*S*)-*N*,*N*-dimethyl-α-methylbenzylamine-2*C*,*N*}-{(2-aminoethyl)butylphenylphosphine}] and [Pd{(*S*)-*N*,*N*-dimethyl-α-methylbenzylamine-2*C*,*N*}-{(2-aminoethyl)diphenylphosphine}] (·····).

be assigned to the (*S*)-configuration. This assignment coincides with the previous one based on the ^1H NMR and CD spectra of the bis(acetylacetonato)cobalt(III) complex of (2-aminoethyl)butylphenylphosphine obtained from the same **1a** isomer.[7]

The CD spectra of diastereomers, **1a** and **1b** are nearly enantiomeric to each other over the whole region (Fig. 2). This indicates that the CD depends largely on the donating chiral phosphorus atom and little on the chiral cyclometallated amine ligand. In fact, the corresponding (2-aminoethyl)diphenylphosphine complex whose phosphorus atom is achiral shows very weak CD. Thus the absolute configuration of chiral phosphorus atoms of aminoalkylphosphines could be assigned from CD spectra of their dichloro- or more conveniently [(*S*)-*N*,*N*-dimethyl-α-methylbenzylamine-2*C*,*N*]palladium(II) complexes.

This work was supported by Grant-in-Aid for Scientific Research from the Ministry of Education (No. 454194) and The Kurata Research Grant of The Kurata Foundation.

References

1) D. Valentine, Jr., and J. W. Scott, *Synthesis*, **1978**., 329.
2) K. Tani, Leo D. Brown, J. Ahmed, J. A. Ibers, M. Yokota, A. Nakamura, and S. Otsuka, *J. Am. Chem. Soc.*, **99**, 7876 (1977).
3) N. K. Roberts and S. B. Wild, *J. Am. Chem. Soc.*, **101**, 6254 (1979).
4) I. Kinoshita, K. Kashiwabara, J. Fujita, T. Yamane, H. Ukai, and T. Ashida, *Bull. Chem. Soc. Jpn.*, **52**, 1413 (1979).
5) K. Issleib and D. Haferburg, *Z. Naturforschg*, **20b**, 916 (1965).
6) K. Issleib and H. Oehme, *Chem. Ber.*, **100**, 2685 (1976).
7) K. Kashiwabara, I. Kinoshita, and J. Fujita, *Chem. Lett.*, **1978**, 673.

Binuclear Metal Complexes. XXXV.[1] Synthesis and Magnetism of Binuclear Copper(II) Complexes with 3-[2-(Dialkylamino)ethylthio]-1-propanols

Masahiro MIKURIYA, Hisashi OKAWA,* and Sigeo KIDA

Department of Chemistry, Faculty of Science, Kyushu University 33, Hakozaki, Higashi-ku, Fukuoka 812

(Received June 2, 1980)

Synopsis. Binuclear copper(II) complexes with 3-[2-(dialkylamino)ethylthio]-1-propanols, $Cu[R_2N(CH_2)_2S(CH_2)_3O]X$ ($R=CH_3$, C_2H_5; $X=NO_3^-$, ClO_4^-), were prepared and their magnetic properties were investigated in the temperature range 80—300K. The magnetisms were interpreted in terms of the Bleaney-Bowers equation with exchange integral $-J=450$—$495\ cm^{-1}$, which is much larger than the values ($-J=\approx 250\ cm^{-1}$) for $Cu[R_2N(CH_2)_2NH(CH_2)_3O]X$.

As a part of the continuing study on binuclear copper(II) complexes mimic to type III copper,[2] we recently reported the synthesis and spectral and magnetic properties of the binuclear copper(II) complexes with *N*-[2-(alkylthio)ethyl]-3-amino-1-propanols, $Cu[RS(CH_2)_2NH(CH_2)_3O]X$ (abbreviated as Cu(R-sno)X, where R=alkyl, X=anion) (Fig. 1a).[3,4] It was shown that these complexes reveal a stronger antiferromagnetic spin-exchange interaction than the complexes with *N*-[2-(dialkylamino)ethyl]-3-amino-1-propanols (abbreviated as Cu(R-nno)X).[5,6] This suggests that the spin-spin coupling between the copper(II) ions is facilitated by substituting a sulfur donor atom for a nitrogen donor atom.[3,4] In order to examine further the sulfur donation effect on the spin-exchange interaction, we synthesized binuclear copper(II) complexes with 3-[2-(dialkylamino)ethylthio]-1-propanols, $Cu[R_2N(CH_2)_2S(CH_2)_3O]X$ (abbreviated as Cu(R-nso)X, where $R=CH_3$, C_2H_5; $X=ClO_4^-$, NO_3^-) (Fig. 1b) and investigated their magnetic properties in comparison with those of the Cu(R-sno)X and Cu(R-nno)X complexes.

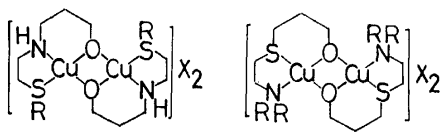

a b

Fig. 1. Structures of complexes.
(a) Cu(R-sno)X and (b) Cu(R-nso)X.

Experimental

Preparation of the Complexes. The ligands, $R_2N(CH_2)_2S(CH_2)_3OH$ ($R=CH_3$, C_2H_5) were prepared after the method described by Clinton *et al.*[7] Preparation of the complexes is exemplified by $Cu(CH_3\text{-nso})ClO_4$. Copper(II) perchlorate hexahydrate (186 mg) and 2,2-dimethoxypropane (2 cm^3) were mixed in absolute ethanol (4 cm^3) and allowed to stand at room temperature for one night in order to decompose water in the solution. This solution was added to a solution of CH_3-nsoH (163 mg) in absolute ethanol (5 cm^3). The mixture was allowed to stand for several days at room temperature to give black needles, which were collected and dried *in vacuo* over P_2O_5. Yield: 75 mg. The $Cu(R\text{-nso})NO_3$ complexes were prepared by a method similar to that for $Cu(R\text{-nso})ClO_4$. Analytical data of the complexes are given in Table 1.

Measurements. Infrared spectra were measured with a Hitachi Grating Infrared Spectrophotometer Model 215 on a KBr disk. Diffuse reflectance spectra were measured with a Shimadzu Multipurpose Spectrophotometer Model MSP-5000. Magnetic susceptibilities were measured by the Faraday method in the temperature range 80—300 K. All the susceptibilities were corrected for the diamagnetism of the constituting atoms by the use of Pascal's constants.[8] Effective magnetic moments were calculated from the equation, $\mu_{eff}=2.828\sqrt{(\chi_A-N\alpha)T}$, where χ_A is the atomic magnetic susceptibility and $N\alpha$ is the temperature-independent paramagnetism.

Results and Discussion

The complexes obtained were sparingly soluble in any conventional solvents. Hence, the electronic spectra of the complexes were measured by reflection on powder samples. The spectra display a fairly broad band centered around $15\times10^3\ cm^{-1}$ which is attributable to d-d transition bands. In addition, the spectra show a band at 22—$24\times10^3\ cm^{-1}$ characteristic of alkoxo-bridged structure.

The infrared spectra of $Cu(R\text{-nso})ClO_4$ showed a strong broad band at 1080—1140 cm^{-1}. Because of little splitting of this band, no coordination of the perchlorate ion to the copper is supposed.[9] The infrared spectra of $Cu(R\text{-nso})NO_3$ show a strong broad band at 1380 cm^{-1} and a sharp band at 820 cm^{-1}. Hence it is assumed that the nitrate ion does not coordinate to the metal.[10] Thus, it is likely that the present complexes possess a binuclear structure with a nearly planar $\overset{S}{N}\!>\!Cu\!<\!\overset{O}{O}\!>\!Cu\!<\!\overset{N}{S}$ skeleton.

Table 1. Analytical data

Complex	C(%) Found (Calcd)	H(%) Found (Calcd)	N(%) Found (Calcd)
$Cu(CH_3\text{-nso})ClO_4$	25.66 (25.85)	4.96 (4.96)	4.29 (4.31)
$Cu(C_2H_5\text{-nso})ClO_4$	30.34 (30.60)	5.80 (5.71)	3.92 (3.96)
$Cu(CH_3\text{-nso})NO_3$	28.90 (29.21)	5.57 (5.60)	9.57 (9.73)
$Cu(C_2H_5\text{-nso})NO_3\cdot 1/2H_2O$	32.99 (33.27)	6.31 (6.51)	8.53 (8.62)

Table 2. Magnetic data of Cu(R-nso)X[a)]

Complex	μ_{eff}/BM (293K)	$2J/cm^{-1}$	$N\alpha$/cgs emu	P
$Cu(CH_3\text{-nso})ClO_4$	0.48	−930	57×10^{-6}	2.2×10^{-2}
$Cu(C_2H_5\text{-nso})ClO_4$	0.58	−900	63×10^{-6}	4.5×10^{-2}
$Cu(CH_3\text{-nso})NO_3$	0.53	−910	59×10^{-6}	3.0×10^{-2}
$Cu(C_2H_5\text{-nso})NO_3\cdot1/2H_2O$	0.72	−990	66×10^{-6}	11.7×10^{-2}

a) For all the complexes $g=2.10$ is assumed.

Magnetic moments per copper atom are very low at room temperature, indicating that a fairly strong antiferromagnetic interaction is operating between copper(II) ions (Table 2). The magnetic susceptibility decreases with lowering of temperature but increases again below 150 K. This feature is most likely due to the binuclear structure and a small amount of mononuclear paramagnetic impurity. Accordingly, the impurity term was added to the Bleaney-Bowers equation[11] giving,

$$\chi_A = \frac{Ng^2\beta^2}{3kT}\left[1+\frac{1}{3}\exp(-2J/kT)\right]^{-1}(1-P) + \frac{0.45P}{T} + N\alpha \quad (1)$$

where χ_A is susceptibility per copper atom, P is the ratio of mononuclear copper(II) ions to total copper(II) ions, and other symbols have the usual meanings.[12] The magnetic data evaluated from the best fit of the experimental data to Eq. 1 are listed in Table 2. The results suggest that these complexes contain an appreciable amount of paramagnetic impurity. Since $Cu(C_2H_5\text{-nso})X$ ($X=ClO_4^-$, NO_3^-) are hygroscopic in the open atmosphere, partial decomposition might take place in these complexes. It is clear that the $-2J$ values for Cu(R-nso)X are more than 900 cm^{-1}. This magnetic behavior is essentially the same as that of Cu(R-sno)X ($-2J=ca.$ 800 cm^{-1}).[3,4] On the other hand, the binuclear copper(II) complexes with *N*-[2-(dialkylamino)ethyl]-3-amino-1-propanols, Cu(R-nno)X, show a weaker spin-exchange interaction; $-2J$ values being evaluated at 500 cm^{-1}.[5,6] Thus, it may be concluded that the binuclear copper(II) complexes with *SNO*- and *NSO*-donor sets exhibit a stronger antiferromagnetic spin-exchange interaction compared with the complexes with *NNO*-donor set.

References

1) Part XXXIV: M. Mikuriya, M. Aihara, Y. Nishi, H. Okawa, and S. Kida, *Chem. Lett.*, **1980**, 795.
2) J. A. Fee, *Struct. Bonding*, **23**, 1 (1975).
3) M. Mikuriya, H. Okawa, and S. Kida, *Inorg. Chim. Acta*, **34**, 13 (1979).
4) M. Mikuriya, H. Okawa, and S. Kida, *Inorg. Chim. Acta*, **42**, 233 (1980).
5) Y. Nishida and S. Kida, *Chem. Lett.*, **1974**, 339.
6) Y. Nishida, F. Numata, and S. Kida, *Inorg. Chim. Acta*, **11**, 189 (1974).
7) R. O. Clinton, C. M. Suter, S. C. Laskowski, M. Jackman, and W. Huber, *J. Am. Chem. Soc.*, **67**, 594 (1945).
8) A. Earnshaw, "Introduction to Magnetochemistry," Academeic Press, London (1968), pp. 5,6.
9) B. J. Hathaway and A. E. Underhill, *J. Chem. Soc.*, **1961**, 3091.
10) B. M. Gatehouse, S. E. Livingstone, and R. S. Nyholm, *J. Chem. Soc.*, **1957**, 4222.
11) B. Bleaney and K. D. Bowers, *Proc. R. Soc. London, Ser. A*, **214**, 451 (1952).
12) K. E. Hyde, G. Gordon, and G. F. Kokoszka, *J. Inorg. Nucl. Chem.*, **30**, 2155 (1968).

Catalysis by Heteropolyacid. V. Catalytic Alkylation of Toluene by Mixed-coordination type, $H_4[SiMo_{12-n}W_nO_{40}]$, Heteropolyacid

Kenji NOMIYA, Hidehiko SAIJOH, and Makoto MIWA*

Department of Industrial Chemistry, Faculty of Engineering, Seikei University, Musashino-shi, Tokyo 180

(Received June 5, 1980)

Synopsis. To compare the specific difference between molybdenum and tungsten ions on the catalytic reaction, we investigated the alkylation of toluene with benzyl chloride by mixed-metal heteropolyacids, $H_4[SiMo_{12-n}W_nO_{40}]$ (n=0, 1, 10, and 11). Molybdenum-rich compound is more active than tungsten-rich one.

Recently it has been reported that protonated form of Keggin-structure heteropolyanion, showing strong Brønsted acidity, catalyzes the polycondensation of benzyl alcohols[1] and the Friedel-Crafts-type reaction.[2] Among those heteropolyacids, the mixed-coordination type, which is constituted from two kinds of metal with original Keggin-framework retained and with the total number of metal unchanged, has been marked in comparison with original type. Not so many mixed-coordination compounds, which behave as Brønsted acid, have been known. Mo–W system is one of such examples. In order to examine the role of the metal constituting the Keggin-unit, we have prepared $H_4[SiMo_{12-n}W_nO_{40}]$-type compounds. The compounds corresponding to n=1, 10, and 11 showed the catalytic activity for the alkylation of toluene with benzyl chloride resulting in *o*- and *p*-tolylphenylmethane. In this paper, the data will be compared with those by saturated compounds of n=0 and 12. Molybdenum and tungsten ions have been known to form similar type of complexes and their chemistry has always been treated as an identical family. The heteropolyanions discussed here show the different catalytic activity, although the cause has not been clarified.

TABLE 1. ANALYTICAL RESULTS

$(n\text{-}Bu_4N)_4[SiMo_{12-n}W_nO_{40}]$	Found (Calcd) (%) C	H	N
n=1	26.03 (26.71	5.09 5.01	1.90 1.95)
n=10	20.59 (20.94	3.93 3.92	1.56 1.53)
n=11	20.42 (20.45	3.95 3.83	1.51 1.49)

TABLE 2. IR DATA OF $H_4[SiMo_{12-n}W_nO_{40}]$ (KBr disk, cm^{-1})

n=0	n=1	n=10	n=11	n=12	Assignment[5]
958	955	971	972	982	$\nu(M\text{–}O_d)$
910	908	915	915	930	$\nu(Si\text{–}O)$
860	855	870	870	885	$\nu(M\text{–}O\text{–}M)$
780	775	790	785	792	$\nu(M\text{–}O\text{–}M)$

The n=0, 1, and 12 compounds were prepared according to the literature,[3,4] and the n=10 and 11 compounds were obtained by its modification from the stoichiometric reaction of Na_2SiO_3, Na_2MoO_4 and Na_2WO_4 in aqueous acidic solution. The heteropolyanions were isolated as tetrabutylammonium salts and analyzed. The results are presented in Table 1. The characteristic IR bands of the anions in 1000—750 cm^{-1} region are listed in Table 2, indicating that the original Keggin-unit is retained. These are distinct from those of the mixtures of the n=0 and 12 compounds with corresponding molar ratios. For example, IR bands of the n=1 compound were shown in Fig. 1. These are clearly different from those of the mixture of the n=0 and 12 compounds with molar ratio of 11 : 1. The four-protonated forms of heteropolyanions identified by IR spectra were used for the alkylation reaction of toluene with benzyl chloride.

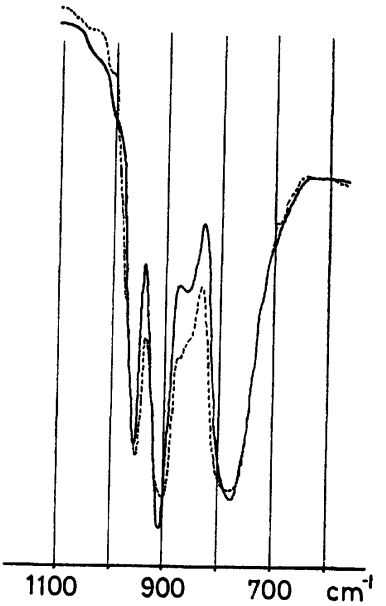

Fig. 1. IR spectra of the n=1 compound and the mixture of n=0 and 12 compounds with molar ratio of 11 : 1; full line : the n=1 compound, broken line : the mixture.

The reaction was performed at *ca.* 110 °C by refluxing the solution of toluene 92 g (1 mol) and benzyl chloride 6.3 g (0.05 mol) in the presence of the heteropolyacid of *ca.* 9.7×10^{-5} mol, where the molar ratio of reactant is designated to avoid the polymerization of benzyl chloride. Although heteropolyacids are undissolved in the solution, they promote the reaction homogeneously. The reaction time was unified to the sufficient time for the lowest active catalyst. After *ca.* 17 h, the reaction was stopped by cooling and the solution once filtered. By shaking the filtrate with chloroform, product and heteropolyacid were separated. Unreacted substrate and chloroform were removed by distillation. The products, *o*- and *p*-tolylphenylmethane, were obtained

Table 3. Experimental conditions and yields

Catalyst $H_4[SiMo_{12-n}W_nO_{40}]$	($\times 10^{-5}$ mol)	Reaction time h	Yields %
$n=0$	9.90	17.5	78
$n=1$	9.68	17.5	71
	9.44	17.0	60
$n=10$	9.92	17.0	56
	9.84	17.0	58
$n=11$	9.61	17.0	58
$n=12$	9.90	17.0	43

by reduced pressure-distillation of the residual solution (8 mmHg, 130 °C). Conditions and yields were presented in Table 3, the yields being estimated from the total amounts of products.

Generally, to compare a reactivity, it is necessary to obtain a rate constant in the initial reaction stage. However, observing the procedure of this experiment, it is not so far from the truth to discuss the activity by the yield at an appropriate time. In Table 3, the $n=0$ compound shows the maximum activity, whereas the $n=12$ compound does the minimum one, and the mixed-coordination compounds do the intermediate and almost equal activity. Moreover, it was shown that (1) all reactions proceed catalytically, (2) Mo-rich compound is more active than that of the W-rich one for the alkylation, however, (3) the activity is not always proportional to the number of exchanged or unexchanged metal.

The pH values of the aqueous solutions of the catalysts studied here have shown no significant difference.

References

1) K. Nomiya, T. Ueno, and M. Miwa, *Bull. Chem. Soc. Jpn.*, **53**, 827 (1980).
2) K. Nomiya, Y. Sugaya, S. Sasa, and M. Miwa, *Bull. Chem. Soc. Jpn.*, **53**, 2089 (1980).
3) E. O. North and W. Haney, *Inorg. Synth.*, Vol. I, p. 127.
4) M. Fiolwitz, R. K. C. Ho, E. G. Klemperer, and W. Shum, *Inorg. Chem.*, **18**, 93 (1979).
5) C. Rocchicciolo-Deltcheff, R. Touvenot, and R. Franck, *Spectrochim. Acta, Part A*, **32**, 587 (1976).

Synthetic Photochemistry. XXI.[1] The Sensitized Photooxygenation of Calarene. A Facile Hock Cleavage of an Allylhydroperoxide and Structure Revision for Aristolenols

Hitoshi TAKESHITA,* Isao SHIMOODA, and Toshihide HATSUI

Research Institute of Industrial Science, 86, Kyushu University, Hakozaki, Fukuoka 812

(Received March 28, 1980)

Synopsis. An allylic hydroperoxide formed by the sensitized photooxidation of calarene causes a Hock cleavage. A revised stereochemistry of an aristolenol is given on the basis of the direction of oxygenation.

Calarene (**1**),[2] an unconjugated vinyl cyclopropane, should be incapable of forming a dioxetane in a sensitized photooxygenation,[3] but its structural complexity may reveal some other features in the reactions. In fact, a keto aldehyde formed in the Methylene Blue (MB)-sensitized photooxidation of **1** was a Hock cleavage product.

When **1** and MB were irradiated in a mixture of chloroform and methanol (30 : 1) under an oxygen atmosphere by means of a tungsten lamp, a neat reaction occurred. The silica gel column separation of products yielded, together with an inseparable mixture of aristoladienes (**2a** and **2b**),[4,5] an allylic hydroperoxide (**3**), the major product, and a keto aldehyde (**4**). The separation of **2** from the hydrocarbon mixture was achieved by silver nitrate-impregnated silica-gel chromatography, and it was shown that the selenium dioxide oxidation of **1** also gave **2**. The structure of **3**, a colorless oil, was obtained by NMR [δ:[6] 0.59—0.85 (2H, m), 1.00 (3H, d, J=7 Hz), 1.03 (6H, s), 1.15 (3H, s), 1.1—2.7 (7H, m), 4.28 (1H, m), 5.56 (1H, m), and 7.62 (1H, s, OOH)] spectroscopy and chemical correlations; the sodium borohydride reduction of **3** yielded an oily allylic alcohol (**5**), which was further converted to an α,β-unsaturated ketone (**6**).[4] On the other hand, **4** was identical with the osmium(VIII) oxide-oxidation product of **1**. However, the photochemical formation of **4** is not related to a dioxetane; it was formed from **3** by either a contact with an acidic silica gel for 8 h or gentle heating in a chloroform solution, indicating it to be a Hock-cleavage product.[7,8]

Next, the Rose Bengal (RB)-sensitized oxygenation of **1** in a mixture of methanol and chloroform (1 : 30) mainly produced an ene-reaction product; a work-up after the sodium borohydride reduction yielded **5** (67%) and another allylic alcohol (**7**) (8.5%), which was subsequently oxidized to a known 1(10)-aristolen-2-one (**8**).[9-11] The stereochemistry of the hydroxy group of **7** is likely to be α-equatorial, judging from the large spin splittings revealed in its NMR spectrum, but it would be difficult to conclude the point from the limited evidence available at present. The absence of *cis*-glycol in this case also ruled out the intermediacy of dioxetane.[12] An attempted oxygenation in the dark resulted in the complete recovery of the starting material.

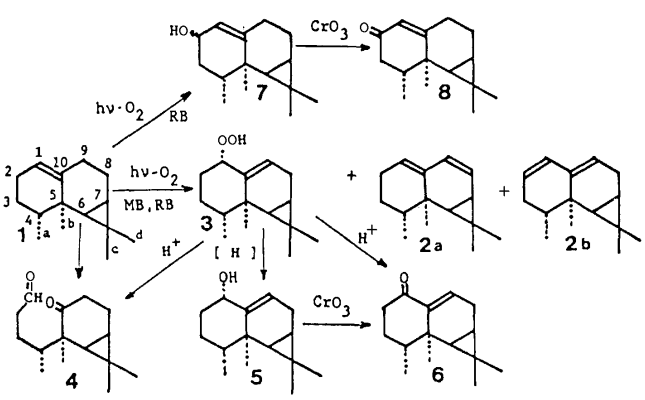

Scheme 1.

For the structure of crystalline allylic alcohol, **A** (designated as **1** in the original paper[4]), isolated from *Nardostachys chinensis* Betalin, Rücker and Kretzchmar have given the structure that we have assigned to **5**. However, the NMR spectrum of **5** taken in dimethyl-d_6 sulfoxide was different from that of **A**,[13] and so **5** might be an isomer of **A**. Mainly, the formulation **A** was deduced from the conformational analysis of the equatorial hydroxyl group. However, for the preferable conformation, an alternative may be possible. On the other hand, the β-configuration of the *gem*-dimethyl cyclopropane ring should prohibit the sterically hindered β-side attack of the oxygen, much as in the case of 2-carene.[14,15] This was supported by the chemical-shift difference for the methyl groups[16,17] on the ring-juncture of **3**, **5**, and **6**; two of the three sets of chemical-shift differences for the singlet methyls between **3** and **5**, $\Delta\delta_n$(3–5), were very small, but $\Delta\delta_b$(3–5), the difference of between the lowest methyl signals which are ascribable to the angular methyls, was significantly large, 1.15—1.23=−0.08. The $\Delta\delta_b$(5–6) value, the difference between **5** and **6**, is +0.16 or +0.24, in accord with only the α-orientation for the oxygen function. Otherwise, the $\Delta\delta_b$(5–6) is estimated to be less than +0.02.

Experimental

MB-sensitized Photooxidation of 1. a): Calarene[18] (**1**, 546 mg) was dissolved in MeOH (1 cm^3) and $CHCl_3$ (30 cm^3) containing MB (77 mg) and irradiated by means of a 500-W tungsten lamp under an oxygen atmosphere for 7 h. Then the mixture was chromatgraphed on a silica gel (Wako Gel C 200) column. From the fractions eluted by hexane we obtained hydrocarbons (**1** and **2**) (147 mg, 27%) and subsequently two colorless oils, **3** (108 mg, 30.5%) [Found: M.W., 236.1772. Calcd for $C_{15}H_{24}O_2$: 236.1776. ν: 3360 cm^{-1}] and **4** (48 mg, 13.5%)[M. W., 236.1802. Calcd for $C_{15}H_{24}O_2$: 236.1776. δ: 0.85 (3H, s), 0.89 (3H, d, J=7 Hz), 1.01 (3H, s), 1.25 (3H, s), 1.1—2.7 (11H, m), and 9.76 (1H, t, J=2 Hz). ν: 2720, 1730, 1710 cm^{-1}]. The hydrocarbon fractions were separated by the use of an $AgNO_3$-impregnated silica-gel column to give **1** (150 mg, 27%) and **2** (a colorless oil, 10 mg, 2.7%) [m/e, 202 (M^+). δ: 0.92 (3H, s), 0.96 (3H, s), 1.00

(3H, d, J=7 Hz), 1.10 (3H, s), 5.25 (1H, m), 5.6—5.9 (2H, m). ν: 1640, 1610, 980 cm^{-1}. λ_{max}^{hex}: 238 nm (ε=27000), 245 (28000)].

b): A mixture of MeOH (1 cm^3), $CHCl_3$ (30 cm^3), **1** (817 mg) and MB (77 mg) was irradiated by means of a tungsten lamp for 13 h under an oxygen atomsphere. The mixture was then diluted with water, extracted with ether, and treated with $NaBH_4$ (20 mg). Subsequent silica-gel chromatography of the product gave, besides the hydrocarbon mixture, two colorless oils **5** (260 mg, 50%) [Found: 220.1827. Calcd for $C_{15}H_{24}O$: 220.1827. δ: 0.5—0.9 (2H, m), 1.00 (3H, d, J= 7 Hz), 1.02 (6H, s), 1.23 (3H, s), 1.0—2.6 (8H, m), 4.17 (1H, m), and 5.42 (1H, m). δ $(CD_3)_2SO$: 0.5—0.8 (2H, m), 0.92 (3H, d, J=6.5 Hz), 0.98 (6H, s), 1.17 (3H, s), 1.07—2.45 (7H, m), 3.98 (1H, m), 4.29 (1H, d, J=2.3 Hz), and 5.28 (1H, m). ν: 3370 cm^{-1}] and **6** (25 mg, 5%) [Found: 218.1672. Calcd for $C_{15}H_{22}O$: 218.1671. δ: 0.6—0.85 (2H, m), 0.99—1.07 (12H, overlapped four methyls), 1.6—2.4 (7H, m), and 6.39 (1H, m). ν: 1690, 1623 cm^{-1}]. Further $AgNO_3$–silica-gel chromatography of the hydrocarbon fractions yielded **1** (333 mg, 41%) and **2** (32 mg, 6.7%).

SeO_2 Oxidation of 1 to 2. To a dioxane solution (15 cm^3) of **1** (175 mg), freshly sublimed SeO_2 (120 mg) was added, after which the mixture was refluxed for 1 h. Then, powdered $Na_2S_2O_3$ was added to the mixture. After the removal of the Se (50 mg) by filtration, the mixture was chromatographed on silica gel to get a hydrocarbon mixture (150 mg). $AgNO_3$-impregnated silica-gel chromatography gave recovered **1** (4 mg) and **2**, a colorless oil (127 mg, 74%). The sample of **2** was identical with those obtained by the photooxygenations (NMR, $AgNO_3$–silica gel, and gas-liquid chromatogram[19]).

RB-sensitized Photooxidation of 1. A mixture of MeOH (1 cm^3), $CHCl_3$ (30 cm^3), **1** (253 mg), and RB (30 mg) was irradiated by means of a tungsten lamp for 8.5 h. After treatment with $NaBH_4$ (50 mg), the mixture was chromatographed on a silica-gel column to give **5** (100 mg, 67%), **7** (colorless crystals, mp 84—86 °C (23 mg, 15%) [M. W., 220.1838. Calcd for $C_{15}H_{24}O$: 220.1827. δ: 0.47—0.8 (2H, m), 0.92 (6H, s), 0.95 (3H, d, J=7 Hz), 1.05 (3H, s), 3.93 (1H, br. m, $W_{h/2}$=14 Hz), 4.51 (1H, d, J=5.5 Hz), and 5.15 (1H, m). ν: 3620—3000 cm^{-1}]) and the recovered **1** (114 mg, 45%).

Conversion of 3 to 4. *a)*: To a hexane solution (5 cm^3) of **3** (25.4 mg), silica gel (Wako Gel C 200, 5 g) was added after which the mixture was kept at room temperature for 7 h. Subsequent extraction with ether gave **4** (12.3 mg).

b): A $CHCl_3$ solution (4 cm^3) of **3** (22.3 mg) was refluxed for 20 min. Subsequent evaporation of the solvent *in vacuo* gave **4** (22 mg).

Osmium(VIII) Oxide Oxidation of 1 to 4. To a solution of **1** (93 mg) in MeOH (5 cm^3), OsO_4 (100 mg) was added, after which the mixture was kept for 24 h. After treatment with $NaIO_4$ (215 mg) and H_2S, the mixture was chromatographed on a silica-gel column to give **4** (43 mg, 40%) which was identical with the sample of photochemical origin.

Jones Oxidation of 5 to Give 6. To a solution of CrO_3 (61 mg) and H_2SO_4 (1 cm^3) in acetone (10 cm^3), **5** (40 mg) was added. After 5 min, the mixture was treated with 2-propanol and extracted with ether. The colorless oil obtained by silica-gel column chromatography was **6**[4] (9 mg, 22%).

Jones Oxidation of 7 to Give Aristolenone (8). Similarly, **7** (12.1 mg) was dissolved in acetone (10 cm^3) containing CrO_3 and H_2SO_4, after which the mixture was oxidized for 5 min. Then, the mixture was treated with 2-propanol and extracted with ether. Silica-gel chromatography of the extract gave colorless crystals (mp 46—47 °C (lit, 39—42 °C,[9] 46.5—47.5 °C[10])), identified as **8** (5.6 mg, 46%), whose NMR NMR [δ: 0.68 (1H, d, J=9 Hz), 0.96 (3H, s), 1.02 (3H, s), 1.06 (3H, d, J=7 Hz), 1.0—2.6 (8H, m), 1.23 (3H, s), and 5.72 (1H, m)] were in accord with the previously reported figures.[9,10]

References

1) Part XX: H. Takeshita, I. Shimooda, and T. Hatsui, *Kyushu Daigaku Sogo Rikogaku Kenkyuka Hokoku*, **2**, 23 (1980).

2) G. Buchi, F. Grenter, and T. Tokoroyama, *Tetrahedron Lett.*, **1962**, 827.

3) For a verification of the dioxetane intermediate in the singlet-oxygen oxidation of the vinylcyclopropanes, see H. Takeshita, T. Hatsui, and H. Mametsuka, *Heterocycles*, **11**, 323 (1978).

4) G. Rücker and U. Kretzuschmar, *Ann. Chem.*, **748**, 214 (1971).

5) One of the isomers (**2b**) has been isolated from *Nardostachys chinensis Betalin*.[4]

6) All the NMR spectra, otherwise specified, were obtained in $CDCl_3$ solutions, and the chemical shifts were expressed in δ values from the internal standard, Me_4Si.

7) G. O. Schenck and K. H. Schulte-Elte, *Ann. Chem.*, **618**, 185 (1958).

8) K. Gollnick, "Advances in Photochemistry," **6**, 1 (1968).

9) G. Rücker, *Ann. Chem.*, **717**. 221 (1968).

10) R. Nishida and Z. Kumazawa, *Agric. Biol. Chem.*, **37**, 341 (1973).

11) G. Rücker and U. Kretzschmar, *Ann. Chem.*, **748**, 211 (1971).

12) H. Takeshita and T. Hatsui, *J. Org. Chem.*, **43**, 3080 (1978).

13) We are grateful to Professor G. Rücker for sending us copies of the spectral charts of **A** and the related compounds.

14) K. Gollnick and G. Schade, *Tetrahedron Lett.*, **1966**, 2335.

15) H. Takeshita and I. Kouno, *Kyushu Daigaku Seisan Kagaku Kenkyusho Hokoku*, **65**, 13 (1977).

16) a) W. Zürcher, *Helv. Chim. Acta*, **44**, 1380 (1961); **46**, 2054 (1963).

17) K. Tori and K. Aono, *Ann. Rept. Shionogi Research Lab.*, **14**, 136 (1964).

18) The starting material, **1**, was isolated from an unspecified luan oil, a generous gift of Professor Kyoichi Suga and Dr. Shoji Watanabe, Chiba University, to whom our thanks are due.

19) Gas-liquid chromatography on a glass capillary column (tricresyl phosphate at 115 °C) showed two peaks. However, **2** was rather unstable under the preparative chromatographic conditions. An attempted separation by means of a high-pressure liquid chromatograph (Micropolasil–hexane) was unsuccessful.

Application of the MTPA Method to Determination of Abusolute Stereochemistry. The Hydroxymethyl-substituted Chiral Carbon of Carbocycles

Yayoi SUGIMOTO, Takahiko TSUYUKI, Yoshihiko MORIYAMA,† and Takeyoshi TAKAHASHI*

Department of Chemistry, Faculty of Science, The University of Tokyo, Hongo, Bunkyo-ku, Tokyo 113

†*Institute of Chemistry, Kyoto Prefectural University of Medicine, Taishogun, Kita-ku, Kyoto 603*

(Received May 23, 1980)

Synopsis. Application of the MTPA method is extended to determination of the absolute configuration of primary alcohols such as furanoeremophilan-14-ol and 17β-(hydroxymethyl)androst-5-ene with a hydroxymethyl group on the chiral ring carbon atom of carbocycles.

Recently Yamaguchi and Yasuhara have developed a new convenient method for determination of the absolute configurations of secondary alcohols[1] and primary alcohols with the chiral center at the 2-position.[2] An optically active alcohol was converted to the corresponding (*R*)-(+)-α-methoxy-α-(trifluoromethyl)phenylacetic acid [(*R*)-(+)-MTPA; Mosher's reagent] ester (**A**) and (*S*)-(−)-MTPA ester (**B**) according to Mosher's method.[3] The magnitude of lanthanoid induced shift (LIS) by Eu(fod)$_3$-d_{27} for the methoxyl group of the (*R*)-(+)-MTPA ester (**A**) is larger than that of the (*S*)-(−)-MTPA ester (**B**) when the chiral center is in *R*-configuration. This generality is applicable to many optically active alcohols. However, successful application of this method to primary alcohols is limited to only acyclic carbinols having the chiral carbon atom at 2-position. In connection with a structural study of nigakialcohol,[4] we examined an applicability of this method for optically active primary alcohols in which a hydroxymethyl group is situated on the chiral ring carbon atom of a carbocycle. In this report, we wish to describe a successful application of this method to furanoeremophilan-14-ol (**1**) and 17β-(hydroxymethyl)androst-5-ene (**2**) with known absolute configurations.

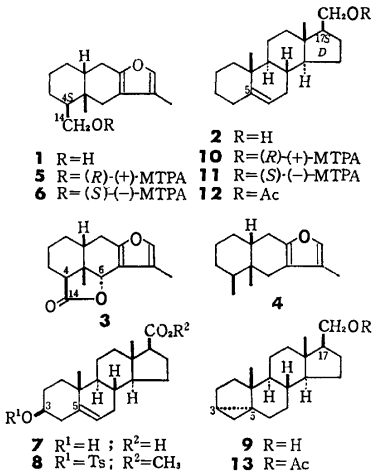

Furanoeremophilan-14,6α-olide (**3**), isolated from *Ligularia Hodgsoni* HOOK, f., has been converted to furanoeremophilan-14-ol (**1**),[5] whose absolute stereochemistry at C-4 has been established to be *S* by conversion of **1** into a known furanoeremophilane (**4**).[5] The primary alcohol (**1**) was transformed into the corresponding (*R*)-(+)-MTPA ester (**5**) and (*S*)-(−)-MTPA ester (**6**) by Mosher's method.[3] The LIS values of the methoxyl groups of **5** and **6** were given in Table 1. The ΔLIS_{OMe} value was negative (−0.97) for the diastereomeric MTPA esters of the alcohol (**1**), indicating that the chiral center at C-4 of **1** is in an *S*-configuration, in accordance with the reported stereochemistry.[5]

A cyclopentane D-ring of 17β-(hydroxymethyl)-androst-5-ene (**2**) has an asymmetric carbon atom at C-17 position which bears a hydroxymethyl group, the absolute configuration of this carbon atom being established to be *S*. This alcohol (**2**) was prepared from 3β-hydroxyandrost-5-ene-17β-carboxylic acid (**7**).[6] Esterification and tosylation gave methyl 3β-(tosyloxy)-androst-5-ene-17β-carboxylate (**8**), which on treatment with lithium aluminium hydride afforded a mixture of 17β-(hydroxymethyl)androst-5-ene (**2**)[7] and 17β-hydroxymethyl-3α,5α-cycloandrostane (**9**) in a ratio of *ca.* 1 : 1. Reduction with lithium triethylborohydride in tetrahydrofuran (Super-Hydride) gave the same mixture (**2** and **9**) in a ratio of *ca.* 2 : 1. The ΔLIS_{OMe} value of (*R*)-(+)- and (*S*)-(−)-MTPA esters (**10** and **11**) of 17β-(hydroxymethyl)androst-5-ene (**2**) was negative (−0.36) as shown in Table 1. This indicates that the asymmetric center at C-17 is in an *S*-configuration. From these observations, it is concluded that application of the MTPA method can be extended to primary alcohols such as **1** and **2** with a hydroxymethyl group on the chiral ring carbon of carbocycles.

TABLE 1. LANTHANOID INDUCED SHIFT (LIS) VALUES OF THE METHOXYL GROUP IN THE ACID MOIETY FOR (*R*)-(+)- AND (*S*)-(−)-MTPA ESTERS OF **1** AND **2**

Original alcohol	Furanoeremophilan-14-ol (**1**)		17β-(Hydroxymethyl)androst-5-ene (**2**)	
MTPA esters in CCl_4 (mmol/ml)	(*R*)-(+)- (**5**) 0.12	(*S*)-(−)- (**6**) 0.14	(*R*)-(+)- (**10**) 0.18	(*S*)-(−)- (**11**) 0.17
LIS_{OMe} value[a]	6.81	7.78	5.30	5.66
ΔLIS_{OMe} value	−0.97		−0.36	
Absolute configuration	(4*S*)		(17*S*)	

a) Determined at the molar ratio of Eu(fod)$_3$-d_{27}/each MTPA ester (1 : 1) at 60 MHz.

Experimental

Melting points were measured on a Mel-temp capillary melting point apparatus (Laboratory Devices) and were uncorrected. IR spectra were measured using a Hitachi 260-30 spectrometer. Mass spectra (MS) were taken on a Hitachi RMU-6-Tokugata mass spectrometer at 70 eV with a direct inlet system and high resolution mass spectra on a JMS-D300 (JEOL) mass spectrometer. Relative intensities are expressed in % in parentheses. ^{1}H NMR spectra were measured on a Hitachi R-20B (60 MHz) or a Varian EM-390 (90 MHz) spectrometer with TMS as an internal standard. Thin layer chromatography (TLC) was carried out on Kieselgel GF_{254} (E. Merck). Wakogel C-200 (Wako) was used for silica gel column chromatography.

(R)-(+)- and (S)-(−)-MTPA Esters (5 and 6) of Furanoeremophilan-14-ol (1). Furanoeremophilan-14-ol[5] (**1**; 21.6 mg and 18.7 mg) was converted into (*R*)-(+)-MTPA ester (**5**; 17.3 mg, 42% yield) and (*S*)-(−)-MTPA ester (**6**; 27.1 mg, 75% yield) by the usual method.[3] (*R*)-(+)-MTPA ester (**5**): an oil, IR (liq) 1742, 1640, and 1562 cm^{-1}; ^{1}H NMR (60 MHz) δ (CCl_4) 1.00 (3H, s), 1.87 (3H, d, J=2 Hz), 3.53 (3H, $-OCH_3$), *ca.* 4.2—4.6 (2H, m), 6.95 (1H, m), and *ca.* 7.3—7.7 (5H, m); MS *m/e* 450 (M^+) and 189 (100). (*S*)-(−)-MTPA ester (**6**): an oil, IR (liq) 1742, 1642, and 1562 cm^{-1}; ^{1}H NMR (60 MHz) δ (CCl_4) 1.01 (3H, s), 1.88 (3H, d, J= 2 Hz), 3.53 (3H, $-OCH_3$), *ca.* 4.0—4.8 (2H, m), 6.95 (1H, m), and *ca.* 7.3—7.7 (5H, m); MS *m/e* 450 (M^+) and 189 (100).

Methyl 3β-(Tosyloxy)androst-5-ene-17β-carboxylate (8). Methyl 3β-hydroxyandrost-5-ene-17β-carboxylate (30.4 mg), prepared from pregnenolone *via* 3β-hydroxyandrost-5-ene-17β-carboxylic acid (**7**),[6] was treated with tosyl chloride (45.4 mg) in pyridine (8 ml) at room temperature overnight. To the reaction mixtrure, dichloromethane was added and the solution was washed with dilute hydrochloric acid. The organic layer was worked up as usual and the residue was subjected to separation by preparative TLC (developed with diethyl ether–hexane, 1 : 1) to give a tosylate (**8**; 40.5 mg), mp 143.5—144.5 °C (from diethyl ether); IR (Nujol) 1707, 1198, and 1172 cm^{-1}; ^{1}H NMR (90 MHz) δ ($CDCl_3$) 0.67, 0.98, 2.44, 3.67 (each 3H, s), 4.30 (1H, m), 5.28 (1H, m), and 7.30 (2H, d, J=8.5 Hz); MS *m/e* 314 (M−TsOH)$^+$ and 299. No molecular ion peak was observed.

17β-(Hydroxymethyl)androst-5-ene (2). Super-Hydride (0.5 ml; 1 M lithium triethylborohydride solution in tetrahydrofuran, Aldrich) was added to a solution of the tosylate (**8**; 30.0 mg) in tetrahydrofuran (2 ml) and the solution was refluxed for 3 h under nitrogen. Usual work-up afforded a mixture (17.0 mg) of 17β-(hydroxymethyl)androst-5-ene (**2**) and 17β-hydroxymethyl-3α,5α-cycloandrostane (**9**) in a ratio of *ca.* 2 : 1. To the mixture acetic anhydride (3 ml) and pyridine (10 drops) were added and the reaction mixture was stirred overnight at room temperature. After the usual work-up, the reaction product was purified by preparative TLC (developed with hexane–diethyl ether, 4 : 1) to give a mixture (20.3 mg) of acetates (**12** and **13**). This procedure was repeated and two crops of the acetate mixture (**12** and **13**) were combined. The combined mixture (39.7 mg) was subjected to separation by column chromatography on silica gel (15 g) impregnated with 20% silver nitrate. Elution with a mixture of hexane–diethyl ether (19 : 1) gave 5-ene acetate (**12**; 21.3 mg), 3α,5α-cyclo acetate (**13**; 10.2 mg), and a mixture (10.0 mg) of **12** and **13**. **12**: mp 78—79.5 °C (from hexane); IR (Nujol) 1742 cm^{-1}; ^{1}H NMR (90 MHz) δ ($CDCl_3$) 0.67, 1.00, 2.01 (each 3H, s), 4.03 (2H, d-like, J=7 Hz), and 5.23 (1H, m); MS *m/e* 330 (M^+; 92), 270 (26), and 255 (100); Found: *m/e* 330.2568. Calcd for $C_{22}H_{34}O_2$: M, 330.2558. **13**: mp 60—64 °C (from hexane); IR (Nujol) 1742 cm^{-1}; ^{1}H NMR (90 MHz) δ ($CDCl_3$) 0.20—0.55 (3H, m), 0.67, 0.91, 2.02 (each 3H, s), and 4.12 (2H, dd, J=15 and 6 Hz); MS *m/e* 330 (M^+; 77), 270 (32), and 255 (100); Found: *m/e* 330.2555. Calcd for $C_{22}H_{34}O_2$: M, 330.2558.

17β-(Acetoxymethyl)androst-5-ene (**12**; 90 mg) was heated with an excess of lithium aluminium hydride in tetrahydrofuran (5 ml) under reflux for 30 min. The reaction mixture was worked up as usual to give 17β-(hydroxymethyl)androst-5-ene (**2**; 78.4 mg) quantitatively, mp 136—137.5 °C (from diethyl ether–hexane); IR (Nujol) 3380 cm^{-1}; ^{1}H NMR (90 MHz) δ ($CDCl_3$) 0.67, 1.01 (each 3H, s), 3.60 (2H, m), and 5.25 (1H, m); MS *m/e* 288 (M^+; 100), 273 (96), and 255 (38); Found: C, 83.47; H, 11.19%. Calcd for $C_{20}H_{32}O$: C, 83.27; H, 11.18%.

(R)-(+)- and (S)-(−)-MTPA Esters (10 and 11) of 2. (*R*)-(+)-MTPA ester (**10**; 36.9 mg, 96% yield) and (*S*)-(−)-MTPA ester (**11**; 30.4 mg, 87% yield) were prepared from 17β-(hydroxymethyl)androst-5-ene (**2**; 22 mg and 20 mg, respectively).[3] **10**: IR (liq) 1751 cm^{-1}; ^{1}H NMR (60 MHz) δ (CCl_4) 0.68, 0.97 (each 3H, s), 3.49 (3H, $-OCH_3$), 4.20 (2H, m), 5.15 (1H, m), and *ca.* 7.2—7.6 (5H, m); MS *m/e* 504 (M^+; 100) and 255 (63). **11**: IR (liq) 1751 cm^{-1}; ^{1}H NMR (60 MHz) δ (CCl_4) 0.62, 0.97 (each 3H, s), 3.51 (3H, $-OCH_3$), 4.18 (2H, m), 5.16 (1H, m), and *ca.* 7.1—7.6 (5H, m); MS *m/e* 504 (M^+; 87) and 255 (100).

References

1) S. Yamaguchi and F. Yasuhara, *Tetrahedron Lett.*, **1977**, 89; S. Yamaguchi, F. Yasuhara, and K. Kabuto, *Tetrahedron*, **32**, 1363 (1976).

2) F. Yasuhara and S. Yamaguchi, *Tetrahedron Lett.*, **1977**, 4085.

3) J. A. Dale and H. S. Mosher, *J. Am. Chem. Soc.*, **85**, 512 (1973); J. A. Dale, D. L. Dull, and H. S. Mosher, *J. Org. Chem.*, **34**, 2543 (1969).

4) Y. Sugimoto. T. Sakita. Y. Moriyama, T. Murae, T. Tsuyuki, and T. Takahashi, *Tetrahedron Lett.*, **1978**, 4285; Y. Sugimoto, T. Sakita, T. Ikeda, Y. Moriyama, T. Murae, T. Tsuyuki, and T. Takahashi, *Bull. Chem. Soc. Jpn.*, **52**, 3027 (1979).

5) Y. Ishizaki, Y. Tanahashi, T. Takahashi, and K. Tori, *Chem. Commun.*, **1969**, 551; Y. Ishizaki, Y. Tanahashi, T. Tsuyuki, T. Takahashi, and K. Tori, *Bull. Chem. Soc. Jpn.*, **52**, 1182 (1979).

6) J. Staunton and E. J. Eisenbraun, *Org. Synth.*, **42**, 4 (1962).

7) Reduction of 17β-methoxycarbonyl group of androst-5-ene and 5α-androstane derivatives with lithium aluminium hydride gives 17β-hydroxymethyl derivatives. *Cf.* J. Hora and V. Cerny, *Collect. Czech. Chem. Commun.*, **30**, 1169 (1965); F. Sallmann and Ch. Tamm, *Helv. Chim. Acta*, **39**, 1340 (1956).

The Direct Alkylamination of 1-Aminoanthraquinone Promoted by Cobalt(II) Chloride

Katsuhira Yoshida,* Masaru Matsuoka,*,† Yoshio Yamashita, Shoichi Nagamori, and Teijiro Kitao†

Department of Chemistry, Faculty of Science, Kochi University, Akebono-cho, Kochi 780

†*Department of Applied Chemistry, College of Engineering, University of Osaka Prefecture, Sakai, Osaka 591*

(Received May 28, 1980)

Synopsis. The reaction of 1-aminoanthraquinone with primary aliphatic amines in the presence of cobalt(II) chloride under atmospheric oxygen preferentially gave the corresponding 1-amino-4-(alkylamino)anthraquinones. The reaction did not proceed with aqueous ammonia, bidentate amines, secondary aliphatic amines, and primary arylamines. While, with alicyclic amines the reaction mainly afforded 1-amino-2,4-bis(alkylamino)anthraquinones.

In our previous paper,[1] we have reported a novel direct 4-butylamination of 1-aminoanthraquinone (**1**) promoted by metal ions and proposed the possible mechanism of the reaction: the formation of a metal complex, in which the 1-amino and 9-carbonyl groups of **1** coordinate to the metal ion, increases the electrophilicity of the substituted anthraquinone nucleus and facilitates the nucleophilic attack of butylamine to the 4-position. This direct amination appeared to be a convenient method to introduce amino groups to the anthraquinone nucleus of **1**.

In this paper, similar reactions of **1** with various amines in the presence of cobalt(II) chloride under atmospheric oxygen are examined. The results are summarized in Table 1.

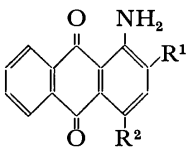

Compd No.	Substituent R¹	Substituent R²
1	H	H
2	H	NH_2
3	H	NHMe
4	H	*n*-BuNH
5	H	*s*-BuNH
6	H	$CH_3(CH_2)_7NH$
7	$CH_3(CH_2)_7NH$	H
8	H	$C_6H_{11}NH$
9	H	$PhCH_2NH$
10	piperidino	piperidino
11	morpholino	morpholino

The reaction of **1** with aqueous ammonia was unsuccessful, while almost primary aliphatic amines reacted with **1** to give the corresponding 1-amino-4-(alkylamino)anthraquinones, which are valuable as dyes and dye intermediates. The reaction of **1** with 40% aqueous methylamine gave 1-amino-4-(methylamino)anthraquinone (**3**) in 39% yield along with a 47% recovery of **1** after 26 h at 30 °C. 1,4-Diaminoanthraquinone (**2**) formed by the demethylation of **3** was also obtained in 8.2% yield. The dealkylation of alkylamino group in 1-amino-4-(alkylamino)anthraquinone was generally observed in the other cases. Especially, with benzylamine the reaction gave **2** (29% yield), the dealkylation product of **9**, much more than the expected 1-amino-4-(benzylamino)anthraquinone (**9**) (5.5%). The reaction of **1** with 1-octylamine was also successful. From the column chromatography of the products, unchanged **1** (45%), 1-amino-4-(octylamino)anthraquinone (**6**) (34%), 1-amino-2-(octylamino)anthraquinone (**7**) (2.4%), and a trace amount of **2** were isolated. The formation of **7**, though only a small amount, suggests that not only the 4-position but also the 2-position of **1** is activated by the formation of a chelate complex between **1** and the cobalt(II) ion. However, with the other primary aliphatic amines the reaction gave only the 4-aminated products but not the 2-aminated products.

The preferential 4-amination may be assisted by the formation of hydrogen-bonding between the *N*-hydrogen atom of alkylamino group and the oxygen atom of the 10-carbonyl group, as suggested in our previous paper.[1]

The amination proceeded smoothly with primary aliphatic amines, while, with bidentate amines such as

Table 1. Alkylamination of 1-aminoanthraquinone (**1**) in the presence of $CoCl_2$[a]

Run	Amine	Temp °C	Time h	Recovery/% (**1**)	Aminated products/% Yield: 4-Isomer	2-Isomer	2,4-Isomer	(**2**)
1	CH_3NH_2[b]	30	26	47	(**3**) 39	0	0	8.2
2	*n*-$BuNH_2$	30	8	0	(**4**) 79	0	0	trace
3	*s*-$BuNH_2$	30	50	47	(**5**) 38	0	0	trace
4	$CH_3(CH_2)_7NH_2$	30	30	45	(**6**) 34	(**7**) 2.4	0	trace
5	$C_6H_{11}NH_2$	40	20	44	(**8**) 52	0	0	trace
6	$PhCH_2NH_2$	40	12	53	(**9**) 5.5	0	0	29
7	Piperidine[c]	30	70	13	—	—	(**10**) 58	0
8	Morpholine[c]	40	48	83	—	—	(**11**) 9.1	0
9	Morpholine[c]	40	170	49	—	—	(**11**) 23	0

a) Reactant **1** (9 mmol) was stirred in pyridine (20 ml) with amine (30 ml) and $CoCl_2$ (9 mmol). b) 40% Aqueous methylamine solution (60 ml) was used as reactant and pyridine (60 ml) was added as solvent. c) Piperidine (50 ml) or morpholine (50 ml) was used as reactant without solvent. An addition of pyridine as solvent rather depressed the yields of products.

ethylenediamine and 2-aminoethanol the amination did not proceed. It is reasonable to consider that the cobalt ion is preferentially combined with bidentate amines than with **1**, because the bidentate amines can act as an effective chelating agent. Therefore, the formation of the cobalt complex of **1** was disturbed and the amination was inhibited.

Aromatic amines also did not react with **1**. This lack of reactivity is probably due to the lower nucleophilicity of arylamines compared to the alkylamines. These facts support the nucleophilic attack of alkylamines to the substituted anthraquinone nucleus activated by the formation of a cobalt complex. With diethylamine the amination was also unsuccessful and no amination products were obtained. The lack of reactivity of diethylamine may be attributed to a steric hindrance.

The attack of alkylamine at the 4-position of **1** would cause a considerable steric crowding. Therefore, the increase in the size of the alkyl residue may decrease the reactivity of the amine. For example, *s*-butylamine was much less reactive than *n*-butylamine in spite of their similar basicities. Thus, both the basicity and the size significantly affected the reactivity of amines.

Reaction of **1** with alicyclic amines was very specific and afforded the corresponding 1-amino-2,4-bis(alkylamino)anthraquinones. Trace amounts of some by-products were also noted on chromatography but could not be identified.[2] The cause of the differences in the amination products between primary aliphatic amines and alicyclic amines are not yet clear.

The structure of compounds (**10** and **11**) were confirmed by the elementary analysis, ^{1}H-NMR spectra, and the alternative synthesis of the compounds from 1-amino-2,4-dibromoanthraquinone with the corresponding amines.

Experimental

All the melting points are uncorrected. The visible spectra in methanol solution were measured using a Hitachi EPS-3T spectrometer.

The ^{1}H-NMR spectra were taken on a JEOL Model MH-100 spectrometer with TMS as an internal standard. Elemental analyses were recorded on a Yanaco CHN recorder MT-2. Column chromatography was carried out on activated alumina (Sumitomo KCG-30) using xylene as an eluent.

Reaction Procedure. The general procedure is as follows. A mixture of **1** (9 mmol), $CoCl_2$ (9 mmol), amine (30 ml), and pyridine (20 ml) was stirred in an open flask. After the reaction, the solvent and the excess amine were distilled off under reduced pressure. The mixture was poured into an aqueous NaOH solution (pH=10), and then H_2S gas was introduced into the solution to decompose a chelate complex of the products. The separated precipitate was filtered, washed with water and dried. The crude products were extracted with xylene, separated by column chromatography and recrystallized from benzene.

Characterization and Identification of Products. Compound **2** was identified by comparison with the authentic sample obtained from commercial source. Some properties of the compounds (**3**,[3] **4**,[1] and **8**[4]) were already known, and these were identified by the data described in the literature together with additional following data.

3: ^{1}H-NMR ($CDCl_3$) δ=3.07 (3H, d, $-CH_3$), 6.8—7.2 (4H, m, $H^{2,3}$, and NH_2), 7.68 (2H, m, $H^{6,7}$), 8.30 (2H, m, $H^{5,8}$), 10.45 (1H, b, N<u>H</u>-Me).

8: ^{1}H-NMR ($CDCl_3$) δ=1.0—2.3 (10H, m, $-(CH_2)_5-$), 3.64 (1H, m, -NH-C<u>H</u>-), 6.9—7.4 (4H, m, $H^{2,3}$ and NH_2), 7.85 (2H, m, $H^{6,7}$), 8.50 (2H, m, $H^{5,8}$), 11.12 (1H, b, -N<u>H</u>-).

1-Amino-4-(s-butylamino)anthraquinone (5): Mp 135—136 °C. UV_{max} (CH_3OH), nm, 573 (ε 15400), 616 (ε 18100). Found: C, 73.61; H, 6.33; N, 9.27%. Calcd for $C_{18}H_{18}N_2O_2$: C, 73.45; H, 6.16; N, 9.52%. ^{1}H-NMR ($CDCl_3$) δ=1.03 (3H, t, $-CH_3$), 1.34 (3H, d, $-CH_3$), 1.71 (2H, m, $-CH_2-$), 3.76 (1H, m, -CH-), 7.0—7.4 (4H, m, $H^{2,3}$ and NH_2), 7.80 (2H, m, $H^{6,7}$), 8.46 (2H, m, $H^{5,8}$), 11.06 (1H, b, N<u>H</u>- *s*-Bu).

1-Amino-4-(octylamino)anthraquinone (6): Mp 112.5—113.5 °C. UV_{max} 573 (ε 14400), 617 (ε 17000). Found: C, 75.49; H, 7.54; N, 7.63%. Calcd for $C_{22}H_{26}N_2O_2$: C, 75.40; H, 7.48; N, 7.99%. ^{1}H-NMR ($CDCl_3$) δ=0.84 (3H, t, $-CH_3$), 1.1—1.9 (12H, m, $-(CH_2)_6-$), 3.32 (2H, q, -NH-C<u>H</u>$_2$-), 6.8—7.2 (4H, m, $H^{2,3}$ and NH_2), 7.64 (2H, m, $H^{6,7}$), 8.30 (2H, m, $H^{5,8}$), 10.73 (1H, b, N<u>H</u>-Octyl).

1-Amino-2-(octylamino)anthraquinone (7): Mp 197—198 °C. UV_{max} 539 (ε 10700). Found: C, 74.88; H, 7.67; N, 7.78%. Calcd for $C_{22}H_{26}N_2O_2$: C, 75.40; H, 7.48; N, 7.99%. ^{1}H-NMR (DMSO-d_6) δ=0.89 (3H, t, $-CH_3$), 1.0—1.9 (12H, m, $-(CH_2)_6-$), 3.20 (2H, q, NH-C<u>H</u>$_2$-), 6.13 (1H, b, N<u>H</u>-Oc), 6.56 (1H, d, H^3), 7.59 (1H, d, H^4), 7.70 (2H, m, $H^{6,7}$), 8.0—8.4 (4H, m, $H^{5,8}$ and NH_2).

1-Amino-4-(benzylamino)anthraquinone (9): Mp 167.0—167.5 °C. UV_{max} 571 (ε 13800), 613 (ε 15200). Found: C, 76.62; H, 4.90; N, 8.17%. Calcd for $C_{21}H_{16}N_2O_2$: C, 76.81; H, 4.91; N, 8.53%. ^{1}H-NMR ($CDCl_3$) δ=4.62 (2H, d, $-CH_2-$), 6.7—7.2 (4H, m, $H^{2,3}$ and NH_2), 7.32 (5H, s, C_6H_5), 7.71 (2H, m, $H^{6,7}$), 8.36 (2H, m, $H^{5,8}$), 11.00 (1H, b, -NH-).

1-Amino-2,4-dipiperidinoanthraquinone (10): Mp 145—145.5 °C. UV_{max} 580 (ε 8200). Found: C, 73.85; H, 7.04; N, 10.34%. Calcd for $C_{24}H_{27}N_3O_2$: C, 74.01; H, 6.99; N, 10.79%. ^{1}H-NMR ($CDCl_3$) δ=1.5—2.0 (12H, m, $-(CH_2)_3\times 2$), 2.8—3.3 (8H, m, N-C<u>H</u>$_2\times$4), 7.14 (1H, s, H^3), 7.60 (2H, b, NH_2), 7.78 (2H, m, $H^{6,7}$), 8.42 (2H, m, $H^{5,8}$).

1-Amino-2,4-dimorpholinoanthraquinone (11): Mp 220—221 °C. UV_{max} 565 (ε 8400). Found: C, 67.34; H, 5.83; N, 10.50%. Calcd for $C_{22}H_{23}N_3O_4$: C, 67.16; H, 5.89; N, 10.68%. ^{1}H-NMR ($CDCl_3$) δ=2.9—3.4 (8H, m, N-C<u>H</u>$_2\times$4), 3.8—4.3 (8H, m, O-C<u>H</u>$_2\times$4), 7.16 (1H, s, H^3), 7.56 (2H, b, NH_2), 7.84 (2H, m, $H^{6,7}$), 8.41 (2H, m, $H^{5,8}$).

References

1) K. Yoshida, M. Matsuoka, Y. Yamashita, and T. Kitao, *Bull. Chem. Soc. Jpn.*, **53**, 2552 (1980).

2) From their UV spectra, it was considered that some of them should be 1-amino-2(or 4)-(alkylamino)anthraquinones.

3) *Beilstein*, **14**, 198.

4) T. Tokumitsu and T. Hayashi, *Yuki Gosei Kagaku Kyokai Shi*, **24**, 1060 (1966).

Amine Base-catalyzed H-D Exchange Reaction of 2,3,4-Trimethylthiazolium Iodide in Methanol-d_4

Yumihiko YANO,* Yoshiharu TAMURA, and Waichiro TAGAKI*,†

Department of Chemistry, Faculty of Engineering, Gunma University, Kiryu, Gunma 376

†*Department of Applied Chemistry, Faculty of Engineering, Osaka City University, Sugimoto-cho, Sumiyoshi-ku, Osaka 558*

(Received June 16, 1980)

Synopsis. The rates of amine base-catalyzed H-D exchange of 2-methyl hydrogens of 2,3,4-trimethylthiazolium iodide were measured in deuterated methanol by using following amines: α-picoline, imidazole, 2- and 4-aminopyridine. The results indicated that the reaction was subject to a general base catalysis. The solvent effect is also described.

The acyloin condensation catalyzed by thiazolium salts are known to involve multistep reaction pathways.[1] One crucial step of them is the ionization of initially formed 2-(α-hydroxyalkyl)thiazolium salt (**1**) to form so called "active aldehyde (**2**)" (Eq. 1).

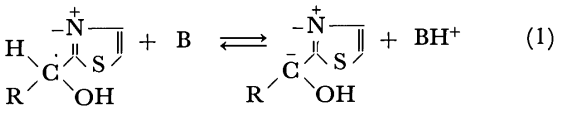

1 **2** (1)

Until recently, the mechanism of this step has been left uncertain whether it is subject to specific base or general base catalysis. Recently, the deprotonation from 2,3,4-trimethylthiazolium and 2-(α-hydroxyethyl)-thiazolium ions has been reported to occur by general base catalysis in aqueous buffer solution.[2,3] In contrast, we were unable to detect general base catalysis by an internal dimethylamino group of thiazolium salt in the benzoin condensation in methanol.[4] Therefore it was desired to examine base catalysis of externally added amines, also in methanol. In this paper, we describe the H-D exchange reaction of 2,3,4-trimethylthiazolium iodide (**3**) in deuterated methanol, catalyzed by several amines.

Results and Discussion

The amines employed were α-picoline, imidazole, 2- and 4-aminopyridine. The rate constants of H-D exchange were determined by following the relative peak area of 2-methyl protons and that of non-exchangeable 3- or 4-methyl protons by NMR. No decomposition products were detected under the present reaction conditions. The results are shown in Table 1. The base concentration was changed for imidazole. The rate constants are linearly dependent on the concentration of imidazole. From the slope, the apparent second-order rate constant for imidazole is calculated to be 6.10×10^{-3} M^{-1} s^{-1}. Since pK_a values of the bases in CD_3OD are not available, the estimated pK_a values in CH_3OH were employed. The estimation is based on the fact that the plots of pK_a values of ammonia and substituted anilines in H_2O against those in CH_3OH give a single straight line. Thus, the pK_a of desired amine in CH_3OH can be estimated from the pK_a in H_2O, as indicated in Table 1 for 2- and 4-aminopyridine. Plots of log k_{app} against the pK_a's of the bases gave a straight line [slope$=0.81(\gamma=0.995)$].[5] This may indicate that a general base catalysis is also important for the present H-D exchange reaction in addition to the lyate ion catalysis.

Table 1. The rate constants of H-D exchange reaction of 2,3,4-trimethylthiazolium iodide[a] in methanol-d_4 at 38 °C

Base	pK_a (in MeOH)	10^2[Base]/M	$10^4 k_{obsd}$/s^{-1}	$10^3 k_{app}$/M^{-1} s^{-1}[b]
α-Picoline	6.11[c]	40	0.967	0.242
2-Amino-pyridine	7.9[d]	10	4.03	4.03
Imidazole	8.10[e]	3.3	2.77	
		6.8	4.44	
		13.6	8.41	
		27.2	16.5	6.10
4-Amino-pyridine	9.9[d]	5.0	146	292

a) [Thiazolium salt]$=0.1$ M. b) Apparent second-order rate constants, $k_{app}=\frac{k_{obsd}}{[Base]}$. c) C.H. Rochster, *J. Chem. Soc., B*, **1967**, 33. d) Estimated values. e) M. Tanaka, "Acid and Base," Shoka-bo, Tokyo (1975), p. 46.

Table 2. The rate constants[a] in CD_3OD–D_2O at 38 °C

CD_3OD (%)	D[b]	$10^4 k_{obsd}$/s^{-1}	Rel rate
100	32.6	146	128
50	58.5	21.1	18
10	75.0	1.60	1.4
0	78.5	1.14[c]	1

a) 4-Aminopyridine (0.05 M) was used as a base. b) Dielectric constants in CH_3OH–H_2O system.[7] c) This is the extrapolated value.

In model reactions of thiamine catalysis, it has been shown that all kinetically significant steps proceed faster in ethanol than in water.[6] This suggests that in many thiamine pyrophosphate dependent enzymatic reactions, the catalysis is in large part to occur through the binding of the thiazolium portion of the coenzyme in a hydrophobic region of the protein. Therefore, more detailed solvent effects were also examined for the present exchange reaction, by changing the composition of D_2O in CD_3OD as shown in Table 2.

Regarding this solvent effect, it may be of interest to see a relationship between the dielectric constants and the composition of CH_3OH–H_2O mixture. Albright *et al.* reported that the dielectric constant increases linearly with the increase of water content.[7] As shown in Table 2, log k_{obsd} decreases linearly with the increase

of the apparent dielectric constants. Thus, less polar solvent is more favorable for the present H-D exchange reaction. This may be accounted for by an accepted view that the ionic structure of the reactant state is stabilized more in a polar solvent and the neutral zwitter ionic carbanion is stabilized more in a less polar solvent. This suggests that the enzyme-mediated reaction of thiamine occurs in a relatively nonpolar environment. The results of the above model reaction also support the occurrence of a general base catalysis for the carbanion formation at the α-carbon of 2-(α-hydroxyethyl)thiazolium ion, especially under hydrophobic conditions. Thus, it is tempting to speculate that aminopyrimidine moiety of thiamine would act as an internal base in step of the carbanion formation from 2-(α-hydroxyethyl)thiazolium ion. However, it should also be kept in mind that previous failure to observe internal base catalysis in benzoin condensation has been still left unanswered.

Experimental

NMR spectra were recorded on a Varian A-60 spectrometer.

Materials. Deuterium oxide (99.75%, Merck) and methanol-d_4 (99%, Merck) were used. 2- and 4-Aminopyridines were purified by recrystallization from diethyl ether–hexane, mp 58 °C (lit,[8] mp 58 °C) and mp 156—158 °C (lit,[9] mp 157 °C). Imidazole (Wako Pure Chemical Co.) was used without further purification. Imidazole hydrochloride was prepared from imidazole and HCl in EtOH. Purification was performed by recrystallization (MeOH–diethyl ether). α-Picoline was purified by distillation.

2,3,4-Trimethylthiazolium Iodide was prepared from 2,4-dimethylthiazole and methyl iodide. Mp 250 °C (EtOH), NMR (CD_3OD), δ 2.58 (3H, s), 2.98 (3H, s), 3.96 (3H, s), and 7.60 (1H, s). Found: C, 28.30; H, 3.97; N, 5.46%. Calcd for $C_6H_{10}INS$: C, 28.25; H, 3.95%; N, 5.48%.

Exchange Kinetics. The salt (5×10^{-2} mmol) was weighed accurately in NMR tube and 0.45 ml of CD_3OD was added. This was placed in the probe of the NMR spectrometer for 10 min. The reaction was initiated by adding 0.05 ml of the base solution by a microsyringe. 2-Methyl protons (2.98 ppm) were followed by integration as a function of time, relative to the 3- or 4-methyl protons, which was found not to be exchangeable under the present reaction conditions. The rate constants were calculated as described in the previous paper.[10]

References

1) R. Breslow, *J. Am. Chem. Soc.*, **80**, 3719 (1958); *Ann. N. Y. Acad. Sci.*, **98**, 445 (1962).

2) a) A. A. Gallo and H. Z. Sable, *J. Biol. Chem.*, **251**, 2564 (1976); b) J. A. Zoltewicz and S. Sridharan, *J. Org. Chem.*, **43**, 3785 (1978).

3) Y. Yano, Y. Tamura, Y. Hoshino, and W. Tagaki, *Bull. Chem. Soc. Jpn.*, **53**, 2340 (1980).

4) Y. Yano, Y. Tamura, and W. Tagaki, *Bull. Chem. Soc. Jpn.*, **53**, 740 (1980).

5) This is not the Brönsted β value. In separate experiments, the buffer concentration (imidazole–imidazole hydrochloride) was changed with a constant buffer ratio. The rate constants were linearly dependent on the concentration of free imidazole.

6) J. Crosby, R. Stone, and G. E. Lienhard, *J. Am. Chem. Soc.*, **92**, 2891 (1970); J. Crosby and G. E. Lienhard, *ibid.*, **92**, 5707 (1970).

7) L. J. Gosting and P. S. Albright, *J. Am. Chem. Soc.*, **68**, 1061 (1946).

8) "The Merck Index," ed by P. G. Stecher, Merck and Co., N. J. (1968), p. 485.

9) T. Ishii, *J. Pharm. Soc. Jpn.*, **72**, 1315 (1952).

10) Y. Yano, T. Okonogi, and W. Tagaki, *J. Org. Chem.*, **38**, 3919 (1973).